CLIMA 2022

EYE ON 2030

Towards digitalized, healthy, circular and energy efficient HVAC

REHVA 14th HVAC World Congress

22nd - 25th May, Rotterdam, The Netherlands

PROCEEDINGS

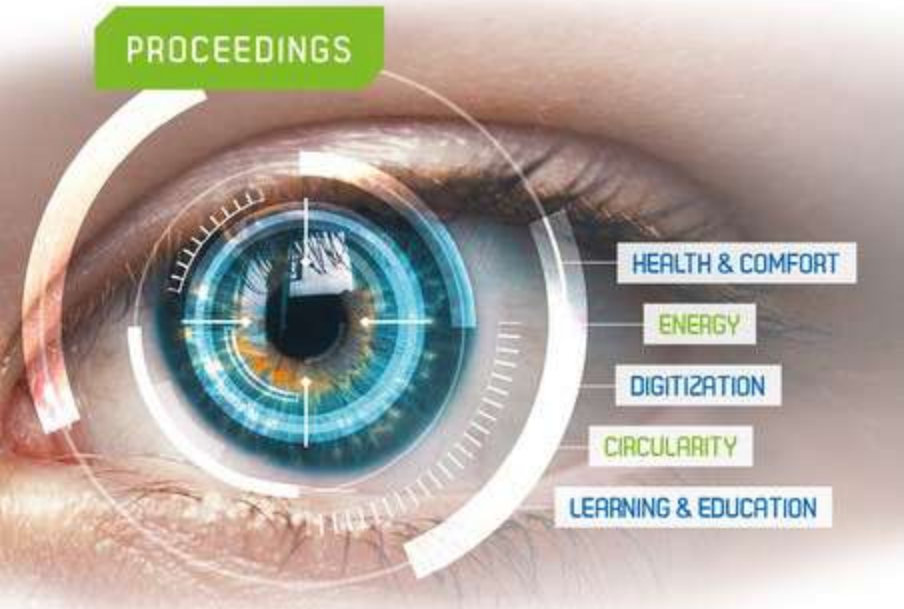

PROCEEDINGS.OPEN.TUDELFT.NL/CLIMA2022

TU Delft OPEN

Colophon

Proceedings CLIMA2022 | 14th REHVA HVAC World Congress, 22-25 May 2022, Rotterdam

Editors:
Laure Itard[1], Lada Hensen-Centnerová[2], Atze Boerstra[1], Philomena Bluyssen[1], Jan Hensen[2], Tillmann Klein[1], Marcel Loomans[2], Pieter Pauwels[2], Christian Struck[3], Martin Tenpierik[1], Bob Geldermans[4]

[1]Delft University of Technology (TU Delft), Faculty of Architecture and the Built Environment
[2] Eindhoven University of Technology (TU/e), Department of the Built Environment
[3] Saxion University of Applied Sciences, Research Group Sustainable Building Technology
[4]University of Antwerp, Faculty of Design Sciences

Keywords:
Advanced HVAC Systems; Indoor Environmental Quality; Indoor Infection Risks; Indoor Air Quality; Thermal Comfort; High Energy Performance Buildings; Circular Buildings; Building & HVAC Simulation models; Smart Buildings; Smart & Predictive Control; Intelligent Building Energy Management Systems; Zero-energy Buildings; Energy Transition; Energy Systems for Cities; HVAC Learning Communities; Digitization in Buildings; CLIMA2022; REHVA World Congress

Published by:
TU Delft OPEN Publishing | Delft University of Technology, The Netherlands

DOI: https://doi.org/10.34641/mg.33
ISBN: 978-94-6366-564-3

Copyright statement:

This work is licensed under a Creative Commons Attribution 4.0 International (CC BY 4.0) licence
© 2022 published by TU Delft OPEN on behalf of the editors & authors

Electronic version of this book is available at https://proceedings.open.tudelft.nl/clima2022

Cover design made by TVVL (www.tvvl.nl)
Copyright clearance made by the TU Delft Library copyright team

Disclaimer:
Every attempt has been made to ensure the correct source of images and other potentially copyrighted material was ascertained, and that all materials included in this book have been attributed and used according to their license. If you believe that a portion of the material infringes someone else's copyright, please contact Laure Itard (l.c.m.Itard@tudelft.nl).

TU Delft OPEN

Executive Scientific Committee

Chairs & Congress vice-presidents
Lada Hensen-Centnerová, *TU/e*
Laure Itard, *TUDelft*

Theme chairs
Philomena Bluyssen, *Health & Comfort, TUDelft*
Jan Hensen, *Energy, TU/e*
Tillmann Klein, *Circularity, TUDelft*
Pieter Pauwels, *Digitization, TU/e*
Christian Struck, *Learning & Education, Saxion University of Applied Sciences*

Theme co-chairs
Jan-Jaap Blum, *Energy, Alba Concepts, TVVL*
Annemarie Eijkelenboom, *Health & Comfort, EGM-Architecten*
Bob Geldermans*, Circularity, University of Antwerp*
Jan Kerdel, *Digitization, Kerdel Business Development*
Olaf Oosting, *Circularity, Valstar & Simonis, TVVL*

Organization
Atze Boerstra, *Congress President, TUDelft, BBA Binnenmilieu b.v.*
Froukje van Dijken, *Interactive Sessions, BBA Binnenmilieu b.v*
Marcel Loomans, *Programming, TU/e*
Martin Tenpierik, *Guidelines, TUDelft*

Peer review Statement

The editors of the proceedings warrant that 1) they adhere to TU Delft OPEN Policy on publishing integrity and good scientific publishing practices; 2) all papers have been subject to double blind review by at least 2 reviewers from an International Scientific Committee of 200 reviewers, administered by the editors; 3) Reviews were conducted by expert referees who were requested to provide unbiased comments aimed at improving the work.

Data Statement

The Executive Scientific Committee and the authors warrant to have made every reasonable effort to make the datasets (generated and/or analyzed during the research and described in these Proceedings) publicly available in recognized research data repositories.

REHVA & TVVL

CLIMA2022 is the 14th REHVA HVAC World Congress. REHVA is the Federation of European Heating, Ventilation and Air Conditioning associations and is an umbrella organization that represents over 120,000 HVAC designers, building services engineers, technicians and experts across 26 European Countries.
TVVL, the Dutch Society for Building Services and Technology, is the Dutch Member association of REHVA and has over 1000 personal members and 500 company members.

Congress Sponsors

REHVA, TVVL,

Delft University of Technology

Eindhoven University of Technology

Carrier HVAC Europe,

Daikin Europe, Georg Fisher, Oy Halton Group, Siemens Schweiz, Wij Techniek

Belimo Automation, De Nieman Groep, Velux, Eurovent Certita Certification, Priva Building Automation, Systemair, Smay

ACIN Instrumenten, Arçelik , BBA Binnenmilieu, Clockworks Analytics, Eko Instruments Europe, Grundfos Nederland, UTCB, Valstar Simonis

CONTENTS

1 Preface…… 6
2 Theme Health & Comfort…… 8
3 Theme Energy…… 984
4 Theme Circularity…… 2095
5 Theme Digitization…… 2141
6 Theme Learning & Education…… 2625

Preface

The 14th REHVA HVAC World Congress CLIMA2022 challenges advances in technologies for smart energy transition, digitization, circularity, health and well-being in buildings. How can we create circular buildings, fully heated, cooled and powered by renewable energy? How can we design human-centered indoor environments while mastering life-cycle costs? How can we also include their integration into infrastructure for energy, health, data and education? The congress is organized around 5 themes.

Theme 1: Health & Comfort

The achievement of health and comfort of people in the built environment, whether at home, at work, at school, or enjoying free time, is a complex subject that involves physics, behaviour, physiology, energy conservation, climate change, architecture, engineering and technology. The way people feel, experience and behave in their environment is related to the quality of their environment, described by the thermal, air, lighting and sound qualities, but also to the ability of the buildings and systems to respond to people's changing needs and preferences and the ability of people to respond to new buildings and systems. As shown by the outbreak of the COVID-19 pandemic, building systems have to provide a resilient environment not only on the long term (as climate change is evolving) but also in the short term (for example during a pandemic). CLIMA2022 challenges advances in intelligent interfaces and interaction between building, indoor climate systems and humans and seeks for new approaches to health & comfort in relation to low-energy buildings, energy-efficient retrofit and pandemics.

Theme 2: Energy

CLIMA2022 considers fossil-free energy use in the built environment of vital importance. Development of building services systems using heat, cold and electricity from renewable resources is accelerating, creating a need for flexibility and therefore for energy storage and inter-building energy exchanges. Following this there is also a need for innovative HVAC products and for performance optimization via improved design, operation and maintenance of the various integrated mechanical and electrical sub-systems. This typically includes reduction and balancing of the energy demands for heating, cooling and ventilation. While this is not exactly trivial in new buildings, it poses huge technical, social, economic and political challenges for existing buildings. Obviously the solutions will vary across countries. Exchanging experiences and learning from each other are the main objectives of CLIMA2022. When homes become small energy plants, or when large building complexes start to exchange energy, or when smart data companies control energy consumption, then the government, grid operators, energy companies, financial institutions and our sector need to respond.

Theme3: Digitization

CLIMA2022 considers digital solutions that encourage the energy transition in the built environment. Solutions are expected in the areas of (predictive) digital twinning, data-driven smart buildings, data management, and continuous commissioning. Nowadays digital solutions must be capable of handling a wide variety of HVAC systems and even be self-learning in detecting trends and process anomalies. Stand-alone (add-on) or embedded solutions are possible, but system architectures must include large scale deployment. Monitoring strategies are needed that also bridge the gap between Building Automation and Control Systems (BACS) and Building Information Modeling (BIM), and enable lifetime-cost control using system and building-contextual data. Large-scale monitoring of energy, comfort and life-cycle cost performances at an affordable cost level are needed in support of business cases and policies. Finally, the recent COVID-19 pandemic has triggered research on digital-focused design, monitoring and control of ventilation systems, in relation to overall comfort and health. This includes AI algorithms for fault detection and diagnosis, pattern recognition and anomaly detection.

Theme 4: Circularity

As a result of a growing population worldwide and the need for comfortable and healthy indoor environments, a massive building challenge lies ahead with the development of new building projects as well as the need to upgrade the existing building stock. To ensure a future-proof, sustainable economy for future generations, the reduction of the use of primary resources is essential. Circularity aims at closing and connecting material, water and energy flows while eliminating waste and reducing the demand for primary resources. The HVAC sector has a particularly high potential to contribute to circularity. Cycling energy, air and water flows is its core business. Components are frequently subject to upgrades and change. The retention and reuse of valuable materials and components offer business opportunities. However, the associated benefits have not yet translated into a large-scale market breakthrough. The sector needs a clear vision on how to achieve circularity goals, based on innovative strategies and an integrated approach with regard to circular design, product technology, business models, and management.

Theme 5. Learning & Education

The European targets around the energy transition in the built environment are huge. To realize the transition towards an energy-efficient, circular, digitized and healthy built environment, an upscaling of solutions is urgently needed. Dissemination of technical innovations and proven knowledge and approaches is needed. The building services sector is essential for realizing this transition: next to delivering the workforce for designing, placing and maintaining all energy and indoor climate equipment in buildings and neighborhoods, the sector also acts as innovator and is the axis between the construction, energy, IT and health sectors, integrating knowledge from these fields. Rapid changes in energy and HVAC engineering techniques and systems and in contracts and processes make it necessary to accelerate the uptake of knowledge in these areas. This means that continuous professional development of the current workforce and the education of new employees is necessary. There is a growing need for in-company, sectoral and cross-sectoral learning communities.

Enjoy these Proceedings!

The Editors

HEALTH & COMFORT

Simulation of the effect of windcatchers on air quality inside courtyards

Hayder.M. Khan [a], Gregory. F. Lane-Serff [b], Jonathan Dewsbury [b]

[a] Department of Civil and Architectural Engineering, Sultan Qaboos University, Muscat, Oman,123.

[b] School of Mechanical, Aerospace and Civil Engineering, the University of Manchester, Manchester, UK, M13 9PL.

Abstract. The courtyard is an essential traditional building element for sustainable construction in hot arid areas. However, there are some limitations in using it for future sustainable buildings. One of these is air quality, where previous research indicates that the courtyard provides thermal comfort to its residents by generating a microclimate that isolates the courtyard from external air, but this can reduce the building's ventilation potential. Traditional houses in the Middle East use windcatchers as a solution to this problem. This paper shows the results of a numerical simulation of a courtyard with windcatchers in traditional houses. The results indicate that windcatchers can provide enough fresh air for ventilation. It can also reduce the outdoor air temperature by using the thermal mass of the windcatcher wall and earth cooling, but will not provide low enough temperatures to maintain the microclimate, which suggests the need for more research in this field.

Keywords. Windcatcher, CFD, Traditional houses.
DOI: https://doi.org/10.34641/clima.2022.280

1. Background

The courtyard house is the traditional form of housing in the Middle East and has been subject to much research in thermal comfort and building energy. Much of this research concludes that a house with a deep courtyard will have a microclimate with a better thermal environment than outdoors for the house's residents [1–3]. However, the work of Hall et al [1] shows that a deep courtyard will have the highest concentration of pollution, as shown through practical measurement in a wind tunnel. Furthermore, traditional houses in the Middle East are usually built-in dense cities and are next to a narrow alleyway where air quality is unsatisfactory. In addition, the house's windows overlooking the outside are few or non-existent [4, 5]. Also, the courtyard is usually covered to reduce the solar irradiation on the courtyard as shown in the book of Reynolds [6] which further isolates the courtyard.

Thus, we need to increase the outdoor airflow toward the courtyard by using a windcatcher. The windcatcher (also called a wind tower, badgeers or malkafs) can be defined as a "*structure built onto the roofs of buildings with open vents at their head facing in the direction of the cooler prevailing wind. Air caught in the vent is channelled down through a shaft in the building into the room below which are cooled ventilated*" [7]. A windcatcher's function is inducing airflow and cooling the air passing through the windcatcher by passive means such as thermal mass and earth cooling (geothermal cooling). The shape of a windcatcher is shown in Figure (1) where the windcatchers in Baghdad (Iraq) are usually short and have a lower external surface area to reduce exposure to solar radiation. The dimensions of a windcatcher as given in references are shown in Table (1) where the height of a wind catcher is around the height of the external parapet with dimensions (L x D) as shown in Figure (1) for section equal to (1 x 0.4 m) and has a section with a rectangular shape, which is common in Baghdad [8]. The windcatchers in Figure (1) have only one opening directed towards the predominant wind [9].

Copyright ©2022 by the authors. This conference paper is published under a CC-BY-4.0 license.

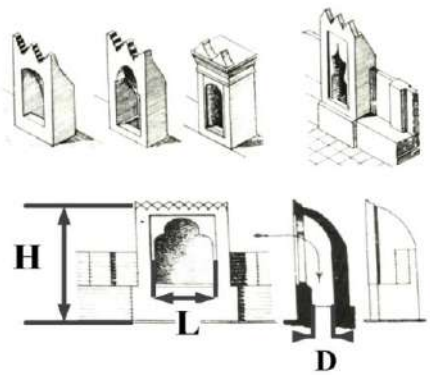

Fig 1- Various windcatcher designs from [4], the notation for dimensions is from Table (1)

Tab 1- Review for the dimensions of a windcatcher

Reference	Height (over the roof) (m)	Depth (D)(m)	Length(L) (m)
[9]	1.5 ~ 2.5		
[10]		0.2	1
[4]	To the highest point of an external parapet	0.15~0.2	0.5
[8]	2	0.3~0.4	1

Furthermore, to take advantage of earth cooling (geothermal cooling), the windcatcher guides the air from the top of the tower to the basement, so it is cooled by geothermal cooling and is then expelled into the courtyard. In this case, the ground is used as a heat sink, and it must have a sufficient difference in temperature between the earth and the ambient air above it.

This paper will focus on the windcatcher's role in enhancing the air quality inside the courtyard house and its effect on its thermal condition. We used Computational Fluid Dynamics (CFD) for the numerical simulation because it is less expensive than a full-scale model and gives satisfactory results and high-resolution details compared with other numerical models.

2. Methodology

In this paper, we simulated the pollutants through calculating the concentration of gas carbon dioxide (CO_2). The concentration of CO_2 gas was used as an indicator for the air quality because it is a by-product of the house residents' respiration. Furthermore, CO_2 gas cannot be filtered or absorbed (like an odour or emissions), and it will affect human health if its concentration exceeds a specific limit. The accepted limits for CO_2 in indoor air ranges are 3500-5000 ppm [11], also in the book of Awbi [12] explains that for cases that include an extended stay (i.e. several hours), a concentration less than 1000 ppm is preferable to avoid discomfort and headaches.

The concentration of CO_2 inside the courtyard was predicted using CFD software STAR CCM+. It models the flow in and around the courtyard, and the airflow was modelled as turbulent flow using Renolds Averaged Navier Stokes (RANS) model, with a two-layer realizable k-ε model. The radiation effect is included to show the impact of solar radiation. The air is treated as a non-participating medium in radiation transfer due to the air's low emissivity in dry weather. CFD is used to calculate the flow by dividing the domain into cells and solving the Navier-Stokes equations (conservation of momentum), the continuity equation (conservation of mass), the energy equation (conservation of energy); the initial and boundary conditions are listed in Table (2). Extra transport equations need to be solved for simulations that examine the air quality by finding the concentration of CO_2. Air quality was represented through the concentration of CO_2. It is emitted during the process of respiration. A source point is used to release gas in the same quantity as a human, with a density of occupants in the courtyard equal to 1 person /m^2 [13]. The software measures the CO_2 released during the simulation, not the ambient CO_2 (whose concentration depends on the area's pollution levels). All the drawings show the concentration of CO_2 release only. The computational model is set according the recommendations from guide book of Franke et al [14] and as shown in Figure (2). The geothermal cooling effect on the windcatcher was simulated by setting the soil temperature using the following equation from [15]

$$T(z,t) = T_{avg} + T_{amp}\exp(-z * G_c) * \cos(\frac{2\pi t}{365} - z\,G_c - 1.02\pi)$$

here z (m) is the depth below the surface, and t is time in days beginning from 1st Jan; T_{avg} is the average soil temperature (25 °C), T_{amp} is the annual amplitude of surface soil temperature (22 °C) and G_c is a coefficient that depends on the thermal diffusivity for the sand and the time cycle (0.83 (1/m). This equation will be used to determine the temperature in the soil which is in contact with the windcatcher. The computational domain is extended by only 1 m. This limited thickness was chosen because the heatwave inside soil tends to be stored in the ground surface rather than penetrating it. The simulations were done on three houses with different courtyard ratios between height to width (Aspect Ratio); the ratios used are AR4, AR2, AR 1.

The mesh used is an unstructured, polyhedral mesh with a prism layer and local refinements for a

specific region. The number of grids reaches over a million. The accuracy of the solution was compared with published works of other researchers, as shown in Figure (3) where the model has well predicted the velocity distribution within the courtyard.

Table 2-The boundaries and parameters of the simulation**.**

Walls, roof, floor	Brick with thermal conductivity = 0.69 W $K^{-1}m^{-1}$, specific heat = 840 J kg^{-1} K^{-1}, density= 1600 kg m-3, thickness =0.2 m, emissivity = 0.8 and reflectivity =0.2. All the external surfaces are insulated by extruded polystyrene with thermal conductivity = 0.032 W $K^{-1}m^{-1}$ and reflectivity =1.0
Initial conditions	Room air temperature =300 K, outside air temperature =313 K, Walls's temperature = 300 K
Boundary conditions	Wind speed at 10m from ground = 5 m s^{-1} , the air velocity, turbulent dissipation and kinetic energy for the boundaries of CFD domain. Velocity inlet and pressure outlet, are set using equation from [16]
Time step and total time	3 seconds and continues for 3600 s
Date and time	Summer solstice day 21 Jun 2012, 12 PM
Place of the simulation	Baghdad city, Latitude 33.3° and longitude 44.3°
Soil	$\rho = 1470(\mathrm{kg\ m^{-2}})$, $k = 1.7(\mathrm{W\ m^{-1}K^{-1}})$and $Cp = 1000(J\ kg^{-1}K^{-1})$ [17]

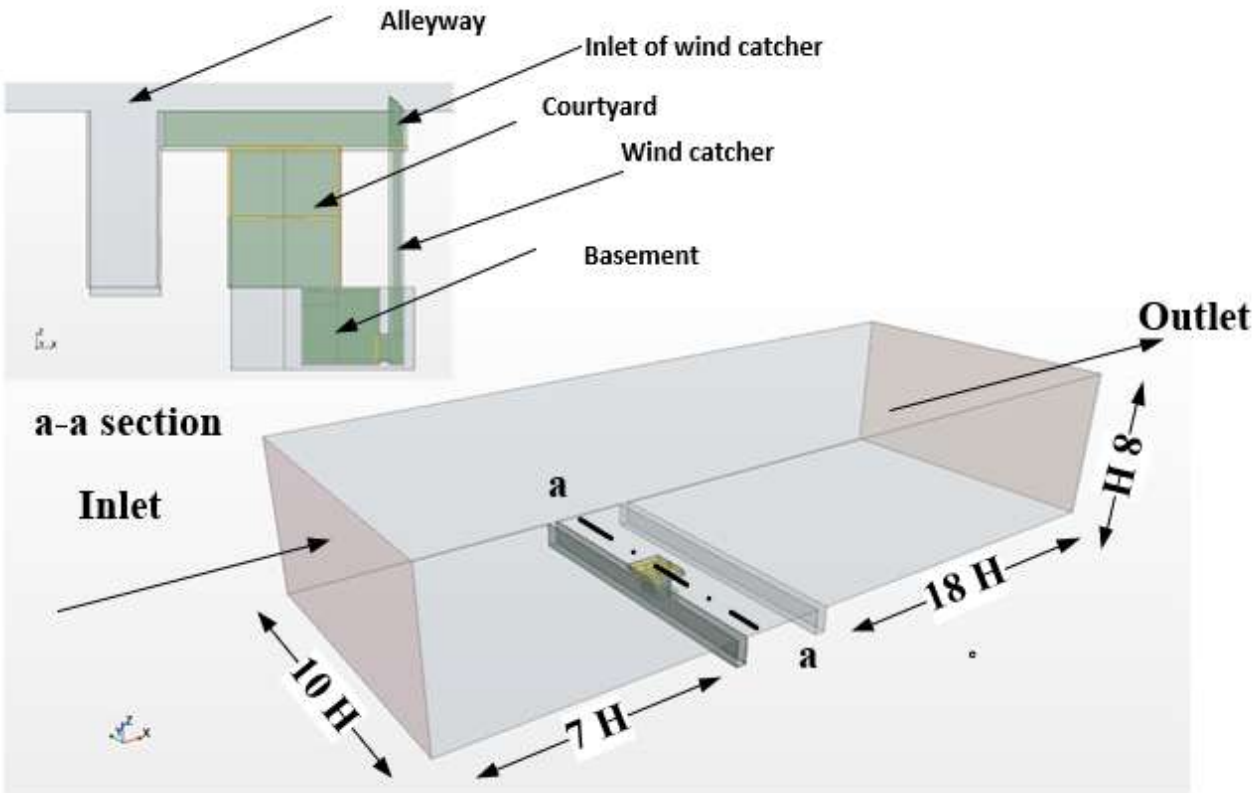

Fig 2-The computational model.

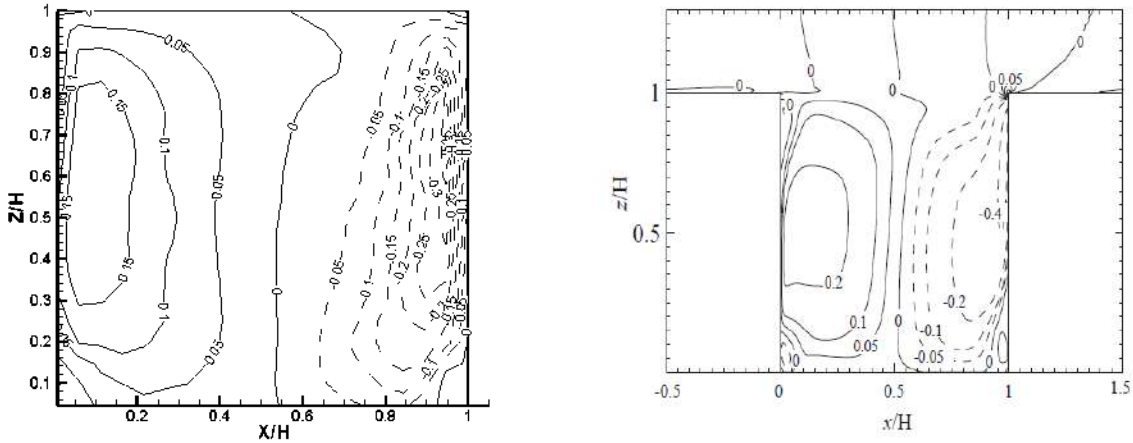

Courtyard with AR=1.0

Fig 3- The comparison for the results of spatial contours of the dimensionless mean streamwise velocity w/Uat 10 metres between the current research (left) and the results from work by **[18]** right (note dashed line is negative pressure).

3. Results

The results show the effect of courtyard isolation on the air quality, and simulations were done with CO_2 gas emitted to represent outputs of the process of respiration from several persons. The case chosen is for a courtyard without any opening and which is covered from the top.

Figure (4) shows how the average volume of CO_2 concentration in the ground level is escalated through time to be seven times above the acceptable limit (1000 ppm). The CO_2 concentrations in the first level are much lower than those in the ground level, suggesting that convection between the ground and first level is limited. The local concentration for CO_2 in two of the courtyards is shown in Figure (5). The concentration near the ground can reach even higher levels, especially with a narrow courtyard (*AR*4). This indicates that a number of people cannot inhabit the courtyard for a long time without an extra means of ventilation, especially given the arrangement of the windows.

The building is attached to other houses from three directions and overlooks a narrow alleyway, and this restricts the windows to only overlook the courtyard. Windcatcher can represent a short path from outdoor air at the top of the house to the courtyard, through the basement (Figure (6)).

A windcatcher provides fresh air to the courtyard and increases the connection between the courtyard levels. Figure (7), shows an increase in the level of CO_2 in the first level in comparison with cases without windcatcher and this is due to the moving of air with CO_2 from the ground to the first level. Where the windcatcher is capable of delivering fresh air through the basement with a flow rate equal to 1 m^3/s (for wind speed equal to 5 m/s) and the concentration of CO_2 in the basement is similar to the ambient air. The figure also shows that the levels of CO_2 are within acceptable limits and that they are stable.

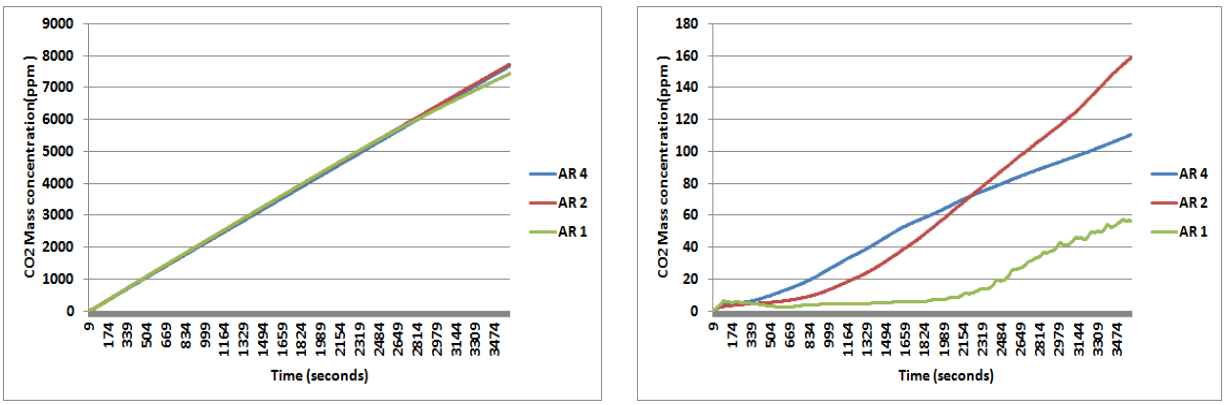

Ground Level First Level

Figure 4- The local concentration for CO_2 inside the courtyard.

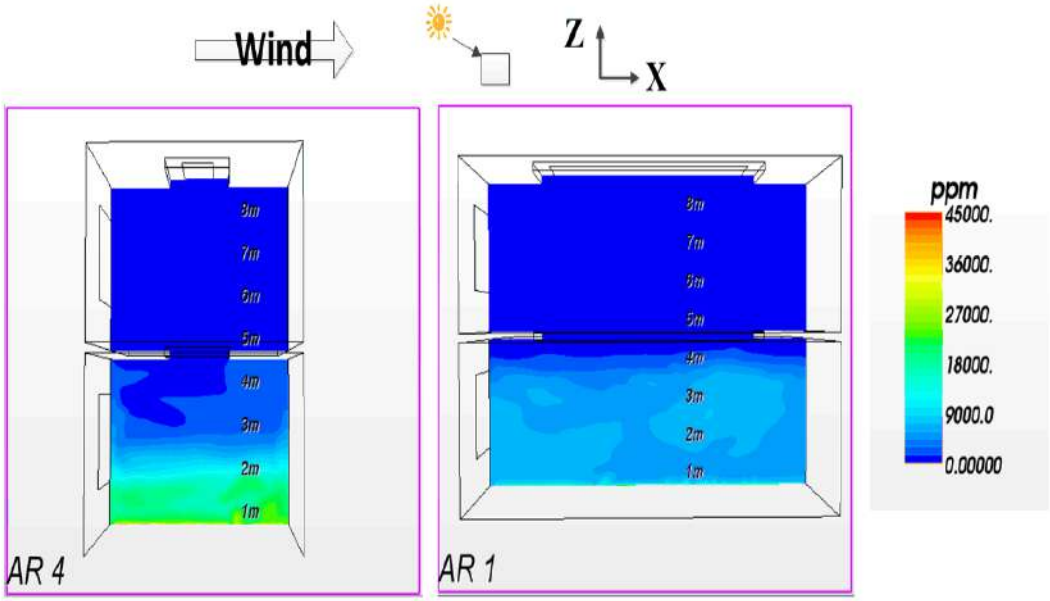

Figure 5- The local concentration for CO_2 inside the courtyard.

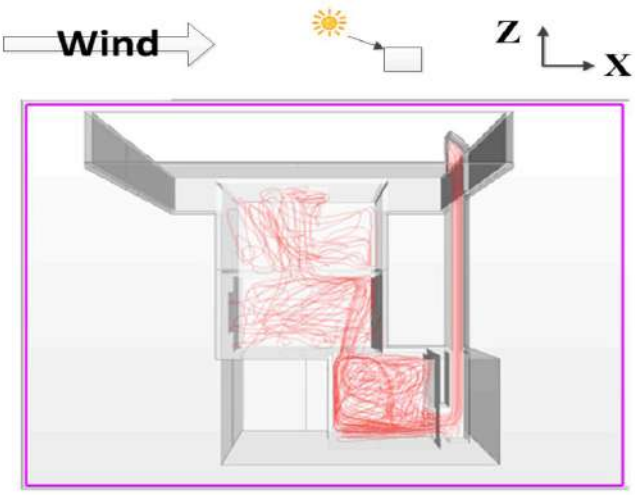

Figure 6- The airstream for a house with a windcatcher and a basement.

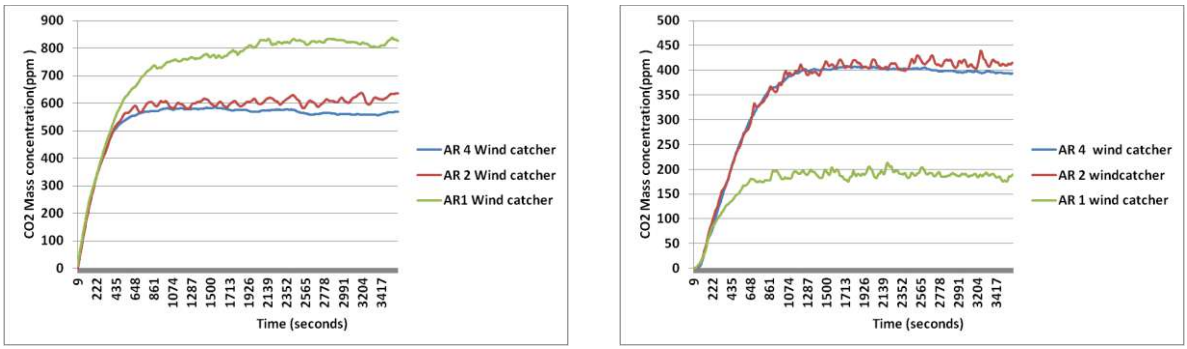

Ground Level First Level

Figure 7- Volume average with time for CO_2 inside the courtyard with a windcatcher.

Though there is clear enhancement in air quality, the windcatcher would reduce the thermal comfort by introducing the outdoor warm air to the courtyard, where the air temperature increases by two degrees in the case of using a windcatcher for an hour between 12 PM to 1 PM. However, the temperature in the courtyard, without a windcatcher, only increases by less than half-degree, as shown in Figure (8). This increase in courtyard temperature was even with air which had been cooled down by three to four degrees in the basement by earth cooling and with a thermal mass of the windcatcher, and this can explain why in traditional houses the windcatcher is usually closed in the afternoon and courtyard usage becomes less at that time, according to [19]. Other researchers such as [20] suggest using evaporative cooling to increase the windcatcher's cooling potential. However, using evaporative cooling in hot arid areas becomes limited due to water scarcity. More research is needed to use other passive cooling alternatives, such as a windcatcher with phase change materials to store the heat during the day and release it at night. However, we can achieve an acceptable indoor air quality by opening the access between the courtyard and basement (which is connected with the windcatcher). The access opening is happing when the concentration of CO_2 reaches a limit (800 pp,) and closes at 500 ppm. This process was controlled using Java code and the result for a number of hours during the afternoon is shown in Figure (9). The figure shows that opening the windcatcher for a few minutes is enough to reduce the CO_2 concentration in the basement, and this can also temporarily increase the air temperature by more than two degrees; however, it will subsequently return to the average temperature.

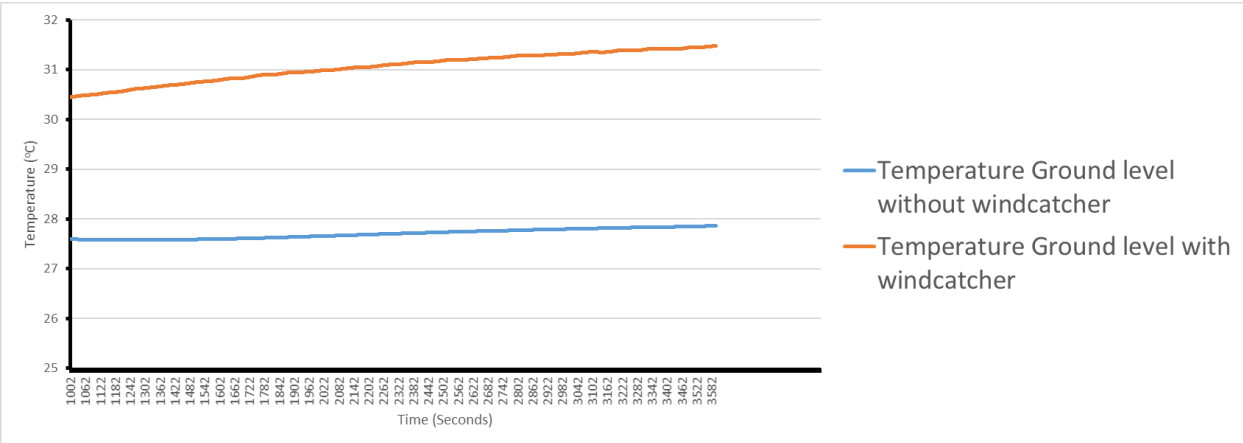

Figure 8-The increase in air temperature at ground level for cases with and without a windcatcher.

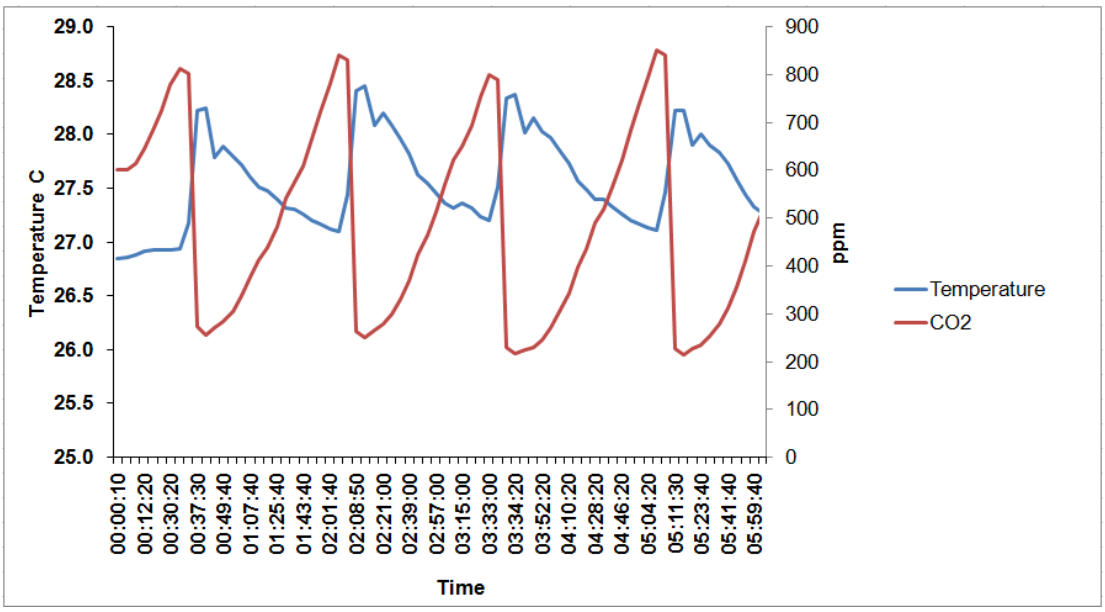

Figure 9- the air temperature with CO_2 concentration represented by ppm for a basement with attached wind catcher (the data are from a house with *AR2*)

4. Conclusion

This paper has discussed the use of CFD for numerical simulations of windcatchers attached to the courtyards of traditional houses. The courtyard is usually not well-ventilated. The simulations show that pollutions represented by CO_2 gas can reach many times the acceptable limit within a short period (one hour). It concentrates mainly on ground levels, where they will be away from the courtyard's opening and with weak convection between the levels. This is more apparent in cases with narrow and deep courtyards.

The traditional builder has found a solution for this problem using a windcatcher; a shaft connecting an air scoop at the roof to the basement and delivering fresh air from the roof levels to the ground levels. CFD simulates this building element, and we found it achieves an acceptable level of air quality but with some effect on the courtyard's microclimate. The thermal mass of the windcatcher and the earth cooling was used to reduce the temperature, but they were not enough to cool down the outdoor air to the level of thermal comfort. It requires more research to find alternatives to achieve enough pre-cooling for air to maintain thermal comfort in the house.

5. References

[1] Hall DJ, Walker S, Spanton AM. Dispersion from courtyards and other enclosed spaces. *Atmos Environ* 1999; 33: 1187–1203.

[2] ALVAREZ S, F S, J.L. M. Air flow pattern at courtyards. In: *PLEA '98*. Lisbon, Portugal: James & James Science Publishers Ltd, 1998, pp. 503–506.

[3] Dunham D. THE COURTYARD HOUSE AS A TEMPERATURE REGULATOR. *Ekistics* 1961; 11: 181–186.

[4] Warren J, Fethi I. *Traditional Houses in Baghdad*. Coach Publishing House, https://books.google.com.om/books?id=p_nVAAAAMAAJ (1982).

[5] Akbar JA. *Support for court-yard houses : Riyad, Saudi Arabia*. Thesis, Massachusetts Institute of Technology, https://dspace.mit.edu/handle/1721.1/15808 (1980, accessed 28 August 2019).

[6] Reynolds J. *Courtyards: aesthetic, social, and thermal delight*. John Wiley, 2002.

[7] Roaf S. The Wind Catchers of the Middle East. In: *Islamic Architecture and Urbanism*. Dammam: King Faisal University Press, 1983.

[8] Al-Haidary A. *The Baghdad house*. Damascus: Al-Mada P.C., 2008.

[9] Reuther O, Kabībū M. *البيت العراقي: في بغداد ومدن عراقية أخرى*. شركة دار الوراق للنشر المحدودة المملكة المتحدة, https://books.google.com.om/books?id=2d1vIgAACAAJ (2006).

[10] Jawadi MH. Model of house design responsive to hot-dry climate. 2011; 35: 171–183.

[11] ASHRAE. *2009 ASHRAE Handbook: Fundamentals*. American Society of Heating, Refrigeration and Air-Conditioning Engineers, 2009.

[12] Awbi HB. *Ventilation of Buildings*. Taylor & Francis, 2003.

[13] Littlefield D. *Metric Handbook*. Taylor & Francis, https://books.google.com.om/books?id=SnfLCoIswIUC (2012).

[14] Franke J, Hellsten A, Schlünzen H, et al. The COST 732 Best Practice Guideline for CFD simulation of flows in the urban environment: A summary. *Int J Environ Pollut* 2011; 44: 419–427.

[15] Abbas TR, Abbas RR. Variation of Soil Temperature with Time and Depth in Karbala Region. *J Kerbala Univ* 2009; 7: 170–175.

[16] Richards PJ, Hoxey RP. Appropriate boundary conditions for computational wind engineering models using the k-ϵ turbulence model. *J Wind Eng Ind Aerodyn* 1993; 46–47: 145–153.

[17] Bash AlMaliky S, Maliky A. Investigation of the Readiness of Ground Soils for the Installation of Ground Heat Exchange Systems in Baghdad City. *J Geogr Geol*; 3. Epub ahead of print 31 August 2011. DOI: 10.5539/jgg.v3n1p200.

[18] Li X-X, Liu C-H, Leung DYC. Development of a k–ε model for the determination of air exchange rates for street canyons. *Atmos Environ* 2005; 39: 7285–7296.

[19] Al-Azzawi SHA. *A Descriptive, Analytical and Comparative Study of Traditional Courtyard Houses and Modern Non-courtyard Houses in Baghdad: (in the Context of Urban Design in the Hot-dry Climates of the Sub-tropics)*, https://books.google.com.om/books?id=R2PU

jwEACAAJ (1984).

[20] Bahadori MN. An improved design of wind towers for natural ventilation and passive cooling. *Sol Energy* 1985; 35: 119–129.

Data Statement

Data sharing not applicable to this article as no datasets were generated or analysed during the current study.

Evaluation of "ventilation resilience" in mid-sized office buildings

Douaa Al Assaad [a], *Hilde Breesch* [a]

[a] Building Physics and Sustainable Design, Department of Civil Engineering, Ghent Technology Campus, KU Leuven, Ghent, Belgium

Abstract. In industrialized countries, people spend 80-90% of their times indoors, thus, providing them with clean spaces that preserve their wellbeing and productivity is critical. This can be done by delivering scheduled or demand-driven amounts of clean air that dilute the concentration of generated pollutants to adequate levels. However, the building and its ventilation system might be subjected to unpredictable shocks or disturbances (i.e., sudden failure in system components) that compromise the efficiency of the ventilation design, deteriorate indoor air quality and lead to acute exposure events. The ability of the building and its ventilation system to withstand and absorb the shock and maintain the IAQ design conditions is termed as "ventilation resilience". In this work, a typical open-plan office equipped with a balanced variable-air-volume mechanical ventilation system, is considered. Its ventilation resilience was assessed against power outage shocks and additional occupancy beyond expected peaks. Two types of pollutants were considered (exhaled CO_2 and formaldehyde from exhalation and office surfaces). To conduct this study, a Building simulation model was developed for the office and AHU in Modelica using Dymola. Results showed that for the considered shocks, no VOC violations were noted due to low emission rates. This was not the case for CO_2: For power outage shocks, the building/ventilation system were resilient for up to 15 minutes of shock and for 1 additional occupant in the space. Beyond those limits, the building/ventilation system are no longer resilient. For 60 minutes of power outage shock, CO_2 violations (>900 ppm) of 2 hours were noted with peaks of 1240 ppm while for 6 additional occupants, CO_2 violations of 2 hours were noted with peaks of 1150 ppm. A combined shock of these two cases caused 3 hours of violation and peak concentrations of 1747 ppm.

Keywords. Ventilation resilience, office buildings, indoor air quality, building simulation.
DOI: https://doi.org/10.34641/clima.2022.238

1. Introduction

In today's generations, humans are mostly 'indoor dwellers', conducting their daily activities within enclosed workspaces, located in air-tight building envelopes (1). These spaces are characterized by a chemically diverse and complex indoor air quality (IAQ), due to the presence of multiple pollutants of either gaseous nature (volatile organic compounds (VOCs) (2), CO_2(3), bio-effluents (4)) or aerosol particulate matter (5). Pollutants can infiltrate indoors from the outside environment though the mechanical ventilation system (6) or are generated indoors due to endogenous sources (i.e., occupants' respiratory activities) (7) or exogenous sources (i.e., office equipment (8)).

With the lack of proper source control or inefficient IAQ management techniques, contaminants' concentrations can quickly build-up at the breathing level, increasing occupants' exposure. Acute exposure trends are either short-term (few minutes to few hours) to peak pollutants' concentrations, or long-term (years to decades) to upper-limit concentrations (9). These trends can cause adverse health effects from a lower life quality due to illnesses, and diseases (e.g., infections, pulmonary infections), to a decrease in life years' expectancy or mortality (10). To mitigate acute exposures in buildings, it is important to implement smart, energy-friendly ventilation strategies (i.e., scheduled, demand-controlled) with well-designed air distribution systems (11). These ventilation strategies are usually designed based on well-known indoor/outdoor conditions (i.e., outdoor, and indoor pollution sources, emission rates, occupancy schedules, etc.). In a field study, Merema et al. (12) monitored the performance of a demand-controlled ventilation system in educational buildings and landscape offices, driven by IAQ measurements (i.e., CO_2). Their results showed that demanded-controlled ventilation was able to maintain good IAQ levels even at reduced airflow rates. Additionally, it reduced energy use compared to a

Copyright ©2022 by the authors. This conference paper is published under a CC-BY-4.0 license.

constant air volume system. Similar conclusions can be made for dynamic ventilation rates driven by pre-defined occupancy schedules (13).

Nevertheless, throughout a building's lifetime, there is a probability that indoor and outdoor conditions might shift unexpectedly from their pre-defined values (e.g., sudden increase in outdoor air pollution, unexpected rise in occupancy beyond expected peak)(6,14). Under such unprecedented and unavoidable circumstances – defined as "shocks" or "disturbances", the IAQ can shift quickly from its design conditions to unsatisfactory levels possibly causing instances of acute short-term exposures to harmful contaminants (e.g., VOCs, particles, CO_2). With the possible increase in shock occurrence (15), existing ventilation systems and strategies should be able to maintain good IAQ levels, not only under anticipated conditions but also in the case of extreme events. This characteristic is defined as "ventilation resilience". So far, in the literature, the resilience of current ventilation strategies in the non-residential sector has not been studied yet.

The aim of this work is to investigate the "ventilation resilience" of a scheduled ventilation strategy, a smart ventilation strategy considered as a simplified form of demand-controlled ventilation. supplying clean air to a multi-occupied office space. To reach this objective, a model of the office space and ventilation system will be developed using Modelica. The model will be simulated under normal operation (no shocks) and two types of shocks: a mechanical shock (power outage) shock and a spatial shock (increase in occupancy beyond peak values). The IAQ performance of the ventilation system will be assessed and compared between the cases.

2. Methodology

2.1 Office and system description

A typical single-zone medium-sized office based on the *medium office model of the commercial reference buildings* provided by the DOE, was considered (16,17). The office (16 m × 5.3 m × 2.7 m) location is in Brussels, Belgium (climate zone 4A) (18)(**Fig. 1**). The envelope consists of two external walls located on the south-west and north-eastern façades (U-value = 0.15 W/m^2.K) (passive house standard). Each wall has a triple-glazed window with a window to wall ratio of 0.48 and a U-value of 0.65 W/m^2.K). The rest of the boundaries (walls, floor, ceiling) were considered as internal or 'adiabatic' to represent a zone within a larger floor plan with other floors above and below. The envelope is air-tight with a rate of 0.3 h^{-1} (n-value). The space was conditioned by a mixing ventilation (MV) system, creating homogeneous conditions of temperature and IAQ (**Fig. 1**). The MV system is served by its own air handling unit (AHU) that supplies clean conditioned outdoor air to the space.

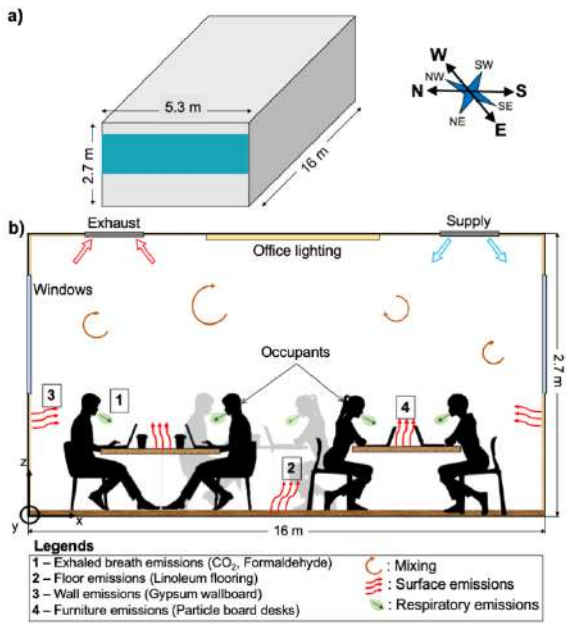

Fig. 1 – Schematic of occupied office space and associated sources of pollutants.

The ventilation rates Q (l/s) vary throughout the day depending on the occupancy schedule (**Fig. 2**). An occupant density of 0.07 person/m^2 was considered(20). According to ASHRAE standard 62.1 (21), Q (l/s) was determined by equation (1) below:

$$Q\ (t) = R_p P_z(t) + R_a A_z \qquad (1)$$

where R_p is the required airflow rate per person (7 l/s in the case of this study), P_z is the number of occupants at each time t (**Fig. 2**), R_a is the required outdoor airflow rate per unit area (0.3 l/s.m^2 recommended for offices) (21) and A_z(m^2) is the floor area.

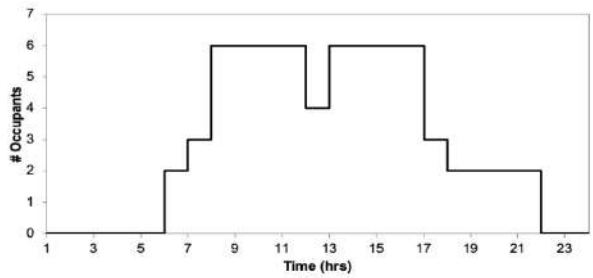

Fig. 2 – Occupancy schedule.

2.2 Pollution sources

Two sources of pollution were considered in the space. The first source is CO_2 resulting from occupants' exhalation flow (generation of 0.0048 l/s for adults at sedentary office activities, MET=1.2 (22)) (**Fig. 1**) and from outside air (400 ppm). According to a royal decree on indoor working conditions (21), a threshold of 900 ppm should be maintained for CO_2. Violations are allowed for 5% of the time over a maximum of 8 hours (24 minutes of violation). The second source of pollutants indoors is VOCs emissions, namely formaldehyde (CHOH), a common compound found in non-residential buildings (24). The sources of formaldehyde in the space are occupant exhalation (2.8 μg/h.person assuming an adult of 1.8 m high, 70 kg, body surface area of 1.89 m^2 and exhaled flow rate of 0.55 m^3/h)

(25), linoleum flooring (0.01384 mg/h.m^2), gypsum wallboard walls and ceiling (0.001235 mg/h.m^2) and particle board tables (75 μg/h.m^2) (26) (**Fig. 1**). For simplification purposes, constant emission rates were assumed from surfaces. Outdoor formaldehyde concentrations of 0.002 ppm were considered (27). An intervention value of 0.08 ppm was recommended by the Flemish indoor environment decree (28).

2.3 Shocks and disturbances

Shocks and disturbances are unpredictable events that occur outside or inside the building envelope and that can compromise IAQ by causing it to shift from its design conditions. During such events, if the ventilation or source control strategies can maintain IAQ within the recommended levels of violation, then the building and associated systems can be characterized as resilient. Note that to be characterized as shocks, the events must occur suddenly; in a way that the occupants or building owner have no time to take preventive measures. To test the resilience of the current case, two types of shocks were considered:

- **Shock I:** A power outage shock due to an interruption of electricity supply from the grid. Interruption can be due to extreme weather conditions (i.e., heat waves, severe storms)(29) or equipment damage (30). Information on current and future trends of sudden power outages (in Belgium) are scarce. Hence, there is at this moment no typical duration to consider for power outage shocks. Thus, in this work, a power outage shock varying from few minutes to 1 hour was considered to cover a wide range of possible scenarios. The shock was considered to occur during peak occupancy at 9:00 AM.
- **Shock II:** An occupancy shock due to additional occupants (i.e., additional sources of pollution: CO_2 and CHOH) entering the office. The number of additional occupants varied from 1 to 6 (e.g., each occupant in the office had a visitor). The additional occupants were considered to enter the office at the same time during peak occupancy at 9:00 AM and stay there for 1 hour.

The effect of combined shocks on IAQ will be also assessed for an extreme case (maximum power outage and additional occupants).

2.4 Office space model

To assess the effects of shocks on IAQ (i.e., contaminants' concentrations in the space) and the ventilation resilience, a model was developed for the office space and the AHU. The building simulation tool Dymola (31) with the integrated District Energy Assessment by Simulation (IDEAS) library, was used due to its ability to accurately simulate models that combine the building environment and its envelope, the heating ventilation and air conditioning system as well as advanced controllers (32). The model assumes uniform thermal and IAQ conditions in the space (single node).

Figure 3 below illustrates the model as seen in the Dymola environment with its different components (1 to 8). Components (1) and (2) constitute the inputs to the model which consist of the typical meteorological year (TMY) weather data for Brussels (dry bulb temperature, solar radiation) embedded in Dymola (33) as well as outdoor species' concentrations (CHOH, CO_2, water vapor). Components (3) and (4) constitute the AHU and associated control. The AHU consists of a supply/exhaust fans with the ventilation schedule (equation (1)), a heat recovery unit with an efficiency of 75%, as well as a simplified ideal cooler/heater that conditions (according to a PID control), the outdoor clean air to supply temperatures that provide comfortable indoor setpoints of 23±0.5°C in the space. Component (5) illustrates the building envelope (walls, ceiling, floor, windows), and the air zone model. Component (6) is the occupancy schedule (**Fig. 2**) with associated sensible and latent heat and CO_2 gains. It also includes office equipment gains (30 W/person: each occupant has is considered to have a laptop) and lighting gains (LED) which are only active in the case of occupancy. Note that in the power outage shock, the lights were considered to turn off as well. Component (7) constitutes the VOC (CHOH) emission rates to the space and component (8) is a set of CO_2, CHOH sensors to monitor IAQ in the office.

2.5 Simulation cases

The developed model will be simulated for a base case with no shock and for the case of the two shocks (**shock I** & **II**) and the combined shock (section 2.3). The simulations will be conducted for one representative day (August 1st). As the focus of this work is IAQ and ventilation resilience rather than thermal resilience, the choice of period of simulations is not critical to this study.

2.6 IAQ assessment

To assess ventilation resilience, and its effect on IAQ, the ppm.hours index will be used as seen in equation (2) below:

$$ppm.hours = \int C_s(t)dt \quad (2)$$

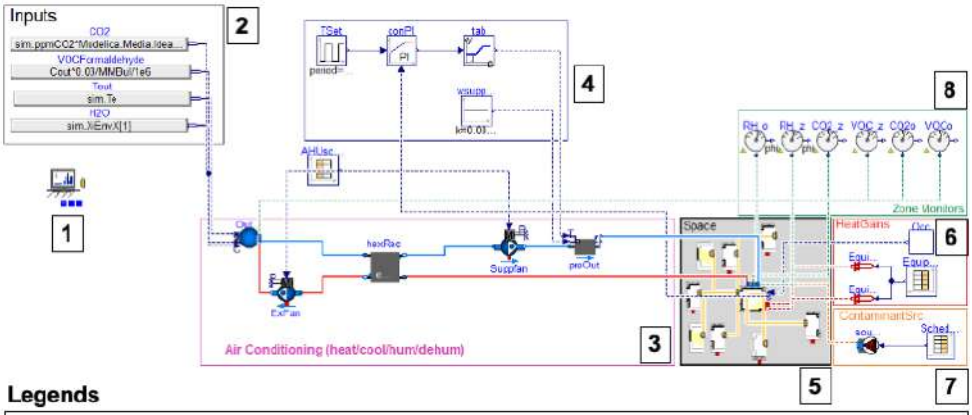

Legends

1 – Simulation and Information manager for handling time and climate data
2 – Model inputs: Weather data (T_{db}(°C), $\omega_a(kg/kg)$), outside pollutants (CO_2, Formaldehyde) concentrations (ppm)
3 – Simplified air handling unit (AHU) model
4 – AHU Control (Supply temperature, humidity)
5 – Office zone model (single-node lumped conditions) with envelope (walls, windows)
6 – Heat gains due to occupancy and office equipment (W) + CO_2 production due to exhalation
7 – Formaldehyde emission rates (kg/s) due to respiratory activities and surface emissions
8 – IAQ Sensors (RH(%), CO_2 (ppm), Formaldehyde (ppm))

Figure 3 Illustration of the office space model as seen in Dymola.

where C_s is the temporal variation of the concentration of either CO2 or CHOH. The ppm.hours will be calculated for concentrations above 900 ppm for CO2 and above 0.08 ppm for CHOH.

3. Results and discussion

3.1 Base Case (no shock)

For the base case scenario where no shocks occur (normal operation), the concentrations of CO_2 and CHOH are within the recommended guidelines (**Fig. 4, base case**). CO_2 concentrations increase during the day with increasing number of occupants and reach a maximum of 850 ppm at 12:00 during peak occupancy (<900 ppm threshold). Concentrations decrease during break hours (12:00-13:00) only to increase again when employees return to the office. After 17:00, concentrations start to decrease back to ambient concentrations (400 ppm) due to end of work shift and occupants gradually leaving the office.

As for CHOH concentrations, it is first noted that throughout the entire day, the threshold value (0.08 ppm) is never reached. Concentrations are higher during the early morning before occupancy starts. This is due to low ventilation rates and the constant CHOH surface emissions from flooring, walls and tables. When occupants start to come into the office, ventilation rates increase causing CHOH concentrations to decrease reaching minimum of 0.007 ppm at 12:00 when ventilation rates were the highest. This occurs despite the CHOH exhalation emissions from occupants. This is since the increment in CHOH concentration due to exhalation is not as significant as the dilution effect of the surface emissions by the increased amounts of clean air by the ventilation system. Subsequently, during break hours (12:00-13:00), an increase in CHOH concentration to 0.008 ppm is noted due to reduced ventilation rates. Concentrations reduce again during shift time at 13:00 and increase after the shift starts to end at 17:00 and occupants leave the office (**Fig. 4**). Note that during all times, the CHOH concentrations were well below the guideline value of 0.08 ppm.

3.2 Effect of Shocks

Figure 4 illustrates the temporal variation of CO_2 and CHOH concentrations from 6:00 – 17:00 for the base case scenario and the case of power outage shocks (5 min, 30 min and 60 min). **Figure 5** illustrates the temporal variation of CO_2 and CHOH concentrations from 6:00 – 17:00 for the base case scenario and the additional occupancy shocks (+2, +4 and +6) and **Figure 6** shows the cumulative ppm.hours for a) Power outage shock and b) Occupancy shock.

3.2.1 Shock I: Power outage

According to **Fig. 4**, when the power outage shock occurs, the ventilation system stops supplying air to the space. This causes CO_2 and CHOH concentrations to build up. For up to 10 minutes of power outage, the CO_2 concentrations remain below the guideline value of 900 ppm (ppm.hours = 0, **Fig. 6**). At 15 minutes of shock, concentrations increase beyond 900 ppm for 24 minutes reaching a maximum of 940 ppm (4% increase w.r.t threshold). Hence, for up to 15 minutes of power outage, the space remains within the allowed violation threshold of CO_2 (ppm.hours = 9.3, **Fig. 6**). However, for longer shocks (>15 minutes), violations become longer and more intense, deviating outside the allowed limits. For example, for a power outage of 60 minutes, concentrations remain above 900 ppm for 2 hours reaching a peak of 1240 ppm towards the end of the shock (27% increase w.r.t threshold) (**Fig. 4**) (ppm.hours = 381, **Fig. 6**). Such concentrations can cause sick building syndromes (lethargy, drowsiness, nausea, fatigue).

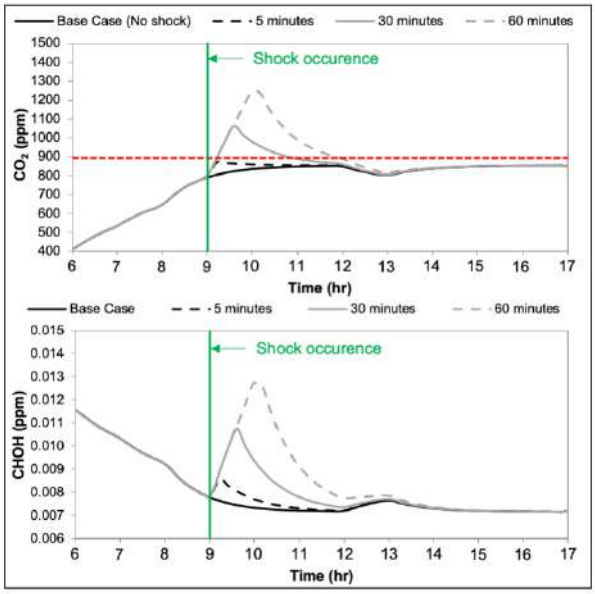

Fig. 4 – Illustration of the temporal variation of CO_2 and CHOH concentrations (ppm) for the base case and power outage shocks from 6:00 – 17:00.

As for CHOH, similarly during the power outage shocks, concentrations increase to reach peaks 0.013 ppm at 60 minutes. However, they remain way below the intervention value of 0.08 ppm and the thresholds of mild sensory irritation.

Consequently, during power outage shocks below 15 minutes, the building can be considered as resilient. However, this is not the case for longer shocks. The building is no longer resilient especially against high-emission pollutants like CO_2 (4% of exhaled air volume). Note that the building is always resilient against power outage shocks that cause peaks in VOC emissions. This is since VOC emission rates are much lower than CO_2 emission rates.

3.2.2 Shock II: Additional occupants

According to **Fig. 6**, for 1 additional occupant in the space, CO_2 concentrations remain well below 900 ppm (ppm.hours = 0). Therefore, an additional occupant is equivalent to [0-10] min power outage shock. For 2 additional occupants, concentrations increase beyond 900 ppm for 56 minutes reaching a peak of 940 ppm (4% increase w.r.t threshold) (**Fig. 5**) (ppm.hours = 17.5, **Fig. 6**). The violation duration and intensity increased with additional occupancy even long after the shock was over (additional occupants left the office after 1 hour). For example, for 6 additional occupants, violation duration increased to 2 hours with peak concentrations of 1150 ppm (ppm.hours = 251.5, **Fig. 6**).

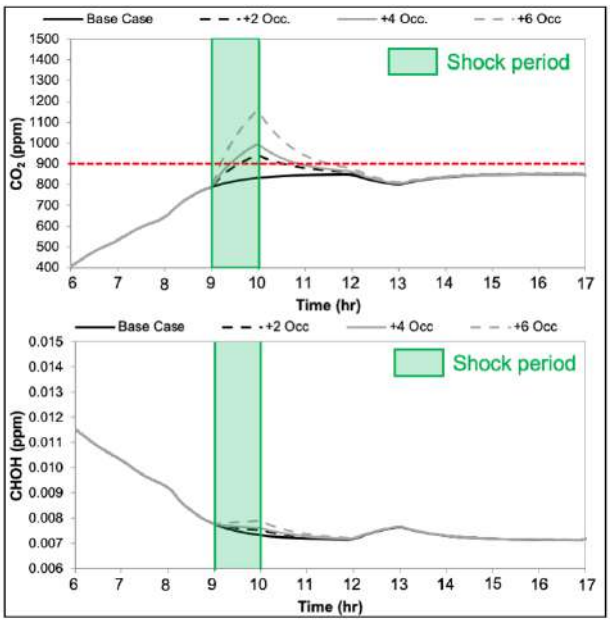

Fig. 5 – Illustration of the temporal variation of CO_2 and CHOH concentrations (ppm) for the base case and occupancy shocks from 6:00 – 17:00.

As for CHOH, concentrations increase during shocks, however much less than the power outage shock. For example, the peak concentration reached 0.0079 ppm during the maximum shock of 6 additional occupants. This is since the exhalation emission rates of CHOH from occupants are not that significant when compared to surface emissions especially from linoleum flooring (5 times lower), and particle board tables (27 times lower).

Consequently, the building remains resilient against CO_2 for 1 additional occupant. However, for more than 1 occupant, it is no longer resilient. Note that the building is always resilient against occupancy shocks that cause peaks in VOC emissions.

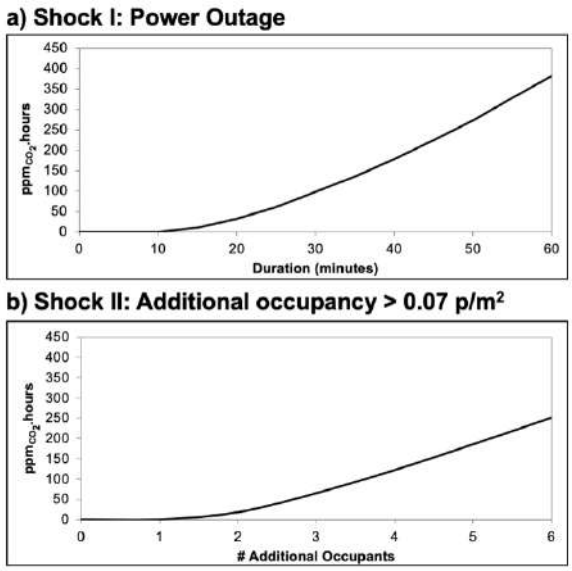

Fig. 6 – Illustration of CO_2 ppm.hours violations for the : a) Power outage and b) Occupancy shocks.

3.2.3 Combined shocks

For the case of combined power outage shock of 60 minutes and 6 additional occupants (extreme cases), as expected the building and system are not resilient. CO_2 violations lasted for 3 hours and concentrations reach peaks of 1747 ppm. The corresponding ppm.hours is 1061. No violations were noted for formaldehyde.

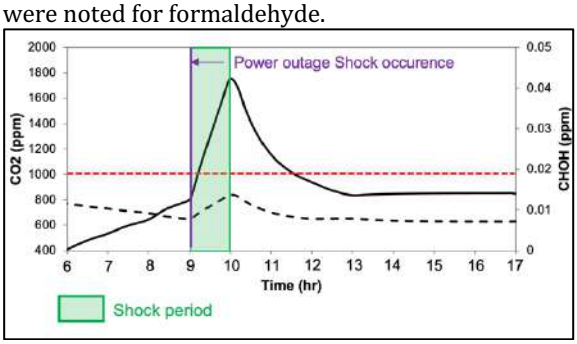

Fig. 7 – Illustration of the temporal variation of CO_2 and CHOH concentrations (ppm) for combined power outage (60 min) and additional occupancy (+6 occ) from 6:00 – 17:00.

4. Conclusion

In this work, the ventilation resilience of an office space equipped with scheduled ventilation was tested against power outage shocks and additional occupancy beyond expected peaks. Two types of pollutants were considered (exhaled CO_2 and formaldehyde from exhalation and surfaces to represent common indoor VOC). Simulation results showed that for power outage shocks, the building/ventilation system were resilient for up to 15 minutes of shock and for 1 additional occupant in the space. Beyond those limits, the building/ventilation system were no longer resilient (especially against high emission pollutants like CO_2) and additional interventions are needed (e.g., backup generator, battery-powered actuators to open windows, etc.). Therefore, as a standalone smart ventilation strategy, scheduled ventilation is not enough to withstand shocks of high intensity and duration.

Future work includes testing ventilation resilience against other types of shock (i.e., outdoor pollution), more critical contaminants like particulate matter, other types of spaces (i.e., educational buildings) and other ventilation strategies. Moreover, other aspects of ventilation resilience will be assessed and quantified along with shock impact (absorptivity and restorative capacity) as well as quantifying the shocks (degree of shock) by developing mathematical indicators.

5. Acknowledgement

The authors would like to acknowledge the Agency Innovation & Entrepreneurship (VLAIO), Flanders, Belgium, for funding the strategic basic research (SBO) Flux50 project "Towards Smart Ventilation in mid-sized buildings" to which this current work contributes.

6. References

1. Schweizer C, Edwards RD, Bayer-Oglesby L, Gauderman WJ, Ilacqua V, Juhani Jantunen M, et al. Indoor time–microenvironment–activity patterns in seven regions of Europe. Journal of Exposure Science & Environmental Epidemiology 2007 17:2
2. Mølhave L. Volatile Organic Compounds, Indoor Air Quality and Health. Indoor Air (4):357–76.
3. Du B, Tandoc MC, Mack ML, Siegel JA. Indoor CO2 concentrations and cognitive function: A critical review. Indoor Air;30(6):1067–82.
4. Zhang X, Wargocki P, Lian Z. Effects of Exposure to Carbon Dioxide and Human Bioeffluents on Cognitive Performance. Procedia Engineering. 2015 Jan 1;121:138–42.
5. Braniš M, Řezáčová P, Domasová M. The effect of outdoor air and indoor human activity on mass concentrations of PM10, PM2.5, and PM1 in a classroom. Environmental Research. 2005 Oct 1;99(2):143–9.
6. Stasiulaitiene I, Krugly E, Prasauskas T, Ciuzas D, Kliucininkas L, Kauneliene V, et al. Infiltration of outdoor combustion-generated pollutants to indoors due to various ventilation regimes: A case of a single-family energy efficient building. Building and Environment. 2019 Jun 15;157:235–41.
7. Fenske JD, Paulson SE. Human Breath Emissions of VOCs, Journal of the air & waste management association, 2011 49(5):594–8.
8. Destaillats H, Maddalena RL, Singer BC, Hodgson AT, McKone TE. Indoor pollutants emitted by office equipment: A review of reported data and information needs. Atmospheric Environment. 2008 Mar 1;42(7):1371–88.
9. Spengler JD, Sexton K. Indoor Air Pollution: A Public Health Perspective. Science. 1983 ;221(4605):9–17.
10. Smith KR, Mehta S. The burden of disease from indoor air pollution in developing countries: comparison of estimates. International Journal of Hygiene and Environmental Health. 2003 Jan 1;206(4–5):279–89.
11. Guyot G, Sherman MH, Walker IS. Smart ventilation energy and indoor air quality performance in residential buildings: A review. Energy and Buildings. 2018;165:416–30.
12. Merema B, Delwati M, Sourbron M, Breesch H. Demand controlled ventilation (DCV) in school and office buildings: Lessons learnt from case studies. Energy and Buildings. 2018 Aug 1;172:349–60.
13. Rackes A, Waring MS. Modeling impacts of dynamic ventilation strategies on indoor air quality of offices in six US cities. Building and Environment. 2013 ;60:243–53.
14. Shivakumar A, Welsch M, Taliotis C, Jakšić D, Baričević T, Howells M, et al. Valuing blackouts and lost leisure: Estimating electricity interruption costs for households across the European Union. Energy Research & Social Science. 2017;34:39–48.

15. Lopes JAP, Madureira AG, Matos M, Bessa RJ, Monteiro V, Afonso JL, et al. The future of power systems: Challenges, trends, and upcoming paradigms. Wiley Interdisciplinary Reviews: Energy and Environment 2020;9(3):e368.
16. Ko WH, Schiavon S, Brager G, Levitt B. Ventilation, thermal and luminous autonomy metrics for an integrated design process. Building and Environment. 2018 Nov 1;145:153–65.
17. Commercial Reference Buildings | Department of Energy.https://www.energy.gov/eere/buildings/commercial-reference-buildings
18. British Standards Institution. BS EN 16798-1:2019 Energy performance of buildings - Ventilation for buildings. British Standards Institution. 2019.
19. ANSIASHRAE Standard 62.1-2016: Ventilation for Acceptable IAQ
20. Persily A, de Jonge L. Carbon dioxide generation rates for building occupants. Indoor Air. 2017 Sep 1;27(5):868–79.
21. Nieuwe eisen luchtverversing werklokalen-aangepaste CO2-waarden https://werk.belgie.be/nl/themas/welzijn-op-het-werk/arbeidsplaatsen/basiseisen#toc_heading_3
22. Wolkoff P. Trends in Europe to reduce the indoor air pollution of VOCs. Indoor Air (2003)
23. Moser B, Bodrogi F, Eibl G, Lechner M, Rieder J, Lirk P. Mass spectrometric profile of exhaled breath—field study by PTR-MS. Respiratory Physiology & Neurobiology. 2005 Feb 1;145(2–3):295–300.
24. Won D;, Shaw CY, Won D. Investigation of building materials as VOC sources in indoor air;173–80.
25. Bruinen De Bruin Y, Koistinen K, Kephalopoulos S, Geiss O, Tirendi S, Kotzias D. Characterisation of urban inhalation exposures to benzene, formaldehyde and acetaldehyde in the European Union: Comparison of measured and modelled exposure data. Environmental Science and Pollution Research 2008 15(5):417–30.
26. Indoor Environment Decree - Decree of the Flemish Government of 11 June 2004 concerning measures to combat health risks due to pollution of the indoor environment - Care and Health https://www.health.belgium.be/sites/default/files/uploads/fields/fpshealth_theme_file/shc_8794_advice_iaq_.pdf
27. Añel JA, Fernández-González M, Labandeira X, López-Otero X, de la Torre L. Impact of Cold Waves and Heat Waves on the Energy Production Sector. Atmosphere 2017, Vol 8, Page 209
28. Vinogradov A, Vinogradova A, Bolshev V. Analysis of the quantity and causes of outages in LV/MV electric grids. CSEE Journal of Power and Energy Systems. 2020 Sep 1;6(3):537–42.
29. Dymola - Dassault Systèmes® https://www.3ds.com/products-services/catia/products/dymola/
30. Jorissen F, Reynders G, Baetens R, Picard D, Saelens D, Helsen L. Implementation and verification of the IDEAS building energy simulation library. 11(6):669–88.
31. TMY generator | EU Science Hub https://ec.europa.eu/jrc/en/PVGIS/tools/tmy

Individual control of the frequency of intermittent personalized ventilation and its effect on cross-contamination in an office space

Elvire Katramiz [a], Nesreen Ghaddar [a], Kamel Ghali [a]

[a] Department of Mechanical Engineering, Maroun Semaan Faculty of Engineering and Architecture, American University of Beirut, Beirut, Lebanon, efk06@mail.aub.edu, farah@aub.edu.lb, ka04@aub.edu.lb

Abstract. The transmission of respiratory diseases is influenced to a great extent by the ventilation in the space, mainly localized ventilation near the infection source (i.e. the infected person): One of the strategies that has been proven efficient in providing occupants with protection indoor are source control strategies. Personalized Ventilation (PV) is such strategy that delivers conditioned clean air towards the breathing zone of the user, thus providing protection while procuring acceptable levels of thermal comfort. In recent studies, PV applications varied the supplied cool clean air intermittently, mimicking natural outdoor conditions in order to enhance occupants' thermal comfort and improve energy efficiency. Such system operation is referred to as Intermittent PV (I-PV). The highly turbulent oscillatory jet may however promote the dispersion of contaminants, especially when the user is infected. Furthermore, the individual preferences of IPV frequency also affects the contaminants' transport. To the authors' knowledge, such effect has not been tackled in literature. Therefore, this work investigates the impact of individually controlling the frequency of an I-PV system on cross-contamination between occupants in an office space. An infected person is considered seated in a tandem (i.e. back-to-face) position with respect to a healthy person, located at a distance of 1.5 m. This seating configuration is usually the most critical when using PV. The contamination source is the breathing of the infected person. The IPV is considered to operate at an average flowrate of 10 l/s, with a minimum of 4 l/s. The IPV users are free to control the frequency of flow delivery in a range of [0.3 Hz – 1 Hz]. A validated computational fluid dynamics (CFD) model of an office space equipped with IPV and background mixing ventilation is used to assess the cross-contamination between the occupants. A comparison between IPV frequencies is conducted to highlight the influence of IPV frequency control on contaminants dispersion and the resulting exposure level of the healthy occupant.

Keywords. Intermittent Personalized Ventilation, Individual Control, Cross Contamination, Breathing, Indoor Air Quality.
DOI: https://doi.org/10.34641/clima.2022.192

1. Introduction

The transmission of airborne infectious diseases is a critical threat to human health, and needs to be thoroughly mitigated. One of the main sources of such transmissions in indoor spaces is the dispersion of infectious expelled airborne particles due to the respiratory activities of an infected person such as breathing (1). The transmission of such airborne contaminants is mainly influenced by room ventilation (2). Total volume ventilation strategies like mixing ventilation (MV) provide a uniform environment in the space – thus, they do not guarantee the simultaneous provision of high ventilation efficiency for each individual, nor do they provide people with their favoured thermal comfort level, failing thereby to meet the different preferences of all occupants. Therefore, many researchers have shed light on the concept of localized air-conditioning: personalized ventilation (PV). This system usually assists the traditional air conditioning systems, providing cool clean air to the breathing zone (BZ) of the occupant, which enhances the inhaled air quality and provides the desired thermal comfort levels (3). Recently, different studies considered a PV system supplying a dynamic airflow fluctuating between a minimum and a maximum at a characteristic frequency. This system is known as intermittent PV (I-PV). Such operation provides the user with enhanced thermal comfort states while ensuring good levels of breathable air quality (4, 5).

Copyright ©2022 by the authors. This conference paper is published under a CC-BY-4.0 license.

However, the I-PV system creates a non-uniform environment in the microclimate of occupants, resulting in an undesirable transport of exhaled contaminants when an infected person is using the I-PV, hence enhancing cross contamination between occupants. Furthermore, considering the individual preferences of I-PV users, the control of the frequency of the flow delivery and the resulting turbulence levels may affect the level of contaminants transport. The effect of the individual control of the I-PV frequency on the dispersion of exhaled contaminants, and resulting exposure of the healthy occupant has not been tackled yet in literature to the authors' knowledge. Thus, it is of value to investigate it thoroughly.

In this work, a desk-mounted I-PV system is assisting a MV system in conditioning a typical office space. The objective is to study the effect of frequency fluctuation of I-PV on the transport of particles generated by an infected user due to breathing. The infected person is considered seated in a tandem (i.e. back-to-face) position with respect to a healthy person, located at a distance of 1.5 m. The I-PV is operating at an average flowrate of 10 l/s, with a minimum of 4 l/s. The users are free to change the frequency of the I-PV flow in the range of 0.3-1 Hz. Note that such range is proven in literature to provide acceptable levels of thermal comfort for PV users (5). A 3-D computational fluid dynamics (CFD) model is used to simulate the potential contaminants' transport and assess the resulting exposure levels.

2. Research Methods

This work considered a two-workstation office space of dimensions 4.8 m (length) × 3.4 m (width) × 2.6 m (height), conditioned by a MV+I-PV system (**Fig. 1**). The MV system consisted of two supply diffusers at ceiling level and an exhaust diffuser at mid-upper part of the wall. The PV system consisted of computer-mounted panel supplying conditioned clean air horizontally towards the face of the occupants. The PV inlet was of diameter of 10 cm, located at a typical horizontal distance of 40 cm from the face (3, 6). Each ventilation system was served by its own air-handling unit. An infected person was located 1.5 m (7) in front of a healthy occupant, in a back-to-face seating configuration (i.e. tandem seating) (see **Fig. 1**). Both occupants were considered using I-PV that supplied a sinusoidal air flowrate $\dot{m}_{I-PV}$ with a minimum of 4 l/s and an average of 10 l/s at a specific frequency f_{I-PV}. The users had the freedom to change this frequency between 0.3 and 1 Hz. These limits consisted of the typical minimum and maximum operating frequency values that ensure thermal comfort as reported by previous I-PV studies (4, 5). Thus, nine simulations were considered as presented in **Tab. 1** where f_{I-PV_i} is the frequency adopted by the infected person and f_{I-PV_h} is the frequency preferred by the healthy person. Note that the delivered air temperature of the PV system was fixed at 23 °C (8). The contamination source was considered the nose-exhaled breath of the infected person. The periodic breathing pattern followed a sine curve consisting of 3 s of inhalation and 3 s of exhalation, with a maximum velocity of 1.33 m/s (9). The pulmonary ventilation was 8.4 l/min with a 10 times per minute breathing cycle, representing a normal person at low activity level (10). The nostrils were round openings with diameter of 12 mm, similar to those of healthy adults (11). The exhaled flow contained passive contaminants (i.e. species) (12). The temperature of the exhaled air was reported in literature to be around 32 °C (13).

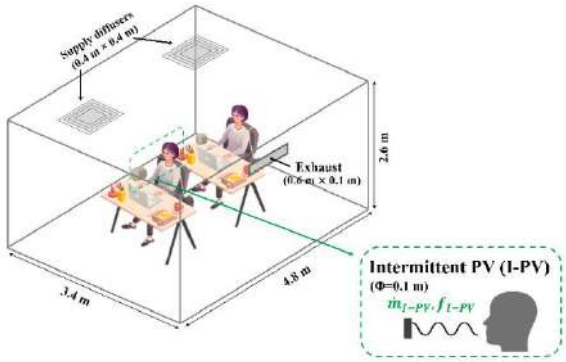

Fig. 1 - Schematic of the office space layout with the intermittent personalized ventilation.

Tab. 1 - Different considered operation scenarios.

f_{I-PV_i} (Hz)	f_{I-PV_h} (Hz)
	0.3
0.3	0.5
	1
	0.3
0.5	0.5
	1
	0.3
1	0.5
	1

3. Numerical Methods

A 3-D CFD model was developed in the study of Katramiz et al. (8) for the considered office space using the commercial software ANSYS Fluent (version 19.2) (14). The model was used to simulate the transport of the expelled contaminants produced by breathing upon the use of I-PV. **Fig. 2** presents the computational domain used in Fluent, with the proper mesh configuration that was selected to capture the flow physics, especially in front of the face of each occupant where a sphere of influence was created. After performing a grid independence test, the adopted mesh consisted of 1.5/2 cm face sizing on the manikin and walls respectively, resulting in 3,713,769 elements (8). Note that the

developed model was experimentally validated by Katramiz et al. (8), where good agreement was reported between the experimental and numerical results, with a maximum relative error of 7.5 % in terms of exposure level of the healthy occupant.

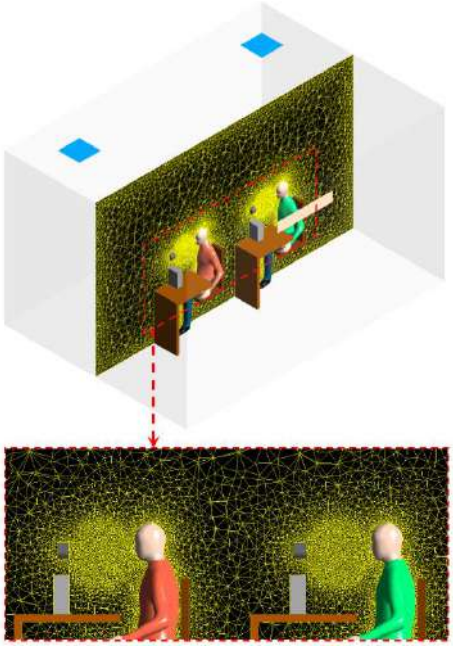

Fig. 2 - Illustration of the computational domain used in the CFD model and the mesh at the cross-sectional mid-plane (x = 0 m).

3.1 Airflow model

High turbulence levels were present in the space due to the I-PV flow and breathing flow nature; thus, the renormalization group (RNG) k-ε turbulence model with enhanced wall treatment and full buoyancy effects was used to solve for the turbulent kinetic energy k and its rate of dissipation ε in the continuum phase (i.e. room airflow). This model was employed in similar studies due to its relatively low computational cost, and robustness when describing indoor airflows with contaminant distribution (15). The Boussinesq approximation was used to account for the buoyancy effects. For the pressure equation, the "PRESTO!" scheme was used as it considers pressure gradients near boundaries (4, 5). The Pressure-Implicit with Splitting of Operators (PISO) algorithm was employed to couple the velocity and pressure fields due to its suitability for transient flows (4). The exhaled passive contaminants were considered as species, following the airstream and were thus simulated using the tracer gas "Nitrous oxide N_2O" - typically used in literature for exhaled infectious contaminants' representation (16, 17). The species' transport equation was therefore employed to solve for the tracer gas concentration in the space. The second order upwind scheme was employed to discretize the mass, momentum, energy, k, ε and turbulence equations. The solver was set to transient as the conditions in the space were time dependent; and a second order implicit time stepping was adopted with a time step of 0.05 s. It is noteworthy to mention that a solution is considered convergent when the scaled residuals reach 10^{-5} for all parameters except energy that should be less than 10^{-7}, with the mass and heat balance ensured in the space.

3.2 Boundary conditions

Adequate selection of the boundary conditions in the CFD model is crucial to obtain accurate results from the numerical simulations concerning airflow and concentration fields. The adopted boundary conditions for the different domain boundaries in the CFD model are presented in **Tab. 2**. Both supply diffusers of the MV system were set to a constant velocity inlet and the MV exhaust was assigned as a pressure outlet. Both PV inlet and nose of the infected person were set to a velocity inlet: the I-PV flow and the exhaled jet were each properly defined by a user-defined function (UDF). The rate of N_2O generation during exhalation was defined by a mass fraction of 5% (18, 19).

Tab. 2 - Boundary conditions of the CFD model.

Boundary condition	CFD boundary conditions
MV inlet	Velocity inlet - V = 0.3 m/s - T = 20 ^{0}C
MV exhaust	Pressure outlet - Zero-gauge pressure
I-PV inlet	Velocity inlet - UDF of I-PV air velocity - T = 23 ^{0}C
Nose opening	Velocity inlet - UDF of breathing velocity - T = 32 ^{0}C
Walls, Ceiling, thermal manikin, PC	Wall, constant heat flux: - Walls: 15 W/m^2 - Ceiling (lights): 10 W/m^2 - Thermal manikin: 39 W/m^2 - PC: 100 W

3.3 Cross-contamination assessment

The airflow field near the occupants resulting mainly from the I-PV flow may cause the transport of the exhaled contaminants by the infected person towards the healthy occupant sitting in the back, causing cross-contamination. The effect of the I-PV on cross-contamination between occupants is measured by the inhalation intake fraction (iF) index presented in equation (1): $\overline{C_{BZ}}$ is the average contaminants concentration at the BZ of the exposed (healthy) person when steady periodic conditions are reached (after around 20 mins from the initiation of the breathing, i.e. after 200 breathing cycles of the infected person), and $\overline{C_S}$ is the average concentration of exhaled contaminants at the source (i.e. at the nose of the infected person). Note that the BZ is defined as a spherical control volume having a diameter of 2 cm, located 2.5 cm away from the nose of the occupant (4).

$$iF = \frac{\overline{C_{BZ}}}{\overline{C_S}} \quad (1)$$

4. Results and discussion

This work investigates the effect of using I-PV at different frequencies on the dispersion of exhaled contaminants in the space and resulting cross-contamination towards a healthy person sitting at 1.5 m distance from the infected person in a tandem position. Thus, nine simulations considering the entire f_{I-PV} range were conducted (as presented in **Tab. 1**) in the aim of assessing the exposure level of the healthy occupant for all possible individual f_{I-PV} control scenarios. When accounting for the personal preferences of I-PV users, the efficiency of the I-PV in protecting the users from potential cross-contamination might differ with respect to the adopted frequency. This was assessed by obtaining the *iF* for all the possible operation scenarios as presented in **Tab. 3**.

With the increase in the frequency adopted by the infected person (f_{I-PV_i}), the turbulence level of the I-PV flow increases, aggravating thereby the transport of contaminants towards the back. This results in an increase in the exposure of the healthy person: for example, for a fixed f_{I-PV_h} of 0.5 Hz, the *iF* increased by 62.6 % when f_{I-PV_i} increased from 0.3 to 1 Hz (**Tab. 3**). On the other hand, when the frequency adopted by the healthy person (f_{I-PV_h}) increases from 0.3 Hz to 0.5 Hz, the concentration of contaminants at the BZ decreases due to the increased rate of clean air supply overcoming the increased turbulence and mixing effects as presented in **Fig. 3**: for a fixed f_{I-PV_i} of 1 Hz, the increase in f_{I-PV_h} from 0.3 to 0.5 Hz provided more clean air towards the BZ which increased the protection effect. However, further increasing f_{I-PV_h} from 0.5 to 1 Hz at a fixed f_{I-PV_i} caused a pronounced entrainment of contaminants into the supplied I-PV jet to the healthy person, which jeopardized the air quality at the BZ. This is seen in **Fig. 3 (b)** and **(c)** for a f_{I-PV_i} of 1 Hz. As a result, the *iF* increased from 11.97×10^{-4} at $f_{I-PV_h} = 0.5\ Hz$ to 20.08×10^{-4} at $f_{I-PV_h} = 1\ Hz$ (**Tab. 3**).

From the above-mentioned observations, and keeping in mind that one cannot know a priori who is infected and who is healthy in the space, it is clear that the increase in the frequency of I-PV for both all users is in general unfavourable, as it amplifies the cross-contamination between them due to the increased turbulence and entrainment of contaminants into the delivered PV jet. Thus, it is recommended to operate the I-PV in the lower range of [0.3 - 0.5] Hz for enhanced protection level.

It is noteworthy to mention that for the same space configuration (seating position, breathing pattern, PV system etc.), a **steady PV supply of 10 l/s** for both users resulted in an *iF* of approximately 11.5×10^{-4} (8). Comparing this value with the obtained results in **Tab. 3** for different I-PV frequencies, it is clear that the operation of PV at the recommended low frequency range of [0.3 - 0.5] Hz ensures lower exposure levels (i.e. lower iF values). Thus, operating the PV system in an intermittent way at low frequency range provides better protection against cross-contamination than operating it in a steady way.

Tab. 3 - Summary of *iF* for all the considered cases.

	iF ($\times 10^{-4}$)		
$f_{I-PV_i} \setminus f_{I-PV_h}$	**0.3 Hz**	**0.5 Hz**	**1 Hz**
0.3 Hz	7.55	7.36	8.21
0.5 Hz	8.72	8.44	11.65
1 Hz	12.21	11.97	20.08

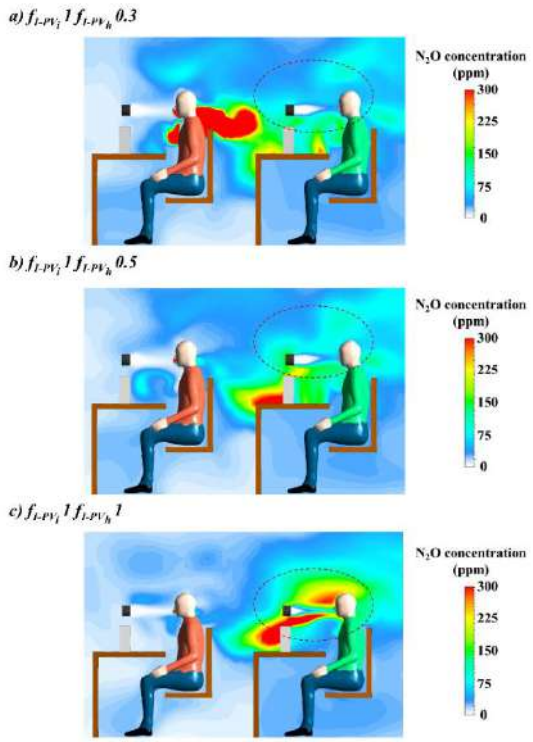

Fig. 3 - N_2O concentration contours at the cross-sectional mid-plane during highest exposure levels for the cases of: a) f_{I-PV_i}**1** f_{I-PV_h}**0.3**, b) f_{I-PV_i}**1** f_{I-PV_h}**0.5** and c) f_{I-PV_i}**1** f_{I-PV_h}**1**.

5. Conclusions

This work studied the effect of individually controlling the frequency of the I-PV flow on the dispersion of exhaled contaminants in the space and the resulting cross-contamination. A two-workstation office space was considered to be occupied by one healthy occupant and another infected occupant contaminating the space via nose breathing. A validated 3-D CFD model was thus used to simulate the different f_{I-PV} operation scenarios. Results showed that when considering cross-contamination, the increase in the frequency of I-PV for users is generally undesirable, as it increases the

turbulence and entrainment of contaminants into the delivered jet, which puts the healthy occupant at increased risk of exposure. It is thus recommended to operate the I-PV in the lower range of [0.3 - 0.5] Hz for enhanced protection level.

6. Limitations and Future Work

This work highlighted the effect of fluctuation the frequency of the I-PV flow on the potential cross-contamination in a two-workstation office where one of the occupants was infected. The latter was considered breathing from the nose. Furthermore, typical office settings were considered: a MV background ventilation, a common PV air terminal device (computer-mounted panel of 10 cm diameter (4)), a tandem seating layout, a typical distance of 1.5 m between occupants (7), and occupants' head always facing the PV air terminal device outlet. Such configurations are not fixed in real-life scenarios, and changing any of these settings may affect the dispersion of contaminants and the resultant cross-contamination. This will be a topic of future investigations.

7. Acknowledgement

The authors would like to acknowledge the financial support of the Munib and Angela Masri Institute of Energy and Natural Resources at the American University of Beirut grant award. In addition, the American University of Beirut PhD scholarship to Ms. Katramiz is highly acknowledged.

8. References

1. He Q, Niu J, Gao N, Zhu T, Wu J. CFD study of exhaled droplet transmission between occupants under different ventilation strategies in a typical office room. Building and Environment. 2011;46(2):397-408.
2. Qian H, Zheng X. Ventilation control for airborne transmission of human exhaled bio-aerosols in buildings. Journal of Thoracic Disease. 2018:S2295-S304.
3. Melikov AK. Personalized ventilation. Indoor air. 2004;14:157-67.
4. Katramiz E, Al Assaad D, Ghaddar N, Ghali K. The effect of human breathing on the effectiveness of intermittent personalized ventilation coupled with mixing ventilation. Building and Environment. 2020:106755.
5. Al Assaad D, Ghali K, Ghaddar N, Habchi C. Mixing ventilation coupled with personalized sinusoidal ventilation: Optimal frequency and flow rate for acceptable air quality. Energy and Buildings. 2017;154:569-80.
6. Melikov AK, Cermak R, Majer M. Personalized ventilation: evaluation of different air terminal devices. Energy and Buildings. 2002;34(8):829-36.
7. Xiaoping L, Jianlei N, Naiping G. Spatial distribution of human respiratory droplet residuals and exposure risk for the co-occupant under different ventilation methods. HVAC&R Research. 2011;17(4):432-45.
8. Katramiz E, Ghaddar N, Ghali K, Al-Assaad D, Ghani S. Effect of individually controlled personalized ventilation on cross-contamination due to respiratory activities. Building and Environment. 2021:107719.
9. Bulinska A, Bulinski Z. A CFD analysis of different human breathing models and its influence on spatial distribution of indoor air parameters. Computer Assisted Methods in Engineering and Science. 2015;22:213-27.
10. Junjing Y, Sekhar C, Cheong D, Raphael B. Performance evaluation of an integrated Personalized Ventilation–Personalized Exhaust system in conjunction with two background ventilation systems. Building and Environment. 2014;78:103-10.
11. Grymer LF, Hilberg O, Pedersen O, Rasmussen T. Acoustic rhinometry: values from adults with subjective normal nasal patency. Rhinology. 1991;29(1):35-47.
12. Villafruela JM, Olmedo I, Ruiz de Adana M, Méndez C, Nielsen PV. CFD analysis of the human exhalation flow using different boundary conditions and ventilation strategies. Building and Environment. 2013;62:191-200.
13. Bjørn E. Simulation of human respiration with breathing thermal manikin: Department of Building Technology and Structural Engineering, Aalborg University; 2000.
14. Fluent A. ANSYS Fluent Software - CFD simulation [Available from: https://www.ansys.com/products/fluids/ansys-fluent.
15. Li X, Niu J, Gao N. Co-occupant's exposure to exhaled pollutants with two types of personalized ventilation strategies under mixing and displacement ventilation systems. Indoor Air. 2013;23(2):162-71.
16. Cermak R, Melikov AK. Protection of occupants from exhaled infectious agents and floor material emissions in rooms with personalized and underfloor ventilation. Hvac&R Research. 2007;13(1):23-38.
17. Bjørn E, Nielsen PV. Dispersal of exhaled air and personal exposure in displacement ventilated rooms. Indoor air. 2002;12(3):147-64.
18. Gao N, Niu J, Morawska L, editors. Distribution of respiratory droplets in enclosed environments under different air distribution methods. Building simulation; 2008: Springer.
19. Shen C, Gao N, Wang T. CFD study on the transmission of indoor pollutants under personalized ventilation. Building and Environment. 2013;63:69-78.

Data Statement

The datasets generated during and/or analysed during the current study are not available because they are contained within the article.

Carbon capture from indoor air as an alternative ventilation technique

Jean Paul Harrouz[a], Kamel Ghali[b], Mohamad Hmade[c], Nesreen Ghaddar[d]

[a] Department of Mechanical Engineering, Faculty of Engineering and Architecture, American University of Beirut, Beirut, Lebanon, jeh15@mail.aub.edu

[b] Department of Mechanical Engineering, Faculty of Engineering and Architecture, American University of Beirut, Beirut, Lebanon, ka04@aub.edu.lb

[c] Department of Chemistry, Faculty of Arts and Sciences, American University of Beirut, Beirut, Lebanon, mh210@aub.edu.lb

[d] Department of Mechanical Engineering, Faculty of Engineering and Architecture, American University of Beirut, Beirut, Lebanon, farah@aub.edu.lb

Abstract. A polluted indoor space is a serious problem for the occupants especially for office workers who require high attentiveness levels. Indoor pollutants, especially carbon dioxide (CO_2), reduce the workers performance by increasing sickness risk and impairing cognitive abilities needed to make informed decisions. Typically, indoor air quality is improved by diluting indoor contaminants with fresh outdoor air. However, the outdoor air should be dehumidified and cooled before it is entrained into the office, especially in hot and humid climates. Nonetheless, this solution is energy intensive since conventional systems use vapor compression-based air-conditioning. This increases the building electricity consumption as well as its carbon footprint. To mitigate the danger of global warming emerging from the increased carbon emissions, sustainable ventilation techniques must be conceived. The use of the recirculated indoor air, characterized by lower temperature and humidity levels than the outdoor air, could reduce the ventilation load. However, the indoor air suffers from increased CO_2 levels generated by the occupant. To overcome this problem, adsorption-based CO_2 removal from the room air can be a good solution. Recently, this system has become more promising due to the emerging of new generation of solid adsorbents, the metal-organic frameworks (MOF). They can be produced to exhibit high capacity and affinity towards carbon dioxide and can be regenerated at low temperature energy such as solar and waste energy. CO_2 capture by adsorption reduces the ventilation load by reducing the outdoor air requirement to modest levels needed to maintain healthy levels of VOCs and O_2. A sustainable cooling system is developed using MOF-packed adsorption beds for CO_2 capture to treat the indoor air and resupply it to the space. A numerical model simulating the heat and mass transfer in the adsorbent bed is developed and used to size the adsorption system for a case study of a typical office in the hot and humid climate of Beirut, Lebanon. The proposed ventilation system reduced the outdoor air requirements and ventilation load by 72.6 % and 36 %, respectively during the peak load month of August.

Keywords. Carbon capture, sustainable ventilation system, metal organic frameworks, indoor air quality.
DOI: https://doi.org/10.34641/clima.2022.49

1. Introduction

Concerns about acceptable indoor air quality (IAQ) in the workplace environment are rapidly increasing [1]. This is due to the IAQ's direct effect on the workers' well-being and their decision-making abilities [2, 3]. A healthy environment is thus provided by diluting air contaminants level below a certain threshold [4, 5]. Although not a direct contaminant, high CO_2 concentration leads to dizziness and fatigue sensation. Similarly, high indoor relative humidity (RH) levels cause mould growth [6] and affect the thermal comfort perceived by the occupants [7]. Moreover, indoor spaces are typically characterized by high concentrations of VOCs, such as formaldehydes that are generated

Copyright ©2022 by the authors. This conference paper is published under a CC-BY-4.0 license.

from furniture and surface finishes among others [8, 9]. Outdoor air is used to dilute these contaminants; however, it requires excessive dehumidification and cooling, especially in hot and humid climates [10]. Conventionally, such air-conditioning has been achieved using vapor compression-based cooling systems, which run on high amount of electricity [11]. Subsequently, ventilation and air-conditioning systems consumes more than half of the building's electrical energy [12]. Since more than 80 % of electricity is produced from fossil fuels [13], there is pressing need to pursue more sustainable ventilation techniques. This is important to move towards a more productive workplace while also limiting the building's carbon footprint.

A prominent solution is the use of indoor recirculated air with adsorption-based CO_2 treatment techniques [10, 14]. Using adsorbent materials, excess CO_2 is removed from the room air before it is resupplied to the space [15]. The saturated adsorbent is then regenerated by increasing its temperature to the desorption temperature [16]. Conventional adsorbents such as zeolites suffers from low capacity for CO_2 at the dilute levels required in indoor spaces (<1,000 ppm), which is further degraded in presence of water vapor [17]. Amine-functionalized adsorbents are insensitive to water presence and have high capacities for dilute CO_2; however, they require high regeneration energy to desorb the chemically bonded CO_2 [18, 19]. The limitations of these conventional sorbents can be overcome by using the metal organic framework (MOF), a new generation of porous material [20, 21]. MOF are synthesized from metal ions clusters connected using organic linkers, called ligands [22]. With the appropriate choice of the metal ions and ligands, MOF can be produced to exhibit the required properties for efficient CO_2 treatment of the return air [18]. Such properties include high capacity and affinity for CO_2 at dilute levels, low H_2O selectivity over CO_2 and low regeneration temperature and energy to enable the use of low-grade thermal energy [23, 24]. Nonetheless, the use of such advanced materials is currently hindered by its high investment cost. It is important thus for the selected MOFs to be commercially available at economic prices. MOF-74- Mg is therefore a suitable candidate due to its low price and regeneration temperature and good capacity for dilute CO_2 in dry conditions. It can be used in conjunction with a low-price, and low regeneration temperature desiccant, such as silica gel, to remove the competition with H_2O present in the return air [25].

A ventilation system is proposed that incorporates desiccant and MOF adsorbents for the treatment of the return air through a sequential removal of excess water vapor and CO_2. This system can reduce the outdoor air requirements to minimal levels needed to maintain acceptable indoor VOCs levels as well as replenish the consumed O_2 by the occupants. Therefore, it is important to evaluate the performance of this proposed system in the reduction of the vapor compression cooling system' s outdoor air intake and the subsequent energy consumption. For this reason, a mathematical model is developed for the heat and mass transfers in the water and CO_2 adsorbents as well as in the indoor space. The models are then integrated and used for a case study of a typical occupied office space located in the hot and humid climate of Beirut, Lebanon. The system's energy consumption is evaluated over the peak load month of Beirut's cooling season and compared to that of the conventional air-conditioning system.

2. System description

In this work, a typical air-tight office space is considered located in Beirut. A mixing ventilation system is adopted to supply cool, dry, and CO_2-lean air. Thermal comfort is achieved by regulating the indoor air temperature and RH between 20 – 24 °C and 40 – 60 %, respectively. In addition, acceptable IAQ is provided by maintaining CO_2 levels below 1,000 ppm [26], while those of formaldehyde, representer of the VOCs family [14], should be kept below 8 ppb [8]. Additionally, O_2 levels above 19.5 % must be ensured for the office workers [10]. These indoor conditions are achieved using the proposed ventilation and air-conditioning system that integrates two adsorption beds in series that are packed silica gel and MOF-74-Mg followed by the evaporator coil of a vapor compression cooling system as shown in **Fig. 1(a)**.

The psychrometric process of the supply air using the proposed system is shown in **Fig. 1(b)**. The extracted room air at state (2) is divided into 3 streams: a part $\dot{m}_{oa}$ is exhausted to the outdoor environment, a part $\dot{m}_{ta}$ is treated in the adsorption beds and the remaining bypasses them. $\dot{m}_{ta}$ is first dehumidified to state (3) in the silica gel packed bed. The hot and dry air is then passes in the MIL-101-Cr packed bed to remove the excess CO_2. The resulting air stream at state (4) is mixed with the outdoor air at state (1) and flowrate $\dot{m}_{oa}$. The air mixture at state (5) is mixed with the bypassed air at state (2), forming the supply airstream $\dot{m}_{sa}$ at state (6) that is cooled to the supply temperature at state (7).

The system operation is regulated in terms of the supply, outdoor and treated air flowrates ($\dot{m}_{sa}$, $\dot{m}_{oa}$, $\dot{m}_{ta}$) to remove the space' s both latent and sensible load as well as meeting the needed IAQ constraints for the different species at minimal thermal regeneration energy consumption and minimal electric power consumption for both the bed's blowers and the compressor of the cooling system.

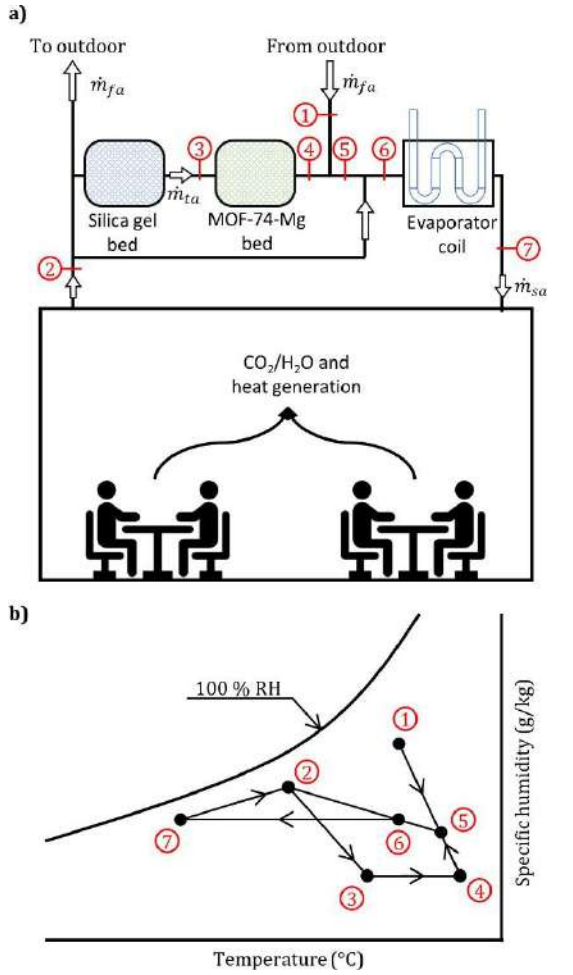

Fig. 1 – Schematic of a) the proposed ventilation system and b) the psychrometric process of the supply airflow.

3. Methodology

Mathematical models are developed for the heat and mass balances taking place in the adsorption bed as well as the office space. The models are integrated and used to size the different packed beds and evaluate the proposed system's energy consumption over the peak load month of Beirut's climate and compare it to that of conventional cooling system.

3.1 Adsorption model

Packed beds are used to selectively remove either H_2O or CO_2 from the room recirculated air. Such process is exothermic, requiring thus coupled heat and mass balances [27, 28]. A transient-one dimensional model is developed to predict the heat and species transfer between the airstream and the adsorbent. Due to the dilute nature of both H_2O and CO_2, the loss in species' mass does not affect the overall flowrate, enabling the assumption of a constant velocity along the flow path with plug flow pattern [29, 30]. Using these assumptions, the species mass balance considers the transient or storage effect, the convective and diffusive mass fluxes as well as the sink/source terms related to adsorption/desorption stages as given by [27, 28]:

$$\frac{\partial x_i}{\partial t} + u\frac{\partial x_i}{\partial z} - D_{zi}\frac{\partial^2 x_i}{\partial z^2} + \left(\frac{1-\varepsilon_b}{\varepsilon_b}\right)\rho_s\frac{\partial \bar{q}}{\partial t} = 0 \quad (1)$$

where x_i (kg/m³) and $\frac{\partial \bar{q}}{\partial t}$ (kg/kg·s) are the concentration and the average adsorption rate of species "i" (H_2O or CO_2) in the gas phase, u (m/s) is the flow velocity, ρ_s (kg/m³) is the adsorbent density, respectively. ε_b (-) is the bed void fraction. D_{zi}(m²/s) is the axial diffusion coefficient. $\frac{\partial \bar{q}}{\partial t}$ is given by the linear driving force model [27, 28]:

$$\frac{\partial \bar{q}}{\partial t} = k_{LDFi}(\bar{q}_i - \bar{q}) \quad (2)$$

where K_{LDFi} (s⁻¹) is the linear driving force model time constant, and $\bar{q}_i$ (kg/kg) is the equilibrium concentration evaluated at the adsorbent temperature and the species partial pressure in the airstream. The energy balances on the airstream and adsorbent takes into consideration the transient storage effect, diffusive heat flux and heat source/sink due to the exchange of heat of adsorption during adsorption/desorption stages. In addition, the airstream energy balance considers the convective heat flux. These equations are detailed by Myers et al. [27] and are not reported here for simplicity.

Based on the packed bed dimensions and inlet air conditions, the adsorption model yields the outlet air conditions in terms of temperature and species (H_2O or CO_2) concentration.

3.2 Office space indoor air model

The validated indoor air model developed by Yassine et al. [31] is adopted in this work. It considers the heat and species balances inside the office, where the air conditions are assumed homogeneous (well mixed assumption). The heat balance considers the heat generated internally by the occupants, lighting, and electrical equipment. In addition, the heat balance accounts for the heat gain from the office envelop and the heat removed by advection using the ventilation and air conditioning system. For the mass balance, the adopted model considers the net species transfer by advection from the ventilation and air-conditioning system as well as the internal generation of H_2O/CO_2 by the occupants, formaldehyde by the indoor furniture, and the rate of consumption of O_2.

Based on the office envelop characteristics, occupancy and equipment schedules, the indoor air temperature and species concentrations are determined.

3.3 Numerical methodology

The conservation equations are solved numerically using the finite volume method. For the disctrization, backward Euler scheme is used for temporal gradients, while first order upwind and second order

central difference schemes are used for first and second order sapctial gradients. A time step independence test results in a 1×10^{-5} s time step for the integrated model. Convergence is reached when the relative error between two consecutive iterations falls below 1×10^{-6} for all calculated parameters. Note that the adsorption model is validated by the authors as presented in [25, 32].

4. Case Study

This work considers a case study of a typical office space (5 m × 5 m × 3 m) located Beirut, in the coastal region of Lebanon characterized by hot and humid climate. The weather conditions during the cooling season of Beirut are adopted from typical meteorological year database as presented by El Loubani et al. [33]. The office envelope properties and occupancy schedule are adopted Katramiz et al. [34]. Each occupant is responsible for the generation of 11.57 mg/s of H_2O [35], 10.8 mg/s of CO_2 [36] and the consumption of 9.92 mg/s O_2 [10]. The formaldehyde generation rate from the different office is set to 30 mg/h [8, 9].

The beds are sized to capture the maximum H_2O during the peak load month and the maximum CO_2 mass during peak occupancy. Based on Beirut weather and the office maximum occupancy of 4 occupants, it was found that design $\dot{m}_{ta}$ is 0.03 kg/s and that August is the peak load month. Accordingly, the required silica gel and MOF-74-Mg masses are 4.1 kg/bed and 4.0 kg/bed respectively. The packed bed diameter and length are 0.2 m and 0.1 m, respectively for silica gel, and 0.25 m and 0.15 m, respectively for MOF-74-Mg. Note that the sizing is based on a regeneration temperature of 75 °C and 50 °C with feed-to-purge airflow ratio of 0.6 and 0.45 for the silica gel and MOF-74-Mg, respectively.

5. Results and discussion

The proposed system operation is regulated in terms of the supplied outdoor air ($\dot{m}_{oa}$) and the treated air ($\dot{m}_{ta}$) in the adsorption beds, and the supply air ($\dot{m}_{sa}$) to the space. The resulting hourly variation of these parameters along with the corresponding thermal and electrical energy requirements are presented in **Fig. 2**.

During the occupied hours, the supplied flowrate varied between 0.35 kg/s and 0.45 kg/s (**Fig. 2(a)**) that ensured an indoor temperature within the comfort range. The minimum was needed at *8:00 hr* when the space load was low, while the maximum was needed during peak load hour (*15:00 h*). Due to the night-time infiltration of outdoor air, the initial CO_2 levels were near the ambient levels (400 ppm). This enabled the system to completely bypass the adsorption bed during the first occupied hour with a $\dot{m}_{oa}$ of 0. 04 kg/s to meet the IAQ constraints of CO_2, VOCs and O_2 (**Fig. 2(a)**). After *8:00 h*, $\dot{m}_{oa}$ was reduced to a minimum of 0.01 kg/s that was dictated by the formaldehyde generation rate (**Fig. 2(a)**). Consequently, the O_2 levels were also above the allowable threshold of 19.5 %. Simultaneously, $\dot{m}_{ta}$ was increased to 0.1 kg/s between *9:00 h* and *14:00 h* when the outdoor humidity was low. However, it was increased to 0.15 kg/s for the remaining occupied hours (**Fig. 2(a)**). This is necessary to dilute the water vapor levels in the supply stream, which are caused by the increase in the outdoor humidity during the afternoon.

The resulting thermal energy consumption (E_t) for the bed regeneration varied between 1.36 kWh and 2.1 kWh (**Fig. 2(b)**). The electrical energy consumed by the packed bed fans ($E_{e,fans}$) varied between 0.86 kWh and 1.64 kWh (**Fig. 2(b)**). Moreover, the electrical energy consumed by the compressor of the air-conditioning system ($E_{e,coil}$), which reflects the proposed system ventilation load, varied between 1.55 kWh and 1.84 kWh (**Fig. 2(b)**). The variation pattern of E_t and $E_{e,fans}$ followed that of $\dot{m}_{ta}$, whereas the variation of $E_{e,coil}$ depended largely on $\dot{m}_{sa}$.

For comparison purposes, a vapor compression air-conditioning system with a COP of 3.2 is adopted. In addition, the conventional system is operated with the same $\dot{m}_{sa}$ since the space load does not depend on the choice of the system. Furthermore, the conventional system is operated with $\dot{m}_{oa}$ of 0.05 kg/s throughout the occupied hours to enable the same level of IAQ created by the proposed system. Accordingly, it can be concluded that the proposed system was able to reduce the outdoor air flowrate requirements and the ventilation load on the cooling coil by 72.6 % and 36 %, respectively.

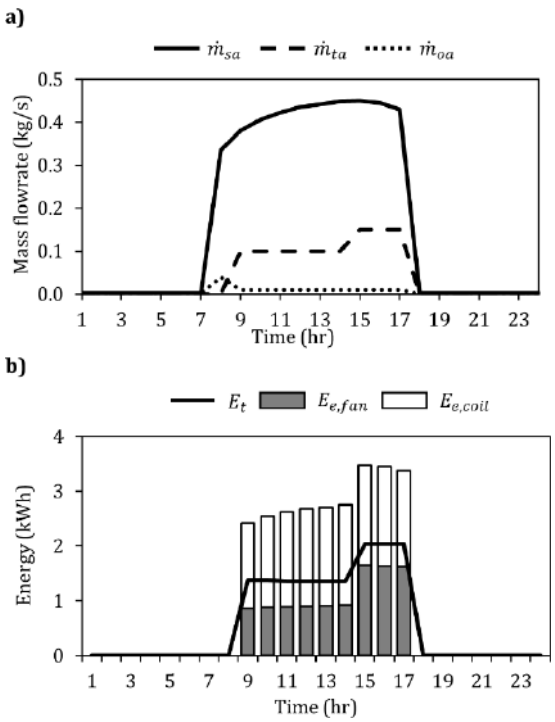

Fig. 2 – The hourly variation of a) the system's operating parametrs and b) the corresponding electrical and thermal energy cosumptions.

6. Conclusion

In this work, the performance of sustainable ventilation system is studied for a case study of a typical office in the hot and humid climate of Beirut, Lebanon. The proposed system integrates adsorption beds packed with either silica gel or MOF-74-Mg to sequenially treat the room recirculated air and reduce the outdoor air intake. Numerical models for the heat and mass transfers were developed to assess the performance of this system vis-a-vis the vapor compression-based ventilation and cooling systems. The model is used to determine the system operation in terms of required outdoor and treated air flowrates that meet the office indoor air constraints at minimal energy consumption. The hourly operation reduced the outdoor air intake and ventilation load by 72.6 % and 36 % as compared to that of a conventional system maintain the same indoor air conditions.

7. Acknowledgement

The authors would like to acknowledge the financial support of the American University of Beirut – Masri Institute of Energy and Natural Resources. The findings achieved herein are solely the responsibility of the authors.

8. References

[1] Burroughs H, Hansen SJ. Managing indoor air quality: River Publishers; 2020.
[2] Wang C, Zhang F, Wang J, Doyle JK, Hancock PA, Mak CM, et al. How indoor environmental quality affects occupants' cognitive functions: A systematic review. Building and Environment. 2021:107647.
[3] Du B, Tandoc MC, Mack ML, Siegel JA. Indoor CO2 concentrations and cognitive function: A critical review. Indoor air. 2020;30(6):1067-82.
[4] Yuan J, Chen Z, Zhong L, Wang B. Indoor air quality management based on fuzzy risk assessment and its case study. Sustainable Cities and Society. 2019;50:101654.
[5] Mannan M, Al-Ghamdi SG. Indoor Air Quality in Buildings: A Comprehensive Review on the Factors Influencing Air Pollution in Residential and Commercial Structure. International Journal of Environmental Research and Public Health. 2021;18(6):3276.
[6] Du C, Li B, Yu W. Indoor mould exposure: characteristics, influences and corresponding associations with built environment—a review. Journal of Building Engineering. 2021;35:101983.
[7] Jing S, Li B, Tan M, Liu H. Impact of relative humidity on thermal comfort in a warm environment. Indoor and Built Environment. 2013;22(4):598-607.
[8] Salthammer T. Formaldehyde sources, formaldehyde concentrations and air exchange rates in European housings. Building and Environment. 2019;150:219-32.
[9] Salthammer T, Mentese S, Marutzky R. Formaldehyde in the indoor environment. Chemical reviews. 2010;110(4):2536-72.
[10] Kim MK, Baldini L, Leibundgut H, Wurzbacher JA, Piatkowski N. A novel ventilation strategy with CO2 capture device and energy saving in buildings. Energy and Buildings. 2015;87:134-41.
[11] Maheswari A, Singh MK, Prajapati YK, Kumar N, Singh V. Experimental Analysis of a Thermoelectric Air-Conditioning System with Desiccant Dehumidification. Recent Advances in Industrial Production: Springer; 2022. p. 419-28.
[12] Pérez-Lombard L, Ortiz J, Pout C. A review on buildings energy consumption information. Energy and Buildings. 2008;40(3):394-8.
[13] Balat M. Electricity from worldwide energy sources. Energy Sources, Part B. 2006;1(4):395-412.
[14] Chu Y, Xu P, Jia Y, Lin M, Peng C, Dou Q. An adsorption-based CO2 treatment unit for ultra-low fresh air HVAC system using solid amine. Energy and Buildings. 2021;247:111148.
[15] Major C, Sollami B, Kammermeyer K. Carbon dioxide removal from air by adsorbents. Industrial & Engineering Chemistry Process Design and Development. 1965;4(3):327-33.
[16] Lee TS, Cho JH, Chi SH. Carbon dioxide removal using carbon monolith as electric swing adsorption to improve indoor air quality. Building and Environment. 2015;92:209-21.
[17] Sinha A, Thakkar H, Rezaei F, Kawajiri Y, Realff MJ. Direct Air Capture of CO2 in Enclosed Environments: Design under Uncertainty and Techno-Economic Analysis. In: Eden MR, Ierapetritou MG, Towler GP, editors. Computer Aided Chemical Engineering. 44: Elsevier; 2018. p. 2179-84.
[18] Wang J, Huang H, Wang M, Yao L, Qiao W, Long D, et al. Direct capture of low-concentration CO2 on mesoporous carbon-supported solid amine adsorbents at ambient temperature. Industrial & Engineering Chemistry Research. 2015;54(19):5319-27.
[19] Gelles T, Lawson S, Rownaghi AA, Rezaei F. Recent advances in development of amine functionalized adsorbents for CO2 capture. Adsorption. 2020;26(1):5-50.
[20] Eddaoudi M, Zaworotko MJ, Nugent P, Burd S, Luebke R, Belmabkhout Y, et al. Metal-organic materials for c02 adsorption. Google Patents; 2017.
[21] Zhou D-D, Zhang X-W, Mo Z-W, Xu Y-Z, Tian X-Y, Li Y, et al. Adsorptive separation of carbon dioxide: From conventional porous materials to metal–organic frameworks. EnergyChem. 2019;1(3):100016.
[22] Sumida K, Rogow DL, Mason JA, McDonald TM, Bloch ED, Herm ZR, et al. Carbon dioxide capture in metal–organic frameworks. Chemical reviews. 2012;112(2):724-81.
[23] Yang Q, Vaesen S, Ragon F, Wiersum AD, Wu D, Lago A, et al. A water stable metal–organic framework with optimal features for CO2 capture. Angewandte Chemie. 2013;125(39):10506-10.
[24] Bhatt PM, Belmabkhout Y, Cadiau A, Adil K, Shekhah O, Shkurenko A, et al. A fine-tuned fluorinated MOF addresses the needs for trace CO2 removal and air capture using physisorption. Journal of the American Chemical Society. 2016;138(29):9301-7.
[25] Harrouz JP, Ghali K, Hmadeh M, Ghaddar N, Ghani S. Feasibility of MOF-based carbon capture from indoor spaces as air revitalization system. Energy and Buildings. 2021:111666.
[26] Ashrae A, Standard A. 62.1. 2007, Ventilation for Acceptable Indoor Air Quality. American Society of Heating, Refrigerating and Air-Conditioning Engineers, Inc, Atlanta, GA. 2007.
[27] Myers TG, Font F, Hennessy MG. Mathematical modelling of carbon capture in a packed column by

adsorption. Applied Energy. 2020;278:115565.
[28] Ben-Mansour R, Habib M, Bamidele O, Basha M, Qasem N, Peedikakkal A, et al. Carbon capture by physical adsorption: materials, experimental investigations and numerical modeling and simulations–a review. Applied Energy. 2016;161:225-55.
[29] Dantas TL, Luna FMT, Silva Jr IJ, de Azevedo DC, Grande CA, Rodrigues AE, et al. Carbon dioxide–nitrogen separation through adsorption on activated carbon in a fixed bed. Chemical Engineering Journal. 2011;169(1-3):11-9.
[30] Hwang KS, Lee WK. The adsorption and desorption breakthrough behavior of carbon monoxide and carbon dioxide on activated carbon. Effect of total pressure and pressure-dependent mass transfer coefficients. Separation science and technology. 1994;29(14):1857-91.
[31] Yassine B, Ghali K, Ghaddar N, Srour I, Chehab G. A numerical modeling approach to evaluate energy-efficient mechanical ventilation strategies. Energy and Buildings. 2012;55:618-30.
[32] Harrouz JP, Katramiz E, Ghali K, Ouahrani D, Ghaddar N. Comparative analysis of sustainable desiccant–Evaporative based ventilation systems for a typical Qatari poultry house. Energy Conversion and Management. 2021;245:114556.
[33] El Loubani M, Ghaddar N, Ghali K, Itani M. Hybrid cooling system integrating PCM-desiccant dehumidification and personal evaporative cooling for hot and humid climates. Journal of Building Engineering. 2021;33:101580.
[34] Katramiz E, Ghaddar N, Ghali K. Daytime radiative cooling: To what extent it enhances office cooling system performance in comparison to night cooling in semi-arid climate? Journal of Building Engineering. 2020;28:101020.
[35] Mossolly M, Ghali K, Ghaddar N. Optimal control strategy for a multi-zone air conditioning system using a genetic algorithm. Energy. 2009;34(1):58-66.
[36] Persily A, de Jonge L. Carbon dioxide generation rates for building occupants. Indoor air. 2017;27(5):868-79.

9. Data availability

The datasets generated during and/or analysed during the current study are not publicly available because they are contained within the article but are/will be available upon request.

Nearly Zero Energy Buildings as a Standard of 21st Century – Velux RenovActive

Anna Predajnianska [a], Eva Švarcova [a], Imrich Sánka [a], Dušan Petraś [a]

[a] Slovak University of Technology in Bratislava, Faculty of Civil Engineering, Department of Building Services, Slovakia

Abstract. Most residential buildings in Slovakia, built in the 20th century, do not meet current requirements for energy efficiency. Therefore, nationwide remedial measures have been taken to improve the energy efficiency of these buildings and reduce their energy consumption. That is why Velux has created a RenovActive project to make this possible. The goal of renovations is to ensure today´s strict conditions for the energy consumption of buildings and thus achieve nearly zero energy buildings. In this article, we focused on the reconstruction of an old family house, which was built in 1960. The family house has been uninhabited for decades and was in a desolated state. We created three different options of reconstruction for the family house, each with different materials and technical equipment. Part of the article is also a comparison of the need for energy in each variant of reconstruction. We also processed a comparison of investment costs required for individual variants. The article also describes the current state of the family house. Currently, the house is inhabited by a young family and measurements of the basic quantities of internal well-being take place in the house. The aim of this project was to turn an old family house into a nearly zero energy building and ensure the required internal well-being at the level of 21st century.

Keywords. Family house, RenovActive, energy evaluation, nearly zero energy building.
DOI: https://doi.org/10.34641/clima.2022.135

1. Introduction

The recast the Energy Performance of Buildings Directive (EPBD) (2010/31/EU) was approved by the Parliament and the Council at the end of 2009 and contains number of changes. An important one is that as of 31 December 2020, all new buildings in the EU will have to consume "nearly zero" energy and the energy should to a significant extent be covered from renewable sources [2]. Kurnitski et al. (2011) outlined this general definition of a nearly zero energy building (nZEB): „A nZEB is typically a grid connected building with very high energy performance. nZEB balances its primary energy use so that the primary energy feed-in to the grid or other energy network equals to the primary energy delivered to nZEB from energy networks. Annual balance of 0 kWh/(m2.a) primary energy use typically leads to the situation where significant amount of the on-site energy generation will be exchanged with the grid." Before the nearly zero energy building type was defined in the EPBD, several commercial low energy building types had been defined in Europe. Some of them were so successful that they had been fully or partially implemented into national legislations. The overview of the low energy building types and their state of definition per 1 January 2010 is shown in Table 1.1. One particularly successful low-energy building type is a so-called Passive house, characterized by an extremely low specific energy demand. The passive house can be defined as a building, for which thermal comfort can be achieved solely by post-heating or post-cooling of the fresh air mass, which is required to achieve sufficient indoor air quality conditions – without the need for additional recirculation of air [1].

One of the prerequisites so that the building can be qualified as a nearly zero energy building is very low energy consumption for heating. This should be achieved by an excellent level of thermal insulation and an excellent air tightness to decrease heat losses by transmission and infiltration, resulting in a very low energy need for heating. To evaluate the whole heating system, and not only the level of thermal insulation of the building envelope, heat losses and auxiliary energy for the technical systems need to be added to the energy need for heating. The resulting energy performance indicator is called the energy use. If the calculation methodology follows the rules of energy certification as defined in the Regulation 364/2012 Coll., the heating system can be classified in one of the energy efficiencies classes A to G.

The same classification system applies for the energy use for domestic hot water (DHW). The total energy use for a building presents the sum of all energy uses for the respective building technical system. For apartment buildings, only space heating and DHW are considered, for other buildings also lighting and if applicable ventilation and cooling must be included. The criteria on

Copyright ©2022 by the authors. This conference paper is published under a CC-BY-4.0 license.

the specific total energy use for different types of buildings as defined in Regulation 364/2012 Coll. are shown in Tab. 1. The total energy use is calculated by a simple summation of the energy need and energy losses of the heat emission and distribution systems [1].

Tab. 1 – Energy classes to classify the total energy use [1, 10].

Energy performance classes	Family houses	Apartment houses	Office buildings
A	≤54	≤40	≤58
B	55-110	41-79	59-115
C	111-165	80-119	116-166
D	166-200	120-158	167-218
E	221-275	159-198	219-272
F	276-330	199-237	273-327
G	>330	>237	>327

The generation efficiency and renewable sources are considered in the delivered energy, which is defined as the energy content, expressed per energy carrier, supplied to the building through the system boundary, to satisfy the uses considered (heating, cooling, ventilation, DHW, lighting, appliances etc.) or to produce electricity [11].

This delivered energy is a necessary input to calculate the primary energy, which is the global indicator and presents the energy that has not been subject to any conversion or transformation process. The primary energy is calculated using primary energy factors, which are given at the national level and vary for different energy carriers. The scales of primary energy classes are shown in Tab. 2 [1].

Primary energy presents the global indicator that serves for the overall classification of the building. Until the end of 2015, the minimum requirement on the overall energy performance of new buildings, as expressed by the global indicator, was the upper boundary of the energy class B.

The minimum requirement on energy performance (global indicator) of new buildings built after 31 December 2015 was the upper boundary of the energy class A1. After 31 December 2018, new public buildings, and after 31 December 2020 also all other new buildings must fulfil the requirement of class A0 for the global indicator. Energy class A0 represents the nearly zero energy level of the building energy performance [1].

Tab. 2 – Energy classes to classify the primary energy [1, 10].

Energy performance classes	Family houses	Apartment houses	Office buildings	
A0	≤54	≤32	≤60	
A1	55-108	33-63	61-120	
B	109-216	64-126	121-240	
C	161-324	127-189	241-360	
D	325-432	190-252	361-480	
E	433-540	253-315	481-600	
F	541-648	316-378	601-720	
G		>648	>378	>720

2. Typical family houses in Slovakia

There are more than 900,000 family houses in Slovakia. About 100,000 of them were built in the 1950s to 1970s. These family houses have a typical square floor plan, almost identical layout, and material design of internal and external structures. From the point of view of the rising standards and requirements for thermal insulation and energy performance requirements of buildings, these family houses are not in satisfactory and needs reconstruction [2, 3, 4, 5, 6, 7, 8]. Some typical houses are shown in Fig. 1.

Fig. 1 – Sample of the family house in Slovakia built in the 1950s and 1970s [2, 3, 4].

Family houses built between 1950 and 1970 had a typical square floor plan and material composition. At present, many of them are inhabited, but they do not meet today´s thermal-technical requirements. The interior and exterior finishing of the walls, ceilings, and floors are in unsatisfactory conditions. Single or double windows with simple glazing were used in these houses.

The ceilings were made of wooden beams. In many cases, the floor is degraded by time, especially due to weather conditions. The project documentation of these family houses was drawn by hand, as no drawing software was used at that time. A sample project documentation can be seen on Fig. 2.

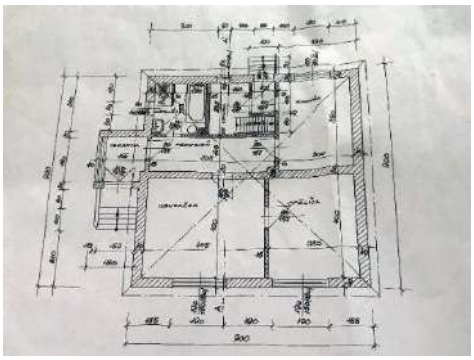

Fig. 2 – Layout of the family houses in Slovakia built in the 1950s to 1970s [2, 3, 4].

These family houses do not meet the energy efficiency requirements of buildings, which are currently very strict. According to the regulations, buildings with almost zero energy demand are required. Therefore, it is necessary to renovate unsuitable family houses. In this article, we will introduce an exemplary reconstruction of a family house, which applies to most of the family houses built between 1950 to 1970.

3. Renovation of a representative family house

The biggest disadvantage of the old family houses is that they were not thermally insulated due to the requirements at the time. The first step in reconstruction is to ensure building modifications in the form of a change in layout, changes in the material design of walls and ceilings. Due to the thermal-technical requirements valid today, thermal insulation of external constructions is required. The original simple windows, which have only minimal insulation ability, need to be replaced by modern window. We are talking here about plastic, plastic-aluminium or wooden windows, which have good thermal insulation properties and are secured with insulating glass. Tab. 3 shows two possibilities of renovation of family houses. The first renovation met energy performance requirements that complied with the values valid after 2016. With this reconstruction, it would be possible to achieve an ultra-low-energy building. The second renovation meet energy performance requirements that have been in force after 2020. With these requirements it is possible to ensure nearly zero energy building. Of course, there are many other ways of renovations. It is important to maintain the thickness of the thermal insulation so that the building meets today´s building conditions with almost zero energy consumption. This step precedes a satisfactory energy evaluation of the building. Heating system, DHW preparation system and other building environment technology positively contribute to achieving a satisfactory energy evaluation of the building.

Tab. 3 – Summary of renovations details [9].

	Renovation 1	Renovation 2
Thermal-technical evaluation regarding values valid after year	2016	2020
Windows, doors	Plastic-aluminium or wooden windows with insulating glass	Plastic-aluminium or wooden windows with insulating glass
Thermal insulation of external walls	160 mm	180-250 mm
Thermal insulation of the roof	320 mm	380-400 mm
Thermal insulation of the floor	120 mm	120 mm
Heating system	Gas condensing boiler, floor heating, control based on climate	Heat pump air-air, photovoltaic panels, and solar collectors on the rooftop
Domestic hot water preparation system	Storage heating system of DWH	Storage heating system of DHW
Ventilation	Natural	Natural, Hybrid
Heat recuperation from exhaust air	No	Yes
Fireplace	Yes	Yes

4. Energy evaluation of buildings

As part of the energy evaluation, the building is classified based on energy demand for heating, DHW, mechanical ventilation and cooling, also based on total energy demand, primary energy, and CO2 emissions. The result of the energy evaluation of previous renovations are summarized in Table 4. The table also shows the energy evaluation of the original condition of the house before renovation. Within the total energy demand, the building falls into class G which represents circa 387 kWh/(m2.a). The primary energy classifies the building into class D which represents almost 426 kWh/(m2.a).

Tab. 4 – Results of energy evaluation of two levels of house reconstruction [9].

	Original state	Renovation 1	Renovation 2
Space heating (kWh/m².a)	353,0 G(>258)	53,7 B(43-86)	40,8 G(<42)
DWH preparation (kWh/m².a)	34,0 C(25-36)	15,4 B(13-24)	12,2 A(< 13)
Total energy demand (kWh/m².a)	387,9 G(>258)	69,1 B(55-110)	53,0 A(< 54)
Primary energy (kWh/m².a)	425,7 D(325-432)	76,0 A1(55-108)	33,2 A0(< 54)
Emission CO_2 (kg/m².a)	117,9	21,1	6,4

It is clear from the results of the energy evaluation that the renovation has a positive effect on the energy intensity of the house. For comparison, we see that the primary energy indicator improves sharply. The first renovation shifts the house to the energy class A1, which is an ultra-low-energy building. With the second renovation, it is possible to attain energy class A0, which is a nearly zero energy building.

5. State of family house before and after renovation

Before the renovation of the family house, an architectural competition was launched, in which several architectural studios participated. In the second round of the competition, the architects presented their studies, and the commission unanimously determined Architectonic Studio Ddak as a winner of architectural competition. The design of the reconstruction preserves the current expression of the family house, but nevertheless the reconstruction improves the quality of life in the house in an economical and feasible way. The architecture of the family house is very fine and clean lines predominate. Neutral colours for exteriors and interiors were chosen. State of the house in exterior before and after renovation are showed in Fig. 3 and Fig. 4.

Fig. 3 – State of the house before renovation [2, 3, 4].

Fig. 4 – State of the house after renovation [2, 3, 4].

A wooden terrace was built in the garden of the family house. Part of the terrace is in interior and is made as a wooden building. The second part of the terrace is exterior with a pleasant sitting area. The family house is an ideal home for a family.

Fig. 5 – View of the family house from the garden before renovation [2, 3, 4].

View of the family house from the garden before and after renovation can be seen in Fig. 5 and Fig. 6.

Fig. 6 – View of the family house from the garden after renovation [2, 3, 4].

A significant renovation also took place in the interior of the family house. The degraded truss was removed and a new one was built. This creates a residential attic and two children´s rooms and a bathroom.

In the residential attic, wooden columns have been preserved, which are part of the truss, which elegantly fits into the architecture of the house. The old degraded wooden truss and new children room created in residential attic can be seen in Fig. 7 and Fig. 8.

Fig. 7 – The old degraded wooden truss before renovation of the house [2, 3, 4].

Construction work on the project was completed in July 2019. To the family moved into the house in September 2019. Over the next years, key parameters will be measured in cooperation with the Department of Building Services of the Slovak University of technology in Bratislava to verify the functionality of the renovated house. The unfavourable pandemic situation currently does not allow us to install measuring devices in the family house and record the necessary key values needed to assess the indoor climate of the renovated space.

Fig. 8 – Children´s room in new residential attic [2, 3, 4].

6. Conclusion

A large part of houses and other buildings in Slovakia was built between the 1950s and 1970s. These buildings do not meet today´s strict criteria, either of the energy efficiency of buildings or the quality of the indoor environment. By increasing the energy efficiency, it is possible to ensure that less energy is needed to provide the service.

Increasing energy efficiency not only allows individuals and organizations to reduce capital and operating costs and can also reduce fuel consumption. It can reduce greenhouse gasses emissions and thus preventing climate change. Almost two-thirds of countries still do not have any energy regulations in place. This contribution showed the possibility of obtaining a building with an ultra-low-energy or ever nearly zero energy demand for a 50-year-old building. This was achieved through modern thermal insulation, space heating, DHW, and ventilation technologies [9]. This home managed to breathe a second life. We will also pay attention to the urgent need to renovate other houses in Slovakia by creating healthy and energy-efficient and affordable homes that bring a healthy indoor environment to their users.

7. Acknowledgement

This article was supported by the Ministry of Education, Science, Research and Sports of Slovak Republic through a grant VEGA 1/0303/21, VEGA 1/0304/21 and KEGA No. 005STU-4/2021.

8. References

[1] Krajčík. M. (2015) Energy Balance and Indoor Environment of Building with Low-Exergy Heating and Cooling Systems, Habilitation thesis, Slovak University of Technology in Bratislava, Faculty of Civil Engineering, Department of Building Services.

[2] Predajnianska, A., Sánka, I. (2020) Energy evaluation of renovated family house, In Proceedings of the Conference Facility management 2020, SSTP, Bratislava, ISBN 978-80-89878-63-5, pp. 109-112.

[3] Sánka, I, Predajnianska. A. (2019) Possibilities of improving the energy efficiency of family houses, In Proceedings of the Conference Heating 2019, SSTP, Bratislava, ISBN 978-80-89878-42-0, pp. 439-446.

[4] Sánka, I, Predajnianska, A., Petráš, D. (2019) Comprehensive renovation of family house to the standard of 21st century, In Proceedings of Conference Comprehensive renovation of residential buildings 2010, ZSVTS, Bratislava, ISBN 978-80-972493-8-0, pp. 33-37.

[5] Bekö G., Földváry V., Langer S., Arrhenius K. (2016) Indoor air quality in a multifmily apartment building before and after energy renovation. Proceedings of the 5th International Conference on Human-Environment System, ICHES 2016 Nagoya, Japan

[6] Sánka, I, Földváry, V., Petráš, D. (2017) Experimental measurements of the toxic substance of indoor climate of building before and after renovation of the family house, TZB Haustechnik, Vol. 26, 2/2017, pp. 32-35.

[7] Földváry V., Bekö G., Petráš D. (2015) Seasonal variation in indoor environmental quality in non-renovated and renovated multifamily dwellings in Slovakia. Proceedings of Healthy Buildings Europe 2015, Eindhoven, Paper ID 242.

[8] Sánka I., Földváry V., Petráš D. (2017) Evaluation of Indoor Environment Parameters in a Dwelling before and after renovation. Magyar épűletgépészet Vol, 65, pp. 29-33.

[9] Predajnianska, A, Sánka, I., Petráš, D. (2021) Environmental technology for nearly zero energy buildings, In Proceedings of Conference Heating 2021, SSTP, Bratislava, ISBN 978-80-89878-72-7, pp. 423-426.

[10] Regulation 364/2012 Ministry of Transport, Construction and Regional Development of the Slovak Republic, implementing Act No. 555/2005 Coll. On the energy performance of buildings and on the amendment of certain laws

[11] Standard STN EN 15603/NA: 2012 Energy efficiency of buildings. Total energy demand and definition of energy assessment. National Annex, 2012, 32 pp.

Data Statement

The results of the energy assessment o the buildings were created by the authors who are part of the RenovActive project. The output data is published with the consent of Velux, which covers the project.

Acknowledgement

This work was supported by the Ministry of Education, Science, Research and Sports of the Slovak Republic through a grant VEGA 1/0303/21, VEGA 1/0304/21 and KEGA 005STU-4/2021.

Personal comfort model for automatic control of personal comfort systems

Dragos-Ioan Bogatu[a], Ongun B. Kazanci[a], Futa Watanabe[b], Yosuke Kaneko[b], and Bjarne W. Olesen[a]

[a] International Centre for Indoor Environment and Energy – ICIEE, Department of Civil Engineering, Technical University of Denmark, Nils Koppels Allé, Building 402, 2800 Kgs. Lyngby, Denmark, drabo@byg.dtu.dk

[b] Mitsubishi Electric Corporation, 5-1-1 Ofuna, Kamakura, Kanagawa 247-8501, Japan.

Personal comfort models could be used for the development of automatic controls for personal environmental comfort systems (PECS). These models often use indoor environment and physiological indicators as attributes for estimating the subjective response of occupants. Traditional indoor thermal environment research and standardization recommend 7-point scales for thermal comfort or thermal sensation estimation. However, many studies apply transformations to the response, thus oversimplifying the scales and generating controversy. The aim of this study is to determine the relevance of different indicators for the development of personal comfort models while investigating the implications and resulting model accuracy when using different thermal sensation scale discretization. Two simple machine learning algorithms, namely logistic regression and Naïve Bayes, were used in a multi-class setting to predict the overall thermal sensation of individual subjects when occupying a heated or cooled chair in steady state conditions. Multiple models were generated depending on the variables included in the feature set. Additionally, two response vectors were generated based on the thermal sensation vote, a three class and a seven class one, the latter being generated by further discretizing the hot and cold spectrum of thermal sensation. Both models performed better than a random guess at identifying thermal sensation classes and reached accuracies of up to 72% when predicting the overall thermal sensation of people using PECS. Including information of the PECS operation in the model, i.e. seat temperature, increased the prediction accuracy by up to 5%. The overall accuracy was higher when using three classes for the thermal response, as implementing seven classes led to a decrease of up to 21 percentage points. Nevertheless, the latter provided a finer adjustment without affecting the model's ability to distinguish between the cold and hot spectrum, which may be an advantage for personal comfort systems that condition the microenvironment of the occupant.

Keywords. Personal environmental comfort system, automatic control, thermal sensation vote, machine learning, response scale.
DOI: https://doi.org/10.34641/clima.2022.120

1. Introduction

Personal environmental comfort systems (PECS) are a topic of interest because they could improve comfort by dealing with the inter-personal differences between people [1], [2]. Their implementation could lead to energy savings [1], [2]. However, for an optimal operation, automatic controls based on machine learning algorithms are becoming attractive as an alternative to manual interaction between the occupant and the PECS.

Monitoring and including physiological indicators such as skin temperature and heart rate in the control of the indoor environment has the potential to suplement or replace occupant feedback [3]. By including these indicators alongside environmental parameters in thermal comfort prediction models based on machine learning algorithms can achieve accuracies of up to 98% [4][5]. However, it is still

Copyright ©2022 by the authors. This conference paper is published under a CC-BY-4.0 license.

unclear which algorithms, indicators, or response scale should be used [1], [2], especially for PECS. Katić et al. [6] found that mean skin temperature, hand skin temperature, and PECS control intensity influence thermal comfort and should be included as features when PECS is in use. By integrating wrist, forehead, nose, and cheek skin temperature, Aryal et al. [7] managed to obtain accuracies of up to 85% for thermal comfort prediction when using no PECS, a fan, or a heater if the models were trained using only the data for each specific system. However, although both studies registered thermal sensation using the ASHRAE 7-point scale [8], it was discretized into three classes when using it as a response vector for the thermal comfort models as in other studies [2].

The goal of the present study was to assess whether machine learning algorithms could be used for the automatic control of PECS and which indicators and thermal response scale should be used. The prediction power of two algorithms, namely logistic regression and Naïve Bayes, when used to estimate overall thermal sensation while using a PECS under steady-state conditions was investigated. Different models were built with different sets of variables to assess their relevance for thermal comfort prediction when using a PECS. By discretizing thermal sensation into three or seven classes and retraining the models, the resulting differences could be compared.

2. Methods

2.1 Dataset

The dataset consisted of 980 observations of the operative temperature (Top), the seat temperature (Tseat), the skin temperature, and the overall thermal sensation (TSV). The data were obtained from twenty human subjects (ten females and ten males) in experiments in climate chambers with a heated/cooled seat. The subjects were university students with a body mass index (BMI) between 20 and 30. Clothing was maintained constant throughout each session but differed depending on the chamber temperature, between 0.5 clo when hot and 1 clo when cold.

In all, three scenarios were emulated: hot summer (44°C), cold winter (10°C), and near comfort (20°C). The seat was designed to heat or cool depending on the chamber temperature, cold or hot respectively to maintain comfort. The seat temperature was set to 40°C when heating, 20°C when cooling, and 34°C when close to comfort (Fig. 1). The measurement of

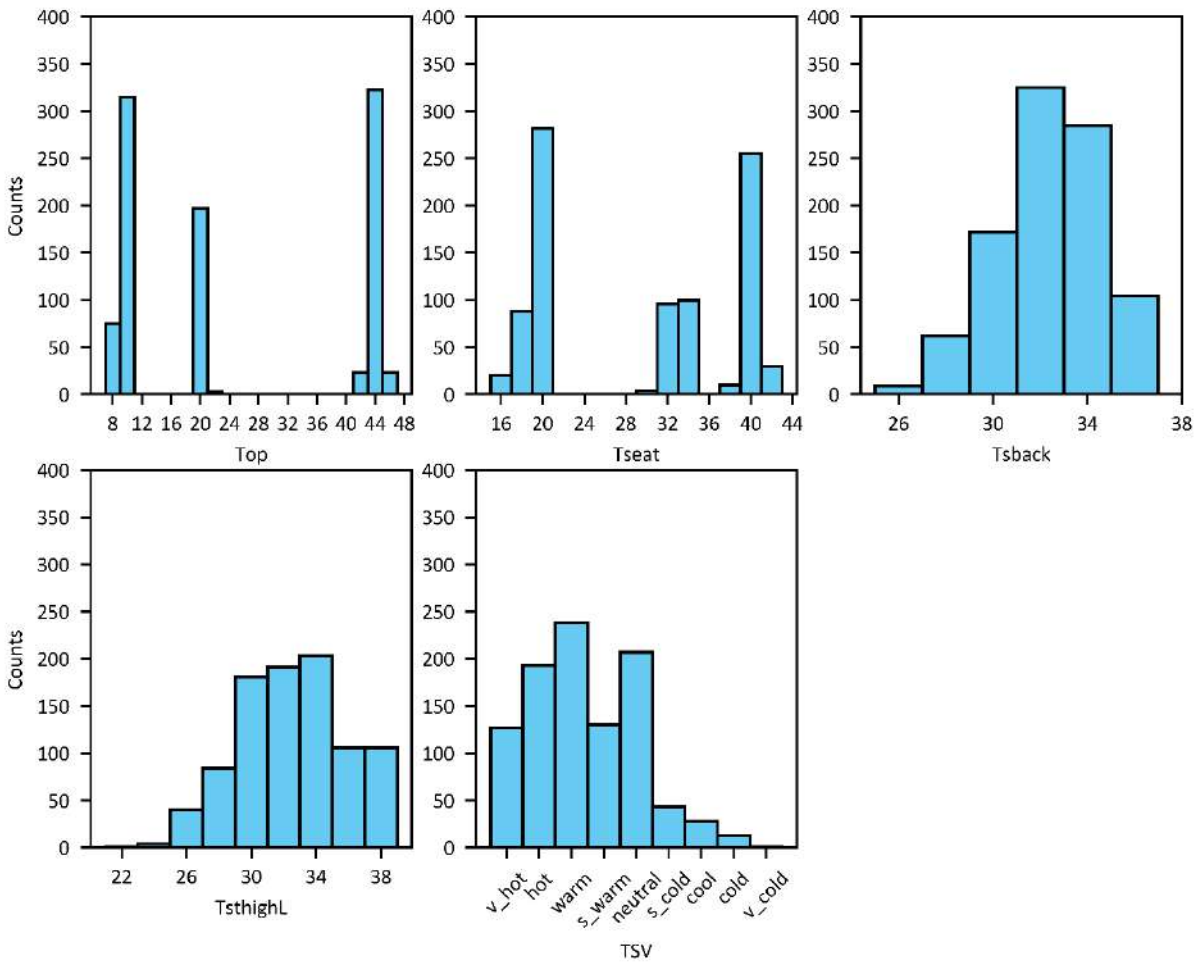

Fig. 1 - Histogram of variables in the dataset: operative temperature (Top), seat temperature (Tseat), skin temperature of the back (Tsback), left thigh (TsthighL), and left palm (TspalmL), and the overall thermal sensation of the subjects (TSV).

the operative temperature and the seat temperature had a five-minute resolution.

The skin temperature was monitored at two different points on the body, namely the back (Tsback), the left back thigh (TsthighL), both body parts in contact with the heated/cooled chair. The skin temperature had a resolution of one minute. As shown in Fig. 1, all skin temperatures were negatively skewed. The thermal sensation votes (TSV) followed a 9-point scale, namely very hot, hot, warm, slightly warm, neutral, slightly cold, cool, cold, and very cold. The TSV was positively skewed with very few "very cold" votes registered. In total ten thermal sensation votes were registered per condition from each subject.

2.2 Models

Due to the discrete and nominal nature of the multi-class predicted variable, namely the TSV, the problem represented a classification task. A logistic regression (Logit) and a Naïve Bayes (NB) algorithm were therefore selected for the study.

Six different sets of variables were used. The base set contained the operative temperature and the subject identification (sID). Three additional sets were generated by including the remaining variables, namely the seat temperature and the skin temperature of the back and thigh, in an alternating sequence. Two additional sets contained either the seat temperature and the sID or all variables except for the TSV. The sID, which indicates to which subject the variable refers, was always included since the aim was to generate an individual thermal comfort model.

For all models, the overall thermal sensation represented the response vector. However, the thermal sensation was simplified to either three (TSV3) or seven categories (TSV7). For both response vectors, the slightly hot and slightly cold classes were merged in the neutral class, as they are usually perceived as acceptable. Two other classes, hot and cold, were created in the TSV3 response by merging all the remaining hot and cold sensations, respectively. The rest of the remaining classes were kept separate for TSV7.

In total, seven different models were created for each algorithm. The first six used the TSV3 and each of the six sets of variables. For the last model, the TSV7 was used with the set containing all of the other variables in order to compare the results with the three-category scale of thermal sensation. In all instances, the performance of the two algorithms was compared to a baseline. The baseline represented a model that predicted everything as belonging to the class with the highest frequency in the response vector.

2.3 Training and test

Training and testing of the algorithms was carried out on the entire dataset in Python version 3.8.5. A two-level K-fold cross validation was used, with K_1=K_2=10 at each level. The data were shuffled before splitting them into the train and test sets. At the inner level (K_1), the respective complexity control parameter of each algorithm was optimized using only the training set of the outer level (K_2). In the regularized logistic regression algorithm (L2 penalty), the regularization parameter λ was tuned. In the NB algorithm Laplace smoothing was included, where α>0 was chosen as a complexity controlling parameter and optimized.

At the outer level, the optimized algorithm was trained and tested using the entire dataset, thus estimating the generalization error. The optimized model was retrained at the outer level to avoid overestimating the generalization error [9]. The error rate, equal to the number of misclassified observations divided by the number of test observations, was used as a performance indicator at each level. The accuracy, precision, recall, and F1-score were computed for each model using Equations 1 to 5. The precision, recall, and F1-scores were computed using the weighted average due to the class imbalance observed in the data (Fig. 1), where the weight represented the number of true instances for each label:

$$Precision_c = \frac{TP_c}{TP_c+FP_c}, c \in [1, C] \quad (1)$$

$$Recall_c = \frac{TP_c}{TP_c+FN_c}, c \in [1, C] \quad (2)$$

$$Precision = \sum_{c=1}^{C} \frac{1}{n_c} \cdot Precision_c \quad (3)$$

$$Recall = \sum_{c=1}^{C} \frac{1}{n_c} \cdot Recall_c \quad (4)$$

$$F1 = \sum_{c=1}^{C} \frac{1}{n_c} \cdot \frac{2 \cdot Precision_c \cdot Recall_c}{Precision_c + Precision_c} \quad (5)$$

where TP is the number of true positives, FP the number of false positives, and FN the number of false negatives. C indicates the number of classes, and n represents the number of observations. In order to assess and compare the models, a pairwise statistical t-test was used [10][9].

3. Results

3.1 Correlation between the variables

The correlation (Pearson's correlation coefficient) between the variables (Top, Tseat, Tsback, TsthighL) and the response (TSV) is shown in Fig. 2. The dark blue colour represents a strong negative correlation, while the dark red colour represents a strong positive correlation. A value close to 0 indicates no correlation.

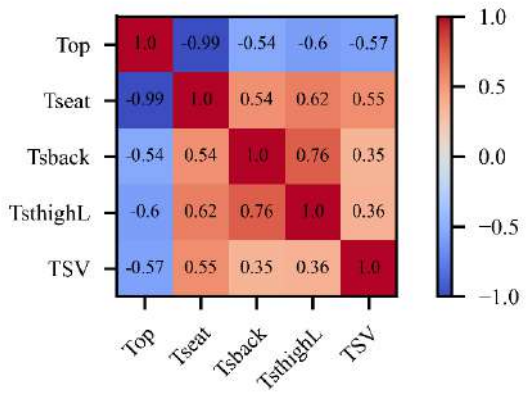

Fig. 2 - Pearson correlation between variables.

An almost perfect linear correlation was found between the Top and Tseat since when the operative temperature was low (10 °C) the seat temperature was high (40 °C) and vice-versa. All attributes were correlated with the TSV, with the Top and Tseat having a stronger correlation than the Tsback and TsthighL. The only negatively correlated attribute with the TSV was the operative temperature due to the scale's characteristics, as it spanned from very hot (0) to very cold (100). Since the back and the left thigh were in contact with the seat, the skin temperature (Tsback and TsthighL) was positively correlated with the seat temperature while negatively correlated with the operative temperature. This also meant that the two skin temperatures were linearly correlated.

3.2 Model performance

Tab. 1 shows the results of the models obtained from the two-level K-fold cross validation by algorithm and variable set. In order to quantify their ability to predict thermal sensation, the weighted precision, recall, and F1-score are given together with the overall accuracy of each model. The performance of the Baseline model was the same for each set of variables. However, it was dependent on the response vector, TSV3 or TSV7, since the most frequent thermal sensation was in the hot class for the former and in the neutral class for the latter.

Tab. 1 – Accuracy and weighted precision, recall, and F1-score by algorithm, feature set, and response used.

Algorithm	Feature set	Response	Precision	Recall	F1-score	Accuracy
Baseline		TSV3	0.32	0.57	0.41	0.57
Logit	Top, sID	TSV3	0.66	0.67	0.66	0.67
NB			0.65	0.66	0.61	0.66
Logit	Tseat, sID	TSV3	0.64	0.67	0.65	0.67
NB			0.6	0.63	0.6	0.63
Logit	Top, sID, Tseat	TSV3	0.71	0.72	0.71	0.72
NB			0.71	0.68	0.67	0.68
Logit	Top, sID, Tsback	TSV3	0.67	0.68	0.67	0.68
NB			0.73	0.69	0.69	0.69
Logit	Top, sID, TsthighL	TSV3	0.66	0.67	0.67	0.67
NB			0.71	0.67	0.68	0.67
Logit	Top, sID, Tseat, Tsback, TsthighL	TSV3	0.72	0.72	0.72	0.72
NB			0.71	0.68	0.67	0.68
Baseline		TSV7	0.15	0.39	0.22	0.39
Logit	Top, sID, Tseat, Tsback, TsthighL		0.56	0.57	0.56	0.57
NB			0.43	0.47	0.42	0.47

Both the Logit and the NB algorithms outperformed the Baseline. The accuracy of the Logit algorithm was higher by 0.1 to 0.15 when TSV3 was used as a response vector. Moreover, with the seven-point scale the difference increased by 0.18. The NB algorithm surpassed the Baseline by only 0.6 to 0.12 and 0.8 depending on the scale of the response, three or seven categories respectively.

For the same response vector, TSV3, the inclusion of both Top and Tseat in the feature set led to the highest accuracy, 72%. However, changing the operative temperature for the seat temperature as a model variable when predicting thermal sensation made little difference. Additional features, i.e. the skin temperatures, did not improve the accuracy of any of the algorithms.

The precision, recall, and F1-score were always between 60% and 72% for the Logit and NB when the response had only three classes. The model was able to identify a great degree of samples from each class while mismatching few samples [11], [12]. In general, the Logit algorithm obtained higher values. Values below 60% were observed when the response vector had seven classes. Still, with both three or seven classes, the precision and recall improved. With three classes for the TSV, the precision approximately doubled while the recall improved by up to 0.15 compared to the Baseline. When the response was changed to seven classes, the precision and recall increased by 0.41 and 0.18 for the Logit and by 0.28 and 0.8 for the NB. This led to an F1-score increase of 0.34 for the Logit and 0.2 for the NB algorithms.

Fig. 3 shows the confusion matrices for some of the Logit models. By comparing Fig. 3 a and b it was observed that the number of class matches (grey) increased while the number of critical mismatches between the cold and hot spectrum (red) decreased with the inclusion of additional variables. Additionally, although the overall mismatches increased when the response was categorized in seven classes, the number of misclassified observations between the hot and cold spectrum remained almost constant (Fig. 3 c).

3.3 Statistical evaluation

The performance of the three models relative to each other, i.e. Logit vs. Baseline, Logit vs. NB, and NB vs. Baseline, was evaluated using pairwise statistical t-tests. The 95% confidence intervals (CI), α=0.05, and the p-values are shown in Tab. 2. The performance differs for a p-value < 0.05, i.e. the probability that the two classifiers would predict differently given the number of different predictions made.

a

TRUE \ PREDICT	Hot	Neutral	Cold
Hot	444	112	2
Neutral	166	206	8
Cold	10	26	6

b

TRUE \ PREDICT	Hot	Neutral	Cold
Hot	446	110	2
Neutral	135	239	6
Cold	5	17	20

c

TRUE \ PREDICT	V_Hot	Hot	Warm	Neutral	Cool	Cold	V_Cold
V_Hot	81	28	5	13	0	0	0
Hot	32	89	36	35	0	1	0
Warm	11	25	89	112	0	1	0
Neutral	5	10	70	289	2	4	0
Cool	1	0	2	12	11	2	0
Cold	0	1	0	8	2	2	0
V_Cold	0	0	0	0	0	1	0

Fig. 3 - Confusion matrices of different logistic regression models with features: a) Top, sID, TSV3, b) Top, sID, Tseat, Tsback, TsthighL, c) Top, sID, Tseat, Tsback, TsthighL. The correctly classified and the misclassified observations between the warm and cold spectrum are highlighted in grey and red, respectively.

Tab. 2 – The pairwise statistical t-test results between the three algorithms, Logit, NB, and Baseline.

Test	Feature set	Response	Confidence interval (CI)	p-value
Logit vs. Baseline	Top, sID	TSV3	[0.06; 0.15]	$2 \cdot 10^{-4}$
	Tseat, sID		[0.05; 0.15]	$3 \cdot 10^{-4}$
	Top, Tseat, sID		[0.09; 0.19]	$4 \cdot 10^{-6}$
	Top, Tsback, sID		[0.07; 0.14]	$1 \cdot 10^{-5}$
	Top, TsthighL, sID		[0.06; 0.15]	$4 \cdot 10^{-5}$
	Top, Tseat, Tsback, TsthighL, sID		[0.1; 0.19]	$1 \cdot 10^{-6}$
	Top, Tseat, Tsback, TsthighL, sID	TSV7	[0.12; 0.25]	$5 \cdot 10^{-6}$
Logit vs. NB	Top, sID	TSV3	[0.01; 0.06]	$8 \cdot 10^{-3}$
	Tseat, sID		[0.02; 0.07]	$5 \cdot 10^{-3}$
	Top, Tseat, sID		[0.02; 0.07]	$5 \cdot 10^{-4}$
	Top, Tsback, sID		[0.01; 0.07]	$1 \cdot 10^{-2}$
	Top, TsthighL, sID		[0.02; 0.06]	$7 \cdot 10^{-4}$
	Top, Tseat, Tsback, TsthighL, sID		[0.02; 0.07]	$3 \cdot 10^{-3}$
	Top, Tseat, Tsback, TsthighL, sID	TSV7	[0.04; 0.15]	$1 \cdot 10^{-3}$
NB vs. Baseline	Top, sID	TSV3	[0.06; 0.12]	$1.3 \cdot 10^{-6}$
	Tseat, sID		[0.04; 0.1]	$2 \cdot 10^{-4}$
	Top, Tseat, sID		[0.05; 0.18]	$2 \cdot 10^{-3}$
	Top, Tsback, sID		[0.05; 0.17]	$6 \cdot 10^{-4}$
	Top, TsthighL, sID		[0.06; 0.16]	$1 \cdot 10^{-4}$
	Top, Tseat, Tsback, TsthighL, sID		[0.07; 0.17]	$1 \cdot 10^{-6}$
	Top, Tseat, Tsback, TsthighL, sID	TSV7	[0.05; 0.14]	$2 \cdot 10^{-4}$

Tab. 2 shows that none of the 95% confidence intervals (CI's) of the pairwise t-tests contain zero. Thus, there was strong evidence that both the Logit and the NB had a higher accuracy than the Baseline. Although there was still evidence that the Logit had a higher accuracy than the NB, the effect was not as significant in this case. For all three pairwise comparisons, the p-values are significantly smaller than the chosen level, 0.05. In general, the lower and upper bounds of the confidence interval moved further away from zero as more variables were included.

4. Discussion

The focus of this study was to determine whether machine learning algorithms could be used for the control of personal comfort systems and which indicators should be used as input. Two simple algorithms, logistic regression and Naïve Bayes, were used to assess their ability to predict the overall thermal sensation based on the operative temperature, the seat temperature, and the skin temperature in contact with the seat, namely of the back and thigh, was assessed.

The Logit and NB algorithms managed to reach accuracies up to 72% for a three class TSV response, supporting the values previously reported in literature [13], [14]. Although this only meant an increase of up to 15 percentage points from the Baseline, the use of the two algorithms actually reduced the misclassification rate while increasing the models' effectiveness at identifying each class, as seen in the increase in recall and precision. Moreover, the high accuracy of the Baseline was a consequence of the skewness in thermal sensation votes, which were concentrated on the warm side. This could be due to the high heating and low cooling effectiveness of the chair as shown by the distribution of the subjects' votes. Therefore, even at low or high operative temperatures the subjects rarely reported feeling cold. The actual performance of the models when used with a more balanced dataset requires further investigation.

The highest overall increase in performance was observed when both Top and Tseat were included in the input set, confirmed by the statistical evaluation. Even though the two variables were collinear, they had an opposite effect on the TSV as the chair was

supposed to counter the loss in thermal comfort caused by the change in operative temperature. Moreover, since the back side of the body was in contact with the chair while the front side was directly exposed to the ambient thermal conditions it was expected that both would be correlated almost equally although inversely with the TSV, thus providing additional information to the model.

Having the skin temperatures from the two body parts in contact with the heated/cooled chair in the set of input variables did not improve the model performance. As observed both the Tsback and TsthighL showed a weak correlation with TSV. At the same time, they were not perfectly correlated with each other, most likely due to the non-uniform seat temperature and area of contact. Moreover, since the skin temperature was measured at points in direct contact with the chair, these variables were providing the same information to the model as the seat temperature. As previous research showed, there could be other physiological and environmental indicators, e.g. relative humidity, heart rate, and the heat flux between the seat and the occupant that could improve the prediction of the TSV [15]–[18]. Additionally, in a dynamic environment the time constant of the heating or cooling element of the chair might make these aforementioned indicators more relevant.

When investigating the effect of the response scale it was determined that an increased discretization led to a decrease in performance, and this applied also to the Baseline model. Even with a higher discretization the model maintained the same distinction power between hot and cold sensations. The problem was though differentiating between the neutral and the warm or cool sensations and the increase in computational power. A higher discretization may provide additional information regarding the intensity of the thermal sensation and increased flexibility for the control but questions remain on the optimality of the scale and its discretization for thermal comfort prediction [2].

The difference in performance between the two algorithms, Logit and NB, is inherently due to the way the two operate. The logistic regression is a linear model while the relationship between environmental and physiological indicators and thermal sensation is complex [1]. The NB assumes the variables are conditionally independent [1], [9], which could also be the reason for the slightly worse performance of the NB in the present dataset. Other algorithms such as decision trees, support vector machines, and artificial neural networks should be considered since previous research has shown that they are useful for thermal comfort estimation [1], [19]. Including feature transformations such as the gradient or mean of different variables should also be considered in future model development.

5. Conclusion

Both algorithms, the Logistic Regression and the Naïve Bayes, achieved a sub-optimal performance registering an accuracy of up to 72% when predicting the thermal sensation of subjects using a PECS. However, the models performed better than a random guess.

Information on the operation of the PECS should be included in the set of input variables as the prediction accuracy increased by up to 5% when the seat temperature was added to the operative temperature. This is in line with the findings of Katić et al. [6] and Aryal et al. [7] who showed that the PECSs' settings should be used as input variables in personal comfort models as they influence individual thermal preference. However, the skin temperature of any body parts in direct contact with the PECS may not provide any useful additional information for thermal sensation prediction. These findings support the idea that control signals and measurements of the PECS output, which are easier to obtain than physiological indicators, could be used to improve the predictive accuracy of personal comfort models.

The benefit of having additional classes and hence a more accurate control came at a greater computational cost. Nevertheless, this did not affect the model's ability at distinguishing between the cold and hot spectrum.

Dataset

The datasets generated during and/or analysed during the current study are not available because of a non-disclosure agreement but the authors will make every reasonable effort to publish them in near future.

Acknowledgement

This study was financially supported by Mitsubishi Electric Corporation and by the International Centre for Indoor Environment and Energy (ICIEE), Technical University of Denmark (DTU).

References

[1] J. Kim, S. Schiavon, and G. Brager, "Personal comfort models – A new paradigm in thermal comfort for occupant-centric environmental control," *Build. Environ.*, vol. 132, no. January, pp. 114–124, 2018, doi: 10.1016/j.buildenv.2018.01.023.

[2] M. André, R. De Vecchi, and R. Lamberts, "User-centered environmental control: a review of current findings on personal conditioning systems and personal comfort models," *Energy Build.*, vol. 222,

2020, doi: 10.1016/j.enbuild.2020.110011.

[3] A. Ghahramani, G. Castro, B. Becerik-Gerber, and X. Yu, "Infrared thermography of human face for monitoring thermoregulation performance and estimating personal thermal comfort," *Build. Environ.*, vol. 109, pp. 1–11, 2016, doi: 10.1016/j.buildenv.2016.09.005.

[4] F. Salamone *et al.*, "Integrated method for personal thermal comfort assessment and optimization through users' feedback, IoT and machine learning: A case study," *Sensors (Switzerland)*, vol. 18, no. 5, 2018, doi: 10.3390/s18051602.

[5] S. Lu, W. Wang, S. Wang, and E. C. Hameen, "Thermal comfort-based personalized models with non-intrusive sensing technique in office buildings," *Appl. Sci.*, vol. 9, no. 9, 2019, doi: 10.3390/app9091768.

[6] K. Katić, R. Li, and W. Zeiler, "Machine learning algorithms applied to a prediction of personal overall thermal comfort using skin temperatures and occupants' heating behavior," *Appl. Ergon.*, vol. 85, no. February, 2020, doi: 10.1016/j.apergo.2020.103078.

[7] A. Aryal and B. Becerik-Gerber, "Thermal comfort modeling when personalized comfort systems are in use: Comparison of sensing and learning methods," *Build. Environ.*, vol. 185, no. August, p. 107316, 2020, doi: 10.1016/j.buildenv.2020.107316.

[8] ASHRAE, "ASHRAE 55-2017 Thermal Environmental Conditions for Human Occupancy." 2017.

[9] T. Herlau, M. N. Schmidt, and M. Mørup, *Introduction to Machine Learning and Data Mining*. 2021.

[10] A. Benavoli, G. Corani, J. Demšar, and M. Zaffalon, "Time for a change: A tutorial for comparing multiple classifiers through Bayesian analysis," *J. Mach. Learn. Res.*, vol. 18, pp. 1–36, 2017.

[11] M. Sokolova and G. Lapalme, "A systematic analysis of performance measures for classification tasks," *Inf. Process. Manag.*, vol. 45, no. 4, pp. 427–437, 2009, doi: 10.1016/j.ipm.2009.03.002.

[12] M. Grandini, E. Bagli, and G. Visani, "Metrics for Multi-Class Classification: an Overview," pp. 1–17, 2020, [Online]. Available: http://arxiv.org/abs/2008.05756.

[13] S. Liu, S. Schiavon, H. P. Das, M. Jin, and C. J. Spanos, "Personal thermal comfort models with wearable sensors," *Build. Environ.*, vol. 162, no. July, p. 106281, 2019, doi: 10.1016/j.buildenv.2019.106281.

[14] D. Li, C. C. Menassa, V. R. Kamat, and E. Byon, "HEAT - Human Embodied Autonomous Thermostat," *Build. Environ.*, vol. 178, no. March, 2020, doi: 10.1016/j.buildenv.2020.106879.

[15] T. Chaudhuri, D. Zhai, Y. C. Soh, H. Li, and L. Xie, "Random forest based thermal comfort prediction from gender-specific physiological parameters using wearable sensing technology," *Energy Build.*, vol. 166, pp. 391–406, 2018, doi: 10.1016/j.enbuild.2018.02.035.

[16] Z. Deng and Q. Chen, "Development and validation of a smart HVAC control system for multi-occupant offices by using occupants' physiological signals from wristband," *Energy Build.*, vol. 214, p. 109872, 2020, doi: 10.1016/j.enbuild.2020.109872.

[17] I. Pigliautile, S. Casaccia, N. Morresi, M. Arnesano, A. L. Pisello, and G. M. Revel, "Assessing occupants' personal attributes in relation to human perception of environmental comfort: Measurement procedure and data analysis," *Build. Environ.*, vol. 177, no. March, p. 106901, 2020, doi: 10.1016/j.buildenv.2020.106901.

[18] Y. F. Zhang, D. P. Wyon, L. Fang, and A. K. Melikov, "The influence of heated or cooled seats on the acceptable ambient temperature range," *Ergonomics*, vol. 50, no. 4, pp. 586–600, 2007, doi: 10.1080/00140130601154921.

[19] N. Ma, D. Aviv, H. Guo, and W. W. Braham, "Measuring the right factors: A review of variables and models for thermal comfort and indoor air quality," *Renew. Sustain. Energy Rev.*, vol. 135, no. August 2020, p. 110436, 2021, doi: 10.1016/j.rser.2020.110436.

Development and initial testing of a Personalized Environmental Control System (PECS)

Ongun B. Kazanci [a,], Jun Shinoda [a], Hang Yin [c], Dragos-Ioan Bogatu [a], Futa Watanabe [b], Yosuke Kaneko [b], Bjarne W. Olesen [a]*

[a] International Centre for Indoor Environment and Energy, Department of Environmental and Resource Engineering, Technical University of Denmark, Koppels Allé, Building 402, 2800 Kgs. Lyngby, Denmark (* onka@byg.dtu.dk)

[b] Mitsubishi Electric Corporation, 5-1-1 Ofuna, Kamakura, Kanagawa 247-8501, Japan

[c] Department of Civil and Environmental Engineering, Norwegian University of Science and Technology, Trondheim, Norway

Abstract. Personalized Environmental Control Systems (PECS) condition the immediate surrounding of occupants in contrast to conventional HVAC systems. PECS have several advantages including allowing occupants to adjust their immediate surroundings according to their preferences, which could improve their satisfaction with the indoor environment, which may lead to higher productivity. PECS can also lead to noticeable energy savings, if implemented effectively in buildings. The present study explains the development process and initial testing of a novel PECS. The PECS had heating, cooling, and ventilation functions, together with the possibility of adjusting lighting color and brightness. Ventilation and cooling were provided from a desktop air terminal device, and heating was provided by a curved panel covering the lower body from the thigh to the lower leg of a seated occupant. A thermal manikin was used to quantify the heating and cooling performance of the different versions of the PECS. The most recent prototype was able to provide a cooling effect up to 6 K (calculated by the manikin-based equivalent temperature difference) to the left side of the face, and a heating effect of up to 5 K to the left and right thighs. The cooling and heating effect of the whole body was up to 0.3 K and 1.3 K, respectively. A Peltier element was introduced to lower the supply air temperature from the PECS, but had limited effect on the cooling effect despite the large increase in power use. When implementing a Peltier element in PECS, the generated waste heat must be handled so that it does not interfere with the cooling.

Keywords. Personalized system, ventilation, cooling, thermal manikin, equivalent temperature
DOI: https://doi.org/10.34641/clima.2022.239

1. Introduction

There are large differences among occupants in terms of thermal preference, air movement preference, clothing level, activity, ventilation and air quality preference and also their physiological and psychological responses [1]. Therefore, Personalized Environmental Control Systems (PECS) allow controlling the localized environment at occupant's workstation by their preference instead of conditioning an entire room to uniform conditions. This has the potential to improve comfort, health, and productivity of the occupants, and has the potential to improve the energy efficiency of the entire heating, ventilation and air-conditioning (HVAC) system substantially.

Personalized ventilation will also protect against cross contamination, which is critical in open-plan offices and work places with close distance [1]. There is currently an increasing interest for PECS as buildings are needed to be pandemic-proofed. The application is for work places with mainly sedentary activity such as open-plan offices, banks, and control centers. Due to the COVID-19 pandemic, where many people have been working from home, there will also be an increase in home working places where PECS could be a solution as well.

In these regards, PECS has advantages in large spaces such as open-plan offices where it substantially improves the local comfort and the energy efficiency of the entire system [2]. Generally, PECS is more energy-efficient and economically-feasible than conventional HVAC systems because it can extend the standardized temperature range related to HVAC, which is specified in ISO 7730 [2], [3]. Previous studies pointed out that with the suitable application of PECS, it is possible to achieve comfort (dissatisfaction lower than 20%) in a temperature

Copyright ©2022 by the authors. This conference paper is published under a CC-BY-4.0 license.

range between 18 and 32°C [4].

Despite the proven benefits, there are currently a very limited number of commercially-available PECS and their applications have not reached the broader market. Therefore, development and performance specifications of new types of PECS are needed.

The present study reports the results from physical measurements of a newly developed PECS prototype. A thermal manikin was used to evaluate the heating and cooling performance of the PECS on a human body. The obtained results were also compared with measurement data of previous prototypes, and to their respective power use for each of their function.

2. Methodology

2.1 PECS prototypes

Three prototypes of a desk-type PECS have been developed until now. Each prototype was evaluated based on its heating and cooling performance using the manikin-based equivalent temperature at different operation settings. The measurement procedure will be described in the following subsection.

The first prototype (v1) had an air terminal device (ATD) for cooling and ventilation, and three separate heating panels to heat the lower body. The ATD recirculated the room air, and was equipped with a simple filter. Cooling was provided by increasing the air supply, and hence the velocity, from the ATD. For heating, one panel was placed above the thighs of the occupant (i.e., the bottom side of the table), another panel was placed perpendicular to the floor, facing the lower leg of the occupant, and the other panel was placed on the floor where occupants would place their feet.

In the following prototype (v2), improvements were mainly made to the ATD. A Peltier element was introduced to provide additional cooling. Therefore, the ATD could be operated in both "ventilation" and "cooling" modes. During the ventilation mode, room air was recirculated through a filter in the ATD. The Peltier element was turned on during the cooling mode, and the waste heat from the Peltier element was dissipated to the room air through the sides of the ATD (not interacting with the supply air from the ATD).

The heating panels of v2 consisted of three panels, similar to that of v1. In parallel to the measurements of the two prototypes, a mockup of an alternative system to integrate the three panels into one panel was developed and tested. The mockup (flexible heating panel, FHP) consisted of a single curved surface that covered the lower body from the thighs to the lower leg, with a flexible heating element pasted on the surface. This heating element heated all of the lower body parts simultaneously.

The most recent prototype (v3) integrated the improvements made in v2 and the FHP. The heating panels were integrated into a single, flexible panel with a similar geometry as the FHP. The ATD had a Peltier element but water pipes were installed to remove the waste heat. The recirculated air for ventilation was cleaned by means of ultraviolet germicidal irradiation (UVGI). The ventilation setting could be adjusted from 1 to 10, the cooling setting could be adjusted from 1 to 5 (only when the ventilation was turned on), and the heating setting could be adjusted from 1 to 10. The overview and its setup is shown in Fig. 1.

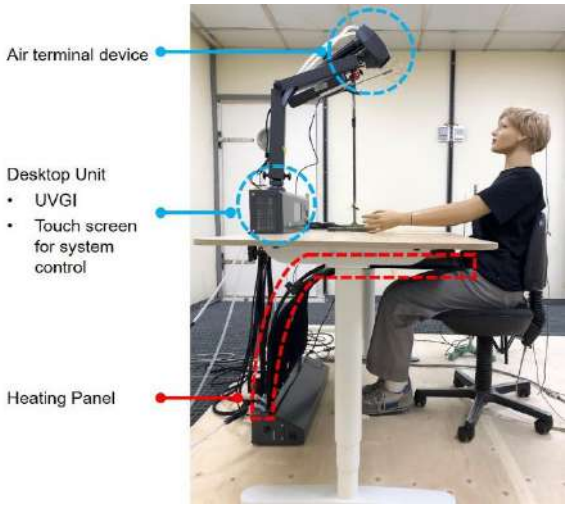

Fig. 1 – Overview of developed PECS (v3) and its setup in the chamber.

It must be noted that the "ventilation" function in all the prototypes provides recirculated air cleaned by filters and/or UVGI, and does not provide fresh air (outdoor air). The term "ventilation" is used for simplicity within the text, and air quality was not analyzed in the present study.

2.2 Measurement setup

Measurements were conducted in a climate chamber at the Technical University of Denmark. The chamber had a floor area of 28 m^2 and a height of 2.5 m. A displacement ventilation system supplied air at a very low velocity from the floor to the chamber. Air was also supplied between the wall and finishing fabric so that the surrounding surface temperatures would be nearly equal to the room air temperature. PECS v3 was mounted on a desk with dimensions of 160 × 80 × 80 cm ($L \times W \times H$). The floor beneath the PECS was covered with a wooden board with dimensions of 2.44 × 2.44 m to reduce the effects of the ventilation system on the measurement results.

A thermal manikin was used to study the heating and cooling effects of the PECS on the human body. Only the thermal performance was analyzed, and indoor air quality was not within the scope of the present study. The manikin had a body shape representing an average Scandinavian female with a height of 1.7 m.

The manikin had 24 individually controlled body parts: left and right foot, left and right low leg, left and right front thigh, left and right back thigh, pelvis, back side, crown, left and right face, back of neck, left and right hand, left and right forearm, left and right upper arm, left and right chest, and left and right back. An illustration of the body parts is shown in Fig. 2 (note that the back of the manikin was divided into two parts in the current measurements). The manikin was seated on an office chair with a clothing insulation corresponding to 0.10 clo [5]. The manikin was dressed in light summer clothes in cooling mode measurements, and in medium winter clothes in heating mode measurements. The clothing insulation for the different clothes are listed in Table 1.

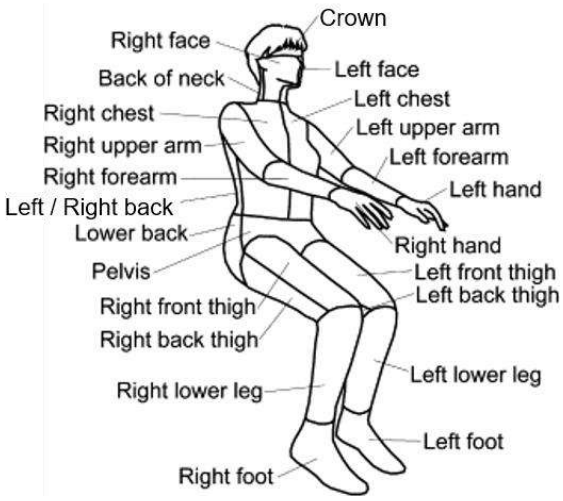

Fig. 2 – Body parts of the thermal manikin (based on the illustration from Watanabe et al. [6]).

A PT100 temperature sensor with an accuracy of ±0.03 K was positioned next to the desk at a height of 0.6 m for room temperature monitoring. Air and operative temperature sensors were positioned 0.5 m behind the manikin at the height of 0.6 and 1.1 m. A watt meter was used to monitor the system power use during the measurement.

2.3 Experimental conditions

Table 2 summarizes the experimental conditions with PECS. Measurements were conducted for both cooling and heating scenarios. For each room temperature setting, thermal manikin measurements were conducted with the PECS turned off, which was used as the reference case. For the test cases with PECS turned on, at each room temperature setting, 12 cases were conducted with the cooling scenario and 20 cases with the heating scenario. Each test case was conducted at steady state, and the average value over 5 min was used for analysis. All measurement equipments were logging at 10 s intervals. Prior to the measurements, a smoke visualization was conducted to determine the optimal position of the ATD. The position of the ATD was fixed at a position in which the supply air reaches the breathing zone (mouth) of the manikin.

Table 1 – Clothing insulation (*Icl*) values for different clothes

Garment	*Icl* (clo)
Light summer clothes	
T-shirt (short sleeves)	0.09
Normal trousers	0.25
Socks	0.02
Shoes (thin soled)	0.02
Panties	0.03
Standard office chair	0.10
Total	0.51
Medium winter clothes	
Normal shirt (long sleeves)	0.25
T-shirt (short sleeves)	0.09
Normal trousers	0.25
Socks	0.02
Shoes (thin soled)	0.02
Panties	0.03
Standard office chair	0.10
Total	0.76

Table 2 – Experimental conditions with PECS

Tested component/ Room condition	Operational Settings
Cooling scenario (light summer clothes)	
Room temperature	23, 24, 26, 28, 30 °C
Ventilation (ATD)	1, 5, 7, 10
Cooling (ATD)	0, 1, 5
Heating scenario (medium winter clothes)	
Room temperature	16, 18, 20, 22, 23 °C
Ventilation (ATD)	0, 1, 5, 7, 10
Heating (Panel)	2, 4, 7, 10

2.4 Data analysis

The thermal manikin gives the surface temperature and power use to maintain that surface temperature (which can be interpreted as the heat loss for a given condition) for each of the 24 body segments. The output was then used to calculate the manikin-based equivalent temperature (t_{eq}) for each body segment. ISO 14505-2 [7] defines the equivalent temperature to be a "temperature of a homogeneous space, with mean radiant temperature equal to air temperature and zero air velocity, in which a person exchanges the same heat loss by convection and radiation as in the actual conditions under assessment". The

following equations were used to calculate t_{eq}.

$$h_{bp} = \frac{P_{bp}}{t_{bp} - t_a} \quad (1)$$

$$t_{eq} = t_{bp} - \frac{P_{bp}}{h_{bp}} \quad (2)$$

Where:

h_{bp} : combined heat transfer coefficient for the body part (W/(m²·K))

P_{bp} : heat loss from the body part (W/m²)

t_a : reference room temperature (°C)

t_{bp} : surface temperature of the body part (°C)

Equation (1) was used to calculate the combined heat transfer coefficients of each body part of the reference cases (without PECS) in all room temperature conditions. The average value for each body part was used in equation (2) to calculate t_{eq} in all measurement cases. To show the cooling and heating effect of the PECS, the equivalent temperature difference (Δt_{eq}) was calculated by subtracting the t_{eq} of the reference case from the t_{eq} of the cases with the PECS turned on.

3. Results and Discussion

3.1 Power use

Tables 3 and 4 list the power use during the cooling and heating cases. The values are the average over all the tested conditions. The power use of the ventilation (without cooling) was in the range of 8 – 11 W, and turning on the cooling function added another 8 – 57 W to the power use. The power use for the heating panel was in the range of 25 – 128 W.

3.2 Manikin-based equivalent temperature

Fig. 2 shows the manikin-based equivalent temperature difference for the cooling scenario, at a room temperature of 28 °C. Negative values indicate cooling, and positive values indicate heating. The largest cooling effects were seen around "L. Face" (left part of the face), "R. Face" (right part of the face), and "Back of Neck". Among these body parts, the left side of the face was cooled the most due to the design of the ATD, as it was positioned to the left side of the PECS unit instead of at the center. In lower room temperature settings, the cooling effect to the left side of the face increased to about Δt_{eq} = -5 K, and also a small cooling effect (up to Δt_{eq} = -1 K) was seen at "L. Chest" (left part of the chest). In general, the cooling effect became larger in lower room temperature settings as the supply air from the ATD becomes lower as the room temperature decreases.

The comparison between the cooling settings and the no cooling settings (only ventilation) suggests that the cooling provided from the Peltier element at the ATD had a limited or negligible cooling effect on the manikin (occupant). However, the results in these figures were conducted at steady state, meaning the PECS had been running in each operational setting for at least 30 minutes. A slight decrease in the supply air temperature during the first few minutes of operation was observed, which could result in a difference in actual use (with humans at dynamic conditions). This aspect will be investigated further.

Table 3 – Power use of all cooling cases (V: ventilation, C: cooling settings)

Setting	Power [W]	Setting	Power [W]
V10-C5	68	V5-C5	65
V10-C1	19	V5-C1	13
V10-C0	11	V5-C0	10
V7-C5	66	V1-C5	64
V7-C1	18	V1-C1	16
V7-C0	10	V1-C0	8

Table 4 – Power use of all heating cases (H: heating, V: ventilation settings)

Setting	Power [W]	Setting	Power [W]
H10-V10	137	H4-V10	62
H10-V7	137	H4-V7	61
H10-V5	136	H4-V5	61
H10-V1	134	H4-V1	59
H10-V0	128	H4-V0	51
H7-V10	98	H2-V10	36
H7-V7	98	H2-V7	35
H7-V5	96	H2-V5	35
H7-V1	95	H2-V1	34
H7-V0	88	H2-V0	25

Despite the cooling effect on the face, the equivalent temperature difference of the overall body was nearly zero in all cases. This is due to the small surface area of the cooled body segments compared to the total surface area of the manikin. However, as the breathing zone and the head area is being cooled, it is possible that an actual person will perceive a larger cooling effect than that indicated by the manikin based equivalent temperature.

Fig. 3 shows the manikin-based equivalent temperature difference for the heating scenario, at a room temperature of 18 °C (both heating and ventilation without cooling was active). The largest heating effects were seen around the "L. Front thigh" and "R. Front thigh", with an equivalent temperature

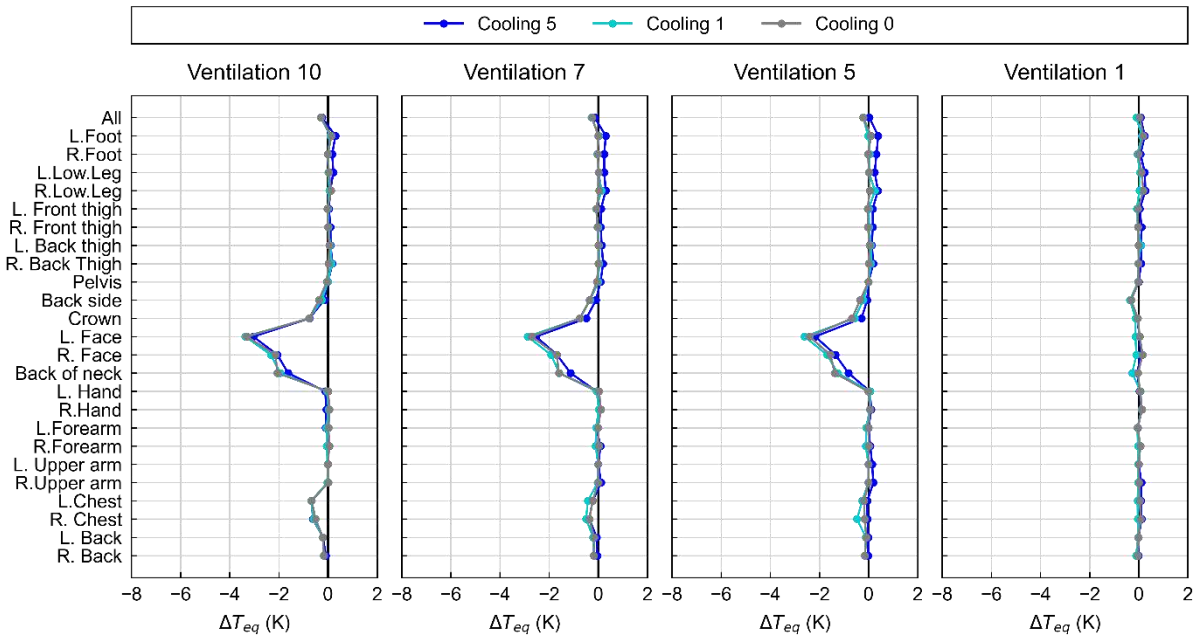

Fig. 2 – Equivalent temperature difference at 28 °C room temperature (cooling scenario).

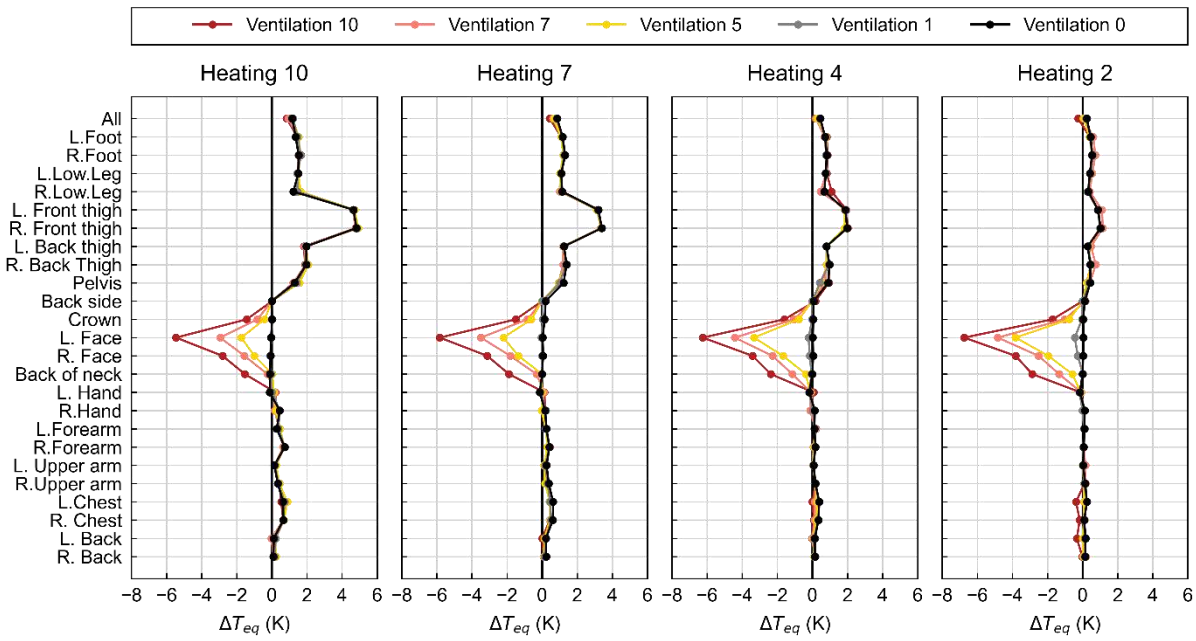

Fig. 3 – Equivalent temperature difference at 18 °C room temperature (heating scenario).

difference up to about 4 – 5 K. For the other lower body parts, such as the "L./R. Foot", "L./R. Low Leg" and "L./R. Back Thigh", the heating effect was up to 1 – 2 K. In higher heating settings (i.e., 7 or 10), a slight increase in the equivalent temperature difference can be seen around the chest, which could be the effect of warm air from the heating panel below the desk.

During the combined use of the ventilation and heating, no interaction was seen between the operations of the two components. The heating effect was uninfluenced by the ventilation setting, and the cooling effect from the ventilation followed the same trend as seen the cooling scenario. Therefore, it was concluded that the heating component does not interfere with the airflow to the breathing zone.

3.3 Power use and equivalent temperature difference

The extent of cooling or heating PECS can provide is a critical characteristic for the system. The amount of power required to provide the cooling or heating is also a key parameter. Therefore, the comparison of the power use and equivalent temperature difference can be a viable option to compare different PECS. Sections 3.1, 3.2 reported the results of the measurement for PECS v3. The same measurement procedure with the same room temperature settings

were conducted for the previous prototypes (v1, v2, and FHP), and therefore a comparison could be made.

Fig. 4 shows the comparison of the power use and equivalent temperature difference in the cooling scenario, using all the collected measurements from each prototype (v1 – v3). The equivalent temperatures of the whole body, left and right face, crown and back of neck were selected. Each point represents the measured value at different conditions, i.e., room temperature and operation settings of the fan or cooling. For example, for PECS v3, the measurement data with the combination of a room temperature setting of 23 – 30 °C, fan setting of 1 – 10, and cooling setting of 1 and 5 was plotted (i.e., the cooling scenario in Table 2). The cases with cooling were distinguished from the cases with air flow only (ventilation cases).

From the ventilation cases, it can be seen that the power use between different ventilation settings were small. Using the cooling function of the PECS resulted in a large increase in the power use but with little to no enhancement of the cooling (in terms of equivalent temperature difference). This was observed for both PECS v2 and v3. For v3, the average power use for the ventilation cases was 10 W, while the average power use for the cooling cases at the maximum setting was 66 W. For v2, the corresponding average power use were 4 W and 44 W, respectively. The power use of v3 was higher than the previous versions due to the UVGI for ventilation, whereas the others only had a simple filter.

Despite not having a dedicated active cooling function, v1 was able to provide the largest cooling effect. The differences with the other prototypes were the air velocity and the shape of the ATD. This suggests that further improvement in the air distribution (both in terms of air velocity and flow pattern) would be possible.

The comparison of different body parts show that the cooling effect of v3 was mostly to the left and right sides of the face, with a cooling effect up to about 6 and 4 K, respectively. The cooling effect to the crown was up to about 2 K, and about 3 K for the back of the neck. It can also be seen that v3 had the widest range of equivalent temperature differences for the face and back of neck, which would mean that occupants could have a better control over the PECS.

Fig. 5 shows the comparison of the power use and equivalent temperature difference in the heating scenario, using all the collected measurements from each prototype and mockups (v1 – v3 and FHP). The equivalent temperatures of the whole body, left and right front thigh, and left and right lower leg were selected. As was with the cooling scenario, each point represents the measured value at different conditions, i.e., room temperature and operational settings of the heaters, including the operation of different heating panels in v1 and v2. The v3

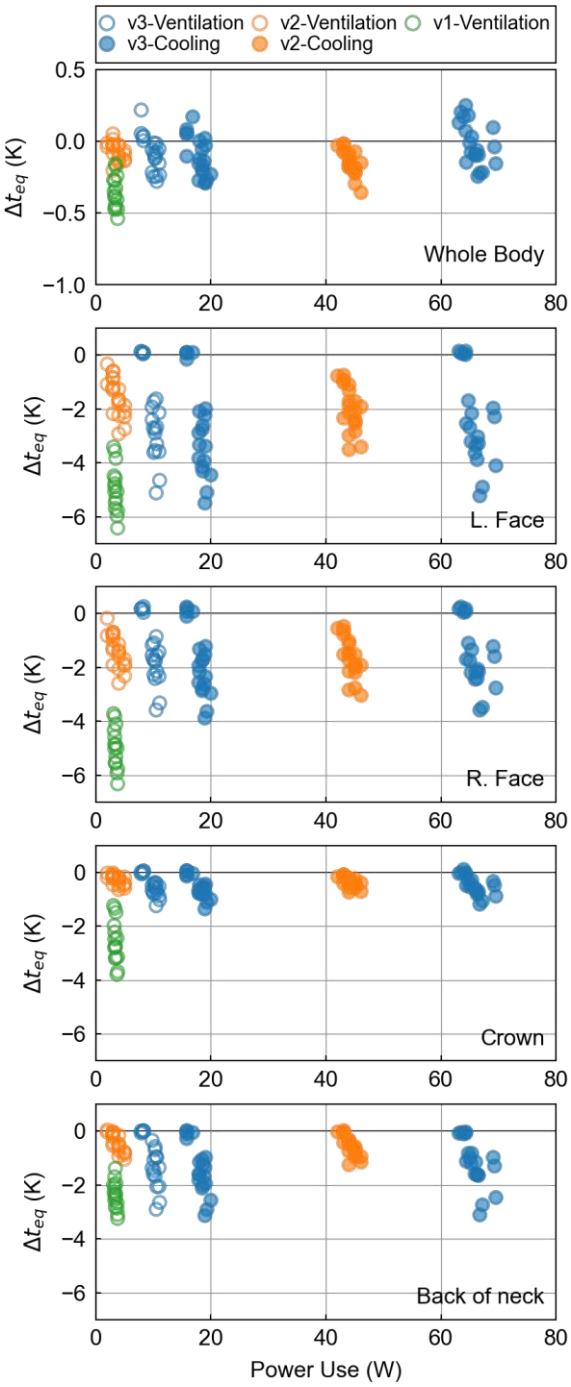

Fig. 4 – Power use and equivalent temperature difference in cooling scenario.

measurement cases with the combined use of the ventilation system and the heater was excluded to limit the comparison to the heating output of the heaters.

The results show that the heater of PECS v3 was able to replicate the performance of the FHP both in terms of power use and equivalent temperature difference of the manikin. It can also be seen that the FHP and PECS v3 was able to provide more heating to the whole body (mainly on the lower body), resulting in an equivalent temperature difference up to about 0.5 K higher than those of v1 and v2. For the individual body parts, as v1 and v2 had multiple panels that

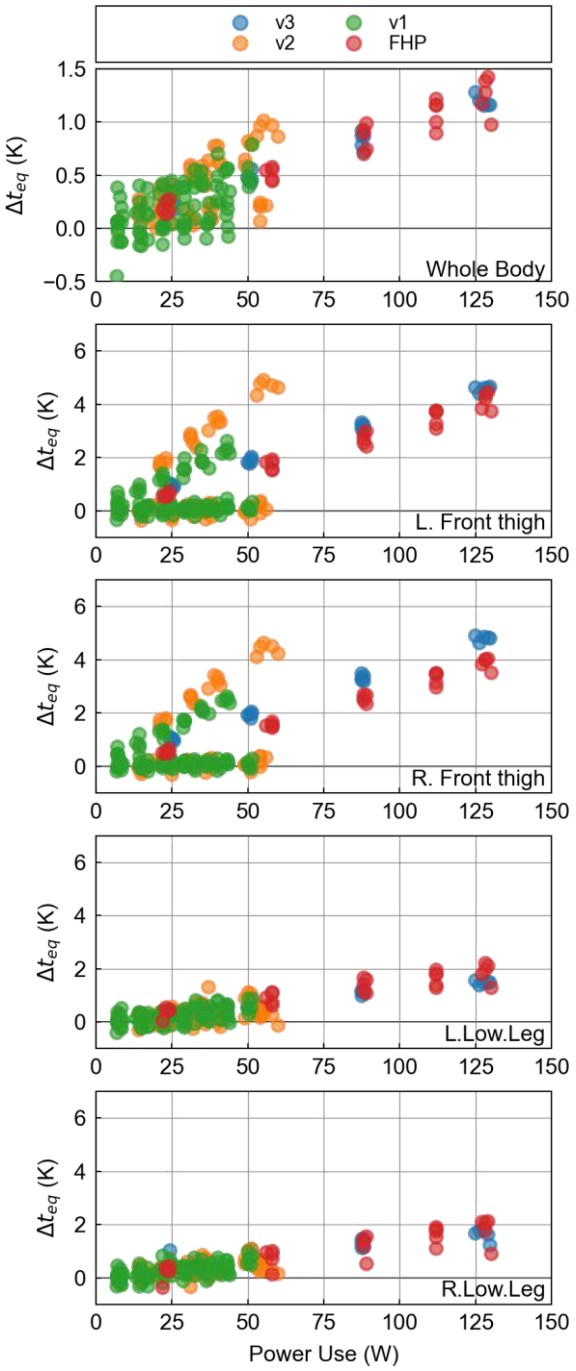

Fig. 5 – Power use and equivalent temperature difference in heating scenario.

heated different parts of the body, in some cases they were able to provide up to 5 K of heating to the front thighs with less power use as compared to v3 or FHP. The relationship between the power use and heating effect was similar across all prototypes, but v3 and FHP were able to provide more heating with the use of more power.

It should be noted even though a thermal manikin is a viable tool for studying the effects of the PECS, the actual heating and cooling effects might be much larger in reality, as the heating has focused on the lower body parts and the cooling has focused on the head region. This requires further studies with human subject experiments.

4. Conclusion

Thermal manikin measurements were conducted in a climate chamber to evaluate the cooling and heating effect of a prototype of a novel PECS on the human body. The thermal performance of the ventilation, cooling and heating components were evaluated based on their power use and manikin-based equivalent temperature. A comparison was made with previous prototypes to evaluate the improvements made during the development process.

The cooling component of the developed PECS provided a cooling effect of up to 6 K to the left side of the face, 2 K to the crown, 3 K to the back of the neck, and 0.3 K to the whole body. The heating panel was able to provide a heating effect of up to 5 K to the front thighs, 1 K to the lower legs, and 1.3 K to the whole body.

For the ventilation component, the power use increased by about 5 W due to the added UVGI. The use of a Peltier element for cooling the supply air increased the power use by about 66 W. However, little to no enhancement of the cooling performance in terms of equivalent temperature was observed. When implementing a Peltier element for cooling within the PECS, the generated waste heat must be handled so that it does not interfere with the cooling. For the heating panels, introducing a curved panel covering the thighs and lower leg was able to provide heating up to about Δt_{eq} = 1.3 K, showing clear improvement from the previous prototypes.

The results presented in the present study are interim results and further development on the PECS is ongoing. Human subject measurements are planned to be conducted to evaluate the performance of PECS v3. Both subjective and objective outputs from the human subjects will be collected and compared with the results reported in this paper.

5. Acknowledgements

This study was financially supported by Mitsubishi Electric Corporation and by the International Centre for Indoor Environment and Energy (ICIEE), Technical University of Denmark (DTU). The authors would like to thank Nico Henrik Ziersen for his help with preparing the experimental setup.

6. Data Access Statement

The datasets generated during and/or analyzed during the current study are not available because of a non-disclosure agreement but the authors will make every reasonable effort to publish them in near future.

7. References

[1] Melikov, A.K. Personalized ventilation. Indoor Air. 2004; 14(7): 157-167.

[2] Warthmann, A., Wölki, D., Metzmacher, H., van Treeck, C., Personal Climatization Systems – A Review on Existing and Upcoming Concepts. Applied Sciences. 2018; 9(1):35.

[3] EN ISO 7730. Ergonomics of the thermal environment - Analytical determination and interpretation of thermal comfort using calculation of the PMV and PPD indices and local thermal comfort criteria. European Committee for Standardization, Brussels. 2005.

[4] Rawal, R., Schweiker, M., Kazanci, O.B., Vardhan, V., Jin, Q., Duanmu, L. Personal comfort systems: A review on comfort, energy, and economics. Energy and Buildings. 2020; 214:109858.

[5] Rupp, R.F., Kazanci, O.B., Toftum, J. Investigating current trends in clothing insulation using a global thermal comfort databse. Energy and Buildings. 2021. 252: 111431.

[6] Watanabe, S., Melikov, A.K., Knudsen, G.L. Design of an individually controlled system for an optimal thermal microenvironment. Building and Environment. 2010. 45(3): 549-558.

[7] ISO 14505-2. Ergonomics of the Thermal Environment – Evaluation of Thermal Environment in Vehicles – Part 2: Determination of Equivalent Temperature. International Organization for Standardization, Geneva, Switzerland. 2004.

Revisiting radiant cooling systems from a resiliency perspective: A preliminary study

Ongun B. Kazanci, Jun Shinoda, Bjarne W. Olesen

International Centre for Indoor Environment and Energy – ICIEE, Department of Environmental and Resource Engineering, Technical University of Denmark, Koppels Allé, Building 402, 2800 Kgs. Lyngby, Denmark

Abstract. Radiant heating and cooling systems have been proven to be an energy-efficient and resource-effective heating and cooling solution for buildings. One of the key features of radiant systems is the possibility of activating and controlling the thermal mass. This feature allows spreading the heat removal from indoor spaces over a longer period, compared to more conventional systems e.g., air-conditioning. This feature of radiant systems could be particularly beneficial under heat wave and power outage events. The present study investigated the performance of Thermally Active Building Systems (TABS) and Packaged Terminal Air Conditioners (PTAC) in terms of controlling indoor temperatures under future typical weather files, and under future heat wave and power outage events. The simulations were carried out for Copenhagen, Denmark. For future typical meteorological years, TABS performed better with heavyweight construction, but PTAC had little influence from the construction type. During heat waves, both systems were able to maintain a generally comfortable temperature range but with a slightly overall higher temperature. When a heat wave and power outage occurred at the same time, the cases with heavyweight construction had lower temperatures regardless of the cooling system. With TABS and heavyweight construction, the room temperature was maintained within the comfort range of 26°C for 16 hours after the heat wave and power outage started. After the power outage was over, TABS with heavyweight construction was able to reduce the room temperature to the comfort condition of 26°C faster than PTAC by 18 – 71 hours. Results obtained from this initial set of simulations suggest TABS could be a better solution than PTAC in terms of its resiliency to heat waves and power outages although both systems could have different advantages depending on the operation, building type and building use.

Keywords. Heat wave, power outage, resiliency, Thermally Active Building System (TABS), Packaged Terminal Air Conditioner (PTAC).
DOI: https://doi.org/10.34641/clima.2022.241

1. Introduction

There are several passive and active cooling systems that are widely used in buildings. The cooling performance (in this context, keeping indoor temperatures within desired or required comfort limits) of these systems vary depending on several factors such as physical principles, operation, control and geography.

One of the critical selection criteria for these cooling systems is their resiliency i.e., resiliency against heat waves and power outages. International Energy Agency (IEA), Energy in Buildings and Communities Programme (EBC) Annex 80 – Resilient Cooling of Buildings [1] is working on defining resiliency and its key concepts in terms of building cooling [2] [3], developing qualitative and quantitative key performance indicators [4], and evaluating different cooling systems based on these indicators. One of the critical tasks of the Annex is to develop future typical meteorological year weather files and future heat wave weather files [5].

Radiant cooling systems have been proven to be an energy-efficient and resource-effective cooling solution for buildings [6]. One of the key features of radiant systems is the possibility of activating and controlling the behavior of the thermal mass. This feature allows spreading the heat removal from indoor spaces over a longer period, compared to more conventional systems e.g., air-conditioning. This feature of radiant systems is particularly important under heat wave and power outage events.

Copyright ©2022 by the authors. This conference paper is published under a CC-BY-4.0 license.

Table 1 – Physical properties of building materials. [8]

Construction	Material	Thickness [mm]	Density [kg/m³]	Conductivity [W/(m·K)]	Thermal Capacity [Wh/(kg·K)]	Emissivity [-]
Floor/ceiling	Screed	45	2000	1.4	0.28	0.94
	Acoustical insulation	20	50	0.04	0.42	
	Concrete	180	2400	2.1	0.28	
Outside wall (light)	Aluminium	2	2600	200	0.28	0.3
	Insulation	100	30	0.04	0.28	
	Aluminium	2	2600	200	0.28	
Outside wall (heavy)	Plaster	8	1000	0.7	0.28	0.82
	Insulation	80	40	0.04	0.42	
	Sand lime brick	240	1200	0.56	0.28	
	Plaster	15	1200	0.35	0.28	
Internal wall (light)	Plasterboard	25	900	0.21	0.28	0.82
	Insulation	60	20	0.04	0.28	
	Plasterboard	25	900	0.21	0.28	
Internal wall (heavy)	Plaster	15	1200	0.35	0.28	0.82
	Sand lime brick	115	1800	0.99	0.28	0.93
Window	Wooden frame, 30% Glass	Frame thermal transmittance: 2.1 W/(m²·K) Glass thermal transmittance: 1.1 W/(m²·K) Window thermal transmittance: 1.4 W/(m²·K) g-value: 0.58				

Radiant cooling systems and air-conditioning systems are commonly used in buildings and they are also a part of the studied cooling systems in IEA EBC Annex 80. Therefore, the present study compared the performance of Thermally Active Building Systems (TABS) and Packaged Terminal Air Conditioners (PTAC) in terms of controlling indoor temperatures under future typical weather files, and under future heat wave and power outage events.

2. Methodology

2.1 Building Model

Simulations were conducted with TRNSYS version 18 [7]. The model was based on the simulation model used by Olesen and Dossi [8] and Kolarik et al. [9] The model consists of east and west facing office rooms (floor area of 19.8 m² each) with a corridor (floor area of 8.6 m²) in between them. The east and west walls were external walls, and all other surfaces were adjacent to another zone with the same temperature. Both heavyweight and lightweight constructions were modelled. Fig. 1 shows the section view of the building model and the physical properties of the building materials are listed in Table 1.

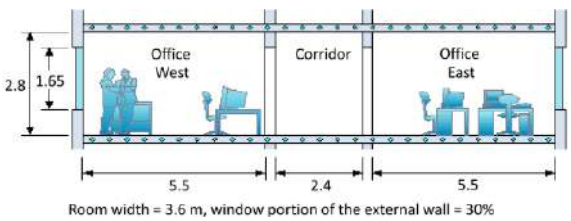

Fig. 1 – Section view of building model (units: m) [10].

Each room was assumed to be a two-person office, and the room was occupied on weekdays from 8:00 to 17:00 with a lunch break between 12:00 and 13:00. The sensible load during occupancy was 550 W (27.8 W/m²), corresponding to two occupants, two computers, a printer and lights. The sensible load during the lunch break was reduced to 350 W (17.7 W/m²). Moisture production of 0.1 kg/h was given during occupancy. The infiltration was set to 0.3 h^{-1}. A shading factor of 0.5 was given to the windows when there was direct solar radiation during occupancy.

The corridor had a constant air volume (CAV) system supplying air with an air change rate of 0.5 h^{-1} at a constant temperature of 19 °C. The CAV was operating on weekdays from 6:00 to 18:00. The infiltration was set to 0.3 h^{-1}.

2.2 Cooling systems

Two types of systems were modelled for comparison: a thermally activated building system (TABS) and a packaged terminal air conditioner (PTAC). All the values and settings presented in this section were taken from [8] and [9], unless otherwise stated.

The TABS piping was embedded in the center of the concrete slab, i.e., 90 mm from both sides of the slab. The pipes had an outside diameter of 20 mm, and a spacing of 150 mm. The supply water pump to the TABS was operating for 24 hours every day. The pump flow rate was fixed at 350 kg/h with an on/off control with a deadband of 23 – 24 °C. The deadband was increased by 1 K to prevent overcooling. The supply water temperature was modulated based on

the outdoor temperature with equation (1) [8]. An air-cooled chiller was selected as the cooling source for the chilled water. A simulation with ideal supply water conditions calculated by equation (1) was conducted to obtain the maximum system load, and the chiller was sized with a capacity 15% higher than the maximum load as a buffer.

$$T_{water\ supply} = 0.35 \cdot (18 - T_{outdoor}) + 18 \qquad (1)$$

Where:

$T_{outdoor}$: Outdoor air temperature (°C)

An air-to-air heat recovery unit with a constant flow of 2 L/(s·m^2) to each office zone was used for ventilation for the TABS cases. This ventilation rate is based on two-people in the office rooms of a non low-polluting building [11]. The ventilation system was turned on between 7:00 and 18:00 on weekdays. The sensible and latent efficiency of the heat recovery unit was set to 0.85.

For the PTAC cases, the default component provided by TRNSYS was used [12]. The outdoor air was fixed to 2 L/(s·m^2) per zone and was mixed with recirculated air, supplying a total of 7.2 L/(s·m^2) to each zone. The supply air flow rate was calculated internally within the component based on ASHRAE Standard 90.1 [13]. The deadband for the supply air temperature control was set to 24.5 ± 1.5 °C, corresponding to Category II of EN 16798-1 [11]. A simulation with ideal cooling was conducted to obtain the maximum room cooling load, and the PTAC was sized with a capacity 15% higher than the maximum load as a buffer.

2.3 Weather files and simulation cases

Weather files created by the IEA EBC Annex 80 Weather data task force were used for the simulations. The weather data is based on the European Coordinated Regional Downscaling Experiment (EURO-CORDEX) [14]. The methodology for creating the weather data is reported by Machard et al. [15]. Weather files were created in EPW format for each representative climatic zone and city.

Weather files were generated for three periods i.e., contemporary (2001 – 2020), medium-term future (2041 – 2060), and long-term future (2081 – 2100). For each period, a typical meteorological year (TMY) file was created. In addition, heat wave year (HWY) files were created for each period. Multiple heat waves with different characteristics were created. The heat waves were characterized by its intensity (maximum temperature), duration (length of heat wave), and severity (combined evaluation of temperature and duration, i.e., degree days).

Table 2 lists the simulated weather files. The weather file for Copenhagen, Denmark was used for the analysis. The selection of the cases follow the simulation guideline developed by IEA EBC Annex 80 [16]. Typical meteorological years for three different periods were used. For the heat wave years, the most severe heat wave years for the contemporary, medium-term future, and long-term future were each selected. All simulations were conducted between 1. May and 30. September with a simulation time step of 15 min. Load calculations for sizing the TABS and PTAC were conducted with the typical meteorological year 2001 – 2020.

For the heat wave cases, simulations were conducted both with and without a power outage. According to the simulation guideline developed in the Annex, simulations are to be conducted with power outage throughout the entire duration of the heat wave (worst case scenario) [16]. During the power outage, TABS (and the ventilation system) and PTAC were both turned off. The internal heat gain during the heat wave was limited to equipment load (i.e., 12 W/m^2).

Table 2 – Simulated weather files.

Type	Year / Category	Power outage
TMY: Typical Meteorological Year	2001 – 2020	No
	2041 – 2060	No
	2081 – 2100	No
HWY: Heat wave year, Most severe	Contemporary	Both with and without power outage
	Medium-term future	
	Long-term future	

3. Results and Discussion

3.1 Indoor temperatures without power outage

Fig. 2 shows the distribution of operative temperature in the west office during occupied hours. The west office was selected as higher temperatures were observed and therefore was more critical than the east office. The cases without power outage was selected. For TMY files, the results were evaluated from 1. June, and for HWY files, results were evaluated from 1 week before to 1 month after the heat wave. The temperature range shaded in green represents the default indoor operative temperature values for office spaces according to Category II of EN 16798-1 [11] in the cooling season.

The simulation result of the typical meteorological year cases show that both TABS and PTAC can maintain the indoor operative temperature within a comfortable range in most cases. TABS had a tendency of a larger range of room operative temperature in lightweight construction. For TABS, a lightweight construction results in less precooling during unoccupied hours, which causes more room

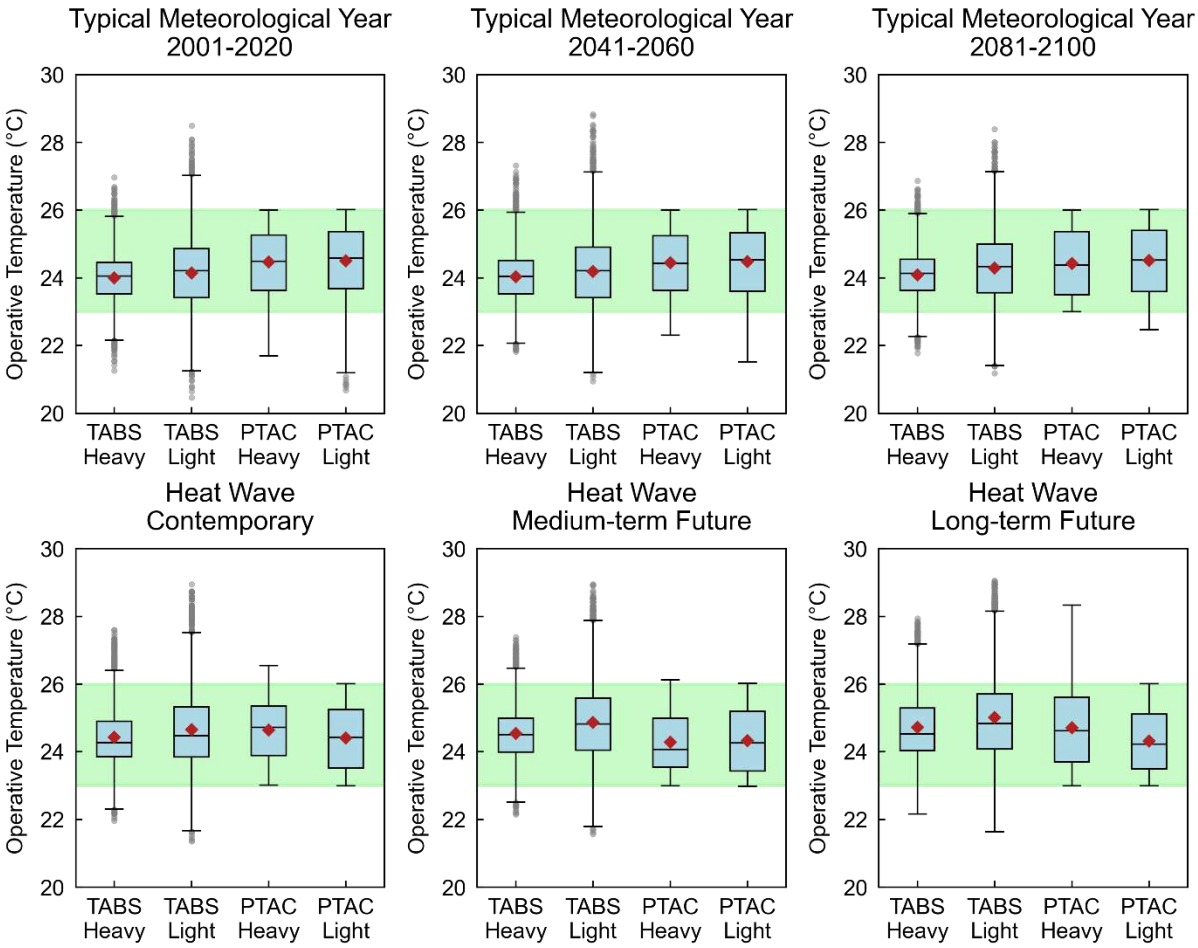

Fig. 2 – Distribution of operative temperature in the west office during occupied hours.

temperature fluctuation during occupied hours. For both systems and building types, the time period of the TMY files had minimal effects on the simulation outcome.

It can be seen that under the heat wave conditions, overall room temperatures increased, which was an expected result. The differences in the room temperatures due to the different heat removal mechanisms of the two systems can be seen by comparing the TABS Heavy and the PTAC Heavy cases. In the long-term future weather case, higher room temperatures compared to other cases are observed for the PTAC Heavy cases. The PTAC system is struggling to remove the heat from the room as there is also heat accumulated in the building thermal mass. TABS on the other hand is cooling the building structure (i.e., thermal mass) and also cooling the room through cooled surfaces and it is more effective in keeping the room temperatures within the desired range.

Overall, PTAC with lightweight building construction had the most of the occupied hours within a comfortable range. TABS with heavyweight construction was also able to have most of the hours within the same range, but temperatures were occasionally outside of those ranges. However, it must be noted that the most common operating principle of TABS allows the fluctuation of the indoor temperature and does not aim to control at a fixed temperature throughout the day.

3.2 Indoor conditions with power outage

Fig. 3 shows the operative temperature of the west office under contemporary heat wave conditions with power outage. The red line indicates the 26 °C comfort limit [16].

During the heat wave and power outage, the cases with heavyweight construction maintained a temperature generally lower than the lightweight construction cases; however, this difference between the heavyweight and lightweight cases became smaller as the heat wave continued. TABS with heavyweight construction had the lowest room temperatures, and was able to maintain a room temperature below 26 °C for the longest time after the heat wave and power outage. At the final day of the heat wave (20 days), the temperature of the TABS and PTAC heavyweight cases had similar temperatures. After the heat wave and power outage, the four scenarios showed a different trend in their temperature recovery. TABS with lightweight construction was the fastest to reach 26 °C, and PTAC with heavyweight construction was the slowest.

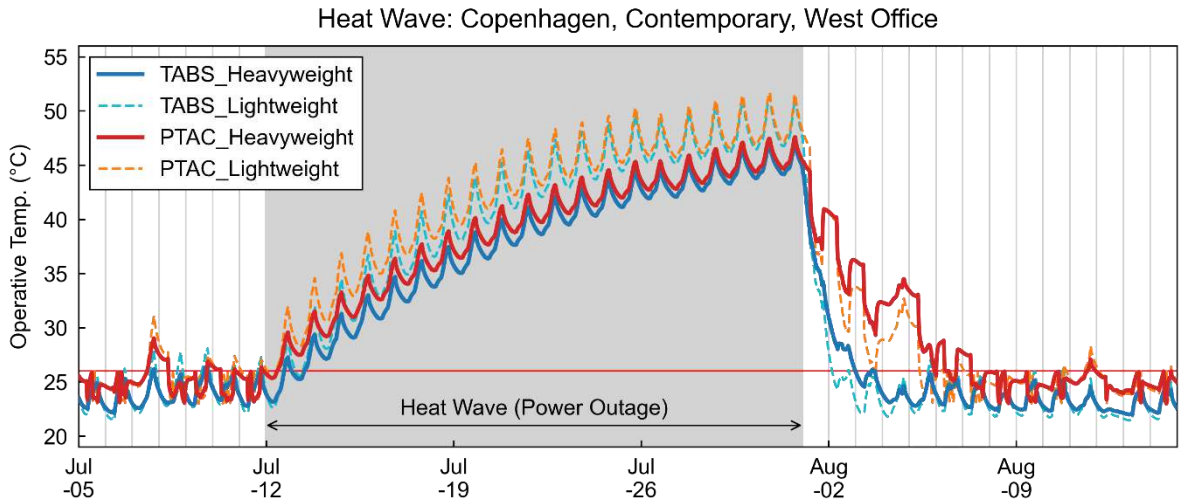

Fig. 3 – Operative temperature of west office under contemporary heat wave conditions with power outage.

Figs. 4 and 5 show a closer look at the operative temperature of the west office for 3 and 7 days from the beginning of the heat wave and power outage. Horizontal lines were drawn at 26, 27, 28 °C as a reference for different comfort limits. TABS with heavyweight construction was able to maintain a temperature below 26 °C for 16 hours after power outage, and for 40 hours when the comfort limit was set to 28 °C. PTAC with heavyweight construction was able to maintain a temperature below 26 °C for 10 hours, but the temperature increased to nearly 30 °C in the evening.

The difference in the daily peak temperature between the heavyweight and lightweight cases increased gradually to about 5 K for both TABS and PTAC. On the first day of the heat wave and power outage, TABS heavyweight case had a peak temperature 1.9 K lower than the lightweight case, and the difference increased to 4.8 K on the seventh day. For PTAC, the corresponding temperature differences were 2.4 K and 4.9 K, respectively. When comparing the same heavyweight construction cases, TABS had a peak temperature lower than PTAC by 2.3 K on the first day, and the difference decreased to 1.4 K on the seventh day. In the comparison of lightweight cases, the corresponding peak temperature differences were 2.8 K and 1.5 K, respectively. As the systems were not operating during the power outage, the difference by the cooling systems became smaller each day.

Figs. 6 and 7 show a closer look at the operative temperature of the west office for 3 and 7 days after the end of the heat wave and power outage. For TABS, the lightweight construction was able to lower the room temperature to 26 °C after 27 hours and after 48 hours for the heavyweight construction. For PTAC, the room temperature reached 26 °C in 66 hours for the lightweight construction and 119 hours for the heavyweight construction. Table 3 summarizes the hours each system maintained below a certain baseline temperature and the hours it took to recover to the baseline after the heat wave.

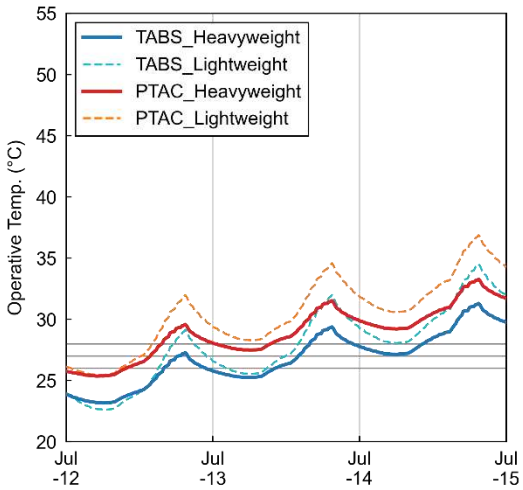

Fig. 4 – Operative temperature of west office for the first 3 days of the heat wave (contemporary, with power outage).

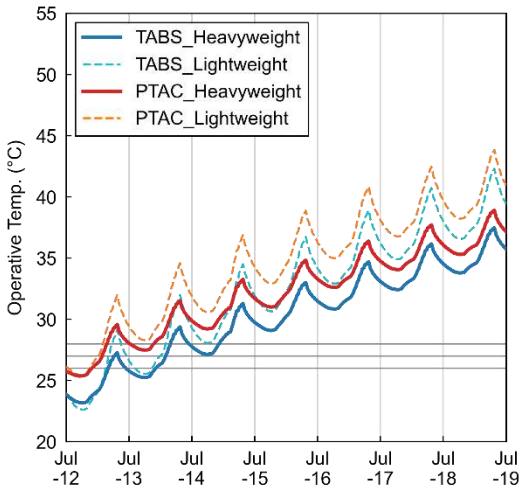

Fig. 4 – Operative temperature of west office for the first 7 days of the heat wave (contemporary, with power outage).

Table 3 – Hours below baseline (at the beginning of heat wave) and hours until baseline (after heat wave).

Baseline (°C)	TABS		PTAC	
	Heavy	Light	Heavy	Light
Hours maintained below baseline temperature				
26	16	15	10	0
27	19	16	14	12
28	40	18	16	14
Hours until baseline temperature is reached				
26	48	27	119	66
27	45	25	117	61
28	38	24	108	59

4. Overall Discussion

In this study, a series of simulations were conducted for a simple comparison of TABS with consistent operation and PTAC with intermittent operation. The systems simulated in this study were sized with the typical meteorological year file of 2001 – 2020, but did not result in a substantial difference in the operative temperature of the cases with future weather files. This suggests that sizing a system based on future weather files may not provide a clear advantage, though it should be noted that the capacity of the cooling plants was 15% higher than the maximum load as a buffer. It should also be noted that in reality the sizing of the chiller for a TABS and for a PTAC system would be different.

Though the present results suggest that TABS with heavyweight construction is a better solution than PTAC under heat wave and power outage conditions, further studies should be performed, especially for the control strategies and the heat source. Different control strategies of TABS (e.g., varying the supply water temperature or operation during night time only) and PTAC (e.g., precooling) would likely result in a different outcome. As this was a preliminary study, relatively simple control strategies were used for both systems. Future studies will investigate optimized control strategies.

Both of the studied systems intend to condition the entire indoor space. The combination of these ambient control systems with a personalized environmental conditioning system (PECS) to offset the comfort conditions could also be an alternative solution and could help occupants get back to the buildings sooner

In the studied boundary conditions, the selection of the heat source is likely to have a large impact to the simulation results. Another possibility would be to consider the use of renewable energy, such as geothermal heat. While systems that rely on outdoor air temperature will be directly affected by the

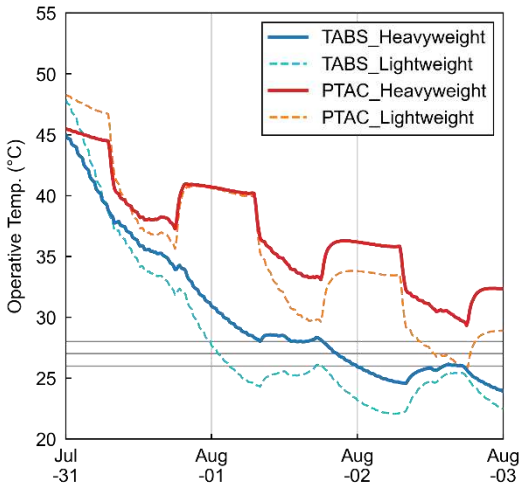

Fig. 6 – Operative temperature of west office 3 days after the heat wave (contemporary, with power outage).

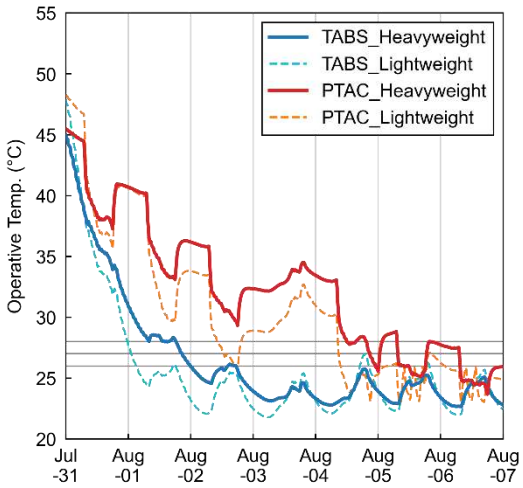

Fig. 7 – Operative temperature of west office 7 days after the heat wave (contemporary, with power outage).

temperature rise during the heat wave, the ground temperature is likely to be less influenced. However, the effect of the increasing yearly average temperature of the site (and thus the ground) must be considered.

5. Conclusion

Simulations were conducted to re-evaluate radiant cooling systems from the resiliency perspective. Thermally Active Building Systems (TABS) with consecutive operation and packaged terminal air conditioners (PTAC) with intermittent operation were compared. Future weather files of typical meteorological years (TMY) and heat wave years (HWY) were used.

For future typical meteorological years, both TABS and PTAC were able to provide an indoor temperature within a comfortable range. TABS performed better with heavyweight construction, but PTAC had little influence from the construction type. During heat waves (but with power available),

both systems were able to maintain a generally comfortable temperature range but with a slightly overall higher temperature.

On the first day of the power outage with heavyweight construction cases, TABS was able to maintain a peak temperature 2.3 K lower than with PTAC. This difference became gradually smaller, and became 1.4 K after one week. With lightweight construction, TABS kept the peak temperature lower than that of PTAC by 2.8 K on the first day of the power outage, and 1.5 K lower after one week.

When a heat wave and power outage occurred at the same time, the cases with heavyweight construction had lower temperatures regardless of the cooling system. With TABS and heavyweight construction, the room temperature was maintained within the comfort range of 26°C for 16 hours after the heat wave and power outage started. After the power outage was over, TABS with heavyweight construction was able to lower the room temperature to the comfort condition of 26°C faster than PTAC by 18 – 71 hours. Results obtained from this initial set of simulations suggest TABS could be a better solution than PTAC in terms of its resiliency to heat waves and power outages although both systems could have different advantages depending on the operation, building type and building use.

6. Acknowledgement

This research was a part of IEA EBC Annex 80 – Resilient Cooling of Buildings and was financially supported by Det Energiteknologiske Udviklings- og Demonstrationsprogram (EUDP) under grant no. 64018-0578.

7. Data Access Statement

The datasets generated during and/or analyzed during the current study are not available because of a non-disclosure agreement but the authors will make every reasonable effort to publish them in near future.

8. References

[1] IEA EBC Annex 80 - Resilient Cooling of Buildings. [Online]. Available: https://annex80.iea-ebc.org/. [Accessed 2022].

[2] Attia S., Levinson R., Ndongo, E., Holzer, P., Kazanci, O.B., Homaei, S., Zhang, C., Olesen, B.W., Qi, D., Hamdy, M., Heiselberg, P. Resilient cooling of buildings to protect against heat waves and power outages: Key concepts and definition. Energy and Buildings. 2021; 239: 110869.

[3] Miller, W., Machard, A., Bozonnet, E., Yoon, N., Qi, D., Zhang, C., Liu, A., Sengupta, A., Akander, J., Hayati, A., Cehlin, M., Kazanci, O.B., Levinson, R. Conceptualising a resilient cooling system: A socio-technical approach. City and Environment Interactions. 2021; 11: 100065.

[4] Zhang, C., Kazanci, O.B., Levinson, R., Heiselberg, P., Olesen, B.W., Chiesa, G., et al. Resilient cooling strategies – A critical review and qualitative assessment. Energy and Buildings. 2021; 251: 111312.

[5] Machard, A., Pourabdollahtootkaboni, M., Gaur, A., Salvati, A. Annex 80 - Weather Data Task force - Workshop to generate present and future weather files and heat wave data for building simulations Methodology overview. 2020.

[6] Kazanci, O.B. Low Temperature Heating and High Temperature Cooling in Buildings. PhD Thesis. Kgs. Lyngby: Technical University of Denmark. 2016.

[7] TRNSYS version 18. [Online]. Available: https://sel.me.wisc.edu/trnsys/index.html.

[8] Olesen, B.W. and Dossi, F. C. Operation and control of activated slab heating and cooling systems. in Procedings of CIB World Buildings Congress 2004. Toronto, Canada. 2004.

[9] Kolarik, J., Toftum, J., Olesen, B.W., Jensen, K. L. Simulation of energy use, human thermal comfort and office work performance in buildings with moderately drifting operative temperatures. Energy and Buildings. 2011; 43: 2988-2997.

[10] Li, R., Yoshidomi, T., Ooka, R., Olesen, B.W. Case-study of Thermo Active Building Systems in Japanese Climate. Energy Procedia. 2015; 78: 2959-2964.

[11] EN 16798-1 Energy Performance of buildings – Ventilation for buildings – Part 1: Indoor environmental input parameters for design and assessment of energy performance of buildings addressing indoor air quality, thermal environment, lighting and acoustics. European Committee for Standardization. 2019.

[12] Thermal Energy System Specialists, LLC. TRNSYS 18 Documentation 10. Examples. 2017.

[13] ANSI/ASHRAE/IES Standard 90.1. Energy Standard for Buildings Except Low-Rise Residential Buildings. 2019.

[14] Jacob, D., Petersen, J., Eggert, B., et al. EURO-CORDEX: new high-resolution climate change projections for European impact research. Regional Environmental Change. 2014; 14: 563-578.

[15] Machard, A., Inard, C., Alessandrini, J.-M., Pelé, C., Ribéron, J. A Methodology for Assembling Future Weather Files Including Heatwaves for Building Thermal Simulations from the European Coordinated Regional Downscaling Experiment (EURO-CORDEX) Climate Data. Energies. 2020; 13: 3424.

[16] Zhang, C., Kazanci, O. B., Attia, S., Lee, S. H., Holzer, P., Salvati, A., Machard, A., Pourabdollahtootkaboni, M., Gaur, A., Olesen, B. W., Heiselberg, P.K. IEA EBC Annex 80 - Dynamic simulation guideline for the performance testing of resilient cooling strategies. Aalborg University. 2021.

Baby beds' sleep micro-environment in day care centres

Wim Zeiler

Faculty of Architecture and the Built Environment, Eindhoven University of Technology, Eindhoven, the Netherlands, w.zeiler@bwk.tue.nl.

Abstract. Concerns are emerging about potential adverse effects of indoor air pollutants on children's health and development, since young babies are exceptionally more sensitive to chemical exposures than children and adults. Day care centres (DCCs) are the most important place besides their home as babies spend up to 11 hours inside the DCCs, of which half of the time in their beds during the first six months. Especially during the first year their developing lungs are highly sensitive to pollutions. Ventilation within the baby bed themselves is rarely studied however insufficient IAQ conditions at DCCs were unanimously confirmed in t previous studies. Therefore, the main aim of this paper is to state the importance of improving the indoor air quality at day-care centres, especially in sleep micro-environment of the baby beds. The paper presents an overview to emphasize the importance for the health of babies.

Keywords. Day-care centres, cribs, sleep micro-environment
DOI: https://doi.org/10.34641/clima.2022.123

1. Introduction

The moment you are born you start breathing for the first time. Immediately the developments of your lungs continue in a new phase depending for the first time on the Indoor Air Quality. To date, air pollution, a world-recognized threat to human health, has been documented to be responsible for various health problems (e.g., respiratory diseases, asthma, cancer, etc.) and even shorten lifespans, both indoors and outdoors. Concerns are emerging about potential adverse effects of indoor air pollutants on children's health and development, since young babies are exceptionally more sensitive to chemical exposures than children and adults. Day care centres (DCCs), the first program for the social development of young children, is the most important place besides their home. Babies spend up to 11 hours inside DCCs and spend more than half of the time in their beds during the first six months. Especially during the first year their lungs are developing rapidly and therefor highly sensitive to the Indoor Air Quality. the needs for DCCs have increased considerably around the world over the last few years. For example, within the Netherlands, from 344,280 children in 2015 to 454,660 children in 2018 have registered at DCCs (increased by 32%), (CBS 2020). There are more than 100.000 twin baby beds in the Netherlands, which means that on average daily around 120.000 babies spend half of their time with sleeping in one of these twin baby beds. These beds are close on 5 sides and only there is a front with bars that allow air to come in, see Fig. 1.

Fig. 1 – Most used baby bed in modern Dutch DCCs, fully closed on all sides only open at the from by bars

Adequate ventilation within the baby bed themselves has not been studied before however, it is extremely important for the babies and their healthy development. Especially within the sleep micro-environment, the source-proximity effect would become the most dominant, that is, pollutant concentrations above the crib mattress are greater than those in the bulk air of the sleeping room. When you also consider the layout of most of the modern DCCs, see Fig. 2, where they put as many beds in a room as possible it immediately becomes clear that

Copyright ©2022 by the authors. This conference paper is published under a CC-BY-4.0 license.

there might be a problem with the adequate ventilation of these twin baby beds.

Fig. 2 – Most common set-up on modern day care centres; 2 rows of 6 baby beds, with just enough space between them

Therefore, the main aim of this study is to explore the air quality within the baby bed and determine influencing factors related to the indoor air quality. This especially for the position of the baby in the bed and the difference between lower and upper bunk bed in sleep microenvironment with the double baby bunk beds at DCCs. This article represents an overview of the research on baby beds over the last decades.

2. Health aspects and IAQ

2.1 Development of the lungs

To date, air quality, a world-recognized threat to human health, has been documented to be responsible for various health problems (e.g., respiratory diseases, asthma, cancer, etc.) and even shorten lifespans, both indoors and outdoors (EEA, 2017). Recently, World Health Organization (WHO) also stated that air pollutants, both indoor and outdoor, the biggest environmental threat to health, contribute to one-ninth of deaths annually in the world (WHO 2016).

DCCs are the most important place besides their home of young children (generally aged 0-4 years old). Concerns are emerging about potential adverse effects of indoor air pollutants in DCCs on children's health and development. Worse, available evidence (Zheng et al 2022) indicates young children's attendance in DCCs increases the risk of respiratory and gastrointestinal infections (Bradley 2003, Ferng and Lee 2002, Hagerhed-Engman et al. 2006, Koopman et al. 2001, Louhiala et al. 1995, Nafstad et al. 2005).

Young children are exceptionally more sensitive to chemical exposures than higher-grade children and adults (Ferguson and Solo-Gabriele 2016, Gabriel et al. 2020, WHO 2005). This is because of their developing organ systems (particularly lungs), incomplete metabolic systems, immature host defences, the higher inhalation rates per unit of body weight, and their greater surface-to-volume ratios (Brent and Weitzman 2004, Burtscher and Schüepp 2012, Oliveira et al 2019, WHO 2005). Baby's breath 10 times more air per body mass than adults and have skin surface area to body mass ratio three times greater than that of adults.

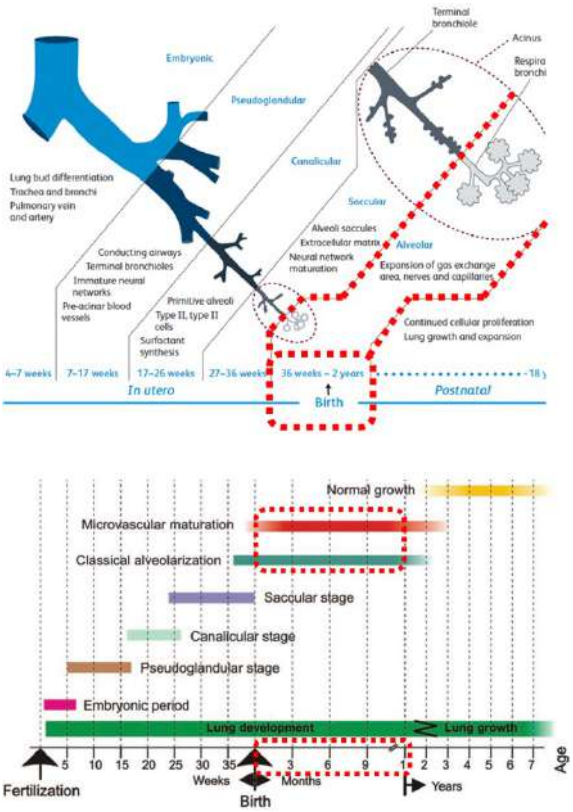

Fig. 3. Top Principal stages of lung development in humans [Holgate 2016] and timing [Schittny and Burri 2008].

2.2 IAQ within DCCs

On a global scale, there has been a certain body of studies about IAQ investigations at DCCs over the last decade. More specifically, a total of 122 IAQ-related studies were performed at DCCs from 2010 to 2020(Zheng et al. 2022). Measured types of indoor air pollutants covered physical parameters (temperature and relative humidity), chemical (VOC, SVOC, O_3, CO_2, CO, NO_2, SO_2, Radon, PM), biological contaminants (bacteria, fungi/moulds, allergens, pollen, pet dander).

There are significant space-related contaminants, including diapers, arts-and-crafts supplies, and

cleaning agents (ANSI/ASHRAE, 2019). Apart from that, it's worth mentioning that the level of exposure to indoor air pollutants may be elevated due to the source-proximity effect specific to children's activity patterns (e.g., playing or crawling on the ground; sleeping in the crib; more mouth breathing; more oral ingestion via hands-to-mouth-transfer) (Boor et al. 2014, Boor et al. 2017, Liang and Xu 2014). Especially, within the sleep micro-environment, the source-proximity effect would become the most dominant. Pollutant concentrations within the crib mattress are greater than those in the bulk room air (Furtaw et al. 1996, Laverge et al. 2013, Spilak et al. 2014, Boor et al. 2014, Boor et al. 2015, Kim et al., 2015, Zheng et al. 2022), which may also be a significant influence on exposures to the sleep micro-environment at DCCs.

2.3 Micro-climate DCCs' Baby beds

Mattress dust is found to contain a diverse spectrum of biological particles and particle-bound chemical contaminants and their concentrations in dust can span many orders of magnitude among bed samples (Boor et al 2014). Furthermore, mattress foam and covers, pillows, and bed frames can emit a variety of volatile and semi volatile organic compounds, and emission rates can increase due to localized elevations in surface temperature and moisture near the bed due to close contact with the human body (Boor et al 2014). Emissions can emit more organic compounds (VOCs) due to the increase in surface temperature by the baby's body and humidity (leaking diapers). This is specifically in the places where the material is in contact with the body. Therefore, good ventilation levels inside the baby beds are of extreme importance to remove the pollutants and create a healthy sleep microenvironment for the babies. Crib mattresses have also been indicated as a major source of VOC concentrations in a room. The emission rates of mattresses are comparable to those of flowing materials, wallcoverings, and plastic toys. (Boor et al 2015) This is a concern as the source of VOCs is within the breathing zone of the babies when put in bed.

Despite the severity of the situation inside the baby beds, only a few studies were performed to focus on the air quality of sleep microenvironment within the beds at DCCs (Da Silva et al. 2005). These studies only investigated CO_2 levels or mite levels, which would be far insufficient to characterize the overall IAQ since other air pollutants can be dominant. Unfortunately, insufficient IAQ conditions, based on CO_2 measurements at DCCs were unanimously confirmed in the previous studies (Ferng and Lee 2002, Versteeg 2009, Mendes et al 2014, le Grand and Duijm 2017, Prussin et al. 2019). Similar to a home, various indoor pollutant sources exist in the DCCs (Junaidi et al. 2019, Lee et al. 2018, Yu et al., 2019, Zheng et al. 2022). The air quality might not be the same throughout a ventilated space. What really counts for the occupants is the air quality in the breathing zone. Such an inhomogeneity of the air quality in space has an impact on the ventilation requirement, especially in the case of the sleep microenvironment within baby bunk beds at DCCs. So clearly, more interesting are the conditions inside the baby beds, they only measurements we could find beside our own measurements [Offermans 2020], were by le Grand and Duijm (2017). To determine whether our results were in line with their results we compared them, see Fig. 4. Both trendlines have a factor of slightly more than 1.2, meaning that on average the CO_2 concentration in the baby bed is around 20% more than in the sleeping room itself. However, there is a weaker correlation in the measurements in the Eindhoven DCC compared to that of the results by le Grand and Duijm [2017]. This probably because of more different occupancy rates of babies in the sleeping room in Eindhoven.

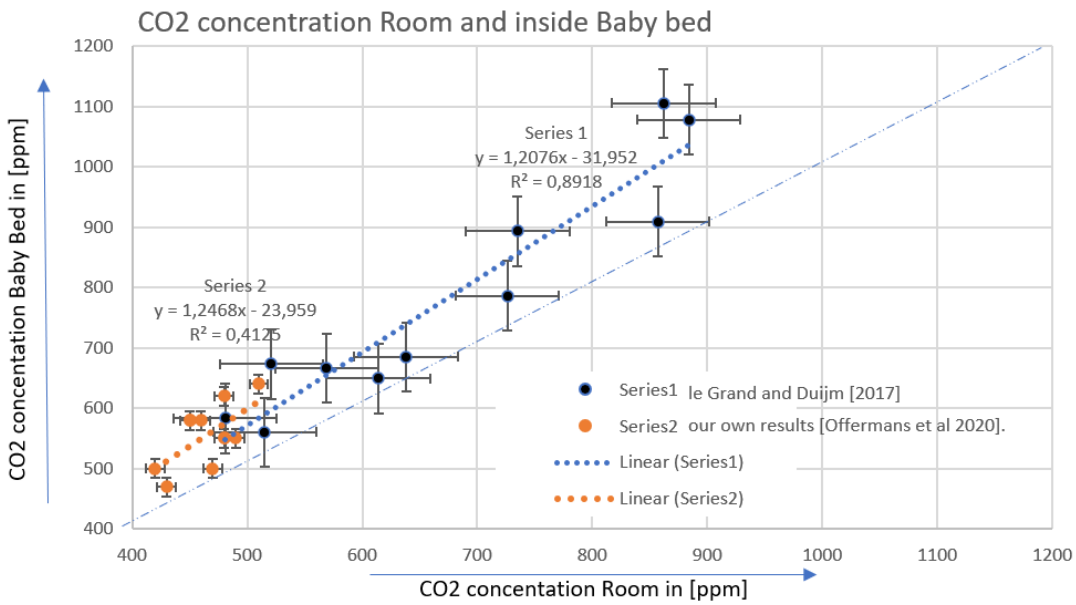

Fig. 4 -Results measurements within the baby beds

3. Methodology measurements

It is clearly necessary to get more and detailed insight in the IAQ in sleep microenvironment with the baby bunk beds at DCCs.

3.1 Influence of the position of the bed

Especially, interesting is to see whether there is a significance difference in IAQ between the upper and lower bed of a baby bed bunk. Therefore, the CO2 concentration were measured in the upper baby bed as well as in the lower baby bed in the real situation of a DCC, see Fig. 5.

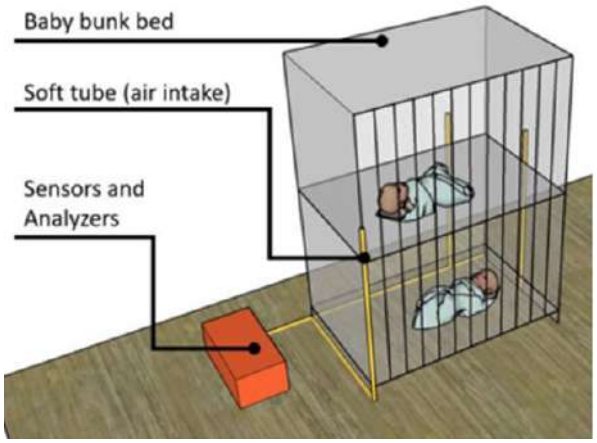

Fig. 5 - Measurement setup indoor air quality in the upper and lower baby bunk beds (Offermans et al 2020)

Also, interesting is whether the position of the baby within the bed itself would have a large influence on the CO2 concentrations inside the bed. However, due to privacy reason it was not allowed to monitor the positions of real babies in their beds, therefore an experimental set-up was built. A baby doll was used, in which the breathing of a baby was simulated by a ventilator and valve mechanism. In this way a mixture of air and CO2, just like the breathing of a baby, was generated, see Fig. 6-8. Experiments were performed representing a bottom bunk bed and a bedstead.

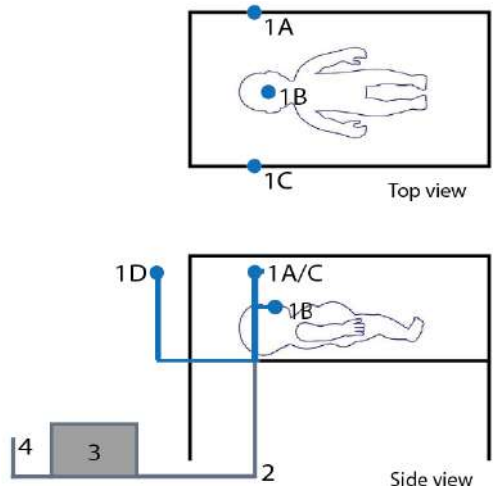

1. Four CO_2 sensors 2. Cable bundler 3. Central box 4. Main's supply

Fig. 6 - Experimental measurement to simulate different positions for the baby doll inside the baby beds(Braun and Zeiler 2019)

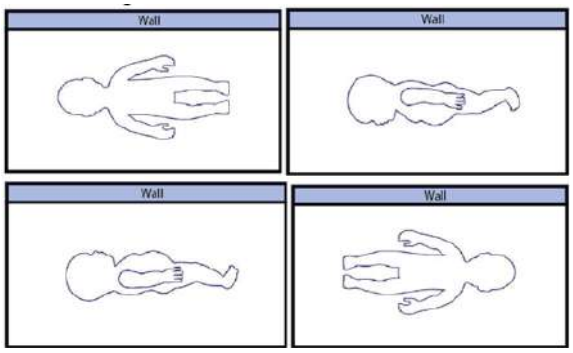

Fig. 7 - Measurement positions for the baby doll inside the baby beds: supine, lateral facing room, lateral facing wall and prone (Braun and Zeiler 2019)

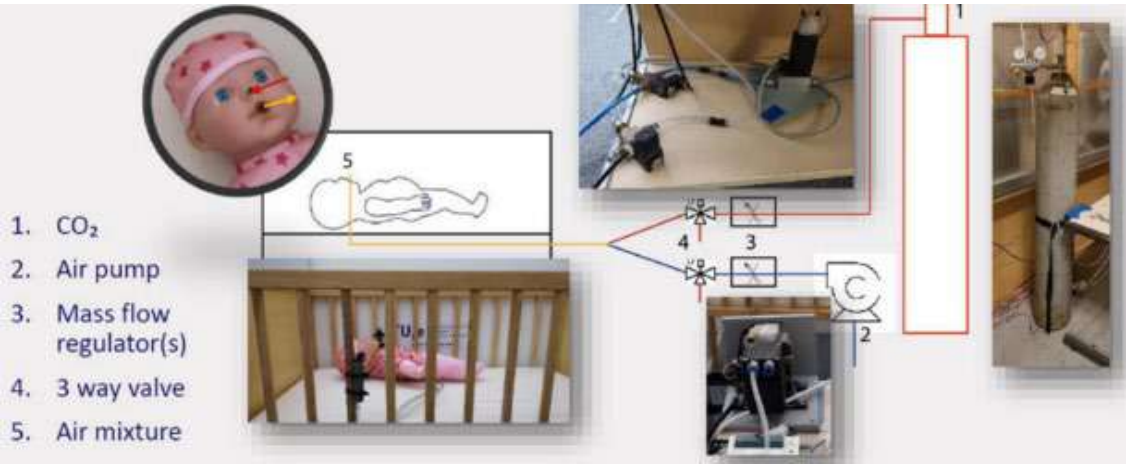

Fig. 8 - Breathing simulator and baby doll in a bedstead at TU/e (Braun and Zeiler 2019)

4. Results

The effects of the different location of the bed (upper or lower bed), as well as the different positions of the baby itself in the bed on the CO_2 concentrations are displayed in this paragraph.

4.1 Influence of the position of the bed

In the bottom bunk bed and upper bunk bed the average measured CO_2 concentration were determined. These are displayed in Table 1, where it can be seen that the CO_2 concentrations are higher for the position in the upper bunk bed and therefore lower in the lower bunk bed. Unfortunately, there were different occupancies in the sleeping room during our measurements.

Table 1. Difference between bottom and top position in baby bunk bed with 3 and 5 babies in the sleeping room (max. 6) in ppm CO_2

Bottom bunk bed - back of bed					Top bunk bed - back of bed			
min	average	max	P98	babys	min	average	max	P98
474	592	739	679	3	446	543	644	600
426	517	609	568	3	400	536	704	652
420	501	655	557	3				**μ = 626**
			μ = 601					
455	536	623	585	5	449	563	705	***635***
409	475	612	559	5				
			μ = 572					

As can be seen there is a significant difference, the top position is worse than the bottom position by 5 to 10 % CO_2 concentration.

4.2 Influence of the position of the baby

In the second series of experiments different fixed positions of a baby were simulated. It was found that the bottom bunk bed with more closed surroundings led to an average increase of around 220 percent relative to the background level compared to a bedstead where the increase was 160 percent, see Fig. 9. In both situations the increases are significant and even more significant for the measurements at the wall side, here the increase in the bottom bunk bed was on average around 270 percent and for the bedstead it was around 210 percent. Therefore, it can be concluded that the more closed the surroundings of a crib are, the higher the CO_2 concentrations will be.

The position of the baby doll also had a significant effect on the measurements. For example, with the bottom bunk bed when the baby is facing the wall the rise in the average CO2 concentrations was around 270 percent, however when the baby was facing the room (bars) the CO2 concentrations only rose by nearly 30 percent. Facing the roof led to an average increase of around 80 percent. Therefore, it is concluded that the position of the baby has a significant effect on the measured values. When the mouth of the baby is facing an open surrounding the average CO2 concentrations of the inhaled air decreased significantly compared to when a baby was facing a more closed surrounding. Thus, it is concluded that it is not sufficient to only measure the CO2 concentrations in the sleeping room as the conditions will significantly deviate from those in a bedstead.

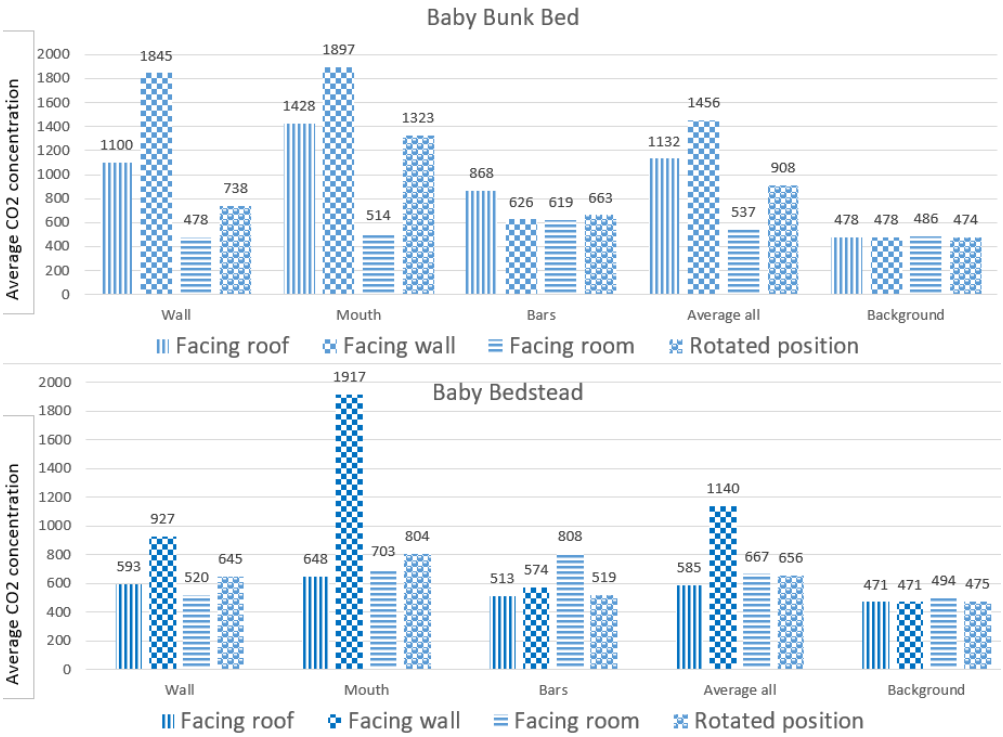

Fig. 9 – Bottum bunk bed versus bedstead average CO_2 concentration

5. Discussion

Concerning the measurements in relation to the position of the baby within the bed, it would be best to perform measurements in a real setting. However, this is not allowed due to privacy rules within the DCCs.

The research clearly showed the importance to monitor inside the baby bed and not take the average IAQ of sleeping room conditions of DCCs which as such is currently the common practice. Unfortunately, insufficient IAQ conditions at DCCs were unanimously confirmed in our studies. Especially within the sleep micro-environment, the source-proximity effect is most dominant, that is, pollutant concentrations within the crib mattress are greater than those in the bulk room air. The ventilation effectiveness inside the baby bed of the typical double baby bunk beds is considerable worse and it is therefore that more effort is necessary to come up with solutions to improve this.

The number of measurements which were done to determine the difference in IAQ between bottom and top position in the baby bunk bed is rather limited, so more measurements are needed to determine whether this is significant enough or not.

6. Conclusions

The main aim of this paper is to state the importance of improving the indoor air quality at DCCs especially inside the sleep microenvironment of the most used type of double baby bunk beds in the Netherlands.

The research on the indoor air quality at bed level and sleeping room level at DCCs ultimately can give a clear picture of the indoor air quality level at the bedroom and baby bunk bed in the Netherlands. It can lead to develop effective and efficient control strategies for the ventilation system to guarantee adequate indoor air quality at DCCs. Additionally, the result of this study should be used as a useful evidence base for the formulation and targeting of new standards, or guidelines for improving IAQ at DCCs.

Data access statement

The datasets generated during and/or analysed during the current study are not available because of privacy reasons but the authors will make every reasonable effort to publish them in near future.

References

ANSI/ASHRAE (2019) ANSI/ASHRAE Standard 62.1-2019 -- Ventilation for Acceptable Indoor Air Quality. American Society of Heating, Refrigerating and Air-conditioning Engineers (ASHRAE).

Boor B.E., Järnström H., Novoselac A., Xu Y. (2014) Infant exposure to emissions of volatile organic compounds from crib mattresses. Environmental Science and Technology 48, 3541-3549.

Boor B.E., Spilak M.P., Corsi R.L., Novoselac A. (2015) Characterizing particle resuspension from mattresses: chamber study. Indoor Air 25, 441-456.

Boor B.E., Spilak M.P., Laverg, J., Novoselac A., Xu Y. (2017) Human exposure to indoor air pollutants in sleep microenvironments: A literature review. Building and Environment 125, 528-555.

Bradley R.H. (2003) Childcare and common communicable illnesses in children aged 37 to 54 months. Archives of pediatrics & adolescent medicine 157, 196-200.

Braun G.J., Zeiler W. (2019) CO_2-concentration of the surrounding air of sleeping infants inside a crib, Proceedings 40th AIVC Conference: From Energy crisis to sustainable indoor climate–40 years of AIVC. Air Infiltration and Ventilation Centre (AIVC), Gent, Belgium.

Brent R.L., Weitzman M. (2004) The Vulnerability, Sensitivity, and Resiliency of the Developing Embryo, Infant, Child, and Adolescent to the Effects of Environmental Chemicals, Drugs, and Physical Agents as Compared to the Adult: Preface. Pediatrics 113, 933-934.

Burtscher H., Schüepp K. (2012) The occurrence of ultrafine particles in the specific environment of children. Paediatric respiratory reviews 13, 89-94.

CBS, (2020) StatLine - Formele kinderopvang; kinderen, uren, soort opvang, vorm opvang, regio. Dutch Central Bureau of Statistics

Da Silva D.R., Binotti R.S., Da Silva C.M., De Oliveira, C.H., Condino-Neto, A., De Capitani, E.M. (2005) Mites in dust samples from mattress surfaces from single beds or cribs in the south Brazilian city of Londrina. Pediatric Allergy and Immunology 16, 132-136.

EEA (2017) National Emission Ceilings (NEC) Directive reporting status (2017): The need to reduce air pollution in Europe. European Environment Agency, Copenhagen, Denmark.

Ferguso, A., Solo-Gabriele H., (2016) Children's Exposure to Environmental Contaminants: An Editorial Reflection of Articles in the IJERPH Special Issue Entitled, "Children's Exposure to Environmental Contaminants". Multidisciplinary Digital Publishing Institute.

Ferng S.F., Lee L.W. (2002) Indoor air quality assessment of daycare facilities with carbon dioxide, temperature, and humidity as indicators.

Journal of Environmental Health 65, 14-18.

Gabriel M.F., Felgueiras F., Fernandes M., Ribeiro C., Ramos, E., Mourao Z., de Oliveira Fernandes, E. (2020) Assessment of indoor air conditions in households of Portuguese families with newborn children. Implementation of the HEALS IAQ checklist. Environ Res 182, 108966.

Grand A. le, Duijm F. (2017) Onderzoek binnenmilieu kinderdagverblijven, GGD Groningen, Groningen, Netherlands

Hagerhed-Engman L., Bornehag C.G., Sundell J., Aberg, N. (2006) Day-care attendance and increased risk for respiratory and allergic symptoms in preschool age. Allergy 61, 447-453.

Holgate S., Royal College of Physicians (2016) Every breath we take: the lifelong impact of air pollution. Report of a working party, London: RCP.

Furtaw Jr.J.F., Pandian M.D., Nelson D.R., Behar J.V. (1996) Modelling indoor air concentrations near emission sources in imperfectly mixed rooms. Journal of the Air & Waste Management Association 46, 861-868.

Junaidi E.S., Jalaludin J., Tualeka A.R. (2019) A Review on the Exposure to Benzene among Children in Schools, Preschools and Daycare Centres. Asian Journal of Atmospheric Environment 13, 151-160.

Kim K.-H., Pande, S.K., Kim Y.-H., Sohn J.R., Oh J. (2015) Emissions of amides (N, N-dimethylformamide and formamide) and other obnoxious volatile organic compounds from different mattress textile products. Ecotoxicology and Environmental Safety 114, 350-356.

Koopman, L.P., Smit H.A., Heijnen M.-L.A., Wijga A., van Strien R.T., Kerkhof M., Gerritsen J., Brunekreef B., de Jongste J.C., Neijens H.J. (2001) Respiratory infections in infants: interaction of parental allergy, childcare, and siblings-the PIAMA study. Pediatrics 108, 943-948.

Laverge J., Novoselac A., Corsi R., Janssens A. (2013) Experimental assessment of exposure to gaseous pollutants from mattresses and pillows while asleep. Building and Environment 59, 203-210.

Lee J.Y., Kim C., Kim J., Ryu S.H., Bae G.N. (2018) Exposure assessments for children in homes and in daycare centers to NO2, PMs and black carbon. Asian Journal of Atmospheric Environment 12, 204-214.

Liang Y., Xu Y. (2014) Emission of phthalates and phthalate alternatives from vinyl flooring and crib mattress covers: The influence of temperature. Environmental Science and Technology 48, 14228-14237.

Louhiala P.J., Jaakkola N., Ruotsalainen R., Jaakkola J. (1995) Form of day care and respiratory infections among Finnish children. American Journal of Public Health 85, 1109-1112.

Mendes A., Aelenei D., Carreiro-Martins P., Agular L., Pereira C., Neves P., Azevedo S., Cano M., Prooenca C., Viegas J., Siva S., Mendes D., Neuperth N., Teixeira J.P. (2014) Environmental and ventilation assessment in Child Day Care Centres in Porto: the ENVIRH Project, J.Toxicol Environ Health A:77(14-16): 931-943

Nafstad P., Jaakkola J.J., Skrondal A., Magnus P. (2005) Day care center characteristics and children's respiratory health. Indoor Air 15, 69-75.

Offermans A., Zheng H., Zeiler W. (2020) Indoor Air Quality conditions within the baby bunk beds at Dutch daycare centers indicate the necessity for an improved ventilation ndesign, Proceedings 16th Conference of the International Society Indoor Air Quality & Climate, Indoor Air 2020, COEX, Seoul

Oliveira M., Slezakova K., Delerue-Matos C., Pereira M.C., Morais S. (2019) Children environmental exposure to particulate matter and polycyclic aromatic hydrocarbons and biomonitoring in school environments: A review on indoor and outdoor exposure levels, major sources and health impacts. Environment International 124, 180-204.

Pagliano L., Armani R., Sangalli A., Causone F., Pietrobon M. (2016) Analysis of ventilation strategies for nearly zero energy retrofit of a day care center, Proceedings Clima 2016, Aalborg, Denmark

Prussin A.J., Torres P.J., Shimashita J., Head S.R., Bibby K.J., Kelley S.T., Marr L.C. (2019) Seasonal dynamics of DNA and RNA viral bioaerosol communities in a daycare center. Microbiome 7.

Schittny J.C., Burri P.H. (2008) Development and growth of the lung. In: Fishman A.P., Elias J A , Fishman J.A., Grippi M.A., Kaiser L.R., Senior R.M. (eds) Fishman's pulmonary diseases and disorders, vol 1. McGraw-Hill, New-York, pp 91–114

Spilak, M.P., Boor B.E., Novoselac A., Corsi R.L. (2014) Impact of bedding arrangements, pillows, and blankets on particle resuspension in the sleep microenvironment. Building and Environment 81, 60-68.

Versteeg H. (2009) Onderzoek binnenmilieu kindercentra, LBP|Lichtveld Buis & Partners

Wargocki P., Hviid C.A., Skupien A. (2016) Do New Renovated Schools and Kindergartens Secure Sufficient High Indoor Environmental Quality?, Proceedings Clima 2016, Aalborg, Denmark

WHO (2005) Effects of air pollution on children's health and development: a review of the evidence. World Health Organization, Regional Office for Europe, Copenhagen, Denmark (No. EUR/05/5046027).

WHO (2016) Ambient Air Pollution: A Global Assessment of Exposure and Burden of Disease. World Health Organization, Geneva, Switzerland 978-92-4-151135-3.

Yu K.P., Lee Y.C., Chen Y.C., Gong J.Y., Tsai M.H. (2019) Evaluation of PM1, PM2.5, and PM10 exposure and the resultant health risk of preschool children and their caregivers. Journal of Environmental Science and Health Part a-Toxic/Hazardous Substances & Environmental Engineering 54, 961-971.

Zeiler W. (2018) CO_2-concentration of the surrounding air of sleeping infants inside a crib, Proceedings Roomvent & Ventilation 2018, June 2-5, Aalto University, Espoo, Finland

Zheng H., Walker S., Zeiler W. (2022) IAQ aspects of Daycare Centers: Lungs and the Exposure to Particular Matter, ASHRAE and AIVC, submitted to IAQ 2020 conference, Athens, Greece

Evaluation of the ventilation situation in Dutch schools using the QuickScan method

Vinayak Krishnan [a], Marcel Loomans [a], Shalika Walker [a], Wim Zeiler [a]

[a] Department of the Built Environment, Eindhoven University of Technology, Eindhoven, the Netherlands,

v.krishnan@tue.nl

Abstract.
The COVID19 pandemic has brought especially the health aspect to the forefront and the need to improve ventilation in Dutch schools. To assess the ventilation in schools during the pandemic, the QuickScan method was developed by a large National consortium called 'Masterplan Ventilatie'. The method contains a list of instructions for users to quickly evaluate the quality of ventilation. As part of this study, 25 TU Eindhoven bachelor students were provided with the QuickScan documentation and children and teacher questionnaires were added to assess the ventilation systems, each in a different Dutch school. These results have been used to identify the possibilities and limitations of the QuickScan method and provide information on the current ventilation status in the investigated schools. Firstly, administrative (i.e., information gathering and reporting) and functional (i.e., measurements and data analysis) groups of steps are distinguished. Secondly, scoring criteria are defined to rate each individual step of the QuickScan performed by the students. The questionnaires pointed at uncomfortable winter conditions, limited possibilities for ventilation control, poor air quality, and inadequate cleanliness for schools. The measurements show that 50% of the schools, which indicated maximum CO_2 levels during occupancy, recorded levels above 1200 ppm. About 67% of the studies, which reported the ventilation capacity for the worst or winter operating conditions, recorded insufficient ventilation. The balanced mechanical ventilation system rated better based on the teacher questionnaires while the children questionnaires indicated no preference for a specific ventilation system. The QuickScan evaluation highlighted that 100% of the studies achieved at least 60% completion for the administrative steps and only 52% of the studies achieved at least 60% completion for the functional steps. This study is the first to apply the QuickScan method, report results, and provide an approach to evaluate and suggest improvements to the QuickScan method.

Keywords. Schools, Ventilation, Materplan Ventilatie, QuickScan method, Evaluation.
DOI: https://doi.org/10.34641/clima.2022.282

1. Introduction

Schools have a typical indoor environment where there is high occupancy throughout the year. If they are not properly ventilated it can lead to increase in CO_2 concentration and other pollutants which come from both indoor and outdoor non treated sources. There are many sources of such pollutants and there is a complex interplay which can impact the child wellbeing [1]. A bad indoor environment can significantly impact the health and the learning capacity of children [2]. Most schools in the Netherlands are financed and controlled by the government. Budgets generally are limited, and policy implementation can take time as they must be applied throughout the Netherlands. There are still many classrooms in the Netherlands today that rely on natural ventilation to meet their fresh air needs. This becomes a challenge especially during winter when the temperatures are too low. The windows are then kept closed to avoid thermal comfort problems. This in turn leads to an increase in indoor pollutants. A recent study in 54 classrooms at 21 schools in the Netherlands found out that measures to improve air quality conditions in classrooms are needed [3]. As a result of the COVID-19 pandemic, the issue of ventilation in Dutch schools has been brought to the forefront and there is an urgent call for action also by the government. The Landelijk Coördinatieteam Ventilatie in Scholen (LCVS) was incorporated to assess the situation in schools and found that at

Copyright ©2022 by the authors. This conference paper is published under a CC-BY-4.0 license.

least 2194 school buildings still need to assess their ventilation systems to check whether they match the relevant standards or not [4]. With this urgent need in mind, the Masterplan Ventilatie – Quickscan COVID-19, 2020 [4] was devised by a consortium of TVVL, Binnenklimaat Nederland, ISSO and VCCN. The method entails a list of instructions that the user can follow for a fast-track assessment of the ventilation in a (Dutch) school.

However, the QuickScan method is new and has not been tested before. Therefore, an assessment based on its actual application in the field is beneficial to check its current effectiveness and shortcomings. To get an assessment of the QuickScan and the status of Dutch schools, TU Eindhoven (TU/e) students conducted field studies in schools. Keeping this in mind, the primary objectives of this study are formulated as follows:

1. To find the status of ventilation in Dutch schools using the QuickScan method

2. To evaluate the QuickScan method

2. Method

To achieve the objectives of this study, the following steps were followed. As a first step, students from TU/e conducted studies in schools using the QuickScan method and questionnaires. The results from these QuickScan studies and questionnaires are used to firstly prepare a summary of the current situation in schools. Secondly, the studies are used for an assessment of the QuickScan based on a rating criterion developed to evaluate the QuickScan method.

2.1 Field studies using the QuickScan Method

In total 25 schools of Lucas Onderwijs, were studied by 25 TU/e students. The students gathered important information from field visits during the period of November and December 2020 and compiled a report each with detailed analysis of the school ventilation as per the QuickScan. The year of construction of the schools varied from 1892 to 2006 and almost all schools were in and around the Hague, the Netherlands. Out of the total 25 studied, 19 schools were primary schools with children ages between 4 and 12 years, and the other 6 schools were Secondary schools with children ages between 12 and 18 years. The different ventilation systems (Types) and their percentage out of the total 25 schools studied are:

A (40%): Natural inlet and Natural exhaust
B (4%): Mechanical inlet and Natural exhaust
C (40%): Natural inlet and Mechanical exhaust
D (16%): Mechanical inlet and Mechanical exhaust

It is to be noted that some of the systems assigned as type A could be type C, in cases where there is a Mechanical exhaust provided in the corridor which can also exhaust the classroom airflow via the vents provided in the door or by door opening. However, for this study this detail is not considered. The QuickScan method consists of 3 main steps: A-Preparation, B-On the spot investigation, C-Analysis. A detailed description of each step can be found in [4].

2.2 Teacher and Student Questionnaires

In addition to the QuickScan, the TU/e students were provided with questionnaires for both school children and teachers to obtain their perception of the ventilation. Both the children and teacher questionnaires are based on a 7-point rating scale. The teacher questionnaires were more elaborate with 28 questions (indicators) about various aspects relating to the classroom air quality, thermal comfort, health, cleanliness, winter and summer conditions, and ventilation controllability. The children questionnaires were less extensive with 7 questions (indicators) about the winter and summer thermal comfort and air quality. The children questionnaires were filled in almost all cases by the children from the classroom where measurements were conducted. To get more responses, the teacher questionnaires were filled in by teachers from the same and different classrooms when possible. The questionnaires were filled in anonymously.

2.3 Assessment of the QuickScan Method

An important aim of this report is to assess the QuickScan method. The QuickScan steps [4] are divided into an administrative part, which is about information gathering and reporting, and a functional part, which is about measurements and data analysis, for ease of assessment. The QuickScan identifies steps by a capital alphabet and number, e.g. A1, however, for ease of identification of each important step or sub-step, additional letters and numbers are added in this study, refer **Tab. 1.** Step C 2 (a) [iii] is an addition made for this study. The assessment of the Quickscan method will be made by giving each of the student reports a score with respect to the administrative steps and functional steps of the QuickScan. The distribution of the scores for correctly performing each step is mentioned for both the administrative and functional steps in **Tab. 1**. Based on the scores, an overview of how correctly the school assessments were preformed according to the QuickScan will be determined. The errors that were encountered will also be reported and its significance will be discussed. Based on this, suggestions for improving the QuickScan method will be proposed.

An additional remark is that there are cases where the scoring of a step is dependent on a previous step. For e.g., if there is no CO_2 measurement reported (B 5 (c) [i]|), then all the points for the rest of the steps related to using CO_2 data are also lost. Moreover, there are cases where the step cannot be evaluated as it is not applicable for the study. For e.g., if there were no vents present in the classroom,

the steps for information collection and vent capacity determination will become redundant and, for such steps, full points are provided in the assessment. The same is the case for a ventilation system type D, where capacity determination via windows and vents is not necessary and hence the relevant steps are marked with full points for these cases.

Tab. 1: Rating criteria for the Administrative and Functional steps of the QuickScan method

QuickScan step Number	QuickScan steps in brief	Total Points	Rating method	Part
A 1 (a)	Preparation: Ventilation system	9	All Points lost if not reported	Administrative
A 1 (b)	Preparation: Year of construction	9		
A 1 (c)	Preparation: Floor plan	9		
A 1 (d)	Preparation: Pictures	9		
B 2	On the spot: Determine measurement method	9		
B 4 (a)	On the spot: Occupancy & age	9		
B 4 (b)	On the spot: Classroom details	9		
B 4 (c)	On the spot: Ventilation devices	9		
B 4 (d)	On the spot: Classroom marked on school map	9		
C 3 (a)	Assessment for each Building: Tabulate the results	9		
C 3 (b) [i]	Assessment for each Building: Action points mentioned	5		
C 3 (b) [ii]	Assessment for each Building: Action points selected from the provided list	5		
Maximum score		100		
B 5(a)	On the spot: Information for capacity determination via windows as per NEN 8087:2001 [5]	10	All Points lost if not reported. 5 points lost for incorrect data collected.	Functional
B 5(b)	On the spot: Information for Capacity determination via Vents as per NEN 8087:2001 [5]	10		
B 5 (c) [i]	CO_2 measurement reported	8	All Points lost if not reported	
B 5 (c) [ii]	CO_2 measurement reported during occupancy	8		
C 1 [i]	Determine the test values for Ventilation rate	8		
C 1 [ii]	Determine the test values for CO_2 levels	8		
C 2 (a) [i]	Analyse the measurement data: Capacity determination via vents	8		
C 2 (a) [ii]	Analyse the measurement data: Capacity determination via windows	8		
C 2 (a) [iii]	Analyse the measurement data: Worst case considered (*extra step added for this study*)	8		
C 2 (b) [i]	Analyse the CO_2 measurement data: Report 98th percentile	8		
C 2 (b) [ii]	Analyse the CO_2 measurement data: Correct the value for design occupancy (only if there are at least 5 less people compared to design occupancy)	8		
C 2 (b) [iii]	Analyse the CO_2 measurement data: Asses if it was a representative measurement day (KNMI [6])	8		
Maximum Score		100		

3. Results

3.1 Results from Field Studies & Questionnaires

When available, only the maximum CO_2 levels measured during occupancy have been reported in **Tab. 2**. Nine studies reported the ventilation capacity via the vents and windows for the worst-case or winter operating conditions for ventilation types A and C. The ventilation capacity computed using NEN 8087:2001 [5] for the windows and vents did not meet the requirements for 6 out of these 9 schools.

Tab. 2: Summary of Results about the maximum CO_2

School Number	Max CO_2 levels (ppm)	Occupancy during measurement
2	1356	no information
10	904	17
12	1250	no information
14	1150	21
17	1434	29
19	869	19
22	1320	25
24	1193	31

The results from the Children Questionnaires were analysed using box plots with the rating for each indicator on the y axis and the School number on the x axis. A student questionnaire box plot example for one indicator (TS1) out of the total 7 is shown in **Fig. 1**. The data from 21 schools which were available are presented in the box plots with the red line representing the median, the box representing the 2nd and 3rd quartile and the end of the box to the whiskers (in black) representing the 1st and the 4th quartiles respectively. The small back circles represent the outliers. The different ventilation systems are also marked in the plots on the x axis between brackets. The indicators are graded such that the highest values represent a comfortable situation, and a lower score represents an uncomfortable situation. For school number 15 and 22 only the median values were available.

The results from the teacher questionnaires for 21 schools whose data was available, are presented in **Fig. 2**. The data per school is not presented as the number of teachers filling the questionnaires were insufficient, and only one in some cases. To remove subjectivity, the data from all the schools is plotted in a bar graph to give a general assessment of the school ventilation perception by the teachers for the investigated schools. Similar to the children questionnaires, the lower values represent an uncomfortable situation, and a high value represents a comfortable situation. The x axis represents the different indicators investigated, 28 in total. Additionally, in colour, the results are plotted per ventilation system A, C and D. Eighteen teachers filled in the questionnaires for type A schools, 34 for type C schools and 11 for type D schools. Only the median values are presented.

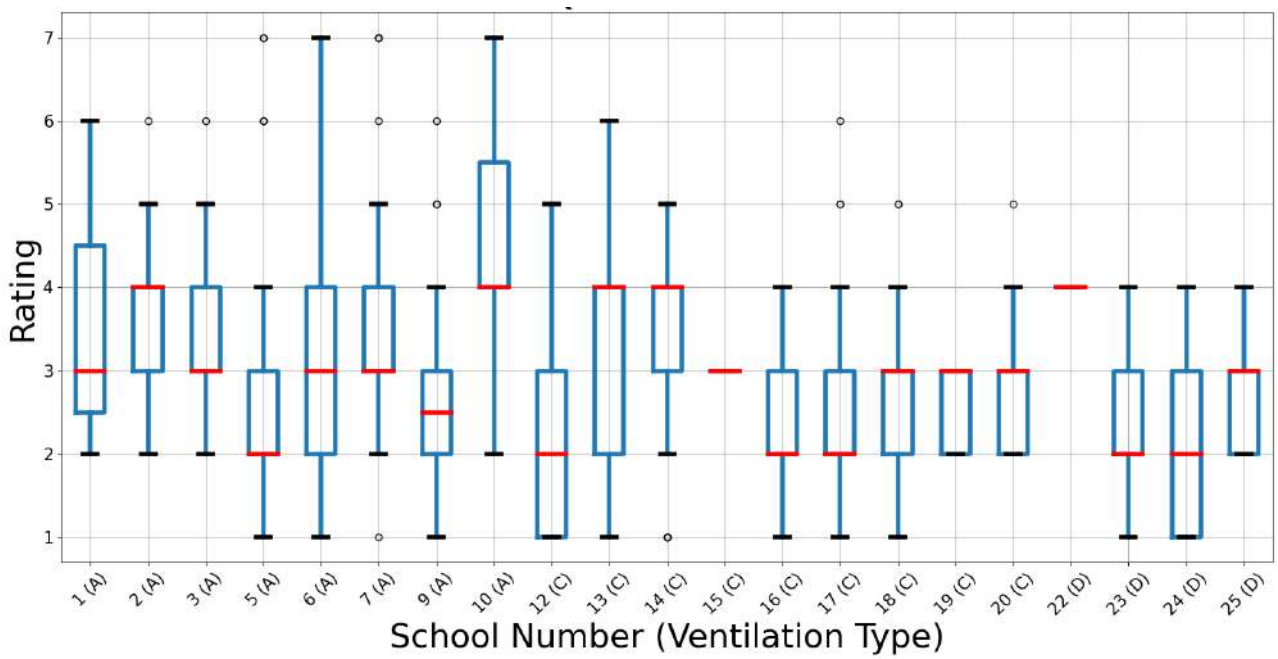

Fig. 1: Results from the Children questionnaires: Temperature Summer (TS1) – Rating 1 = Too Hot, Rating 4 = Not warm and not cold; Rating 7 = Too Cold. Ventilation types are added in brackets adjacent to the school number

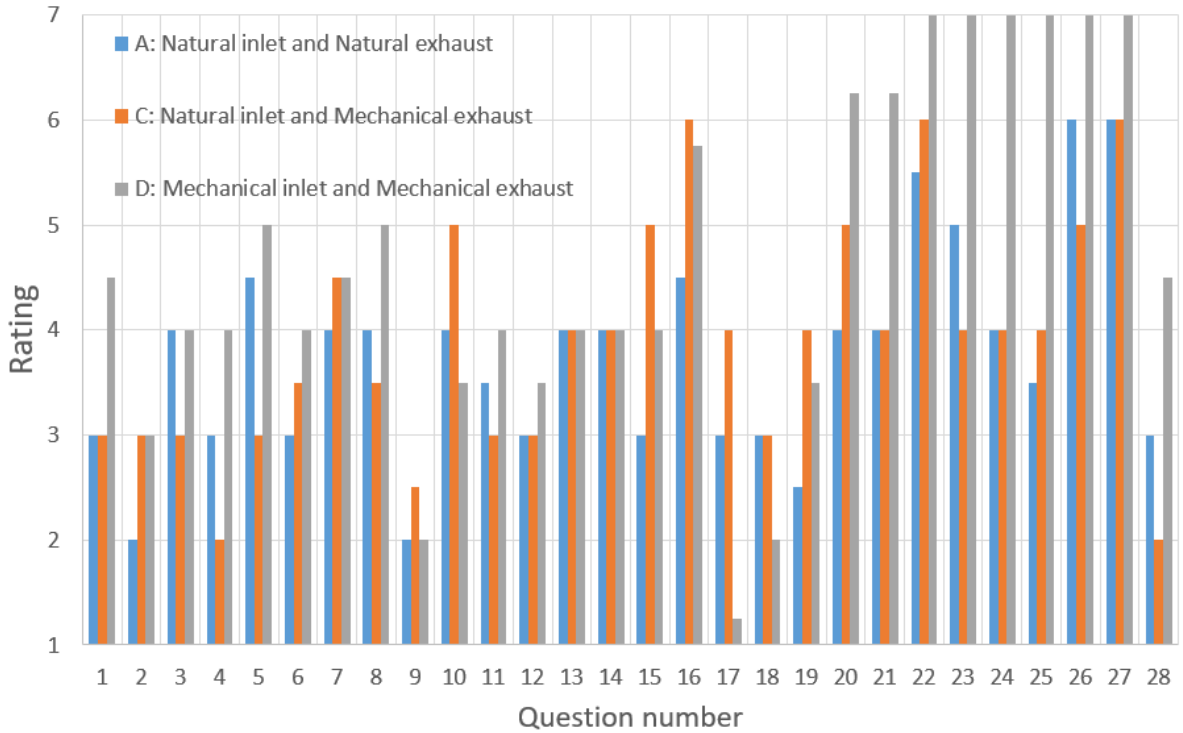

Fig. 2: The results of the teacher questionnaires with the median values presented as per different ventilation system types – **1/8.** Winter/Summer temperature - Uncomfortable (1), Comfortable (7); **2/9.** Winter/Summer temperature - Too Cold (1/7), Too hot (7/1); **3/10.** Winter/Summer temperature - Varying (1), Stable (7); **4/11.** Winter/Summer Air Quality - Dry (1), Moist (7); **5/12.** Winter/Summer Air Quality – Not Fresh (1), Fresh (7); **6/13.** Winter/Summer Air Quality – Uncomfortable (1), Comfortable (7); **7/14.** Winter/Summer Air Quality – Stinky (1), No Smell (7); **15.** Draft – Very much (1), None (7); **16.** Noise - Very much (1), None (7); **17.** Temperature Controllability - None (1), Complete (7); **18.** Ventilation Controllability - None (1), Complete (7); **19.** General Experience – Cold (1), Hot (7); **20.** Headache – A lot (1), Little (7); **21.** Drowsiness– A lot (1), Little (7); **22.** Trouble breathing – A lot (1), Little (7); **23.** Dry eyes – A lot (1), Little (7); **24.** Children Headache – A lot (1), Little (7); **25.** Children Drowsiness– A lot (1), Little (7); **26.** Children Trouble breathing – A lot (1), Little (7); **27.** Children Dry eyes – A lot (1), Little (7); **28.** Cleanliness – Unsatisfactory (1), Satisfactory(7); (in bold the question numbers to which the description applies)

3.2 Results from the QuickScan evaluation

A summary of ratings given for both the Functional and Administrative aspects in terms of percentage is shown in **Tab. 3.** The summary is based on the rating criteria presented in **Tab. 1.**

Tab. 3: Percentage of studies that were completed as per the Rating definition for both Administrative and Functional steps

Rating definition	% Completion	Admin. part (% studies meeting rating)	Functional part (% studies meeting rating)
complete and correct	100	0	0
partly	80 - 99	60	4
partly with some mistakes	60 - 79	40	48
partly with several mistakes	40 - 59	0	36
incomplete and insufficiently	0 - 39	0	12

The error prone steps are displayed in terms of the percentage of studies encountering this error in **Tab 4.** Only steps where at least 40% of the studies encountered an error are mentioned.

Tab 4: QuickScan error prone steps in terms of % of studies encountering error (>40% of studies)

Step number	% Studies	Part
B 2	40	Administrative
C 3 (a)	80	
C 3 (b) [ii]	100	
B 5 (c) [i]	44	Functional
B 5 (c) [ii]	68	
C 1 [i]	68	
C 1 [ii]	68	
C 2.a [iii]	44	
C 2.b [i]	72	
C 2.b [ii]	64	
C 2.b [iii]	96	

4. Discussion

4.1 Status of School ventilation

The natural ventilation capacity computed from the windows and vents as per NEN 8087:2001 is variable based on the number of windows opened or closed and their opening area (partially or fully open). The best-case scenario is all the windows and vents staying fully open. The worst case, which generally occurs during winter, is almost all windows closed or partially closed. It was found from the study that the ventilation is insufficient for 67% (6 out of 9) of the cases when considering the worst-case scenario of window and vent operation. A worst-case assessment with windows and vents closed was not explicitly stated in the QuickScan, but is important to be noted, because in winter most schools with natural supply of fresh air have a high chance of being operated in this worst-case scenario.

With regards to the maximum CO_2 levels reported in **Tab. 2**, the students relied on the measurements by the CO_2 meters in the classroom which was not easily accessible during working times. However, there are some schools for which the CO_2 levels are available during occupancy. For 50% (4 out of 8) of these cases the maximum CO_2 levels are above the limit set by Frisse Scholen Class C of 1200 ppm [7]. When converting all levels reported in **Tab. 2** from current occupancy to design occupancy, more measurements could overshoot the limits of 1200 ppm. This raises concerns about the CO_2 levels, and therefore the ventilation levels, at least in the cases where measurements were reported during occupancy.

An example result from the student questionnaire is shown in **Fig. 1**. On an average, the summer temperature is perceived too hot by the children. In general children prefer lower temperatures than predicted by most used comfort models like the PMV (predictive mean vote)[8]. However, children still consider the summer temperature to be bearable in most schools. The winter temperature is perceived too cold by most children, and they find it to be very uncomfortable as well. This is a cause of concern seen in almost all the schools during winter, which can incite actions to close the windows thereby reducing the ventilation in the classroom. A note must be made that, due to the COVID-19 pandemic, schools were strongly advised to keep windows frequently open to ensure sufficient ventilation. As a result, thermal comfort was compromised as the results clearly indicate. The children do not indicate any issues with the classroom air quality.

When looking at the ratings for the 7 children questionnaire indicators for the different ventilation types, the children don't seem to prefer any one type of ventilation system. One would have expected the type C and D to perform much better than A, but it seems the children perceive all of them in the same way. In some cases, D performs even worse than A. However, the teacher questionnaire results in **Fig. 2** indicate that the ventilation type D performs better or at least equal to other types in most cases, especially for the health aspects. This gives confidence on the use of type D Mechanical ventilation systems in the schools. However, the system D scores low for the control indicators and hence, the control should be an important aspect to deal with when considering such systems.

From **Fig. 2** it can be deduced that the winter conditions, in line with the children, are noted as uncomfortable by almost all teachers and the summer temperature is assessed as very hot by almost all teachers. The air during both summer and winter is considered dry in general and in summer it is perceived as not being fresh. The teacher still has a problem about the ventilation controllability and the cleanliness is not considered adequate.

4.2 QuickScan evaluation & improvements

From **Tab. 3**, it can be observed that most studies lag with respect to the functional aspects. It can be observed that no study was completed perfectly with a score of 100. Most of the administrative steps were completed partly and the rest completed partly with some mistakes. For the functional steps most studies were completed partly with some mistakes or with several of mistakes. There were also some studies regarded insufficient. This indicates that there is a definite scope for improving the QuickScan implementation, especially with respect to the functional steps.

To better identify the causes of incompleteness of the studies, the number of errors recorded per QuickScan step is mentioned in **Tab 4**. It can be observed that certain steps are more error prone than others. To filter out the most error prone steps, only the errors reported in more than or equal to 40% of the studies are tabulated. The main improvement points for the QuickScan highlighted from the error prone steps are:

- <u>Step B2, C3(a), C3(b)[ii], C1[i], C1[ii]:</u> In the QuickScan, it needs to be clearly stated that the report template which is provided with the QuickScan is to be used to report the results. This makes it part of the QuickScan steps and clear to the user about how to present the data, such as, e.g., B2 or C3(a). It also creates uniformity. Special attention needs to be given to clarify to the user that there is also a list of action points that the user can choose from while preparing an action plan for the assessed school.
- <u>Step B5(c)[i], B5(c)[ii]:</u> The collection of equipment required for the measurements should be added in the preparation part (A) so that they are not missed during the campaign. The accuracy and other equipment details can also be specified

here. It can also be added in the preparation part (A) that special permissions need to be sought from the school for measuring during occupancy. Such measurements have the highest value.

- C2(a)[iii]: Since all windows and vents may not be open fully for naturally ventilated classrooms during winter, it is necessary to explicitly mention that the capacity determination using NEN 8087:2001 needs to be performed for the worst-case operating states. The measurement condition therefore should resemble everyday practice as much as possible.
- C2(b)[i], C2(b)[ii], C2(b)[iii]: As per the QuickScan report template [4], only the CO_2 98th percentile needs to be reported and corrected for design occupancy, if applicable. However, in the detailed descriptions (QuickScan disclosures [4]), the ventilation capacity is to be calculated from the CO_2 levels for both the measurement and design occupancy. This ventilation capacity based on CO_2 levels is not part of the conclusions and hence is not clear why the capacity is required to be derived in an alternative manner. E.g., the ventilation capacity is calculated using the NEN 8087:2011 for naturally ventilated cases and air flow measuring devices in Mechanically ventilated cases. The CO_2 based ventilation capacity calculation can be used when there is no possibility of measurement of the ventilation flowrate in the classroom. It may also serve as a check for comparing with the outcomes from the measured flowrates. However, this needs to be clarified in the QuickScan.

Some other suggestions for improvement for the QuickScan implementation are as follows:

- Communication with schools: CO_2 sensor data, if available, can be requested from each school for a longer period. The measurement team can request selection of a classroom based on their preferences.

- Capacity determination from windows and vents as per NEN 8087:2001: The capacity determination using NEN 8087:2001 does not consider the actual indoor and outdoor conditions which are the main drivers of the flow through windows and vents. The pressure difference across the window plays an important part in determining the flowrate [9][8]. Moreover, using a constant value for the discharge coefficient for different cases leads to an inaccurate prediction of window airflow capacity [9]. The velocity can also vary considerably across the vent cross section and is also highly unsteady with a lot of fluctuations [10]. However, according to NEN 8087:2001 a constant air velocity is assumed throughout the vent. This can lead to inaccurate (too positive) estimates of the airflow computed through vents as well. Therefore, it should be explicitly mentioned that the QuickScan is only for a preliminary evaluation and cannot guarantee proper natural ventilation in the classroom even if the results meet the requirement. CO_2-measurement data can give a first impression whether the natural ventilation is working properly.

- Capacity determination from vents and windows for type C ventilation system: The ventilation flowrate for type C cannot be only computed by the capacity determination from windows and vents as per NEN 8087:2001, because there is also a mechanical exhaust which is the main driver of the ventilation. The computation of the ventilation flowrate for type C needs to be clarified, possibly it can be measured directly from the exhaust grille.

- Questionnaires: The QuickScan currently does not have a perception evaluation and it is recommended to include that using questionnaires. Moreover, the QuickScan currently misses measurements to assess thermal comfort in the schools, which can also be addressed using questionnaires. This method allows for additional information on the ventilation when measurements are not easy to perform.

4.3 Limitations of the study

The main assumptions and limitations of this study are:

- It is assumed that the students used the QuickScan excel tool properly for all computations, especially for the ventilation rates from windows and vents.
- The students did not have their own CO_2 or flow measuring equipment. Because of this some steps could not be fully performed.
- There are some QuickScan steps excluded from the evaluation as they could not be performed by the students because of logistic or accessibility issues. Hence, the

final evaluation method is intended to highlight the areas of improvement rather than providing a final rating for the QuickScan.

- The QuickScan assessment has a subjective component and is mainly intended to identify possible sources of errors when trying to use the QuickScan method.
- It is assumed that the students interpreted and clearly understood the intent of the QuickScan and reported all the results correctly. Since Scans are not necessarily performed by professionals, it is assumed to provide for a good representation of potential users of the QuickScan.

5. Conclusions

The idea of the QuickScan is to make a fast-track assessment of the ventilation in Dutch schools. Therefore, it must be as minimally ambiguous as possible with clear instructions that anyone can follow. By considering the students who are not subject experts, the QuickScan method was tested for a critical case. The QuickScan method was evaluated by dividing it into an administrative and functional part. It was found that the administrative part has a better chance of completion as compared to the functional part. Based on the evaluation results, the QuickScan steps that have a higher risk of not being completed have been identified. Based on the identified error prone steps, concrete improvements for the QuickScan have been suggested.

50% of the studies reported maximum CO_2 levels during classroom occupancy above the limit of 1200 ppm. Out of all studies that reported the ventilation capacity for the worst case or winter operation (type A & C ventilation system), 67% reported insufficient ventilation. The questionnaires were not part of the QuickScan but were specially used for this study. The questionnaires pointed at uncomfortable winter conditions, limited possibilities for ventilation control, poor air quality, and inadequate cleanliness for schools. The results give confidence in using Mechanical ventilation systems in schools instead of naturally ventilated systems. The questionnaires have proved to be a valuable addition to the QuickScan.

Acknowledgement

The authors would like to acknowledge the support from Lucas Onderwijs for providing access to their schools for the QuickScan studies, and the teachers and children for participating in the study.

References

[1] Salthammer, T., Uhde, E., Schripp, T., Schieweck, A., Morawska, L., Mazaheri, M., ... & Kumar, P. Children's well-being at schools: Impact of climatic conditions and air pollution. Environment international, 2016; 94, 196-210.

[2] Bluyssen, P. M. Health, comfort and performance of children in classrooms–new directions for research. Indoor and Built Environment, 2017; 26(8), 1040-1050.

[3] Bluyssen, P. M., Zhang, D., Kurvers, S., Overtoom, M., & Ortiz-Sanchez, M. Self-reported health and comfort of school children in 54 classrooms of 21 Dutch school buildings. Building and Environment, 2018; 138, 106-123.

[4] Masterplan Ventilatie – Quickscan COVID-19 en Ventilatie in Scholen – November 2020. https://www.masterplanventilatie.nl/

[5] NEN 8087:2001 'Ventilatie van gebouwen; Bepalingsmethoden voor bestaande gebouwen.'

[6] Klimatologie - Metingen en waarnemingen, KNMI, https://www.knmi.nl/nederland-nu/klimatologie-metingen-en-waarnemingen

[7] Programma van Eisen Frisse Scholen 2021, RVO. https://www.rvo.nl/sites/default/files/2021/06/PvE-Frisse-Scholen-2021.pdf

[8] Sander ter Mors, Jan L.M. Hensen, Marcel G.L.C. Loomans, Atze C. Boerstra, Adaptive thermal comfort in primary school classrooms: Creating and validating PMV-based comfort charts, Building and Environment, Volume 46, Issue 12, 2011, Pages 2454-2461, ISSN 0360-1323,

[9] Heiselberg, P., Svidt, K., & Nielsen, P. V. Characteristics of airflow from open windows. Building and Environment, 2001, 36(7), 859-869.

[10] Jansen, D. W. L., Loomans, M. G. L. C., Wit, de, M. H., & Zeiler, W. . Boundary conditions for natural supply ventilation. In O. Seppänen, & J. Säteri (Eds.), Proceedings of the SCANVAC Roomvent 2007 Conference, 13-15 June 2007, Helsinki, Finland FINVAC.

Data Access Statement

The datasets generated during and/or analysed during the current study are not publicly available *because they are provided by a company and has to be kept private owing to privacy and security concerns* but are/will be available if *the concerned parties contact us and explain the reason for the data requirement, but the final decision lies with the company and access cannot always be guaranteed.*

Development of a Non-contact Modular Screening Center (NCMSC) for COVID-19

Jinkyun Cho [a], Jinho Kim [b], Jongwoon Song [c], Seungmin Jang [a]

[a] Department of Building and Plant Engineering, Hanbat National University, Daejeon, Republic of Korea, jinkyun.cho@hanbat.ac.kr

[b] Department of Fire Protection, Safety and Facilities, Suwon Science College, Hwasung , Republic of Korea, jinho.kim@ssc.ac.kr

[c] E-SOLTEC Co., Ltd, Gwangju, Korea, kb9503@hanmail.net

Abstract. Under the global landscape of the prolonged COVID-19 pandemic, the number of individuals who need to be tested for COVID-19 through screening centers is increasing. However, there is a risk of cross-infection at each stage of the screening process. To address the risk of cross-infection in the screening center during the COVID-19 testing process, a non-contact modular screening center (NCMSC) was developed that uses biosafety cabinets and negative pressure booths to improve the problems of existing screening centers and enable safe, fast, and convenient COVID-19 testing. The main purpose of this study is to evaluate the effect of the cross-infection prevention of viruses and ventilation performance for rapid virus removal from the indoor space using both numerical analysis and experimental measurements. Computational fluid dynamics (CFD) simulations were used to determine the ventilation rate and pressure difference. We also characterized the airflow dynamics of NCMSCs using the particle image velocimetry (PIV). Moreover, design optimization was performed with three alternatives based on the air change rates and the balance of supply air (SA)/exhaust air (EA) as a ventilation strategy for preventing viral transmission.

Keywords. COVID-19, Screening center, Cross-Infection, Ventilation strategy, CFD, PIV.
DOI: https://doi.org/10.34641/clima.2022.283

1. Introduction

In the past, most types of viruses that reached the pandemic level were respiratory infections such as influenza and coronavirus [1]. As shown in **Fig. 1**, influenza viruses mutate continuously and the antigenic shift occurs every 40 to 50 years, leading to a pandemic situation. Particularly, the coronavirus causes a pandemic every 5 to 10 years [2]. The WHO (word health organization) declared COVID-19 a global pandemic in 2020, which persists at the present. There is a possibility that the COVID-19 outbreak started from a hospital and transmitted to the community because HCWs (health care workers) are positioned at the interface between the medical environment and local community [3], [4]. Therefore, medical institutions isolate symptomatic patients from general patients through screening centers. The screening center plays a primary role in screening suspected patients of COVID-19. According to the Ministry of Health and Welfare of Korea, as of August 2021, more than 600 screening centers have been installed and are under operation in Korea. Temporary, drive-through and walk-through screening centers have been installed as top-priority countermeasures to overcome the challenges of this situation. However, there are no clear criteria and guidelines for the design, installation, and operation of these screening centers worldwide. In this study, a novel NCMSC (non-contact modular screening center) was developed that addresses the problems of existing screening centers and the risk of cross-infection in screening centers during the COVID-19 testing process. This facility aims to evaluate the effect of the cross-infection prevention of the viruses and ventilation performance for rapid virus discharge from indoor spaces.

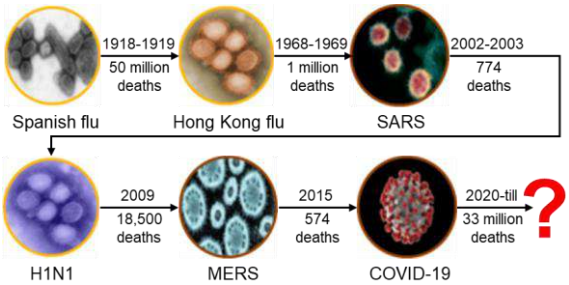

Fig. 1 - Brief outline of respiratory viral disease outbreaks.

Copyright ©2022 by the authors. This conference paper is published under a CC-BY-4.0 license.

2. Methodology

The initial step includes the classification of the different types of COVID-19 screening centers currently in operation and a novel NCMSC was proposed. The design optimizations of the space configuration and ventilation system are key factors in reducing the risk of cross-infection. The principal function of the ventilation strategy based on the NCMSC setup is to effectively block the movement of indoor aerosol that transmits the COVID-19 virus to other spaces and to discharge the viral particles quickly. The CFD (computational fluid dynamics) analysis of the ventilation system was performed using three design alternatives with different ventilation rates and balance of SA (supply air) and EA (exhaust air). The evaluation of the ventilation performance confirms the effect of the cross-infection prevention of the COVID-19 virus, which can be indirectly evaluated by analysis of airflow profiles of velocity and pressure differential in the rooms. And full-scale field measurements were performed under similar conditions as the numerical analysis to overcome the lack of experimental data on indoor airflow patterns. In addition, the results of the measurements were compared and verified using the results of the CFD simulation. The experiment was performed using PIV (particle image velocimetry), which can simulate virus particles.

3. Development of a NCMSC

A NCMSC was developed that uses biosafety cabinets and negative pressure booths to address the problems of existing screening centers and enable safe, fast, and convenient COVID-19 testing. NCMSC is a mobile modular building that can be quickly moved, installed, and operated in the required area depending on the COVID-19 testing demand. This type of medical modular facility can reduce the risk of cross-infection between rooms by achieving the airtightness performance of the structure. In particular, a non-contact automated system was applied to the entire testing process, from medical interviews and body temperature measurements to specimen transport, to prevent infection from the source. NCMSC increases the accessibility of patients to the screening center and provides adequate protection for HCWs.

NCMSC is a safe medical facility equipped with negative pressure zones, namely the AR (anteroom) and SCB (specimen collection booth), and positive pressure zones, such as the ER (examination room), as shown in **Fig. 2**. Moreover, it implemented two-stage negative pressure control to prevent virus leakage. The air change rate was set to 12 ACH [5], [6] or above, which is the standard for an airborne infectious isolation room, and the pressure differential was set to maintain 25 Pa or above. Subsequently, the ER maintained positive pressure, and a low-noise fan and high-performance air filter (PM2.5 99.97%) were applied to prevent infection among HCWs.

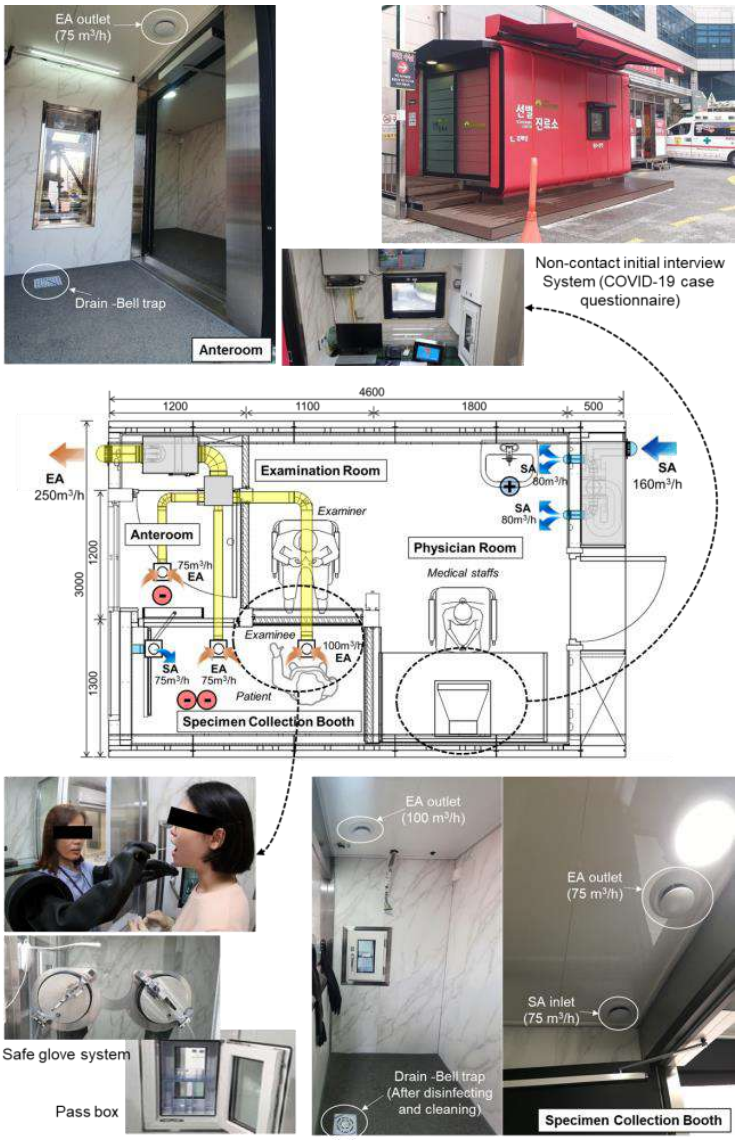

Fig. 2 - Layout of the NCMSC and location of SA/EA for the ventilation system.

This pressure differential is based in the case in which the door is closed and not when the door is opened or with the movement of people. The total air change rate was set to be 12-30 ACH for an effective discharge of viruses that can be produced in SCB. The screening center ventilation system provides a safe air environment for HCWs and individuals to be tested against infection. Therefore, the appropriate arrangement of the SA and EA outlets of the ventilation system is an important consideration for adequate indoor airflow. The ventilation system and pressure differential performance should be reviewed and the airtightness and the area of opening of the structure

should be optimized to maintain pressure differential through simulation analysis results and prevent aerosol viral diffusion and infection between rooms for SCB and ER in NCMSC. On the other hand, the indoor space needs to be comparted into zones, and the plan should be simplified when performing CFD analysis that can investigate the inter-zonal air movement from the SCB to the ER. In addition, three ventilation strategies and operating conditions were presented to evaluate the ventilation performance based on the SA and EA conditions of each room.

4. Numerical analysis

A quantitative analysis of the effect of the COVID-19 virus cross-infection prevention and a ventilation strategy to prevent the transmission are needed and should be established in the developed NCMSC. In this study, the airflow that can cause the diffusion of the COVID-19 virus was analyzed using STAR CCM+ CODE for CFD analysis of the NCMSC ventilation system. The effects of the airflow velocity and room pressure control based on the operation of the ventilation system on the viral transmission were investigated. The safe location of the ER, where HCWs were present, was also determined.

4.1 CFD modelling

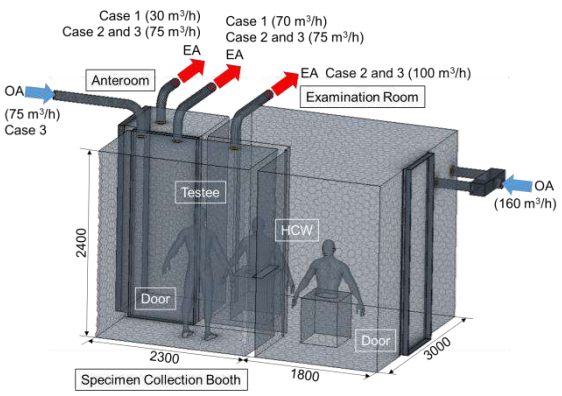

Fig. 3 - NCMSC mesh of the CFD model.

The dimension of the CFD domain was 4100 × 3000 × 2400 mm (L × W × H). **Fig. 3** shows the division of SCB, AR, and ER. The EA outlet was located on the ceiling of the SCB and AR to avoid its effect on the airflow generated from the door, and the SA inlet was installed in the ER that required a positive pressure. Both SA and EA systems were applied in the SCB for effective ventilation. On the other hand, the SA flowrate of the ER and the two circular diffusers placed on the upper wall was set to 160 m^3/h (6 ACH). An EA outlet was installed on the ceiling in AR. In particular, the airflow rate of EA was 30 m^3/h (12 ACH) for Case 1, and 75 m^3/h (30 ACH) for Cases 2 and 3. Meanwhile, an EA outlet was installed in the SCB with an EA flowrate of 75 m^3/h (12 ACH) for Case 1. In addition, two EA outlets were installed for Cases 2 and 3 with an EA flowrate of 175 m^3/h (30 ACH). Furthermore, Case 3 applied the SA system in which a circular diffuser was installed on the ceiling with a flowrate of 75 m^3/h. The negative pressure control was performed in SCB, and analyses were performed with all doors closed. The shortage of SA for EA was supplemented through door gaps of adjacent rooms, and the direction of airflow was from the ER to the SCB. Finally, a relief damper was installed to prevent backflow.

The mesh density was adjusted by dividing the analysis domain to consider the importance of the analysis domain. The total number of grid cells was 8,176,419. The analysis and convergence conditions were set to a residual range of 10^{-4}, and the turbulence analysis model was based on the standard k–ε model. The boundary conditions of the simulations are listed in **Tab. 1**.

Tab. 1 – CFD boundary conditions with airflow rates.

	Case 1 (Baseline)	Case 2	Case 3
Supply (ER)	160 m^3/h	160 m^3/h	160 m^3/h
Transfer (ER to SCB)	25 m^3/h	40 m^3/h	30 m^3/h
Supply (SCB)	N/A	N/A	75 m^3/h
Exhaust (SCB)	70 m^3/h	175 m^3/h	175 m^3/h
Exhaust (AR)	30 m^3/h	75 m^3/h	75 m^3/h
Transfer (AR to SCB)	45 m^3/h	135 m^3/h	70 m^3/h
Lying manikins	Uniform heat flux: 62 W, no slip boundary		
Walls	2 and 1 W/m^2 at ceiling/floor, no slip boundary		
Bedside	Adiabatic wall boundary condition		
Grid cells	8,176,419		
Turbulence model	Standard k–ε model		

4.2 Simulation results

In this study, the velocity of air supplied through the SA inlet and gap of the door, the velocity of air exhausted through the EA outlet, and the pressure differential between rooms were evaluated for the steady-state airflow in the rooms using the standard k–ε model. Then, the ventilation performance through which the virus is assumed to be an aerosol of SCB is predicted. **Tab. 2** lists the CFD analysis results for NCMSC that were derived for the three ventilation cases by combining different air change rates and SA/EA methods.

4.2.1 Airflow velocity

Fig. 4 shows the horizontal airflow velocity profile at a height of 1.5, and 2.2 m from the floor for each Case. The air change rates for AR and SCB in Case 1, which only applied the EA system, was set to 12 ACH. The velocity values were in the range of 0.0374 to 0.0506 m/s by examining the average airflow velocity distribution for each height of the SCB, indicating that the airflow progressed slowly and the air was gradually exhausted. The total airflow rate of EA, AR, and ER were 67.7, 24.2, and

43.5 m³/h, respectively. Specifically, in the case of AR, the air was exhausted at an air flowrate of 29.0 m³/h with a similar velocity of approximately 0.0365~0.0414 m/s with some of the air moved to the SCB.

Tab. 2 – CFD simulation results of the airflow profile; velocity and pressure differential.

Room	Velocity (m/s)	Case 1 (Baseline)	Case 2	Case 3
SCB	Z = 0.5m	0.0506	0.0945	0.1756
	Z = 1.5m	0.0442	0.0852	0.1781
	Z = 2.2m	0.0374	0.0861	0.1236
	Y = 0.5m	0.0743	0.1125	0.1201
	Y = 1.0m	0.0937	0.1095	0.1454
	X = 0.5m	0.0526	0.1150	0.1152
	Average	0.0587	0.1122	0.1786
AR	Z = 0.5m	0.0414	0.0977	0.1166
	Z = 1.5m	0.0365	0.0931	0.1086
	Z = 2.2m	0.0406	0.1003	0.1110
	X = 0.5m	0.0379	0.0857	0.1167
	Average	0.0410	0.0988	0.1166
ER	Z = 0.5m	0.1499	0.1469	0.1470
	Z = 1.5m	0.1412	0.1381	0.1405
	Z = 2.2m	0.2825	0.2591	0.2814
	Y = 0.5m	0.0748	0.0838	0.0755
	Y = 1.0m	0.0783	0.0826	0.0818
	Average	0.1652	0.1664	0.1638
Pressure differential (Pa)		Case 1 (Baseline)	Case 2	Case 3
SCB ↔ ER		-14.62	-18.17	-25.25
SCB ↔ AR		-1.39	-1.87	-3.02

On the other hand, the air change rates for AR and SCB in Case 2, which only applied the EA system were set to 30 ACH. The average air velocity profile for each height of the SCB was in the range of 0.0852 to 0.0945 m/s, indicating that the airflow velocity was increased twice than in Case 1, and the air was exhausted at an air flowrate of 169.2 m³/h. At this time, air was introduced from AR and ER at an air flowrate of 38.7 and 169.2 m³/h, respectively. The air in the AR is exhausted at an air flowrate of 72.5 m³/h with a velocity range of 0.0931 to 0.1003 m/s with some of the air moves to the SCB.

Furthermore, the air change rates for AR and SCB in Case 3, which applied both EA and SA systems in the SCB were set to 30 ACH. The average airflow velocity, SA airflow rate, and EA airflow rate were from 0.1236 to 0.1781 m/s, 72.5 m³/h, and 169.2 m³/h, respectively. The average airflow velocity profile for each height increased by approximately 1.7 times than in Case 2. At this time, air was introduced from AR and ER at an air flowrate of 29.0 and 67.6 m³/h, respectively. The air in AR was exhausted at an air flowrate of 72.5 m³/h with a velocity ranging from 0.1086 to 0.1166 m/s, and some of the air moves to the SCB.

4.2.2 Pressure differential

The pressure differential is another factor that can determine the effect of COVID-19 cross-infection prevention on NCMSC. A negative pressure should be maintained in the contaminated zone (SCB) and a positive pressure should be maintained in the clean zone (ER) to ensure that the aerosol COVID-19 viruses in SCB do not flow to the ER.

Fig. 5 shows the pressure differential profile for each height of 0.5 and 1.5 m from the floor for each case in which the key parameter is the pressure differential between SCB and ER. It is less likely that

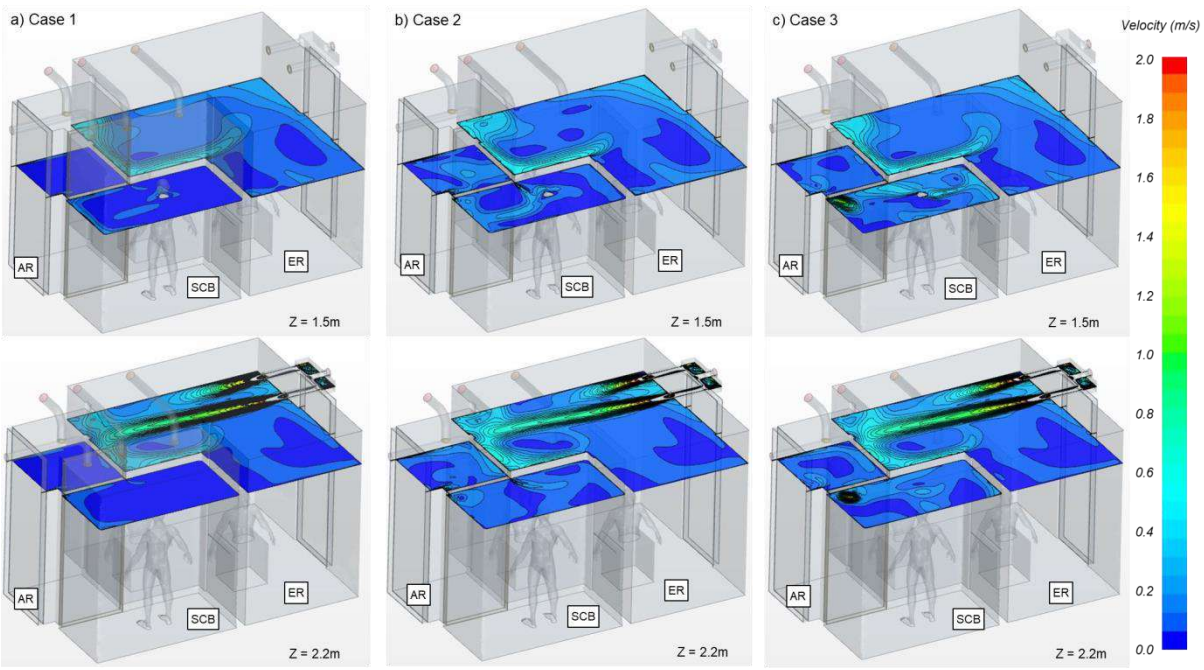

Fig. 4 - Velocity magnitude contours at the cross-sections (Z = 1.5m and 2.2m) in NCMSC for different ventilation conditions.

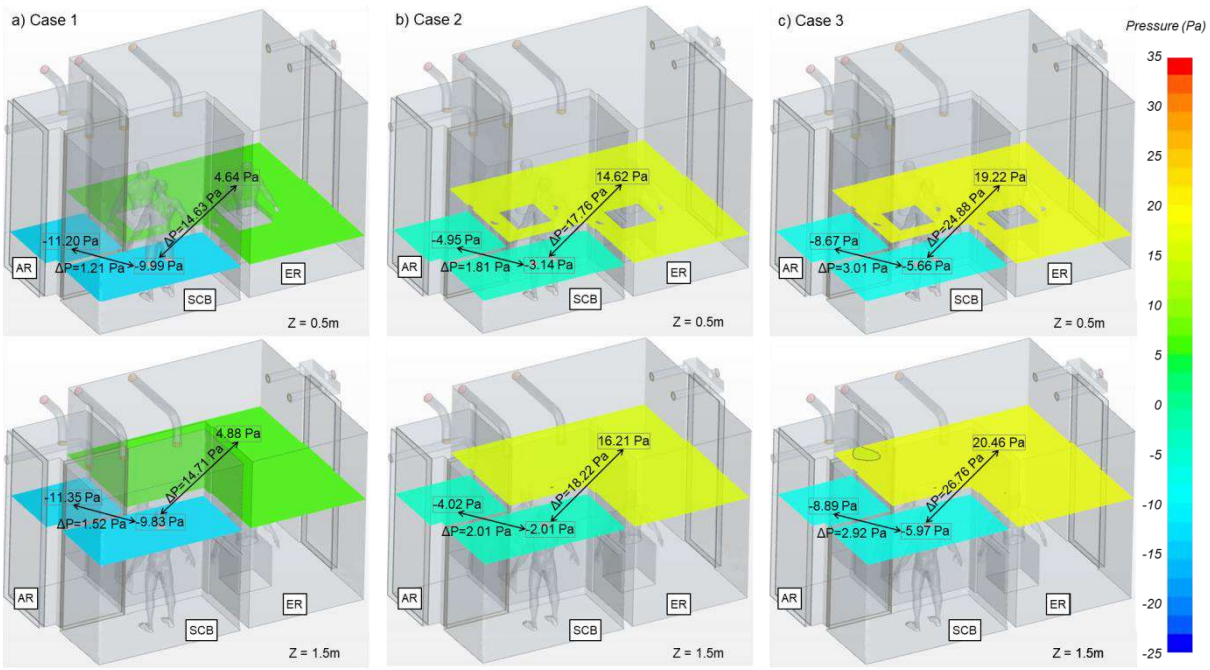

Fig. 5 - Pressure magnitude contours at the cross-sections (Z = 0.5m and 1.5m) in NCMSC for different ventilation conditions

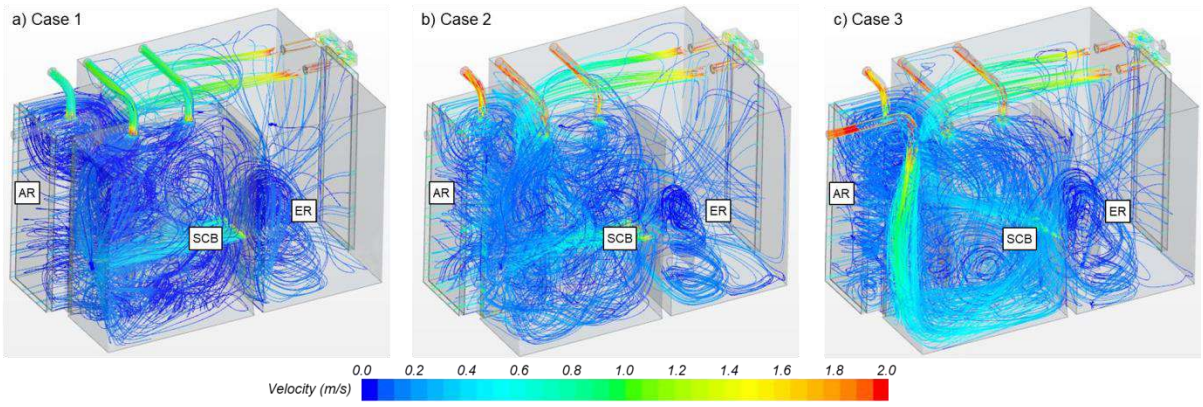

Fig. 6 - Streamline visualization of the velocity field in NCMSC for different ventilation conditions.

COVID-19 viruses migrate from SCB to the ER if the pressure is great between these two rooms. The average pressure differential for Cases 1, 2, and 3 were -14.62, -18.17, and -25.25 Pa, respectively. The analysis showed that the SCB was properly controlled for all cases to maintain the negative pressure. In addition, the effect of the cross-infection prevention of COVID-19 entering the ER is considerably enhanced because the pressure differential increases from Case 1 to Case 3. The pressure differential between the SCB and AR functions were also tested to prevent the cross-infection of other individuals to be tested waiting outside. The average pressure differential for Cases 1, 2, and 3 were -1.39, -1.87, and -3.02 Pa, respectively. Moreover, both SCB and AR maintain a negative pressure. However, the pressure differential values for Cases 1 and 2 are not within the appropriate range of the recommended pressure differential of at least -2.5 Pa based on the criteria applied to the airborne infectious isolation room [7]. Therefore, Case 3 was found to be the most effective method for preventing COVID-19 cross-infection.

4.2.3 Ventilation

Fig. 6 shows the airflow streamlines across the entire MCMSC space. It is apparent that for SCB, which applied both SA and EA systems in Case 3, the ventilation is active across the entire room compared to Cases 1 and 2, which only applied the EA system. The airflow velocity results of 0.0587 m/s for Case 1 and 0.112 m/s for Case 2 were obtained by examining the overall average airflow velocity of the room, indicating that the velocity of Case 2 increased by 1.9 times than Case 1. In addition, the airflow velocity was 0.1786 m/s for Case 3, indicating a velocity increase of 1.6 times than Case 2 and 3.0 times than Case 1. It is expected that Case 3 will enhance the ventilation performance and facilitate an effective discharge of the aerosol COVID-19 viruses.

5. Experimental analysis

This experimental study analyzes the airflow pattern based on the application of both SA and EA systems to facilitate ventilation in SCBs. The airflow patterns based on the CFD analysis may be different depending on the placement of the SA inlet and EA outlet and open-closed status of the door. Full-scale field measurements were performed under similar conditions used in the numerical analysis. PIV (particle image velocimetry) was used to conduct experiments for airflow behavior characterization and examination of the leakage area through visualization of particles simulating viruses in SCB and to verify the safety of the developed NCMSC against cross-infection. PIV is a non-intrusive measurement method that allows the application of all optical approaches to airflow by adjusting various parameter constraints, including image and recording characteristics, laser sheet properties, and analysis algorithms [8].

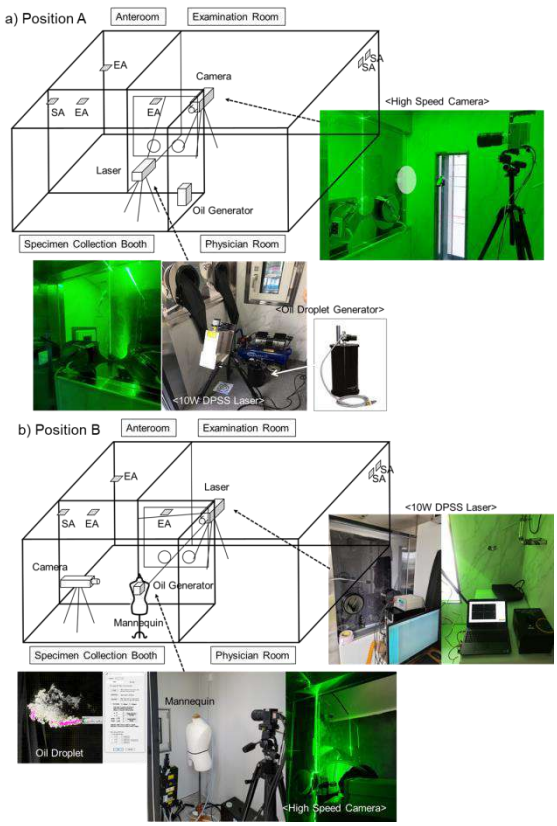

Fig. 7 - Experimental set-up for the PIV.

5.1. Experimental set-up

The purpose of the experimental study was to obtain information on airflow patterns between the SCB and ER. **Fig. 7** shows the experimental setup and perspective view of the PIV set-up. Two-dimensional flow fields were measured at different positions of the camera and laser. First, the camera was installed in the ER, and the laser and oil droplet generator were installed in the SCB. The overall airflow in the rooms adjacent to the tested individual was observed at Position A. Moreover, at Position B, the laser was installed at the ER and the camera. Then, at the same position, the oil droplet generator was installed in the SCB to ensure that the droplet came out from the mouth of the manikin, a simulation model of the individual to be tested. Subsequently, the exhaust airflow was observed.

Four different PIV measurements were performed for four different combinations, as shown in **Tab. 3**. First, the PIV measurement was performed at Position A for Case 2, where only the EA system was applied, and Case 3, where both EA and SA systems were simultaneously applied in the ventilation system of the SCB, that were analyzed in the CFD simulation. Subsequently, the experimental setup was changed and the ventilation performance at Position B was examined with the door between the AR and SCB closed and open for Case 3. In principle, all doors are closed during the COVID-19 testing. However, the doors were opened and ventilation was performed before the next individual to be tested entered the SCB after each examination. Therefore, the ventilation effect in this situation was investigated.

Tab. 3 - Measuring cases with the PIV equipment.

Measurement	Cases	Position	Door between SCB and AR
PIV A1	Case 2	A	Closed
PIV A2	Case 3	A	Closed
PIV B1	Case 3	B	Closed
PIV B2	Case 3	B	Open

5.2. Measurement results

In Case 2, the PIV experiment was conducted only with the EA system applied in SCB, while both SA and EA systems were used in Case 3. The pressure differentials of SCB and ER with the ventilation system turned on are ΔP = -21.8 and -29.3 Pa, respectively. The negative pressure in the SCB was properly maintained for both cases (Cases 2 and 3). **Tab. 4** lists the time-averaged airflow velocity profiles in the SCB. The experimental results were divided into two parts based on the location of the PIV measurements.

Tab. 4 – PIV measurement results of airflow velocity.

Measurement	Cases	Velocity (m/s)		
		Mean	Min	Max
PIV A1	Case 2	0.0098	0.0031	0.0607
PIV A2	Case 3	0.0541	0.0120	0.2531
PIV B1	Case 3	0.0536	0.0238	0.1124
PIV B2	Case 3	0.1042	0.0117	0.1747

Moreover, **Fig. 8** shows the experimental results for the vertical airflow velocity. The velocity vector consists of two time-averaged velocity components V_x(m/s) and V_y(m/s) along the X- and Y-axes, respectively. All the results presented are based on the map of the average velocity vectors. **Fig. 8a)** shows the average velocity of Case 2 for Position A

(i.e., PIV A1). The particle movement velocity in the SCB was found to be very slow with almost no airflow for a maximum airflow velocity of 0.0607 m/s and an average airflow velocity of 0.0098 m/s. The air exhaust efficiency is lowered because the air flowing in from the AR is not sufficient due to the high airtightness of the structure. On the other hand, the average airflow velocity of PIV A2 in Case 3 shown in **Fig. 8b)**, where SA and EA systems were applied to the SCB, was 0.0541 m/s, indicating a four-time increase than PIV A1. In addition, the generated particles were smoothly discharged through the upper EA outlet. The make-up air was smoothly supplied to improve the exhaust efficiency. In addition, the result after the examination of the leakage area showed that there were no particles generated inside the SCB that escaped through the gap in the wall in contact with the ER. Therefore, the cross-infection by viruses is not expected to occur since there was no airflow from the contaminated zone (SCB) to the clean zone (ER) in PIV A1 and PIV A2.

Fig. 8c) shows the average velocity of Case 3 for Position B (i.e., PIV B1). The maximum airflow velocity of PIV B1 was 0.1124 m/s and the average airflow velocity was 0.0536 m/s, indicating that the average velocity of the particles generated in the SCB is the same as that in PIV A1. This result is expected because they were both performed under the same conditions except for the measurement position Finally, **Fig. 8d)** shows the average velocity of Case 3 for Position B (PIV B2). The same condition was applied to PIV B2 as PIV B1, but the door to the AR was opened. In this case, the results showed that the maximum airflow velocity was 0.1747 m/s, the average airflow velocity was 0.1042 m/s, and the velocity of the generated particles increased more than twice than that of PIV B1, confirming the improvement in the ventilation performance. However, it is a principle to close the door during specimen collection to prevent airflow in adjacent rooms. Therefore, it is recommended to operate the ventilation system with the door open before the next individual to be tested enters to increase the cleaning and disinfection effect after collecting the specimen.

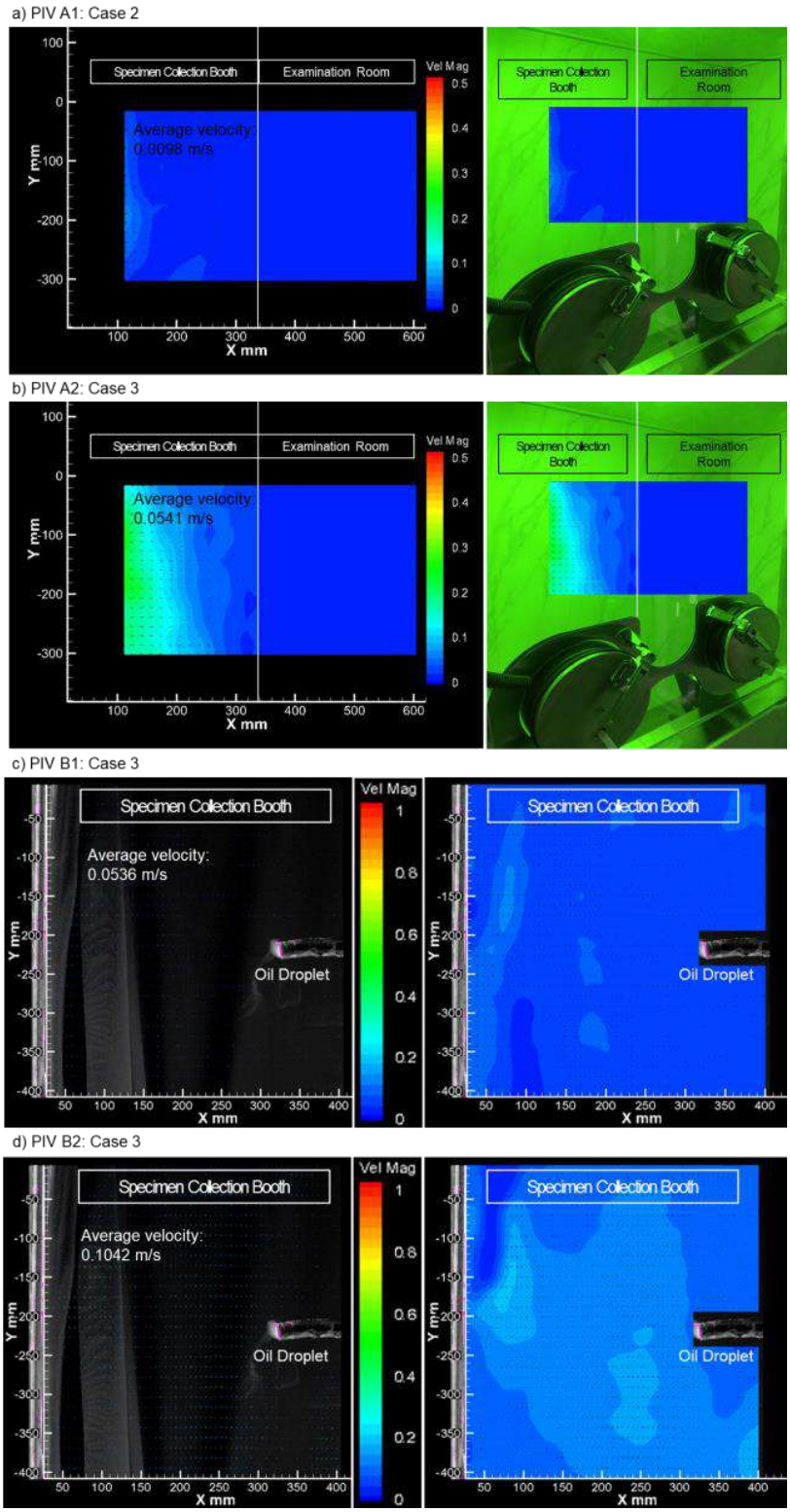

Fig. 8 - Time-averaged air distribution under PIV cases.

6. Conclusion

A novel non-contact modular screening center (NCMSC) was developed to address the potential risk of cross-infection in screening centers during COVID-19 testing. The main aim of this study was to evaluate the effects of virus cross-infection prevention and ventilation performance on rapid virus discharge based on an actual project and to

employ both numerical analysis and experimental measurements. The main findings of this study are as follows.

(1) In the proposed NCMSC, the space configuration that enables non-contact specimen sampling between HCWs and tested individuals were implemented, and the pressure differential control such as maintaining negative-positive pressure were reflected. In addition, the proposed SCB design allows sufficient ventilation for safe use by the next patient to be tested.

(2) Furthermore, design optimization was performed using three alternatives by combining different air change rates in each room and applying the SA/EA system for the ventilation strategy of NCMSC to prevent the transmission of the COVID-19 virus.

(3) The results of the CFD analysis showed that the effect of cross-infection prevention was the most significant in Case 3 in the SCB, where the negative pressure must be maintained, at the ventilation rate of 30 ACH and a pressure differential of -25 Pa or more between ER using both SA and EA systems. Compared to Case 2, in which only the EA system was applied under similar ventilation rate conditions, the airflow velocity in the room increased by approximately 0.6 times. Moreover, compared to Case 1, in which only the EA system was applied with a ventilation rate of 12 ACH, the airflow velocity increased by more than two times. This demonstrated the improvement of the ventilation performance in Case 3.

(4) The result of the PIV experiments in Case 3 shows that the pressure differential between an ER of -30 Pa or more was maintained, and the effect of cross-infection prevention was excellent compared to -22 Pa in Case 2, and the ventilation performance with an increase in airflow velocity by four times was also achieved.

Based on the results of this study, the standards for the installation and operation of the COVID-19 screening centers are proposed. It is necessary to implement space configuration and secure airtight performance to ensure that all tests can be performed using non-contact methods. To maintain the negative pressure of SCB and prevent cross-infection between HCWs and individuals to be tested, a ventilation rate of 30 ACH, and a pressure differential of -15 Pa or higher is recommended. In addition, a simultaneous application of both SA and EA systems is effective in facilitating a smooth discharge of the airborne COVID-19 virus.

7. Acknowledgement

This work is supported by the Korea Agency for Infrastructure Technology Advancement (KAIA) grant funded by the Ministry of Land, Infrastructure and Transport (21TBIP-C161839-01).

8. References

[1] Lim, T., Cho, J., Kim, B.S. The predictions of infection risk of indoor airborne transmission of diseases in high-rise hospitals: Tracer gas simulation. Energy Build. 2010;42(8):1172-1181.

[2] Noor, R., Maniha, S.M. A brief outline of respiratory viral disease outbreaks: 1889-till date on the public health perspectives. Virusdisease. 2020;31(4): 441-449.

[3] Asad, H., Johnston, C., Blyth, I. Holborow, A., Bone, A., Porter, L., Tidswell, P., Healy, B. Health Care Workers and Patients as Trojan horses: a COVID19 ward outbreak. Infect Prev Pract. 2020;2(3):100073.

[4] Hassan, A.M., Megahed, N.A. COVID-19 and urban spaces: A new integrated CFD approach for public health opportunities. Build. Environ. 2021;204:108131.

[5] CDC, Guidelines for preventing the transmission of mycobacterium tuberculosis in health-care facilities. US Department of Health and Human Services, Public Health Services, Federal Register. 1994.

[6] Cho, J., Woo, K., Kim, B.S. Removal of airborne contamination in airborne infectious isolation rooms. ASHRAE J. 2019;61(2):8-21.

[7] Cho, J. Investigation on the contaminant distribution with improved ventilation system in hospital isolation rooms: Effect of supply and exhaust air diffuser configurations. Appl. Therm. Eng. 2019: 148:208-218.

[8] Cao, X., Liu, J., Jiang, N., Chen, Q. Particle image velocimetry measurement of indoor airflow field: A review of the technologies and applications. Energy Build. 2014;69:367-380.

The Indoor Air Quality, Ventilation and Energy Nexus in the COVID-19 Context

Talie Tohidi Moghadam [a], Carlos E. Ochoa Morales [b], Maria Lopez Zambrano [b], Ken Bruton [a], Dominic T. J. O'Sullivan [a]

[a] Intelligent Efficiency Research Group (IERG), University College Cork, Cork, Ireland, 120222839@umail.ucc.ie (T.T.M.); ken.bruton@ucc.ie (K.B.); dominic.osullivan@ucc.ie (D.O.).

[b] International Energy Research Centre (IERC), Tyndall National Institute, Cork, Ireland. carlos.ochoa@ierc.ie (C.E.O.) maria.lopez@tyndall.ie (M.L.Z)

Abstract. In the face of the Covid-19 pandemic and environmental crises, ventilation plays a critical role in the removal of infectious pathogens. A building ventilation paradigm results in excessive energy consumption to ensure indoor air quality. At the time of writing this paper, several studies have been conducted regarding COVID-19 and ventilation; however, the energy challenges of ventilation operation under the pandemic condition has not been fully addressed by previous studies. This paper is based on a literature review of publications, using an internet-based search in different scientific databases. A data-driven keyword analysis on bibliographic data was performed based on English-language textual data of more than 267 publications downloaded from Dimensions website and using VOSviewer, a freely available software tool for analysing bibliographic data. Via analysis of co-occurrence of the specific terms in the field of COVID-19 ventilation, the trends in research publications were illustrated. The study aims to review the scientific literature of the indoor spread of SARS-CoV-2; clarify the effect of ventilation systems on airborne transmission of the virus; identify the impacts of COVID-19 mitigation measures on the energy consumption of mechanical ventilation systems; define the research gaps and future challenges. This investigation reveals a strong need for more scientific studies in reduction of the transmission risks of the SARS-CoV-2 virus through ventilation systems without compromising buildings' energy performance. The implications of this study will establish a foundation for engineering control strategies and future energy-targeted investigations for virus transmission reduction and the enhancement of indoor air quality.

Keywords. COVID-19, indoor air quality, mechanical ventilation system, building energy performance, healthy indoor environments.
DOI: https://doi.org/10.34641/clima.2022.285

1. Introduction

The COVID-19 pandemic has exposed areas requiring urgent development to provide a healthy indoor environment [1]. Given that most of the documented spread of the disease has happened in indoor environments [2], control of indoor air is essential to reduce the risk of airborne pathogens [3]. Engineering controls through heating, ventilation, and air-conditioning (HVAC) systems are considered a higher level of precaution than physical containment methods for creating healthy indoor environments [4; 5; 6; 7; 8]. Ventilation is the primary control measure for indoor transmission of airborne particles [1]. Existing ventilation systems in buildings are designed to remove heat and pollution loads in normal conditions. However, ventilation systems should also be able to eradicate the transmission of airborne particles during serious outbreaks [9]. In addition, an inadequate ventilation rate and inappropriate ventilation strategy are associated with inferior health outcomes for the occupants.

Energy consumption linked with control of the indoor environment is a critical concern, given that buildings consume over 36% of energy globally [10]. New ventilation criteria, proposed by industry professionals, have mainly focused on indoor air quality improvements to guarantee occupants' health. However, the associated energy consumption was an afterthought; this has resulted

Copyright ©2022 by the authors. This conference paper is published under a CC-BY-4.0 license.

in high energy consumption as a result of increased volumes of fresh air being treated and delivered during the pandemic [11]. Higher ventilation rates required to flush air out of a space in a short period exceed the capacity of most of the existing mechanical ventilation systems and might result in discomfort to occupants as well as non-optimal performance from a cost perspective. In regard to this matter, Lipinski et al. (2020) assessed the current ventilation strategies intending to decrease the risk of pathogen transmission and to adapt ventilation measures to new threats posed by pandemics [3]. Melikov (2020) proposed a paradigm shift in the design of future ventilation with a specific focus on the occupant but not space [12]. Thus, the challenge is how to balance the ventilation energy use and the prevention of infection risk in the indoor environment and to recommend strategies that help to deliver a healthy yet sustainable indoor environment [8].

Although many papers have been published regarding indoor air quality, ventilation and COVID-19 spread, very few of them have mentioned the energy challenges of ventilation operation due to these requirements. Aiming to identify the impacts of COVID-19 on the energy consumption of mechanical ventilation systems, this paper reviews the research, conducted on:

1. the couplings of reducing infection risks of SARS-CoV-2, operating ventilation systems and reducing energy consumption;

2. the scientific literature of the indoor spread of SARS-CoV-2 and the transmission routes are also reviewed and the effect of ventilation systems on airborne transmission of the virus is then clarified;

3. the gaps of adaptation on the three aforementioned areas (Figure 1).

Aiming to demonstrate the evolution of the scientific landscape of COVID-19 ventilation and energy efficiency through bibliometric analysis, the implications of this research lead to a new discussion of the assessment of operating ventilation systems in relation to the connected energy consumption and healthy indoor environment. This could be essential for proposing effective and energy-efficient solutions for adapting ventilation systems to the pandemic context.

1.1 The indoor spread of SARS-CoV-2 and transmission

To understand the role of ventilation systems in keeping indoor environments virus-free and reducing energy consumption, it is important to know the characteristics of SARS-CoV-2 and its trajectories. This section elaborates the indoor spread of this virus and its transmission routes.

SARS-CoV-2 belongs to the betaCoVs category. Considering that the virus has a diameter of approximately 60–140 nm [13], it can be easily transmitted by aerosol droplets in the air and stay float for a period depending on factors like heat and humidity [3; 14]. Many studies suggested SARS-CoV-2 may be airborne and is stable on aerosols for 3 hours, and can travel a long distance in the closed and open environments [9; 12; 14; 15; 16] via three main routes, including droplet, contact, and airborne routes. The airborne route (also called aerosol transmission) happens when exhaled respiratory droplets are small enough to remain suspended that they can be inhaled into the respiratory system of other people [1; 3; 17; 18; 19].

The distance particles move away from the infected person depend on several factors, including the size of the particles, initial momentum they are expelled (i.e., type of respiratory activity), the position of the head and the body of the person generating the particles, strength (velocity), structure (turbulent or laminar), direction, temperature and humidity of the surrounding air flow, individual differences between people regarding respiratory activities, etc. [3; 20; 21; 22; 23; 24; 25]. Li et al. (2021) measured the main influencing factors of the exposure risk of SARS-CoV-2, namely the occupant density, dwell time, and fresh air volume per person, in retail buildings [26].

Also, successful infection depends on exposure (inhaled dose of particles with viruses) and time. With regard to the distance between infected and exposed persons, short-range exposure to large and small particles and long-range exposure mainly to small airborne particles can be defined. The risk for short-range exposure is much higher than long-range exposure. Research shows that a rise in outdoor air supply to occupied spaces can reduce the risk of long-range exposure but is less effective in reducing the short-range exposure [12].

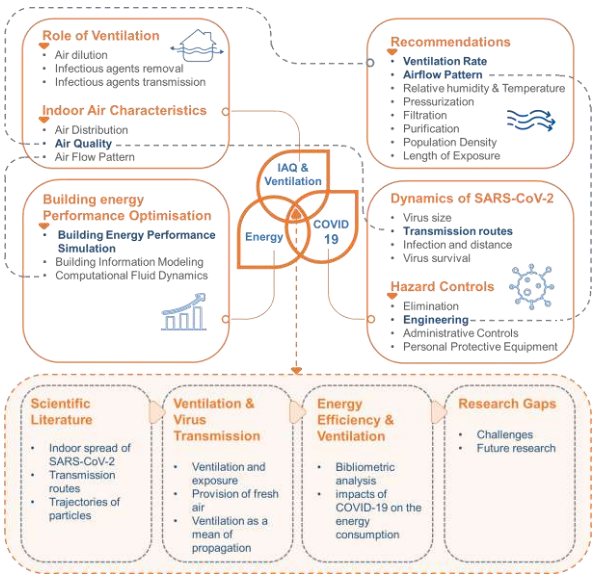

Fig. 1 – Structure of the research.

1.2 Effect of Ventilation Systems on Airborne Transmission of the Virus

Ventilation can be defined as "the process of introducing and distributing outdoor and/or properly treated recycled air into a building or a room" [27] or "the process by which "clean" air (normally outdoor air) is intentionally provided to space and stale air is removed" [28]. Due to the short-fall in the stable wind pressure, natural ventilation systems are usually used for auxiliary purposes and mechanical ventilation systems are largely utilized to meet requirements for indoor air quality [8]. In the recent research, Nembhard et al. (2020) reviewed the role of building ventilation in minimizing the risk of SARS-CoV-2 transmission in non-medical settings [6]. Also, Blocken et al. (2021) measured the aerosol particle removal by mechanical ventilation and mobile air cleaning units in a gym. They concluded that the combination of existing ventilation supplemented with air cleaning is energy efficient and can also be applied to other indoor environments [29].

The principle of ventilation to control the airborne transmission of viruses mainly includes two aspects, namely, diluting viral concentration and blocking virus transmission [9; 30]. The dilution is managed either by supplying outdoor air mixing with the existing indoor air; or by attempting to enter the outdoor air into the occupied zone of the building space in a relatively unmixed state and then "displace" any air polluted by airborne virus particles back outdoors [31; 32]. The Air Changes per Hour (ACH) is a measurement of how much fresh/clean air replaces indoor air in 1 hour [33], which is more widely adopted in engineering to determine if ventilation and air conditioning systems can provide adequate ventilation rate to guarantee a low infection probability [34]. The recently updated guidelines for the reduction of airborne infection recommend a substantial increase in the ventilation rate [35; 36]. In this matter, Dai & Zhao (2020) estimated the link between the infection probability and ventilation rates with the Wells–Riley equation for some typical scenarios, including offices, classrooms, buses, and aircraft cabins [34]. Pease et al. (2021) evaluated the concentrations and probabilities of infection and concluded that increasing the fraction of virus-free outdoor air is helpful unless outdoor air is infective [37].

2. Research Methods

2.1 Bibliometric analysis

The bibliographic data was collected from 267 publications published from December 2019 to July 2021 from the Dimensions bibliographic database [38]. It must be noted that several search query words with "AND" as a Boolean operator were used to create a total of 5 combinations of specific query wording of "SARS-CoV-2" AND "ventilation" AND "COVID-19" AND "indoor air quality" AND "energy." Data-driven keyword analysis on bibliographic data was performed using VOSviewer, a freely available software tool for analysing bibliographic data [39].

Through analysis of co-occurrence of field-specific terms, this software visualises the trends in research publications. Out of a total of 7418 terms identified occurring in the titles and abstracts, the terms with a minimum of five occurrences and the top 15 according to relevance were extracted from English-language textual data, unrelated words were eliminated, and abbreviations were replaced by full terms. It is important to mention that although the bibliographic tools greatly reduce the time spent analysing bibliographical sources, human supervision on the results is still needed. In this paper, we analysed and elaborated the results obtained from the software analysis. This produced a network visualisation of terms, where each circle represents a term and the label and circle size of a term determines its importance (the higher the importance, the larger the label and circle); the link corresponds to a connection between two terms, and its strength represents the strength of co-occurrence; The distance between two terms is

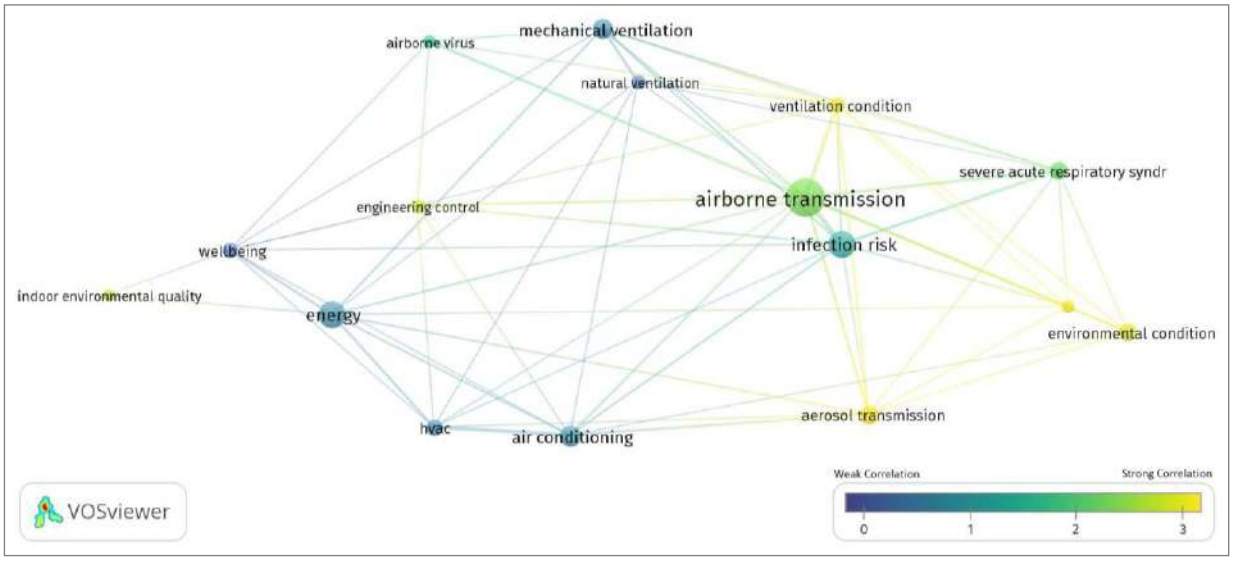

Fig. 2 - Keyword network visualization of terms.

representative of their relatedness; terms that co-occur a lot tend to be located close to each other in the visualization. Finally, the network was colour-overlaid where the colour assigned shows the strength of co-occurrence, enabling the analysis of the importance of the term in the literature (Figure 2). Analysing Figure 2, it could be determined that:

- The core topic in the literature with the highest link strength is the airborne transmission SARS-CoV-2.
- There is a strong link between the terms aerosol transmission, ventilation, and environmental condition with the assigned yellow colour, indicating a rise in awareness of the importance of these couplings.
- Decreasing the occurrence of the terms energy, mechanical ventilation, air conditioning, and well-being demonstrates insufficient studies and research on the topics on which this paper is focusing.
- There is a multi-faceted and multi-dimensional character of this particular scientific field.

3. The impact of COVID-19 on the energy consumption of mechanical ventilation systems

Although measures provided by various industry associations and HVAC operators have the potential to reduce infection risks, they need extra energy use by the HVAC system, which might simply be wasting energy without providing a meaningful reduction in transmission risk [4; 9].

Higher ventilation means higher energy use [30]; ventilation should be adequate to the demand but not unnecessarily high [30; 40; 41]. If future ventilation systems are designed to supply a large amount of outdoor air during the pandemic, they will not operate economically under normal conditions (no pandemic) with a greatly reduced supply airflow rate [12]. On this matter most of the papers have focused on high-density indoor environments. More specifically, the following three papers have targeted the building occupants as the transmission source of infection diseases by applying the occupant-related information, in particular, occupant presence schedule. Wang et al. (2021) proposed an intelligent, low-cost ventilation control strategy based on an occupant-density-detection algorithm that can actively self-adjust the ventilation rate when experiencing different occupant densities considering both infection prevention and energy efficiency. Melikov et al. (2020) proposed an improved control strategy based on source control, which would be achieved by implementing intermittent breaks in a typical classroom [42]. Through a multi-objective optimization, Mokhtari & Jahangir (2021) examined the optimum occupant distribution models that account for the lowest number of infected people and minimum energy use in a university building [43].

Concerning other high-density environments, a large number of studies have focused on educational buildings, in particular, school and university classrooms using experimental and numerical investigations [42; 43; 44; 45; 46]. In their findings, Balocco & Leoncini (2020) showed that it is possible to obtain healthy school environments by means of an optimal compromise between energy savings and proper management of mechanical ventilation systems for indoor air quality [44].

Ascione et al. (2021) proposed a comprehensive approach for the retrofit design of university classrooms through both experimental studies and by the coupling of different numerical methods of investigations and building performance simulations [45]. Aviv et al. (2021) analysed the energy consequences of increasing the fresh air delivered through typical commercial building recirculating ventilation systems. Their results suggested the coupling of natural ventilation and radiant systems [47]. On the matter of energy efficiency of ventilation systems in school classrooms, Schibuola & Tambani (2021) investigated the possibility of containing COVID-19 contagion in indoor environments via increased ventilation rates obtained through high energy efficiency systems combining thermal recovery by a heat exchanger and thermodynamic recovery by a heat pump [46]. The controlled parameters studied in these papers have been mostly and commonly based on the indoor distribution of microclimatic parameters (i.e., air temperature, air velocity and flow fields, indoor thermal comfort, age of air) [44; 45; 47; 48] indoor/outdoor CO2 concentrations [46] and their effects on the indoor infection probability and energy consumption [4; 11; 49]. The effects of these parameters were mainly studied in indoor environments with high occupancy, where infection probability is high [42; 43; 44; 45; 46; 47; 49]. However, in terms of the building type, there is a gap to study the energy performance of the ventilation system and indoor air quality in low-occupancy buildings such as homes and small offices. Table 1 summarises the reviewed papers in this field. Reviewing the abovementioned papers and analysing Table 1, it could be determined that:

- As most of the papers have focused on high-density indoor environments such as educational buildings where infection probability is high, there is small diversity of case studies in the published literature and very few preliminary studies in low-occupancy indoor environments.
- Several studies have highlighted improved ventilation control strategies based on source control and the optimum occupant distribution.
- There has been considerable interest in studying the indoor distribution of

microclimatic parameters, pollutant concentration and infection probability in the literature.

4. Discussion

Through the above review and discussions, the research gaps of adaptation on the three aforementioned areas were highlighted in this section. According to these gaps, attention should be paid to adapting ventilation designs to the normal and pandemic situations simultaneously and to operating HVAC systems in a relatively low energy consumption mode during the pandemic period. HVAC system auxiliary equipment should also be developed for energy savings and improving indoor air quality. Optimization of ventilation systems, indoor air quality, and energy efficiency is another significant gap in this nexus. Additional studies are also required on the energy efficiency assessment of novel mechanical ventilation methods and control strategies that can significantly improve effective ventilation performance in different building types with varying occupancy densities. Figure 3 represents the gaps found in the literature.

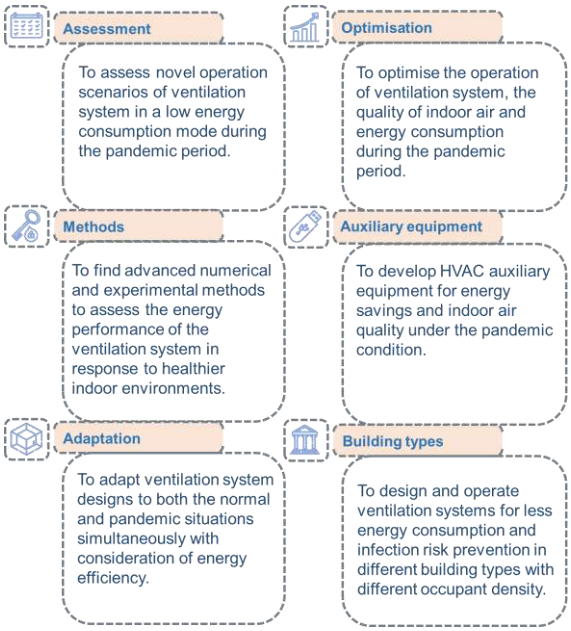

Fig. 3 - Research gaps in the literature.

5. Conclusion

The pandemic mitigation set of measures forces the adaptation of existing buildings and changes to new paradigms, where health is preferred over energy efficiency. The current approach would result in higher energy consumption, in buildings in a post-COVID-19 period. It is crucial to identify the most influential research channels and major concerns of the design and operation of effective ventilation systems and energy consumption to meet future challenges. This article presented an up-to-date bibliometric analysis to describe and assess the scientific landscape of COVID-19 ventilation and energy consumption. The results of bibliometric analysis demonstrates insufficient studies and research on the topics on which this paper is focusing.

Through reviewing the most cited publications in this literature, and analysing the main theme, method, results, parameters and the building type investigated in these papers, the research gaps and future challenges are highlighted and summarised in six main categories including the assessment and optimisation of ventilation operation during the pandemic period; the advanced numerical and experimental methods of assessing the energy performance of the ventilation system; the development of HVAC auxiliary equipment for better energy savings and indoor air quality; the adaptation of ventilation system design to both normal and pandemic situations; and to consider these items in diverse building types with different building densities.

Given the struggle between energy sustainability and occupant wellness, it is essential to make indoor air quality a priority parameter in the design of a building. If the design and operation of the mechanical ventilation systems are oriented towards the health of the users, the virus transmission can be significantly reduced. Thus, greater integration is needed to ensure that energy efficiency interventions are carried out simultaneously, with indoor air quality provision. This is very much the key component in future attempts to overcome the conflicts between energy efficiency and indoor air quality.

6. Acknowledgement

This research was part-funded by Science Foundation Ireland (SFI) through MaREI, the SFI Research Centre for Energy, Climate, and Marine and specially the Centre for Doctoral Training in Energy Resilience and the Built Environment (ERBE) (grant no: 12/RC/2302_P2), with supporting funding obtained from UK Engineering and Physical Sciences Research Council (EPSRC) (grant EP/S021671/1) and FlexTECC: Flexible Timing of Energy Consumption in Communities Innovation Fellowship (grant EP/S001670/1).

Data access statement: The datasets generated and analysed during the current study are not publicly available in the Dimensions Website because the access requires login credentials; but the data will be available by creating an account and inserting search string terms as discussed in the Research Methods section.

Tab. 1 - Overview of research in energy efficiency of ventilation systems in the context of COVID-19.

Reference	Methodology	Results	Building Type	Main Theme	Studied Parameter
[4]	• Modelling the transmission rate by considering the airborne concentration of infectious particles. • Estimating the energy consumption by considering the change in HVAC variables and applying standard models.	• Underlying transmission risk and the energy-optimal disinfection strategies can vary significantly from building to building and from space to space.	• Not specified	• Infection rate • Energy consumption	• Concentration of infectious particles, activity, dimensions of the space, HVAC operation • Flow rates and temperatures
[11]	• Comparing energy consumption, CO2 emissions and operations costs in nine US climate zones between the previous and post COVID-19 scenarios using BES.	• Climate zones above mixed-humid type tend to increase relative energy use intensity by 21.72%, but below that threshold the zones decrease relative energy use intensity by 11.92%.	• High-rise office buildings	• Energy consumption • CO2 emissions • Operation costs	• Cooling & heating • Lighting • Fans &Plug & equipment, pumps, SWH • CO2 emissions
[41]	• Different factors and strategies are reviewed and discussed. • Suggested mitigations and solutions are provided.	• Need for in situ experimental studies to understand the different scenarios of the virus spread. • The human factor should also be considered.	• Not specified	• Technological solutions for HVAC systems	• Underfloor air distribution • Chilled beams & Radiant ceiling panels, Laminar flow systems • HEPA filter & UV light
[42]	• Aerosols concentration prediction. • Evaluation of the risk of airborne cross-infection calculating the time-averaged intake fraction.	• An improved control strategy based on source control, can be achieved by implementing intermittent breaks in room occupancy.	• Classroom	• Occupant presence schedule • risk of air-borne cross-infection	• Supply flow rate • Schedule of lessons and breaks • Density, Room height • Number of source
[43]	• A multi-objective optimization used with the objectives of energy consumption and COVID-19 infected people, using NSGA-II algorithm.	• An optimal population distribution can reduce the number of infected people and energy consumption.	• University building	• Energy consumption • COVID-19 infection	• Occupant presence schedule • ACH • Class duration • Working hours
[44]	• Transient simulations.	• Correct behaviour, together with proper management and maintenance of a mechanical ventilation guarantee indoor air quality and healthy environments.	• Schools	• Demand-controlled mechanical ventilation	• Indoor Air Temperature • Air Change per Hour (ACH) • Energy Cost
[45]	• A numerical model of a University building was proposed and the design of refurbishment was performed by coupled numerical methods, Building Energy Simulation (BES) and Computational Fluid Dynamics (CFD).	• New scenarios and evidenced the usefulness of HVAC systems, equipment and suitability of some strategies for the air distribution systems compared to traditional ones.	• University classrooms	• Energy impacts • Indoor distribution of microclimatic parameters	• Annual & monthly primary energy demand • Indoor distribution of microclimatic parameters & thermal comfort • Age of air
[46]	• Evaluation of the infectious risk by using measurements of indoor/outdoor CO2 concentrations to calculate actual ACH.	• There is possibility to achieve a reduction in energy consumption as a result of installing an autonomous high efficiency air handling unit (HEAHU).	• Schools classroom	• Energy consumption	• ACH • Indoor/outdoor CO2 concentrations
[47]	• Analysing the energy consequences of increasing the fresh air and the potential of alternative radiant and convective systems to compensate using thermal comfort models combined with global weather data.	• It is possible to add up to 100 days' worth of natural ventilation while saving energy, when coupling natural ventilation and radiant systems.	• Typical commercial building	• HVAC energy cost	• The increasing outdoor air ratio • Thermal comfort indoors
[48]	• Optimization of the in-duct Ultra Violate Germicidal Irradiation (UVGI) system using CFD simulation and energy simulation.	• Identifying two energy-efficient UVGI system designs as references during the COVID-19 pandemic.	• Not specified	• Germicidal source output • UV rate constant • System inactivation efficiency • System energy consumption	• Air temperature • Air velocity • Relative humidity
[49]	• YOLO (You Only Look Once) algorithm was applied for occupancy detection.	• Infection probability reduction and energy saving increase.	• Public transportation buildings	• Occupant density	• Infection probability • Energy consumption
[50]	• Editorial Review	• Risk reduction of exposure and virus contamination through focusing on the health of the users	• Not specified	• Energy efficiency • Indoor air quality	• Not specified

7. References

[1] Burridge, H.C. Johnson-Llambias, Marco-Felipe King,Oleksiy Klymenko, Alison McMillan, Piotr Morawiecki, Thomas Pennington, Michael Short,David Sykes, Philippe H. Trinh, Stephen K. Wilson,Clint Wong, Hayley Wragg, Megan S. Davies Wykes,Chris Iddon,AndrewW.Woods, Minjoo Noh, Neeraja Bhamidipati, HuwWoodward,Clive Beggs, Hywel Davies, Shaun Fitzgerald, Christopher Pain & P. F. Linden. The ventilation of buildings and other mitigating measures for COVID-19: A focus on winter 2020. In arXiv. arXiv. 2021. https://doi.org/10.1098/rspa.2020.0855

[2] Hamner, L., Dubbel, P., Capron, I., Ross, A., Jordan, A., Lee, J., Lynn, J., & Ball, A. High SARS-CoV-2 attack rate following exposure at a choir practice. Morbidity and Mortality Weekly Report. 2020; 69(19). https://www.cdc.gov/mmwr/volumes/69/wr/mm6919e6.htm

[3] Lipinski, T., Ahmad, D., Serey, N., & Jouhara, H. Review of ventilation strategies to reduce the risk of disease transmission in high occupancy buildings. International Journal of Thermofluids. 2020; 7–8. https://doi.org/10.1016/j.ijft.2020.100045

[4] Risbeck, M. J., Bazant, M. Z., Jiang, Z., Lee, Y. M., Drees, K. H., & Douglas, J. D. Quantifying the Tradeoff Between Energy Consumption and the Risk of Airborne Disease Transmission for Building HVAC Systems. 2021.https://doi.org/10.1101/2021.06.21.21259287

[5] Ren, Y. F., Huang, Q., Marzouk, T., Richard, R., Pembroke, K., Martone, P., Venner, T., Malmstrom, H., & Eliav, E. Effects of mechanical ventilation and portable air cleaner on aerosol removal from dental treatment rooms. Journal of Dentistry. 2021; 105. https://doi.org/10.1016/j.jdent.2020.103576

[6] Nembhard, M. D., Burton, D. J., & Cohen, J. M. Ventilation use in nonmedical settings during COVID-19: Cleaning protocol, maintenance, and recommendations. Toxicology and Industrial Health. 2020; 36(9): 644–653. https://doi.org/10.1177/0748233720967528

[7] Rolloos, M. HVAC Systems and Indoor Air Quality. Indoor and Built Environment. 1993; 2(4): 204–212.https://doi.org/10.1177/1420326X9300200403

[8] Ding, J., Yu, C. W., & Cao, S. J. HVAC systems for environmental control to minimize the COVID-19 infection. Indoor and Built Environment. 2020; 29(9): 1195–1201. https://doi.org/10.1177/1420326X20951968

[9] Zheng, W., Hu, J., Wang, Z., Li, J., Fu, Z., Li, H., Jurasz, J., Chou, S. K., & Yan, J. COVID-19 Impact on Operation and Energy Consumption of Heating, Ventilation and Air-Conditioning (HVAC) Systems. Advances in Applied Energy. 2021; 3, 100040. https://doi.org/10.1016/j.adapen.2021.100040.

[10] UN Env. and IEA. Towards a zero-emission, efficient, and resilient buildings and construction sector. In Global Status Report. 2017. www.globalabc.org

[11] Cortiços, N. D., & Duarte, C. C. COVID-19: the impact in US high-rise office buildings energy efficiency. Energy and Buildings. 2021; 111180. https://doi.org/10.1016/j.enbuild.2021.111180

[12] Melikov, A. K. COVID-19: Reduction of airborne transmission needs paradigm shift in ventilation. In Building and Environment. 2020; (Vol. 186). Elsevier Ltd. https://doi.org/10.1016/j.buildenv.2020.107336

[13] Cascella, M., Rajnik, M., Cuomo, A., Dulebohn, S. C., & Di Napoli, R. Features, Evaluation and Treatment Coronavirus (COVID-19). StatPearls. 2020. http://www.ncbi.nlm.nih.gov/pubmed/32150360

[14] van Doremalen, N., Bushmaker, T., Morris, D. H., Holbrook, M. G., Gamble, A., Williamson, B. N., Tamin, A., Harcourt, J. L., Thornburg, N. J., Gerber, S. I., Lloyd-Smith, J. O., de Wit, E., Munster, V. J. Aerosol and Surface Stability of SARS-CoV-2 as Compared with SARS-CoV-1. New England Journal of Medicine. 2020; 382(12): 1177–1179. https://pubmed.ncbi.nlm.nih.gov/32182409/

[15] Santarpia, J., Rivera, D., Herrera, V., & Morwitzer, M. Transmission potential of SARSCoV-2 in viral shedding observed at the University of Nebraska Medical Center (pracetak). MedRxiv, 2020; 1–12.

[16] Wang, J., & Du, G. COVID-19 may transmit through aerosol. Irish Journal of Medical Science. 2020; 189(4): 1143–1144. https://doi.org/10.1007/s11845-020-02218-2

[17] World Health Organization (WHO), Modes of Transmission of Virus Causing COVID-19. 2020; 1921. doi:10.1056/NEJMc2004973.Cheng.

[18] Mittal, R., Ni, R., & Seo, J. H. The flow physics of COVID-19. Journal of Fluid Mechanics. 2020; 894: 1–14. https://doi.org/10.1017/jfm.2020.330

[19] Ferretti, L., Wymant, C., Kendall, M., Zhao, L., Nurtay, A., Abeler-Dörner, L., Parker, M., Bonsall, D., & Fraser, C. Quantifying SARS-CoV-2 transmission suggests epidemic control with digital contact tracing. Science. 2020; 368(6491), 0–8. https://doi.org/10.1126/science.abb6936

[20] Li, Y., Leung, G. M., Tang, J. W., Yang, X., Chao, C. Y. H., Lin, J. Z., Lu, J. W., Nielsen, P. V., Niu, J., Qian, H., Sleigh, A. C., Su, H. J. J., Sundell, J., Wong, T. W., & Yuen, P. L. Role of ventilation in airborne transmission of infectious agents in the built environment - A multidisciplinary systematic review. Indoor Air. 2007; 17(1): 2–18. https://doi.org/10.1111/j.16000668.2006.00445.x

[21] Shiu, E. Y. C., Leung, N. H. L., & Cowling, B. J. Controversy around airborne versus droplet transmission of respiratory viruses. Current Opinion in Lipidology. 2019; 30(4): 300–306. https://doi.org/10.1097/QCO.0000000000000563

[22] Memarzadeh, F., Olmsted, R. N., & Bartley, J. M. Applications of ultraviolet germicidal irradiation disinfection in health care facilities: Effective adjunct, but not stand-alone technology. American Journal of Infection Control. 2010; 38(5 SUPPL.). https://doi.org/10.1016/j.ajic.2010.04.208

[23] Shajahan, A., Culp, C. H., & Williamson, B. Effects of indoor environmental parameters related to building heating, ventilation, and air conditioning systems on patients' medical outcomes: A review of scientific research on hospital buildings. Indoor Air. 2019; 29(2): 161–176. https://doi.org/10.1111/ina.12531

[24] Prussin, A. J., Schwake, D. O., & Marr, L. C. Ten questions concerning the aerosolization and transmission of Legionella in the built. 2018; 684–

695. https://doi.org/10.1016/j.buildenv.2017.06.024
[25] Qian, H., & Zheng, X. Ventilation control for airborne transmission of human exhaled bio-aerosols in buildings. Journal of Thoracic Disease. 2018; 10(Suppl 19): S2295–S2304. https://doi.org/10.21037/jtd.2018.01.24
[26] Li, C., Tang, H., Wang, J., Zhong, Z., Li, J., & Wang, H. Field study to characterize customer flow and ventilation rates in retail buildings in Shenzhen, China. Building and Environment. 2021; 197. https://doi.org/10.1016/j.buildenv.2021.107837
[27] Etheridge, D., & Sandberg, M. Building Ventilation: Theory and Measurements, Wiley. 1996; 13: 978-0471960874
[28] AIVC, Air Infiltration and Ventilation Centre, International Energy Agency. Retrieved on 11 May 2020, https://www.aivc.org/resources/faqs/what-ventilation
[29] Blocken, B., van Druenen, T., Ricci, A., Kang, L., van Hooff, T., Qin, P., Xia, L., Ruiz, C. A., Arts, J. H., Diepens, J. F. L., Maas, G. A., Gillmeier, S. G., Vos, S. B., & Brombacher, A. C. Ventilation and air cleaning to limit aerosol particle concentrations in a gym during the COVID-19 pandemic. Building and Environment. 2021; 193. https://doi.org/10.1016/j.buildenv.2021.107659
[30] Kurnitski, J., Kiil, M., Seppanen, O., Boerstra, A., Seppänen, O., Wargocki, P., Olesen, B., & Morawska, L. Preprint-A new ventilation criterion based on respiratory infection risk of COVID-19 Energy efficient buildings. 2021. https://doi.org/10.13140/RG.2.2.35510.83524
[31] Bhagat, R. K., & Linden, P. Displacement ventilation: a viable ventilation strategy for makeshift hospitals and public buildings to contain COVID-19 and other airborne diseases. Clinical Infectious Diseases. 2020; 71(9): 2311–2313. https://doi.org/10.1093/cid/ciaa939
[32] Mingotti, N., & Woods, A. W. On the transport of heavy particles through an upward displacement-ventilated space. Journal of Fluid Mechanics. 2015; 772: 478–507. https://doi.org/10.1017/jfm.2015.204
[33] Sherman, M. H., & Wilson, D. J. Relating actual and effective ventilation in determining indoor air quality. Building and Environment. 1986; 21(3–4). https://doi.org/10.1016/0360-1323(86)90022-3
[34] Dai, H., & Zhao, B. Association of the infection probability of COVID-19 with ventilation rates in confined spaces. Building Simulation. 2020; 13(6): 1321–1327. https://doi.org/10.1007/s12273-020-0703-5
[35] ASHRAE. Position Document on Infectious Aerosols. Atlanta, Georgia. 2020.
[36] REHVA. COVID-19 guidance document. How to operate HVAC and other building service systems to prevent the spread of the coronavirus (SARS-CoV-2) disease (COVID-19) in workplaces. Ago. 2020.https://www.rehva.eu/fileadmin/user_upload/REHVA_COVID-19guidance_document_V3_03082020.pdf.
[37] Pease, L. F., Wang, N., Salsbury, T. I., Underhill, R. M., Flaherty, J. E., Vlachokostas, A., Kulkarni, G., & James, D. P. Investigation of potential aerosol transmission and infectivity of SARS-CoV-2 through central ventilation systems. Building and Environment. 2021; 197: 107633. https://doi.org/10.1016/j.buildenv.2021.107633
[38] Dimensions. Going beyond traditional databases | Dimensions Data. 202.
[39] van Eck, N. J., & Waltman, L. Software survey: VOSviewer, a computer program for bibliometric mapping. Scientometrics. 2010; 84(2): 523–538. https://doi.org/10.1007/s11192-009-0146-3
[40] Sun, Y., Wang, Z., Zhang, Y., & Sundell, J. In China, students in crowded dormitories with a low ventilation rate have more common colds: Evidence for airborne transmission. PLoS ONE. 2011; 6(11). https://doi.org/10.1371/journal.pone.0027140
[41] Sleiti, A. K., Ahmed, S. F., & Ghani, S. A. Spreading of SARS-CoV-2 via heating, ventilation, and air conditioning systems-an overview of energy perspective and potential solutions. Journal of Energy Resources Technology, Transactions of the ASME. 2021; 143(8). https://doi.org/10.1115/1.4048943
[42] Melikov, A. K., Ai, Z. T., & Markov, D. G. Intermittent occupancy combined with ventilation: An efficient strategy for the reduction of airborne transmission indoors. Science of the Total Environment. 2020. https://doi.org/10.1016/j.scitotenv.2020.140908
[43] Mokhtari, R., & Jahangir, M. H. The effect of occupant distribution on energy consumption and COVID-19 infection in buildings: A case study of university building. Building and Environment. 2021; 190. https://doi.org/10.1016/j.buildenv.2020.107561
[44] Balocco, C., & Leoncini, L. Energy cost for effective ventilation and air quality for healthy buildings: Plant proposals for a historic building school reopening in the covid-19 era. Sustainability (Switzerland). 2020;12(20):1–16. https://doi.org/10.3390/su12208737
[45] Ascione, F., De Masi, R. F., Mastellone, M., & Vanoli, G. P. The design of safe classrooms of educational buildings for facing contagions and transmission of diseases: A novel approach combining audits, calibrated energy models, building performance (BPS) and computational fluid dynamic (CFD) simulations. Energy and Buildings. 2021; 230. https://doi.org/10.1016/j.enbuild.2020.110533
[46] Schibuola, L., & Tambani, C. High energy efficiency ventilation to limit COVID-19 contagion in school environments. Energy and Buildings. 2021; 240. https://doi.org/10.1016/j.enbuild.2021.110882
[47] Aviv, D., Wee Chen, K., Teitelbaum, E., Sheppard, D., Pantelic, J., Rysanek, A., & Meggers, F. A Fresh (Air) Look at Ventilation for COVID-19: Estimating the global energy savings potential of coupling natural ventilation with novel radiant cooling strategies. Applied Energy. 2021; 116848. https://doi.org/10.1016/j.apenergy.2021.116848
[48] Luo, H., & Zhong, L. Ultraviolet germicidal irradiation (UVGI) for in-duct airborne bioaerosol disinfection: Review and analysis of design factors. Building and Environment. 2021; 107852. https://doi.org/10.1016/j.buildenv.2021.107852
[49] Wang, J., Huang, J., Feng, Z., Cao, S. J., & Haghighat, F. Occupant-density-detection based energy efficient ventilation system: Prevention of infection transmission. Energy and Buildings. 2021; 240. https://doi.org/10.1016/j.enbuild.2021.110883
[50] Settimo, G., & Avino, P. The Dichotomy between Indoor Air Quality and Energy Efficiency in Light of the Onset of the COVID-19 Pandemic. Atmosphere. 2021; 12(6): 791. https://doi.org/10.3390/atmos12060791

Simulation-Aided Development of a Compact Local Ventilation Unit with the Use of CFD Analysis

Petr Zelenský [a,b], Martin Barták [a,b], Vladimír Zmrhal [a,b], Juraj Mázik [c]

[a] Department of Environmental Engineering, Faculty of Mechanical Engineering, Czech Technical University in Prague, Czech Republic, petr.zelensky@cvut.cz

[b] University Centre for Energy Efficient Buildings, Czech Technical University in Prague, Czech Republic.

[c] RECUAIR, Kralupy nad Vltavou, Czech Republic

Abstract. The current emphasis on the renovation of existing buildings to meet EU energy efficiency targets brings, in addition to energy savings and related CO2 reduction, also some negative issues. One of them can be the lack of fresh air supply caused by increased air tightness of the building envelope after its insulation and renovation or change of windows. The easy solutions are decentralized units for local ventilation, which can be installed during fast renovations in selected rooms without major building modifications. Controlled ventilation then ensures the delivery of a sufficient amount of fresh air to meet current standards and, at the same time, creates a healthy and comfortable environment for occupants. The paper demonstrates the practical use of CFD simulations for the development of a new type of compact small ventilation unit for local ventilation of rooms with heat and humidity recovery. An increase in the device efficiency and a reduction in acoustic power, while maintaining its very compact dimensions, were achieved with the help of the numerical study. The paper shows the possibility of using CFD analysis during the development of new HVAC appliances. It describes the preparation of the numerical model of the device, presents the simulation approach, including the calculation settings, and discusses device optimization based on variant numerical analyses in ANSYS Fluent. The initial prototype design of the unit was optimized following the findings from the numerical analysis, and it was verified by CFD study that the proposed adjustments were appropriate and that the expected results were achieved. In a separate CFD study, the use of different types of diffusers at the air outlet from the supply duct to the room was addressed. It was recommended to use adjustable nozzles, which allow one to direct the air flow into the room according to the user's preference. Consequently, it was verified that the ventilation unit meets the hygienic noise limits, both for day operation and for night operation with reduced power.

Keywords. Local ventilation, compact ventilation unit, development, optimization, CFD, numerical analysis.
DOI: https://doi.org/10.34641/clima.2022.194

1. Introduction

The lack of fresh air supply caused by the increase in the air tightness of the building envelopes after their renovation is a major concern of HVAC engineering today. Additional insulation of walls and renovation or change of windows of existing building stocks is driven by the EU energy efficiency targets that lead to energy savings and related CO_2 reduction. However, in some cases of fast renovations that target only the building envelope, proper ventilation and fresh air delivery can be ignored. This leads to inadequate indoor air quality, humidity problems, and other related issues. The easy solutions to improve indoor environment quality are decentralized local ventilation units, which can be installed during such fast renovations, without major building modifications. Controlled ventilation then ensures the delivery of a sufficient amount of fresh air to meet current standards and, at the same time, creates a healthy and comfortable environment for the occupants.

The paper demonstrates the practical use of computational fluid dynamics (CFD) simulations for the development of the compact ventilation unit for local ventilation of rooms. It is a decentralised unit without the need for condensation drainage and any necessary connections to other building systems. The visible part of the unit (Fig. 1, top) is located on the inner wall of the room and contains supply and exhaust fans, air filters, and control system of the

Copyright ©2022 by the authors. This conference paper is published under a CC-BY-4.0 license.

unit. The cylindrical part on the back side of the unit (Fig. 1, bottom) passes through the external wall of the building and ends on the facade.

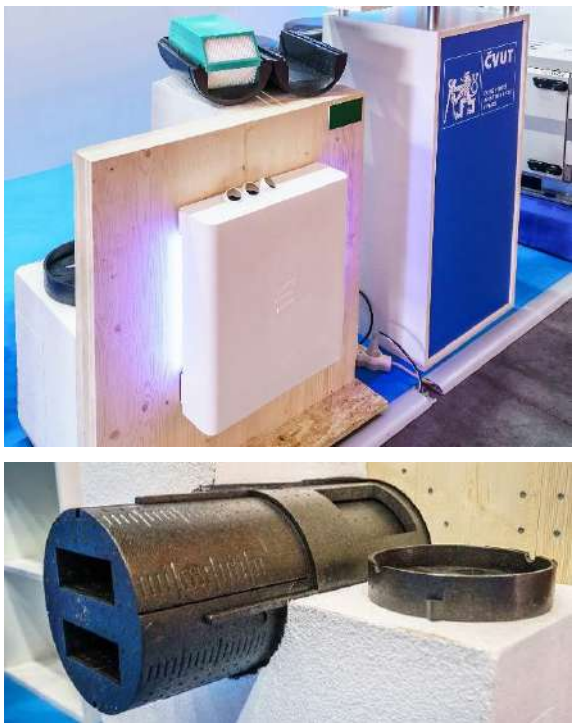

Fig. 1 - Compact ventilation unit [1]

The cylindrical part of the unit houses a rotary recuperation heat exchanger driven by an actuator, which turns it 180° at intervals determined according to the outdoor air temperature. This way, an alternation of the flow of supply outdoor air and exhaust degraded air is ensured, which enables humidity recovery throughout the year and prevents icing of the exchanger in the winter season. High efficiency of heat and moisture recovery is achieved all year round.

A numerical CFD study of airflow in a complex system of supply and exhaust air channels of the ventilation unit was performed. CFD simulations provide detailed information about pressure, velocity, turbulence, and other quantities on the network of computational cells (control volumes) that divide the area of interest. The motivation for using this method was to reduce the cost of the development, manufacturing, and operation of the device. Effective optimization of the complex geometry of supply and exhaust air channels of the ventilation unit would be very challenging without the use of CFD simulations, which provide otherwise inaccessible information and relatively easy possibility to analyse and compare variant design solutions.

The paper describes the preparation of a numerical model of the device for CFD simulation, presents the simulation approach, including the calculation settings, and discusses the device optimization based on variant numerical analyses in ANSYS Fluent. The methods of simulation of the fan impeller rotation and approximation of the filtration material in the model are discussed in detail. The results of the numerical analysis served as feedback to the design team during the development and optimization of the prototype device. It provided the basis for changes in the internal arrangement of the unit, the purpose of which was to minimize the occurrence of local pressure losses and possible sources of aerodynamic noise. It helped the design team to reach a design solution that brings higher energy efficiency and lower acoustic power generated by the device, taking into account the compact dimensions of the unit.

The numerical analysis described in this paper was followed by a measurement of the noise and volume flow rate of the unit under laboratory conditions. The study was part of a project supported by the EU under the Operational Program Enterprise and Innovation for Competitiveness.

2. Numerical model of the unit

The numerical model of the examined device was created on the basis of the 3D prototype geometry provided by the design team; see Fig. 2. The dimensions of the device were 455 × 425 × 105 mm, the cylindrical part had diameter of 260 mm.

The variant numerical analysis was solved iteratively, following these seven steps:

1. import of the CAD design geometry into the ANSYS SpaceClaim software;
2. adjustment of the geometry for CFD simulations (software: SpaceClaim);
3. preparation of the numerical mesh (software: ANSYS Fluent Meshing);
4. CFD simulations of airflow (software: ANSYS Fluent);
5. analysis and discussion of the results;
6. proposal of device design optimization;
7. CFD analysis of the optimized geometry (repeating steps 1 to 6).

Fig. 2 - Prototype geometry of the ventilation unit

2.1 Preparation of the model for CFD

The prototype geometry was available in the universal format STEP and could be imported directly into the ANSYS SpaceClaim as a spatial model. The initial geometry was adjusted for the CFD simulations. After quality control of the obtained spatial model and correction of minor deficiencies (especially colliding bodies), the simplifications listed below were made. It was expected that the simplifications and geometry adjustments should have minimal influence on the airflow in the ventilation unit. The modified geometry is shown in Fig. 3.

- All the bolts were removed; the empty holes for the removed parts were filled;
- technological fillets and cutouts of sheet steel parts of the device were removed;
- the cylindrical part of the unit housing the heat exchanger was removed (heat exchanger was approximated in the simulation by a boundary condition);
- overlapping surfaces were corrected;
- small surfaces of the air channel walls were removed;
- the curved surfaces of the air channel walls were simplified.

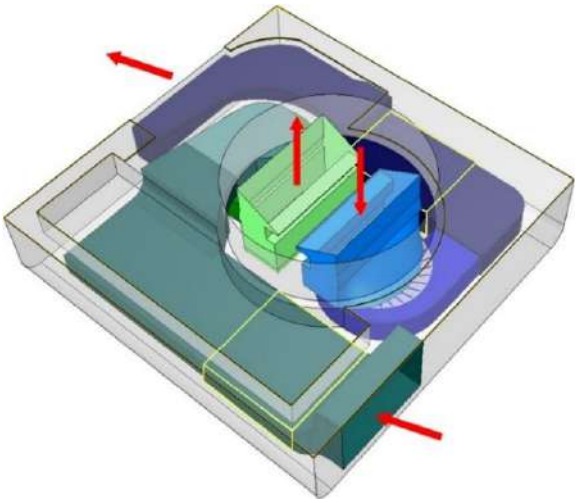

Fig. 3 - Ventilation unit model as adapted for CFD; supply channel (in blue), exhaust channel (in green); domains with filters marked by yellow line; airflow direction marked by red arrows

The simulation study analysed the airflow in the supply channel (see Fig. 3, in blue) and the exhaust channel (Fig. 3, in green). The geometry of the air channels is quite complex. The supply air is drawn on the façade and passes through the heat exchanger through the wall of the building. Then it flows through a small radial fan and is distributed to the room by a supply channel containing a filter. Exhaust air is drawn from the room on the opposite side of the ventilation unit. It passes through the exhaust channel with the filtration material and flows through the exhaust fan and heat exchanger, where it transfers its heat to the supply air, to the façade outlet. It is discharged to the outdoor environment.

The aim of the study was to predict the characteristics of the airflow in the ventilation unit, including the airflow through the rotating radial fans and the air filters. Both channels have a unique geometry to maintain as compact dimensions of the unit as possible and at the same time achieve sufficient noise attenuation (their walls are partially lined with noise-absorbing material, although with limited thickness). The CFD study indicates critical points of the geometry with risk of increased generation of aerodynamic noise, such as regions with local increase of velocity, points of air flow separation, etc.

2.2 Preparation of the numerical mesh

CFD simulations are usually based on the finite volume method, i.e., division of the investigated domain into a large number of consecutive control volumes and the solution of conservation equations of mass, momentum, and energy for each of them. The quality of the numerical mesh significantly affects the convergence of the simulation and the accuracy of the results. Therefore, attention must be paid to the meshing part of the model preparation.

The geometry of the supply and exhaust air channels was imported into the ANSYS Fluent Meshing. The volumetric model was automatically converted to a set of surfaces meshed by a triangular grid with predefined parameters. The surface mesh serves as a basis for the following discretization of the domain volume. Therefore, it must be sufficiently fine to capture all the important geometric details. It is also necessary to check its quality and, if necessary, repair problematic cells.

As the next step, a hybrid polyhexcore volume mesh with a prismatic boundary layer mesh on the selected surfaces was created. The mesh combines high-quality octree hexahedron in the bulk region, and isotropic polyhedral cells near the walls; see for example Fig. 4.

Each of the channels was meshed and simulated separately (airflows in the channels do not affect each other). The maximum size of mesh cells was globally set to 2 mm; at critical locations for simulation, the general cell size was manually corrected to provide a finer computational mesh (e.g., around radial fans, near the walls, etc.). The smallest cell size was 0.2 mm. A prismatic mesh region was created, with a height of 10 cells on the fan blades and a height of 6 cells on the surfaces of the fan housings and on the walls of the channels. The resulting mesh had $6{,}5 \cdot 10^6$ million computational cells for the case of the supply channel and $8{,}3 \cdot 10^6$ million cells for the case of the exhaust channel.

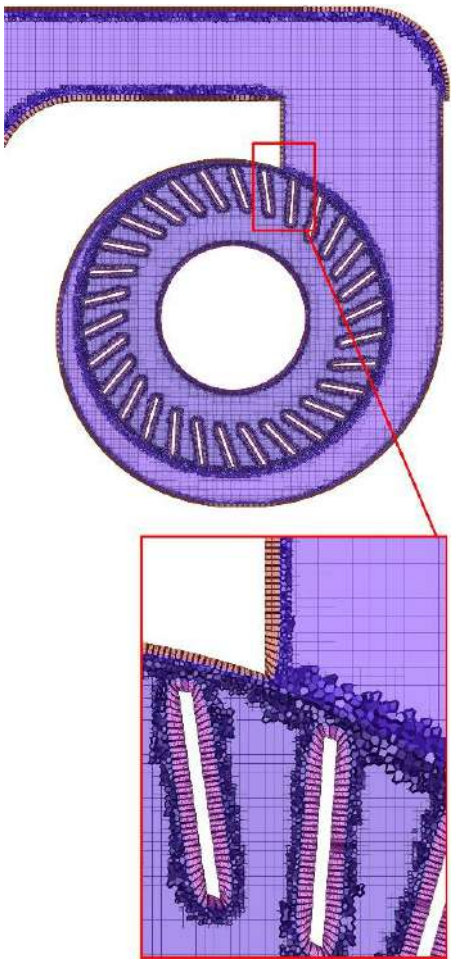

Fig. 4 - Computational mesh for CFD simulations

3. Numerical solution

The CFD simulations were solved using the software ANSYS Fluent 19.0. as a flow of incompressible air, without considering the energy equation. The two-equation model k-ε according to Shih et al. [2] (so called k-ε Realizable) was used for all calculations. It was previously shown to be optimal for simulation of similar types of devices with rotating fan impellers [3]. The flow in the near-wall regions was calculated by integration of the governing equations in the viscous sublayer, with the use of the Enhanced Wall Treatment method. The PRESTO! scheme was chosen for the discretization of the pressure equation as it is recommended for solving rotary machines [4]. The convective terms of the equation were solved using second order upwind scheme. The pressure and velocity fields were coupled by the SIMPLE algorithm.

The pressure loss of the filters was approximated in the simulation by porous layers added to the numerical models. The characteristics of the porous elements were established on the basis of documentation provided by the filter manufacturer. The PorZo software add-on [5], an ANSYS Customization Toolkit (ACT) extension of the Fluent software, was used to prescribe the characteristic pressure-volume curve of the filter to the porous layers.

The pressure loss of the heat exchanger was determined according to the manufacturer's documentation. The RecAir RS220 exchanger was used in the prototype of the device. The pressure drop was prescribed as boundary conditions at the inlet to the supply channel and at the outlet from the exhaust channel.

The boundary conditions facing the room were considered as open space, that is, the static pressure at the inlet to the exhaust channel and the outlet from the supply channel was 0 Pa, the intensity of turbulence was 0.1 % and the turbulent viscosity ratio 0.01.

The correct approximation of the fan impeller rotation is the fundamental part of the CFD simulation of the ventilation unit. There are two different methods available in ANSYS Fluent [4, 6, 7, 8], while the MRF method was used for the approximation of the fan impeller rotation in the presented study:

- **Multiple Reference Frame (MRF)** – airflow is calculated in one single moment of the rotation, i.e. in one single impeller position (the method can also be referred to as the "frozen rotor approach"). It does not account for the relative motion of a moving zone with respect to adjacent zones. The impeller rotation is approximated by prescribing the tangential components of the velocity to the specified volume rotating at a chosen angular velocity. The result of the simulation is a stationary image of the flow in the domain. The MRF method is not recommended to be used in unsteady simulations.
- **Sliding Mesh** – airflow is considered as unsteady. The rotation of the wheel is simulated directly, that is, the relative motion of a moving zone (fan impeller) with respect to adjacent zones is considered, and continuous change of the geometry occurs in the CFD simulation. The advantage of this method compared to the MRF approach is the potential higher accuracy of the results obtained. The disadvantage is considerably higher demand on computational time and difficult post-processing of the obtained results arising from the large number of data files obtained for individual positions of the fan impeller during its rotation.

4. CFD Simulation and evaluation of first Results

All simulations were calculated for one operation point of the ventilation unit with the required airflow of 45 m^3/h through both channels, which was the maximum design airflow of the prototype unit. The corresponding pressure loss of the heat exchanger was 112.5 Pa and the fan speed was 3,920 RPM. The numerical study was divided into

two separate tasks: (i) simulation of the supply channel and (ii) simulation of the exhaust channel. The velocity fields were analysed for each of the channels.

Fig. 5 shows the velocity isosurfaces in the supply channel. The airflow velocity at the fan impellers reaches approximately 33 m/s. The velocity in the channel is in range from 1.5 to 12 m/s, while high velocities can be observed especially in the restricted part of the channel before the outlet to the room and near the 90° bend of the channel behind the fan. Moreover, the 90° bend has a sharp inner corner. Fig. 6 shows the disturbance of the airflow trajectories in the mentioned areas.

Another concern was the noise generated by the fan and its propagation through the supply channel to the room, as it was not possible to equip the unit with silencers. Noise attenuation was addressed by adding a layer of noise-absorbing material on the inner walls of the channels and by considerate design of the internal airways. The position of the fan in the prototype geometry was found to be not optimal and the issue was further addressed during the optimization of the ventilation unit.

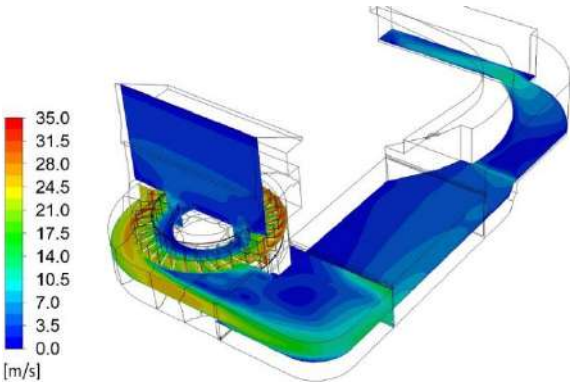

Fig. 5 – Velocity isosurfaces in the supply channel

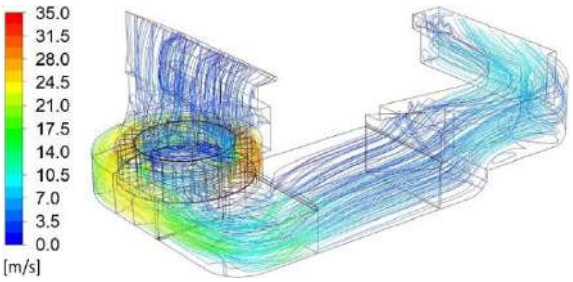

Fig. 6 - Airflow pathlines in the supply channel

The complex geometry of the supply channel near the outlet of the ventilation unit to the room was studied in detail. The narrow part of the channel and sharp bend before the outlet to the room lead to relatively high air flow velocity of up to 9 m/s; see Fig. 7. This brings a risk of high aerodynamic noise. Furthermore, the velocity profile of the airflow at the outlet opening is not uniform. With the given geometry of the supply channel, some areas show a very high outlet velocity, while only the minimum airflow is achieved in the remaining area of the outlet. Moreover, the bend of the channel before the outlet causes a high directivity of airflow into the room. These issues were faced during the optimization phase of the study.

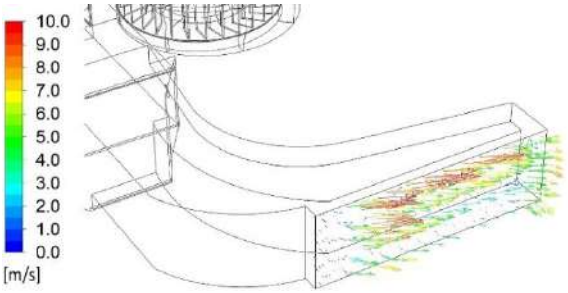

Fig. 7 - Detail of the velocity field at the outlet to the room

The geometry of the exhaust channel is less complex in comparison to the geometry of the supply channel. Also, most of the channel is on the suction side of the fan. Thus, it shows a more uniform airflow, see Fig. 8. Significant disturbance of airflow is apparent only at the section after the fan, before the inlet to the heat exchanger. It was recommended to round the sharp corners of several bends in this region. The velocity of airflow in the channel is in range from 3 to 5 m/s, the velocity at the fan reaches 33 m/s.

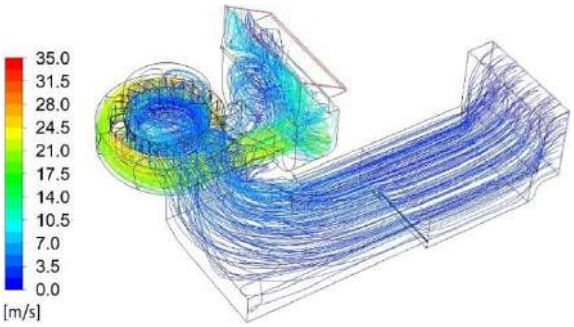

Fig. 8 - Airflow pathlines in the exhaust channel

5. Ventilation unit optimization

Critical points of the prototype geometry were identified on the basis of the initial CFD simulations and modification of the supply and exhaust channel geometry was proposed. The effect of the modifications on airflow was analysed by a subsequent numerical study.

Compared to the prototype geometry of the unit, the following optimizations were applied (see also Fig. 9):

1. geometry modification at the inlet from the room;
2. fillets on the sharp edges of the exhaust channel in front of the fan;
3. fillet on the sharp corner of the supply channel after the fan;
4. change of the supply channel fan orientation (the fan was rotated by 90° in order to reduce the noise emitted to the room);

5. adding an air diffuser at the outlet of the ventilation unit to the room; a separate variant study was performed to choose an optimal air diffuser, while four different configurations were compared; see Fig. 10:
   a) outlet without a diffuser (original solution);
   b) outlet with a perforated diffuser;
   c) outlet with directional vanes;
   d) outlet with adjustable nozzles.

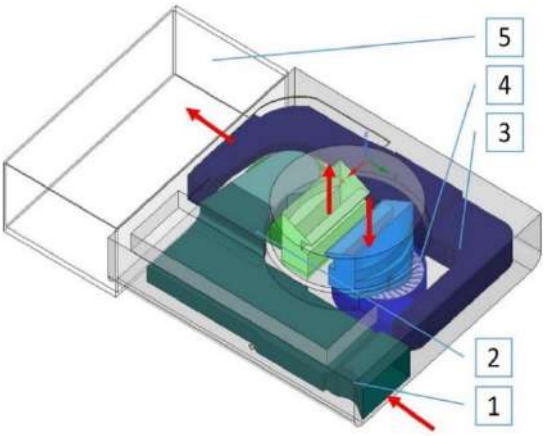

Fig. 9 - Optimized geometry of the ventilation unit

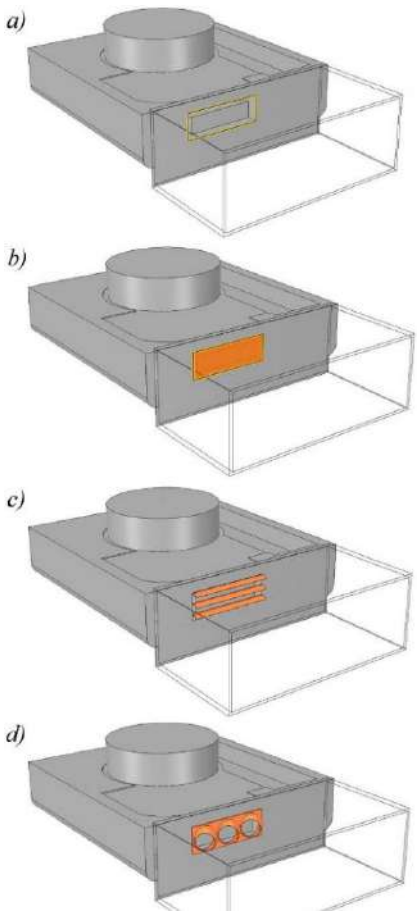

Fig. 10 - Variant study of different HVAC diffusers

The numerical study of the airflow after geometry optimization was carried out following the same methodology as the CFD simulations with the prototype geometry. The spatial model of the supply channel was extended by a part of the surrounding space, to study the directional characteristics of the airflow into the room. The numerical mesh was created with the same parameters. In the case of the supply channel, it had $11 \cdot 10^6$ computational cells and in the case of the exhaust channel $8.1 \cdot 10^6$ computational cells. The CFD simulations were set identically. Calculations were performed for one operating state of the unit, with volume air flow rate through the device of 45 m^3/h and corresponding pressure loss of the heat exchanger of 112.5 Pa.

6.3 CFD analysis of the optimised design

By optimization of the supply channel geometry, a more uniform airflow was achieved, see Fig. 11 and Fig. 12. The velocity in the channel is in the range from 1.5 to 15 m/s, similar to the simulation with the prototype geometry. However, a high velocity can be observed mainly in the narrow part of the channel immediately behind the fan. This region is, due to the rotated position of the fan, shielded from the outlet to the room. The fan noise as well as the aerodynamic noise of the fast airflow are more effectively absorbed by the walls, which are lined by the sound insulation material.

However, even after the geometry optimization, the airflow at the outlet to the room was still not optimal, with very high directionality. This issue was solved in a separate variant study presented in the following chapter.

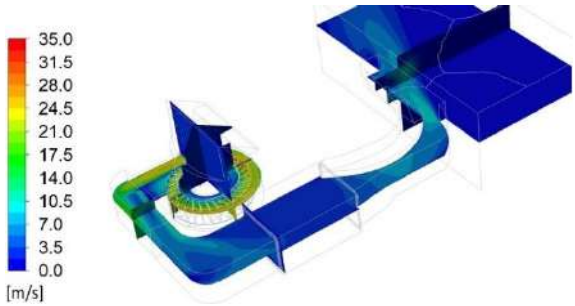

Fig. 11 - Velocity isosurfaces in the supply channel after optimization

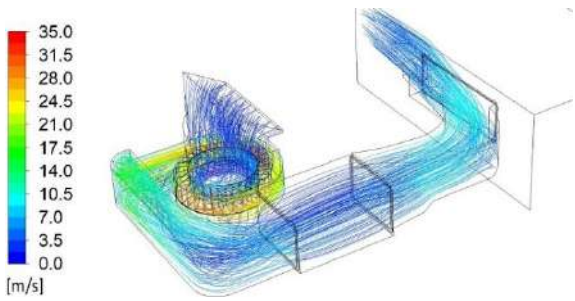

Fig. 12 - Airflow pathlines in the supply channel after optimization

In the case of the exhaust channel, the applied optimisations did not have a significant effect on the airflow, as the flow was already uniform in the previous case of the prototype geometry. The airflow pathlines after the geometry optimization shows Fig. 13.

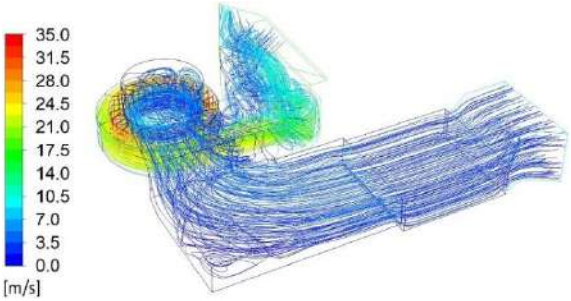

Fig. 13 - Airflow pathlines in exhaust channel after optimization

6.3 Variant study of the outlet diffusers

A separate numerical study was carried out to assess the performance of various types of HVAC diffusers at the outlet to the room. Four different configurations of the ventilation unit were simulated; see Fig. 10: outlet without any diffuser, outlet with a perforated diffuser, outlet with directional vanes, and outlet with three adjustable nozzles. The main aim of the study was to choose the optimal outlet diffuser to:

- improve airflow distribution on the outlet opening (optimally reach uniform airflow velocity at the whole cross-section of the outlet);
- improve the directional characteristics of the airflow to the room (optimally reaching airflow direction normal to the outlet opening).

The change in pressure conditions at the diffuser was reflected in the study by increasing the fan rotation speed in the individual simulations, so the constant volume flow rate of 45 m^3/s was maintained for all four simulated cases.

Fig. 14 shows the pathlines of the airflow at the outlet to the room, for the three cases with HVAC diffusers. On the basis of the variant study, the configuration of the unit with the three nozzles was recommended for further use. This configuration leads to the best airflow distribution in the outlet opening and the best directional characteristics of airflow to the room. Furthermore, the nozzles are adjustable and allow one to change the direction of the air flow according to the user's preference. See also Fig. 15, showing in detail the flow velocity vectors at the outlet from the device to the room.

6.3 Experimental measurement

A physical prototype of the ventilation unit was manufactured, with the optimized geometry, following the numerical study. A measurement of the noise and volume flow rate was conducted under laboratory conditions. The main objective was to confirm that the noise generated by the unit does not exceed the limits given by current regulations and to test the unit under different operating conditions.

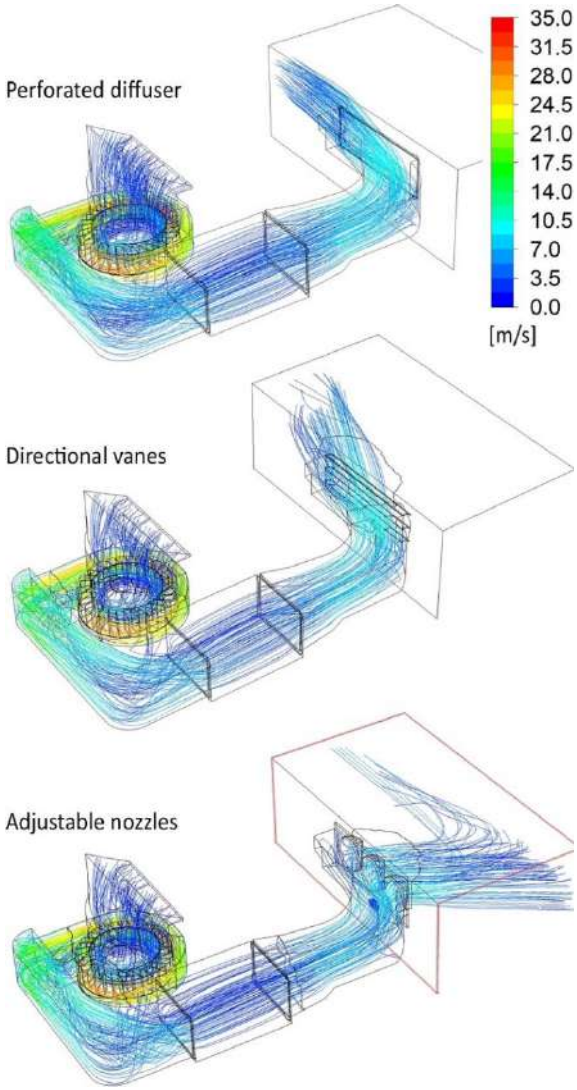

Fig. 14 - Pathlines of airflow to the room – unit equipped with various HVAC diffusers

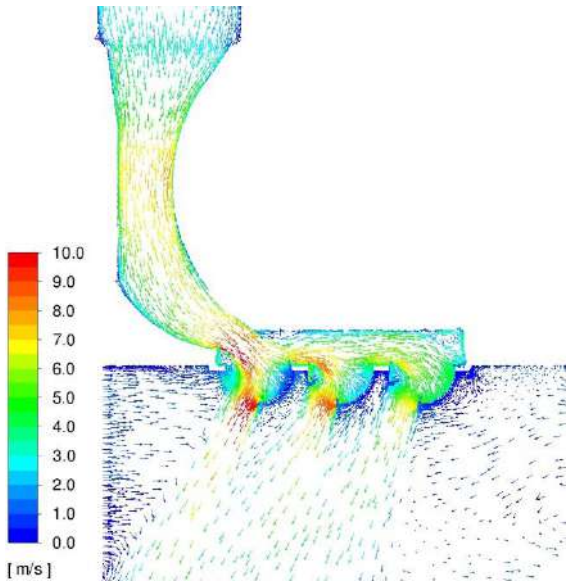

Fig. 15 - Velocity vectors of airflow to the room – unit equipped with adjustable jet nozzles

Following initial measurements in the noise laboratory, the prototype of the unit was further adapted. Selected parts of the sound absorbing material were removed from the walls of the channels. This adjustment had only a small negative effect on the noise attenuation, but the cross section of the channels increased, reducing their pressure losses. Thus, the required airflow was achieved with a lower rotation speed of the fans, which improved the acoustic performance of the device.

It was tested that the ventilation unit reaches the required operational volume flow rate from 15 to 40 m^3/h. It was achieved with the rotation speed of the fans from 1,600 to 3,250 RPM. The corresponding A-weighted levels of acoustic pressure ranged from 15 to 32 dB (measured 3 m from the unit). The values meet the current regulations. It was advised to run the ventilation unit in the low power setting during the night, as it does not exceed the A-weighted level of acoustic pressure 25 dB (measured 1 m from the unit), as requested by the Government Regulation No. 272/2011 on protection of health from adverse effects of noise and vibrations.

6. Conclusion

The main aim of the paper was to demonstrate the practical use of variant numerical analysis for the development of new HVAC appliances. The CFD simulations were used to support the development of a new decentralized compact ventilation unit for local ventilation of rooms.

The numerical model of the ventilation unit was prepared on the basis of the prototype geometry. The Multiple Reference Frame (MRF) method was used to approximate the rotation of the fan impellers. The filtration material was represented in the models by porous media, while the pressure-volume characteristic curve of the filters was prescribed to the model with the use of the PorZo ACT extension.

The initial design of the unit was optimized following the findings of the numerical analysis. Critical points of the prototype geometry were identified and adjusted. These were imperfections in the geometry of the air channels and not optimal orientation of the supply channel fan. It was verified by CFD study that the proposed adjustments were appropriate and that the expected improvements were achieved. In a separate variant CFD study, the use of different types of diffusers at the outlet to the room was addressed. It was recommended to use adjustable nozzles, which allow one to direct the airflow into the room according to the user's preference.

Consequently, it was experimentally verified that the ventilation unit meets the technical requirements. It was tested that the it reaches the operational volume flow rate of 15 to 40 m^3/h with the corresponding A-weighted levels of acoustic pressure in the range from 15 to 32 dB. Thus, the unit meets the noise limits set by current regulations. However, it was advised to run the ventilation unit in low power setting during the night operation, so it does not exceed the requested A-weighted level of acoustic pressure of 25 dB

The outcome of the research is a new type of compact small ventilation unit for local ventilation of rooms with heat and humidity recovery. An increase in device efficiency and a reduction in its acoustic power were achieved, with the help of CFD simulations, while maintaining its compact dimensions.

7. Acknowledgement

This study was supported by the European Union, the European Regional Development Fund, the Operational Program Enterprise and Innovation for Competitiveness.
No. CZ.01.1.02/0.0/0.0/17_107/0012492

8. References

[1] Ryszawy, J. Photos of the ventilation unit, VIC ČVUT, Prague, Czech Republic. 2019

[2] Shih, T., Liou, W., Shabbir, A., Yang, Z., Zhu J. A new eddy viscosity model for high Reynolds number turbulent flows. Computers & Fluids 1995; (24): 227–238.

[3] Zelenský, P., Barták, M., Zavřel, V., Zmrhal, V., Krupa, R. Numerical Analysis of Airflow in a Modular Fan Unit Using CFD Simulation. Proceeding of the 13th REHVA World Congress CLIMA 2019. Bucharest, Romania. 2019.

[4] ANSYS Inc. ANSYS Fluent User's Guide. ANSYS Inc. Canonsburg (USA). 2013.

[5] SVS FEM PorZo ACT Extension. Available from: https://www.svsfem.cz/produkty/aplikace-ansys-act/porzo (11. 7. 2020)

[6] Gullberg, P., Sengupta, R. Axial Fan Performance Predictions in CFD, Comparison of MRF and Sliding Mesh with Experiments. Proceeding of the 11th European Conference on Turbo-machinery Fluid Dynamics and Thermo-dynamics. Istanbul, Turkey. 2011.

[7] Gullberg, P., Löfdahl, L., Adelman, S., Nilsson, P. A correction method for stationary fan CFD MRF models. Proceeding of the SAE World Congress & Exhibition. Detroit, USA. 2009.

[8] Moreau, S., Henner, M., Brouckaert, J.F., Neal, D. Numerical and Experimental Investigation of Rotor-Stator Interaction in Automotive Engine Cooling Fan Systems. Proceeding of the 7th European Conference on Turbomachinery Fluid Dynamics and Thermodynamics. Athens, Greece. 2007.

Ventilation and air conditioning for school buildings

Pavol Štefanič [a], Zuzana Straková [b]

[a] Department of Building Services, Faculty of Civil Engineering, Slovak University of Technology in Bratislava, pavol.stefanic@stuba.sk

[b] Department of Building Services, Faculty of Civil Engineering, Slovak University of Technology in Bratislava, zuzana.strakova@stuba.sk

Abstract. One of the basic problems of school buildings is the unsatisfactory thermal insulation properties of peripheral building structures. Unsatisfactory, especially in terms of the creation and long-term maintenance of microclimatic conditions in the classroom, is the complete absence of mechanical ventilation systems. In almost all schools, ventilation is based on the natural exchange of air through windows. Such a solution is no longer satisfactory today. In the old school buildings, the old ventilation shafts were usually abolished and in the new schools, there are no such shafts at all. In general, in many places, it is also forbidden to open windows during breaks for safety reasons. In addition, the method of window ventilation is based only on the subjective feelings of teachers and students; and since the human factor is unable to determine sufficient air quality with the help of its organs, the result is that the interior is not sufficiently ventilated. This also results in an unacceptable concentration of CO_2 in the classroom, a high level of resistance, an increasing level of relative humidity, and dust content in the indoor air. This is an unacceptable situation for teachers 'and students' health. The quality of the indoor environment of school buildings directly impacts the ability to concentrate and the attention of teachers and students. In this article, we will take a closer look at 6-week experimental measurements of the indoor microclimate in kindergarten. The measurement took place in two rooms, a playroom and a bedroom, where there were 22 children plus 1 or 2 adults at the same time. The measurement results for some quantities are acceptable, but in particular, the concentration of carbon dioxide is unacceptable.

Keywords. Ventilation, indoor microclimate, kindergarten, children, school, students.
DOI: https://doi.org/10.34641/clima.2022.257

1. Introduction

Facilities for children and youth are established in a health-friendly environment, which is protected from harmful environmental factors, especially against noise and air pollution sources, and the environment is protected from negative educational influences [1]. As well as the building of schools should be a non-toxic environment, also the school building itself, to be a wholesome environment for pupils and students [2]. However, most school buildings were established in the last century. Some have been reconstructed, but the condition of the indoor microclimate is still unsatisfactory. The microclimate conditions in schools must be as good as possible for the proper functioning of the classroom. Natural ventilation through windows is a good habit, but it does not guarantee sufficient air exchange and is counterproductive for schools located in busy areas. It is also not a good solution in terms of energy savings and the risk of children's exposure to disease, due to low temperatures [3].

2. Requirements for internal microclimates in education buildings in legislation

Microclimate conditions for school buildings can be found in several Slovak legal regulations, which are binding. The most important is the subsequent documents.

2.1 decree of the Ministry of Health of the Slovak Republic no. 259/2008 Coll. the title

Decree of the Ministry of Health of the Slovak Republic no. 124/2017 Coll. amendment to decree no. 259/2008, which lays down details on the requirements for the indoor environment of buildings and the minimum requirements for lower standard flats and accommodation facilities. In the Decree of the Ministry of Health of the Slovak Republic no. 259/2008 Coll., the table defines exactly what parameters of microclimate for school buildings.

Copyright ©2022 by the authors. This conference paper is published under a CC-BY-4.0 license.

Tab. 1 - Parameters of microclimate for rooms with special requirements [4].

Space	t_0 (°C)	φ (%)	n (h^{-1})
Facilities for children and youth			
playrooms and bedrooms for children up to 6 years of age	at least 22	30 to 70	5
washrooms and toilets for children under 6 years of age	at least 24	30 to 70	8
classrooms, games rooms, living rooms	20 to 24	30 to 70	3 to 8
gyms	15	30 to 70	5
changing rooms at gyms	at least 20	30 to 70	5
washrooms and toilets at gyms	at least 24	30 to 70	8
other changing rooms, corridors, toilets	at least 15	30 to 70	5
Schools, pre-school facilities			
gyms	15 to 17	30 to 70	5
nursery and kindergarten bedrooms	18 to 20 c)	30 to 70	5
classrooms, games rooms, living rooms	20 to 24 c)	30 to 70	3 to 8
isolation room	22 to 24	30 to 70	5

c) In pre-school facilities, t_0 values are determined 0.5 m above the floor.

2.2 decree of the Ministry of Regional Development of the Slovak Republic no. 527/2007 Coll.

Which lays down details on requirements for facilities for children and youth. The abovementioned document, specifically in §6 Operation of facilities for children and youth, sets out the conditions for heating, air exchange and also defines the supply of drinking water.

Heating - paragraph 2: In the preschool facility and the establishment for the care of preschool children, the temperature in the playroom and bedroom was ensured to be at least 22 °C and in the washroom and toilet at least 24 °C, in the facilities for children and young people, in addition to the facilities for children and youth mentioned in the previous point, the temperature was ensured: Classrooms and other rooms in which pupils work for four hours or more, at least 20 °C, rooms intended for teaching physical education at least 15 °C, changing rooms set up in areas intended for teaching physical education at least 20 °C, changing rooms and other areas for storing pupils' outer clothing at least 15 °C, corridors and toilets at least 15 °C. Air exchange – paragraph 4: In classrooms 20 to 30 m^3/h per student, in areas intended for teaching physical education 30 m^3/h per student, in changing rooms and other areas intended for storing outer clothing 20 m^3/h in one place, in washrooms 30 m^3/h per washbasin, showers 150 m^3/h up to 200 m^3/h for one shower, toilets 50 m^3/h per cubicle and 25 m^3/h per urinal [5].

Non-binding but professionally recommended technical norms include: Energy performance of buildings - Ventilation for buildings - Part 1: In-door environmental input parameters for design and assessment of energy performance of buildings addressing indoor air quality, thermal environment, lighting, and acoustics - Module M1-6

Because the creation of an indoor environment with centrally conditioned air requires large air distribution systems and relatively high energy requirements, in the vast majority of cases it is customary to design the volume of air handling unit only on the so-called hygienic minimum, which means ensuring that the legislation provides sufficient fresh air for people [6].

In each of the above documents, you can find a mention of why, how, and when to ventilate. The mentioned technical standard STN EN 16798-1: 2019 defines how school premises should be ventilated (**Tab. 2**).

Tab. 2 - Examples of recommended operating temperature design values for the design of buildings and environmental engineering systems [7].

Type of building (space)	Category	Operating temperature (°C)	
		Minimum for heating (winter season) ~ 1.0 clo	Maximum for cooling (summer season) ~ 0.5 clo
Offices and rooms with similar activities (classrooms) sedentary activities 1.2 met	II	20.0	26.0

3. Experimental measurement

Measurement of selected parameters of the indoor environment lasting 42 days was performed in the kindergarten.

3.1 measurement target

The aim of the experimental measurement was:

Verify that the indoor air temperature, relative indoor air humidity and carbon dioxide (CO_2) concentration in the kindergarten premises meet the requirements set out in the relevant legal documents and technical standards.

Assess whether legal and standard requirements are met, otherwise determine the reasons for noncompliance.

3.2 methodology in terms of measured parameters of the internal environment

The most important of the measured parameters was the indoor air temperature. All used recorders were equipped with a sensor for measuring the temperature and relative humidity of the indoor air.

The criterion for the thermal environment in the cold period is the lower limit value of the operating temperature t_0 of the indoor air. The following applies to the calculation of the operating temperature:

$$t_0 \cong (t_a + t_{mr})/2 \quad (°C) \qquad (1)$$

where:
t_a is the air temperature (°C),
t_{mr} is the mean radiant temperature of the surrounding surfaces (°C).

If the temperature of the surfaces in the room is approximately the same as the temperature of the indoor air in the room, the operating temperature can be exchanged for the indoor air temperature during practical measurements.

3.3 methodology in terms of measuring instruments

Measurements of indoor air temperature, indoor air relative humidity, and CO_2 concentration were performed using Comet (U3430) recorders (**Fig. 1**).

Fig. 1 - Recorder Comet U3430.

Measuring range and measuring accuracy of sensors:

Temperature sensor: -20 to +60 °C, ±0.4 °C,
Humidity sensor: 0 to 100 % RH, ±1.8 % (at a temperature of 23 °C in the range of 0 to 90 % RH),
CO_2 sensor: 0 to 5000 ppm, ± (50 ppm + 3 % of measured value) at 25 °C.

3.4 methodology in terms of time and measurement conditions

The measurement of selected quantities took place in the period from 22.03.2021 to 03.05.2021, i.e. 42 full calendar days, including weekends. Values were recorded at minute intervals. Due to the ongoing pandemic situation, the premises could be used by fewer children than usual.

3.5 methodology in terms of sensor placement

The measuring points were selected based on an agreement with the principal of the kindergarten. At the same time, the purpose of the measurement was the even distribution of recorders and recording of measured quantities in different types of rooms (in the bedroom and game room).

Recorders intended for continuous measurement were placed mainly on tables and cabinets. One of the recorders was hung in the middle of the room. All were informed about the ongoing measurements and were asked to take extra care to avoid shifting or damage to the measuring recorders.

Fig. 2 – Location of recorders.

4. Analysis of measurement results

4.1 requirements for indoor microclimate

The measurement was focused on the assessment of the microclimate as well as the quality of indoor

air in selected rooms. The most significant factors that affect the microclimate are the temperature and relative humidity of the indoor air. In air quality, the decisive measured quantity was the concentration of carbon dioxide CO_2.

Tab. 3 - Optimal conditions of indoor microclimate and air quality.

Season of the year	Temperature of indoor air *t* (°C)			Permissible air velocity *v* (m/s)	Permissible relative humidity *φ* (%)	Carbon dioxide concentration (ppm)
	optimal	permissible				
		min.	max.			
warm V to IX	23 to 27	20	28	≤ 0.25	30 to 70	350 to 1500
cold IX to V	20 to 24	18	26	≤ 0.20	30 to 70	350 to 1500

4.2 measurement results

The results of measurements in the game room are shown in the graphs in the following figures. The thermal state in the game room at the individual measuring points by the requirements defined in legal and technical regulations was acceptable, as the indoor air temperature during the entire measurement period in the cold period was 20 to 24 °C (**Fig. 3**). However, at certain measuring points in the cold season, the indoor air temperature was exceeded at certain times during the day, when the temperature dropped below 18 °C or rose above 24 °C. In tab. 3 shows that the maximum allowable temperature is 26 °C. In this context, the environment can be characterized in terms of the thermal state as acceptable, but not ideal.

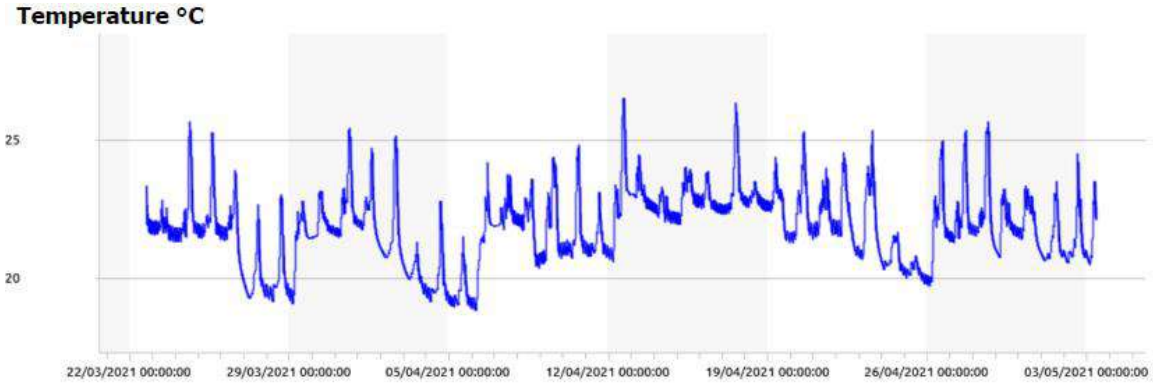

Fig. 3 - Graphs of temperature - Game room.

The humidity in the game room at the individual measuring points in connection with the requirements defined in legal and technical regulations was acceptable, as the relative humidity of the indoor air during the entire measurement period was in the range of 30 to 70 % (**Fig. 4**).

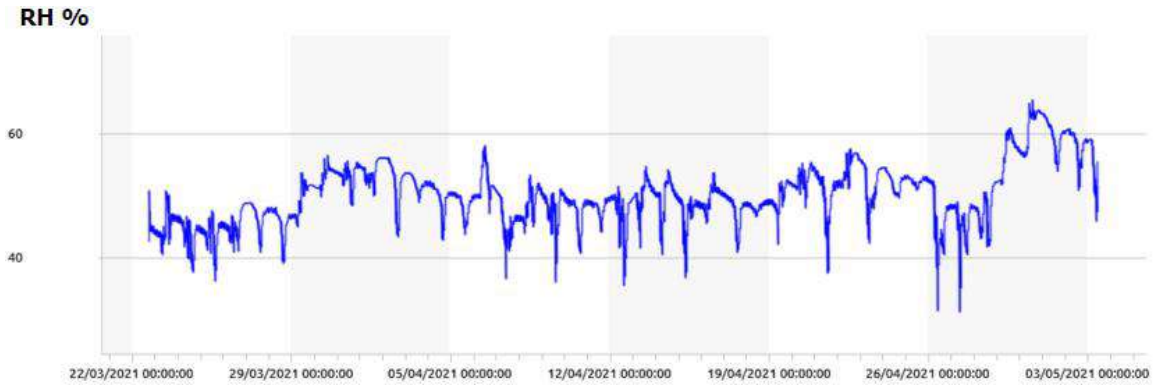

Fig. 4 - Graphs of humidity - Game room.

The quality of the indoor air at the individual measuring points by the requirements defined in the legal and technical regulations was partially acceptable, as at certain points the CO_2 concentration values were higher than the recommended limit value of 1500 ppm (**Fig. 5**) [8, 9].

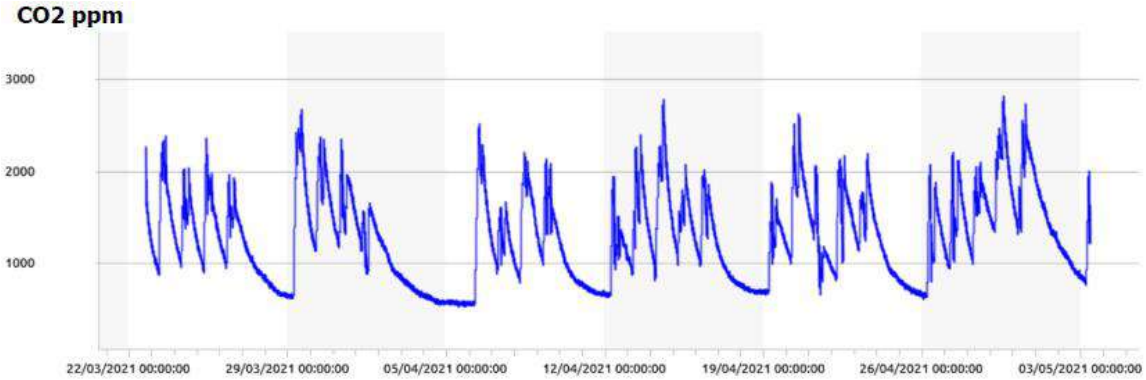

Fig. 5 - Graphs of concentration of carbon dioxide - Game room.

5. Conclusion

Some of the measured points show an acceptable state of both microclimate and indoor air quality, while others reach this state only in certain time intervals, but there are measured values where the state of the indoor environment is unacceptable. One of the solutions that can significantly improve indoor air quality in the school classroom is mechanical decentralized ventilation with a very unconventional location (under the sill) of the air handling unit. These are not local (room) ventilation units, this is a new solution that is still in the development phase.

6. Acknowledgement

This research was supported by the Ministry of Education, Science, Research and Sport of Slovak Republic grant VEGA 1/0303/21, VEGA 1/0304/21, and KEGA 005STU-4/2021.

7. References

[1] Act no. 355/2007 Coll. Of the Slovak Republic on the protection, promotion, and development of public health and the amendment of certain.

[2] Rubina, A. Větrání v době pandemie koronaviru. (Ventilation during a coronavirus pandemic.) TZB-info. Praha: Topinfo s.r.o., 2020. s. 1 (1 s.). ISSN: 1801-4399. (in [Czech language])

[3] Kassai, M., Kajtar, L. "Cooling energy saved investigation of air-to-air heat and energy exchangers", In Proceedings Express 2016, 8th International Symposium, Subotica, Serbia, 2016, pp. 6-10, ISBN 978-86-919769-0-3. [online] Available at: https://www.epget.bme.hu/docs/Kutatas/Konferencia/expres2016/.

[4] Decree No. 259/2008 Coll. Ministry of Health of the Slovak Republic on the details of the requirements for the indoor environment of buildings and the minimum requirements for lower standard flats and accommodation facilities.

[5] Decree 527/2007 Coll. Ministry of Health of the Slovak Republic on details of requirements for facilities for children and youth.

[6] Čurik, M. The Required Air Exchange in Buildings – How to be acquainted with current legislation. In: TZB Haustechnik 4/2010, 48-50, ISSN 1210-356X.

[7] STN EN 16798-1: 2019, Energy performance of buildings - Ventilation for buildings - Part 1: Indoor environmental input parameters for design and assessment of energy performance of buildings addressing indoor air quality, thermal environment, lighting, and acoustics - Module M1-6.

[8] Kapalo, P., Domnita, F., Lojkovics J. "Methodology for Calculating the Fresh Air Ventilation Airflow Rate Based on CO_2 Concentration" In Pollack Periodica, volume 9, issue 2, 2014, pp. 89-97. ISSN 1788-1994. https://doi.org/10.1556/Pollack.9.2014.2.9.

[9] Ferstl, K., Masaryk M. "Prenos tepla - príklady, 3. časť – Prenos tepla sálaním a odparovaním vody", (Heat transfer book - calculation samples, Part 3 - Heat radiation and water evaporation), Publisher STU, Bratislava, Slovakia, 2018, ISBN 978-80-227-4841-4. (in [Slovak language]).

The consent to the citation of standards was granted by the institute Slovak Office of Standards, Metrology, and Testing under number UNMS/00427/2020-702/000364/2020.

Data Statement

The datasets generated during and/or analyzed during the current study are available in the "Ulož.to" repository, https://ulozto.sk/file/XVZmKyN4RVpz/game-room-23-xlsx#!ZGWuZwR1MJSuMTZ1LwyvAmp1ZGHlraOJHx1zK3tkrxS2LmVl.

Application of Adapted Tracer Gas Test for Ventilation Assessment in Two Locations

Sarah L. Paralovo [a,b], Marianne Stranger [b], Borislav Lazarov [b], Maarten Spruyt [b], Jelle Laverge [a]

[a] Research Group Building Physics, Department of Architecture and Urban Planning, Ghent University, Ghent, Belgium, sarah.limaparalovo@vito.be.

[b] Unit HEALTH, Flemish Institute for Technological Research, Mol, Belgium.

Abstract. In the wake of the current worldwide COVID crisis, the vital role of ventilation in keeping healthy indoor environments has become increasingly clear. But even before that, researchers have been pointing out how crucial ventilation is in avoiding the accumulation of pollutants in indoor spaces and in interpreting indoor air quality (IAQ) data. Given the importance of ventilation, especially in estimating pollutant sources' strength and proposing remediation actions, it is imperative that IAQ assessments quantify the actual building ventilation rates. However, many IAQ field studies found in the literature do not report ventilation rates adequately. This paper describes the application of an alternative method to passively measure the average ventilation in two different locations. This alternative method consists of an adaptation of the traditional tracer gas test (TGT) used for long-term average air change rates (ACH) measurement. This adapted TGT employs an alternative tracer gas (decane-D_{22}) that is more adequate than the currently employed SF_6 and perfluorocarbons. The selected tracer can be co-captured and co-analysed with commonly assessed VOCs by commercial passive IAQ-sampling. A passive source design of decane-D_{22}, optimized in lab, provides stable and repeatable emission rates unaffected by varying RH and ACH. The actual source emission rate is determined from the average room temperature via an exponential prediction curve derived in lab. Results from the two field experiments described in this paper show the satisfactory applicability of the proposed adapted TGT in different types of environments and settings. The ultimate research goal is to provide an accessible enough method to quantify ventilation that it may encourage researchers, contractors and building owners to perform appropriate ventilation assessments more often and with a good degree of accurateness.

Keywords. Ventilation, passive sampling, tracer gas test, air change rate.
DOI: https://doi.org/10.34641/clima.2022.255

1. Introduction

The quality of the air present in indoor spaces has an undeniable influence over the health and well-being of occupants, and one of the key factors impacting indoor air quality (IAQ) is ventilation [1][2][3][4]. In the wake of the COVID-19 pandemic, the vital role of ventilation in controlling the spread of airborne diseases became clearer than ever before [5]. But even disregarding SARS-CoV-2, a myriad of other different pollutants of concern is ubiquitous to most buildings [2][3]. Therefore, assessing the contamination level in the air of all indoor spaces designed for human occupancy is crucial to assure its quality is enough to promote a healthy environment. For such assessments to be significant, measurements of ventilation rates must be included. Ventilation data is crucial in interpreting IAQ, studying pollutant sources, evaluating the performance of ventilation systems and proposing remediation actions if needed [6]. Especially in energy-efficient, more airtight buildings, it is of utmost importance to monitor the ventilation rates of the occupied spaces to make sure that a healthy level of ventilation is kept.

Despite the vital role ventilation plays in the field of IAQ, however, many IAQ assessments found in the literature do not report ventilation rates. Even when they do, in many cases the measurement approaches are not described in sufficient detail to evaluate their quality or applicability to the study design [7]. Among the many possible reasons for such a lack of adequate reporting on ventilation, it can be pointed out that the current methods available to measure ventilation rates are limited. While some are not suitable for application in the presence of occupants, others require the use of expensive and complex

Copyright ©2022 by the authors. This conference paper is published under a CC-BY-4.0 license.

equipment and/or environmentally-unsafe substances. Moreover, the existing ventilation measurement methods are generally disconnected from the indoor pollutants' concentration measurements, hindering the inter-comparison and co-interpretation between the ventilation and IAQ data.

In this this paper, an alternative method to quantify ventilation is applied in two different locations. This alternative method consists of an adaptation of one of the most common methods used to measure ventilation rates, the tracer gas test (TGT). In the TGT technique, an easily identifiable substance (tracer gas) is injected by a source to the indoor air, and then the total air change rate (ACH) in the space is inferred from the tracer air concentration and injection rate. This technique is the only one capable of directly measuring the actual total ACH in a room (i.e. from natural and mechanical ventilation, either intentional or from infiltration) [8]. Furthermore, TGTs in general are inherently simpler and more convenient than other ACH measurement methods.

However, the TGTs currently employed by IAQ researchers and practitioners have important limitations that are often overlooked. The method applied in this paper incorporates a few key adaptations to the classic TGT method in order to address some important limitations identified in the literature. Ultimately, the research goal is to propose a ventilation quantification method as simple, accurate and accessible as possible, so that it may encourage researchers, contractors and building owners to perform appropriate ventilation assessments more often in the future.

2. Materials and methods

2.1 the adapted TGT employed for ACH measurement

The three most important shortcoming commonly related to TGTs in the literature are: 1) Limited comparability between IAQ and ventilation data, as most TGTs provide short-term results while the concentrations of indoor pollutants are commonly measured using long-term sampling techniques that report time-averaged results; 2) Use of inadequate substances as tracer gases, e.g. sulphur hexafluoride (SF_6) or perfluorocarbons (PFTs), which are potent greenhouse gases with very long lifetimes in the atmosphere [9]; 3) Potential bias in the measurements arising from indiscriminate perfect-mixing assumption (i.e. if the air mixing is limited, the tracer distribution will be spatially heterogeneous across the assessed room; thus the placement of sources and samplers may bias the measurements of tracer concentration and, consequently, the calculated ACH) [8][10].

Therefore, the adaptations proposed for the new TGT applied in this research focus in 1) exclusive use of passive techniques (i.e. based solely on diffusive processes, excluding the use of pumps or any type of forced airflows, either for the injection or sampling of the tracer gas), 2) the use of standard, commercially available passive samplers commonly used in IAQ studies to capture the tracer gas simultaneously with IAQ pollutants of interest (automatically matching the IAQ and ventilation data timescales and rendering them comparable), 3) the employment of an alternative and more adequate substance as tracer gas and 4) the inclusion of a pre-TGT planning phase in which the TGT is simulated beforehand in the space to be assessed. Moreover, considering that the presence of occupants may significantly impact the indoor environment, the adapted TGT also aims for occupancy compatibility.

Based on these guidelines, the adapted TGT utilizes an alternative substance as tracer gas (the solvent decane-D_{22}) and an adapted passive tracer source design to measure long-term average ventilation rates. These proposed adaptations have previously been extensively tested in lab conditions and successfully validated in a controlled field test (against an active TGT using artificially-injected CO_2 as tracer). Details on the development and testing of the adapted TGT can be found elsewhere [11]. In summary, the alternative tracer decane-D_{22} is non-reactive, non-toxic, not found naturally in the atmosphere and does not adhere/absorb significantly to common indoor surfaces. The adapted passive source of decane-D_{22} consists of a very simple design that provides stable and repeatable tracer emission rates unaffected by varying RH and ACH (emission tests under varying RH/ACH were performed in previous development stages and are not shown, results were reported elsewhere [11]). The source design is shown in Figure 1; it consists of one single 1ml glass vial filled with ~0,5 ml of liquid decane-D_{22} and capped with a metal cap, with the rubber stop substituted by a PE filter disk (through which the tracer that volatilizes inside the vial diffuses to the air).

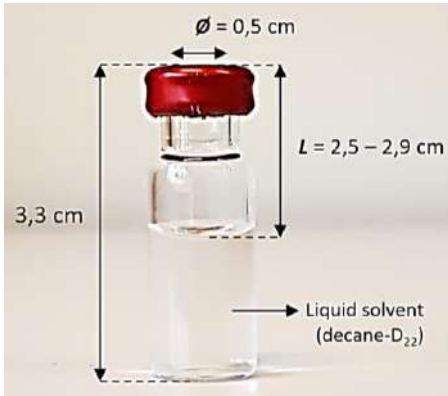

Fig. 1 - Tracer source design employed in the adapted TGT.

The source emits tracer gas at a known rate until the room concentration reaches a steady state (if the ACH is constant), from which the total ACH can be inferred using Equation 1.

$$q = \frac{G}{VC_S} \quad (1)$$

where q is the ACH (h^{-1}), G is the source emission rate (mg h^{-1}), V is the total volume of the assessed space (m^3) and C_s is the steady-state tracer concentration (mg m^{-3}). In a normal long-term passive TGT, however, neither q, G nor C_s can be assumed as constant. G and C_s will assume the average values of tracer emission and concentration over the whole sampling period. Thus, Equation (1) is still valid, but in that case the calculated q represents the average ACH over the total period.

In this newly proposed TGT, the average tracer emission rate from the passive source (G) is either determined gravimetrically in lab or estimated from the average room temperature measured during the TGT via an exponential prediction curve (Figure 2), derived after several controlled lab tests.

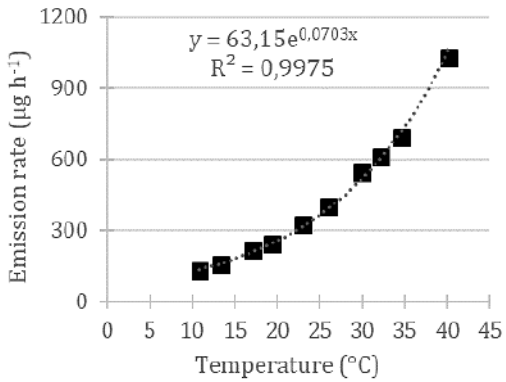

Fig. 2 - Tracer source emission rate as a function of room temperature for sources with 2,9 cm > L > 2,5 cm. Regression equation and linearity are also presented.

During the application of the TGT, the decane-D_{22} concentration in the indoor air is measured passively with Radiello® VOC samplers (for chemical desorption). Samplers and source(s) are left in the studied space for the pre-defined sampling period (usually 7 consecutive days), and then retrieved for analysis in lab. The passive samples obtained in the test are analysed by means of gas chromatography coupled to mass spectrometry detection (GC-MS), after extraction using carbon disulphide (CS_2) as solvent. All samples, calibration solutions and blanks are spiked with the same amount of internal standard (2-fluortoluene) to improve the precision and accuracy of the results.

Another adaptation proposed in the TGT employed in this paper is the addition of a simulation-based planning phase before the actual application of the TGT onsite. This is intended mostly to evaluate the air mixing in the space to be assessed and thus aid in the positioning of sources and samplers to avoid bias in the final ACH calculations. However, the field test previously performed for validation of the adapted TGT suggested that the air in indoor spaces can be in fact very well-mixed, and thus satisfactorily simulated using simple multizone software tools like CONTAM (as opposed to more computationally-demanding CFD tools) [11]. Therefore, the field tests described in this paper have also the aim of evaluating the adequateness of using perfect-mixing assumption to simulate different field settings.

2.2 sampling sites and testing setups

Unoccupied building: The first of the two tests described in this paper was performed in an unoccupied low-energy building located in Ostend (Belgium), the so-called E-Cube. The E-Cube is a zero-energy house of 265 m^3 that has been designed by team of students from UGent in 2011, during their participation in the U.S. Department of Energy Solar Decathlon 2011 competition [12]. After the competition, the structure was rebuilt in the Greenbridge Science Park in Ostend (Belgium), where it is currently used as a testing facility. All characteristics and HVAC systems of this building are well-known [13] and, as it is subject to real environmental conditions, the E-cube is ideal for measurements providing data for validation of simulation models and methods in general. Due to the open-plan design, the building behaves as a single-zone even though it has a ground and first floor. Figure 3 shows a picture of the exterior façade of the E-Cube as well as an interior view of the building.

Fig. 3 - Exterior (top) and interior (bottom) view of the E-Cube (Source: [14]).

The E-Cube was ventilated continuously during the experiment by the installed mechanical ventilation system, set to "low ventilation" configuration (design airflow rate = 110 m^3 h^{-1}[13]). The building's thermal and ventilation behaviour over one year had been thoroughly simulated in CONTAM as part of a previous experiment [12], and therefore no new simulation was performed during this field test. The previous simulation was executed to study the effect of varying outdoor environmental conditions over

the indoor environmental conditions via leakage and uncontrollable exchanges through the building envelope, i.e. without any forced air flow. From the results of that simulation, the ACH in the E-Cube ranges between 0,1 and 0,5 h^{-1} without the aid of the mechanical ventilation system, with the lowest ventilation rates during summer months and the highest during the winter months. The experiment was executed in April, when an intermediate unintentional ACH of 0,2 h^{-1} is expected. Adding the (intentional) contribution of the mechanical ventilation system (which, from the design ventilation and the internal building volume, should be of approx. 0,4 h^{-1}), the total ACH during the experiment was expected to be around 0,6 h^{-1}.

The ventilation assessment was executed alongside a parallel experiment by Ghent University, intended to study aldehydes emissions from the building materials (reported elsewhere [12]). Since it was known from previous experiments that the indoor conditions of the E-Cube were highly influenced by sunlight, a minimum indoor temperature of 30°C was set and a fixed schedule of air humidification was deployed in order to minimize the fluctuations of indoor temperature and relative humidity.

The newly proposed TGT was performed simultaneously with an active, constant-emission TGT, employing artificially-injected CO_2 as tracer gas. The complete duration of the two tests was 4 consecutive days. One pressurized CO_2 cylinder was placed outside the E-Cube, and a long flexible tube connected it to the interior of the building, with the end of the tube at a 1,3 m height. A pressure nozzle and a mass flow controller kept the CO_2 emission rate tightly at 0,5 l min^{-1}. One decane-D_{22} source was weighed uncapped with the microbalance in lab one day before and one day after the test for determination of the average emission rate (0,8 mg h^{-1}). Four CO_2 automatic loggers and four Radiello® passive samplers were distributed in the interior of the E-Cube (centre of the ground floor, next the window close to the backdoor and on the first floor) to check the indoor air mixing, and one sampler for each tracer was placed outdoors. Due to time and logistics constraints, the passive decane-D_{22} source was placed (with PE filter cap) in the E-Cube only 30min before the placement of the passive samplers. During these 30min, the CO_2 source and sensors were also placed.

Occupied apartment: The second experiment described in this paper was performed in a 1st-floor residential apartment occupied by one couple and one cat. The apartment is 52 m^2 and has no mechanical ventilation system, except for one extraction hood in the kitchen and another one in the bathroom, both of which manually activated by the occupants. Except for these local on-demand extraction points, the ventilation on the dwelling relies on natural ventilation through the openable windows (and ventilation grills over the windows). The TGT was applied in the part of the dwelling most intensively occupied by the dwellers: the living room/kitchen. In this apartment, there is no physical limit between the living room and the kitchen, and the open space acts like a single-zone. This space is also fully merged to the entrance hall/corridor. The TGT was performed employing two decane-D_{22} sources and three passive samplers scattered around the room to evaluate the air mixing. The sources were placed 3h before the samplers. Two sensor boxes for CO_2 and T active monitoring were also placed in the room. Figure 4 shows a sketch of the studied space and the test setup.

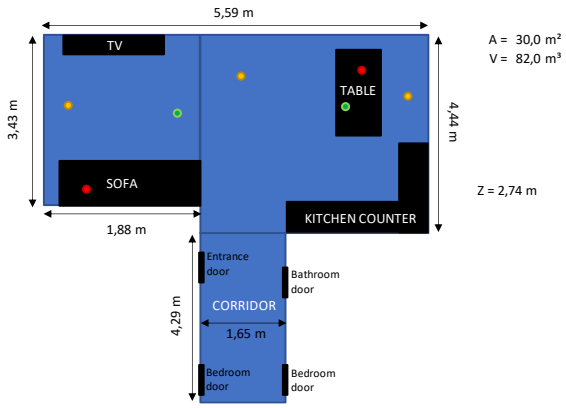

Fig. 4 - Sketch of the test space, along with the TGT setup in the occupied apartment. Green dots represent the decane-D_{22} sources, the yellow dots represent the passive samplers and the red dots represent the CO_2/T loggers. Distances in figure not to scale.

Before the application of the TGT, the test space was modelled in CONTAM (Figure 5). Since the space would be normally occupied and the occupancy-dependent patterns (e.g. presence/absence of occupants, windows opening, activation of extraction hoods) were unpredictable, the model was then intended to predict the lowest ventilation in the space, resulting from infiltration and exchanges through closed doors and windows. From the previous simulations performed until this point, the same simplifications were applied (closed doors and windows modelled as forced flow openings of 6 and 5 m^3 h^{-1}, respectively).

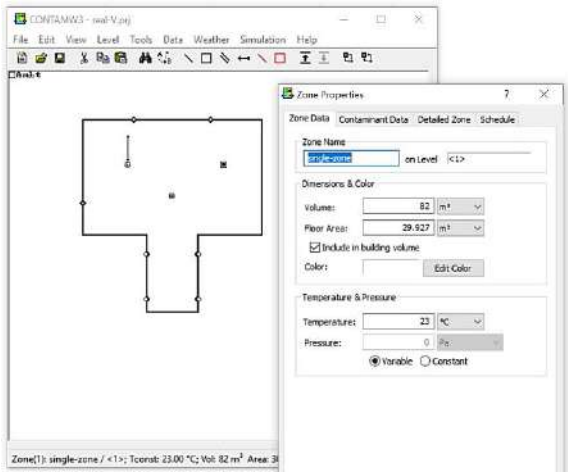

Fig. 5 - The apartment assessed during the TGT, as modelled in CONTAM.

The temperature was set to the average expected inside the apartment during the experiment. One source of decane-D_{22} was modelled with a constant emission rate of 0,72 mg h^{-1}, corresponding to twice the emission rate expected from a tarcer source at 23°C (according to the prediction curve from Figure 2). From the simulation results, the minimum ACH in the studied space should be 0,44 h^{-1} and the steady state decane-D_{22} concentration should be 20,0 µg m^{-3}. According to the simulation, 90% of the steady-state concentration would be reached in the space after 5h of source placement.

In an occupied setting such as the apartment in this experiment, the application of an active CO_2 constant-emission TGT is hindered both for technical and for practical reasons. Since the occupants act like mobile CO_2 sources of unknown (and hardly calculable) emission rate, neither CO_2 emission rate nor concentration can be kept at a minimally constant level during the test, and thus the average ACH cannot be calculated. Moreover, the transportation and installation of a pressurized cylinder (plus the necessary flow controllers) and the potential noise arising from the gas injection would cause great disturbance to the daily-routine of the occupants. Nevertheless, the CO_2 concentration was monitored throughout the experiment. In combination with specific activities annotations from the occupants, short periods in which the occupants were absent from the test space (e.g. left the apartment or went to bed with closed door) and the ventilation conditions were clearly stated could be carefully selected for applying a decay test calculation to the CO_2 concentration to determine the ACH in that short period. In a decay testing, there is no emission/injection of tracer into the space, thus the tracer concentration decays exponentially. The ACH in the space is thus derived from plotting the natural logarithm (ln) of the concentration difference between the CO_2 concentration and the background versus time. The coefficient of the linear regression obtained is equal to ACH in the space.

3. Results and discussion

3.1 Unoccupied building

Figure 6 shows the concentration of CO_2 measured over the 4-days test at the 4 indoor and 1 outdoor locations in the E-Cube, together with the temperature measured indoors.

The graph in Figure 6 shows that the air inside the E-Cube was well-mixed all throughout the experiment, with the 4 indoor sensors recording very similar CO_2 concentrations between themselves the whole time. Although a stark temperature difference can be noted between the indoor and outdoor environments during the experiment, the strategy adopted to minimize indoor temperature variation worked, as it did vary much less than the outdoor temperature, even with a very sunny weather over the whole week (75th-percentile global horizontal irradiation = 623 W m^{-2}). It is noticeable that there was an inverse correlation between the CO_2 concentration and the recorded outdoor temperature, indicating that the leakage was inversely proportional to the temperature difference, differently from what would be expected.

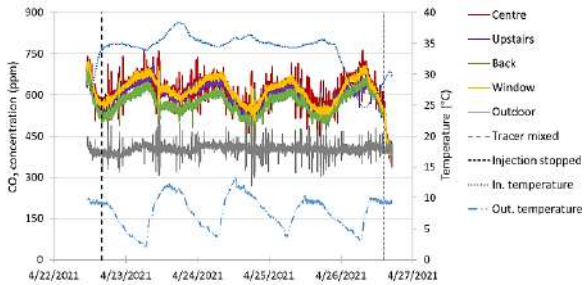

Fig. 6 - CO_2 concentration and temperature recorded over the 4-days experiment in the E-Cube.

Regarding the passive sampling results, the average decane-D_{22} concentration measured by the 4 samplers was 3,8 µg m^{-3} with an RSD = 3,7%, once again indicating an excellent level of air mixing in the E-Cube during the experiment. This result is another good indication that most indoor spaces are in fact well-mixed, regardless of size (the E-Cube is approx. 7 times larger in internal volume than the office assessed in by Paralovo et al. [11]) and occupancy status (researchers tend to assume that occupancy is one of the driving forces of air mixing, but it was not a factor in this experiment). Figure 7 shows the ACH calculated from both the active and passive TGTs (ACH calculation method described in greater detail in Paralovo et al. [11]).

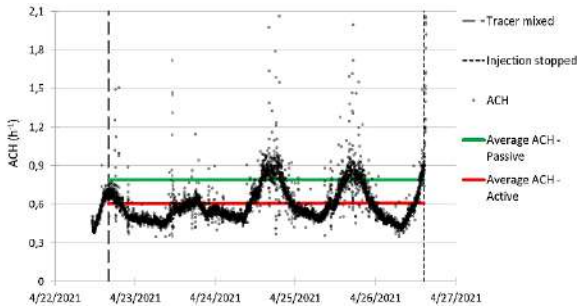

Fig. 7 - ACH calculated from the measured concentrations of CO_2 (active) and decane-D_{22} (passive).

The results displayed in Figure 7 show that the ACH in the E-Cube fluctuated mostly between 0,3 and 0,9 h^{-1} over the 4-days experiment. The average calculated from the active CO_2 measurements (black dots, represented by the straight red line) was 0,61 h^{-1}, almost exactly the same value that was expected from the theoretical evaluation, indicating that the previous model of the building leakage [12] is adequate and that the design flow rate of the ventilation system at "low ventilation" configuration is satisfactorily maintained in practice.

On the other hand, the average ACH calculated from the passive decane-D_{22} measurements (0,79 h^{-1}) was

22,9% higher than the value calculated from the active CO_2 measurements. Considering the intrinsic passive sampler uncertainty (10,5%) and the error arising from imperfect air mixing in this experiment (3,7%), the decane-D_{22} average concentrations measured in the E-Cube experiment had a global uncertainty of 14,2%. Thus, the 22,9% difference between the active and passive results, although low, is significant. There are two potential explanations for this ACH overestimation: 1) the underestimation of the true decane-D_{22} average concentration in the studied space and 2) the overestimation of the actual source emission rate. The likelihood of (1) is small but considerable, as it is known that passive samplers can be sensitive to concentration peaks (they need more time to be able to capture enough analyte mass to reflect the actual concentration increase — time by which the concentration peak itself is already decreasing), i.e. they have a natural tendency to underestimate the actual averages when the target contaminant concentration fluctuates significantly during the sampling time. Besides, in this particular experiment, the total sampling time (4 days) was shorter than the recommended by the manufacturer (1 week), which can also influence the accuracy of the analysis when the average concentration is overall low. Thus, it is recommended that the minimum sampling time of 7 consecutive days is respected in future TGTs and, especially in larger spaces, that multiple tracer sources are employed to reach higher levels of tracer concentration.

On the other hand, the likelihood of (2) is a bit more prominent. While it is preferable to measure the emission rate of the source gravimetrically using a micro-balance, potential losses of tracer from inside the source during transportation cannot be ruled out. For the E-cube experiments, the source had to be weighed one day before the start of the experiment and then one day after its finish, as its transportation between the lab and the E-Cube site took 3h. During the 6h in the car rides (for the complete round-trip), the source position could not be controlled, and the liquid tracer in the source was subject to the car movement and vibrations, getting into full contact with the rubber-septum in the vial cap. It is possible that small amounts of liquid tracer were adsorbed in the rubber septum, and therefore lost when the cap was substituted by a new one with a PE filter disk (and also when the second rubber-cap for the trip back was removed for the final weighing). Therefore, not all the weight difference measured can be attributed to the actual tracer volatilization during the TGT.

Another potential evidence of (2) is the fact that the emission rate measured gravimetrically was around 12% higher than the value predicted by the Figure 2 prediction curve (0,70 mg h^{-1}) from the average temperature measured in the E-Cube. That prediction curve was derived from more than 20 separate experiments using several replicate sources simultaneously, and applying different environmental conditions. Even when the conditions to which the sources were subjected varied during the experiment, the final gravimetric measurements still showed excellent agreement with the prediction curve (considering the average temperature). If the predicted source emission rate is used for the ACH calculation in the E-cube test instead of the gravimetrically measured one, the calculated ACH (0,70 h^{-1}) becomes then only 13% different than the ACH calculated from the active CO_2 measurements, a value below the global uncertainty of the passive sampling for this experiment (14%), i.e. with this method of calculation, the new TGT can be considered validated also in a larger space. Therefore, the recommendation for future applications of this new TGT is to determine the source emission rate either via the prediction curve shown in Figure 2 or gravimetrically with an on-site scale (minimum accuracy of 0,1 mg), to avoid potential tracer losses during transportation.

3.2 Occupied apartment

Figure 8 shows the CO_2 concentration monitored during the 7 days in the occupied apartment, along with three periods selected for the decay test calculations and the ACH calculated for each period.

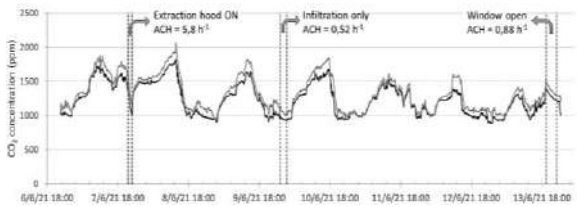

Fig. 8 - CO_2 concentration measured by two active logging sensors during the TGT in the occupied apartment. The straight dashed lines mark 3 short periods right after the occupants exited the test space, and when distinct ventilation characteristics were in place.

Figure 8 shows that the CO_2 concentration in the apartment oscillated greatly during the experiment, mostly between 900 and 2000 ppm, reflecting both the ventilation variations and the CO_2 sources (i.e. occupants) movement. Hence why an accurate CO_2-based TGT would be impractical in this setting. Despite this issue, the three well-characterized periods highlighted in Figure 8 provide a few insights for further analysis of the decane-D_{22} TGT results. According to Figure 8, the infiltration-only portion of the ventilation in the studied space amounts to an ACH = 0,52 h^{-1}, a value only 15% higher than the predicted by the CONTAM simulation. The ventilation in the space is increased tenfold (ACH = 5,8 h^{-1}) when the extraction hood over the kitchen counter is activated on full-power. An intermediate ventilation level (ACH = 0,88 h^{-1}) is achieved when one of the windows is open. Since it is not possible to know with certainty the actual weight the ventilation strategies held during the experiment, any passively-calculated average ACH between 0,5 and 5 h^{-1} should be considered at least realistic in this case.

The average decane-D_{22} concentration measured by

the three passive samplers was 13,4 µg m^{-3} with a very low RSD between them (1,6%), indicating that the studied space was very well-mixed during the experiment period. As was observed during the E-Cube experiments, the sources' emission rates measured gravimetrically (509 mg h^{-1}) were higher than the value predicted with the Figure 2 curve by the same factor of 12%. This suggests that, when the liquid tracer gets in contact with the vial cap during transportation, a specific minimum amount of tracer is adsorbed by it, leading to an overestimation of the average emission rate by at least 12%. Thus, the value theoretically predicted by the curve from the average temperature measured during the TGT (26°C) was applied to both sources (450 mg h^{-1}).

Therefore, by applying these measured and estimated values to Equation 1, the average ACH calculated from the passive TGT is of 0,82 h^{-1}. This value is in line with the predictions based on the CO_2 concentration, and in fact very close to the ACH calculated from the CO_2 decay when the window was open. Therefore, it can be considered that the TGT can provide realistic estimations of ACH in occupied naturally-ventilated spaces as well.

4. Conclusion

This paper presented two successful applications of a newly proposed TGT to measure average ventilation rates over long-term periods in varied types of buildings. The proposed test is passive, more affordable and practical than commonly applied active pressurization tests, e.g. the blowerdoor test. Moreover, it is also more environment-friendly when compared to the currently employed long-term passive TGTs, which use known potent greenhouse gases (PFTs) as tracers. The first application reported in this paper took place in an unoccupied building, and the second one in an occupied apartment. Results from both experiments showed reasonable agreement with predictions previously done with CONTAM multizone simulations, indicating a good level of air mixing inside both studied buildings. Additionally, results yielded by the newly proposed TGT in both settings demonstrated the accuracy of the tracer emission rates estimated with the lab-derived prediction curve (Figure 2). More applications of this proposed TGT are recommended to further evaluate its appropriateness to different and more complex settings in the future, so that the main goal of providing a reliable, accessible and accurate alternative to researchers, contractors and buildings owners to assess ventilation in a wide range of buildings is achieved.

5. Acknowledgement

The authors would like to acknowledge the support of colleagues from VITO who, although not directly involved in this project, assisted and facilitated our work immensely. Special thanks to the UGent colleague Klaas De Jonge for the partnership developed during the E-Cube experiments. No potential competing interest is reported by the authors.

6. References

[1] WHO. Burden of disease from the joint effects of household and ambient air pollution for 2012. 2014. Geneva, Switzerland.

[2] Carrer, P., E. d O. Fernandes, H. Santos, O. Hänninen, S. Kephalopoulos, P. Wargocki. On the development of health-based ventilation guidelines: Principles and framework. International Journal of Environmental Research and Public Health. 2018; 15 (7):1360. doi:10.3390/ijerph15071360

[3] Fernandes, E. D. O., M. Jantunen, P. Carrer, O. Seppänen, P. Harrison, S. Kephalopoulos. EnVIE - Co-ordination Action on Indoor Air Quality and Health Effects. Project no. SSPE-CT-2004-502671, IDMEC/European Commission. 2009.

[4] Heinrich, J. Influence of indoor factors in dwellings on the development of childhood asthma. International Journal of Hygiene and Environmental Health. 2011; 214 (1):1–25. doi:10.1016/j.ijheh.2010.08.009

[5] REHVA. COVID-19 guidance document 4.1, April 15th 2021. REHVA, 2021.

[6] Persily, A. K., Levin, H. Ventilation measurements in IAQ studies: Problems and opportunities. In Proceedings of Indoor Air 2011, 12th International Conference on Indoor Air Quality and Climate, Austin, TX, USA: ISIAQ. 2011.

[7] Persily, A. K. Challenges in developing ventilation and indoor air quality standards: The story of ASHRAE Standard 62. Building and Environment. 2015; 91:61–9. doi:10.1016/j.buildenv.2015.02.026

[8] Lunden, M., D. Faulkner, E. Heredia, S. Cohn, D. Dickerhoff, F. Noris, J. Logue, T. Hotchi, B. Singer, M. H. Sherman. Experiments to evaluate and implement passive tracer gas methods to measure ventilation rates in homes. LBNL-5984E, Ernest Orlando Lawrence Berkeley National Laboratory, Berkeley, CA, USA. 2012.

[9] IPCC. 2.10.2 Direct Global Warming Potentials. Climate Change 2007: The Physical Science Basis: Contribution of Working Group I to the Fourth Assessment Report of the IPCC. Cambridge, UK:Cambridge University Press. 2007.

[10] Liu, Y., P. K. Misztal, J. Xiong, Y. Tian, C. Arata, W. W. Nazaroff, A. H. Goldstein. Detailed investigation of ventilation rates and airflow patterns in a northern California residence. Indoor Air. 2018; 28 (4):572–84. doi:10.1111/ina.12462

[11] Paralovo, S. L., M. Stranger, B. Lazarov, M. Spruyt, J. Laverge. Adapted tracer gas test for passive measurement of total air change rates using alternative tracer substance. Science and Technology for the Built Environment. 2021; 0:1-15. doi:10.1080/23744731.2021.1997061

[12] De Jonge, K., Laverge, J. Modeling Dynamic Behavior of Volatile Organic Compounds in a Zero

Energy Building. International Journal of Ventilation. 2020; 1-11.
[13] Vermeir, T., P. J. De Loof, T. Delameillieure, R. Rottiers, D. van de Walle, M. Arens, W. Wuyts, C. Vyncke. Project Manual: Solar Decathlon 2011. Team Belgium - Ghent University: E-Cube. UGent, Ghent, Belgium, 2011.
[14] Ghent University. E-Cube: Zero Energy Testing House. Ghent University, Ghent, Belgium, 2021.

Data Statement

The datasets generated and analysed during the current study are not publicly available because they are owned by VITO, but can be shared on an individual basis via direct contact with the authors.

Effects of supply air temperature and pollutant location on concentration characteristics with a night-time ventilation in a school classroom

Sami Lestinen [a], Panu Mustakallio [b], Risto Kosonen [a,c], Simo Kilpeläinen [a], Juha Jokisalo [a]

[a] Department of Mechanical Engineering, School of Engineering, Aalto University, 02150 Espoo, Finland, sami.lestinen@aalto.fi, simo.kilpelainen@aalto.fi, risto.kosonen@aalto.fi, juha.jokisalo@aalto.fi

[b] Halton Oy Ltd., Haltonintie 1–3, Kausala, 47400, Finland, panu.mustakallio@halton.com.

[c] Department of HVAC, College of Urban Construction, Nanjing Tech University, Nanjing 211899, China, risto.kosonen@aalto.fi.

Abstract. Night-time ventilation is used to remove indoor pollutants before the occupied periods. However, a lack of knowledge exists on how well a minimum level of ventilation can dilute pollutants during the night, and how a location of a polluting source and a supply air temperature affect the concentration levels with a typical mixing ventilation strategy. Therefore, the constant polluting source of 12 mg/h was defined on the floor (60 m^2), sidewall (17 m^2), and floor-corner (1 m^2) describing a low-polluting floor material of 0.2 mg/h,m^2 (EN 15251:2007). The objective of the study was to demonstrate a minimum night-time ventilation scenario of 0.15 L/s,m^2 with the isothermal supply air, underheated supply air (-4°C), and overheated supply air (4°C) compared to indoor air initial temperature. Furthermore, the temporal and spatial concentration characteristics were considered. The daytime ventilation was 3 L/s,m^2 with the underheated supply air temperature. Both the night and the day periods lasted 12 hours. The room air distribution was arranged by using 2 corridor wall supply air grilles and 4 exhaust air valves. However, only 1 grille and 2 valves were used at night. ANSYS CFX tools were used for numerical modelling. The RANS and URANS simulations were carried out with the implicit pressure-based multigrid coupled solver. The second-order discretization schemes were used in space and time and the SST-model was chosen to model turbulence with the automatic wall treatment. The convection-diffusion equation was used in scalar transportation. The measured data were used as boundary conditions and the computational grid adaptation was applied to improve accuracy. The results show that the underheated supply air provided the lowest concentration level in the occupied zone because the low-temperature supply air flowed down to the floor and dilute well the occupied zone. The overheated supply air, in turn, provided the largest concentration level in the occupied zone because the heated air was not mixed well in the room. The isothermal supply air provided a circulating airflow pattern increasing the concentrations beyond the supplied airflow region. The daytime ventilation decreased the cumulated night concentrations to one-tenth within an hour.

Keywords. night-ventilation, school, pollutants, CFD, IAQ.
DOI: https://doi.org/10.34641/clima.2022.251

1. Introduction

Ventilation is an important matter in reducing pollutants from the indoor environment [1]. Generally, the main target is providing clean air for people and maintaining indoor air quality and thermal comfort. Therefore, the air distribution flows and their interactions with surroundings are important matters to investigate. Night-time ventilation is typically used to remove indoor pollutants before the occupied periods. Finnish building code instructs that the minimum ventilation is 0.15 L/s per floor square for the unoccupied hours of non-residential buildings. European Standard EN 15251:2007 [2] recommends 0.1-0.2 L/s per floor square for the unoccupied hours or 2 air volume changes before occupancy. However, a lack of knowledge exists on how well a minimum level of ventilation rate can

Copyright ©2022 by the authors. This conference paper is published under a CC-BY-4.0 license.

dilute and remove the pollutants during the night, and how the location of a polluting source and the supply air temperature affect the concentration characteristics.

Earlier studies have found that the increased TVOC concentrations in the mornings in non-residential buildings may occur due to off-gassing of building materials because the ventilation is not used at night [3], [4]. Consequently, the objective of this study was to investigate the effects of minimum ventilation level on different classroom pollutant sources. The study demonstrates a minimum night-time ventilation scenario of 0.15 L/s,m^2 with the isothermal, underheated (-4°C) or overheated (4°C) supply air. The research question was how the night-time ventilation should be used with the minimum ventilation.

CFD-simulation is a common modelling method while investigating indoor airflows [5]-[8]. In many cases, the Newtonian viscous incompressible flow equations are discretized by a system of linear algebraic equations at discrete locations in space and time [9]. The boundary conditions are then implemented to define the desired airflow field, and the initial conditions are used for describing a beginning moment of time-dependent computation. A numerical solution of linear algebraic equations is generally obtained by conducting the iterative methods.

The Reynolds-averaged Navier–Stokes (RANS) modelling has been commonly used to simulate a time-averaged indoor airflow field. In RANS, the Reynolds-averaged momentum equations provide nonlinear stress terms that must be modelled, because each unknown variable needs an equation. Therefore e.g. many well-known two-equation eddy viscosity models have been developed, in which the turbulent viscosity is added to reduce the kinetic energy from the predicted flow field. The turbulence affects remarkably the indoor airflow field by enhancing the heat and mass transfer and by increasing the flow disturbances and losses in the air jets and mixing layers. This may typically mean that the predicted air jets become wider, and the mixing layers increase faster downstream than without using the turbulence models. However, this depends greatly on the initial air jet velocity levels and interacting buoyancy flows in the airflow field.

In this study, the airflow field of a school classroom was modelled by using CFD-simulations. Three constant and equal total emission sources were placed in the different locations in the classroom. In addition, different supply air temperature levels were examined. The novelty of the study is in the effects of night-time ventilation use on the pollutant concentration characteristics in indoor air before space usage.

The CFD model was based on the previously created CFD model that was validated by comparing the experiments in a laboratory test room [10], [11]. The computational grid and the computational models were updated to meet new test cases.

2. Methods

2.1 classroom

The simplified classroom is shown in Fig. 1. The classroom is 10 m long, 6 m wide and 3.3 m high. The height of the suspended ceiling at the corridor side-wall was 3 m. Furthermore, the outer side-wall had a window.

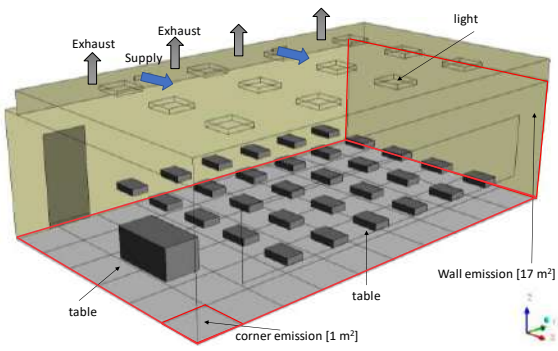

Fig. 1 The school classroom model.

2.2 pollutant sources

The three equal emission sources of 12 mg/h were placed to the different locations in the classroom. Each source describes a low-polluting material installed on the entire floor with an emission flux of 0.2 mg/h,m^2 [2]. In this study, these equal total source rates were located on the floor (60 m^2), on the side-wall (16.8 m^2), and on the floor-corner (1 m^2) which can be seen in Fig. 1. Therefore, the emission flux was the largest in the floor-corner source and the smallest in the floor source.

2.3 CFD-simulations

ANSYS CFX tools [12] were used for numerical modeling. The RANS and URANS simulations were carried out with the implicit pressure-based multigrid coupled solver. The second-order discretization schemes were used in space and time and the SST-model [13] was chosen to model turbulence with the automatic wall treatment. The convection-diffusion equation was used in scalar transportation. The measured data were used as the boundary conditions and the computational grid adaptation was applied to improve accuracy. In this way, the computational grid was automatically refined in the mixing layers of high-velocity gradients. The indoor air was ideal gas and pollutants were modelled as scalars, because tiny particles were considered. RANS simulations were used mainly in pre-simulations to test air distribution and computational grid levels. URANS-simulations were performed in 12-hour simulations.

2.4 air distribution

The ventilation method was mixing ventilation (Fig. 2). The daytime ventilation airflow rate was 3 L/s, m^2 with the underheated supply (dT=-4°C). This corresponds to the ventilation level of 6 L/s per person. Furthermore, this means around 3 indoor air changes per hour. The supplied airflow jet from the wall-grille device was 15 degrees upwards attaching to the ceiling due to pressure losses on the surface layer. The velocity profile at the grille boundary was provided by the device manufacturer (Halton Oy) that was applied to the given ventilation airflow rate. The change in speed level due to simplification of the terminal device was corrected by using a momentum source in front of the device. The ventilation was started smoothly such that the nominal level was achieved after 40 seconds from the start. In addition, the correct mass flow rate levels of exhaust valves were verified during the simulation.

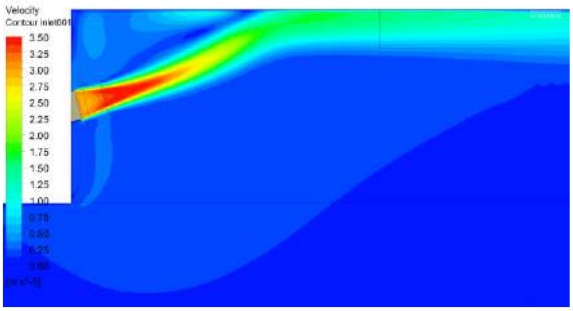

Fig. 2 The day-time ventilation supply air jet from the wall-grille device.

The day-time air distribution was arranged with 2 corridor wall-grilles and 4 exhaust valves. The night-time air distribution was arranged with 1 grille and 2 valves. Both the night and the day periods lasted 12 hours. The night-time ventilation was 0.15 L/s,m^2 with the isothermal, underheated (-4°C) or overheated (4°C) supply air. Fig. 3 shows the airflow streamlines from the supply air grille and the exhaust air valves. The difference arises from gravity.

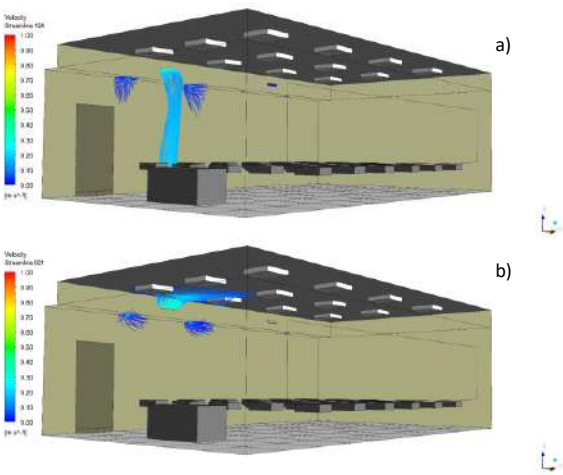

Fig. 3 The night-time supply air jet: a) underheated and b) overheated supply air.

2.5 Test cases

The test cases for the night-time ventilation were the isothermal, underheated (-4°C), and overheated (4°C) supply air. The night-time ventilation of 12 hours and the day-time ventilation of 12 hours were simulated by using URANS. In addition, the floor pollutant source, the wall pollutant source, and the corner pollutant source were compared. URANS time-step size was 1 s for the day-time ventilation and 10 s for the night-time ventilation. 3 internal iterations were used in each time-step. The wall boundary conditions were 22°C, window 21°C and the initial temperature of indoor air 21°C. The pollutant concentration characteristics of the school classroom was considered.

3. Results

3.1 concentration characteristics

Fig. 4 shows the predicted night-time increase of pollutant concentration level with the minimum ventilation of 0.15 L/s, m^2. In the graph, the concentration begins from the zero-concentration level and the pollutant source was the entire floor. Each curve represents a location in the middle of the room, inside the rectangle.

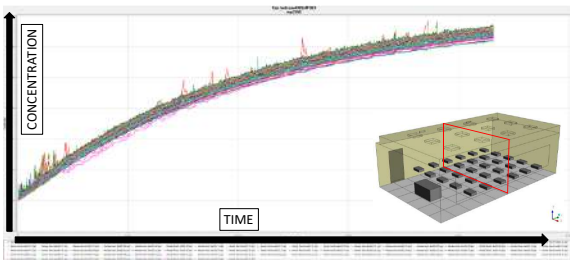

Fig. 4 Concentration characteristics in the middle of the room (marked with a rectangle). Transient simulation (URANS) for the 12 hour ventilation of 0,15 L/s,m^2. Floor emission 0.2 mg/h,m^2, dT_{supply}= -4°C.

In this case, the concentration was approaching stable conditions after 12 hours of minimum ventilation. The concentration characteristics are not linear but had a curved shape as approaching a balance with the ventilation. This describes the scenario where the pollutants from the floor material (12 mg/h) will increase the indoor air concentration during the night, and the minimum ventilation of 0.15 L/s,m^2 removes and dilutes the pollutant concentrations.

Generally, the spatial concentration differences between the different locations during the temporal development remained quite small with the mixing ventilation, which is seen as the distance between the curves on the vertical axis. When the day-ventilation is started, the concentration levels decrease rapidly. Fig. 5 shows the decay curve of concentration after the day-ventilation was started.

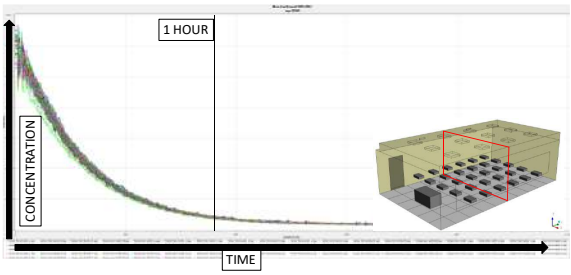

Fig. 5 Decay curve of floor emission of 0.2 mg/h, m². The day ventilation 3 L/s,m² was started up after 12 hour pollution.

The results show that the day-time ventilation decreased concentrations to 10% within an hour. Therefore, the results indicate that a 2-hour criterion for ventilation operation before the space usage is sufficient.

3.2 supply air temperature

Fig. 6 shows the dimensionless concentration level after 12 hours from the floor emission if the ventilation was not used at night. The predicted concentration level rises to about 5-7E-4 highlighting the regions near walls.

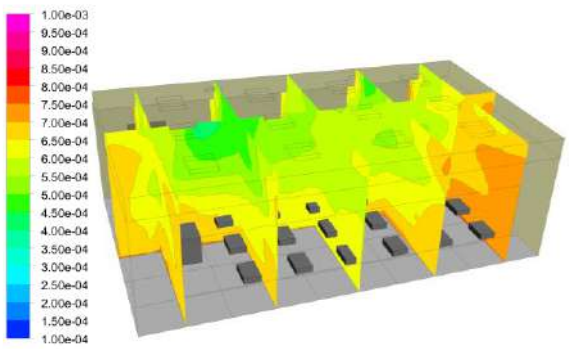

Fig. 6 The concentration characteristics without the ventilation from the floor emission 0.2 mg/h, m².

When the ventilation was used at night, the concentration levels decrease. The supply air temperature also affects the results because the gravity accelerates underheated supply air to the floor zone and the overheated supply air to the ceiling zone. Fig. 7 shows the corresponding concentration characteristics after 12 hours of minimum ventilation.

The results reveal that the underheated supply air flows on the floor by diluting the concentrations in the occupied zone. Consequently, the low-temperature supply air provided a rather well-mixed concentration field in the classroom.

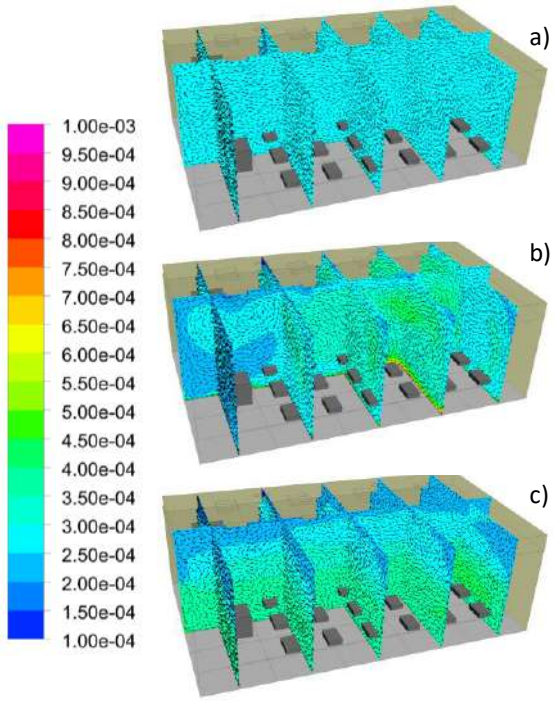

Fig. 7 The concentration characteristics with the floor emission after 12 hours of minimum night-time ventilation: a) the underheated supply air, b) the isothermal supply air and c) the overheated supply air.

The concentration range was larger with the isothermal supply air. The increased concentration levels were obtained beyond the supply airflow region, on the other side of the room. However, near the supply airflow, the concentration was at a low level. This is because the isothermal supply caused a rotating airflow pattern in the cross-section of the room, from the supply air device to the opposite wall side, affecting the concentration levels in this side of the room.

However, the highest concentration levels in the occupied zone were achieved with the overheated supply air because the warm air flows up to the ceiling zone and does not mix well with the indoor air. Consequently, the largest concentration range was achieved with the overheated supply air, while the smallest one was obtained with the underheated supply air.

3.3 location of pollutant source

Fig. 8 shows the pollutant concentration characteristics from the floor emission after the 12 hours of minimum night-time ventilation. The figure shows the volumes where the dimensionless concentration level was greater than 3E-4. The volumes show conveniently the differences between each test case.

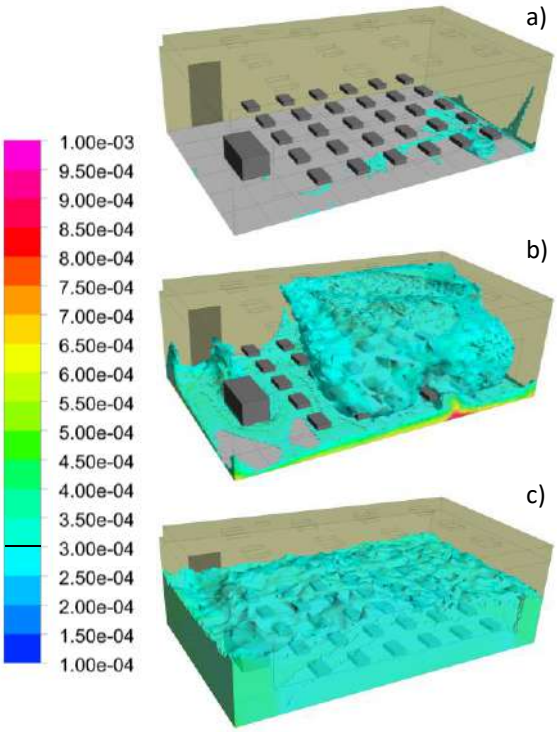

Fig. 8 The pollutant concentration (above 3E-4) with the floor emission after the 12 hours of minimum night-time ventilation: a) the underheated supply air, b) the isothermal supply air and c) the overheated supply air.

The results show that the underheated supply air provided the lowest concentration levels to the indoor air whereas the largest concentration levels occurred with the overheated supply air that was emphasizing the corners.

Fig. 9 shows the concentration characteristics from the wall emission. At the wall pollutant source (16.8 m^2), the underheated supply air increased the pollutant concentrations in the ceiling zone, while with the overheated supply air, the concentrations in the occupied zone increased. With the isothermal supply air, the increased concentration levels were more equally created beyond the supply airflow region, on the other side of the room.

The results reveal that the underheated supply is a reasonable choice when limiting the night-time concentration levels in the occupied zone before the day-ventilation is started.

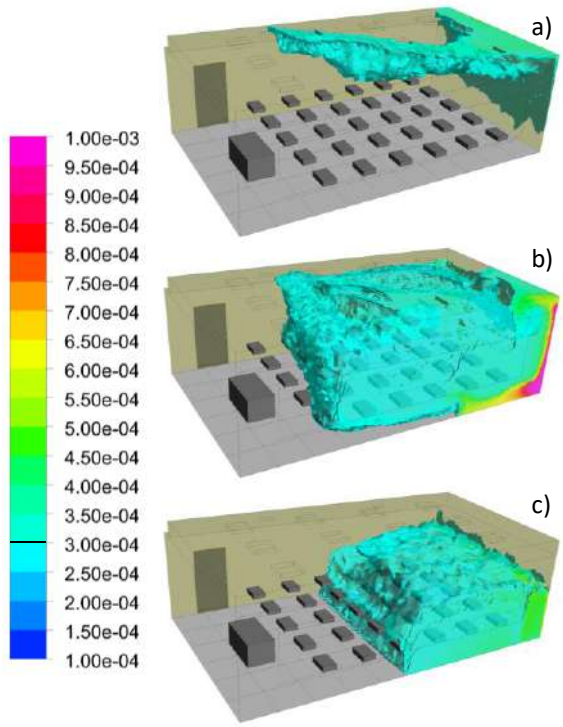

Fig. 9 The pollutant concentration (above 3E-4) with the wall-emission after the 12 hours of minimum night-time ventilation: a) the underheated supply air, b) the isothermal supply air and c) the overheated supply air.

Fig. 10 shows the concentration characteristics from the floor corner emission. With the underheated supply air, the high concentration levels existed near the corner and in the roof zone towards the supply airflow device. With the isothermal supply air, the increased concentration area became narrower than in the case of wall pollution source. With the overheated supply air, the increased concentration region occurred in the source corner side of the room. The concentration gradients increased greater towards the source than in the case of the wall pollutant source or the floor pollutant source.

The results indicate that the smallest concentration field was reached by using the underheated supply air due to better mixing of indoor air, while the concentration range increased with the isothermal and the overheated supply air. With the corner source, the isothermal supply air provided the largest low concentration region in the backside of the room. This was because the supply air was distributed from the pollutant corner side, and therefore, preventing the pollutants to spread so much to the other side of the room. By using the overheated supply air, the corresponding low concentration area existed in the roof zone.

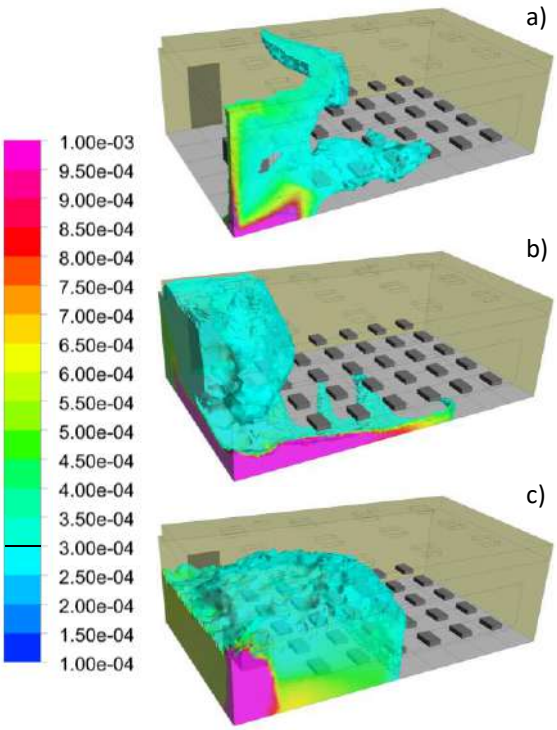

Fig. 10 The pollutant concentration (above 3E-4) with the floor-corner emission after the 12 hours of minimum night-time ventilation: a) the underheated supply air, b) the isothermal supply air and c) the overheated supply air.

The results show that the location of the pollutant source and its surface area affect the pollutant concentration characteristics. All the sources had the same emission rate in the room [mg/s], and therefore, the emission flux was the greatest in the floor corner ($1m^2$) and the lowest in the floor source ($60m^2$) [mg/s, m^2]. It follows that the highest concentration gradients exist near the smallest pollutant source and the smallest gradients near the largest pollutant sources due to those flux differences.

4. Discussion

Night-time ventilation is typically used to increase indoor air quality before space usage in public buildings. The study investigated the effects of supply air temperature and location of pollutant sources on the concentration characteristics of the school classroom by using the minimum level of night-time ventilation. Generally, the minimum level means the low ventilation airflows, and as a consequence, the supplied air jets are not behaving similarly than that of the day-time ventilation ones. Furthermore, the results showed clearly that the supply air temperature matters because the buoyancy forces accelerate the underheated supply air to the floor level and the overheated supply air to the ceiling zone. The overall conclusion is that the night-time ventilation may fasten a threshold time before the space usage in the mornings. In addition, night-time ventilation should be used with low supply air temperature levels. However, these results support the general 2-hour ventilation criterion before space use.

CFD-simulations showed that although the airflow rate is low, the night-time ventilation has an effect on the indoor airflow field. The underheated supply airflows dilute and mix with the surrounding air by decreasing the pollutant concentrations in the occupied zone. Consequently, the concentration levels were lower than that of the isothermal supply airflow or the overheated supply airflow. However, the isothermal supply airflow may prevent the pollutants to spread to the other side of the room. This means that even a low airflow may affect the pollutant dispersion in the room. Furthermore, it shows clearly that air distribution matters.

The different locations of pollutant source provided the different concentration characteristics in indoor air. The large floor emission with the lowest emission flux generated the lowest concentration gradients in the occupied zone whereas the smallest corner source with the highest emission flux generated the largest concentration gradients in the occupied zone, especially towards the source. Generally, the location of emission sources had negligible effects on the occupied zone when the low supply air temperature was used, because the indoor air was well-mixed in predictions.

5. Conclusions

The results indicate that the 2-hour criterion of ventilation is sufficient before the space usage. In predictions, the daytime ventilation reduced the pollutant concentrations to one-tenth within an hour.

The underheated supply air provided the lowest concentration levels in the occupied zone because the supplied air flowed down to the floor and diluted and mixed the indoor air in the occupied zone. Therefore, the night-time ventilation should be used with the low supply air temperature.

The overheated supply air was not mixed in the classroom, because the supplied air flowed to the ceiling zone. Therefore, the concentration levels were greatest in the occupied zone with the overheated supply air.

The isothermal supply air provided a circulating airflow pattern that was increasing the concentrations beyond the supplied airflow region.

The location of emission sources had negligible effects on the occupied zone when the low supply air temperature was used.

The spatial concentration differences between the different locations remained quite small with the mixing ventilation during the temporal development.

6. Acknowledgement

The authors acknowledge the Finnish Work Environment Fund, the Aalto University Campus & Real Estate (ACRE), the Senate Properties and the cities of Helsinki, Espoo and Vantaa, for the financial support. The authors wish to acknowledge the Halton Oy for supporting the CFD-model of school classroom.

7. Data access statement

The datasets generated during and/or analysed during the current study are not publicly available because the data are very case-specific and their applicability in other studies is limited, but the authors will make every reasonable effort to publish them in near future.

8. References

[1] Müller D., Kandzia C., Kosonen R., Melikov A.K., Nielsen P.V. Mixing Ventilation, Guide on mixing air distribution design. REHVA, 2013.

[2] CEN European Standard EN 15251:2007. In Indoor Environmental Input Parameters for Design and Assessment of Energy Performance of Buildings Addressing Indoor Air Quality, Thermal Environment, Lighting and Acoustics. European Committee for Standardization. 2007. Brussels, Belgium.

[3] Montgomery, J.F., Storey, S., Bartlett, K. Comparison of the indoor air quality in an office operating with natural or mechanical ventilation using short-term intensive pollutant monitoring. Indoor Built Environ. 2015; 24:777–787.

[4] Chao, C., Hu, J. Development of a dual-mode demand control ventilation strategy for indoor air quality control and energy saving. Build. Environ. 2004; 39:385–397.

[5] Nielsen, P.V., Allard, F., Awbi, H.B., Davidson, L., Schälin, A. Computational fluid dynamics in ventilation design. REHVA Guidebook no 10. 2007. ISBN 2-9600468-9-7.

[6] Chen, Q. Ventilation performance prediction for buildings: A method overview and recent applications. Building and environment, 2009;44(4):848-858.

[7] Li, Y., Nielsen, P.V. CFD and ventilation research. Indoor Air. 2011;21(6):442-453.

[8] Nielsen, P.V. Fifty years of CFD for room air distribution. Building and Environment. 2015;91:78-90.

[9] Ferziger J.H., Peric M. Computational methods for fluid dynamics. 3rd edition, Springer-Verlag. 2002. ISBN 3-540-42074-6.

[10] Mustakallio, P., Kosonen, R. Modelling Indoor Climate in Classroom with Different Air Distribution Methods. In Proceedings of 12th International Conference on Indoor Air Quality and Climate 2011. ISIAQ.

[11] Kosonen, R., Mustakallio, P. Ventilation in classroom: a Case-study of the performance of different air distribution methods. In Proceedings of 10th REHVA World Congress-Clima. 2010.

[12] ANSYS Inc. ANSYS CFX-Solver Theory Guide, release 17.0. 2016. Canonsburg, USA.

[13] Menter F.R., Two-equation eddy-viscosity turbulence models for engineering applications. AIAA-Journal. 1994;32(8):1598-1605.

Impact of night-time ventilation on indoor air quality in kindergartens and schools

Simo Kilpeläinen [a], Sami Lestinen [a], Risto Kosonen [a,b], Maria Valkonen [c], Juha Jokisalo [a]

[a] Department of Mechanical Engineering, Aalto University, Espoo, Finland; simo.kilpelainen@aalto.fi, sami.lestinen@aalto.fi, risto.kosonen@aalto.fi, juha.jokisalo@aalto.fi

[b] Department of HVAC, Nanjing Tech University, Nanjing, China

[c] Department of Health Security, Finnish Institute for Health and Welfare (THL), Kuopio, Finland; maria.valkonen@thl.fi

Abstract. In Finland, the public sector employs about 30% of the total employment and the building users include just under a million children and students. Therefore, a good indoor climate in public buildings and the proper use of ventilation systems are important. Night ventilation is commonly used to improve indoor air quality in educational buildings before the premises are used. A typical use has been to turn off the ventilation after using the facilities and restart it about 2 hours before reusing those facilities. Another option is to keep night ventilation running at minimum ventilation. The third option is to use night ventilation intermittently. Although current technology allows ventilation systems to be monitored and controlled using air temperature, carbon dioxide, and presence sensors, it is very common to keep ventilation units running continuously, even if it significantly increases the energy consumption of ventilation. In this study, the pre-started, continuous, and intermittent ventilation strategies were compared by assessing indoor air quality in field measurements during different seasons in 2019 and 2020. The daytime ventilation was kept as usual. Each test period lasted for 2 weeks. Indoor air quality was assessed by measuring TVOC with the metal oxide semiconductor method and microbes by using the quantitative PCR method. Also, CO2, pressure over building envelope, and thermal conditions were measured. The results indicate that the average TVOC concentrations were similar during mornings with all the ventilation strategies. TVOC concentrations were higher during the day than at night. This indicates that the use of the facilities had the greatest effect on TVOC concentrations. The microbial concentration was usually only a few percent of the corresponding outdoor air concentration. The used strategy of night ventilation did not have a systematic effect on indoor microbial concentrations.
In general, the natural variation of the measured physical quantities was greater during the test periods than could be observed with different night ventilation operating strategies. The working conditions at the measured buildings were at normal levels. The results show that 2 hours of ventilation before the premises are used is sufficient, and thus continuous ventilation at night is not necessary.

Keywords. Night ventilation, pollutant sources, indoor air quality, kindergarten, school
DOI: https://doi.org/10.34641/clima.2022.288

1. Introduction

Poor indoor air quality in schools and kindergartens has been widely reported in research literature [1-4], and it is often connected to difficulties in learning [5-7]. To improve the situation, ventilation use patterns have been altered in public buildings. The European standard 16798-1:2019 recommends that the ventilation system is pre-started before space usage or is run continuously at a minimum power during unoccupied times to ensure that there are no contaminants present when the space usage begins.

In Nordic countries, this recommendation has been applied in three ways. One method has been to stop the ventilation when the building is not in use and pre-start it two hours before the occupied periods. Another common method has been to run the fans at partial power during unoccupied periods to ensure the removal of contaminants. Finally, a third strategy has been to intermittently ventilate the spaces during unoccupied periods by running the fans for an hour or two.

While it is well-known that insufficient ventilation during unoccupied time can lead to accumulation of contaminants originating from building materials and furniture [8-9], the effects of different night-time ventilation strategies have not been studied. There have been concerns from the public that if the fans are not run continuously, contaminant concentrations and humidity in the spaces could reach alarming levels during occupied hours. Continuous operation of ventilation systems, however, considerably increases the building energy consumption and thus is not a preferable strategy unless ensuring sufficient indoor air quality demands it.

The purpose of this study was to fill the knowledge gap on how different night-time ventilation

Copyright ©2022 by the authors. This conference paper is published under a CC-BY-4.0 license.

strategies affect the indoor air quality. To assess this, field measurements were conducted in educational buildings. Interventions applying the three common night-time ventilation strategies were conducted in the buildings, and total volatile organic compound (TVOC) and microbial concentrations were measured. None of the case buildings had reported indoor air quality or thermal problems and all were in normal use during the study. The objective was to find out the optimal ventilation strategy which ensures good indoor air quality during occupied hours without unnecessarily increasing energy consumption. The comprehensive results of the study have been published in [10] and this paper rep the main findings.

2. Research methods

2.1 Case buildings

The measurements were conducted in 11 educational buildings in southern Finland during different seasons in 2019 and 2020. Five of the buildings were kindergartens, five schools and one a university building. Six buildings had a constant air volume (CAV) and five a variable air volume (VAV) ventilation system. The building use and ventilation were normal during the occupied hours, and during unoccupied hours three different ventilation strategies were applied: pre-started, continuous, and intermittent.

2.2 Measurements

The main measured quantities were TVOC and microbial concentrations. TVOC was continuously monitored whereas biological samples were gathered throughout each two-week intervention and collected at the end. In addition, CO_2 concentrations, thermal conditions, and pressure differences over the building envelope (where applicable) were measured.

TVOC concentration was measured with a Nuvap N1 IEQ monitor. The N1 deploys a metal oxide semiconductor (MOS) sensor to measure the organic compounds and the sampling is done three to four times per hour. Thermal conditions were monitored with TinyTag plus 2 TGP-4500 loggers and another type of TinyTag (TGE-0011) was used to capture the CO_2 concentrations. A cloud-based solution equipped with Sensirion SDP816 differential pressure probes was used to monitor the pressure differences over building envelope. An overview of the instruments is shown in Table 1.

Tab. 1 – Sensors used in the measurements.

Sensor	Measured Quantity	Accuracy
Sensirion SDP816	diff. pressure	±3% / ±0.08 Pa
TinyTag TGP-4500	T / RH	±0.5°C / ±3% RH
TinyTag TGE-0011	CO_2	±3% / ±50 ppm
Nuvap N1	TVOC	±15%

To study the biological contaminants, settled dust samples were collected from indoors and outdoors on eight petri dishes adjacent to each other. The dishes inside were placed on shelves at a height of 2-2.5 m, and the outside ones were put in an open plastic box sheltered from rain and wind. The quantitative polymerase chain reaction (qPCR) technique was used to determine the micro-organisms present in the samples. The collection period for each sample was two weeks after which they were sent to the Finnish Institute for Health and Welfare (THL) laboratory in Kuopio, Finland for storage and analysis.

As the analysis for all the biological samples was done in one batch, the samples had to be stored prior to it. The samples were prepared for seven days following the arrival in the laboratory. The dust in each collector was swiped into a cotton swab moistened with a dilution solution (sterilized water + 0.05% Tween 20). After this, the swabs were put into tubes containing glass beads to prepare for DNA isolation. Blanks were inserted every 20 samples as a control measure. All the samples were then stored at -80°C.

The DNA isolation was done with a DNA Chemagic DNA plant kit (Perkin Elmer, Germany) according to manufacturer instructions with a KingFisher insulation robot (ThermoFisher, Finland). Salmon sperm DNA (Sigma-Aldrich, USA) was added to the samples as an internal standard prior to isolation. The samples and the glass beads were milled in a bead mill to disrupt the microbial cell walls before the DNA extraction. The extracted DNA was then stored at -20°C before the qPCR analysis was performed.

The actual analysis was done with the qPCR method using assays for three different groups: unifung [11], *Penicillium, Aspergillus* and *Paecilomyces* group [12], and Gram-positive/Gram-negative bacteria [13]. For sample pipetting a Piro pipetting robot (Dornier, Germany) was used, and the analysis was done on a Stratagene Mx3005P qPCR system (Agilent, USA). The salmon sperm DNA along with positive and negative controls for both bacterial and fungal assays were used to ensure the quality of the analysis. The results were calculated according to [12] and reported as cell equivalent per square meter per day ($CE/m^2 \cdot d$).

3. Results

3.1 TVOC

Figure 1 shows the TVOC concentration during morning hours in two of the case buildings (one school, one kindergarten). As can be seen from the figure, there were clear differences in TVOC concentrations between the three night-time

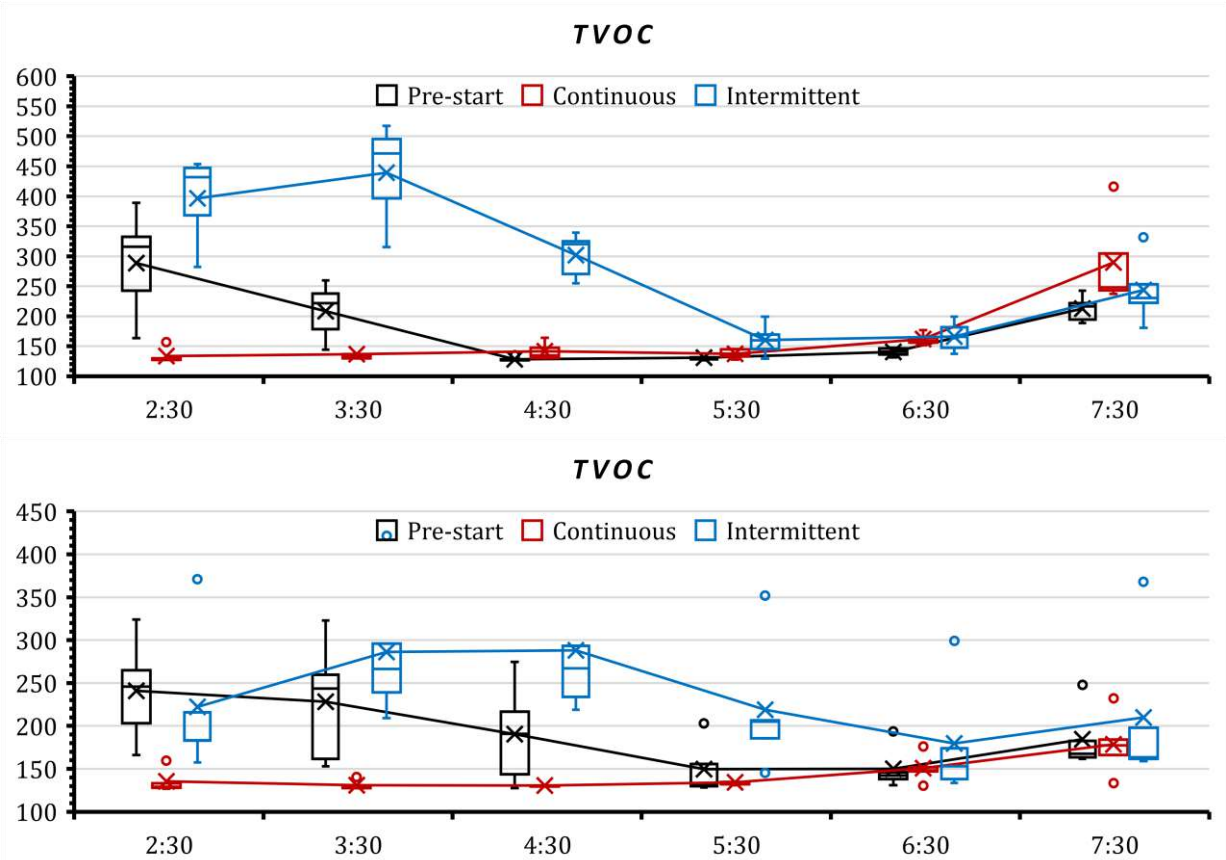

Fig. 1 – TVOC concentration [ppb] during weekday mornings in one of the kindergartens (a) and schools (b). The lines follow the average concentration. [10]

ventilation strategies during the night. As expected, the levels were lowest with continuous ventilation.

T[illegible] ghest levels were found with intermittent v[illegible]tion. This is most likely due to internal pressure differences between ventilation system service areas as the interventions were only applied to one area and the others were operating normally. In the morning when the occupied time began, the TVOC levels were very similar with all three strategies, leading to the conclusion that night-time ventilation does not have a large role in TVOC concentrations during mornings, if the ventilation is started two hours before space use begins. Similar results were obtained from the other case buildings not shown here.

The occupied time TVOC concentrations for one c[illegible]uilding (a school) are depicted in Figure 2 along with the CO_2 concentration which is used to assess occupancy. Similar trends were visible with the other case buildings as well. The peaks in TVOC coincide with those of CO_2, showing that most VOCs originate from the space use. It is also worth noting that the TVOC levels during daytime are similar regardless of the night-time ventilation strategies so night-time ventilation does not have a major role in daytime TVOC concentrations either.

3.2 Microbes

The indoor/outdoor ratios for three of the

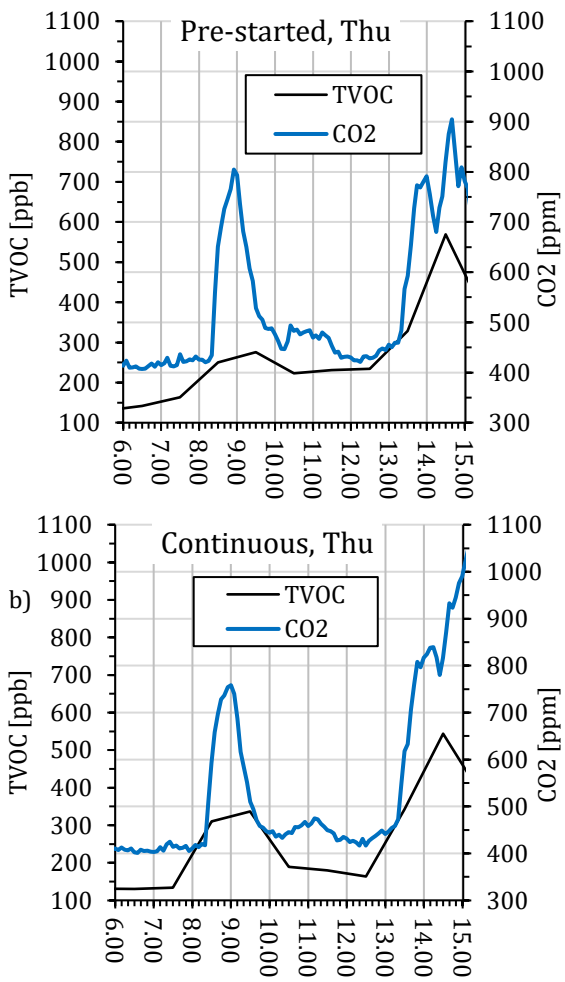

a)

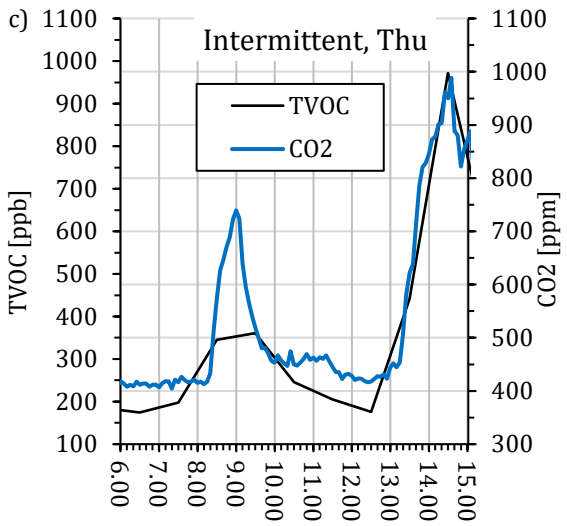

Fig. 2 – TVOC and CO_2 concentrations during a Thursday morning in a school for (a) pre-started, (b) continuous, and (c) intermittent night-time ventilation operation modes.

measured groups (Unifung, Pen./Asp., and Gramneg,) are shown in Figure 3 for one school and one kindergarten. Grampositive bacteria were omitted from this analysis due to outdoor samples having issues, most likely due to inhibiting organic material such as pollen. The ratios were generally very small for most of the groups regardless of the night-time ventilation strategy, and rarely exceeded 10%. This is normal and can be explained by filtration of the supply air. From the data it can be deduced that none of the applied night-time ventilation strategies had a systematic effect on the

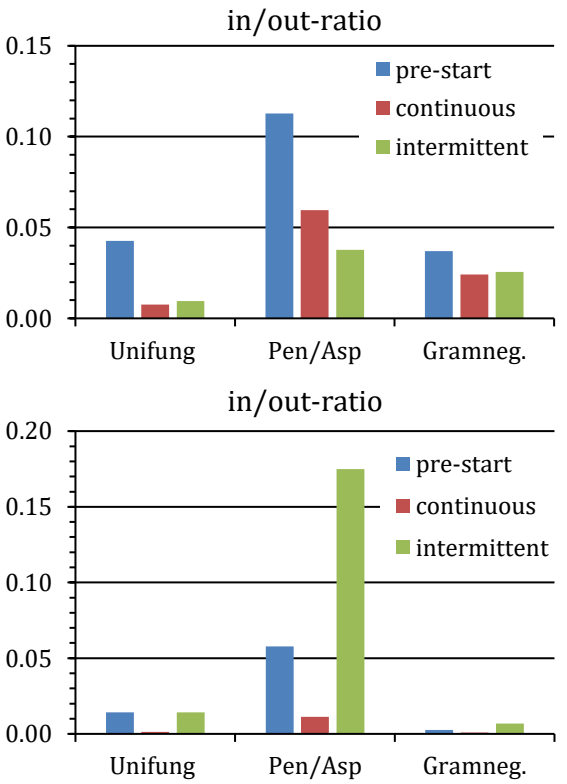

Fig. 3 – Indoor/outdoor ratios of the microbial content in the collected dust samples for one kindergarten (a) and one school (b).

indoor/outdoor ratios of any of the analyzed groups.

Overall microbial content for indoor samples divided by groups can be found in Figure 4. This data is a combination from two schools, three kindergartens and the university building. The unifung fungal group and both bacterial groups (grampus., gramneg.) behaved similarly with the contents being highest with pre-started ventilation and lowest with intermittent. The mold group (Pen./Asp.) expressed different behavior and with that the intermittent night-time ventilation was giving the highest values and pre-started the lowest.

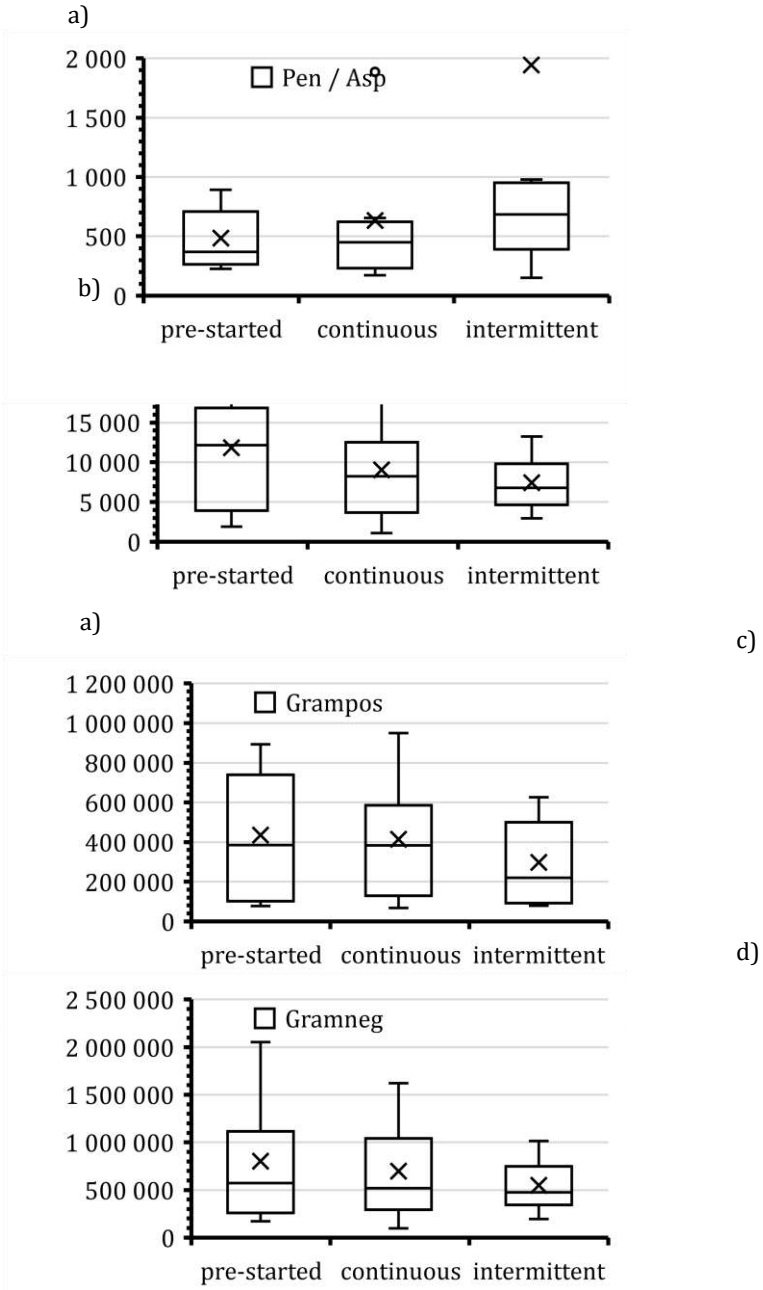

Fig. 4 – Microbial content [CE/m²·d] of indoor dust samples by group: Unifung (a), Pen / Asp (b), Grampos (c), and Gramneg (d). The sample includes three kindergartens, two schools and a university building.

4. Conclusions

In this study, three different night-time ventilation strategies (pre-started, continuous, and intermittent) were compared by making interventions at field sites and assessing the indoor air quality. The main motivation of the study was to assess how different night-time ventilation strategies affect the indoor air quality during occupied times and especially in the mornings. The measurements were conducted in different seasons in 2019 and 2020. The results showed that most pollutants originate from daytime activities in the buildings, and the effect of night-time ventilation on TVOC and microbial concentrations was minimal if the ventilation was pre-started two hours prior to occupied time. Hence, the hypothesis of having to run the ventilation continuously throughout the night to ensure good indoor air quality was proven wrong. The differences seen in the measured quantities between the three night-time ventilation strategies were smaller than that of normal variation produced by differences in space use and seasonal weather conditions.

5. Acknowledgements

This study was a part of the "Effect of ventilation schedules on working conditions and indoor air quality in public buildings" project funded by the Finnish Work Environment Fund. The authors acknowledge the Finnish Work Environment Fund, Aalto University Campus & Real Estate (ACRE), the Senate Properties, and the cities of Helsinki, Espoo, and Vantaa for the financial support. The authors would like to thank Research Analyst Heli Martikainen from the Finnish Institute for Health and Welfare for the laboratory analyses of microbiological samples.

6. Data access

The datasets generated during and/or analysed during the current study were not made publicly available because the data are very case-specific and their applicability in other studies is limited. However, the data are available from the authors upon request.

7. References

[1] Wargocki P., Sundell J., Bischof W., Brundrett G., Fanger P.O., Gyntelberg F., et al. Ventilation and health in non-industrial indoor environments: Report from a European Multidisciplinary Scientific Consensus Meeting (EUROVEN). Indoor Air. 2002;12:113-128.

[2] Daisey J.M., Angell W.J., Apte M.G. Indoor air quality, ventilation and health symptoms in schools: An analysis of existing information. Indoor Air. 2003;13:53-64.

[3] Mendell M.J., Heath G.A. Do indoor pollutants and thermal conditions in schools influence student performance? A critical review of the literature. Indoor Air. 2005;15:27-52.

[4] Chatzidiakou L., Mumovic D., Summerfield A.J. What do we know about indoor air quality in school classrooms? A critical review of the literature. Intell. Build. Int. 2012;4:228-259.

[5] Haverinen-Shaughnessy U., Shaughnessy R.J., Cole E.C., Toyinbo O., Moschandreas D.J. An assessment of indoor environmental quality in schools and its association with health and performance. Build. Environ. 2015;93:35-40.

[6] Wargocki P., Wyon D.P. The effects of outdoor air supply rate and supply air filter conditions in classrooms on the performance of schoolwork by children. HVAC&R Res. 2007;13:165-191.

[7] Bakó-Biró Z., Clements-Croome D., Kochhar N., Awbi H., Williams M. Ventilation rates in schools and pupils' performance. Build. Environ. 2012;48:215-223.

[8] Montgomery J.F., Storey S., Bartlett K. Comparison of the indoor air quality in an office operating with natural or mechanical ventilation using short-term intensive pollutant monitoring. Indoor Built Environ. 2015;24:777-787.

[9] Chao C., Hu J. Development of a dual-mode demand control ventilation strategy for indoor air quality control and energy saving. Build. Environ. 2004;39:385-397.

[10] Lestinen S., Kilpeläinen S., Kosonen R., Valkonen M., Jokisalo J., Pasanen, P. Effects of Night Ventilation on Indoor Air Quality in Educational Buildings – A Field Study. Appl. Sci. 2021;11:4056-4075.

[11] Haugland R., Vesper S.U.S. Identification and Quantification of Specific Fungi and Bacteria. U.S. Patent Patent No. 6,387,652. 2002, 5, 14.

[12] Haugland, R.A., Varma, M., Wymer L.J., Vesper S.J. Quantitative PCR Analysis of Selected Aspergillus, Penicillium and Paecilomyces Species. Syst. Appl. Microbiol. 2004;27:198-210.

[13] Kärkkäinen P.M., Valkonen M., Hyvärinen A., Nevalainen A., Rintala H. Determination of bacterial load in house dust using qPCR, chemical markers and culture. J. Environ. Monit. 2010;12:759-768.

The relation between occupant's mood state and thermal sensation

Cihan Turhan [a], Neşe Alkan [b], Aydın Ege Çeter [c], Mehmet Furkan Özbey [c,d]

[a] Energy Systems Engineering Department, Atılım University, Ankara, Turkey, cihan.turhan@atilim.edu.tr

[b] Department of Psychology, Atılım University, Ankara, Turkey, nese.alkan@atilim.edu.tr

[c] Graduate School of Nature and Applied Sciences, Atılım University, Ankara, Turkey, aege.ceter@gmail.com, m.furkanozbey@gmail.com

[d] Mechanical Engineering Department, Atılım University, Ankara, Turkey, m.furkanozbey@gmail.com

Abstract. Thermal comfort is mainly evaluated by the Fanger's Predicted Mean Vote/Predicted Percentage of Dissatisfied (PMV/PPD) method and adaptive thermal comfort approaches. PMV/PPD method takes four environmental (such as indoor air temperature, relative humidity, mean radiant temperature and air velocity) and two personal parameters (basic clothing insulation and metabolic rate) into account for calculations. On the other hand, adaptive approach adds human behaviours to the thermal comfort models. However, none of these models includes the effect of the mood state of the occupants on thermal sensation. To this aim, this study investigates the relationship between occupant's mood state and thermal sensation as a case study. Pre-test-Post-test Control (PPC) experimental design is conducted on the students in a university study hall in Turkey. Profile of Mood States (POMS) is used to examine the effect of mood state on the thermal sensation while the Actual Mean Vote (AMV) is obtained via developed mobile application. Simultaneously, the PMV is calculated in order to obtain the difference from the AMV. The results showed that there is a strong relationship between the mood state and thermal sensation. The outcome of this study would enlighten the HVAC engineers and specialists in order to understand the gap between PMV and AMV caused by the mood state.

Keywords. Profile of Mood States, Thermal Sensation, Psychology
DOI: https://doi.org/10.34641/clima.2022.261

1. Introduction

Thermal comfort mainly depends on four environmental parameters such as indoor air temperature (T_i), relative humidity (RH_i), mean radiant temperature (T_r) and air velocity (v_a) and two personal parameters as basic clothing insulation (I_{cl}) and metabolic rate (met) [1]. International standards such as ASHRAE 55 [2] and ISO 7730 [3] still use Fanger's Predicted Mean Vote/Predicted Percentage of Dissatisfied (PMV/PPD) method as thermal comfort index [1]. The method uses the parameters above and runs seven-point thermal comfort scale from -3 (represents very cold scale) to +3 (represents very hot scale). In addition, zero (0) PMV value claims that the occupant is fully comfortable in a given environment. In other words, neutral thermal comfort, not thermal sensation, is obtained in an environment. Considering the definition of the thermal comfort in the ASHRAE 55 [2], as "*the condition of mind that expresses satisfaction with the thermal environment and is assessed by subjective evaluation*", it is obvious that thermal sensation not only depends on physiological parameters but also psychological ones. The side of the "State of the Mind" in the definition should be explained in detail. Recent studies showed that thermal sensation also depends on psychology, stress levels, culture and climate adaptation etc. [4-8]. For instance, Rohles [5] conducted an experiment with two different occupants in two different rooms with the same architectural configuration. However, there was a heater in one of the rooms and no heater was existed in another, however, both occupants were informed by the researchers as there was a heater in the room. According to the outcomes of the study, both occupants stated that they felt warm in the room. In another study by Turhan and Özbey [8], the effect of one of the psychological parameters; stress level was investigated on the thermal sensation of students. The authors stated that there was a strong relationship between the stress level and thermal sensation. Similar to the Turhan and

Copyright ©2022 by the authors. This conference paper is published under a CC-BY-4.0 license.

Özbey's study [8], Jones [9] considered that absence of psychological variables in thermal comfort models caused the gap between measured and actual thermal comfort since thermal sensation was highly related to the psychological variables as well as physical parameters. The effect of the psychological parameters especially increases in unconditioned or mixed-mode buildings. For instance, Singh et al. [10] concluded that the reason of the gap between thermal comfort and sensation was psychological parameters in unconditioned buildings.

Mood state is one of the affective states in psychology field [11]. For instance, Muller et al. [12] stated that in cold environments, occupants felt negative mood states and as a conclusion, were triggered to alter their human cognition, daily activities and wellbeing. Ibrahim et al. [13] conducted virtual settings-based experiments to investigate the effect of mood states on human evaluation of the thermal environment. The participants were requested to use the PANAS-X pre-mood test [14] before watching a video that targeted eliciting predetermined mood states: anger and happiness. By using linear models, the researchers concluded that happy and angry occupants voted different thermal sensation scale in the same environment. However, none of the studies included all of the mood states as a psychological rating scale used to assess transient and distinct mood states. The experiments in a real and living buildings are essential.

This study aims to investigate the relationship between occupant's mood state and thermal sensation with experiments conducted in a university study hall in Turkey.

2. Materials and Methods

The method of the study includes objective measurements, such as PMV, T_i, RH_i and T_r, and subjective measurements from online surveys in order to learn basic clothing insulation (I_{cl}) value, thermal preferences (AMV) and Profile of Mood States (POMS) score of the occupants.

2.1 design of experiments

The experiments are conducted in a Turkish university study hall in Csb climate zone according to the Köppen Geiger Climate classification [15]. The total capacity of the study hall is 912 occupants, however, the experiments are conducted in a 10 m^2 zone of the total zone (Fig.1). The average outdoor temperatures for the building location is -3.3°C and 14°C for winter and summer seasons, respectively [16]. In the building, there is no mechanical ventilation in the hall while the heating is obtained by four radiators with a fixed 22°C set-temperature value of each. Moreover, there is no mechanical system for cooling, thereby, the occupants prefer to open the doors for fresh air and cooling purposes.

A hundred two apparently healthy and normotensive male and female occupants are included in the study. As an example, Table 1 depicts the main characteristics of the occupants included in the experimental and control group. For the experiments, the study hall is used by students, researchers and academicians during experiments between 15th of July, 2021 and 1st of November, 2021. Occupants are selected from different majors such as Engineering, Architecture, Psychology and Fine Arts. Pre- and Post- Control (PPC) tests are conducted in the experiments. For this reason, the students are split into two equal groups (control and experimental groups). The experiments are conducted before and after activities. A total of 102 occupants is attended to the study. As a first step, permissions are taken from the Ethics Committee of the University and the occupants are informed of the aim and experimental procedures.

Tab. 1 - Main characteristics of the occupants in experimental and control groups.

Experimental Group			
Gender	Average Age	Age Range	Total Number
Male	24.1	18-67	35
Female	22.8	18-54	16
Total	23.5	18-67	51
Control Group			
Male	24.2	18-67	35
Female	22.6	18-54	16
Total	23.6	18-67	51

Then, the occupants are requested to rest for thirty minutes since high metabolic rates after arriving the study hall could affect their thermal sensations and mood states. Likewise, the authors ensure that the occupants never take caffeine based drinks and alcohol before the experiments by interview method. In the study, experiments are conducted on pre-and post- periods with one-hour time interval (Fig.1).

Fig. 1 - Snapshot of pre-and post-experiments.

The occupants are requested to use mobile application while environmental parameters are measured by objective sensors. The environmental parameters to be measured are chosen as PMV, T_i, T_o, RH_i, RH_o and T_r. All measurement devices are placed at 1.1 m above the ground. The list of measurement devices and their specifications are given in Table 2. The measurements are taken with 1-minute interval during experiments.

Tab. 2 – Measurement devices and specifications

Device	Model	Aim of the usage	Specifications
Thermal Comfort Sensor	Delta Ohm [17]	PMV, T_i,RH_i, T_r	Measuring range: -10-100 °C. Accuracy: ±0.1°C Resolution: 0.1°C
Temperature and Relative Humidity Sensor	Onset HOBO [18]	T_o and RH_o	Measuring range: −40-80°C Accuracy: <±0.5°C Resolution: 0.1°C

For the experiments such as obtaining mood state and/or thermal sensation, occupants should not be in close contact with other occupants since the mood state can be affected by occupants that stay close. For this reason, the experimental zone is isolated from the other occupants. On the other hand, occupants in control group do not study any major, instead, they are requested to read their favourite books with underlining the all sentences of the book. The reason of underlining sentences is to obtain same metabolic rate with experimental group. On the other hand, occupants in experimental group study their majors.

Finally, the metabolic rate of the students are assumed as 1.1 met regarding to seated-typing (65 W/m^2) position [2].

2.2 assessing mood state of occupants

In the study, Profile of Mood States (POMS) test is used to assess mood state of the occupants. The POMS test is a self-reported questionnaire in order to obtain mood state of the occupants developed by McNair et al [19]. The test includes 65 mood states which load on six different sub- scales such as depression, anxiety, fatigue, vigour, tension, and confusion. Total Mood Disturbance (TMD) is calculated by subtracting positive feelings from negative feelings. Negative feelings include the sum of the scores of Tension-Anxiety (TA), Anger-Hostility (AH), Depression-Dejection (DD), Fatigue-Inertia (FI), and Confusion-Bewilderment (CB), while the positive feeling is only represented by Vigor-Activity (VIG). After finding the value of the raw scores of the TMD, they are converted into normalized T-scores [19] with a mean equal to 50 and a standard deviation equal to 10 [20,21] by equation 1.

$$T - Score = 50 + \frac{10\times(n-m)}{s} \quad (1)$$

Here, n represents the raw scores, m defines the mean, and s is the standard deviation [19, 22]. Increasing T-score could indicate a worsening of the mood. More information on the usage of the POMS in thermal comfort field can be found in [8]. One-tailed *t-test* is used in order to understand the relationship between mood state and thermal sensation. Experiments are conducted to verify null hypothesis (H0: $\tau i = 0$) below;

"There are no positive and significant relationships between mood state and thermal sensation".

The hypothesis is analyzed for occupants at a 5% significance level ($\alpha = 0.05$). The null hypothesis is assumed to be rejected if p-value is found to be lower than 0.05. Alongside the statistical tests, it is also worth to analyze effect size (d_{ppc}), which interprets practical significance, in order to assess the size of differences between experimental group and control group for repeated experiments. Detail information on the calculation of effect size is given in [8, 23, 24]. The SPSS statistical computer package is used to analyze the results [25].

2.3 development of mobile application

A mobile application is developed for smartphones and tablet computers to obtain subjective values such as AMV, mood state score and basic clothing insulation value. Four interfaces are developed for the study. In first interface, main characteristics (gender, nationality, weight and height etc.) of the occupants are asked while garments are simultaneously asked in order to calculate "clo" value of the occupants in the second interface. The occupants are requested to pick their garments in the list developed from the ASHRAE 55 clothing list [2]. Thus, the mobile application easily calculates basic clothing insulation value of the occupant. In third interface, the POMS test asks positive and negative feelings of the occupants by referring a scale where "0 star" means "not at all" and "5 stars" means "extremely". In final interface, the occupant is asked to fill the AMV section by selecting their thermal preferences from the ASHRAE 7-point scale which runs between cold (−3) and hot (+3). The collected data are then stored in a web-server. An example screenshot of the developed mobile application is depicted in Fig.2.

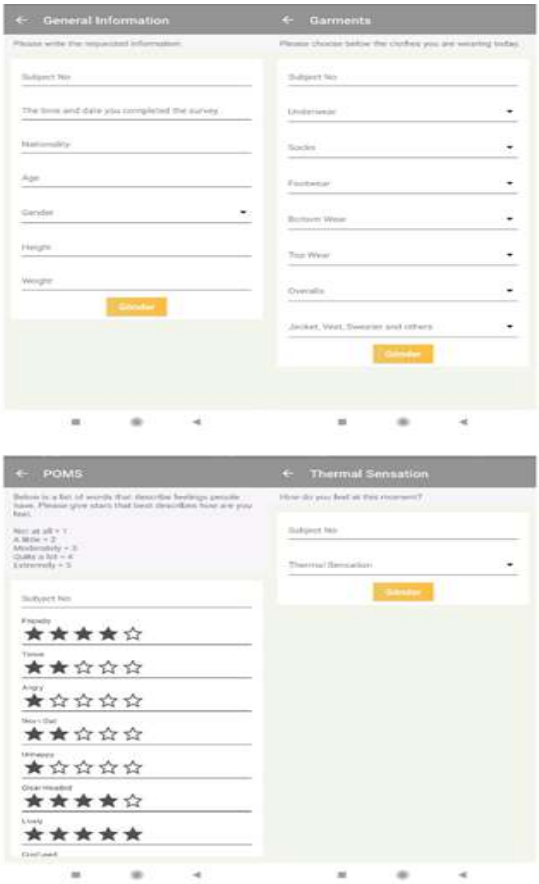

Fig. 2 – Example screenshot of the developed mobile application

3. Results and Discussions

The environmental parameters are measured during pre- and post- experiments and the results are depicted in Table 2.

Tab. 2 – The results of objective measurements during experiments

parameter	Average	SD
PMV	-0.47	0.38
T_i	23.8	2.4
T_o	24.1	4.6
RH_i	35.8	10.4
RH_o	30.9	10.1
T_r	23.9	2.1

The average PMV values are measured as -0.47 on the cooler side. Moreover, average indoor air temperature is obtained as 23.8°C. It is worth to remind that there are minor temperature and relative humidity differences between pre- and post-test experiments. However, this difference can be neglected in the study.

Fig.3 depicts the sub-scales of the POMS items on abscissa for both groups while their T-scores are represented on y-axis. The figure clearly indicates that T-scores of the negative mood states (TA+AH+DD+FI+CB) of the control groups are lower than the experimental groups for post-test results. In addition, positive mood states (VIG) of the experimental group are lower than control group. This result indicates that studying a major increases stress level as a conclusion of increasing negative mood states. On the other hand, total score of the positive mood states are declining while studying a major in a study hall. Total T-score of the experimental group is found as 52.7 and 68.4 for pre-and post-tests, respectively. The result shows that negative mood states are dominant compared to positive mood states for post-test data. Similarly, one can compare the pre- and post- tests results of control group. The figure depicts that total T-score of the control group does not differ for pre-and post- tests data. This result concludes that mood state of the control group does not change while the mood state of the experimental group worsens.

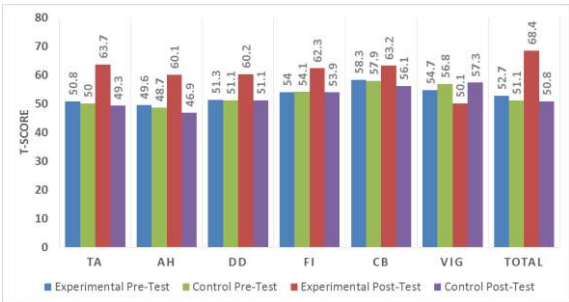

Fig. 3 – Pre- and Post- Tests T-scores for control and experimental groups

Table 3 represents the evaluation of the T-scores in POMS between control and experimental groups. There are no significant difference between two groups on the pre-test experiments. On the other hand, statistical results conclude that there are some significant differences between the control and experimental groups in the T-score of the POMS for the post-test. It is found that total T-score of the mood state is significant at 1% level, while other sub-scales are found to be significant at 5% level.

Tab. 3 –Scores of Profile of Mood States (POMS) in the control and experimental groups

Control versus Experimental groups				
Pre-Test	T-score	t-value	p-value	significance
TA	50±3	0.91	0.18	(-)
AH	49±4	0.80	0.21	(-)
DD	51±2	0.86	0.19	(-)
FI	54±3	0.61	0.27	(-)
CB	58±2	0.41	0.35	(-)
VIG	56±4	0.26	0.41	(-)
Total	51±3	1.21	0.11	(-)
Post-Test	T-score	t-value	p-value	significance
TA	61±4	1.91	0.03	**
AH	58±4	2.16	0.02	**
DD	56±3	2.17	0.02	**
FI	58±2	1.89	0.03	**
CB	60±1	1.91	0.03	**
VIG	54±2	1.93	0.03	**
Total	63±2	3.11	0.003	***

Note: *** = significance at 1%, ** = significance at 5%, (-) is considered as not significant

3.1 correlations of POMS score with AMV

Correlations of mood state with thermal sensation are summarized in Table 4. Pre-test and Post-test data of experimental group are used together in the correlation. The results represent that the AMV is highly correlated with the total T-score of the POMS (R^2 of 0.87). Furthermore, the parameter is found to be significant in 1%. Similarly, subscales of the POMS test including TA, AH, DD, FI, CB and VIG are correlated with the AMV at 5% interval. However, the effect of the VIG subscale is lower than the others. The reason could be the small variation of the VIG score in the post-test experiments. Studying the majors in a study hall lowers occupant's the VIG score and occupants prefer to be in similar T-score of the VIG. On the other hand, aversive mood states increase for the occupants (Fig.4).

Tab. 4 –Correlations between mood state and the AMV

Experimental group				
AMV	R^2	t-value	p-value	significance
TA	0.81	2.9	0.002	***
AH	0.84	2.9	0.002	***
DD	0.85	3.1	0.001	***
FI	0.79	2.1	0.019	**
CB	0.76	2.1	0.021	**
VIG	0.71	1.9	0.030	**
Total	0.87	3.1	0.001	***

The results also show the difference between the PMV and AMV values related to the mood states changes (Fig.4). For instance, at PMV= -0.4, the AMV of the occupants with the total T-score of 50, is -0.37. However, the occupants with the total T-score of 68 feels warmer (AMV=-0.21) than the normal ones. On the other side, if the positive mood state score increases (left hand-side in the figure), the occupants feel warmer (AMV=-0.32) again. The reason could be overproduction of "Adrenaline" which causes blood pressure increase.

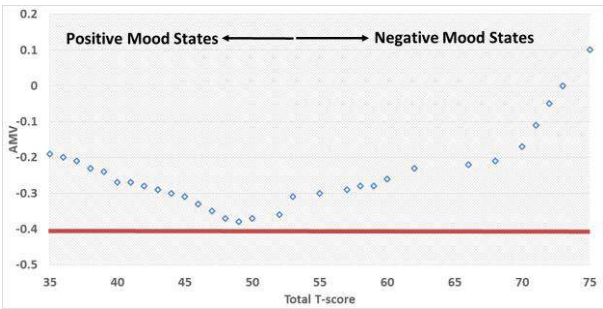

Fig. 4 – The change of the AMV related to mood state of the occupants on the same PMV value of -0.4.

3.2 effect size control

As a supportive analysis, effect size control is conducted for the study since statistical significance could be affected from different population parameters. For pre- and post-test control experiments, it is worth to conduct effect size control which indicates the size of differences between experimental group and control group [23]. The value under 0.2 means small effect, between 0.2 and 0.5 depicts medium effect and values above 0.8 represents large effects. Similar to the statistical results, effect sizes of the parameters show medium and large effects between control and experimental groups. Thereby, the results are considered as consequential.

Tab. 1 – Effect size control results

parameters	d_{ppc}
TA	0.65
AH	0.71
DD	0.86
FI	0.74
CB	0.77
VIG	0.56
Total	1.1

3.3 limitations

This study aims to show the relationship between the mood state of the occupants and thermal sensation. However, some limitations should be considered in the study. The first limitation is the number of the occupants used in the study. Only 102 occupants are participated in pre-and post-test experiments. A fairly large data sets are needed to verify the correlations above.

Moreover, due to the global pandemic of Covid-19, the occupants wear face masks which could affect thermal sensation and even their current mood states. Additionally, clothing insulation of the face mask is neglected in the study. As a further study, the effect of face mask on thermal sensation and mood states will be studied in detail.

Cultural differences may alter the personal selections in the POMS questionnaire and may affect the results directly. Even though, all occupants are selected as Turkish, the occupants may have different cultural background.

In the study, raw scores are subjected to T-score transformations with a standard scale of standard deviation and mean. Even though the results of Turkish occupants in the experiments obey this standard scale with a mean of 50 and a standard deviation of 10, larger data sets should be investigated.

This study is conducted at study hall of engineering department. Thus, female participants are lower than male ones. Female and male occupant size should be equal to verify the correlations.

Some potential moderating parameters such as age and gender could affect the results. However, these differences of T-score depending on gender and age, are not investigated in this study.

4. Conclusions

The relationship between occupant's mood state and thermal sensation is investigated with pre- and post-control experiment design strategy in this study. Statistical analysis results show that the AMV is related to the mood states of the occupants.

The present findings suggest that mood states of the occupants can increase the gap between the PMV and AMV. Thereby, researchers should take psychological parameters such as mood state into account while determining thermal sensation of the occupants.

Future research might investigate normative values of mood states for other specific populations.

5. Acknowledgement

The Scientific and Technological Research Council of Turkey (TÜBİTAK) funded this research and their contribution is gratefully acknowledged (Project Number: 120M890). Moreover, the authors would like to thank all participants for the contribution to this study.

It is worth to note that this study is conducted under the Approval of Ethics Committee of Atılım University as result of meeting on 14.11.2019.

6. References

[1] Fanger, P.O. Thermal Comfort: Analysis and Applications in Environmental Engineering, Danish Technical Press, Copenhagen, 1970.

[2] ASHRAE Standard 55, Thermal Environmental Conditions for Human Occupancy, ASHRAE, Atlanta, Geo., USA, 2017.

[3] ISO 7730:2005 Ergonomics of the thermal environment. Analytical determination and interpretation of thermal comfort using calculation of the PMV and PPD indices and local thermal comfort criteria, CEN, Switzerland, 2005.

[4] de Dear, R. Brager, G.S. Developing an adaptive model of thermal comfort and preference. ASHRAE Trans. 1998:104 (1):1-18.

[5] Rohles, F.H. Temperature & Temperament. A Psychologist Looks at Comfort. ASHRAE February Journal.2017: 14-22.

[6] Nikolopoulou, M., Baker, N., Steemers, K. Thermal comfort in outdoor urban spaces: understanding the human parameter. Solar energy. 2001; 70(3): 227-235.

[7] Zabetian, E., Kheyroddin, R. Comparative evaluation of relationship between psychological adaptations in order to reach thermal comfort and

sense of place in urban spaces. Urban Climate. 2019; 29: 100483.

[8] Turhan, C., Özbey, M.F. Effect of pre-and post-exam stress levels on thermal sensation of students. Energy and Buildings. 2021; 231: 110595.

[9] Jones, B.W. Capabilities and limitations of thermal models for use in thermal comfort standards. Energy Build. 2002; 34 (6):653-659.

[10] Singh, M.K., Mahapatra, S., Atreya, S.K. Adaptive thermal comfort model for different climatic zones of North-East India. Appl. Energy. 2011; 88 (7): 2420-2428.

[11] Ladiun, S.D., Abu Talip, N.K., Nikol, L., Kram, S., Mon, D.D. Comparison of Mood State between Team Sports and Individual Sports among Young Athletes. Jurnal Psikologi Malaysia. 2021; 35(2):23-33.

[12] Muller, M.D., Muller, S.M., Kim, C.H., Ryan, E.J, Gunstad, J., Glickman, E.L. Mood and selective attention in the cold: the effect of interval versus continuous exercise. EurJ Appl Physiol. 2011; 111: 1321–1328.

[13] Ibrahim, A., Ali, H., Zghoul, A., Jaradat, S. Mood state and human evaluation of the thermal environment using virtual settings. Indoor and Built Environment. 2021; 30(1):70–86.

[14] Watson, D., Clark, L.A. The PANAS-X: manual for the positive and negative affect schedule-expanded form. Iowa: The University of Iowa, 1999.

[15] World Map of Koppen-Geiger Climate Classification, 2006.

[16] Turkish State Meteorological Service, www.mgm.gov.tr/veridegerlendirme/il-ve ilceleristatistik. aspx?m=ANKARA, (Access Date: 18.10.2021).

[17] Delta Ohm, HD32.3TC – HD32.3TCA – Thermal Microclimate PMV-PPD / WBGT, 2021.

[18] Onset Dataloggers Retrieved from: https://www.onsetcomp.com/products/data-loggers/u12-012, Retrieved date: 28 August 2020

[19] McNair, D.M., Lorr, M., Droppleman L.F. Manual for the Profile of Mood States Educational and Industrial Testing Services. 1971: San Diego, CA.

[20] Lin, S., Hsiao, Y. Y., Wang, M. Test review: the profile of mood states 2nd edition. 2014.

[21] Terry, P. C., Lane, A. M. Normative values for the profile of mood states for use with athletic samples. Journal of applied sport psychology. 2000; 12(1): 93-109.

[22] Heuchert, J. P., McNair, D. M. Profile of Mood States 2nd Edition. 2012.

[23] Cohen, J. Statistical Power Analysis for the Social and Behavioural Sciences (2nd Ed.). 1988. Lawrence Erlbaum Associates, U.S.A.

[24] Morris, S.B., DeShon R.P. Combining effect size estimates in meta-analysis with repeated measures and independent-groups designs. Psychol. Methods. 2002; 7 (1): 105-125.

[25] IBM Corp. Released 2020. IBM SPSS Statistics for Windows, Version 27.0. Armonk, NY: IBM Corp.

Data Statement

The datasets generated during and/or analysed during the current study are not available because the project (Project Number: 120M890) is still in process but the authors will make every reasonable effort to publish them in near future.

Age of Air Measurement in Air-recirculating Systems Applying Dynamic Steady-state Concentration Theory

Haruki Taguchi [a], Takashi Kurabuchi [b], Jinya Takeuchi [c], Hajime Yoshino [d], Yoshihiro Toriumi [e], Masaki Shimizu [f]

[a] Tokyo University of Science, Japan, haruki.t7.03@gmail.com.

[b] Tokyo University of Science, Japan, kura@rs.tus.ac.jp.

[c] Akita Prefectural University, Japan, jtakeuchi@akita-pu.ac.jp.

[d] Nippon Institute of Technology, Japan, yoshino.hajime@nit.ac.jp.

[e] Tokyo Denki University, Japan, toriumig@gmail.com.

[f] Tokyo University of Science, Japan, masaki.jpn3047@gmail.com.

Abstract. In open air systems which is rooms with ventilation by fresh air, the evaluation of an indoor air environment based on age of air measurement, such as a stepdown method using tracer gas, is widely applied. However, in a ventilation room with air-recirculating systems such as multiple packaged air conditioning unit systems, the concentration continues to increase endlessly when there is no ventilation with fresh air. Thus, it is not possible to measure the air age using the conventional experimental method, as noted. Therefore, in previous studies, a tracer gas experiment was established by applying a dynamic steady-state concentration theory. The dynamic steady-state concentration is the concentration transition of each single source, assuming that the steady-state concentration is composed of the difference between the room source and the recirculating source. Previous studies have confirmed that the dynamic steady-state concentration agrees with the equivalent steady-state concentration in the ventilation room of an open air system. In addition, simulations by computational fluid dynamics (CFD) analysis and tracer gas experiments in the laboratory showed that the dynamic steady-state concentration of only the recirculating part of the source equals the age of air. With all these methods and studies, we attempted to extend to a real space with air-recirculating systems using the tracer gas experimental method based on dynamic steady concentration. First, we measured the air age in a real space with multiple packaged air-conditioning unit systems. We thereafter confirmed the distribution property of the multiple packaged air conditioning unit systems and verified the validity of the quantitative evaluation using CFD analysis.
Our findings were as follows:

1. The age of the air measurement in a room with two or more recirculating parts was clarified by applying the dynamic steady-state concentration theory.

2. The tracer gas experiment of the dynamic steady-state concentration enabled the quantitative evaluation of the air distribution characteristics of the multiple-packaged air-conditioning unit system in real space.

Keywords. age of air, air-recirculating systems, dynamic steady-state concentration, multiple packaged air conditioning unit systems, tracer gas experiments

DOI: https://doi.org/10.34641/clima.2022.250

1. Introduction

In ventilated rooms, tracer gas has been used to evaluate fresh air distribution properties and polluted air emission efficiency. With the introduction of the concept of "the age of air" by Sandburg et al.[1][2], pulse, step-up, and step-down measurement methods have been proposed, and measurement devices have been developed[3]-[6]. However, although experiments with tracer gas can be performed in open air systems which is rooms with ventilation by fresh air, experimental methods for air-recirculating systems where exhausted air is recirculated. have not been established. For

Copyright ©2022 by the authors. This conference paper is published under a CC-BY-4.0 license.

example, dust collectors in smoking rooms, air purifiers in rooms with drifting pollen and house dust, and air conditioners without ventilation are in high demand to investigate these air conditions.
Thus, we developed a method to measure the concentration distribution of pollutants and the age of air in a room by tracer gas experiments in air-recirculating systems.[7] In addition, owing to COVID19, it is strongly desirable to be able to quantitatively evaluate the effect of improving indoor air quality in air-recirculating systems.

In this study, using the dynamic steadystate which will be described later, we understand the air distribution of two air conditioners (hereinafter, for simplicity, multiple packaged air conditioning unit systems are referred to as air conditioners.). The purpose of this study is to confirm the validity of the results by comparing them with computational fluid dynamics (CFD) analysis.

2. Dynamic steady-state concentration theory

2.1 Dynamic steady-state concentration theory with perfect mixing condition

Air-recirculating systems with leakages have room source M, volume V, airflow Q, and leakage air flow q, as shown in Fig. 1(a). Air-recirculating systems have a recirculating part source βM, as shown in Fig. 1(b), where β denotes the room source removal efficiency. For simplicity, the concentration of the leakage (in) was assumed to be zero in both cases. Assuming that room concentration is a perfect mixing condition, the concentrations of leakage (out) are C_P and C_N. Substituting Equation (2) from Equation (1), we obtain Equation (3). This is illustrated in Fig. 1(c).

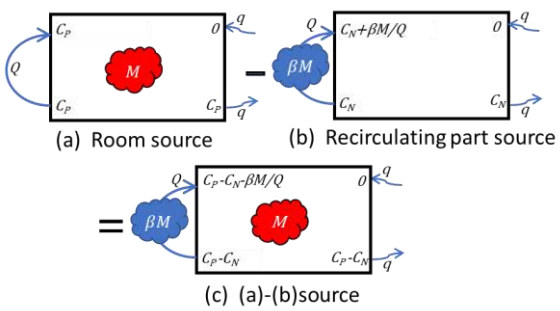

Fig. 1- Tracer gas experimental method with leakage

We subtracted the concentration in Fig. 1(b) from that in Fig. 1(a) according to β at the right time. Equation (4) is established, and the right side of Equation (3) becomes zero. Under these conditions, C_P - C_N becomes a steady-state concentration. This is shown in Fig. 2. Equations (1) and (2) change with time until they reach the steady-state concentration. However, C_P - C_N remained constant at $(1 - \beta)M/q$. The steady-state concentration distribution in the open air system is represented by the difference between the room source and the recirculating part source of the air-recirculating system. The time-varying concentration transition of the room source and recirculating part source, which constitutes the steady-state concentration distribution, is known as the dynamic steady-state concentration.

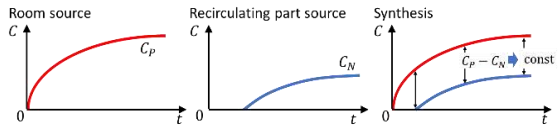

Fig. 2 – Dynamic steady-state concentration transition

$$V\frac{dC_P}{dt} = M - C_P q \quad \cdots (1) \qquad V\frac{dC_N}{dt} = \beta M - C_N q \quad \cdots (2)$$

$$V\frac{d(C_P - C_N)}{dt} = (1-\beta)M - (C_P - C_N)q \quad \cdots (3)$$

$$C_P - C_N = (1-\beta)\frac{M}{q} \quad \cdots (4)$$

2.2 Dynamic steady-state concentration theory with non-perfect mixing condition

Next, we consider the case with non-perfect mixing condition. A block model of the air-recirculating systems divided by microvolume elements is shown in Fig. 3, where the air flow from element i to j is Q_{ij}, room source is $m_{p,i}$, recirculating part source is $m_{n,i}$, leakage air flow from element i to the outside is q_i, and concentrations are $C_{p,i}$ and $C_{n,i}$, respectively.

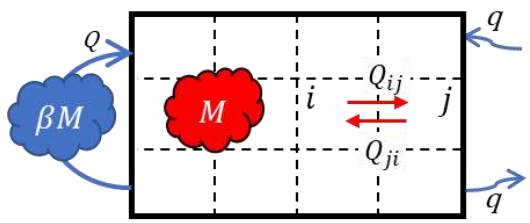

Fig. 3 – Block model of the air-recirculating systems divided by micro volume elements

Their concentration changes are shown in Equations (5) and (6), respectively. The sum of $m_{p,i}$ is M and that of $m_{n,i}$ is βM. The average concentrations were C_P and C_N, and the average concentrations (room to outside by leakage) were $C_{P,ex}$ and $C_{N,ex}$. When Equations (5) and (6) were summed over the entire space, they were obtained from Equations (1) and (2), respectively. If Equation (4) is satisfied, the spatial average concentration difference, C_P-C_N, does not change with time. We assume α_i is independent of the source generation points and is determined by each point in space. If Equations (7) and (8) are satisfied, then $C_{P,i}$ - $C_{N,i}$ is a steady-state concentration. To achieve this, the average concentration must be approximated by Equation (9), using $T = V/q$. Under this condition, by transforming Equation (5) using Equations (7) and (9), α_i becomes the solution of Equations (10) and

(11). In particular, without leakage, $q_i = 0$ and $T \to \infty$; therefore, the solution to Equations (10) and (11) is $\alpha_i = 1$ for all i. This implies that the rate of change in concentration with time is constant at each point in space. Equation (11) becomes $\alpha_i \approx 1$ because $V = \sum v_i$ is valid. Therefore, we can expect $\alpha_i \approx 1$ under the condition that $q << Q$.

$$v_i \frac{dC_{P,i}}{dt} = \sum_j C_{P,j} Q_{ji} - \sum_j C_{P,i} Q_{ij} + m_{P,i} - C_{P,i} q_i \quad \cdots (5)$$

$$v_i \frac{dC_{N,i}}{dt} = \sum_j C_{N,j} Q_{ji} - \sum_j C_{N,i} Q_{ij} + m_{N,i} - C_{N,i} q_i \quad \cdots (6)$$

$$\frac{dC_{P,i}}{dt} = \alpha_i \frac{dC_P}{dt} \cdots (7) \qquad \frac{dC_{N,i}}{dt} = \alpha_i \frac{dC_N}{dt} \cdots (8)$$

$$C_P = C_{P0} e^{-t/T} + C_\infty \left(1 - e^{-t/T}\right) \quad \cdots (9)$$

$$\left(\sum_j Q_{ij} + q_i - \frac{v_i}{T}\right) \alpha_i - \sum_j Q_{ji} \alpha_j = 0 \cdots (10)$$

$$V = \sum_i v_i \alpha_i \quad \cdots (11)$$

2.3 Relation between dynamic steady-state concentration and age of air

This is the block model of the airrecirculating part source, as shown in Fig. 4.

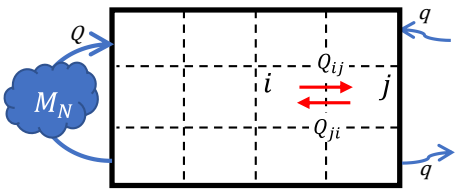

Fig. 4 - Block model of the air-recirculating systems divided by micro volume elements (recirculating part source)

Without leakage, Equation (6) becomes Equation (12). Because $\alpha_i = 1$, if $\beta = 1$, the change in concentration is constant, which becomes Equation (13). The sum of the air inflow and outflow for each microvolume element was $\sum_j Q_{ij} = \sum_j Q_{ji}$. Therefore, Equation (13) becomes Equation (14). C_0 is an arbitrary value.The age of air is $\tau_i = C_0 - C_{N,j}$, which is the steady-state concentration in the room under $M \propto V$ conditions. The term C_0 refers to the correction for setting the age of air in the supply air to zero.

With leakage, Equation (14) becomes Equation (15). When a tracer step-up experiment is conducted in air-recirculating systems with leakage, the recirculating part source is consumed by the increase in the concentration and leakage, as expressed in Equation (2). The term γ represents the fraction spent on increasing the concentration, which was 1 → 0. Therefore, under q << Q and just after the start of the experiment, Equation (15) is nearly equal to Equation (14); therefore, the dynamic steady-state concentration is expected to approximate the age of air.

$$v_i \frac{dC_{N,i}}{dt} = \sum_j C_{N,j} Q_{ji} - \sum_j C_{N,i} Q_{ij} + m_{N,i} \quad \cdots (12)$$

$$0 = \sum_j C_{N,j} Q_{ji} - \sum_j C_{N,i} Q_{ij} + m_{N,i} - v_i \frac{M}{V} \quad \cdots (13)$$

$$0 = \sum_j (C_0 - C_{N,j}) Q_{ji} - \sum_j (C_0 - C_{N,i}) Q_{ij} - m_{N,i} + \frac{v_i}{V} M \quad \cdots (14)$$

$$0 = \sum_j (C_0 - C_{N,j}) Q_{ji} - \sum_j (C_0 - C_{N,i}) Q_{ij} - m_{N,i} + C_0 p_i - (C_0 - C_{N,i}) q_i + \gamma \alpha_i \frac{v_i}{V} M \quad \cdots (15)$$

2.4 Measuring method of age of air with multiple recirculating part sources by dynamic steady-state concentration

Fig. 5(a) and (b) shows the situation after the correction. Because the concentration transition is linear, the concentration distributions in (a) and (b) are multiplied by correction factors k1 and k2, respectively. Figure 5(c) shows the situation in which they were synthesized. Equation (16) is the condition for setting the blowing concentration to zero, and Equation (17) is the condition for the total source volume to be equal to the source volume V (in a room under M ∝V conditions). Equations (16) and (17) are quadratic equations with k1 and k2 as unknowns, and we can obtain k1,k2 using these equations. Figure 5(d) shows the situation after the correction of Fig. 5(c).

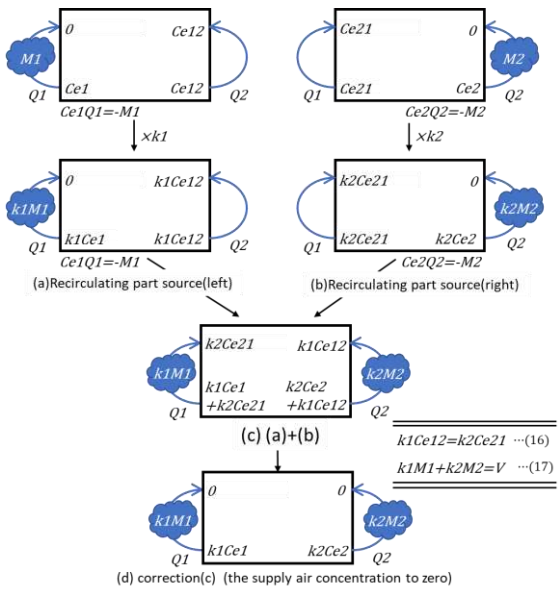

Fig. 5 - Correction method with two recirculating parts

3. Experiment

3.1 Outline of experiment

Fig. 6(a) and (b) show the plan and A-A' sectional views of the target room and positions of the air conditioners. We placed 4 × 4 highly responsive CO_2 concentration measuring instruments on the same

plane ($h = 700$). Tracer gases were generated by air conditioners (plan view painted in red or blue). Figure 6(c) shows the details of the air conditioners.

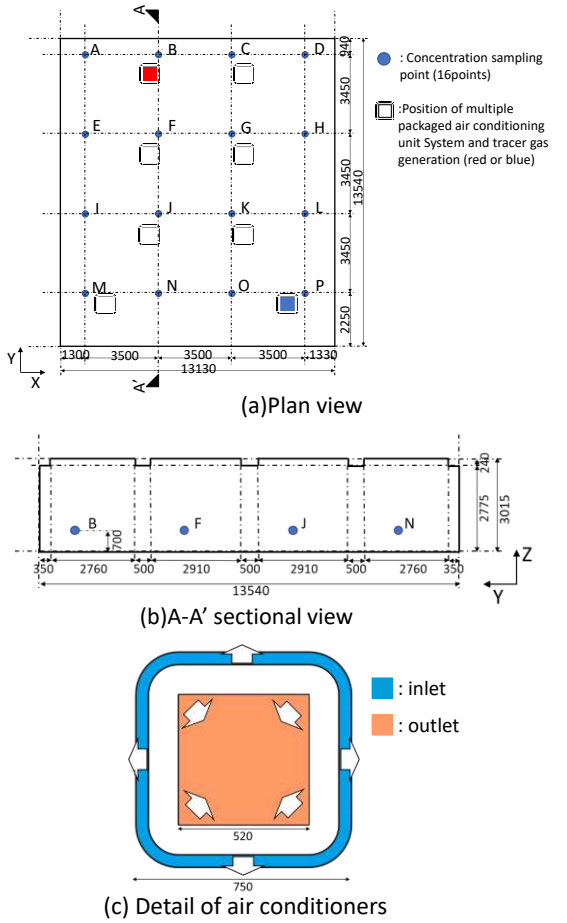

Fig. 6 - Target room overview and detail of air conditioners

Fig. 7 shows the results of the airtightness measurement and the allowable leakage time. We perfromed a concentration decay method using tracer gas in the target room. The ventilation rate was used as the leakage rate in the target room, and the leakage rate was *0.0233 times/h*. Equation (18) expresses the change in concentration in a room with ventiration rate n in an open air system. The rate of increase in concentration is obtained from Equation (19). If we allow a 5% error, we must use data up to $nt = 0.05$, implying that the measurement limit in the target room is approximately 2.1 h. Tab.1 lists the case studies. The four cases depend on the generation point and airflow.

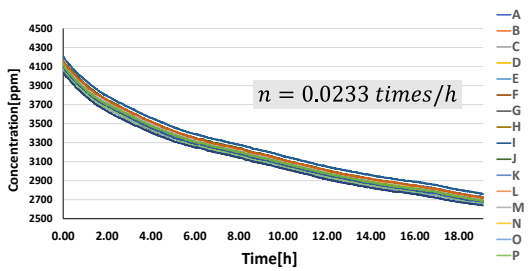

Fig. 7 – Airtightness measurement results

$$C = \frac{M}{q}\{1 - \exp(-nt)\} \quad \cdots (18)$$

$$V\frac{dC}{dt} = V\frac{d}{dt}\left\{-\frac{M}{q}\exp(-nt)\right\} = V\frac{M}{q}\frac{q}{V}\exp(-nt) = M \cdot \exp(-nt) \quad \cdots (19)$$

$$V\frac{dC}{dt} \fallingdotseq M \quad \cdots (20)$$

Tab. 1 – Study case

Case	Tracer Gas Generation	Airflow [m³/(h*one)]	Blowing Angle
Case A_1	Red	612	30°
Case A_2	Blue		
Case B_1	Red	1138	30°
Case B_2	Blue		

3.2 Experimental result

Fig. - 8 shows the concentration transition of the four cases and the sampling time. The previous studymust measure the air age at approximately 1/2 of the nominal ventilation time (V/Q) after the formation of the concentration distribution[8]. However, in case A_2, we measured the concentration at the time when it was stable because the concentration was not stable at the measurement points K, L, O, and P.

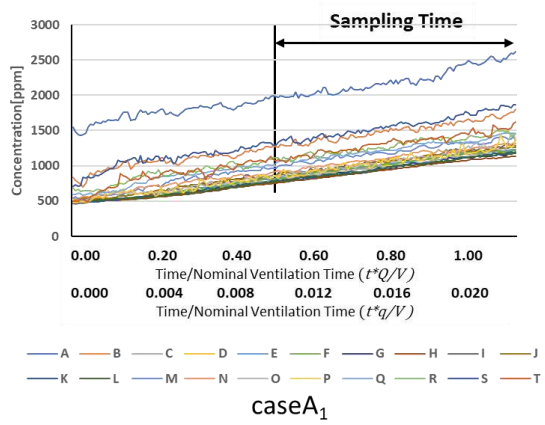

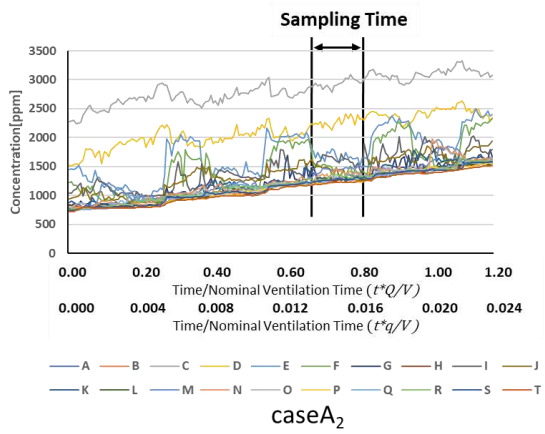

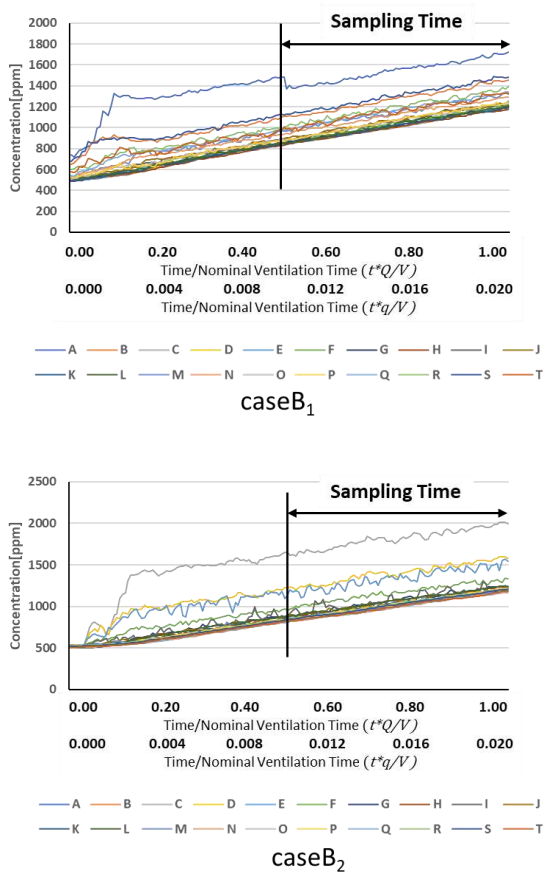

Fig. 8 – Concentration transition of the four cases

Fig. 9 shows the results for the four cases. The values are the SVE3 of each concentration, with the blowing concentration corrected to zero. In all cases, the age of the air near the generation point is better, and the age of the air becomes worse as it moves away from the generation point. When comparing cases A_1 and B_1, the values were generally the same. However, when comparing A_2 and B_2, the values near the generation location are the same, but B_2 is better at a distance from the generation location. In case A_2, the concentration transition near the generation location (K, L, O, and P) was not stable, but the values in A_2 and B_2 were generally the same; therefore, the results were not affected.

Fig. 10(a) and (b) shows the synthesis results for A_1 and A_2, and B_1 and B_2, respectively. Comparing (a) and (b), the distributions are almost the same and the value of (b) is better than that of (a). We confirmed a difference in the range of forces depending on airflow.

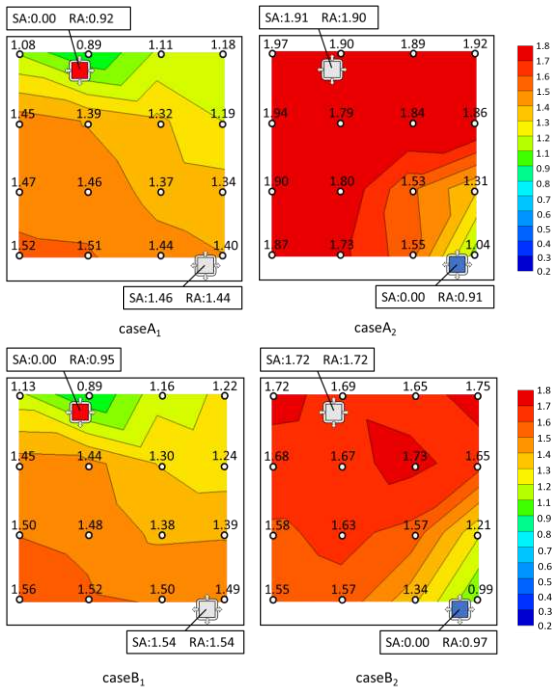

Fig. 9 – Experiment result : age of air

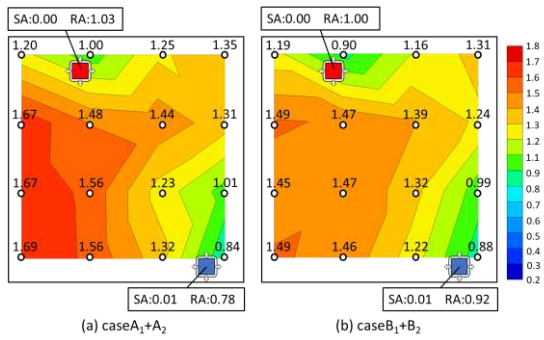

Fig. 10 – Synthesized results : age of air

4. CFD analysis

4.1 Outline of CFD analysis

Tab. 2 lists the analytical conditions, and Fig. 11 shows the analytical model. The age of air in the air-recirculating systems is equal to the age of air in the equivalent open air system. A steady-state analysis was performed with two air conditioners as the source locations under open conditions.

Tab. 2 – CFD analysis conditions

Software	STAR-CCM+(2020.3)
Analysis Area[㎥]	13.54(x)*13.13(y)*3.015(z)
Total Mesh Size	1,503,668
Turbulence Model	Standard k-εModel
Airflow Analysis	2nd-order upwind scheme
Passive Scalar Analysis	1st-order upwind scheme

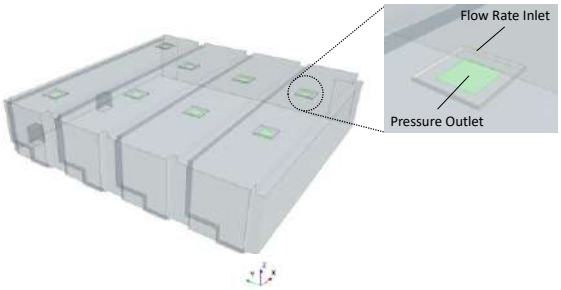

Fig. 11 – CFD analysis model

Fig. 12 shows the CFD results and Fig. 13 shows the correlation between the CFD results and the experiment. Comparing Fig. 12(a) and Fig.10(a), the values in Fig. 12(a) in the upper right corner of the room are higher than those in Fig. 10(a), but the values near the generation point are approximately the same. Although the distributions were generally consistent, there was a slight difference in the RMSE = 0.154. Fig. 12(b) and the experimental data exhibit a similar trend, dispite *RMSE = 0.109*

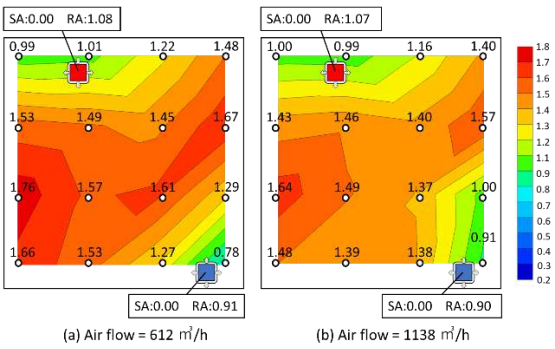

Fig. 12 – CFD analysis results

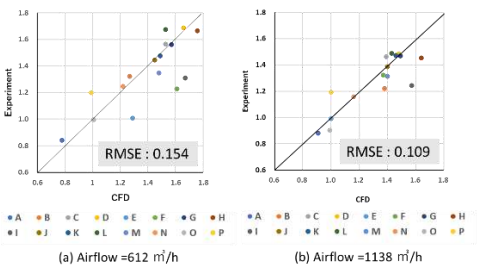

Fig. 13 - Correlation between the CFD results and the experiment

The problem is that the only way to measure the air-blowing angle of the air conditioner is by visual measurement, and case studies are conducted by changing the angle in the analysis. Therefore, a future task is to improve the accuracy of the analysis of air conditioners with oblique blowing angles.

5. Conclusion

1. The age of air measurement in a room with two or more recirculating parts was clarified by applying the dynamic steadystate concentration theory.

2. The tracer gas experiment of the dynamic steady-state concentration enabled the quantitative evaluation of the air distribution characteristics of the multiple-packaged air-conditioning unit in a real space.

6. Acknowledgement

We would like to thank Editage (www.editage.com) for English language editing.

7. References

[1] Mats Sandberg. What is ventilation efficiency?, Building and Environment, Volume 16, Issue 2, 1981:123-135.

[2] Mats Sandberg, Mats Sjöberg. The use of moments for assessing air quality in ventilated rooms, Building and Environment, Volume 18, Issue 4, 1983:181-197.

[3] ANSI. Measuring Air—Change Effectiveness, American Society of Heating, Refrigerating, and Air—Conditioning Engineers（07—Apr—1997）, ASHRAE 129—1997,1997,4:1-19.

[4] ANSI. American Society of Heating, Refrigerating, and Air—Conditioning Engineers（31—Dec—2004）, ASHRAE 62．1—2004：Standard 62 Ventilation for Acceptable Indoor Air Quality,2004:12.

[5] The Society of Heating, Air-Conditioning and Sanitary Engineers of Japan , Field Measurement Methods for Ventilation Effectiveness in Rooms. SHASE—S115—2002.2002;1-20

[6] The Society of Heating, Air-Conditioning and Sanitary Engineers of Japan, Ventilation Rate Measurement of a Single Room Using Tracer Gas Technique. SHASE—S116—2003.2003;1-33

[7] Kurabuchi T et al. Dynamic steady-state concentration distribution realized in air recirculating systems with leakage part 1 theoretical consideration. ROOMVENT 2020.2021,2:254-297.

[8] Sato K et al. Dynamic steady-state concentration distribution realized in air recirculating systems with leakage part 2 experimental verification. ROOMVENT 2020.2021,2:246-249.

c.The datasets generated during and/or analysed during the current study are not available because authers take time to organeze the data but the authors will make every reasonable effort to publish them in near future.

Numerical and experimental studies on a hybrid panel element for heating, cooling and ventilation

Lars Schinke [a], André Schlott [b], Maximilian Beyer [a], Joachim Seifert [a]

[a] Chair of Building Energy Systems and Heat Supply, Institute of Power Engineering, Technische Universität Dresden, Dresden, Germany, lars.schinke@tu-dresden.de.

[b] Fraunhofer Institute for Manufacturing Technology and Advanced Materials IFAM, Branch Lab Dresden, Dresden, Germany, andre.schlott@ifam-dd.fraunhofer.de.

Abstract. The use of surface heating systems will become even more important in the future. On the one hand, the systems can be operated at lower system temperatures and thus represent an energy optimisation. On the other hand, such a system is very well recognised by the user in terms of thermal comfort. In addition, due to the hermetic construction of the buildings, a ventilation system is needed to ensure the necessary supply of fresh air. Considering the Covid-19 pandemic and the reduction of the risk of infection, the importance of fresh air supply is even higher. To meet these requirements, a hybrid panel element was designed and prototyped. The area of application includes new construction as well as the modernisation of residential and commercial buildings. The hybrid panel element combines the advantages of surface heating in winter with cooling in summer and all-season ventilation. The prototypes were used to carry out extensive measurement tests. This made it possible to prove the functionality of the hybrid surface system and to make statements regarding the performance parameters (transferable heat flux via the surface to the room and transferable heat flow to the air). In addition, a parameter study on influencing variables (e.g. material selection, arrangement of air channels) was carried out by means of numerical simulation.

Keywords. hybrid panel element, heating, cooling, ventilation, open-cell porous metals, numerical simulation, temperature distribution
DOI: https://doi.org/10.34641/clima.2022.410

1. Introduction

Radiant heating and cooling are well known in residential and non-residential buildings and will become even more important in the future. The good thermal comfort means that such a system is accepted by the users. Additionally, such systems represent an energy optimization by using lower system temperatures to operate. Recent buildings are more and more hermetic which introduces the need of a ventilation system to ensure the necessary supply of fresh air. This is even more important considering the current Covid-19 pandemic and the need to reduce infection risks. Up to now, the heating and ventilation of rooms have mainly been considered separately in terms of construction. For example, to simplify installation and media routing during building refurbishment, hybridising the room climate tasks of heating, cooling and ventilation in one component can be a clear advantage. The focus of the presented study is a modular element that fulfils the functions of surface heating or surface cooling and ventilation. Several research projects have already been carried out on this hybrid approach in the past, some of which also took thermal comfort into account in addition to functional and energy-related aspects. Investigations related to the application on the floor is available in [1]. For use on the ceiling, results can be found in [2-4]. The approach presented in this article is a single component/element that is used as surface heating/cooling as well as for conditioning the room supply air (therefore called hybrid panel element). This is to be used primarily on the ceiling. In the following, the various analyses (measurements and simulation) of this hybrid element are presented. A significant difference to systems available on the market is the use of open-cell porous metals in the hybrid element.

2. Description of the hybrid panel element

The element has a compact design consisting of a

Copyright ©2022 by the authors. This conference paper is published under a CC-BY-4.0 license.

water-carrying pipe system, which can deliver heat to the room (heating mode) and is able to absorb heat (cooling mode). At the same time, air is conditioned regarding its temperature before it is supplied to the room. As a special feature, cellular metallic materials (metal foam or metal fibre structures) are used in the element to improve the thermal properties and to realise a lightweight construction. This gives the element the following advantageous properties:

- fulfilment of all HVAC tasks incl. cooling
- lightweight and compact design
- very good heat distribution and, therefore, reduction of thermal inertia compared to classic underfloor heating
- thus, possibility to increase pipe distance at a nearly constant mean surface temperature
- very low surface temperature ripple
- variable installation options (ceiling or wall)

In recent years, extensive research on open-cell porous metals (OCPM) has taken place in materials science. Examples are the metal foam and the metal fibres, described in [5, 6]. These materials have various advantages for use in building energy technology, as shown in [7, 8]. The metal foam and the metal fibres were considered more closely as OCPMs and incorporated into the hybrid element. Both OCPM have different advantages for the intended use. A comprehensive thermal analysis of a composite of OCPM and a pipe is documented in [9].

In the first step, the dimensions of the hybrid element were based on the grid size 625 mm x 625 mm, which is common in grid ceiling construction. To have the greatest possible variety during the examinations, four channels were provided for the airflow in the element. These can be switched off separately depending on requirements. Fig. 1 shows an example of a hybrid element.

Fig. 1 – Example of a hybrid element

Various preliminary investigations have shown that the integration of the individual components (pipe, OCPM, air channel) especially poses some challenges from a manufacturing point of view. At this point, for example, the manufacturing tolerances of the individual components as well as the connection of the components (bonding, pressing) should be mentioned. For this reason, eight different demonstrators were manufactured. These differ in terms of the OCPM (metal foam (MFO)/metal fibre (MFI)/no OCPM), the position and material (copper/polyethylene (PE)) of the tube in the OCPM and the manufacturing quality. Tab. 1 summarises the demonstrators investigated.

Tab. 1 – Properties of the built demonstrators

No.	OCPM	position of tube related to OCPM	tube material	manufacturing accuracy
V01	MFO	on	copper	low
V02	MFO	in	copper	low
V03	-	-	copper	low
V04	MFI	on	copper	low
V05	MFI	in	copper	low
V06	-	-	PE	high
V07	-	-	copper	high
V08	MFI	on	copper	high

3. Thermal investigations

The thermal investigation was divided into an experimental and a numerical simulations part. With the help of the experimental investigations, the various demonstrators had been analysed by measurement. Influences such as manufacturing tolerances and pipe material are shown by means of numerical simulations.

3.1 Experimental investigation

A test stand was designed and built for the experimental investigations (see Fig. 2).

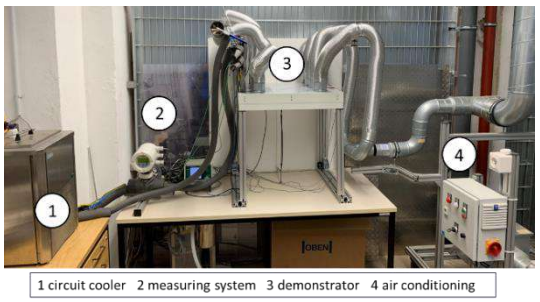

Fig. 2 – Test stand for experimental investigation

The water flowing through the pipes of the demonstrator (3) is tempered and the water volume flow is controlled with a circuit cooler (1). The air volume flow, which is guided through the air channels of the demonstrator (3), is realised by means of an air conditioning unit (4) consisting of a heater and a fan. With the aid of the measuring system (2), the water flow parameters (inlet and outlet temperature $\vartheta_{W,i}$ and $\vartheta_{W,o}$, water volume flow $\dot{V}_W$), air flow parameters (inlet and outlet temperature $\vartheta_{air,i}$ and $\vartheta_{air,o}$ per air channel and the total air volume flow $\dot{V}_{air}$) as well as the specific heat flux density on the room-facing side of the demonstrator are acquired. To be able to achieve meaningful results, the influencing parameters air volume flow, water volume flow and water inlet temperature are varied within a suitable range.

For the evaluation of the experiments, thermography

is used to analyse the surface temperature distribution on the room-facing side of the demonstrator. The caloric balances are drawn up for the media water and air in order to determine the respective heat fluxes. Furthermore, the specific heat flux from the element to the air on the room-facing surface is determined with heat flux measuring plates.

3.2 Numerical simulation

A 3D simulation was done using COMSOL Multiphysics. The model included the thermal modelling of all solid materials and the fluid flow of the air through the four channels. The geometric model was derived from the construction data of the demonstrators, which is shown in Fig. 3. The design represents the ideal thermal contact and neglects necessary manufacturing tolerances in most parts. This ideal case, which ignores the thermal resistances that occur in practice, serves to determine the target size for further optimisation.

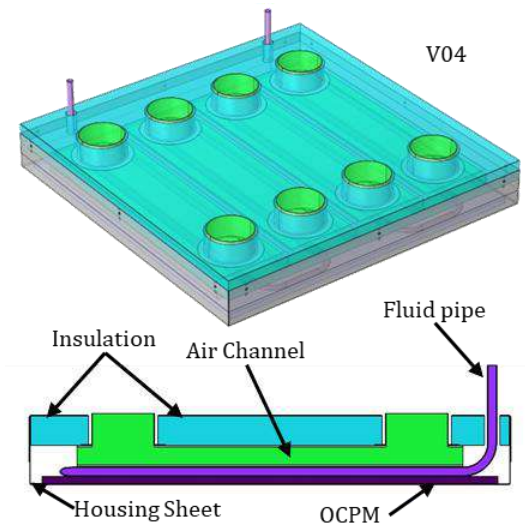

Fig. 3 – Geometric simulation model in transparent 3D (top) and 2D slice (bottom)

Special attention was paid to the connection between the fluid pipe and the OCPM. Since manufacturing tolerances lead to enormous thermal contact resistances, these tolerances were modelled to investigate their influence. Therefore, the tolerance range between the pipe and the air channel was filled in constructively and made accessible to the simulation (Fig. 4). The effect of these tolerances was approximated by varying the material data. Air is defined and examined as the worst case and aluminium as the ideal contact.

The boundary conditions were adapted so that they largely correspond to the experimental conditions. To include the convective heat transfer the basic characteristic [10] is used. The flow inside the air channels is also considered. The flow rate was varied between $\dot{V}_{air} = 0...75\ \mathrm{m^3/h}$. This corresponds to the experimental possibilities. To extrapolate higher volume flows, an air volume flow of $\dot{V}_{air} = 150\ \mathrm{m^3/h}$ was also simulated. The fluid flow inside the pipe was also set to $\dot{V}_W = 0.5\ \mathrm{L/min}$ according to the experimental conditions and kept constant for all variations.

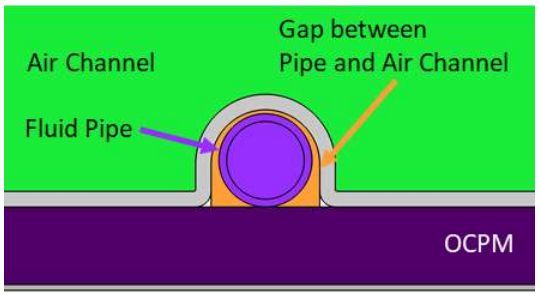

Fig. 4 – Detail of the filled tolerance space between heat transfer tube and air channel

The simulations were conducted with the element variants V03, V04 and V05 (see Tab. 1). The geometric differences are shown in Fig. 5 below.

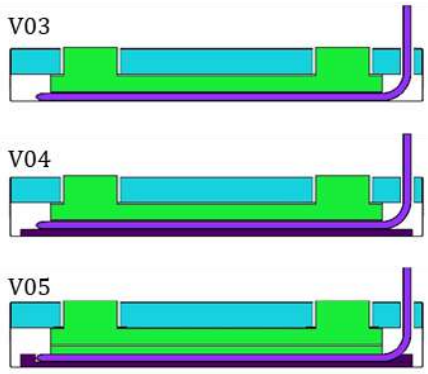

Fig. 5 – Simulated element variants

In element V03, there is no OCPM present and therefore this variant is the reference case. In elements V04 and V05 the fluid pipe is located on the OCPM or inside the OCPM, respectively. As an extension to the experimental investigations, the air channels used for air flow were varied. As shown in Fig. 3, there are 4 channels within the model. When all 4 channels are used the variants are labelled 4C. Variants then only use the inner two channels or outer two channels are labelled CI and CO, respectively. Air channels not used would not be present when the element is built and replaced by insulation. Therefore, unused air channels are simulated as insulation by assigning the corresponding material properties to the channel itself and the volume inside the unused channel. Furthermore, two application variants were investigated: heating case and cooling case. The corresponding temperature levels for the simulations are shown in Tab. 2.

Tab. 2 –Temperatures used in application variants

Study Case	Temperature Room	Air inlet	Fluid inlet
Heating	20 °C	20 °C	50 °C
Cooling	26 °C	26 °C	16 °C

To establish grid-independence, a mesh refinement

study was performed for the element V03 with constant parameters. The mesh giving sufficiently accurate results considering the computational time has about 741,000 elements and a computational time of about 4.5 hours. The results of the simulation were compared with the measurement results and the required agreement of less than 15 % deviation was achieved for these investigations.

4. Results

As given in Tab. 1, 8 demonstrators were built. The numerical simulations were done with many parameters. Therefore, selected results are presented and correlations explained. Due to the limited space, only the heating case is presented. The cooling cases were equally evaluated leading to analogue results.

4.1 Experimental investigation

In the first step, the surface temperature distribution on the room-facing side of the demonstrator was analysed using thermography. Fig. 6 shows the demonstrator V03 with no air volume flow and with an air volume flow of $\dot{V}_{air} = 20$ and 75 m^3/h. It can be seen very clearly that at no and low airflow the surface temperature is higher because less heat is transferred to the air and thus more heat is transferred to the room-facing surface. Since no OCPM is installed in this demonstrator, the contact points of the pipe and sheet metal are very clearly visible in all the conditions investigated. This results in thermal hotspots on the surface.

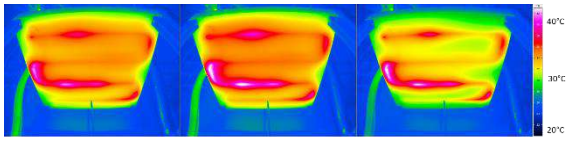

Fig. 6 – Thermography of the room-facing side demonstrator V03 at $\vartheta_{W,i} = 50$ °C, $\dot{V}_W = 0.5$ L/min and $\dot{V}_{air} = 0$ m^3/h (left), 20 m^3/h (centre), 75 m^3/h (right)

The influence of the metal foam can be seen in Fig. 7 showing demonstrator V02. The OCPM improves the heat distribution from the pipe to the room-facing surface. The thermal hotspots only occur in places at the pipe bends and are relatively smaller. Furthermore, with no or low air volume flow, a more homogeneous surface temperature distribution occurs compared to the maximum volume flow.

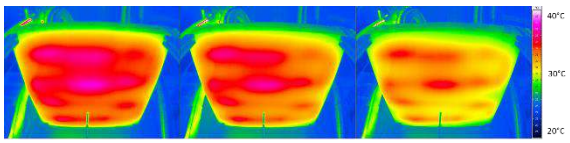

Fig. 7 – Thermography of the room-facing side demonstrator V02 at $\vartheta_{W,i} = 50$ °C, $\dot{V}_W = 0.5$ L/min and $\dot{V}_{air} = 0$ m^3/h (left), 20 m^3/h (centre), 75 m^3/h (right)

With the use of metal fibres as OCPM in demonstrator V05, a significant increase in surface temperature as well as a more homogeneous distribution can be achieved, see Fig. 8. This is caused by the better heat conduction properties of the metal fibres compared to the metal foam.

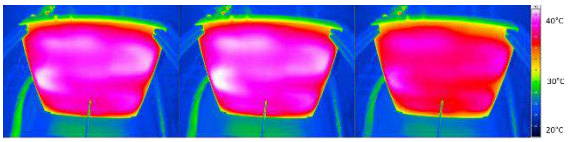

Fig. 8 – Thermography of the room-facing side demonstrator V05 $\vartheta_{W,i} = 50$ °C, $\dot{V}_W = 0.5$ L/min and $\dot{V}_{air} = 0$ m^3/h (left), 20 m^3/h (centre), 75 m^3/h (right)

The fact that the manufacturing quality has a very high influence on the thermal properties of the hybrid element can be seen in Fig. 9. The surface temperature is significantly higher and more homogeneously distributed compared to demonstrator V03 in Fig. 6.

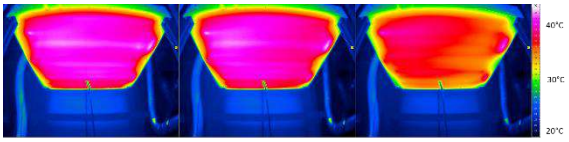

Fig. 9 – Thermography of the room-facing side demonstrator V07 at $\vartheta_{W,i} = 50$ °C, $\dot{V}_W = 0.5$ L/min and $\dot{V}_{air} = 0$ m^3/h (left), 20 m^3/h (centre), 75 m^3/h (right)

Fig. 10 shows a comparison of the heat flow emitted by the water $\dot{Q}_W$ for all demonstrators as a function of the air flow rate $\dot{V}_{air}$. All demonstrators tend to behave quite similarly - the increase in air flow rate provides an increased heat flux, which is given off by the water. The reference case V03 lies approximately in the middle of all demonstrators.

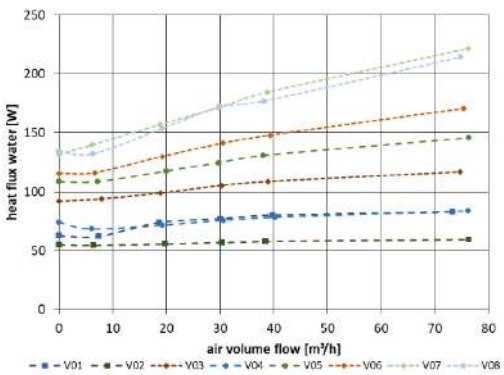

Fig. 10 – Course of the heat flux water $\dot{Q}_W$ in comparison of all demonstrators at $\vartheta_{Wi} = 50$ °C, $\dot{V}_W = 0.5$ L/min

The demonstrators below have either the metal foam as the OCPM (V01, V02) or the pipe lies on the OCPM metal fibres (V04). Here it can be seen that the metal foam worsens the heat transport due to its properties (e.g. thin webs, relatively large air content) and that with an unfavourable arrangement of the OCPM and tube, the OCPM acts as an additional thermal resistance. This has a clear effect on the performance of the demonstrator. In demonstrator V05, the tube is placed inside OCPM metal fibres and therefore has much better thermal contact. This is also reflected in the performance curve. Again, better

thermal properties of the hybrid element can be achieved with a higher manufacturing quality, see demonstrators V06, V07 and V08.

Regarding the heat flux density on the room-facing surface, the same statements can be made. The demonstrators with the OCPM metal foam and the demonstrator with the tubes on the OCPM metal fibres have significantly lower specific heat flux densities (Fig. 11). Comparing the heat flux densities to the reference element V03, the specific heat flux density on the room-facing surface without air volume flow can be increased to values of $\dot{q}_{room}$ = 120 ... 130 W/m^2 (V07, V08). It can also be seen that the drop in heat flux density of the elements V05, V07, V08 at the highest air volume flow rate is still at the level of the heat flux density of the reference element V03 without air volume flow rate. This means that despite a high air volume flow and the associated heat absorption of the air, the hybrid element can achieve a high value for the function as surface heating.

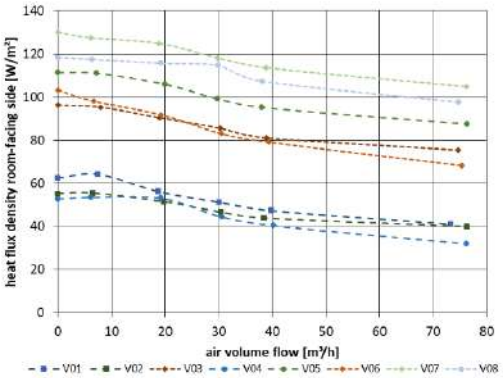

Fig. 11 – Course of the heat flux density on the room-facing side $\dot{q}_{room}$ in comparison of all demonstrators at $\vartheta_{W,i} = 50$ °C, $\dot{V}_W = 0.5$ L/min

Fig. 12 shows the change in air temperature as a function of the air flow rate for all demonstrators. Also from this point of view, the demonstrators behave as described above. With the demonstrators V06 to V08, changes in the air temperature as a function of the air volume flow of $\Delta\vartheta_{air} = 7.5$ ... 11 K are possible under the present boundary conditions.

It should be noted that this change in air temperature occurs over the 625 mm length of the hybrid element. By connecting several elements in series or by using a longer element, higher temperature changes are possible.

The influence of the water volume flow on the thermal performance of the hybrid element is small. Due to the very good heat transfer from the water to the pipe wall, this thermal resistance is negligible compared to the other heat transfer resistances in the element. In comparison, the water inlet temperature has a significant influence on the thermal behaviour of the hybrid element. The higher it is, the greater the heat fluxes that can be transferred.

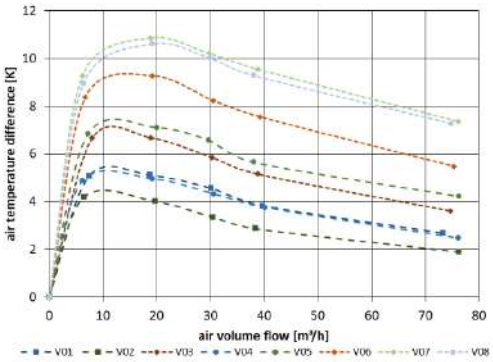

5

Fig. 12 – Course of air temperature difference $\Delta\vartheta_{air}$ in comparison of all demonstrators at $\vartheta_{W,VL} = 50$ °C, $\dot{V}_W = 0.5$ L/min

4.2 Numerical simulation

With all the different variations described in chapter 3.2, there are 168 parameter cases for each of the 3 geometric variants simulated. This leads to a total of 504 numerical investigated variants. For all the variants, the caloric change of the air flow and heat transfer medium was evaluated as well as the minimal, maximal and average temperatures of all surfaces. Additionally, all corresponding heat fluxes are calculated. Due to the enormous number of variants, exemplary results are discussed in the following. Presented are the results of element V03, where the differences between different variants are greatest. Subsequently, general statements and conclusions are formulated from the simulation results.

Fig. 13 shows heat flux to the air (top) $\dot{Q}_{air}$ and out of the heat transfer medium (centre) $\dot{Q}_W$ as well as the heat flux to the room (bottom) $\dot{q}_{room}$ as a function of the air flow $\dot{V}_{air}$ of element V03 with 4 air channels. The heat flux to the air and to the room are considered positive. The heat flux out of the medium is considered negative to correspond with the other heat flux directions. Note that the heat flux to the room $\dot{q}_{room}$ is given in W/m^2. This is to enable a simple comparison with other, commercially available systems. But the given values cannot be added according to the energy balance of the element. The left edge of the diagrams corresponds to operation as a pure radiant heating system with no air flow so no heat flux to the air is calculated. The designation of the respective curves compiles the pipe material (e.g. Cu, PE) and then the material in the tolerance range between pipe and air channel (e.g. Air, Alu). The combination "Cu/Alu" indicates a copper pipe with aluminium as gap filler in the tolerance space.

The curves show the expected pattern. As the air flow rate increases, the heat flow transferred to the air increases steadily. Thus, the corresponding temperature difference is getting smaller (not shown). The heat transfer medium shows the same behaviour, but with the opposite sign as mentioned before. The cooling of the fluid increases

continuously, as does the heat flux. This temperature change of the heat transfer fluid consequently leads to a reduced temperature of the surface facing the room, which results in a lower average excess temperature and, thus, also a lower heating output.

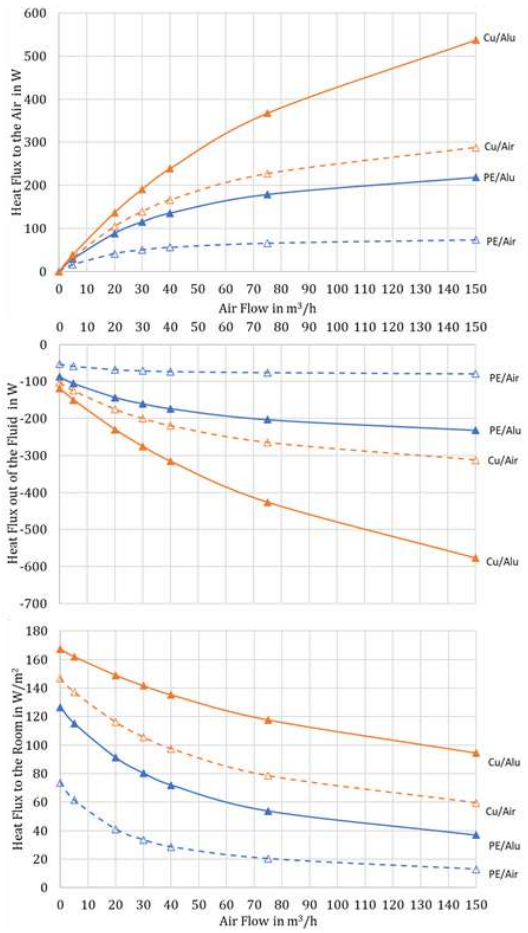

Fig. 13 – Heat flux in the air, out of the heating fluid to the room (model V03, 4 air channels, heating case)

The influence of the tolerance range between the tube and the air channel as well as the tube material is also as expected. The copper tube performs significantly better than PE tube due to the lower thermal resistance through the tube wall. If there is air between the pipe and the air channel, lower heating capacities occur as expected. Due to the direct contact between the pipe and the surfaces facing the room, the resulting differences between the tube materials are unambiguous.

This unambiguity is partially lost when OCPM is used as a heat spreader between the pipes and the surface facing the room, as considered in element V04. Fig. 14 shows the same curves for geometry variant V04. Here the variant with plastic tube and very good thermal contact (PE/Alu) approaches the combination of copper tube with air gap (Cu/Air) or performs minimally better. The combination of metallic copper pipe with ideal thermal contact is also far ahead in this case and the plastic tube with air gap performs correspondingly poorly.

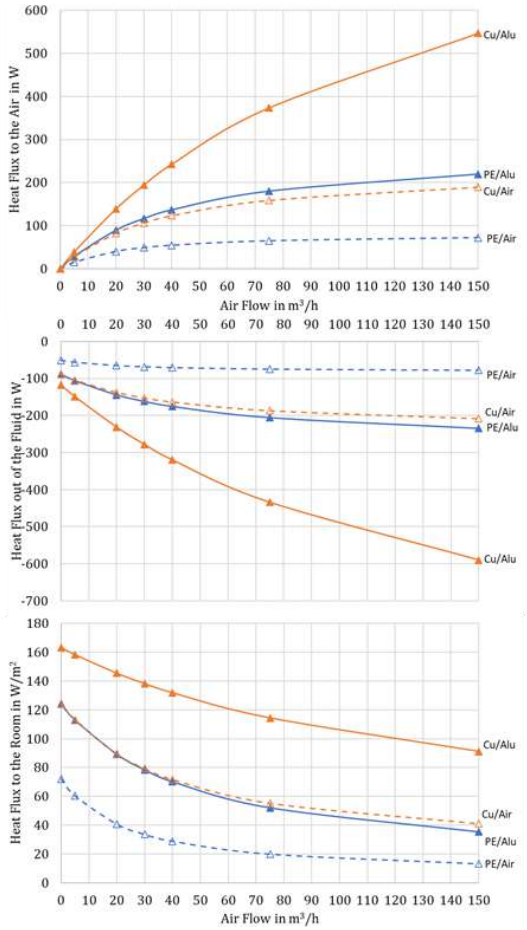

Fig. 14 – Heat flux in the air, out of the heating fluid to the room (model V04, 4 air channels, heating case)

When looking at the curves of geometry variant V05 in Fig. 15, the deviating scale values should be noted. The heating of the air and, thus, also the heat flow transferred to the air are significantly reduced. In order to achieve a clear assignment of the curves and to increase the readability of the diagrams, the axes have been adjusted. The same applies to the heat transfer fluid. However, the scaling of the axes for mean excess temperature and heat flow of the surface facing the room is unchanged.

In comparison, all 3 variants show comparable values regarding the average excess temperature of the surface facing the room and the possible heat flux. The differences in the internal structure are not visible in this illustration, but they do influence the temperature distribution and the minimum and maximum temperatures that occur.

Fig. 16 shows the temperature spread of the room facing surface for geometry variant V03 (top) and V05 (bottom) for the combination of copper pipe with air as filler. The curves show the minimum, average and maximum temperatures of the surface. In this case, when OCPM is omitted (V03), the maximum surface temperature is approximately equal to the fluid temperature. This maximum temperature is found around the inlet of the heat carrier fluid. There is a line contact between the tube and the casing sheet. Because of the air gap, the air

channel is not able to distribute the heat to the casing sheet so that the minimum surface temperature is only slightly above the room temperature. This results in spreads of up to 27 K, i.e. overheated and cold areas are formed.

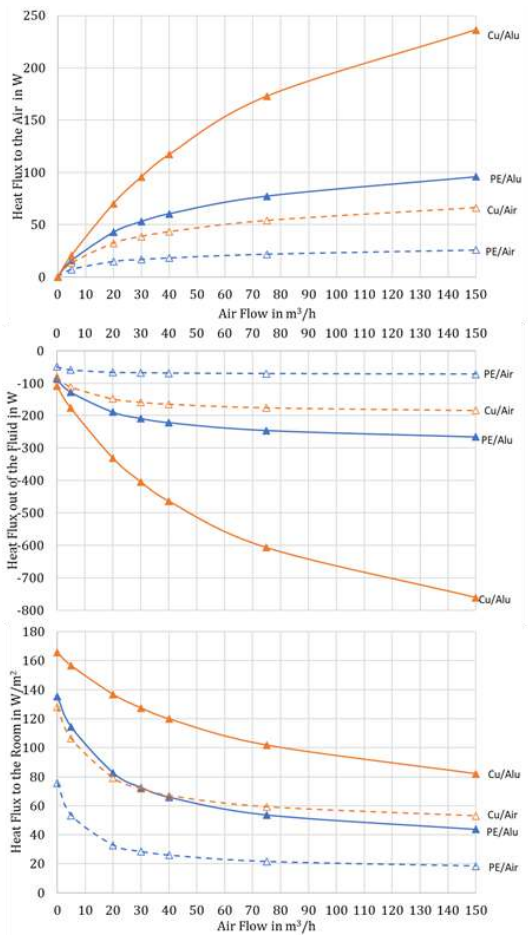

Fig. 15 – Heat flux in the air, out of the heating fluid to the room (model V05, 4 air channels, heating case)

If OCPM is installed (V05), the average surface temperatures drop by up to approximately 5 K due to the additional thermal resistance, but the spread between minimum and maximum temperature at the surface is halved to approximately 13 K.

From this it can be concluded that the use of an open-cell porous metal results in a significantly more uniform surface temperature, particularly in the case of high manufacturing tolerances, whereby the reduction in the area-specific heating power can be neglected. The previous explanations always refer to the case where all existing air channels are in use. However, it is possible to use only two air channels These can be located at the outer edge (labelled CO) or in the centre of the module (labelled CI). Fig. 17 shows the heat flux out of the heating fluid with different pipe materials and tolerance materials for model V03. The heat flux out of the fluid is lower with the same air volume flow with only two active air channels. The position of the air channels is not relevant. Corresponding results are shown by all other investigated geometries.

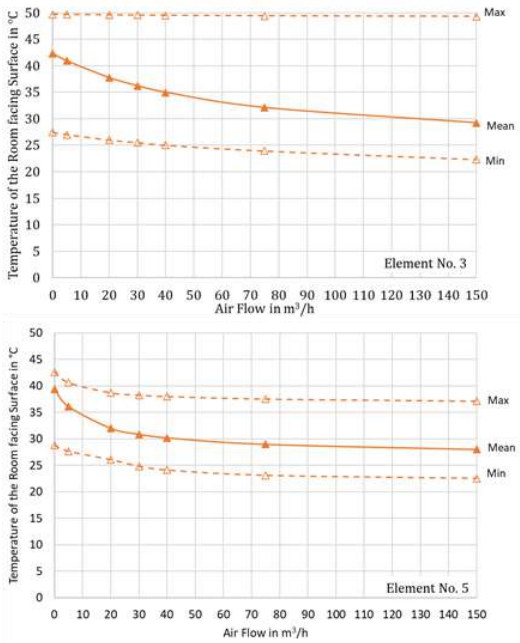

Fig. 16 – Minimum, average and maximum temperature of the room facing surface for model V03 (top) and V05 (bottom) (copper tube, air filled gap)

Identical evaluations were done for the cooling case. The signs of temperature differences and the heat fluxes are reversed. This time the fluid absorbs heat and its temperature rises. The air releases heat accordingly and cools down. The excess temperature of the room facing surface is also negative, as temperatures below the room temperature must be realised to cool the room. With this in mind, identical statements can be made about the tendencies of the temperatures and heat fluxes.

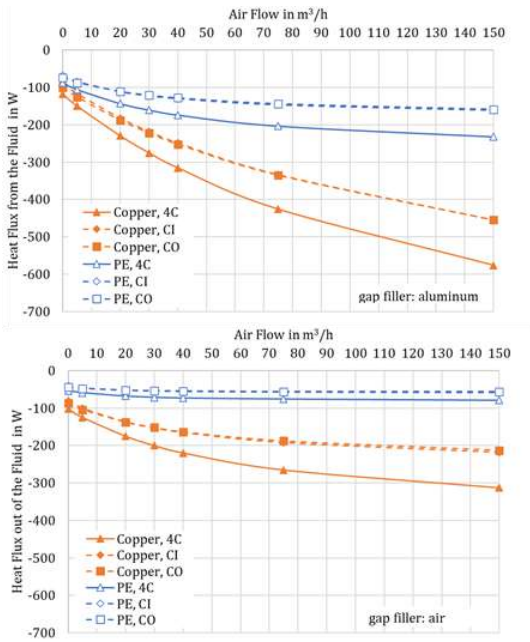

Fig. 17 – Heat flux from the heat transfer fluid for model V03

Also in the cooling case, good contact between the tube and the air channel is important for the performance of the system. The Cu/Alu case is therefore to be preferred in the cooling case. The

same applies to the comparisons between the geometry variants.

5. Conclusions

The study presented consists of experimental and extending numerical investigations. The geometrical models were comprehensively analysed and compared in terms of their thermal and energetic behaviour in heating. The given results for the heating case equally apply to the cooling case. As a result, the intended functional principle of implementing a surface heating/cooling with simultaneous conditioning of an air volume flow could be proven. Furthermore, influencing parameters on the thermal performance such as air volume flow, water volume flow and flow temperature of the water were worked out. The results of the experimental investigations under the given boundary conditions show that in the heating case an area-specific heating capacity of $\dot{q}_{room} = 130$ W/m^2 at the room facing surface can be achieved with a heating fluid of $\vartheta_{W,i} = 50$ °C. The same hybrid element extracts up to $\dot{q}_{room} = 30$ W/m^2 from the room with a fluid temperature of $\vartheta_{W,i} = 16$ °C in the cooling case. Depending on the design of the demonstrator, heat flux densities of up to $\dot{q}_{air} = 500$ W/m^2 can be transferred to the air at maximum air flow rate which results to a temperature increase of the air between $\Delta\vartheta_{air} = 7.5$ K … 11 K. Regarding the planned modes of operation, the potential control range can be defined on the basis of the course of the heat flux density to the air. The simulations carried out provided detailed findings on the influence of the thermal contact resistances between the tube and the surrounding OCPM or air channel. It is imperative to avoid high manufacturing tolerances to avoid unnecessary thermal resistances to the overall system. A very well-connected PE pipe achieves similar performance values as a copper tube with an air gap caused by manufacturing tolerances. Therefore, a lighter plastic pipe can be used if the heat transfer pipe is very well contacted. Using an OCPM reduces the possible surface temperatures by approximately $\Delta T = 5$ K, but forms a much more uniform temperature field where the spread between minimum and maximum surface temperature is reduced from $\Delta\vartheta_{SF} = 27$ K to only $\Delta\vartheta_{SF} = 13$ K in extreme cases. The heat transferred to the air flow is directly dependent on the number of active air channels, thus the position of the air channels inside the demonstrator is not relevant. The scalability of the element, the control and system integration into the building, the interaction with the user and an extensive field test are seen as the next steps.

6. Acknowledgement

This research was supported by the German Federal Ministry for Economic Affairs and Energy under the project number 03ET1512A-D

7. References

[1] Causone F., Baldin F., Olesen B. W., Corgnati S. P. Floor heating and cooling combined with displacement ventilation: Possibilities and limitations. Energy and Buildings. 2010;(42):2338-2352

[2] Riffat S. B., Zhao X., Doherty P. S. Review of research into and application of chilled ceilings and displacement ventilation systems in europe. International Journal of Energy Research. 2004;(28):257-286

[3] Khan Y., Khare V. R., Mathur J., Bhandari M. Performance evaluation of radiant cooling system integrated with air system under different operational strategies. Energy and Buildings. 2015;(97):118-128

[4] Hao X., Zhang G., Chen Y., Zou S., Moschandreas D. J. A combined system of chilled ceiling, displacement ventilation and desiccant dehumidification. Building and Environment. 2007;(42):3298-3308

[5] Andersen O., Kostmann C., Stephani G., Korb G. Application-related properties of sintered metallic fiber structures. MetFoam. 2003;481-486

[6] Fink M., Andersen O., Seidel T., Schlott A. Strongly orthotropic open cell porous metal structures for heat transfer applications. Metals. 2018;8(7):554

[7] Zhao C.Y. Review on thermal transport in high porosity cellular metal foams with open cells. Int. J. Heat Mass Tansf. 2012;55(13-14):3618-3631

[8] Veyhl C., Fiedler T., Andersen O., Meinert J., Bernthaler T., Belova I. V., Murch G. E. On the thermal conductivity of sintered metallic fibre structures. Int. J. Heat Mass Transf. 2012;55(9-10):2440-2448

[9] Schinke L., Schlott A., Beyer M., Seifert J., Fink M. Investigations on a hybrid element with cellular metallic material for heating, cooling and ventilation. E3S Web of Conferences 111, 01095 (2019), DOI:10.1051/e3sconf/201911101095.

[10] Glück, B. „Heizen und Kühlen mit Niedrigexergie (LowEx), Abschlussbericht, FKZ 0327370B," Westsächsische Hochschule Zwickau, Zwickau, 2008.

Data Statement

The datasets generated and analysed during the current study are not available because patent protection law votes are currently being carried out but the authors will make every reasonable effort to publish them in near future.

Relationship between bioaerosol particle size and ventilation removal for airborne infections

Yuta Muto [a], Sihwan Lee [b], Jaeung Hwang [a]

[a] Graduate Student, Faculty of Engineering, Shinshu University, Japan.

[b] Associate Professor, Graduate School of Environmental Studies, Nagoya University, Japan.

Abstract. It is now suggested that COVID-19 can cause airborne infection by fine particles called droplet nuclei and reducing the risk of indoor infection through ventilation is attracting attention as a part of countermeasures against infectious diseases. However, indoor ventilation planning does not take into account the deposition of fine particles on the floor due to gravitational settling or on the wall due to inertia, and thus there is an urgent need to establish appropriate ventilation rate and methods. Therefore, this study aimed to clarify the effect of gravitational settling of suspended particles and ventilation characteristics by natural ventilation using the temperature difference between indoor and outdoor, and evaluated the outflow characteristics and removal efficiency of suspended particles by natural ventilation using CFD analysis. When the outdoor temperature is 5 ºC, particles with a diameter of 80-100 μm are deposited on the floor by gravitational settling in about 20 seconds and are almost completely removed. Particles with diameters of 10 to 70 μm are also deposited by gravitational settling, but some of them are carried by the circulating flow generated in the room by natural ventilation, so the decay of concentration is slow. When the outdoor temperature is 35 ºC, particles with diameters of 30 to 100 μm are almost completely removed from the space in about 30 seconds due to gravitational settling and floor deposition by downward flow generated near the opening. Particles with a diameter of 10 to 20 μm are partially transported by the circulating flow, so that the concentration decay is slow.

Keywords. Virus, Particle, Ventilation, Gravitational Sedimentation, CFD
DOI: https://doi.org/10.34641/clima.2022.198

1. Introduction

The first case of coronavirus infection (COVID-19) was reported in Wuhan in December 2019, and then in March 2020, WHO considered COVID-19 a global pandemic based on the spread and severity of the infection. In November 2021, the cumulative number of infected people worldwide was more than 250 million, and the cumulative number of deaths was more than 5 million, and the disease continues to rage. Infectious diseases, such as COVID-19, SARS, MERS, and H1N1, cause symptoms when microorganisms invade and multiply in the human body. Infectious particles emitted by an infected person are dispersed into the air by sneezing, coughing, vomiting, talking, etc., and are then transmitted to the infected person. The size of droplets has a wide distribution, roughly from 1 to 1000 μm in size. The droplets of about 100 μm fall to the floor in a short time. However, droplets of 10 μm in size drift in the air and are transported by air currents, although not for a long time. In addition, it has been confirmed that many droplet nuclei with a diameter of 0.5 to 5.0 μm exist in the respiratory tract of an infected person, and are discharged into the air in the form of particles by coughing, etc., and remain floating in the room for a long time, increasing the risk of infection to the infected person. Ventilation rate and airflow patterns play an important role in airborne transmission of viruses in indoor environments. Currently, many organizations provided COVID-19 ventilation guidance including the Federation of European Heating, Ventilation and Air Conditioning Associations (REHVA). However, the guidance does not take into account floor deposition of fine particles such as droplet nuclei due to gravitational settling or wall deposition due to inertial forces, and thus cannot be said to be appropriate ventilation rate or ventilation methods. Therefore, the purpose of this study is to clarify the effect of gravitational settling of suspended particles and ventilation characteristics by natural ventilation using the temperature difference between indoor and outdoor, which is the simplest ventilation method, and to evaluate the outflow characteristics and removal efficiency of suspended particles by natural ventilation by CFD analysis.

Copyright ©2022 by the authors. This conference paper is published under a CC-BY-4.0 license.

2. Research methods

2.1 CFD analysis Model

Fig. 1 shows the CFD analysis model for the study, and Tab. 1 shows the CFD analysis model and boundary conditions. The model consists of an indoor space of 2.5(x) × 2.5(y) × 2.5(z) m and an outdoor space of 10.0(x) × 10.0(y) × 10.0(z) m. The outflow flow of polluted air and particulate matter from the indoor space is calculated through an opening of 2.1(y) × 0.8(z) m. The turbulence model is the Low-Re k-ε turbulence model, and the buoyancy force is the Boussinesq approximation. The concentration of polluted air and particles are uniformly distributed in the room as the initial conditions, and the time variation of the concentration of polluted air and particles in the room for 100 seconds is evaluated by unsteady CFD analysis. The indoor temperature is set to 20 ºC, and the outdoor temperature is 5 ºC and 35 ºC.

2.2 Boundary Conditions

The boundary conditions are Reflect for the indoor ceiling and walls and Escape for the indoor floor. The boundary conditions are shown in Fig. 2. In reflect boundary condition, the particle bounces off the boundary surface with a change in momentum defined by the repulsion coefficient. The normal coefficient of restitution defines the amount of momentum in the direction normal to the wall that is retained by the particle after the collision with the boundary. In escape boundary condition, the particle is reported as having "escaped'' when it encounters the boundary in question.

2.3 Passive Scalar and Discrete Phase Model

Tab. 2 shows the passive scalar and DPM. The initial concentration of polluted air in the room is set to be 1 as a passive scalar. About 530,000 particulate matter is uniformly distributed in the indoor space at intervals of 30 mm from a point 50 mm away from the inner surface of the indoor. The particles are water molecules with a diameter of 10-100 μm, and a non-evaporating model is adopted in this study.

As a preliminary study, the number of particles to be generated in a room space is examined. The particle spacing is set to 40-240 mm and particles are uniformly distributed in the indoor space (Tab. 3). The particle size is set to 10 μm, the indoor temperature is 20 ºC, and the outdoor temperature is 0 ºC. Fig. 3 shows the indoor concentration. As the number of particles increases, the concentration transition of the passive scalar tends to approach the concentration trend of the chemical species. The particle spacing of 30 mm, which is applied in the CFD analysis of regarding particle size, is considered to be a reasonable condition, as it appears to approach the concentration trends of passive scalar more closely.

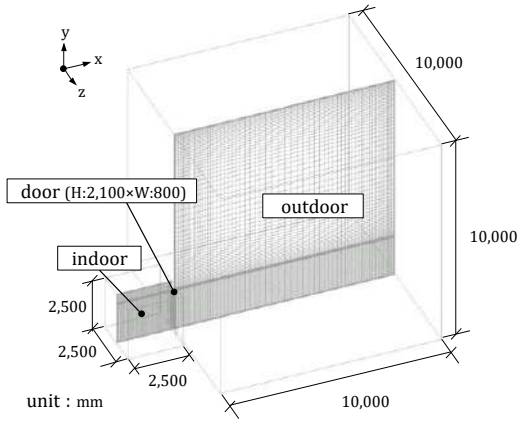

Fig. 1 - CFD analysis model.

Tab. 1 - Models and Boundary Conditions.

Models	
Scale	indoor: 2.5(x) × 2.5(y) × 2.5(z) outdoor: 10(x) × 10(y) × 10(z)
Turbulent	Low-Re k-ε turbulence model
Mesh	1,406,920 ea
Time step	Transient calculation (0.05 [s] × 2000 time steps)
Temperature	Indoor： 20 [ºC] ① Outdoor: 5 [ºC] (in winter) ② Outdoor: 35 [ºC] (in summer)
Buoyancy	Boussinesq approximattion
Boundary Conditions	
Wall, Top	Reflect
Floor	Escape

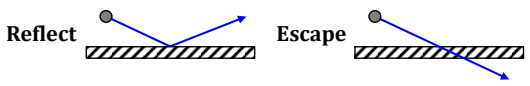

Fig. 2 - DPM Boundary Conditions.

Tab. 2 - Passive Scalar and Discrete Phase Model.

Passive Scalar	
Initial Concentration	Indoor: 1 Outdoor: 0
Discrete Phase Model	
Diameter	10-100 [μm]
Quantity	53,1441
Density	998.2 [kg/m^3]
Type	Inert
Material	Water-liquid
Drag law	Spherical

3. Results

3.1 In winter (outdoor: 5 ºC)

Fig. 4 shows the transition in indoor concentration of polluted air and particles by the natural ventilation system in winter (outside air: 5 ºC), Fig. 5 shows the behavior of particles. Particles with a diameter of 80-100 µm are deposited on the floor by gravitational settling in about 20 seconds, and they are almost completely removed from the space. Particles with a diameter of 10 to 70 µm are also affected by gravitational settling, but some of them are carried away by the circulating flow generated in the room by natural ventilation, so the concentration decay becomes slower.

3.2 In summer (outdoor: 35 ºC)

Fig. 6 shows the transition of indoor concentration of polluted air and particles by the natural ventilation system in summer (outside air: 35 ºC), Fig. 7 shows the behavior of particles. Particles with a diameter of 30 to 100 µm are almost completely removed from the space after about 30 seconds due to gravitational settling and deposition on the floor by the downward flow generated near the opening. Particles with a diameter of 10 to 20 µm are also affected by gravitational settling and downward flow, but as in the case of winter, some of them are carried away by the circulating flow, so the concentration decay becomes slow.

4. Conclusions

The results indicate that the particle removal efficiency of the natural ventilation methods across single-side opening depends on particle size and airflow characteristics. Large particles with diameters of 80-90 µm were deposited on the floor surface and removed in a short time due to the effect of gravitational settling, while small particles with diameters of 10-20 µm tended to decrease outflow to the outdoor by the circulating airflow, resulting in slow concentration decay.

5. References

[1] X. Xie, Y. Li, H. Sun, L. Liu. Exhaled droplets due to talking and coughing: J. R. Soc. Interface. 6. 2009: 703–714.

[2] C.-R. Du et al. Effect of ventilation improvement during a tuberculosis outbreak in underventilated university buildings: Indoor Air 30. 2020: 422–432.

[3] T. A. Myatt et al. Detection of airborne rhinovirus and its relation to outdoor air supply in office environments: Am. J. Respir. Crit. Care Med. 169. 2004: 1187–1190.

[4] J. Kurnitski. REHVA Covid guidance document 4.0: REHVA Eur. HVAC J., vol. 57, no. 6, 81–93.

Tab. 3 – Particle space.

Space [mm]	Quantity
240	1,331
200	2,197
160	4,096
120	9,261
80	29,791
40	226,981

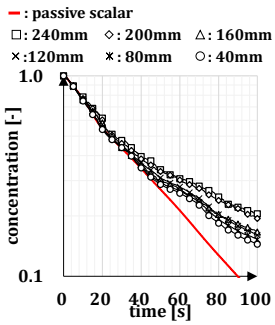

Fig. 3 – Concentration.

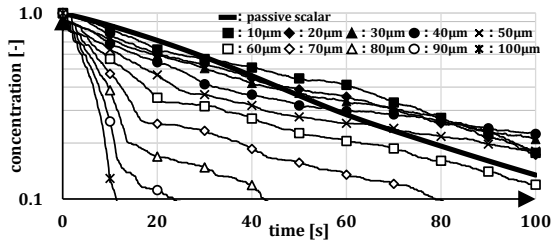

Fig. 4 - Concentration (in winter).

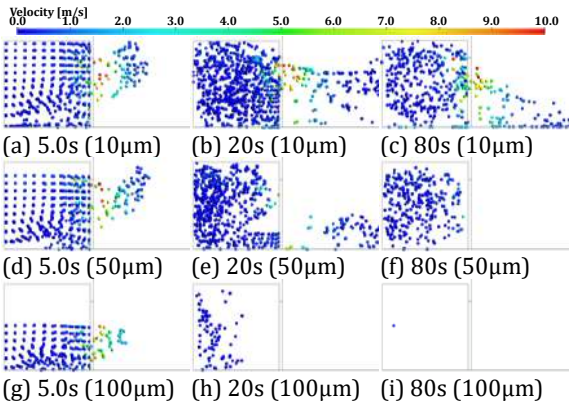

Fig. 5 - Particle behavior (in winter).

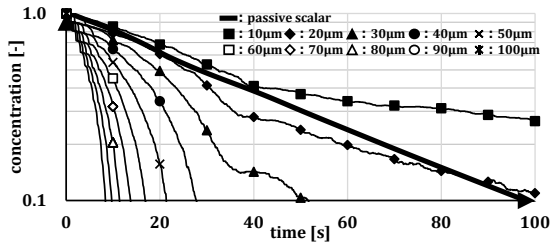

Fig. 6 - Concentration (in summer).

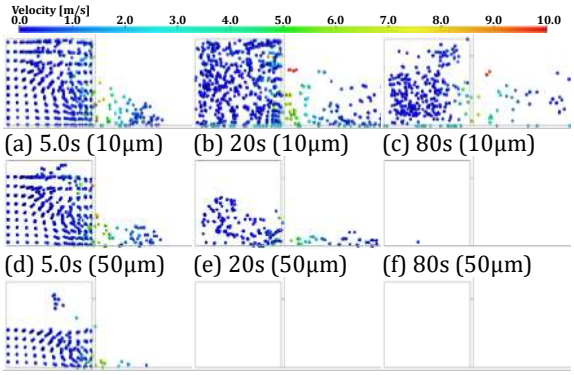

Fig. 7 - Particle behavior (in summer).

Development of an automatic sliding window system to control adequate ventilation rate

Akane Tsutsumi [a], *Sihwan Lee* [b]

[a] Graduate Student, Department of Engineering, Graduate School of Science and Technology, Shinshu University, Japan, email address [22w5013c@shinshu-u.ac.jp].

[b] Associate Professor, Graduate School of Environmental Studies, Nagoya University, Japan, email address [shany@nuac.nagoya-u.ac.jp].

Abstract. Under the influence of COVID-19, it is recommended to ventilate to reduce the risk of infection in the room. In an air-conditioned room, window open can increased the ventilation rate that caused by indoor and outdoor temperature difference. However, there is a concern that opening the window in the air-conditioned room will increase the heating and cooling loads due to air leakage. In addition, it is difficult to maintain the appropriate ventilation rate, because the outdoor air temperature changes from time to time. To solve this problem, we have developed an automatic window opening system to control the natural ventilation rate. This system can be controlling the appropriate ventilation rate for the room by adjusting the opening area of window automatically. In this study, actual measurements were conducted to understand the operating performance of the system, and its effect on the indoor thermal environment. The measurements were conducted in summer and winter season, and the results were compared between the developed window opening system and 95 mm width opened ordinary window. As a result, it was confirmed that the ventilation rate could be controlled by this system. In addition, in the case of the developed window opening system, the system controlled the ventilation rate when there was a large difference in indoor and outdoor temperatures, which prevented the deterioration of the indoor thermal environment and reduced the heating load compared to the ordinary window.

Keywords. Natural ventilation, Window, Ventilation measurement, Temperature.
DOI: https://doi.org/10.34641/clima.2022.264

1. Introduction

It has been reported by ASHRAE[1)] and others that securing adequate ventilation is effective to reduce the risk of infection such as COVID-19 in the room. Natural ventilation by opening windows and doors (see **Fig. 1**) is the simplest method to increase the ventilation rate when there is an indoor and outdoor temperature difference. However, there are concerns that opening the window in the air-conditioned room may be affected by the outdoor air temperature, resulting in poor heating and cooling efficiency and deterioration of the indoor thermal environment. Also, excessive ventilation may increase the heating and cooling load and power consumption. In addition, it is difficult to maintain the appropriate ventilation rate, because the outdoor air temperature changes from time to time. As a preliminary study, CONTAM was used to analyse the natural ventilation rate at a single opening. The opening conditions were as shown in **Table 1**, the outdoor condition was August 3, 2021, Nagano, and the indoor temperature was 26 ˚C. **Fig. 2** shows the results of the calculation using CONTAM. The ventilation rate exceeds 30 m^3/h during the daytime when the outdoor air temperature is high, but it does not meet the required ventilation rate during the hours when

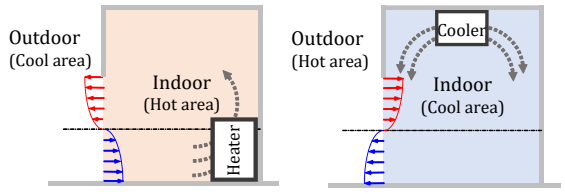

a) During cooling b) During heating
Fig. 1 - Natural convection in a single aperture.

Tab. 1 - Aperture conditions in CONTAM.

Model Summary	
Type	Two-way flow
Formula	One-opening
Model Parameters	
Height	2 m
Width	40 mm
Discharge coefficient	0.6

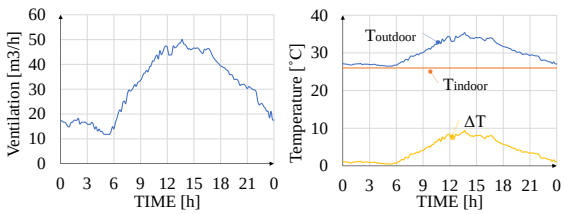

a) Ventilation rate b) Temperature
Fig. 2 - Calculation of ventilation rate by CONTAM.

Copyright ©2022 by the authors. This conference paper is published under a CC-BY-4.0 license.

there is little indoor and outdoor temperature difference. This indicates that it is not easy to maintain the proper ventilation rate by manually opening and closing the windows.

The purpose of this study was to develop an automatic window opening system to control the natural ventilation rate according. This system (see **Fig. 3**) can be controlling the appropriate ventilation rate for the room by adjusting the opening area of the window automatically. From the equation of Brown[2] (**Equation (1)**), we calculated the opening width when the required ventilation rate per person is 30 m^3/h[3) 4) 5)].

2. Methods

In this study, actual measurements were conducted to understand the operating performance of the system. To confirm the indoor thermal environment, measurements were taken in summer and winter. Results were compared between the automatic window opened by this system and the ordinary window opened at 95 mm in width. The width of the automatic window opened by this system was adjusted every 30 seconds. Also, there are two types of window openings: constant opening and intermittent opening. In the case of intermittent opening, the concentration of pollutants in the room increases while the window is closed. So, the actual measurements were conducted with the window constantly open.

Fig. 4 shows the target experimental building in Takaoka city, Toyama, and **Fig. 5** shows the temperature measurement points. Both rooms have a floor area of 6.25 m^2, a room volume of 15 m^3, and a window height of 2 m. The ventilation rate using the constant concentration method, indoor temperature distribution, and power consumption were measured. In addition, to understand the external environment, the outdoor temperature, wind direction and speed, and solar radiation were measured.

3. Results of the study in summer

The measurement was conducted on September 11, 2021, and all air conditioners in both rooms and the corridor were set at 22 ˚C.

3.1 ventilation rate

Fig. 6 shows the measured ventilation rate. **Fig. 7** shows the results of the temperature changes, and the opening width of the window using this system. According to the results, in the case of the automatic window opened by this system, the ventilation rate was generally maintained at 30 m^3/h throughout the day. The daily average ventilation rate was measured to be about 28.9 m^3/h. On the other hand, in the case of the ordinary window opened at 95 mm in width, the ventilation rate increased during high outdoor temperatures. The average ventilation rate during the daytime (9:00 to 18:00) was measured to be

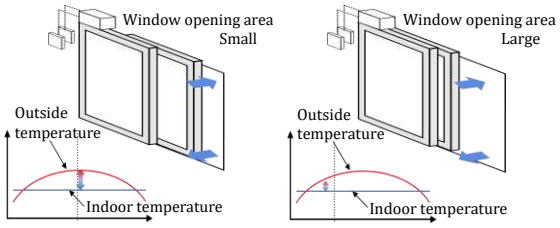

a) ΔTemperature large b) ΔTemperature small

Fig. 3 – The automatic window opening system.

Eq. 1 - The equation of Brown[2].

$$Q = \frac{\alpha A}{3}\sqrt{\frac{2\Delta P}{\rho}} \qquad (1)$$

where Q is the ventilation rate [m^3/s], α is the flow coefficient [-], A is the window opening area [m^2], ρ is the fluid density of air [kg/m^3], and ΔP is the pressure difference between indoor and outdoor [Pa].

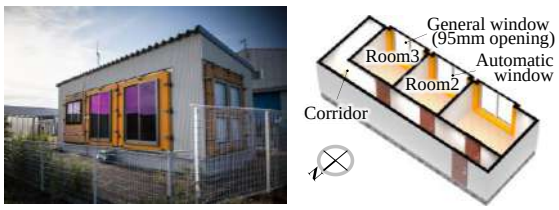

a) External view b) Interior view

Fig. 4 - Overview of the experimental building.

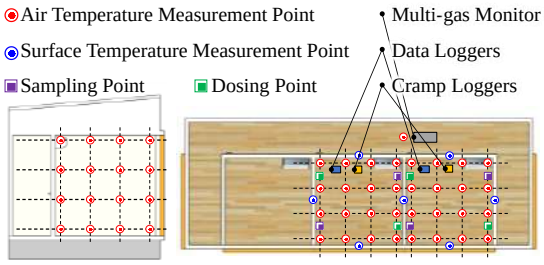

Vertical section Horizontal section temperature

Fig. 5 - Temperature measurement points.

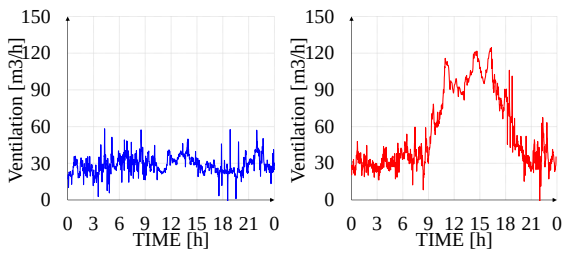

a) Automatic window b) Ordinary window

Fig. 6 - Ventilation rate.

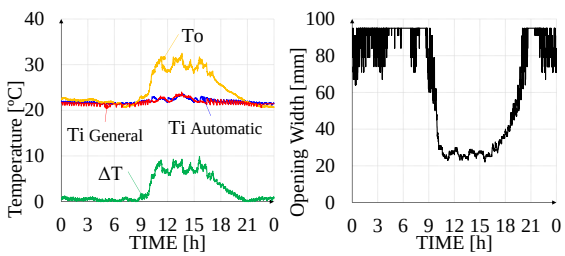

a) Temperature b) Opening width

Fig. 7 - Temperature changes and opening width.

about 65.6 m³/h. The system adjusted the opening width according to the indoor and outdoor temperature difference. It was confirmed that the ventilation rate could be controlled by using this system.

3.2 indoor thermal environment

Fig. 8 shows the horizontal temperature distribution in the room at 10:00 and 13:00, and **Fig 9** shows the vertical temperature distribution in the cross-section of the opening at 13:00. In both rooms, the indoor temperature was generally maintained at the set temperature of 22 ˚C. However, in the case of the ordinary window opened at 95 mm in width, the indoor temperature increased slightly due to the high outdoor temperature and increased air leakage. The maximum indoor and outdoor temperature difference was measured at 9.9 ˚C in the room with the automatic window opened by this system.

3.3 power consumption

Fig. 10 shows the power consumption of the air conditioner in each room. There was no significant difference between the two rooms, and the air conditioner operated at about 0.1 kW to 0.15 kW during the daytime when power consumption was high. However, in the case of the ordinary window opened at 95 mm in width, it operated at about 0.18 kW from 13:00 to 14:00. Due to increased air leakage, the cooling load temporarily increased.

4. Results of the study in winter

The measurement was conducted on December 5, 2021. The air conditioner was set at 28°C to provide indoor and outdoor temperature difference.

4.1 ventilation rate

Fig. 11 shows the measured results of the ventilation rate. **Fig. 12** shows the results of the temperature changes, and the opening width of the window using this system. According to the results, in the case of the automatic window opened by this system, the ventilation rate was controlled throughout the day. Although the daily average ventilation rate was measured to be about 46.3 m³/h, which was about 16 m³/h higher than the controlled rate of 30 m³/h. Based on the results of the opening width, the ventilation rate was calculated to be about 28.4 m³/h by the theoretical formula. It was confirmed that this system was working properly. In winter, when the indoor and outdoor temperature difference is large, the opening width becomes very small, so errors are likely to occur. Also, the ventilation rate may have increased due to the influence of the window frame. On the other hand, in the case of the ordinary window opened at 95 mm in width, the daily average ventilation rate was measured to be about 184.5 m³/h. It was because the difference in indoor and outdoor temperatures was large that the ordinary window was always had excessive ventilation. During the daytime, the outdoor temperature rise,

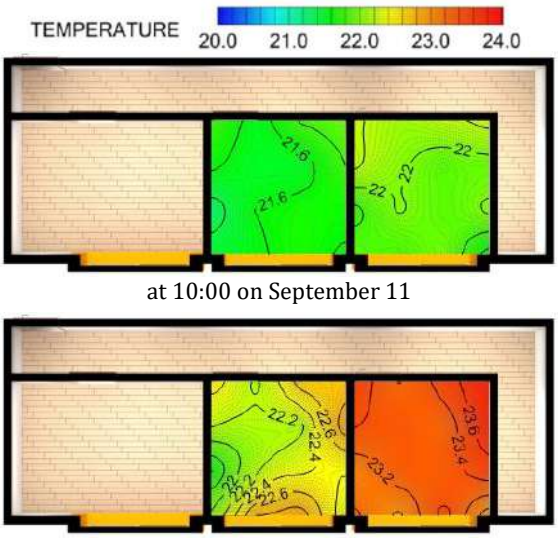

at 10:00 on September 11

at 13:00 on September 11

Fig. 8 - Horizontal temperature distribution.

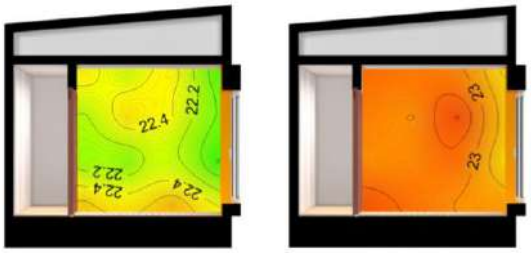

a) Automatic window b) Ordinary window

Fig. 9 - Vertical temperature distribution.

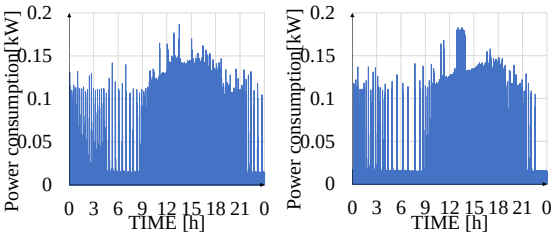

a) Automatic window b) Ordinary window

Fig. 10 - Power consumption of the air conditioner.

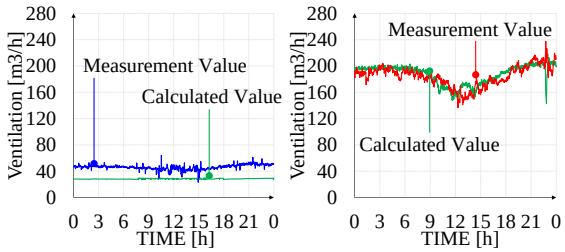

a) Automatic window b) Ordinary window

Fig. 11 - Ventilation rate.

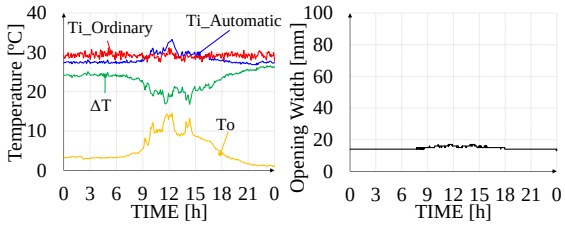

a) Temperature b) Opening width

Fig. 12 - Temperature changes and opening width.

and the indoor and outdoor temperature difference became smaller, so the ventilation rate decreased.

4.2 indoor thermal environment

Fig. 13 shows the horizontal temperature distribution in the room at 13:00 and 22:00. In both rooms, during the daytime when the outdoor temperature was high, the indoor temperature was around 28 °C, which is the set temperature. However, as the outdoor temperature decreased, the indoor temperature near the openings also decreased. Especially in the case of the ordinary window opened at 95 mm in width, the indoor temperature was affected by the outdoor temperature due to increased air leakage. The temperature difference in the room was large, and the indoor temperature near the opening was lower by about 6 ˚C or more. **Fig. 14** shows the vertical temperature distribution in the cross-section of the opening at 22:00. In the case of the ordinary window opened at 95 mm in width, cold drafts occur due to large air leakage. In winter, the occurrence of cold drafts was reduced by using this system.

4.3 Power consumption

Fig. 15 shows the power consumption of the air conditioner in each room. In the case of the automatic window opened by this system, the air conditioner operated at about 0.2-0.4 kW. On the other hand, in the case of the ordinary window opened at 95 mm in width, the air conditioner operated at about 0.5-1.1 kW during other the hours when the indoor and outdoor temperature difference was large. It indicated that using this system prevented the increase of heating load due to excessive ventilation, and saved energy compared to the ordinary window opened at 95 mm in width.

5. Conclusion

In this study, we developed an automatic window opening system to control the natural ventilation rate. The following findings were obtained from the study.

(1) This system was able to control the ventilation rate, and the daily average ventilation rate was about 28.9 m^3/h throughout the day in summer. However, in winter, the daily average ventilation rate was controlled at about 46.3 m^3/h.

(2) The ventilation rate controlled by this system prevented the deterioration of the indoor thermal environment and the occurrence of cold drafts, in winter.

(3) By controlling the ventilation rate to prevent excessive air leakage, the heating load was reduced, and power consumption was reduced.

6. Acknowledgement

We would like to express our gratitude to Sankyo Tateyama,Inc. SankyoAlumi-Company for their cooperation in conducting this study.

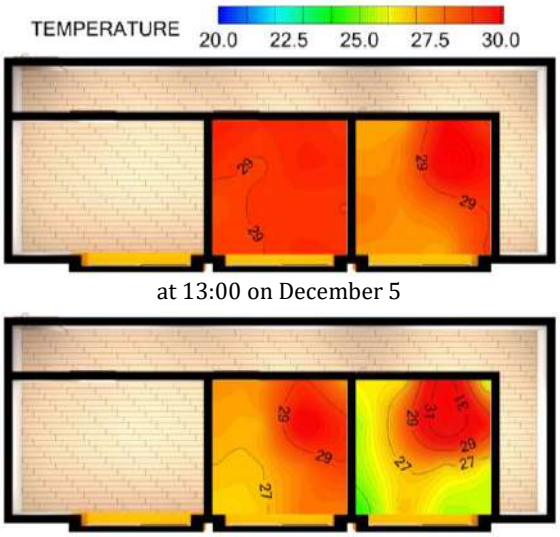

at 13:00 on December 5

at 22:00 on December 5

Fig. 13 - Horizontal temperature distribution.

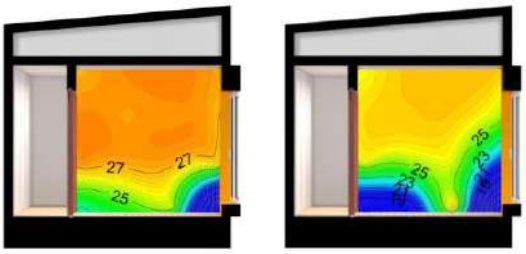

a) Automatic window b) Ordinary window

Fig. 14 - Vertical temperature distribution.

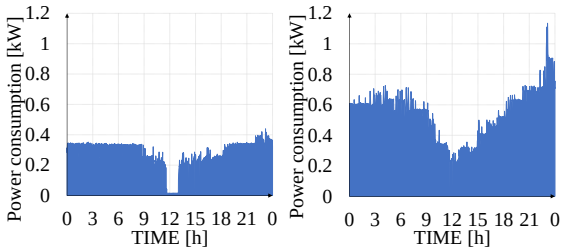

a) Automatic window b) Ordinary window

Fig. 15 - Power consumption of the air conditioner.

7. References

[1] ASHRAE Epidemic Task Force: Residential building guidance, 2020.

[2] Brown W.G., Solvason K.R., 1962, Natural convection through rectangular openings in partitions Pt. 1: Vertical partitions, International Journal of Heat and Mass Transfer, 5, p.859-868.

[3] ASHARE: ASHRAE Standard 62.1 2019, Ventilation for Acceptable Indoor Air Quality, 2019.

[4] REHVA COVID-19 guidance document, August 3, 2020.

[5] Ministry of Health Labour, and Welfare. For managers of commercial and other facilities: ventilation methods to improve closed space with poor ventilation. April 3, 2020.

Review of health and well-being aspects in Green Certification Protocols

Cécile Berquand[a], Verena M. Barthelmes[a], Giorgia Spigliantini[b], Giulia Vergerio[b], Cristina Becchio[b], Stefano P. Corgnati[b], Dolaana Khovalyg[a]

[a] Integrated Comfort Engineering (ICE), École polytechnique fédérale de Lausanne (EPFL), Switzerland

[b] TEBE-IEEM Research Group, Energy, Politecnico di Torino, Italy

Abstract. Over the past decades, the world-leading Green Certification Protocols have paid increasing attention to health-related aspects of buildings. However, the way and the extent to which green certifications currently account for these aspects vary largely. This paper aims to review and compare four certification protocols, namely LEED v4, BREEAM 2018, WELL v2, and MINERGIE-ECO v1.4, and to provide insights on how aspects related to occupants' health and well-being and their influencing factors are accounted for and assessed. To that scope, indicators used to assess the users' health and well-being are extracted from each certification and compared. Indicators traditionally used to evaluate IEQ in buildings (thermal, indoor air quality, visual and acoustic) based on international or national standards were found in all certifications. However, the analysis highlights that their assessment and verification stage (e.g., pre- vs. post-occupancy) significantly differs from one label to another. More "advanced" indicators, which are related to mind, promotion of physical activities, and community engagement, have come to light. While a comprehensive approach to the evaluation of well-being might include a combination of objective (e.g., measurement-based evaluations) and subjective components (e.g., people's subjective evaluation), the review highlighted that only in one protocol (i.e., WELL), direct feedback from occupants is kept in the loop for further optimization of the building management during operation. Otherwise, indicators are mainly verified through quantitative measurements, reports, or implemented policies.

Keywords. Indoor Environment, Green Certification, Health, Well-being
DOI: https://doi.org/10.34641/clima.2022.322

1. Introduction

As stated in the ASHRAE guidelines, humans spend up to 90% of their day inside buildings [1]. Providing an adequate level of indoor environment quality (IEQ) is then crucial to the users' health and well-being. As demonstrated by past studies, a low IEQ can trigger a range of negative effects, from loss of productivity to illnesses such as Sick Building Syndromes (SBS). Buildings should then not only be designed to be energy efficient but to provide a positive impact on their occupants. In this context, well-being and health-related aspects are becoming a growing concern in Green Certifications. However, the notions of health and well-being are complex to measure as they can differ from one person to another. For this reason, there is growing attention in shifting from traditional Key Performance Indicators (KPIs) of buildings behaviour to Health Performance Indicators (HPIs) of the whole occupant-building system. HPI can be defined as "quantifiable measures of human health that can be used to identify drivers of negative and positive impacts of buildings on health, productivity and well-being of occupants." [2] They can be direct or indirect, depending on whether they measure people or the building, respectively. Indeed, the experience of users is considerably impacted by the quality of the indoor environment that depends on air quality, sound protection, thermal comfort, lighting, security, water quality, and view quality. The current study aims to identify the various indicators influencing the user well-being that are deployed in Green Certifications schemes. To do so, a review of three main certifications used worldwide, BREEAM v3 2018 [3], LEED v4 2014 [4-5], WELL V2.2018 [6] was done. Additionally, a national certification Minergie-Eco v1.4 2018 [7-8] was also reviewed as it is the main one used in Switzerland. The indicators to assess the users' health and well-being were extracted from each certification and compared. Traditional indicators related to indoor air quality, sound protection, thermal comfort, lighting were

Copyright ©2022 by the authors. This conference paper is published under a CC-BY-4.0 license.

found in all certifications. Advanced categories such as mental health, promotion of physical activities, and support of the users, were introduced to a different extent in LEED v4 2014, BREEAM v3 2018, and mostly in WELL V2.2018. A comparison of how each indicator is meant to be assessed in each label and at which stage was also done. The methodology of the review approach is described in Section 2. Individual protocols are critically described in Section 3, and Section 4 reports the main results. Finally, the main conclusions are outlined in Section 5.

2. Methodology

This study was performed in two stages. Firstly, an analysis of individual certificates was done to better understand each of the selected Green Protocols. The individual analysis allowed to compare the assessment method, rating system, and references used by the certifications (Section 3). Additionally, all health-related categories and indicators were extracted from the protocols. The list of indicators was classified into different categories and indicators individually studied to assess how (e.g., type of evidence needed) and at which stage (e.g., pre- vs. post-occupancy) they were treated in each protocol (Section 4). Two different levels of comparison were, thus, used to explore the similarities and differences of the health and well-being approach of studied protocols:

- *Large scale (Section 3):* it assesses the different health-related categories included in each protocol, their rating method, and, finally, the main standards and references used by the certification schemes.

- *Indicator Scale (Section 4)*: it highlights the different ways performances indicators were treated in each protocol and at which stage.

It must be mentioned that only online open-source descriptions of selected Protocols were used for the review. Additional information can be provided once the project is launched. It is the case, for example, for the LEED certificate where an additional guide is obtained when a project is launched and gives all the information for the project team to achieve the credits. [9]

3. Overview of selected Green Protocols

BREEAM v3 2018

Launched in 1990 by the Building Research Establishment (BRE), this label represents the world's first sustainability rating scheme for the built environment. It proposes an environmental assessment method to optimize and reduce the impact of the built environment. This protocol is mainly based on International, European and British Standards. The version studied is the third one set in 2018 for New Constructions. It is composed of 9 categories: Management, Health & Well-being, Energy, Transport, Water, Resources, Resilience, Land Use & Ecology, and Pollution. Overall, 49 issues are treated, 6 of them concern Well-being. Then, each issue is decomposed into different criteria and linked to a number of credits. The six health issues are linked to the following credits: visual comfort (5 credits), indoor air quality (6 credits), thermal comfort (3 credits), acoustic performance (3 credits), security (1 credit), and safe & healthy surroundings (2 credits). Four of the six issues deal with the environmental hazard, with special importance given to the visual comfort and indoor air quality, representing 11 of the 20 available credits. The other two issues are more advanced by dealing with the security on-site and the surroundings of the project (outdoor space and site access). Overall, the health and well-being category is the third most important category with a weight of 14% behind the energy (16%) and material (15%) ones. Nevertheless, to obtain the certificate, a project must achieve a certain number of points and respect 11 minimum criteria. However, none of them are health-related, and no minimum amount of points is required per category. Hence, even if the weighting of the health category is important, a project could obtain the certification without dealing with many health-related criteria.

The assessment method is composed of two main phases, one at the design stage and a final one at the post-construction stage, during which the final grade is given. For each stage, the project team has to provide diverse evidence. The final grade is calculated as the sum of the ratio between the number of credits achieved and available ones in each category times the weight of the category. Then, according to the grade, a certain level of certification is reached: Pass (30-45%), Good (45-55%), Very Good (55-70%), Outstanding (>85%)

LEED v4 2014

The first pilot of LEED was launched in 1998 by the US Green Building Council, created in 1993. LEED is the most used green building rating system. The certification focuses not only on the building energy performance but also on its surroundings and sustainability. The aim is to realize healthy, highly efficient, and cost-saving green buildings. A variety of protocols have been developed through the years dealing, for instance, with Building Design and Constructions, Interior Design and Construction, Operations and Maintenance. In the current review work, the protocol V4 launched in 2014 for Building Design and Construction was studied.

The protocol includes 6 main categories divided into mandatory prerequisites and optimizations, which provide a certain amount of points. Tab. 1 describes the distribution of preconditions (P), optimizations (O), and the available points, respectively, for each concept of the LEED v4. Specific evidence is required for each criterion to obtain the credits. The

assessment method is divided into two phases: an intermediate evaluation at the design stage and a final evaluation post-construction.

There is a significant difference in points granted per category. The Location & Transportation category, as well as the Energy & Atmosphere category, contribute 28.7% each to the global weighting, while the other categories do not exceed 10%. The Indoor Environmental Quality (IEQ) is only composed of two prerequisites dealing with the minimum indoor air quality performance and tobacco smoke control. However, IEQ category is also composed of 8 optimizations. Its total weight is around 14%, which shows fewer points are granted for these optimizations compared to the ones from other categories. Other well-being and health-related aspects are found, for instance, in the Sustainable Site category (e.g., environmental site assessment, outdoor thermal comfort, access to nature) or the Location & Transportation category (e.g., promotion of walking and cycling, site location).

Tab.1 – LEED distribution of precondition (P), optimization (O), points, and weight [4]

	P	O	Points	Weight
Integrative process	1	1	1	0,87%
Location & Transportation	0	8	33	28,70%
Sustainable Site	2	6	10	8,70%
Water Efficiency	3	4	11	9,57%
Energy and Atmosphere	4	7	33	28,70%
Materials and Resources	3	5	11	9,57%
IEQ	2	8	16	13,91%

As for BREEAM, the rating system is point-based and different levels of certification are granted according to the number of points achieved: Bronze (40), Silver (50), Gold (60), Platinum (80). Additionally, all prerequisites are mandatory and should be respected. However, conversely to BREEAM, the weight of each category does not interfere with the final grade. This has a consequent impact on how health and well-being could be considered by the rating system in each protocol. Indeed, the point-based rating system presents a strong disadvantage that the different categories could be unequally treated in a project. By introducing, the weight of each category in the final grade, the project team is encouraged to treat all the categories to not strongly diminish its final grade. Nevertheless, the project could still obtain the certificate. Besides this difference, the two protocols appear very similar (see Tab 4) as they present the same assessment methods, which are mostly based on national and international standards.

WELL V2.2018

The certification was first introduced in 2014 by the International WELL Building Institute (IWBI). A second version was launched in 2018, and it is the one used for the current review. WELL proposes a unique scheme with a human-focused approach. The protocol does not only aim at providing a healthy and comfortable environment to building occupants but also at influencing them to adopt healthier behaviour. It is based on the expertise of WELL users, practitioners, public health professionals, and building scientists around the world. Therefore, it is established not only on international, national standards or regulations but also on a large pool of scientific research.
The protocol is divided into 10 concepts. Each of them is a combination of *mandatory preconditions* (P) and *optimizations* (O) that provide a certain amount of points. The distribution is shown in Tab 2. A visible concern is given to more advanced concepts as they represent almost 50% of the weights: community (19,4%), mind (9,7%), nourishment (8,2%), and movement (10,7%). Conversely, less weight is given to more established in other schemes categories such as water quality. This might be explained by the fact that in many countries, several conditions on different concepts would be already met by international and national regulations. Hence, the protocol gives more importance to health-related aspects not or little present in standards.

Tab.2 – WELL distribution of precondition (P), optimization (O), points and weight [2]

	P	O	Points	Weight
Air	4	10	18	9,2%
Water	3	6	14	7,1%
Nourishment	2	12	16	8,2%
Light	2	7	18	9,2%
Movement	2	9	21	10,7%
Thermal Comfort	1	8	18	8,2%
Sound	1	8	18	9,2%
Material	3	9	19	9,2%
Mind	2	9	19	9,7%
Community	4	14	38	19,4%

The rating system is point-based. However, in order to assure the project team does not focus on specific concepts only, a maximum and a minimum level of points can be achieved in each category. A maximum of 12 points is set for all the categories. All mandatory preconditions should be achieved as well. Then, according to the number of points obtained, the following level of certification is given (Tab 3).

Tab. 3 - WELL level attainment according to the number of points and minimum points per concept achieved [2]

Points achieved	Minimum Points per concept	Level
40	0	Bronze
50	1	Silver
60	2	Gold
80	3	Platinum

The grade is granted after the final assessment, at which the project team must provide evidence foreach optimization pursued. However, conversely

Tab. 4 – Large scale comparison of the 4 green certifications

	HEALTH AND WELL-BEING DOMAINS												
	Visual	IAQ	Water	Acoustic	Thermal Comfort	Material	Safety	Movement	Nourishment	Mind	Community	Method	References
BREEAM	x	x	x	x	x	x	x					Point – based system Category weighting Mandatory criteria	British (BS), European (EN) and International (ISO) Standards, CIBSE
WELL	x	x	x	x	x	x	x	x	x	x	x	Point – based system Minimum points per concept Mandatory criteria	British(BS), European (EN) and International (ISO) Standards, CIBSE World Health Organisation, ASHRAE, US Green Council LEED and scientific researches
MINERGIE-ECO	x	x	x	x	x	x						Traffic light system Mandatory criteria	SIA, MoPEC
LEED	x	x	x	x	x	x	x					Point – based system Mandatory criteria	ASHRAE, European (EN) and International (ISO) Standards, CEN, ASTM

to other schemes such as Minergie-Eco, even after the certification, spot or annual measures, reports, monitoring data, or even surveys should be reported. In all aspects presented (see Tab 4), WELL appears more advanced on the approach of health and well-being related aspects. Indeed, almost all "advanced" domains (Movement, Nourishment, Mind, Community) are only included in WELL. Additionally, the protocol differentiates itself by including scientific research and requiring minimum points per concept, thus, balancing the treatment of each category.

MINERGIE-ECO v1.4 2018

Minergie is a Swiss Label launched in 1998 which focuses on the building's energy efficiency. Through the years, different versions of the certification appeared: Minergie P (2003), Minergie A (2011). These versions treat the building performances and hence, in a certain way, users' comfort. The studied protocol is the extension Minergie-Eco, which was created in 2006 to deal with specific aspects of health (optimized daylight condition, low noise emissions) and ecology of the construction. Conversely to the other protocols, the label is mostly based on the Swiss norms SIA and the national regulations such as MoPEC [7]. Therefore, the Green Protocol could be seen as a continuation of the Swiss regulations and is focused on the Swiss-built environment.

As for the other labels, the protocol includes minimal criteria, called *excluding criteria*, needed to be respected to obtain the certifications. The Green Protocol is then divided into two main categories dealing with health and building ecology. Each of these categories is then divided into different sub-categories. The health sub-categories deal with daylight, noise protection, and indoor climate. Each of these subsections includes diverse criteria. Overall, the certification includes 81 criteria, with 12 excluding ones and 69 non-prerequisites.

The latter ones are distributed in two categories, with 36 in the health category and 33 dealing in the building construction ecology one. Most of the health criteria deal with indoor climate and noise protection. [8] The assessment method consists of two stages, one during the design phase and one in the post-construction phase. During the design phase, a provisional certificate is given, and it lasts for 3 years. After the construction, an evaluation of the project is done, and a permanent certificate is granted. Conversely to other protocols, the system is not point-based but uses a traffic light system. For each subcategory, a colour is given according to the percentage of requirements achieved: Red: ≤50%, Orange: 50-70%, Green: ≥70%. To obtain the certification, all *excluding criteria* should be fulfilled, and the colour obtained by the subcategory should not be red and at least 3 of them should obtain a green colour. This rating system differentiates from the point-based one used in all the other studied certificates as all the criteria must be treated to a certain extent. It represents an upgrade for health and well-being as energy efficiency categories are usually prioritized.

4. Indicators scale critical review

By extracting well-being and health-related indicators from the analysed Green Protocols, an important diversity of health-related aspects could be observed. Indeed, these ones were considered differently and at different stages by the Green Certifications. Therefore, a final table (Tab.6) was designed to report all the health-related indicators organised in different categories, indicate the type of evidence required, and whether it was verified at pre- or/and post-occupancy. The different types of evidence are summarized in Tab.5; mandatory requirements are highlighted in orange (e.g., o).

The extracted list of indicators could be divided into three main groups: Environmental Hazard, Building

and Architectural Design, and Social Factor. Environmental Hazard is addressed in all the studied certifications, while the other two groups seem more advanced. This can be explained by the fact that the former concerns traditional and well-known health and comfort aspects such as indoor air quality, thermal comfort, or acoustic.

Concerning the identified HPIs, with regard to the Building and Architectural Design, they can be grouped into three sub-categories, namely material selection, physical activities promotion, and site environment. The material selection takes part of the pollutant source management approach present in all the studied Green Protocols. Most of its indicators are related to lowering the exposure to pollutants and material transparency. The other two sub-categories are less represented in the certification as they are included in an approach of not only considering the design of the building itself but also its surroundings and how to influence the users to increase their physical activities. This approach is mostly embodied by the WELL certification. The most innovative group observed is the Social Factor one, as it considers how to improve the users' behaviour and mental health thanks to supporting, programs, or prevention. It considers the daily life in the building and not only the design and operation of the building.

This observation represents a key point as two distinct approaches are taken by the certifications. The first approach is focused on the building characteristics and how they directly impact the occupants. For instance, indoor air quality is provided thanks to source control of pollutants (e.g., material selection) and efficient management of pollutants (e.g., ventilation design, pollutant concentration monitoring). However, a complementary second approach observed is rather human-focused and consists in how the occupant could be influenced to adopt healthier behavior. For instance, the practice of physical activities could be encouraged by promoting the use of stairs but also cycling thanks to the presence of bike storage, on-site showers, or the connection to a qualitative bicycle network. This second approach also inspects how the user will behave and feel in the building; mental as well as physical well-being are both considered. This mix of approaches is characteristic of the WELL label, which is human-focused and even integrates the implementation of policies to increase the occupants' well-being. Conversely, the other certifications BREEAM, Minergie-Eco, and LEED seem more traditional as they focus mostly on the building itself. LEED mostly focuses on the site environment and connection to mobility, such as access to mass transit or bicycle/pedestrian access. BREEAM as well considers the safety and quality of the access to the project. These criteria are mostly concerned the users' arrival and departure from the building. No specific regulations or policies are planned for the post-occupancy and how the users will feel or act in the building. This difference is also stressed by the fact that WELL is the only protocol assessing the post-occupancy stage. As WELL is a more human-centered protocol, it highlights certain limits of Green Certifications when it comes to measuring and assessing people's health and well-being in buildings. Focusing on *when* (pre/post occupancy) and *how* (i.e., types of evidence) health and well-being are assessed, a lack of post-occupancy management and subjective measures such as occupants' feedback or surveys is observed through most of the protocols. Several reasons could explain this as Minergie-Eco tends to be a continuity of the Swiss norms and focuses on the building performances. The label only requests reports or measurement types of evidence. No post-occupancy management is considered, however, the protocol reserves the right to proceed to a spontaneous evaluation during the 5 years of post-certification. Concerning BREEAM and LEED, other schemes could be available to assess the post-occupancy stage, but it would mean for the project team additional work and costs. On another level, BREEAM does not require specific evidence for each criterion but proposes a list of evidence possible to the project team that could also show a will to simplify the procedure for the project team.

Tab. 5 - Legend used in the tables Tab. 6 to distinguish the different type of evidence

Type of Evidence	Frequency: Punctual	Frequency: Multiple
Report (photo, document, calculations, simulations, maintenance report)	o	oo
Measure (data report)	x	xx
Subjective measure (survey)	§	§§
Implemented policy and schedule		Δ

5. Conclusions

A distinct list of Health Performance Indicators was extracted from the review of four selected Green Certification Schemes in this work. The list was organised into 3 main domains, with a traditional one concerning the Environmental Hazard treated by all protocols. Fewer protocols consider Building and Architectural Design as this domain is mostly assessed with material selection in BREEAM and Minergie-Eco. Finally, only WELL treats the Social Factor domain.

Even though health-related aspects are a growing concern in Green Certifications, improvements still need to be done. Important limits could be pointed out concerning the point-based rating systems. Indeed, even if preconditions are mandatory, they do not necessarily concern health-related aspects (e.g., BREEAM). Furthermore, conversely to WELL, BREEAM and LEED protocols do not set a minimum and maximum amount of points achieved by

categories. Therefore, a project team could mainly focus on building energy efficiency and cost savings. However, a minimum of points required per category only interferes when at least the silver level of WELL is reached. Additionally, only 1 to 3 points are required per concept, which seems little considered to the number of points available through all the concepts. Regardless, WELL seems more user-centered, and more explicitly focused on health and well-being aspects. A lack of post-occupancy management, as well as subjective measurements, are also pointed out. The impact of this lack should be further studied. As this study only used open-source documents, the present review can be complemented with more details once the full text of the certification documents are available (for example, for a specific project going after green certification). Finally, since BREEAM and LEED certifications both include a post-occupancy scheme, a further analysis of these ones should be done.

6. References

1. US EPA O. Indoor Air Quality [Internet]. 2017 [cited 2021 Dec 18]. Available from: https://www.epa.gov/report-environment/indoor-air-quality
2. Allen JG, MacNaughton P, Laurent JGC, Flanigan SS, Eitland ES, Spengler JD. Green Buildings and Health. Curr Environ Health Rep. 2015 Sep;2(3):250–8.
3. BREEAM: the world's leading sustainability assessment method for masterplanning projects, infrastructure and buildings [Internet]. BREEAM. 2018 [cited 2021 Jun 28]. Available from: https://www.breeam.com/
4. LEED | Leadership in Energy & Environmental Design [Internet]. [cited 2021 Jun 28]. Available from: http://leed.usgbc.org/leed.html
5. LEED v4.1 | U.S. Green Building Council [Internet]. 2014 [cited 2021 Jun 28]. Available from: https://www.usgbc.org/leed/v41?creative=340432438239&keyword=building%20certificate&matchtype=b&network=g&device=c&gclid=EAIaIQobChMInY_ggb268QIVi7d3Ch2i9A67EAAYASAAEgKiNPD_BwE
6. Standard | WELL v2 [Internet]. 2018 [cited 2021 Jun 16]. Available from: https://v2.wellcertified.com/wellv2/en/water/feature/6
7. En bref - MINERGIE Schweiz [Internet]. [cited 2021 Jun 28]. Available from: https://www.minergie.ch/fr/a-propos-de-minergie/en-bref/
8. Kellenberger D. MINERGIE-ECO® 2011 – definition of thresholds in an LCA-based building label. 2018;8.
9. LEED Reference Guide for Building Design and Construction | U.S. Green Building Council [Internet]. 2013 [cited 2022 Jan 7]. Available from: https://www.usgbc.org/resources/leed-reference-guide-building-design-and-construction

Tab 6 - List of health-related indicators present in the selected Green Certifications Protocols. The types of evidence needed to assess the different indicators are listed in table 5.

		Indicators	Required evidence							
			BREEAM		MINERGIE - ECO		WELL		LEED	
			Pre	Post	Pre	Post	Pre	Post	Pre	Post
Environmental Hazard	Visual- Lighting	Visual lighting design (light level, illuminance)	o				o		o	
		Natural daylight design (illuminance, daylight factor, circadian rhythm)	o		o		o		o	
		Design - Building : enveloppe glazing area Interior : distance between individual units and enveloppe glazing	o				o		o	
		Internal and external lighting - illuminance, comfort level	o				o		o	
		Internal lighting - light color rendering	o				o		o	
		Glare control	o				o		o	
		Electric light quality	o				o			
		Circadian lighting design					o,x			
		Lighting control	o				x,o		o	
	Visual - View	Window / Opening surface and room depth	o						o	
		Adequate view out								
		Direct sky view, visual balance	o							
		Direct sight to outdoor	o		o				o	
	IAQ	IAQ Plan	o						o	
		Ventilation rate	o				o		o	
		Air filtration	o				o	oo	o	
		Ventilation pathway	o				o		o	
		Natural Ventilation - Openess of the windows and vents considered for ventilation requirements					o			
		Outdoor Particulate Matter level (PM2.5,PM10)					x			
		Natural Ventilation - Outdoor conditions PM level, temperature, humidity					o,x	o		
		Enhanced ventilation design: displacement / personalized					o			
		CO2 level			x		x	xx	o	
		VOC - Formaldehyde concentration	x		x		x	xx	x	
		VOC - Benzene , Toluene					x	xx	x	
		Other individual VOC							x	
		TVOC concentration	x		x		x	xx	x	
		Radon concentration			x		x	xx		
		Ozone, Carbon monoxide, Particulate Matter (PM2.5,PM10) concentration					x	xx	x	
		Building flush-out							o	
		Monitoring of 3 indoor air pollutant					o	xx		
		Monitoring of IAQ - accuracy of sensors					o			
		Ventilation system cleaning and hygene inspection and maintenance			x		o	o		
		Non-Ionizing Radiation			x					
		Air treatment - humidification, dehumidification			x					
		Air treatment - Carbon filters, media filters , UVGI					o	oo		
		Prohibition of indoor and outdoor smoking			x		o,Δ	Δ	o	
		Protection of the ventilation system during construction					o		o	
		IAQ management plan during construction							o	
		Operable windows					o		o	
	Acoustic	Sound Insulation	x		x		x,o		o	
		Indoor ambient and airborn noise level	x		x		x			
		Impact noise level	x		x		x	§		
		Room acoustic	x		x		x,o			
		Technical installation noise			x				x	
		Outdoor noises			x					
		Sound mapping					o			
		Sound reducing surfaces	x				o			
		Hearing health conservation						Δ,§		
		Speech intelligibility					o	Δ,§	x	
		Reverberation time	x		x		x,o		x	
	Thermal Comfort	Thermal modelling	o		x				o	
		PMV , PPD	x				x		o	
		Thermal comfort survey						§		
		Thermal zoning	o				o			
		Temperature control	o		x		o			
		Summer heat protection			x					
		Overheating hours	o		x					
		Thermal parameter monitoring: dry-bulb temperature, relative humidity					o	xx		
		Individual heating and cooling control	o				o	Δ		
		Radiant heating and cooling					o			
		Manage relative humidity					o	xx		
		Windows with multiple opening modes					o	§		
		Outdoor thermal comfort					o	§	o	
		Adptability of the building design to adapt with futur outdoor conditions	o							
	Water Quality	Legionella risk management	o		o		x,o	xx,oo		
		Turbidity and coliforms level					x			
		Chemical composition of drinking water					x/o			
		Drinking water taste and quality management					x			
		Drinking water promotion					o	Δ		
		On site non-potable water reuse					o	oo, §		
		Moisture management					o	oo, Δ		
		Quality of water in cooling towers							o	

Tab 6 - List of health-related indicators present in the selected Green Certifications Protocols. The types of evidence needed to assess the different indicators are listed in table 5.

		Indicators	Required evidence							
			BREEAM		MINERGIE - ECO		WELL		LEED	
			Pre	Post	Pre	Post	Pre	Post	Pre	Post
Building and Architectural Design	Material selection	Emission limit of TVOC or VOC , Formaldehyde for: wood based products , paints and coating, floor emission, insulation material	x		o		o		o	
		Interior adhesive emission limit of TVOC or VOC , Formaldehyde	x				o		o	
		Emission limit of carcinogens for: wood based products , paints and coating, floor emission, insulation material, interior adhesive	x							
		Mineral fibers			o					
		Transparency of the materials and products used			o		o			
		Construction material restriction of solvant			o					
		Reduce exposure from entryways					o		o	
		Emission limit - Asbestos, Lead, Mercury					o			
		Manage Polychlorinated Biphenyl (PCB) and CCA					o			
		Pesticide management						Δ		
		Contact reduction					o	§		
	Physical activities Promotion	Ergonomic workstation					o	Δ		
		Ergonomic program						Δ,§		
		Circulation network. visibility and promotion of staircases					o			
		Cycling infrastructure (storage , showers ...)					o		o	
		Site with pedestrian friendly access					o			
		Offer physical activities opportunities and promote health self-monitoring						Δ		
		Access to a space dedicated to physical activities					o	Δ		
		Physical Activity Incentives (use of the incentives have to exceed 50%/y or increase of 10% annualy)					o	oo		
	Site Environment	Environmental assessment	o				o		o	
		Monitoring and remediation of outdoor contaminant					oo		o	
		Waste management						Δ		
		Outdoor space with external amenity	o						o	
		Surrounding density and distance to other facilities (retail, service, community) ; connection to pedestrian and bicycle network							o	
		Site with access to mass transit					o		o	
		Reduce outdoor pollution exposure					o			
		Parking design - reduced capactity to encourage other transport modes and use of green cars							o	
Social Factor	Security	Security needs assessment	o				o		o	
		Implementation of security requirements for physical security, technological security(alarms, control system...)	o							
	Surrounding Safety	Safe access and pedestrian paths	o							
	Hygiene Accomodation	Bathroom and handwashing accomodation					o			
		Cleaning products and protocols						Δ		
	Nourishment	Fruit and vegetables provision and promotion, nutritional transperancy , food allergens					o,Δ	Δ		
		Special diets and composition of food (limitation of sugar, fired or artificial ingredients)					o,Δ	Δ		
		Promote healthy portions of food					o			
		Nutrition education					o,Δ	Δ		
		Space and time for eating					o,Δ	Δ		
		Space to prepare on-site meal					o			
		Local food sourcing					o	Δ		
		Food production - gardening space					o			
		Local food access					o	o		
		Limit red and processed meat					o	Δ, §		
	Mind	Promotion of mental health and well- being (courses, dedicated space for relaxation...)						Δ		
		Incorporate natural element in the design					o			
		Offer of mental health service						Δ,§		
		Mental health education and training for managers						Δ		
		Stress management plan					o			
		Restorative opportunities , programmes and dedicated spaces					o	Δ		
		Substance use / tabacco cessation policy , education					o	Δ		
		Nature access	o				o		o	
	Community	Quaterly communication about health resources, programs, amenities and policies available						Δ		
		Stakeholders engagement, promote health oriented project					o	Δ		
		Emergency preparedness plan					Δ			
		Occupant survey - experience and self-reported health/ well-being						§§		
		Support for new parents, new mother , family , victims of domestic violence					o	Δ		
		Promote community and diversity engagement					o	Δ		
		Universal design					o	Δ		
		Promote business continuity , emergency resilience , facilitate healthy re-entry						Δ,§		
		Promote housing equity					o	§		
		Responsible labor practises					o	Δ,§		
		Health service (free service health and health benefits plan, sick leave)						Δ		

Reproduction of Thermal Plume above Commercial Cooking Gas Stove using CFD Analysis

Takao OSAWA [a], Takashi KURABUCHI [b], Yoshihiro TORIUMI [c], Sihwan LEE [d], Yuki SHIMANUKI [e], Ami KUDO [f]

[a] Graduate Student, Department of Architecture, Faculty of Engineering, Tokyo University of Science, Japan, takao1089@gmail.com

[b] Professor, Department of Architecture, Faculty of Engineering, Tokyo University of Science, Japan, kura@rs.tus.ac.jp

[c] Professor, Division of Architectural, Civil and Environmental Engineering School of Science and Engineering, Tokyo Denki University, Japan, toriumi@g.dendai.ac.jp

[d] Associate Professor, Graduate School of Environmental Studies, Nagoya University, Japan, shany@nuac.nagoya-u.ac.jp

[e] Researcher, TOKYO GAS CO.,Ltd, Japan, n-yuki@tokyo-gas.co.jp

[f] M.Technol. Manag. , TOKYO GAS CO.,Ltd, Japan, Kudo_ami@tokyo-gas.co.jp

Abstract. In commercial kitchens, the working environment of cooks deteriorates because of the generation of large amounts of heat and vapor. Ventilation is required to improve the environment, and the accompanying increase in air-conditioning energy becomes an issue. Therefore, a proper ventilation design is required to reduce the risk of contaminated air, thereby deteriorating the indoor environment. When planning ventilation and air conditioning for commercial kitchens, the heat generated by cooking products can be efficiently exhausted to reduce the air conditioning load and maintain good air quality in the workspace. Computational fluid dynamics (CFD) analysis was used to predict the air conditioning load and air quality. It is important to accurately evaluate the heat generated from the cooking equipment and the exhaust collection performance of cooking products. At that time, the accuracy of reproducing the thermal updraft is important, but when the capture efficiency is predicted using the simple gradient diffusion hypothesis model, which is widely used for indoor airflow analysis, the capture efficiency is excess owing to insufficient diffusion. Several studies on the thermal plume on gas stoves have been conducted thus far[1]–[4], and previous studies have clarified that there is a problem in the reproducibility of the production term G_k owing to the buoyancy of the turbulent kinetic energy. It is possible to improve the accuracy using the generalized gradient diffusion hypothesis (GGDH), which uses the gradient of the average flow other than the diffusion direction as the approximation method for the turbulent heat flux in G_k. In this study, we investigated the reproducibility of CFD analysis with a GGDH on an open fire. First, we measured the thermal plume and capture efficiency. Subsequently, as a result of attempting to reproduce the thermal plume with CFD and then perform capture efficiency analysis, it was confirmed that the actual measurement results were consistent with the analysis results. Because the actual measurement and CFD results were in agreement, we believe that it would contribute to comfort and energy savings in a commercial kitchen.

Keywords. Capture efficiency, Commercial kitchen, Thermal plume, CFD
DOI: https://doi.org/10.34641/clima.2022.324

1. Introduction

An appropriate ventilation design is required to maintain the optimum working environment in a commercial kitchen, and the recovery efficiency of the hood exhaust is an important index.

The capture efficiency of the hood exhaust indicates the amount of pollutant generated by kitchen equipment that can be collected by the exhaust hood.

The purpose of this research is to examine the reproducibility of computational fluid dynamics (CFD) from the temperature measurement and capture efficiency measurement of the heat updraft in the direct flame and to propose a CFD analysis when the pot is placed in the future.

Copyright ©2022 by the authors. This conference paper is published under a CC-BY-4.0 license.

2. Reproduction of thermal plume

2.1 Measurement overview

The temperature and velocity distributions were obtained by measuring the temperature of the thermal plume. **Figure 1** shows a plan view of the environmental test room used for the measurement.

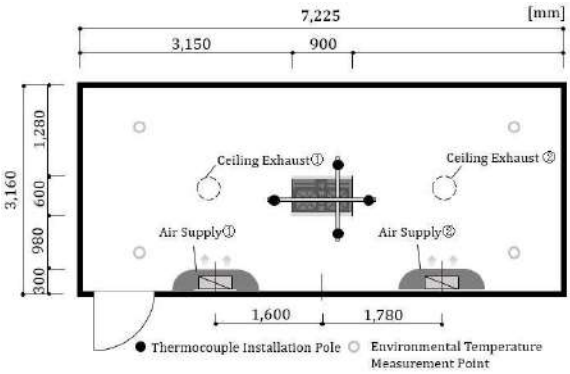

Fig. 1 – Environmental test room (floor plan)

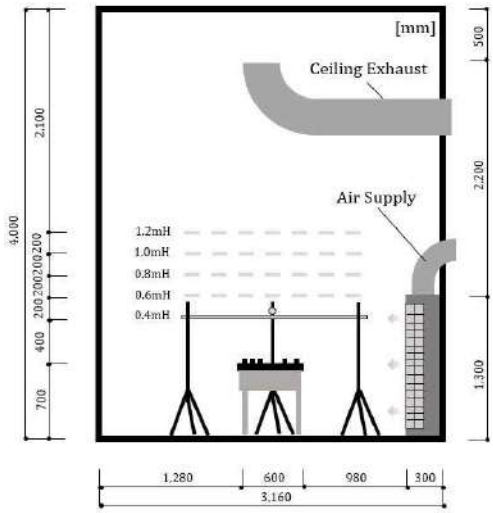

Fig. 2 – Environmental test room (cut open)

A commercial gas stove is installed at the center of the room, and one of the three is used for measurement. **Figure 2** shows a cross-sectional view. The measurement heights were 0.4, 0.6, 0.8, 1.0, and 1.2 m from the burner. **Figure 3** shows the locations of the measurement points.

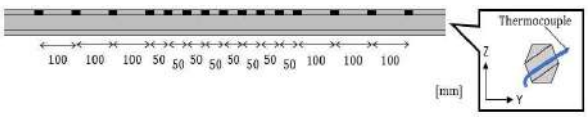

Fig. 3 – Installation position of thermocouple

Based on the lower heating value of 12.7 kW corresponding to the rated output, the thermal power was set to three conditions of 9.2 and 4.6 kW, which correspond to two-thirds and one-third of the rated output, respectively. For velocity distribution, the central velocity v_c was calculated using **Eq. (1)**, where the low calorific value of the city gas is taken as the retained calorific value H of the plume, ρ denotes the density, c_p is the specific heat, t_c is the temperature difference on the central axis, and v_c is the velocity on the central axis. The distribution widths R_t and R_v denote the radial distances of the points where the central axis temperature and central axis velocity are 1/e, and the ratio of R_t and R_v expressed in **Eq. (2)** is 0.9.

$$H = \pi \rho c_p t_c v_c \frac{R_t^2 R_v^2}{R_t^2 + R_v^2} \quad \cdots(1)$$

$$\lambda = R_t / R_v \quad \cdots(2)$$

The measurements were performed under the condition of an open fire without a pot.

2.2 Boundary conditions for CFD analysis

Figure 4 shows an outline of the analysis model, and **Tab. 1** lists the boundary conditions for plume analysis.

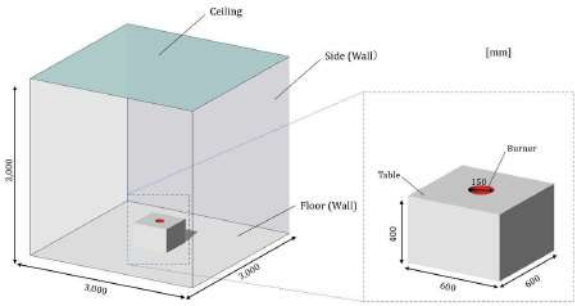

Fig. 4 – CFD analysis model of thermal plume

Tab. 1 – Boundary conditions (plume analysis)

Boundary	Type		
burner	4.6 kW	Temperature	516 °C
		Velocity	1.16 m/s
	9.2 kW	Temperature	810 °C
		Velocity	2.00 m/s
	12.7 kW	Temperature	1002 °C
		Velocity	2.62 m/s
	Material: Air Turbulent intensity: 0.25 Turbulent length scale: 0.10 m		
Floor	All dependent variable : 0 gradient condition		
Ceiling	Boundary (Pressure: 0.00 Pa)		
Side	All dependent variable : 0 gradient condition		
Table	All dependent variable : 0 gradient condition		

The boundary conditions for plume analysis were set based on the actual experimental results. The burner diameter was set to 0.15 m. The temperature of the burner was 516 °C when the calorific value was 4.6 kW. In addition, based on the similarity rule of Maele et al.[5], we set the stove temperature to 1002 °C at 12.7 kW, and calculated the velocity at each thermal power by back calculation from **Eq. (3)**.

$$H = c_p \rho A v \Delta\theta \quad \cdots(3)$$

Table 2 lists the analysis conditions. The total number of meshes was 980,000 meshes.

Tab. 2 – Analysis conditions

	Analysis conditions
Software	Simcenter STAR-CCM+ 2020.3
Turbulence	Standard k-ε Model Generalized k-ε Model
Density	Incompressible ideal gas
Algorithm	Time dependent
Mesh	980,000 meshes
Analysis area	3,000mm(X)×3,000mm(Y)×3,000mm(Z)

2.3 Turbulence model

The turbulence model used in this study is explained. Simple gradient diffusion hypothesis (SGDH) and generalized gradient diffusion hypothesis (GGDH) were used as the turbulence models, and the reproducibility of the thermal plume was compared with the measured results. **Table 3** lists the turbulence model formula. **Equation (4)** is the transport equation for the turbulent kinetic energy k, and **Eq. (5)** is the transport equation for the turbulent dissipation rate, ε. The term P_k is the production term of turbulent energy due to the Reynolds stress. The term G_k is the production term of the turbulent energy by buoyancy. The buoyancy production term G_k is expressed in **Eq. (6)**, and the turbulent heat flux $-\overline{\theta u_j}$ in the equation is modeled by **Eq. (7)** in SGDH. As a remedy, it is conceivable to newly model $-\overline{\theta u_j}$ in **Eq. (9)**. In the GGDH analysis, the Reynolds stress $-\overline{u_i u_j}$ was set to **Eq. (10)** such that G_k is modeled using **Eq. (11)**, and the horizontal temperature–velocity gradient is also considered.

Tab. 3 – Turbulence model

$$\frac{\partial k}{\partial t}+\frac{\partial k U_i}{\partial x_i}=\frac{\partial}{\partial x_i}\left[\left(\nu+\frac{\nu_t}{\sigma_k}\right)\frac{\partial k}{\partial x_i}\right]+P_k+G_k-\varepsilon \quad \cdots(4)$$

$$\frac{\partial \varepsilon}{\partial t}+\frac{\partial \varepsilon U_i}{\partial x_i}=\frac{\partial}{\partial x_i}\left[\left(\nu+\frac{\nu_t}{\sigma_\varepsilon}\right)\frac{\partial \varepsilon}{\partial x_i}\right]+\frac{\varepsilon}{k}\left[C_{\varepsilon 1}(P_k+C_{\varepsilon 3}G_k)-C_{\varepsilon 2}\varepsilon\right] \cdots(5)$$

$$G_k=-\beta g_i\overline{\theta u_i} \quad \cdots(6) \qquad -\overline{\theta u_i}=\frac{\nu_t}{P_t}\frac{\partial \Theta}{\partial x_i} \quad \cdots(7)$$

$$G_k=-\beta g_z\frac{\nu_t}{P_t}\frac{\partial \Theta}{\partial z} \quad \cdots(8) \qquad -\overline{\theta u_i}=\frac{3\nu_t}{2P_t k}\overline{u_i u_j}\frac{\partial \Theta}{\partial x_j} \quad \cdots(9)$$

$$-\overline{u_i u_j}=\nu_t\left(\frac{\partial U_i}{\partial x_j}+\frac{\partial U_j}{\partial x_i}\right)-\frac{2}{3}\delta_{ij}k \quad \cdots(10)$$

$$G_k=-\beta g_z\frac{3\nu_t}{2P_t k}\left(\overline{wu}\frac{\partial \Theta}{\partial x}+\overline{wv}\frac{\partial \Theta}{\partial y}+\overline{ww}\frac{\partial \Theta}{\partial z}\right) \quad \cdots(11)$$

ν: Kinematic viscosity$[m^2/s]$	ν_t: Eddy kinematic viscosity$[m^2/s]$
σ_k,σ_ε,C_{ε_1}, C_{ε_2}, C_{ε_3} : model constants	$\sigma_k=1.0, \sigma_\varepsilon=1.3$, $C_{\varepsilon_1}=1.44, C_{\varepsilon_2}=1.92$, $C_{\varepsilon_3}=0.2$
C_μ: model parameter [=0.09]	
g_i: Gravitational acceleration vector [m^2/s^2]	
P_t: Turbulent Prandtl number [-]	
δ_{ij}: Kronecker delta dimensionless [-]	

2.4 Comparison of measurement and CFD analysis

Focusing on the installation height of the exhaust hood (1.0 m), we compared the analysis and actual experimental results. **Figure 5** shows the temperature difference distribution. From **Eq. (12)**, the temperature is arranged by an approximate equation based on the difference t between the plume and environmental temperatures and the radial distance r from the center of the thermal plume. The maximum temperature difference of the measured data was taken as the central axis temperature t_c, and the temperature distribution width R_t was determined using the least-squares method.

$$t/t_c=e^{-(r/R_t)^2} \quad \cdots(12)$$

When GGDH was used for all thermal powers, the CFD results were closer to the experimental results than SGDH. At a thermal power of 4.6 kW, the analysis results using the GGDH were almost in agreement with the experimental results. **Figure 6** shows the velocity distribution. The analysis values and the experimental results corresponded to each other for all thermal powers, but the results demonstrated that the analysis values using the GGDH diffused.

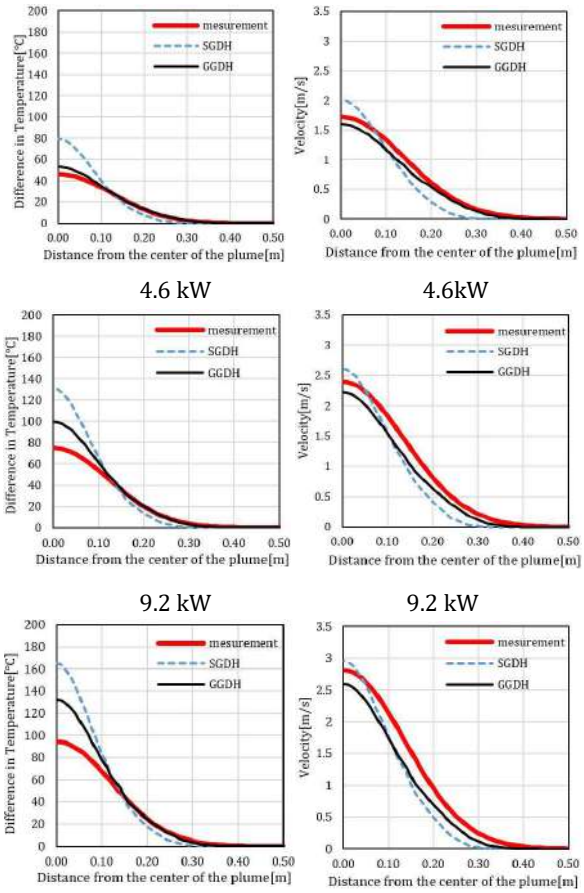

Fig. 5 - Difference in temperature

Fig. 6 – Velocity

Figures 7 and **8** show the temperature difference and velocity on the central axis under the condition of a thermal power of 4.6 kW. **Figures 9** and **10** also show the results of plotting R_t and R_v at each height. The GGDH exhibited a value close to the measured result compared with the SGDH. The central axis velocity approached the experimental results as the height increased. From these findings, it can be concluded that the prediction accuracy was improved by CFD in an open flame.

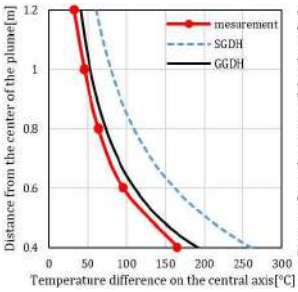

Fig. 7 - Temperature Difference on the central axis

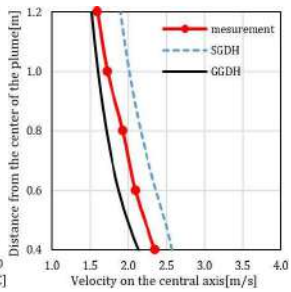

Fig. 8 – Velocity on the central axis

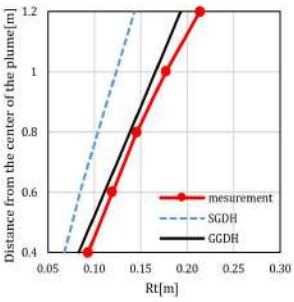

Fig. 9 - Temperature distribution width

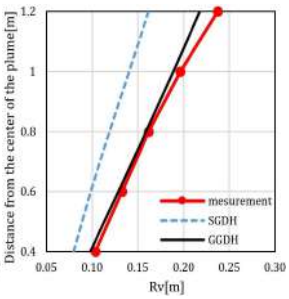

Fig. 10 – Velocity distribution width

3. Reproduction of Capture Efficiency

3.1 Measurement overview

The capture efficiency of the exhaust hood was measured according to the JSTM standards[6]. The capture efficiency of hood exhaust is measured separately for combustion exhaust gas generated from a gas-cooking appliance and for cooking products such as water and oil. For the combustion exhaust gas, carbon dioxide emitted from the gas-cooking appliance was used as a tracer gas. The capture efficiency of the hood exhaust was calculated using **Eq. (13)**.

$$\eta_C = \frac{C_{h,\infty}}{C_{h,100}} \quad ...(13)$$

The term η_C denotes the capture efficiency of the hood exhaust, $C_{h,\infty}$ is the average of the 10 min exhaust duct concentration, $C_{h,100}$ is the exhaust duct concentration measured with 100% capture of contamination from cooking equipment (complete collection state). **Figure 11** shows a section view of the test room used for the collection rate measurement. An exhaust hood of 0.90 m × 1.2 m × 0.68 m in height was installed on the gas stove.

The same commercial gas stove as in **Chapter *2.1*** was installed, and the target burners and thermal power were set under the same conditions.
The ventilation rates of the exhaust hood were determined as 391.5, 522, 652.5, and 783 m^3/h.

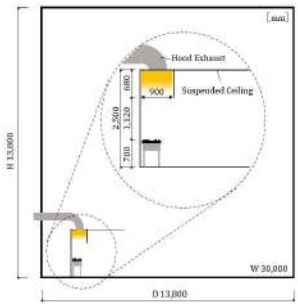

Fig. 11 – Test room

3.2 Overview of CFD analysis of capture efficiency

Figure 12 shows the analysis model. To reduce the analysis load, a part of the laboratory in the large space to be analyzed was targeted for analysis, and a wall surface other than the side wall adjacent to the gas stove was set as a slip boundary.

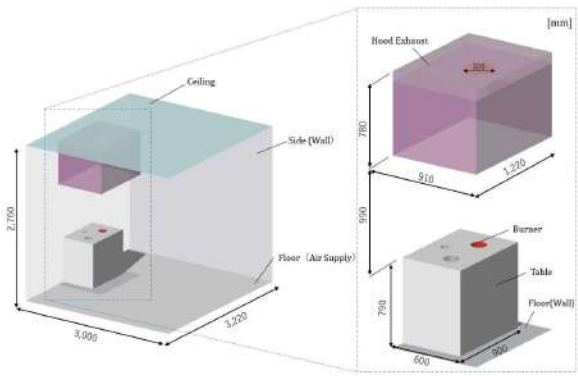

Fig. 12 – CFD analysis model of capture efficiency

Tab. 4 lists the boundary conditions. The floor surface was supplied with air, air was blown vertically upward at 0.10 m/s, and the ceiling surface was used as the pressure boundary. The boundary conditions for the burner were the same as in **Chapter *2.2*.**

Tab. 4 – Boundary conditions (capture efficiency)

Boundary	Type		
Burner	4.6 kW	Temperature	520 ℃
		Velocity	1.16 m/s
	9.2 kW	Temperature	814 ℃
		Velocity	2.00 m/s
	12.7 kW	Temperature	1006 ℃
		Velocity	2.62 m/s
	Material : Air Turbulent intensity : 0.25 Turbulent length scale : 0.10 m		
Floor	Velocity inlet (Temperature: 20℃, Velocity: 0.1 m/s, Turbulent intensity : 0.01 Turbulent length scale : 0.10 m)		
Ceiling	Boundary (Pressure: 0.00 Pa)		
Side Table	All dependent variable : 0 gradient condition		

3.3 Comparison of measurement and CFD analysis

Figures 13, 14, and **15** show a comparison of the results for capture efficiency. Under all thermal power conditions, CFD analysis using the SGDH as the turbulence model tended to overestimate the capture efficiency. In addition, the analysis results using the GGDH exhibited values close to the actual experimental results. In particular, under the conditions of thermal power of 9.2 and 12.7 kW, it was confirmed that the measurements were almost the same as those of GGDH regardless of the ventilation volume.

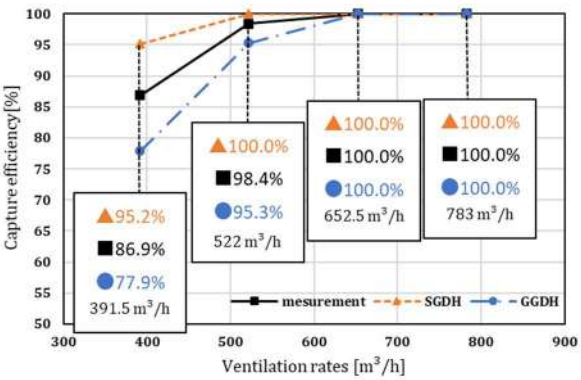

Fig. 13 - Comparison of capture efficiency of 4.6 kW

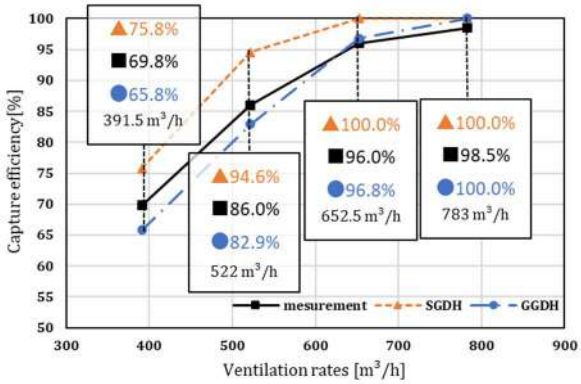

Fig. 14 - Comparison of capture efficiency of 9.2 kW

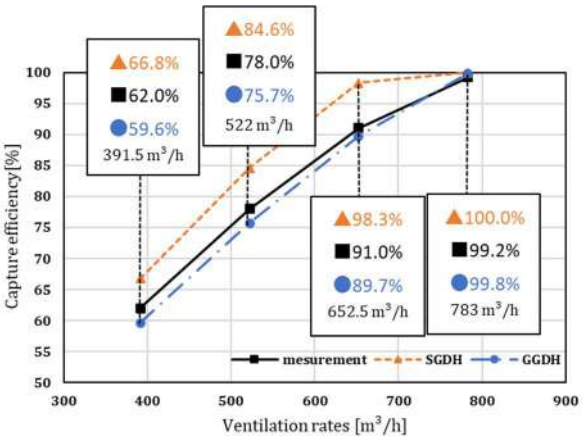

Fig. 15 - Comparison of capture efficiency of 12.7 kW

4. Conclusions

The following findings were obtained from this study:

(1) Using the generalized k–ε model (GGDH), it was confirmed that the temperature distribution of the thermal plume was closer to the measured value than that of the standard k–ε model (SGDH).

(2) Using the GGDH, it was confirmed that the collection rate of the exhaust hood was close to the measured value.

(3) When predicting the exhaust collection rate by CFD analysis in a commercial kitchen, it is important to use the GGDH as a turbulence model.

Reproducing the capture efficiency by CFD will be a material for future modeling and will significantly contribute to the comfort and energy saving of commercial kitchens in the long run.

In the future, boundary conditions should be set when the pot is installed on the stove. It is important to reflect the heat-transfer phenomena observed around the pot in CFD and improve the reproducibility of the plume. In addition, this research may be reflected in the actual Japanese kitchen environment in the future.

5. References

[1] Y. Kondo et al., Study on Air-Conditioning and Ventilation System od Kitchen (Part4) Numetrical Simulations of Flow and Temperature Distributions and Ventilation Efficiency, The Society of Heating, Air-Conditioning and Sanitary Engineers of Japan, proceedings, C-17, 1994, 201-204

[2] T. Momose et al., Measurement and Modeling of Plume above Commercial Cooking Stoves, The Architectural Institute of Japan's Journal of Environmental Engineering, No.567, 2003, 49-56

[3] J. Sakaguchi et al., Study on the Themal Environment and Air Flow Distribution in the House Kitchen by CFD analysis, Architectual Institute of Japan, Summaries of technical papers of annual meeting, 2008

[4] H.Kiyosuke et al., Study on reproduction of heat updraft on gas stove by CFD, Architectual Institute of Japan, Summaries of technical papers of annual meeting, 2018

[5] K. Van Maele et al., Application of two buoyancy-modified k–ε turbulence models to different types of buoyant plumes, Engineering Applications of Computational Fluid Mechanics, 2006

[6] JSTM V 6201: Measurement method for capture efficiency of exhaust hoods in commercial kitchens, 2017

Analysis of occupant satisfaction with IEQ in residential buildings

Quinten Carton [a], *Jakub Kolarik* [b], *Hilde Breesch* [c]

[a] Building Physics and Sustainable Design, Ghent Technology Campus, Department of Civil Engineering, KU Leuven, Belgium, quinten.carton@kuleuven.be.

[b] Department of Civil Engineering and Mechanical Engineering, Technical University of Denmark, Kongens Lyngby, Denmark, jakol@byg.dtu.dk.

[c] Building Physics and Sustainable Design, Ghent Technology Campus, Department of Civil Engineering, KU Leuven, Belgium, hilde.breesch@kuleuven.be.

Abstract. Multiple studies have shown that occupants' satisfaction with the indoor environmental quality (IEQ) is not always as high as expected from standards. Furthermore, consensus on methods for quantification of occupant satisfaction is still missing. Therefore, satisfaction assessment and further investigations into the relationships between occupant satisfaction and measured IEQ are needed.

This paper investigated the relationships between satisfaction ratings and IEQ parameters in mechanically ventilated residential buildings. This study used data from Belgian dwellings with a demand-controlled extraction system that was accompanied by a mobile phone application, enabling the users to adapt the ventilation system settings.

In this study, we evaluated the residents' satisfaction with the IEQ in their main living room. The satisfaction assessment approach consisted of (1) a retrospective survey and (2) the implementation of satisfaction rating scales into the mobile application of the ventilation system, allowing the residents to evaluate their satisfaction with the thermal environment or IAQ. The satisfaction rating option was active for two weeks during winter conditions. Simultaneously, IEQ-related parameters (i.e., air temperature, relative humidity and CO_2 concentration), and residents' interactions with their ventilation system (e.g., changing airflow rates or CO_2-thresholds) were monitored. We investigated the relationships between the satisfaction ratings and the IEQ- and interaction-related parameters through mixed-effect model analysis.

130 residents filled in the retrospective survey, and over 800 satisfaction ratings were submitted by approximately 60 different dwellings. Results of the retrospective survey and satisfaction ratings show that the participating residents were in general satisfied with the IEQ in their living room. The mixed-model analysis shows that the indoor temperature was the main parameter affecting residents' satisfaction with both IAQ and thermal environment. Furthermore, the results illustrate that the satisfaction ratings are mostly related to the specific resident, making it challenging to determine an aggregated model without personal and contextual information.

Keywords. Occupant satisfaction, indoor environmental quality, residential buildings, mixed-effect models
DOI: https://doi.org/10.34641/clima.2022.125

1. Introduction

The occupants' satisfaction with the indoor environmental quality (IEQ) is not always as high as expected and often does not reach the 80%-requirement of standards [1], [2]. The main reason for this performance gap is that occupants' satisfaction with the IEQ is complex to predict since it is influenced by both IEQ- and non-IEQ related parameters, e.g. demographic information, perceived control, time of day [2]. Becker and Paciuk [3] found a discrepancy between the thermal comfort expected with the PMV-PPD method and the actual thermal comfort of residents. The discrepancy is attributed to contextual factors such as control over the IEQ and local climate. The study of Zalejska-Jonsson and Wilhelmsson [4] also showed differences in residents' satisfaction based on characteristics of the building and resident. At present, most studies regarding occupants' satisfaction focus on

Copyright ©2022 by the authors. This conference paper is published under a CC-BY-4.0 license.

commercial buildings like offices while satisfaction in residential buildings remains underexplored [1], [5]. Therefore, further investigation in residents' satisfaction with attention to personal and context-related factors is needed.

This paper evaluates occupants' satisfaction with the IEQ in residential buildings in Belgium. In addition, this study investigates which IEQ- and context-related parameters influence the residents' satisfaction with the IEQ and how personalized residential satisfaction is. Lastly, this paper determines if residents' interactions with their ventilation system (e.g., changing airflow rates or CO_2-tresholds) can be used as a predictor for satisfaction with IEQ.

2. Methods

This study focusses on residents' satisfaction with the IEQ in one representative space of a house, i.e. the main living room. The living room was chosen as monitoring room type since the IEQ in this space is the least influenced by specific occupant activities (e.g., cooking in kitchen, showering in bathroom) and we assumed it is the room in which residents spend the most time in when awake and not doing active tasks. Our study was performed during heating season conditions.

2.1 Ventilation system and user application

All participating dwellings of this study were equipped with a mechanical demand-controlled exhaust ventilation system. In these dwellings, outside air was supplied through inlet grilles above the windows and air was mechanically extracted in different rooms of the house. Extraction grilles were mostly present in the bathroom, toilet, kitchen and bedroom in the majority of the dwellings. The ventilation system was also accompanied by a mobile application consisting of multiple functions that the residents could use, e.g., viewing historical data, adapting CO_2-thresholds, changing ventilation flow rates.

The ventilation system measured four IEQ parameters, namely, air temperature, relative humidity, CO_2 and VOC. The IEQ parameters of the extraction air were measured by the extraction valve in the ventilation system unit. Different types of extraction valves were used each measuring different IEQ parameters. The type of extraction valve used, was depending on which room type the air was extracted from. Air temperature and relative humidity were measured in all rooms, in contrast to the CO_2 and VOC-levels. CO_2-levels were only monitored in the kitchens, living rooms and bedrooms, while VOC-levels were only measured in the bathrooms and toilets. The ventilation systems were online connected and the IEQ data was stored with a timestep of 5 minutes in a database.

2.2 Satisfaction surveying and IEQ monitoring

Both subjective satisfaction ratings and objective IEQ parameters were gathered in this study in order to analyse the parameters influencing the residents' satisfaction. A two-step approach was used, firstly, a retrospective survey was designed and distributed among the ventilation system users. The retrospective survey started with an informed consent procedure in which the residents could indicate if they were willing to participate in the study. Only residents who gave their informed consent were able to fill in the retrospective survey. The survey was divided into three main parts: (1) resident demographics, dwelling and house information, (2) residents' perception and satisfaction with the IEQ in their living room during past winter period and (3) residents' usage of the user application. At the end of the survey, residents were given the option to indicate whether they wanted to participate further with the study using the satisfaction rating options. The retrospective survey was distributed among all residents using the mobile application. The survey was active from 06/04/2021 until 18/04/2021. Each resident could fill in the retrospective survey only once.

Secondly, two satisfaction rating options were implemented in the mobile application of the residents, who indicated to be willing to participate in this next step. The results of the latter were combined with IEQ monitoring data coming from the connected ventilation systems that were present in the dwellings. The two satisfaction rating options were implemented from 26/04/2021 until 10/05/2021. During this period the residents were able to evaluate their immediate satisfaction with the thermal environment and IAQ in their living room on a 5-point ordinal scale. Up to six evaluation ratings could be casted each day, three regarding the thermal environment and three regarding the IAQ. One of the two rating options appeared randomly on the screen of the user application when the resident opened the application. Before the implementation of the rating options, participating residents were informed about the procedure and asked to use the rating option at least three times throughout the day, i.e., morning, afternoon and evening.

2.3 Dataset construction and cleaning

In total 839 valid satisfaction scores were gathered from unique 62 residents during the two-week long satisfaction surveying. These raw satisfaction data were combined with IEQ data. The combined dataset consisted of the residents' satisfaction ratings and the nearest IEQ measurement in time. Only IEQ data measured from extraction air from living rooms, open or closed kitchens were used. Preference was given to measurements from living rooms. However, a majority of the dwellings did not have an extraction grille in their living room. In this case measurements of the extraction airflow from the open kitchen were taken. If measurements of both the living room and

the open kitchen lacked, the data from the closed kitchen were used. One dwelling did not have IEQ measurements of one the three rooms available, as a result, 32 datapoints were deleted out of the dataset.

The dataset contained some repetitive datapoints, which could be due to an error in the system or due to the resident quickly responding to the same rating option multiple times in a row. To eliminate bias due to this effect, satisfaction ratings on the same IEQ-domain (thermal environment or IAQ) that were passed on by the same resident within 10 minutes, were excluded from the dataset. As a result, 182 datapoints were dropped out of the dataset. Afterwards, the time between the casting of the satisfaction rating and the nearest IEQ measurement was calculated and checked. One datapoint was excluded due to a large time difference which exceeded four hours. This was the result of a gap in the IEQ data monitoring. Lastly, it was checked if the IEQ measurements had realistic values. One datapoint, which consisted of an unrealistic high airflow rate, was excluded from the dataset. The final dataset consisted of 623 datapoints of both a satisfaction score and the nearest IEQ-related parameters. The cleaned dataset was separated into two datasets of IAQ and thermal satisfaction scores containing 308 and 315 datapoints, respectively.

2.4 Statistical analysis

The survey results and IEQ data were further analysed to investigate the statistical relationships between the residents' satisfaction with the IEQ. The following parameters were included: demographics and context-related information (e.g., gender, age, building type of house), IEQ-related parameters (i.e., air temperature, relative humidity and CO_2-concentration) and residents' interactions with their ventilation system (e.g., boosting ventilation flow rate, adapting CO_2-thresholds, activating a silent ventilation operation). The results of the statistical tests were determined to be statistically significant if a $p<0.05$ was obtained. Statistical analyses were performed using R software [6].

Firstly, a non-parametric correlation analysis was performed to determine the relationships between the different retrospective survey questions, i.e., residents' perception and satisfaction with the IEQ. The retrospective survey primarily consisted of questions answered on a Likert scale, which resulted in ordinal data. The Spearman's ρ correlation coefficient was used for the correlation analysis, since it is suitable for ordinal data [7]. The effect sizes of Spearman's ρ were categorized as follows: neglectable ($\rho < 0.2$), weak ($0.2 < \rho < 0.5$), moderate ($0.5 < \rho < 0.8$) and strong ($\rho > 0.8$) [7]. The correlation matrix was visualized using the ggcorrplot [8] package.

The relations between the context-related parameters and the residents' satisfaction in their living room was analysed using the results of the retrospective survey. The non-parametric Kruskal-Wallis H and Mann-Whitney U tests were used to determine whether there was a significant difference in the satisfaction scores, casted on 5-point ordinal scales, between the subgroups of the context-related categories (e.g., gender, age group, and building type). The first test was for context-related categories with more than two groups, the latter was used to determine a statistical difference between two groups (i.e., male vs female). If the Kruskal-Wallis test showed a statistically significant difference among the subgroups of a context-related category, a post-hoc test was done to find out, which of the subgroups were significantly different. The post-hoc pairwise comparison consisted of a Mann-Whitney U test with a Bonferroni correction [9].

The influence of IEQ- and interaction-related parameters on the residents' satisfaction with the thermal environment or IAQ in the living room were analysed using the dataset from the longitudinal satisfaction surveying and IEQ monitoring. The dataset consisted of dependent datapoints, since the same residents could cast multiple ratings during the two-week period. Furthermore, the amount of casted ratings was different for each resident. Therefore, a mixed-effect approach was used in which the residents' unique ID was used as a random effect and the IEQ- and interaction-related parameters as fixed-effects variables (see **Table 1**). By using the unique ID as a random effect, the models also considered the differences between the residents, such as personal preferences. Mixed-effect regression analysis has been used in other studies to investigate occupant satisfaction [10], [11] and behaviour [12], [13].

The IAQ and thermal satisfaction ratings, assessed on a 5-point ordinal scale, were used as dependent variables. The 'clmm' function from the 'ordinal' package [14] was used to fit ordinal logistic mixed-effect regression models. A forward selection procedure was done using Akaike information criterion (AIC) [15], which balances the model's complexity and goodness of fit, as an evaluation metric. A lower AIC-value represents a better model fit. Furthermore, the intraclass correlation coefficient (ICC) was used to quantify the proportion of variance due to the grouping of the random effect, which was in this case the residents' ID [16]. The forward selection procedure started with the null model which consisted of no fixed effects and only a random intercept with the residents' ID as random effect. In step 1, models with one fixed effect variable (see **Table 1**) and the residents' ID as random intercept were fitted and evaluated. It was determined if the difference in AIC of the fitted models in step 1 and the null model were statistically significant. Furthermore, it was required that all fixed effects in the models are statistically significant. In the following steps, the most suitable model, the model with the lowest AIC, from the last step was made more complex by adding one of the remaining fixed effects to the model. This process was repeated until no statistically significant improvement can be

achieved. The last step in the selection procedure, step X, consisted of the addition of one or more random slopes to the most suitable model. The model fit was again evaluated by the AIC. The model selection procedure was done two times, i.e., for thermal satisfaction and IAQ satisfaction as dependent variable. Afterwards, the satisfaction ratings were recoded into binary variables, i.e., ratings <3 were coded as "Dissatisfied" and ratings ≥3 as "Satisfied". The same selection procedure was repeated for thermal and IAQ satisfaction ratings as binary variables, in order to analyse the distinct difference between satisfaction and dissatisfaction. The 'glmer' function of the 'lme4' package [17] was used to fit binary logistic mixed-effect models.

Table 1. - Overview fixed-effect variables in mixed model analysis. Including indication of variable types C= continuous variable, B= Boolean and Cat= categorical.

Category	Name	Description	Unit	Type
IEQ-related variables	T	Indoor air temperature	°C	C
	RH	Relative humidity	%	C
	EA	Specific air enthalpy	kJ/kg	C
	CO_2	CO_2-concentration	ppm	C
	AF	Airflow rate	m^3/h	C
Interaction-related variables	Boost	Temporarily increase/ decrease AF	/	B
	Breeze	Passive cooling function which increases AF at a user-defined temperature setpoint	/	B
	Silent	User function to temporarily decrease AF	/	B
	Program	Set nominal AF to 70%, 100% or 120% of the standard AF	/	Cat
	CO_2_min	Lower CO_2-concentration threshold set by user	ppm	C
	CO_2_max	Upper CO_2-concentration threshold set by user	ppm	C

Multicollinearity among the fixed-effects variables was checked using the variance inflation factor (VIF). The VIF values exceeded the threshold of 5 when T, RH and EA were all three included in the model, showing the occurrence of multicollinearity. Therefore, models with all three predictors (i.e., T, RH and EA) were not further analysed.

3. Results - Analysis of retrospective survey

3.1 Residents demographics

Table 2 gives an overview of the demographics and context-related parameters of the 130 residents that completed the retrospective survey. The total amount of residents using the ventilations system and accompanying mobile application exceeds 6000, however, only around 600 residents are frequent users, leading to an acceptable response rate of approximately 21.6%.

Table 2. – Overview demographics and context-related parameters of residents participating in retrospective survey (n=130)

	Options	Rate [% of residents]
Residents gender	Male	82.3
	Female	17.7
Residents age	18 – 29 years	20.00
	30 – 39 years	36.2
	40 – 49 years	21.5
	50 – 59 years	9.2
	60 – 69 years	9.2
	70+ years	3.9
Dwelling size	1 person	12.3
	2 persons	35.4
	3 persons	20.8
	4 persons	20.0
	5 persons	9.2
	6 persons	1.5
	20 persons	*0.8*
Average daytime occupancy	0	14.6
	1	38.5
	2	36.2
	3	6.1
	4	4.6
Building type	Apartment	29.2
	Terraced house	13.1
	Semi-detached house	25.4
	Detached house	32.3
Residents' mindset*	Energy efficiency	3.1
	Comfort	13.8
	Equally important	83.1
	No opinion	0

* Statement that was most important for resident: house must be as energy efficient as possible, IEQ must be as comfortable as possible, energy efficiency and comfort are equally important, no opinion

3.2 Survey data reliability

Prior to the data analysis of the retrospective survey, the reliability of the survey data is evaluated through

a Cronbach's alpha calculation. Cronbach's alpha is a metric to determine the internal consistency or scale reliability [18]. An alpha value of >0.7 is required to categorize the results as reliable. A Cronbach's alpha of 0.77 is obtained, showing an acceptable consistency among the different satisfaction questions scales. Thus, the survey data can be considered as reliable.

3.3 IEQ and control satisfaction overview

Figure 1 shows the frequency of the satisfaction scores from the retrospective survey. The satisfaction with the overall IEQ, IAQ, user application control, thermal, acoustic and visual comfort is assessed on a 5-point ordinal scale. The residents were in general very satisfied with the IEQ in their living room and the control possibilities in the user application during winter conditions. Residents were the least and most satisfied with the acoustic and visual (e.g. daylight, lighting) comfort of their living room respectively. The main cause for acoustic dissatisfaction was noise from outside the building. This effect is probably due to the air inlet grilles that are situated above the windows, which are typical for extraction ventilation systems.

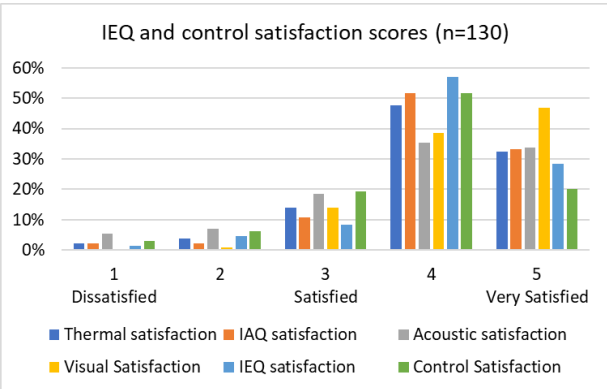

Figure 1. - IEQ and control satisfaction scores from retrospective survey – the votes correspond to the living room

The survey also asked the residents in which rooms of their house they were the least satisfied with the IEQ. The 'others' option gave residents the opportunity to clarify which room they were the least satisfied. However, 13 residents did not mention a room and filled in answers as 'none' or 'not applicable'. These 13 answers are not considered in the overall voting rates in **Table 3**.

Table 3. - Overview answers room least satisfied with IEQ (n=117)

Room	Rate [% of answers]
Living room	15.4
Dining room	1.7
Kitchen	7.7
Bedroom	29.1
Bathroom	23.9
Others (e.g., storage, attic, toilet, garage,…)	22.2

Table 3 shows that bedroom was the room with least satisfaction, followed by bathroom. Different room types were mentioned under 'Others' option, none of the other room types were mentioned more than the living room. Therefore, living room was the third in rank of rooms in which the residents were the least satisfied with the IEQ. The main reasons for dissatisfaction with the IEQ in the bedroom were noise nuisance (27.1%), a too warm (17%) or too cold (15.3%) environment and stuffy air (11.9%).

3.4 Correlation analysis

A Spearman correlation analysis was performed to investigate the relationship between questions of the retrospective survey related to occupants' satisfaction and perception of the IEQ. The results of the correlation analysis are visualized by a correlation matrix in **Figure 2**. The highest effect size was found between the occurrence of noise and acoustic satisfaction (ρ = 0.64), which shows that

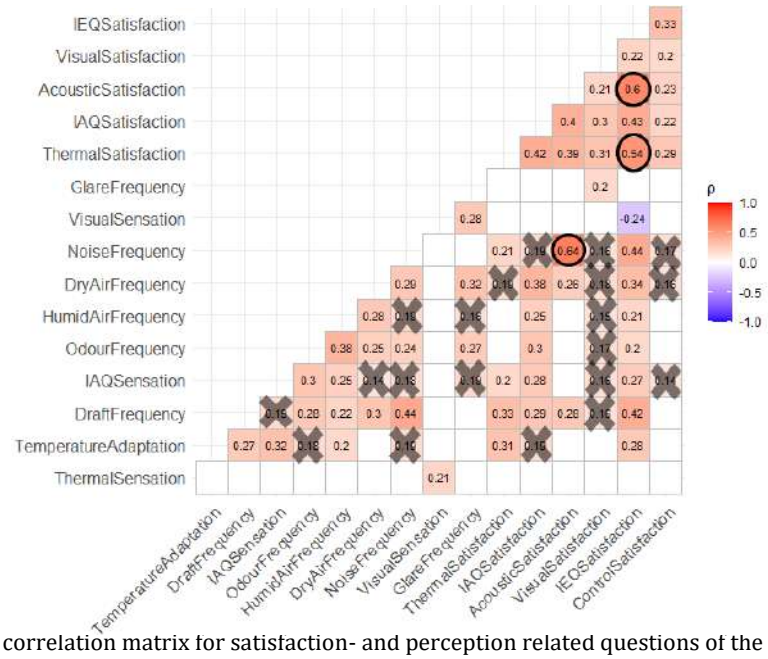

Figure 2. - Spearman correlation matrix for satisfaction- and perception related questions of the retrospective survey in which negligible and moderate effect sizes are crossed out and encircled, respectively. (p<0.05)

residents who perceive noise less often are more satisfied with the acoustic comfort in their living room. Residents' satisfaction with the overall IEQ in their living room was the strongest related to the satisfaction with the acoustic (ρ = 0.6) and thermal (ρ = 0.54) environment. The overall IEQ satisfaction was also related to the IAQ (ρ = 0.43), control (ρ = 0.33) and visual (ρ = 0.22) satisfaction. This ranking of IEQ domains on the overall IEQ satisfaction is in line with the determined weighting for dwellings by Leccese et al. [19].

3.5 Context-related differences

The Kruskal-Wallis H test shows that there are statistically significant differences in the mean IEQ satisfaction scores among the subgroups of "Average daytime occupancy" (p=0.031) and "Building type" (p=0.005). Furthermore, the non-parametric test determines a statistically significant difference in the mean control satisfaction scores among the subgroups of "Building type" (p=0.021) and "Residents' mindset" (p=0.019). No other statistically significant differences in IAQ, thermal, acoustic and visual satisfaction scores were found for the context-related categories. The post-hoc test results show no statistically significant difference in the mean IEQ satisfaction scores between two of the subgroups of "Average daytime occupancy", i.e., 0, 1, 2, 3 and 4. **Table 4** shows the remaining subgroups for which the post-hoc test was statistically significant together with the mean satisfaction score for that subgroup.

Table 4. - Results of the post-hoc test with the mean satisfaction score for the subgroup

	Building type	Residents' mindset
IEQ satisfaction	Apartment (3.7) ~ Detached house (4.3)	/
Control satisfaction	Apartment (3.4) ~ Semi-detached house (4.0)	Equally important (3.7) ~ Comfortable indoor climate (4.3)

Table 4 shows that the type of building in which the resident lives, is the only resident-related information that affects the overall IEQ satisfaction and the control satisfaction. The residents living in apartment buildings show lower satisfaction levels with the overall IEQ and control satisfaction compared to detached and semi-detached houses, respectively. However, the mean differences in satisfaction scores are minor. Residents who prioritize comfort over energy efficiency are slightly more satisfied with their control possibilities compared to residents who ranked comfort and energy efficiency as equally important. It should be mentioned that the number of residents who indicated comfort as the most important characteristic is far lower than the number of residents indicating that energy efficiency and comfort are equally important (see **Table 2**).

4. Results - Analysis of longitudinal surveying

4.1 Data overview

Figure 3 shows the distribution of the gathered satisfaction votes during the longitudinal surveying period. As with the results of the retrospective survey, the majority of the votes represent satisfaction (score ≥ 3) with the thermal environment and IAQ in the living room.

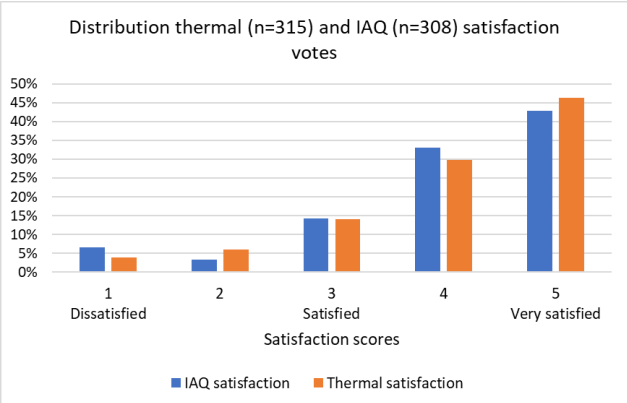

Figure 3. - Overview thermal and IAQ satisfaction scores during longitudinal study

4.2 Parameters influencing occupants' satisfaction

We performed a mixed-effects regression analysis to determine which IEQ and interaction-related parameters influenced the occupants' satisfaction. The results of the forward model selection procedure are summarized in **Table 5**.

Table 5. - Forward model selection summary showing the statistically significant fixed effects (FE), AIC and ICC. NS = non-significant model improvement
NC = no model convergence

FE AIC ICC	Thermal satisfaction		IAQ satisfaction	
	Ordinal	**Binary**	**Ordinal**	**Binary**
Null model	/ 691.02 0.496	/ 170.47 0.627	/ 627.65 0.6	/ 123.06 0.928
Step 1	T 685.69 0.452	T 165.71 0.490	T 619.8 0.58	T 119.02 0.919
Step 2	NS	NS	NS	NS
Step X	NS	NS	NC	NS

Based on the results in **Table 5** it can be stated that the indoor temperature has the strongest relationship with thermal and IAQ satisfaction of all IEQ and interaction-related variables. The addition of a random slope to the models did not improve the

model fit, which indicates that, although the residents casted different satisfaction ratings at the same indoor temperature, the trend between indoor temperature and thermal and IAQ satisfaction is likewise among the different residents. All models have a negative relationship between the indoor temperature and the residents' satisfaction, meaning that a higher indoor temperature leads, in this case, to a higher probability of residents' dissatisfaction with the thermal environment and IAQ.

The assumption for mixed effect models is legitimate based on the high ICC values which vary from 0.496 to 0.928 for the null models. The high ICC values show that a major part of the variance in the models is explained by the random effect, in this case, the residents' ID. The ICC is higher for the binary models than for the ordinal models in which the dependent variable was the 5-point satisfaction rating. This indicates that the residents during the two-week long monitoring period changed their satisfaction rating, but that it mostly stayed within the same category, i.e., satisfied (3 – 5) or dissatisfied (1-2). This is especially the case for the IAQ satisfaction in which the ICC has values above 0.9 for the binary models, indicating that nearly all IAQ satisfaction ratings were the same (satisfied or dissatisfied) for a resident. The addition of indoor temperature as a fixed effect did just marginally decrease the ICC for the IAQ models compared to the thermal satisfaction models. The high ICC values could also be due to short monitoring period in which IEQ parameters did not change dramatically. Therefore, a longer monitoring campaign is needed to investigate the potential change in residents' satisfaction due to varying IEQ conditions.

The high ICC-values among the different fitted models demonstrate that the probability of satisfaction with IEQ is mostly influenced by the residents' ID instead of environmental or interaction-related parameters. Consequently, it is quite difficult to establish an aggregated model to explain residents' satisfaction with IEQ, while a resident-specific approach that considers personal and contextual information would be more appropriate. The study of Langer et al. [20] made a similar conclusion, stating that information regarding residents and building type helped to explain residents' perception of the IAQ. Therefore, the use of personal comfort models [2], which focusses on identifying personal comfort preferences, could be beneficial to more accurately determine residents' satisfaction with IEQ.

5. Conclusion

In this paper we analysed occupants' satisfaction with the IEQ in the living rooms of residential buildings equipped with a demand-controlled extraction ventilation system. Satisfaction data was gathered in two steps, firstly, through a retrospective survey, secondly, by two rating options that were implemented in a mobile application used by the respondents. The latter was combined with indoor environmental parameters, measured by valves of the ventilation system, into one dataset.

Results showed that the inhabitants of the participating dwellings were in general satisfied with the indoor environment in their living rooms during the survey period. Residents living in apartment buildings were slightly less satisfied with the overall IEQ and control possibilities compared to residents living in detached and semi-detached houses. Correlation analysis showed that acoustic and thermal satisfaction had the strongest relation with the overall IEQ satisfaction.

The logistic mixed-effect regression analysis showed that the indoor air temperature was the most influencing parameter for IAQ and thermal satisfaction. Interaction-related variables were not found to be suitable predictors for residents' satisfaction in this case. A large proportion of the variance in the mixed-effects regression models was due to the random-effect of the residents' ID, which shows the importance of accounting for resident-specific information in determining a satisfactory IEQ. However, it should be noticed that the monitored IEQ parameters in this study were rather limited and the dataset fairly small. More data from different dwellings and during different weather conditions are needed to generalize the insights of this paper. Furthermore, this study only focused on residents' satisfaction in the main living room, while residents' preferences regarding the IEQ could change depending on the room type. Therefore, further research should investigate other types of rooms than the main living room to get an overall assessment of residents' satisfaction with IEQ in their homes.

6. Acknowledgments

The authors would like to thank all participating residents. Furthermore, the authors acknowledge the support of the Renson Chair: "Data-driven servitization in creating healthy spaces". This work has also been supported by the Flemish Agency for Innovation and Entrepreneurship (VLAIO) in the Flux50 project Towards Smart Ventilation in Mid-Sized Buildings (HBC.2020.2520).

7. Data access statement

The datasets generated and analysed during the current study are not available because of ethical and legal restrictions but the authors will make every reasonable effort to publish them in near future.

8. References

[1] L. t. Graham, T. parkinson, and S. schiavon, "Lessons learned from 20 years of CBE's occupant surveys," *Build. Cities*, vol. 2, no. 1, pp. 166–184, 2021, doi: 10.5334/bc.76.

[2] J. Kim, S. Schiavon, and G. Brager,

"Personal comfort models – A new paradigm in thermal comfort for occupant-centric environmental control," *Build. Environ.*, vol. 132, pp. 114–124, 2018, doi: 10.1016/j.buildenv.2018.01.023.

[3] R. Becker and M. Paciuk, "Thermal comfort in residential buildings - Failure to predict by Standard model," *Build. Environ.*, vol. 44, no. 5, pp. 948–960, 2009, doi: 10.1016/j.buildenv.2008.06.011.

[4] A. Zalejska-Jonsson and M. Wilhelmsson, "Impact of perceived indoor environment quality on overall satisfaction in Swedish dwellings," *Build. Environ.*, vol. 63, pp. 134–144, 2013, doi: 10.1016/j.buildenv.2013.02.005.

[5] M. S. Andargie, M. Touchie, and W. O'Brien, "A review of factors affecting occupant comfort in multi-unit residential buildings," *Build. Environ.*, vol. 160, no. April, p. 106182, 2019, doi: 10.1016/j.buildenv.2019.106182.

[6] R Core Team, "R: A Language and Environment for Statistical Computing." Vienna, Austria, 2020, [Online]. Available: https://www.r-project.org/.

[7] C. J. Ferguson, "An Effect Size Primer: A Guide for Clinicians and Researchers," *Prof. Psychol. Res. Pract.*, vol. 40, no. 5, pp. 532–538, 2009, doi: 10.1037/a0015808.

[8] A. Kassambara, "ggcorrplot: Visualization of a Correlation Matrix using 'ggplot2.'" 2019, [Online]. Available: https://cran.r-project.org/package=ggcorrplot.

[9] P. Dalgaard, *Introductory Statistics with {R}*, Second. New York: Springer, 2008.

[10] S. Lechner, C. Moosmann, A. Wagner, and M. Schweiker, "Does thermal control improve visual satisfaction? Interactions between occupants' self-perceived control, visual, thermal, and overall satisfaction," *Indoor Air*, no. April, pp. 1–21, 2021, doi: 10.1111/ina.12851.

[11] T. Cheung, S. Schiavon, L. T. Graham, and K. W. Tham, "Occupant satisfaction with the indoor environment in seven commercial buildings in Singapore," *Build. Environ.*, vol. 188, no. October 2020, 2021, doi: 10.1016/j.buildenv.2020.107443.

[12] F. Haldi, D. Calì, R. K. Andersen, M. Wesseling, and D. Müller, "Modelling diversity in building occupant behaviour: a novel statistical approach," *J. Build. Perform. Simul.*, vol. 10, no. 5–6, pp. 527–544, 2017, doi: 10.1080/19401493.2016.1269245.

[13] M. Schweiker, M. Hawighorst, and A. Wagner, "The influence of personality traits on occupant behavioural patterns," *Energy Build.*, vol. 131, pp. 63–75, 2016, doi: 10.1016/j.enbuild.2016.09.019.

[14] R. H. B. Christensen, "ordinal---Regression Models for Ordinal Data." 2019, [Online]. Available: https://cran.r-project.org/package=ordinal.

[15] H. Akaike, "A New Look at the Statistical Model Identification," *IEEE Trans. Automat. Contr.*, vol. 19, no. 6, pp. 716–723, 1974, doi: 10.1109/TAC.1974.1100705.

[16] S. Nakagawa, P. C. D. Johnson, and H. Schielzeth, "The coefficient of determination R2 and intra-class correlation coefficient from generalized linear mixed-effects models revisited and expanded," *J. R. Soc. Interface*, vol. 14, no. 134, 2017, doi: 10.1098/rsif.2017.0213.

[17] D. Bates, M. Mächler, B. Bolker, and S. Walker, "Fitting Linear Mixed-Effects Models Using {lme4}," *J. Stat. Softw.*, vol. 67, no. 1, pp. 1–48, 2015, doi: 10.18637/jss.v067.i01.

[18] M. Tavakol and R. Dennick, "Making sense of Cronbach's alpha," *Int. J. Med. Educ.*, vol. 2, pp. 53–55, 2011, doi: 10.5116/ijme.4dfb.8dfd.

[19] F. Leccese, M. Rocca, G. Salvadori, E. Belloni, and C. Buratti, "Towards a holistic approach to indoor environmental quality assessment : Weighting schemes to combine effects of multiple environmental factors," *Energy Build.*, vol. 245, p. 111056, 2021, doi: 10.1016/j.enbuild.2021.111056.

[20] S. Langer, O. Ramalho, E. Le Ponner, M. Derbez, S. Kirchner, and C. Mandin, "Perceived indoor air quality and its relationship to air pollutants in French dwellings," *Indoor Air*, vol. 27, no. 6, pp. 1168–1176, 2017, doi: 10.1111/ina.12393.

Local heating and cooling effectiveness - an evaluation method based on calculated local and overall thermal state

Mohamad Rida [a], Dolaana Khovalyg [a]

[a] Integrated Comfort Engineering (ICE), Ecole Polytechnique Fédérale de Lausanne (EPFL), Switzerland.

Abstract. The application of Personal Comfort Systems (PCS) in the buildings demonstrated their potential to improve thermal comfort and reduce energy use by the HVAC systems. With its personal controllability PCS is a practical solution to tackle the diversity in perceiving thermal comfort between occupants. The differences in thermal perception can be due to physiological and psychological factors, such as metabolic rate, acclimatization, body composition, gender, and age. In addition to the primary purpose of improving individual thermal comfort, it allows for a wider set point temperature of the HVAC system conditioning the space, which may lead to an extensive reduction in energy use.

Several PCS device options have already evolved, but incorporating these devices into building conditioning faces lots of restrictions. The PCSs are categorized between movable, portable, and fixed devices, and PCS devices can function with different means of heat exchange.

In this study, the capability of local heating and cooling to correct the individual's thermal state toward thermal neutrality when the rest of the body is exposed to cold or heat was evaluated. A detailed physiology model was applied to evaluate the impact of the nonuniform environment from PCS on local skin, heat flux, and thermal comfort. Different locations of the human body (head, hands, feet, legs, thighs, back, and pelvis) have been tested since the heat exchanged at local body parts differs in its effectiveness in improving the overall thermal state. Different operative temperature relaxations have been tested with a base cooling setpoint of 25°C and heating of 24°C. Multiple simulations have been conducted to account for multiple local environmental settings. We have evaluated the influence of local heating and cooling of different body parts on correcting the whole-body thermal state toward thermal neutrality. Results showed that the thigh could be a promising prominent body part for both cooling and heating, followed by the hands and feet, which are good responders to local heating. The percentage of correction toward thermal neutrality varies with background temperature and local heating or cooling power, and can range from 50–80% for hands and feet to 60–100% for the thigh.

Keywords. Personal comfort system, Local heating and cooling, Energy efficient system, Human thermo-physiology.
DOI: https://doi.org/10.34641/clima.2022.267

1. Introduction

It is a fact that people spend the majority of their time indoors in urbanized areas, which makes indoor environmental quality (IEQ) accountable in new and existing buildings for assuring the well-being of the occupants [1]. IEQ is characterized by environmental categories such as thermal comfort, air quality, lighting, and acoustics. While each category is equally important for the comfort and well-being of occupants, thermal comfort has repeatedly been determined to be the primary factor in people's overall satisfaction with indoor environmental quality [2]. Studies have shown that good indoor thermal comfort plays an important role in determining people's well-being, health and productivity. Therefore, indoor temperatures are typically set in buildings with the aim of providing thermal comfort to occupants by keeping their thermal sensation around thermal neutrality (the

Copyright ©2022 by the authors. This conference paper is published under a CC-BY-4.0 license.

state when a human body primarily maintains its core body temperature with minimal metabolic regulation) [3]. However, the practice of setting the indoor temperature at a narrow range is achieved by the use of heating, ventilation, and air conditioning systems. HVAC, on the other hand, has repeatedly been criticized for its excessive energy use that reaches almost 40% of operational energy use in buildings [4]. Furthermore, it has been found to be difficult to satisfy individual thermal comfort due to individual differences such as gender, age, body composition, and personal preference [5,6]. As a result, it is difficult to thermally satisfy all building occupants using the common practice of uniform indoor temperature created by an HVAC system [7]. Therefore, in the quest to improve the well-being of occupants and limit energy use in buildings, indoor energy-efficient personal comfort systems (PCSs) have been widely employed to increase occupant thermal comfort and acceptance under a variety of thermal circumstances.

A PCS delivers heating and cooling to local body parts rather than whole surroundings, allowing for specific heating and cooling to suit the real occupant's need [8,9]. As a result, the ambient temperature range can be broader beyond the temperature range specified by regulations, which potentially saves energy. When using the appropriate PCSs, a reduction of 4% to 60% of the energy used is expected [10,11,12]. Different PCS devices have already been presented and tested individually in the literature; each device can target one or more body areas. When it comes to PCS that directly target a body part, it's important to distinguish between a covered and uncovered body part with cloth. Furthermore, the format of heat transmission between the body surface and the heating/cooling device/surface varies.

Based on the literature, PCSs can be categorized as fixed and attached to the workplace (furniture) such as radiant heating and cooling desks, personal ventilation systems, movable such as heating and cooling chairs, portable heaters, and foot mattresses, and wearable such as wristbands, active clothes, shoe insoles, and gloves. In most of the studies reported in the literature, the effectiveness of the PCS is evaluated based on the subjective tests by evaluating the occupants' votes on thermal sensation, thermal comfort, and thermal acceptance. These methods require a large number of subjects to derive a statistically valid answer [13].

Different characteristics that influence the heat transfer from the skin of a body part to local heating or cooling devices. Starting from the skin surface area, to the body part (mass) or layer composition, to the different heat generation distribution. The skin blood flow plays the main role in transferring heat between the different layers and different body parts. For example, hands/ limbs skin temperature has always a bigger range of temperature fluctuation compared to the head and torso skin temperature. Therefore, the comparison of local thermal sensitivity becomes more challenging.

According to the literature review conducted by [14], in terms of local thermal perception, the head shows the largest heating-induced local thermal sensation response to a warm stimulus in a neutral environment, whereas the extremities appear to have the least. On the other hand, the local perception of a cold stimulus differs between research studies. Face cooling resulted in the greatest increase in whole-body comfort in a hot climate [15]. Abdomen cooling is the least recommended [15]. In a cold climate, face warming is regarded as less comfortable than heating on the chest, abdomen, and thighs, with abdominal warming providing the most comfort [15]. [16] In an experiment involving 24 subjects, they found that the legs, thighs, and back were the key body segments for local cooling in summer. In the winter, the primary segments for local heating were the leg, thigh, back, and upper arm. Due to the differences in evaluation between studies, as some tend to point to heat flow and others rely on the user's thermal perception, it is hard to draw a conclusion on the most influential body part. For example, [17] pointed out that the legs and thighs are the most influential body parts, when other studies claimed that the lower body parts are the least influential.

Most of the multi-node HTPMs are based on Stolwijk's model [18], and one of the latest models called JOS3 segments the human body into 17 parts [19]. The model is based on the energy balance between the environment and the human body; thus, it includes heat transfer between the skin layer and the environment through 3 modes of heat transfer in addition to conduction between the different layers and convection due to the blood circulation between layers and body parts. Using a detailed human thermo-physiology to project the changes and influences of local heating and cooling on the whole body could be a potential approach. This approach can help in addressing several questions in order to properly design, select and improve a PCS system.

In the extensive literature review of [14] they tried to answer the basic question of which body parts should be targeted. The literature showed a significant contradiction between the studies and for that the question has yet to be resolved. This research seeks to answer this issue by methodically examining the impact of local body parts heating and cooling on the entire body.

Luo et al. [14] defined the three different factors that affect the effectiveness of a personal comfort system as: 1) environmental factors, 2) user factors, and 3) system factors. In our simulation, we considered the effect of different background operative temperatures as an environmental factor, as well as the differences between a male and female and the different clothing insulation representing two seasons, winter and summer. Local heating and cooling were represented as an imaginary system

that could provide an ideal operative temperature uniformly distributed around the targeted body part. The influence of power has been represented as a different local operative temperature. In addition, the influence of the body thermal state before activating the local cooling and heating has been considered in our study which can be added as an additional environmental factor to what has been reported in [14].

The model has been validated by a set of data from a pilot study. In the experiment, a temperature drift from 24°C to 16°C has been conducted in a climatic chamber during winter. The subjects were sitting relaxed, wearing winter clothing with a total insulation value of 0.8 clo. In the HTPM simulation, we specified all local environmental parameters from the detailed experimental measurements. In addition, we used dynamic EE data directly from the experiments rather than estimating metabolic rate.

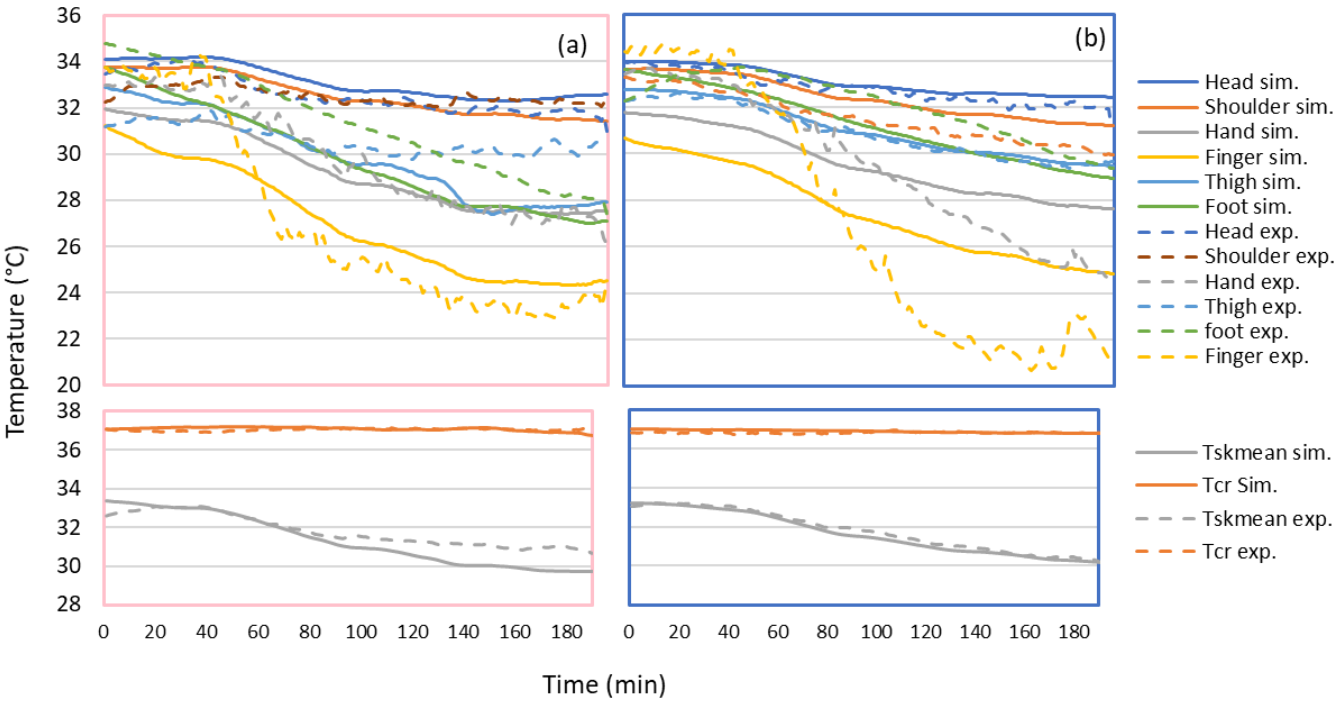

Fig. 1- Experimental results vs. HTPM Simulation in a drift environment from 24°C to 16°C.(a) are the results from a female and (b) for a male subject

2. Simulation

2.1 Thermo-Physiology model

In this study we have adopted the human thermo-physiology model JOS3 as an open source model developed by [19]. The model initially includes 17 body parts including the head, neck, chest, back, pelvis, right and left shoulders, arms, hands, thighs, legs, and feet. We have further improved the model to account for the 10 fingers.

The simulation has been conducted on two mid aged healthy subjects a male and female subject the body composition of each subject are presented in table 1

2.2 Model improvement

We have improved the model by including the fingers as separate body parts from the hands. We believe that hands including fingers are sensitive to the changes in the environment as most of the time bare skin body parts, and as extremities the skin temperature fluctuate the most in a wider range.

2.3 Model validation

Tab. 1- Subjects body composition

Sex	Age	Hight (m)	Weight (Kg)	Fat percent. %	Body surf. area (m2)
F	37	1.64	62	35.2	1.69
M	36	1.78	85	28.8	2.06

Figure 1 presents the results of the mean skin temperature, core temperature, as well as some local skin temperatures for 2 subjects, a female (a) and a male (b). We personalized inputs such as age, gender, fat percentage, height, and weight as mentioned in table 1. The local experimental results were compared with the simulation results from the HTPM for the head, shoulder, thigh, hand, and foot.

According to the results, both subjects showed an acceptable MSE for mean skin temperature, with a value of less than 0.5°C and a core temperature with an MSE of 0.1°C. Furthermore, the results showed

that the skin temperature of the female subjects' hands and fingers correlated better with the simulation, with an MSE of less than 0.5 °C when compared to male subjects, which could be attributed to female participants' lower BMI. Contrarily, the results of the foot showed a slightly better agreement in the male subject compared to the female. The actual foot skin temperature was higher in both subjects than the predicted foot skin temperature. The head showed an acceptable result for both subjects, with an MSE of 0.5°C for the female and 0.2 for the male. Females had better agreement on the shoulder, with an MSE of 0.5 °C. The skin temperature of the thigh predicted from the HTPM simulation was compared with the averaged anterior and posterior thigh skin temperature from the experiment, where the results were in alignment with each other.

Although the results showed an acceptable agreement, there is still some deviation in the local skin temperature of the extremities, especially the feet. This highlights some limitations of the model in extreme environments. As the HTPM follows the changes in the environment correctly, we believe that using the model to study the effect of local heating and cooling on the thermal state of the whole body can be valid.

2.4 Mean skin temperature

Mean skin temperature is essential to represent the thermal state of the whole body. For example, during a cold exposure, vasoconstriction at the extremities occurs before a noticeable change in core temperature, giving the mean skin temperature an additional advantage as a better indicator of the whole-body thermal state [20].

In most of the research, the mean skin temperature is calculated based on a number of local skin temperatures from specific body parts. Some used measurements from only one side, either the left or right side of the body. For example, [21] calculated the mean skin temperature using seven body locations, whereas others used a fourteen-point method [20]. In this study, we intended to consider all body parts included in the model and the weight of each body part calculated by the weighted surface area. All local weights are presented in table 2. It is the purpose of having a consistent influence on the locals.

$$T_{mean} = \sum_{i=1}^{27} (f_{weight,i} \times T_{local,i})$$

Tab. 2- Body parts weighting factor

Body part	Weight factor
Head	0.059
Neck	0.015
Chest	0.094
Back	0.086
Pelvis	0.118
Shoulder x2	0.051
Arm x2	0.033
Hand x2	0.013
Finger x10	0.003
Thigh x2	0.112
Calf x2	0.06
Foot x2	0.03

3. Results

The results from the thermo-physiology model simulations represent an ideal situation as the ambient and local environments are considered uniform, thereby limiting the various influences on human thermoregulation to only influences from local heating or cooling.

The differences between the gender or, in another word, the effect of the different body composition has been considered. All simulations have been repeated for a male and a female subject considered, the body characteristics are reported in table 1. With a fixed metabolic rate of 1.2 met representing office work, and winter clothing of 0.8 clo and summer clothing of 0.6 clo.

3.1 Steady-state results

We have conducted several simulations that all started from the same initial conditions as reported in table 3. Simulations were grouped into two categories: one represents a cold exposure with local heating and the second is a hot exposure with local cooling. Three different ambient environments have been selected for each cold and hot exposure correspondingly, as follows: cold exposure at 16°C, 18°C, and 20°C; hot exposure at 28°C, 30°C, and 32°C.

Tab. 3- Neutral environmental conditions

Neutral environment	Winter	Summer
Operative temperature(°C)	24	25
Air velocity (m/s)	0.1	0.1
Relative humidity %	50	50

Four different powers of local heating and cooling have been tested, with the power represented by the local temperature. For local heating, we considered 34°C, 36°C, 38°C, and 40°C, and for cooling, we considered 16°C, 18°C, 20°C, and 22°C. Each body part was locally heated or cooled while the other body parts were exposed to either cold or hot temperatures. The difference of mean skin temperature resulted to the neutral case has been calculated. The mean skin temperature was taken after 60 min of exposure. Figure 2 shows the heat map results from the local heating and cooling of the hands, feet, head, chest, back, thigh, and pelvis in addition to some combinations of multiple body local

backgroud	24°C	16 [°C]					18 [°C]					20 [°C]				
Body part	Neutral	No Local H/C	$T_{op,local}$34°C	$T_{op,local}$36°C	$T_{op,local}$38°C	$T_{op,local}$40°C	No Local H/C	$T_{op,local}$34°C	$T_{op,local}$36°C	$T_{op,local}$38°C	$T_{op,local}$40°C	No Local H/C	$T_{op,local}$34°C	$T_{op,local}$36°C	$T_{op,local}$38°C	$T_{op,local}$40°C
Hands	33.5	-2.9	-2.2	-2.1	-2.0	-2.0	-2.2	-1.5	-1.5	-1.4	-1.3	-1.5	-0.9	-0.8	-0.7	-0.7
Feet	33.5	-2.9	-2.5	-2.4	-2.4	-2.4	-2.2	-1.8	-1.8	-1.8	-1.7	-1.5	-1.2	-1.1	-1.1	-1.1
Hand+Feet	33.5	-2.9	-1.8	-1.7	-1.6	-1.5	-2.2	-1.2	-1.1	-1.0	-0.9	-1.5	-0.6	-0.5	-0.4	-0.3
Head	33.5	-2.9	-2.5	-2.4	-2.4	-2.3	-2.2	-1.8	-1.8	-1.7	-1.6	-1.5	-1.1	-1.1	-1.0	-0.9
Chest	33.5	-2.9	-2.3	-2.3	-2.2	-2.1	-2.2	-1.7	-1.6	-1.6	-1.5	-1.5	-1.0	-1.0	-0.9	-0.9
Back	33.5	-2.9	-2.3	-2.3	-2.2	-2.2	-2.2	-1.7	-1.7	-1.6	-1.5	-1.5	-1.1	-1.0	-0.9	-0.9
Pelvis	33.5	-2.9	-2.4	-2.3	-2.3	-2.2	-2.2	-1.7	-1.7	-1.6	-1.5	-1.5	-1.1	-1.0	-0.9	-0.9
Pelvis+Back	33.5	-2.9	-1.8	-1.7	-1.6	-1.5	-2.2	-1.2	-1.1	-1.0	-0.9	-1.5	-0.6	-0.5	-0.4	-0.3
Thigh	33.5	-2.9	-1.5	-1.4	-1.2	-1.1	-2.2	-1.0	-0.8	-0.7	-0.5	-1.5	-0.4	-0.3	-0.1	0.1
Pelvis+Thigh	33.5	-2.9	-1.0	-0.8	-0.6	-0.4	-2.2	-0.5	-0.3	0.0	0.2	-1.5	0.1	0.3	0.6	1.0
Thigh+Back	33.5	-2.9	-1.0	-0.8	-0.6	-0.4	-2.2	-0.5	-0.3	0.0	0.2	-1.5	0.1	0.3	0.6	0.9
Thigh+Back+Pelvis	33.5	-2.9	-0.5	-0.2	0.2	0.5	-2.2	0.1	0.4	0.9	1.2	-1.5	0.7	1.1	1.4	1.6

backgroud	25°C	28 [°C]					30 [°C]					32 [°C]				
Body part	Neutral	No Local H/C	$T_{op,local}$16°C	$T_{op,local}$18°C	$T_{op,local}$20°C	$T_{op,local}$22°C	No Local H/C	$T_{op,local}$16°C	$T_{op,local}$18°C	$T_{op,local}$20°C	$T_{op,local}$22°C	No Local H/C	$T_{op,local}$16°C	$T_{op,local}$18°C	$T_{op,local}$20°C	$T_{op,local}$22°C
Hands	33.2	1.6	0.9	1.1	1.2	1.3	2.0	1.9	1.9	2.0	2.0	2.2	2.1	2.1	2.1	2.2
Feet	33.2	1.6	1.2	1.3	1.4	1.4	2.0	1.9	1.9	1.9	2.0	2.2	2.1	2.1	2.1	2.1
Hand+Feet	33.2	1.6	1.0	1.1	1.2	1.3	2.0	1.8	1.8	1.9	1.9	2.2	2.3	2.3	2.3	2.2
Head	33.2	1.6	1.0	1.1	1.2	1.3	2.0	1.8	1.9	1.9	2.0	2.2	2.1	2.1	2.1	2.1
Chest	33.2	1.6	1.0	1.1	1.2	1.3	2.0	1.8	1.9	1.9	2.0	2.2	2.1	2.1	2.1	2.1
Back	33.2	1.6	0.3	0.5	0.7	1.0	2.0	1.3	1.5	1.7	1.8	2.2	1.9	1.9	1.9	2.0
Pelvis	33.2	1.6	1.0	1.1	1.2	1.3	2.0	1.8	1.9	1.9	1.9	2.2	2.1	2.1	2.1	2.1
Pelvis+Back	33.2	1.6	0.4	0.6	0.8	1.0	2.0	1.3	1.4	1.6	1.8	2.2	1.9	2.0	2.0	2.0
Thigh	33.2	1.6	-0.2	0.1	0.3	0.6	2.0	0.4	0.8	1.3	1.5	2.2	1.5	1.7	1.8	1.9
Pelvis+Thigh	33.2	1.6	-0.2	0.1	0.3	0.6	2.0	0.4	0.8	1.3	1.5	2.2	1.5	1.7	1.8	1.9
Thigh+Back	33.2	1.6	0.4	0.6	0.8	1.1	2.0	1.5	1.7	1.8	1.9	2.2	1.9	2.0	2.0	2.1
Thigh+Back+Pelvis	33.2	1.6	-0.6	-0.3	0.0	0.4	2.0	-0.1	0.2	0.6	1.1	2.2	0.4	1.0	1.5	1.7

Fig. 2- Heat map of the mean skin temperature shift from neutrality for different local heating and cooling settings

heating and cooling, such as the pelvis+back, pelvis+thigh, thigh+back, thigh+back+pelvis, and hands+feet.

From the results, we could see that the effect of both cooling and heating of the thigh as a single body part has the most influence on the mean skin temperature compared to the other body parts. On the other hand, the hands showed a higher or similar impact compared to the head, chest, and back. Based on the environmental conditions and local heating and cooling power presented in this study, we could see that only cooling or heating the thigh as a single body part could bring the mean skin temperature closer to the mean skin temperature at neutrality, especially at moderate background temperatures of 20°C and 28°C. It is clear that heating or cooling multiple body parts has more potential for bringing the body toward thermal neutrality. The results showed that both hands and feet could be equally compared to the back and pelvis. According to the findings, the thigh is the most important component in shifting any combination toward thermal neutrality and, in some cases, overheating, as in the case of heating the back, pelvis, and thigh at 38°C and 40°C at all three background temperatures, and over cooling when the local temperature was 16°C and 18°C for a background temperature of 28°C.

Tab. 4- Percentage of effectiveness achieved toward

Local temperature	Thigh	Pelvis +Back	Hand +Feet	Thigh +Back +Pelvis
T_16°C	33	38	25	106
T_18°C	25	29	17	89
T_20°C	18	19	12	72
T_22°C	13	13	8	44
T_34°C	56	44	45	104
T_36°C	63	49	51	119
T_38°C	69	54	56	140
T_40°C	75	60	61	158

thermal neutrality from local heating and cooling at 30°C and 18°C background environment

The simulations have been repeated for both male and female where results showed that the female subject showed slightly closer values compared to the men. Here we should acknowledge the influence of the differences in body composition between the male and female subjects that is mainly behind the

differences in the mean skin temperature results. Table 4 presents the percentage of effectiveness of different local cooling and heating body parts in terms of bringing the mean skin temperature back to neutrality which can range from 50–80% for hands and feet to 60–100% for the thigh.

3.2 Dynamic results

The thermal state in which the body is just before applying local heating or cooling in HTPM has a big influence on the time required to reach steady state again. Here, in this simulation example, we present the dynamic result of the mean skin temperature changing with time as the environmental parameters change. Figure 3 presents the mean skin temperature for the different cases. All simulations began in a neutral environment defined as 24°C for winter clothing and 25°C for summer clothing. After reaching a steady state, the environmental temperature changed to either 18°C with the winter clothes or 30°C with the summer clothes. Followed by two different cases, first one the solid lines where local heating or cooling started immediately with the cold or hot exposure, second case is when local cooling or heating introduced after one hour of full body heat or cold exposure. The results highlight that the thermal state of the body is in a better position when applying local heating and cooling from the beginning of the cold or hot exposure, and that compared with the delayed local heating and cooling mean skin temperature required even more than 30 min to reach the mean skin temperature of the first case local H/C from the beginning.

a hot exposure (red frame) with local cooling and the second represent a cold exposure (blue frame) with local heating. The graph also presents the local results from two different local heating or cooling strategies, Figure 4-I the hands and feet cooling or heating and Figure 4-II the back, pelvis and thigh local heating at 36°C and cooling at 18°C. The rate of heat losses in the case of back pelvis thigh is more than double the rate of heat loss in the hands and feet.

Skin blood flow in all cases for local body parts has gone back to similar range as thermal neutrality. Looking at local skin temperature, in the local heating case the hands and feet were effective as much as the back pelvis and thigh but not in the local cooling case.

4. Conclusion

In order to assess the human thermal state for individuals and in non-uniform environments, the thermophysiology model become the most suitable tool in this case. The model gives physiological responses to the environmental changes locally and overall. To obtain a high percentage of occupant thermal satisfaction in a building while reducing energy usage for heating and cooling, occupant physiological activity must be more carefully taken into consideration. Individual variables in human physiology (age, gender, and body composition) impact the thermal state of the body and physiological reactions, potentially resulting in differences in thermal comfort and thermal preferences among occupants.

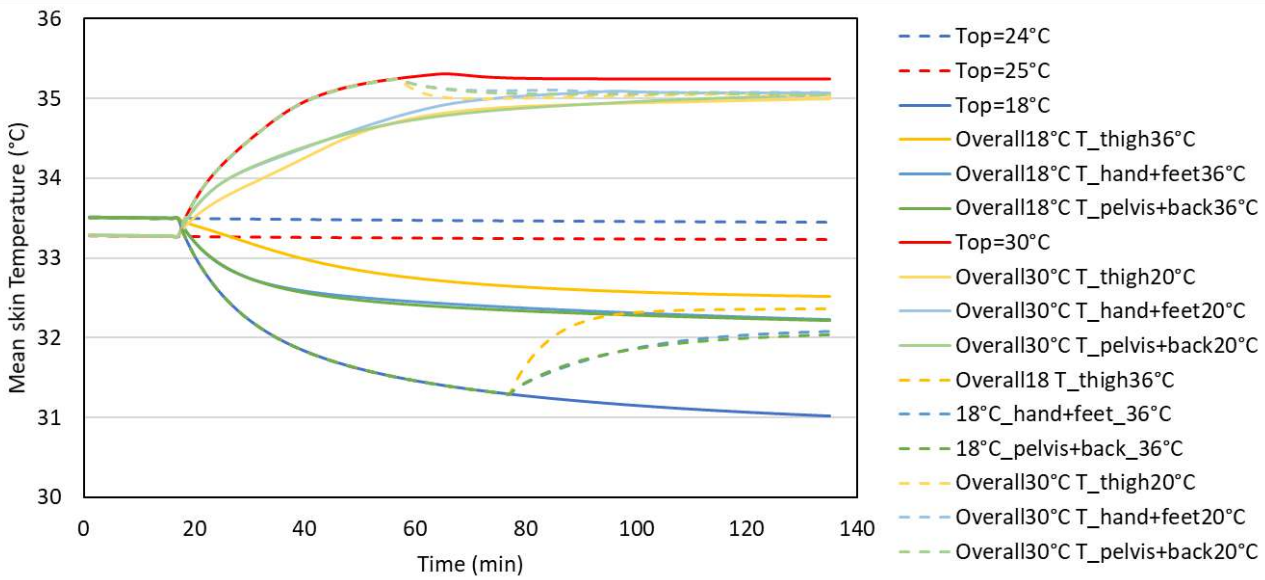

Fig. 3- Dynamic respons of the mean skin temperature during different environmental scenario

3.3 Physiological parameters changes

In this section of the results analyses we focused on the physiological changes happening in local body parts such as the local skin temperature, local skin blood flow and local heat losses compared to thermal neutrality at the start of the simulation. Two sets of data are presented in Figure 4 I and II, first represent

Localized heating or cooling can be an energy-efficient method because it does not require conditioning of the entire room. Further, if occupant comfort can be maintained by heating or cooling a specific body segment with a local heating or cooling device, more energy savings potential can be obtained.

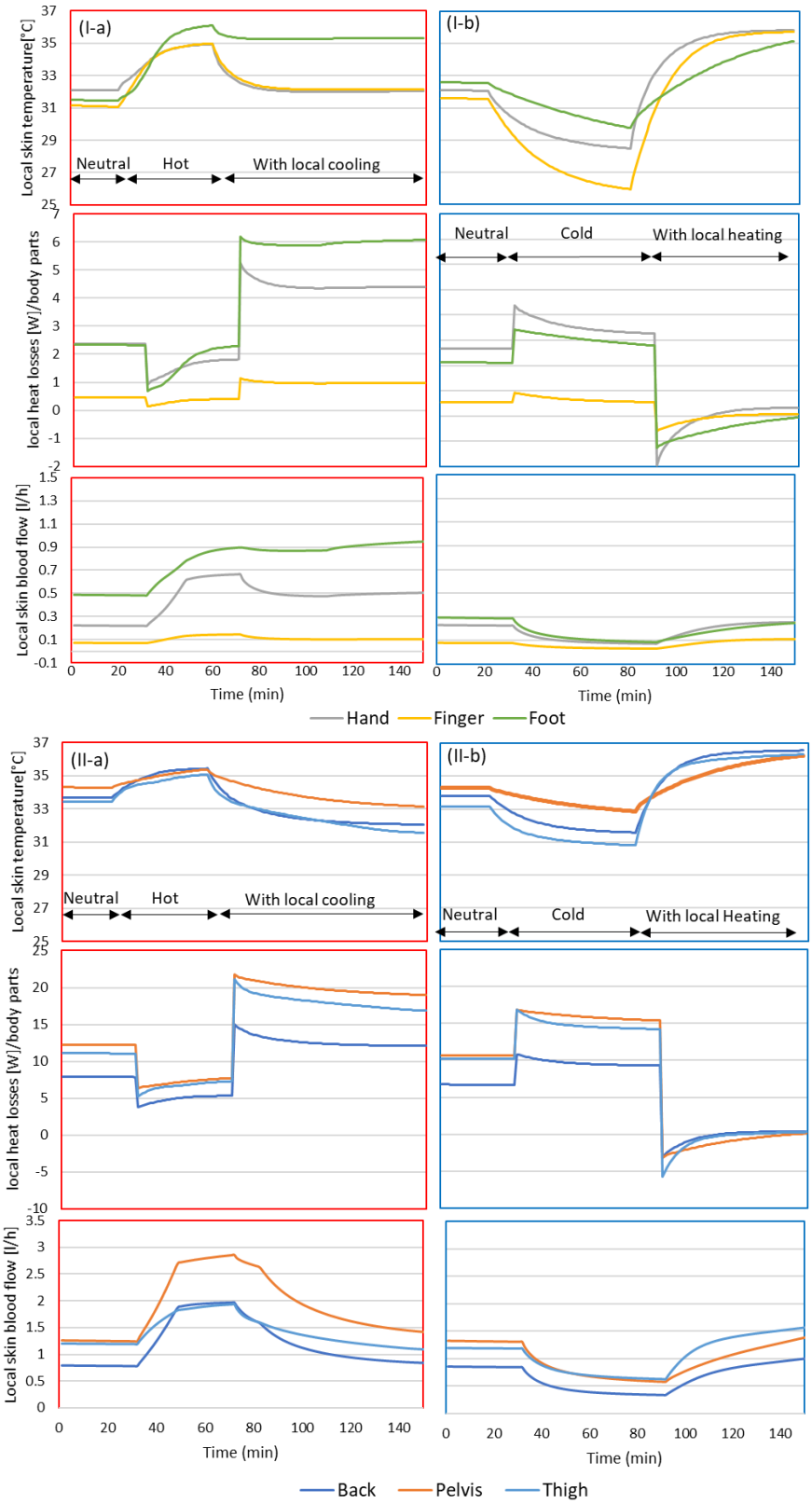

Fig. 4- Physiological parameters of hand, finger and foot (I a,b) and back, pelvis, thigh (II a,b) during locally cooling at 18°C and local heating at 36°C

This study is based on the results from the human thermo-physiology model. Although those models are usually criticized for their accuracy in prediction, we believed that in this study we were able to project the effect of local heating and cooling on the whole body. The results showed the influence of the non-uniform environment on the total thermal state of the human body, as well as the influence of the power of local heating and cooling. We have also highlighted the transient effect and the initial condition before introducing the local heating and cooling on the time required to reach a steady state. For further

development, the model requires further improvement to increase its accuracy individual subjects. Moreover, differentiating between the different mean of heat transfer needs to be highlighted in order to see the effect of heat transfer mode.

5. References

[1] Neil E K., Nelson W., Ott R., Robinson J P., Tsang A., Switzer P., Behar J., Hern S., and Engelmann W. The national human activity pattern survey (nhaps): a resource for assessing exposure to environmental pollutants. Journal of Exposure Science & Environmental Epidemiology, 11(3):231–252,2001.

[2] Frontczak, M., & Wargocki, P. (2011). Literature survey on how different factors influence human comfort in indoor environments. *Building and environment*, *46*(4), 922-937.

[3] Kingma B., Frijns A., Lisje Schellen, and Wouter D van Marken Lichtenbelt. Beyond the classic thermoneutral zone. Temperature, 1(2):142–149, 2014. PMID: 27583296.9

[4] Luis P´erez-Lombard, Jos´e Ortiz, and Christine Pout. A review on buildings energy consumption information. Energy and Buildings, 40(3):394–398, 2008.

[5] Marcel Schweiker, Gesche M. Huebner, Boris R. M. Kingma, Rick Kramer, and Hannah Pallubinsky. Drivers of diversity in human thermal perception – a review for holistic comfort models. Temperature, 5(4):308–342, 2018. PMID: 30574525.

[6] Zhe Wang, Richard de Dear, Maohui Luo, Borong Lin, Yingdong He, Ali Ghahramani, and Yingxin Zhu. Individual difference in thermal comfort: A literature review. Building and Environment, 138:181–193, 2018.

[7] Monika Frontczak and Pawel Wargocki. Literature survey on how different factors influence human comfort in indoor environments. Building and Environment, 46(4):922–937, 2011.

[8] H. Zhang, E. Arens, Y. Zhai, A review of the corrective power of personal comfort systems in non-neutral ambient environments, Build. Environ. 91 (2015) 15–41, https://doi.org/10.1016/j.buildenv.2015.03.01.

[9] M. Vesely´, W. Zeiler, Personalized conditioning and its impact on thermal comfort and energy performance - A review, Renew. Sustain. Energy Rev. 34 (2014) 401–408, https://doi.org/10.1016/j.rser.2014.03.024.

[10] Yang B., C. Sekhar, A.K. Melikov, Ceiling mounted personalized ventilation system in hot and humid climate - an energy analysis, Energ Build 42 (12) (2010) 2304–2308.

[11] Pan C.S., H.C. Chiang, M.C. Yen, C.C. Wang, Thermal comfort and energy saving of a personalized PFCU air-conditioning system, Energ Build 37 (5) (2005) 443–449.

[12] Schiavon S., A.K. Melikov, Energy-saving strategies with personalized ventilation in cold climates, Energy Build 41 (5) (2009) 543–550.

[13] Song, W., Zhang, Z., Chen, Z., Wang, F., & Yang, B. (2022). Thermal comfort and energy performance of personal comfort systems (PCS): A systematic review and meta-analysis. *Energy and Buildings*, *256*, 111747.

[14] Luo, W., Kramer, R., de Kort, Y. and van Marken Lichtenbelt, W., 2021. Effectiveness of personal comfort systems on whole-body thermal comfort–a systematic review on which body segments to target. *Energy and Buildings*, p.111766.

[15] Nakamura, M., Yoda, T., Crawshaw, L.I., Yasuhara, S., Saito, Y., Kasuga, M., Nagashima, K. and Kanosue, K., 2008. Regional differences in temperature sensation and thermal comfort in humans. Journal of applied physiology, 105(6), pp.1897-1906.

[16] Wang, L., Tian, Y., Kim, J., & Yin, H. (2019). The key local segments of human body for personalized heating and cooling. *Journal of thermal biology*, *81*, 118-127.

[17] L. Wang, Y. Tian, J. Kim, H. Yin, The key local segments of human body for personalized heating and cooling, J. Therm. Biol. 81 (2019) 118–127, doi: 10. 1016/j.jtherbio.2019.02.013.

[18] Katić, K., Li, R., & Zeiler, W. (2016). Thermophysiological models and their applications: A review. *Building and Environment*, *106*, 286-300.

[19] Takahashi, Y., Nomoto, A., Yoda, S., Hisayama, R., Ogata, M., Ozeki, Y., & Tanabe, S. I. (2021). Thermoregulation model JOS-3 with new open source code. Energy and Buildings, 231, 110575.

[20] Zhang, H. (2003). Human thermal sensation and comfort in transient and non-uniform thermal environments. University of California, Berkeley.

[21] Hardy, J. D., Du Bois, E. F., & Soderstrom, G. F. (1938). The technic of measuring radiation and convection: one figure. *The Journal of Nutrition*, *15*(5), 461-475.

Thermal environment in simulated office rooms generated by active ceiling diffuser with radiant panels

Panu Mustakallio [a], Pekka Kanerva [b], Yuxin Wu [c], Risto Kosonen [d, e]

[a] Halton Oy, Kausala, Finland, panu.mustakallio@halton.com.

[b] Halton Oy, Kausala, Finland, pekka.kanerva@halton.com.

[c] School of Civil Engineering and Architecture, Zhejiang Sci-Tech University, Hangzhou, Zhejiang, China, wuyuxin1988@foxmail.com.

[d] Department of Mechanical Engineering, Aalto University, Espoo, Finland, risto.kosonen@aalto.fi.

[e] College of Urban Construction, Nanjing Tech University, Nanjing, 210009, China.

Abstract. Ventilation airflow rates are typically controlled based on occupancy, air quality and heat load levels in office rooms with variable air volume (VAV) system. Additional water-based cooling is often the most energy efficient to use when air cooling does not cover heat gains. This can be done by air-water system, by combining ceiling diffusers with radiant panels. The operation can be challenging especially with non-uniform heat loads. In the earlier study, it was concluded that active ceiling diffusers were able to generate a more uniform thermal environment than static ceiling diffusers. The thrown pattern is not constant with the static diffuser, but with the active diffuser, it is more uniform. This study was continued by analysing differences between the design of all-air and air-water systems with active diffusers and investigating higher heat load situations enabled by air-water system. The novelty of this research is to confirm the usability of the air-water system with active ceiling diffusers in an office environment. Office room situations were measured earlier in a full-scale test room with partial occupancy for studying differences between air distribution. Now that was done with CFD simulations. The same 3-person office room case without and with radiant panels was modelled first to validate CFD-simulation in all-air system case, and then to simulate the performance of the design with air-water system. Then 10-person meeting room case with air-water system was simulated with a higher, design heat load level. The thermal environment in the same office room cases measured in the full-scale test and modelled in the CFD simulation was near to each other. Supply air diffuser was modelled in CFD simulation with detailed geometry and other boundary conditions were similar to in full-scale test situation. RANS simulation method was used with SST turbulence model and with a fine computational grid. CFD simulations with higher heat load levels brought new findings for the air distribution with radiant panels. The increase of heat loads also increased room air velocities, but still local thermal environment remained at a good level. This confirms the usability of air-water system with active ceiling diffusers in variable conditions.

Keywords. Office, Thermal environment, Air distribution, Radiant panel
DOI: https://doi.org/10.34641/clima.2022.148

1. Introduction

Ventilation airflow rates are typically controlled based on occupancy, air quality and heat load levels in office rooms with variable air volume (VAV) system. Additional water-based cooling is often the most energy efficient to use when cooling by cold ventilation air for occupancy and indoor air quality does not cover heat gains. This can be done by air-water system, by combining ceiling diffusers with radiant panels. The target of operation of these room units is to maintain a good thermal environment for occupants and stable supply air distribution in varying occupancy/heat load levels. This can be

Copyright ©2022 by the authors. This conference paper is published under a CC-BY-4.0 license.

challenging especially with non-uniform heat loads. In the earlier study, it was concluded that active ceiling diffusers were able to generate a more uniform thermal environment than static ceiling diffusers [1]. The thrown pattern is not constant with the static diffuser, but with the active diffuser, it is more uniform due to constant supply air velocity. This study was continued by analysing differences between the design of all-air and air-water system with active diffusers and investigating higher heat load situations enabled by air-water system. The novelty of this research is to confirm the usability of the air-water system with active ceiling diffusers in the office environment.

2. Method

Office room cases were measured earlier in a full-scale test room with partial occupancy for studying differences in air distribution with different ceiling diffusers. Now that was done with CFD simulations in the cases with active ceiling diffusers without and with radiant panels. With CFD simulations more detailed view of the performance was possible to obtain. The geometry of the same measured and simulated test room setups is shown in Fig. 1. The dimensions of the test room were 6.1 m × 4.4 m x 2.7 m (L x W x H), with a floor area of 26.6 m^2. The operating principle of the active diffuser (595x595 mm attached to the suspended ceiling) is based on two air adjustment dampers: Fig. 2-1 A) adjustment for the constant static pressure level of the duct and B) active adjustment of supply airflow rate with linear movement of adjustment blade. The plenum of the active diffuser is sound attenuated so additional sound attenuator or VAV damper are not needed. Diffusers were selected with the manufacturer's design tool [2] for sound pressure level maximum 30 dB(A) with suitable supply air jet throw length for having a realistic design case. Additional 4 radiant panels (2995x595 mm attached to the suspended ceiling) are shown in Fig. 2-2 and Fig. 8.

Studied heat load levels and supply airflow rates are listed in Tab. 1 and 2. The same measured 3-person office room case (46 W/m^2floor) without and with radiant panels was modelled first to validate CFD-simulation in all-air system case O3AA (4.3 l/s,m^2floor), and then to simulate the performance of the design in the air-water system case O3AW (1.8 l/s,m^2floor). Then 10-person meeting room case with air-water system M10AW (4.3 l/s,m^2floor) was simulated with CFD in the higher, design heat load level (81 W/m^2floor) situation.

The thermal environment was measured with calibrated air velocity, turbulence and temperature sensors in steady-state conditions. The measurement grid is shown in Fig. 3. Sensors were at heights 0.1, 0.6, 1.1, 1.7, 2.1 and 2.5 m from the floor (total 270 measurement points). Sensors included in the occupied zone started from 0.5 m distance from walls and up to 1.7 m height from floor (total 100 measurement points). Velocity and turbulent intensity were measured with omni-directional hot sphere anemometers HT412 (accuracy +/- 0.02 m/s and +/- 1 % of readings with velocities 0.05 - 1.0m/s), and temperature with PT100 sensors (accuracy +/- 0.2 °C). Readings were three minutes average values.

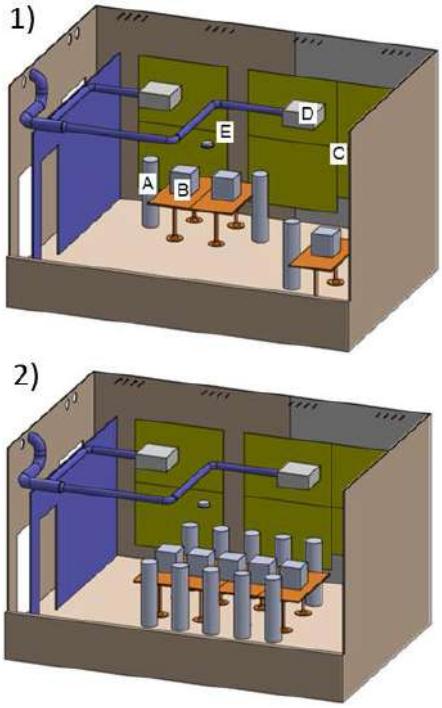

Fig. 1 - Geometry of the measured and simulated test room setups. Heat loads presented in office room setup: A) occupants, B) computers and C) simulated warm windows. Also supply air ductwork, D) diffusers and E) exhaust air valve.

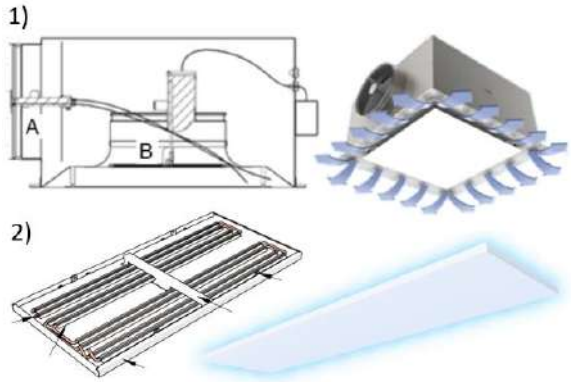

Fig. 2 – 1) Active radial ceiling diffusers and 2) radiant panels used for supply air distribution and cooling.

CFD simulations were done with Ansys CFX 2021 R2. An unstructured computational grid was constructed of 7.5 – 8.2 million elements (1.4 – 1.5 million nodes). Finer grid resolution was used near the supply air diffusers. Grid element edge length varied from 0.0015 m to 0.2 m with a growth rate of 1.2. Visualization of the grid is shown in Fig. 4. Supply air diffusers were modelled in CFD simulation cases with detailed geometry. Boundary conditions were

similar to the full-scale test situation. Heat gains were modelled as wall heat fluxes based on the electrical power or manufacturer's cooling capacity data for radiant panels. The steady-state RANS simulation method was used. Turbulence was modelled by using the SST model with automatic wall treatment. Buoyancy was modelled by using air ideal gas with gravity. Radiation was modelled with the discrete transfer model. Cases were solved with high numerical resolution (2nd order with blend factors). Validation results will be published also separately with grid independence study [3].

Tab. 1 - Heat gains in measured and simulated cases.

Case	O3AA	O3AW	M10AW
Room type	Office	Office	meeting
Occupants	225 W	225 W	750 W
Computers	300 W	300 W	750 W
Lighting	112 W	112 W	112 W
Window solar load	600 W	600 W	549 W
Tot. gains	1237 W	1237 W	2161 W
Tot. gains / floor area	46 W/m^2	46 W/m^2	81 W/m^2

Tab. 2 – HVAC system operating data in measured and simulated cases.

Case	O3AA	O3AW	M10AW
HVAC system	All-air	Air-water	Air-water
Supply airflow	115 l/s	48 l/s	115 l/s
Supply airfl. / floor area	4.3 l/s,m^2	1.8 l/s,m^2	4.3 l/s,m^2
Fully-mixed CO_2 predict.	545 ppm	747 ppm	883 ppm
Design room temperature	25 °C	25 °C	25 °C
Supply air temperature	16 °C	16 °C	16 °C
Supply air cooling power	1242 W	518 W	1242 W
Radiant panel cooling power	0 W	719 W	919 W
Radiant panel cooling power / panel area	0 W/m^2	67 W/m^2	85 W/m^2
Total cooling power	1242 W	1237 W	2161 W

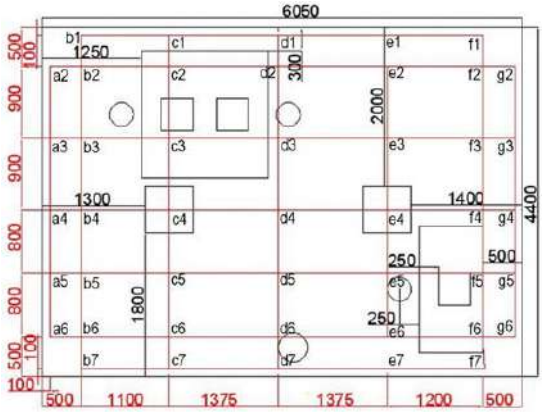

Fig. 3 - Measurement pole locations in office and meeting room cases: marked with letter a..g and number 1..7.

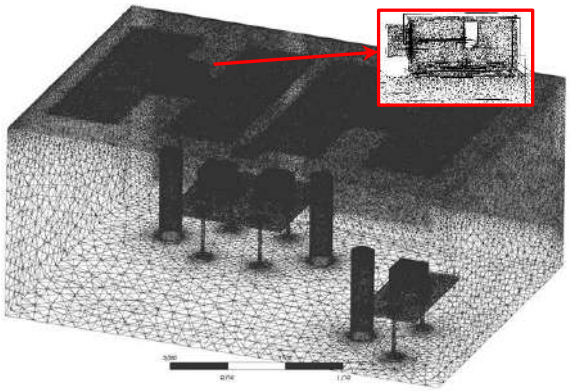

Fig. 4 – Visualization of the computational grid used in simulated cases with diffuser model grid magnified

3. Results

Measured air velocities and temperatures in all 270 measured locations are presented and compared to CFD simulation results in Fig. 5. This comparison was done by collecting data from the same locations and sorting it in ascending sequence. The thermal environment in the same office room cases measured in the full-scale test and modelled in the CFD simulation was near to each other. That analysis does not take into account if that specific velocity or temperature level occurred exactly at the same location. It can be seen that in the CFD results the velocity and temperature ranges were a bit wider. Still, overall trends were very near to each other. The average difference of absolute values between measured and CFD simulated velocity in the curve is 0.02 m/s and in the same location 0.05 m/s. The average difference of absolute values of temperatures in the curve is 0.13 °C and in the same location 0.34 °C.

Air temperature, velocity and draught rate distribution in the occupied zone are shown in Fig. 6. The occupied zone was defined by including values from 0.5 m from walls. Pole locations e5 and d5 were excluded in the meeting room case (overlapping with occupants), and only points at 0.1 m were included

from pole locations c4, d4 and e4 (meeting room table was located there). These graphs show both measured and simulated cases. The highest draught rate levels were a bit underestimated in CFD simulation when compared to measurement results. The thermal environment in the case O3AW was slightly better than in the case O3AA (same heat load situations). Air velocity level was a bit lower, temperature more uniform and draught rate level lower. A clear increase in the air velocity level was seen in the M10AW case when compared to office room cases. The air temperature distribution was now similar to the O3AA case. The draught rate level was also clearly increased. Still, the draught rate in the occupied zone stayed below 20%, which indicated that local thermal comfort was at a good level (even if maximum measured draught rate levels would have been slightly higher like seen in O3AA curves).

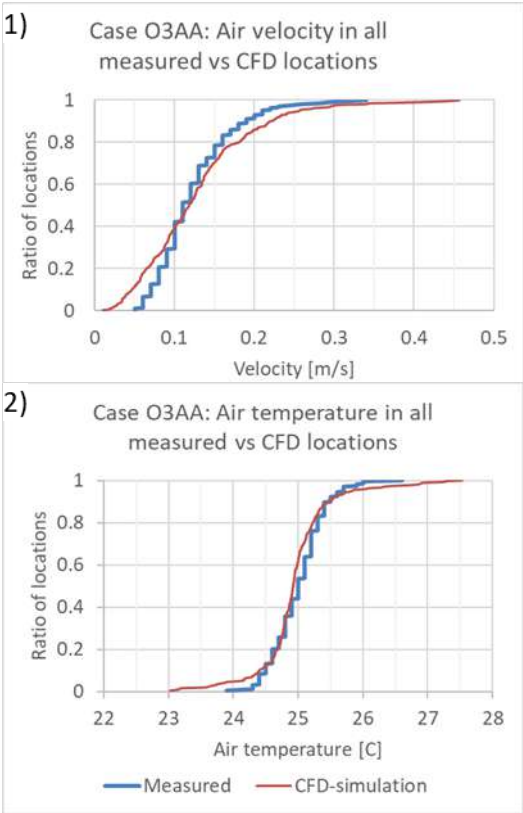

Fig. 5 - Measured and CFD simulated 1) air velocities and 2) temperatures in all measured locations.

Measured and simulated draught rate distributions on a cross-section plane in the middle of the room parallel to the simulated window wall are shown in Fig. 7. Scales in the measured and simulated distributions differ slightly, but colours are at similar levels for comparison. According to this, the CFD simulations predicted a similar flow field than in the measured case O3AA. Slightly smaller draught rate levels were visible in the case O3AW as seen earlier from the velocity distribution curves (Fig. 6). Clearly higher draught rate levels in the case M10AW were seen and that can be compared with case O3AA where the same supply airflow rate was used, but with a lower heat load level and without radiant panels.

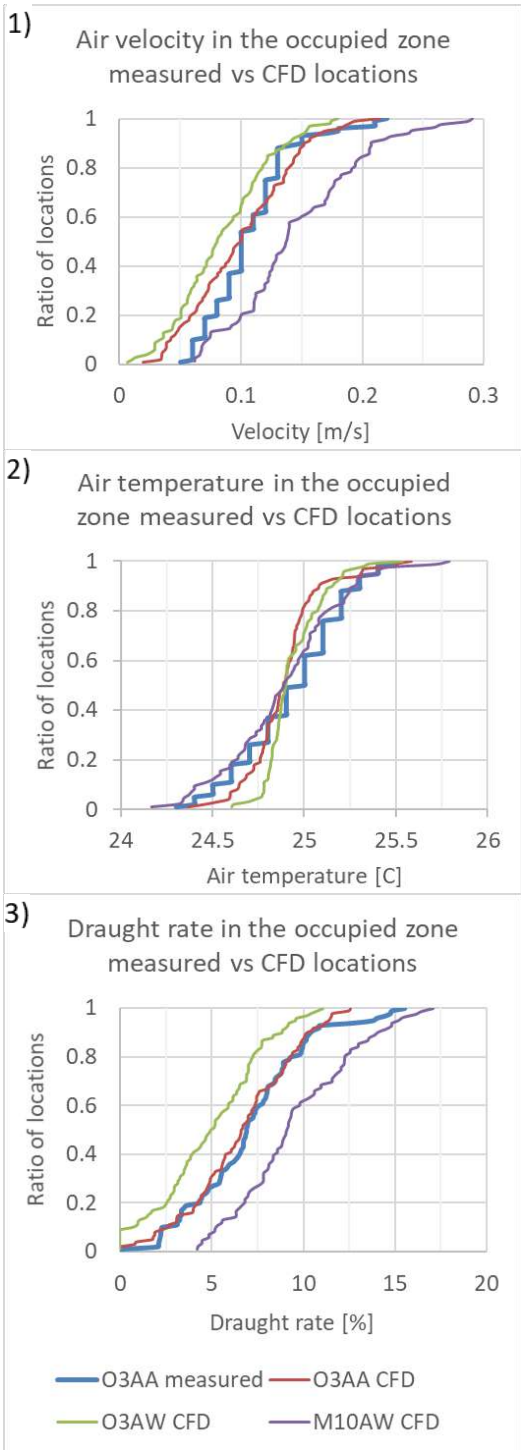

Fig. 6 - Measured and CFD simulated 1) air velocities, 2) temperatures and 3) draught rate levels in measured locations of the occupied zone.

Room air velocities over 0.20 m/s in CFD simulation cases are visualized in Fig. 8. There can be seen higher velocity level in the room in cases with higher supply airflow rate. This was especially clear in case M10AW with higher heat load level (with same supply airflow rate than in case O3AA) as discussed earlier. Even if an active ceiling diffuser provided a constant supply air velocity level at different VAV situations. It should be noted that the momentum of the supply air jet was higher with a higher supply airflow rate. This can be beneficial for uniform air distribution also in the cases

with higher heat load levels and thus stronger convection flows in the room.

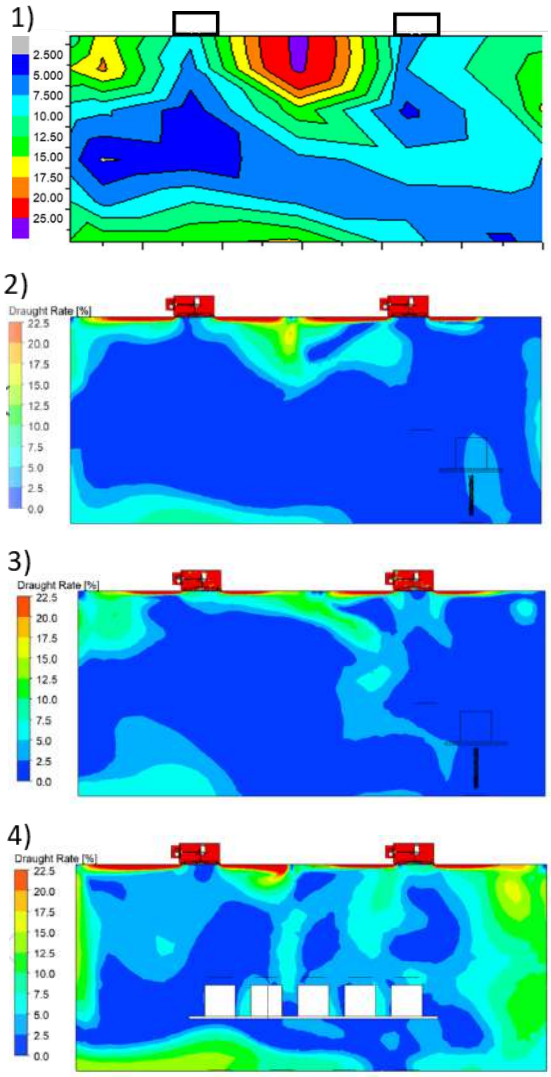

Fig. 7 –Draught rate distribution 1) in measured case O3AA and in CFD simulation cases 2) O3AA, 3) O3AW and 4) M10AW

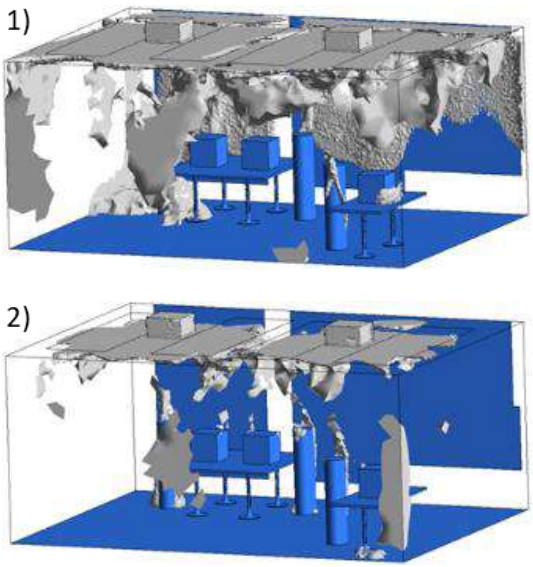

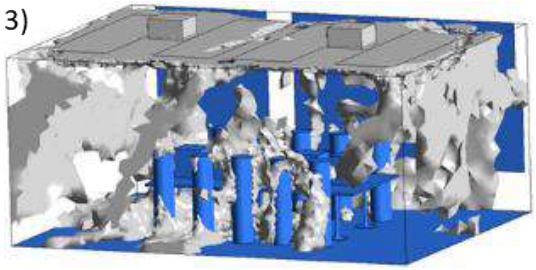

Fig. 8 – Room air velocity over 0.20 m/s in simulated cases 1) O3AA, 2) O3AW and 3) M10AW

4. Conclusions

The thermal environment in the same office room cases measured in the full-scale test and modelled in the CFD simulation was near to each other. This was based on the comparison of measured air velocities and temperatures in 270 measured locations with CFD simulation results.

The thermal environment in the same office room case with ceiling diffusers and radiant panels for cooling was slightly better than cooling with only supply air distribution. Room air velocity level was a bit lower, temperature more uniform and draught rate level lower.

A clear increase in the room air velocity level was seen in the meeting room case with high heat loads when compared to office room cases. The draught rate level was also clearly increased. Still, the draught rate in the occupied zone stayed below 20%, which indicated that local thermal comfort was at a good level also in the high heat load case. This confirms the usability of air-water system with active ceiling diffusers and radiant panels for providing a good thermal environment in variable conditions.

5. Acknowledgement

This research was supported by Business Finland.

6. References

[1] Wu Y., Mustakallio P., Kosonen R., Kaukola T., Chen J., Liu H., Li B. Experimental study of five different VAV air terminal devices under variable heat gain conditions in simulated office and meeting rooms. Building and Environment 2022;209:108641.

[2] Halton HIT Design product selection tool, 2019, Halton Oy, Finland.

[3] Kanerva P., Mustakallio P. Comparison of CFD analyses and experiments of active ceiling diffusers. In: Indoor Air 2022 (submitted). 2022 Jun 12-16; Kuopio, Finland.

DATA ACCESS STATEMENT

The datasets generated during and/or analysed during the current study are not available because they contain detailed product drawings of the diffusers, but the authors will make every reasonable effort to publish them in near future.

Impact of future climate on the performances of ground-source cooling system

Abantika Sengupta [a], Pieter Proot [b], Tom Trioen [b], Hilde Breesch [c], Marijke Steeman [d]

[a] PhD student, Faculty of Engineering Technology, KU Leuven, Belgium, email address -abantika.sengupta@kuleuven.be

[b] Master Thesis student, Faculty of Engineering Technology, KU Leuven, Belgium, email address- pieter.proot@telenet.be, tom.trioen@gmail.com

[c] Associate Professor, Faculty of Engineering Technology, KU Leuven, Belgium, email address - hilde.breesch@kuleuven.be.

[c] Associate Professor, Department of Architecture and Urban Planning, Ghent University, Belgium, email address - marijke.steeman@ugent.be

Abstract. Newly constructed and renovated dwellings in Belgium are designed for the current climate context. However, due to the effects of global warming, extreme weather conditions like warmer summers and frequent heatwaves are expected in future climate scenarios. Future climate scenarios are nowadays not taken into consideration during the building and HVAC design process. This paper studies a case study dwelling equipped with a ground-water heat pump coupled with a heat exchanger to provide passive floor cooling, derived from two vertical boreholes with a depth of 100 meters. The aim of this study is to evaluate the impact of future climate scenario on the thermal comfort and the performance of radiant floor cooling system in a Belgian dwelling. Monitoring of the case study building (April-October 2020) and Building Energy Simulations (BES) in Open studio and EnergyPlus were conducted. Future weather files (future mid-term-2050s and future long-term-2090s according to the RCP8.5-scenario) were developed in the framework of IEA EBC Annex 80 Resilient Cooling of Buildings. The performance of the floor cooling system was analysed for four different climate scenarios for Melle, Belgium: typical historical-2010s, 2020 including a heatwave (observational data obtained from RMI), typical future mid-term-2050s and long-term 2090s. The evaluation was based on two parameters, (1) thermal comfort and (2) cooling capacity of the ground heat exchanger. Results demonstrate that in the future (long-term)weather scenario, the current design of the building including the floor cooling system is inadequate to provide a good thermal comfort. Due to the rising indoor and ground temperatures, the maximum cooling capacity will decrease 22,5% in future long-term scenario compared to the typical historical weather scenario. Results also confirm that the occupancy has a big impact on the thermal comfort, especially in thebedrooms. This study also indicates the importance of implementing shading as a good solution to obtain a better thermal comfort in future climate scenarios.

Keywords. Climate Change, Future climate scenarios, Passive cooling strategies, Cooling capacity, Thermal Comfort.
DOI: https://doi.org/10.34641/clima.2022.326

1. Introduction

IPCC's Special Report on Global Warming of 1.5°C concludes there is a growing risk of overheating in buildings and an increase in severity of heatwaves in future climate scenarios (1). As seen in Figure 1, if the current trend of global greenhouse gas emissions continues, that is Business as Usual (BAU), RCP8.5, by 2100 an increase of the outdoor temperature of approximately 5°C in Belgium is expected (2). An increase of the outdoor temperature will have an enormous impact on the environment, soil and indoor climate. Europe has witnessed in the last two decades, 18 of the warmest years and an increase in the frequency and intensity of extreme weather events (3). Mitigating the adverse effects of climate change is a high priority for the EU. Studies on the Future of Cooling by IEA shows that, by 2050, without action, the cooling demand will be more than triple and around 2/3rd of the world's households

Copyright ©2022 by the authors. This conference paper is published under a CC-BY-4.0 license.

will have an air conditioner (4). To reduce the sensitivity of highly insulated dwellings to overheating, cooling systems (active or passive) are needed and will have an important role in the future (5)(6)(7). In recent years, policies in Europe and worldwide focused on the energy efficiency of both new and renovated buildings. Energy Performance of Buildings Directive (EPBD) (9) required that from 2020, all new buildings in the EU have to be nearly zero-energy buildings (nZEB).

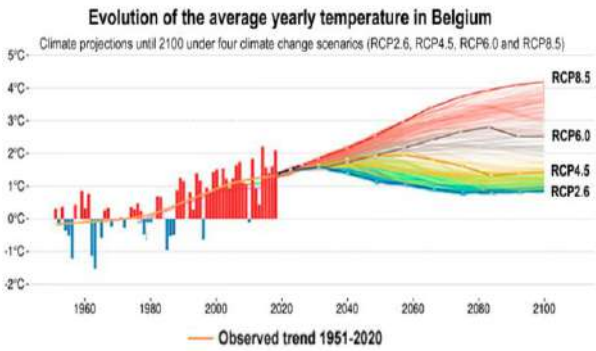

Fig. 1. Evolution of the average annual temperature in Belgium (2)

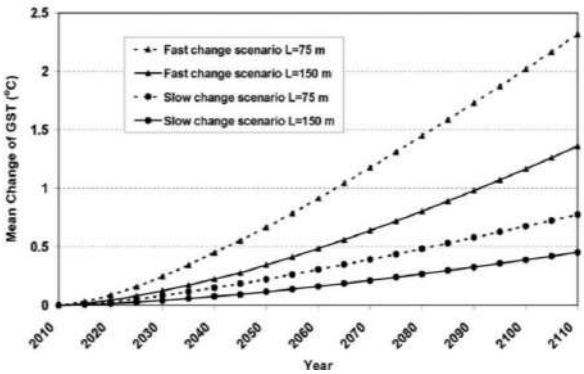

Fig. 2. Evolution of ground temperature in future climate scenario(8)

The European Green Deal(10) and the "Flemish Climate Policy Plan (2013-2020)"(11) are aligned towards combating the climate change, adapt and improve the ability to defend against the effects of climate change. They aim at a climate-neutral Europe and carbon-neutral technologies, encouraging a transformation towards new, more efficient energy systems. To avoid excessive increase of energy use for cooling, there is a need to examine alternative cooling concepts and passive cooling strategies in order to achieve the goals of the EU's Climate Change mitigation policies(12). In new dwellings in Flanders, built between 2006 and 2018(13), between 15-20% of new dwellings are equipped with a heat pump, out of which 30% are ground-water heat pump. Even though currently they are mainly used for heating, these numbers suggest a high potential for ground-source cooling. Ground-source cooling systems are gaining significant market share amongst low energy cooling technologies(14)(15). The working principle of ground-source cooling is based on the fact that the ground temperature below approximately 10 m remains fairly constant all year round at about mean annual ambient air temperature (16). It rejects heat to the ground by circulating a working fluid through ground heat exchangers. Ground-source cooling can be classified as direct ground cooling (passive) or ground source heat pump (active). As seen in Figure 1 and Figure 2, in future climate scenarios, the outside air temperature and ground temperature will be higher, this will affect the cooling capacity of ground-source cooling(8). Rising ground temperatures lead to the decrease in performance of a ground-water heat pump, as shown by a decrease in COP value during the summer. In the winter the COP will increase(17)(18).

The objective of this study is to assess the performance of passive cooling strategy, in this case, a radiant floor cooling in future climate scenarios. This study aims to evaluate the increase in cooling energy need in future climate scenarios, even in moderate climates. The effect of climate change (increase in outdoor air temperature, solar radiation and ground temperature) is assessed to evaluate the performance of the floor cooling to ensure robust thermal summer comfort in a dwelling in Flanders (Belgium). In the following section, the case study building, model validation and methodology are described in detail, followed by a discussion of the main results and conclusions.

2. Materials and Methods

2.1. Case Study Building

The case study building examined is a terraced dwelling, located in Geel, Belgium and constructed in 2014. This building is also a part of the SCOOLS-project (2018-2021) which aims to evaluate the performance of low-energy cooling systems (19). The building is South-West oriented and designed for a family consisting of 4 people. Figure 3, shows the (southwest) facade of the building.

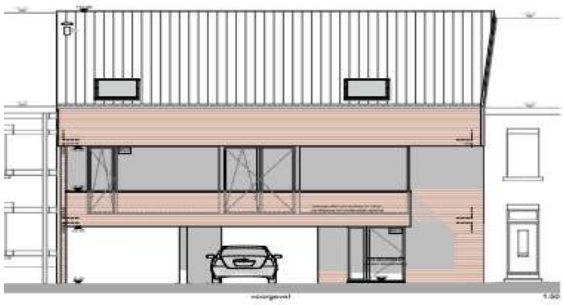

Fig. 3. South-West facade of the case study building

Table 1. U-values of construction elements

Construction	U-value (W/m²K)
Ground Floor slab	0.21
External Wall	0.19
Common Wall	0.31
Internal Wall	2.39
Pitched Roof	0.13
Flat Roof	0.15

The building, apart from the parking in the ground floor, consists of two floors (3 m high each), with a total volume of 825 m^3, an external surface of 440 m^2 and a compactness ratio (Surface area/gross heated volume) of 0.53. The dwelling is well-insulated and has a heavy thermal mass (calculated based on NBN EN ISO 52016-1) (20). The average U-value of the construction is 0.42 W/m^2K. The U-values of the construction elements are given in Table 1. The windows and the doors have a g-value of 0.55. The U-value of the fixed window and the skylights are 1.11 W/m^2K and 1 W/m^2K respectively. The glazing to floor ratio is 14%. As seen in Figure 4, the case building is equipped with a geothermal heat pump of 8kW capacity coupled with a heat exchanger to provide floor heating in winter and during summer period, passive floor cooling from two vertical boreholes with a depth of 100 meters. One drilling of 100 m provides a cooling capacity of 2.5 kW and a heating capacity of 5 kW. Furthermore, a balanced mechanical ventilation system with total Airflow of 275m^3/h, with heat recovery is installed, which allows free cooling during the night.

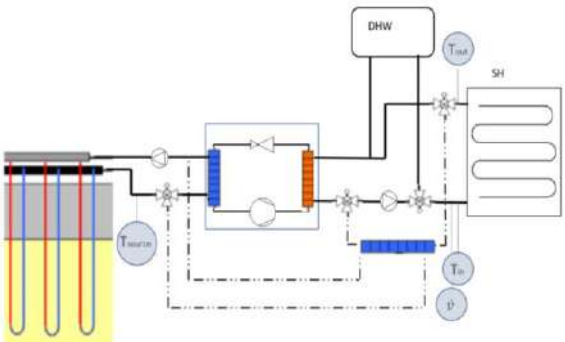

Fig. 4. The scheme of the geothermal heat pump and the measurement locations

2.2. Simulation Model

OpenStudio and EnergyPlus was used to perform the dynamic simulations (21)(22). First, the building envelope is drawn in SketchUp using the OpenStudio SketchUp Plugin(23). Then loads, schedules, HVAC-systems etc. are modelled in accordance with the real building, to set up a detailed simulation model.
The building was divided into 3 main floors, where: (a) ground floor was for entrance and storage, (b) first floor (day use)-living room, kitchen and (c) second floor (night use)- 3 bedrooms, bathroom, attic. However, for the simulation, the building has been divided into 13 thermal zones (see Fig. 4 and Table 2).

The internal loads are assigned for each zone and correspond to the heat gains due to occupancy, lighting and equipment (see Table 3). The occupancy is scheduled separately for weekday, weekend and summer vacations (See Figure 6 for a typical weekday Schedule). Four people are assumed to be at work/school from 9h to 17h from Monday to Friday except Wednesday afternoon from 13h. Hours of occupancy are 132h/week. The 'radiant fraction' is set to 0.5 for the persons, electrical equipment and lighting. This value is recommended by EN ISO 52016-1when performing simulations(24).

Hours of occupancy in a space is a crucial factor impacting thermal comfort. In zone 2 and 3(living room), it is assumed that the spaces are occupied during the daytime. Concerning zone 6(bedrooms), two different scenarios are created for simulation. In the first scenario, the bedrooms are only occupied during the night (11 p.m. – 7 a.m.). For the second scenario, an occupancy from 4 p.m. till 7 a.m. is assumed. Since the case study building was not equipped with solar shading, a simulation scenario to evaluate the impact of solar shading on thermal comfort was implemented.

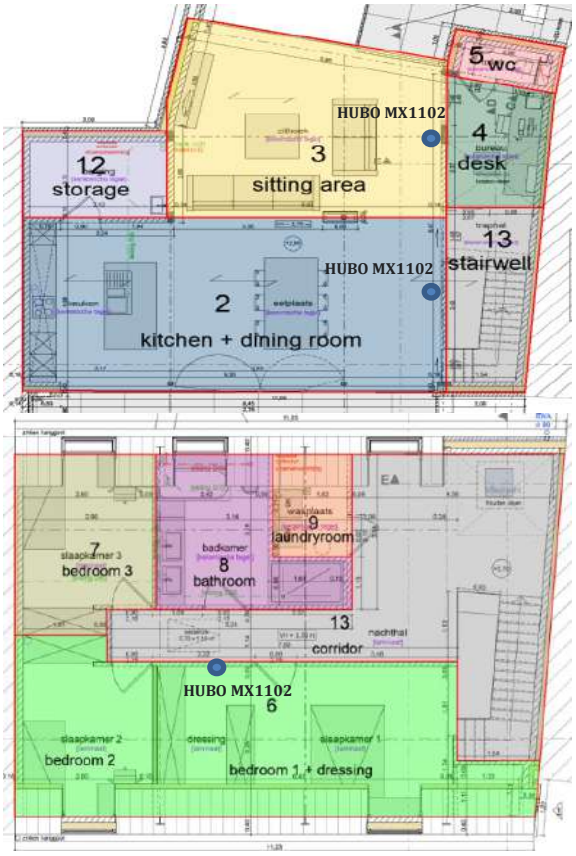

Fig. 5. Thermal Zones

Table. 2 – Thermal Zones and Ventilation flow rates

Thermal Zone	Ventilation Flow rates (m^3/h)
Zone 1 (Entrance hall)	-
Zone 2 (Kitchen + dining) + Zone 3 (Living Room)	112.1
Zone 4 (Home Office/ Desk)	39.1
Zone 5 (Toilet-WC)	39.1
Zone 6 (Bedroom 1&2+ Dressing)	75
Zone 7 (Bedroom 3)	32.8
Zone 8 (Bathroom)	75
Zone 9 (Laundry)	62.6

An automatic solar shading with g-value of 0.55 has been implemented in the simulation model. The solar shading is only applied to the windows located on the

south-west side of the building, both for the bedrooms (thermal zone 6) and the living space (thermal zone 2 and 3). The solar shading is modelled to be ON, when the global solar radiation on the window reaches exceeds a value of 250 W/m^2. It remains ON for 15 min, after which the control checks the radiation on the window. If the solar radiation on the window exceeds 250 W/m^2, the shading remains ON and if the value is lower than the threshold value of 250W/m^2, the shading is turned OFF.

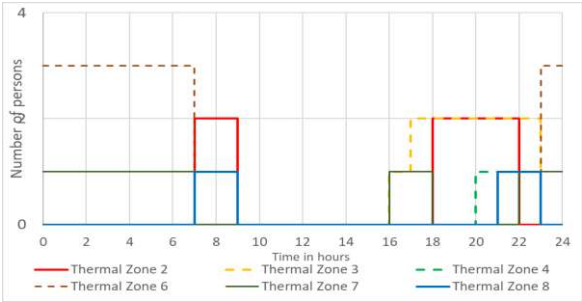

Fig. 6. Weekday occupancy schedule

Table. 3 – Internal loads for each space for heat gains(24).

	Loads			
	Room	Persons (number)	Lighting (W/m^2)	Equipment (W)
level 1	Desk (Zone 4)	1	2	250
	Living area (Zone 3)	2	2	330
	Dining + kitchen (Zone 2)	2	1.7	108
level 2	Bedroom 1 + dressing (Zone 6)	2	2	0
	Bedroom 2 (Zone 6)	1	2	30
	Bedroom 3	1	2	30
	Bathroom	1	4.6	0
	Laundry room	0	0	3200

2.3. Model Validation

Before evaluating the impact of future climate scenarios on the performance of the floor cooling system, the simulation model must be validated. To do this, the indoor temperatures obtained from the model are compared with the indoor temperatures measured by sensors on site. For this reason, the operative indoor zone temperatures (from the model) are compared with the data from measuring devices placed on-site. A weather station TMK was placed with 2 minutes time step for monitoring the outdoor dry bulb temperature, relative humidity and solar radiation. Sensor HUBO MX1102 with time step 10 minutes was placed in the bedroom (See Figure 5 for the position of the sensor in the bedroom) to monitor the temperature, relative humidity, CO_2 and dew point temperature. This sensor has a range between 0°C to 50°C with an accuracy of ± 0.21°C in the given range. The comparison is performed for two periods of 10 days in July (6.07-16.07) and August (17.08-27.08-post heat wave period) of the year 2020 (see the weather data from July and August 2020 in Figure 7).

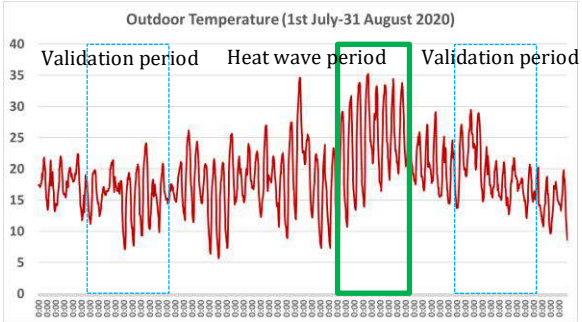

Fig. 7. Weather data from 1st July to 31st August 2020 indicating the heat wave period in the beginning of August

Table. 4 – Adaptations in the simulation model for model validation

	Adaptation	Description
1	Floor Cooling	Setpoint cooling : 23°C±1°C Supply temperature : 18°C Measure operative temperatures Max Flow rate cooling: 1200l/h Check parameters of circulation pump and heat exchangers
2	Air Flow	Measure: Add zone mixing Object Adjustments in the air flows between zones
3	Infiltration	N50=2h$^{(-1)}$
4	Ground Heat Exchanger	Ground Thermal conductivity: 2.1 W/Mk Ground thermal heat capacity: 3400000 PA:K Ground Temperature : 13°C Pipe thermal conductivity: 0.42 W/mK U_tube distance: 0.06 m Pipe Thickness: 0.003 m Flow rate loop: 0.00032 m^3/s

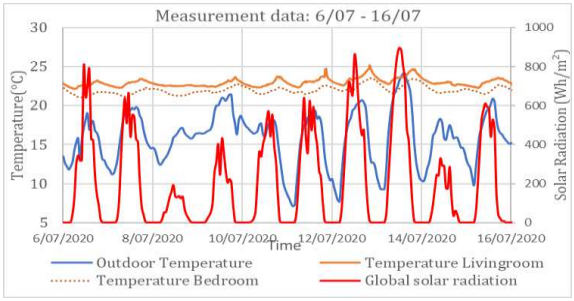

Fig. 8. Measured outdoor and indoor temperature between 6th to 16th July 2020

Figure 8 shows the measured data between 6th to 16th July 2020. The outdoor temperature reaches a maximum of 24.1°C on 13/07/2020 at 2 pm. The maximum indoor temperature for bedroom (23.5°C) and living room (25.2°C) was observed on 12/07/2020 at 8.11 pm. Improvements on the simulation model were made on parameters of the floor cooling system, airflows, infiltration rates and

ground heat exchanger to obtain the best result (see Table 4). The entire summer period of measured temperatures and simulated temperatures is compared (1st July -14th September 2020) . There are two conditions that the results of the simulation model must meet to be considered that the indoor temperatures as validated-(a) The MAE (Mean absolute value of error) should be less than 1°C and (b)RMSE (Root mean squared error) should be less than 1.5°C (25).

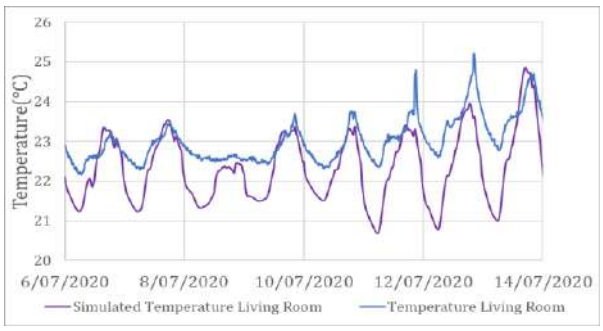

Fig. 9. Comparison of the measured and Simulated temperature of the living room

Table. 5 – Model validation (Summer period : 1st July-14th September 2020)

	Difference between simulated and measured temperature	Validation condition	Status
MAE living bedroom	0.80°C 0.83°C	< 1°C <1°C	Validated
RMSE living bedroom	1.03°C 1.03°C	<1.5°C <1.5°C	Validated

2.4. Climate Scenarios

The impact on the performances of a floor cooling system is assessed for four possible climate scenarios, representing historical, extreme weather data (heatwave period) and future weather data (midterm-2050s and longterm-2100s). The historical weather data of 2010 represent a moderate climate and are used as the reference scenario. The rising ground temperature is also taken into consideration for the dynamic-simulations. The weather data of Melle, for Scenario 1, 3 and 4 are based on RCP8.5 and developed adopting the methodology IEA EBC Annex 80-Resilient Cooling of Buildings(26). Weather data of Melle for scenario 2 is based on the observations by RMI for year 2020 (27).

Table. 6 – Climate scenarios used for performance assessment

Scenarios	Description
1	Historical weather data 2010s (2000-2020)
2	Weather data -Melle 2020 (heatwave)
3	Future mid-term 2050s (2040-2060)
4	Future long-term 2090s (2080-2100)

In Figure 10, we can observe, the average temperatures of the summer months (April-August). The figure indicates, increase in the average temperature trend between historical (2010s)and future weather scenario(2050s and 2090s). This indicates warmer summers in future years. However, the year 2020, was an exceptionally warm year with heat waves in July and August and the observed weather data of 2020 had higher maximum temperature for the summer months than mid-term (2050s) climate scenario. However, for radiation, the variation between the 2 scenarios (historical and midterm) in summer months are not significant. But for 2020, heat wave scenario, the solar radiation is significantly higher compared to the long-term scenario.

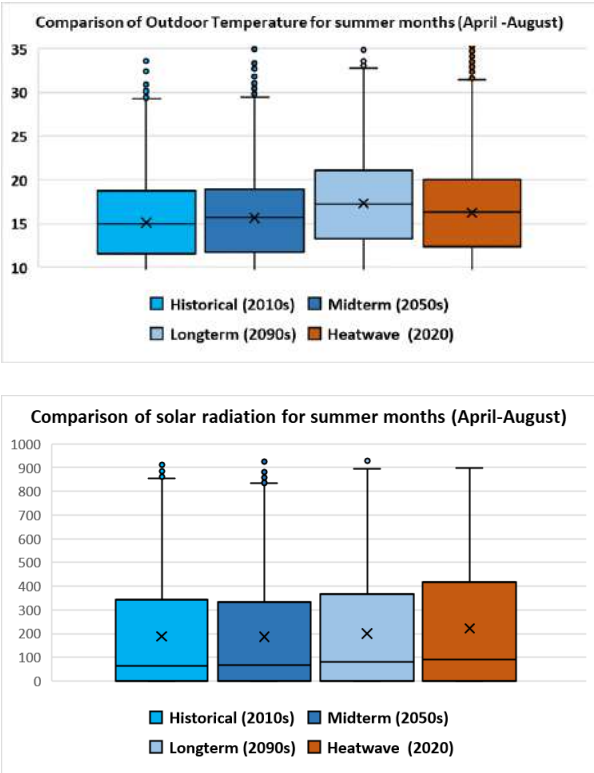

Fig. 10. Temperature and solar radiation trends for the summer months for all 4 climate scenarios

The OpenStudio/EnergyPlus manual shows that weather data (excluding specific ground temperatures) only has an impact on the ground temperature at the surface (up to 0.5m). The ground heat exchanger is placed to a depth of 100 meters. It is therefore crucial that the ground temperature for the ground heat exchanger is manually adjusted for the future climate scenarios. For climate scenario 1 and 2, the ground temperature 13°C, 13.7°C for scenario 3 and 14.7°C for scenario 4 has been implemented. With boreholes up to 100 m deep, the choice was made to follow the fastest increasing scenario at a depth of 75 m (8).

2.5. Thermal Comfort and Cooling Capacity Assessment

Method A as described in Annex F of the EN 16798-1 is used for the evaluation of the thermal comfort

(28). For this study, the percentage of occupied hours when the operative indoor temperature is above 25°C, 26°C and 28°C is evaluated for a period from the 1st of April until 31st October. The temperature thresholds also verify with the heat stress impact on human body, studied by(29). The analysed period is an extension of the meteorological summer because, assuming future climate scenarios, summers can be longer. If the percentage above 25°C is lower than 5%, the thermal comfort is considered acceptable while lower than 3% is considered good.
The cooling capacity is calculated using the energy equation (1). The cooling capacity of the floor cooling system is affected by the outlet temperature of the ground heat exchanger (2 vertical boreholes).

$$Q = \dot{m} * c * \Delta T \ (1)$$

For the calculations on the supply side of the heat exchanger, the following parameters have been extracted from the simulation model (per time step of 1 hour):

- heat exchanger: inlet temperature (°C)
- heat exchanger: Outlet temperature (°C)
- Flow rate flowing through the heat exchanger (kg/s)

To evaluate the thermal comfort, only the most critical zones (living space (2&3) and bedrooms (6)) are considered. To improve the thermal comfort, the impact of solar shading is also investigated for all the zones.

3. Results and Discussion

3.1. Thermal comfort assessment

3.1.1. Bedroom (Zone 6)

Zone 6 (Bedroom) is only occupied during the night. Two types of occupancy profile (11pm to 7 am) and (4 pm to 7 am) has been simulated. Both the occupancy scenarios are simulated with and without solar shading interventions.

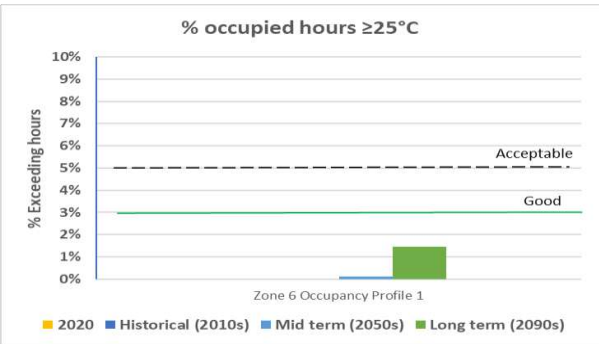

Fig. 11. % occupied hours >25°C occupancy between 11 pm to 7 am, with and without shading

As seen in Figure 11, a good thermal comfort can be guaranteed in all 4 climate scenarios with a maximum of 1,4% of occupied hours above 25°C in the long term scenario. Occupancy profile 1 (11pm to 7 am) do not have any occupied hours above 26°C and 28°C threshold with or without shading. However, when the bedrooms are occupied for a longer period (4 am to 7 am), the percentage of occupied hours above 25°C in long-term scenario increases to 7,1%(see Figure 12). With higher occupancy, the percentage of exceeding hours in Future long-term scenario can be decreased from 7.1% to 3.5% with the intervention of solar shading(see Figure 12). For the climate scenarios-2020, historical and also midterm, solar shading decreases the exceeding hour percentage by 50%. There are no exceeding hours above 28°C with solar shading. However without solar shading, there are 3.1% occupied hours exceeding 26°C, and 1.8% occupied hours exceeding 28°C.

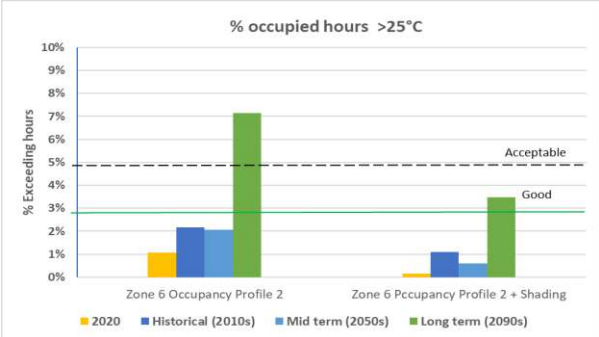

Fig. 12. % occupied hours >25°C (Zone 6- Bedroom with Occupancy between 4 pm-7 am, with and without shading)

3.1.2. Living Room (Zone 2&3)

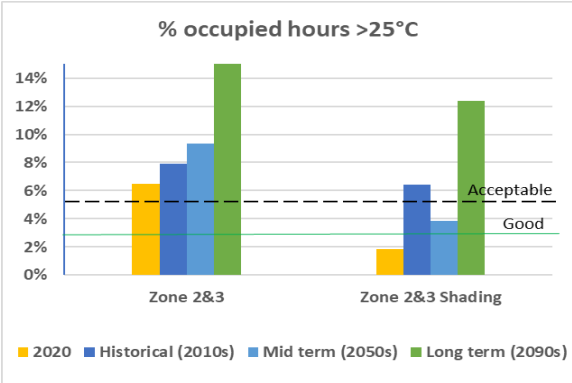

Fig. 13. % occupied hours >25°C (zone 2&3) without and with shading

Zone 2&3 (Kitchen+ dining and Living room) is occupied during the day. Zone 2 &3 is simulated with and without solar shading interventions. As seen in Figure 13, without solar shading, the percentage of occupied hours above 25°C is higher than the acceptable limit in all 4 climate scenarios. The percentage of occupied hours above 25°C threshold reaches up to 14.5 % in the long term scenario.
With the intervention of solar shading, the percentage of occupied hours in historical and mid-term scenario can be improved and brought back below the acceptable 5% limit. However, even with solar shading, percentage of occupied hours above 25°C is above the acceptable level for the year 2020 (heat wave period) and for long-term climate scenarios (see Figure 13).
Figure 14 illustrates the percentage of occupied hours above 26°C threshold in Zone 2 &3, without and with shading. Without shading, only in long-term scenario, the percentage of occupied hours are above

acceptable limit (9.8%). Historical and mid-term scenario are in good limits (below 3%), whereas year 2020 is 3.5%. However, with the intervention of shading, all 4 scenarios are within the acceptable limit.. Thus Solar shading will reduce 50% of occupied hours above 26°C% for the long-term scenario and will guarantee a good thermal comfort in the other scenarios. In the long-term, the indoor temperature will rise above 28°C (0.5%) without solar shading. With shading, no indoor temperatures above 28°C are measured.

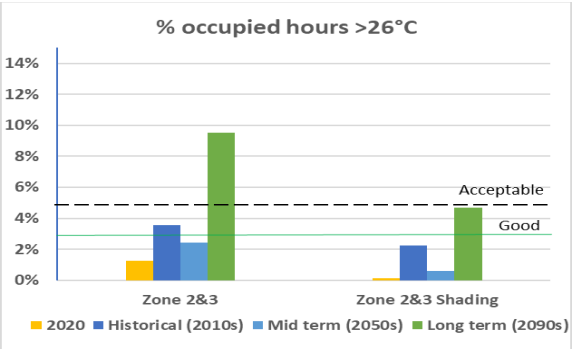

Fig. 14. % of occupied hours in Zone 2 & 3 above 26 without and with solar shading

3.2. Cooling capacity assessment

The impact of future climate scenarios on the cooling capacity of a ground source heat pump without any mechanical cooling is illustrated in Figure 15. The results from the simulation confirm, climate change will have a negative impact on the cooling capacity, even for cooling devices used in this case study.

However, the technical data sheet of the system shows a peak cooling capapcity of 5kW. This value was never exceeded during all 4 climate scenarios, proving the current system should be able to deliver the peak cooling capapcity in future climate scenarios. Howver, peak cooling power decreases 1 kW over 80 years. This is due to the rising ground temperature as a result of global warming. Figure 16 illustrates the inlet and outlet temperatures on the supply side of floor cooling. The supply temperature of the floor cooling system was set at 18°C to avoid condensation and this setpoint was used in the actual system on site as well. For climate scenarios 2, 3 and 4, this supply temperature can no longer be guaranteed. There is a rise in the inlet temperature (0.15°C) for 2020, 0.16°C during mid-term and almost by 1°C for the long-term scenario.

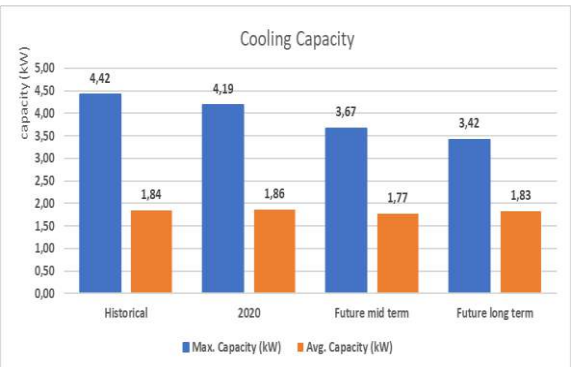

Fig. 15. Cooling Capacity heat exchanger

Analysis of the cooling capacity shows that the maximum power output will decrease in the future climate scenarios. For example, the maximum power output will decrease by approximately 17% by 2050 and 22.5% by 2090. The average cooling capacity will remain approximately the same. The decrease in maximum cooling capacity is due to the faster increase of the outlet temperature compared to the inlet temperature of the heat exchanger. For example, in climate scenario 4 (2090) the supply temperature of 18 degrees cannot be guaranteed over the entire period. On average, the supply temperature rises to almost 19°C, which is the result of a rising source temperature in the boreholes.

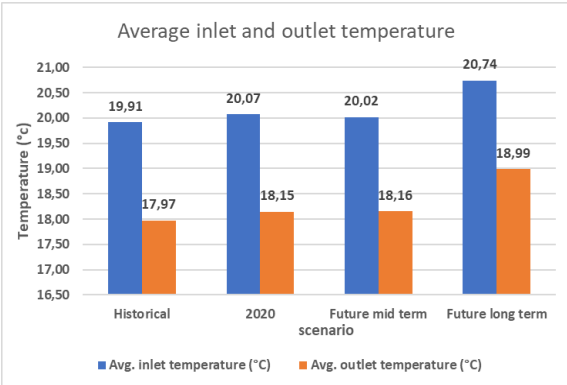

Fig. 16. Average inlet and outlet temperature(Floor cooling)

4. Conclusions

The results of the thermal comfort show that occupancy has a major impact on whether or not the predetermined upper limits are exceeded. If the analysis is performed for the living space with an upper limit of 25°C, good thermal comfort cannot be guaranteed for any climate scenario. If the upper limit is raised to 26°C, the floor cooling system will only fail in 2090 and in rest 3 climate scenarios, it can guarantee acceptable hours of thermal comfort. In the long term, only 0.5% of occupied hours was measured, with the indoor temperature exceeding the upper limit of 28°C. For the bedroom, assuming occupancy only at night in the bedrooms, good thermal comfort is achieved for all climate scenarios. With the occupancy profile from 4 pm to 7 am, good thermal comfort cannot be guaranteed 7.1% occupied hours above 25°C in 2090. In the bedroom, assuming an upper limit of 25°C for both occupancy patterns, good thermal comfort can still be guaranteed. However, implementation of solar shading shows much improvement in the thermal comfort in the bedroom and especially in the living-dining room (Zone 2 &3).In the living space, good thermal comfort is only obtained if the comfort temperature limit is raised to 26°C, even in historical climate scenario. However, with intervention of solar shading this can be improved for the 4 climate scenarios. This verifies the necessity of solar shading especially in highly glazed and south or west facing zones in the buildings.

The decrease in cooling capacity of the floor cooling in mid-term climate scenario is 17%. In the long

term, the impact of climate change is greater. Even assuming an upper limit of 26°C, good thermal comfort is not obtained With regard to the cooling capacity of the floor cooling, the decrease is also greater-22.5% compared to the existing condition. In the future, the system will therefore have to be dimensioned differently, for example by increasing the flow rates or additional (active or passive) cooling systems will have to be implemented. In the long-term, the current design of this dwelling including the floor cooling system will not be able to reduce the temperature below 26°C in each thermal zone. The inlet temperature of 18°C can't be guaranteed in future climate scenarios, which results in a lower maximum cooling capacity.

Thus it can be concluded that in future climate scenarios, shading is indispensable. Also the cooling systems needs to be dimensioned keeping in mind the rise in air and ground temperature to guarantee good thermal comfort to the users.

5. Acknowledgement

This study was conducted as part of the curriculum for Master thesis of students Pieter Proot and Tom Trioen under the supervision of Prof. Hilde Breesch and PhD student Abantika Sengupta. The data of the case study building and the monitoring data was provided by Thomas More University of Applied Sciences as a part of their sCOOLS project. This study is part of IEA EBC's Annex 80-Resilient Cooling of Buildings.

6. References

1. IEA/EBC. Ventilative Cooling (State-of-the-art review) Annex 62. IEA - EBC Program [Internet]. 2015;Annex 62:213.
2. KMI. Klimaatrapport 2020 -
3. European Commission. Going climate-neutral by 2050. Facilities.
4. OECD/IEA. The Future of Cooling Opportunities for energy-efficient air conditioning Together Secure Sustainable. 2018;92.
5. Sengupta A, Steeman M, Breesch H. Analysis of Resilience of Ventilative Cooling Technologies in a Case Study Building. iCRBE Procedia.
6. Pradyumna A, Guinto R. Climate change and health. Lancet. 2016;
7. Zhang C, Kazanci OB, Levinson R, Heiselberg P, Olesen BW, Chiesa G, et al. Resilient cooling strategies – A critical review and qualitative assessment. Energy Build. 2021
8. Kharseh M, Altorkmany L, Nordell B. Global warming's impact on the performance of GSHP. Renew Energy
9. EPBD. Directive 2010/31/EU on the energy performance of buildings (recast). 2010.
10. Commission E. Communication Green Deal.
11. Flemish Government. The Flemish Climate Policy Plan 2013-2020,.
12. Hatamipour MS, Abedi A. Passive cooling systems in buildings: Some useful experiences from ancient architecture for natural cooling in a hot and humid region. Energy Convers Manag.
13. VEA. EPB-CIJFERRAPPORT Procedures , resultaten en energetische karakteristieken van het Vlaamse gebouwbestand - periode 2006 - 2018. (in Dutch). 2019;
14. Oxizidis S, Papadopoulos AM. Performance of radiant cooling surfaces with respect to energy consumption and thermal comfort. Energy Build [Internet]. 2013;57:199–209.
15. Jeong CH, Yeo MS, Kim KW. Feasibility of a Radiant Floor Cooling System for Residential Buildings with Massive Concrete Slab in a Hot and Humid Climate. Int J Concr Struct Mater [Internet]. 2018;12(1).
16. Popiel CO, Wojtkowiak J, Biernacka B. Measurements of temperature distribution in ground. Exp Therm Fluid Sci. 2001
17. Jungqvist G, Oni SK, Teutschbein C, Futter MN. Effect of climate change on soil temperature in Swedish boreal forests.
18. Zhang Y, Chen W, Smith SL, Riseborough DW, Cihlar J. Soil temperature in Canada during the twentieth century: Complex responses to atmospheric climate change. J Geophys Res D
19. SCoolS - Home [Internet]. [cited 2020 Feb 28].
20. MyNBN - Ro PdfMeta
21. OpenStudio | OpenStudio [Internet].
22. Olesen BW. Revision of EN 15251: Indoor Environmental Criteria: REHVA [Internet]. Vol. 49, The REHVA European HVAC Journal. 2012. 6–14 p. Available from: http://www.rehva.eu/publications-and-resources/hvac-journal/2012/042012/revision-of-en-15251-indoor-environmental-criteria/
23. 3D Design Software | 3D Modeling on the Web | SketchUp [Internet]. [cited 2021 Nov 19]. Available from: https://www.sketchup.com/
24. ISO - ISO 52016-1:2017 - Energy performance of buildings — Energy needs for heating and cooling, internal temperatures and sensible and latent heat loads — Part 1: Calculation procedures [Internet]. [cited 2021 Dec 9].
25. Jain N, Burman E, Stamp S, Mumovic D, Davies M. Cross-sectoral assessment of the performance gap using calibrated building energy performance simulation. Energy Build [Internet]. 2020;224:110271. Available from: https://doi.org/10.1016/j.enbuild.2020.110271
26. IEA EBC || Annex 80 || Resilient Cooling [Internet]. [cited 2020 Feb 28]. Available from: http://annex80.iea-ebc.org/
27. Weather Belgium - RMI [Internet]. [cited 2021 Nov 23]. Available from: https://www.meteo.be/en/belgium
28. EN 16798-1:2019 - Energy performance of buildings - Ventilation for buildings - Part 1: Indoor [Internet]. [cited 2021 Dec 9]. Available from: https://standards.iteh.ai/catalog/standards/cen/b4f68755-2204-4796-854a-56643dfcfe89/en-16798-1-2019
29. Buildings CR. Climate Resilience Buildings : Guideline for management of overheating risk in residential buildings. 2021;

Influence of a portable air cleaner location on the exposure to exhaled contaminants in hospital rooms

José Luis Sánchez-Jiménez [a], *M. Ruiz de Adana* [a]

[a] Departamento de Química-Física y Termodinámica Aplicada, Escuela Politécnica Superior, Universidad de Córdoba, Campus de Rabanales, Antigua Carretera Nacional IV, km 396 14014 Córdoba, España, jlsanchez218@gmail.com; manuel.ruiz@uco.es

Abstract. Indoor environments with a deficient mechanical ventilation, could increase exposure to exhaled contaminants. This situation is critical in hospital environments such as hospital rooms. In this situation, a portable air cleaner system based on high efficiency air filters maybe a solution by itself or combined with mechanical ventilation systems to reduce the concentration of aerosols in hospital room environments.

In this study the influence of the location of a portable air cleaner based on high efficiency air filters on the exposure to exhaled contaminants of a health worker close to a patient lying on a bed was investigated.

The experimental setup consists of a hospital room (40.84 m^3) with two breathing thermal manikins, BTM. One BTM was lying on the bed (patient) and the other BTM was stand up near the bed (health worker). Each BTM has its own independent breathing system with the capability of performing different breathing flows. Both BTM inhale and exhale through the mouth with a respiration frequency of 17.90 min-1 (inhalation) and 16.43 min-1 (exhalation). Both has minute volume 9.46 (l/min) and tidal volume 0.55 l. The BTM lying on a bed, simulated the source of exhaled contaminants and exhales particles sized 0.57-0.76 µm.

A total air flow rate of 150 m^3/h (3.67 ACH) was used in all experimental tests. The total air flow rate was generated only by the air cleaner, only by the ventilation system or using a combination of the air cleaner and the ventilation system. The concentration of particles was measured in the inhalation of the standing BTM close to bed, and in other points of the room to analyse the influence of air cleaner location on the exposure to airborne contaminants.

The results suggest that the air diffusion plays an important role in the exposure to exhaled contaminants in a hospital room. In these indoor environments, low values in the exposure to exhaled contaminants can be obtained using a combination of a portable air cleaner located near the source of contaminants and the ventilation system or using only 100% air flow rate in the ventilation system.

Keywords. Air cleaner, exhaled contaminants, airborne contaminants exposure, hospital rooms
DOI: https://doi.org/10.34641/clima.2022.328

1. Introduction

The patients in hospital rooms exhale particles when they speak, cough or sneeze. In hospital rooms there are infected patients and healthy people as worker or family members which are interacting continuously with each order therefore it is necessary to create safe hospital environments through different ventilation strategies.

Ventilation in hospital rooms is necessary to create a safe environment. Clean air can be supply in the room through a ventilation mechanic system or ventilation natural. Some authors have been developed previous studies about ventilation in hospital rooms. The effect of different ventilation systems on particles in a hospital room [1]. Influences of ventilation on the exposition to particles generated by patient and medical staff [2]. This study indicates that localized ventilation can be a solution to combine to ventilation system to reduce cross infection risks between patient and medical staff. Separate and combined effects of ventilation rate, airflows interaction of manikin on the distribution of particles in a single-bed hospital room [3]. Use of four different mixing ventilation configurations in hospital rooms based on ventilation performance and health workers exposure to the contaminants released by an infected patient [4][14].

Copyright ©2022 by the authors. This conference paper is published under a CC-BY-4.0 license.

There are situations where a hospital room has a poor ventilation. A solution to control the exposure of particles may be the use of portable air cleaners. A portable air cleaner control and reduce the exposure of particles. A portable air HEPA cleaner assist to reduce the risk of exposure of particles. Portable air cleaner increases the effective clean airflow rate in the hospital rooms. The influence of the portable HEPA air cleaner on the airflow was studied through of Computational Fluid Dynamics, CFD, simulations [5]. Recent studies evaluate the efficiency of portable air cleaner based on Clean Air Delivery Rate, CADR [6][7] and different positions inside the room [6][7][8][9].

The combination of a ventilation system and a portable air cleaner has been studied by several authors. In [5] raises that a portable air HEPA cleaner increase the effective airflow rate of the hospital room. The study [8] indicates that combination between two portable air HEPA cleaners and ventilation system reduced overall exposure by up to 90%. The portable air HEPA cleaners were most effective when they were close to aerosol source.

The objective of this study was to investigate the exposure of particles in a hospital room under different ventilation strategies: only a portable air cleaner active, only a ventilation system active or a combination of both systems. Influence of the position of the air cleaner in the room was also investigated. Experimental tests were carried out in an experimental chamber that simulate a hospital room where two breathing thermal manikins, BTM, were used to simulate a lying infected patient and a standing exposed healthy worker.

2. Methodology

2.1 Setup

The experimental study was carried out in a controlled environmental chamber at the Universidad de Cordoba [4][14].

(a)

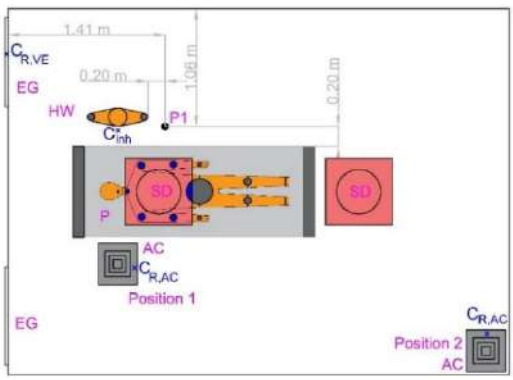

(b)

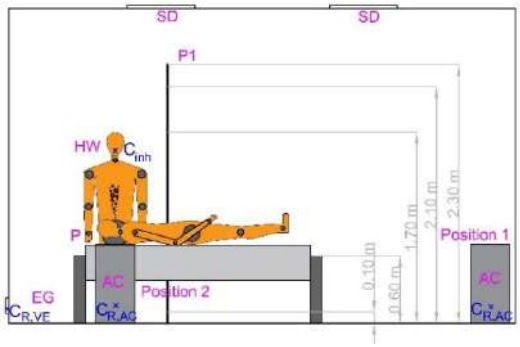

Fig. 1 – Experimental setup (a) Layout view (b) Side view.

The experimental chamber simulates a hospital room. The dimensions of the chamber are length 4.5 m, width 3.3 m and height 2.8 m. Inside the chamber, there were two breathing thermal manikins, three particles measurement equipment, a portable air cleaner and a temperature pole. The experimental setup is shown in Fig.1.

2.2 Breathing thermal manikins

Two breathing thermal manikins, BTM, [4][14] with a surface temperature of 34ºC were placed in the room. One of the manikins represented a patient, P, lying in bed, and the other represented a health worker (HW) standing 0.2 m from the bed side. Both manikins breathed through their mouth or their nose. The P and HW manikins generated a heat gain of 70 W and 80 W respectively, which correspond to a man of 70 kg weight and 1.7 m height. The breathing function was configured based on the research carried out by Gupta [16]. A breathing cycle of 0.55 l of tidal volume, a respiration frequency 17.90 min^{-1} of inhalation and 16.43 min^{-1} of exhalation and a minute volume of 9.46 l/min was used for both breathing thermal manikins.

Particles were injected in the breathing air to simulate emission of contaminants through the exhaled air in the P manikin. P manikin is considered source manikin and HW manikin is considered as an exposed person. A portable test aerosol generator (3073, TSI) was used to generate particles. Di-Ethyl-Hexyl-Sebacat (DEHS) was used to generate particles in the generator. The average exhaled concentration, C_0, was measured, in the P manikin exhalation. The average exhaled concentration, C_0, was 12647 #/cm^3 in the experimental tests.

2.3 Experimental conditions

Clean air is supplied to the chamber through two 400x16 mm swirl diffuser, SD, (VDW, Trox, Germany) placed on the ceiling of the chamber. The air is exhausted through two 400x140 mm wall grilles, EG, (AEH, Trox, Germany) placed on the lower part of the wall. At the same time a portable air cleaner, AC (Pure Airbox Home, Zoneair 3D), was used to supply clean air to the chamber through a 280x280 mm square diffuser (DLQ, Trox, Germany).

Before each experimental test, the ventilation HEPA H14 filtered air was supplied to the experimental chamber until the concentration of particle was reduced to a minimum value. Experimental tests were carried out once stationary air temperature conditions, 22ºC, were obtained inside the chamber. Experimental ambient conditions were considered stationary when the variation in the air temperature inside the experimental chamber remain under 0.5ºC.

2.4 Measurement equipment

Five temperature sensors were placed in a pole P1 at different heights, see fig. 1. Each temperature sensor consists of a J-type thermocouple with an accuracy of 2% in the range 15ºC to 45ºC.

Particle concentration measurements were carried out in three points in the experimental chamber. One particle measurement point was placed near of BTM mouth, see C_{inh} in fig. 1. A particle measurement point was placed in the exhaust wall grill, see $C_{R,VE}$. A last particle measurement point was placed in the exhaust AC, see $C_{R,AC}$. The particle concentration in the range of 0.57 to 0.76 µm, was measured every second with three optical particle device (Optical Particle Sizer 3330, TSI), OPS. The OPS measurement equipment has an uncertainly of 5%.

2.5 Case studies

Seven experimental tests were carried out using only the ventilation system, only the portable air cleaner or using a combination of both systems. In each case, the total air flow was set to 150 m^3/h (3.67 ACH) see table 1. The total airflow was distributed between the ventilation system and the air cleaner using different percentages in each case study. Case study 1 correspond to 100% air flow rate using only the portable air cleaner. A 100% air flow rate was used in the ventilation system in the case study 4. A distribution of 60% of the total air flow for air cleaner and 40% for the ventilation system, was used in case study 2, or vice versa, in the case study 3. Moreover, in each case study two locations of the air cleaner in the chamber were used, near of bed, N, and faraway of bed, F, see figure 1. As a result, seven experimental tests were performed, see table 1.

Tab. 1 – Experimental test carried out.

Case study	Experimental Test	ACH (h^{-1})	
		Ventilation system	Portable air cleaner
1	1F	0	3.67
	1N		
2	2F	1.47	2.20
	2N		
3	3F	2.20	1.47
	3N		
4	4	3.67	0

3 hours experimental tests were performed to ensure that the particles concentration in the measurement points was stationary. 15 minutes of stationary concentration measurements were selected at the end of each experimental test to calculate the contaminants exposure indices.

2.6 Contaminants exposure indices

To evaluate the exposure to exhaled contaminants in a hospital room setup, two contaminants exposure indices were used: a modified personal exposure index and the intake fraction index.

The personal exposure, ε, [11][12][13][14][15], is defined as the ratio between the average concentration of contaminants in the inhalation of an exposed person, such as HW manikin, and the average concentration of contaminants in the exhaust of the ventilation system:

$$\varepsilon = \frac{\int_0^t \dot{Q}_{inh} \cdot C_{inh}}{\int_0^t \dot{Q}_{R,VE} \cdot C_{R,VE}} \quad (1)$$

Different experimental tests were performed with the combination of a portable air cleaner and a ventilation system in this study. So, two different exhaust systems were active simultaneously: the exhaust of the portable air cleaner and the exhaust of the ventilation system. Thus, a modified personal exposure index, ε_c, was used in this study to evaluate the personal exposure in the exposed person, manikin HW:

$$\varepsilon_c = \frac{\int_0^t \dot{Q}_{inh} \cdot C_{inh}}{\int_0^t \dot{Q}_{R,AC} \cdot C_{R,AC} + \int_0^t \dot{Q}_{R,VE} \cdot C_{R,VE}} \quad (2)$$

where C_{inh}, is the average concentration of particles measured in the inhalation of HW manikin, $\dot{Q}_{inh}$, is the inhalation air flow rate of HW manikin, $C_{R,AC}$, is the average concentration of particles measured in the exhaust of portable air cleaner, $\dot{Q}_{R,AC}$, is the air flow rate in the exhaust of portable air cleaner, $C_{R,VE}$, is the average concentration of particles measured in the exhaust of ventilation system, $\dot{Q}_{R,VE}$, is the air flow rate in the exhaust of the ventilation system and, t, is the time.

The intake fraction, IF, defines the proportion of particles that an exposed person inhales, HW manikin, referred to the particles exhaled by a source person, P manikin [11], which can be expressed as:

$$IF = \frac{\int_0^t \dot{Q}_{inh} \cdot C_{inh}}{\int_0^t \dot{Q}_0 \cdot C_0} x100 \quad (3)$$

where C_0 is the average concentration of particles exhaled by P manikin and $\dot{Q}_0$, is the air flow rate

exhaled by the P manikin. The concentration of particles in the mouth section of P manikin, C_0, was carefully measured at the beginning of each experimental test.

2.7 Clean Air Delivery Rate

The performance of the ventilation system, the air cleaner and the combination of both systems was evaluated using the Clean Air Delivery Rate, CADR [10]. After each experimental test, the injection of particles was inactivated, whereas the portable air cleaner and/or the ventilation system were maintained active to obtain the CADR using the decay method for each experimental test.

The decay constant k_n and decay natural constant k_s in the experimental chamber were obtained using the equation:

$$C_{(t)} = C_i e^{-kt} \quad (4)$$

where $C_{(t)}$ is the concentration measure at the instant t, C_i is the concentration measure at the instant $t = 0$, t is the time, k_n is the decay constant for each test and k_s is the natural decay constant of the experimental chamber.

Then, the CADR was calculated as:

$$CADR = V(k_n - k_s) \quad (5)$$

where V is the volume of the experimental chamber.

3. Results

3.1 Temperature conditions

The experimental tests were carried out with an average air temperature of 22 ºC inside the experimental chamber.

3.2 Modified personal exposure index

Average values of the modified personal exposure index, ε_c, are represented in fig. 2 for different experimental tests. All the experimental results were carried out using a total airflow rate of 150 m^3/h (3.67 ACH).

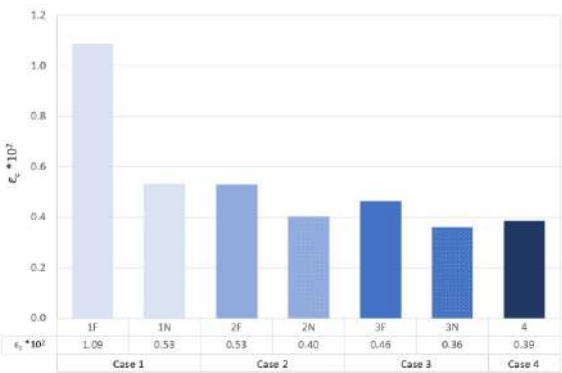

Fig. 2 – Experimental results of modified personal exposure index, ε_c.

The higher value, 1.09 10^{-2}, of modified personal exposure index, ε_c, was found using only the air cleaner in the position far away from the bed with an air flow rate of 3.67 ACH, see experimental test 1F in fig. 2.

However, if the air cleaner is located near the bed using the same air flow rate of 3.67 ACH, experimental test 1N in fig. 2, the modified personal exposure index, ε_c, is reduced from 1.09 10^{-2} to 0.53 10^{-2}. The same value, 0.53 10^{-2}, of the modified personal exposure index, ε_c, was found using the same air flow rate of 3.67 ACH but with a distribution of 60% of the total air flow for air cleaner and 40%for the ventilation system, see experimental test 2F in fig. 2.

Lower values in the modified personal exposure index, ε_c, were found using the same air flow rate of 3.67 ACH but with a distribution of 60% of the total air flow for air cleaner and 40% for the ventilation system, see case study 2 in fig. 2. In this case, values of 0.53 10^{-2} and 0.40 10^{-2} of modified personal exposure index, ε_c, were found locating the air cleaner far away from the bed, experimental test 2F, and near the bed, experimental test 2N, respectively. Similar value, 0.39 10^{-2}, of the modified personal exposure index, ε_c, was found using only the ventilation system, see experimental test 4 in fig. 2.

These experimental results in the modified personal exposure index, ε_c, are very close to those obtained with a distribution of 40% of the total air flow for air cleaner and 60% for the ventilation system, see case study 3 in fig. 2. In this situation, values of 0.46 10^{-2} and 0.36 10^{-2} of modified personal exposure index, ε_c, were found locating the air cleaner far away from the bed, experimental test 3F, and near the bed, experimental test 3N, respectively.

These results suggest that it is possible to obtain low values in the modified personal exposure index, ε_c, if the air cleaner is located near source of contaminants, manikin P or if a 100% air flow rate is used in the ventilation system. These reduced values of exposure are obtained if the air cleaner or ventilation system are used alone or if the air cleaner is used in combination with the ventilation system using different percentages of distribution of the total air flow rate.

3.3 Intake fraction

Average values of the intake fraction index are represented in fig. 3. All the experimental results were carried out with an airflow rate of 150 m^3/h (3.67 ACH).

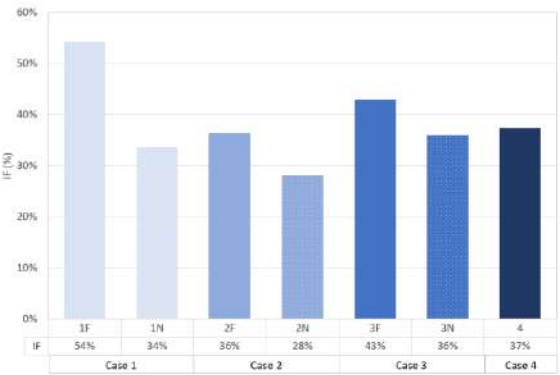

Fig. 3– Experimental results of intake fraction index, IF.

The higher value of intake fraction, 54% is obtained when the air flow rate is generated only by the air cleaner and it is located far away from the bed, see experimental test 1F in fig. 3. However, the IF can be reduced to 34% if the air cleaner is located near the bed using the same air flow rate. So, the closer the air cleaner is located to the source of contaminants, P manikin, the lower is the IF in the HW manikin.

Higher values of IF values were found when a distribution of 40% of the total air flow for air cleaner and 60% for the ventilation system, see case study 3 in fig. 3, than those with a distribution of 60% of the total air flow for air cleaner and 40% for the ventilation system, see case study 2 in fig. 3. In these case studies, IF values of 43% and 36% were found when the air cleaner is located far away from the bed and IF values of 36% and 28% were found when the air cleaner is located near the bed. Again, a reduction of IF can be found in both case studies if the air cleaner is located near the source of contaminants, P manikin.

Similar values of IF, 37%, was found using only the ventilation system, as shown in fig. 3. Slightly lower values in IF were found using a combination of the ventilation system and the air cleaner when the air cleaner is located near the bed, 28%, 34% and 36% for the experimental tests 2N, 1N and 3N respectively.

3.4 Normalized decay curve and Clean Air Delivery Rate

Normalized decay curves are represented in fig.4. All the experimental tests were carried out using an airflow rate of 150 m^3/h (3.67 ACH).

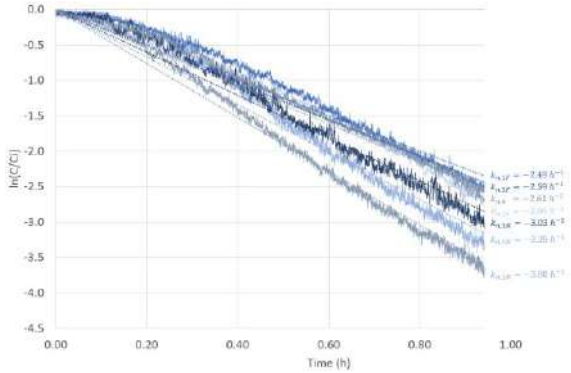

Fig. 4 – Experimental results of normalized decay curve.

Experimental tests 1F, 3F, 4 and 2F show a slope of the normalized decay curve lower than rest of tests, with a decay constant k_n of -2.49, -2.59, -2.61 and -2.69 h^{-1} respectively, as shown in fig. 4.

The higher slope in normalized decay curve is obtained in experimental tests 3N, 2N and 1N, with a decay constant k_n of -3.03, -3.35 and -3.80 h^{-1} respectively, as can be seen in fig. 5. These results show that if the air cleaner is located near the source of contaminants, P manikin, it can be obtained a faster reduction of contaminants in HW manikin.

A natural decay constant, k_s, of the experimental chamber of -0.15 was determined in different experimental tests.

Clean Air Delivery Rate was calculated using equation 5. CADR results are represented in fig. 5 for all the experimental tests. All the experimental results correspond to an airflow rate of 150 m^3/h (3.67 ACH).

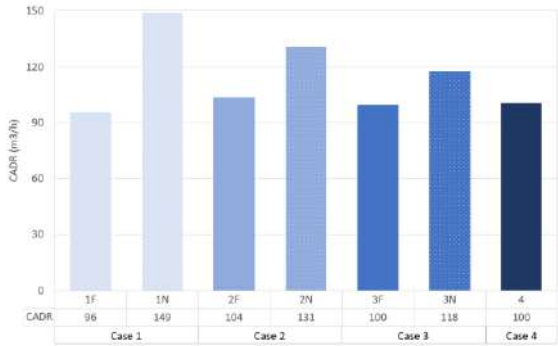

Fig. 5– Experimental results of CADR.

Fig. 5 show that if the portable air cleaner is placed far away of bed, experimental tests 1F, 2F, 3F or there is only ventilation system active, experimental test 4, the CADR values are similar, 96, 104, 100 and 100 m^3/h respectively.

If the portable air cleaner is placed near of bed the CADR values are higher compared to the rest of the tests, experimental tests 1N, 2N and 3N, see fig. 5, showing values of 149, 131 and 118 m^3/h

respectively.

These results suggest that a reduction on exposure to airborne contaminants can be obtained using only the air cleaner, experimental test 1N, or a combination of the air cleaner and the ventilation system, experimental tests 2N and 3N. Higher values of CADR are found in these situations if the air cleaner is near the source of contaminants, manikin P.

4. Study limitations

In this study a set of experimental tests is performed in a hospital room setup using three different particle concentration measurements equipment. A more detailed study could be performed if there were available more particle concentration measurement points. Moreover, the effect of different air flow rates and other combination of the air cleaner and the ventilation systems should be investigated. Exhaled contaminants behaviour can differ of that observed using DEHS particles in this study. Convective air flows could be different if the considered heat gains in the hospital room were changed. In these situations, the results of this study should be completed.

5. Conclusions

The exposure to exhaled contaminants in a hospital room under different ventilation strategies using a portable air cleaner active in combination with a ventilation system has been carried out in an experimental chamber using two breathing thermal manikins. Different experimental tests were carried out using a total air flow rate of 150 m^3/h (3.67 ACH).

Based on the results obtained, the following conclusions can be drawn:

- Low values in the exposure indices can be obtained if the air cleaner is located near the source of contaminants in a hospital room environment or if it is used only the ventilation system. In these cases, high CADR values were obtained, using only the air cleaner, 149 m^3/h or a combination of the air cleaner and the ventilation system 131 and 118 m^3/h respectively.

- If it is used only the air cleaner and it is located far away the source of contaminants in a hospital room environment, a low value in the CADR, 96 m^3/h, and high values of modified exposure index, 1.09 10^{-2}, and intake fraction index, 54%, were obtained.

- A significant reduction in the modified exposure index, 1.09 10^{-2} to 0.53 10^{-2}, and in the intake fraction index, 54% to 34% were found when it is used only the air cleaner and it is changed from a far location to a near location to the source of contaminants, in manikin P.

- Similar results in exposure indices were found with a distribution of 60% of the total air flow for air cleaner located far away the contaminant source and 40% for the ventilation system, a distribution of 40% of the total air flow for air cleaner located far away the contaminant source and 60% for the ventilation system, or a 100% air flow rate in the ventilation system. In these cases, were obtained values of the modified exposure index, 0.53 10^{-2}, 0.46 10^{-2} and 0.39 10^{-2} respectively, the intake fraction index, 36%, 43% and 37% respectively, and the CADR, 104, 100 and 100 m^3/h respectively.

These results suggest that low values in the exposure to exhaled contaminants can be obtained using a combination of a portable air cleaner located near the source of contaminants and the ventilation system or using only the ventilation system. Both the air diffusion and the incomplete air mixing play an important role in the exposure to exhaled contaminants in a hospital room environment.

Further studies should be carried out to completely investigate the influence of these issues in the exposure to exhaled contaminants in hospital room environments using a combination of a portable air cleaner and a ventilation system.

The datasets generated during and/or analysed during the current study are available in the ZENODO repository, 10.5281/zenodo.6334442.

6. Acknowledgements

The authors acknowledge the financial support received from the Spanish Ministry of Science, Innovation and Universities to the National R&D project BIORISK with reference RTI2018-094703-B-I00, entitled "*Bioaerosols in hospital environments. Control and evaluation of the infection risk*". This project is financed by the European Regional Development Fund (ERDF).

7. References

[1] Kong X., Guo C., Lin Z., Duan S., He J., Ren Y., Ren J. Experimental study on the control effect of different ventilation systems on fine particles in a simulated hospital ward. Sustainable Cities and Society. 2021, October: Volume (73): 103102.

[2] Li H., Zhong K., Zhai Z. Investigating the influences of ventilation on the fate of particles generated by patient and medical stall in operating room. Building and Environment. 2020, August: Volume (180): 107038.

[3] Bivolarova M., Ondrácek J., Melikov A., Zdímal V. A comparison between tracer gas and aerosol

particles distribution indoors: The impact of ventilation rate, interaction of airflows, and presence of objects. Indoor Air. 2017, April: 315760.

[4] Berlanga F.A., Olmedo I., Ruiz de Adana M., Villafruela J.M., San José J.F., Castro F., Experimental assessment of different mixing air ventilation systems on ventilation performance and exposure to exhaled contaminants in hospital rooms. Energy & Buildings. 177:(2018):207-219.

[5] Qian H., Li Y., Sun H., Nielsen P.V., Huang X., Zheng X. Particle removal efficiency of the portable HEPA air cleaner in a simulated hospital ward. Build simul. (2010) 3: 215-224.

[6] Küpper M., Christof A., Schneiderwind U., Finger H., Spiegelhoff D., Schumacher S. Testing of an Indoor Air Cleaner for Particulate Pollutants under Realistic Conditions in an Office Room. Aerosol and Air Quality Research, 19: 1655-1665, 2019.

[7] Noh K.C., Yook S.J. Evaluation of clean air delivery rates and operating cost effectiveness for room air cleaner and ventilation system in a small lecture room. Energy and Buildings. 119 (2016) 111-118.

[8] William L., Raymond D., Jayme C., Stephen M., Kenneth M., Francoise B., Donald B., Brooks J., Boots T., Noti J. Efficacy of Portable Air Cleaners and Masking for Reducing Indoor Exposure to Simulated Exhaled SARS-CoV-2 Aerosols. Morbidity and Mortality Weekly Report. 2021, July 9: Volume (70) No. 27.

[9] Curtius J., Granzin M., Schrod J. Testing mobile air purifiers in a school classroom: reducing the airborne transmission risk for SARS-CoV-2. Aerosol Science and Technology (2021).

[10] AHAM AC-1 Method for Measuring Performance of Portable Household Electric Room Air Cleaners (2020).

[11] Ai Z., Hashimoto K., Melikov A. Airborne transmission between room occupants during shot-term events: Measurement and evaluation. Wiley (2019).

[12] Villafruela J.M., Castro F., San José J.F., Saint-Martin J. Comparison of air change efficiency, contaminant removal effectiveness and infection risk as IAQ indices in isolation rooms. Energy and Buildings 57 (2013) 210-219.

[13] Krajcik M., Simone A., Olesen B.W. Air distribution and ventilation effectiveness in an occupied room heated by warm air. Energy and Buildings 55 (2012) 94-101.

[14] Berlanga F.A., Ruiz de Adana M., Olmedo I., Villafruela J.M., San José J.F., Castro F. Experimental evaluation of thermal comfort, ventilation performance indices and exposure to airborne contaminant in an airborne infection isolation room equipped with a displacement air distribution system. Energy and Buildings 158 (2018) 209-221.

[15] Tomasi R., Krajcik M., Simone A., Olesen B.W. Experimental evaluation of air distribution in mechanically ventilated residential rooms: Thermal comfort and ventilation effectiveness. Energy and Buildings 60 (2013) 28-37.

[16] Gupta J.K., Lin C.H., Chen Q. Characterizing exhaled airflow from breathing and talking. Indoor Air 20 (2010) 31-39.

Droplet Concentration Produced during Expiratory Activities and Evaluation of Relative Infection Risk

Arisu Furusawa [a], Takashi Kurabuchi [b], Jeongil Kim [c], Masaki Shimizu [d], Haruki Taguchi [e]

[a] Tokyo University of Science, Tokyo, Japan, arisu.f.0919@yahoo.ne.jp.

[b] Tokyo University of Science, Tokyo, Japan, Kura@rs.tus.ac.jp.

[c] Tokyo University of Science, Tokyo, Japan, jeongil.kim@rs.tus.ac.jp.

[d] Tokyo University of Science, Tokyo, Japan, masaki.jpn3047@gmail.com.

[e] Tokyo University of Science, Tokyo, Japan, haruki.t7.03@gmail.com.

Abstract. The outbreaks caused by COVID-19 have prompted researchers to quantitatively assess the risk of infection. Since airborne transmission is caused by inhalation of droplet from infected persons, it is important to understand the droplet concentration and size distribution of aerosols. In this study, we examined the size distribution of droplets produced by various expiratory activities, compared the results with previous studies, and tested the consistency of a simple measurement method. We realized the measurement by conducting the experiment in a clean room with low background concentration, using an optical particle counter and a device that can constantly ventilate the generated droplets. Quanta emission rate is a method of evaluation the risk of infection. Among the variables in the equation to determine it, we measure droplet concentration and inhalation rate, which we can measure, and from the product we get the relative risk of infection for each of the various expiratory activities. In the expiratory activities, in addition to the same cases as in the previous study, we conducted conversations and vocalizations while wearing a mask. In this study, we mainly analysed particles smaller than 1μm, based on the theory that viruses are highly proliferative and pose a high risk of infection. The concentration of droplets generated by exhalation activity is dominated by particles smaller than 1 μm in number concentration, but only a small percentage in mass concentration. In addition, the risk of infection increased in proportion to the volume of voice, and loud vocalizations showed a prominent risk of infection. Furthermore, it was confirmed that the risk of infection was reduced by wearing a mask, and the degree of reduction depended on the method of wearing the mask.

Keywords. Evaluation of SARS-CoV-2 (COVID-19), Expiratory-aerosol, Particle size distribution of droplets, Coronavirus, Masks effect
DOI: https://doi.org/10.34641/clima.2022.153

1. Introduction

In order to evaluate the risk of infection via aerosols, it is important to understand the droplets concentration and the size distribution of aerosols in infected individuals. Therefore, we first examined the particle size distribution of droplets produced by various expiratory activities. Buonanno proposed the quanta emission rate, expressed in equation (1), as a method to evaluate the risk of contagion [1].

$$ER_q = c_v \cdot c_i \cdot IR \cdot V_d \qquad (1)$$

Where c_v is the viral load in the sputum (RNA copies mL^{-1}), c_i is the amount of virus expressed in terms of viral RNA copies corresponding to 1 quanta (quanta RNA copies^{-1}), IR is the inhalation rate (m^3 h^{-1}), V_d is the droplet volume concentration (mL m^{-3}). In this study, we measure IR and V_d, which we can measure, and use the product ($IR \cdot V_d$) to evaluate the relative risk of infection for various vocalization patterns and when wearing a mask.

2. Experimental methods

2.1 the droplet measurement methods

To achieve the objective, a low background environment was required, so we conducted our experiments in an ISO standard class 5 clean room. The measurement of droplet due to expiratory

Copyright ©2022 by the authors. This conference paper is published under a CC-BY-4.0 license.

activities is done by Morawska [2] using a small wind tunnel in which the subject can put their head and in which a built-in HEPA filter provides a clean environment. In this experiment, a zinc-based duct with a ventilation fan was installed in the clean room to enable simple measurements. **Fig. 1** shows the measurement device. By ventilating the air in the duct with a fan attached to the duct at 48.5 m^3h^{-1}, it was assumed that the droplet concentration in the duct is uniform a few seconds after the utterance. To confirm that the air in the duct was in a steady state, we measured the CO_2 concentration, which indicated that 80~90% of the air was in a steady state at the position where the particle counter was measured. An optical particle counter is installed inside the duct to measure the steady-state concentration in the duct. The inlet of the particle counter is placed at 15 cm from the mouth. The air mixed with the droplets sucked in by the fan is exhausted outside the room. **Tab. 1** shows a comparison of measurement methods with Morawska.

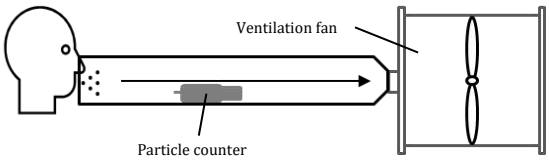

Fig. 1 - Measurement device.

2.2 measurement protocol

This study was conducted by five subjects, two males and three females. In order to match the volume of the voice of each subject, the measurement was performed while constantly checking the value of the sound level meter placed right next to the face. The vocalizations were performed for 2 minutes, and the activity intervals were defined for each expiratory activities and measured using a metronome to avoid differences in the number of vocalizations between subjects.

Three major types of expiratory activities are performed and are shown in **Tab. 2**. The details of each activity are described below.

1. Comparison with previous studies

We performed expiratory activities like those performed in Morawska's study to examine the accuracy of a simple measurement method.

- Nasal breathing:
  Breathe in through the nose and out through the nose.
- Breathing:
  Breathe in through the nose and out through the mouth.
- Whispered:
  Counting in Japanese for 10 s at a whisper.
- Voiced:
  Counting in Japanese for 10 s at normal voice.
- Unmodulated:
  Unmodulated vocalization with "aah".

2. Vocalization for conversation

The Japanese greeting *"ohayougozaimasu"* was uttered at three levels of voice volume.

3. Vocalizing while wearing a mask

A total of six cases of nasal breathing, mouth breathing, and normal voice greetings were performed, with the mask firmly in place and with only the nose out. The masks were made of non-woven fabric with a VFE test of 99%, and all the subjects used the same size.

Tab. 2 – Type of expiratory activities, its volume, and how the mask is worn.

	Activity	Volume	3. Mask
1.	Nasal breathing	—	—
			Nose out
			Cover all
	Breathing	—	—
			Nose out
			Cover all
	Whispered	40dB	—
	Voiced	60dB	—
	Unmodulated	90dB	—
2.	Vocalization for conversation	40dB	—
			—
		60dB	Nose out
			Cover all
		90dB	—

Tab. 1 – Comparison of measurement methods with Morawska.

	This study	Morawska[2]
Instrument and Particle size	Particle counter (KANOMAX model 3889) The instrument has a minimum measurement interval of 6 s and measure s the particles in the diameter range 0.3-0.5 μm, 0.5-1.0 μm, 1.0-3.0 μm, 3.0-5.0 μm, 5.0-10.0 μm, 10.0 μm ≤. Details of the four particle sizes shown in the results : 0.3-1.0 μm, 1.0-3.0 μm, 3.0-5.0 μm, 5.0-10.0 μm	Particle sizer (APS TSI model 3312A) The instrument measures the particles in the diameter range 0.5-20.0 μm and detects particles as small as 0.3 μm. Details of the four particle sizes shown in the results : ≥0.8±0.08 μm, 1.8±0.3 μm, 3.5±0.7 μm, 5.5±1 μm
Vocalization method	・Breathe in through the nose and out through the mouth (Breathe for 3.24 s per set for 2 min) ・Counting in Japanese for 10 s (Count from 1 to 10 in 3.75 s per set for 20 sets) ・Unmodulated (Vocalize "aah" for 3 s per set for 20 sets) Since the instrument reports the sum of 6 s, the duration of the vocalizations was determined by metronome rhythm, which can be performed in 6 s or less. When the subjects finished voiced, they held their breath until the next 6 s measurement began, and then took 20 6 s measurements, for a total of 2 min.	・Breathe in through the nose and out through the mouth (Breathe at a natural pace for 2 min) ・Counting in English for 10 s (Alternate 10 s of counting and 10 s of natural breathing for 2 min) ・Unmodulated (Alternate 10 s of vocalization "aah" and 10 s of natural breathing for 2 min) The subjects were given a demonstration on how to vocalize, and the timing of the activity was determined by looking at the second hand on an analog clock.
Calculation method	To compare with previous studies, the values obtained in this experiment were converted using the following equation. Droplet number concectration per vocalization = Measured number concentration $\times \frac{T_i}{T_v} \times \frac{Q_f}{IR}$ T_i : Minimum measurement interval of the instrument T_v : Vocalization time for each case Q_f : Airflow rate of ventilation fan(m^3h^{-1}) IR : Inhalation rate(m^3h^{-1})	The number concentration was obtained by multiplying the dilution factor (D) calculated from the following two equations to indicate the concentration in the upper respiratory during expiration (1) $D = \frac{AH_0}{AH_s - AH_{BG}}$ (2) $AH = \frac{RH}{100} \frac{P_{sat}\, MW_{H2o}}{RT}$ AH_0 : the water vapor concentration in the respiratory tract AH_s : the water vapor concentration in the sample AH_{BG} : the background air water vapor concentration RH : relative humidity(%) P_{sat} : the saturation vapour pressure of water at T MW_{H_2o} : the molecular weight of water R : the gas constant T : the temperature(K)
Background number concentration	Measurements without a subject : $3 \times 10^{-3}(cm^{-3})$ Measurement in the presence of a subject : $7 \times 10^{-3}(cm^{-3})$	Background concentrations were measured by adjusting the airflow in the wind tunnel so that the subject's breath was directed away from the probe. Measurements without a subject : $5 \times 10^{-4}(cm^{-3})$ Measurement in the presence of a subject 10 cm from the subject's face : $1.5 \times 10^{-3}(cm^{-3})$ Right in front of the subject's eyes : $6 \times 10^{-3}(cm^{-3})$

In this experiment, the subjects had to prove negative by PCR test beforehand to avoid infection.

2.3 the inhalation rate measurement methods

We used the Aero monitor AE-3105 to measure the inhalation rate. The measurement is performed by connecting a transducer with a special mask attached. This device can acquire data every 0.1 s.

2.4 analysis methods

When comparing with previous studies, the values obtained in this experiment were multiplied by the airflow rate of the fan ventilating the duct and divided by the inhalation rate to convert the number concentration per exhalation 1 cm^3.
Santarpia has performed an analysis on the presence of RNA and proliferative potential of the virus for patients with covid19. The presence of RNA was confirmed in all particle sizes, but the statistical superiority of RNA replication was observed in particle sizes less than 1 μm, with a 90~95% confidence level in the 1~4 μm range, and no superior replication above 4.1 μm [3]. Morawska et al. also proposed that the size of droplets depends on where they are produced, with 1 μm in the bronchi, 5 μm in the pharynx, and 50 μm in the oral cavity, and the risk of infection for particles less than 1 μm produced in the bronchi [4]. Based on these theories, we mainly analysed particles smaller than 1 μm in calculating the relative risk of infection.
In order to calculate the relative risk, the volume concentration of droplets was calculated by assuming a spherical shape based on the average diameter of each particle size range, and the mass concentration was calculated by multiplying the volume concentration by the density of water, assuming that droplets are water molecules.
Moreover, all the results were calculated by subtracting the background concentration from the measured concentration, and the background concentration was measured with the face close to the duct and without exhaling, just as during vocalization. When calculating the effect of the mask, the background concentration measured with the mask on was used.

3. Results and discussion

3.1 comparison with previous studies

The measurement results of this study were converted to the number concentration per exhalation 1 cm^3 and compared with previous studies in **Tab. 3**. As a result, the trend of values in this study and the previous studies was generally the same, confirming the reliability of the data of the simple measurement method. The results for 0.8 μm and 1.8 μm in this study are larger than those in the previous study, but the error in the conversion of 1.8 μm is thought to be caused by the difference in classification between the measurement equipment used in the previous study and the equipment used in this study.

Tab. 3 – Comparison of droplet number concentrations (cm^{-3}) with previous studies.

Particle size	0.8μm	1.8μm	3.5μm	5.5μm
Morawska[2]				
Breathing	0.084	0.009	0.003	0.002
Whispered	0.110	0.014	0.004	0.002
Voiced	0.236	0.068	0.007	0.011
Unmodulated	0.751	0.139	0.139	0.059
This study				
Breathing	0.135	0.058	0.000	0.000
Whispered	0.157	0.028	0.003	0.000
Voiced	0.271	0.115	0.003	0.000
Unmodulated	1.183	0.890	0.066	0.018

The results for each subject are shown in **Fig. 2**. This result shows that droplet concentration varies from individual to individual and that some subjects generate more droplets than others. However, the result of Fig. 2 multiplied by IR to the number of droplets per hour (**Fig. 3**) shows that the result for another subject is the highest. Subject C has a high droplet concentration and a high inhalation rate, while subject B has a low inhalation rate in relation to the droplet concentration, which is probably the reason for the extremely high value. The inhalation rate would not be negligible since it is the Number concentration per hour that is related to the risk of infection.

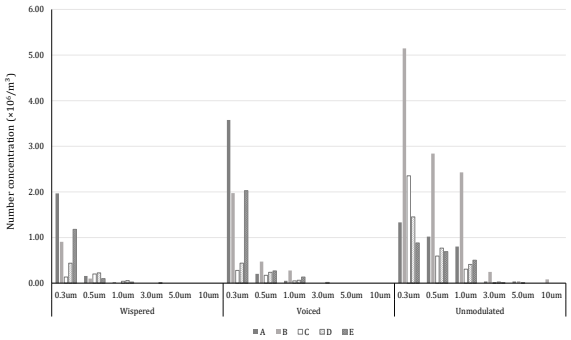

Fig. 2 - Number concentration per exhalation 1 cc for each subject and each particle size.

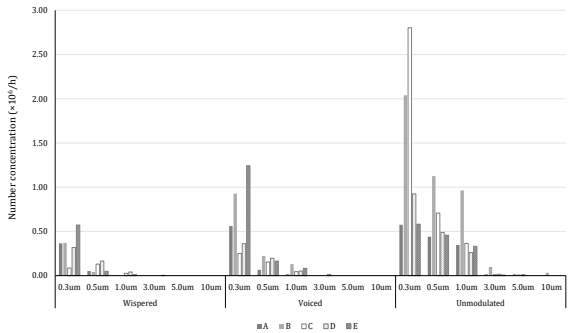

Fig. 3 - Number concentration per hour for each subject and each particle size.

3.2 vocalization for conversation

The sum of the mass concentrations per hour of particles less than 1 μm is shown in **Fig. 4**. From this result, it can be said that the droplet concentration is roughly proportional to the loudness of the voice. Next, **Fig. 5** shows the sum of the mass concentration of particles of all sizes. In this graph, the droplet concentration when speaking at 90 dB is prominent. This result suggests that although there are individual differences, large diameter droplets are generated when the voice is loud, and the generation of large diameter particles has a significant effect on the results when converted in terms of mass concentration.

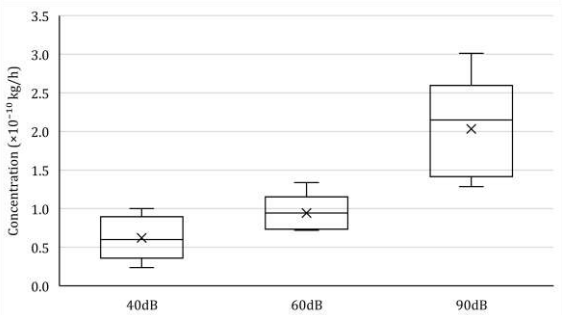

Fig. 4 - Mass concentration of particles less than 1 μm per volume of voice.

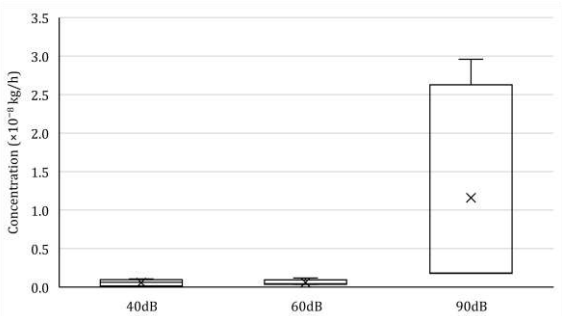

Fig. 5 - Mass concentration of particles of all sizes per volume of voice. Error bars show the standard error of the mean.

The comparison with the previous study in the previous section shows that particles smaller than 1 μm account for most of the total generation in terms of number concentration, while **Fig. 6** shows that their ratio is negligible in terms of mass concentration.

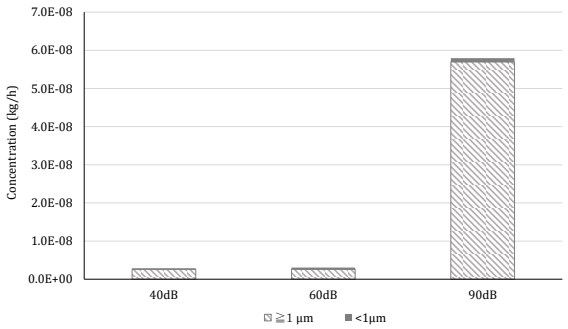

Fig. 6 - Comparison of mass concentrations of particles less than 1 μm and larger particles.

3.3 vocalization while wearing a mask

Fig. 7 shows the droplet generation volume with the mask on divided by the droplet generation volume without the mask on. This shows the extent to which the generated droplets penetrate the mask. Particles with a diameter of 3 μm or more were completely collected by the mask, indicating that the smaller the particle size, the more virus leaked through the mask. In addition, when the mask was worn so that the nose was exposed, the transmission rate increased slightly compared to when it was completely covered.

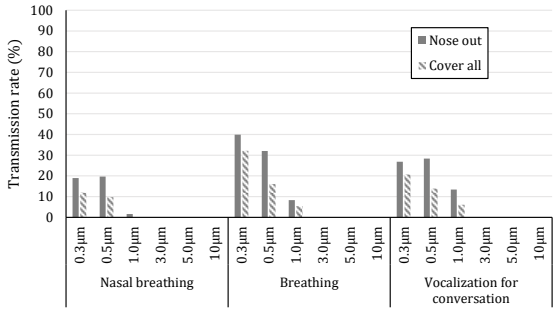

Fig. 7 - Average transmittance of the mask for all subjects, by particle size.

3.4 relative risk from expiratory activities

The average value of $IR \cdot V_d$ for nasal breathing without wearing a mask was set to 1. The results calculated for total particle size are shown in **Fig. 8**, and those calculated for particles less than 1 μm are shown in **Fig. 9**. For particles less than 1 μm, there was no difference in the risk of infection from activity compared to particles of all sizes, but both results showed that vocalization without a mask was several times riskier than breathing, with the risk increasing with the volume of the voice. Furthermore, wearing a mask reduced the risk of infection in all expiratory activities. For particles less than 1 μm, for which infection risk has been proposed, the reduction in infection risk by wearing masks is clear.

4. Conclusions

The results of this study showed that even a simple method can generally identify trends the droplets concentration and the size distribution of aerosols. The droplet concentration during the expiratory activities varied considerably among the subjects, but in all subjects, particles with a diameter of 1 μm accounted for a large percentage when converted to number concentration, and the percentage was very small when converted to mass concentration. The droplet concentration was proportional to the loudness of the voice for all particle sizes, but the droplet concentration for large particle sizes was much higher when the voice was loud. The smaller the particle size, the more difficult it is for the mask to collect infectious particles, but it was confirmed that the mask reduced the risk of infection for particles less than 1 μm in diameter. Moreover, to further reduce the risk of infection, it is important to wear a mask in the correct way.

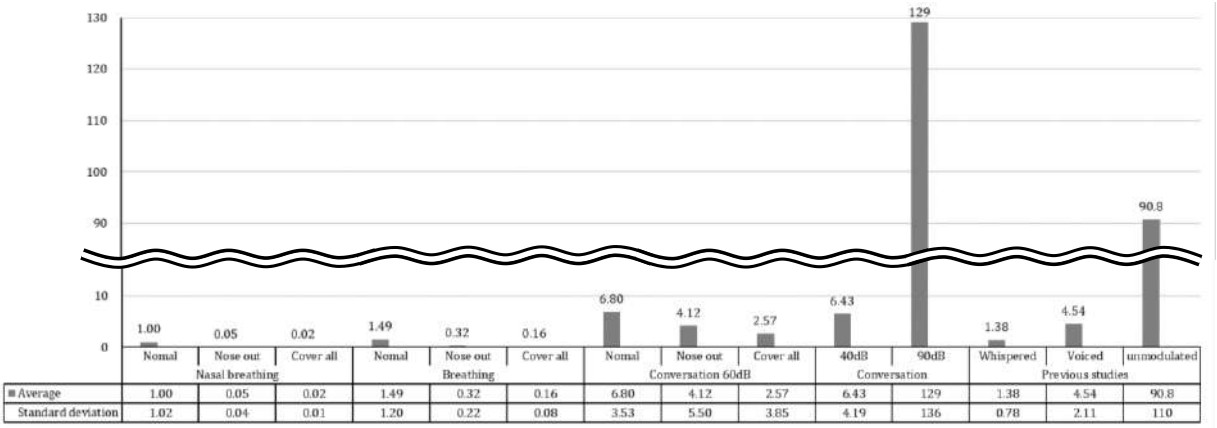

Fig. 8 - Relative risk of infection for each expiratory activities at all particle sizes, with the mean value of all subjects in $IR \cdot V_d$ for nasal breathing set to 1.

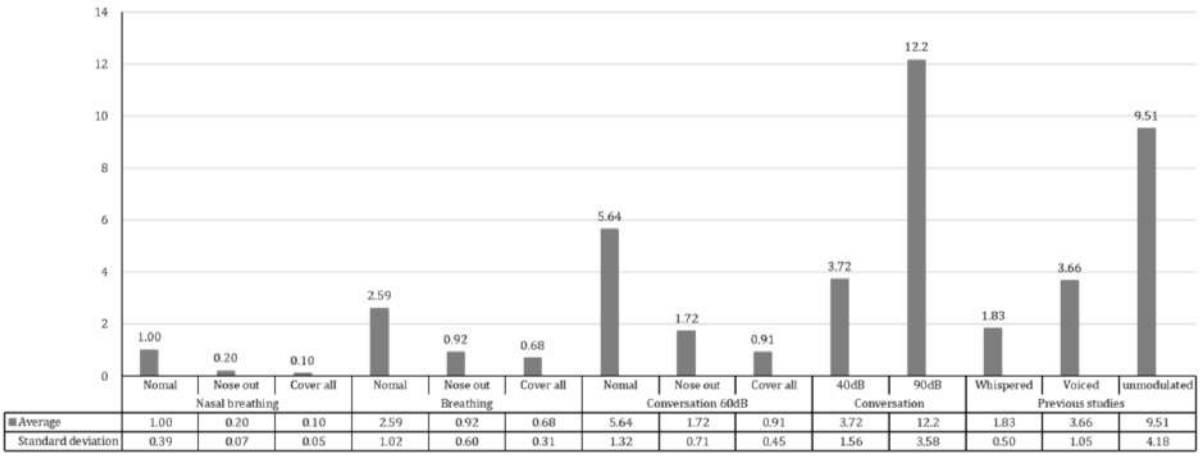

Fig. 9 - Relative risk of infection for each expiratory activities at particle sizes less than 1 μm with the mean value of all subjects in $IR \cdot V_d$ for nasal breathing set to 1.

5. Acknowledgement

The authors thank the students at Shinshu University for their cooperation in the experiment, Professor Lee of Shinshu University for his valuable comments and the Daidan Institute of Technology for lending us their clean room.

6. References

[1] Buonanno G.: Quantitative assessment of the risk of airborne transmission of SARS-CoV-2 infection: Prospective and retrospective applications. J. Environment International. 2020

[2] Morawska L., et al.: Size distribution and sites of origin of droplets expelled during expiratory activities. J. Aerosol Science. 2009;40(3)

[3] Santarpia J.L. et al.: The Infectious Nature of Patient-Generated SARS-CoV-2 Aerosol. medRxiv Cold Spring Harbor Laboratory Press. 2020

[4] Morawska L., Buonanno G.: The physics of particle formation and deposition during breathing. Nat Rev Phys. 2021

c. The datasets of this study are not available because authers take time to organeze the data but the authors will make every reasonable effort to publish them in near future.

Determination of ventilation effectiveness with tracer gas methods under COVID-19 conditions

Beat Frei [a], Heinrich Huber [b], Moritz Bienz [b], Kevin Bucheli [b]

[a] FREI WÜEST EXPERT, Willisau, Switzerland, beat.frei@frei.expert

[b] Institute of Building Technology and Energy, University of Applied Sciences and Arts, Lucerne, Switzerland, heinrich.huber@hslu.ch

Abstract. We report in this paper on the use of tracer gas methods and two tracer gases to determine ventilation effectiveness under COVID-19 conditions in a large concert hall in Lucerne, Switzerland. The occupancy of the concert hall was simulated by using thermal dummies and partial occupancy of people because of the COVID-19 protection regulations. Contaminants are removed very efficiently in the parquet (by factors better than with mixed ventilation). On the stage and balconies, the local ventilation effectiveness with displacement ventilation is partly comparable to mixed ventilation or even lower. The ventilation of balconies and galleries is demanding and must be carefully assessed in the case of pandemic risks. For the assessment of infection risk through aerosol transmission, a characteristic value for the entire room is not sufficient. The ventilation effectiveness and contaminant removal effectiveness depend very strongly on local boundary conditions and the prevailing flow conditions when dosed locally. The investigations show that the tracer gases sulphur hexafluoride (SF_6) and 2,3,3,3-tetrafluoropropene (R1234yf) provide comparable results in determining the air exchange rate and ventilation effectiveness. With both tracer methods, it is possible to gain knowledge about the operation of the ventilation system (e.g. volume air flows, heat recovery leakage).

Keywords. Tracer methods, Ventilation effectiveness, SARS-Cov-2 aerosols
DOI: https://doi.org/10.34641/clima.2022.199

1. Introduction

Lucerne University of Applied Sciences and Arts has been using tracer gas methods to determine large volume flows in road tunnels and buildings for 20 years. These methods are also used to investigate the ventilation effectiveness in occupied rooms of buildings. The COVID-19 pandemic triggered the authors of this paper to start thinking about this issue long before. The discussions about aerosol transport suggested a fundamental investigation of transport mechanisms through indoor air flow. The resulting questions about the ventilation of occupied rooms and the transport of pollutants led to a bachelor thesis [1] being initiated by the authors Frei and Huber at the beginning of 2021 and carried out by the co-authors Bienz and Bucheli. Clarifications and preliminary investigations into the replacement of the tracer gas sulphur hexafluoride were already carried out beforehand. For climate protection reasons, the use of the otherwise ideal tracer gas sulphur hexafluoride (SF_6) is no longer opportune, as it has a high global warming potential. The bachelor thesis and the associated preliminary work have shown that the tracer gas 2,3,3,3-tetrafluoropropene (R1234yf) is a suitable substitute for SF_6. The determination of the ventilation effectiveness leads to comparable results. The equipment used for dosing and detecting the tracer gas can still be used. The investigations carried out so far include the parliament chamber of a government building, several classrooms and a large concert hall.

2. Building

2.1 Description

The Culture and Convention Centre Lucerne (KKL) is a multifunctional building that was opened in 1998. It contains a large concert hall, a multifunctional hall, an art museum, various restaurants and several congress and meeting rooms. The KKL was built according to the plans of the architect Jean Nouvel. The large concert hall, which is famous for its acoustics, is the centrepiece of the KKL [2].

2.2 Geometry and Occupation

The room volume of the large concert hall is variable and can be adapted to the different acoustic

Copyright ©2022 by the authors. This conference paper is published under a CC-BY-4.0 license.

requirements of the musicians and orchestras. The room volume without the echo chamber is 19'000 m³. Taking the echo chamber into account, the room volume is 26'000 m³.

The geometric dimensions of the concert hall

- Total height 23 metres
- Hall width 23 metres
- Total length 46 metres

Number of seats (total at full occupancy 1839 seats)

- Parquet 725 seats, incl. Parquet gallery
- 1st balcony 228 seats, incl. gallery
- 2nd balcony 214 seats, incl. gallery
- 3rd balcony 234 seats, incl. gallery
- 4th balcony 314 seats

Organ loft on level 1st balcony 124 seats (rarely for visitors)

Number of musicians on stage: max. 120 musicians

2.3 Heating, Ventilation, and Air Conditioning

The concert hall is conditioned by two air-conditioning units of equal size installed in the attic. The supply air is centrally humidified and dehumidified. The reheating takes place in three zones each. Heat and humidity recovery is achieved with rotating heat exchangers. The supply air is routed via a pressure chamber and flows in at the bases of the seats. The exhaust air is discharged at a total of four exhaust air inlets on the hall ceiling. According to the system documentation, the target value of the supply air volume flow in concert mode is 29'290 m³/h per air handling unit. The basic setting of the room air temperature is 22°C. The target value of the room air humidity is set to 55 % RH.

3. Research methods

Experimental methods will be used to demonstrate the effectiveness of ventilation and the removal of pollutants in the concert hall under realistic conditions. Two tracer gases and aerosol mist are used. This conference paper reports on the use of normative tracer gas methods [3]. The tracer gas method of pulsed emission was used to investigate how the release of SARS-Cov-2 aerosols in spatially distributed positions can be quantified by releasing the tracer gas SF_6. On the one hand, the time lag of the pulse from release to local detection is of interest. On the other hand, the local exposure can be determined from the ratio of the tracer gas mass released in a pulse and the tracer gas mass inhaled locally. The tracer mass released with a rectangular pulse was recorded with a thermal mass flow sensor. The time-dependent evolution of the tracer gas concentration was detected by means of fast Fourier transform infrared spectroscopy (FTIR). The results were evaluated and interpreted by numerically integrating the tracer gas concentration over time. The tracer method of constant emission was used to investigate how the removal of SARS-Cov-2 aerosols in spatially distributed positions can be quantified by releasing the tracer gas R1234yf. For this purpose, first a defined tracer gas mass flow was dosed into the space to be investigated over a fixed period of time. Afterwards, the decay behaviour of the tracer gas concentration at local positions was detected by means of non-dispersive infrared spectroscopy (NDIR).

3.1 Dosing of tracer gas

The tracer gases SF_6 and R1234yf were used. For all doses, the tracer gas mass flows were kept constant according to **Tab. 1.**

Tab. 1 – Tracer gases used in this study.

Description	Symbol	Tracer	
		Sulphurhexa-fluoride	Tetrafluor-propene
Chemical		SF_6	$C_3H_2F_4$
Formula			R1234yf
Density	ρ_N	6.63 kg/m³	4.8 kg/m³
[a]	GWP	23'900	4
Mass flow	$q_{m,tr}$	110 mg/s	77 mg/s

[a] Global warming potential (GWP)

R1234yf was dosed in the concert hall with constant emission. SF_6 was mainly used in pulsed emission mode.

3.2 Constant emission tracer method

Equation (1), formulated by Frei and Kägi [4], allows to calculate the volume flow of air, $q_{V,air}$, at the measuring point from the measured concentration of tracer gas and its mass flow at the dosing point.

$$q_{V,air} = 10^6 ppm \cdot \frac{1}{\rho_{air}} \cdot \frac{R_{tr}}{R_{air}} \cdot \frac{q_{m,tr}}{c_V} \; [m^3/s] \qquad (1)$$

where

$q_{m,tr}$ mass flow of tracer at the dosing point in kg/s

R_{tr} specific gas constant of the tracer in J/(kg K)

R_{air} specific gas constant of the air in the exhaust duct in J/(kg K)

c_V volumetric tracer gas concentration at the measuring point in ppm

ρ_{air} density of the moist air at the measuring point in kg/m³

3.3 Pulsed emission tracer method

A tracer gas pulse with a mass flow rate of $q_{m,tr}(t)$ is injected upstream or locally in the room and the time-dependent tracer gas concentration c(t) is measured downstream or locally elsewhere in the room. For mass flow calculations it is essential that the tracer gas is well mixed with the air. Furthermore, the whole amount of tracer gas must have left the duct at the time t_2. If that is the case the following integral mass balance, equation (2), reported by Persily and Axley [5], is applicable.

$$\int_{t1}^{t2} q_m(t) \cdot c(t) \cdot dt = \int_{t1}^{t2} q_{m,tr}(t) \cdot dt; \quad q_m(t) \geq 0 \tag{2}$$

Assuming a constant air mass flow, q_m, during the observed time interval, and assuming that the mass flow of the tracer gas is negligible compared to the air mass flow, the mass flow of air can be calculated according to equation (3):

$$\overline{q}_m(\xi) = \frac{\int_{t1}^{t2} q_{m,tr}(t) \cdot dt}{\int_{t1}^{t2} c(t) \cdot dt} \quad t_1 \leq \xi \leq t_2 \tag{3}$$

Considering the volumetric concentration rather than the mass concentration of the tracer gas in the air, equation (3) is transformed to the following:

$$\overline{q}_{m\ air} = 10^6 \ \frac{R_{tr}}{R_{air}} \cdot \frac{\int_{t1}^{t2} q_{m,tr}(t) \cdot dt}{\int_{t1}^{t2} c_V(t) \cdot dt} \tag{4}$$

where

$c_V(t)$ measured volumetric tracer gas concentration at time t in ppm

$q_{mTracer}(t)$ mass flow rate of tracer gas at time t in kg/s

Equation (4) is equivalent to equation (1) with the difference that the mass flow of the tracer gas at the dosing point as well as the measured concentration are no longer constant and must be integrated over time.

3.4 Decay tracer method

The tracer gas is metered in at a constant emission rate either locally in the room or centrally via the supply air. It is important that the tracer gas is well mixed with the room air. Depending on the time, a steady-state concentration will be reached if the boundary conditions remain constant. After that, the tracer gas dosing can be stopped. The mechanically or naturally induced air exchange will reduce the initial tracer gas concentration in the room air. Depending on the time, the tracer gas concentration will decay. The air exchange rate over time can be calculated from the decay behaviour [6].

3.5 Supply air volume flow and concentrations in the equilibrium state

The supply air volume flows were determined by dosing tracer gas in the outdoor air of the two air handling units (monoblocs) of the concert hall. The concentrations were measured in the supply air and exhaust air.

The exhaust air transfer rate of the rotational heat recovery units (rotors) was estimated on the basis of various measurements in which the concentration in the exhaust air was above 0.5 ppm for at least half an hour. Due to their coating, the rotors transfer a higher proportion of tracer gas R1234yf than of air. For the tracer gas SF_6, it is known from the literature that the transfer rate is the same as for air.

The outdoor air flow rate supplied to the room is calculated using equation (1), assuming that there is no tracer gas concentration in the outdoor air (less than 0.002 ppm).

The supply air flow rate supplied to the room is calculated with equation (5), assuming that there is no tracer gas concentration in the outdoor air (less than 0.01 ppm).

$$\boldsymbol{q_{v,ODA} = q_{v,tr} \cdot \frac{1 - TGTR}{(c_{SUP} - c_{ETA}) \cdot TGTR} \cdot (1 - OATR) \cdot 10^6} \tag{5}$$

where

$q_{v,ODA}$ Outdoor air volume flow in m^3/h
$q_{v,tr}$ Volume flow rate of tracer gas in m^3/h
c_{ETA} Tracer gas concentration in the exhaust air in ppm
c_{SUP} Tracer gas concentration in the supply air in ppm
$TGTR$ Tracer gas transfer ratio from exhaust air to supply air
$OATR$ Outdoor air transfer ratio into the exhaust air

$$\boldsymbol{q_{v,SUP} = \frac{q_{v,ODA}}{(1 -\cdot EATR)}} \tag{6}$$

where

$q_{v,SUP}$ Supply air volume flow in m^3/h
$q_{v,ODA}$ Outdoor air volume flow in m^3/h
$EATR$ Exhaust air transfer ratio into the supply air

3.6 Ventilation effectiveness

In this paper, we use the term "ventilation effectiveness" to express the quality of a ventilation system in how it reduces the risk of transporting pollutants from an emitter (issue position) to a receiver (immission position) (see **Fig. 1**). This definition is not found in the literature, but we consider it meaningful in the context of an infection risk from aerosols.

In the case of **constant dosing (step-up)** with tracer gas, the ventilation effectiveness corresponds to the ratio of the tracer gas concentration in the extract air to the tracer gas concentration at a certain point in the room that is in a steady state. The concentration of the supply air must be subtracted from the measured values.

$$\varepsilon_{C,i} = \frac{c_{ETA} - c_{SUP}}{c_{IDA,i} - c_{SUP}} \tag{7}$$

where

$\varepsilon_{C,i}$ Ventilation effectiveness at the position i

c_{ETA} Tracer gas concentration of the exhaust air in ppm

$c_{IDA,i}$ Tracer gas concentration of the room air at the position i in ppm

c_{SUP} Tracer gas concentration of the supply air in ppm

With **pulsed emission dosing**, the ventilation efficiency is determined with:

$$\varepsilon_{C,i} = \frac{m_{tr,em}}{q_{m,tr,ETA}} \cdot \frac{C_{ETA} - C_{SUP}}{\sum(\Delta C_{IDA,i}(t) \cdot \Delta t)} \quad (8)$$

where

$m_{tr,em}$ tracer gas mass emitted at the emission position in g

$q_{m,tr,ETA}$ Tracer gas mass flow to achieve c_{ETA} in g/s

c_{ETA} Tracer gas concentration in the exhaust air at equilibrium (at tracer gas mass flow $q_{m,tr,ETA}$) in ppm

$\Delta c_{IDA}(t)$ Difference caused by the pulse in the tracer gas concentration in the room air (at immission position i) compared to the background concentration at time t, in ppm

Δt Time step in s

The ventilation effectiveness indicates the factor by which fewer pollutants (e.g. aerosols) are transferred from the issue position to the immission position than with an ideal room air mixture. Thus, with a value greater than 1, fewer pollutants are transferred than with an ideal mixture and with a value less than 1, more. This means that the higher the value $\varepsilon_{C,i}$ the better the ventilation effectiveness. The definition of ventilation effectiveness used always applies only to the transmission direction from one spatially defined issue position to a second spatially defined immission position. The transmission rate in the other direction can be significantly different. This can be illustrated, for example, if the issue position were directly in front of the supply air diffuser. In this case, a ventilation efficiency of ≤ 1 would be expected. In the opposite direction, however, the ventilation efficiency would be >>1.

With **pulsed emission dosing**, the time lag between the release of the pulse and its arrival at the immission position is also determined (**Fig. 1**)

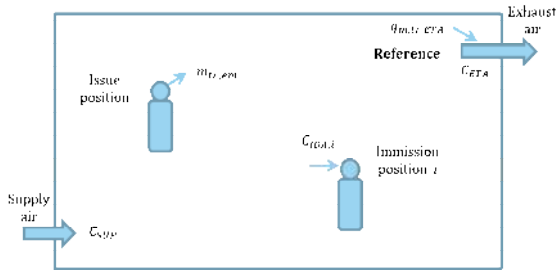

Fig. 1 – Model for ventilation effectiveness.

3.7 Short description of measurements

The measurement campaign was carried out over two days. The focus of the first measurement day was on the stage and the stalls of the concert hall. On the second day, the balconies of the concert hall were examined.

Fig. 2 shows the placement of dummies, spotlights and people as internal loads in the concert hall on the first day of measurement.

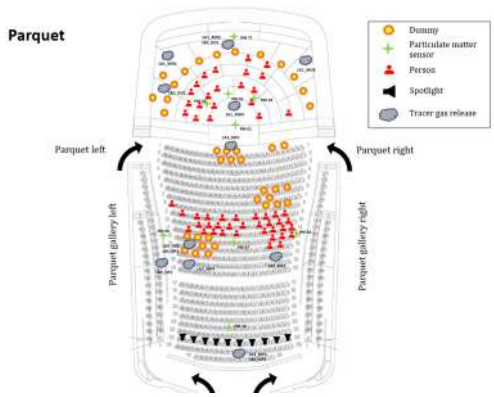

Fig. 2 – Disposition of internal loads in the concert hall.

3.8 Boundary conditions

Tests for the ventilation efficiency were carried out with an audience, that was simulated with locally distributed thermal loads and partial occupancies. The air flow rates were determined without internal heat load. The orchestra rehearsed to a reduced extent during the measurement campaign.

3.9 Occupancy and heat loads

The heat loads and occupancy on the first measurement day are listed below. The values in brackets apply to the second measurement day.

Persons:

25 (22) orchestra

40 (35) audience (1st to 3rd balconies and galleries)

8 (8) staff

Other heat loads:

46 dummies stalls (2nd to 4th balconies) (7.1 kW)

10 luminaires in the parquet (10 kW)

7 luminaires in 1st balcony (7 kW)

Measuring devices (approx. 0.5 kW)

Total sensible heat load in the hall approx. 30 kW (29.6 kW) (both without hall lighting) or equivalent approx. 420 (415) persons.

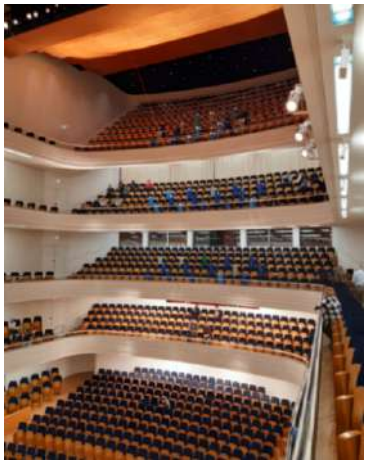

Fig. 3 – Balconies of the concert hall with dummies.

4. Results

4.1 Supply air volume flows

Tab. 2 summarises the determination of the air volume flows (referred to 20°C) of the two air handling units. It is assumed that the Outdoor air transfer ratio (OATR) is the same as the Exhaust air transfer ratio (EATR). The measurement uncertainty of the air volume flows is estimated at 5 %.

Tab. 2 - Determination of the air volume flows

Symbol	AHU LC01 Concert hall west	AHU LC02 Concert hall east	Sum for both AHU units
-	SF_6	R1234yf	-
EATR	0.035	0.035	-
TGTR[a]	0.035	0.045	-
$q_{v,ODA}$	28'300 m³/h	28'100 m³/h	56'400 m³/h
$q_{v,SUP}$	29'300 m³/h	29'100 m³/h	58'400 m³/h

[a] Tracer gas transfer ratio from exhaust air to supply air (TGTR)

4.2 Concentrations in the equilibrium state

Tab. 3 lists the theoretical tracer gas concentrations in the equilibrium state that result from homogeneous mixing with the total air volume flow of both air handling units and when the tracer gas mass flows are metered in according to **Tab. 1**
For the assessment of the ventilation effectiveness in the concert hall, the differences between supply and extract air are used.

Tab. 3 - Theoretical tracer gas concentrations in the equilibrium state

Designation	Symbol	Tracer gas SF_6	Tracer gas R1234yf
Concentration in the supply air	c_{SUP}	1.30 ppm	1.17 ppm
Concentration in the exhaust air	c_{ETA}	0.05 ppm	0.05 ppm
Difference in concentration of supply and exhaust air	$\Delta c_{SUP-ETA}$	1.25 ppm	1.12 ppm

4.3 Air exchange rate of concert hall

Measurements with constant dosing with the tracer gas R1234yf in the concert hall were concluded to be a difference between supply and extract air of 1.07 to 1.10 ppm rather than the value listed in the table. One reason for the difference is the measurement uncertainty. However, it is also possible that the total extract air volume flow is slightly higher than the total supply air volume flow. A rounded value of 1.1 ppm is used in the evaluations. The measurements were carried out with closed echo chambers. According to the client, the volume of the concert hall is 19'000 m³. The supply air spaces under the stalls are not included.
The air exchange rate of the supply air volume flow in relation to the room volume is 3.07 h⁻¹. The nominal time constant (reciprocal value of the air exchange rate) is 0.325 h.

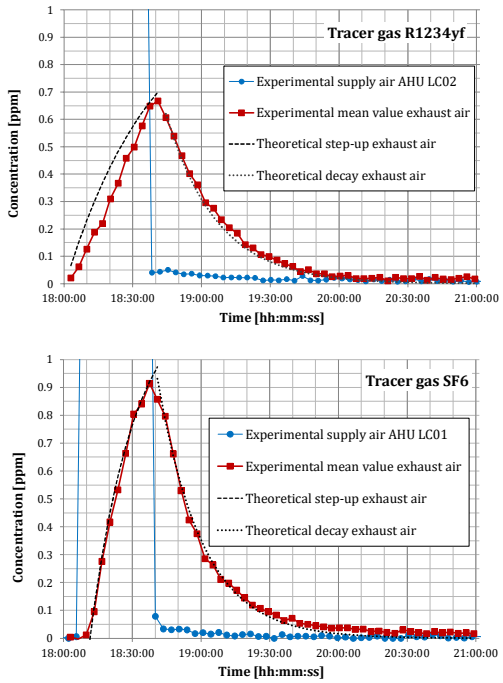

Fig. 4 – Constant emission of tracer gases R1234yf and SF_6, decay of tracer concentrations, without internal loads.

Fig. 4 shows the step-up dosing of the tracer gases R1234yf and SF_6 into the outdoor air of the air handling units LC01 and LC02. The decrease of the tracer gas concentration in the exhaust air of the concert hall for both tracer gases is shown depending on time. Due to the large volume of the concert hall and the time available, the state of equilibrium could not be achieved.

For comparison, the theoretical course of the tracer gas concentration during dosing and removal through the ventilation system is shown. The model of ideal mixed ventilation and the measurements agree very well. The concentration in the exhaust air is practically at an ideal mixed ventilation.

After that, the time lag of the tracer gas in the room obviously increases.

4.4 Ventilation effectiveness

Tab. 4 to Tab. 7 show experimentally determined values for ventilation effectiveness at the stage, on the parquet and on the balconies. The ventilation effectiveness was determined using the constant emission method (R1234yf) and the pulsed emission method (SF_6). In addition, the pulsed emission method was used to determine the time lag for tracer propagation from the source to the target.

The duration of a single pulse of SF_6 was 60 s and the injected tracer gas mass was 6.3 g in each case.

The measurements were carried out with person occupancy and heat loads (dummies) on the stage and in the stalls.

5. Discussion

5.1 Supply air volume flows

By dosing tracer gas into the outdoor air, the following supply air volume flows (referred to 20°C) of the two air handling units LC01 and LC02 of the concert hall were determined

Concert Hall West unit (LC01) 29'300 m^3/h

Concert Hall East unit (LC02) 29'100 m^3/h

Total of both units 58'400 m^3/h

These air volume flows are practically identical to the target values according to the system documentation.

The air exchange rate in relation to the room volume is thus 3.07 h^{-1}. The nominal time constant (reciprocal value of the air exchange rate) is 0.325 h.

5.2 Ventilation effectiveness

The ventilation effectiveness on the balconies is obviously strongly influenced by heat loads (upward currents). Ventilation effectiveness can occur that are significantly worse than with ideal mixed ventilation. In four cases, however, better ventilation efficiencies were also observed. The high relative standard deviations in the measurements with constant dosage indicate unstable flow conditions (swath behaviour). This is also evident in comparison with the pulse measurements. When dosing in the parquet and measuring in the 1st balcony, row 2, there were markedly different ventilation effectiveness with constant dosing and pulse dosing. Possible causes are unsteady currents and locally strongly differing conditions at the dosing points (which, however, had a distance of max. 2 m). Furthermore, the two pulse measurements with the transmission from the 1st balcony in the front to the 2nd balcony, row 4, also showed clear differences.

In conclusion, the indoor air flow in the area of the balconies can be described as unstable and hardly locally predictable.

5.3 Air handling units

The two air handling units (AHU) of the concert hall are equipped with rotating heat recovery units (rotors). From the tracer gas measurements, it was estimated that 3.5 % of the exhaust air volume flow is transferred to the supply air (EATR). This value is in a good range and can be considered uncritical from a hygienic point of view. According to the system documentation, the exhaust air is filtered with class F7 fine dust filters. Depending on the filter product and condition, around 80 to 90 % of the aerosols contained in the exhaust air are retained in the exhaust air filters. This means that only about 0.5 % of the aerosols get into the supply air. Since the exhaust air has the characteristics of ideal mixed ventilation, the average age of these aerosols is about 20 minutes. The potential transmission of virus copies via this route is thus about two orders of magnitude lower than the (very low) potential transmission from the stage to an audience member in the parquet.

The F7 filters used correspond to the state of the art in ventilation hygiene guidelines. It is recommended to keep this filter class.

6. Conclusions

6.1 Concert Hall KKL

Contaminants are removed very efficiently in the parquet (by factors better than with mixed ventilation). On the stage and balconies, the local ventilation effectiveness is partly comparable to mixed ventilation or even lower. It is interesting to know what proportion of the emitted particles is inhaled. This is calculated by dividing the inhaled air volume flow by the supply air volume flow. This ratio is divided by the ventilation effectiveness according to equation (7) or (8).

Tab. 4 – Ventilation efficiency at four positions in the stage and parquet area

Position measurement	Ventilation efficiency with standard deviation at position dosing Centre stage	Parquet, row 1	Comment Constant dosing with tracer gas R1234yf
Conductor	(close range)	0.23±0.32[a]	"Overflow"
Orchestra left	1.23±0.16	0.84±0.19	Approximately mixing ventilation
Parquet, row 1	2.3±1.5	(close range)	Approximately mixing ventilation
Parquet, row 7	8±5	108±50 (approx.)	Displacement ventilation

[a] The standard deviation does not result from a measurement uncertainty, but from non-stable conditions (unsteady flow conditions, swath behaviour).

Tab. 5 – Pulse measurements with tracer gas SF_6 on stage, with personal exposure and heat sources: time lag and ventilation effectiveness

Position measurement	Ventilation effectiveness/ time lag for dosing position Orchestera back	before conductor	Comment Pulse dosing with tracer gas SF_6
Orchestra right	5.7 / 5'20"	-	Good contaminant removal
Orchestra centre back	-	2.3 / 3'34"	Approximately mixing ventilation

Tab. 6 – Ventilation effectiveness for positions on the balconies

Position measurement	Dosing on parquet at the rear, row 24 without thermal load	with thermal load	Comment Constant dosing with tracer gas R1234yf
1st balcony, row 2	1.3±0.4	4.7±3.5[a]	Approximately mixing ventilation[a]
2nd balcony, row 2	0.76±0.11	0.40±0.08	Transfer from parquet to balcony
3rd balcony, row 4	0.58±0.13	0.59±0.09	Transfer from parquet to balcony
4th balcony, row 5	2.0±0.9	1.1±0.1	Approximately mixing ventilation

Tab. 7 – Measurements with pulsed emission tracer method, with personal exposure and heat sources: time lag and ventilation effectiveness

Position measurement	Position dosing	Time lag mm:ss	Ventilation effectiveness	Comment Pulsed emission with tracer gas SF_6
1st balcony, row 2	Parquet back	02:16	0.28	Possibly swaths
2nd balcony, row 4	1st balcony front	03:05	1.0	Approximately mixing ventilation
2nd balcony, row 4	1st balcony back	03:20	2.4	Good ventilation effectiveness
3rd balcony, row 4	3rd balcony front	04:39	0.63	Rather low ventilation effectiveness
4th balcony, row 5	1st balcony back	06:53	0.85	Approximately mixing ventilation

Thanks to the large supply air volume flow, with a ventilation effectiveness of 1 and an assumed breathing air volume flow of 0.5 m^3/h (person in the audience), only 9 out of 1million emitted particles are inhaled. In the measurement with the least favourable ventilation effectiveness, the number of particles inhaled is around 30 out of 1 million.

It is not the purpose of this paper to assess the infection risk. However, this was done by a hygienist in the course of the accompanying investigation of the tracer gas measurements and is documented in the overall report of the investigation [7]. According to this assessment, there is generally a low risk when masks are worn.

6.2 Tracer gas methods

Working with two tracer gases makes sense in complex rooms and installations. New tracer gas R1234yf has proven itself for measurements in large rooms (requires safety awareness). The disadvantage of R1234yf is its high flammability. This requires safety measures and trained personnel. Both the pulsed emission dosing method and constant dosing method are justified. In the concert hall of the KKL Lucerne and in a preliminary study in a parliament hall, the tracer gas measurements led to the same conclusions as a parallel conducted aerosol measurement study. The investigation has shown that with both tracer gases, a concentration of 1 ppm is sufficient to obtain qualitatively and quantitatively meaningful results when using high-quality measuring equipment.

6.3 General considerations

Fig. 5 – 3rd Balcony of the concert hall with dummies and sampling points, view down to stage.

The ventilation of balconies and galleries is demanding and must be carefully assessed in the case of pandemic risks. For the assessment of infection risk through aerosol transmission, a characteristic value for the entire room is not sufficient. An aeorosol transmission from point A to B is not equal to the transmission from B to A (see **Fig. 6**).

Further research and efforts are needed to clarify these issues.

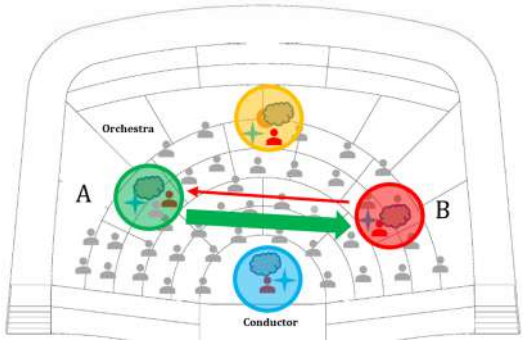

Fig. 6 – Considerations for aerosol transport.

7. Acknowledgement

We would like to thank the management of the KKL Luzern for funding the study. We thank our colleagues Dr. Michael Riediker and Dr. Benoit Sicre for the professional exchange.

8. References

[1] Bienz M., Bucheli K., Erprobung des klimafreundlichen Tracergases HFO-1234yf zur Bestimmung der Luftwechselrate und der Lüftungseffektivität in belegten Räumen unter Covid-19 Randbedingungen. Bachelor thesis, Hochschule Luzern – Technik & Architektur, Horw/Lucerne, 2021, (in german).

[2] Kultur- und Kongresszentrum Luzern (KKL), Wikipedia, https://de.wikipedia.org/wiki/Kultur-_und_Kongresszentrum_Luzern (07.01.2022).

[3] SN EN ISO 12569, Thermal performance of buildings and materials – Determination of specific airflow rate in buildings – Tracer gas dilution method, European Committee for standardization, Brussels, 2012.

[4] Frei B., Kägi A., Recent developments and applications of tracer gas methods in road tunnels. 5th International Conference Tunnel Safety and Ventilation, Graz, 2010.

[5] Persily A.; Axley J., Measuring Airflow Rates with Pulse Tracer Techniques, in ASTM paper: Air Change Rate and Air tightness in Buildings; ISBN 0-8031-1451-6, 1990.

[6] Mundt E. (Hrsg.), Mathisen H.M., Nielsen P.V., Moser A., Ventilation Effectiveness, REHVA Guidebook No 2, Brussels, 2004.

[7] Huber H., Riediker M., Sicre B., Untersuchung der Lüftungswirksamkeit bezüglich einer Exposition durch Aerosolemissionen von Personen, Bericht Nr: HP-212120, Hochschule Luzern – Technik & Architektur, Horw/Lucerne, 2021, (in german).

Health and energy assessment of a demand controlled mechanical extraction ventilation system

Janneke Ghijsels [a], Klaas De Jonge [a,b], Jelle Laverge [a]

[a] Ghent University

[b] FWO Flanders Research Foundation

Abstract. Today, the assessment of residential demand controlled ventilation systems only considers the perceived indoor air quality in terms of comfort, with CO_2 and humidity as the main parameters to investigate. However, the ventilation system and its controls also have an impact on the health aspect of Indoor Air Quality (IAQ) due to the higher exposure to unhealthy pollutants (Volatile Organic Compounds (VOCs), fine dust particles, e.g. $PM_{2.5}$). In this paper, two demand controlled mechanical extraction ventilation systems (DCV) and a continuous mechanical extraction ventilation system (MEV) of a typical Belgian apartment are modelled using Modelica. This allows to simulate the combined effect and interaction of temperature, airflow and IAQ. The model includes sources of CO_2, humidity, VOCs and $PM_{2.5}$ to the indoor air. The combined approach using Modelica allows to do an in-depth analysis of the indoor air quality. A two-stage assessment method is performed, resulting in an overall performance (in terms of IAQ and energy use) of a DCV system in relation to the performance of the MEV reference system.

Keywords. Smart ventilation system, Indoor Air Quality, VOC, health and energy assessment.
DOI: https://doi.org/10.34641/clima.2022.155

1. Introduction

In the recent decades there has been an increasing awareness that the energy demand for buildings must be greatly reduced. Today, our buildings are better insulated and high-temperature heating is replaced by low-temperature surface-heating. The stricter insulation standards ensure an energy reduction and a better thermal comfort. The disadvantage is that, if we only focus on the thermal comfort, an adverse effect will be induced on the indoor air quality (IAQ) of our homes. In old houses there is natural ventilation through cracks and crevices [1] but in more modern houses, that are build more airtight, the pollutants will accumulate in the indoor air. This creates a greater risk of concentration problems, fatigue and other serious health effects. Therefore, there is a need for a designed ventilation system that brings fresh air in and evacuates polluted air out of the home, preferably in a comfortable way.

A continuous, constant, airflow ventilation system will guarantee a good IAQ but will also provide more cold airflow that needs to be heated then strictly necessary to ensure comfort. This results in an increase of the energy use. Therefore, researchers have developed new ventilation strategies that have led to demand controlled ventilation systems (DCV) that only supply and/or extract the amount of air when and where necessary. It is stated that a DCV system can reduce the heating energy related to ventilation and elektricity use of the ventilation system by 20 to 50% [2].

Nowadays, the assessment of a DCV system only considers the perceived IAQ in terms of comfort criteria (such as CO_2, humidity and odour) [3]. However, the big disadvantage of a DCV system is the accumulation of indoor pollutants in times of low occupancy. When the airflow rates are reduced, the VOC emissions of building materials and furniture will accumulate in the indoor air, resulting in harmful VOC concentrations and a poor IAQ. Therefore, the assessment of a DCV system must be extended from only comfort criteria to both comfort and health criteria.

2. Research methods

2.1 Simulation model

The simulation model is made in Dymola, an integrated environment for developing models in the Modelica language. This allows to simulate the combined effect of heat, moisture, airflow and indoor concentrations. In this study, the IDEAS library [4] is used in combination with proprietary models for modelling the airflows and pollutant sources. Figure 1 shows the floor plan of the modelled three-bedroom apartment. This typical Belgian apartment

Copyright ©2022 by the authors. This conference paper is published under a CC-BY-4.0 license.

has already been used several times and has been described in Heijmans, Van Den Bossche, Janssens (2007); Laverge, Janssens (2013) and De Jonge, Janssens, Laverge (2018). During modelling, a lot of attention is paid to the multi-zone representation of the apartment, the building envelope, the elements of the various ventilation systems, the occupant schedules, the ventilation controls, the emissions from the occupant activities and the emissions from the building materials and furniture.

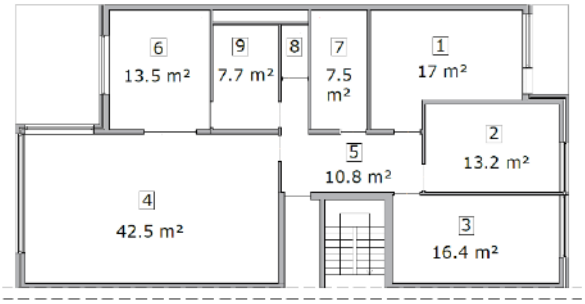

2.2 Investigated DCV systems

The performance of two demand controlled mechanical extraction ventilation systems (DCV) are being compared to the performance of a continuous mechanical extraction ventilation system (MEV). The two DCV systems follow the same principles: fresh air is naturally brought into the dry spaces through trickle vents and will be mechanically extracted in the wet spaces. The first DCV system **(DCV1)** is a theoretical control system based on controls that can currently be found on the Belgian market. The ventilation flow rates (Q) are adapted on the one hand by a local detection and a local control in the wet areas. The bathroom is controlled on humidity, the kitchen on CO_2 and the toilet on VOC. Additionally, there are also extra CO_2 sensors in the dry spaces that will increase the extraction flow rate in the wet spaces if the CO_2 concentration in the dry spaces becomes too high. For the increase of the extraction flow rate only the dry space with the maximum CO_2 concentration will be considered. The increase of extraction creates negative pressure in the building which force more fresh air through the trickle vents resulting in a larger supply of fresh air in the dry spaces.

The second DCV system **(DCV2)** is also a theoretical control system based on controls that can currently be found on the Belgian market. The ventilation flow rates (Q) are, just like DCV1, adapted by a local detection and local control in the wet spaces. Supplementary to these extraction in the wet spaces, there is an additional extraction in the dry spaces based on local CO_2 sensors. Due to the direct extraction in the dry spaces, the amount of supply through the trickle vents can be guaranteed. In addition, the extraction works in two zones, namely the bedrooms and the living space. The zone with the highest CO_2 concentration will be controlled based on this concentration and the flow rate of the other zone is lowered to the minimal flow rate. In that way, the zone with the highest occupation, receives the highest ventilation flow rate.

The working principles of both DCV systems is graphical represented in figure 2. The nominal ventilation flow rates according to the NBN-D50-001 are represented for each zone in table 1. Q_{nom} are the nominal flow rates for both systems and $Q_{nom_addition}$ are the nominal flow rates for the additional extraction in the dry spaces for DCV2. The zones are numbered like the floor plan in figure 1. Lastly, the different sensors and their controls on the ventilation flow rates are represented in table 2. The first four controls are for both DCV systems. The fifth and sixth control are respectively for DCV1 and DCV2.

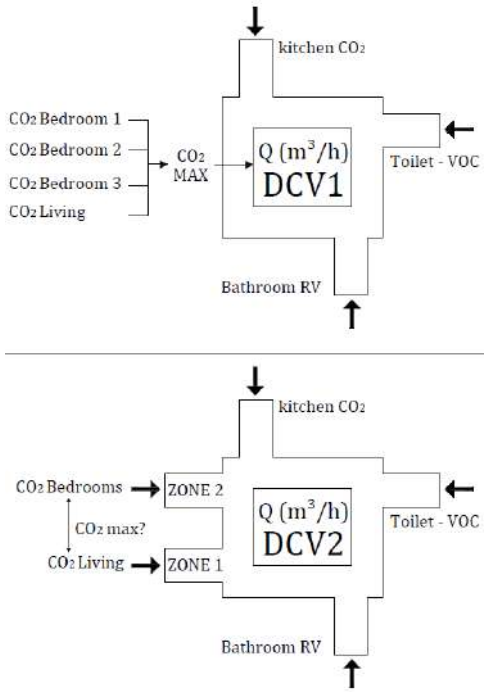

Fig. 2 – Graphical representation of the working principle of DCV1 and DCV2

Tab. 1 – Ventilation flow rates

Zone	Q_{nom} (m^3/h)	$Q_{nom_addition}$ DCV2 (m^3/h)
1: Bedroom	43.92	25
2: Bedroom	35.26	25
3: Bedroom	38.88	25
4: Living room	108.32	60
5: Hall	16	-
6: Kitchen	60	-
7: Bathroom	60	-
8: Toilet	30	-
9: service room	60	-

Tab. 2 – Controls

Sensor	Control	Q (m^3/h)
1. RV – Bathroom and service room	RV < 30%	10 %
	30% < RV < 65%	30 %
	65% < RV < 95%	60%
	RV > 95%	100%
2. RV – Bathroom	ΔRV > 2% in 5min	100%
3. CO_2 (ppm) Kitchen	CO_2 > 850	10%
	850 < CO_2 < 950	Linear
	CO_2 > 950	100%
4. VOC – Toilet	No presence	10%
	Presence	100%
5. CO_2 (ppm) **DCV1** Max. of dry spaces	CO_2 < 1000	10%
	1000 < CO_2 < 1200	Linear
	CO_2 > 1200	100%
6. CO_2 (ppm) **DCV2** Dry spaces extraction		
Zone 1: zone with maximum CO2-concentration.	CO_2 > 850	10%
	850 < CO_2 < 950	Linear
	CO_2> 950	100%
Zone 2: zone with smaller CO2-concentration	-	10%

2.3 Pollutants of concern and their emissions

More than 100 indoor pollutants are currently identified as (potentially) hazardous to our health. To obtain a priority list of target pollutants, 7 large studies are reviewed, each a conclusion of many other studies. The most important study is the AIVC-CR17 [5] study where, for Belgium, the concentrations of harmful pollutants were measured in more than 400 homes. As a result, 6 indoor pollutants and 3 outdoor pollutants are prioritized for the Belgian residential application, namely benzene, formaldehyde, naphthalene, limonene, toluene and particulate matter ($PM_{2.5}$) as indoor pollutants and $PM_{2.5}$, nitrogen dioxide (NO_2) and ozone (O_3) as outdoor pollutants. The concentration of the outdoor pollutants will be modelled as constants. In the future, this can be further investigated.

To allow a clear representation of which emissions are implemented for each pollutant, the emissions will be divided into three categories. namely emissions from building materials and furniture, emissions from occupants and emissions from occupant activities.

A. Emissions from building materials and furniture

To determine the emissions of the building materials and furniture, it is assumed that the apartment is refurbished or newly built so that can be concluded that the floor and furniture are new. Therefore, all the emissions will be determined after a lifetime of 28 days. The furniture is calculated for an occupancy of two adults, two children and two babies. The furniture is considered wood, synthetic or gypsum. This means that only the pollutants benzene, formaldehyde, naphthalene and toluene are considered for these emissions. All the emissions of building materials and furniture are determined using the Pandora Database [6]. The summary of these emissions is given in table 3. All these emissions are assumed to have a constant emission rate. One exception is made for the formaldehyde emission by the floor. The emission rate of the flooring is a dynamic source model based on the air temperature and relative humidity in the zone [7].

B. Emissions from occupant activities

The impact of the occupant activities on the VOC concentrations is significant. To determine which activities must be implemented, the original occupant schedules, used in Belgian simulation studies for the determination of ventilation legislation [8], were reviewed. The original activities were cooking, showering and washing clothes and only the emission of moisture was recorded. Eventually, the activities were expanded with cleaning, washing dishes and using deodorant spray. The emissions of the activities, including the original activities, were expanded with limonene, naphthalene and particulate matter emissions. Existing research on emission values is very limited, which means that assumptions often must be made. When newer or more accurate research is published, the emission values can easily be adjusted in the model.

For cooking, $PM_{2.5}$ emissions were added based on the relationship to the moisture emission in the study of Poirier et al (2021) [9]. Extensive cooking results in a greater moisture and $PM_{2.5}$ production. Important is that the cooking emissions are considerably reduced by the implementation of a cooker hood with a flow rate of $200m^3/h$ and a capture efficiency of 0,7. This means that 70% of the emissions are captured by the cooker hood. For the activity of showering, the use of shampoo and shower gel was added, resulting in limonene [10] and naphthalene [11] emissions. For the activity of washing clothes, the use of washing liquid (wash pods of 27 gram) was added, resulting in limonene emissions [12]. For the use of deodorant, a $PM_{2.5}$ [13] and limonene [14] emission was added to the occupant itself. The occupant uses the deodorant 3 times a day (0,5 gram) and carries these emissions around the house. Also, the emissions for the activity cleaning, were added to the occupant itself. When the occupant is cleaning, moisture [15] and limonene [6] emissions are released into the air where the occupant is situated.

All these emissions are summarized in table 4. The references are given in the text and in the table. For a more in-depth explanation on how the emissions are obtained, reference is made to "*Health-based assessment method for residential DCV systems*" by Janneke Ghijsels (2022).

Tab. 3 – Summary of the emissions from building materials and furniture for each pollutant

Emission [ug/h/m^2]	formaldehyde	benzene	naphthalene	toluene
Floor (wood)	9,91	negligible	negligible	negligible
Furniture (wood)	3,06	1,40	5,68	-
Door (wood)	4,50	-	-	-
Other furniture (synthetic)	3,00	2,00	-	11,00
Carpet	4,27	0,21	0,47	0,20
Walls (gypsum)	negligible	negligible	negligible	0,50

Tab. 4 – Summary of the emissions from building materials and furniture for each pollutant

Emission [ug/h/m^2]	moisture	limonene	naphthalene	PM2.5
Cleaning (3)	5,00 g/m^2(floor) [15]	1912 ug/h/m^2(floor) [6]	-	-
Cooking	0,60 L/s *	-	-	1260 ug/min [9]
	1,00 L/s *			1910 ug/min
	1,50 L/s *			2550 ug/min
Washing dishes	4,20 e-04 L/s	24,8 ug/h	-	-
Showering	0,50 L/s *	1200 ug/h [10]	3,76 ug/h [11]	-
Deodorant use	-	1438 ug/use [14]	-	12 ug/use [13]
Washing clothes	6,50 x e-2 L/s *	7833 ug/h [12]	-	-

* CEN 14788: Ventilation of buildings - Design and dimensioning of residential ventilation systems

C. Emissions from occupants

Occupants produce both CO_2, H_2O and human odour. The CO_2 and H_2O emissions are shown in table 4 for a metabolism (the degree of activity) equal to 1,6 met (very active). In the simulation these productions are scaled according to the metabolism of each occupant at each timestep.

Tab. 5 – Emissions by occupants themselves

Production	1,6 met (light activity)
CO2-production	
- Adult	19,0 l/h *
- Child	12,6 l/h [16]
- Baby	6,7 l/h *
H2O-production	
- Adult	55,0 g/h *
- Child	41,3 g/h [17]
- Baby	18,3 g/h *

* Norm CEN 14788

2.4. Assessment method

To make a complete analysis of the impact of a DCV system on IAQ, the assessment method will be divided into two stages. The first stage is a **health performance checklist** that will rule out the possibility that the exposure concentrations cause harmful health effects for the occupants. If this criterion is not met, the controls can be adapted (e.g increasing the nominal flow rates, increasing the minimal flow rates or adjusting the boundaries.)

When the quality of the indoor air is sufficient for the health of the occupants, the DCV system can be analysed by the second stage of this assessment method, namely the **overall performance rating** in terms of health and energy. A comparison will be made with the performance of the MEV reference system. In this way, a pareto optimum can be explored for each DCV system in which both the energy and health performance are better than the performance of the MEV reference system.

A. Health performance checklist

For the assessment of the health performance, a checklist will be followed in which first the exposure concentrations of each pollutant will be compared with the limit concentrations of the chosen exposure metrics. Both acute and chronic exposure concentrations will be checked to exclude both acute and chronic health effects.

The peak concentrations will be checked by the 10-minute AEGL-1 value (obtained by U.S. EPA) [18] and the average exposure concentrations over a time interval of 1 hour and 8 hours will be checked by the acute REL values (obtained by OEHHA) [19]. The chronic exposure concentrations will be checked by the chronic REL value. The summary of these limit concentrations is given in table 6.

After the control of the exposure concentrations, the lifetime average daily dose (LADD) is calculated for each pollutant [20]. The formula of the LADD is given in equation (1). Because the LADD considers both body weight and inhalation rate it is possible to obtain an estimation of the health effects for sensitive occupants, for example babies.

Tab. 6 – Emissions by occupants themselves.

Reference $C_{exposure}$ (ug/m^3)	10 min AEGL-1	Acute REL-1h	Acute REL-8h	Chronic REL
Benzene	415.000	27	3	3
Formaldehyde	1105	55	9	9
Naphthalene	-	-	9	9
Limonene	-	-	-	9000
Toluene	252.000	-	800	400
$PM_{2.5}$	-	-	25 (24h) *	10*

* WHO guidelines : air quality guidelines for particulate matter, ozone, nitrogen dioxide andsulfur dioxide : summary of risk assessment

Babies will have a higher lifetime average daily dose than an adult, even though the exposure concentrations of the pollutants are the same.

$$LADD = \frac{E_i \, x \, IR \, x \, E_f \, x \, E_d}{BW \, x \, A_t} \, x \, \epsilon \qquad (1)$$

Where E_i is the timeweighted exposure (ug/m^3), IR is the inhalation rate (m^3/day) [21], E_f is the exposure frequency (day/year), E_d is the exposure duration (day), BW is the bodyweight (kg) where in this study 70kg is used for adults, 23kg for children and 11kg for babies. A_t= is the simulation time, in this study 365 days and ϵ is the absorption factor of each pollutant (for example 0,9 for formaldehyde).

The use of LADD makes it possible to exclude non-carcinogenic health effects by calculating the hazard quotient (HQ), given in equation (2). The LADD is compared by the reference doses (RfD) (obtained by U.S. EPA) [22]. When HQ is less than 1, the risk of non-carcinogenic health effects is considered negligible.

$$HQ = \frac{LADD}{R_f D} < 1 \text{ Health effects are negligible} \qquad (2)$$

B. Overall performance rating

If the DCV system passes the health performance checklist, it is evaluated by the second part of this assessment method. In this assessment method, the DALY-index (Disabled Adjusted Life Years) is used as health indicator. It quantifies the total years lost due to death or disability due to poor IAQ. It scales the harmfulness of the different VOC and $PM_{2.5}$ concentrations to allow a general health rating. The total DALYs are calculated based on the study of Logue et al. (2012) [23]. The DALYs of the outdoor pollutants (i.e $PM_{2.5}$, NO_2 and O_3) are calculated using the IND-method. The DALYs of the indoor pollutants (i.e. benzene, formaldehyde, naphthalene, limonene and toluene) are calculated using the ID-method where the study of Huijbrechts et al. (2005) [24] provides the information on the *(∂D/∂I)*-factors.

When the total DALYs are calculated for each DCV system, this health indicator can be compared with the energy use of each DCV system. In that way it is possible to rate the overall performance of the DCV system. The performance of a DCV system is considered sufficient when there is a pareto optimum compared to the continuous MEV reference system. This means that both the energy use and the health impact of the DCV system must be lower than those of the reference system.

3. Results – Assessment method

Each DCV system and their controls are modelled in the Modelica model together with the different emissions and the activity schedules of the occupants. For each ventilation system 10 different families are simulated. The results are average exposure concentration of these 10 scenarios.

3.1 Health performance checklist

In this paper, the focus will be on one constant emission source (i.e. formaldehyde) and on one emission source that depends on the activities of the occupants (i.e. $PM_{2.5}$), because these two pollutants show to have the highest impact on our health. In figure 2 the exposure concentration of formaldehyde is compared for the two DCV systems and the MEV reference system. The acute concentration limit of 55 ug/m^3 is not exceeded by any system. The chronic concentration limit of 9 ug/m^3 is exceeded by the two DCV systems. DCV1 has a chronic exposure concentration of 11 ug/m^3, while DCV2 has a much larger chronic exposure concentration of 18.8 ug/m^3.

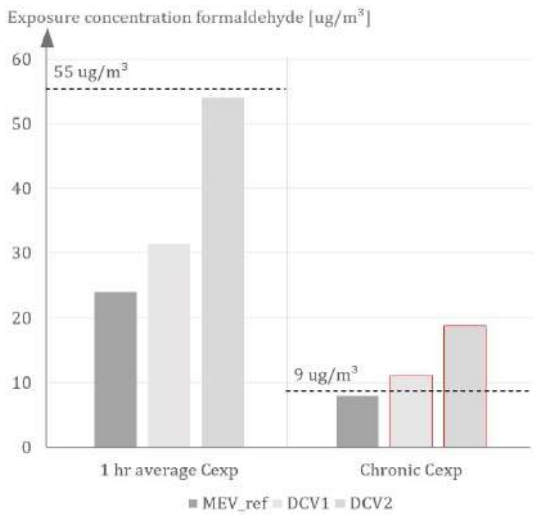

Fig. 2 – Comparison of the exposure concentration of formaldehyde between DCV1, DCV2 and MEV_ref.

Figure 3 shows the exposure concentration of $PM_{2.5}$ for the three systems. The acute exposure concentration is compared with the 24 hours limit concentration of the WHO and is only exceeded by DCV2. The chronic exposure concentration is exceeded by all the ventilation systems. This is a result of a constant outside $PM_{2.5}$-concentration of 14 ug/m^3 (according to MIRA 2019) [26]. In the future, it can be important to change the approach of the outside pollutants to more variable concentrations according to the environment (e.g. temperature) and the location (e.g. nearby industry, heavy traffic).

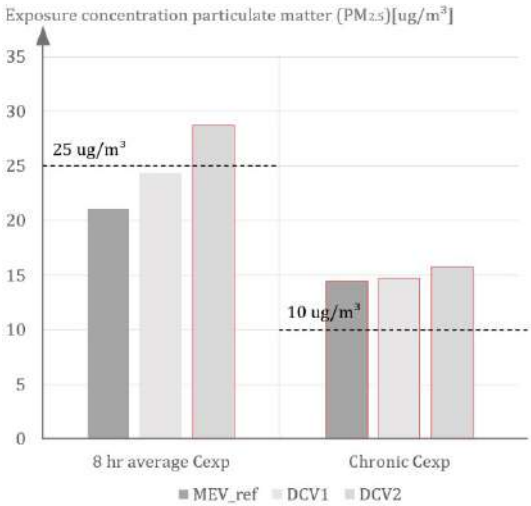

Fig. 3 – Comparison of the exposure concentration of $PM_{2.5}$ between DCV1, DCV2 and MEV_ref.

In table 7 all the concentrations of the pollutants of concern are summarized. DCV2 scores too high for formaldehyde and $PM_{2.5}$. DCV2 has also higher exposure concentrations for all the other pollutants than DCV1.

	Maximum Cexp	1 hour average Cexp	8 hour average Cexp	Chronic Cexp
MEV_ref				
Formaldehyde	21,94	24,03	19,15	7,92
Benzene	1,66	1,55	1,22	0,66
Limonene	565,41	581,52	-	12,56
Naphthalene	5,24	-	3,78	1,83
Toluene	11,15	11,12	8,64	5,55
PM2.5	187,61	-	21,08	14,46
DCV1				
Formaldehyde	35,72	31,43	24,76	11,02
Benzene	2,77	2,27	1,65	0,87
Limonene	694,99	651,46	-	15,97
Naphthalene	8,69	-	5,13	2,42
Toluene	18,87	18,07	12,55	7,50
PM2.5	215,70	-	24,35	14,70
DCV2				
Formaldehyde	73,01	54,07	42,75	18,84
Benzene	4,51	3,91	2,57	1,37
Limonene	856,91	736,12	-	22,12
Naphthalene	14,77	-	7,90	3,81
Toluene	35,87	34,80	25,80	12,16
PM2.5	229,66	-	28,75	15,79

Tab. 7 – Summary of all the acute and chronic exposure concentrations of the pollutants of concern for DCV1, DCV2 and MEV_ref.

To ensure that the IAQ, caused by system DCV2 does not cause any health effects on the sensitive occupants, the LADD is calculated. Subsequently the HQ of each pollutant is calculated by comparing the LADD to the reference dose (obtained by U.S. EPA). An example is worked out for benzene. In table 8 the average LADD of benzene of the 10 scenarios simulations is calculated for each occupant in the simulation. For DCV2, the LADD of benzene is higher than the reference dose (8,57 x 10^{-3}mg/kg/day) for both the smaller children. Therefore, DCV2 will not ensure a good IAQ for the sensitive occupants.

LADD Benzene	Adult 1	Adult 2	Child 1	Child 2	Baby 1	Baby 2
MEV_ref	0.00203	0.00254	0.00198	0.00195	0.00423	0.00400
DCV1	0.00278	0.00350	0.00264	0.00260	0.00564	0.00538
DCV2	0.00483	0.00599	0.00452	0.00408	0.01062	0.00915

Tab. 8 – Summary of all LADD of benzene for each occupant in the simulation for MEV_ref and the two DCV systems

It is necessary to **adjust DCV2** to meet the minimum requirements of the health performance checklist. A **new simulation** is carried out where the minimum flow rates are increased from 10% to 30% of the nominal flow rates. This adaptation changes the LADD of benzene for occupant 5 (Baby 1) from 0,01062 to 0,00784 mg/kg/day and for occupant 6 (Baby 2) from 0,00915 to 0,00676 mg/kg/day. All the average daily doses are now below the reference doses. Hence, it can be said that no important negative health effects will occur due to a poor IAQ. In the next paragraph, it is examined whether there is a pareto optimum between the two DCV systems, incl. the new DCV2 system and the MEV-reference system. The overall performance of the DCV systems, both in terms of energy and health, should perform better than the overall performance of the MEV reference system.

3.2 Overall performance rating

The total DALYs per 100.000 persons per year are calculated for each pollutant using the IND and ID method. The results are given in figure 4. It becomes clear that the total DALYs are for more than 80% caused by $PM_{2.5}$. The second major pollutant is formaldehyde. All the other VOCs seem to have a very small impact and are therefore less harmful for our health. DCV1 has the smallest total number of DALYs. Even smaller than the reference system. This is caused by the smaller influence of the outdoor pollutants in periods of less ventilation. DCV2 has the largest total number of DALYs. This is caused by the higher formaldehyde concentrations and the higher $PM_{2.5}$-concentration in the kitchen during cooking periods.

The **new DCV2 system**, where the minimum flow are adapted to 30% of the nominal flow rates (instead of 10%) reduces the total number of DALYs from 41,1 to 32,8 DALYs per 100.000 persons per year. This is a reduction of more than 20% (8,3 DALY).

Now that the total DALYs are known, it is possible to generate an overall performance rating of the DCV systems. In figure 5 the total number of DALYs are

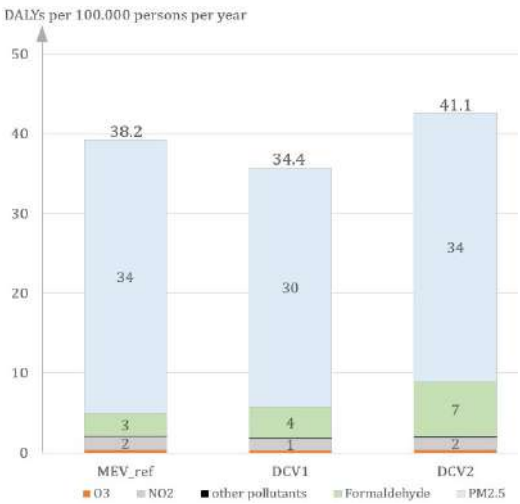

Fig. 4 – The share of each pollutant in the total number of DALYs (the health indicator in this research) per 100.000 persons per year compared for the two original DCV systems and the MEV reference system.

compared with the energy use (electricity use of the fans and ventilation heat losses) of the ventilation system. To create a pareto optimum it is necessary that the DCV systems perform better in terms of health and energy. This means that the DCV systems must be located in the green frame shown in figure 5. The system that is situated on the bottom, left, is the system that generate the best pareto optimum. At first, system DCV2 had a very low energy use. After the adaptation, the IAQ is improved with 20% (8,3 DALY) and the energy use increased with 35% (1040 kWh/year). This increase in energy use seems very high, but the total energy use is still 40% (1845kWh/year) lower than the energy use of the reference system with continuous flow rates. The overall performance of the new DCV2 is even better than the overall performance of DCV1. It is stated that with correct adaptions, it is possible to find a pareto optimum for each DCV system.

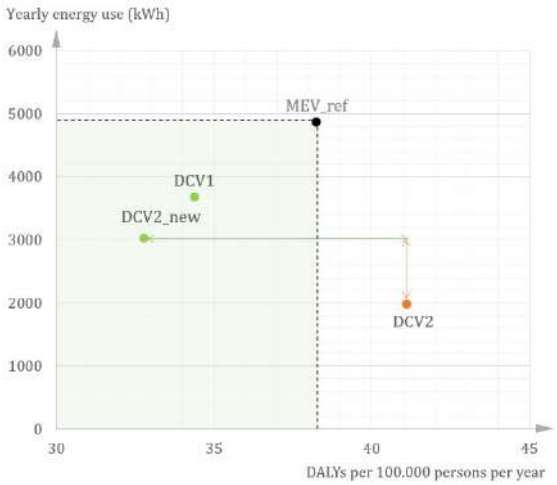

Fig. 5 –The overall performance of a DCV system in terms of energy and health compared to the MEV reference system. The overall performance of a DCV system is sufficient if there is a pareto optimum compared to the MEV reference system. DCV2_new scores best on the overall performance.

4. Discussion and conclusion

In this research, a very extensive emission model was combined with a dynamic temperature and occupancy model in the Dymola software. This allows an assessment of IAQ at every timestep for the different occupants with different ages, habits and metabolisms. Based on the determination of the exposure concentration at each time step and for each occupant, both the average daily dose (LADD) and the intake can be calculated. These two parameters are both very important in the assessment method that was developed to determine whether a system ensures a good indoor air quality. The necessity for such an assessment method is high since the DCV systems are nowadays only assessed on comfort criteria such as CO_2, humidity and odour. Because the danger lies in the increased VOC concentrations in times of less ventilation, it is necessary that a DCV system, designed to ensure an energy saving, also ensures a sufficiently IAQ in terms of health.

The health and energy assessment method was designed as a two-stage assessment method in which first the exposure concentrations are checked on health risks for the occupants. The peak concentrations, acute concentrations and chronic concentrations are compared with the corresponding limit concentration from relevant exposure metrics. In this paper, the limit concentrations of the reference exposure levels [19] were used. It is possible to use other limit concentrations of exposure metrics that are for example drawn up in function of a legislation in the country where the research is being conducted.

The second stage of the assessment method is an overall performance rating where one health indicator, the total DALYs, is used as general health indicator of the system. The total DALYs scales the harmfulness of exposure to the different pollutants. In that way, the health performance of a system that ventilates more in the kitchen and induces lower $PM_{2.5}$ concentrations, can be compared to the health performance of a system that ventilates more in the living rooms and induces lower formaldehyde concentrations. The total DALYs for each system are compared with the energy use of each system, resulting in an overall performance of the DCV system in comparison to the MEV reference system.

The conclusion of the two DCV systems is that, if there is minimum air flow rate of 10%, DCV1 ensures a better indoor air quality. This means that increasing the extraction flow rate by using CO2-sensors in the dry spaces, works sufficient. The disadvantage is that DCV1 only ensures an energy reduction of around 25% (1200 kWh/year) in comparison to the continuous MEV system, which is rather low. When the minimal flow rates of DCV2 are increased to 30%, it guarantees a better IAQ and a higher energy reduction then DCV1. That's why the adaption of a DCV system that initially guarantees a

high energy reduction but a low IAQ, ensures mostly an improvement to the health/energy contradiction. In comparison to the continuous MEV system, the energy reduction of DCV2_new is around 40% (1845 kWh/year) and the improvement of IAQ is around 15% (5,5 DALY).

The investigated cases show that DCV systems can be an effective measure to save energy and provide a healthier indoor air. Both systems, DCV1 and DCV2_new, guarantee a pareto optimum in comparison to the continuous reference system. It is stated that for every DCV system, an optimalisation can be found where the health/energy contradiction disappears.

References

[1] Fazli T., Stephens B. "Development of a nationally representative set of combined building energy and indoor air quality models for U.S. residences". Building and Environment. 2018;136, table 5

[2] Savin J., Berthin S. and Jardinier M. "Demand Controlled ventilation: 20 years of in-situ modelling in the residential field". 32ste AIVC and 1ste TIGHTVENT conference. 2011

[3] Hänninen O. e.a. "Hallvent Project : Reducing burden of disease from residential indoor air exposures in Europe". The 11th International Conference on Urban Health. 2014

[4] Jorissen F. e.a. (2018). "Implementation and Verification of the IDEAS Building Energy Simulation Library". Journal of Building Performance Simulation. 2018. 11(6), p. 669–688

[5] Abadie M.O. e.a. "Indoor Air Quality Design and Control in Low-energy Residential Buildings" Annex 68 | Subtask 1: Defining the metrics. AIVC-CR17. 2017.

[6] Abadie M.O. and Blondeau P. "Pandora database: A compilation of indoor air pollutant emissions". HVAC & R Research. 2011. 17(4), p. 602–613 (database url: https://db- pandora. univ- lr.fr)

[7] De Jonge K. "The impact of demand-controlled ventilation on indoor VOC exposure in Belgian dwellings". 2017

[8] Heijmans N., Van Den Bossche N and Janssens A. "Berekeningsmethode gelijkwaardigheid voor innovatieve ventilatiesystemen in het kader van de EPB-regelgeving". 2007

[9] Poirier B. e.a. "Pollutants emission scenarios for residential ventilation performance assessment: A review". Journal of Building Engineering. 2021.42

[10] Yeoman A. M. e.a. (2020). "Simplified speciation and atmospheric volatile organic compound emission rates from non-aerosol personal care products". Indoor Air. 2020.30(3), p. 459–472.

[11] Kang D.H. e.a. "Household materials as emission sources of naphthalene in Canadian homes and their contribution to indoor air". Atmospheric Environment. 2012. 50, p. 79–87

[12] NICNAS. "Priority Existing Chemical : Assessment Report : Limonene". 22, p. 18–25.

[13] Schiavon M. e.a. (2015). "Domestic activities and pm generation: a contribution to the understanding of indoor sources of air pollution". International Journal of Sustainable Development and Planning Vol 10.No. 3, p. 347–360.

[14] Rastogi S.C., Jensen G.H. and Johansen J.D. "Survey and risk assessment of chemical substances in deodorants". Survey of Chemical Substances in Consumer Products No. 86. 2007

[15] TenWolde A. and Pilon C. L. "The Effect of Indoor Humidity on Water Vapor Release in Homes". 2007

[16] Persily A. and de Jonge L. (2017). "Carbon dioxide generation rates for building occupants". Indoor Air. 2017. 27(5), p. 868–879

[17] Johansson P., Pallin S. and Shahriari M. "Risk Assessment Model Applied on Building Physics: Statistical Data Acquisition and Stochastic Modeling of Indoor Moisture Supply in Swedish Multi-family Dwellings". IEA/ECBCS Annex 55 meeting. 2010

[18] U.S.EPA. "Chemical Priority Lists for Acute Exposure Guideline Levels (AEGLs)". 2014

[19] OEHHA. "Acute, 8-hour and Chronic Reference Exposure Level (REL) Summary". 2019

[20] ATSDR. "Public Health Assessment Guidance Manual. Appendix G: Calculating Exposure Doses". 2005

[21] Moya J., Phillips L. and Schuda L. (2011). "Inhalation rates". Exposure Factors Handbook. Cap.6, p. 348–443

[22] U.S.EPA. "A review of the reference dose and reference concentration processes". 2002

[23] Logue J.M. e.a. (2012). "A Method to Estimate the Chronic Health Impact of Air Pollutants in U.S. Residences". Environmental Health Perspectives. 2012. 120(2), p. 216–222.

[24] Huijbregts M.A.J. e.a. (2005). "Human-toxicological effect and damage factors of carcinogenic and noncarcinogenic chemicals for life cycle impact assessment". Integrated Environmental Assessment and Management. 2005. 1(3), p. 181–244.

[25] U.S.EPA. "Guidelines for Carcinogen Risk Assessment". 2005.

[26] Milieurapport Vlaanderen (MIRA) : Luchtkwaliteit : Jaar-gemiddelde concentraties van buitenstoffen. 2019.

Study on Ventilation Efficiency and Infection Probability in the Outbreak at Restaurant

Nobuhide Ashiki [a], Takashi Kurabuchi [b], Jeongil Kim [c]

[a] Tokyo University of Science, Tokyo, Japan, ashiki@juutaku.co.jp.

[b] Tokyo University of Science, Tokyo, Japan, Kura@rs.tus.ac.jp.

[c] Tokyo University of Science, Tokyo, Japan, jeongil.kim@rs.tus.ac.jp.

Abstract. With the spread of the coronavirus infection, ventilation efficiency, new design styles, air conditioning and ventilation operation methods, existing building improvement plans, and other building infection risk reduction methods need to be systematized. This study used computational fluid dynamics (CFD) to recreate a series of cases in which nine out of 89 people were infected at a restaurant in Guangzhou, China. Although the importance of ventilation has been reaffirmed, when making a general ventilation plan, ignore the pollutant concentration distribution in the room and calculate the required ventilation volume assuming complete ventilation in the room. In a real space, the generation of pollution sources are local, and the airflow properties in the room, arrival/distribution of fresh air, and discharge properties of the generated pollutants differ greatly; thus, non-uniform concentration fields, ventilation efficiency distributions, and infection probability distributions also occur. A series of cases infected at a restaurant in Guangzhou was evaluated by Scale for Ventilation Efficiency 3,4 (SVE3, SVE4). SVE3 is corresponding to the traveling time of air from the supply outlet to each point. SVE4 indicates the contribution ratio of a supply opening to air at a point in a room.
In addition, the Wells–Riley model (WRM) is a typical model for quantitatively evaluating the risk of airborne infections, and cases of numerical analysis have been reported in various countries worldwide.
However, WRM assumes that the distribution of indoor droplets is uniform and the droplet concentration is stable, and that floating fine particles with a nonuniform concentration field from the active state of the virus, gravity sedimentation, and a non-uniformly distributed pollution source. A diffusion phenomenon is possible, but there is a problem that has not been addressed. Previous studies have excluded diffusion phenomena from their evaluation because gravity sedimentation is significantly less than inactivation, and the cause of local cluster formation is inadequate.This study aims to establish a predictive flow for infection control using CFD.

Keywords. Airborne transmission, Coronavirus, COVID-19, Room air distribution, Transient analysis, Ventilation efficiency
DOI: https://doi.org/10.34641/clima.2022.75

1. Introduction

Currently, owing to the influence of COVID19, there is a need for a method to accurately confirm the distribution of indoor air. In this study, the infections were reproduced using computational fluid dynamics (CFD) simulation (**Fig. 1**) of a restaurant in Guangzhou, China, where a local cluster was generated. A series of cases infected was evaluated by SVE3, SVE4.
Therefore, considering the spillover effect, we will demonstrate the effects of each factor of ventilation efficiency evaluation and inactivation, gravity sedimentation, and collection rate to construct an infection control prediction flow.

Copyright ©2022 by the authors. This conference paper is published under a CC-BY-4.0 license.

Fig. 1 - Plan of Guangzhou Restaurant

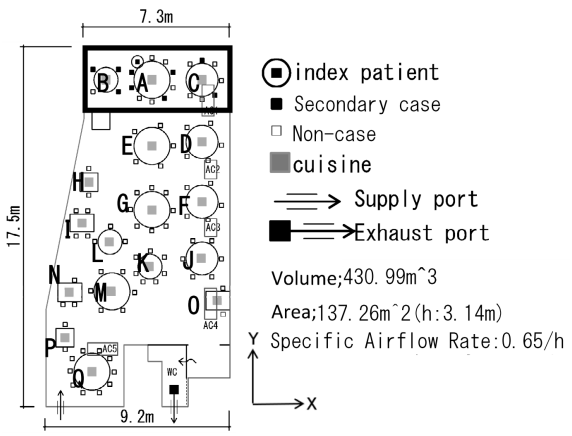

2. Methods

The research methods and procedures of this study are as follows:

1) To clarify the cause of cluster formation, ventilation efficiency indices (SVE3 and SVE4) were evaluated using CFD simulations.
2) Using CFD simulations, we examined the concentration decay due to inactivation, along with the concentration transition due to gravity sedimentation and collection rate.
   Through unsteady CFD analysis, the concentration increase and transition were clarified, and the amount of quanta produced in each case determined. In this study, the exhalation of a primary infected person was modeled using a passive scalar. The gravity sedimentation rate was determined as 8E-04 m s^{-1} by Buonanno et al. , the inactivation rate was 0.63h-1 by Li et al. , and the collection rate was 20%.

3. Results and discussion

3.1 Assessment of ventilation efficiency sections and subsections

It is presumed that the cause of the occurrence of local clusters is a small ventilation volume ranging from 2.7 to 3.7 $m^3 h^{-1}$, a short circuit of ventilation by the air supply port and the exhaust port of the toilet by the fire door, and the generation of the retention area by the air conditioning airflow. **Tab. 1** shows the analysis cases of SVE3 defined by the average arrival time of the outlet air to a specific area based on the discharge concentration of the suction port and SVE4 defined by the range of force of each outlet. **Fig. 2** shows the distribution of SVE3 when Z = 1.1 m, and the analysis results with poor ventilation efficiency are shown in the local cluster generation space region. To rationally control the indoor air environment locally, it is necessary to specifically evaluate the force range of the blown airflow, which is a control factor. **Tab. 2** shows the contribution rate of each air conditioner, air supply port, and exhaust port to the space. In the area where regional clusters occurred, 42.43% of the air conditioning airflow became circulating airflow, and it was confirmed that a flow field with less air exchange was formed. **Fig. 3** shows the distribution of SVE4 in the horizontal cross-section with respect to the center of the height direction of the air outlet and air supply port of each air conditioner. It is a distribution map based on each outlet. **Fig. 4-7** show contour maps of the vertical section of SVE4. This indicates that the local cluster was created by the airflow properties in the room where it was generated.In order to control the indoor air environment locally and rationally, it is necessary to specifically evaluate the range of force of the blowing airflow, which is the control element.

Tab. 1 – Types of ventilation efficiency (SVE3, SVE4), types of air supply / exhaust ports and air conditioning outlets, its amount.

Case	Ventilation efficiency	3. Mask
1.	SVE3	Supply :280$m^3 h^{-1}$ Exhaust:280$m^3 h^{-1}$ AC1-5 :4080$m^3 h^{-1}$
2－1.	SVE4	AC1 :960$m^3 h^{-1}$
2－2.		AC2 :600$m^3 h^{-1}$
2－3.		AC3 :600$m^3 h^{-1}$
2－4.		AC4 :960$m^3 h^{-1}$
2－5.		AC5 :960$m^3 h^{-1}$
2－6.		Supply :280$m^3 h^{-1}$

Fig. 2 - Contour diagram for SVE3 [h](Z = 1.1 m)

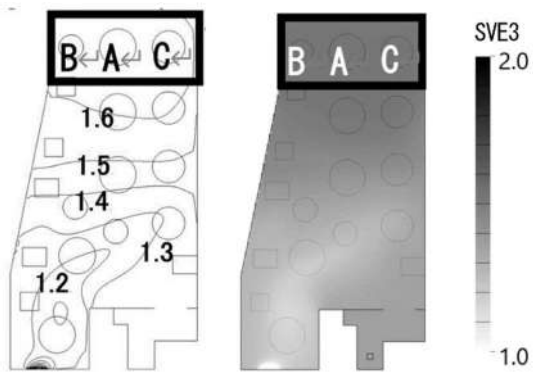

Tab. 2 - Percentage of power range for each SVE4 analysis case.

	Case2-1	Case2-2	Case2-3	Case2-4	Case2-5	Case2-6
AC1	42.43	23.09	11.99	5.68	6.35	3.85
AC2	23.71	27.59	19.62	9.87	11.01	6.68
AC3	13.87	20.04	22.73	15.05	16.63	10.38
AC4	7.92	11.67	17.92	21.15	22.02	18.81
AC5	4.70	6.86	10.95	26.29	21.63	38.84
Exhaust	7.38	10.74	16.79	21.96	22.36	21.44
Total[%]	100	100	100	100	100	100

Fig. 3 - Contour diagram for each SVE4 case.

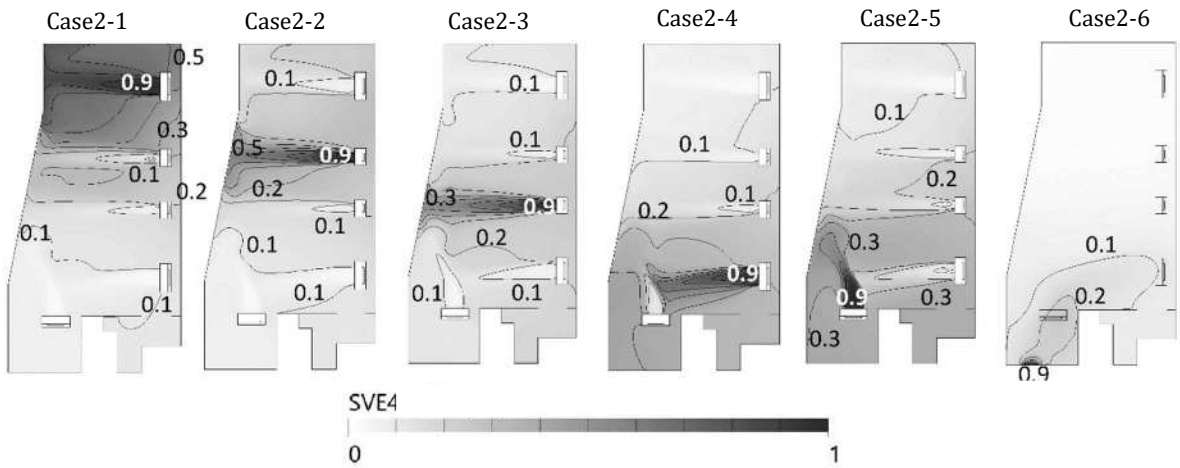

Fig. 4 - Target diagram

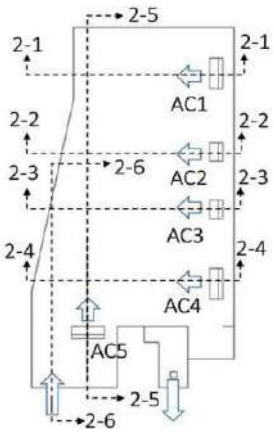

Fig. 5 - Case2-1 section

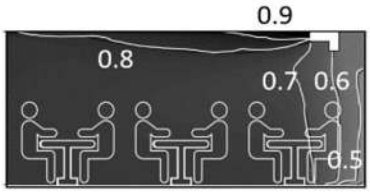

Fig. 6 - Case2-2 section

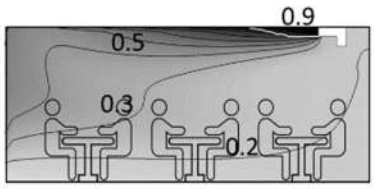

Fig. 7 - Case2-5 section

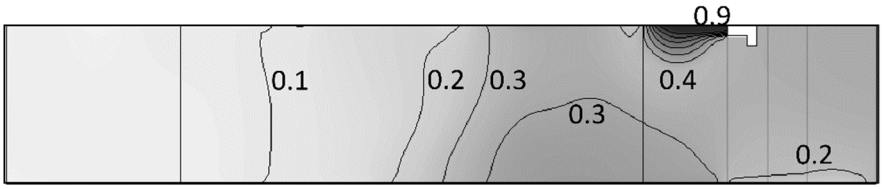

3.2 Changes in the concentration of each Table standardized by A1

The turbulence model was the standard k–ε model; The scheme is Quick and the exhalation model is a passive scalar. The number and duration of exposures were reported in primary infected individuals and in Tables A, B, C, and other tables in which secondary infections occurred. Tables A, B, C and other tables in **Fig. 8** show the same monitoring points as in the experiment. **Fig. 9** shows the effects of all elements standardized by A1 and the concentration transitions in each table. Table A shows the decay tendency and damping effect of each element after the concentration increases until the visit to the store for 82 minutes. The dotted line shows the case where the concentration transition is compared with the collection rate and gravity sedimentation to investigate the effect of inactivation. Since there are temporary infected persons in Table A, it was confirmed that Table B and Table C showed the maximum attenuation effect and were affected by inactivation. The other tables also aimed to reduce the inactivated concentration and had no effect. Including the analysis results of SVE3 and SVE4 above, Tables A, B, and C show that when the ventilation efficiency decreases, the formation of a non-uniform concentration field and the circulation airflow of the air conditioner occur.

Fig. 8 - Monitoring points for tables A, B, C, and other tables

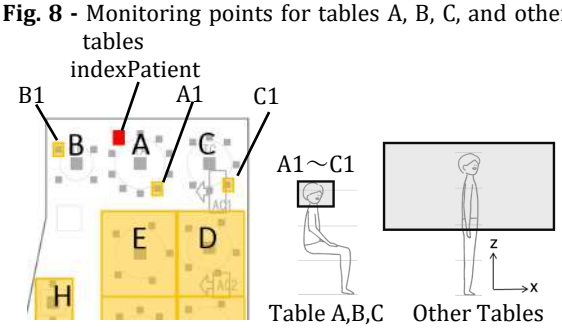

Fig. 9 - Changes in the concentration of each Table standardized by A1

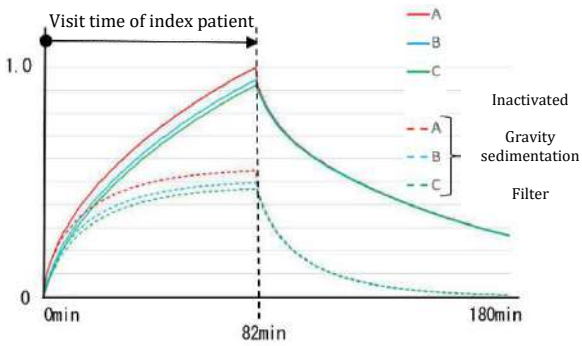

4. Conclusions

In real space, the analysis result of ventilation efficiency by SVE3 was effective because it is displayed in the local cluster generation space area. SVE4 shows the contribution rate of each air conditioner, air supply port, and exhaust port to the space. In order to control the indoor air environment locally and rationally, it was effective to specifically evaluate the range of the force of the blowing airflow. These ventilation efficiency assessments are useful for planning layout plans, suggestions for improving existing buildings, and suggestions for air conditioning and ventilation. Assuming a practical level, we adopted the Euler method passive scalar in consideration of its spread. The difference from previous studies was the difference in Quanta concentration. In the future, we believe that it will be necessary to compare the passive scalar method of the Euler method, which is a respiratory model approach, with the Lagrange method in the infection control flow. In addition, it is confirmed in Tables D to Q that no secondary infection has occurred.

5. References

[1] Riley EC, Murphy G, Riley RL. Airborne spread of measles in a suburban elementary school. Am. J. Epidemiol. 1978; 107: 421-432

[2] REHVA COVID-19 Ventilation Calculator for estimation of ventilation effect on COVID-19 airborne infection, https://www.rehva.eu/covid19-ventilation-calculator,2022

[3] This is not a citation, it is a comment. It seems that two papers are referenced ("2020a, b") Possibly, these are:
Buonanno, G., Stabile, L. and Morawska, L., 2020. Estimation of airborne viral emission: Quanta emission rate of SARS-CoV-2 for infection risk assessment. Environment international, 141, p.105794.
Buonanno, G., Morawska, L. and Stabile, L., 2020. Quantitative assessment of the risk of airborne transmission of SARS-CoV-2 infection: prospective and retrospective applications. Environment international, 145, p.106112.

[4] Lu et al.: COVID-19 Outbreak Associated with Air Conditioning in Restaurant, Guangzhou, China, 2020, Emerging Infectious Diseases, Vol/26, No.7 July 2020 Research Letter

Effects of airing behaviours on bedroom air pollutants during sleep

Chenxi Liao [a], Xiaojun Fan [b], Mariya Petrova Bivolarova [b], Anna Mainka [c], Chandra Sekhar [d], Jelle Laverge [a], Li Lan [e], Mizuho Akimoto [f], Pawel Wargocki [b]

[a] Department of Architecture and Urban Planning, Ghent University, Belgium, Chenxi.Liao@UGent.be, Jelle.Laverge@UGent.be

[b] Department of Environmental and Resource Engineering, Technical University of Denmark, Denmark, xiafan@byg.dtu.dk, mbiv@byg.dtu.dk, paw@byg.dtu.dk

[c] Department of Air Protection, Faculty of Energy and Environmental Engineering, Silesian University of Technology, Poland, Anna.Mainka@polsl.pl

[d] Department of the Built Environment, National University of Singapore, Singapore, bdgscs@nus.edu.sg

[e] Department of Architecture, School of Design, Shanghai Jiao Tong University, Shanghai, China, lanli2006@sjtu.edu.cn

[f] Department of Architecture, Waseda University, Japan, mizuho.akimoto@gmail.com

Abstract. Higher ventilation rates were verified to have a positive impact on indoor air quality and therefore benefit sleep quality. However, how does ventilation influence bedroom air quality if the outdoor air quality is poor? Whilst ventilation helps to reduce indoor pollution it inadvertently brings outdoor pollution indoors, such as NO_2, which is from vehicular emission. In this study, we collected the info of window and door status during sleep and measured carbon dioxide (CO_2), nitrogen dioxide (NO_2), volatile organic compounds (VOCs) and particulate matter ($PM_{2.5}$ and PM_{10}) among 38 bedrooms while occupants were sleeping during nights. Meanwhile, the air change rate (ACR) was calculated. The experiments were conducted in the heating season (September to December 2020) in the capital region of Denmark. The median values were 981.8 ppm (mean CO_2 level during sleep), 0.6 h^{-1} (ACR), 3.4 $\mu g \cdot m^{-3}$ (NO_2), 166.2 $\mu g \cdot m^{-3}$ (VOCs), 11.0 $\mu g \cdot m^{-3}$ (PM_{10}) and 2.8 $\mu g \cdot m^{-3}$ ($PM_{2.5}$). CO_2 levels were positively correlated with VOCs levels, whereas negatively correlated with NO_2 levels in bedrooms. ACR was also negatively correlated with VOCs. CO_2 levels were significantly higher whereas NO_2 levels were lower with both window and door closed compared to them with either window or door open. With higher ventilation rates, while occupants would be less exposed to indoor pollution of VOCs, they would be increasingly exposed to NO_2. Future studies of bedroom ventilation and sleep quality should consider outdoor air quality.

Keywords. pollutant, indoor air quality, CO_2, air change rate, NO_2, VOCs, PM, window, door.
DOI: https://doi.org/10.34641/clima.2022.128

1. Introduction

Indoor air quality (IAQ) is influential to sleep quality among human beings [1-9]. Subjective assessment of bedroom IAQ or measurement of CO_2 (only as a marker of ventilation) is typically considered as the criteria of IAQ for the majority of the studies regarding the association between bedroom IAQ and sleep quality. A recent study reviewed 15 studies with 133,695 subjects involving the association between ambient air pollutants and sleep quality. That epidemiological and experimental evidence underlines that exposure to ambient air pollutants, such as nitrogen dioxide (NO_2), particulate matter (PM_{10} and $PM_{2.5}$, particles with a diameter below 10 and 2.5 μm, respectively), might have detrimental effects on sleep quality [10]. Nevertheless, these air pollutants were generally not considered when it comes to the effects of IAQ on sleep quality. There are also limited studies involving how ventilation impacts bedroom IAQ.

Mattress dust, mattress foam and covers, pillows, and bed frames can emit a variety of volatile organic compounds (VOCs), which are also essential to understand the occupant exposure on them during sleep [11].

Canha et al. (2021) [12] reviewed bedroom IAQ in real-life conditions based on 22 articles from 2003 to

Copyright ©2022 by the authors. This conference paper is published under a CC-BY-4.0 license.

2020. 77% of the studies reported CO_2 levels, followed by $PM_{2.5}$ and PM_{10}, while only 18% of the studies reported volatile organic compounds (VOCs) or other air pollutants. 86% of studies reported $PM_{2.5}$ levels higher than the air quality guideline of the World Health Organisation (WHO, 2010) of 10 $\mu g \cdot m^{-3}$. However, no specific info regarding NO_2 levels in bedrooms was reported by previous studies.

Canha et al. (2017) also assessed the IAQ during sleep under different ventilation patterns. The highest levels of CO_2, VOCs, PM_{10} and $PM_{2.5}$ were found under the ventilation setting with door and window closed in summer in Portugal. The other 3 scenarios of natural ventilation in the bedroom were either window or door open [13].

The present study aimed to examine four air pollutants (NO_2, VOCs, PM_{10} and $PM_{2.5}$) and the impact of ventilation on bedroom IAQ. A marker of ventilation – CO_2, air change rate and "window and door status" during sleep were parameters or factors of ventilation in this study.

2. Method

2.1 Experimental design

Field measurements of bedroom environmental parameters were conducted from September to December 2020 in the capital region of Denmark. The monthly average outdoor temperature in the capital region of Denmark during the experiment period was 15.1 °C (3.5 – 26.9 °C) September, 11.2 °C (1.6 – 18.6 °C) October, 8.1 °C (-1.4 – 17.2 °C) November, and 4.8 °C (-4.5 – 9.4 °C) December [14].

2.2 Measurements

Bedroom environmental parameters were measured using an instrument box that was delivered to the participants on Sundays during the experiment period along with, the instructions and a consent form. The instrument box contained the devices of FLOW (Plume Labs, France) and GMW22 (Vaisala, Finland) and the sleep tracker. The participants were asked to place the box about one meter away from the head at the same height as the bed during sleep.

The concentrations of air pollutants were determined by FLOW, an inexpensive (< $200) personal air pollution device that tracks air quality in its immediate surroundings. In 60-second intervals, FLOW provides an estimate of the major air pollutants NO_2, VOCs, PM_{10} and $PM_{2.5}$. According to the manufacturer, the tests obtained by the reference devices in laboratory conditions point to the coefficients of correlation in the range 84% to 99% for NO_2, 68% to 72% range for VOCs, 87% to 95% for PM_{10} and 92% to 97% for $PM_{2.5}$. CO_2 concentrations were measured by GMW22.

Bedtime and wake-up time was recorded by the sleep tracker of Fitbit Alta. Fitbit, which determines awakenings and sleep stages based on movement and cardiac sensors [15], was reported to have good agreement with polysomnography, a gold standard to measure sleep quality, in differentiating wakefulness from sleep [16].

The participants were asked not to enter the bedroom for at least half an hour the next morning after leaving and keep the windows and door the same status as they were sleeping since air change rates (ACRs) would be calculated by the CO_2 decay in the morning.

In addition, the window and door status of "open" and "closed" during sleep was asked to be recorded the second morning of sleep.

2.3 Statistical analysis

Mean levels of the environmental parameters during sleep were calculated based on bedtime and wake-up time.

The Mann-Whitney *U* test was used to analyse the difference of environmental parameters between the different window and door status. Spearman's correlation coefficients were used to analyse the correlations between any two of the variables.

Statistical analyses and plots were performed by using "scipy" and "matplotlib" packages in Python (version 3.7.3). All analyses were considered statistically significant when the *p*-value was less than 0.05 (2-tailed).

3. Results & discussion

The levels of environmental parameters of 38 bedrooms were measured. The results are represented from three parts, which are bedroom ventilation, bedroom air pollutant, and correlation of bedroom ventilation and air pollutants. Statistical descriptions of the parameters and their levels between window and door status are displayed.

3.1 Bedroom ventilation and airing behaviours

Tab. 1 shows the statistical description of mean CO_2 level and air change rate (ACR) during sleep. The median CO_2 level during sleep was 981.8 ppm with an interquartile range (IQR) between 638.0 and 1547.6 ppm. The median ACR during sleep was 0.6 h^{-1} (IQR, 0.3 – 1.5 h^{-1}).

CEN standard specifies total ventilation (including infiltration) of 0.6 h^{-1} (CO_2 level of 1250 ppm) and 2.0 h^{-1} (1000 ppm) for whole dwellings and bedrooms, respectively, for Category (Cat.) II [8], which is the normal level used for operation and design [17]. However, the majority of the bedrooms did not achieve the required ACR, and CO_2 levels of more than half of the bedrooms exceeded 1000 ppm. Overall, IAQ in bedrooms based on CO_2 levels or ACR during sleep was generally poor.

Tab. 1 – Statistical description of CO_2 and air change rate (ACR) during sleep.

	Mean	Std.	min	Percentile			max
				25th	50th	75th	
Mean CO_2 (ppm)	1305.3	942.4	427.5	638.0	981.8	1547.6	4803.7
ACR (h^{-1})	1.1	1.3	0.1	0.3	0.6	1.5	4.9

Regarding bedroom airing behaviours during sleep, 31.6% of the participants slept with both window and door closed, while 68.4% slept with either window or door open. Fig. 1 and Fig. 2 show the mean CO_2 levels and air change rate (ACR) of two "window and door status" during sleep. As expected, mean CO_2 levels during sleep were significantly higher with window and door closed, compared to them with either window or door open. However, no significant difference between the two "window and door status" was found, although the ACRs were generally higher with either window or door open.

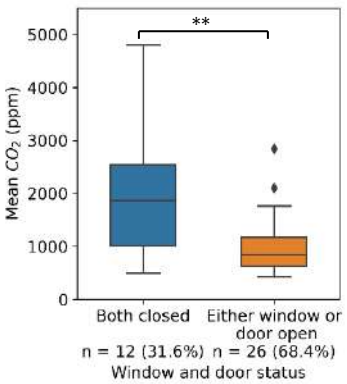

Fig. 1 – Mean CO_2 levels between two "window and door status" during sleep. ** *p*-value < 0.01.

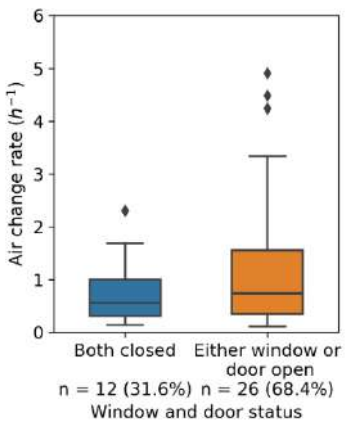

Fig. 2 – Air change rate between two "window and door status" during sleep.

3.2 Bedroom air pollutants

Tab. 2 shows the statistical description of bedroom pollutants during sleep. The median NO_2, VOCs, PM_{10} and $PM_{2.5}$ levels during sleep were 3.4 ppb (IQR, 1.7 – 7.1 ppb), 166.2 ppb (146.7 – 204.0 ppb), 11.0 μg·m^{-3} (7.1 – 36.4 μg·m^{-3}) and 2.8 μg·m^{-3} (2.3 – 7.1 μg·m^{-3}), respectively.

The WHO (2021) reported recommended a long-term $PM_{2.5}$ air quality guideline (AQG) level of no more than 5 μg·m^{-3}, PM_{10} no more than 15 μg·m^{-3}, and NO_2 no more than 10 ppb [18]. The WHO did not recommend AQG value for VOCs, while a previous study reported the reference value was 600 ppb from the Portuguese air quality standard [12]. Based on these standards, the NO_2, VOCs, PM_{10} and $PM_{2.5}$ levels were acceptable in the majority, all, more than half of the bedrooms, respectively.

Tab. 2 – Statistical description of bedroom pollutants during sleep.

	Mean	Std. Dev.	min	Percentile			max
				25th	50th	75th	
NO_2 (ppb)	5.7	5.9	0.2	1.7	3.4	7.1	30.2
VOCs (ppb)	187.7	80.9	84.1	146.7	166.2	204.0	445.9
PM_{10} (μg·m^{-3})	24.5	26.0	3.9	7.1	11.0	36.4	99.4
$PM_{2.5}$ (μg·m^{-3})	5.0	4.0	2.0	2.3	2.8	7.1	19.5

VOCs, volatile organic compounds; PM, particulate matter.

Fig. 3 shows the mean levels of four air pollutants. Only NO_2 levels were significantly different between the two "window and door status". Higher concentration with either window or door open point to the significant influence of outdoor or indoor sources other than the bedroom (e.g. kitchen or garage). The median values of mean VOCs, PM_{10} and $PM_{2.5}$ with window and door closed was slightly higher compared with it with either window or door open. However, the difference was not statistically significant.

Opening doors or windows had an effect on CO_2 levels indicating that there was an improved dilution, whereas VOCs, PM_{10} and $PM_{2.5}$ were not significantly different between the two window and door status since the dilution could be due to outdoor air or air from other parts of the dwellings having lower CO_2 levels than bedrooms at night. This and other mixed factors influencing the effects of window and door status on air pollutants levels would be one of the reasons why no significant differences of VOCs, PM_{10} and $PM_{2.5}$ levels between the window and door status were shown in Fig. 3.

Although NO_2 levels were significantly higher with either window or door open, the levels were still below 10 ppb for most of the bedrooms.

Fig. 4 shows the mean NO_2 levels during sleep among different housing locations and "window and door status". The NO_2 level was significantly higher among bedrooms with either window or door open (urban, 6.8 ppb (4.0 – 13.3 ppb); rural, 5.5 ppb (2.7 – 8.9 ppb)), compared to the bedrooms located in rural areas with window and door closed (1.8 ppb (1.3 – 3.0 ppb)). Window and door status had a more dominant impact on NO_2 levels than housing areas.

A.

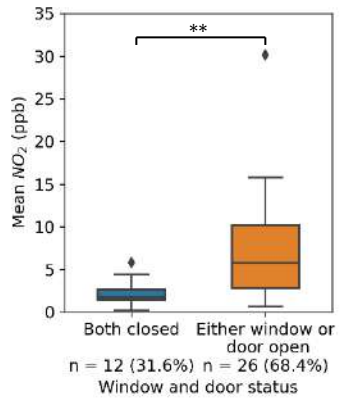

B.

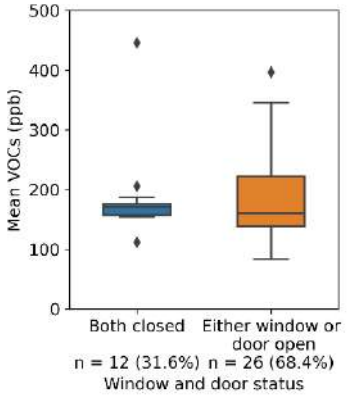

C.

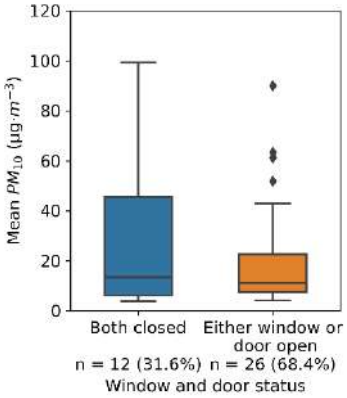

D.

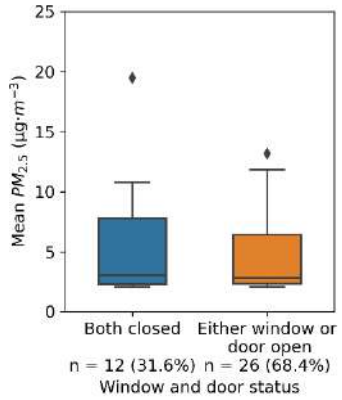

Fig. 3 – Mean levels of indoor pollutants during sleep between two "window and door status". A, NO_2; B, VOCs; C, PM_{10}; D, $PM_{2.5}$. NO_2, nitrogen dioxide; VOCs, volatile organic compounds; PM, particulate matter. ** *p*-value < 0.01.

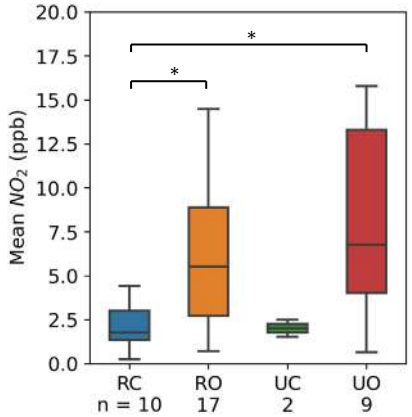

Fig. 4 – Mean NO_2 levels during sleep among different housing areas and "window and door status". RC, rural + window and door closed; RO, rural + either window or door open; UC, urban + window and door closed; UO, urban + either window or door open. ** *p*-value < 0.01.

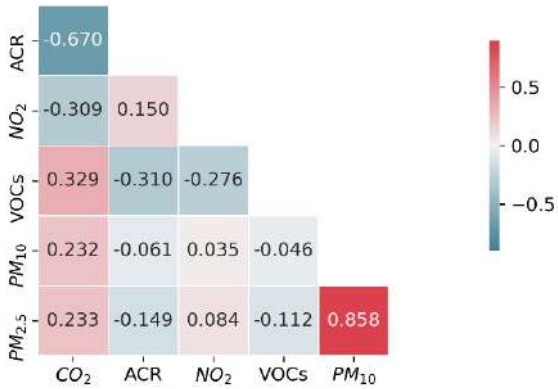

Fig. 5 – Spearman's correlation coefficients between any of the two parameters of bedroom ventilation (CO_2 and ACR) and air pollutants (NO_2, VOCs, PM_{10} and $PM_{2.5}$). ACR, air change rate; NO_2, nitrogen dioxide; VOCs, volatile organic compounds; PM, particulate matter.

3.3 Correlation of bedroom ventilation and air pollutants

Fig. 5 shows the correlation between any of the two parameters of bedroom ventilation and air pollutants. CO_2 levels were moderately correlated with ACR (*p*-value < 0.05) and weakly correlated with VOCs (*p*-value < 0.05) and NO_2 levels (*p*-value < 0.1). ACR was only weakly correlated with VOCs (*p*-value < 0.1).

PM_{10} and $PM_{2.5}$ levels were highly correlated (*p*-value < 0.05), while NO_2 and VOCs levels were weakly correlated (*p*-value < 0.1).

The correlations in Fig. 5 could be influenced by many other factors as well. For example, opening doors might not change $PM_{2.5}$, PM_{10} or VOCs if sources were other places than the bedroom. Estimation of ACR might have errors and could be

inaccurate. This might explain some weak correlations.

CO_2 decay and the reference of ambient CO_2 levels were utilized to calculate ACR. However, there are uncertainties by this method since a mix of outdoor CO_2 levels and the other parts of the dwellings could be the reference instead of the ambient CO_2 levels. A more accurate method to calculate ACR should be used in future studies. Future studies should figure out the correlation between bedroom ACR and air pollutants by using a more accurate method.

Previous studies performed the association between bedroom ventilation (IAQ) and sleep quality mostly using CO_2 as a marker of ventilation [1-9]. However, that the relevant contaminants of VOCs and the other pollutants measured in the present study were only weakly or even not correlated with CO_2 levels in the present study stipulates that CO_2 is a poor marker of VOCs levels, as well as the other pollutants measured in this study.

3.4 Strengths and limitations

Although the present study reported the levels of four air pollutants in the occupants' bedrooms during sleep, this work was a relatively small study with only 38 bedrooms. The uncertainties of ACR could not be captured. Only roughly correlations were made and other factors were not adjusted. Ventilating bedrooms by opening windows or doors could be with outdoor air or the air coming from other parts of the dwellings, while it was uncertain. These limitations could influence the outcomes.

4. Conclusion

The levels of CO_2, air change rate (ACR), NO_2, VOCs, PM_{10} and $PM_{2.5}$ were measured in bedrooms during sleep in the heating season in Denmark. The infiltration of NO_2 into bedrooms is significant and thus it should be included in future research. CO_2 levels were only weakly correlated with VOCs levels in bedrooms during sleep, while not correlated with the other pollutants. ACRs were only correlated with VOCs in the present study.

Air pollutants potentially related to sleep quality, such as PM and NO_2, are necessary to be measured when it comes to the topic of bedroom IAQ (and its effects on sleep quality). Sleep parameters will be included in our future analyses and the results will be reported later.

5. Acknowledgement

The authors would like to thank all the participants. This work was supported by the ASHRAE research project on bedroom ventilation and sleep quality [grant number 1837]; VLAIO research project on smart ventilation [grant number HBC.2020.2520]; the Research Foundation – Flanders (FWO), Belgium [grant number V409120N]; the National University of Singapore [financial support for Chandra Sekhar during his sabbatical visit to DTU, September 2019 – February 2020]; the China Scholarship Council (CSC) and DTU Civil Engineering Department [financial support for Xiaojun Fan of his PhD study]; the National Agency for Academic Exchange of Poland [grant number PPI/APM/2018/1/00004 for financial support for Anna Mainka during her visit to DTU, August – September 2021] and Fonden af 20. december (155808-15) for the scholarship to Assoc. Prof. Pawel Wargocki.

6. References

[1] Strom-Tejsen P., et al. The effects of bedroom air quality on sleep and next-day performance. Indoor Air. 2016;26(5):679-686.

[2] Mishra A.K., et al. Window/door opening-mediated bedroom ventilation and its impact on sleep quality of healthy, young adults. Indoor Air. 2018;28(2):339-351.

[3] Liao C., et al. A survey of bedroom ventilation types and the subjective sleep quality associated with them in Danish housing. The Science of the total environment. 2021;798:149209.

[4] Liao C., et al. Effects of window opening on the bedroom environment and resulting sleep quality. Science and Technology for the Built Environment. 2021;27(7):995-1015.

[5] Xiong J., et al. Associations of bedroom temperature and ventilation with sleep quality. Science and Technology for the Built Environment. 2020:1-11.

[6] Laverge J., A. Janssens. Analysis of the influence of ventilation rate on sleep pattern.

[7] Zhang X., et al. Associations of bedroom air temperature and CO2 concentration with subjective perceptions and sleep quality during transition seasons. Indoor air. 2021.

[8] Sekhar C., et al. Bedroom ventilation: Review of existing evidence and current standards. Building and Environment. 2020:107229.

[9] Akimoto M., et al. Reviewing How Bedroom Ventilation Affects IAQ And Sleep Quality. ASHRAE Journal. 2021;63(4):56-58,60.

[10] Cao B., Y. Chen, and R.S. McIntyre. Comprehensive review of the current literature on impact of ambient air pollution and sleep quality. Sleep Medicine. 2021;79:211-219.

[11] Boor B.E., et al. Human exposure to indoor air pollutants in sleep microenvironments: A literature review. Building and Environment. 2017;125:528-555.

[12] Canha N., et al. How Is Indoor Air Quality during Sleep? A Review of Field Studies. Atmosphere. 2021;12(1).

[13] Canha N., et al. Indoor air quality during sleep under different ventilation patterns. Atmospheric Pollution Research.

2017;8(6):1132-1142.
[14] DMI T.D.M.I. Weather archive. 2020.
[15] Beattie Z., et al. Estimation of sleep stages using cardiac and accelerometer data from a wrist-worn device. Sleep. 2017;40:A26-A26.
[16] Haghayegh S., et al. Accuracy of Wristband Fitbit Models in Assessing Sleep: Systematic Review and Meta-Analysis. Journal of Medical Internet Research. 2019;21(11).
[17] Aguilera Benito P., et al. Ventilation for Residential Buildings: Critical Assessment of Standard Requirements in the COVID-19 Pandemic Context. Frontiers in Built Environment. 2021;7(113).
[18] World Health Organization. WHO global air quality guidelines: particulate matter ($PM_{2.5}$ and PM_{10}), ozone, nitrogen dioxide, sulfur dioxide and carbon monoxide. 2021, Geneva: World Health Organization.

Holistic operating room hygiene control for air and surface cleanliness

Kim Hagström[a], Ismo Grönvall [a]

[a] Halton Technology, Halton Oy, Kausala, Finland

Abstract. Surgical site infections pose a severe risk for patients entering in a surgery. Surgical site infections are caused when microbes are entering to operation wound during surgery. Treatment of surgical site infections is very difficult and expensive, and it is expected that this will be even more difficult in the future due increased number of antibiotic resistant bacteria, such as MRSA, in hospitals.

The microbes may penetrate to patient wound principally through two routes: through air in a form of airborne microbes or by physical contact. In the later case the infection may be caused if an operating person touch a contaminated surface before accessing to the wound. Thus, to minimize surgical site infections it is utmost important to ensure that both operating room air and surfaces are maintained clean both during the operation and between consecutive operations.

The air cleanliness may be ensured with an appropriate ventilation system that is able to react according to surgical schedule also between operations. A throughout surface cleaning by cleaning staff is typically applied at the end of the day and additional cleaning takes place between operations. However, mechanical cleaning may leave some surfaces that are not fully cleaned and especially surfaces that are hard to reach or have complicated structures may remain untouched. To ensure better cleaning result it is possible to back up mechanical cleaning with a radiant disinfection. A blue light-based disinfection method can provide a safe to people cleaning both during operating room downtime and also between operations.

A novel, holistic integrated operating room cleaning system is developed to address simultaneously challenge of both air and surface cleaning. This system is managed by an intelligent control system that can automatically manage both air and surface cleaning processes through seamless interfacing with medical operations management system. Coordinated dimensioning is described to provide simultaneously optimal cleaning result of both airborne and surface bacteria. It is also described how the control system is set to provide cleaning cycles, personnel safety and comfort, and energy efficiency according to operational schedule.

Keywords. Operating Room, Hygiene control, Integrated design, Indoor environment
DOI: https://doi.org/10.34641/clima.2022.342

1. Introduction

Operating rooms are used for surgical interventions to human patients. The focus is to provide safe environment for operations to minimize the adverse health effects caused to the patient during operation. In relation to indoor environment and ventilation this means a clean environment with low level of airborne microbes during operation that could cause an infection to the patient. The level of cleanliness needed is depending on the type of the operation and the general health condition of the patient.

In modern hospitals it is quite common to design most of the operating rooms for general use covering wide variety of operations, while specialized operating rooms are less in numbers. This necessitates the need to understand the different operational needs, when defining the design targets. Operating rooms with extensive use or imaging medical devices, so call hybrid operating

Copyright ©2022 by the authors. This conference paper is published under a CC-BY-4.0 license.

rooms, enabling minimally invasive surgeries are increasing in numbers as well.

This paper discusses on the design challenges and infection routes in modern operating rooms and describes a holistic building services system that is designed taken into account the acknowledged challenges.

2. Operating room design challenge

Traditional thinking has been that the actual operational activity (clean zone) is taking place in the centre of the room, while most of the room is less used. This, however, is too simplistic approach in modern operating rooms, where the operational activity and the sterile instruments may occupy an extensive area of the room depending on the type of the operation.

Medical Installations occupy space in the ceiling and cause obstruction for airflow in the operation room. It is important to understand the medical layout and analyse it's effect to the design. The challenge does not only concern newbuild, but also the life-cycle of operation rooms – medical processes and development of medical technology drive need for flexibility for room renewal.

Thus, in modern operating rooms it is imperative to design ventilation and all building services systems in such a way that maximum space is given to current and future medical activities and installations. Ideally systems should also be made adaptable to medical operations rather than set requirements for medical staff.

A more detailed description of Operating room design challenges and design process is given in /1/

3. Infection routes in operating rooms

The main source of contamination in operation rooms is operating personnel or other persons entering operating room during and between operations. Other potential sources relating to ventilation is air leakage, especially during door openings. Eventual introduction of contaminated equipment and supplies to operating environment should be eliminated by medical protocols.

Infection carrying particles have multiple routes to patient wound, where they can potentially cause an operational infection.

The principal routes how infection carrying particles may enter into operating room air and ultimately to patient wound are illustrated in figures 1 and 2.

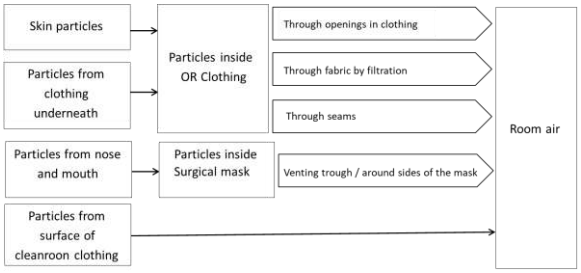

Fig. 1 – Airborne contamination routes in operating environment

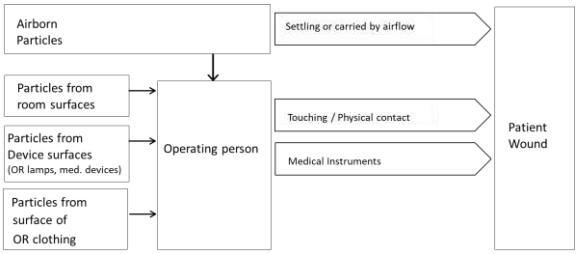

Fig. 2 – Potential routes for infectious particles to patient wound.

It is evident that for operative infection both airborne and physical contact routes are important. Both of these can be impacted by means of ventilation, but it is also important to ensure that surface cleanliness is properly maintained.

Surface cleanliness in operating rooms are carried by physical manual cleaning at the end of working day and between operations according to planned schedules in hospitals. Despite distinct protocols manual work has always natural variance in its quality and especially complex structures for example in medical devices or lamps may leave spots that are not so easily reachable and may not get as well cleaned. This quality variance was recognized for example in Norway where the quality of hospital bed cleaning was studied.

4. Operating room ventilation principles

So called laminar flow ceilings have been common in ultraclean operating rooms, while for standard operation rooms more simple mixing ventilation systems have been commonly used. In traditional thinking there has been very big difference between two approaches and for example the airflow rate has typically been 5 to 6 times bigger in laminar flow systems.

The latest development in operating rooms, such as use of whole room area, new medical practices and equipment have, however, challenged old mantras and brought to stage the challenges and needs that traditional systems are no able to meet. In addition to cleanliness requirements in current operating room design maybe the most important customer need is flexibility, both operational and for unspoken future upgrade needs during life cycle. Also, the need to ensure staff wellbeing and comfort

is gaining higher emphasis.

To address both traditional and future needs of ultra-clean operations a new ventilation approach, controlled dilution ventilation system was developed. Figure 3 shows an illustration of such ventilation system, a more detailed description and information about the performance validation can be found from /2/.

Fig. 3 – Illustration of controlled dilution flow system airflow pattern.

One of the significant new advantages of the new ventilation approach is that it leaves much more ceiling space and flexibility for medical installations than traditional laminar flow system.

5. Surface disinfection in operating rooms

As mentioned earlier mechanical cleaning may leave some surfaces that are not so well cleaned, which may serve as bases for microbial growth.

Currently there are advanced technologies that may be used to enhance surface cleaning and disinfection. In cleanrooms for example UV -light fixtures and gas cleaning, such as H2O2, has been used to enhance the room cleanliness. Gas cleaning has been typically used as a periodic disinfection method, while UV – light has sometimes been used more for daily cleaning during shut-down period. The advantage of irradiation is that it can penetrate also to areas that may not be easily reachable by manual cleaning.

Use of traditional UV – light for such purpose is not trouble free, because precautions have to be implemented to protect users from entering the space during cleaning period, which limits its usage. UV has also effect on surfaces and materials that may wear out due to UV irradiation.

One, very promising new technology is to use visible blue light for surface disinfection. It is proven that specific wavelengths of visible blue light are capable of eliminating microbes from the surfaces. /3,4/ Figure 4 illustrates the efficiency of photon disinfection in inactivation of *Staphylococcus aureus* (ATCC 6538) at low intensity (blue light 0,7 mW/cm2).

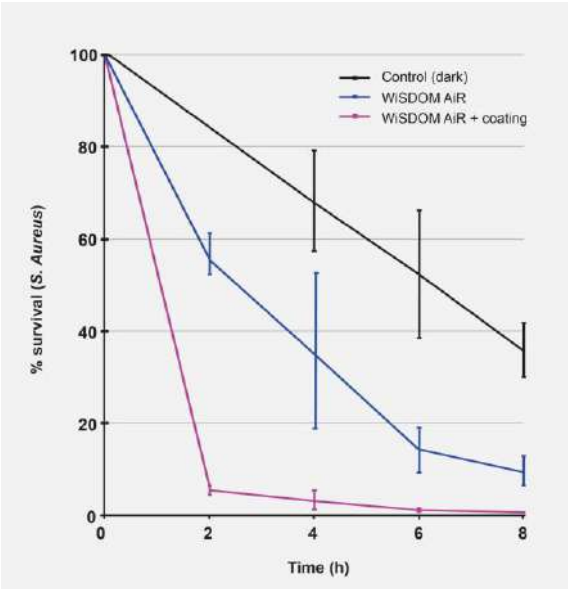

Fig. 4 – Blue light efficiency in inactivation of S. aureus bacteria (blue curve - blue light only, purple curve – blue light with catalytic coating)/4/

The advantage of blue light compared to UV irradiation is that blue light is not causing any harm for people nor surfaces. Thus, even if it is not recommended to use strong blue light irradiation during occupation it is not dangerous to enter the space. This makes blue light much more usable in operating rooms, where the entrance control is not as tight as in cleanrooms and allows the use of such disinfection except during shut-down period also during the day between operations.

As a next evolution of future fit operating room system a blue light disinfection system has been integrated into control dilution flow ventilation terminal in such a way that both ventilation and surface disinfection performance are simultaneously optimized. By integration it is possible to add more value for the end users without using even more critical ceiling space to be used for medical installations. A module of integrated unit is shown in Figure 5.

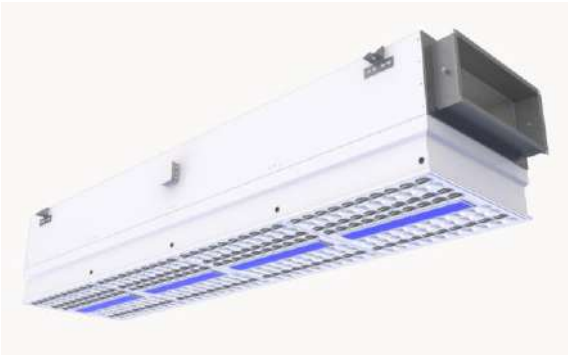

Fig. 5 – Integrated terminal for operating room ventilation and surface cleaning

The blue light disinfection system was designed to provide 99% disinfection performance during 3,5 hours in the whole operating room and even in 1 hour in the most critical room center. A simulation of the system performance in 7,0m by 8,7m size operating room is shown in Figure 6.

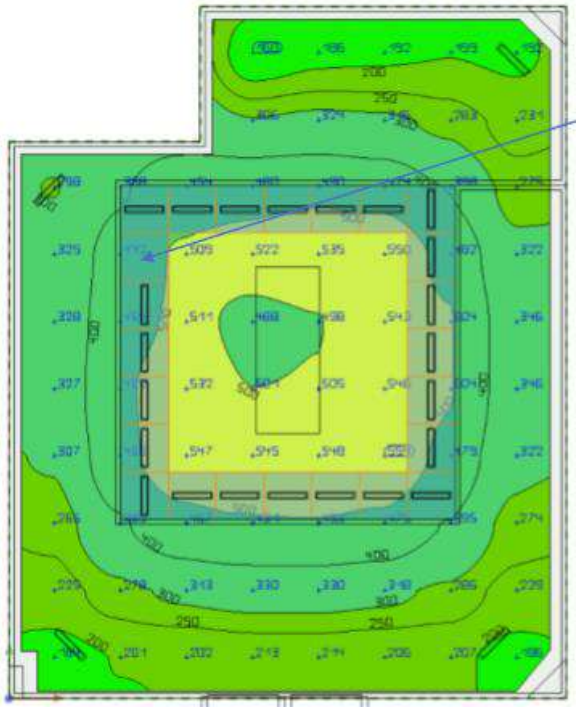

Fig. 6 – Performance of the integrated blue light disinfection system

6. Total OR Environment concept

6.1 Integrated Building services

In addition to ventilation, also general lighting is a major ceiling space occupier in operating rooms. Thus, also integrating also the general OR lighting as part of the integrated disinfection development was taken as a target. This added one more optimisation challenge to ensure that the performance of all utilities, ventilation, surface disinfection and general lighting are functioning according to customer demands. This was solved by developing an integrated light fixture that can provide both high quality general lighting and by changing operational mode also blue-light disinfection.

This was ensured by light simulation and ultimately by measurements of physical installation. An illustration of lighting simulation is shown in Figure 7.

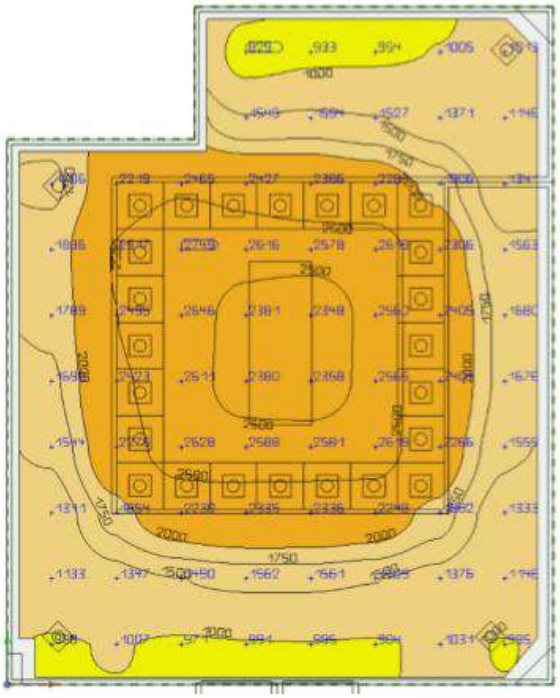

Fig. 7 – General lighting simulation of operating room with integrated building services unit

Available ceiling space with integrated building services unit can be further increased by 20 % compared to disintegrated services, see Figure 8.

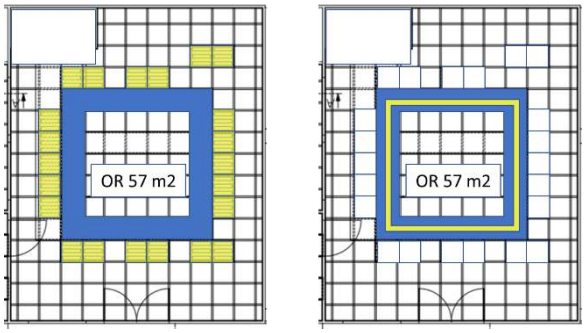

Free area: 40,4 m2 Free area: 48,4 m2

Fig. 8 – Available ceiling space with integrated building services unit compared to disintegrated services. Yellow squares on the left hand layout show the location of separate light fixtures in the ceiling.

6.2 Operating room control system

In earlier stage, a comprehensive on-demand management system integrating predictive cleanliness and controlled dilution flow ventilation system was developed, which enables improved safety and sustainability. /2,5/ With the help of controlled flow principle it is possible to implement safely demand based ventilation also in operating environment. This is made by utilizing the knowledge of the operational clothing quality and it's influence on microbial source strength in operation./6/T o enhance usability of the system it has also been integrated to general operating room

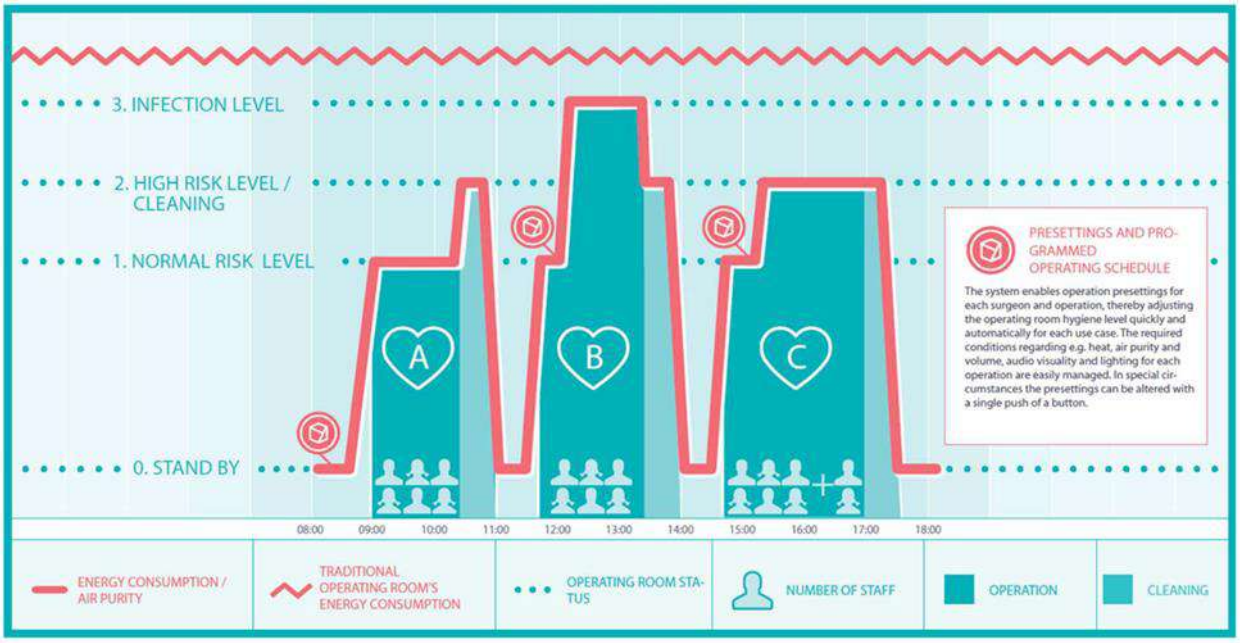

Fig. 9 – Illustration of operation mode based control.

process management system. This integration enables usage of operation mode-based system control by activation of medical personnel depending on their stage of work. The principle of operation mode based control is presented in Figure 9.

This same system can now be extended to control the whole integrated building services system of ventilation, blue-light disinfection, and general lighting, which simplifies the working process of operation room personnel and enables optimal use of room with integrated building services based on the actual operation mode.

7. Acknowledgement

We want to acknowledge our partner Merivaara Oy for integrated control development and partner Led Tailor Oy for joint development of integrated blue light disinfection solution.

8. References

[1] Hagström K., Grönvall I. Operating Room Ventilation. Industrial Ventilation Design Guidebook, Vol 2: Engineering Design and Applications. 2021, ISBN:978-0-12-816673-4; 492-505.

[2] Hagström, K., Grönvall, I., Kaukola, T., & Koskinen, V. (2015). Validation of vita OR space solution using simulated operation, Ventilation 2015 Conference on Industrial Ventilation. Shanghai, China.

[3] Wang, Y., Wang, Y., Wang, Y., Murray, C. K., Hamblin, M. R., Hooper, D. C., & Dai, T. (2017). Antimicrobial blue light inactivation of pathogenic microbes: State of the art. Drug Resistanceupdates. https://doi.org/10.1016/j.drup.2017.10.002

[4] Efficiency of photon disinfection luminaires (LED Tailor, Wisdom Air) in inactivation of Staphylococcus aureus (ATCC 6538). 3rd party laboratory test report, MetropoliLab (FINAS accredited), 2020.

[5] Halton Vita OR VMS technical description.

[6] Ljunqvist, B., & Reinmuller, B. (2013). People as a contamination source, report no. D2013:03. Göteborg, Sweden: Chalmers University of Technology.

Data sharing not applicable to this article as no datasets were generated or analysed during the current study.

Dynamics of metabolic rate in male individuals due to the meal and regular office activities

Dolaana Khovalyg [a], Jiyoung Kwak [a]

[a] Laboratory of Integrated Comfort Engineering (ICE), School of Architecture, Civil and Environmental Engineering (ENAC), Ecole Polytechnique Fédérale de Lausanne (EPFL), Fribourg, Switzerland, dolaana.khovalyg@epfl.ch

Abstract. Metabolic rate is one of the main parameters affecting the thermal balance of the human body and perception of thermal comfort. Typically, we consider a constant value for a specific type of activity (sitting quiet, standing, etc.) despite the time of the day and body built of a person. In this study, we challenged this by undertaking minutely metabolic rate measurements of 3 men in a realistic office layout at 23-27°C operative temperature. The type of activity (sitting and standing quiet work) and their timing were standardized, and the meal ingested (breakfast and lunch) by the participants was also the same. We also measured temporal changes in the heart rate and skin temperature to understand the variation of physiological parameters. A whole day session was split into four 1.5-hour-long sessions, two in the morning (08:30-12:00) and two in the afternoon (13:00-16:30). Thermal comfort between sessions varied within ±1 per ASHRAE seven-point thermal sensation scale, based on the surveys. The metabolic rate varied throughout the day, even for the same activity type, with an apparent effect of the activity performed upon arrival in the morning (e.g., commute to the office) and the thermic effect of food. After a standardized normal-protein lunch, the metabolic rate was about 15% higher for the same activity for all three men. The effect of the prior physical activity on the metabolic rate was smaller than the meal effect. These results revealed that people's metabolic rate is dynamic, and it can be elevated not only because of physical activity but also by diet-induced thermogenesis. All in all, this work is intended to draw attention to the metabolic rate variation in daily life that has been overlooked so far in the field of ergonomics of the indoor environment and to outline possible future perspectives for smart buildings if personalized metabolism could be known.

Keywords: metabolic rate, energy expenditure, indirect calorimetry, thermal comfort, dynamic environment
DOI: https://doi.org/10.34641/clima.2022.412

1. Introduction

It is well known that thermal comfort is defined as "*conditions of mind that express satisfaction with the thermal environment and is assessed by subjective evaluation*" [1]. The satisfaction comes mainly from the thermal balance of the body with the surrounding environment when there is no thermal discomfort that could disturb a person's mind. Predicted Mean Vote/ Predicted Percentage Dissatisfied (PMV/PPD) method typically used to predict thermal sensation considers the energy balance of the person where the metabolic rate (i.e., heat production or energy expenditure), is one of the main parameters driving this balance. Metabolic rate is measured in *met* which is energy expenditure divided by the overall body skin surface area *W/m²* (1 *met* = 58.2 W/m²). International standard ISO 8996:2004 [2] provides different methods (referred to as levels) of determining the metabolic heat production of humans. **Level 1** called "*screening*" is the simplest one, and it provides a classification of metabolic rate values per occupation (method 1A) or per kind of activity (method 1B). **Level 2** is "*observational*"; time-weighted average metabolic rates based on the noted transient activity types are calculated using the classification determined in level 1. Metabolic rate is determined indirectly from heart rate recording in **Level 3** called "*analysis*". Finally, "*expertise*" **Level 4** outlines 3 methods for measuring metabolic rate in humans directly: (4A) based on the oxygen consumption measurements (indirect calorimetry), (4B) using doubly labelled water (applicable for 1-2 weeks of measurements), (4C) direct calorimetry. Level 4 methods are the most precise but the most complex ones, while level 1 is the least accurate but the simplest one to use in practice. Therefore, practitioners and many researchers in the comfort field use *met* values prescribed for various activities in standards ASHRAE 55:2020 [1] and ISO 7730-2006 [3], as listed in **Tab. 1**.

Copyright ©2022 by the authors. This conference paper is published under a CC-BY-4.0 license.

Tab. 1 – Standardized metabolic rates of different activities (*met* values in parenthesis are calculated more precisely by considering 1 *met* = 58.2 W/m²).

Activity type	*met*	W/m²
ISO 7730-2006:		
Reclining	0.8 (0.79)	45
Seated, relaxed	1.0 (1.00)	58
Sedentary activity (office, dwelling, school, laboratory)	1.2 (1.20)	70
Standing, light activity (shopping, laboratory, light industry)	1.6 (1.60)	93
ASHRAE 55-2020:		
Reclining	0.8 (0.77)	45
Seated, quiet	1.0 (1.03)	60
Reading, seated	1.0 (0.95)	55
Typing	1.1 (1.12)	65
Filing, seated	1.2 (1.2)	70
Filing, standing	1.4 (1.37)	80

The standardized values in **Tab. 1** are based on the work by Durin & Passmore (1967) [4], and they were not challenged for nearly 50 years. Recently, Zhai et al. (2018) [5] and Yang et al. (2021) [6] re-evaluated *met* values of typical office activities using indirect calorimetry (level 4A per ISO 886:2004). Measurements on 30 males and 30 females for different office activities at 26°C from Zhai et al. (2018) and sedentary 20 females and 20 males exposed to 14-32°C from Yang et al. (2021) demonstrated that standard *met* values at neutrality did not match with measurements, and metabolic rate was affected by ambient temperature. Although the works fundamentally questioned the *met* values used to design the indoor environment and predict the thermal sensation of occupants, the research methodology did not consider metabolic rate variance potentially due to the time of the day and the meal effect (the meal intake of participants was not standardized).

Generally, the metabolism of humans is comprised of 3 main components (i) resting metabolic rate, (ii) thermic effect of food, (iii) activity-induced thermogenesis [7]. With the current advancements in dynamic HVAC controls and personalized sensing, understanding the dynamics of metabolic rate is an important step forward toward personalized and occupant-centric buildings. While resting metabolic rate largely depends on the relatively constant fat-free mass of individuals [8], time-scale is important for the post-prandial (after-meal) thermogenesis as it is a transient phenomenon, and residuals of metabolism from the previous meal intake superimpose any further activities [9]. Since our understanding of the metabolic rate variation during daily activities is still limited, this work demonstrates *met* values variation that can be observed in 3 males during a full-day experiment imitating typical office routines. To this aim, indirect calorimetry was used for continuous measurements of metabolic rate in recruited participants during sedentary and standing work. The meal was standardized to observe comparable post-prandial effects across participants. In addition, measured metabolic rates of individuals are compared to standard approaches to determining *met* values; thus, demonstrating potential discrepancies when standard methods are used.

2. Methodology

The study was conducted in February 2021, and it was approved by the Cantonal Commission for the Ethics of Research on Human Beings (Switzerland). Hereafter, details of participants, experimental procedures, sensing approach, and surveying are provided.

2.1 Participants

We originally planned to conduct experiments with 3 males and 3 females; thus, 6 participants were recruited. However, the experiments with 2/3 females failed, and only the results for males are provided in this paper. Anthropological characteristics and basal metabolic rate (BMR) of male participants are listed in **Tab. 2**. The body composition analyzer InBody 720 was used for weight, fat-free mass (FFM), and BMR measurements. BMR measured in *kcal* converted to *W/m²* and *met* is also provided in Tab. 2. Two participants S2-S3 were nearly identical in terms of BMI, FFM, and BMR, while S1 was slightly heavier. Nevertheless, the FFM percentage was quite similar in all of them (76-81%). The body surface area (BSA) was determined using the DuBois formulation [10]. Typically, the average BSA of an adult is considered 1.7 m² (1.9 m² for adult males). In our sample size, the BSA of S2 was close to the average one, the BSA of S3 was close to the average for males, and S1 was off the average values.

Tab. 2 – Anthropological characteristics of participants

Parameter	S1	S2	S3
Age (y. o.)	36	29	29
Height (cm)	178	166	175
Weight (kg)	85.6	67.5	73.1
FFM (%)	76.8	81.9	76.7
BMI (kg/m²)	26.8	24.5	23.9
BSA (m²)	2.02	1.73	1.86
BMR (kcal/day)	1790.5	1564.0	1582.3
BMR (W/m²)	42.9	43.8	41.2
BMR (met)	0.73	0.75	0.71

2.2 Overview of the experimental design

The experimental protocol had objectives to determine the day-long dynamics of metabolic rate variation of individuals during typical office activities such as sitting and standing work. Each participant performed a specific sequence of office activities, as listed in the experimental timeline in **Fig. 1,** from 8:30 till 16:30. There were four 1.5- hour sessions in total (2 in the morning and 2 in the afternoon), each session had alternating sitting and standing work, 30 min each. An electric height adjustable desk was used in the study for an easy switch between sitting and standing positions. Participants were allowed to do the work of their choice (2/3 of participants were working on their laptop, while 1 participant was reading and taking notes occasionally). There was a 30-min long morning (10:00-10:30) and afternoon (14:30-15:00) break when a person could have some refreshments of their choice (water, tea, and coffee), the amount of liquid intake was not limited. During the lunch break, a standardized lunch meal was provided. Participants were free to go out of the research facility during the breaks.

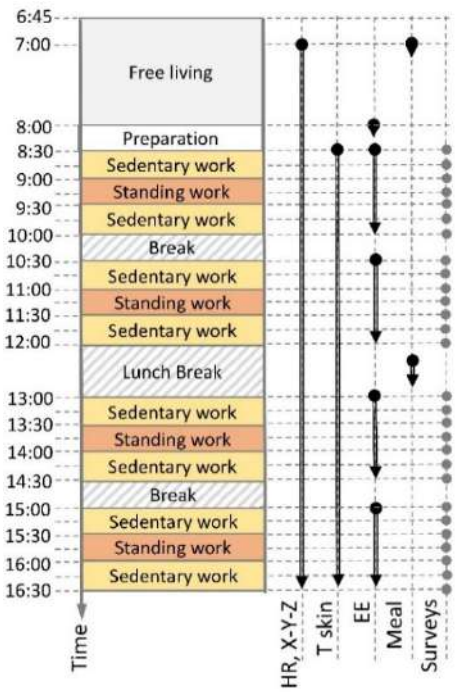

Fig. 1 – Experimental timeline with an indication of activities and measurements.

A day before the experiment, every participant was instructed to avoid any strenuous physical activity, alcohol, and any medication. It was advised to consume a regular-sized evening meal no later than 19:30 and to go to sleep no later than 23:30. On the day of the experiments, subjects were asked to wake up no later than 6:45. Upon arousal, they needed to put on a heart rate monitor and an accelerometer (abbreviated as X-Y-Z in Fig. 1) provided in advance. Participants were instructed to consume at 7:00 a standardized breakfast meal with a glass of water. Subjects were asked to arrive at the research facility by 8:00 on foot or by car/bus. Right upon arrival at the research facility, a participant put on a silicon face mask for metabolic measurements for a few minutes (this session is hereafter called "pre-session"). During this time, a participant completed a short arrival questionnaire. Afterward, a subject was asked to change into the standardized clothing of 0.8 clo (a cotton T-shirt, thick ankle socks, a cotton sweater, cotton jeans, and sneakers were provided, a contribution of the mesh chair was also included). Finally, skin temperature sensors were placed using medical tape at selected locations. After the preparations, a participant was guided inside the experimental office room a couple of minutes prior to 8:30. Once a participant was comfortably seated at the office desk, metabolic rate measurements were restarted. During each experimental session, the participant was alone in the room.

2.3 Sensing overview

Two groups of sensors were used in the study – *wearable sensors* to measure physiological parameters and *environmental sensors* to monitor the environment around participants.

Wearables: Real metabolic rate of each participant was determined using the indirect calorimeter COSMED Quark CPET by sampling oxygen consumption and carbon dioxide production of the person (accuracy of gas sampling ± 3%) and applying Wier's formulation [11]. The frequency of gases sampling was 5 s. Local skin temperature (T_{skin}) was measured using rugged iButton® temperature loggers DS1922L (accuracy ± 0.2°C, calibrated in-house); the temperature at each site was measured every 10 s. We used a 14-point scheme per ISO 9886:2004 [12] to determine the mean skin temperature ($T_{skin,mean}$) variation. The temperature difference between the right chest and the right fingertip ($\Delta T_{chest\text{-}fingertip}$) was used to determine the magnitude of vasomotion and potential deviation of the participant's thermal state from neutrality. Heart rate (HR) was measured by using the wireless ECG recorder Camntech Actiheart 5 every 30 sec.

Environmental sensing: To characterize the thermal environment surrounding the person, operative temperature T_{op} (accuracy ± 0.5 °C) was measured at 12 positions in the vicinity of the participant using two vertical stands. Four sets of sensors at heights of 0.1, 0.6, 1.1, 1.7 m, as suggested by the ISO 7726:1998 [13], were placed on each stand. Each set had a shielded dry-bulb temperature sensor PT100, a globe temperature sensor (a grey ball 38 mm with the PT100 inside), and an omnidirectional anemometer (Sensor Electronic) connected to H HOBO UX120-006M (Onset) data logger. The frequency of measurements was 1 s. The placement of comfort stands is illustrated in **Fig. 2**. Relative humidity was measured in the center of the room using a HOBO U12-012 (Onset). The mean operative temperature (averaged over 12 locations) is used to illustrate the dynamics of the thermal environment during the experiments.

Fig. 2 – Photo of the experimental setup and placement of comfort stands (S window with direct solar exposure, the office desk behind the calorimeter stand)

2.4 Experimental facility and temperature regulation

An experimental office room of 20 m^3 (3 x 6.3 m^2 floor area) was used for mock-up office activities. It had two large windows (N and S oriented). To avoid direct sunlight on participants from the S window, external shades were lowered, and the slats were half-open, as seen in **Fig. 2**. Radiant ceiling panels were used to maintain the temperature setpoint in the room, while fresh air (1.15 ACH) was supplied already pre-conditioned. The initial intention was to keep the operative temperature in the room relatively neutral (around 24^oC). Due to the dynamic variation of solar radiation and significant internal heat gains from the experimental equipment, indoor temperature tended to drift towards higher values (up to 27^oC in some cases) during morning sessions. To avoid significant heating indoors, the side section of the N window was slightly opened after the temperature drift was noted. In terms of airspeed in the room, it was below 0.2 m/s in the vicinity of the participant during all experimental sessions; therefore, there was no risk of the draft.

2.5 Surveys

Thermal comfort votes (TCV) and thermal sensation votes (TSV) were surveyed every 15 min starting 8:30 until 16:30 (**Fig. 1**). There were 7 discrete response options for both questions:

- TSV: cold (-3), cool (-2), slightly cool (-1), neutral (0), slightly warm (+1), warm (+2), hot (+3)
- TCV: very uncomfortable (-3), uncomfortable (-2), slightly uncomfortable (-1), neutral (0), slightly comfortable (3), comfortable (+2), very comfortable (+3).

2.6 Standardized meal

Two standardized normal-protein meals were provided to participants. The *breakfast* consisted of 2 slices of toast (121 kcal) with butter (108 kcal) and jam (49 kcal), and a 200 ml of protein drink (250 kcal). The total energy value was 528 kcal. The *lunch* meal included 1 serving of pasta Bolognese (589 kcal), a pack of whole-grain crackers (172 kcal), and a bottle of orange juice (123 kcal). The total amount of calories was 884 kcal.

2.7 Methods for metabolic rate comparison

The primary method of determining the metabolic rate of people in this study is based on indirect calorimetry. This method is classified as "level 4A, *expertise*" per ISO 8996:2004. For the comparison of the metabolic rate with other simplified methods, we denote as M1 actual metabolic rate measurements converted to W/m^2 (further converted to units of *met*) using the actual BSA of each participant. Four more additional metabolic rate options (M1-M4, M0) were defined. As M2 and M3, we denote metabolic rates calculated based on indirect calorimetry measurements, but with the BSA of an average adult (1.7 m^2) and an average adult male (1.9 m^2), respectively. As M4, we used the "level 3, analysis" approach based on HR measurements which are supposed to be more precise compared to the classification of the metabolic rate based on the activity type. At last, "level 1, *screening*" was considered, denoted as M0, where sedentary work was considered as 1.2 *met* and standing work was considered as 1.4 *met*.

3. Results

First of all, we present the dynamics of parameters from the experiments. This includes metabolic rate and T_{op}, HR, $T_{skin,mean}$, $\Delta T_{chest\text{-}fingertip}$, and TSV & TCV responses. A comparison of metabolic rates determined per different methods is provided afterward.

3.1 Dynamics of experimental data

Experimental results are presented in **Fig. 3.** Seven parameters are plotted as a function of time from 7:30 till 17:00. Four experimental sessions and pre-session (8:00-8:30) are highlighted using different color schemes. Three intervals of different activities types within each session and the break time are also marked. To understand what could be the metabolic rate of individuals upon their arrival to the office, as described in section 2.2, metabolic rate was briefly measured during the pre-session. It was measured for 3 min for a participant S2 (8:00-8:03) and for 8 minutes for participants S1 and S3 (8:00-8:08). The duration of measurements was not standardized; thus, it was not homogenized between participants (the duration was determined ad-hoc). Continuous measurements of T_{op}, HR, $T_{skin,mean}$, and $\Delta T_{chest\text{-}fingertip}$ are also shown during the pre-session and breaks to explain some variation in metabolic rate right afterward.

Metabolic rate: Measured 5-sec data points are interpolated using the 3^d degree of the polynomial

shown as bold lines in **Fig. 3**. It is obvious that the metabolic rate is elevated upon arrival. In participants S1-S2 (all sessions) and S3 (only sessions 1 and 4), we can observe the tendency of the metabolic rate to drop during sedentary work and to increase during standing work. The degree of the drop and increase depends on the time of the day and on the activity prior to the session. During the 1st sitting activity of almost every session, metabolism is elevated, and it gradually drops towards the end of the 30-min session. Once the participant stands up, the metabolic rate increases reaching its peak in the middle of the 30-min long activity. During the sitting work after the standing one, the metabolic rate reaches the minimum of the session. The trends are the most pronounced during morning session 1, which can be explained by the elevated metabolic rate of participants upon arrival to the facility on foot. The metabolic rate during the morning session 2 is lower compared to the 1st one, perhaps, due to the reduced activity in-between and faded thermic effect of food past 3.3 hours after the breakfast intake. An increase in the metabolic rate during the 3d session (after lunch) is due to the combination of the increased activity prior to the session (all participants went outside the facility during the lunch break) and the thermic effect of the lunch meal. We observe similar dynamics during the last session as in the 2nd session but at higher metabolic rate values. Elevated metabolic rate in the afternoon compared to the morning session is due to the thermic effect of a larger meal compared to the breakfast meal. The spikes in raw *met* values within the sessions are due to the participants changing their posture from sitting to standing and from standing to sitting.

Heart rate: HR variation during experimental sessions is similar to metabolic rate dynamics. It is increased during standing work, and it is decreased during sitting work. HR is slightly lower during the 2nd session compared with the 4th one in participants S1 and S3, while it is obviously higher in participant S2. Relatively constant HR between sessions 2-3 in participant S3 can be explained by reduced physical activity at lunch break. The participant went outside the facility at the beginning of the break, but came back shortly and was working seated on his laptop from 12:30-13:00. Generally, three participants spent their lunch break differently (S1 was relatively active during the entire break, S2 was walking around during the 2nd half of the break, S3 walked only at the beginning of the break), and this influenced their metabolism right after lunch. For example, there was no increase in metabolic rate in participant S3 during the 3d session which can be due to the reduced lunch break activity and individual metabolic response to the meal. These HR

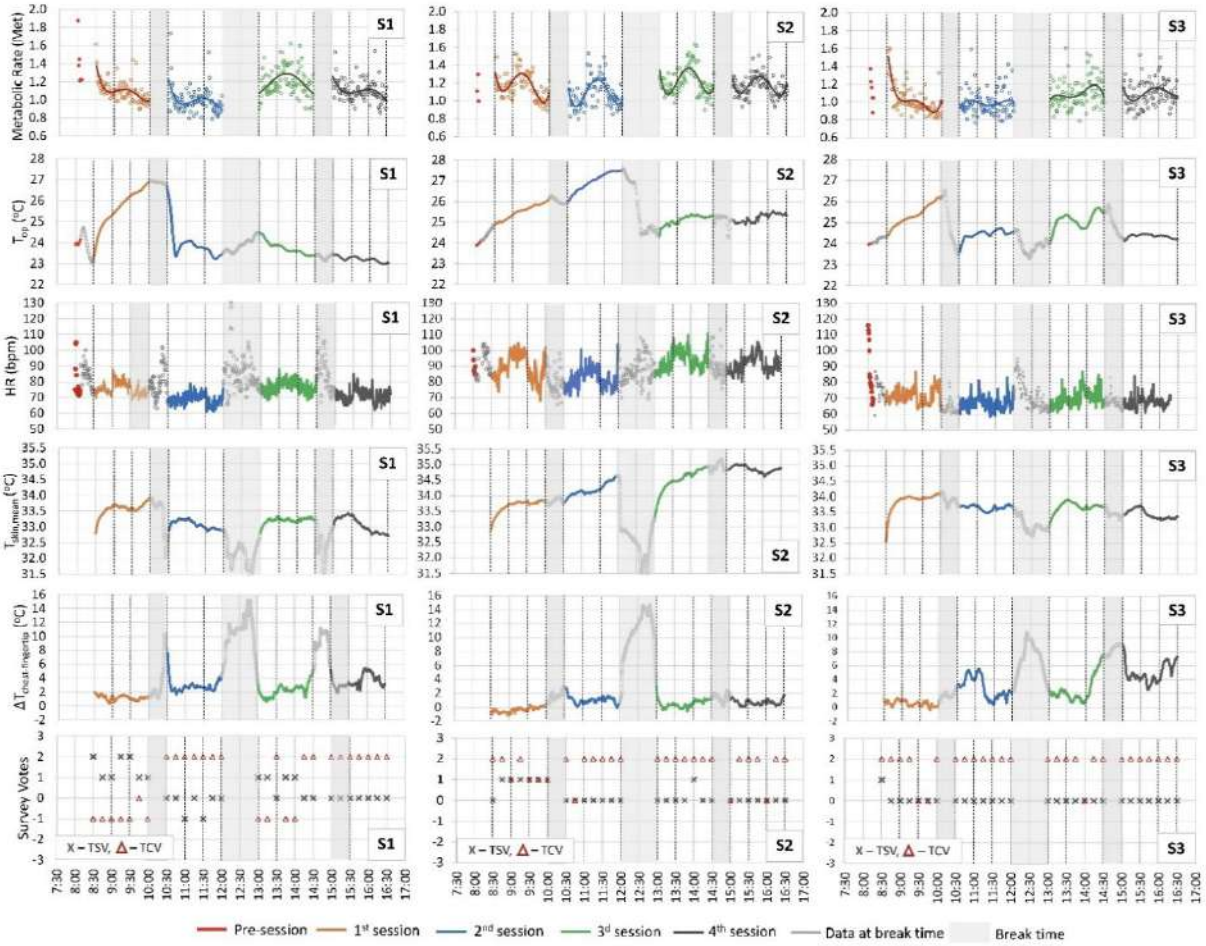

Fig. 3 - Dynamics of metabolic rate, indoor operative temperature, heart rate, mean skin temperature, chest-fingertip temperature difference, and comfort/sensation votes during experiments with 3 participants S1-S3

measurements are used further to determine the metabolic rate per "level 2, analysis". The minimum heart rate at rest required for calculations is taken as the minimum value observed in the experiments

Thermal environment: Mean operative temperature T_{op} variation inside the experimental room shown in Fig. 3 indicates that the temperature climbed up in the mornings (in session 1 of participants S1 and S3, and sessions 1-2 of participant S2). As described in section 2.4, there was little control of the temperature during the direct sunlight exposure on the S-oriented window in the mornings. There was better control of the temperature in the afternoons, the thermal environment was relatively stable in all 3 experiments. Of course, a substantial temperature increase in the mornings could have an effect on metabolic rate due to the triggered thermoregulatory adjustments when the body is beyond neutrality. However, this contribution might be small compared to the physical activity effect and thermic effect of food, as we see from metabolic rate dynamics.

Skin temperature and thermal comfort: $T_{skin,mean}$ and $\Delta T_{chest\text{-}fingertip}$ can be objective indicators of the thermal state of the person. Thus, they are plotted in **Fig. 2** together with the survey votes on TCV and TSV. Mean skin temperature $T_{skin,mean}$ plotted in Fig. 2 shows that it follows a variation of the mean operative temperature T_{op} in participants S1 and S3. It is elevated during the 1st session, and relatively stable during the following sessions 2-4 ($T_{skin,mean}$ of S1 was 0.5°C lower than S3). Although participant S1 felt slightly warm and slightly uncomfortable during the 1st session in the morning, there was a negligible difference between his right chest and right fingertip skin temperature $\Delta T_{chest\text{-}fingertip}$. The same was observed in S3 that, oppositely to S1, felt comfortable and neutral during all 4 sessions. $\Delta T_{chest\text{-}fingertip}$ increased up to 4-6°C in the later afternoon in both participants. In participant S2, $T_{skin,mean}$ had a tendency to increase towards the end of the day, a similar pattern can be observed in his HR measurements, despite the stable mean operative temperature of 25-25.5°C in the afternoon. His $T_{skin,mean}$ reached 35°C in the afternoon, the highest value among all 3 participants. Interestingly, there was a negligible difference between the right chest and right fingertip temperature $\Delta T_{chest\text{-}fingertip}$ for S2 in all 4 sessions. TCV and TSV-related responses also indicate that the person was feeling neutral, and the temperature was found to be comfortable in sessions 2-4, while there was a slight warm discomfort during the morning session 1.

3.2 Met comparison with standard methods

Effect of individuals' BSA: The measured metabolic rate indicates that it varies dynamically, and averaging it over a prolonged time interval (for instance, 30 min) will not appropriately show this. Therefore, for the comparison of metabolic rates determined per different methods M1-M3, the data was averaged over 10-min intervals. The averaged values are compared with the standard values of 1.2 *met* for sedentary work, and 1.4 *met* for standing work (M0 method). The percentage of met variations for 3 participants is presented in **Fig. 4**. Generally, the measured *met* values considering individuals' BSA (method M1) are lower than what we typically consider for a particular activity type. Only on a few occasions (first 10 min of session 1 for S1 and S3, and the first 10 min of the 3d part of sessions 3 and 4 or S3) were measured *met* values are slightly greater (<8%). In the rest of the cases, the measured values were lower (i) standing work: 35.5% for S1, 22.2% for S2, and 38.8% for S3, (ii) sedentary work: 24.1% for S1, 21.6% for S2, 24.2 for S3. As illustrated on the plot, the percentage of variation in met is activity-, time-, and person-specific. If we consider the average adult BSA of 1.7 m² (method M2) or specifically adult *male* BSA of 1.9 m² (method M3), the percentage of variation decreases. It actually increases for S1 per method M2 up to 22%. For participants S2-S3, *met* values per M2 are the closest to standardized values. Consideration of average adult BSA reduces the percentage variation in *met*, while consideration of average *male* BSA is not so straightforward. For instance, the metabolic rate of participant S3 does not differ much between M1 and M3 since his actual BSA (1.86m²) is close to the average male one. Overall, our analysis demonstrates that individuals' BSA needs to be considered to have more precise *met* values.

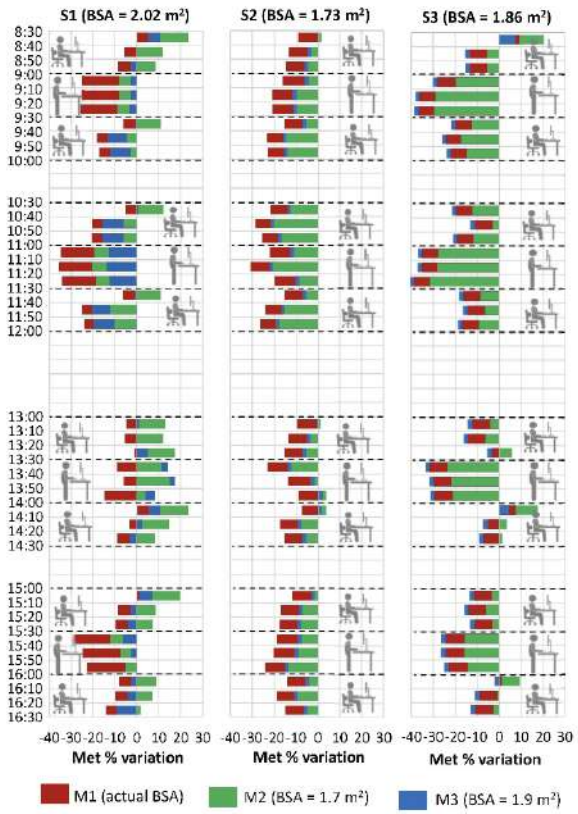

Fig. 4 – Metabolic rate percentage variation for 3 approaches of determining met rates M1-M3 compared to the M0 approach (classification of activity types)

HR-based evaluation: In method M4, we used measured HR data to evaluate *met* values. Activity-

type comparison (30-min averaged) is provided in **Tab. 3**. Generally, HR-based evaluation of *met* values is substantially higher than what was actually measured using an indirect calorimeter. Although the expected accuracy is supposed to be ±10% per ISO 8996:2004, it is substantially lower in our experiments. In HR-based met calculations, age, weight, heart rate at rest (HR_o), and metabolic rate at rest (M_o) are considered. Since age and weight are determined precisely, small errors might be coming from (i) HR_o estimation as the minimum from our experimental measurements, (ii) M_o considered as BMR from InBody measurements (see **Tab. 2**). If actual HR_o is greater than what we considered (61 *bpm* for S1, 66 *bpm* for S2, and 58 *bpm* for S3), then *met* values increase. An increase is also expected if M_o is greater than what we've taken (42.9 *met* for S1, 43.8 *met* for S3, 41.2 *met* for S3). Therefore, the source of significant discrepancy is not on actual the subject-specific values we considered but rather on the conditions that the method could be applicable. It is noted in ISO 8996:2004, that the HR-based method should be applied for HR values in a neutral climatic environment. As discussed in section 3.1, there were moments in the mornings when the indoor temperature was high; however, this did not result in increased HR. Therefore, there was no thermal stress that could affect HR-based *met* values estimation. To further investigate the source of discrepancy, it might be necessary to go to the original source of the method described in the standards to better understand underlying assumptions that are not explicitly mentioned in the text of the standard.

Tab. 3 – Comparison of metabolic rates determined by methods M0-M4 (30-min averaged per each activity)

Participant	Method	Session 1			Session 2			Session 3			Session 4		
		8:30-9:00	9:00-9:30	9:30-10:00	10:30-11:00	11:00-11:30	11:30-12:00	13:00-13:30	13:30-14:00	14:00-14:30	15:00-15:30	15:30-16:00	16:00-16:30
Work Type		Sitting	Standing	Sitting	Sitting	Standing	Sitting	Sitting	Standing	Sitting	Sitting	Standing	Sitting
All	M0	1.20	1.40	1.20	1.20	1.40	1.20	1.20	1.40	1.20	1.20	1.40	1.20
S1	M1	1.16	1.10	1.03	1.01	0.98	0.98	1.15	1.28	1.17	1.17	1.10	1.07
	M2	1.38	1.30	1.22	1.20	1.16	1.16	1.37	1.52	1.39	1.39	1.30	1.27
	M3	1.23	1.16	1.10	1.08	1.04	1.04	1.22	1.36	1.24	1.24	1.16	1.14
	M4	1.89	2.32	1.77	1.31	1.62	1.24	1.90	2.34	1.95	1.95	1.81	1.47
S2	M1	1.16	1.28	1.05	0.99	1.22	1.03	1.15	1.34	1.14	1.14	1.26	1.11
	M2	1.18	1.31	1.06	1.00	1.24	1.05	1.17	1.36	1.16	1.16	1.28	1.13
	M3	1.05	1.17	0.95	0.90	1.11	0.94	1.05	1.22	1.04	1.04	1.15	1.01
	M4	2.36	3.20	2.10	1.80	2.40	1.81	2.55	3.32	2.79	2.79	3.12	2.44
S3	M1	1.13	1.00	0.94	1.00	0.96	1.01	1.08	1.04	1.18	1.18	1.11	1.12
	M2	1.24	1.09	1.02	1.09	1.05	1.10	1.18	1.13	1.29	1.29	1.22	1.22
	M3	1.11	0.97	0.91	0.98	0.94	0.99	1.06	1.01	1.15	1.15	1.09	1.10
	M4	1.77	1.74	1.74	1.33	1.39	1.34	1.39	1.67	1.67	1.67	1.45	1.26

4. Discussion

Our experimental measurements of three individuals' metabolic rates confirm its transient nature that depends on the physical activities and time of meal intake. While the indoor thermal environment was not strictly controlled during the experiments, and we even had a temperature up to 27°C, participants found the environment acceptable and most of the time comfortable, except for a warm discomfort in the mornings. The same is confirmed from objective measurements of the skin temperature difference chest-fingertip that was relatively low despite the elevated indoor temperature. Per standardized requirements, typical indoor temperature setpoints are much lower than what we had during our experiments. For instance, in Switzerland, the operative temperature setting in offices in winters should be 21°C according to the national standard SIA 180:2017 [14] guided by temperature recommendations in ISO 7730:2015. To determine how much thermal sensation could be off neutrality due to the elevated indoor temperatures, we determined dynamic variation of PMV by accounting for measured environmental parameters and *met* values for each individual using the PMV/PPD model. Surprisingly, results plotted in **Fig. 5** show that most of the time PMV values were within the comfortable interval of [-0.5; +0.5]. Interestingly, the cool sensation is supposed to be expected in subjects S1 and S3 during session 2, when the metabolic rate was at the minimum. However, the sensation is near neutrality during the remaining sessions, even during morning session 1 when the indoor temperature was increasing. Overall, our study shows that: (i) dynamics of the metabolic rate and indoor thermal environment observed during the experiments are beyond what we typically consider based on standardized recommendations, (ii) the thermal state of people was near neutrality even when the indoor temperature was beyond the standard comfortable range due to the dynamics of the metabolic rate. Thus, constant values of metabolic rates that have been used so far based on the classification of activity types should be used with a great degree of caution. Dynamics of the metabolic rate should be accounted for in the design and operation of buildings and indoor climate systems to advance the transition toward a human-centric built environment.

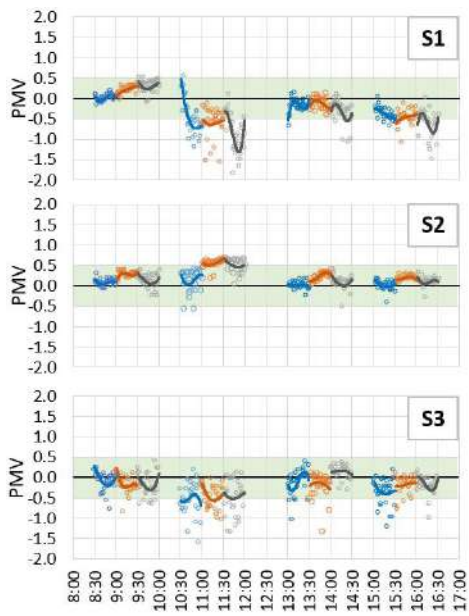

Fig. 5 – Dynamics of PMV variation using measured metabolic rates and environmental parameters

5. Conclusions

The human metabolism considerably impacts the body's thermal balance with its surrounding environment and, consequently, affects the individual's thermal sensation. The metabolic rate estimation based on the classification of activity types is less accurate compared to the measurements using indirect calorimetry that we performed in our experiments with 3 male subjects. Despite the lack of gender consideration, our results still demonstrate that the metabolism of individuals varies throughout the day, not only due to physical activities but also due to the thermic effect of food. Therefore, we could expect that metabolic rates might also vary from day to day depending on the kind of meal eaten and individual specifics of the digestion system. Dynamics of subjects' metabolism and indoor thermal environment in our experiments resulted in their neutral sensation most of the time, despite the fact that the actual metabolic rate was lower than what we typically consider, and indoor temperature was higher compared to what we typically set in office buildings. To further investigate the magnitude of metabolic rate variation in individuals, more participants should be involved to reach statistically significant results. In addition, the timing of meal intake and all activity types should be standardized for a firm comparison. Our study, even with limited participants, points out the importance of considering individuals' metabolism and its daily dynamics if we want to transition towards the design of human-centric indoor spaces. The major challenge of considering the min-by-min change in metabolic rate in practice is how to measure it non-invasively and even remotely. With the availability of low-cost wearable sensors, estimation of human metabolism is more feasible nowadays than a decade ago. However, while HR-based predictions of human metabolism are widespread, they hardly can capture the thermic effect of food. Still, it is the parameter that directly affects intra-day and inter-day variability of metabolic rate in humans. Overall, if transience the individuals' metabolism could be indirectly measured, it could be used as input to climate controls in future human-centric buildings.

6. Data statement

The datasets generated during and/or analyzed during the current study are not available because of privacy issues, but the authors will make every reasonable effort to publish them in the near future in anonymized form.

7. Acknowledgment

We thank Prof. Y. Ravussin and Prof. A. Dulloo from the University of Fribourg for providing the indirect calorimeter and their precious advice during metabolic data processing; Prof. J.-P. Montani for assisting in screening participants; I. Scerri for training on the indirect calorimeter. Last but not least, we want to thank our participants for providing valuable data.

8. References

[1] ANSI/ASHRAE/IES Standard 55: Thermal Environmental Conditions for Human Occupancy. American Society of Heating, Ventilation, Refrigeration and Air Conditioning Engineering, Atlanta, GA, 2020.

[2] ISO 8996, Ergonomics of the thermal environment – Determination of metabolic heat production. International Organization for Standardization, Geneva, 2004.

[3] ISO 7730, Ergonomics of the thermal environment - Analytical determination and interpretation of thermal comfort using calculation of PMV and PPD indices and local thermal comfort criteria. International Organization for Standardization, Geneva, 2005.

[4] Durin G.A., Passmore R. Energy, Work and Leisure. London: Heinemann Educational Books, Ltd. London, 1967.

[5] Zhai Y., Minghui L., Gao S., Yang L., Zhang H., Arens E., Gao Y. Indirect calorimetry on the metabolic rate of sitting, standing and walking office activities. Building and Environment. 2018; 145:77-84.

[6] Yang L., Zhao S., Gao S., Zhang H., Arens E., Zhai Y., Gender differences in metabolic rates and thermal comfort in sedentary young males and females at various temperatures. Energy and Buildings. 2021;251:111360.

[7] Lam Y.Y., Ravussin E. Analysis of energy metabolism in humans: A review of methodologies. Molecular Metabolism, 2016; 5(11):1057–1071.

[8] Pontzer H., et al. Daily energy expenditure through the human life course. Science. 2021;373(6556):808-812

[9] Ruddick-Collins C.L, King A.N, Byrne N.M, Wood R.E. Methodological considerations for meal-induced thermogenesis: measurement duration and reproducibility. British journal of nutrition. 2013;110(11):1978–1986.

[10] Dubois D., Dubois E.F. formulation A formula to estimate the approximate surface area if height and weight be known. Archives of Internal Medicine. 1916; 17:863-871.

[11] Weir J. B. New methods for calculating metabolic rate with special reference to protein metabolism. The Journal of Physiology. 1949;109(1e2):1e9.

[12] ISO 9886, Ergonomics – Evaluation of thermal strain by physiological measurements. International Organization for Standardization, Geneva, 2004.

[13] ISO 7726, Ergonomics of the thermal environment – Instruments for measuring physical quantities. International Organization for Standardization, Geneva, 1998.

[14] SIA 180, Wärmeschutz, Feuchteschutz und Raumklima in Gebäuden. Schweizerischer Ingenieur- und Architektenverein, Zurich, 2014

A Methodology to assess economical impacts of poor IAQ in office buildings from DALY and SBS induced costs

Louis CONY[a], Jelle LAVERGE[b]

[a] Department of Architecture, Gent University, Gent, Belgium, louis.cony@ugent.be.

[b] Department of Architecture, Gent University, Gent, Belgium, jelle.laverge@ugent.be.

Abstract. Indoor air quality is a major issue that concerns everyone. Indeed, human being spend more than 70% of time in indoor environment. Indoor pollutants are responsible for many chronic diseases such as lung cancer or leukaemia, but it also has short-term outcomes, it can cause headache, coughing, running nose, etc, it affects daily concentration and productivity of office workers. Considering the numerous consequences of indoor pollution, a will to quantify induced costs seems logical. In 2003 a study conducted in US concluded a global 41 billion € cost, in France, total cost of indoor pollution for the whole nation was estimated around 19 billion € in 2014. Nonetheless, for an individual person or a whole building, the point of view is not the same, and therefore, integrated costs will differ from those for a nation. This work aims at proposing a methodology to estimate IAQ costs in office buildings, with a function that accounts for pollutants concentration and number of workers. This proposed methodology permits calculation of costs for Disability Adjusted Life Years (DALY). A distinction is made for each individual pollutant cost, accounting for healthcare costs, life years lost and productivity loss. An original part of this work consists in also integrating Sick Building Syndrome (SBS) costs. Preliminary results show a higher cost for SBS compared to DALY.

Keywords. Indoor Air Quality, office buildings, economical cost, DALY, SBS.
DOI: https://doi.org/10.34641/clima.2022.297

1. Introduction

People spend more than 70% of their time in indoor environments [1]. Indoor air is often more polluted than outdoor air. Therefore, its preoccupation is of major concern. Long-term exposure to chemical substances may cause chronic diseases with more or less severity, such as, asthma, bronchitis, pneumonia, lung cancer or leukemia… On a short term perspective, it is also responsible for headaches, eyes or nose irritations… Those acute reversible effects are known as Sick Building Syndrome (SBS) [2]. As indoor Air Quality (IAQ) may lead to a need for medical treatment, incapability to work or even loss of productivity, [3,4], there is a financial consequence. Economic impact of indoor air quality has already been studied in the past, globally [5,6,7], in schools [8,9], in residential buildings [10] . As it is a complex task that has a wide range of impacts, choices have to be made to select the various costs as well as a way to quantify their financial impacts, depending on selected point of view (global costs for a nation, building scale or individual costs). Usually, estimations are made from the point of view of a government by associating costs to a general quantity of Disability Adjusted Life Years (DALY) lost. Identified costs are medical costs, life quality lost, research and measurement studies as well as productivity lost. Some studies include willingness to pay. Depending on the studies, a negative cost (gain) can also be included if people die prematurely due to poor IAQ while living at the expense of society (e.g: savings realized by unpaid pensions, insurances for retired or unemployed person). Those previous studies include a complete range of parameters and set the basis of IAQ socioeconomical assessment. Nevertheless, in order to identify specific financial losses for an individual person, a building or a company, methodologies proposed require to be modified. This paper aims at proposing a new complementary approach designed to fulfill these needs in office buildings, applicable both at building or individual scale. Although, the proposed formula can afterward be readapted to the purpose of other building types (schools, dwellings, retirement houses…), this investigation focuses only on office buildings. Indeed, working environment represents a strategic point as well from the time spent inside as for the financial income it is associated to.
In average, people work 1744h per year, which represents 19.9% of their total annual time. This

Copyright ©2022 by the authors. This conference paper is published under a CC-BY-4.0 license.

percentage of time spent in working environment differs lightly from one industrialized country to another, it ranges from 15.5% (Germany) to 25.5% (Mexico), in Belgium, people work 1574h per year(18%) [11]. Any disturbance in working environment could possibly have a significant negative economic impact Those costs impact both workers, companies that employ them and insurances.
This work is part of the project flux50 Smart Ventilation that aims at qualifying ventilation in mid-sized buildings.
In this study, we will start discussing methodologies proposed in the past (available in french or english litterature) as well as a few results published. Then we will explain our new approach based on DALYs lost, and an original aspect that consists in implementing a Sick Building Syndrome (SBS) cost. A set of first results from a dwelling measurement campaign is finally presented before concluding with perspectives and limitations of this actual work.

2. Basics of IAQ economics previously established

Unfortunately, the literature rather poor and dated when it comes to assess and quantify costs induced by indoor air quality. This evaluation process is a complex task that requires to make assumptions and proposals. Nevertheless, the work of ANSES [5] propose a complete analysis and identified several costs (medical, research studies and measurements, productivity, …) . They concluded a total cost of 19 billion € per year for the whole French nation.

The methodology used was to quantify all the DALYs lost due to poor indoor air quality by analysing global burden disease (GBD) data and medical costs for various diseases associated to it. Authors also determined a life year cost and a yearly productivity. As they adopt the point of view of a government, all financial fluctuations (positive or negative) are included. For each DALY lost, an annual sum of money is calculated, corresponding to a combination of resources produced by work and pensions paid by government (unemployed or retired, refunding of medical costs by insurances…). If applied consecutively to different types of populations, such chosen parameters may lead to unusual situations. For example, employees having a sickness is considered as a much larger loss to the nation , than people living at its expanses and then dying prematurely, as soon as the sickness decreases worker's productivity. Indeed, second category fluctuations also induce a gain because savings are realized on pensions that should be paid. Even if it remains an objective observation of money incomes and outcomes designed for the purpose of a government it raises ethical questions and is not applicable as it is, to the scale of a building or a person.

A second major contribution in this field is the work of Sherman et al. [6]. In this review study they suggest monetization of DALYs or Health Adjusted Life Years (HALY) as a suitable solution. Including only the cost of a life year, they estimate the value of 150,000US$ per DALY in developed country. In 2005, CalEPA estimated to 41 billion € total IAQ cost in California [12] based on willingness to pay.

DALY calculation is possible as a function of pollutant concentration, therefore it is possible to adapt previous works to evaluate costs induced locally, at building scale.

In the next section, we will explain our method based on DALY cost calculation associated to a SBS cost.

3. Calculating indoor quality impacts in office buildings from DALY and SBS induced costs

In this section, we shall propose a way to estimate IAQ cost with a concentration response function in office buildings. Two combined approaches will be used, DALY and Sick Building Syndrome (SBS) costs calculations.

3.1 Health impact assessment with DALY approach

A bad environment can sometimes cause sickness or severe diseases. It is therefore necessary to assess the costs related to health issues. In order to do so, it is first needed to estimate health impact.
An existing approach consists in counting Disability Adjusted Life Years (DALY) lost due to exposure to chemical substance. The unit for this metric is the number of healthy years lost. In the initial formulation [13], two methodologies (depending on available information) are proposed to calculate a dose response function for a large range of chemical species.
The first one is the Intake Incidence Daly (IND) approach (equations (1) &(2)), based on human epidemiologic data.

$$\boldsymbol{DALYs = DALY\ f\ X\ disease\ inc} \qquad (1)$$

$$\boldsymbol{disease\ inc = pop\ X\ y0\ \mathrm{X}\ (1 - e^{-\beta Cexp})} \qquad (2)$$

Where $DALY\ f$ is DALYs lost per incidence, $disease\ inc$ is the disease incidence, y0 is the baseline prevalence of illness per year, β is the coefficient of the concentration change, $Cexp$ is the exposure-related concentration, and pop is the number of persons exposed.
The second approach is the Intake Daly (ID) method that is based on animal toxicological data (equations (3)(4) &(5)) .

$$\boldsymbol{DALYs = \frac{\partial DALY}{\partial intake} X\ intake} \qquad (3)$$

$$\frac{\partial DALY}{\partial intake} = \frac{\partial DALY}{\partial intake} c\ X\ AF + \frac{\partial DALY}{\partial intake} nc \quad (4)$$

$$intake = C\ X\ time\ X\ air\ intake\ X\ day \quad (5)$$

Where ∂DALY/∂intake are the cancer *(c)* and noncancer *(nc)* mass intake-based DALY factors, C is the indoor concentration, time is the percentage of time spent in the environment per day, air intake is the volume of air inhaled per day, day is the considered number of day , and AF is the age-dependent adjustment factor for cancer exposure.

3.2 DALY cost calculation

To associate DALY to a cost, a cost per DALY has to be determined for each pollutant. In literature, 5 main categories were identified:

- Mortality and life cost
- Medical costs
- Productivity cost
- Research, prevention and regulation costs
- Willingness to pay

In the Flux50 project, we are aiming to define a cost that can be applied at the scale of an individual person or a building, so that each ventilation strategy can be studied independently.

Cost related to willingness to pay, research, prevention and regulation should not be accounted in office buildings.

In a previous socio-economical study, life year (LY) cost was estimated around 115 000€ per year per person [13].

Average national productivity (P_{cost}) is estimated around 145 000 € per year per person [5], this value corresponds to average French productivity. When applied individually to a specific building, P_{cost} should be recalculated, based on average employees productivity inside building.

Medical costs vary from one pollutant to another as the diseases induced are also different.

Concerning the productivity cost due to DALY, we consider that the proportion of productivity loss is equal to the life quality loss (e.g, a person suffering a disease that induces a 20% life quality lost, would have a 20% productivity loss). We are conscient that this may induce a bias because some diseases may have a low quality life lost and yet induce a working stop.

Average medical cost per DALY is proposed for studied pollutants [14] in Table **Tab. 1**. For pollutants whose medical cost could not be found, authors arbitrarily selected a cost of 40,000€ (Average + 10,000€ marge).

Tab. 1 - Medical cost induced by pollutants (€)

Pollutant	Medical cost (€)
Benzene	46 000
Trichloroethylene	70 971
Radon	25 526
PM	10 402
CO	1 085

Finally DALY cost of a pollutant *i* is the sum of concerned medical cost ($\boldsymbol{H\ cost_i}$), productivity loss ($\boldsymbol{P_{cost}}$) as well as life cost (***LY cost***), as detailed in equation *(6)*

$$Daly\ cost_i = LY\ cost + P_{cost} + H\ cost_i \quad (6)$$

3.3 Calculation of global productivity loss by SBS

Although there is already a productivity loss integrated in the DALY calculation, it is important to also integrate a global productivity loss. Productivity loss associated to DALY cost is due to severe chronic diseases (that will obviously impact working productivity). Nevertheless, a bad environment can cause concentration disturbance and productivity loss without leading to severe diseases. For one person that may suffer severe disease, there may a proportion of other employees who feel uncomfortable and are therefore less efficient at work due to temporary acute effects.

An original part of this study consists in proposing a calculation of SBS cost. Nevertheless, influence of SBS is difficult to assess numerically since it is an information that mainly comes from questioner. When having an in situ inquiry it is possible to ask the Percentage of Occupants Presenting at least 1 (SBS) Symptom in a persistant way (from 1 to 3 days a week) during the last 4 weeks (POPS) or at least 2 symptoms (POPS2). A correlation was proposed [16] between POPS and IAPI [17] index as well as another one between POPS2 and IEI [18].

$$Mean\ IAPI = 0.25 \times Mean\ POPS - 14.3 \quad (7)$$

$$Mean\ IEI = 0.30 \times Mean\ POPS2 - 14.6 \quad (8)$$

Productivity loss for POPS is assumed to be twice lower than productivity loss for POPS2. Therefore, cost due to SBS can be estimated as follows.

$$SBS_{cost} = P_{cost} \times \left[(P_{loss} \times POPS2) + \left(\frac{P_{loss}}{2} \times (POPS - POPS2) \right) \right] \quad (9)$$

By reusing equations *(7)* and *(8)*, we can write:

$$SBS_{cost} = P_{cost} \times P_{loss}\left(\frac{IEI + 14.6}{0.60} + \frac{IAPI + 14.3}{0.5}\right) \times \frac{2}{5} \quad (10)$$

As POPS and POSPS2 describes persisting symptoms as occurring from 1 to 3 times a week, a coefficient of $\frac{2}{5}$ was added to ponderate Productivity loss and consider it occurs 2 days in working week of 5 days. As IEI is dependant of IAPI (equation (11)),

$$IEI = \frac{IAPI + IDI}{2} \quad (11)$$

$SBS\ cost$ is finally calculated as described in equation *(12)*.

$$SBS_{cost} = P_{cost} \times P_{loss}(0.83 + 2.83IAPI + 0.83IDI) \times \frac{2}{5} \quad (12)$$

Productivity decrease due to SBS in office buildings is assumed to be 6% for POPS2 and 3% for POPS, which is relevant with findings of Wargocky et al. [3]

3.4 Global cost

Finally, to assess global cost due to IAQ in office buildings, we sum DALY and SBS as described in equation *(13)*

$$IAQ_{Cost} = \sum_{i}^{p} Daly_i \times Daly\ cost_i + SBS_{cost} \quad (13)$$

This solution proposes a cost per year per employee with a dose-response function. In order to estimate costs in an entire building, simply multiply per number of employees in the building.

4. Results and discussion

As authors did not have access to office measurement campaign, the proposed methodology was applied to values of dwelling measurement campaign conducted from 2003 to 2005 in France [19]. For lack of better, assumption is made that concentration levels have same order of magnitude in dwellings and offices. Estimated costs per year and per person for each pollutants studied, total DALYs cost, SBS cost and total cost are presented in Fig. **1**.

Concerning pollutants, we notice that Acetaldehyde, Benzene, Styrene, Tetrachloroethylene, Toluene, Trichloroethylene and Xylenes have a maximum value lower than 5€/year/person which is relatively low compared to Formaldehyde, Acrolein and PMs. As expected, cost induced by PMs is major when measured (91% of total DALY). Total DALY cost ranges from 0.07 to 3,200€/year/person because PMs are not measured in every situation. Costs related to DALYs are relevant with literature although PMs importance is higher than results obtained by ANSES[5]. This can be explained by the fact that their study include a negative cost of 136.5 billion euros for this pollutant because of unpaid pensions (65,3% of total gains), which considerably lowers the impact of PMs.

SBS cost ranges from 1,300 to 2,900€/year/person. Average (2,300€) value is higher than for any other category. This first value tends to prove the importance of considering SBS in future works.

Total costs ranges from 1,842 to 6,300€/year/person in office buildings. Even if the data originates from a dwelling measurement campaign, costs assessed in this study are relevant enough to be applied to office purpose (SBS function is limited by 2 extremities). Total cost is impacted mainly by daily productivity decrease reported from SBS (50,5%), followed by DALY cost of PM (45,5%).

All costs included, and with the selected parameters, one DALY costs 265,250€ in average.

5. Discussion, limitations and perspectives

The methodology proposed in this document allows quantification of costs induced by indoor air quality issues in building offices by including medical costs, life year costs and productivity costs associated to DALY lost as well as acute SBS costs. This solution is designed to be used at the scale of an individual person or a whole building.

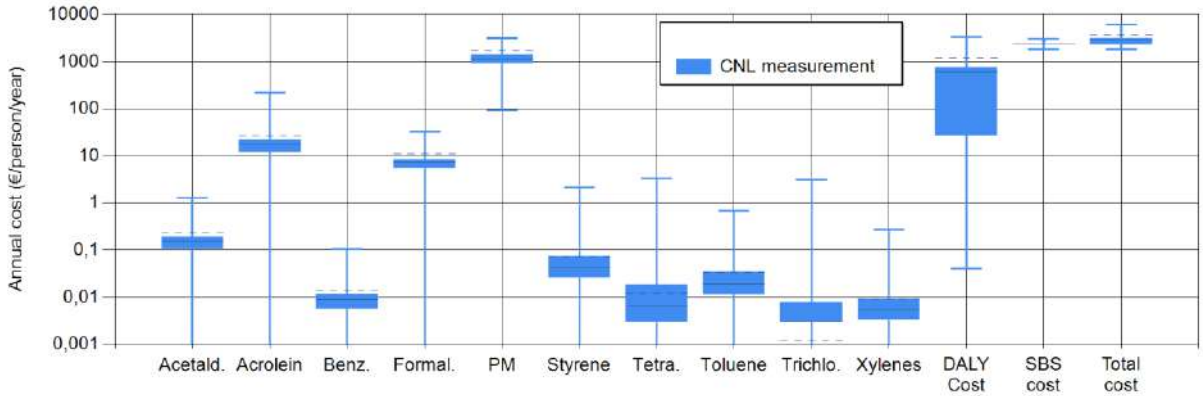

Fig. 1 - Estimated costs of indoor air quality in France, for major pollutants, DALY and SBS cost.

5.1 Discussion

Assessment of costs obtained in this work show that indoor air quality has a very important economical. Therefore, taking special precautions to improve IAQ is a major issue that could directly profit to everyone. Similar conclusions were found in previous studies [3,20,21]. In worst situations we estimate the possibility to reach 3000€/year/person of benefit.
This methodology can be applied to various cases and most parameters can be adapted to the context of a specific study. With more detailed information (medical insurance cover rate, company insurance rate, salary, company policies…), a further step would be to differentiate resulting costs by the category of population they directly impact. A company will be impacted by SBS cost and maybe a part of DALYs if it has to pay for a part of absent while sick employee salary. A worker will be impacted by a varying part of DALYs (productivity used must be replaced by perceived salary), depending on his/her health insurance covering for medical costs and maybe a part of SBS if revenues are not only a fixed salary, but also productivity related.

5.2 Limitations of the study

Some of the assumptions made induce limitations.
Although results obtained are expressed by €/year/person, if the methodology is applied to a small scale sample, results may highly differ from reality. Indeed, all parameters are estimated from statistical values which means that every costs are pondered by their probability of occurrence and passed on every one. In reality, costs will differ highly from one individual to another, depending on his constitution, resilience, type of work done…
As explained earlier, percentage of productivity decrease related to DALY is assumed to be proportional life quality lost. Nevertheless, in some situations, a disease may result to a work interruption whereas life quality lost remains lower. Therefore DALY cost might be underestimated by this bias.
Data used to produce results is from 17 years old measurement campaign. It may be possible that a more recent measurement campaign would show lower concentration levels.

5.3 Perspectives of this work

The methodology proposed in this study is a further step to assessment of economic impact of indoor air quality, yet, it remains a proposal that can be improved.
With better knowledge, medical costs associated to each pollutant can be refined (diseases and their incidence, up to day costs…), as well as the associated productivity lost.
It could be possible to establish new correlations more accurate between SBS and objective measurements.
More studies conducted about productivity lost at work due to IAQ would refine the productivity decrease parameters used.

5.4 Future works

This study was conducted in the frame of Flux50 Smart ventilation project. The objective of this project is to qualify ventilation in mid-sized buildings accounting for various aspects. Buildings studied are not limited to offices. Therefore, this methodology will be readapted to fit purposes of residential buildings, retirement houses and schools.
A simulation based on a coupling between CONTAM and TRNSYS softwares is currently being developed, accordingly to procedure described in work form Cony [22], to produce transient concentration files for all types of buildings.
As IAQ is not the only included field in this project, members of the project are actually collaborating to extend this methodology and adapt it to all concerned categories (acoustic comfort, sleep quality, hygrothermal comfort and user satisfaction, resilience, installation and maintenance costs as well as energy consumption).

6. Conclusion

This work proposes a new complementary approach to estimate IAQ costs in office for individual person or building scale. An original aspect of this study is to include SBS costs corresponding to the global population suffering reversible acute effects that lightly (but daily) impact work productivity.
Result obtained for DALY cost are relevant with results found in literature. Importance of PMs (1,150€/year/person in average) remains major as they account for a majority of DALYs (around 90%). Economic impact induced by SBS (2,300€/year/person in average) appears to be even higher than health impact. All costs included, authors estimate that one DALY costs 265,250€ in average. Higher preoccupation of IAQ issues in building conception and refurbishment is once again confirmed to be of major importance.

7. Acknowledgement

This work has been supported by the Flemish Agency for Innovation and Enterpreneurship (VLAIO) in the Flux50 project Smart Ventilation (HBC.2020.2520).

8. References

[1] Tsang A.M., Klepeis N.E.. Descriptive statistics tables from a detailed analysis of the National Human Activity Pattern Survey (NHAPS) data. Lockheed Martin Environmental Systems and Technologies, Las Vegas, NV ...; 1996.

[2] Tham K.W. Indoor air quality and its effects on humans—A review of challenges and developments in the last 30 years. Energy and Buildings.

2016;130:637–50.

[3] Wargocki P., Wyon D.P., Fanger P.O. Productivity is affected by the air quality in offices. In: Proceedings of Healthy Buildings. 2000. p. 635–40.

[4] Dorgan C.E., Dorgan C.B.. Assessment of link between productivity and indoor air quality. In: Creating the productive workplace. Taylor & Francis; 2006. p. 141–63.

[5] ANSES. Etude exploratoire du coût socio-économique de l'air intérieur. 2014.

[6] Walker I., Sherman M., Jones B. Economics of Indoor Air Quality. 2018;

[7] Duflo E., Greenstone M., Hanna R. Indoor air pollution, health and economic well-being. SAPI EN S Surveys and Perspectives Integrating Environment and Society. 2008;(1.1).

[8] Wargocki P., Foldbjerg P., Eriksen K.E., Videbæk L.E. Socio-economic consequences of improved indoor air quality in Danish primary schools. Proceedings of Indoor Air. 2014;2014.

[9] Jalas J., Karjalainen K., Kimari P. Indoor air and energy economy in school buildings. In: Proceedings of Healthy Buildings. 2000. p. 273.

[10] Dymond A., Mealing S., McMaster J, Holmes H, Owen L. Indoor Air Quality at Home—An Economic Analysis. International journal of environmental research and public health. 2021;18(4):1679.

[11] Inc C. Working hours by country and industry [Internet]. Clockify. [cited 2022 Jan 13]. Available from: https://clockify.me/working-hours

[12] California EPA. Indoor air pollution in California. 2005;

[13] Quinet E., L'évaluation socioéconomique des investissements publics. 2014.

[14] INCA. Analyse économique des coûts du cancer en France. 2007

[15] Logue J.M., Price P.N., Sherman M.H., Singer B.C. A method to estimate the chronic health impact of air pollutants in US residences. Environmental health perspectives. 2012;120(2):216–22.

[16] Kirchner S., Arenes J.-F., Cochet C., Derbez M., Duboudin C., Elias P. État de la qualité de l'air dans les logements français. Environnement, Risques & Santé. 2007;6(4):259–69.

[17] Sofuoğlu S.C., Moschandreas D.J. The link betweensymptoms of office building occupants and in-office air pollution: the Indoor Air Pollution Index. Indoor Air. 2003;

[18] Moschandreas D.J., Sofuoglu S.C. The indoor environmental index and its relationship with symptoms of office building occupants. Journal of the Air & Waste Management Association. 2004;54(11):1440–51.

[19] Kirchner S., Derbez M., Duboudin C., Elias P., Gregoire A., Lucas J.-P., Indoor air quality in French dwellings. In: Indoor Air 2008. 2008. p. Paper-ID.

[20] Boulanger G., Bayeux T., Mandin C., Kirchner S., Vergriette B., Pernelet-Joly V. Socio-economic costs of indoor air pollution: A tentative estimation for some pollutants of health interest in France. Environment international. 2017;104:14–24.

[21] Wargocki P. Improving indoor air quality improves the performance of office work and school work. 2008;

[22] Cony L. Élaboration et développement d'un indice de la qualité sanitaire de l'habitat: outil de quantification de la «favorabilité» à la santé [PhD Thesis]. Université de La Rochelle; 2020.

Temperature calibration and Annual performance of cooling for ceiling panels

Seyed Shahabaldin Seyed Salehi[b], Karl-Villem Võsa[b], Jarek Kurnitski[a,b,c], Martin Thalfeldt[a,b]

[a] FinEst Centre for Smart Cities (Finest Centre), Tallinn University of Technology, 19086 Tallinn, Estonia

[b] Nearly Zero Energy Buildings Research Group, Ehitajate tee 5, 19086 Tallinn, Tallinn University of Technology, Estonia

[c] Aalto University, School of Engineering, Rakentajanaukio 4 A, FI-02150 Espoo, Finland

Abstract. In this paper, the annual energy usage and emission efficiency of ceiling panels for cooling were assessed with IDA ICE building performance simulation software. The models were calibrated against measurements carried out in the autumn of 2021 at the nZEB test facility in Tallinn University of Technology. Calibrated models were then used to investigate the energy performance of the systems with annual simulations with the Estonian test reference year and energy simulation input data for office buildings in EN 16798-1:2019.
The simulations were conducted on a room model with fixed geometry and boundary conditions. The goal of the control strategy was to maintain a specified operative temperature within the room. The annual cooling energy need of the test room was compared with the same value obtained using an ideal cooler with 100% convective heat emission. Additionally, a single-value performance indicator in the form of an air temperature set-point deviation was obtained for the device and each configuration, as the result of this research, to be used in further hourly, monthly, or annual cooling energy usage calculations. The imperfections in air stratification within the room (temperature gradient), the surface temperature of the panels, and additional temperature deviation from the set-point to achieve the desired operative temperature level are the effective parameters on the performance indicator. Further analysis is needed to determine if room temperature set-point deviation can be applied with varying room geometry, boundary conditions, and cooling control principles.

Keywords. Cooling, Cooling design, Cooling device performance, Cooling simulation, thermal comfort, ceiling panel, thermal stratification
DOI: https://doi.org/10.34641/clima.2022.344

1. Introduction

The recent analysis and trends of climate change show a warmer pattern in Europe's climate, while the heatwaves are lasting longer, resulting in more cooling demand in the buildings. [1] This results in higher energy consumption for cooling and an increase in the importance of emission efficiency and accurate calculation and energy simulation of cooling devices. For cooling ceiling panels, there are three main aspects of accuracy measurement, vertical room temperature profile, cooling power output, and ceiling panel surface temperature. [2]

In this paper, the emission efficiency of the cooling ceiling panels is assessed. The European standard EN 15316 [3] presents a method for quantifying the influence of various system components, such as the effect of the emitter system on room air stratification and the effect of the system on thermal comfort (considering the operating temperature). This quantification takes the form of additional set-point increments to the initial room air temperature set-point to account for the energy difference necessary to overcome the effects of these components.

The purpose of this work is to compute such set-point increments using experimental data collected at the Tallinn University of Technology's nZEB test facility. These measurements are utilized to calibrate the IDA ICE 4.9.9 [4] model of the same nZEB facility room at Tallinn University of Technology. The necessary parameters are subsequently used in the model for yearly simulations. The set-point difference is then computed based on the energy need. This method was originally conducted in 2019 [5] as a contribution to the CEN TC 130 standardization technical committee's agenda for the determination of the experimental input and model calibration data required for dynamic simulations.

2. Methods

In this paper, the annual cooling energy need of ceiling panels was analyzed. For this purpose, these steps were followed:

1. The simulation model is created in IDA ICE

Copyright ©2022 by the authors. This conference paper is published under a CC-BY-4.0 license.

4.9.9 software package. The CFD-free zone model [6] is used to model the air temperature in horizontal 0.2 meter layers (total 15 layers). Models with low and high cooling capacity ceiling panels were created.

2. The modelled temperature at different heights were compared to measured values provided in [7] for model calibration.
3. The simulation model calibrated against the measurements by minimizing a mean square equation function using two main variables:
    a. Kfin, thermal resistance of the coolant which effects the rate of heat transfer between the surface and the environment and consequently influences the surface temperature of the ceiling panels
    b. Extra heat loss introduced as thermal bridge to correct the temperature magnitude.
4. Annual cooling energy is simulated with the calibrated model with pre-defined input data from EN16798-1 [8] using the Estonian test reference year climate file [9].
5. The cooling need dependency from room temperature setpoint is assessed with an identical model with an ideal cooler instead of ceiling panels. The cooling temperature set-point increment was identified so that the cooling needs of the models with ceiling panels and ideal cooler were equal.

2.1 Test room and conditions

Ceiling panels are installed in the largest room of the facility located on the East side of the building. The general view of the inside of the room is shown in **Fig. 2**. The room is 30 m² and has four windows, two on the East-facing external wall and one on each North and South facade. The test room has a false ceiling, and the whole building has a ventilated crawlspace.

The room temperature during experiments was free-floating and the temperature developed based on the the heat balance of internal heat gains, ventilation air flow, heat transfer from/to the outdoor environment and adjacent rooms and cooling capacity of ceiling panels. The exterior venetian blinds of South- and East-oriented windows were drawn to minimize the uncertainty due to solar heat gains. Chilled water with constant flow rate and supply temperature was supplied to the ceiling panels.

The airflow rate of the room was 45 l/s (approximately 1.46 l/(s·m²)), and the air handling unit supply air temperature is measured every 10 seconds for the period of the tests with an average of 20.2°C.

Fig. 1 – Tallinn University of Technology nZEB test facility

Fig. 2 – General view of the testing premises.

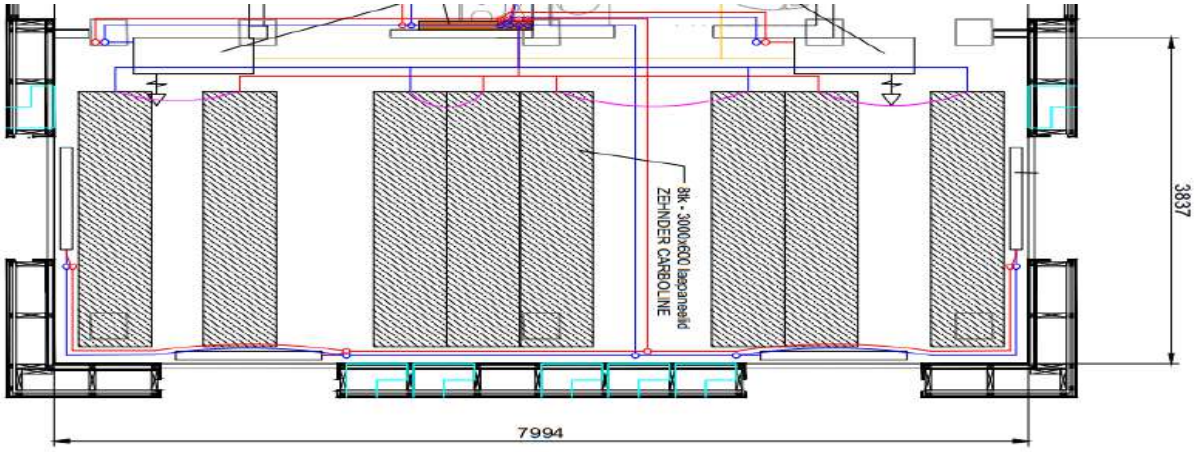

Fig. 3 – Positioning of ceiling panels and supply (blue) and return (red) pipes.

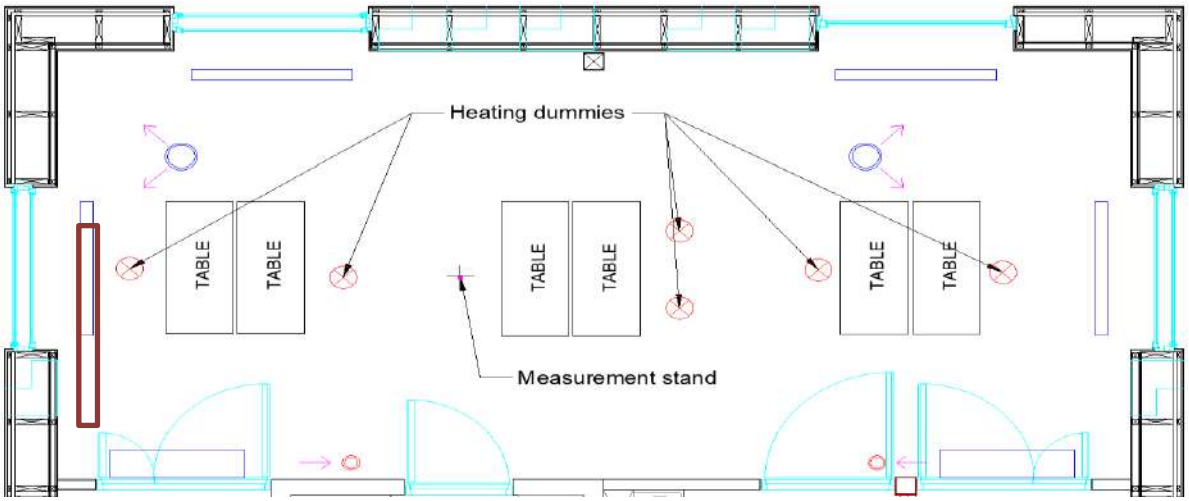

Fig. 4 - Room setup and positioning of heating dummies.

Necessary temperature sensors were installed in the room to measure the temperatures needed for the calibration. For supply and return temperature, ceiling and floor temperature, ceiling panels surface temperature, and the air stratification in the room.

Internal heat gains in the form of 6 thermal dummies were placed in the test room consisting of 3 incandescent lamps with a rated output of 3x60 W per dummy. There was no specific profile, and all heating dummies were always on to the full power. As an extra heat source, one radiator was also working with a rated power of 1000W. Positioning of the dummies and the room radiators can be seen in **Fig. 4**, while the only working radiator is the one with red color.

2.2 Ceiling Panels

The specifications for testing are briefly provided here. detailed information regarding the tests is available in the experimental study. [7]

Eight ceiling panels with a size of 600 x 3000 mm and a nominal cooling output of 172 W at 8°C logarithmic temperature difference installed under the ceiling using suspension cables at the height of 2.85 m from the floor and the upper side of the ceiling panels which can emit toward the ceiling is insulated by the manufacturer using mineral wool. Ceiling panels are installed in four pairs, and each pair of panels are connected in series. The detailed geometry and positioning of the panels are indicated in **Fig. 3**. The tests have been done at two nominal outputs named High and Low in this paper. The detailed specifications of each test are listed in **Tab. 1**. For each case, 1 hour of consecutive data has been measured with time steps of 10 seconds. Such data is then imported to the calibration models for boundary conditions and supply air temperature for the air handling unit.

Tab. 1 - Ceiling panels test specifications.

Parameter	Value	
	Low	High
Supply temperature, °C	18.50	15.09
Return temperature, °C	20.64	17.96
Chilled water flow rate, l/h	337	335
Cooling output per pair, W	205	282

2.3 Measured air temperature and surface temperatures

Surface temperatures were measured at several locations, and the average temperatures for the duration of the tests are written in **Tab. 2**. 1st series refers to the ceiling panels that had chilled water inlet connected to them, and 2nd in series refers to the ones with returned water pipe connected to them.

Tab. 2 – Measured surface temperatures.

Device	Sensor	Temp., °C
Ceiling panels HIGH	1st in series	16.30
	2nd in series	17.75
Ceiling panels LOW	1st in series	19.36
	2nd in series	20.38

The air stratification profile is measured at some data points, and the temperature in the other heights is interpolated. Measured air temperatures in different heights are used to compute vertical temperature gradients inside the zone.

$$G = \frac{t_2 - t_1}{h}, \quad (1)$$

Where t_2 and t_1 are temperatures from the two consecutive temperatures from the measured layers,

and h is the height difference between the two layers.

2.4 Model Calibration

For the calibration, a variable is defined based on the root mean square errors (RMSE) method in order to achieve the lowest possible error between measured temperatures and simulation results. Such minimization will lead to calibrated simulation models. The objective function is written as:

$$f(x) = \sum_{m=1}^{M} \sqrt{\left(\frac{\sum_n (\hat{t}_n^{air} - t_n^{air})^2}{N}\right)} + \sqrt{\left(\frac{\sum_n (\hat{t}_n^{surf} - t_n^{surf})^2}{N}\right)} \quad (2)$$

Where $\hat{t}_n^{air}$ and t_n^{air} are the simulated and measured air temperatures in layer m (m defines the number of the layer in gradient, e.g., m=1 for the temperature at the height of 3m) and $\hat{t}_n^{surf}$ and t_n^{surf} are the surface temperatures of the ceiling panels from simulated and measured results.

The calibration process is written in the steps below:

- The temperature gradients generated, and then plotted together with the temperature gradients from the measurements to create a visual comparative chart.

- The temperature profiles from simulations then compared to the measured profiles. Using RMSE method, two variables are adjusted for calibration.

- The variables *Kfins* and the extra loss factor are adjusted in to minimize the RMSE formula. *Kfins* parameter has impact on surface temperature of the ceiling panels and by adjusting the *Kfins* parameter using RMSE method, the gap between simulated and measured temperature is reduced.

- The profiles with the minimum RMSE are called calibrated models in which *Kfins* and extra loss factor are closer to the real values in experiments.

- Those values then used in annual energy simulations

The cooling capacity parameters are calculated based on the power formula. The formula that is used for power calculations is as follow:

$$P = Kc \times LMTD^N \quad (3)$$

Where P is cooling power, Kc is power law coefficient for cooling, LMTD is the logarithmic mean temperature difference between the air temperature at the height of the panels, supply and return water temperature, and N is power law exponent.

- In the formula, the parameter N is used as the constant provided by the manufacturer, LMTD calculated based on the measured temperatures and cooling power is the average of Kc in LOW and HIGH cases calculated using the power formula based on measured values during the experiments.

In **Fig. 5** and **Fig. 6 t**here are temperature differences between different layers of the air temperature gradients when we compared the measured data to the simulation data, specifically on the layers close to the ceiling. That is due to the fact that IDA ICE 4.9.9 gradient temperature calculations are all based on horizontal layers using the so-called transient zonal model. [10] while the temperature sensors during the tests were in specific point that could have a different temperature than the average of the whole layer in that height.

2.5 Annual Energy Simulation

The parameters used in the simulations are according to EN 16798-1:2019 [8] that are listed below:

- The number of occupants sitting and working in the office is 1.81 (17 m^2/person), the equipment and lighting power are 12 W/m^2 and 6 W/m^2, respectively,

- Air Handling Unit (AHU) supplies air with a constant temperature of 20 °C,

- The office has a Constant Air Volume flow of 2 Litre per second per square meter during office hours (workdays 6 a.m. to 7 p.m.)

- There is no shading for the simulations,

- Windows will never open,

- The operative temperature set-point at the location of the occupant is 26°C, and since such set-points usually results in oversized cooling systems, 3% deviation from this during the cooling period was acceptable for the annual energy calculation.

The resulted cooling energy need from annual energy simulation using the ceiling panels then compared to the energy simulation using an ideal cooler with the same requirements (26°C operative temperature with 3% deviation) in order to identify what air temperature set point using ideal coolers should be used for the annual energy simulations instead of modelling the ceiling panels in details and such difference will be reported as a temperature increment. The emission efficiency of the ceiling panels then calculated by simulating the model with the same parameters using ceiling panels and ideal

cooler. The resulted cooling energy usage using Ideal cooler then divided by energy usage of ceiling panels, to provide the emission efficiency of the ceiling panels.

The formula that is used for emission efficiency calculations is as follow:

$$\text{Efficiency} = \frac{E_{Ic}}{E_C} \tag{3}$$

Where E_C is the annual energy usage of the ceiling panels and E_{Ic} is the annual energy usage of the ideal cooler.

3. Results and discussion

3.1 Model Calibration

The temperature gradients from simulation results and test results for two LOW and HIGH cases are presented in **Fig. 5**. Qualitatively, the absolute values for the LOW case temperature profile is closer to the measurements compared to the HIGH case, while the main temperature difference in the upper layer has offset from the measured values in both cases. However, the shape of the temperature profiles was more similar to the measurements for the HIGH case, but there was an offset of 1.8°C. The absolute temperature of the lower layers fits quite well in the LOW case compared to the HIGH case. The reason for such difference in the upper layer between test measurements and the simulation results in both cases is the fact that the temperature sensors were located in the middle of the two coupled panels in the test, but in the simulation model, such location does not exist. The temperature of the surrounding area of the ceiling panels is lower than points further, resulting in lower temperatures measured in the real test, while IDA ICE 4.9.9 gradient temperature calculations are all based on horizontal layers using the so-called transient zonal model. [7]

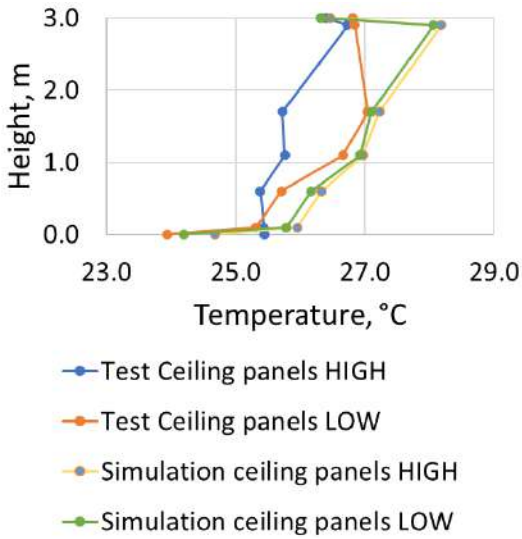

Fig. 5 - The temperature gradient in the test room from sensors measurements and simulation before calibration using MSE method.

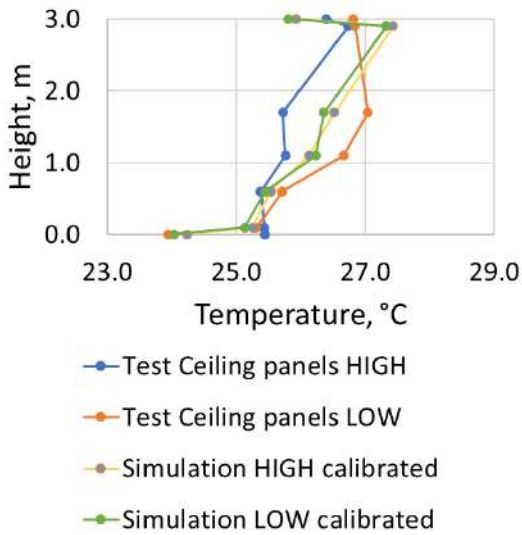

Fig. 6 - The temperature gradient in the test room from sensors measurements and simulation after calibration.

The calibration process using MSE resulted in extra heat loss from room boundary. The result of optimization process and the added heat loss is presented in **Fig. 7**. The temperature gradient profiles after calibration using RMSE method are presented in **Fig. 5** and **Fig. 6.** The calibration is done by minimizing the sum of the squared differences between each of the temperature data points in every height. The surface temperatures of the ceiling panels after calibration are also shown in **Fig. 9** . The surface temperature of the ceiling panel, which is connected to the chilled water input in the coupled system, is lower than the second panel. The measured values are from a point on the ceiling panels, while the simulation results are an average of the temperature on the whole panel. The thermal image of the panels **Fig. 8** shows that the temperature is different at different points of the panels, and such difference can be up to 1 degree.

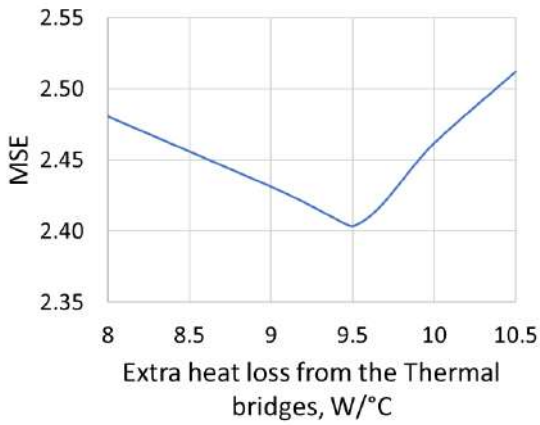

Fig. 7 - The Extra heat loss from thermal bridges resulted from optimization process using MSE.

The surface temperatures and resulting temperature in the height of 2.9m, which is important for cooling capacity and surface temperature calibration, can be summarized in **Fig. 9**. The temperature difference between the surface temperature and air temperature are close for both simulation and test

results, while as it is demonstrated, the temperatures of the upper layer from the simulations are higher.

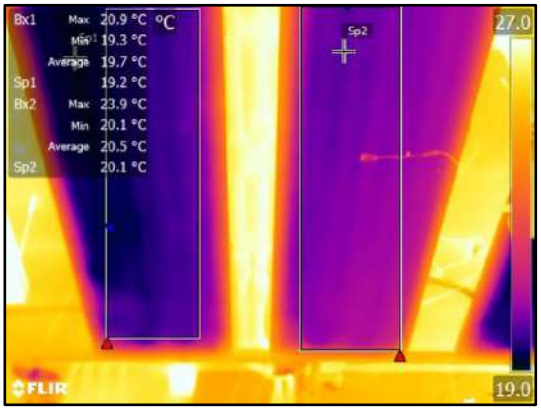

Fig. 8 - Thermal image of the ceiling panels, LOW case.

The *Kc* for each case calculated using the *N* parameter provided in manufacturers handbook (using the power calculation formula provided in the Methods part). The cooling power output of the eight ceiling panels from both LOW and HIGH cases is shown in **Fig. 10**. The *Kc* used in the simulations is the average of *Kc* from LOW and HIGH cases, together with *N* provided by the manufacturer. They both used to generate the Energy simulation results.

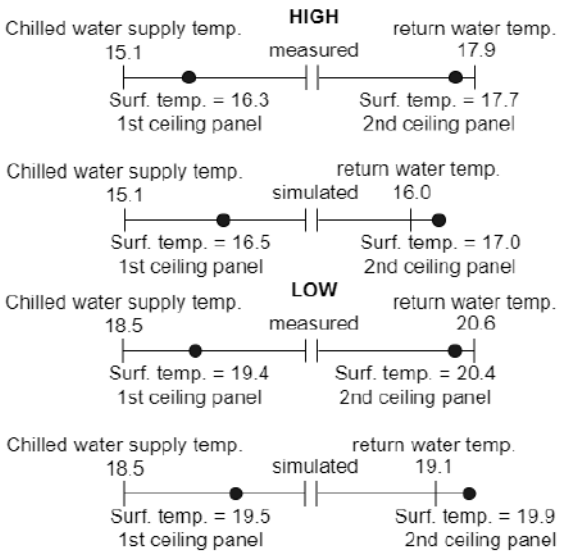

Fig. 9 – The graphical comparison for ceiling panels temperature and resulting air temperature between test results and simulation results.

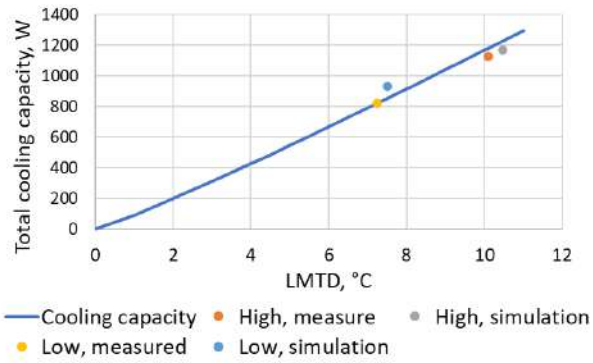

Fig. 10 – The average total cooling power for 8 ceiling panels measured from experiments and calculated in the simulations measured or expected average temperature difference between coolant and room air.

3.2 Annual Energy Simulation

The annual cooling energy use was simulated using two types of controls, PI controller and On/Off controller. The set-point has been adjusted for each type of controller. The adjusted set-points are shown in **Fig. 11**. The duration curves for temperatures from annual energy simulations are indicated in **Fig. 12** for each control strategy.

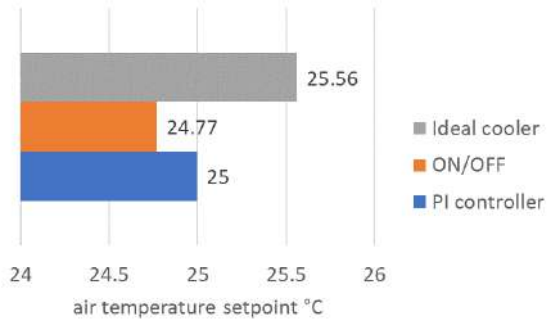

Fig. 11 – air temperature set-points to keep the operative temperature lower than 26 °C during 97% of the cooling period.

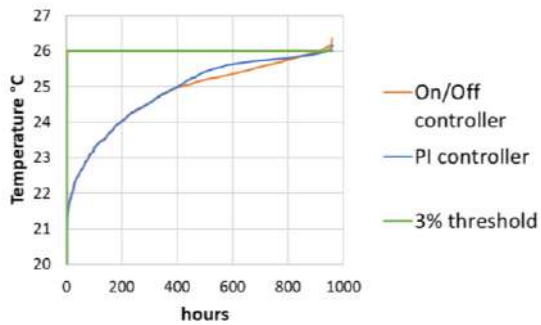

Fig. 12 – Duration curve for occupied hours during cooling months. PI controller and ON/OFF controller

The annual energy usage for each type of control system and their corresponding set-points in the chart of annual energy consumptions using the ideal cooler are shown in **Fig. 13**. As a result, the Total set point increment for the cooling ceiling panel with two different control systems are -0.79 for the ON/OFF controller and -0.56 for the PI controller.

In **Fig. 11**, we showed the resultant set-point rise in air temperature to keep the room at the appropriate operating temperature. This difference in temperature indicates the less energy necessary to overcome inaccurate indoor air stratification and the additional air temperature rise required to attain the desired operating temperature inside the space. This temperature increment is intended to be used in estimations and simulations of cooling energy use with ceiling panels on a monthly, annual, and hourly basis.

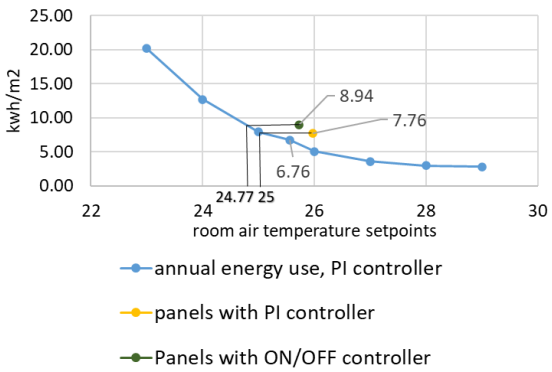

Fig. 13 – annual cooling energy usage curves resulted from simulations with ideal coolers and annual cooling energy usage points resulted from ceiling panels with different control systems.

The emission efficiency of the ceiling panels can be calculated from the annual cooling energy simulations using the ceiling panels and the ideal cooler. The annual energy results are derived from simulation and the emission efficiency can be calculated as follow:

$$\text{Efficiency, PI controller} = \frac{6.76}{7.76} = 87\%$$

$$\text{Efficiency, ON/OFF controller} = \frac{6.76}{8.94} = 76\%$$

3.3 Limitation and future work

The measurements conducted during autumn months between September and November, which are not the main cooling seasons in Estonia, but this timing helped us to reduce the impact of uncontrollable boundary conditions, e.g. solar gains. The internal heat gains were virtually applied using heating dummies and an electric radiator to simulate the real case scenario in summer. These loads are static, while the real internal heat gains vary by time, and therefore the system's inertia and the dynamic cooling loads' effects on the control parameters are not compared with simulation results. Further studies can be conducted to evaluate the possibility of using the room temperature set-point deviation for varying geometry, boundary conditions and control strategies.

In the future, such study can be conducted for other types of cooling systems. Furthermore, the measurements points can be increased to give us a better overview of the temperature gradients and average surface temperatures.

4. Conclusions

Annual energy usage and emission efficiency of ceiling panels for cooling using PI and ON/OFF controllers were assessed with IDA ICE building performance simulation software. The models were then compared to measurements carried out in the autumn of 2021 at the nZEB test facility at Tallinn University of Technology to reflect the accuracy of the building simulation model. The cooling capacity of the ceiling panels was then calibrated in models using actual values from the experiments, which were then used to investigate the energy performance of the systems with annual simulations with the Estonian test reference year and energy simulation input data for office buildings in EN 16798-1:2019.

During the calibration process the unknown values of Kfin and heat loss from the room's boundary were changed in order to have the minimum RMSE value for the temperature profiles measure from tests and calculated in the simulations. The IDA-ICE 4.9.9 [4] zonal model well reproduced the measured air temperatures at different heights in the test room.

The annual cooling energy need of the test room was compared with the same value obtained using an ideal cooler with 100% convective heat emission. Additionally, a single-value performance indicator in the form of an air temperature set-point deviation was obtained for the device and each configuration, as the result of this research, to be used in further hourly, monthly, or annual cooling energy usage calculations. Such increments for the ceiling panels are -0.79 for the ON/OFF controller and -0.56 for the PI controller. The imperfections in air stratification within the room (temperature gradient), the surface temperature of the panels, and additional temperature deviation from the set-point to achieve the desired operative temperature level are the effective parameters on the performance indicator.

Further analysis is needed to determine if room temperature set-point deviation can be applied for different cooling system devices and with varying room geometry, boundary conditions, and cooling control principles.

5. Acknowledgment

This work has been supported by the Estonian Ministry of Education and Research, European Regional Fund (grant 2014-2020.4.01.20-0289), the Estonian Centre of Excellence in Zero Energy and Resource Efficient Smart Buildings and Districts, ZEBE (grant 2014- 2020.4.01.15-0016) funded by the European Regional Development Fund, by the European Commission through the H2020 project Finest Twins (grant No. 856602), the Estonian Research Council grant (PSG409), the Association of the European Heating Industry EHI member companies Irsap Spa, REHAU AG + Co and Zehnder Group International AG.

6. References

[1] Ürge-Vorsatz D, Cabeza LF, Serrano S, Barreneche C, Petrichenko K. Heating and cooling energy trends and drivers in buildings. Renewable and Sustainable Energy Reviews 2015 Jan;41:85–98.

[2] Li R, Yoshidomi T, Ooka R, Olesen BW. Field

evaluation of performance of radiant heating/cooling ceiling panel system. Energy and Buildings 2015, Jan, 13;86:58–65.

[3] EN 15316-2:2017, "Energy performance of buildings. Method for calculation of system energy requirements and system efficiencies. Part 2: Space emission systems (heating and cooling), Module M3-5, M4-5,." CEN, Standard, (2017).

[4] EQUA, "IDA ICE - Indoor Climate and Energy," EQUA, Stockholm, Sweden, Tech. Rep., (2013). http://www.equaonline.com/iceuser/pdf/ice45eng.pdf.

[5] Võsa K-V, Ferrantelli A, Kurnitski J. Annual performance analysis of heat emission in radiator and underfloor heating systems in the European reference room. E3S Web of Conferences 2019;111:04009.

[6] Eriksson L, Grozman G, Grozman P, Sahlin P, Havgaard Vorre M, Ålenius L. CFD-Free, Efficient, Micro Indoor Climate Prediction in Buildings. Building Simulation and Optimization Conference. 2012

[7] Võsa K-V, Eist E, Kurnitski J. Experimental study on the cooling emission efficiency of ceiling panels, underfloor cooling, and fan-assisted radiators. CLIMA2022. 2022

[8] Standard - Energy performance of buildings - Ventilation for buildings - Part 1: Indoor environmental input parameters for design and assessment of energy performance of buildings addressing indoor air quality, thermal environment, lighting and acoustics - EN 16798-1:2019.

[9] Kalamees T, Kurnitski J. Estonian test reference year for energy calculations. Proceedings of the Estonian Academy of Sciences Engineering. 2006;12(1):40.

[10] Georges L, Thalfeldt M, Skreiberg Ø, Fornari W. Validation of a transient zonal model to predict the detailed indoor thermal environment: Case of electric radiators and wood stoves. Building and Environment 2019 Feb;149:169–81.

Unsteady Ventilation in a Scaled Room Model with Swirl Ceiling Diffusers

Eva Mesenhöller [a,b], Steffen Jacobs [a,c], Peter Vennemann [a], Jeanette Hussong [c]

[a] Department of Energy, Building Services, and Environmental Engineering, FH Münster, Steinfurt, Germany, eva.mesenhoeller@fh-muenster.de, s.jacobs@fh-muenster.de, vennemann@fh-muenster.de.

[b] Chair of Hydraulic Fluid Machinery, Faculty of Mechanical Engineering, Ruhr-University Bochum, Bochum, Germany.

[c] Institute for Fluid Mechanics and Aerodynamics, Faculty of Mechanical Engineering, Technical University Darmstadt, Darmstadt, Germany, hussong@sla.tu-darmstadt.de.

Abstract. Mechanical ventilation of buildings is generally based on steadily operating systems. This field is well known and established. But, an approach based on time-varied supply flow rates might improve indoor air quality, comfort, and energy consumption. Typical time-scales of the variation are in the order of seconds or minutes. Until now, the effects of unsteady ventilation scenarios are not fully described and so, reliable dimensioning rules are missing. Hence, with a better understanding of the flow in unsteady ventilation, systems can be calculated and optimised. To understand the effective mechanisms and derive functional relations between the flow field and variation parameters, full-field optical flow measurements are executed with a particle image velocimetry (PIV) system. Experiments are conducted under isothermal conditions in water in a small-scale room model (1.00 m × 0.67 m × 0.46 m) with two swirl ceiling diffusers, Reynolds-scaling assures similarity. In a series of experiments, the effects of different unsteady ventilation strategies on the flow fields are investigated and compared to steady conditions with the same mean exchange rate. Mean exchange rates, signal types, periods, and amplitudes are varied. Time-averaged normalised velocity fields already indicate notable differences between steady and unsteady cases especially for lower exchange rates: the distribution is more homogeneous in unsteady scenarios compared to steady conditions, and low-velocity areas are reduced while the mean velocity of the room increases. So, unsteady ventilation might be beneficial in terms of improved ventilation and energy savings in partial-load operation. Fast Fourier Transformation (FFT) analyses of the mean velocity for each field over the whole series detect the main frequency of the volume flow variation. By dividing the velocity field into smaller areas, this main frequency is still detected especially in the upper part of the room, but side frequencies play a role in the room as well.

Keywords. unsteady ventilation, PIV, room airflow, mixing ventilation.
DOI: https://doi.org/10.34641/clima.2022.200

1. Introduction

Ventilation and air conditioning are an important technology in modern, highly-insulated and airtight buildings – not only about preventing mould by ensuring a sufficient air exchange but also about maintaining good indoor air quality for occupants. As a result of the Covid-Pandemic, the focus has shifted to ventilation and air conditioning systems and hygienically necessary air exchange rates to prevent the virus concentration in the occupied zone from rising above a critical level at which occupants can become infected. But also climate change and resulting higher outdoor temperatures are contributing factors for an increasing demand for air conditioning in buildings. However, despite improved building standards and well-established approaches to reduce the energy consumption of ventilation and air conditioning systems, such as heat recovery, speed-controlled fans, or demand-controlled ventilation rates, the energy consumption for ventilation and air conditioning in buildings is increasing [1–3].

A newer approach with potential for reducing the energy consumption of ventilation and air conditioning could be found in so-called unsteady ventilation systems, where supply flow rates or temperatures are varied in short time intervals (seconds, minutes). Kaup [4, 5] for example

Copyright ©2022 by the authors. This conference paper is published under a CC-BY-4.0 license.

registered energy savings in the range of up to 20 % (heat) and up to 40 % (electricity) while improving the room airflow and comfort. Additionally, energy savings can be achieved in scenarios with high temperatures, as set-point temperatures can be increased because occupants still feel comfortable at higher temperatures due to the air movement (e.g. [6–8]). Scientific and industrial studies indicate that this mode of operation can furthermore improve comfort (e.g. [9–11]), mixing, and velocity/ temperature/pollutant distributions (e.g. [12–15]). More detailed descriptions of the state of the art in science and technology at national and international level are summarised in a review article [16]. Complete scientific explanations for the observed effects have not yet been derived. A first explanatory attempt for enhanced mixing through vortex structures was reported by Sattari [13] and Fallenius [17]. A wide use in practice is currently prevented due to the lack of design rules, standardised systems, or suitable software. Hence, the identification and explanation of effective mechanisms and functional relations between parameters and room airflow are essential for developing such design rules and calculation bases.

Room airflows are usually analysed by punctual measurements of velocities or temperatures. So, information about conditions in the room is only of a discrete type, or simply visualised with smoke gas experiments. Through full-field measurements using PIV combined with computational fluid dynamics (CFD), flow structures can be recorded and analysed entirely with a high level of detail at different points in time. Measurement and simulation data confirm and support each other. Statistical design of experiments offers the possibility not only to find the effects of single parameters on the flow, but also to uncover interactions between different parameters. With the help of the results from both approaches, a better understanding of room airflow in unsteady ventilation is to be gained to derive practice recommendations.

The purpose of this article is to describe findings from two-dimensional PIV-measurements on flow structures and velocity fields in a scaled model room under isothermal conditions and to draw comparisons between steady and unsteady modes of operation at different mean exchange change rates. The unsteady mode of operation was generated by varying the supply volume flow over time, using two different signal types. In addition, diffuser types, cycle durations, and amplitudes of the signals were varied. Pulse lengths of high and low volume flows were of equal duration. The focus of these measurements is on the effects of previously described operating parameters on the flow field in the entire room, especially the large-scale structures. Inlets used in the investigations described in this article were scaled swirl ceiling diffusers. Within the scope of the investigations, the following questions are to be clarified:

- Do flow structures in unsteady ventilation differ from those in steady-state ventilation?
- Do velocities and flow structures follow the volume flow variation?
- Is the velocity distribution more homogeneous in the unsteady case?

Finally, the article shall give hints on where to set the focus in future experiments.

2. Research Methods

2.1 Scale Model

For the investigation of the entire flow field in the room with a PIV-system, smaller dimensions than in real facilities must be considered. Scale models are an established method in fluid mechanics to guarantee similar conditions. Here, relevant dimensionless parameters have to be kept constant in real and scaled setups. There are no heat sources or temperature differences between supply and room in the experimental setup, leading to almost isothermal conditions without buoyancy effects. Hence, the relevant dimensionless parameter is the Reynolds-number according to Posner et al. [18], and Anderson and Mehos [19]. Thus, it is possible to analyse the effects of different unsteady ventilation strategies on the “basic” flow structures.

The model room (1.00 m × 0.67 m × 0.46 m) is geometrically related to the air-conditioning test room at FH Münster (6.22 m × 4.19 m × 2.86 m). Water is used instead of air in the scaled model. As dimensions and kinematic viscosity decrease in the model, velocities and times have to be multiplied by the factors from Tab. 1 to obtain quantities in the non-scaled room. Reynolds numbers in the experiments mentioned are between 14 900 and 22 300.

Tab. 1 – Scale factors (test room / scale model).

	dimensions	time	velocity	kin. viscosity
factor	6.25	2.73	2.29	14.33

Two supply inlets are symmetrically arranged in the ceiling at the room’s centre line. Five smaller return outlets are located in the room’s rear wall above the floor. The room is placed inside a 1 m^3 water tank. A pump in the tank transports the water through pipes and valves from the tank to the supply inlets. Flow rates can be regulated by three valves, where the pneumatic valve generates the flow rate variations in unsteady cases. Magnetic-inductive flow metres in each supply pipe measure the flow rates. Valves and flow metres are connected to a PLC control and flow rates are recorded during PIV-measurements. The setup is shown in Fig. 1. 3D-printed models of real swirl ceiling diffusers are used as inlets with an effective opening area of 0.0011 m^2. The pipe diameter is constantly reduced with 3D-printed nozzles in front of the diffusers.

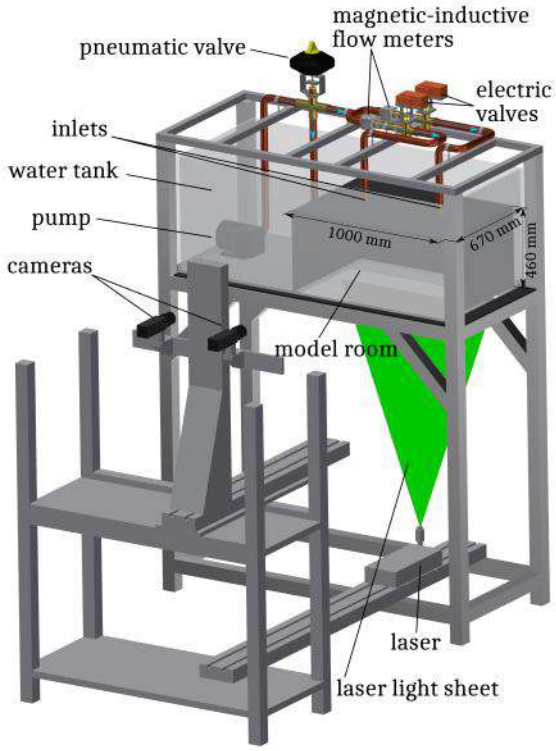

Fig. 1 – Experimental setup. PIV-system consisting of two cameras in front of the model room (one for each half of the room) and a laser under the water tank generating a light sheet. Seeded water is pumped through the pipe system to the diffusers in the ceiling of the model room. A pneumatic valve creates flow rate variations. Blue arrows indicate the flow direction.

2.2 Particle Image Velocimetry (PIV)

Two-dimensional PIV is used to investigate the flow field in the model room. It is a non-invasive, optical measuring technique with which entire flow fields can be analysed. The flow has to be seeded with small particles. The basic principle of PIV is described as follows [20, 21]: a light source generates two flashes to illuminate particles inside a measurement plane and a camera takes pictures of the particles simultaneously to the flashes. Simultaneity is guaranteed by a timing unit. The images are divided into smaller areas, so-called interrogation windows. Inside these interrogation windows, particle patterns in the image pairs are evaluated by cross-correlation algorithms to obtain the local shift. Velocities are then calculated by the known time interval between the acquisitions, resulting in a velocity field with high resolved information that can be used to derive further quantities.

In the experiments, the light source is a 200 mJ double-pulsed Nd:YAG laser (Litron Nano PIV L) with a wavelength of 532 nm. Images are acquired by two side-by-side arranged 5 Mpx double-frame CCD-cameras (LaVision Imager Pro SX 5M) with 7 Hz acquisition rate. Wide-angle lenses (Nikon AF Nikkor 35mm 1:2D) were used. The magnification factor was 4.33458 px mm^{-1}. Vestosint 1101 by Evonik was used as tracer particles (particle size distribution: 100 % <250 µm, ≥45 % <100 µm, ≤2 % <32 µm). The measurement plane is located in the centre line of the room right under the supply inlets, as can be seen in Fig. 1. A 90° deflection element and light-sheet optics (*f*=*-9.7* mm) were used to generate the measurement plane. The time between the exposures of the first and the second frame depends on the flow properties; here it is between 9 ms (maximum exchange rate) and 15 ms (minimum exchange rate). This time was chosen as a compromise between resolving higher velocities at the diffusers and lower velocities in the room. If the chosen time delay is too long, higher velocities cannot be calculated since the particles have moved out of the interrogation window, but lower velocities can be resolved with good accuracy. This is also a problem if there is a high out-of-plane motion. If the chosen time delay is too short, lower velocities cannot be resolved any more as the particles seem to have no motion, but higher velocities can be calculated. The setup was calibrated by using LaVision's software DaVis 8.4 with a calibration plate of the size of the measurement plane placed at the location of the light sheet. To guarantee a correct mapping of the processed vector fields, there has to be an overlap area acquired by both of the cameras with a size of at least 10 % of the measurement width. The size of the interrogation windows is decreased from 64 px × 64 px to 16 px × 16 px during the multi-pass processing procedure. The overlap was 50 % and two passes were selected for each step. Spurious vectors in the velocity fields were identified by using the universal outlier detection by Westerweel and Scarano [22] and removed during multi-pass processing. In the last step, the processed vector fields of both cameras are merged to create one vector field for the whole model room.

2.3 Experimental Design

Five different factors were identified for possibly influencing the flow; three of a quantitative nature (a-c), and two of a qualitative one (d, e):
a) offset (mean supply flow rate) (OFF)
b) amplitude (AMP)
c) cycle duration (CYC)
d) inlet type (INL)
e) signal type (SIG)
Test planning is based on fractional factorial design of experiments, as it enables both main effects and twofold interactions between factors to be identified. Higher-order interactions are negligible [23]. A 2^{5-1} design was chosen with two settings for each factor, extended by centre point testing. For the full study, 16 different experiments, completed by eight centre point tests (each combination of qualitative factors tested twice at the centre point settings of the quantitative ones) had to be performed to identify possible deviations from linearity. So there were three different settings for each quantitative factor and two for the qualitative ones. This article presents one part of the complete study. Tab. 2 shows the relevant extract of the experimental design and related factor settings.

Tab. 2 – Overview of the experimental design for experiments in the scale model. - and + are factor settings of the 2^{5-1} design, o is the centre point setting.

No.	OFF	AMP	CYC	INL	SIG
-	3.33 m^3h^{-1}	0.25	0.05	nozzle	sine
o	4.16 m^3h^{-1}	0.5	0.125	/	/
+	4.99 m^3h^{-1}	0.75	0.2	swirl	square
1	-	-	-	+	-
2	-	-	+	+	+
3	-	+	-	+	+
4	-	+	+	+	-
5	+	-	-	+	+
6	+	-	+	+	-
7	+	+	-	+	-
8	+	+	+	+	+
9	o	o	o	+	-
10	o	o	o	+	+
11	o	o	o	+	-
12	o	o	o	+	+

Additionally, measurements of the corresponding steady scenarios with comparable mean exchange rates were conducted. The offset was derived by typical mean exchange rates, respectively 4 h^{-1}, 5 h^{-1} and 6 h^{-1} in non-scaled dimensions. The corresponding nominal time constants in the scaled model are 330 s, 264 s, and 220 s. All values in Tab. 2 are based on the scaled model. Parameters for the amplitude in Tab. 2 represent the proportion of the smallest difference between offset value and the total maximum/ minimum of the system to realize the maximum possible fluctuation range, see Fig. 2 for a graphical explanation of the procedure.

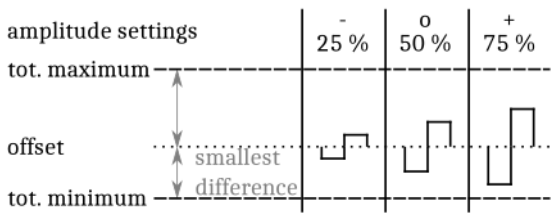

Fig. 2 – Amplitude definition for the settings -, o, and + from Tab. 2. Percentage values refer to the proportion of the smallest difference between offset and total minimum/maximum.

Parameters for the cycle duration in Tab. 2 indicate the proportion of the nominal time constant used for the variation, analogous to the definition of van Hooff and Blocken [14]. Using the proportions from Tab 2, the actual settings for amplitude and cycle duration in Tab. 3 can be calculated.

Tab. 3 – Actual settings for factors AMP and CYC for different offsets in the scale model.

OFF	AMP [m^3h^{-1}]			CYC [s]		
[m^3h^{-1}]	-	o	+	-	o	+
3.33	0.67	-	2.00	16.5	-	66.0
4.16	-	0.92	-	-	33.0	-
4.99	0.25	-	0.76	11.0	-	44.0

3. Results and Discussion

3.1 Prerequisites

For sine wave signals, the acquisition was started at the offset (on the downward slope of the wave), and for square waves, it was started at the beginning of the low period. Spurious vectors were removed before further analyses of the vector fields and replaced by the median of their neighbours. The definition of the occupied zone is based on DIN EN 16798-3 (0.05-1.8 m height, 0.5 m to walls): It is located between $y/H=-0.98$ and $y/H=-0.37$ and $x/L=0.08$ and $x/L=0.92$, where y is the actual height and H is the full height of the room and x is the actual length and L is the full length of the room.

3.2 Time-Averaged, Normalised Velocity Fields

To ensure comparability between the cases, the following velocity fields are presented in normalised form. The normalisation is based on the time-averaged velocity at the supply inlets during the measurements. Colours indicate the velocity magnitude and arrows show the flow direction. To ensure good visibility of the lower velocities in the model room, maximum normalised velocity in the contour plots was set to $u/u_0=0.15$, where u is the actual velocity and u_0 is the mean velocity at the inlets. Time-averaged velocity fields in steady cases are based on 250 single pictures, and in unsteady cases on the number of pictures acquired during three full cycle durations.

Fig. 3, 4 and 5 show the time-averaged normalised velocity fields at minimum, medium and maximum mean exchange rates; the reference cases with steady conditions are shown in subfigures a). Mean normalised velocity fields of all cases presented show expectable flow structures: the inlet flow radially spreads out under the ceiling after exiting the swirl diffusers in the model room. The mean flow direction changes at the walls and in the middle of the room where the jets merge. Differences between the average velocity fields of steady and unsteady scenarios are present especially in case of minimum exchange rates, as can be seen in Fig. 3.

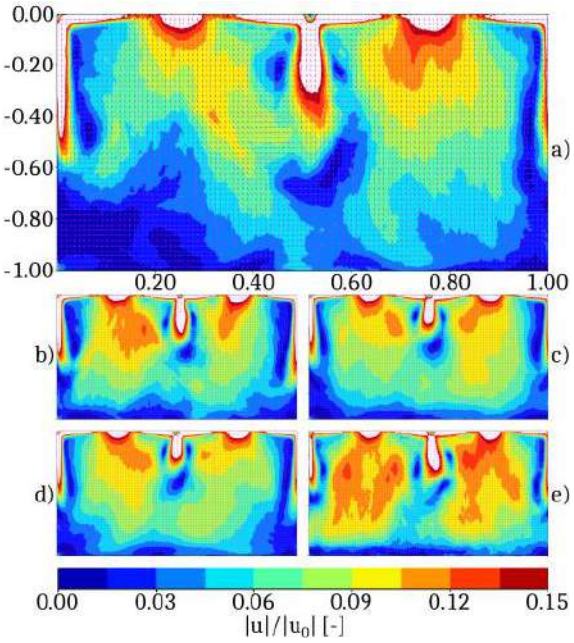

Fig. 3 – Time-averaged, normalised velocities for minimum exchange rates: a) steady case Ref. 1, b) Exp. No. 1, c) Exp. No. 4, d) Exp. No. 2, e) Exp. No. 3.

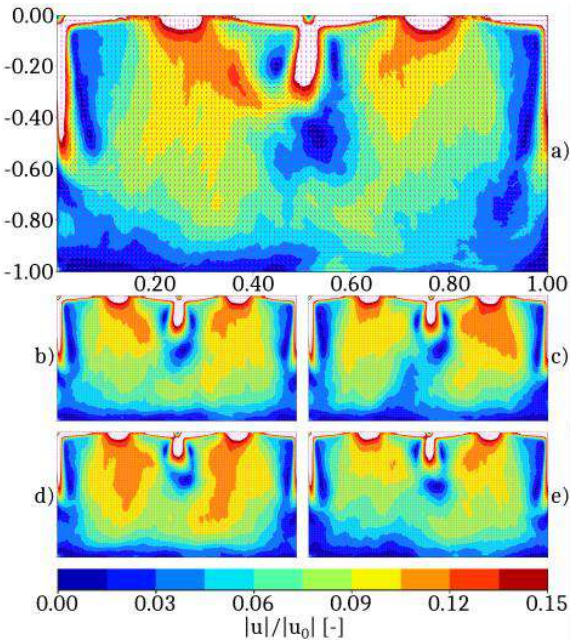

Fig. 4 – Time-averaged, normalised velocities for medium exchange rates: a) steady case Ref. 2, b) Exp. No. 9, c) Exp. No. 11, d) Exp. No. 10, e) Exp. No. 12.

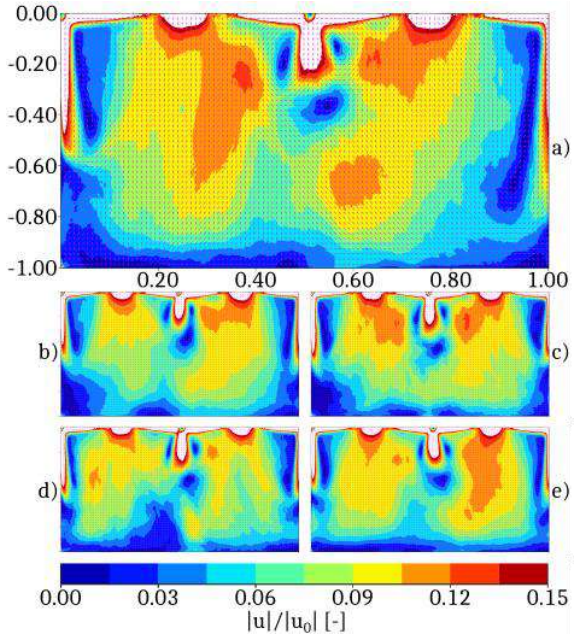

Fig. 5 – Time-averaged, normalised velocities for maximum exchange rates: a) steady case Ref. 3, b) Exp. No. 6, c) Exp. No. 7, d) Exp. No. 5, e) Exp. No. 8.

Tab 4 presents a summary of the mean velocities at the inlets (v_{in}), mean (v_{mean}), and median velocity (v_{median}), the difference between 95 % percentile and 5 % percentile ($p_{95\text{-}5}$) of the whole velocity field, and the relative deviation of $p_{95\text{-}5}$ in unsteady cases related to the steady cases (Δ).

Tab. 4 – Statistical data of time-averaged, normalised velocity fields; Exp. No. refer to Tab. 2.

No.	v_{in} [ms^{-1}]	v_{mean} [ms^{-1}]	v_{median} [ms^{-1}]	$p_{95\text{-}5}$ [ms^{-1}]	Δ [%]
Ref.1	0.43	0.066	0.059	0.129	-
1	0.43	0.073	0.069	0.126	-2.33
2	0.43	0.072	0.071	0.111	-13.95
3	0.43	0.085	0.088	0.110	-14.73
4	0.43	0.073	0.073	0.114	-11.63
Ref.3	0.64	0.080	0.079	0.116	-
5	0.64	0.075	0.075	0.118	+1.72
6	0.64	0.075	0.074	0.115	-0.86
7	0.64	0.079	0.080	0.124	+6.90
8	0.64	0.080	0.080	0.116	0.00
Ref.2	0.54	0.073	0.069	0.117	-
9	0.54	0.076	0.076	0.117	0.00
10	0.53	0.080	0.083	0.110	-6.00
11	0.54	0.075	0.074	0.120	+2.56
12	0.54	0.072	0.071	0.114	-2.56

Mean and median velocities increase for all unsteady cases with a minimum exchange rate compared to the steady scenario. This behaviour can also be found for medium exchange rates, except for Exp. No. 12. The highest increase can be recognised for Exp. No. 3 (minimum exchange rate), and Exp. No. 10 (medium mean exchange rate). For maximum exchange rates, the velocities tend to decrease under unsteady conditions, except for Exp. No. 8. Taking the difference between 95 % percentile and 5 % percentile into account, a reduction can be recognised for unsteady cases with a minimum exchange rate. This can be interpreted as a more homogeneous velocity distribution under unsteady conditions as the range of velocities gets smaller. For medium and maximum exchange rates, reductions can be detected only for some cases.

3.3 Frequency Analysis of Instantaneous Velocity Fields

Instantaneous velocity fields are analysed via FFT to check for main and secondary frequencies. The sampling frequency of 7.0 Hz was considerably higher than the frequency required according to the Nyquist-Shannon theorem to correctly detect the frequencies of the volume flow variations. The following questions should be answered after analysing the frequencies of the velocity fields:

- Is it possible to detect the variation frequency in the mean velocity of the whole velocity field?
- In which areas of the velocity field are the main frequencies detected strong?

For answering these questions, the following analyses were performed:

- FFT-analysis of the series of mean velocities in each velocity field
- FFT-analysis of the series of mean velocities in small areas in each velocity field (in the further course called "regional FFT")

In a first step, a mean velocity was calculated for each instantaneous velocity field of the full series and analysed via FFT. As expected, steady scenarios did not show remarkable magnitudes, while unsteady scenarios did. The frequency of the flow rate variations was detected as the frequency with the highest magnitudes in all cases except for Exp. No. 5, see Tab 5. In Exp. No. 5, the magnitudes themselves were of a low level (between 0.13 and 0.17) and there is a region without a clear peak between the frequencies 0.030 s^{-1} and 0.121 s^{-1}. A low peak level of the FFT-results was also present for Exp. No. 1, 3, 6, and 7 with the highest magnitudes smaller than 1.0. In experiments with the same cycle durations, magnitudes of the FFT were higher for cases with higher amplitudes. Experiments with the same mean exchange rates showed the highest magnitudes for those cases with longer cycle durations. Magnitudes for all centre point experiments varied between 1.98 and 2.50 with slightly higher peaks for square wave signals.

Tab. 5 – Highest magnitudes and related frequencies of the FFT-analyses of mean velocities.

No.	Magnitude [-]	Frequency [s^{-1}]
1	0.35	0.061
2	5.79	0.015
3	0.96	0.061
4	12.54	0.015
5	0.17	0.061
6	0.87	0.023
7	0.42	0.091
8	4.14	0.023
9	1.98	0.030
10	2.27	0.030
11	2.17	0.030
12	2.50	0.030

Results of the regional FFT-analyses with the highest peaks for each mean exchange rate (see Tab. 5) are displayed in Fig. 6. Velocity fields were divided into small regions of the size of 20 mm × 18.4 mm (50 boxes in x-direction and 25 boxes in y-direction). Mean velocities per box were calculated for the whole series and FFT-analyses were performed for each region. The colours of the boxes in Fig. 6 indicate the magnitude of the FFT for the main frequency. Highest magnitudes are detected in the upper centre of the room in the merging area of the jets, but the occupied zone is also influenced by the variation frequency. Secondary frequencies may influence other parts of the room.

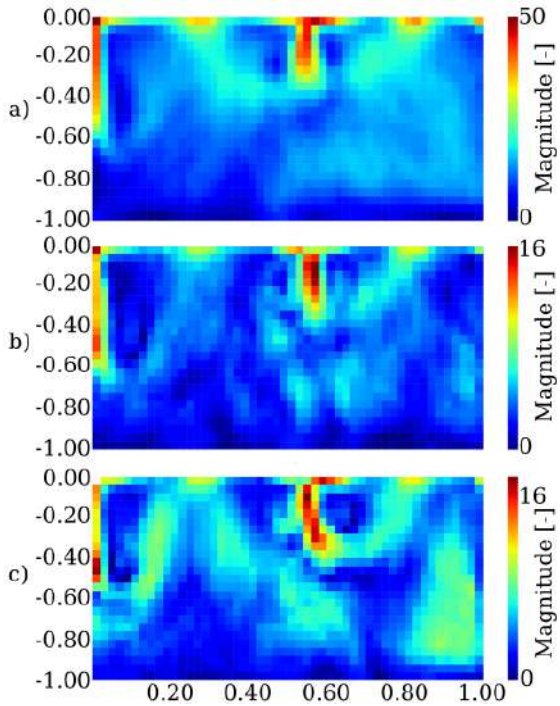

Fig. 6 – Regional magnitudes of the main frequency: a) Exp. No. 4, b) Exp. No. 12, c) Exp. No. 8.

4. Conclusions

Average velocity fields of steady and unsteady cases already showed differences in local velocities. Single velocity fields of all steady reference cases did not vary over time and showed comparable structures to average velocity fields, which is also proved by a constant standard deviation. Single velocity fields of the unsteady cases differed in time, depending on the conditions of the supply flow rate. The frequency of the supply flow rate variations could also be detected as the main frequency in the velocity changes. Consequently, it is inevitable, that instantaneous velocity fields and not averaged values have to be taken into account for analysing the effects of unsteady ventilation scenarios. This kind of ventilation seems to have a stronger impact under lower mean exchange rates.

Taking into account the results presented in this article, the three main questions asked in the introduction can be answered as follows:

1. Do flow structures in unsteady ventilation differ from those in steady-state ventilation?

Flow structures in the room are influenced by supply flow rate variations, which can already be seen in time-averaged velocity fields, especially for minimum exchange rates. Here, also the lower part of the room seems to be affected by the variable flow rates, as velocities in unsteady cases increase in this part.

2. Do velocities and flow structures follow the volume flow variation?

FFT analyses of the velocity fields detect the frequency of the flow rate variation as the dominating frequency in the room, but secondary frequencies can be identified in some cases as well. Regional FFT shows that especially the merging zone of the jets is affected by the variation frequency.

3. Is the velocity distribution more homogeneous in unsteady cases?

Time-averaged velocity fields indicate a more homogeneous velocity distribution and higher mean velocities, especially for minimum exchange rates. In this article, a difference between 5 % and 95 % percentile is used to derive a measure of homogeneity. This quantity was compared to steady conditions and varied between -2.33 % and -14.73 % for minimum exchange rates meaning that the spread of velocities decreases.

5. Outlook

This study gives first indications that the effects of supply flow rate variations are stronger in lower exchange rates. This can be inferred by comparing the difference in percentiles and mean velocities to the reference cases. If the greatest effects occur at lower exchange rates, this would support an improvement of the ventilation in part-load operation and energy-savings. In further investigations, the focus should therefore be set on low exchange rates.

Furthermore, it is necessary to derive functional relations between unsteady ventilation scenarios and flow quantities to draw conclusions that are beneficial for a wider practical application of unsteady ventilation scenarios. Subsequently, the experimental data will be used to validate a CFD model. With the help of this model, further parameter studies will be carried out via simulations under isothermal conditions. Effects and interactions of factors will be evaluated after finishing the whole series of experiments to draw conclusions, derive functional relations, and develop dimensioning rules or application recommendations. Effects of contrary supply flow rates and non-equally timed high and low periods should also be considered in future experiments.

The results presented in this article indicate the necessity of using time-resolved measurements, e.g. for vortex tracking. As the flow has a strong three-dimensional property, three-dimensional velocity measurements using particle tracking velocimetry (PTV) would help to gain a deeper understanding of the mechanisms and development of flow structures in the ventilated room.

6. References

[1] Diefenbach N., Cischinsky H., Rodenfels M., et al. Datenbasis Gebäudebestand: Datenerhebung zur energetischen Qualität und zu den Modernisierungstrends im deutschen Wohngebäudebestand. IWU Darmstadt. 2010.

[2] Bettgenhäuser K., Boermans T., Offermann M., et al. Klimaschutz durch Reduzierung des Energiebedarfs für Gebäudekühlung. UBA Dessau-Roßlau. 2011.

[3] Koch M., Kenkmann T., Winger C., et al. Klimatisierungsbedarf und dafür abgerufener Stromverbrauch für Wohngebäude in Deutschland von 2020 bis 2050. Öko-Institut e.V. Freiburg. 2017.

[4] Kaup C. Impulslüftung für bessere Luftqualität. Instationäre RLT-Anlage zur intermittierenden Raumlüftung. Tech am Bau. 2012; 43: 54–59.

[5] Kaup C. Höhere Luftqualität mit geringerer Luftmenge. TGA Fachplaner. 2013; 1–8.

[6] Huang L., Ouyang Q., Zhu Y. Perceptible airflow fluctuation frequency and human thermal response. Build Environ. 2012; 54: 14–19.

[7] Kabanshi A. Experimental study of an intermittent ventilation system in high occupancy spaces. 2017.

[8] Zhou X., Ouyang Q., Lin G., et al. Impact of dynamic airflow on human thermal response. Indoor Air. 2006; 16: 348–355.

[9] Luo M., Yu J., Ouyang Q., et al. Application of dynamic airflows in buildings and its effects on perceived thermal comfort. Indoor Built Environ. 2018; 27: 1162–1174.

[10] Wigö H. Effects of intermittent air velocity on thermal and draught perception -A field study in a school environment. Int J Vent. 2013; 12: 249–255.

[11] Zhu Y., Luo M., Ouyang Q., et al. Dynamic characteristics and comfort assessment of airflows in indoor environments: A review. Build Environ. 2015; 91: 5–14.

[12] Lichtner E., Kriegel M. CFD-Studien zur intermittierenden Belüftung von Räumen – Potenzialanalyse und vereinfachte Modellierung. In: BauSIM. 2014; 536–540.

[13] Sattari A. Investigations of Flow Patterns in Ventilated Rooms Using Particle Image Velocimetry. KTH Royal Institute of Technology. 2015.

[14] van Hooff T., Blocken B. Mixing ventilation driven by two oppositely located supply jets with a time-periodic supply velocity: A numerical analysis using computational fluid dynamics. Indoor Built Environ. 2020; 29: 603–620.

[15] Backes C., Kaup C. Möglichkeit zur Luftmengenreduzierung. Steigerung der Effektivität der Verdünnungsströmung durch Intermittierende Raumlüftung - Teil 1. HLH. 2016; 67: 17–21.

[16] Mesenhöller E., Vennemann P., Hussong J. Unsteady room ventilation – A review. Build Environ. 2020; 169: 106595.

[17] Fallenius BEG., Sattari A., Fransson JHM., et al. Experimental study on the effect of pulsating inflow to an enclosure for improved mixing. Int J Heat Fluid Flow. 2013; 44: 108–119.

[18] Posner JD., Buchanan CR., Dunn-Rankin D. Measurement and prediction of indoor air flow in a model room. Energy Build. 2003; 35: 515–526.

[19] Anderson R., Mehos M. Evaluation of indoor air pollutant control techniques using scale experiments. In: ASHRAE Conference IAQ. 1988; 193–208.

[20] Adrian RJ., Westerweel J. Particle image velocimetry. Cambridge University Press. 2011.

[21] Raffel M., Willert C., Wereley ST., et al. Particle Image Velocimetry (3rd ed.). Springer. 2018.

[22] Westerweel J., Scarano F. Universal outlier detection for PIV data. Exp Fluids. 2005; 39: 1096–1100.

[23] Kleppmann W. Versuchsplanung - Produkte und Prozesse optimieren (8th ed.). Hanser . 2013.

Data Statement

The datasets generated during and/or analysed during the current study are not publicly available because they are part of a comprehensive study, which will be published in the near future in an aggregated form, but are/will be available after contacting the author in the meantime.

CO_2 levels as an indicator of ventilation performance in mechanical ventilated buildings

Natalia Lastovets [a], Piia Sormunen [a], Ksenia Ruuska [a]

[a] Faculty of Built Environment, Tampere University, Tampere, Finland, natalia.lastovets@tuni.fi, piia.sormunen@tuni.fi, ksenia.ruuska@gmail.com

Abstract. The current COVID-19 pandemic has attracted considerable attention from the general public and researchers. To increase this resilience toward global pandemics, we urgently need a deeper understanding of effective protection strategies. During the COVID-19 pandemic, more evidence confirms that airborne transmission plays an essential role in spreading pathogens. The ventilation systems play an important role in removing pathogens from indoor air. The current paper focuses on examining the air ventilation performance of the existing building stock before Covid 19 pandemic. The study was carried out in mechanical ventilated 440 spaces in four different building types by comparing the obtained individual CO_2 concentration data with the maximum concentration values given by official regulations, recommendations and guides. The data was obtained from the property maintenance program for one month at 5-15 minutes intervals. The risk spaces were studied in detail, and the risk analysis was conducted by applying the Wells-Riley approach. The research proposes recommendations for utilising air ventilation systems in different applied cases.

Keywords. Indoor air quality, Carbon dioxide, COVID-19, Ventilation system
DOI: https://doi.org/10.34641/clima.2022.113

1. Introduction

The COVID-19 disease caused by the pathogen identified as severe acute respiratory syndrome coronavirus 2 (SARS-CoV-2) has spread worldwide, resulting in a global pandemic. Studies have revealed that SARS-CoV-2 is spread human-to-human through close contact, respiratory droplets, fomites, and contaminated surfaces predominately in indoor environments [1]. Therefore, ventilation of the premises is of great importance in controlling Covid-19 infection. Poorly ventilated places are considered a high risk of infection and occupants' exposure [2].

Carbon dioxide can be considered an indirect but very objective indicator of indoor air pollution [3]. Concentrations of carbon dioxide in indoor air are mainly due to two factors such as carbon dioxide concentrations in outdoor air (about 400 ppm) and the metabolism of people in the premises (exhaled air about 50,000 ppm). Without proper ventilation, CO_2 concentrations in premises will rise rapidly to high levels. In previous studies, carbon dioxide monitoring has been used to identify measures to improve ventilation in settings such as schools and offices [4]. However, excessive carbon dioxide levels have also been connected to headaches, fatigue and reduced work capacity [5]. In addition to that, the risk of indoor airborne infection transmission could be directly estimated via measurements of CO_2 in well-mixed conditions [6].

The Wells–Riley model has been widely used for quantitative infection risk assessment of respiratory infectious diseases in indoor premises [6]. The method has been already adopted to calculate the infection risk for different activities and rooms using a standard airborne disease transmission Wells-Riley model calibrated to COVID-19 with the correct source strength (quanta emission rates) [7]. In this study, the Wells–Riley model is applied to predict the risk to get infected by coronavirus calculated with quanta values for the Delta variant of the virus.

This study aims to show the preliminary approximate results on the effect of ventilation on the spread of coronavirus by air. In addition, the carbon dioxide concentrations in the indoor air are under consideration. Finally, the study provides a general overview of the predicted risk of coronavirus in different building types.

2. Methods

This study aims to review current regulations, guidelines, and recommendations regarding the CO_2 concentrations in premises and design airflow rates. The research also focuses on how the CO_2 concentrations measured before the corona pandemic in the different building types relate to the recommendations for maximum CO_2 concentrations. The study compared measured individual CO_2 concentration data with the maximum CO_2 concentrations given by official

Copyright ©2022 by the authors. This conference paper is published under a CC-BY-4.0 license.

regulations, recommendations and guides. The recommended limit of 800 ppm issued by REHVA guidelines [7] and Decree 1009/2017 [8] was used as a starting point for evaluating the carbon dioxide concentration data.

2.1 guidelines related to CO_2 levels

As part of the study, current government regulations, guidelines, guides and studies were reviewed. Table 1 summarises the maximum concentrations of CO_2 following regulations, standards, guides and recommendations.

Table 1 summarises the most relevant regulations, guidelines, and recommendations that affect ventilation design and carbon dioxide levels in buildings. [7-11]. The carbon dioxide concentrations recommended by REHVA in the Covid-19 pandemic [7] are in line with the maximum concentrations of the current regulation 1009/2017 [8], 545/2015 [9] and the indoor air classification S1 and S2 indoor climate categories [10] and building code [11].

Tab. 1 - Maximum levels for carbon dioxide.

Guidelines, regulation		CO_2 level (maximum)
Regulation	1009/2017; 5 §	800 ppm (1 450 mg/m³)
	545/2015; 8 §	1 150 ppm (2 100 mg/m³)
Building code	D2 National Building Code of Finland	1 200 ppm (2160 mg/m³)
Guidelines	Valvira's Environmental Health	1 150 ppm (2 100 mg/m³)
	Healthy facilities (Terveelliset tilat)	1500 ppm (tyydyttävä taso)
Recommendations	Finnish classification of Indoor climate	
	indoor climate category S1	350 ppm + outdoor concentration
	indoor climate category S2	550 ppm + outdoor concentration
	indoor climate category S3	800 ppm + outdoor concentration
	REHVA COVID-19 Guidance	
	- minimum area/person 7 m²	800 ppm
	- minimum area/person 10 m²	1 000 ppm

Exposure to indoor air via Covid-19 aerosols is very high in poorly ventilated rooms. Therefore, REHVA recommends maximum concentration limits of 800 ppm and 1000 ppm during a Covid-19 pandemic, depending on other factors in the space. Table 2 summarises the design air volumes for the room types covering the measurement data. At the air volumes in the table, the CO_2 concentrations should not exceed the CO_2 concentrations in the regulations.

Tab. 2 – Design airflow rates.

Room type	Design airflow rate dm³ / s / m²
Office / Open Office	1 / 2
Restaurant	10
Class 1 / Class 2	3 / 4
Library	2
Patient Room 1 / Patient Room 2 / Operating Room	2,5 / 1,5 / 30
Retail space 1 / Retail space 2	2 / 4
Meeting room 1/Meeting room 2	3 / 4
Educational building	
minimum area/person 7 m²	2
minimum area/person 10 m²	1

Carbon dioxide data for February 2019 were available for the research project. The measurement data is obtained from Granlund Manager software, cloud-based property management and energy management software. Due to the anonymous processing, no precise building data are known for the CO_2 concentrations of the obtained premises. Therefore, the following information has been used for the measurement data: date and time, room type, sensor name, and CO_2 concentration. The interval of the measurement data is from 5 minutes to 15 minutes, depending on the status. The measurement time is 01.02.2019 - 28.02.2019. The time before the corona pandemic with ordinary usage of indoor premises was chosen as the time of measurement. Table 3 shows the number of spaces and measuring points by building type.

Tab. 3 - Number of spaces and measuring points by type of building.

Building type	Series	Spaces	Measurement points
Office	A	67	193 114
Office	D	88	722 112
Shopping centre	B	44	157 199
Shopping centre	C	7	88 704

Hospital	E	3	14 415
Educational building	F	231	661 174

2.2 Wells–Riley approach for infection risk assessment

The Wells–Riley equation [6] is based on the concept of a hypothetical infectious dose unit: 'the quantum of infection'. A 'quantum' is a core value and a specific term for this method. Wells defines it as the representation of infectious dose, where inhalation of one quanta leads to a probability of infection of 63%. The current study applied the quanta emission rates (66th percentile) for the Delta variant of SARS-CoV-2 and breathing rate values depending on time-weighted averages of occupant's activities [7]. The model calculates the individual probability of infection of susceptible persons for which acceptable values can be calculated from the event reproduction number (R).

3. Results

The facilities and their measurement data were examined by choosing a carbon dioxide concentration limit of 800 ppm. Table 4 summarises the number of premises by building type with carbon dioxide concentrations <800 ppm and ≥800 ppm. Measurement data were observed for the entire measurement period. If the concentration limit of 800 ppm was reached momentarily in the premises, it was considered to be above the concentration limit of 800 ppm (≥ 800 ppm).

Tab. 4 - Number and share (%) of premises by the building type with a CO_2 emission limit of 800 ppm

Building type	Carbon dioxide concentration	
	≥ 800 ppm	< 800 ppm
Office, Series A	41 (62 %)	26 (39 %)
Office, Series D	33 (38 %)	55 (63 %)
Shopping centre, Series B	9 (21 %)	35 (80 %)
Shopping centre, Series C	0 (0%)	7 (100 %)
Hospital, Series E	1 (33 %)	2 (67 %)
Educational building, Series F	164 (71 %)	68 (29 %)

The CO_2 concentrations above 800 ppm were temporarily reached in all room types. In the shopping centre premises, the average level of the concentrations was the lowest. In 80% of the shopping centre premises, the concentration limit of 800 ppm was never reached during the measurement period. The worst situation was in the teaching facilities, where only nearly 30% had carbon dioxide concentrations below 800 ppm. For hospital facilities, measurement data were available for only three facilities. Therefore, the results are too limited to make some valuable conclusions. However, it should be noted that the time taken to exceed the concentration of 800 ppm is not taken into account.

3.1 CO_2 concentration profiles

The next step in processing the measurement data is to focus on periods when the steady-state concentration exceeds 800 ppm in the office (series A), shopping centre (series B) and educational building (series F). Figures 1-3 depict the concentration profiles measured at the same day measured in different premises. The premises are marked with the measurement series letter (A, B or F) and the sensor number. Every space is presented by one CO_2 sensor. The general occupancy period is marked with dash lines to differentiate the occupied and unoccupied periods.

The carbon dioxide concentration measurements in the office premises (Fig.1) show typical occupation profiles with two main working periods (3-4 hours) and a lunch break (about an hour). Apparently, the occupancy schedule depends on the use of the office premises and working regime. In most cases, after the occupancy period, the CO_2 concentration returns to the lever before the occupancy.

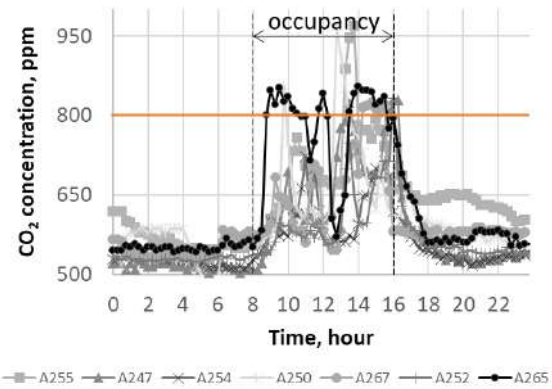

Fig. 1 - CO_2 concentration profiles in the office building

The occupancy varies during the working day in the educational building (Fig. 2a, b). The active period lasts about 4 hours in general. The results revealed the premises with different ventilation schedules. In some cases (Fig. 2a), the CO_2 concentration returns to the initial values after the occupancy period. In the other cases (Fig. 2b), the concentrations grow a certain time after the occupancy period. Different ventilation schedules could influence ventilation schedules when in the other cases (Fig. 2b), the ventilation airflow rate is significantly reduced or turned off during the unoccupied time.

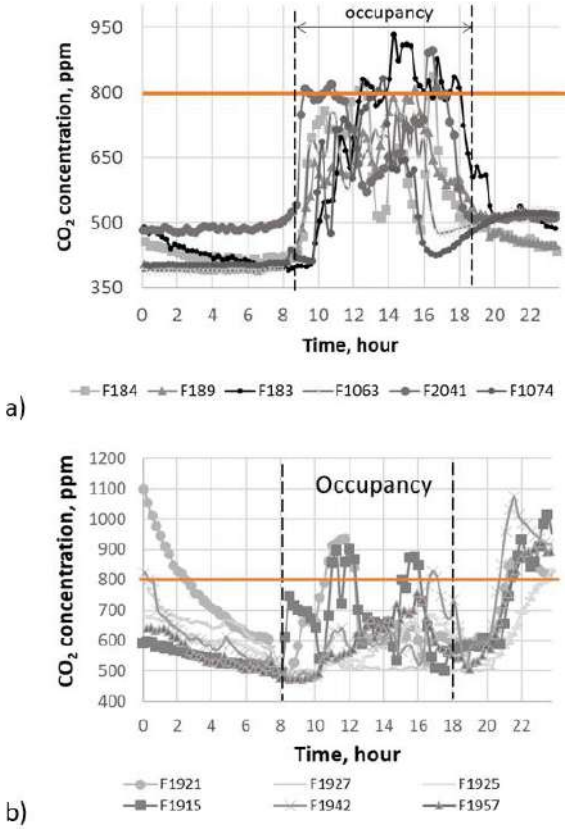

Fig. 2 - CO_2 concentration profiles in the educational building

The CO_2 concentrations in the shopping centre rise steadily, depicting the gradual growth of the occupancy with the typical maximum values between 4-6 pm. After the occupancy time, the concentration steadily returns to the unoccupied period values.

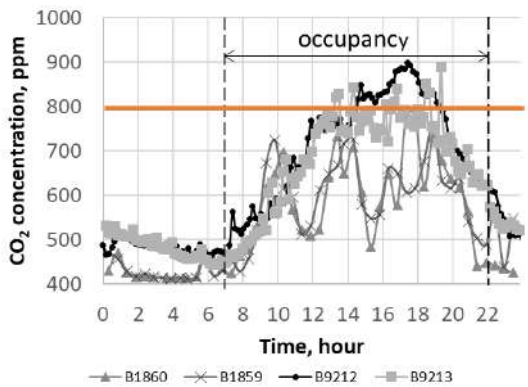

Fig. 3- CO_2 concentration profiles in the shopping centre

The growth of CO_2 concentration indicates the population density in all the studied cases, which enables the estimation of occupancy. In contrast, the exceeded CO_2 levels during the unoccupied time could result from insufficient ventilation schedules.

3.2 Infection risk assessment with the Wells–Riley approach

Since the measurement data are not enough to directly apply the Wells–Riley risk assessment method, there is a need to assume the initial data for the Wells–Riley approach to risk assessment (Table 5). The room size in all the cases is the same, the room area is 80m^2, and the room height is 3 m. The specific airflow rates are selected from the current building codes based on the assumption that the ventilation systems have been designed according to them. Finally, the measurements of carbon dioxide concentration gave information about the average occupancy time and the number of occupancies.

The measurement results marked with black are used later for the occupancy assessment from carbon dioxide measurements. The occupancy assessment is based on a fully-mixed dynamic mass balance model simplified by the steady-state assumption [12]. The final number of occupants should give the closest fit to the measurement data. The study applies the generally accepted assumption for ventilation sizing purposes that one infectious person stays in the room throughout the event. The occupancy time in offices and educational buildings is estimated based on the analysis of CO_2 concentration profiles. The average occupancy time in the shopping centre is assumed based on the research data [13].

Tab. 5 – Estimated parameters of the rooms

Room	Ventilation rate, L/(s m^2)	No of susceptible persons	Occupancy time, hour
Office	1.125	8	3
Educational building	4	28	4
Shopping centre	1.5	7	0.5

The results (Table 6) show the significant effect of the quanta value and averaged breathing rate on the probability of infection. The higher quanta and breathing rate values in educational buildings than in offices result in a higher probability of infection. At the same time, the event reproduction number highly depends on the calculated occupancy time.

Tab. 6 – Probability of the infection

Room	Quanta emission rate, quanta/h	Breathing rate, m^3/h	Probability	R event
Office	5	0.65	0.015	0.12
Educational building	3.2	0.6	0.004	0.15
Shopping centre	8.4	1.32	0.004	0.03

Figure 5 shows the calculated rise of the probability of infection and event reproduction number during 8

hours. However, the probability of infection in the education building remains the lowest compared to the office building and shopping centre results. At the same time, the event reproduction number in the office and education building showed comparable values during the chosen period.

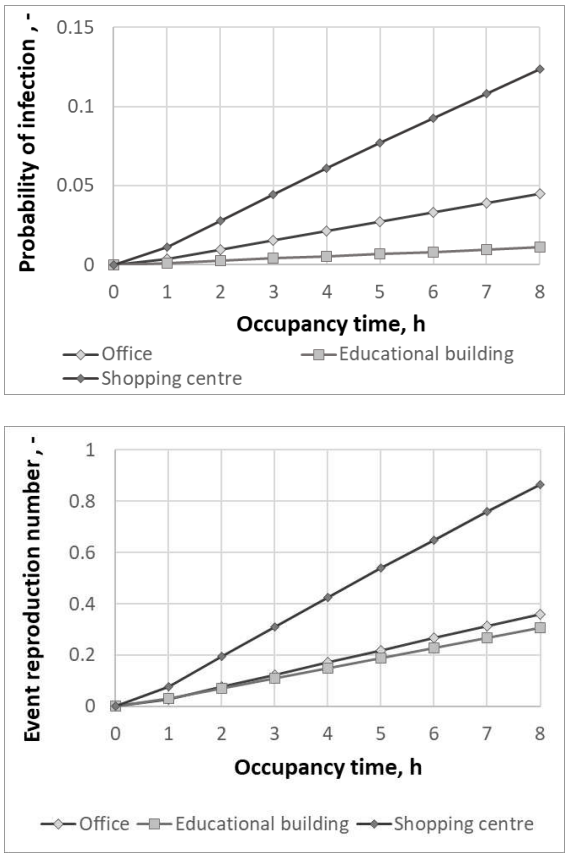

Fig. 4- Probability of the infection and the even reproduction number for the studied cases

4. Discussion

The measurements of CO_2 concentration give general information about ventilation efficiency and approximate occupancy. However, risk assessment of coronavirus infection needs to consider other essential parameters [14]. For example, crowded indoor environments and air exchange rates could also lead to the reproduction number R0 > 1 with reduced exposure times. In addition, occupants' expiratory and physical activities could lead to high quanta concentrations and breathing rates, resulting in increased infection risk. Thus, the comparatively highest carbon dioxide levels during the measured period in the educational building did not lead to the highest risk of infection because the quanta concentrations and breathing rates were the lowest in this case. Nevertheless, in general cases, the real-time monitoring of carbon dioxide concentrations can be applied to ensure adequate air ventilation, which prevents SARS-CoV-2 transmission [15].

The methods presented in the study include some limitations and uncertainties related to the lack of measurement data and the Wells–Riley method. The Wells–Riley equation assumes steady-state conditions. It requires measurement of ventilation airflow rates and occupancy, which are frequently difficult to measure, often vary with time, and in many cases are inaccessible because of security reasons.

Carbon dioxide monitoring could be not fully efficient in situations where exhalation is not the only CO_2 source [16]. Furthermore, CO_2 monitoring is not able to consider the mechanisms for the removal of infectious aerosols, such as virus deactivation, deposition, and filtration. In addition, the virus generation mechanisms through coughing, loud talking and singing might not correlate with corresponding CO_2 generation [17]. Thus, further studies are needed for monitoring carbon dioxide to quantify the risk of indoor airborne transmission of coronavirus infection. Nevertheless, the results give a general overview of the probability of infection considering the limitations mentioned above.

5. Conclusions

Even though the measures to prevent SARS-CoV-2 transmission were recommended in all European countries following the WHO, the exceeded contaminant levels are observed in many buildings due to high occupancy density inside enclosed environments for several hours a day. It could result in relatively high SARS-CoV-2 transmission probability. Therefore, ventilation systems should be adopted to guarantee more effective fresh air exchanges. The measurement data considered in this study were anonymous, and only the state type, sensor, time, and measured CO_2 concentration were known. It was not known, for example, the year of construction, address or opening hours of the holding. There are significant differences between the different room types based on the measurement data. In the case of shopping centre premises, about 80 per cent of the premises remain below the concentration limit of 800 ppm throughout the measurement period. However, in teaching premises, the same situation is present in less than 30%. Based on the CO_2 concentration results, conclusions can be made related to the ventilation efficiency concerning the use of the premises.

The results show the significant effect of the quanta value and averaged breathing rate on the probability of infection. The higher quanta and breathing rate values in educational buildings than in offices result in a higher probability of infection. As the study progresses, the situations where specific expiratory and physical activities should be considered can lead to high quanta concentrations and risk in large and closed environments.

6. Acknowledgement

The study is a part of the Licence to Breathe project funded by Tampere University.

7. References

[1] World Health Organization. Coronavirus disease (COVID-19) technical guidance: Infection prevention and control. Geneva: World Health Organization; 2020. Available from: https://www.who.int/emergencies/diseases/novel-coronavirus-2019/technical-guidance/infection-prevention-and-control

[2] Bhagat R., Davies Wykes M., Dalziel S., Linden P. Effects of ventilation on the indoor spread of COVID-19. Journal of Fluid Mechanics 2020; 903.

[3] Ha W., Zabarsky T. F., Eckstein E. C., Alhmidi H., Jencson A. L., Cadnum J. L., Donskey C. J. Use of carbon dioxide measurements to assess ventilation in an acute care hospital. American journal of infection control 2020; 1.

[4] Zhang D., Ding E., Bluyssen P. M. Guidance to assess ventilation performance of a classroom based on CO_2 monitoring. Indoor and Built Environment 2022; 0(0): 1–20

[5] Rudnick S.N., Milton D.K. Risk of indoor airborne infection transmission estimated from carbon dioxide concentration. Indoor Air 2003; 13: 237–245.

[6] Foster A., M. Kinzel, Estimating COVID-19 exposure in a classroom setting: A comparison between mathematical and numerical models. Phys. Fluids 2021;33. Available at https://aip.scitation.org/doi/full/10.1063/5.0040755 (Accessed: 23.01.2022).

[7] REHVA COVID-19 guidance document version 2.0 2021, August 1. Available at https://www.rehva.eu/activities/covid-19-guidance/rehva-covid-19-guidance (Accessed: 23.01.2022).

[8] Ympäristöministeriö. 1009/2017 Ympäristöministeriön asetus uuden rakennuksen sisäilmastosta ja ilmanvaihdosta 2017. Available at: https://www.finlex.fi/fi/laki/alkup/2017/20171009 (Accessed: 23.01.2022).

[9] Sosiaali- ja terveysministeriön asetus asunnon ja muun oleskelutilan terveydellisistä olosuhteista sekä ulkopuolisten asiantuntijoiden pätevyysvaatimuksista. Sosiaali- ja terveysministeriön asetus 545/2015. Available at https://www.finlex.fi/fi/laki/alkup/2015/20150545 (Accessed: 23.01.2022).

[10] RT 07-11299, Sisäilmastoluokitus 2018. Sisäympäristön tavoitearvot, suunnitteluohjeet ja tuotevaatimukset

[11] Ympäristöministeriö. D2 Rakennusten sisäilmasto ja ilmanvaihto, määräykset ja ohjeet 2012. Available at https://www.finlex.fi/data/normit/37187-D2-2012_Suomi.pdf (Accessed: 23.01.2022).

[12] Zuraimi M. S., Pantazaras A., Chaturvedi K. A., Yang J. J., Tham K. W., Lee S. E. Predicting occupancy counts using physical and statistical CO_2-based modeling methodologies. Building and Environment 2017; 123: 517-528.

[13] Choi Y., Yoon H., Kim D. Where do people spend their leisure time on dusty days? Application of spatiotemporal behavioral responses to particulate matter pollution. The Annals of Regional Science 2019; 63(2): 317-339.

[14] Su W, Yang B, Melikov A, Liang C, Lu Y, Wang F, Angui Li, Zhang Lin, Xianting Li, Guangyu Cao and Kosonen, R. (2022). Infection probability under different air distribution patterns. Build-ing and Environment, 207, 108555.

[15] Di Gilio A., Palmisani J., Pulimeno M., Cerino F., Cacace M., Miani A., de Gennaro G. CO2 concentration monitoring inside educational buildings as a strategic tool to reduce the risk of Sars-CoV-2 airborne transmission. Environmental research 2021; 202: 111560.

[16] Li Y. 2021. Hypothesis: SARS-CoV-2 transmission is predominated by the short-range airborne route and exacerbated by poor ventilation. Indoor Air, 31(4), 921-925.

[17] Li Y, Qian H, Hang J, Chen X, Cheng P, Ling H, Wang S, Liang P, Li J, Xiao S and Wei J. 2021. Probable air-borne transmission of SARS-CoV-2 in a poorly ventilated restaurant. Building and Environment, 196, 107788.

A Study on the effect of the Wind Catcher in Apartment Buildings

Kotaro Ishikawa [a], Takashi Kurabuchi [b], Jeongil Kim [c]

[a] Department of Architecture, Graduate School of Engineering, Tokyo University of Science, Tokyo, Japan, ishidra.0206@gmail.com.

[b] Department of Architecture, Faculty of Engineering, Tokyo University of Science, Tokyo, Japan, kura@rs.tus.ac.jp.

[c] Department of Architecture, Faculty of Engineering, Tokyo University of Science, Tokyo, Japan, Jeongil.kim@rs.tus.ac.jp.

Abstract. In recent years, there has been growing emphasis on natural ventilation for energy conservation and intellectual productivity. However, in urban areas with a high building density, it is difficult to let in fresh outdoor air into the room, and installing a wind catcher (WC) is considered an effective solution. In this study, we conducted wind tunnel experiments and computational fluid dynamics (CFD) analysis to verify the ventilation-enhancing effects of installing WC in apartment buildings.
Two models are used in this study. In the initial stages of wind tunnel testing and CFD analysis, we used a model without adjoining rooms to determine the correspondence of the wind tunnel test values to the CFD analysis values. Subsequently, CFD analysis was performed using the model with an adjacent room, and comparisons were made with the model without an adjacent room. Using the model with an adjacent room, we also studied the difference in the ventilation volume depending on the wind direction and ventilation volume with a single-sided opening. Consequently, we determined the following:

1. The pressure difference between the inlet and outlet openings was smaller in the model with an adjacent room than in the model without an adjacent room, and the ventilation volume was smaller. In other words, installing a WC in an apartment building can create a pressure difference, which is considered effective in promoting ventilation.
2. The WC works effectively for the wind flowing parallel to the opening.

Keywords. CFD analysis, natural ventilation, wind catcher, wind tunnel experiment
DOI: https://doi.org/10.34641/clima.2022.203

1. Introduction

To improve the thermal and air environment in houses, it is important not only to use air conditioning equipment but also to let in fresh outdoor air to save energy and improve intellectual productivity. In addition, with the recent outbreak of COVID-19, letting in fresh outdoor air into rooms as a measure to prevent infection has become an issue. However, in urban areas, where buildings are densely constructed, it is often difficult to obtain sufficient ventilation through wall-to-wall openings. To address this issue, previous studies have shown the effect of wind catcher (WC) in promoting ventilation, and it is expected that an increasing number of buildings will attempt to do so in the future (Fig. 1). [1]

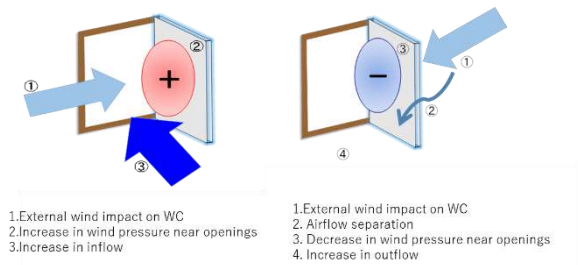

Fig. 1 – Working mechanism of WC

The purpose of this study was to confirm the effect of WCs through wind tunnel experiments and numerical simulation of flow (hereinafter referred to as computational fluid dynamics (CFD) analysis), to confirm the performance of each WC installation pattern by CFD analysis, and to understand the factors influencing ventilation performance.

Copyright ©2022 by the authors. This conference paper is published under a CC-BY-4.0 license.

2. Method

2.1 wind tunnel experiment

The experiment was conducted using an Eiffel-type wind tunnel at Tokyo Polytechnic University. The experimental model was a room in an apartment complex, and the adjacent dwelling was omitted (Fig. 2). The model eave height was set as the reference height (Z_0 = 226.6 mm), eave height wind velocity of the approaching flow (V_0 =7 m/s) was set as the reference velocity, and dynamic pressure based on the reference velocity was set as the reference pressure P0. The wall and room pressures near each opening were measured from the pressure measurement points placed on the model (Fig. 3), and the ventilation volume Q was calculated using Equation (1). Q[m^3/s] denotes the ventilation volume, α [-] is the flow coefficient, A[m^2] is the opening area, ρ[kg/m^3] is the air density, and ΔP[Pa] is the pressure difference.The calculation assumes that α is 0.6, which is the value for a typical opening. The approaching flow is the profile according to the 1/4 power law assuming an urban area, the study cases are the six cases shown in Fig. 4, and the wind direction is the direction of the arrow in Fig. 4.

Fig. 2 - Wind Tunnel Experiments model

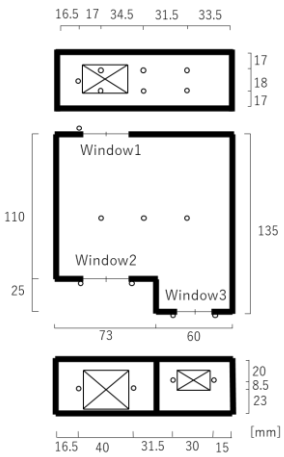

Fig. 3 - Pressure measurement point of the model

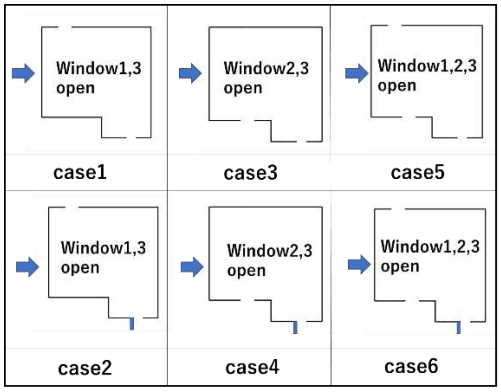

Fig. 4 – Study case

$$Q = \alpha A \sqrt{\frac{2}{\rho}\Delta P} \quad (1)$$

The measurement results for the mainstream and spanwise components of the approaching flow are shown in Fig. 5. The measured values of the former generally agreed with the distribution of the 1/4 power law at each height, whereas the measured values of the latter were generally 0 m/s.

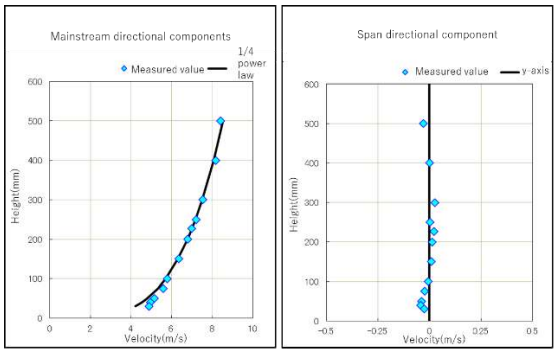

Fig. 5 - Approach flow measurement results

2.2 CFD analysis

An analytical model was constructed to simulate an experimental wind tunnel model. The turbulence model was a standard k–ε model, and the inflow condition was the approaching flow measured in the wind tunnel experiment (Tab. 1 and, Fig. 6).

Tab. 1 - CFD boundary conditions

boundary	Boundary conditions
Inlet surface	Profile based on 1/4 power law $U = U_0(Z/Z_0)^{0.25}$ Standard wind speed (U_0 = 1.0m/s) Eave height (Z_0 = 1.0m)

Outlet surface	Free flow
Top and sides	Free slip
ground	Wall function based on the general logarithmic law

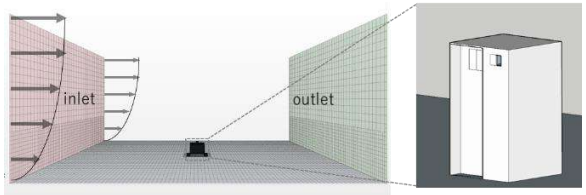

Fig. 6 – CFD analysis model

3. Validation

Fig. 7 shows a comparison between the ventilation rate obtained from the pressure measurements in the wind tunnel experiment and the CFD analysis. The standardized ventilation volume is the product of the wind speed at each eave height and the square of the eave height. From the results, it is observed that there are some differences between the wind tunnel experimental values and the CFD analysis, although the trend of the ventilation volume conversion was consistent. In the CFD analysis, the wind pressure at the apertures was measured using a shield model with the apertures blocked, and the flow coefficient α for each aperture was calculated as α1 = 0.39, α2 = 0.41, and α3 = 0.52. In the wind tunnel experiment, the flow coefficient α was fixed at 0.6 and the ventilation volume conversion calculated from the wind pressure may have been overestimated. Fig. 7 also shows that the ventilation volume decreased when the WC was installed in the full opening pattern. It is expected that the installation position of the WC in the case under consideration will obstruct ventilation in the opposite direction.

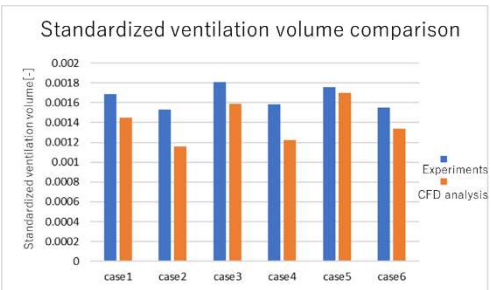

Fig. 7 - Standardized ventilation volume comparison

4. Additional study

4.1 Outline

Because the ventilation enhancement effect of the WC installation was not obtained in the wind tunnel experiment, an additional study was conducted using CFD. Based on the pressure distribution in the wind tunnel experiment, it was expected that window 3 was the inflow opening and windows 1 and 2 were the outflow openings. Therefore, based on case 1, the WC was installed at a position that increased the pressure at window 3 and decreased the pressure at window 1 (Fig. 8), and the wind direction angle was determined by the wind tunnel experiment. The wind direction angle was the same as that used in the wind tunnel experiment.

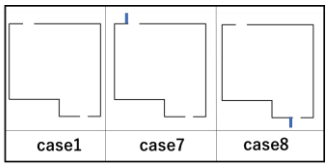

Fig. 8 - Study case

4.2 Result

Figure 9 shows the results of the ventilation volume comparison. Cases 1 and 7 show a decrease in ventilation volume, indicating that the WC installed on the windward side of window 1 had no effect on ventilation. The results of the comparison between cases 1 and 7 show that the amount of ventilation decreased, and the WC installed on the windward side of window 1 had no effect on ventilation.

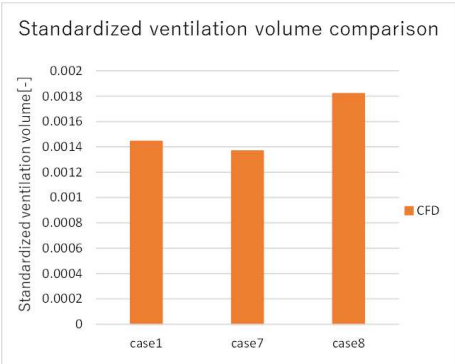

Fig. 9 - Standardized ventilation volume comparison

4.3 Discussion

The pressure contour diagram is shown in Fig. 10. From this, it can be confirmed that in case 8, the wind collided with the WC installed on the leeward side of window 3, the pressure near the opening increased, and the pressure near window 1 was significantly negative. Consequently, the pressure difference between the inflow and outflow openings increased, leading to an increase in the ventilation volume. Next, in case 7, by installing the WC on the upwind side of window 1, the peeling pressure of the airflow is blocked and the negative pressure at

the outflow opening cannot be built up. This reduced the pressure difference between the inflow and outflow apertures, leading to a decrease in the ventilation volume.

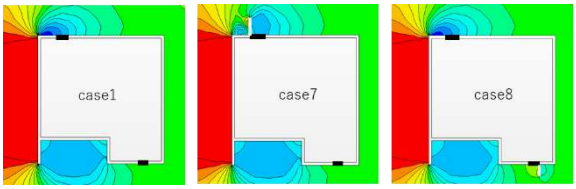

Fig. 10 - Pressure contour diagram

5. Study in a model with adjacent rooms

5.1 Outline

The CFD analysis was performed using a model with an adjacent room on the upwind side of the target room (Fig. 11), which could not be performed in the wind tunnel experiment. The items to be studied were the comparison of ventilation volume by different WC installation patterns and the comparison of ventilation volume by wind direction in the model with adjacent rooms.

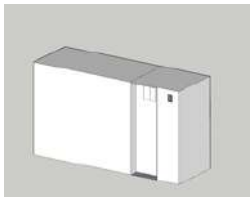

Fig. 11 - Model with adjacent rooms

5.2 Result for different WC installation patterns

The four studied cases are shown in Fig. 12. The ventilation volume comparison results for each case are shown in Fig. 13. In the model with an adjacent room upwind, the ventilation rate was significantly lower in the case with no WC (case 9). Next, looking at the standardized ventilation volumes for cases with WC upwind of window 1 (case 10) and downwind of window 3 (case 11), the values increased significantly in both cases. The largest value was obtained when the WC was installed both upwind of window 1 and downwind of window 3 (case 12).

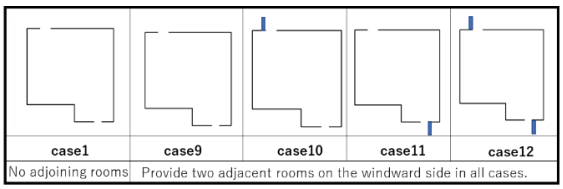

Fig. 12 - Study case

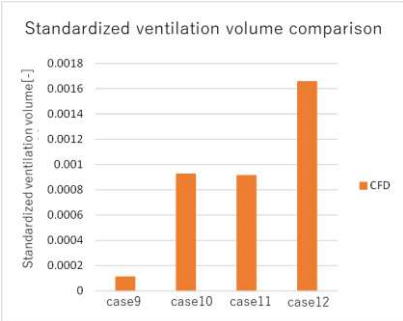

Fig. 13 - Standardized ventilation volume comparison

5.3 Discussion

The pressure contour diagram is shown in Fig. 14. The pressure contour diagram for case 9 shows that there is almost no pressure difference between the inlet and outlet openings. Referring to the pressure contour diagram of cases 10 and 11, we observe that the pressure difference is caused by the installation of the WC. It is observed that when the WC is installed on both the windward side of window 1 and leeward side of window 3 (case 12), the pressure difference between the inlet and outlet openings is the largest, and the ventilation rate is the highest. This indicates that the installation of a WC in a single building, which is susceptible to airflow separation, may decrease the ventilation volume; however, in a long building such as an apartment building, it is easy to obtain the ventilation promotion effect by installing a WC.

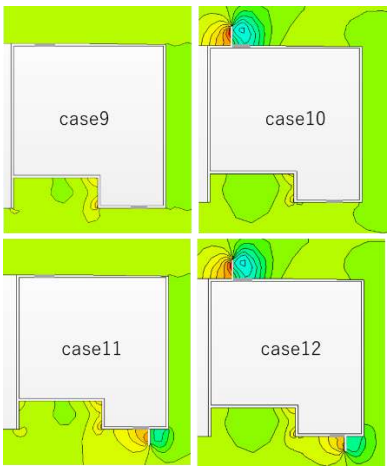

Fig. 14 - Pressure contour diagram

5.4 Result for different wind directions

We compare the ventilation rate by wind direction using a model with adjacent rooms. The study cases are cases 9 and 11 shown in Fig. 12. The wind direction is shown in Fig. 15. The results of the ventilation rate comparison are shown in Fig. 16, and the wind-speed vector diagrams for each case are shown in Fig. 17. From these figures, the ventilation rate is highest when the wind direction angle was 0°. When the wind direction angle was 0°, the ventilation enhancement effect of the WC could not be confirmed. In contrast, when the wind direction angles are 90° and 270°, the ventilation

rate is remarkably low in the case without a WC, but in the case with a WC, there is an improvement in the ventilation rate.

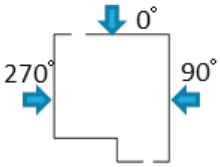

Fig. 15 - Wind direction angle

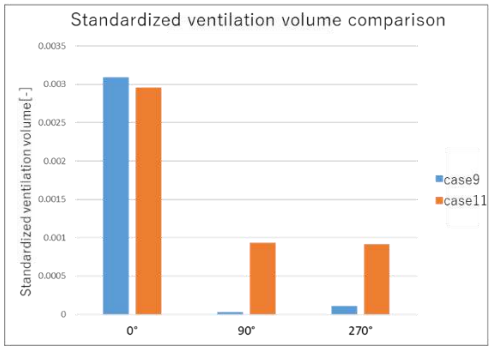

Fig. 16 - Standardized ventilation volume comparison

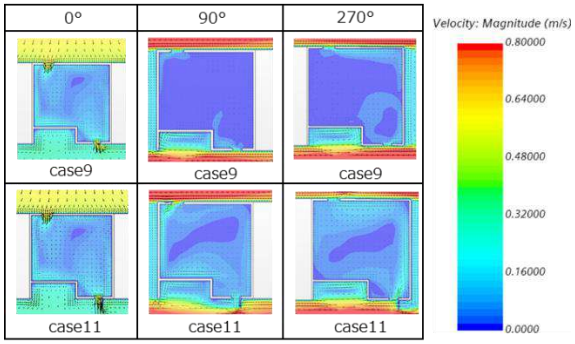

Fig. 17 - Wind velocity vector diagram

6. Conclusion

1. The pressure difference between the inlet and outlet openings was smaller in the model with an adjacent room than in the model without an adjacent room, and the ventilation volume was smaller. In other words, installing a WC in an apartment building can create a pressure difference, which is considered effective in promoting ventilation.

2. A WC works effectively for wind flowing parallel to the opening

7. References

[1] Oda T et al. Effects of Wind Cather on Improvement in Cross-Ventilation Performance, Roomvent 2014

c. The datasets generated during and/or analysed during the current study are not available because it is currently in preparation, but the authors will make every reasonable effort to publish them in near future.

Monitoring (N)ZEB dwellings in the Netherlands Lessons learned from current practices

Olivia Guerra-Santin[a], Twan Rovers[b], Laure Itard[c]

[a] Department of the Built Environment, Eindhoven University of Technology, o.guerra.santin@tue.nl

[b] Chair of Sustainable Building Technology, School of Business, Building & Technology, Saxion University of Applied Sciences, Enschede, the Netherlands, t.j.h.rovers@saxion.nl

[c] Faculty of Architecture and the Built Environment, Delft University of Technology, Delft, the Netherlands, S.Marchionda@tudelft.n, L.C.M.Itard@tudelft.nl.

Abstract. Monitoring the energy performance of very low and zero energy buildings is fundamental to evaluate the efforts made to transition into an energy neutral built environment. Post occupancy monitoring has been embedded into current practice, supported by the availability of smart meters and affordable sensor technology. However, there is still a lack of standardised monitoring guidance, which complicates the comparison between projects. In this study, we reviewed reports and publicly available documents related to the monitoring of low energy and zero energy projects in the Netherlands. A total of 12 studies reporting on 65 projects containing 4,400 dwellings were analysed. These included both new and renovated housing built in the last decade. This study aims to provide an overview of actual energy performance in energy renovation projects across the Netherlands. It also analyses the difference with predicted energy performance and analyses the perceptions of residents involved in low and zero energy renovations. It answers questions such as: What energy and behavioural data is being gathered through energy monitoring in the residential sector (related to monitoring low and zero energy buildings/dwellings)? How is the data currently being utilized? What does the data tell us about actual energy use and resident perceptions? How can monitoring be improved to help develop better energy models, and help building owners optimize their investments in energy renovation projects? The results indicate that even though monitoring building performance in the Netherlands could be considered common practice, the results are seldomly reported or communicated. Furthermore, very few projects monitor indoor conditions and occupants' behaviour. As a consequence, the performance gaps found in these projects are not fully understood. These findings are summarised to provide an overview of the main goals for monitoring from a practical point of view. These findings are used to provide recommendations for monitoring setups according to the final goals.

Keywords. Energy monitoring, (n)zeb dwellings, occupant behaviour, performance gap
DOI: https://doi.org/10.34641/clima.2022.206

1. Introduction

In the Netherlands, a significant amount of final energy consumption is used by households, the majority of which is used for space and water heating. In 2019, the Dutch government introduced a suite of policies and plans to support the transition to a carbon-free built environment via the Climate Plan, the National Energy and Climate Plan (NECP) and the National Climate Agreement [1]. Approximately 75% of the housing stock required in 2050 already exists today [2]. Therefore, a significant focus will be placed on energy efficiency renovations in the coming years to achieve the national targets. The Dutch government estimates that to achieve 2030 targets, over 50,000 existing homes should be renovated per year, beginning in 2021. By 2030, the rate of energy efficiency renovations should be 200,000 homes per year. Working toward these objectives, the number of low and zero energy renovations have accelerated in recent years. Although many projects report on innovative approaches and techniques for the renovation of residential buildings, for instance through the Topsector Energie Database [3], few projects report on the actual realized energy efficiency. However, building monitoring campaigns in energy renovations and new net-zero energy housing projects is becoming

Copyright ©2022 by the authors. This conference paper is published under a CC-BY-4.0 license.

increasingly common in the building sector to evaluate actual energy performance in energy renovation projects. The gathered data can be utilized for a range of purposes, which can be categorised in four main goals: 1) data can be used to determine parameters for building models, with the goal of predicting more accurately the energy saving potential of buildings; 2) data can be used to determine the energy performance of buildings (e.g. in energy performance contracts) to evaluate the renovation concepts and to continuously monitor and manage actual and agreed performance; 3) monitoring is used to test and improve renovation concepts and products to help building owners, contractors, installers and technology companies make better decisions, save money and improve the experience of residents; and 4) data can be used as input in continuous fault detection to ensure proper operation of the systems. In this study, we mostly focus on monitoring campaigns for purpose 2: determining building performance to evaluate renovation concepts and improve their performance.

This study aims to provide an overview of actual energy performance in energy renovation projects across the Netherlands, by analysing the difference with predicted energy performance and the perceptions of residents of low and zero energy renovations. It answers the following questions: What energy and behavioural data is being gathered through energy monitoring in the residential sector? How is the data currently being utilized? What does the data tell us about actual energy use and resident perceptions?

2. Scope & Methodology

The report draws on energy monitoring campaigns, providing a data-driven approach to analysing energy efficiency measures and concepts. Reports and documents containing specific reference to at least one project and seriously targeting the occupants were considered. The focus of this study is on thermal energy renovation measures and concepts, including space and water heating and ventilation, concepts that targeted a low energy outcome (energy label B or better), measures based on technologies expected to become predominant in the future, studies carried out in the recent past (approximately 10 years), and renovation projects in both the social and private housing sector across the Netherlands. The information searched for with respect to the energy monitoring campaigns includes: What building characteristics were reported?, What aspects of energy performance were considered?, What aspects of occupancy were considered, and in which part of the renovation process?, What methods of data collection and analysis were used?, Which data was collected, with which time step and during which period?, How were other performance aspects (such as indoor environmental quality (IEQ)) considered?

Renovation projects and energy monitoring campaigns referenced in this study were identified through desktop research, where on a non-exhaustive search for reports and information about renovation projects where monitoring data (both quantitative and qualitative) was gathered. The report is therefore based on an analysis of existing data, results and publications which have been publicly reported. In total, 12 studies representing 65 Dutch renovation projects, and 4.404 houses were identified. From these houses, only 3.695 houses, from 10 different studies, reported on the results and could be accounted for in the analysis of energy performance or user experience. From these, only three projects reports combined all needed information on both energy performance and occupant perspective. The remaining 709 houses, belonging to a project without a written report, have been considered in a short analysis of how data is used (see section 3.3) through non-structured interviews/discussions with the ones processing the data.

Table 1 contains an overview the studied projects in which monitoring data or energy bills or occupants' related data were used to assess the energy performance and/or occupants' satisfaction of the dwellings. In total, the results from 10 studies were analysed.

3. The actual energy efficiency of renovated dwellings

Eight studies provided data on energy performance (see Table 1). The results are summarised in this section.

Quickscan huurderstevredenheid EPV [4]

The electricity generation exceeded the electricity consumption in 42 of the 46 dwellings, after correcting for the use of appliances and ventilation (a standard electricity use of 3,000 kWh was used), and in a reference climate year. In one dwelling, more energy was used for domestic hot water (DHW), and in three dwellings more energy was used for space heating. Ten out of 20 dwellings were monitored. After correcting for the use of appliances and ventilation, six of these dwellings were found to be net-zero energy or positive energy in a reference climate year. Building installations did not function correctly, causing the electricity use for heating to be higher than expected.

Thermal Compartmentation [5]

For three of the dwellings, annual electricity

generation exceeded the electricity consumption with approximately 1,100, 1,500 and 800 kWh in a reference climate year, despite the fact that heat pumps had lower efficiencies than expected. One dwelling had an annual net energy use of approximately 600 kWh per year, which is at least partially the result of a dysfunctional heat pump.

Concepten nul op de meter en 80% besparing – Kerkrade [6]

For a number of the 153 renovated dwellings in Kerkrade, the gas and electricity use were analysed. User related energy use (for appliances, ventilation, domestic hot water and cooking) and electricity generation was lower than anticipated. The energy use for space heating was higher than expected. The difference is attributes to the calculation method for space heating in the EPC being too positive for heat pumps, or to the efficiency of the heat pump itself.

2nd SKIN (Demonstrator) [7]

Twelve Simplex buildings were renovated. During the first two years, a net energy surplus was measured due to the high yield of the PV-panels.

Tolhuis 1590 [8]

A net energy surplus of 1,300 kWh was measured in the heating season 2015/2016.

NOM-Zoetermeer

On average there was an annual surplus of energy of 2,300 kWh. Indoor parameters, temperature, humidity and CO_2 were mostly part of the time within good comfort range in the winter season. However, high temperatures were recorded during the summer season. The houses are well insulated, and they have not been equipped with external shading devices.

NOM renovation Heerhugowaard [9]

The total energy consumption, electricity generation, and energy use of the heat pumps of 55 buildings was monitored from 1 January 2015 to 22 December 2015. Due to issues with the monitoring systems in nine of the buildings, the energetic results of only 46 dwellings are reported. In 2015, all 46 dwellings were found to be positive energy. In a reference climate year (NEN 5060), 42/46 dwellings would be positive energy. 43/46 Dwellings used less energy for DHW than anticipated. 33/46 Dwellings used less energy for space heating than anticipated.

NOM renovation Tilburg [10]

Eighteen buildings were renovated, for ten of which monitoring data of sufficient quality was available. The total energy consumption, the electricity generation and the energy use of the heat pump was monitored from July 2015 to March 2016. For 2015, 8/10 dwellings were found to be at least net-zero energy. In a reference climate year (NEN 5060), 6/10 dwellings would be at least net-zero energy. The energy use for space hating is higher than anticipated.

4. Occupants' experiences in renovated dwellings

A considerable share of the variation in energy use is known to be due to variations in occupant behaviour. Previous research has shown that household composition, heating, cooling and ventilation practices, and lifestyle have a large effect on energy consumption and indoor air quality [11, 12]. These differences can contribute to the performance gap and to uncertainties regarding the financing of renovation projects.

Next, this study summarizes the existing knowledge regarding the role of the occupants in the success of zero energy and low energy renovation projects in the Netherlands, from a practical perspective, that is: focusing on the practices followed in current energetic renovations of dwellings.

In total, six public documents as well as non-public reports were analysed. In these reports, we found a focus on the overall results of the renovation, the information given to the occupants, and the performance of the building in terms of (energy) costs, thermal comfort, indoor air quality, noise, and the interaction of the people with the building's installations.

Four types of data collection and analysis methods were found in the projects reviewed in this study: surveys and interviews with residents, building monitoring, interviews with professionals, and desk studies based on previously documented cases. All of the cases in which building monitoring was carried out also included some method to obtain information from the residents (Concepten nul op de meter en 80% besparing [6,13], NOM Renovation – Heerhugowaard [9] and NOM – Tilburg [10]), while one project presented the results of a very elaborated residents survey (ZEN Nieuwbouwwoningen [14]). Other analyses focused on the review of previous studies (Quickscan Huurderstevredenheid EPV [4]) and interviews with experts on the topic but focusing on the residents' perspective. In this section, the results of the reviewed projects are summarised.

The aspects that are evaluated are the residents' satisfaction with communication (after care), quality of information (is it understandable), easiness of use and maintenance of the systems, energy costs, energy use, thermal comfort and indoor air quality, noise and odour complaints, and overall satisfaction with the final product (the renovated home). The fact that in most projects the communication, easiness of use, thermal comfort, indoor air quality and noise are investigated and reported, highlights how important these aspects are for both occupants, housing corporations and builders.

Communication (follow up)

The main reported sources of dissatisfaction regarding communication seem to be due to differences in expectation from part of the residents (showroom vs. prototype), the performance contract, and responsibilities for maintenance and malfunctions after the delivery of the house. The residents seem to experience the information about installation as complex or too technical. Since information is delivered in a short period of time, they are overwhelmed with it. Some expressed to require more personalized information.

Quality of information (understanding)

Residents in the different projects reported good understanding on how to use the systems from 54% to 79%, depending on the system. Residents in the different projects reported good understanding on how to maintain the systems from 20% to 76%, depending on the system.

Easiness of use and maintenance

Two reports state that most residents reported that they knew how to use the systems, but those that do not, are often dissatisfied with their comfort. Residents find more difficulties in the control of non-traditional systems such as low temperature heating systems (e.g.underfloor heating and convectors). They feel that it cannot be properly regulated, and the heat cannot be felt properly. In Heerhugowaard [9], residents had to deal with initial installation problems of the heat pump. In Kerkrade and Zorgeloos Wonen [6], up to 34% of households have the ventilation on the lowest level. There are complaints about noise, too cool air, and draughts. The Quickscan and the ZEN project [4, 14] reported complains about the usability of the ventilation system.

Thermal comfort and air quality

Most residents were satisfied with indoor climate (67-90%), especially in comparison with the previous situation (95%). Overheating seemed to be a problem in many cases, especially in bedrooms (10 to 44%). Measurements in Kerkrade, Montferland and RijswijkBuiten [6] confirmed the overheating problem. In projects with active cooling and an air heat pump to cool the ground floor, overheating complaints are reduced. However, there were complaints on too low temperatures in the winter and fluctuating temperatures in the summer. A small number of residents (5%) suffered from indoor air being too dry.

Noise

Residents experience less noise from outside, but more noise from neighbours and installations (ventilation system and heat pump). The measurements in Zorgeloos Wonen, Amsterdamse Buurt-Haarlem and Montferland [6] confirm the statements from residents.

Overall result (home)

Residents are mostly satisfied with their homes (78 to 95%). Residents appreciate when the exterior of the homes, as well as kitchens and bathrooms are also renovated. Projects in which this was investigated [9], report that most residents recognize the advantages (on energy and IEQ) of a NOM or energy efficiency home.

5. Takeaways

5.1 Reported energy performance

In most of the renovation projects reviewed in this report, the actual energy consumption was lower than was predicted or expected after correction for degree days. The monitoring periods were long enough to ensure a reliable estimation of the annual energy use. However, the targeted performance in these projects was not expressed in terms of energy savings but in terms of being 'net-zero' energy which may also explain the positive outcome.

Although the positive results are very promising, it may be useful to realize that more positive results may have been published than negative results. The higher-than-expected energy performance is surprising in comparison to the results from previous research on the Dutch housing stock [15-18] where it was found that deep renovation generally perform much worse than expected. However, monitoring campaigns were not conducted in these previous studies. It might also be that in projects where energy monitoring is being carried out, the data helps to acquire early insights in the functioning of building installations. Repairs may then be completed, and results may only be reported after adjustments have been made. Additionally knowing that monitoring will take place could influence positively the quality of the studied projects.

In the data reported on the energy monitoring campaigns associated with the renovation projects, it is often not clear why projects are outperforming or underperforming. More data, particularly from sub-

meters, is essential for developing an understanding about why buildings are performing the way they do. For example: in the Thermal Compartmentation and Kerkrade projects, it was found that in reality, less energy was used for DHW, ventilation, lighting and appliances than anticipated. In the Thermal Compartmentation project, it was furthermore found that the efficiencies of the heat pumps were lower than expected (i.e. more energy was used for the heat pumps than anticipated). In the Quickscan huurderstevredenheid EPV project [4], monitoring revealed dysfunctional building systems.

Satisfaction of residents

All the projects covered concluded some success on achieving occupants' satisfaction, in comparison to their situation before the renovation or as low/zero energy projects. The satisfaction does not always have to do with energy performance, but has to do with a previous situation, a better indoor quality, upgraded services and exterior look of the dwellings.

In all projects there were some dissatisfied occupants. The causes for dissatisfaction were mostly related to residents not understanding the use or maintenance of the systems (ventilation, low temperature heating) that in some cases led to discomfort situations, and to complains about noise from the systems (heat pump and ventilation system). Where these aspects were investigated, it was concluded that there is a need for better introduction to the home's systems, better manuals and follow up information and support to the residents.

Where the satisfaction with the renovation process was also investigated, it was concluded that in most cases, the residents were not satisfied with the process. In two of the projects, it was also concluded that these issues after delivery could be affecting their satisfaction on a longer term (up to 1 year after completion). Issues affecting this dissatisfaction are extended or changed plans, lack of information, nuisance, lack of trust, and mismanagement of residents' expectations.

How is energy data used?

From non-structured interviews and discussions during IEBB partner meetings it seems that it is becoming more common to collect energy data. However, this data is used at a high aggregation level only. While energy meter data are collected, sometimes on a monthly basis, sometimes per hour or at 15 minute intervals, it seems that only aggregated data is used for yearly performance analysis and sometimes to roughly track malfunctioning in HVAC systems. In general, the largest part of the data is not used and there seems to be a need for methods and standards on the analysis of the data. As noted by an interviewee from an organization having collected data before and after renovation, the organization lacks time, capability and workforce to analyse the data. This was even more the case for data relating to occupant preferences and behaviour.

Some companies/organizations are working together with students and teachers at universities of applied sciences to make progress in their analyses. The remarks here were that in few projects a lot is measured, and even used to improve some parts of the system, like heat pumps. But in general, the students were the first ones to make detailed analysis and to find out that sometimes sensors were wrongly placed, or wrongly tagged, or that submetering data needed for the diagnostic of malfunctioning were not present.

Finally, in discussions with two companies selling and installing monitoring equipment for energy and indoor air quality, they both indicated that developments regarding the use and analysis of the data were urgently needed.

Satisfaction and opinions vs. measured data

Most reports focus on satisfaction of the residents on different stages of the process (before, during or after), as well as satisfaction on the final result (the product). Several aspects related to building performance were investigated, but with more attention to residents' satisfaction, experiences, and opinions regarding the easiness of use and maintenance of the new installed technologies, as well as perceptions regarding thermal comfort, noise, and air quality. The actual indoor environmental quality such as temperature, CO_2 concentration, noise levels, presence of draughts, etc., are often not investigated. Energy is monitored in some projects, which is used to assess whether a project performs within the expectations or the performance contract. However, in cases in which higher energy use is demonstrated and some users are dissatisfied, there is rarely the intention, or possibility, to investigate further the reasons for such deviations.

Qualitative vs. quantitative data collection and analysis

More than half of the reviewed reports focused on qualitative data from interviews and surveys with the residents. In addition, two reports were based on interviews with experts about the residents (second-hand information). The projects that also measured indoor temperatures or setpoint, and/or energy use were able to provide more insight in the performance of the buildings. However, it is difficult to assess what exactly causes poor performance (indoor environmental quality / energy use), since information on indoor environmental quality and energy submetering is rarely collected. In the reports, the experts were often able to estimate the cause of the performance gap, which was often attributed to technical malfunctions or poor quality of the construction. However, in many instances a

non-technical reason could be also attributed to the perception, understanding or satisfaction of the residents regarding the technologies, for example, experiences in a previous home (new users), pre-renovation situation (very high energy bills or very bad indoor quality), previous problems with installations, etc. In all but one report, the role of occupants' behaviour was not explored. For example, the actual needs and preferences of the residents (e.g. regarding heating setpoint) were not investigated, and there was little reporting on thermostat use, heating setpoints and thermostat setbacks, which are known to have a large impact on comfort and energy use. On the other hand, a great deal of importance was given to the use of ventilations systems, which are also known to be problematic in terms of noise and user interaction.

6. Conclusions

Current energy models do not accurately predict energy savings in dwellings. The discrepancy between predicted and actual energy consumption is a main result of: 1) Models that do not consider occupant behaviour (number of occupants, ventilation behaviour, temperature settings, use of sun shading, maintenance, and settings of appliances); 2) Parameters and inputs of the models that cannot be well-determined (like infiltration flow rates or even R_C- and U-values); 3) Issues with the systems based on how they are installed and commissioned.

Based on data that is currently collected at a housing stock [15-18] and individual housing level, it is difficult to determine the exact causes of the discrepancies. Better models – digital twins – are therefore needed to predict the actual energy performance of renovation measures in dwellings. The goal of this study was to determine the performance of specific renovation concepts in practice and how the projects are monitored and evaluated. Building owners, contractors and technology providers are increasingly gathering data to assess the performance of net-zero energy renovation technologies and concepts. In this study, we found that the nature of the data gathered and reported varies significantly. For example, some organizations gather data on energy performance, some on indoor climate, some on resident preferences and opinions, but none are examining the complete picture, which makes it difficult to determine the actual performance of the renovation concepts. In cases where renovation concepts outperformed or underperformed compared to expectations, there was often insufficient data to determine the reasons. However, from the point of view of energy performance, many monitored project appeared to perform as expected or even better than expected. This may be a direct result of the monitoring and/or the result of expressing targeted performance in terms of absolute energy usage instead of energy savings.

In all studied cases, monitoring was generally not at the level that it could be used to diagnose and solve technical problems in a standardised way. The desk research also shows that the satisfaction of residents with the renovation process was often monitored, but not at a level allowing for a good understanding of their needs and interactions with the technical systems.

7. Recommendations

Recommendation 1: Renovation pojects that complete monitoring campaigns are better positioned to evaluate real energy savings and occupant satisfaction. Building owners and operators should therefore develop monitoring campaigns early in the renovation process. This could also help ensuring that results are realised and can support quicker diagnosis of (rough) malfunctioning.

Recommendation 2: More transparency is needed from parties involved in energy renovations about underperformance. With more information researchers, installers and producers can undertake targeted monitoring and even solve problems beforehand. This would also help in the development of more accurate energy prediction models.

Recommendation 3: More research/transparency is needed about what makes a successful renovation project. This could positively influence the market by making companies aware of what works well and creating positive dynamics.

Recommendation 4: More sub-metering data should be collected and disclosed by building owners, contractors and/or technology providers. With more sub-metering data, researchers and contractors will be better able to fix malfunctions as soon as possible malfunctioning. This would also help researchers explain the differences between the anticipated and actual energy efficiency of a building after renovation in such a way that better predictions can be made.

Recommendation 5: Develop GDPR-proof standards for sub-metering and data collection. In addition to smart meter data, sub-metering data should include: 1) Splitting gas use in space heating, domestic hot water (DHW) and cooking; 2) splitting electricity use in space heating, DHW, ventilation, cooking and appliances; 3) splitting electricity production of PV-cells in on-site energy used, and delivery to grid, 4) splitting net electricity use in electricity from grid, from PV-cells and electricity delivered to grid; 5) setpoint temperatures of the systems, especially when heat pumps are involved; 6) air temperature and CO_2 sensors; and 7) additional data like radiant temperature, humidity, air velocity, opening of windows and doors and residence presence are also useful in explaining higher or lower energy use and thermal (dis)comfort.

Recommendation 6: Develop guidance on how to analyse data from smart meters and other indoor

environment meters should be developed by experts in the field, considering different objectives.

Recommendation 7: Those involved in energy renovation projects should ensure clear communication towards the residents about the renovation process. This is needed to keep the burden low during the renovation.

Recommendation 8: Those involved in energy renovation projects should provide residents with (long-term) follow up information about the use and maintenance of systems, . While clear manuals are important, they are not enough.

Recommendation 9: Building owners and managers should take resident's complaints seriously and investigate further possible malfunctioning of components and installations and mismatches with their use.

Recommendation 10: Those involved in energy renovations should ensure that a process is in place to investigate resident satisfaction and experience as well as actual indoor environment quality and energy. This is essential for deepening our understanding about why expected performance is achieved or not and what determines whether residents are satisfied or not.

Recommendation 11: The investigation of the non-technical reasons for underperformance of systems should be standardized. This includes resident's experiences and needs before the renovation, and their actual needs regarding heating and ventilation setpoints, as well as how they interact with these systems. This could strongly enrich existing simulation models.

Recommendation 12: Develop standardized methods for a) analysis of pre-renovation experiences and needs b) actual needs and interaction with systems.

8. Acknowledgement

This project is executed with the support of the MMIP 3&4 grant from the Netherlands Ministry of Economic Affairs & Climate Policy as well as the Ministry of the Interior and Kingdom Relations. This study has been developed as part of the Integrale Energietransitie in Bestaande Bouw (IEBB) Theme 2 - Data-driven Optimization of Renovation Concepts project. The project is a multi-year, multi-stakeholder program focused on developing affordable and user- friendly renovation concepts for residential buildings.

9. References

[1] Ministry of Economic Affairs and Climate. (2019, June 28). National Climate Agreement.
[2] Visscher, H., Meijer, F., Majcen, D., & Itard, L. (2016). Improved governance for energy efficiency in housing. Building Research & Information, 44, 552-562.
[3] Topsector Energie. (2020). Topsector Energie Projecten.
[4] Van den Brom, P. (2020). Energy in Dwellings: A comparison between Theory and Practice. Delft: Delft University of Technology.
[5] Van den Brom, P., Hansen, A., Gram-Hanssen, K., Meijer, A., & Visscher, H. (2019). Variances in residential heating consumption–Importance of building characteristics and occupants analysed by movers and stayers. Applied Energy, 250, 713-728.
[6] Majcen, D. (2016). Predicting energy consumption and savings in the housing stock. Delft: Delft University of Technology.
[7] Majcen, D., Itard, L., & Visscher, H. (2013). Theoretical vs. actual energy consumption of labelled dwellings in the Netherlands: Discrepancies and policy implications. Energy Policy, 54(C), 125-136.
[8] De Jong, F., & Borger, D. (2018). Eindrapport quickscan huurderstevredenheid EPV. Utrecht: Atrivé. -over-epv
[9] Salemink G., Rovers, T. (2021) Compartimenteren woningen met binnen isolatie op maat. Aanvulling Openbaar Eindrapport: Monitoring van het energiegebruik over 2020. 22 March, 2021. Saxion Hogeschool.
[10] Jacobs, P., Liedelmeijer, K. Borsboom, W.A., van Vliet, M.R.A., de Jong P. (2015). Concepten nul op de meter en 80% besparing. Energiesprong.
[11] Guerra-Santin O & Silvester S. (2016) Development of Dutch occupancy and heating profiles for building simulation. Building Research & Information 45:4, 396-413.
[12] Guerra-Santin O., Romero Herrera N, Cuerda E & Keyson D. (2016). Mixed methods approach to determine occupants' behaviour –Analysis of two case studies. Energy and Buildings 130 546-566.
[13] Cozijnsen, E., Leidelmeijer, K., Borsboom, B., van Vliet, M. (2015). Resultaten uit monitoring over: Tevreden bewoners. Energiesprong.
[14] Silvester S., et al. (2016) Report: 2ndSKIN zero energy apartment renovation via an integrated façade approach. TKI energo. Technical University Delft.
[15] De Gemeenschap. (n.d.). Tolhuis 1590: Hoogwaardige renovatie - woonkwaliteit gedreven. Nijmegen: Woningbouwstichting De Gemeenschap.
[16] Borsboom, W., Leidelmeijer, K., Vliet, M., de Jong, P., & Kerkhof, H. (2016). Resultaten uit monitoring: Bewonerservaringen En Meetresultaten Uit Nul Op De Meter Woningen In Heerhugowaard (BAM). Utrecht: Energiesprong.
[17] Borsboom, W., Leidelmeijer, K., Vliet, M., de Jong, P., Schouten, K., & Engelmoer, W. (2017). Resultaten uit monitoring: Bewonerservaringen En Meetresultaten Nul Op De Meter In Tilburg. Utrecht: Energiesprong.
[18] de Jong, E. (2019). Woonbelevingsonderzoek bij bewoners van ZEN nieuwbouwwoningen. Lente-akkoord.

Tab. 1 – Overview of analysed projects

	Project	Energetic aim of the renovation	Sector	# monitored dwellings	Renovation concept used and goal of the monitoring campaign
1	Quickscan Huurderstevredenheid EPV [4]	NOM / Net-Zero Energy	Social	51 (3100 homes)	Monitoring of the energy use for one year after the renovation. Satisfaction with the EPV
2	Thermal Compartmentation [5]	NOM / Net-Zero Energy	Social	4	Insulation, airtightness and ventilation measures to kitchen and living room. Insulated floor between the living room and bedrooms
3a	Kerkrade [6,11]	80% reduction in energy use	Social	153	Prefab façades, ventilation ducts into timber frame. Prefab roof elements with PV-panels.
3b	Zorgeloos Wonen [6,11]	A or A+	Social	115	Insulated facades, insulation of the roof and ground floor, high- performance windows and doors.
3c	Amsterdamse Buurt – Haarlem [6,11]	B to A+	Social	108	Internal wall insulation, high-performance glazing and PV panels.
3d	Energiesprong Montferland [6,11]	N/a	Social	61	Air source heat pumps, low-temperature underfloor heating and convectors.
3e	RijswijkBuiten [6,11]	NOM New Build	Private	5	Ground-source heat pumps, solar panels, high-efficiency ventilation and a well-insulated shell.
4	2nd Skin Demonstrator [7]	NOM/Net-Zero Energy	Social	9	Testing user-centered methodologies for monitoring and data analysis Improved insulation, balanced mechanical ventilation, ground source heat pump, low-temperature convectors.
5	Tolhuis 1590 - Nijmegen [8]	NOM/Net-Zero Energy	Social	1	Monitoring to evaluate the efficacy of the ActiveWarmth electrical wall heating system
6	NOM – Zoetermeer	NOM/Net-Zero Energy	Social	120	Monitoring the energy and comfort performance, and to ensure the proper functioning of the energy system. Integrated Climate Energy Module (iCEM) of Factory Zero.
7	NOM Renovation – Heerhugowaard [9]	NOM/Net-Zero Energy	Social	55	Prefabricated facade and roof. Natural gas connection was disconnected, and PV panels were installed at the front and rear.
8	NOM Renovation – Tillburg [10]	NOM/Net-Zero Energy	Social	18	Modular building systems: prefabricated facade elements, new roof and floor insulation. Balanced ventilation system with heat recovery, heat pump, boiler, control box, monitoring system and a solar power inverter. No gas connection.
9	Zen Nieuwbouwwoningen [12]	NOM/Net-Zero Energy or Low-Energy	Social and private	31 projects and 302 residents engaged	measure the satisfaction of homebuyers, to investigate the experiences of residents of a ZEN home. Survey

Technology concepts for rapid renovation using adaptable lightweight façade systems

Daniel Adamovský [a], Jan Vcelak [a], Pavel Mlejnek [a], Jaume Colon [b], Zuzana Prochazkova [c], Constantinos Tsoutis [d], Daniel Philippen [e], Maria Founti [f]

[a] University Centre for Energy Efficient Buildings, Czech Technical University in Prague, Bustehrad, Czechia, daniel.adamovsky@cvut.cz, jan.vcelak@cvut.cz, pavel.mlejnek@fel.cvut.cz

[b] Denvelops, Igualada - Barcelona, Spain, jaumec@denvelops.com

[c]PichArchitects,Barcelona,Spain,z.prochazkova@picharchitects.com

[d] AMSsolutions, Irakleio, Greece, constantinos.tsoutis@amsolutions.gr

[e] Institute for Solar Technology SPF, Eastern Switzerland University of Applied Sciences OST, Rapperswil-Jona, Switzerland, daniel.philippen@ost.ch

[f] Lab. of Heterogeneous Mixtures & Combustion Systems, School of Mechanical Engineering, National Technical University of Athens, Athens, Greece, mfou@central.ntua.gr

Abstract. H2020 project PLURAL (Plug-and-Use Renovation with Adaptable Lightweight Systems) proposes prefabricated, modular and adaptable lightweight façade systems for rapid renovation of existing buildings providing high-performance, cost-effective and fast renovation solutions. This paper presents the early stage technology concepts of three different core systems representing Plug-and-Use (PnU) building envelope kits. The PnU kits couple the lightweight façade module concept with ecological coating materials, integrated energy systems such as photovoltaics, heating, cooling, and ventilation. The paper describes in detail technical solutions of three innovative core systems and presents real and virtual demonstration buildings. Also shows calculated energy performance for real buildings when one of PnU kits is applied for renovation.

Keywords. Building renovation, energy performance, nZEB, façade panel, HVAC integration.
DOI: https://doi.org/10.34641/clima.2022.42

1. Introduction

The existing building stock calls for high-performance, cost-effective and fast renovation solutions to significantly decrease energy consumption [1], [2]. The answer to this challenge regarding residential buildings is the PLURAL project, which targets to design, validate and demonstrate a palette of versatile, adaptable, scalable, off-site prefabricated "plug and play" facades accounting for user needs (named "Plug-and-Use" - PnU kits). Technologies integrated in prefabricated panel solutions in the framework of local nZEB requirements need to fulfil requirements for: fast retrofitting process, renovation cost reduction, high level of prefabrication, use of eco-friendly and sustainable construction materials and in total provide high indoor environment quality. All these aspects will be validated in the frame of the PLURAL project for three demonstration sites (called real demonstration) and three additional buildings where the PnU kits will be "virtually" installed accounting for specific design and climatic requirements and their performance will be validated using computational tools (virtual demo sites).

In the second year of PLURAL we present the three basic PnU kits:

- "SmartWall" – a multifunctional prefabricated wall panel,
- "eWHC" – an external prefabricated Wall Heating and Cooling module panel,
- "eAHC" – a prefabricated module with air handling unit with Advanced Heat/Cool recovery system.

The goal of this paper is to present developed technology concepts of above mentioned three different PnU kits. The project is in the stage of preparation of real demonstrations, the paper presents only calculated results for two of them.

Copyright ©2022 by the authors. This conference paper is published under a CC-BY-4.0 license.

2. Overview of the core systems

PLURAL renovation aims to ensure that the retrofitted buildings reach criteria of nZEB, according to each country's nZEB directives. It is important to note that the target level is a comparison of the retrofitted building with the nZEB definition for new buildings. This is because the requirements for retrofitted buildings are often lower.

The PLURAL approach is in line with the EU energy strategies for 2050. Heat losses through the envelope will be minimized through improved insulation of the façade components, reaching U-values of less than 0.23 W/(m²·K) and building primary energy consumption less than 60 kWh/m². In addition, through the installation of the prefabricated panels, the cost of renovation is aimed to be reduced by 58 % and the time of renovation by 50 %. Energy performance, renovation time and costs will be validated via extended monitoring campaigns at the three real demo sites.

Each of the core systems described below has a unique structure; "SmartWall" is a welded steel frame structure, "eWHC" is a timber frame structure and "eAHC" is a stainless-steel line structure.

2.1 SmartWall

The SmartWall is a unique compact versatile prefabricated wall panel, which can be installed externally or internally in existing building envelopes, introducing an innovative and flexible solution for light and/or deep buildings' retrofitting. Fig. 1 illustrates its three basic components, which are the frame, insulation material and finishing layers.

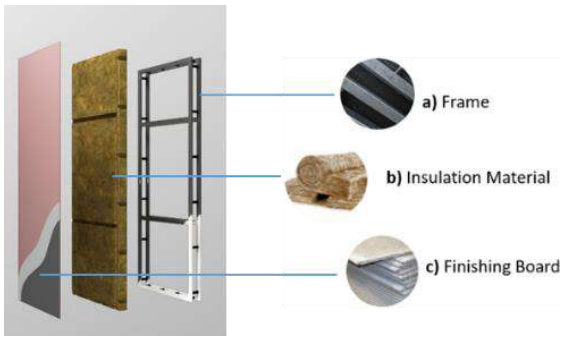

Fig. 1 – Fundamental components of "Smartwall".

The basic material for the frame is steel S245, using lightweight 50 x 50 mm members welded in a frame. The "Smartwall" can be easily manufactured using alternative materials such as timber, industrial plastic, aluminium or carbon fibre. Due to various materials and technologies that can be integrated in the "Smartwall", a large variety of panel sizes with various frame strengths can be designed and manufactured

Among insulation materials possible alternatives are rockwool, glass wool, EPS, cellulose and VIP (backside of a convector). Finishing surfaces differ according to the use of the PnU kit in interior or exterior of a wall. Large variety of boards contains cement, gypsum, fibre, timber, etalbond, etc. Most of the aforementioned boards can also be treated with PCM-multifunctional coatings enhancing their properties with energy storage, self-cleaning, IR reflective, anti-bacterial, self-healing etc., characteristics, produced by project partner AMS [3].

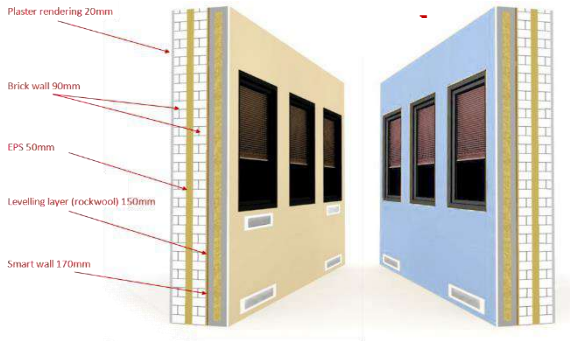

Fig. 2 – "Smartwall" solutions for interior (left) and exterior (right) integration.

The conceptual idea of "SmartWall" PnU kits, is to integrate various prefabricated elements such as windows, doors, and balcony doors, in order to reduce installation time and construction faults during installation. Also, a wide range of technologies for heating and / or cooling could be integrated in the SmartWall, e.g. fan coils, split units, air ducting systems, radiators and convectors. Optional features for exterior "Smartwall" PnU kits are PV panels including local batteries.

Fig. 3 – General example of "Smartwall" application.

2.2 eWHC

The eWHC PnU kit is specifically designed to be used in colder climatic zones such as continental and alpine. Therefore, the high requirements are set on the thermal isolation properties and airtightness. Fundamental material for the frame is timber because of low carbon footprint, high flexibility in

shape, dimensions and variety of connection techniques.

Outer layers serve as load bearing timber and include the main thermal insulation (see parts 1 – 4 in Fig. 4). Next comes a flexible layer made from an insulation material (5). Its purpose is to ensure best and maximum contact of the heating/cooling pipes (8) with the existing façade wall accounting for wall irregularities (7). This enables the element to adapt to uneven sections of the wall. After investigations the most appropriate materials are selected that include the group of organic (wood fibre, sheep wool, hemp wool) and mineral (glass and rock wools) materials. The nut and washer (12), attached to the L-profile via a threaded rod will provide the horizontal force to push the PnU kit against the wall.

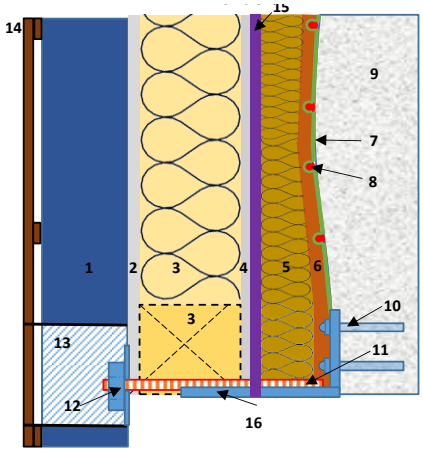

Fig. 4 – Section of "eWHC" kit (1 – insulation + weathering membrane, 2 – upper fermacell board, 3 – beams and insulation, 4 – lower fermacell board, 5 – flexible layer, 6 – soft board, 7 – metal heat fin, 8 – heating/cooling pipe, 9 – original wall, 10 – anchor, 11 – threaded rod, 12 – nut + washer, 13 – access, 14 – outer cladding, 15 – vapor barrier, 16 – L profile).

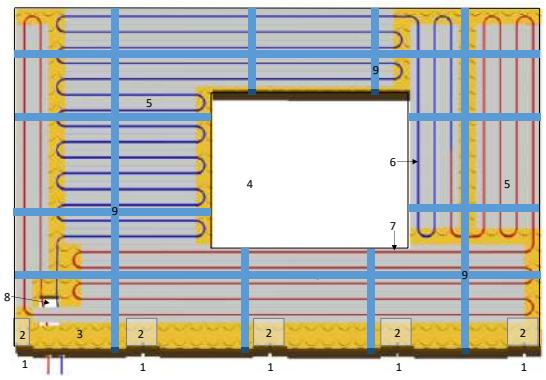

Fig. 5 – Heating layer in "eWHC" kit (view from original wall; 1, 2 – slots and space for L-profile, 3 – soft fibreboard, 4 – recess for a window, 5 – metal fins, 6 – return flow, 7 – supply flow, 8 – opening for pipes, 9 – belts)

The eWHC, as described above, integrates a heating and cooling layer in its composition creating a dynamic HVAC feature. The construction of the heating/cooling pipe network (Fig. 5) is done with standard materials of a radiant floor heating systems. The flexible and structured board (6 – Fig. 4) has slots for the metal fins (7) and the composite heat pipe (8). The metal fins are essential to ensure a sufficient heat distribution throughout the wall.

The "eWHC" PnU kit can easily integrate a local air-handling unit with heat recovery in order to supply fresh air to a single room.

Integration of windows as well as window frame integrated units is possible above or below the "eWHC". The "eWHC" system is ready to integrate standard types of windows with double or triple glazing configurations depending on climatic zones and local nZEB requirements.

2.3 eAHC

The "eAHC" PnU kit is a ventilated façade prefabricated system that can integrate a large range of functionalities. The base is the system developed by the project partner company Denvelops, composed of vertical stainless-steel guide lines and connectors, that allow to attach and bear the loads of the cladding [4]. The thermal insulation is made of mineral wool and is protected by a weathering layer. Both are attached to the system vertical guidelines in order to achieve the required thermal and water-tightness performance. Thickness 100 mm with declared thermal resistance of 2.90 ($m^2 \cdot K$)/W is considered as the optimum passive measure according to simulations and includes at least 50% of recycled material. The mineral wool is covered by a glass-fibre layer that can protect against mechanical damage.

The cladding of the façade is made with painted aluminium cladding tiles with 1 mm thickness and a resistant powder coating. PV panels are integrated in the façade, replacing locally the final cladding. These panels are composed of 2 layers of tempered glass and amorphous PV cells with overall thickness of 4 mm and width of the module 200 mm. The peak power of the cell with height of 800 mm is 19,4 W.

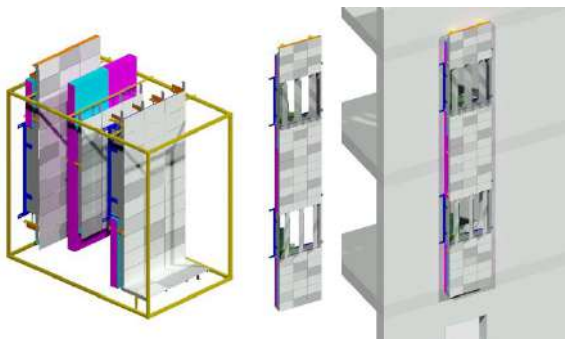

Fig. 6 – Vertical transport and straight frames for installation of eAHC kit.

The main HVAC component integrated in the façade is the "eAHC" ventilation unit. The unit is located in

vertical position, thus needs to have a very low depth (160 mm). It contains two stage heat recovery, the first is regular plate heat exchanger, the second is active heat exchanger with thermoelectric modules and provide supply air temperature control. The unit is connected with the interior space via supply and extract channels. Due to maintenance reasons, the ventilation unit must be located next to a window side. (Fig. 7).

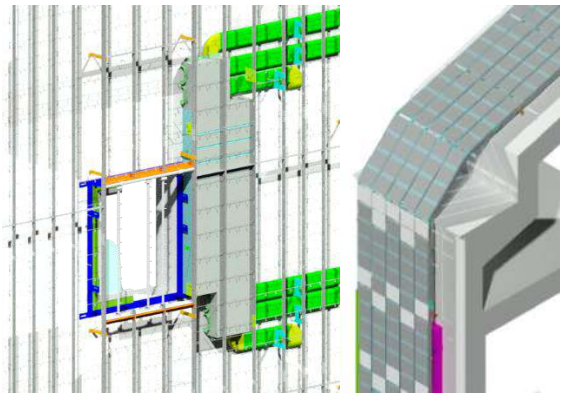

Fig. 7 – Ventilation unit and air channels (left) and PV panels (right) in eAHC kit.

3. Real and virtual demonstration

The PnU kits are planned for real (Table 1) and virtual application (Table 2) to verify their design and performance on various types of buildings in different climate zones in Europe.

Tab. 1 – Overview of real demonstration sites.

Description	Photo
Greece, Athens, Voula *Mediterranean climate (hot summer)* 2 of 10 flats - "SmartWall".	
Spain, Barcelona, Terrassa *Mediterranean climate (mild summer)* 1 block of 2 – "eAHC".	
Czech Republic, Kašava *Continental climate (warm, humid)* Whole building – "eWHC"	

Tab. 2 – Overview of virtual demonstration sites.

Description	Photo
Germany, Berlin *Continental climate* "SmartWall".	
Sweden, Väsby *Boreal climate* "eWHC"	
Switzerland, Bern *Alpine climate* "eWHC"	

Each real demonstration building faces different challenges and objectives given by the local law requirements, owner plans, inhabitants expectations, etc.

3.1 Czech pilot – Kašava

The Czech pilot project in Kašava is a detached double dwelling house built in 1962. Renovation doesn´t include only improving of thermal insulation of external walls and windows and installation of renewable energy sources. The Czech strategy for the building energy efficiency retrofit prefers complex solutions for the whole thermal envelope. PnU kits are not used only on outer walls, but modified prefabricated elements are used on new walls and roof construction. The volume of the roof is changed to improve internal flat distribution and to minimize surface of external thermal envelope. New volume has been designed to avoid thermal bridges that are joined with traditional mode of energy efficiency refurbishment.

Regarding HVAC, the existing gas boiler will be replaced by air-to-water heat pump as heating and cooling source for the wall integrated "eWHC" system. Integration of BIPV system on building's roof is essential to achieve nZEB. Also, each room will be equipped with local ventilation unit with heat recovery.

Tab. 4 – Overview of preliminary energy performance for renovation of Kašava building [5] (green – nZEB criteria passed, red – nZEB criteria failed, need update).

nZEB indicators	Kašava building	Building retrofit	nZEB 2022
Average U value of envelope (W/m².K)	**0.21**	0.41	0.29
Total delivered energy (kWh/a)	**18579**	44272	34094
Specific delivered energy (kWh/(m².a))	**93**	161	124
Total non-renewable primary energy (kWh/a)	**-10943**	46320	19383
Specific non-renewable primary energy (kWh/(m².year))	**-39.8**	169	71

Table 4 summarizes the expected energy performance of the Kašava building after renovation with the eWHC PnU kits. It is significant in preliminary design that because of heat pumps replacing old gas boiler and heat recovery ventilation, the overall delivered energy decreased. Furthermore, due to PV system on the roof, non-renewable primary energy fell into negative values.

3.2 Spanish pilot – Barcelona

The Spanish pilot project in Barcelona (Terrassa) is renovation of one of the two blocks of a residential social housing built in 2008. The project is specific for the specific requirements by the building owner in order to improve the management of the building and match with the user needs. These requirements are at technical, social, economic and building controls' level. The final scenario involves renovating the East and West façades of the selected building block using the "eAHC" PnU kit, counting it as an intervention to the thermal envelope, as well as using the roof area facing East in order to install photovoltaic panels for RES production, using the same PnU solution as for the façade, but without affecting the thermal properties of the roof. Important emphasis is on installation of new windows with outer folding blinds and ventilation units for each apartment.

The recent HVAC systems include local electric heaters and electric hot water tanks. According to the building owner, these will not be replaced.

Table 5 summarizes the expected energy performance of the Bercalona building after renovation with the eAHC PnU kits. Main issue for this building is very high portion of non-renewable energy because all electric HVAC. Therefore, the entire energy savings must be provided via active measures in the "eAHC" PnU kits.

Tab. 5 – Overview of energy performance with various PLURAL measures of Barcelona building (green – nZEB criteria passed, red – nZEB criteria failed).

Simulated Cases	Description	EP_{nren} [kWh/(m² a)]	EP_{total} [kWh/(m² a)]
Base case	Existing building before PLURAL	103	137
PLURAL passive	PLURAL passive solutions (1st and 2nd floor)	**83**	**113**
PLURAL passive + active	PLURAL passive solutions (1st and 2nd floor), active solutions eAHC + PV installation to accomplish regulations	**70**	**105**
PLURAL passive + active nZEB	PLURAL passive solutions (1st and 2nd floor) active solutions eAHC + PV installation to accomplish nZEB for a new building	**38**	**76**

To accomplish local regulations [6] for a building renovation, it is necessary to reduce the consumption of non-renewable primary energy (EP_{nren}) to 12.8 kWh/(m²·a) and total consumption of primary energy (EP_{total}) to 7.6kWh/(m²·a). This will be done through the "eAHC" ventilation unit and PV system. To be an nZEB building in terms of Spanish definition, as for a new building, active measures, especially the PV system, have to reduce EP_{nren} for 44.8 kWh/(m²·a) as well as EP_{total} for 36.6 kWh/(m²·a).

3.3 Greek pilot – Athens

The Greek pilot project in Voula, Athens is a multi-floor residential social dwelling for elderly people built in 1971. Local municipality divide the overall renovation in two stages, mainly for budget reasons, as well as, to minimize tenant's reallocation in other buildings, as the building provides accommodation to elderly people with limited financial capabilities. The 1st renovation stage works in the semi-basement and ground floor have already been completed since September 2020. The 2nd renovation stage is focused on the ETICS installation on all external envelope of the building; roof renovation and insulation; refurbishment of the apartments, common areas, corridors, staircases, lift etc.

Application of the "Smartwall" PnU kit targets to refurbish and upgrade each apartment with recyclable and eco-friendly materials, upgrade all energy systems in order to reduce energy consumption to reach the Greek KENAK nZEB standard (5) and ameliorate the thermal, acoustic and visual comfort of the residents. In order to meet the Greek nZEB standards [7], primary energy consumption should be between 31 and 99 kWh/(m^2·a) or lower. Unfortunately, no data are available at the moment.

4. Conclusion

The target of this paper is presentation of three prefabricated versatile "plug and play" facades (PnU kits) for building retrofit to nZEB level of a new building. The overview presents a path for cost-effective and fast retrofit of buildings which provide very large variety of panel structures with integrated technologies. One or more of the three basic PnU kits is capable to provide a solution for renovation of residential buildings across Europe from Mediterranean to Cold climate.

At the moment are available only calculated data from evaluation according to local nZEB requirements. They indicate abilities of proposed PnU kits. But it is important to notice also limits of energy savings, when the renovation targets only the building envelope. This is seen in the case of Czech demonstration building, which meet requirements for retrofit, but to reach requirements for new buildings deeper optimization of envelope is necessary. In the case of Spanish demonstration building is seen limitation when focus is only on façade and not to existing HVAC systems in the building. This results in significant increase of PV system in façade.

5. Acknowledgement

Research project Plug-and-Use Renovation with Adaptable lightweight Systems – PLURAL funded from the European Union's Horizon 2020 research and innovation programme under Grant Agreement No. 958218. See more on https://www.plural-renovation.eu/

6. Appendices

List of PLURAL partners in alphabetical order: Advanced Management Solutions, Agència de l´Habitatge de Catalunya, BG Tec Bergamo Tecnologie Sp.z o.o., Czech Technical University in Prague, Daikin Airconditioning Hellas SA, DENVELOPS TEXTILES S.L., FENIX TNT s.r.o, Institute for Solar Technology SPF of Eastern Switzerland University of Applied Sciences OST, INTRASOFT International S.A, Municipality of Vari-Voula-Vouliagmeni, National Technical University of Athens - Project coordinator, Obec Kašava, Pich Architects, RD Rymarov, RECUAIR s.r.o, The Catalonia Institute for Energy Research, The Catalonia Institute of Construction Technology, ZRS Architekten.

7. References

[1] Directive (EU) 2018/844 amending Directive 2010/31/EU on the energy performance of buildings and Directive 2012/27/EU on energy efficiency, 30 May 2018.

[2] Proposal for a directive (EU) on the energy performance of buildings (recast), 15.12.2021. Available at: https://ec.europa.eu/energy/sites/default/files/proposal-recast-energy-performance-buildings-directive.pdf

[3] AMS coatings and advanced materials, Available at: https://amsolutions.gr/materials/, visited January 13 2022.

[4] Denvelops smart system, Available at: https://www.denvelops.com/new-construction-system/, visited January 13 2022.

[5] Decree No. 264/2020 on the energy performance of buildings, 5 May 2020 (in Czech).

[6] CTE DB-HE 2019 Building technical regulations – Energy savings (in Spanish).

[7] Regulation on the Energy Performance of Buildings (KENAK), March 2018 (in Greek).

Thermal comfort perception and indoor climate: Results from the OPSCHALER project

Arjen Meijer [a], Anastasia Petropoulou [a], Andrea Joseph Thaddeus [a], Laure Itard [a]

[a] Faculty of Architecture and the Built Environment, Delft University of Technology, Delft, the Netherlands, A.Meijer@tudelft.nl.

Abstract. The average energy consumption for heating of dwellings in the Netherlands has been decreasing over the last decades as a result of increasing thermal performance of new and renovated dwellings. However, this decrease is found to be lower than energy performance models predicted. One of the possible reasons is the behaviour of the residents, which is partially determined by the thermal comfort preferences of these residents. In this paper, the relationship between thermal comfort perception, indoor climate and energy consumption is investigated using high-resolution measurement data in 93 dwellings in the Netherlands. In the OPSCHALER project, data about thermal comfort perception, indoor climate and operational energy consumption were collected in 93 dwellings in the Netherlands during periods ranging from two to twelve months over a period of two years. Comfort perception was registered using the Comfort App, an application where users record their comfort data. Indoor climate data were collected per five minutes using sensors for temperature, relative humidity and CO2 concentration in the living room, kitchen and bedrooms of the dwellings. The Comfort App asked the residents for the room they are in, their comfort perception, their activities during the last half hour and the amount of clothing they wear. Significant relationships were found between thermal sensation and thermal preference, clothing level, metabolic activity level, activities related to thermal comfort taken in the last half hour, and indoor air temperature. These data can be used to compare the comfort level registered by the residents with the comfort level predicted by the PMV model, and link this to the indoor climate and the energy consumption for heating. This information can help to understand the relations between user preferences, indoor climate and energy consumption for heating.

Keywords. Thermal comfort, indoor climate, dwellings, comfort theory
DOI: https://doi.org/10.34641/clima.2022.167

1. Introduction

According to the European Commission, buildings are responsible for approximately 40% of the EU energy consumption and 36% of the CO_2 emissions. The residential building sector takes 63% of this share [1]. To meet the goals for reduction of CO_2 emissions as stated in the Paris Agreements [2], a significant effort is needed to reduce energy consumption in the residential sector, both in new and in existing houses. However, energy renovations in existing houses were found to result often in lower energy savings than estimated from energy models. One of the reasons are differences in energy consumption of dwellings with similar characteristics. It has been shown that the energy consumption of similar dwellings may differ up to 3 times [3,4]. At the same time, several studies have concluded that there is a difference between the actual and the predicted energy consumption, the so-called "energy performance gap", with differences reaching up to a factor of 2 [5-7]. Current simulation software is simplified and does not take residents' energy related behaviour largely into account [8]. This behaviour is largely related to the comfort perception of the residents.

The most widely used thermal comfort models for assessing thermal sensations are Fanger's Predictive Mean Vote or the PMV model [9] and the adaptive thermal comfort model [10]. These theories have been tested in the past on small scale, but large testing using large scale monitoring campaigns in many dwellings over an extended period has not often been carried out. These monitoring campaigns can yield data that can be used to test the comfort perception models, which can then be used to improve energy consumption models for dwellings.

In this paper, the relationship between thermal comfort perception, resident characteristics and indoor

Copyright ©2022 by the authors. This conference paper is published under a CC-BY-4.0 license.

climate is investigated using high-resolution measurement data in 93 dwellings in the Netherlands.

2. Methodology

2.1 Data collection

In the OPSCHALER project, data about thermal comfort perception, indoor climate and operational energy consumption were collected in 100 dwellings in the Netherlands during periods ranging from two to twelve months over a period of two years (2017-2019). The dwellings are privately owned houses, located in several areas in mid, west and southwest Netherlands. The choice of the dwellings was based on the willingness of the residents to participate with the monitoring campaign and on the presence of a smart meter for gas and electricity consumption.

The thermal comfort perception was monitored using a tailor-made app (ComfortApp) that the residents could use on their phone or tablet. In the ComfortApp, residents were able to fill in various subjective data such as:

- Perceived comfort level (thermal sensation) on a 7-point scale, from -3 (very cold) via 0 (neutral) to +3 (hot), as well as preferred comfort level (thermal preference), from -1 (cooler) to +1 (warmer)
- The room they are occupying when filling in the log
- Clothing level (6 levels)
- Metabolic activity level: lying /sleeping, relaxed sitting, doing light deskwork, walking, jogging, running.
- Actions taken during the past half hour related to comfort and energy consumption

The residents of the houses were asked to fill in the app a few times per day (preferably in the morning, midday and evening), but no reminders could be given, so the input in the ComfortApp depended on the initiative of the residents. For each dwelling, two accounts for the ComfortApp were available, but in most cases, only one family member used the ComfortApp. The data from the ComfortApp were directly stored in a central project database.

Indoor climate was monitored using sensors developed by Honeywell that monitor temperature, relative humidity, CO_2 concentration and presence in the room. The sensors were installed in four rooms (of available, else fewer sensors were installed) in each dwelling: living room, kitchen and two bedrooms. The measuring frequency of all sensors was 5 minutes. The value recorded for each 5-minute interval was the average of the readings during that interval. Further information on the sensors can be found in [11].

The operational energy consumption was monitored using the smart meter for gas and electricity consumption that was present in each house, provided by the grid operator and used for billing. The meter readings and actual power were collected from the available data port on the meter (P1 port) using a wireless device called Cloudia. This device, developed By Technolution, send the data to a central server of this company, which directly sends the data to the database of the research project. The meter readings for the electricity consumption are collected once per 10 seconds, and for the gas consumption once per hour.

Additional characteristics of the dwellings (installations, insulation, room size, etc.) were gathered during a visual inspection round by the project workers during installation of the sensors. The list of data collected during this inspection was sufficient to determine the energy label of the dwellings [12].

Finally, the resident characteristics were investigated using a survey that the residents filled in during the installation of the sensors. In this survey, questions on the residents, daily presence in the dwelling, use of the installations and other energy-related questions were asked.

All data were treated as privacy sensitive data, meaning that the data analysis and reporting were done anonymously and that the dwellings in the reporting cannot be traced back to the actual dwelling or resident.

2.2 Data analysis

Before data analysis, the data were cleaned from illogical or (possibly) incorrect datapoints. The thermal comfort perception data were cleaned by removing the first two datapoints on the date of installation, which may be entered as imaginary data during the demonstration of the ComfortApp to the residents. Dwelling which after this step had no thermal comfort data were excluded from this research.

Indoor climate data were cleaned by removing empty values and values that are above a certain threshold (35 °C for temperature, 100% for relative humidity), or far below the background concentration (400 ppm for CO_2 concentration). For the dwelling inspection, contradictory findings were removed.

The thermal comfort data were divided between datapoints taken in winter (October-March) or taken in summer (April-September). This distinction was made because during winter months, a relatively warm environment is often considered less a problem in summer than in winter, and in summer, outdoor temperatures are usually higher, leading to a different thermal sensation. Because of the relatively low number of

dwellings in this analysis, all individual datapoints for thermal comfort were regarded; no aggregation on dwelling level were made, because the thermal comfort perception of an individual can change during the day.

Indoor air temperatures in the living room and in the kitchen of the last half hour were averaged for each datapoint and used for the comparison with the thermal comfort and thermal sensation.

The thermal sensation was plotted against the month of the year, the thermal preference at the moment that the datapoint was registered, and the indoor air temperature in the living room. The thermal preference was also plotted against the indoor air temperature in the living room. The significance of the relations between the thermal sensation and the thermal preference, thermal sensation and clothing level, thermal sensation and metabolic activity level, and thermal sensation and activities related to thermal comfort that were done in the last half hour before the datapoint was taken, were tested using a Pearson's Chi-square test. The relation between thermal sensation and indoor air temperature, and between thermal preference and indoor air temperature, was tested using a multinominal logistic regression.

3. Results

3.1 Data cleaning and overview

The data collection could not or partially take place in a few dwellings because of several practical reasons such as malfunctioning of equipment or mistakes in inspections. Therefore, for several data types there are date for fewer than the 100 dwellings in the project. An overview of the available data is given in Table 1.

3.2 Thermal comfort

Figure 1 shows the total number of datapoints for the thermal comfort perception per month (winter months in blue, summer months in red). In winter, 3486 datapoints were taken, and in summer, 4268 datapoints were taken for thermal comfort perception.

Tab. 1 – Available data in OPSCHALER dataset.

Type of data	Number of dwellings
Thermal comfort perception	83
Indoor climate	81
Energy consumption	78
Dwelling inspection	83
Resident survey	83

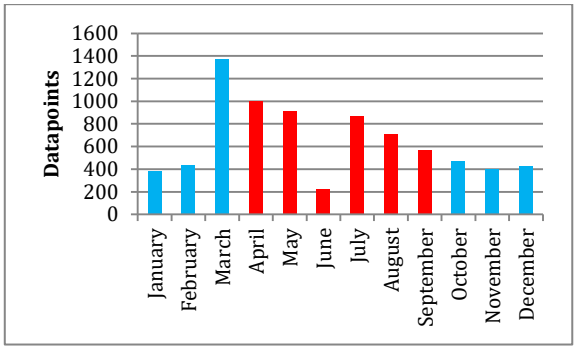

Fig. 1 – Number of datapoints for thermal comfort perception (blue: winter; red: summer).

Figure 2 shows the distribution of thermal sensation in winter, and Figure 3 shows it for summer. The distribution of thermal comfort perception levels in both winter and summer shows roughly a bell curve, which is in line with the thermal comfort perception theories [9, 10].

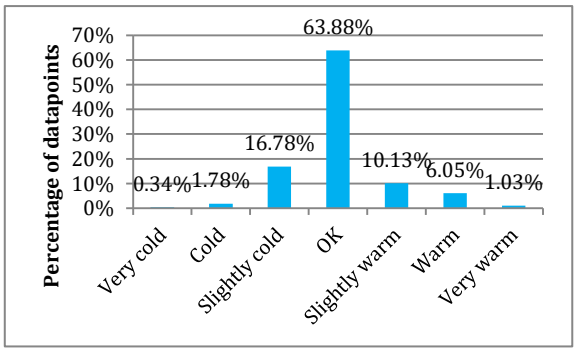

Fig. 2 – Percentage of datapoints for thermal sensation per perception level (winter).

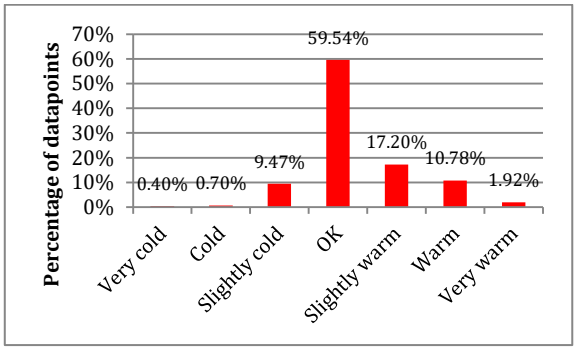

Fig. 3 – Percentage of datapoints for thermal sensation per perception level (summer).

Figure 4 shows the share of comfort preference per datapoint for thermal comfort perception in winter, and Figure 5 shows it for summer.

In winter, the majority of residents that feel warm are OK with this, with a small share having the preference to feel colder. The majority of residents that feel cold, however, have a preference to feel warmer, except for residents that feel very cold. The large share of residents that feel very cold but are OK with it is possibly a bias caused the low number of datapoints (12) in that category.

In summer, a large share (23-57%) of the residents that feel warm have a preference to feel cooler, and the majority of the residents that feel cold have a preference to feel warmer, except of residents that feel very cold (possibly a bias caused by the low numer of datapoints (17) in that category.

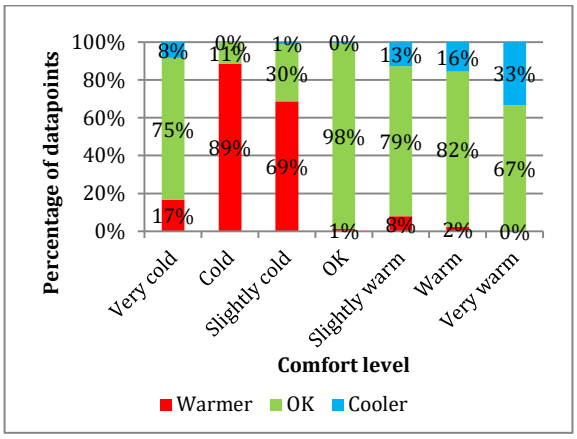

Fig. 4 – Percentage of thermal preference per thermal sensation level (winter).

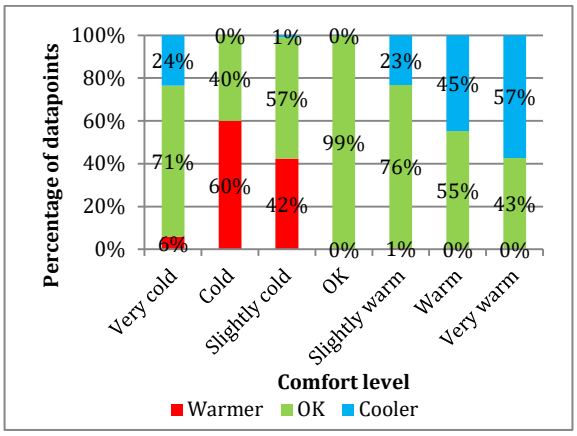

Fig. 5 – Percentage of thermal preference per thermal sensation level (summer).

A Chi-square test was performed on the relation between the thermal sensation level and thermal preference. The null hypothesis was: "The thermal sensation is not related with the thermal preference". The crosstabulation table is given in the analysis report [11]. The test results of the Chi-square test are given in Table 2. All requirements for the Chi-square tests are satisfied. For a significance level of 0.05, both for winter and summer the p-value is 0.000, which is below 0.05, and the null hypotheses are rejected. This means that there is a significant relationship found between thermal sensation and thermal preference for the dwellings in this research.

Tab. 2 – Chi-square test results for the relation between thermal sensation and thermal preference for winter and summer.

	X^2 value	df	Asymptotic significance (2-sided)
Winter			
Pearson Chi-square	2286.219[a]	8	0.000
N of valid cases	3486		
Summer			
Pearson Chi-square	2741.655[b]	8	0.000
N of valid cases	4268		

[a]: 1 cells (6.7%) have expected count less than 5. The minimum expected count is 2.27.

[b]: 2 cells (13.3%) have expected count less than 5. The minimum expected count is 2.26.

The thermal sensation has also been tested using a Chi-square test against the clothing level of the residents, the metabolic activity levels, and actions taken during the half hour before the reporting of the thermal sensation. Details of these analyses can be found in [11]. The conclusions of these tests are given in Table 3. All requirements for the Chi-square tests are satisfied. For all relationships tested and for a significance level of 0.05, both for winter and summer the p-value is 0.000, which is below 0.05, and the null hypotheses are rejected. This means that there is a significant relationship found between thermal sensation and clothing level, metabolic activity level and actions taken during the half hour before the reporting of the thermal sensation.

Tab. 3 – Chi-square test results for thermal sensation and clothing level, metabolic activity level and actions taken during the half hour before the reporting of the thermal sensation, in winter and summer.

	X^2 value	df	Asymptotic significance (2-sided)	N of valid cases	# cells with expected cound <5	Minumum expected count
Thermal sensation – clothing level (winter)	191.947	12	0.000	3486	0 (0.0%)	5.71
Thermal sensation – clothing level (summer)	420.704	12	0.000	4268	1 (5.0%)	1.96
Thermal sensation – metabolic activity level (winter)	172.189	20	0.000	3486	1 (3.3%)	1.80
Thermal sensation – metabolic activity level (summer)	93.747	20	0.000	4268	2 (6.7%)	1.01
Thermal sensation – actions taken in past half hour (winter)	902.970	44	0.000	6627	8 (13.3%)	0.52
Thermal sensation – actions taken in past half hour (summer)	417.859	44	0.000	8175	7 (11.7%)	0.84

3.2 Relation between thermal comfort and indoor climate

Figure 6 shows the relation between thermal sensation and indoor air temperature (averaged over the half hour before the datapoint was collected) in the living room for all dwellings in the dataset. Figure 7 shows the relation between thermal preference and indoor air temperature (averaged over the half hour before the datapoint was collected) in the living room for all dwellings in the dataset. The width of the line shows the relative number of datapoints for that particular thermal comfort/temperature datapoint. The thermal sensations and thermal preferences were used without considering activities or metabolic rates of the residents. It was found that in most of the dwellings, the temperature is between 15°C and 30 °C. For datapoints with thermal sensation warmer than average, the average indoor temperature seems slightly higher than for datapoints with thermal sensation colder than average. The average indoor temperature is slightly higher for datapoints where the thermal preference is 'cooler', and slightly lower for datapoints where the thermal preference is 'warmer'.

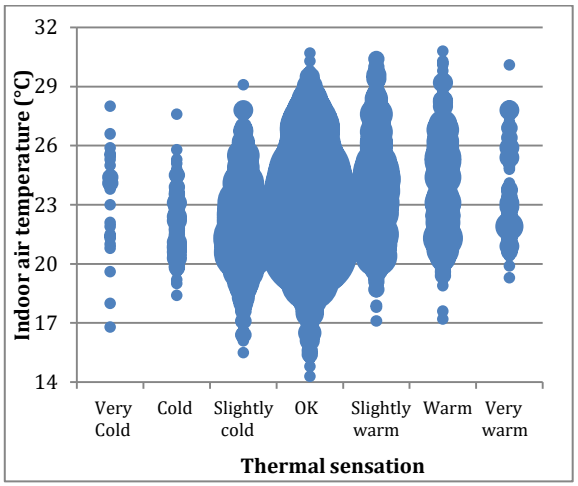

Fig. 6 – Indoor air temperature in living room for all thermal comfort datapoints, given per thermal perception level. The width of a datapoint shows the relative number of datapoints at that coordinate.

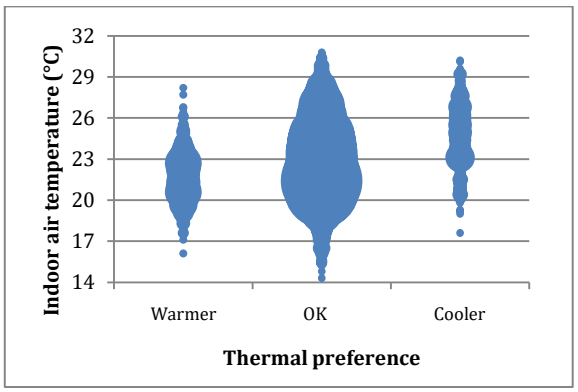

Fig. 7 – Indoor air temperature in living room for all thermal comfort datapoints, given per thermal sensation level. The width of a datapoint shows the relative number of datapoints at that coordinate.

The significance of the relation between thermal sensation and indoor air temperature, and between thermal preference and indoor air temperature, was tested using a multinominal logistic regression. The null hypotheses for these tests are respectively "The thermal sensation is not related with the indoor air temperatures" and "The thermal preference is not related with the indoor air temperatures.". The regression results are given in Table 4 for the thermal sensation and Table 5 for the thermal preference. The column 'Sig.' gives the significance of the relation, and the column 'Exp(B)' gives the factorial increase or decrease of the probability compared with the value for 'OK'. The significance for the regression results are all below the significance level of 0.05, except for the difference between the thermal sensation level 'very cold', which is possibly caused by the low number of datapoints in this category. The null hypotheses for the relations between indoor air temperature and both thermal sensation and thermal preference can therefore be rejected, and there is found a significant relationship between indoor air temperature and both thermal sensation and thermal preference.

Tab. 4 – multinominal logistic regression results for the relation between thermal sensation and indoor air temperature in the living room of all project dwellings.

								95% Confidence interval for Exp(B)	
Preference		B	Std. error	Wald	Df	Sig.	Exp(B)	Lower bound	Upper bound
Very cold	Intercept	-6.245	1.961	10.148	1	0.001			
	Temperature	0.054	0.084	0.410	1	0.522	1.056	0.895	1.245
Cold	Intercept	-0.262	1.107	0.056	1	0.813			
	Temperature	-0.158	0.050	9.898	1	0.002	0.854	0.774	0.942
Slighlty cold	Intercept	2.119	0.392	29.206	1	0.000			
	Temperature	-0.162	0.018	84.461	1	0.000	0.850	0.821	0.880
Slighlty warm	Intercept	-5.122	0.393	169.567	1	0.000			
	Temperature	0.152	0.017	83.449	1	0.000	1.164	1.127	1.203
Warm	Intercept	-5.640	0.477	139.751	1	0.000			
	Temperature	0.154	0.020	58.959	1	0.000	1.167	1.122	1.214
Hot	Intercept	-7.131	1.026	48.268	1	0.000			
	Temperature	0.148	0.043	11.747	1	0.001	1.159	1.065	1.262

Tab. 5 – multinominal logistic regression results for the relation between thermal preference and indoor air temperature in the living room of all project dwellings.

								95% Confidence interval for Exp(B)	
Thermal sensation		B	Std. error	Wald	Df	Sig.	Exp(B)	Lower bound	Upper bound
Warmer	Intercept	3.235	0.445	52.781	1	0.000			
	Temperature	-0.240	0.020	139.220	1	0.000	0.797	0.756	0.819
Cooler	Intercept	-9.548	0.582	268.919	1	0.000			
	Temperature	0.297	0.024	147.721	1	0.000	1.333	1.272	1.396

4. Discussion

This paper shows that several significant relationships were found between different thermal comfort parameters regarding the resident indoor and air temperature were found. However, the conclusions should be drawn with care, because of limitations in the data and in the research set-up.

The first limitation is the relatively low number of

dwellings. The project dwellings are common dwellings that can be found in many places in the Netherlands, but are not a good cross-section of the Dutch housing stock in terms of dwelling type, ownership (most dwellings in the project are owner-occupied) or age, and can differ significantly from dwellings in other countries. Therefore, generalisations of the results presented in this paper should be made with care.

There is some uncertainty regarding the separation of the data between winter and summer. The separation was made based on the theory that heating of the dwellings is required from October till March not in April till September, but this is not always the case.

The analysis of the thermal comfort data was done without regarding the room of the dwelling or the time of the day of the reported thermal sensation. Most datapoints were reported by the residents while being in the living room and were quite uniformly distributed throughout the day with most data points in the evening.

The thermal comfort data were registered by the residents themselves using the ComfortApp. This means that the data on presence in which room, the clothing level and activities taken are self-reported and could deviate from the actual situation, leading to small errors in the comfort data. It is assumed, however, that these errors do not change the outcomes significantly.

For simplification, for the analysis of the indoor air temperature it was assumed that the living room and kitchen had about the same temperatures and therefore the mean of these two rooms was used for the analysis. This assumption is applicable for some dwellings, but it might be not true for dwellings. It is assumed that these errors do not change the outcomes significantly. Also, all indoor air temperature points taken during the whole day are taken into account in the analysis. However, the thermal sensation might be different during different times of the day. An analysis of the relation between indoor air temperature and thermal sensation for different times of the day may give insight in the magnitude of this effect.

The relation between indoor air temperature and thermal sensation was investigated. However, a better measure for assessing thermal comfort is the operative temperature which is derived from air temperature, mean radiant temperature and air velocity. In this study, mean radiant temperature and air speed were not measured, and thus the operative temperature could not be calculated and indoor air temperature was used instead in the analysis. This makes it difficult to compare the results of this study with the PMV model. Also the relatively low number of data points, especially in the upper and lower extremes of the thermal sensation scale, makes comparison between predicted and actual percentage of dissatisfied difficult. For example, Figures 4 and 5 show that the percentage dissatisfied in the category 'very cold' is lower than in the category 'cold', which is not expected. Furthermore, the relations between indoor air temperature and thermal sensation and between indoor air temperature and thermal preference were assessed without considering activities or metabolic rates of the residents. By considering activities or metabolic rates in the analyses, better insight in the relation between indoor air temperature and thermal comfort could be gained.

5. Conclusion

In this paper, the relationship between thermal comfort, resident behaviour and indoor air temperature was investigated. Significant relationships were found between thermal sensation and thermal preference, clothing level, metabolic activity level, activities related to thermal comfort taken in the last half hour, and indoor air temperature in the living room. A significant relation was also found between thermal sensation and indoor air temperature in the living room. In further research, the relation between thermal comfort perception and operational energy consumption and dwelling characteristics can be investigated to improve the knowledge on the relation of thermal comfort with energy consumption and energy saving in dwellings.

These data can be used to compare the comfort level registered by the residents with the comfort level predicted by the PMV model, and link this to the indoor climate and the energy consumption for heating. This information can help to understand the relations between user preferences, indoor climate and energy consumption for heating.

6. Acknowledgement

The OPSCHALER project was financed by the Netherlands Enterprise Agency (RVO).

7. References

[1] Balaras, C.A., Gaglia, A.G., Georgopoulou, E., Mirasgedis, S., Sarafidis, Y. and Lalas, D.P. European residential buildings and empirical assessment of the Hellenic building stock, energy consumption, emissions and potential energy savings. Building and environment, 2007;42(3), pp.1298-1314.

[2] United Nations. Paris Agreement. United Nations, 2015.

[3] Rosso, F., Pisello, A.L., Cotana, F. and Ferrero, M. Integrated thermal-energy analysis of innovative translucent white marble for building envelope application. Sustainability, 2014; 6(8): 5439-5462.

[4] de Gracia, A., Navarro, L., Coma, J., Serrano, S., Romaní, J., Pérez, G. and Cabeza, L.F. Experimental set-up for testing active and passive systems for energy savings in buildings–lessons learnt. Renewable and Sustainable Energy Reviews, 2018; 82: 1014-1026.

[5] Jeeninga, H., Uyterlinde, M. and Uitzinger, J. Energy Use of Energy Efficient Residences, Report. ECN and IVAM, Pelten; 2001.

[6] De Wilde, P. The gap between predicted and measured energy performance of buildings: A framework for investigation. Automation in construction, 2014; 41: 40-49.

[7] Rinaldi, A., Schweiker, M. and Iannone, F. On uses of energy in buildings: Extracting influencing factors of occupant behaviour by means of a questionnaire survey. Energy and Buildings, 2018; 168: 298-308.

[8] Boomsma, C., Jones, R.V., Pahl, S. and Fuertes, A. Do psychological factors relate to energy saving behaviours in inefficient and damp homes? A study among English social housing residents. Energy Research & Social Science, 2019; 47: 146-155.

[9] Fanger, P. Assessment of man's thermal comfort in practice. Occupational And Environmental Medicine, 1973; 30(4): 313-324.

[10] De Dear, R. and Brager, G.S. Developing an adaptive model of thermal comfort and preference. UC Berkeley: Center for the Built Environment, 1998.

[11] Petropoulou, A. Understanding thermal comfort and heating energy use in Dutch dwellings: Analysis of smart meter data, indoor climate and comfort in 78 Dutch dwellings. Master thesis, Delft University of Technology, 2021.

[12] ISSO. Energieprestatie woningen en woongebouwen. Report 82.1, ISSO, Rotterdam, 2020.

The datasets generated during and/or analysed during the current study are not publicly available because of data agreements made in the OPSCHALER project, but can be made available after agreement with the authors on an individual basis.

Summer comfort in residential buildings and small offices, using sustainable cooling systems

Margot De Pauw [a], Jeroen Van der Veken [b]

[a] Thomas More Kempen, Kenniscentrum Energie, Geel, Belgium; margot.depauw@thomasmore.be

[b]. Belgian Building Research Institute, HVAC laboratory, Limelette, Belgium; jvdv@bbri.be

Abstract Summer comfort gains attention due to climate change and increasing frequency of heat waves, also in small office buildings and even in residential dwellings. Active cooling systems, using an electric compressor and standard refrigerants, are widely used because of the high cooling power and comfort level they can guarantee. However, given the energy use and refrigerants inherent to those cooling systems, other more sustainable cooling systems should be considered in the first place. To accelerate the acceptance of sustainable cooling systems such as evaporative cooling or free geothermal cooling combined with high temperature emitters, and to ensure a large scale rollout of those systems, a more profound insight is needed into their performance and the provided level of comfort.

In the framework of the CORNET project SCoolS the performance of different sustainable cooling systems is evaluated for a set of residential buildings and small offices by means of TRNSYS simulations. To do so, a new future climate file for Belgium has been constructed and comfort classes were defined. A parameter study varying insulation, thermal capacity, window percentage and orientation of the building was performed. Furthermore, the impact of adding passive cooling strategies like solar shading and intensive ventilation by window opening were analyzed. The SCoolS project resulted in a decision support tool for sustainable cooling systems. This article presents the preconditions and results with focus on the non-residential cases. Results show that in office buildings the necessary cooling loads are higher than in dwellings due to more concentrated heat gains during the day and often also more solar gains due to larger window surfaces. However, also in office buildings a combination of passive cooling strategies and sustainable cooling systems (coupled to floor or ceiling cooling) proves to be able to deliver excellent summer comfort.

Keywords. Summer comfort, climatic data, sustainable cooling systems, high temperature cooling, office HVAC
DOI: https://doi.org/10.34641/clima.2022.289

1. Introduction

1.1 Sustainable cooling systems

Due to climate change and increasing frequency of heat waves, cooling in residential buildings gains importance. The most common way of cooling in buildings is active cooling with the use of 'split units' or central air-conditioning systems, using an electric compressor and standard refrigerants. However, these systems have a relative high energy consumption, and the European parliament has called a phasedown for many of the existing refrigerants. Sustainable cooling systems with higher performance and less or no refrigerants can therefore be a superior alternative for conventional systems. These systems are however not often applied due to a lack of real performance data and guidelines for the correct selection and dimensioning. This problem was addressed in the CORNET project SCoolS, where an accessible decision support tool for cooling systems was developed. A screenshot of the main output of the tool is shown in Fig. 1. The tool is aimed to be user friendly and gives insight in the different options and applicability of sustainable cooling systems. After the selection of a limited number of descriptive input building parameters, the main graph gives an indication of the energy consumption (height of the bars) and an assessment of the comfort level (color of the bars) for different cooling systems. Another graph (not on the figure) gives the specific cooling load for each room.

The considered sustainable cooling systems are evaporative cooling systems as well as systems with free geo-cooling coupled to different high temperature emitters such as floor or ceiling cooling

Copyright ©2022 by the authors. This conference paper is published under a CC-BY-4.0 license.

or large water-air heat exchangers. Compared to classical low temperature air cooling systems (with the possibility of latent cooling), they typically cause a risk of condensation problems. The high temperatures with, in addition, the control strategies that are necessary to avoid condensation, result in limited emission capacity. The results for a classical air cooling system are added to the tool as a reference.

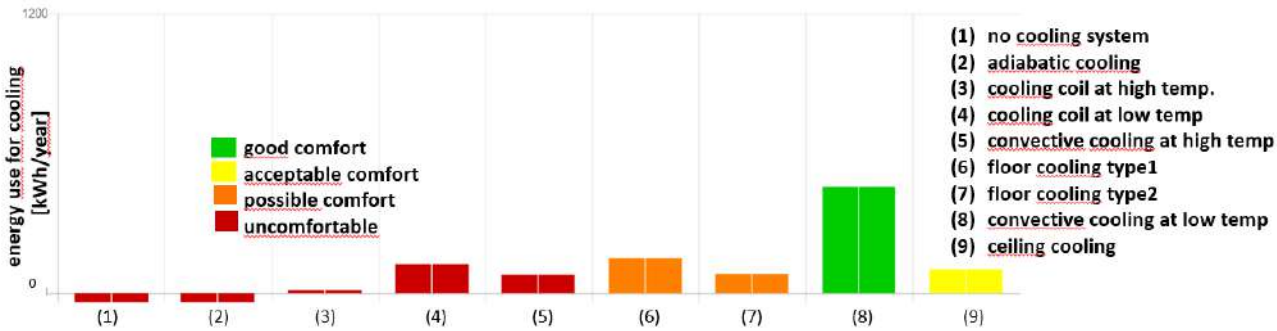

Fig. 1 – Decision support tool for sustainable cooling systems: screenshot of main output graph.

1.2 State-of-the-art

The assessment of summer comfort against future climate scenario's has gained extensive international attention. In the framework of Annex80 focus is on climate resilience of buildings. Resilience, as defined in [2], is assessed against different criteria like vulnerability, resistance, robustness and recoverability, including specifically a vulnerability assessment that considers future climate scenarios (using average, extreme, future and worst future weather conditions and short-term disruptions including brief heat waves). In [3] the importance of using future heatwaves in building thermal simulations is pointed out and a methodology is proposed to re-assemble future weather files using data from EURO-CORDEX. In the meantime weather files are constructed for Belgium according to this methodology, but unfortunately this work was not finished at the start of the simulations. An overview of available future weather data for Belgium was made in [4]. [5] presents the decrease/increase of future heating and cooling degree days for Belgium, again showing the importance of the weather files that are used for dynamic simulations.

The determination of thermal comfort is set by several different standards, but only few of them are appropriate when evaluating sustainable cooling in residential buildings under extreme weather conditions. The PMV model (EN ISO 7730) for instance was intended for application by the HVAC industry in the creation of artificial climates in controlled spaces (Fanger PO [6]).
In free running buildings where occupants have free access to operable windows and where they are relatively free to adjust their clothing, two approaches can be found to determine relevant thermal comfort limits. The first one is a fixed temperature limit, amongst others described in CIBSE Guide A [7]. This standard establishes a fixed maximum temperature for bedrooms (<26°C) and other living quarters (<28°C).
The second method is an adaptive temperature limit that relates the indoor comfort temperature to outdoor conditions. It was found by de Dear *et al.* [8] that higher indoor temperatures are acceptable in free running buildings because of a person's thermal adaptability, which is related to the outdoor temperature of that particular day and of preceding days. This is the fundament of the adaptive comfort requirements as described in EN 16798-1 (2019), ASHRAE standard 55, EN 15251 Annex A2 or CIBSE TM 51.

Chen [9] also points out that there is a risk in using the comfort assessment as defined in CIBSE TM52 and TM59 with respect to the uncertainty surrounding the used climate file: both TM52 and TM59 require the use of local Design Summer Year (DSY) weather files, defined as the year with the third highest average dry-bulb temperature within a period of 20 years. However, existing files are soon outdated with recent record-breaking summers. Moreover, this selection process based on average temperatures may exclude crucial heat waves and it could underestimate the overheating risks.

For this particular study the assessment of thermal comfort in contemporary buildings in the (near) future is therefore mainly based on the recent 'Themablad Thermisch Comfort' [10]. This method is specifically targeted towards residential buildings and future summer comfort. It contains a list of the most important boundary conditions and it demonstrates how '2018T1' can be used for the creation of a relevant climate file by collecting all the hottest months of the last 20 years.

2. Research Method

2.1 Simulation-based

The decision support tool is based on a database with simulation results. For a large set of more than 8000 cases, energy consumption and temperature exceeding hours on an annual basis were calculated using TRNSYS17 simulations, with a room-by-room approach. The model is verified by comparing the simulation results with 2 measured cases within the project and the BESTEST data on the Fraunhofer twin house. The different cases as well as the simulation model with his various preconditions are described in detail in [1] with respect to the residential buildings. A summary of the chosen typologies and varied simulation parameters is given in the text below. For the office rooms, the simulation model and preconditions deviate in a number of respects, for instance concerning hygienic ventilation, internal gains and the control of the passive cooling strategies. These aspects are described in more detail.

A parameter study has been undertaken by simulating 7 different building types (5 typical residential buildings, a small office and a conference room) , variated by insulation level, thermal capacity, window percentage and orientation of the building/room. The main characteristics of the buildings are shown in Table 1.

Tab. 1 – Building characteristics: net volume Vnet, surface area A, cooled floor area Afl, window/floor percentage W

	Vnet [m^3]	A [m^2]	Afl [m^2]	W [%]
row house	393	253	119	18
modern	486	697	169	21/30
semi det house	460	348	137	19/25
2 façade ap	206	58	62	21
3 façade ap	203	88	62	25/30
small office (2 pers)	47	12	18	32
conference room (10 pers)	97	25	38	31

The different building parameter values are described in detail in [1] and summarized Table 2.

Tab. 2 – building parameter values

Building parameter	values
insulation	current/passive standard
thermal mass	high(solid construction)/low (timber frame construction)
window percentage	depends on building type, see Tab. 1
orientation	N/S/E/W

For the assumed building variants, an assessment was made of the performance of different cooling systems and emitters, optionally combined with passive cooling strategies. More precisely, systems with free geo-cooling coupled with floor cooling, ceiling cooling, fan coils or cooling coils (in the ventilation supply air), as well as indirect adiabatic cooling systems are considered and compared with a classic air conditioning system.

Two different types of floor cooling are considered, with different thermal mass and thermal resistance, and with a nominal power of 30 W/m^2 and 20 W/m^2 respectively. Because of the high latent gains in the office rooms and the increasing risk for condensation that this entails, a dewpoint control is added: the supply temperature is not allowed to be lower than the dewpoint temperature of the room air (*Tsupply* = max (16°C, *Ti_dewpoint*)). The ceiling cooling has a nominal power of 45 W/m^2 and the same dewpoint control as for the floor cooling.

For the convective cooling devices, we distinguish between 2 systems. The first one can be representative for any active cooling system at low temperature and has a maximum power of 50 W/m^2 for the residential buildings, 100 W/m^2 for the small office room and 150 W/m^2 for the conference room. The second is aimed to represent a system with fan coils working at high temperature (which are assumed to be sized based on the heat demand). For the latter system a dewpoint control is added in the office rooms. As the convective system is modelled in TRNSYS as an ideal cooling system, only characterized by his setpoint and maximum power, it is not possible to adjust the water supply temperature as a function of the dewpoint *Ti_dwp*. So the dewpoint control consists of an adjustment of the maximum specific power *Pmax* [W/m^2], according to equation (1):

$$Pmax = \max(0, 15/8 * (Ti - \max(16, Ti_dwp) - 1)) \quad (1)$$

Three cooling systems operating on the ventilation unit are analyzed: a cooling coil in the supply air working at high or at low temperature and an indirect adiabatic cooling system. In the non-residential cases the extraction air is assumed to be saturated at 100% RH after the evaporation unit (whereas the saturation process was limited to a RH of 70% for the residential cases). This results in a better approach of the efficiency of higher performance evaporative systems that are on the market nowadays.

Concerning the passive strategies, solar shading devices and intensive ventilation or less intensive night cooling by opening of windows can be applied. The occupant behavior with respect to the control of solar shading and window opening is supposed to follow logical rules. For the non-residential cases the operation of solar blinds and the opening of windows is automatic, so no presence is required. The windows are opened if 3 conditions are fulfilled:

- the room temp *T_room* is > 23°C,
- *T_room* -1°C > Te (outside temp)
- *Te* > 16°C, during working hours

Windows are closed if

- or *T_room* < 21°C
- or *T_room* < Te -2°C
- or Te < 14°C, during working hours

Solar shading is operated as follows:

- Screens go down if *T_room* > 23°C and solar radiation > 125W/m^2 on the window
- Screens go up if *T_room* < 20°C or at sundown

Finally, these conditions should be true for 30 min before action is taken.

A demand controlled mechanical ventilation system with a flow rate of 25 m^3/h/pers is assumed. To maximize cooling potential a maximum flow rate is imposed between 4h and 8h in the morning. The ventilation system has a heat exchanger with an efficiency of 75%, which can be bypassed during the cooling period. The air that passes the ventilation unit heats up with 0.5K to take into account the heat gains from the ventilator.

Internal heat gains are imposed based on profiles (and other boundary conditions) developed by Witkamp et al. (2019). They are mainly due to the presence of persons, equipment and lighting during working hours (8h – 17h). For the small office 2 persons are taken into account, the conference room is occupied by 8 people most of the time (lower occupancy at noon and beginning and end of working day). At full occupancy, heat gains for lighting are 5W/m^2 and 200 W and 300W for equipment in respectively the small office and the conference room.

The office rooms are on an intermediate floor, no air or heat exchange with adjacent rooms is assumed.

2.2 assessment of summer comfort and climatic data

For this project, a new climate file has been constructed based on a selection of the most severe heat waves of the recent 10 years (2010-2020) using the official weather station data of Belgium in Uccle. This could seem a bit extreme, but the authors found a good overlap with the very recently constructed 2040-2060 weather files in the framework of Annex80 Task A (IEA 2020).

Based on literature review, a.o. IEA (2018), EN16798 (2019), ISO 7730 (2005), and given the scope of the simulations, the comfort range is expressed in terms of operative temperature (instead of PMV) and based on the individual room temperature (instead of a mean building temperature) and room occupancy. Concerning the temperature limits a difference is made between residential and non-residential cases.

For the non-residential cases the temperature limits depend on the type of building, according to EN 16798-1 (2019). For beta buildings fixed temperature limits are used. The comfort classes are indicated by the horizontal lines in Fig. 2. They correspond to comfort categories 1,2,3 of EN 16798-1 and depend on the fixed temperature limit Tlim that is not exceeded: good (*Tlim* = 26°C), acceptable (*Tlim* = 27°C), possible (*Tlim*=28°C), uncomfortable.

For alfa buildings, adaptive temperature limits are applicable. In Fig. 2 the adaptive temperature limits as a function of the running mean outdoor temperature, are indicated with the dotted sloped lines. They show the upper and lower boundaries of the comfort categories 1,2 and 3. When compared with the fixed limits of the different categories, it appears that the adaptive limits fall below the fixed limits at low outside temperatures. To avoid this, the fixed temperature limits are applied as an upper boundary, resulting in the comfort classes indicated by the green, yellow, orange, red area in Fig. 3.

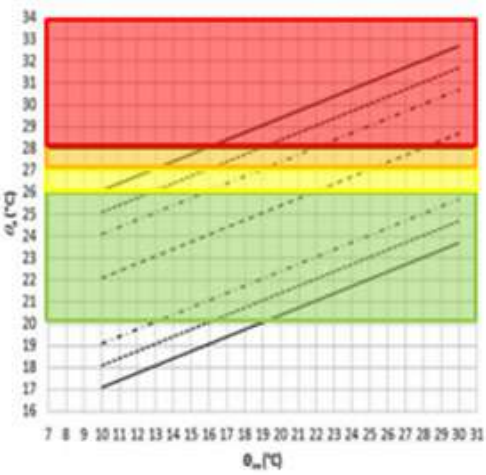

Fig. 2 – Comfort classes for beta buildings.

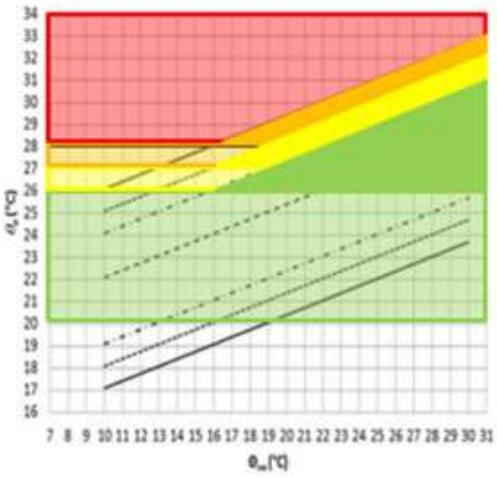

Fig. 3 – Comfort classes for alfa buildings.

One of the criteria to distinguish between alfa and beta buildings according to EN 16798-1 is the perceivability of the cooling system by the occupants. If the cooling system is clearly perceivable, the building is considered as a beta building. This means that different comfort criteria are used for, on the one hand, the cases with active cooling or fan coils and where the cooling system is thus clearly perceived (beta building) and, on the other hand, the cases with sustainable cooling systems in the ventilation unit or with floor and ceiling cooling (alfa building).

It is not certain if these adaptive criteria as described in EN 16798-1 (2019) can be applied straightforward to residential cases: the comfort limits seem very wide, especially during heat waves and compared to comfort methods using fixed limits. However it was found that these last objections are less the case if the the adaptive temperature limits of Van der Linden et al. [11] are applied. Therefore the authors chose to work basically with absolute comfort criteria. The absolute comfort criteria of CIBSE Guide A (2015) are used [7], because they distinguish between bedrooms (<26°C) and other living quarters (<28°C). Then, the following comfort classes were determined based on the exceeding hours: good (<33h), acceptable (<100h), possible (< 250h), uncomfortable. As described in [1] these boundaries implies that the 'good comfort' band corresponds with the absolute comfort boundary for the bedrooms in the CIBSE TM52 and TM59 (1% of the night time). By adding the 'average' and 'possible comfort' bands, only 0.1% of the dwellings that are in comfort band A (following Van der Linden et al. 2006) are declared as 'not comfortable'.

3. Results and discussion

3.1 General results office buildings

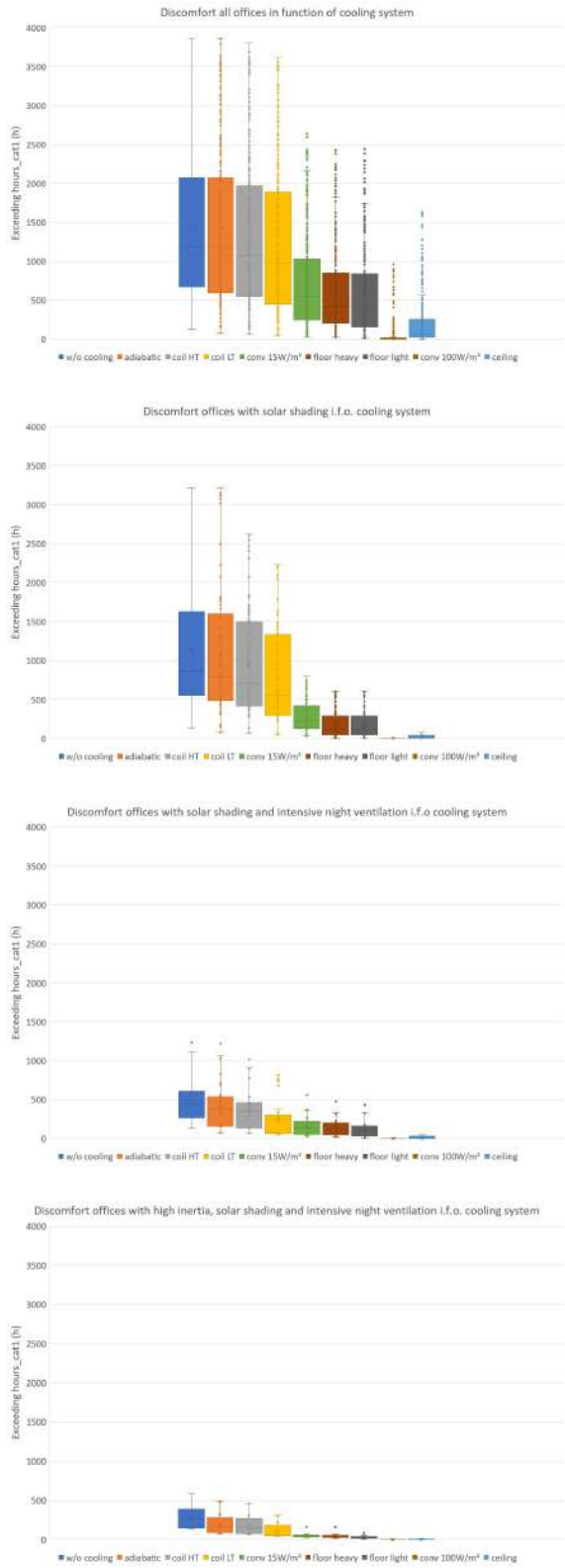

Fig. 3 – Discomfort results (exceeding hours outside comfort category 1) for different office cases in function of the implemented cooling system. The upper graph shows all offices, followed by the offices with solar shading, solar shading and intensive night ventilation, and finally the lower graph for the offices with high inertia, solar shading and intensive night ventilation.

Previous graphs sum up the discomfort scores for all simulated office building variants. The different

simulated cooling systems are on the graph from left to right represented with (in general) increasing cooling capacity:

- no cooling system
- adiabatic cooling on ventilation system
- cooling coil at high regime temperatures
- cooling coil at lower regime temperatures
- convective cooling system at HT (15 W/m^2)
- heavy floor cooling (30 W/m^2)
- lightweight floor cooling system (30 W/m^2)
- standard convective cooling (100 W/m^2)
- and finally ceiling cooling (45 W/m^2).

If we compare all the systems, we see that for the office buildings it is generally quite difficult to obtain good comfort results with cooling systems that have lower cooling capacities. Certainly for the offices without any passive cooling strategies (solar shading, ventilative cooling) we need up to 100W/m^2 and more; the convective cooling that can deliver this 100W/m^2 reaches in 77% of all office cases the best comfort band (below 26°C since it is a beta building in these cases) and only in 4% cases temperatures above 28°C are attained. With dropping cooling capacity, the risk at bad thermal comfort increases; 18% for ceiling cooling, already 77% for convective cooling systems at 15W/m^2 and coiling coils and 92% of the offices without cooling system.

However, when applying solar shading the comfort of the offices is greatly improved; 100% of the cases attain the best comfort for the convective systems at 100 W/m^2, but also sustainable systems that are coupled with ceiling cooling can reach this best comfort band in 74% of the cases. Ceiling cooling and floor cooling can make sure that no office buildings with solar shading reaches temperatures outside category 3 (the red zone in Figure 3). For the cooling coils on the ventilation system, this is still the case; more than 50% of the cases have bad comfort risks.

If solar shading is combined with an intensive night cooling schedule, the situation improves further for the systems with lower cooling capacities. Certainly if finally only the buildings with more inertia are taken and coupled with these passive cooling strategies, the comfort can be well maintained; in 100% of these cases the ceiling cooling can maintain in the best comfort band, while this is also in 70% of the floor cooling cases. For floor cooling, but also for the convective cooling systems at high temperatures and 15W/m^2 and the cooling coils at lower regime temperatures 0% of the cases reaches the worst comfort band. Obviously if these passive cooling measures are taken, more and more choice is coming available when selecting a fitting sustainable cooling system.

3.2 comparison between residential and office buildings

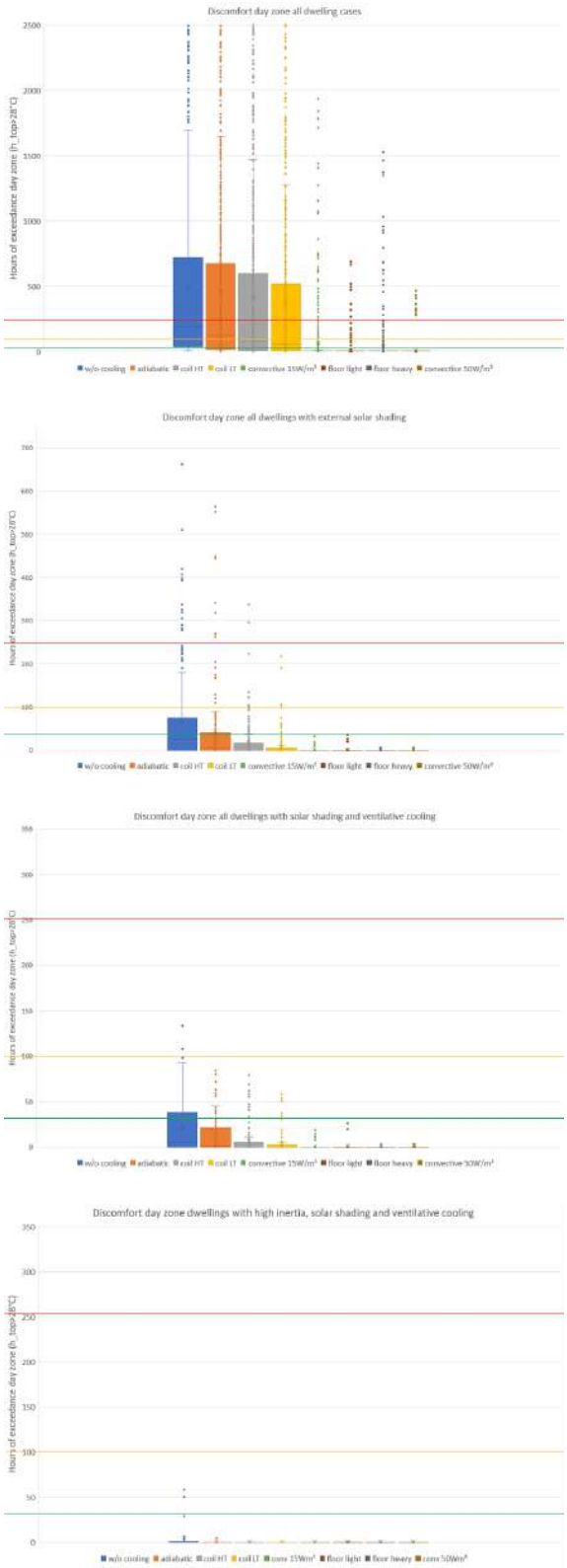

Fig. 4 – Discomfort results (exceeding hours for operative temperatures above 28°C in the day zone) for residential cases in function of the cooling systems. The upper graph shows all dwellings, followed by dwellings with solar shading, solar shading and moderate night ventilation, and finally the lower graph for the dwellings with high inertia, solar shading and night ventilation

If we compare the office simulation results with these from the dwellings (see also [1]), we see that the (sustainable) cooling systems with lower capacities reach more easily the best comfort criteria. Already all dwellings that have solar shading reach the best comfort band with floor cooling systems and the convective systems at high regime temperatures (delivering only 15 W/m^2). The situation improves further when night cooling is applied and certainly when only the massive dwellings are considered. For these last dwelling combinations all cooling system are able to maintain good comfort and even the dwellings without any system can maintain a reasonable summer comfort.

One should notice that the comfort criteria are different, but they are adapted to the use of the buildings, so that the comparison can still be made. The difference between office buildings and dwellings are caused by on the one hand larger window areas and the other hand higher heat gains that are more concentrated during the working hours in the day time. This causes a peak in heat gains that is more difficult to handle with low capacity cooling. It is clear that the combination with passive cooling strategies helps and that also more thermal inertia helps to spread the load over the whole day.

3.4 Peak demand and dimensioning

Regarding the insulation thickness, the influence works in two directions; during a heat wave the better insulated (not actively cooled) dwellings and offices reach indoor temperatures that are lower compared to less insulated buildings. However, after the heat wave, the indoor temperatures are maintained during a longer time and the cooling season will be longer if cooling systems are applied. Regarding the peak power, these are lower for the better insulated buildings.

Finally, when comparing the lower cooling capacities of sustainable cooling systems that show good comfort results in many buildings (that contain more or less passive cooling strategies), with the cooling capacities that result from the classical cooling load calculations, such as the methods prescribed by ASHRAE, VDI, or ATIC in Belgium, we see that these calculated values are often much higher. This is due to the assumptions in the cooling load calculations that a fixed temperature is to be maintained and that all excess heat will be cooled away (by air cooling systems). For surface cooling systems with high inertia and/or buildings where more fluctuations in the indoor temperature are allowed, cooling capacities can be much lower. In the new project "koeling 2.0" we will focus on a new dimensioning tool for these sustainable systems with lower cooling capacity.

Conclusions

A new decision tool has been made to compare different (sustainable) cooling systems and passive cooling strategies in dwellings and typical office zones. To make it future proof, a new (extreme) climatic data file was constructed. However, the selection of the comfort criteria showed to be difficult.

In general, the simulations show that a lot of sustainable cooling systems, although their lower specific power, can provide good comfort in most of the residential buildings, and also a great deal of the office buildings, provided that the window surfaces are not exaggerated and passive cooling strategies can be applied when necessary. Without any cooling system only the dwellings with the combination of high inertia, the best solar shading and ventilative cooling are able to maintain a reasonable comfort during the heat waves. For office buildings this will become difficult since indoor heat gains are higher and more concentrated during the day, resulting in higher cooling needs.

4. Acknowledgements

This research is funded by the CORNET-project SCoolS sponsored by the Flemish government (www.vlaio.be).

5. References

[1] Wuyts T., De Pauw M., Van Der Veken J. Indoor summer comfort: a study into the practical useability of sustainable cooling systems. Eceee summer study; 2021

[2] Attia S., Levinson R., Ndongo E., Holzer P., Berk Kazanci O., Homaei S., Zhang C., W. Olesen B., Qi D., Hamdy M., Heiselberg P. Resilient cooling of buildings to protect against heat waves and power outages: Key concepts and definition. Energy & Buildings. 2021

[3] Machard A., Inard C., Alessandrini J.M., Pelé C., Ribéron J. A Methodology for Assembling Future Weather Files Including Heatwaves for Building Thermal Simulations from the European Coordinated Regional Downscaling Experiment (EURO-CORDEX) Climate Data. Energies. 2020

[4] Ramon, D., Allacker, K., De Troyer, F., Wouters, H., & van Lipzig, N. P. (2020). Future heating and cooling degree days for Belgium under a high-end climate change scenario. *Energy and Buildings*, *216*, 109935.

[5] Ramon, D., Allacker, K., van Lipzig, N. P., De Troyer, F., & Wouters, H. (2019). Future weather data for dynamic building energy simulations: overview of available data and presentation of newly derived data for Belgium. *Energy Sustainability in Built and Urban Environments*, 111-138.

[6] Fanger PO, 1970, Thermal comfort. Danish Technical Press, Copenhagen, Denmark.

[7] CIBSE Guide A: Environmental design. London: Chartered Institution of Building Services Engineers, 2015

[8] R. de Dear, G. Brager, D. Cooper, Developing an Adaptive Model of Thermal Comfort and Preference, Final Report, ASHRAE RP/884,1997

[9] Chen D. Overheating in residential buildings: challenges and opportunities, Indoor and Built environment (2019)

[10] Energielinq, 2019. Themablad Thermisch Comfort by Energielinq and Stroomversnelling, https://energielinq.stroomversnelling.nl/kwaliteitskaders/nieuwe-methode-voorkomt-oververhitting-woningen/

[11] A.C. van der Linden et al Adaptive temperature limits: a new guideline in the Netherlands A new approach for the assessment of building performance with respect to thermal indoor climate. Energy and Buildings 38 (2006) 8-17

Data Statement

The datasets generated during and/or analysed during the current study are not publicly available because of the large size and form of the data but specific information can be obtained by e-mailing the authors of this paper.

New developments in odour testing: Adapter connects emission test chamber and funnel

Simone Brandt [a], Frank Brozowski [b], Wolfgang Horn [c], Wolfgang Plehn [b], Birgit Müller [a]

[a] Building Energy and Information Technology (Sustainable Building Engineering, Faculty of School of Engineering – Energy and Information, University of Applied Sciences, HTW Berlin, Germany, simone.brandt@htw-berlin.de

[b] Section for Substance-related Product Issues, German Environment Agency, Dessau-Roßlau, Germany, frank.brozowski@uba.de

[c] Materials and Air Pollutants, Bundesanstalt für Materialforschung und -prüfung, Berlin, Germany, wolfgang.horn@bam.de

Abstract. Healthy and energy efficient buildings must be free from disturbing odours. Odour emissions from building materials can be measured with the well-known and accepted standard ISO 16000-28 "Indoor air – Part 28: Determination of odour emissions from building products using test chambers". For commonly used emission test chambers the sample air is collected in containers (bags) and presented to a group of panel members for the purpose of evaluating the odour. A standard sets requirements for the on-demand presentation in detail. These include the validation procedure for container materials, pre-treatment of bags, details on storage of filled bags and how to carry out the measurements. However, although these measures are proven in practice, incorrect measurements are still possible. Also errors can occur due to a very complex measurement procedure. So, there is a great need for research into how the odour samples are presented.

The proposal planned to be presented will introduce a new development in sample provision by using an adapter which enables collection and provision of sample air without storage or transport of bags. The adapter is a sample container which is permanently positioned on the emission test chamber´s outlet and continuously filled with sample air flowing through it. The flow is briefly interrupted at the time when a sample is taken by a panel member for the test.

The size of the container is sufficient to provide enough sample air for evaluation by at least one panel member via a funnel. Since sampling and presentation are technically connected, it means you can almost do away with storage or transportation and thus it can be presented almost unchanged to the panelmembers. The aim is to reduce measurement errors in the odour samples provision process and the improvement of measurement reproducibility. The paper presents the construction of the adapter as well as the results of emission and odour tests carried out so far.

Keywords. Building materials, odour, emission, test chamber, perceived intensity, bags, sample provision system, adapter.
DOI: https://doi.org/10.34641/clima.2022.168

1. Introduction

Building products used indoors such as floor coverings, paints and adhesives should be low-emission and hardly noticeable in terms of odour. This protects the health and well-being of those people who spend time in these rooms. Unfortunately, odour nuisance and the associated health complaints, e.g. irritation of the eyes or headaches, are among the most frequently mentioned impairments of indoor spaces [1]. The resulting dissatisfaction in office buildings can also lead to lower productivity [2, 3].

The use of low-emission and low-odour products is becoming increasingly important, as the European Union's goal of achieving greenhouse gas neutrality by 2050 [4] also focuses on the energy efficiency of buildings. With buildings accounting for 40% of the total annual energy demand, Member States have committed to enhancing building renovation. New should be constructed to the nearly-zero energy standard [5, 6]. Due to energy-efficient construction, accompanied by better thermal insulation of façades and tightly closing windows and doors, the building envelope is becoming increasingly airtight. If users try to ventilate unpleasant odours out of the room, e.g. by frequently opening windows, the building's heating energy demand inevitably increases [7]. In addition, the users' comfort can decrease due to

Copyright ©2022 by the authors. This conference paper is published under a CC-BY-4.0 license.

falling room temperatures or undesirable drafts, which in turn can lead to health problems [8]. The testing and use of low-emission and low-odour products is therefore essential for healthy indoor air and energy-efficient building operation. The ISO 16000-28 standard for odour testing has been available since 2012. It comprehensively describes the odour testing options for building products using an emission test chamber [9]. The building product to be tested is measured under standard conditions (23°C, 50% relative humidity and an air exchange rate of 0.5 h-1). The sample air from the emission test chamber is then evaluated using the criteria acceptability or perceived odour intensity Π. The perceived intensity describes the strength of an odour perception and is evaluated with the help of a reference. For this purpose, different acetone concentrations in air are set on the so-called comparative scale and offered for comparison to a specially trained group of panel members. The hedonic note, i.e. how pleasant or unpleasant an odour is perceived, can be added to the evaluation as a further measurand. The olfactory measurands and the comparative scale have been described in detail in various publications [10, 11].

To evaluate the sample air, it must be ensured that a sufficient and constant air flow rate of 0.6 to 1.0 l/s is made available to the panel members. This prevents ambient air from mixing with the sample air during smelling. Another requirement according to EN 16516 is to establish an air exchange rate of 0.25 to 2.0 h-1 in the emission test chamber [12]. Due to these requirements, sample provision on a funnel directly connected to the emission test chamber is only possible with very large test chambers (from a size of 3 m^3) and is thus rather the exception. In the smaller test chambers normally used, sample containers are filled with sample air from the emission test chamber and presented to the panel for odour evaluation. The tested and ISO 16000-28 approved materials polyvinyl fluoride (brand name: Tedlar®) and polyethylene terephthalate (brand name: Nalophan®) serve as sample containers [9].

As various studies show, the type of sample provision can influence the result of the odour measurement. The results of the perceived intensities can be different in direct evaluation compared to those from sample container-based evaluation because the sample air changes in the sample container [13–16]. Overall therefore, there is a great need to preferably use direct sample provision. The adapter presented here offers this possibility.

2. Research Method

2.1 Development of the adapter

In sample container assessment, sample air is first collected in a sample container and then placed in a sample provision system for assessment by the panel (Figure 1).

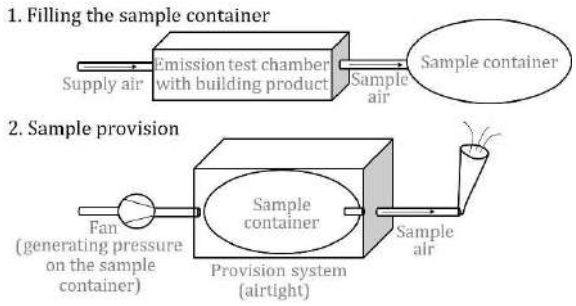

Fig. 1 - Sample provision setup using sample containers according to ISO 16000-28 (two sub-steps).

The adapter enables the collection and provision of sample air in only one step (Figure 2) by connecting the emission test chamber to the funnel. It is capable of buffering a sufficient amount of air for assessment by a panel member and providing it at the moment of sampling with a flow rate of 0.6 to 1.0 l/s.

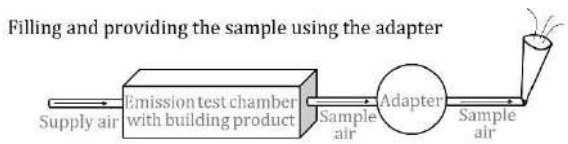

Fig. 2 - Sample provision setup using adapter (single step).

2.2 Adapter design and functioning

The adapter consists of a sample container (Tedlar or Nalophan bag) and the necessary accessories to allow alternating its operation between the filling process and sample air provision (Figure 3). During filling, the supply air valve is opened and the exhaust air valve is closed. As soon as the sample container is filled, the excess air flows to the funnel via the bypass. This prevents the flow conditions in the emission test chamber from being affected. The adapter is connected at least one hour before sampling to flush the sample container sufficiently with sample air. During emptying, i.e. at the time of sampling, the supply air valve is closed and the exhaust air valve is opened. The panel member can operate a blower with the help of a button, which exerts pressure on the sample container within the airtight box. This causes the sample container to empty towards the funnel. The blower speed can be controlled with the help of an orifice plate so that the desired constant volume flow rate (between 0.6 and 1 l/s) is provided at the funnel. The panel member can take sample air several times for evaluation. At the end of sampling, the exhaust valve is closed and the supply valve is opened to start the next filling process. During the emptying of the container, it must be ensured that the flow conditions in the emission test chamber are not influenced. This can be achieved by opening a sampling point to remove excess air.

The size of the sample container is about 15 l and is sufficient to provide sample air for evaluation by at least one panel member. Afterwards, the sample

container is filled again ready for the next person to evaluate. The exact frequency of how quickly the adapter becomes available for the next panel member depends on the air exchange rate of the emission test chamber. For very small chambers, this may well take several minutes.

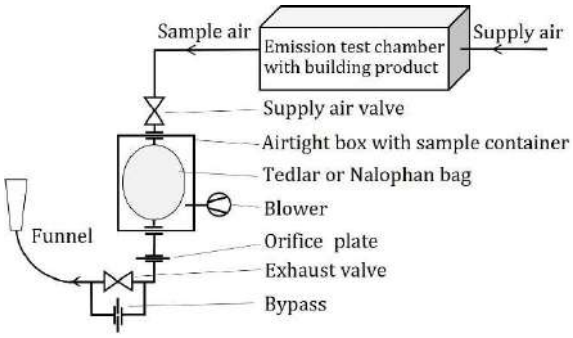

Fig. 3 - Adapter setup and positioning.

2.3 Carrying out experimental tests

To test and prove the applicability of the adapter, analytical and olfactory tests were carried out.

Analytical measurements

The aim of the analytical measurements was to check whether the sample air provided to the panel members when using the adapter had the same composition as when sampling directly. Figure 3 shows the measurement setup for sampling the air from the adapter. For the measurement, the adapter was connected to a 1 m^3 chamber that contained a varnish sample with various volatile organic components added artificially and operated with an air exchange rate of 1.1 h-1. An approx. 15 l Tedlar bag was used, which was baked out at 80 °C for 4 hours according to the requirements of ISO 16000-28. The bag was then rinsed with sample air for 12 hours. For sampling, another completely empty Tedlar bag, which had also been baked at 80 °C for 4 hours, was placed over the funnel and an emptying procedure was then carried out with the help of the blower (as described in 2.2). Thus the sample air flowed out of the bag in the adapter into the second Tedlar bag and filled it with sample air. Directly afterwards, a Tenax tube was loaded both from the emission test chamber and from the bag filled with sample air. The sampling volume was 1 l each at a flow rate of 100 ml/min. The substances were determined using thermodesorption and gas chromatography coupled with mass spectrometry measurements (TDS/GC/MS).

Olfactory measurements

Olfactory measurements have the aim of checking whether similar results have been achieved in an evaluation using the adapter as in the direct evaluation. Several tests were carried out, of which an investigation of a varnish sample artificially doped with additional VOCs is presented here as an example. The emission test chamber used was the 44 l CLIMPAQ (Chamber for Laboratory Investigations of Materials, Pollution and Air Quality), which is widely used in Northern Europe and is supplied with conditioned air (temperature and humidity according to ISO 16000-28) by an air conditioning system. The chambers comply with the requirements of ISO 16000-9 [17]. Loading was selected so that a distinct odour could be detected. All components that come into contact with sample air are made of glass or stainless steel. For direct evaluation, the air from the CLIMPAQ is fed directly to a glass funnel at a flow rate of 0.9 l/s.

For an evaluation using the adapter, the air flow is diverted and channelled to the adapter. The sample container made of Nalophan was rinsed with sample air for one hour before the test. The flow rate at the funnel was also set to 0.9 l/s for the sampling.

The study comprised the determination of the perceived intensity and the hedonic note by 9 trained panel members based on ISO 16000-28. The minimum size of 12 panel members required by the standard could not be met when performing the measurements due to the Corona pandemic. For the evaluation, the arithmetic mean was calculated from the individual values determined by the panel members. The 90% confidence intervals prescribed by ISO 16000-28 were ± 2.0 pi for perceived intensity and ± 1.0 for hedonics. The bag was filled for approx. 30 s after sampling. This time is sufficient for a 15 l sample container and a flow rate of 0.9 l/s.

3. Results

Analytical measurements

Table 1 shows the results of the analytical measurements.

Tab. 1 - Air composition in the emission test chamber and in the Tedlar bag filled via the funnel. Substance-specific determination of the components.

Components *(CAS number)*	Emission test chamber	Tedlar bag
	Concentration in µg/m^3	
Toluene *(108-88-3)*	23	17
Propylene glycol *(57-55-6)*	980	860
Butyl acetate *(123-86-4)*	3	1
Styrene *(100-42-5)*	27	23
Camphene *(79-92-5)*	14	13
Benzaldehyde *(100-25-7)*	21	20
Phenol *(108-95-2)*	24	19
Decane *(124-18-5)*	5	3
Acetophenone *(98-86-2)*	24	21

The air in the Tedlar bag has the same qualitative composition as the air in the emission test chamber, only the concentrations are somewhat lower for all substances. It is generally known that the concentrations in sample containers are lower. Analytically, however, except for propylene glycol, no significant distinction can be made between acetophenone concentrations such as 24 and 21 µg/m^3. The accuracy of the method in this measurement range is about 20%. Consequently, both values are in each other's uncertainty range.

Olfactory measurements

Figure 4 shows the results of perceived intensity and hedonics for direct evaluation and evaluation using an adapter.

The calculated mean value of the perceived intensity is 11.3 pi for the adapter i.e. lower than 13.1 pi obtained in direct evaluation. The difference of 1.8 pi shows that the results, compared with each other, are within the measurement uncertainty of the method. Despite the low number of panel members (9), the required 90% confidence interval has been met by the direct evaluation and just missed by the method using an adapter. The number of panel members and the standard deviation influence the confidence interval. Having the same number of panel members, the standard deviation is significantly greater in the adapter method since the values recorded by the individual panel members are very different: they are between 7 and 15 pi. Hedonics is rated the same at -2.2 in the direct evaluation and in the test using the adapter. The 90% confidence interval of the hedonics is also almost the same for both tests: 0.7 and 0.8.

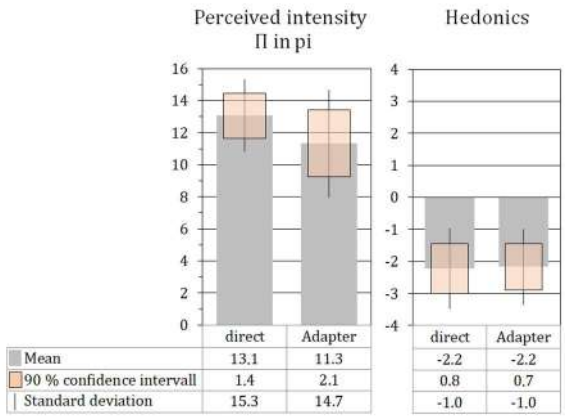

Fig. 4 - Perceived intensity and hedonics – directly determined and using an adapter.

4. Discussion

The results of the analytics show, as expected, that the sample air has a very similar composition at the funnel as in the emission test chamber and that the adapter is a suitable device in terms of analytics. The measurements will be repeated in the course of the study with a sample that emits higher substance concentrations that will help the system to achieve the more accurate measuring range of the GC/MS method. The Tedlar bag, which is placed over the funnel, should also be rinsed with sample air beforehand to increase accuracy. The measurements will also be carried out using Nalophan sample containers.

The results of the olfactory measurements, one of which was presented here as an example, show overall that the intensities determined using the adapter are often reported as lower and the standard deviations are higher. Further investigations have shown that an air backflow via the funnel into the sample container of the adapter may be the cause. As soon as a panel member stops pressing the button for the blower, air flows back because the emptied sample container exerts a suction effect. The sample air is thus provided in different compositions for the individual panel member. The adapter is currently being optimised so that a non-return valve can be installed between the funnel and the sample container. The measurements will be repeated after the modification and a larger number of panel members will be employed.

Overall, it can be assumed that all sampling systems without mechanical backflow prevention can lead to sample air dilution. The smaller the sample containers are and the more frequently the fan is operated by the testers to empty the bag, the more noticeable this becomes in the olfactory measurements.

The adapter should be used on test chambers from approx. 250 l size as the exhaust air volume at these chambers is still sufficiently large to fill a bag within an acceptable time. With a 15 l bag, an air exchange rate of 0.5 h-1 is achieved and after being completely emptied by a panel member, a bag can be completely refilled in approx. 8 minutes.

The advantage of the adapter over the commonly used sampling systems is that the air in the bags does not remain for a longer period of time and thus experiences little change. The procedure can be carried out in laboratories where odour assessment is feasible in close proximity to the emission test chamber. When planning the measurement, the filling time of the bags must be taken into account. If several samples need to be evaluated on one day, a fresh adapter must be available for each sample.

The adapter can help to further develop the odour measurement method according to the ISO 16000-28 procedure and reduce the influence of the type of sampling inasmuch as results comparable to direct evaluation can be achieved using the adapter. Overall, this will further increase the acceptance of ISO 16000-28. As a result, the dissemination of odour measurements for indoor building products can be further advanced for the benefit of health and energy-efficient building operation.

5. References

[1] VDI 4302 Part 1:2015-04. Sensory testing of indoor air and determination of odour emissions from building products - Fundamentals. Verein Deutscher Ingenieure e.V.

[2] Wargocki P., Wyon D.P., Baik Y.K., Clausen G., Fanger P.O. Perceived Air Quality, Sick Building Syndrome (SBS) Symptoms and Productivity in an Office with Two Different Pollution Loads. Indoor air 9 (3), S. 165-179.

[3] Lagercrantz L., Wistrand M., Willén U., Wargocki P., Witterseh T., Sundell J. Negative impact of air pollution on productivity: previous Danish findings repeated in new Swedish test room. Proceeding of Healthy Buildings 2000:653–8.

[4] A European Green Deal. https://ec.europa.eu/info/strategy/priorities-2019-2024/european-green-deal_en. European Commission. Link last checked 2021-12.

[5] DIRECTIVE 2012/27/EU OF THE EUROPEAN PARLIAMENT AND OF THE COUNCIL of 25 October 2012 on energy efficiency, amending Directives 2009/125/EC and 2010/30/EU and repealing Directives 2004/8/EC and 2006/32/EC.

[6] DIRECTIVE 2010/31/EU OF THE EUROPEAN PARLIAMENT AND OF THE COUNCIL of 19 May 2010 on the energy performance of buildings (recast): EPBD.

[7] Panaskova J. Olfaktorische Bewertung von Emissionen aus Bauprodukten [Dissertation]. RWTH-Aachen. 2012.

[8] Fisk W., Seppanen O. Providing Better Indoor Environmental Quality Brings Economic Effects. FINFVAC, Helsinki. Proceedings of Clima 2007.

[9] ISO 16000-28:2020-11. Indoor air - Part 28: Determination of odour emissions from building products using test chambers. International Organisation for Standardisation.

[10] Panaskova J., Müller D., Müller B. Olfaktorische Messgrößen für die geruchliche Bewertung von Emissionen aus Bauprodukten. GI - Gebäudetechnik, InnenraumKlima. 2014:61–9.

[11] Brosig L., Horn W., Pyza L., Jann O., Plehn W. Round robin test for the implementation of odour measurement according to DIN ISO 16000-28 into the assessment of emissions from building products. Gefahrstoffe - Reinhaltung der Luft. 2013;73:441–5.

[12] EN 16516:2020-10. Construction products: Assessment of release of dangerous substances - Determination of emissions into indoor air. European Committee for Standardization.

[13] Müller B., Mertes A., Scutaru AM. Innenraumluftqualität nach Einbau von Bauprodukten in energieeffizienten Gebäuden. Hg. Umweltbundesamt. Dessau-Roßlau; 2016.

[14] Müller B., Panaskova J., Danielak M., Horn W., Jann O., Müller D. Sensorische Bewertung der Emissionen aus Bauprodukten: Integration in die Vergabegrundlagen für den Blauen Engel und das Bewertungsschema des Ausschusses zur gesundheitlichen Bewertung von Bauprodukten. Hg. Umweltbundesamt. Dessau-Roßlau; 2011.

[15] Salthammer T., Schulz N., Stolte R., Uhde E., Bartsch J. Evaluierung einer Methode zur sensorischen Bewertung von Bauprodukten für Innenraumanwendungen unter Praxisbedingungen. Fraunhofer WKI. Braunschweig; 2016.

[16] Müller B., Mertes A., de Lima Vasconcelos S., Jann O., Horn W., Brosig L.. Emissions- und geruchsarme Bauprodukte für energieeffiziente Gebäude - Entwicklung von Anforderungen und Konzepten für den Blauen Engel aus Klimaschutzsicht. Hg. Umweltbundesamt. Dessau-Roßlau; 2017.

[17] ISO 16000-9:2006-02. Indoor air — Part 9: Determination of the emission of volatile organic compounds from building products and furnishing — Emission test chamber method. International Organisation for Standardisation.

The datasets generated during the current study are not publicly available because the study is still ongoing but will be available after the study is completed.

Simulation aided development of a façade-integrated air handling unit with a thermoelectric heat exchanger

Vojtech Zavřel [a], Petr Zelenský [a], Jordi Macia [b], Angelos Mylonas [b], Jordi Pascual [b]

[a] University Centre for Energy Efficient Buildings, CTU Prague, Prague, Czech Republic;
vojtech. zavrel@cvut.cz, petr.zelensky@cvut.cz

[b] Thermal Energy and Building Performance Group, IREC – Catalonia Institute for Energy Research, Barcelona, Spain;
jpascual@irec.cat, jmacia@irec.cat, amylonas@irec.cat

Abstract. The paper presents a simulation aided development of a new type of a façade-integrated air handling unit for local ventilation of rooms. The unit is developed as a part of the Plug-and-Use (PnU) concept within the H2020 project PLURAL. Unlike conventional local ventilation units designed solely for ventilation, the developed air handling unit has a two-stage heat recovery that combines a passive and an active heat exchanger. The active heat exchanger consists of an array of thermoelectric elements and provides the flexible and energy efficient capability of temperature control of supplied ventilation air. The paper demonstrates the practical use of building energy simulations for the development of the unit. A combined simulation approach was used, while the IDA ICE software addressed the indoor CO_2 concentration and related ventilation volume flow rates used for the TRNSYS software, which predicted energy performance and indoor thermal conditions. In the TRNSYS, a numerical representing the initial prototype of the air handling unit was prepared. This sub-model was integrated into the TRNSYS building model of the real installation demo site, namely, the Terrassa building, Barcelona, Spain. A variant numerical analysis was performed with two different compositions of the building envelope (pre- and post-renovation) and several ventilation control strategies and air handling unit operation settings. The performed simulations were capable to predict the performance of the innovative device in the real-case arrangement, under various scenarios, on the scale of the entire building. The simulation analysis demonstrated that the façade integrated air handling unit can clearly improve the IAQ conditions and reduce the overheating in the case when no other cooling system is available. The simulations provided an important navigation for the design team to further develop the innovative device.

Keywords. PLURAL, local **v**entilation**,** façade unit, thermoelectric cell**,** design, simulation, TRNSYS
DOI: https://doi.org/10.34641/clima.2022.207

1. Introduction

The implementation of ambitious EU energy efficiency targets within the Renovation Wave Strategy [1] calls for high-performance, cost-effective, and fast renovation solutions to rapidly reduce energy demand of existing building stock [2]. Prefabricated add-on façade modules represent a suitable solution that allows, in addition to increased insulation of the building envelope, the integration of best-practice technologies such as photovoltaic panels or in-facade ventilation units.

The goal of such integration is to upgrade the performance of existing buildings in the shortest possible renovation time, as the prefabrication and modular approach decrease the duration of the on-site production and installation phases, lower the overall cost, ensure maximum comfort standards and at the same time reduce the operational energy consumption. While standard ways of building envelope renovation opting mainly for better energy efficiency (increased insulation, new windows, etc.) may lead to overheating risk and unacceptable IAQ quality [3], the more complex solutions integrate other systems to mitigate these potential risks.

The paper is focused on the simulation aided development of a Plug-and-Use (PnU) façade module providing additional insulation and visual improvement of the building façade and integration of advanced building systems. The module may integrate photovoltaic panels and an air handling unit (AHU) with thermoelectric air-conditioning capability. The prefabricated façade module presented in this study acts as an 'add-on' panel that is mounted on the existing building envelope. The panel development is carried out within the

Copyright ©2022 by the authors. This conference paper is published under a CC-BY-4.0 license.

framework of the H2020 project PLURAL (Plug-and-Use Renovation with Adaptable Lightweight Systems), see www.plural-renovation.eu. As the proposed PnU solution combines several non-standard and innovative features, the simulation analysis helps the design team to better understand the overall PnU module performance and the impact to the indoor environment and energy use of the dwelling during the initial design phase, before manufacturing of the prototype and consequent final product. This study is focused mainly on the integrated AHU and its operational regimes. The paper demonstrates the practical use of building energy simulations for the development of the proposed system and prediction of the AHU positive impact on the IAQ and thermal comfort indoors. The developed solution is tested with use of a numerical model of the real demo-site where it will be installed, i.e., Terrassa apartment building located in Barcelona, Spain.

2. Combined simulation approach and simulated scenarios

A combined simulation approach was used to predict airflows and related indoor air quality (IAQ), which is represented by CO_2 concentration here, as well as the energy performance considering the innovative and non-standard components. While the IDA ICE software addressed air-flow network simulation and predicted the indoor CO_2 concentration in the simulated dwellings, TRNSYS software predicted energy performance and thermal comfort. Both simulation software used the same weather file and the boundary conditions of the model, which enabled the combination of the results from the different simulation tools.

The following steps were taken during the combined numerical study, see also Fig. 1, to simulate performance of the two representative flats in the installation demo site of Terrassa building. First, the identical weather file was imported to each software. Second, the IDA ICE software was used to predict the infiltration and related indoor CO_2 concentration in the simulated dwellings for both natural and mechanical ventilation. In case of mechanical ventilation, the required ventilation volume flow rates were exported for energy simulation. Third, the results of IDA ICE were imported into the TRNSYS software, for the simulation of influence of AHU operational regimes.

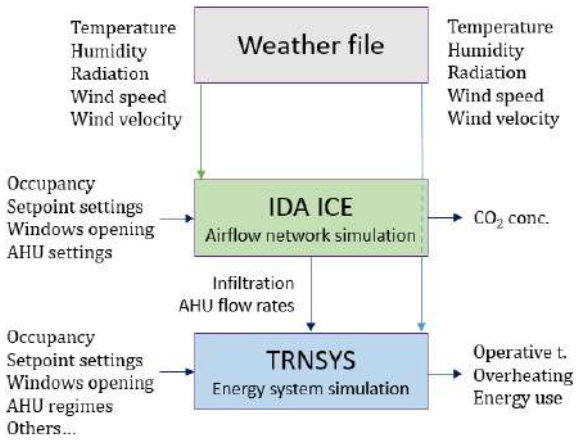

Fig. 1 – Combined simulation approach

Eleven scenarios combining various building model configurations and control strategies were simulated, as described in Tab 1. The building was simulated in two pre-renovation (Pre) scenarios and nine post-renovation (Post) scenarios, with the following ventilation strategies:

- Ventilation only by infiltration and opening of windows at night;
- Occupancy controlled ventilation; i.e. required fresh air delivery according to occupancy (following current standards);
- CO_2 controlled ventilation with the limit of 1,000 ppm (following the Pettenkofer criteria);
- CO_2 controlled ventilation with the limit of 1,000 ppm; AHU running in AC mode, that is, full

Tab. 1 – Simulated Scenarios

Nr.	Scenario	Ventilation strategy
1	Pre – realistic	infiltration and opening of windows at night
2	Pre – hypothetical	occupancy required fresh air delivery
3	Post – no AHU	Infiltration and opening of windows at night
4	Post – passive HX	occupancy req. fresh air delivery, without active heat exchanger
5	Post – active	occupancy req. fresh air delivery
6	Post – active	occupancy req. fresh air delivery, AC mode during overheating hours
7	Post – active	occupancy req. fresh air delivery, AC mode during overheating hours, night cooling mode
8	Post – passive HX	CO_2 controlled ventilation, without active heat exchanger
9	Post – active	CO_2 controlled ventilation
10	Post – active	CO_2 controlled ventilation, AC mode during overheating hours
11	Post – active	CO_2 controlled ventilation, AC mode during overheating hours, night cooling mode

power during overheating hours.

- CO_2 controlled ventilation with the limit of 1,000 ppm; AHU running in AC mode and overnight cooling mode with partial load for noise reduction.

The post-renovation scenarios targeted various operating modes of the AHU. In the scenario 3 the unit was disabled and in the scenarios 4 and 8 the active heat exchanger was not used. In the scenarios 6 and 10, the unit was running in AC mode, i.e., with full possible cooling capacity during the overheating hours. In the scenarios 7 and 11 the night cooling mode was enabled and the AHU ran continuously to pre-cool the dwelling overnight. The ventilation flow rate was limited to 30 % during the night, in order to reduce the noise emission. The cooling power of the AHU was not adjusted.

3. Façade-integrated air handling unit

To provide mechanical ventilation for the building after renovation, each dwelling will be served by the compact ventilation unit integrated into the prefabricated façade module as an inbuilt system. Unlike conventional local ventilation units designed solely for ventilation, the developed AHU has a two-stage heat recovery (active and passive). Aside of the passive and active heat exchangers, the unit is equipped with a controlled bypass system, filtration, and supply and exhaust fans, see Fig. 2.

The main innovation is an active heat exchanger, that consists of an array of thermoelectric elements providing both cooling and heating capability. The use of the thermoelectric element has several advantages such as (i) compact size, (ii) no mechanical parts, (iii) reliability due to the absence of liquid refrigerant circuit, i.e., without risk of leakage and related low maintenance requirements (iv) direct current device suitable for energy supply from PV panels and (v) universal application, where the same device can be used for heating and cooling purpose by reversing the current polarity. The main disadvantages are lower efficiency and limited temperature drop in comparison to refrigerant based solutions [4].

A numerical model of the initial prototype design of the unit was prepared in the TRNSYS simulation software. This sub-model representing the AHU was integrated to the TRNSYS model of the Terrassa building. The cooling and heating power of the active heat exchanger depends on the electric current and the temperature difference between the supply and exhaust air. It was modelled with the use of a performance map, which was prepared according to the characteristics of the installed thermoelectric cells.

The maximum volume flow rate of the ventilation air through the AHU is 150 m^3/h. The maximum heating power of each unit is 340 W, with COP approx. 2.5. The maximum cooling power is 250 W with EER approx. 0.65.

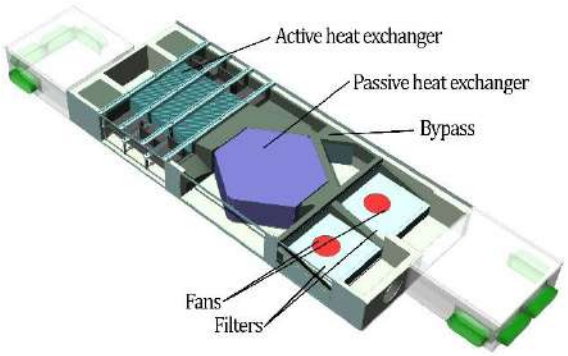

Fig. 2 – Integrated air handling unit

4. Real-Case scenario of Terrassa building Spain

One of the PLURAL targets is to install the developed PnU façade modules during a real demo site renovation and test them under real conditions. As a demo site for the presented type of the PnU façade module was selected the Terrassa building, located in Terrassa, Barcelona, Spain; i.e., a typical Spanish multi-family block of flats, see Fig. 3 and Fig. 4. The same building was considered for the numerical study.

This four-storey building with a basement used as car parking was completed in 2008 and consists of 18 existing dwellings; 6 dwelling per floor, while levels 3 and 4 are connected by 6 double-storey flats with underroof zones. The total area of the building is 1,280 m^2. The east façade faces the street, the west façade faces an inner courtyard. The longitudinal axis of the building is oriented 9° east.

According to the Spanish Energy Performance regulation, the building reached label D for CO_2 emissions and label E for primary non-renewable energy consumption. Thus, it is a good candidate for renovation with the use of PLURAL technologies.

Fig. 3 – Terrassa building demo site, aerial view

Fig. 4 – Terrassa building demo site, east façade

The 3D model of the building was prepared in the SketchUp geometry modeller. The model follows the real building topology, i.e., four storeys with 18 dwellings and a basement. However, the internal arrangement of the building was adjusted in the model, in order to simplify it. Zones with similar characteristics were merged (i.e., rooms within one dwelling, divided building corridors, etc.), resulting in the total number of 39 simulated zones.

Two representative dwellings were modelled and simulated in detail (including subdivisions into individual rooms), while the surrounding zones acted as boundary conditions. These two dwellings were significant in terms of boundary conditions and the results of their simulation could be extrapolated to the rest of the PLURAL affected building spaces. Both dwellings are located at the first floor; the first one faces the courtyard (ZA1-court), while the other faces the street (ZA1-street), see Fig. 5. The purple colour indicates either external solar shading volumes representing surrounding buildings in the model or adiabatic boundary conditions.

The building model for the TRNSYS software was prepared with the use of the TRNSYS Type 56. The location was considered identical to the real demo site, and the weather file used for the simulations was Meteonorm Terrassa TMY-2. Only the aforementioned dwellings were modelled in the IDA ICE environment.

The model was prepared in two configurations: pre-renovation and post-renovation, after the installation of the PLURAL PnU façade modules, i.e., with additional thermal insulation, new windows, building integrated PV system and façade integrated AHUs. For the pre-renovation building envelope characteristics, see Tab. 2. In the Tab. 3 are shown differences due to the renovation. The infiltration Equivalent Leakage Area (ELA) [5] has been calculated according to the Spanish regulation for residential buildings [6]. In addition to infiltration, the windows opening schedule was considered during the occupancy, where the opening ratio was determined with respect to outdoor temperature.

3.1 Configuration of the building model

For all simulated scenarios, identical profiles of occupancy, exhaust ventilation, internal heat gains, and basic dwelling technical systems were considered, see below. However, the ventilation control strategies differ, as described in Chapter 2.

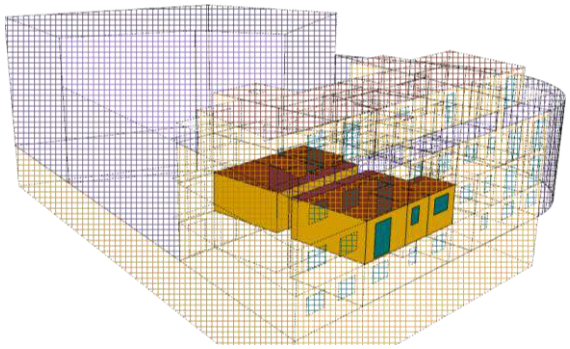

Fig. 5 – Building model, representative dwelling

Tab. 2 – Pre-renovation building envelope

Construction	Characteristics
Ceiling	0.37 W/m²·K
Floor	0.43 W/m²·K
External wall	0.49 W/m²·K
Partition Wall	0.69 W/m²·K (between buildings)
Internal wall	1.81 W/m²·K (between flats)
	1.71 W/m²·K (towards corridor)
Glazing	2.72 W/m²·K, G-Value 50 %
Window frame	2.27 W/m²·K, 20 % frame area
Window blinds	0.66 W/m²·K, 0 - 100% opening
ELA	500 cm²

Tab. 3 – Post-renovation building envelope (changes)

Construction	Characteristics
External wall	0.20 W/m²·K
Glazing	1.00 W/m²·K, G-Value 53 %
Window frame	2.27 W/m²·K, 20 % frame area
Window blinds	0.66 W/m²·K, 30 - 60% opening
ELA	200 cm2

Occupancy profiles

The occupancy profiles follow the realistic behaviour of the inhabitants, with respect to three different zone types in the simulated dwellings: common area, bedroom and bathroom; see Tab. 4. The profiles are related to the total number of occupants in each dwelling, while three people are considered in each of the two representative dwellings.

Tab. 4 – Occupancy profiles for different zones

Zone type	Occupancy
Bathroom	100 % at 7-8 h; 14-15 h; 22-23 h
Bedroom	100 % at 23-7 h
Common area	30 % at 7-10 h and 14-17 h 80 % at 17-23 h

Internal gains

Three types of internal heat gains were defined in the model: lighting, appliances and occupants. The heat gains were related to the floor area of the particular zone. The heat gain from occupants was calculated according to the occupancy schedule in each zone and considered as 2.15 W/m² [7]. Tab. 5 shows the internal gains from the lighting and white appliances, with respect to the zone type.

Tab. 5 – Internal heat gains schedule

Zone type	Occupancy
Lighting (common area)	0.1 W/m² at 7-18 h 0.5 W/m² at 18-19 h 0.8 W/m² at 19-23 h
Lighting (bedroom)	0.5 W/m² at 7-8 h 0.5 W/m² at 17-23 h
Appliances (common area)	0.03 W/m² at 22-8 h and 9-20 h 0.08 W/m² at 8-9 h and 21-22 h 0.2 W/m² at 20-21 h

Exhaust ventilation

Forced exhaust ventilation was considered in the open kitchen areas of the dwellings and in the bathrooms with total flow rate of 125 m³/h. It was operated during the following periods: 7-8 h at 50 %, and 20-21 h at 100 %. The exhaust ventilation is part of the air-flow network calculation, thus during these periods the total infiltration is increased (similar to the windows opening schedule).

Dwelling technical systems

A standard electric heating by electrical radiators was used in the simulated dwellings. The heating power was limited to 5.6 kW, corresponding to the real systems installed in the building. The heating setpoint was set to 21 °C between 7-10 h and 17-23 h. During the remaining time, the heating was operating with lower setpoint of 18 °C. There was no cooling considered, aside the cooling of ventilation air provided by the AHU's active heat exchanger.

The domestic hot water was prepared in electric tank heater with a volume of 80 l and 1.5 kW power. Daily hot water consumption in each dwelling with 3 occupants was considered 122 l.

Photovoltaic systems (post-renovation only)

A building integrated photovoltaic system was used in the post-renovation scenarios. The areas of 80 m² on the roof (inclination of 17°) and 100 m² on the east facade (inclination of 90°) of ONYX GL.01.MONO panels with 15% efficiency were considered. The produced energy was evenly divided among the dwellings with respect to their floor area.

5. Results of the simulation study

The main objective of the numerical study was to assess the benefit of PLURAL façade kits and to estimate the performance of the façade integrated AHU under different conditions. Indoor environment quality and energy consumption were evaluated and compared for 11 simulated scenarios. The realistic pre-renovation scenario (scenario nr. 1) was considered as a baseline for the comparison, as it represents the current conditions of the Terrassa building.

5.1 Indoor environment quality

Fig. 6 and Fig. 7 show the IAQ and operative temperature, respectively. The results are displayed for the dwelling ZA1-street and for the most relevant scenarios, for the sake of simplicity. The ZA1-street dwelling is the one more exposed to direct sun radiation and therefore the one more susceptible to overheating. It represents the more unfavourable case of the two representative dwellings. The figures show yearly conditions and conditions during four extreme days. Red dashed lines indicate the CO_2 concentration limit of 1,500 ppm (in Fig. 6) and the operative temperature limit of 27 °C (in Fig. 7).

From Fig. 6 it is apparent that the CO_2 concentrations in the two scenarios without controlled ventilation exceed the hygienic limit – in baseline scenario nr. 1 for approx. 11% of the occupied time and in scenario nr. 3 for 23%. This happens especially during the winter season, when ventilation by opening of windows is restricted due to the low outdoor temperatures. The maximum concentration of CO_2 exceeds 3,000 ppm in the baseline scenario and 4,400 ppm in the scenario 3, after the renovation of the building envelope, without the AHU. These concentrations are more than twice higher than the recommended limit for a good indoor environment.

The IAQ for all scenarios with AHU is sufficient throughout the year. The graph of CO_2 concentration during the extreme period of the year shows the differences in operation of AHU with various ventilation control strategies. CO_2 controlled ventilation (here scenario nr. 8) generally leads to higher concentrations in the dwelling, reaching the limit of 1,000 ppm. In such case, the ventilation volume flow rate is lower, which may lead to better energy efficiency, as discussed in the next chapter.

In all the scenarios, the operative temperature in the dwelling frequently exceeds 27 °C during the summer season, see Fig. 7. The graph for the extreme period (on the right) shows that the renovation of the building envelope with additional ventilation to meet the required fresh air delivery can lead to operative temperatures over 30 °C, if not done properly. This risk of overheating was mitigated by AHU temperature conditioning of the fresh air and an

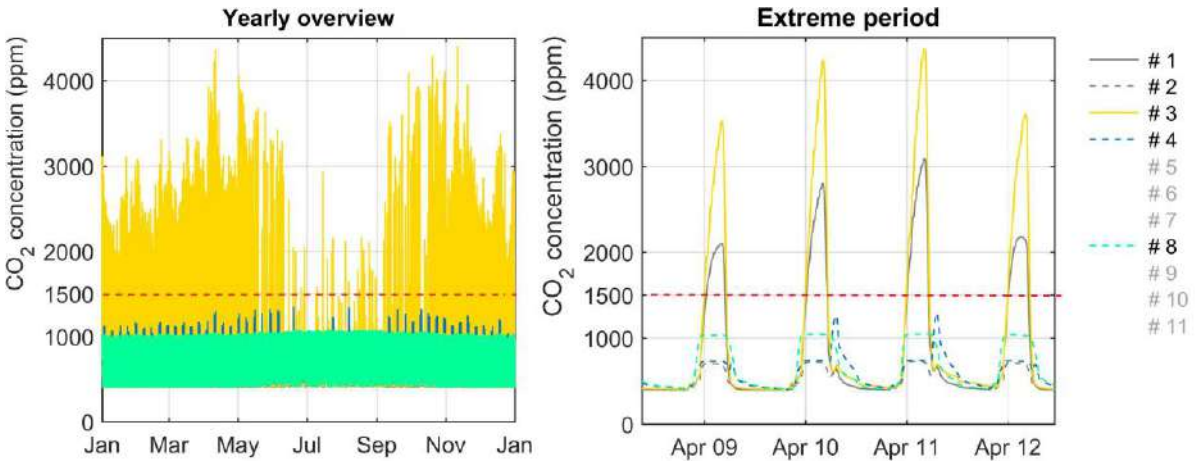

Fig. 6 – IAQ (represented by CO_2 concentration), dwelling ZA1-street, bedroom; red dashed lines indicated CO_2 limit

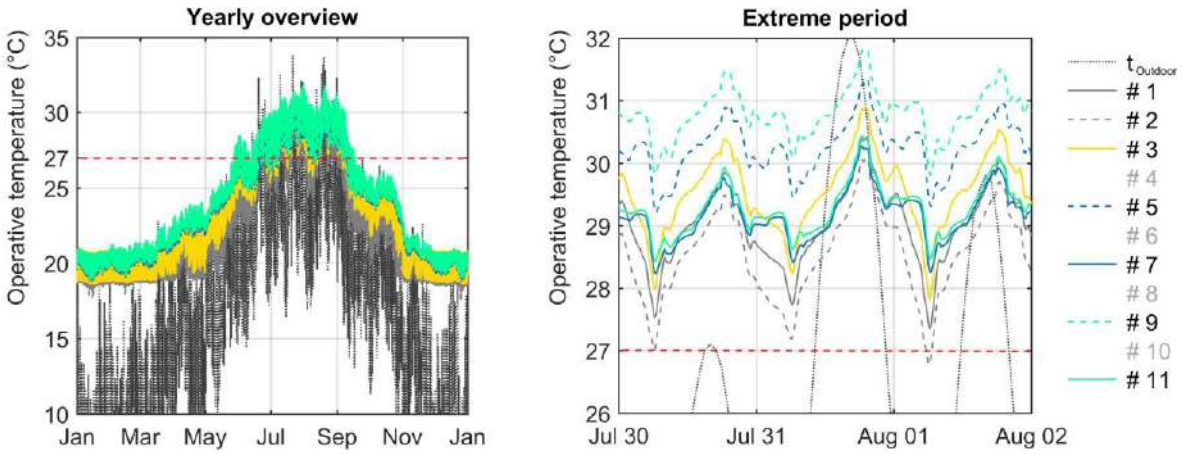

Fig. 7 – Indoor operative temperature, dwelling ZA1-street, average temperatures in the dwelling; red dashed lines indicate indoor operative temperature limit

appropriate ventilation control strategy. From the compared PLURAL scenarios, the lowest indoor temperatures were achieved in scenarios 7 and 11, when the AHU operated in AC mode, with overnight pre-cooling. Although the temperatures were slightly higher than in the baseline case (scenario nr. 1), the indoor CO_2 concentration was much better.

The indoor environment quality in both representative dwellings (ZA1-street and ZA1-court) was evaluated in Fig. 8 in the form of annual discomfort hours (overheating and IAQ – left axis) and annual discomfort degree-hours (right axis). It is evident that the pre-renovation conditions (scenario nr. 1) are not optimal. With ventilation only by infiltration and opening of windows, the CO_2 concentration frequently exceeds the desired limit of 1,500 ppm (for more than 660 hours per year). The additional ventilation flow rates must be delivered to satisfy the hygiene standards of IAQ. Scenario nr. 2 represents the situation prior renovation, when the required airflow is delivered via infiltration and represent secondary baseline for energy calculation.

The PLURAL renovation solution by the PnU façade modules was tested in the other 9 scenarios. Scenario nr. 3 (new windows, thermal insulation of the building envelope and PVs, without local AHU) leads to a significant increase in the number of discomfort hours with CO_2 concentration exceeding 1,500 ppm (for nearly 1,300 hours per year). This is due to the increased airtightness of the building envelope. The results of the study indicate that integrated AHU should be used as a part of the PLURAL solution, to maintain hygienic IAQ with desirable CO_2 concentrations.

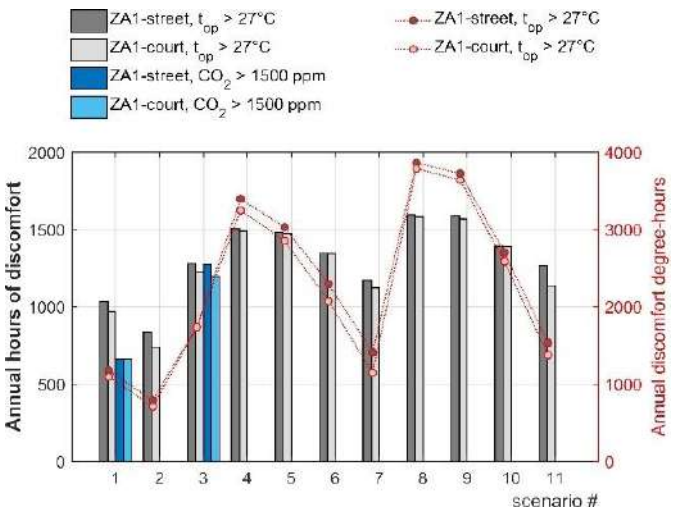

Fig. 8 – Indoor environment quality

All scenarios with the AHU (nr. 4 to nr. 11) show that, with controlled ventilation, the CO_2 concentration does not exceed the desired limit. However, ventilation by warm outdoor air results in the increase in the number of hours with indoor operative temperature exceeding 27 °C, as well as related number of the annual discomfort degree-hours. This negative effect can be addressed by cooling of the delivered fresh air and suitable ventilation control strategy. The best post-renovation environment quality was achieved in two scenarios with AHU operating in AC mode during overheating hours and providing night cooling. The best scenario was nr. 7 with the occupancy controlled ventilation, followed by the scenario nr. 11 with the CO_2 controlled ventilation. However, in both scenarios the number of overheating hours was still over 1,000, as the AHU is designed mainly for ventilation, with additional ability to condition the temperature of the delivered fresh air, rather than an actual air-conditioning device. Therefore, its cooling power is not sufficient to cool the whole dwelling.

5.2 Energy consumption

The energy consumption of the dwelling ZA1-street was evaluated in the form of total electricity use and total primary energy consumption related to the floor area of the dwelling. Results from all simulated scenarios are summarized in Fig. 9.

At first, it was checked that the distribution of the consumption among the building systems in the pre-renovation scenario (nr. 1) corresponds to the common situation in Spanish dwellings of a similar type [8]. This indicated that the building model was set in a reasonable way.

The comparison of energy consumption of the post-renovation scenarios clearly demonstrates the contribution of the PLURAL solution to the energy savings. The reduction of the total energy use was from 13 to 37 %, depending on the ventilation control strategy. The reduction of the total primary energy consumption was in the range of 34 to 59 %, considering building integrated photovoltaic system. Scenario nr. 11 (that is, CO_2 controlled ventilation and AHU running in AC mode during overheating hours, with night cooling mode) can be advised as the most favourable, with the best indoor environment quality, as discussed in the previous chapter, 17% reduction of total electricity use and 38% reduction of the total primary energy consumption.

5.3 Building integrated PV system

For all the scenarios with building integrated PV system, the self-sufficiency (demand coverage by PV production) and self-consumption (PV production matching) ratios were evaluated, see Tab. 6. While the self-sufficiency ratio is around 0.2 in all the scenarios, the self-consumption differs significantly. The scenarios with the AHU running in AC mode (scenarios nr. 6, 7, 10 and 11) indicate the best on-site matching of the electric energy delivery from the PV system with the energy demand of the building systems. The self-consumption ratios are 0.78 for scenarios 6 and 7 and 0.75 for scenarios 10 and 11. The high values are reached due to the AHU operating with the maximum cooling power during the hot periods of the day, when the intensity of solar radiation is usually high. This situation is the most favourable for the utilization of the PV generated electric energy.

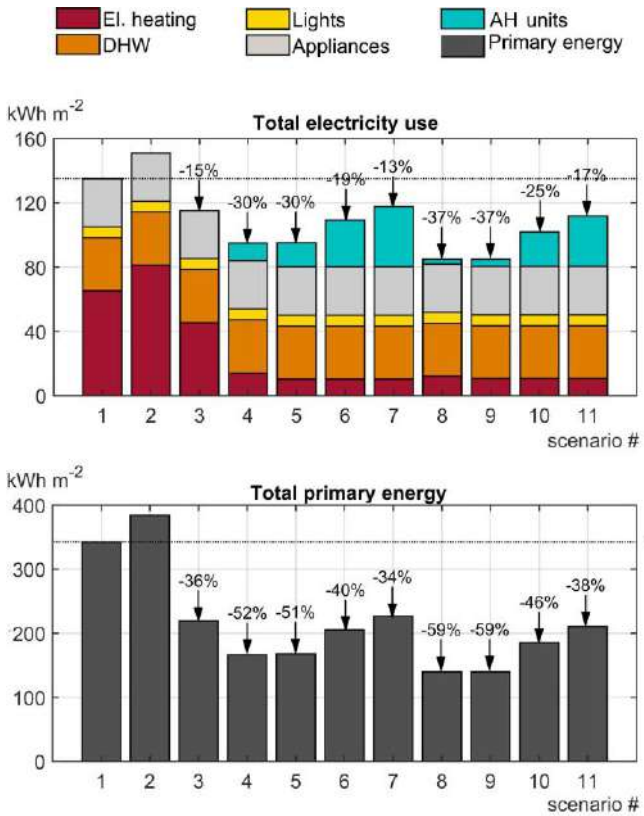

Fig. 9 – Energy consumption

Tab. 6 – PV electric energy indicators

Scenario	Self-sufficiency	Self-consumption
1	No PV	No PV
2	No PV	No PV
3	0.13	0.47
4	0.18	0.56
5	0.19	0.58
6	0.22	0.78
7	0.20	0.78
8	0.18	0.49
9	0.18	0.50
10	0.22	0.75
11	0.21	0.75

6. Conclusion

The paper demonstrates the risks related to the building envelope renovations aiming solely at better energy efficiency, i.e., increase of thermal insulation and change of windows, without considering proper ventilation strategy. It shows that such renovations may lead to overheating and unacceptable IAQ, with very high CO_2 concentrations. A new type of a façade module was introduced as a suitable solution that allows, in addition to increased insulation, the integration of other technologies such as photovoltaic panels and a controlled ventilation system. The integrated AHU provides the ability to condition the temperature of the air supplied for local ventilation of rooms by an active thermoelectric heat exchanger. The façade module is developed as a part of the Plug-and-Use concept within the H2020 project PLURAL and the simulation study helped the design team to better understand its performance during the yearly operation, before the manufacturing phase.

Combined simulation study with the use of IDA ICE and TRNSYS software was elaborated. Eleven scenarios of the Terrassa building Spain, real-case demo site for installation and testing of the developed façade module, were simulated. The building was simulated in two pre-renovation scenarios and nine post-renovation scenarios, with various ventilation control strategies. The integrated AHU was controlled according to the occupancy, CO_2 concentration, indoor air temperature (i.e., with cooling during overheating hours) and with over-night cooling mode. The main target was to predict the performance of the developed PLURAL systems. The indoor environment quality and energy indicators were evaluated.

It was demonstrated that without proper ventilation, the CO_2 concentration in the simulated dwellings exceeds the required limits, both in the pre-renovation case and in the post-renovation case without controlled ventilation system. The limit of 1,500 ppm was frequently exceeded especially during winter season, when ventilation by opening of windows is restricted due to the low outdoor temperature. The façade module with integrated AHU mitigates this risk and ensures good IAQ, with CO_2 concentration below 1,500 ppm thorough the year. However, in the summer season, the controlled ventilation by warm fresh air results in the increase in the number of hours with indoor operative temperature exceeding 27 °C. This negative effect was addressed by cooling of the delivered fresh air.

From the nine post-renovation scenarios, the one with ventilation flow rate controlled by CO_2 concentration indoors, AHU operating in AC mode, i.e., maximum cooling power during overheating hours, and with night cooling seems to be the most favourable. It indicates good IAQ during the year and one of the lowest numbers of overheating hours and related overheating degree-days. In this scenario, 17% electricity saving and 38% reduction of the primary energy consumption was achieved, in comparison with the baseline pre-renovation scenario. Also, the self-consumption ratio of the PV generated electric energy revealed the complementarity of the combined PV - AHU system, where the self-consumption was increased from approximately 0.50 to 0.75.

7. Acknowledgement

This project has received funding from the European Union's Horizon 2020 research and innovation programme under grant agreement No 958218

8. References

[1] A Renovation Wave for Europe - greening our buildings, creating jobs, improving lives. European Commission. 2020

[2] Factsheet: 97% of buildings in the EU need to be upgraded. Buildings Performance Institute Europe. 2017. Available from: ww.bpie.eu/wp-content/uploads/2017/12/State-of-the-building-stock-briefing_Dic6.pdf (5.1.2022)

[3] Attia, S. et al. Overview and future challenges of nearly zero energy buildings (nZEB) design in Southern Europe. Energy and Buildings. 2017; 155: 439–458.

[4] Martín-Gómez, C, María Ibáñez-Puy, Javier Bermejo-Busto, José Antonio Sacristán Fernández, Juan Carlos Ramos, and Alejandro Rivas. Thermoelectric Cooling Heating Unit Prototype. Building Services Engineering Research and Technology. 2016; 37 (4): 431–449.

[5] Sherman, M.H. Grimsrud, D.T. Infiltration-Pressurization Correlation: Simplified Physical Modeling. ASHRAE Transactions, 1980; 86(2): 778-803.

[6] Documento basico CTE-HE Ahorro de energía. Ministry of Development of Spain (Ministerio de Fomento). 2019.

[7] Proyecto SECH-SPAHOUSEC – Análisis de Consumos Energéticos del Sector Residencial en España. Eurostat. 2011.

[8] Consumos del Sector Residencial en España, Resumen de Información Básica. The Institute for Diversification and Saving of Energy, the Ministry of Industry, Energy and Tourism, Spain. 2012. Available from: www.idae.es/uploads/documentos/documentos_Documentacion_Basica_Residencial_Unido_c93da537.pdf (5.1.2022)

NUMERICAL ANALYSIS OF GERMICIDAL UV-C LAMP AIR DISINFECTION SYSTEM

Tunahan Akış [a], Ziya Haktan Karadeniz [b], Orhan Ekren [a]

[a] Ege University, Solar Energy Institute, İzmir Turkey, tunahannakis@hotmail.com, orhanekren@gmail.com

[b] Department of Energy Systems Engineering, İzmir Institute of Technology, haktankaradeniz@iyte.edu.tr

Abstract. In this study, four germicidal UV-C lamps that are in a 600x600 square duct are numerically investigated. Also an UV reactor design is investigated for high resistive microorganisms. Air flow in the duct has 3000 m3/h volumetric flow rate. Simulations are conducted with commercial computational fluid dynamics solver ANSYS-FLUENT. In square duct, Lamps has 75 W UV power and their electrical efficiency depends on UV radiation generation, lamp surface temperature, contact air humidity, lamp working hours, lamp surface pollution. The radiation intensity around the lamps in the channel is evaluated by the using discrete ordinates method depending on the location. After that, the air flow on the lamps are modelled and particle motion simulation is carried out with the DPM model. The amount of UV dose received by these particles is calculated at the duct outlet, and the inactivation ratio for the general coronavirus family is examined. As a result, D90 inactivation performance is achieved in the system. The radiation distributions obtained depending on the UV power and the dose map in the duct outlet section depending on UV power are parametrically examined and presented.

Keywords. UV-C disinfection, germicidal lamp, computational fluid dynamics, indoor air quality,
DOI: https://doi.org/10.34641/clima.2022.294

1. Introduction

The concept of indoor air quality has gained importance in recent years. The pandemic caused by the SARS-CoV-2 virus, which threatens humanity today, has once again shown the importance of focusing on this concept. The most common ways of infection of this virus, which has a great impact on the design and operating conditions of air conditioning and ventilation systems, can be summarized as follows [1].

(i) Large droplets and aerosols (when sneezing, coughing, or talking), with close contact of 1-2 m,

(ii) Airborne by aerosols (dried small droplet nuclei) that can stay in the air for hours and be carried over long distances (released when breathing, talking, sneezing, or coughing).

(iii) Through surface contact (hand-to-hand, hand-to-surface, etc.)

(iv) Fecal-respiratory.

The most effective transmission is through droplet (i) with 21%, with viruses suspended in the air (airborne) with 64%, adhered to other parks or clustered or alone (ii) and contact with (iii) 15%.

As it is known, particles suspended in the air circulation in heating, cooling, ventilation, and fresh air distribution systems. This situation brings up the fact that any microorganism or virus will be included in this flow. Therefore, considering the pandemic conditions we are in today, the design of ventilation and air conditioning systems has become more important than ever. There are three basic inactivation methods known to reduce the effectiveness of the aerosols in the airflow:

(i) Removal by mechanical ventilation

(ii) Filtration

(iii) UV-C Disinfection

It is possible to produce optimum solutions for disinfection by using these methods, which we call "Total Disinfection Management", together.

In the literature, there are recent studies dealing with the use of UV-C lamps in the air flow. F. Atci et al. [2] examined the in-duct disinfection with

Copyright ©2022 by the authors. This conference paper is published under a CC-BY-4.0 license.

numerical methods in their study. They considered four different lamp arrays in 61x61x183 cm channel dimensions and modelled the particles in the air flow with the DPM algorithm and analysed the air flow with the SIMPLE and PRESTO! algorithm. The UV radiation distribution in the channel is analysed using the discrete ordinates method. For the lamp arrays they examined, they observed that the particles in the air are exposed to a UV dose of 19.12 J/m^2 in the best scenario. They stated that this dose value inactivated the MS2 Bacteriophage virus at the rate of 56.05% at the duct outlet. A. Capetillo et al. [3] compared EPA tests with CFD simulations and interpreted that the results are in good agreement with experimental results for different microorganisms and viruses. In their analysis for a single lamp, they stated that only 6.2% of the particles in the channel are exposed to double the average dose, while the remaining particles could only receive half the average dose. They stated that this situation had significant effects on the total efficiency of the UV disinfection system. W.J. Kowalski et al. [4] proposed a solution method for modelling UVGI systems. They are confirmed their findings with experimental studies with a margin of error of ±%15. On the other hand, they stated that the effects of air relative humidity in UV-C disinfection are not yet understood. On the other hand, the rate constants of pathogens to UV radiation are an issue that needs to be investigated to determine the inactivation performance. Capetillo et al. [5] discussed the use of UVC lamps for in-duct air disinfection in their study. The amount of UV dose to which the particles suspended in the air flow are exposed is calculated using computational fluid dynamics simulations. They created their numerical models with the inputs of the UV disinfection tests performed by the EPA (Environmental Protection Agency) agency. They compared their findings with EPA agency test results, which revealed test results with different UV lamp numbers and configurations. As a result of the comparison, they observed that the UV radiation distribution findings are in good agreement with the experimental data. The study reveals that the UV resistance coefficient unique to each microorganism, which reveals the resistance of different microorganisms to UV radiation, should be investigated in more detailly. For some microorganisms, it is suggested that although the accuracy that can be a reference in the verification of the numerical model results has been determined, this coefficient has not been determined with sufficient accuracy for other microorganisms. This situation shows that there can be misconceptions when questioning the adequacy of the UV disinfection system. Yi Yang et al. [6] developed a new model to determine the UV radiation field based on the view factor model in their study. The model results are well agreed with the experimental data. In the computational fluid dynamics simulations, they carried out investigations on the inactivation efficiency of the model for E. coli bacteria. They observed that the amount of inactivation decreased for increasing air flow rate and increased for increasing lamp size. On the other hand, the local dynamic loss coefficient of the UV lamp for the air flow is calculated as 0.085 by them. Yi Yang et al. [7], in their study, a numerical model that includes multiple physics by determining the trajectories of particles in the air using the Langrangian method is proposed. Their model based on the view factor model developed with their previous studies. In their findings, they calculated the inactivation amount of S. Marcencens bacteria as 100%, the inactivation amount of MS2 bacteriophage as 54.43%, and the inactivation amount of B. atrophaeus bacteria as 0%. When they compared their findings with the EPA test reports, they reported that they calculated 100% accuracy for S. marcescens bacteria, 15% deviation for MS2 bacteriophage, and 100% accuracy for B. atrophaeus bacteria.

In this study, the design steps of UV disinfection systems are explained. Calculation of the average dose amount does not provide clear evidence for the adequacy of the system design. For this reason, the dose distribution at the duct outlet is also presented in this study. In addition, when the dose distributions are examined, it reveals the necessity of examining numerical methods in system design with UV disinfection. Inactivation performance also depends on the type of microorganism examined. A reactor design for fungal spores, which are the most difficult to inactivate, is also considered within the scope of the study, and the dose distribution and inactivation performance in the outlet channel section are presented. In addition, the effects of these systems on power consumption are discussed.

2. Material and Method

In this section, the system design stages, and the content of these steps are detailed. Also, sample designs are shown. As can be seen in Fig. 1, the mathematical model of the system is created in the first step. The model structure is divided into finite volumes (meshing) and turned into a numerical model. The numerical model uses three different equations, (i) discrete ordinates method, (ii) continuity, momentum and k-ε turbulence model (iii) discrete phase model (DPM). SIMPLE algorithm is implemented as iterative solver. Boundary conditions and governing equations is explained under cont'd subsections.

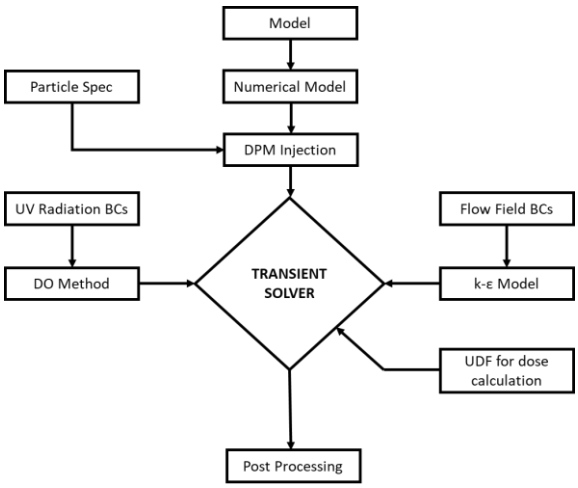

Fig. 1 – Numerical System Design Algorithm

2.1 Discreate Ordinates Method

Discrete Ordinates (DO) method is used for solving radiation distribution emitted from UV-C lamps. Governing equation for DO is represented with Equation-1 [8].

$$\nabla(I(\vec{r},\vec{s})\vec{s}) + (a+\sigma_s)I(\vec{r},\vec{s}) = \frac{an^2(\sigma T^4)}{\pi} + \frac{\sigma_s}{4\pi}\int_0^{4\pi} I(\vec{r},\vec{s'})\phi(\vec{s}\,\vec{s}')d\Omega' \quad (1)$$

In Equation-1, the first term on the left is the emission term, and the term on the right is the scattering term. Here **r** is the position vector and **s** is the direction vector. **s'** is the scattering vector and s is the distance. I is defined as the radiation intensity. Angular scattering and pixelization are important here. For this analysis, angular scattering and pixelization values are used as 5x5 and 3x3, respectively.

2.2 k-ε Turbulence Model

Solving the airflow in duct, the standard k-ε turbulence model is implemented to Navier Stokes equation. For solving governing equations with turbulence dissipation ANSYS – FLUENT solver is used. Second order upwind scheme is selected as discretization scheme and SIMPLE algorithm is implemented as solver. Three dimensional continuity and Navier-Stokes equations are discretised and governing equations are [8]:

$$\frac{\partial\rho}{\partial t} + \nabla(\rho\vec{v}) = 0 \quad (2)$$

$$\frac{\partial}{\partial t}(\rho\vec{v}) + \nabla(\rho\vec{v}\vec{v}) = -\nabla p \quad (3)$$

$$\frac{\partial}{\partial t}(\rho k) + \frac{\partial}{\partial x_i}(\rho k u_i) = \frac{\partial}{\partial x_j}\left[\left(\mu + \frac{\mu_t}{\sigma_k}\right)\frac{\partial k}{\partial x_j}\right] + G_k - \rho\epsilon \quad (4)$$

$$\frac{\partial}{\partial t}(\rho\epsilon) + \frac{\partial}{\partial x_i}(\rho\epsilon u_i) = \frac{\partial}{\partial x_j}\left[\left(\mu + \frac{\mu_t}{\sigma_\epsilon}\right)\frac{\partial\epsilon}{\partial x_j}\right] + \frac{C_{1\epsilon}\epsilon G_k}{k} - \frac{C_{2\epsilon}\rho\epsilon^2}{k} \quad (5)$$

$$\mu_t = \frac{\rho C_\mu k^2}{\epsilon} \quad (6)$$

Here, k is turbulence kinetic energy, and ε is energy dissipation. G_k represents generation of turbulence kinetic energy by mean velocity gradient. $C_{1\epsilon}$, $C_{2\epsilon}$ are constants, σ_k and σ_ϵ are the turbulent Prandtl numbers for k and ε respectively.

2.3 DPM Model

DPM (Discreate Phase Model) can predict trajectory of a discreate phase particle by integrating force balance on the particle [4]. For z direction of model used in this study, force balance can be written as,

$$\frac{du_p}{dt} = F_D(u-u_p) + \frac{g_z(\rho_p-\rho)}{\rho_p} \quad (7)$$

where $F_D(u-u_p)$ is drag force per unit particle mass can be written as,

$$F_D = \frac{18\mu}{\rho_p d_p^2}\frac{C_D Re}{24} \quad (8)$$

Here u is fluid velocity, u_p is particle velocity, μ is viscosity of fluid, ρ is fluid density, ρ_p particle density, d_p particle diameter. Re is relative Reynolds number, calculated as,

$$Re = \frac{\rho d_p|u_p-u|}{\mu} \quad (9)$$

2.4 Dose and Inactivation

It should be ensured that the particles injected into the air flow receive a sufficient dose. For this, the amount of dose taken by a particle during its movement in the air flow must be determined. The dose amount can be determined by Equation – 10 [1].

$$D = \int_{t_0}^{t} I(x, y. z)dt \qquad (10)$$

Here t_0 is the starting time and t is the time until the particle leaves the channel. I is local radiation density [W/m^2] that depends on particle's location. After calculating the UV radiation dose received by each particle during the channel movement, the total dose received by the particles can be calculated and the average dose amount of the disinfection system can be calculated as,

$$\overline{D} = \sum_{i=1}^{n} \frac{D(n)}{\Delta T} \qquad (11)$$

Where $\overline{D}$ is the average dose and ΔT is the mean duration of motion, n is the number of particles injected into the channel. By determining the average dose amount, the inactivation performance (removal rate) of the disinfection system can be calculated with Equation - 12.

$$RR = 1 - S \qquad (12)$$

Here S is removal rate which can be evaluated as,

$$S = \exp(-k\overline{D}) \qquad (13)$$

Here k is inactivation constant that is specific for injected microorganism type to ventilation duct. In this study, a user defined function (UDF) is used that records the local radiation distribution at each time step to determine the dose.

2.5 Sample Designs

There are four UV-C lamps in a ventilation duct which can be seen in Fig. 2a and Fig. 2b at two different models. Also, a reactor design which can achieve D90 in activation for high-resistant to UV-C radiation (fungal spores) is shown in Fig. 2c.

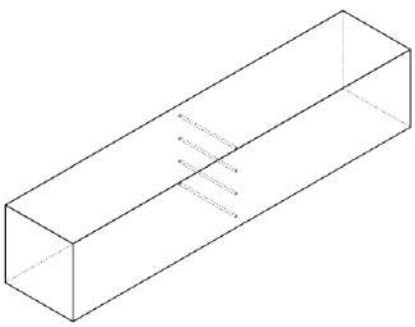

Fig. 2a – Sample Design-1 (Far Arrangement)

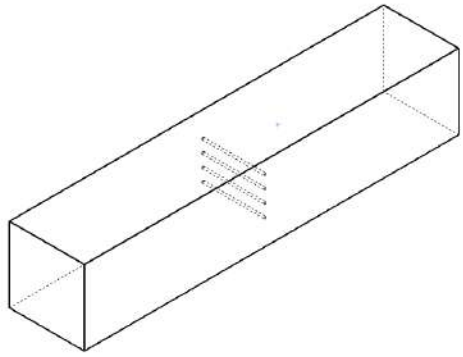

Fig. 2b – Sample Design-2 (Close Arrangement)

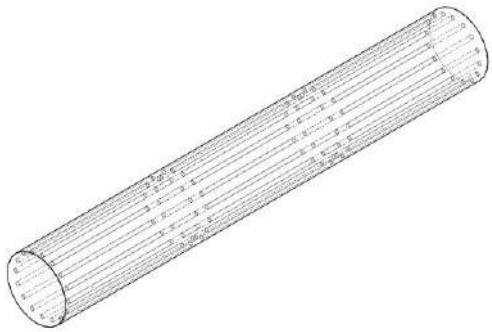

Fig. 2c – Sample Design-3 (Reactor Design)

Sample designs which are given in Fig-2a and Fig-2b contain the same number of lamps. The diameters of the lamp are 16mm. and arc length is 500 mm. Channel dimensions are 600x600x5000. these square channel sample designs are taken from the ISO 15714-2019 [9] standard, a standard for the test procedure of UV-C disinfection systems. The difference between them is the central distance between the lamps in the middle plane where the lamps are located. The central distance between the lamps is 125 mm in the design with far arrangement given in Fig - 2a, the central distance between the lamps is 100 mm in the design with close arrangement given in Fig-2b. In Fig-3c, the sample design geometry for the disinfection of microorganisms which resistive to UV radiation is given. There are 48 lamps with 38 mm diameter and 1.5 m arc length in the relevant geometry. The duct cross-sectional area is taken at the same ratio as the square duct cross-sectional area to make a well comparison. Channel length is 5000 mm

2.6 Validation

The validation of the numerical model is carried out by validating the irradiation field created by the UV lamp with radiation distribution experimental data. A drawing of the validation model is given with Fig - 3. Validation model Kowalski et al. [5] taken from his 2001 study. In Fig G25T8 Philips UVC lamp located in the air volume.

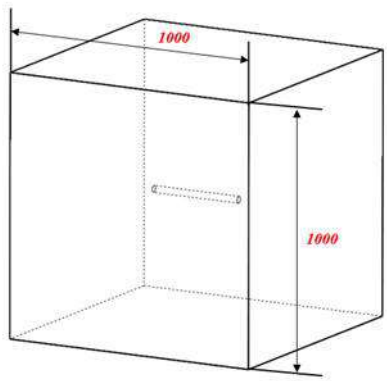

Fig. 3– Validation Model

The G25T8 Philips UVC lamp used has a power of 6.6 W. The arc length of the lamp is 35.56 mm and its radius is 1.27 mm.

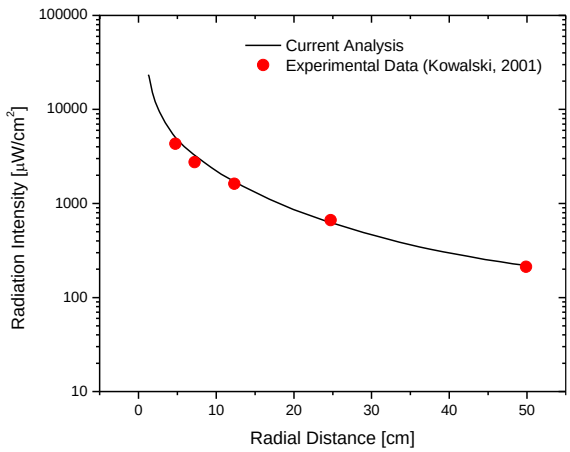

Fig. 4– Comparison with Experimental Data

As can be seen with Fig-4, the results obtained with the present analysis well agreed with the experimental data. For the analysis, 1399143 mesh numbers were used. Convergence criteria are given in Tab-1. Each analysis for the square channel took an average of 187 minutes. For the reactor, it took 76 hours and 37 minutes.

Tab. 1 – Convergence Criteria

Model	Value
DO Discretization	$1x10^{-12}$
Continuity	$1x10^{-6}$
k- ε Standard Equation	$1x10^{-6}$
Momentum	$1x10^{-6}$

2.7 Boundary Conditions

A total of 7 analyses are carried out at different lamp UV powers within the scope of the study. The air flow rate is considered as a constant 3000 m^3/h for each analysis. UV power of 75W is determined for the lamps (for reactor lamps has 135 W UV power). The channel outlet is at an absolute pressure of 0 Pa. Inactivation is examined for the general coronavirus family, and the inactivation coefficient is 0.009716 [m^2/J] [1]. However, the inactivation coefficient of fungal spores, which has a very high resistance to UV radiation, is considered in the reactor design (k=0.0009 m^2/J). In each analysis, 400 particles were injected into the channel in a homogeneous distribution from the channel inlet section. The duct inner surface reflectivity is considered as 50% as recommended in the ISO 15714-2019 standard.

The energy efficiency of UV lamps can be calculated by Equation - 14.

$$\eta_{tot} = \eta_{UVC}\eta_T\eta_\phi\eta_a\eta_f \qquad (14)$$

Here, η_{UVC} is the efficiency of the lamp to produce ultraviolet radiation at a wavelength of 253.7 nm, η_T is efficiency depending on lamp surface temperature, η_ϕ efficiency depending on the humidity of the air carrying the virus, η_a is depending on lamp operating hours (ηa), and η_f is efficiency due to surface contamination. Considering the applications, the average UVC radiation efficiency of the lamps is around 35%. Also the temperature efficiency can be between 40%-90% depending on the location of the UVC system in a practical sense. No information is found in the literature on cleaning efficiency. However, for a safe design, it is considered appropriate to take an average of 99%, provided that the lamp is cleaned frequently. Although there are some experimental studies on moisture efficiency, these studies are for a certain microorganism and special radiation distributions. It is an area that needs to be studied for any microorganism. For operating hours efficiency, using the performance of the lamp at the end of the renewal life given by the lamp manufacturer will be appropriate in terms of safe design (this value is around 60%). When all these efficiency parameters are considered, it is seen that the total efficiency is around 15-20%. the best efficiency at 25°C temperature, 40-50% relative humidity and 2.5 m/s air velocity. Efficiency analyzes is carried out under these assumptions by reverse engineering. More detailed studies should be done in the future.

3. Results

3.1 Far Arrangement Sample Design

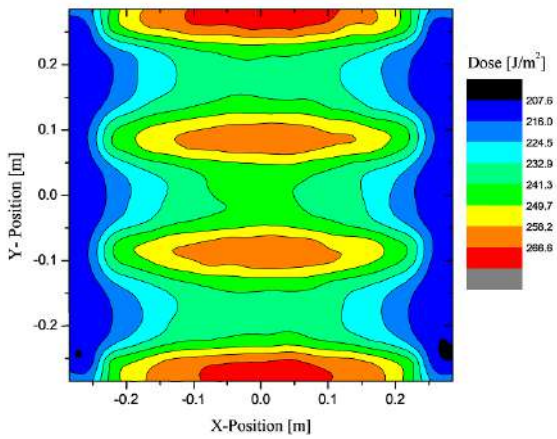

Fig. 5– Far arrangement sample design duct outlet dose map

In Fig-5 duct outlet dose map is given for close arrangement sample design. It can be said that the amount of dose received by the particles are more regularly distributed compared to the closely spaced design. In addition, as expected, the particles in the flow around the lamp receive a higher dose than the particles in other parts of the flow.

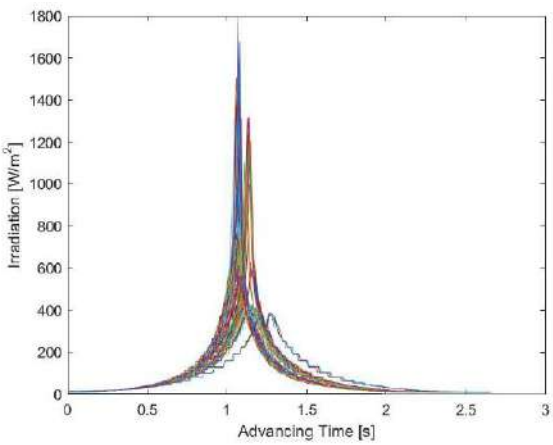

Fig. 6– Far arrangement sample design the intensity of radiation to which particles are exposed during their movement.

In Fig. 6, the radiation intensity that each particle is exposed to during its movement is given depending on time. For this design, it is observed that a particle moving near the lamps in the middle section of the duct is exposed to a maximum radiation intensity of 1800 W/m². For the general coronavirus family, the average dose value obtained in this design is 237.51 J/m². When the inactivation amount of this design is calculated with Equation-13, it can be said that the inactivation amount is 90.05%. However, when Fig. 7 is examined, there are particles that have not received sufficient dose in the outlet section. Fig. 7 shows that particles that have received enough dose in the outlet section with the green area (%36.75), and the particles that have not received the enough dose with the red area (%63.25). For this reason, it is incomplete to question the adequacy of a UV system design with only the average dose amount.

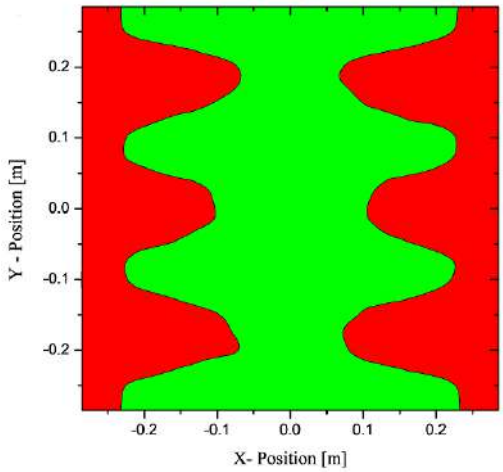

Fig. 7– Far arrangement sample design duct outlet safe zone investigation

3.2 Close Arrangement Sample Design

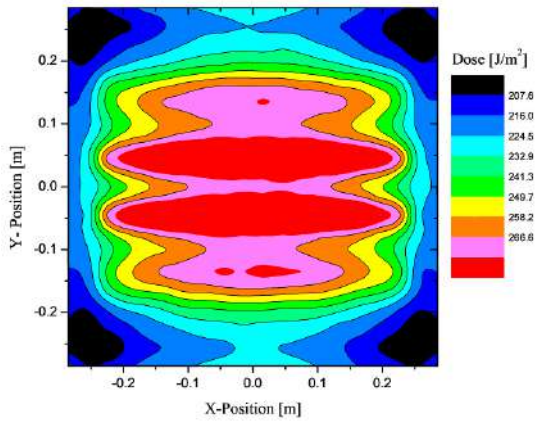

Fig. 8– Close arrangement sample design duct outlet dose map

Fig. 8 shows the dose distribution of the particles in the outlet section of the close arrangement sample design. Particles exposed to intense radiation is concentrated at the midpoint of the cross-section, in contrast to the far arrangement sample design. In Fig. 9, the radiation intensity that each particle is exposed to during its movement is given depending on time. For this design, it is observed that a particle moving near the lamps in the middle section of the duct is exposed to a maximum radiation intensity of 2500 W/m² as expected.

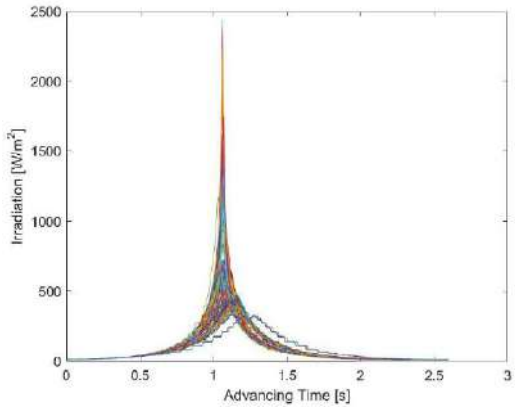

Fig. 9– Close arrangement sample design the intensity of radiation to which particles are exposed during their movement.

The distribution of the safe zone in the outlet section of the arrangement sample design is given in Figure 10. While the safe zone area indicated in green on the exit section is 46%, the risk zone area is 54%.

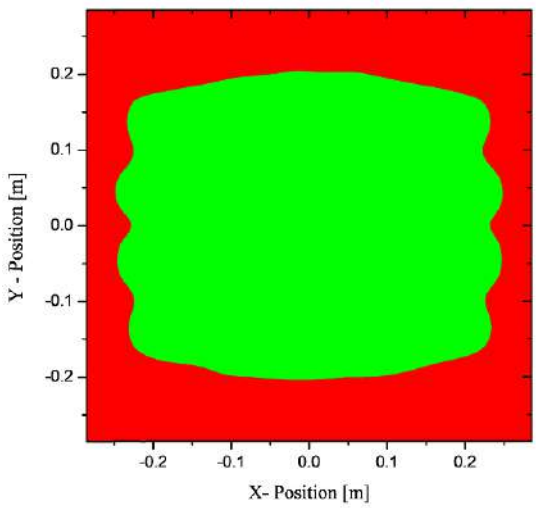

Fig. 10– Close arrangement sample design duct outlet safe zone investigation

3.3 Reactor Design

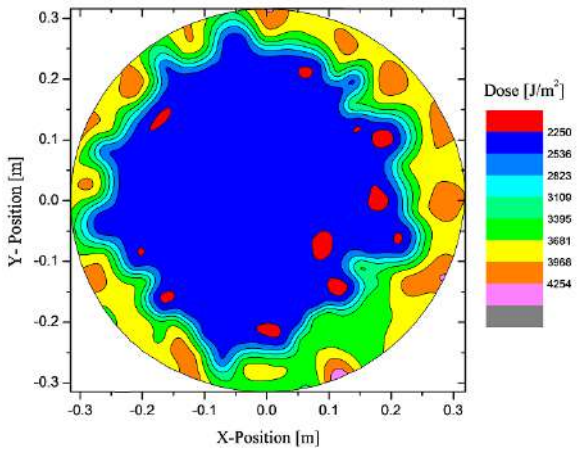

Fig. 11– Reactor design duct outlet dose map

In the reactor design for UV-resistant microorganisms, the dose distribution at the outlet is observed as in Fig. 11. The findings show that the dose amount of the particles increases around the radially arranged lamps and decreases along the channel center axis. Main reason of this, it can be said that the particles close to the center move approximately 1.5 times faster than the other particles, considering the fully developed velocity profile.

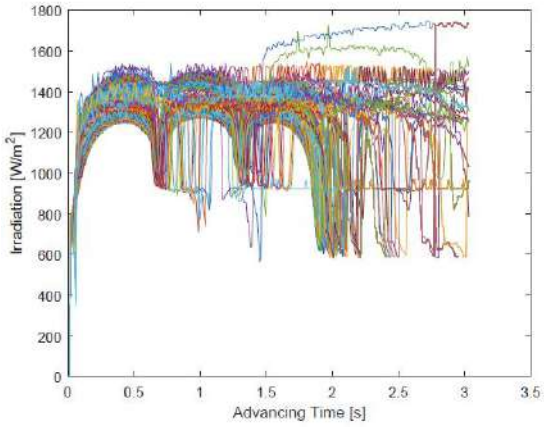

Fig. 12– Reactor design the intensity of radiation to which particles are exposed during their movement.

In Fig. 12, the radiation distribution of the particles in the reactor during their movement is given. As can be seen in the findings, the amount of radiation exposed between the lamp sets placed at 3 levels reached the maximum level. In addition, some particles were attached to the lamp side surfaces and could not exit through the flow channel.

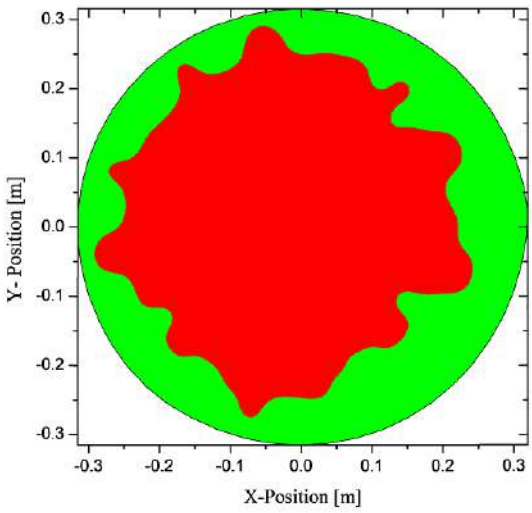

Fig. 13– Reactor design duct outlet safe zone investigation

In Figure-13, the safe zone distribution of the outlet section in the reactor design is given. Here, while the safe zone area, which is determined by the green color and concentrated around the lamps, is 41.91%, the risk zone area is 58.09%. On the other hand, a total power consumption of 37.2 kW is required for

the operation of this system. The average dose value calculated for this power consumption is 2930.4 J/m^2. Again, when Equation -13 is applied, D90 inactivation can be achieved.

4. Conclusions

Within the scope of this study, the inactivation performance of four UV lamps with 75 W UV power, positioned perpendicular to the air flow in two different layouts (far and close arrangement), are investigated in the air duct. In addition, a reactor design for inactivation of microorganisms with high resistance to UV radiation is investigated. The important results can be summarized as follows;

- The average dose obtained with four lamps with 75 W UV radiation is 237.51 J/m^2. D90 inactivation performance is achieved. However, when the dose distribution at the duct outlet and the safe zone are examined, it can be say that there are particles that leave the channel without receiving sufficient dose.
- In the proposed designs, moving the lamps away from each other allows a more regular dose distribution in the output section. However, the safe zone area decreases from 46% to 36.75%.
- A more detailed design should be considered for microorganisms resistant to UV radiation. Although an average of 2930.4 J/m^2 UV dose is obtained in the examined design and D90 performance is achieved, when the outlet section is examined, it is observed that a risky zone area is formed around the axis of the air duct.
- For the reactor design, the system power consumption is calculated as 37.2 kW. (Total UV efficiency is %20)
- In the reactor design made by the authors [1], the examination in previous studies differs in the outlet section dose and safe zone area found by this study. The main reason for this is the assumption that the UV dose distribution and the safe zone area calculated in the duct outlet within the scope of the previous study are assumed to move along a straight line with a constant and the same with inlet velocity. Within the scope of this study, particle analyzes are carried out with the DPM model and the particles carried out their movements in accordance with the velocity profile formed in the in-channel flow. The uniform distribution of the lamps around a radial path, limits the channel cross-sectional area through which the particles will move. This caused an increase in the velocity of the air flow along the channel axis and shortened the exposure time of the particles to UV radiation. On the other hand, the problem being solved is a Hagen - Poiseuille flow and when the air flow velocity profile is examined, it can be observed that the maximum velocity is along the duct axis. This explains the difference with the authors' previous work. For this reason, particle analyzes should be done in modeling the UV-Disinfection system and more realistic results / predictions should be obtained with these analyzes.

In addition to all these, another aim of the study is to present how UV systems should be analyzed with numerical methods, with a scientific methodology. Inspections in which different disinfection systems such as climatic data of the air and filtering and UV systems are used together should also be carried out in the duct. The most important parameter among the specified climatic data is the relative humidity of the air. The detailed effects of relative humidity on both system inactivation efficiency and power consumption can be discussed in future studies.

5. References

[1] TTMD, 2021, UVC ile Dezenfeksiyon: Örnek Tasarımlar, 99-101, Ultraviyole Işınım ile Dezenfeksiyon, TTMD İç Çevre Komitesi UVC Çalışma Grubu, İzmir, 132s.

[2] Atci, F., Cetin, Y. E., Avci, M., & Aydin, O. Evaluation of in-duct UV-C lamp array on air disinfection: a numerical analysis. Science and Technology for the Built Environment. (2020); 27(1), 98-108.

[3] Capetillo, A., Noakes, C. J., & Sleigh, P. A. Computational fluid dynamics analysis to assess performance variability of in-duct UV-C systems. Science and Technology for the Built Environment, (2015);21(1), 45-53.

[4] Kowalski, W. J., Bahnfleth, W. P., & Mistrick, R. G. A specular model for UVGI air disinfection systems. IUVA News, (2005); 7(1), 19-26.

[5] Capetillo, A., Noakes, C., & Sleigh, P. A. CFD analysis to assess performance of multi-lamp in-duct UVGI air disinfection systems. In Proceedings of Healthy Buildings Europe. (2017); International Society of Indoor Air Quality and Climate (ISIAQ).

[6] Yang, Y., Zhang, H., Chan, V., & Lai, A. C. Development and experimental validation of a mathematical model for the irradiance of in-duct ultraviolet germicidal lamps. Building and Environment. (2019); 152, 160-171.

[7] Yang, Y., Zhang, H., & Lai, A. C. Lagrangian modeling of inactivation of airborne microorganisms by in-duct ultraviolet lamps. Building and environment, (2021).;188, 107465.

[8] Fluent, 2009, " Documentation," ANSYS, 12.0/12.1, ANSYS Inc., Canonsburg, PA.

[9] ISO, 2019, Method of evaluating the UV dose to airborne microorganisms transiting in-duct ultraviolet germicidal irradiation devices, International Standarts Organization, 17p.

Evaluation of preventive measures in mitigating the risk of airborne infection of COVID-19

Yunus Emre Cetin[a], Martin Kriegel [a]

[a] Hermann-Riestchel-Institut, Chair of Energy, Comfort and Health in Buildings, Technische Universitaet Berlin, Berlin, Germany, y.cetin@tu-berlin.de

Abstract. In this study, a systematic approach for estimating the infection probability under different infection control strategies is presented for several indoor cases. Increased airflow rates, ventilation schemes, air cleaning equipment, disinfection systems, and face masks are considered according to existing guidelines and standards. These strategies are implemented to care facilities, schools, and offices with varying scenarios. Infection probability calculations are conducted based on the widely used Wells-Riley model. The possible variation of the input parameters is evaluated by employing the Monte Carlo approach to increase the representativeness of the findings. Results show that the infection risk reduction of 15 to 99% is possible depending on the measure preferred.

Keywords. Indoor air quality, COVID-19, preventive measures, Wells-Riley model.
DOI: https://doi.org/10.34641/clima.2022.299

1. Introduction

The novel coronavirus Covid-19 pandemic impinged millions of people [1]. Overwhelming numbers of reported cases brought into attention the importance of preventive strategies to alleviate the propagation of extremely infectious diseases. Multiple guidelines have raised the concern on the indoor airborne transmission of Covid-19 and many recommendations have been released by organizations [2–4]. These recommendations and strategies in terms of building, room, and personal scale have been reviewed and discussed from different perspectives [5–7]. In this context, infection risk assessment is considered a useful tool that may help to quantify and compare the effectiveness of corresponding infection control measures.

Wells-Riley [8,9] and dose-response models are known as two fundamental approaches in infection risk modeling for ventilated indoor enclosures. In general, the infection risk is characterized by a probability between 0 to 1. Models preferred can provide a quantitative risk assessment to deal with the ongoing epidemic and help to comprehend possible results of varying circumstances. The Wells-Riley model is a simple and quick approach based on the quantum concept, which also considers infectivity and source strength. The infection risk prediction with the Wells Riley assumes that the pathogens are homogeneously distributed in a room. The dose-response model on the other hand can provide more precise and realistic outputs than the Wells-Riley model. Nevertheless, this model is less handy since it requires infectious dose data to construct the dose-response relationship [10,11].

The Wells–Riley model and its modifications have been extensively used for the investigation and evaluation of the infection risk of numerous ventilated environments from different perspectives [12–17]. In corresponding studies, key parameters of the Wells-Riley model like quantum generation and breathing rate are evaluated mostly as a constant. In fact, these fundamental parameters have a varying character and considering them as a constant may result in misleading conclusions. Also, the effect of preventive measures on infection risk mitigation was rarely inspected and compared in a quantitative way. Hence, the motivation of this study is to evaluate the effect of different infection preventive strategies by employing the Wells-Riley model in which the probability distributions of unknown parameters are considered. For this purpose, the stochastic Monte Carlo approach is used to broaden the representativeness of the results. The effect of displacement ventilation, standalone air cleaners, installing partition, upper room UVGI systems, and wearing N95 masks are evaluated. The findings can be used in the ongoing struggle against Covid-19 by helping to understand effective countermeasures in infection.

2. Methods

2.1 Infection risk model

The Wells-Riley equation is mainly described as

Copyright ©2022 by the authors. This conference paper is published under a CC-BY-4.0 license.

follows:

$$P_0 = \frac{D}{S} = 1 - e^{-IqQ_b t/Q} \quad (1)$$

where P_0 is the probability of infection, D is the number of cases, S is the number of susceptible, I is the number of infectors, q is the quanta emission rate by one infector ($quanta/h$), Q_b is the breathing rate of the susceptible person (m^3/h), and Q is the volume flow rate of pathogen free air (m^3/h). In this study, the above version of the Wells-Riley equation is modified to include the use of N95 masks, air cleaners, displacement ventilation, partition, and UVGI system. The modified equation is given as follows:

$$P = 1 - e^{-(1-\eta_s)(1-\eta_I)\frac{IqQ_b t}{V\alpha}} \quad (2)$$

In this equation, η_s and η_I represents the mask filtration efficiency of the susceptible and infected persons respectively. V is the volume of the room (m^3) and α expresses the equivalent air change rate (given in Eq. 3) which depends equivalent ventilation air change rate (λ_{vent}), inactivation rate of ultraviolet germicidal irradiation (k_{UV}), and natural inactivation (k_{inact}).

$$\alpha = \lambda_{vent} + k_{UV} + k_{inact} \quad (3)$$

The equivalent ventilation rate (λ_{vent}) includes the air supply rate of the HVAC system (λ_{HVAC}) and portable air cleaners (λ_{PAC}). Here, in order to reflect the imperfect mixing case in different ventilation concepts like displacement ventilation an additional ventilation parameter (ε_{HVAC}) is also included to this equation as seen below. This additional ventilation parameter is equal to one for a perfect mixing situation which is one of the main assumptions in Wells-Riley consideration. A similar factor is also employed in another modification of Wells-Riley by Sun and Zhai [14].

$$\lambda_{vent} = \lambda_{HVAC}\varepsilon_{HVAC} + \lambda_{PAC} \quad (4)$$

Air supply rate of the HVAC system (λ_{HVAC}) is composed of supplied air flow rate of outdoor air ($\lambda_{outdoor}$) and recirculated air ($\lambda_{recirculated}$). It is given in the following form:

$$\lambda_{HVAC} = \lambda_{outdoor} + \lambda_{recirculated}\eta_{filter} \quad (5)$$

where η_{filter} is the filtration efficiency of the filters.

2.2 Cases considered

Three different base cases namely an elderly nursing home, a waiting area at the doctor's office, and a classroom are evaluated. Layouts, occupancy levels, duration of stay, ventilation configurations are assigned based on literature and the most typical real practices. Definitions and details regarding corresponding cases are given in Table 1.

2.3 Model parameters

Two critical parameters in the Wells-Riley equation are quanta generation rate (q) and breathing rate (p). The quantum generation rate depends on disease type, infector activity, etc., and varies significantly [18]. In this study, the quantum generation rate is adapted from the studies of Shen et al. [19], Millet et al. [20], and Hartmann et al. [21]. Breathing rates are assigned up to the activity levels. In each scenario, only one infectious pathogen emitter exists. It is also assumed that the infectious aerosols become evenly distributed throughout the space promptly. Quantum generation and breathing rates are assumed to follow the normal distribution. Variations of these inputs are applied by using the stochastic Monte Carlo approach on the calculations. In every setup, 50.000 trials are simulated.

Minimum outdoor ventilation rates are calculated in accordance with Ashrae Standard 62.1 [22]. In these calculations space area and occupant number are taken into account as seen in the following form:

$$\lambda_{outdoor} = R_p P_z + R_a A_z \quad (6)$$

where R_p is the outdoor airflow rate required per person (L/s), P_z is the occupant number, R_a is the outdoor airflow rate required per unit area (L/s), and A_z is the net floor area (m^2). Required airflow rates are determined by the minimum ventilation rates presented in Ashrae Standard 62.1 [22].

For the base cases mixing ventilation ($\varepsilon_{HVAC} = 1$) is applied. The fraction of outdoor ventilation on the air supply rate of the HVAC system is specified as 25% [23]. The filtration efficiency of the filters (η_{filter}) in recirculation is considered as 70 % [22]. Natural inactivation is assumed to have a uniform distribution between 0 and 1 h^{-1}.

Tab. 1 - Settings of the studied cases.

Space	Elderly nursing home	Waiting area at doctor's office	Music lesson in a classroom	Corridor in a school	Gym in a school
Duration of stay (min)	60	60	60	15	90
Number of total people	2	10	25	40	25
Volume of space (m^3)	3x4x2.7	4x5x2.7	5x8x3.2	30x1.25x3.2	15x27x5.5
Outdoor ventilation rate (l/s)	8.6	44	137		452.5
Quanta generation (h^{-1})	58±31	58 ± 31	970±390	251±134	492±270
Breathing rate (m^3/h)	0.3±0.2	0.3± 0.2	1.3±0.85	1.3±0.85	2.5±1.75

At first, infection probability is calculated for the

base cases. Then, six different mitigation strategy is applied, and the effect of these strategies is evaluated individually. Proposed strategies are as follows:

-Increased outdoor ventilation rate is analysed by employing 100 % outdoor air.

-Air distribution patterns affect the ventilation factor (ε_{HVAC}) considerably. Displacement ventilation has the potential to reduce the exposure in the breathing region so it is considered with a factor of 1.2 to 2 [24].

-Installing partition is considered by a factor of 1.1 – 3 [24].

-Portable air cleaners are becoming popular recently. The use of such air cleaners is assumed to supply clean air with a rate of 12 m3/h per square meter, which is suitable with the current EPA guide [25].

-Proper use of an upper room UVGI system is assumed to provide an air change rate of 2 to 6 h^{-1} [26].

-N95 masks can filter the droplets significantly. Filtration efficiency for both susceptible and infected persons is assumed as between 70% to 95% [27,28].

3. Results and discussion

The calculated infection rates for the base cases are shown in Table 2. The infection probabilities over 10% are considered as high risky spaces and these values are bolded. As it is observed, infection rates indicate a large variation in considered cases. The least risky space is found as the waiting area at the doctor's office. As a result of the excessive quanta generation rate the music class configuration shows the highest infection risk potential (40%) among evaluated scenarios. As a result, it can be said that without any mitigation strategy all the cases apart from the waiting area show a considerable risk in terms of infection probability.

Tab. 2 - Infection probabilities for base cases.

Space	Infection probability (%)	
	Mean	SD
Elderly nursing home	**14**	**11**
Waiting area at doctor's office	3.4	2.8
Music lesson in a classroom	**40**	**23**
Corridor in a school	**32**	**22.6**
Gym in a school	**24**	**18.4**

Infection risk probabilities under different mitigation measures for the nursing home, waiting area, classroom, corridor, and gym are depicted in Fig.1, Fig.2, Fig.3, Fig.4, and Fig.5 respectively. Mean value of the situational reproduction number ($R_S = P\ .\ S$) [28] in each case is also given in these figures. R_S points out the infection spreading in community. If $R_S > 1$ it is considered that an epidemic occurred.

In general, it is seen that all the measures help to decrease the infection probability to some extent. For the nursing home shown in Fig.1, the average infection probability decreases about 17% when the supply air is 100% outdoor originated. Nevertheless, in this case, the average infection risk is still higher than the threshold level with an 11.6% infection probability. All the other measures help to reduce the infection risk between 30% to 98%. In all these cases average infection risk is reduced to below 10% and the limit is met. Also, since the $R_S < 1$ in all cases the spread of the disease is unlikely for the nursing home.

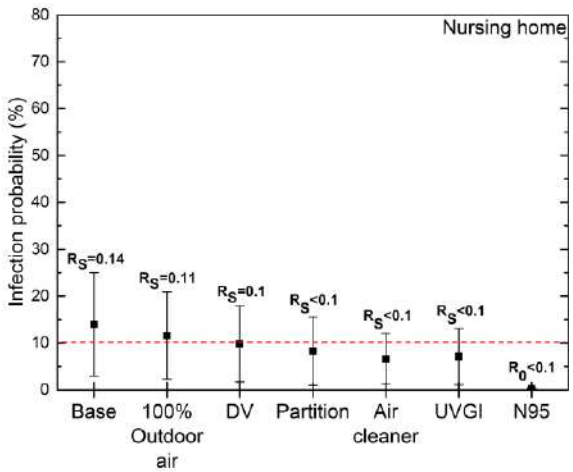

Fig. 1 - Infection risk predictions for the nursing home.

As seen in Fig.2, in the case of the waiting area considered measures alleviated the infection probability in the range of 23-99%. In this case, the lowest risk reduction is obtained with the use of 100% outdoor air, and the highest reduction is with the N95 face masking as expected. Both the values of infection probability and R_S point out that the lowest risk is obtained for the waiting area at doctor's office.

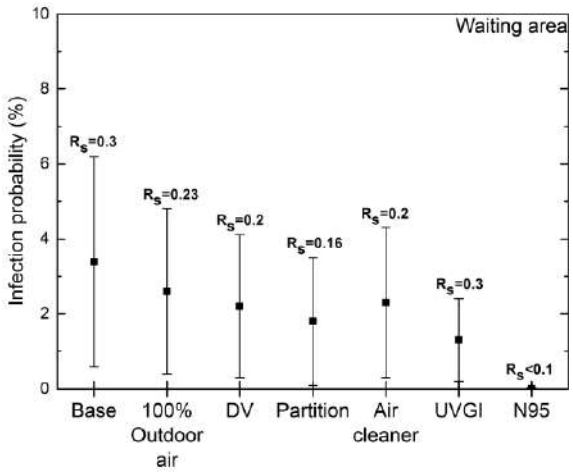

Fig. 2 - Infection risk predictions for the waiting area.

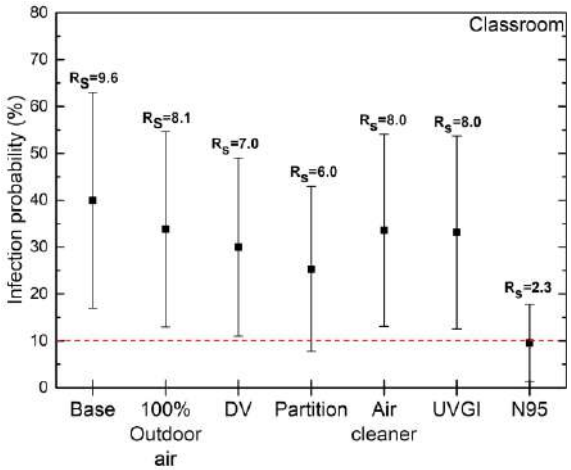

Fig. 3 - Infection risk predictions for the classroom.

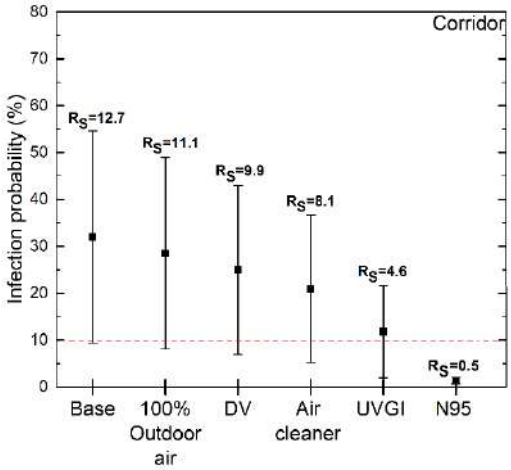

Fig. 4 - Infection risk predictions for the corridor.

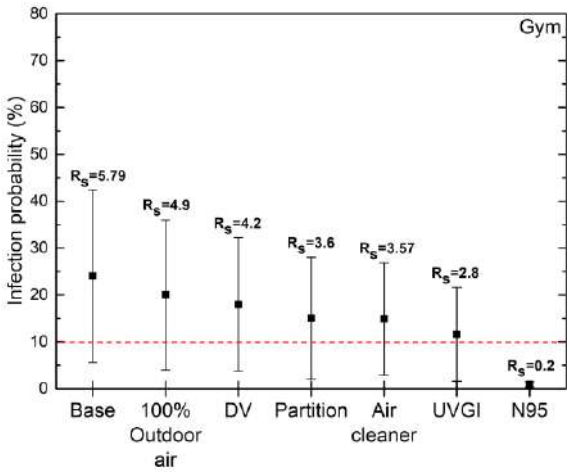

Fig. 5 - Infection risk predictions for the gym.

Infection risk predictions for the classroom, corridor and the gym are given in Fig.3, Fig.4 and Fig.5 respectively. It is deduced from the findings that the evaluated measures are not adequate in terms of attaining the threshold limit mostly. In all three cases high reproduction number ($R_S > 1$) points a risk of serious outbreak. In every evaluated configuration, the use of N95 masks meets the threshold value and stands as the only solution for the lowest infection probability. Still, it should be noted that it might not be a feasible solution in a music class. Also, for a deeper analysis of the mask efficiency leakage during inhalation and exhalation can be considered in terms of personal protection related factor [28]. For an efficient reduction of the infection risk, the combined effect of the multiple measures can also be evaluated with including feasibility and cost considerations.

4. Conclusions

In the present paper, possible infection preventive measures were analysed for five different settings by employing the well-known Wells-Riley model. Increased outdoor ventilation rate, displacement ventilation, installing partition, portable air cleaners, UVGI systems, and N95 face masks were evaluated. Related model parameters were determined based on the literature and practices. The stochastic Monte Carlo approach was used in calculations in order to include the variations of the input parameters. Future studies can evaluate the combined effect of different risk-mitigating factors from a feasibility and cost standpoint.

Important outcomes are summarized below:

-Predicted infection risk values show a deviating figure depending on the boundary conditions of the cases.

-Based on the evaluated measures risk reduction is possible between 15.5 to 99%.

-Infection risk-mitigating measures lower the probability although this may not be sufficient to achieve the predetermined limit for some cases.

-The use of N95 masks may reduce the infection risk remarkably. This potential can be considered as an easy option for complicated cases at first instance.

5. Acknowledgement

This study is supported by The Federal Institute for Research on Building, Urban Affairs and Spatial Development with funding code of SWD-10.08.18.7-20.02.

6. References

[1] WHO. WHO Coronavirus (COVID-19) Dashboard https://covid19.who.int/.

[2] REHVA. COVID-19 Guidance Document v4.1. Brussels: 2021.

[3] ASHRAE. Core Recommendations for Reducing Airborne Infectious Aerosol Exposure 2021. https://www.ashrae.org/file library/technical resources/covid-19/core-recommendations-for-reducing-airborne-infectious-aerosol-exposure.pdf.

[4] RKI. Alle Daten und Empfehlungen des RKI www.rki.de/covid-19.

[5] Bu Y, Ooka R, Kikumoto H, Oh W. Recent

research on expiratory particles in respiratory viral infection and control strategies: A review. Sustain Cities Soc 2021;73:103106.
[6] Agarwal N, Meena CS, Raj BP, Saini L, Kumar A, Gopalakrishnan N, et al. Indoor air quality improvement in COVID-19 pandemic: Review. Sustain Cities Soc 2021;70:102942.
[7] Zivelonghi A, Lai M. Mitigating aerosol infection risk in school buildings: the role of natural ventilation, volume, occupancy and CO2 monitoring. Build Environ 2021;204:108139.
[8] Riley EC, Murphy G, Riley RL. Airborne spread of measles in a suburban elementary school. Am J Epidemiol 1978;107:421–32.
[9] Wells WF. Airborne Contagion and Air Hygiene. Cambridge MA: Cambridge University Press; 1955.
[10] Sze To GN, Chao CYH. Review and comparison between the Wells-Riley and dose-response approaches to risk assessment of infectious respiratory diseases. Indoor Air 2010;20:2–16.
[11] Zhang S, Lin Z. Dilution-based evaluation of airborne infection risk - Thorough expansion of Wells-Riley model. Build Environ 2021;194:107674.
[12] Escombe AR, Oeser CC, Gilman RH, Navincopa M, Ticona E, Pan W, et al. Natural ventilation for the prevention of airborne contagion. PLoS Med 2007;4:0309–17.
[13] Kriegel M, Buchholz U, Gastmeier P, Bischoff P, Abdelgawad I, Hartmann A. Predicted infection risk for aerosol transmission of sars-COV-2. MedRxiv 2020:2020.10.08.20209106. https://doi.org/10.1101/2020.10.08.20209106.
[14] Sun C, Zhai Z. The efficacy of social distance and ventilation effectiveness in preventing COVID-19 transmission. Sustain Cities Soc 2020;62:102390.
[15] Srivastava S, Zhao X, Manay A, Chen Q. Effective ventilation and air disinfection system for reducing coronavirus disease 2019 (COVID-19) infection risk in office buildings. Sustain Cities Soc 2021;75:103408.
[16] Foster A, Kinzel M. Estimating COVID-19 exposure in a classroom setting: A comparison between mathematical and numerical models. Phys Fluids 2021;33.
[17] Khankari K. Analysis of spread of airborne contaminants and risk of infection. ASHRAE J 2021;63:14–20.
[18] Buonanno G, Stabile L, Morawska L. Estimation of airborne viral emission: Quanta emission rate of SARS-CoV-2 for infection risk assessment. Environ Int 2020;141:105794.
[19] Shen J, Kong M, Dong B, Birnkrant MJ, Zhang J. A systematic approach to estimating the effectiveness of multi-scale IAQ strategies for reducing the risk of airborne infection of SARS-CoV-2. Build Environ 2021;200:107926.
[20] Miller SL, Nazaroff WW, Jimenez JL, Boerstra A, Buonanno G, Dancer SJ, et al. Transmission of SARS-CoV-2 by inhalation of respiratory aerosol in the Skagit Valley Chorale superspreading event. Indoor Air 2021;31:314–23.
[21] Hartmann A, Lange J, Rotheudt H, Kriegel M. Emission rate and particle size of bioaerosols during breathing , speaking and coughing. Preprint 2020:1–5.
[22] ASHRAE. ASHRAE Standard 62.1-2019 Ventilation for Acceptable Indoor Air Quality 2019.
[23] Persily A, Gorfain J. Analysis of Ventilation Data from the U.S. Environmental Protection Agency Building Assessment Survey and Evaluation (BASE) Study. 2004.
[24] Zhang J. Integrating IAQ control strategies to reduce the risk of asymptomatic SARS CoV-2 infections in classrooms and open plan offices. Sci Technol Built Environ 2020;26:1013–8.
[25] U.S. EPA. Guide to Air Cleaners in the Home. 2018.
[26] ASHRAE. ASHRAE Handbook - HVAC Applications. 2019.
[27] Dugdale CM, Walensky RP. Filtration Efficiency, Effectiveness, and Availability of N95 Face Masks for COVID-19 Prevention. JAMA Intern Med 2020;180:1612.
[28] Kriegel M, Hartmann A, Buchholz U, Seifried J, Baumgarte S, Gastmeier P. SARS-CoV-2 Aerosol Transmission Indoors: A Closer Look at Viral Load, Infectivity, the Effectiveness of Preventive Measures and a Simple Approach for Practical Recommendations. Int J Environ Res Public Health 2021;19:220.

Parametric Modelling Using the Operative Temperature Map for Façade Design of Office Buildings

Yu Chen Lin [a], *Yaw Shyan Tsay* [b]

[a] Department of Architecture, National Cheng Kung University, Tainan, Taiwan, e74036085@gs.ncku.edu.tw.

[b] Department of Architecture, National Cheng Kung University, Tainan, Taiwan, tsayys@mail.ncku.edu.tw.

Abstract. Controlling incoming solar radiation to a building is one of the main targets of sustainable architecture designers because it decreases HVAC energy consumption and maximizes thermal comfort and usable daylight. The introduction of parametric design has allowed designers to expand their approaches to explore possibilities in façade forms and systems. However, most solar shading designs with complex geometries have been rejected by such building performance simulation software as *Energyplus* when assessing the calculation of thermal loads.

To overcome this limitation, this research introduced a new framework using the Rhinoceros platform to simulate radiant discomfort across spaces with various types of parametric façades. The framework was established based on the ASHRAE55 appendix and improved the longwave MRT calculation by using the Radiance-based pre-processing method. The use of an operative temperature (OT) map was then highlighted as a measure of the combined effect of mean radiant and air temperatures considering the conditions of air velocity and relative humidity in office layouts. Designers were able to compare the hourly intensity of solar radiation passing through a façade between different design cases. Furthermore, the metric of Annual Thermal Discomfort Hours (ATDHs) and the Spatial Thermal Comfort Availability (sTCA) index were proposed for assessing the effect of solar radiation throughout a space. These dynamic indexes were adopted to evaluate different scenarios using the local climate thermal comfort statistics. Eventually, the simulation framework was validated by a field experiment which showed a high accuracy by R^2=0.91. By the proposed study, designers can involve critical thermal sensation factors in the early design stage regardless of the complexity of the parametric facades.

Keywords. Indoor thermal comfort, solar radiation, subtropical.
DOI: https://doi.org/10.34641/clima.2022.301

1.Introduction

As an improvement to office building design in order to increase natural daylight, floor-to-ceiling glazing on the façade in office design is gaining favor with modern architects. However, with the warm subtropical climate in Taiwan, large openings create serious issues by admitting large amounts of solar, especially shortwave, radiation indoor [1]. The landing of uncontrolled solar radiation directly on occupants can lead to considerable indoor thermal discomfort that the HVAC system cannot handle. Therefore, in buildings with a high wall-to-window ratio (WWR), the critical assessment for thermal comfort is the daylit perimeter zone near the facades [2].

Radiant temperature is of great importance when assessing thermal comfort. Incoming solar radiation, which comes in the form of direct, diffuse, and reflected beams, is responsible for solar heat gains absorbed by building envelopes, as well as localized temperature rise in the overly lit area, consequently leading to an increase of the mean radiant temperature (MRT). The occupants are thus forced to deploy additional shading; otherwise, the thermal perceptions may change beyond the acceptable range. Due to a lack of simulation methods and standards, not until recently did the ASHRAE55-2017 adopt the Solar Calculation Method based on Arens's study [3], which was then implemented in Ladybug Comfort Component [4] to provide a parametric module for designers.

External shadings attaching to the façade can simultaneously shade the solar radiation and improve a building's energy efficiency, while still maintaining a high level of architectural and aesthetic quality [5]. Thus, designers in Taiwan embrace double skin façade such as perforated metal

Copyright ©2022 by the authors. This conference paper is published under a CC-BY-4.0 license.

board, louvers and expanded metal lathes. On top of that, parametric software that acts as a graphical algorithm editor and allows designers to generate parametric forms has also been introduced and has been used to combine different dimensions and proportions with building performance simulation plugins [6]. However, when encountering complex forms, designers need to conduct considerable simulation work and often fail to import a model that restricts the function and accuracy of the simulation results.

In this research, a new simulation framework is illustrated based on the Rhinoceros-Grasshopper platform to expand the possibility of the simulation process when encounter complex double skin façade geometries.

2.Method

2.1 Simulation Framework

In this section, the workflow (**Error! Reference source not found.**) is presented to introduce the Diva plugins into the calculation of adjusted MRT (ΔMRT) and explain how to post-process the results to assess the thermal comfort index using spatial distribution and a climate-based adaption model.

We first defined complex façade geometries and chosen location, which were later transformed by the presented pre-processor. Consequently, the performance of the facade on MRT was calculated using the *SOLcal* model and *EnergyPlus* heat balance method, which generate both the effect of shortwave and longwave solar radiation. Finally, the results presented in operative temperature (OT) were processed into dynamic indexes to assess thermal comfort.

2.2 Description of the test case scenario

The model replicates a single-room office space located in Taipei (latitude 25.1054°N, longitude 121.5973°E). A reference model measuring 15 m×10 m and 4m in height was modelled using Rhinoceros-Grasshopper software, as shown in **Fig. 2**. The west wall was set as a floor-to-ceiling glaze since this study was focused on the solar radiation effect of

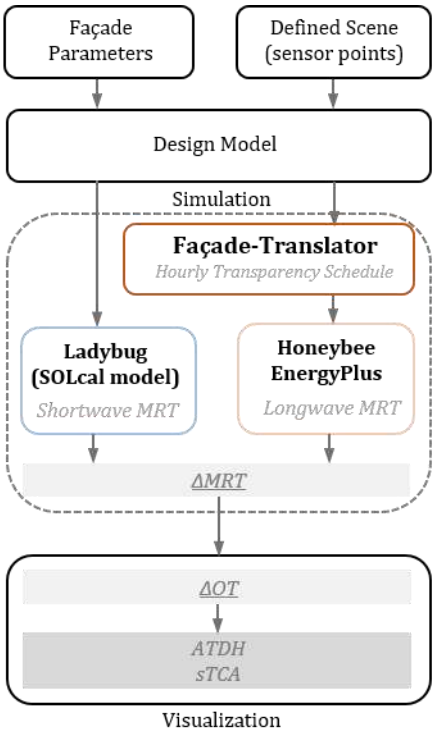

Fig. 1 - Simulation framework

façade design.

The target surface was set to 0.75 meter from the floor to represent the central point of the sitting human body. The lifted surface was a frame with a grid of 0.5× 0.5 m, which divided the space by human scale.

The thermal and radiative properties set for the elements are shown in **Error! Reference source not found.**. In order to guarantee a thermally neutral starting condition, an ideal HVAC was modelled with $T_{heating}$ = 23°C, $T_{cooling}$ = 26°C. All windows were assumed to be closed, and the infiltration rate was set to as low as 0.0001. According to office use, internal load density is defined as equipment (10W/m^2), lighting (20 W/m^2), and people (0.2 ple/m^2), considering working hours of 9:00 to 18:00. The hourly schedules for the internal heat sources were illustrated in **Fig. 3**.

2.3 pre-processor

In order to model the thermal performance of the

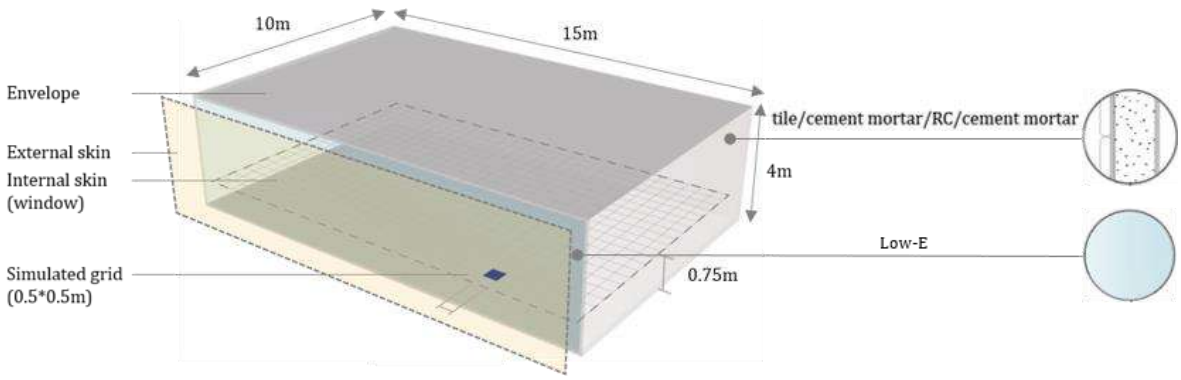

Fig. 2 - Description of the base model

Tab. 1 - Base model material properties

Element	description	Value/ properties
Exterior wall	Solar reflectance	0.5
	Material	adiabatic
Floor	Solar reflectance	0.2
	Material	adiabatic
Ceiling	Solar reflectance	0.8
	Material	adiabatic
Glaze	Solar reflectance	0.7
	Visible transmittance	0.542
	Solar heat gain coefficient	0.424
	Thermal transmittance(U-value)	1.81W/m^2
Façade shading	Solar reflectance	0.7
	Material	Hourly Transparency Schedule

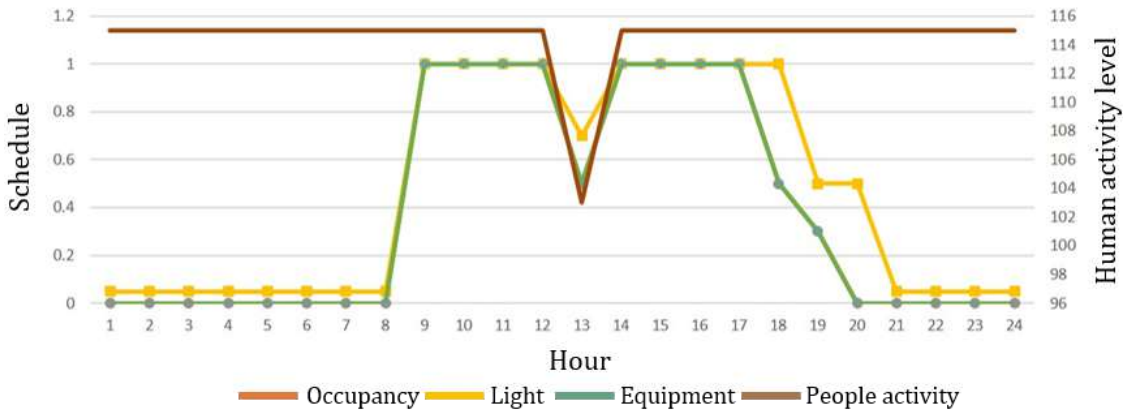

Fig. 3 - Occupancy Schedule

double skin façade, we developed a specific calculation process that coupled the advantages of Energyplus software with the potential of DIVA plugins concerning characterizing complex geometries with ray tracing methods. First, solar radiation was simulated using the TMY3 weather file (.EPW) on a vertical mesh attached to the glazed façade with 160 sensors arranged in the grid of 0.5 m × 0.5 m, as shown in **Fig. 4(a).** Secondly, the shading transparency coefficient was generated according to the ratio of the value of solar radiation with and without the portion of façade. The closer the coefficient value was set to 0, the more effective the thermal efficiency of the façade was (**Fig. 4(b)**). The annual radiation transparency schedule was then compiled into an hourly transparency schedule with 8760 value and connected to the HB_context module in the Honeybee plugins. The Honeybee plugins work as an interface to connect parametric design platform (Rhino-grasshopper) with Energyplus.

2.4 Solar-adjusted MRT calculation

This study applies the Solar Calculation model (SOLcal) developed by Arens in 2015 [3] to calculate the solar-adjusted MRT (ΔMRT). The radiation derived from the sun was split into direct, diffuse and reflected radiation and consequently translate into an effective radiant field and into ΔMRT.

Operative temperature aligned with ASHRAE55 and ISO standards is a modified temperature for the feeling of the thermal environment. It states that air velocity and relative humidity were assumed to be stable in air-conditioned spaces such as office buildings. Therefore, OT is chosen to be a reasonable indicator of thermal comfort indices that represent the effect of both air temperature and ΔMRT.

We use the "indoor micro-climate map" component in the Ladybug module [7] to calculated the ΔMRT

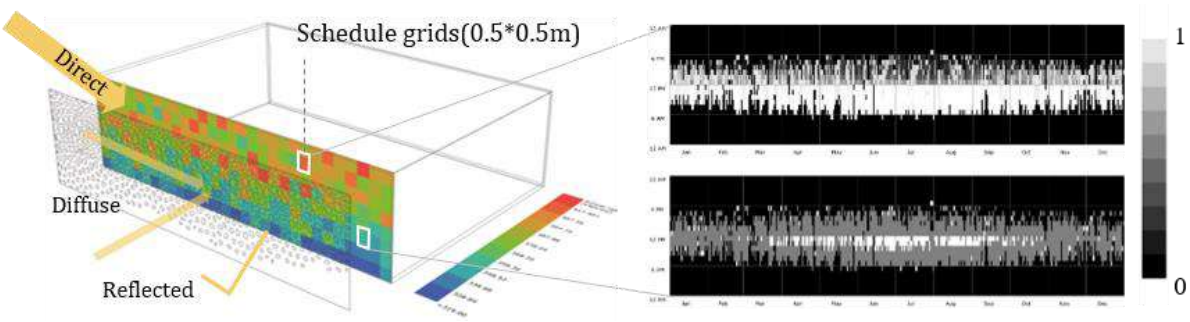

Fig. 4- Pre-processor:(a)schematic diagram of daylight transmission (b) hourly transparency schedule

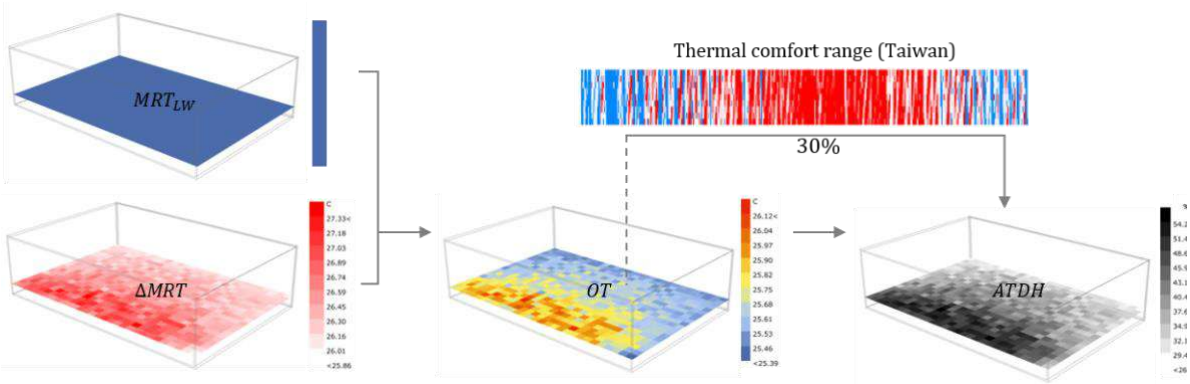

Fig. 5 - Detailed procedure of the OT and ATDHs map

based on the simulation framework described in paragraph 2.3. Significant variations of the distribution of the indoor OT were found according to the example façade pattern, as shown in **Fig. 5**

2.5 thermal comfort assessment

Adapted thermal comfort range varies depending on several essential factors, climate zones, race and gender, for instance. Accordingly, the acceptable thermal comfortable range was defined based on the field experiments, conducted in 29 air-conditioned offices with 650 individuals in Taiwan [8]. Responses from those subjects suggest a comfort temperature range of 23.8–27.5ºC that shifts to slightly warmer temperatures by about 0.5ºC as compared to the comfort zone recommended in ASHRAE standard 55 [9].

Performance metrics can be used for comparative studies to guide building design or to benchmark a building against a pool of other buildings. On top of that, dynamic metrics such as sDA and ASE include spatial and temporal consideration can better adopted by building certification systems.

The annual thermal discomfort hour (ATDH) was then developed as a dynamic index [10]. This metric can be described as the percentage of working hours that are above the acceptable thermal comfortable range. This comfort range indicates that occupants in Taiwan have adapted to the area's hot and humid climate. For acclimatized people, ATDHs can be applied as shown in equation (1).

$$\text{ATDH} = \frac{\sum_n (wf_i \times t_i)}{\sum_n t_i} \in [0,1]$$

$$\text{wfi} = \begin{cases} 1 & \text{if Cot} \notin [23.8 - 27.5°\text{C}] \\ 0 & \text{if Cot} \in [23.8 - 27.5°\text{C}] \end{cases} \quad (1)$$

where t_i is each occupied hour in a year, and C_{ot} is the hourly value of operative temperature for each point presented in the grid.

To assess the annual scenario between various façade design candidates, an example of the spatial map of ATDH is presented in **Error! Reference source not found.**(a). Without the influence of air velocity and relative humidity, indoor thermal indices were dominated by solar radiation, where the occupants near the façade were forced to apply extra

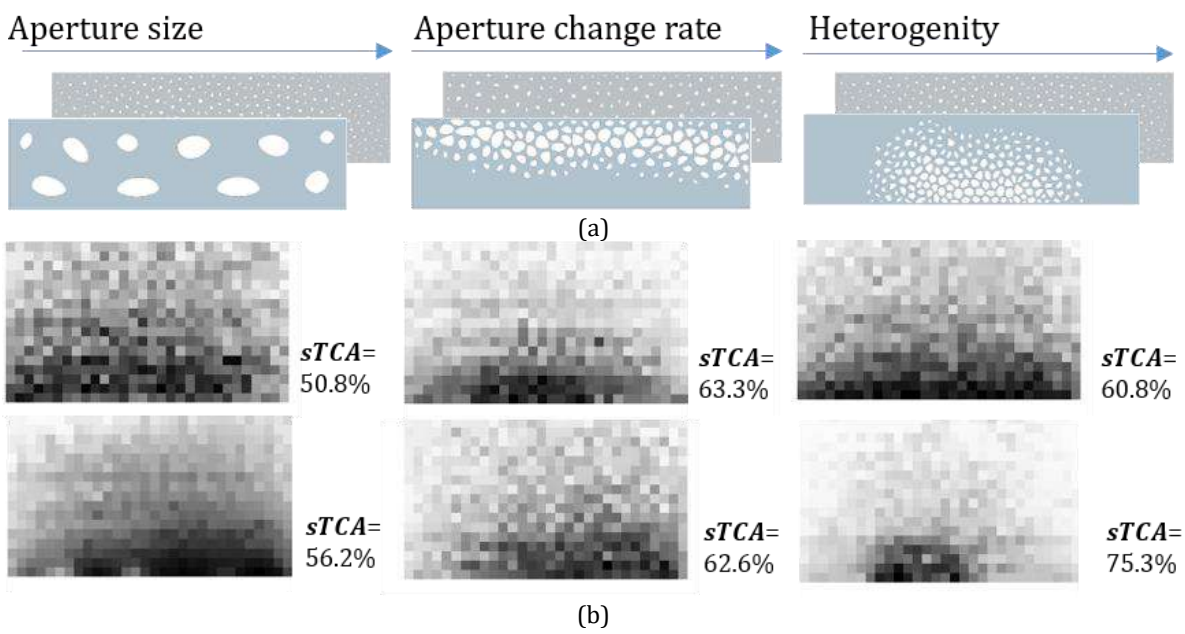

Fig. 6 - (a) The diversification of the Façade (b) Examples of indoor ATDHs distribution

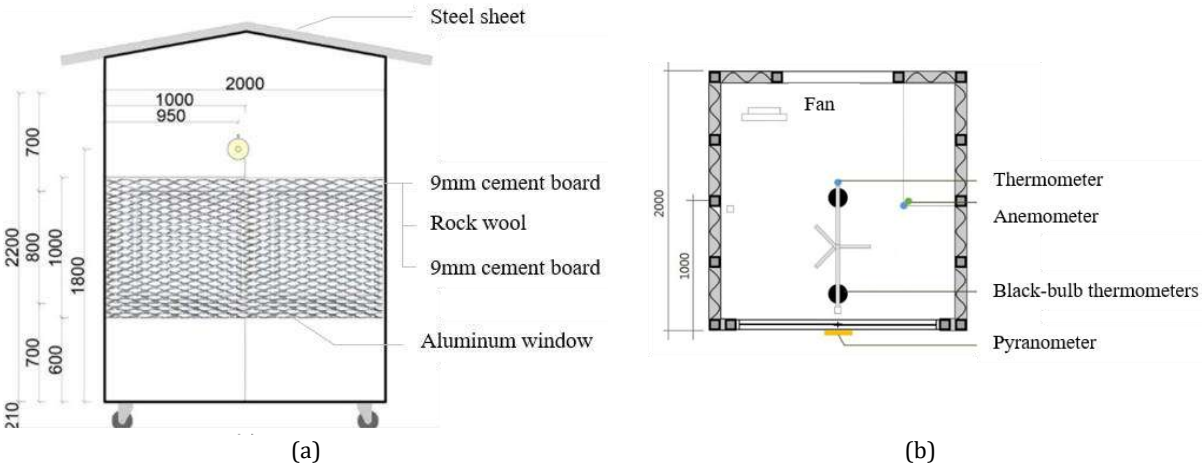

Fig. 7 - Field measurement configuration: (a)material and dimensions, (b)plan and equipment

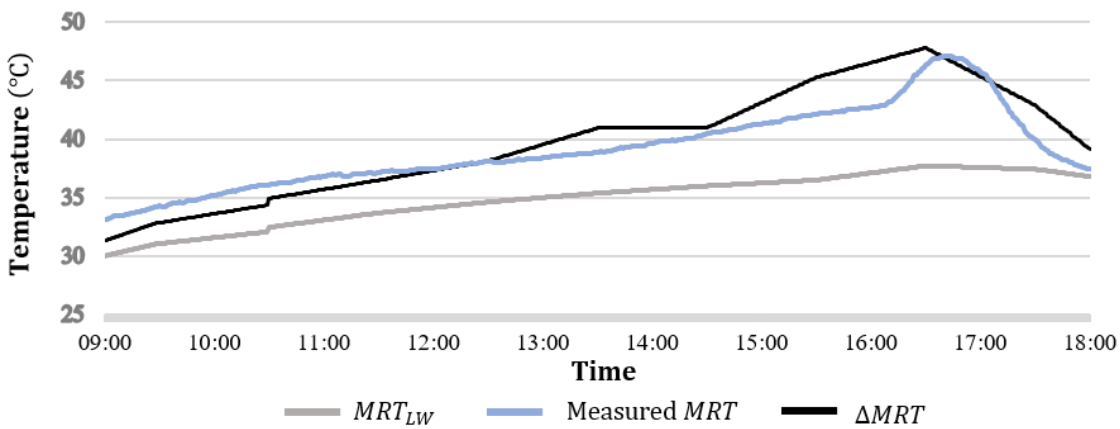

Fig. 8 - MRT comparison between field measurement and simulation

shading.

Furthermore, the results obtained with the thermal comfort range were compared by means of the long-term metrics -of Spatial Thermal Comfort Availability (sTCA) shown in equation (2). The sTCA expresses the partition of space with a threshold comfort range, which is 80% of perception according to a previous study [11]. This metric could significantly benefit architects and owners. Architects can use sTCA analysis to evaluate different design alternatives to determine which concept provides a better thermal environment in the interior, as shown in **Fig. 6**(b).

$$sTCA_{80} = \sum_{i}^{N} wfi \frac{1}{N} \in [0,1]$$

$$Wf_i = \begin{cases} 1 \text{ if } ATDHi < 10\% \\ 0 \text{ if } ATDHi > 10\% \end{cases} \quad (2)$$

3.Validation

3.1 validation of the simulation model

To verify the simulation framework, we conducted a field measurement at National Cheng Kung University, Tainan. An experimental house was constructed with the dimensions of 2 m×2 m×2.2 m. The only opening of the house is 1.9 m×1 m covered with an expanded aluminum mesh, and the orientation was set to the west. The perforated rate of the metal mesh was 70%. The MRT was measured through two black-bulb thermometers, two thermometers, and one anemometer, which were arranged as shown in Error! Reference source not found.. The time interval of data collection was ten minutes, and the experiments were carried out from 9:00 to 18:00 on October 10.

The simulation model replicated the experimental house and was tested using the proposed framework. The TMY3 data was replaced by measured data when the simulation was implemented.

Error! Reference source not found. shows the comparison of the measured results and the simulation outputs, with and without shortwave radiation. Both of the simulation results were in line with the increase of the MRT from 9:00 to 18:00. However, the black-bulb thermometer was affected by the direct radiation around 16:00, which caused a rapid increase in MRT value. The results of the proposed workflow were highly correlated to the measured value, with an R^2 value of 0.91.

4. Conclusions and Future Works

The results presented in the previous section prove the feasibility of the workflow. Parametric modelling façades were programmed in the Rhinoceros-Grasshopper platform, and the effectiveness of the double-skin facades were pre-processed into grids with an hourly transparency schedule, which overcame the limitation of Energyplus software when facing complex geometries. Furthermore, we established a thermal comfort model considering climate adaptation, which allows local designers to predict more applicable thermal sensations of the occupants across the room. Using an hourly operative temperature map and Annual Thermal Discomfort Hours distribution, early-stage performance evaluations are possible in combination with energy and daylight optimization by using parametric design.

The framework described in this paper opens up new research questions:

First, coupling the CFD simulation that introduces the impact of air flow may help to include the influence of wind velocity on thermal comfort in order to predict more realistic heat stress conditions.

Secondly, introducing such machine learning methods as random forest and artificial neural network with specific local data may reduce simulation time and accelerate the design process.

5. References

[1] Wong Nyuk Hien, Wang Liping, Aida Noplie Chandra, Anupama Rana Pandey, Wei Xiaolin. Effects of double glazed facade on energy consumption, thermal comfort and condensation for a typical office building in Singapore, Energy and Buildings, Volume 37, Issue 6,2005,Pages 563-572.

[2] Arens, Edward & Heinzerling, David & Paliaga, Gwelen. (2018). Sunlight and Indoor Thermal Comfort. ASHRAE Journal. 60. 12-21.

[3] Edward Arens, Tyler Hoyt, Xin Zhou, Li Huang, Hui Zhang, Stefano Schiavon. Modeling the comfort effects of short-wave solar radiation indoors, Building and Environment, Volume 88, 2015, Pages 3-9.

[4] Sadeghipour Roudsari, Mostapha; Pak, Michelle. "Ladybug: A Parametric Environmental Plugin for Grasshopper to Help Designers Create an Environmentally-Conscious Design." In Proceedings of the 13th International conference of Building Performance Simulation Association. Chambery, France, Aug 25-28 2013

[5] Amrita Ghosh, Subhasis Neogi. Effect of fenestration geometrical factors on building energy consumption and performance evaluation of a new external solar shading device in warm and humid climatic condition. Solar Energy, Volume 169,2018,Pages 94-104.

[6] Fang, Yuan. Optimization of Daylighting and Energy Performance Using Parametric Design, Simulation Modeling, and Genetic Algorithms." A dissertation submitted to the Graduate Faculty of North Carolina State University. San Francisco, USA, Spring , 2017.

[7] Sadeghipour Roudsari, Mostapha & Pak, M.. (2013). Ladybug: A parametric environmental plugin for grasshopper to help designers create an environmentally-conscious design. Proceedings of BS 2013: 13th Conference of the International Building Performance Simulation Association. 3128-3135.

[8] Hwang, Ruey-Lung & Cheng, Ming-Jen. Field Survey on Human Thermal Comfort Reports in Air-Conditioned Offices in Taiwan. The Open Construction and Building Technology Journal. 107. 8-13.

[9] ANSI/ASHRAE Standard 55-2017. Thermal environmental conditions for human occupancy. Atlanta, GA: American Society of Heating, Refrigeration and Air Conditioning Engineers, Inc., 2017. Parsons, KC

[10] Jorge Conejo-Fernández, Francesca Cappelletti, Andrea Gasparella. Including the effect of solar radiation in dynamic indoor thermal comfort indices, Renewable Energy, Volume 165, Part 1,2021,Pages 151-161.

[11] Zani, Andrea & Richardson, Henry & Tono, Alberto & Arens, Edward. (2019). Annual Radiation Discomfort: A New Climate-Based Framework For Modeling Short-Wave Solar Radiation In Indoor Spaces. 2426-2433.

Data Statement

Data sharing not applicable to this article as no datasets were generated or analysed during the current study.

MITIGATING THE HIGH RADON CONCENTRATION IN EXISTING HOMES

Ion-Costinel MAREŞ[1], Tiberiu CATALINA[1]

[1] Faculty of Engineering Installations, Technical University of Civil Engineering of Bucharest, Bucharest, Romania, maresioncostinel@gmail.com, tiberiu.catalina@gmail.com

Abstract. The article presents the experimental study of the efficiency of mitigating the high level of radon in existing homes using a centralized mechanical ventilation system with heat recovery. The measurements were performed both initially and after the installation of mechanical ventilation systems. The efficiency of reducing the radon level in the house was analysed, calculating the energy saved due to the heat recovery system compared to the conventional one (natural ventilation). The study concludes with a cost-benefit analysis, which shows the payback period of the investment.

Keywords: Indoor air quality, Mitigation systems, Experimental campaign, Centralized ventilation, Heat recovery.
DOI: https://doi.org/10.34641/clima.2022.276

1. Introduction

The impact of the quality of the indoor environment on the occupants has been the subject of much research in various fields. Their purpose was unique, to create a healthy and safe indoor environment. Previous studies have identified numerous indicators of indoor environment quality: indoor air quality, thermal, visual and acoustic comfort.

Poor quality of the indoor environment has been shown to contribute to diseases, which for prolonged exposure, can even have a fatal effect (1). The accumulation of indoor pollutants leads to the appearance of the sick building syndrome. Many studies have shown the connections between indicators of the quality of the indoor environment and the health of its occupants (2, 3).

According to international organizations reports, the World Health Organization (WHO) and the International Atomic Energy Agency (IAEA), radon is considered the main source of human exposure to ionizing radiation due to its inhalation. WHO estimates that between 3 and 14% of lung cancer cases in a country are due to radon (4).

Radon (222Rn) is a naturally occurring radioactive gas from the decomposition of natural uranium present in the ground or rocks. In Eastern Europe, the radon problem is increasingly being researched, becoming a priority for both researchers and the general population (5, 6).

Burghele et al. conducted the first attempt to identify and map radon after performing a series of measurements carried out on soil and drinking water (7). The results of the study were represented in the following figure, laying the foundations of the radon map for updating the European radon map.

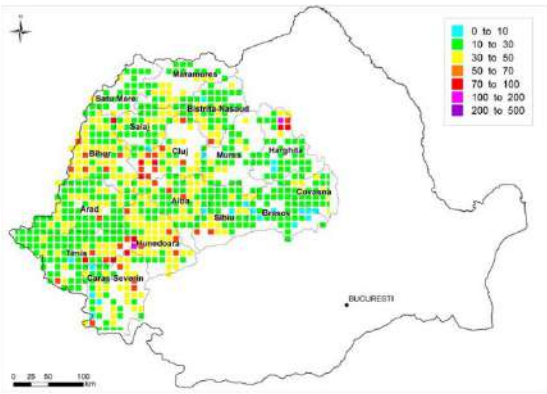

Figure 1 - Romania radon map (kBq/m^{-3} for soil gas)(7)

As we can see in figure 1, the values of radon in the soil vary between 0,2 kBq/m−3 and 179 kBq/m−3, being comparable to those reported for typical European soils (8).

2. International methods and analysis

In Romania, important steps have been taken in determining the effectiveness of methods for

Copyright ©2022 by the authors. This conference paper is published under a CC-BY-4.0 license.

reducing the level of radon in homes.

Cosma et al. have experimented with several techniques to mitigate the radon levels for a home in the northwest of the country. Active and passive sub-slab depressurization techniques with gas extractors and cellar ventilation were used. The results showed efficiency of remediation systems values up to 86% (9).

Burghele et al. analysed several methods to mitigate the radon level in homes, through experimental tests. They achieved radon mitigation efficiencies of up to 92% for the active sub-slab depressurization solution, combined with a decentralized ventilation system (10).

Istrate et al. analysed two similar classrooms, from a high school in Bucharest, demonstrating the importance of achieving mechanical ventilation of spaces. The results showed that in the mechanically ventilated room, radon and VOC concentrations decreased 7-8 times compared to the naturally ventilated room (11).

(Vázquez et al. 2011) performed a series of simulations on a pilot house, based on the principles of basement depressurization through collectors. They obtained very good remedial efficiency values (12).

The problems caused by radon have been carefully debated through numerous studies (13, 14) each of them focusing on radon level remediation. Some of these studies are neglecting the energy efficiency of the home, the costs for implementing the remediation system, the thermal comfort in the dwelling and other secondary benefits of using the remediation system.

The house is located in the western part of the country, an area with a strong potential for radon in the soil (15, 16). It is a detached house consisting of 3 bedrooms, 2 living rooms, two cellars, kitchen, hall and two bathrooms. It is a construction made of masonry of brick walls, covered on the outside with expanded polystyrene 50 mm thick, the exterior carpentry is made of PVC with double glazing, with low air permeability.

Tunyagi et al. have developed a revolutionary system for measuring and controlling radon in homes capable of continuous monitoring for a series of indoor parameters (radon, VOCs, CO_2, CO, temperature, relative humidity). The equipment is connected to a server, being able to be access any measurement information at any time (real time or period export). All the data regarding previous mentioned parameters, figured in this article, has been measured using this smart equipment (17, 18).

3. Measuring campaign - initial conditions

To find out the preliminary diagnosis of radon, two smart equipment (described above) were installed for monitoring and controlling the radon level, which would serve both sectors (TM01, respectively TM167) of the house. The daily evolution of radon was monitored for 3 months in the cold season, obtaining an average value of approximately 365,5 Bq/m3 (for TM01), respectively 402,5 Bq/m3 (for TM167), values that exceed the threshold imposed by European directives (19).

Even before the installation of equipment for continuous monitoring of radon levels, some preliminary measurements were made to determine the potential of radon. Starting from that point, the occupants of the house became aware of the danger they are exposed to and tried to remedy it through natural ventilation. As we can see in the figure 2 and figure 3, despite attempts to ensure natural ventilation, the limit of 300 Bq/m3 is frequently exceeded.

Figure 2 - Radon concentration 24.01.2019 - 24.04.2019, TM167

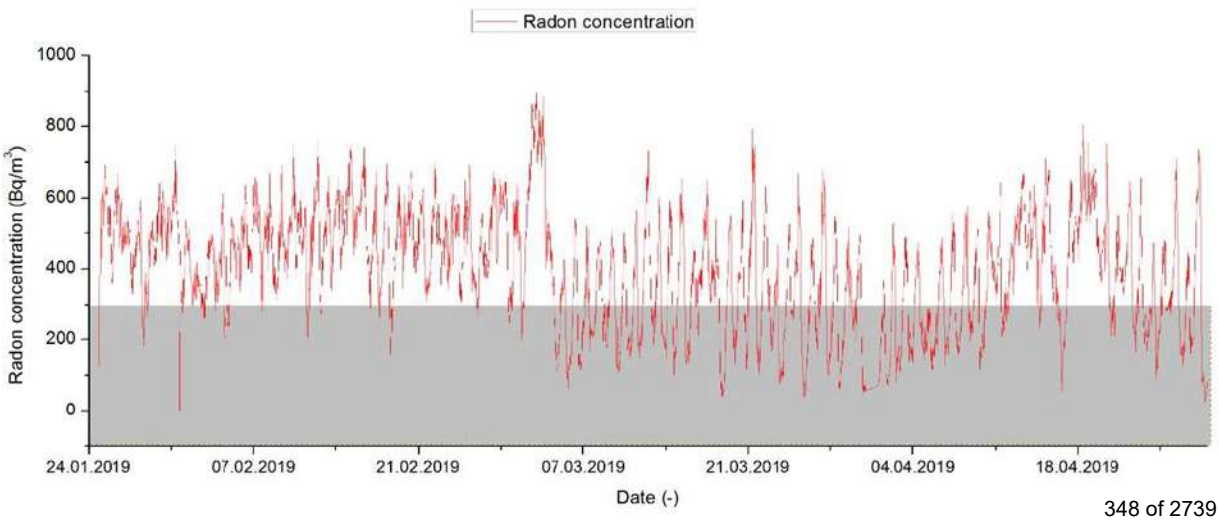

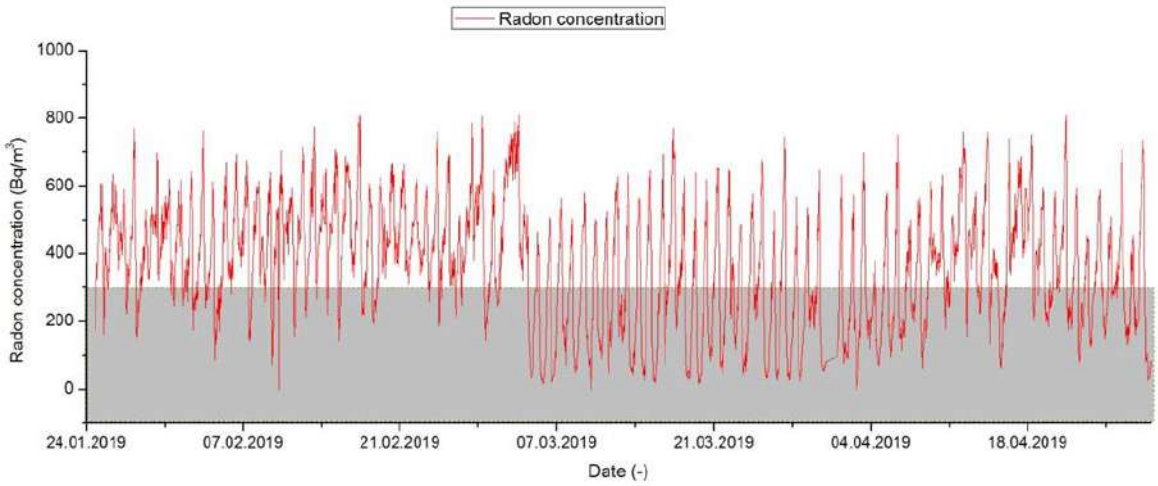

Figure 3 - Radon concentration 24.01.2019 - 24.04.2019, TM 01

Analysing the graphs presented above, can be observed the daily variation of radon due to the use of natural ventilation. This solution can be effective for short periods of time, not being a long-term option. On the other hand, this habit of natural ventilation of the spaces can also affect the level of indoor temperature and relative humidity.

4. Mitigation method and results

The mitigation solution chosen was to install two mechanical ventilation plants, which will serve each part of the house. This equipment has an introduction flow of 150 m3/h, respectively 350 m3/h realizing a good ventilation of the whole house. These ventilation plants are equipped with heat recuperators that positively impact energy consumption, limiting unnecessary losses due to natural ventilation.

The results of the implementation of the ventilation system were remarkably, remedying both the problem due to the high level of radon in the house, and the problems caused by the presence of other pollutants and temperature differences.

As can be noticed in figure 4, the radon concentration level has improved considerably, stabilizing around 165,5 Bq/m3, remaining below the maximum allowed limits, with occasional exceedances.

In the other part of the house, operating at nominal parameters of the equipment for mechanical ventilation, the radon level is maintained at values below the maximum allowed limit. The average value remains below the maximum limit, being approximately 219 Bq/m3, which indicates that this equipment has a good remedial efficiency. The peaks recorded for short periods of time highlight the moments when the centralized mechanical ventilation equipment with heat recovery did not work for various reasons.

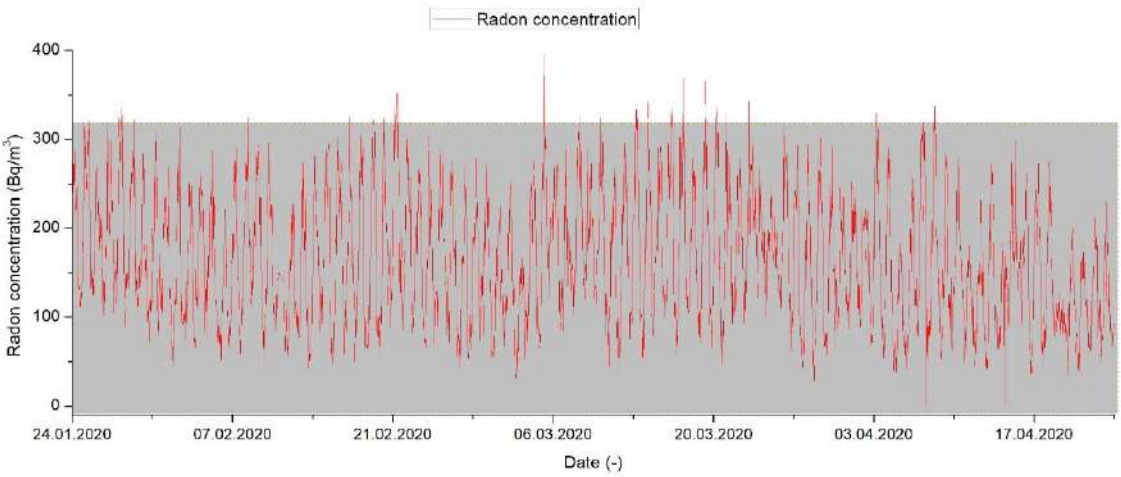

Figure 4 - Radon concentration 24.01.2020 - 24.04.2020, TM01 (after mitigation)

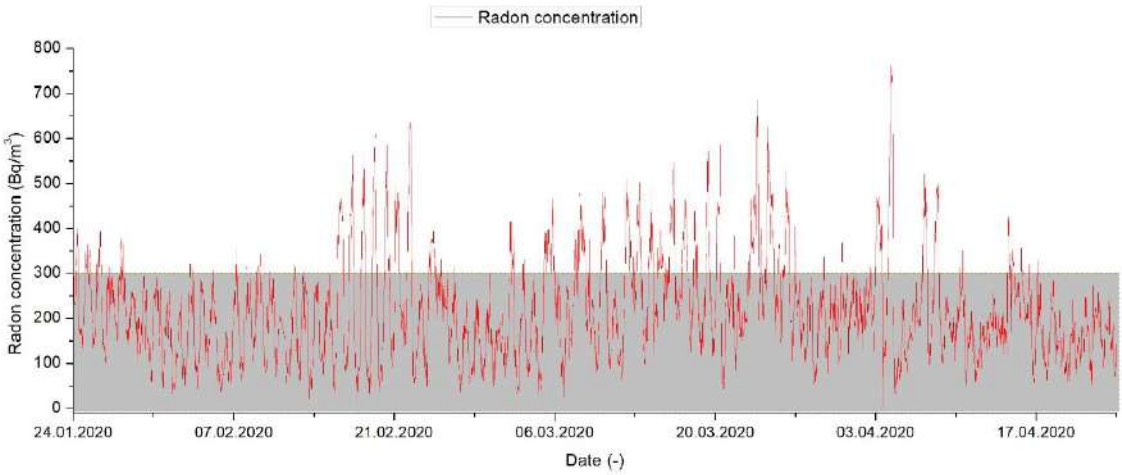

Figure 5 - Radon concentration 25.01.2020 - 01.02.2020, TM167 (after mitigation)

As we can see in figure 4 and figure 5, operating at nominal parameters of the equipment for mechanical ventilation, the radon level is maintained at values below the maximum allowed limit. The average value remains below the maximum limit, being approximately 219 Bq/m3, which indicates that this equipment has a good remedial efficiency. The peaks recorded for short periods of time highlight the moments when the centralized mechanical ventilation equipment with heat recovery did not work for various reasons.

5. Numerical simulation

In order to determine the thermal loads necessary to maintain an optimal indoor thermal comfort, a simulation was performed by a numerical simulation program, reproducing the normal conditions, respecting the specifications of the thermal comfort standards (20).

Figure 6 - Points of view for the analysed house

The simulation provided the real conditions to maximize the correctness of the results obtained. Thus, the data used for the simulation are:

- Construction materials;
- The heating system consists of a natural gas thermal power plant, with an efficiency of 80%;
- The same system was used to prepare domestic hot water;
- A model was established considering only the natural infiltration with a rate of 0.1 air changes per hour;
- The efficiency of the heat recuperator was considered 70%.

To establish the thermal loads for each scenario, a series of simulations presented below were performed:

The first simulation was performed considering only the infiltration rate, not considering any kind of ventilation in the analysed house. As presented above, the lack of ventilation of indoor spaces damages the quality of indoor air. Following the first set of simulations, the thermal load presented in the graph below was obtained through the black line, being able to make the comparison between the scenario in which the house is naturally ventilated and the scenario when the house is not ventilated at all. Significant differences can be observed, which impact the costs of heating the house.

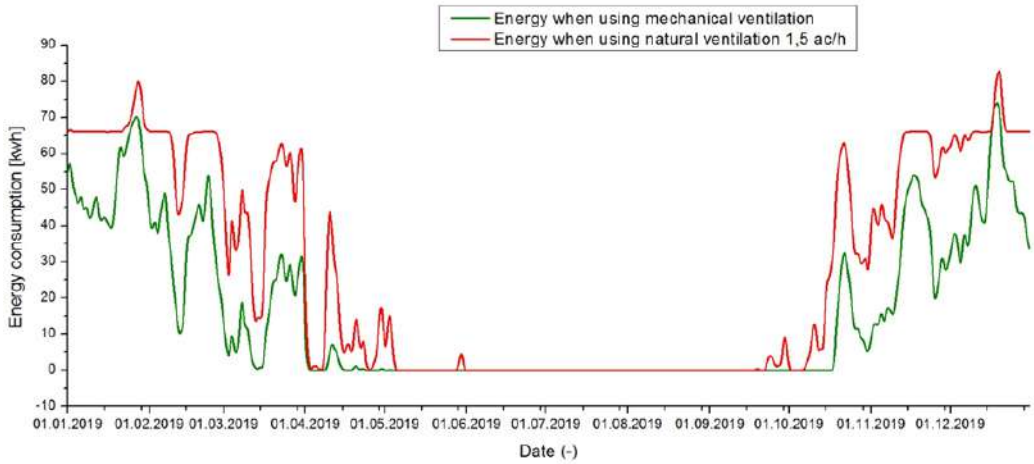

Figure 7 - Energy consumption 01.01.2019 - 31.12.2019

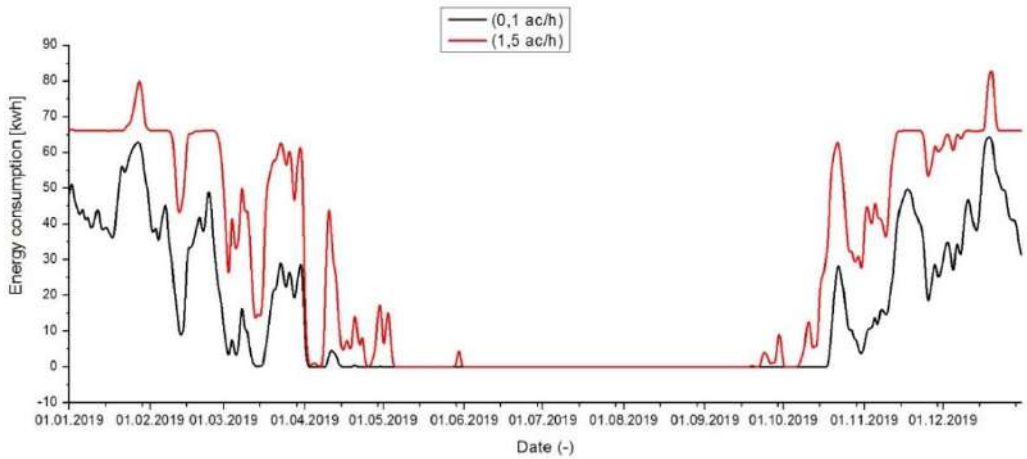

Figure 8 – Energy consumption comparison (01.01.2019 – 31.12.2019)

Considering this problem, an energy simulation was performed using centralized mechanical ventilation to remedy the increased radon level in the analysed home.

The graph presented in figure 7 shows the difference in heating thermal load when the house is naturally ventilated and the thermal load when the house is mechanically ventilated by a centralized mechanical ventilation equipment.

To determine the value of energy savings and cost savings following the implementation of the solution, the monthly gas consumption was exported from the design builder program, for a period of one year, when using both mechanical ventilation with heat recovery and natural ventilation. In the simulation, a gas thermal power plant with an average efficiency of 0.8 was used as heat source

Table 1 - Heating cost analysis

Costs	January	February	march	April	may	June	July	August	September	October	November	December	Total/ year
	€	€	€	€	€	€	€	€	€	€	€	€	€
Monthly fee (ventilation with heat recovery)	427	262	127	9	0,1	0	0	0	0	58	240	388	1509
Monthly fee (natural ventilation)	555	462	360	83	89	0	0	0	0	189	440	548	2647
Money savings/year													1137

6. Conclusions and discussions

Considering all the above, the problem of high levels of radon in homes can be solved by using centralized mechanical ventilation with heat recovery. This method brings multiple benefits, from reducing the level of indoor pollutants (including radon), maintaining the indoor temperature at a constant level, maintaining relative humidity at normal values. All these benefits can be obtained with relatively low energy costs, compared to the use of conventional methods as natural ventilation. The above calculation highlights how the costs, generated by the purchase and installation of equipment to remedy the high level of radon, will be amortized in a short time, compared to the costs of natural ventilation.

7. Acknowledgement

The study is part of the project called Smart Systems for Public Safety through Control and Mitigation of Residential Radon linked with Energy Efficiency Optimization of Buildings in Romanian Major Urban Agglomerations SMART-RAD-EN.

The datasets generated during and/or analysed during the current study are available in the SmartRADON repository, http://app.smartradon.ro.

References

1. Organization WH. WHO guidelines for indoor air quality: selected pollutants. 2010.
2. Chan IY, Liu AM. Effects of neighborhood building density, height, greenspace, and cleanliness on indoor environment and health of building occupants. Building and Environment. 2018;145:213-22.
3. Megahed NA, Ghoneim EM. Indoor Air Quality: Rethinking rules of building design strategies in post-pandemic architecture. Environmental Research. 2021;193:110471.
4. Organization WH. WHO handbook on indoor radon: a public health perspective: World Health Organization; 2009.
5. Cucoş A, Dicu T, Cosma C. Indoor radon exposure in energy-efficient houses from Romania. Rom J Phys. 2015;60(9–10):1574-80.
6. Mareș I-C, Catalina T, Istrate M-A, Cucoș A, Dicu T, Burghele BD, et al. Research on Best Solution for Improving Indoor Air Quality and Reducing Energy Consumption in a High-Risk Radon Dwelling from Romania. International Journal of Environmental Research and Public Health. 2021;18(23):12482.
7. Burghele B, Ţenter A, Cucoş A, Dicu T, Moldovan M, Papp B, et al. The FIRST large-scale mapping of radon concentration in soil gas and water in Romania. Science of the Total Environment. 2019;669:887-92.
8. Beaubien S, Ciotoli G, Lombardi S. Carbon dioxide and radon gas hazard in the Alban Hills area (central Italy). Journal of Volcanology and Geothermal Research. 2003;123(1-2):63-80.
9. Cosma C, Papp B, Cucoş A, Sainz C. Testing radon mitigation techniques in a pilot house from Băiţa-Ştei radon prone area (Romania). Journal of environmental radioactivity. 2015;140:141-7.
10. Burghele B, Botoș M, Beldean-Galea S, Cucoș A, Catalina T, Dicu T, et al. Comprehensive survey on radon mitigation and indoor air quality in energy efficient buildings from Romania. Science of The Total Environment. 2021;751:141858.
11. Istrate M-A, Catalina T, Cucos A, Dicu T. Experimental measurements of VOC and Radon in two Romanian classrooms. Energy procedia. 2016;85:288-94.
12. Vázquez BF, Adán MO, Poncela LSQ, Fernandez CS, Merino IF. Experimental study of effectiveness of four radon mitigation solutions, based on underground depressurization, tested in prototype housing built in a high radon area in Spain. Journal of environmental radioactivity. 2011;102(4):378-85.
13. Groves-Kirkby CJ, Denman AR, Phillips PS, Tornberg R, Woolridge AC, Crockett RG. Domestic radon remediation of UK dwellings by sub-slab depressurisation: evidence for a baseline contribution from constructional materials. Environment international. 2008;34(3):428-36.
14. Ashry A, Abou-Leila M, Abdalla A. Measurement of radon permeability through polyethylene membrane using scintillation detector. Radiation measurements. 2011;46(1):149-52.
15. Cosma C, Cucoș-Dinu A, Papp B, Begy R, Sainz C. Soil and building material as main sources of indoor radon in Băiţa-Ştei radon prone area (Romania). Journal of environmental radioactivity. 2013;116:174-9.
16. Cucoş A, Cosma C, Dicu T, Begy R, Moldovan M, Papp B, et al. Thorough investigations on indoor radon in Băiţa radon-prone area (Romania). Science of the total environment. 2012;431:78-83.
17. Tunyagi A, Dicu T, Cucos A, Burghele B, Dobrei G, Lupulescu A, et al. An innovative system for monitoring radon and indoor air quality. 2020.
18. Tunyagi A, Dicu T, Szacsvai K, Papp B, Dobrei G, Sainz Fernández C, et al. Automatic system for continuous monitoring of indoor air quality and remote data transmission under SMART_RAD_EN project. 2017.
19. COUNCIL DIRECTIVE 2013/59/EURATOM, (2013).
20. De Dear RJ, Brager GS. Thermal comfort in naturally ventilated buildings: revisions to ASHRAE Standard 55. Energy and buildings. 2002;34(6):549-61.

Perceived and measured indoor environment in educational buildings

Tuomo Ojanen [a], Esa Nykänen [b], Teemu Vesanen [c]

VTT Technical Research Centre of Finland Ltd,
[a] tuomo.ojanen@vtt.fi, [b] esa.nykanen@vtt.fi, [c] teemu.vesanen@vtt.fi .

Abstract. In educational buildings there is strong variation of the user-caused loads on indoor air during the working days. The challenge is to energy efficiently maintain comfortable indoor environment allowing good working and learning conditions for the building users. The objective was to define the main factors having effect on the user experience of indoor environment and to evaluate what range of measured factors are found comfortable in different building user groups. Three educational buildings representing different grades and one day care center were studied at least for a one-year period to find the main factors affecting the perceived indoor environment comfort in these spaces. Altogether 30 selected spaces were monitored, and perceived comfort of the users was collected through a novel real-time feedback system. The users could give their feedback concerning the perceived thermal comfort, humidity, air freshness and cleanliness, odours, lighting, noise and capability to work and learn. The feedback was based on the targets presented in the classification of the indoor environment [1] using Likert-scales [2) in questions. Each feedback of the experienced indoor environment condition had the space and time identification for the comparison with the corresponding monitored values. All the four sites had modern building technology systems. Only a weak correlation could be found between measured temperatures and the primary goal, i.e. good learning and working conditions. However, stronger correlation was found with the lighting, noise/acoustics, air freshness and humidity. With the humidity levels, both too low and too high levels affected the comfort. The effect of the total VOC-level on the comfort depended on the case - only in the day care center it had a strong negative effect. One relevant finding was that there was no difference between the user comfort in a case with full time ventilation compared to a case where the ventilation that was shut down during unoccupied hours to save energy. This paper presents the analysed findings for the measured and feedback data for these cases.

Keywords. Indoor air quality, indoor environment, educational buildings, schools, ventilation, learning conditions, working conditions
DOI: https://doi.org/10.34641/clima.2022.386

1. Introduction

Indoor environment has strong effect on the perceived working and learning capability. Educational buildings are quite demanding in that connection while the internal loads and user demand may vary strongly depending on the occupational rate and user age and activities. Mere measurements can very seldom give reliable data about the user comfort. The user feedback information should be collected as real-time as possible. The question about indoor comfort can be reliably answered only about current situation, not that from the day or week before. The applied novel system collected momentary feedback data, which is unique compared to typical questionnaires. Each given feedback could be connected to the indoor conditions measured at the same time. These principles were applied in this study aiming to find out the factors for comfortable indoor environment conditions in educational buildings. The presented study and results are based on a project reported on 2021 [3]. The results are mainly valid for the studied sites, but some findings may have wider relevance when evaluating the correlation between user experience and indoor environment.

Copyright ©2022 by the authors. This conference paper is published under a CC-BY-4.0 license.

2. Monitored sites

Four buildings, three educational buildings and one day care center, located in Helsinki and Espoo cities in the southern coast of Finland were monitored. All the buildings were renovated during the recent years and they had modern HVAC -systems.

Altogether 30 room spaces, mainly class rooms, were monitored and the user feedback was collected from these spaces. The indoor conditions of these selected room spaces were monitored using the data from the existing HVAC -automation system, additional measurement set-ups and space user surveys. The sensors of the additional measurements were placed close to the occupation zone of the room spaces, which gives supplementary information about the indoor conditions. Tab. 1 represents the monitored sites, the age groups of the pupils and the number of the monitored room spaces in each site. There was one feedback device in each of the monitored space.

Tab. 1 – Monitored buildings.

Building code	Purpose	Ages and number of pupils	Monitored room spaces
#1	Secondary and high school	12-18 (900)	6
#2	Day care center	0–5 (150)	4
#3	Primary school	6–13 (390)	10
#4	Vocational school	15–19 (900)	10

Typical classrooms (from 4 – 10 from each site) were selected for this analysis. The indoor environment feedback system was used by the personnel and the school children. More than 2000 persons were able to give feedback about the indoor environment of the spaces.

At least one year measurement and feedback data was collected from these sites during years 2019 - 2020. There were some interruption periods in the use of the school sites due to Covid-19 epidemic, but sufficient data could be collected for the analysis.

3. Indoor condition measurements

The indoor environment conditions were monitored in each space that had the user comfort feedback system. The condition data was collected from the HVAC automation system and using additional sensors placed in the occupation zones of the studied spaces. Typical data measured for the HVAC system were: Indoor temperature, CO2 -content, ventilation inlet and outlet air flow rates and temperatures. Additional measurements were carried out to ensure proper indoor data from the occupation zones of the room spaces. These measurements, collecting data every 10 minutes, included: Air temperature and humidity, CO2 -content, total content of volatile compounds (tVOC), particle contents of the air in three size categories (PM 1.0, PM2.5 and PM10). In some sites the pressure difference over the building envelope was monitored.

4. Feedback system

The feedback system tablet terminals were placed in the selected room spaces. They all had the same set of questions and answering categories. The feedback could be given for all or only for selected questions. Typically the feedbacks were given before and after the 45 or 90 minute class period, representing the perceived indoor environment when entering the space and during the working period.

4.1 Feedback evaluation classes

The feedback system asked about how the respondent finds out the current

- Temperature
- Humidity
- Freshness
- Odours
- Cleanliness
- Lighting
- Acoustics and voices
- Capability to work and learn.

The answering was based on defined representative choices. In the analysis, each choice was given a number. The following tables present some typical choices for the answers.

Tab. 2 present the choices for thermal comfort. Level 0 corresponds to comfortable conditions, higher values to warmer and negative to chilly or cold conditions.

Tab. 3 present the choices for air freshness. Level 0 corresponds to still tolerable conditions (not fresh/ stuffy), higher values to better and fresh conditions, negative to stuffy conditions.

Tab. 4 present the choices for the experienced capability to work and learn. Level 0 corresponds to still tolerable conditions (not good/bad), higher values to better, negative to worse conditions.

The same systematic way all the answering choices were formed.

It is obvious that the user experience of working and learning ability depends on several factors apart from indoor environment. The general atmosphere while working and teaching, the level of activities, how many pupils and teachers occupy the space, etc. have effect on the feedback. In this limited study

these factors were not evaluated, and the feedback was compared with the measured indoor conditions.

Tab. 2 – Choices for the answers about thermal comfort.

Definition	Number
Hot	3
Warm	2
Slightly warm	1
Comfortable	0
Slightly chilly	-1
Chilly	-2
Cold	-3

Tab. 3 – Choices for the answers about air freshness.

Definition	Number
Fresh	2
Slightly fresh	1
Not fresh, not stuffy	0
Slightly stuffy	-1
Stuffy	-2

Tab. 4 – Choices for the answers about capability to work and learn.

Definition	Number
Good	2
Relatively good	1
Not good, not bad	0
Slightly bad	-1
Bad	-2

4.2 Real time feedback

Each feedback entry was attached to the exact entry time. This made it possible to link the given feedbacks with the monitored indoor environment conditions for the same time periods. The time interval for the measured data collection was typically 10 minutes. Each feedback could be connected to measured conditions during the last 10 minutes.

5. Analysis of the results

The measured and feedback data were combined to form correlations between different conditions and measurements. In the following only some of the clearest and most interesting findings are presented. Because the buildings were recently renovated, the HVAC systems performed quite well and, for example, the indoor temperature and CO2 -levels remained mainly close to the common comfort zone. Therefore, the perceived conditions very seldom had the utmost values and these correlations remained mostly quite weak.

The feedback level of each indoor environment factor was given a number corresponding to the level of comfort (Tables 2 - 4). The distributions of the feedback classes were formed and for each level of comfort the concurrent measured average values of different indoor environment factors could be solved. The correlations were formed using this data. For example, when the indoor conditions were experienced hot (perceived indoor temperature level = 3), the average of all the measured concurrent conditions could be solved. Each experienced condition level corresponds to certain concurrent average measured factors.

The presented results are preliminary. Proper statistic approach was not yet applied, partly due to the strong variation on the number of feedbacks for different factors.

5.1 Correlations between perceived conditions

Correlations between the different feedback conditions reveal how the different factors affect each other. In schools and offices one of the most important factor is the user experience about how well and effectively one can work and learn in such conditions. This feedback question gives the best overall number for the indoor environment quality.

The cross tabulation of the feedback results shows clear correlations between the *capability to work and learn* with the perceived *lighting* and *acoustics* conditions, and also some correlation with the *freshness* of the air. Tab. 5 present the correlations between the different factors of indoor environment derived from the feedback data.

Tab. 5 – Correlations between the different experienced conditions.

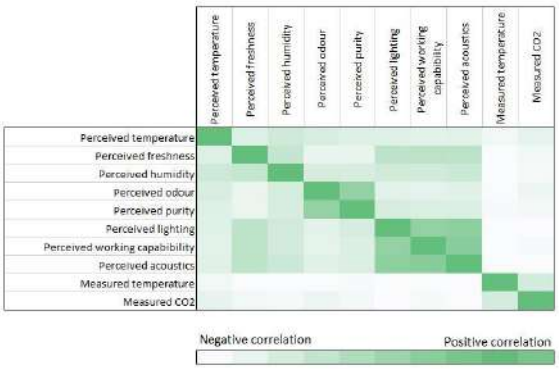

The recently renovated HVAC systems maintained relatively stabile and comfortable conditions throughout the monitored periods, which reduced the possibility to define the effect of wide range of conditions, for example with temperature and CO2 -contents clearly close or out of comfort boundaries.

5.2 Correlations between feedback and measurements

The age categories of the building users varied from building to building and, also the activities in the

buildings differed from each other. The main results from each building are presented separately.

Two measured values represent two measurement sites from the living space of each room. Typically one close to occupation zone and one close to air outlet device. This gives an idea of the distribution of the inside conditions.

School #1

The feedback for school #1 during the year 2019 was compared to the measured values and the main findings are presented in the following figures. Measurements are typically from two sites from the living space of each room to show the distribution of the inside conditions.

Fig. 1 present the dependency of the temperature and relative humidity levels on the experienced indoor temperature and Fig 2 presents the correlation between thermal comfort and indoor air enthalpy. Low increase in the average relative humidity and enthalpy level increased the feedback proportion in classes too warm or hot.

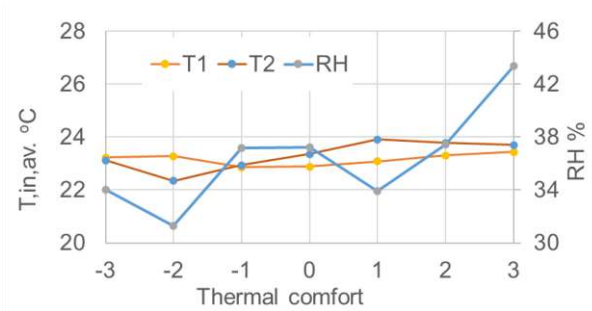

Fig. 1 – Dependency of the temperatures and relative humidity levels on the thermal comfort conditions in all the monitored spaces of the school #1 during 2019.

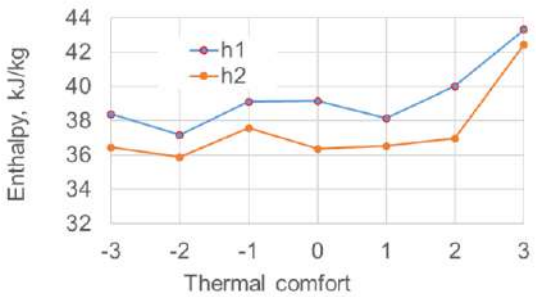

Fig. 2 – Dependency between the indoor air enthalpy and the thermal comfort conditions in all the monitored spaces of the school #1 during 2019.

Increased enthalpy level affected the experienced freshness of the indoor air (Fig. 3)). This is in line with the publications [4 and 5]. Also, higher CO2 -levels contributed to feeling of the stuffy air (Fig. 4). This correlation is most probably indirectly under these CO2-contents and it is related to other loads in the air.

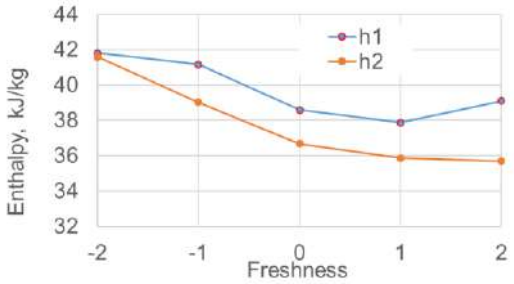

Fig. 3 – Dependency between the indoor air enthalpy and the user perceived freshness of indoor air of all the monitored spaces of the school #1 during 2019.

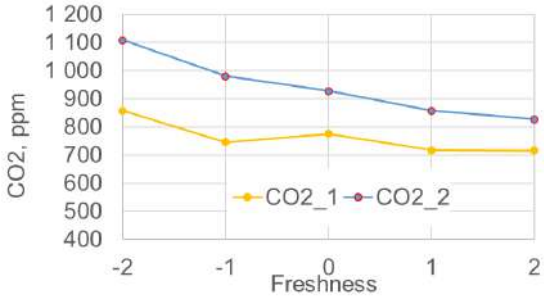

Fig. 4 – Dependency between the indoor air CO2 -content and the perceived freshness of indoor air of all the monitored spaces of the school #1 during 2019.

The correlations between *the ability to work and learn* with the measured factors of indoor air were not very clear. About 97 % of the feedbacks for the capability to work and learn (n=201) were in the level 'reasonable' or better (numbers 0 – 2). Due to marginal number of negative experiences, no good correlations could be found for this factor. Fig. 5 shows how the distribution of three factors - *the capability to work and learn, lighting and acoustics* – are almost identical.

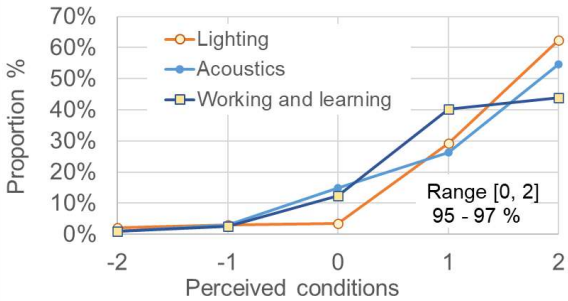

Fig. 5 – Distribution of the perceived conditions of lighting, acoustics and capability to work and learn in all the monitored spaces of the school #1 during 2019.

Day care center #2

The feedback was collected only from the personnel of the day care center. The feedback for the year 2020 was compared to the measured indoor environment values and the main findings are presented in the following figures.

The perceived thermal comfort was relatively sensitive to the indoor air enthalpy level (Fig. 6). The variation of enthalpy was mainly caused by the relative humidity.

The experienced capability to work depended on the indoor air CO2 -levels (Fig. 7). This most probably linked to other factors than only CO2-level that was on an average quite low. While the CO2-level refers to the occupation rate of the room space, some other factors may have affected the working capability when the room was more crowded. This is partly supported by the dependence on total VOC -content. The lowest experienced capability to work was found with the highest tVOC -levels (Fig. 8).

The experienced air freshness was clearly reduced with higher air enthalpy and CO2 -levels (Figs. 9 and 10)

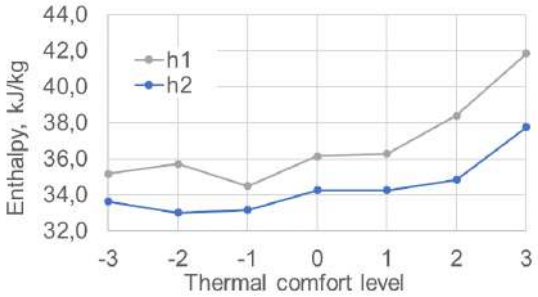

Fig. 6 – Dependency between the indoor air enthalpy and the thermal comfort conditions in all the monitored spaces.

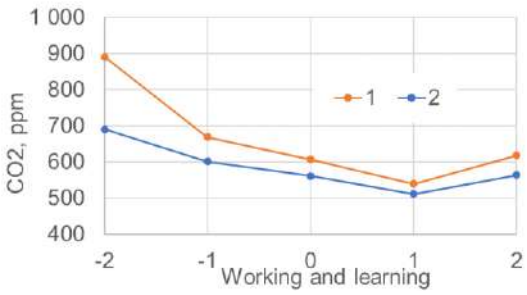

Fig. 7 – Dependency between the CO2 -content and the capability to work and learn in all the monitored spaces.

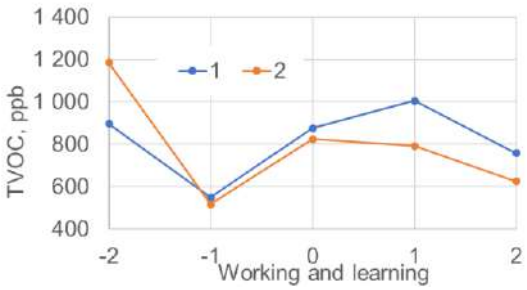

Fig. 8 – Dependency between the total VOC -content and the capability to work and learn in all the monitored spaces.

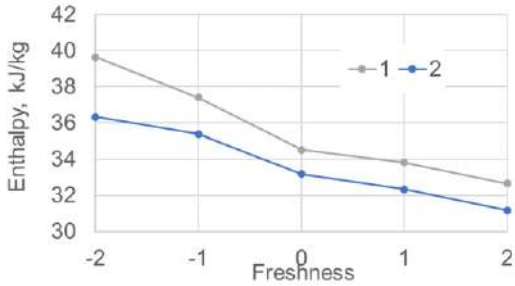

Fig. 9 – Dependency between the enthalpy level and the perceived freshness of indoor air.

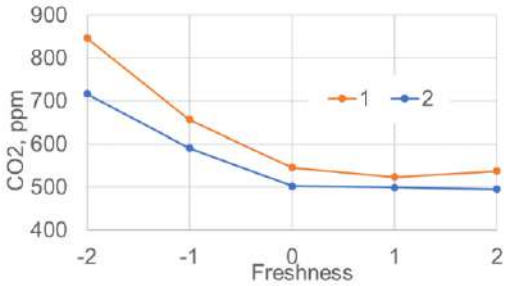

Fig. 10 – Dependency between the CO2 - level and the perceived freshness of indoor air.

Primary school #3

The following represents the comparison between the feedback and measured factors in a Primary school #3 during the year 2019 and partly during 2020. The feedback was collected both from the pupils and school personnel.

This school was a good example about well performing, adaptive HVAC -system. The feedback referred to relatively good conditions and it was distributed so that no clear correlations with indoor air conditions could be found. As examples, the dependency between thermal comfort (n = 4142) and indoor thermal measurements (T, RH, enthalpy) are presented in Fig. 11 and that between the experienced freshness (n=1993) and CO2-level in Fig. 12. In both figures the measured conditions varied in a very low range and apparently corresponded relatively well to comfortable indoor conditions.

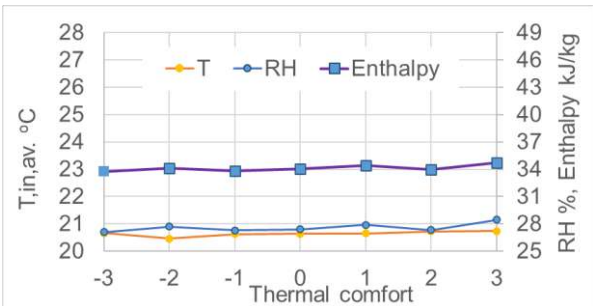

Fig. 11 – Dependency between the indoor air temperature, humidity and enthalpy levels with the thermal comfort conditions in the monitored spaces.

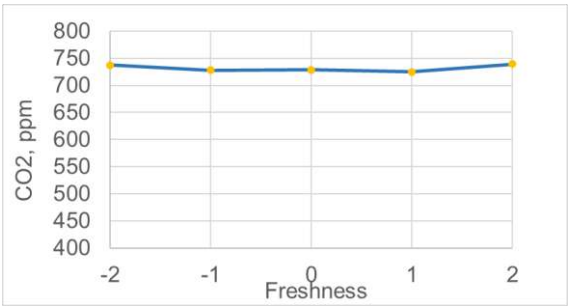

Fig. 12 – Dependency between the CO2 - level and the perceived freshness of indoor air.

Vocational school # 4

In the vocational school the results mostly corresponded to that with the Primary school #3, no clear correlations could be shown between the feedback and measured values. This was partly due to the relatively stabile indoor conditions.

Some interesting findings can be presented. The experienced capability to work and learn (82 % from feedbacks , n=147, found it satisfying or better) that has a positive dependence of total VOC content. This was quite the opposite that was expected or what was found in the day care center. Fig 13 presents the average results for all the monitored spaces and one space 144 meant for hair dressing practices. It seems that some VOCs were positively linked to learning and practicing in this school.

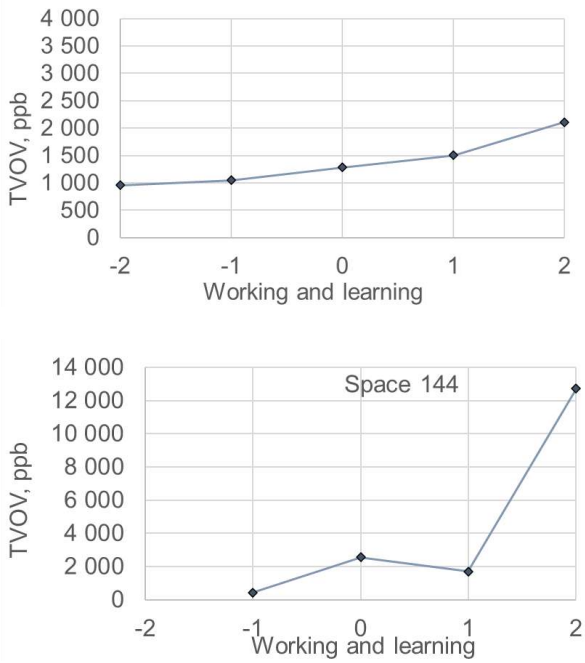

Fig. 13 – Unexpected dependence of working and learning capability with the total volatile compound contents. Above the average for all the monitored spaces and below the for the space for hair dressing practices.

The experienced working and learning capability had some negative correlation with the direct solar radiation measured in the in the weather station close to the site (Fig. 14). The building has large window areas facing south. The effect of solar radiation could not be clearly seen in thermal conditions, but maybe the solar radiation caused possible glare that affected the experienced working conditions.

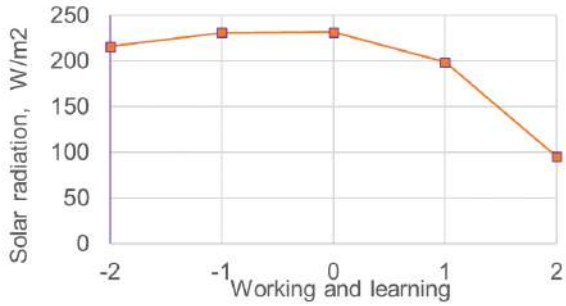

Fig. 14 – Dependence of working and learning capability with the direct solar radiation measured in the weather station close to the site.

5.2 Normal vs. full time ventilation

In all the sites during the occupation hours ventilation is controlled based on the CO2 -levels of the spaces. For energy saving purposes the ventilation is closed outside the occupation times and it is started two hours before the daily working begins.

By mistake, the ventilation in the Primary school #3 was used full time without interruptions (24/7) for a 16 days period (27.8.–12.9.2019). The users didn't know about this. This occurrence made it possible to compare how the different ventilation modes affected the user experience of the indoor climate.

The following results present the comparison of the feedback results between the full time (24/7) and typical intermittent ventilation schemes. The normal, intermittent ventilation periods were taken from both sides of the 24/7 ventilation period (6.–26.8. and 13.–30.9.2019).

The following figures (Figs. 15 – 19) present the comparison between indoor air user experience from the normal and 24/7 periods. The comparison is presented as a sum of the perceived level of satisfaction starting from the best experienced conditions on the left of the x-axis. The proportion level represent which portion of the feedbacks correspond to the experienced level on x-axis or are better than that.

For example, the perceived temperature (Fig. 15) was best possible (neutral, value 0) in case with normal ventilation scheme in about 30 % of the total number of feedbacks during to selected period. The conditions were acceptable (between -1, 1) in about 47 % of the feedbacks, meaning that about 53 % considered the indoor conditions to be too warm or cold. The distribution of all the other experienced conditions are presented in the same way in Figs. 16 – 19.

The difference between the experienced temperature condition in 24/7 and normal ventilation cases was very low.

The only difference between the cases was detected in the feedback levels of the cleanliness of the air (Fig. 17), where the normal ventilation scheme showed better (higher values in lower values indicating better cleanliness) user comfort than the 24/7 scheme. This difference remained inexplicable, but could be partly due to the low number of feedbacks for this question. The 11-step scale used in the cleanliness and odour feedbacks was not clear enough and caused some focus on the maximum value.

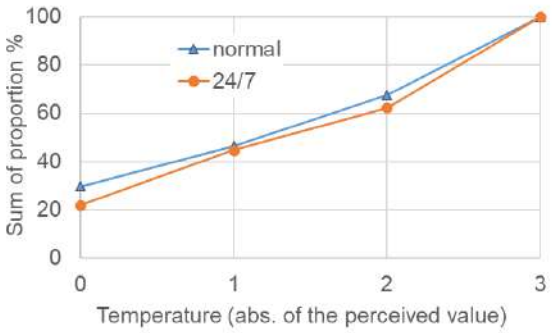

Fig. 15 - Distribution of the temperature feedbacks presented as a sum starting from the best conditions.

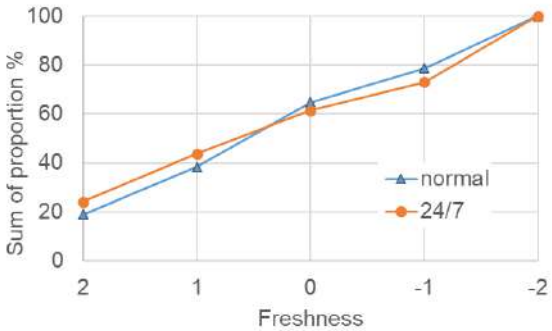

Fig. 16 - Distribution of the air freshness feedbacks presented as a sum starting from the best conditions.

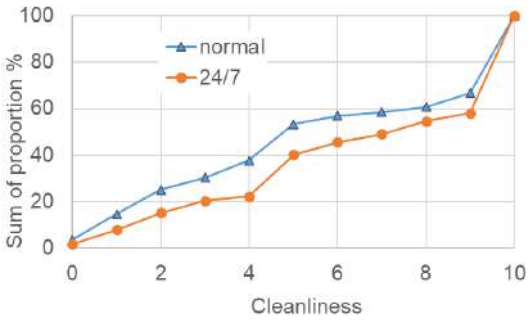

Fig. 17 - Distribution of the air cleanliness feedbacks presented as a sum starting from the best conditions.

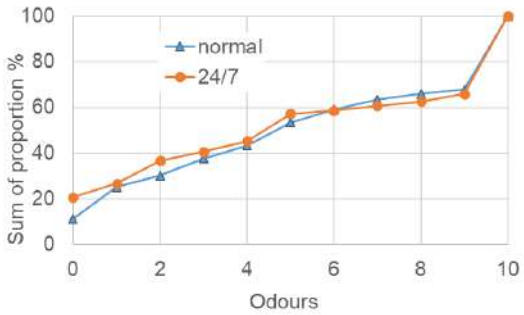

Fig. 18 - Distribution of the feedbacks about odours presented as a sum starting from the best conditions.

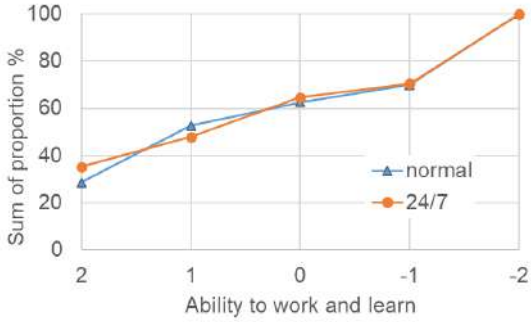

Fig. 19 - Distribution of the feedbacks about capability to work and learn presented as a sum starting from the best conditions.

6. Discussion and conclusion

The capability to work and learn is one of the main goals of user experience. This is emphasised in educational buildings, and the same criteria is applicable also in offices, homes and other buildings.

In this study three educational buildings representing different grades and one day care center were studied at least for a one-year period to find the main factors affecting the perceived indoor environment comfort. In total, the indoor conditions of 30 selected room spaces were monitored and the perceived comfort of the users was collected through a novel real-time feedback system. Each feedback could be connected to the right indoor conditions measured at the same space and at the same time range.

The selected buildings had been recently renovated HVAC -systems with adapting ventilation systems. Therefore, the utmost conditions of at least air temperature and CO2 -content, were missing and the analysis is based mainly on the conditions close to typically known comfort zones.

The results are mainly valid for the studied sites, but some findings may have wider relevance when evaluating the correlation between user experience and indoor environment.

The experienced feedback results showed clear correlations between the capability to work and learn with the perceived lighting and acoustics

conditions, and some correlation with the freshness of the air.

While the indoor temperature levels remained mostly in reasonable levels in the studied buildings, the thermal comfort depended mainly on the relative humidity levels. The correlation between thermal comfort and indoor air enthalpy (energy level combining temperature and relative humidity) level was even more clear. Typically, the thermal comfort was reasonable until some level of enthalpy, and with higher values the feeling of too warm condition increased clearly. This turning point value depended on the use of the building and the age and activity of the users. Compared to the comfort zones presented in ASHRAE [5 and 7] the comfort conditions in these buildings remained in the lower side of temperature and humidity. High indoor air enthalpy levels also affected the perceived air freshness.

The total VOC -levels didn't have much effect on the perceived air freshness. Even unexpected positive correlation between the capability to work and learn and the tVOC-levels were found, which partly reveals the uncertainty with respect to the interpretation of the total VOC -measurement results.

One important finding was that there were no difference in the experienced indoor conditions when comparing a case with full time ventilation with a typical case where the ventilation was shut down outside the working hours. This finding supports the energy efficient use of the ventilation system.

The applied methodology where the real-time feedback results are combined with the concurrent measured indoor data seems to be reliable when evaluating the factors having effect on the experienced indoor environment. Further studies with buildings having older technical systems, different user activities and separating the seasonal effects are needed to broaden the perspective for the factors of good indoor environment.

7. Acknowledgement

This work is based on the results from Indoor Air 2020 -project (Sisäilma-2020, 2019 -2020) that was funded by the Cities of Helsinki, Espoo and Vantaa and by VTT Technical Research Centre of Finland Ltd.

8. References

[1] RT 07-11299, Classification of Indoor environment 2018. Indoor environment target values, design guidelines and requirements for products (in Finnish). 24 p.

[2] Likert scale. https://en.wikipedia.org/wiki/Likert_scale

[3] Ojanen, T., Vesanen, T., Kannari, L., Piira, K., Nykänen, E., Tuomainen, M., Naumi, H., Lumme, T., Melender, M., Vene, E., Markkanen, P., Åberg, J. & Mattila, J., Indoor climate 2020: Factors for good indoor environment in schools and daycare centers (in Finnish) 2021, VTT Technical Research Centre of Finland. 137 p. (VTT Technology; No. 388).

[4] Fang, L., Clausen, G. and Fanger P.O. Impact of temperature and humidity on the perception of indoor air quality. *Indoor air 8*. 1998. pp. 80 – 90.

[5] Fang, L., Clausen, G. and Fanger P.O. Impact of temperature and humidity on chemical and sensory emissions from building materials. *Indoor air 9*. 1999. pp. 193 – 201.

[6] ANSI/ASHRAE Standard 55-2010. Thermal Environmental Conditions for Human Occupancy.

[7] Tartarini, F., Schiavon, S., Cheung, T., Hoyt, T., 2020. CBE Thermal Comfort Tool : online tool for thermal comfort calculations and visualizations. SoftwareX12,100563. https://doi.org/10.1016/j.softx.2020.100563

Research, standards, practice: Necessary conditions for occupant-centric indoor environments

Christiane Berger [a], Veselina Bochukova [b], Ardeshir Mahdavi [b]

[a] Department of Architecture, Design and Media Technology, Aalborg University, Aalborg, Denmark, chbe@create.aau.dk.

[b] Department of Building Physics and Building Ecology, TU Wien, Vienna, Austria, amahdavi@tuwien.ac.at, veselina.bochukova@tuwien.ac.at.

Abstract. The precise definition of appropriate indoor-environmental conditions for human occupancy is not trivial. Practitioners in the building delivery process frequently rely on applicable standards and guidelines to identify the relevant performance variables and their required values. In this context, recent inquiries have pointed out a number of gaps in our knowledge. Certain aspects of these gaps can be explored in terms of the following three basic questions: *i)* Are current codes/standards compliance processes limited to meeting formal criteria and minimum requirements, thereby losing sight of the essential task of producing high-quality indoor environments? *ii)* Do currently deployed standards entail a clear, transparent, and evidence-based logic underneath their recommended or mandated quality requirements? In other words, have the results of scientific research on indoor environment been adequately translated into the language of codes and standards? *iii)* What is the degree of precision and validity of the indoor-environmental research results? In other words, are we asking the right questions and using the right methods to answer them? To address these questions, the present contribution considers a number of common indoor-environmental quality standards pertaining to thermal and visual comfort, as well as indoor air quality. The outcome of this preliminary appraisal point to gaps in the chain of evidence from research to standards. The results also point to a number of areas in which the scientific research on indoor-environmental quality could benefit from a strategic rethinking of a number of its underlying methodological premises.

Keywords. Indoor-environmental quality, standards, evidence.
DOI: https://doi.org/10.34641/clima.2022.369

1. Introduction

Indoor-environmental quality (IEQ) standards and guidelines represent important sources of reference for those involved in the building delivery process. They are expected to represent the state of knowledge regarding building performance requirements, including those related to occupant needs. Performance criteria cover, at a basic level, elementary mandates relevant to occupants' health and comfort. Specifically, they define acceptability criteria for thermal, visual, acoustic, and air quality conditions in indoor environments. Note that the evaluation of what is assumed to be a healthy or comfortable environment is not a trivial matter. Particularly the perception of the comfort level of an environment involves a considerable number of subjective factors.

Aside their function as a source of knowledge and guidance for professionals, standards are also relevant with regard to accountability and compliance (quality assurance, liability) issues in the building delivery process [1]. But this does not mean that all content entailed in standards and guidelines must be assumed to be completely objective and entirely evidence-based. Rather, in the IEQ domain too, the scientific basis and technical validity of standard-based requirements must be regularly scrutinised, amended, and updated.

2. Requirements and rationale

The inquiry after the evidentiary basis of IEQ standards and guidelines is at times met with the following objection. Standards, we are told, are comparable with legal documents. As such, they do not need to provide a justification for the requirements entailed. Their justification is argued to be based on the circumstance that they have been developed and issued by a body of entrusted experts. We consider this claim an obvious instance of *argumentum ab auctoritate* and hence clearly fallacious.

It can be of course argued that standards and guidelines are primarily meant to guide professional in the relevant domain and as such must not explicitly

Copyright ©2022 by the authors. This conference paper is published under a CC-BY-4.0 license.

include their evidentiary basis in the respective contents. But it seems reasonable to expect that there would be a traceable and unbroken chain of reference from the standards' content to underlying supportive documents (e.g., technical publications, research reports).

In the specific case of standard-based IEQ mandates, a reasonable assumption would be that their scientific basis could be traced back to the findings of studies in fields such as biology, physiology, psychology, neuroscience, and ergonomics. However, a cursory look at most IEQ standards does not confirm this expectation. Rather, neither the standards nor the modes of their application appear to the evidence for or the uncertainty of entailed performance requirements. The downside of this circumstance lies in the risk of limiting the deployment of standards to compliance and liability issues only. This would be a missed opportunity, in the sense of focusing on minimum requirements instead of reaching for truly high-quality indoor environments.

An important issue in this discussion is the state of knowledge regarding the mechanisms by which indoor environment conditions influence occupants' health, comfort, well-being, and productivity. Thereby, the causal factors in such mechanisms are not only postulated in "classical" IEQ codes and standards, but also in an increasing number of building quality evaluation and certification schemes and systems. Yet searching for explicit theoretical basis and empirical evidence in these schemes and systems is no more fruitful than looking in the standards. This point can be exemplified based on the case of two common building rating/certification systems, namely LEED [2] and DGNB [3].

As illustrated in Figure 1, these systems frequently do not explicitly include IEQ requirements, but refer to various other national or international standards [1]. Occasionally, the referenced standards themselves refer to further standards for specific requirements and perhaps provide a list of technical literature, without making the mandates-to-references clear and transparent. There are rather few instances, where IEQ standards and codes entail direct and explicit evidence to justify the requirements regarding preferable or necessary indoor-environmental conditions. However, even in these instances, it is not a simple matter to locate, in the referenced scientific publications, the explanatory reasoning behind the standard-based IEQ mandates.

3. Approaches to specification of IEQ requirements

Arguably, the main utility of IEQ standards for building professionals and other relevant stakeholders lies in establishing the definitions and values of suitable performance indicators. In case of certain IEQ-related variables (e.g., concentration of pollutants in indoor air, presence of glare in working spaces, background noise levels in offices) it would be meaningful to establish maximum permissible values. In case of some other variables (e.g., task illuminance levels, air change rates) minimum necessary values could be specified.

Prescription of specific maximum and/or minimum values for performance indicators is especially helpful to the practitioners in connection with quality assurance questions and compliance checking procedures. Ideally, the expected values of relevant performance variables could be part of contractual framework. As such, the actual values of these performance variables could be objectively measured in the course of the commissioning process. This would provide, at least in theory, a rational approach to accountably address and resolve potential liability issues.

A further modus of IEQ-related performance specification involves the definition of multi-variable "zones". For instance, indoor air temperature, mean radiant temperature, air flow velocity, and indoor air humidity are considered concurrently to define a recommended thermal comfort zone. Generally speaking, recommended or mandated values of performance indicators are typically specified as a function of other, mostly indoor-environmental, variables. Illustrations of this approach are provided in Figures 2 and 3, which generically depict the dependency of desired operative temperature or maximum acceptable air flow speed on outdoor temperature, indoor air temperature, and turbulence intensity.

This approach is in principle not much different from the one adopted in basic building-related codes, when variables such as minimum dimensions of doors, stairways, or corridors are specified. The difference is that, in the latter cases, the reasoning behind the requirements may be explained in a more straight-forward manner (e.g., reference to dimensions of the human body or wheelchairs). In contrast, the reasoning behind most IEQ-related mandates is more complex. The complexity, however, does not absolve us from looking for the scientific evidence underlying the performance mandates in IEQ standards.

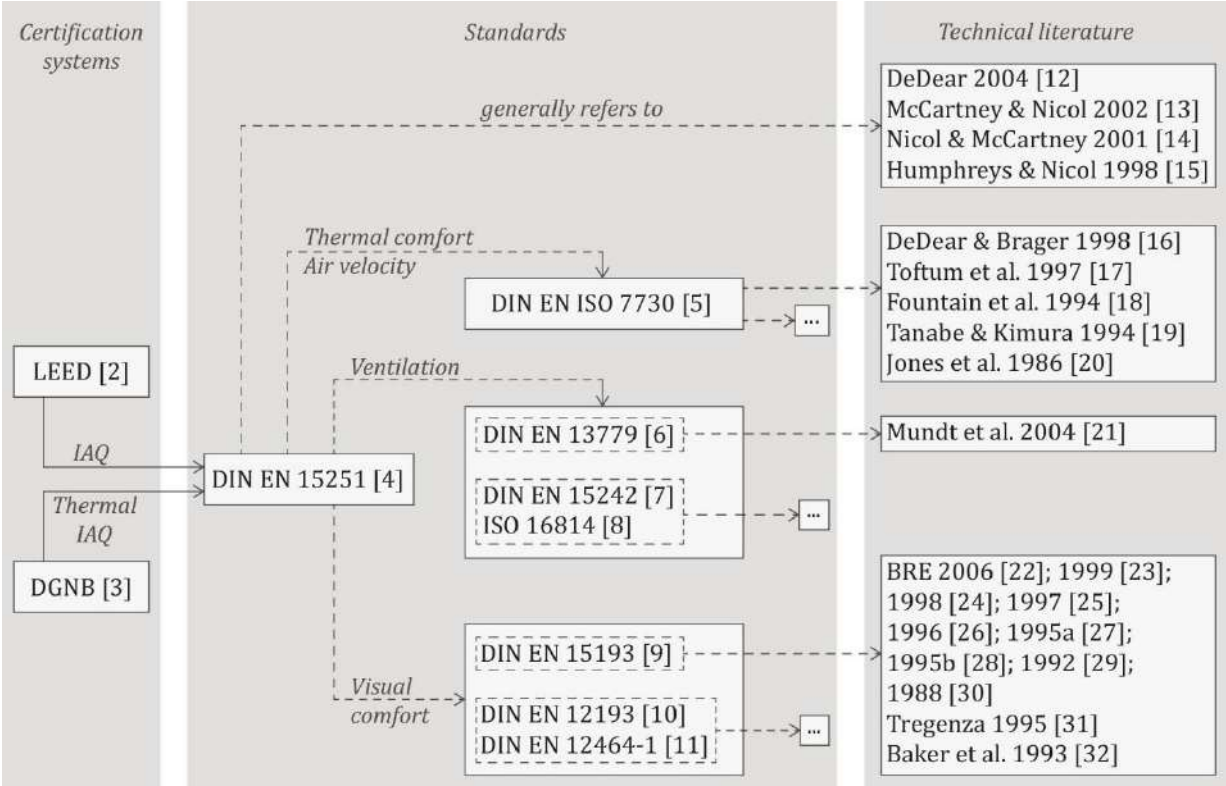

Fig. 1 – Exemplary illustration of chain of references from certification systems to standards and technical literature.

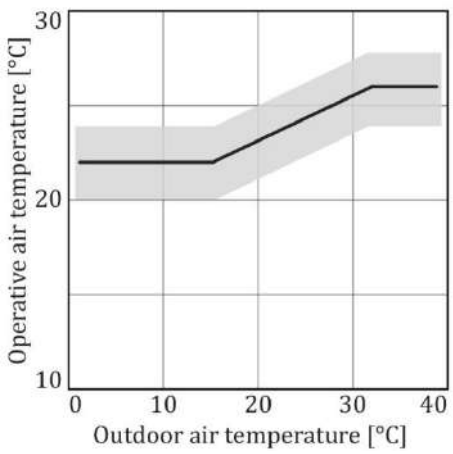

Fig. 2 – Standard-based declaration of the dependency of the recommended values of operative air temperature on the outdoor air temperature (DIN EN 15251 [4], DIN EN ISO 7730 [5]).

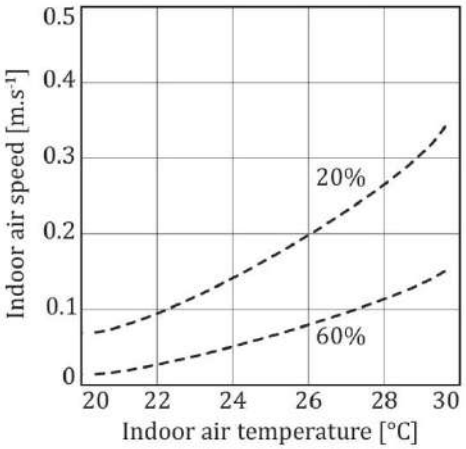

Fig. 3 - Standard-based specification of the dependency of the maximum permissible values of indoor air speed on the indoor air temperature depicted for two turbulence intensity levels (20% and 60%) (DIN EN 15251 [4], DIN EN ISO 7730 [5]).

4. From expectation to reality

It was already indicated that various prescriptive mandates are included in typical IEQ standards, for which rather little supporting evidence is explicitly provided. It was also noted before that, when dealing with specific performance requirements, building certification and rating systems typically refer to standards. The referenced standards may in turn refer to further standards. In some instances, standards do refer to scientific publications and technical reports. But it is often quite difficult to establish a direct and explicit link from such resources back to the requirements entailed in the standards. The provided technical literature appears frequently to act as a rather general bibliography. But the search therein for evidentiary basis of standard-based mandates is rather arduous and frequently inconclusive. Let us consider some of the factors that could have contributed to this situation:

- As mentioned earlier, for many practitioners, standards are not sources of scientific information or educational material, but rather sources of practical guidance and regulative norms.

- There is arguably a key difference between standards in core areas of building construction and building structures on the one side and IEQ standards on the other sides. Whereas standards in the former category need to rely mainly on engineering sciences, those in the latter category need to address information and insights from human and social sciences (i.e., biology, physiology, ergonomics, psychology, and sociology). The path from material science and statics to building structure codes is presumably much more straight-forward than the process by which the results from health and comfort sciences are to be translated into IEQ standards' content. The complexity of the latter translation lies to a large part in the inherently qualitative and subjective factors involved in how people perceive, evaluate, and react to conditions in indoor environments.

- General statements about codes and standards relevant to the building design, construction, and operation processes should be made with care, given their broad spectrum and diversity. Nonetheless, it should be noted that, similar to standards in other areas, IEQ standards do not necessarily come about in the course of an entirely systematic and meticulously structured process. For better or worse, the standardization process does not only address occupants' health and comfort requirements, but is also influenced by factors such as financial considerations, policy constraints, and special interests. Hence, the process requires that the stakeholders involved, be those from governmental bodies, industry representatives, or academic experts, are open to consent and compromise. The point is that objective scientific evidence is not the only aspect driving the final formulation of standard-based IEQ performance mandates.

These points are of course not meant to suggest that IEQ standards and their recommendations are not scientifically based. Rather, the point is that whatever their underlying evidentiary basis is, it is rarely included as an explicit component of the standards. As alluded to before, this may or may not be considered appropriate. But be that as it may, it is important to note that IEQ standards do entail implicit clues with regard to the principles they follow and the approaches they adopt. This suggests that one could, through a kind of reverse engineering of IEQ standards' terminology and composition, arrive at the underlying theoretical reasoning of their requirements.

5. Derivation of IEQ standards' comfort constructs

The underlying logic of the various comfort constructs in IEQ standards cannot be covered here. However, we can exemplify one common approach adopted by such standards, using the case of indoor-environmentally relevant comfort equations in thermal and visual comfort standards. The ingredients of such comfort equations are schematically illustrated in Figure 4. The approach involves the identification of a set of physical parameters that act as the independent variables in the comfort equations. Using information obtained from empirical psycho-physical studies involving human participants, these independent variables are mapped onto dependent variables (constructs) that are meant to capture occupants' level of comfort [33]. The values of the independent (physical) variables typically result from measurements. Values of dependent variables, on the other hand, are determined based on people's subjective statements. Examples for the constructs emerging from this process are provided in Table 1. They are suggested to reflect subjective evaluations pertaining to thermal and visual comfort (or discomfort) obtained from human participants.

In thermal comfort standards, various measurable (physical) variables are identified as relevant independent variables (e.g., ambient air temperature, air velocity, water vapour concentration). On the other hand, the values of constructed thermal comfort indicators are determined via participants' subjective evaluations. To this end, typical physiological scales (e.g., thermal sensation scale) are deployed. The mapping logic from independent variables to comfort constructs is primarily accomplished based on two sources. One source stems from descriptions of physiological processes. For instance, the function of the thermo-regulatory system of human's body toward maintaining a stable body core temperature plays a central role in understanding the processes related to people's evaluation of thermal comfort [34]. The operationalization of this theoretically relevant source requires a second, empirical source. Specifically, participants' thermal comfort responses in the course of controlled experimental studies (conducted under varying indoor-environmental conditions) provide the information necessary to test and calibrate the physiologically-based theoretical model.

To reiterate, in care of thermal comfort equations, the physiological knowledge of the thermo-regulatory processes in the human body represents the key aspect. Experimental studies with human participants capture subjective evaluations of the prevailing conditions and thus facilitate the operationalization of the physiological process model. Likewise, in the visual domain, the physiological understanding of glare-inducing processes (such as light scattering) is an important component of the theoretical comfort (or discomfort) model. Non-comfortable visual circumstances are evaluated via participants' subjective judgements.

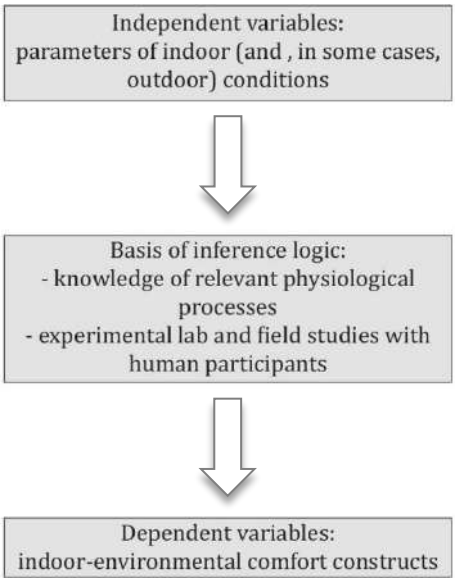

Fig. 4 – Schematic depiction of the derivation process of indoor-environmental comfort equations.

Tab.1 - Independent and dependent parameters with regard to thermal comfort and visual discomfort.

	Key indoor-environmental comfort parameters (independent parameters)	Indoor-environmental comfort constructs related to users' subjective evaluation (dependent parameters)
Thermal comfort	Air temperature, water vapour concentration, air velocity, MRT	Predicted mean vote, Predicted percentage of dissatisfied
Visual comfort	Background luminance, luminance of the glare source	UGR (unified glare rating), VCP (visual comfort probability)

6. Conclusions and discussion

Our investigation so far suggests that IEQ codes and standards rarely state, in explicit terms, the reasoning for the performance mandates they entail. Some of the reasons for this circumstance were alluded to before. It is difficult to precisely define – and subsequently arrive at constructs and proxies for – notions such as health, comfort, and well-being. Whereas the basic tendency of common IEQ standards is to address performance mandates in isolated domains (e.g., thermal, visual, auditory), exposure situation in actual indoor environments is always multi-domain. Building occupants are diverse in terms of their capabilities and requirements, and the nature of these requirements is not static, but changes continuously. The working processes in standardization bodies are complex and are not guided solely by purely scientific considerations.

Nonetheless, our observations so far do reveal recurrent logical patterns common in fields involving medicine, physiology, and psychology. IEQ standards frequently identify a number of indoor-environmental variables as relevant to occupants' health and comfort. The relationship between indoor-environmental states on the one side and occupants' comfort on the other side is established via *i)* psychologically or physiologically based theories, and *ii)* results of experimental studies involving human participants. In some cases (thermal, visual) comfort equations are established explicitly in order to compute the necessary combination of the value ranges of pertinent indoor-environmental variables. In other cases, explicit comfort models are not provided. Rather, it is suggested that compliance to applicable standards is demonstrated as long as the values of certain indoor-environmental parameters (such as carbon dioxide concentration) are kept in mandated ranges.

Given the preceding discussion, a number of observations concerning the current and future IEQ-related codes and standards can be formulated as follows:

- Our review of IEQ standards thus far suggest that it is frequently difficult – or even infeasible – to track back from standards to the specific body of evidence that would explain the formulation of entailed performance mandates. A potentially negative corollary of this circumstance would be to look at standards not as primary sources of technical guidance, but as mere regulatory constraints that must be addressed to avoid contractual or legal issues. It is important to understand what is not suggested here. It is certainly not suggested here that standards must routinely include in detail all theoretical and evidentiary details relevant to their requirements and recommendations. In fact, it is fairly obvious that codes and standards need to be specific and focused on operational and regulative fronts. Nonetheless, the link – or the chain of references – between formulated mandates and scientifically-based arguments for their validity is important and should be, in principle, traceable.
- The paucity of explicit references to theories and data that would unambiguously substantiate the standard-based performance requirements is perhaps not entirely a matter of documentation. Doing science in the domain of human health, comfort, and well-being has its own challenges. Research in this area has generated much in terms of valuable results, but it has to deal with serious sources of uncertainty. Having these uncertainties in mind, serious scientists working in this domain typically abstain from doctrinal claims. But regulative bodies and standardization organizations are expected to deliver, despite insufficiently certain knowledge,

clear and specific rules and mandates. Hence, it appears that living with certain levels of inconclusiveness in the results of scientific studies is perceived as a price to be paid, if codes and standards are to reliably address the accountability and liability matters in the building delivery process.

- There are indeed considerable gaps in the scientific areas expected to support the formulation of IEQ-related performance requirements. It is not always fully clear what features of indoor-environmental conditions are the right variables affecting occupants' comfort and health. The definition and verification of comfort and health constructs can rarely cover all psychological, physiological, and social aspects of exposure situations. Progress in this area is also hampered by the difficulty to obtain sufficient (detailed and long-term) observational data toward validation of theories of human perception and behaviour. Further challenges pertain to the aforementioned multi-domain nature of indoor-environmental exposure situations and the inadequacy of treating these situations in terms of isolated IEQ domains. Likewise, the increasing appreciation of the diversity of the occupants and the highly dynamic of their perceptual processes has not sufficiently reflected the scope and attitude of current IEQ standards.

The contribution could only accommodate a relatively brief and high-level treatment of IEQ-related standards and guidelines. Nonetheless, the discussion of these resources highlights not only a number of their inherent – and in part understandable – limitations, but points also to existing gaps in our scientific understanding of people's health and comfort requirements regarding indoor-environmental conditions. What is needed is an improved and more readily trackable procedure for the translation of the available knowledge in this area (with all its limitations and uncertainties) into IEQ standards and guidelines. Furthermore, our understanding of how occupants perceive and evaluate indoor-environmental conditions and how these conditions influence their health, comfort, and well-being, needs to be both expanded and enhanced.

7. References

[1] Mahdavi A., Berger C., Bochukova V., Bourikas L., Hellwig R. T., Jin Q., Pisello A. L., & Schweiker M. Necessary Conditions for Multi-Domain Indoor Environmental Quality Standards. Sustainability. 2020;12(20).https://doi.org/10.3390/su12208439

[2] LEED Rating System | U.S. Green Building Council. Available online: https://www.usgbc.org/leed (accessed on 19 December 2021).

[3] DGNB System—Sustainable and Green Buildings. Available online: https://www.dgnb-system.de/en/ (accessed on 19 December 2021).

[4] German Institute for Standardization (DIN). DIN EN 15251. Indoor Environmental Input Parameters for Design and Assessment of Energy Performance of Buildings Addressing Indoor Air Quality, Thermal Environment, Lighting and Acoustics. Berlin: Beuth Verlag GmbH; 2012.

[5] German Institute for Standardization (DIN). DIN EN ISO 7730. Ergonomics of the Thermal Environment—Analytical Determination and Interpretation of Thermal Comfort Using Calculation of the PMV and PPD Indices and Local Thermal Comfort Criteria. Berlin: Beuth Verlag GmbH; 2006.

[6] German Institute for Standardization (DIN). DIN EN 13779. Ventilation for non-residential buildings-Performance requirements for ventilation and room-conditioning systems. Berlin: Beuth Verlag GmbH; 2007.

[7] German Institute for Standardization (DIN). DIN EN 15242. Lüftung von Gebäuden — Berechnungsverfahren zur Bestimmung der Luftvolumenströme in Gebäuden einschließlich Infiltration. Berlin: Beuth Verlag GmbH; 2007.

[8] International Standardization Organization (ISO). ISO 16814. Building environment design – Indoor air quality – Methods of expressing the quality of indoor air for human occupancy. Geneva: ISO; 2008.

[9] German Institute for Standardization (DIN). DIN EN 15193. Energetische Bewertung von Gebäuden — Energetische Anforderungen an die Beleuchtung. Berlin: Beuth Verlag GmbH; 2007.

[10] German Institute for Standardization (DIN). DIN EN 12193. Licht und Beleuchtung — Sportstättenbeleuchtung. Berlin: Beuth Verlag GmbH; 2008.

[11] German Institute for Standardization (DIN). DIN EN 12464-1. Light and Lighting—Lighting of Work Places—Part 1: Indoor Work Places. Berlin: Beuth Verlag GmbH; 2008.

[12] DeDear R. Thermal comfort in practice. Indoor Air. 2004;14(7):32-39.

[13] McCartney K. J., & Nicol J. F. Developing an Adaptive Control Algorithm for Europe: Results of the SCATs Project. Energy And Buildings,. 2002;34(6):623-635.

[14] Nicol F., & McCartney K. Final report (Public) Smart Controls and Thermal Comfort (SCATs), Report to the European Commission of the Smart Controls and Thermal Comfort project (Contract JOE3-CT97-0066). Oxford: Oxford Brookes University; 2001.

[15] Humphreys M. A., & Nicol J. F. Understanding the Adaptive Approach to Thermal Comfort. ASHRAE Transactions. 1998; 104(1):991-1004.

[16] DeDear R., & Brager G. S. Developing an adaptive model of thermal comfort and preference. ASHRAE Transactions. 1998; 104(1a):145–167.

[17] Toftum J., Zhou G., & Melikov A. Airflow direction and human sensitivity to draught. Proceedings of CLIMA 2000. 1997; Brussels, Belgium.

[18] Fountain M., Arens E., DeDear R., Bauman F., & Miura K. Locally controlled air movement preferred in warm isothermal environments. ASHRAE Transactions. 1994;100(2):937–952.

[19] Tanabe S., & Kimura K. Effects of air temperature, humidity, and air movement on thermal comfort under hot and humid conditions. ASHRAE Transactions. 1994; 100(2):16.

[20] Jones B. W., Hsieh K., & Hashinaga M. The Effect of Air Velocity on Thermal Comfort at Moderate Activity Levels. ASHRAE Transactions. 1986;92(2B):761–769.

[21] Mundt E., Mathisen H. M., Nielsen P. V., & Moser A. Ventilation Effectiveness. Brussels: 2004; Guidebook no. 2. REHVA.

[22] Littlefair P. J. BRE Digest 498. Selecting lighting controls. Bracknell: BRE; 2006.

[23] Littlefair P. J. BRE Information Paper IP2/99. Photoelectric control of lighting, design, setup and installation aspects. Bracknell: BRE; 1999.

[24] Littlefair, P. J., & Aizlewood, M. BRE information paper IP3/98.Daylight in atrium buildings. Bracknell: BRE; 1998.

[25] BRECSU for Department of the Environment. Electric lighting controls — a guide for designers, installers and users. Good Practice Guide 160. London: BRECSU; 1997.

[26] Littlefair P. J. BRE Report BR 305. Designing with innovative daylighting. Bracknell: BRE; 1996.

[27] Littlefair P. J. BRE Information Paper IP10/95. Daylighting design for display screen equipment. Bracknell: BRE; 1995a.

[28] Bell J., & Burt W. BRE report. Designing buildings for daylight. Bracknell: BRE; 1995b.

[29] Littlefair P. J. BRE report. Site layout planning for daylight and sunlight - a guide to good practice. Bracknell: BRE; 1992.

[30] Littlefair P. J. BRE Information Paper 15/88. Average daylight factor - a simple basis for daylight design. Bracknell: BRE; 1988.

[31] Tregenza P. R. Mean daylight illuminance in rooms facing sunlit streets. Building And Environment. 1995;30(1):83-89.

[32] Baker N., Fanchiotti A., & Steemers K. Daylighting in architecture. (Eds.). London: James & James; 1993.

[33] Mahdavi A. Explanatory stories of human perception and behavior in buildings. Building And Environment. 2020;168. https://doi.org/10.1016/j.buildenv.2019.106498

[34] Mahdavi A. The human factor in sustainable architecture. In K. Al-Sallal (Ed.), Low Energy Low Carbon Architecture: Recent advances & future directions (pp. 177-198). London: CRC Press; 2017.

Data Statement

Data sharing not applicable to this article as no datasets were generated or analysed during the current study.

Estimating Long-Term Indoor $PM_{2.5}$ of Outdoor and Indoor Origin using Low-Cost Sensors

Tongling Xia [a], Yue Qi [b], Xilei Dai [c], Ruoyu You [d], Dayi Lai [e], Junjie Liu [c], Chun Chen [a,f]

[a] Department of Mechanical and Automation Engineering, The Chinese University, tlxia@mae.cuhk.edu.hk

[b] Shanghai Research Institute of Building Sciences (Group) Co., Ltd, Shanghai 201108, China, qiyue@sribs.com

[c] Tianjin Key Lab of Indoor Air Environmental Quality Control, School of Environmental Science and Engineering, Tianjin University, Tianjin, 300072, China, xileidai@tju.edu.cn, jjliu@tju.edu.cn

[d] Department of Building Services Engineering, The Hong Kong Polytechnic University, Kowloon, 999077, Hong Kong SAR, China, ruoyu.you@polyu.edu.hk

[e] School of Design, Shanghai Jiao Tong University, Shanghai 200240, China, dayi_lai@sjtu.edu.cn

[f] Shenzhen Research Institute, The Chinese University of Hong Kong, Shenzhen 518057, China, chunchen@mae.cuhk.edu.hk

Abstract. To evaluate the separate impacts on human health and establish indoor control strategies, it is crucial to estimate the contribution of outdoor infiltration and indoor emission to indoor $PM_{2.5}$ in the built environment. This study applied an algorithm to automatically estimate the long-term time-resolved indoor $PM_{2.5}$ of outdoor and indoor origin in real apartments with natural ventilation. The inputs for the algorithm were only the time-resolved indoor/outdoor $PM_{2.5}$ concentrations and occupants' window actions, which were easily obtained from the low-cost sensors. This study first applied the algorithm in an apartment in Tianjin, China. The indoor/outdoor contribution to the gross indoor exposure and time-resolved infiltration factor were automatically estimated using the algorithm. Due to the year-round monitoring, the probabilistic distribution of the time-resolved $PM_{2.5}$ infiltration factor and indoor $PM_{2.5}$ emission can be given over a year. The influence of outdoor $PM_{2.5}$ data source on the estimated results was compared using the data from the low-cost light-scattering sensor and official monitoring station. Besides, the sensitive parameters to the algorithm were analyzed and their effects on the indoor emission contribution and estimated infiltration factor were investigated. Through the analysis, this study identified the practical applications that robust long-term outdoor $PM_{2.5}$ monitoring for a specific building can use the data from nearest official monitoring station. This study demonstrated an algorithm for estimating long-term time-resolved indoor $PM_{2.5}$ of outdoor and indoor origin in real naturally ventilated apartments with only the time-resolved indoor/outdoor $PM_{2.5}$ concentrations and window behaviors.

Keywords. Indoor $PM_{2.5}$ exposure, indoor emission, real building monitoring, I/O ratio, year-round distribution, natural ventilation
DOI: https://doi.org/10.34641/clima.2022.367

1. Introduction

Exposure to particulate air pollution poses one of the greatest risks to human health around the world [1]. In recent decades, $PM_{2.5}$ (particulate matter with a diameter less than 2.5 μm) has been proven to have a strong association with various diseases, on the basis of a large amount of epidemiological data [2-4]. Given that people spend a significant fraction of their time in indoor environments [5], it is essential to reduce indoor exposure to $PM_{2.5}$. Many studies have used the outdoor $PM_{2.5}$ concentration as an indicator to estimate the indoor exposure to $PM_{2.5}$ [6-7]. However, even when indoor $PM_{2.5}$ originates outdoors, the concentration of outdoor $PM_{2.5}$ is not a suitable indicator, because building-specific parameters such as air tightness and window-opening behavior would also influence the exposure [8-9]. Moreover, the existence of indoor $PM_{2.5}$ emissions, such as those from cooking and smoking, would further differentiate ambient $PM_{2.5}$ and indoor $PM_{2.5}$. Therefore, it is crucial to estimate the contribution of outdoor infiltration and indoor emissions to indoor $PM_{2.5}$ for evaluating the

Copyright ©2022 by the authors. This conference paper is published under a CC-BY-4.0 license.

separate risk effects on human health.

With the rapid development of low-cost light-scattering $PM_{2.5}$ sensors, it is now straightforward to monitor time-resolved outdoor and indoor $PM_{2.5}$ concentrations. Our previous study proposed an algorithm that automatically differentiates the indoor $PM_{2.5}$ of outdoor and indoor origin using time-resolved indoor-to-outdoor $PM_{2.5}$ concentration ratio and window status. The method was validated in a small-scale chamber in a laboratory with a low relative error of 0.32% [10]. However, its performance in real buildings is still unclear. Therefore, to facilitate practical applications, it is worthwhile to assess the performance of the method in differentiating indoor $PM_{2.5}$ of outdoor and indoor origin in real buildings.

This study aimed to differentiate the indoor $PM_{2.5}$ of outdoor and indoor origin in real apartments with natural ventilation to demonstrate the robustness of the differentiation method proposed in our previous study [10]. Three inputs, the time-resolved concentrations of outdoor $PM_{2.5}$ and indoor $PM_{2.5}$ and window/door status, were monitored for a one-year period in 2017. The concentrations of indoor and outdoor $PM_{2.5}$ were monitored by a low-cost light-scattering $PM_{2.5}$ sensor, while official data from the national monitoring station near the target building were also obtained as alternative for the concentrations of outdoor $PM_{2.5}$. The occupants' window and door action was also monitored using low-cost sensors. Based on the differentiation method, the time-resolved indoor $PM_{2.5}$ of outdoor and indoor origin and their contributions to the total indoor exposure were estimated. The time-resolved infiltration factors were also obtained.

2. Research Methods

2.1 Original data

This study first focused on a naturally ventilated apartment located in Tianjin, China. The apartment was on the 16th floor of an 18-floor residential building. The indoor and outdoor $PM_{2.5}$ concentrations were recorded in the living room and the neighborhood, respectively, from January to December of 2017 using two low-cost light-scattering sensors with a time resolution of 1 min. In addition, the window/door-opening/closing actions were monitored with window/door sensors. The details of the monitoring setup can be found in a previous study [11]. However, it was found that a significant amount of data were missing from the outdoor low-cost $PM_{2.5}$ sensor due to bad weather and unstable power supply. Therefore, as an alternative, the outdoor $PM_{2.5}$ concentrations with a time resolution of 2 h were also obtained from the nearest official monitoring station, Binshui West Road station, operated by the China National Environmental Monitoring Center.

2.2 Data pre-processing

The low-cost light-scattering sensor for indoor $PM_{2.5}$ monitoring was first calibrated by a standard gravimetric instrument under a controlled environment. Since previous studies found that an increase in relative humidity can result in an increase in $PM_{2.5}$ concentration as measured by a light-scattering sensor, the indoor $PM_{2.5}$ concentrations were further calibrated based on the relative humidity [11].

Note that the original indoor $PM_{2.5}$ data were recorded once every minute. However, our previous study found that a time step size smaller than 10 minutes would result in significant errors in the differentiation algorithm [10]. Therefore, after the calibration, the concentrations of indoor $PM_{2.5}$ were averaged every 10 minutes, so that the time step size was in line with that of the differentiation algorithm. The sensitivity analysis about the time step size will be discussed in Section 3.4. In general, the low-cost sensor used indoors was stable. Over 94% of the indoor $PM_{2.5}$ data were successfully recorded throughout the year. Due to the relatively harsh environment, around 60% of the outdoor $PM_{2.5}$ data from the low-cost sensor were missing. Only were the data in February to April relatively complete for the analysis. As an alternative, this study also obtained the outdoor $PM_{2.5}$ data recorded once every two hours from the official monitoring station. Linear interpolation was used to convert the official monitoring outdoor $PM_{2.5}$ data to that with a time step size of 10 minutes. This study first used both outdoor $PM_{2.5}$ data from the low-cost sensor and the official monitoring station to estimate the indoor $PM_{2.5}$ of outdoor and indoor origin in February to April, and discussed the differences. We then used the outdoor $PM_{2.5}$ data from the official monitoring station to calculate the year-round indoor $PM_{2.5}$ of outdoor and indoor origin to demonstrate of the proposed algorithm.

Since the time step size was set at 10 minutes, this study counted effective window behavior with a time interval longer than 10 minutes from the previous and subsequent actions.

Besides, any time periods with mechanical ventilation or air cleaners turned on were removed since the algorithm is applicable for natural ventilation. Furthermore, this study applied the differentiation algorithm to each day individually. The results would be unsatisfactory for periods shorter than four hours [10]. Thus, this study removed the data that were recorded in any period shorter than four hours. Furthermore, if the results from the differentiation algorithm indicated that indoor $PM_{2.5}$ emissions occurred continuously throughout a whole day, there was no way to estimate the indoor $PM_{2.5}$ of outdoor and indoor origin, then such days were also removed. With these considerations, there were 40 days with valid input data for the analysis using the outdoor $PM_{2.5}$ data measured by the low-cost sensor in February to April. For the year-round estimation using the

official monitoring outdoor $PM_{2.5}$ data, there were 275 days with valid inputs in this study.

2.3. Differentiation algorithm

After the data pre-processing, the three inputs, concentrations of outdoor $PM_{2.5}$ and indoor $PM_{2.5}$ and window action, were used with the differentiation algorithm to estimate indoor $PM_{2.5}$ of outdoor and indoor origin. This sub-section briefly describes the differentiation algorithm developed in our previous study [10].

Step 1 is to obtain indoor-to-outdoor $PM_{2.5}$ ratio. To consider the change in concentrations of outdoor and indoor $PM_{2.5}$ simultaneously, this study utilized the indoor-to-outdoor ratio time-resolved $PM_{2.5}$ concentration (I/O ratio), IO(t), to start the differentiation method:

$$IO(t) = \frac{C_{in}(t)}{C_{out}(t)} \quad (1)$$

where $C_{in}(t)$ and $C_{out}(t)$ ($\mu g/m^3$) are the averaged indoor and outdoor $PM_{2.5}$ concentrations, respectively, in the t-th time step. The size of time step was set at 10 minutes [10].

Step 2 is to process the change-point analysis. Normally, indoor $PM_{2.5}$ emissions can affect indoor $PM_{2.5}$ concentrations. The method of change-point analysis was used to detect significant changes in the time-series I/O ratios statistically [12]. The method also provided the confidence level for each change point. The details of the change-point analysis method can be found in [10]. Note that except for indoor emission of $PM_{2.5}$, window actions and fluctuations in infiltration rate can make a difference in the time-series I/O ratios and result in the change points as well. Therefore, this step was taken mainly to identify candidates for change points due to indoor $PM_{2.5}$ emissions.

Step 3 is to handle time periods no window status change. For the periods without window actions, significant increases in the I/O ratio were ascribed to either the indoor emission of $PM_{2.5}$ or the change of infiltration rate. To differentiate these two scenarios, three criteria were employed. First, when the I/O ratio was greater than 1, the period must have had an indoor emission of $PM_{2.5}$. Second, if the outlier was more than 1.5 interquartile over the third quartile in the I/O ratio, the period was considered to contain an indoor emission. Third, a detected change might arise from either a sudden increase in infiltration rate or an indoor $PM_{2.5}$ emission. Sudden increase in infiltration rate would increase the indoor concentration smoothly, while an indoor emission would increase the concentration with relatively strong fluctuations [10]. In a large-scale simulation, Shi et al. [9] obtained the infiltration rate distribution in Beijing residences with a 15th percentile of 0.09 h^{-1} and an 85th percentile of 0.32 h^{-1}. Considering a relatively extreme case in which the infiltration rate suddenly increased from 0.09 to 0.32 h^{-1}, the infiltration factor would increase by 0.22 (from 0.40 to 0.62), assuming the penetration factor and deposition rate to be 0.8 and 0.09 h^{-1}, respectively. Namely, if a detected change is caused by a sudden increase in infiltration rate, it is unlikely that the I/O ratio would increase by 0.22. Therefore, when the difference between the maximum and minimum values of the I/O ratio in the period was over an empirical threshold of 0.22, the period was regarded as containing an indoor $PM_{2.5}$ emission.

Step 4 is to handle the time periods having window status change. For the periods with window behavior, the I/O ratio would follow an exponential regression deducted from the mass balance equation without indoor particle emission [13]:

$$IO(t) = c_1 + c_2 \cdot e^{-c_3(t-t_0)} \quad (2)$$

where c_1 (unitless), c_2 (unitless), and c_3 (h-1) are constants as a function of the air exchange rate, $PM_{2.5}$ deposition rate and penetration factor. If the time-series I/O ratio fitted very well with equation (2), it is likely that there was no indoor source. Therefore, the R^2 value of the regression was used to determine the existence of indoor emission of $PM_{2.5}$. If the data fitting yielded a satisfactory R^2 value above 0.8, an empirical value according to Xia and Chen [10], then the period was regarded as free of indoor-generated $PM_{2.5}$. Otherwise, there existed indoor emission of $PM_{2.5}$.

Step 5 is to estimate the indoor $PM_{2.5}$ of outdoor and indoor origin. For the periods without indoor $PM_{2.5}$ emissions, the infiltration factor, F_{in}, was equal to the I/O ratio. For the periods with indoor $PM_{2.5}$ emissions, the infiltration factor was estimated with the use of equation (2), as demonstrated by Xia and Chen [10]. The indoor $PM_{2.5}$ of outdoor origin, $C_{in,out}$, in the periods with indoor $PM_{2.5}$ emissions was then calculated by:

$$C_{in,out}(t) = F_{in}(t) \cdot C_{out}(t) \quad (3)$$

The indoor $PM_{2.5}$ of indoor origin, $C_{in,in}$, can be expressed as:

$$C_{in,in}(t) = C_{in}(t) - C_{in,out}(t) \quad (4)$$

To compare the contributions of outdoor infiltrated $PM_{2.5}$ and indoor emitted $PM_{2.5}$, we calculated the ratio of indoor exposure to $PM_{2.5}$ of outdoor and indoor origin, respectively, to the gross indoor exposure for each day, denoted as the "indoor contribution" and "outdoor contribution", respectively, as follows:

$$\frac{E_{in,in}}{E_{in}} = \frac{\int_{t_{start,d}}^{t_{end,d}} C_{in,in}(t)dt}{\int_{t_{start,d}}^{t_{end,d}} C_{in}(t)dt} \quad (5)$$

$$\frac{E_{in,out}}{E_{in}} = \frac{\int_{t_{start,d}}^{t_{end,d}} C_{in,out}(t)dt}{\int_{t_{start,d}}^{t_{end,d}} C_{in}(t)dt} \quad (6)$$

where $E_{in,out}$ and $E_{in,in}$ ((μg·10min)/m³) are the daily indoor exposure to $PM_{2.5}$ of outdoor and indoor origin, respectively, and Ein ((μg·10min)/m³) is the daily gross indoor exposure to $PM_{2.5}$. The start time, $t_{start,d}$, and end time, $t_{end,d}$, of the daily gross indoor exposure are the start and end of an effective day. Here it was assumed that the occupant stayed indoors all the time. For different occupancy schedules, the corresponding exposures can be calculated accordingly based on the estimated concentrations of indoor $PM_{2.5}$ of outdoor and indoor origin.

Note that the indoor $PM_{2.5}$ sensor was placed in the living room. The indoor $PM_{2.5}$ emissions that occurred in other rooms, e.g., the kitchen and bedroom, may have contributed to the $PM_{2.5}$ concentration in the living room. In the differentiation algorithm, although the non-living-room $PM_{2.5}$ emissions were also detected, the estimated emission strength was equivalent to the portion that actually influenced the living room. In other words, these $PM_{2.5}$ emissions were also regarded as indoor sources that were located in the living room.

3. Results and discussion

3.1. Examples of estimated indoor $PM_{2.5}$ of outdoor and indoor origin

Fig. 1 illustrates the estimated time-resolved concentrations of indoor $PM_{2.5}$ of outdoor and indoor origin and the infiltration factor on Feb 21, Feb 14, and Mar 19. The inputs, outdoor and indoor $PM_{2.5}$ concentrations, are also shown in the figure. The area under the estimated indoor $PM_{2.5}$ of outdoor origin line (in orange) represents the daily indoor exposure to $PM_{2.5}$ of outdoor origin ($E_{in,out}$). The area under the indoor $PM_{2.5}$ line (in green) represents the daily gross indoor exposure to $PM_{2.5}$ (E_{in}). The total area of the four purple shaded zones represents the daily indoor exposure to $PM_{2.5}$ of indoor origin ($E_{in,in}$). equations (5) and (6) were used to calculate the daily indoor and outdoor contribution to the total indoor exposure, respectively. On Feb 21, four indoor emission events were detected with the differentiation algorithm, as shown in Fig. 1(a). The latter three detected $PM_{2.5}$ emissions were likely attributed to cooking considering the normal time periods for preparing breakfast, lunch, and dinner. In this apartment, the occupants often prepare late-night snacks. Therefore, the first emission might be from a late-night cooking activity. Based on the algorithm, the daily indoor and outdoor contribution was 32.5% and 67.5%, respectively. However, it should be noted that the first detected emission was weak, which might be a misclassification. If this weak emission was not considered as a real emission, the daily indoor and outdoor contribution would be altered by only 1.7%. Namely, the detected small emission did not alter the results of indoor/outdoor contribution in a major way. By characterizing the indoor $PM_{2.5}$ emission, the differentiation algorithm can then calculate the time-resolved infiltration factor ($F_{in}(t)$). As shown in Fig. 1(a), the real-time infiltration factor fluctuated in a wide range from 0.16 to 0.51. The daily averaged infiltration factor was 0.34±0.09. Similar results can be found on Feb 14, as shown in Fig. 1(b). The indoor emission events were also likely from cooking activities for late-night snack, breakfast, lunch, and dinner. After breakfast and lunch, there might be cleaning or other activities leading to emissions. The estimated daily indoor and outdoor contribution was 19.1% and 80.9%, respectively, and the averaged infiltration factor was 0.23±0.08. On Mar 19, the algorithm only detected one indoor emission event, which was likely from preparing the lunch. Since Mar 19 was a weekend, the occupants might get up late and skip the breakfast, and have their dinner in a restaurant. The estimated daily indoor and outdoor contribution was 3.0% and 97.0%, respectively, and the averaged infiltration factor was 0.45±0.11. The plausible explanation for the detected indoor emissions in these examples can partially support the feasibility of the algorithm.

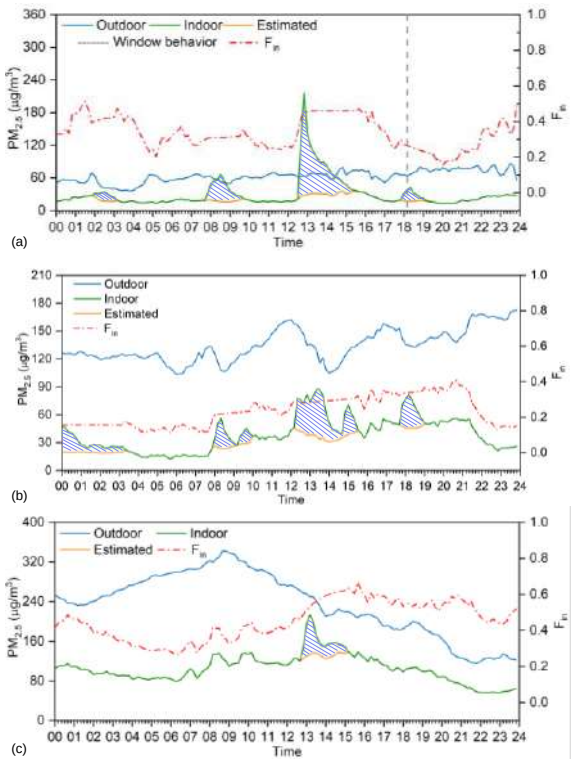

Fig. 1 - Estimated concentrations of indoor $PM_{2.5}$ of outdoor and indoor origin and infiltration factor on (a) Feb 21, (b) Feb 14, and (c) Mar 19 using the differentiation algorithm. (The purple shading represents indoor exposure to $PM_{2.5}$ of indoor origin.)

3.2. Comparison of results based on outdoor low-cost sensor and official monitoring station

As discussed, due to bad weather and unstable power supply, the outdoor $PM_{2.5}$ data from the low-cost light-scattering sensor were only available in February to April. The alternative was the outdoor $PM_{2.5}$ data recorded from the nearest official monitoring station. The mean ± standard deviation of the outdoor $PM_{2.5}$ data measured by the light-scattering sensor in February to April (68.9 ± 71.4 μg/m^3) was close to that measured by the official monitoring station (69.4 ± 60.7 μg/m^3). This study first compared the results based on the 1-min outdoor low-cost sensor and 2-h official monitoring station in February to April. Both datasets were averaged or interpolated to a 10-min resolution. Fig. 2 compares the probabilistic distribution of the daily indoor/outdoor contribution estimated based on the two outdoor $PM_{2.5}$ datasets. The general distributions were similar, but discrepancies can also be observed. It was estimated that, on average, the indoor $PM_{2.5}$ emissions and outdoor $PM_{2.5}$ infiltration contributed 23.2% and 76.8% of the daily total indoor exposure, respectively, if the outdoor $PM_{2.5}$ data from the low-cost sensor were used. When using the data from the official monitoring station, the average indoor and outdoor contribution was estimated to be 17.8% and 82.2%, respectively. Interestingly, the indoor contribution over 70% only occurred when the low-cost light-scattering sensor was used and the outdoor $PM_{2.5}$ concentrations were low. The outdoor $PM_{2.5}$ concentrations at the low level tended to be under-reported by the light-scattering sensor, which would result in a higher indoor contribution. The under-reported outdoor $PM_{2.5}$ concentration by the low-cost light-scattering sensor could be another possible reason for the long continuous indoor emission. In conclusion, the proposed algorithm can effectively differentiate indoor $PM_{2.5}$ of outdoor and indoor origin and estimate their contributions to the total indoor exposure. However, the average results of daily indoor/outdoor contributions estimated based on the two outdoor $PM_{2.5}$ datasets had an around 5% difference.

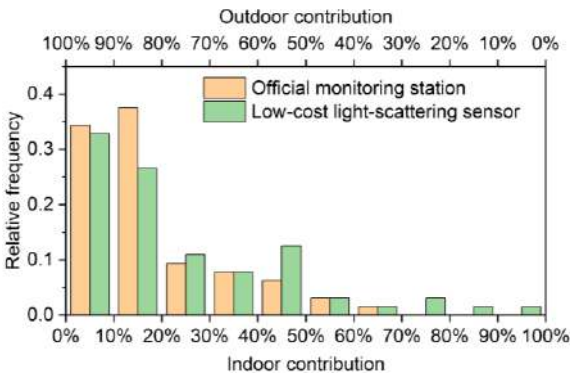

Fig. 2 - Comparison of the probabilistic distribution of the daily indoor/outdoor contribution estimated based on the outdoor $PM_{2.5}$ data from the low-cost sensor and official monitoring station in February to April 2017.

Fig. 3 compares the probabilistic distribution of the time-resolved infiltration factor estimated based on the outdoor $PM_{2.5}$ data from the low-cost sensor and official monitoring station in February to April. Again, the general distributions were similar, but discrepancies can be observed. The average infiltration factor estimated using the outdoor $PM_{2.5}$ data from the low-cost sensor was 0.46, which was equal to that estimated based on the official monitoring data, 0.46. Therefore, the proposed algorithm can effectively calculate the time-resolved infiltration factor using only the inputs of time-series indoor/outdoor $PM_{2.5}$ concentrations and window behavior. Furthermore, the average infiltration factors obtained from the two outdoor $PM_{2.5}$ datasets were similar, but discrepancies can be observed in terms of the probabilistic distribution.

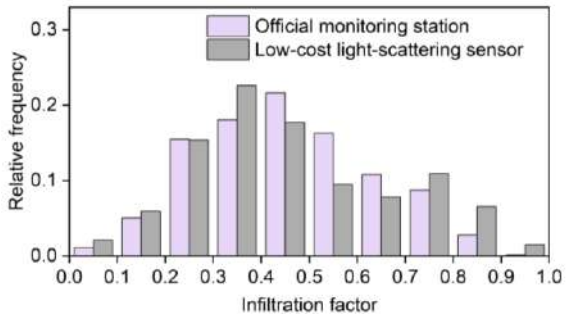

Fig. 3 - Comparison of the probabilistic distribution of the time-resolved $PM_{2.5}$ infiltration factor estimated based on the outdoor $PM_{2.5}$ data from the low-cost sensor and official monitoring station in February to April 2017.

Theoretically, using the same light-scattering sensors with careful calibration for both indoor and outdoor $PM_{2.5}$ monitoring would yield more accurate results than using the official monitoring outdoor data since the light-scattering sensor can effectively capture the peak outdoor $PM_{2.5}$ concentration with a 10-min time step size but the official monitoring data with a 2-h sampling interval cannot. In addition, the nearest official monitoring station may still be far away from the target building, which would result in inaccurate input of outdoor $PM_{2.5}$. Therefore, from the theoretical perspective, we would recommend using the same low-cost light-scattering sensors with careful calibration for both indoor and outdoor $PM_{2.5}$ monitoring.

However, using the low-cost light-scattering sensor to monitor long-term outdoor $PM_{2.5}$ in a neighborhood is practically challenging for general customer use. Several problems were identified in the monitoring of this study. First, the current low-cost light-scattering sensors available on the market suffers from severe data loss due to bad weather, unstable power supply, or even accidental damage. The general users, such as the participants in this study, would not spend time on regular

maintenance for the outdoor sensor. Furthermore, most of them do not have the technical skills to fix a light-scattering sensor. Second, the outdoor sensor should be placed somewhere in the neighborhood which is a public area. Thus, the outdoor monitoring requires the permission from the neighborhood committee, which would become impractical if a lot of residents request a public area for outdoor monitoring. Therefore, from the practical perspective, we would recommend using the outdoor $PM_{2.5}$ data from the nearest official monitoring station as the input for the algorithm if the year-around results are to be obtained.

In the future, efforts should be made in the following aspects to facilitate the practical application of the proposed algorithm by using low-cost light-scattering sensor for outdoor $PM_{2.5}$ monitoring. First, the sensors should be further developed for robust and stable long-term measurements in relatively hash environments. Currently, there are some well-designed $PM_{2.5}$ monitors specifically for outdoor monitoring available on the market. However, the cost would be too high for general customer use. Low-cost solutions would significantly facilitate the practical applications. Second, the neighborhood-based outdoor $PM_{2.5}$ monitoring should be conducted by the neighborhood property manager and the data should be shared in real-time with all the residents in the neighborhood. This would require both technical development in terms of data sharing and policy development in terms of neighborhood-based air quality monitoring.

3.3. Year-round results

Based on the discussion above, this study then used the outdoor $PM_{2.5}$ data from the official monitoring station to calculate the year-round indoor $PM_{2.5}$ of outdoor and indoor origin as a full demonstration of the proposed algorithm. Furthermore, the seasonal characteristics were analyzed in addition to the year-round results. Division of the time into four seasons was based on the five-day moving average temperature according to the definition of climatic season in Chinese national standard QX/T 152-2012 [14]. According to this standard, in 2017, spring in Tianjin was from March 16 to May 10, summer from May 11 to October 2, autumn from October 3 to November 11, and winter from January 1 to March 15 and November 12 to December 31.

Fig. 4 displays the year-round distribution of the daily indoor/outdoor contribution for the 275 days, with a wide range from 0 to 94.2%. On average, the indoor $PM_{2.5}$ emissions and outdoor $PM_{2.5}$ infiltration contributed 26.3% and 73.7% of the daily total indoor exposure, respectively. In other words, for most of the time, the outdoor $PM_{2.5}$ infiltration contributed to the indoor $PM_{2.5}$ more than the indoor emission did. The results demonstrated that the proposed algorithm can automatically differentiate indoor $PM_{2.5}$ of indoor and outdoor origin and estimate their contributions to the total indoor exposure, even for a whole year. The automated estimation of indoor and outdoor contributions would support the large-scale exposure and health risk assessment as well as the development of effective strategies for controlling indoor particulate air pollution.

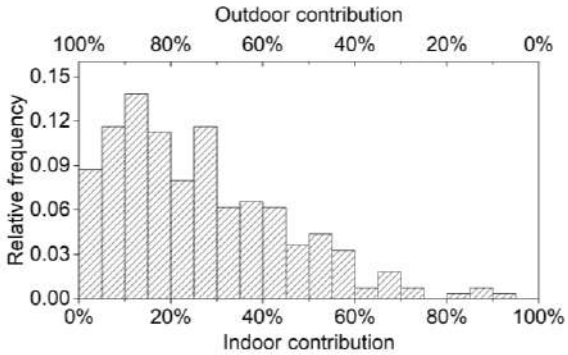

Fig. 4 - Year-round probabilistic distribution of the daily indoor/outdoor contribution to total indoor exposure in 2017.

Fig. 5 shows the year-round probabilistic distribution of the time-resolved $PM_{2.5}$ infiltration factor with a mean value ± standard deviation of 0.56 ± 0.22. The median value was 0.55. The results were comparable to the annual-averaged infiltration factor for residences in Beijing, 0.48 ± 0.07 [9]. The year-round infiltration factor showed a great span ranging from 0.001 to 0.993 in the same apartment. The great variation in the infiltration factor was attributed to the window behavior, outdoor wind speed, etc. Note that measuring time-resolved infiltration factor in a real building with indoor $PM_{2.5}$ sources is very challenging using the existing methods in the literature [13]. However, with the approach proposed in this study, the real-time $PM_{2.5}$ infiltration factors can be obtained by using only the concentrations of outdoor $PM_{2.5}$ and indoor $PM_{2.5}$ and window actions.

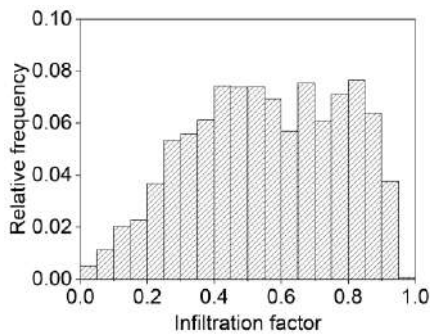

Fig. 5 - Year-round probabilistic distribution of the time-resolved $PM_{2.5}$ infiltration factor in 2017.

3.4. Sensitivity analysis

The sensitivity analysis in this study was to test how the empirically determined setting parameters, i.e., time step size, infiltration factor range (in Step 3),

and R^2 value (in Step 4), would alter the results of indoor/outdoor contribution and infiltration factor based on the outdoor low-cost sensor data shown in Section 3.2.

Time step size: In general, a smaller time step size would result in greater uncertainties due to data fluctuation, while a larger time step size would result in greater error in quantifying indoor emission. The validation using the ground truth data in the laboratory tests in our previous study [10] indicated that the time step size of 10 min yielded the best estimation of the indoor/outdoor contribution. This study further tested how the time step size of 2, 5, 10, 15, and 20 min affected the results in the Tianjin apartment. The average daily indoor contribution increased with the time step size, while the infiltration factor decreased. The change point analysis in Step 2 may generate more change points with a smaller time step size due to data fluctuation. If a real indoor emission was divided into several time periods by the additional change points, the algorithm might misclassify these short time periods as without emission. Consequently, the average daily indoor contribution would be underestimated, while the infiltration factor would be overestimated. On the other hand, a larger time step size might result in the overestimation of indoor contribution when calculating the integral in the numerator of equation (5). As a result, the average daily indoor contribution would be overestimated, while the infiltration factor would be underestimated. When the time step size ranged from 5 to 15 min, the average daily indoor contribution in the range of 21.3% to 24.1% with an absolute difference of 2.8%, and the average infiltration factor was in the range of 0.47 to 0.50 with an absolute difference of 3%. Therefore, if an uncertainty of 5% in indoor/outdoor contribution is acceptable, the time step size can be set between 5 to 15 min. Furthermore, the time step size between 5 to 15 min is also suitable considering the light-scattering $PM_{2.5}$ sensor performance and typical indoor emission duration [10].

Infiltration factor range threshold: The infiltration factor range threshold of 0.22 in Step 3 was determined according to the reasonable inputs from the literature. The validation using the ground truth data in the laboratory tests [10] also indicated that the threshold of 0.22 yielded the best estimation of the indoor/outdoor contribution. This study tested how the threshold of 0.15, 0.19, 0.22, 0.28, and 0.35 affected the results in the Tianjin apartment in February to April. These values corresponded to the $75^{th}/25^{th}$, $80^{th}/20^{th}$, $85^{th}/15^{th}$, $90^{th}/10^{th}$, and $95^{th}/5^{th}$ percentiles of the upper/lower limits of the infiltration rate, respectively [9]. A larger infiltration factor range threshold resulted in a lower the indoor contribution and a higher infiltration factor. When the infiltration factor range threshold ranged from 0.15 to 0.35, the average daily indoor contribution was in the range of 21.7% to 24.8% with an absolute difference of 3.1%, and the average infiltration factor was in the range of 0.47 to 0.48 with an absolute difference of only 0.01. Therefore, the results were insensitive to the infiltration factor range threshold between 0.15 and 0.35.

R^2 value: The algorithm used an R^2 value of 0.8 in the data regression analysis in Step 4 for identifying whether there was $PM_{2.5}$ emission in a period with a window-opening action. Again, the validation using the ground truth data in the laboratory tests [10] also indicated that the R^2 value of 0.8 yielded the best estimation of the indoor/outdoor contribution. This study tested how the R^2 value of 0.65, 0.7, 0.8, 0.9, and 0.95 affected the results in the Tianjin apartment in February to April. when the R^2 value range threshold ranged from 0.65 to 0.95, both the average daily indoor contribution and the average infiltration factor almost remain unchanged. Therefore, the results were insensitive to the R^2 value in the range of 0.65 to 0.95.

4. Conclusions

This study used an indoor/outdoor $PM_{2.5}$ differentiation algorithm in real residential apartments to automatically estimate the long-term time-resolved indoor $PM_{2.5}$ of outdoor and indoor origin. The inputs for the differentiation algorithm were only the concentration values of outdoor and indoor $PM_{2.5}$ and occupants' window actions, which were easily obtained from the low-cost sensors. The indoor/outdoor contribution to the gross indoor exposure and the time-resolved infiltration factor were calculated using the algorithm. Within the scope of this study, the following conclusions can be made:

1. The proposed algorithm can automatically estimate the long-term time-resolved indoor $PM_{2.5}$ of outdoor and indoor origin in naturally ventilated buildings using only the inputs of time-resolved indoor/outdoor $PM_{2.5}$ concentrations and window behavior.

2. The indoor/outdoor contribution to the gross indoor exposure and time-resolved infiltration factor can also be automatically estimated using the algorithm.

3. This study identified several directions for further development, such as robust long-term outdoor $PM_{2.5}$ monitoring using low-cost light-scattering sensors, which would facilitate the practical applications of the algorithm.

5. Acknowledgement

This work was supported by the National Natural Science Foundation of China (Grant No. 51708474) and the Early Career Scheme of Research Grants Council of Hong Kong SAR, China (Grant No. 24208518).

6. References

[1] GBD 2017 Risk Factor Collaborators. Global, regional, and national comparative risk assessment of 84 behavioural, environmental and occupational, and metabolic risks or clusters of risks for 195 countries and territories, 1990 – 2017: a systematic analysis for the Global Burden of Dis. Lancet. 2018;392:1923–94.

[2] Guo Y, Zeng H, Zheng R, Li S, Barnett AG, Zhang S, et al. The association between lung cancer incidence and ambient air pollution in China: A spatiotemporal analysis. Environ Res. 2016;144:60–5.

[3] Pope CA, Ezzati M, Dockery DW. Fine particulate air pollution and life expectancies in the United States: The role of influential observations 2013;63:129–32.

[4] Weichenthal S, Hatzopoulou M, Goldberg MS. Exposure to traffic-related air pollution during physical activity and acute changes in blood pressure, autonomic and micro-vascular function in women: A cross-over study. Part Fibre Toxicol. 2014;11.

[5] Klepeis NE, Nelson WC, Ott WR, Robinson JP, Tsang AM, Switzer P, et al. The National Human Activity Pattern Survey (NHAPS): A resource for assessing exposure to environmental pollutants. J Expo Anal Environ Epidemiol. 2001;11:231–52.

[6] Dockery DW, Pope CA, Xu X, Spengler JD, Ware JH, Fay ME, et al. An Association between Air Pollution and Mortality in Six U.S. Cities. N Engl J Med. 1993;329:1753–9.

[7] Vanos JK, Hebbern C, Cakmak S. Risk assessment for cardiovascular and respiratory mortality due to air pollution and synoptic meteorology in 10 Canadian cities. Environ Pollut. 2014;185:322–32.

[8] Chen C, Zhao B, Weschler CJ. Indoor Exposure to "Outdoor PM10": Assessing Its Influence on the Relationship Between PM10 and Short-term Mortality in U.S. Cities. Epidemiology. 2012;23:870–8.

[9] Shi S, Chen C, Zhao B. Modifications of exposure to ambient particulate matter: Tackling bias in using ambient concentration as surrogate with particle infiltration factor and ambient exposure factor. Environ Pollut. 2017;220:337–47.

[10] Xia T, Chen C. Differentiating between indoor exposure to PM2.5 of indoor and outdoor origin using time-resolved monitoring data. Build Environ. 2019;147:528–39.

[11] Liu J, Dai X, Li X, Jia S, Pei J, Sun Y, et al. Indoor air quality and occupants' ventilation habits in China: Seasonal measurement and long-term monitoring. Build Environ. 2018;142:119–29.

[12] Taylor WA. Change-Point Analysis: A Powerful New Tool For Detecting Changes. Analysis. 2000;1–19.

[13] Chen C, Zhao B. Review of relationship between indoor and outdoor particles: I/O ratio, infiltration factor and penetration factor. Atmos Environ. 2011;45:275–88.

[14] China Meteorological Administration, QX/T 152-2012, Definition of Climatic Season 2012.

Ray-tracing MRT and human thermophysiology model combination for local discomfort prediction

Mohamad Rida [a], Miaomiao Hou[c,b], Arnab Chatterjee [a], Eric Teitelbaum [d], Forrest Meggers [d], Dorit Aviv [b], Dolaana Khovalyg [a]

[a] Integrated Comfort Engineering (ICE), Ecole Polytechnique Fédérale de Lausanne (EPFL), Switzerland.

[b] Thermal Architecture Lab (TAL), Weitzman School of Design, University of Pennsylvania, USA.

[c] College of Architecture and Urban Planning, Tongji University, China.

[d] CHAOS Lab, Andlinger Center for Energy and the Environment, Princeton University, Princeton, NJ, USA.

Abstract. Thermal comfort and discomfort based on the local sensation of different body parts have been an important development in thermal comfort studies from the past decade. The human thermophysiology model can be a handy tool to predict local skin and core temperatures, which can then be projected into diverse human's local and overall thermal sensation and comfort. When local environmental parameters are incorporated in the thermophysiology model, the degree of modeling information improves. One of the important input parameters is the mean radiant temperature. Variations in radiant heat fluxes when shortwave radiation is present in the room can be significant. Combining novel scanning and thermography methods together with ray-tracing simulation, we derived a high-resolution thermal model to fully characterize the variations of radiant heat fluxes experienced by different body parts of a human, both longwave (LW) and shortwave (SW). The shortwave heat flux varied in the range of 0-216 W/m2 throughout the day in the experiments conducted in an office room prototype on 23/02/2021 in Fribourg, Switzerland. The radiant temperature experienced by different body parts varied widely, from 24 °C to 58 °C, due to uneven exposure to solar radiation through a window, while the air temperature remained relatively uniform, as it was controlled by a mechanical system. To demonstrate the importance of combining detailed MRT modeling together with the thermophysiology model, we input detailed MRT distribution into the human thermophysiology model, along with the environmental parameters from the experimental measurements. The calculated skin temperatures were compared with the measured ones using iButtons and thermal sensation and comfort values with the survey results collected from the human subject. A combination of these detailed methods can be used as a design tool to assess local (dis)comfort and thermal perception of an occupant exposed to shortwave radiation and for dynamic shading and personalized comfort systems control strategies.

Keywords. Solar radiation, Local MRT, Human thermal comfort, Human thermo-physiology.
DOI: https://doi.org/10.34641/clima.2022.371

1. Introduction

Even in a well-conditioned building, our thermal environment is frequently transient and non-uniform because of the different zonal environments and the solar radiation propagated through the windows. The determination of microclimate conditions of a person inside a space is required in order to achieve a high standard thermal comfort quality in the space where the human activity is undertaken.

Solar radiation passing through a transparent construction has a significant impact on thermal comfort and the indoor thermal environment. Consequently, unshaded windows exposed to excessive sun irradiation can cause overheating as well as undesirable thermal environments in particular areas of the interior space [1]. The massive use of glass as an architectural component in modern buildings, as well as the associated solar radiation, leads to an increase in serious indoor thermal discomfort issues [2]. In contrast, the primary premise of passive solar designs is to increase the use

Copyright ©2022 by the authors. This conference paper is published under a CC-BY-4.0 license.

of solar gain and day lighting in order to reduce the energy used for heating during the winter season without compromising the occupant's thermal comfort. Otherwise, people usually react to the thermal discomfort from the solar radiation by pulling the shading system ON if they have control over it . Finally, indoor thermal comfort in buildings with a large glazing façade is heavily dependent on the direct component of solar radiation on the human body [3].

The Predicted Mean Vote (PMV) established by Fanger is generally used to predict persons' thermal sensation and has been included in the ISO7730 standard [4]. Solar radiation, on the other hand, was not taken into consideration in Fanger's PMV where only the long-wave radiation heat transfer between humans and surroundings is considered. The average values of microclimatic environmental parameters are commonly used to assess occupant global thermal comfort conditions. However, in many situations, the preceding approach does not result in an accurate assessment of individual environmental quality because the variability of environmental parameters around the human body, as well as its transient nature, should be considered in the assessment.

The short-wave radiation fell on the human body has a heating effect, which lead to an increase of the outer surface temperature of the human body and consequently, leads to local warm sensation. Furthermore, local thermal discomfort that is happening due to unpleasant local heating or cooling of a particular area of the body can lead to global thermal discomfort [5]. This can be mainly caused by the stratification height, a high variation in vertical temperature, a large and significant air draft, or radiant asymmetry. The human thermal sensation is the person's thermal perception of the environment, which is related to the local environmental parameters, personal parameters specified as activity level and clothing insulation, as well as the specific body composition such as gender, body fat and BMI.

Therefore, approaches that address this issue require the use of thermophysiological models that can predict human thermal response as a function of both physiological factors and variables that define the surrounding thermal environment. A detailed human thermal model (HTPM) is usually used in order to address the variability in the local thermal environment over the body parts. These models are capable of assessing the skin temperature dynamically as well as other physiological responses. Local skin temperature is the main factor to evaluate in order to project a person's local thermal sensation. HTPMs represent the thermodynamics of human body interaction with the environment and are defined as a set of energy balance equations at each layer of a body segment. These models take the local environmental parameters as inputs, and it's up to the modeller to either consider a uniform or non-uniform environment based on the studied situation. Direct solar radiation on separate body parts is rarely accounted for, but some researchers considered it in the calculation of mean radiant temperature [6], while others used the heat flux directly to the corresponding body part [7].

The multi-node multi-segment HTPM segments the human body into multiple body parts, each part in multiple concentric layers, and all body parts are connected by a blood circulatory system [7-11]. All these models were initially based on the model of Stolwijk [12]. Taking the radiant asymmetric factor into account increases the detailed level of modelling. Furthermore, the results predicted are highly dependent on the subject's posture, the position of the person inside the spaces as well as other individual physiological factors which are variable among individuals. Individual variability has been accounted for in some models such as [7,9]. The contribution of solar radiation to the global thermal comfort and local thermal comfort conditions for a person sitting near a glass window in a building is sometimes underestimated. In this study, the effects of transmitted direct solar radiation, transmitted diffuse solar radiation, inside glass surface temperature, as well as all surrounding surface temperatures have been considered to calculate the local MRT distribution on a 3D scanned human body. A detailed human thermo-physiology model has been used to predict the local skin temperatures, which has been compared with the experimental results. Moreover, a local thermal sensation has been projected based on the person's thermal state from the HTPM simulation.

2. Methodology

The purpose of the simulation is to propose a method that can be relied upon in the design of comfortable indoor spaces where glass and non-opaque facades exist. Solar radiation can be a source of discomfort, especially in warm weather.

We can reduce the number of measurements required by simulating the real-world scenario, especially those that require the person to wear a sensor or answer surveys.

Finding the human local and overall thermal sensation can be achieved by the use of a detailed thermo-physiology model combined with a detailed thermal sensation model.

2.1 Experimental setup

The experiment has been conducted in a facility which can be described as a 1-story office building, that consists of two geometrically identical rooms. The rooms' dimensions are 3.07m width x 6.23m length x 3.10m height. Each room has two double-glazed windows of 2.52m width x 1.83m height, one window is facing north and the other facing south.

The overall U-value of the opaque walls is 0.139 w/m2k, and the windows has a g-value 65%, and average transmittance of 36% over 285-3000nm. Each window has an internal textile roller blind as well as an external Venetian blind.

The room has three radiant ceiling panels. Each panel has the following dimensions of 0.33 m x 3.75 m, and the distance between the panels is 0.31 m. The fresh air is supplied through a circular diffuser located on the east wall with a flow rate of 68.5 m3/h.

2.2 Personal and environmental parameters

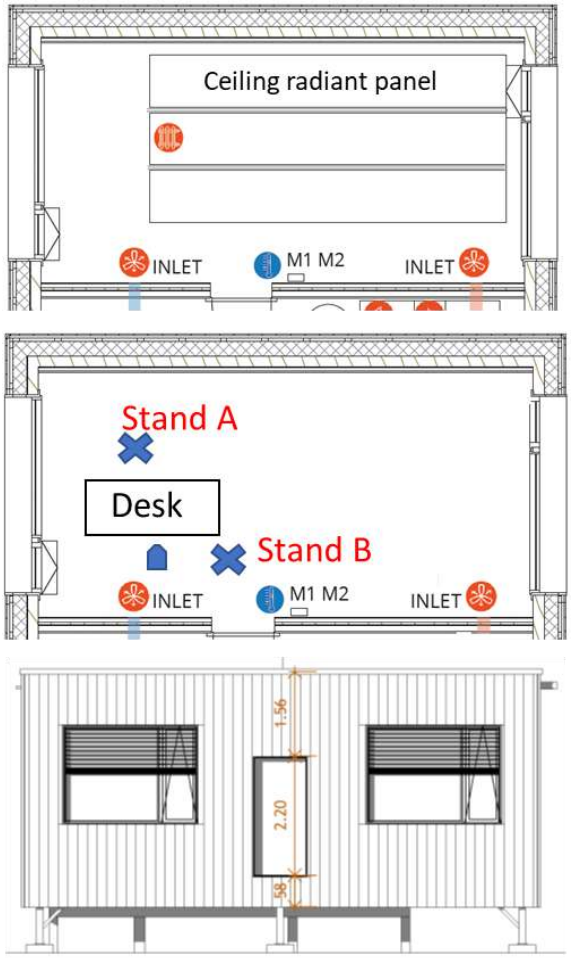

Fig. 1- Representation of the experimental set-up and an exterior and interior image of the facility.

In the experiment, multiple environmental sensors were used. The SPN1 pyranometer (Delta-T, UK) was used to measure outdoor direct, normal, and diffuse horizontal irradiance with an accuracy of ±10 W/m2. The dry bulb temperature and air speed were measured every second on two vertical stands 0.2 m distant from the right of the subject, and 1.2m in front-left of the subject, as shown in Figure 1, and at four different heights (0.1, 0.6, 1.1, 1.7 m), and relative humidity was measured in the centre of the room. Figure 1 depicts the general configuration of the room's environmental sensors as well as an exterior and interior schematic of the facility.

To improve the accuracy of radiant temperature readings, two digital, non-contact longwave measuring equipment were employed. The Scanning Mean Radiant Temperature (SMART) Sensor is a spatially resolved thermal imager that consists of a melexis 90614 five-degree field of view non-contacting medical grade surface temperature sensor (accuracy 0.5°C) and a Garmin LidarLite module (2 cm over 40 m). The sensor rotates on perpendicular axes and records the angular position of the servos, which are then rebuilt using Lidar and temperature data to build a thermal point cloud of the surface temperatures in the scanned area.

The temperature of the skin was recorded at 24 positions of the body, iButton® temperature loggers DS1922L were used (MAXIM Integrated, USA) which has an accuracy of 0.25°C. 14 out of the 24 sensors position were chosen as recommended in the standard ISO 9886:2004 which can be used to do the 14-point weighting scheme. The other locations were used to check the differentiation between left and right. Figure 2 presents a schematic of the skin temperature sensor's position on the human body. During the experiment the subject was wearing a short-sleeve T-shirt, denim pants, sneakers, ankle socks, and underwear with an overall clothing insulation of 0.57 clo.

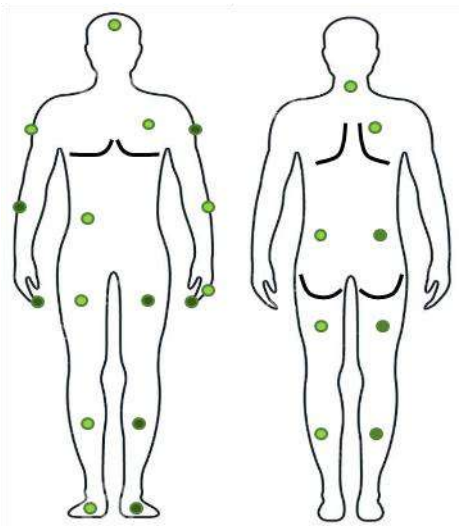

Fig. 2- skin temperature sensor location front and back and image of the subject during the experiment.

The metabolic rate was considered to be 1.2-1.4 met as the person was sitting performing office work. The variation in metabolic rate between the morning and afternoon was considered in addition to the effects of brake activity.

The subject body compositions are stated in table 1.

Tab. 1 - The subject's body composition.

Sex	Age	Hight (m)	Weight (kg)	Fat Percent. %	Body surf. area (m^2)
M	29	1.75	72.9	28.2	1.98

2.3 Experimental scenarios

The averaged environmental parameters of the three experimental scenarios are presented in table 2. The three scenarios can be described as follows, in all the three experiments the blinds of the north window were set down. The blinds were kept up in the south window for both experiment I and II but were down in experiment III. In each experiment the subject was sitting for one hour during each session the SMART sensor scans all the surfaces twice (once every half-hour). The three experiments were conducted during one day and the time of each session is shown in table 3.

Tab. 2 - The inputs of the parameters for the PMV thermal comfort model.

	Exp I		Exp II		Exp III	
T_air (°C)	23.3	24	25.1	26	24.7	24.5
V_air (m/s)	0.05	0.05	0.1	0.1	0.04	0.05
RH %	25	25	21	22	23	24

Tab. 3 - Time of the experiments in the day

	Session	Time of the day
Exp I	a	10:17-10:47
	b	10:52-11:22
Exp II	a	13:12-13:42
	b	13:47-14:17
Exp III	a	15:34-16:04
	b	16:15-16:45

2.4 Simulation setup

In this study we chose to consider local air temperature and air velocity data measured from the experiment although those values could be calculated through a CFD model.

Three separate sessions have been performed in the experiment, where all measured skin temperature data has been compared to simulation results. In the simulation, the initial conditions are always required, and to simplify, we ran the HTPM model over the whole day, considering that breaks are conducted in a uniform environment of 25°C operative temperature.

2.5 Local air temperature

In the simulation we took the detailed air temperature distribution from the experimental results at four different heights to assign the local body air temperatures. Local air temperature was measured in the experiment using two poles located to the subject's right and front left. Figure 3 shows the air temperature corresponding to each body part.

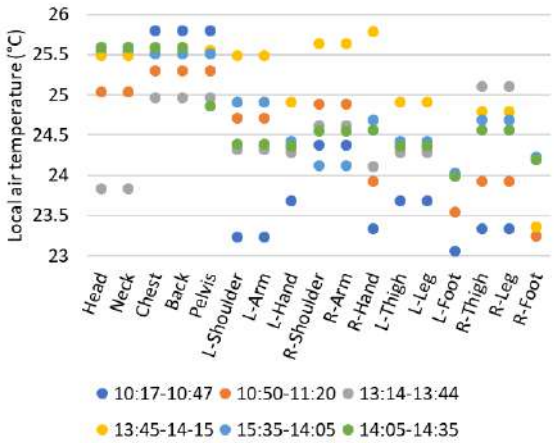

Fig 3- Local air temperature

2.6 Mean radiant temperature

The local mean radiant temperature was calculated through a sophisticated ray-tracing method in the Grasshopper algorithmic modelling tool within the Rhino 3D environment, allowing for five-phase radiation bounces within the room. The radiant heat transfer model accounts for the interreflections from room surfaces with the use of high-resolution geometric models combined with material properties and surface temperature of all exposed surfaces in the room. For each test point on the body surface, heat flux vectors emanating from the point are traced through bounces, during which the radiant heat exchange at each intersection with the surrounding surfaces can be calculated. The details of this method can be found in our previous papers [13].

The 3D room mesh model was built in Rhino with a 0.1 m × 0.1 m grid size. The human 3D body model was obtained from performing a 3D scan and subdivided into 3,916 surfaces based on the 17 segments used in the thermo-physiology model. The reflectivity of the main surfaces indoors can be different for shortwave or longwave radiation, e.g. floor-0.05 for LW, 0.16 for SW; wall and ceiling-0.1 for LW, 0.7 for SW. The transmittance of the glazing that allows solar radiation coming in is 0.36.

The simulation contains shortwave and longwave components, which need different inputs. For the longwave irradiance simulation, the surface temperature was majorly measured with a high-resolution thermal array scanning and mapping platform named SMART [15], which can spatially resolve surface temperature into 3D thermal point clouds. Together with the use of thermocouples and

thermography, surface temperature of all exposed surfaces were obtained and connected to the geometric model in a 3D environment. The body skin and clothes temperature were measured with wearable temperature sensors and the surface temperature of the clothed body of 14 locations were used to create the body temperature mesh. In the shortwave component, an environmental plugin in Grasshopper named Honeybee was used to calculate the shortwave irradiance on every body surface of a specific date and time with additional inputs of geographic location and measured solar irradiance.

For each body surface, the radiant temperature can be derived from the combination of shortwave and longwave portions. The radiant temperature of smaller segments varied from 24.8 to 58.5 °C across the body, and the range was narrowed to 26.4-43.1°C when averaging the data of small segments within every one of the 17 segments. Figure 4a shows the local mean radiant temperature of the 17 body parts, which correspond with the body part segmentation shown in Figure 2. The areas exposed to direct sunlight from the left, e.g. left side of the head, abdomen and both arms, had significantly higher radiant temperature than other parts. By averaging the radiant temperature of all segments with the surface area of the segments as weighted coefficients, the whole-body MRT can be calculated. The human subject had the highest MRT above 33 °C in the second session and the lowest in the third session, as is shown in Figure 4b.

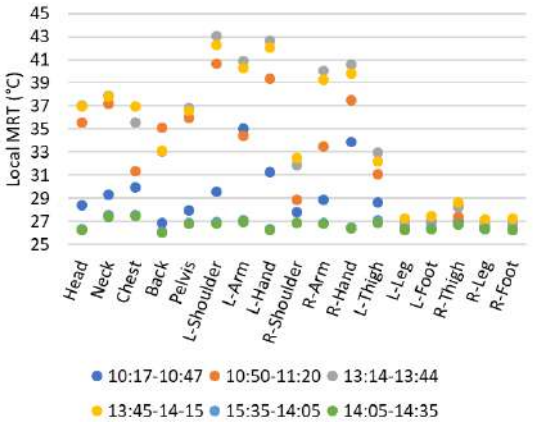

Fig 4b- Local radiant temperature for different segments at different time steps

2.4 Human thermo-physiology model

In this study we have adopted the human thermo-physiology model JOS3 as an open source model developed by [7]. The model initially includes 17 body parts including the head, neck, chest, back, pelvis, right and left shoulders, arms, hands, thighs, legs, and feet. We have further improved the model to account for the 10 fingers. The model is personalized by taking the age, gender, height, weight and body fat of each subject into account. As mentioned in Table 1 all the body composition has been considered in the simulation. By evaluating the local (Tskin,i) and mean skin temperature (Tskin,mean) output from the HTPM, we can project

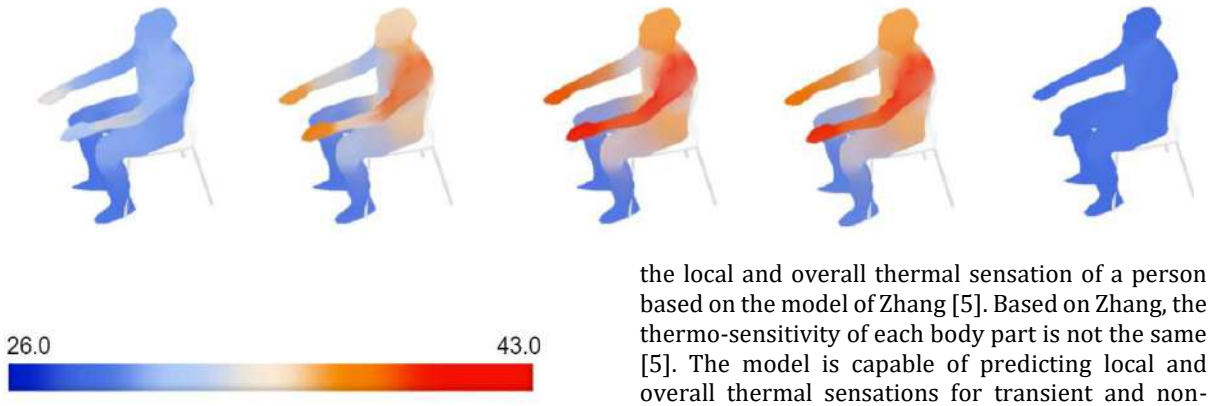

Fig 4a- Illustration showing body segment planar radiant temperature variations during the experiments

the local and overall thermal sensation of a person based on the model of Zhang [5]. Based on Zhang, the thermo-sensitivity of each body part is not the same [5]. The model is capable of predicting local and overall thermal sensations for transient and non-uniform environments. Where the local sensation is a function of local skin temperature and is given by the following equation:

$$S_{body\ seg} = 4 * \left(\frac{2}{1+e^{-C_1\left(T_{part,skin}-Tset_{part,skin}\right)-K_1\left[\left(T_{part,skin}-T_{mean,skin}\right)-\left(Tset_{part,skin}-Tset_{mean,skin}\right)\right]}} - 1 \right) + C_{2i}\frac{dT_{part,skin}}{dt} + C_{3i}\frac{dT_{core}}{dt}$$

Where S is the local sensation and $body\ part\ C$ are cold and warm coefficients 1, $K1$, $C2i\ and\ C3i$ based on Zahng's model [12].

3. Results

3.1 Local and mean skin temperature

To evaluate our simulation results, we have compared the mean skin temperature along with the local skin temperatures to the measured ones from the experiment. As mentioned previously, three different sessions represent three different times of the day with different solar radiation intensities affecting the subject. Figure 5 represents the temperature comparison between the simulation and experimental data. The figure has 6 sub-figures, each representing the data corresponding to one experimental set-up. From the results, we can see that the thermo-physiology prediction showed some agreement with the experimental results in multiple body parts. Where the head skin temperature showed an acceptable agreement, especially in the first and last sessions, in the second session the difference exceeded one degree centigrade. The hand skin temperature showed good agreement in the second session but deviated at the end of the first session as well as in the third session, where results showed the largest discrepancy. The shoulder skin temperature showed acceptable agreement in the second and third sessions, but differences were greater in the first session. In general, the mean skin temperature, on the other hand, was acceptable in the three sessions, with less than 0.5°C in the third session and the highest discrepancy of around 1°C in the second session.

Those differences could be due to multiple reasons, where the most come from the detailed physiology model, since the physiology model considers a generalised physiological set point and we are comparing it to one specific subject. Secondly, the MRT calculation has been conducted on a half-hour basis and it is considered constant in the simulation during that time.

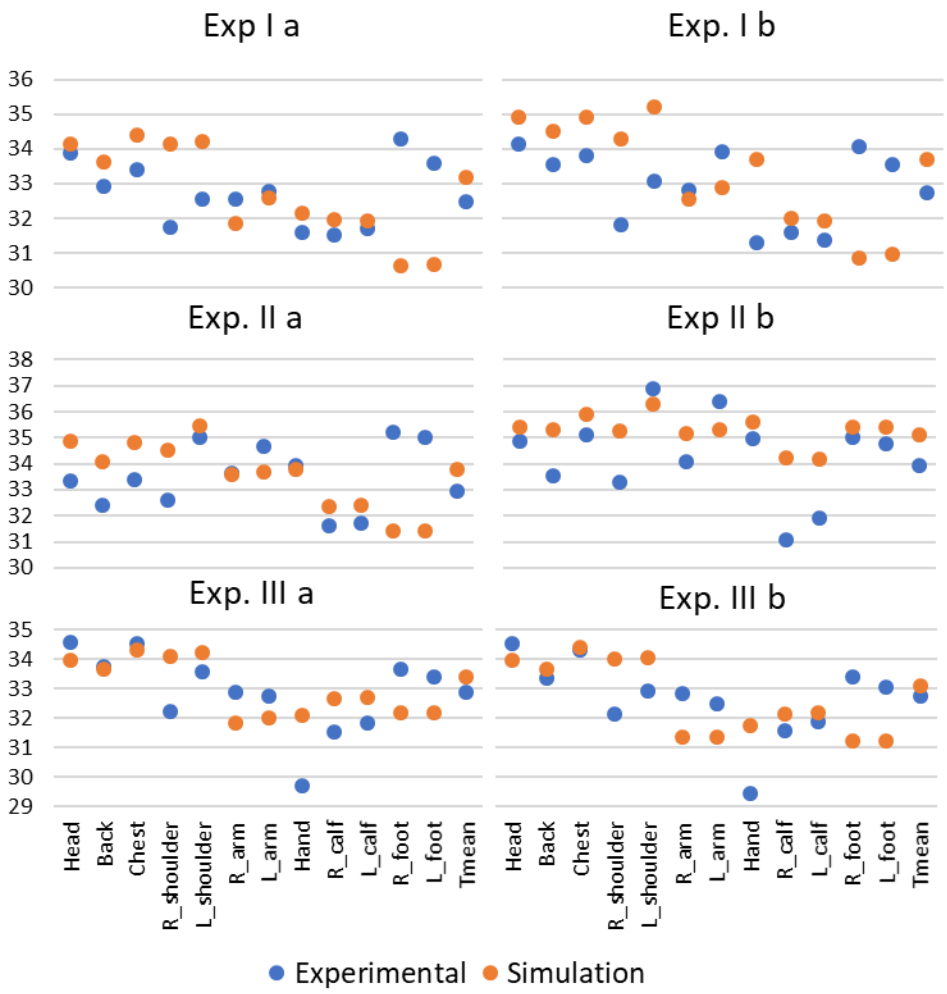

Fig 5- Experimental vs. simulation results at different body parts

4.2 Local and overall sensation

The physiology model has been linked to a detailed local sensation model of Zhang (2010). The results from the model showed that during the first session when MRT showed elevated values in the second half-hour of the session reached 31 °C, the overall sensation increased from neutral to warm with a value of 2 on the 9-point scale. In the second session, MRT was high during the whole period, and that was reflected in the overall sensation with a value of +3,

which corresponds to "Hot". As for the third session, the solar radiation was almost negligible, with MRT values fluctuating around 1°C higher than the air temperature, the overall sensation was in the neutral range. Looking at the local sensation values as Figure 6 shows, the sensation of the head was the highest and the most sensitive body part toward the elevated temperature. The differences between the left and right can be seen in the shoulders, where sensation has higher values for the left shoulder, especially during exposure to solar radiation. The difference in sensation between the left and right shoulders was around one point on the nine-point scale, moving the shoulder from neutrality to slightly warm.

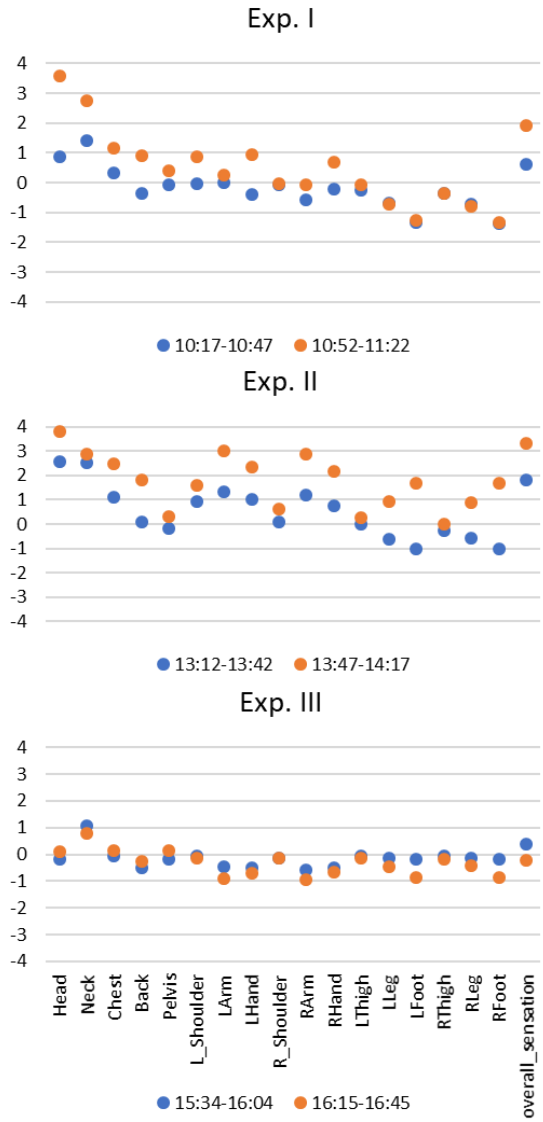

Fig. 6 Local thermal sensation and overall sensation prediction over the different experimental sessions.

4. Discussion

Based on the local skin temperature, it is clear that the effect of solar radiation had more influence on the left part of the subject. The shoulders showed the highest difference in experiment II-b, where the solar intensity was the highest. The differences between left and right were clearer in the simulation from Experiment I-b, especially between the arms and shoulders. During the experiment, the subject conducted a survey of thermal sensation and thermal comfort. From his voting, it seems the environment was neutral in both exp. I and III, but exp. II showed a warmer sensation. The subject felt warm in the following body parts: head, chest, back, left shoulder, left arm, and left hand. Based on the thermal sensation results, we can see that the simulation indicated a warm environment in the second half of the experiment I, overall sensation in experiment II, showed warm and hot results. In the third experiment, the results showed a neutral thermal sensation, which is expected due to the non-presence of solar radiation. In general, the results comparison shows that although there are some discrepancies in the local results, the model still follows the physiological response behaviour of the human subject.

5. Conclusion

The indoor environment is heterogeneous and non-uniform, and consequently, accounting for the non-homogeneous nature of the environment in the design process increases the accuracy and the expectation of the design. The heat stress that can occur as a result of direct exposure to solar radiation places the occupant in an uncomfortable situation. Even in the case of partial body exposure to solar radiation, this can affect the whole-body thermal state, as our results showed. This paper presented a detailed approach to calculating the local MRT of a person seated close to a window.

The simulation results showed an acceptable correlation with the experimental results. Even so, there is still room for improvement in order to achieve better accuracy. For instance, the model needs to be tested on multiple subjects, for which different subjects need to be included in the experiment. Moreover, the MRT calculation was happening every 30 minutes, and that could be improved by shortening the duration to 10 minutes in order to better account for the variability of the environment. A thorough investigation and development needs to be conducted on the human thermo-physiology model in order to achieve better accuracy in local skin temperature as some body parts showed higher values compared to the experimental ones.

6. References

[1] Arens E, Hoyt T, Zhou X, et al. (2015). Modeling the comfort effects of short-wave solar radiation indoors. Building and Environment, 88: 3–9.

[2] Arens E, Heinzerling D, Paliaga PE (2018). Sunlight and indoor thermal comfort. ASHRAE Journal, 2018(7): 12–21.

[3] La Gennusa, M., Nucara, A., Pietrafesa, M., & Rizzo, G. (2007). A model for managing and evaluating solar radiation for indoor thermal comfort. Solar Energy, 81(5), 594-606.

[4] ISO, ISO7730. "7730: Ergonomics of the thermal environment Analytical determination and interpretation of thermal comfort using calculation of the PMV and PPD indices and local thermal comfort criteria." Management 3.605 (2005): e615.

[5] Zhang, H. (2003). Human thermal sensation and comfort in transient and non-uniform thermal environments. University of California, Berkeley.

[6] Staiger, H., & Matzarakis, A. (2020). Accuracy of Mean Radiant Temperature Derived from Active and Passive Radiometry. Atmosphere, 11(8), 805.

[7] Takahashi, Y., Nomoto, A., Yoda, S., Hisayama, R., Ogata, M., Ozeki, Y., & Tanabe, S. I. (2021). Thermoregulation model JOS-3 with new open source code. Energy and Buildings, 231, 110575.

[8] Huizenga, C., Hui, Z. and Arens, E., 2001. A model of human physiology and comfort for assessing complex thermal environments. Building and Environment, 36(6), pp.691-699.

[9] KINGMA, B. R. M. Human thermoregulation: a synergy between physiology and mathematical modelling. 2012.

[10] Tanabe, S. I., Kobayashi, K., Nakano, J., Ozeki, Y., & Konishi, M. (2002). Evaluation of thermal comfort using combined multi-node thermoregulation (65MN) and radiation models and computational fluid dynamics (CFD). Energy and Buildings, 34(6), 637-646.

[11] Fiala, D., Lomas, K. J., & Stohrer, M. (1999). A computer model of human thermoregulation for a wide range of environmental conditions: the passive system. Journal of applied physiology, 87(5), 1957-1972.

[12] Stolwijk, J.A., 1971. A mathematical model of physiological temperature regulation in man (No. NASA-CR-1855). NASA.

[13] Aviv, D., Gros, J., Alsaad, H., Teitelbaum, E., Voelker, C., Pantelic, J., & Meggers, F. (2022). A data-driven ray tracing simulation for mean radiant temperature and spatial variations in the indoor radiant field with experimental validation. Energy and Buildings, 254, 111585.

[15] Guo, H., Aviv, D., Loyola, M., Teitelbaum, E., Houchois, N., & Meggers, F. (2020). On the understanding of the mean radiant temperature within both the indoor and outdoor environment, a critical review. Renewable and Sustainable Energy Reviews, 117, 109207.

Towards the integration of air chemistry and building simulation models IAQ assessment

Jeroen van 't Ende [a, b], Mihalis Lazaridis [b], Christian Struck [a], Annemarie Weersink [a]

[a] Chair of Sustainable Building Technology, School of Business, Buildings & Technology, Saxion University of Applied sciences, Enschede, the Netherlands, j.a.n.vantende@saxion.nl.

[b] Faculty of Environmental Engineering, Technical University of Crete, Chania, Greece.

Abstract. To limit greenhouse gas emissions, energy efficiency measures are applied at a large scale resulting in buildings becoming more airtight. Indoor environmental quality depends strongly on ventilation rates. Whilst controlled ventilation contributes to the reduced use of fossil fuel, too little ventilation increases the risk of health-damaging concentrations of pollutants in the indoor environment. There are three primary sources for pollutants indoors (1) ventilated outside air, (2) emissions from activities such as cooking and cleaning and (3) longitudinally emitted pollutants from people, building components and furnishings. Some accepted primary pollutants to assess indoor air quality are CO2, Volatile Organic Compounds (VOC) and OH. However, indoor chemistry studies indicate the presence of a great amount of complementary secondary pollutants with potentially health-damaging effects. Secondary pollutants indoors are the result of chemical reactions of pollutants with solar radiation as an energy source and ozone/other oxidants. Little is known about the type of resultant secondary pollutants and their effect on human health. One approach to assess the effect of secondary pollutants on indoor environmental quality is to integrate chemical box models with building simulation models, e.g. computational fluid dynamics. In this contribution, the authors provide an overview of the state of the art in integrated simulation models of air chemistry with building performance. A reduced-order case study will be presented comparing methods and identifying key parameters for indoor air quality, including selected secondary pollutants. Additionally, a conceptual framework is presented for assessing the impact of secondary pollutants on human health.

Keywords. CFD, Adverse health effects, simulation, breathing, mannequin
DOI: https://doi.org/10.34641/clima.2022.374

1. Introduction

In atmospheric models, chemical models such as Master Chemical Mechanism (MCM) [5] can be used to describe the breakdown of compounds in the open atmosphere. A tool like [1] combined with [19] can easily run "chamber" experiment simulations. In indoor air quality assessments, such models are not available and detailed chemical analysis, in general, is not applied. The current state of indoor air quality and key priorities to focus on were identified by [9], among others, it was found that indoor gas-, solid- and liquid-phase chemistry potential needs to be assessed. In the European Union (EU) VOC are defined as:

"VOC shall mean any organic compound having at 293,15 K a vapour pressure of 0,01 kPa or more, or having a corresponding volatility under the particular conditions of use."[2]. The standards used are similar but still widely different, there is no agreement on what VOC exactly are. One example, formaldehyde, is considered to have strong adverse health effects and is also measurable in most indoor environments. This pollutant is primarily emitted by furniture, glues, paints, resins and wood.

Human activities such as sports, cooking and cleaning will also cause increased levels of pollutants. When using liquid cleaning agents to clean the floor, a large surface area is covered in a thin film. This promotes evaporation of the cleaning agent. Limonene is commonly used as a solvent in cleaning products, therefore this is a realistic scenario. It is also used as a flavouring agent and is known as the "fragrance" of oranges. In [12] an experiment has been conducted under controlled conditions: the limonene concentration and reaction products under oxidative stress of ozone are simulated through a Computational Fluid Dynamics (CFD) package. To gain more information about the healthiness of indoor air, toxicological databases are available. This combined with known reaction constants and pathways for breakdown makes it

Copyright ©2022 by the authors. This conference paper is published under a CC-BY-4.0 license.

possible to simulate these effects on a relatively small scale.

1.1 Research objective

The objective is to specify a way to translate the air chemical content to a health effect index. One objective(s) that can be distilled from above is: to provide a methodology to study indoor gas-phase chemistry. This includes primary pollutants introduced by ventilation (or surface emissions) and secondary pollutants introduced through chemical reactions. This is one of the main concerns of this effort.

1.2 Species of interest

Lower Ozone concentrations are found indoors compared to the outdoor environment [14], therefore it is an interesting gas to monitor that is likely involved in the breakdown of VOC. Furthermore, Limonene is studied because it is widely available. Since the Smart Tiny Lab (STL) building is new, it is suspected that formaldehyde is being emitted from new building materials like Oriented Strand Board (OSB). The methodology described will be limited to the chemicals **Limonene**, **Ozone** and **Formaldehyde** bur is not limited to these chemicals, it is applicable in a wider context.

2. Literature

In classical terms, Indoor Air Quality (IAQ) is defined as a combination of temperature, humidity and (chemical) pollution. In terms of pollution, it is common to look at CO2 or VOC concentrations. Open Field Operation And Manipulation (OpenFOAM) [21] can be used to model air. OpenFOAM has many built-in solvers and examples, the general workflow is to find an example that is close to your problem and adjust a copy of the example case to your custom case. For more advanced problems, the solver can be changed/rewritten. Depending on what you want to simulate, different simplifications can be made. OpenFOAM does this by providing the end-user with different solvers which are set up for specific simplifications such as incompressible flow, no heat transfer, particle tracking, transient or steady-state, multi-species, combustion, chemical reactions and more.

2.1 CFD model

The most sophisticated models applied here, use the rhoReactingBuoyantFoam "standard application" from OpenFOAM. This is a multi-species, density-based solver which supports chemistry.

A Reynolds-averaged-Simulation (RANS) with K-epsilon model is used for Momentum transport, this model can be applied when the phenomena of interest are far away from turbulent phenomena. All eddies are averaged out. So make sure that Reynolds numbers are low, and well in the laminar region. Or make sure that the turbulent phenomena do not matter.

2.2 Material emissions

In [18] different sources of formaldehyde are identified and investigated with Monte-Carlo methods. The generated normal distributions can be used to assign emissions to wall elements in the room model. Wall coverings have been found to emit 0.5 $\frac{\mu g}{m^2 h}$. For OSB material mean emissions of 43$\frac{\mu g}{m^2 h}$ have been found. Since the structure is well known, these emissions can be taken into account. In [12], chemical equation (1) is used, all reaction products are summarized in C_{prod}.

$$C_{10}H_{16} + O_3 = C_{prod} \qquad (1)$$

$$k(T) = Ae^{\frac{-B}{T}}\left(\frac{T}{300}\right)^n \qquad (2)$$

The Arrhenius equation (2) and the following constants $A = 1.752e^{-15}$ $[cm^3 mole^1 s^{-1}]$, $B = 0$ and $T = 770$ allow for accurate concentration profiles. See Chapter 3 for more details. The Arrhenius rate constants are found in [15]. Note that the found A value has to be converted through Avogadro's constant: N_a = $6.022141 \cdot 10^{23}[mol^{-1}]$ to work correctly with OpenFOAM.

2.4 Respiration model

For the second simulation shown in chapter 3.2, A breathing model needs to be incorporated. The mannequin generating tool DINED [4] is suitable for generating the required 3D geometry. The tool allows the user to generate a realistic 3D human model based on a large number of 3D scans.

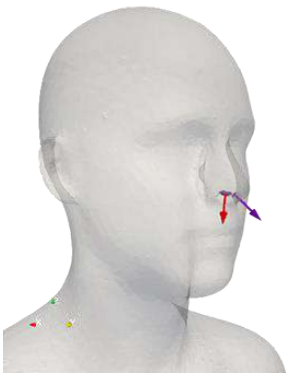

Fig. 1 - Normal vectors for the involved flow areas, respectively: 4.47332 · 10−5[m2] of the left, purple area. and 2.38476 · 10−5[m2] for the right, red area.

Since the 3D models generated by DINED are realistic, the existing geometry around the nose can be used to determine the involved flow areas. This is shown in **Fig. 1.** The total flow-area, from and to which the breathing occurs needs to be combined with a changing speed vector. The combination of these will lead to airflow in $[L \cdot min^{-1}]$. The total "breathing" area is $4.47332 \cdot 10^{-5} + 2.38476 \cdot 10^{-5} = 6.85808[m^2]$

This airflow should line up with standard figures that can be found for normal human breathing under rest conditions [8]. The breathing volume per minute ranges from 6[L] to 8[L] per minute. The average adult takes 12-15 breaths per minute [8]. The breathing rate has been set to 0.23 Hz, which equals 1/0.23 = 4.34 seconds for one breathing cycle, and 60/4.34 = 13.8[$breaths\cdot min^{-1}$]. Combining all the above characteristic numbers, a simple breathing model was made and has been visualized in **Fig. 2**, the green line shows the accumulated exhaled air over one minute, where the red and blue lines show the inhalation rate, and total breathing cycle rate. The last value of the green line,

5.37[$L\cdot min^{-1}$] equals the breathing rate per minute.

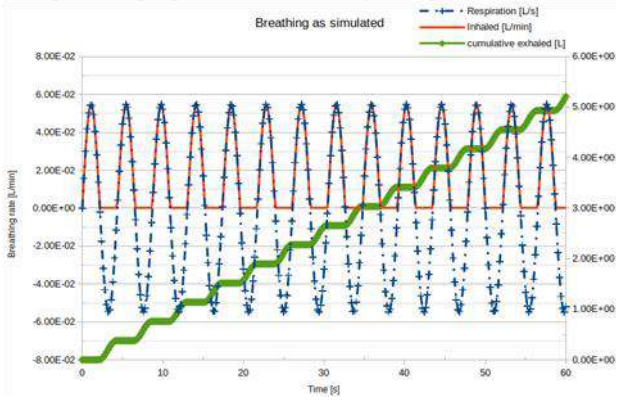

Fig. 2 - Breathing rate as simulated in OpenFOAM with a target volume of 650[L·min^{-1}].

2.5 Toxicity indexes

With toxicological dose descriptors, the relationship between effects and the dose is described. To describe different effects, different dose descriptors have been called into life by toxicologists. Some important ones are:

1. Lethal Concentration 50% (LC50) in [$mg\cdot L^{-1}$] or [ppm] and sometimes [$mg\cdot L^{-1} \cdot 6h^{-1} \cdot day^{-1}$]. These values are used for gases.
2. No Observed Adverse Effect Level (NOAEL) or *NOAEC* for gases.
3. Lowest Observed Adverse Effect Level (LOAEL) or *LOAEC* for gases.

Repeated dose Toxicity tests provide valuable information about chemicals. NOAEL or LOAEL can be derived and specific target organ toxicity can be determined. In **Tab. 1,** 6 categories of toxicity tests are given, in general, the above-mentioned dose descriptors can be categorized under one of those 6 categories.

Data availability

One of the biggest challenges in IAQ and toxicology is the vast amount of chemicals from which the exact properties are required. The availability of good and reliable measurements varies widely from species to species and in general data availability is sparse, unless it concerns a common species. Nonetheless, multiple systems try to index all available information, the following list shows sources that have been consulted and proved useful.

1. Pubchem [17] and Pubmed [7] contain chemical and medical information for most species.
2. Eurochamp [3] contains gas-phase reaction-rate constants.
3. Comptox [22] Computational toxicology chemicals dashboard.
4. GenRA [11] Generates Read-Across predictions by looking at properties of nearest k neighbours.

In particular, the GenRA tool is very useful, it can generate predictions of toxicological values by looking at similar chemicals. This is *not* accurate or realistic, but most probably better than a random guess. To generate a ReadAcross prediction for a given compound, the following steps are taken with genRA:

1. select the chemical of interest (in this example Ozone)
2. Evaluate the proposed analogues and check data availability from different databases
3. Data gap analysis, possibly filter analogues that contradict the majority
4. generate genRA prediction for the chemical of interest and export data

It is expected that with time, the predictions of genRA will improve if new measurements of toxicological effects are continued to be added to the database. This means that this method of calculating a health index will also gain some accuracy.

2.6 Health index calculation method

In the GenRA [11] database, the effect types as shown in **Tab. 1** can be found. These effects cannot be ranked on *severity*, since there is an overlap between effects. Still, it is clear to see that the long-term consequences of **MGR** effects are by far the worst. The first 3 effects can "cross" to offspring, which gives it a higher score. Where **CHR** is the worst for the individual according to this created rating. The severity rating will later be used as a weight to scale to the total.

Tab. 1 - Toxicity testing types normally used to determine Derived No Effect Levels.

Effect types	severity	Explanation
MGR	1	Multigenerational reproductive toxicity
REP	0.9	reproduction/developmental toxicity

DEV	0.8	Prenatal Developmental toxicity
CHR	0.7	Chronic toxicity
SUB	0.6	Subchronic toxicity
SAC	0.5	Sub-acute repeat dose toxicity

For each of the mentioned types in **Tab. 1**, there are between 1 to 129 different toxicity effects defined, ranging from specific organ toxicity to death.

It is good to realize that there is a lot of information behind the 6 categories in 2.1, note that *none* of the effect types has all 129 effects defined, this is a product of the subset that has been selected. Most predictions have high p-values and are not considered significant, p-values might go down in the future when more measurements are added to the database.

Overall values will be calculated for the 6 categories and per gas. The Adverse Effect Index (AEI), AEI_{test} value essentially consists of 3 calculated values.:

1. A reliability weight to compensate for low data availability, and thus more uncertainty.
2. A positive-test weight to incorporate the predicted values from genRA.
3. The severity weight(s),$S_{gas,test}$, mentioned **Tab. 1** to account for the range of severeness.

$$\eta_{gas,test,rel} = \frac{129}{Tox_{gas,test,available}} \quad (3)$$

The reliability weights are calculated through equation (3). The total amount of effects for $Tox_{O3,CHR,available}$ would be 101 according to figure 2.4, the 129 comes from the maximum amount of tests possibly available in the genRA database.

$$P_{gas,test} = \frac{Tox_{gas,test,available}}{\Sigma(Tox_{gas,test,magnitude})} \quad (4)$$

The positive-test weights are calculated in equation (4) The total amount of effects for the test category and gas are divided by the sum of available magnitudes for the same combination of gas and test. With the above example into consideration, the weight would become: $P_{O3,CHR} = \frac{101}{\ldots+0.872+\ldots}$ where *0.872* is part of the sum.

$$AEI_{gas,test} = P_{(gas,test)} \cdot S_{gas,test} \cdot \eta_{gas,test,rel} \quad (5)$$

Now the 3 weights can be multiplied as shown in equation (5) and all $AEI_{gas,test}$ can be calculated.

$$x_i = \frac{X_{max} - X_i}{X_{\max} - X_{min}} \quad (6)$$

As the last step, the found weights will be normalized through equation(6), where X_{max} and X_{min} will be taken from all found *AEIgas,test*.

2.7 Health index concept result

An example matrix where the above method was applied is shown in **Fig. 13**, the matrix represents the strength of the effect type definitions from **Tab. 1**. The matrix has been normalized because this method relies on working with non-physical weights, for this to work, concentration data also needs to be normalized before being post-processed with this matrix.

The steps are as follows to apply this matrix to a CFD simulation where gas concentrations are available:

1. Normalize the CFD gas concentrations through equation (6).
2. Normalize over the time of interest (multiple time steps, larger set for finding X_{max} and X_{min}) or only one timestep of interest.
3. Multiply the normalized concentrations with the coefficients for the same gas, do this per *Effectgroup*/test.
4. A positive-test weight to incorporate the predicted values from genRA.
5. The weight(s),$S_{gas,test}$, mentioned in table 2.1 to account for the range of severeness.
6. Take the average of the *Effectgroups* per gas, this gives you a total health index on gas-level.
7. Take the average of all the gas-level health indexes for a specific location and a true *AEI* index is defined.
8. As a final step, the average for a complete simulation/space can be taken to get a total average.

It is important to be aware of the limitations of this technique, no absolute *limits* or *concentrations* are calculated so it should not be used to determine absolute limits. It can be used to assess the *relative* healthiness of different locations within the same space, simulation, or at least under very similar conditions. The current categorization can be improved by expert knowledge, the scripts used for generating above have taken this into account and can easily be adjusted to alternate categorization schemes.

3. Experiments

2 Simulations have been conducted with OpenFOAM .org Version 9. The first simulation is briefly shown below in **Fig. 3**. The shown simulation involves A coarse human breathing model The mannequin is used to study the effects of humans on indoor air.

At the Saxion university of applied sciences, a test room is available. Limonene concentration from cleaning activities will be simulated and Formaldehyde emissions from the building materials.

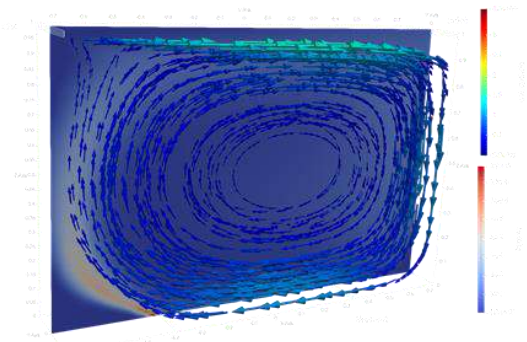

Fig. 3 - Geometry overview of the reproduced case study [12]

The case study presented in [12] has successfully been repeated with similar results. Proving that the chosen toolchain, OpenFOAM and ParaView are capable of solving similar problems. Reaction constants have been retrieved from [15]

3.2 Smart tiny lab summary

It has been established in chapter 3.1 that the developed model is adequately accurate to approach indoor species concentrations. In this chapter, the details of the case study will be shown

A building for testing the integration and overall performance of building coupled installations and IAQ test lab has recently been built at the Saxion University of Applied Sciences.

A mesh model of the STL for CFD purposes has been created initially with a 5 cm grid-scale. There are no simplifications in terms of 2D-case or mirroring possible within the room. The test chambers are geometrically identical, so results can be mirrored for the right test room (room 2). A graphical representation of the room is shown in **Fig. 4**.

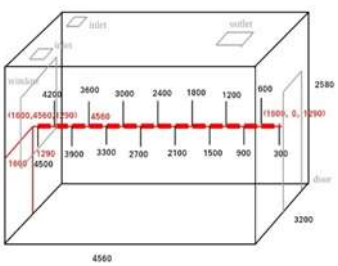

Fig. 4 - Schematic drawing and central line

3.3 Experiment 4: Breathing model

In this simulation, human breathing is simulated, see **Fig. 5** for the geometry. The following contour plots are taken from the other side, facing the mannequin. The groundwork for the breathing model is shown in 2.4.

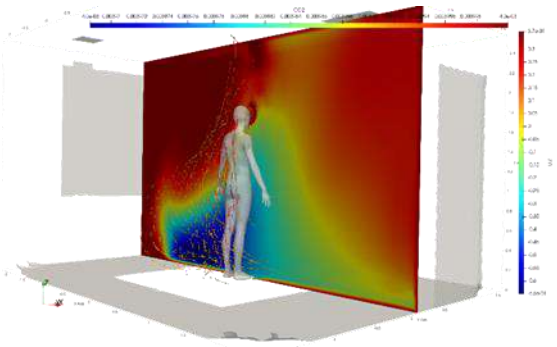

Fig. 5 - Visualization of simulation, the mannequin has a body temperature of 306.95[K], the exhaled air has a temperature of 309.15[K].

There are several reasons why it is interesting to simulate a mannequin with a realistic body temperature and breathing cycle.:

1. A realistic body temperature can be set, this will cause free convection and significantly alter the exposure.
2. By simulating the change of chemical content, CO2 levels will increase over time, another known gas with adverse health effects
3. The simulations that were generated before will be significantly different with density-driven free-convection, caused by the mannequin body temperature.
4. It requires more computational power to do these simulations, mainly because of the more complex geometry.

The mix of exhaled air needs to be adjusted, according to [20] the exhaled CO_2 concentrations under normal breathing are around 4 ≈ 5%. The exhaled water content is also slightly higher, all increases in exhaled gas concentrations are deducted from the exhaled oxygen since this is the gas being used in the process. The mix for exhaled air is shown in **Tab. 2**.

Tab. 2 - Respired gas concentrations

Concentrations		
Gas	Respired	Gas
CO_2	4.0 %	CO_2
O_2	17.09 %	O_2
H_2O	1.5 %	H_2O

Fig. 6 shows the breathing cycle measured at the emitting surface. It can be seen that this can be used to determine exposure more realistically. The inhaled CO_2 can be calculated through equation (11), or directly through the breathing rate of 5.1[$L{\cdot}min^{-1}$] from **Fig. 2**.

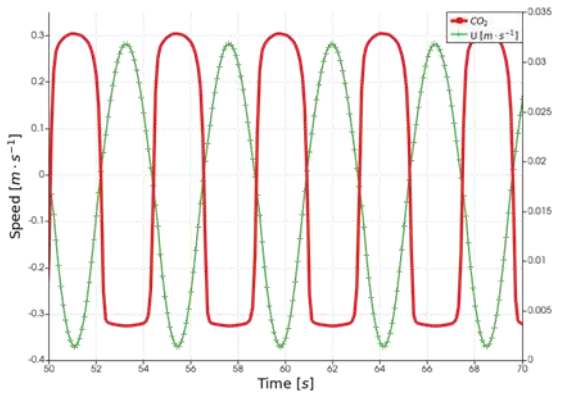

Fig. 6 - Speed U left, CO2 right. Note that the CO2 concentration fluctuates between 3.8% (exhaled) and 0.42% (inhaled)

$$\sum Cgas,i \cdot \Delta ti \qquad (11)$$

The variable Δt_i in equation (11) stands for the time interval of the data, $C_{gas,i}$ denotes the specific gas concentration at that time. This can be applied only where the speed vector is negative, $U < 0$.

Fig. 7 shows the inhaled/exhaled gas concentration, these coincide perfectly with **Tab. 2**. Since the ozone concentration is initialized as zero, it can be observed that the concentration increases with each breathing cycle.

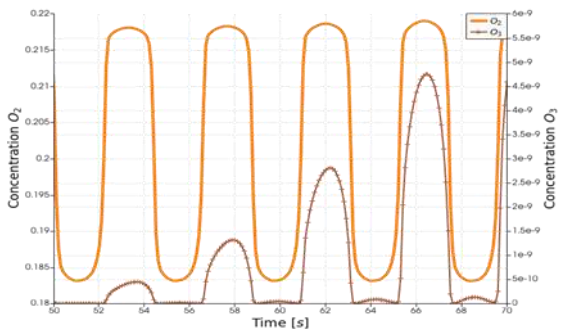

Fig. 7 - Inhaled/exhaled gas, Concentration oxygen left, ozone right. Note the difference in inhaled/exhaled oxygen.

Concentration over time

Fig. 8 shows how ozone and Limonene rapidly shoot up in the first time-steps. After around 25[s] the concentrations are high enough for the reaction towards C_{prod} to kick in.

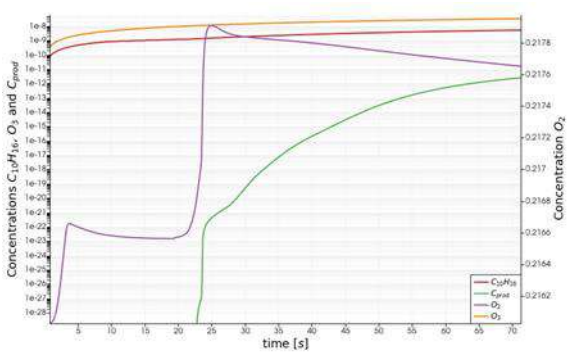

Fig. 8 - Note that the right axis of 3.10 is zoomed in, these initialization effects are less visible on larger scales.

Contour Plots

The contour plots shown below can be compared to the AEI contour plots to understand how concentrations and AEI relate. In **Fig. 9**, Higher concentrations of Ozone are visible close to the inlet and moving towards the person.

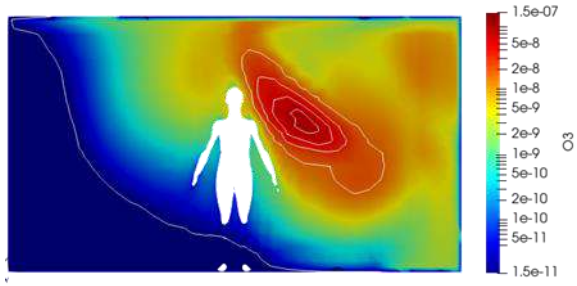

Fig. 9 - Ozone concentrations location Mid-Y

Fig. 10 shows high concentrations close to the emission surface at the floor and along with the mannequin towards the outlet, the simulated body temperature of the mannequin considerably aids convection, gas velocities close to the mannequin are up to 0.2[$m{\cdot}s^{-1}$] in the Z-direction.

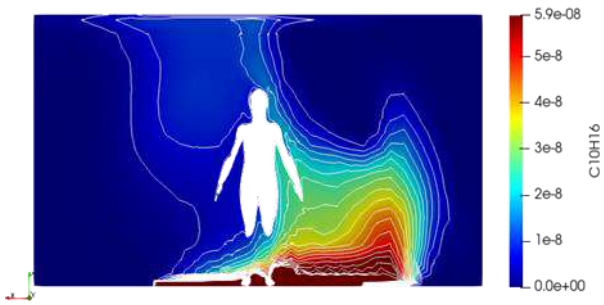

Fig. 11 - Limonene concentrations location Mid-Y

The CO_2 plot in **Fig. 12** is taken at the Inlet-1 surface, this visualizes the breathing better. It is noticeable that CO_2 tends to build-up closer to the inlet. Concentration differences are minimal, so the effect is small

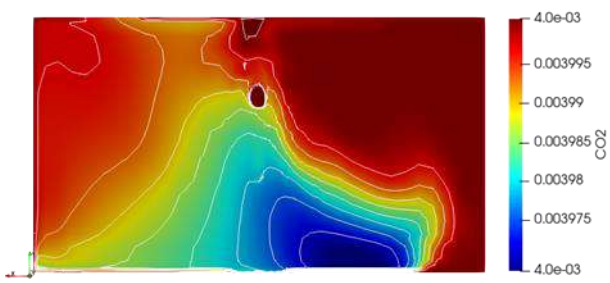

Fig. 12 - CO_2 concentrations location Mid-Y

3.3 Applying Adverse Effect Index

The matrix used is shown in **Fig. 13**. Because C_{prod} is a collection of species, it is roughly estimated that

$C_p rod$ consists largely of *IPOH*, 6−*MHO* and *Acetaldehyde*[16], so the average of those 3 is taken, since information can be found in[11].

The steps explained in section 2.7 are still numerous if the total amount of gases mentioned in **Fig. 13** has to be processed.

Sum - Normalized AEI_rel		Effectgroup						
formula	Name	CHR	DEV	MGR	REP	SAC	SUB	Total Result
Cprod	C_Intermediate product	0.720	0.302	0.706	0.803	0.958	0.436	3.925
C10H16	D-Limonene	0.370	0.702	0.656		0.923	0.348	2.998
C10H16O2	3-Isopropenyl-6-oxo-heptanal	0.851	0.229	0.918	0.753	1.000	0.593	4.345
C8H14O	6-Methyl-5-hepten-2-one	0.871	0.134		0.753		0.397	2.155
CH2O	Formaldehyde	0.533	0.495	0.637		0.687	0.099	2.450
CH3CHO	Acetaldehyde	0.437	0.543	0.494	0.902	0.916	0.319	3.611
CO2	Carbon dioxide	0.010	0.379	0.626		0.770	0.184	1.969
N2	Nitrogen	0.196	0.711	0.951			0.468	2.325
O3	Ozone	0.408	0.431	0.770		0.768	0.383	2.760
Total Result		3.676	3.623	5.051	2.409	5.064	2.790	22.613
		0.488	0.436	0.7195	0.803	0.8603	0.3585	

Fig. 13 - AEI matrix weights used in the final calculation

For this reason, a python macro has been written for ParaView[6]. This script assumes you opened a .csv file in ParaView only containing a title header and the coefficients per gas and effect. It then asks the user for a comma-separated list of formula's to process, and it will apply the calculation.

3.4 final result

The method described in section 2.6 is now finally applied to the fourth simulation, **Fig. 14** shows the final result, the opacity of the planes and "clouds" are scaled to the applied AEI. The shown AEI is the fully collapsed version, where the average of all gases at that position is taken into account. The separate health effects per chemical are still available if desired.

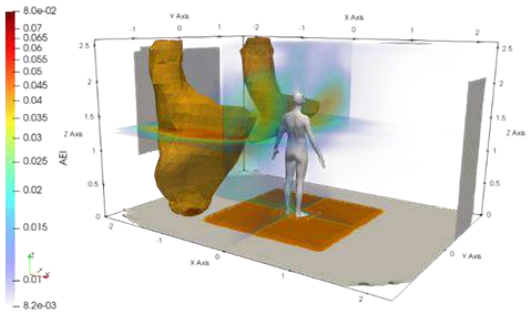

Fig. 14 – Opacity based on strength of AEI.

In **Fig. 14** it is visible that Ozone and Limonene cause the biggest hotspots, the orange blobs from the ceiling and at the floor have the lowest opacity and are most polluted. Note that it is very little, looking at the scale. But in relative terms this still holds. It stands out that lightly polluted blobs are visible around the mannequin. The slices in **Fig. 15** and **Fig. 16** show more clear where the hotspots are situated, primarily in front, behind and to the left of the mannequin. This is most likely caused by the positive updraft in the centre of the room, caused by simulated body temperature.

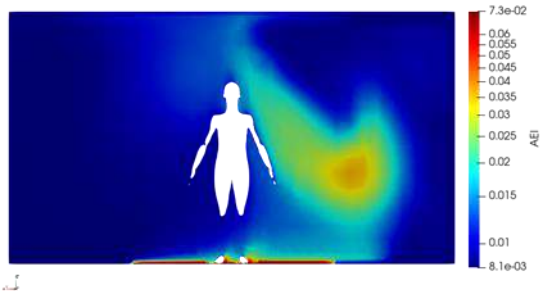

Fig. 15 - Adverse Effect Index location Mid-Y

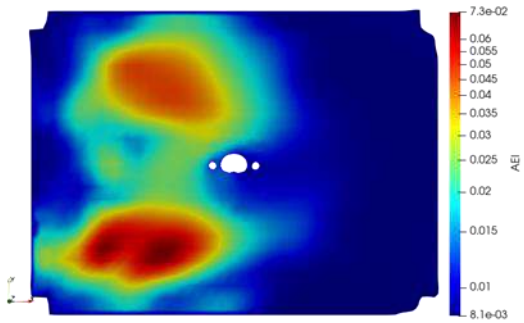

Fig. 16 - Adverse Effect Index, location Mid-Z

The blob to the left (shown on the right in **Fig. 15**) of the mannequin is primarily caused by C_{prod}, so this is the area where Limonene and Ozone first react. The 2 blobs in **Fig. 16** are caused by Ozone, coming down relatively straight down from the inlets. The areas in front of and behind the mannequin are caused by C_{prod} and CO_2.

4. Conclusion

4.1 discussion

1. A lot of data is missing, finding rate constants, Janaf coefficients, Sutherland coefficients or toxicity values like NOAEL are in general very hard to find.
2. the used database, genRA has many gaps and low p-values. For now, the results are unreliable.
3. Indoor gas-phase chemistry has not been studied as thorough yet as atmospheric chemistry, as a result, knowledge is taken from atmospheric chemistry, which leads to at best uncertainty for the moment.
4. A better categorization could be thought of for the Adverse Effect Index, or maybe a more flexible approach.
5. The AEI momentarily only says something about the *relative* toxicity within one set of data. If you want to compare 2 buildings, the data *must* be normalized and considered together as a whole.

Throughout the document, multiple problems were solved, which all build towards the modelling of the indoor environment in detail. In chapter 1 different kinds of simulations were considered, and the species of interest were selected. The decision was made to continue focusing on OpenFOAM because it

is free, well documented, capable and flexible. The chemicals Ozone, Formaldehyde and Limonene were selected as species of interest.

In chapter 2 different problems were solved to successfully apply an OpenFOAM model. First, the steep learning curve of CFD was undertaken and documented. Material (surface) emissions were determined and different ways to convert values from literature to OpenFOAM. To be able to simulate a breathing human, and the effects on the distribution of gases, a breathing model has been set up in section 2.4. Finally, the Adverse Effect Index, AEI was designed in section 2. A python script was developed for this purpose. The AEI builds on an online Generalized Read-Across toxicity database.

In Chapter 3, two simulations were executed. The first simulation was used as a validation tool, to prove that the selected OpenFOAM model performs well. The second simulation added a mannequin with a body temperature and simple breathing pattern, this model requires much finer mesh sizes and is ±100 times more computationally expensive compared to simulation 1.

Finally, the AEI was applied in section 3.3, a python macro script was developed for ParaView to apply the AEI fast and efficiently to any simulation with chemical concentrations that is accessible by ParaView. The results seem to be in line with the simulation and do provide a sane indication of healthier and less healthy spots within a given space.

Data Access Statement

The datasets generated during and/or analysed during the current study are available in the AAEI Github repository, https://github.com/Kwabratseur/AAEI.

5. Acknowledgement

This work has been inspired by COST action CA17136 Indoor Air Pollution Network (INDAIRPOLLNET), we thank the contributors for their support.

6. References

[1] BOXMOX - box model extensions to KPP | Atmospheric Chemistry Observations & Modeling (ACOM).

[2] Council Directive 1999/13/EC of 11 March 1999 on the limitation of emissions of volatile organic compounds due to the use of organic solvents in certain activities and installations.

[3] Database for the Kinetics of the Gas-Phase Atmospheric Reactions of Organic Compounds – Eurochamp Data Center.

[4] Dirken, J. M. (Creator), Steenbekkers, L. P. A. (Creator), Daanen, .. (Creator), Voorbij, A. (Creator), Molenbroek, J. F. M. (. (Creator) (2018). Dutch adults (DINED - anthropometric database). TU Delft - 4TU.ResearchData. 10.4121/UUID:1B214A8F-F59C-460F-8EB9-3EF8DB5E85EE

[5] Jenkin et al., Atmos. Environ., 31, 81, 1997 [doi:10.1016/S1352-2310(96)00105-7]

[6] Ahrens, James, Geveci, Berk, Law, Charles, ParaView: An End-User Tool for Large Data Visualization, Visualization Handbook, Elsevier, 2005, ISBN-13: 978-0123875822

[7] PubMed. https://pubmed.ncbi.nlm.nih.gov.

[8] Kim E. Barrett and William F. Ganong, editors. *Ganong's Review of Medical Physiology*. A Lange Medical Book. McGraw-Hill Med, 24. ed edition.

[9] Gabriel Bekö, Nicola Carslaw, Patrik Fauser, Violeta Kauneliene, Sascha Nehr, Gavin Phillips, Dikaia Saraga, Coralie Schoemaecker, Aneta Wierzbicka, and Xavier Querol. The past, present, and future of indoor air chemistry. 30(3):373–376.

[10] Alessandro D'Amico, Agnese Pini, Simone Zazzini, Daniela D'Alessandro, Giovanni Leuzzi, and Edoardo Currà. Modelling VOC Emissions from Building Materials for Healthy Building Design. 13(1):184.

[11] George Helman, Imran Shah, Antony J. Williams, Jeff Edwards, Jeremy Dunne, and Grace Patlewicz. Generalised Read-Across (GenRA): A workflow implemented into the EPA CompTox Chemicals Dashboard. 36(3):462–465.

[12] Kazuhide Ito, Masaru Abuku, Shinsuke Kato, and Shuzo Murakami. CFD and Model Experiment with Chemical Reaction.

[13] N. E. Klepeis, W. C. Nelson, W. R. Ott, J. P. Robinson,

[14] A. M. Tsang, P. Switzer, J. V. Behar, S. C. Hern, and W. H. Engelmann. The National Human Activity Pattern Survey (NHAPS): A resource for assessing exposure to environmental pollutants. 11(3):231–252, 2001 May-Jun.

[15] Yingjun Liu, Pawel K. Misztal, Caleb Arata, Charles J. Weschler, William W. Nazaroff, and Allen H. Goldstein. Observing ozone chemistry in an occupied residence. 118(6).

[16] Max R. McGillen, William P.L. Carter, Abdelwahid Mellouki, John J. Orlando, Bénédicte Picquet-Varrault, and Timothy J. Wallington. Database for the kinetics of the gas-phase atmospheric reactions of organic compounds.

[17] A. W. Nørgaard, J. D. Kudal, V. Kofoed-Sørensen, I. K. Koponen, and P. Wolkoff. Ozone-initiated VOC and particle emissions from a cleaning agent and an air freshener: Risk assessment of acute airway effects. 68:209–218.

A review of thermal comfort modeling of elderly people

Minzhou Chen[a], Risto Kosonen[a,b], Simo Kilpelainen[a], Ru Ming[c]

[a] Aalto University, Department of Mechanical Engineering, Finland

[b] College of Urban Construction, Nanjing Tech University, China

[c] School of civil engineering, Chongqing University, China

Abstract. With the global warming and aging of society, the analysis of thermal comfort of elderly people is becoming more important. One example is during heat wave period, the elderly are exposed to a hot environment for a long time, the probability of health problems (cardiovascular disease, mental confusion, etc.) may increase, and even death may occur. The thermal comfort model can predict the human thermal response and evaluate the ambient thermal environment. Therefore, thermal comfort models have a significant effect to improve the thermal sensation of occupants in a built environment. But models being established with adults' data may not be accurate enough in predicting the thermal response of the elderly. This paper reviews the existing thermal comfort models for the elderly and summarizes different types of thermal comfort models, including the thermoregulatory model, the thermal comfort model, and the machine learning model. The differences and the applicable conditions of models are summarized. This paper provides evidence from literature for the difference in thermal response between the elderly and young people, and also provides a reference for the establishment of a thermal comfort model for the elderly in the future.

Keywords. thermal comfort model, elderly people, human thermoregulation.
DOI: https://doi.org/10.34641/clima.2022.56

1. Introduction

The impact of climate change on human body has been concerned [1], including mortality and morbidity caused by hot weather. More scholars began to focus on heat-related vulnerability and conducted researches [2]. According to the published literatures from different countries, it is found that the mortality of the elderly account for a high proportion [3,4]. Two issues can be extracted from these data: global aging and warming.

On the one hand, the global ageing society is accelerated growth [5,6]. Ageing means the functional decline of body organs and systems, suffering from various chronic diseases [7]. In terms of heat-related health, this degradation is mainly manifested in a preference for a warm environment and a reduced thermoregulatory response, which means less sensitive to changes in ambient thermal conditions. There may even be dangerous situations in which an appropriate response cannot be made to maintain the core temperature under some extreme weather [8,9]. Generally accepted reasons include: 1) Changes in body composition; 2) Lower metabolic rate; and 3) Decreased cardiovascular function [10]. On the other hand, global warming makes heat waves and extreme weather more frequent [11]. Some scholars have predicted the future heat-related mortality through modeling, and believe that the mortality will increase [12,13], while population aging will amplify this situation [3].

Facing the above problems, it is possible to alter the elderly's living environment to fulfill their comfort and health requirements, thereby reducing the threat of hot weather. The use of thermal comfort models can achieve the purpose of predicting the thermal response of the elderly. At present, scholars divide thermal comfort models into human thermoregulatory model, adaptive model and the latest machine learning model [14-16]. This paper mainly summarizes thermoregulatory models and

Copyright ©2022 by the authors. This conference paper is published under a CC-BY-4.0 license.

adaptive models. However, most of the existing human thermal comfort models are established using the data of average adults (age between), which can not predict older people's response accuratly enough. Therefore, the human thermal comfort model of older people should be established specialy [10].

This paper reviews and summarizes the existing thermal comfort models for the elderly, and analyzes the characteristics and applicability of different models. At the same time, the important physiological parameters involved in the model are also summarized. This article identifies the current knowledge gaps, It provides some directions for the future research on thermal comfort and health of the elderly.

2. Thermoregulatory models for elderly people

Human thermoregulatory model includes a passive system and an active system. The skin temperature distribution and core temperature distribution of human body in different thermal environments can be predicted by inputting the ambient environment parameters and some human related parameters. In addition, combining this kind of model with thermal sensation model can predict the human thermal sensation at the same time. The models for the elderly are usually based on the existing thermoregulatory models for average adults, but modified some physiological parameters. A summary of these models is shown in **Tab. 1**.

Tab. 1 - Thermoregulatory models for elderly people

Model	Age	Basic model	Modification	
			Passive system	Active system
Novieto [17]	>75	Fiala's model	Modify Weight, Height, Body fat, Basic metabolic rate , Cardiac output	The coefficients of the equation are modified by Neural algorithm
Takahashi (JOS-3) [22]	>60	JOS-2 model	Modify Weight, Height, Basic metabolic rate, Body fat, Age, Sex, Add heat gain by shortwave solar radiation, Change the nodes of the pelvis	Add aging effect factors; Add non–shivering thermogenesis caused by brown adipose tissue
Rida [23]		Karaki's model	Modify Basic metabolic rate , Body fat(skin), Blood flow max(skin), Blood flow min(skin), Fat skin thickness	Modify sweat factor; Cold shivering factor; Threshold of thermoregulatory action; Arterial radii
Itani [25]	>60	Rida's model	Modify abdomen fat thickness	Modify body fat (skin) and the threshold of sweating are affected by the body water losses; Metabolic rate, heart rate and cardiac output are affected by the body core temperature
Hirata [26]	mean: 67.8 (elderly) 73.9 (aged)	Nagaoka's model	–	Modif sweating in the limbs(legs); Sensitivity of the skin due to aging affects the threshold of sweating
Zhou [30]	40-60	Fiala's model	Modify Weight, Height, Age, Sex, Segments' length and radius	–
Ma [35]	>60	Zhou's model	Modify Weight, Height, Age, Sex, Segments' length and radius(models for men and women separately)	–

Coccarelli [38]	<80	Coccarelli's previous model	Modify Age, Vessel wall elasticity, Heart rate, End-diastolic elastance, End-systolic elastance, End-diastolic pressure, Bone density, Segments' length and radius	Modify Thermal sensitivity factor; The maximum and minimum skin blood flow; The threshold of sweating

Based on the IESD-Fiala model [19], Novieto and Zhang [17, 18] modified the weight, height, percentage of body fat, basal metabolic rate and cardiac output of the passive system in the original model into the corresponding parameters of the elderly through literature research, and recalculated the body surface area through height and weight. For the active system, they did not change the node temperature set point in the original model, but modified the coefficients of the controling formulas in the original model through the Genetic algorithm [20]. This model was verificated in the 5-42°C conditions through the existing data in literatures. It was found that the accuracy of the model in predicting the core temperature was higher than that of the mean skin temperature.

Tanabe established a Jointed Circulation System (JOS) model for women and the elderly based on Stolwijk's model. The input parameters of the model include age, gender, basal metabolic rate and percentage of body fat. The AVA mechanism of hands and feet and the heat transfer in the superficial venous of limbs were also considered in the passive system. After that, the research team improved the JOS to the JOS-2 model [21]. JOS-2 model redivided the node of head in the passive system. In the active system, JOS-2 proposed different aging factors which would change the human thermal response, but did not give specific values. Recently, the research team updated JOS-2 to JOS-3 model [22]. In the passive system, the pelvic node was modified, and the heat production of short wave radiation was included, so that the model could more accurately predict the human body temperature in the solar radiation environment. Meanwhile, the non-shifting thermogenesis caused by human brown adipose tissue was added to the active system, making the prediction of metabolic rate more accurate. In addition, the model gave the specific value of aging factors proposed in JOS-2. The model was verified by simulation in steady and unsteady conditions. It is considered that it can more accurately predict the thermal response of young and older men in cold environment than JOS-2.

Rida et al. [23] established a biothermal model for elderly people based on the bioheat model of Karaki [24]. The passive system of this model considered a blood circulation model based on cardiac output and limb blood flow (including arterial and venous blood circulation, limb AVA mechanism and skin blood perfusion). Particularly, reseachers modeled each finger as independent segments to predict the finger temperature more accurately. In addition, the regulated skin blood perfusion coefficients, the metabolic rate during hot and cold conditions, and the cardiac output were also modified.It is verified that the model has certain accuracy in cold/heat stress environment. The Rida's model was further improved [25], to made it can be applied to predict the thermal response of the elderly in extremely hot environment. In the active system of this model, the changes of skin blood flow and sweating threshold caused by body water loss and the changes of heart rate, cardiac output and metabolic rate caused by the increase of core temperature were considered.

The model established by Hirata et al. [26] can predict the body temperature and sweating of elderly people exposed to passive heat. The passive system of the model was based on a voxel model [27], which had an anatomically realistic shape of human body. The passive system adopted Pennes's bioheat equation [28]. But when calculating the blood temperature, the total blood volume was simplified to 7% of the weight of the corresponding part. And for the blood perfusion rate, it was assumed that only the increased cardiac output can meet the increased demand for skin blood flow, while ignoring the potential redistribution of blood flow from internal organs to skin [29]. In addition, the model considers the change of sweating threshold caused by the change of skin sensitivity caused by aging in the active system. The model considers the maximum possible evaporation heat loss under hot conditions, and can predict the sweating rate and core temperature of the elderly.

Zhou et al. [30] modified some physiological parameters in the passive system of Fiala's model [31]. In particular, metabolic rate, percentage of body fat and cardiac output in the model were not independent input parameters, but calculated by gender, age, height and weight [32-34], which makes the model more personalized. Ma et al. [35] further modified Zhou's model [36, 37], refined the

physiological parameters to each body segment in passive system, and made the model suitable for the elderly over 60 years old. Coccarelli et al. [38] built the model based on their previous thermoregulatory model [39], considered the changes of vascular elasticity, cardiac contraction and bone mineral density in the passive system caused by aging, as well as the changes of blood flow and sweating threshold in the control system.

3. Other models for elderly people

Different from the above temperature regulation and thermal sensation models, the adaptive thermal comfort model is based on the data measured in the field test, which focuses on reflecting the relationship between human thermal response (thermal comfort temperature, clothing insulation, regulation behavior, etc.) and outdoor climate parameters, reflecting the adaptability of different people to the local environment. The research results fully show the significant correlation between comfort temperature and outdoor temperature, that is, with local climate characteristics, especially with outdoor temperature [40]. A summary of these models is shown in **Tab. 2**.

Yang et al. [41] studied the effect of seasonality on the thermal comfort of the elderly in the elderly care center and found that the comfort range of the elderly was wider than expected by PMV. The elderly prefer warm or slightly hot indoor temperature. The linear regression equation between 4-day weighted running mean of outdoor temperature and clothing insulation of the elderly was established, Showing that the clothing insulation distribution of the elderly in mid season is wider and more diverse. And elderly people were more sensitive to outdoor temperature.

Wang et al. established an adaptive thermal adaptation model for older people (ATCO) through field investigation of a nursing home [42]. Comparing the Atco model with the neutral temperature of the elderly obtained by the adaptive model provided by ASHRAE and EN15251, it is found that the Atco model predicts a lower neutral temperature in the cold outdoor environment and a higher neutral temperature in the warm outdoor environment, which is more accurate than the other two models. The paper also compares the adaptive models of the elderly and adults, and finds that the neutral temperature of the elderly is higher. In the follow-up study, the research team established an adaptive model [43] for the middle-aged and elderly people in the house. It is considered that the acceptable temperature range for the elderly is 14.1-19.4 ℃ in winter and 23.8-27.0 ℃ in summer. In addition, the clothing model of the elderly in winter [44] is also established. It is pointed out that the wrong estimation of the thermal insulation of the typical winter clothing of the elderly may lead to the deviation of the predicted average skin temperature of about 1.3 ° C or the deviation of heat loss of about 26%.

Tab. 2 - Adaptive models for elderly people.

Model	Region	Age	Outdoor parameter	Thermal response
Yang [41]	Korea	>65	4-day weighted running mean of outdoor temperature	clothing insulation
Wang [42]			7-day weighted running mean of outdoor temperature	Neutral temperature
Jiao [43]	Shanghai, China	>70	Prevailing mean outdoor air temperature	Neutral temperature
Tang [44]			Outdoor air temperature	Clothing insulation
Wu [45]	Chongqing, China	>60	Outdoor air temperature	Thermal sensation vote, Proportion of air-conditioned, Proportion of windows opened, Proportion of fans used

Giamalaki [46]	Crete, Greece	>65	Monthly average temperature	–

Wu et al. [45] studied the elderly in residential buildings and nursing homes in Chongqing, and obtained the adaptability model of the elderly in this area. It is found that the thermal sensation of the elderly is affected by outdoor air temperature more than indoor air temperature. The elderly can sense the relative humidity of indoor and outdoor air. Moreover, in terms of adaptive behavior, natural ventilation (opening and closing windows) is the main way for the elderly.

Giamalaki et al. [46] considered the increase their expenditure of heating and cooling in the Adaptability Study of the elderly in Greece, and found that in the hot season, the elderly most often open windows to adapt to the environment, while in the cold season, they adapt by adjusting clothes. The elderly may first adopt strategies that do not require energy consumption, and then adopt methods to increase expenditure (such as using portable heaters and fans). However, the functional relationship between outdoor parameters and thermal behavior is not given, and only frequency statistics are carried out.

The research of Wang et al. [47] is based on the adaptive model APMV proposed by Yao et al. [48, 49]. Based on the survey and questionnaire survey of the elderly in Guiyang, China, the adaptive coefficient is obtained λ= 0.32. The actual thermal comfort temperature of the elderly is higher than that predicted by PMV model.

Machine learning model is the latest model, which depends on computer and sensor technology. The traditional thermal comfort model usually adopts the white box approach, while the machine learning model prefers to use the black box approach (e.g. linear SVM, radial basis function (RBF) SVM and random forest) to process a large number of data to predict human thermal comfort. Some studies show that the accuracy of the black box approach is better than that of the white box approach [50]. Few of the existing machine learning models [51-53] are suitable for the elderly. Wang et al. [54] established a machine learning model suitable for the elderly, using four environmental variables (air temperature, speed, CO2) concentration and illumination plus two human related variables (health status and residence time in nursing home) as input parameters to predict the thermal sensation of the elderly. It is verified that the accuracy of this model is 24.9% higher than that of PMV model.

4. Conclusion

For thermoregulatory models, based on the Fiala multi-node model, by correcting the height, weight, basal metabolic rate, body fat, segments' length and radius, blood vessel distribution in the passive system (among which, the basal metabolic rate, body fat and cardiac output are considered as a sensitive parameter), and the threshold of sweating and shivering temperature in the control system can more accurately predict the physiological parameters of the elderly (skin temperature, core temperature, sweating, etc.). Through these physiological parameters, thermal sensation can be predicted. Thermoregulatory models are widely applicable because they take environmental factors into account and include a detailed biological model of the human body. Although thethermoregulatory model takes clothing insulation into account, it lacks a dynamic model for clothing changes in the elderly and components for other behavioral responses, such as opening windows or not, using cooling devicest or not. In addition, the parameters used in the model are the average value of the older people, and lack of personalized parameters, so it cannot be better used to predict individual responses.

For thermal adaptation models, the connection between the outdoor environment and human behavioral responses is mainly established. At present, there are few studies, and they are mainly aimed at the elderly group in a certain climate environment or region, so the scope of application is small. In addition, the models rarely involve physiological parameters, so they lack a certain degree of objectivity. But the human behavior included in the thermal adaptation model may complement the thermoregulatory model.

Different from thermal regulation models and thermal adaptation modesl, machine learning models take more parameters (such as CO_2 concentration, individual health, etc.) as input parameters, and found that the black box method can predict thermal sensation more accurately than the white box method. However, the black box method cannot observe the intermediate process, which makes the output results difficult to interpret and affects the reliability of the model. In addition. These

models require a large amount of data to support, and there are still few studies on thermal comfort of the elderly, so there are few machine learning models, and the scope of application is limited.

In general, among the existing thermal comfort models for the elderly, the thermoregulatory model can better predict the changes in the physiological parameters of the elderly, the thermal adaptation model can predict the behavior changes of the elderly, and machine learning models have higher accuracy in predicting changes in psychological parameters such as thermal sensation. Future research may consider the combination of models to predict the thermal response of the elderly more comprehensively and accurately.

Acknowledgement

This study is part of the following project: HEATCLIM (Heat and health in the changing climate, Grant Numbers. 329306, 329307) funded by the Academy of Finland within the CLIHE (Climate change and health) programme. Also, the authors gratelfully acknowledge financial support from China Scholarship Council.

Reference

[1] Qian Xing, ZhaoBin Sun, Yan Tao, Xiaoling Zhang, Shiguang Miao, Canjun Zheng, Shilu Tong, Impacts of urbanization on the temperature-cardiovascular mortality relationship in Beijing, China, Environmental Research, Volume 191, 2020, 110234, ISSN 0013-9351

[2] Dominic Royé, Raquel Codesido, Aurelio Tobías, Margarita Taracido, Heat wave intensity and daily mortality in four of the largest cities of Spain, Environmental Research, Volume 182, 2020, 109027, ISSN 0013-9351

[3] Yang J, Zhou M, Ren Z, et al. Projecting heat-related excess mortality under climate change scenarios in China[J]. Nature communications, 2021, 12(1): 1-11.

[4] Centers for Disease Control and Prevention. Heat-Related Deaths--United States, 1999-2003[J]. MMWR: Morbidity and mortality weekly report, 2006, 55(29): 796-798.

[5] Li J, Han X, Zhang X, et al. Spatiotemporal evolution of global population ageing from 1960 to 2017[J]. BMC public health, 2019, 19(1): 1-15.

[6] Wang S. Spatial patterns and social-economic influential factors of population aging: A global assessment from 1990 to 2010[J]. Social Science & Medicine, 2020, 253: 112963.

[7] Bunker A, Wildenhain J, Vandenbergh A, et al. Effects of air temperature on climate-sensitive mortality and morbidity outcomes in the elderly; a systematic review and meta-analysis of epidemiological evidence[J]. EBioMedicine, 2016, 6: 258-268.

[8] N. Wongsurawat, B.B. Davis, J.E. Morley Thermoregulatory failure in the elderly. St. Louis University Geriatric Grand Rounds J. Am. Geriatr. Soc., 38 (1990), pp. 899-906

[9] C.M. Blatteis Age-dependent changes in temperature regulation–a mini review Gerontology, 58 (4) (2012), pp. 289-295

[10] J. van Hoof, L. Schellen, V. Soebarto, J.K.W. Wong, J.K. Kazak, Ten questions concerning thermal comfort and ageing, Building and Environment, Volume 120, 2017, Pages 123-133,

[11] C. Schleussner, P. Pfleiderer, E. Fischer In the observational record half a degree matters Nat. Clim. Chang., 7 (2017), pp. 460-462

[12] S. Zacharias, C. Koppe, H.-G. Mücke Climate change effects on heat waves and future heat wave-associated IHD mortality in Germany Climate, 3 (1) (2015), pp. 100-117

[13] Chen K, Vicedo-Cabrera A M, Dubrow R. Projections of ambient temperature-and air pollution-related mortality burden under combined climate change and population aging scenarios: A review[J]. Current environmental health reports, 2020, 7(3): 243-255.

[14] Qiantao Zhao, Zhiwei Lian, Dayi Lai, Thermal comfort models and their developments: A review, Energy and Built Environment 2 (2021) 21–33.

[15] Ming Fu, Wenguo Weng, Weiwang Chen, Na Luo,Review on modeling heat transfer and thermoregulatory responses in human body, Journal of Thermal Biology, Volume 62, Part B, 2016, Pages 189-200

[16] Diana Enescu, A review of thermal comfort models and indicators for indoor environments, Renewable and Sustainable Energy Reviews, Volume 79, 2017, Pages 1353-1379

[17] Novieto D T, Zhang Y. Thermal comfort implications of the aging effect on metabolism, cardiac output and body weight[J]. Adapting to change: new thinking on comfort, 2010: 1-9.

[18] Novieto D T, Zhang Y. Towards thermal comfort prediction for the older population: a review of aging effect on the human body[C] Proceedings of IESD PhD Conference. De Montfort University, Leicester. 2010: 35-48.

[19] Fiala D, Lomas K J, Stohrer M. Computer prediction of human thermoregulatory and temperature responses to a wide range of environmental conditions[J]. International journal of biometeorology, 2001, 45(3): 143-159.

[20] Novieto, Divine Tuinese, PhD Thesis, Adapting a human thermoregulation model for predicting the thermal response of older persons, 2013

[21] Yutaka Kobayashi, Shin-ichi Tanabe, Development of JOS-2 human thermoregulation model with detailed vascular system, Building and Environment, Volume 66, 2013, Pages 1-10,

[22] Takahashi Y, Nomoto A, Yoda S, et al. Thermoregulation model JOS-3 with new open source code[J]. Energy and Buildings, 2021, 231: 110575.

[23] Rida M, Ghaddar N, Ghali K, et al. Elderly bioheat modeling: changes in physiology, thermoregulation, and blood flow circulation[J]. International journal of biometeorology, 2014, 58(9): 1825-1843.

[24] Karaki W, Ghaddar N, Ghali K, et al. Human thermal response with improved AVA modeling of the digits[J]. International journal of thermal sciences, 2013, 67: 41-52.

[25] Itani M, Ghaddar N, Ghali K, et al. Bioheat modeling of elderly and young for prediction of physiological and thermal responses in heat-stressful conditions[J]. Journal of thermal biology, 2020, 88: 102533.

[26] Akimasa Hirata, Tomoki Nomura, Ilkka Laakso, Computational estimation of body temperature and sweating in the aged during passive heat exposure, International Journal of Thermal Sciences, Volume 89, 2015, Pages 154-163.

[27]T. Nagaoka, S. Watanabe, K. Sakurai, E. Kuni eda, M. Taki, Y. Yamanaka Development of realistic high-resolution whole-body voxel models of Japanese adult males and females of average height and weight, and application of models to radio-frequency electromagnetic-field dosimetry Phys. Med. Biol., 49 (2004), pp. 1-15

[28] H.H. Pennes Analysis of tissue and arterial blood temperatures in the resting human forearm J. Appl. Physiol., 1 (1948), pp. 93-122

[29] J.A.J. Stolwijk Mathematical Model of Physiological Temperature Regulation in Man (1971) NASA Contractor Reports

[30] X. Zhou, Z. Lian, L. Lan An individualized human thermoregulation model for Chinese adults Build. Environ., 70 (2013), pp. 257-265

[31] D. Fiala, K.J. Lomas, M. Stohrer A computer model of human thermoregulation for a wide range of environmental conditions: the passive system J Appl Physiol, 87 (5) (1999), pp. 1957-1972

[32] H.Y. Liu, Y.F. Lu, W.J. Chen Predictive equations for basal metabolic rate in Chinese adults: a cross-validation study J Am Diet Assoc, 95 (12) (1995), pp. 1403-1408

[33] Y. Zhen Physiology Higer Education Press, Beijing (2010)

[34]P. Deurenberg, K. Ge, J.G.A.J. Hautvast, J. Wa ng Body mass index as predictor for body fat: comparison between Chinese and Dutch adult subjects Asia Pac J Clin Nutr, 6 (2) (1997), pp. 102-105

[35] Ting Ma, Jing Xiong, Zhiwei Lian, A human thermoregulation model for the Chinese elderly, Journal of Thermal Biology, Volume 70, Part A, 2017, Pages 2-14,

[36] Zhou, X., Lian, Z., Lan, L., 2013. An individualized human thermoregulation model for Chinese adults. Build. Environ. 70, 257 – 265.

[37] Zhou, X., Zhang, H., Lian, Z., Zhang, Y., 2014. A model for predicting thermal sensation of Chinese people. Build. Environ. 82, 237 – 246.

[38] Coccarelli A, Hasan H M, Carson J, et al. Influence of ageing on human body blood flow and heat transfer: a detailed computational modelling study[J]. International journal for numerical methods in biomedical engineering, 2018, 34(10): e3120.

[38] Coccarelli A, Boileau E, Parthimos D, et al. An advanced computational bioheat transfer

model for a human body with an embedded systemic circulation[J]. Biomechanics and modeling in mechanobiology, 2016, 15(5): 1173-1190.

[40] A. Mendes, et al. Indoor air quality and thermal comfort in elderly care centers Urban Clim., 14 (2015), pp. 486-501

[41] Jinho Yang, Insick Nam, Jong-Ryeul Sohn, The influence of seasonal characteristics in elderly thermal comfort in Korea, Energy and Buildings, Volume 128, 2016, Pages 583-591.

[42] Zi Wang, Hang Yu, Yu Jiao, Qi Wei, Xiangyang Chu, A field study of thermal sensation and neutrality in free-running aged-care homes in Shanghai, Energy and Buildings, Volume 158, 2018, Pages 1523-1532,

[43] Jiao Y, Yu H, Yu Y, et al. Adaptive thermal comfort models for homes for older people in Shanghai, China[J]. Energy and Buildings, 2020, 215: 109918.

[44] Tang Y, Yu H, Wang Z, et al. Typical winter clothing characteristics and thermal insulation of ensembles for older people in China[J]. Building and Environment, 2020, 182: 107127.

[45] Wu Y, Liu H, Li B, et al. Thermal adaptation of the elderly during summer in a hot humid area: Psychological, behavioral, and physiological responses[J]. Energy and Buildings, 2019, 203: 109450.

[46] Marina Giamalaki, Dionysia Kolokotsa, Understanding the thermal experience of elderly people in their residences: Study on thermal comfort and adaptive behaviors of senior citizens in Crete, Greece, Energy and Buildings, Volume 185, 2019, Pages 76-87,

[47]Zu Wang, Liang Xia, Jun Lu, Development of Adaptive Prediction Mean Vote (APMV) Model for the Elderly in Guiyang, China, Energy Procedia, Volume 142, 2017, Pages 1848-1853,

[48] Runming Yao, Baizhan Li, Jing Liu, A theoretical adaptive model of thermal comfort – Adaptive Predicted Mean Vote (aPMV), Building and Environment, Volume 44, Issue 10, October 2009, Pages 2089-2096.

[49] Runming Yao, Baizhan Li, Jing Liu, A theoretical adaptive model of thermal comfort – Adaptive Predicted Mean Vote (aPMV), Building and Environment, Volume 44, Issue 10, October 2009, Pages 2089-2096.

[50] Hu W, Wen Y, Guan K, et al. itcm: Toward learning-based thermal comfort modeling via pervasive sensing for smart buildings[J]. IEEE Internet of Things Journal, 2018, 5(5): 4164-4177.

[51] Andrei Claudiu Cosma, Rahul Simha, Machine learning method for real-time non-invasive prediction of individual thermal preference in transient conditions, Building and Environment, Volume 148, 2019, Pages 372-383,

[52] A. Rajith, S. Soki and M. Hiroshi, "Real-time optimized HVAC control system on top of an IoT framework," 2018 Third International Conference on Fog and Mobile Edge Computing (FMEC), 2018, pp. 181-186

[53] Mansur V, Carreira P, Arsenio A. A learning approach for energy efficiency optimization by occupancy detection[C]//International Internet of Things Summit. Springer, Cham, 2014: 9-15.

[54] Wang Z, Yu H, Luo M, et al. Predicting older people's thermal sensation in building environment through a machine learning approach: Modelling, interpretation, and application[J]. Building and Environment, 2019, 161: 106231.

Special Systems of Foul Water Stacks in High-Rise Buildings

Martin Sokol [a], Jana Peráčková [b], Taťjana Jánošková [c]

[a] Department of Building Services, Faculty of Civil Engineering, Slovak University of Technology in Bratislava, Slovakia martin.sokol@stuba.sk.

[b] Department of Building Services, Faculty of Civil Engineering, Slovak University of Technology in Bratislava, Slovakia jana.perackova@stuba.sk.

[c] Department of Building Services, Faculty of Civil Engineering, Slovak University of Technology in Bratislava, Slovakia tatjana.janoskova@stuba.sk.

Abstract. Due to maximum usage of building lands in cities, the construction of high-rise buildings is currently having the greater importance. High-rise buildings are buildings that, due to their height, must be designed in a different technical, technological and constructional way. In addition to height, the dominant element of high-rise buildings compared to buildings with a smaller number of floors is the usable area, which is an important factor for an investor. The more floors a building has, the more complicated it is to provide requirements of hygiene and quality of sanitary installations. In sanitary technology, the biggest problem is in the design of foul water stacks, which must be given higher attention. The issue of foul water stacks in high-rise buildings is a relatively complex and demanding topic, due to the complicated hydraulic conditions in the flow of foul water in drainage pipes. The design must be based mainly on research and knowledge, which is obtained mainly from foreign sources. This topic is not so developed in our country. Stacks must be designed in such a way that the negative pressure and the overpressure created in them do not cause suction of water from traps. When there is no water in the trap, an annoying smell from the drainage occurs in the building. Extraction of water from traps is not the only one problem. Other problems are excessive vibration and noise spreading from stacks through building structures to the interior. This can be caused, for example, by an incorrectly chosen system, piping material, anchoring, or offset of the stack. Special fittings and systems have been designed for high-rise buildings, which eliminates most of disadvantages of conventional solutions. The paper deals with the analysis of modern technical solutions that favourably affect the hydraulic conditions in stacks and thus help to improve the comfort users of building.

Keywords. high-rise buildings, foul water stacks, hydraulic, pressure fluctuation.
DOI: https://doi.org/10.34641/clima.2022.29

1. Introduction

Nowadays, high-rise buildings are coming into the forefront in urban development of cities, because it mininaze necessary build-up area. With increase of number ofhigh-rise buildings, large demand for new solutions in the field of technical equipment of buildings come into the foreground. Qualitative development in the design of all parts of drainage systems began. In sanitary technology, the biggest problem in high-rise buildings occurs in the design of stacks, which must be given higher attention. The biggest changes are in the design and installation of stacks in buildings with 9 – 16 floors belonging to the 1st group, Tab. 1.

Tab. 1 – Types of high-rise buildings [7]

The class	Number of floors	Height (m)
Multi-storey – I. group	9 - 16	< 50
Multi-storey – II. group	17 - 25	50 - 70
Multi-storey – III. group	26 - 40	75 - 120
High	41 - 60	120 - 200
Very high	> 60	> 200

Stacks must be designed so, that the negative pressure and the overpressure achieved in them do not cause suction of water from traps. If is no water in the trap, an annoying smell occurs in the building. Another problematic part of vertical piping is

Copyright ©2022 by the authors. This conference paper is published under a CC-BY-4.0 license.

direction change of stack (offset), which causes excessive vibration and noisiness.

Conventional stacks systems are stacks with direct vent and stacks with additional vent pipe, which are insufficient for high-rise buildings. The reasons are higher investment piping costs for bigger piping diameter, fire stop elements, and piping anchoring. To achieve higher quality of distribution systems for high-rise buildings, special systems and fittings have been developed. Properly designed fittings ensure optimal water flow in stacks. Special systems for stacks in high-rise buildings are:

- stacks with flow-optimized Sovent fitting which is suitable solution for buildings with more than 5 floors, Fig. 1a,
- stacks equipped with elements of active protection which is suitable solution for buildings with more than 10 floors, Fig. 1b.

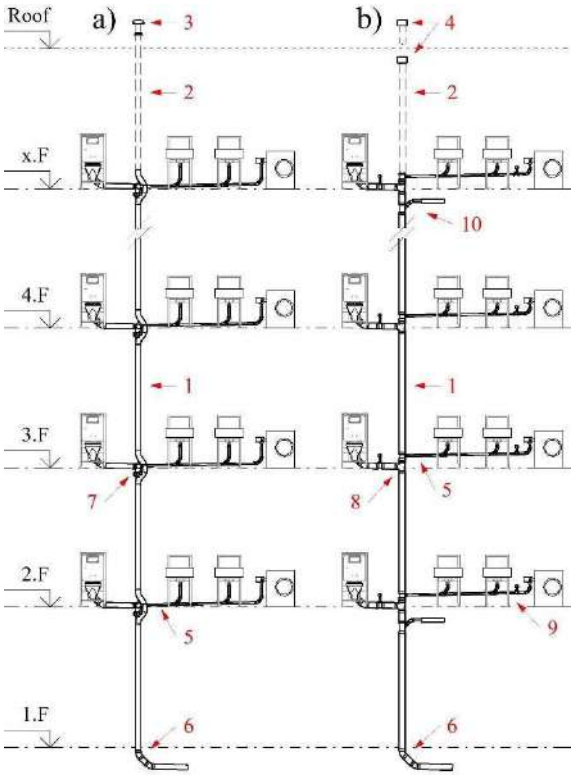

Fig. 1 – Special stack systems

a) stack with Sovent fitting, b) stack equipped with active protection elements, 1 – stack, 2 – vent pipe, 3 – vent head, 4 – air admittance valve on the stack (above or below a roof), 5 – branch pipe, 6 – transition to the drain (2 x 45° bend, base), 7 – Sovent fitting, 8 – simple Y-branch, 9 – air admittance valve on a branch pipe, 10 – positive air pressure attenuator

2. Water flow and hydraulic conditions in a foul water stack

The water in the stack flows around the inner wall of the pipe and forms a cylinder with an air core in the middle of it, Fig. 2. At the connection of the branch pipe with a larger flow, the air core can be closed (interrupted) and piston effect occurs, which causes a negative pressure. During the piston effect large amount of air is sucked to the stack from the vent pipe. Incorrect design of the stack can cause, an air can be sucked from branch pipes, which causes the extraction of water from traps.

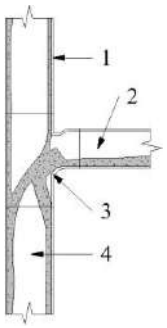

Fig. 2 – Water flow in the stack

1 – water flow around the inner wall of the stack, 2 – water flow from the branch pipe, 3 – occuring of the piston effect, 4 – air core

In the case of low water flow or no water flow in the stack, air flows through the stack from the bottom up to the exterior. The pressure loss which occurs at the airflow is main reason which causes exceeding of maximum negative pressure in the stack.

Fluctuation of pressure in the stack is by the system of stack venting, by used branch fittings, by offsets and the accessories used in the stack affected.

If the direction of the stack changes for more than 45°, hydraulic jump occurs which is caused by sudden change of velocity of the water flow. The water stops flowing around the inner wall of the pipe and the pipe begins to fill up. Above the direction change is an overpressure and below the change of direction is negative pressure. Besides that, the water which hits the inner wall of the bottom bend will cause excessive vibration and noisiness.

2.1 The velocity of water flow in foul water stacks

Fig. 3 shows two cases of falling velocity of water in the stack. Curve one shows the theoretical falling velocity according to Torricelli´s law. Curve two shows real falling velocity of water in the stack which includes friction losses and the air resistance in the stack.

Curve two shows that after approximately 20 meters, the falling velocity of water reaches 12 m/s. Increasing of velocity is not significant for higher stacks. After approximately 35 meters, water reaches maximal velocity of 13 m/s and does not increases due to air resistance and friction losses in the stack.

From the Fig. 3 it's clear, that it is not important to design offsets on the stack in order to reduce the falling velocity of water. The biggest increasing of falling velocity is in the highest 10 meters of the stack.

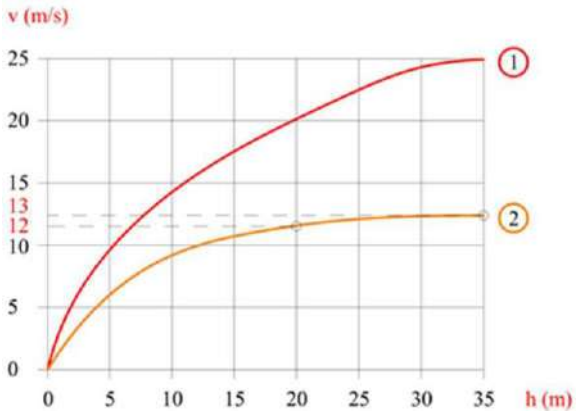

Fig. 3 – Theoretical falling velocity and real falling velocity in the stack [2]

1 – theoretical falling velocity, 2 – real falling velocity in the stack (water film with air column), v – falling velocity (m/s), h – height of the fall (m)

3. Technical solutions of special systems and fittings for stacks

Special systems and fittings for stacks in high-rise buildings ensure a significant reduction of pressure fluctuation in stacks, vibration and noisiness and also an optimal foul water flow in the stack. Other benefits of these solutions are lower piping costs due to smaller dimensions, lower anchorage costs, and lower fire protection costs.

3.1 Stack with Sovent fitting

The Sovent fitting is designed to prevent hydraulic blockage from forming and creating a piston effectin the stack, Fig. 1a. The swirl of the flow creates a rotation that allows the flow of foul water to move along the inner wall of the fitting and forms a continuous air column along the entire height of the stack, Fig. 4.

Fig. 4 – Simulation of swirl flow in the Sovent fitting [10]

This flow effect increases the discharge rate of the stack by 30 %, in comparison to conventional systems, Tab. 2. The main flow of wastewater in the stack is adjusted around the connection points of the branch pipes by divider. Incoming wastewater from branch pipe has time to switch to the vertical main flow, Fig. 5a. This minimises collision turbulences and reduces the pressure fluctuation in the system. This solution is intended to reduce the water velocity, which limits the kinetic pressure.

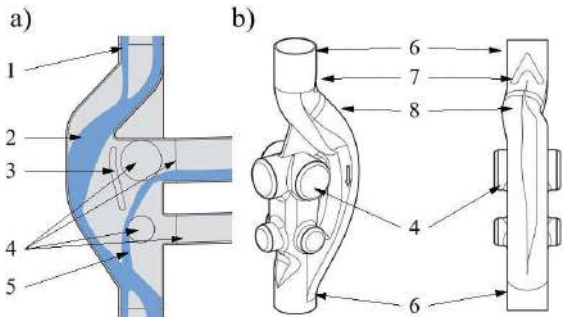

Fig. 5 – Sovent fitting [10]

a) function of the fitting, b) zones of the fitting,
1 – main flow falling around the inner wall, 2 – directed flow, 3 – protection against collision of two streams,
4 – connection points of branch pipes, 5 – flow of wastewater from branch pipe, 6 – connection to the stack, 7 – flow divider, 8 – swirl zone

Tab. 2 shows maximum flow rate Q_{max} in the stack with Sovent fitting and discharge units (DU) for the drainage factor K = 0,5.

Tab. 2 – Maximum flow rate in the stack with Sovent fitting [10]

Nominal diameter of the stack DN	Maximum ∑DU (l/s) for K = 0,5	Maximum flow rate Q_{max} (l/s)
100	576	12,0
150	1156	17,0

3.2 Stack with active protection elements

The stack can be supplemented (equipped) with active protection elements which protect the stack from critical negative pressure and overpressure. The elements of active protection are following:

- positive air pressure attenuator on the stack, Fig. 1d, and Fig. 6a,
- air admittance valve on each branch pipe, Fig. 1d, and Fig. 6b,
- air admittance valve on the stack, Fig. 1d, and Fig, 6c.

Correct design of the stack with elements of active system prevents the stack from exceeding the limit values of negative pressure and overpressure. Air admittance valves installed at the branch protects traps against increasing of limit negative pressure in the stack, which causes suction of water. Air admittance valves should be placed at the stack on each floor, to be able to suck the necessary amount of air at any place. The air admittance valve on the stack placed in exterior prevents creation of critical negative pressure due to the wind, which flows above the roof of a high-rise building. The valve opens only when an negative pressure occurs in the stack. A positive air pressure attenuator prevents overflowing of water from sanitary appliance due to overpressure, which arises mainly above the offset of the stack.

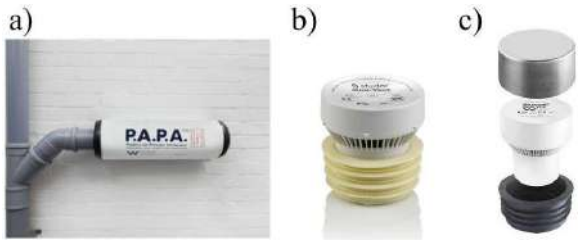

Fig. 6 – Elements of active protection [11]

a) positive air pressure attenuator, b) air admittance valve for the branch pipe, c) air admittance valve for the stack with aluminum cover for external usage

For sufficient protection of whole system, main requirements for the placement of the positive air pressure attenuator are given in the Tab. 3.

Tab. 3 – Requirements for installation of the positive air pressure attenuator connected to one stack [11]

Number of floors	Placement of the positive air pressure attenuator
5 - 10	one unit at the base
11 - 15	one unit at the base and one in the middle of the stack
16 - 25	one unit on the base, one unit on 5th floor, one unit between 5th floor and the end of the stack
26 - 50	two units in series on the base, then one unit on every 5th floor to the 25th floor, then every 10th floor
50 +	a necessary consultation with the supplier

It is possible to connect two stacks to one positive air pressure attenuator, what saves lot of initial investment costs. In this case, it is not possible to apply requirements from the Tab. 3.

Tab. 4 – Maximum flow in the stack with active protection elements [11]

Nominal diameter of the stack DN	Maximum ∑DU (l/s) for K = 0,5	Maximum flow rate Q_{max} (l/s)
100	213	7,3
125	400	10,0
150	1339	18,3

While using active protection elements, it is possible to design transitions of stacks to the drain in high-rise buildings more economical. Tab. 4 shows maximum discharge units for stacks with active protection elements and the calculated maximum flow rate Q_{max} for the drainage factor K = 0,5.

4. Experimental measurements of hydraulic conditions in stacks

The following part of the paper describes experimental measurements which were made for evaluating negative pressure and overpressure in stacks in various stacks systems. Experimental measurements were performed by two foreign companies:

- in the company Geberit in Switzerland was pressure fluctuation in stacks with Sovent fittings and a 88,5° single Y- branches compared,
- in the company Studor in China was pressure fluctuation in stacks with direct vent and stacks with the active protection elements compared.

U-tube pressure manometers are used to measure the negative pressure in stacks and are placed on each floor at the connection points of branch pipes. When the flow condition is complete, the water drop in manometers is read in mm of the water column and then converted to Pa. After the reading is recorded, the water level in the manometers is replenished and the measurements are repeated. In the following figures the maximum allowed negative pressure of - 464 Pa is indicated. This value represents the water level in the trap after 2 weeks without using of the sanitary appliance. When is this limit exceeded, there is no water in the trap which would prevent the interior for annoying smell from the drainage.

4.1 The Pressure fluctuation in the stack with Sovent fitting and 88,5° simple Y-branch

In the company Geberit were two different experimental measurements preformed:

I. Measurement of pressure fluctuation in the stack with DN 100 in the 6-floor building using Sovent fittings and the stack with 88,5° simple Y-branches were compared, Fig. 7. Two flow states were applicated. In the first flow state the WC on 5th floor was flushed, Fig. 7a. In the second flow state the WC on the 5th floor was flushed and the steady flow of 0,5 l/s from the 6th floor was simulated, Fig. 7b.

II. Measurement consisted of monitoring of pressure fluctuation in the stack in the 20-floor building with Sovent fittings; where flushing of WC was simulated with toilet paper on the marked floors Fig.8.

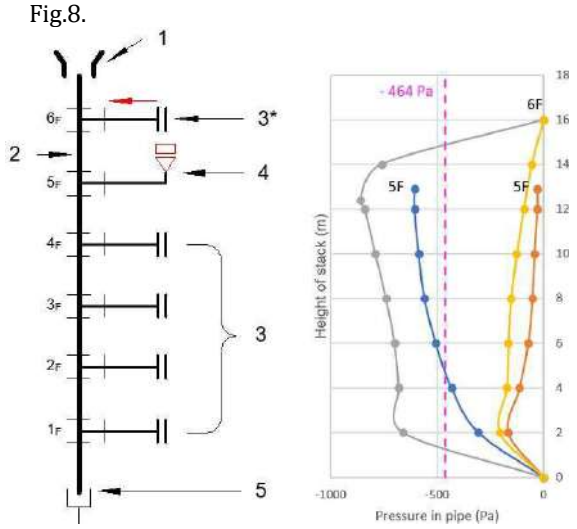

Fig. 7 – Pressure fluctuation in the stack with Sovent fitting and 88,5° simple Y-branch [10]

Fig. 7 description:
a) flushing the WC on 5th floor: ● 88,5°simple Y-branch, ● Sovent fitting,
b) flushing the WC on 5th floor and steady flow 0,5 l/s from 6th floor: ■ 88,5°simple Y-branch, ● Sovent fitting,
1 – air inlet, 2 – stack DN 100, 3 – branch pipes without flow, 3* – branch pipe on the 6th floor with steady flow, 4 – branch pipe with WC, 5 – free discharge

In the first flow state, the pressure in the stack with 88,5° simple Y-branches exceeded the maximum negative pressure of - 464 Pa between 2nd to 5th floor. The pressure in the stack with the Sovent fitting did not significantly change Fig. 7a. During the second flow state in the stack with 88,5° simple Y-branches, a negative pressure of - 900 Pa reached at mostly whole height of the stack Fig. 7b. Negative pressure in the stack with the Sovent fitting did not significantly change, fig. 7.

The best results were achieved in the stack with Sovent fitting.This fitting significantly eliminates the risk of extraction of water from traps. Maximum negative pressure was - 250 Pa.

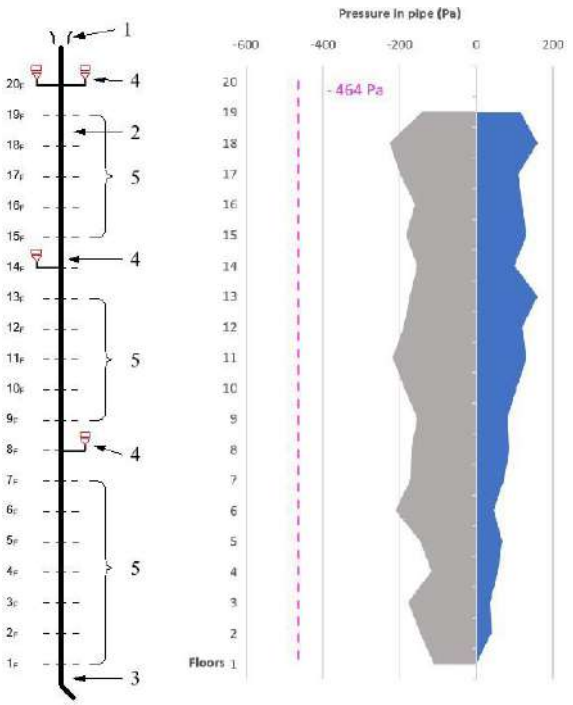

Fig. 8 – Pressure fluctuation in the stack in 20 floor building with Sovent fitting [10]

1 – air inlet, 2 – stack DN 100, 3 – transition to the drain, 4 – branch pipe with WC, 5 – branch pipe without flow

Fig. 8 shows the pressure fluctuation in the stack with Sovent fittings which were installed on each floor. WC´s were installed on the 20th floor (two WC´s), 14th and 8th floor. By flushing was toilet paper used. Pressure characteristic of the flow of water in various flushing mode was analysed. The area chart, which was created when the individual pressure curves were overlapped. The maximum allowed negative pressure was not exceeded. The pressure in the stack fluctuated approximately in the range of -250 to +180 Pa.

By comparing the drainage stack system with direct vent with 88,5° simple Y-branches and the system with Sovent fittings, diameter of conventional system must have been around DN 150 which is not economical solution.

4.2 Pressure fluctuation in the stack with direct vent and stack with active protection elements

In the company Studor was an experimental measurement in a 33-story building with different type of the stack DN100 performed. The stack with direct vent and the stack with active protection elements were compared. Construction of the stack with active protection is described in the chapter 3.2. Water flow was simulated from branch pipes on the 30th to 33th floor. The maximum water flow in the stack was 6,0 l/s.

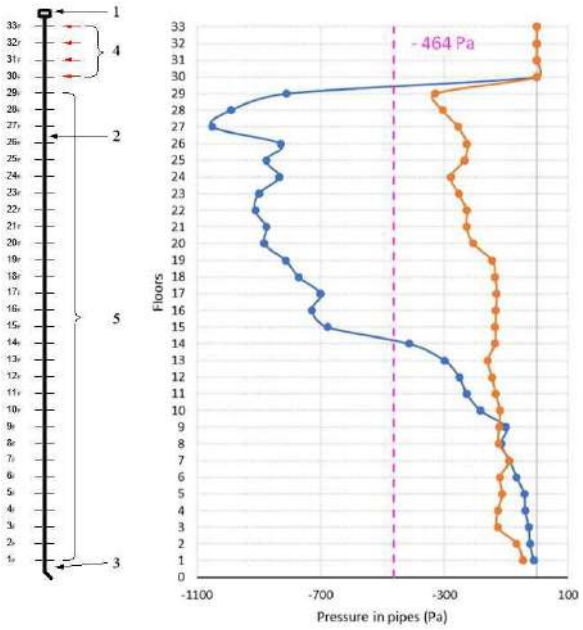

Fig. 9 – Pressure fluctuation in the stack with direct vent and the stack with active protection elements [8]

● stack with direct vent, ● stack with active protection elements,
1 – air admittance valve, 2 – stack DN 100, 3 – transition to the drain, 4 – branch pipes with flow, 5 – branch pipe without flow

Fig. 9 shows the stack with direct vent where the maximum negative pressure exceeded between 15th to 29th floor. The maximum negative pressure was - 1050 Pa. In the stack with active protection elements the maximum negative pressure didn't occur. The best results were achieved by the stack equipped with active protection elements. The active elements eliminate the risk of extraction of water from traps. The maximum negative pressure was - 350 Pa.

To avoid the high negative pressure in the stackwith direct vent, the dimension of the stack must have been at minimum DN 200. Comparing with the stack

with active elements DN 100 this would be an uneconomical solution.

5. Conclusion

From the analysis of special drainage systems and fitting for stacks in high-rise buildings, it is possible to state:

• special systems and fittings for stacks ensure optimal flow of foul water while comparing with conventional systems,

• stacks equipped with special systems and fittings can be designed for much bigger flow than conventional stack systems,

• the Sovent fitting ensures a continuous column of air along the entire height of the stack,

• the biggest increasing of falling velocity in the stack is in the highest 10 m, for this reason, it is not important to design offsets on stacks to reduce the velocity,

• above the offset of the stack overpressure occurs, and under offset negative pressure occurs.

The issue of hydraulic conditions of wastewater flow in stacks is a challenging and extensive topic, especially in high-rise buildings. To avoid the problem with high overpressure and negative pressure in stacks, with spreading of nosiness and vibration, it is necessary to follow the principles from standards and installation regulations.

Due to increasing of height of buildings also the requirements on drainage piping systems became more important. Therefore, new technical and material solutions are necessary to improve the quality of drainage systems.

6. Acknowledgments

This work was supported by the Ministry of education, science, research and sport of Slovak Republic through the Scientific Grant Agency VEGA 1/0303 and KEGA n.005STU-4/2021.

7. Resources

[1] Cheng, L. Ho, C. Lu, H. Current Desiggn of High-Rise Building Drainage System in Taiwan. CIB W062 Symposium 2004.

[2] Heinrichs, F. Rickmann, B. Sondergeld, K. Störrlein, K. Kommentar zum DIN 1986-100 and EN 12056-4. Gebäude und Grund stucksentwässerung: 2010, DIN Deutsches Institut für Normung, s. 126–127 ISBN 978-3-410-20533-3.

[3] Öngören, A. Materna, R. Tanner, M. Investigation of the effect of swept entry configuration on the air entertaiment and self-siphoning behaviour in gravity drainage systems. CIB W062 Symposium 2005 s. 2 - 4.

[4] Öngören, A. Weiss, R. Principles of a genuine high flow waste water fitting with an in-pipe integrated ventilation. CIB W062 Symposium 2018 s. 17 - 24.

[5] Pomogaeva, V. Matechko, L. Prokofiev, D. Narezhnaya, T. Investigation of the motion processes of wastewater in sewerage of high-rise buildings. E3S Wew of Conferences 2018 s. 1 – 9.

[6] Valášek, J.: Vnútorná kanalizácia. Komentár k ČSN 73 6760. Dimenzovanie potrubia vnútornej kanalizácie (Design of drainage pipes): 1986, Vydavatelství úradú pro normalizaci a měrení, s. 21-30 ISBN 59-313-83.

[7] Valášek, J.: Vodovody a kanalizácia vo vysokých budovách (Water supply and drainage in high-rise buildings). Bratislava: Alfa 1982, s. 131-157 ISBN 63-021-82.

[8] While, S. Hill, T. High-rise Testing of Active Drainage System Compared with Conventional Venting on Two Test Wowers. CIB W062 Symposium 2015 s. 11 - 29.

[9] Yabe, S. Otsuka, M. Kawaguchi, T. Sugimoto, R. An Experimental Investigation of the Influence of Different Offset Piping Methods on the Drainage Performance of a Drainage Stack. CIB W062 Symposium 2015 s. 30 - 55.

[10] GEBERIT – company documents and videos.

[11] STUDOR – company documents.

[12] STN EN 12056 – 2002: Gravitačné kanalizačné systémy vnútri budov (Gravity drainage systems inside buildings).

- STN EN 12056 – 1: Všeobecné a funkčné požiadavky.

- STN EN 12056 – 2: Potrubia pre splaškové odpadové vody. Navrhovanie a výpočet.

- STN EN 12056 – 5: Inštalácia a skúšanie, pokyny na prevádzku, údržbu a použitie.

[13] STN 73 6760 – 2009: Kanalizácia v budovách (Drainage inside buildings).

Data Statement

Data sharing not applicable to this article as no datasets were generated or analyzed during the current study.

Comparing Fast Numerical Methods and Conventional CFD for Mixing Ventilation Flows

Eugene Mamulova [a], *Twan van Hooff* [a]

[a] Eindhoven University of Technology, Eindhoven, the Netherlands, e.mamulova@tue.nl.

Abstract. Computational fluid dynamics (CFD) provides detailed information on the flow inside a room and can thus be used for detailed analyses of the influence of design variables, such as the placement of ventilation openings. As a result, CFD is well-suited to the optimization of ventilation at room level. However, the high computational cost and level of expertise required for implementation constitute bottlenecks in the engineering sector. In this research, a number of fast numerical techniques such as voxel-based CFD (vCFD) and coarse grid CFD (cCFD) are implemented as alternatives to conventional CFD. The methods are used to predict the velocity field for a generic mixing ventilation case and their accuracy and speed are compared. Reynolds-averaged Navier-Stokes simulations using RNG $k-\epsilon$ closure are performed, using ANSYS Fluent, in series and in parallel. The vCFD simulation is executed using the commercially available software ANSYS Discovery 2021 R2, which utilizes a proprietary algorithm that runs on GPU. The results show that, for the isothermal case, the fast numerical methods (FNMs) are two orders of magnitude faster than CFD. The accuracy of vCFD, cCFD and CFD is very similar: All cases yield RMSE and FAC1.3 values in a similar range. Current results show that vCFD and cCFD offer accelerated performance when compared to CFD, while maintaining similar accuracy. FNMs offer a distinct advantage over engineering tools, in the form of spatial information, which decreases the uncertainty of local comfort calculations prescribed by building standards. Ongoing thermal simulations for, among other things, a displacement ventilation case, using CFD, vCFD and cCFD are expected to offer additional insight into the feasibility of FNMs in the context of ventilation design optimization.

Keywords. fast numerical methods, ventilation design, coarse-grid CFD, voxel-based modeling, computational fluid dynamics.
DOI: https://doi.org/10.34641/clima.2022.303

1. Introduction

Building ventilation quality has a large impact on the comfort, health and performance of building occupants [1]. Thus, the act of optimizing a ventilation design is of paramount importance to the engineer. Optimization criteria at room level include variables such as opening location and the shape of the supply openings [2,3]. There are three common approaches that may be employed in the act and they are outlined in **Fig. 1**. Engineering tools, computational fluid dynamics (CFD) and fast numerical methods (FNMs) each possess a characteristic trade-off between accuracy, computational cost and level of numerical expertise required for implementation.

The use of CFD for simulating indoor flows was pioneered by Nielsen in the 1970s [4]. CFD is capable of providing high-quality information on momentum, energy and mass transfer within a room. CFD methods range from transient large eddy simulations to steady-state Reynolds-averaged Navier-Stokes (RANS) simulations, the latter of which consume less resources. Nevertheless, steady RANS remains very costly, impeding its adoption in day-to-day design practices [5].

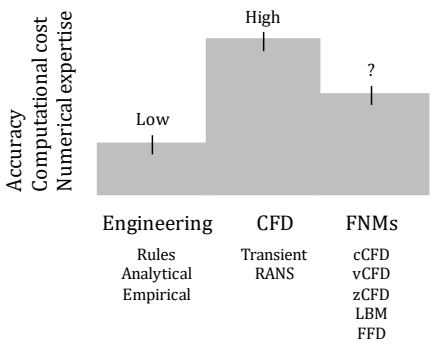

Fig. 1 – Qualitative accuracy-cost-expertise trade-off for engineering tools, CFD and FNMs.

Copyright ©2022 by the authors. This conference paper is published under a CC-BY-4.0 license.

Common engineering tools include rules of thumb, as well as analytical and empirical models that allow ventilation designers to make quick decisions and perform the calculations necessary for compliance with building quality standards. In contrast to CFD, engineering tools are very easy to apply and do not require any computational resources. However, the accuracy of the aforementioned methods is lower, as is the resultant spatial information.

Fast numerical methods constitute a compromise between the aforementioned approaches, such that they may potentially yield accuracies higher than engineering tools and most likely lower than CFD, while demanding less computational resources and modelling expertise than the latter [5]. Past studies encompass a vast variety of fast numerical methods, some of which are well-suited for indoor applications [6]. Fast numerical methods of interest include coarse-grid CFD (cCFD) [7], voxel-based CFD (vCFD) [8], zero-equation turbulence modeling (zCFD) [9], Lattice Boltzmann methods (LBM) [10] and fast fluid dynamics (FFD) [11]. The focus of this paper is on the application of cCFD and vCFD, which are both based on conventional CFD. cCFD makes use of a sub-optimal grid, yielding a solution that cannot be considered grid-independent. The reduced number of cells decreases the computation time, at the expense of accuracy. vCFD uses a voxel-based, Cartesian grid that is automatically generated [12]. The GPU-based implementation is expected to significantly speed up the computation.

The inclusion of FNMs in current ventilation design methodologies could potentially improve the quality of the design outcome. However, a comparative assessment of conventional CFD, fast numerical methods and empirical approaches is not yet available in literature, hindering the prospective development of an effective workflow for ventilation design. Moreover, the potential of fast numerical methods in terms of ensuring ventilation design quality has not yet been quantified. The main objective of this research is to test the speed and accuracy of vCFD, cCFD and CFD for an isothermal mixing ventilation case. This study compares the performance of empirical models, fast numerical methods and conventional CFD, in the aim to discuss whether the implementation of fast numerical methods in current engineering practice can improve ventilation design quality, as it is prescribed by current building standards.

2. Isothermal validation study

The isothermal case is based on measurement data collected by Nielsen [13]. The case involves a three dimensional enclosure with one inlet and one outlet. The measurements are performed for Re = 5000 and a kinematic viscosity v of $15.3 \times 10^{-6} \mathrm{m}^2/\mathrm{s}$, at an air temperature of $20^{o}C$. The setup captures the flow penetration and recirculation that is characteristic of mixing ventilation, which makes it well-suited for the validation of mixing flow simulations. The geometry modeled in ANSYS Design Modeler is shown in **Fig. 2**. The length L, width W and height H are equal to $9\ m$, $3\ m$ and $3\ m$, respectively. The inlet height h is equal to $0.168\ m$. The outlet height t is equal to $0.480\ m$. Inlet and outlet length l is equal to $3\ m$.

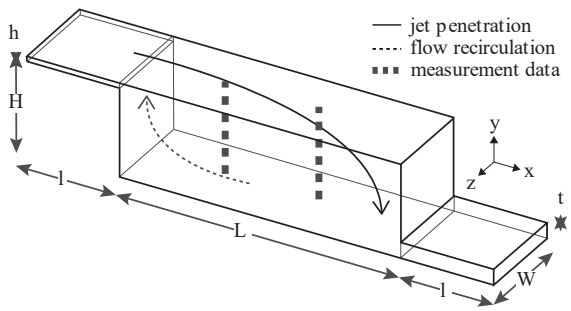

Fig. 2 – Room geometry including two measurement locations at z = 0.5W.

Validation data consists of 25 measurement points at x = H and 25 measurement points at x = $2H$. The data is used to test the accuracy of the numerical methods. The validation metrics used, i.e. root-mean square error (RMSE) and factor of 1.1 of observations (FAC1.1) are defined in equations (1) and (2), where y_{CFD} and y_{EXP} represent simulated and measured values, respectively. In addition to FAC1.1, FAC1.2 and FAC1.3 are calculated. The equations are not shown for the sake of brevity.

$$\mathrm{RMSE} = \sqrt{\left(\sum_{n=1}^{N} \frac{(y_{CFD} - y_{EXP})^2}{N}\right)} \tag{1}$$

$$\mathrm{FAC1.1} = \frac{1}{N}\sum_{n=i}^{N} n_i,\ \ n_i = \begin{cases} 1\ for\ 0.91 \leq \frac{y_{CFD_i}}{y_{EXP_i}} \leq 1.1 \\ 0\ else \end{cases} \tag{2}$$

2.1 CFD methodology

The domain is discretized into hexahedral cells using ANSYS Meshing, as shown in **Fig. 3a**. A grid-sensitivity analysis is performed in order to establish a grid resolution that provides a nearly grid-independent solution. **Tab. 1** summarizes the key characteristics of the grids. Coarse is the coarsest possible grid to satisfy the requirement $y^* < 5$ for low Reynolds number modeling.

Tab. 1 – Summary of the computational grids.

Grid	Cell count	$y*_{max}$	$\overline{y^*}$
Coarse	265,650	6	4
Basic	766,250	4	3
Fine	2,211,863	3	2

The inlet velocity, $U_o = 0.455 m/s$, is obtained using the relation $Re = hU_o/v$. The static gauge pressure at the outlet is $0\ Pa$. The boundary conditions at the walls are no-slip. The turbulent kinetic energy k_0 and turbulent dissipation rate ϵ_o are scaled according to the inlet and outlet heights, using equations (3) and (4), where the turbulent length scale l_0 is taken to be 10% of the opening height and C_μ is a model constant, equal to 0.09.

$$k_0 = 1.5(0.04 \cdot U_0)^2 \quad (3)$$

$$\epsilon_0 = \frac{k_0^{1.5}}{l_0} \quad (4)$$

The resultant k_0 and ϵ_0 at the inlet are set to $5.0 \times 10^{-4}\ m^2/s^2$ and $6.6 \times 10^{-4}\ m^2/s^3$. Similarly, backflow k_0 and ϵ_0 are equal to $5.0 \times 10^{-4}\ m^2/s^2$ and $2.3 \times 10^{-4}\ m^2/s^3$, respectively.

The simulations are performed using the steady solver in ANSYS Fluent 2021 R1. The RANS equations are closed via the RNG $k - \epsilon$ model and low Reynolds number modeling is used for near-wall treatment. The settings are based on a comparison of experimental results with the results obtained using a range of RANS turbulence models, which is omitted for the sake of brevity. Pressure and velocity are coupled using the SIMPLE algorithm and the former is interpolated via the second order discretization scheme. The remaining terms are computed using the second order upwind scheme. Steady statistics are enabled after 1000 iterations and the sampling interval is set to 1. The under-relaxation factors for momentum, pressure, density, body forces, turbulent kinetic energy, turbulent dissipation rate and turbulent viscosity are set to 0.3, 0.6, 0.6, 0.3, 0.5, 0.5 and 0.6, respectively.

Due to oscillations in the residual values, the mean x-velocity component U_x is monitored at several points in the domain. The percentage deviation D between two iterations, 1000 iterations apart, is calculated and convergence is assumed when $D \leq 0.1$ %. Absolute convergence criteria for momentum, velocity and turbulence terms are not defined but all residual terms level off and drop by at least three orders of magnitude before the aforementioned convergence criteria for U_x are satisfied. The simulations are stopped after 35,000 iterations.

The grid-sensitivity analysis focuses on the dimensionless x-velocity profiles at $x = H$ and $x = 2H$, as shown in **Fig. 4**. The grid convergence index (GCI) is calculated using equation (5), where r is the linear grid refinement factor, equal to 2, p is the formal order of accuracy, equal to 2, and F_s is the safety factor, which takes the value 1.25 for a sensitivity analysis involving three or more grids.

$$GCI_{basic} = F_s \frac{r^p[(U_{basic} - U_{fine})/U_0]}{1 - r^p} \quad (5)$$

The results show that the coarse grid provides almost grid-independent results. The coarse grid is shown in **Fig. 3a**. The maximum and average GCI_{coarse} values at $x = H$ are 0.02 and 0.07 and the maximum and average GCI_{coarse} values at $x = 2H$ are 0.01 and 0.07, respectively.

2.2 cCFD methodology

The boundary conditions used for cCFD are identical to those used for CFD. The cCFD simulations are also performed using the steady solver in ANSYS Fluent 2021 R1. The RANS equations are closed via the RNG $k - \epsilon$ model and wall functions are used for near-wall treatment. Pressure and velocity are coupled using the Coupled scheme and the former is interpolated via the second order discretization scheme. The remaining terms are computed using the second order upwind scheme. Steady statistics are enabled after 1000 iterations and the sampling interval is set to 1. The under-relaxation factors for momentum, pressure, density, body forces, turbulent kinetic energy, turbulent dissipation rate and turbulent viscosity are set to default values of 0.5, 0.5, 1, 1, 0.8, 0.8 and 1, respectively. Convergence is assumed when all residual terms level off and drop by at least three orders of magnitude. The simulations are stopped after 1,500 iterations.

The meshing procedure consists of coarsening the CFD mesh while maintaining a smaller cell size closer to the wall and ensuring the presence of distinct cells at validation points $x = H$ and $x = 2H$. The cell count decreases from 265,650 cells for CFD to 4,401 cells for cCFD. The y^* values at the ceiling range from 5 to 12. The cCFD grid is shown in **Fig. 3b**.

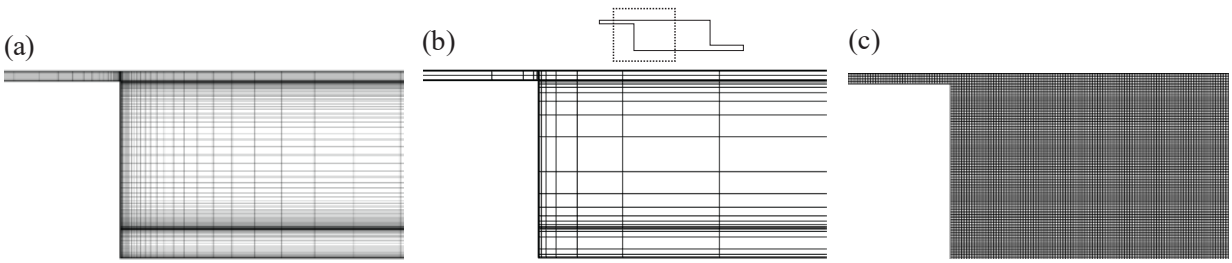

Fig. 3 – Two-dimensional, close-up view of the computational grids: (a) CFD, (b) cCFD, and, (c) vCFD.

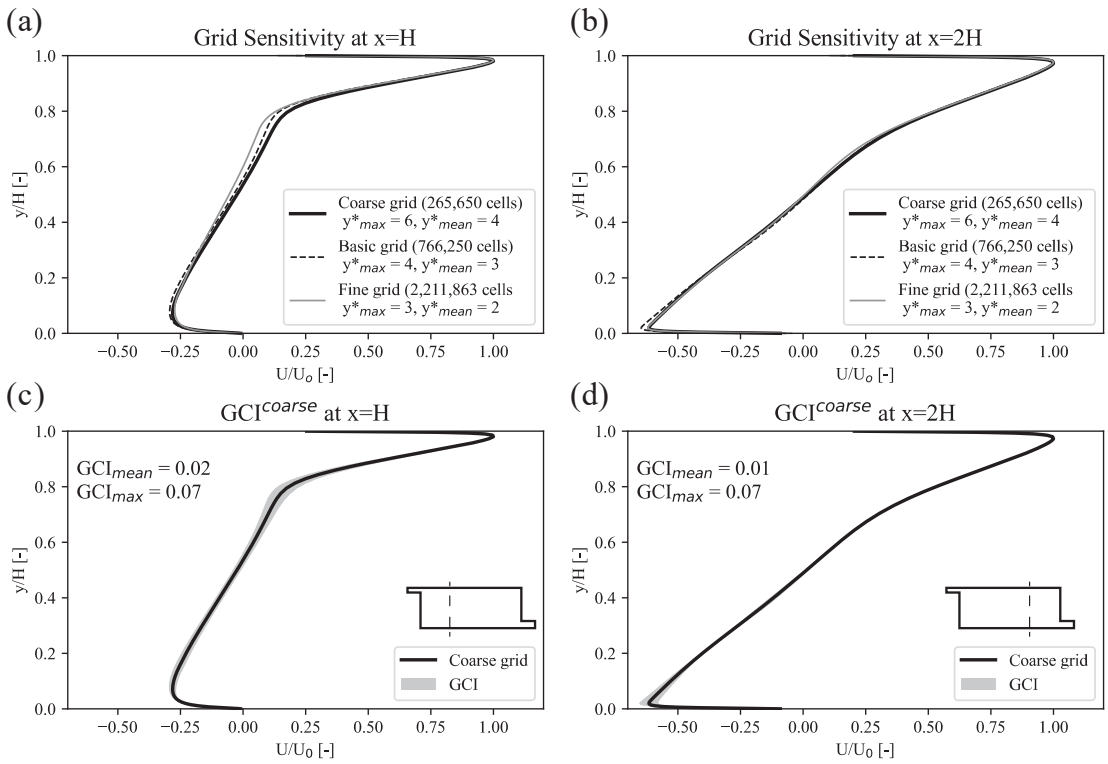

Fig. 4 –Grid-sensitivity analysis at (a) x=H, (b) x=2H. GCI plot at (c) x=H, (d) x=2H.

2.3 vCFD methodology

The vCFD simulations are performed via the steady solver in ANSYS Discovery 2021 R2. The software requires basic input in the form of boundary conditions. The solver settings cannot be adjusted and several proprietary aspects of the software remain undisclosed. Turbulence modeling is performed using the Standard $k - \epsilon$ model. Pressure and velocity are coupled via the use of a SIMPLE-like algorithm. Simulation convergence is determined automatically.

The voxel-based grid is sized according to the available video memory (VRAM). The highest fidelity setting discretizes the domain using 40.21 mm voxels. The total count is equal to 1,338,095 voxels. The vCFD grid is shown in **Fig.3c**.

3. Hardware configurations

All simulations are performed on a HP Zbook Studio G5 laptop, equipped with an Intel® Core™ i7-9750H central processing unit (CPU) and 16 GB of random access memory (RAM). The CPU consists of six physical cores and six logical processors, which run at a base clock speed of 2.60 GHz. Hyperthreading is disabled to ensure efficient use of physical cores. The laptop is equipped with an NVIDIA Quadro P2000 graphical processing unit (GPU) with 4 GB video memory (VRAM). Six CFD configurations and six cCFD configurations are tested using 1-6 physical cores and one vCFD simulation is run on GPU. The computational domain is divided into n partitions, corresponding to the number of active CPU cores.

4. Ventilation design quality

While there exist multiple ways to evaluate the quality of a given design, most engineers refer to standards for quality assurance. Using the available experimental data, the draught rate DR is computed using equation (6), where T_a = 20℃ is the air temperature, v is the mean velocity magnitude and I is the turbulence intensity.

$$\mathrm{DR} = (34 - T_a)(v - 0.05)^{0.62} \qquad (37 \cdot I \cdot v + 3.14) \tag{6}$$

DR is then computed via vCFD, cCFD and CFD and compared to a hand calculation (EMP), based on a series of engineering assumptions. The maximum velocity in the occupied zone u_{rm} is obtained using the empirical formula stated in equation (7), where the decay constant for a plane wall jet K_p is 3.5 [14], the decay constant in the recirculation region K_{rm} is 0.7 [15] and the distance from the virtual origin of the diffuser x_0 is 3 m.

$$\mathrm{u_{rm}} = \mathrm{K_p K_{rm} u_0} \sqrt{\frac{\mathrm{h}}{\mathrm{L + x_o}}} \tag{7}$$

Given that turbulence intensity information is unavailable for vCFD and EMP, $10\% \leq I \leq 90\%$ is used to account for the range of values that may be used as input. The results are used to discuss the potential contribution of FNMs towards ventilation design, beyond that of engineering tools.

5. Results

5.1 isothermal validation study

Fig. 5a-5b show the dimensionless mean velocity profiles obtained using vCFD, cCFD and CFD, in comparison with the available experimental data. The results show that all three numerical methods capture the primary characteristics of the mixing ventilation flow, such as the high-velocity region near the ceiling and the recirculation flow in the occupied zone. **Fig. 5c-5d** compare the accuracy of the three numerical methods. No single numerical method outperforms the others across all metrics. The RMSE values for vCFD, cCFD and CFD are 0.05, 0.09 and 0.05, respectively, suggesting that the accuracy of vCFD and CFD is comparable. The FAC1.1 values for vCFD, cCFD and CFD are 0.26, 0.26 and 0.32, indicating that CFD gives the best agreement with the experimental data. The FAC1.2 values are 0.60, 0.50 and 0.68 and the FAC1.3 values are 0.62, 0.60 and 0.60, respectively. The best performing method differs per metric and, given that the relative difference in performance is small, the accuracy of vCFD, cCFD and CFD for this validation case is considered commensurate. **Fig. 5e** shows the computational time per simulation, in minutes. The results show that the fast numerical methods are two orders of magnitude faster than CFD. Moreover, the decrease in computational time obtained from parallel processing is almost linear as the number of cores is increased but exhibits stagnant behaviour after a certain number of cores. The stagnation may be attributed to a number of hardware or software related factors [16], one of which is the low cell count used for this validation case. It is concluded that fast numerical methods are significantly faster than conventional CFD and that shared-memory parallel simulation does not change the outcome in favor of using CFD for ventilation design optimization.

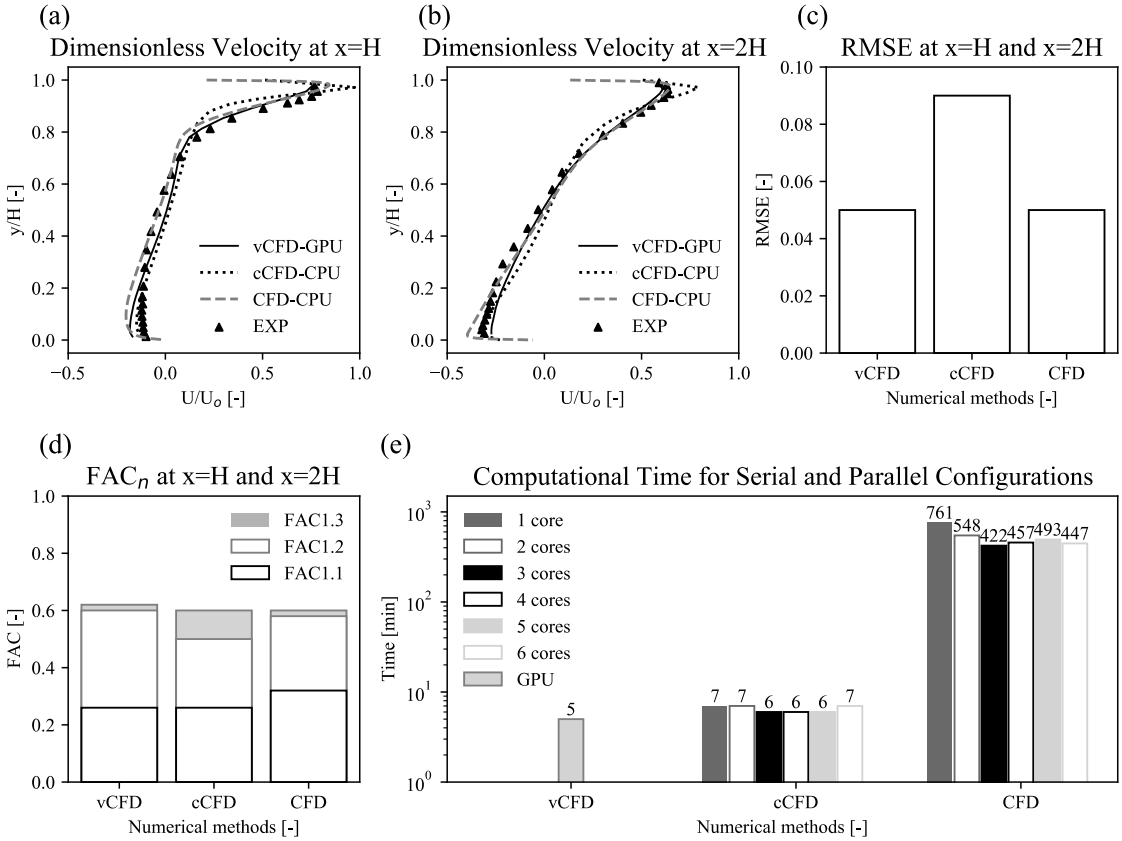

Fig. 5 – Results for vCFD, cCFD and CFD. (a)-(b) Dimensionless velocity profiles at x=H and x=2H. (c) RMSE for vCFD, cCFD and CFD. (d) FAC1.1, FAC1.2 and FAC1.3 for vCFD, cCFD and CFD. (e) Computation time for vCFD, cCFD and CFD.

5.2 ventilation design quality

Tab. 2 reports the maximum DR in the occupied zone, computed according to equation (6), as well as the maximum velocity in the occupied zone u_{rm} and the turbulence intensity I. For the CFD-based methods, the search for u_{rm} and maximum DR is conducted at z = 0.5W. For EMP, u_{rm} is computed via equation (7). The empirical model yields the lowest $u_{rm} = 0.14\ m/s$, followed by vCFD, CFD and cCFD at $0.18\ m/s$, $0.20\ m/s$ and $0.24\ m/s$, respectively. The latter three values are relatively comparable in magnitude and are located near the outlet. Meanwhile, EMP assumes that u_{rm} occurs at $x = 2H$. It is not possible to validate the accuracy of the u_{rm} calculations due to the absence of measurement data. However, the discrepancy in location suggests that EMP does not have the spatial sensitivity to predict u_{rm} and that FNMs allow for more effective optimization of local comfort parameters. The maximum DR values lie above 10% (categories II-III) for all methods. The results for cCFD and CFD are

23% and 19%, placing them in categories III and II, respectively. The results for EMP and vCFD span both categories, given the range $10\% \leq I \leq 90\%$ used for the calculation. This illustrates that, in the absence of numerical data, ventilation design quality is sensitive to user input, which can lead to uncertainty in ventilation design quality. For this validation case, such dependency can be reduced through the use of cCFD, which provides spatial information at a low computational cost.

Tab. 2 – Default criteria, according to [17], and calculated values related to the draught rate *DR* in the occupied zone.

Variable		EMP	vCFD	cCFD	CFD
u_{rm} $[m/s]$		0.14	0.18	0.24	0.20
I [%]		10-90	10-90	17	19
DR	[%]				
I	<10	-	-	-	-
II	<20	11-24[a]	14-31[a]	-	19
III	<30			23	-

[a] Note that the results are within categories II and III.

It is important to mention that each method has its advantages and disadvantages. For example, vCFD is performed using a commercially available software with a simple graphical user interface that could soften the barrier of entry for the engineering sector. However, the software is relatively new and further developments are ongoing. Meanwhile, cCFD can be performed using any CFD software, which allows the user flexibility in obtaining detailed spatial information. On the other hand, the implementation of cCFD implies a very similar level of CFD knowledge as conventional CFD, thereby increasing the level of expertise required for its implementation. In summation, it is highly unlikely that one method will maintain an advantage for every given case. A potential strategy for integrating FNMs in design practices is to approach the methods as components in a workflow or toolkit, perhaps even alongside engineering tools and conventional CFD.

6. Limitations and future research

This study presents first results in a larger research effort on FNMs as a toolkit for ventilation design. It is subject to several limitations which may be addressed via future research efforts:

- The validation case is based on a geometry that captures mixing flow characteristics but is too simple to be representative of a real design scenario.
- The absence of validation data inhibits the validation of important design criteria, such as the draught rate *DR*.
- The isothermal study does not account for significant influences such as windows, people and other heat sources, which will be included in ongoing and future studies.
- Other FNMs, such as zCFD, LBM and FFD, are not included in this study but are worth including in the future.

7. Conclusion

This study presents preliminary results in an effort to evaluate the potential of FNMs for improving ventilation design quality. An isothermal mixing ventilation case is simulated using vCFD, cCFD and conventional CFD. The results are compared to existing measurement data and are further used to evaluate the draught rate *DR* in the occupied zone. The outcomes are compared to that of an empirical calculation. This study offers a comparison between engineering tools, CFD, vCFD and cCFD, which, to the best knowledge of the authors, has not been made before. The following conclusions are made:

- Both conventional CFD and FNMs capture the principal characteristics of mixing ventilation flow.
- FNMs are two orders of magnitude faster than conventional CFD, for this case.
- For this validation case, the accuracy of vCFD and cCFD is comparable to that of CFD.
- The spatial resolution of vCFD, cCFD and CFD is better-suited to evaluate local parameters, such as u_{rm} and *DR*, compared to empirical models.
- In order to calculate *DR* using EMP and vCFD, an assumption for I is required. Dependency on user input introduces uncertainty in the ventilation design quality, as shown by the large variability in *DR*. In this case, cCFD offers a distinct advantage to vCFD.
- To extrapolate, the results suggest that the choice of numerical method is case-dependent. The authors do not encourage the pursuit of a one-size-fits-all.

8. Acknowledgement

The authors gratefully acknowledge the partnership with ANSYS. The authors acknowledge the support of the Flemish Agency for Innovation and Entrepreneurship (VLAIO) in the Flux50 project Smart Ventilation (HBC.2020.2520).

9. Data access statement

Data sharing is not applicable to this article as no datasets were generated or analyzed during the current study.

10. References

[1] Awbi, H.B. Ventilation systems: Design and performance. 2007; Chapter 2: 62-104.

[2] Morsli S., Ramenah H., El Ganaoui M., and Bennacer R. Effect of aligned and misaligned

ventilation openings affecting energy demand and air quality in buildings. EPJ Applied Physics. 2018; 83(1).

[3] Staveckis, A., Borodinecs, A. Impact of impinging jet ventilation on thermal comfort and indoor air quality in office buildings. Energy and Buildings. 2021; 235(5).

[4] Nielsen P.V. Strømningsforhold i luftkonditionerede lokaler (English translation: Flow in Air Conditioned Rooms). Phd Thesis. Technical University of Denmark. 1974.

[5] Morozova N., Trias F.X., Capdevila R., Pérez-Segarra C.D., Oliva A. On the feasibility of affordable high-fidelity CFD simulations for indoor environment design and control. Building and Environment. 2020; 184(May).

[6] Hosain M.L., Fdhila R.B. Literature Review of Accelerated CFD Simulation Methods towards Online Application. Energy Procedia. 2015; 75: 3307–3314.

[7] Wang H., Zhai Z. Application of coarse-grid computational fluid dynamics on indoor environment modeling: Optimizing the trade-off between grid resolution and simulation accuracy. HVAC and R Research. 2012; 18(5), 915–933.

[8] Papp B., Kristóf G., Gromke C. Application and assessment of a GPU-based LES method for predicting dynamic wind loads on buildings. Journal of Wind Engineering and Industrial Aerodynamics. 2021; 217.

[9] Chen Q., Xu W. A zero-equation turbulence model for indoor airflow simulation. Energy and Buildings. 1998; 28(2): 137–144.

[10] Khan M.A.I., Delbosc N., Noakes C.J., Summers J. Real-time flow simulation of indoor environments using lattice Boltzmann method. Building Simulation. 2015; 8(4): 405–414.

[11] Liu W., Van Hooff T., An Y., Hu S., Chen C.W. Modeling transient particle transport in transient indoor airflow by fast fluid dynamics with the Markov chain method. Building and Environment. 2020; 186(September).

[12] ANSYS Inc. Discovery 2021 R2. January 2021.

[13] Nielsen P.V., Rong L., Olmedo I. The IEA Annex 20 Two-Dimensional Benchmark Test for CFD Predictions. 2010.

[14] Nielsen P.V. Lecture slides on Mixing Ventilation. University of Aalborg. Accessed on 14 Dec 2021.

[15] Nielsen P.V. Numerical Prediction of Air Distribution in Rooms – Status and Potentials. University of Aalborg. 1988.

[16] ANSYS Inc. Parallel Processing Guide. 2021.

[17] NEN-EN 16798-1: 2019 - Energy performance of buildings - Ventilation for buildings - Part 1: Indoor environmental input parameters for design and assessment of energy performance of buildings addressing indoor air quality, thermal environment, lighting and acoustics - Module M1-6. 2019.

Ventilation and COVID-19 transmission risks on board of Dutch governmental ships

Atze Boerstra [a,b], *Mark Verlinde* [a]

[a] bba binnenmilieu, The Hague, the Netherlands, email: ab-bba@binnenmilieu.nl.

[b] Faculty of Architecture and the Built Environment, Delft University of Technology, Delft, the Netherlands,

Abstract. The Dutch government (specifically the 'Rijksrederij', the governmental shipping company) owns a fleet of just under 100 ships that are equipped to service the internal waterways and parts of the North Sea. Think in this context of e.g. Coast Guard ships, ships that help to fight oil accidents or ships that maintain buoys. Just after the COVID-19 pandemic had started the 'Rijksrederij' decided that it was necessary to investigate to what extent the fleet might pose a risk for cross-contamination of this new disease on board. This was approached with a specific focus on ventilation and the airborne route. The objective was to find out whether the most important spaces on board of the ships were adequately ventilated and to evaluate how ships can be made or kept 'COVID-resistant' as far as the airborne route is concerned. A sample of 16 ships of different types, most of them mechanically ventilated, were surveyed. This included a general inspection, an inspection of relevant HVAC system characteristics and measurements of e.g. air supply flows. Also, ships were equipped with monitors that measured CO_2 concentration (e.g. in galleys and wheelhouses) that were left on board for at least one week. As reference for the supply flow measurement outcomes we used ISO 7547 guideline values and the Germanischer Lloyd ventilation requirements. On board of 6 of the 16 ships that were investigated we found serious problems with the fresh air supply and/or measured CO_2 concentrations. On the positive side, the majority of the ships had ventilation capacities in line with the two reference standards, and almost all did not use central recirculation. We also found that many of the ships had adequate options, at room level, for individual control of both fresh air supply and temperature. The results of the study will be used to further improve 'COVID safety' on board of the whole fleet and to ameliorate future, new ships and their HVAC systems.

Keywords. Airway infections, cross contamination, Corona disease, CO_2 concentration, dilution, fresh air supply, recirculation.
DOI: https://doi.org/10.34641/clima.2022.175

1. Introduction

At the beginning of the COVID pandemic (spring 2020) the Rijksrederij (Dutch governmental shipping company, linked to the Directorate General for Public Works and Water Management) conducted general risk evaluations related to COVID-19 AND occupational health on board. One conclusion was that it made sense to further evaluate the effectiveness of the ventilation systems of the ships.

It is well known that ships are particular vulnerable when it comes to cross infection risks of airway diseases in general and COVID-19 specifically (see e.g. [1] and [2]). Not surprisingly as on board of ships people have limited personal space, while from the general literature [3] [4] we know that viruses are easily transmitted from person to person especially when people spend a lot of time together in relative small spaces. This is even more likely when these spaces are poorly ventilated and people are in relatively close distance to each other. For good reason Japan has developed, in this context, the so-called 3 C policy [5] stating that to avoid cross infection people should avoid i. Closed spaces with poor ventilation, ii. Crowed places with many people nearby, and iii. Close contact settings with e.g. close-range conversations.

The Rijksrederij operates just under 100 ships, some smaller (used for day trips) and some larger (used for 'over-the-horizon' patrols that can last for up to one week). See figure 1 for an impression.

Copyright ©2022 by the authors. This conference paper is published under a CC-BY-4.0 license.

Fig. 1 - Two example ships used by the Rijksrederij; the upper one is for week patrols, the lower one is for day patrols

The Rijksrederij already had taken several 'regular' measures to decrease cross-infection risks on board of these ships, related to handwashing, mask wearing and e.g. cleaning in between shifts. Apart from that, the organisation was determined to further improve 'COVID safety' by addressing the airborne route and thereby focusing on ventilation.

The core objective of this study was to find out whether the most important (most intensively used) spaces on board of the ships were adequately ventilated and to evaluate how the ships can be kept or made more 'COVID-resistant' as far as the airborne route is concerned.

The research questions were as follows:

1. Is the fresh air supply in line with the ISO and Germanischer Lloyd requirements?

2. Are there any other airway infection risks related to the design, operation and maintenance of the ventilation systems?

3. Which measures could be taken to further improve the situation on board of these ships and future new ships?

Note that the focus was to not only measure mechanical fresh air supply but also to investigate options for natural ventilation, possible issues with recirculation etc..

2. Research Methods

2.1 General approach

A total of 16 ships (this is about 1 in 6 of the total amount of ships) were evaluated. These ships came from different home ports all over The Netherlands (from Harlingen in the upper North to Vlissingen in the South). The ships were selected with the different subgroups (ship types e.g. large vs. small) in mind, also taking into account patrol schedules and general availability.

The surveys on board were conducted during the winter of 2020/2021. Each time we went through the following steps:

1. Beforehand relevant technical documentation of the ship was studied (desk research).

2. Next an on board inspection was conducted; this involved a general survey of relevant spaces, inventory of normal use practices (e.g. amount of people on board), a check-up of relevant technical appliances (air handling units etc.) and short on-site interviews with contact persons (e.g. the captain or a marine engineer in charge of on-board technology). In this context we used the REHVA COVID-19 guidance document [6] and the WHO ventilation roadmap document [7] as base references.

3. During the inspection day we also measured air supply rates in randomly selected spaces (with a calibrated ACIN flow finder device); this was done in the most intensely used spaces (especially messrooms, wheel houses and sleeping quarters). Before the measurements started we asked those present to put the ventilation system in 'the setting normally used when out on patrol'.

4. At the end of the inspection day, one or more CO_2 loggers were placed in the living spaces at breathing zone height (Aranet 4 Pro devices). These loggers where retrieved about one week later (sometimes after 2 weeks depending on patrol schedules).

5. Afterwards, all data and qualitive findings were analyzed. First for the ships individually, at the end of the project for the batch as a whole.

Note that some ships did not have a mechanical ventilation system (only natural supply and exhaust). In those cases we only measured the CO_2-concentration.

2.2 Reference values measurements

Beforehand we had to decide what reference levels to use when interpreting the air flow and CO_2 concentration measurements. In that context we first made an inventory of relevant legal requirements specifically applicable for marine vehicles and inland vessels.

Article 73 of the Dutch 'Schepelingenbesluit' (Sailors Decree) for example states: 'All on board spaces for personnel shall be effectively ventilated in such a way that the air indoors remains in a satisfactory condition.'

Article 11.07 of the Dutch 'Binnenschepenbesluit' (Inland Vessel Decree) asks for something similar, also without specific requirements in terms of minimum amount of fresh air that should be provided at room level or per person.

More concrete reference requirements are presented in an ISO standard for marine vehicles that is often used e.g. when new ships are being built: ISO 7547: 2005 'Air-conditioning and ventilation of accommodation spaces on board ships, Design conditions and basis of calculations' [8]. Also the Germanischer Llyod document 'Rules for classification and construction of seagoing ships' [9] gives some clues about what is considered 'adequate ventilation' in the shipbuilding context. Note that the ISO requirements are stated in terms of minimum requirement fresh air supply per person (in l/s) and that the German Lloyd requirements are stated in terms of minimum allowed air exchange rates (with different values for sleeping quarters and non-sleeping quarters). The quantitative requirements of the two standards are summarized in table 1.

Tab. 1 – Reference values.

	ISO 7547	Germa-nischer Lloyd
Minimum fresh air supply per person	8 l/s = 28,8 m^3/h	-
Minimum Air Exchange Rate messrooms, offices	-	12 h^{-1}
Minimum Air Exchange Rate sleeping quarters, wheel houses	-	6 h^{-1}

In the context of COVID cross-transmission via the airborne route one might pose the question whether these values are high enough to substantially mitigate infection risks. The World Health Organisation stated spring 2021 (at a time that the Omicron variant did not exist yet) that normally speaking, in 'standard work situations' 10 l/s fresh air supply per person and a minimum Air Exchange Rate (AER) of 6 should be enough to at least provide some level of safety [7]. The reference values that we used, that are mentioned in table 1 are quite in line with that.

The reference level that we used when interpreting the continuous CO_2 measurements was 1000 ppm. This is the steady-state concentration that will occur when a fresh air supply is provided in accordance with the previously mentioned ISO standard. That is assuming an outdoor (above-sea) CO_2 concentration of 350 ppm, a metabolism of not more than 1,4 met and a CO_2 production of 0,006 l/s or less [10]. Also assuming an error margin of 10%. Moreover, this 1000 ppm also tunes in with the often used reference value (in the Netherlands) when investigating indoor climate problems in offices.

3. Results & discussion

First we present the quantitative results. The air flow measurement data are presented in paragraph 3.1, the CO_2 measurement outcomes are presented in paragraph 3.2. After that, in paragraph 3.3 the qualitative results of the survey are presented. The results per ship are presented using codes like L-A2 and S-R1. This has been done to ensure confidentiality.

3.1 Results air flow measurements

The results of the air flow measurement are presented in Table 2.

A special note in relation to the 8 smaller ships that are used for day patrols (bottom half of table 2): the main space on board here was the wheel house (often with an integrated pantry). No measurements were conducted in messrooms or sleeping quarters as these smaller boats did not have those kind of spaces. Some of the smaller ships were not equipped with a mechanical ventilation system: these were ventilated naturally via sliding windows and / or air scoops (elbow pipes). This applies specifically to the ships S-A1, S-C1 and S-S1, This explains why no measurement data are presented for those three ships in Table 2.

As far as the Air Exchange Rates (AER's) in table 1 are concerned: Conclusion in relation to the 8 larger ships for week patrols was that the ventilation performance varies significantly from ship to ship. The best ships allow for Air Exchange Rates (AER's) at room level of about 15-25; while in the worst ventilated spaces AER's were as low as 2-3. As far as air supply per persons on the larger ships is concerned: also here a large variation was found: with e.g. less than 20-30 m3/h air supply person in some spaces and more than 300 m3/h in others.

Conclusion in relation to the 8 smaller ships for day patrols: AER's in the wheel houses in the 5-10 range; air supply per person in the 50-200 m3/h range.

Median values of AER's and per person air supply rates for can be found in the last row of Table 2. In two of the 16 ships (both larger ones) the ISO and/or Germanischer Lloyd ventilation requirements are clearly not met: this applies to L-M2 and L-Z1. In two others (L-T1 and L-W1) we identified suboptimal ventilation only in the mess rooms.

Tab. 2 – Results air flow rate measurements. Suboptimal values (not in line with ISO / Germanischer Lloyd reference values) are indicated in bold. Ships that mainly had suboptimal outcomes are highlighted with grey backgrounds.

	ship	wheel house		mess room		sleeping quarters	
		AER	m^3/h pp	AER	m^3/h pp	AER	m^3/h pp
	reference	*6*	*28,8*	*12*	*28,8*	*6*	*28,8*
Larger ships (week patrols)	L-A2	**5,9**	597	**10,3**	43	**5,8**	107
	L-B1	23,7	424	13,4	84	**4,9**	113
	L-I1	14,7	271	13,0	34	17,7	184
	L-M2	**3,1**	112	**1,9**	**16**	**1,6**	38
	L-R2	**5,1**	215	16,7	184	12,8	338
	L-T1	7,2	186	**5,9**	46	9,1	124
	L-W1	6,1	211	**4,1**	31	9,5	48
	L-Z1	**3,3**	44	**10,6**	48	**2,5**	64
Smaller ships (day patrols)	S-A1	-	-	-	-	-	-
	S-C1	-	-	-	-	-	-
	S-M1	8,7	77	-	-	-	-
	S-R1	9,7	79	-	-	-	-
	S-R3	5,7	62	-	-	-	-
	S-R4	8,6	226	-	-	-	-
	S-R5	6,3	167	-	-	-	-
	S-S1	-	-	-	-	-	-
	Median	6,3	186	10,5	45	7,5	110

Tab. 3 – Results CO_2 concentration measurements (measurement duration: at least 1 week; results presented are the most representative day in that week). Suboptimal values (not in line with ISO / Germanischer Lloyd reference values) are indicated in bold. Ships that mainly had suboptimal outcomes are highlighted with grey backgrounds.

	ship	wheel house		mess room		sleeping quarters	
		max. (P95) CO_2 conc. repr. day	minutes >1000ppm per 24 h	max. (P95) CO_2 conc. repr. day	minutes >1000ppm per 24 h	max. (P95) CO_2 conc. repr. day	minutes >1000ppm per 24 h
	reference	*1000*	-	*1000*	-	*1000*	-
Larger ships (week patrols)	L-A2	520	0	810	0	630	0
	L-B1	**1030**	**10**	960	0	900	0
	L-I1	840	0	800	0	860	0
	L-M2	**1480**	**110**	**1500**	**690**	**1010**	**10**
	L-R2	670	0	900	0	650	0
	L-T1	650	0	720	0	560	0
	L-W1	**1050**	**30**	**1320**	**50**	930	0
	L-Z1	640	0	780	0	810	0
Smaller ships (day patrols)	S-A1	880	0	-	-	-	-
	S-C1	**1620**	**190**	-	-	-	-
	S-M1	**1870**	**500**	-	-	-	-
	S-R1	1070	30	-	-	-	-
	S-R3	**>2000**	**300**	-	-	-	-
	S-R4	890	0	-	-	-	-
	S-R5	910	0	-	-	-	-
	S-S1	850	0	-	-	-	-
	Median	900		855		835	

3.2 Results CO_2 measurements

The CO_2 measurement results are presented in table 3. Not every ship was used every day during the measurement period. Also: we found that the CO_2 - concentration fluctuated over time substantially (more than e.g. in an average office or class room) because people moved around on the ships quite a bit. Due to these two reasons we selected, for each ship, a *representative* day (a day with normal use) within the sampling period for analysis. See table 3, One column in the table describes the maximum concentrations that were measured (P95 values) and one column describes the amount of minutes (during the whole period of 24 hours) that the upper limit of 1000 ppm was exceeded.

Conclusion in relation to the 8 larger ships (upper half of table 3): in 5 of the 8 ships CO_2 concentrations stayed well below the limit of 1000 ppm. Two ships (L-M2 and L-W1) showed serious exceedances of the limit value, especially in the mess rooms. The last large ship showed performance around reference value level. We found peak values of 1500-2000 ppm in the less favourable spaces and 500-700 ppm in the best ventilated spaces. In one case (mess room L-M2) the limit of 1000 ppm was exceeded more than 10 hours (600 minutes). For other cases that were less well ventilated, exceedance was limited to half an hour up to 2 hours.

Conclusion in relation to the 8 smaller ships are comparable: in 5 of the 8 smaller ships CO_2 concentrations stayed well below the limit of 1000 ppm. Three ships (S-C1, S-M1 and S-R2) showed serious exceedances of the limit value (in their main space, the mess room). Here we found peak values of a 1500 ppm till well over 2000 ppm in the less favourable spaces. In the better ventilated smaller ships peak levels were in the 800-1000 ppm range. In the mess rooms of the three smaller ships that were under ventilated we found that the limit of 1000 ppm was exceeded more than 3 hours, in one case this occurred more than 8 hours.

3.3 Qualitative results

Below the most relevant qualitative findings are summarized:

Overall maintenance

The on-board ventilation systems were inspected both in terms of technical functionality and overall (internal) hygiene. Despite an adequate amount of fresh air (par. 3.1), if outside air is transported via polluted air handling units and ventilation ducts towards living spaces than the end-result is still suboptimal indoor air quality. The inspections identified very little general issues with overall maintenance or internal hygiene problems. With just one exception: on board of one of the smaller ships we found a (small) air handling unit that was internally polluted (with rust, unidentified debris, sooth). Also in all ships, filter sections were found to be in good shape. Filter exchange frequencies were also in line with manufacturer's instructions. The overall conclusion was that the systems on board of the ships were well-maintained, especially when compared with standard HVAC maintenance levels in offices and schools.

Recirculation

The majority of the ships that were surveyed were not equipped with central air recirculation sections or had central recirculation sections that were indefinitely in '100% outside air mode'. Though, there were exceptions: one of the larger ships used recirculation, only when in 'heat-up' mode before patrols started (usually with 50% outside air). Another ship was equipped with a 100% recirculation option that was only used when this ship was involved in oil spill cleaning / chemical disaster mitigation (to prevent polluted air from entering the ship).

As far as decentral recirculation (at room level) is concerned: this was quite common especially in wheel houses, both in the larger and the smaller ships. Often decentral recirculation was part of an separate cooling system (split unit) that could be operated independent of the ventilation system (Fig. 2). Such decentral recirculation are seen as less of a problem than central recirculation [6]. That is, as long as 'other systems' (the basis ventilation systems) provide for adequate fresh air amounts independent of whether additional cooling systems are on or off (independent of outside whether).

Personal control of mechanical air supply

On board of most ships we found quite adequate options for end-users to control the mechanical air supply. For example, in many sleeping quarters of the larger ships, we found *adjustable* supply grills integrated in the ceiling (figure 3). This is positive as we know from several studies, that when people are provided with effective options to finetune fresh air supply and e.g. temperature that people are more satisfied with their indoor climate and less likely to develop certain health symptoms [11]. On the other hand, in many of the living spaces there was no option for additional natural ventilation (see also under 'operable windows').

Moreover, nearly all ships had good options at central level to influence ventilation for the ship as a whole: in all cases overall air supply for all living spaces could be manipulated in the wheelhouse from a central HVAC system dashboard. Sometimes this was an advantage and sometimes not: none of the rooms were equipped with CO_2 monitors to help those on board to timely identify underventilation situations. Also in once specific case (ship S-M1) we found that ventilation control knobs were used sub

optimally due to noise problems: ventilation capacity of the system in place here was very adequate (with fresh air supply of 77 m^3/h per person with system in highest setting) but this generated such high installation noise levels that in real live situations people decided to keep the system in a very low setting, resulting in in CO_2 levels far above 1000 ppm despite an 'adequate' (but noisy) system in place.

Other examples related to central manual operation of the on board ventilation system: in three of the 16 ships we found problems related to issues with inappropriate use of control knobs for i. the central ventilation system and ii. a decentral, locally recirculating cooling system (split system). Especially with warm weather it probably happens a lot that people turn on the cooling system (recirculation) only, but do not switch on the fresh air supply. This leads to high CO_2 and human bio effluent concentrations that are not easy to detect with the human nose [12]. A situation that should also be avoided as far as cross infection risks during pandemics and epidemics are concerned [4][13].

Operable windows

Most of the 16 ships were not equipped with operable port-holes or other types of operable windows. On the one hand this does not make sense as the ships involved, when on patrol, find themselves in excellent outside air (e.g. at sea). Nevertheless, operable parts in ships nowadays often are avoided due to insurance requirements and to avoid that ships take in too much spray- and rainwater during stormy, rainy weather. We found that the wheel houses, especially those of smaller ships, often did have operable windows (see figure 4) and/or doors with access to the deck. Some of these were well-designed (with devices that helped to keep windows and doors fixed in certain positions also with fluctuating winds), some lacked such devices.

Cross flow grills

To ensure that supplied air is distributed well within a ship as a whole it is essential not just to ensure enough air supply in living spaces and adequate exhaust 'further down the hall' (for example in the galley, in toilets and in bathrooms), but also that air can flow from living spaces to the adjacent hall. This is especially important on board of the larger ships that were only provided with mechanical supply *and* exhaust at room level. To enable cross-ventilation it is essential that internal doors are equipped with overflow grilles in entrance doors or substantial cracks under those doors. On many of the larger ships we noticed a lack of such 'overflow options'. In one case we found cross flow grills in cabin-doors that were adjustable but that according to end-users were often closed as they were perceived as not well sound-insulated.

Fig. 2 - Example of additional, separately operated, cooling system in wheel house of one of the smaller ships for day patrols (fan coil unit).

Fig. 3 - Example of supply grill in the mess room of one of the larger ships; note the red handle that can be used to influence the amount of air supply.

Fig. 4 - Example of on-board operable window

4. Study Limitations

This field study has a few limitations.

We worked with a sample that is supposed to given insight in the situation on board of the whole fleet (97 ships). To be able to do this, it is necessary that the objects studies were selected truly ad random. This in real live was only partly possible because of practical aspects (e.g. patrol schedules, non-proximity to some harbours that are used by the Rijksrederij). This is something that should be kept in mind when interpreting the results.

Also, the indirect assumption during this study was that when one ventilates in accordance with the ISO and Germanischer Lloyd requirements that this implies a space was 'safe enough' in terms of COVID-19 transmission risks (as far as the airborne route is concerned). In real live it is not just air supply per person that matters but also aspects like in-between-person distance that can be kept, ceiling height, overall space volume, air distribution patterns etc that determine how 'safe' spaces are. [4] [13] Another aspect that should be kept in mind when interpreting the results.

As far as the calculated fresh air supply per person is concerned (see table 2): we calculated these values based on the overall air supply that we measured in each space (for all supply grilles combined) and divided that by the amount of persons that normally should be present in a 'full use' situation (full use as normal during the COVID period). These occupancy estimates were made based on on-site verbal information provided by the captain or marine engineer. The actual occupancy at times in the different spaces of course could differ a bit from our estimated occupancy. Yet another aspect that should be taken into account.

A remark related to the CO_2 measurements: these were primarily done to objectify olfactory discomfort and to identify possible issues with actual fresh air supply during patrols. Elevated CO_2 concentrations, that people are exposed to for a considerable amount of time, also influence task performance negatively [14]. Something that is especially important e.g. in the wheel houses. In that context we reported back to the Rijksrederij that in some of their ships (4 of the 16 ships that we investigated) they had task performance risks related to suboptimal fresh air supply. An extra reason (apart from the COVID-19 airborne transmission risk) to 'repair' the situations on these 4 ships.

As far as actual infection risks on board are concerned: we also calculated the theoretical probability of airborne cross-infection making use of the Wells-Riley method making used of a method as described in [15]. These results will be published at a later stage and are outside the scope of this article. Just to get an idea of orders of magnitude, however: we found P-values (probabilities of infection with I=1; one infected person in the room) in the range of 10-30% in the worst ventilated wheel houses and mess rooms (assuming 4 hour shifts in wheel houses and 2 hour dinner/relax session in mess rooms). In well ventilated larger wheel houses and mess rooms P-values often were < 1%. As far as the living quarters were concerned: often P-values were 0% as in most situations people slept alone in a cabin. There were people did share cabins we found P-values >50%. (Input values used for the Wells Riley calculations were as follows: virus type assumption: original Wuhan variant; source strength assumption 25 quanta/hour (assuming that people on board now and then talk with each other); breathing volume assumption 0,6 m^3/hour; other assumptions: no mask wearing on board; nobody vaccinated or immune).

5. Conclusions

Objective nr. 1 was to find out whether the most important spaces on board of the ships were adequately ventilated or not. We found out that 3 of the 8 larger ships and 3 of the smaller ships suffered from too little fresh air supply and elevated CO_2 concentrations. This implies, assuming a representative sample, that about 65% of the whole fleet is ventilated adequately (in line with ISO / Germanischer Lloyd requirements) but that 35% is not.

The 2nd objective was to find out whether there were any other ventilation related risk factors of importance on board. On the positive side: many of the ships had adequate options, at room level, for individual control of fresh air supply (e.g. with adjustable ceiling grills). We also found that central recirculation was shut off or absent anyhow on most ships. Installation noise was an issue on a few boats, especially in wheel houses. Leading to people shutting off systems. Sometimes control knobs for i. fresh air supply and ii. separate, local cooling were mixed up / not used optimally. Operable windows were not available in most cases for additional natural ventilation at will. And in some of the larger ships cross ventilation from living space to hall to e.g. galley was hampered by overflow grills in cabin-doors that were closed at all times.

6. Recommendations

Apart from tailored improvement measures for the 6 ships that scored suboptimal, the following general advice was presented (for whole fleet):

1. We recommended that all wheelhouses and ideally also all mess rooms should be equipped with CO_2 monitors to provide feedback to the end-user. Additionally personnel would have to be instructed to keep CO_2 levels below 1000 ppm, ideally below 800 ppm. This should help people to better make use of both existing (adjustable) mechanical ventilation systems and of operable windows and doors.

2. We also instructed the Rijksrederij to try to organize multiple day patrons in such a way that people were able to sleep alone in separate spaces (not with 2 or 4 persons in one cabin sharing the same air all night), especially during pandemics and epidemics. A recommendation that is easier to follow in the newer ships than in the older ones as the newer ones mostly only had 1-person cabins.

3. Furthermore we recommended that a general 'indoor climate & ventilation guideline should be developed for the governmental ships. Normally when a new ship is built or when an existing one is renovated the shipyards decide what requirements to use. To make sure that in the long run the health and comfort performance of the on-board installations is in line with what the 'Rijksrederij' would like to achieve, a dedicated own standard works better.

Apart from this, we also suggested to start a pilot-project on e.g. three of the larger ships for week patrols with additional, stand-alone, recirculating air cleaning devices with HEPA or electrostatic filters. This could further reduce COVID-19 infection risks especially there where occupant density is high and people spend a lot of time, like in mess rooms.

7. Acknowledgements

This article presents data and insights that were gathered during a field study that was commissioned by the Dutch Directorate General for Public Works and Water Management, specifically the 'Rijksrederij' (governmental shipping company). We would like to express our gratitude to the governmental employees that helped us to conduct the surveys on board, especially the captains and marine engineers who provided us with both technical information and more general information about 'life on board during corona times'.

8. References

[1] Almilaji O. Air Recirculation Role in the Spread of COVID-19 Onboard the Diamond Princess Cruise Ship during a Quarantine Period. Aerosol Air Qual. Res.. 2021;21(4):200495.

[2] Malone JD. USS Theodore Roosevelt, COVID-19, and Ships: Lessons Learned. JAMA Netw. Open. 2020;3(10):2022095.

[3] Morawska L., Allen J., Bahnfleth W., Bluyssen P.M., Boerstra A., Buonanno G., et al. A paradigm shift to combat indoor respiratory infection. Science. 2021;372(6543):689-691.

[4] Nazaroff W.. Indoor aerosol science aspects of SARS-CoV-2 transmission. Indoor Air Journal. 2021; 00:1-31.

[5] Business Insider. Japan avoided a lockdown by telling everyone to steer clear of the 3 C's. Here's what that means. Business Insider US. 2020;May 28th.

[6] REHVA. REHVA COVID-19 guidance document, version 4.1. 2021. Federation of European Heating, Ventilation and Air Conditioning Associations (REHVA).

[7] World Health Organisation (WHO). Roadmap to improve and ensure good indoor ventilation in the context of COVID-19. 2021; March 1st.

[8] International Organization for Standardization (ISO). ISO 7547, Air-conditioning and ventilation of accommodation spaces on board ships - Design conditions and basis of calculations. 2002. ISO, Geneva, Switzerland.

[9] Germanischer Lloyd / DNV GL SE. Rules for Classification and Construction, Chapter 21. Ventilation. 2014. DNV GL SE, Hamburg, Germany.

[10] Persily A. & De Jonge L., 2017. Carbon dioxide generation rates for building occupants. Indoor Air Journal. 2017;27:868-879.

[11] Boerstra A.C.. Personal Control over indoor climate in offices (PhD thesis). Bouwstenen TU Eindhoven, The Netherlands.

[12] Fang L., Wyon D.P, Clausen G. & Fanger P.O.. Impact of indoor air temperature and humidity in an office on perceived air quality, SBS symptoms and performance. Indoor Air journal. 2004; 14(7):74-81.

[13] Loomans M.G.L.C., Boerstra A.C., Franchimon F. & Wisse C.J., Rekenen aan het risico op infecties. TVVL magazine 5. 2020; october:42-47.

[14] Satish U., Mendell M.J,, Shekhar K., Hotchi T., Sullivan D., Streufert S. & Fisk W.J.. Impact of CO_2 on human decision making and productivity. Env. Health Persp.. 2012;120(12):1671-1677.

[15] Kurnitski J., Kiil M'., Wargocki P., Boerstra A., Seppänen O., Olesen B. & Morawska L. Respiratory infection risk-based ventilation design method. Journ. Build Environ.. 2021;206:108387.

Data Statement

The datasets generated during the current study are not publicly available due to confidentiality issues. In specific situations the data are available from the corresponding author, assuming permission of the Dutch Directorate General for Public Works and Water Management.

Improving the indoor / outdoor ratio of (ultra)fine particles in a school

Froukje van Dijken [a], Marije te Kulve [b], Bob Ursem [c]

[a] bba binnenmilieu, The Hague, the Netherlands, fd-bba@binnenmilieu.nl.

[b] bba binnenmilieu, The Hague, the Netherlands, mk-bba@binnenmilieu.nl.

[c] Faculty of Applied Sciences, Delft University of Technology, Delft, the Netherlands, W.N.J.Ursem@tudelft.nl.

Abstract. Buildings located close to busy roads, industry or stock farms, are of risk of increased indoor particle concentrations, which negatively impacts the health of the building occupants. In order to reduce the exposure of the building occupants, it is important to take measures to reduce the concentration of particulate matter indoors. Solutions for existing buildings include application of improved filters in the air handling units, using local air cleaners and limit the use of operable windows. However, little is known about the overall effectiveness of these measures in existing buildings that are in use. The aim of our study was to quantify the effectiveness of particle reducing measures in buildings at high traffic locations. We performed a field study in a school in a neighbourhood between highways. In this school the effect of improved filters in the air handling unit, a HEPA filter at room level as well as the combination of both interventions on the particle concentrations indoors were studied. We quantified the effect of the interventions by momentary measurements of PM2,5 and ultrafine particles (≥4 nm). Moreover, PM2.5 was continuously measured outdoors and indoors. The ePM1 85% filters in the AHU seemed effective on the reduction of (ultrafine) particles (nearly 75% reduction of PM2,5). The use of a HEPA filter was not effective in our test situation.

Keywords. PM2.5, ultrafine particles, filter, classroom
DOI: https://doi.org/10.34641/clima.2022.84

1. Introduction

Exposure to particulate matter over a longer period of time poses significant health risks. Exceeding the air quality guidelines for particulate matter of the World Health Organization (WHO) [1] can lead to acute and chronic health complaints, including throat and nose irritations, asthmatic complaints and (aggravation of) cardiovascular diseases [2].

Epidemiological studies show that no safe levels can be demonstrated at which no harmful health effects of particulate matter occur. This means that health benefits can be expected with any reduction in the particulate matter concentration (also indoors), regardless of the nature or composition of the particulate matter [3].

For ultrafine particles, there are no health-related guidelines yet. However, several epidemiological studies show a link between exposure to ultrafine dust and health effects, such as asthma, in children [4].

Exposure to particulate matter does not only occur outside: in particular, the small fractions of particulate matter (PM2.5 and ultrafine particles) that is present in the outside air can easily enter through cracks and seams in the façade and via ventilation. This is especially true for buildings located close to busy roads, air traffic, industry or stock farms.

It is important to take measures to reduce the exposure to particulate matter indoors. Solutions for existing buildings include application of improved filters in the air handling unit (AHU) and local air cleaners. However, little is known about the overall effectiveness of this kind of measures in a building that is in use.

The aim of our study was to quantify the effect of particle reducing measures in a school building at a high traffic location.

2. Research methods

2.1 location

We performed a field study in a primary school

Copyright ©2022 by the authors. This conference paper is published under a CC-BY-4.0 license.

building located in a neighbourhood surrounded by highways. The study was caried out between April and October 2021. The school has two identical buildings next to each other. The distance from the road and the orientation of the windows was equal. Both buildings have their own ventilation system with CO_2-based demand-driven mechanical supply with a sensor for each classroom and (limited) mechanical exhaust. The maximum air change rate of the classrooms was approximately 950 m^3/h. The AHU's were both equipped with ePM2,5 70% filters. The classrooms on the second floor have a cooling system.

2.2 interventions

The following interventions were investigated:

I. Improved filters in the air handling unit (AHU). We replaced the standard ePM2.5 70% filters by ePM1 85% filters in one of the school buildings.

II. HEPA filter at room level. We used two Camfil City M units with H14 filters with an efficiency of 99.995% for particles between 0,1 and 0,25 µm. The maximum capacity of the unit is 433 m3/h (level 6). In the experiments, we used the filter at level 4 (127 m3/h) due to noise. The rooms in which the filters were tested have a floor area of ±50 m2 and a volume of ±140 m3. The circulation rate of the unit was around 0.9. The filter was turned on continuously throughout the test period. This situation was tested in combination with the standard ePM2.5 70% filter and both with open and closed windows.

III. Combination of intervention I and II. This situation was tested only with open windows.

2.3 momentary measurements

The effect of the interventions was quantified by means of momentary measurements in empty classrooms. We first explored the baseline situation in both buildings. Then, the interventions were tested simultaneously with the baseline situation. This was possible since the school has two identical buildings.

Measurements of the PM2.5 mass concentration were carried out using a TSI Sidepak personal aerosol monitor (TSI AM520). At each measuring location, the mass concentration of these particles was measured for 10 minutes with an interval of 1 second.

Measurements of the ultrafine particles were performed using a TSI Condensation Particle Counter (TSI 3775). The device measures particles of 4 nm in diameter and larger in a bandwidth of 0 to 107 particles per cubic centimeter of air. The measurements were carried out over a period of 10 minutes with a set interval of 10 seconds.

These measurements were performed successively indoors and outdoors. During the momentary measurements the air change rates in the classrooms were comparable: the CO_2-based demand-driven ventilation system in the school was overruled, so the classrooms were all ventilated at maximum capacity. The HEPA filter was in operation for at least one hour before the measurements.

The table below shows the number of measurement series per intervention.

Table 1 – Overview of measurements

Situation	Number of locations	
	PM2,5	Ultrafine
Baseline	10	10
Intervention I	9	9
Intervention II	5	5

2.4 continuous measurements

The PM2.5 concentration was been monitored continuously during the research period. These measurements were performed simultaneously indoors in multiple rooms (Siemens QSA2700 room sensors) and outdoor at the air intake of the AHU (Siemens QSM2100 duct sensor). An interval of 5 minutes has been used.

2.5 data analysis

The impact of the interventions was evaluated by comparing the indoor/outdoor (I/O) ratios during the different situations. The I/O ratio was calculated using the measured particle concentration in the building divided by the concentration outside.

For the momentary measurements, the average PM2.5 concentration and ultrafine particle concentration were calculated per measurement location, indoors and outdoors, over the measurement period of 10 minutes. For the PM2.5 measurement the standard deviation was calculated as well. Only measurements performed with outdoor PM2.5 concentrations above 5 µg/m^3 were included in the analysis.

With an unpaired t-test, it was investigated whether the average I/O ratios in a situation with improved filters (intervention I) differ significantly from the situation without intervention. A p-value <0.05 was considered to be statistically significant. The static analyses were performed in Microsoft Excel version 2102. The data of the other interventions could not be statistically tested, due to the limited number of momentary measurements.

Continuous measurements were used to underpin the findings of the momentary measurements. The hourly average on schooldays of both concentrations and I/O ratios were visually presented in graphs.

3. Results

3.1 improved filters in the AHU

The I/O ratio in the situation with an ePM1 85% filter is compared with the standard ePM2.5 70% filter (Figure 1). The median of the average I/O ratios of all measurements was 0.27 in the situation with an improved filter, which is significantly lower (p=0.026) than with a standard filter (0.38). With an improved filter, the average of all measurements was between 0.24 and 0.30. With a standard filter, this was between 0.27 and 0.82.

The median I/O ratios of the ultrafine particle concentration were comparable (0.28 vs 0.26) (Figure 2). The range of the I/O ratio is wider for the standard filter; the P75 for the standard filter is 0.55 whereas it was 0.28 for the improved filter. The difference is not significant (p=0.104).

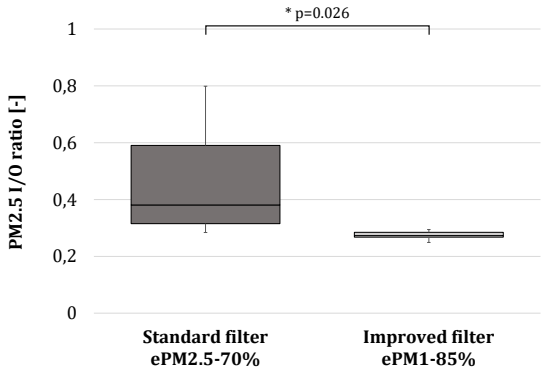

Fig. 1 – Boxplot of the average I/O ratio of PM2.5 comparing the situation with a standard filter (n=8) and a classroom with an improved filter (n=5).

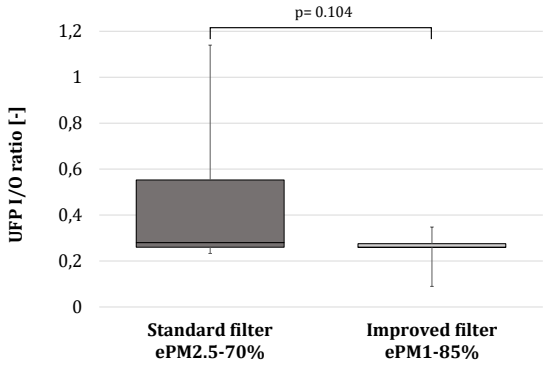

Fig. 2 – Boxplot of the average I/O ratio of ultrafine particles comparing the situation with a standard filter (n=8) and a classroom with an improved filter (n=5).

The continuous measurements showed a clear difference between the concentration and I/O ratio in classrooms in the building with the standard filter and the building with the improved filter (Figure 3).

Remarkably, we also found differences between classrooms within the same building (Figure 4). These differences were observed between the classrooms on the ground floor (higher indoor concentrations) and the first and second floor (lower indoor concentrations).

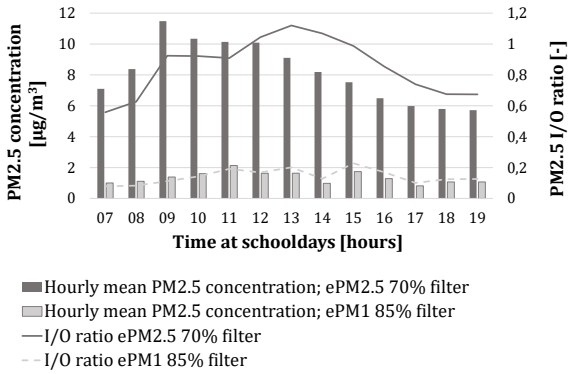

Fig. 3 – Continuous measurements comparing a classroom with a standard filter (ePM2.5 70%) and a classroom with an improved filter (ePM1 85%).

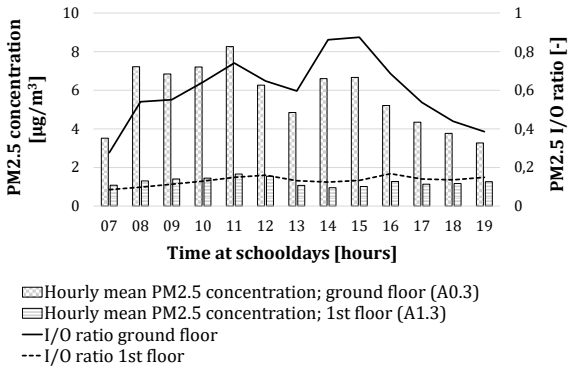

Fig. 4 – Continuous measurements comparing two classrooms with an improved filter (ePM1 85%); one on the ground floor and one on the first floor.

3.2 HEPA filter at room level

The average I/O ratios were 0.75 and 0.82 without HEPA filter and 0.63 and 0.75 with HEPA filter in the room in a situation with closed windows (Figure 5). The difference was not significant (p=0.158).

With open windows, the average I/O ratios were 0.67 and 0.84 without HEPA filter and 0.75 and 0.78 with HEPA filter in the room (Figure 5).

The measurements of ultrafine particles (Figure 6) show a comparable trend.

In line with these observations, no differences were observed based on the continuous measurements in two in adjacent classrooms with and without a HEPA filter during school hours (Figure 7). However, it is clear that the PM2.5 concentrations are lower in the rooms with a HEPA filter in the evening and at night, when the ventilation system is turned off and the room is not occupied.

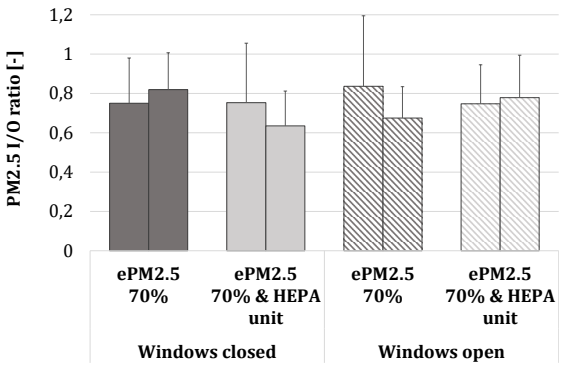

Fig. 5 – Bar diagram of the I/O ratio of PM2.5 (average and standard deviation) for the intervention with a HEPA filter at room level.

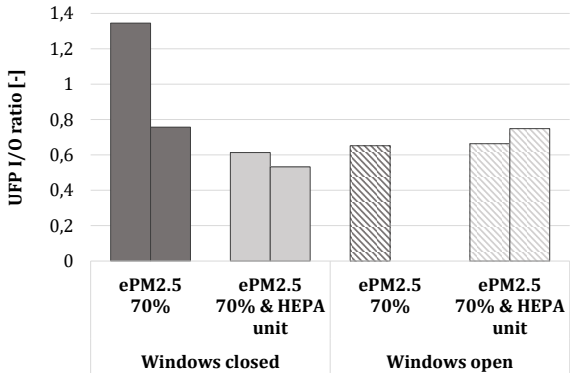

Fig. 6 - Bar diagram of the I/O ratio of ultrafine particles (average) for the intervention with a HEPA filter at room level.

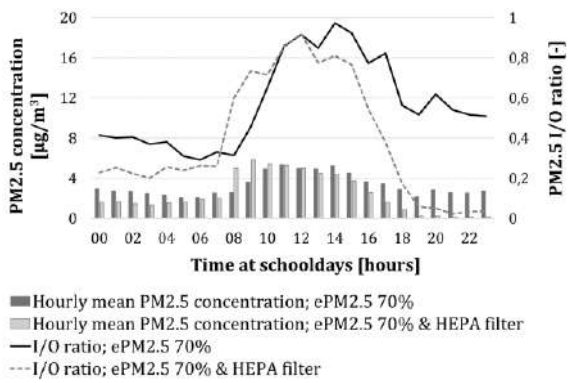

Fig. 7 - Continuous measurements comparing a classroom with a standard filter only and a classroom with a standard filter and HEPA filter.

3.3 improved filters and HEPA filter

The average I/O ratios were 0.30 and 0.33 when the AHU is provided with an improved ePM1 80% filter and 0.32 and 0.37 when the classroom additionally is provided with a HEPA filter; both in a situation with windows open (Figure 8). The combination of an improved filter and a HEPA filter did not reduce the indoor concentration as compared to the situation with only an improved filter.

Similarly, the results of the ultrafine particles (Figure 9) show no impact of the HEPA filter when combined with an improved filter in the AHU.

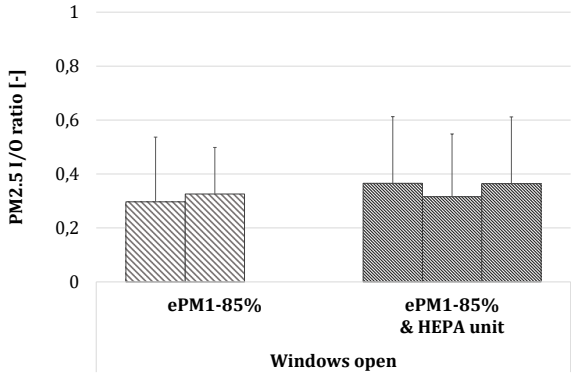

Fig. 8 - Bar diagram of the I/O ratio of PM2.5 (average and standard deviation) for the intervention with both improved filters and a HEPA filter.

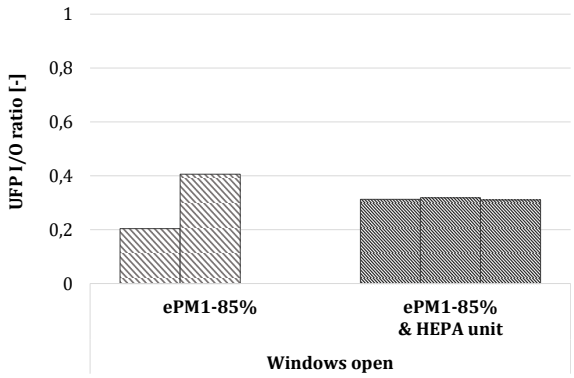

Fig. 9 - Bar diagram of the I/O ratio of ultrafine particles (average) for the intervention with both improved filters and a HEPA filter.

The combined effect of the improved filters and the HEPA filter was evaluated using the continuous measurements. The hourly average concentration during the day in the building with the improved filter in the AHU is comparable in the situation with and without mobile HEPA filter (figure 10). In contrast to the situation where the HEPA filter was combined with a standard filter (figure 7), no lower PM2.5 concentrations were observed in the evening or night.

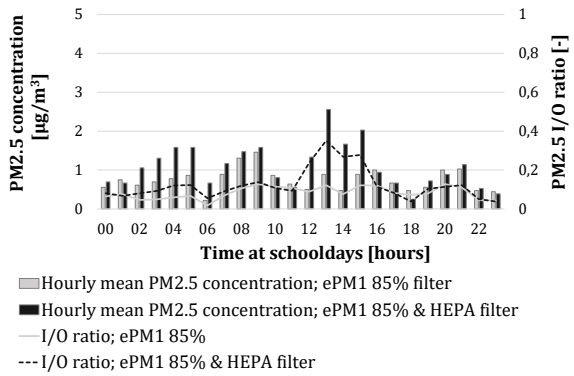

Fig. 10 – Continuous measurements comparing a classroom with an improved filter only and a classroom with an improved filter and HEPA filter.

4. Discussion

4.1 methodology

The field study was carried out to get a better understanding about particulate reducing measuring in a school in use. Thereby confounding factors such as opening windows were explored. Because of that numerous combinations were possible leading to limited number of momentary measurements for each situation. This makes it difficult to prove the effectiveness, since the power is too small to statistically compare the situations. Especially when the impact of the intervention is small, effects are not clearly visible.

In this field study we had to cope with changing outdoor conditions, like outdoor particle concentrations and wind speed and direction, affecting the I/O ratio. Low outdoor concentrations (<5 μg/m^3) during the momentary measurements reduced the number of valid measurements. In the continuous measurements we only compared classrooms with identical orientations to minimize the effect of the outdoor situations.

For the continuous measurements we used the PM2.5 room sensors connected to the building management system. Unfortunately, the range of these sensors seemed too broad, making the results unusable for this study. The sensors were replaced, but data from a vast period of the study is missing.

4.2 effect improved filters

The measurement data show a clearly improved I/O ratio in the building where the improved filter (ePM1 85%) is placed in the AHU compared to the building with the standard filter (ePM2.5 70%). This is in line with the required performance of the filters: the improved filter should reduce the outdoor concentration by 85% while the standard filter is only rated on the efficiency for PM2.5 which should be reduced by 70%.

Although the overall findings are clear, we found remarkable differences between classrooms within the same building, as illustrated by the results in figure 4. The I/O ratio in the classrooms on the ground floor (I/O on average 0.45) seemed much higher than on the 1st and 2nd floor (I/O average 0.20). This is, to some extent, expected: Traffic related particles are known to distribute at lower altitudes. As a result, the outdoor air at ground level is more polluted than on the first floor. Though, the difference could also be explained by the different settings of demand-driven ventilation in combination with the opening of windows. All rooms are equipped with demand-driven ventilation based on the CO_2 concentration. When conducting the measurements, we noticed that the windows were often open, especially in the classrooms on the ground floor. This ensures that the ventilation system in classrooms on the ground floor may not be switched on much or not at all, because sufficient air exchange already takes place through open windows (natural ventilation). Probably, these rooms were regularly ventilated with unfiltered air, leading to higher I/O ratios. Moreover, in some rooms on the 1st floor, the ventilation settings were disturbed and air is continuously supplied at a fixed (maximum) flow rate. These classrooms always receive filtered air, whether the windows are open or not.

In order to gain more insight into the effect of demand-driven ventilation, the ventilation system was overruled for several weeks and the results of continuous measurements in the period with and without demand-driven ventilation were compared.

Table 2 – Statistics of the I/O ratios (7-19h) for two measurements periods: average ± stdev.

	Period 1 (1- 20 sept)	Period 2 (22 sept - 4 oct)	Delta Period 1 - period 2
	Demand-driven	Overruled	
Ground floor A0.1	0,62 ± 0,17	0,08 ± 0,04	0,54
Ground floor A0.2	0,60 ± 0,16	0,07 ± 0,04	0,52
Ground floor A0.3	0,65 ± 0,22	0,26 ± 0,15	0,39
1st floor A1.1	0,19 ± 0,04	0,06 ± 0,03	0,13
1st floor A1.3*	0,13 ± 0,02	0,04 ± 0,02	0,09
1st floor A1.5	0,14 ± 0,05	0,03 ± 0,02	0,12
2nd floor A2.1	0,24 ± 0,06	0,09 ± 0,03	0,15
2nd floor A2.3	0,22 ± 0,07	0,05 ± 0,02	0,17

** continuously overruled*

The results of these measurements (table 2) show that the I/O ratios of the PM2.5 concentrations in the rooms on the ground floor are significantly lower (average Δ=0.48) when the ventilation system is continuously switched on (overruled) compared to the situation with demand-driven ventilation. Also in the other classrooms a small improvement was observed.

Further research is required to learn more about the effect of operable windows on particle concentrations in buildings.

4.3 effect HEPA filter

The HEPA filter has a higher efficiency than a ePM1

80% filter, and it theory may therefore be a more effective solution than the installation of improved filters in the AHU. Moreover, the unit should be able to filter particles entering the room through open windows (in schools opening windows is very important for passive cooling), in contrary to a filter in the AHU. However, we found that the relative contribution of the local HEPA filter was too small to achieve a clear reduction of particulate matter.

Measurements near the outlet of the filter proved that the HEPA filter is effective. Measured values of PM and UFP at the outlet of the unit are lower than the average concentrations in the room. The limited effectiveness of the HEPA filter can be explained by the flow rate of the unit. At the setpoint used, 127 m3 of air is filtered per hour (circulation rate of approx. 0.9). The mechanical ventilation system, on the other hand, supplies approximately 950 m^3 of filtered air per hour (ventilation rate of approx. 6.8 h^{-1}). This means that filtration via the HEPA filter is more than a factor of 7 lower than by the mechanical ventilation system. The filter unit needs a higher flow rate to become effective. With the risk of an increased noise level as a result, which is unacceptable during lessons.

4.4 effect improved filters and HEPA filter

We expected that the HEPA filter could further reduce the exposure to (ultra)fine particles when windows were opened. Though, we didn't see any effect of the presence of the HEPA filter in combination with improved filters in the AHU.

5. Conclusions

Application of an improved filter in the air handling unit seemed the most effective measure to reduce the number of particles coming from outdoors to the indoor environment compared to a HEPA filter in the classrooms.

In the building with an improved filter (ePM1 85%) the I/O ratios were significantly lower as compared to the building where the standard filter (ePM2.5 70%) was used.

Local air cleaning by a HEPA filter in the room seemed ineffective in a school. Both with the windows open and closed. And independent from the type of filter in the AHU (ePM2.5 70% or ePM1 85%). The HEPA filter does remove contaminants from the air, but since the ventilation flow rate in classrooms is about 7 times higher than the circulation flow rate of the HEPA filter, it is fighting a running battle. At a higher flow rate, the noise level of the filter unit becomes critical.

The results imply that the particulate concentration in schools can significantly be reduced using adequate filters. Still, other pollutants in polluted areas can negatively impact the indoor air quality. Moreover, children are also exposed when playing outside. Therefor the most important measure to reduce exposure to traffic related pollutants is to pay attention on the outdoor air quality when choosing a location to build new schools.

6. Acknowledgements

The study was funded by TVVL and VCCN. The interventions are sponsored by Camfil. Siemens installed PM2,5 sensors for continuous monitoring in the school. We are grateful that the school allowed us to perform this study in their buildings.

7. References

[1] World Health Organization. WHO global air quality guidelines: particulate matter (PM2,5 and PM10), ozone, nitrogen dioxide, sulfur dioxide and carbon monoxide. WHO. 2021

[2] Gezondheidsraad. Gezondheidseffecten luchtverontreiniging. Gezondheidsraad. 2018.

[3] World Health Organization. Health Effects of Particulate Matter: Policy implications for countries in eastern Europe, Caucasus and central Asia. WHO. 2013.

[4] García-Hernández C., Ferrero A., Estarlich M., Ballester F. Exposure to ultrafine particles in children until 18 years of age: a systematic review. Indoor air. 2020;30(1):7-23.

Data Statement

The datasets generated during and/or analysed during the current study are not publicly available because the project is privately funded. The data that support the findings of this study are available from the corresponding author, and with permission of TVVL/VCCN, upon reasonable request.

Assessing Thermal Comfort in Nursing Home Using Heart Rate Measurement

Anne Sørensen [a], Steffen Petersen [a]

[a] Department of Civil and Architectural Engineering, Faculty of Technical Sciences, Aarhus University, Aarhus, Denmark, asv@cae.au.dk, stp@cae.au.dk.

Abstract. The ratio of dementia amongst the residents in nursing homes makes it practically impossible to conduct traditional questionnaire-based comfort analyses. Besides, there are uncertainties in the residents' cognitive capabilities to respond to a questionnaire, since residents with dementia can be very sensitive to the smallest changes in their everyday life. Therefore, there is a need for alternative investigation methods when conducting comfort studies in nursing homes, such as indirect measurements or observational studies. Based on a pilot study in two Danish nursing homes, this paper demonstrates how thermal comfort can be estimated using the heat balance-based comfort equation of P.O. Fanger, using the metabolic rate of residents calculated from a simple heart rate measurement. This estimate is then compared to the Predicted Mean Vote (PMV), using standard metabolic rates to investigate how well the estimated thermal comfort fits the PMV theory.
The proposed method, based on heat rate measurements, has minimum impact on the test persons and requires no cognitive activity. Furthermore, it enables a more dynamic perspective on thermal comfort. The study results indicate that the metabolism of elderly people (+75 years of age) living in nursing homes can be at a lower level than what can be counterbalanced by a lower heat loss, as it is normally assumed.
The conclusion is that the proposed method is promising but needs further development and validation concerning the conversion of heart rate to metabolism and how to account for age-related physiological changes.

Keywords. Metabolism, Thermal comfort, Field study, Nursing home.
DOI: https://doi.org/10.34641/clima.2022.177

1. Introduction

Conducting thermal comfort analyses in nursing homes entails a number of challenges, from the impact of the residents' physical- and mental disabilities to the general differences between the typical users (residents and employees).

Despite national differences in age and degree of physical- and/or mental disabilities of persons who becomes a nursing home resident, dementia often plays a role. In western Europe 50-80% of nursing home residents suffer from dementia [1]. People with dementia belongs to a category of particularly vulnerable adults, who are unable to express the need for adjustments of the thermal environment or conduct the right correctional action [2]. This cognitive impairment often leads to an exclusion of dementia sufferers from environmental studies in nursing home. Simply because they do not have the cognitive abilities to complete the used questionnaire [3], [4].

This exclusion of dementia sufferers can question whether it, in practical terms, is possible to form a group of test subjects that is representative of the resident-population in a typical nursing home. Alternatively, comfort analyses must be altered in a way that allows dementia sufferers to participate.

An example of such an alteration is the 10-month behavior study of agitation among nursing home residents with dementia, which have shown a direct link between the average indoor temperatureand the occurrence of agitated behavior [5]. Observational studies running for several months will in many cases be too time consuming to be a realistic alternative, and the response time exclude the possibility of using the response to adjust the thermal indoor environment.

Another alternative way of conducting comfort studies that allows dementia sufferers to participate, is by measuring parameters related to the human thermoregulation. In other studies, infrared thermography (IRT) have been used for measuring skin temperature [6]. In relation to dementia sufferers, IRT could be challenged by placing the cameras correctly without introducing a forint object in the living space. A third alternative could be to use the relation between heart rate and metabolism, as done in [7]. The particular measuring devices used in

Copyright ©2022 by the authors. This conference paper is published under a CC-BY-4.0 license.

this study could not be used for either onside measurements or test subjects with dementia. During the last decade there has been a great development in wearable devices capable of measuring heart rate. Simple devices intended for athletes, which means that measuring heart rate could be done with an impact of a test subject that is comparable to wearing a wristwatch.

When assessing thermal comfort in nursing homes, another question that is often raised [2] has to be taken into account:

- Is the age of the test subjects a factor of importance?

P.O. Fanger originally stated that age related reduction of the metabolic rate did not have a significant impact on the validity of the comfort equation, because the decrease in the metabolic rate is counterbalanced by a lower heat loss - provided that comfort analyses are based on tabular values of the metabolic rate. In other studies of this specific question, no consistent answer has been given, but in some field studies a significant age related difference have been detected [8].

It is also worth noticing, that in nearly all the conducted age related studies, the test subjects are described as healthy and often significantly younger than the average nursing home residents. A person moving into a nursing home in Denmark is in average 84 years old and suffers from one or more chronical illnesses [9].

2. Research Methods

A pilot study was conducted in November 2019 in two different Danish nursing homes. The scope was to determine if it is possible to evaluate thermal comfort, based on simple heart rate measurement, without consideration to dementia amongst the test subjects. The measuring period at each nursing home consisted of five consecutive weekdays.

The conceptual idea is to calculate the ideal operative temperature for each test subject. This is defined as the temperature that provide equilibrium in P.O. Fanger's Comfort equation, corresponding to a PMV scorer of 0 on the 7-point Ashrae scale according to DS/EN/ISO 7730 [10], by using a Metabolic rate calculated from measured heart rate (comparable with level 3 analysis DS/EN/ISO_8996 [11]).

Finally, the calculated temperature is compared to operative temperatures, defined from observed activity levels and measured room temperatures.

2.1 Test Subjects and Registrations

Test subjects are selected amongst both residents and employees to be able to detect age related deviations in the results.

Test subjects have been selected in two different ways, depending on the subject's status as resident or employee. Employees could volunteer, if they had one or more work shifts in the measuring period. Potential test subject amongst the residents have been pointed out by the General Manager.

Prior to volunteering, all test persons and legal guardians for persons suffering from dementia have received information of the study and signed a consent form to participate. As part of the consent, a test subject gives the following information:

Employees: age, sex and work function.

Residents: age, sex, if they are diagnosed with dementia or use beta blockers.

Height and weight gets registered for all test subjects. Height and weight of the employees got measured as part of the introduction to the measuring equipment. Measuring height and weight of the residents is part of the weekly routine, and is provided by the nursing homes.

The test subjects are anonymized and consists of 13 residents (see Tab. 1) and 17 employees (see Tab. 2)

Tab. 1 - Essential parameters of the resident test subjects, information on dementia and Beta-blogger not included.

ID	Sex	Age [year]	Height (h) [cm]	Weight (w) [kg]
R01	M	93	178	68
R02	F	81	153	53
R03	M	75	183	85
R04	M	87	183	91
R05	F	85	167	80,4
R06	M	86	182	65,5
R07	F	93	166	58,9
R08	M	91	175	72
R09	M	92	162	80,1
R10	F	67	169	91,5
R11	F	69	160	63
R12	M	88	163	66,4
R13	M	69	180	88,7

2.2 Observations

During day and evening hours, clothing- and activity level of the test subjects were registered based on visual observations. The observations were conducted by following the participating employees in the common area of the nursing home. The observer registered time of observation, description of the observed activity and estimated clothing level.

The registration was noted in predefined forms for each test subject.

To protect the integrity of the residents, the observer only enters private living spaces based on direct invitation from the resident. Activities in the private living spaces are therefore mainly based on observations trough open doors and the employees' descriptions of the work conducted in the private living spaces.

The observations were conducted in collaboration with engineering students, specialized in indoor environment.

Tab. 2 - Essential parameters of the employee test subject.

ID	Sex	Age [year]	Height (h) [cm]	Weight (w) [kg]
E01	F	57	161	69
E02	F	58	156	58
E03	F	25	164	57,7
E04	F	22	169	64,8
E05	F	22	189	95,5
E06	M	51	175	93,5
E07	F	64	169	63
E08	F	37	162	61,7
E09	F	39	160	54
E10	F	58	171	81,5
E11	F	20	167	58,7
E12	F	45	167	67,9
E13	F	42	176	75
E14	F	46	172	79,5
E15	F	55	167	75,6
E16	F	49	166	61,2
E17	F	37	177	131

2.3 Measuring Heart Rate and Room Temperature

For residents it is essential that the measuring equipment affect the subject's everyday life as little as possible. Therefore, measurements are conducted using Garmin vivosmart® 4 Fitness Activety tracker worn around the wrist, as a normal wristwatch (see Fig. 1).

Hygiene requirements states that employees are not allowed to wear anything on their arms below the elbow, beside clothing. This excludes the wrist worn measuring device. Instead, the heart rate of employee test subjects are measured using Garmin HRM-Dual, Heart Rate Monitor with Chest Strap, in combination with iPhone 5 (or newer) or IOS 8 (or newer) (see Fig. 1). The phones act as data loggers, because Garmin HRM-Dual do not have a build in memory.

Fig. 1-On the left, Garmin vivosmart 4 worn by a test subject beside the subject's own wristwatch. On the right, measurement equipment for the employee.

The residents carried the Garmin vivosmart activity tracker around the clock during the measuring period, while the employees carried the equipment during one or several work shifts.

Room temperatures were measured using Tinytags, placed out of sight and out of reach in both common areas and private living spaces of the nursing homes (see Fig. 2).

The Tinytags were set to log temperature every third minute during the measuring period.

Fig. 2 – Example of placement of Tinytags in the common area.

2.4 Converting Heart Rate to Metabolic Rate

It is presumed that the relation between heart rate (HR) and metabolism (M) given in (DS/EN/ISO 8996) [11] can be used with a satisfactory accuracy, despite the potential effect of psychological factors with heart rates below 120 beats pr. minute (BPM). The relation between HR and M is defined as:

$$HR = HR_0 + RM \cdot (M - M_0) \quad (1)$$

Where:

M_0 Metabolic rate at rest, defined from tabular values related to age (a) and weight (w), (Tab. 3).

HR_0 Heart rate at rest under neutral thermal condition.

RM Increase in heart rate per unit of metabolic rate.

Tab. 3 - Metabolic rate at rest based on age and weight (w), given in MJ/day [12].

Age	Female	Male
19-30	0,0615 w + 2,08	0,0640 w + 2,84
31-60	0,0364 w + 3,47	0,0485 w + 3,67
61-75	0,0386 w + 2,88	0,0499 w + 2,93
>75	0,0410 w + 2,61	0,0350 w + 3,43

Conversion from MJ/day given in Tab. 3, to W/m² in formula (1) is based on the body surface area of the test persons defined as:

$$A = 0{,}202 \cdot h^{0{,}725} \cdot w^{0{,}425} \quad (2)$$

For residents HR_0 is defined as the average of the measured HR between midnight and 4 am. Whereas for employees, HR_0 is given as the mean value for persons with an average fitness and a fitness level above average(se Tab. 4). Notice that an exception has been made if the value is less than 8 BPM lower than the average measure heart rate. In these cases, HR_0 is defined as 90% of the average measure heart rate.

RM is found, as defined in (DS/EN/ISO 8996) [11], to:

$$RM = \frac{HR_{maks} - HR_0}{MWC - M_0} \quad (3)$$

Where

HR_{maks} Maximum heart rate based on age (a) as given in equation (4)

MWC Maximum working capacity based on age (a) and weight (w) as given in equation (5)

$$HR_{maks} = 205 - 0{,}62 \cdot a \quad (4)$$

$$MWC = \begin{cases} male = (41{,}7 - 0{,}22 \cdot a) \cdot w^{0{,}666} \left[\frac{W}{m^2}\right] \\ female = (35{,}0 - 0{,}22 \cdot a) \cdot w^{0{,}666} \left[\frac{W}{m^2}\right] \end{cases} \quad (5)$$

2.5 Calculating Operative Temperature

Based on the general time factor involved in regulating the room temperature, the ideal operative temperature for each test subject is calculated based on the average metabolic rate of the test subject.

Tab. 4 - Heart rate at rest based on age, sex and general fitness [13], F=Female, M=Male, AF=Average fitness, AaF=Above average Fitness.

Age	F-AF	F-AaF	M-AF	M-AaF
18-25	74-78	70-73		
26-35	74-76	69-72		
36-45	75-78	70-73		
46-55	74-77	70-73	72-76	68-71
56-65	74-77	69-73	72-75	68-71
65+	74-76	69-72	70-73	66-69

The ideal operative temperature is defined as the temperature which provides equilibrium in P.O. Fanger's heat balance-based comfort equation:

$$(M - W) - 3{,}05 \cdot 10^{-3} \cdot (5733 - 6{,}99 \cdot (M - W) - p_{da}) - 0{,}42 \cdot \big((M - W) - 58{,}15\big) - 17 \cdot 10^{-6} \cdot M \cdot (5867 - p_{da}) - 1{,}4 \cdot 10^{-3} \cdot M \cdot (34 - t_a) = 39{,}6 \cdot 10^{-9} \cdot f_{cl} \cdot ((t_{cl} + 273)^4 - (t_r + 273)^4) + f_{cl} \cdot \alpha_k \cdot (t_{cl} - t_a) \quad (6)$$

Where:

M The average calculated metabolic rate

W Effective mechanical power - Assumed from observing activities

I_{cl} Clothing insulation calculated from observed clothing levels, as described in [14].

t_r Mean radiation temperature

t_a Air temperature

t_{cl} Clothing temperature found from equation (7)

α_k Convective heat transfer coefficient given in equation (8)

f_{cl} Clothing area surface factor calculated in equation (9)

P_a Water vapour patial pressure set for a relative humidity at 50%, at the calculated air temperature

$$t_{cl} = 35{,}7 - 0{,}0275 \cdot (M - W) - \Big((M - W) - 3{,}05 \cdot 10^{-3} \cdot (5733 - 6{,}99 \cdot (M - W) - p_{da}) - 0{,}42 \cdot \big((M - W) - 58{,}15\big) - 17 \cdot 10^{-6} \cdot M \cdot (5867 - p_{da}) - 1{,}4 \cdot 10^{-3} \cdot M \cdot (34 - t_a)\Big) \quad (7)$$

$$\alpha_k = Higest\ value\ of \begin{cases} 2{,}38 \cdot (t_{cl} - t_a)^{0{,}25} \\ 12{,}1 \cdot {v_{ar}}^{0{,}5} \end{cases} \quad (8)$$

Where:

v_{ar} is the relative air velocity found from equation (10)

$$f_{cl} = \begin{cases} 1{,}00 + 1{,}290 \cdot I_{cl} & for\ I_{cl} \leq 0{,}078 \\ 1{,}05 + 0{,}645 \cdot I_{cl} & for\ I_{cl} > 0{,}078 \end{cases} \quad (9)$$

$$v_{ar} = v_a + 0{,}005 \cdot (M - 58) \quad (10)$$

Where:

v_a Air velocity assumed to be equal to 0,15m/s.

The participating nursing homes are relatively new, well insulated and mechanically ventilated. It is therefore assumed, that the mean radiation temperature is equal to the air temperature, which makes the operative temperature equal to the air temperature.

3. Results

The given result is a condensed overview of conducted observations and calculations.

3.1 Observed Activity and Clothing

In general, the observed activity level of the residents is significantly lower than the activity level of the employees, in particular employees handling care tasks.

For the residents, a typical day consists of different sedentary activities in the private living spaces of the nursing home, e.g. watching TV, using a computer or doing needlework. These activities are estimated to be equal to the activity level "seated, relaxed", giving an expected metabolic rate of 58 W/m^2. During the day the general sedentary activity is replaced by short periods of physical activity consisting of walking (if capable of it) to the common room for the main meals, or participating in common activities, such as singing, church service or chair gymnastics.

From an activity point of view, the employees can be divided into two groups depending on work function.

Employees primarily conducting administrative tasks, are evaluated to have an activity level comparable to sedentary office work, with short brakes of walking around in the common areas. This gives an expected metabolic rate of 70 W/m^2. The activities of employees primarily providing care of the residents are described as active work without heavy lifting and no running. The observed activities primarily consist of standing and walking in both private living spaces and common areas. Due to a general focus on self-empowerment of the residents and prevention of injuries amongst the employees, heavy lifting is conducted using assistive devises. The observed work activities are estimated to be comparable with "walking on level ground 2-3 km/h", giving an expected metabolic rate of 125 w/m^2.

Based on the observed activities, the effective mechanical power for all test subjects are assumed to be negligible, whereby W=0.

Fig. 3 shows examples of typical clothing levels for both employees and residents.

Fig. 3 – Examples of typically observed clothing levels, left to right: Employee, female resident and male resident.

The observed clothing levels show big individual differences amongst the residents. Both from test subject to test subject, but also as variations during the day; from fully dressed to dressing gown and pyjamas. In general, the registered clothing levels of the residents arefound to vary from 0,63 clo to 1,18 clo, with an average of 0,83 clo.

The employees are wearing uniforms with some possibilities for adaptation to individual preferences. The uniform consists of either a shirt with short sleeves in combination with trousers or a dress with short sleeves. The employees have free choice of footwear, and it is possible to combine the general uniform with a light jacket. The chosen combinations are evaluated to give a combined clothing level of the employees that vary from 0,3 clo to 0,82 clo, with an average of 0,5 clo.

3.2 Measured Heart Rate

With the continuously logged heart rate, it becomes clear that the heart rate changes very rapidly during the day for both residents and employees. The measured heart rates also show significant differences from individual to individual, both in terms of the average heart rate and the deviation. These are differences that cannot be related to either age, sex, or group of test subject.

Deviding the test subjects into tree groups, some general differences can be detected. As shown in Fig. 4, the residents have the lowest average heart rate, while the caregiving employees have the highest. The employees that primarily conduct administrative

work are more compareable to the residents based on the average heart rate.

Heart rates below 50 BPM are defined as low, but normal, and can be the result of a fitness level above average, heart disease or medication [15]. Therefore, the very low heart rates amongst the residents are not ruled out as measuring errors.

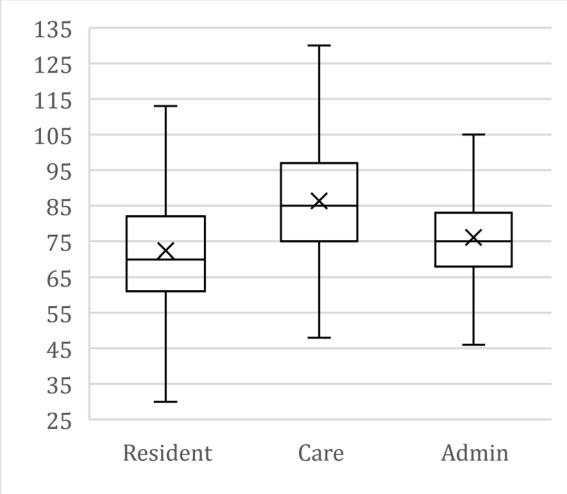

Fig. 4 – All measured heart rates (BPM) sorted according to groups of test subjects; Residents, Employees (care), Employees (administration)

3.2 Measured Room Temperatures

In general, the variation in the individual measuring points troughout the nursing home are very low. The maximum and minimum temperatures in Tab. 5 can be seen as temperature variations between rooms rather than variations over time.

Tab. 5 – Average, maximum and minimum temperatures, measured in both private living spaces and common areas of the participating nursing homes.

Location	Average [^{0}C]	Min [^{0}C]	Max [^{0}C]
Privat	23,5	21,1	25,6
Common	23,0	21,4	26,3

3.3 Metabolism

Based on the measured heart rate, the metabolic rate is calculated for each time step, and sorted according to subject groups. This gives, as illustrated in Fig. 5, a picture quite similar to the heart rate, where the residents have the lowest average metabolic rate and the caregivers have the highest. It is necessary to note that all three groups have minimum values below zero, which is not possible. This could be caused by the widening of the scope of the calculation method, or be an indication of a need for validation of the method used for estimating values of, for instance, heart rates at rest.

To minimize the effect of undetected uncertainties, all further analyses is therefore strictly based on the average of the calculated metabolic rate for each test subject.

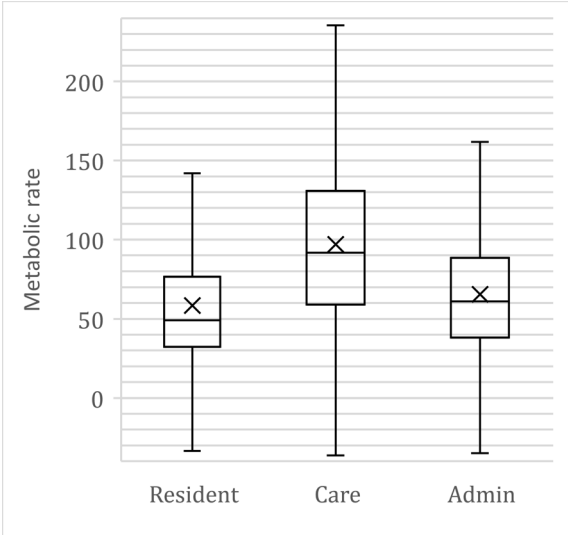

Fig. 5 – Calculated metabolic rate sorted according to groups of test subjects; Residents, Employees (care), employees (administration).

When plotting the calculated metabolic rate for each test subject according to age, some interesting tendencies are worth noticing, despite a low correlation to the linear regression (see Fig .6).

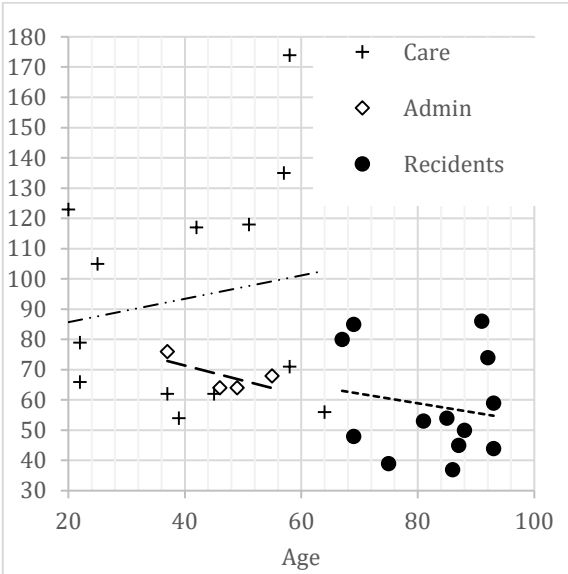

Fig. 6 – Average metabolic rate for each test subject in relation to the age of the test subject.

It could look like a part of the test subject identified as caregivers have more administrative work tasks than registered in the observations. The calculated metabolic rate also indicates a tendency to decrease with age. For 50% of the resident test subjects, the average metabolic rate is below 50 W/m^2, which is significantly lower than the metabolic rate for the activity level "seated relaxed" of 58,15 W/m^2 used in equation (6).

3.4 The Operative Temperature

For each test subject the ideal operative temperature is found based on calculated metabolic rate and the estimated clothing level. This gives a variation of the ideal temperature for each subject group as given in Tab. 6.

Tab. 6 – Average, maximum and minimum values of the calculated operative temperature based on the metabolic rate calculated from the measured heart rate.

Subject group	Average [^{0}C]	min [^{0}C]	max [^{0}C]
Resident	24,1	20,1	27,6
care	22,7	13,9	27,9
Admin	24,5	20,5	26,1

This is a wide range, but when the calculated temperature is put in relation to the calculated metabolic rate, a nearly linearly relation is found for each subject group (see Fig. 7).

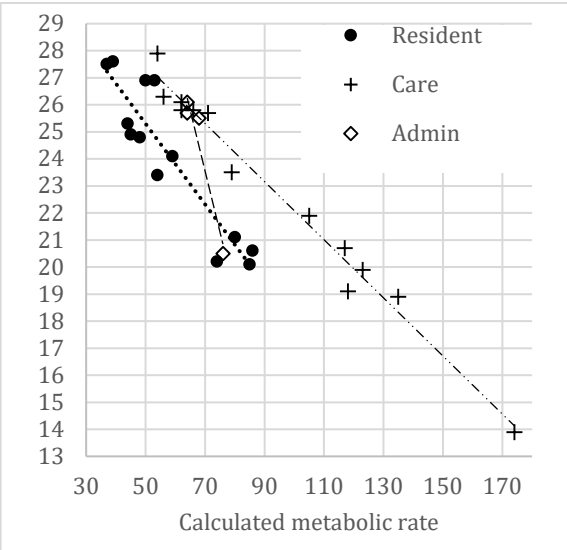

Fig. 7 – Optimal operative room temperature based on the calculated metabolic rate for each test subject.

For comparison to standardized investigation methods, the operative temperature, for the three groups of test subjects, is found based on tabular values for metabolic rate of the observed activities to the values given in Tab. 7

Tab. 7 – Average, maximum and minimum values of the calculated operative temperature based on table values of the metabolic rate for the observed activities.

Subject group	Average [^{0}C]	min [^{0}C]	max [^{0}C]
Resident	24,1	22,7	26,4
care	19,3	18,1	20,8
Admin	24,3	21,4	25,4

By using the tabular values for the observation based activity estimations, the deviation in the optimal temperature becomes smaller and the individual differences in activity cannot be taken into account. Notice the close correlation of the average ideal temperatures for the resident and administrative test subject in Tab. 6 and Tab. 7.

4. Discussion

This study contains several assumptions and simplifications which can influence the results or indicate requirements of further investigations.

None of the test subjects fulfill the required minimum heart rate of 120 BPM, that makes the mental component in relationship to the metabolic rate negligible according to [11]. This could question whether the used widening of the scope of the heart rate to metabolic rate conversion is acceptable. Meanwhile the focus of this study was not to increase precision of the determined metabolic rate, but to evaluate whether or not a simple heart rate measurement, can be used as an indicator for thermal comfort when working with test subjects that are not cognitively capable of answering a classical questionnaire.

Only a single resident test subject chose to stop wearing the activity tracker before time. This indicate that the intended minimum impact is obtained, even though the residents were wearing the activity tracer around the clock.

The accuracy of the proposed method has to undergo further investigation. This include finding an explanation of the negative values of the calculated metabolic rate. It could be caused by; a systematic error in the equipment, inaccuracies in the determination of heart- and metabolic rate at rest or because the correlation between heart rate and metabolic rate is significantly different for activities with a heart rate below 120 BPM.

P.O. Fanger's comfort equation have been used in the original form, even though it is clearly stated that it is not valid for field studies or measured metabolic rate. In lack of a better solution, this widely used deviation [2] is also accepted as valid for this study, based on the purpose of the study.

Before the method can be used, the correlation between the calculated metabolic rates and P.O. Fanger's Comfort equation has to be investigated further. Particularly because this study does not include systematic subjective evaluation of the thermal indoor environment from the test subjects. This is a significant drawback in relation to evaluating the method's ability to predict a PMV score, or defining a set point for the operative temperature.

The number of test subjects and the length of the measuring period is too small to provide the

statistical foundation for a modification of any parameters in the process. It only provides the possibilitie to test and illustrate pros and cons in the conceptual idea and determine relevant focus points for future studies.

5. Conclusion

This pilot study has shown that it could be possible to use simple heart rate measurement to determine metabolic rate with a precision, at least comparable with general observation. Furthermore, the method has the potential to provide a more detailed description of the activity level of the individual test subject, and thereby an individually based regulation of the thermal indoor environment in the future.

The study has also demonstrated that the impact on the individual test subject, by wearing the wrist worn activity tracer, makes it possible for persons suffering from dementia to be enrolled as test subjects.

6. Acknowledgement

Cathrine Schermer Riis and Amalie Dokkedal Jensen for systematic and qualified work in the measuring period.

Innobyg for financial support.

Aarhus Friplejehjem and Meta Marie Hjemmet, for cooperation in finding test subjects and allowing the measurements to take place in their facilities.

7. References

[1] Helvik A-S, Engedal K, Benth JŠ, Selbæk G. Prevalence and Severity of Dementia in Nursing Home Residents. Dementia and geriatric cognitive disorders. 2015;40(3-4):166-77.

[2] Van Hoof J. Forty years of Fanger's model of thermal comfort: comfort for all? Indoor air. 2008;18(3):182-201.

[3] Zhan H, Yu J, Yu R. Assessment of older adults' acceptance of IEQ in nursing homes using both subjective and objective methods. Building and environment. 2021;203:108063.

[4] Tartarini F, Cooper P, Fleming R. Thermal perceptions, preferences and adaptive behaviours of occupants of nursing homes. Building and environment. 2018;132:57-69.

[5] Tartarini F, Cooper P, Fleming R, Batterham M. Indoor Air Temperature and Agitation of Nursing Home Residents With Dementia. American journal of Alzheimer's disease and other dementias. 2017;32(5):272-81.

[6] Tejedor B, Casals M, Gangolells M, Macarulla M, Forcada N. Human comfort modelling for elderly people by infrared thermography: Evaluating the thermoregulation system responses in an indoor environment during winter. Building and environment. 2020;186.

[7] Choi J-H, Loftness V, Lee D-W. Investigation of the possibility of the use of heart rate as a human factor for thermal sensation models. Building and environment. 2012;50:165-75.

[8] Wang Z, de Dear R, Luo M, Lin B, He Y, Ghahramani A, et al. Individual difference in thermal comfort: A literature review. Building and environment. 2018;138:181-93.

[9] Socialudvalget. Liskvalitet og selvbestemmelse på plejehjem. Social og integrationsministeriet: Kommission om livskvalitet og selvbestemmelse i plejebolig og plejehjem; 2012.

[10]DS/EN/ISO_7730. ERgonomics of the thermal environment - Analytical determination and interpretation of thermal comfort using calculation of the PMV and PPD indices and local thermal comfort criteria. Dansk Standard; 2006.

[11]DS/EN/ISO_8996. Ergonomics of the thermal environment - Determination of metabolic heat produktion. Dansk Standard2004.

[12]Bertelsen AS, Andersen MR. Basalstofskifte: University of cobenhagen Department of Nutrition, Exercise and Sports; 2013 [updated 6/7 2017. Available from: https://nexs.ku.dk/forskning/vidensbanken/basalstofskifte/.

[13]www.aktivtraening.dk. Mål din maks- og hvilepuls Aktiv træning: Bonnier Publications International; 2020 [Available from: https://aktivtraening.dk/traening/maal-din-maks-og-hvilepuls.

[14]DS/EN/ISO_9920. Ergonomics of the thermal environment - Estimation of the thermal insulation and wather vapour resistance of a clothing ensemble. Dansk Standard; 2009.

[15]Lassen JF. Bradykardi (langsom puls) 2020 [Available from: https://www.sundhed.dk/borger/patienthaandbogen/hjerte-og-Blodkar/sygdomme/hjertearytmier/bradykardi-langsom-puls/.

Data Statement

The datasets, generated during and/or analysed during the current study, are not publicly available because of GPDR but will be available in anonymized form by contact to the main author.

Safe indoor work-outs during the COVID-19 pandemic

Marije te Kulve [a], Francesco Franchimon [b], Vincent Vons [c], Eliane Khoury [d]

[a] bba binnenmilieu, The Hague, the Netherlands, mk-bba@binnenmilieu.nl

[b] Franchimon ICM, Berkel en Rodenrijs, the Netherlands, francesco@franchimon-icm.nl

[c] Virus Free Air Solutions, Schiedam, the Netherlands, vincent.vons@vfatechnology.com.

[d] Virus Free Air Solutions, Schiedam, the Netherlands, eliane.khoury@vfatechnology.com.

Abstract. Many people go to the gym to work-out or take part in classes to remain in good physical health. During the COVID-19 pandemic, gyms in most countries across the world were obliged to close to prevent the virus from spreading during indoor work-outs. Indeed, the risk of aerosol virus transmission during high intensity exercise is significantly increased due to the increased aerosol production of a potentially infected person and the increased breathing volume of susceptible individuals. However, doing physical workouts is of great importance to stay healthy and enhance the immune system, especially during the pandemic, since it is known that overweight people and people with underlying diseases are at increased risk. Therefore, the objective of this project was to design a ventilation and air cleaning system that significantly reduces the risk of aerosol virus transmission in indoor sport environments. The project aims to contribute to establishing requirements for indoor sport facilities in terms of ventilation and air cleaning such that, during a next lockdown, gyms that fulfil these requirements can remain open. To achieve this objective, a literature survey was conducted to map the current knowledge on the aerosol transmission of COVID-19 and the characteristics of different types of exercise. Based on that, requirements were set for different intensity group classes to maintain the CO_2 concentration below 1200 ppm and the theoretical Wells Riley-infection risk below 5%. In addition, the importance of ventilation efficiency to dilute released contaminated aerosols was well understood in order to apply the Wells Riley-model. A lab- and field study were conducted to test if the model assumptions were met. Also, the possibility to measure aerosols in the field was investigated. Based on these outcomes, a prototype consisting of a ventilation system, air cleaning system and cooling system combined with a smart control algorithm, was designed and installed in a room for group classes. The performance of the systems was tested during exercise classes of yoga, zumba and indoor cycling (spinning).

Keywords. COVID-19, Aerosols, Exercise, Ventilation, Air cleaning.
DOI: https://doi.org/10.34641/clima.2022.178

1. Introduction

To remain in good physical health, many people go to the gym to exercise. Especially during a pandemic, like the COVID-19 pandemic, this is of great importance since overweight people and people with underlying diseases are at increased risk of getting severe symptoms after infection with the SARS-Cov-2 virus [1]. Besides overweight lower cardiorespiratory fitness and higher waist circumference appaers to be predictors of severe COVID-19 [2]. Moreover, physical activity attributes to the immune system of humans [3]. Although obliged closures of gyms to reduce the reproduction number, there are good reasons to consider a strategy to exclude closures in the strategy for this necessary reduction. However, due to the increased aerosol production of any infected person in a gym and the increased breathing volume of susceptible individuals, the risk of aerosol virus transmission is significantly increased in gyms. Indeed, there are a few outbreak cases in indoor sport facilities [e.g. 4, 5]. The potential additional risk of virus transmission in gyms and the reported cases were probably a driving force to close gyms in most countries across the world during waves of infections.

The objective of this project was to design a ventilation and air cleaning system that significantly reduces the risk of aerosol virus transmission, potentially containing virions, in indoor sport environments. The project aims to contribute to establishing ventilation and air cleaning requirements for indoor sport facilities such that, during a next lockdown, gyms that fulfil these requirements can remain open.

To achieve this objective, a literature survey was conducted to map the current knowledge on the aerosol transmission of COVID-19 and the characteristics of different exercise activities. Based on that, requirements were set for different intensity group classes. A lab- and field study were conducted to test if the model assumptions were met. Also, the possibility to measure aerosols in the field was investigated. Based on these outcomes, a prototype consisting of a ventilation system, an air cleaning system and a cooling system combined with a smart

Copyright ©2022 by the authors. This conference paper is published under a CC-BY-4.0 license.

control algorithm, was designed and installed in a room for group classes. The performance of the systems was tested during group classes of yoga (holistic), zumba (aerobic) and indoor cycling (cardio).

2. Requirements for gyms

Starting point for the requirements of the adaptive system is that the following functional demands are met:
1. The theoretical risk of airborne transmission is sufficiently low when one of the persons present is infected.
2. The indoor air quality has no negative impact on health as compared to limits for public health.
3. The temperature in the room is adjusted to the physical intensity of the exercise performed.
These functional demands are translated to performance criteria based on literature as described below.

2.1 Theoretical risk of airborne transmission

The theoretical risk of airborne transmission can be estimated using the Wells-Riley equation [6, 7]. The risk for each individual in a room to get infected (P), can be estimated based on the ventilation (Q), the number of infected persons present in the room (I), virus emission of susceptible persons (q) the breathing volume (p) and the duration of exposure (t) using equation (1).

$$P = 1 - exp\left(-\frac{Iqpt}{Q}\right) \quad (1)$$

Thereby it is assumed that all people are equally likely of getting infected, their breathing volume is equal and the time spent in the room is the same. Also, it is presumed that the air is fully mixed and a steady state concentration has been reached. By doing so, the estimated risk of persons close to the infected person might be underestimated [8], while the assumption of a steady state might overestimate the risk, especially in rooms with a low ventilation rate, since it takes some time to reach steady state.

Apart from ventilation, other factors that inactivate the virus and/or remove virions, can be included in the model [9]. Filtering of the air can be included based on the air cleaning flow rate (Q_r) and the air filtering efficiency (η). The individual risk of infection can then be calculated according to equation (2).

$$P = 1 - exp\left(-\frac{Iqpt}{Q + Q_r\eta}\right) \quad (2)$$

To calculate the required amount of ventilation and other factors that inactivate the virus and/or remove virions ($Q+Q_r*\eta$), all other parameters of equation 2 need to be addressed.

The limit for the theoretical risk of airborne transmission (P) is set at 5%.

Number of infected persons (I): the model is based on the assumption that one of the athletes or instructors is infected.

Virus emission of infected person (q): the virus emission is expressed in quanta per hour, where one quantum represents a virtual amount of virus that is enough (with a probability of 63%) to infect an average healthy person. Principles for quanta production of the SARS-Cov-2 virus have been published and show large differences between breathing during light and intense activity, talking and screaming [10]. In this model the P95 values as reported by Buonanno are used [10]. The assumption here is that athletes in holistic exercise (yoga, Pilates) talk 10% of the time and in other sports a maximum of 20% of the time. For instructors, the assumption is that they are talking 50% of the time (fitness, holistic exercise) or yelling 50% of the time (aerobics, cardio). For the latter, the aerosol production was calculated with and without the use of a microphone to reduce quanta production. For the virus emission, the time-averaged value has been taken for the hourly-averaged quanta production (Table 1).

Breathing volume (p): the breathing volume is dependent on the intensity of the physical activity. The assumption for the breathing volume during the different types of exercise, has been based on the data published by Salonen et. al. that include the relation between physical intensity and breathing volume [11], (Table 1). Compared to the study of Ramos et al, might be slightly on the low side [12].

Time of exposure (t): in determining the required capacity of the ventilation system in the room for group classes, time of exposure is assumed 1 hour.

2.2 Indoor air quality and health

A limit value of 1200 ppm is used for the CO_2 concentration, which is in line with the National Institute for Public Health and the Environment in the Netherlands [13]. The ventilation required per person for this depends on the CO_2 production and thus the intensity of the athlete or instructor. The intensity of the activities is expressed in MET. For the various categories in, the MET value was determined on the basis of the compendium [14]. In this case, we assume an average basal metabolic rate (BMR) of 6.94 MJ/day, based on an equal distribution between men and women and age (range: 16 and 70 years old) and a respiratory coefficient (RQ) of 0.85 [15]. The resulting CO_2 production per person for the defined exercise intensities [M=MET] was calculated (equation 3). The outcome and the required flow rates are shown in Table 2.

$$V(CO_2) = BMR * M * 0{,}484 * 10^{-3} \quad (3)$$

Tab. 1 – Overview of the estimated values used for the parameters included in the WR-equation based on different exercise activities (wild corona variant).

Activity	Virus emission (q) [quanta/hour]	Breathing volume (p) [m³/ hour]
Athlete: holistic	30	1.2
Athlete: aerobic	40	1.8
Athlete: Cardio	40	2.4
Instructor: holistic	50	1.2
Instructor: aerobic	193 (98[a])	1.8
Instructor: cardio	240 (145 [a])	2.4

[a] when using a microphone.

Tab. 2 – Overview of the required ventilation flow rate per person to keep the CO_2 concentration in the room below 1200 ppm.

Activity & corresponding estimated metabolism in [MET]	CO_2 production [l/s / person]	Ventilation rate [m³/ hour per person]
Athlete: holistic, 4	0.013	60
Athlete: aerobic, 6	0.020	90
Athlete: Cardio, 8	0.027	120
Instructor: holistic, 4	0.013	60
Instructor: aerobic, 6	0.020	90
Instructor: cardio, 8	0.027	120

For the particulate matter, a limit values has been set based on the daily average exposure limit by the WHO of 15 µg/m^3 [16]. This value is adjusted for the breathing volume and thereby the increased dose (concentration * volume), due to the increased breathing volume caused by an increased metabolism during exercise (eq. 4). This results in a limit for the PM2.5 concentration of 6 µg/m^3, 4 µg/m^3 and 3 µg/m^3 for respectively holistic exercise (MET=4), aerobics (MET=6) and cardio (MET =8).

$$Limit\ avg.PM_{2.5} = \frac{1{,}5}{MET} * 15\ \mu g/m^3\ )(4)$$

2.3 Thermal comfort

In Europe, there are no specific standard that prescribe the thermal environment in sporting facilities. Also in other parts of the world, standards often have only general recommendation for the thermal indoor environments in sport facilities [17]. Sporting federations for indoor sport facilities as recognized by the International Olympic Committee (IOC), describe guidelines for specific games, but these vary widely among different games: for example 16°C-20°C for basketball and 18°C-30°C for badminton [14]. Therefore, it was decided to evaluate thermal comfort and based on that adjust the setpoint where needed. The limits for the temperature were initially set at 16-20°C.

2.4 Overall requirements

Based on the findings in literature, the requirements for the room were calculated for the three different types of group classes. To calculate the required capacity of the ventilation equivalent, the worst-case scenario was used (i.e. the instructor is infected, but was required to wear a microphone to reduce the required voice volume and subsequently the aerosol production) to keep the probability of infection below 5%. Then the required ventilation rate was calculated to keep CO_2-concentration below 1200 ppm in case of occupation of 20 athletes. In case the required fresh air supply is lower than the ventilation equivalent, the remaining is provided using air cleaning. Table 3 shows the required design criteria in terms of the ventilation equivalent, the fresh air supply and the amount of air cleaning.

Tab. 3 – Overview of the required ventilation equivalent, fresh air supply and air cleaning

Activity & estimated metabolism in [MET]	Ventilation equivalent (Q+Qr*η) [m³/ h]	Ventilation rate (Q) [m³/ h]	Additional air cleaning [Qr*η] [m³/ h]
Holistic, 4	1180	1200	0
Aerobic, 6	3440	1800	1600
Cardio, 8	6800	2400	4400

3. Verify model assumptions

3.1 Lab measurements

Experiments were carried out in a small indoor test room to determine whether it is feasible to measure (an indication of) the aerosol production during exercises.

Method

In a test room of 27 m^3 (3.2 x 3.3 x 2.6 meter) measurements were performed when riding a spinning bike at two intensities. The protocol consisted of cycling at moderate intensity (±70% of the maximum heartrate) and high intensity (±90% of the maximum heartrate). During each intensity measurements were performed with a FFP2 mask and repeated without the mask so that the difference could be used as an estimation of the aerosol production while correcting for other factors influencing the particle concentration. Without wearing the mask, the athlete was silent for 6 minutes, talking for 6 minutes and singing loudly for 6 minutes to increase the aerosol production. During all experiments particle concentrations were measured using a GRIMM 1.109 Optical Particle Counter (OPC). All measurement were performed during one day.

There was no ventilation in the room (infiltration ± 9 m^3/hour) during the experiments. Between different experiments, the room was ventilated and cleaned using a large air cleaner to remove airborne particles so that each experiment started with low background concentrations.

Results and discussion

Except for the measurement when the athlete was singing and cycling at high intensity, the increase in the number of particles (0.250-30µm) per second during one experiment was smaller during the course of the day (Figure 1). A similar pattern was observed for the increase in PM1 concentration. Based on these results, the larger increase during singing at high intensity might be attributed to the increased aerosol production. However, the differences between cycling experiments with and without mask, appears to be not the only factor of concern. It is hypothesized that the bicycle itself or infiltration of surrounding air were sources of particles in the experimental chamber, sources for which the contribution decreased during the day. This confounding effect appears to be larger than the aerosol production of the athlete (except for singing at high intensity).

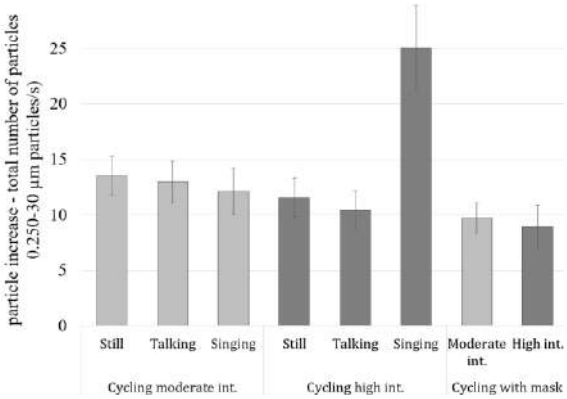

Fig. 1 – Particle increase per second during the different experiments during the course of the day (chronological) (average ± 95% confidence interval).

Already in this tightly controlled experiment, without ventilation, and with a standardised protocol, the aerosol production by the athlete is overruled by other (not constant) sources. Also the contribution of bioaerosols released by the athlete is relatively small: the increase in PM1 during high activity and singing, corresponds with an increase of 3,8 µg/m^3 per hour if no particles settle and there is no ventilation at all. In practise it will therefore not be possible to attribute an increase of particles to an increase aerosol production.

3.2 Field measurements

Based on the outcomes from literature and lab study, a prototype combining ventilation, air cleaning and cooling coupled to a smart control algorithm, was designed and installed in a room for group classes. The performance of the system was first tested in an empty room that is normally used for group classes.

The objectives of the measurements were:

- Determine the obtained ventilation and air cleaning performance.
- Determine the ventilation efficiency.

The system was installed in a room for group classes with a volume of 477 m3 (Figure 2 and 3). The system consists of an air handling unit (AHU) which provides fresh air to the room via four textile air ducts (Figure 2). Dependent on the required ventilation equivalent, air from the room is recirculated and mixed with the fresh air and filtered and cleaned using an ASPRA cylindrical Electrostatic Air Precipitator (ESP) combined with an open structure static filter: particles are charged inside the ESP section, and captured directly on the filter. Additionally, a standalone fancoil unit was used for cooling, heating and cleaning (ASPRA cylindrical ESP) recirculated air.

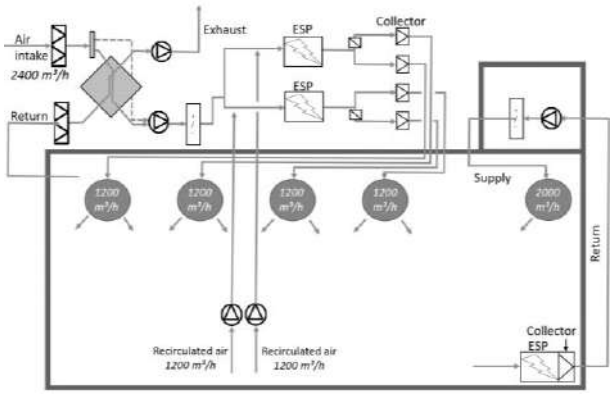

Fig. 2 – Schematic illustration of the principle

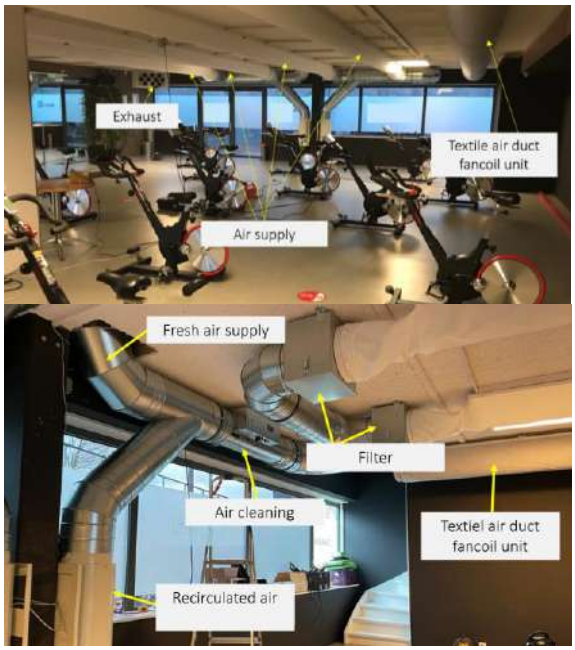

Fig. 3 – Room where the system was installed.

Performance of the ventilation and recirculation system was determined a grid of CO_2 sensors placed in the room and a GRIMM 1.109 Optical Particle Counter (OPC) (Figure 4).

The air change per hour (ACH) of the ventilation and air cleaning was determined based on the decay rate (equation 5). CO_2 extinguishers were used to generate CO_2 and thus determine the decay rate at each measurement location. The ventilation rate was calculated as the average of the ACH per location. To determine the total ventilation equivalent, a smoke machine was used to generate particles, to ensure a high PM1 concentration as a starting point. The decay rate was calculated and based on that the air change rate was determined. Note, the decay rate of CO_2 determines the ventilation rate and the decay rate of particles the air changes (equivalent ventilation).

$$Concentration\ time = t\ (C_t) = C_0 * e^{-\lambda t} \quad (5)$$

C_0 = concentration at time [ppm of µg/m^3]
t = time [hours]
λ = ventilation (equivalent) rate (ACH) [hours^{-1}]

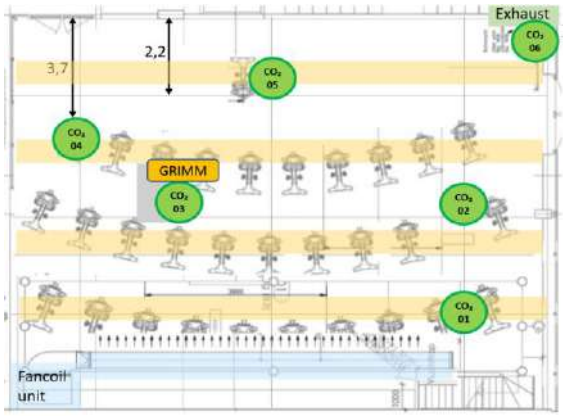

Fig. 4 – Locations of the CO_2-sensors and GRIMM (schematic).

Whether the air in the room is well mixed, was determined based on the Air Change Effectiveness (ACE) index [18] using equation (6).

$$\text{ACE } index = \frac{ACH\ location}{ACH\ room} = \frac{\lambda}{\tau} \quad (6)$$

The measurements of the ventilation and ventilation equivalent were performed in the setting for the high intensity activity (8 MET). Outdoor measurements of the air temperature CO_2-concentration, relative humidity and PM2.5 were performed on April 7th 2021, had a duration of 8 minutes and a measurement interval of 1 second (PM2.5) and 1-minute (Temp, CO_2 and RH) (Table 4).

Tab. 4 – Outdoor conditions during measurements

	Average	Standard deviation	Unit
PM2.5	17	9	µg/m^3
CO_2 concentration	428	5	ppm
Relative Humidity	46	2	%
Temperature	11	0.3	°C

The results of the measurements show that the air was well mixed within the room: ACE is between 0,96 and 1.07 (Table 5). The measured ventilation rate is slightly (9%) lower as compered the design value.

Figure 5 illustrates the decay of the PM1 concentration. As illustrated the natural logarithm of this decay shows a linear drop during the first 8 minutes, this interval is used to determine the slope (0.215 min^{-1} = 12.9 h^{-1}). Thereby providing a representative value of the ACH of the ventilation equivalent. Similar to the ventilation rate, the ventilation equivalent is 10% lower as compared to the design value (Table 5).

Tab. 5 – Comparison between the required and measured performance of the system during the cardio settings.

	Cardio / high intensity	
	design	measured (avg ± stdev)
Ventil. rate 20 ath. [m^3/h]	2400	2195 ± 98
ACH ventilation (h^{-1})	5.0	4.6 ± 0.2
ACE index (range)	0.90 – 1.10	0.96 – 1.07
Ventilation equiv. [m^3/h]	6800	6142
ACH Ventilation equiv. (h^{-1})	14.3	12.9

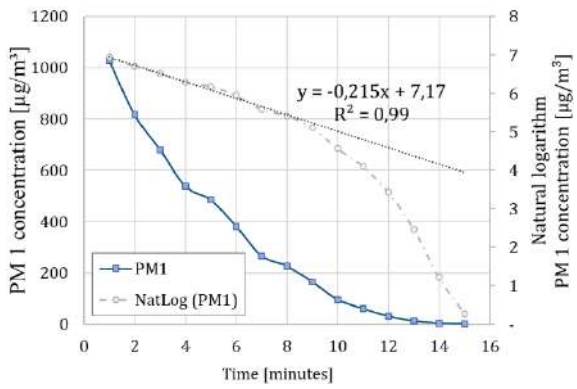

Fig. 5 – Decay of the PM1 concentration (primary x-axis) and the natural logarithm (secondary x-axis).

Conclusion

Based on the measurements it can be concluded that the air in the room is well-mixed, but the decay rate of CO_2 and the PM 1 showed a slight underperformance. However, the ventilation rate is still within acceptable limits for a field environment.

4. Prototype

To test whether the system performed as expected during occupation, field measurements were carried out to evaluate the indoor environmental parameters and the experiences of the athletes. Also, the data was used to validate the assumed MET values per sport.

4.1 Method

Measurements were performed during two days, whereby the same program was carried out each day. This program consisted of three types of group classes: yoga (holistic ±4 MET), zumba (aerobic ±6 MET) and spinning (cardio ±8 MET). During the first day, the "standard settings" were used: fixed ventilation rate based on the national guidelines (1200 m^3/ hour, so that 20 persons can participate), air cleaning switched off, and cooling system switched on. During the second evening the settings as specified in Table 3 were used for the "prototype". All classes had a duration of 45 minutes.

During each classes, 20 athletes could participate (partly the same participants during both days). Of each person, the age, gender, weight and length was collected to calculate the expected BMR using the Harris and Benedikt Formula [19], see table 6. After each class, participants were asked to fill out an online questionnaire to indicate how they experienced the indoor environment. The results of the questionnaire were compared using a t-test. P-values <0.05 were considered significant (indicated with * and p<0.01 **), p-values <0.1 were considered a trend (indicated with #).

During all classes temperature, relative humidity CO_2-concentration and PM1, PM2.5 and PM10 were measured continuously.

Tab. 6 – Number of athletes per class and their calculated BMR (average).

	Average BMR [kcal/day]	Number of athletes (incl. instructor)
Yoga day 1	1393	17
Yoga day 2	1516	17
Zumba day 1	1471	18
Zumba day 2	1394	18
Spinning day 1	1618	20
Spinning day 2	1620	20

4.2 Results

During the zumba class and spinning class the peak CO_2-concentrations were lower on day 2 (prototype settings) as compared to day 1 (standard settings). Still 1200 ppm CO_2 was exceeded during spinning on day 2 and achieved at the end of the class (Figure 6). The difference between both Yoga classes were more equal due to the same setting of the ventilation rate.

Temperature was significantly lower at day 2 (19.0 ± 0.37) as compared to day 1 (20.3 ± 0.70) (Figure 7). During the standard settings temperature increased during the evening with a median temperature of 20.8°C during spinning class. At day 2 temperature during the all classes was around 19.0°C.

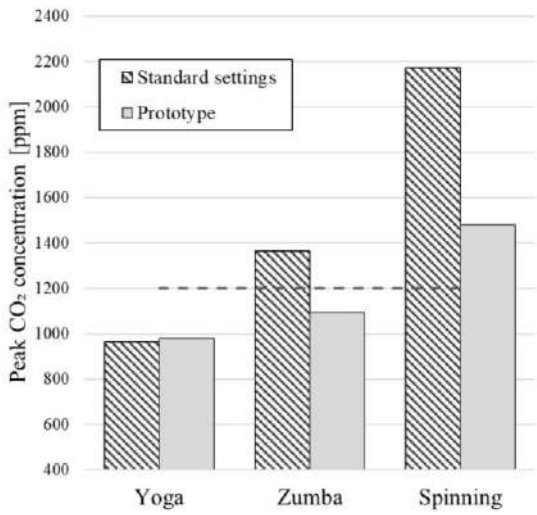

Fig. 6 – Peak CO_2-concentration during each class.

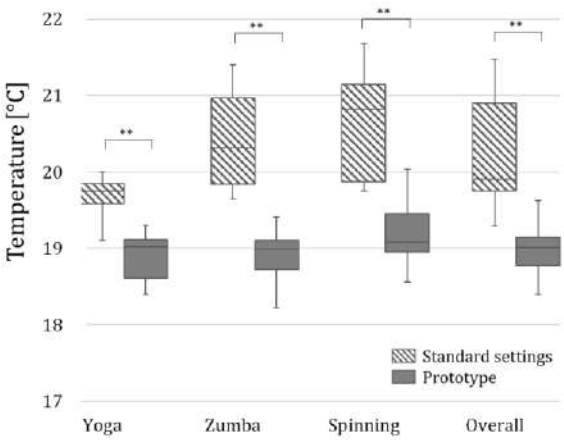

Fig. 7 – Air temperature day 1 (standard settings) versus day 2 (prototype).

In line with the measurements of CO_2-concentration and temperature, the participants of the zumba and spinning class were significantly more satisfied with the indoor air quality and temperature when the settings of the prototype were used as compared to the standard settings (Figure 8 and 9). For the yoga class participants did not experience a difference but were on average satisfied with the temperature and indoor air quality during both sessions. Also, the thermal sensation was closer to neutral during the zumba and spinning class when the settings of the prototype were used (Figure 10).

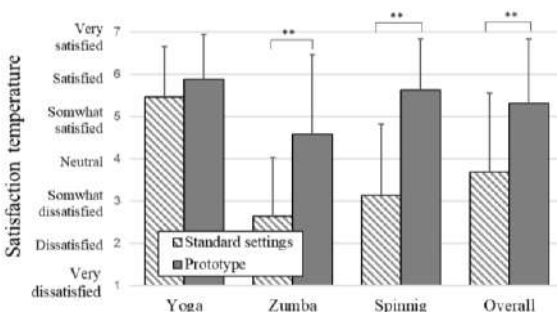

Fig. 8 – Satisfaction with the air quality.

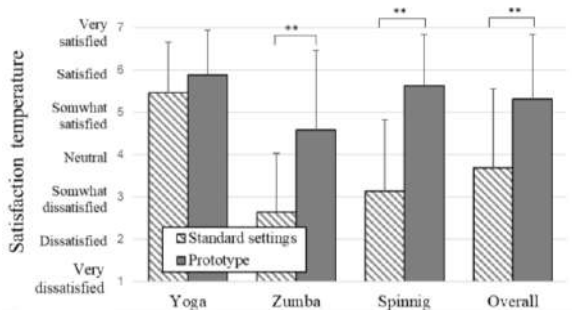

Fig. 9 – Satisfaction with the temperature.

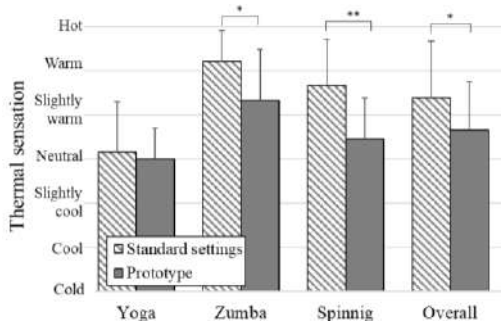

Fig. 10 – Thermal sensation of participants.

Based on the peak CO_2-concentrations at t=45 minutes, the CO_2-production of the athletes was calculated for each class (Table 7). For the yoga and zumba classes the assumed MET values of 4 and 6 seemed to be adequate estimates. However, for the spinning class 8 MET underestimated the physical activity of the participants: at day 1 the calculated MET value was on average around 10 and at day 2 on average 10,5.

4.3 Conclusion

The new settings of the prototype improved the indoor air quality as compared to the standard settings. Based on the data it was concluded that the participants of the spinning class had an average MET value of around 10, which is higher than the assumed 8 MET. As a result, the CO_2-concentrations exceeded the 1200 ppm during this lesson. Still the subjective response about the indoor air quality and temperature of the participants of the Zumba and spinning class significantly improved as compared to the standard settings.

5. Conclusion

Due to the increased breathing volume and quanta production, indoor exercising poses an increased risk of transmission of viruses in case of insufficient ventilation. Especially when the intensity is high, ventilation rates need to be extremely high to sufficiently reduce the risk of transmission of the SARS-Cov 2 virus. A theoretical approach for determining the required ventilation equivalent is recommended since explorative measurements indicate that it is not possible to measure the aerosol production during exercise in the field. A combination of ventilation and air cleaning can both ensure a good indoor air quality and a safe environment in an energy efficient way. It must be noted that mutation of the virus and changing infectivity of the virus, may change the required performance.

Moreover, the results show that the general guidelines for the amount of ventilation per person are insufficient for moderate and high intensity activities. Dynamic settings based on the intensity of the activities performed, are needed to provide an adequate indoor climate, both in terms of temperature and indoor air quality.

The study demonstrates that it is possible to anticipate on the transmission of viruses by increasing ventilation and air cleaning rates in sport accommodations, thereby allowing safe indoor exercising during a pandemic when staying physically healthy is of upmost importance.

Tab. 7 – Calculated MET value using the measured CO_2 concentrations, the average BMR, the occupation and the ventilation rate.

	Ventilation rate [m^3/hour]	CO_2 production MET=1 / pers. [m^3/min]	Number of athletes [-]	Peek CO_2 concentration [ppm]	Calculated sport intensity [MET]
Yoga day 1	1200	0.000169	17	964	3.8
Yoga day 2	1200	0.000184	17	981	4.0
Zumba day 1	1200	0.000179	18	1364	6.7
Zumba day 2	1800	0.000169	18	1093	6.7
Spinning day 1	1200	0.000197	20	2172	10.1
Spinning day 2	2400	0.000197	20	1480	10.7

6. Acknowledgement

The study was funded by SBIR, on behalf of Sportinnovator, the Dutch Ministry of Economic Affairs and Climate and the Dutch Ministry of Health, Welfare and Sport.

7. References

[1] Ko, J. Y., Danielson, M. L., Town, M., Derado, G., Greenlund, K. J., Kirley, P. D., ... & Kim, L. (2021). Risk factors for coronavirus disease 2019 (COVID-19)–associated hospitalization: COVID-19–associated hospitalization surveillance network and behavioral risk factor surveillance system. Clinical Infectious Diseases, 72(11), e695-e703.

[2] Ekblom-Bak, E., Väisänen, D., Ekblom, B., Blom, V., Kallings, L. V., Hemmingsson, E., ... & Lönn, A. (2021). Cardiorespiratory fitness and lifestyle on severe COVID-19 risk in 279,455 adults: a case control study. International Journal of Behavioral Nutrition and Physical Activity, 18(1), 1-16.

[3] Dorneles, G. P., Dos Passos, A. A., Romão, P. R., & Peres, A. (2020). New insights about regulatory T cells distribution and function with exercise: the role of immunometabolism. Current pharmaceutical design, 26(9), 979-990.

[4] Brlek, A., Vidovič, Š., Vuzem, S., Turk, K., & Simonović, Z. (2020). Possible indirect transmission of COVID-19 at a squash court, Slovenia, March 2020: case report. Epidemiology & Infection, 148.

[5] Jang, S., Han, S. H., & Rhee, J. Y. (2020). Cluster of coronavirus disease associated with fitness dance classes, South Korea. Emerging infectious diseases, 26(8), 1918.

[6] Wells, W.F. (1955) Airborne Contagion and Air Hygiene, Cambridge MA, Cambridge University Press. 117–122

[7] Riley 1982 indoor airborne infection, Env Int

[8] Noakes CJ, Sleigh PA (2008) Applying the Wells–Riley equation to the risk of airborne infection in hospital environments: the importance of stochastic and proximity effects, In: Proceedings of Indoor Air 2008, International Conference on Indoor Air Quality and Climate, Paper ID: 42, Copenhagen, 17–22 August 2008

[9] Sze To, G. N., & Chao, C. Y. H. (2010). Review and comparison between the Wells–Riley and dose-response approaches to risk assessment of infectious respiratory diseases. Indoor air, 20(1), 2-16.

[10] Buonanno, G., Morawska, L., & Stabile, L. (2020). Quantitative assessment of the risk of airborne transmission of SARS-CoV-2 infection: prospective and retrospective applications. Environment international, 145, 106112.

[11] Salonen, H., Salthammer, T., & Morawska, L. (2020). Human exposure to air contaminants in sports environments. Indoor air, 30(6), 1109-1129.

[12] Ramos, C. A., Reis, J. F., Almeida, T., Alves, F., Wolterbeek, H. T., & Almeida, S. M. (2015). Estimating the inhaled dose of pollutants during indoor physical activity. Science of the Total Environment, 527, 111-118.

[13] Dusseldorp et al, (2002) Gezondheidskundige advieswaarden binnenmilieu. RIVM Rapport 609021029/2004

[14] Ainsworth, B. E., Haskell, W. L., Leon, A. S., Jacobs Jr, D. R., Montoye, H. J., Sallis, J. F., & Paffenbarger Jr, R. S. (1993). Compendium of physical activities: classification of energy costs of human physical activities. Medicine and science in sports and exercise, 25(1), 71-80.

[15] Persily, A., & de Jonge, L. (2017). Carbon dioxide generation rates for building occupants. Indoor air, 27(5), 868-879.

[16] World Health Organization. (2021). WHO global air quality guidelines: particulate matter (PM2. 5 and PM10), ozone, nitrogen dioxide, sulfur dioxide and carbon monoxide.

[17] Fantozzi, F., & Lamberti, G. (2019). Determination of thermal comfort in indoor sport facilities located in moderate environments: An overview. Atmosphere, 10(12), 769.

[18] Whyte, W. M., & Ward, S. (2018). Ventilation effectiveness in cleanrooms and its relation to decay rate, recovery rate, and air change rate. European Journal of Parenteral and Pharmaceutical Sciences, 23(4), 126-134.

[19] Roza, A. M., & Shizgal, H. M. (1984). The Harris Benedict equation reevaluated: resting energy requirements and the body cell mass. The American journal of clinical nutrition, 40(1), 168-182

Conflict of interest

Conflict of interest: EK and FF are co-founders of iVention, which is a commercially available HVAC solution which emerged from this research project.

Data Statement

The datasets generated and analysed during the current study are not publicly available because it was collected to test the effectiveness of the described innovation. The paper presents the relevant outcomes. Upon reasonable request, the data that support the findings are available from the corresponding author.

Limiting the spread of long-range airborne diseases in Long Term Care Facilities

J.M.A de Kort [a], M.G.L.C. Loomans [b], L. Havinga [c]

[a] Faculty of Architecture, Building and Planning, Eindhoven University of Technology, Eindhoven, the Netherlands, j.m.a.d.kort@student.tue.nl; j.m.a.d.kort@gmail.com

[b] Faculty of Architecture, Building and Planning, Eindhoven University of Technology, Eindhoven, the Netherlands, m.g.l.c.loomans@tue.nl

[c] Faculty of Architecture, Building and Planning, Eindhoven University of Technology, Eindhoven, the Netherlands, l.c.havinga@tue.nl

Abstract. In the next decades the number of aging people living with dementia and requiring intensive care will increase significantly. With this increasing number, due to their frailty, new challenges arise, including a higher risk of infection due to long-range aerosols that contain pathogens. This study sought an answer to the question of how the risk of (potentially lethal) infection through such transmissions can be limited, and the quality of life improved. The study looked at improving the basic health of residents and at additional measures to reduce the risk of infection in long term care facilities (LTCF). The focus group within this research was demented aging people living in small scale care facilities with 24-hour guidance. By means of an iterative design process and the In2health method, a building design was realised in which additional measures concerning ventilation and air-cleaning were applied. These measures were tested against different future scenarios concerning the spread of viruses in LTCFs. Based on various calculations using the Wells-Riley method, it was concluded that the building design can reduce the risk of infection without affecting the quality of life. This, however, does take a lot of additional devices, services and measures per building. Further research should include measurements in long term care facilities to ensure the specific effectiveness of the measures. Furthermore, specific air quality regulations should be designed for long term care facilities, including calculations based on risk for infection.

Keywords. Health, ventilation, Covid-19, pathogen transmission, dementia, care facilities.
DOI: https://doi.org/10.34641/clima.2022.41

1. Introduction

The number of aging people in the Netherlands rises quickly. Within that population, 280,000 persons are suffering from dementia, 80,000 of whom are currently living in nursing homes with intensive care. In the next 25 years, this number is expected to double[1]. When people are getting old, especially when having dementia, new challenges emerge, including 1) an alternative perception of an indoor environment, 2) a higher vulnerability to air pollution due to a declining immune system and weakened host defence, 3) and a sensitivity to too high and too low temperatures [2].

When focussing on indoor air quality (IAQ), not only poor air quality causes health issues, but air can also be seen as a transfer medium for pathogens and airborne diseases. As there are no specific guidelines for IAQ in Long Term Care Facilities (LTCF), it is still not well understood on how to create a healthy environment for this specific target group concerning the spread of infectious airborne diseases.

According to a research of Te Kulve et al. [3], the chance for an outbreak of an infectious disease in a LTCF depends on building characteristics, indoor air quality and the basic health of residents (based on underlying diseases). Subsequently, the spread can be divided into contact transmission and airborne transmission (long-range and short-range).

At the moment not much research has yet been conducted on designing small-care facilities for aging people with dementia, concerning the airborne transmission of infectious diseases. However, with the introduction of Covid-19 there has been an increasing discussion on the state of care homes in terms of indoor air quality, focused on the quality of life versus the chance for infection by airborne transmission [4].

Copyright ©2022 by the authors. This conference paper is published under a CC-BY-4.0 license.

Because there is a lack of research within the field of building design, this study looks at how the quality of life can be improved in a small care facility, minimising the risk of infection by long-range airborne transmission, while increasing the quality of life for aging people with dementia in a LTCF. The aim of the study is to identify design measures that contribute to limit the risk for infection, and with that develop a building design that takes both the building and services design into account, as well as the quality of life.

2. Method

The research is based on the In2Health [5] method and is divided into four different stages: 1) formulating the design challenge, 2) conceptual design, 3) embodied design and 4) detailed design. Formulating the design challenge consists of a literature review on the long-range transmission of airborne diseases, with Covid-19 as a case study. With the help of this literature review, Key Indoor Performance Indicators are formulated which form a guideline for the design of the building. In the concept design, embodied design and detailed design, an iterative process is followed, in which a small scale LTCF is designed, analysed, and evaluated into a final design. In this paper, the main outcomes of the literature review and the final design results are shown.

2.1 In2Health method

When working in a care-environment, many stakeholders are involved. This makes the design process complex and dynamic. However, a structured approach can be applied by making use of design-support models and evidence-based design. Evidence-based design is an approach for the design of health care facilities, basing design choices on scientific data [6]. A suitable method to implement evidence-based design in the design of healthcare environments is by making use of the In2Health-method [5], see Fig. 1. This philosophy looks into 'wholes' of technology, meaning that the building does not only function as a care facility, but also as a home and work environment. In Fig. 1 an overview is given of this method combined with the steps for an iterative design process. It makes use of three models: the ontology of Dooyeweerd, the International classification of functioning, disability and health (ICF) and the model of integrated building design (MIBD).

The ontology of Dooyeweerd states that first the disorder -which is in this case dementia- should be understood before the design process can be started. This is consistent with the concept of ICF, which looks at, in this case, environmental factors that affect human functioning. During this evaluation, both the perspectives of residents and care givers should be considered. As the study is conducted from a technical point of view, subject-specific knowledge on dementia is not investigated in depth. For this reason the tool OAZIS [7] combined with literature has been used whereby wishes and demands of a healing environment are translated into practical guidelines for designing a LTCF for aging people with dementia. Using this strategy, the disorder can be understood in a more practical way.

Next MIBD is applied (see Fig. 1). During this step a translation has to be made from the value framework to specific design strategies which contain the so-called six S's (stuff, space, services, skin, structure and site). The value framework indicates what the main purpose is of the building. It is a balance between the performances demanded by the user and performances delivered by the building.

The third step is the evaluation of the design per conceptual, embodied and detailed design to check if the building design meets the requirements set by the In2health method. Ultimately a final design is realized.

2.2 Stakeholders

Many stakeholders are involved in the design of a LTCF. As in this case the study is about the spread of long-range airborne diseases, the group of aging people with dementia is considered as most important as they should be protected from infectious diseases and a lacking IAQ on the one hand, and protected from social isolation to prevent high levels of stress and unmanageable behaviour by residents on the other hand [8]. Furthermore, preferences of care givers, including nurses and family, should be incorporated in the design too. The

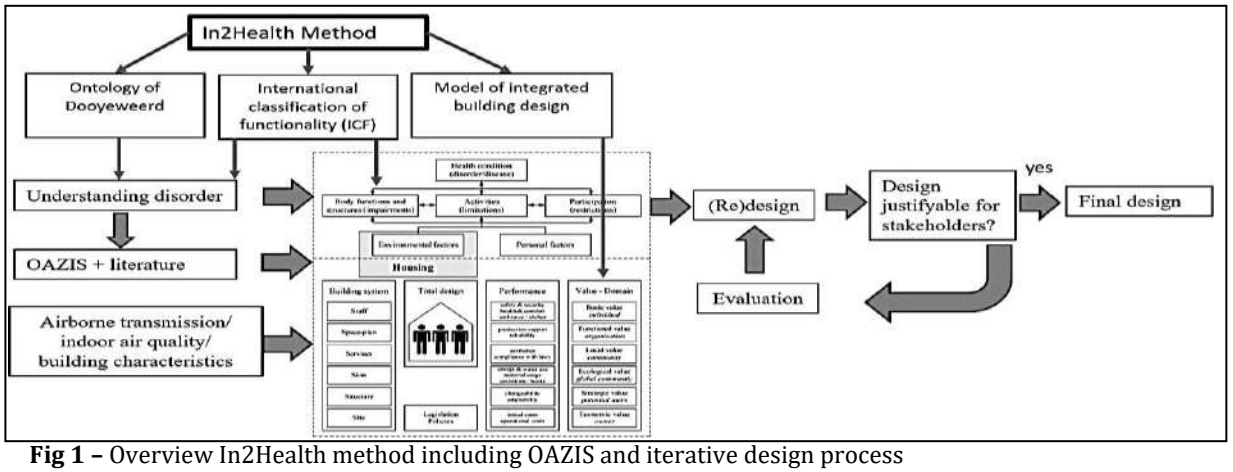

Fig 1 – Overview In2Health method including OAZIS and iterative design process

main goal of this target group is to improve the quality of life of the residents by supporting them in their daily activities, independence and social care.

2.3 MIBD – value framework

The value framework in the MIBD model has a strong relationship with the stakeholders. Based on reference studies ([2], [5], [6]) it can be stated that the basic value and the functional value are most prominent for this case. The basic value includes safety & security, Health & Comfort, and Ambiance & Shelter. This value is based on the relationship between an individual and their sense of physiological and physical well-being. The functional value includes Production, Support & Reliability. It mostly focusses on how daily activities and care giving/taking processes, taking place in the building, are supported. For residents this means that the building should facilitate the resident's way of living and for caregivers it means that they should be able to provide care in the most optimal way [2].

3. Results

An iterative design process has been applied. In this paper the most important outcomes of the literature study and the final results are shown.

3.1 Literature review

Airborne diseases originating from humans can be spread through the air as droplets or aerosols. An aerosol is a collection of solid or liquid particles suspended in gas and can be spread by breathing, coughing and talking [9]. These particles can survive in the air within a range of a couple of hours to a couple of days, depending on their size [10]. It makes the transportation of airborne aerosols possible over a long distance. In this paper only long-range transmission is considered, which will be the case when an aerosol travels at least beyond the short-range distance of 1-2 meters and is controlled by the air. In this case the assumption is made that a fully mixed situation exists.

The focus of the study is on the spread of the SARS-CoV-2 virus, causing Covid-19 disease. It causes febrile respiration infection and atypical pneumonia and can be transmitted via the air.

Spread of airborne diseases

The movement of aerosols through space is influenced by two main mechanisms: 1) the expiratory flow and 2) dispersion via room air flow. The expiratory flow depends on human activities, including among other things: coughing, talking and breathing in a certain direction. The survivability of aerosols by dispersion via room air flow depends on room characteristics, including temperature, air circulation patterns and the operation of the HVAC system, possibly supported by local mitigation manners through air cleaning [11]. Relative humidity is less important for Covid-19, as effects only start to occur at humidity levels outside the normal comfort conditions, e.g. above 70% [12].

Taking a closer look at room characteristics, there are signs that the recirculation of air at building level by a heat recovery system may contribute to the spread of aerosols through the building [12]. Secondly, recirculation at room level can also be seen as a possible polluting source when no air cleaning methods are applied in the room. Furthermore, ventilation has an effect on the deposition of particles on surfaces [13] and determines the direction of air flow in the room [14]. Displacement ventilation can be considered as a more efficient option for ventilation. However, this method is not always better for the dispersion of aerosols at a long distance, because air particles can remain longer in a stratified layer of air [13]. Using mixed ventilation, contaminated air will be diluted while limiting the chance of a direct air flow between two person, assuming vortex flows will not occur in the room [15].

Indoor air quality (IAQ)

IAQ refers to the air quality within and around buildings and structures, with the health and comfort of building occupants in mind [16]. It includes different sorts of indoor chemicals or substances. The importance of each pollutant depends on its potential effect on health and, the emission rate into the (indoor) environment and at what time span: continuously or temporarily [17]. Furthermore, the accumulation of emissions also depends on the degree of ventilation in the building and the infiltration of outdoor conditions into indoors or from one room to another room [16].

The quality of the indoor air has an influence on the basic health of residents. The likelihood of getting ill from infectious diseases increases when a person's health is deficient [3]. Aging people experience a faster deterioration of immune defences and long function, resulting in an increased risk of infection. According to a study of Bentayeb et al. [18] risks for regular breathlessness and cough were found with an elevated level of PM_{10} and NO_2. Furthermore, a relation was found between COPD-type of symptoms and high ratios of $PM_{0.1}$. Even at low levels of pollution, the IAQ affected respiratory health of aging people permanently living in nursing homes. Additionally, there is a suspicion that there is a link between CO_2-levels >800 ppm, as proxy for the IAQ, and restlessness behaviour during sleep for people with Alzheimer's disease [19].

Guidelines indoor air quality

At present, no specific guidelines exist for the indoor air quality of a LTCF for aging people with dementia [3]. However, there are general guidelines that can be considered as a reference point. Using Praktijkboek Gezonde gebouwen [20] ventilation requirements, ventilation rates and limits for CO_2 can be set based on three classifications: A (very good), B (moderate), C (minimum – slightly better than Dutch Building decree). Ventilation rate class C has a minimum of 8.3 l/s p.p. (30 m^3/h), class B 11.1 l/s p.p. (40 m^3/h) and class A 17 l/s p.p. (60 m^3/h). For CO_2 the reference

value for class A is 800 ppm (400 ppm outdoors + 400 ppm indoors).

To include risk for infection, the Wells-Riley method can be used. This method calculates the risk for infection and is divided into three categories in this study: <1%, 1-5% and 5-20% risk for infection [21], [22]. The chance for infection is the chance that a non-infected person will get infected in a room with one infected person.

Using this method, the needed mitigation options (e.g. ventilation rate) can be determined that have to be applied in the room to reduce the risk for infection. Limitations of the method include the uncertainty of the exact amount of quanta emitted by a person and it assumes a well-mixed ventilated room. Furthermore, peaks of the virus concentration are left out of consideration [21]. Therefore, the method only has been used as a method, to compare design solutions.

Design Long Term Care Facility

The physical environment has a significant influence on the perception of people with dementia [23]. Traditionally, the design of a LTCF can be directed towards a traditional nursing home ward or a small scale living. In this research the focus is on a stand-alone small scale care facility.

The fit between the environment and an individual's cognitive and physical activities is associated with the ability to age in place in a LTCF. This means that the building should be an environment that positively influences people's autonomy, support their quality of life and well-being, and attain the best possible potential of independence.

For the assessment of the building the tool OAZIS 1.0 has been used [7], [23]. This tool can be used to examine the effect of the building on the perception of residents and staff members, and gives guidelines for evaluating the design of a care institution. The model is based on evidence based design and the healing environment concept. Ultimately, this model is used to create a design that suits the wishes and demands of the resident the best. The statements being made in the OAZIS tool are validated with additional studies of Prevosth et al. [24], Verbeek et al. [25] and Heumen et al. [26].

OAZIS provides suggestions on different categories: 1) privacy and autonomy, 2) Nature, windows and view, 3) Comfort and control, 4) Facilities, 5) Orientation and Routing, 6) interior and 7) Staff. Within each category, different statements can be assessed using a 5-point system, where 5 stands for 'fully agree/ fully applied' and 1 for 'fully disagree/ not applied'. In the end, all the points in each category

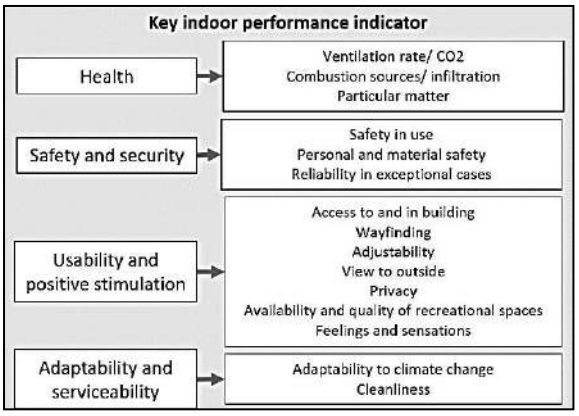

Fig 3 – Key indoor performance indicators

are added up and these determine the final score for the component. When making different variants for the building design, these different scores can therefore be compared in order to arrive at the most optimal design.

OAZIS only provides statements for creating a healing environment and does not give an indication on functional rooms and sizes. Therefore, additional studies ([25]–[29]) are used to determine the required room functions and room sizes in a small scale LTCF.

3.2 Scenario development

A standard LTCF design is based on a scenario when no residents are infected with an airborne disease. This is not always the case. It may happen that residents in the building are infected and can therefore infect others. A distinction can be made between diseases that are contagious, but do not immediately pose a serious risk to other residents and staff members (e.g. influenza virus and Norovirus), and a situation in which a deadly virus spreads, causing the possibility for both residents and caregivers to become seriously to lethally ill (e.g. Covid-19). In this research a design has been created that functions during normal and extreme cases. Therefore, three scenarios are defined, shown in Fig. 2.

1: Scenario: Alert

This scenario is based on a standard situation. The risk for infection is very low. Additional measures do not apply. However, residents are monitored for infections.

2: Scenario: Alarming

In this scenario one or multiple residents are infected with an essentially non-lethal airborne virus. In scenario 2A) an infected individual will be separated from the group for a short amount of time, or 2B) a

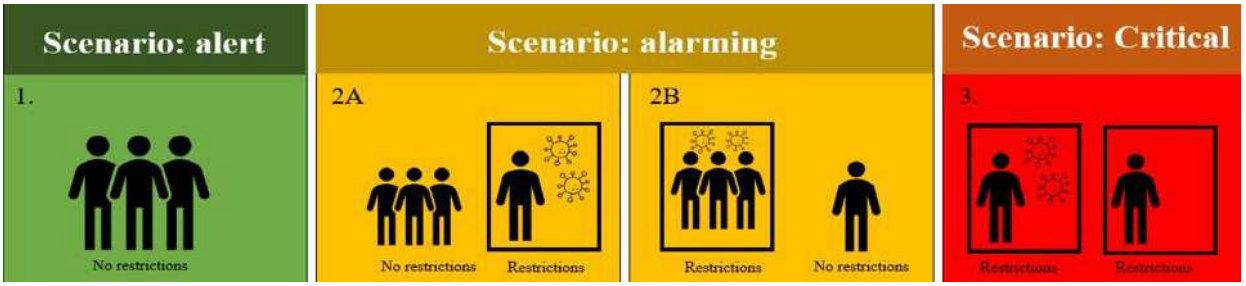

Fig 2 – Scenario development for possible future circumstances concerning restrictions for residents depending on the type of virus

group of infected people will be separated from an individual.

3: Scenario: Critical

In this scenario, a pandemic like Covid-19 would occur. In this case, the number of people in a room and in contact with others should be limited as much as possible. This means that people should be separated from each other individually by keeping enough distance between residents, care takers and visitors. The risk for infection must be very low.

Ultimately, for each scenario, the best design solution is sought for preventing the spread of infectious diseases versus the quality of life. For this purpose, Key Performance Indicators are weighted against all scenarios, resulting in one best design solution.

3.3 Key Indoor performance indicators

In Fig. 3 a simplified version of the Key Indoor Performance Indicators (KIPI) is shown, with the most important indicators at the top of the figure. The KIPIs for health are evaluated based on: 'minimum', 'moderate' and 'good'. For the other KIPIs the KIPIs are evaluated using the tool of OAZIS. For this tool inclusive data will be evaluated using the scale from one to five. The minimum standard is a score of 3/5, moderate a score of 4/5 and good a score of 5/5 per statement.

3.4 Model of integrated building design

In Fig. 4 the KIPIs are linked to the basic and functional values of the value framework of MIBD. Focus was given to private rooms of residents and communal spaces including the living and dining room.

Building design LTCF

On the left side of Fig.4 it is shown that the design of the building has a strong relationship with the KIPIs as presented in Fig. 3. Especially wayfinding [30], access in and around the building [24], simple adjustability of the building, personal privacy [7] and connectability are important aspects for the usability of the building and for the increase in autonomy and self management of aging persons with dementia. Concerning infections in the building, especially adjustability of the building is very important. Based on the scenarios shown in Fig.2, rooms are opened or closed. The restrictions that apply to autonomy and

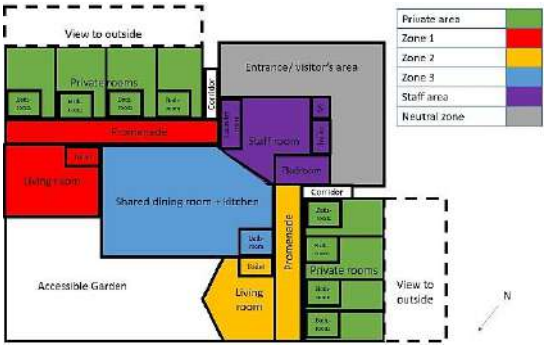

Fig 5 – Conceptual design (plan) for zoning in building. Private area: Private rooms/ isolation rooms; Zone 1/2: Communal space zone 1/2; Zone 3: Communal space that can be added to zone 1 or zone 2; Staff area: Staff room + functional rooms; Neutral zone: Zone where direction towards zone 1, zone 2 or staff area is determined.

self-determination, for instance the choice which room they enter, should be as natural as possible to improve the quality of life.

Ventilation design

The ventilation design has a direct link with the infection degree. When there are no infections in the building, standard guidelines can be applied. However, when scenario 2 or 3 occurs, the ventilation strategy has to shift towards ventilation based on risk of infections. The spread of air should also be on personal level and the interaction with other rooms should be included as well. To set reasonable limits for the risk for infection, the results as shown in Tab.1 are used.

3.5 Final design and strategies

Concluding from the previous sections, the building must not only meet the conditions concerning usability and autonomy, but must also reduce the risk of infection by improving the indoor air quality

For the building design zoning must be used in order to separate infected residents from non-infected residents, when needed. In this study a building design concept is created as an example how different zones in a building can be included. In Fig.5 an overview of the design is shown.

In scenario 1 (alert) zone 1, zone 2 and zone 3 are accessible for all residents. They can move freely through the building. In scenario 2A, the infected person remains in the private area, while other

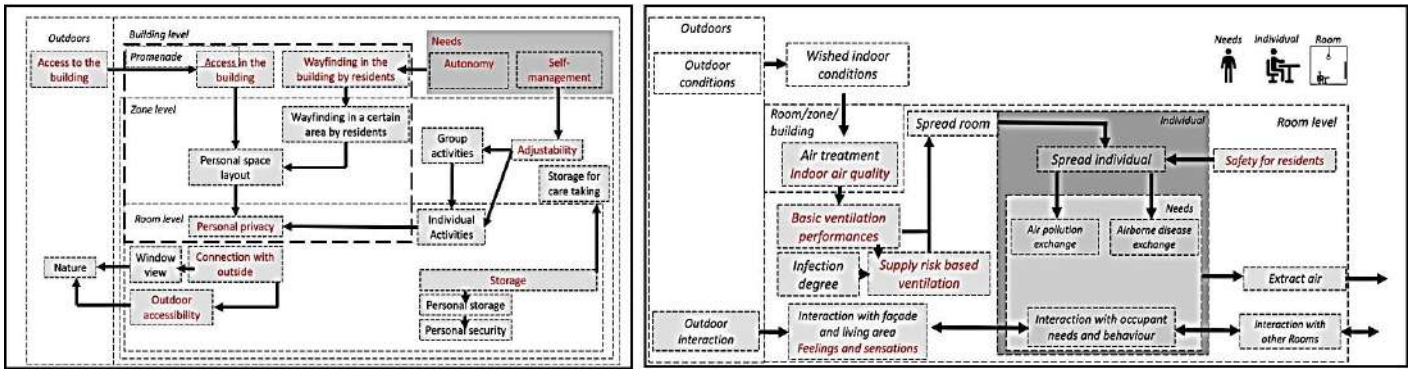

Fig 4 – Key Indoor Performance Indicators linked to Model of integrated building design

residents can enter the same zones as in scenario 1. In scenario 2B, the building can be split into two zones, where a distinction can be made between zone 1 and zone 2, and partially zone 3. Zone 3 can be split in half to create a dining space for both zones. In scenario 3, all zones will be separated, so that a limitation in number of persons per room can be guaranteed. In this case non-infected residents can meet visitors in a separated communal room or in their private room. The zones can be created using moveable walls and closing doors.

For the ventilation design in scenario 1, ventilation calculations are based on the maximum allowable CO_2-levels set to class A of praktijkboek gezonde gebouwen [20]. For scenarios 2 and 3, calculations are based on the Wells-riley equation and linked to a risk for infection (RFI) specified for each scenario. In Tab. 1 an overview is shown of a potential RFI that can be applied per scenario. This, however, strongly depends on the wishes and demands of the building owners and occupants. Considering scenario 1, the maximum value of CO_2 in the room is set to 800 ppm, which comes down to a ventilation rate of 17 l/s per person based on a CO_2-production of 0.005 l/s per person [20]. For aging people this rate can be lower 0.0034 – 0.0041 l/s p.p. depending on the body activity.

For scenario 2A, 2B and 3 various calculations have been made. Using only ventilation in the building as the main source of limiting the risk of infection, very high ventilation rates are needed. In case of this design challenge, the ventilation rates are set to 120 l/s in private rooms for which an infection risk of <1% has been set during a 1-hour visit. When using 17 l/s per person, a maximum of 2 visitors in the room and an infection risk set to 1%, only a visit by family or staff of 30 minutes is possible. This, however, does not improve the quality of life, which means that additional measures have to be taken. This can be done using air cleaning methods. In total five different air cleaning methods are investigated: 1) Portable Air purifier with HEPA filter ($\overline{CADR}$: 361 m3/hr [31]), 2) Huv: HEPA Air Cleaner with UV-ABC lamps. ($\overline{CADR}$: 934 m3/hr.), 3) cHuv: Ceiling mounted HEPA Air Cleaner with UV-C lamps ($\overline{CADR}$:: 1700 m3/hr.), 4) UVGI: upper-room Ultraviolet germicidal irradiation ($\overline{CADR}$:: 1392 m3/hr.), 5) Huv-MP UVGI@100%($\overline{CADR}$: 2373 m3/hr). The ventilation rate in the room remains at a full capacity of 17 l/s per person. The main ventilation method is mixed ventilation complemented with personalized ventilation in the private rooms and dining rooms.

Ultimately, two results can be obtained for the private rooms and the communal spaces. In scenario 2A a HuV-MP UVGI@100% system will be turned on in all rooms combined with ventilation turned at full capacity. In the infected room the UVGI-system will be combined with a Huv system and the air lock - in terms of low pressure (-) in the infected room and high pressure (+) in the hallway of a private room - will be turned on. This increases the visiting time in the room to 4 hours at a 1% risk of infection. In the communal spaces the cHuv system will be turned on. the communal spaces up to 16 hours at a 5% risk of infection, which creates a normal environment for non-infected residents.

In scenario 2B multiple residents are infected with a non-lethal disease. In this scenario the CO_2-based ventilation will be switched to risk-based controlled ventilation. This also means that windows may not be opened anymore, due to the fact that the building will be regulated using (extreme) under and over pressure. In all the private rooms the UVGI-system should be turned on and in the infected rooms a Huv system should be placed and airlocks - in terms of low pressure (-) in the infected room, high pressure (+) in the hallway of a private room and higher pressure (++) in the hallways between the apartments - should be turned on to create an air barrier between the corridor and the private rooms. In the communal spaces it depends on the risk of infection set and the activities in the building what system should be turned on. Assuming that the cHuv-system will be turned on per zone, a 2-hour visit may be possible with a 1%risk of infection and a 11-hour visit may be possible with a 5% risk of infection.

In scenario 3 in all private rooms the HuV-MP UVGI@100% system will be turned on. When residents receive visitors, a Huv system can be placed inside the room. For the infected rooms, the air lock will be turned on. Furthermore, both living rooms will be closed. When visitors want to come by, they have to be sent to the private rooms. This option is more beneficial concerning infection rates than using all communal spaces. Furthermore, both dining rooms will be separated from each other. By using a cHuv system, 4 residents and 2 staff members can dine together as a 2-hour visit to the dining room is possible, assuming the infection risk. This prevents total social isolation. Note that assumed risk for infection is only possible when the distance between residents is large enough. Short-range and contact transmission are not included in the design.

Discussion

The main goal of this research was to see what design measures must be taken to limit the risk for infection in a LTCF as much as possible. In addition, the design

Tab 1 - Ventilation based on praktijkboek gezonde gebouwen (PGG) and risk for infection (RFI) linked to scenario 1, 2A, 2B and 3.

	Scenario 1	Scenario 2A	Scenario 2B	Scenario 3
Private bedroom	Fully accesible Ventilation: PGG	RFI: <1% in infected rooms <5% in non-infected rooms	RFI: <1% when multiple persons are infected.	RFI: <1%.
Dining room	Fully accesible Ventilation: PGG	RFI: 5-20% Restricted for infected residents	RFI: 1-5% Restricted for infected residents	RFI: <1%.
Living room	Fully accesible Ventilation: PGG	RFI: 5-20% Restricted for infected residents	RFI: 1-5% Restricted for infected residents	RFI: <1%.

should contribute to a good quality of life, which is why the human perspective is the most important starting point. When other starting points, such as acquisition costs, energy consumption or the flexibility of the system, are regarded more important, this research is no longer entirely relevant. It is therefore necessary to consider what the focus will be when designing a building, as this has a major effect on the applicability of systems. This also accounts for the risk of infection. Using strict measures to keep the risk for infection as low as possible asks for major interventions in a building. It depends on the stakeholders which measures should be taken to see which chance of infection best suits the situation.

Secondly, the calculations are based on the wild variant of SARS-CoV-19 of October 2020 [22]. Other variants of the virus have emerged in the meantime that are more (or less) infective. This indicates that when sizing systems a position should be taken on the infectivity when using the Wells-Riley method for a design. The method for designing such a building including the risk of infection, however, does not change.

Thirdly, the method explains the In2Health Method. The In2Health method is a derivative of the Model of Integrated Building Design (MIBD). The method describes that an in-depth investigation of the client's requirements must first be carried out, before design principles are adopted that relate to the design of the building. This in-depth investigation is supported by the OAZIS tool. This tool is a basic tool in which the starting points of a healing environment are included in the design. Because these are basic assumptions, a number of statements have been expanded with literature studies. Because the OAZIS tool is based on practical experiences in cooperation with research agencies, and because the basic assumptions in the tool are based on a literature study, it is assumed that it is a valid tool in the context. A note on the OAZIS tool is that it is based on a scoring system where points need to be allocated. By linking the scoring to the literature study, the validity of the results can be determined to some extent. It is assumed that the tool gives enough handles to make a design with this system, which makes the method of the study valid.

Conclusion

Using the In2Health method and the Wells-riley method, a solution was sought for reducing the risk of infection in a small-scale long-term care facility. A number of conclusions can be drawn:

- In order to reduce the risk of infection, the indoor air quality should already be at a healthy level to maintain the basic health of the residents and thus prevent a more serious risk of infection.
- Different scenarios should be considered when designing the building. The building must be able to adapt quickly to these changing scenarios at building and ventilation level.
- By using the In2Health method in combination with MIBD and OAZIS, targeted solutions can be devised that meet the needs of the residents and carers.
- The Wells-Riley method can be used to calculate the risk of infections. This has shown that extra sink terms, such as the cHuv and Huv-MP UVGI@100% system, reduce the risk of infection in residents and increase the visiting time. This increases the quality of life and reduces the risk of infection. Only using ventilation as a strategy does not fulfil the requirements under severe circumstances, given the infectivity assumed.
- The risk of infection drastically affects the visiting time and the additional measures. Therefore, it is important to talk to the stakeholders to see what infection risk is regarded acceptable.
- For the building design, a combination of different systems was made. This combination fits best when designed from a health perspective.
- The final design satisfies requirements concerning health. For the requirements on energy, purchase costs and maintenance, this design is not the best option and could therefore be improved.
- In the upcoming years more attention should be paid to specific guidelines for long term care facilities including ventilation rates and additional measures to 1) keep the air as clean as possible to maintain health of residents at a high level and 2) to limit the chance for infection using for instance calculations based on the Wells-Riley method.
- This study focuses on long-range transmission of aerosols. A completely mixed situation has been assumed, so that the Wells-Riley method could be applied. Situations also occur in a nursing home in which short-range transmission takes place. This falls outside the scope of this study, but could be a good addition for a follow-up study by modelling such issues. Combined results of long-range and short-range transmission have the potential to lead to a more realistic result in practice. However, solely modelling long-range emissions can already gives some insight in the drastic measures that are needed to create both a healthy and practical home environment.

Data access statement

Data sharing is not applicable to this article as no datasets were generated or analysed during the current study.

References

[1] Alzheimer Nederland, “Factsheet cijfers en feiten over dementie,” *Factsheet cijfers en feiten over dementie [Factsheet numbers and facts about dementia]*. https://www.alzheimer-nederland.nl/factsheet-cijfers-en-feiten-over-dementie.

[2] J. van Hoof, H. S. M. Kort, M. S. H. Duijnstee, P. G. S. Rutten, and J. L. M. Hensen, “The indoor

environment and the integrated design of homes for older people with dementia," *Build. Environ.*, vol. 45, no. 5, pp. 1244–1261, 2010, doi: 10.1016/j.buildenv.2009.11.008.

[3] M. te Kulve, M. G. L. C. Loomans, E. R. C. M. Huisman, and H. S. M. Kort, "A systematic approach to assessing indoor air quality of long term care facilities," *Gerontechnology*, vol. 16, no. 4, pp. 224–238, 2018, doi: 10.4017/gt.2017.16.4.004.00.

[4] D. C. Anderson, T. Grey, S. Kennelly, and D. O'Neill, "Nursing Home Design and COVID-19: Balancing Infection Control, Quality of Life, and Resilience," *Journal of the American Medical Directors Association*, vol. 21, no. 11. pp. 1519–1524, 2020, doi: 10.1016/j.jamda.2020.09.005.

[5] J. van Hoof and M. J. Verkerk, "Developing an integrated design model incorporating technology philosophy for the design of healthcare environments: A case analysis of facilities for psychogeriatric and psychiatric care in The Netherlands," *Technol. Soc.*, vol. 35, no. 1, pp. 1–13, 2013, doi: 10.1016/j.techsoc.2012.11.002.

[6] J. van Hoof, P. G. S. Rutten, C. Struck, E. R. C. M. Huisman, and H. S. M. Kort, "The integrated and evidence-based design of healthcare environments," *Archit. Eng. Des. Manag.*, vol. 11, no. 4, pp. 243–263, 2015, doi: 10.1080/17452007.2014.892471.

[7] OAZIS and TNO, "OAZIS 1.0." 2015, [Online]. Available: https://oazis.nl/oazis-web/wp-content/uploads/2013/06/OAZIS-1.0.xls.

[8] X. Y. Huali Wang, Tao Li, Paola Barbarino, Serge Gauthier, Henry Brodaty, Jose Luis Molinuevo, Hengge Xie, Yongan Sun, Enyan Yu, Yanqing Tang, Wendy Weidner, "Dementia care during COVID-19," *Lancet*, vol. 395, no. 10231, pp. 1190–1191, 2020, [Online]. Available: https://doi.org/10.1016/S0140-6736(20)30755-8.

[9] R. M. Jones and L. M. Brosseau, "Aerosol transmission of infectious disease," *J. Occup. Environ. Med.*, vol. 57, no. 5, pp. 501–508, 2015, doi: 10.1097/JOM.0000000000000448.

[10] GAEF, "Who is the Gesellschaft für Aerosolforschung ? Gesellschaft für Aerosolforschung," no. December, 2020.

[11] L. Morawska, "Droplet fate in indoor environments, or can we prevent the spread of infection?," *Indoor Air*, vol. 16, no. 5, pp. 335–347, 2006, doi: 10.1111/j.1600-0668.2006.00432.x.

[12] F. Franchimon, "COVID-19 in relatie tot gebouwen," no. 02, pp. 12–17, 2020.

[13] M. Li, Y.; Nielsen, P.V.; Sandberg, "No Displacement ventilation in hospital environments," *ASRAE*, pp. 86–88, 2011.

[14] J. Wei and Y. Li, "Airborne spread of infectious agents in the indoor environment," *Am. J. Infect. Control*, vol. 44, no. 9, pp. S102–S108, 2016, doi: 10.1016/j.ajic.2016.06.003.

[15] P. V. Loomans, M.G.L.C..; de Leeuw, J.J.M.; middendorf, J.G.; Nielsen, "Corona-virus en recirculatie," *TVVL Mag.*, no. 05, pp. 14–17, 2020.

[16] Environmental Protection Agency USA, "Indoor Air Quality (IAQ)." https://www.epa.gov/indoor-air-quality-iaq/introduction-indoor-air-quality (accessed Mar. 08, 2021).

[17] World Health Organisation, "WHO guidelines for air quality - selected pollutants," 2010.

[18] M. Bentayeb *et al.*, "Indoor air quality, ventilation and respiratory health in elderly residents living in nursing homes in Europe," *Eur. Respir. J.*, vol. 45, no. 5, pp. 1228–1238, 2015, doi: 10.1183/09031936.00082414.

[19] B. Cremers and Z. G. Nederland, "Effect of CO2 on restlessness of an Alzheimer patient," no. October, pp. 41–44, 2015.

[20] ISSO, "ISSO praktijkboek gezonde gebouwen; Cahier T1," 2002.

[21] M. G. L. C. Loomans, A. Boerstra, F. Franchimon, and C. J. Wisse, "Rekenen aan het risico op infecties," no. 05, pp. 3–6, 2020.

[22] Masterplan Ventilatie, "Achtergronddocument : Indicator besmettingskansen via aerosolen," 2021.

[23] B. de Boer, H. Beerens, M. Katterbach, M. Viduka, B. Willemse, and H. Verbeek, "The Physical Environment of Nursing Homes for People with Dementia: Traditional Nursing Homes, Small-Scale Living Facilities, and Green Care Farms," *Healthcare*, vol. 6, no. 4, p. 137, 2018, doi: 10.3390/healthcare6040137.

[24] M. D. J. Prevosth, T. van der Voordt, "Het creëren van een healing environment," *Facil. Manag. Mag.*, pp. 22–27, 2013.

[25] H. Verbeek, E. Van Rossum, S. M. G. Zwakhalen, G. I. J. M. Kempen, and J. P. H. Hamers, "Small, homelike care environments for older people with dementia: A literature review," *Int. Psychogeriatrics*, vol. 21, no. 2, pp. 252–264, 2009, doi: 10.1017/S104161020800820X.

[26] S. van Heumen, H. Straatsma, L. Huibers, A. Jans, and E. Krijger, *Kleinschalig wonen: een full-servicepakket*. 2009.

[27] E. Huisman, R. Appel-Meulenbroek, and H. Kort, "A structural approach for the redesign of a small-scale care facility as a guideline for decision-makers," *Intell. Build. Int.*, vol. 12, no. 1, pp. 32–43, 2020, doi: 10.1080/17508975.2018.1493569.

[28] LOC, "Programma van Eisen (PvE) voor een kleinschalige woonvorm voor mensen met dementie en/of meervoudige problematiek," 2014.

[29] W. Achterberg, "Kleinschalig wonen voor mensen met dementie," *Tijdschr. voor Ouderengeneeskd.*, no. September 2010, 2010, doi: 10.1007/s12500-010-0015-7.

[30] G. Marquardt, "Wayfinding for people with dementia: A review of the role of architectural design," *Heal. Environ. Res. Des. J.*, vol. 4, no. 2, pp. 75–90, 2011, doi: 10.1177/193758671100400207.

[31] B. Zhao, Y. Liu, and C. Chen, "Air purifiers: A supplementary measure to remove airborne SARS-CoV-2," *Building and Environment*, vol. 177. 2020, doi: 10.1016/j.buildenv.2020.106918.

A Multi-Domain Approach to Explanatory and Predictive Thermal Comfort Modelling in Offices

Eugene Mamulova [a], Henk W. Brink [a, b], Marcel G. L. C. Loomans [a], Roel C. G. M. Loonen [a], Helianthe S. M. Kort [a]

[a] Eindhoven University of Technology, Eindhoven, the Netherlands, e.mamulova@tue.nl.

[b] Hanze University of Applied Sciences, Groningen, the Netherlands, h.w.brink@pl.hanze.nl.

Abstract. It is well known that physical variables, such as temperature, exert a significant influence on occupants' thermal comfort in office buildings. Despite this knowledge, models that are currently used to predict thermal comfort fail to do so accurately, resulting in a mismatch between design conditions and actual thermal comfort conditions. The assumption is that exclusive attention to physical variables is insufficient for understanding or predicting thermal comfort. Contextual, social and personal variables may also affect thermal comfort in office buildings and interact with each other. The question arises as to how a multi-domain approach can aid in explaining and predicting thermal comfort in offices. In this study, a unique dataset containing indoor environment, demographic, occupancy and personality related variables is used to construct two types of thermal comfort models. The dataset contains 524 observations, collected during summertime in two office buildings in the Netherlands. Firstly, structural equation modelling (SEM) is used to construct an explanatory model, with the aim to identify significant variables affecting thermal comfort, as well as the interactions between them. Secondly, machine learning is used to train four binary classification models to predict thermal discomfort. For the investigated cases, SEM suggests that thermal discomfort is significantly affected by (i) temperature, (ii) sound pressure level, (iii) the interaction between temperature, sound pressure level and illuminance, and (iv) the interaction between gregariousness and occupancy count. The four predictive models are subsequently trained using only the significant variables. Nevertheless, the weighted F_1-score for all four models ranges between 0.55 and 0.59, indicating weak predictive performance. The results show that significant influencers are not necessarily good predictors of thermal discomfort. Future researchers are encouraged to combine explanatory and predictive modelling techniques, in order to test whether variables that are relevant to the domain are useful for prediction.

Keywords. Thermal comfort, multi-domain, personal domain, interaction effects, structural equation modelling, machine learning.
DOI: https://doi.org/10.34641/clima.2022.181

1. Introduction

Thermal comfort is that condition of mind that expresses satisfaction with the thermal environment [1]. Building engineers refer to building standards to predict the thermal comfort conditions for a given design [1,2]. However, current standards do not always produce adequate thermal comfort predictions [3]. For example, the most prominent model for predicting thermal comfort in office buildings, Fanger's PMV, does not consider the influence of non-thermal influences and does not account for interactions between influences [4]. Recent research efforts have focused on multi-domain approaches that treat thermal comfort as a combination of variables belonging to four domains, which are outlined in **Fig. 1** [5].

1.1 research background

Researchers in the field of thermal comfort seek to understand and predict thermal comfort. The former deploy explanatory models, while the latter use predictive models. Explanatory models typically employ statistical techniques that provide insight into what influences thermal comfort in offices. Predictive models are built to forecast the thermal comfort conditions for a given office space. The relevance of social, contextual and personal factors is apparent but their presence in existing thermal comfort models is limited [6]. The combined presence of all four domains is almost non-existent [6]. Moreover, the majority of existing studies focus on explanatory modelling [6]. As a result, the research community has yet to identify a prominent

Copyright ©2022 by the authors. This conference paper is published under a CC-BY-4.0 license.

multi-domain model for predicting thermal comfort in offices. The absence of a comprehensive predictive model causes stagnation in the engineering sector, as building engineers rely on sub-optimal models to meet thermal comfort regulations.

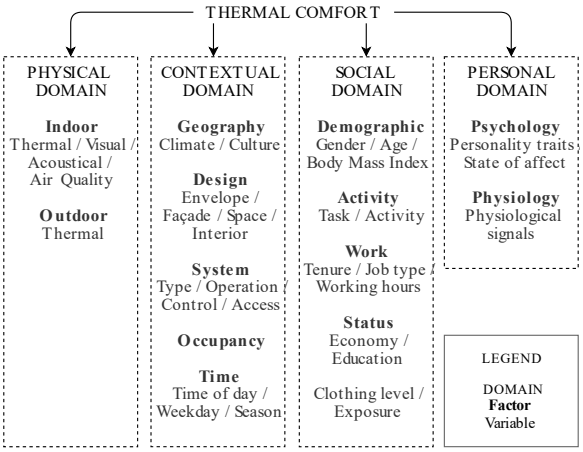

Fig. 1 - Physical, social, contextual and personal variables present in literature, adapted from [5].

The rift between design conditions and real-world thermal conditions is in part attributable to the absence of a suitable thermal comfort model. In consequence, it is important to pursue better prediction of thermal comfort in office buildings and it is worthwhile doing so using the multi-domain approach. This study looks at existing thermal comfort models to identify potential variables from multiple domains that may aid in better explaining and prediciting thermal comfort in offices.

1.2 thermal comfort variables

Existing multi-domain studies identify several variables that are of interest to thermal comfort modelling. A list of main effects and interaction effects that are supported or rejected by existing research on multi-domain thermal comfort in offices is composed [6]. Based on these findings, a series of hypotheses on the direct effects M_i and the indirect effects I_i on thermal (dis)comfort are constructed. For example, existing studies suggest that sound exerts a direct effect on thermal discomfort. Existing research also suggests that the effect of temperature dominates other physical aspects. Several studies show that individual personality traits, such as extraversion, may have both a direct and indirect influence on thermal discomfort. The current study uses gregariousness and assertiveness to represent extraversion. Occupant assertiveness is a facet of extraversion that reflects a person's willingness to take charge, while occupant gregariousness is a facet of extraversion that reflects a person's disposition to be sociable.

The focus of the study is on thermal discomfort during the cooling season and the hypotheses are:

$M1$: Air temperature exerts a positive, exponential, effect on thermal discomfort.

$M2$: Sound pressure exerts a positive effect on thermal discomfort.

$M3$: Occupant gregariousness exerts a negative effect on thermal discomfort.

$I1$: Air temperature exerts a negative effect on the interaction effect between sound pressure level and illuminance on thermal discomfort.

$I2$: Occupant assertiveness exerts a positive effect on the effect of air temperature on thermal discomfort.

$I3$: Occupancy count exerts a positive effect on the effect of occupant gregariousness on thermal discomfort.

The aforementioned hypotheses are tested via an explanatory model, using field measurement data. The results are used to train a model that aims to predict whether office employees are experiencing thermal comfort or discomfort. The articulation of the modelling outcome is unprecedented in current literature, covering three physical variables (air temperature, illuminance and sound pressure level), one contextual variable (occupancy count), two personal variables (occupant assertiveness and gregariousness) and one social variable (gender), in the interest of testing whether such a multi-domain approach can aid in a better understanding or prediction of thermal (dis)comfort in offices.

2. Research methods

The data was collected prior to this study, in two office buildings in the Netherlands. The cross-sectional campaign was conducted during the years 2015-2018. The applied measurement protocol is described in a publication by Brink and Mobach [7]. The data points used in this study are limited to the warmer months of June and July 2016. 623 office employees participated in the measurements. A summary of the demographics is available in Appendix A. The final sample size is equal to 522, of which 493 participants have a sedentary occupation. Their metabolic rate is assumed to be constant. The clothing insulation value is calculated according to the ASHRAE-55-2017 standard [1]. Adaptive opportunities such as clothing ($N = 352$), temperature control ($N = 125$) and operable windows ($N = 515$) are available to the participants. However, perceived control and adaptive behaviour are not recorded and are thus excluded from the study. The measurement procedure consists of objective and subjective measurements. Most objective measurements, such as physical and contextual observations, are performed by the experiment leader. Subjective data concerning the social and personal domains, as well as occupants' thermal perception, is collected via an online questionnaire. The items are available in appendix B.

2.1 explanatory modelling

Explanatory modelling is performed via structural equation modelling (SEM); a covariance-based technique that enables the inclusion of observable and unobservable variables. The latter is important, since the model includes personality traits, which are unobservable constructs, modelled using a set of questionnaire items. An additional advantage of SEM is the graphical aspect that allows the user to visualize relationships between the variables. This is done using standard LISREL matrix notation [8]. The computation is performed via the lavaan package [9].

Tab. 1 provides an overview of the variables used, along with their notation. Variables T_{in}, SPL, E and N_{occ} are continuous. Variables $a_1 - a_2$ and $g_1 - g_4$ are ordinal. All variables are normalized using min-max feature scaling. To account for multivariate non-normality, robust diagonally weighted least squares (DWLS) estimation, known as weighted least square mean and variance adjusted estimation (WLSMV) in lavaan, is used to compute the parameter estimates, robust standard errors and fit indices. Several fit indices are used to evaluate DWLS estimation for ordinal data, namely the Root Mean Square Error of Approximation (RMSEA), the Bentler Comparative Fit Index (CFI) and the Standardized Root Mean Square Residual (SRMSR).

2.2 predictive modelling

The predictive model takes the form of a binary classifier that predicts whether a participant is experiencing thermal comfort or discomfort. The variables included in the model are listed in **Tab.2**. Two linear and two non-linear classification algorithms are selected and trained using the scikitlearn Python library [10]. P_0 is used for linear algorithms, while P_1 is used for non-linear algorithms, as the latter are expected to capture non-linear relationships. The linear algorithms are logistic regression (LR) and linear support-vector machine (L-SVM), while the non-linear algorithms are random forest ensemble (RF) and non-linear support-vector machine that uses the radial basis function kernel (RBF-SVM).

The four models are trained using 231 observations and validated using 77 observations. A search space is proposed for each model, with the objective to maximize the weighted F_1-score, while also tuning the models' respective regularization coefficients. The search is performed on the training set, with 5-fold cross validation yielding the average weighted F_1-score to be maximized. It is performed using the popular Tree of Parzen Estimators (TPE) algorithm which suggests future hyper-parameter choices based on the previous results [11]. 3,000 hyper-

Tab. 1 – Direct and indirect effects included in the SEM model.

Effect	Domain	Symbol	SEM	Variable	Range [unit]
Direct	Physical	$exp^{T_{in}}$	x_8	Air temperature	20 – 26 [^oC]
		SPL	x_9	Sound pressure level	40 – 70 [$dB(A)$]
		E		Illuminance[a]	0 – 2,000 [lx]
	Personal	g_1	x_1	Gregariousness	
		g_2	x_2	Gregariousness	
		g_3	x_3	Gregariousness	
		h_1	y_1	General body discomfort	
		h_2	y_2	Lower body discomfort	
		h_3	y_3	Upper body discomfort	
Indirect	Physical	$SPL \cdot E \cdot T_{in}$	x_{10}	Sound, illuminance and temperature	
	Physical and personal	$T_{in} \cdot a_1$	x_4	Temperature and assertiveness	
		$T_{in} \cdot a_2$	x_5	Temperature and assertiveness	
	Contextual and personal	$N_{occ} \cdot g_1$	x_6	Occupancy count and gregariousness	$N_{occ} < 20$
		$N_{occ} \cdot g_4$	x_7	Occupancy count and gregariousness	$N_{occ} < 20$

[a] The direct effect of illuminance is excluded but illuminance is used to compute $SPL \cdot E \cdot T_{in}$.

parameter choices are evaluated for each model and the highest score is selected. During the testing phase, the four models are retrained on 308 observations, comprising the training and validation sets, and are then tested on the remaining 77 observations. Common classification metrics such as the F_1-score, accuracy (ACC) and the area under the ROC curve (AUC) are used. The aforementioned metrics are based on elements of the confusion matrix; true-positive predictions (TP), true-negative predictions (TN), false-positive predictions (FP) and false-negative predictions (FN). The higher the number of true predictions, the higher the scores.

Tab. 2 – Variables used for prediction.

Variable	Symbol
Indoor temperature exponent	P_0
Indoor temperature	P_1
Sound pressure level	P_2
Sound × illuminance × temperature	P_3
Gregariousness × occupancy count	P_4
Gender	P_5

3. Results

3.1 structural equation modelling

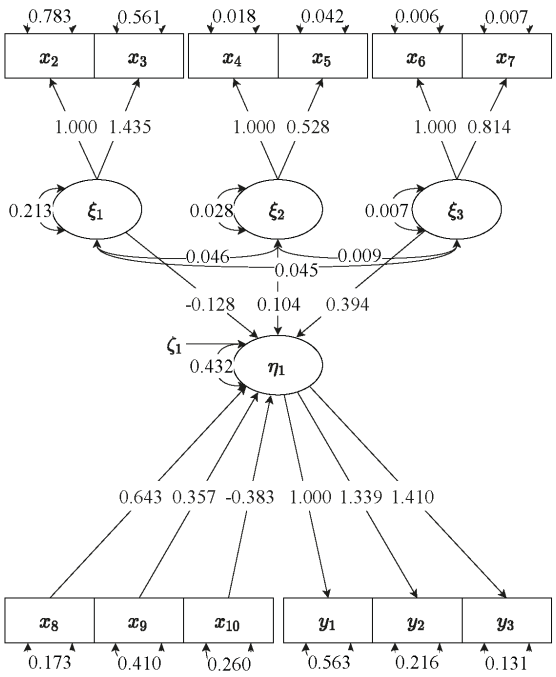

Fig. 2 - Graphical representation of model estimation.

The outcome of the explanatory modelling phase is a SEM model. **Fig. 2** shows the parameter estimates, variance/covariance estimates and factor loadings for the explanatory model. The model fit is summarized in **Tab. 3**. According to the fit indices, the model constitutes an acceptable fit, indicating that the model is capable of explaining thermal comfort in relation to the data.

Tab. 3 – Fit indices used to evaluate the SEM model.

Fit Index	Value
CFI	0.956[a]
$RMSEA$	0.075[b]
CI_{low}	0.064[b]
CI_{high}	0.087[a]
$SRMR$	0.037[a]

[a] Good.
[b] Acceptable.

The parameter estimates are shown in **Tab. 4.** The exponent of air temperature x_8 is expected to have a positive effect on thermal discomfort η_1. According to the results, the effect of x_8 on η_1 is positive (see Fig. 2) and significant at 99.9% confidence (z>3.09, p<0.001). Sound pressure level x_9 is expected to exert a positive effect on η_1. The main effect of sound pressure level x_9 is found to be positive and significant at approximately 98% confidence (z>2.33, p<0.02).

Tab. 4 – Parameter estimates for the thermal comfort variables included in the SEM model.

	Estimate	SE	Z	P(<|z|)
x_8	0.643	0.203	3.177	0.001[a]
x_9	0.357	0.151	2.368	0.018[b]
x_{10}	-0.383	0.196	-1.951	0.051[c]
ξ_1	-0.128	0.174	-0.736	0.462
ξ_2	0.104	0.382	0.272	0.785
ξ_3	0.394	0.198	1.988	0.047[c]

[a] CI – 99.9%.
[b] CI – 98%.
[c] CI – 95%.

The interaction between indoor temperature, sound pressure level and illuminance x_{10} is expected to exert a negative effect on η_1, such that an increase in indoor temperature will result in a decreased audio-visual influence. The parameter estimate for the three-way interaction x_{10} is found to be negative and significant at 95% confidence (z>1.96, p<0.05). Gregariousness x_1 is expected to exert a negative effect on η_1. The effect of x_1 on η_1 is found to be negative but it is not found to be significant. The interaction between assertiveness and indoor temperature x_2 is expected to be positive, to the extent that an increase in temperature will result in an increased influence of assertiveness on η_1. The two-way interaction x_2 is found to be positive but it is not found to be significant. The interaction between gregariousness and occupancy count x_3 is expected to be positive, such that an increase in occupancy count will result in an increased influence of gregariousness on η_1. The two-way interaction x_3 is found to be significant at approximately 95% confidence (z>1.96, p<0.05). As a result, hypotheses $M1$, $M2$, $I1$ and $I3$ are not rejected.

3.2 binary classification

The outcome of the predictive modelling phase are four models; LR, L-SVM, RF and RBF-SVM. LR is fitted as shown in equation (1). The polarity of the parameter estimates is consistent with hypotheses $M1$, $M2$, $I1$ and $I3$, suggesting the model learned a similar pattern to the one captured using SEM.

$$P(Y = 1|X) = \frac{exp(-0.27+0.29X_0+0.30X_2-0.13X_3+0.17X_4+0.23X_5)}{1+exp(-0.27+0.29X_0+0.30X_2-0.13X_3+0.17X_4+0.23X_5)} \quad (1)$$

Fig. 3 shows the confusion matrix, obtained by running LR, L-SVM, RF and RBF-SVM on the test set. The number of true predictions for the four models ranges between 42 and 46. The large number of false negative predictions, ranging between 19 and 25, suggests that all four models have difficulty predicting thermal discomfort.

Actual value	Predicted value: 1		Predicted value: 0	
	TP		FN	
Discomfort: 1	LR	22	LR	25
	L-SVM	28	L-SVM	19
	RF	23	RF	24
	RBF-SVM	25	RBF-SVM	22
	FP		TN	
Comfort: 0	LR	9	LR	21
	L-SVM	12	L-SVM	18
	RF	11	RF	19
	RBF-SVM	11	RBF-SVM	19

Fig. 3 – Confusion matrix for the test set.

Tab. 5– Performance metrics (validation and testing).

Model	Set	*AUC*	*ACC*	F_1
LR	Valid	0.58	0.56	0.53
	Test	0.68	0.56	0.56
L-SVM	Valid	0.58	0.61	0.61
	Test	0.67	0.55	0.55
RF	Valid	0.62	0.60	0.60
	Test	0.64	0.58	0.59
RBF-SVM	Valid	0.57	0.52	0.48
	Test	0.66	0.57	0.58

The performance metrics for the validation and testing phases are reported in **Tab. 5**. The difference in performance across the models is very slight and all four models yield similar scores across all three metrics. While L-SVM and RF show better *ACC* and weighted F_1 on the validation set, they no longer outperform the other models on the test set. The increase in ACC during the testing phase for all four predictive models could be attributed to random variation between data splits. The predictive performance of the models is just above random guessing (= 0.50) and is not sufficient for predicting thermal (dis)comfort.

4. Explaining thermal comfort

The interpretation of the SEM model addresses the hypotheses $M1 - M3$ and $I1 - I3$. The model estimates do not reject $M1, M2, I2$ and $I3$, leading to several implications that may be of interest to the understanding of thermal comfort in offices:

- During the cooling season, an increase in indoor temperature results in an exponential increase in thermal discomfort.
- An increase in sound pressure level results in an increase in thermal discomfort.
- An increase in air temperature decreases the effect that the interaction between sound pressure level and illuminance has on thermal discomfort, resulting in a negative three-way interaction.
- An increase in occupancy count increases the effect of occupant gregariousness on thermal discomfort, resulting in a positive two-way interaction.

The fit indices and the polarity of the parameter estimates support the notion that the model may be used to explain thermal comfort. However, the existence of a near-equivalent model is likely. The reliability of the subjective data, particularly assertiveness and gregariousness, is questionable. A better fit may be achieved via the use of a more extensive and well-known scale, such as the IPIP-NEO-120 [12].

5. Predicting thermal comfort

The SEM model suggests that P_0-P_5 significantly affect thermal comfort in offices. Yet, the four predictive models are not capable of adequately predicting thermal (dis)comfort. Looking at all four outcomes, the quality of the data may have introduced noise, masking the patterns necessary for making reliable predictions. However, real-world data is noisy and constitutes a pitfall for even the most prevalent models. A predictive model can be expected to perform even worse in practice than it does on the mother data set. The results show that thermal comfort is a complex, multi-domain construct that is difficult to predict. However, the performance of the four predictive models does not cast a definitive shadow over the prospect of accurate prediction. Predictive models that include a larger number of thermal comfort variables and higher quality subjective measurements may yield better predictions. Moreover, other, more advanced modelling techniques, such as stochastic modelling, may be better suited for thermal comfort prediction.

6. Conclusion

This study applies the multi-domain approach to thermal-comfort modelling. An explanatory model is constructed using SEM. The specified model examines the influence of indoor temperature, illuminance, sound pressure level, occupancy count, gregariousness and assertiveness on thermal discomfort. The SEM model is unique, as it is the first explanatory model, derived from field measurements, to include multiple physical and personal variables, while also including contextual variables. The following conclusions are derived from the explanatory model:

- Thermal discomfort increases at higher indoor temperatures and higher sound pressure levels, suggesting that both should be optimized and maintained during the design and operation phase.
- Uncomfortably high indoor temperatures decrease the effect that sound pressure level and illuminance otherwise have in a comfortable thermal environment. This highlights the importance of designing for optimal temperature conditions and constitutes a basis for the use of personalized heating and cooling strategies to optimize individual temperature conditions.
- Gregarious individuals may be more thermally comfortable than non-gregarious individuals when there are many occupants in the room. While it is not feasible to obtain information on personality traits during the design phase, designers are encouraged to account for inter-individual differences by providing flexible working conditions.

Four predictive models LR, L-SVM, RF and RBF-SVM are trained using significant variables P_0-P_5. The models examine the predictive potential of the explanatory model. All models struggle to predict thermal (dis)comfort, despite the inclusion of significant thermal comfort variables. The results bring to light several conclusions:

- Significant thermal comfort influences are not always adequate predictors thereof.
- Researchers are advised to precede future thermal comfort studies with explanatory modelling, to facilitate the creation of predictive models that contain a large variety of physical, contextual, social and non-social variables.
- Combined use of explanatory and predictive modelling is necessary, to test whether variables considered in thermal comfort research hold theoretical relevance, predictive potential, both or, perhaps, neither.

This study is part of a broader research effort to achieve better prediction of thermal comfort in offices, which is an essential step in the building design process. The results formulate a basis for further research on the influence of indoor climate, occupancy and personality traits on thermal comfort in offices, as well as the interaction between the different influences. Moreover, the findings have direct implications for the engineering sector, as they suggest that influences such as sound pressure level, occupancy and personality traits, should be considered when designing for optimal thermal conditions.

6.1 limitations

This research is subject to several limitations, the mitigation of which is encouraged in the future. Firstly, prominent variables such as correlated colour temperature and air velocity are not included in the study. Similarly, variables such as age, relative humidity, clothing insulation and metabolic rate are excluded due to insufficient variability in the measured data. Secondly, extreme indoor conditions are not observed during field measurements. In addition, the measurements are limited to summer conditions in the context of the Netherlands and are not representative of cooler conditions or other climate regions. Due to this limitation, the relationship between temperature and thermal discomfort is assumed to be exponential. Future studies are encouraged to include cold sensation data and thereby model a parabolic relationship between temperature and thermal discomfort, where thermal discomfort increases at lower and higher temperatures both. Thirdly, the internal consistency of the personal variables is poor and they are not sufficiently representative of the Big Five personality traits. Lastly, the quality of the predictive models may be improved via the use of advanced hyper-parameter tuning, a larger variety of machine learning algorithms and more advanced modelling methods.

7. Acknowledgement

The data is provided by the research group of Mark Mobach at the Hanze University of Applied Sciences. The authors acknowledge the contribution of Yasin Toparlar, Deerns Groep B.V.

8. Data access statement

The dataset generated and analysed during the current study is available in the 4TU repository [13].

Appendix A

Tab. A1 – Demographics for offices 1 and 2.

Gender		Office 1		Office 2	
		$\mu \pm \sigma$	N	$\mu \pm \sigma$	N
Male			154		88
	Age	43 ± 10		47 ± 8	
	Clo	0.5 ± 0.1		0.4 ± 0.1	
Female			170		112
	Age	43 ± 10		45 ± 8	
	Clo	0.5 ± 0.1		0.5 ± 0.2	

Appendix B

Tab. B1 - Items, item scales and reliability concerning thermal comfort constructs.

Construct	Item	Likert scale	Cronbach's alpha α
Thermal discomfort			0.83
General discomfort (heat)	It is too hot in here now.	5-point	0.87
Lower body discomfort	I have warm feet.	5-point	0.71
Upper body discomfort	I have warm hands.	5-point	0.69

Tab. B2 - Items, item scales and reliability concerning personality facets.

Construct	Item	Likert scale	Cronbach's alpha α
Gregariousness			0.55
	I prefer to work in a completely open space with several people.	5-point	0.43
	I prefer to work alone in a room. (excluded)	5-point (R)	0.40
	I love working with others. (excluded)	5-point	0.47
	I involve my colleagues in carrying out my work.	5-point	0.57
Assertiveness			0.46
	I can always communicate in an open way.	5-point	
	I adjust my job to the work of my colleagues.	5-point	

9. References

[1]ANSI/ASHRAE. Standard-55-2017 Thermal Environmental Conditions for Human Occupancy. 2017.

[2]I. O. for Standardization. ISO 7730 2005-11-15 Ergonomics of the Thermal Environment: Analytical Determination and Interpretation of Thermal Comfort Using Calculation of the PMV and PPD Indices and Local Thermal Comfort Criteria. International standards. 2005.

[3]Van Hoof J. Forty years of Fanger's model of thermal comfort: Comfort for all? Indoor Air. 2008; 18: 182–201.

[4]Fanger P. O., Thermal comfort: Analysis and applications in environmental engineering. Copenhagen: Danish Technical Press. 1970.

[5]Schweiker M., Ampatzi E., Andargie M. S., Andersen R. K., Azar E., Barthelmes V. M., Berger C., Bourikas L., Carlucci S., Chinazzo G., Edappilly L. P., Favero M., Gauthier S., Jamrozik A., Kane M., Mahdavi A., Piselli C., Pisello A. L., Roetzel A., Rysanek A., Sharma K., Zhang S. Review of multi-domain approaches to indoor environmental perception and behaviour. Build. Environ. 2020.

[6]Mamulova E., A Multi-Domain Approach to Thermal Comfort in Office Buildings. Master thesis. Eindhoven University of Technology, Eindhoven, The Netherlands. 2021. https://pure.tue.nl/ws/portalfiles/portal/167630476/Mamulova_1371118_BPS.pdf

[7]Brink H. W, Mobach M.P., Quality and satisfaction of thermal comfort in Dutch offices. Proc. 15th EuroFM Res. Symp. 2016; 162-171.

[8]Newsom J. LISREL Matrix Notation. 2012.

[9]Rosseel Y. lavaan: An R Package for Structural Equation Modeling. J. Stat. Softw. 2012: 48.

[10]Pedregosa F., Varoquaux G., Gramfort A., Michel V., Thirion B., Grisel O., Blondel M., Prettenhofer P., Weiss R., Dubourg V., Vanderplas J., Passos A., Cournapeau D., Brucher M., Perrot M., Duchesnay E. Scikit-learn: Machine learning in Python. J. Mach. Learn. Res. 2011; 12: 2825–2830.

[11]Bergstra J., Bardenet R., Bengio Y., Kégl B. Algorithms for hyperparameter optimization. Advances in Neural Information Processing Systems. 2011; 24: 2546-2554.

[12]J. A. Johnson J. A. Measuring thirty facets of the Five Factor Model with a 120-item public domain inventory: Development of the IPIP-NEO-120. J. Res. Pers. 2014; 51: 78–89.

[13]Mamulova E., Brink H. Dataset for SEM analysis. 4TU.ResearchData. Dataset 2022. https://doi.org/10.4121/19403912

The value of user feedback to improve the indoor environment in offices

Merlijn Huijbers [a], *Marije te Kulve* [b]

[a] DGMR B.V., The Hague, The Netherlands, mhu@dgmr.nl.

[b] bba binnenmilieu, The Hague, The Netherlands, mk-bba@binnenmilieu.nl.

Abstract. A healthy, stimulating and comfortable office building positively influences health and the productivity of employees. To determine the indoor environmental quality of a building, indoor environmental parameters in buildings are often measured. While measurements are important, they do not give full insight in the indoor environmental quality of a building and often do not provide complete insight in the causes of potential problems.
Since the requirements for a good indoor environment depend on the type of activities that take place in the building and on the preferences of individuals, the feedback of the building occupants should be included in the assessment. Moreover, this contributes to the interpretation of indoor environmental data. We have started collecting data on user feedback, in which building characteristics and the approximate location of users is included, in a systematic way. This makes it possible to easily compare the results of different buildings. The results show among others that the motive to apply the survey appears to be, to a certain extent, a predictive factor in the satisfaction rates: buildings that aim for sustainability- or health certification score highest. The lowest satisfaction rates for indoor environmental parameters are observed for temperature and acoustics. For all parameters, respondents were more satisfied when they perceived control over it. Sharing a workplace with an increasing number of people decreases satisfaction with acoustics and people report a negative impact on concentration. This observation calls for re-evaluation of modern office layouts. In case studies, the results of the questionnaire can be combined with the characteristics of the building to obtain insight in possible risk factors and provide solutions to indoor environmental challenges. Overall, all data collected will be used to define a reference value. By expanding the database, more analyses can be performed to better understand the relation between building characteristics, indoor environment and user satisfaction.

Keywords. User-feedback, offices, indoor environment, health, comfort, risk factors
DOI: https://doi.org/10.34641/clima.2022.311

1. Introduction

What defines a comfortable building and how to design one? It would be great if one could present a clear definition and a set of golden design rules that, by applying them correctly, would always lead to an office building in which building occupants are satisfied with the indoor environment and where their activities and mood are positively affected. In practice this unfortunately is not always the case: overall satisfaction with the indoor environment in offices is often low (e.g. [1-2]) The requirements for a good indoor environment largely depend on the type of activities that take place in the building and on the preferences of the building occupants.

1.1 Measuring and monitoring

A comfortable office building positively influences health and the productivity of employees. To demonstrate whether a building is comfortable, measurements of indoor environmental parameters such as temperature, humidity, CO_2-concentration, fine particles, light intensity and Volatile Organic Compounds (VOC's) are performed. These measurements are important and give valuable information about the indoor environment. They do however not give full insight in the building performance, since a lot of parameters that also affect the employee experience are not included. When combined with user feedback, collected indoor environmental data becomes much more valuable. As a result, expensive measurements to identify problems in a building and to confirm hypotheses

Copyright ©2022 by the authors. This conference paper is published under a CC-BY-4.0 license.

regarding the cause of these problems, can be applied more targeted. This approach is also known as the building in use method [3].

When adding user feedback, the collected data of the measurements can be interpreted better and the perceived quality of aspects that are difficult to measure during occupation, such as quality of light and acoustics, can be determined.

Continuously changing working methods, office layouts, building characteristics combined with cultural differences, result in time- and place-dependent outcomes of user feedback surveys. Because of these continuously changing factors it is important to keep including contemporary data to the databases. A database such as that of the Healthy Building Index can be used to learn which aspects are important for user satisfaction and which building characteristics might be labelled as risk factors.

1.2 Collecting user feedback

To collect user feedback in a systematic way, use of a thorough survey tool is recommended. For our research we used the "Healthy Building Index tool", in which user feedback on four indoor environmental parameters (light, temperature, indoor air quality and acoustics) is collected. Based on the results a Healthy Building Index of the building is determined that expresses the satisfaction of the building users with the indoor environment in their building, figure 1. The index varies between 100 and 1000 and, to give an idea of the value of the score in comparison to that of an average office building, the reference value of the database is included.

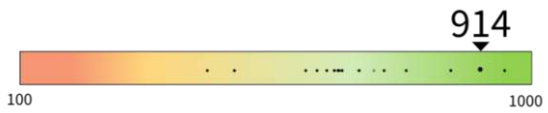

Fig. 1 – The Healthy Building Index

For each indoor environmental category the satisfaction rate is defined and presented to the building owner and/or -occupants, figure 2.

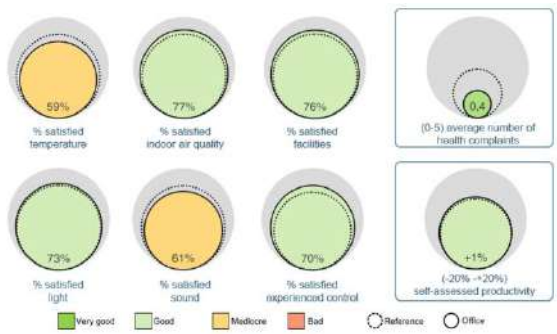

Fig. 2 – Partial results of the Healthy Building Index tool

1.3 Research objectives

What can we learn from the data collected? The purpose of this data analysis is to:

- provide insight into the satisfaction rates within the buildings.
- provide insight into the factors that influence satisfaction with the indoor environment.
- show the added value of collecting contemporary user feedback in order to continue to realize healthy and comfortable buildings.
- Determine the implications for future building design.

2. Method

2.1 Data collection

From the start of 2020 user feedback was collected from 710 respondents in thirteen office buildings using an online survey tool (*name will be added after review*) about their satisfaction with the indoor environment. The motivation to apply the survey differed between the buildings investigated. From all buildings evaluated, two buildings aimed for a WELL building certificate, six buildings were evaluated to map the indoor environmental status of the building, four buildings used the survey as input for their planned renovation and in one building the survey was used to systematically map the complaints about the indoor environment in order to take measures to solve possible problems. Respondents were invited via email to complete the questionnaire within two weeks. An overview of the buildings investigated and the number of respondents is indicated in Table 1.

Tab. 1 – Motivation to apply survey.

Building	Number of respondents	Motivation to apply survey
#1	21	Complaints
#2	56	Pre-renovation
#3	30	Pre-renovation
#4	41	Pre-renovation
#5	49	Pre-renovation
#6	16	IEQ status
#7	36	IEQ status
#8	139	IEQ status
#9	108	IEQ status
#10	56	IEQ status
#11	20	IEQ status
#12	58	WELL
#13	80	WELL

2.2 Survey

In all buildings the same questionnaire was used. The questionnaire focusses on four indoor environmental parameters: temperature, air quality, light and acoustics. Respondents were asked how satisfied they were with each parameter at their workstation on a 7 point scale from "Very dissatisfied" (1) to "very satisfied" (7). If respondents indicated they were not satisfied, score 1, 2 or 3, they were asked which aspects contributed to their dissatisfaction. For each theme, satisfaction rates per building were calculated; being the percentage of respondents who answered "neutral"(4) or higher, as applied in the CBE questionnaire [2]. Additionally building users were asked if they suffered from building related health symptoms (yes or no). If yes, a list of symptoms was provided, in which they could indicate which symptoms they suffered from. Finally respondents were asked to indicate how important each indoor environmental parameter is to them (1 "not important" to 5 "extremely important") and how much control they experience over each indoor environmental parameter (1 "no control at all" to 7 "full control"). The survey furthermore includes questions regarding the general location and characteristics of the workplace, the activities carried out and the amount of time spent in the building.

2.3 Data analyses

Data was analysed to map the average satisfaction rates with the indoor environment and to obtain insight in factors that influence the experience with the indoor environment. Using the satisfaction rate (percentage of people satisfied with one parameter) of each building, the average satisfaction rate for all indoor environmental parameters was calculated. Differences between parameters were compared using a two tailed t-test.

To analyse differences between groups, based on the answers given in the questionnaire (for example number of people who work together in a room), a two tailed t-test was used for the ordinal variables. Bi-nominal variables were compared using a Chi-squared test. A p-value <0.05 was considered to be statistically significant and indicated with * in the figures. The static analyses were performed in Microsoft Excel version 2102.

3. Results

3.1 Overall satisfaction rates

Based on the average satisfaction rates per building, it was observed that satisfaction of the respondents per indoor environmental parameter significantly differs. The percentage of respondents who indicated being satisfied with 'light' (77%) and 'air quality' (69%) at their workplace was higher compared to 'temperature' (56%) and 'acoustics' (52%). (Figure 3).

The motive to apply the survey appears to be, to a certain extent, a predictive factor in the satisfaction rates. Explorative analysis of the data shows that from all buildings evaluated, the two buildings that aimed for a WELL building certificate had the highest satisfaction rates for temperature, indoor air and acoustics, followed by the buildings that were evaluated to map the indoor environmental status of the building (except for acoustics) (Figure 4). Third are the buildings that used the survey as input for their planned renovation. As expected, in the building (n=1) in which the survey was used to systematically map the complaints about the indoor environment in order to take measures to solve possible problems, the satisfaction rates were the lowest. The differences are most pronounced for the satisfaction rates of temperature and indoor air quality. The satisfaction rates of light do not seem to be different among these groups. The number of buildings in each group was too small to perform statistical analyses.

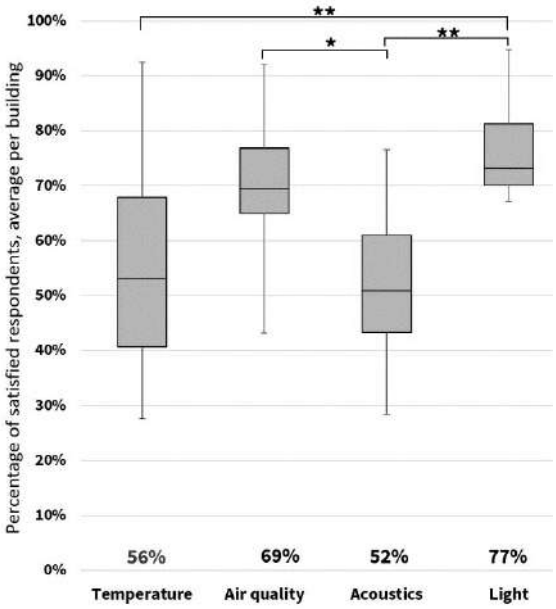

Fig. 3 – Box plots show the average satisfaction rates per theme based on the average per building.

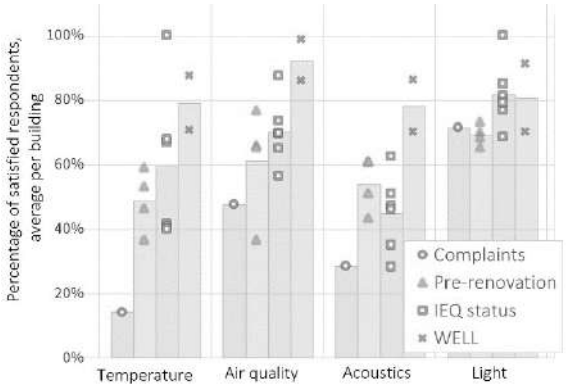

Fig. 4 – Satisfaction rates per theme differentiated among motives of applying the survey.

3.2 Importance and perceived control

The respondents rated "temperature" and "indoor air quality" as being the most important indoor environmental parameters. Differences among the parameters were small. Still "light" and "acoustics" were rated slightly but significantly less important ($p<0.05$ for all comparisons) (Figure 5). Surprisingly, the parameter "control over the indoor environment" was rated least important ($p<0.01$).

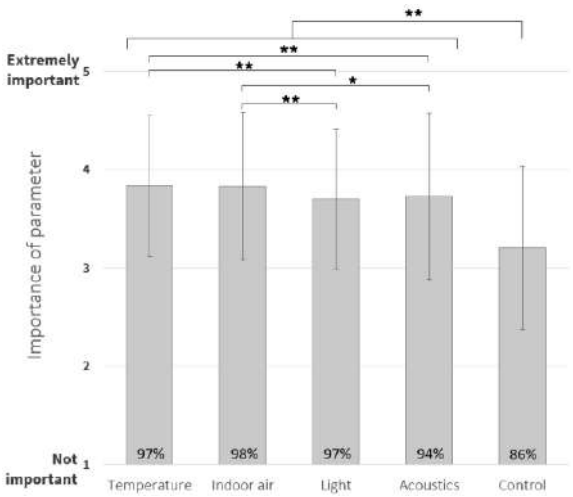

Fig. 5 – Importance of each indoor environmental theme. Percentage indicate rating "3" or higher.

The relation among the indicated importance and the satisfaction rate of each parameter is illustrated in figure 6. It shows, for all parameters, that the percentage of respondents that is satisfied, is highest for the respondents that indicated that parameter to be "not important" or "somewhat important'". The percentage of people satisfied is lowest for the respondents that indicated the parameter to be "extremely important".

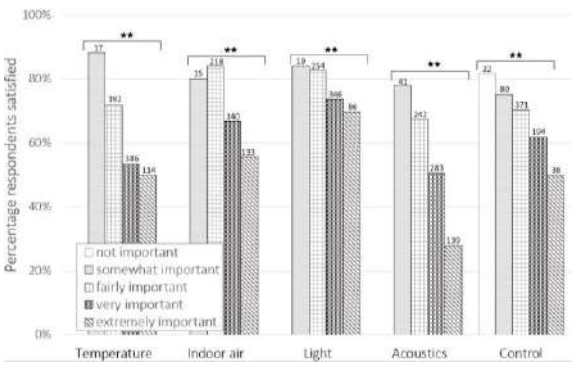

Fig. 6 – Importance of each indoor environmental parameter compared to satisfaction rates per parameter.

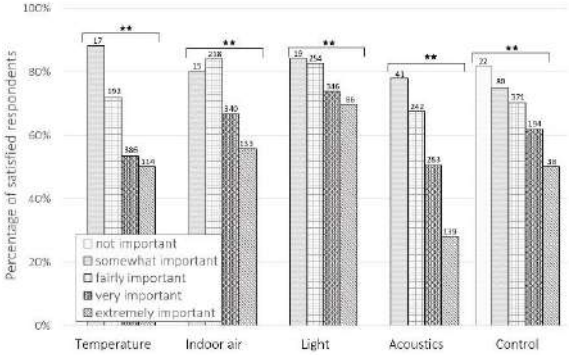

Fig. 7 – Perceived control over the indoor environment and corresponding satisfaction rates.

The level of perceived control affects the satisfaction rates per theme (Figure 7). For all parameters, respondents were significantly more satisfied when they indicated to have "reasonable control" (5), "high level of control" (6) and "full control" (7) as compared to "some control" (4) or "no control" (1) to "little control" (3) (Table 2 a - c).

3.3 Impact number of people working together

The number of people that work together in one room, significantly affects satisfaction with acoustics in the workplace (Figure 8). The more people working together in the same work space, the lower the satisfaction rate. However, the size of the standard deviation illustrates that more factors are involved. Satisfaction with the parameters temperature, light and air quality, was not affected by the number of people working in the room, see table 3.

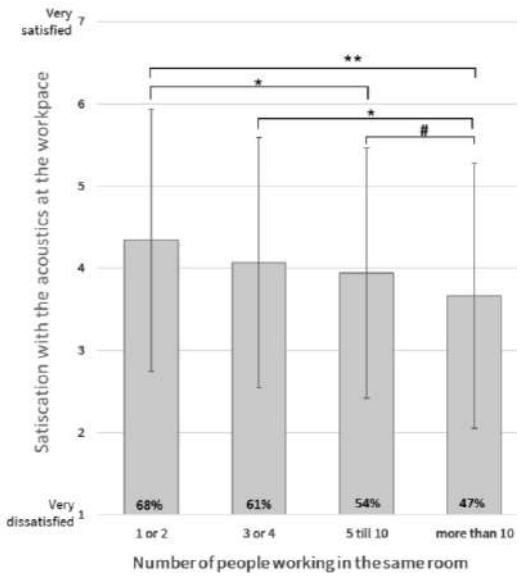

Fig. 8 – Satisfaction with the acoustics at the workplace. Percentages indicate the satisfaction rates.

Tab. 2a – Satisfaction scores of respondents experiencing "no control" to "little control".

		Group A	
		No control (1) to little control (3)	
		Avg ± stdev	**N**
Satisfaction	Temperature	3,6 ± 1,6	399
	Indoor air	4,1 ± 1,4	402
	Light	4,4 ± 1,5	352
	Acoustics	3,3 ± 1,3	413

Tab. 2b – Satisfaction scores of respondents experiencing "some control". Significant differences are indicated in bold.

		Group B		
		Some control (4)		
				A vs B
		Avg ± stdev	**N**	**p-value**
Satisfaction	Temperature	4,3 ± 1,4	183	**<0,01**
	Indoor air	4,4 ± 1,3	135	**0,02**
	Light	4,6 ± 1,3	203	0,73
	Acoustics	4,4 ± 1,3	185	**<0,01**

Tab. 2c – Satisfaction scores of respondents experiencing "reasonable control" to "full control". Significant differences are indicated in bold.

		Group C		
		reasonable (5) - full control (7)		
				B vs C
		Avg ± stdev	**N**	**p-value**
Satisfaction	Temperature	5,4 ± 1,4	123	**<0,01**
	Indoor air	5,6 ± 1,3	93	**<0,01**
	Light	5,8 ± 1,1	145	**<0,01**
	Acoustics	5,6 ± 1,2	97	**<0,01**

Tab. 3 – Satisfaction score (average ± standard deviation) of all respondents grouped by the number of people working together in one room. Observations that significantly differ from the other categories for one parameter are indicated in bold.

	Number of people working in the same room			
	1 or 2	3 or 4	5 to 10	more than 10
Temp.	4,1 ± 1,6	4,4 ± 1,5	**3,8 ± 1,6**	4,2 ± 1,7
Indoor air	4,3 ± 1,6	4,4 ± 1,4	4,2 ± 1,4	4,4 ± 1,5
Light	4,6 ± 1,7	4,7 ± 1,6	4,8 ± 1,5	4,7 ± 1,5
Acoust.	**4,3 ± 1,6**	**4,1 ± 1,5**	**3,9 ± 1,5**	**3,7 ± 1,6**

Conversations in adjacent rooms, conversations in the own room and disturbing reverberation of voice were indicated most often as being (one of) the cause(s) for dissatisfaction with the acoustics in the room. These causes for dissatisfaction were, together with noise from installations, mentioned more often by respondents that shared a work place with an increasing number of people (figure 8).

People working in larger rooms reported a higher amount of concentration problems (figure 10). Though a tendency was observed that people that work in larger rooms, more often have one or more building related health symptoms, this difference was not significant (figure 11).

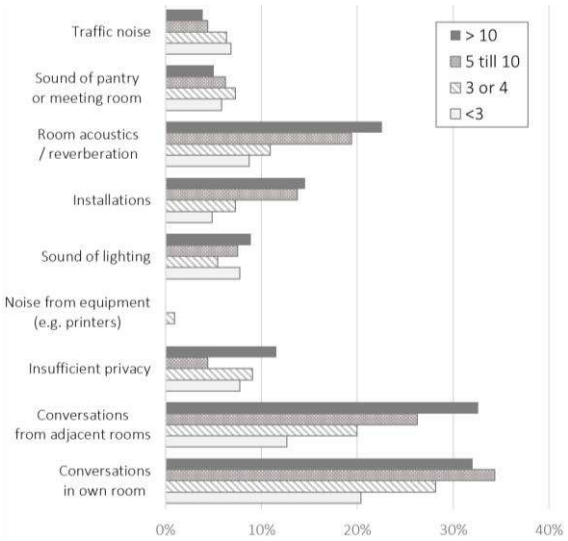

Fig. 9 – Reasons indicated to be dissatisfied with the acoustics, grouped by number of people working in one room.

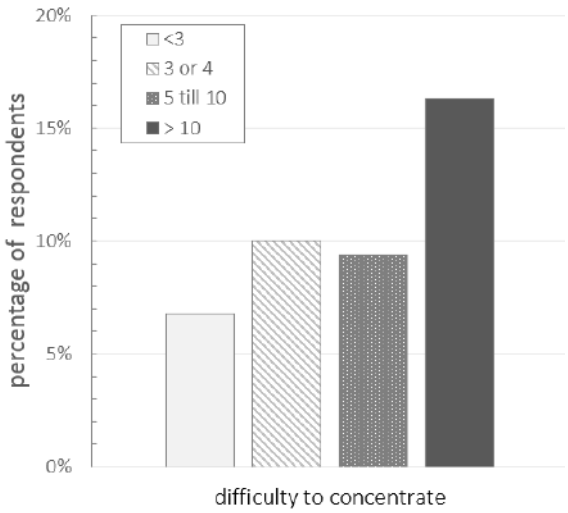

Fig. 10 – Impact of number of people working together on reported concentration problems

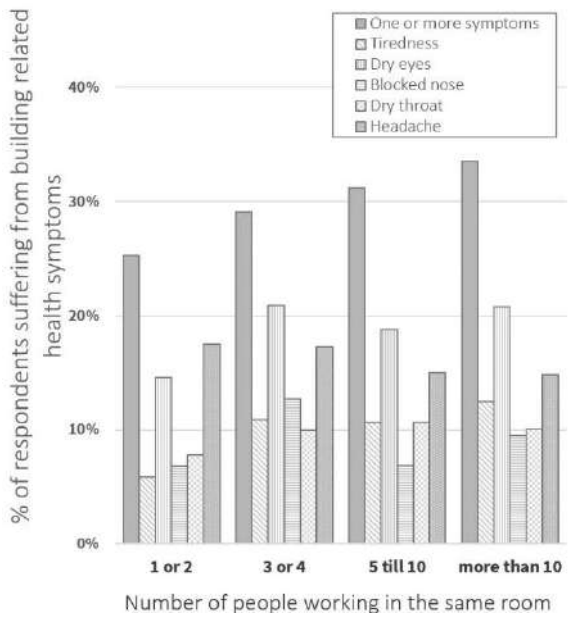

Fig. 11– Impact of number of people working together on reported health problems

4. Discussion

Based on the data analysed, the lowest satisfaction rates were observed for temperature (56%) and acoustics (52%). These parameters are also rated lowest in de CBE database. The satisfaction rates of the current study are lower as compared to the data from occupant surveys by CBE (containing approximately 90.000 respondents from 900 buildings): satisfaction with sound privacy (46%), temperature (61%) and noise level (66%) [2]. In both databases satisfaction rates of indoor air quality and light were higher. Due to the relative small number of buildings in the database analysed, the average values might be affected by the type of buildings included. Already within this small dataset, we observed a tendency that satisfaction rates are lower when user feedback is used as input for renovation of the building or to solve indoor environmental problems as compared to buildings that aim for a WELL Building Certificate or that want to map the satisfaction with the indoor environment just to obtain insight in the current status. This might not be surprising, but it illustrates the importance of a representative sample when drawing general conclusions based on satisfaction rates in office buildings.

Outcomes of the survey show that there is a relation among how important respondents rate a certain indoor environmental parameter and their satisfaction about that parameter. In general, respondents indicate to be less satisfied about the parameters they rate as being most important at their workplace. Whether this is because parameters become more important when you are not satisfied or because one is more critical about aspects which are important to him/her (or both) remains to be explored. The impact of control on the satisfaction rates are in line with the data analyses of the HOPE database [4] and an explorative study on the role of perceived control [5], the results show a clear positive impact of perceived control over the indoor environment on the satisfaction ratings with the indoor environment. Moreover, a recent field study in 167 buildings Europe, indicates the importance of control over the indoor environment on overall comfort and building-related symptoms [6] and self-estimated productivity [7]. These observations advocate for control opportunities over the indoor environment. Though it should be noted that care should be taken that available control opportunities also lead to an increased perception of control.

As expected, it was observed that lower satisfaction with acoustics is related to sharing a work place with a large number of people. These findings call for a careful reassessment of the layout of larger office spaces in future designs to improve user satisfaction, with attention to the type of work that will be performed and the required privacy for the employees. Especially conversations of colleagues in the same (30%) or adjacent rooms (26%) are factors that negatively affect user satisfaction. These percentages are in line with a 30-year old field study in 61 Dutch offices, containing 7000 respondents, that observed a complain rate of 33% about conversation in the same room and 20% in adjacent rooms [8].

The current database used for the analysis in this paper is still growing but already offers insights in experience of the indoor environment in offices and influencing factors. To be able to study the influence of building related factors, the dataset needs to be extended to a larger number of buildings with characteristics that are representative for current office buildings. The aim is to expand the number and type of buildings assessed to enable including the effect of building characteristics such as HVAC- and heating systems on user satisfaction in future analyses.

Next to conducting new analyses, it is recommended

to combine the results of the questionnaire with measurements of the indoor environment of the buildings. The combination of both sources of indoor environmental data will lead to an even better understanding of buildings.

5. Conclusion

A systematic approach to collect user feedback allows for meta analyses of the data to gain insight in user satisfaction and causes for dissatisfaction. In the current analyses, it was observed that average satisfaction rates are likely to differ among different type of buildings (for example pre and post renovation). Also, perceived control over- and self-rated importance of the indoor environmental parameters relate to user satisfaction. Expanding the database and including building characteristics and continuous measurements in the analyses, enables risk factor analyses.

As stated at the beginning of this paper, without user feedback some indoor environmental parameters (especially light and acoustics) are hard to map using continues measurements. Therefore it is not possible to make adjustments to better meet the needs of the building users regarding these parameters. In the buildings discussed in this paper, satisfaction about acoustics was low. Through the use of the survey this information has become available, including the most important causes for dissatisfaction per building. This allows for tailor-made measures for each office regarding acoustics, in order to better suit the requirements of the building users. This will likely benefit their health, well-being and productivity.

The coming years, the database will be expanded to be able to conduct more targeted and extensive follow-up research, among others on the correlation between perceived and available control and health related symptoms. With a more robust database, satisfaction- and complaint rates can be used to define a custom made, contemporary reference for office buildings. In practice, these references are of great value in communicating with managers / owners about the quality of the indoor environment in their building. Both follow-up research and an updated reference building will contribute to improving the quality and overall user satisfaction rates of the contemporary office building.

6. Acknowledgement

[Will be added in the after double review.]

7. References

[1] Brunia, S. and Beijer, M. (2014) Trends in werkplekbeleving. Center for people and buildings.

[2] Graham, L.T., Parkinson, T., Schiavon, S. (2020). Lessons learned from 20 years of CBE's occupant surveys.

[3] Vischer, J. C. (2018). Building-in-use assessment: Foundation of workspace psychology. In Building Performance Evaluation (pp. 129-139). Springer, Cham.

[4] Boerstra, A., Beuker, T., Loomans, M., & Hensen, J. (2013). Impact of available and perceived control on comfort and health in European offices. Architectural Science Review, 56(1), 30-41

[5] Hellwig, R. T. (2015). Perceived control in indoor environments: a conceptual approach. Building Research & Information, 43(3), 302-315.

[6] Sakellaris, I., Saraga, D., Mandin, C., de Kluizenaar, Y., Fossati, S., Spinazzè, A., ... & Bartzis, J. (2019). Personal control of the indoor environment in offices: Relations with building characteristics, influence on occupant perception and reported symptoms related to the building—The officair project. Applied Sciences, 9(16), 3227

[7] Chen, C. F., Yilmaz, S., Pisello, A. L., De Simone, M., Kim, A., Hong, T., ... & Zhu, Y. (2020). The impacts of building characteristics, social psychological and cultural factors on indoor environment quality productivity belief. Building and Environment, 185, 10718

[8] Zweers, T., Preller, L., Brunekreef, B., & Boleij, J. S. M. (1992). Health and indoor climate complaints of 7043 office workers in 61 buildings in the Netherlands. Indoor Air, 2(3), 127-136.

The datasets generated during and/or analysed during the current study are not available, because when obtaining the data it has been confirmed to the clients, based on privacy regulations, that the data will not be published or will not be accessible to anyone but the organisation that performed the user feedback survey.

Assessment of the infection risk distribution of COVID-19 and ventilation energy consumptions in indoor environments

Marco Marigo [a], Giacomo Tognon [a], Michele De Carli [a], Angelo Zarrella [a]

[a] Department of Industrial Engineering, University of Padova, Italy. E-mail: marco.marigo.3@studenti.unipd.it

Abstract. The energy use for ventilating buildings involves high economic and primary energy consumption costs. Nevertheless, ventilation is essential, especially in public places, to ensure acceptable Indoor Air Quality (IAQ) levels and reduce the risk of airborne virus infection. The latter aspect has recently increased because of the ongoing COVID-19 pandemic. In this paper, a model that couples a zonal ventilation model with infection risk calculation is integrated with an energy consumption model to analyse the energy consumption and infection risk from COVID-19 at different ventilation flow rates for three case studies: an office room, a high school and a university classroom. The main results show that the increase in ventilation flow rate involves reducing risk, but it increases energy consumption. Moreover, the mask-wearing resulted in having a relevant effect, whereas the effect of the relative position difference inside the room was not detected with the proposed discretisation.

Keywords. HVAC, risk assessment, COVID-19, ventilation, indoor air quality, energy consumption, building energy model.
DOI: https://doi.org/10.34641/clima.2022.80

1. Introduction

Buildings are one of the leading energy consumption sectors in Europe. In 2018, they were responsible for 40% of final energy use and the consequent greenhouse gas emissions into the atmosphere, leading to a significant environmental impact [1].

People spend most of their time in indoor spaces, so fulfilling a good indoor environmental quality (IEQ) is primarily important to guarantee their wellness. Thermal comfort and indoor air quality (IAQ) are provided by the HVAC system of the building. In particular, the supply of outdoor air by ventilation is fundamental to replace stale indoor air, thus removing pollutants. In the case of mechanically ventilated buildings (full-air or primary air systems), the consumptions are those related to air handling unit operation, namely thermal energy required at the heating and cooling coils and fan electrical absorption to supply it to the indoor environment.

The salubrity of indoor environments has become the main topic with the beginning of the COVID-19 pandemic, caused by the spread of SARS-CoV-2, whose existence was first reported to the WHO Country Office in China on 31st December 2019 [2]. According to the current knowledge, the disease transmission mainly occurs by contact with infected subjects or contaminated surfaces (fomites) and large exhaled droplets [3]. The airborne transmission caused by suspended virus-laden microdroplets is a third possibility. Its relevance in indoor environments is increasingly recognised after the documentation of COVID-19 outbreaks [4,5].

The airborne infection route is the result of subsequent phases: infectious aerosol generation, transport and inhalation [6]. Droplet nuclei are generated by the infected subject through common respiratory activity, such as breathing, talking, coughing, sneezing. Ventilation and air distribution systems play a key role in transporting pathogens, determining their spread across the available space, dilution and removal. Therefore, ventilation has been immediately recommended as a suitable mitigation strategy against the airborne transmission of the disease, along with personal protection devices and social distancing [3].

Different approaches have been proposed to model the airborne transmission of respiratory diseases in indoor spaces. All methods aim at determining the concentration of infectious material that a susceptible individual could inhale. The most accurate analyses are provided by CFD simulations, as they can define precisely the airflow patterns, but they require high computational resources [7]. On the other hand, simple mathematical models have been developed to calculate the airborne infection risk and investigate the effectiveness of the countermeasures. Among these, the Wells-Riley

Copyright ©2022 by the authors. This conference paper is published under a CC-BY-4.0 license.

equation and its modifications are widely used for the current pandemic. It is based on the concept of infectious quantum, a hypothetical dose unit that makes 63.2% of an exposed population sick. The indoor space is considered as perfectly mixed and an exponential probability equation is used to calculate risk [8]. Despite their simplicity, they can be used to quickly estimate suitable ventilation rates for risk mitigation in a given situation.

Nevertheless, risk models do not consider the energy needs for air handling associated with an increase in the air change rates. Recently, several researchers have focused on the double effect of ventilation rate on infection and energy consumptions trends. Schibuola and Tambani estimated the reproduction number (number of secondary infections per infected person) in two naturally ventilated Italian schools, by monitoring the CO_2 concentration. They proposed an high efficiency air handling unit to achieve both risk mitigation and contained energy needs [9]. Wang et al. analysed the effectiveness of a smart ventilation control based on occupant density in mitigating the airborne transmission of SARS-CoV-2 and saving ventilation energy. Compared to a traditional system with fixed outdoor air ratio, the infection probabilty was lowered up to 2 %, and 11.7 % of consumptions saving was obtained [10].

This paper evaluates the effect of outdoor air supply on infection risk and energy consumption. For the first aspect, a risk zonal model for assessing the infection probability from COVID-19 in indoor environments is presented. It originates from the need to abandon the usual assumption of a well-mixed space since it involves a macro-discretisation of the interested domain into different cells, as proposed in [11]. The main purposes are analysing the effect of increasing the ventilation flow rate on airborne transmission and observing the spatial variation of risk. Successively, the rise in the energy needs for air handling is determined to investigate the drawbacks of this mitigation strategy. The model has also been applied to verify the benefits of wearing masks in lowering infection risk. In Section 2, the model and calculation method are illustrated. The procedure is applied to three different single rooms; the case studies are presented in Section 3. Finally, the obtained results and considerations are summarised in Section 4.

2. Method

In this section, the development of a risk zonal model is presented. It couples a zonal ventilation model to the infection risk calculation. The former applies a macro-discretisation of the indoor space into multiple cells in order to define the interzonal airflows transporting the infectious aerosols. The second step assesses the airborne infection probability within each cell through a risk equation.

2.1 Zonal ventilation model

The application of the zonal model is aimed at the definition of the air movements within the environment concerned. It provides an intermediate approach between nodal modelling and CFD analyses [12]. The POMA model (Pressurized ZOnal Model with Air Diffuser) was applied in this work (Haghighat et al., 2001), whose principle is to subdivide the geometrical domain into well-mixed cells or zones.

The model is founded on some basic assumptions. The discretisation grid comprises parallelepiped-shaped cells, so there are only vertical and horizontal interfaces. Each zone is well-mixed in temperature and density, whereas the pressure is hydrostatically distributed, starting from a reference value at the bottom level. The thermodynamic properties are correlated by the ideal gas law.

Regions affected by thermal plumes and wall boundary layers are not modelled. Jets model does not consider the spatial effect, but supply and return airflows are assumed as input parameters in the mass balances of the zones where diffusers and grilles are placed. Therefore, each cell is surrounded by two types of boundary surfaces: normal interfaces of separation with adjacent zones, and, for the outer zones, wall boundaries interested only by heat exchanges. Mass and heat flows are modelled for each boundary.

As regards the interzonal mass flows, they are calculated as a function of the static pressure difference across the normal boundary, through the well-known Power Law (Eq. (1)):

$$\dot{m} = \rho\, k\, A\, \Delta P^n \qquad (1)$$

Parameters k and n are the flow coefficient (i.e., permeability of the boundary) and the flow exponent, respectively. For k, a value of 0.83 m s^{-1} Pa^{-n} is taken from previous studies [13], while for n a value of 0.5 is assigned considering turbulent airflow.

The horizontal boundaries present a constant pressure difference along the interface, between the reference pressure of the upper zone and the pressure at the summit of the lower one. Conversely, vertical boundaries are characterised by a variable pressure difference along the surface due to the linear pressure distributions at both sides (Fig.1).

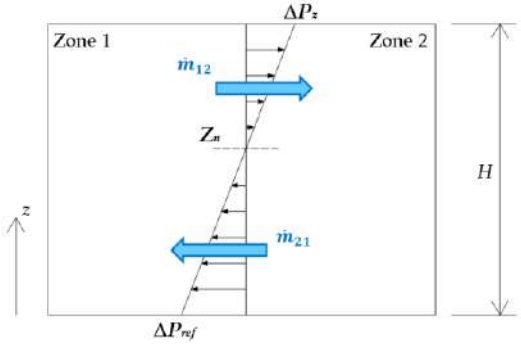

Fig. 1 – Vertical pressure distribution and neutral plane between adjacent cells.

In this case, a neutral plane Z_n is defined as the height at which opposite pressures equalise, leading to a null horizontal airflow across that point. The neutral plane position is determined through Eq. (2), and the mass flowrates, above and below it, are calculated integrating the Power Law along the vertical coordinate (Eqs. (3)-(4)):

$$Z_n = \frac{\Delta P_{ref}}{g\ \Delta\rho} \tag{2}$$

$$\dot{m}_{0-Z_n} = \rho_{0-Z_n}\ k\ L\ |g\ \Delta\rho|^n\ \frac{|Z_n|^{n+1}}{n+1} \tag{3}$$

$$\dot{m}_{Z_n-H} = \rho_{Z_n-H}\ k\ L\ |g\ \Delta\rho|^n\ \frac{|Z_n-H|^{n+1}}{n+1} \tag{4}$$

where L is the depth of the vertical interface, $m_{0\text{-}Zn}$ is the mass flowrate crossing the interface portion from 0 to Z_n, whereas $m_{Zn\text{-}H}$ is that crossing the section from Z_n to H.

In energy transfers, radiative heat exchanges and solar radiation are neglected. The contribution of internal heat gains (people, electrical appliances) is neglected. Referring to each i-th cell, the only heat flows are those related to the enthalpy carried by the interzonal mass flowrates (Eq. (5)) and the heat exchange with the outdoor environment through the building envelope by conduction and convection (Eq. (6)).

$$q_{ji} = \dot{m}_{ji}\ c_{p,air}\ \left(T_j - T_i\right) \tag{5}$$

$$q_{transm,i} = U\ A_{wall}\ \left(T_i - T_{air,ext}\right) \tag{6}$$

U is the thermal transmittance of the building structure and $T_{air,ext}$ is the external air temperature.

For each zone i, along with the ideal gas law, mass and energy balance equations are set under steady-state conditions (Eqs. (7)-(8)), obtaining a nonlinear system.

$$\sum \dot{m}_{ji} - \sum \dot{m}_{ij} + \dot{m}_{sup} - \dot{m}_{rem} = 0 \tag{7}$$

$$\sum q_{ji} - q_{transm,i} = 0 \tag{8}$$

After solving the system, the interzonal mass and volumetric flow rates can be explicitly computed reapplying the Power Law equations.

2.2 Risk assessment model

The airborne infection risk calculation is performed for each cell. The amount of aerosolised pathogens is expressed in terms of quanta. It is assumed that outdoor air does not contain infectious quanta. The infected source quanta exhalation rate is specific for the considered disease and indoor air becomes the carrier for the spread of these fictitious particles across the space. A quanta concentration balance (Eq. (9)) is set for each i-th cell:

$$V_i \frac{\mathrm{d}C_i}{\mathrm{d}t} = ER_i I_i - Q_{oi} C_i - \sum Q_{ij} C_i + \sum Q_{ji} C_j \tag{9}$$

where C is the zonal quanta concentration, ER is quanta emission rate for the disease, I is the number of infected people in the zone, Q_o is the exhaust air flow rate. The terms Q_{ij} and Q_{ji} represent the volumetric interzonal flow rates calculated from the zonal model.

Quanta concentrations represent the infectious material available at the breathing zone of a susceptible subject. Following the formulation given by Wells [8], the zonal infection risk $P_{I,i}$ for the susceptible individual is calculated through an exponential probability equation:

$$P_{I,i} = 1 - \mathrm{e}^{-p \int C_i(t)\mathrm{d}t} \tag{10}$$

where p is the breathing flow rate and t_{exp} is the exposure time interval. The exponent in Eq. (10) represents the intake dose of the susceptible subject.

2.3 Energy consumption calculation

A separate model was used for energy calculations. In addition, it was decided to distinguish between thermal and electrical consumptions; for this reason, two different calculation methods were defined and will be explained in this section.

The first step for the energy calculations was the definition of the HVAC system layout. In all the simulated environments, an ideal hydronic heating system was considered, which maintains the indoor conditions at 20°C temperature and 50% relative humidity; in addition to the heating system, a primary air mechanical ventilation system provides fresh external air to ensure high indoor air quality levels and infection risk mitigation. According to recent recommendations on airborne infection by the leading associations dealing with HVAC [14], the considered system does not include the possibility of air recirculation. Instead, the air is taken from outdoor and, after filtering, enters the air-handling unit (AHU), where it undergoes appropriate transformations. In heating conditions, the external air meets a crossflow heat exchanger where sensible heat recovery occurs, pre-heating coils, adiabatic saturator and post-heating coils, which bring it to the inlet conditions. Air is supplied to the room through two wall air diffusers, and two wall exhaust grilles near the floor were considered; inlets and outlets are placed at opposite sides of the room.

Inlet conditions were set and considered constant during the heating season: the air was supposed to enter the room at 20°C and 50% relative humidity. As for external conditions, monthly-average values were assumed for the external air temperature and the partial vapour pressure from the Italian Standard for Padova [15]. The values used for calculations are reported in Tab. 1.

Tab. 1 – Monthly average external air temperatures and vapour partial pressure.

Month	$p_{v\ ext}$	$T_{ext\ air}$
January	591 Pa	1.9 °C
February	652 Pa	4.0 °C
March	609 Pa	8.4 °C
November	934 Pa	8.2 °C
December	677 Pa	3.6 °C

According to the AHU layout, air undergoes four transformations. Among them, three sensible heating processes occur. The first one is due to the heat recovery (recuperator efficiencies η range between 80% and 98% as function of the volumetric flow rate), the other two when the air meets the pre- and post-heating heat exchangers. Finally, the humidification process is carried out between the pre- and post-heating processes by a saturator, working at constant efficiency (ε) equal to 90%.

Thermal energy demand consists of the energy supplied to the fresh air by the two heating coils. The energy used by the saturator has been neglected. The total energy supplied to the air is shown in Eq. (11).

$$E_{heating} = \dot{m}_{air}\,[(h_R - h_B) + (h_{IN} - h_C)]\,t \quad (11)$$

where $\dot{m}_{air}$ is the supply mass flow rate, h is the air specific enthalpy after the heat recovery (subscript R), after pre-heating coils (subscript B), after adiabatic saturator (subscript C) and after post-heating coils (subscript IN) and t is the operating time.

The electrical consumption was calculated assuming two variable speed fans for supply and return paths. The pressure drop due to continuous and localised effect was calculated; their aggregation provided a final value of the pressure drop, which was used for the choice of the electrical fans used for energy calculation.

Concerning distributed pressure drops, the airflow rate in a circular pipe was considered. According to the volume of the case study and, consequently, to the volumetric flow rates required, different duct diameters were chosen from commercial catalogues in order to maintain air velocities below a typical threshold of 10 m/s. Considering all cases, a range between 0.5 and 9 m/s was kept with this selection. In both supply and return paths, the pipe length was considered equal to 10 m. The choice of the same pipe length for all the considered AHUs is aimed at the comparison between different consumptions; therefore, it does not necessarily represent a realistic value for the considered system.

The components of the AHU were considered to generate a localised pressure drop that has been calculated assuming a quadratic relationship with mass flow rate (Eq. (12)):

$$\Delta P = \lambda\, Q^2 \quad (12)$$

The λ-values were extracted from datasheets of commercially available components. The pressure drop for each AHU can be seen in Tab. 2. For energy calculations, two different fans were considered for the supply and return paths; for the sake of simplicity, values reported in the table are the sum between them, considering both distributed and concentrated pressure drop.

Tab. 2 – Pressure drops in the supply and return paths of the AHU.

Air Changes per hour [h^{-1}]	Office Room	High school classroom	University classroom
0.5	23 Pa	28 Pa	43 Pa
1	53 Pa	72 Pa	97 Pa
1.5	94 Pa	132 Pa	150 Pa
2	145 Pa	223 Pa	229 Pa
2.5	198 Pa	321 Pa	324 Pa
3	258 Pa	445 Pa	434 Pa
3.5	332 Pa	598 Pa	560 Pa
4	422 Pa	760 Pa	710 Pa

3. Case Studies

3.1 Description and boundary conditions

The model described in the previous section was applied to three different case studies, representing an office room, a school classroom and a university classroom in heating conditions.

In all the analysed cases, the rooms are considered square or rectangular plants, with one vertical wall facing outside, whose thermal transmittance is equal to 0.3 $Wm^{-2}K^{-1}$. The presence of windows is not considered in the model, and infiltrations are also neglected. Dimensions and geometrical characteristics of the case studies are summarised in Tab. 3. As it can be seen, the three analysed volumes are very different from each other to evaluate the incidence of the proposed solutions in different volume rooms. Different occupancy profiles were applied according to the intended use of the building, as shown in Tab. 3. As explained in Section 2.1, the presence of occupants is only aimed at the infection risk assessment.

For all the case studies, the risk zonal model has been applied subdividing the geometrical domain into four identical well-mixed cells with a cross-section on the plan view, as shown in Fig. 2.

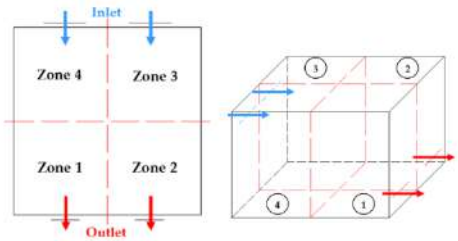

Fig. 2 – Discretisation grid applied to all case studies.

The same inputs of the risk model are set for all the analysed cases. The presence of one COVID-19 asymptomatic infected subject in Zone 1 is considered. The occupants' exhalation characteristics are assumed considering a sedentary activity, following [16]; thus, their breathing flow rate was set at 0.54 m^3 h^{-1} and, for the infected subject, a pathogen emission of 20 quanta/h was considered. The exposure time for the analysed cases was established according to the room final use, dealing with 8, 5 and 2 hours exposure time for the office workers, the high school and university students, respectively.

3.2 Sensitivity analysis

A sensitivity analysis was performed to highlight the influence of different aspects on ventilation costs and risk assessment. Despite the room volume, already mentioned in the previous section, the impact of varying renewal air flowrate and mask use was studied.

For each analysed case, the ventilation flowrate was ranged between 0.5 h^{-1} and 4 h^{-1}, with 0.5 h^{-1} steps. As already pointed out in Section 2.3, all the indicated air changes per hour assume 100% outdoor air.

Three different scenarios were outlined for the mask impact: in the first one, it was assumed that occupants were not wearing a mask; in the other two cases, the wearing of surgical and FFP2 masks was considered. For FFP2 masks, a penetration of the filter material of 6% and a leakage factor of 11% were obtained from European Standard [17]. According to Standard EN 14683:2019, surgical masks have a bacterial filtration efficiency of 95% in exhalation [18]. For the inhalation efficiency, the Standard does not indicate a value; for this reason, a precautionary value of 20% was chosen. Finally, a leakage factor of 27% for surgical masks was adopted according to [19].

4. Results and Discussion

4.1 Flow rate effect on risk and energy need

The effect of different ventilation flow rates in both the energy consumption and infection risk is analysed in this section. The probability of infection reported is the average between the values of the airborne infection risk in the four zones. This approach is justified by the similarity between risk values of the four cells; this aspect will be further discussed in Section 4.2. A permanent stay of both the susceptible subjects and the infective source inside the considered place for the duration of exposure time is assumed. As for energy consumption, the values reported for both thermal and electrical parts are calculated considering the seasonal operation of the AHU in steady conditions and at fixed mass flow rate. Daily consumption was calculated based on the exposure time for each case study; hence, monthly and seasonal consumptions were derived from the aggregation of daily values.

The simulation results for the office room are shown in Fig. 3. As the ventilation rate increases, there is a significant drop in the infection risk from 95% for 0.5 h^{-1} to 35% with 4 h^{-1}. Two relevant aspects can be highlighted in this case: the energy consumption grows significantly, up to almost ten times, but they represent only part of the total consumption, as they neglect the expenditure for heating purposes; moreover, it can be observed that, despite the high ventilation rate (considering 4 workers inside the office, the maximum flow rate analysed corresponds to about 13 L/s per person), with 8 hours continuous occupancy, the AHU alone cannot ensure enough fresh air to guarantee a healthy and safe workplace. For this reason, in cases of little offices similar to the analysed one, not only good ventilation must be provided, but also the correct use of personal protective equipment (PPE) must be observed. The specific thermal energy demand goes from about 10 kWh per person with 0.5 h^{-1} (1.7 L/s per person) to 102 kWh per person with 4 h^{-1} (13.4 L/s per person), whereas the specific electrical energy consumption goes from 0.5 to 81 kWh per person.

In the high school classroom (Fig. 4), the trend is the same respect to the office case: the increase of ventilation rate from 0.5 to 4 h^{-1} (e.g. from 0.8 to 6.1 L/s per person) leads to a decrease of infection risk (from 37% to 7%) with the annual consumption rising from 89 kWh to 948 kWh for thermal and from 2 kWh to 608 kWh for electrical share.

Tab. 3 – Case studies characteristics.

Room end-use	Dimensions					Occupancy
	L [m]	W [m]	H [m]	A_{floor} [m^2]	V [m^3]	
Office	4	4	3	16	48	4
High school classroom	8	6	3	48	144	26
University classroom	20	10	5	200	1000	151

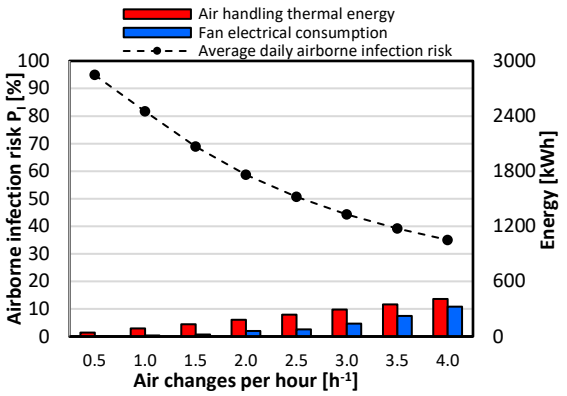

Fig. 3 – Daily infection risk (%), seasonal air handling thermal energy and fan electrical consumption (kWh) in the office case study.

The corresponding range of the specific energy demand lies between about 3 and 34 kWh per person for the required heating at the AHU finned coils, and between 0.1 and 23 kWh per person for fan absorption. Differently from the previous case, lower infection risk is detected; therefore, in this case, the volume effect is positive in terms of risk mitigation. On the other hand, it involves more considerable energy costs due to the higher volumetric flow rates needed to satisfy the required hourly changes.

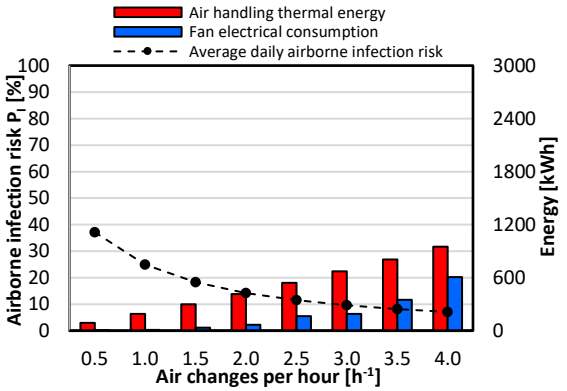

Fig. 4 – Daily infection risk (%), seasonal air handling thermal energy and fan electrical consumption (kWh) in the high school classroom.

The university classroom (Fig. 5) is the higher volume indoor environment simulated. As already shown for the other cases, the risk of infection is much lower than in the other rooms and energy consumption are greater. However, it should be noticed that the exposure time was considered equal to 2 h: this contributes to low values of infection probability, but extending the operation to other hours of the day, as is probable when considering a classroom used all day, would result in a further increase in consumption. As regards energy costs, the increase of ventilation flow rate from 0.5 to 4 h^{-1} (from 0.9 to 7.4 L/s per person) takes to an estimation of the specific thermal energy demand ranging from about 2 to 16 kWh per person and an electrical absorption between 0.1 and 10 kWh per person.

Similarly to the other cases, it can be concluded that the increase of the ventilation flow rate takes to higher energy costs but involves a decrease in the infection risk which passes from 1.3% to 0.3%.

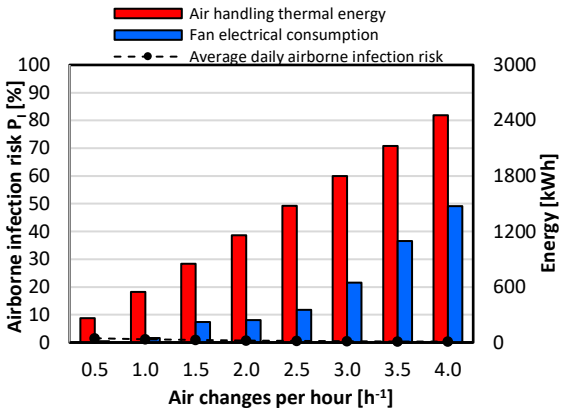

Fig. 5 – Daily infection risk (%), seasonal air handling thermal energy and fan electrical consumption (kWh) in the university classroom.

In this analysis, the occupants were considered not wearing masks; this aspect will be treated in the next section. Another aspect was not considered in this work: in higher volume places, the infection risk seems not crucial; however, high occupancy is likely to make it less realistic to employ only one infected person in the environment.

4.2 Relative position and mask effect

This section deals with assessing the probability of infection from COVID-19 obtained applying the zonal model. The risk extent is affected by different parameters, and their relevance is investigated.

As shown by the results reported in Section 4.1, an increase in the supply of outdoor air and higher room volumes lead to significant benefits in terms of infection risk since they promote the dilution of the airborne infectious material within the indoor space lowering its concentration to less harmful levels.

On the other hand, Fig. 6 shows the effect of the relative position between the infected source and the susceptible subjects, highlighting the spatial distribution of infection risk across the adopted grid through the zonal approach. The results are only reported for the single office room considering the extreme ventilation regimes (0.5 and 4 h^{-1}). Intermediate situations are trivially detected for the other flow rates.

The adopted calculation mesh defines a perfectly mixed environment. Therefore, the final infection risk is almost uniform within the space, and people's relative positions have limited effect. However, it can be noticed that spatial distribution of risk is slightly more heterogeneous with higher ventilation flow rates. Similar outcomes have been observed for the other case studies.

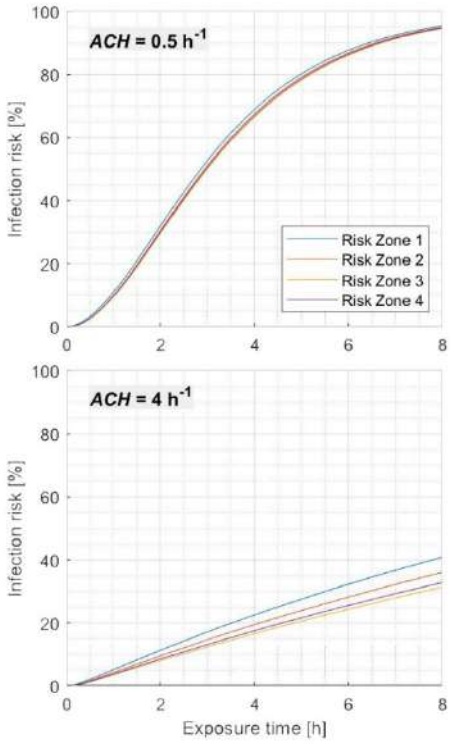

Fig.6 - Spatial distribution of risk in the office room.

Finally, Fig. 7 displays the risk curves obtained with both the infected and the susceptible subjects wearing the same type of mask. The shown situation is the worst one, i.e., a single office room (smallest volume) with an air change rate of 0.5 h^{-1} (lowest supply flow rate) and susceptible subject in Zone 1 (where the infected source is located).

The positive effect of using personal protective equipment is evident, even in this case. The infection spread is drastically reduced from a probability of 95 % without masks to 55 % with surgical masks and 8 % with FFP2. However, Fig. 7 points out that masks use must be coupled with adequate ventilation to maintain the risk below an acceptable threshold for smaller rooms.

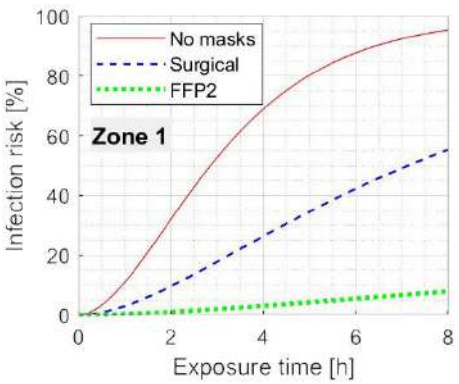

Fig. 7 – Influence of mask use on infection risk (office room, 0.5 h^{-1}, Zone 1).

For all the other situations, the benefits of masks are even more remarkable, also when the same exposure time is considered for comparison. Making the use of FFP2 devices mandatory could bring some advantages in energy consumption because lower flow rates would be sufficient to mitigate the airborne transmission of COVID-19. However, this aspect is out of the scope of this work.

5. Conclusions

In this work, the relationship between ventilation flow rate, energy consumptions and the risk of COVID-19 airborne infection was studied in three different indoor environments, a 48 m^3 office room, a 144 m^3 high school classroom and a 1000 m^3 university classroom. The effects of occupants' relative position inside the room, mask use and room volume on risk were also evaluated. For this purpose, a risk zonal model and an energy consumption model were applied to the considered case studies.

The following results emerged from this study:

- The increase of ventilation flow rate is an effective way to reduce the infection risk in indoor environments; however, it involves significant increases in energy consumption.
- With 8 hours exposure time, in the office case study the ventilation alone is not able to guarantee a safe and healthy workplace; in this context, the mask use can reduce the infection risk from 95% to 55% considering surgical masks and less than 10% with FFP2 masks (with 0.5 h^{-1} ventilation flowrate).
- The analysis of risk variation with relative position highlights a substantially uniform environment; to further analyse this aspect, a more discretised grid should be used in the model.

The proposed model presents some limitations and needs further improvements. A spatial modelling of jets and thermal plumes from heat sources can be included and a denser discretisation grid would be more appropriate to determine their effect on the mixing level of the indoor air. Additionally, the respiratory jets were not modelled, since people were considered as point sources of infectious aerosol; including information about temperature and momentum of exhalation jet would be suitable to get more accurate results from this type of analysis. Moreover, the likelihood of having more than one infected source in spaces with high occupancy should be considered.

6. Nomenclature

SYMBOL

A	Boundary surface area	m^2
ACH	Air changes per hour	h^{-1}
C	Quanta concentration	quanta m^{-3}
c_p	Specific heat at constant pressure	J kg^{-1} K^{-1}
E	Energy	kWh
ER	Quanta emission rate	quanta h^{-1}
g	Gravitational acceleration	m s^{-2}
h	Air specific enthalpy	kJ kg_{da}^{-1}
I	Number of infected sources	-

λ	Overall friction factor	Pa m^{-3} h
k	Flow coefficient	m s^{-1} Pa^{-n}
L	Depth of vertical boundary	m
$\dot{m}$	Mass flow rate	kg s^{-1}
P_I	Airborne infection probability	%
p	Breathing flow rate	m^3 h^{-1}
p_v	Partial vapour pressure	Pa
Q	Volumetric flow rate	m^3 h^{-1}
q_h	Heat flow	W
T	Temperature	K
t	Time	h
U	Thermal transmittance	W m^{-2} K^{-1}
V	Room volume	m^3
X	Mask filtration efficiency	%
Y	Leakage factor	%
Z_n	Height of the neutral plane	m
ΔP	Pressure difference	Pa
$\Delta\rho$	Air density difference	kg m^{-3}

Subscript

exh	exhalation
exp	exposure
ext	external
i	*i*-th zone
inh	inhalation
j	*j*-th zone
ref	reference level of zones (bottom level)
sup	supplied

7. References

[1] Eurostat, Energy data 2020 edition: Statistical book.

[2] Morawska L., Cao J. Airborne transmission of SARS-CoV-2: The world should face the reality. Environ. Int. 2020;139:105730.

[3] Morawska L., Tang J.W., Bahnfleth W., et al. How can airborne transmission of COVID-19 indoors be minimised? Environ. Int. 2020;142:105832.

[4] Buonanno G., Stabile L., Morawska L. Estimation of airborne viral emission: Quanta emission rate of SARS-CoV-2 for infection risk assessment. Environ. Int. 2020;141:105794.

[5] Miller S.L., Nazaroff W.W., Jimenez J.L., Boerstra A., et al. Transmission of SARS-CoV-2 by inhalation of respiratory aerosol in the Skagit Valley Chorale superspreading event. Indoor Air. 2021;31:314–323.

[6] Aliabadi A.A., Rogak S.N., Bartlett K.H., Green S.I. Preventing Airborne Disease Transmission: Review of Methods for Ventilation Design in Health Care Facilities. Adv. Prev. Med. 2011;2011:1–21.

[7] Ai Z.T., Melikov A.K. Airborne spread of expiratory droplet nuclei between the occupants of indoor environments: A review. Indoor Air. 2018;28:500–524.

[8] Sze To G.N., Chao C.Y.H. Review and comparison between the Wells-Riley and dose-response approaches to risk assessment of infectious respiratory diseases. Indoor Air. 2010;20:2–16.

[9] Schibuola L., Tambani C. High energy efficiency ventilation to limit COVID-19 contagion in school environments. Energy Build. 2021;240:110882.

[10] Wang J., Huang J., Feng Z., Cao S.J., Haghighat F. Occupant-density-detection based energy efficient ventilation system: Prevention of infection transmission. Energy Build. 2021;240: 110883.

[11] Noakes C.J., Sleigh P.A. Mathematical models for assessing the role of airflow on the risk of airborne infection in hospital wards. J. R. Soc. Interface. 2009;6:791-800.

[12] Lu Y., Dong J., Liu J. Zonal modelling for thermal and energy performance of large space buildings: A review. Renew. Sustain. Energy Rev. 2020;133:110241.

[13] Haghighat F., Li Y., Megri A.C. Development and validation of a zonal model - POMA. Build. Environ. 2001;36:1039–1047.

[14] Kurnitski J., Boerstra A., Franchimon F. COVID19 HVAC Guidance version 4.1. REHVA. 2021.

[15] Italian Organisation for Standardisation. Heating and cooling of buildings - Climate data: UNI 10349:2016.

[16] Buonanno G., Morawska L., Stabile L. Quantitative assessment of the risk of airborne transmission of SARS-CoV-2 infection: Prospective and retrospective applications. Environ. Int. 2020;145:106112.

[17] European Committee for Standardization - CEN. Respiratory protective devices - Filtering half masks to protect against particles - Requirements, testing, marking: EN 149:2001+A1:2009.

[18] European Committee for Standardization - CEN. Medical face masks. Requirements and test methods: EN 14683:2019.

[19] Mueller A.V., Eden M.J., Oakes J.M., Bellini C., Fernandez L.A. Quantitative Method for Comparative Assessment of Particle Removal Efficiency of Fabric Masks as Alternatives to Standard Surgical Masks for PPE. Matter. 2020;3:950–962.

Data Statement

Data sharing not applicable to this article as no datasets were generated or analysed during the current study.

Effects of daytime cool vs warm exposure on evening thermal perception and thermoregulation

Hannah Pallubinsky [a,b], Rania Christoforou [a], Kai Rewitz [c], Janine Bardey [a,d], Tobias Burgholz [c,d], Mahmoud El-Mokadem [c], Dirk Müller [c,d], Marcel Schweiker [a]

[a] Research and Teaching Area Healthy Living Spaces, Institute for Occupational, Social and Environmental Medicine, Medical Faculty, RWTH Aachen University, Germany, hpallubinsky@ukaachen.de

[b] Department of Nutrition and Movement Sciences, School of Nutrition and Translational Metabolism Research (NUTRIM), Maastricht University, the Netherlands

[c] Institute for Energy Efficient Buildings and Indoor Climate, E.ON Energy Research Center, RWTH Aachen University, Aachen, Germany

[d] Heinz Trox Wissenschafts gGmbH, Aachen, Germany

Abstract. Thermal conditions experienced during daytime can be different from those experienced after working hours outdoors or at home. Since most dwellings in Central and Western Europe in the temperate climate zone are naturally ventilated (NV), while public spaces and offices are often air-conditioned (AC), a substantial gap between daytime and evening thermal exposure can occur. This thermal gap likely reduces acclimation to the more 'natural' climate outdoors and in NV spaces, and therefore may affect thermoregulation and thermal perception. Structural information on how thermal conditions experienced during daytime (e.g. in offices) influence thermal perception and physiology in the evening (at people's private homes). Therefore, the present study seeks to assess the impact of staying in cool vs. warm environments during daytime working hours on thermal perception and thermophysiology in the evening at home.

In this hybrid laboratory and field study, 31 participants (41±17 years, BMI: 24±3 kg/m^2) were exposed to a simulated workday in either 21 °C (cool) or 28 °C (warm) at two separate occasions. Thermal sensation, thermal preference and mean skin temperature were measured at eight timepoints throughout the day (lab) and evening (home) until the following morning.

Preliminary results suggest that daytime thermal conditions affect people's thermal perception and thermophysiology after working hours at home. The effect is most pronounced just after arriving at home and decreases over time. Importantly, our results raise the question whether conditioning of work places solely based on on-site productivity and comfort, but without considering the impact on comfort and well-being during leisure and recovery time at home, is the way to go in the future.

Keywords: Thermal perception, air conditioning, natural ventilation, thermoregulation.
DOI: https://doi.org/10.34641/clima.2022.404

1. Introduction

People working in public and commercial spaces are often exposed to thermal conditions that are more or less independent from naturally-occurring outdoor temperatures, as many of them are air-conditioned (AC). In Germany, only about 2% of residential buildings, but about 50% of non-residential, e.g. office buildings, are equipped with AC [1]. For both types of buildings, numbers are expected to rise sharply within the upcoming years, according to the International Energy Agency [2]. Particularly in the Asian and North American region, the use of AC is already much more widespread, in both residential and non-residential buildings, than in Europe [2].

Thermal conditions in AC spaces are usually strictly controlled and uniform, based on indoor environmental standards such as ASHRAE 55 [3]. In contrast, in naturally ventilated (NV) dwellings, thermal conditions vary within the time of a day and night, as well as through different seasons of the year.

Copyright ©2022 by the authors. This conference paper is published under a CC-BY-4.0 license.

Consequently, people who spend the majority of their daytime in AC spaces may perceive more 'natural' thermal environments as less comfortable, which may also include their homes. In contrast, people working in NV spaces (or even outdoors) are likely to benefit from natural acclimatisation effects and may thus be better adapted to the fluctuating conditions of a specific time and season. A person's individual thermal physiology and thermal perception may be influenced by factors including, but not limited to, age, BMI, physical fitness, thermal preference, and thermal acclimatisation.

The widespread availability of AC in public and commercial buildings as well as offices is likely also affecting people's choices and behaviours at home: if natural acclimatisation in spring and summer during daytime is prevented by the use of AC, it may be hypothesised that people would be more inclined to the usage of AC at home. Considering the progress of climate change, which brings along an increase in global average temperature, but also increasingly frequent and more intense summer heat waves, it is likely that many people will want to acquire an AC unit for their homes, to reproduce the controlled conditions they are used to from their work environments. Unfortunately, this will cause an increased energy demand, which counteracts the need to reduce our environmental impact, and can further worsen the issue of overheated cities and the heat island effect [2, 4].

To avoid getting drawn deeper into this vicious circle, it is important to assess whether being exposed to particular thermal conditions during daytime working hours will influence human thermal physiology and perception in the later course of the day. This knowledge brings us a step ahead in the design and implementation of sustainable, comfortable, and healthy indoor environmental conditions, in order to make both people and buildings more resilient. Hitherto, structural information on the interaction of daily thermal history on thermal physiology and perception, is lacking. Therefore, the present study seeks to evaluate the effect of cool vs warm conditions in a simulated office environment, on thermoregulation and thermal perception in the evening at home. We hypothesise that staying in a cool environment during the day will result in higher (thus warmer) thermal perception of natural summer conditions after working hours at participants' homes. The measurements described in this article are part of a larger study. For the purpose of this conference paper, the analysis of a limited set of measurements obtained will be presented.

2. Methods

2.1 Study design

To assess the effects of a cool vs warm environment during the workday on thermoregulation and thermal perception in the evening at home, a hybrid study with a controlled laboratory part and an observational field part was set up: a simulated workday at the laboratory and subsequent field observations at the participants' private homes. To account for differences in the order of exposures, a cross-over design was selected, where all participants underwent one cool (C, 21 ˚C) vs one warm (W, 28 ˚C) laboratory condition, followed by the observational part at the participants' homes. Wherever possible with respect to scheduling, two participants were coupled with each other for both sessions, and sat together in the simulated office environment throughout the day. Others were at the laboratory by themselves for both sessions.

2.2 Participant characteristics

A sample of 32 healthy male and female participants (one dropout for personal reasons, thus n=31 for analysis; age: 41±17 years, BMI: 24±3 kg/m^2) was recruited for the study based on an a-priori sample size calculation (G*power [5]) with α=.05, β=.8, η2=.5 (medium effect size). This calculation resulted in a total population of 27, which we increased by 20% to include drop-out. Participants were screened for their general health status to assess eligibility for the study. Amongst other things, exclusion criteria included the intake of medication as well as acute and active diseases that are known to affect thermoregulation.

2.3 Study procedures and measurements

Participants arrived at the laboratory in the morning at 08:00 a.m.. Upon arrival, their COVID-19 vaccination status was checked, and an antigen test was performed if necessary. After ensuring the participants were either fully vaccinated or tested negative, they were equipped with sensors to mean skin temperature at 4 ISO-defined sites [6] using wireless temperature sensors (iButtons®, Maxim Integrated, USA) over one-minute intervals. Whole-body thermal sensation was assessed using the ASHRAE 7-point scale (−3=cold, −2=cool, −1=slightly cool, 0=neutral, 1=slightly warm, 2=warm, 3=hot) and thermal preference using a 7-point scale (−3=much cooler, −2=cooler, −1=slightly cooler, 0=no change, 1=slightly warmer, 2=warmer, 3=much warmer) at eight time points throughout the day: 1. 9:00h, 2. 11:00h, 3. 13:00h, 4. 14:00h, 5. 16:00h (1-5 at the laboratory), 6. 18:00h, 7. 22:00h, and 8. 7:00h the following morning (6–8 at participants' homes). During the two experimental days, participants were asked to wear the same clothes both days (long-sleeved light top or short-sleeved light top, long trousers, underwear, socks, and low shoes). Thermal conditions in the laboratory room were assessed using a commercially available air temperature sensor (Testo 480, Probe 0632 1543, Titisee-Neustadt, GER). Moreover, participants were equipped with a tailormade portable environmental monitoring station to be used at their homes, to control for environmental conditions during the observational part of the study. Participants were instructed to keep it in close (but not too close) proximity of their whereabouts. They were instructed to carry the device with them whenever

they changed a room for more than 10 minutes. The device did not have a display in order to avoid any influence of environmental measurements on subjective perception and survey results. Participants were instructed to go home after the laboratory part of the study without delay, with minimal physical activity (preferably by car or public transport) and to prevent extreme thermal exposure (such as direct sun radiation or strong draft).

2.4 Statistics

Mean skin temperature, thermal sensation and thermal preference were compared over the eight designated time points between condition C and W using Wilcoxon Signed Rank tests for non-parametrical data in the software R. A difference with p<.05 was considered as statistically significant, and a trend towards significant difference was assumed at p<.10. Data is presented as mean±standard deviation.

3. Results

Ambient temperature in the laboratory during condition C was 22.4±1.7 ˚C and 27.7±1.6 ˚C during condition W. Temperatures observed at people's homes at the day of condition C ranged 23.4±1.9 ˚C [min 19 and max 29.7 ˚C] and 23.5±1.65 ˚C [min 18.9 and max 31.5 ˚C] at the day of condition W (p>.05). Throughout the day and evening until the following morning of condition C, mean skin temperatures of 29.8± 5.1˚C [range 17–39.3 ˚C], thermal sensation of −1 (median) [min −3 and max 3] and thermal preference of 1 (median) [min −3 and max 3] were observed. Throughout the day and evening until the following morning of condition W, mean skin temperatures of 29.8±6 ˚C [range 13.3–37 ˚C], thermal sensation of 1 (median) [min −2 and max 3] and thermal preference of −1 (median) [min −3 and max 1] were measured.

3.1 Mean skin temperature

Mean skin temperature was statistically significantly lower during condition C compared with condition W for timepoints 1–5 (V=0 for timepoints 1–5, all p<.000, effect sizes range=0.88–0.90 for timepoints 1–5, Fig. 1). At timepoint 6, a trend was observed towards higher mean skin temperatures in condition C compared with condition W (V=110.5, p=.094, effect size=0.32). There was no significant difference in mean skin temperature at timepoints 7 and 8 between C and W.

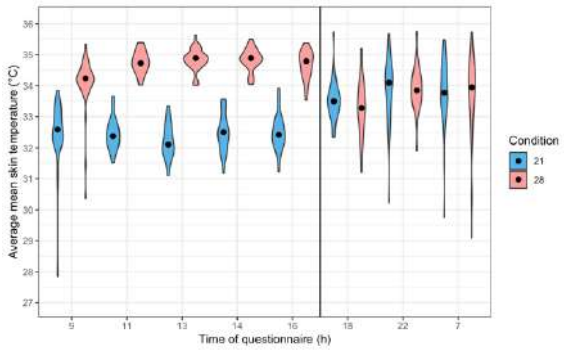

Fig. 1 – Mean skin temperature at the questionnaire times for the cool (21 ˚C) and warm (28 ˚C) condition.

3.2 Thermal sensation

Thermal sensation was significantly lower during condition C compared with condition W for timepoints 1–5 (V=0 for timepoints 1–5, all p<.000, effect size=0.88 for timepoints 1–5, Fig. 2). At timepoint 6, the first observed at participants' homes, thermal sensation was significantly higher at condition C compared with condition W (1.4±0.9 vs 0.7±0.6, V=129, p<.000, effect size=0.64). At timepoint 7, the difference was no longer statistically significant. At timepoint 8, a trend towards significantly higher thermal sensation in the morning after condition C compared with condition W was observed (V=124.5, p=.079, effect size=0.39).

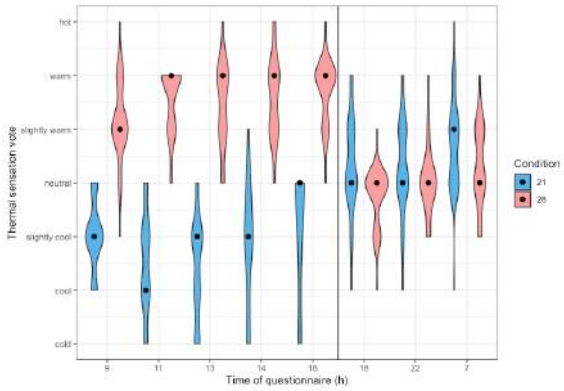

Fig. 2 – Thermal sensation votes at the questionnaire times for the cool (21 ˚C) and warm (28 ˚C) condition.

3.3 Thermal preference

Thermal preference was significantly higher during condition C compared with condition W for timepoints 1–5 (V_1=300, V_2=496, V_3=496, V_4=496, V_5=351; all p<.000, range effect size=0.87–0.88 for timepoints 1–5; Fig. 3). At timepoints 6–8, thermal preference was not different between condition C (0.8±0.7) and W (0.9±0.7).

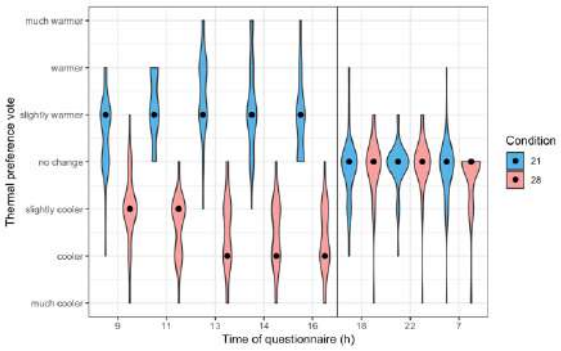

Fig. 3 – Thermal preference votes at the questionnaire times for the cool (21 °C) and warm (28 °C) condition.

4. Discussion and conclusion

The present paper aimed at establishing the effect of daytime (workplace) thermal exposure on thermal perception in the evening (at home). Preliminary analysis shows a significant effect of circadian thermal history on whole-body thermal sensation, where exposure to a cool (21 °C) environment during the day produced higher (meaning warmer) thermal sensation at the participant's private home, one hour after leaving the laboratory environment. In contrast, when participants were exposed to a warm (28 °C) environment during the day, thermal sensation was lower at the participants' private home, one hour after leaving the laboratory environment. The effect diminished until five hours after leaving the lab, even though a trend towards a difference in thermal sensation was observed in the morning after exposure to a cool vs warm environment. Even though no significant differences in measured physical thermal conditions were detected, thermal sensation was significantly different after participants arrived at home. As thermal perception (thermal comfort and sensation) is closely related to thermoregulatory behaviour (such as changing clothes, opening and closing windows, or operating a thermostat or an AC unit) [7, 8], it may be anticipated that higher thermal sensation at home, particularly in summer, would lead to a desire for (artificial) cooling. In accordance with our hypothesis, it may thus be expected that people who also work in air-conditioned offices are more inclined towards the use of AC at their homes, to counteract the higher thermal perception.

Alongside with the significant increase in thermal sensation one hour after leaving the lab on the day of the cool condition, a trend towards higher mean skin temperatures was observed. It is well-established that thermal sensation is related to skin temperature [9]. Both absolute mean skin temperature, but also the rate of change of skin temperature, play roles in this relationship. As expected, mean skin temperature was lower in the cool laboratory condition and higher in the warm laboratory condition, which also produced the corresponding thermal sensation (lower in cool and higher in warm condition). After the first part of the experiment, which took place in the controlled laboratory environment, participants left for their private homes. Interestingly, at this point, a trend towards higher mean skin temperatures after the cool condition vs lower mean skin temperatures after the warm condition was observed, which is also reflected in thermal sensation. It might be speculated that this reversal could be due to thermoregulatory behaviour (e.g. seeking relatively warmer or cooler environments, in spite of the instructions provided by the researchers), or even a change in physical activity (i.e. more physical activity to generate warmth after the cool condition). Since thermoregulatory behaviour is a very natural automatic act (think of rolling up sleeves for better cooling or a hunched posture with crossed arms in front of the chest for heat retention), participants might not even have noticed this, let alone had the intention to actively warm up or cool down and thus resist the instructions. Analysis of these potential confounders will be part of the ongoing analysis. Moreover, as the latter part of the experiment was of observational character and in real-life circumstances, the environment was not controllable. This led to differences in thermal exposure from participant to participant and from day to day, which may have also played a role in this context.

When interpreting the above results, it should be considered that opposed to thermal sensation, thermal preference was not different in the second, observational part of the study, in the hours after the cool vs the warm laboratory condition. Interestingly, participants even indicated to prefer warmer temperatures during the cool condition, which may enhance the comfort feeling related to the higher thermal sensation after returning home, based on thoughts related to thermal alliesthesia [10]. Thermal alliesthesia describes the pleasure perceived when moving from an uncomfortably cold or hot environment to the respectively opposite condition, e.g. standing in front of a lit fireplace after returning home from a winter walk, or jumping into cold water on a hot summer day. The state of alliesthesia is, however, usually not very long-lasting, but rather attenuates as soon as the body has returned to a state of thermal equilibrium. With respect to our results, the cool vs warm laboratory conditions could explain the higher thermal sensation after the cool condition, and the lower thermal sensation after the warm condition (with no change in thermal preference, due to higher respectively lower sensation and skin temperatures in cool vs warm), as well as the diminishment of this effect over time. Deeper analysis of this relationship is warranted.

The results presented in this paper are part of a larger study and the analysis has not been finalised, which is why the presented findings may not be the final conclusion of the investigation. The original idea of the study was to assess the effect of daytime air-condition exposure on thermal perception in

naturally-ventilated spaces in warm summer evenings. Unfortunately, the summer of 2021, when the measurements took place (end of June till beginning of October) was much cooler than expected based on the record-breaking summers of the preceding years. Even though our collected dataset does not necessarily reflect what we originally wanted to investigate, the data still points towards the same original hypothesis: being exposed to (overcooled) air-conditioned spaces for the major part of the day (in this case ~8 hours) influences the thermal sensation of warmer (outdoor or naturally ventilated) spaces in the evening.

In conclusion, we have observed higher thermal sensations at home after being exposed to cool daytime environments, and the other way around. Further analysis is needed to unravel the underlying relationships between skin temperature and thermal perception and influences of confounding variables as well as to relate our findings to the available knowledge on short-term acclimation and seasonal adaptation.

5. Acknowledgements

This study was funded by the VILLUM FONDEN (21055) and under the Excellence Strategy of the Federal Government and the Länder

6. References

1. Bettgenhaeuser, K., et al., Climate protection by reducing cooling demands in buildings; Klimaschutz durch Reduzierung des Energiebedarfs fuer Gebaeudekuehlung. 2011.
2. IEA, I.E.A., *The Future of Cooling*. 2018: Paris.
3. ASHRAE, *Thermal Environmental Condition for Human Occupancy*, in *Standard 55-2020*. 2020, American Society of Heating, Refridgerating and Air Conditioning Engineers: Atlanta GA.
4. Salamanca, F., et al., Anthropogenic heating of the urban environment due to air conditioning. Journal of Geophysical Research: Atmospheres, 2014. **119**(10): p. 5949-5965.
5. Faul, F., et al., G*Power 3: A flexible statistical power analysis program for the social, behavioral, and biomedical sciences. Behavior Research Methods, 2007. **39**(2): p. 175-191.
6. ISO7730, *Ergonomics of the Thermal Environment - Analytical Determination and Interpretation of Thermal Comfort Using Calculation of the PMV and PPD Indices And Local Thermal Comfort Criteria*, in *ISO 7730:2005*. 2005, International Standards Organization: Geneva.
7. Schlader, Z.J., et al., Characteristics of the control of human thermoregulatory behavior. Physiology & behavior, 2009. **98**(5): p. 557-562.
8. Flouris, A.D., Functional architecture of behavioural thermoregulation. Eur J Appl Physiol, 2011. **111**(1): p. 1-8.
9. Gagge, A.P., J.A. Stolwijk, and J.D. Hardy, Comfort and thermal sensations and associated physiological responses at various ambient temperatures. Environ Res, 1967. **1**(1): p. 1-20.
10. Parkinson, T. and R. de Dear, Thermal pleasure in built environments: physiology of alliesthesia. Building Research & Information, 2015. **43**(3): p. 288-301.

Data access statement

The datasets generated and/or analysed during the current study are not yet available, as they are still being processed. However, the authors will make every reasonable effort to publish the datasets as soon as possible in the near future.

The effect of thermal comfort conditions during work hours on social disconnection

Rania Christoforou [a], Hannah Pallubinsky [a,b], Janine Bardey [a,d], Kai Rewitz [c], Mahmoud El-Mokadem [c], Tobias Burgholz [c,d], Dirk Müller [c,d], Marcel Schweiker [a]

[a] Research and Teaching Area Healthy Living Spaces, Institute for Occupational, Social and Environmental Medicine, Medical Faculty, RWTH Aachen University, Aachen, Germany, rchristoforo@ukaachen.de

[b] Department of Nutrition and Movement Sciences, School of Nutrition and Translational Metabolism Research (NUTRIM), Maastricht University, the Netherlands

[c] Institute for Energy Efficient Buildings and Indoor Climate, E.ON Energy Research Center, RWTH Aachen University, Aachen, Germany

[d] Heinz Trox Wissenschafts gGmbH, Aachen, Germany

Abstract. Studies have focused on people's physiological reactions to thermal conditions in indoor environments, neglecting the social consequences that could arise from them. Therefore, there is a gap in literature how these thermal comfort conditions could influence psychosocial aspects of our lives, such as how disconnected we feel from other people around us or how connected we feel with them, especially after being exposed to these conditions for many hours within an occupational context. This study attempted to address this gap in literature by exposing participants to two thermal conditions: a warm condition (28 ˚C) and a cool condition (21 ˚C) in a simulated office environment. The purpose of the study was to observe possible social consequences arising from a day at work under either of those conditions by focusing on social distance and empathy levels. 31 participants were recruited and exposed to both conditions, each condition at a different day (gap between days of at least one day for washout), and were asked to remain in the temperature-controlled environment for eight hours (between 9 a.m. and 5 p.m.). Additionally, they were asked to complete a series of questionnaires, investigating their levels of social disconnection and empathy before and after both testing days. The temperature of the room was monitored throughout the process. The difference observed between pre- and post-measures for both conditions was not significantly different with regards to the feelings of social disconnection, despite the difference in responses observed within the raw data for each condition. In contrast, the difference observed in empathy levels between pre- and post-measures was significantly different between conditions. Individuals exposed to the cool condition reported lower levels of empathy after exposure, while participants exposed to the warm condition exhibited higher empathy levels after exposure. The results suggest that thermal conditions could influence people's levels of empathy, which could have consequences both within a work environment and in private life. Further research is needed to support this. Implications of these outcomes and recommendations for further research are discussed.

Keywords. temperature, social disconnection, empathy, work
DOI: https://doi.org/10.34641/clima.2022.405

1. Introduction

Considering indoor environmental conditions and their consequences is of primary importance within an occupational context. Several studies have looked at the association between environmental conditions and health-related issues [1, 2]. However, the relationship between indoor environmental conditions and social relationships between colleagues has received less attention within the indoor environment literature [3]. Studies have shown that social support at work can be related to higher control over work and reduction in depression levels [4], highlighting the value of investigating the effect of indoor environmental conditions on social relationships.

Indoor environmental conditions are characterized by four different dimensions: 1) air quality, 2) temperature, 3) light, and 4) acoustics. Although all dimensions are considered essential when investigating the indoor environment, the current

Copyright ©2022 by the authors. This conference paper is published under a CC-BY-4.0 license.

paper will focus on the effects of indoor temperature (operative temperature) on social connection, as it is hypothesized by the authors to have the strongest association to social variables compared to the other environmental dimensions. Additionally, temperature has been rated by building occupants as the most important aspect of the indoor environment compared to visual and acoustic comfort, and air quality [5].

Temperature has been found to have a bidirectional relationship with social variables; especially social warmth/connection [6]. People report higher levels of physical warmth when reading messages reflecting social connection with another person, and they feel more connected when holding a warm pack (peripheral body temperature [7]). Additionally, Inagaki and Eisenberger [7] found that there is a shared neural mechanism underlying physical and social warmth, suggesting that modification in one of the variables will probably lead to the modification of the other.

According to Bargh and Shalev [6], people who experience physical coldness are feeling significantly more lonely than individuals with physical warmth. Additionally, people who score higher on loneliness tend to take more frequent warm baths/showers [6]. The aforementioned associations make us wonder how this could be translated within an occupational context and to the indoor temperature. In a study conducted by Kolb, Gockel and Werth [8], student participants demonstrated more customer-oriented behaviour and gave more discounts when they were exposed to lower temperatures compared to when exposed to higher temperature. However, there is still a gap in literature on how temperature conditions within a work environment can influence feelings of social connectedness.

The majority of studies investigating the effect of temperature on social connectedness have focused on the haptic experience of temperature (peripheral body temperature), instead of the actual indoor temperature, leading to weak and inconclusive findings with regards to the effects of indoor temperature on social connectedness [9]. Furthermore, studies have investigated internal body temperature conditions, which demonstrate a positive association with social connectedness [10, 11]. This contradicts the negative association demonstrated between indoor temperature conditions and prosocial behaviours in the Kolb, Gockel and Werth [8] study. Distinguishing internal thermal conditions from external thermal conditions and their effects, reminds us of the saying "cold hands, warm heart", which further supports the existence of these contradictory thermal conditions.

In addition to social connectedness, temperature has been associated to changes in empathy levels. Interestingly, Salazar-Lopez et al. [12] found a positive association between facial temperature changes and empathy scores. In general, empathy positively predicts social connectedness [13]. Consequently, investigating the association of indoor temperature with empathy levels could provide insights into an underlying pathway leading to social connectedness or a moderator to the association. However, taking into consideration the difference observed between indoor temperature and body temperature and their association with social variables, it is not yet known whether indoor temperature could have an effect on empathy levels. Empathy is a core social characteristic, which develops early in life, hence, it might require a targeted empathy training to modify it [14]. A possible explanation of the observed effect in the Salazar-Lopez et al. [12] study could be that the shared neural mechanism is driving the facial temperature changes as an outcome of the empathic responses. Consequently, investigating the effect of indoor temperature on empathy levels in this study could provide important preliminary outcomes for future studies.

People evaluate a wide range of indoor conditions as thermally neutral before perceiving them as too cold or too hot. This range is depending on a variety of variables, like air temperature, air velocity, clothing, metabolic rate, running mean outdoor temperature, among others. In addition, thermal conditions within office spaces have a wide range, too, easily ranging between 21 °C and 28 °C and beyond, depending strongly on the type of building. However, it is not yet known if this wide range of thermal conditions people experience at work is reflected in social relationships, too, particularly with respect to social connectedness and empathy.

The current study aimed to investigate the effects of indoor temperature on social connectedness and empathy, by exposing participants to two distinct thermal conditions (21 °C vs. 28 °C) during the summer.

Based on the Kolb, Gockel and Werth [8] study, it was hypothesized that:

1) A negative association will be observed between social connectedness and indoor temperature.

2) A negative association will also be observed between empathy and indoor temperature.

2. Research Methods

2.1 Procedure and ethical considerations

After ethical approval was granted by the relevant ethics committee, a sample of 32 participants was recruited via convenience sampling from participant lists, snowball sampling and via adverts on social media platforms and local amenity shops during summer 2021. One of the participants did not complete the study for personal reasons. A pre-screening assessment was conducted before

participating in the study. Participants were excluded if they: 1) were active cases of COVID-19, 2) had a medical condition that could interact with thermoregulation and/or cognitive performance, 3) were suffering from insomnia, 4) had an unstable body weight, 5) exhibited high alcohol consumption (more than 2 servings per day for men and more than one serving per day for women) and 6) were regular smokers in the past 12 months. Women were also excluded if they were pregnant, or in case they were in the older age group, if they were not in a stable post-menopausal stage, since this could interfere with the measurements. Participants who were eligible to participate in the study were invited to attend a two-day hybrid study involving eight hours in the laboratory and field assessment at home on both study days. Before participation, written informed consent was obtained. During the two experimental days, participants were asked to wear similar clothes (long-sleeved light top or short-sleeved light top, long trousers, underwear, socks and low shoes) and they were exposed to two temperature conditions, a cool condition (21 ℃) and a warm condition (28 ℃) in a cross-over design. A gap of at least one day was maintained between the two experimental days to ensure the washout of any effects from the preceding condition.

Visual, acoustic and air quality aspects were kept constant for both temperature conditions and only indoor temperature varied. Indoor temperature and thermal perception were monitored throughout the day during both conditions. Pre-post measurements of social disconnection and empathy were collected for both conditions and were analysed at the end of the study.

2.2 Demographics

During the pre-screening process, participants' demographic data was collected. The demographic data included participants' sex (male, female), year of birth, nationality and employment status.

2.3 Indoor temperature

Indoor temperature was recorded in degrees Celsius every minute throughout the experimental days using a commercial air temperature sensor. However, for the purposes of this study, only the average indoor temperature, which represented the condition, was used for the analysis.

2.4 Thermal perception

Thermal perception was assessed using one of the most prominent scales for thermal sensation, the ASHRAE 7-point scale. Items assessed participants' thoughts on the thermal environment (acceptable vs. unacceptable), how they felt (on a scale from cold to hot), their perception of the environment (on a scale from very comfortable to very uncomfortable), how they would prefer it (on a scale from much cooler to much warmer), if they shivered (Yes, No), if they were sweating (Yes, No) and if they would change the temperature if they had the opportunity (Yes, No). The analysis of these variables will be presented in a different paper.

2.5 Social disconnection

Feelings of social disconnection were assessed using a 5-item scale, previously used in the Inagaki and Eisenberger [15] study. Items included questions on how close the participants feel and want to be with other people, which were rated on a 5-point Likert scale from 1 (Not at all) to 5 (Very strongly). Higher scores indicate stronger feelings of social disconnection.

2.6 Empathy

Empathy levels were assessed using specific scenarios, which were developed for the purposes of this study. Similar scenarios were used and validated in other studies [16], but were addressing a different population (i.e. child victims) and hence, they only served as an example for the development of these empathy scenarios, which the authors plan to validate in the future. The scenarios investigated participants' reaction to: 1) returning home after work and finding their partner or family member having a bad day, 2) returning home tired from work and being informed that their partner/family member had to stay longer at work because of a deadline, missing in this way important plans for the afternoon and 3) returning tired from work and finding their partner/family member lying on the sofa/bed looking very ill. Answers were scored from 0 to 2 points depending on the response and were summed to form a total score. Higher scores indicate greater expression of empathy.

2.7 Statistical analysis

Outcomes were analysed using R Studio and descriptive statistics were calculated using the "psych" package. In order to identify differences between baseline data and post-testing day data and differences in the outcomes between conditions, a series of Wilcoxon-Signed Rank tests were conducted.

3. Results

3.1 Participant characteristics

The sample included 16 female participants (51.6%) and 15 males (48.4%), of whom 13 participants (41.9%) were considered in the older participants category (i.e. between the age of 50–71 years) and 18 participants (58.1%), formed the young participant group (i.e. between the age 20–35 years old). The average age of all participants was 40.7 years old (*SD*=16.5). The majority of the participants had a German nationality (90%), one participant was Greek, one was Belgian and one was Portuguese, all of whom had a native or close to native German language proficiency. The majority of younger participants were university students, while older

participants were employed at a wide range of sectors, such as engineering, law, psychology, medicine, business and insurance. Participants had an average Body Mass Index (BMI) of 23.8 (*SD*=3.2).

3.2 Thermal perception

A series of Wilcoxon-Signed Rank tests demonstrated that participants reported significantly different thermal sensation votes during the two experimental conditions, with participants being exposed to the 21 °C stating that the room was cold and participants exposed to the 28 °C stating that the room was warm. Additionally, participants exposed to the 21 °C expressed the preference for a warmer environment, while participants exposed to the 28 °C expressed the preference for a cooler environment. Still, on average, participants reported that both conditions were acceptable and just comfortable for them.

3.3 Social disconnection

The Wilcoxon-Signed Rank tests demonstrated that there were no significant differences between baseline data on feelings of social disconnection before being exposed to the two experimental conditions on the two different days (V=161, p= .98, Effect size=0.02). Additionally, there were no significant differences between conditions on post-testing day measures of social disconnection (V=132, p= .42, Effect size=0.14). The difference between pre- and post- outcomes was also found to be not significantly between the two conditions (V=162.5, p= .75, Effect size=0.05), although a small difference is demonstrated in Figure 1, with participants being exposed to the 21 °C demonstrating more variation in levels of social disconnection after the experimental day than after the 28 °C.

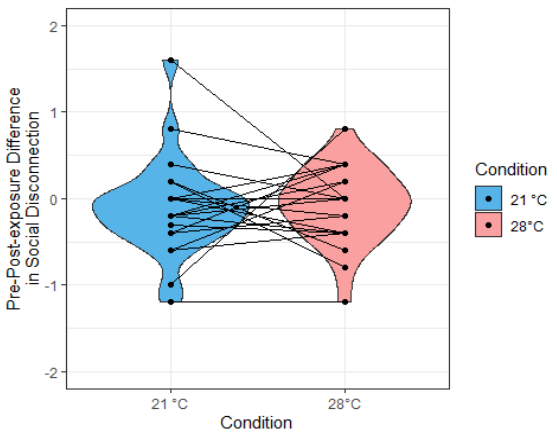

Fig. 1 - Difference between pre- and post-measures of social disconnection for both experimental conditions (21 °C vs. 28 °C). Note: Lower values represent lower levels of social disconnection.

3.4 Empathy

Similarly to the social disconnection outcomes, the Wilcoxon-Signed Rank test demonstrated no significant differences in empathy levels in pre-testing day measures between the two conditions (V=13.5, p=.59, Effect size=0.02). However, a difference very close to significance was observed in the post-testing day measures between the two conditions (V=15, p=.05, Effect size=0.34). The difference between pre- and post-measures was found to be significantly different between the two conditions (V=15, p=.03), with the outcomes indicating a moderate effect (Effect size=0.42). The difference between the two conditions is indicated in Figure 2.

Supplementary analyses indicated that the difference in empathy levels between pre- and post-exposure measures was only significant for the cool condition (21 °C; Z=−2.27, p=.02), since the difference between pre- and post-exposure measures for the warm condition (28 °C) was not significant (Z=−1.31, p=.19).

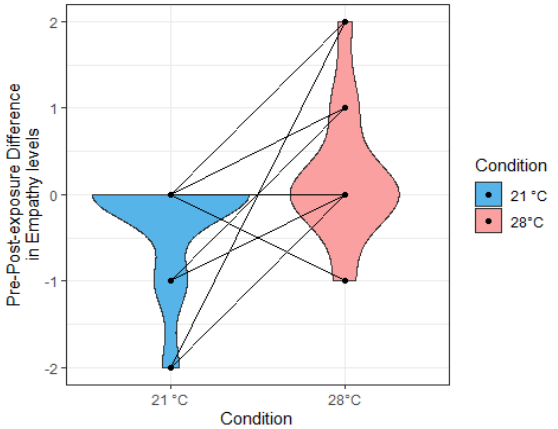

Fig. 2 - Difference between pre- and post-measures of empathy for both experimental conditions (21 °C vs. 28 °C). Note: Lower values represent lower levels of empathy.

4. Discussion

The study followed a cross-over design to investigate differences in social disconnection and empathy between pre- and post-exposure measures, and between warm and cool conditions in a simulated office environment. The findings indicated no significant differences between conditions for social disconnection, although a greater variation of responses was observed for the social disconnection scale in the cool condition compared to the warm condition. When taking into consideration the whole sample, participants demonstrated both increases and decreases in feelings of social disconnection after exposure to both conditions. However, more participants demonstrated an increase in social disconnection after exposure to the 21 °C, compared

to the 28 ℃. The difference in empathy levels between the pre- and post-exposure outcomes was significantly different between the two conditions. Participants reported lower empathy levels after exposure to the cool condition and higher empathy levels after exposure to the warm condition.

The findings for empathy levels are not consistent with the Kolb, Gockel and Werth [8] study, which found that more prosocial behaviours were exhibited after exposure to lower temperatures compared to higher temperatures. Our findings indicate a positive association between indoor temperature and empathy, which is in accordance to the positive association between peripheral temperature and empathy found in the Salazar-Lopez et al. [12] study. This outcome could provide additional support to the shared neural mechanism suggested by Inagaki and Eisenberger [7] between physical and social warmth, although further research is needed to support this.

Additionally, contrary to the hypotheses of this study, there were no significant differences between conditions with regard to changes in feelings of social disconnection after exposure to the two thermal conditions. This could be attributed to the observed bidirectional change in social disconnection presented within our sample under both conditions, which could have overshadowed the differences observed in the raw data. When exposed to the cool condition, some of the participants reported reduction in feelings of social disconnection (i.e. they were feeling more socially connected). At the same time under the same condition, some other participants reported increased feelings of social disconnection (i.e. less socially connected). This contradiction within outcomes, which is probably a consequence of an uncontrolled variable, could mask the change in feelings of social disconnection driven by the indoor temperature. This bidirectional change in social disconnection could be explained by other variables, influencing the association between indoor temperature and social disconnection, which are affected particularly by cool temperature conditions, since the variation in social disconnection ratings after exposure to the warm condition was less compared to the cool condition. A potential variable influencing this association could be the presence of another participant within the room or the general social network availability of the participants. According to the social thermoregulation theory, body temperature could be regulated based on social connections, a process more prominent under cool conditions [17]. However, further research is needed to investigate these potential moderating effects on the association between indoor temperature and social disconnection.

Taking into consideration the outcomes of this study, supporting the influence of indoor temperature on social behaviours, such as empathy, it is suggested that controlling indoor temperature within an office environment might provide the necessary conditions for a more socially-friendly environment. Although further research is needed to support the outcomes, higher temperatures might be preferred to encourage more empathy between colleagues, where preferable.

This study, however, is not without limitations. The assessment of social disconnection and empathy relied heavily on self-report data, which are prone to several biases, such as desirability bias [18]. Additionally, the study was conducted only in the summer, and hence, seasonal effects on the experience of temperature could not be controlled. When considering thermal comfort of indoor environments, it is recommended to take into account the outdoor conditions and the seasonal effects that might influence outcomes [5]. Moving from a warm outdoor environment will make a cool indoor environment to be perceived cooler than it is, which could also have an effect on the association between temperature and social connectedness and empathy levels. Unfortunately, though, summer 2021 was also cooler than expected during the data collection (end of June until beginning of October 2021), therefore, typical summer conditions could not be taken into consideration.

Nevertheless, the study provided some preliminary outcomes on the association between indoor temperature, social disconnection and empathy, which could form the basis for future and more elaborate research.

5. Conclusions

In conclusion, a laboratory study was conducted, which investigated the effect of indoor temperature on measures of social disconnection and empathy. Differences between pre- and post-exposure to thermal conditions were reported for empathy levels between the cool (21 ℃) and warm (28 ℃) condition. However, no significant differences were observed for social disconnection. Further research is needed to assess the role of thermoregulation in these associations. However, the outcomes have already implications in the preferred temperature conditions that an office should hold to maintain prosocial behaviours between colleagues, favouring higher temperature conditions.

6. Acknowledgements

This research was funded under the Excellence Strategy of the Federal Government and the Länder and supported by a research grant (21055) by VILLUM FONDEN.

7. References

1. Tham S, Thompson R, Landeg O, Murray K, Waite T. Indoor temperature and health: a global systematic review. Public Health. 2020;179:9-17.
2. Jones AP. Indoor air quality and health. Atmospheric environment. 1999;33(28):4535-64.

3. Rashid M, Zimring C. A review of the empirical literature on the relationships between indoor environment and stress in health care and office settings: Problems and prospects of sharing evidence. Environment and behavior. 2008;40(2):151-90.
4. Park K-O, Wilson MG, Lee MS. Effects of social support at work on depression and organizational productivity. American journal of health behavior. 2004;28(5):444-55.
5. Frontczak M, Wargocki P. Literature survey on how different factors influence human comfort in indoor environments. Building and environment. 2011;46(4):922-37.
6. Bargh JA, Shalev I. The substitutability of physical and social warmth in daily life. Emotion. 2012;12(1):154.
7. Inagaki TK, Eisenberger NI. Shared neural mechanisms underlying social warmth and physical warmth. Psychological science. 2013;24(11):2272-80.
8. Kolb P, Gockel C, Werth L. The effects of temperature on service employees' customer orientation: An experimental approach. Ergonomics. 2012;55(6):621-35.
9. Lynott D, Corker KS, Connell L, O'Brien KS. The effect of haptic and ambient temperature experience on prosocial behavior. Archives of Scientific Psychology. 2017;5(1):10.
10. Inagaki TK, Human LJ. Physical and social warmth: Warmer daily body temperature is associated with greater feelings of social connection. Emotion. 2020;20(6):1093.
11. Inagaki TK, Irwin MR, Moieni M, Jevtic I, Eisenberger NI. A pilot study examining physical and social warmth: Higher (non-febrile) oral temperature is associated with greater feelings of social connection. PloS one. 2016;11(6):e0156873.
12. Salazar-López E, Domínguez E, Ramos VJ, De la Fuente J, Meins A, Iborra O, et al. The mental and subjective skin: Emotion, empathy, feelings and thermography. Consciousness and cognition. 2015;34:149-62.
13. Alam A, Rafique R, Anjum A. Narcissistic Tendencies, Forgiveness and Empathy as Predictors of Social Connectedness in Students from Universities of Lahore. Dialogue (Pakistan). 2016;11(2).
14. Teding van Berkhout E, Malouff JM. The efficacy of empathy training: A meta-analysis of randomized controlled trials. Journal of counseling psychology. 2016;63(1):32.
15. Eisenberger NI, Inagaki TK, Mashal NM, Irwin MR. Inflammation and social experience: an inflammatory challenge induces feelings of social disconnection in addition to depressed mood. Brain, behavior, and immunity. 2010;24(4):558-63.
16. Schaefer GA, Feelgood S. Empathy for children scale. Handbook of sexuality-related measures. 2011;40:7.
17. IJzerman H, Lindenberg S, Dalğar İ, Weissgerber SS, Vergara RC, Cairo AH, et al. The Human Penguin Project: Climate, social integration, and core body temperature. Collabra: Psychology. 2018;4(1).
18. Donaldson SI, Grant-Vallone EJ. Understanding self-report bias in organizational behavior research. Journal of business and Psychology. 2002;17(2):245-60.

Data access statement: The datasets generated during and/or analyzed during the current study are not available because the authors are still processing the data, but the authors will make every reasonable effort to publish them in near future.

Simulated thermal comfort in renovated houses with low temperature heating

Victor Ghering [a], Paula van den Brom [b], Laure Itard [c], Roel Schipper [d]

[a] ABT bv, Junior Specialist Building Physics, Delft ,the Netherlands, VictorGhering@gmail.com.

[b] Faculty of Architecture and the Built Environment, Delft University of Technology, Delft, the Netherlands, P.I.vandenBrom@tudelft.nl.

[c] Faculty of Architecture and the Built Environment, Delft University of Technology, Delft, the Netherlands, L.C.M.Itard@tudelft.nl.

[d] Faculty of Civil Engineering and Geosciences, Delft University of Technology, Delft, the Netherlands, H.R.Schipper@tudelft.nl.

Abstract. Low Temperature Heating (LTH) of buildings is a key feature when switching to renewable energy. Even when the capacity of LTH is high enough, LTH may adversely affect indoor thermal comfort in case buildings are not suitably insulated. This paper goes deeper into methodological issues when conducting a thermal comfort assessment. Thermal comfort is either quantified by Fanger's Predicted Mean Vote (PMV) or ranked in building comfort classes in the adaptive model. In both cases, one of the main parameters influencing comfort is the Mean Radiant Temperature (MRT). This study addresses issues with common MRT and PMV calculations in energy simulation software. The case study is TRNSYS 17. Several MRT and PMV calculation methods are compared, showing possible draw-backs and deviations from comfort standards NEN-EN ISO 7726 and 7730. For instance, in the standard heating settings in TRNBuild only the total heating capacity is specified. The radiative part is then distributed area-weighted over opaque surfaces. A more detailed option in TRNBuild is to specify the locations of radiative gains as points. In both cases, the MRT at a comfort sphere is calculated with Gebhardt-factors instead of view-factors. The standard settings may be considered too simplified for detailed comfort studies whereas the detailed model shows deviations from comfort standards NEN-EN ISO 7726 and 7730. Therefore, two additions to these models are proposed to increase accuracy. One addition is an ordinary detailed model with radiative gains as point sources in order to retrieve all surface temperatures during a desired period of time. In the second addition walls with radiators are split-up and planes are added at the locations of radiators to generate a view-factor matrix. This can be done in TRNBuild, but also in other view-factor calculation software. From model 1 all surface temperatures are retrieved. Combined with the view-factors from model 2, the MRT can be calculated.

Keywords. Thermal Comfort, low temperature heating, dwellings, energy transition
DOI: https://doi.org/10.34641/clima.2022.219

1. Introduction

In 2021, around 75% of the building stock in the European Union was considered to be energy inefficient, whilst 90% of these buildings are expected to still be standing in 2050 [1]. Energy labels in The Netherlands further substantiate the claim that buildings are still performing relatively poor in terms of their energy use, with an average label of C for all residences in 2019. Especially older dwellings, with construction years <1980, have poor energy labels of D or lower. Yet the vast majority of the residential building stock consists of these older dwellings [2].

In dwellings, energy is used for several purposes. The main categories that can be distinguished for energy use in The Netherlands are: space heating, cooking, hot tap water, lighting and 'other'. The largest share of energy is used for space heating but in recent years also cooling has become an increasing factor of the total energy demand. The main source of energy in The Netherlands, but also in the UK, is natural gas. The total natural gas consumption has been decreasing between 1995 and 2015 but has since then stagnated [3], whilst a further reduction (if not complete elimination) is strongly desired.

In order to pull these older, energy inefficient

Copyright ©2022 by the authors. This conference paper is published under a CC-BY-4.0 license.

dwellings through the energy transition, a mix of interventions can be carried out. Whilst a demolish and rebuild option of the old building stock is an option, renovations often require less resources and time and impose less intrusion on residents and are therefore often preferred where possible [4].

An effective way to reduce the primary energy demand from finite resources for space heating, is adding insulation (reducing the heat loss of the building) combined with the use of low temperature heating (LTH) opposed to high temperature heating (HTH). In order to effectively and comfortably use LTH and further reduce energy demand, a sufficient level of insulation should be present. In older dwellings, this is often not the case, leading to uncomfortable situations due to a capacity deficit of LTH systems.

This paper aims to evaluate the use of TRNSYS 17 for a comfort assessment. First a literature review on LTH, Thermal comfort and TRNSYS will be presented. Then the results will be provided followed by a discussion and conclusion.

2. Literature

In this chapter the results of a literature review on LTH, thermal comfort and TRNSYS 17 will be presented in order to further elaborate the reasons for this paper.

2.1 Low Temperature Heating

In colder climates, like The Netherlands, space heating is one of the main energy consuming factors of buildings [3]. Increasing insulation values of the building envelope reduces the amount of heat loss to the environment and thus the amount of energy required for space heating. It also enables temperatures of the heating system as a whole to be lowered. This further reduces the required primary energy demand and enables more efficient and renewable heat energy sources such as heatpumps, geothermals etc..

The energy for space heating is often supplied in the form of warm water. The heat is transferred to the room via a delivery system such as radiators or underfloor heating. The energy the water can deliver to the delivery system can be determined with [5]:

$$Q = \dot{m} * C_p * (T_h - T_c) \qquad (1)$$

Where: Q = capacity (W), $\dot{m}$ = mass flor rate of the water, C_p = specific heat capacity of water (J/kg °C), T_h = inlet water temperature (°K), T_c = outlet water temperature (°K)

From this equation it becomes clear the capacity of the radiator is not dependent on the temperature of the water, but the temperature difference of hot inflowing and cold outflowing water. The heat from the radiator is transferred to the room via convection and radiation. For convection, the heat transfer equation is [6]:

$$Q_{conv} = h * A * (T_{rad} - T_{air}) \qquad (2)$$

Where: Q_{conv} = capacity of the convective part (W), h = convective heat coefficient (W/m² °C), A = surface area of radiator (m²), T_{rad} = temperature of the radiator (°K), T_{air} = air temperature (°K)

For the radiative part, heat transfer happens through [6]:

$$Q_{rad} = \varepsilon * \sigma * A * T_{rad}^4 \qquad (3)$$

Where: Q_{rad} = capacity of the radiative part (W), ε = emissivity (-), σ = Stefan Boltzmann constanc ($5.67*10^{-8}$ W/m² °K), A = surface area of radiator (m²), T_{rad} = temperature of the radiator (°K)

From these equations, it can be seen that the heat delivery of the radiator is dependent on the surface area of this radiator and the temperature of the radiator. In this instance, LTH will reduce the capacity compared to HTH if this is not mitigated through the surface area or the convective coefficient of the installed radiator. This means that in most cases, the heating delivery system will also need to be adjusted when changing to LTH.

2.2 Thermal Comfort

Thermal Comfort is defined as

"the condition of mind the expresses satisfaction with the thermal environment and is assessed by subjective evaluation" [7]

In The Netherlands, thermal comfort is formulated in NEN-EN ISO 7730 [8]. This standard is based on Fanger's Predicted Mean Vote (PMV). This comfort theory is based on the following energy balance:

$$M = P_c + P_{zv} + P_g + P_{ma} + P_d + P_s + P_{av} + P_{al} \quad (4)$$

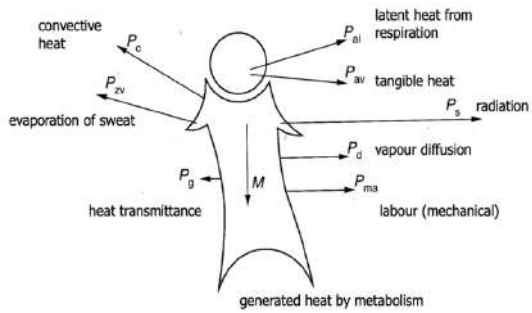

Fig. 1 – PMV principle [9]

Calculate the PMV using Equations (1) to (4):

$$PMV = [0{,}303 \cdot \exp(-0{,}036 \cdot M) + 0{,}028] \cdot \left\{ \begin{array}{l} (M - W) - 3{,}05 \cdot 10^{-3} \cdot [5\,733 - 6{,}99 \cdot (M - W) - p_a] - 0{,}42 \cdot [(M - W) - 58{,}15] \\ -1{,}7 \cdot 10^{-5} \cdot M \cdot (5\,867 - p_a) - 0{,}0014 \cdot M \cdot (34 - t_a) \\ -3{,}96 \cdot 10^{-8} \cdot f_{cl} \cdot \left[(t_{cl} + 273)^4 - (\bar{t}_r + 273)^4 \right] - f_{cl} \cdot h_c \cdot (t_{cl} - t_a) \end{array} \right\}$$

$$t_{cl} = 35{,}7 - 0{,}028 \cdot (M - W) - I_{cl} \cdot \left\{ 3{,}96 \cdot 10^{-8} \cdot f_{cl} \cdot \left[(t_{cl} + 273)^4 - (\bar{t}_r + 273)^4 \right] + f_{cl} \cdot h_c \cdot (t_{cl} - t_a) \right\}$$

$$h_c = \begin{cases} 2{,}38 \cdot |t_{cl} - t_a|^{0{,}25} & \text{for} \quad 2{,}38 \cdot |t_{cl} - t_a|^{0{,}25} > 12{,}1 \cdot \sqrt{v_{ar}} \\ 12{,}1 \cdot \sqrt{v_{ar}} & \text{for} \quad 2{,}38 \cdot |t_{cl} - t_a|^{0{,}25} < 12{,}1 \cdot \sqrt{v_{ar}} \end{cases}$$

$$f_{cl} = \begin{cases} 1{,}00 + 1{,}290 I_{cl} & \text{for } I_{cl} \leqslant 0{,}078\ m^2 \cdot K/W \\ 1{,}05 + 0{,}645 I_{cl} & \text{for } I_{cl} > 0{,}078\ m^2 \cdot K/W \end{cases}$$

where

M is the metabolic rate, in watts per square metre (W/m^2);

W is the effective mechanical power, in watts per square metre (W/m^2);

I_{cl} is the clothing insulation, in square metres kelvin per watt ($m^2 \cdot K/W$);

f_{cl} is the clothing surface area factor;

t_a is the air temperature, in degrees Celsius (°C);

$\bar{t}_r$ is the mean radiant temperature, in degrees Celsius (°C);

v_{ar} is the relative air velocity, in metres per second (m/s);

p_a is the water vapour partial pressure, in pascals (Pa);

h_c is the convective heat transfer coefficient, in watts per square metre kelvin [$W/(m^2 \cdot K)$];

t_{cl} is the clothing surface temperature, in degrees Celsius (°C).

NOTE 1 metabolic unit = 1 met = 58,2 W/m^2; 1 clothing unit = 1 clo = 0,155 $m^2 \cdot °C/W$.

Fanger's theory states that if the incoming energy from the metabolic rate is equal to the sum of the outgoing energy fluxes, a comfortable situation is reached resulting in a PMV of 0. If the outgoing energy is greater than the incoming energy, a sensation of coldness will occur, resulting in a negative PMV. A positive PMV is achieved when the sum of the incoming energy is larger than the outgoing energy and is linked to a sensations of being warm. The PMV results are scaled between -3 (cold) to +3 (hot).

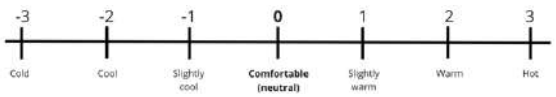

Fig. 2 – PMV scale

In order to provide an insight into how people experience the PMV score, the Percentage of People Dissatisfied (PPD) was developed. This PPD is directly linked to the PMV. At a PMV of 0, the PPD shows that still 5% of people will be uncomfortable. A building performs well if 10 % of people are dissatisfied, resulting in a PMV of 0.5. The PMV should not exceed 0.7 resulting in a PPD of 15 %.

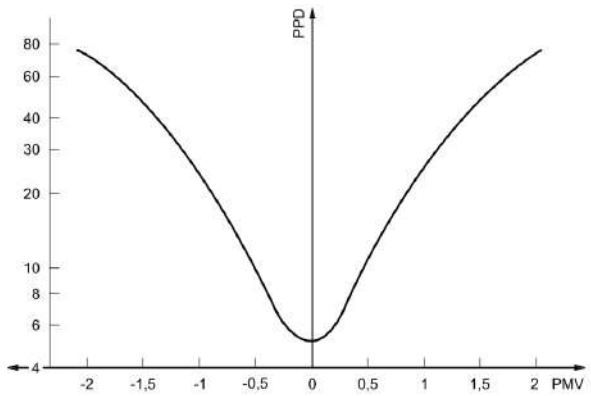

Fig. 3 – PPD link to PMV [9]

A second way to assess thermal comfort is the adaptive thermal comfort model. This model assumes that people can take actions to mitigate thermal discomfort. These actions involve, among others, changing attire, opening windows or changing the activity they partake in.

The adaptive model is based on the operative temperature, which is formulated based on the mean radiative temperature (MRT) and the indoor air temperature. This operative temperature is plotted against the running mean external temperature which takes the last 7 days into account. This is done to discount for weather deviations per day [9].

The plotted points are evaluated against 3 bandwidths. If all points fall within the narrowest bandwidth, a building is qualified as a class A(B) building and is deemed comfortable.

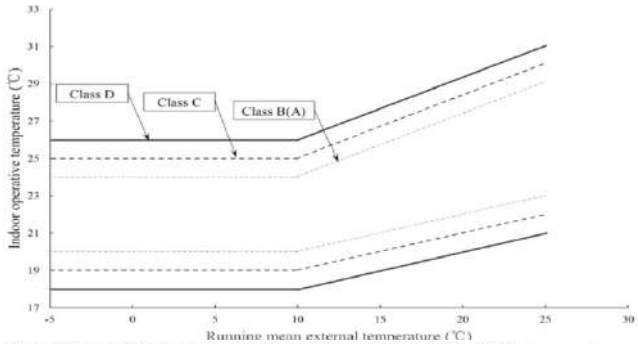

Class A	"High level of expectation. Select this category as a reference when designing spaces for people with limited lead capacity (for instance, sensitive people or persons who are diseased) or when there is a higher demand for comfort".	Max 5%	–	–
Class B	"Normal level of expectation. Select this category as a reference when designing or measuring new buildings or in the case of substantial renovations".	Max 10%	−0.5 to +0.5	–
Class C	"Moderate level of expectation. Select this category as a reference in the case of limited renovations or when measuring older existing buildings".	Max 15%	−0.7 to +0.7	–
Class D	"Limited level of expectation. Select this category as a reference in the case of temporary buildings or limited use (for instance, one to two hours of occupation per day)".	Max 25%	−1.0 to +1.0	–

Fig. 4 – Adaptive comfort [10]

Whether thermal comfort is determined via the PMV or adaptive model, the Mean Radiant Temperature of the surfaces in a thermal zone are of significant impact on the comfort sensation. This MRT is calculated not only based on the temperatures of the planes, but also their relative orientation to the comfort sensor. This sensor is usually a sphere, which can accurately resemble a seated person.

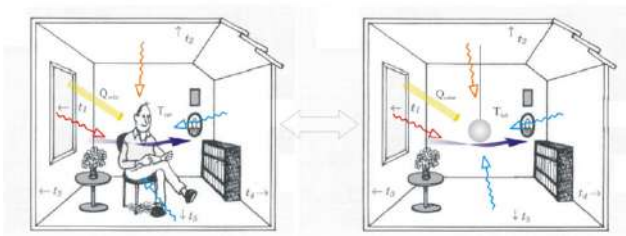

Fig. 5– MRT principle [11]

In The Netherlands NEN-EN ISO 7726 [12] prescribes how the MRT should be calculated. The most elaborate but also most thorough method is via view factors. The MRT can then be calculated through:

$$MRT = \left(\sum_{i=0}^{n} T_i^4 * F_{p \to i}\right)^{\frac{1}{4}} \qquad (5)$$

Here T_i is the surface temperature of surface i and $F_{p\rightarrow i}$ is the view factor from the comfort sphere to surface i. The view factors are dependent on orientation and surface areas of the individual planes.

2.3 TRNSYS 17

TRaNsient SYStems 17 (TRNSYS 17) is a validated and widely used program to simulate energy flows in a variety of systems through a set timeframe. Originally the program focused on solar energy systems but over years it has been elaborated to carry out a variety of simulations [13]. One addition is the option to simulate a full dwelling. A geometry can be set up in Sketchup 2014 with the plugin TRNSYS3D. TRNSYS3D can read the geometry and assign boundaries to planes. These boundaries can either be another thermal zone, ground or the outdoors. The geometry can be inputted into TRNBuild where properties can be added to the individual planes, ventilation and infiltration regimes can be assigned to thermal zones and a heating system can be implemented.

All this information is linked to the TRNSYS simulation studio in the Type 56 component [14]. Individual components can be linked to form a closed energy loop. The simulation studio is also where the time settings can be adjusted. Examples of time settings are the desired time period the simulation runs, the time steps and tolerances for the solver. In addition, weather and ground temperature data can be loaded into the project here.

The components are all open source. This ensures a 'black-box' idea can be avoided. The comfort calculation in TRNSYS 17 is however carried out in the 'Type 56: multi-zone building' component. This Type is more elaborate than the other Types and has its own interface in the form of TRNBuild. The functionality of this Type is explained in TRNSYS manual Volume 5. Here it is stated that the PMV and PPD are calculated via NEN-EN ISO 7730. The MRT is however not based on view factors but on Gebhardt factors [14]. These factors take view factors into account but also add a component that states the emissivity of the surrounding surfaces.

$$T_{MR} = \left(\sum_{i=0}^{n} T_i^4 * G_{s,i}^{LW}\right)^{\frac{1}{4}} \qquad (6)$$

$$G_{ir} = (I - F\rho_{ir})^{-1} F\varepsilon_{ir} \qquad (7)$$

Where:

G_{ir}	The Gebhardt factor matrix
I	Identity matrix
F	View Factor matrix
ρ_{ir}	Hemispherical Longwave reflectivity
ε	emissivity matrix

Radiators cannot be implemented as planes in TRNSYS 17. The first and most simplified way to implement radiators is to add a certain maximum heating capacity to a thermal zone where TRNSYS will assign the radiative part of the heating system area-weighted to the individual planes. If the locations of the radiators are to be specified, this can be done through infinitesimal points. A point source view factor matrix is then created with the use of solid angles.

Outputs of the simulations can either be directly displayed in graphs and charts or stored in CSV files.

3. Method

In order to assess the functioning of the comfort simulations in TRNSYS 17, an existing terraced dwelling in The Netherlands was modelled. One of reasons for choosing this dwelling was the availability of measured data. In the months of November and December, measurements of air and surface temperatures were taken. The measured data was used to calibrate the model in TRNSYS. The air temperatures were measured at the green dots in figure 6 whilst surface temperatures were measured at the red dots. Three comfort sensors were modelled at the blue dots.

Fig. 6– Floorplans case study dwelling

Radiators are modelled as point sources in the heart of the existing radiators. Their respective capacities are derived from the data based on their size and type. View factors are calculated through a work-around.

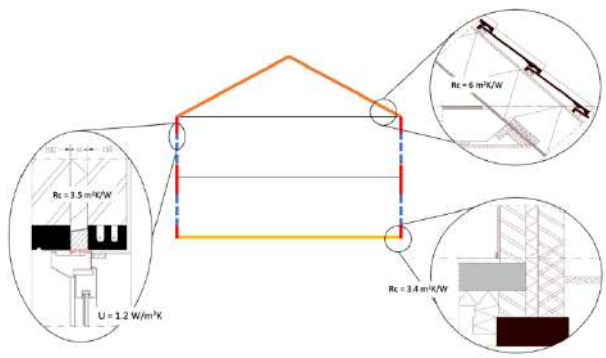

Fig. 7– Thermal insulation studied dwelling

The properties of the shell of the dwelling were derived from a previous survey. The heating system used for the calibration closely resembles a common HTH system in The Netherlands where a central heating unit is connected to a set of radiators. A central pump is the driving force to ensure waterflow and a thermostat regulates the setpoints.

During heating season, the setpoint was set at 18,5 °C

and raised to 20 °C between 15:00 and 22:00 hours. This temperature profile was chosen to match the settings the residents used at the time of measurement. For the heat recovering ventilation unit, flow rates were matched to the Bouwbesluit 2012. Infiltration was set to match class 2 'Good' standards for airtightness of building. The weather input data was linked to a weather file from the KNMI from the year 2020. Timesteps were set to 0.01 hour (6 seconds).

The metabolic rate was determined at 1.2, the clothing factor at 1, external work at 0 and the air velocity at 0.1. The ventilation

The outcomes of the TRNSYS 17 model were then compared to the measured data. Unknown properties of the heating system were adjusted (within realistic boundaries) until a close match was found between the measured an modelled data.

4. Results

In this chapter the results will be presented. First the results of the calibration process will be given. Then the comfort assessment of TRNSYS 17 will be evaluated against 4 other calculation tools.

Figure 8 shows the measured air temperatures in the living room and the modelled temperatures. Figure 9 shows the measured and modelled surface temperatures as measures. Except for the surface temperature of the façade, the measured an modelled data are deemed to be a close enough resemblance to perform a comfort comparison. Deviations most likely occur due to thermostat settings by the residents. This goes especially for the period between 21-11-2020 and 23-11-2020 where the residents were absent and lowered the thermostat in the meantime.

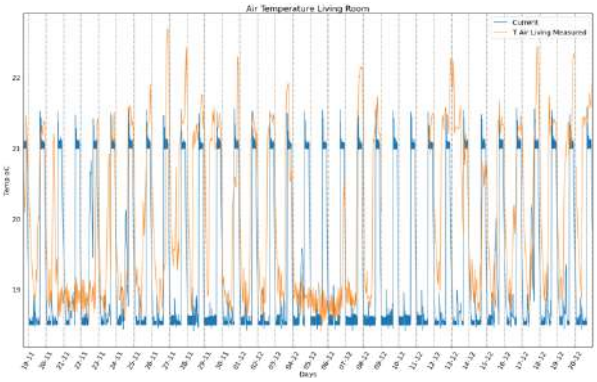

Fig. 8– Measured and modelled air temperatures

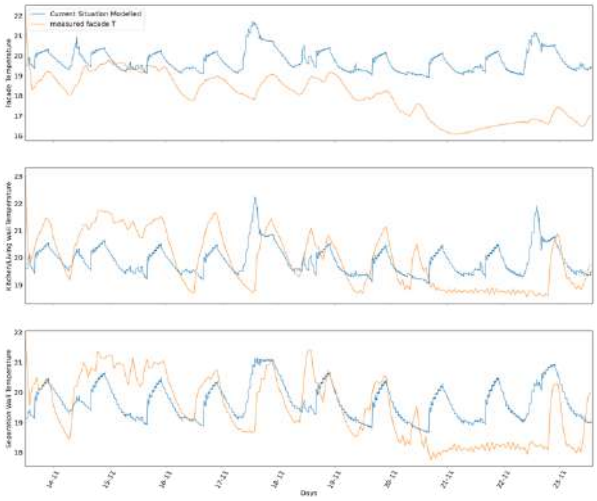

Fig. 9 – Measured and modelled surface temperatures

The surface temperature of the façade is higher in the model than what was measured. A possible explanation is the relatively low thermal conductivity (0.02 W/mK) stated by the manufacturer of the cavity insulation. resulting in an Rc value 3,5 m^2K/W. For a cavity of 6 cm a more realistic Rc value after cavity insulation is 1,1 m^2K/W. The modelled surface temperature with a façade insulation of 1,1 m^2K/W was also carried out and provided a much closer match to the measured data. It was however not deemed proven that the manufacturers claims were faulty since also execution or the state of the cavity could affect the insulation values.

For all time steps, the PMV and individual comfort parameters determined by TRNSYS were loaded into a CSV file. These parameters include the air temperature (°C), mean radiant temperature (°C) (calculated with Gebhardt factors), relative humidity (%) and air speed (m/s).

These parameters were used to compare the PMV results created by TRNSYS 17 to three other tools based on ISO 7730 and one based on EN-16798. The calculation tools included the calcPMVPPD function in the comf R-package [15] an MS Excel tool developed by the Faculty of Mechanical Engineering at the University of Coimbra [16], an Online comfort tool developed by the Centre for the Built Environment at the University of Berkeley [17] and a Python function developed by the author of this paper based on NEN-EN ISO7730. The results of the comfort calculators are presented below.

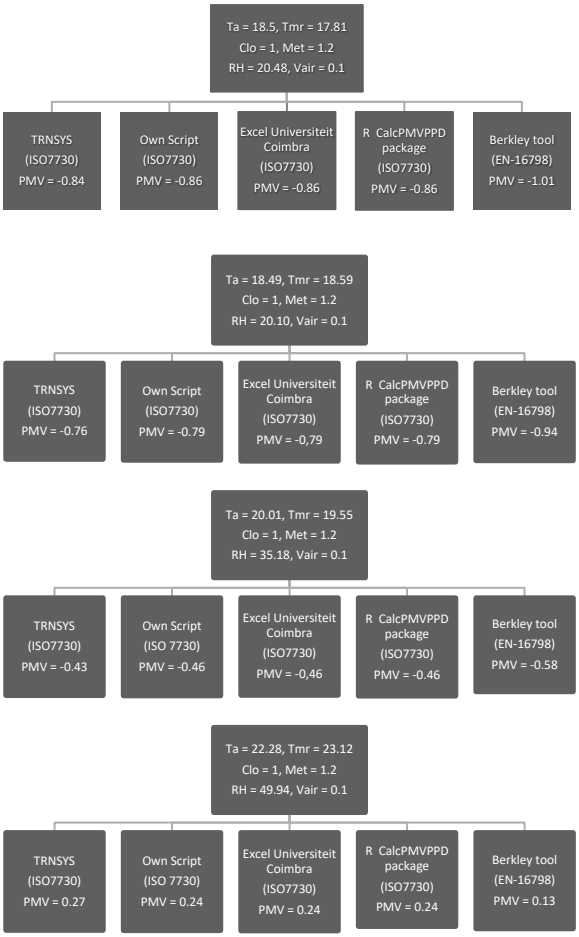

Fig. 10 – PMV calculated for 4 situations with 5 calculators

From these outcomes, it is clear that the PMV calculated by TRNSYS 17 shows an overestimation of the PMV compared to the outcomes of the three other calculators based on NEN-EN ISO7730, with the exact same input. A comparison for the PMV calculated by TRNSYS 17 and the Python function throughout the simulated year is presented in figure 11. The overestimation of the PMV calculated by TRNSYS 17, varies between 0.036 and 0.026 with a mean overestimation of 0.028.

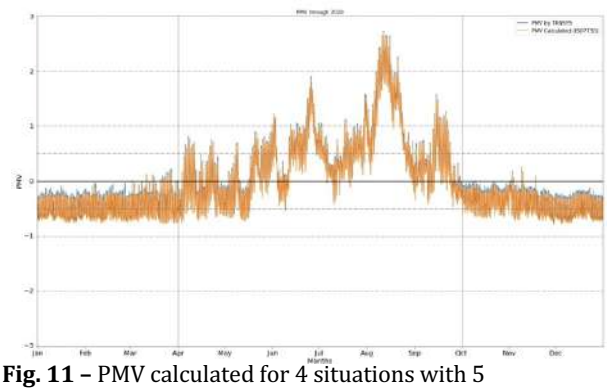

Fig. 11 – PMV calculated for 4 situations with 5 calculators

5. Discussion

The PMV scale of -3 to +3 is a large scale and often not expressed in more than 1 decimal place. A mean difference of 0.028 could also be considered trivial, especially given the accuracy of temperature measurements in general. Often, thermometers have accuracies of 0.25 °C, which will provide different PMV results.

However, since the PMV formulas are so specifically documented and have been around for so long, a difference of 0.028 should not occur at all. An attempt was made to discover a possible reason for the different outcomes. Different solvers for the clothing temperature factor were tried and rounding differences were tested. Solar radiation was also eliminated as a possible reason for overestimation since this is also not taken into account in the PMV calculation of TRNSYS.

It could not be explained why this program calculates a small but persistent difference in the PMV. This makes the program function as a 'black-box', which should always be avoided when executing simulations. Furthermore, the MRT calculation through Gebhardt factors instead of view factors, is a deviation from standards by TRNSYS 17. Additionally, the absence of a function to simulate radiators as planes can create an error in the MRT calculation. Therefore TNRSYS 17 is not deemed a suitable program for extensive thermal comfort assessments of buildings. Although it is a well-documented, validated and commonly used energy simulation program, thermal comfort should be assessed with different packages. Especially in long-term thermal comfort assessment, the difference of 0.03 might make a building pass thermal quality controls, where it actually preforms below standard.

When using TRNSYS 17 for energy simulations in buildings, thermal comfort should be assessed via a work around. A proposed method is to start with 2 TRNSYS 17 models. In one model, the radiators are simulated as points in the centre of the radiators. This model is used to perform the actual energy simulation. From this model, all surface temperatures, air temperatures and relative humidity can be retrieved for each time step.

A second model is then created where radiators are modelled with their actual sizes. If this is done in TRNSYS 17, these planes can only be added inside other surfaces. If these planes were to be added as active layers, this would mean a section of the façade would not be modelled accurately, which would affect the heat loss through this part of the façade and thus the energy demand. This model is only suitable for retrieving the view factors from the comfort sphere to the individual planes (now including the radiators).

With the parameters from model 1 and the view factors from model 2, the MRT can now be calculated

line with NEN-EN ISO7726 for each time step through for example a Python script or the Comf R-package. Subsequently, the PMV can also be calculated through a Python or R script in line with NEN-EN ISO7730.

A preliminary comfort study, carried out with the proposed work-around in TRNSYS 17, showed that the lowered peak capacity of efficient LTH systems can create uncomfortable situations. With HTH systems, it is not uncommon to have lower temperatures at times of absence or at night and increase the air temperature by over 2 °C for short periods of time. HTH often has an abundance of capacity, enabling systems to reach higher temperatures in a relatively short period of time. LTH systems on the other hand are most efficient if their capacities are closely matched to the required maximum. This also means temperature rises are slower, even when heat losses are minimized (though increased insulation and decreased infiltration rates). Less fluctuation in the temperature regime is therefore advised [18]. Further research could point out what the influence of the LTH heating systems and the used temperature settings is on the indoor thermal comfort and energy use.

Alternative software packages for comfort assessments are not abundant, but present nonetheless. One option is the PMV calculator in IES. Also VABI elements has a pre-build PMV calculator. Another option that was identified was the PMV calculator in the Ladybug/Honeybee extension for Grasshopper. This has an added benefit of enabling parametric engineering. This could be useful when attempting to determine the relative effect of insulation versus infiltration on thermal comfort for example. It should however be mentioned that all three of the named examples should also always be validated before use in a particular simulation.

6. Conclusion

With increased complexity of models and simulations, increased caution is required. When changing to LTH in dwellings in an efficient manner, new heating systems should be installed and often more insulation should be added. In order to find optimized solutions in terms of energy demand reduction with minimal material use, it is important to conduct a thorough and correct comfort assessments. Not only the absolute air temperature is of importance, but also relative humidity, air speed and the mean radiant temperature of the surrounding surfaces play a significant part in the comfort sensation. All these factors are taken into account by the PMV assessment. This increases complexity, but also the possibility to depend on outcomes to be in line with reality.

Although energy simulation software for dwellings should provide the required parameters to also conduct a comfort calculation, this has proven not be the case for TRNSYS 17. With a terraced dwelling in The Netherlands in 2020 as a case study, TRNSYS 17 overestimated the PMV with a mean of 0.028 throughout the year. Although this deviation might seem small, it should not be there at all. This was proven by the use of 3 other PMV calculation tools based on NEN-EN ISO 7730, which all showed the same results. T

7. References

[1] European Commission. A Renovation Wave for Europe - greening our buildings, creating jobs, improving lives. Brussels: European Commission. 2020

[2] CBS. Voorraad woningen; gemiddeld oppervlak; woningtype, bouwjaarklasse, regio. Retrieved December 2020, from opendata.CBS.nl: https://opendata.cbs.nl/statline/#/CBS/nl/dataset/82550NED/table?ts=1607695178923. 2020

[3] Rijksdienst voor Ondernemend Nederland. Monitor Energiebesparing Gebouwde Omgeving. 2018

[4] Najah, M. Conserveren, renoveren, transformeren of sloop, gevolgd door vervangende nieuwbouw? Eindhoven: TU Eindhoven. 2012

[5] Engineering Toolbox. Heat Capacity. Retrieved from Engineering Toolbox: https://www.engineeringtoolbox.com/heat-capacity-d_338.html. 2021

[6] Itard, L., & Rasooli, A. ME45110. Indoor Climate Fundamentals. Delft, Zuid-Holland, Netherlands: TU Delft. 2020

[7] ASHRAE. ANSI/ASHRAE Standard 55-2017. ANSI/ASHREA. 2017

[8] NEN-EN-ISO 7730. Ergonomics of the thermal environment - Analytical determination and interpretation of thermal comfort using calculation of the PMV and PPD indices and local thermal comfort criteria. Delft: NEN. 2005

[9] van der Linden, A., Kuijpers-Van Gaalen, I., & Zeegers, A. Building Physics. Amersfoort: Thieme Meulenhoff. 2018

[10] Carlucci, S., Bai, L., de Dear, R., & Yang, L. Review of adaptive thermal comfort models in built environmental regulatory documents. Building and Environment, 73-89. 2018

[11] Frenzel, C., Gröger, S., Hiller, M., Kessling, W., & Müllner, K. 12th Conference of International Building Performance Simulation Association. SIMULATION OF THERMAL COMFORT IN

SOCCER STADIA USING TRNSYS 17 (pp. 972-979). Sydney: Proceedings of Building Simulation. 2011

[12] NEN-EN-ISO 7726. Ergonomie van de thermische omgeving - Instrumenten voor het meten van fysische grootheden (ISO 7726:1998,IDT). Delft. 2001

[13] Solar Energy Laboratory. TRNSYS 17: a TRaNsient SYstem Simulation program. Wisconsin: University of Wisconsin. 2009

[14] Solar Energy Laboratory. TRNSYS 17 a TRaNsient SYstem Simulation program Volume 5: Multizone Building modeling with Type56 and TRNBuild. Wisconsin: University of Wisconsin. 2012

[15] Schweiker M., Mueller S., & Sarwar S. calcPMVPPD: PMV and PPD. Retrieved from rdrr.io: https://rdrr.io/cran/comf/man/calcPMVPPD.html. 2021

[16]Gameiro da Silva M. PMV_PPD_MC_english_Prot. Coimbra, Portugal. .d.

[17] Tartarini F., Schiavon S., Cheung T., & Hoyt T. CBE Thermal Comfort Tool: Online tool for thermal comfort calculations and visualizations. SoftwareX. 2020

[18] Ghering V., Facade renovations of dwellings for high comfort with low temperature heating. 2021.

The datasets generated during and/or analyzed during the current study are not publicly available but are/will be available upon request with the first author of this paper.

The effects of novel personal comfort systems on thermal comfort and thermophysiology

Wei Luo[a], Rick Kramer[a,c], Yvonne de Kort[b], Pascal Rense[a], Wouter van Marken Lichtenbelt[a]

[a] Department of Nutrition and Movement Sciences, NUTRIM, Maastricht University, Maastricht, P.O. Box 616, 6200MD, The Netherlands

[b] Department of Industrial Engineering and Innovation Sciences, Eindhoven University of Technology, P.O. Box 513, 5600MB, Eindhoven, The Netherlands

[c] Department of the Built Environment, Eindhoven University of Technology, P.O. Box 513, 5600MB, Eindhoven, The Netherlands

Abstract. Allowing more indoor temperature variations may stimulate human physiological thermoregulation and benefit (metabolic) health. However, thermal comfort may be compromised. To investigate possible solutions for balancing thermal comfort and health, we evaluated a novel personal comfort system (PCS) in moderately drifting ambient temperatures (17-25˚C). This PCS targets the most sensitive body parts (hands, underarms and feet in cold and the head in warm conditions), leaving the rest of the body exposed to the ambient dynamic temperature. A cross-over, randomized study was conducted in an office-like laboratory. Eighteen participants (nine male and nine female) were enrolled and performed two scenarios on separate days, one with the PCS and another scenario without the PCS in 17-25˚C. Skin temperature, skin blood flow and thermal perception were measured. The skin temperature is used to indicate thermoregulation as it is an important driver for thermoregulation while skin blood flow indicates vasomotion. The results show that the designed PCS significantly affected the skin temperature of targeted body parts while it had no significant effects on the skin temperature of most non-targeted body parts. Moreover, the skin blood flows of the hands and feet were not affected by the designed PCS in 17-21˚C. On the other hand, the designed PCS significantly changed thermal sensation and improved thermal comfort in cold to neutral conditions (17-23˚C). Therefore, the PCS may maintain the effectiveness of the cold temperature drift on vasomotion and thermoregulation, while significantly improving thermal perceptions. These findings imply that the designed PCS, combined with cold ambient conditions, potentially balances thermal comfort and health in office environments.

Keywords. personal comfort systems, thermal comfort, thermophysiology, health, drifting temperatures
DOI: https://doi.org/10.34641/clima.2022.407

1. Introduction

One of the main health concerns worldwide is the metabolic syndrome. The prevalence of the metabolic syndrome has been suggested to be associated with temperature exposures [1–3]. For example, diabetes incidence appears to be positively related to the ambient temperature [3]. One of the possible reasons for the association between metabolic syndrome and temperature is that residing mostly in a thermal neutral condition indoors minimizes thermogenesis, in combination with other factors, contributing to obesity [4,5]. On the other hand, excursions outside the neutral temperature range may elicit important (metabolic) health benefits. Firstly, exposure to cold conditions and warm conditions increases human metabolism [6,7], beneficial for preventing or combatting overweight. Moreover, regularly activating human thermoregulation in mild cold and warmth improves insulin sensitivity and reduces the risk of cardiovascular diseases [8]. Humans spend 80-90% of their time indoors. Thus, using indoor temperature variations to stimulate human thermoregulation may be a viable way to enhance human metabolic health.

Indoor temperature design should, however, meet occupants' thermal comfort as well. The practice of indoor temperature variation is challenging because

Copyright ©2022 by the authors. This conference paper is published under a CC-BY-4.0 license.

it may induce thermal discomfort. Furthermore, thermal discomfort also drives people's behaviour to reduce healthy thermal stimuli. However, recent advances in the insight in thermal comfort research may provide some potential solutions. Previous studies have shown that a moderately drifting temperature (17-25˚C with a temperature ramp around ±2 °C/h) can exercise thermoregulation without leading to thermally unacceptable conditions [9,10]. In addition, a personal comfort system (PCS) can extend the comfortable ambient temperature range down to 14°C and up to 32°C [11,12]. The PCS heats/cools body segments locally (e.g. hand, feet and torso) and allows personal control, thus, it potentiates offering individual thermal comfort. Most essentially, the PCS may precisely target the most sensitive body parts that cause thermal discomfort while leaving the rest of the body exposed to the dynamic ambient temperatures, and hence, activate thermoregulation. Taken together, a drifting temperature and/or a PCS may balance thermal comfort and thermoregulatory activation in office environments.

To date, most PCS studies focus on thermal comfort and were conducted in a stable ambient thermal environment. Given the potentials as outlined above, it is worthwhile to investigate the effect of a novel PCS on thermal comfort and thermophysiology in a drifting temperature. It was previously reported that extremities are the most uncomfortable body parts in the cold whereas the head is the most sensitive body part in warm conditions [13]. Thus, a PCS design that targets those local body parts being most uncomfortable may induce a large improvement in whole-body thermal comfort. Meanwhile, this PCS design only conditions small body areas (hands, feet and head), therefore, it may retain thermal stimulations to the rest of the body (i.e. the torso). The combination between a drifting ambient temperature profile and the designed PCS may provide a solution for the future to create a healthy and comfortable environment.

In this study, we tested a novel PCS for an office context that targets only the extremities and head under drifting ambient temperatures (17-25˚C). Thermophysiology and thermal comfort were measured. Skin temperature was used to indicate thermoregulation as it is an important driver for thermoregulation.

2. Methods

2.1 Personal comfort system

To warm the extremities in cold conditions and cool the head in warm conditions, a PCS was developed, consisting of a heating feet mat, a heating desk and two personal fans. The participants were able to adjust each device to four levels: off, low, medium and high.

2.2 Study design

Eighteen participants were enrolled (nine males and nine females) and completed two 8-hours scenarios on two separate days (with-PCS scenario and no-PCS scenario). The sequence of the scenarios was randomized. The experimental procedures of the two scenarios were identical, except for the availability of the PCS.

During the test days, the participants wore standard clothing (0.8 clo) and multiple sensors that measure skin temperature and skin blood flow. Afterwards, the participants rested in a thermally neutral condition for 30 min. Based on ISO 9886 [14], skin temperatures were assessed on fourteen sites by wireless thermometers (iButtons, Maxim Integrated Products, California, USA, Accuracy: ±0.5°C). The skin blood flows were gauged at the dorsal site of the left hand and feet by laser doppler flowmetry (PF5000, Perimed AB, Sweden).

The participants were transferred to a climate chamber around 9:00 h, where a drifting temperature profile was applied (Fig. 1). First, the temperature remained at 17˚C for 30 min to habituate participants to the environment. Then, the ambient temperature increased from 17˚C to 25˚C at a rate of change of 1.5˚C/h. Meanwhile, the participants were able to control the PCS freely in the with-PCS scenario. Every 2˚C rise, the participants did a measurement, including keeping still for 5 min to measure skin blood flow and filling in a questionnaire to rate their thermal perceptions. For thermal perceptions, thermal comfort and thermal sensation were assessed using visual analogue scales according to ISO standard 10551 [15]. Once the temperature reached 25˚C, it was maintained at 25˚C for 130 min and measurements were completed every 65 min. In total, participants resided in the climate chamber for 8 h. Participants' activities and food intake were standardized.

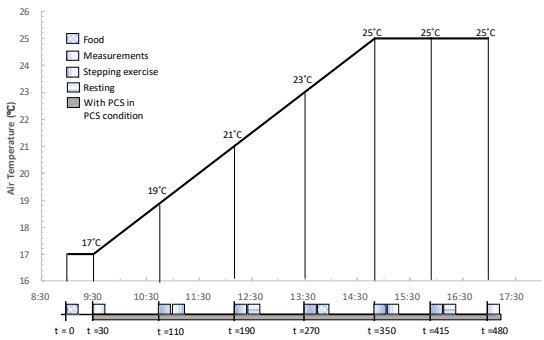

Fig. 1 – Protocol of the scenarios (the figure is adopted from [16])

2.3 Data analysis

The skin temperature was continuously monitored. Thus, the data of 10 min before submission of the questionnaire were averaged as a representative value. For skin blood flow, the average of 5 min keeping still data was used. The differences between the two scenarios were tested using a linear mixed

effects model, with participant as a random factor, and the scenarios and timepoint as fixed factors. The significance level was set at 0.05.

3. Results

3.1 Thermal perceptions

The thermal comfort and sensation data have been previously reported [16]. In the NOPCS scenario, there was a steady rise in thermal sensation from 17˚C to 25˚C and it generally followed the temperature profile (Fig 2). The thermal comfort increased in 17-21˚C and levelled off afterwards in the NOPCS scenario (Fig 3). In comparison to the NOPCS scenario, the PCS significantly increased thermal sensation in cold to neutral conditions. Also, thermal comfort significantly improved. In warm conditions (25˚C), no significant thermal perception difference between the two scenarios was found.

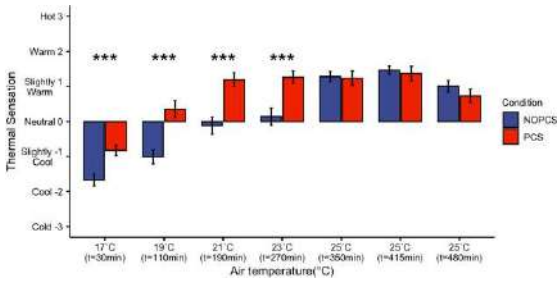

Fig. 2 – Thermal sensation votes over time (the data were adopted from [16]. *, **, *** indicate p<0.05, p<0.01, p<0.001 respectively.)

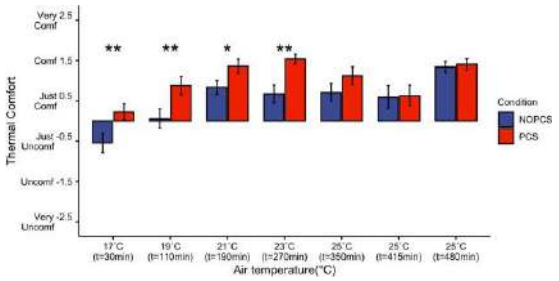

Fig. 3 – Thermal comfort votes over time (the data were adopted from [16]. *, **, *** indicate p<0.05, p<0.01, p<0.001 respectively.)

3.2 Skin temperatures

In cold to neutral conditions, the participants mainly manipulated the heating desk and heating feet mat. The PCS significantly increased skin temperature of the targeted body parts in 19-23˚C while no significant differences were found at 17˚C (hand, underarm and feet, Table 1). For most non-targeted body parts (head, neck, upper arm, torso, upper leg), the use of the PCS did not affect the skin temperature (Table 1). On the other hand, the skin temperature of the lower leg was significantly higher in the PCS scenario (19-23˚C, Tab. 1).

At 25˚C, the personal fan was generally used to cool the head region. As expected, the PCS successfully cooled the head and neck (Table 2). However, feet and lower leg skin temperatures were higher in the PCS scenario at 25˚C, t = 350min and t = 415 min (Tab. 2). For other non-targeted body parts (upper arm, underarm, hand, torso and upper leg), the skin temperatures were unaffected by the PCS.

Table 1 – Significance levels of the skin temperature differences in local body parts between two scenarios in 17-23˚C (X, *, **, *** indicates p>0.05, p<0.05, p<0.01, p<0.001 respectively. ↑/↓ indicates a higher/lower skin temperature compared to the NOPCS scenario.)

	17˚C (t=30)	19˚C (t=110)	21˚C (t=190)	23˚C (t=270)
Head	X	X	X	X
Neck	X	X	X	X
Upper arm	X	X	X	X
Under arm	X	↑, ***	↑, ***	↑, ***
Hand	X	↑, ***	↑, ***	↑, **
Torso	X	X	X	X
Upper leg	X	X	X	X
Lower leg	X	↑, **	↑, *	↑, **
Feet	X	↑, ***	↑, ***	↑, ***

Table 2 – Significance levels of the skin temperature differences in local body parts between two scenarios at 25˚C (X, *, **, *** indicate p>0.05, p<0.05, p<0.01, p<0.001 respectively. ↑/↓ indicates a higher/lower skin temperature compared to the NOPCS scenario.)

	25˚C (t=350)	25˚C (t=415)	25˚C (t=480)
Head	↓, ***	↓, ***	↓, ***
Neck	↓, **	↓, ***	↓, **
Upper arm	X	X	X
Under arm	↑, ***	X	X
Hand	X	X	X
Torso	X	X	X
Upper leg	X	X	X
Lower leg	↑, ***	↑, **	X
Feet	↑, ***	↑, **	X

3.3 Skin blood flow

The skin blood flows of the hands and feet showed different patterns in the NOPCS scenario (Figures 4 and 5). The hand skin blood flow increased with the rise of ambient temperature (Fig. 4). In contrast, the feet skin blood flow remained stable across 17-23°C, but showed an increase at 25°C (Fig. 5). Overall, the PCS did not significantly affect the skin blood flow of hands and feet, except for a rise in hand skin blood flow using the PCS at 23°C.

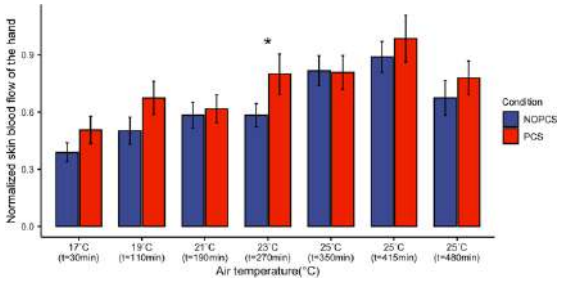

Fig. 4 – Normalized skin blood flow of the hands over time (the data were adopted from [16]. *, **, *** indicate p<0.05, p<0.01, p<0.001 respectively.)

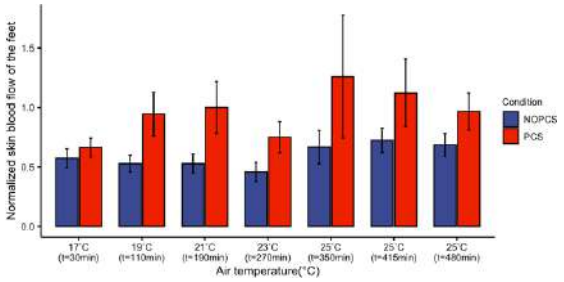

Fig. 5 – Normalized skin blood flow of the feet over time (*, **, *** indicate p<0.05, p<0.01, p<0.001 respectively.)

4. Discussion

The purpose of this study was to determine the effect of a novel PCS on thermophysiology and thermal comfort under drifting ambient temperatures. We found that thermal perceptions were significantly improved using the PCS in 17-23°C (Fig. 2 and 3, [16]). The PCS significantly manipulated the skin temperature of targeted body parts, but it did not affect non-targeted body parts in most cases (Tables 1 and 2). Moreover, the skin blood flows of the hands and feet were generally similar between the two scenarios (Fig. 4 and 5).

By targeting the most sensitive local body parts, the PCS successfully improved thermal comfort in 17-23°C. This improvement is comparable to Zhang's study [17], where the participants also felt more comfortable by heating hands and feet at 18°C. Given the fact that the designed PCS only cooled/heated a small area of the body (extremities or the head area), it was assumed that the non-targeted body segments would not be influenced by the PCS. The present results validate this assumption. The PCS did not affect the skin temperature of the major non-targeted body segments. This finding was also reported in other studies [18,19]. Interestingly, the PCS significantly increased the skin temperature of the lower leg in 17-23°C. The reason may be that the heating mat caused an unintentional elevation of the ambient temperature near the lower leg. Moreover, the increased skin temperature of the lower legs and feet in the PCS scenario continued until 25°C. This may be attributed to the fact that some participants still used the feet heating mat at 25°C.

Skin temperature feeds an important signal to our brains used for thermoregulation [20]. Considering that skin temperatures of non-targeted body segments were similar between the two scenarios in most cases, we can reasonably assume that the thermoregulatory responses were also similar between the two scenarios. The present results confirm this. Indeed, there were no significant differences in hands and feet' skin blood flow. This indicates that vasomotion, one of the thermoregulatory responses, remained unchanged when using the PCS. In general, it seems that the designed PCS did not reduce the effectiveness of the cold temperature drift on thermoregulation and vasomotion.

5. Conclusion

In this study, the effects of a novel PCS on thermophysiology and thermal comfort were studied. The main conclusions are that: 1) the designed PCS significantly improved thermal comfort in cold to neutral conditions [16]. 2) the designed PCS did not affect the skin temperature of non-targeted body parts in most cases. 3) The PCS did not generally affect vasomotion indicated by the unchanged skin blood flow of the hands and feet. These findings suggest that the designed PCS has a great potential to balance thermal comfort and health under cold ambient conditions in office environments.

6. Acknowledgement

This work is financially supported by the TKI project "PERDYNKA— dynamic light and indoor climate for office", project number: 1507503. The authors would like to thank Michiel Moonen, Luc Schlangen, Marc Souren, Paul Schoffelen, and the companies Royal Ahrend and Almende for their help.

7. Data availability statement

The data that support the findings of this study are available from the corresponding author, [W.L.], upon reasonable request.

8. References

[1] Keith SW, Redden DT, Katzmarzyk PT, Boggiano MM, Hanlon EC, Benca RM, et al. Putative contributors to the secular increase in obesity: Exploring the roads less traveled. Int J Obes.

2006;30(11):1585–94.

[2] McAllister EJ, Dhurandhar N V., Keith SW, Aronne LJ, Barger J, Baskin M, et al. Ten putative contributors to the obesity epidemic. Crit Rev Food Sci Nutr. 2009;49(10):868–913.

[3] Speakman JR, Heidari-Bakavoli S. Type 2 diabetes, but not obesity, prevalence is positively associated with ambient temperature. Sci Rep. 2016;6(August):30409.

[4] Van Marken Lichtenbelt WD, Kingma BR. Building and occupant energetics: A physiological hypothesis. Archit Sci Rev. 2013;56(1):48–53.

[5] Van W, Lichtenbelt M, Kingma B, Van Der Lans A, Schellen L. Cold exposure-an approach to increasing energy expenditure in humans. Trends Endocrinol Metab. 2014;25(4).

[6] Celi FS, Brychta RJ, Linderman JD, Butler PW, Alberobello AT, Smith S, et al. Minimal changes in environmental temperature result in a significant increase in energy expenditure and changes in the hormonal homeostasis in healthy adults. Eur J Endocrinol. 2010;163(6):863–72.

[7] Pallubinsky H, Schellen L, van Marken Lichtenbelt WD. Exploring the human thermoneutral zone – A dynamic approach. J Therm Biol. 2019 Jan; 79:199–208.

[8] van Marken Lichtenbelt W, Hanssen M, Pallubinsky H, Kingma B, Schellen L. Healthy excursions outside the thermal comfort zone. Build Res Inf. 2017;45(7):819–27.

[9] Ivanova YM, Pallubinsky H, Kramer R, van Marken Lichtenbelt W. The influence of a moderate temperature drift on thermal physiology and perception. Physiol Behav. 2021;229:113257.

[10] Schellen L, van Marken Lichtenbelt WD, Loomans MGLC, Toftum J, de Wit MH. Differences between young adults and elderly in thermal comfort, productivity, and thermal physiology in response to a moderate temperature drift and a steady-state condition. Indoor Air. 2010;20(4):273–83.

[11] Zhang H, Arens E, Zhai Y. A review of the corrective power of personal comfort systems in non-neutral ambient environments. Build Environ. 2015 Sep;91:15–41.

[12] Veselý M, Zeiler W. Personalized conditioning and its impact on thermal comfort and energy performance - A review. Renew Sustain Energy Rev. 2014;34:401–8.

[13] Arens E, Zhang H, Huizenga C. Partial- and whole-body thermal sensation and comfort - Part I: Uniform environmental conditions. J Therm Biol. 2006;31(1-2 SPEC. ISS.):53–9

[14] ISO 9886. Ergonomics-Evaluation of thermal strain by physiological measurements. International Organization for Standardization; 2004

[15] 10551 I. Ergonomics of the physical environment - Subjective judgement scales for assessing physical environments. International Organization for Standardization; 2019

[16] Luo W, Kramer R, Kort Y, Rense P, Marken Lichtenbelt W. The effects of a novel personal comfort system on thermal comfort, physiology and perceived indoor environmental quality, and its health implications - Stimulating human thermoregulation without compromising thermal comfort. Indoor Air. 2021;(September):1–17.

[17] Zhang H, Arens E, Kim DE, Buchberger E, Bauman F, Huizenga C. Comfort, perceived air quality, and work performance in a low-power task-ambient conditioning system. Build Environ. 2010;45(1):29–39.

[18] Luo W, Kramer R, de Kort Y, van Marken Lichtenbelt W. Effectiveness of personal comfort systems on whole-body thermal comfort – a systematic review on which body segments to target. Energy Build. 2021;111766.

[19] Veselý M, Molenaar P, Vos M, Li R, Zeiler W. Personalized heating – Comparison of heaters and control modes. Build Environ. 2017 Feb;112:223–32.

[20] Romanovsky AA. Skin temperature: Its role in thermoregulation. Acta Physiol. 2014;210(3):498–507.

Simulating indoor air quality in London hospitals: A building-based bottom-up method

Shih-Che Hsu [a], Ian Hamilton [a], Anna Mavrogianni [b], Rob Liddiard [a]

[a] UCL Energy Institute, University College London, United Kingdom, shih-che.hsu.15@ucl.ac.uk

[b] UCL Institute for Environmental Design and Engineering, University College London, United Kingdom

Abstract. Healthcare premises are energy-intensive buildings, and their operation and performance are critical to healthcare delivery and the protection of patients. A key step towards ensuring people's wellbeing and facilitating recovery is establishing the distributions of indoor air pollutants and temperature, and associated exposures in hospitals. Microenvironment pollutant concentrations are determined by the generation of indoor sources of pollution and the penetration of outdoor air to the indoors. In hospitals, the conditions for air pollution are typically highly controlled to deliver clean environments; however, building ventilation systems may still be subject to harsh external environments that impact on indoor environmental conditions. The aim of this study is to enhance understanding of how building operations and energy efficiency improvements will impact indoor hospital environments whilst reducing potential harmful pollutant exposures and energy demand. To achieve this, the ventilation conditions and corresponding $PM_{2.5}$ penetration of London hospitals were simulated. The baseline data of building stock physics (building types, construction periods, floor levels, room functions, total floor area and energy performance ratings) for hospitals were aggregated from the building typologies and room functions of the London 3DStock model to analyse the effect of built configurations on air ventilation and pollutant transfer using the CONTAM tool. The simulation results show that recently built or retrofitted hospital buildings are more airtight and energy-efficient but also need to carefully maintain intentional ventilation and filtration to ensure adequate air quality conditions to prevent the ingress of outdoor-sourced air pollutants. The simulations also show that COVID operating procedures may greatly increase airflow and a corresponding need for additional air filtration to meet guidance on pollution levels.

Keywords. Indoor Air Quality, Healthcare Premises, Optimization and Modelling, Building Envelope, CONTAM.
DOI: https://doi.org/10.34641/clima.2022.408

1. Introduction

The UK's 2050 climate target of net zero carbon emissions [1] prompts the urgent need for building retrofits to improve building energy efficiency and reduce carbon emissions, especially in public buildings. To reduce the heat loss, requires the improvement of the building envelope which will significantly modify ventilation characteristics, such as air tightness. As a result, research and policy interest in Indoor Air Quality (IAQ) and the potential health impacts of indoor air pollutant exposure has been gradually increasing in recent years. When estimating indoor air quality, both the infiltration of outdoor air pollutants and building air exchange play significant roles [2].

The healthcare sector has been estimated to be responsible for 4 to 5% of the carbon footprint and about a fifth of public sector emissions in England [3]. Actions of the healthcare sector will be instrumental in delivering the Net Zero Strategy (NZS) by 2050. Although the National Health Service (NHS) has made significant progress in reducing carbon emissions by 26% between 1990 and 2019 [4], to-date the pace of improvement is insufficient to meet the 2050 target. Therefore, there must be an acceleration of related work to deliver a net zero healthcare sector. Hospitals are energy-intensive buildings, but their operation and performance are critical to healthcare delivery and the protection of patients. A key step towards ensuring people's wellbeing and facilitating recovery is establishing the distributions of indoor air pollutants and temperature, and associated exposure in hospitals. However, there are significant knowledge gaps around the impact of building retrofits on IAQ within UK healthcare premises, and more generally their

Copyright ©2022 by the authors. This conference paper is published under a CC-BY-4.0 license.

indoor environmental conditions are not well described.

This study aims to understand the impact of building physics and energy performance on air penetration rates for ventilation prediction and indoor air quality modelling in London healthcare buildings. London healthcare premises were retrieved from a 3-dimensional model of London, providing the opportunity to develop bottom-up physics-based models to simulate indoor air quality and energy demand. Hospitals, surgeries, clinics, and health centres (including dentists) were modelled, and offices and wards in the premises were focused upon as they are the main room types where people spend time in hospitals.

CONTAM 3.2 was employed to simulate IAQ in London healthcare buildings. CONTAM, as a well-validated multizone indoor air quality and ventilation analysis computer program, created by the National Institute of Standards and Technology (NIST) of the U.S. Department of Commerce, can determine: (1) airflows; (2) indoor contaminant concentrations; (3) personal exposure to indoor air pollution [5]. To-date only a few studies have applied CONTAM to healthcare environments [6, 7, 8] and the modelling outputs of these studies were mainly for a single building, which may be difficult to generalise across multiple spaces in multiple buildings. Moreover, previous studies, using either computational fluid dynamics (CFD) simulation [9, 10] or a modelling approach based on in-situ measurements [11] to estimate hospital ventilation, were also from very specific cases. This study employing bottom-up large-scale building modelling of healthcare premises provides an innovative way to address the limitation of generalisation by using information aggregated from across London.

2. Method

2.1 3DStock: aggregation of healthcare environments in London

The London 3DStock model, which was developed by a team at the UCL Energy Institute led by Professor Philip Steadman, is a method for modelling London's whole building stock. Great Britain Ordnance Survey digital maps, commercial property taxation data from the Valuation Office Agency (VOA), and Light Detection and Ranging (LiDAR) data from the UK Environment Agency were assembled into a 3D model [12]. The characteristics of individual domestic, non-domestic and mixed-use premises in all 33 boroughs of the Greater London area and the floor-by-floor activities, room-level sub-activities and floor areas from the VOA's non-domestic premises surveys were held in a PostgreSQL database. This large dataset has been mainly used in analysing and estimating population-level energy demand [13, 14]. In this research, for simulating indoor air quality based on energy performance and building characteristics, 3DStock was used to aggregate basic building characteristics of existing healthcare buildings in London. Simple archetypes representing healthcare building typologies in different construction periods were proposed, based on the aggregation.

The building information extracted from the 3DStock model for CONTAM model development were building types; construction periods; floor levels; room functions; floor areas and energy performance ratings. The classes of each building characteristic are listed below:

(1) Building type: Four typical building types were used, which are Detached, Semi-detached, End-terrace and Mid-terrace forms. These types refer to the attachment of a building to other buildings, and are not a reference to residential use. Those without a record of building type, were denoted 'N/A'.

(2) Construction period: Four periods were used to present the building age, which are Pre-1914, 1918-1939, 1945-1980, Post-1980. Those without a record of construction year, were denoted 'N/A'.

(3) Floor level: Floor level was recorded for each premises in 3DStock up to the fiftieth floor. Numbers 0 to 50 denote ground floor to fiftieth floor. Basements, lower ground floors and mezzanines are also identified. Those without a record of floor level, were denoted 'N/A'.

(4) Room function: Detailed sub-activities within each premises are provided in 3DStock, largely based on the VOA's sub-activity classification system. In this research, healthcare sub-activities are grouped into 14 types: Consulting Room; Facilities (such as x-ray rooms, computer rooms); Kitchen (including staff/mess/common rooms and tea points); Office; Reception (including lobby, hall and porch); Retail Zone; Storage (including file/ report rooms; Surgery (including dental surgeries); Toilet (including changing area, shower rooms, restrooms); Treatment Room (including clinics); Waiting Room (free space excluding reception area); Ward (including pre-/post-surgery rooms); Utility Room (such as garages, cleaning rooms); Other (Including mix-used rooms and rooms hard to classify).

(5) Floor area of sub-activity was recorded in square metres (m^2) in 3DStock. In this research, healthcare premises were rounded to show the statistics of different bands of building total floor area.

(6) Energy performance: 3DStock contains records for Energy Performance Certificates (EPCs), which are a theoretical energy performance indicator based on the building and the standardised use of its fixed services (heating,

lighting etc.). EPCs grade performance from 'A' (best) to 'G' (worst). Where the premises do not have an EPC, a 'virtual EPC' (vEPC) has been created, based on nearby premises with similar non-EPC derived characteristics. To cope with mixed-use buildings, 3DStock also aligns and aggregates non-domestic EPCs and vEPCs to their domestic equivalents [9], presenting as "rvEPCs" for healthcare premises with a scale of 1 to 100 from the worst to the best energy performance. Henceforth, rvEPCs are simply denoted as EPCs. This provides a metric applicable across all building types in the stock and a general idea of energy performance, but it is not 100% accurate.

Depending on the building statistics, basic models were created to simulate ventilation and penetration of outdoor air pollution indoors in CONTAM by estimating building air exchange rates (Air Changes per Hour, ACH) for each archetype.

2.2 CONTAM: simulation of ventilation and air pollution in London healthcare environments

CONTAM determines room-to-room airflows driven by exterior wind pressure, buoyancy effect of indoor-outdoor temperature difference and intentional mechanical ventilation. In hospitals, the conditions for air pollution are typically highly controlled to deliver clean environments; however, building ventilation systems may still be subject to harsh external environments that impact on indoor environmental conditions. This work includes both unintentional infiltration and intentional ventilation to simulate hour-by-hour indoor $PM_{2.5}$. Here, indoor-sourced $PM_{2.5}$ was ignored and only outdoor-sourced $PM_{2.5}$ was assumed to affect indoor microenvironment pollutant concentrations.

The U.S. Department of Energy defined sixteen reference buildings, and CONTAM models of the 16 reference buildings were created to support physics-based airflow calculations and indoor air quality analysis [15]. Two types of reference building of healthcare environments have been identified: hospital and outpatient health care. These were further classified into subtypes based on the construction year, pre-1980, post-1980 and newly built after 2004. In this research, only the type "hospital" was applied for simplicity, and parameters in CONTAM libraries and building variables were adjusted accordingly for London healthcare buildings. For alignment with the construction years of healthcare premises in 3Dstock, only pre-1980 and post-1980 CONTAM models were used. Summer weather was set as the warmest July and winter weather as the coldest January, according to the UK typical meteorological status [16]. Based on the typical meteorology features, hourly airflows, and time-average ventilation rates and indoor $PM_{2.5}$ were subsequently simulated in the building form of hospital environments for January and July in the Pre-1980 and Post-1980 reference buildings.

Figure 1 from NIST Technical Note 1734 shows the layout of floors in a hospital where (a) patient rooms (wards) and (b) offices are located [12]. The ambient environment surrounding the building was set following the weather file converted from Typical Meteorological Year 2 (TMY2) in London for transient analysis. The zones in CONTAM sketchpad were assigned with the aggregate floor areas by room use type, construction periods and energy performance. According to the Chartered Institute of Building Services Engineers recommendations, the workplace temperature was set at 18 °C in hospitals [17] and the ward was set at 20 °C. Other settings were kept default when running simulations. The single patient room 8 at the top-left corner in figure 1 (a) and the single office 3 at the top-left corner in figure 1 (b) were the target rooms to be modelled in this research.

Fig. 1 - Layout of floors in hospitals where (a) wards and (b) offices are located on (adapted from [15]).

CONTAM was also used to estimate room-to-room indoor infiltration of $PM_{2.5}$ concentrations only originating from the environment surrounding the building, which were investigated under the pollution scenario related to the London Average Air Quality Levels. Indoor sources of $PM_{2.5}$ were not

considered in this study at this stage. The London Average Air Quality Levels, available from the London Datastore for the period 01/01/2008 – 31/07/2019, shows background and roadside average pollutant levels (ug/m^3) for $PM_{2.5}$ by hour of day per month [18]. This research used the 2019 London mean background $PM_{2.5}$ levels. The contaminant species properties of $PM_{2.5}$ were set with a molecular weight of 8 kg/kmol, diffusion coefficient 2×10^{-5}-m^2/s and specific heat 1000 J/kgK, and a sink of $PM_{2.5}$ was set in each room in the deposition rate model with the deposition rate 0.19 per hour for transient simulation. Other settings of Contaminant Numerics in CONTAM models, including Linear Contaminant Solver, CVODE Non-Linear Contaminant Solver, Convergence for Cyclic Simulations and 1D Options, were kept as default settings.

The COVID-19 pandemic has shown the importance of indoor air quality and ventilation controls, especially in facilities where reducing viral exposure is required, such as hospitals. COVID-19 guidance from UK Health Security Agency [19] was examined in an attempt to evaluate the impacts on indoor pollution level. However, as the guidance is only general in nature and contains no information on proposed rates of ventilation/infiltration, the effects of the guidance could not be evaluated.

3. Results and discussion

3.1 3DStock model aggregation results

The 3DStock model can provide information regarding the distribution of building types, building physics and room features of healthcare buildings in London. The Sankey diagram in Figure 2 illustrates the breakdown of room-level healthcare premises in London by building archetype, storey count, room use, room area, floor level, and construction period. The majority of London healthcare premises were found in mid-terrace and detached buildings of less than four storeys. Office, Surgery, Storage, Toilet and Consulting rooms were the top five room uses, which were found mainly at ground and first floor level. Very few activities were found higher than the fifth floor. Most of these rooms were no more than 20 m^2 and located in the buildings built before 1940 or with no construction year record.

In all, 11,028 room-level units of healthcare premises were present in the building dominated by non-domestic activities in the 3DStock model and Table 1 summarises their energy performance in different construction periods. Most London healthcare premises are EPC grade D (44%) or grade E (27.9%), and EPC grade D dominates all construction periods. The mode of EPC grades was D within the 3DStock samples, which is the same for England's existing properties as found in the Live tables on Energy Performance of Buildings Certificate [20]. It was also found post-1980 healthcare premises have better energy performance than other periods, with more EPC grade B and C than EPC grade E, F, and G. Other periods have higher percentages of EPC grade E, F, and G than EPC grade B and C. This could also suggest that the more recently built hospital premises, modelled in the research, might have higher airtightness and less leaky building envelopes bringing better energy performance.

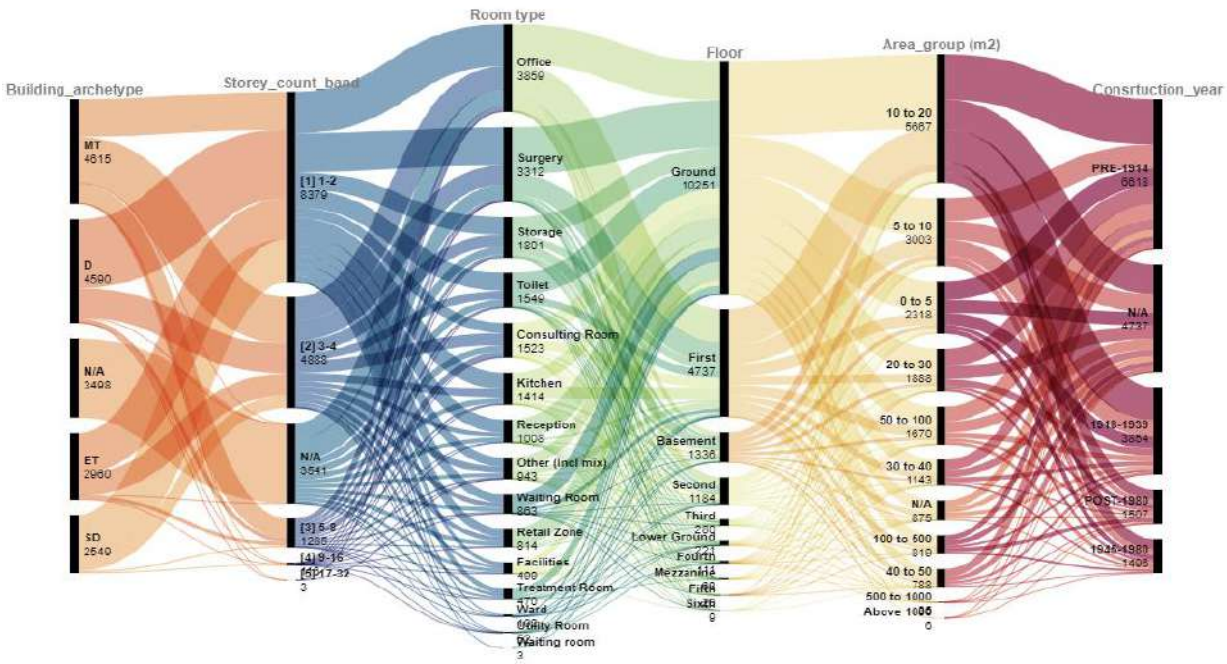

Fig. 2 - Sanky diagram of London healthcare premises created by RAWGraphs data visualization framework [21].

Tab. 1 - Energy performance of London healthcare premises in different construction periods.

EPC Periods	A N(%)	B N(%)	C N(%)	D N(%)	E N(%)	F N(%)	G N(%)	N/A N(%)	Total N(%)
N/A	1 (0.0)	42 (0.4)	172 (1.6)	351 (3.2)	192 (1.7)	115 (1.0)	52 (0.5)	91 (0.8)	1016 (9.2)
PRE-1914	0 (0.0)	92 (0.8)	482 (4.4)	1984 (18.0)	1472 (13.3)	325 (2.9)	93 (0.8)	398 (3.6)	4846 (43.9)
1918-1939	0 (0.0)	27 (0.2)	189 (1.7)	1601 (14.5)	938 (8.5)	144 (1.3)	85 (0.8)	80 (0.7)	3064 (27.8)
1945-1980	0 (0.0)	6 (0.1)	117 (1.1)	516 (4.7)	291 (2.6)	58 (0.5)	28 (0.3)	56 (0.5)	1072 (9.7)
POST-1980	0 (0.0)	137 (1.2)	173 (1.6)	401 (3.6)	180 (1.6)	24 (0.2)	50 (0.5)	65 (0.6)	1030 (9.3)
Total	**1 (0.0)**	**304 (2.8)**	**1133 (10.3)**	**4853 (44.0)**	**3073 (27.9)**	**666 (6.0)**	**308 (2.8)**	**690 (6.3)**	**11028 (100)**

3.2 CONTAM model simulation results

Based on the 3DStock aggregate information, CONTAM building layouts were adjusted for hospitals in pre-1980 and post-1980 buildings. Table 2 shows the mean floor area per room use type in two periods, which were input to CONTAM zone floor area for each room use type. For example, the mean office floor area in pre-1980 is 37m^2 and in post-1980 is 72m^2. Using the table, it was found that all room types except for the Facilities rooms are more spacious in post-1980 buildings than in pre-1980 buildings.

Tab. 2 - The mean floor area of different room use types in pre-1980 and post-1980 healthcare premises.

Year Room type	Pre-1980 Area (m^2)	Post-1980 Area (m^2)	N/A Area (m^2)	Total % of N	Total Area (m^2)
Consulting Room	33	37	55	8.4	39
Facilities	14	12	22	2.7	17
Kitchen	10	11	11	7.8	10
Office	37	72	47	21.2	43
Reception	20	37	25	5.5	23
Retail Zone	23	71	27	4.5	26
Storage	12	19	13	9.9	13
Surgery	34	75	35	18.2	37
Toilet	4	6	7	8.5	5
Treatment Room	20	32	26	2.6	23
Utility Room	6	12	10	0.3	8
Waiting Room	18	35	23	4.8	21
Ward	39	128	33	0.6	47
Other (Incl mix)	37	117	52	5.2	52
Total	**26**	**54**	**32**	**100**	**30**

Figure 3, below, is the example of simulated airflow rate distribution of the target patient room (ward) of pre-1980 hospitals, during 1st January to 7th January. Sixteen grey lines indicate the balanced airflows through all airflow paths coming from outdoors (positive values) and blowing out of (negative values) the room. The red line is the sum of all sixteen flow rates, and the sum was used to estimate the air exchange of a room. In wintertime, the maximum ventilation rate in the pre-1980 hospital ward was 351.0 m^3/h at 8 am on 3rd January, which gives 2.1 ACH after being divided by the volume of the ward 166.5 m^3. For summertime, the maximum ventilation rate of the pre-1980 hospital ward was 132.7 m^3/h at 1pm on 22nd July and lead to 0.8 ACH. Comparing to the results of the post-1980 hospital, larger ward floor areas lead to lower air change rate, 0.6 ACH in winter and 0.2 ACH in summer. As for the offices in hospitals, the maximum air change rates from an airflow path were: 5.5 ACH in winter and 2.6 ACH in summer in the pre-1980 hospitals and 1.7 ACH in winter and 0.8 ACH in summer in the post-1980 hospitals. It was found the air change rates in the post-1980 hospitals are less than half those in the pre-1980 hospitals. The average ACH in an office was higher than in a ward, 2 – 4 times depending on the time of day and month of the year.

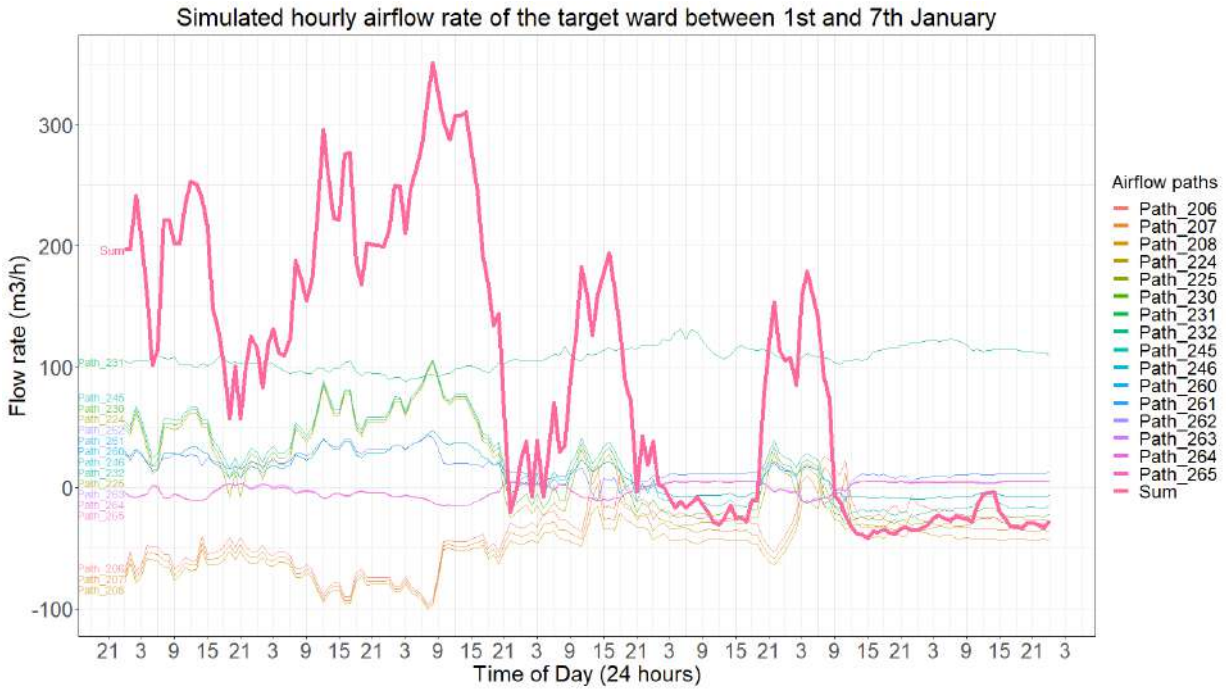

Fig. 3 - Simulated airflow rate of the target patient room of London hospitals between 1st January and 7th January. Sixteen lines stand for the balanced airflows through all airflow paths coming from outdoors and blowing out the room.

With different levels of ventilation rate resulting from conditioned simulation, air pollutants from outdoors are accumulated and removed at a different pattern for each room in healthcare environments. In this research, transient concentrations of $PM_{2.5}$ (μg/m³) in each room are simulated based on the temporal resolution of transient weather data and transient contaminant data, which are both on an hourly basis.

Figure 4 shows the example of simulated hourly $PM_{2.5}$ concentration of the target office and ward in the pre-1980 hospitals from 1st January to 7th January and 1st July to 7th July respectively. It was found, in wintertime, offices (10.9 – 15.2 μg/m³) and wards (11.1 – 15.8 μg/m³) both have higher indoor $PM_{2.5}$ concentrations than the WHO air quality guideline for $PM_{2.5}$, 10 μg/m³ annual mean (WHO 2006) in the pre-1980 hospitals, while in summertime the $PM_{2.5}$ for the office (8.3 – 9.5 μg/m³) and for the ward (8.4 – 9.6 μg/m³) are both lower than the WHO air quality guideline. As for the post-1980 hospitals, the overall indoor $PM_{2.5}$ concentrations are close to, but slightly lower than, the ones in the pre-1980 hospitals: in wintertime the offices are 10.9 – 15.2 μg/m³ and the wards are 11.1 – 14.9 μg/m³; in summertime the offices are 7.9 – 9.5 μg/m³ and the wards are 8.4 – 9.4 μg/m³.

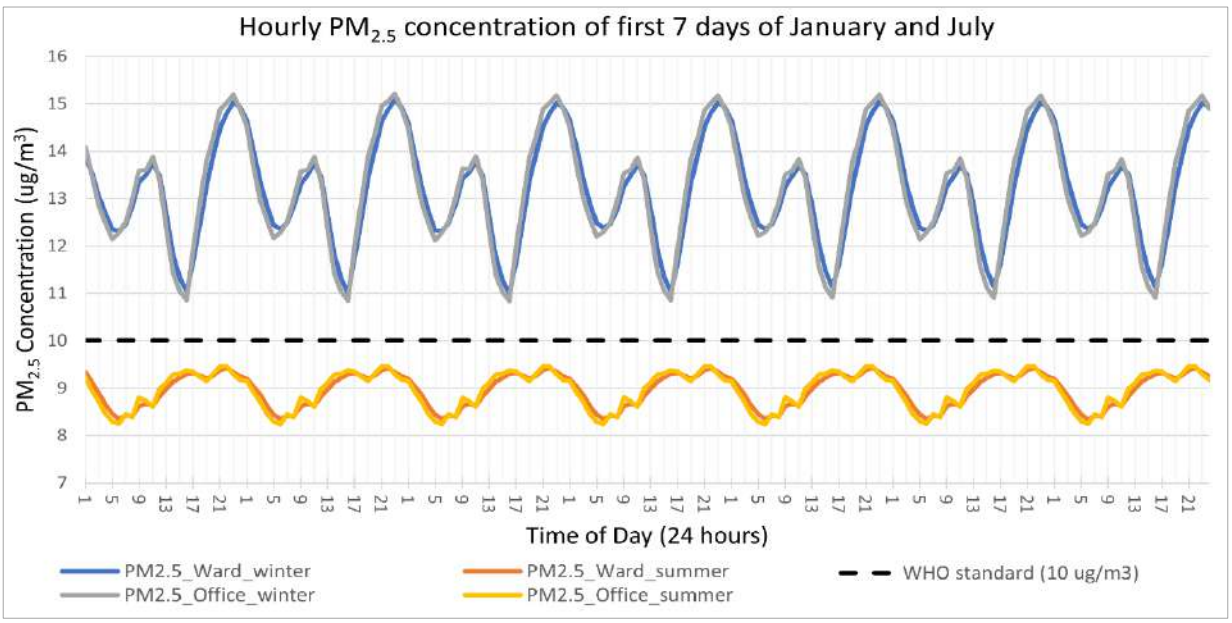

Fig. 4 - Hourly $PM_{2.5}$ concentration of the target office and patient rooms in the pre-1980 hospitals during 1st to 7th January and 1st to 7th July. The dashed line shows the WHO air quality guideline for $PM_{2.5}$, 10 μg/m³ annual mean.

3.3 Discussion

The air change rate of the hospital zones was shown to be affected by not only external ambient conditions in different seasons but also by building features, spatial configuration, floor area, construction year and energy-related features. However, both the 3DStock and CONTAM models are still under development, so some building characteristics were not available in 3DStock and were assumed in the simulations; for example, the space arrangement of rooms. The simulation results of London hospital models presented here indicate the air change rate is lower in post-1980 premises than in the pre-1980 premises, which implies recently built or retrofitted buildings are both more airtight and more energy efficient, as would be hoped from the evolution of Building Regulations.

The observed association between simulated indoor $PM_{2.5}$ concentrations and ventilation rate in rooms also implies the importance of both external ambient conditions and building characteristics. Wintertime weather, with a high ventilation rate, may increase the risk of people being exposed to the outdoor-sourced $PM_{2.5}$ moving indoors, but a recently built or retrofitted building with more airtightness and an appropriate operating schedule of openings could, on the contrary, lower the risk. Also, mechanical ventilation may further limit the penetration of outdoor $PM_{2.5}$ to the indoors. Our results show low ventilation may decrease indoor $PM_{2.5}$ exposure from outdoor $PM_{2.5}$, but the airtightness may prevent indoor-sourced $PM_{2.5}$ (which were not considered in this study but should be included in the future) from flowing out through openings. On the contrary, during the COVID-19 pandemic, the UK Health Security Agency guidance asks to keep fresh air coming into homes and workspaces through both natural and mechanical ventilation, which may lead to more outside-sourced $PM_{2.5}$ exposure. Therefore, a filtering system or air-purifying device might reduce both $PM_{2.5}$ and virus exposure.

DOE CONTAM models of reference buildings provide us with an opportunity to apply London settings to develop London hospital models, applicable to similar spaces across entire portfolios of buildings. However, the feasibility of DOE models, designed for the U.S. healthcare environments, still need to be examined when the representative information becomes available in the 3DStock or from other building stock surveys, in the future.

4. Conclusion

The deterioration of indoor air quality, due to increasingly airtight buildings (assumed to result from improved construction quality), may cause adverse exposure to indoor air pollutants, so we need to enhance our understanding of how improvement to energy efficiency-related features affects indoor air quality. This study contributes knowledge of how building physics and energy-related features interact in terms of airflow ventilation and penetration by outdoor air pollutants. Furthermore, the method is applied at the individual room or building scale across an entire building stock, providing a high-level but relatively detailed model, without the need for individual surveys. As more information becomes available, the large-scale inventories of healthcare buildings can provide an opportunity for bottom-up indoor air quality modelling to eliminate indoor air pollutants.

5. Acknowledgement

The authors gratefully acknowledge support from UK Research and Innovation through the NERC APEx: An Air Pollution Exposure model to integrate protection of vulnerable groups into the UK Clean Air Programme [NE/T001887/1] and the EPSRC Centre for Research into Energy Demand Solutions (grant reference EP/R035288/1).

Valuation Office Agency (VOA) data contain public-sector information licensed under the Open Government Licence v1.0. Environment Agency LiDAR data contain public sector information licensed under the Open Government Licence v3.0. Ministry of Homes, Communities and Local Government (MHCLG): Energy Performance Certificate and Display Energy Certificate data are licensed under the Open Government Licence v3.0.

6. References

[1] UK Legislation. Climate Change Act 2008 [cited 2022 Jan 1]. Available from: https://www.legislation.gov.uk/ukpga/2008/27

[2] Shi S., Chen C., Zhao B. Air infiltration rate distributions of residences in Beijing. Building and Environ. 2015;92:528-537.

[3] NHS England. Greener NHS campaign to tackle climate 'health emergency'. 2020 [updated 2020 Jan 25; cited 2022 Jan 1]. Available from: https://www.england.nhs.uk/2020/01/greener-nhs-campaign-to-tackle-climate-health-emergency/.

[4] Tennison I., Roschnik S., Ashby B., et al. Health care's response to climate change: a carbon footprint assessment of the NHS in England. The Lancet Planetary Health. 2021;5(2):84-92

[5] NIST. CONTAM User Guide and Program Documentation Version 3.2. Technical Note (NIST TN) – 1887. 2015.

[6] Verijkazemi K., Mansouri N., Moattar F., et al. Evaluation of Indoor PM Distribution by CONTAM Airflow Model and Real Time Measuring: Model Description and Validation. Avicenna J Environ Health Eng. 2018 June;5(1):4.

[7] Emmerich S., Heinzerling D., Choi J., et al. Multizone modeling of strategies to reduce the spread of airborne infectious agents in healthcare facilities. Building and Environment. 2013;60:105-115.

[8] Nakano V. M., Croisant Jr. W. J., Abraham D. M. Methodology to Assess Building Designs for Protection against Internal Chemical and Biological Threats. Journal of Computing in Civil Engineering. 2009;23(1):14-21.

[9] Balocco C. Hospital ventilation simulation for the study of potential exposure to contaminants. Build Simul 2011;4:5–20.

[10] Beaussier M., Vanoli E., Zadegan F., et al. Aerodynamic analysis of hospital ventilation according to seasonal variations. A simulation approach to prevent airborne viral transmission pathway during Covid-19 pandemic. Environment International 2022;158:106872.

[11] Chamseddine A., Alameddine I., Hatzopoulou M., et al. Seasonal variation of air quality in hospitals with indoor–outdoor correlations. Building and Environment 2019;148:689–700.

[12] Steadman P., Evans S., Liddiard R., et al. Building stock energy modelling in the UK: the 3DStock method and the London Building Stock Model. Buildings and Cities. 2020;1(1):100-119.

[13] Hamilton I., Summerfield A., Oreszczyn T., et al. Using epidemiological methods in energy and buildings research to achieve carbon emission targets. Energy and Buildings. 2017;154(1):188-197.

[14] Liddiard R., Godoy-Shimizu D., Ruyssevelt P., et al. Energy use intensities in London houses. Buildings and Cities. 2021; 2(1): 336-353.

[15] Ng L. C., Musser A., Persily A. K., et al. NIST Technical Note 1734 – Airflow and Indoor Air Quality Models of DOE Reference Commercial Buildings. 2012.

[16] MET Office. Seasons [cited 2022 Jan 1]. Available from: https://www.metoffice.gov.uk/weather/learn-about/weather/seasons/

[17] UNISON. Health and safety information sheet –Temperature at work. 2014 [updated 2014 August; cited 2022 Jan 1]. Available from: https://www.unison.org.uk/content/uploads/2 014/08/TowebTemperature-at-Work-Information-Sheet-Aug14-update2.pdf.

[18] GLA. London Datastore – London Average Air Quality Levels. [cited 2021 Oct 1]. Available from: https://data.london.gov.uk/dataset/london-average-air-quality-levels

[19] UK Health Security Agency. Ventilation of indoor spaces to stop the spread of coronavirus (COVID-19). [updated 2021 Sep 15; cited 2022 Jan 1]. Available from: https://www.gov.uk/government/publications/covid-19-ventilation-of-indoor-spaces-to-stop-the-spread-of-coronavirus/

[20] Smith C. Energy Performance Building Certificates (EPC) in England and Wales. MHCLG: London. Live tables Q2 2020.

[21] Mauri M., Elli T., Caviglia G., et al. RAWGraphs: A Visualisation Platform to Create Open Outputs. In Proceedings of the 12th Biannual Conference on Italian SIGCHI Chapter. New York. USA: ACM. 2017; 28:1–5.

Data Statement

The datasets generated during and/or analysed during the current study are not available because data licence agreements do not allow publication of the raw data but the authors will make every reasonable effort to publish them in near future.

Indoor Air Quality Evaluation of guests' rooms in hotel building: a Case Study of Turówka Hotel

Marek Borowski [a], Klaudia Zwolińska [a], Bernadetta Ryba [a]

[a] Faculty of Civil Engineering and Resource Management, AGH University of Science and Technology, Kraków, Poland, borowski@agh.edu.pl (M.B.), kzwolinska@agh.edu.pl (K.Z.), bryba@agh.edu.pl (B.R.).

Abstract. The advancement of civilizations and the development of society increase the amount of time that a person spends indoors. Currently, people spend up to 80-90% of their lives in buildings, which is why it is so important to ensure proper thermal conditions and high indoor air quality. Air exchange in the rooms is a necessary process for comfort due to the concentration of oxygen and carbon dioxide and the removal of heat and pollutants. The presence of users is a source of pollution in the form of carbon dioxide and heat emitted. An insufficient supply of fresh air may lead to the increase of dioxide concentration to levels that disturb the proper functioning of the body. Installations in hotel buildings must be designed and operated in such a way as to ensure high comfort and meet the high requirements of customers in terms of the internal environment, safety, and reliability of the system. The study aimed to analyse air quality and thermal comfort in hotel rooms. The research was conducted in a historic hotel located in southern Poland. The building consists of four above-ground stories and the basement. The building has 50 double rooms, a conference room for 40 people, and a restaurant with 90 seats for guests. Temperature, humidity, and carbon dioxide concentrations were measured in the rooms. The analysis was conducted based on data from the daily and weekly cycles and included the influence of external factors. Measurements in hotel rooms were carried out continuously with a sampling period of 1 minute, both in the presence and absence of guests. The paper presents an analysis of the variability of air parameters in a daily and weekly cycle and the influence of external factors on the measured values. On this basis, it will be possible to assess the air quality inside hotel rooms and propose solutions to improve internal conditions.

Keywords. Indoor air quality, comfort assessment, carbon dioxide concentration, hotel building.
DOI: https://doi.org/10.34641/clima.2022.67

1. Introduction

Indoor air quality (IAQ) refers to the environmental characteristics inside buildings that may influence the health and comfort of residents. Physical and chemical properties affect it in various ways and on various scales. Air temperature and relative humidity are the fundamental parameters of the assessment of indoor conditions. ASHRAE [1] recommends that relative humidity be maintained below 65%. There is no requirement for a minimum level of relative humidity. Although, low values can cause discomfort to users, including reduced resistance to infection, skin problems, xerosis and dry mucous membranes. The relative humidity should be greater than 30%. The operating temperature depends on thermal insulation and humidity. It should be in the range of about 19-26°C for clothing insulation of 1.0 clo and 23.5-28°C for 0.5 clo [2]. Carbon dioxide is also one of the most popular indicators of air quality and ventilation system performance. The CO_2 concentration increases over time, depending on the building's tightness, the number of occupants, and the type of ventilation. Carbon dioxide at high levels indoors can cause drowsiness, headaches, reduced work efficiency, and impaired concentration. The concept of "Pettenkofer number" can be found in the literature [3]. It is the hygienically acceptable concentration of carbon dioxide in a room. Pettenkofer assumed that air with a concentration of carbon dioxide above 1000 ppm is not suitable for users. In rooms intended for a permanent human residence, this concentration should not exceed 700 ppm. ASHRAE Standard 62.1 [1] also highlights the risk to human health from high concentrations of carbon dioxide. The document assumes that a carbon dioxide concentration of no more than 700 ppm above the outdoor CO_2 concentration will satisfy the vast majority of the population.

Copyright ©2022 by the authors. This conference paper is published under a CC-BY-4.0 license.

Air quality in hotel rooms is crucial for the comfort of users, which consequently also translates into the popularity of the facility. Customer complaints and dissatisfaction can directly affect the financial losses of the hotel. The comfort of the hotel's customers is strictly related to the parameters of the air in the rooms. It is essential to maintain the thermal and humidity parameters while ensuring a low concentration of carbon dioxide in the room. Hotel facilities are very complex cases to analyze air quality. There are many factors that directly affect indoor parameters in guestrooms. Particularly difficult in the analysis is to consider factors such as irregular use of rooms and users' preferences or habits.

In the literature, many papers [4-7] focus on the assessment of indoor air quality. However, only a small number of them consider the hotel buildings. Asadi et al. [5] presented the results of air measurements in a hotel building, including temperature, humidity, and indoor pollutants, including particulate matter, carbon dioxide (CO_2), carbon monoxide (CO), formaldehyde (HCHO), and total volatile organic compounds (TVOCs). The results indicate, among other things, inadequate ventilation and significant indoor air pollution. A similar study for newly opened hotels was conducted by Chan et al. [6]. The authors studied both the physical parameters of the air and the pollutants in it. The results showed that most of the studied hotels were not able to provide a completely comfortable indoor environment. Shen et al. [7] instead focused on indoor environmental quality as assessed by guests in Chinese budget hotels. Authors considered user comfort in four categories: acoustic environment, luminous environment, indoor air quality (IAQ), and thermal environment. Of all air quality problems, acoustic environment problems were the most common. The authors also noted the significant impact of the season and climate region of the hotel in reducing occupant quality. For example, the indoor air quality complaint rate drops significantly in winter, and the thermal environment complaint rate is much higher in regions with lower temperatures. Moreover, differences in the perception and evaluation by different customer groups were also noted.

The paper presents an analysis of the parameters inside the hotel rooms. The hotel is located in southern Poland. Variability of internal parameters in the daily and weekly cycles is presented. The analysis includes temperature, relative air humidity, and carbon dioxide concentration. The dependences of these parameters on external conditions, including air temperature, wind speed, precipitation, and insolation, were also checked.

2. Research Methods

2.1 Case of the study

The measurements were carried out in a hotel located in a town within the Kraków metropolitan area in Poland. The building is a reconstruction of a historic salt store from 1812. The five-story hotel has been entered to the register of monuments. The building consists of four floors above ground and underground. Figure 1 shows the hotel's appearance.

Fig. 1 - The appearance of the analyzed hotel.

The hotel has 49 double rooms, one single room, and a suite. There is also a restaurant, a hotel bar, a drink bar, a conference room, and a swimming pool. During the measurements, a constant airflow was supplied to the guest rooms.

2.2 Data collection

The measurements included both conditions inside the rooms and external conditions directly on the premises of the analyzed facility. The tests were conducted continuously with a reading period of 1 minute and during normal hotel operations. Measurements inside the guests' rooms include air temperature, air relative humidity, and carbon dioxide concentration. Figure 2 presents the appearance of the room with the location of the measuring sensor.

Fig. 2 - View of a hotel room with location of measuring sensor.

The outdoor air parameters measured during the study are temperature, wind speed, rainfall occurrence (on a scale of 0 - no rain, 1 - rain), and insolation.

Data from two double guest rooms located on the second floor were used for analysis. Room R1, with an area of 31.3 m², is located on the northwest side of the building. Room R2 (21.7 m²) is located almost on the other side of the corridor (south-east side). The floor plan with the indicated rooms is presented in Figure 3.

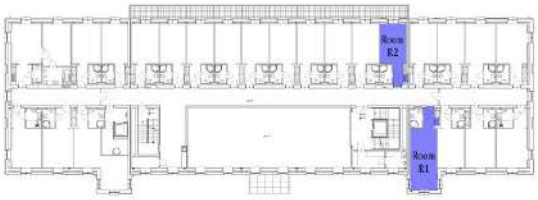

Fig. 3 - Floor plan with room locations.

The measurements have been carried out in 2020. However, due to the pandemic, restrictions in Poland, temporary closure of the hotel, and reduced tourist traffic, not all of the collected data fully reflect the characteristics of the facility and indoor air quality. The months with the low outdoor temperatures were chosen. The two months, November and December of 2020, were adopted as the analyzed period. In the summer, users are much more likely to leave the windows open, which in turn affects the assessment of air quality and ventilation efficiency in the facility. Therefore, the authors deliberately chose months with low temperatures when the opening of windows and balconies is limited. Figure 4 shows the variation in outdoor temperature over the analyzed period, highlighting the periods included in the detailed analysis.

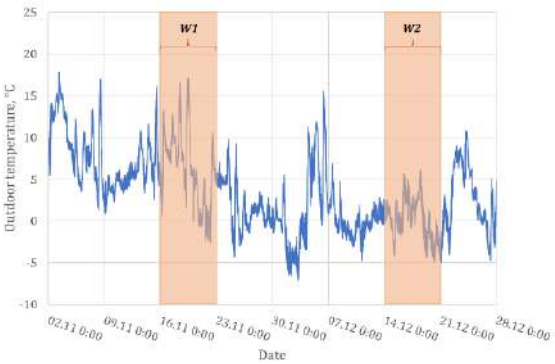

Fig. 4 - Outside temperature distribution of November-December 2020 period highlighting the analyzed periods.

The weeks covered by a more detailed analysis are marked in orange in figure 4. The first week, including a period from 16 to 23 November, is referred to as "W1". As can be seen, this period is characterized by large temperature amplitudes and high maximum readings reaching over 15 °C. The second of the selected periods is referred to as "W2" in further analysis and covers the week from 14 to 21 December. During this period, lower outside temperatures are observed. Moreover, the daily and weekly temperature variations are less than during the W1 week.

2.3 Analysis methods

The obtained data were averaged to 5-minute periods to facilitate further analysis and to eliminate the influence of momentary signal outages or extreme readings. The prepared dataset was further analyzed in both daily and weekly cycles. Additionally, the dependence between indoor conditions and outdoor parameters was checked. For this purpose, correlation coefficients and correlation charts were used.

3. Results and discussion

This chapter presents the main results and their discussion. As described in Section 2.3, this part of the study is divided into four sections.

3.1 Preliminary data analysis

Firstly, the initial analysis of the collected data from both study weeks was conducted. For this purpose, the minimum, maximum and average values of each measured parameter were determined. Table 1 presents a statistical summary of the outdoor air parameters for the two weeks analyzed. The table does not include the parameter determining the occurrence of precipitation. This parameter was measured on a two-level scale, where 0 means no precipitation and 1 indicates the rainy period.

Tab. 1 – Statistical summary of external conditions data.

Parameter	Min	Max	Avg
	Week W1		
Sunlight, lux	1.00	999.00	357.37
Temp, °C	-2.50	16.78	6.09
Wind, m/s	0.00	4.46	1.02
	Week W2		
Sunlight, lux	1.00	999.00	306.61
Temp, °C	-4.80	5.74	0.05
Wind, m/s	0.00	2.66	0.47

Similarly, a summary of internal parameters was prepared. Due to the analysis of two separate rooms, the data were prepared individually for rooms R1 and R2. The obtained values are summarized in Table 2 and Table 3, respectively.

Tab. 2 – Statistical summary for data from room R1 for both analyzed periods.

Parameter	Min	Max	Avg
	Week W1		
Temp, °C	22.3	23.6	23.1
RH, %	30.0	42.0	38.2
CO_2, ppm	400.0	914.0	493.1
	Week W2		
Temp, °C	20.2	22.5	22.0
RH, %	28.0	39.0	31.7
CO_2, ppm	400.0	1126.0	595.9

Tab. 3 – Statistical summary for data from room R2 for both analyzed periods.

Parameter	Min	Max	Avg
	Week W1		
Temp, °C	16.8	24.8	23.0
RH, %	25.0	45.0	34.4
CO_2, ppm	400.0	3296.0	626.3
	Week W2		
Temp, °C	21.8	25.0	23.3
RH, %	24.0	35.0	28.3
CO_2, ppm	400.0	4079.0	703.5

Already on the preliminary stage of the analysis, it was noticed that the rooms have different characteristics and the range of the obtained values of parameters vary greatly. Both air temperature, relative humidity, and CO_2 concentrations vary in a wide range in room R2. Moreover, low temperatures below 17°C and very high concentrations of carbon dioxide above 3000 ppm were recorded in room R2 during the measurement period.

3.2 Weekly analysis

In the next step, analysis was performed based on the data from tested weeks. Results were examined separately for both rooms. Figure 5 presents the variation of air parameters inside room R1 for the first test week.

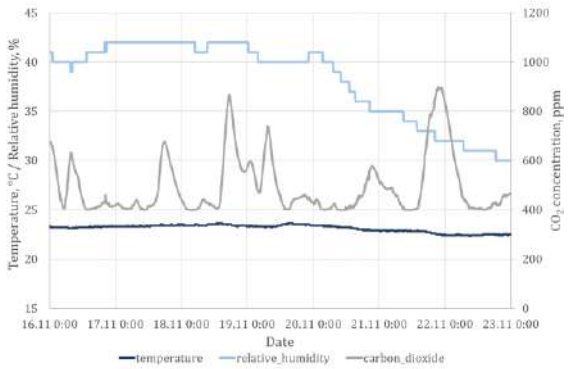

Fig. 5 - Variability of internal parameters of air in room R1 for the first measuring week W1.

The graph shows variations in carbon dioxide concentrations ranging from 400 to over 900 ppm, with no clear trend of variability in the week cycle. On some days, there is a visible increase in concentration in the evening hours and then its slow decline into the morning hours. This decrease may be the effect of the daily sleeping timetable of the average user. Human emits a much smaller stream of carbon dioxide during sleep. The temperature inside the room is kept relatively constant. On the other hand, the relative air humidity significantly decreases at the end of the week from over 40% to 30%. The fluctuations in the values of these parameters for the R2 week are presented similarly. The graph is given in Figure 6.

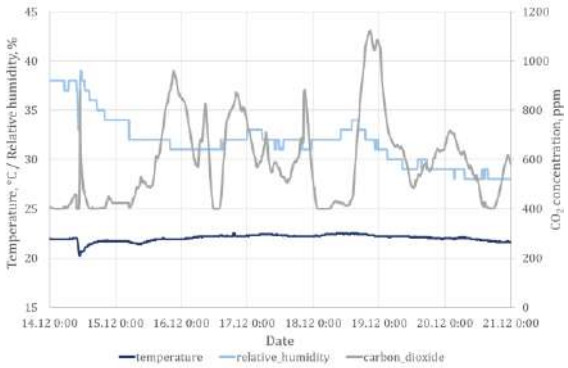

Fig. 6 - Variability of internal parameters of air in room R1 for the second measuring week W2.

Similar to the first week, there is also a trend of increasing carbon dioxide concentration during the evening. The concentration during this period exceeds 1000 ppm but does not rise above 1200 ppm, which can be considered correct conditions for use. On 14 December, a decrease in temperature to 20 °C is noticeable. Given the suddenness of the drop, it may be the result of opening a window. The rapid decrease of the carbon dioxide concentration also confirms this theory. Similar to the first week, the relative humidity also decreases during the week.

An analogous procedure was carried out for the second in hotel rooms. Figure 7 shows a plot of the variation in indoor conditions in room R2 during week W1.

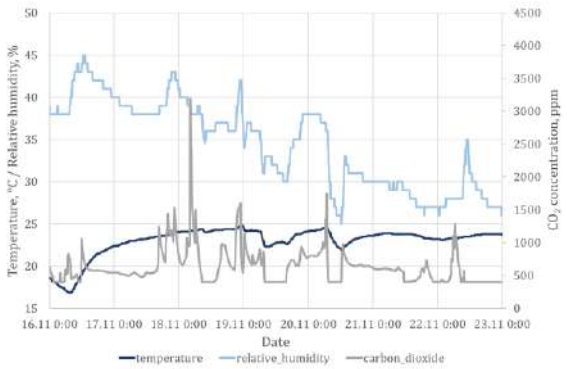

Fig. 7 - Variability of internal parameters of air in room R2 for the first measuring week W1.

In this case, significant variability is noted for each parameter. The decrease in temperature on the first of the analyzed days may be due to the guests' preference for low air temperatures or to the absence of users. However, a temperature of 17°C, as observed on 16 December, is associated with a high probability of feeling cold among users. As can be seen, carbon dioxide concentrations as high as 1000 ppm were recorded at the same time, so we assume that users were nevertheless present in the room. As in the previous examples, there is also a decrease in relative humidity values. Figure 8 shows the variation of these parameters for week W2.

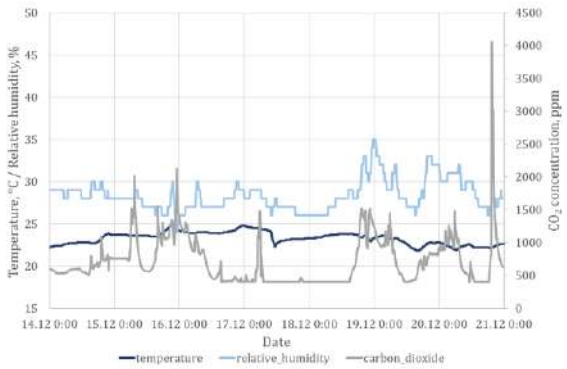

Fig. 8 - Variability of internal parameters of air in room R2 for the second measuring week W2.

It is noticeable in the figure that the temperature varies from 22 to 25°C during the week. On 17 December, the temperature drops quickly by about 2 degrees. No other sudden temperature changes were noted. However, significant fluctuations can be observed in the case of carbon dioxide concentration. The concentration increases several times to the level of about 1500 ppm. On 21 December a sudden increase to the level of 4000 ppm is noticed. Such indications significantly exceed the level considered as comfortable.

3.3 Daily analysis

The next step focused on the variability of indoor parameters in the analyzed rooms over a daily cycle. From the research period, one day from each of the rooms was selected for the detailed analysis. The selection was based on the high variability of parameters. At the same time, periods with CO_2 concentrations observed above 500 ppm were selected, which may indicate the presence of indoor users. Figure 9 shows the distribution of indoor parameter variability in room R1 on 17 December (Thursday).

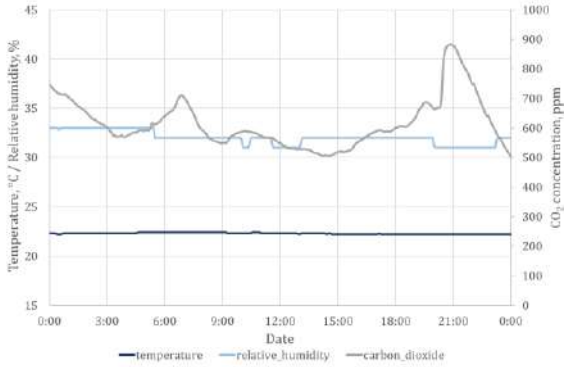

Fig. 9 - Variability of internal air parameters in room R1 on the example of December 17.

As can be seen in the graph above, the concentration of carbon dioxide varies from 500 to just under 900 ppm, which can be considered an acceptable level for comfortable use. Temperature and relative humidity fluctuate within a small range and are maintained at a comfortable level. Figure 10 shows the distribution of indoor parameter variability in room R2 on 15 December (Tuesday).

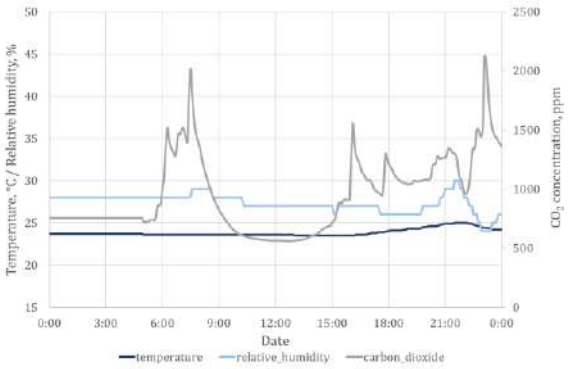

Fig. 10 - Variability of internal air parameters in room R2 on the example of December 15.

In the case of room R2, we see significantly higher variability in all measured parameters. The concentration of carbon dioxide varies from over 500 to over 2200 ppm. An increase in temperature and humidity is also noticed after 20:00. The decrease in these two values after 22:00, and the subsequent decrease in carbon dioxide concentration, may indicate that a window was opened in the room.

3.3 Analysis of the external factors

In the next stage, the authors decided to check the relationship between the values of individual indoor air parameters and the values measured outside the building. Further analysis was conducted jointly for both measurement weeks to get a more general view of the relationship between the parameters.

Tab. 4 – Correlation coefficients of room R1.

Outdoor conditions	Temp, °C	RH, %	CO_2, ppm
Rain	-0.008	0.093	-0.144
Sun	0.042	0.031	-0.291
Temp	0.761	0.757	-0.336
Wind	0.318	0.280	-0.431

The determined correlation coefficients show a clear relationship between the individual values inside the room and the temperature measured outside the facility. For the relationships of two parameters: air temperature and relative humidity and the outside air temperature, the values of the coefficients are above 0.75. Moreover, for room R1, the influence of wind speed on the concentration of carbon dioxide was noticed, and the determined correlation coefficient was -0.431. The above-mentioned dependencies with the highest correlation coefficients are presented on graphs. Figure 11 shows the relationship between the temperature inside room R1 and the outdoor temperature. In addition, the graph shows the trend line as a second-order polynomial and the coefficient R2.

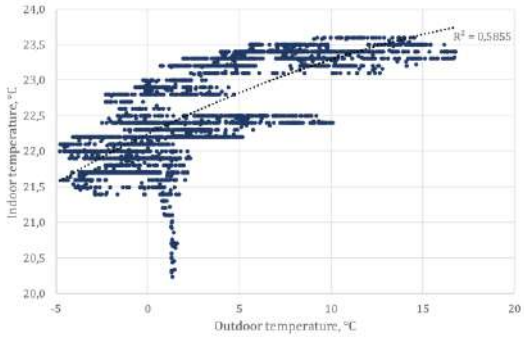

Fig. 11 - Relationship of indoor temperature to outdoor temperature for room R1 in both weeks.

As can be seen, several measurements' points do not fit into the trend noted. These records were obtained at outdoor air temperatures around 1-2 °C. Likely, this is the result of the periodic ventilation of the room by opening the window. Similar to previous charts, Figure 12 shows the relationship between indoor relative humidity and outdoor temperature.

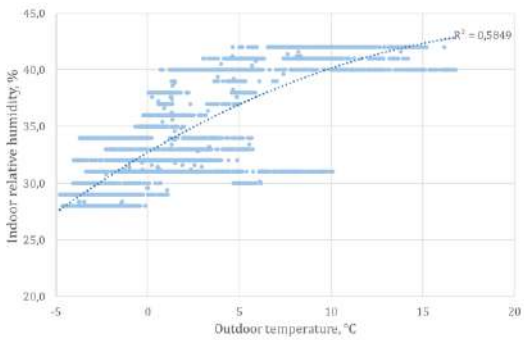

Fig. 12 - Relationship of indoor relative humidity to outdoor temperature for room R1 in both weeks.

As in the case of the previous chart, a group of values deviates from the determined trend. Nonetheless, the relationship is noticeable. As mentioned before, an interesting relation between the concentration of carbon dioxide in room R1 and the wind speed was noticed. The results in the form of a graph are presented together with the trend line in Figure 13. As above, a second-order polynomial relationship was used.

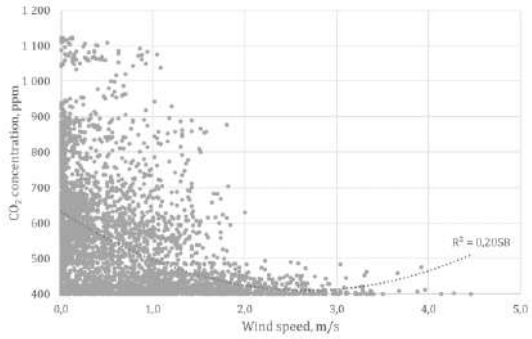

Fig. 13 - Relationship of indoor CO_2 concentration to wind speed for room R1 in both weeks.

The presented dependence is much weaker than the previous two relations. Nevertheless, there is a noticeable tendency for the concentration of carbon dioxide to decrease at high wind speeds. Of course, the presence of users and their activities are the key factors that affect changes in carbon dioxide concentration. However, it was noted that the increased windiness, and hence air infiltration, may dilute indoor air pollutants. This fact may be related to the leakage of window frames and the location of the room on the west side because, in the Polish climate, the winds blow from the west direction most often. This analysis does not include the direction of the wind. It may result in a weaker relationship between these quantities. Likewise, the dependence coefficients were also estimated for room R2. The results are summarized in Table 5.

Tab. 5 - Correlation coefficients of room R2.

Outdoor conditions	Temp, °C	RH, %	CO_2, ppm
Rain	-0.076	0.018	-0.051
Sun	-0.124	-0.018	-0.267
Temp	-0.045	0.634	-0.231
Wind	0.018	0.167	-0.158

In this case, the highest values of the coefficient were obtained for the relation between indoor air humidity and external temperature. The remaining values for the R2 room take low values, not exceeding the level of 0.3 in absolute terms. As can be seen, the dependence of carbon dioxide concentration on wind speed, in the case of this room, is characterized by a much lower correlation coefficient. As mentioned above, it may result from the location of the rooms on both sides of the corridor, where room R1 is on the

north-west side, and room R2 is on the south-east side. The relationship that obtained the best result with the trend line is shown in Figure 14. As in the above cases, a second-order polynomial function was used.

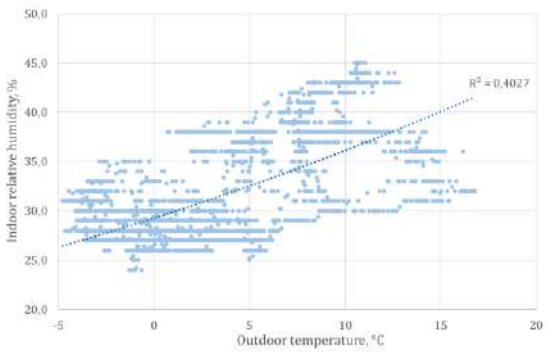

Fig. 14 - Relationship of indoor relative humidity to outdoor temperature for room R2.

Among the analyzed relationships, only the relationship between indoor relative humidity and outdoor temperature is noticeable for both of the analyzed rooms. Hence, the relationship between these two parameters for both rooms is shown in Figure 15.

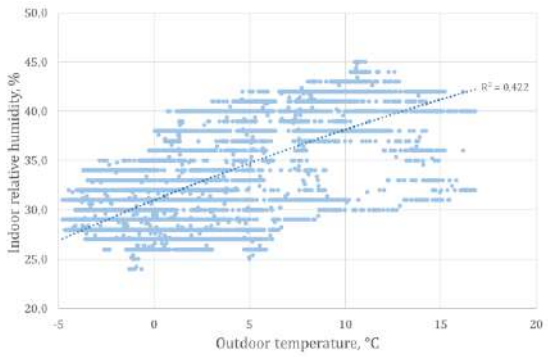

Fig. 15 - Relationship of indoor relative humidity to outdoor temperature for both rooms.

4. Conclusion

Analysis of indoor environmental quality is crucial, particularly in rooms where users spend a significant part of their day. The measurements were carried out in two guest rooms located on the first floor of a hotel in southern Poland. The conducted analysis showed that the conditions inside the rooms are highly variable with time. Moreover, the levels of carbon dioxide are many times higher than the recommended values, especially for room R2. An increase in the ventilation flow rate for room R2 should be considered to improve indoor air quality. As can be seen, both rooms, despite their location in the same building, have quite different characteristics and dynamics of air parameters changes. Room R1 is over 30% larger, therefore with the same number of users, the increased concentration of carbon dioxide is not surprising. However, the level of the CO_2 concentration is significantly high, temporarily reaching values that threaten the health and comfort of the users. Periodic air humidification would also be appropriate, as a drop in humidity below 30% may cause discomfort to users.

There are several problems noted in the measurements and analysis of indoor air quality in hotel buildings. The most important of them include individual preferences of users and irregular periods of actual hotel guests' presence. At the stage of further analyses, the conducted research should be supplemented with the measurements of user presence in the examined room.

During the analysis, clear relations between the indoor air parameters and the external conditions were noticed. Especially for room R1, the determined correlation coefficients took high values, considering that the correlations were checked individually for the relationships of each parameter. Once the data were supplemented with the occupant presence factor, the developed dependencies could provide an excellent basis for further multi-parametric analysis. For example, authors could implement artificial intelligence to develop a prediction model. In this way, ventilation and heating systems could automatically respond before indoor conditions deteriorate.

5. Acknowledgement

The research was carried out in the project entitled „Opracowanie zintegrowanego systemu umożliwiającego precyzyjną kontrolę mikroklimatu w dużych obiektach użytkowych w celu spełnienia wymagań dotyczących budynków o niemal zerowym zapotrzebowaniu na energię (nZEB)" no. POIR.01.01.01-00-0720 / 16 co-financed by the EU European Union from the Regional Development Fund under the Intelligent Development Operational Program for 2014-2020.

6. References

[1] ASHRAE Standard 62.1-2019 Ventilation for Acceptable Indoor Air Quality American Society of Heating, Refrigerating and Air-conditioning Engineers, Inc, Atlanta, GA. 2019.

[2] ASHRAE Standard 55-2020 Thermal Environmental Conditions for Human Occupancy. The American Society of Heating Refrigerating and Air Conditioning Engineers, Atlanta, GA. 2020.

[3] Von Pettenkofer, M. Über den Luftwechsel in Wohngebäuden; Der, J.G., Ed.; Cotta'schen Buchhandlung: München, Germany, 1858.

[4] Borowski M., Łuczak R., Halibart J., Zwolińska K., Karch M. Airflow Fluctuation from Linear Diffusers in an Office Building: The Thermal Comfort Analysis. Energies. 2021; 14(16):4808.

[5] Asadi E., Costa J.J., Gameiro da Silva M. Indoor air quality audit implementation in a hotel building in Portugal. Build Environ. 2011;46(8):1617-1623.

[6] Chan W., Lee S-C., Chen Y., Mak B., Wong K., Chan C-S., Zheng C., Guo X. Indoor air quality in new hotels' guest rooms of the major world factory region. International Journal of Hospitality Management. 2009;28(1):26-32.

[7] Shen Z., Yang X., Liu C., Li J. Assessment of Indoor Environmental Quality in Budget Hotels Using Text-Mining Method: Case Study of Top Five Brands in China. Sustainability. 2021; 13(8):4490.

Data Statement

The datasets generated during and analysed during the current study are not publicly available due to privacy restrictions but are available on request from the corresponding author.

Numerical investigation of the transmission route of infectious particles produced by human

Wonseok Oh [a], Ryozo Ooka [b], Hideki Kikumoto [c], Sihwan Lee [d]

[a] Institute of Industrial Science, The University of Tokyo, Tokyo, Japan, oh-ws@iis.u-tokyo.ac.jp

[b] Institute of Industrial Science, The University of Tokyo, Tokyo, Japan, ooka@iis.u-tokyo.ac.jp

[c] Institute of Industrial Science, The University of Tokyo, Tokyo, Japan, kkmt@iis.u-tokyo.ac.jp

[d] Department of Architecture, Shinshu University, Japan, shany@shinshu-u.ac.jp

Abstract. This study aims to investigate the major factors to influence the respiratory transmission occurred by infectious particles from a human in an indoor environment. Identifying the critical factors of respiratory transmission is important for taking a countermeasure to control its spread. However, it is difficult to track large numbers of infectious particles generated by a human and floating in a room by the experimental method. Therefore, the transient jet airflow by human cough was numerically reproduced, and the trajectories of particles were investigated using the Lagrangian method. In the numerical analysis, two persons sitting and facing each other in a small office room were considered assuming that one person produced infectious particles by cough, and another was exposed to the infection. The trajectory of the dispersed infectious particles was calculated to confirm the proportion of particles that were directly inhaled by a person, attached to the human body surface, adhered to the floor, removed by ventilation, and suspended in the air. Also, the size of particles (1, 5, 10, 20, 40, and 80 μm) produced by the infector, the ventilation rate (6 m^3 h^{-1}·$person^{-1}$, equivalent to air changes per hour is 0.5 h^{-1}), and the distance between individuals (0.9 m (3 ft) and 1.8 m (6 ft)) were investigated as an influential major factor to affect the spread of transmission. As a result, it was confirmed that the effects of gravity and inertia increased with larger particles, resulting in a greater rate of adhered particles to the floor. On the other hand, when the size of particles was smaller, they were able to be removed more effectively by increasing the ventilation rate. Further, when the individuals were spaced 1.8 m apart, particles larger than 20 μm had no significant effect on droplet transmission. However, the smaller particles less than 10 μm were highly likely to be inhaled directly and cause droplet transmission. Therefore, for smaller particles less than 10 μm, practical measures to avoid infections such as social distancing is necessary.

Keywords. droplet dispersion, Lagrangian method, coughing, breathing, particle fate
DOI: https://doi.org/10.34641/clima.2022.411

1. Introduction

Our lives are severely affected by the risk of infection during the coronavirus disease 2019 (COVID-19) pandemic, which is caused by the SARS-CoV-2 virus. Infectious respiratory diseases have severe negative effects on public health, society, and the economy. Various types of respiratory viruses are known, such as the measles virus, influenza A virus, respiratory syncytial virus, rhinoviruses, coronaviruses, and adenoviruses. Respiratory diseases can be spread via naturally produced droplets and droplet nuclei from an infected person by breathing, speaking, coughing, and sneezing. The droplets consist of 98.2% H_2O and 1.8% nuclei (mass ratio) [1], and small droplets evaporate quickly and become droplet nuclei. Respiratory viruses can be spread via three transmission routes: contact (direct or indirect), droplet, and airborne transmission [2,3]. Washing hands and wearing masks are effective ways to prevent contact and droplet transmission [4,5]. However, it is known that droplet nuclei smaller than 5 μm may remain in the air for a long time, causing airborne infection [2]. Samples of SARS-CoV-2 RNA have recently been detected in the air and on the surfaces in COVID-19 wards [6,7]. However, although direct evidence of an infectious infection is difficult to obtain, Yu et al. presented reasonable evidence of aerosol infection by showing the predictability of viral infections through analyses of airflow and contaminant dispersion using computational fluid dynamics (CFD)

Copyright ©2022 by the authors. This conference paper is published under a CC-BY-4.0 license.

[8]. Zhu and Kato examined the diffusion characteristics of droplets of various sizes using CFD [9]. Droplets with a diameter of less than or equal to 30 μm ($d_p \leq 30$ μm) were affected very little by inertia and gravity and tended to diffuse randomly into the room. Wan et al. experimentally investigated the importance of mechanical ventilation in reducing respiratory infection risk in a hospital ward [10].

The characteristics of airflow, droplets, and droplet nuclei can be used to understand and predict the spread of infection. Gupta and colleagues measured subjects' airflow characteristics during breathing and talking [11] and proposed flow rate model coughing [12]. Several researchers tried to measure the maximum air velocity and direction produced by coughing using the particle image velocimetry (PIV) technique [13,14]. Recently, an attempt has been made to analyze the distribution of airflow caused by coughing [15]. The flow rate variations during coughing and breathing could be represented as a combination of gamma probability distributions and sine waves, respectively. Xie et al. inferred the size distribution of droplets produced by coughing and talking using an experimental method [16]. Additionally, the particle size distributions of subjects were confirmed by Chao et al. for coughing and speaking [13] and by Johnson et al. for breathing [17]. Nishimura et al. employed PIV to visualize the movement of particles released by coughing and sneezing and measured the dynamics of droplets and droplet nuclei [18].

Using a simple physical model, Xie et al. estimated how far droplets produced by various respiratory activities can travel [19]. The maximum distances were 6, 2, and 1 m for sneezing, coughing, and breathing, respectively. The maximum distance traveled by droplets can be used as a reference index for social distancing, which can be used to avoid the spread of infection. Liu et al. developed a theoretical model that can be used to estimate the size and dispersion of droplets and droplet nuclei considering evaporation [20]. The droplets became droplet nuclei with 32% of their initial size by evaporation.

CFD analysis is most commonly used to understand the dispersion of droplets and droplet nuclei. The dispersion of cough droplets and droplet nuclei considering evaporation was investigated and validated by CFD analysis using the Eulerian–Lagrangian method [21,22]. Yang et al. investigated the dispersion of droplets in a crowded bus to understand the ventilation effectiveness and effects of environmental factors [23]. Zhang and Li investigated the dispersion of droplets from a coughing person in a rail cabin. They found that increasing the air changes per hour (ACH) was not the best way to reduce the risk of airborne infection [24]. Higher-velocity air movement delivers droplets and droplet nuclei more rapidly and diffuses them more widely, exposing more people to the risk of infection.

The most important factor for preventing airborne infection in an indoor environment is maintaining a high ventilation rate to quickly remove potentially infectious particles. Mui et al. investigated the dispersion and diffusion of droplet nuclei 0.1 and 10 μm in size in an indoor environment under displacement ventilation and mixing ventilation conditions [25]. They used a drift flux model to calculate the distribution of the droplet nuclei concentration in the room and estimate the infection risk. Zhao and Wu evaluated the deposition of particles on indoor surfaces experimentally and verified the results by comparison with numerical analysis [26]. In addition, various ventilation systems were reviewed using numerical analyses to investigate airborne infection [27,28]. However, most studies utilized the drift flux model to confirm the distribution of droplets and droplet nuclei. Therefore, it is necessary to track the route of infectious particles and confirm the fate of the particles for identifying the key factors of the infection route and taking a countermeasure against infectious diseases in an indoor environment.

2. Methodology

2.1 Eulerian model

The three-dimensional transient Reynolds-averaged Navier-Stokes equations for the conservation of mass, momentum, and energy of a continuous fluid inside a room were solved using the realizable k–ε model as summarized in **Tab. 1** [29].

A second-order upwind scheme was used as the convection term in the discretization scheme. The pressure–velocity coupling for the continuous fluid was solved using the SIMPLE algorithm [30]. The realizable k–ε model has been used and validated in many previous studies to investigate particle dispersion and shown to agree well with experimental results [31–34].

Tab. 1 - Numerical methods used for simulation.

Commercial code	STAR-CCM+ ver. 14.06
Turbulence model	Realizable k–ε model
Convection	Second-order upwind scheme
Solver	SIMPLE algorithm
Buoyancy	Boussinesq approximation
Particles	Lagrangian model
Mesh	Polyhedral with prism layer mesh (approx. 1,100,000 cells)
Time	Implicit unsteady state ($\mathrm{d}t = 0.05$ s)

2.2 Lagrangian model for particles (droplet and droplet nuclei)

The dispersion of particles in the continuous fluid was calculated using the Lagrangian model. The conservation of the linear momentum of the particle is balanced by the surface and body forces. This study considered the drag ($\vec{F}_{\mathrm{D}}$), pressure ($\vec{F}_{\mathrm{P}}$), and gravitational forces ($\vec{F}_{\mathrm{G}}$) as expressed in Equations (1)–(4).

$$m_{\mathrm{p}} \frac{\mathrm{d}\overrightarrow{u_{\mathrm{p}}}}{\mathrm{d}t} = \vec{F}_{\mathrm{D}} + \vec{F}_{\mathrm{P}} + \vec{F}_{\mathrm{G}} \tag{1}$$

$$\vec{F}_{\mathrm{D}} = \frac{1}{2}\frac{C_{\mathrm{D}}}{C_{\mathrm{C}}}\, \rho_{\mathrm{f}}\, A_{\mathrm{p}}\, \left|\overrightarrow{u_{\mathrm{f}}} - \overrightarrow{u_{\mathrm{p}}}\right| \left(\overrightarrow{u_{\mathrm{f}}} - \overrightarrow{u_{\mathrm{p}}}\right) \tag{2}$$

$$\vec{F}_{\mathrm{P}} = -V_{\mathrm{p}}\, \nabla P \tag{3}$$

$$\vec{F}_{\mathrm{G}} = V_{\mathrm{p}}\, \left(\rho_{\mathrm{p}} - \rho_{\mathrm{f}}\right) \vec{g} \tag{4}$$

Here, m_{p} is the particle mass; $\overrightarrow{u_{\mathrm{f}}}$ and $\vec{u}_{\mathrm{p}}$ are the continuous velocity vectors of the fluid and particle, respectively, and ρ_{f} and ρ_{p} are the density of the continuous fluid and particle, respectively. A_{p} is the projected area, and V_{p} is the volume of the particle. ∇P is the gradient of the static pressure in the continuous fluid, and $\vec{g}$ is the gravitational acceleration vector.

The Schiller–Naumann correlation [35] was used to calculate the drag coefficient of the particle (C_{D}) in Equation (5). C_{D} depends on the Reynolds number of the particle ($\mathrm{Re_p}$) in Equation (6). The Cunningham slip correction factor (C_{C}) for droplets in small size was defined in Equation (7). The Cunningham effect occurs on particles smaller than 10 μm.

$$C_{\mathrm{D}} = \begin{cases} \dfrac{24}{\mathrm{Re_p}}\left(1 + 0.15\,\mathrm{Re_p}^{0.687}\right), & \mathrm{Re_p} \le 10^3 \\ 0.44, & \mathrm{Re_p} > 10^3 \end{cases} \tag{5}$$

$$\mathrm{Re_p} = \frac{\rho_{\mathrm{f}}\, d_{\mathrm{p}}\, \left|\overrightarrow{u_{\mathrm{f}}} - \vec{u}_{\mathrm{p}}\right|}{\mu_{\mathrm{f}}} \tag{6}$$

$$C_{\mathrm{C}} = 1 + \frac{2\lambda}{d_{\mathrm{p}}}\left(1.257 + 0.4\exp\left(-\frac{1.1\, d_{\mathrm{p}}}{2\lambda}\right)\right) \tag{7}$$

Where d_{p} is the particle diameter, and μ_{f} is the dynamic viscosity of the continuous fluid. λ is the mean free path of the air molecular (i.e. $\lambda = 0.0673$ μm at 23 °C and 1 atm air [36]).

In the simulation, the turbulent dispersion of particles was considered because turbulent motion significantly affects the particles with small sizes. The stochastic model similar to the random walk model was used [37]. The velocity of the continuous fluid ($\overrightarrow{u_{\mathrm{f}}}$) was calculated by adding the fluctuating velocity component ($\overrightarrow{u_{\mathrm{f}}'}$) to the local Reynolds-averaged velocity of the continuous fluid ($\overrightarrow{\overline{u_{\mathrm{f}}}}$), as shown in Equation (8). The fluctuating velocity component was randomly sampled by the Gaussian probability density function (p) with the standard deviation ($\sigma = \sqrt{2k/3}$) and zero mean in Equation (9) [9]. Here, k is the turbulent kinetic energy.

$$\vec{u}_{\mathrm{f}} = \overrightarrow{\overline{u_{\mathrm{f}}}} + \overrightarrow{u_{\mathrm{f}}'} \tag{8}$$

$$p\left(\overrightarrow{u_{\mathrm{f}}'}\right) = \frac{1}{\sqrt{2\,\pi\,\sigma^2}}\exp\left(-\frac{\overrightarrow{u_{\mathrm{f}}'}^{\,2}}{2\,\sigma^2}\right) \tag{9}$$

2.3 Case study description

Indoor space of the typical small office with a size of 3.6 × 2.7 × 2.5 m³ (width × length × height) was considered for the simulation. Mechanical ventilation by the displacement ventilation system was investigated as illustrated in **Fig. 1**. The ventilation rate was set as 6 m³ h⁻¹·person⁻¹, and two occupants were considered (equivalent ACH is 0.5 h⁻¹). One was assumed as an infected person and the other was set as a susceptible person. Two thermal manikins in a seated position with a height of 1.21 m were placed in the center of the room. The furniture was not considered because its various types and locations can interfere an indoor airflow and may have a significant effect on the results [38]. The present study analyzed the independent influence of the infectious particles generated from the person.

Further, different cases of social distancing were investigated as an influential major factor to affect the spread of the transmission by setting the several distances between individuals (Case A: 0.9 m (3 ft) and Case B: 1.8 m (6 ft)). The distances between individuals were modeled by measuring nose-to-nose distance.

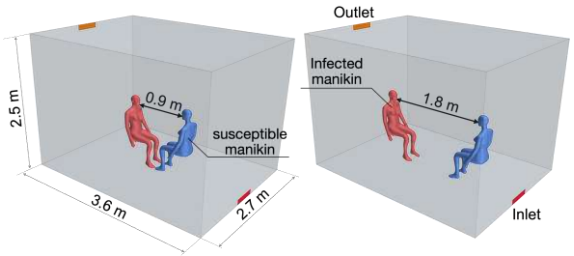

(a) Case A (b) Case B

Fig. 1 - Different cases of social distancing in a typical small office.

The detailed boundary conditions for the calculation can be found in **Tab. 2**. A boundary condition of velocity inlet was applied for the inlet of the room. Supplying air temperature was set at 18 °C. The opening of the inlet and outlet were assumed to have the same size of 0.45 × 0.1 m². The outlet was a pressure outlet with zero static pressure. The constant temperature of 24 °C was set to all indoor walls. The boundary condition of the infected and susceptible manikins was set as a constant heat flux of 23 W/m².

For coughing and breathing behaviors, boundary condition at the mouth opening was set as velocity inlet, and a time-series velocity profile for each behavior was applied. The temperature of the airflow due to exhalation was set at 34 °C, and a turbulence intensity was set at 10% [39]. Validation calculations were conducted to determine a statistically appropriate number of particles, and for this simulation, 5,000 particles were chosen for each size.

Tab. 2 – Boundary conditions.

Inlet opening	velocity inlet: according to 1.0 ACH temperature: 18 °C turbulence intensity: 5% turbulence length scale: 7% of hydraulic dimeter d_h size: 0.45 × 0.1 m^2
Outlet opening	pressure outlet: static pressure = 0 size: 0.45 × 0.1 m^2
Wall	Dirichlet condition, T_w = 24 °C two-way all-y+ wall treatment no-slip boundary condition
Surface of infected / susceptible manikin	Neumann condition, q_s = 23 W/m^2 two-way all-y+ wall treatment no-slip boundary condition
Mouth opening of infected / susceptible manikin	velocity inlet • infected manikin: cough airflow at first time and follow the breath cycle (equation (10)) • susceptible manikin: follow the breath cycle (equation (10)) temperature: 34 °C turbulence intensity: 10% turbulence length scale: 7% of d_h
Particles	d_p: 1, 5, 10, 20, 40, and 80 μm 5,000 particles for each size

2.4 Boundary conditions for particles

The deposition on the surface is a major removal mechanism of particles, and thus, stick condition on the floor, and the surface of infected and susceptible manikins was considered [40]. The ceiling and vertical walls were set as a rebound condition. An escape condition was applied to the outlet opening and mouth openings of infected and susceptible manikins, and the fate of particles was tracked.

2.5 Cough model for infected manikin

The direction of the cough airflow was set to 27.5 ° downward as shown in **Fig. 2**, and the time-series velocity profile obtained from the experiment [41] was adopted as the boundary condition in the mouth of the infected manikin (**Fig. 2**(b)).

Water droplets quickly equilibrate with the surrounding environment and its evaporation process is very rapid. The equilibrium size of the droplet is reduced to about half its initial expiratory size [42]. In this study, the size of the droplet in the equilibrium state, not the initial size of the droplet, was considered to reduce the computational load in the calculation, and the evaporation process was not conducted.

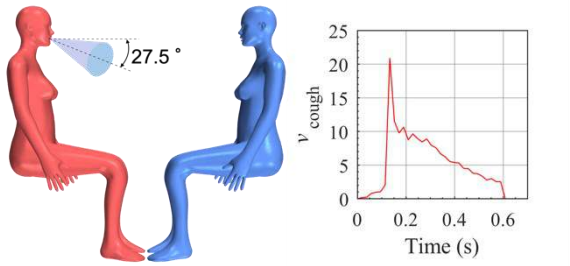

(a) Direction of cough (b) Velocity profile

Fig. 2 - Cough model for infected manikin.

2.6 Breath model for infected and susceptible manikin

In the breath model, the airflow rate of inhalation and exhalation was assumed to be a sine wave. Tidal breath flow rate (inhalation or exhalation) and its frequency were assumed as 1 L and 3 s, respectively, as described in Equation (10). The mouth opening area of 123 mm^2 was considered, and the infected manikin started coughing at the beginning of the simulation calculation and the coughing was last for 0.6 s. Further, during the simulation, the breath model was started after the cough model was completed.

$$V_{\text{breath}}(t) = \frac{\pi}{6}\sin\left(\frac{\pi}{3}t\right), [\text{L/s}] \quad (10)$$

2.7 Validation of proper number of particles

It is necessary to set a proper number of particles for statistical analysis for the Lagrangian simulation. The motion of the particle is greatly affected by turbulence as the particle size is smaller. Therefore, the appropriate number of particles was investigated firstly with the particle size of 1 μm, and the same number of particles was applied to all particles. Various numbers of particles of 1,000, 5,000, 10,000, and 20,000 were considered, and the ratio of the time series particle fates to the initial number of particles was confirmed. There were no significant differences in more than 5,000 particles, and thus, 5,000 particles were investigated in this study.

3. Results and Discussion

3.1 Indoor Airflow distribution

Fig. 3 displays the results of indoor airflow distributions during the coughing and breathing stage. The rising airflows due to the heat of the human body were formed adjacent to both manikins. The velocity of cough airflow showed over 10 m/s at 0.2 s. Also, the formed exhaled airflow by breathing can be confirmed at 2.0 s after the infected manikin finished the coughing behavior. The respiratory airflow of susceptible manikin was directed forward, but the expiratory airflow was warmer than the ambient air temperature and raised due to the buoyancy effect.

In Case A (social distancing with 0.9 m), the airflow by coughing tended to reach the susceptible manikin. However, when the social distancing was doubled in Case B (1.8 m), it was difficult to reach the airflow to the opponent.

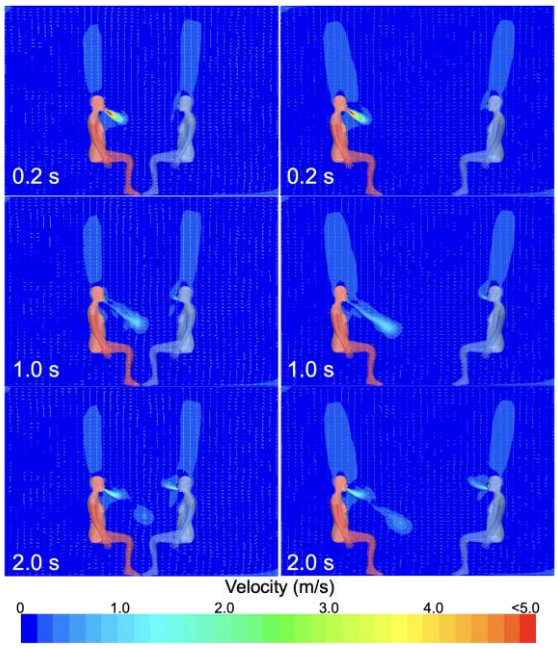

(a) Case A (b) Case B

Fig. 3 - Indoor airflow distribution with cough and breath model.

3.2 Particle dispersion in the room

Fig. 4 shows the results of particle dispersion generated by coughing behavior over time. In Case A (social distancing with 0.9 m), the released particles reached the opponent's body around 5 seconds after coughing. However, when the social distancing was doubled to 1.8 m in Case B, particles did not reach the opponent. Also, it was found that particles with large sizes such as 80 μm headed to the bottom relatively quickly. On the other hand, particles of small size such as 1.0 μm descended more slowly and tended to rise along the thermal plume of the body.

The upward airflow by the human body was greater in Case A where two occupants were set closer to each other than Case B, showing a tendency that particles smaller than 40 μm were more easily to rise to the ceiling and diffuse into the room.

During the simulation from 100 seconds to 300 seconds, particles of 20 μm or less suspended in the air were gradually removed by deposition on the floor, exhaust by ventilation, adhesion to the human body surface, and intake by respiration.

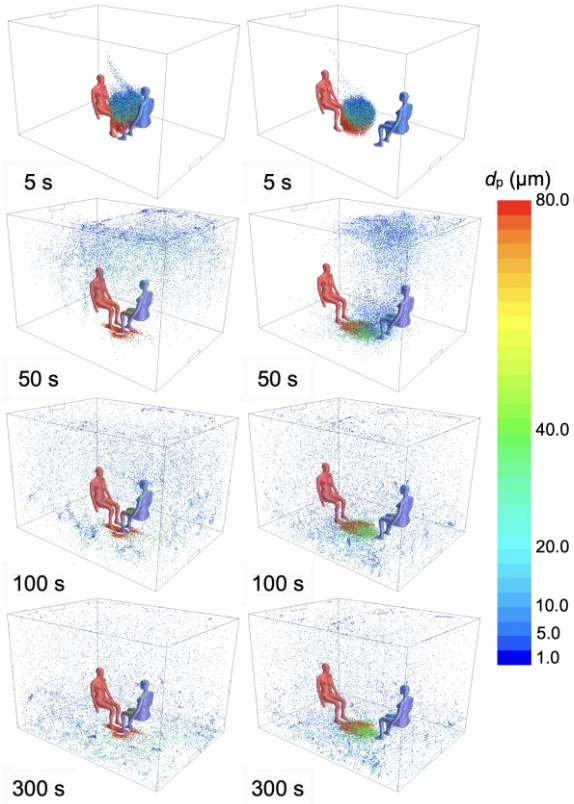

(a) Case A (b) Case B

Fig. 4 - Results of particle dispersion in each case of social distancing in a typical small office.

3.3 Calculated particle fates

Tab. 3 shows the fates of infectious particles generated by coughing after 300 seconds of the simulation according to the particle sizes and distances between individuals. To understand the characteristics of the movement path by the particle sizes, the ratio for each particle size was analyzed.

The smaller size of particles tended to float and be suspended in the room regardless of the distance between individuals. The larger size of particles showed to easily deposit on the surface of the floor (F) or susceptible body (S_{sk}).

In case of a short social distancing (0.9 m in Case A) between two persons, 45.5% of the 40 μm size of the particles and 38.1% of the 80 μm size of the particles generated from the infected person were

deposited on the susceptible manikin (S_{sk}) and 39.8% on the floor (F). However, when the distance between individuals became doubled, only 4.8% of the 40 μm size of particles were attached to the surface of the susceptible manikin (S_{sk}), the 80 μm size of the particles could not reach the surface of the susceptible manikin (S_{sk}), and most of the particles (94.4–97.7%) were removed by deposition to the floor (F).

The droplet transmission and airborne transmission by ingestion of infectious particles (S_m) could occur when the particle size was less 40 μm, however, the probability of transmissions was not significantly influenced by the distance between individuals and size of particles. However, as the distance between individuals increases, range of particle sizes, which can cause the droplet and airborne transmissions, could be reduced.

In general, infectious particles can be removed by the exhaust by ventilation and deposition on the floor. However, regular sterilization should be carried out to prevent a contact transmission possibly occurring by the deposited infectious particles. Also, particles smaller than 20 μm tend to be suspended in the air for a long time, hence, they should be rapidly removed by increasing the ventilation rate and the utilization of the air purifier to lower the risk of airborne transmission.

Tab. 3 - Particle fates released from infected manikin for 300 s.

Distance (m)	d_p (μm)	I_{sk} (%)	I_m (%)	S_{sk} (%)	S_m (%)	E (%)	F (%)	A (%)
0.9	1	1.9	0.1	9.2	0.5	1.0	7.9	79.4
	5	1.5	0.1	9.3	0.8	0.8	17.5	70.0
	10	0.8	0.2	9.6	0.9	1.0	37.5	50.0
	20	1.1	0.2	14.0	0.7	0.5	66.5	17.1
	40	5.5	0.5	45.5	0.7	-	46.8	1.0
	80	21.9	0.1	38.1	-	-	39.8	0.1
1.8	1	2.1	0.2	6.2	0.7	2.2	4.3	84.3
	5	1.7	0.1	6.6	1.0	2.8	10.6	77.2
	10	1.2	0.1	7.6	0.8	1.7	28.7	59.9
	20	0.7	0.1	13.3	0.9	0.5	67.7	16.8
	40	0.8	-	4.8	-	-	94.4	-
	80	2.2	0.1	-	-	-	97.7	-

Note: d_p is the diameter of the particle, and I and S represent the infected and susceptible manikins. Subscripts of sk and m indicate the particles attached to the surface of the manikins and the particles inhaled by respiration, respectively. E, F, and A represent discharged particles by outlet opening by ventilation, deposited particles on the floor, and suspended particles in the air, respectively.

4. Conclusion

This study investigated the probability of exposure to the respiratory infection of a susceptible person by tracking the spread of infectious particles caused by the coughing of an infected person in a ventilated indoor office. As a result, it was found that the arrival of infectious particles can be significantly prevented when the distance between the individuals is maintained from 0.9 m to 1.8 m. Also, the small size of infectious particles capable of causing airborne transmissions was independent of the distance between individuals. Therefore, further studies are necessary to explore the countermeasures against airborne transmissions by appropriately increasing the ventilation rate and the utilization of air purifiers.

5. Acknowledgement

This work was supported by the Japan Society for the Promotion of Science (JSPS) KAKENHI Grant Number 21K18763.

6. References

[1] M. Nicas, W.W. Nazaroff, A. Hubbard, Toward understanding the risk of secondary airborne infection: Emission of respirable pathogens, J. Occup. Environ. Hyg. 2 (2005) 143–154.

[2] J.S. Kutter, M.I. Spronken, P.L. Fraaij, R.A. Fouchier, S. Herfst, Transmission routes of respiratory viruses among humans, Curr. Opin. Virol. 28 (2018) 142–151.

[3] Y. Bu, R. Ooka, H. Kikumoto, W. Oh, Recent research on expiratory particles in respiratory viral infection and control strategies: A review, Sustain. Cities Soc. (2021) 103106.

[4] P. Anfinrud, V. Stadnytskyi, C.E. Bax, A. Bax, Visualizing Speech-Generated Oral Fluid Droplets with Laser Light Scattering, N. Engl. J. Med. 382 (2020) 2061–2063.

[5] K.F. Ho, L.Y. Lin, S.P. Weng, K.J. Chuang, Medical mask versus cotton mask for preventing respiratory droplet transmission in micro environments, Sci. Total Environ. 735 (2020) 139510.

[6] K. Razzini, M. Castrica, L. Menchetti, L. Maggi, L. Negroni, N. V. Orfeo, A. Pizzoccheri, M. Stocco, S. Muttini, C.M. Balzaretti, SARS-CoV-2 RNA detection in the air and on surfaces in the COVID-19 ward of a hospital in Milan, Italy, Sci. Total Environ. 742 (2020) 140540.

[7] A. Kenarkoohi, Z. Noorimotlagh, S. Falahi, A. Amarloei, S.A. Mirzaee, I. Pakzad, E. Bastani, Hospital indoor air quality monitoring for the detection of SARS-CoV-2 (COVID-19) virus, Sci. Total Environ. 748 (2020) 141324.

[8] I.T.S. Yu, Y. Li, T.W. Wong, W. Tam, A.T. Chan, J.H.W. Lee, D.Y.C. Leung, T. Ho, Evidence of airborne transmission of the severe acute

respiratory syndrome virus, N. Engl. J. Med. 350 (2004) 1731–1739.

[9] S. Zhu, S. Kato, J.H. Yang, Study on transport characteristics of saliva droplets produced by coughing in a calm indoor environment, Build. Environ. 41 (2006) 1691–1702.

[10] M.P. Wan, C.Y.H. Chao, Y.D. Ng, G.N. Sze To, W.C. Yu, Dispersion of expiratory droplets in a general hospital ward with ceiling mixing type mechanical ventilation system, Aerosol Sci. Technol. 41 (2007) 244–258.

[11] J.K. Gupta, C.H. Lin, Q. Chen, Flow dynamics and characterization of a cough, Indoor Air. 19 (2009) 517–525.

[12] J.K. Gupta, C.H. Lin, Q. Chen, Characterizing exhaled airflow from breathing and talking, Indoor Air. 20 (2010) 31–39.

[13] C.Y.H. Chao, M.P. Wan, L. Morawska, G.R. Johnson, Z.D. Ristovski, M. Hargreaves, K. Mengersen, S. Corbett, Y. Li, X. Xie, D. Katoshevski, Characterization of expiration air jets and droplet size distributions immediately at the mouth opening, J. Aerosol Sci. 40 (2009) 122–133.

[14] S.-B. Kwon, J. Park, J. Jang, Y. Cho, D.-S. Park, C. Kim, G.-N. Bae, A. Jang, Study on the initial velocity distribution of exhaled air from coughing and speaking, Chemosphere. 87 (2012) 1260–1264.

[15] M. Han, R. Ooka, H. Kikumoto, W. Oh, Y. Bu, S. Hu, Measurements of exhaled airflow velocity through human coughs using particle image velocimetry, Build. Environ. 202 (2021) 108020.

[16] X. Xie, Y. Li, H. Sun, L. Liu, Exhaled droplets due to talking and coughing, J. R. Soc. Interface. 6 (2009).

[17] G.R. Johnson, L. Morawska, Z.D. Ristovski, M. Hargreaves, K. Mengersen, C.Y.H. Chao, M.P. Wan, Y. Li, X. Xie, D. Katoshevski, S. Corbett, Modality of human expired aerosol size distributions, J. Aerosol Sci. 42 (2011) 839–851.

[18] H. Nishimura, S. Sakata, A. Kaga, A new methodology for studying dynamics of aerosol particles in sneeze and cough using a digital high-vision, high-speed video system and vector analyses, PLoS One. 8 (2013).

[19] X. Xie, Y. Li, A.T.Y. Chwang, P.L. Ho, W.H. Seto, How far droplets can move in indoor environments – revisiting the Wells evaporation–falling curve, Indoor Air. 17 (2007) 211–225.

[20] L. Liu, J. Wei, Y. Li, A. Ooi, Evaporation and dispersion of respiratory droplets from coughing, Indoor Air. 27 (2017) 179–190.

[21] X. Li, Y. Shang, Y. Yan, L. Yang, J. Tu, Modelling of evaporation of cough droplets in inhomogeneous humidity fields using the multi-component Eulerian-Lagrangian approach, Build. Environ. 128 (2018) 68–76.

[22] Y. Yan, X. Li, J. Tu, Thermal effect of human body on cough droplets evaporation and dispersion in an enclosed space, Build. Environ. 148 (2019) 96–106.

[23] X. Yang, C. Ou, H. Yang, L. Liu, T. Song, M. Kang, H. Lin, J. Hang, Transmission of pathogen-laden expiratory droplets in a coach bus, J. Hazard. Mater. 397 (2020) 122609.

[24] L. Zhang, Y. Li, Dispersion of coughed droplets in a fully-occupied high-speed rail cabin, Build. Environ. 47 (2012) 58–66.

[25] K.W. Mui, L.T. Wong, C.L. Wu, A.C.K. Lai, Numerical modeling of exhaled droplet nuclei dispersion and mixing in indoor environments, J. Hazard. Mater. 167 (2009) 736–744.

[26] B. Zhao, J. Wu, Effect of particle spatial distribution on particle deposition in ventilation rooms, J. Hazard. Mater. 170 (2009) 449–456.

[27] Z. Lin, J. Wang, T. Yao, T.T. Chow, Investigation into anti-airborne infection performance of stratum ventilation, Build. Environ. 54 (2012) 29–38.

[28] Q. He, J. Niu, N. Gao, T. Zhu, J. Wu, CFD study of exhaled droplet transmission between occupants under different ventilation strategies in a typical office room, Build. Environ. 46 (2011) 397–408.

[29] T.-H. Shih, W.W. Liou, A. Shabbir, Z. Yang, J. Zhu, A new k-ϵ eddy viscosity model for high Reynolds number turbulent flows, Compurers Fluids. 24 (1995) 227–238.

[30] B.P. Leonard, A stable and accurate convective modelling procedure based on quadratic upstream interpolation, Comput. Methods Appl. Mech. Eng. 19 (1979) 59–98.

[31] C. Gromke, B. Blocken, W. Janssen, B. Merema, T. van Hooff, H. Timmermans, CFD analysis of transpirational cooling by vegetation: Case study for specific meteorological conditions during a heat wave in Arnhem, Netherlands, Build. Environ. 83 (2015) 11–26.

[32] T. van Hooff, B. Blocken, Coupled urban wind flow and indoor natural ventilation modelling on a high-resolution grid: A case study for the Amsterdam ArenA stadium, Environ. Model. Softw. 25 (2010) 51–65.

[33] H. Montazeri, B. Blocken, J.L.M. Hensen, Evaporative cooling by water spray systems: CFD simulation, experimental validation and sensitivity analysis, Build. Environ. 83 (2015) 129–141.

[34] H. Montazeri, Y. Toparlar, B. Blocken, J.L.M. Hensen, Simulating the cooling effects of water spray systems in urban landscapes: A computational fluid dynamics study in Rotterdam, The Netherlands, Landsc. Urban Plan. 159 (2017) 85–100.

[35] L. Schiller, A. Naumann, Über die grundlegenden berechnungen bei der schwerkraftaufbereitung, Zeitschrift Des Vereines Dtsch. Ingenieure. (1933).

[36] Y.S. Cheng, M.D. Allen, D.P. Gallegos, H.C. Yeh, K. Peterson, Drag force and slip correction of aggregate aerosols, Aerosol Sci. Technol. 8 (1988) 199–214.

[37] A.D. Gosman, E. Ioannides, Aspects of computer simulation of liquid-fueled combustors, J. Energy. (1983).

[38] P. V. Nielsen, Computational fluid dynamics and room air movement, Indoor Air. 14 (2004) 134–143.

[39] N. Dudalski, A. Mohamed, S. Mubareka, R. Bi, C. Zhang, E. Savory, Experimental investigation of far-field human cough airflows from healthy and influenza-infected subjects, Indoor Air. 30 (2020) 966–977.

[40] H. Qian, Y. Li, Removal of exhaled particles by ventilation and deposition in a multibed airborne infection isolation room, Indoor Air. 20 (2010) 284–297.

[41] W. Oh, R. Ooka, H. Kikumoto, M. Han, Numerical modeling of cough airflow: Establishment of spatial–temporal experimental dataset and CFD simulation method, Build. Environ. 207 (2022) 108531.

[42] H. Holmgren, B. Bake, A. Olin, E. Ljungström, Relation between humidity and size of exhaled particles, J. Aerosol Med. Pulm. Drug Deliv. 24 (2011) 253–260.

Control of the bed thermal environment by a ventilated mattress: human subject response

Ge Song [a], Mariya Petrova Bivolarova [b], Guoqiang Zhang [a], Arsen Krikor Melikov [b]

[a] Hunan University, China, songgee@hnu.edu.cn

[b] Technical University of Denmark, Denmark

Abstract. Bioeffluents emitted from person lying down in bed can be removed by ventilated mattress (VM) before mixing with the room air. VM is designed to suck air through an exhaust opening located near the feet and move the sucked air inside the mattress. The air moves through the whole mattress and is removed to the exhaust or cleaned and discharged back to the room. The VM can change the thermal conditions in the bed micro-environment and provide uncomfortable local cooling of the person in the bed. Therefore, the design of the ventilated mattress is further improved by incorporating local heating. The response of people to the bed thermal environment generated by the mattress was studied at three room air temperatures – 19°C, 23°C and 28°C. 30 human subjects (15 males, 15 females) of age 20 - 29 years old and body mass index in the range 18 - 27 were exposed to the bed thermal environment provided by the VM. The subjects were covered with a thin duvet (2.9 clo) at room temperature 19°C, a double cotton sheet at 23°C and a single cotton sheet was used at 28°C. The subjects were dressed with pajama (short-sleeve shirt, shorts) and underwear. Thermal sensation assessment was collected through standardized questionnaires. The subjects answered questions regarding their whole body thermal sensation and local thermal sensation of separate body parts including face, head, neck, chest, back, arms, hands, thighs, lower legs, and feet. The bed thermal micro-environment was adjusted by the exhaust flow rate through the ventilated mattress and the localized heating depending on the acceptability of the subjects' thermal sensation collected every 7 minutes. The results show that the applied control of the bed thermal environment increased the acceptability of the whole body thermal sensation votes and the risk of local cold discomfort (especially on the feet and hands) decreased over time. Local heating at the feet will be needed to achieve thermal comfort in room temperatures below 23°C. Local heating incorporated in the VM or separate and the airflow through the mattress can be controlled based on physiological signals of the person's body.

Keywords. Ventilated mattress, bed thermal environment, thermal sensation, thermal acceptability, physiological parameters.
DOI: https://doi.org/10.34641/clima.2022.415

1. Introduction

Thermal comfort is a critical factor that effects sleep quality [1]. A good bed micro-environment can ensure high sleep quality, which directly affects the daytime productivity and mental state of people. In addition, the bed is one of the places where people may stay for a long time, especially in healthcare facilities. An important factor affecting the bed micro-environment is the various airborne odorous contaminants (bio-effluents) emitted from lying people's bodies. These pollutants are difficult to remove by room background ventilation before they mixed with the air near the bed [2].

The main method to solve the pollution problem in the bed micro-environment is by source control. For this purpose, a ventilated mattress (VM) was designed to remove body-emitted pollutants by sucking a small amount of air near the feet of a lying person [2]. A detailed description of the VM can be found in [2]. Although the VM is highly efficient to remove body bio-effluents, it has been found that its design may cause local cold discomfort to the users [3]. Bivolarova et al. [3] found out local body cooling of a thermal manikin's body segments in contact with the surface of the VM. It was concluded that large differences in the body local thermal sensation might be expected when the VM is used. Therefore, human subject experiments are needed to identify the effect

Copyright ©2022 by the authors. This conference paper is published under a CC-BY-4.0 license.

Tab. 1 - The interquartile range (IQR) and median of the age, height, weight and BMI of the subjects.

Gender	Number	Age(year)	Height(cm)	Weight(kg)	BMI(kg/m2)
		Median(IQR)	Median(IQR)	Median(IQR)	Median(IQR)
Male	15	25(22-27)	175(172-178)	72(66-75)	22.3(19.9-22.59)
Female	15	25(23-27)	168(165-170)	57(55-65)	21.5(21.59-24.2)
Total	30	25(23-27)	171(168-175)	65(56-72)	22.0(20.31-23.96)

of the non-uniformity in the local body cooling on the overall thermal sensation of people. There are no relevant studies until now related to the risk of local cold discomfort of people using the VM. The ventilated mattress is a similar system to a personalized environment control system (PECS), aimed to maintain good inhaled air quality and preferred thermal comfort of users [4]. Previous studies on PECS have shown the need for more flexible and sensitive control strategies [5, 6]. To save energy, the overall building temperature is usually set lower in winter and higher in summer when PECS are used [7]. This suggests that people need extra personalized heating or cooling system (radiant heater, fan, personalized ventilation) to reach the individual comfort level. There are some automatic control systems based on time or motion sensors used with PECS, but manual control is still the most accepted method. Compared with the traditional HVAC control systems, people are more willing to spend personal time to control PECS in order to obtain preferred individual micro-environment. Gao et al. (2013) designed a smart system that considers the individual thermal preference and can balance energy conservation with personal thermal comfort in an office environment (SPOT) according to the Predicted Mean Vote (PMV) model of ISO 770 standard [8]. Kim et al. [9] predicted individuals' thermal preference using occupant heating and cooling behaviour and machine learning. Zhu et al. [10] produced an occupant-centric air-conditioning system for recognition and control of thermal preference in the personal micro-environment. These previous studies discussed the application of several control logics for personal comfort systems in office environments where people are mostly sitting. The control of the bed thermal microenvironment generated by the VM is different and has not been analysed so far.

The aim of this study was to investigate the performance of the ventilated mattress combined with local heating for providing thermal comfort in bed. For this purpose, the thermal sensation and acceptability response of thirty subjects was studied. The bed thermal micro-environment (BTME) was adjusted by manually controlling the exhaust airflow rate of the ventilated mattress and the local heating based on the acceptability votes of the subjects' thermal sensation. This study adds new knowledge of the control strategies of the bed thermal microenvironment.

2. Methodology

2.1 Human subjects

In this study, thirty young and healthy human subjects were recruited. The subjects were asked not to drink alcohol and caffeine drinks prior to the experiment and to be rested on the days of the experiment. The experimental procedure and subjective questionnaires were explained to the subjects in advanced. During the experiment, they were wearing pajamas consisting of short-sleeve shirt (0.17 clo) and shorts (0.06 clo) and underwear (0.03 clo (women), 0.04 clo (men)). The basic physical characteristics of the subjects are shown in Table 1.

2.2 Experimental facilities and Measurements

A typical bedroom environment was simulated in a climate chamber with dimensions of 4.7 m × 4.7 m × 2.6 m (W×L×H). The room was ventilated with three air changes per hour of clean air supplied and exhausted by ceiling mounted diffusers. The air was distributed in a way that the air speed in the occupied zone was less than 0.1 m/s. The chamber was arranged to resemble a bedroom. A bed (1.6 m wide and 2 m long) with six cm thick mattress was used. On top of the regular bed mattress, it was placed the ventilated mattress (Fig. 1). Air temperature and relative humidity were measured in the room close to the bed at 0.8 m and 1.2 m above the floor. In addition, the air temperature and relative humidity were measured under the cover around the lying subject at three locations – between the feet, between the thighs and between the torso and the right arm.

The skin temperature was measured at 10 points: forehead, right scapula, left upper chest, right upper arm, left lower arm, left hand, right anterior thigh, left calf, right instep, and left instep. The equipment used in this experiment is shown in Table 2.

The continuous ASHRAE seven-point scale was used to assess the overall and local body thermal sensation including the body parts face, top of the head, neck, chest, back, arms, hands, thighs, lower legs, and feet [11]. The thermal sensation scale was from "cold" to "hot", where hot = +3, warm = +2,

Tab. 2 - Environmental and physiological parameter measuring equipment.

Parameters	Instruments	Accuracy
Air temperature	Sensirion EK-H4 kit, SHT31 sensor	±0.2°C (5°C – 60 °C)
Air humidity		±3% (20 %RH – 80 %RH)
Skin temperature	ibutton DS1922T	±0.5°C (20 -70°C)

slightly warm = +1, neutral = 0, slightly cool = -1, cool = -2, and cold = -3. Acceptability of the thermal sensation was assessed using the acceptability scale. The acceptability scale consists of two continuous scales (Fig.3 right scale) from "clearly unacceptable = -1" until just "unacceptable = -0.01" and from "just acceptable = +0.01" until "clearly acceptable = +1". Each question was shown on a flat screen hanged from the ceiling in front of the bed, on which the subjects were able to see the question and provide their answer.

2.3 Experimental procedure and conditions

The subjects were exposed to three room air temperatures: 19°C, 23°C and 28°C. The relative humidity in the chamber was not controlled. It was in the range of 35 - 50% during all experimental sessions. Each subject participated in three experimental sessions. One session lasted 2 hours as shown in Fig. 2. Each participated in all three sessions at the same time of the day. After entering the chamber, the subject changed clothes, attached the ten skin temperature sensors, and their body parameters (weight, body fat, bone mass, body water, muscle mass physique rating, BMR, metabolic age, visceral fat) were measured on a digital scale before going to the bed to start the acclimation period. During the acclimatization period, the subject adopted a comfortable position, and answer the first questionnaire (Q1) regarding how many hours they slept during the previous night. Afterwards, the temperature sensors for measuring in the bed were placed, as shown in Fig. 1, and the subject was covered up to his/her neck. Most subjects kept their arms below the cover. Only few subjects put their arms above the cover during the session at 28°C. The subjects were covered with a thin duvet (2.9 clo) at 19°C. A double cotton sheet was used at 23°C and a single cotton sheet was used at 28°C. Only one female subject requested to be covered with a blanket on top of the double cotton sheet at 23°C. The thermal insulation of the blanket was 0.65 clo. After the acclimatization period, the ventilated mattress was started at 3 L/s (amount of air exhausted through the mattress). Since, the VM suction openings were at the feet some subjects were experiencing local cooling at their feet. In that case, a small heated mat was placed on top of the feet over the cover until the subject needed it. If a subject was feeling warm, then the flow rate of the VM was increased. The flow rate of the VM at 19°C and 23°C varied for each subject between 3 L/s – 6.5 L/s and at 28°C between 3 L/s – 19.5 L/s. The subjects were asked to lay only on their backs, and they were allowed to move.

During the exposure time in the bed, the subjects were asked every 10 min to answer the second questionnaire (Q2) regarding their thermal sensation and acceptability. The flow rate and heating power of the local heating device were adjusted every 10 min according to the human subjects thermal preferences.

Fig. 1 - View of a subject lying on the VM and the three temperature sensors positioned around the subject (placed inside green protectors). The white surfaces near the feet are where the suction openings of the VM were.

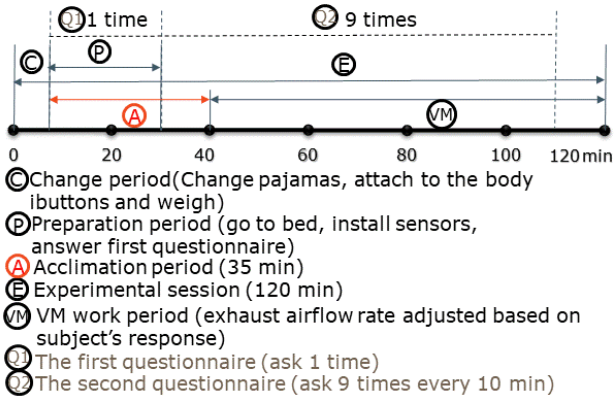

Fig. 2 - Experiment procedure.

2.4 Data Analyses

A total of 90 experiments were conducted with 30 subjects, 830 questionnaires were answered, and 27390 votes were obtained to ensure the statistical significance of the data. Statistical analyses were performed using SPSS version 24.0 for Windows (SPSS Inc., Chicago, IL, USA). The box plots were made to show the results from the overall thermal sensation and acceptability at the three studied room temperatures. The sum of the thermal sensation votes (TSVs) of the subjects were used to show the effect of the VM's control on whether it is effective to provide subjects with acceptable thermal sensation. The following equation was used to calculate the sum of the thermal sensation votes separately for the fifteen female participants and the fifteen male participants:

$$Y_i = \sum_{k=1}^{15} X_{k,i} \quad (1)$$

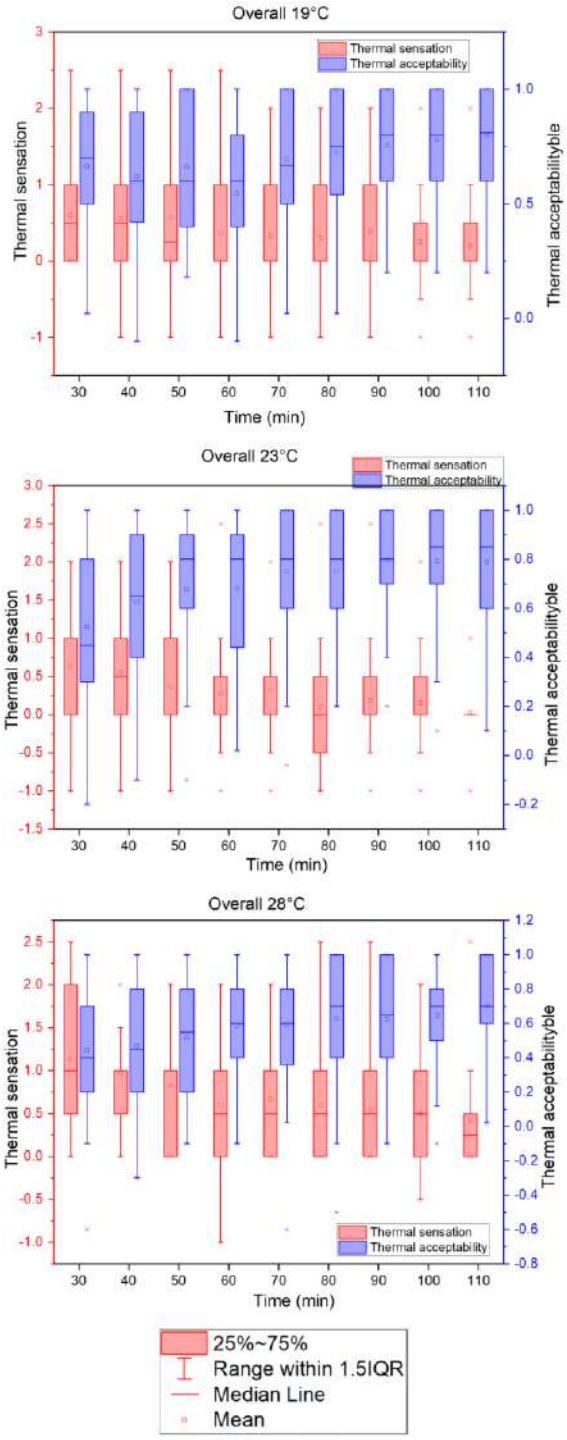

Fig. 3 - The distribution of the overall thermal sensation and acceptability votes of the 30 subjects as a function of the exposure time in the bed at room air temperature 19°C, 23°C, and 28°C.

Where $X_{k,i}$ is the overall or separate body part thermal sensation vote of a subject at the time i of answering the questionnaire Q2.

3. Results

The distribution of the overall thermal sensation and acceptability votes of all 30 subjects is shown in Fig. 3 for each experimental room condition. According to the medians and mean values, the thermal acceptability gradually approached almost 1 (clearly acceptable) at the end of the exposure time as the thermal sensation approached almost neutral sensation (equal to 0). This trend can be observed for the three studied room air temperatures. Overall, during the whole exposure time of all experimental conditions the subjects' acceptability of the overall thermal sensation was above just acceptable. These results suggest that the ventilated mattresses combined with local heating can effectively control the bed thermal microenvironment.The fastest increase of thermal acceptability of the subjects was achieved (after 20 min) in the neutral room temperature environment (23°C), where the subjects thermal sensation was between neutral and slightly warm. This means that the bed microenvironment's control may face more challenges when the indoor temperature is cold (19°C) or hot (28°C) than when the room conditions are within the comfortable range (21 - 24°C). Therefore, focus not only on the subjective response but also on the response of the users' physiological parameters such as skin temperature is needed. In this way the time response of the bed microenvironment to meet the users' thermal preferences can be determined.

Fig. 4 shows the sum of the TSVs for the whole body (overall) and different body parts of the participants as a function of time. Fig. 4 shows the separate results for female and male subjects obtained at all three room conditions (19°C, 23°C and 28°C). The overall thermal sensation as well as thermal sensation of the back, arms, thighs, and feet always approached zero at the end of the exposure time in the bed with VM working. This trend is observed for both men and women's thermal sensation. This means that the control of the VM and the local heating at the feet was effective, and the thermal sensation tended to be neutral (equal to zero in Fig. 4). The results for the thermal sensation for the body parts top of head, face, chest, hands, and lower legs showed the same trend of reaching almost neutral thermal sensation at the end of the experimental session. Fig. 4 shows also that the overall thermal sensation of the women was lower than that of the men; especially the differences were large at 19°C. Similar results can be observed for the individual body parts. It was found out that the sum of TSVs for the face of the women were lower than 0 during the entire exposure time at 19°C. The sum of the TSVs of the women in the last 10 min of the exposure time were less than 0 for the arms and feet at 23°C. Whereas, for the men only the thermal sensation at the feet was less than 0 in the beginning and at the end of the exposure at 19°C and at the end of the exposure time at 23°C. The sum of the overall thermal sensation votes and the neck for both the men and the women were higher than 0 during the three studied room temperatures. But a trend moving towards 0 from the start of the exposure until the end of the exposure time can be observed. Furthermore, the sum of TSVs of the body parts in contact with the VM (back, arms, thighs, and lower legs) were higher than neutral throughout the exposure time in the bed at all three room conditions. But due to the VM's cooling effect, the TSVs

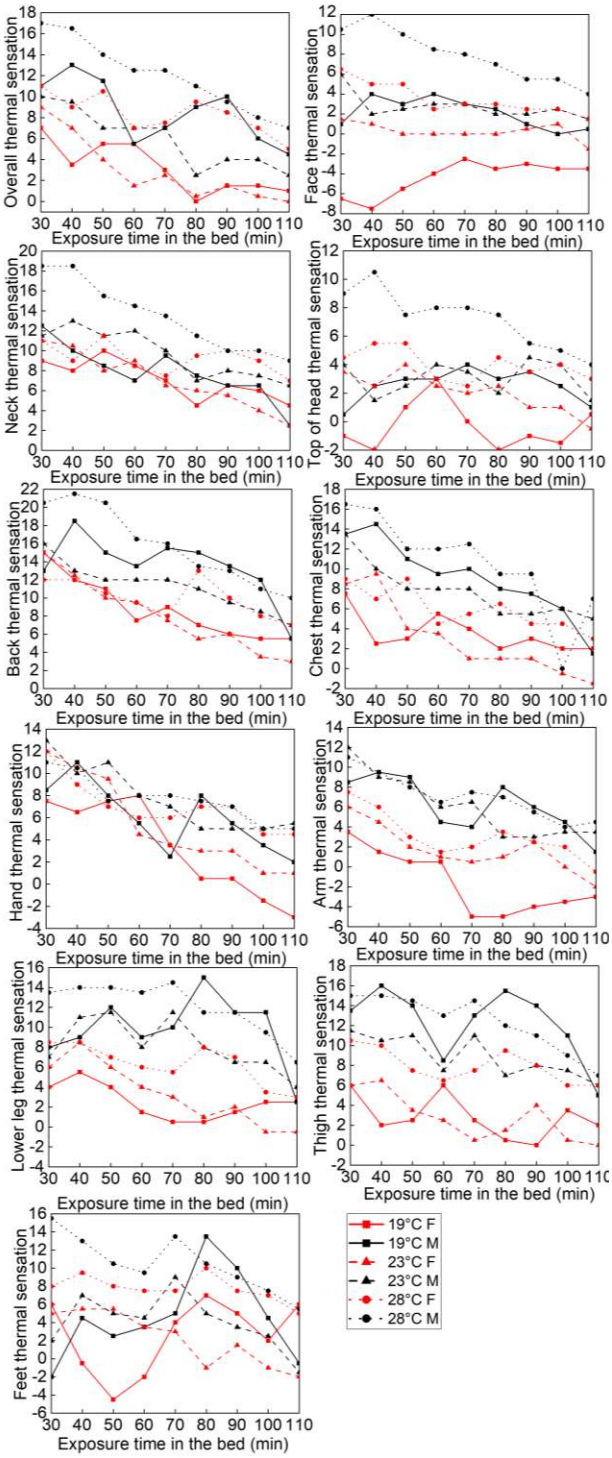

Fig. 4 - Subjects' overall and body parts thermal sensation as a function of time at room air temperature of 19°C, 23°C and 28°C, where F = female and M = male.

approached neutral at the end of the exposure, which proves that the application of the VM has a positive effect to create neutral BTME. The higher TSV for the neck may cause local hot thermal discomfort, but the resulting cooling of the body parts in contact with the mattress seems to be able to reduce this discomfort.

4. Discussion

In this study, the BTME was adjusted according to the feedback of the subjects, which was collected by questionnaires. The whole experiment process was in a state of variable conditions, and the subjects were almost exposed to a neutral micro-environment all the time. This study aims at creating a comfortable BTME for people as much as possible. This study proves the necessity of real-time control of the VM based on the response of the user for creating comfortable BTME. The ultimate goal of control is to integrate an intelligent control of the VM, which requires the VM to recognize the comfort needs of the occupants and adjust its flow rate and surface temperature in time. Therefore, focus not only on the subjective response but also on the users' physiological parameters such as skin temperature is needed. In this way, the time response of the bed microenvironment to meet the users' thermal preferences can be determined. Furthermore, a bio-signal from people, which can be used as an indicator for thermal sensation, should be identify. Our study only examined the thermal response of people while they were lying on their back and did not account for different body positions. This factor may have an impact on the amount of heat transfer from the body to the environment. This needs to be studied. How to identify the comfort needs of occupants and how to control them in time are the research directions for the development of the VM intelligent control systems in the future.

5. Conclusion

The present study used real-time control of the BTME by the VM combined with local heating device installed on the feet and the response of 30 subjects to the BTME was examined. The following conclusions were drawn:

1) At 19°C and 23°C, uncomfortable local cooling was reported and therefore, local heating was needed.

2) Local thermal sensation at feet improved for most of the subjects. For some of the subjects, the applied local heating was not so sufficient.

3) At 28°C, the ventilated mattress provided beneficial cooling although it required substantial increase of the ventilation flow through the mattress for the majority of the subjects.

4) The need for local heating was reported with some delay (20 - 40 min) after exposure to the bed micro environment.

6. Acknowledgement

This research was supported by the Bjarne Saxhof's Foundation for Support of Danish Research, project No 26946.

7. References

[1] X. Zhang, G. Luo, J. Xie, and J. Liu, "Associations of bedroom air temperature and CO2 concentration

with subjective perceptions and sleep quality during transition seasons," Indoor air, 2021.

[2] M. P. Bivolarova, A. K. Melikov, C. Mizutani, K. Kajiwara, and Z. D. Bolashikov, "Bed-integrated local exhaust ventilation system combined with local air cleaning for improved IAQ in hospital patient rooms," Building and Environment, vol. 100, pp. 10-18, 2016/05/01/ 2016.

[3] M. P. Bivolarova, A. K. Melikov, M. Kokora, and Z. D. Bolashikov, "Local cooling of the human body using ventilated mattress in hospitals," in Proceedings of the 13th International Conference on Air Distribution in Rooms–Roomvent, 2014, pp. 19-22.

[4] A. K. Melikov, "Personalized ventilation," Indoor air, vol. 14, pp. 157-167, 2004.

[5] J. Kaczmarczyk, A. Melikov, Z. Bolashikov, L. Nikolaev, and P. O. Fanger, "Human Response to Five Designs of Personalized Ventilation," HVAC&R Research, vol. 12, pp. 367-384, 2006/04/01 2006.

[6] Q. Zeng, J. Kaczmarczyk, A. Melikov, and P. O. Fanger, "Perceived air quality and thermal sensation with personalized ventilation system," in Proceedings of roomvent, 2002, pp. 61-64.

[7] S. Schiavon and A. K. Melikov, "Energy-saving strategies with personalized ventilation in cold climates," Energy and Buildings, vol. 41, pp. 543-550, 2009.

[8] P. X. Gao and S. Keshav, "SPOT: a smart personalized office thermal control system," in Proceedings of the fourth international conference on Future energy systems, 2013, pp. 237-246.

[9] J. Kim, Y. Zhou, S. Schiavon, P. Raftery, and G. Brager, "Personal comfort models: Predicting individuals' thermal preference using occupant heating and cooling behavior and machine learning," Building and Environment, vol. 129, pp. 96-106, 2018/02/01/ 2018.

[10] Zhu, Mingya, et al. "An occupant-centric air-conditioning system for occupant thermal preference recognition control in personal micro-environment." Building and Environment 196 (2021): 107749.

[11] R. A. S. o. Heating, A. C. Engineers, and G. Atlanta, ASHRAE handbook: fundamentals: ASHRAE, 2009.

Control of the bed thermal environment by a ventilated mattress

Rinsa Kunnathummal [a], Mariya P. Bivolarova [a], Arsen K. Melikov [a]

[a] Department of Environmental and Resource Engineering, Technical University of Denmark, Denmark, mbiv@byg.dtu.dk.

Abstract. Thermal comfort affects the sleep quality and well-being of people. The effect of a ventilated mattress (VM with integrated localized heating on providing the necessary thermal conditions for comfort in the bed-microenvironment was studied. The VM has an exhaust opening located under the feet of a lying person. Air is sucked and transported inside the mattress by a small fan connected to the mattress. The benefit of using such a mattress is that it sucks and removes body-emitted bio-effluents, which prevents the pollutants to spread in the room. The air movement inside the mattress provides cooling to the body, which makes the bed micro-environment comfortable during the cooling season but may cause discomfort during the heating season. Therefore, the VM was further developed by implementing local heating. Full-scale experiments were performed in a climate chamber furnished with a single bed equipped with the VM. A full-size thermal manikin was used to simulate a person lying in the bed. The performance of the VM with regard to the provided body heating/cooling was studied at room air temperatures of 19, 23, and 28 °C. The control of the thermal conditions in the bed-microenvironment was tested when the VM was operating at different airflow rates and local heating power. A reference condition at 23 °C without the VM in operation was assumed to provide thermal comfort in the bed. The performance of the VM was evaluated based on a comparison of the body dry heat flux from the segments and the whole body of the thermal manikin obtained with the VM in operation and during the reference condition. The results show that it was possible to achieve the same body heat flux at all studied room temperatures using the VM with localized heating as in the reference condition. The use of the VM combined with localized heating with control based on the individual needs of the user can be an efficient method for providing thermal comfort in a bed at a wide range of room air temperature. Energy can be saved by expanded lower and upper room temperature limits recommended in the standards.

Keywords. Bed microenvironment, ventilated mattress, local body heating and cooling, thermal comfort.
DOI: https://doi.org/10.34641/clima.2022.434

1. Introduction

The indoor environment highly influences the health, productivity, and comfort of the occupants. Therefore, a healthy and comfortable environment is necessary for the quality performance of the occupants. However, there are several sources of pollutants in buildings. Among these pollutants, humans are one of the main sources of bio-effluents that can substantially reduce indoor air quality. In addition, sensory pollution load from people, such as body odour from sweat and the skins' sebaceous secretions, foul breath, and gases from the digestive tract, can be present in the indoor air [1].

Removing pollutants at the source before mixing with the room air is an effective way to reduce the pollutants concentration in the room. An advanced air distribution (AAD) based on providing a personalized microenvironment is a promising solution [2] both for energy saving and higher IAQ. One of the most efficient locations for integrating the local ventilation system is the bed, considering one third of the time we spent sleeping. The AAD solution integrated in a bed can considerably remove air pollution before it is mixed with the room air, thus improving the occupant perceived air quality.

An AAD solution with source control in the bed, named VM (Ventilated Mattress) has been shown to remove effectively polluted air in the bed microenvironment and increase room air quality [3]. Furthermore, the study conducted with a thermal manikin lying on a VM showed that the cooling effect

Copyright ©2022 by the authors. This conference paper is published under a CC-BY-4.0 license.

by the movement of air sucked through the mattress can enhance the bed thermal microenvironment and can improve the occupant's thermal comfort in warm indoor environments [4]. However, the study also concluded that the cooling effect of the VM is nonuniform, which can potentially cause thermal discomfort for the occupant, especially during the heating season. In this regard, utilizing a local heating solution for the VM could be beneficial in improving thermal comfort. In this paper, the application of the VM combined with a localized heating method to improve the thermal perception of the human body is examined.

2. Methods

2.1 Experimental Facilities

The experiment was performed in a full-scale test room arranged as a single bedroom of size 4.68 m × 4.7 m × 2.6 m (W × L × H). The room background was ventilated by total volume mixing ventilation. Diffusers for air supply and exhaust were a perforated square diffuser and a circular diffuser, respectively. The diffuser was supplying clean outdoor air in one way as shown in Figure 2-1. A 50 L/s (3 ACH) ventilation rate was set, which is a typical air change rate (ACH) for ventilating general patient rooms in hospitals according to the ASHRAE standard [5].

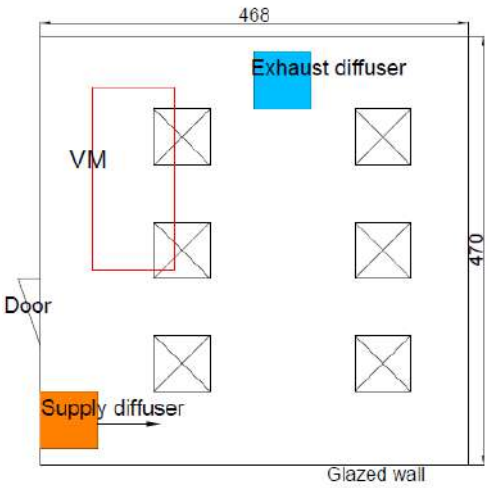

Figure 2-1:Ceiling arrangement with light and diffusers

The VM's was made up of synthetic fiber, which is permeable for air. With the use of an exhaust fan, the air was moved through the VM starting from the exhaust opening at the feet and was taken out from the top of the mattress through exhaust ducts at the left and right sides of the VM, as shown in Figure 2-2. The exhaust opening at the feet was covered with a polyester mesh. An additional, regular mattress of 6 cm thickness was placed below the VM.

Figure 2-2: Ventilated mattress(VM)

A thermal manikin consisting of 23 body segments was used to simulate an occupant in bed. The thermal manikin had the shape of an average Scandinavian female with a height of 1.68 m, weight 22 kg and size 38. During the experiments, so-called Comfort mode in the Manikin software was used to control the surface temperature of manikin segments to be the same as the skin temperature of an average person in the state of thermal comfort [6]. The evaluation of the local cooling effect was conducted using the manikin with different clothing levels, including naked condition, dressed with long sleeve pyjama, short sleeve pyjama, and short pyjama. Two local heating sheets of size 50 cm x 60 cm were used for the study, and the sheets were placed below the feet and below the back, inside the VM below the supporting mesh, as shown in Figure 2-3. One of the local heating sheets was placed below the manikin's feet due to high heat loss at the feet. The local heating sheet below the feet could also heat up the exhaust air flowing through the VM. The second local heating sheet was placed below the back as the back of the manikin had the largest contact area with the VM. The power of each local heating sheet was adjusted using a transformer.

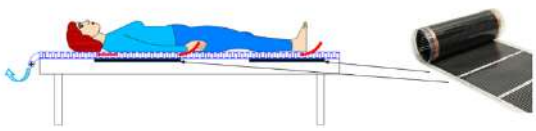

Figure 2-3:Location of the local heating sheet in the VM

In addition, carbon fiber heating elements were placed below the arms to compensate for the high local heat loss, as shown in Figure 2-4. The heating level control of the carbon fiber heating elements was done using an adjustable DC supply.

Figure 2-4:Carbon fiber heating element

The temperature in the room near the bed at 0.6 m and 1.1 m was constantly monitored to verify a stable room temperature (Figure 2 5). The surface temperature of the VM was measured at five different locations, such as below the left and right thigh of the manikin, close to the bottom part, below back, below upper back. Also, the exhaust air temperature was monitored by one sensor placed inside the VM at the exhaust duct.The temperature measurements were recorded every minute using EK-H4 evaluation kit from Sensirion. The digital sensors SHT31 with a measurement accuracy of ±0.2 °C can measure the temperature in the range of 0°C to 90°C. The temperature sensors were attached on the mattress and insulation was used to isolate the sensors from the side exposed to the microenvironment or in contact with manikin's body.

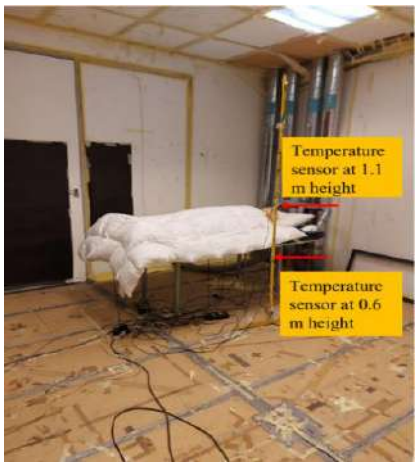

Figure 2-5:Temperature sensors location in the room

The velocity in the room around the bed was measured to ensure the air speed was low around the bed. The air speed around the bed, 20 cm from the bed, was measured using a multichannel low-velocity thermal anemometer AirSpeed 5000, which uses a sensoAnemo 5100SF transducers. The transducer was equipped with a probe that includes omnidirectional air speed and temperature sensors. The range of air speed measurement by the sensor was 0.05 m/s to 3 m/s with an accuracy of ±0.02 m/s ± 1%.

2.2 Experimental Conditions

Various standards define comfortable indoor temperatures. For instance, according to the ASHRAE standard [5], the ideal temperature for thermal comfort in a general patient room is 20°C - 24°C. According to the Danish standard DS/ISO/TR 17772-:2018 [7] for bedrooms in residential buildings with indoor environmental quality (IEQ) of category I and II, the recommended design values of the indoor operative temperature in winter and summer are 21°C (for winter, IEQ I), 25.5°C (for summer IEQ I), and 20°C (for winter, IEQ II) and 26°C (for summer, IEQ II) respectively. In this regard, a room temperature of 23°C was assumed to be thermally acceptable for the person lying down naked. Therefore, a naked manikin covered with a 600 g duvet without using VM at a room temperature of 23°C was chosen to be the reference case in this study.

A summer period with a room temperature of 28°C ±0.5°C and a winter period with a room temperature of 19°C ±0.5°C were considered in the experiment. The winter and summer room temperatures were chosen to be slightly below and over the minimum and maximum standard values of 20°C and 26°C (IEQ II) [8]. It was hypothesized that the VM can provide thermal comfort at extended lower and upper room temperature limits than the recommended in the standard DS/ISO/TR 17772. Extending the room temperature range is a well-known strategy to achieve energy savings in buildings [9] [10]. Clothing and bedding for the manikin was adapted to different room conditions. For instance, a 600 g down duvet was utilized at 23°C room temperature condition, whereas, a thicker 1055 g down duvet was used for the case simulating winter conditions (19°C) and a thin cotton sheet was used during the summer conditions (28°C). The manikin was placed in a supine position, with a pillow for a headrest. At room temperatures of 19°C and 23°C, the manikin was clothed with long sleeve pajamas and short sleeve pajamas respectively. A short pajama including a singlet and shorts was used during the conditions at 28°C. At the three room temperatures (19°C, 23°C, 28°C), experiments were performed at an exhaust flow rate of 1.5 L/s, 3 L/s, 4.5 L/s, 6 L/s, and 10 L/s without local heating and 3 L/s exhaust flow rate (optimum to remove bioeffluents) with local heating.

2.3 Experimental Procedure and Data analysis

The room ventilation system and the manikin were both operational at all times to maintain a steady room air temperature. After the temperature reached steady state, the measurements were started. Firstly, the air velocity in the room around the bed was measured to ensure that the air speed around the bed was less than 0.1 m/s. At the beginning of experiments, the temperature in the room was set to 23°C, which was the reference condition. For each of the performed experiments (referred in the following as cases) the segmental and whole-body cooling effect on the manikin was assessed by comparing the manikin's segmental heat flux data obtained from the particular experimental condition with that of the reference case (at 23°C,

naked manikin, no VM). If the heat flux of the segments was higher than the heat flux of the respective segments in the reference case, the local heating was provided for compensation. The local heating power was adjusted using a transformer to reduce the body heat flux and make it closer to the reference case.

During the whole experiment, the temperature below the manikin's left and right thighs, close to the bottom part, below the back, below the upper back as well as the exhaust air temperature were measured. Furthermore, the power required for the local heating elements were recorded.

2.3.1 Data analysis

The average of the logged dry heat flux was calculated for a ten minutes interval after the manikin reached a steady state. The cooling effect of the VM was evaluated by comparing the data of the average dry heat flux obtained for each body segment for the cases with a different exhaust flow rate of the VM against the reference case data. The difference between the average dry heat flux of each body segment and the average heat flux obtained in the reference case of the respective body segment (designated as ΔQ) was calculated first. ΔQ was used to define ΔQmax. Where ΔQmax of the measured case is the maximum value of the differences ΔQ for each body segments. It was assumed in this study that for an acceptable thermal environment, the difference between the average heat flux of the manikin during a case with VM turned ON and the reference case without VM should be less than 6 W. That is, the condition for the acceptable thermal environment is defined as

$$\Delta Q_{max} < 6W \quad (1)$$

3. Results

The measured heat flux at the reference case is shown in Figure-3-1. The differences in the heat flux of the various body segments was due to the difference in the thermal insulatilon for each body segments. For example, the heat flux of the body parts in contact with the duvet (pelvis, chest, front things) was lower compared to the other body parts. The heat flux measured at 23 °C with the VM in operation for the cases with different exhaust airflow rate are shown in Figure 3-2. For every case, the average dry heat flux of the body segments of the undressed manikin measured at the studied exhaust airflow rates of the mattress - 1.5 L/s, 3 L/s, 4.5 L/s, and 6 L/s - was compared with the average dry heat flux at the reference case without the VM.

Figure 3-2 depicts the ΔQ for different exhaust flow rates of the VM at 23°C room temperature. It can be seen that the average dry heat flux of the manikin's body segments increased as the exhaust airflow rate increased, which demonstrates the cooling effect introduced due to the airflow of the VM. It can also be seen from Figure 3-2 that ΔQ is more substantial at certain body segments, especially at the lower segments of the body and the body segments in contact with the mattress, namely backside, arms, feet, legs, and back. A nonuniform ΔQ across the body segments suggests potential risk of local thermal discomfort.

Similarly, the same trend was observed at 19°C room temperature at the studied exhaust airflow rates of the VM. The results are shown in Figure 3-3. The surface temperature of the mattress at the studied exhaust flow rates at 19°C is shown in Figure 3-4. The results are in agreement with the results of the local cooling effect and nonuniform heat flux loss from the body segments. The highest temperature deviation from the reference case temperature occurred below the back, below the left thigh, and close to the bottom part. The temperature difference and heat flux below the left thigh were different than the one below the right thigh. Such a difference is possibly due to asymmetry in the airflow of the VM or asymmetrical contact of the respective body segments with the VM. An attempt to eliminate the local cooling effect of the VM by utilizing local heating was applied (shown in Figure 2-3). The objective of the local heating method was to make the heat flux of the different manikin body segments closer to the heat flux in the reference case and meet the defined acceptable thermal environment criteria given by equation (1). Heating

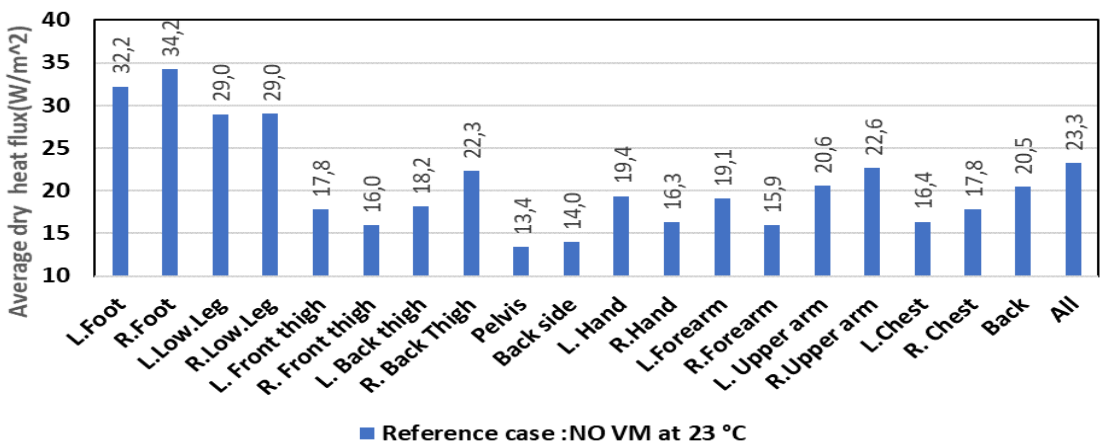

Figure-3-1: Manikin's average dry heat loss at reference case

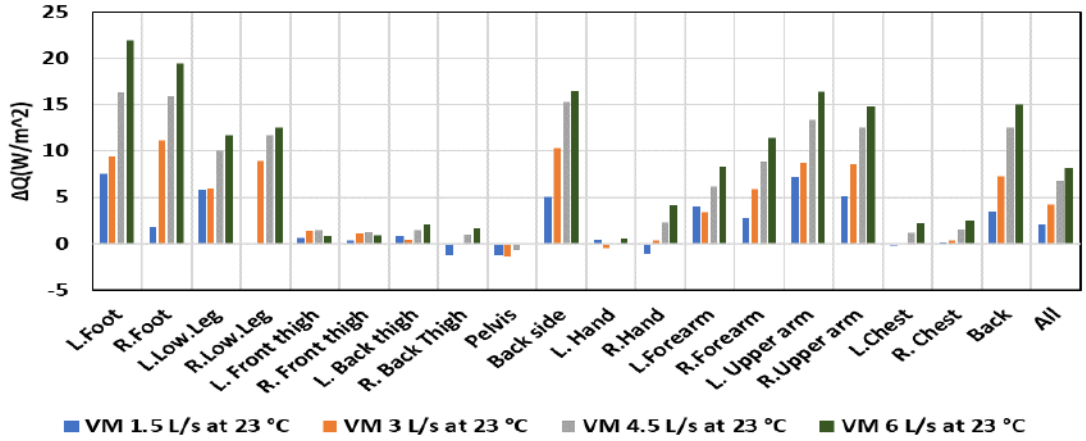

Figure 3-2:Average dry heat flux for different exhaust flow rates of the VM at 23 °C

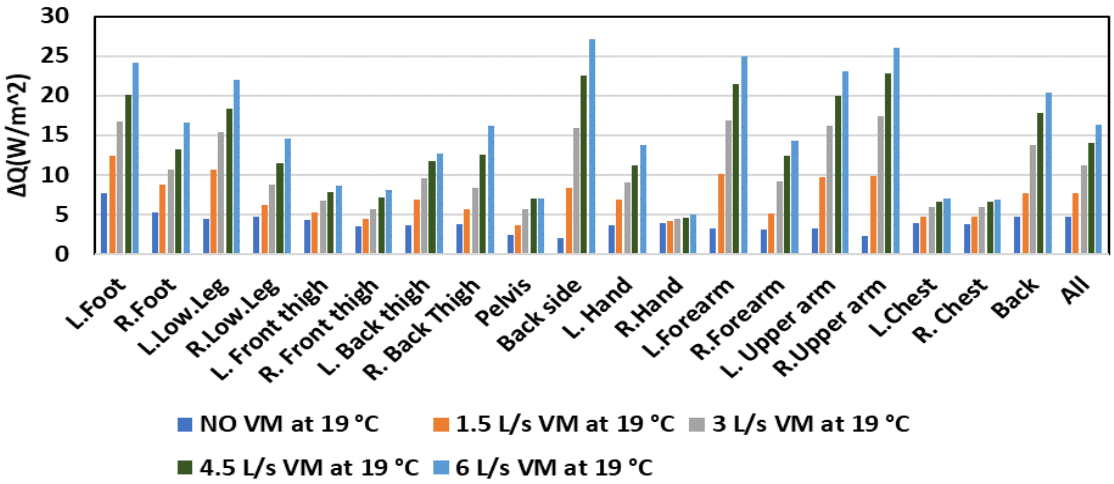

Figure 3-3:Average dry heat flux for different exhaust flow rates of the VM at 19 °C

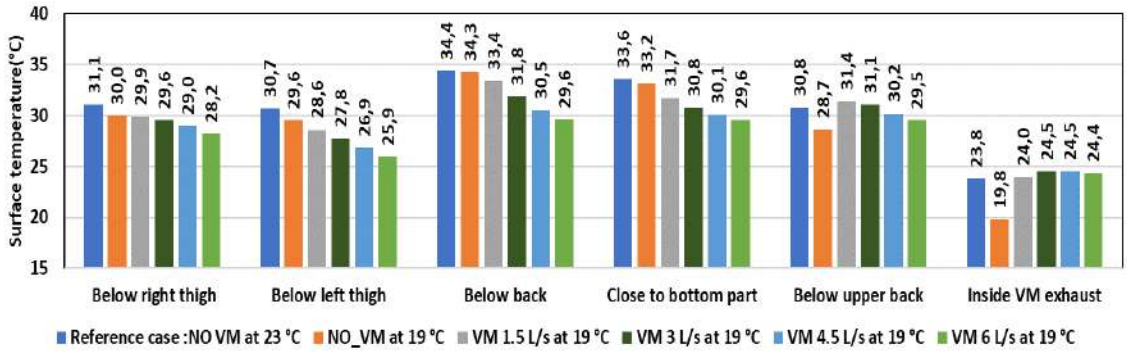

Figure 3-4:Surface temperature at different exhaust flow rate at 19°C

compensation was carried out for the VM operating at 23°C and at 3 L/s exhaust. After multiple iterations by adjusting the heating levels, the 8 Watts heating at the feet and 9 Watts at the back was the most optimal choice. The results in this case are shown in Figure 3-5. It can be seen that it is possible to make the heat flux of different manikin body segments closer to the heat flux in the reference case when local heating is applied. Furthermore, it was found out that by dressing the manikin with a long sleeve pajama and with added insulation on top of the mattress, no extra local heating was required to compensate for the heat loss (Figure 3-5, bars in orange). However, for both cases in Figure 3-5, the heat flux at the arms was higher than the maximum acceptable deviation (ΔQmax) from the reference case and still needed to be adjusted. Thus, the Carbon fiber heating method was required below the arms to provide the necessary heat to the arms.

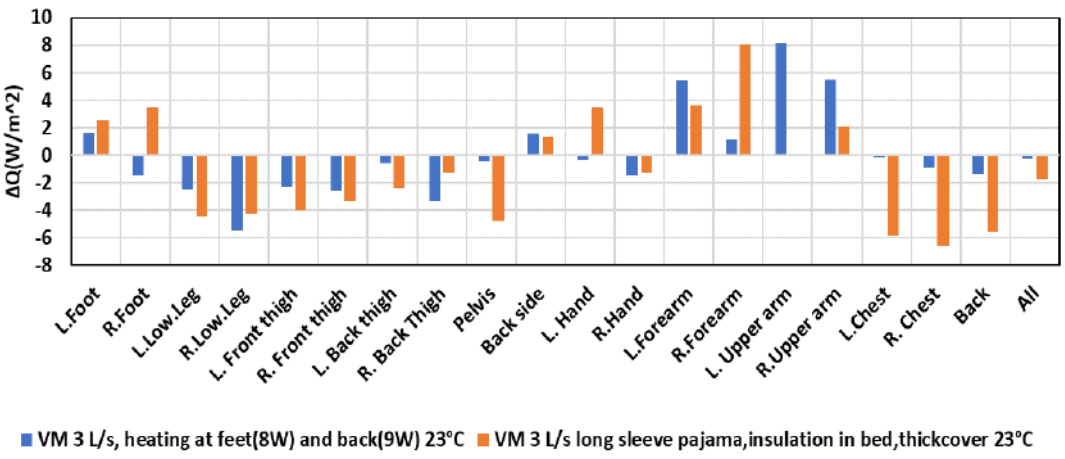

Figure 3-5: Heating compensation at 3 L/s VM case at 23ºC

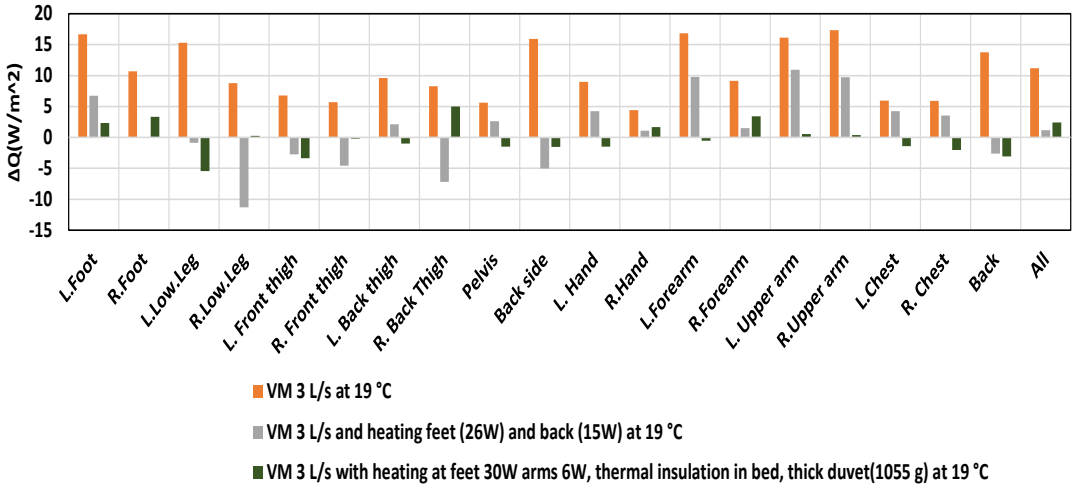

Figure 3-6: Heating compensation at 3 L/s VM case at 19ºC

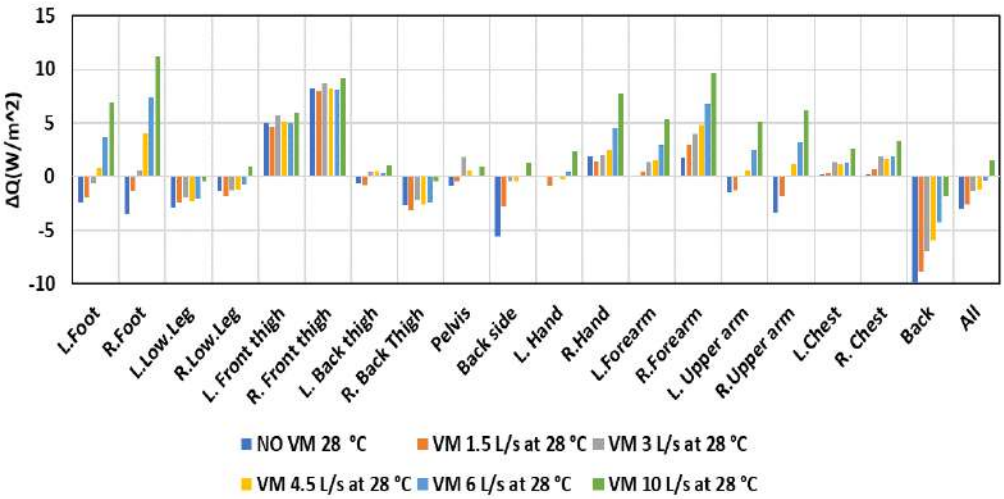

Figure 3-7:Average dry heat flux for different exhaust flow rates of the VM at 28 ºC

Figure 3-6 depicts the local heat flux of the body segments for the case of 3 L/s exhaust flow rate of the VM with the local heating sheet (as shown in Figure 2-3) at 19°C room temperature. The results indicate that it is possible to use the VM at 3 L/s exhaust flow rate at 19°C room temperature and mitigate the cooling effect of the VM for all body parts except at arms when providing local heating of 26 W at the feet and 15 W at the back. In addition, the ΔQ for the right low leg was greater than 6 W, i.e. the acceptable range considered. This measurement could be a possible outlier due to unwanted infiltration from the room due to the air gap between the duvet and the VM. Excluding the arms and the outlier, the ΔQmax was less than 6 W, i.e., in the range of the defined acceptable thermal condition for this study. To compensate for the heat loss at the arms, a carbon fiber heating element, as shown in Figure 2-4, was placed below both arms along with the thermal insulation on top of the VM and the local heating sheet below the feet. The experiments were then repeated with the local heating sheet, and the result of the heat flux at the arms is shown in the Figure 3-6. It can be seen that using the local heating sheet and the carbon fiber heating element below the arms can effectively compensate for the heat loss due to the VM.

Figure 3-7 shows the average dry heat flux of the manikin's body segements with the VM in operation at 28°C room temperature. The manikin was dressed with short pajama and covered with a thin sheet. Similar to the other room temperatures, the cooling effect of the VM at 1.5 L/s, 3 L/s, 4.5 L/s, 6 L/s, and 10 L/s exhaust flow rate of the VM at 28°C room temperature were assessed. It can be seen that the VM operating at 3 L/s can provide a cooling effect which can reduce substantially the difference in the heat flux with the reference case (ΔQ).

4. Discussion

The experimental results showed that the dry heat flux from the body segments of the manikin increases with the exhaust flow rate of the VM at all studied room temperatures. The heat flux was higher with a higher exhaust flow rate because a higher exhaust flow rate means more air in the bed microenvironment is displaced with cooler ambient room air at a higher velocity, thus increasing the convective heat transfer. The suction of the VM continuously displaces the air in the bed microenvironment, and it was replaced by the air under the cover at ambient temperature, which was lower than the manikin segment temperature. This difference in temperature coupled with the airflow leads to increased heat transfer by convection between the manikin and air in the bed microenvironment.

In addition, higher airflow rate through the VM also means that the mattress's effective thermal insulation was reduced, increasing conductive heat loss in the body segments in contact with the mattress. The measured surface temperature of the VM also decreased with an increase of the exhaust flow rate through the VM. The largest drop in surface temperature with respect to increasing the VM's exhaust flow rate was observed below the back of the manikin and close to the bottom part. As explained, these body segments are firmly in contact with the VM. Thus, the drop in surface temperature also implies that the heat flux of these body segments are primarily due to conduction.

The different body segments of the manikin were exposed to nonuniform cooling in the bed, leading to different heat flux loss. Even inside the bed microenvironment, which was covered with a duvet, there were differences in the heat loss of the body segments. For example, the chest, pelvis, and front thigh were in contact with the duvet, and heat loss occured by convection to the air below the duvet and conductive heat loss to the duvet. The backside, back, and back thigh were firmly in contact with the mattress; hence conductive heat loss to the mattress was dominant. However, some areas of these segments may not be in contact with the mattress, therefore, convection heat loss for these areas occured. On the other hand, feet, legs, and arms had a larger exposure to the airflow in the bed microenvironment, thus has a high convective heat loss and limited conductive heat loss. In addition, using thermal insulation, the conduction heat loss through the VM can be reduced, but still there was a non-uniform heat loss, particularly in the arms.

The VM cooling effect can be beneficial during summer temperatures (28°C). With an increased exhaust flow rate of the VM, it is possible to increase the heat loss from the manikin's body segments.

This paper demonstrates the possibility of using local heating to improve the occupant's thermal comfort with the VM. With the local heating solutions employed in this paper, the temperature difference between the body and the surface of the VM was reduced, resulting in decreased heat loss from the body. An increase in the surface temperature of the VM in contact with the manikin segment with local heating can directly compensate for the conductive heat loss. However, compensating with the local heating was more challenging for body segments with primarily convective heat loss, which are not in firm contact with the VM, such as arms and feet.

The key function of the VM is pollution (body bio-effluents) source control which results in improved room air quality and energy reduction. To that end, it could be beneficial to explore changes in VM design that can reduce the undesired cooling effect in winter and thereby reduce the local heating while ensuring source control. One option could be to change the exhaust connection location during winter. For instance, if the exhaust connection location is placed exactly below the suction opening of the VM instead of being at the opposite end of the mattress near the head, it is possible to limit the cooling effect at upper body parts because there is no air movement through the VM.

Finally, the study presented in the paper is performed on a specific configuration of the VM with a manikin lying in the supine position. Thus, the study is limited when deriving general conclusions

about the VM. Also, only one position of the manikin was tested, but in reality, people lying on the bed have different positions. Therefore, the cooling effect of the VM and the effectiveness of the local heating with different positions of the lying person can also be verified during the human subject experiment.

5. Conclusion

The potential local thermal discomfort for the occupant due to cooling effect induced by the air movement in the VM is addressed in the paper. In addition, a localized heating method is suggested to improve the thermal perception of the human body. The key conclusions of the study are:

- The body segments where the local cooling is critical are the feet, back, and arms. This discomfortable cooling effect can be eliminated by the studied local heating methods;
- At 23°C room temperature, the local heating can compensate the local cooling at the studied flow rate (3 L/s) through the mattress. However, with the addition of thermal insulation on top of the VM, the local cooling effect can be reduced. Even though local heating below the arms is required to eliminate the nonuniform cooling effect;
- At 19°C room temperature, the addition of thermal insulation on top of the VM reduced the need for local heating. However, local heating at the feet was necessary to obtain thermal comfort;
- At 28°C room temperature, the cooling effect of the VM can be beneficial to obtain thermal comfort for the occupant in bed. It is observed that no local heating was needed to compensate the cooling effect of the VM.

6. Acknowledgement

This research was supported by the Bjarne Saxhof's Foundation for Support of Danish Research, project No 26946.

References

[1] P. Wargocki, «Sensory pollution sources in buildings,» *Indoor air*, vol. 14, pp. 82-91, 2004.

[2] A. K. Melikov, «Advanced air distribution: improving health and comfort while reducing energy use,» *Indoor air*, vol. 26, pp. 112--124, 2016.

[3] M. P. Bivolarova, A. K. Melikov, C. Mizutani, K. Kajiwara Z. D. Bolashikov, «Bed-integrated local exhaust ventilation system combined with local air cleaning for improved IAQ in hospital patient rooms,» *BAE*, vol. 100, pp. 10-18, 2016.

[4] M. P. Bivolarova, A. K. Melikov, M. Kokora e Z. D. Bolashikov, «Local cooling of the human body using ventilated mattress in hospitals,» in *Proceedings of the 13th International Conference on Air Distribution in Rooms-Roomvent*, 2014.

[5] A. N. S. I. ASHRAE, *ASHRAE/ASHE Standard 170-2008 Ventilation of health care facilities*, Atlanta, 2008.

[6] Manikin – manual, «pt-teknik.dk/files/manual.pdf,» [Online]. Available: http://pt-teknik.dk/files/manual.pdf. Accessed 29 03 2022.

[7] Danish Standards Association, «DS/ISO/TR 17772-2:2018 Energy performance of buildings -- Overall energy performance assessment procedures -- Part 2: Guideline for using indoor environmental input parameters for the design and assessment of energy performance of buildings,» 2018.

[8] Danish Standards Association, «DS/EN ISO 7730 Ergonomics of the thermal environment –Analytical determination and interpretation of thermal comfort using calculation of the PMV and PPD indices and local thermal comfort criteria,» 2006.

[9] J. Khodakarami e I. Knight, «Thermal comfort requirements in Iranian hospitals,» in *Citeseer*, 2007.

[10] R.-L. Hwang, T.-P. Lin, M.-J. Cheng e J.-H. Chien, «Patient thermal comfort requirement for hospital environments in Taiwan,» *Building and environment*, vol. 42, pp. 2980--2987, 2007.

[11] «long infrared underfloor heating film building material,» [Online]. Available: https://www.banggood.com/da/50CMX2M-220V-Far-Infrared-Floor-Heating-Film-Building-Material.

[12] T. Hoyt, K. H. Lee, H. Zhang, E. Arens e T. Webster, «Energy savings from extended air temperature setpoints and reductions in room air mixing,» *hoyt2005energy*, 2005.

[13] S. Schiavon e A. K. Melikov, «Energy-saving strategies with personalized ventilation in cold climates,» *Energy and Buildings*, vol. 41, pp. 543-550, 2009.

[14] « DSF/FprCEN/TR 16244 Ventilation for hospitals,» 2011.

Recognition and Analysis of Air-conditioner Operation Based on Basic IAQ-monitoring

Yuanchen Wang [a], Florian Frey [a], Dirk Schwede [a], Konstantinos Stergiaropoulos [a]

[a] Institute for Building Energetics, Thermotechnology and Energy Storage (IGTE), University of Stuttgart, Stuttgart, Germany, dirk.schwede@igte.uni-stuttgart.de

Abstract. Building performance simulations are particularly important for the development of various building energy efficiency strategies. However, the accuracy of these building simulations is often greatly influenced by real occupant behaviour, which leads to deviations between expected and measured performance. The occupant behaviour varies greatly from region to region and even within the same region due to the differences in cultural, climatic and socio-economic contexts and building characteristics. Therefore, typical occupant behaviours and usage patterns in local buildings should be considered to improve the accuracy of the building simulations. To achieve this purpose, sufficient occupant data is needed to derive these typical behaviours. The cost of data collection and analysis as well as privacy concerns, are the main challenges that must be addressed. This study proposed a simple method to recognise the use of individual split-air-conditioning units based on basic environmental parameters (indoor air temperature, humidity and CO_2-concentration) collected by IAQ-sensors in residential buildings. This method was used to analyse the air-conditioning (AC) usage patterns of 98 rooms in 49 residential apartments over one year in Hanoi, Vietnam and validated through comprehensive occupant surveys and on-site measurements. While deriving typical behaviours, deviations from measured room temperature and AC set temperature were observed and discussed in detail. The highlights of the proposed method are as follows: a) The data on AC operation can be determined without labour-intensive manual processing; b) The necessary input data can be collected by using standard IAQ-monitoring instruments, which minimises the cost of data collection and the invasion of occupant privacy; c) Missing information about AC usage can be added to data sets of previous studies for further analysis.

Keywords. Occupant behaviour, Residential building, Air conditioning, Operation recognition, Case study.
DOI: https://doi.org/10.34641/clima.2022.419

1. Introduction

The use of air conditioners (AC) for space cooling accounts for nearly 20% of the total electricity consumption in buildings worldwide today, which places a huge burden on the grid and increases CO_2 emissions [1]. Meanwhile, the AC's household penetration rate in many emerging countries with hot climate zones is currently low, for example, nearly 50% of urban households and 80% of rural households in Vietnam are not yet equipped with AC [2]. With rising living standards, population growth and more frequent heatwaves, the AC ownership is expected to increase significantly, especially in the Asian region [1] [3]. Therefore, it is important to improve the energy efficiency of the buildings there to reduce the energy consumption and emissions related to air conditioning. Many studies have revealed that occupant behaviour significantly impacts energy consumption and is a major factor in the building performance gap [4]-[7]. Different cooling behaviour can significantly differ in AC-related energy consumption, even in the same building [8]. The effectiveness of building performance improvement actions differs under diverse occupant behaviour, so it is essential to quantify its impact on energy efficiency measures [7]. In order to gain insight into cooling behaviour, a large amount of AC operating data, such as on/off-states (AC events) and cooling setpoints, is required to determine typical AC usage patterns and derive occupant behaviour models. In previous studies, researchers have used different methods to directly or indirectly obtain the data on the AC operation. Measurement parameters such as indoor air temperature (1), AC power consumption (2), AC supply air temperature (3) and infrared (IR) control signals of AC remotes (4) are often used to determine

Copyright ©2022 by the authors. This conference paper is published under a CC-BY-4.0 license.

the AC operating status as illustrated in. **Fig. 1**. Advantages and disadvantages of these methods are listed in **Tab. 1**.

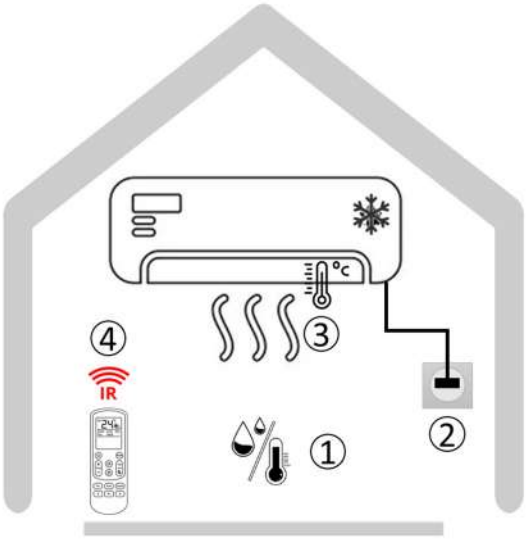

Fig. 1 - Common measurement parameters for monitoring the AC on-off state

Zhang et al. [9] monitored the indoor climate with temperature/humidity data loggers. The AC events were determined by directly observing the change in the room temperature. The indoor air temperature measured after the cooling process has become stable is estimated as the cooling set temperature. Although the parameters required for this method can be obtained with low-cost measuring instruments, the manual processing is labour-intensive. Furthermore, night ventilation or air exchange with adjacent air-conditioned rooms can also lead to changes in indoor climate that may interfere with the results. In contrast, by monitoring the AC power consumption, Ren et al. [10] determined the AC on/off-state more accurately and obtained the actual AC-related energy consumption

data. However, indoor climate, such as air temperature and humidity, as well as the cooling setpoints must be measured separately. In addition, the power measuring instruments also increase the costs and are not suitable for some scenarios, e.g., in some households investigated in this study, the AC power supply cable is enclosed in the wall and cannot be connected to an external power meter. Song et al. [11] also determined the air conditioning events by observing temperature changes, but the difference is that they used the temperature measured at the AC supply air vent. When the AC state changes, the change in the air supply air temperature is more noticeable than the change in room temperature, thereby avoiding false recognition caused by other cold/heat sources. However, the AC events were still manually recognised and the indoor climate needs to be measured by other instruments. Mun et.al. [12] adopted a more direct method to determine the AC operating status by collecting and analysing the infrared control signals from the AC remote. In this way, the on/off-state and the AC operating mode (incl. the cooling setpoint and the fan speed) can be obtained accurately. During the pre-processing of the signals collected by the IR receiver, signals from other home appliances must be excluded. Moreover, due to the different protocols, the AC control signals for each AC unit must be analysed individually.

A common disadvantage of these methods mentioned above is the labour-intensive manual processing. In addition, the data collection in residential buildings is very challenging, not only due to the cost of the measuring instruments but also because of the intrusion of long-term measurements on the occupants. Therefore, the data collection and processing process must be improved to make it more implementable in practice.

Tab. 1 - AC event recognition methods used in previous studies

	Measuring instruments/ key parameters/sample size	**Pros & Cons**
Zhang et al. (2013) [9]	• T/RH data logger • Indoor air temperature • 10 dormitories (bedroom) in Guangzhou, China (January 2009 – January 2010)	(+): Low-cost and low-complexity (-): Manual recognition is labour-intensive. (-): Recognition may be affected by night ventilation or air exchange with adjacent rooms.
Ren et al. (2014) [10]	• Power meters • Power of AC • 34 households (living room and bedroom) in 8 different cities in China, (mid-July – mid-September 2013)	(+): AC energy consumption can also be measured (-): Additional costs for power meters and possible limitations on installation (-): Indoor climate must be measured separately.
Song et al. (2018) [11]	• Temperature logger • Supply air temperature of AC • 43 households (living room and bedroom) in Tianjin, China (May – November 2016)	(+): The change in the air supply temperature can indicate the AC on/off state more obviously. (-): Manual recognition is labour-intensive. (-): Indoor climate must be measured separately.
Mun et al. (2019) [12]	• Infrared receiver • Control signal of AC remote • 4 households (living room) in Seoul, South Korea (late July – early September 2017)	(+): AC settings can be accurately obtained (-): Pre-processing procedure is labour-intensive (-): Indoor climate must be measured separately

With the development of sensor technology and the growing concern for comfort and health, measuring instruments for indoor environment monitoring are becoming more popular in people's daily life. Key parameters in the indoor environment such as air temperature, humidity and carbon dioxide (CO_2) concentration can be long-term measured with an integrated IAQ sensor. Thanks to IoT technology, measurement data can be uploaded to cloud servers and accessed remotely. Considering these advantages, this study proposes a simplified method for determining the operating status of split-AC using cloud-based IAQ data loggers. To improve the efficiency of data analysis, automatic recognition algorithms have been developed based on a long-term investigation of 49 households in Hanoi, Vietnam.

2. Methodology

2.1 Direct observation (DO)

The use of AC is accompanied by significant changes in indoor climate. By directly observing the rate of change of the relevant parameters, e.g. temperature gradients, it is possible to manually recognise the space cooling events and determine the AC on/off moments as adopted by Zhang et al. (2013) [9] in their study. However, rapid drops in outdoor temperature (e.g. due to rainfall) or in adjacent rooms (e.g. due to space cooling) can also cause similar changes in room temperature with air exchange. Determining the AC on/off-state with room temperature alone is unreliable in some cases. Long-term observations of indoor climate data have shown that when the AC is turned on the humidity in a room usually drops significantly, sometimes even more sensitively than the temperature (especially under hot and humid conditions). In addition, most occupants only use AC in the rooms they occupy and close the windows during the cooling process, which leads to an increase of the CO_2-concentration in these rooms. Therefore, the humidity change rate and CO_2-concentration in the indoor air were introduced as additional parameters to manually determine the AC operating status in this study. **Fig. 2** illustrates the working principle of the DO-method with an example of a bedroom. Since rapid simultaneous drops and rises of room temperature (red curve) and absolute humidity (blue curve) may indicate that the AC is on and off respectively, the AC on/off moments can be first determined by observing the sudden changes in the time series (black dashed lines). The occupancy status of this room can be estimated from the CO_2-concentration (yellow curve). When the CO_2-concentration continuously exceeds 500 ppm it can be considered as evidence that the room is occupied. The estimated occupancy profile (green dotted step curve) indicates on the one hand that the room is poorly ventilated when the AC is in use (blue zone), and on the other hand confirms that the change in indoor climate is not caused by airflow from other rooms or from outdoor.

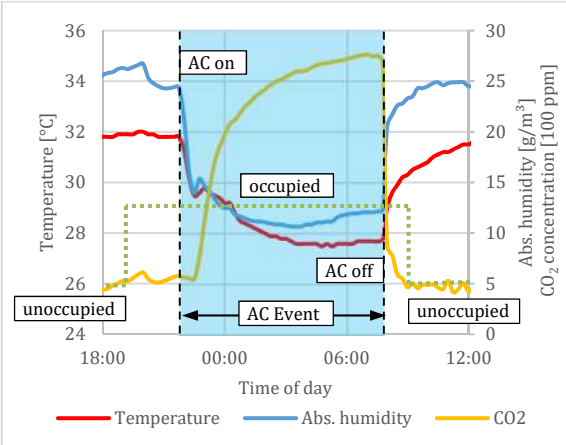

Fig. 2 - Principle of the direct observation method

Manual processing can ensure accurate recognition of AC events, especially under complex conditions (e.g. when indoor environment fluctuates greatly), but it is very labour-intensive and inefficient. Three representative households in this study were analysed using this method to validate and compare the following two automatic recognition algorithms.

2.2 Local extrema analysis (LEA)

The first algorithm for automatic recognition of AC events is also based on finding sudden changes (local extremes) in the time series of room temperature and absolute humidity. Although **Fig.** 2 demonstrates that CO_2-concentration is also correlated with AC use, it cannot be used as a criterion for the automatic determination of AC on/off moments, as changes in occupant CO_2 generation rate and the operation of doors and windows may interfere with the results. However, the estimated room occupancy status can be used to correct the recognition result under certain conditions, e. g. according to the occupant survey, the AC is always turned off when the room is unoccupied.

In order to introduce the rate of change (ROC) of room temperature and absolute humidity as criteria in the recognition process, they are first normalised by their maximum ROC over the period in question and then combined according to **equation (1)**.

$$nROC_{indoor} = \frac{\frac{d}{dt}\rho_V}{max\left(\frac{d}{dt}\rho_V\right)} + \frac{\frac{d}{dt}\vartheta}{max\left(\frac{d}{dt}\vartheta\right)} \qquad (1)$$

Where,

$nROC_{sum}$: Sum of normalised ROC
ρ_V: Absolute humidity
ϑ: Room temperature

Fig. 3 illustrates the working principle of the LEA-method using the same indoor climate data as in **Section 2.1**. The sum of the normalised rates of change of room temperature and absolute humidity ($nROC_{sum}$) deviates significantly at the moment when the AC operating status is changed. The AC on/off state recognition is therefore equivalent to finding

local minima and maxima (valleys and peaks) in the $nROC_{sum}$ time series. In this study, this task was performed with the "Find Local Extrema" function available in the software MATLAB R2020b [13]. The parameter "prominence", which measures how the valley/peak at the AC on/off moment stands out with respect to its depth/height and location relative to other valleys/ peaks, has to be set to a reasonable value. A high parameter value can improve the recognition accuracy but will reduce the sensitivity, resulting in some AC events cannot be recognised, especially those events with short duration (2 – 3 h). A low parameter value, on the other hand, will increase the number of misrecognised AC events. Since there is no universal parameter value that can be applied in all cases, it is necessary to manually select a relatively reasonable values and to fine-tune it in some special cases. In order to correct misrecognised events, an automatic checking procedure is needed to remove frequent AC on/off events (fluctuation) that occur in a very short period of time. In addition, typical room temperature and humidity values observed during the use of AC are used as reference values to check each AC event.

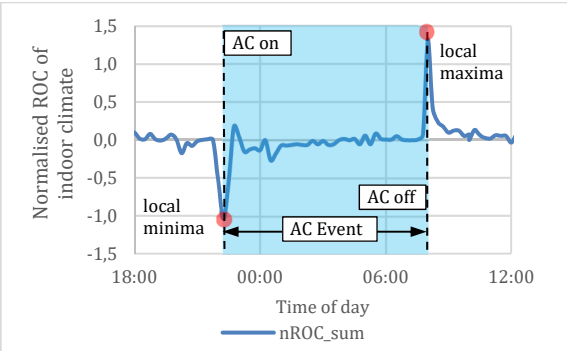

Fig. 3 - Principle of the local extrema analysis

2.3 Deviation monitoring (DM)

As the method presented in **section 2.2** requires manual parameter adjustment and its recognition performance is not very stable, another method "DEM" has been developed to improve efficiency, robustness and accuracy in the recognition processing. It is based on dynamic monitoring the deviation of the measured temperature and absolute humidity from their baselines (see **Fig. 4**). The baselines used to calculate the dynamical temperature deviation (DevT) and humidity deviation (DevH) are defined as the moving mean of the daily maximum values of the corresponding parameters. When a room is being mechanically cooled, the room temperature and humidity will deviate significantly from their respective baselines at the same time. Therefore, comparing whether the deviation exceeds a certain threshold can be used as a basis for determining the AC operating status of in that room. The threshold is defined as the product of the threshold factor and the mean dynamic deviation for the period in question. If the climatic and building conditions are similar, a uniform threshold factor can be used, e.g. in this study 1.5 and 2.5 are used to determine the DevT-threshold and DevH-threshold respectively. Since the mean dynamic deviation is calculated separately for each room, this method allows for self-tuning of parameters to suit different rooms. This method applies to "part-time occupant AC behaviour", which means that the room is not constantly air-conditioned. This AC behaviour is typical in most residential buildings.

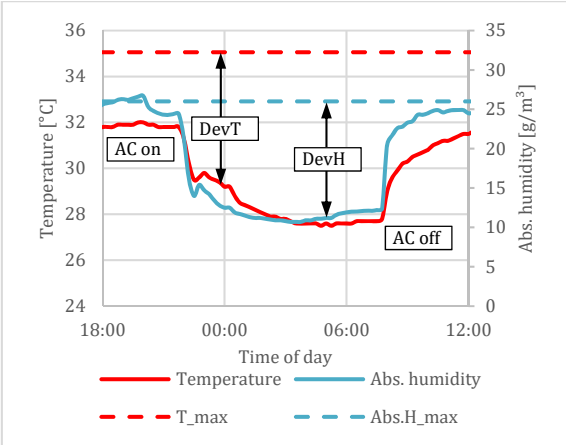

Fig. 4 - Determination of the dynamic deviation

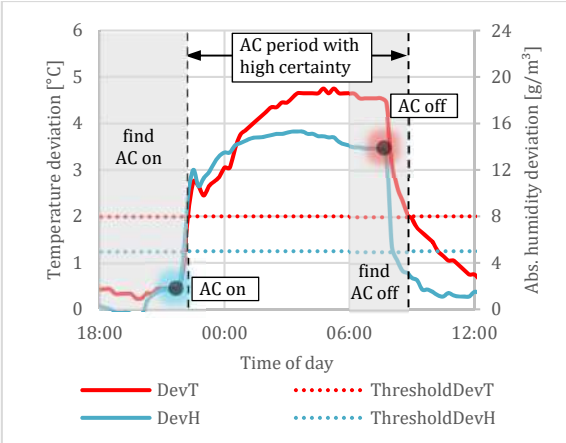

Fig. 5 - Principle of the deviation monitoring

A concrete example is presented in **Fig. 5** to show how this method works. Whenever DevT and DevH simultaneously exceed and fall below their respective thresholds again after a certain time, the air conditioner is considered to be in use during this time period. In contrast to the LEA-method, the AC event is determined first rather than the AC on/off moments. The advantage is that the misrecognition rate can be reduced by increasing the threshold factor. Although the preliminary derived AC event time period will be narrower than the actual one, it is more reliable. The AC on/off moments are then searched additionally by finding the local extreme value of room temperature and absolute humidity in the area near the edge of each AC event (grey area). Although the recognition can already be improved by using this method, a checking procedure is still used to reduce the misrecognition rate further.

2.4 Performance evaluation

Fig. 6 illustrates the workflow used to evaluate the

two automatic recognition algorithms (LEA and DM). The direct observation method is first used to analyse indoor climate data collected from long-term monitoring to prepare a reference dataset for a quantitative comparison of results based on the other two automatic recognition methods. Next, information on occupant AC usage collected through online and telephone surveys was used to verify the accuracy of the reference dataset generated. However, the data on AC operation obtained through the questionnaire is in fact a summary of the AC usage over a period of time and cannot be compared directly with the time series AC on/off dataset. The frequency of AC usage, the duration of each AC operation and the typical cooling setpoints were therefore statistically analysed based on the recognition results to make a semi-quantitative comparison with the occupant survey. Although AC operation data obtained by direct measurements (i.e. power measurements) would be more suitable for evaluation, in this study it was not possible to install such measurement devices because the AC power cables were all enclosed in the wall.

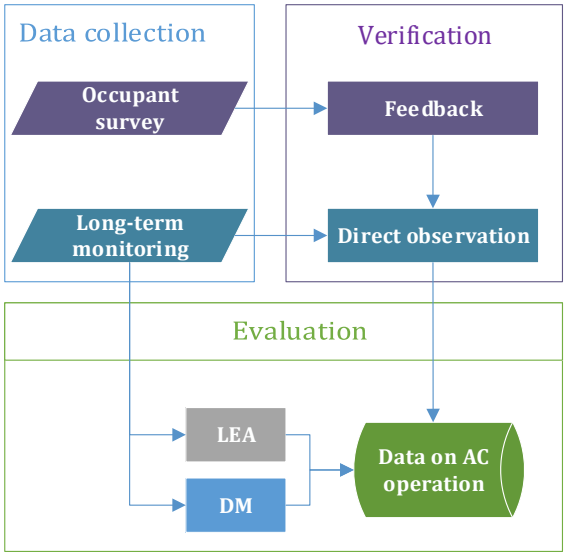

Fig. 6 - Workflow of the performance evaluation

In previous studies [14], [15] on AC-related energy consumption, the operating rate (OR) of AC and F_1 score are commonly used as important evaluation indices. They were introduced in this study to analyse the performance of the recognition algorithms. OR, calculated according to **equation (2)** is the ratio of the sum of the AC running time (t_{AC_on}) to the total observed time period (t_{total}).

$$OR = \frac{\sum t_{AC_on}}{t_{total}} \tag{2}$$

The F_1 score is calculated from precision and recall (see **Tab. 1**) using **equation (3)**, where the precision is the number of true positive results divided by the number of all positive results, including those not recognised correctly **(Eq. 4)**, and the recall (known as sensitivity) is the number of true positive results divided by the number of all samples that should have been recognised positive **(Eq. 5)**.

Tab. 1 - Precision and recall

		Reference result (DO)	
		AC on	*AC off*
LEA & DM	*AC on*	True positive (TP)	False positive (FP)
	AC off	False negative (FN)	True negative (TN)

$$F_1 = 2 \times \frac{precision \times recall}{precision + recall} \tag{3}$$

$$precision = \frac{TP}{TP + FP} \tag{4}$$

$$recall = \frac{TP}{TP + FN} \tag{5}$$

3. Study cases

As a part of the research project CAMaRSEC [16], a comprehensive technical survey campaign with accompanying measurements was conducted in 49 households living in high-rise buildings in urban Hanoi, Vietnam from June 2020 to June 2021.

Indoor climate data (air temperature and humidity, CO_2 concentration, ambient pressure) were collected from 49 living rooms and 49 bedrooms using wall-mounted WiFi data loggers testo 160 IAQ with a measurement interval of 15 minutes. (see **Tab. 2**).

Tab. 2: - Technical data of the measuring instrument

Parameter	***Range***	***Accuracy***
Temperature	0 ~ 50 °C	± 0.5 °C
Relative Humidity	0 ~ 100 % (non-condensing)	± 2.0 % at 20 ~ 80 %RH (±3.0% at remaining range)
Ambient CO_2	0 ~ 5000 ppm	± 50 ppm
Atmospheric Pressure	600 ~ 1100 mbar	± 3 mbar

Hanoi features a warm and humid subtropical climate, with summer lasting from May to September. Winters in Hanoi are generally mild. This climate results in a large demand for space cooling using AC in summer and relatively low heating demand in winter. Based on this AC usage characteristic, measurements from June to November 2020 were defined as the observation period in this study. According to the household survey, the frequency of AC use in Summer in the 98 rooms investigated was categorised as 'rarely', 'sometimes' and 'often'. Three bedrooms (BR) and a living room (LR) from three households (No. 17; No. 25; No. 34) were chosen as representative rooms to evaluate the performance of the recognition algorithms. The basic information about these rooms is listed in **Tab. 3.**

Tab. 3: - Basic information about the selected rooms and the AC usage in them based on the household survey

Room	Floor area [m²]	Main orientation	Window size [m²]	Location of data logger	AC usage frequency	Typical months for using AC	Typical time for using AC
17LR	36.1	NW	2.5	Internal wall, without direct sun irradiation	rarely	-	-
17BR	14.8	NW	4.1	Internal wall, opposite the window	often	May to Oct	Sometimes in the afternoon, always overnight
25BR	11.5	W	2.3	Internal wall, opposite the window	often	May to Aug	Overnight
34BR	14.3	E	1.2	Internal wall, without direct sun irradiation	sometimes	May to Jul	Overnight (9pm – 4am)

4. Results and discussion

4.1 Summary of direct observed AC events

Fig. 7 shows the monthly AC operating rates for the four selected rooms from June to November 2020, derived from direct observation of indoor climate data.

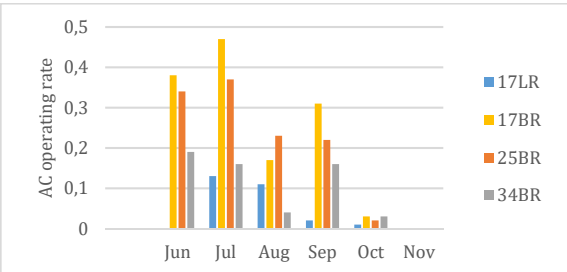

Fig. 7 - Overview of monthly AC operating rate derived by observation of indoor climate data (01.06 – 30.11)

July 2020 is the hottest month in Hanoi and this is well reflected in the usage of air conditioners. 25BR and 17BR have a significantly higher OR than 34BR and 17LR, which is consistent with the results of the occupant survey shown in **Tab. 3**. It is noticeable that although occupants responded in the survey that they rarely use AC in 17LR, the OR observed in this room in July and August exceeded 0.1. A further occupant survey revealed that one visitor slept in the living room during those two months, and sometimes, only the AC in the 17LR was turned on at night to cool the whole apartment. It can also be observed that the AC running time in the bedrooms significantly dropped in August, which could be a result of lower room occupancy due to holidays. This is confirmed by additional occupant surveys and low levels of CO_2 (< 500 ppm) in those rooms over a long period of time.

By comparing the operating rates in **Fig.** 7 with the occupant feedback for typical AC months in **Tab. 3**, it can be determined that the results derived from the direct observation of indoor climate data generally match the occupant responses. However, there are deviations in some details. For example, the occupant answered that the AC was usually used from May to July, but a similar AC usage frequency can be observed in September. This means that data on AC operation obtained from occupant surveys can only give a rough overview of AC usage information and is not suitable for analyses that require more detail.

To compare the results of direct observation with the occupant feedback at a higher temporal resolution, the AC operating probabilities over time were calculated from the derived AC operation data. Since the operating probability of AC is closely related to the month, two typical cooling months, June and July, are used for the comparison.

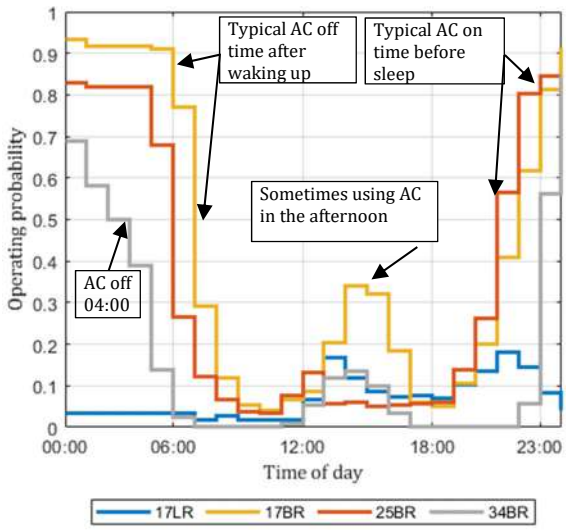

Fig. 8 - AC operating probabilities over time derived by observation of indoor climate data (01.06 – 31.07)

Responses from three households regarding the typical time for using AC in the bedroom are all "overnight", which can also be clearly seen in **Fig. 8.** Both 17BR and 25BR have a probability of turning on the AC after 22:00 of more than 0.8, coinciding with occupant responses regarding the AC usage frequency ("often"). The occupant specified that the AC in 17BR was sometimes used in the afternoon, which is also well represented in the diagram. After 04:00, the AC operating probability in 34BR drops significantly, which matches the typical AC off time given by the occupant. However, the typical AC time

for this room, as derived from the diagram, should be after 23:00, later than the 21:00 given by the occupants. This may be due to a discrepancy between the response of the occupants and the actual situation or because the AC cannot immediately change the indoor climate in hot and humid environments.

The cooling setpoint is the last parameter used to compare the derived data on AC operation with the occupant responses. The indoor air temperature measured after the cooling process has become stable is estimated as the cooling setpoint for each AC event. **Fig. 9** presents the boxplots of estimated cooling setpoints for the different rooms from 1 June to 31 July 2021.

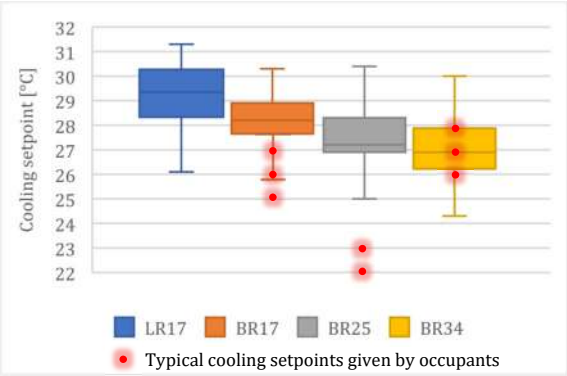

Fig. 9 - Comparison of the derived cooling setpoints with the occupant responses (01.06 – 31.07)

According to the occupant survey, the common cooling setpoints in 34BR are 26 to 28 °C, which is in line with the statistics for the typical AC months. However, it is noticeable that the cooling setpoint statistics for 17BR and 25BR are generally higher than the occupant responses. In particular, in 25BR, the estimation results completely deviate from the occupant responses. By analysing the room information in **Tab. 3**, it can be seen that the data loggers in both rooms are located on internal walls that are exposed to direct sunlight in the afternoon. This causes the walls to gain and store a lot of heat. As the data logger is mounted on the wall, its temperature measurement is also influenced by the wall surface. When the room is not cooled by the AC, the deviation of the temperature measured by the sensor from the actual indoor air temperature is not apparent. However, when the room is in the cooling phase, the temperature in the near-wall region will be higher than the temperature in the AC dominated area, resulting in an overestimation of the cooling setpoint. At this point the temperature measured by the wall-mounted data logger is closer to the operative temperature. In addition, the AC temperature set by the occupant does not mean that the room can actually be cooled to that temperature, which also depends on the cooling capacity and control accuracy of the AC, as well as the cooling load and the thermal performance of the room.

Another reason that causes the estimated cooling temperature to be sometimes higher than the actual set temperature is the short operating time. **Fig. 11** presents the indoor climate measured in 17BR around a typical afternoon short AC event. The increase in CO_2-concentration in the room after the AC has been turned on indicates that the occupant has closed the internal door and windows to cool down the room quickly. With the AC running, the humidity in the room also drops very significantly. However, the hot and humid indoor environment makes it impossible for the AC to cool the room to the set temperature in such a short time. This also explains why in the same apartment, the measured (estimated) cooling setpoints in 17LR are generally higher than that in 17BR, since **Fig. 8** shows that the 17LR is usually cooled only briefly in the afternoon or evening rather than overnight.

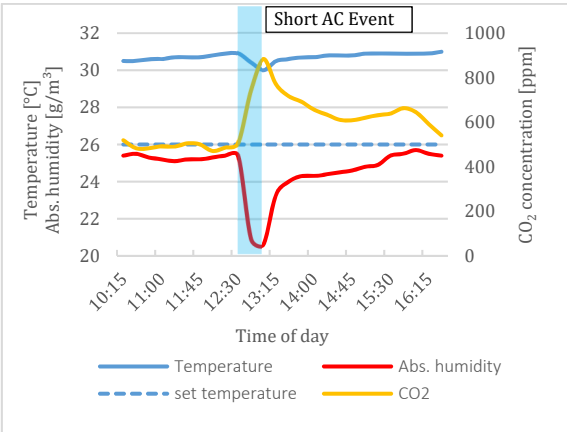

Fig. 10 - Indoor climate measured in 17BR around a short AC event

The AC operation data derived by the direct observation method generally matches the occupant feedback regarding the typical AC time and usage frequency, which can be used as a reference to evaluate the performance of the other two recognition algorithms.

4.2 Evaluation of the recognition algorithms

Data from 1 June to 30 September 2021 was chosen for the performance evaluation as the period after October is no longer a typical AC usage period. As shown in **Fig. 11**, for all four representative rooms, the AC operating rates derived from the two automatic recognition algorithms are very close to the reference (DO), and the performance of the DM-method is slightly better.

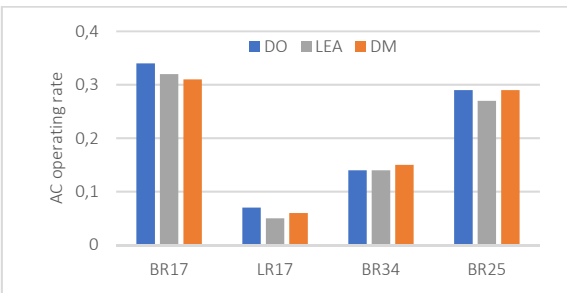

Fig. 11: - Comparison of OR derived by different methods (01.06 – 30.09)

Tab. 4 shows a comparison of the F_1 scores, precision and recall of the two developed algorithms,

assuming the reference data derived by the DO-method as the true result. The F_1 scores for the DM are overall higher than those for the LEA. Although the LEA has higher precision scores, this comes at the cost of reduced sensitivity. This means that some AC operations are ignored, especially in rooms where the AC is not used regularly, such as 17LR.

Tab. 4 - The results of F1 scores for different methods

	LEA	**DM**
	F_1/precision/recall	*F_1/precision/recall*
17LR	*0.78/0.88/0.71*	*0.82/0.80/0.84*
17BR	*0.85/0.89/0.82*	*0.90/0.82/0.86*
25BR	*0.84/0.89/0.80*	*0.86/0.87/0.86*
34BR	*0.86/0.86/0.87*	*0.87/0.84/0.90*

5 Conclusion

Occupant AC behaviour plays an essential role in the indoor environment and energy consumption in residential buildings in hot and humid regions. However, collecting and processing data on AC operation can be very challenging in practice. To improve the efficiency of data processing and analysis regarding AC operations, two algorithms have been developed to automatically recognise AC events based on the analysis of indoor climate data. To evaluate the performance of the two algorithms, AC operation data for four representative rooms were determined using direct observation of indoor climate data and verified by comparing with occupant responses. The results show that both algorithms perform well in analysing OR, while the DM has higher F_1 scores. Compared to the LEA, the DM is easier to adapt to process different cases and its result is more robust (without repeated on/off events within a short time period). Therefore, the DM algorithm will be used in the further work to analyse the AC operation in all measured rooms. In addition, the preliminary derived AC usage patterns differ from the "full time" (always on) patterns commonly used in building simulations. It would therefore be more reasonable to introduce these "part-time" AC usage patterns into the building simulation.

6 Acknowledgement

The study is founded by the funding initiative "CLIENT II – International Partnerships for Sustainable Innovations" by the German Ministry of Education and Research (No. 01LZ1804). The authors are particularly grateful to Ms. Hoa, Dr. Ha and Mr. Binh from Hanoi University of Civil Engineering for their assistance with the surveys.

7 References

[1] IEA (2018). The Future of Cooling. Available at: https://www.iea.org/reports/the-future-of-cooling (Accessed: 20.12.2021)

[2] General Statistics Office of Vietnam. Completed results of "The 2019 Viet Nam Population and Housing Census". 2020.

[3] JRAIA (2019). World air conditioner demand by region. Available at: https://www.jraia.or.jp/english/World_AC_Demand.pdf (Accessed: 20.12.2021)

[4] Paone, A., and Bacher, J.-P. The Impact of Building Occupant Behavior on Energy Efficiency and Methods to Influence It: A Review of the State of the Art. Energies. 2018; 11(4): 953.

[5] Zhang, Y., Bai, X., Mills, F.P., and Pezzey, J.C. Rethinking the role of occupant behavior in building energy performance: A review. Energy Build. 2018; 172: 279-294.

[6] Wang, X., Feng, W., Cai, W., Ren, H., Ding, C., and Zhou, N. Do residential building energy efficiency standards reduce energy consumption in China? – A data-driven method to validate the actual performance of building energy efficiency standards. Energy Policy. 2019; 131: 82-98.

[7] Sun, K., and Hong, T. A framework for quantifying the impact of occupant behavior on energy savings of energy conservation measures. Energy Build. 2017; 146: 383-396.

[8] Hu, S., Da, Y., and Qian, M. Using bottom-up model to analyse cooling energy consumption in China's urban residential building. Energy Build. 2019; 202: 109352.

[9] Zhang, Y., Chen, H., and Meng, Q. Thermal comfort in buildings with split air-conditioners in hot-humid area of China. Build Environ. 2013; 64: 213-224.

[10] Ren, X., Yan, D., and Wang, C. Air-conditioning usage conditional probability model for residential buildings [online]. Build Environ. 2014; 81: 172-182.

[11] Song, Y., Sun, Y., Luo, S., Tian, Z., Hou, J., Kim, J., Parkinson, T., and Dear, R. de. Residential adaptive comfort in a humid continental climate – Tianjin China. Energy Build. 2018. 170: 115-121.

[12] Mun, S.-H., Kwak, Y., and Huh, J.-H. A case-centered behavior analysis and operation prediction of AC use in residential buildings. Energy Build. 2019; 188-189: 137-148

[13] MATLAB. 9.9.0.1592791 (R2020b). Natick, Massachusetts: The MathWorks Inc.; 2020.

[14] Zhou, X., Tian, S., An, J., Yang, J., Zhou, Y., Yan, D., Wu, J., Shi, X., & Jin, X. Comparison of different machine learning algorithms for predicting air-conditioning operating behavior in open-plan offices. Energy Build. 2021; 251: 111347.

[15] Xia, D., Lou, S., Huang, Y., Zhao, Y., Li, D. H. W., & Zhou, X. A study on occupant behaviour related to air-conditioning usage in residential buildings. Energy Build. 2019; 203: 109446.

[16] Schwede, D., Wang, Y. CAMaRSEC: Climate-adapted Material Research for the Socio-economic Context in Vietnam. Pacific Geographies. 2019; 52: 18-19.

The datasets generated during and/or analysed during the current study are available from the corresponding author on reasonable request.

Development and performance analysis of a novel multi-zone hybrid desiccant cooling system

*Shuo Liu [a], Chang-Ho Jeong [b], Myoung-Souk Yeo *[c]*

[a] Department of Architecture and Architectural Engineering, Graduate School, Seoul National University, Seoul, Korea, 2019-34430@snu.ac.kr

[b] Division of Architecture for Urban Planning & Real Estate Development, The University of Suwon, Hwaseong, Korea, chjeong@suwon.ac.kr

[c] Institute of Construction and Environmental Engineering, Department of Architecture and Architectural Engineering, Seoul National University, Seoul, Korea, msyeo@snu.ac.kr

Abstract. This study proposed a novel multi-zone applicable hybrid desiccant cooling system (MHDC) that uses condensing heat from the condenser to regenerate the solid desiccant and applied it as an outdoor air unit (OAU) with demand-controlled ventilation (DCV) in order to control the indoor humidity and air quality (IAQ). Indoor temperature and humidity control effect and system energy use were analysed compared to a conventional packaged terminal air-conditioning (PTAC) system with the heat recovery wheel (HRW) assisted OAU. The simulation result shows that in a typical high-rise building with high air tightness, The CO_2 concentration in bedrooms can reach up to 3686 ppm when PTACs operate without fresh air. Without the dehumidification process, the introduction of fresh air will increase the relative humidity most of the occupancy time. The MHDC system adopted DCV can maintain IAQ except for a short period of cooking time and can handle the fresh air latent load while controlling indoor humidity without a separate regeneration heat source. However, due to the air volume limitation of OAU, the instantaneous dehumidification capacity of the MHDC system is not sufficient, resulting in a short time required to process the indoor humidity to 50 % level when the system initially started. Although the operation of the MHDC system increases the energy use of the OAU, the decrease in the latent load of zone level PTACs makes the total energy use is almost equal to the PTAC system with HRW assisted OAU, 606 kWh and 605 kWh respectively, while obtaining better indoor thermal comfort and IAQ. This study can prove that the proposed MHDC system is a possible alternative system to a conventional multi-zone air-conditioning system that can provide energy savings and thermal comfort.

Keywords. Multi-zone air conditioning system, demand-controlled ventilation, outdoor air unit, Indoor air quality, Dehumidification, energy use.
DOI: https://doi.org/10.34641/clima.2022.188

1. Introduction

Indoor environment control is one of the most significant indicators to evaluate the performance of an air conditioning system. Indoor humidity control should be considered while performing an effective indoor temperature control. It is demonstrated that the growth of human health-related bacteria and melds can be effectively inhibited under 40 ~ 60 % relative humidity conditions [1]. The mismatch between the indoor sensible heat ratio (SHR) and sensible heat ratio of general air conditioning unit leads to the problem associated with indoor humidity control [2]. In addition, the proportion of latent load to total indoor load is increasing due to the requirement of fresh outdoor air and changing lifestyle of occupants [3]. Therefore, discomfort caused by humidity has gradually become the main problem of indoor comfort control because general domestic air-conditioning units do not possess an effective dehumidification capacity. Currently, condensation dehumidification systems are widely used in practical applications due to their compact system structure and convenience maintenance. Generally, direct expansion (DX) cooling coils or chilled water-cooling coils are used to reduce the air temperature below the dew point temperature. The cooling coil operates in a wet coil state, which causes the growth of fungi and affects indoor air quality and personnel health [4]. And the sub-

Copyright ©2022 by the authors. This conference paper is published under a CC-BY-4.0 license.

cooling and re-heating process in the condensation dehumidification system causes unnecessary energy use [5]. Focusing on the possibility of miniaturization and dehumidification capacity, this study assesses the solid desiccant dehumidification system which mainly absorbs the moisture through the solid desiccant composed desiccant wheels. Existing studies have discussed the thermal comfort and energy-saving effects of various solid desiccant dehumidification systems and combined desiccant wheels with various cooling equipment to become a hybrid solid desiccant cooling system (HDC). In addition to responding the indoor load, the cooling equipment has to handle the adsorption heat generated by the dehumidification process. Mainstream cooling equipment includes DX cooling coil, direct evaporative cooler (DEC), in-direct evaporative cooler (IEC), and regenerative evaporative cooler (REC). These HDC systems can effectively control temperature and humidity; however, a separate heating coil provides the heat required for desiccant regeneration, which reduces the system's energy efficiency and structural advantages [6-9]. The energy use of the regeneration electric heater accounts for more than 45% of the system's total energy use [10]. The regeneration temperature of most desiccants is mainly in the range of 60 ^{o}C and 90 ^{o}C. Even if desiccants exist with regeneration temperatures lower than 50 ^{o}C, they cannot be regenerated by outdoor high-temperature air [11]. Therefore, in addition to the development of low-temperature regeneration desiccant [12] the use of renewable energy and low-grade waste heat become a significant research direction to solve the regeneration heat consumption. Ali et al. [13, 14] proposed a decoupling cooling system that combined the solar energy regenerated solid desiccant system with a radiant cooling system and optimized the design parameters of the solar collectors. Additionally, they experimentally investigated indoor thermal comfort during winter. However, solar collectors may not produce adequate regeneration heat output under high outdoor humidity and low solar radiation [15]. Therefore, focusing on the trade-off between the simple system structure and stable regeneration heat output, this paper assessed the heat-pump assisted hybrid solid desiccant cooling system (HPDC) that regenerated the desiccant wheel through the condenser's condensation heat. Some extant studies have focused on HPDC systems with the evaporator located downstream of the desiccant wheel (HPDC-D). Sheng et al. [16] studied the effect of outdoor conditions on the regeneration temperature and proposed that the COP of the heat pump increases with increasing outdoor temperature. Jia et al. [17] analysed the effect of different inlet air conditions and regeneration temperature on the sensible heat ratio of a heat pump in the HPDC-D system. Nie et al. [18, 19] observed that the increase in outdoor humidity caused increased heat pump energy use and a decrease in COP. Ge et al. [20] analysed the HPDC-D system and condensing dehumidification system regarding their exergy efficiency and clarified the relationship between regeneration air humidity and regeneration temperature. The HPDC system with the evaporator located upstream of the desiccant wheel (HPDC-U) is proposed to improve the dehumidification performance and reduce the dehumidification load by pre-cooling and pre-dehumidification. Belguith et al. [21] observed the negative effect of humidity on dehumidification performance and suggested the issue of ineffective supply air temperature control. In a previous study [22], the performances of HPDC-U, HPDC-D, and condensation dehumidification systems were compared regarding their energy use and energy efficiency.

Current research on dehumidification systems mainly focuses on the performance of systems with different system structures and the temperature and humidity control effect for a single space or experimental space. For air conditioning systems serving multi zone, how to effectively control the humidity of each space while ensuring indoor air quality (IAQ) is a research issue that needs more attention. To ensure the IAQ in each space, separated outdoor air units are usually installed, and the minimum outdoor air volume is usually determined by the building type and the number of people in the room. Demand controlled ventilation (DCV) is an effective approach to reduce the outdoor air cooling/heating load compared to constant volume ventilation systems by reducing the outdoor air volume during most of the operation time, which provides a great opportunity to reduce the energy use of fan operation and HVAC system. [23]. Luigi et al. [24] demonstrated a 33 % reduction in total annual primary energy use for air handling units (AHUs) with the DCV compared to conventional constant flow ventilation. In the case study about four school and office buildings, Bart et al. [25] showed that the fan energy use could be reduced by 50 % to 55 % with the DCV due to its variable outdoor air volume. Sun et al. [26] implemented a CO_2 based adaptive DCV in a multi-zone office building in Hong-Kong and also demonstrated that the fan energy use under the DCV strategy is significantly lower compared to the constant air flow system.

In view of the high energy use in outdoor air treatment process and the multi-zone humidity control problem, it is necessary to investigate the feasibility of a multi-zone applicable hybrid desiccant cooling (MHDC) system combined HPDC-U with DCV. The following innovative research is conducted in this paper. As a reference group, indoor humidity control and IAQ problems in the commonly used packaged terminal air conditioning units (PTAC) without outdoor air are demonstrated. The effects of adopting DCV on indoor environment are also discussed. This study verifies the accuracy of the desiccant wheel model based on the analytic solution. The improvement of indoor humidity

environment by combining HPDC-U system with DCV is analyzed and the system energy use is compared to the outdoor air unit (OAU) with heat recovery wheel (HRW).

2. Research methodology

2.1 System configurations and control logics

Case1: conventional PTAC without the outdoor air.

The conventional PTAC mainly consists of a direct expansion cooling coil, which is responsible for regulating the indoor temperature in summer, and an electric auxiliary heater which is designed for heating in winter. PTACs are installed in each room and there is no OAU. The distribution of the PTAC is shown in Fig. 1. (The outdoor unit placed outside is not shown in the figure.) Case 1 is intended to serve as a reference group to illustrate the problems of indoor humidity control and IAQ in conventional household air conditioner.

Case2: conventional PTAC with heat recovery wheel assisted DCV approach OAU.

Compared to conventional PTACs, IAQ in buildings with OAU can be effectively controlled. However, the introduction of outdoor air increases the cooling load of the cooling equipment, therefore, a heat exchanger wheel is used to induce the heat exchange between the outdoor air and the indoor return air as shown in the Fig. 2. The outdoor air after heat exchange is then mixed with the indoor return air and cooled by PTACs. Considering the impact of outdoor air cooling load on the system energy efficiency, the outdoor fresh air volume is controlled by DCV method to reduce the energy use while meeting IAQ.

Case3: conventional PTAC with HPDC-U assisted DCV approach OAU

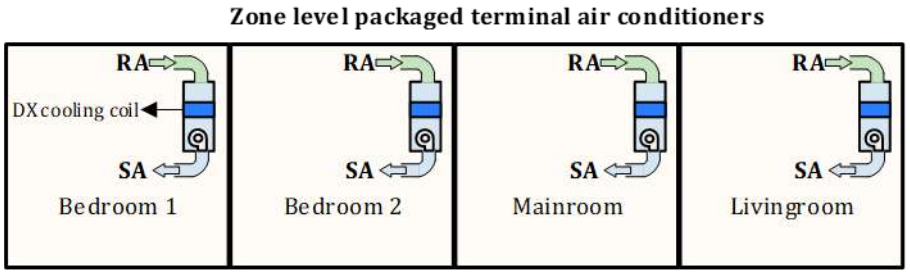

Fig. 1 - The distribution of the PTAC.

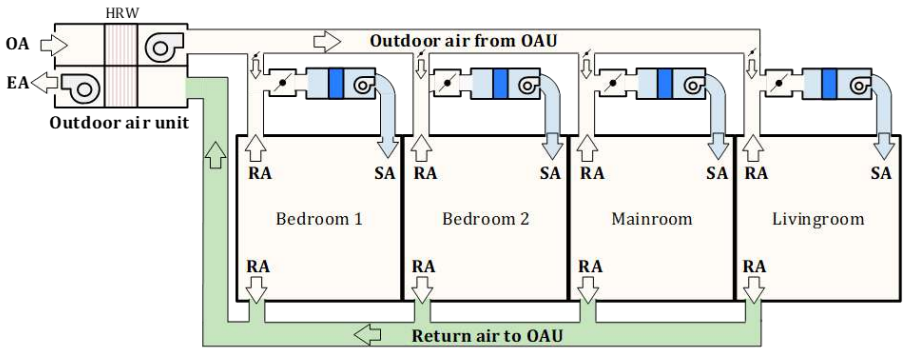

Fig. 2 – Diagram of zone level PTACs and the heat recovery wheel assisted OAU.

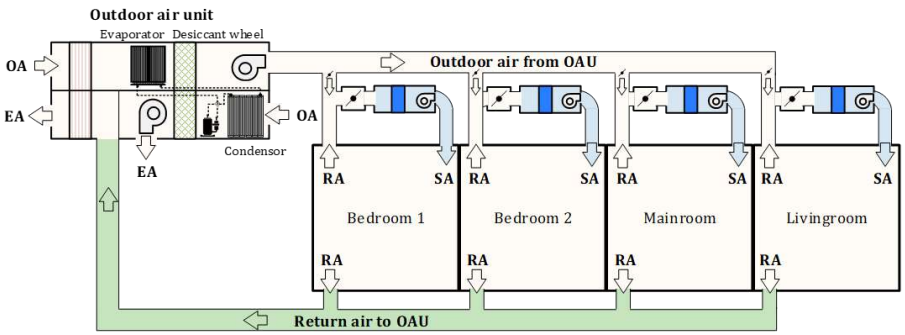

Fig. 3 – Diagram of the HPDC-U assisted OAU.

Although previous studies have demonstrated the ability of HPDC-U systems to effectively control indoor humidity in a single-zone, for HPDC-U systems serving multi-zone with variable latent load profile and total outdoor air volumes, the multi-zone humidity control effect and stability of the regeneration process need to be proven through dynamic simulations. Similar to case2, the same heat exchanger is placed upstream of the HPDC-U system. After heat transfer, outside air is cooled and dehumidified by the DX cooling coil and then further dehumidified by the desiccant wheel. The dry air is mixed with the return air and delivered to the PTAC for temperature regulation. Fig. 3 shows the system configuration and air handling process in the psychrometric chart.

2.2 Building model and simulation setup

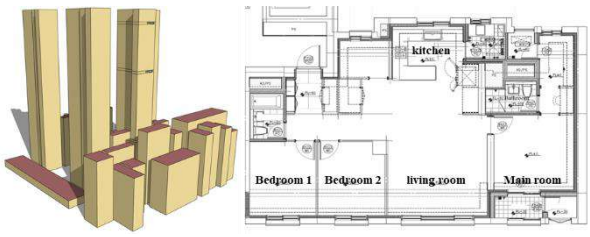

Fig. 4 – Building geometry and multi-zone floor plan.

Tab. 1 - Details of the target building.

Conditions	Detail setting
Simulation period	8/1 – 8/7
U-value (W/m^2·K)	wall: 0.211
	ceiling: 0.768
	floor: 0.768
	window: 0.834
Internal gain	people: 120 W/person
	light: 6.19 W/m^2
	household equipment: 160 W
	cooking: 15 W
Infiltration	maximum: 0.3 ACH
Internal carbon dioxide source	people: 3.82E-8 m^3/s·W
	cooking: 9.465E-5 m^3/s
Indoor T/RH	26 °C and 50 %
People schedule	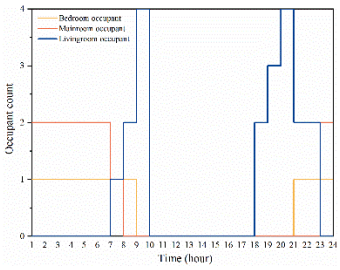

HPDC-U systems with a small size and simple structure can be potentially used in residential buildings with a low sensible and latent load. There is a tendency for residential buildings to develop into high-rise buildings, and the strengthening of airtightness in high-rise buildings makes it difficult to discharge indoor moisture. Therefore, we choose a three-bedroom apartment on the 69th floor of a high-rise building with high airtightness as the object of multi-zone analysis. The building geometry and room distribution are shown in the Fig. 4. Information about the building envelope and internal heat sources is summarized in Tab. 1. The carbon dioxide generation rate per unit of activity level is set at 3.82E-8 m^3/s·W according to the ASHRAE standard 62.1, and the carbon dioxide generation rate during cooking is taken as 9.465E-5 m^3/s and released for ten minutes with reference to the research results of Yujiao Zhao et al. [27]. Seoul (37° 33'N, 126°58'E) were selected as the outdoor conditions where has higher outdoor humidity in the summer than other cities with the same latitude, and the outdoor temperatures is below 30 °C most of the time which means that low outdoor temperatures are more conducive to the verification of the effect of condensing heat regeneration. We choose the week with the highest outdoor temperature and humidity as the simulation period (8/1-8/7), while the system energy use analysis is done for the entire summer (6/1-9/30).

3. System modelling and validation

3.1 Desiccant wheel modelling

$$\begin{bmatrix} T'_{ro} \\ w'_{ro} \end{bmatrix} = \begin{bmatrix} i_2 & i_3 & i_4 & i_5 & i_6 & i_7 & i_8 \\ j_2 & j_3 & j_4 & j_5 & j_6 & j_7 & j_8 \end{bmatrix} \begin{bmatrix} w_{ri} \\ T_{ri} \\ w_{ri}/T_{ri} \\ w_{pi} \\ T_{pi} \\ w_{pi}/T_{pi} \\ u \end{bmatrix} + \begin{bmatrix} i_1 \\ j_1 \end{bmatrix} \quad (1)$$

EnergyPlus mainly uses the dehumidification performance curve to establish the desiccant wheel model. Dehumidification performance curves are as shown in equation (1), reflecting the relationship between the inlet and outlet air state of both sides of the desiccant wheel. Where w is the air humidity ratio in kg/kg DA, T is the air temperature in °C, and u is the air flow rate in m/s. The subscript pi, po, ri, ro in following equations represents the inlet and outlet of the dehumidification side and regeneration side of the desiccant wheel. The curve coefficients i and j can be obtained by fitting measurement data or the results from other mathematical models that accurately reflect the performance of a balanced flow desiccant heat exchanger.

This regeneration side outlet air state is the state when the desiccant wheel is operated under full load condition. For part load operation, the actual regeneration side outlet air state could be modified by the part-load ratio (PLR) as shown from equation (2) to equation (4). ΔT_r and Δw_r are the

temperature difference and humidity difference of regeneration side under the full load condition, respectively.

$$\begin{bmatrix}\Delta T_r\\ \Delta w_r\end{bmatrix}=\begin{bmatrix}T'_{ro}-T_{ri}\\ w'_{ro}-w_{ri}\end{bmatrix} \tag{2}$$

$$PLR=\frac{w_{pi}-w_{setpoint}}{\Delta w_r} \tag{3}$$

$$\begin{bmatrix}T_{ro}\\ w_{ro}\end{bmatrix}=\begin{bmatrix}T_{ri}+\Delta T_r\times PLR\\ w_{ri}-\Delta w_r\times PLR\end{bmatrix} \tag{4}$$

Then, the sensible heat and latent heat change in the regeneration side of the desiccant wheel can be obtained by equation (5). Where $c_{p,r}$ and h_v are the specific heat of regeneration air and the latent heat of vaporization of water, respectively.

$$\begin{bmatrix}Q_{sensible,\ Reg}\\ Q_{latent,\ Reg}\end{bmatrix}=\begin{bmatrix}m_r c_{p,r}(T_{ro}-T_{ri})\\ m_r h_v(w_{ro}-w_{ri})\end{bmatrix} \tag{5}$$

In addition, the dehumidification side outlet air state can be accordingly calculated using the principle of mass and energy conservation as shown in equation (6), where $c_{p,p}$ is the specific heat of process air.

$$\begin{bmatrix}T_{po}\\ w_{po}\end{bmatrix}=\begin{matrix}T_{pi}-\dfrac{Q_{sensible,\ Reg}}{m_p c_{p,p}}\\ \left\lfloor W_{pi}-\dfrac{Q_{latent,\ Reg}}{m_p h_v}\right\rfloor\end{matrix} \tag{6}$$

3.2 Direct expansion coil modelling

DX cooling coil model in EnergyPlus is used since the heat pump operates only in the cooling mode. In EnergyPlus, the actual operational state of the DX cooling coil is determined by the total cooling capacity (TCC) modification curve (MC) and energy input rate (EIR) modification curve. Equation (7) and equation (8) depict the performance curves related to the inlet wet bulb temperature of the evaporator (T_{w_ei}), inlet dry bulb temperature (T_{ci}) of the condenser, and airflow rate (V).

$$\begin{bmatrix}MC_{TCC_T}\\ MC_{EIR_T}\end{bmatrix}=\begin{bmatrix}a_1\\ c_1\end{bmatrix}+\begin{bmatrix}a_2 a_3 a_4 a_5 a_6\\ c_2\, c_3\, c_4\, c_5\, c_6\end{bmatrix}\begin{matrix}T_{w_ei}\\ T_{w_ei}^2\\ T_{ci}\\ T_{ci}^2\\ \lfloor T_{w_ei}T_{ci}\rfloor\end{matrix} \tag{7}$$

$$\begin{bmatrix}MC_{TCC_F}\\ MC_{EIR_F}\end{bmatrix}=\begin{bmatrix}b_1\\ d_1\end{bmatrix}+\begin{bmatrix}b_2 & b_3\\ d_2 & d_3\end{bmatrix}\begin{bmatrix}V\\ V^2\end{bmatrix} \tag{8}$$

The coefficients of the modification curve are the same as those used in the prior study [22].

3.3 Heat exchanger wheel modelling

Generally, heat-exchanger effectiveness for balanced flow is evaluated by equation (9).

$$\varepsilon=\frac{T_i-T_o}{T_i-T_e} \tag{9}$$

where T_i and T_o are the inlet and outlet air temperature of the supply flow side. T_e is the inlet air temperature of the secondary flow side.

As the equation (10) and equation (11), the model in this study determines the actual sensible (latent) heat transfer effectiveness by linear interpolation or extrapolation of the 100% flow and 75% flow sensible (latent) heat transfer effectiveness values, ε_{s_100} (ε_{l_100})and ε_{s_75} (ε_{l_75}). These values used in this study are obtained from the Air-Conditioning and Refrigeration Institute's Certified Product Directory for Air-to-Air Energy Recovery Ventilation Equipment and listed in Tab. 3. HX_{fr} is the ratio of the average operating volumetric air flow rate [(supply flow + exhaust flow)/2] to the norminal supply air flow rate.

$$\varepsilon_{op_s}=\varepsilon_{s_75}+(\varepsilon_{s_100}-\varepsilon_{s_75})\left(\frac{HX_{fr}-0.75}{1-0.75}\right) \tag{10}$$

$$\varepsilon_{op_l}=\varepsilon_{l_75}+(\varepsilon_{l_100}-\varepsilon_{l_75})\left(\frac{HX_{fr}-0.75}{1-0.75}\right) \tag{11}$$

Tab. 3- Effectiveness values of heat recovery wheel.

	Heating	Cooling
ε_{s_75}	0.75	0.75
ε_{s_100}	0.72	0.72
ε_{l_75}	0.73	0.73
ε_{l_100}	0.7	0.63

According to the equation (12) to (14), the supply air conditions (T_{1o} and w_{1o}) leaving the heat exchanger are determined using the operating effectiveness calculated above, the ratio of the air stream with the minimum heat capacity rate, $\dot{m}c_{p,min}$, to the supply air stream heat capacity rate, $\dot{m}c_{p,1}$, and the difference in temperature or humidity ratio between the supply and exhaust inlet air with subcript 1i and 2i, respectively.

$$\dot{m}c_{p,min}=\min(\dot{m}c_{p,1},\dot{m}c_{p,2}) \tag{12}$$

$$T_{1o}=T_{1i}+\varepsilon_{op_s}\cdot\left(\frac{\dot{m}c_{p,min}}{\dot{m}c_{p,1}}\right)\cdot(T_{2i}-T_{1i}) \tag{13}$$

$$w_{1o}=w_{1i}+\varepsilon_{op_l}\cdot\left(\frac{\dot{m}c_{p,min}}{\dot{m}c_{p,1}}\right)\cdot(w_{2i}-w_{1i}) \tag{14}$$

4. Simulation results

4.1 Indoor humidity and IAQ in case 1

Fig. 5 shows the variation of indoor humidity during the PTAC operation and the shaded areas in different colours represents the people schedule of each room. Since the two bedrooms have the same orientation, size and number of people, the humidity variation in the bedroom remains almost the same. Except for a brief increase in humidity caused by an increase in the number of people, the humidity in

the room can be continuously reduced due to the wet coil state operated DX cooling coil in PTACs. For a bedroom with only one person, indoor humidity can be reduced to 50 % in a short time. For the livingroom with a brief high people density and the mainroom with two persons, the indoor humidity is unable to be dropped below 50 % within the occupancy time. In addition, since the bedroom has a relatively small area and good airtightness, the indoor CO_2 concentration tends to increase and can reach up to 3686 ppm. The CO_2 concentration exceeds the recommended level all of the occupancy period. The CO_2 concentration in other large rooms can reach up to 2158 ppm and 3246 ppm respectively. Moreover, the time that indoor CO_2 concentration exceeded the recommended level accounts for 94 % and 74 % of the total occupancy time for livingroom and mainroom.

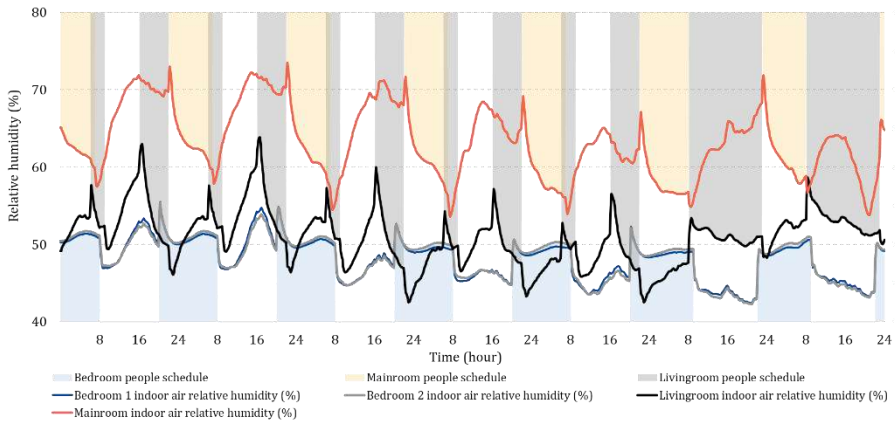

Fig. 5 – Variation of the indoor humidity during PTACs operation.

4.2 The effect of DCV on indoor humidity and IAQ

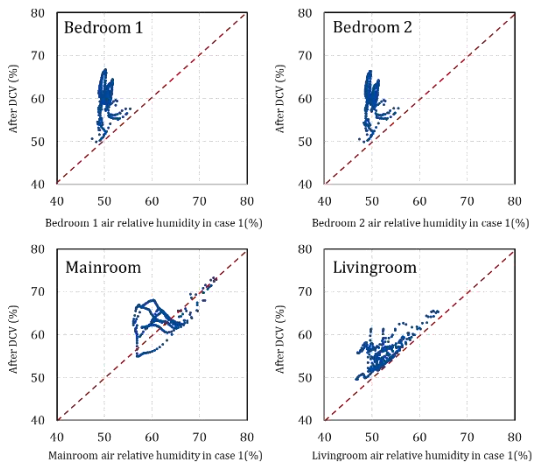

Fig. 6 –Indoor relative humidity after the introduction of outdoor fresh air during occupancy period.

After the introduction of outdoor fresh air, there is a significant increase in indoor humidity in each room compared to case1 during the occupancy period as shown in Fig. 6. There is a situation that the indoor humidity in the mainroom is lower than case1, which is mainly due to the fact that the outdoor humidity ratio is lower than the indoor humidity ratio during the night ventilation, therefore it achieves a certain free-dehumidification effect.

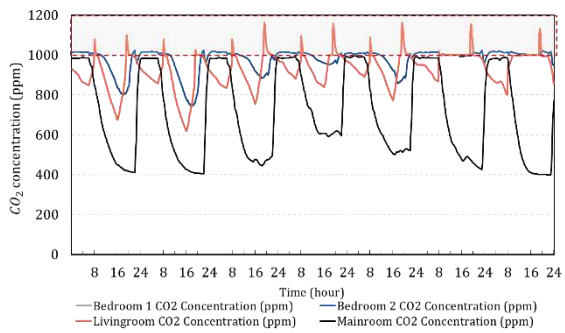

Fig. 7 – Changes in indoor CO_2concentration after the introduction of outdoor fresh air.

Fig. 7 indicates that the DCV method can effectively control the CO_2 concentration in each room. For the livingroom, the CO_2 generated during cooking for a short period of time can cause the CO_2 concentration to spike, however, the time that the CO_2 concentration exceeds the recommended level only accounts for 8 % of the total occupancy time. Therefore, we propose the multi-zone applicable HPDC-U system that can maintain the indoor humidity environment while controlling IAQ by DCV method.

4.3 Indoor environment control effect and energy use of the HPDC-U system

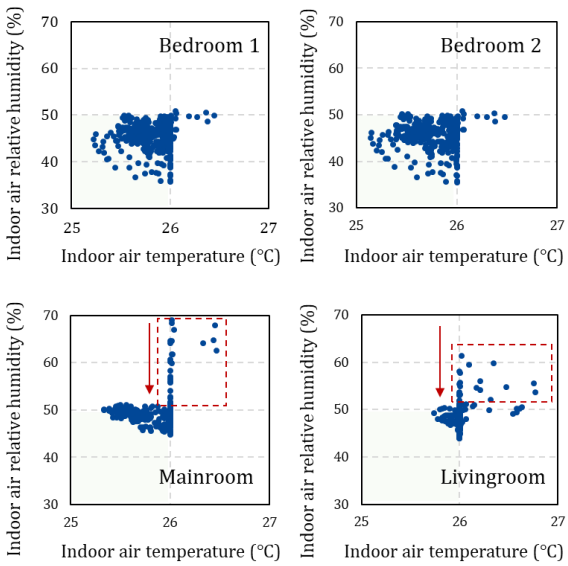

Fig. 8 – Indoor temperature and humidity state during the occupancy period.

Fig. 8 shows the state of indoor temperature and humidity during the occupancy period in each room. For bedrooms with small changes in indoor sensible and latent loads, the indoor temperature and humidity control is relatively stable, with only a brief temperature rise of about 0.5 °C when people enter. Limited by the DCV determined outdoor air volume, the HPDC-U system has insufficient instantaneous dehumidification capacity for multi-zone applications, allowing the indoor humidity in the mainroom and livingroom to decrease from high humidity to 50 % level over a period of time. The descent process corresponds to the data in the red box line in Fig. 8. The indoor temperature in each room is sometimes lower than the indoor design temperature. Under low indoor sensible and latent load conditions, after the pre-cooling and pre-dehumidification process in HPDC-U systems, the air humidity meets the demand of indoor latent load. Therefore, the desiccant wheel does not need to be started. The PTAC in each room also does not require re-cooling of the air, and the approximately 22 °C mixed air is directly supply into the room which leads to the low indoor temperature.

From the Fig. 9, it can be seen that the maximum monthly energy use of both case3 and case2 occurs in August when the outdoor temperature and humidity are high. The monthly energy use of case3 is slightly lower than that of case2 in June and September, while it is higher than that of case2 in July and August as the humidity increases. The total energy use in summer of case2 and case3 is 605 kWh and 606 kWh, respectively, which means that the setup of the HPDC-U system does not lead to an increase in the total system energy use.

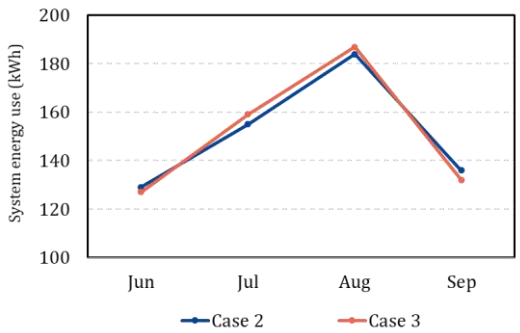

Fig. 9 – Monthly energy use comparison between case2 and case3.

Fig. 10 indicates the energy use comparison of each energy consuming component in the two systems. With the HPDC-U system, the energy use of PTACs in each room is able to be reduced significantly due to the fact that the desiccant wheel can reduce the latent heat treated by the PTAC and increase the sensible heat ratio of PTACs (SHR) and the dry coil state operation time. Energy use of the PTAC in the livingroom with higher latent load can be reduced by 40 %. However, the total energy use of the HPDC-U system as an OAU is much greater than that of the heat recovery wheel assisted OAU, therefore, the total energy use of the OAU and zone level PTACs in both cases is almost equal. The ability of case3 to maintain the indoor thermal environment and IAQ without increasing energy use proves that it is a viable alternative system for existing systems in multi-zone.

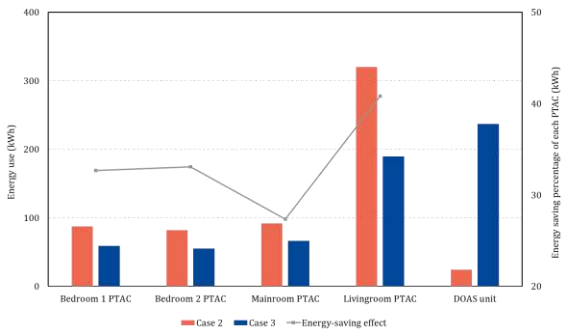

Fig. 10 – Energy use comparison of OAU and PTACs for case2 and case3.

Acknowledgement

This work was supported by the National Research Foundation of Korea grant (2021R1A2C1014415) funded by the Ministry of Science and ICT (South Korea) (MIST). We thank Humaster Co. for technical data support in desiccant wheel modelling.

References

[1] Arundel A V., Sterling EM, Biggin JH, Sterling TD. Indirect health effects of relative humidity in indoor environments. Environ Health Perspect. 1986; 65(3):351–61.

[2] Li Z, Chen W, Deng S, Lin Z. The characteristics of space cooling load and indoor humidity control

for residences in the subtropics. Build Environ. 2006;41(9):1137–47.
[3] Katili AR, Boukhanouf R, Wilson R. Space Cooling in Buildings in Hot and Humid Climates—A Review of the Effect of Humidity on the Applicability of Existing Cooling Techniques. Proc 14th Int Conf Sustain Energy Technol. 2015;(August):25–7.
[4] Bakker A, Siegel JA, Mendell MJ, Peccia J. Building and environmental factors that influence bacterial and fungal loading on air conditioning cooling coils. Indoor Air. 2018;28(5):689–96.
[5] Fong KF, Lee CK, Chow TT, Fong AML. Investigation on solar hybrid desiccant cooling system for commercial premises with high latent cooling load in subtropical Hong Kong. Appl Therm Eng. 2011;31(16):3393–401.
[6] Jani DB, Mishra M, Sahoo PK. Performance studies of hybrid solid desiccant-vapor compression air-conditioning system for hot and humid climates. Energy Build. 2015;102:284–92.
[7] Hwang WB, Choi S, Lee DY. In-depth analysis of the performance of hybrid desiccant cooling system incorporated with an electric heat pump. Energy. 2017;118:324–32.
[8] Kashif Shahzad M, Ali M, Ahmed Sheikh N, Qadar Chaudhary G, Shahid Khalil M, Rashid TU. Experimental evaluation of a solid desiccant system integrated with cross flow Maisotsenko cycle evaporative cooler. Appl Therm Eng. 2018;128:1476–87.
[9] Elgendy E, Mostafa A, Fatouh M. Performance enhancement of a desiccant evaporative cooling system using direct/indirect evaporative cooler. Int J Refrig. 2015;51:77–87.
[10] Jani DB, Mishra M, Sahoo PK. A critical review on solid desiccant-based hybrid cooling systems. Int J Air-Conditioning Refrig. 2017;25(3):1–10.
[11] Shamim JA, Hsu WL, Paul S, Yu L, Daiguji H. A review of solid desiccant dehumidifiers: Current status and near-term development goals in the context of net zero energy buildings. Renew Sustain Energy Rev. 2021;137(September 2020):110456.
[12] Yao Y, Dai L, Jiang F. Photo-crosslinked nanofibrous membranes as advanced low-temperature regenerative desiccant. Polym Test. 2019;78.
[13] Habib MF, Ali M, Sheikh NA, Badar AW, Mehmood S. Building thermal load management through integration of solar assisted absorption and desiccant air conditioning systems: A model-based simulation-optimization approach. J Build Eng. 2020;30(February):101279.
[14] Kashif A, Ali M, Sheikh NA, Vukovic V, Shehryar M. Experimental analysis of a solar assisted desiccant-based space heating and humidification system for cold and dry climates. Appl Therm Eng. 2020;175(April).
[15] Li H, Dai YJ, Köhler M, Wang RZ. Simulation and parameter analysis of a two-stage desiccant cooing/heating system driven by solar air collectors. Energy Convers Manag. 2013;67:309–17.
[16] Sheng Y, Zhang Y, Deng N, Fang L, Nie J, Ma L. Experimental analysis on performance of high temperature heat pump and desiccant wheel system. Energy Build. 2013;66:505–13.
[17] Jia CX, Dai YJ, Wu JY, Wang RZ. Analysis on a hybrid desiccant air-conditioning system. Appl Therm Eng. 2006;26(17–18):2393–400.
[18] Nie J, Fang L, Zhang G, Sheng Y, Kong X, Zhang Y, et al. Theoretical study on volatile organic compound removal and energy performance of a novel heat pump assisted solid desiccant cooling system. Build Environ. 2015;85:233–42.
[19] Nie J, Li Z, Hu W, Fang L, Zhang Q. Theoretical modelling and experimental study of air thermal conditioning process of a heat pump assisted solid desiccant cooling system. Energy Build. 2017;153:31–40.
[20] Ge F, Wang C. Exergy analysis of dehumidification systems: A comparison between the condensing dehumidification and the desiccant wheel dehumidification. Energy Convers Manag. 2020;224(September):113343.
[21] Belguith S, Slama R Ben, Chaouachi B, Meddeb Z. Performance analysis of hybrid solid desiccant-vapor compression air conditioning system: Application and comparative study. 11th Int Renew Energy Congr IREC 2020. 2020;(Irec).
[22] Liu S, Jeong CH, Yeo MS. Effect of evaporator position on heat pump assisted solid desiccant cooling systems. Energies. 2020;13(22):1–21.
[23] Afroz Z, Higgins G, Shafiullah GM, Urmee T. Evaluation of real-life demand-controlled ventilation from the perception of indoor air quality with probable implications. Energy Build. 2020;219.
[24] Schibuola L, Scarpa M, Tambani C. CO2 based ventilation control in energy retrofit: An experimental assessment. Energy. 2018;143:606–14.
[25] Merema B, Delwati M, Sourbron M, Breesch H. Demand controlled ventilation (DCV) in school and office buildings: Lessons learnt from case studies. Energy Build. 2018;172:349–60.
[26] Sun Z, Wang S, Ma Z. In-situ implementation and validation of a CO2-based adaptive demand-controlled ventilation strategy in a multi-zone office building. Build Environ. 2011;46(1):124–33.
[27] Zhao Y, Li A, Gao R, Tao P, Shen J. Measurement of temperature, relative humidity and concentrations of CO, CO2 and TVOC during cooking typical Chinese dishes. Energy Build. 2014;69:544–61.

Human Body Cooling Effect of Local Non-Isothermal Airflow during Natural Ventilation

Yoshihide Yamamoto [a]

[a] Architecture Course, Faculty of Engineering, Tokyo Polytechnic University, y.yamamoto@arch.t-kougei.ac.jp

Abstract. In recent years, the natural ventilation system has been attracting attention not only as an energy saving method but also as a countermeasure method for COVID-19 in a building with poor ventilation. However, during natural ventilation, the outside air temperature has a large effect on the indoor environment, which causes fluctuations in the indoor thermal environment. In such a situation, it is effective to positively utilize the indoor airflow generated during natural ventilation as a method of utilizing the advantages of natural ventilation while maintaining the thermal comfort of the room. Most of the airflow generated by natural ventilation is non-isothermal airflow lower than room temperature, but there are few previous studies on non-isothermal airflow compared to isothermal airflow. In addition, in the actual measurement survey conducted by the author, it was found that the whole body does not receive the airflow uniformly during natural ventilation, but often receives the airflow locally such as the upper body. Therefore, the purpose of this paper is to clarify the effect of local non-isothermal airflow generated during natural ventilation to cool the human body. To achieve this goal, we conducted experiments with thermal manikin in a climate chamber. The amount of heat loss for each human body segments was measured under 28 conditions with clothes, room temperature, airflow temperature, and airflow velocity as parameters. As a result, the following findings were obtained.

Keywords. Natural ventilation, Thermal manikin, Local non-isothermal airflow, Thermal comfort sensation

DOI: https://doi.org/10.34641/clima.2022.427

1. Introduction

Recently, the natural ventilation system has been garnering considerable attention, not only as an energy saving method, but also as a countermeasure method against COVID-19 in a building with poor ventilation. However, during natural ventilation, the outdoor air temperature has a significant effect on the indoor environment, which causes fluctuations in the indoor thermal environment. As an example, although the energy-saving and cooling effects of the outdoor air increase as the introduced outdoor air temperature decreases, there are cases where residents near the natural ventilation inlet may complain, thereby leading to the suspension of the natural ventilation operation [1]. In other words, from the perspective of saving energy, it is desirable to relax the outside air conditions that allow natural ventilation; however, the range is limited by the balance with indoor comfort. Therefore, it is important to operate natural ventilation considering the comfort of residents. In the survey of permit conditions for natural ventilation in actual buildings, there were few cases in which comfort was adopted as the permit condition [2].

Various standards and studies already exist on indoor airflow, and it is recommended to keep the still air in the room when operating mechanical air conditioning. The ASHRAE standard recommends that the indoor airflow should be less than 0.2 m/s to prevent cold drafts, and should not exceed 0.8 m/s even when the airflow can be adjusted [3]. However, it has been reported that when the room temperature is relaxed by Cool Biz in the summer or when the airflow temperature is not negligible, a positive feeling of comfort can be obtained by the airflow owing to the natural wind. Xing et al. [4] reported that the practical temperature decreases by 0.55 °C was owing to the increase in the airflow by 0.15 m/s on the surface of the human body in a hot environment. Several other studies have been conducted on isothermal airflow exposed to the entire body [5]. Although these studies are aimed at isothermal airflow that is uniform throughout the body, in an actual natural ventilation building, it is possible to obtain an airflow lower than room temperature that hits the human body locally (local non-isothermal airflow). It is necessary to accumulate further knowledge on such local non-isothermal airflow. In addition, several studies on the effects of natural wind on the human body are

Copyright ©2022 by the authors. This conference paper is published under a CC-BY-4.0 license.

conducted by subject experiments, and only a few studies quantitatively evaluate the cooling effect of the human body under the condition of local non-isothermal airflow. Therefore, in this study, experiments were conducted using thermal manikins at various room temperature and airflow conditions under the natural ventilation of an actual building. Accordingly, the effect of cooling the human body by local non-isothermal airflow was quantitatively evaluated. Furthermore, subject experiments were conducted at temperatures of 22 °C and 29 °C to evaluate comfort.

2. Research methods

2.1 Experiment outline

This experiment was conducted in the artificial climate room of the Wind Engineering Research Centre, Tokyo Polytechnic University. An inverter fan was installed for airflow control in the artificial climate room, while a spot air conditioner and blowout temperature control were employed to generate airflow with varying wind speeds and blowout temperatures; in addition, the amount of loss at each part was measured using a thermal manikin.

Fig. 1 illustrates the plan and composition of the artificial climate chamber. Furthermore, Fig. 2 presents the cross sections of the artificial climate chamber, manikin installation position, and measurement position. Here, a box was installed on the suction side of the inverter control fan, while the outlet temperature was adjusted by mixing the cold air from the spot air conditioner with the outlet temperature control function and the room air in the box. Photo. 1 illustrates a case of the manikin and fan room in the artificial climate room. In addition, as illustrated in Photo. 2, The thermal manikin is installed sideways in a sitting position 2 m away from the inverter control fan, and one unit is located on the third stage from the floor (a 0.9-m height from the floor level). The measurement was performed under the condition that a local air flow was applied from the side to the upper body using a fan. Only the fans surrounded by the white frame in the photo were operated. Such measurement conditions reproduce the effects of the perimeter's occupants in a naturally ventilated building.

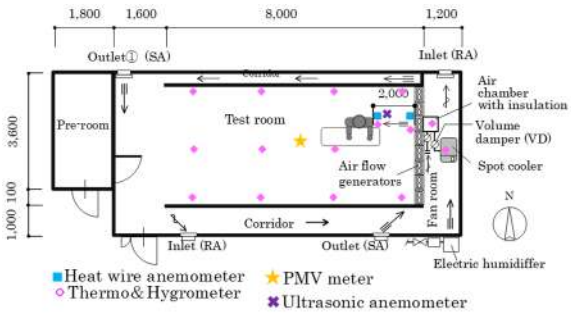

Fig. 1 Climate-controllable wind tunnel

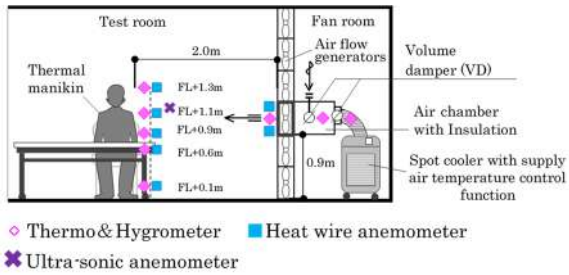

Fig. 2 Measurement points (sections)

(1) Thermal manikin in the chamber (2) Fan room
Photo. 1 Climate chamber experiment

2.2 Measurement condition

In this experiment, a thermal manikin manufactured by MTNW and an Asian male model were utilized. The manikin specifications and their measurement conditions are presented in Tables 1 and 2, respectively. The measurements were performed under the conditions of long-sleeved clothing at 22 °C, short-sleeved clothing at 29 °C, and long- and short-sleeved clothing at 26 °C. Photo. 3 presents an illustration of the clothes. The CLO value of the clothes were measured based on AIJES-H0005-2015 [6]; accordingly, 0.76 and 0.49 CLO values were obtained for the long and short sleeves, respectively. The thermal manikin was measured under 28 conditions by setting 4 conditions for the combination of room temperature and clothing, 3 conditions for wind speed, and 3 conditions for airflow temperature. The temperature of the thermal manikin was controlled to a constant temperature, and the set temperature was 33 °C, which was the skin temperature at the time of thermal neutralization by Gagge et al. [7].

2.3 Experimental procedure

The artificial climate chamber was sufficiently air-conditioned before commencing the experiment, the thermal manikin was preheated for 2 h or more, and the measurements started after the skin surface temperature was stabilized at 33 °C. The measurements were performed twice or more under one condition, and the average value obtained was calculated after verifying that the difference was negligible. Furthermore, to make the manikin's posture the same in each experiment, the positions in which the chair, desk, and manikin's hands were placed were marked, and the distance between each part of the manikin and chair or desk was measured beforehand.

Photo. 2
Measurement position

Table 1 Thermal Manikin specifications

USA	MTNW Corp. Newton 20-Zone Sweating Thermal Manikin
	Asian male model 168.5cm・30kg 20 divisions (face, head, chest, shoulders, back, stomach, upper arms, forearms, hands, hip, thigh, calf, foot) Total body surface area: 1.71m²

(1) Long sleeve（0.76clo） (2) Short sleeve（0.49clo）
Photo.3 Clothing conditions

Table 2 Measurement Condition

Item	Set point	
Room temperature	22 °C, 26 °C, 29 °C	
Average radiation temperature	Operate the air conditioner until the average radiation temperature is equal to room temperature	
Relative humidity	40% RH	
Thermal manikin control	Constant skin surface temperature control (33 °C)	
Fan control conditions	Operate one fan in the third row from the bottom and the third row from the left, and perform measurements under three conditions: (1) Stop, (2) 0.6 m/s, (3) 0.8 m/s.	
Airflow temperature conditions	Airflow temperature was measured near the fan and the following three conditions were used: (1) isothermal (2) 2 °C lower than room temperature, (3) 4 °C lower than room temperature,	
Combination of room temperature and clothes	Room temp.: 22 °C/26 °C	Long sleeve clothing
	Room temp.: 26 °C/29 °C	Short sleeve clothing
Long-sleeve clothing	Pants, shirts, long-sleeved shirts, jackets, slacks, socks, and leather shoes	
Short-sleeve clothing	Pants, shirts, short-sleeved shirts, slacks, socks, and leather shoes	

3. Experimental results

3.1 Indoor thermal environment

In the experiment, the representative room temperature was controlled within the set room temperature of ±0.2 °C, while the relative humidity was controlled within the range of ±2%. Fig. 3 and 4 presents the results obtained from measuring the wind speeds and temperatures of FL + 0.1 m, 0.6 m, 0.9 m, 1.1 m, and 1.3 m from the floor, at a position 10 cm away from the manikin. According to the measurement results, the FL + 1.1 m and 1.3 m airflows, which are close to the height of the outlet, were the fastest in the isothermal airflow, while the FL + 0.6m airflow was the fastest in the non-isothermal airflow. The airflow velocity was slightly slower than the wind speed at the outlet. Regarding the distribution of the airflow temperature, it can be verified that the temperature of the airflow, which is 22 °C at the outlet, increases by approximately 2 °C near the manikin to 24 °C. Photo. 4 presents the results obtained from a laser visualization experiment on the changes in airflow properties due to airflow temperature. In the isothermal airflow, the airflow from the outlet moves straight and hits the shoulders and head; however, in the non-isothermal airflow, the turbulence becomes large and tends to hit the upper arm and armpit. Table 3 presents the results obtained from measuring the wind speed and the degree of turbulence at a height of 1.1 m near the manikin using ultrasonic wind speed. It can be observed that the isothermal airflow has a large average wind speed and a small degree of turbulence, while the non-isothermal airflow has a small average wind speed and a large degree of turbulence.

3.2 Whole body heat loss due to local non-isothermal airflow

Table 4 presents the results of the total heat loss of the thermal manikin for each case. The whole-body heat loss in each case ranged from 23.9 to 68.4 W/m². It was 40.1 W/m² in a still air at 26 °C (short sleeves), which appears to be close to the neutral state. When the airflow temperature was 4 °C lower than room temperature and the wind speed was 0.8 m/s, the systemic heat loss increased by 13.8 to 18.9 W/m² from the still air. It was also verified that the amount of heat loss can be adjusted between 5.9 and 11 W/m² by changing clothes from long sleeves to short sleeves.

Although the amount of heat loss in the entire body is suitable for comparing the cooling effect of each airflow pattern on the human body, it is impossible to directly evaluate the thermal sensation or comfort. Therefore, the whole-body equivalent temperature $t_{eq,whole}$ was obtained from the amount of whole-body heat loss using Equations (1) and (2).

$$t_{eq,whole} = t_{s,whole} - R_{t,cal,whole} \cdot Q_{t,whole} \quad (1)$$

$$R_{t,cal,whole} = \left(t_{s,cal,whole} - t_{a,cal}\right)/Q_{t,cal,whole} \quad (2)$$

SET* was calculated under the conditions of air temperature and average radiation temperature for the entire body, metabolism amount of 1.0 MET, cloth amounts of 0.76 CLO for long sleeves and 0.49 CLO for short sleeves, airflow of 0.1 m/s, and relative humidity of 50%. From the experiment, the thermal resistance values $R_{t,\,cal,\,whole}$ from the skin surface to the environment in the standard environment calculated using the Equation (2) were 0.166 m²K/W

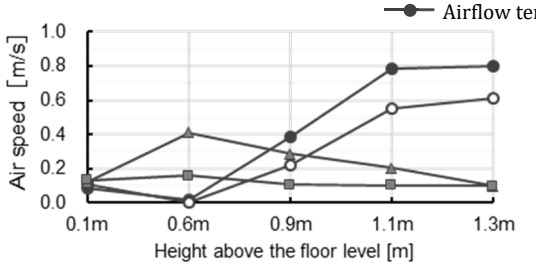

Fig. 3 Air speed distribution near the thermal manikin (Room temperature: 26 °C)

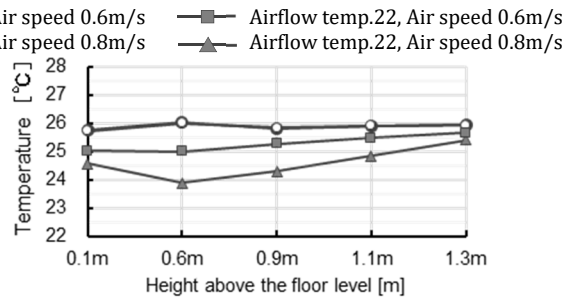

Fig. 4 Airflow temperature distribution near the thermal manikin (Room temperature: 26 °C)

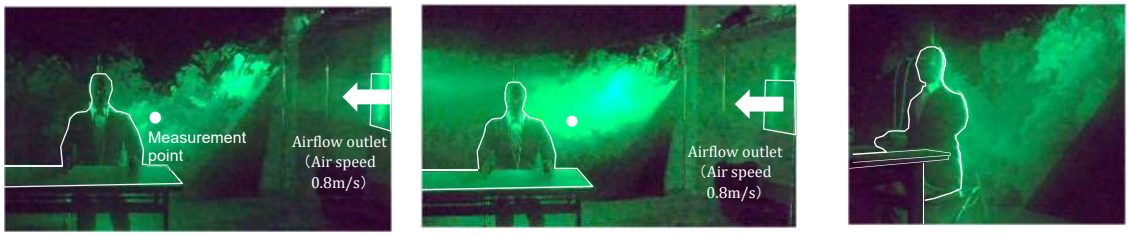

(1) Low temperature airflow at 23 °C, Front (2) Isothermal airflow at 26 °C, (3) Low-temperature airflow at 23 °C diagonally forward

Photo. 4 Airflow visualization (room temperature: 26 °C, air speed: 0.8 m/s)

Table.3 Average air speed [m/s] and airflow turbulence [%]

Airflow temp, Wind speed	Room temp. 26℃		Room temp. 29℃	
Isothermal, 0.6m/s	0.52m/s	26.7%	0.40m/s	39.0%
Isothermal, 0.8m/s	0.79m/s	17.3%	0.73m/s	21.8%
Room temp.−2℃, 0.6m/s	0.40m/s	43.1%	0.31m/s	55.6%
Room temp.−2℃, 0.8m/s	0.55m/s	39.8%	0.56m/s	38.0%
Room temp.−4℃, 0.6m/s	0.19m/s	46.8%	0.18m/s	46.1%
Room temp.−4℃, 0.8m/s	0.31m/s	49.3%	No data	No data

Table.4 Whole body heat loss of thermal manikin

	Whole body heat loss [W/㎡]			
	22℃ (Long sleeves)	26℃ (Long sleeves)	26℃ (Short sleeves)	29℃ (Short sleeves)
Still air	53.1	34.2	40.1	23.9
Isothermal, 0.6m/s	58.1	36.0	44.0	25.1
Isothermal, 0.8m/s	60.8	37.4	46.0	26.6
Room temp.−2℃, 0.6m/s	60.5	39.7	49.3	31.3
Room temp.−2℃, 0.8m/s	65.6	42.5	52.4	33.0
Room temp.−4℃, 0.6m/s	62.1	41.8	49.9	32.5
Room temp.−4℃, 0.8m/s	68.4	48.0	59.0	38.6

and 0.203 m²K/W under the short- and long-sleeve conditions, respectively.

3.3 SET in local non-isothermal airflow*

Fig. 5 presents the whole-body equivalent temperature obtained from the whole-body heat loss under each experimental condition, while Fig. 6 shows SET*. It was demonstrated that SET* decreased by a maximum of 2.9 °C owing to the local non-isothermal airflow compared to the calm state at each room temperature. Fig. 7 presents the change in SET* when the blowout temperature and wind speed change by 1 °C and 1.0 m/s, respectively. The numerical value presented in the legend represents the rate of change of SET* obtained from the slope of the approximate straight line of the measurement data. From the results of (a) and (b), it can be observed that SET* decreases in the range of 0.19–0.58 °C when the airflow temperature is lowered by 1 °C. The decrease in the airflow temperature is particularly significant at a temperature of 29 °C, where the temperature difference from the skin surface temperature is negligible. It was deduced that when the wind speed was increased by 1 m/s in (c), SET* decreased in the range of 0.54–1.72 °C. At a temperature of 22 °C, the difference from the skin surface temperature was significant; hence, the rate of decrease in SET* tended to be large, and the rate of decrease in short-sleeve conditions with more exposed parts tended to be greater than that of long-sleeve conditions.

From the experimental results obtained by Xing et al., it is considered that when the wind speed on the surface of the human body increases by 1.0 m/s, the practical temperature drops by approximately 3.7 °C; however, in this experiment, it was 1.72°C. This difference is considered to be due to the difference in the exposure range of the airflow, and it can be deduced that the data of this experiment are obtained from the evaluation of the airflow during natural ventilation under conditions close to actual conditions.

3.4 Amount of heat loss by site

Fig. 8–11 present a comparison of the amount of heat loss by site. Fig. 8 shows the results of isothermal airflow while Fig. 10 presents the results of non-isothermal airflow 4 °C lower than room temperature. When the temperature of the room drops from 29 °C to 22 °C, the temperature difference on the skin surface increases, and the amount of heat loss at each site generally increases. At a temperature of 29 °C, the difference between parts is negligible; however, when the temperature of the room drops to

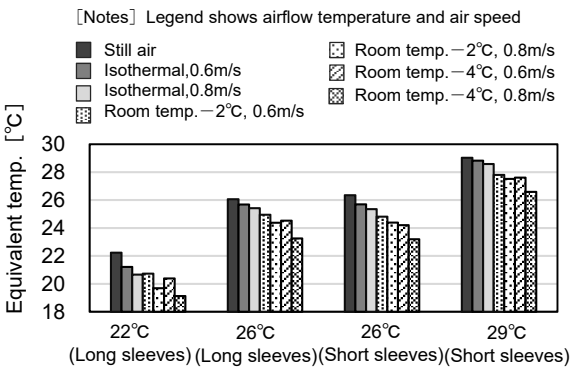

Fig. 5 Equivalent temperature

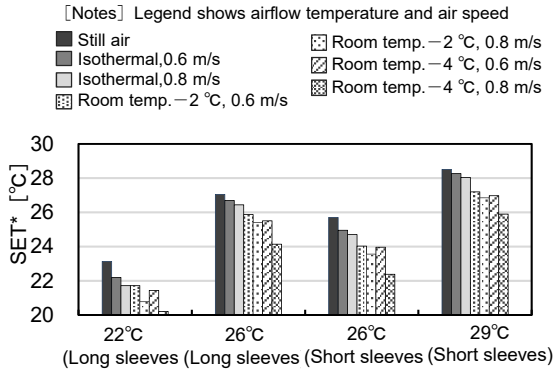

Fig. 6 SET* obtained from the equivalent temperature and room temp.

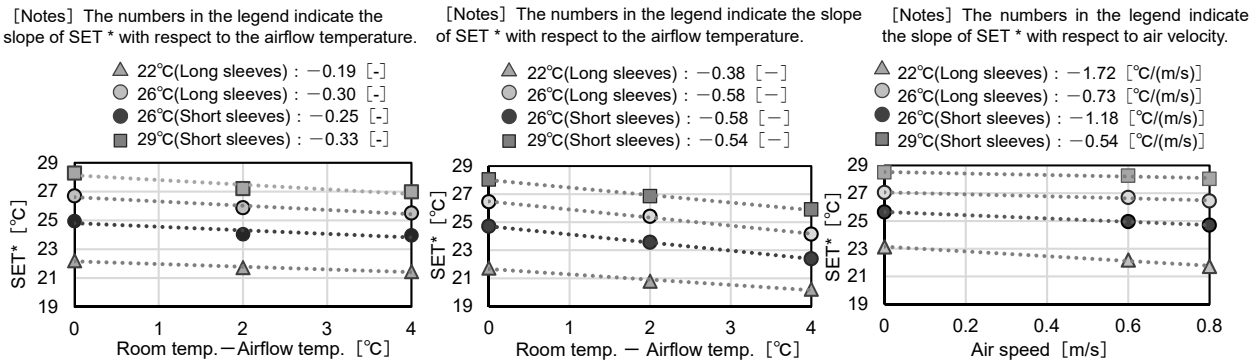

(a) Temperature difference and SET* (Air speed: 0.6 m/s)

(b) Temperature difference and SET* (Air speed: 0.8 m/s)

(c) Isothermal airflow speed and SET*

Fig. 7 Rate of decrease of sensible temperature due to airflow temperature and air speed

26 °C and 22 °C, the amount of heat loss in the undressed head, forearms, hands, and thighs increases. From Fig. 10, it can be observed that in non-isothermal airflow, the amount of heat loss in the upper and lower arms increases significantly when the clothes are changed from long sleeves to short sleeves.

Compared to the exposed parts of the upper body and the lower body, the chest, shoulders, stomach, back, and hip were less affected by the temperature of the room and airflow. It is expected that this is owing to the heat insulating effect of clothes and the difference in how the airflow hits the body. In addition, when the temperature of the room drops, the rate of increase in the amount of heat loss in the lower body becomes larger than that in the upper body parts such as the chest, shoulders, and abdomen. The reason for this is hypothesized to be the difference in heat insulation between the upper and lower body clothing and the heat plume of the human body.

Fig. 9 illustrates the relationship between the airflow temperature at a temperature of 29 °C and the amount of heat loss for each part. At a 29-°C temperature, which is close to the skin surface temperature, the cooling effect due to the air speed is negligible, while the cooling effect due to the airflow temperature is significant. As the airflow temperature decreases, the cooling effect of the lower body, such as the thighs, increases in addition to the exposed parts such as the upper arms and hands.

Fig. 11 presents the results of exposure to an isothermal airflow at a temperature of 22 °C and exposure to a non-isothermal airflow of 22 °C at a room temperature of 26 °C. Although the airflow temperature is the same as 22 °C, in an isothermal airflow with a room temperature of 22 °C, the airflow is less turbulent and is primarily exposed to the head; hence, the amount of heat loss on the head and face is significant. Conversely, in the non-isothermal airflow, the turbulence of the airflow is significant, and the part below the shoulder is cooled. In particular, under the short sleeve condition, the amount of heat loss in the arm part is substantial.

4. Comparison with subject experiments

4.1 Subject experiment outline

In the thermal manikin experiment, the effect of cooling the human body by the airflow during natural ventilation was demonstrated. However, it is necessary to verify the actual thermal sensation and comfort felt by subject experiments. Therefore, a subject experiment was conducted in an artificial climate room under the same conditions as the manikin experiment. The subjects included eight

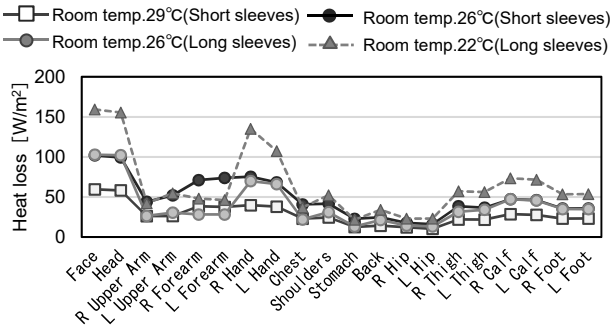

Fig. 8 Room temperature/clothes and heat loss by site (Air speed: 0.8 m/s, isothermal)

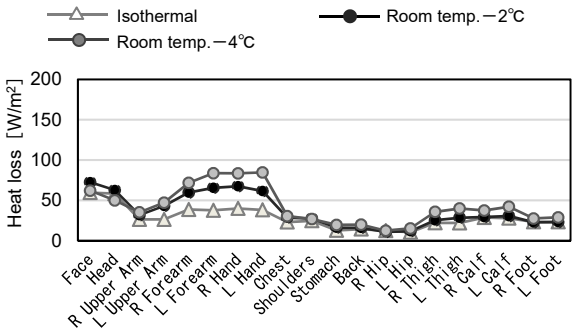

Fig. 9 Airflow temperature and heat loss by site (Room temp.: 29 °C, air speed: 0.8 m/s, short sleeves)

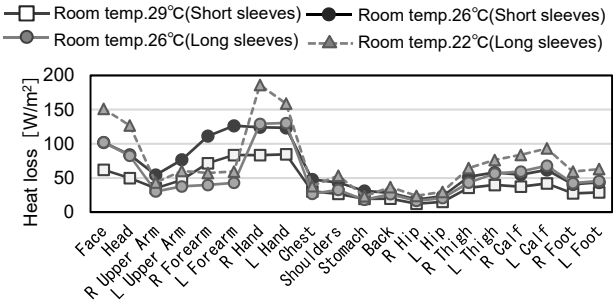

Fig. 10 Room temperature/clothes and heat loss at different sites (Air speed:0.8 m/s, room temp.: −4 °C)

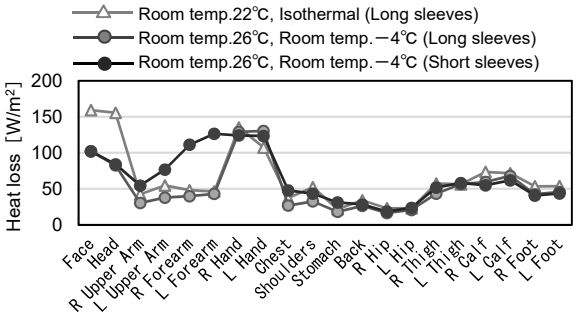

Fig. 11 Airflow temperature: 22 °C, air speed: 0.8 m/s, and heat loss at different sites

adult males, and the survey was conducted from September to October 2021. The experimental cases are presented in Table 5.

The room temperatures were 22 °C and 29 °C, while the relative humidity was 40%. However, for 29 °C, a case with a relative humidity of 70%RH was included. There were nine experimental cases in total, and eight subjects participated in all nine experimental cases. The state of the experiment is presented in Photo. 5, while the experimental procedure is illustrated in Fig. 12. Three cases of the experiments were conducted per day, and the subjects were asked to do step-up exercises during the experiments to maintain their metabolic rate at 1.2 MET. During the experiment of Case 1, the questionnaire on the feeling of warmth, coldness, and comfort was reported thrice. The three questionnaires were the same and attempted to verify the change in the subject's feelings over time. In the experiment, in addition to the questionnaire, the skin surface temperature of each part was also measured.

Table 5 Experimental cases

	Subject	Climate chamber		Air flow	
	Clothing [clo]	Room temp. [℃]	Relative humidity [%]	Air speed [m/s]	Air temp. [℃]
Case 1-1	0..49	29	40	0.8	29℃ (Isothermal)
Case 1-2					27℃(-2℃)
Case 1-3					25℃ (-4℃)
Case 2-1			70		29℃ (Isothermal)
Case 2-2					27℃(-2℃)
Case 2-3					25℃ (-4℃)
Case 3-1	0.76	22	40		22℃ (Isothermal)
Case 3-2					20℃(-2℃)
Case 3-3					18℃ (-4℃)

Table 6 Measurement condition of wet mode

Item	Set point
Set point of sweat flow (ml/min)	Head:53, Face:30, Upper Arm:8, Forearm:14, Hand:41, Chest:15, Shoulders:40, Back:73, Hip:60, Thigh:30, Calf:50, Foot:18
Thermal manikin control	Constant skin surface temperature control (33 °C)

Photo. 5 State of the experiment

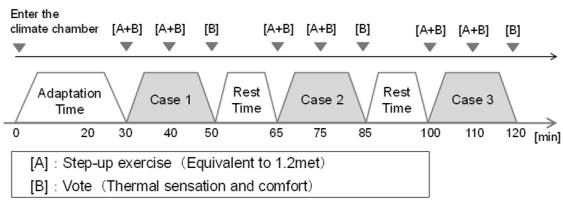

Fig.12 Experimental procedure

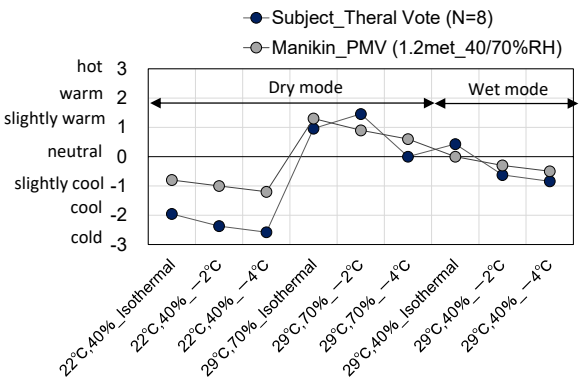

Fig. 13 Thermal sensation vote and PMV calculated from measurement data

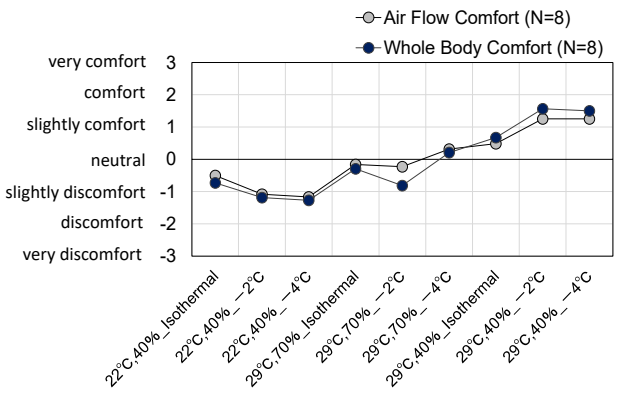

Fig. 14 whole body and airflow comfort

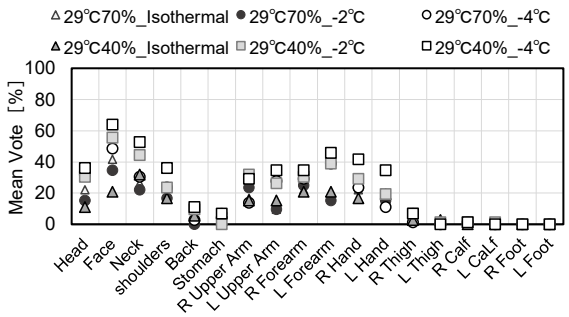

Fig. 15 The part where the subject feels the air flow (Room temperature 29℃)

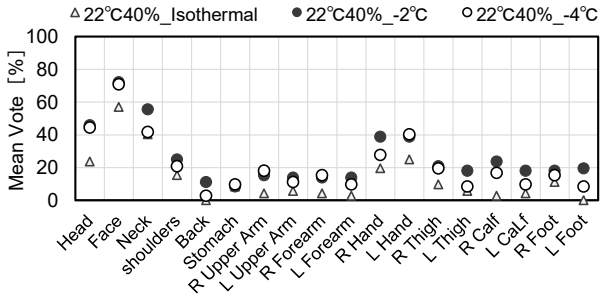

Fig. 16 The part where the subject feels the air flow (Room temperature 22℃)

4.2 Thermal sensation vote

Fig. 13 presents the results obtained from the thermal sensation vote report by the subject experiment. To compare the results of the subject experiment with the thermal manikin, the predicted mean vote (PMV) was calculated using the equivalent temperature obtained from the thermal manikin data. For the cases of 22 °C, 40%RH and 29 °C, and 70%RH, the amount of heat loss measured by the thermal manikin under dry conditions was adopted. In addition, at 29 °C and 40%RH, which are significantly affected by latent heat evaporation, the amount of heat loss was measured again with a sweating thermal manikin, and the obtained data were utilized. Photo. 5 and Table 6 present the measurement conditions for the sweating thermal manikin. The CLO value of the clothing including a fabric skin was calculated, and PMV was calculated from the equivalent temperature. PMV was calculated using the equivalent temperature of the entire body as the air temperature and average radiation temperature, and the metabolic rate was 1.2 MET, the amount of clothes was 0.76 CLO for long sleeves, 0.49 CLO for short sleeves, the indoor wind speed was 0.15 m/s, and the relative humidity was 40%. RH and 70% RH were adopted.

In addition, Fig. 14 presents the results of a questionnaire regarding whole-body and airflow comfort. At 29 °C (70% RH) the thermal sensation vote was slightly warm, and comfort vote was slightly unpleasant. The results were slightly cool and slightly comfortable under the conditions of 29 °C (40% RH). Under these conditions, the PMVs obtained from the amount of heat loss in the thermal manikin and the subject's thermal sensation vote were close to each other. At 22 °C (40% RH), the subject's vote was between cool and cold, which was slightly unpleasant. There was a significant difference between the results of the thermal manikin at 22 °C and 40% and the subject's vote, which is considered to be owing to the effect of local discomfort.

4.3 Airflow sensation by site

Fig. 15 and 16 present the results of the declaration regarding the part where the subject feels the air flow. At a room temperature of 29 °C, it can be observed that the head, neck, shoulders, and arms feel the airflow, centering on the upper body, because the clothes are short-sleeves. At a room temperature of 22°C, it was deduced that airflow was felt in the head, neck, hands, and lower body owing to the long-sleeved clothes. It is considered that the discomfort of the airflow related to these parts affects the whole-body warmth and discomfort at 22 °C. There was a difference in how the lower body felt the airflow between 29 °C and 22 °C. Fig. 17 presents the results of the requests for changes in the wind speed and temperature of the airflow. At a room temperature of 29°C, there were several requests to strengthen the airflow and reduce the airflow temperature; however, in a room of 29 °C and 40% RH, when the airflow temperature was at a room temperature of -4 °C, the ratio at which it was acceptable was the largest. At a room temperature of 22 °C, there were several requests to weaken the airflow and increase the entire airflow temperature.

4.3 Skin surface temperature

Fig. 18 presents the average skin surface temperature of the subjects. At a room temperature of 29 °C, the skin surface temperature was in the range of 32–35 °C, and the skin surface temperatures of the stomach and foot, which were not directly exposed to airflow, were slightly higher than those of other parts. There was also a tendency for the skin surface temperature of the upper arm and hand to decrease in low-temperature airflow compared to isothermal airflow. At a room temperature of 22°C, the temperature was in the range of 28–32 °C, and the skin surface temperatures of the Back of the hand and foot tended to be slightly low. The entire skin surface temperature appears to be generally low, which seems to affect the results of the subject's vote, slightly cold.

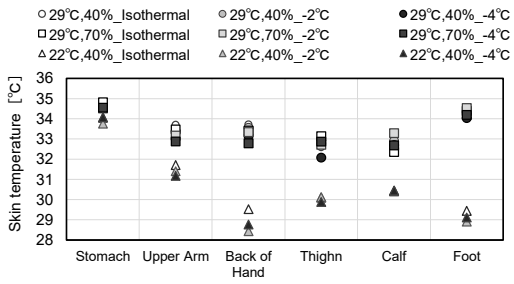

Fig. 18 Average skin surface temperature

5. Discussion

From the results of the subject experiment, it was inferred that the room temperature of 22 °C was cold and uncomfortable under the experimental conditions that reproduced the natural ventilation, and it appeared unsuitable as an indoor environment during natural ventilation where the indoor airflow is generated. In addition, although the airflow was centered on the upper body, the coldness of the lower body tended to increase. Furthermore, it was expected that the subject feels colder than the amount of cooling heat obtained by the thermal manikin, owing to local discomfort. However, it was confirmed that when the room relative humidity was low at a room temperature of 29 °C, positive comfort was obtained from the air flow. The room temperature range that allowed natural ventilation was generally in the range of 22–26 °C; however, if the airflow from the natural ventilation inlet can be utilized, a higher room temperature setting, such as 24–28 °C, should be adopted. It is assumed that this approach will provide comfort.

6. Symbols

$R_{t,cal,whole}$: Total cloting insulation[(m² · K)/W]
Short sleeves 0.166[(m² · K)/W],
Long sleeves 0.203[(m² · K)/W]

$Q_{t,cal,whole}$: Amount of sensible heat loss from the whole body under standard conditions [W/m²]

$Q_{t,whole}$: Amount of sensible heat loss from the whole body [W/m²]

$Q_{t,segment}$: Amount of sensible heat loss by site [W/m²]

$t_{eq,whole}$: Whole body equivarent temperature [°C]

$t_{s,whole}$: Skin surface temperature [°C] =33

7. Acknowledgement

This work was supported by JSPS KAKENHI Grant Number JP 20K14888 (Research Leader: Yoshihide Yamamoto).

8. References

[1] Yoshihide Yamamoto, Masatoshi Kuboki, Hiromasa Suzuki, Shin-ichi Tanabe. Investigation on management of natural ventilation system. Journal of Environmental Engineering (Transactions of AIJ). 2007,9； No.619:9-16.

[2] Yoshihide Yamamoto, Shin-ichi Tanabe. The Criteria of Outdoor Conditions for Operating Natural Ventilation Openings. Journal of Environmental Engineering (Transactions of AIJ). 2016.4 ；Vol.81.No.722：375-384.

[3] ASHRAE Standard 55-2017. Thermal Environmental Conditions for Human Occupancy. ASHRAE. 2017.10.

[4] Xing Su, Xu Zhang, Jun Gao. Evaluation method of natural ventilation system based on thermal comfort in China. Energy and Buildings. 2009.1 ；Volume 41, Issue 1：67-70.

[5] E Arens, S Turner, H Zhang, G Paliaga. Moving air for comfort. ASHRAE Journal. 2009.5 ：p.18-28,

[6] Architectural Institute of Japan environmental standards: AIJES-H0005-2015 Standards for evaluation of indoor thermal environment using thermal manikin. Maruzen. 2015.2.

[7] A.P.Gagge, J.A.J.Stolwijk, J.D.Hardy. Comfort and thermal sensations and associated physiological responses at various ambient temperatures, Environmental Research. 1967.6；Volume1, Issue 1： 1-20.

Data Statement

Data sharing not applicable to this article as no datasets were generated or analysed during the current study.

Thermal inactivation of the corona virus (SARS-CoV-2) in air volumes

André Schlott [a], Thomas Hutsch [a], Eileen Sauer [b], Jens Wetschky [b], Jana Hessel [b], Susanne Bailer [b], John Laubert [c], Stefan Lösch [c]

[a] Fraunhofer Institute for Manufacturing Technology and Advanced Materials IFAM, Branch Lab Dresden, Dresden, Germany, andre.schlott@ifam-dd.fraunhofer.de

[b] Fraunhofer Institute for Interfacial Engineering and Biotechnology IGB, Stuttgart, Germany, jens.wetschky@igb.fraunhofer.de

[c] Fraunhofer Institute for Manufacturing Technology and Advanced Materials IFAM, Bremen, Germany, john.laubert@ifam-dd.fraunhofer.de

Abstract. To control the spread of viruses (e.g., SARS-CoV-2) and other pathogens in a pandemic situation, slowing down the rate of spread is an essential goal that can be achieved by interrupting transmission chains. According to the current state of knowledge, SARS-CoV-2 is mainly transmitted by droplet infection through virus-containing aerosol clouds in the air. These aerosol clouds are mainly produced by exhalation and can be reduced by wearing medical masks. In closed rooms, there is an increased probability of infection by aerosols. Countermeasures include various recently developed air cleaning technologies. Most of these technologies available on the market are based on filters with a limited lifetime to remove the virus load from the air or different sterilisation methods like UV irradiation. The air cleaning technology presented focuses on the thermal inactivation of viruses beyond their temperature sensitivity by heating the air. In the developed apparatus, the potentially germ-carrying ambient air is sucked in and conditioned in such a way that it is exposed to a certain temperature for a defined period of time. Before the inactivated / hygienised air is returned to the environment, it is cooled down to almost room temperature. The recovered heat remains in the system and is used to heat the intake air. The use and combination of different technologies enable the most efficient air disinfection possible. Four different experiments were conducted. After determining a base line, the air was solely passed through the pump, through the whole »Virus-Grill« pressure free and with an elevated pressure of 1.5 bar. In all experiments (except the baseline) the number of active viruses were reduced below the limit of detection.

Keywords. Health, Thermal Sterilisation, Thermal Inactivation, Air Treatment, Air Cleaning Technology, Virus Inactivation, SARS-CoV-2, COVID-19, Heat Recovery, Energy Efficiency
DOI: https://doi.org/10.34641/clima.2022.214

1. Introduction

Aerosols containing viruses can accumulate indoors and lead to superspreading events [1]. Therefore, slowing down the rate of spread is an essential goal in order to control the pandemic spread of viruses (e.g. SARS-CoV-2) and other pathogens. That can be achieved by interrupting transmission chains.

Researchers all over the world work on air purification technologies. Possible air purifying technologies include filtration with HEPA filters, where the viruses are removed from the air volume. This is a common approach to reduce contamination in the surrounding air. With light in UV-C spectrum (200 to 280 nm), viruses are deactivated through critical damage to the genomic system of the microorganism by absorbing photons [2, 3]. With UV light, surfaces, e.g. door knobs, are sterilized [4]. To clean air volumes, an upper-room mounting of UV lights is possible [5]. Additionally, UV lights are installed in HVAC channels. A third method is the plasma air cleaning, which uses high-voltage electrodes to create ions in the air [6].

The developed apparatus »Virus-Grill« reduces the probability of droplet infection by inactivating viruses. This inactivation is achieved by heating the viruses beyond their temperature sensitivity. (e.g.

Copyright ©2022 by the authors. This conference paper is published under a CC-BY-4.0 license.

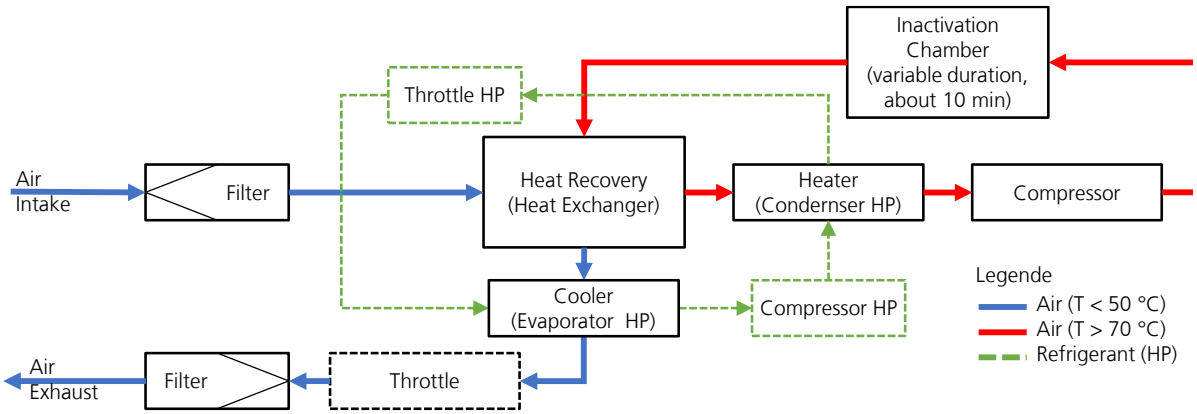

Fig. 1 - Flow chart of the sterilization process

70 °C), the virus proteins, especially the surface proteins needed to dock to receptor molecules on the host cell membranes, are denaturized.

If this targeted process is carried out continuously, it can be used as a kind of "virus sink". In order to return the inactivated air to the room, the air must be cooled down to nearly room temperature. The use of a heat pump enables efficient temperature control within the apparatus. The interaction of the components is ensured by a regulation and control software.

The aim was to construct and build up a test rig for the proof of the inactivation of viruses using a safety workbench. The developed principle itself can be integrated into climatization systems for closed volumes like rooms (bureau; waiting rooms; class rooms; passenger areas in aircrafts, hotels and ships)

2. Principle of Thermal Inactivation

The concept of the »Virus-Grill« is that a partial quantity is extracted from a closed volume of air by the compressor and is specifically exposed to a higher temperature (e.g. more than 70 °C) in the apparatus for at defined dwell time (e.g. 10 minutes in a dwell chamber). Before the air reaches this chamber, it is heated in three steps as shown in Fig. 1. The heating steps one and two utilize the already treated and still hot air. While the first step is a passive heat recovery system, the second step uses an active heat pump to heat the air. The final heating step is the compressor itself, where the air reaches the temperature needed during compression. After that, the compressed air is stored in a heated chamber to inactivate the viruses. The viruses will stay in the treated air but because they are not infectious anymore, the air is considered inactivated/ purified.

After releasing the sterilized air from the chamber, it goes through the heat recovery and the evaporator of the heat pump to reduce its temperature. Before leaving the apparatus, a throttle reduces the pressure of the air. Therefore, the air leaves the »Virus-Grill« apparatus at ambient pressure and almost at ambient temperature.

3. Experimental Test Rig – The »Virus-Grill« Apparatus

The set-up was done considering the planned tests with surrogate viruses in a safety workbench to characterise the effectiveness of the »Virus-Grill«. Because of the limited space in the workbench, the test rig had to adhere to certain dimensions. Also, the required air volume of the aerosol generator and available electrical connection were considered at the design process of the test rig.

Fig. 2 shows the set-up of the »Virus-Grill« during the trials for the proof of efficacy. The following components are marked: (1) aerosol generator, (2) virus chamber, (3) compressor, (4a-4c) holding chambers, (5) clean chamber, (6) heat pump, (7) measuring computer with control software, (8) safety workbench (sterile bench).

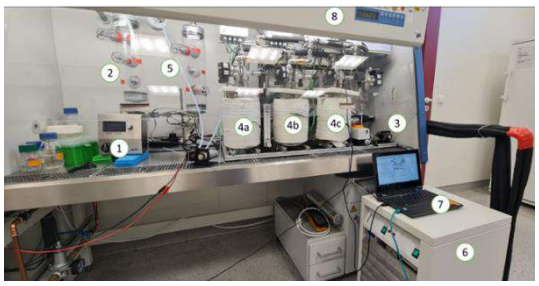

Fig. 2 – Prototype of the »Virus-Grill« in the sterile bench environment to characterise the efficacy in terms of inactivation of aerosol-borne viruses.

The individual components play a special role in this process, the sum of which can achieve effective inactivation. The compressor works according to the principle of a piston compressor. This causes pressure (change) and temperature to act for a short time. In addition, the pressure-resistant dwell chambers (here 3 bar) are tempered to a certain temperature by an external heater. In order to use energy more efficiently, the heat pump supports the heat recovery unit used. The developed system of solenoid valves enables almost continuous operation through appropriate control. The question of effectiveness was addressed as a complete unit as well as in partial component tests.

The »Virus-Grill« control includes the collection and processing of numerous temperature and pressure sensor data and adjustable process parameters. Valves and compressor are controlled by control electronics containing market available and self-developed components. The »Virus-Grill« is monitored by 16 temperature sensors (PT1000) and 16 pressure transmitters, whose data are processed by the controller. Switching operations on solenoid valves and air compressors as well as power control of the heat pump components are made possible by means of a Mosfet driver circuit and an external power supply. The control of the chamber heating is realised via standardised interfaces.

A microcontroller board is used as the central element of the control system, which has sufficient computing power and supports all necessary connections. The necessary firmware was programmed in C++ and processes the measurement data, interprets process parameters and gives corresponding control signals. A wireless LAN access point including a webserver enables the user to interact with the »Virus-Grill«.

A control software developed in C# establishes the necessary connection and displays the measurement data using a circuit diagram of the »Virus-Grill« (Fig. 3). The measurement data are stored in parallel for later evaluation. It is also possible to adjust the process parameters of the »Virus-Grill«.

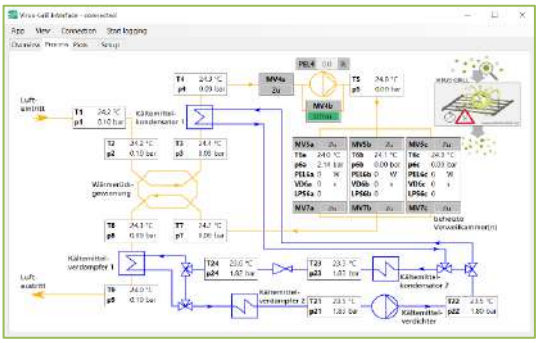

Fig. 3 – GUI of the control software.

In order to take suitable samples, aerosol samples must be collected from a closed system, such as the virus and clean chamber, without manipulating the atmosphere in the system or allowing air contaminated with viruses to escape. Therefore, a small airlock for swabs was developed and four polycarbonate 3D printed components were created for each airlock, which were assembled with UV-resistant adhesive.

The construction is shown in Fig. 4. The three-part airlock consists of a handpiece, a piston insert and the actual airlock chamber as well as the piston. The handpiece serves as a carrier/holder for the swab and at the same time as the "outer sluice gate". The piston insert combines inner and outer sluice gate including the necessary piston seals. The piston itself determines the volume of air exchanged when opening and closing the airlock.

The greatest difficulty in the CAD-supported development was the sealing ability of the piston rings. The tubes used, made of special solvent-resistant and UV-permeable acrylic glass, showed strong geometric tolerances, so that commercially available sealing solutions with rubber rings and lubricants and sealants did not achieve sufficient sealing. Therefore, piston sealing rings made of flexible filament were developed and manufactured by means of 3D printing, with which tolerances could be compensated and a sufficient seal achieved at both sluice gates. These are shown in red in Fig. 4. Smooth sliding of the piston insert was also ensured.

To close the sluice gates securely, neodymium magnets are used to magnetically attract a metal ring on the handpiece itself or on the outer end of the piston, depending on the position of the handpiece. These metal rings required precise manufacturing in order to minimise the gap between the magnets and the metal ring so that the neodymium magnets can generate a sufficiently large magnetic attraction force.

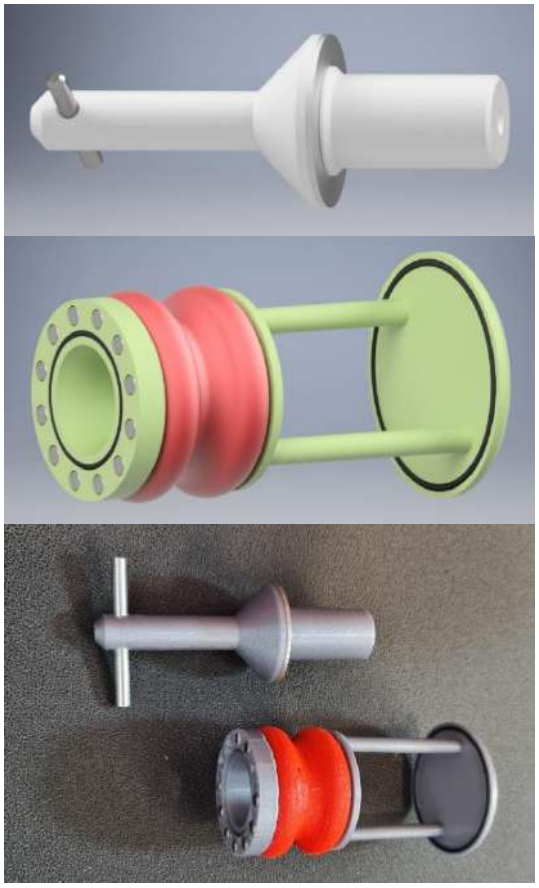

Fig. 4 – Three-part airlock for sampling (above: Handpiece/swab holder; middle: piston insert with sealing ring; bottom: printed components)

4. Virological Test Setup

The current and still ongoing pandemic situation regarding SARS-CoV-2 requires standardised methods for the detection and analysis of airborne viruses in the form of aerosol. Since SARS-CoV-2 is classified as a biosafety level 3 virus, the number of

laboratories that can culture and analyse infectious viruses is severely limited and the experiments require a high level of security measures for containment. For this reason, the bacteriophage Phi6 was established as a surrogate virus. Phi6 shows a high degree of similarity to SARS-CoV-2 in particle size, external structure, and the type of genome. In contrast to other surrogate viruses, Phi6 is a bacteriophage that only infects bacteria and poses no danger to humans, animals or plants. In order to assess the effectiveness of disinfection measures, two parameters were applied. i) The number of viral genomes that accounts for all viruses whether dead or alive, was determined by the molecular biological method of qPCR. ii) The viral activity or infectivity that accounts the number of infectious viruses was determined by the plaque assay.

4.1 Sample Preparation of surrogate viruses

The bacteriophage Phi6 was used as surrogate virus for the evaluation of the »Virus-Grill«. Phi6 was propagated using its host bacterium *Pseudomonas syringae*. Stock solutions of Phi6 and *P. syringae* were kindly provided by Prof. Dr. Martin Hessling and Dr. Petra Vatter (Technische Hochschule Ulm). For propagation of the surrogate virus, *P. syringae* was cultivated overnight in tryptic soy broth (TSB) at 25 °C and 170 rpm. Bacterial culture was subcultivated in fresh TSB for starter culture. At an optical density of 0.3, Phi6 was added 1:10 followed by incubation to an optical density of 0.08. To obtain pure phage lysate, the culture was centrifuged to pellet the bacteria, and supernatant was filtered through a 0.45 µm filter (Fisher Scientific).

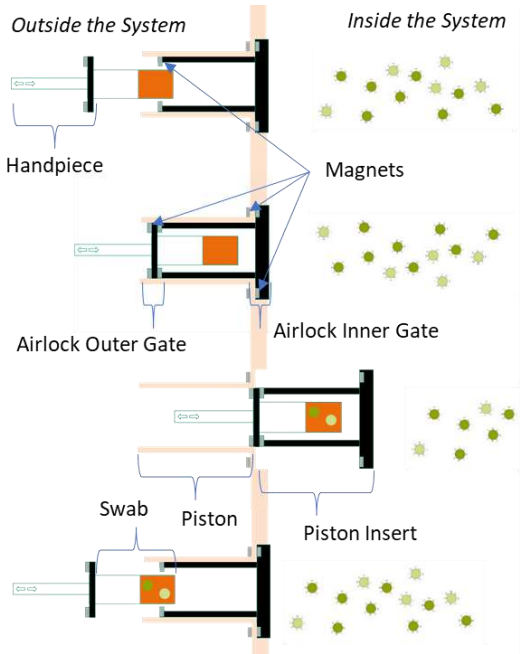

Fig. 5 – Sampling concept with airlock and swab

For all experiments performed, Phi6 lysate was rebuffered in water. The titer of the obtained Phi6 stock lysate was determined using a bacterial plaque Assay [7] and stored at 4 °C until further usage. For the experimental procedures, the stock lysate was adjusted to 1 x 10^{10} PFU/mL and used for aerosolization.

4.2 Virological Data Acquisition

The individual steps of sampling with this airlock are shown in Fig. 5. After inserting the swab into the handpiece, it was mounted in the piston insert. At the same time, the outer airlock is closed. For sampling, the entire piston insert is guided into the interior of the system, exposing the swab to the aerosols. When the piston insert is pulled out, the inner lock closes and the handpiece with the swab can be removed again. The escape of aerosols can thus be reduced to a minimum.

5. Measurements and Results

For the experimental set-up, a droplet aerosol with an average droplet size of 0.15 µm was generated from a phosphate-buffered saline (PBS) containing Phi6. The aerosol was collected and analysed at three positions before the experimental setup (virus chamber) and after the experimental setup (clean chamber) using swabs moistened in PBS. All samples were analysed for virus activity and total virus count.

Four different experiments were conducted to examine partial components of the »Virus-Grill« and finally the entire test rig. In the first experiment (Exp. 1), the virus-containing aerosol was sucked from the virus chamber into the clean chamber. The pump was behind the clean chamber. This was done to find a baseline of surrogate viruses in the virus chamber and clean chamber with no treatment whatsoever. In the second experiment (Exp. 2), the virus-containing aerosol was pumped from the virus chamber through the pump into the clean chamber. In the third experiment (Exp. 3), the virus-containing aerosol was pumped pressure-free from the virus chamber through the »Virus-Grill« into the clean chamber. Again, the pump was located at the end of / after the clean chamber. And in the fourth experiment (Exp. 4), the virus-containing aerosol was pumped from the virus chamber through the »Virus-Grill«, through the pump into the clean chamber at room temperature and 1.5 bar overpressure.

The results of the detection of the virus activity and the determined virus genome count are shown in Fig. 6 and Fig. 7. It was shown that only in experiment 1, in which the viruses were sucked directly from one chamber to the other, were active viruses detectable in the clean chamber.

The detected virus genomes in Fig. 7 show an increasing reduction of virus genomes when using the pump in experiment 2, the flow through the »Virus-Grill« in experiment 3 up to the greatest reduction of virus genomes when operating the »Virus-Grill« at room temperature and a system pressure of 1.5 bar in experiment 4.

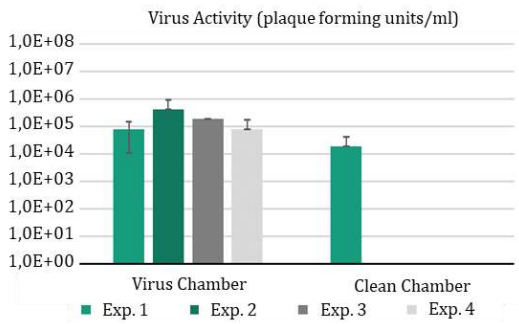

Fig. 6 – Comparison of virus activity in virus chamber and clean chamber.

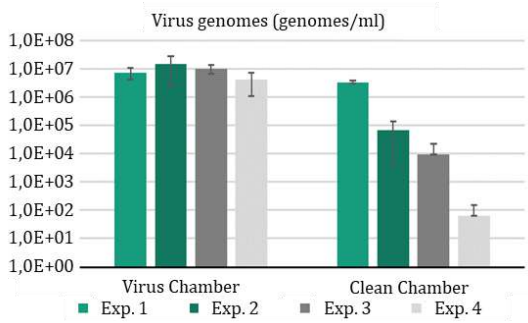

Fig. 7 – Detected viral genomes in virus chamber and clean chamber The viral genomes detect both inactivated and infectious viruses.

Taken together, it was possible to aerosolise surrogate viruses in the experimental set-up, to transport them from the virus chamber into the clean chamber and to detect them. The use of the pump already leads to complete inactivation of the viruses used. This leads to the hypothesis that continuous inactivation is possible by using compressors based on the principle of the piston compressor for SARS-CoV-2. Furthermore, the use of the »Virus-Grill« was able to reduce the total number of virus genomes.

6. Conclusions and outlook

The efficacy of the »Virus-Grill« was validated with four experiments. Experiment 1 defined a baseline of viruses reaching the clean chamber with no treatment whatsoever. Experiments 2 to 4 tested different »Virus-Grill« configurations. Experiment 2 pulls the virus-containing aerosol only through the piston pump into the clean chamber. In experiments 3 and 4 the contaminated air flows through the complete »Virus-Grill« at ambient pressure and at an elevated pressure of 1.5 bar, respectively. The number of active viruses were reduced below the limit of detection in all three cases. The number of viral genomes in the clean chamber shows that there are inactivated viruses carried through the »Virus-Grill«.

This process has very high potential in applications that dispense mechanical filtration. Here, maritime applications and integration into existing ventilation systems are mentioned in particular. The concept can also be adapted in the medical field for the ventilation of patients. Thus, a wide range of flow rates from a few l/min to several m^3/min can be addressed through suitable design and scaling of the components.

7. Acknowledgement

The presented work was part of the project AVATOR and funded by the Fraunhofer-Society within the Fraunhofer vs. Corona campaign which is gratefully acknowledged.

8. References

[1] Miller, S.L., et al., Transmission of SARS-CoV-2 by inhalation of respiratory aerosol in the Skagit Valley Chorale superspreading event, Indoor Air 31 (2020), p. 314-323, DOI: 10.1111/ina.12751

[2] Raeiszadeh, M., et.al., A Critical Review on Ultraviolet Disinfection Systems against COVID-19 Outbreak: Applicability, Validation, and Safety Considerations, ACS Photonics 2020, 7, 11, 2941–2951, DOI: 10.1021/acsphotonics.0c01245

[3] Fukui, T. et.al., Exploratory clinical trial on the safety and bactericidal effect of 222-nm ultraviolet C irradiation in healthy humans, PLoS ONE 15(8): e0235948., DOI: 10.1371/journal.pone.0235948

[4] Storm, N., et al. Rapid and complete inactivation of SARS-CoV-2 by ultraviolet-C irradiation. Sci Rep 10, 22421 (2020). DOI: 10.1038/s41598-020-79600-8

[5] Beggs C. B., et.al., Upper-room ultraviolet air disinfection might help to reduce COVID-19 transmission in buildings: a feasibility study, PeerJ 8:e10196, DOI: 10.7717/peerj.10196

[6] Fennelly M, et al. Effectiveness of a plasma treatment device on microbial air quality in a hospital ward, monitored by culture, J Hosp Infect. 2021; 108:109-112. doi:10.1016/j.jhin.2020.11.006

[7] Kropinski, A.M., et al., Enumeration of bacteriophages by double agar overlay plaque assay, in Bacteriophages. 2009, Springer. p. 69-76.

Data Statement

The datasets generated and analysed during the current study are not available because of the ongoing validation and up-scaling process but the authors will make every reasonable effort to publish them in near future.

Dynamic evaluation method for assessing households' thermal sensation using parametric statistical analysis: A longitudinal field study in the South-eastern Mediterranean climate

Hasim Altan [a], Bertug Ozarisoy [b]

[a] Department of Architecture, Faculty of Design, Arkin University of Creative Art and Design (ARUCAD), Kyrenia, Cyprus
hasimaltan@gmail.com

[b] Graduate School, School of Architecture, Computing & Engineering, University of East London (UEL), London, United Kingdom,
ozarisoybertug@gmail.com

Abstract. Climate change is causing a wide range of impacts, including more frequent and brutal climate events, such as long-term heatwaves while compound effects of extreme weather events can dramatically disrupt indoor thermal conditions, causing increased mortality risks, especially for vulnerable populations with health conditions. Comfort standards do not give clear guidelines to determine the minimum or ideal range of continuous measurements, considering the climate change projections to determine neutral thermal comfort thresholds in 2030s, 2050s and 2080s. The aim of this study is to evaluate the predictive skills of existing long-term thermal comfort indices from the ASHRAE RP-884-II database and to propose new indices based on continuous, in-situ physical environmental measurements and subjective evaluations of social householders in naturally ventilated multi-family houses in the South-eastern Mediterranean basin. A meta-analysis of ASHRAE Global Thermal Comfort Database II showed that the acceptable temperatures extend across a wide range of conditions and vary depending on building type and climate. The results revealed that the Predicted Mean Vote (PMV) is the upper limit in ASHRAE standard-55's 0.5 clothing value (*clo*) summer comfort zone stretches all the way to 27°C at 50% relative humidity with air speeds below 0.2 m/s. The results prove that the neutral mid-point of the summer comfort zone is at about 25.5°C regardless the neutral temperature was 28.5°C, and the upper limit of the comfort range in warm indoor air temperature conditions was 31.5°C in the South-eastern Mediterranean region. Our analysis reappraises the scope of applicability of the adaptive comfort standard, assess potential regional differences by considering the detrimental impact of climate change in adaptive thermal comfort responses, and propose mitigation strategies to adaptive comfort theory, the adaptive comfort model and standard and sustainable building design. Finally, we suggest that building operations should better regulate occupant's psychological behaviour to adapt to warmer indoor conditions by implementing adaptive comfort algorithms to optimise occupants' thermal comfort against the warming climate conditions. This could lead to improving energy performance of naturally ventilated buildings without sacrificing the occupant comfort.

Keywords. Adaptive model, ASHRAE database, Climate change, Thermal comfort, Thermal history
DOI: https://doi.org/10.34641/clima.2022.422

1. Introduction

1.1 Knowledge Gap

The provision of thermal comfort for building occupants stands out as one of the largest end-uses of energy in the built environment, bearing significant responsibility for greenhouse emissions (GHG) and their destabilising effects on our global climate system. One of the more common architectural answers to these challenges is climate-responsive or passive design of buildings where natural ventilation (NV) is substituted for mechanical conditioning to deliver comfortable indoor environments while at the same time minimising the energy demand for heating, ventilation, and air-conditioning (HVAC).

Copyright ©2022 by the authors. This conference paper is published under a CC-BY-4.0 license.

In light of the changing landscape of adaptive thermal comfort research over the last two decades, and the release of the ASHRAE Global Thermal Comfort Database II - into the public domain, a follow-up analysis of the adaptive concept seems timely. The availability of a large volume of new data from diverse climatic and regional contexts provides an opportunity to revisit the original ASHRAE 55 adaptive comfort standard. Typical of that era is the 'neutral' adaptive thermal comfort model developed for detailed and more reliable (evidence-based) thermal comfort studies that would go on to form the ASHRAE RP-884 database, from which the first adaptive thermal comfort standard.

Comfort standards do not give clear guidance to determine the minimum or ideal range of continuous in-situ physical measurements of indoor environment conditions of buildings. Long-term assessment criteria found in ISO 7730 (ergonomics of the thermal environment - Analytical determination and interpretation of thermal comfort using calculation of the predicted mean vote (PMV) and the predicted percentage of dissatisfied (PPD) indices and local thermal comfort criteria), EN 16798 (energy performance of buildings - ventilation for buildings - Part 1: Indoor environmental input parameters for design and assessment of energy performance of buildings addressing indoor air quality, thermal environment, lighting and acoustics) and ASHRAE 55 Standard simply state that the environmental monitoring (EM) period should be representative of the in-vivo experience of longitudinal field studies. Given that most of the existing indices found in current international comfort standards do not correlate well with long-term thermal satisfaction, there is a need to propose new thermal comfort thresholds for benchmarking criteria that better forecast occupants' evaluations of indoor environments.

None of the previous studies in the literature review demonstrated clear impacts of thermal history and expectations on thermal comfort in buildings that are shared by multiple occupants who have grown up in diverse climate conditions. Whilst the general adaptive principle has been repeatedly demonstrated across diverse settings world-wide, region-specific adaptive models are not universally applicable. ASHRAE's Standard 55 adaptive thermal comfort model and the European Union counterpart of EN 15251 were transformative because of their generalisability, the empirical basis of which was vastly more comprehensive than anything preceding the development of 'neutral' adaptive thermal comfort for each region across the world.

1.2 Study Focus

This study will leverage the largest global thermal comfort database to date, and explore the effects of available demographic, contextual factors and their interaction effects on building occupants' thermal sensation in the indoor environment, aiming to contribute to the current understanding of drivers of diversity in human thermal perception. The aim of this study is to reappraise the scope of applicability of the adaptive comfort standard, assess potential regional differences in adaptive comfort responses, and propose nudges to adaptive comfort theory, the adaptive comfort model and standard, and building design and operational conventions.

In the interest of nudging on current understanding of adaptive theory, the existing adaptive comfort model, and the application of adaptive principles to building operational strategies, the objectives of this study are as follows:

- To assess differences in adaptive comfort principles across broad regions of the world;
- To provide an evidence-based methodological workflow to extend the limits of applicability of the adaptive comfort model beyond naturally ventilated buildings as currently specified in ASHRAE Standard 55-2021;
- To develop the potential for nudging building optimisation strategies to incorporate adaptive comfort theory as an energy-reduction strategy.

This study addresses the following research questions: "Is there any relationship between thermal comfort perception and long-term thermal history in environments accommodating occupants with diverse climatic backgrounds?" and "How does the occupant's climatic background (long-term thermal history) influence their in-the-moment thermal comfort assessments inside their condominiums in different climate characteristics worldwide?".

2. Literature Review

This section reviews previous scholars' thermal comfort assessment criteria to provide thorough guidance for the development of "neutral" adaptive thermal comfort thresholds in the South-eastern Mediterranean climate of Cyprus. Scholars have applied and developed different methods of design to measure occupants' thermal sensation in order to identify their PMV, but none of these scholars have clarified the differences between the selection of thermal sensation as either an ordinal or continuous variable type, or they haven't accurately undertaken parametric statistical analysis in the building engineering field.

In the present study, throughout the development stages of the statistical analysis, it was found that the differences between ordinal and continuous variable types of thermal sensation should be addressed. This is supported by the conventional methods of design applied by previous studies on thermal comfort, as listed in **Tab. 1**.

Tab. 1 - Worldwide Studies on Thermal Comfort Assessment.

References	Sample Size	Statistical Method	Thermal Comfort Assessment
Rupp *et al.* (2021) [1]	Data extracted from the ASHRAE Global Thermal Comfort Database II (n = 107,583).	Regression coefficient	Griffiths constant/occupant's thermal sensitivity theorem applied.
Wang *et al.* (2018) [2]	Three different experiments were conducted in the climate chamber by using a discrete scale of 2 votes per subject, a discrete scale of 5 votes per subject, and a continuous scale for thermal sensation and satisfaction with 5 votes per subject.	- Frequency statistics - Normalised standard uncertainty - Descriptive statistics - Box plot distribution - Bar chart distribution	Humphreys and Nicol's (2002) theorem was applied by investigating subject respondents' PMV and PPD.
Haldi and Robinson (2008) [3]	- A dataset of some 5,908 entries from 60 participants was used. - The dataset was built on a comprehensive longitudinal field survey conducted during the warm summer of 2006.	- Histograms were used for the distribution of temperature measurements in the database. - Logistic regression techniques were used. - G-statistics differences were reported by using Nagelkerke's statistical tradition.	Nicol and Humphreys's (2004) theorem was applied to assess occupants' thermal comfort votes.
Haghighat and Donnini (1998) [4]	A total of 877 subjects participated in the questionnaire survey during the summer and winter of 1996.	- Descriptive statistics - Pearson's correlation coefficient - Bar chart diagram distribution	ASHRAE Standard 62-89R and ASHRAE Standard 55-92 were used for the benchmarking criteria.
Brager *et al.* (2004) [5]	A total of 1,000 survey responses were integrated into the dataset.	- Descriptive statistics - Scatter plot diagrams - Bar chart distribution - Linear regression analysis - Histograms	ASHRAE RP-884 and ASHRAE RP-1161 datasets were used for the benchmarking criteria.

Many scholars have debated the identification of accurate statistical analysis criteria for the convention of the initial thermal comfort assessment scale that was developed by Bedford in 1936. This assessment used a 7-point Likert scale and was later applied and proved by Fanger in the 1970s; it has since become the widely used conventional method of design, and was applied, among others, by Griffiths in the 1990s. Its scale was also made popular by Nicol in the 2000s and since then many top-notch scholars in thermal comfort research, such as Brager in 2008, de Dear in 2010 and Parkinson in 2016, have continued developing this reliable thermal comfort assessment criterion based on the conventional methods of design applied and developed by previous scholars.

De Dear in 2010 and Parkinson in 2016, as well as their colleagues in thermal comfort studies, established the ASHRAE Global Thermal Comfort Databases I and II. This open-source international global database allows researchers to identify the appropriate method of thermal comfort assessment criteria for their studies (i.e. using thermal sensation as either an ordinal or continuous variable).

Rupp *et al.* published an article in 2021 entitled "The Impact of Occupants' Thermal Sensitivity on the Adaptive Thermal Comfort Model". In this paper, 107,583 samples were extracted from the ASHRAE Global Thermal Comfort Database II to conduct a regression analysis using a p-value of < 0.001 to determine the significance factor within the variables. Rupp *et al.* (2021) used the [-3, +3] thermal comfort assessment criteria as a continuous variable to run statistical analysis with in-situ measurements (i.e. indoor operative temperature and indoor air temperature) [1].

Wang *et al.* (2018) stress that the use of different measurement criteria in thermal comfort studies has led to misunderstandings when interpreting the findings in accordance with statistical conventions [2]. To avoid any further misunderstanding by the scholars who are not experts in thermal comfort studies, Wang *et al.* (2018) recommend the most appropriate thermal sensation assessment criteria as shown in **Fig. 1**.

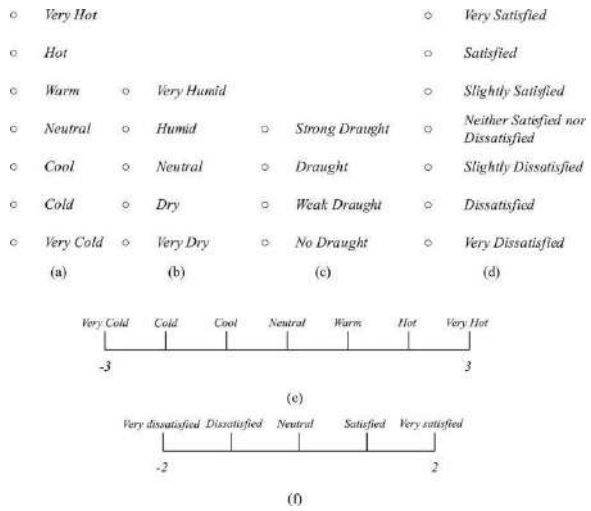

Fig. 1 - Thermal sensation scale on the questionnaire. (a) 7-point discrete thermal sensation scale; (b) 5-point discrete humidity sensation scale; (c) 4-point discrete draught sensation scale; (d) 7-point discrete thermal sensation scale; (e) 7-point continuous thermal sensation scale; (f) 5-point continuous thermal sensation scale. Source: Wang *et al.* (2018)

Wang *et al.* (2018) used a climate chamber to control thermal variables and determine the most appropriate design for their thermal sensation scale. They provide a list of the acceptable variable types to be used when assessing any type of variable related to thermal comfort studies, which is shown in **Tab. 2**.

Tab. 2 - Variables for Thermal Comfort Assessment.

Subjective thermal indicators	Points on rating scale	Subjective rating scale
Thermal sensation	Fig.2 (a)	Discrete
Humidity sensation	Fig.2 (b)	Discrete
Draught sensation	Fig.2 (c)	Discrete
Thermal satisfaction	Fig.2 (d)	Discrete
Thermal sensation	Fig.2 (a)	Discrete
Thermal satisfaction	Fig.2 (d)	Discrete
Thermal sensation	Fig.2 (e)	Continuous
Humidity sensation	Fig.2 (b)	Discrete
Draught sensation	Fig.2 (c)	Discrete
Thermal satisfaction	Fig.2 (f)	Continuous
Source: Adapted from Wang *et al.* (2018)		

Haldi and Robinson (2008) conducted a longitudinal field survey to assess occupants' thermal comfort [3]. They conducted a multiple logistic regression analysis to identify neutral adaptive thermal comfort; the assessment criteria were presented by using the thermal scale band [-3, +3]. Another pilot study was conducted by Haghighat and Donnini (1998) to investigate the psycho-social factors affecting occupants' thermal sensation by using in-situ measurements of indoor air environment conditions [4]. They used descriptive statistics to report the monitored indoor air environment conditions by using the continuous variable type. Haghighat and Donnini also used Pearson's correlation analysis to measure occupants' thermal sensation and the measured/recorded variables for their statistical analysis. In their study, occupants' thermal sensation was coded by using the conventional tradition of [-3, +3] parameters. Additionally, Haghighat and Donnini (1998) presented the questionnaire survey items set out as ordinal variables in bar chart formatting to demonstrate the survey findings according to their research hypothesis.

Brager *et al.* (2004) conducted a longitudinal survey by using a sample size of 105 for the warm season and 93 for the cool season to assess occupants' thermal sensation [5]. By using this method, they were following a similar method of design to that developed by Haghighat and Donnini (1998) to report on-site measurement findings by using the EM dataset as a continuous variable and occupants' thermal sensation votes coded as a continuous variable ranging between -3 and +3 for accuracy in their linear regression analysis.

The present study follows the conventional method of design that was developed and conducted by previous scholars. To identify the neutral adaptive thermal comfort thresholds in the South-eastern Mediterranean climate of Cyprus, it codes thermal sensation as [-3, +3] and conducts a Pearson's correlation analysis. The following section presents the stages of data collection undertaken to assess domestic energy use and occupants' thermal comfort in this longitudinal field study.

3. Materials and Methods

This section presents the research methodology by explaining the rationale of the research hypotheses, aims and objectives. It illustrates the case study and explains the research design model adopted to approach the research problem. It also explains the selection criteria of base-case representative residential tower blocks (RTBs) and presents the data collection methods used, the field work procedures and the data analysis and interpretation. The present study fully explains the mixed methods research design approach through three different sets of methods developed before stating some limitations of the study.

The outdoor air temperature (OAT) and relative humidity (RH) levels of the environmental conditions were monitored between July 28 and September 3, 2018 to assess the overheating risk issues of the flats interviewed and measured in this research context. This monitoring period overlapped with the 2018 heatwave period, during which the Meteorological Office of Cyprus recorded the highest temperatures across Europe since 1976 [6]. The outdoor thermal conditions, including the outdoor air temperature, relative humidity and heat stress index, were monitored by a Wireless Vintage Pro 2 weather station from Davis Instruments. The

monitoring of OAT and RH levels in the case study provides an in-depth understanding of the indoor environment conditions and validates the results from a simulation analysis of the occupied spaces in which the measured rooms reported relatively high indoor temperatures inappropriate for their occupants' thermal comfort [7].

The indoor air temperature (IAT) was recorded using a thermometer (resolution 0.1°C), the globe temperature was recorded using a globe thermometer, which is a 15 cm diameter thin-walled copper sphere painted black (resolution 0.1°C), the relative humidity was recorded using the Heat Stress WBGT Meter model HT200 by Extech Instruments (resolution 0.1°C) and the black globe temperature (TG) was recorded. In order to validate these findings, additional spot measurements were carried out using a forward-looking infrared radiometer (FLIR) infrared thermographic camera to assess the occupants' decisions on thermal comfort preference votes (TPVs) and thermal sensation votes (TSVs) [8].

This section discusses the spaces in which the occupants mostly spent their time at home, the warmest space in summer, and the occupants' thermal comfort experience in the interviewed flats; the significant variables strongly correlate with the occupants' thermal comfort. At the same time, additional comments on several aspects of the measured IAT and RH of the households' living rooms were considered in relation to the questionnaire results. During the questionnaire survey, the households in the interviewed and measured RTBs were selected randomly, based on a door-to-door survey. Correlations among the different parameters were calculated using SPSS version 28, and the significance level of the analysis was set to both $p < 0.01$ and $p < 0.05$. This means that the statistical results were significant at the indicated p-values for the questionnaire variables. First, a descriptive analysis was used on the interview findings to report the occupants' reasons for discomfort, taking into account the building orientation and floor level differences to assess the overheating risk of the interviewed and measured flats. Then, correlation analysis methods were used on the findings to evaluate the correlations between different parameters, and for this, Pearson's rank correlation analysis (two-tailed) was conducted.

4. Analysis and Results

This section focuses on linking all the results from both the general survey and thermal comfort survey findings, on-site environmental monitoring, in-situ measurements, as well as findings from the overheating analysis, to understand the current energy performance of the flats and the thermal comfort of their occupants. The outcome of the EM carried out at the social housing development estate during the summer conditions is presented. The variables measured during the survey are discussed in order to understand the environmental conditions of measured flats for assessing their occupants' thermal comfort level and the risk of overheating experienced in summer. Furthermore, the findings of the accelerators used to measure the air temperature and relative humidity of the occupants' living room spaces are highlighted.

4.1 Questionnaire Survey Findings

Questionnaires were administered to the occupants of the measured flats. Out of 200 questionnaires distributed to the households in the 36 RTBs across the social housing development, 100 of them were successfully completed. A breakdown of the completed questionnaires shows that 36% of them were returned from south-facing blocks, 33% from northeast-facing blocks, 18% from southwest-facing blocks, 11% from southeast-facing blocks, and 4% from northwest-facing blocks. Of the households, 18% were recruited from ground floor flats, 28% were from the first floor, 19% were from the second floor, 3% were from the third floor, 23% were from the fourth floor, and 9% were from fifth-floor flats. Of the completed questionnaires, 33% male and 67% female responses were received. An analysis of age distribution votes across the interviewed households suggests that 48% of the respondents were between 55 and 65 and 65 or over, as shown in **Fig. 2** a, b and c, respectively.

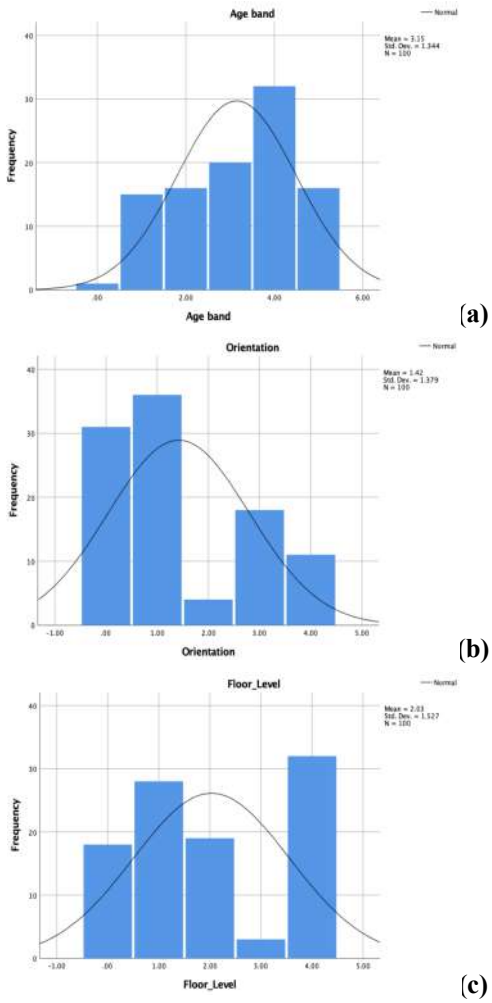

Fig. 2 - (a) frequency distribution of the households' age

groups; (b) frequency distribution of the households' age band, taking into consideration the RTBs' orientation; (c) frequency distribution of the households' age band, taking into consideration the flats' floor level differences; the households' age band scale runs from 0 "20–25" to 5 "65 or over;" the recruited households from different orientations with the age band scale runs from 0 "northeast" to 4 "southeast;" the recruited households from the floor level differences with the age band scale runs from 0 "ground" to 4 "fourth". **Tab. 3** highlights the frequency and percentage of age distribution from the questionnaires from the households.

Tab. 3 - Age distribution of the thermal comfort survey questionnaires returned from the RTBs.

	Age frequency distribution					
Orientation	**20-25**	**25-35**	**35-45**	**45-55**	**55-65**	**65 or over**
Northeast	1	8	4	4	9	5
South	0	6	8	9	6	7
Northwest	0	0	0	0	3	1
Southwest	0	0	2	4	10	2
Southeast	0	1	2	3	4	1
Total	1	15	16	20	32	16
Floor level	**20-25**	**25-35**	**35-45**	**45-55**	**55-65**	**65 or over**
Ground	0	1	2	2	10	3
First	1	2	3	7	9	6
Second	0	4	5	3	3	4
Third	0	1	1	0	0	1
Fourth	0	7	5	8	10	2
Total	1	15	16	20	32	16

The distribution of occupancy type and responses indicate 84% ownership status and 16% private tenancy status. These response rates according to the different tenure types indicate that ownership status may influence the occupants' perceptions of the thermal environment. The occupancy duration of the residents in the interviewed flats indicates that 14% of the households have been living in their flats between 2 and 5 years while the majority of the residents in the development have been living there for more than 10 years as of the time of the survey. The responses also indicate that the southwest-facing block, number 21, which was built in phase two in the 1990s, has the highest density of occupants per household in the RTBs. This may be a result of the location of the block and the tenancy status available in the interviewed flats as most of the residents in number 21 were either private housing owners or private renters.

This section presents the second phase of the questionnaire in line with the interpretation of the general survey findings that emerged from the first phase of the study. The main survey results are discussed, focusing on the topics presented in **Tab. 4**. From the survey findings, the mean average age of the households was 51.37 years old; the oldest surveyed household member was 84 years old and the youngest was 23 years old. In addition, the number of rooms examined in the residences ranged between 2 and 5 rooms; most of the households participating in the survey had 5 rooms, which they mostly occupied on weekdays and at weekends. In the 20 blocks examined, there were five-storey buildings and 15 four-storey buildings; 32 flats were located on the ground floor, 32 flats were on the fourth floor (top floor flats), and 40 flats were on the fifth floor (top floor flats). Finally, a noteworthy result emerging from the survey is that most of the flats do not have any form of insulation.

In this survey, the households' types of heating and cooling systems were examined. Most of the households were using combinations of heating and cooling systems to achieve better thermal conditions in their properties [9]. Furthermore, they preferred to use each available system based on their needs to improve their thermal comfort and achieve maximum energy savings. Therefore, it was found that there were a lot of adaptive solutions developed by the elderly households in their properties to withstand the cold winters and extremely hot summers in these inefficiently built RTBs in this particular Mediterranean climate.

In the general survey findings, it emerged that in the heating season, most of the households used heating systems that were gas cylinder domestic appliances (frequency = 32), wall-mounted air-conditioning systems (frequency = 7) and wood-burning stoves (frequency = 5). From these results, it can be seen that gas cylinder heaters proved to be the most commonly used energy to supplement the main heating system in most of the flats; these are used because they are a high-temperature and affordable heat source, but they are not fuel-efficient or low-carbon heating systems. In addition, wood-burning stoves as well as wood and oil biomass heating with other systems (wall-mounted air-conditioning systems, wood burners, oil-fired heaters etc.) were used in all but 21% of the households, where portable electrical heaters were the main heating system.

In the cooling season, the most commonly used cooling systems were portable fans (frequency = 28) and wall-mounted air-conditioning systems (frequency = 18); in two of the flats examined, there were no cooling systems used, either due to economic reasons or because the occupants stated that they did not need them (e.g. they spent more time sitting on the balcony or on an outdoor patio in the ground floor flats). It is worth noting that these social housing blocks are located in a densely built city centre, indicating the possibility of a different thermal experience in the cooling season for the elderly people and the homes with young children present. In addition, 39% of the households preferred to use both wall-mounted air-conditioning systems and portable fans for cooling purposes while in the rest of the homes, air conditioning with or without fans was used.

4.2 Relationships for the Identification of Thermal Comfort

Cross tabulations using chi-square analysis explored the reasons for thermal discomfort in respect to the household age, the orientation of the RTBs and the different floor levels in each occupied space based on the collected data from the respondents. This analysis was conducted because socio-demographic characteristics have been shown to be a significant factor in people's behaviour in any setting. Considering the age band in this cross tabulation analysis was necessary because nearly half (48%) of the households were in the 55–65 and 65-years-of-age and older age groups, it is important to consider the impact of age on thermal comfort in these measured flats.

In conjunction with households' socio-demographic analysis, the different RTB orientations and floor levels were taken into consideration. The results of interviews highlight that 24% of the occupants complained about high humidity in the southwest-facing RTBs in summer, and 17% complained about incoming sun. This indicated that the occupants may have experienced thermally uncomfortable conditions due to the high outdoor-air temperatures and humid conditions in this south-eastern Mediterranean climate. This became clear when the study determined that there were negative relationships between the occupants' reasons for thermal discomfort and the different floor levels for their respective flats, as shown in **Tab. 4**.

Tab. 4 - Relationships between reasons for thermal discomfort and household age band, RTB orientation, and floor level.

Research Question and Variables	Measure	Discomfort	Age Band	Orientation	Floor Level
Q 35: How would you best describe the source of this discomfort?	Cramer's V	1	0,203	0,405**	0,233
	Significance	—	0,416	<0,001	0,062
Age Band	Cramer's V	0,203	1	0,229	0,211
	Significance	0,416	—	0,202	0,347
Orientation	Cramer's V	0,405**	0,229	1	0,197
	Significance	<0,001	0,202	—	0,234
Floor Level	Cramer's V	0,233	0,211	0,197	1
	Significance	0,062	0,347	0,234	—

Household age band scale ran from 0 (20–25) to 5 (65 and over)
RTB orientation: 0 (north-east), 1 (south), 2 (north-west), 3 (south-west), and 4 (south-east)
Different floor levels: 0 (ground), 1 (first), 2 (second), 3 (third), 4 (fourth) and 5 (fifth)
Age band scale ran from 0 (20–25) to 5 (65 and over)
Reasons for thermal discomfort – Floor level, χ^2 (9) = 16,26, p = 0,062, Cramer's V = 0,233
Reasons for thermal discomfort – Orientation, χ^2 (9) = 49,33, p = 0,000, Cramer's V = 0,405
Reasons for thermal discomfort – Age bands, χ^2 (12) = 12,38, p = 0,416, Cramer's V = 0,203
Age bands – Floor level, χ^2 (12) = 13,31, p = 0,347, Cramer's V = 0,211
Age bands – Orientation, χ^2 (12) = 15,77, p = 0,202, Cramer's V = 0,229
Orientation – Floor level, χ^2(9) = 11,65, p = 0,234, Cramer's V = 0,197

As shown in **Tab. 4**, the results indicate a moderate-strong relationship between orientation and reasons for thermal discomfort (χ^2 = 49,327, p < 0,001, Cramer's V = 0,405). A greater proportion of participants living in south-facing RTBs felt thermal discomfort due to humidity than participants living in the southwest. A greater proportion of participants living in the southwest selected incoming sun as thermal discomfort than participants living in the other areas; this was due to the poor window design in the RTBs, which prevented NV into the indoor occupied spaces. This

led to a difference of 2–3°C between the ground and upper floor level flats due to a lack of NV and as a result the upper floor receives the intense horizontal radiation on the roof surfaces. Thus, it appeared that the occupants' habitual adaptive behaviour in window-opening patterns also played a crucial role in their TSV decisions. Nevertheless, reasons for thermal discomfort were not significantly related to age and floor levels. From the field survey results, it was found that the occupants were very dissatisfied with their thermal environment in summer, with the highest levels of dissatisfaction in the south- and southwest-facing RTBs. The mean distribution of votes suggests that occupants were dissatisfied with their thermal environment in the winter, at more than two-thirds (34%) of participants, indicating a slightly uncomfortable indoor environment in their flats. However, the highest level of dissatisfaction during winter was observed in the northeast-facing RTBs, particularly on the first and top floor flats, and there was a positive strong correlation found between occupancy hours and TSVs in the winter ($r = 0.540$, $p < 0.01$). Comparing overall thermal comfort in the winter and taking into consideration the RTBs' orientation differences, there was no significant correlation found, but a negative moderate correlation was found with floor level differences in summer ($r = -0.244$, $p < 0.05$) as occupants in the ground floor flats were slightly more comfortable in the indoor occupied spaces in summer than the occupants living in the top floor flats. It is noteworthy to mention that building occupants are likely to spend most of their time in the spaces that provide the best environmental living conditions [6]. From the survey results, 62% of the respondents indicated that they mostly spent their time in the living room while 69% of the respondents reported the bedroom as the warmest space across the interviewed and measured flats, with the highest number of responses coming from the south-facing RTBs, at 26%. A comparison of the findings from the surveys suggests higher thermal satisfaction of the occupants in the south-facing RTBs than the households who lived in the upper floor flats despite the higher temperatures observed in the southwest-facing RTBs. In addition, it is concluded that overheating occurs in these flats, and the occupants were thermally dissatisfied due to the higher indoor air temperatures observed in the RTBs in summer. Overall, the respondents indicated a preference to be much cooler in summer when the outdoor air temperatures increase.

5. Conclusions

The output of this work can contribute to identifying the thermally comfortable and energy efficient environmental criteria for the development of evidence-based passive cooling design strategies by selecting archetype housing stock as base-case scenario development. Furthermore, information on the thermal comfort requirements of different climatic background groups can help to suggest appropriate environmental and design solutions, which can offer a comfortable and satisfactory thermal environment. To test the research hypothesis that greater adaptive opportunities in buildings is associated with a wider range of indoor temperature (i.e. wider comfort zone), statistical analysis would be applied to the development of an adaptive model defining the comfort zone of each climatic region across the world. The results support the development of the long-term thermal history for the adaptation of human's physiological body adaptation.

6. Acknowledgement

The authors would like to acknowledge the Graduate School, School of Architecture, Computing & Engineering (ACE), London, United Kingdom.

Data Access Statement: The datasets generated during and/or analysed during the current study are publicly available at - https://repository.uel.ac.uk/item/89zv1

7. References

[1] Rupp, R. F., Parkinson, T., Kim, J., Toftum, J., & de Dear, R. (2021). The impact of occupant's thermal sensitivity on adaptive thermal comfort model. *Building and Environment*. https://doi.org/10.1016/j.buildenv.2021.108517

[2] Wang, Z., de Dear, R., Luo, M., Lin, B., He, Y., Ghahramani, A., & Zhu, Y. (2018). Individual difference in thermal comfort: A literature review. Building and Environment. Elsevier Ltd. https://doi.org/10.1016/j.buildenv.2018.04.040

[3] Haldi, F., & Robinson, D. (2008). On the behaviour and adaptation of office occupants. *Building and Environment*, *43*(12), 2163–2177. https://doi.org/10.1016/j.buildenv.2008.01.003

[4] Haghighat, F., & Donnini, G. (1999). Impact of psycho-social factors on perception of the indoor air environment studies in 12 office buildings. *Building and Environment*, *34*(4), 479–503. https://doi.org/10.1016/S0360-1323(98)00034-1

[5] Brager, G., Paliaga, G., & De Dear, R. (2004). UC Berkeley Envelope Systems Title Operable windows, personal control and occupant comfort. Permalink https://escholarship.org/uc/item/4x57v1pf Publication Date. Retrieved from www.ashrae.org

[6] Constantinidou, K., Zittis, G., & Hadjinicolaou, P. (2019). Variations in the simulation of climate change impact indices due to different land surface schemes over the Mediterranean, Middle East and Northern Africa. Atmosphere, 10(1).

[7] Földváry Ličina, V., Cheung, T., Zhang, H., de Dear, R., Parkinson, T., Arens, E., … Zhou, X. (2018). Development of the ASHRAE Global Thermal Comfort Database II. Building and Environment, 142, 502–512. https://doi.org/10.1016/j.buildenv.2018.06.022

[8] De Dear, R., Xiong, J., Kim, J., & Cao, B. (2020). A review of adaptive thermal comfort research since 1998. Energy and Buildings. Elsevier Ltd. https://doi.org/10.1016/j.enbuild.2020.109893

[9] Indraganti, M., & Rao, K. D. (2010). Effect of age, gender, economic group and tenure on thermal comfort: A field study in residential buildings in hot and dry climate with seasonal variations. Energy and Buildings, 42(3), 273–281. https://doi.org/10.1016/j.enbuild.2009.09.003

The conceptualization of exhalation in buildings

Sara Dorregaray-Oyaregui [a], Arturo Ariño [b], Leonardo Andrade De Brito [d], Amaia Zuazua-Ros [a], Juan Carlos Ramos [c], Robiel Manzueta [a], Bruno Sánchez Sáiz-Ezquerra[a], César Martín-Gómez [a]

[a] Universidad de Navarra, Department of Construction, Building Services and Structures, Campus Universitario, 31009, Pamplona, Spain.

[b] Universidad de Navarra, Department of Environmental Biology, Campus Universitario, 31009, Pamplona, Spain.

[c] Universidad de Navarra, TECNUN School of Engineering, Department of Mechanical Engineering and Materials, Thermal and Fluids Engineering Division, Paseo de Manuel Lardizábal 13, 20018 San Sebastián, Spain.

[d] Department of Rural Engineering. Federal University of Santa Catarina. Florianopolis-SC, 88034-000, Brazil.

Abstract. Among the sources of urban air pollution, the gases and airborne particles coming out from residential buildings through normal ventilation outlets are often neglected or poorly understood. Yet, it carries the potential to deeply affect urban air quality, given the universal ubiquity and function of dwellings. The climate emergency declaration approved by the European Parliament on November 28th, 2019, calls for urgent science-based action to curtail it. Our research explores the concept of building exhalation, through research aimed at characterizing and quantifying pollutants leaving residential buildings through their ventilation systems, and how such exhalation impacts urban air quality both outside and, through recapture, inside dwellings. We have set an intensive monitoring system in residential buildings in Pamplona (Spain) to obtain hard data about selected pollutants and their exhalation from buildings, thereby helping define the complete impact of buildings as inhabited units in cities. The verification of this main statement lays on the resolution of several future research questions, which are stated in order to set the boundaries and define the path of this text, developing the concept of exhalation of buildings and the factors involved. To confirm the validity of this hypothesis, an experimental campaign is being carrying out in the city of Pamplona (Spain), which has the goal of quantifying the pollutants exhaled by residential buildings through the ventilation systems. This project is included in the global concern about the unknown pollutants sources and the need of defining the complete impact of buildings as inhabited units in cities.

Keywords. pollutant emissions; ventilation systems; residential buildings; I/OAQ.
DOI: https://doi.org/10.34641/clima.2022.424

1. Introduction

For more than one-third of humankind, breathing in their homes can eventually lead to disease and even death from chronic exposure to contaminants such as toxic gases and particles (1). Ventilation is a way to reduce the concentration of such pollutants in dwellings, but it is evident that (i) indoor air may be fouled by external contaminant sources through ventilation exchange; that (ii) the same used, polluted indoor air that sickens people will thus be ultimately expelled to the environment, that is, the city for urban buildings, and that (iii) once outside, some of this polluted air may re-enter the building if dissipation does not act fast or long enough, cycling back to (i). How much is thus the outdoor air pollution generated by a building? What are the pollutants that are exhaled by the buildings? Can we develop the concept of 'exhalation of buildings'? Our research project aims at contributing to solve these questions.

The results should allow the establishment of strategies to e.g. minimize the emission of such pollutants into the atmosphere by mimicking the action of vehicle catalyzers in fossil fuel engines, or recapture useful components such as residual methane (CH_4), which will also be measured in this project.

1.1 Proposal motivation in the scientific and technical context

Numerous studies have been carried out in relation to the air quality from different perspectives and in different environments, but most often air quality has been contextualized in terms of its impact in public health.

Copyright ©2022 by the authors. This conference paper is published under a CC-BY-4.0 license.

According to the World Health Organization (WHO), air pollution may be the greatest environmental risk to health in the (3). A recent study (2019) developed by the Forum of International Respiratory Societies' Environmental Committee suggests that air pollution affects many organs beyond the lungs (1) and "although air pollution affects people of all regions, ages, and social groups, it is likely to cause greater illness in those with heavy exposure and greater susceptibility". A similar conclusion is achieved in (4), where the interpretation of the results states that "ambient air pollution contributed substantially to the global burden of disease in 2015, which increased over the past 25 years, due to population ageing, changes in non-communicable disease rates, and increasing air pollution in low-income and middle-income countries." Thus, it becomes a transversal matter affecting the whole society, emphasizing inequalities.

The relation between the outdoor and indoor air has also been subject of several studies. Even though indoor air is certainly affected by indoor sources, outdoor air has been proven a major contributor to indoor levels of pollutants, through building infiltration and mechanical ventilation systems (5).

The effect of outdoor pollution on indoor air quality appears to have worsened over the years. One of the factors that might cause this decrease in air quality is the construction of buildings designed to be more airtight. These solutions can cause a reduced regeneration of the indoor atmosphere, in order to improve energy efficiency (6). This type of construction might also contribute to unpredicted inequality, since it has been recently found that families with a higher socioeconomic status are at greater risk of being exposed to chemical contaminants such pesticides. On the contrary families with a lower socioeconomic status are at risk of being exposed to other type of contaminants, such as lead (7).

The air quality in indoor environments is a risk for the human health as human beings spend between 80 and 90% of their time indoors (8), where they are exposed to different types of chemical pollutants, which in low concentrations can cause headache, dizziness, fatigue, nausea, and in the long-term produce harmful effects on health.

In indoor spaces, the sources of pollutants are diverse, with emissions coming from construction materials, decoration, tobacco smoke, cleaning products, and external or internal activities. On the other hand, inadequate ventilation favors the increase in pollutant levels, which depend on the emitting source and the dilution caused by the ventilation (9). These air contaminants of indoor air have prompted numerous epidemiological researches related to building uses and typologies, such as those involving the schools and children contaminants exposure and health (10) and other studies state the health impact due to air quality (indoor/outdoor), especially respiratory diseases.

1.2 Hypothesis and research questions

Based on the context outlined above, the following hypothesis is proposed: The exhaled air from buildings contains pollutants that become another source of contamination, affecting the global air quality of cities.

The verification of this main statement lays on the resolution of several future research questions, which are stated in order to set the boundaries and define the path of the research area, being each research question related to a general objective:

1. What do we mean by 'exhalation of buildings', and what are the factors involved?

2. How does the residential buildings polluted air extracted comply the Spanish Regulation CTE HS?

3. Is it possible to mitigate, minimize, or eliminate the amount and variety of environmental pollutants exhaled by buildings to the urban environment? How can it be achieved?

From these starting points, the following sections of this document inform about the potentials of this project proposal as an effective and efficient study in terms of the use of human resources and of existing material resources.

2. Exhalation of buildings

2.1. Ventilation systems

As the energy performance of the building improves as a result of the regulations that require buildings to be more airtight, it has an inevitable impact on indoor air quality (11).

Two recently built residential buildings have been selected to measure the air exhalation given two main reasons. On the one hand, the lower air exchanges per hour and the smaller and more airtight spaces in residential buildings, as compared to other building typologies such as offices, commercial buildings or schools, might cause higher pollutant concentration indoors that must eventually be released, making them priority. On the other hand, given the sizable residential building stock, to start these measurements in residential typology is considered primary.

As it will be shown, four identified, localized air exhalation sources come in handy to lay out the pollutant measurement strategies: dwelling ventilation, kitchen exhaust ducts, garage ventilation and drain-waste-ventilation. The project is designed around the classification of ventilation according the Spanish regulations. Specifically, the reference is made to the following sections of the

Spanish Regulation CTE: CTE DB HS: Healthiness; HS3 Indoor Air Quality; HS 5 Water Evacuation (12).

-Dwelling ventilation: The increasing airtightness of our home's places new demands on residential ventilation, such as ensuring occupants a good indoor ambient at low energy consumption, which combined with the expected adequate ventilation, presents a challenge in the market (13). The CTE-HS3 stipulates that, buildings will have means to adequately ventilate their indoor spaces, eliminating the pollutants that occur regularly during normal use, meaning that an enough outdoor air flow of can be provided and their extraction and expulsion can be guaranteed. The dwelling ventilation is the mechanical ventilation that ensures a certain air changes per unit time within the dwelling apartments. The current regulation for residential buildings in Spain specifies the requirement for air changes in indoor spaces. Two types of ventilation systems can provide the necessary changes per hour. (1) Single-flow controlled mechanical ventilation: In these systems air is introduced passively throughout the apartment, e.g. through micro-ventilation slits in windows and infiltration while it is extracted mechanically to the roof through the wet rooms (kitchen and bathrooms). (2) Dual-flow controlled mechanical ventilation: These systems both introduce and extract the air mechanically, usually from the facades, through a heat recovery unit.

-Kitchen exhaust ducts: This ventilation is independent from the house ventilation. The regulation states that in the cooking area of kitchens the installation of a system that allows the extraction of fumes produced when cooking is mandatory.

-Garage ventilation system: While the ventilation of the garage could be either natural or mechanical, we are considering only the more common mechanical system given that natural ventilation requires openings in opposed facades. The extraction of the garage exhaust air is made through the rooftop and the regulations require both minimum ventilation rates and a carbon monoxide detection system to activate the fans when attaining a threshold concentration.

-Drain-waste-ventilation system: This ventilation system ensures the air a proper removal of blackwater allowing air entering the plumbing system. According to the Spanish regulations, the buildings must have ventilation subsystems depending on the height, all of them extended up to the roof. Special attention will be paid to the presence of methane in these systems.

Residential buildings complying with current regulations will be selected for the experimental study. They tend to be more airtight and better insulated in order to meet the passive house standards and energy requirements. It is initially proposed to focus the study on the Soto de Lezkairu neighborhood in Pamplona **Fig.1**. It is a newly created neighborhood with a high density ratio (approximately 70 dwellings per hectare).

Fig. 1 – Image of some residential buildings already constructed of the neighborhood of Soto de Lezkairu in Pamplona, Spain (sept. 2018).

2.2. Pollutants

In an indoor space, there is a wide variety of pollutants: carbon dioxide, carbon monoxide, nitrogen oxides, sulfide oxide, ozone, volatile organic compounds, particles… and so on.

They come from various sources: materials used to the construction, improper or excessive use of cleaning and hygiene products, combustion gases, standing water and the environment itself, where outside pollutants come in through the air renewal system or by infiltration. Given the wide variety of contaminants, the following factors have been use to select those to be evaluated.

Those factors are: 1. Impact on health. Pollutants that have the greatest known effects on human health. 2. Impact on the environment. Pollutants likely significant for environmental change, e,g. methane. 3. Preponderance of use. Contaminants linked to building materials, cleaning products and accessories, associated with the characteristics of the building, the environment and human activities.

3. Description of the analyzed buildings

The two buildings selected in Soto de Lezkairu are named as AC building and AB building. Both were designed with the current Spanish regulation. Their high-rise typology aids to have a higher concentration of analyzable houses.

The dwelling area, at the roof, follows a replicable structure that provides an easy working and mobility for systematic measuring.

3.1 Building AB

AB building, located at Adela Bazo street, is an 8-storey building. It contains 36 flats with an average

area of approximately 75 m^2, distributed in a lineal typology around two vertical communication systems. The main typology is a two-bedroom apartment with a kitchen, living room and two bathrooms. Ducts are located in two different areas of the house. One for kitchen ducts, and the other for bathroom and fecal (see **Fig.2**).

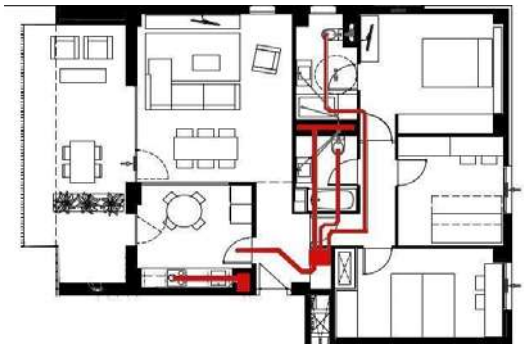

Fig. 2 – Image of AB house typology. Ventilation system in red.

3.2 Building AC

AC building, located at Calle Cataluña 16 is a nine-floor building with two garage floors. Each level has four flats, connected through a vertical communication system. Each flat has three bedrooms, a living room, two bathrooms and a kitchen The average floor area is around 80 m (see **Fig.3**). Ducts are located in one shaft per vertical aggrupation of houses. So in the roof will be found four ventilation shaft terminals. The particularity is that on the ground floor there is a commercial area, that modifies the floor connection making independent the tower and the underfloor levels. Garage ventilation goes independently and exhales at the roof of the commercial area.

Fig. 3 – Image of AC house typology. Ventilation system in red.

4. Methodology

It is essential to take into account the plans, the typology and the structure of the building, since twelve independent tubes needs to be located.

The measured gases are: methane ($CH_4$4), carbon monoxide (CO), carbon dioxide (CO_2), water (H_2O) and volatile organic compounds (TVOC), each of them has different properties and will be affected independently by the surrounding atmosphere given natural phenomena. The initial data analysis served to ensure the reliability of the data acquired and to determinate the measuring points. Besides, it is essential to register or collect the information about the atmospheric conditions during the measurements (wind, temperature, rain…) and to be aware of the surrounding activities and traffic. These factors are the main variables that need be evaluate and take into account during the measurements interpretation.

The measurements have been done with a Gasera One combined with a Multipoint and a Dekati® eFilter™. Gasera One is a "photoacoustic multi-gas analyzer platform that can be configured to a wide variety of research and industrial applications. The performance is based on a photoacoustic infrared spectroscopy engine with a patented ultra-sensitive cantilever pressure sensor." The Dekati® eFilter™ is a unique instrument that combines a standard gravimetric filter holder and sensitive real-time PM detection in one compact instrument.

Actual shafts aren´t prepared to be monitored nether manually nether technologically. The identification of each type of duct is done by plans and by knowledge of installations function. Dwelling ventilation normally plastic ducts with no mechanical needs, can be circular or square. Kitchen exhaust ducts, circular metallic or high resistant to fire plastic with double butterfly valves. Drain-waste ventilation circular plastic ducts characterized of the smell.

Fig. 4. – Taking measurements in AB Building.

Fig. 5. – Taking measurements in AC Building.

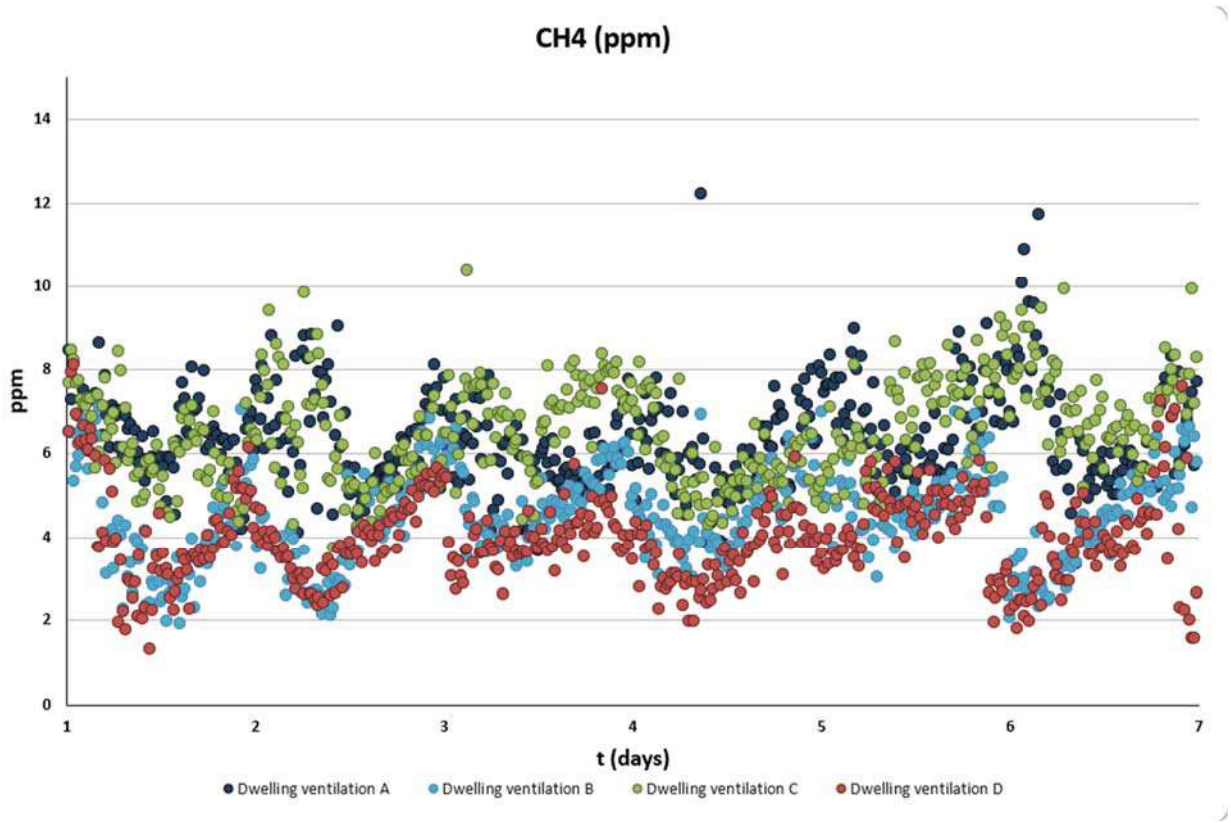

Fig. 6 – Image of methane fluctuation during a week.

After all measurable elements are identified. Cables will be located and properly introduced at ducts, (**Fig. 4, Fig. 5**) they will be fixed with temporal elements, searching a secure measure sample of each element. The sampling is collected during one minute and half at periods of twelve minutes.

5. Preliminary results and conclusions

The information that has been received from the measuring equipment needs to be meticulously analyzed to discard the spurious measurements. The amount of data registered is relevant, thus, the work needs to be slow and justified. The process supposes a comprehension of the environment and the conditions under which the measurements were carried out.

The measured pollutants are methane (CH_4), carbon monoxide (CO), carbon dioxide (CO_2), water (H_2O) and volatile organic compounds (TVOC). During one month at each building. The image below is a graphical representation of measured fluctuation of methane gas during one week at AC building such as an example of the results, (see **Fig. 6**)

As can be seen in **Fig. 6**, the values and the variation of the methane in dwelling ventilation is similar for the 4 apartments of Building AC. The highest values are obtained during the three first days of the week and with low fluctuations. After Thursdays, the fluctuation is higher with peak values on the middle hours of the day**.**

This paper has presented the theoretical parameters that define the concept of building exhalation, the methodology for the data monitoring and an example of the preliminary results obtained.

In any case, this research continues to record and analyze data within the project in which it is enrolled and which is scheduled to end in 2024. So, the results are still being analyzed and interpreted. Searching variables that could affect in the future and comparing with other measures.

6. Acknowledgement

Ministerio de Ciencia, Innovación y Universidades. Proyectos de I+D+i Retos Investigación. n. PID2019-104083RB-I00 "Cuantificación de parámetros contaminantes de la exhalación de los edificios en entornos urbanos EXHAL Quantifying pollutants originated by the exhalation of buildings in urban environments".

Federal University of Santa Catarina for financial support during the postdoctoral fellowship of Dr. Leonardo de Brito Andrade at Escuela Técnica Superior de Arquitectura of Universidad de Navarra.

Ayudas para la Formación de Profesorado Universitario (FPU2020) of Ministerio de Universidades (Spain) received by Robiel Manzueta.

The datasets generated during and/or analysed during the current study are not available because it is on process of study but the authors will make every reasonable effort to publish them in near future.

7. References

1. Schraufnagel DE, Balmes JR, Cowl CT, de Matteis S, Jung S-H, Mortimer K, et al. Air Pollution and Noncommunicable Diseases. Chest [Internet]. 2019 Feb;155(2):409–16. Available from: https://linkinghub.elsevier.com/retrieve/pii/S0012369218327235

2. WHO. WHO guidelines for indoor air quality: selected pollutants. World Health Organization. 2010. 484.

3. WHO. World health statistics 2016: monitoring health for the SDGs, sustainable development goals. World Health Oraganization (WHO). Switzerland; 2016.

4. Cohen AJ, Brauer M, Burnett R, Anderson HR, Frostad J, Estep K, et al. Estimates and 25-year trends of the global burden of disease attributable to ambient air pollution: an analysis of data from the Global Burden of Diseases Study 2015. The Lancet [Internet]. 2017;389(10082):1907–18. Available from: http://dx.doi.org/10.1016/S0140-6736(17)30505-6

5. Hänninen O, Goodman P. Outdoor Air as a Source of Indoor Pollution. In: Issues in Environmental Science and Technology [Internet]. Royal Society of Chemistry; 2019 [cited 2021 Jun 7]. p. 35–65. Available from: http://ebook.rsc.org/?DOI=10.1039/9781788016179-00035

6. Gil Hormazábal L, Adonis M. Calidad de aire de interiores: contaminantes y sus efectos en la salud humana. Revista Panamericana de Salud Pública. 1998;4(6).

7. Montazeri P, Thomsen C, Casas M, de Bont J, Haug LS, Maitre L, et al. Socioeconomic position and exposure to multiple environmental chemical contaminants in six European mother-child cohorts. International Journal of Hygiene and Environmental Health [Internet]. 2019;222(5):864–72. Available from: https://doi.org/10.1016/j.ijheh.2019.04.002

8. Klepeis NE, Nelson WC, Ott WR, Robinson JP, Tsang AM, Switzer P, et al. The National Human Activity Pattern Survey (NHAPS): A resource for assessing exposure to environmental pollutants. Journal of Exposure Analysis and Environmental Epidemiology. 2001;11(3):231–52.

9. Gallego E, Roca FJ, Perales JF, Guardino X. Experimental evaluation of VOC removal efficiency of a coconut shell activated carbon filter for indoor air quality enhancement. Building and Environment. 2013 Sep 1;67:14–25.

10. Annesi-Maesano I, Baiz N, Banerjee S, Rudnai P, Rive S. Indoor air quality and sources in schools and related health effects. Journal of Toxicology and Environmental Health - Part B: Critical Reviews [Internet]. 2013 Nov 17 [cited 2021 May 25];16(8):491–550. Available from: https://www.tandfonline.com/action/journalInformation?journalCode=uteb20

11. Seppänen OA, Fisk WJ, Mendell MJ. Association of Ventilation Rates and CO2 Concentrations with Health andOther Responses in Commercial and Institutional Buildings. Indoor Air [Internet]. 1999 Dec;9(4):226–52. Available from: https://doi.org/10.1111/j.1600-0668.1999.00003.x

12. Of SM of H. CTE - Spanish Building Technical Code [Internet]. 2007. Available from: https://www.codigotecnico.org/DocumentosCTE/DocumentosCTE.html

13. Händel C. Residential Ventilation – Needs, Trends and Expectations. REHVA Journal [Internet]. 2017 [cited 2020 Oct 5];6:11–7. Available from: https://www.rehva.eu/rehva-journal/chapter/residential-ventilation-needs-trends-and-expectations

Patterns and Profiles for understanding the indoor environment and its occupants

Philomena Bluyssen[a]

[a] Chair Indoor Environment, Faculty of Architecture and the Built Environment, Delft University of Technology, Delft, the Netherlands, p.m.bluyssen@tudelft.nl.

Abstract. Research has shown that, even though the indoor environmental conditions seem to comply with current guidelines and those conditions seem 'comfortable' enough, staying indoors is not good for our health. Reasons for this discrepancy might be the fact that these guidelines are based on single-dose response relationships to prevent negative effects, and that the criteria are determined for an average adult person. A more complex model that accounts for all stressors, both positive and negative, interactions, and preferences and needs of the individual for different scenarios and situations was introduced. To validate this 'new' model, several field studies have been executed to determine patterns of stressors and profiles of people for different scenarios (office workers and their workplace; students and their homes; primary children and their classrooms; employees of outpatient areas in hospitals). The outcome shows that it is possible to determine patterns of stressors for different scenario's based on multivariate regression analysis of a survey of the occupants and the buildings they are occupying. Moreover, people differ in their preferences and needs, and it seems possible to distribute them into clusters based on TwoSteps cluster analysis of preferences and needs acquired through a questionnaire. It is concluded that all possible stressors, negative or positive, are important to consider when studying a certain disease or disorder; and that both profiles of IEQ-clusters and profiles of psychosocial clusters are important parts of this 'complex' model. Next steps should focus on interactions at human and environmental level, and how to account for those in the 'New' model.

Keywords. indoor environmental quality, preferences and needs, profiles, patterns of stressors.
DOI: https://doi.org/10.34641/clima.2022.417

1. Introduction

Although most people are aware of the importance of the outdoor environment, especially in relation to climate change issues but also related more directly to our health, the effects of indoor environment quality are not that common knowledge. There are many diseases and disorders related to staying indoors, such as mental illnesses, obesity, cardio-vascular and chronic respiratory diseases (for example asthma with children and COPD with adults), cancer [1-4], and more recent COVID-19 [5].

Relationships between indoor building conditions and wellbeing of occupants of different buildings are complex (e.g. homes: [1]; offices: [6]; schools: [7]]. 'Bad' indoor building conditions have been associated with discomfort (annoyance), building-related symptoms (e.g. headaches, nose, eyes, and skin problems, fatigue etc.), building-related illnesses (e.g. legionnaires disease), productivity loss and decrease in learning ability [8)] Indoor environmental stressors can cause their effects additively or through complex interactions: thermal factors (e.g. draught, temperature), lighting aspects (e.g. reflection, view, luminance ratios), air quality (e.g. odours, mould, chemical compounds, particulates) and acoustical aspects (e.g. noise and vibration) [9-10]. From these findings, it seems that staying indoors is not good for our health. Even when the conditions seem to comply with the current guidelines for thermal, lighting, acoustical and air quality, people feel uncomfortable and get sick [11]. Those guidelines, such as maximum concentrations of certain pollutants, ventilation rate, and temperature ranges, are meant to prevent diseases and disorders rather than focusing on positive effects; and these guidelines and standards are mainly based on single-dose response relationships [11-12]. IEQ assessment is based on effect modelling of dose or indoor environment related indicators: for each parameter or indicator its effect is determined separately. This tends to work well for health threatening exposures for which a clear dose-response relationship has been determined. However, complexity, number of indoor environmental parameters and lack of knowledge, make a total performance assessment using only

Copyright ©2022 by the authors. This conference paper is published under a CC-BY-4.0 license.

threshold levels for single environmental-related parameters difficult. It is clear, that we are in need of a more complex model to determine IEQ. A model that accounts for different scenarios (such as homes, offices, schools), possible problems, interactions, people and effects [8]. A model that focuses on situations rather than single-dose response relationships. A model that uses all stressors and factors, whether of psychological, physiological, personal, social or environmental nature, whether with a positive or negative effect. A model that contains other indicators that the environmental or dose-related indicators. Other indicators are available to assess indoor environmental quality: a) indicators concerned with buildings and its components, such as certain measures or characteristics of a building and its components (for example the possibility of mould growth), or even labelling of buildings and its components; b) indicators focused on the occupant such as sick leave, productivity, and number of symptoms or complaints [8;13]. In the category building and its components certain measures or characteristics of a building can be used, while in the category occupants, the emphasis should be on indicators that can give us information on the effects of stress: indicators that can tell us something on changes in the bodily systems and experience of people [8].

In 2014, a first concept of this 'new' model was introduced [8]; an improved version followed five years later [14] (Figure 1). The model takes account of the individual preferences and needs of the occupants (profiles) and the combined effects of stress factors in buildings on people (patterns) for different scenario's, different situations (for example sleeping/eating; meeting/concentrated work; getting lessons); and interactions at human and environmental level.

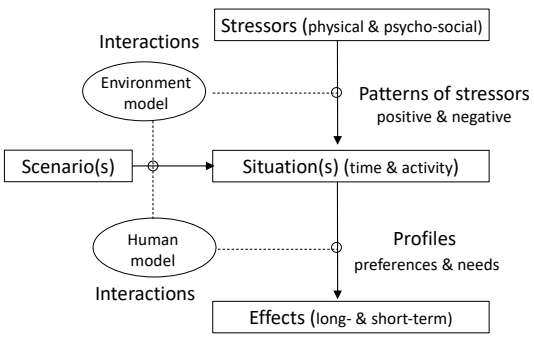

Fig. 1. - New model [14].

This model features the individual differences in needs and preferences (profiles of people as shown in the Human model, Figure 2) and the stress factors caused by the (indoor) environment that a person is exposed to (represented by patterns of stressors and the Environment model, Figure 3), depending on their situation (activity and time).

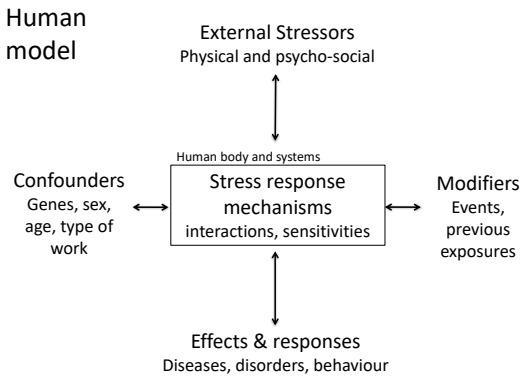

Fig. 2. - The Human model [14].

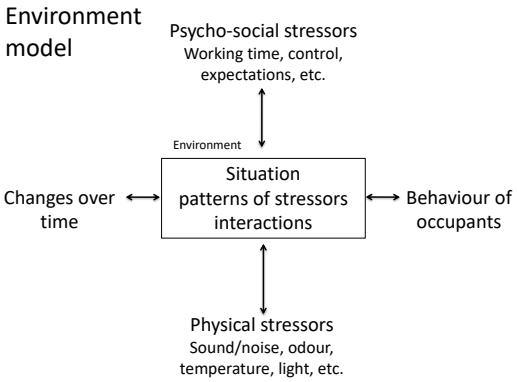

Fig. 3. - The Environment model [14].

For the determination of patterns of stressors of importance to people in different situations, identification of other factors and stressors than the environmental parameters used in guidelines [e.g. 12] is needed [15]. While for the determination of profiles of people for different scenarios and situations, identification of preferences and needs of individuals is needed [15].

Therefore, to validate this 'new' model, several field studies have been executed to determine profiles of people and patterns of stressors for different scenarios.

2. Methods

2.1 Study design

In the field studies, several scenarios were studied: 1) office workers and their workplace; 2) students and their homes; 3) primary school children and their classrooms; 4) employees of outpatient areas in hospitals.

For each scenario, occupant-related indicators and building-related indicators were collected through a questionnaire and checklist(s) to associate patterns of building-related stressors to occupant-related

indicators (health: symptoms; comfort: complaints); and to determine clusters of occupants and their profiles.

For each scenario, except for the 'Students and their homes' scenario, a survey was conducted comprising of a questionnaire and a building inspection with the use of checklists (at building and room level). For 'Students and their homes', only a questionnaire was developed, including also questions on building-related indicators, because visiting the homes was not feasible.

For each scenario, except for the 'primary school children and their classrooms' scenario, the questionnaire was digitally distributed. The questionnaire for the children was handed out and collected during the visit to the schools.

The checklists (building and room) focused on the indoor and built environment through characteristics of building, systems and rooms (e.g., operable or no windows, type of HVAC system, lighting system, solar screens, reflection on desks, surfaces of ceiling, floor and walls, sources of noise, dampness, mould growth, condensation, pollution sources, and control system), characteristics of the built environment (e.g., busy road and rural/ surroundings), and processes to maintain and operate the building and its activities (e.g., cleaning activities/schedule, renovation and retrofitting activities, and maintenance of HVAC system). The questionnaire included questions about personal data, psychosocial environment, psychological characteristics, events, physical effects, and preferences and needs for IEQ and in some cases also for psychosocial comfort.

2.2 Patterns of stressors

To find patterns of stressors, multivariate analysis was performed on data of 7441 office workers and 167 office buildings [16-17], 396 students and their homes in the Netherlands [18] and of 682 students and their homes in different countries [19], 949 primary school children and 45 classrooms [20], and 556 employees of outpatient areas in six Dutch Hospitals [21].

To examine the relations between an indicator for health or comfort and building characteristics, multivariate linear regressions were fitted, taking into account potential confounders and/or risk factors. First univariate analysis was performed for the building-related aspects, unadjusted and adjusted for confounding variables. Variables associated with a P-value less than 0.20 in bivariate analyses were included. The full model was reduced by sequential elimination of terms for which P-value > 0.20. Collinearity among variables in the model was measured by the variance inflation factor (VIF). No multicollinearity was detected for VIF<4.

2.3 Profiles of clusters

To determine clusters and their profiles, 2-steps cluster analysis was performed based on comfort, health, preferences and needs of 1014 office workers in 20 office buildings in the Netherlands [22], of 949 primary school children of 45 classrooms [23]; 556 employees of outpatient areas in six Dutch hospitals [24], and of 502 employees of 10 office buildings in the Netherlands [25].

Before performing the TwoStep cluster analysis, correlation analysis and Principal Component Analysis (PCA) was performed for all studies except for the OFFICAIR study [22], to statistically strengthen the models. Correlation analysis, the strength between perceived comfort and preferences, were performed to decide if both perceived comfort and preferences could be included in the cluster analysis; multicollinearity may affect the weight of constructs in cluster analysis [26]. PCA was conducted to reduce the number of original variables into fewer independent components [27]. As recommended by Tabachnick and Fidell [28], the number of components was determined by an Eigenvalue greater than 1; sample adequacy with Kayser-Meyer-Olkin was greater than 0.6; for the rotation method a Varimax orthogonal rotation was selected; and strength was determined by loadings within components > 0.4, loadings between components < 0.4 [29].

For the TwoStep analysis, the final sets of components resulting from the PCA were used to conduct the analysis. This clustering technique was used as opposed to other clustering methods, as it allows for the handling of both continuous and categorical data, the optimal number of clusters are automatically selected by the method; and the method is suitable for large data sets [30-31]. Final model validation was carried out with the fulfilment of four conditions [31]: a silhouette of above 0.2; variables predictor importance greater than 0.02; ensuring statistical significance ($p< 0.05$) between variables by conducting Chi^2 tests; applying the model to two random halves of the sample and ensuring that the results are similar.

3. Results

3.1 Patterns of stressors

The building-related patterns of stressors followed from the multivariate regression analysis, taking account of specific confounding factors, for each of the field studies performed are presented in Table 1.

3.2 Profiles of clusters

The outcome of the clustering (including PCA-analysis and TwoSteps cluster analysis) for each of the surveys performed, are presented in Table 2.

Table 1 - Patterns of building-related stressors for different health and/or comfort indicators.

Study	Building-related pattern of stressors	Adjusted/confounding factors
OFFICAIR 2012: 167 office buildings in 8 EU countries with 7441 office workers [16]	**Overall satisfaction**: acoustical solutions, mould growth, complaints procedure, cleaning activities **Health (BSI-5)**: number of occupants, lack of operable windows, presence of carpet and cleaning activities	gender, age mean, current smoker percentage, ERI (Effort-Reward Imbalance), overcommitment and negative affect means
OFFICAIR 2012: 167 office buildings in 8 EU countries with 7441 office workers [17]	**Dry eyes**: proximity (<100 m) to potential sources of outdoor air pollution, absence of operable windows, portable humidifiers in the offices, exposed concrete and/or plaster and dispersion and/or emulsion paint as wall covering in offices and cleaning surfaces at least once per week.	gender, age, level of education, smoking status, alcohol consumption, number of hours working with a VDU, ERI, overcommitment and negative affect means
Student homes 2015: 396 students and homes in the Netherlands [18]	**Rhinitis**: biological pollutants (caused by pets), chemical pollutants (caused by MDF less than 1 year old in bedroom), ventilation (opening window in bedroom) and workout	gender, family rhinitis, smoking status, alcohol consumption, and PANAS negative and positive
Students international 2019: 682 students and their homes in 5 cities [19]	**Rhinitis**: biological pollutants (caused by pets), chemical pollutants (caused by open bookshelves and lack of sweeping floors) **Headaches**: biological pollutants (caused by pets)	gender, age, family rhinitis, smoking status, negative events gender and age, negative events, PANAS negative
Schools 2017: 949 children of 45 classrooms (17 primary schools) [20]	**Health (PSI-9)**: location of school building, heating system, solar devices hampering opening windows **Comfort (PCI-7)**: ventilation type, window frame colour, floor material and vacuum cleaning frequency	mood during completion of questionnaire
Hospitals 2019: 556 outpatient workers of 6 hospitals [21]	**Dry eyes:** rotating heat exchanger, having no windows, type of workplace (office vs consultation room), more than 1 person in room. **Headaches**: having no windows, type of workplace (office vs consultation room)	gender, age, smoking status, alcohol consumption; ERI and over commitment gender, age, suffering from migraine

notes: BSI-5 = Building Symptom Index based on five symptoms: dry eyes, blocked or stuffy nose, dry/irritated throat, headache, and lethargy [32]; ERI = the Effort Reward ratio [33]; PANAS = Positive Affect Negative Affect Scale [34]; PSI-9 is defined based on 9 symptoms: dry eyes, itching or watery eyes, blocked or stuffy nose, running nose, sneezing, dry throat, difficulty breathing, dry, irritated or itching skin, and headache; PCI-7, is defined based on 7 classroom conditions: thermal discomfort, temperature changes, wind/draught, smells, noise, sunlight and artificial light.

Table 2 - Studies performed with clusters and their profiles.

Name study	Profiles
OFFICAIR 2012 NL: 1014 office workers in 20 office buildings in the Netherlands [22]	3 profiles clustered on IEQ-related complaints (comfort): · Healthy and satisfied workers · Moderate healthy and noise-bothered workers · Unhealthy and air and temperature-bothered workers
Schools 2017: 949 children of 45 classrooms (17 primary schools) [23]	6 profiles clustered on self-reported IEQ-comfort and IEQ-preferences: Sound concerned, Smell and sound concerned, Thermal and draught concerned, Light concerned, All concerned, and Nothing concerned.
Hospitals 2019: 556 outpatient workers of 6 hospitals [24]	6 profiles clustered on self-reported on IEQ-comfort and IEQ-preferences 3 profiles clustered on self-reported psychosocial comfort and preferences for psychosocial aspects.
MyWorkplace 2020: 502 employees of 10 office buildings in the Netherlands [25]	4 profiles clustered on self-reported preferences for IEQ and 6 profiles clustered on self-reported preferences for psychosocial comfort

4. Discussion and conclusions

4.1 'New' model

Research has shown that, even though the conditions seem to comply with current standards for indoor environmental quality based on single-dose response relationships, staying indoors is not good for our health. There is a need for understanding the indoor environment and its occupants; we need to acknowledge the fact that we are dealing with people who are different in their needs and preferences and that the indoor environmental quality is more than the sum of its parts.

A 'new' model which takes account of the combined effects of positive and negative stress factors in buildings on people (patterns), interactions at and between different levels (human and environment) over time, as well as the (dynamic) preferences and needs of occupants (profiles) in different scenarios and situations, is needed.

Several field studies were performed to determine profiles of people and patters of stressors for different scenarios, as suggested in Almonte et al. 2020 [15].

4.2 Patterns of stressors

From the field studies presented it can be concluded that it is possible to determine patterns of stressors for different scenario's based on multivariate regression analysis of a survey of the occupants and the buildings they are occupying.

After full adjustment, the regression models in all of the studies for health effects confirmed their multifactorial character. Moreover, the studies resulted in 'other' factors and stressors than used in guidelines, confirming the importance of considering all possible stressors when studying a certain disease or disorder. Several building-related stressors, personal factors and psycho-social factors, showed to be related to a disease or disorder.

The outcome, therefore, highlights the importance of considering all possible stressors, negative or positive, when studying a certain disease or disorder.

4.3 Profiles of clusters

From the field studies presented it can be concluded that people can differ in their preferences and needs, and that it seems possible to distribute them into clusters based on TwoSteps cluster analysis of preferences and needs for IEQ and psychosocial comfort acquired through a questionnaire.

Moreover, in a follow-up qualitative study of outpatient workers' preferences and needs, comparing preferences and needs before and during COVID-19 pandemic, it was concluded that occupants' preferences changed over time and were situation-related [35].

The outcome indicates that preferences and comfort of IEQ are related to health; preferences of workers are situation- and gender-driven; and that both the profiles of IEQ-clusters and the profiles of the social clusters are important to study.

4.4 Next steps

For validation and completion of the 'new' model, besides the 'patterns of stressors' and 'profiles of clusters', possible interactions at and between different levels (human and environment) over time need to be explored for different scenarios and situations (e.g. [9], [10], [15]).

Previous studies show that, at environmental level interactions or actions by occupants occur over time, which may affect the needs and preferences of the occupants (e.g. [9], [36]0.

Also, at human level interactions between different acoustical, olfactory, and visual stressors may occur (e.g. [10], [37]). However, more research is needed to explain all of these interactions, and to account for those in the 'New' model.

4.5 Concluding remark

The 'new' model will make it possible to match profiles of people with patterns of positive and negative stressors for a certain situation. The model can also help to create personal indoor environments that can both improve health and comfort of the individual. Clustering of the occupants of different scenario's, each with their own profile, can help designers of building and architects, to anticipate to changing preferences and needs of office workers, students, school children, etc. at cluster level. How the number of clusters vary, how the profiles of these clusters change over time, and how depended these profiles are on the scenario and situation, will need to be studied.

5. References

[1] Bonnefoy X., Annesi-Maesona I., Aznar L., Braubachi M., Croxford B., Davidson M., Ezratty V., Fredouille J., Ganzalez-Gross M., van Kamp I., Maschke C., Mesbah M., Moisonnier B., Monolbaev K., Moore R., Nicol S., Niemann H., Nygren C., Ormandy D., Röbbel N., Rudnai P. Review of evidence on housing and health. 2004. Copenhagen. Denmark.

[2] Fisk W.J., Lei-Gomez Q., Mendell M.J. Meta-analysis of the associations of respiratory health effects with dampness and mold in homes. Indoor Air. 2007; 17:284-96.

[3] Lewtas J. Air pollution combustion emissions, Mutat. Res-Rev. 2007; 636:95-133.

[4] Houtman, I., Douwes M., de Jong T., Meeuwsen J.M., Jongen M., Brekelmans F., Nieboer-Op de Weegh M., Dick Brouwer, van den Bossche S.,

Zwetsloot G., Reinert D., Neitzner I., Hauke A., Flaspöler E., Zieschang H., Kolk A., Nies E., Brüggemann- Prieshoff H., Roman D., Karpowicz J., Perista H., Cabrita J., Corral A. New forms of physical and psychological health risks at work. European Parliament. 2008; IP/A/EMPF/ST/2007-19, PE 408.569. Brussels, Belgium.

[5] Morawska L, Tang J., Bahnfleth W., Bluyssen P.M., Boerstra A., Buonanno G., Cao J., Dancer S., Floto A., Franchimon F., Haworth C., Hogeling J., Isaxon C., Jimenez J.L., Kurnitski J., Li Y., Loomans M., Marks G., Marr L.C., Mazzarella L., Melikov A.K., Miller S., Milton D., Nazaroff W., Nielsen P.V., Noakes C., Peccia J., Querol X., Sekhar C., Seppänen O., Tanabe S., Tellier R., Tham K.W., Wargocki P., Wierzbicka A., Yao M. How can airborne transmission of COVID-19 indoors be minimised? Env. Int. 2020; 142:105832.

[6] Kim J. and de Dear R. Nonlinear relationships between IEQ factors and overall workspace, Build. Environ. 2012; 49:33-40.

[7] Bluyssen P.M. Health, comfort and performance of children in classrooms – new directions for research. Indoor Built Environ. 2017; 26(8): 1040-50.

[8] Bluyssen P.M. What do we need to be able to (re) design healthy and comfortable indoor environments? Intell. Build. Int. 2014; 6(2):69-92.

[9] ASHRAE. Guideline 10P, Interactions affecting the achievement of acceptable indoor Environments. 2016. Atlanta, USA.

[10] Torresin S., Pernigotto G., Cappelletti F., Gasparella A. Combined effects of environmental factors on human perception and objective performance: A review. Indoor Air 2018; 28:525-38.

[11] Bluyssen P.M. The Healthy Indoor Environment, How to assess occupants' wellbeing in buildings. 2014. Taylor & Francis, London, UK.

[12] CEN. EN 16798-1:2019, Energy performance of buildings - Ventilation for buildings - Part 1: Indoor environmental input parameters for design and assessment of energy performance of buildings addressing indoor air quality, thermal environment, lighting and acoustics - Module M1-6, 2019. CEN-CENELEC Management Centre, Brussels, Belgium.

[13] Bluyssen P.M. Towards new methods and ways to create healthy and comfortable buildings, Build. Environ. 2010; 45:808-18.

[14] Bluyssen P.M. Towards an integrated analysis of the indoor environmental factors and its effects on occupants. Intell. Build. Int. 2020; 12(3):199-207.

[15] Allomonte S., Allen J., Bluyssen P., Brager G., Heschong L., Loder A., Schiavon S., Veitch J., Wang L., Wargocki P. Ten questions concerning well-being in the indoor environment, Build. Environ. 2020; 180:106949.

[16] Bluyssen P.M., Roda C., Mandin C., Fossati S., Carrer P., de Kluizenaar Y., Mihucz V.G., de Oliveira Fernandes E., Bartzis J. Self-reported health and comfort in 'modern' office buildings. Indoor Air 2015; 26:298-317.

[17] Kluizenaar de Y., Roda C., Dijkstra N.E., Rossati S., Mandin C., Milhucz V.G., Hanninen O., de Oliveira Fernandes E., Silva G.V., Carrer P., Bartzis J., Bluyssen P.M. Office characteristics and dry eye complaints in European workers – The OFFICAIR study, Build. Environ. 2016; 102:54-63.

[18] Bluyssen P.M., Ortiz M., Roda C. Self-reported rhinitis of students from different universities in the Netherlands and its association with their home environment. Build. Environ. 2016; 110:36-45.

[19] Bluyssen P.M., Zhang D., Ortiz-Sanchez M. Self-reported rhinitis and headaches of students from universities in Taiwan, Chile, Suriname, China and the Netherlands, and its association with their home environment. Intell. Build. Int. 2021; 1964424.

[20] Bluyssen P.M., Zhang D., Kurvers S., Overtoom M., Ortiz M. Self-reported health and comfort of school children in 54 classrooms of 21 Dutch school buildings. Build. Environ. 2018; 138:106-23.

[21] Eijkelenboom A., Ortiz M., Bluyssen P.M. Building characteristics associated with the prevalence of dry eyes and headaches of outpatient workers in six hospital buildings in the Netherlands, Indoor Built Environ. 2021; 1420326X211023125.

[22] Kim D.H. and Bluyssen P.M. Clustering of office workers from the OFFICAIR study in the Netherlands based on their self-reported health and comfort, Build. Environ. 2020;176: 106860.

[23] Zhang D., Ortiz M., Bluyssen P.M. Clustering of Dutch school children based on their preferences and needs of the IEQ in classrooms, Build. Environ. 2019; 147:258-66.

[24] Eijkelenboom A. and Bluyssen P.M. Profiling outpatient workers based on their self-reported comfort and preferences of indoor environmental quality and social comfort in six hospitals. Build. Environ. 2020; 184:107220.

[25] Ortiz M. and Bluyssen P.M. Profile office workers based on their self-reported preferences of indoor environmental quality at their workspace during COVID-19. Build. Environ. 2022; 211:108742.

[26] Ketchen D.J. and Shook C.L. The application of cluster analysis in strategic management research: an analysis and critique. Strat. Manag. J. 1996;17(6):441-58.

[27] Wold S., Esbensen K., Geladi P. Principal component analysis. Chemometr. Intell. Lab. Syst. 1987; 2:37-52.

[28] Tabachnick B.G. and Fidell L.S. Using Multivariate Statistics. 2007. Pearson Education.

[29] Howard M.C. A review of exploratory factor analysis decisions and overview of current practices: what we are doing and how can we improve? Int. J. Hum. Comput. Interact. 2016; 32(1):51-62.

[30] Tkaczynski A. Segmentation using two-step cluster Analysis. in: Dietrich T., Rundle-Thiele S., Kubacki K. (Eds.), Segmentation in Social Marketing: Process, Methods and Application, 2017:109-125. Springer Singapore, Singapore.
[31] Norusis M.J. IBM SPSS Statistics 19 Statistical Procedures Companion. 2012 Prentice Hall.
[32] Raw G.J., Roys M.S., Whitehead C., Tong D. Quesitonnaire design for sick building syndrome: an empirical comparison of options, Environ. Inter. 1996; 22:61-72.
[33] Siegrist, J., Starke D., Chandola T., Godin I., Marmot M., Niedhammer I., Peter R. The measurement of effort-reward imbalance at work: European comparisons. Soc. Sci. Med. 2004; 58:1483-99.
[34] Thompson E.R. Development and validation of an internationally reliable short-form of the positive and negative affect schedule (Panas). J. Cross-Cultural Psychol. 2007; 38:227-42.
[35] Eijkelenboom A., MA. Ortiz, P.M. Bluyssen Preferences for indoor environmental and social comfort of outpatient staff during the COVID-19 pandemic, an explanatory study, International Journal of Environmental Research and Public Health 2021; 18:7353.
[36] Zhang D and Bluyssen PM Actions of primary school teachers to improve the indoor environmental quality of classrooms in the Netherlands, Intell. Buildings Int. 2019; 13(2):103-115.
[37] Bluyssen PM, Zhang D, Kim DH, Eijkelenboom A, Ortiz M First SenseLab studies with primary school children: exposure to different environmental configurations in the Experience room, Intelligent Buildings International 2019; 13(4):275-292.

Data access statement

Data sharing not applicable to this article as no datasets were generated or analysed during the current study. All studies reported have been published.

Influence of temperature and relative humidity on subjective and objective air quality data in shopping centers

Mahmoud El-Mokadem [a], Kai Rewitz [a], Dirk Müller [a]

[a] RWTH Aachen University, E.ON Energy Research Center, Institute for Energy Efficient Buildings and Indoor Climate (EBC), DE-52074 Aachen, Germany

Abstract. Germany has 493 shopping centers mostly located in urban cities. According to STASTICA, the number of shopping centers was doubled in the last two decades .For consumers, good indoor air quality (IAQ) is a basic requirement for their shopping experience. This leads to very high air exchange rates for current operation of HVAC systems in shopping centers. Accordingly, achieving good IAQ in combination with increasing energy efficiency is a main issue for operation. Thus, previous studies were done to evaluate the intensity of shopping product emissions. Trained subject panels evaluated the emissions from retail products by using an intensity comparative scale.

In this paper, we analyze the IAQ parameters not only by trained human panel, but also by analyzing the volatile organic compounds (VOC) through objective tests. In a first step, we cluster five different product groups: books, clothing, shoes, coffee and perfume. For these groups, we measure the emissions through a multi VOC sensor system and a trained human panel, depending on two main parameters: temperature and relative humidity. The multi VOC sensor system consists of electrochemical sensors which resistivity changes according to the oxidation reactions that happens on the surface of the sensors at high temperatures. We use the results to investigate the correlation between the intensity of VOCs in respect to the two main parameters. Finally, we used the subjective data along with the objective data, to evaluate the perceived odor intensity and correlate the evaluations with the measured VOC concentrations by the multi VOC sensor system. The evaluation and visualization is done in principle of statistical data analysis methods such as Friedman test. The results show the potential for the metal oxide semiconductor sensors technology for detection of VOCs and for prediction of perceived intensity based on objective data. Moreover, a product specific regression leads to better prediction results, which shows that different limit values are required for different shop types.

Furthermore, the results show an influence of air temperature and humidity on subjective perception. Thus, for all products investigated, the perceived intensity and the percentage of dissatisfied people increases with rising temperature and relative humidity.

Keywords. Indoor air quality, shopping center, total volatile organic compounds, E-Nose, VOC
DOI: https://doi.org/10.34641/clima.2022.418

1. Introduction

Currently, air quality control in shopping centers is largely based on the measured CO_2 concentration of the indoor air. The CO_2 sensors used in this process usually measure the CO_2 concentration in the room increased by the emissions of the human organism. The advantage of CO_2 sensors is that the measured value can be calibrated to known source strengths with proven effects on humans. The use of absolute threshold values (e.g. Pettenkofer number: 1000 ppm CO_2) simplifies the control of ventilation systems in many applications. However, in shopping centers, controlling the ventilation system based on only one parameter (CO_2) may not be sufficient from an energy and air quality perspective. For example, odors and contaminants emitted from food courts, building materials, or products from inside the stores cannot be detected by CO_2 sensors. As a result, air quality can be perceived as inadequate, even though the CO_2 parameter recorded to control the ventilation system has been set according to standards for good air quality.

Odors perceived by humans can often be traced back to so-called volatile organic compounds (VOCs). These substances occur in the air in the form of gases and vapors and are of organic origin. Even low VOC emissions are often associated with significant odor perceptions and can lead to health problems (irritation of the respiratory tract, headaches, nausea, poor concentration, sleep disturbances). In contrast to CO_2 sensors, VOC sensors are able to detect mixtures of substances in the room air with a characteristic signal [2]. However, the control of ventilation with VOC sensors is relatively rarely carried out, since no specific limit value is defined that could be used to control a ventilation system.

Due to the large number of VOC emissions in shopping centers, the goal is therefore to define acceptable objective limits for different zones of a shopping center or for different product groups. This should allow an extension of current CO_2 based regulations by VOC-based regulations according to the needs.

Copyright ©2022 by the authors. This conference paper is published under a CC-BY-4.0 license.

2. Methodology

2.1 E-Nose: Sensor Methodology

Different sensor types can be used to detect gas concentrations. Possible sensor types are metal oxide semiconductor sensors, and infrared optical gas sensors. In this study, metal oxide semiconductor sensors are selected for the detection of volatile organic compounds. Their operating principle is based on the dependence of the electrical conductivity of metal oxides on the gas concentrations and gas types present. Metal oxide semiconductor sensors can be divided into thin-film and thick-film sensors and exhibit, among other things, high sensitivity to low gas concentrations, a long service life and a low price, making them potentially suitable for use in the demand-based control of ventilation systems. On the other hand, there are non-linear sensor characteristics depending on the gas concentration, which make calibration difficult, as well as drift and aging behavior that cannot be neglected. Furthermore, there is a cross-sensitivity of additional parameters such as relative humidity and air temperature. Due to the high operating temperatures of 300 °C - 900 °C, these sensors can also have a comparatively high energy consumption of more than 1 watt, which can, however, be reduced to almost 90% by an optimized design [3].

2.2 E-Nose: Sensor system development

For the setup of the VOC sensor system, different metal oxide semiconductor sensors of the MQ sensor series are used to enable the detection of several gases.

Tab. 1 – Overview of the detectable chemical components of the sensors used.

E-Nose Sensor	Description
BME680	Industrial sensor (TVOC)
MQ-2	Hydrogen, methane, propane, i-butane, LPG , alcohol, smoke
MQ-3	Alcohol, ethanol, smoke
MQ-7	Carbon monoxide
MQ-9	Carbon monoxide, flammable gasses
MQ-135	NH_3,NO_x, alcohol, benzene, smoke, CO_2
HCHO	Benzene, toluene, alcohol, formaldehyde gas, hydrogen
DHT22	Temperature and humidity sensor

The MQ sensors are connected to a single board Arduino Mega microcontroller for power supply as well as data transfer. In addition, a temperature sensor and a humidity sensor are integrated to compensate for cross-sensitivities to these parameters. With the help of a TVOC sensor, the sum of volatile organic compounds can be recorded and thus a total air pollution can additionally be estimated [4]. **Tab. 1** gives an overview of the used sensors. **Fig. 1** shows the schematic for the developed E-Nose.

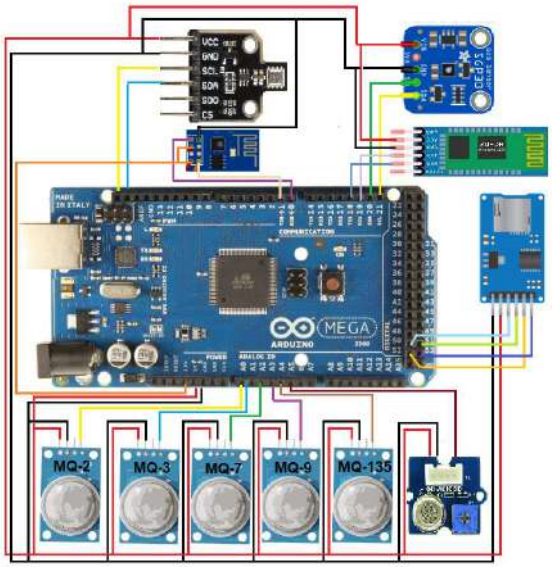

Fig. 1 – Schematic of the developed E-Nose.

Fig. 2 – Developed E-Nose.

An SD card is connected to the microcontroller for local data storage. In addition, the sensor system has a Bluetooth module to establish a wireless connection to other devices. **Fig. 2** shows the final VOC sensor system including an optimized housing as well as the circuit diagram of the system.

2.3 Subjective and objective tests

According to previous studies, Fangers Group, conducted a series of subjective tests. These studies confirm the significant decrement of the acceptability with increasing temperature and humidity [5–8].

The aim of the study is to collect both subjective and objective data for the evaluation of odors or air quality for selected product groups and to derive possible limit values. In particular, the influences of air temperature and relative humidity are to be analyzed. The objective evaluation is carried out with the developed VOC sensor system. The subjective evaluation is carried out with a group of test persons trained according to DIN ISO 16000-28 with regard to acceptance and perceived intensity by using a acetone comparative scale [9].

2.3.1 Emission chambers

The study is conducted in the air quality laboratory of the Institute for Energy Efficient Buildings and Indoor Climate (EBC). The product groups are divided into 5 categories: clothing, books, shoes, perfume and coffee.

Fig. 3 – Positioning of the E-Nose and the product inside the emission chamber.

These are filled into so-called emission chambers. These chambers are made of stainless steel in order to minimize the influence of oxidation reactions on the air. In addition, these chambers have both a connection for the introduction of conditioned supply air via a central ventilation unit and an outlet fitted with a glass cylinder at which the group of test subjects can evaluate the air quality. A control of the supply air volume flow with a measurement of the actual condition via an orifice plate allows a precise adjustment of the air exchange in the emission chambers. In order to achieve good mixing even at low air changes, an additional fan, which circulates the air in the chamber, is installed in each case. **Fig. 3** shows an example of the positioning of the clothing and the sensor system in one of the emission chambers. The sensor system is positioned directly in front of the fan.

A total of three emission chambers can be used in parallel in the EBC air quality laboratory, shown in **Fig. 4**. An exhaust hose is positioned above each cylinder of the emission chambers to prevent contamination of the room air by the outflowing air from the chambers. In addition, each chamber is equipped with a laptop computer on which subjects can enter their subjective ratings regarding acceptance and perceived intensity. In addition, one of the three VOC sensor systems is positioned in each of the chambers.

Fig. 4 – Emission chambers in the EBC air quality laboratory.

2.3.2 Acetone comparative scale and subject panel

In order to be able to evaluate the intensity of the air, an acetone comparative scale is used according to DIN ISO 16000-28, see also **Fig. 5**. The concentration of the acetone-air mixture at the different cylinders can be reproducibly adjusted with this test rig. According to DIN ISO 16000-28, the acetone concentration in mg/m^3 can be converted into PI. Here, 0 PI corresponds to the odor threshold concentration or an acetone concentration of 20 mg/m^3. The increase by 1 PI corresponds to a linear increase of the acetone concentration of 20 mg/m^3 (e.g. 15 PI = 320 mg/m^3).

Fig. 5 – Acetone comparative scale in the EBC air quality laboratory.

In previous investigations Hegemann et. al used a maximum intensity of 14 PI for a shopping center product (shoes) [10]. Since the current study also tests other products such as perfume, for which significantly higher ratings are expected, the upper end of the comparative acetone scale is extended to 28 PI (580 mg/m^3). In choosing this value, the stated National Institute for Occupational Safety and Health (NIOSH) limits of 590 mg/m^3 (250 ppm) and Emergency Exposure Guidance Levels (EEGLs) of 2400 mg/m^3 (1000 ppm) for exposure over 24 hours are met [11].

According to DIN ISO 16000-28, the minimum size of a group of testers (hereinafter referred to as the subject group), for the evaluation of acceptance is 15 persons (untrained) and for the evaluation of perceived intensity is 8 persons (trained). In order to increase the statistical significance of the results, the training of a larger group of subjects is aimed at. Out of a total of 26 participants, 17 persons successfully completed the 5-day training.

2.3.3 VOC classes for shopping center products and method of detection

Tab. 2 shows a classification of product groups from shopping centers or their emissions with respect to different VOC classes. As relevant and suitable product groups for the main study, shoes, clothing, books, perfume and, representing the food courts, coffee are identified. In **Tab. 2**, sensors with correspondingly high sensitivity are also assigned to the VOC classes. For example, formaldehyde can be emitted from new clothing, new shoes, or new books. The HCHO sensor is suitable for detecting formaldehyde [12]. Sanaeifar et al. use the MQ-135 sensor for the detection of aromatic compounds emitted from food [13]. Perfumes and detergents contain alcohols, which can be detected with the MQ-3 sensor. Cosmetics containing alkanes can be detected with the MQ-2 sensor [14].

Since only three emission chambers are available, the study is divided into two sub-studies. In the first sub-study, clothing, shoes and perfume (variant 1) are evaluated. In the second sub-study, books, coffee and perfume (variant 2) are evaluated. Perfume is rated in two variants, as the highest ratings were recorded here. The second variant corresponds to a 60 % reduction in source strength compared to the first variant. In each sub-study, the group of test subjects is also divided into two sub-groups due to hygiene protection with regard to the Corona pandemic, so that the first sub-group participated in the study in the morning and the second sub-group in the afternoon.

Tab. 2 – VOC classes and assignment to product groups of shopping centers and suitable sensors for detection.

Product group	VOC class	Detecting sensor
Clothes Shoes Books	Formaldehyde	HCHO
Food Furniture Polishes	Aromatics	MQ-135
Perfumes Cleaning Agent	Alcohols	MQ-3
Cosmetics	Alkanes	MQ-2

2.3.4 Test procedure

The test procedure is shown schematically in **Fig. 6**. One setting is selected per day for the air temperature and the relative humidity of the supply air, which is not varied during the day. Two hours before the arrival of the group of test subjects, the test stand is switched on to create stationary boundary conditions. After a welcome and brief acclimation of the subject group, the evaluation begins. Once an evaluation is completed for all three emission chambers, the volumetric flow rate or air exchange rate is varied. During the test run, the subject group is almost exclusively in the air quality laboratory. After all assessments are completed, the subject group is dismissed.

The parameter variations carried out are included in **Tab. 3**. This corresponds to a total of 36 evaluations per subject and product. The temperature and humidity were chosen to be inside the acceptable thermal comfort range boundaries [15].

In addition to evaluating the perceived intensity, an additional question is used to determine the percentage of dissatisfied subjects. For this purpose, the 17 trained subjects are asked the question: "Imagine you were exposed to the air from the emission test chamber for several hours a day. Would you rate the odor as acceptable?" "Yes" and "No" are

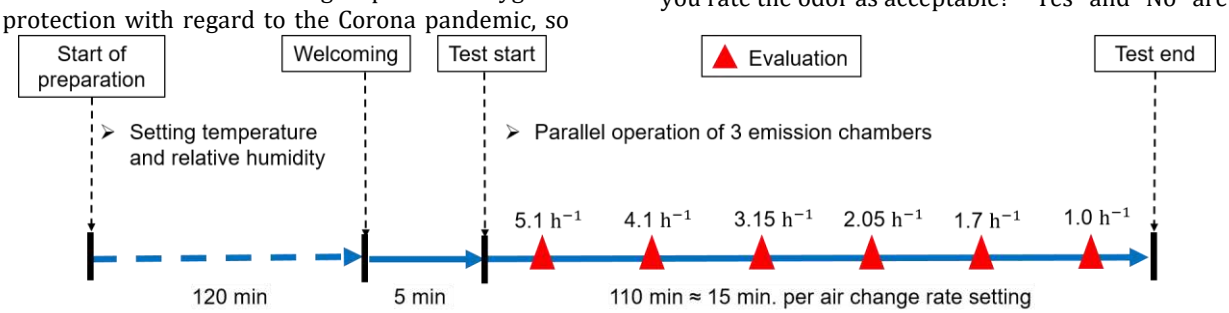

Fig. 6 – Test procedure.

available as response options. The proportion of no ratings is defined as the proportion of dissatisfied. The evaluation is carried out for each parameter variation, so that a total of 36 evaluations per product and test person are recorded here as well.

Tab. 3 – Overview of parameter variation.

Parameter	Value
Air temperature in °C	20; 23; 27
Relative humidity	30 %; 50 %
Air change rate in 1/h	1; 1.7; 2.05; 3.15; 4.1; 5.1

3. Results

3.1 Influence of temperature and humidity on the perceived intensity

In **Fig. 7**, the ratings per air exchange setting averaged over all test subjects are plotted against temperature. These mean values are shown as colored circles per product group. The relative humidity is 50 % for the evaluation. Based on the results, a slightly proportional relationship between air temperature and perceived intensity can be seen. Thus, the perceived intensity increases with increasing air temperature. The slope of the regression lines varies slightly between the individual product groups. Furthermore, it can be seen that the difference in perceived intensity due to the product groups is significantly higher than the influence of temperature. Perfume (variant 1) has by far the highest ratings between about 19 and 27 PI. The reduced source strength for perfume (variant 2) leads to a reduction to values between approx. 12 and 16 PI. The ratings for coffee are at a similar level to perfume (variant 2). Shoes and books are significantly lower, at about 10 to 12 PI and about 6 to 10 PI, respectively. The lowest ratings, between about 5 and 7 PI are observed for clothing.

Fig. 8 shows, as an example for the perfume product group (variant 1), the ratings averaged over all test subjects per air change rate setting plotted against temperature. The data for the relative humidity of 30 % are shown as red circles and for 50 % as black crosses. In addition, the regression lines are drawn. Both regression lines run almost parallel with the same slope. However, the ratings at 50 % humidity are shifted upward by about 2 PI compared to 30 % humidity. The results for the other product groups show a similar behaviour.

Overall, it can be concluded that as temperature and humidity increase, the perceived intensity also increases. The influence of temperature differs slightly for the different product groups, but is of the same order of magnitude as the influence of relative humidity for the value ranges considered.

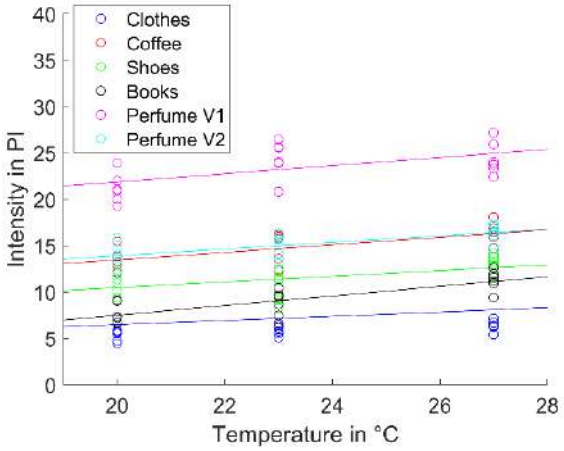

Fig. 7 – Influence of temperature on the perceived intensity at 50 % relative humidity.

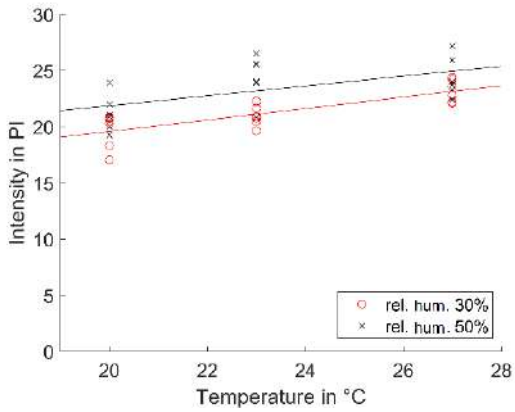

Fig. 8 – Influence of relative humidity on the perceived intensity for perfume (variant 1).

In order to evaluate whether the variation of temperature and humidity leads to a statistically significant difference with respect to the subjects' evaluation, the Friedman test is used. The Friedman test is a statistical test suitable for the evaluation of non-parametric data, so it does not assume a normal distribution of the data [16]. As a result of the test statistic, the "p-value" is output, which is compared with the previously determined significance level α. The significance level indicates the probability with which the null hypothesis is falsely rejected, even if it is actually true. This is called a first kind error or α-error. In this paper, a significance level $\alpha = 0.05$ is chosen for this purpose. If $p>\alpha$, the null hypothesis cannot be rejected and a difference between the sample distributions cannot be detected. However, if $p<\alpha$ holds, the null hypothesis is rejected and the alternative hypothesis is accepted, i.e., a significant difference exists.

The results of the p-value are included for the analysis of temperature differences in **Tab. 3**. All values are smaller than the defined significance level, so that statistically significant differences due to the variation in temperature can be assumed. An analysis for the influence of relative humidity leads also to p-values < 0.05.

Tab. 4 – p-value results of the Friedman test for a comparison of subjective ratings as a function of temperature.

50 % relative humidity 20 – 23 – 27 °C		30 % relative humidity 20 – 23 – 27 °C	
SC product	p-value	SC product	p-value
Perfume (Variant 1)	$1.39e^{-41}$	Perfume (Variant 1)	$7.24e^{-46}$
Perfume (Variant 2)	$1.05e^{-53}$	Perfume (Variant 2)	$1.40e^{-40}$
Books	$4.30e^{-47}$	Books	$3.79e^{-35}$
Coffee	$6.95e^{-55}$	Coffee	$8.79e^{-17}$
Shoes	$4.30e^{-47}$	Shoes	$3.30e^{-13}$
Clothes	$7.79e^{-41}$	Clothes	$4.42e^{-36}$

3.2 Influence of temperature and humidity on acceptance

Fig. 9 shows an example of the percentage of dissatisfied people for the perfume product (variant 1) across the different scenarios. The values in each case represent an average value over all test subjects and set air change rates. It can be seen that the percentage of dissatisfied people increases with rising air temperature and rising relative humidity. The influence of the temperature is higher at a relative humidity of 50 % than at 30 %.

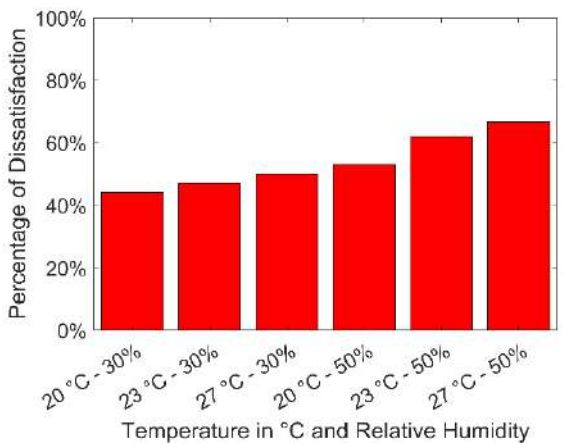

Fig. 9 – Influence of temperature and humidity on percentage of dissatisfied for perfume (variant 1).

In **Fig. 10**, the percentage of dissatisfied people is plotted against the Perceived Intensity. The colored symbols are mean values of the 17 evaluations by the test persons for each combination of product, temperature, relative humidity and air change rate. It can be seen that the range of ratings for the products studied varies. The highest ratings for perceived intensity and the proportion of dissatisfied persons exist for the product perfume (variant 1). The lowest ratings occur for clothing and books, with an intensity of approximately 5 PI resulting in a proportion of dissatisfied of approximately 20 %. It can be seen from the data that the proportion of dissatisfied people increases in principle with perceived intensity. In addition, a linear regression function is plotted in red through the data cloud. It should be noted, however, that the data show a high degree of scatter, especially in the middle range between about 10 and 17 PI, so that the proportion of dissatisfied people varies by about 30 % for the same intensity.

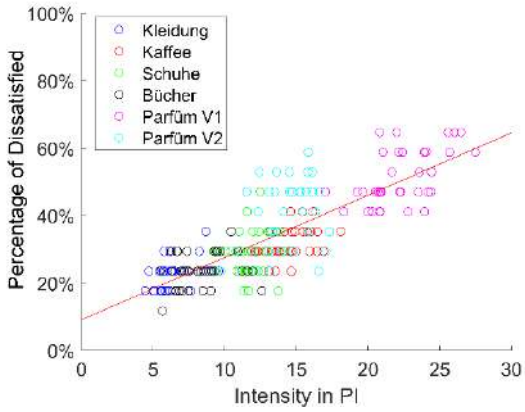

Fig. 10 – Correlation between perceived intensity and percentage of dissatisfied.

3.3 Influence of temperature and humidity on the sensor signal

In the following, the results for the MQ-3 sensor are presented exemplarily, since it has the highest sensitivity to the products investigated. **Fig. 11** shows the sensor signal as a function of temperature for various products at a relative humidity of 50 % for the MQ-3 sensor. For all products except clothing, the sensor signal increases with increasing air temperature.

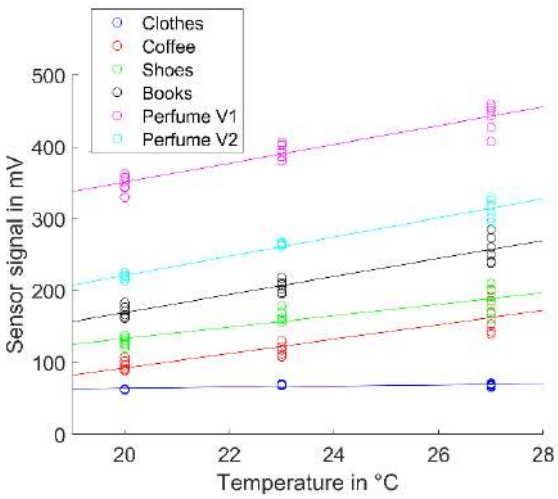

Fig. 11 – Influence of temperature on the sensor signal at 50 % relative humidity for MQ-3 sensor.

Comparing this with the subjective data from **Fig. 7**, a similar behaviour can be seen for the sensor signal

as a function of temperature. When looking at the order of the perceived intensities with the measured sensor signals, it can also be seen that these are the same except for position 3 and 5, see also **Tab. 5**. The subjects rate coffee as more intense than shoes, books and clothing, whereas the sensor signal is only weaker for clothing than for coffee.

Fig. 12 shows an example of the sensor signal as a function of temperature for perfume (variant 1) at a relative humidity of 30 % and 50 % for the MQ-3 sensor. It can be seen that the sensor signal increases with increasing relative humidity. This behavior is similar to the observation for the evaluation of perceived intensity in **Fig. 8**.

Tab. 5 – Ranking of the SC-Product according to perceived intensity and to the sensor signal of MQ-3.

SC-Product	Perfume V1	Perfume V2	Books	Shoes	Coffee	Clothes
Subjective Test	1	2	3	4	5	6
Objective Test	1	2	5	4	3	6

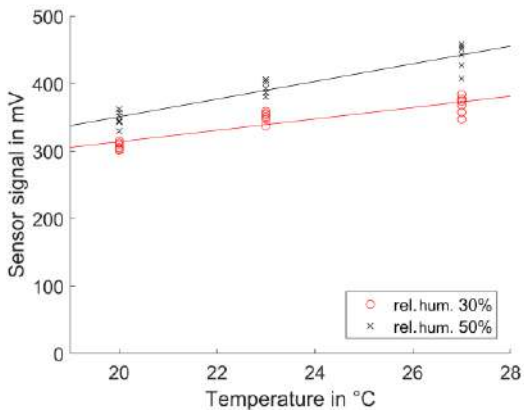

Fig. 12 – Influence of relative humidity on the sensor signal for perfume (variant 1) for MQ-3 sensor.

3.4 Correlations between objective and subjective evaluation

In order to use VOC sensors for advanced demand-controlled ventilation in shopping centers, limit values are needed that can be used as set points for the controlled variables. In **Fig. 13**, the perceived intensity is plotted against the sensor signal for the MQ-3 sensor. In addition, the investigated product groups are shown with different coloured markers.

It can be seen that for the different product groups the point clouds in the diagram have different positions. From this, it can be seen that the correlation of the perceived intensity and the objective sensor signal should be done depending on the product groups. For example, the evaluation of the intensity of coffee is significantly stronger than that of shoes or books for the same sensor signal. In addition, linear regression lines are shown on the basis of the five product groups investigated, whose functions, the coefficients of determination R^2 and the root mean square error (RMSE) are contained in **Tab. 6**. In each case, a linear regression approach is used to derive a correlation between the sensor signal in mV and the perceived intensity in PI. It can be seen that the coefficient of determination for the separate analysis of the product groups books, coffee, clothing and shoes is smaller compared to a regression over all data, but the RMSE can be reduced from 3.2 PI to as low as 0.9 PI. It is noticeable that for books, coffee and shoes the slope of the regression function is the same and only the Y-axis intercept differs.

Tab. 6 – Derived correlations between sensor signal in mV (x) and perceived intensity in PI (y).

Data	Correlation	R^2	RMSE
All data	$y = 0.05 \cdot x + 4.75$	0.65	3.2 PI
Books	$y = 0.026 \cdot x + 3.72$	0.40	1.4 PI
Coffee	$y = 0.026 \cdot x + 11.48$	0.30	1.5 PI
Clothes	$y = 0.053 \cdot x + 3.39$	0.40	0.9 PI
Perfume	$y = 0.05 \cdot x + 5.20$	0.65	2.5 PI
Shoes	$y = 0.026 \cdot x + 7.09$	0.20	1.5 PI

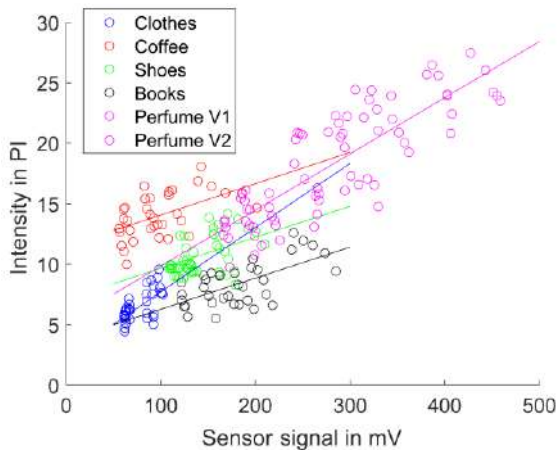

Fig. 13 – Correlation between the sensor signal of MQ-3 and the perceived intensity

In **Fig. 14**, the percentage of dissatisfied persons is plotted against the sensor signal of the MQ-3 sensor for the product groups investigated. The strong scattering of the data along the regression line drawn in red can be seen. This makes it difficult to derive an exact objective limit value.

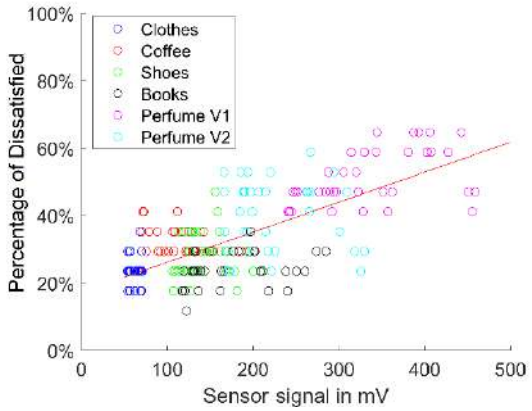

Fig. 14 – Correlation between the sensor signal of MQ-3 and the percentage of dissatisfied.

4. Conclusion

Currently, CO_2 sensors are mainly used in shopping centers for demand-based volume flow control of HVAC systems. In order to additionally detect emissions from building materials and products, VOC sensors are suitable in principle. Depending on their design and measuring principle, these sensors exhibit cross-sensitivities to air temperature and humidity as well as low selectivity, so that interpretation of the sensor signals is not trivial. However, based on the results of the study carried out with the metal oxide semiconductor sensors used, it is in principle possible to correlate the objective sensor signals with subjective evaluations for individual product groups. However, the definition of exact limit values is not possible due to the scattering of the data. Nevertheless, the results show in principle the potential of such sensor technology. With a larger amount of data, which would require further studies, it would also be possible to use machine-learning methods to analyze the data. With these, it might be possible to derive correlations between the sensor signals and the subjective evaluations much more easily and robustly. Important findings were also obtained in connection with the influence of air temperature and humidity on subjective perception. Thus, for all products investigated, the perceived intensity and the proportion of dissatisfied persons increases with rising temperature and relative humidity. This should be taken into account when selecting set points for the control of temperature and humidity, especially if there are complaints from the people present.

5. References

[1] Koptyug E. Number of shopping centers in Germany from 1965 to 2021: Statista; 2021. Available from: URL: https://www.statista.com/statistics/523100/number-of-shopping-centers-in-germany/.

[2] Beuth. Ventilation for non-residential buildings - Performance requirements for ventilation and room-conditioning systems. Available from: URL: https://www.beuth.de/en/standard/din-en-13779/94054008.

[3] Wöllenstein, J Semiconductor gas sensors in thin and thick film technology: IPM, Fraunhofer-Institut für Physikalische Messtechnik.

[4] Molhave L, Clausen G, Berglund B, *et al.* Total Volatile Organic Compounds (TVOC) in Indoor Air Quality Investigations*. Indoor Air 1997; 7(4): 225–40 [https://doi.org/10.1111/j.1600-0668.1997.00002.x]

[5] Berglund LG, Cain WS. Perceived air quality and the thermal environment. In: ASHRAE, editor. Perceived air quality and the thermal environment; 1989; 93–9.

[6] Berglund LG. Comfort and Humdity. ASHRAE Journal 1998; (August): 35–41.

[7] Gunnarsen L, Fanger PO. Adaptation to indoor air pollution. Environ Int 1992; 18(1): 43–54.

[8] Fang L, Clausen G, Fanger PO. Impact of Temperature and Humidity on Perception of Indoor Air Quality During Immediate and Longer Whole-Body Exposures. Indoor Air 1998; 8(4): 276–84 [https://doi.org/10.1111/j.1600-0668.1998.00008.x]

[9] DIN. Indoor Air Pollution - Part 28: Determination of odour emissions from building products using an emission test chamber (ISO 16000-28:2012).

[10] Mathis P, Freitag H, Hegemann D, Schmidt M, Müller D. New concepts for the ventilation of shopping centers: Reducing air change rate, applying active chilled beams and elevating cold water supply temperature. Indoor and Built Environment 2017; 26(2): 208–25 [https://doi.org/10.1177/1420326X16677571]

[11] The National Institute for Occupational Safety and Health (NIOSH). Immediately Dangerous to Life or Health Concentrations (IDLH) for Acetone; 1994.

[12] European Chemical Agency. Investigation Report: Formaldehyde and Formaldehyde Releasers; 2017

[13] Sanaeifar A, Mohtasebi SS, Ghasemi-Varnamkhasti M, Ahmadi H, Lozano J. Development and application of a new low cost electronic nose for the ripeness monitoring of banana using computational techniques (PCA, LDA, SIMCA and SVM). Czech J. Food Sci. 2014; 32(No. 6): 538–48

[14] Cosmetic Ingredient Review. Safety Assessment of Alkane Diolsas Used in Cosmetics; 2018. Available

[15] ANSI/ASHRAE. Thermal Environmental Conditions for Human Occupancy: ANSI/ASHRAE Addendum a to ANSI/ASHRAE Standard 55-2010.

[16] Friedman M. The Use of Ranks to Avoid the Assumption of Normality Implicit in the Analysis of Variance. Journal of the American Statistical Association 1937; 32(200): 675–701

Data Statement

The datasets generated during and/or analysed during the current study are not available because the authors are still processing the data, but the authors will make every reasonable effort to publish them in near future.

Students' self-reported health and psychosocial status at home before and during COVID-19

Amneh Hamida [a], Dadi Zhang [b], Marco A. Ortiz [c], Philomena M. Bluyssen [d]

[a] Chair Indoor Environment, Faculty of Architecture and the Built Environment, Delft University of Technology, the Netherlands, A.B.Hamida@tudleft.nl.

[b] Chair Indoor Environment, Faculty of Architecture and the Built Environment, Delft University of Technology, the Netherlands, D.Zhang-2@tudelft.nl.

[c] Chair Indoor Environment, Faculty of Architecture and the Built Environment, Delft University of Technology, the Netherlands, M.A.OrtizSanchez@tudelft.nl.

[d] Chair Indoor Environment, Faculty of Architecture and the Built Environment, Delft University of Technology, the Netherlands, P.M.Bluyssen@tudelft.nl.

Abstract. During the COVID-19 outbreak, university courses were shifted online and students spent the majority of their time inside their homes. However, staying indoors can affect students' health due to the exposure to several environmental stressors, such as background noise, and/or inefficient ventilation, and/or insufficient lighting. Previous studies showed that the indoor environmental factors may cause health effects on students (physiological and psychological). Therefore, this research aimed at investigating the differences in students' health and psychosocial status between before and during COVID-19. An online questionnaire survey was completed by first-year undergraduate university students in March 2019, 2020, and 2021. This questionnaire includes questions about time spent at home, psychosocial status, diseases, and home-related symptoms. The mean number of hours that students spent at home during the weekdays and on weekends were calculated, respectively. Besides, occurrence frequencies of psychosocial statuses were calculated for each year. Furthermore, a statistical analysis, including one-way ANOVA and Chi2, were performed to examine the differences between the three groups in terms of time spent at home, psychosocial statuses, diseases, and home-related symptoms. It is worthwhile to note that students spent significantly more time at home, during the COVID-19 pandemic in March 2021. Another notable result is that students' mood and emotional states changed significantly over the three years; for example, fewer students reported to be active and inspired in 2021. Moreover, the home-related symptoms, such as headache and tiredness, significantly increased in 2021, compared with the other two years.

Keywords. Indoor environmental quality, self-reported health, home-related symptoms, students' home, psychosocial status, COVID-19 pandemic
DOI: https://doi.org/10.34641/clima.2022.189

1. Introduction

During the COVID-19 outbreak, individuals spent the majority of their time inside their homes because one of the most common imposed lockdown measures is "staying at home" [1–3]. However, it has been indicated that staying indoors for a long time is not beneficial for individuals' well-being [4]. This is due to the number of environmental stressors which could affect individuals' well-being, including health and comfort. These stressors (e.g. noise, insufficient air quality) are related to the indoor environmental quality (IEQ), including air quality, acoustical quality, lighting quality, and thermal quality [5–7]. Also, the lockdown measures might cause social isolation and health issues, such as anxiety, and affect students' well-being [8]. For example, in a study conducted by Cao *et al.*, it was found that 21% of university students were suffering from anxiety during the COVID-19 pandemic, which suggested that the mental health of students is essential to be monitored [9]. Hence, this study aimed at investigating the differences in students' health and psychosocial status while staying at home before and during the COVID-19 outbreak.

Copyright ©2022 by the authors. This conference paper is published under a CC-BY-4.0 license.

2. Methods

2.1 questionnaire design

An online-based questionnaire was built in the *Qualtrics XM* platform in English and Dutch languages. Parts of this questionnaire, such as the psychosocial status (e.g. emotional state, PANAS) and the building-related symptoms, are based on the OFFICAIR questionnaire developed by Bluyssen *et al.* [10]. In this study, four sections of this questionnaire were analysed: 1) demographics, 2) time spent at home, 3) psychosocial status, and 4) self-reported health. In terms of the demographic section, two items were considered: gender and students' house type (student residence or parents' home). The question of the number of hours (including sleeping hours) spent at home was divided into two parts: weekdays and weekend. Pertaining to the psychosocial status, three items were considered: emotional states (e.g. relaxed, calm, sad), positive/ negative events (e.g. wedding and funeral) experienced recently, and the Positive and Negative Affect Schedule (PANAS) developed by Thompson [11] (e.g. active and upset). The self-reported health section included two questions: diseases and home-related symptoms. The diseases questions covered 17 types of diseases (e.g. anxiety), while the home-related symptoms questions included 11 home-related symptoms (e.g. dry eyes).

2.2 sample size

The questionnaire has been sent to first-year bachelor students in the faculty of Architecture and the Built Environment in Delft University of Technology, the Netherlands. The questionnaire was completed by 1132 students: 374 students in March 2019, 349 students in March 2020, and 409 students in March 2021. The students were asked to give consent before they started to process the survey.

2.3 data management and analysis

Data were exported from Qualtrics XM and stored in IBM-SPSS version 25. For the data analysis, percentages or mean values of the answers, were calculated with descriptive statistics. Additionally, Chi-squared tests (Chi^2) and analysis of variance (one-way ANOVA) were performed to compare the three groups of students (2019, 2020, and 2021) in terms of their time spent at home, psychosocial status, and health. In the case in which $p<0.05$ was found between the student groups (year) and the selected items, it was considered that there was a significant difference between the groups.

3. Results and Discussion

3.2 students' characteristics

The percentages of students' characteristics in terms of their gender and house types were calculated through the descriptive statistics and sorted in **Tab. 1.** There was no statistically significant difference in these two items among the three groups.

Tab. 1 – Students' characteristics.

Characteristics			Percentage
Gender	Male	2019	44.7%
		2020	45.6%
		2021	41.0%
	Female	2019	55.3%
		2020	54.4%
		2021	59.0%
House type	Student residence	2019	58.7%
		2020	54.3%
		2021	54.3%
	Parents' home	2019	41.3%
		2020	45.7%
		2021	45.7%

3.1 time spent at home

The mean number of hours the three groups of students spent at their homes during the weekdays and weekend is illustrated in **Fig. 1**. It is clear that students in 2021 spent more time (mean 20.0 hours) in their homes on the weekdays compared to the 2020 (mean 13.9 hours) and 2019 (mean 16.0 hours) groups. Also, the results of the ANOVA analysis showed that there was a significant difference between the three groups in terms of the number of hours spent on the weekdays ($p<0.001$), and weekends ($p<0.001$).

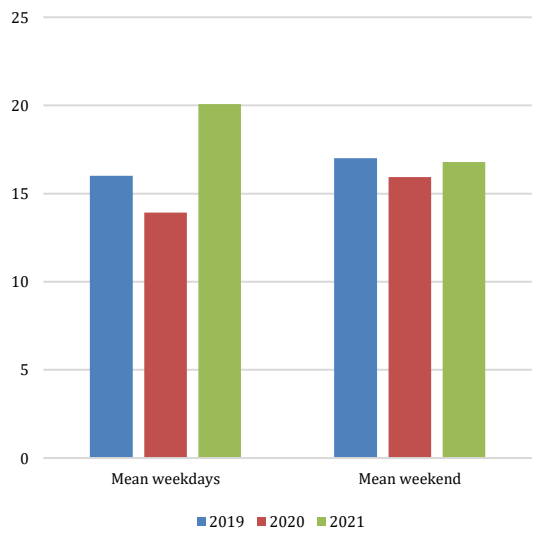

Fig. 1 – Students' time spent at home.

3.3 students' psychosocial status

The students' psychosocial statuses were analysed with regards to their emotional state, recently experienced events, and PANAS. Pertaining to the students' emotional states, **Fig. 2** demonstrates the emotional states of the three groups of students while they were answering the questionnaire. As can

be seen, the students in 2021 were feeling more bored and sad, as well as less calm, cheerful, and relaxed than the other two groups. It is worthwhile to note that the results from Chi2 revealed that there was a statistical difference among the three groups of students in their emotional states (*p<0.001*).

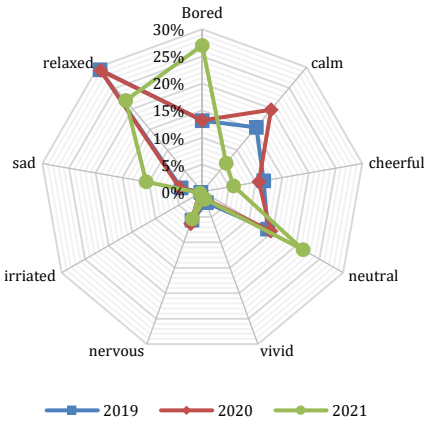

Fig. 2 – Students' emotional states while completing the questionnaire.

Fig. 3 indicates the percentages of students that have recently experienced positive and negative events. Generally speaking, the number of students who recently experienced positive events in March 2021 and 2020 were less than in 2019. Also, a significant difference among the three groups regarding their recently experienced positive event was observed (*p=0.015*).

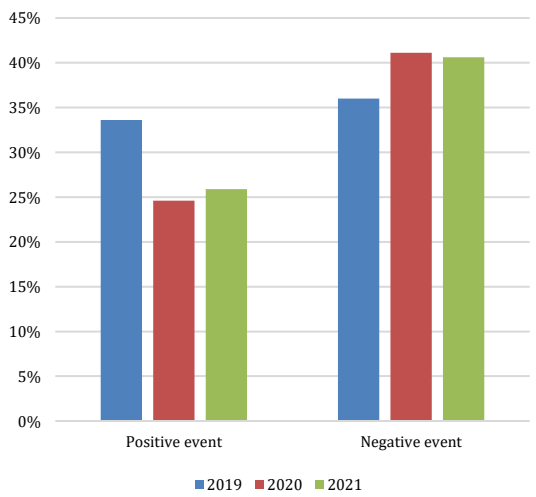

Fig. 3 – Students' experiences of recent positive and negative events.

Fig. 4 shows the students' emotional states related to the 10 PANAS items. It can be noted that there were significant less students in 2021 who selected the positive items which are inspired (*p=0.024*), attentive (*p=0.009*), and active (*p=0.007*). Furthermore, three negative PANAS items, nervous (*p=0.001*), upset (*p=0.018*), and anxious (*p=0.013*), were reported significantly more by students in 2021.

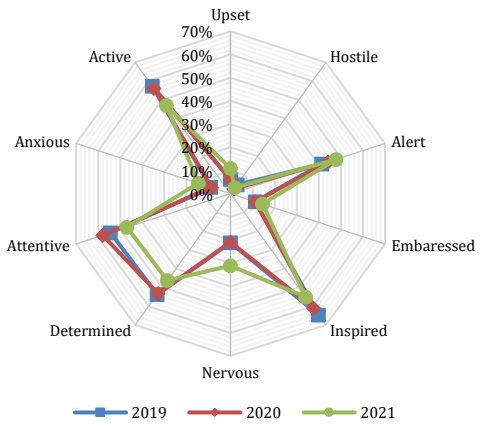

Fig. 4 – Students' emotional states based on PANAS.

3.4 students' self-reported health

The students' self-reported health was identified through analysing the data related to diseases and home-related symptoms. In terms of diseases, **Fig. 5** shows the percentages of students who suffered from them in the last 12 months. Four diseases showed to be significantly different among the three groups. These were bronchitis/pneumonia (*p=0.001*), wheezing (*p=0.005*), hay fever (*p=0.001*), and allergic rhinitis (*p=0.004*).

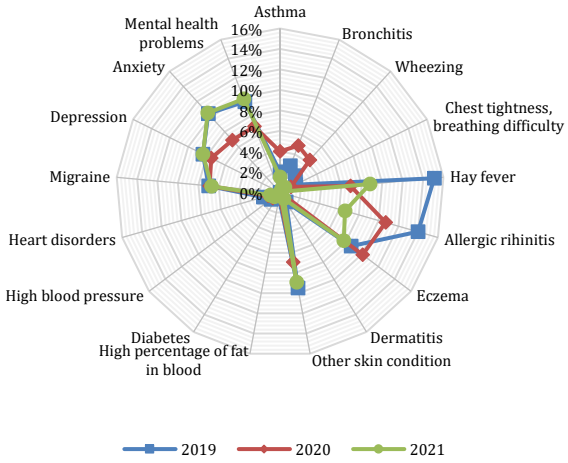

Fig. 5 – Percentages of students suffered from the disease in the last 12 months.

Regarding the home-related symptoms, **Fig. 6** illustrates the percentages of students who suffered from these while at home. For dry eyes (p<0.001), itchy or watering eyes (p=0.001), lethargy or tiredness (p<0.001), headache(p<0.001), there were significantly more students in 2021 suffering from them than in the other two years. Moreover, there were significantly less students in 2021 who suffered from blocked or stuffy nose (p=0.001) and there were significantly less students in 2019 who suffered from breathing difficulties (p=0.007).

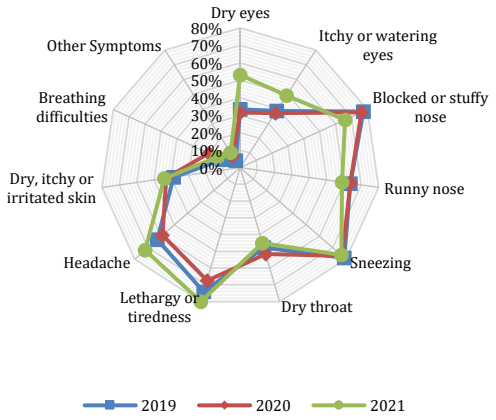

Fig. 6 – Percentages of students suffered from the home-related symptoms.

4. Discussion and Conclusion

This study examined the differences among university students' health and psychosocial status while at home before and during the COVID-19 pandemic. This was done by surveying three groups of students in March for three years: 2019, 2020, and 2021. The results showed that there was a significant difference in the number of hours that students stayed at home. The students during the COVID-19 pandemic recorded the highest number of hours during the weekdays (20 hours). In addition, there were significant differences found among the three groups regarding their psychosocial status. One of the key findings was that students in 2021 reported to be less inspired, active, and attentive, as well as they were more upset, anxious, and nervous than students before the COVID-19 pandemic. Moreover, the 2021 students were found to be more bored and sad, as well as less relaxed than the other two groups (2019 and 2020). In a previous study conducted by Aristovnik *et al.* [12] students were found to be suffering from boredom, anxiety, and frustration during the COVID-19 pandemic. Similarly, Son *et al.* [13] concluded that reported stress and anxiety of 71% of students increased during this pandemic. In addition, it was indicated that social distancing was one of the factors that affected the students.

In the current study, the students' health significantly differed among the three groups of students. For instance, the students in 2021 reported to suffer more from headaches and tiredness. This can be associated with the long time that students in 2021 used to stay at home. Also, Bluyssen *et al.* [14] found that staying at home was related to students' reported headache. Moreover, Zhang *et al.* [15] revealed that the indoor pollutants in homes such as dampness and mould were associated with the reported building-related symptoms such as headache and fatigue.

Thus, it can be concluded that during the COVID-19 pandemic more students suffered from both psychosocial as well as health related effects.

5. References

[1] Torresin S, Albatici R, Aletta F, Babich F, Oberman T, Elzbieta A, et al. Indoor soundscapes at home during the COVID-19 lockdown in London – Part I : Associations between the perception of the acoustic ´ activity and well-being environment , occupants. Appl Acoust 2021;183:108305. https://doi.org/10.1016/j.apacoust.2021.108305.

[2] Dzhambov AM, Lercher P, Stoyanov D, Petrova N, Novakov S, Dimitrova DD. University students' self-rated health in relation to perceived acoustic environment during the covid-19 home quarantine. Int J Environ Res Public Health 2021;18:1–21. https://doi.org/10.3390/ijerph18052538.

[3] Tong H, Aletta F, Mitchell A, Oberman T, Kang J. Science of the Total Environment Increases in noise complaints during the COVID-19 lockdown in Spring 2020 : A case study in Greater London , UK. Sci Total Environ 2021;785:147213. https://doi.org/10.1016/j.scitotenv.2021.147213.

[4] Bluyssen PM. The need for understanding the indoor environmental factors and its effects on occupants through an integrated analysis. IOP Conf. Ser. Mater. Sci. Eng., 2019. https://doi.org/10.1088/1757-899X/609/2/022001.

[5] Bluyssen PM. Towards an integrated analysis of the indoor environmental factors and its effects on occupants. Intell Build Int 2020;12:199–207.

[6] Bluyssen PM. The Indoor Environment Handbook: How to Make Buildings Healthy and Comfortable. Earthscan; 2009.

[7] Bluyssen PM. The healthy indoor environment: how to assess occupants' wellbeing in buildings. London;New York; Routledge/Taylor & Francis Group; 2014.

[8] Smith BJ, Lim MH. How the COVID-19 pandemic is focusing attention on loneliness and social isolation. Public Heal Res Pr 2020;30:2–5.

[9] Cao W, Fang Z, Hou G, Han M, Xu X, Dong J, et al. The psychological impact of the COVID-19 epidemic on college students in China. Psychiatry Res 2020;287:112934. https://doi.org/10.1016/j.psychres.2020.112934.

[10] Bluyssen PM, Roda C, Mandin C, Fossati S, Carrer P, de Kluizenaar Y, et al. Self-reported health and comfort in ' modern ' office buildings : first results from the European OFFICAIR study. Indoor Air 2016;26:298–317. https://doi.org/10.1111/ina.12196.

[11] Thompson ER. Development and validation of an internationally reliable short-form of the positive and negative affect schedule (PANAS). J Cross Cult Psychol 2007;38:227–42.

https://doi.org/10.1177/0022022106297301.
[12] Aristovnik A, Keržič D, Ravšelj D, Tomaževič N, Umek L. Impacts of the COVID-19 Pandemic on Life of Higher Education Students: A Global Perspective. Sustain 2020;12:1–34. https://doi.org/10.3390/su12208438.
[13] Son C, Hegde S, Smith A, Wang X, Sasangohar F. Effects of COVID-19 on college students' mental health in the United States: Interview survey study. J Med Internet Res 2020;22:1–14. https://doi.org/10.2196/21279.
[14] Bluyssen PM, Zhang D, Ortiz M. Self-reported rhinitis and headaches of students from universities in Taiwan , Chile , Suriname , China and the Netherlands , and its association with their home environment. Intell Build Int 2021;0:1–11. https://doi.org/10.1080/17508975.2021.1964424.
[15] Zhang X, Norbäck D, Zhang Y, Li B, Zhao Z, Huang C, et al. Dampness and mold in homes across China : Associations with rhinitis , ocular , throat and dermal symptoms , headache and fatigue among adults. Indoor 2019:30–42. https://doi.org/10.1111/ina.12517.

Data Statement

The datasets generated during and/or analysed during the current study are not available because further analysis will be carried out but the authors will make every reasonable effort to publish them in near future.

Review on Overheating Evaluation Methods in National Building Codes in Western Europe

Ramin Rahif, Deepak Amaripadath, Shady Attia

Sustainable Building Design Lab, Dept. UEE, Faculty of Applied Science, Université de Liege, Belgium

Abstract. Due to the current rate of global warming, overheating in buildings is expected to become more intense and frequent. High indoor temperatures affect occupants' comfort, productivity, and health. In the last twenty years, the "time-integrated overheating evaluation methods" have been introduced in the standards to describe the extent of overheating over some time and prevent the uncomfortable phenomena. In this paper, we critically review those methods found in the national and regional building codes based on the Energy Performance of Building Directive (EPBD) in Belgium, France, Germany, the UK, and the Netherlands. The methods are analysed according to eight measures including, 1) dependency on comfort model, 2) dependency on comfort categories, 3) symmetric or asymmetric, 4) all hours or occupied hours, 5) normalization to occupied hours, 6) short-term or long-term criteria, 7) single-zone or multi-zone, and 8) comfort-based or heat balance-based. We found that the occupant adaptation is largely neglected in the reviewed building codes except for France. We also found that the building codes in Belgium (Wallonia and Flanders), Germany, the UK, and the Netherlands have only or at least one criterion based on the steady-state heat balance equations. The study outcomes also provide practical recommendations for policymakers to improve the regional and national overheating evaluation methods towards climate change-proof residential buildings.

Keywords. EPBD, discomfort, Thermal comfort, Regulations, Temperate climate, building.
DOI: https://doi.org/10.34641/clima.2022.357

1. Introduction

The extreme outdoor temperatures have become more intense and frequent during the last decades. In the sweltering summer of 2003, the maximum outdoor air temperatures between 35-40.2°C are recorded in the Netherlands, France, Belgium, the UK, and Germany [1–4]. The Situation is expected to worsen with the current rate of global warming. The European Environment Agency (EEA) predicted a rise in the annual average air temperature between 2.5-4°C over Europe by the end of this century.

The increase in outdoor temperatures will exacerbate the overheating incidents in buildings. High indoor temperatures affect occupants' comfort, productivity, and health [5,6]. In total, over 35,000 people died during the summer 2003 heatwaves [7]. To prevent health issues for the occupants and ensure comfort in buildings, it is necessary to properly define overheating and its criteria in the regulations.

There exists several methods that attempt to assess the human response to the surrounding thermal environment [8]. They aim to assess the human thermal perception from an exposed environment. There is a new group of indices that emerged to describe, synthetically, the extend of overheating and thermal comfort qualities of buildings over time. Those indices are termed as *"time-integrated comfort/discomfort evaluation methods"* [9].

Carlucci et al. [10] classified 15 time-integrated discomfort indices into four homogenous families (i.e., percentage indices, cumulative indices, risk indices, and averaging indices). Carlucci [11] performed quantitative analysis on 16 time-integrated discomfort indices focusing on overheating discomfort applied on an office building. The study results indicate that different indices identify different variants (in total 54 variants were analysed) as the optimal case. Zero Carbon Hub (an organization to execute zero energy homes policy in the UK) [12] reviewed the overheating assessment methods in different regulatory sources such as Standard Assessment Procedure (SAP), CIBSE Guide A (2006), CIBSE Guide A (2015), CIBSE TM52, Passive House, BB 101, and Part L2A of the UK building regulation. In addition, the UK National House-Building Council (NHBC) [13] published a review report investigating overheating criteria in different regulatory and guidelines in the UK.

There is a limited number of studies [14] that particularly reviewed and analyzed the overheating calculation methods introduced in national or regional implementations of the Energy Performance of Building Directive (EPBD). In 2012, a legislative framework by European Commission

Copyright ©2022 by the authors. This conference paper is published under a CC-BY-4.0 license.

(EC) is established that includes the EPBD [15]. The EPBD targets energy efficiency and carbon emission as well as ensuring a comfortable environment in the European building stock. The overarching legislation introduced by the EPBD must be interpreted and implemented by the Member States within the national or regional building policies.

In this paper, we narrow our scope to the overheating calculation methods in the EPBD regulations of five European countries, including Belgium, France, Germany, the UK, and the Netherlands. Those countries form a large portion of the temperate regions, and together contain 47% of the total population and 30% of the total area considering the EU and the UK [16–18].

This paper provides recommendations for policymakers to improve the building codes towards climate change-proof buildings.

2. Review methodology

2.1 Boundary conditions

Towards providing an in-depth qualitative assessment, we set some boundary conditions. First, this study targets the regulations proposed for the residential buildings since, a) most of the European building stock is composed of the residential units; the share of residential buildings is between 60-89% over the EU and the UK according to the European Union (EU) buildings factsheet, b) people, especially vulnerable elderly people, spend most of the time at homes [13], c) overheating during the sleeping time in the bedrooms is reported as a major concern for the occupants' health [12,19].

The second boundary condition relies on the focus on temperate regions. The building design in such regions is more into maintaining the heat during the heating season to reduce the total building energy consumption [20]. This leads to the prevention of heat loss during the cooling season and thus aggravates the overheating problems.

2.2 Measures

Some measures were introduced in a previous study by Carlucci et al. [10] such as dependency on a comfort model, dependency on comfort categories, symmetric/asymmetric, and inclusion/exclusion of comfort thresholds. This paper includes these measures along with a set of newly defined ones. Overall, the measures of the assessment are as follows,

- **Dependency on comfort model:** this measure evaluates whether the method is based on a comfort model. In case there exists any underlying comfort model, which of the adaptive and static comfort models is specified.

- **Dependency on comfort categories:** this measure investigates whether the underlying comfort model is presented in different categories. The shift from one category yields discontinuities and different results.

- **Symmetric or asymmetric:** this measure evaluates whether the discomfort index quantifies overheating (asymmetric), overcooling (asymmetric), or both (symmetric). The symmetric indices do not imply whether the discomfort is arising from the overheating or overcooling incidents.

- **All hours/occupied hours in a period:** this measure evaluates whether the method is extended over all hours or only the occupied hours. Inclusion of all hours adds the effect of unoccupied hours that is not of interest.

- **Normalization to occupied hours:** this measure assesses whether the method is normalized to the occupied hours. The normalized metrics allow comparing the comfort conditions in buildings with different occupancy profiles.

- **Short-term or long-term criteria:** short-term criteria are maximum threshold values to limit the short-term (i.e., hourly, daily, and weekly) overheating events during the heatwaves. Long-term criteria are maximum threshold values to limit the extensive overheating during monthly, seasonal, and yearly periods.

- **Single-zone or multi-zone:** this measure assesses whether the method is considering the building as a single-zone or has a multi-zone approach in overheating evaluations.

- **Comfort-based or heat balance-based:** this measure shows whether the method is based on comfort parameters (i.e., air temperature, radiant temperature, relative humidity, air velocity, metabolic rate, and clothing factor) or heat balance between the indoor and outdoor environments.

3. Results

In this section, we provide the results of review and analysis on overheating evaluation methods in Belgium, France, Germany, the UK, and the Netherlands. A general description of each method is provided followed by a qualitative assessment based on the eight previously defined measures (see Section 2.2).

3.1 Belgium

In Belgium, each region (i.e., Wallonia, Flanders, and Brussels) oversees the implementation of the EPBD in their regional building codes. Brussels as the first region that adopted the overheating criteria defined by the Passive House standard [21,22]. The Passive

House standard contains an asymmetric index called Percentage of hours Outside the Range (*%PhOR*) [-],

$$\%PhOR = \frac{\sum_{i=1}^{annual\ hours} wf_i . h_i}{\sum_{i=1}^{annual\ hours} h_i} \times 100$$
$$\text{where} \begin{cases} wf_i = 1 & ; \quad T_{a,i} > 25°C \\ wf_i = 0 & ; \quad T_{a,i} \leq 25°C \end{cases} \tag{1}$$

wf_i [-] is the weighting factor, h_i [h] is the hour counter, and $T_{a,i}$ [°C] is the indoor air temperature. A fixed temperature limit of 25°C is defined above the overheating starts. To comply with the overheating requirements, it is required that the *%PhOR* does not go beyond 5% (10% in the Passive House standard) during a year in all living areas.

In Wallonia and Flanders, a quasi-steady-state heat balance method based on ISO 13790 is utilized for overheating calculations in new and renovated residential buildings without active cooling [23,24]. Accordingly, the I_{overh} [Kh] is defined that sums up the normalized monthly excess of heat gains $Q_{excess\ norm,\ m}$ [Kh] based on a predefined setpoint temperature,

$$I_{overh} = \sum_{m=1}^{12} Q_{excess\ norm,m} \tag{2}$$

$$Q_{excess\ norm,m} = \frac{(1 - \eta_{util,overh,m}) . Q_{g,overh,m}}{H_{T,overh} + H_{V,overh,m}} . \frac{1000}{3,6} \tag{3}$$

$\eta_{util,overh,m}$ [-] is the utilization factor concerning the monthly heat gains and heat losses, $Q_{g,overh,m}$ [MJ] is the sum of monthly internal and solar gains, $H_{T,overh}$ [W/K] is the conduction heat transfer coefficient, and $H_{V,overh,m}$ [W/K] is the ventilation heat transfer coefficient. To comply with the overheating criteria, a range 1000 Kh<I_{overh} <6500 Kh is specified. If a building exceeds the 6500 Kh the probability of installing the active cooling system becomes 100%.

3.2 Germany

The national building code in Germany is translated into DIN 4108-2 [25] to calculate the overheating. DIN 4108 sets two criteria as follows,

Criterion (1): it is a simplified method based on some standard boundary conditions. It requires that the summer overheating in the most critical room/zone of the building is ensured via solar transmittance S_{vorh} [-] index that is calculated by,

$$S_{vorh} = \frac{\sum_j (A_{W,j} \times g_{tot,j})}{A_G} \tag{4}$$

$A_{W,j}$ [m²] is the window area of zone j, $g_{tot,j}$ [-] is total energy transmittance of the glazing including sun protection of zone j, and A_G [m²] is the net floor area. The calculated S_{vorh} [-] then is compared to a maximum threshold value S_{zul} [-],

$$S_{zul} = S_1 + S_2 + S_3 + S_4 + S_5 + S_6 \tag{5}$$

The S_1 to S_6 are solar input parameters that are given in DIN 4108. To comply with criterion (1), the calculated S_{vorh} should be equal or less than S_{zul}.

Criterion (2): this criterion is based on the Degree hours (*Dh*) [Kh] index that should be calculated for the most critical room of the building by using dynamic simulations. The *Dh* is derived by,

$$Dh = \sum_i (T_{op,i} - T_{max,comf,th}) \times h_i \tag{6}$$

$T_{op,i}$ [°C] is the indoor operative temperature at the time *i*, $T_{max,comf,th}$ [°C] is the maximum comfort threshold, and h_i [h] is the hour counter. The maximum threshold for the calculation of *Dh* is climate-specific (25°C for "Klimaregion A" Rostock, 26°C for "Klimaregion B" Potsdam, and 27°C for "Klimaregion C" Mannheim). The compliance is achieved if the *Dh* value does not exceed 1200 Kh during the year.

3.3 France

In France, the overarching EPBD regulation is translated into a national standard called "*Règlementation Environnementale (RE2020)*" [26]. The RE2020 evaluates the overheating by using the *Dh* (see equation (6)) index in new residential buildings during the summer season. The underlying comfort threshold for the calculation of *Dh* (i.e., $T_{max,comf,th}$) must be derived from the Category II of the adaptive comfort model in EN15251 using the equations below,

$$T_{max,comf,th} = 0.33 T_{rmo} + 18.8 + 3$$
$$where\ 10°C \leq T_{rmo} \leq 30°C \tag{7}$$

T_{rmo} [°C] is the running mean outdoor air temperature calculated by,

$$T_{rmo} = (1 - \alpha) . \{T_{ed-1} + \alpha T_{ed-2} + \alpha^2 T_{ed-3+\cdots}\} \tag{8}$$

α [-] is the weighting factor between 0 and 1 (recommended value is 0.8 by ISO and EN standards), T_{ed-i} [°C] is the daily mean outdoor air temperature for i-th previous day. The calculated *Dh* value shall not exceed the maximum threshold of 1250 Kh during a summer weather scenario similar to that of 2003. It corresponds to a period of 25 days when the indoor operative temperature is at 30°C during the day and 28°C during the night. The same criterion applies to all climate zones across the

country.

3.4 UK

In the UK, the overheating calculation method for the EPBD is established for new buildings in Approved Document L1B [27]. The Approved Document L1B enforces Standard Assessment Procedure (SAP) [28] to establish the overheating calculation method and criteria. In Appendix P of the SAP, the buildings must comply with the so-called *"overheating check"*. Accordingly, the internal threshold index ($T_{threshold}$) is defined to quantify the overheating during the summer season. The $T_{threshold}$ [°C] is used to assess the likelihood of high internal temperatures that can be calculated by summing up the mean external temperature during the summer month (T_e^{summer}) [°C], the ratio between the monthly heat gains G [W] and losses H [W], and an increment factor concerning the building's thermal mass ΔT_{mass},

$$T_{threshold} = T_e^{summer} + {}^{G}/_{H} + \Delta T_{mass} \quad (9)$$

$$\Delta T_{mass} = 2.0 - 0.007 \times TMP \text{ if } TMP < 285 \quad (10)$$

TMP [kJ/m2K] is the thermal mass factor of the building envelope components. The $T_{threshold}$ must be calculated for June, July, and August. The resulted value should be compared with the ranges specified in Table 1 to estimate the likelihood of high indoor temperatures during hot weather conditions.

Table 1. – The ranges of $T_{threshold}$ corresponding to the liklihood of high internal temperatures.

$T_{threshold}$ [°C]	Likelihood of high internal temperatures during hot weather
> 20.5°C	Not significant
20.5°C – 22°C	Slight
22°C – 23.5°C	Medium
≥ 23.5°C	High

3.5 Netherlands

The EPBD legislation in the Netherlands is interpreted and included in the standard NTA 8800 [29]. It containts the overheating assessment method specified for Almost Energy Neutral Buildings (BENG) (in Dutch *"Bijna Energie Neutrale Gebouwen"*). For this aim, a dimensionless metric TO_{juli} [-] (Criterion 1) is defined depending on the facade surface per orientation. The TO_{juli} should be calculated for the month of July as follows,

$$TO_{juli;or,zi} = \frac{(Q_{C,nd,juli,or,zi} - Q_{C,HP,juli,or,zi}) \times 1000}{(H_{C,D,juli,or,zi} + H_{gr,an,juli,or,zi} + H_{C,ve,juli,or,zi}) \times h_{juli}} \quad (11)$$

Where,

- $Q_{C,nd,juli,or,zi}$ [kWh] is cooling demand for orientation or in zone zi.
- $Q_{C,HP,juli,or,zi}$ [kWh] is the extracted energy from the cooling unit by the booster heat pump for orientation or in zone zi.
- $H_{C,D,juli,or,zi}$ [W/K] is direct heat transfer coefficient by transmission between the heated space and the outdoor air except for the ground floor for orientation or in zone zi.
- $H_{gr,an,juli,or,zi}$ [W/K] is the direct heat transfer coefficient by the transmission for building elements in thermal contact with the ground for orientation or in zone zi.
- $H_{C,ve,juli,or,zi}$ [W/K] is the direct heat transfer coefficient through ventilation for orientation or in zone zi.
- h_{juli} [h] is the total time over July.

The TO_{juli} should not exceed the maximum limit value of 1. It should be mentioned that if the building is provided by space cooling, there is no need for the estimation of TO_{juli}.

In addition, NTA 8800 introduces the Weighted Limit Temperature (GTO) [-] (Criterion 2) for more accurate calculation of overheating once the TO_{juli} slightly exceeds its maximum value. In this method, the hours of when the actual or calculated Predicted Mean Vote (PMV) [-] exceeds the value of +0.5 are weighted proportional to the Predicted Percentage Dissatisfied (PPD) [%]. The formula to calculate the GTO is,

$$GTO = \sum Wf_{i,NTA\ 8800} \quad (12)$$

$Wf_{i,\ NTA\ 8800}$ [-] is the weighting factor (see Table 2). A maximum limit value of 450 is set for GTO.

Table 2. - The $Wf_{i,\ NTA\ 8800}$ corresponding to the PMV and PPD values for the calculation of GTO.

PMV [-]	PPD [%]	$Wf_{i,\ NTA\ 8800}$ [-]
0	5	0
0,5	10	1,0
0,7	15	1,5
1,0	26	2,6

In Table 3, we listed the overheating assessment

methods in the five above-mentioned countries and analyzed them based on eight measures specified in Section 2.2.

4. Conclusions

This paper analyses the overheating evaluation methods in five European countries including Belgium, France, Germany, the UK, and the Netherlands. In total, eight measures are utilized as, 1) dependency on comfort model, 2) dependency on comfort categories, 3) symmetric or asymmetric, 4) all hours or occupied hours, 5) normalization to occupied hours, 6) short-term or long-term criteria, 7) single-zone or multi-zone, and 8) comfort-based or heat balance-based.

To summarize the main findings of this paper we provide the list below:

1. The occupant adaptation to the exposed thermal environment (via physiological, psychological, and behavioural actions) is largely neglected in the reviewed standards except for France.

2. The building codes in Belgium (Wallonia and Flanders regions), Germany, and the UK have only or one criterion based on the heat balance equations. Such an approach is unable to perfectly represent the occupant thermal sensation that is determined by six main factors (i.e., air temperature, radiant temperature, relative humidity, air velocity, metabolic rate, and clothing).

3. In Belgium (Wallonia and Flanders) and the UK, the overheating evaluation is performed by considering the whole building as a single zone. This approach includes the effect of trivial zones (e.g., attic, warehouse, etc.) in the assessments and prevents the identification of the most/least critical zones.

4. The building codes define the annual (long-term) criterion in Belgium, annual and seasonal (long-term) criteria in Germany, annual (long-term) criterion in France, monthly (long-term) criterion in the UK, and monthly (only for July) (long-term) criterion in the Netherlands. Hence, the short-term (hourly, daily, and weekly) criteria are neglected.

5. Non-of the reviewed regulations include provisions regarding climate change. Hence, there is a need for climate change-sensitive overheating evaluation methods and indices [30] to be embedded in the building codes to prevent the increasing risk of overheating in the future.

To summarize the main recommendations and future research ideas of this paper we provide the list below:

- We recommend considering full criteria (i.e., short-term and long-term) in the building design and operation policies. This not only prevents overheating during the short-term heatwave events but also ensures year-round comfort.

- We recommend the inclusion of comfort-based overheating evaluation methods in future revisions of the building codes to better represent the occupant thermal sensation. The new methods should be normalized to the occupied hours enabling the evaluation and comparison of comfort in buildings with different occupancy profiles.

- As future research ideas, we recommend further investigation of the overheating calculation methods using quantitative approaches. Also, future research is recommended to explore the building codes for non-residential buildings as well as for the other Member States across Europe.

5. Acknowledgement

This research was funded by the Walloon Region under the call 'Actions de Recherche Concertées 2019 (ARC)' (funding number: ARC 19/23-05) and the project OCCuPANt, on the Impacts Of Climate Change on the indoor environmental and energy PerformAnce of buildiNgs in Belgium during summer. The authors would like to gratefully acknowledge the Walloon Region and the University of Liege for funding. We would like to also acknowledge the Sustainable Building Design (SBD) lab at the Faculty of Applied Sciences at the University of Liege for valuable support during the content analysis and curation of the data. This study is a part of the International Energy Agency (IEA) EBC Annex 80 – “Resilient cooling of buildings” project activities to define resilient cooling in residential buildings.

Table 3. – Summary of overheating assessment methods in national building codes based on the EPBD.

Country (region)	Regulatory document based on the EPBD	Static (S) / Adaptive (A)	Category-based	Symmetric (S) / Asymmetric (A)	All hours (A) / Occupied hours (O)	Normalized to occupied hours	Short-term (S) / Long-term (L)	Single-zone (S) / Multi-zone (M)	Heat balance-based (H) / Comfort-based (C)
Belgium (Brussels)	Réglementation sur la Performance Energétique des Bâtiments (PEB Brussels)	S	×	A	A	×	L	M	C
Belgium (Wallonia and Flanders)	Réglementation sur la Performance Energétique des Bâtiments (PEB Wallonia) Energieprestatie en Binnenklimaat (EPB Flanders)	S	×	A	A	×	L	S	H
Germany	Deutsches Institut für Normung (DIN) 4108-6	S	×	A	A (Criterion 2)	×	L (Criterion 2)	M	H (Criterion 1) & C (Criterion 2)
France	Règlementation Environnementale (RE2020)	A	×	A	A	×	L	M	C
UK	Approved Document L1A	S	×	A	A	×	L	S	H
Netherlands	Netherlands Technical Agreement (NTA) 8800	S	×	A	A	×	L	M	H (Criterion 1) & C (Criterion 2)

6. References

[1] Garssen J, Harmsen C, De Beer J. The effect of the summer 2003 heat wave on mortality in the Netherlands. Eurosurveillance 2005;10:13SP 557-14. https://doi.org/10.2807/esm.10.07.00557-en.

[2] Perry M, Golding N. Range of environmental temperature conditions in the United Kingdom. Met Office, Department of Transport, Exeter, UK; 2011.

[3] Pirard P, Vandentorren S, Pascal M, Laaidi K, Le Tertre A, Cassadou S, et al. Summary of the mortality impact assessment of the 2003 heat wave in France. Eurosurveillance 2005;10:7–8.

[4] Fink AH, Brücher T, Krüger A, Leckebusch GC, Pinto JG, Ulbrich U. The 2003 European summer heatwaves and drought–synoptic diagnosis and impacts. Weather 2004;59:209–16.

[5] Lan L, Tsuzuki K, Liu Y, Lian Z. Thermal environment and sleep quality: A review. Energy and Buildings 2017;149:101–13. https://doi.org/10.1016/j.enbuild.2017.05.043Get.

[6] Hooyberghs H, Verbeke S, Lauwaet D, Costa H,

Floater G, De Ridder K. Influence of climate change on summer cooling costs and heat stress in urban office buildings. Climatic Change 2017;144:721–35. https://doi.org/10.1007/s10584-017-2058-1.
[7] Brücker G. Vulnerable populations: lessons learnt from the summer 2003 heat waves in Europe. Eurosurveillance 2005;10:1–2. https://doi.org/10.2807/esm.10.07.00551-en.
[8] Enescu D. A review of thermal comfort models and indicators for indoor environments. Renewable and Sustainable Energy Reviews 2017;79:1353–79. https://doi.org/10.1016/j.rser.2017.05.175.
[9] Rahif R, Amaripadath D, Attia S. Review on Time-Integrated Overheating Evaluation Methods for Residential Buildings in Temperate Climates of Europe. Energy and Buildings 2021;252:111463. https://doi.org/10.1016/j.enbuild.2021.111463.
[10] Carlucci S, Pagliano L. A review of indices for the long-term evaluation of the general thermal comfort conditions in buildings. Energy and Buildings 2012;53:194–205. https://doi.org/10.1016/j.enbuild.2012.06.015.
[11] Carlucci S. Thermal comfort assessment of buildings. Springer 2013. https://doi.org/10.1007/978-88-470-5238-3.
[12] Zero Carbon Hub. Impacts of Overheating: Evidence Review. Zero Carbon Hub, London, England; 2015.
[13] NHBC. Overheating in new homes: A review of the evidence. National House-Building Council, UK.; 2012.
[14] Attia S, Rahif R, Fani A, Amer M. Comparison of overheating risk in nearly zero-energy dwelling based on three different overheating calculation methods, KU Leuven; 2021, p. 30147–53.
[15] Recast E. Directive 2010/31/EU of the European Parliament and of the Council of 19 May 2010 on the energy performance of buildings (recast). Official Journal of the European Union 2010;18:2010.
[16] European Commission (EC). Eurostat - Tables, Graphs and Maps Interface (TGM) table. 2017.
[17] United Nations (UN). World Population Prospects - Population Division". United Nations; 2019.
[18] United Nations (UN). Demographic Yearbook - Table 3: Population by sex, rate of population increase, surface area and density. United Nations Statistics division; 2014.
[19] Kovats RS, Hajat S. Heat Stress and Public Health: A Critical Review. Annu Rev Public Health 2008;29:41–55. https://doi.org/10.1146/annurev.publhealth.29.020907.090843.
[20] Yannas S, Rodríguez-Álvarez J. Domestic overheating in a temperate climate: Feedback from London Residential Schemes. Sustainable Cities and Society 2020;59:102189. https://doi.org/10.1016/j.scs.2020.102189.
[21] IBGE. Performance Energétique des Bâtiments: Guide des exigences et des procédures de la réglementation Travaux PEB en Région de Bruxelles Capitale. Brussels, Belgium: 2017.
[22] Feist W, Kaufmann B, Schnieders J, Kah O. Passive house planning package. Passive House Institute, Darmstadt, Germany 2015.
[23] Gouvernement Wallon. Méthode PER 2018: MÉTHODE DE DÉTERMINATION DU NIVEAU DE CONSOMMATION D'ÉNERGIE PRIMAIRE DES UNITES RESIDENTIELLES. Wallonia, Belgium: 2018.
[24] Vlaams Energie- en Klimaatagentschap. Bijlage V Bepalingsmethode EPW: BEPALINGSMETHODE VAN HET PEIL VAN PRIMAIR ENERGIEVERBRUIK VAN RESIDENTIËLE EENHEDEN. Flanders, Belgium: 2020.
[25] Fux V. Thermische Gebäudesimulation zum sommerlichen Wärmeschutz nach DIN 4108-2: 2013. Hochschule Für Technik Stuttgart 2013.
[26] Ministère de la transition écologique. Réglementation environnementale RE2020. France: 2020.
[27] HM Government. The Building Regulations 2010: Conservation of fuel and power in new dwellings, Approved Document L1A. 2013 Edition Incorporating 2016 Amendments, UK: 2016.
[28] BRE (DECC). SAP 2012: The Government's Standard Assessment Procedure for Energy Rating of Dwellings. Watford, UK: 2012.
[29] NTA 8800. NTA 8800: Energieprestatie van gebouwen-Bepalingsmethode. Royal Netherlands Standardization Institute, Delft, Netherlands; 2019.
[30] Rahif R, Hamdy M, Homaei S, Zhang C, Holzer P, Attia S. Simulation-based framework to evaluate resistivity of cooling strategies in buildings against overheating impact of climate change. Building and Environment 2021:108599. https://doi.org/10.1016/j.buildenv.2021.108599.

Learning from innovative climate concepts in schools

Stijn van der Horst [a], Froukje van Dijken [b]

[a] bba binnenmilieu, The Hague, the Netherlands, sh-bba@binnenmilieu.nl.

[b] bba binnenmilieu, The Hague, the Netherlands, fd-bba@binnenmilieu.nl.

Abstract. Newly designed buildings should be energy efficient as well as comfortable. To achieve both, new HVAC concepts are designed. Unfortunately, the introduction of new HVAC concepts is not always successful, leading to discomfort and even health complaints among the occupants.
In this paper we describe three cases that we investigated recently: 1) A school with concrete core heating/cooling and natural air supply and mechanical exhaust. 2) A school with an all-air system with VRF units and heat pumps. 3) A monumental school building (secondary school) with pressure regulated ventilation (BaOpt) and ground heat pump. The occupants had the following complaints in the three cases: 1) complains about cold air draught and cold feet in the winter, spring and autumn and heat in the summer season. 2) complaints about air draughts, fluctuating temperatures, bad air quality and unpleasant odours. 3) Complaints concern heat in summer, cold in winter and intermediate season, and stuffy and dry air. The causes found for the indoor climate problems for the three cases: 1) The combination of natural air supply and low temperature heating. A heating pipe was installed in front of the air inlet but was unable to prevent the draught. 2) The central AHU did not have heating or cooling sections. In defrosting mode of the air heat pump, fluctuating air inlet temperatures were measured. When defrosting, the ventilation system switched to recirculation, with implications for the IAQ. Different zoning of the ventilation system and the heating and cooling system exacerbated the problems. 3) Due to the low air tightness of the building envelope, the ventilation system did not perform as intended. Only the classrooms near the air handling unit got fresh air. The ground heat pump did not function due to underground leakages, therefor the school did hardly have heating and no cooling. From these cases we learn that it is crucial to bring together technical / theoretical knowledge, practical expertise and the user perspective when working on innovative solutions. In this way we learn from practical experience which hopefully lead to improved and robust HVAC-systems.

Keywords. HVAC concept, ventilation, concrete core activation, variable refrigerant flow, BaOpt, classroom
DOI: https://doi.org/10.34641/clima.2022.149

1. Introduction

School buildings should promote learning performance and health and must be comfortable and energy-efficient as well. Current challenges include net zero energy buildings [1] and the Dutch energy transition as well as climate change. Besides the current pandemic asks for new ventilation regimes [2]. To achieve all these aims, new HVAC concepts are designed. Unfortunately, in practice we see that buildings with innovative climate concepts do not always perform as expected, which leads to complaints about the indoor climate. It is important that we learn from those cases.

The aim of this paper is to discuss and share lessons from practical experience that we learned from school buildings with failing innovative HVAC concepts, in order to avoid problems in future buildings. We believe that it is crucial to bring together technical / theoretical knowledge, practical expertise and the user perspective when working on innovative solutions.

2. Method

In this paper we describe three cases of school buildings that we investigated in the past years.

The schools discussed in this paper all have innovative climate concepts (Table 1).
Moreover, in all these buildings occupants have complaints about the indoor climate. The schools asked us to investigate the complaints of the occupants in relation to the indoor climate.

Copyright ©2022 by the authors. This conference paper is published under a CC-BY-4.0 license.

Tab. 1 – HVAC systems of the case studies.

	case 1	case 2	case 3
Heating	Ground heat pump	Air heat pump	Ground heat pump
Heating output	Concrete core	VRF system	Floor heating
Cooling	Ground heat pump	Air heat pump	Ground heat pump
Cooling output	Concrete core	VRF system	Floor cooling
Venti-lation	Natural air supply and mechanical exhaust	Mechanical ventilation system	BaOpt (mechanical ventilation)

For our indoor climate investigations, including the case studies in this paper, we use the Building-in-Use (BiU) approach [3]. This is a method of indoor climate research that has been specially developed to map complex indoor climate problems in an efficient way. Within this approach an inventory of user experiences and a thorough inspection of the building, work places and HVAC systems for risk factors for indoor climate problems are essential. An investigation takes the following steps:

1. *Questionnaire.* The complaints of the employees were collected through an online survey.
2. *Building/workplace survey*. During an on-site investigation, the relevant building and workplace factors are mapped out. For example, building physical characteristics, furnishing materials and use.
3. *Installation survey.* Based on random samples, it was investigated to what extent the climate installations are functioning properly. For example, the general operation, control settings and the hygienic condition of the AHU.
4. *Measurements.* Relevant parameters are measured in several rooms. For example, instantaneous measurements of the amount of fresh air supply/exhaust or long-term measurements of the room temperature, air inlet temperature and/or CO_2 concentration.
5. *Analysis of building documentation.* For example, design specificities or commissioning reports.

3. Results

The paragraph is structured as follows for each case. First, the climate system is briefly explained. Second, we summarized the main complaints from the online survey. Finally, we describe the causes found for the indoor climate problems at the building and installation survey in combination with the (long-term) measurements and documentation were linked to the complaints.

3.1 case 1: concrete core activation and natural air supply

This school building (elementary school) is built in 2009. It has a ground heat pump and is heated and cooled with a concrete core system. The ventilation system is natural air supply and mechanical exhaust ventilation (see figure 1). Fresh air enters the room through baffle chambers above the windows. In front of the ventilation registers, a heating pipe is installed to prevent draught. Moreover, the ventilation system is occupancy driven. An occupancy sensor in the classroom detects if the room is in use. When motion in the room is detected, a signal is sent to open the exhaust air damper for the classroom.

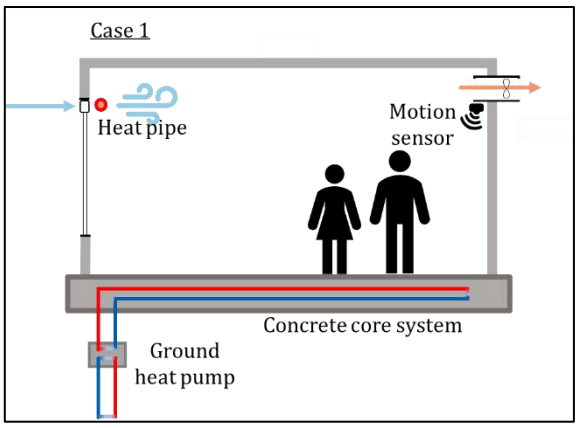

Fig. 1 – Case 1, schematic representation of climate concept.

In this school, the employees complain about cold air draught and cold feet in the winter, spring and autumn and heat in the summer season. Besides the employees have a sensation of dryness.

The combination of natural air supply and low-temperature heating causes complaints about draught in the winter period. The heating pipe in front of the registers seems not be sufficient to prevent draught.

The exhaust air damper can only be fully open or closed. When the sensor detects a person, the exhaust damper goes fully open which often doesn't correspond with the actual occupation of the classroom, for example in the morning and afternoon when only the teacher is in the classroom. This means that the amount of ventilation does not always fit the number of people in de classroom. As a result, too much cold air can be supplied into the classroom in the winter, which leads to complaints about cold and draught.

To prevent draught, employees close the ventilation registers above the windows in order to avoid the supply of cold outside air. As effect, the air from the corridor is sucked into the classroom instead of fresh air from outside, leading to a decreased air quality. Moreover, we found that closing both the registers above the windows and the door to the corridor this causes a fairly strong air stream over the floor

through the gap below the door. This air stream contributes to the observed complaints about cold feet.

Because of the concrete core heating and cooling, open suspended ceilings are used. A disadvantage of the open suspended ceiling is that dust collects on top of it, which is detrimental to air quality. Contaminants irritate the mucous membranes, which is experienced as 'dry air' [4]. However, some classrooms suspended ceilings. In these rooms the capacity for heating and cooling was utterly insufficient, leading to thermal comfort complaints.

3.2 case 2: all-air climate system (VRF) with air heat pumps

The second school building (secondary school) is built in 2011. The building has an all-air system with Variable Refrigerant Flow (VRF) units and air heat pumps (see figure 2). The air handling units had recirculation damper but did not have heating or cooling sections.

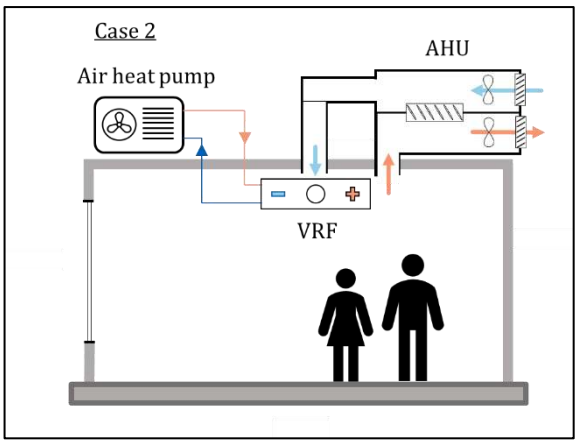

Fig. 2 – Case 2, schematic representation of climate concept.

The main complaints were about cold throughout the year, complaints about air draughts and complaints about fluctuating temperatures. In terms of air quality, there are complaints about 'dry', dusty, stale, stuffy air, and complaints about unpleasant odours.

A VRF system is less suitable for regulating a constant inlet temperature. In this case, the changes in the inlet temperature are larger, because the air handling unit does not preheat or cool the air. Besides this, in winter the air heat pump can turn into the defrosting mode. When the heat pump is defrosting, no heat is delivered to the VRF units in the classrooms. The result is that the inlet temperature can drop by as much as 30°C from 35°C to 5°C within 10 minutes (see figure 3), which, in certain outdoor circumstances, happened several times a day. Both the low inlet temperature and the changes in inlet temperature contribute to the complaints about cold, air draught, and fluctuating temperatures.

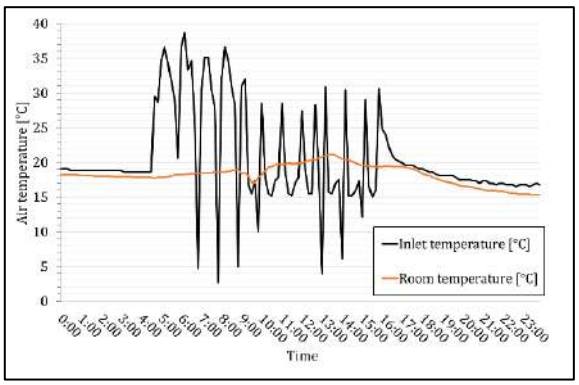

Fig. 3 – Measured inlet temperature and room temperature in a classroom of case 2.

To prevent cold air supply in the rooms when the heat pump is defrosting, the ventilation system can temporarily switch to the recirculation mode, which has a negative impact on indoor air quality in general. Since the exhaust of the toilets was connected to the central ventilation system, exhaust air from the toilets is spread through the building when the ventilation system is in recirculation mode. The odour of the toilets was noticeable in the classrooms, which explains the complaints about unpleasant odours.

Different zoning of the ventilation system and the heating and cooling system exacerbated the problems. The VRF units are divided into two zones: a south and a north zone. The ventilation system is divided into three zones: west, middle, and east. The disadvantage of this layout is that if one of the two air heat pumps must defrost, all air handling units will recirculate the air. As a result, air is recirculated more frequent than necessary during the heating season.

3.3 case 3: monument with pressure regulated ventilation (BaOpt)

The third school is a renovated monumental school building (secondary school). The building is renovated in 2015. The HVAC system is characterised by pressure regulated mechanical ventilation (BaOpt) [5] and a ground heat pump with floor heating and cooling (see figure 4). For the winter season, there are also gas-fired peak boilers.

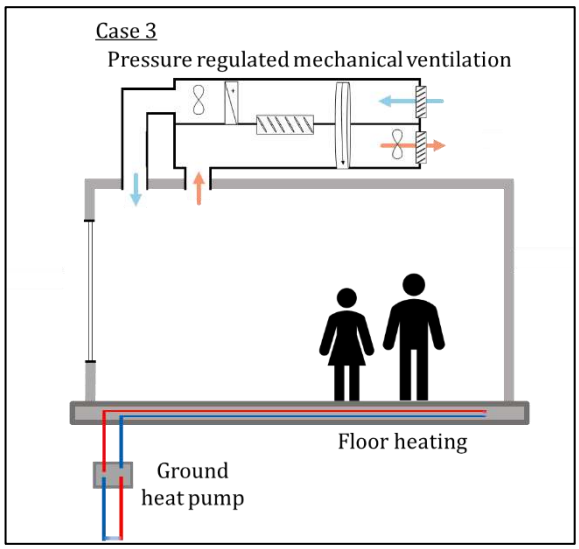

Fig. 4 – Case 3, schematic representation of climate concept.

In this building, the main complaints concern heat in summer, cold in winter and the intermediate season, and complaints about stuffy and dry air.

The complaints about air quality are caused by the fact that the pressure regulated ventilation system is not working properly. Due to the low airtightness of the monumental building envelope, the ventilation system did not perform as intended. The necessary pressure build-up hinders the proper functioning of the ventilation system. As a result, only the classrooms near the air handling unit got fresh air. All other classrooms were generally stale and warm and explain the complaints about stuffy air.

In addition, the air ducts seemed heavily polluted with dust and dirt that seemed to originate from the construction phase. This leads to complaints about 'dry air' (mucosal irritations) [4]. The air handling unit also has various components that are detrimental to air quality (including rotary heat exchanger, recirculation section) [6]. This enhances the complaints about stuffy air or 'dry air'.

To make things worse, the ground heat pump did not function due to an underground leakage. As a result, the school had hardly any heating and no cooling for few years. Because of non-technical issues the lack of heating and cooling capacity was only resolved a few years after the building was taken into occupation.

The lack of cooling and sufficient heating capacity explains the complaints about heat in summer and cold in winter. Because the heater battery also did not get any hot water, the supply air was not preheated. Also, the ventilation system was not working properly with as a consequence the heat recovery was not working. This explains the complaints about draught.

4. Discussion

Below, per case the problems related to the climate systems are discussed, indicating which lessons can be learned in the design of new school buildings.

Case 1 had natural air supply in combination with concrete core conditioning heating. To prevent air draught a heat pipe is installed in front of the registers. The results of the questionnaire shows that the heating pipe in front of the registers did not give the desired effect in preventing air draught. Because the registers can be open and closed by the occupants of the classrooms, the ventilation is not robust for occupant behaviour. From practice, we know that people will close those registers if they feel air draught from the registers, with as a result no fresh air is entering the classroom. Already in the design stage, this kind of problems should be thought out to prevent air draught and lack of ventilation in the classroom.

In a building with a concrete core system, the designer also needs to consider what kind of floor and ceiling can be used. The finishing should not affect the heating and cooling rate of the concrete core. In this case an open suspended ceiling was used. Disadvantage of open ceiling is that it catches a lot of dust. Some classrooms, though, had complete closed suspended ceilings. For those classrooms it seemed to have a serious impact on the cooling rates.

In case 2, several choices were made in the design stage with risks of a poor indoor climate. Fluctuating temperatures of the VRF system and the defrosting cycles of the air heat pump are well known characteristics of these systems. By not applying a heating battery in the air handling unit to cover thermal comfort issues, it is shown that too little attention has been paid to the comfort of the users during the design phase. The same applies to recirculating air in the school, knowing that the toilets are also connected to the same ventilation system. With a different zoning of the ventilation system and the heating and cooling system risks could have been limited.

Also, in case 3 the design stage was taken a risk using a pressure regulated ventilation system in combination with a monumental school building. One of the requirements for a good function this ventilation system is the airtightness of the building. In practice, we know that achieve an airtight building is difficult, especially for old buildings. We are not sure that the designers were aware of the importance of the air tightness of the building envelop with this kind of ventilation system. It seemed that no extra efforts were made to achieve the minimum airtightness needed. Note that opening windows, which is important for the perceived indoor climate in buildings, also affects the pressure differences in the building. Pressure regulated ventilation doesn't work when windows are open.

The combination of an unsuitable ventilation system and the bad luck with the leakage of the ground heat pump made the indoor climate problems even worse.

Some of the complaints about the indoor climate in those three cases, could already be tackled in the design process of the buildings. Assessing the design regarding indoor environment/comfort is not yet a standard procedure in the design process. Also commissioning after completion of the building is not always common, in order to check if the climate system is preforming as designed. Evaluation of climate system in the design phase and a check of the building performance at completion and the first period of occupation by an independent indoor climate specialist seemed successful [7]. Therefore, we need clear and testable agreements about the performance. Finally, attention must also be paid to maintenance and operating costs in the design phase in order to make sure that adequate maintenance takes places in order to sustain the achieved performance.

5. Conclusion

The introduction of new HVAC concepts is not always successful, leading to discomfort and even health complaints among the occupants.

From these cases, we learn that it is crucial to bring together technical / theoretical knowledge as well as practical expertise and the user perspective when working on innovative solutions. In all cases studies already most of the problems which were found during the building investigation could be solved in the design stage of the building.

Moreover, it is important to monitor the performance and occupant satisfaction after introduction of innovative HVAC concepts. Only in this way we can learn from practical experience, leading to improved and robust HVAC-systems.

6. References

[1] Zeiler W. Dutch Efforts Towards Sustainable Schools. Renewable Energy and Sustainable Buildings. 2018; 15:197-207.

[2] Ding E., Zhang D., M. Bluyssen P. Ventilation regimes of school classrooms against airborne transmission of infectious respiratory droplets: A review. Building and Environment. 2022; 207(A)

[3] Vischer J., Building-In-Use Assessment: An Occupancy Feedback. System Workspace Strategies. 1996; 4:66-90.

[4] Sundell, J., Lindvall, T. Indoor air humidity and sensation of dryness as risk indicators of SBS. Indoor Air. 1993; 3:382–390.

[5] Mesenhöller, E., Vennemann, P., & Hussong, J. Unsteady room ventilation–A review. Building and Environment. 2020; 169:106595

[6] Roulet C-A, Pibiri M-C, Knutti R, Pfeiffer A, Weber A . Effect of chemical composition on VOC transfer through rotating heat exchangers. Energy and Buildings. 2002; 34(8):799-807.

[7] GGD Rotterdam-Rijnmond. 5 jaar Frisse Scholen Toets Lessons learned. 2019

Data Statement

Data sharing not applicable to this article as no datasets were generated or analysed during the current study.

Integrating health & comfort into building design. How Active House and other labels can help improve buildings

Bas Hasselaar [a], Merlijn Huijbers [b], Antwan van Haaren [c]

[a] DGMR, BHA@dgmr.nl.

[b] DGMR, MHU@dgmr.nl.

[c] DGMR, HR@dgmr.nl.

Abstract. In the current real estate market, sustainability and wellbeing are no longer seen as something extra, but rather as a point of departure. However, there is a plethora of different sustainability labels focussing on the built environment. This can lead to confusion for architects, developers, commissioners, contractors, and users in general: what label should I use, what label is best suited for my project, why use this or that label, what is the difference? This paper discusses the five best known labels in The Netherlands: BREEAM, WELL, GPR, Active House and Passive house. It explores how they are used, how they differ, and how using them at the design stage can help create more sustainable buildings.

Keywords. BREEAM, WELL, GPR, Active House, Passive House, sustainability, label, design, tool.
DOI: https://doi.org/10.34641/clima.2022.86

1. Introduction

For many people, both end users and professionals in the building industry alike, sustainable building equals energy efficient building. And while it is true that the energy performance is an important aspect of a sustainable building, ultimately we build for people, and buildings should reflect that. This means that, for a truly sustainable building, we should create buildings that offer a healthy and comfortable indoor climate, within the boundary conditions of energy performance and environmental load of the building materials.

Unfortunately, this is less obvious than it should be. Many professionals in the building industry, such as designers, builders, building owners, have insufficient knowledge about healthy and comfortable indoor environments to be able to create truly sustainable buildings, either for new construction or for renovation.

Fortunately, there are instruments to help them make choices beyond adhering to the minimal building code. This paper explains how labels such as Active House, WELL and BREEAM, help create better buildings. All labels have different focus, in this paper we will explain the similarities and differences between them. The aim of this comparison is to inspire and to assist designers and builders in choosing the adequate measures to implement in their sustainable project.

2. Short overview of most relevant labels in the Netherlands

2.1 BREEAM

BREEAM(-NL) is one of the most well-known building labels, aimed at developers and investors. Founded by the BRE in the UK in 1990, it was introduced to and translated for the Dutch market in 2008 by the DGBC (Dutch Green Building Council). The label is internationally recognised as a measure for sustainability and assesses nine categories: energy, health and wellbeing, land use and ecology, materials, management, pollution, transport, waste, and water. A tenth category: innovation, can be used for solutions not covered in the nine previous categories.

Copyright ©2022 by the authors. This conference paper is published under a CC-BY-4.0 license.

Fig. 1 – Example of a BREEAM label.

The tool mainly focuses on commercial real estate, although it is increasingly used by municipalities and to obtain government grants as well. At the building level it is comprehensive and the applicant has to collect a lot of information as a burden of proof to get a label. An independent assessor checks the burden of proof before the DGBC issues a label after a random second check. This complex burden of proof is one of the reasons BREEAM is popular with investors and developers: it offers a degree of assurance about the sustainability of the building. The BREEAM(-NL) label (see also fig. 1) is awarded once for a New construction and Renovation certificate. After that the asset can aim for a certification for BREEAM-in-use which is an assessment method in the operational performance of buildings

2.2 WELL

WELL was launched in 2014 by the International WELL Building Institute (IWBI) in the US and is now also receiving a lot of attention in the Netherlands. It is aimed at developers and building owners and focuses entirely on the health and well-being of the users of a building.

Fig. 2 – Example of a WELL label.

There are ten assessment categories: air, water, nourishment, light, movement, thermal comfort, sound, materials, mind and community. In addition, there is an eleventh category to add innovations that have a positive influence on the wellbeing of the building users. The ambition level set determines how many parameters are tested and achieved.

A certificate is valid for a maximum of three years (see also fig. 2). After that, a new assessment must show whether the building still meets the standard. This ensures that the label is not just a snapshot, but that the building retains the qualities for its users. The burden of proof requires a lot of documentation, including checks in the building itself, before the label is issued. In the Netherlands, this has been done since 2018 by the Blue Building Institute, WELL's local partner, or by DGMR since 2019.

2.3 GPR

GPR has been available since 1995 and is aimed mainly at municipalities (the abbreviation translates as Municipal Practice Guideline) and is used to obtain government grants such as 'MIA/VAMIL'. GPR is the only label that focuses only on the Dutch market. Five categories are assessed: energy, environment, health, user quality and future value. The tool is relatively easy to use and consists of a digital checklist where you can tick building measures. The simplicity of the tool makes it suitable to use as a checklist during the design phase and thus provide insight into the sustainability ambitions and associated measures.

Fig. 3 – Example of a GPR score.

2.4 Active House

Active House celebrated its 10th anniversary in 2021. It is a label aimed at architects, developers and end users. It approaches the categories comfort, energy and the environment as a holistic whole, with the user as the starting point. Active House mainly focuses (in comparison to the other labels) on dwellings, but is also used for other building types, including museums, schools, offices, etc. Nine quantitative aspects are defined for the assessment, in addition to a number of qualitative aspects. Active House is the only label that includes a weighting to distinguish between little and intensively used

spaces in the comfort category.

Fig. 4– Example of an Active House radar.

The performance of a building is visualised in a radar diagram (see fig. 4), that can be used as a communication instrument. The label is relatively simple and accessible and can also be used as a design tool to provide insight into sustainability ambitions.

2.5 Passive House

Passive house is mainly applied to residential buildings, although other building types can also meet the passive standard. The principles date from the 1970s, but the methodology was officially released in Germany in 1996. Passive building is aimed at building as energy-efficiently as possible.

Fig. 4– Example of a passive house label.

Strict limit values are imposed that a passive house must meet if it is to be eligible for a label. A passive house uses as little energy as possible to achieve a pleasant indoor climate, and prescribes which measures must be taken in the field of installations, thermal insulation and crack sealing. Certificates are issued by the Passief Bouwen Foundation.

3. Use in practice

Why is there a market for all these different labels, if the overarching theme is to promote sustainability? In practice, each label is aimed at a different part of the real estate market.

3.1 BREEAM and WELL

For developers of large scale commercial real estate and large commercial companies, often internationally oriented, a sustainable building has more monetary value than a non-sustainable building. Being sustainable, or being associated with sustainability, has transgressed from something for idealists to an image situation, where *not* being associated with sustainability is detrimental to one's credibility and therefore marketability. This is especially important to large corporate companies where the public opinion is vital to their bottom line. Being housed in a building that has a widely accepted sustainability label serves as 'proof' that the company is responsible, trustworthy, and takes care of its employees and the planet as a whole. Because of its monetary importance, the label for these types of buildings needs to be as objective and comprehensive as possible: they need to prove without dispute that the building is sustainable. BREEAM and WELL are the labels of choice for these types of building, because of the large amounts of proof, in the form of data, information, and processes that need to be collected and adhered to before a label is awarded. At the same time, because of the amount of work involved to achieve the label, these labels are the most expensive. The whole process associated with a BREEAM or WELL label can cost upwards of tens of thousands to over a hundred thousand euros, making it viable only for commercial real estate where these added costs can be recovered through higher rent and/or improved public image. This is reflected in the market value of buildings with these labels: in Amsterdam, large scale commercial real estate is expected to have a BREEAM label, not having one will reduce its value, while buildings with a WELL label can command a €50/m^2 higher rent than regular offices, and still experience a waiting list.

In addition, companies are increasingly obliged to record in their policy and to demonstrate which measures they take in the field of ESG. Over the years, this development has shifted from voluntary to obligation and companies have to demonstrate this by means of reports. BREEAM and WELL are then internationally recognized labels to demonstrate that you meet the Environment (E) and Social (S) aspects.

3.2 GPR

Municipalities have a different approach towards labelling of sustainability. They are publicly funded and therefore do not have the deep pockets commercial developers might have. They have a controlling and guiding role in the building process: they can demand better than minimum performance for (mostly) new construction projects. At the same time, dependent on the type of project, they must be careful not to impose higher than necessary costs for building projects, by demanding, for example, a BREEAM label. GPR offers a comprehensive and accessible tool to assess the sustainability of five categories, that can be individually scored. A municipality may, for example, demand a minimum score of 8 (out of 10) for energy and environment, but only a score of 7 for the remaining categories. Or an average score of 7,5 across all categories. The burden of proof for achieving these scores lies with the applicant through textual motivation of the individual measures taken. As such, GPR offers municipalities the possibility to tailor sustainability demands to different projects, while at the same allowing developers and designers a certain level of freedom to choose how they aim to meet the requirements set. Many times, an official GPR label is not even required, just the motivation how the score is achieved is sufficient to substantiate the sustainability potential in the design process. This makes GPR an ideal tool for non-commercial and/or non-corporal real estate, or dwellings that may not have an intrinsic desire to be sustainable, but where the municipality has a clear guiding role. It is relatively low key, low cost, and leads to the required sustainable result.

3.3 Active House

Active House differs from BREEAM, WELL and GPR in that it is aimed more towards the end user, rather than to the rest of the world. Like the previous labels, it reflects a measure of sustainability, but unlike the other labels, its resulting label is a radar diagram where the performance of different aspects of the building is visible at a glance. This radar then can be used as a communication tool towards the building owner, commissioner or potential end-user. Similar to GPR, the tool is relatively straightforward to use. GPR however, is similar to a checklist, where applicable aspects that are included in the building (design) are checked, resulting in a score. Active House defines performance levels, varying from level 1 (best) to 4 (worst), for nine different aspects. It is up to the commissioner or designer to determine where the emphasis lies and how it is met, which leaves a lot of freedom to come up with custom solutions. In addition, Active House puts a weighting on the use of spaces; intensively used spaces are valued more than little used spaces. This means that, in an optimal situation, the user of the building has a direct impact on the layout of the radar diagram, which could change with a different user. Because the creation of an Active House radar is much less complicated and time consuming, making use of many aspects that are part of a regular building permit application, the collection of the required burden of proof, and consequent validation, involves much lower costs than BREEAM or WELL labels. Since end users usually are not interested in investing large sums of money in a label, just for the sake of having one or proving to the outside world how sustainable their building is, Active House is especially suited for buildings that have limited funds (such as dwellings, schools, or other non-commercial buildings), but are intrinsically interested in having better performance than what the building code dictates.

3.3 Passive House

In many respects, Passive House is similar in use to Active House, and many Passive Houses meet the requirements for an Active House. It started in the eighties of last century, when it was founded as a voluntary standard for energy efficiency in buildings. This is still the main driving force behind the label: buildings should use as little energy as possible for climatization, by applying high quality insulation, air tight construction, and heat recovery mechanical ventilation. There are strict limits set for maximum energy requirement for heating and cooling. When properly executed, the resulting building has a comfortable indoor climate all year round, while consuming very little energy. To prove the building is a passive house according to the standard, elaborate energy simulations need to be performed, that give a quite reliable prediction of the real world energy consumption. Similar to Active House, the label is relatively cheap and aimed at non-commercial buildings. It differs from Active House in that it focusses solely on energy performance (and, by extension, thermal environment and air quality), bypassing a number of comfort and environmental aspects that Active House includes. Also, it is more dogmatic in its approach to energy performance: there are strict values that need to be met, whereas Active House allows more leniency, where mediocre energy performance can be offset by very good environmental performance, for example, if desired. The passive house label is widely known for its energy performance, and may even be awarded with lower interest rates for a mortgage at certain banks in the Netherlands.

4. Labels as a design tool

Sustainability is increasingly becoming a commodity. Where it used to be that a building could distinguish itself by being energy efficient, and as such de facto sustainable, this is no longer the case. Sustainability is no longer limited to energy performance alone, but may include topics such as health or wellbeing, social sustainability, and environmental performance. This makes designing sustainable buildings harder, as there is more to choose from, and more to be assessed by.

How then, can the labels described in this paper be

used as a design tool?

4.1 Include the methodologies very early in the design process.

Determine your focus and take a moment at the start of your project to scan through the credits/features of the label(s) of your choice. This will make you aware of many ways in which a building can be sustainable. Some examples:

- Location: BREEAM for instance focusses on the location of the building. Choosing a location which has low ecological value (a location within the city instead of in the middle of a nature reserve), being closer to public transport or close to services such as lunch spots, day care centres or a dry cleaner prevents the need for additional motorised traffic movements and thus increases the sustainable potential of a building.

- Construction site: When judging the sustainability of a building it would not be correct to only assess the completed building. The building process itself can have serious environmental impact as well. Energy management with ambitious goals for energy used on the construction site, responsible use of building materials and meticulous separation and high-quality reuse of waste should also be included in the scope of a sustainable building project, according to BREEAM.

- Materials: WELL, BREEAM, GPR and Active House all put great emphasis on the need to select good materials. Some examples.

    - To reduce environmental impact BREEAM, GPR and Active House reward selecting materials with low 'shadow costs' (Dutch definition for all environmental costs that have to be made in order to produce a material) and for locally produced materials.

    - To minimalize the impact on the health of building users, WELL, BREEAM and GPR reward selecting materials with low to no volatile organic compounds (VOCs).

- Energy: An energy efficient building design, based on the trias energetica, is awarded additional credits in BREEAM, GPR, Active House and Passive House. Next to building related energy efficiency, energy-efficient equipment such as elevators and (kitchen) equipment are rewarded too.

- Comfort: A building that is not comfortable will most likely not be sustainable. This applies to all indoor environmental criteria: indoor air quality, thermal comfort, light conditions and acoustics. All labels have standards to provide improved levels of comfort in the building, thus guiding the designer towards sustainable choices. However, the WELL Building Standard is primarily focused on this.

- Measuring building performance: a sustainable building, designed according to the recommendations mentioned above, might function very well. This however is not guaranteed. Detailed commissioning is always recommended to ensure that all design measures are applied correctly and work well together. BREEAM awards credits when commissioning has been carried out and the results have been included in a detailed report. WELL requires measurements in the building to demonstrate that the measures have led to the required standards.

- Movement and nourishment: Healthy food and sufficient exercise are important to stay healthy. BREEAM and WELL support exercise for instance by rewarding credits to buildings in which signs are placed near elevators that show where the nearest stairs are (BREEAM) and by rewarding buildings that place stairs central and very visible in the entrance area to encourage people to exercise. WELL also encourages to provide healthy food and sufficient tap water spots throughout the building

- Ecology: BREEAM stimulates the mapping of the ecological value of the environment using an ecologist. And to additionally look at which measures can be used to increase the ecological potential of the site and the building.

- Future-proofing: Flexibility and robustness are crucial for sustainable buildings. Both BREEAM and GPR award credits to implementing measures such as:

    - separating core and shell from interior walls for example, making it much easier to transform a building into a new function,

    - designing a building in a way which makes it possible to easily and efficiently be detached at the end of its use,

    - implementing climate adaptation measures: performing overheating calculations using a stricter climate year than usually applied,

preventing the building, even in a warmer future climate, to overheat. And/ or providing sufficient unpaved/ green surfaces for water retention on the building or on site,

  - and designing robust buildings where heavily used areas (entrance areas or areas used for internal transport) are extra protected against possible damage through the use of robust materials or through applying protective measures.

- Use: Active House distinguishes between intensively used spaces in a building, and little used spaces. By differentiating measures according to the intended use, buildings can be designed to make optimal use of resources, such as heating, or daylight.

4.2 Commit and make it official

By entering into the obligation to obtain a sustainability label for a building, it is much more likely that the sustainable ambition will be realised than if only the wish to realise a sustainable building has been expressed.

Obtaining a sustainability label is often seen as a cumbersome and overly time-consuming process and one wonders whether all that paperwork is really necessary. Practice however shows that without contractual obligations it is much more difficult to reach the same level of quality. At the end of the design process, unfortunately there are almost always more wishes than available budget left.

5. Case study

The relevance of labels in sustainable building design becomes apparent in a case study in Amsterdam. Amsterdam has some of the highest real estate prices in The Netherlands, and competition for high profile tenants is high. In this case (the name of the relevant parties shall remain anonymous) the developer purchased an existing building that they planned to renovate and upgrade to appeal to high profile tenants. The building provided a solid basis for a sustainable certificate (accessible location close to a train station, minimal use of materials because of renovation, ample space for PV).

The ambition set by the developer was to use BREEAM Excellent as a guideline. This ambition provided the design team, contractor and, at a later stage, the tenants, with a list of measures that needed to be incorporated not only into the design, but also into their working practice. The measures incorporate a wide range of topics, including and not limited to the energy performance, dimensions of passageways and doors to ensure accessibility, use of non-toxic and sustainably sourced materials, and biodiversity of the surrounding terrain. Because the ambitions increased during the design process, when prospective tenants came into focus, part of the design had to be redone or revised a number of times, to account for changed requirements. Had the ambition been clear from the start, this would have streamlined the design process.

The initial ambition for BREEAM increased from Excellent to Outstanding, and WELL was included at a later stage, (originally Gold but increased to Platinum). The decision to include WELL at a later stage was mainly financial: it was not included from the start because it was still unclear whether it would be a sound financial investment. An early quickscan was made to determine implications for the design, but the decision to obtain a label came later, based on the desire to better distinguish the qualities of the building from its competitors. Because of the increased BREEAM and WELL level ambitions, it was no longer enough to focus on the core and shell of the building alone. The future tenants had to be involved in the decision making process, and the tenants had to sign contracts obliging them to use, for example in this case, sustainable and removable inner walls, and offer healthy and organic alternatives to the regular offerings in their cafeteria. At the same time, the prospective tenants already had their own ambitions (which is partly why they were interested in this development), and want to rent very sustainable office space. The BREEAM and WELL ambitions stimulated them and gave them tools to make their business operations more sustainable.

6. Conclusion

In this paper we discussed the differences and similarities of the main independent sustainability labels in The Netherlands. Although at first glance, they all seem to promote a higher building standard than the building code, and can all be applied to all types of building, in practice there is a clear distinguishment in how and where each label is most optimally used. BREEAM and WELL are the most commercial labels, which translates to application in mostly commercial real estate, can be used for ESG-reporting and obtaining government grants, but the labels are very expensive to obtain. On the other end of the spectrum, Active House and Passive House are mainly aimed at dwellings and non-commercial real estate, where there is less money, but an intrinsic desire for sustainability present. GPR sits somewhere in the middle, being used mainly by municipalities that wish to impose a certain level of sustainability on a project or by profit driven companies to obtain government grants.

To condense the breadth of these label into a single sentence is a gross underestimate of the complexity and wealth of knowledge contained in these labels. But for the sake of simplification and comparison, an attempt is made: BREEAM has a very broad sustainability focus, WELL is aimed mainly at health and wellbeing, GPR is somewhat similar to BREEAM,

but far less complex or strict, Active House focusses on the end user and Passive House on energy performance.

Regardless of the type of label used, setting an ambition at the design stage and meeting that ambition in the finished building, is greatly supported by pursuing an official label. This way, ambition is not only limited to good intentions, but transferred to concrete actions and achievements, because otherwise the desired sustainability level required for the label is not met.

Impact of Climate Change on the Design of Air Handling Units

Christian Fieberg [a], *Dominik Demmelhuber* [b]
[a] Westphalian Energy Institute, Westphalian University of Applied Science Gelsenkirchen, Germany, Christian.Fieberg@w-hs.de.
[b] ZWP Ingenieur-AG, Bochum, Germany, D.Demmelhuber@zwp.de.

Abstract. Air Handling units (AHU) are designed to guarantee a high indoor air quality for any time and outdoor condition all over the year. To do so, the AHU removes particle matter like dust or pollen and adapts the thermophysical properties of air to the desired, seasonal indoor comfort conditions. AHU have a robust design and thus operate for more than fifteen years, sometimes even for decades. An AHU designed today must consider and anticipate the change of user needs as well as outdoor air conditions for the next twenty years. To anticipate the outdoor air condition of coming decades, scientific models exist, which allow the design of peak performance and capacities of the air treatment components. It is most likely, that the ongoing climate change will lead to higher temperatures as well as higher humidity, while the comfort zone of human beings will remain at today's values. Next to the impact of global warming with average rise of mean air temperature local effects will influence the operation of AHU. On effect investigated here is the steep temperature increase in city centres called *urban heat islands*. Heating and cooling capacities as well as water consumption for humidification are investigated for a reference AHU for fifteen regional locations in Germany. These regions represent all climate zones within the country. Additionally, the urban heat island effect was investigated for Berlin Alexanderplatz compared a rural area close by. The AHU was chosen to operate in an intensive care unit of a hospital. The set-up leads to 24/7 operation with 8760 hours per year. The article presents the modelling of current and future weather data as well as the unit set up. The calculated hourly performance and capacity parameters for current (reference year 2012) and future weather data (reference year 2045) yield energy consumption and peak loads of the unit for heating, cooling and humidification. The results are displayed by relative comparisons of each performance value.

Keywords. Air handling unit, climate change, urban heat island, future capacity needs.
DOI: https://doi.org/10.34641/clima.2022.360

1. Introduction

Air Handling units (AHU) are designed to guarantee a high indoor air quality for any time and outdoor condition all over the year. To do so, the AHU removes particle matter like dust or pollen and adapt the thermophysical properties of air to the desired, seasonal comfort conditions by heating, cooling, humidification and dehumidification.

Further, a heat recovery system is uses the energy content of the extract air. AHU have a robust design and thus operate for more than fifteen years, considering refurbishment of components like fans, often more than twenty years.

The design of air conditioning of a building under construction means to consider and anticipate the change of user needs as well as outdoor air conditions for the next twenty years.

To anticipate the outdoor air condition of coming decades, scientific models exist, which allow the design of peak performance and capacities of the air treatment components. It is most likely, that the ongoing climate change will lead to higher temperatures as well as higher humidity, while the comfort zone of human beings will remain at today's values (e. g. 20 – 24 °C, 40 – 60 % r.h.).

Next to the impact of global warming with average rise of mean air temperature local effects will influence the operation of AHU. On effect investigated here is the steep temperature increase in city centres called urban heat islands.

Heating and cooling capacities as well as water consumption for humidification are investigated for a reference AHU for fifteen regional locations in Germany. These regions represent all climate zones within the country. The AHU was chosen to operate

Copyright ©2022 by the authors. This conference paper is published under a CC-BY-4.0 license.

in an intensive care unit of an hospital. The set-up leads to 24/7 operation with 8760 hours per year.

In a first step the generation of weather data for historic and future years is explained. This includes the reginal modelling and the extension to micro climate for urban heat islands. Second, the AHU and its operating and boundary conditions are shown.

In a next step the procedure to calculate the design loads for given weather data is explained and results are presented for test reference years (regional weather) and urban heat islands (urban micro climate), respectively.

Finally, the results for one particular region (Berlin, TRY-region 4) are summarised and evaluated with respect to current and future AHU design rules. Berlin was chosen as the urban heat island effect is well investigated here.

2. Modelling of climate data

Representative weather data for almost any location worldwide is given by test reference years (TRY). These TRY data include hourly values for temperature, humidity, wind speed and direction, rain etc. In Germany, TRY data come from historical weather recordings between 1995 and 2012 (TRY 2012), where representative parts of real weather recordings are used [1]. Further, extreme summer or winter conditions are available. For the investigations here, "summer" TRY data was chosen.

Although, fifteen weather stations in Germany were tested, only the Berlin region will be discussed in this paper, because for Berlin detailed data of urban heat island effects are available. Berlin is located within region 4, Fig. 1. This region is one of the largest in Germany.

The same data structure is available for the weather in 2045. To get these future values, 24 climate models were used to extrapolate the local weather including effects of urbanisation. TRY 2045 is based on projections of global warming with a global radiation increase of 6.0 W/m^2K for the years 2021 until 2060. The time path is called representative concentrations path (RCP) and is explained in the fifth Assessment Report of the Intergovernmental Panel on Climate Change, IPCC [3]. Radiation will increase due to higher concentration of greenhouse gases (GHG). RCP range from 2.0 W/m^2K up to 8.5 W/m^2K with projections of global warming from 1750 until 2100, Fig. 2.

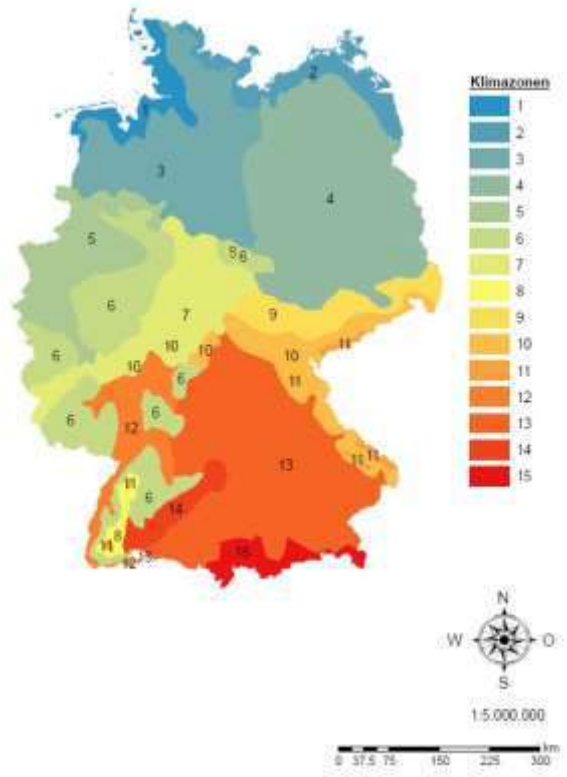

Fig. 1 - Weather (TRY) regions in Germany according to [2]. Berlin = region 4.

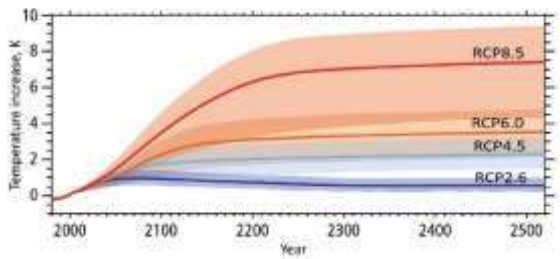

Fig. 2 - Global temperature rise based on RCPs with ±5 % confidence interval according to [4].

Global warming results from higher concentration of GHG like CO_2. According to RCP6 CO_2 concentration will reach a level of 850 ppm compared to 413 ppm today. More pessimistic scenarios like RCP8.5 even end up with a CO_2 concentration of 1370 ppm. In any case, higher CO_2 concentration in the outdoor air will increase minimum air flow rates to keep indoor air quality constant compared to current regulations.

2.1 Weather data overview

As one might expect the mean temperatures and humidity will increase with global warming. The impact for 2045 compared to 2012 is shown for summer (August) and winter (January) for TRY region 4 (weather station Potsdam) including Berlin area in Fig. 3.

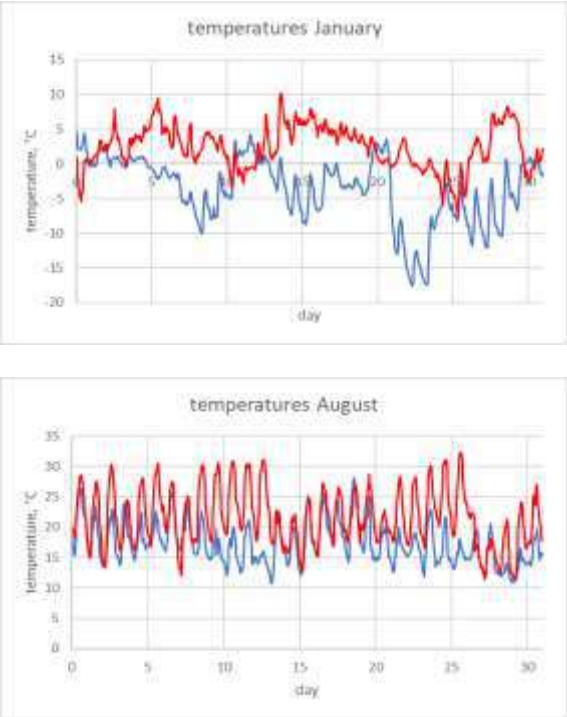

Fig. 3 – Hourly temperatures for region 4 (Potsdam) in January (top) and August (bottom). Blue lines = TRY 2012, red lines = TR 2045.

The average temperature differences between TRY 2012 and TRY 2045 are +4.4 K in August and +6.0 K in January. Both values are extreme. For the complete year the temperature increase in region 4 is only 1.2 K. In general the temperatures increase with TRY 2045, but also have a larger bandwidth within comparable time period (e.g. months).

2.2 Urban heat islands

Additional to the temperature increase due to global warming local effects of urbanisation will modify micro climates in larger cities. Even today, we see a temperature difference of five Kelvin between city and neighbouring, rural areas. As an example, Fig. 4 shows the temperature of one week in July 2020 with up to 4 K higher temperatures in the city centre.

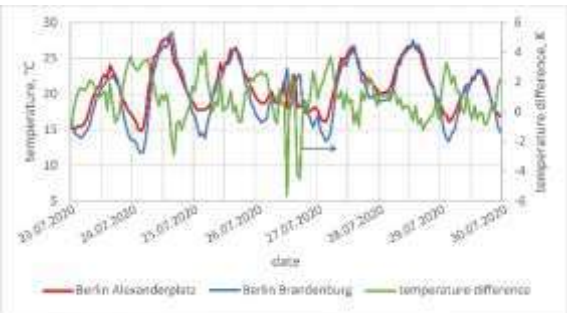

Fig. 4 – Temperatures of one week in Berlin Alexanderplatz and Berlin-Brandenburg (July 23rd – 30th 2020).

Urban heat islands lead to more summer days with temperatures above 30 °C as well as so called tropical nights with temperatures above 20 °C. The frequency is not yet predictable as current summer days and tropical nights are still rare [5]. The impact of climate change will be similar for both urban heat islands and rural areas [6].

Through the day solar radiation heats up the buildings and pavement, where the concrete serves as a heat storage. During the night, the heat is released to warm the outdoor air and thus yields higher air temperatures mainly in early morning hours compared to rural areas.

For Berlin Alexanderplatz in the centre of Berlin the weather data from June 2020 until end of December 2020 were investigated and compared to a rural weather station at Berlin-Brandenburg. The distance between both weather stations is 17.6 km. The weather data is available through the homepage of German Weather Service [7].

The number of hours with a temperature difference of more than four Kelvin is displayed in Fig. 5 where also the time frequency is shown. It is obvious that urban heat island effects are mainly present during the evening and night from 19:00 h until 5:00 h. That means the urban heat island effect is strongest when most building operate with reduced cooling capacity outside of business hours.

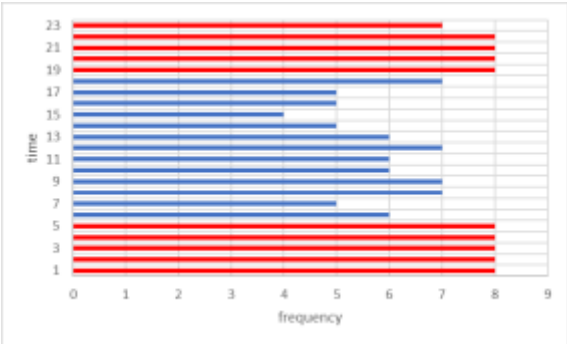

Fig. 5 – Time dependent probability of temperature differences (> 4K) between Berlin Alexanderplatz and Berlin-Brandenburg.

3. Design and operation of a representative air handling unit

A planned air handling unit for an intensive care unit in a hospital in southwest Germany serves as a role model for the performed simulations. The unit model was fed with weather data of fifteen representative weather stations with TRY 2012 and TRY 2045, respectively.

The AHU is designed to supply conditioned air for 20 patient rooms with up to 27 patients and five persons of medical staff. The unit is in operation all the time (24/7) and adapts supply air (SUP) depending on outdoor conditions, Fig. 6. Extract air temperature

(ETA) ranges from 20 °C up to 26 °C in winter and summer, respectively. In any case, the supply air humidity is between 6 g/kg ≤ x_{SUP} ≤ 10.5 g/kg.

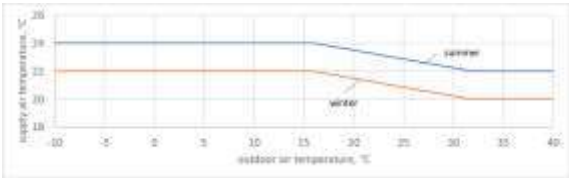

Fig. 6 – Supply air temperatures depending on ODA conditions.

The AHU displayed in Fig. 7 is able to heat, cool humidify and dehumidify outdoor air to the desired conditions. To fulfil current energy requirements a heat recovery system (run-around coil) is used with a heat recovery rate of 72 %.

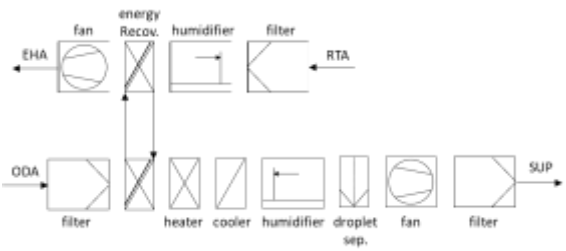

Fig. 7 – AHU set up.

Maximum airflow rate is 6.7 m^3/s with a nominal flow rate of 4.7 m^3/s used in the simulations.

4. Simulation of performance parameters

To gain the actual capacities to achieve the SUP conditions an Excel tool is used which calculates performance and operating hours of all components for each hour of the year. The following flow chart explains the procedure, Fig. 8.

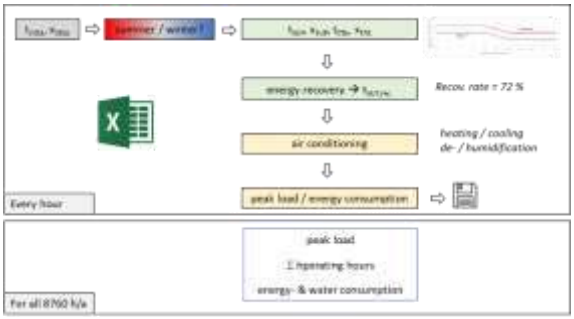

Fig. 8 – Calculation procedure for hourly performance values.

For each hour of the year, the SUP and ETA air condition is determined and the needed energy and capacity to reach the values are calculated. The components of the AHU are not limited performance-wise. Indeed, the max. capacity yields the design size of the heater and cooler as well as water demand for humidification. For full load and part load, the same efficiency parameters are applied. After the hourly calculations maximum and minimum values as well as total energy consumption for the year are calculated

4.1 Validation of the results

TRY weather data files contain a large amount of information and may blur potential errors during processing of the Excel tool. Several quality checks help eliminating potential errors.

Displaying the data in graphs gives a quick overview of the consistency of the input and output data. To do so temperatures and performance data for all components are plotted in a time line as well as in a Mollier h-x diagram. Further, a correlation between outdoor air temperature and performance values show clear trends following the designed boundaries. Finally, thermal balance is displayed for each month.

The following figures show an example of the validation details for TRY 2012 in region 4.

Fig. 9 shows the hourly heating and cooling demand with annual peak load (dotted lines). Cooling and heating curves do not overlap (simultaneous heating and cooling) and correspond to the expected seasonal distribution of the demands.

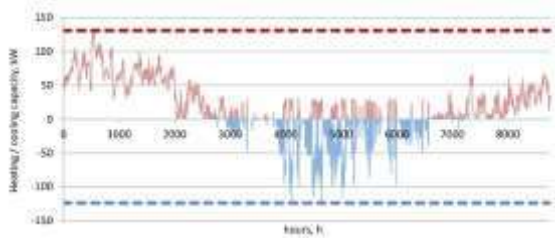

Fig. 9 – Validation of capacity data (Redline = heater, blue line = cooler, dotted lines = maximum capacity).

Fig. 10 shows the energy and water demand as a function of outdoor air temperature. Heating for ODA temperatures above 22 °C results from reheating due to dehumidification.

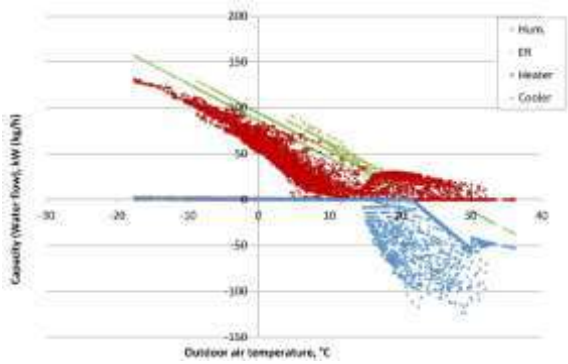

Fig. 10 – Validation of Design parameters vs. ODA.

Fig. 11 sums up the monthly energy and water demands. Electrical power for the fans are constant due to the fixed flow rate. Cooling demand is relevant only for the summer months from June until September.

Fig. 11 – Validation of monthly energy balance.

Testing the tool with constant temperature and humidity values allows a direct comparison with theoretical calculations of temperatures and enthalpies of the system. An addition, sample data for individual hours were calculated manually and checked with the Excel calculations.

5. Results

5.1 Results for TRY 2012 and TRY 2045 in Potsdam region 4

As one example of the absolute results Tab. 1 displays the parameters from region 4 with weather station located in Potsdam.

Tab. 1 - Performance values for region 4 for TRY 2012 and TRY 2045.

Parameter	TRY 2012	TRY 2045
Heating capacity	131 kW	96 kW
Heating energy	216340 kWh	184328 kWh
Heating hours	5625 h	5619 h
Cooling capacity	124 kW	125 kW
Cooling energy	59047 kWh	59423 kWh
Cooling hours	1542 h	1660 h
Water flow rate	109 kg/h	83 kg/h
Water demand	188 m^3	153 m^3
Operating hours	4043 h	4128 h

Potsdam and Berlin are strongly influenced by continental climate with east wind directions from Russia. Thus, the predicted mean climate change towards hotter summers is not clearly seen here.

The following two figures Fig. 12 and Fig. 13 show the changes from TRY 2012 to TRY 2045.

Fig. 12 – Difference in capacity (Blue = TRY 2012, red = TRY 2045).

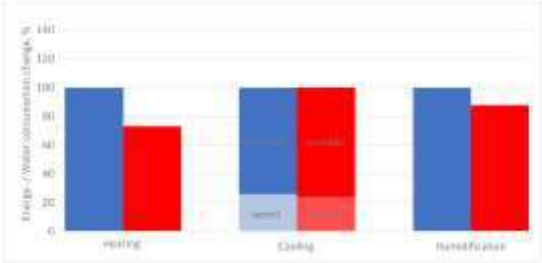

Fig. 13 – Difference in energy and water demand (Blue = TRY 2012, red = TRY 2045).

For the Potsdam region, reduced heating demand is visible, but cooling is not affected at all. As mentioned above, this is a specific result of the climate influence, which keeps summer temperatures at moderate levels. Nevertheless, the average temperature is rising and thus humidity, too. Humidification demand is decreasing accordingly.

5.2 Artificial German weather simulation

In addition to the regional TRY evaluation an area, weighted average weather was created from all fifteen weather stations correlated to the region size. Fig. 14 shows the share of surface area for all fifteen German weather stations according to Fig. 1.

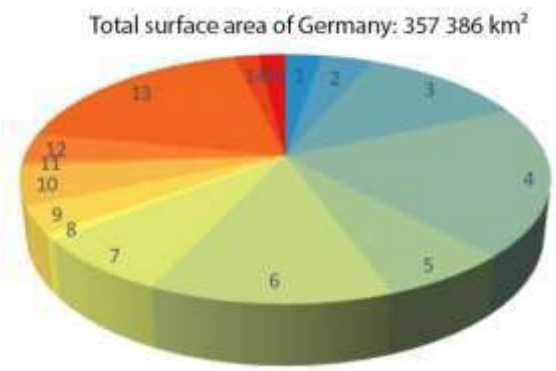

Fig. 14 – Share of surface area for all German TRY-regions

Weighting the TRY data by surface area share of each station, an artificial German weather data set was created and also tested. The following table shows the relative changes from TRY 2012 to TRY 2045 for Germany as a total.

Tab. 2 - Comparison of changes for area-weighted average TRY data (weather stations 1 – 15).

Air conditioning	Performance parameter	Change from 2012 to 2045
Heating	Heating capacity	-16 %
	Heating energy	-17 %
	Heating hours	+5 %
Cooling	Cooling capacity	+2 %
	Cooling energy	+67 %
	Cooling hours	+42 %
Humidifier	Water flow rate	-19 %
	Water demand	-31 %
	Operating hours	-4 %

From Tab. 2 a reduction of heating capacity and demand is obvious as we expect an average temperature increase for the next decades. For cooling, the capacity is almost constant, but the hours, where part load cooling is needed increases by 42 % and thus the overall energy demand. Humidification decreases as higher air temperatures allow higher relative humidity and thus a higher water vapour load.

5.3 Range of German weather simulation

The range of the differences is wide for the fifteen regions including mountain areas as well as seaside locations. Tab. 3 shows the range of changes for all TRY weather regions.

Tab. 3 – Range of changes from TRY 2012 to TRY 2045 for all fifteen regions

Air conditioning	Performance parameter	Deviation range
Heating	Heating capacity	-28 % … + 2 %
	Heating energy	-28 % … -8 %
	Heating hours	-5 % … +8 %
Cooling	Cooling capacity	-29 % … +93 %
	Cooling energy	-9 % … +58 %
	Cooling hours	+4 % … +40 %
Humidifier	Water flow rate	-25 % … +2 %
	Water demand	-38 % … -9 %
	Operating hours	-23 % … +9 %

The changes for all German weather regions show clear trends towards higher temperatures and humidity in TRY 2045. That results in less heating demand and capacity while cooling needs become more important. In some regions the effects leads to almost doubled cooling capacity (+93 %). The number of cooling hours increases, too. The reduction of heating hours due to cool outdoor air temperatures is partly compensated by reheating during dehumidification during warmer und humid air conditions.

5.3 Results for urban heat islands

In contrast to the TRY simulations, we used measured data from two weather stations at Berlin Alexanderplatz and Berlin-Brandenburg from June 14th 2020 until December 2nd 2020, where the summer months July and August are most important for the UHI effect. As the investigation of urban heat islands is quite new, available comparable data with hourly resolution is still limited.

Similar to the TRY results, the diagrams just display differences, but no actual absolute values. Focus is on the differences and not on quantitative performance data.

In case of cooling capacity, no difference is seen which means the same cooler dimension fits for both locations. The heater for Berlin Alexanderplatz needs 5 % less in capacity. Humidification is not needed in the displayed time period and thus not displayed, Fig. 15.

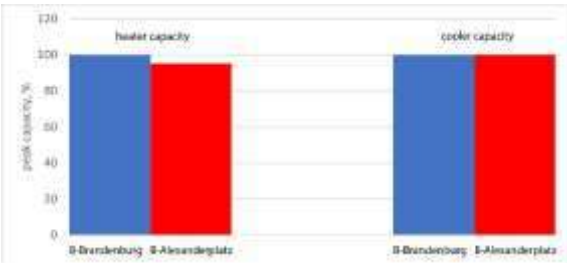

Fig. 15 – Peak capacity for second half of 2020.

As the temperature difference between city centre and rural areas is greatest at night where ODA temperatures are moderate, the effect on cooling capacity is negligible. Peak temperatures are similar for both locations during day time and storage effects of urban structures vanish during the night and early morning hours.

Looking at the energy needed as well as the operating hours, the difference becomes clearer. Here, cooling energy demand as well as operating hours increase by 20 % and 22 %, respectively, Fig. 16.

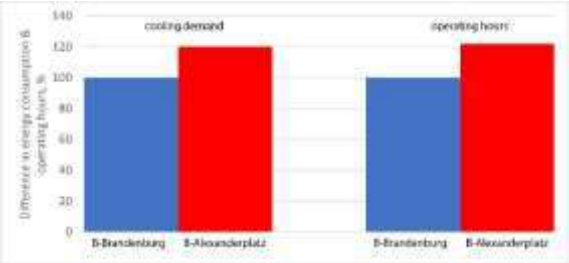

Fig. 16 – Cooling energy difference and difference in operating hours.

Although the database is limited, urban heat islands do not increase peak cooling capacity. Nevertheless, for the AHU of an intensive care unit an increase of operating hours is most likely as cooling demand at night increases.

6. Conclusion and outlook

The predicted climate change and its effects on local weather conditions were introduced and explained for Berlin / Potsdam region in Germany. The influence of urban heat islands on local temperatures was shown for recent weather data.

To make the effects more tangible, an air handling unit for an intensive care unit of a hospital was simulated with TRY-weather data from 2012 and 2045. The results were characterised by heating, cooling and humidification parameters.

The effect of global warming should be part of local climate boundary conditions for the design phase of AHUs. While the maximum cooling capacity just increases by 10 – 15 %, the operating hours will increase stronger. Thus, planers should not only consider additional buffer capacity, but should be aware of higher operating costs due to more operating hours. Although heating capacity is decreasing in the coming years, the effect on current AHUs would lead to a gap in heating capacity in winter. Humidification demand will decrease due to higher humidity in winter and transition periods.

Urban heat islands may not lead to higher cooling capacity, but surely to more cooling hours. As the effect is strongest at night, the impact will mostly affect buildings with a high share of annual operating hours. Office buildings closing at night might only be affected by their cooling strategy of potentially using free cooling during night time. The local effects of urban heat islands are not present yet in the TRY data of the regional weather stations used in this investigation. Nevertheless, DWD has finished a project to calculate local TRY weather data with a resolution of one km^2. Here, UHI is already included in the TRY data [8] and an extension to future TRY data will be soon available.

The results are based on a unit with 24/7 operating hours. Some effects will be similar for office buildings with reduced air conditioning at night, other building types will deviate. Thus, a variety of building and air conditioning types should be further simulated to get the full picture of climate change impact.

7. Acknowledgement

The authors would like to acknowledge the support from Dr. Saskia Buchholz from German Weather Service (DWD), Offenbach, for her kind support to identify available data out of large data files from the DWD homepage as well as detailed explanations about urban heat islands and their integration in future weather data.

8. References

[1] Deutscher Wetterdienst. Test Reference Years. https://www.dwd.de/DE/leistungen/testreferenzjahre/testreferenzjahre.html?nn=507312. Retrieved on 2.08.2021.

[2] VDI 4710-3:2011-03. Meteorological data for the building services.

[3] Stocker, T.F., D. Qin, G.-K. Plattner, M. Tignor, S.K. Allen, J. Boschung, A. Nauels, Y. Xia, V. Bex and P.M. Midgley (eds.): IPCC: Climate Change 2013: The Physical Science Basis. Contribution of Working Group I to the Fifth Assessment Report of the Intergovernmental Panel on Climate Change. Cambridge University Press, Cambridge, United Kingdom and New York, NY, USA. 2013.

[4] Pachauri, R.K., Meyer, L.A. (eds.):IPCC: Climate Change 2014: Synthesis Report. Contribution of Working Groups I, II and III to the Fifth Assessment Report of the Intergovernmental Panel on Climate Change. IPCC, Geneva, Switzerland. 2014.

[5] Früh, B., Koßmann, M., Roos, M. Berichte des Deutschen Wetterdienstes: 237: Frankfurt am Main im Klimawandel – Eine Untersuchung zur städtischen Wärmebelastung. 2011.

[6] Schau-Noppel, H., Koßmann, M., Buchholz, S. Meteorological information for climate-proof urban planning – The example of KLIMPRAX. Urban Climate. 2020; 32.

[7] Deutscher Wetterdienst. Urban Heat Islands. https://www.dwd.de/DE/leistungen/waermeinsel/waermeinsel.html. Retrieved on 3.01.2022.

[8] Krähenmann, S., Walter, A., Brienen, S. et al. Theoretical and Applied Climatology. High-resolution grids of hourly meteorological variables for Germany. 2018 (131): 899–926.

The datasets analysed during the current study are available in the DWD-Klimaberatungsmodul repository, https://kunden.dwd.de/obt/

Air change rates during sleep in Danish bedrooms

Xiaojun Fan [a], Chenxi Liao [b], Mariya Petrova Bivolarova [a], Anna Mainka [c], Chandra Sekhar [d], Jelle Laverge [b], Li Lan [e], Mizuho Akimoto [f], Pawel Wargocki [a]

[a] International Centre for Indoor Environment and Energy, Department of Environmental and Resource Engineering, Technical University of Denmark, Copenhagen, Denmark, xiafan@byg.dtu.dk, mbiv@byg.dtu.dk, paw@byg.dtu.dk

[b] Research Group Building Physics, Construction, and Climate Control, Department of Architecture and Urban Planning, Ghent University, Gent, Belgium, Chenxi.Liao@UGent.be, Jelle.Laverge@UGent.be

[c] Department of Air Protection, Faculty of Energy and Environmental Engineering, Silesian University of Technology, Silesian, Poland, Anna.Mainka@polsl.pl

[d] Department of the Built Environment, National University of Singapore, Singapore, bdgscs@nus.edu.sg

[e] Department of Architecture, School of Design, Shanghai Jiao Tong University, Shanghai, China, lanli2006@sjtu.edu.cn [f] Department of Architecture, Waseda University, Tokyo, Japan, mizuho.akimoto@gmail.com

Abstract. The ongoing project 'Bedroom Ventilation and Sleep Quality' investigates the effects of bedroom ventilation on sleep quality and next-day cognitive performance. As part of the project, 84 bedrooms in the Greater Copenhagen area of Denmark were inspected during the 2020 heating season. In the first week, participants slept under environmental conditions that they typically experienced during sleep; in the second week, they slept with the interventions made by opening/closing either the door, or window, or both. As an essential part of the study, the CO2 concentration in bedrooms was continuously measured. The bedroom window and door status during sleep were obtained the following morning via sleep diary. The air change rates per hour (ACHs) in bedrooms were estimated using the occupant-produced CO2 concentration decay method. Mechanical ventilation was rarely installed in bedrooms; extract ventilation in the bathroom and kitchen was predominant. Participants typically slept with both bedroom window and door closed. The median ACH was 0.40 h^{-1} during sleep under habitual conditions. Opening either the window or door increased bedroom ACH during sleep, but window opening led to better ventilation than the door opening, which was verified by the intervention. These results suggest that the ventilation in most bedrooms is currently insufficient compared with the ventilation requirements prescribed by limited standards, highlighting the urgency to look at its impact on sleep quality and improve bedroom ventilation.

Keywords. Bedroom Ventilation, Air change rate, Airing behaviour, Residential buildings, Sleep
DOI: https://doi.org/10.34641/clima.2022.150

1. Introduction

Sleep is essential for our health and well-being by enabling human bodies to function well. Previous studies have shown that inadequate ventilation in bedrooms adversely affects sleep quality [1–3], which in turn increases the risk of a series of health-related diseases, such as obesity and chronic diseases [4], etc., and reduces the next-day cognitive performance [3,5].

In light of the difficulties in ventilation rate measurements on-site, for example, air mixing indoors and methods limitations, CO_2 concentration during sleep is typically measured in most studies as a proxy of ventilation in bedrooms, as summarized by Akimoto et al. [6]. Limited studies attempted to characterize bedroom ventilation by measuring the air change rate using the tracer gas method as summarized by Sekhar et al. [7]. They found that the mean air change rate (ACH) varied largely from 0.2 to 4.9 h^{-1}. A large number of surveyed bedrooms did not meet the ventilation requirements stipulated by ASHRAE and European Standards [8][9].

Buildings worldwide are being built tightly due to the energy crisis. Consequently, the ventilation rates in dwellings are reduced, especially in areas where the central heating system is installed. Occupants generally sleep with the bedroom door and window closed in these areas during the heating season, further decreasing the bedroom ventilation during

Copyright ©2022 by the authors. This conference paper is published under a CC-BY-4.0 license.

sleep.

This study is part of a large field investigation on the effects of bedroom ventilation on sleep quality and next-day cognitive performance conducted in the Greater Copenhagen area of Denmark during the heating season in 2020. This paper presents the results of the estimated ACHs using the occupant-produced CO_2 concentration decay method to provide an overview of the actual bedroom ventilation and characterize how occupants' airing behaviours affect ACHs during sleep. Other measurements will be reported separately.

2. Method

A cross-sectional field study was conducted from September to December 2020 in the Greater Copenhagen area of Denmark. Eighty-four participants were recruited based on the answers to a recruitment questionnaire, which collected the information on candidates, characteristics of bedrooms and dwellings, and sleep quality over the past month prior to participating in this study. Participants could choose to take part in either one-week or two-week measurements: only weekdays (Monday evening to Friday morning) were considered. The participants were asked to sleep under their habitual sleep conditions in the first week; in the second week, they were instructed to make interventions by opening or closing the bedroom door, or window, or both at night. Among them, 64 participated in two-week measurements.

The CO_2 concentration was measured continuously in bedrooms at an interval of 5 min. Sixteen measuring units, each comprising a CO_2 sensor (GMW90R, Vaisala Corp., Finland) and a data logger (HOBO UX120-006M, Onset Computer Corp., USA), were used in the present study. The measuring range of the sensor was 0-5000 ppm with an accuracy of ±30 ppm + 2% of reading. The air temperature and relative humidity were recorded simultaneously. The CO_2 sensor was calibrated prior to the study.

Each bedroom was installed with one unit. The unit was placed at a similar height of the bed and one meter away from the head region when participants lay down. Participants reported the status of the bedroom door and window via an online sleep diary in the morning, which they were asked to fill out twice, two weekdays' morning of each week.

The ACH was estimated for every weekday night by measuring the decay of the human-produced CO_2 concentration after the participants left the bedrooms assuming that the ACH did not change if the bedroom door and window status were kept the same as the previous night. Participants were asked not to make any changes to the bedroom window and door after waking up and to avoid re-entering the bedrooms at least within 30 min. after leaving to allow the decay of CO_2 concentration to be built up. The outdoor CO_2 concentration throughout the measuring period was not recorded. Instead, the mean value at a steady-state during daytime when the bedrooms were not occupied was used. Otherwise the outdoor CO_2 concentration was assumed to be 420 ppm as used by the previous study to estimate the ventilation rate under different CO_2 levels [10]

3. Results and Discussions

Fig. 1 shows the cumulative probability of estimated ACHs in bedrooms during habitual sleep conditions. The median ACH was 0.40 h^{-1}, ranging from 0.03 h^{-1} to 19.25 h^{-1}, similar to the value measured in 500 children's bedrooms of Denmark [11].

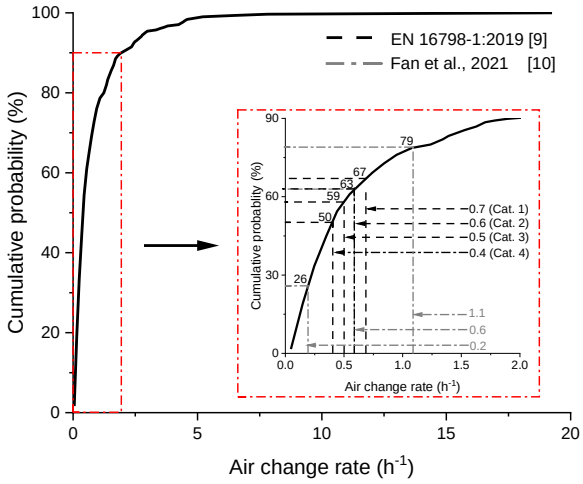

Fig. 1 – Cumulative probability plots of estimated ACHs in bedrooms during habitual sleep conditions. Bedroom ventilation stipulated by EN 16798-1 [9] and recommended by Fan et al. [10] are also presented.

Sekhar et al. reviewed 17 international and national standards and building regulations on ventilation requirements for bedrooms and found that most existing standards do not prescribe specific ventilation requirements for bedrooms; the requirements for bedroom ventilation is simply the application of ventilation requirements for the whole dwellings [7]. Among others, the European standard specifies the total ventilation (including infiltration) of 0.4, 0.5, 0.6, 0.7 h^{-1} for Categories 4 to 1 respectively for entire dwellings [9]. These values are used for benchmarking in the present study.

Half surveyed bedrooms had an ACH lower than 0.4 h^{-1} during sleep, the minimum ventilation requirement stipulated by EN 16798-1 [9]. If an ACH of 0.7 h^{-1} is used as the criterion for bedroom ventilation, 79% of bedrooms did not comply with the ventilation requirement.

Based on the tentative relationship between bedroom ventilation (indicated by CO_2 levels) and sleep quality established by Sekhar et al. [7], Fan et al. recommended the bedroom ventilation rates considering the adverse effects on sleep quality assuming that the CO_2 emission rate during sleep was

11.0 L/h per person [10]. To avoid sleep disturbance, the ventilation rate in bedrooms should be >10 L/s per person, corresponding to a CO_2 level of < 800 ppm. A ventilation rate of < 10 L/s per person may affect sleep; < 5 L/s per person, corresponding to a CO_2 level of >1150 ppm, will affect sleep; <1.5 L/s per person, corresponding to a CO_2 level of >2600 ppm, will affect both sleep quality and next-day cognitive performance. The corresponding ACH was estimated to be 1.1, 0.6, and 0.2 h^{-1} (the median bedroom volume and occupancy during sleep were 32 m^3 and one person in the present study). 79% of bedrooms had an ACH < 1.1 h^{-1} suggesting that occupants sleeping in these bedrooms may suffer from sleep disturbance; 26% was lower than 0.2 h^{-1} indicating that both sleep quality and next-day cognitive performance of occupants sleeping in these bedrooms might be affected already. These results highlight the urgency of improving bedroom ventilation and the importance of investigating its effects on sleep quality.

Window and door opening significantly affect bedroom ventilation [12–14]. According to the habitual airing behaviours, the sample size obtained can be categorized into four different scenarios of natural ventilation in bedrooms: (1) Scenario 1, Window Closed and Door Closed; (2) Scenario 2, Window Closed and Door Open; (3) Scenario 3, Window Open and Door Closed; and (4) Scenario 4, Window Open and Door Open.

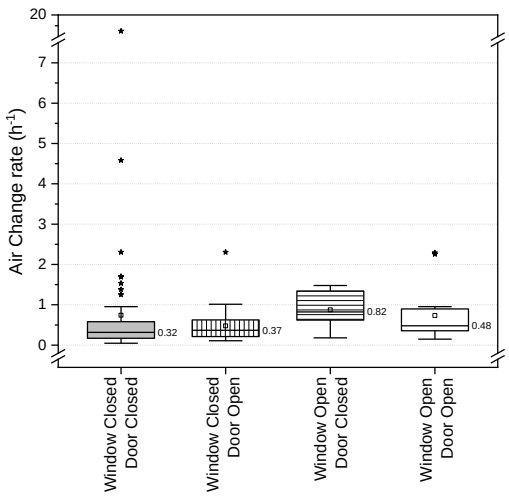

Fig. 2 – Estimated ACHs in different scenarios during the habitual sleep conditions.

Fig. 2 presents the estimated ACHs at different scenarios during the habitual sleep conditions. The lowest ACHs during sleep were found for Scenario 1 with a median value of 0.32 h^{-1} in Scenario 1; while the highest ACHs were observed for Scenario 3 with a median value of 0.82 h^{-1}. Window and door opening improved the bedroom ventilation, as expected. In contrast, the median ACH was 0.48 h^{-1} at Scenario 4 during sleep, which is in between Scenario 2 and 3. Similar results were observed under Scenario 2 and 3 but not Scenario 4 [12]. The plausible explanation for this divergence would be the opposite air movement directions from the window and the door. Further studies are necessary to investigate it.

We estimated the ventilation type in surveyed bedrooms using the information about the air terminals and trickle vents collected by the recruitment questionnaire. Bedrooms with air terminals were considered to have a fully balanced mechanical ventilation system. Bedrooms with trickle vents and exhaust air terminals in the bathroom or kitchen were considered to have mechanical ventilation with exhaust only. Bedrooms with other cases were considered to be ventilated naturally.

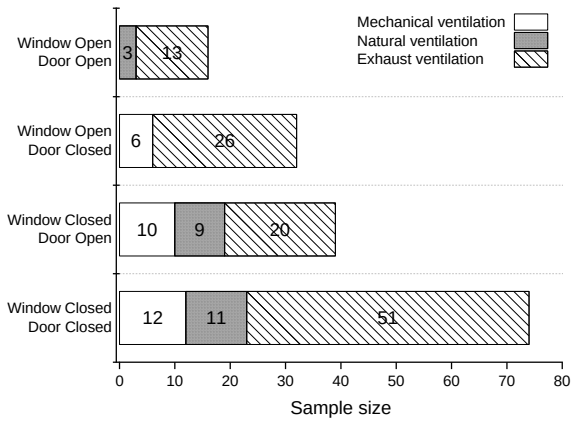

Fig. 3 – The distribution of sample size in terms of the ventilation system of the surveyed bedrooms in different scenarios. The sample size is larger than the number of occupants as more than one sample came from one participant.

The distribution of sample size based on the bedroom ventilation system is shown in Fig. 3. Most ACHs were estimated from bedrooms only with exhaust ventilation; only a few bedrooms were installed with a fully balanced mechanical ventilation system. The choice of opening or closing the window or door seems to be independent of the bedroom ventilation system.

It can also be seen that most samples were from bedrooms in Scenario 1; only a few samples were from bedrooms in Scenario 4; as expected. This study was conducted in wintertime in Denmark when the outdoor temperature was lower. Occupants prefer to avoid air draught and keep the bedroom warm during sleep by closing both the window and door, resulting in poor ventilation. More attention should be paid to bedroom ventilation during sleep, especially in these areas with central heating systems in winter. The sample size from the bedrooms with the door open was similar to those with the window open.

The locations of the surveyed bedrooms were deduced from postcodes collected from the recruitment questionnaire. The distribution of the sample size based on the locations is shown in Fig. 4. Most samples in the present study were from bedrooms located in suburban regions. There was only a small number of samples from bedrooms located in urban regions. The composition of the sample size in each Scenario was similar.

Both the characteristics of the ventilation system in surveyed bedrooms and information on the airing

behaviour during sleep explain the observed low ACHs during sleep under habitual conditions in the present study.

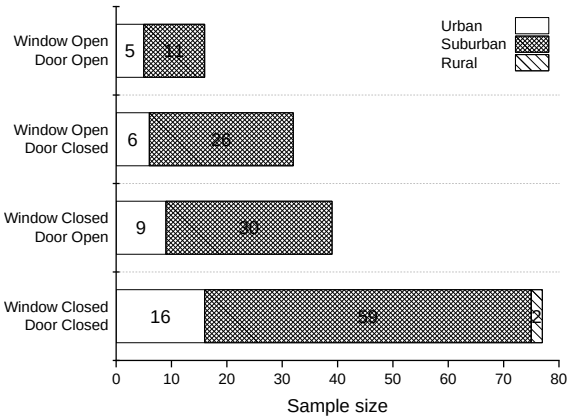

Fig. 4 – The sample size distribution in terms of the locations of the surveyed bedrooms in different scenarios. The sample size is large than the number of occupants as more than one sample came from one participant. The areas of the bedrooms with the first two numbers of postcodes 25 or below are regarded as urban regions; suburban regions refer to the areas with the first two numbers of postcodes 26-31, 34-36, 40, 50-52, 70, 80-82, and 90-92; and the other areas in the Capital Region of Denmark are rural.

The ACHs obtained from two-week measurements with the interventions are depicted in Fig. 5. This analysis is a within-subject comparison. The median ACHs were approx. 0.3 h^{-1} in Scenario 1 during sleep, which was similar to 0.32 h^{-1} measured during habitual sleep conditions. The median ACHs increased from 0.27 h^{-1} to 0.39 h^{-1} in Scenario 2. When opening the window only, the median ACHs increased from 0.32 h^{-1} to 1.14 h^{-1}. The median ACHs were only increased by 27% when opening both the window and door, which was similar to the estimated value under the conditions with the door open.

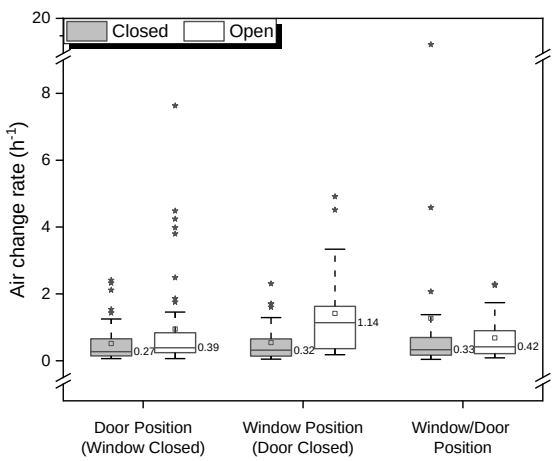

Fig. 5 – Estimated ACHs before and after interventions made by opening or closing either the door, or window, or both.

These results from the intervention part verify the observations from the habitual sleep conditions. The findings of the present study suggest that opening either the door, or the window, or both increases the ACH. However, the open window leads to better ventilation than the open door, as may be expected. Similar results were found by Mishra et al.[13]. It is worth noting that opening both window and door in the present study did not further improve the ventilation in bedrooms compared with only opening the window or door. A follow-up study is necessary to investigate the reasons behind that and the optimal conditions to increase the bedroom ventilation by opening both.

4. Limitation

This study was conducted during the heating season in Denmark, where the outdoor temperature in winter is low. The airing behaviour of participants during sleep may be different in other seasons, resulting in different ventilation. More future studies are needed to investigate it further.

The ACH was estimated by the decay of human metabolically produced CO_2 concentration. Its accuracy depends on the CO_2 measurement, elapsed time for decay, and air mixing in bedrooms. In addition, if the window and door status after sleep is the same as they are during sleep, it is also crucial to estimate the ventilation rate during sleep precisely by the CO_2 decay after sleep. The outdoor CO_2 level was not measured throughout the entire measuring period in the present study. We also did not check the air mixing. It would be useful to monitor the outdoor CO_2 concentration simultaneously and deploy more sensors at the different locations in bedrooms. Besides, we asked participants not to re-enter their bedroom within 30 min. after leaving it, which may lead to large uncertainty of the ACH estimation due to the limited data points available as the CO_2 concentration was registered every five min., especially at the high ventilation conditions where the decay would be quickly established. A more extended decay period could contribute to a more accurate estimation of the ACH.

The ACHs estimated in the present study are the total airflow into the bedroom, including airflows from adjacent spaces, especially when the bedroom door was open as an intervention. In light of no CO_2 measurements conducted in the adjacent spaces, especially outside the bedroom door, we assumed that the CO_2 concentration in the air supplied into bedrooms from adjacent spaces was equal to that in the outdoor air.

Even though we identified the ventilation systems of surveyed bedrooms based on the information about the air terminals and trickle vents, we did not check if they were operated appropriately throughout the entire measuring period. The previous study has shown that the ACH can be further enhanced by operating the exhaust ventilation system when opening the door in bedrooms [15]. In the present study, we did not observe that. It may be because the extraction systems were not in operation during

sleep. It would be helpful to check the operations of the ventilation systems in bedrooms during sleep in future studies to investigate the bedroom ventilation with different ventilation systems installed.

5. Conclusions

This work estimated the ACHs in bedrooms during sleep and explored how bedroom window and door opening affects ventilation. Extract ventilation was predominant in surveyed bedrooms; only a few had mechanical ventilation installed. Most participants slept with both the window and door closed. There was only a small number of participants who kept the bedroom window or door open during sleep, even less with both the window and door open. During habitual sleep conditions, the median ACH was 0.40 h^{-1}, ranging from 0.03 h^{-1} to 19.25 h^{-1}. Bedroom ventilation with closed door and window resulted in the lowest ACH, but window or door opening increased bedroom ACH, and window opening led to better ventilation than the door opening. This was verified by the results from intervention. The median ACH increased from 0.27 h^{-1} to 0.39 h^{-1} by only opening the door and from 0.32 h^{-1} to 1.14 h^{-1} by only opening the window. However, both window and door opening only slightly increased ventilation from 0.33 h^{-1} to 0.42 h^{-1}. During habitual sleep settings, half the surveyed bedrooms did not meet the minimum ventilation requirement prescribed by European Standard; 79% of bedrooms had an ACH of <1.1 h^{-1}, including 26% lower than 0.2 h^{-1}. Future studies are required to investigate whether the sleep quality is disturbed after sleeping under the insufficiently ventilated bedrooms and how window and door opening will affect the bedroom ventilation and sleep quality.

6. Acknowledgment

This research was supported by ASHRAE research project 1837-RP on bedroom ventilation and sleep quality. Xiaojun Fan was supported jointly by the China Scholarship Council (CSC), DTU Department of Civil Engineering (now Department of Environmental and Resource Engineering), Otto Mønsteds Foundation, and S.C. Van Fonden. Chenxi Liao was supported by VLAIO research project on smart ventilation (HBC.2020.2520); the Research Foundation – Flanders (FWO), Belgium (V409120N). Chandra Sekhar received financial support from National University of Singapore for his sabbatical visit at DTU. Anna Mainka was supported by the National Agency for Academic Exchange of Poland (PPI/APM/2018/1/00004). Pawel Wargocki was financially supported by Fonden af 20. december (155808-15). The authors thank Prof. Jørn Toftum for guidance on the construction of the online sleep diary website and the 84 households participating in this study.

Data Statement

The datasets generated during and/or analysed the current study are not publicly available but are/will be available by contacting the first author upon reasonable request.

7. References

[1] L. Lan, Y. Sun, D.P. Wyon, P. Wargocki, Pilot study of the effects of ventilation and ventilation noise on sleep quality in the young and elderly, Indoor Air. 31 (2021) 2226–2238. https://doi.org/10.1111/ina.12861.

[2] X. Xu, Z. Lian, J. Shen, T. Cao, J. Zhu, X. Lin, K. Qing, W. Zhang, T. Zhang, Experimental study on sleep quality affected by carbon dioxide concentration, Indoor Air. (2020) 1–14. https://doi.org/10.1111/ina.12748.

[3] P. Strøm-Tejsen, D. Zukowska, P. Wargocki, D.P. Wyon, The effects of bedroom air quality on sleep and next-day performance, Indoor Air. 26 (2016) 679–686. https://doi.org/10.1111/ina.12254.

[4] M. Miller, F. Cappuccio, Inflammation, Sleep, Obesity and Cardiovascular Disease., Curr. Vasc. Pharmacol. 5 (2007) 93–102. https://doi.org/10.2174/157016107780368280.

[5] X. Fan, H. Shao, M. Sakamoto, K. Kuga, L. Lan, D.P. Wyon, K. Ito, M.P. Bivolarova, C. Liao, P. Wargocki, The effects of ventilation and temperature on sleep quality and next-day work performance : pilot measurements in a climate chamber, Build. Environ. 209 (2022) 108666. https://doi.org/10.1016/j.buildenv.2021.108666.

[6] M. Akimoto, C. Sekhar, M.P. Bivolarova, C. Liao, X. Fan, J. Laverge, L. Lan, P. Wargocki, Reviewing how bedroom ventilation affects IAQ and sleep quality, ASHRAE J. 63 (2021) 56–60.

[7] C. Sekhar, M. Akimoto, X. Fan, M. Bivolarova, C. Liao, L. Lan, P. Wargocki, Bedroom ventilation: Review of existing evidence and current standards, Build. Environ. 184 (2020) 107229. https://doi.org/10.1016/j.buildenv.2020.107229.

[8] ASHRAE 62.2, Ventilation and Acceptable Indoor Air Quality in Residential Buildings, (2019).

[9] EN 16798–1:2019, Energy performance of buildings – Ventilation for buildings – Part 1 : Indoor environmental input parameters for design and assessment of energy performance, (2019).

[10] X. Fan, M. Sakamoto, H. Shao, K. Kuga, K. Ito, L. Lan, P. Wargocki, Emission rate of carbon dioxide while sleeping, Indoor Air. 31 (2021) 2142–2157. https://doi.org/10.1111/ina.12911.

[11] G. Bekö, T. Lund, F. Nors, J. Toftum, G. Clausen, Ventilation rates in the bedrooms of 500 Danish children, Build. Environ. 45 (2010) 2289–2295. https://doi.org/10.1016/j.buildenv.2010.04.014.

[12] N. Canha, J. Lage, S. Candeias, C. Alves, S.M. Almeida, Indoor air quality during sleep under different ventilation patterns, Atmos. Pollut. Res. 8 (2017) 1132–1142. https://doi.org/10.1016/j.apr.2017.05.004.

[13] A.K. Mishra, A.M. van Ruitenbeek, M.G.L.C. Loomans, H.S.M. Kort, Window/door opening-mediated bedroom ventilation and its impact on sleep quality of healthy, young adults, Indoor Air. 28 (2018) 339–351. https://doi.org/10.1111/ina.12435.

[14] J. Few, C. Elwell, Open or Closed ? Use of Windows and Doors at Home : Ventilation Rates in Occupied Dwellings, in: ASHRAE Top. Conf. Proceedings. Am. Soc. Heating, Refrig. Air Cond. Eng. Inc., 2021: pp. 1–8.

[15] C. Sekhar, M. Bivolarova, M. Akimoto, P. Wargocki, Detailed characterization of bedroom ventilation during heating season in a naturally ventilated semi-detached house and a mechanically ventilated apartment, Sci. Technol. Built Environ. 27 (2020) 158–180. https://doi.org/10.1080/23744731.2020.1845019.

Visualisation of the airflow pattern of exhaled droplets in a classroom

Yat Long Liu [a], Marco A. Ortiz [b], Dadi Zhang [b], Philomena M. Bluyssen [b]

[a] Faculty of Civil Engineering and Geosciences, Delft University of Technology, Delft, the Netherlands, marvin.liu93@gmail.com.

[b] Faculty of Architecture and the Built Environment, Delft University of Technology, Delft, the Netherlands, M.A.OrtizSanchez@tudelft.nl.

[b] Faculty of Architecture and the Built Environment, Delft University of Technology, Delft, the Netherlands, D.Zhang-2@tudelft.nl.

[b] Faculty of Architecture and the Built Environment, Delft University of Technology, Delft, the Netherlands, P.M.Bluyssen@tudelft.nl.

Abstract. The airborne transmission of SARS-CoV-2 in educational buildings has raised concerns during the current COVID-19 pandemic. In this study, a portable fog generator system was designed and assembled to visualise the airflow pattern of exhaled droplets in a classroom. The system consists of five components: medium, fog generator, buffer, pump, and manikin head. The medium was made of glycol and demineralised water, which produced a fog composed of droplets. The fog was produced with the fog generator and passed through a pipe into the buffer for build-up. After accumulation, the fog is pumped through another pipe and is exhaled out of the mouth of the manikin. Experiments were conducted with the portable fog generator system in a simulated classroom under four different ventilation regimes: no ventilation, natural ventilation (open windows and door), mixing ventilation (600 m^3/h), and a combination of natural + mixing ventilation. The experiments were recorded with a camera and analysed to determine the horizontal distance of the path taken by the fog and to measure the time it remained visible after exhalation from the mouth. During the experiments, it could be observed with the naked eye that the glycol droplets linger in the air longer than what was captured in the recordings. Not all the droplets were visible with the camera. The recordings showed that with open windows and door (natural ventilation), the droplets travelled the furthest distance (1.8 m) and stayed the longest in the air, while with mixing and natural ventilation, the droplets travelled the shortest (0.5 m) and stayed the least time in the air. These findings confirm that mechanical mixing ventilation increases the removal of aerosols in the air. It is concluded that the portable fog generator system provides a quick method in understanding the duration and distance droplets can travel after being exhaled.

Keywords. Covid-19, SARS-CoV-2, aerosol, respiratory droplets, visualisation, laser, breathing
DOI: https://doi.org/10.34641/clima.2022.361

1. Introduction

Since the beginning of the COVID-19 pandemic, ventilation has been recommended as a measure to reduce transmission of SARS-CoV-2 in indoor environments with a high occupancy, such as educational buildings [1]. In a study initiated by the National Ventilation Coordination Team (LCVS) in which CO_2 monitors were placed in educational buildings, the outcome showed that only 38% of the tested schools (7340 elementary and secondary schools in the Netherlands) meet the ventilation requirements from the Building Decree of 2012 [2]. Furthermore, only a third of the schools have natural ventilation, which is often inadequate to supply enough fresh air in the classroom. Controlling the temperature while the windows are open during periods of cold weather can be challenging as it has a negative effect on thermal comfort. Mechanical ventilation is an option to increase the fresh air supply, while controlling the indoor temperature. Other measures are to reduce the number of occupants, the use of air cleaning devices and/or use of facial masks.

To be able to determine whether in a certain situation additional measures are required, the aim of this study was to design and assemble a portable

Copyright ©2022 by the authors. This conference paper is published under a CC-BY-4.0 license.

fog generator system to visualise the airflow pattern of aerosols produced by pupils in a classroom. This system should mimic human breath and it should be possible to apply at schools, in a classroom. To test whether this fog generator system can be applied, the system was tested in an experimental setting under different ventilation regimes.

2. Research method

2.1 The portable fog generator system

The portable fog generator system consists of five main components: medium, fog generator, buffer, pump, and manikin head. The medium was made of glycol and demineralised water (9:1 ratio). The medium was put inside the container of the fog generator. The fog was produced with the fog generator and passed through a pipe into the buffer for accumulation. The lid of the buffer had to be airtight to prevent leaks. After the built-up, the fog is transferred from the buffer to the mouth of the manikin with a manual pump. The final setup can be seen in Figure 1.

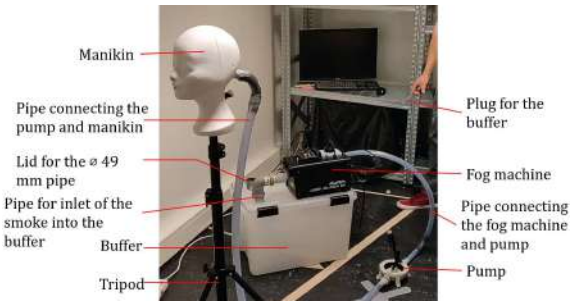

Fig. 1 – Setup of the portable fog generator.

2.2 Ventilation regimes

Four ventilation regimes were applied to visualise how the glycol droplets disperse after exhalation: no ventilation, natural ventilation with windows and door open, mixing ventilation with a ventilation rate of 600 m^3/h and the combination of natural + mixing ventilation. An overview is shown in Figure 2. Two data loggers were placed in the room to examine if the basic indoor parameters deviated too much during the experiment between each attempt and the different ventilation regimes. The baseline measurements (including the air velocity) were measured with the Dantec ComfortSense monitor and HOBO MX1102 data loggers at different locations throughout the Experience room of the SenseLab [3].

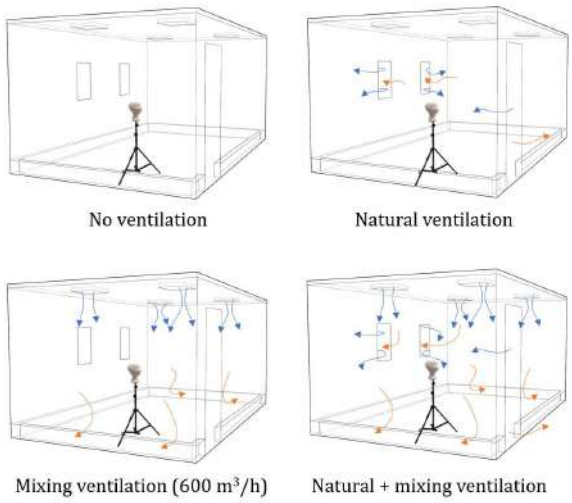

Fig. 2 - Four tested ventilation regimes. The blue arrows indicate air being supplied to the room. The orange arrows are for the air leaving the Experience room.

2.3 Setup for the airflow pattern visualisation

The experiments were conducted in the Experience room of the SenseLab, which is an experimental room decorated as a classroom with the possibility to adjust the indoor environmental conditions. The manikin head was placed at the back of the Experience room (see Figure 3). Five lasers (Huepar BOX-1G) were put on the table, facing towards the ceiling. Another laser was placed at the end of the table. The distances between the manikin's mouth to the lasers were measured with a measuring tape and written on the table. The lights of the room were turned off during the experiment to increase the effect of the lasers. The visualisation of the fog was recorded with a mirrorless camera (E-M10 Mark II) with a wide-angle lens (Lumix G Vario 7-14mm f/4.0 ASPH). Two attempts were taken for each ventilation regime. Each attempt was one minute long. To mimic the respiratory system as realistic possible, the operator based the pumping movement on its breathing. This resulted in 15 breaths per minute.

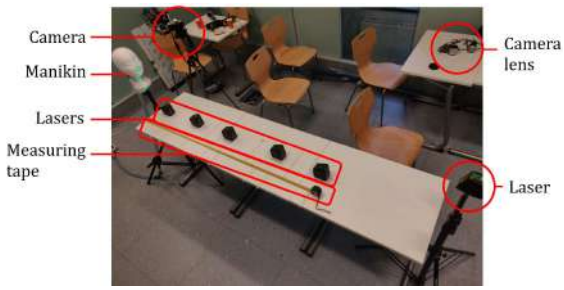

Fig. 3 – Setup of the airflow pattern visualisation experiment.

2.4 Data analysis

The attempts were recorded and reviewed to determine how far the droplets travel in the air, how long it takes before they are no longer visible and the percentage of fog plume visible after each exhalation.

The program VLC was used to review the recordings frame by frame. When the droplets do not progress more than a certain distance after a single exhalation, it is noted as the furthest distance. The duration was measured by how long it took before the droplets were no longer visible in the recording. It was observed with the naked eye that the glycol droplets linger in the air longer than what was captured by the recordings. Therefore, it was decided to time that as well with a stopwatch. To quantify the percentages of the droplets detected by the laser per respiratory cycle an image processing program (named Fiji) was used. The subtraction method was applied to compare each frame with the frame before exhaling the fog plume. This method results in a frame showing only the droplets (depicted in grey/white pixels). The program assigns a value between 0–100% for each frame, depending on the amount of non-black pixels. The mean grey intensity can be computed by summing the grey values of all the pixels in the selection divided by the number of pixels.

3. Results

3.1 Travel distance of glycol droplets

The measurement results of the droplet distances are shown in Figure 4. The corresponding frames of the video which were used to determine the distance can be found in the appendix. The droplets reached a distance of 1.3 metres without any ventilation. By opening the windows and door in the natural ventilation regime, a distance of 1.8 metres was recorded. Applying only mechanical ventilation in the mixing ventilation regime made the droplets travel 0.9 metres. The droplets reached the shortest distance of 0.5 metres in the natural + mixing ventilation regime.

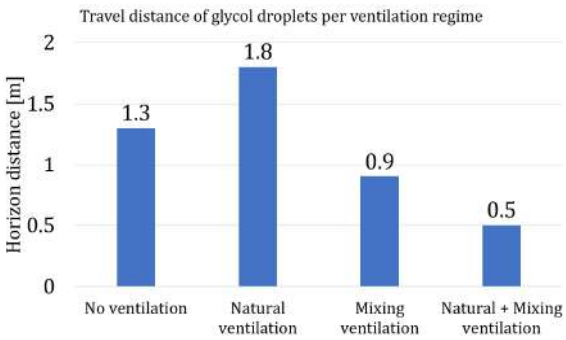

Fig. 4 – The droplets travelled furthest with natural ventilation (1.8 metres) and shortest with natural + mixing ventilation (0.5 metres).

3.2 Visibility time of glycol droplets

Figure 5 presents the time that the glycol droplets were visible for the different ventilation regimes. In the 'no ventilation' regime, the droplets remained suspended in the air for 12.7 seconds according to the video recordings and 15.5 seconds by personal observation. It was observed that the fog plume in the natural ventilation regime was less concentrated than in the no ventilation regime. The droplets lingered in the air for 12.2 seconds according to the video recordings and 13.8 seconds visually. In the only mixing ventilation regime, the fog plume seemed less concentrated and dissipated in both horizontal and vertical directions. It was visible for 9.5 seconds in the video recordings and 11.2 seconds in person. The fog plume disappeared the fastest during the natural + mixing ventilation regime. The droplets travelled upwards and spread even faster when it nearly reached the ceiling, with a lingering time of 5.4 seconds in the video recordings and 7.2 seconds visually.

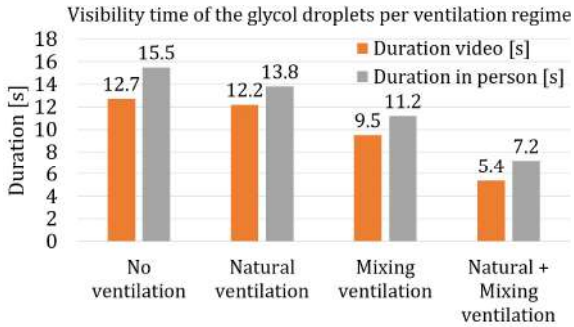

Fig. 5 – The droplets settled or evaporated faster in the recordings than with the naked eye. Increasing the indoor air velocity decreases the visibility of the droplets.

3.3 Percentage of fog plume

Figure 6 presents the mean grey intensity over time, the percentage of fog plume per frame calculated with Fiji. The analysed images with only the fog plumes consisted of almost only black pixels. This resulted in a low mean grey intensity value. The peak and valley in the graph indicate exhalation and inhalation, respectively. The mean grey intensity starts to decrease at t=50s for all ventilation regimes. This is because the amount of fog in the buffer decreased during each exhalation. The natural + mixing ventilation regime had the lowest average mean grey intensity value (0.74%). The fog plume was immediately dispersed by the high air velocity caused by the open door, windows and the presence of mechanical ventilation. Therefore, the majority of the droplets were not detected by the laser. The average mean grey intensity of no ventilation and natural ventilation was 0.86% and 0.90%, respectively. More droplets were detected by the laser in the natural ventilation regime because it passes a longer distance than with no ventilation. The mixing ventilation regime had the highest value (1.22%). The fog plume was mainly dispersed horizontally, causing the total concentration of droplets per exhalation to spread out even more, thus making it easier for the lasers to visualise the droplets.

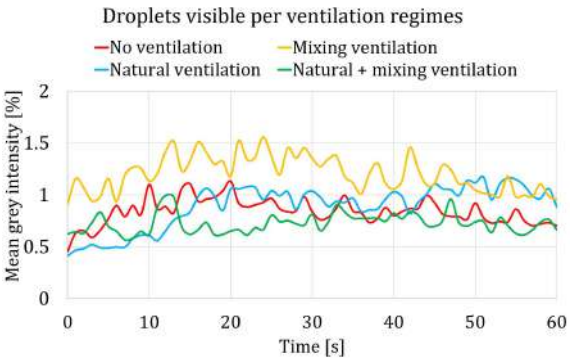

Fig. 6 – The respiratory cycle is represented in the graph with peaks and valleys.

4. Discussion and conclusions

4.1 The portable fog generator

The visualisations of the portable fog generator system provided a quick method in understanding the duration and distance the droplets travel before they settle down. Visualisation studies mostly occurred in hospitals or dental clinics, of which the results were reviewed with numerical studies [8-11]. Others used a more practical approach to examine how well for example face masks obstruct the respiratory jets [12-13]

The reliability of the portable fog generator system may be constrained by the fact that it needs to be manually operated. This results in inconsistent outcomes as it depends on the skill of the operator to use the pump. Although the essence of the airflow pattern of the droplets was recorded in the recordings, we were unable to record all of the exhaled fog plumes. The camera cannot capture single droplets, only clouds of multiple droplets. This makes it impossible to determine the actual droplet sizes from the recordings. The same applies to estimating the time it took for the droplets to evaporate or disappear in the video. Also, timing the experiment with the stopwatch likely caused inaccuracy in time measurements due to human reaction time to mainly start and stop the stopwatch.

4.2 Ventilation and lifespan of the droplets

The chances of getting infected with diseases through airborne transmission are especially high in low ventilation enclosed environments. In such environments, respiratory droplets immediately shrink after exhalation and become droplet nuclei. The majority of the respiratory droplets are smaller than 75 µm and according to Stokes' law, droplets of these sizes can linger in the air from a few seconds to many hours in rooms with low indoor air velocity while holding viable infectious viruses [4]. The results of the airflow pattern visualisation show that the droplets can reach much further than the 1.5 metres guidelines in natural ventilation (1.8 metres). Simultaneously, the droplets lingered the longest in the air. Unfortunately, a third of the Dutch schools only have this type of ventilation, which is often not sufficient to provide adequate indoor air quality for the whole school day [2]. Various research has shown the importance of adequate ventilation in rooms with a high occupancy [5-7].

The findings from this study suggest that there is a correlation between the lifespan and the airflow pattern of droplets under different ventilation regimes. The results showed that the exhaled droplets from the portable fog generator system tend to reach a shorter distance from the source when the airflow pattern becomes more turbulent (characterised by chaotic movements and contains swirling regions), which is visible in the recordings, and the mean grey intensities calculated.

In conclusion, this research contributed to the understanding of how the aerosols and droplets disperse after exhalation under different ventilation regimes. Firstly, it provides awareness and gives direct feedback on the effect of how droplets disperse at different ventilation regimes. Secondly, the fact that the setup is portable creates the convenience of taking it anywhere to visualise the airflow pattern of the droplets. Thirdly, the materials are accessible everywhere and relatively easy to assemble.

5. Acknowledgement

This study is part of the ZonMw funded project "SARS-CoV-2 transmission in secondary schools and the influence of indoor environmental conditions" (no. 50-56300-98-689) coordinated by the University Medical Centre Utrecht in the Netherlands. Participants are the Erasmus Medical Centre in Rotterdam, the University of Utrecht, and the Delft University of Technology in Delft, all in the Netherlands.

6. Appendix

Video frame of the maximum travel distance of glycol droplets per ventilation regime

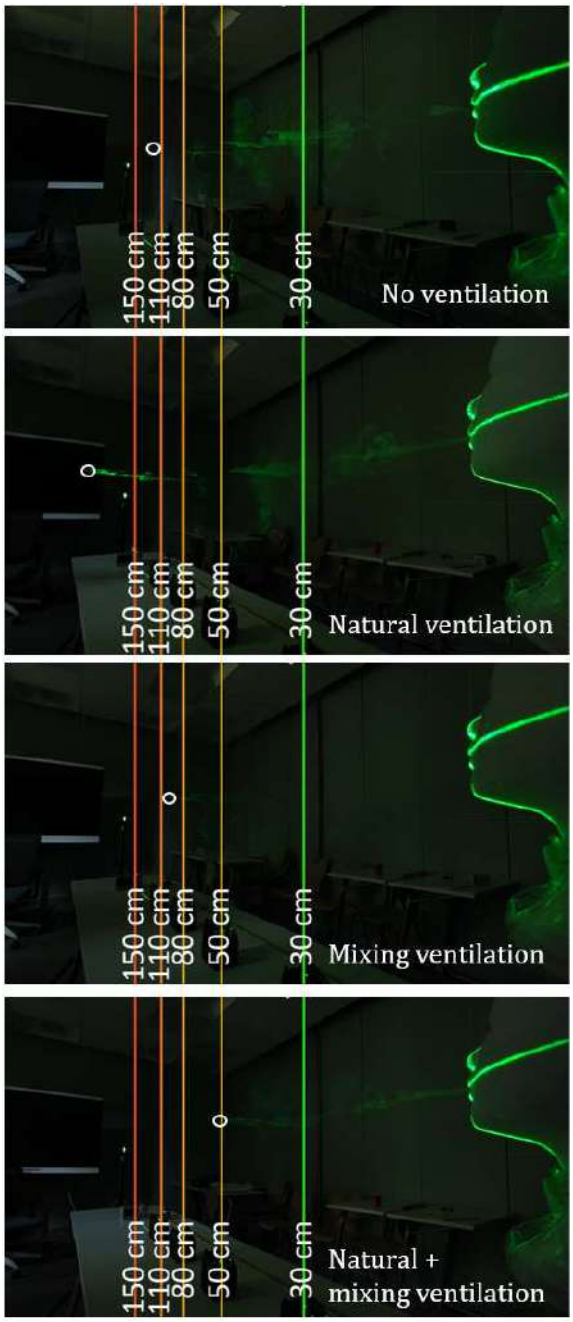

7. References

[1] Morawska, L., Tang, J., Bahnfleth, W., Bluyssen, P.M., et al. 2020. How can airborne transmission of COVID-19 indoors be minimised? Environ. Internat., 142:105832

[2] LCVS. Rijksoverheid. [Online].; 2020. Available from: https://www.rijksoverheid.nl/documenten/rapporten/2020/10/01/eindrapport-landelijk-coordinatieteam-ventilatie-op-scholen.

[3] Bluyssen PM, Zeist Fv, Kurvers S, Tenpierik M, Pont S, Wolters B, et al. The creation of SenseLab: a laboratory for testing and experiencing single and combinations of indoor environmental conditions. Intelligent Buildings International. 2018; 10(1): p. 5-18.

[4] Xie X, Li Y, Sun H, Liu L. Exhaled droplets due to talking and coughing. J. R. Soc. Interface. 2009; 6(6): p. S703-S714.

[5] Schijven J, Vermeulen LC, Swart AMA, Duizer E, de Roda Husman AM. Quantitative Microbial Risk Assessment for Airborne Transmission of SARS-CoV-2 via Breathing, Speaking, Singing, Coughing, and Sneezing. Environmental Health Perspectives. 2021; 129(4): p. 047002.

[6] Somsen GA, van Rijn C, Kooij S, Bem RA, Bonn D. Small droplet aerosols in poorly ventilated spaces and SARS-CoV-2 transmission. The Lancet Respiratory Medicine. 2020; 8(7): p. 658-659.

[7] Verma S, Dhanak M, Frankenfield J. Visualizing the effectiveness of face masks in obstructing respiratory jets featured. Physics of Fluids. 2020 May; 32(6).

[8] Bivolarova M, Ondráček J, Melikov A, Ždímal V. A comparison between tracer gas and aerosol particles distribution indoors: The impact of ventilation rate, interaction of airflows, and presence of objects. Indoor Air. 2017 November; 27(6): p. 1201-1212.

[9] Andersson PA, Hambraeus A, Zettersten U, Ljungqvist B, Neikter K, Ransjö U. A comparison between tracer gas and tracer particle techniques in evaluating the efficiency of ventilation in operating theatres. Epidemiology & Infection. 1983 December; 91(3): p. 509-519.

[10] Bhattacharyya S, Dey K, Paul AR, Ranjib B. A novel CFD analysis to minimize the spread of COVID-19 virus in hospital isolation room. Chaos, Soitons & Fractals. 2020 October; 139: p. 110294.

[11] Teichert-Filho R, Baldasso CN, Campos MM, Gomes MS. Protective device to reduce aerosol dispersion in dental clinics during the COVID-19 pandemic. International Endodontic Journal. 2020 July; 53(11): p. 1588-1597.

[12] Arumuru V, Pasa J, Samantaray SS, Varma VS. Breathing, virus transmission, and social distancing—An experimental visualization study. API Advances. 2021 March; 11(4): p. 045205.

[13] Miller SL, Nazaroff WW, Jimenez JL, Boerstra A, Buonanno G, Dancer SJ, et al. Transmission of SARS-CoV-2 by inhalation of respiratory aerosol in the Skagit Valley Chorale

superspreading event. Indoor Air. 2020 September; 31(2): p. 314-323.

Data Statement

The datasets generated during and/or analysed during the current study are available in the TU Delft Research Repository, http://resolver.tudelft.nl/uuid:73d08938-da05-47c7-89c1-0a497ab990ad.

CO_2 monitoring to assess ventilation rate: practical suggestions from a laboratory study

Dadi Zhang [ab], Er Ding [ac], Philomena M. Bluyssen [ad]

[a] Chair Indoor Environment, Faculty of Architecture and the Built Environment, Delft University of Technology, the Netherlands,

[b] D.Zhang-2@tudelft.nl, [c] e.ding@tudelft.nl, [d] P.M.Bluyssen@tudelft.nl.

Abstract. Several recent studies have demonstrated that ventilation plays an important role in the transmission of SARS-CoV-2 (the coronavirus that causes COVID-19) in public buildings, such as schools. However, there are no clear rules on how to assess the ventilation performance in classrooms, especially during a pandemic. Therefore, the main objective of this study was to develop guidance to assess the ventilation performance under different ventilation regimes. A full-scale laboratory study was conducted in the Experience room of the SenseLab, where CO_2 concentrations were monitored at 19 locations (18 indoors and one outdoors) simultaneously and recorded every 30 seconds by HOBO® CO_2 loggers. The experiment was conducted under four different ventilation regimes: '600 m^3/h mixing', 'open windows', 'no ventilation', and 'open windows and door'. Each regime lasted 50 minutes, which is approximately the duration of one normal lesson at Dutch secondary schools. Six (three males and three females) healthy subjects were invited to participate in this experiment as CO_2 sources. Results showed that CO_2 concentrations varied significantly between different measurement locations in the same classroom, especially under natural ventilation conditions. This demonstrates the need of monitoring the CO_2 concentration, next to outdoors, at more than one location in a classroom. The finding of this study could contribute to a standardized way of monitoring CO_2 concentrations and the assessment of ventilation performance of an occupied space.

Keywords. CO_2 concentration, ventilation regimes, classrooms, monitoring guidance.
DOI: https://doi.org/10.34641/clima.2022.93

1. Introduction

After being proved and confirmed by many scientists, the airborne transmission of SARS-CoV-2 transmission has finally been accepted as the dominant transmission route by the whole world [1-3]. Along with that, people have begun to raise concerns over the indoor air quality (IAQ) and ventilation [4, 5]. Increasing ventilation has been listed as one of the main measures against the spread of SARS-CoV-2 by many governments. However, how do we know whether the ventilation is enough or how to assess the ventilation efficiency? According to previous studies, CO_2 concentration has usually been taken into account as the indicator of the amount of ventilation or for IAQ [6-8]. Because CO_2 measurement devices are easily usable, relatively cheap, and reasonable accurate, CO_2 is widely used to estimate ventilation rate in spaces [8, 9], and the history of using CO_2 as an indicator of the ventilation performance can be traced back to more than 160 years ago [10]. Besides, several studies suggested CO_2 can be seen as the proxy of COVID-19 infection risk [7, 11-13]. because both infected aerosols and CO_2 are mainly originating from human exhalation. For example, by using monitored CO_2 concentrations, Burridge et al. [12] established a predictive and retrospective model to estimate the risk of airborne infection in regularly occupied spaces, such as office or school classrooms.

However, despite the widely use of CO_2-based methods, there is no consistent guidance for CO_2 monitoring. The selection of measurement locations of and number of sensors mainly depends on researchers' personal experiences, and therefore varied a lot among previous studies [14-16]. For example, in some studies the CO_2 concentration was measured at only one indoor location per room [17, 18], while others conducted the measurement at three or four locations to get more accurate ventilation rates [19, 20]. Additionally, the height of measurement point was also not consistent. In studies conducted by Mumovic et al. [21], Clements-Croome et al. [22], and Turanjanin et al. [23], the sensors/devices were placed at the height of 1.1m

Copyright ©2022 by the authors. This conference paper is published under a CC-BY-4.0 license.

above the floor, while the height was set to 1.2m in studies conducted by Hou et al. [17] and Krawczyk et al. [24].

According to the lab study carried out by Mahyuddin et al. [25], CO_2 was not distributed homogeneously in the investigated classrooms, therefore, monitoring CO_2 at only one location might lead to inaccurate result, and the selection of monitoring location should depend on the ventilation regimes. To accurately assess the ventilation rate in an occupied space, a unified and detailed CO_2 monitoring protocol including different strategies that are applicable for different ventilation regimes is needed. Therefore, in this study a full-scale experiment with multiple measurement locations in the SenseLab [26] was conducted to better understand the CO_2 distribution in a room under different ventilation regimes, and developed a consistent CO_2 monitoring guidance, based on the results.

2. Methods

2.1 study design

The full-scale experiment was conducted in the Experience room (6.5 (l) × 4.2 (b) × 2.6 (h)) of the SenseLab [26] (See Fig. 1). Six healthy subjects, including three males and three females, volunteered to participate in this experiment. They were asked to remove their masks after seated [27]. The average age of them was 27 ±2 years old. Prior to the study, all subjects gave informed consent to participate in the experiment, and they were able to leave the Experience room at any time in the case they were not feeling comfortable.

Fig. 1 – Experimental setting.

19 measurement locations (18 indoors and one outdoors) were selected in this study. As shown in Fig. 2, six of them ('D_') were on top of six desks at 1.1m above the floor, two of them were in the centre ('C') / front ('F') of the room at 1.1m and 1.6m respectively, and the last eight of them were on the four walls ('W_'), also at 1.1m and 1.6 m. CO_2 concentrations at all these locations were measured every 30 seconds using HOBO® CO_2 loggers (which have an accuracy of ±50 ppm ±5% of reading in the range of 0-5000 ppm).

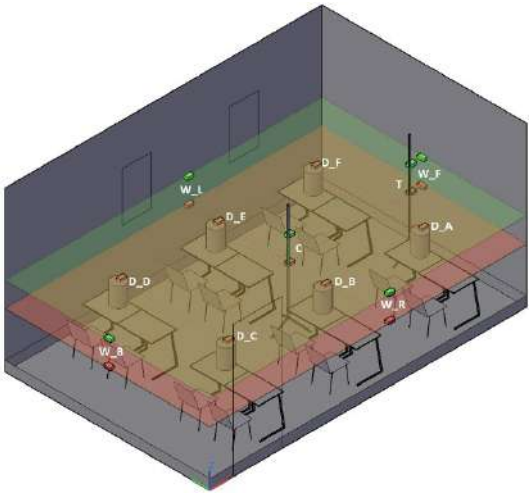

Note: measurement locations at 1.1m were marked in red and at 1.6m were marked in green.

Fig.2 - Measurement locations in the experience room.

The same measurement was repeated four times under four different ventilation regimes: (1) mixing ventilation with a ventilation rate of 600 m^3/h (in which air come from four 600 × 600 mm grills on the ceiling and exhaust from the perforated plinth on the short side of the room); (2) natural ventilation with windows open; (3) no ventilation; and (4) natural ventilation with both door and windows open. Each tested condition lasted 50 minutes. To reset the CO_2 concentration to the default level (close to the outdoor level), a ten-minute break (during which occupants left the room and the ventilation was set as 120m^3/h mixing ventilation) was inserted between each of two test periods. According to the weather report, the outdoor condition on the experiment day was 16 °C, 63%, and with 13 km/h north wind [28].

2.2 Data analysis

All collected data was imported and analysed using SPSS version 26.0 (SPSS Inc. Chicago, IL, USA) in the following steps. First, the average CO_2 concentration of all the indoor locations were compared among the last ten measurements (i.e. the last five minutes) of each test periods using one-way ANOVA to check whether they reach a steady state. Second, the average (standard deviation) CO_2 concentration during the last five minutes of each period at each location was analysed with descriptive statistics. Third, CO_2 concentrations were compared between different ventilation regimes with one-way ANOVA. Then, the average CO_2 concentrations were compared among different horizontal locations at 1.1m and 1.6m, separately, using one-way ANOVA. Finally, using paired samples t-test, the difference of CO_2 concentrations between two heights was compared at five locations (four walls and the centre), separately.

3. Results and Discussion

3.1 CO_2 concentrations under different ventilation regimes

According to the results collected from this study, the trends in CO_2 variation over time at all indoor locations were similar. Take the centre location (1.1m) as an example, as shown in Fig. 3, when the ventilation regime was '600 m^3/h mixing', the CO_2 concentration was relatively steady and low. During 'open windows' regime, the CO_2 concentration increased at the beginning but reached a relatively steady state at the end. When there was 'no ventilation', the CO_2 concentration increased significantly and continuously during the whole period. With the 'open door and windows', the CO_2 concentration was similar to concentration under the '600 m^3/h mixing' condition, but with slightly more fluctuations. According to the one-way ANOVA test result, the CO_2 concentration varied significantly between these four ventilation regimes ($F(3, 676) = 8522$, $p < 0.001$). The Bonferroni test showed that there was a significant difference of CO_2 concentration between almost every two ventilation regimes, except for between '600 m^3/h mixing' and 'open door and windows'. The CO_2 concentration during these two ventilation regimes were much lower than with the other two regimes. This indicated that natural ventilation, under certain conditions, could achieve a similar ventilation effect as mechanical ventilation.

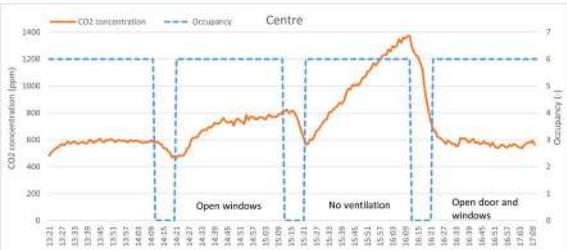

Fig. 3 - CO_2 variation over time at one location.

Additionally, it can be seen from the figure that the CO_2 concentration could reach to a relatively steady state at the end of all test periods, except for the third period- 'no ventilation'; the CO_2 concentration hardly reached a plateau. Nevertheless, the results collected during the last five minutes seemed closest to the steady-state concentration. Besides, results of the one-way ANOVA test showed that the average CO_2 concentration collected from all indoor locations did not vary significantly among the last ten measurements (i.e. last five minutes) of all the periods, which indicated the CO_2 concentration during the last five minutes of all test periods could be considered as stable. Therefore, the following analyses were all based on the results collected during the last five minutes of each test period.

3.2 CO_2 distribution under different ventilation regimes

Fig. 4 illustrates the horizontal distribution of CO_2 concentrations at 1.1m and 1.6m in the Experience room under different ventilation regimes. The diameter of circles represents the difference of the average CO_2 concentration between each indoor measurement location and the outdoor location. Different colours of circles represent different ventilation regimes: red represents '600 m^3/h mixing'; green represents 'open door and windows'; yellow represents 'open windows'; and blue represents 'no ventilation'. As shown in these figures, the CO_2 concentration was not evenly distributed in the Experience room. According to the one-way ANOVA test results (see the values mentioned below the subtitles), the CO_2 concentration did vary significantly between different locations ($p<0.05$), especially under natural ventilation conditions (where higher F-values were found). Generally speaking, CO_2 concentrations measured on the wall were relatively higher than the other locations. Moreover, the lowest CO_2 concentration was always observed at location D_E, while the highest CO_2 concentration on the back wall (W_B), no matter under which ventilation regime.

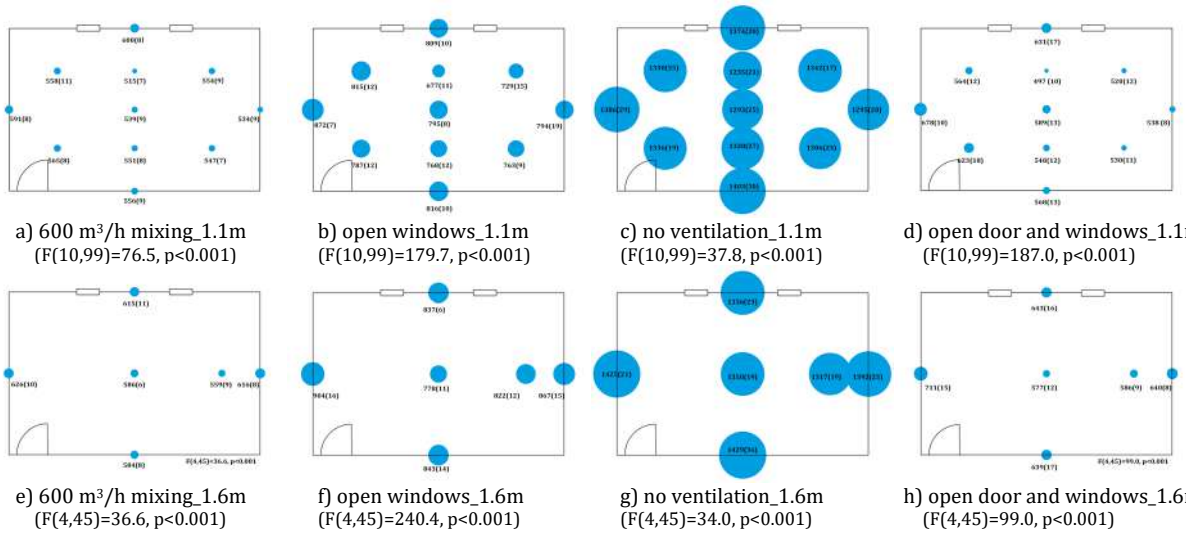

a) 600 m^3/h mixing_1.1m ($F(10,99)=76.5$, $p<0.001$)
b) open windows_1.1m ($F(10,99)=179.7$, $p<0.001$)
c) no ventilation_1.1m ($F(10,99)=37.8$, $p<0.001$)
d) open door and windows_1.1m ($F(10,99)=187.0$, $p<0.001$)
e) 600 m^3/h mixing_1.6m ($F(4,45)=36.6$, $p<0.001$)
f) open windows_1.6m ($F(4,45)=240.4$, $p<0.001$)
g) no ventilation_1.6m ($F(4,45)=34.0$, $p<0.001$)
h) open door and windows_1.6m ($F(4,45)=99.0$, $p<0.001$)

Fig. 4 - CO_2 distribution in the Experience room.

Note: the numbers under the circles are the average (standard deviation) CO_2 concentrations measured at each location during the last five minutes.

To further identify the vertical distribution of CO_2 concentration, results collected from the locations with two different heights were compared with each other (1.1m vs. 1.6m). As shown in Table 1, in most cases, t(9) was negative and the p value was less than 0.05, which means the CO_2 concentration was significantly higher at 1.6m than it at 1.1m, no matter under which ventilation regimes. This vertical distribution might be caused by the thermal plume produced by occupants. Given the fact that students spend most of their time sitting, instead of standing, the CO_2 concentration at 1.1m (the breathing height of a sitting person) should be paid more attention to in field studies.

Tab. 1 - Comparisons of CO_2 concentrations between two heights for different ventilation regimes.

Location	600 m^3/h mixing	Open windows	No ventilation	Open windows and door
C	t(9)=-12.3 (**< 0.001**)	t(9)= 5.2 (**0.001**)	t(9)= -8.8 (**< 0.001**)	t(9)= 2.1 (0.065)
W_F	t(9)=-23.7 (**< 0.001**)	t(9)=-20.9 (**< 0.001**)	t(9)=-14.0 (**< 0.001**)	t(9)=-32.3 (**< 0.001**)
W_R	t(9)=-6.9 (**< 0.001**)	t(9)=-5.8 (**< 0.001**)	t(9)=-5.2 (**0.001**)	t(9)=-16.3 (**< 0.001**)
W_B	t(9)=-8.3 (**< 0.001**)	t(9)=-7.1 (**< 0.001**)	t(9)=-6.8 (**< 0.001**)	t(9)=-6.4 (**0.004**)
W_L	t(9)=-3.6 (**0.006**)	t(9)=-7.0 (**< 0.001**)	t(9) = 2.8 (**0.021**)	t(9)=-3.3 (**0.010**)

Note: all results were obtained from independent t-tests; p-values are shown in paratheses; results in bold means statistically significant difference ($p < 0.05$).

3.3 Proposed CO_2 monitoring guidance

According to the above-mentioned results, the CO_2 concentration was not well mixed, neither horizontally nor vertically, in the Experience room. Therefore, results collected from one measurement location might be inaccurate. However, in occupied classrooms, it is also infeasible to monitor CO_2 concentration at too many locations as this current study did. Thus, if the condition permits, according to the worst-case design principle [29], priorities are suggested to be given to the locations on walls since higher CO_2 concentrations were always measured on walls. If the CO_2 concentration on the wall could meet the requirement, so could the CO_2 concentration in the whole classroom. Moreover, the risk of equipment damage by students was relatively lower on walls than other locations, and in that case, locations on the front wall and back ball were recommended since they are usually farthest from the students' activity zone.

Additionally, to get an accurate result, the outdoor CO_2 concentration should also be monitored, and the number of occupants, open windows and open doors should be recorded during the monitoring period since all this information could cause a remarkable difference in CO_2 concentrations/ventilation rates in classrooms.

4. Conclusions

To understand the CO_2 distribution in a classroom setting, CO_2 concentrations were measured at 18 indoor (and one outdoor) locations simultaneously in the Experience room of the SenseLab, under four different ventilation regimes. Based on the measurement results, this study concluded that only one measurement location might lead to inaccurate results, especially under natural ventilation regimes. Therefore, for future field studies, to get a better understanding of the ventilation/IAQ in classrooms, at least two CO_2 measurement locations on walls (especially the front and the back wall) at 1.1m should be selected in natural ventilated classrooms, while in mechanical ventilated classrooms (with both supply and exhaust), one measurement point seems enough because CO_2 is relatively well-mixed under this ventilation regime. In addition, outdoor CO_2 concentration was also suggested to be monitored, and the number and behaviour of occupants during the measurement should be recorded.

5. Remark

More detailed results and discussion of this study were published in the journal 'Indoor and Built Environment' [30].

6. Acknowledgement

This study is part of the ZonMw funded project "SARS-CoV-2 transmission in secondary schools and the influence of indoor environmental conditions" (no. 50-56300-98-689) coordinated by the University Medical Centre Utrecht in the Netherlands. Participants are the Erasmus Medical Centre in Rotterdam, the University of Utrecht, and the Delft University of Technology in Delft, all in the Netherlands.

7. References

[1] Greenhalgh, T., J.L. Jimenez, K.A. Prather, Z. Tufekci, D. Fisman, and R. Schooley, *Ten scientific reasons in support of airborne transmission of SARS-CoV-2.* The lancet, 2021. **397**(10285): p. 1603-1605.

[2] Dancer, S.J., P.M. Bluyssen, Y. Li, and J.W. Tang, *Why don't we just open the windows?* 2021, British Medical Journal Publishing Group.

[3] Zhang, R., Y. Li, A.L. Zhang, Y. Wang, and M.J. Molina, *Identifying airborne transmission as the dominant route for the spread of COVID-19.* Proceedings of the

National Academy of Sciences, 2020. **117**(26): p. 14857-14863.

[4] Ding, E., D. Zhang, and P.M. Bluyssen, *Ventilation regimes of school classrooms against airborne transmission of infectious respiratory droplets: A review.* Building and Environment, 2022. **207**: p. 108484.

[5] Sun, C. and Z. Zhai, *The efficacy of social distance and ventilation effectiveness in preventing COVID-19 transmission.* Sustainable cities and society, 2020. **62**: p. 102390.

[6] Chatzidiakou, L., D. Mumovic, and A. Summerfield, *Is CO2 a good proxy for indoor air quality in classrooms? Part 1: The interrelationships between thermal conditions, CO2 levels, ventilation rates and selected indoor pollutants.* Building Services Engineering Research and Technology, 2015. **36**(2): p. 129-161.

[7] Bartyzel, J., D. Zięba, J. Nęcki, and M. Zimnoch, *Assessment of Ventilation Efficiency in School Classrooms Based on Indoor–Outdoor Particulate Matter and Carbon Dioxide Measurements.* Sustainability, 2020. **12**(14): p. 5600.

[8] Batterman, S., *Review and extension of CO2-based methods to determine ventilation rates with application to school classrooms.* International journal of environmental research and public health, 2017. **14**(2): p. 145.

[9] Kabirikopaei, A. and J. Lau, *Uncertainty analysis of various CO2-Based tracer-gas methods for estimating seasonal ventilation rates in classrooms with different mechanical systems.* Building and Environment, 2020. **179**: p. 107003.

[10] Olsson, D. *History of ventilation: Carbon dioxide as an indicator of indoor air pollution in 1858!* 2015 [cited 2021 30 May]; Available from: https://www.swegonairacademy.com/2015/12/30/history-of-ventilation-carbon-dioxide-as-an-indicator-of-indoor-air-pollution-in-1858/.

[11] Peng, Z. and J.L. Jimenez, *Exhaled CO2 as a COVID-19 infection risk proxy for different indoor environments and activities.* Environmental Science & Technology Letters, 2021. **8**(5): p. 392-397.

[12] Burridge, H.C., S. Fan, R.L. Jones, C.J. Noakes, and P. Linden, *Predictive and retrospective modelling of airborne infection risk using monitored carbon dioxide.* arXiv preprint arXiv, 2020.

[13] Hartmann, A. and M. Kriegel, *Risk assessment of aerosols loaded with virus based on CO2-concentration.* Technical University of Berlin, Hermann-Rietschel-Institute, 2020.

[14] Shaughnessy, R.J., U. Haverinen-Shaughnessy, A. Nevalainen, and D. Moschandreas, *A preliminary study on the association between ventilation rates in classrooms and student performance.* Indoor Air, 2006. **16**(6): p. 465-468.

[15] Haverinen-Shaughnessy, U., D. Moschandreas, and R. Shaughnessy, *Association between substandard classroom ventilation rates and students' academic achievement.* Indoor Air, 2011. **21**(2): p. 121-131.

[16] Toftum, J., B.U. Kjeldsen, P. Wargocki, H.R. Menå, E.M. Hansen, and G. Clausen, *Association between classroom ventilation mode and learning outcome in Danish schools.* Building and Environment, 2015. **92**: p. 494-503.

[17] Hou, Y., J. Liu, and J. Li, *Investigation of indoor air quality in primary school classrooms.* Procedia Engineering, 2015. **121**: p. 830-837.

[18] Schibuola, L., M. Scarpa, and C. Tambani, *Natural ventilation level assessment in a school building by CO2 concentration measures.* Energy Procedia, 2016. **101**: p. 257-264.

[19] Wargocki, P. and D.P. Wyon, *The effects of moderately raised classroom temperatures and classroom ventilation rate on the performance of schoolwork by children (RP-1257).* Hvac&R Research, 2007. **13**(2): p. 193-220.

[20] Wargocki, P., *Improving indoor air quality improves the performance of office work and school work.* Energy Systems Laboratory (http://esl.tamu.edu), 2008.

[21] Mumovic, D., J. Palmer, M. Davies, M. Orme, I. Ridley, T. Oreszczyn, C. Judd, R. Critchlow, H. Medina, and G. Pilmoor, *Winter indoor air quality, thermal comfort and acoustic performance of newly built secondary schools in England.* Building and Environment, 2009. **44**(7): p. 1466-1477.

[22] Clements-Croome, D.J., H. Awbi, Z. Bakó-Biró, N. Kochhar, and M. Williams, *Ventilation rates in schools.* Building and Environment, 2008. **43**(3): p. 362-367.

[23] Turanjanin, V., B. Vučićević, M. Jovanović, N. Mirkov, and I. Lazović, *Indoor CO2 measurements in Serbian schools and ventilation rate calculation.* Energy, 2014. **77**: p. 290-296.

[24] Krawczyk, D., A. Rodero, K. Gładyszewska-Fiedoruk, and A. Gajewski, *CO2 concentration in naturally ventilated classrooms located in different climates—Measurements and simulations.* Energy and Buildings, 2016. **129**: p. 491-498.

[25] Mahyuddin, N., H.B. Awbi, and M. Alshitawi, *The spatial distribution of carbon dioxide in rooms with particular application to classrooms.* Indoor and Built

Environment, 2014. **23**(3): p. 433-448.
[26] Bluyssen, P.M., F. van Zeist, S. Kurvers, M. Tenpierik, S. Pont, B. Wolters, L. van Hulst, and D. Meertins, *The creation of SenseLab: a laboratory for testing and experiencing single and combinations of indoor environmental conditions.* Intelligent Buildings International, 2018. **10**(1): p. 5-18.
[27] Goverment of the Netherlands. *Wearing of face masks strongly advised*. 2020 [cited 2021 21 June]; Available from: https://www.government.nl/latest/news/2020/10/02/wearing-of-face-masks-strongly-advised.
[28] Time and data. *June 2021 Weather in Delft — Graph*. 2021 [cited 2022 March 17]; Available from: https://www.timeanddate.com/weather/netherlands/delft/historic?month=6&year=2021.
[29] Rustem, B. and M. Howe, *Algorithms for worst-case design and applications to risk management*. 2009: Princeton University Press.
[30] Zhang, D., E. Ding, and P.M. Bluyssen, *Guidance to assess ventilation performance of a classroom based on CO2 monitoring.* Indoor and Built Environment, 2022.

Data Statement

The datasets generated during and/or analysed during the current study are not available because more analysis will be conducted based on these datasets but the authors will make every reasonable effort to publish them in near future.

Modeling the impact of indoor relative humidity on the airborne transmission of several respiratory viruses risk using a modified Wells-Riley model

Amar Aganovic [a], Yang Bi [b], Guangyu Cao [b], Jarek Kurnitski [c], Pawel Wargocki [d]

[a] Department of Automation and Process Engineering, UiT The Arctic University of Norway, Tromsø, Norway, amar.aganovic@uit.no

[b] Department of Energy and Process Engineering, Norwegian University of Science and Technology - NTNU, Trondheim, Norway, yang.bi@ntnu.no

[b] Department of Energy and Process Engineering, Norwegian University of Science and Technology - NTNU, Trondheim, Norway, guangyu.cao@ntnu.no

[c] REHVA Technology and Research Committee, Tallinn University of Technology, Tallinn, Estonia, jarek.kurnitski@taltech.ee

[d] Department of Civil Engineering, Technical University of Denmark, Copenhagen, Denmark, paw@byg.dtu.dk

Abstract. There is good evidence supporting the airborne transmission of many respiratory viruses (measles, influenza A, human rhinovirus and the novel SARS-CoV-2). Relative humidity (RH) is an important factor in understanding airborne transmission as it may impact both airborne survival, inactivation by biological decay, and the gravitational settling of the virus-laden droplets. This study aimed to estimate and compare the impact of indoor relative humidity on the airborne infection risk caused by these viruses using a novel modified version of the Wells-Riley model. To gain insights into the mechanisms by which relative humidity might impact airborne transmission infection risk, we modeled the size distribution and dynamics of airborne viruses emitted from a speaking person in a typical residential setting over a relative humidity (RH) range of 20–80% at a temperature of 20-21 °C. Besides the size transformation of virus-containing droplets due to evaporation and then removal by gravitational settling, the modified model also considers the removal mechanism by ventilation. The direction and magnitude of RH impact depended on the respiratory virus. Measles showed a highly significant RH impact that was as strong as the ventilation impact, as the infection risk was roughly the same at RH of 13.5 % and 6 ACH compared to a higher RH of 70 % and 0.5 ACH. For other viruses, ventilation dominated over RH. In the case of SARS-CoV-2, a very high RH of 83.5% was needed to reduce the infection risk. For rhinovirus, however, the high RH of 80% increased the infection risk. Within the acceptable range of RH of 20-50% indoors, our modeling showed that RH had practically no impact for SARS-CoV-2 and rhinovirus, while the upper RH significantly reduced the infection risk of influenza A at the lowest ventilation rate of 0.5 ACH. This relative impact of RH on infection risk became very weak at higher ventilation rates of 2-6 ACH independently of the virus types (except measles). In conclusion, we showed that in well-ventilated rooms, RH range of 20-50% did not affect the airborne risk of influenza A, SARS-CoV-2, and rhinovirus.

Keywords. Virus airborne transmission, Ventilation, Relative humidity, Indoor environment, Wells-Riley model
DOI: https://doi.org/10.34641/clima.2022.363

Copyright ©2022 by the authors. This conference paper is published under a CC-BY-4.0 license.

1. Introduction

There is good evidence supporting the airborne transmission of many enveloped respiratory viruses (measles [1], influenza A (H1N1) [2], MERS-CoV [3], and the novel SARS-CoV-2 [4]) and certain non-enveloped viruses (human rhinovirus [5]). Airborne infections pose a particular threat to susceptible individuals whenever they are placed together with an infected person in confined spaces [6]. It is therefore important to understand the risks posed by infectious individuals in indoor environments so that interventions can be developed to minimize the spread of airborne infection. In this context, predictive mathematical models and risk assessments can be a fundamental tool for understanding and planning effective infection control strategies in indoor environments. Wells-Riley model is the classic model to quantitatively assess airborne infection risk; it is based on the seminal work of Wells [7] and Riley et al. [8]. The Wells-Riley model has extensively been used to evaluate the airborne infection risk of respiratory diseases [9]. The original Wells-Riley model has been extended to account for three sink or removal mechanisms – ventilation, gravitational settling, and biological decay of the airborne pathogen [10]. However, the removal terms of gravitational settling and biological decay in this model can only be calculated for one specific environmental condition being RH. This is a limitation of the model, as RH may affect the airborne transmission of respiratory viruses via both the deposition loss and airborne decay of infectious droplets [11]. To gain insight into the mechanisms by which relative humidity might impact airborne transmission infection risk, we modeled the size distribution and dynamics of airborne viruses emitted from a speaking person in a typical residential setting over a relative humidity (RH) range of 20–80% and at a temperature of 20-21 °C. Our model advances a mechanistic understanding of the aerosol transmission route, and results complement recent studies on the relationship between humidity and respiratory disease infectivity. It is an extension of the work published earlier investing only the impact of RH on the risk of infection with SARS-CoV-2 [12].

2. Methodology

A schematic representation of the theoretical model assessing the impact of RH on the quanta emission rate of SARS-CoV-2 for infection risk assessment is shown in Fig 1.

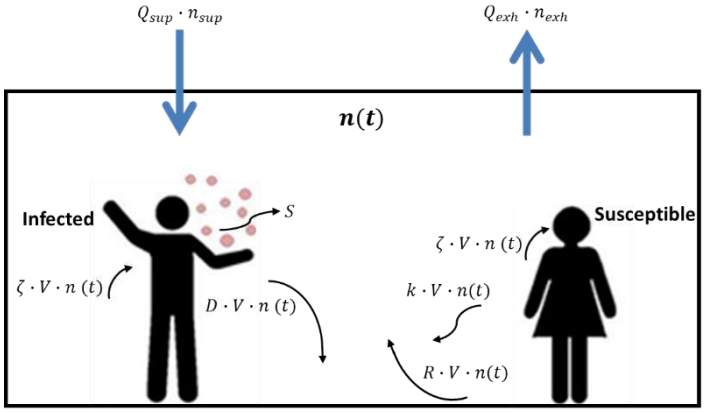

Fig 1. Schematic representation of a simple indoor air mass-balance model in a completely mixed environment including a source term S and removal mechanisms by ventilation, inactivation by biological decay k, deposition by gravitational settling D, resuspension R, and respiratory absorption ζ.

The mass balance model for a completely mixed indoor mechanically ventilated room model can be represented by the following differential equation representing a single-zone model:

$$V \cdot \frac{dn(t)}{dt} = S + Q_{sup} \cdot n_{sup}(t) - Q_{exh} \cdot n_{exh}(t) - k \cdot n(t) \cdot V - D \cdot V \cdot n(t) - R \cdot V \cdot n(t) - 2 \cdot \zeta \cdot V \cdot n(t) \quad (1)$$

To solve equation (1) in the form of a first-order differential equation $\frac{dn(t)}{dt} + n(t) \cdot a = b$, it may be rewritten as follows:

$$\frac{dn(t)}{dt} + n(t) \cdot \left(\frac{Q}{V} + D + k + 2 \cdot \zeta\right) = \frac{S}{V} \quad (2)$$

The unique solution of quanta concentration in an indoor environment with complete mixing ventilation at time t, $n(t)$ is:

$$n(t) = n_0 \cdot e^{-\left(\frac{Q}{V}+D+k+2\cdot\zeta\right)\cdot t} + \frac{S}{V} \cdot \left\{\frac{1}{\frac{Q}{V}+D+k+2\cdot\zeta} - \frac{1}{\frac{Q}{V}+D+k+2\cdot\zeta} \cdot e^{-\left(\frac{Q}{V}+D+k+2\cdot\zeta\right)\cdot t}\right\} \quad (3)$$

where n_0 is the initial quanta concentration ($\frac{quanta}{m^3}$) at time t = 0.

To perform calculations with (9) to predict indoor concentrations of quanta at time t, appropriate expressions for the source term S, deposition rate D, inactivation rate k, and absorption rate ζ must first be known. Regardless of the type of respiratory virus considered, the deposition rate D and absorption rate ζ will be calculated in the same manner. The detailed description of calculating the

impact of RH on deposition rate D can be found in [12], while the calculation of the absorption rate ζ can be found in [13].

The pollutant source emission rate S is defined as the quanta emission rate of respiratory virus generated by infected persons in the room divided into n bins and can be defined by: $S = I \cdot c_v \cdot c_i \cdot IR \cdot \sum_{i=1}(N_i \cdot V_i)$ (4)

I – number of infected persons, -

N_i - droplet number concentration in the ith bin, $\frac{particles}{cm^3}$

V_i – the mean volume of a single droplet (mL) in the ith bin.

$$V_i\,(D) = \frac{\pi \cdot (D_{max}{}^4 - D_{min}{}^4)}{24 \cdot (D_{max} - D_{min})} \qquad (5)$$

where D_{max} and D_{min} denote the bin's lower and upper diameter values [14].
i– size bin of the droplet distribution.

The size distribution for talking is determined experimentally by the works of Morawska et al. [15] for droplet aerosols $\leq 2\ \mu m$ and Chao et al. [16] for respiratory droplets $\geq 2\ \mu m$: both studies measured the size distribution of droplets for talking/voice counting at a distance of 10 mm from the participant's mouth opening.

IR , $\frac{m^3}{h}$– inhalation rate. The inhalation rates for resting and standing averaged between males and females are equal to 0.49 and 0.54 $\frac{m^3}{h}$, respectively [17].

c_v – viral load in the sputum ,$\frac{RNA}{ml}$ or $\frac{\text{TCID50}}{ml}$

c_i – conversion factor is defined as the ratio between one infectious quantum and the infectious dose expressed in viral RNA copies (quanta/RNA) or tissue culture infectious dose ($TCID_{50}$/ml). The mean values for c_i and c_v are given in Tab 1. as derived in a recent study by Mikszewski et al. [18]

Tab 1. Mean viral load c_v and conversion factor c_i values for different respiratory viruses [18] carried by droplets $\leq 5\mu m$ in a dehydrated state

Respiratory virus	Log_{10} c_v	Conversion factor c_i	S (quanta/h)
Measles	3.5 $TCID_{50}$/ml	1.0 quanta/ $TCID_{50}$	$14.79 \cdot 10^{-3}$
Influenzia	6.7 RNA/ml	$7.1 \cdot 10^{-6}$ quanta/RNA	$0.166 \cdot 10^{-3}$
Rhinovirus	3.6 $TCID_{50}$/ml	0.053 quanta/ $TCID_{50}$	$0.99 \cdot 10^{-3}$
SARS-CoV-2	5.6 RNA/ml	$1.4 \cdot 10^{-3}$ quanta/RNA	$2.6 \cdot 10^{-3}$

To characterize the impact of relative humidity on the inactivation rate, experimental data on the survival time of the respiratory viruses in aerosols were used for measured values of k (min^{-1}) at RH = 20%, 50% and 80 % at T = 20–24 °C, as shown in Tab 2.

Tab 2. Mean inactivation rates k $[min^{-1}]$ for the considered respiratory viruses at different RH values

Respiratory virus	Relative humidity (RH %)	Temperature (°C)	Mean inactivation rate k $[min^{-1}]$
Influenza A [19]	21	20-24	$8.68 \cdot 10^{-4}$
	50.5		$9.65 \cdot 10^{-3}$
	81		0.013
Measles [20]	13.5	20-21	0.010
	69		0.112
Rhinovirus [21]	30	20±1	0.066
	50		0.066
	80		$1.21 \cdot 10^{-3}$
SARS-CoV-2 [12]	20	20-25	0.0103
	53		0.0101
	83.5		0.0314

To determine the probability of infection (P, %) as a function of the exposure time (t) of susceptible people, the quanta concentration was integrated over time through the Wells–Riley equation as follows:

$$\boldsymbol{P} = \left(\mathbf{1} - \boldsymbol{e}^{-\boldsymbol{IR}\int_0^T \boldsymbol{n}(t)\boldsymbol{dt}}\right) \quad (\%) \qquad (6)$$

3. Results

We show preliminary results for a 40 m^2 x 3 m room with two occupants, one infected person, and one susceptible person that is distanced by at least 1 m; only droplets less than 5 microns in size before evaporation (dehydrated state) are considered for all cases. Fig 2. shows the impact of RH and ventilation rate on the infection risk when the person is infected with influenza A. The trend is clear - the infection risk decreased with higher RH. However, the overall effect of RH on the infection risk must be interpreted as a function of both the ventilation rate and time. The shorter the time interval and higher the ventilation rate, the less RH has an impact on the infection risk. It can be noted that for higher ventilation rates (6 ACH) the relative impact of RH on the infection risk is very weak.

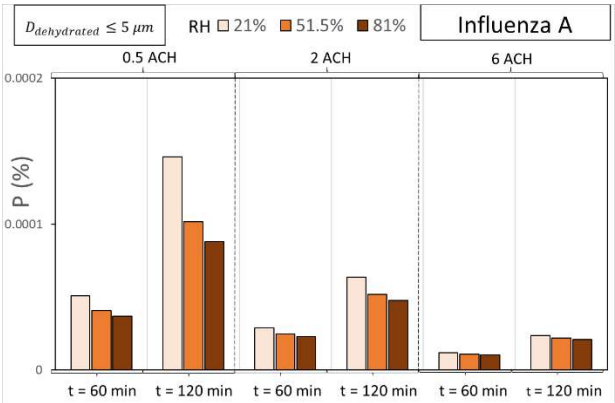

Fig 2. Impact of RH and ventilation (ACH = Air Exchange Rates per Hour) on the infection risk probability P (%) when influenza A infected person with a viral load of $c_v = 10^{6.7}$ RNA/ml is speaking continuously for 60 and 120 min.

The impact of RH on infection risk when a person is infected with measles is similar to the case scenario with influenza A as depicted in Fig 3. Very low RH values of 13.5 % significantly increase the infection risk when compared to a higher RH value of 70 %. Although again the relative impact of RH decreases higher ventilation rate the overall impact of RH is still prominent.

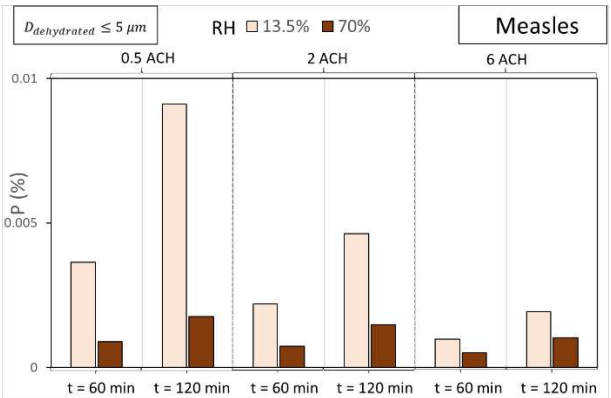

Fig 3. Impact of RH and ventilation (ACH) on the infection risk probability P (%) when the measles infected person with a viral load of $c_v = 10^{3.5}$ $TCID_{50}$/ml is speaking continuously for 60 and 120 min

Compared to influenza A and measles, the impact of RH on the infection risk for rhinovirus is inverse - the infection risk significantly rises for a higher relative humidity of 80 %, while it is lower for RH 30% and 50%. The difference between the calculated infection risks at RH = 30% and 50% is almost non-existent.

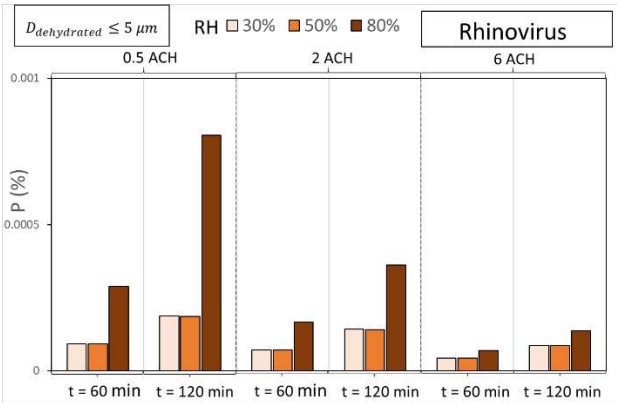

Fig 4. Impact of RH and ventilation (ACH) on the infection risk probability P (%) when a rhinovirus infected person with a viral load of $c_v = 10^{3.6}$ $TCID_{50}$/ml is speaking continuously for 60 and 120 min

Lastly, the impact of RH on SARS-CoV-2 infection risk is shown in Figure 5. The infection risk is lower for high RH values of 83.5 %, but there is no significant difference between infection risks for RH values between 20% and 53%. The difference between the infection risk at all three RH values considered becomes almost non-existent at higher ventilation rates (6 ACH).

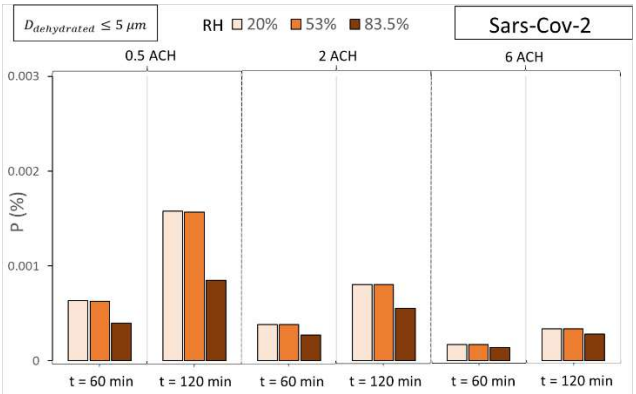

Fig 5. Impact of RH and ventilation (ACH) on the infection risk probability P (%) when a SARS-CoV-2 infected person with a viral load of $c_v = 10^{5.6}$ RNA/ml is speaking continuously for 60 and 120 min

4. Conclusions

The infection risk for four different respiratory. iruses (influenza A, measles, rhinovirus, and SARS-CoV-2) was estimated using the modified Wells-Riley model at different RH levels and different ventilation rates for a specific indoor scenario when an infected person was continuously talking for 120 min. We considered dehydrated droplets having a size lower than 5 microns. We assumed complete mixing and did not examine the impact of RH on susceptibility. The findings of the study can be summarized in the following key points:

- Four respiratory viruses showed different impacts of RH on infection risk regarding the direction of the impact and the magnitude compared to the ventilation rate impact
- For influenza A and SARS-CoV-2, the infection risk decreased with the highest RH values of 81% and 83.5%, but differences were small in the RH range relevant for indoor spaces. While for influenza A the infection risk was slightly lower at RH=51.5% compared to 21%, for SARS-CoV-2 there was practically no effect in the 20-53 RH range.
- Increasing RH from 20 or 30% to 50% had practically no effect in the case of SARS-CoV-2 and rhinovirus and had a small but significant positive effect in the case of influenza A. This impact of RH was more prominent for lower ventilation rates (0.5 ACH) and became very low at higher ventilation rates (6 ACH).
- For rhinovirus, the infection risk significantly rose for a higher relative humidity of 80 %, however, the difference between the calculated infection risks at RH = 30% and 50% was almost non-existent.
- Measles was the only virus for which RH impact was as strong as the ventilation impact, the infection risk was roughly the same at RH of 13.5 % and 6 ACH compared to a higher RH of 70 % and 0.5 ACH demonstrating a highly significant impact of RH.

In conclusion, we showed that maintaining a higher ventilation rate may have a more beneficial effect on reducing the airborne risk of four different airborne viruses than changing RH. Our model advances a mechanistic understanding of the aerosol transmission route, and results complement recent studies on the relationship between humidity and respiratory disease infectivity. The modified model can be used by public health experts, engineers, and epidemiologists when selecting different measures to reduce the infection risk from various respiratory diseases indoors allowing informed decisions concerning indoor environmental control

References

[1] Riley RL, Mills CC, Nyka W, Weinstock N, Storey PB, Sultan LU, Riley MC, Wells WF: Aerial dissemination of pulmonary tuberculosis. A two-year study of contagion in a tuberculosis ward. 1959. Am J Epidemiol. 1995, 142 (1): 3-14.

[2] Tellier : Review of aerosol transmission of influenza A virus. Emerg Infect Dis. 2006, 12 (11): 1657-1662.

[3] Xiao S, Li Y, Sung M, Wei J, Yang Z. A study of the probable transmission routes of MERS-CoV during the first hospital outbreak in the Republic of Korea. *Indoor Air.* 2018;28:51–63.

[4] Morawska and Cao, 2020 L. Morawska, J. Cao Airborne transmission of SARS-CoV-2: The world should face the reality Environ. Int., 139 (2020), p. 105730

[5] Dick EC, Jennings LC, Mink KA, Wartgow CD, Inhorn SL. Aerosol transmission of rhinovirus colds. J Infect Dis. 1987 Sep;156(3):442-8. doi: 10.1093/infdis/156.3.442. PMID: 3039011.

[6] C.C. Wang, K.A. Prather, J. Sznitman, J.L. Jimenez, S.S. Lakdawala, Z. Tufekci, *et al.* Airborne transmission of respiratory viruses Science, 373 (2021)

[7] W. F. Wells, Airborne Contagion and Air Hygiene: An Ecological Study of Droplet Infections (Harvard University Press, 1955).

[8] E. C. Riley, G. Murphy, R. L. Riley, Airborne spread of measles in a suburban elementary school. Am. J. Epidemiol. 107, 421–432 (1978).

[9] Sze To GN, Chao CY. Review and comparison between the Wells-Riley and dose-response approaches to risk assessment of infectious respiratory diseases. Indoor Air. 2010 Feb;20(1):2-16. doi: 10.1111/j.1600-0668.2009.00621.x. Epub 2009 Jul 31. PMID: 19874402; PMCID: PMC7202094.

[10] L. Gammaitoni, M.C. Nucci Using a mathematical model to evaluate the efficacy of TB control measures Emerg. Infect. Dis., 3 (1997), pp. 335-342, 10.3201/eid0303.970310

[11] A. Božič, M. Kanduč Relative humidity in droplet and airborne transmission of disease J. Biol. Phys., 47 (2021), pp. 1-29, 10.1007/s10867-020-09562-5

[12] Aganovic, A., Bi, Y., Cao, G., Drangsholt, F., Kurnitski, J., & Wargocki, P. (2021). Estimating the impact of indoor relative humidity on SARS-CoV-2 airborne transmission risk using a new modification of the Wells-Riley model. *Building and*

Environment, *205*.
https://doi.org/10.1016/j.buildenv.2021.108278

[13] Jones B, Sharpe P, Iddon C, Hathway EA, Noakes CJ, Fitzgerald S. Modelling uncertainty in the relative risk of exposure to the SARS-CoV-2 virus by airborne aerosol transmission in well mixed indoor air. Build Environ. 2021 Mar 15;191:107617. doi: 10.1016/j.buildenv.2021.107617. Epub 2021 Jan 19. PMID: 33495667; PMCID: PMC7816614.

[14] Nicas M, Nazaroff WW, Hubbard A. Toward understanding the risk of secondary airborne infection: emission of respirable pathogens. J Occup Environ Hyg. 2005 Mar;2(3):143-54. doi: 10.1080/15459620590918466. PMID: 15764538; PMCID: PMC7196697

[15]L. Morawska, G.R. Johnson, Z.D. Ristovski, M. Ha rgreaves, K. Mengersen, S. Corbett, C.Y.H. Chao, Y. Li, D. Katoshevski Size distribution and sites of origin of droplets expelled from the human respiratory tract during expiratory activiti**es** J. Aerosol Sci., 40 (2009), pp. 256-269, 10.1016/j.jaerosci.2008.11.002

[16] Chao et al., 2009 C.Y.H. Chao, M.P. Wan, L. Morawska, G.R. Johnson, Z.D. Ristovski, M. Hargreaves, K. Mengersen, S. Corbett, Y. Li, X. Xie, D. Katoshevski Characterization of expiration air jets and droplet size distributions immediately at the mouth opening J. Aerosol Sci., 40 (2009), pp. 122-133

[17] Adams, W.C., 1993. Measurement of Breathing Rate and Volume in Routinely Performed Daily Activities. Final Report. Human Performance Laboratory, Physical Education Department, University of California, Davis. Human Performance Laboratory, Physical Education Department, University of California, Davis. Prepared for the California Air Resources Board, Contract No. A033-205, April 1993.

[18]
A. Mikszewski, L. Stabile, G. Buonanno, L. Morawska The airborne contagiousness of respiratory viruses: a comparative analysis and implications for mitigation Geosci. Front. (2021), p. 101285

[19] Weber TP, Stilianakis NI. Inactivation of influenza A viruses in the environment and modes of transmission: a critical review. *J Infect*. 2008;57(5):361-373. doi:10.1016/j.jinf.2008.08.013

[20] DE JONG, J., WINKLER, K. Survival of Measles Virus in Air. *Nature* **201,** 1054–1055 (1964). https://doi.org/10.1038/2011054a0

[21] Karim YG, Ijaz MK, Sattar SA, Johnson-Lussenburg CM. Effect of relative humidity on the airborne survival of rhinovirus-14. Can J Microbiol. 1985 Nov;31(11):1058-61. doi: 10.1139/m85-199. PMID: 3004682.

Resilient Cooling in Buildings – A Review of definitions and evaluation methodologies

Shady Attia [a], Peter Holzer [b], Shabnam Homaei [c], Ongun Berk Kazanci [d], Chen Zhang [e], Per Heiselberg [e]

[a] Sustainable Building Design Lab, Dept. UEE, Faculty of Applied Science, Université de Liege, Belgium, shady.attia@uliege.be

[b] Institute of Building Research & Innovation, Vienna, Austria, peter.holzer@building-research.at

[c] Department of Civil and Environmental Engineering, NTNU Norwegian University of Science and Technology, Trondheim, Norway, shabnam.homaei@ntnu.no

[d] International Centre for Indoor Environment and Energy – ICIEE, Technical University of Denmark, Denmark,, onka@byg.dtu.dk

[e] Department of the Built Environment, Aalborg University, Denmark pkh@build.aau.dk, cz@build.aau.dk

Abstract. The concept 'Resilience' has gained wide international attention by experts and is now seen as the future target for the design of buildings. However, before using the word 'resilience', we must understand the semantics of the word. Resilience is not 'resistance' and is not 'robustness and is not 'sustainability', it is a more complex definition. As part of the International Energy Agency Annex 80 on resilient cooling in buildings, this paper focuses on formulating a definition for resilient cooling. Resilient cooling is used to denoting low energy and low carbon cooling solutions that strengthen the ability of individuals, and our community as a whole to withstand, and also prevent, the thermal and other impacts of changes in global and local climates; particularly concerning increasing ambient temperatures and the increasing frequency and severity of heatwaves. This paper focuses on the review of most of the existing resilient cooling definitions and the various approaches towards possible resiliency evaluation methodologies. It presents and discusses possible answers to the abovementioned issues to facilitate the development of a consistent resilient cooling definition and a robust evaluation methodology. The paper seeks to impact national building codes and international standards, through a clear and consistent definition and a commonly agreed evaluation methodology.

Keywords. robustness, resistance, discomfort, thermal comfort, ventilation, concepts
DOI: https://doi.org/10.34641/clima.2022.195

1. Introduction

Resilience is a central feature of the United Nations (UN) Sustainability Development Goals (SDGs) and is reflected in a range of SDG targets [1]. According to the UN General Assembly Resolution 71/276 [2], the term "resilience" describes "the ability of a system, community or society exposed to hazards to resist, absorb, accommodate, adapt to, transform and recover from the effects of a hazard in a timely and efficient manner, including through the preservation and restoration of its essential basic structures and functions through risk management."

The need for resilient building design and construction is urgent to anticipate climate change and disruptions caused by weather extremes, increasing carbon emissions, and resource depletion [3]. Our well-being depends on reducing the carbon emissions in our built environment and other sectors [4]. While solving the root-cause problem of climate change, we need to address its effects. Avoiding excessive temperatures induced by overheating is one of the most critical challenges that the building industry will face worldwide in the coming decades [5,6].

Increasing electricity demand during heat stresses can lead to blackouts and grid failures. This can leave buildings out of thermal comfort range and threaten the lives of vulnerable people at risk, as happened during the 2003 Europe heat wave [7]. As building disruptions may have severe and long-term economic impacts, resilient building cooling solutions are an essential strategy to mitigate threats to occupants [8]. There is an urgent need for resilient cooling solutions in buildings to keep comfort despite extreme weather events due to climate change [9]. Meanwhile, the use of fuelintensive mechanical cooling should be reduced

Copyright ©2022 by the authors. This conference paper is published under a CC-BY-4.0 license.

to slow climate change [10]. Greenhouse gas (GHG) emissions from buildings air conditioning stand at around 210–460 gigatonnes of carbon dioxide equivalent (GtCO2e) over the next four decades, based on 2018 levels [11].

It is of principal importance to define buildings' resilient cooling to maintain indoor environmental quality against unexpected events, e.g., extreme weather conditions, heat waves, power outages, etc. However, the definition of resilience and resilient cooling is challenging and complex [12]. Research on resilience associated with human-nature interactions is still in an explorative stage with few practical methods for real-world applications [13,14].

This article presents the main concepts of resilience. It proposes a definition of resilient cooling of buildings based on the discussion taking place in the International Energy Agency (IEA) - Energy in Buildings and Communities Programme (EBC) research project "Annex 80: Resilient Cooling of Buildings" [9]. The essence of this paper is to define resilience against overheating and power outage. It seeks to answer the following research questions:

What are the existing concepts of resilience in the built environment?

How to define resilient cooling of buildings?

The article presents a definition framework based on reviewing almost 90 studies of resilience, including RELi 2.0 Rating Guidelines for Resilient Design and Construction [15]. One of the challenges of this study is to define resilience on the building scale beyond what is present in literature, which mainly addresses the definition of resilience on an urban scale. This reinforces the importance of resilient cooling as an integral approach for building design and operation concerning comfort (including indoor environmental quality), carbon neutrality, and environmental friendliness [4].

2. Methodology

The research methodology is qualitative and relies on literature review, focus group discussions, and follow-up discussions with individuals.

2.1 Data Collection

A literature review was conducted aiming to define resilience against different climate change associated disruptions in the built environment worldwide. The publications included scientific journal articles, books and building rating systems. Our initial Scopus and Web of Science research resulted in almost 90 publications relevant to resilience and resilience criteria in the built environment. To examine the definitions of resilience and the associated resilience criteria such as vulnerability, resistance, robustness and recoverability, we surveyed resilience in ecology, resilience in engineering and resilience in psychology.

2.2 Data Processing

The content of the full text of every identified article was analyzed, and an analysis protocol and coding schema was developed to record its content attributes. The entire text of the full article was read multiple times as the search for coding words was completed by the coders (authors). Coding is a way of indexing or categorizing the text in order to establish a framework of its themes [16]. We used the framework method commonly used for the management and analysis of qualitative data in health research [17], [18].

2.3 Development of definition

For the definition development we used the framework method, which is the most commonly used technique for the management and analysis of qualitative data in health research [17], [18]. The framework method allows systematically analysis of the text data to produce highly structured outputs and summarized data. It can also compare and identify patterns, relevant themes, and contradictory data [17]. We categorized the codes (resilience concepts) by theme. Our classification resulted into four concepts that define resilient cooling of buildings.

2.4. Focus group and follow-up-discussions

Qualitative research is primarily a subjective approach as it seeks to understand human perceptions and judgements. However, it remains a solid exploratory scientific method if bias is avoided. The suggested definition validated through focus group discussions to provide reliable and consistent results. Several validation measures were implemented including member checking, memo logs, and peer examination following the work of Attia et al. [19]. The study validation allowed emphasizing credibility and strengthening the relevance of the conducted study and results. Focus groups were convened during IEA Annex 80's first expert meeting in Vienna, Austria (21 October 2019) and during its second expert meeting, held online (21 April 2020). Each focus group comprised 15 people. The invited experts for the focus-group discussion represented the scientific and professional experts in the field of building performance assessment and comfort. A list of the IEA Annex 80 participants can be found on the Annex website [20]. The goal of the focus-group discussions was to validate the suggested definition and associated main criteria.

Follow-up discussions with RELi steering committee members and UN resilience experts helped articulate and validate the framework and included detailed elaboration of some criteria. The follow-up discussions took place between the first authors and

some of the co-authors via teleconference and emails.

3. Results

3.1 Resilience against what?

One critical prerequisite for a comprehensive definition and assessment of resilience is the identification of threats (shocks) or disruptions to the stability of these systems. An essential question to answer is "resilience against what?".

As shown in Table 1, several types of disruptions or emergencies can lead to the systemic failure of buildings to be resilient—e.g., air pollution, fires, and earthquakes. Disruptions are increasingly presented by unexpected phenomena outside or inside the building [21]. The rate and pace of disturbances that the built environment faces have been accelerating significantly over the past three decades [22]. Understanding and identifying the phenomena that disrupt a building and threaten the well-being of its occupants is fundamental.

Table 1 - Different types of disruptions affecting the built environment

	Description
Air Pollution	- **Outdoor air pollution** refers to the air pollution experienced by populations living in and around urban and rural areas. Air pollution derives from poor combustion of fossil or biomass fuels (e.g., exhaust fumes from cars, furnaces or wood stoves) or wildfires. Buildings require efficient air filters and ventilation systems that mitigate the impact of air pollution.
Fire	- **Wildfires** are sweeping and destructive conflagrations, especially in a wilderness or a rural area, that cause significant damage. Most building codes adequately addresses common fire hazards with mandatory fire-resistant stairwells, fire-resistant building materials, and proper escape methods.
Earthquakes	- **Earthquakes** are the most common disruptions covered in all building codes. Trembling of the ground caused by the passage of seismic waves through earth's rocks. This natural disaster can damage a building by knocking it off its foundations and harm the occupants. Seismic testing should be used on components of buildings to determine their resilience to earthquakes.
Wind storms	- **Hurricane** have the potential to harm lives and property via storm surge, heavy rain, or snow, causing flooding or road impassibility, lightning, wildfires, and vertical wind shear.
Flooding	- **Flooding** is the inundation of land or property in a built environment, particularly in more densely populated areas, caused by rainfall overwhelming the capacity of drainage systems, such as storm sewers.
Heatwaves	- **Heat waves** are a period of excessively hot weather, which may be accompanied by high humidity. They cause overheating in the building and intensify the urban heat island effect. This event can potentially risk the health and lives of occupants if no measures are taken.
Power	- **Power outages** and blackouts are common occurrences that can be caused by natural disasters cited earlier like flood or hurricane. It can lead to overheating in buildings when air conditioners do not operate.
Water	- **Water shortage** is the lack of freshwater resources to meet water demand. Lack of water has a significant impact on irrigation and urban use, degrading food security, public health, and overall stability.
Pandemic	- **Pandemics** can impact the built environment of societies is how spatial and social aspects are intertwined to constitute everyday lives mutually. During active outbreaks, minimizing the risk of disease spread in buildings starts with keeping people out of them. For those who occupy a building, increasing the ventilation and filtration of the inside air is essential.

For our study, we decided to identify heat waves and power outages as the major disruptions that can influence occupant indoor environmental quality conditions on the building scale [4]. The paper is focused on the definition of resilient cooling of buildings as part of the IEA Annex 80 activities that aim to define resilience. Crawley et al. [23] identified heat waves as the significant climate change disruption in buildings. Baniassadi et al. [24] identified the frequency and duration of power outages as a significant cause of disruption for buildings in the near future. Both studies confirmed that the increase of mean outdoor temperatures and the frequent and intensive nature of heat waves disrupt power and degrade comfort.

Disruptions are shocks or events that have an origin, a nature, an incidence, a scale, and duration. Therefore, we define disruptions in buildings as shocks that degrade the indoor environment and, therefore, require resilient cooling strategies and technologies to maintain it [21].

3.2 Resilience: At which scale? And for how long?

The resilience of a system cannot be studied without examining the scale of the system, and the relation between the shock cause and its effect(s). Resilient systems function through the interaction of complex processes operating at different scales and times frames [22]. Therefore, it is essential to characterize the scale of the system that is expected to be resilient in a time-bound way. The definition of resilience should always reflect whether the disturbance affects the performance or operation of

a single building element, or building service or the entire building [23]. As shown in Figure 1, the definition of resilience should always characterize the resilience to disturbance of a system in relation to its scale within a specific time frame for the disturbance.

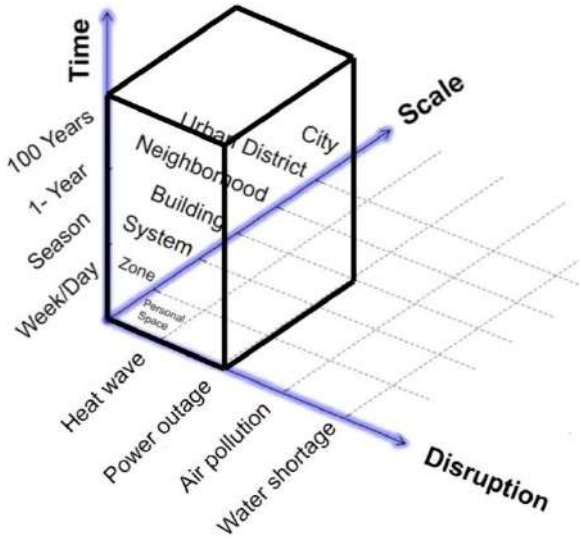

Fig. 1 - the components of a resilience definition within a specific field or domain

For our study, we define heat waves and power outages as the primary disruptive events to be addressed by resilient cooling for buildings. Our proposed definition considers the indoor environmental conditions on the building scale for long periods. Climate scenarios represent historical and future outdoor conditions and consider both short-term and long-term heat waves. Resilience in the building engineering field is strongly associated with long-term climate projections that encompass both the increase in the average temperature due to a global warming effect and a further temperature rise due to the urban heat island effect [27].

Defining and identifying disruptions and specifying their associated events that impact healthy and comfortable buildings is the first step to determine a building's resilience. As shown in Figure 1, heat waves and power outages are events that may impact the thermal conditions in buildings. The identification of heat-wave events is based on their intensity, duration, and frequency coupled with power outages [28]. It is expected that a building with a resistant cooling design (strategy) can withstand short and extensive heat waves. A building with a robust cooling design can withstand short, intense, and prolonged lengthy heat wave. The performance of a building with a resilient cooling design could surpass that of a robust building by reacting to power outages and longer intensive heat waves. The literature review confirms that resilience must be associated with response to system failure [15]. A system is robust when it can continue functioning in the presence of internal and external challenges without a system failure. However, a system is resilient when it can adapt to internal and external challenges by changing its method of operations while continuing to function. The ability of the building to recover after disruptive events is a fundamental feature of resilience. Therefore, the ability to model the occurrence and consequences of discrete heat-wave events is crucial to prepare the building for the response.

The interviewed experts agreed that climate change should be defined as the long-term disruptive event, and that heat waves and power outages should be designated short-term disruptive events. Based on our literature review and following Figure 2, we distinguish four major events categories that can challenge resilient cooling [28]:

- Event 1: Observed and future extreme weather conditions (extended, spanning years)
- Event 2: Seasonal extreme weather conditions (long, spanning months)
- Event 3: Short extreme weather conditions (short, spanning days)
- Event 4: Power outages (spanning hours)

Across the literature, several studies identified extended and long climate change associated temperature increase events (Events 1 and 2) [29], [30]. Other studies investigated the impact of short-term heat waves and power outages on thermal conditions and cooling systems' resilience [31], [32]. For example, the RELi rating system requires thermal safety during emergencies (Events 3 and 4) by maintaining indoor air temperature at or below outdoor air temperature up to seven days [15]. Designers need to demonstrate through thermal zoning and modeling that the building will maintain safe temperatures during a blackout that lasts four days. During a power outage, buildings must provide backup power to satisfy critical loads for 36 hours.

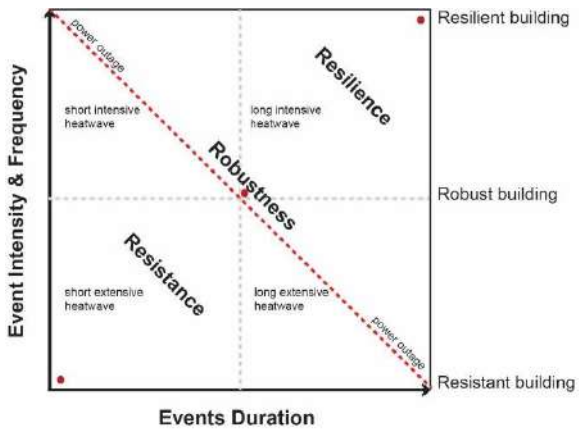

Fig. 2 - the components of a resilience definition within a specific field or domain

We define four major event categories that need to be tested and address in any resilience assessment for comfort in buildings. The following section provides further detailed explanation for Figure 1 in association with Figure 2.

3.3 Definition of "Resilient cooling for buildings"

Resilient cooling is used to denoting low-energy and low-carbon cooling solutions that strengthen the ability of individuals, and our community as a whole to withstand, and also prevent, the thermal and other impacts of changes in global and local climates - particularly concerning rising outdoor temperatures and the increasing frequency and severity of heat waves [33].

Resilient cooling for buildings is a concept that was not approached thoroughly in previous studies. Therefore, we developed the following definition based on the literature review and validated it through the focus group discussion with members of IEA Annex 80:

The cooling of a building is resilient when the capacity of the cooling system integrated in the building allows it to withstand or recover from disturbances due to disruptions, including heat waves and power outages and to adopt the appropriate strategies after failure (robustness) to mitigate degradation of building performance (deterioration of indoor environmental quality and /or increased need for space cooling energy (recoverability).

Resilience is a process that involves several criteria, including vulnerability, resistance, robustness, and recoverability [34]. Therefore, we include those four criteria in the definition formulation shown in Figure 1. The vulnerability involves the sensitivity or propensity of the building's comfort conditions to different disruptions. At this stage, it is vital to define disruptions, as discussed in Sections 3.1 (see Figures 1 and 2).

A resilient building must be conceived based on a vulnerability assessment that takes into account future climate scenarios and prepares the building system, including occupants, to adapt against failures. The vulnerability assessment should test the building performance against long-term disruptions using average weather conditions, extreme weather conditions, future weather conditions, and worst future weather conditions. It should also test the building against short-term disruptions, including brief heat waves and power outages. A vulnerability assessment stage should be part of the design process. A building cooling system is prepared to go through different disruption scenarios engaging different thermal conditions.

The building cooling system should be able to withstand short-term and long-term disruptive events. As shown in Figure 3, resistance involves the ability and the depth of reaction to the shock. Under disruptive events, the building may use performance drop backs to achieve the pre-defined minimal thermal conditions. After failure of the building cooling system, the building's resilience process moves to the most crucial stage—robustness, meaning reaction to failure. Robustness requires the building to be prepared to survive an otherwise-fatal shock by adapting its performance. The survivability of the system relies on its ability to assure the critical thermal conditions to maintain the functional activities of occupants during a crisis. As shown in Figure 5, a robust building will first fail and then adapt its performance conditions meeting critical or minimum thermal requirements to achieve a degree of survivability for occupants depending on the vulnerability assessment decisions made during design. The significant distinction between a resistant building system and a robust building system is that the latter is prepared to adapt based on a backup plan and ecosystem. Robustness involves how the building, including its services and occupants, adjusts and adapts to shocks.

The final stage of resilience involves the recoverability of the system. Recoverability consists of the extent and nature a occupants and building's services to recover, and returns to its equilibrium state and its speed to come back. As shown in Figure 5, recovering has a duration, performance, and learnability. The necessary speed for recovery and the recovery performance curve should be planned during the vulnerability assessment stage. The ability of the users, building, and systems to learn from the event is an integral part of this stage.

While the diagram in Figure 3 is linear, the process of resilience is cyclic and iterative. Resilient cooling of buildings is a continuous process that involves the commissioning and retro-commission of building elements and systems over the building's life cycle. It also includes the continuous education of occupants and the preparation for the adaptive measures during unforeseeable disruptions.

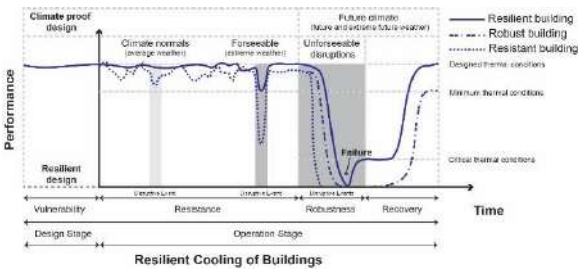

Fig. 3 -The components of a resilience definition within a specific field or domain (for higher resolution check [3])

Figure 4 provides a complementary definition framework that includes the main criteria of resilience. It presents an example of the factors that influence the performance of cooling in buildings

under the four resilience criteria. Depending on the overheating definition and exposure risk, a resilient cooling design for buildings assures that the designed indoor environmental conditions are secured before the disruption. The risk factors should be identified during the design stage to assess vulnerability. Examples of risk factors include climate change scenarios, heat waves combined with power outages, or urban heat island effects. As shown in Figure 4, the resistance stage depends mainly on the building's design features and technologies and their ability to keep the building performing under severe overheating exposure until reaching failure. The failure is the essential disruption to start the third stage of resilience, namely robustness. The robustness of the cooling system the building must adapt to cover the critical thermal conditions temporarily until reaching the recovery stage. The ability to respond in an adaptive way that implements fundamental changes to the original thermal conditions involved occupants and systems adaptability. The presence of energy system backup and an emergency control possibility is part of the building's robustness. This is finally followed by a recovery stage and a shift in the building performance to achieve before designed thermal conditions that reflects adapting to the normal.

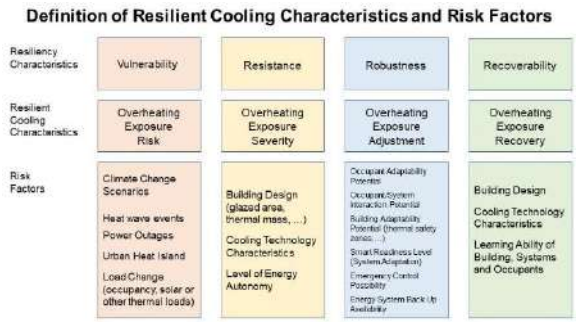

Fig. 4 - Influencing factors of resilient cooling of buildings (for higher resolution check [3])

4. Discussion

The review of the main concepts on resilient cooling for buildings and the proposal for a definition and assessment framework indicates the complexity of the idea. We found varying and inconsistent definitions of resilience in the context of building comfort and in the context of the overall built environment. The following sections discuss possible questions that we answered in this study.

- What are the existing concepts of resilience?
- How to define resilient cooling for buildings?

Few studies and case studies succeeded in defining resilience and applying its principles on a building scale. Across our review, we found some studies that focus mainly on robustness as a proxy for resilience [35-38]. However, none of those reviewed studies embraced a multi-criteria approach for resilience that involves vulnerability, resistance, robustness, and recoverability. Therefore, based on our literature review and focus group discussions, the suggested definition and framework, in this study, is a step forward. The following recommendations can be helpful for designers and building operators that seek to achieve resilient cooling of buildings in a holistic way:

1. Any definition of resilience must be based on the identification of a specific shock or disruption. In the case of resilient cooling of buildings, heat waves and power outages are considered as the main shocks (extreme events). Designers should prepare buildings against those shocks.

2. Any definition of resilience should specify and distinguish, at the same time, the resistance and robustness conditions against heat waves and power outage events. The resistance period involves the building's ability to resist shock(s) with the same pre-shock operation conditions. However, robustness requires failure and adaptation after failure. The robustness mechanism involves building users and building systems adaptation and their ability to adjust after a shock.

3. Thus, the definition of resilient cooling for buildings involves four critical criteria, mainly vulnerability (preparation), resistance (absorption), robustness (adaptation after failure), and recovery (remedy). The building design, construction, and operation processes should address these criteria.

4. Resilient cooling design is an urgent requirement for future proof buildings. Weather extremes must be anticipated to assume well-being. The choice of comfort models is elementary to prepare buildings. Resilient cooling design involves the combination of passive and active cooling design measures, on-site renewable production, and the coupling to storage capacities. Our suggested definition for resilient cooling of buildings can help to develop in the future resilience performance indicators that account for the impacts of global warming for long and short assessment periods. This can allow comparing the carbon emissions and primary energy use at different stages of the building life stages. As part of the activities of IEA - Annex 80, there is a need to assess the performance of conventional and advanced cooling technologies. Without a multi-stage definition, it will be challenging to develop universal indicators that allow assessing the active and passive cooling technologies listed above.

5. Building operation systems and building management systems will play a significant role in applying the adaptation strategies and risk mitigation plans in collaboration with buildings users. For resilient cooling, HVAC systems and envelope features are a prime target for real-time optimization. Different dynamic control strategies with predictive algorithms should be embedded in building operation systems using a deeply coupled

network of sensors. The smart readiness of buildings is part of resilience because it considers the fact that buildings must play an active role within the context of an intelligent energy system [39].

6. Resilience is a process, and its criteria should be addressed following a circular, iterative approach. Extracting learned lessons and integrating user experience during shocks is essential to increase the emergency learnability and feed the preparedness loop.

5. Conclusion

A definition of resilient cooling for buildings is developed and discussed in this paper as part of the IEA Annex 80 research activities. The definition's main concepts and criteria are based on qualitative research methods. The paper presents a set of recommendations to adopt the definition in practice and research. Future research should build on our findings and create more consistent frameworks with useful quantifiable indicators, quantitative metrics, and performance threshold limits. Additional definitions of overheating and modeling of overheating events are required for different building types and climates. The research should be extended to identify benchmarks and case studies with reference values, threshold ranges, and to seek tools and reporting mechanisms for the resilient cooling of buildings. The suggested framework should evolve as research and experience build a greater understanding of resilient and sustainable buildings.

6. Acknowledgemnt

This research was partially funded by the Walloon Region under the call "Actions de Recherche Concertées 2019 (ARC)" and the project OCCuPANt, on the Impacts Of Climate Change on the indoor environmental and energy PerformAnce of buildiNgs in Belgium during summer. The authors would like to gratefully acknowledge the Walloon Region and Liege University for funding.

7. References

[1] A. Jacob et al., 'Transformation towards sustainable and resilient societies in Asia and the Pacific', 2018.
[2] '71/276. Report of the open-ended intergovernmental expert working group on indicators and terminology relating to disaster risk reduction', United Nations, New York, UN General Assembly 71/276 Resolution, 2017.
[3] Attia, S. (2020). Spatial and behavioral thermal adaptation in net zero energy buildings: an exploratory investigation. Sustainability, 12(19), 7961.
[4] Attia, S., et al (2021). Resilient cooling of buildings to protect against heat waves and power outages: Key concepts and definition. Energy and Buildings, 239, 110869.
[5] R. Gupta, L. Barnfield, M. Gregg, Overheating in care settings: magnitude, causes, preparedness and remedies, Build. Res. Inf. 45 (1–2) (2017) 83–101.
[6] T. Kjellstrom, I. Holmer, B. Lemke, Workplace heat stress, health and productivity–an increasing challenge for low and middle-income countries during climate change, Glob. Health Action 2 (1) (2009) 2047.
[7] A. De Bono, Peduzzi, S. Kluser, and G. Giuliani, 'Impacts of summer 2003 heat wave in Europe', 2004.
[8] R. Gupta, M. Kapsali, Empirical assessment of indoor air quality and overheating in low-carbon social housing dwellings in England, UK, Adv. Build. Energy Res. 10 (1) (2016) 46–68.
[9] Holzer and Cooper, 'IEA EBC Annex 80 on Resilient Cooling for Residential and Small Non-Residential Buildings', IEA, Paris, 10.13140/RG.2.2.33912.47368, 2019.
[10] 'The Future of Cooling: Opportunities for energy-efficient air conditioning', IEA, Paris, France, 2018. [Online]. Available: https://www.iea.org/reports/thefuture-of-cooling.
[11] S. O. Andersen et al., 'Cooling Emissions and Policy Synthesis Report: Benefits of Cooling Efficiency and the Kigali Amendment Workplace', 2020.
[12] I. Kelman, J.C. Gaillard, J. Lewis, J. Mercer, Learning from the history of disaster vulnerability and resilience research and practice for climate change, Nat. Hazards 82 (1) (2016) 129–143.
[13] K.-H. Liao, 'A theory on urban resilience to floods—a basis for alternative planning practices', Ecol. Soc., vol. 17, no. 4, 2012.
[14] S.R. Carpenter, C. Folke, Ecology for transformation, Trends Ecol. Evol. 21 (6) (2006) 309–315.
[15] USGBC, RELi 2.0 Rating Guidelines for Resilient Design and Construction, U.S. Green Building Council, Washington, USA, 2018.
[16] G. R. Gibbs, 'Thematic coding and categorizing', Anal. Qual. Data Lond. Sage, pp. 38–56, 2007.
[17] N. K. Gale, G. Heath, E. Cameron, S. Rashid, and S. Redwood, 'Using the framework method for the analysis of qualitative data in multi-disciplinary health research', BMC Med. Res. Methodol., vol. 13, no. 1, p. 117, 2013.
[18] A. Lacey and D. Luff, Qualitative data analysis. Trent Focus Sheffield, 2001.
[19] S. Attia, R. Lioure, and Q. Declaude, 'Future trends and main concepts of adaptive facade systems', Energy Sci. Eng., 2020.
[20] P. Holzer, 'Annex 80 Participants', Annex 80 Participants, 2019. https://annex80.iea-ebc.org/participants (accessed Dec. 01, 2021).
[21] P. De Wilde and D. Coley, The implications of a changing climate for buildings. Elsevier, 2012.
[22] L. Bull-Kamanga et al., 'From everyday hazards to disasters: the accumulation of risk in urban areas', Environ. Urban., vol. 15, no. 1, pp. 193–

204, 2003.
[23]D. B. Crawley, 'Estimating the impacts of climate change and urbanization on building performance', J. Build. Perform. Simul., vol. 1, no. 2, pp. 91–115, 2008.
[24] A. Baniassadi, J. Heusinger, and D. J. Sailor, 'Energy efficiency vs resiliency to extreme heat and power outages: The role of evolving building energy codes', Build. Environ., vol. 139, pp. 86–94, 2018.
[25] T. Swanstrom, 'Regional resilience: a critical examination of the ecological framework', working paper, 2008.
[26] U. Hassler and N. Kohler, Resilience in the built environment. Taylor & Francis, 2014.
[27] M. Palme, L. Inostroza, G. Villacreses, A. Lobato-Cordero, and C. Carrasco, 'From urban climate to energy consumption. Enhancing building performance simulation by including the urban heat island effect', Energy Build., vol. 145, pp. 107–120, 2017.
[28] A. Laouadi, A. Gaur, M. A. Lacasse, M. Bartko, and M. Armstrong, 'Development of reference summer weather years for analysis of overheating risk in buildings', J. Build. Perform. Simul., vol. 13, no. 3, pp. 301–319, 2020.
[29] M. Hamdy, S. Carlucci, P.-J. Hoes, and J. L. Hensen, 'The impact of climate change on the overheating risk in dwellings—A Dutch case study', Build. Environ., vol. 122, pp. 307–323, 2017.
[30] A. Moazami, V. Nik, S. Carlucci, and S. Geving, 'Impacts of the future weather data type on the energy simulation of buildings–Investigating long-term patterns of climate change and extreme weather conditions', 2019.
[31] D. J. Sailor, 'Risks of summertime extreme thermal conditions in buildings as a result of climate change and exacerbation of urban heat islands', Build. Environ., vol. 78, pp. 81–88, 2014.
[32] C. A. MacKenzie and K. Barker, 'Empirical data and regression analysis for estimation of infrastructure resilience with application to electric power outages', J. Infrastruct. Syst., vol. 19, no. 1, pp. 25–35, 2012.
[33] E. Burman, J. Kimpian, and D. Mumovic, 'Reconciling Resilience and Sustainability in Overheating and Energy Performance Assessments of Non-domestic Buildings', 2014.
[34] R. Martin and P. Sunley, 'On the notion of regional economic resilience: conceptualization and explanation', J. Econ. Geogr., vol. 15, no. 1, pp. 1–42, 2015.
[35] R. Kotireddy, P.-J. Hoes, and J. L. Hensen, 'A methodology for performance robustness assessment of low-energy buildings using scenario analysis', Appl. Energy, vol. 212, pp. 428–442, 2018.
[36] S. Homaei and M. Hamdy, 'A robustness-based decision making approach for multi-target high performance buildings under uncertain scenarios', Appl. Energy, vol. 267, p. 114868, 2020.
[37] Homaei, S., & Hamdy, M. (2021). Thermal resilient buildings: How to be quantified? A novel benchmarking framework and labelling metric. Building and Environment, 108022.
[38] Miller, W., Machard, A., Bozonnet, E., Yoon, N., Qi, D., Zhang, C., ... & Levinson, R. (2021). Conceptualising a resilient cooling system: A socio-technical approach. City and Environment Interactions, 11, 100065.
[39] T. Märzinger and D. Österreicher, 'Supporting the Smart Readiness Indicator—A Methodology to Integrate A Quantitative Assessment of the Load Shifting Potential of Smart Buildings', Energies, vol. 12, no. 10, p. 1955, 2019.

SAVINGS ACHIEVED IN OPERATING ROOMS BY IMPLEMENTING VENTILATION AIR FLOW REGULATION STRATEGIES, IN SEVERAL CLIMATIC ZONES OF SPAIN

Rey-Martínez F.J. [a,b], *San José-Alonso J. F.* [a,b], *Velasco-Gómez E.* [a,b], *Tejero-González A.* [a,b], *Esquivias-Fernández P.M.* [a,b], *Arroyo-Gómez, Y.* [a,b] *and Rey-Hernández J.M.* [a,c]

[a] GIRTER Research Unit. (UIC053), Spain

[b] Energy and Fluid Mechanics Department, University of Valladolid (Spain).

[c] Higher Polytechnic School, European University Miguel de Cervantes (Spain)

Abstract. Hospitals are critical environments, characterized by the health and safety of patients and staff. Hospitals have uninterrupted operation of the facilities, thus requiring air conditioning and ventilation, in order to reduce physical, chemical and biological contaminants, such as the current Covid-19. Hospitals have different indoor environments due to the different comfort and health needs of their occupants. These are defined according to the hospital's own standards for IAQ for each specialized area. Currently, most hospital ventilation studies revolve around specialized areas such as operating rooms and infectious and immunosuppressed wards, etc. However, the best practices for achieving an adequate indoor environment are not yet unanimously recognized. This study focuses on the reduction of energy, economic and environmental costs, all of them obtained when a ventilation flow strategy, ventilation controlled by demand, is installed in the operating rooms in a Hospital in Spain. The ventilation air flow rates required in operating rooms, according to Spanish standard UNE 100713, are very high when they are in operation (with a minimum flow rate of 2400 m3/h or 20 ren/h). However, the regulations also allow reducing the air flow during periods of inactivity of the operating room, as long as the safety, availability and asepsis are guaranteed. In this study, experimental data have been collected by monitoring the operation of the air conditioning and ventilation system, as well as the occupancy of the operating rooms of a 900-bed Spanish hospital. With all these acquired data, it has been possible to model the real operation mode of a standard operating room. Due to the implementation of this proposed model, it has been possible to study different ventilation airflow regulation strategies, with the aim of improving hospital IAQ in Spain, in three different climatic zones.

The results obtained in operating rooms, through the implementation of the proposed strategy in ventilation, show that a good IAQ is achieved, reaching energy savings in heating, cooling and electricity consumption, between 20% to 70%. Therefore, the economic costs are drastically reduced, amortizing the investment required for the regulation and control system of the HVAC system in less than a year.

Keywords. Hospital; Operating Room; Ventilation Setback; Heat Recovery; Indoor Overpressure; Energy savings.
DOI: https://doi.org/10.34641/clima.2022.94

1. Introduction

The study is carried out in a surgical area composed of 24 Operating Rooms (OR) of a 900-bed University Hospital Center (UHC), with a built-up area of 136,000 m2. The number of surgeries in 2019 conducted was 24,126, categorized into: scheduled, emergency and cancelled. Moreover they are divided into hospitalized and non-hospitalized, Table 1.

Copyright ©2022 by the authors. This conference paper is published under a CC-BY-4.0 license.

Tab. 1 - Surgical activity of the University Hospital Center in 2019.

	Scheduled	Emergency	Cancelled
Hospitalized	7,710	3,741	303
Non-hospitalized	12,470	205	353

Due to the high number of surgical interventions and operating rooms at the UHC, block three with four operating rooms was selected, corresponding to operating rooms 3.1, 3.2, 3.3 and 3.4, as shown in Figure 1.

Fig. 1 - Surgical block No. 3 with four turbulent flow operating rooms.

Tab. 2 - Average times and Standard Desviation in each operating room in minutes.

Operation Room	Occupation (h/year)	Average (min/Surgery)	Standard deviation (min)
3.1	2,199.4	358.6	11.8
3.2	1,538.0	177.8	7.89
3.3	1,774.2	131.1	9.95
3.4	1,639.3	132.2	9.25
Average	1,787.3	200	9.72

Considering 8,640 hours per year, the occupancy rate amounts to 20.68 % of the annual hours. In spite of the time margins between the intervention and the restitution of the aseptic conditions, it is estimated that the occupancy rate is around 25 %.

The operating rooms have been designed in accordance with the UNE 100713:2005 standard.

Each operating room has an Air Handing Unit (AHU), which has a Supervisory Control And Data Acquisition (SCADA) that manages and controls the operation of the system, a schematic diagram of the AHU is shown in Figure 2.

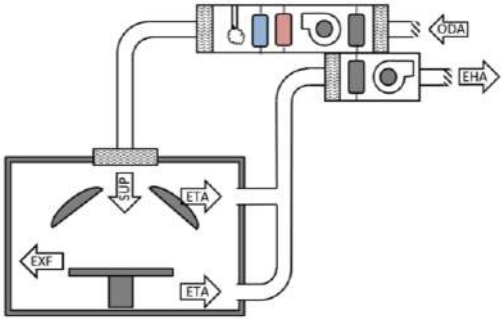

KeyMap.

ODA (Outside air) ***SUP*** (Forced air) ***ETA*** (Inside air) ***EXF*** (EXFiltration air) ***EHA*** (ExHaust Air)

Fig. 2 - Schematic diagram of the operating room' s AHU.

The AHU is regulated on the basis of three strategies that are monitored and recorded by the SCADA system on a 24/7 cycle.

Strategy A. - The thermal comfort of the OR is achieved with temperature and humidity sensors placed inside the OR, which adjust the temperature and humidity of the SUP. The ventilation load is considered as the only load to be compensated in the OR, and the rest of the loads are negligible compared to it. The temperature and humidity conditions are adjusted by the healthcare personnel according to the type of intervention, the comfort of the patient, and the comfort of the healthcare staff.

Strategy B. - SUP flow rate. The standard establishes that the OR must have more than: 20 Air changes per hour (ACH) or 2,400 m3/h. Therefore, the AHU has a nozzle that allows measuring and controlling the SUP flow rate. A frequency variator regulates the impulsion fan to maintain the flow rate when the climatic conditions change, or when the AHU filters become dirty.

Strategy C. - The OR overpressure in relation to adjacent enclosures is set at 20 Pa. For this purpose, a frequency inverter regulates the exhaust fan; when the pressure increases, the inverter regulates the exhaust fan to increase the ETA flow rate, and when the overpressure drops below the set value (20 Pa), the ETA flow rate is reduced.

Tab. 3 - Operating parameters of the ORs under study.

	OR 3.1	OR 3.2	OR 3.3	OR 3.4	Average
Discharge flow rate (m^3/h)	2,280	2,773	2,420	2,396	2,467
Extraction flow rate (m^3/h)	1,505	1,755	1,530	1,630	1,580

Overpressure (Pa)	20.5	22.3	20.9	21.5	21.3
Temperature (ºC)	24.5	23.8	24	24.5	24.2
Relative Humidity (%)	41.1	34.5	42.7	39.7	39.5

To determine the value of the runaround loop efficiency, the parameters recorded by the OR 3.1 SCADA for three months were taken, which means 98,000 records, containing about 400,000 data. The data are analyzed, and allow to determine the efficiency of the runaround loop as a function of the outdoor temperature via a least-squares interpolation. The results are shown in Figure 3.

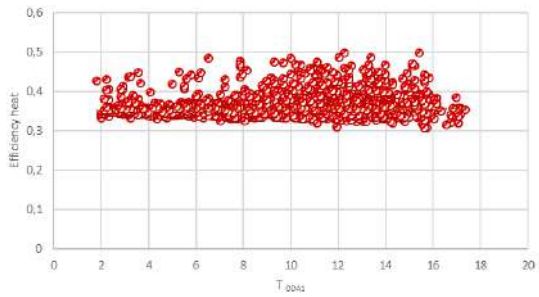

Fig. 3 - Efficiency Heat vs. Outside Temperature.

The equation obtained to determine ε versus T_(〖ODA〗_1) is shown below:

$$\varepsilon=0.0003*T_{ODA1}+0.3522 \quad (1)$$

2. Methodology

The methodology is carried out in this study, taking as outdoor conditions the five reference climates existing in Spain. It considers the indoor conditions in the R_w (Saturation mixing ratio with water) with constant temperature and humidity (24 ºC and 50 % RH), and it considers as a starting situation the operation of the system with a constant ventilation flow rate. Then it is studied by two ventilation flow control strategies: a) by occupancy and b) by schedule. Energy, economic and environmental savings are calculated.

Spain has five climatic zones, which are grouped into climates: Oceanic (C), Continental (D), Mediterranean (B), Mountain (E), and Subtropical (A). Spanish regulations have classified climatic zones according to climatic severity in winter and summer. The climatic harshness is determined according to the degree days and the accumulated solar radiation in winter and summer. Figure 4 shows the different climatic zones in Spain.

Once the climatic zones have been established, reference climates have been developed, which are freely accessible, containing the outdoor conditions hour by hour of a typical year for each zone. This data is the one used in this study.

Fig. 4 - Climatic zones in Spain.

The OR interior conditions depend on the surgical needs of the patient. Usually, 24 ºC and 50% RH are considered. In this study, SUP and ETA air conditions are also considered matching, since the outdoor air treatment is the only thermal load which depends on the outdoor conditions of the OR. The other loads are common to the three strategies under study. This study evaluates the energy, economic and environmental savings, thus they are common to the initial situation and to the strategies under study.

2.1 Ventilation control strategies under study

2.1.1. By occupancy: A presence sensor is installed in the OR.

2.1.2. By schedule: the occupancy of table 2, taking into account that they are not emergency operating rooms.

2.2 Energy demand assessment.

The thermal and electrical energy demand is determined hour by hour in: the standard case, the case of regulation by occupancy, and the case of regulation by schedule. It is shown in the flow chart in Figure 5.

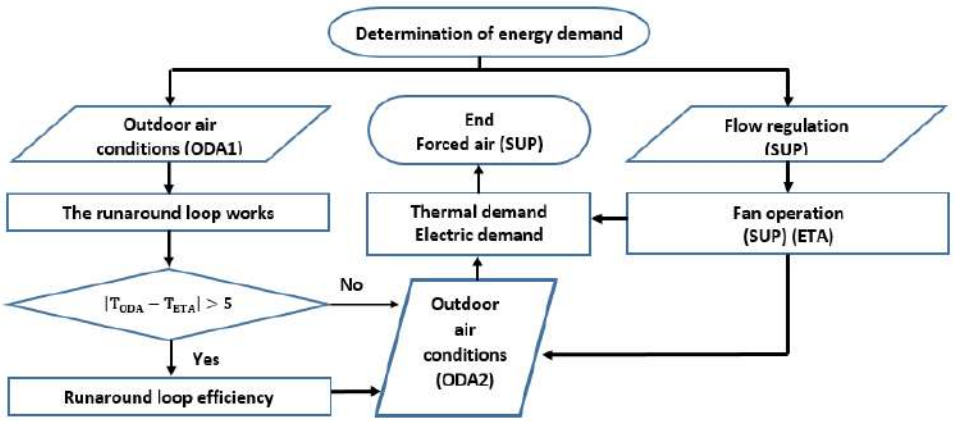

Fig. 5 - Flow chart used to determine thermal and electrical energy demand.

To calculate the thermal demand, the enthalpy of the air at the exhaust air of the ODA2 recovery unit, and the enthalpy of the supply air to the SUP room (24 ºC and 50% RH) are calculated. The heating and cooling needs to be provided to the outside air of the operating room are determined as the difference of enthalpies, multiplied by the supply air flow (Eq. 2)

$$\{\dot{m} * (h_{SUP} - h_{ODA_1})\} \begin{cases} > 0 \rightarrow \text{Heating} \\ \\ <0 \rightarrow \text{Cooling} \end{cases} \quad (2)$$

The standard allows reducing the ventilation flow rate of the operating room to 50% during periods without activity. A minimum air speed must be ensured to avoid the deposition of particles present in the OR, so two strategies can be established: i) establish periods of use of the OR, which together with some periods of restitution/safety, allow programming the system to reduce the flow rate to 50% , and ii) have a presence sensor in the OR, which adjusts the flow rate when the OR is without activity after a safety margin.

3. Analysis & Results.

The study has provided a multitude of data on the energy demand associated with ventilation. Figure 6 shows the heating and cooling demand due to the ventilation of an operating room for the different climatic zones.

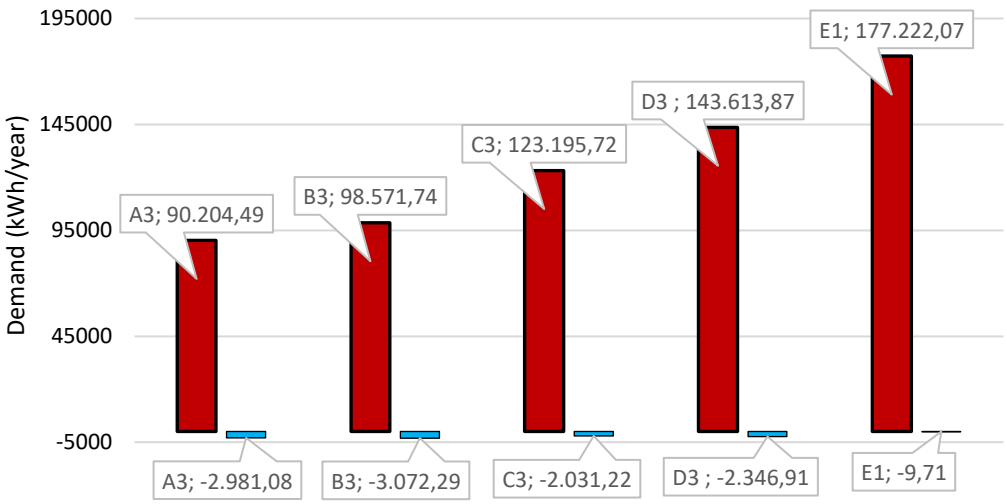

Fig. 6 - Heating and cooling demands for different climate zones.

As shown in Figure 6, it can be observed that the cooling needs are lower than the heating needs.

Table 4 shows the savings on primary energy (kWh/year), CO2 emissions (kg of CO2/year) and economic savings (€/year), using the parameters included in the methodology.

These savings could be extended to the hospital's 30 operating rooms. For the emergency operating rooms, it would be necessary to establish some presence control in order to provide continuous availability.

This would require a presence sensor and a time to restore conditions, which in no case should be more than 5 minutes.

Tab. 4 - Energy, emissions and economic savings from occupancy and schedule control.

	A3	
	Occupation	**Schedule**
Primary energy (kWh)	63,244.45	72,250.24
CO_2 emissions (kg)	12,047.37	13,517.73
Economic (€)	3,604.43	4,301.03
	B3	
	Occupation	**Schedule**
Primary energy (kWh)	67,220.72	76,383.78
CO_2 emissions (kg)	12,884.05	14,385.72
Economic (€)	3,770.95	4,475.71
	C3	
	Occupation	**Schedule**
Primary energy (kWh)	78,501.06	88,074.49
CO_2 emissions (kg)	15,283.71	16,870.98
Economic (€)	4,220.41	4,943.02
	D3	
	Occupation	**Schedule**
Primary energy (kWh)	88,234.12	98,112.69
CO_2 emissions (kg)	17,329.88	18,978.70
Economic (€)	4,629.65	5,367.37
	E1	
	Occupation	**Schedule**
Primary energy (kWh)	103,335.27	113,610.87
CO_2 emissions (kg)	20,561.26	22,293.47
Economic (€)	5,214.70	5,969.18

These savings could be extended to the hospital's 30 operating rooms. For the emergency operating rooms, it would be necessary to establish some presence control in order to provide continuous availability.

This would require a presence sensor and a time to restore conditions, which in no case should be more than 5 minutes.

4. Conclusions

In this study, a simulation has been carried out for the five climates in Spain, making it possible to study the ventilation demand of operating rooms hour by hour, with data from a real Hospital Center. This study allows extrapolating the data and strategies to other operating rooms at Hospital Centers with great accuracy.

A 50% reduction of the supply flow rate has been applied in operating rooms where there is no healthcare activity, in accordance with the Spanish standard, allowing the asepsis of the operating room to be maintained, and the occupancy conditions to be restored in less than five minutes.

The regulation by schedule is shown to be the strategy that allows the greatest energy, emissions and economic savings, although the system by presence has been estimated to have a restitution time of 5% of the annual time.

The installation of a presence sensor in operating rooms would help to reduce this time and improve the scheduled regulation.

The primary energy savings range in the different climatic zones between 72,250 kWh to 113,610 kWh per year per operating room, with schedule control.

Emission savings range in the different climate zones between 13,517 kg CO2 and 22,293 kg CO2 per year per operating room with schedule control.

The economic savings are between €4,300 and €5,969 per year.

5. References

[1] F. J. Wang, T. B. Chang, C. M. Lai, and Z. Y. Liu, “Performance improvement of airflow distribution and contamination control for an unoccupied operating room,” 2012.
[2] M. Porowski, “Energy optimization of HVAC system from a holistic perspective: Operating theater application,” Energy Convers. Manag., vol. 182, pp. 461–496, Feb. 2019.
[3] Antón Cacabelos-Reyes, José Luis López-González, Arturo González-Gil, Lara Febrero-Garrido, Pablo Eguía-Oller and Enrique Granada-Álvarez “Assessing the Energy Demand Reduction in a Surgical Suite by Optimizing the HVAC Operation During Off-use Periods” Appl. Sci., 10, 2233; doi:10.3390/app1007223, 2020.
[4] Guangyu Cao et al. “Experimental measurements of surgical microenvironments in two operating rooms with laminar airflow and mixing ventilation systems”. Energy and Built Environment. 25 August 2020.
[5] Ching-Chieh Liang et al. “Effect of ventilation rate on the optimal air quality of trauma and colorectal operating rooms”. Building and Environment. 16 November 2019.
[6] M. Alsved et al. “Temperature-controlled airflow ventilation in operating rooms compared with laminar airflow and turbulent mixed airflow”. Journal of Hospital Infection. 24 October 2017.
[7] Masab Khalid Annaqeeb et al. “Influence of the surgical team activity on airborne bacterial distribution in the operating room with mixing ventilation system: A case study at St. Olavs Hospital”. Journal of Hospital Infection. 14 August 2021.
[8] Fan et al. “Suitability evaluation on laminar airflow and mixing airflow distribution strategies in operating rooms: A case study at St. Olavs Hospital”. Building and Environment. 12 February 2021.
[9] F. Memarzadeh , A. P. Manning , “Comparison of operating room ventilation systems in the protection of the surgical site” , Build. Eng. 108 (

2002) 3 –15 PART 2 .
[10] W. Whyte , “Sterility assurance and models for assessing airborne bacterial contamination “, J. Parenter. Sci. Technol. 40 (1986) 188 –197 .
[11] O. M. Lidwell , “Sepsis after total hip or knee joint replacement in relation to airborne contamination” , Phil. Trans. Roy. Soc. Lond. B 302 (1983) 583 –592.
[12] T. N. Verma et al. “Numerical Simulation of Air Pollution Control in Hospital”. Air Pollut. Control , Springer Singapore , Singapore , 2018 , pp. 185 –206
[13] P. N. Hoffman et al. “Microbiological commissioning and monitoring of operating theatre suites. a report of a working party of the hospital infection society” , J. Hosp. Infect. 52 (2002) 1 –28 .
[14] S. M. Mchugh et al. “Laminar airflow and the prevention of surgical site infection . More harm than good ? ” , Surg. , J. R. Coll. Surg. Edinburgh Irel. 13 (2014) 52 –58 .
[15] J. G. Whitcomb , W. E. Clapper. “Ultraclean operating room” , Am. J. Surg. 112 (1966) 681 –685
[16] T. Hirsch , et al. “Bacterial burden in the operating room: impact of airflow system”. Am. J. Infect. Contr. 40 (2012) e228 –e232 .
[17] S. Fischer et al. “Reduction of airborne bacterial burden in the OR by installation of unidirectional displacement airflow (UDF) systems” , Med. Sci. Mon. Int. Med. J. Exp. Clin. Res. 21 (2015) 2367 –2374.

Kitchen ventilation system design and its effect on restaurant IAQ

Kamal Moumen [a], Nicolas Delporte [b]

[a] *Halton Foodservice – Research and Development Lab, Bethune, France, kamal.moumen@halton.com*

[b] *Halton Foodservice – Research and Development Lab, Bethune, France, nicolas.delporte@halton.com*

Abstract. It is well established that exposure to high level of Particulate Matter (PM), especially smaller particles below 2,5 micron (PM2.5) has a negative impact on health. We also know that cooking is the major contributor to PM levels in dwellings (Jacobs et al, 2016). A recent field study in restaurants (Kulve et al, 2020) also showed elevated levels of PM exposure, exceeding those recommended by World Health Organization (WHO). It is obvious that ventilation systems do not meet the objective of providing good Indoor Air Quality (IAQ) in restaurants with high level of PM exposure. This presentation addresses ventilation system design and its effect on PM level in the commercial kitchen setting. The study was conducted in a ventilation laboratory setting using a charbroiler and gas fryers cooking hamburgers, and French fries. Two types of ventilation hoods were tested as well as two air distribution strategies: mixing and displacement ventilation. The study replicated elevated levels of PM2.5 concentrations with inadequate ventilation design and demonstrated that properly designed ventilation system can protect kitchen personnel from high PM exposure. The study also emphasized the importance of IAQ sensors in restaurants to guarantee adequate performance of ventilation systems.

Keywords. Indoor Air quality, Ventilation, Commercial Kitchen, PM2.5, Health, Thermal Comfort
DOI: https://doi.org/10.34641/clima.2022.90

1. Introduction

Indoor Environment Quality in commercial kitchens (IEQ) refers to the air quality within and around the working place of kitchen personnel. Commercial kitchen and cooking appliances are major contributors to pollutant releases in the indoor environment. Health effects from indoor air pollutants may be experienced soon after exposure or, possibly, years later (WHO).

It is well established that exposure to high level of Particulate Matter (PM), especially smaller particles below 2,5 micron (PM2.5) has a negative impact on health. It is known that cooking is the major contributor to PM levels in dwellings (Jacobs et al, 2016).

Recent field study in restaurants such as (M Loomans et al 2020) also showed elevated levels of PM exposure exceeding those recommended by World Health Organization (WHO). The study concluded that chefs in professional kitchens are exposed to PM2.5 concentrations well above the daily exposure limit of 25 µg/m^3 as defined by the WHO for the general public (average values ranging from 57-402 µg/m^3, with peaks >1 mg/m^3). The study showed also that cooking activities (such as baking) and the location of the chef (below or next to the hood) are important factors influencing the high values measured in the breathing zone

Known air quality issues related to cooking processes multiplied by the scale in professional kitchens lead to growing concerns about the employees and customers health.

The ventilation system plays a central role in the improvements of the IEQ.

The measurements are meant to evaluate the relative impact of the following parameters on the IEQ in professional kitchens: Exhaust airflow (with/without use of an air curtain system – see description in 2.1), the cooking type and appliance and the air supply method. This last parameter appears to be the least often considered, even if it has a considerable impact as will be shown later in this paper.

To compare the different scenarios, it has been decided that PM 2.5 quantities will be the variable to be compared, as this is a well-known and often shared parameter. It's also common to use the PM2.5 in IEQ studies. Other measurements such us CO^2 and Volatile Organic Compounds (VOCs) have been measured and will be briefly discussed below.

Copyright ©2022 by the authors. This conference paper is published under a CC-BY-4.0 license.

2. Experimental set-up Description

2.1. *Cooking and Ventilation systems*

Extraction and supply

The Extraction hood used was a traditional hood used in the professional kitchen setting.

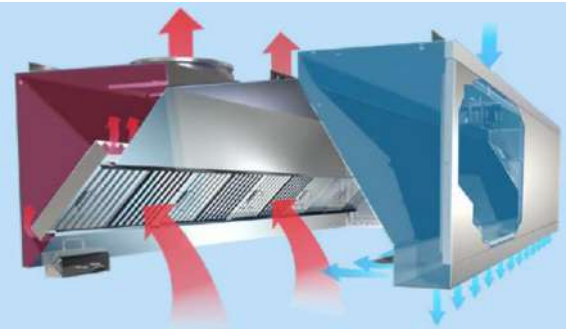

Fig. 1 - Schema of the extraction hood used for the tests

The hood was equipped with an air curtain system that consists of two sets of nozzles, one vertical and one horizontal. The horizontal nozzles push vapours back towards the filters. The vertical nozzles increase the containment volume and prevents vapours escaping from cooking areas. (See Fig.1 air curtain represented with blues arrows). The air curtain system could be enabled / disabled for the front and lateral sides of the hood, respectively and individually.

Two types of supply air systems were tested:

- One was provided by a wall mounted **air displacement unit.** This was done through two sets of grids of 2-OFF *H1900 x L520mm* with low velocity
- The other, using two **ceiling mixing units** that were mounted on the ceiling. they provided the same amount of airflow as the air displacement unit but with higher velocity through circular slots.

Fig 2 – Mixing and displacement units

Airflow Regimes

For each test, 3 airflow regimes were tested: **high, medium, and low**. The high corresponded to the Capture & Containment (**C&C) level** as measured in the laboratory according to the ASTM1704. The medium and low were both conducted at **75% of the C&C level, with (medium) and without (low) the air** curtain system, respectively.

Table 1 – Exhaust air flow regime $[m^3/h]$

Exhaust Regime	Broiler	Fryers
High	2000 + air curtain	1500 + air curtain
Medium	1500 + air curtain	1180 + air curtain
Low	1500 & no air curtain	1180 & no air curtain

Cooking Appliances

Two types of cooking appliances have been used: a gas charbroiler for burgers and 4 deep fryers for frozen French fries.

- **Broiler**: Charbroiler Vulcan (model 36) Griddle's installation at 900mm height

- **Fryers**: gas Electrolux L900xl800xH900

Fig. 3 - Cooking appliances - Fryers and Charbroiler

Cooking Procedure for Burgers

The tests started with a heating period. The griddles were turned on for approximately 30 minutes to reach 300°C. For each test, 5 series of 15 burgers each were cooked. The cooking of burgers was timed to be 3.5 minutes per face. A brushing and reheat to reach 300°C were done after each series.

Cooking procedure for French fries

Oil was pre-heated to 180°C. Each round was done using 2 baskets at the same time which represents around 1kg of French fries. Each batch of French fries were cooked for 10 minutes.

2.2. *Tests Layout*

All the measurements were done in an air-tight lab chamber of dimensions (l x w x h) 9m x 6m x 3.4m.

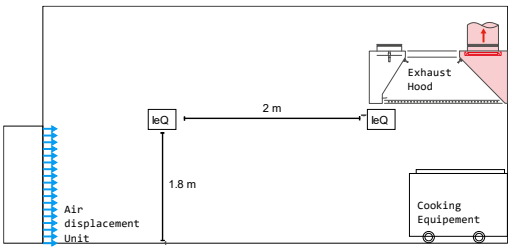

Fig. 4 - Ventilation, appliances, and sensors layout – Displacement air units

IEQ sensors were installed in two positions:

1. **The breathing zone** of the chef under the hood,
2. **2m from the hood** at 1.80m from the floor.

PM 2.5 was measured using the following sensor: FS4408 (Transducer particulate matter / particles, active output (0-10V and 4-20mA)

Table 2 - PM sensor description

Measurement range PM2.5/PM10	0 µg/m^3 ... 1000 µg/m^3
Accuracy PM2.5/PM10	±5 ug/m^3 + max. ±4% FS (@ 20°C, 45% RH., 1013 mbar)
Temperature dependency	±1% FS / 10 K
Response time (t90)	< 10 s
Long term stability	±1% FS/year

3. Results

The results of the tests will be presented in the following order: Tests on the charbroiler and on the fryers with two different air supply modes (displacement and mixing).

PM2.5 levels will be shown under the hood and at 2m distance with 3 different airflow regimes: high, medium, and low.

The Low velocity displacement was installed on the opposite wall situated at 4.8 m from the front of the hood. Mixing air units were situated in the ceiling at 1.2 and 3.2 m from the front of the hood.

3.1. *The Charbroiler with Low Velocity Air Supply (displacement)*

It can be seen that, with C&C airflow level, the PM2.5 concentrations under the hood and in the room stay in average at 9 $\mu g/m^3$ and 4 $\mu g/m^3$ accordingly.

In case of Medium and Low airflow regimes (1500 m^3. h^{-1} with and without air curtain), the PM2.5 concentration are much higher. The tables below summarize the concentration levels.

Tab. 3 - PM2.5 in the breathing zone and in the room – Charbroiler - Displacement [µg/m^3]

	Breathing zone		**In the Room**	
Airflow	**Avg.**	**Max.**	**Avg.**	**Max.**
High	9	412	4	6
Medium	52	718	46	220
Low	118	289	280	636

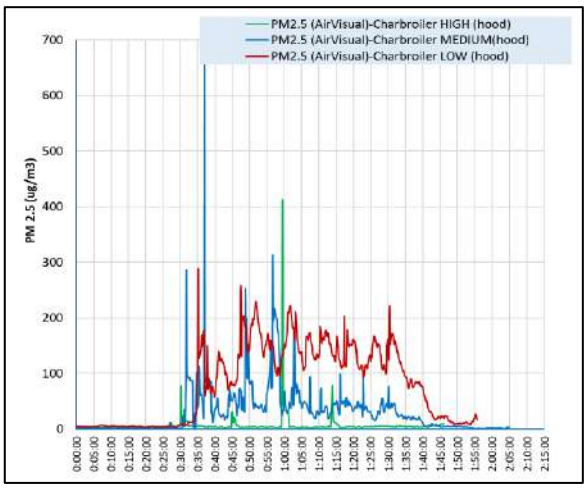

Fig. 5 - PM2.5 measurements **under the hood**, charbroiler with burgers with 3 air flow regimes and displacement air supply

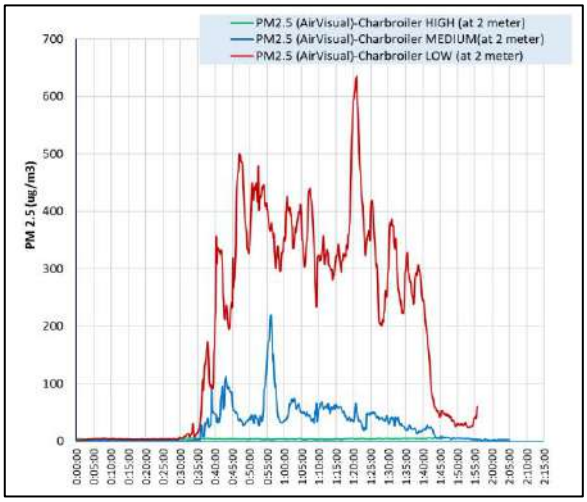

Fig. 6 - PM2.5 measurements at **2m from the hood**, charbroiler with burgers with 3 air flow regimes and displacement air supply

It can be seen that the concentrations in case of Medium and Low airflow regimes are higher than the WHO recommendation (25 $\mu g/m^3$). Levels in the absence of the air curtains were 6x higher in the room and 2x higher under the hood.

The measurements above shows that the air curtain helps to reduce the PM2.5 concentration levels in the room and therefore improve the IEQ in the kitchen (up to 6x times). This improvement is true in case of air supply with low velocity displacement in the room. Later in this paper it will be shown that this is not true for the case of mixing supply from the ceiling.

It was also seen that there were 4 PM2.5 peak events under the hood. That was due to the brushing and cleaning of the broiler. Indeed, after each round, the broiler was brushed with a metal comb to remove residue from the griddles.

3.2. *The Charbroiler with Mixing Air Supply (from the ceiling)*

The second round of test results were obtained following the same procedure as above but using a **mixing air supply from the ceiling.**

The method of supply air introduction was changed whilst all other parameters remained identical. The vertical air mixing supplies nearly the same airflow (90% of the supply) as the displacement method.

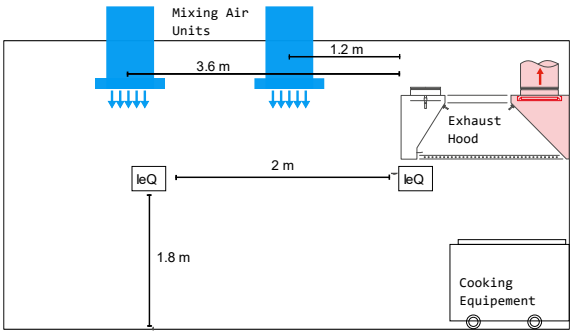

Figure 7 - Ventilation, appliances, and sensors layout – mixing air units

Firstly, it can be seen that there were higher concentrations during the mixing supply test compared to the displacement method test. During the "high" test regime, concentrations under the hood and in the room were on average 32 $\mu g/m^3$ and 17 $\mu g/m^3$, respectively.

Also, it can be seen that, in this case, there was no significant difference between the Medium and Low regimes. This shows that the air curtain doesn't have any impact on reduction of PM2.5 concentrations.

Tab. 4 - PM2.5 in the breathing zone and in the room – Charbroiler - mixing [µg/m^3]

	Breathing zone		In the Room	
Airflow	**Avg.**	**Max.**	**Avg.**	**Max.**
High	32	887	17	41
Medium	344	1001	254	782
High	397	1002	222	470

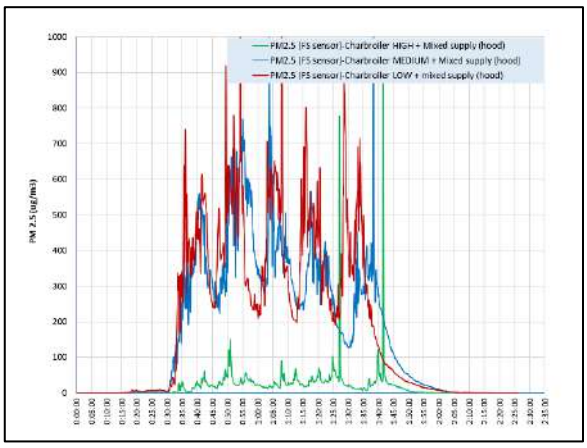

Fig. 8 - PM2.5 measurements under the hood, charbroiler with burgers with 3 air flow regimes and mixing air supply

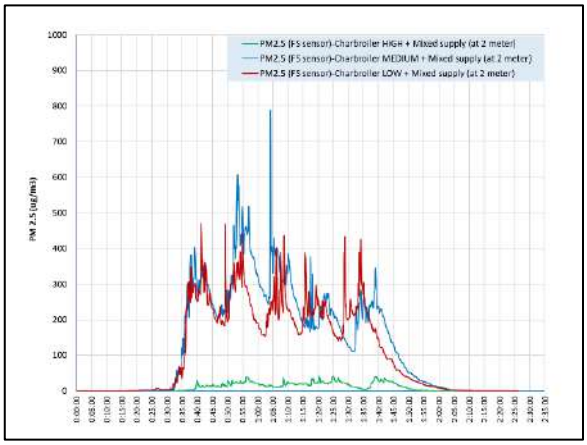

Fig. 9 - PM2.5 measurements at 2m from the hood, charbroiler with burgers with 3 air flow regimes and mixing air supply

3.3. *The Fryer with low velocity air supply (displacement)*

In this case, the max air flow was reduced to be at the appropriate C&C level: 1500 m^3/h.

Firstly, it can be seen that the concentrations were, on average, 10x lower than in the case of the broiler.

Tab. 5 - PM2.5 in the breathing zone and in the room – Fryers - Displacement [µg/m^3]

	Breathing zone		In the Room	
Airflow	**Avg.**	**Max.**	**Avg.**	**Max.**
High	0	1	0	1
Medium	1	3	1	4
Low	7.5	26	12	51

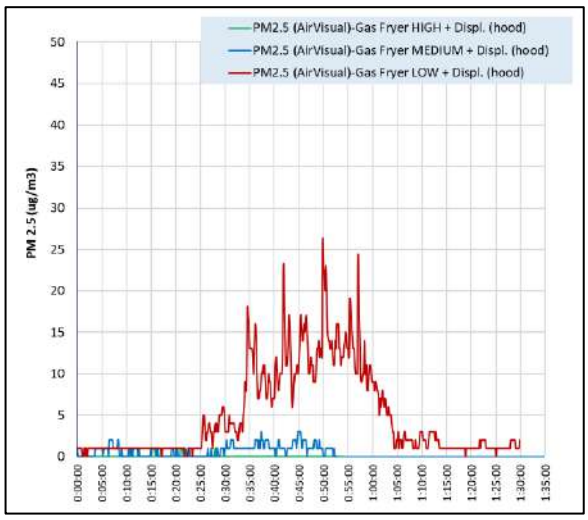

Fig. 10 - PM2.5 measurements under the hood, 2 fryer baskets with 3 air flow regimes and displacement air supply

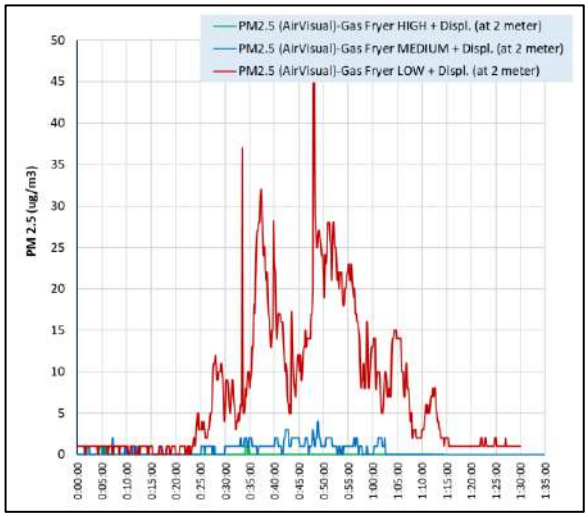

Fig. 11 - PM2.5 measurements 2m from the hood, 2 fryer baskets with 3 air flow regimes and displacement air supply

3.4. *The Fryer with Mixing Air Supply (from the ceiling)*

As per the charbroiler test, all variables apart from the method of supply air introduction remained constant between the different airflow regimes.

Tab. 6 - PM2.5 in the breathing zone and in the room – Fryers - Mixing [µg/m^3]

	Breathing zone		In the Room	
Airflow	**Avg.**	**Max.**	**Avg.**	**Max.**
High	0.2	0.3	0.2	0.4
Medium	1	2.5	1	2.5
Low	7.5	12	7.5	12

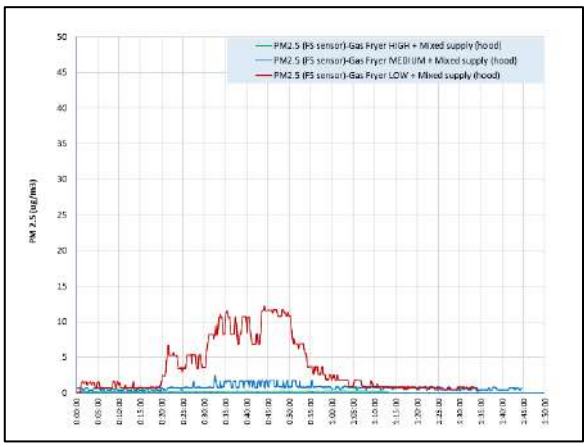

Fig. 12 - PM2.5 measurements under the hood, 2 fryer baskets with 3 air flow regimes and displacement air supply

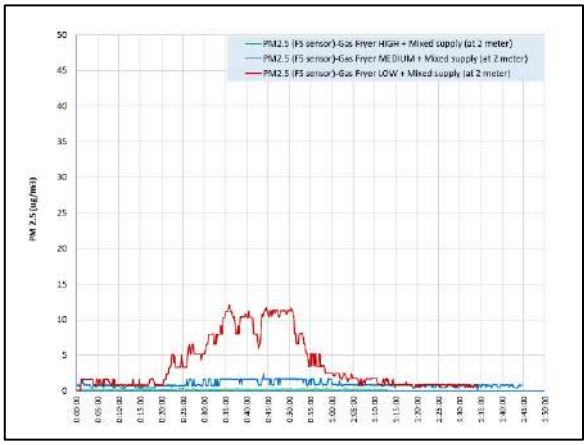

Fig. 13 - PM2.5 measurements 2m from the hood, 2 fryer baskets with 3 air flow regimes and displacement air supply

4. Discussion

4.1. Indoor Air Quality

the results above show that ventilation configuration (exhaust and supply) has a significant impact on the IEQ. The C&C level as determined by the ASTM1704 maximises the extraction efficiency of the hood. Although, frequently the C&C airflow cannot be adequately reached on live job sites. In this case, the IEQ could be heavily deteriorated.

In the case of broiler, we can see that the air curtain system helps improve the IEQ quality in case of air flow lower than C&C. this improvement could be 6x higher, but this could only be obtained by using the appropriate supply system. In our case, the displacement supply air method rather than the mixing air supply method. This could be explained by the turbulences created by the vertical supply. The air velocity in the supply slots is high and one of the supply slots is located close to the front end of the hood (1.2 m). The tables below sum up the results.

In the case of fryers, it was seen that there was no impact of the supply air system on the IEQ. This could be explained by the plume dynamic of the fryer

compared to the charbroiler. The fryer plume tends to follow the backwall due the Coandă effect. That means that the majority of the plume is situated toward the back of the hood; therefore, the wall curtain and supply air system have negligible impact on the plume dispersion.
On the other hand, the charbroiler tends to have a vertically ascending thermal plume and the total depth of the equipment is greater than that of the fryer. (900mm charbroiler depth vs 400mm fryer depth) Therefore, it is more susceptible to air dynamics in front of the hood, as the plume begins closer to the front lip of the hood.

4.2. *Thermal Comfort of the Chef*

Using these measurements, we can also explore the impact on thermal comfort of the chef. Indeed, the temperature at the breathing zone of the chef reached 40°C on average during the fryer tests. That means that even though the chef is protected by the natural rear plume dynamic of the fryers, it still can have a negative impact on the thermal comfort.

We compared temperatures and humidity at the breathing level of the chef with and without the curtain air system.

The following figures show the temperature (in blue) in Relative Humidity (in red) in the beathing zone of the chef. Fig 14. Gaz fryer at 75% of C&C with curtain air system and Fig 15. Is without the curtain air system.

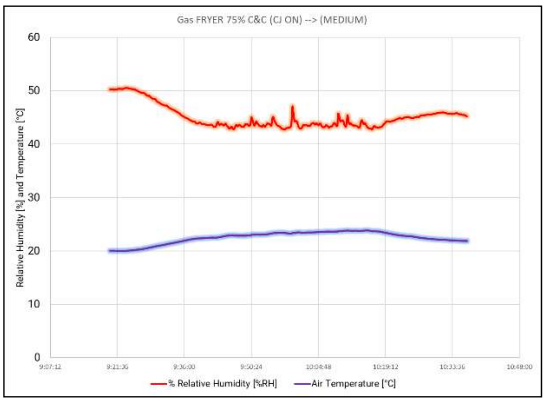

Fig. 14 - Temperature and humidity in the breathing zone with the air curtain system

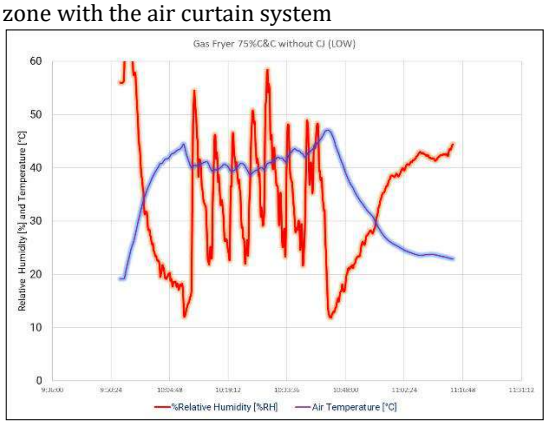

Fig. 15 - Temperature and humidity in the breathing zone without the air curtain system

It can be seen that in the absence of the air curtain system that the temperature is relatively high (average of more than 40°C). The relative humidity fluctuates between 20% and 50%. The fluctuations are correlated to frying series. The French fries are frozen before cooking and thus generate a significant amount of humidity.

When the air curtain is ON, temperature is, on average, equal to 21°C. The humidity is stable and, on average, equal to 45%RH. In this latter situation, the chef cooking is in a better thermal comfort environment.

5. Conclusions and next steps

The objective of this study was to study the impact of ventilation system design and its effect on PM level in commercial kitchens and therefore on the employees' health in these spaces.
3 main parameters have been studied: the cooking appliance type, the airflow settings, and the air supply method.
These three parameters have been found to have a substantial impact on the PM2.5 level in the kitchen and in the breathing zone of the chef.

<u>For cooking appliances:</u> cooking burgers on a broiler has been shown to generate a large effluent load compared to cooking fries with the fryer. At 75% of the C&C airflow without air curtain. The broilers generate up to 394 $\mu g/m^3$ compared to 8 $\mu g/m^3$ for fryers in the breathing zone of the chef.
These levels are 15 times higher than the WHO limit of 25 $\mu g/m^3$.

<u>For airflow settings:</u>
Three airflow regimes have been compared: C&C level, 75% of C&C both with and without air curtain system.
The C&C airflow ensures a good level of IEQ in the kitchen and in the breathing zone.
Degradation of the C&C to 75% deteriorates the IEQ: PM levels increase between 5-15x times dependant on the location, use of the air curtain system and the air supply method.

<u>For air supply method</u>:
Two methods were tested, mixing from ceiling and displacement from the wall. The former method increases the turbulences in front of the hood and reduces the extraction efficiency of the hood.
In the case of 75% of C&C airflow, the air curtain system plays a crucial rule in reducing the propagation of the PM (x6 times), when used with an air displacement unit. In the case of the mixing unit, the IEQ is degraded and the air curtain system has no impact on the reduction of the PM level.

In the case of the fryer, PM appears to be less of an issue because of the plume dynamic, tending to travel toward the back wall and is well captured by the hood. However, the use of the air curtain helps improve the thermal comfort of the chef by reducing temperature and the RH variations.

All of the above shows that the ventilation system is crucial in maintaining a healthy environment in the kitchen.

This study does not include the impact of human behaviour in the kitchen (i.e. hot food stored outside of hoods, doors kept open etc). We would expect that to have a significant impact on IEQ. More field studies will be needed to evaluate this parameter.

For the next studies in the lab, we'll be studying more appliances (Asian woks) and different types of hoods (proximity hood, canopy etc). That should help us to have a deeper understanding of the IEQ in commercial kitchens and how to improve it.

6. References

[Jacobs et al.] Jacobs P., Borsboom,W.A., Kemp R.E.J. PM2.5 in Dutch dwellings due to cooking. ASHRAE and AIVC Conference, 12-14 September 2016, Alexandria, VA, USA

[M Loomans et al. 2020] Loomans M,Te Kulve M, Atze Boerstra A. Particulate matter exposure of chefs in professional kitchens. International Society of Indoor Air Quality and Climate – ISLAQ - 2020

7. Appendices

Hood

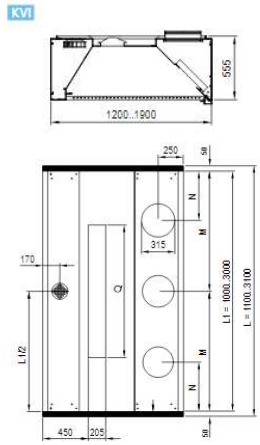

L	M	N
1600	L1/2	450

Mixing units dimensions

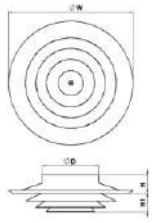

W 457 mm
H 80 – H1 75
D 199

Lab

The laboratory consists of 2 rooms, a test cell and a control command cell. The test cell is approximately 9m long by 6m large by 3.4m high. 2 doors allow installation of equipment and communication to the control command room. Once closed the test cell is airtight.

Exhaust (VFE) and Compensating Air Fans (VFS), with

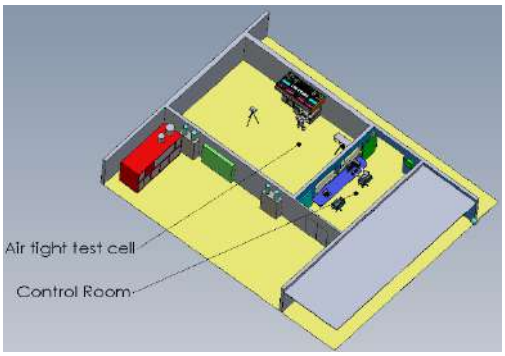

variable-speed drives, to allow for operation over a wide range of exhaust air flow rate from 200m3/h to 7000m3/h. Speed Inverters are controlled by the Datalogger in order to maintain a 0Pa or close to 0Pa pressure difference between outdoor and indoor. The ducting enables multiple configurations, from wall installation (this case) to island.

Air flow rate is measured by Laminar Flow Elements complying with ISO 5167 or equivalent, on ducting of exhaust and air supply.

Temperature and moisture content of exhaust and air supply are monitored, and air supply temperature is tempered by a Chilled or Heat Water system enabling to reach realistic and stable conditions inside the test cell.

Fig. 16 - lab layout – (with charbroiler)

Fig. 17 - Burgers cooking

Fig. 18 - Stir-frying

Sensors PM 2.5 : FS4408 (Transducer particulate matter / particles, active output (0-10V and 4-20mA)

Measurement range PM2.5/PM10	0 µg/m^3 ... 1000 µg/m^3
Accuracy PM2.5/PM10	±5 ug/m^3 + max. ±4% FS (@ 20°C, 45% r.F., 1013 mbar)
Temperature dependency	±1% FS / 10 K
Response time (t90)	< 10 s
Long term stability	±1% FS/year

Assessment of environmental perception of inhabitants of the municipality of Américo Brasiliense on thermal comfort and climate change

João Forte [a], Eva Azevedo [b]

[a] University Institute of Lisbon - ISCTE, Lisbon, Portugal, jota_panagassi@hotmail.com.

[b] Federal University of Pernambuco – UFPE, Caruaru, Brazil, evamoraisazevedo@gmail.com.

Abstract. This research aimed to analyse the environmental perception of climate and the relationship with thermal comfort of adults who have lived in the city of Américo Brasiliense, Brazil. Thus, a questionnaire was created in order to understand the comfort that the participants felt in relation to the environment around them, in addition to the perception of this theme on a global and local scale and how they fit into this context. In this way, it was possible to compare responses and infer the participants' knowledge regarding the concepts of environment and climate comfort in the city. Through the analysis of these aspects in the questionnaire, it was noted that the perception of individuals regarding issues related to the environment, especially in the context of Climate change and the perception of the impact on their comfort and the environment around them, may vary due to the performance of the local government and the involvement of the people in a neighbourhood. It is noticed that respondents related their behaviour and actions in the environment in a different way, when analysed on a global and municipal scale. Therefore, it can be concluded that the sample population can understand the relationship between the environment, thermal comfort and the effect of urban afforestation on local comfort, in addition to the fact that public policies, encouraged by the government, can influence the perception population about the environment in which they live. Another point noticed was the fact that there is an impasse when people think about their roles in relation to the environment and climate change at a local and global level. Part of the interviewees believe that their daily actions in the local environment do not impact the environment when placed on a global scale, which, would be a relevant point that needs to be worked on more deeply.

Keywords. Environment, Thermal Comfort, climate change, environment perception.
DOI: https://doi.org/10.34641/clima.2022.77

1. Introduction

Humanity has been intensifying its urbanization process and its disorderly growth has generated the concentration of populations in cities. This factor increases the diversity and complexity of environmental problems, demonstrating the socio-environmental weaknesses and contradictions of industrial and technological development [1].

From this process of demographic intensification, cities have become predominant factors in the analysis of impact on the environment and climate change. As the population was concentrated in the same spaces, social problems began to arise from the lack of planning and infrastructure that the urban environment had, especially in the historical context of the 20th century. These social problems ended up being added to by environmental problems, among them the lack of basic sanitation and the supply of basic goods and services such as electricity, for example, causing serious problems for the health system.

When looking at the context of the 21st century, there is a worsening of several points described in the last century, a factor that is aggravated due to half of humanity living in urban centres. By 2030, this number will reach 60%, and by 2050, the total should reach around 70%. In Brazil, the urban population already reaches 85%, making the Brazilian panorama different from the rest of the world. As cities grow in size and population, the difficulty of maintaining spatial, social, economic and environmental balance also increases [2].

Copyright ©2022 by the authors. This conference paper is published under a CC-BY-4.0 license.

Thus, it is important to understand the relationship between human beings and the environment, especially when referring to climate changes. Understanding this perspective becomes important to also understand the reason for processes and events by which environmental impacts occur. Therefore, carrying out a study of the environmental perception, focusing on thermal comfort and its impacts on the urban population is fundamental for a better understanding of the human-environment interrelationship, taking into account their expectations, satisfactions and dissatisfactions, judgments and conducts [3].

The definition for the term "environmental perception" can be based on a wide and complex range of concepts. However, it is assumed that its basis starts from a basic principle that is the relationship between man and the environment and, mainly, how each individual perceives, understands and acts within their own environment, according to their cultures and needs [4].

Therefore, It is important also point out that within a study of environmental perception, it is possible to perceive different important aspects of the relationship between man and the environment, and this fact makes it fundamental in terms of an evaluation tool, making that their investigation may provide subsidies for the elaboration of proposals and public policies in different fields [4].

The data from the investigative process of environmental perception come from factors entirely linked to the individual's life history. Among these factors, we can mention: schooling, culture and personal experiences, profession, relationship with the environment, among other factors. From the interpretation of this information, it is possible to understands how each individual live in the environment around them. It is possible to perceive what are its aspects such as ideas, values and identities, and the interaction of all these points allows the recognition of patterns, and environmental issues are not inherent to this fact [5].

1.1 Study area

Américo Brasiliense is a Brazilian municipality located in the central region of the state of São Paulo, located 289 km from the capital (Figure 1). According to IBGE, its population is estimated at 38,701 inhabitants [6].

The sugarcane industry is considered the biggest source of the city's economy. Located in the municipality, São Martinho plant is one of the largest in the country, considering the volume of crushed cane, and serves the national and international sugar and alcohol market. Also finding in the sugarcane residue a great source of energy generation. [7].

The municipality is involved in different historical, economic and cultural problems. As a small municipality, it faces different management problems, mainly related to the search for greater sources of revenue and sufficient technical staff to meet the demand for tasks related to public management.

The region's climate is known for being dry, with high temperatures (above 40ºC, in some summer seasons) and well-defined periods of rain. Being in a tropical climate region, high temperatures are present almost every year, which is one of the main points of thermal discomfort in both winter and summer periods [7].

Therefore, understanding how the population looks at environmental issues becomes a key factor for the creation of effective public policies and for a better structuring of departments to meet the sector demands. Thus, by creating better management for other areas that need technical support.

The present work had the objective of evaluating the opinion of people who live in municipality of Américo Brasiliense about how they understand the concepts that are related to thermal comfort and climate changes. The study sought to understand the relationship between the impacts of citizens' activities on the environment, as well as the cognitive and emotional relationship with it.

2. Research Methods

The present research was developed through the application of online questionnaires during the month of August and September 2020, covering a total of 50 citizens and former residents of the city, chosen at random. Due to Covid-19 pandemic, the questionnaire was only answered online.

Qualitative analyses were performed, due to the subjectivity and context of the responses provided by the participants, but quantitative methods were also evaluated, as the repetition of representative patterns of each response was accounted for. There was no intention to approximate the number of respondents to the universe of inhabitants of the city of Américo Brasiliense, considering that around 38 thousand inhabitants live in the municipality.

The sample number was defined in order to provide greater knowledge about the interviewees regarding thermal comfort in the city. This work does not intend to project generalizations from the data collected, but to qualify the representations of people who live or have lived in the municipality indeed.

Some terms in the questionnaire were replaced, for instance, the term "solid waste", which was now called "garbage" to simplify the understanding of who was responding.

The answers to the questionnaire could be classified in different ways in order to seek the best type of answer for what is being questioned. Questions were

asked to be answered directly (Yes, No, Maybe), some were necessary objective and extensive answers. They were also asked to rate from 0 to 5, where 0 is considered the worst rating and 5 the best.

Each question was prepared and classified as objectively as possible to facilitate the answer of those who are not involved with environmental issues in their daily lives.

In this way, the basis of the structure of all the questions addressed in the questionnaire was planned in order to provide information that would help in the general understanding of how citizens understand some climate change factors and their impacts. Fundamental criteria such as the content, size, organization and clarity of the questions were observed to encourage the informant to respond to the questions addressed [8].

Another factor to be highlighted was in relation to the format and appearance of the questionnaire, which can also significantly influence the rate of return of what is being analysed [9]. The aforementioned authors also emphasize the importance of impartiality, and care must be taken not to influence or induce the subject to answer the questions, which are also observed in the construction of the questionnaire. We sought to elaborate all the questions in order to leave the options open so that the subjects could indicate some other information that they considered important to add in the survey [10].

In addition, they were clarified that they could refuse to participate in the investigation without causing any harm; that such participation would involve no financial cost. They were also informed that anonymity would be guaranteed in the dissemination of the results of this research, in order to seek the most honest opinion possible from the participant and that this academic work would be presented at scientific events and/or journals.

3. Results and discussions

Through the questionnaire, it was possible to reach people from different educational backgrounds (49% with higher education, 44.4% with high school, 4.1% post graduated and 2% others), different age groups and different neighbourhoods of the city.

When analysing the profile of those involved, it can be seen that the most representative age group is adults between 20 and 30 years old, corresponding to approximately 53% of the total number of respondents.

One of the points to be highlighted is the fact that it seeks to represent the majority of neighbourhoods in the municipality, so that it is possible to analyse the perception of people with different points of view, but who live in the same municipality.

Of the approximately 25 neighbourhoods in the city, 18 are represented in the study. Most responses were obtained from 3 neighbourhoods: *Jardim Primavera*, *Centro* and *Vila Cerqueira*. Both correspond to 48% of the participants.

An important point to note is the fact that this questionnaire was applied only to people from the urban area of the municipality. It was not considered participants from rural neighbourhoods, this is because the topics are based on environmental issues through the perception of people who live in urban areas. A different approach is needed for the perception of those who live in rural areas.

Through this questionnaire it was possible to understand what the investigated citizens understand and how they solve some issues related to thermal comfort and climate change in their routine. Important points were also raised regarding specific environmental factors, such as urban afforestation, relation between human being and landscape and environmental public policies.

3.1 Global and local perception about climate change

At first, we sought to analyse how the participants understand the importance of questions about the environment and climate change in a global context, and how important they are in the city context, as well. It was hoped to obtain an overview of the opinion and how important this topic is for the participants.

After analysing the answers, it was noticed that the population differs in the way of understanding on a global and municipal scale. In figure 1, it is shown how the citizens assess the importance of the environment and climate in the world:

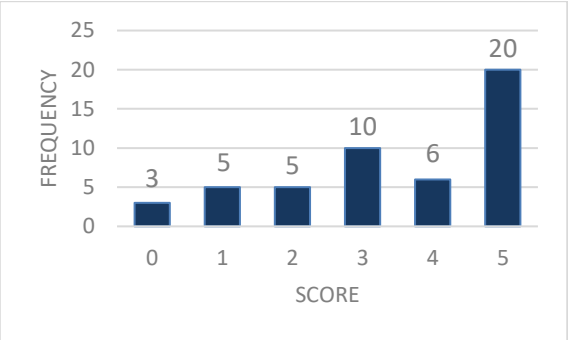

Fig 1 - importance of the environment and climate change in the world.

If you consider 3 a minimally satisfactory grade to clearly consider that people believe that the environment and climate can be considered important, there are 36 people (approximately 73%) who believe those topics are relevant for the planet, of those, 41% evaluating with grade 5 and 12.2% with grade 4. However, the same reality cannot be considered, when analysing people's opinion

regarding the importance of the environment in a local perspective, their opinions vary more significantly. Figure 2 shows that people's opinion changes in relation to the municipal context.

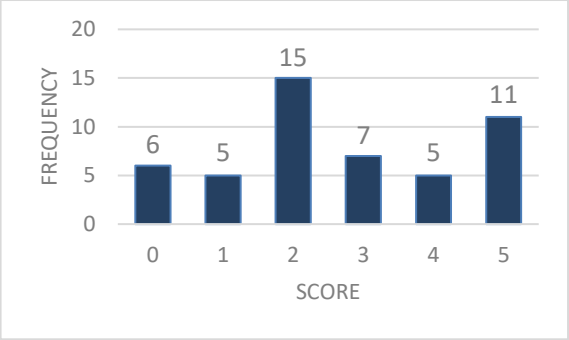

Fig. 2 - Question regarding the importance of the environment and Climate in Américo Brasiliense city.

In this perception, the number of people who gave at least one grade of 3 decreases, being only 23, corresponding to approximately 47% of people (less than the 73% in graph 2). Of these 23, only 11 (22.4%) rated 5 people and 5 people (10.2%) rated 4. Therefore, it is clearer that respondents evaluate differently the importance of the environment and climate to a global scale, than in a local one.

On one hand, those answer may be possible due to the fact that most of the participants do not consider environmental local impacts significant for the city. On the other hand, the global impacts are more significant and easier to be associated with climate changes.

Another relevant point in the questionnaire was the participants' perception of the municipality's environmental and climate policies. For this point, some questions were elaborated for this analysis. First, it was sought to understand how the participants consider to be important for the municipality to include those topics in municipal public decisions. If we consider that a grade of 3 or more is a score that demonstrates that the participant considers the environment and Climate change, at least, relevant, it is possible to see that only 61.2% of the listening population considers them relevant to municipal issues.

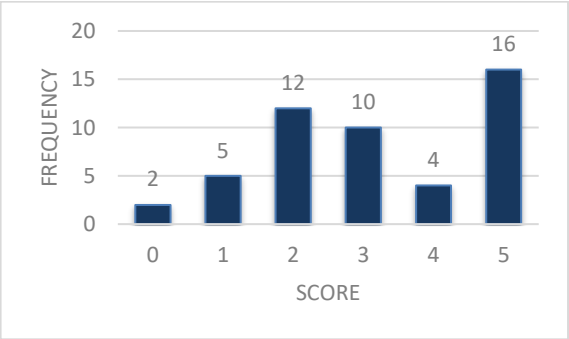

Fig 3 - Importance of the environment and climate changes for the local municipal public policies according to participants.

Another point to be analysed in the political question is how the city's citizens assess the importance that city politicians attribute to environmental issues. For this factor, it was asked, from 0 to 5, how much the participants believe that city politicians (councillors, mayors, among others) are concerned with environmental policies.

When considering, again, an evaluation from 0 to 5, grades 0, 1 and 2 as bad values on an evaluation, one can clearly see the population's discontent regarding the environmental issues that the municipality has been working on throughout its history. Figure 4 shows how the participants assess this context.

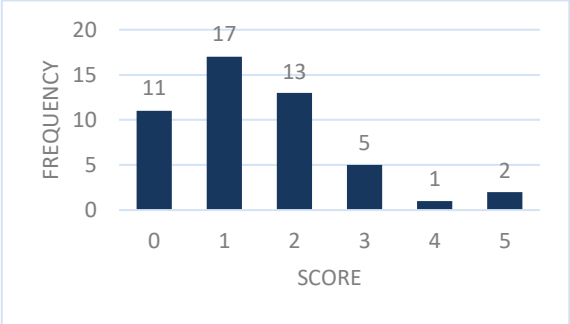

Fig 4 - Politicians' concern for the environment according to the citizens' view.

Taking into account 0, 1 and 2 as bad evaluations, it can be seen that approximately 41 people (83.7%) believe that those responsible for the public administration of the municipality do not care about environmental and climate change issues in the city and they make decisions that not take into account the environmental problems of the municipality.

The environment is an important factor in the context of social well-being, mainly on thermal comfort. The population suffers the consequences of negligence regarding environmental issues, so it is important to understand their point of view regarding these types of problems and find a way to spread knowledge about it.

Therefore, it is necessary to analyse the reasons that lead people to understand why they evaluate those involved in public management in this way, how they look at the environment and how the population understands their impacts on their neighbourhoods.

3.2 Relation between daily actions and consequences on the city's environmental impacts

Often, the relationship with the environment can be conflicting and the individual does not imagine that his actions impact the environment around him - either indirectly or directly. Sauvé states that it is necessary to create a relationship of belonging to the place where one lives, improving the socio-environmental relation between the individual and the environment and, in this way, developing a feeling of belonging to the place, thus establishing a

connection with what happens around you [11].

Therefore, we also sought to question whether the participant considers that their actions have a negative impact on the environment and Climate change.

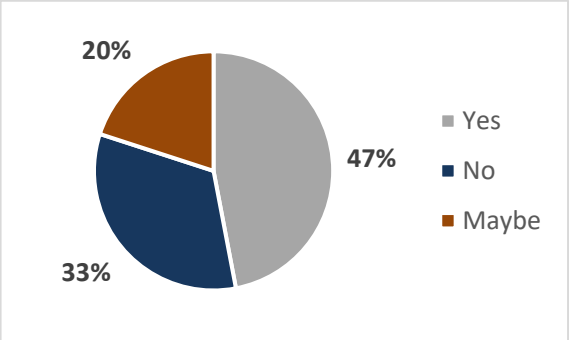

Fig 5 - Result of the question "Do you cause any damage to the environment in your daily life?"

When combining the option "No" and "Maybe", it can be seen that 67% believe that both oh them do not impact the environment around them or do not know how to inform if this occurs. Thus, many people consider that their day-to-day actions are not effective in providing an impact to the environment around them, while only a third of the participants believe that their actions have any impact on their daily actions.

Among those who answered "Yes", the most cited damage to the environment is the production and generation of waste such as: Plastic bags, urban waste, and others such as the use of automobiles and, consequently, the pollution generated by their use.

When talking about thermal comfort, it is clear that some people do not realize whether their actions related to environmental issues can cause any significant impact on what they feel about the environment.

Therefore, they were asked about what they would change in the landscape of the place where they live and most consider urban afforestation as extremely important points to change regarding the surroundings where they are living. This demonstrates how the sample population of this work considers afforestation as a significant factor not only as a necessity, but as a way to change the landscape, making it more pleasant and comforting in terms of temperature.

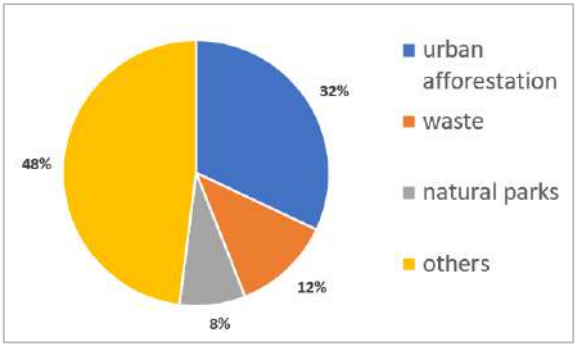

Fig. 6 - Answer to the question "Is there anything you would like to change in the landscape of the place where you live?"

An important fact to comment is that many people responded that they want to change something in the landscape in which they live, but either preferred not to confirm what they were or were not sure how to make this change, in addition to these, 10 people consider themselves satisfied with the place where they live. This variation in the answer can occur due to different factors, among them: Due to the difference in the location in which the participants reside, the time they spend in the place, for having lived at different times in the municipality, for the perception of the space around it and for the way in which interact with the environment and with the people around them. This point related to urban afforestation as a heat reliever can be perceived by the fact that even most of the participants would like to change the place where they live because the heat.

4. Conclusion

Analysing the participants, it was noted that the opinion on some concepts related to the environment varies according to the perception of each involved regarding the questions. People understand the environment as something important to preserve, but they vary in opinion about what to do to protect it.

Due to the fact that the important opinion of 50 people who live in the municipality was collected, it is possible to have an overview of how people perceive the topic addressed in the questionnaire, but it is still not possible to say that this opinion reflects the opinion of the entire local population. More responses are needed for this statement.

In the end, it was observed that the questionnaire provided the opportunity to know how the people of the municipality think about some environmental issues and what they believe are important for local environmental improvement.

In general, people believe that the environment and climate change are important to the world and, indeed, needs to be preserved, but when analysed on a local scale, in which actions can directly affect the environment in which they live, their perception of importance about the impact of their actions have on

the environment decrease significantly.

This can be seen when the environment in which the individual lives is considered less important than the environment in a global scale. Therefore, not assuming that the world is a system that depends on balance and that, by interfering with the surrounding microenvironment, it is also generating an impact on the macroenvironment as a whole.

It is noticed that some of the participants consider the importance of environmental public policies small in their day-to-day. This may reflect the fact that they do not consider that their daily lives are entirely dependent on climate change or environmental policies based on socio-environmental well-being. Therefore, as approximately 98% of respondents are over 18 years of age, it would be important to encourage environmental education policies focused on adults as well.

Because it was an open-ended question, the question "Is there anything you would like to change in the landscape of the place where you live?" demonstrates that 15 people have mentioned the theme of urban afforestation as a factor to be changed in the landscape is very significant. This shows how the government and population, should encourage stronger public policies in this area, as well as incentives to promote and maintain urban afforestation in the municipality as an important heat reliever.

A possible change related to the municipal environmental public policy that local politicians could carry out would be to encourage the planting of native trees in urban spaces through tax incentives. This could bring greater thermal comfort to local citizens, improve the biodiversity of species in the region, in addition to other benefits that would help the citizens' routine.

As future recommendations, it will be necessary to carry out a neighbourhood-by-neighbourhood analysis, with more answers, visits on-site interviews and with specific questions for each theme, in this way the results would be more accurate and more focused on a problem present in each of the locations.

5. References

[1] Ferreira J. Solid Waste and Hospital Waste: An Ethical Discussion. Public Health Notebook, Rio de Janeiro (BR). 1995;11(3):14-20;

[2] Ethos Institute. Sustainable Cities Program. São Paulo (BR). 2011;5(1):3-30.

[3] Villar L., Almeida A., Lima M., Almeida J., Souza L., Paula V. The environmental perception among the inhabitants of the northwest region of the state of Rio de Janeiro (BR). Esc Anna Nery Rev Nursing.2008;1(1):285–90.

[4] Silva B. Evaluation of environmental perception of residents of rural communities of president kubitschek/MG. Dissertation (Master in Agricultural Engineering). Federal University of Lavras (BR), 2017:65-88;

[5] Miranda N., Souza L. Environmental perception in rural properties: Palmas (BR). Mercator. 2011;10(23): 171–186;

[6] Brazilian Institute of Geography and Statistics (IBGE). Database by municipalities in the Immediate and Intermediate Geographical Regions of Brazil [internet]; 2017. [Updated 2021 Nov 12]. Available from: https://www.ibge.gov.br/apps/regioes_geograficas

[7] Brazil. Municipality data - Américo Brasiliense, a sweet city [internet]. Américo Brasiliense (BR); 2021 - [Updated 2021 Oct 2]. Available from: https://www.americobrasiliense.sp.gov.br/site/

[8] Barros P., Lehfeld S. Fundamentals of Methodology: A Guide to Scientific Initialization. São Paulo: McGraw-Hill; 1986: 4 - 7.

[9] Thomas J., Nelson J.; Silverman S. Research methods in physical activities. Brazil. Artmed, 2007;1(1):11-15.

[10] Veiga T., Coutinho S., Takayanagui A. Evaluation of indicators for municipal solid waste management. Electronic Journal Environmental Forum of Alta Paulista (BR). 2015;11(3):1-14;

[11] Sauvé L. Environmental Education: possibilities and limitations. Education and Research. Brazil. 2005;31(2):317-322.

The datasets generated during and/or analysed during the current study are not available because they are in the final stage of evaluation, but the authors will make every reasonable effort to publish them in near future.

Comfort evaluation of a dynamic protective airflow system using human test subjects

Kim Hagström [a], Ismo Grönvall [a], Petri Kalliomäki [b], Henna Maula [b], Arttu Sivula [b]

[a] Halton Technology, Halton Oy, Kausala, Finland, firstname.surname@halton.com.

[b] Research group for Built Environment, Turku University of Applied Sciences, Turku, Finland

Abstract. Amount of sick leave days among nurses is in relatively high level compared to many other occupations. One of the risk factors for nurses at work are respiratory infections.
According to recent studies, there is a high risk for nurses to be exposed to microbes exhaled by patients especially, while they are conducting their work close to patient.
Current ventilation solutions that are used in patient environments are not designed to address this challenge. At best, they are able to dilute the microbial concentrations in the room, but they are not able to affect the nurse's exposure to patients' outbreath close to patients. These may lead to substantially higher exposure levels compared to room air conditions.
To reduce HCW's and especially nurses' exposure and infection risk, a new dynamic protective flow ventilation approach has been developed for patient environments (isolation rooms, intensive care and standard patient rooms). In previous studies, the efficiency of protective flow ventilation as well as thermal comfort has been verified by using breathing thermal manikin and tracer gas experiments.
In this laboratory study done in a simulated patient room, the thermal comfort provided by the protective ventilation solution is studied with human subject experiments. The participants are exposed to indoor environment, both in stable conditions and in a dynamic situation in which patient / nurse interaction is simulated. The thermal comfort is evaluated primarily by questionnaires, which the subjects will complete in different stages of the experiment. Physical measurements are conducted in parallel.
The presentation will outline previous development stages and will especially focus on presenting the results of human subject experiment.

Keywords. HCW, HAI, Infection, Ventilation, Protective airflow, Exposure
DOI: https://doi.org/10.34641/clima.2022.87

1. Introduction

Healthcare workers (HCW) and especially hospital nurses, who are constantly in contact with patients and visitors while treating patients are exposed to multiple occupational health risks in their work. Nurses are exposed to healthcare-associated infections and transmission of highly infectious diseases from infected patient to other patients and HAIs occurs constantly in hospitals and healthcare centres. This challenge has been especially emhasized in relation to certain infective diceases such as tubeculosis and small-box and more recently related to pandemic outbreaks. It has also been acknowledged that some high risk treatment procedures such as suction and incubation pose an inceased risk for infection transmission.

If a patient has or is suspected to have an infectious disease, the patient may be transferred to an infection isolation room that is especially built for such treatment and together with personal protective equipment (PPE) the exposure to and spreading of the infection can be reduced.

However, vast majority of close proximity patient contacts take place during "normal" treatment work in wards. In a pandemic situation personal protection precautions are emphasized and introduced also in wards as infectious patients have to be located there as well due to lack of isolation rooms. But this is a special condition and it may not be realistic to assume PPE's to be used constantly by HCWs. PPE's have been reported to cause adverse health and performance effects during extended usage/1/. Also it has been found that facemasks will increase to CO2 levels inside the mask up to 2000-3000 PPM/2/. HCWs are already acknowledged among

Copyright ©2022 by the authors. This conference paper is published under a CC-BY-4.0 license.

the professions with increased occupational respiratory diseases such as asthma./3/ According some studies the total inward leakage (TIL) of face masks differ remarkably from the material efficiency being in the range of 10%-25% for N95 masks and 25%-50% for surgical masks /4/.

Special ventilation arrangements (like hoods and local supply and exhausts) have been studied and proposed by research for patient wards. Yet, they are not common in hospitals as such arrangements may carry a high additional cost and /or challenge the treatment practices so that they are not considered sufficiently practical for wider use.

The reseach question behind this study is, whether it would be possible to provide better protection while maintaining comfort by means of ventilation and air diffusion with the resources and limitations of current hospitals and treatment processes.

2. Current practices in patient rooms

2.1 Patient Wards ventilation

The ventilation rates in patient wards vary quite much between countries and hospitals. Quite common range in Europe is between 2 ACH to 4 ACH, but even values up to 6 ACH /5/ are recommended. These corresponds in typical 20 m2 single patient ward to 33 l/s, 67 l/s, and 100 l/s outside airflow rate. The typical reasonings for elevated airflow rate are increased amount of odours from patients and medication provided and the treatments given in wards. It is also wort noting that even in one patient ward the occupation varies during the day due to treatments and visitors. Thus, the ideal ventilation arrangements in patient ward would enable minimum ventilation rate for sustainable operation but have flexibility for elevated air flow rate for varying situations in a ward.

Typical patient ward ventilation system is based on mixing ventilation principle without any special considerations. The maximum cooling load in a typical patient ward is about 500W, which means that an additional room cooling is often needed. This is often provided by chilled beams or radiant panels.

2.2 Isolation Room ventilation

A commonly used ventilation rate in European isolation rooms is 12 ACH. Defining the airflow rate based ACH is arbitrary, because ultimately the target of ventilation is to reduce the infection risk caused by a source, which is not depending on the room size. In infection isolation room the source is the patient. In current work within CEN TC156 WG18, Hospital Ventilation standardization workgroup the ventilation rate is defined based on the patient source. /6/ In this way it is possible to determine the targeted protection degree / dilution rate in an isolation room with a patient. With a typical breathing rate of a sedentary person, 15 l/min to reach 1:1000 dilution rate (average, based on complete mixing) a 200 l/s ventilation rate would be required. This air low rate corresponds to 12 ACH in a 60m3 room, but ACH would be different in different size rooms as the ventilation rate should be kept the same to meet the dilution criteria.

The isolation room ventilation system is typically designed to use only outside air apply mixing ventilation principle and thus assuming that the contamination is equal all over the space. In some protective isolation applications, such as burns patient wards, also protective zone ventilation principle is applied. But in such use case the ventilation rate used is much higher.

2.3 HCW work in a patient room

The primary reason for the HCW to enter the patient room is to nurse the patient. This nursing takes place in close proximity of the patient and in acute setting the patient spend most of one's time at patient bed.

As HCWs spend much time close to the patient, it is important to ensure that the exposure is minimized during HCW – patient encounters. The challenge in such situation is that HCW will be directly exposed to exhaled air from patient and vice versa. This is illustrated by a smoke visualization in a breathing mannikin study in Figure 1.

Fig. 1 – HCW exposure to patient exhalation in close proximity treatment situation./ 7/

3. Exposure risk of HCW while treating a patient

3.1 Variation of the HCW Exposure risk in isolation room

The exposure risk of a HCW, while treating patient in an isolation room has been studied in /7,8/. The study was made using breathing mannikins and

tracer gas as well as smoke visualizations.

The research focused on the HCW exposure risk in different locations of isolation room and on the influence of ventilation arrangements in the isolation room. The outdoor ventilation rate during the experiments was maintained at 170 l/s and patient breathing rate 10 L/min..

The HWC exposure risk varies largely depending on the location within the isolation room. While working close to patient the exposure risk can be up to 10 times higher than what can be expected from the exhaust concentration. The results, while using overhead mixing ventilation is presented in Figure 2./7/ Thus, instead of having 1:1000 degree protection HCW may only have compromised 1:100 protection, while working in a typical position close to patient.

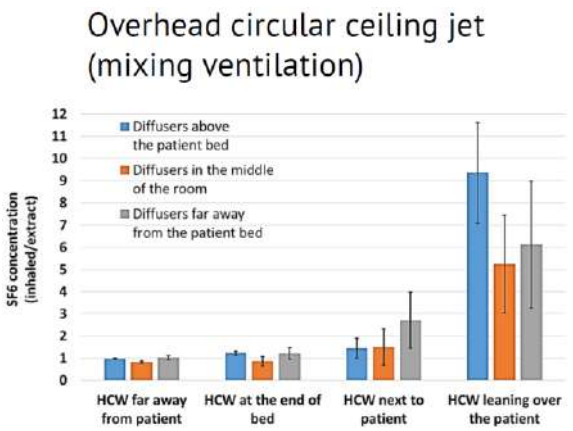

Fig. 2 – Influence of room position and ventilation outlet location on the HCW exposure in an isolation room./7/

Also, local downward flow from the ceiling was studied in the same research. When all the air was supplied on top of patient it was possible to reduce the elevated exposure, but with the consequence of high thermal discomfort, which makes this application impractical.

3.2 Influence of ACH on the HCW exposure

In fully mixed conditions it is assumed that the relative exposure is a function of the air flow rate, in other words doubling the supply airflow rate would half the concentration and thus exposure.

However, in close proximity work this may not be true as the local conditions will impact the exposure. The influence of ACH on the HCW exposure in such conditions has been studied by /8,9/, where Intake fraction, IF, has been used to illustrate relation of inhaled contaminant dose by HCW to total contaminant released to a patient room.

Figure 3 shows results from/8/, where two different air diffusion principles were measured using different air change rates. As a benchmark, in fully mixed conditions, where no direct exposure from patient to HCW occur, the IF fraction for 12ACH, 6ACH and 4 ACH would respectively be 0,1% (= 10 L/min /60s / 170 L/s), 0,2% and 0,3%. Thus, the HCW worker exposure in close proximity during those measurements have been clearly above the calculated overall room exposure. The exposure was approximately 1,5 to 1,7 times higher with the LDV and 3,2 to 5 times higher with the MV compared to calculated fully mixed condition. To put this ratio in scale it is comparable to using a surgical mask instead of N95 mask by HCW (TIL). It can also be noted that in MV situation the relative reduction in exposure, when increasing the airflow, is diminishing.

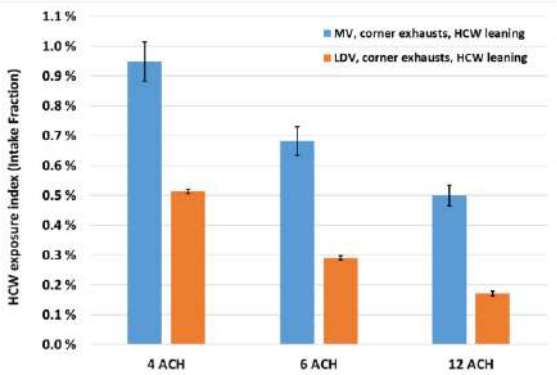

Fig. 3 – Influence of air diffusion principle and ventilation rate on the HCW exposure in an isolation room./8/

4. Development of a protective airflow system for HCW protection

Prior research clearly points out the challenge of increased exposure risk for HCWs in their daily work. Likewise, should the HCW carry an infection they also pose an increased risk to patients. And, especially from the point of ventilation profession it is important to understand that typical general ventilation is incapable to cope with close proximity work. It is not at all sufficient to compensate this gap with general ventilation efficiency indexes as the scale of risk is beyond that.

Thus, specialized ventilation and air diffusion practices should be implemented to provide enhanced protection for HCWs. However, as noted earlier it is challenging to implement any measures in practical hospital projects that would cause significant cost increase and especially would necessitate changes on the work practices of HCW.

Understanding this the targets and boundary conditions were set for the protective airflow system development including; usable airflow rate (Patient Room 30-70 l/s, Isolation room 200 l/s), cooling load requirement taking into account good

comfort air quality and acoustic conditions, and installation and operation of ventilation system in such a way that it don't limit or change HCW practices.

4.1 Protective Airflow system concept

The basic principle of the designed protective airflow system is presented in Figure 4./10/ It is based on the use of parallel air streams supplying air towards patient bed that are created by two adjustable supply air diffusers located on both sides of the patient bed.

Fig. 4 – Protective airflow system concept, patient room. /10/

During the development phase the airflow and temperature parameters have been optimized to provide both optimal protection and comfort conditions.

The same system principle has been applied for both normal ward and isolation room resulting in two variants of the system based on the different boundary conditions.

The patient ward system is based on two inward jets that are integrated with a radiant panel to provide necessary cooling and personal comfort control, like presented in Figure 4. The dynamic airflow is applied to be able to provide sustainable operation for patient only situations and protective conditions for HCW patient interactions.

The isolation room system has slightly different airflow principle; due to high airflow additional airflow patterns are directed towards sidewalls as shown in Figure 5./10/ The isolation room system has also dynamic operation principle to allow sustainable operation, when room is used for normal patients.

Fig. 5 – Protective airflow system concept, Isolation room. /10/

5. Testing of protective airflow system

5.1 Test program

The testing and development of the protective airflow system was conducted in a climate chamber of Turku University of Applied Sciences that was initially built for isolation room testing. Two breathing mannikins were used to allow controlled breathing performance of both patient and HCW as shown in Figure 6.

The research was focused on the close proximity interaction that was in earlier research found to be the most challenging as well as most common situation in patient work. The focus of the research was to measure and minimize the HCW exposure to contaminants exhaled by a patient. Diluted solution of SF6 was used as a marker for contaminant in the same manner as in previous research/7,8/ to make the results comparable. The HCW exposure and protective efficiency of the airflow system was studied with different airflow settings for both patient ward and isolation room.

Airflow pattern was visualized by smoke to illustrate system performance and measurements by omnidirectional sensors were used to ensure desired air movement over patient bed.

The indoor air quality provided by the protective airflow system was studied by means of local mean age of air. In addition to HCW exposure experiments, tracer gas experiments were carried out to measure the local mean age of air in the patient breathing zone (in the inhalation) and in the main exhaust. In the measurements, another tracer gas (N_2O) was released to the supply air duct and hence it spread to the test room with the supply air.

Thermal comfort conditions of the patient were assessed using thermal mannikin. In the experiments, the thermal manikin was lying on the bed on her back with a duvet cover on (see Figure 6). The thermal manikin is equipped with a sensor network capable of measuring thermal comfort. In the test, the manikin was dressed with a typical patient outfit consisting of underwear (underpants

and bra), socks, long pants, and a long sleeved shirt. The clo-value (clothing insulation) of the outfit was measured to be 0.5 clo (K*m2/W). The total clo-value for the manikin lying on the bed (on a mattress) with clothing and duvet cover on was measured to be 1.5 clo. For thermal comfort assessment, the metabolic rate of the manikin was set to 0.8 met, which is close to adults (female) at rest. In the experiments, the whole-body thermal comfort was measured in steady state conditions. The thermal comfort was assessed with predicted mean vote (PMV) and predicted percentage of dissatisfied (PPD) indices.

The room temperature was maintained at 24°C, which is a common value in patient room environments.

5.2 Smoke visualization of the protective airflow

Firstly, smoke visualization was used to demonstrate the protective airflow performance and to show the airflow pattern of protective flow, which is shown on Figure 6.

Secondly smoke visualization was used to demonstrate the impact of the protective airflow to the exhaled air of the patient. Figure 7 shows the outbreath of patient with protective airflow pattern with minimum 30 l/s supply air flow (Test Condition 1 in a regular patient ward situation) and Figure 8 shows the spreading of the exhaled air of the patient, when the protective flow is in use and the ventilation rate is 70 l/s. (Test Condition 2)

Figure 9 shows the exhalation flow pattern, when protective airflow is applied in isolation room conditions with total airflow rate of 200 l/s.

Fig. 6 – Protective airflow pattern at 70 l/s flow rate.

Fig. 7 – Patient outbreath witt protective airflow pattern in isolation room at minimum 30 l/s flow rate.

Fig. 8 – Patient outbreath with protective airflow pattern in isolation room at 70 l/s flow rate.

Fig. 9 – Patient outbreath with protective airflow pattern in isolation room at 200 l/s flow rate.

5.3 Protection efficiency performance of protective airflow system

The protection efficiency indexes for three presented test cases are shown in Table 1.

Tab. 1 – Protection efficiency index, 3 test conditions.

Test Condition	Qsupply [l/s]	ACH	HCW Exposure Ratio (Inhaled/Exhaust)	Intake Fraction IF
1 Patient Ward	30	2	1,7	0,78 %
2 Patient Ward	70	5	0,78	0,17 %
3 Isolation Room	200	14	0,83	0,07 %

The performance of protective airflow with only minimum airflow of 30 l/s is incapable to fully overcome the local exposure challenge – the full mixing indexes with 2 ACH would be for HWC Exposure Ratio 1,0 and Intake fraction, IF, 0,6%. Yet, compared to values from previous research in Figure 3 it can be noted that the Intake Fraction is clearly better than with general mixing ventilation with 4 ACH.

The actual protective airflow mode in patient ward with 70 l/s is able to provide better than fully mixed condition even in the most critical close proximity treatment situation (IF value 0,17% compared to 0,25% in fully mixed condition). Comparing earlier research, it's performance is in the magnitude of 5 times better than mixing ventilation at the same airflow rate and more than 2 times more efficient than LDV system both tested in/8/ and based on the results shown in Figure 3.

In Isolation room test the applied airflow rate was 200 l/s (Test Condition 3) following CEN TC156 WG18 work /6/ leading into 14 ACH in the test room used. Like in the patient ward case the protective airflow performance surpasses the fully mixed condition in close proximity situation. Additionally, it can be seen that, when a functioning protective airflow pattern is in place, it is possible to get full use of the increased airflow – the ratio of the IF factors 0,07%/0,017% is quite close to the ratio of airflow rate between patient ward and isolation room systems.

5.4 Indoor Air Quality performance of protective airflow system

The local mean age of air in the inhalation of the patient was found to be constantly smaller than in the exhaust. Although the differences were small occasionally, the results imply that the supply air distribution was able to provide fresher air locally to the patient bed area compared to the exhaust, even with the lowest flow rate, where no clear downward flow towards the patient was observed by smoke test.

5.5 Thermal comfort performance of protective airflow system

Thermal comfort measurement results for the whole body are shown in Table 2. Despite that all PMV values were slightly negative, generally the measured thermal comfort was on a good level. Such a minor difference is easily adjustable by radiant panel or room temperature adjustment.

Tab. 2 – Thermal comfort indexes, 3 test conditions.

Test Condition	Qsupply [l/s]	Tsup-Trm [°C]	PMV	PPD%
1 Patient Ward	30	-4	-0,4	8 %
2 Patient Ward	70	-4	-0,5	11 %
3 Isolation Room	200	-4	-0,6	13 %

However, before implementing such a special airflow system in real life conditions, it was decided to confirm the thermal comfort evaluation by using human subjects

6. Perception of air movement and thermal comfort in patient room

The purpose of the study was to conduct human subject experiment about perception of air movement and thermal comfort of participants laying in a hospital bed in patient ward with the protective airflow system.

The room conditions during the test were kept the same as in previous test with protective airflow system as the purpose was to validate the acceptability of thermal comfort conditions assessed earlier using thermal mannikin.

6.1 Description of test method

The experiment was done in N Universitys' HVAC laboratory in N, N. A full-scale mock-up simulating a simplified hospital patient room was built into the laboratory. A similar procedure had been developed in earlier patient room testing /11/

Two conditions 1 and 2 were used by varying airflow rate between minimum airflow mode and protective mode. The details of the test procedure is shown on Figure 10 and explained below.

A repeated measures design was used, meaning that each participant went to both test conditions and served as their own control minimizing the effect of participants' individual differences on results.

15 test participants (8 females, 7 males) were used

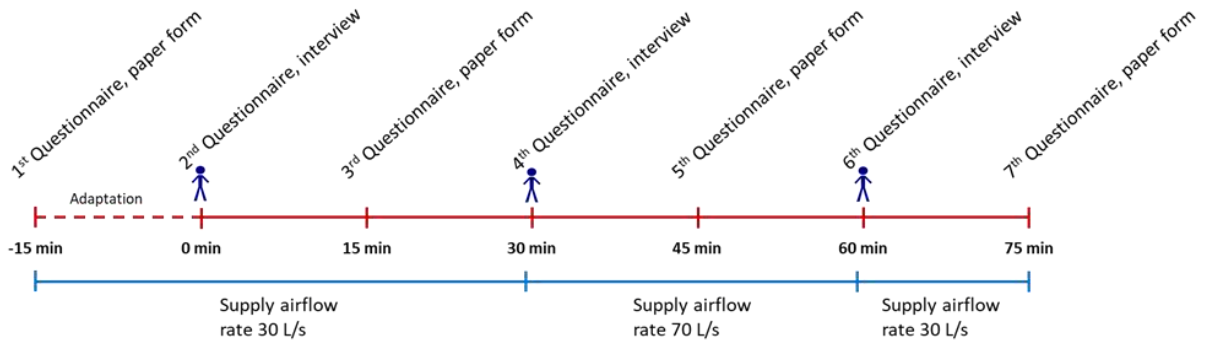

Fig. 10 – Test procedure for air movement and thermal comfort evaluation in patient room.

with mean age 28 years. The subjects used similar standard hospital clothing as was used with thermal mannikin. The thermal isolation of clothing, blanket, pillow and mattress was 1.5 clo, measured with thermal manikin.

The participants were reclining in a hospital bed and listened an audio podcast.

Fig. 11 – Participants' position, clothing and the adjustment of the blanket during the experiment

Overall thermal sensation was asked using seven-point response scale from ISO standard 7730 (2005): Hot (3), Warm (2), Slightly warm (1), Neutral (0), Slightly cool (-1), Cool (-2), and Cold (-3).

Besides overall thermal sensation and comfort, local thermal comfort, thermal satisfaction and pleasantness of the air movement, and perception of airquality was asked.

Symptoms, such as headache, feeling unwell, and nose, throat and eye symptoms were assessed with five-point response scale (1 = Not at all, 2 = Slightly, 3 = To some extent, 4 = Quite a lot 5 = Very much).

In addition, questionnaires included so called "dummy questions" that were used to distract participants focus only on thermal environment. Dummy questions were related to interior design and ergonomics.

6.2 Results - thermal comfort

Thermal comfort results are presented in figure 11 and in tables 3, 4, 5. In figure 12, the box contains the middle 50 % of the votes, the central bold line is the median of the distribution and stars represents outliers. The overall thermal perception by participants was very good for both test cases.

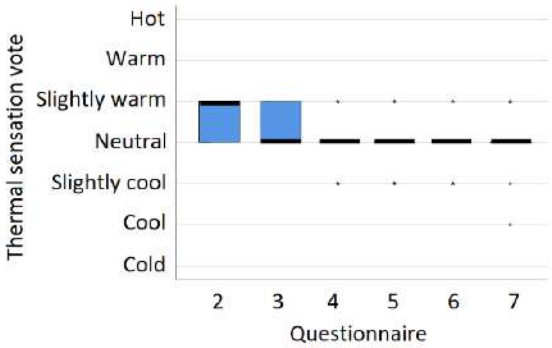

Fig. 13 - The distributions of thermal sensation votes by questionnaires. The distribution is lacking the box if the middle 50 % of the votes are placed on together with the median.

Tab 3. Average thermal comfort results by questionnaire. (TSV = thermal sensation vote, and PD = percentage dissatisfied with the thermal environment).

Questionnaire	2	3	4	5	6	7
TSV	0.5	0.3	-0.1	-0.1	0.1	0.1
PD [%]	0	0	7	20	13	7

Tab 4. Average thermal comfort results by test condition. (TSV = thermal sensation vote, and PD = percentage dissatisfied with the thermal environment).

Test condition	1	2
TSV	0.2	-0.1
PD [%]	5	13

Local thermal sensation was asked using open questions, where face, hands, feet and middle body were mentioned. Both warm and cold sensation was mentioned as well as neutral.

6.3 Results – Perception of air movement and quality

Perception of air movement results are presented on tables 5 and 6. The overall perception by participants was very good for both test cases and felt even more pleasant during test condition 2, which was protective mode.

Table 5. Average perception of air movement by questionnaire. The scale for perception is Very unpleasant (-2), Slightly unpleasant (-1), Not pleasant or unpleasant (0), slightly pleasant (1), Very pleasant (2)

Questionnaire	2	3	4	5	6	7
Participants	7	13	73	87	53	40
Perception	0.0	-0.5	0.1	0.2	0.0	0.3

Table 6. Average perception of air movement by test condition. The scale for perception is Very unpleasant (-2), Slightly unpleasant (-1), Not pleasant or unpleasant (0), slightly pleasant (1), Very pleasant (2)

Test condition	1	2
Participants perceiving air movement [%]	28	80
Perception	0.0	0.2

Local perception of air movement was asked using open questions. Sensation on face and hands were mostly mentioned. Also, sensation on middle body was mentioned by some.

The air quality was perceived rather good in both test conditions (4.4 in test condition 1 and 4.5 in test condition 2, scale: 1= stuffy, 6=fresh).

6.4 Results – Symptoms

The mean values of perceived symptoms in both test conditions are presented in table 7. All mean values are below 2 (slightly) with no difference between test conditions. Minor difference was seen in perception of eye symptoms. However, the practical meaning of this difference is negligible.

Table 7. Perception of symptoms by test condition.

Test condition	1	2
Sweating	1.3	1.3
Nose symptoms	1.1	1.0
Throat symptoms	1.3	1.3
Eye symptoms	1.6	1.7
Feeling unwell	1.0	1.0

7. Conclusions

HCW are exposed to elevated infection risk in their daily work and act as an agent spreading infection within hospitals. The especial concern is work in proximity of patient, where the exposure risk is elevated up to 5-10 times and cannot be eliminated by means of general ventilation. Using constantly personal respiratory protection is not a sustainable solution due to adverse health effects.

A dynamic protective airflow system has been developed to eliminate/reduce exposure even in proximity work and its performance has been studied throughout from HCW protection and patient comfort point of views.

The tested system can provide a cost-efficient and sustainable solution for HCW protection without causing disturbance to daily work of HCWs. The most importantly HCW exposure can be remarkably, even down to 1:5-8, reduced in proximity work. Results also show that this can be made without causing thermal discomfort for a patient, which is a typical challenge for many local ventilation arrangements, such as LDV presented in earlier research.

8. Acknowledgement

The research has been partly funded by Business Finland.

9. References

[1] Ippolito M. et al. Medical masks and Respirators for the Protection of Healthcare Workers from SARS-CoV-2 and other viruses, Review. Pulmonology, Vol. 26, Issue 4, July–August 2020, Pages 204-212.

[2] Geiss O. Effect of Wearing Face Masks on the Carbon Dioxide Concentration in the Breathing Zone. Aerosol and Air Quality Research, Vol 21, Issue 2, 2020.

[3] McDonald J C, Chen Y, et al. Incidence by occupation and industry of acute work related respiratory diseases in the UK, 1992–2001. Occup Environ Med;62:836–842.

[4] Bagheria G, Thiedea B, et al. An upper bound on one-to-one exposure to infectious human respiratory particles, Dec 2021 ,PNAS 2021 Vol. 118 No. 49.

[5] HTM 03-01, Specialised ventilation for healthcare buildings June 2021, NHS, UK.

[6] CEN TC156 WG18, Hospital Ventilation, Working draft document, 2022.

[7] Kalliomäki P., Koskela H, Suojaava ilmanjako sairaaloiden erityistiloissa, Protective Airflow in Hospital isolation rooms (In Finnish), TuAMK Report 244, 66p. 2018.

[8] Kalliomäki P., Koskela H, et al, Assessing the risk to healthcare workers of hospital-acquired infection from patients infected with aerosol-transmissible pathogens, IOSH Research Report, 79p. 2020. https://iosh.com/reducing-hospital-infections

[9] Berlanga F, Olmedo I, Experimental assessment of different mixing air ventilation systems on ventilation performance and exposure to exhaled contaminants in hospital rooms. Energy & Buildings 177 (2018) 207–219.

[10] https://www.halton.com/technology/protective-airflow/

[11] Maula, H., Kalliomäki, P. and Koskela, H. (2021). Thermal comfort in a hospital isolation room – A laboratory study. Proceedings of Healthy Buildings 2021 Europe conference, 21-23 June 2021. Virtual conference.

Data sharing not applicable to this article as no datasets were generated or analysed during the current study.

Comparison of three residential ventilation systems in practical operation

Heinrich Huber, Alex Primas, Claudia Hauri

Institute of Building Technology and Energy, Lucerne University of Applied Sciences and Arts, Horw, Switzerland, heinrich.huber@hslu.ch, alex.primas@hslu.ch, claudia.hauri@hslu.ch.

Abstract. Three mechanical ventilation systems widely used in Swiss apartment buildings were investigated experimentally. The first system is the Central Bidirectional ventilation (CBi), where each dwelling is equipped with an AHU, supply air in bedrooms and extract air in wet rooms. In the second one, the Centralized Unidirectional ventilation (CUn), each dwelling is equipped with a unidirectional ventilation unit, extract air in wet rooms and outdoor air transfer devices in bedrooms. In third system bedrooms and living rooms are equipped with non-ducted Decentralized Ventilation Units (DVU), additional the wet rooms are served by independent extract air fans. The three ventilation systems were investigated in a total of 33 flats in 17 apartment buildings, with a total of 98 supply air rooms and 86 extract air rooms. Multiple products were represented in all systems. The cleanliness of the ventilation systems was assessed visually and the frequency of filter changes was queried.

With few exceptions, the hygienic condition was good to satisfactory. In 80% of the CBi systems and DVU's, filters were changed at least once a year. In the CUn systems, this was done only half as often. The air flows were measured in all rooms as found. Then the filters were changed and the ventilation components were cleaned. Finally, all airflows were measured again. The values in the as-found and clean condition were compared with the requirements of the Swiss standards. Overall, the CBi systems proved to work quite stable and robust. The supply air flow rate was 6% lower in the as-found conditionthan after cleaning. For the other two systems, significant reductions in supply air flow rates dueto clogged filters and devices were observed as well as significant imbalances. One conclusion is that CUn and DVU systems would require significantly more filter changes and cleaning to ensure the same reliable operation conditions as the CBi system. For the CBi, the specific electric power input was determined and compared with measurements in projects carried out 9 and 12 years earlier. The SPI was about one third lower than in the older projects, which was interpreted as product improvements.

Keywords. Residential ventilation. Bidirectional ventilation unit. Unidirectional ventilation unit. Non-ducted ventilation unit. Specific power input (SPI).
DOI: https://doi.org/10.34641/clima.2022.364

1. Introduction

In Swiss apartment houses with continuous running mechanical ventilation, three systems are widely spread:

Central Bidirectional Ventilation (CBi)
Each flat is equipped with a ducted bidirectional air handling unit (AHU) with heat recovery. Bedrooms were served with supply air. Extract air is removed from bathrooms, toilets and kitchens. No supply or extract air is required in the air transfer zone, even if it contains a living space.

Figure 1 shows a simplified scheme of the system.

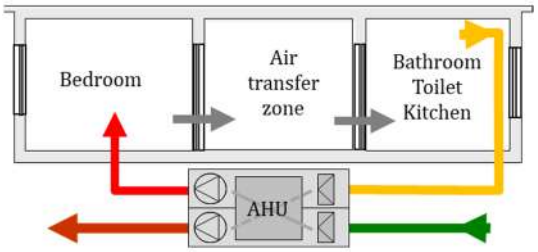

Fig. 1 – Scheme of the CBi system

Copyright ©2022 by the authors. This conference paper is published under a CC-BY-4.0 license.

Central Unidirectional Ventilation (CUn)
Only extract air is mechanically conveyed. For this each flat is equipped with a ducted unidirectional ventilation unit. Alternatively, a central extract air fan serves several or even all flats of an apartment house. Outdoor air is suck in the bedrooms through outdoor air transfer devices (OTD). Figure 2 shows a simplified scheme of the system.

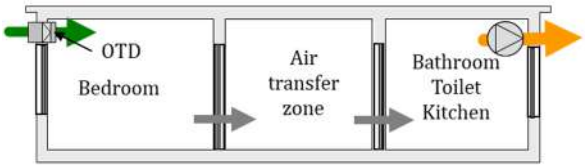

Fig. 2 – Scheme of the CUn system (OTD: outdoor air transfer device)

Decentralized Ventilation Units (DVU)
Bedrooms and living rooms are equipped with non-ducted bidirectional AHUs with heat recovery, the so-called Decentralized Ventilation Units (DVU). Typically, bathrooms and toilets are served by additional exhaust fans. Mostly each wet room has his own exhaust fan, which is switched on only during or after the use of the bath or toilet respectively. Less often a central extract air fan with continuous operation is used. Figure 3 shows a simplified scheme of the system.

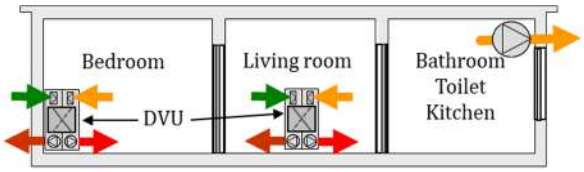

Fig. 3 – Scheme of the DVU system (DVU: non-ducted decentralised ventilation unit)

All three systems are dealt in the old Swiss standard for residential ventilation, the SIA 2023 [1] and the new standard SIA 382/5 [2]. A main area of application for the systems is residential buildings designed according to the Swiss Minergie energy label. Hints, recommendations and specific Minergie requirements for these systems are available in the brochure 'Gute Raumluft' [3] and the Minergie application guide [4]. All publications are available in German, French and Italian.

For owners, planners and operators of residential buildings it is relevant to know the strengths and weaknesses of ventilation systems in practical operation. On the one hand, this is a basis for system evaluation and, on the other hand, it helps to take the right preventive measures for optimal operation. Further, the authorities also have an interest in this information so that the requirements and funding measures can be targeted. Therefore, in 2017 the Conference of the Energy Offices of the Eastern Swiss Cantons launched a project for the investigation of systems CUn and DVU. In 2019 an analogue project for the CBi system was added. The final report of the first project has been published in 2019 [5] and for the second project in 2021 [6].

2. Research method

The aim of the projects was to compare the practical operation of the three ventilation systems on an equal basis. The dwellings for the investigation had been selected so that in each ventilation system products from different manufacturer are represented. Additionally in one housing estate maximum 3 flats were chosen. Finally the objects had to be located in different parts of the main Swiss settlement area, the Swiss Plateau. Table 1 shows selected data from the three ventilation systems.

Tab. 1 – Selected data of the investigated systems

Description	Number in the system		
	CBi	CUn	DVU
Flats	11	13	9
Housing estates	7	6	5
Products	4	4	2
Supply air rooms	29 [a]	26 [a]	[b]
Supply air transfer devices	40	42	16 [c]
Extract air transfer devices	44	31	19

a without rooms in transfer zone, like living rooms
b not recorded, only selected units were measured
c number of selected units

First, the air flow rates of all supply and exhaust air devices were measured in each flat as found. Secondly, the easily accessible parts of the ventilation systems were cleaned, and the filters replaced. At the same time, the hygienic condition was visually assessed. By questioning the caretakers or the residents, it was ascertained how often the filters are changed and when the last filter change took place. Finally, all air flow rates were measured in the clean condition. In both sates the measured air flow rates were compared with the requirements of the Swiss standards. The imbalance of the flat as-found and in the cleaned state was determined and the influence on the efficiency of the heat recovery was calculated.

In the project with the CBi systems, the specific power input (SPI) was evaluated and compared with projects carried out about 10 years earlier.

3. Results

3.1 Maintenance

In the CBi and DVU systems, about 80 % of the flats had a maintenance contract or the filters were changed by the caretaker once or twice a year. In the CUn system, filters were changed at least once a year in only about one-third of the outdoor air transfer devices (OTDs). For another third, this took place about every two years and for the rest every three or

more years. Overall, maintenance was less well organised for the CUn systems than for the other two.

After the filters, the outside air grilles were the most heavily soiled components in all ventilation systems. Overall, the soiling was only hygienically sensitive in 20% of the OTD and in one CBi system with a removed extract air filter. However, the clogging led to additional pressure losses, especially in the OTDs and DVUs, which in some cases massively reduced the air volume flows (for data see the following chapters).

3.2 Air flow rates of the CBi systems

Figure 4 shows the ratio of the measured supply air flow rates of the entire flat in the found and cleaned state, compared with the required minimum of the standard SIA 2023. Since all dwelling were built before 2021 this standard was relevant and not SIA 382/5. For commissioning, a tolerance of 10% for the total air flow rate (of the entire flat) is permissible. 9 out of 11 flats with the system CBi met the total supply air flow of the old Swiss standard both, in the found and the cleaned state. The new standard SIA 382/5 typically requires about 25% lower minimum values. It can be said for the total supply air flow rate, all flats comply with SIA 382/5.

Besides a minimum total air flow rate of the dwelling, SIA 2023 and SIA 382/5 require a minimum supply air flow rate of 30 m^3/h for each supply air room. For commissioning, for this value a tolerance of 15% is permissible. This means a measured supply air flow of 25.5 m^3/h meets the standards. Figure 6 shows for the CBi system the cumulative frequency of rooms with a supply air volume flow below a certain value. Graphs are shown for the found and the clean state.

In the found state 24% of the supply air rooms didn't fulfil the standards. In the clean state the number is 28%. Figure 6 shows that the air volume flow rates generally slightly increased as a result of cleaning. In one flat, which was found with the extract air filter removed, a readjustment of all air volume flows took place, which led to a reduction in 3 supply air rooms. The reason for too low air flow rates (below the lower tolerance) was in about half of the cases bad adjustment. The rest were intentionally undersized, despite the requirements of the standard.

3.3 Air flow rates of the CUn systems

Analogous to Figure 4, Figure 5 shows the ratio of the measured total air flow rates of the flats with the CUn systems in the found and cleaned condition, compared to the required minimum of the SIA 2023 standard.

In the found state only 5 out of 13 flats met the minimum total supply air flow rate of the old Swiss standard. Even in the clean state, only 6 out of 13 comply. With the new standard SIA 382/5 6 flats in the found state and 8 in the clean state would comply. Analogous to Figure 6, Figure 7 illustrates the cumulative frequency of the supply air flow rates in the rooms with the CUn system.

In the CUn system, two thirds of the supply air rooms were equipped with a single OTD. In none of these rooms did the supply air flow rate meet the minimum requirements of the standards. In the remaining supply air rooms, two OTDs were installed. As found, 33% of these rooms did not meet the lower tolerance limit of the standard. In the cleaned state, the value was 13%.

3.4 Air flow rates of the DVUs

For the DVU system the total air flow rate of a dwelling is not relevant, because each room is ventilated individual. Analogue to Figure 6, Figure 8 illustrates for the 16 measured DVUs the cumulative frequency of supply air flow rates in the rooms.

In the as-found condition, 69% of the DVUs did not meet the lower tolerance of the air flow rate of the standard. In the cleaned condition, 56% did not meet the requirements.

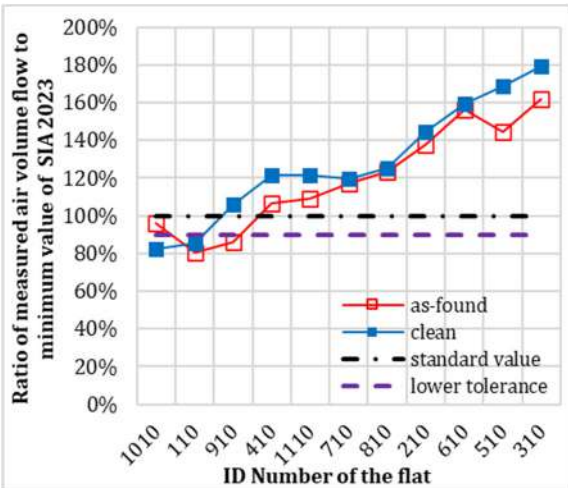

Fig. 4 – Ratio of the measured air flow rates of the flats with a CBi system compared to the requirements of the SIA 2023 standard.

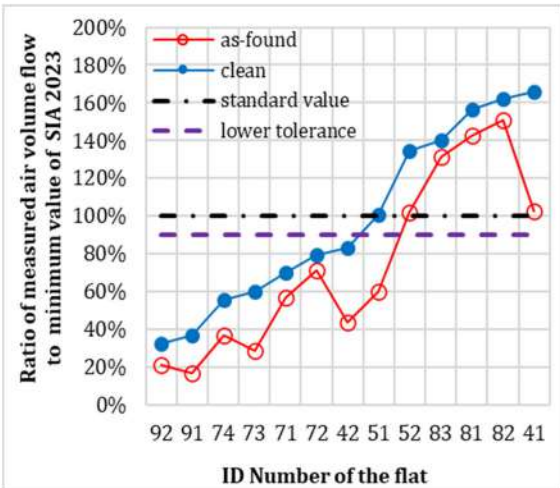

Fig. 5 – Ratio of the measured air flow rates of the flats with a CUn system compared to the requirements of the SIA 2023 standard.

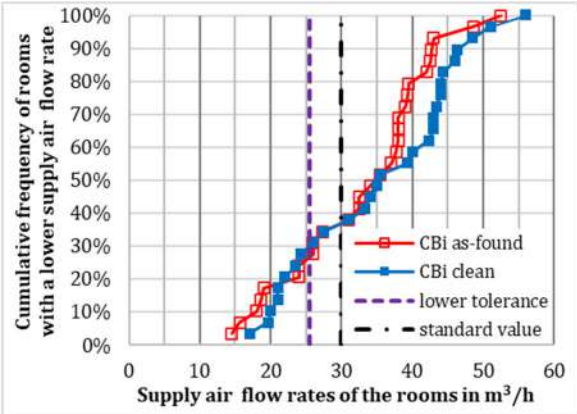

Fig. 6 – Cumulative frequency of supply air flow rates in rooms with the CBi system

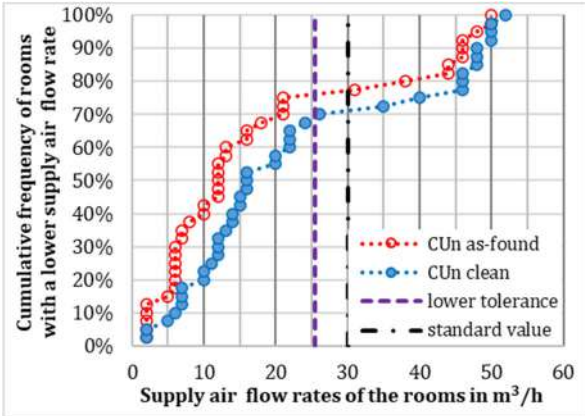

Fig. 7 – Cumulative frequency of supply air flow rates in rooms with the CUn system

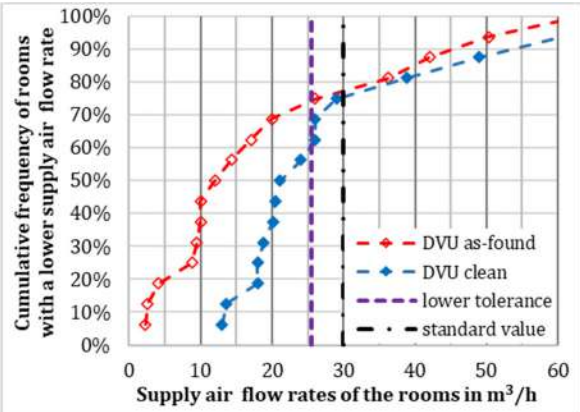

Fig. 8 – Cumulative frequency of supply air flow rates in rooms with DVUs

3.5 Comparison of air flow rates

Table 2 shows the comparison of the measured air flow rates of the three systems. The upper value is the mean value. The values below in brackets show the range between the minimum and maximum measured value.

Tab. 2 – Comparison of the measured air flow rates of the three ventilation systems

Description	CBi	CUn	DVU
Whole flat: Ratio of the measured air flow rate in clean state to the minimum value of SIA 2023	mean 129 % (82 … 179 %)	mean 80 % (27 … 167 %)	[a]
Supply air rooms only: air flow rate in clean state	mean 35 m³/h (17 … 56 m³/h)	mean 24 m³/h (2 … 52 m³/h)	mean 28 m³/h (9 … 64 m³/h)
Ratio of the air flow rates in supply air rooms in the found state to the clean state	mean 94 % (76 … 143 % [b])	mean 83 % (38 … 105 %)	mean 70 % (13 … 98 %)

a For DVU, only single rooms are assessed
b Highest value: The exhaust air filter was removed in the found state.

3.5 Imbalance

The imbalance is the difference between supply and extract air mass flow divided by the higher of the two values. This can be calculated according to Equation (1):

$$f_{imb} = \frac{q_{m,sup} - q_{m,ext}}{max(q_{m,sup}; q_{m,ext})} \quad (1)$$

where $q_{m,sup}$ is the supply air mass flow rate and $q_{m,ext}$ is the extract air mass flow rate.

Regardless of whether the value is positive or negative, any imbalance reduces the benefit of heat recovery. Furthermore, there is additional infiltration or exfiltration and thus higher ventilation heat losses.

Figure 9 shows the imbalance for the CBi systems in the found state and the clean state. In 9 of the 11 flats it was possible to take measurements for the calculation of the imbalance.

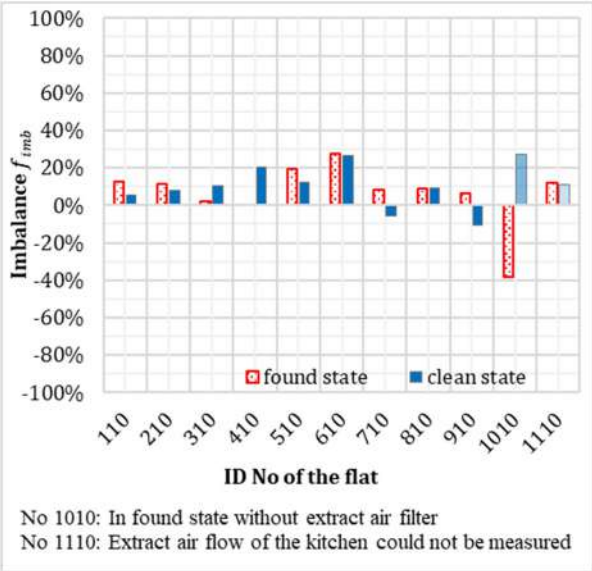

Fig. 9 – Imbalance in the flats with CBi system

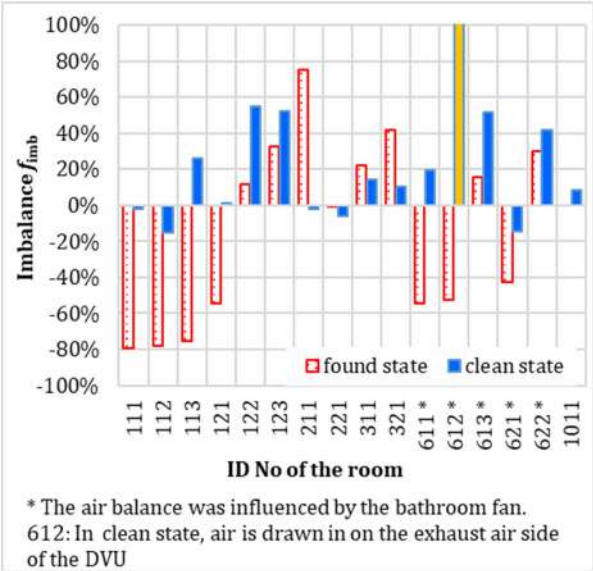

Fig. 10 – Imbalance in rooms with DVUs

In flat No 1110 the extract air transfer device in the kitchen was not accessible. In No 1010, the system was operated without extract air filter in the found state. In the clean state both filters (outside air and exhaust air) were used again. This flat therefore had a large negative imbalance (-38%) in the found state. After inserting the filters and cleaning there was a positive disbalance of 27%.

The mean value of the amount of the imbalance was 12% in both the found and the clean state. In 5 flats, the amount of the imbalance was below 10%, which can be described as a good value. In 2 other flats it was 10 to 20%. In the flats 410, 610 and 1010, an adjustment would be recommended due to the amount of imbalance of higher than 20%.

Figure 10 shows the imbalance for the DVUs in the found state and the clean state. In half of the cases the cleaning and filter replacement led to a clear reduction of the amount of imbalance. However, in five cases the value was higher after cleaning and filter replacement, then in the found state. In 3 cases (No 123, 613 und 622) an imbalance was part of the system design, for a reduction of the sound power level of the DVU. In No 611 to No 622 additional exhaust fans, which could not be switched off by the occupants, influenced the imbalance. In No 612 the exhaust fan of the bathroom caused such a strong negative pressure that after cleaning the outdoor air was sucked through the extract air side of the DVU into the flat.
It's to mention during the measurements for the determination of the imbalance neither strong wind nor high temperature differences was present.

For the evaluation of the impact of the imbalance to the energy efficiency of the heat recovery (HRC), the model shown in Figure 11 is used. Thereby, a room is equipped with a ventilation unit, which runs with imbalance. The difference between the extract air mass flow rate $q_{m,ext}$ and the supply air mass flow rate $q_{m,sup}$ is equal with the air mass flow rate of infiltration $q_{m,inf}$ or exfiltration. In the following, only the infiltration is shown. However, the result, the influence on the energy balance, is the same with infiltration or exfiltration.

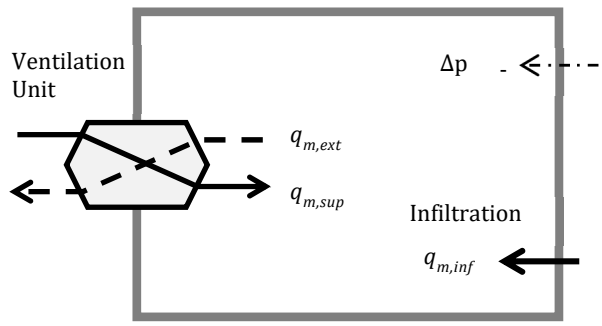

Fig. 11 – Scheme of the model for the influence of imbalance

As quality grade for the impact of the imbalance to the energy efficiency of the heat recovery (HRC) the definition 'system efficiency' is introduced. The system efficiency is the heat gain of the HRC, in relation to the heat losses of a fictional ventilation system without HRC and with an air mass flow rate, which is equal to air mass flow rate of the balanced ventilation unit. With this definition, the system efficiency can be expressed as in Equation (2):

$$\eta_{sys} = \eta_{HRC} \cdot (1 - |f_{imb}|) \qquad (2)$$

where η_{HRC} is the energy efficiency of the HRC with imbalance, and f_{imb} is the imbalance according to Equation (1).

The conversion of the energy efficiency of the HRC with a mass flow ratio of 1 to the energy efficiency with imbalance can be calculated with the NTU model e.g. as described in VDI Heat Atlas [7]. For commercially available ventilation units, the model for counterflow heat exchangers can be used with

good reliability. Figure 12 shows the system efficiency η_{sys} as function of the amount of the imbalance based on calculation according to the mentioned source [7]. The energy efficiency of the HRC with a mass flow ratio of 1 (symbol $\eta_{1:1}$) is the parameter.

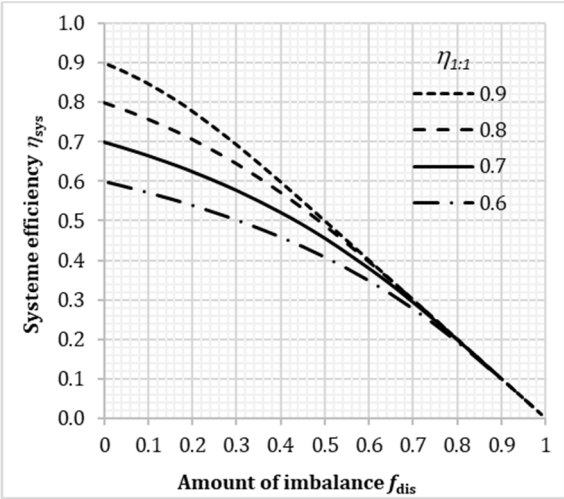

Fig. 12 – System efficiency η_{sys} as function of the imbalance f_{imb} , for different energy efficiencies of the HRC with a mass flow ratio of 1 ($\eta_{1:1}$)

With the DVU system, in addition to the imbalance in normal operation, there is a reduction in energy efficiency in mixed operation mode when the extract air fans in bathrooms and toilets are switched on and cause an additional increased imbalance. Furthermore, for both systems CBi and DVU the frost protection mode can reduce the energy efficiency. Table 3 shows the system efficiency of CBi and DVU systems including imbalance, mixed mode (only DVU) and frost protection. The later two reductions are estimated according to the project report about the practical operation of CUn and DVU systems [5]. The values for frost protection are based on average European climate. In Table 3 the reduction of the system efficiency due imbalance is calculated on base of the average measured imbalance in found state and clean state. Since for CBi systems the imbalance was the same on both states, there is only one column for this system.

3.6 Specific power input of CBi systems

Table 4 shows the comparison of the measured specific electrical power input (SPI) of CBi systems from the measurements of the current project [6] and of two older studies [8] and [9]. The SPI is defined as the electrical power input at design conditions divided by the air flow rate (average of supply and exhaust side). Although no statistically relevant statement is possible due to the small number of AHUs measured, the values can be considered representative for the period under investigation. In all measurement series, widespread AHU types of market leaders were well represented.

Tab. 3 – Estimation of the energy efficiency of CBi and DVU systems with consideration of imbalance and defrosting

Description	System and state		
	CBi [a]	DVU as-found	DVU clean
Average of the amount of the measured imbalances	0.12	0.42	0.21 [c]
Efficiency of heat recovery at mass flow ratio of 1($\eta_{1:1}$)	0.70 … 0.80	0.70 … 0.80	0.70 … 0.80
Reduction of energy efficiency by measured imbalance	0.04 … 0.05	0.17 … 0.24	0.08 … 0.10
Reduction of energy efficiency by additional imbalance caused by mixed mode with extract fans in bathrooms	[b]	approx. 0.05	approx. 0.05
Reduction of energy efficiency by defrosting function	0.00 … 0.03	0.00 … 0.03	0.00 … 0.03
Net annual energy efficiency	0.63 … 0.75	0.45 … 0.51	0.54 … 0.65

a Since for CBi the imbalance was the same on both states, there is only one column for this system
b The CBi system do not have additional fans in bathrooms
c without No 612

Tab. 4 – Comparison of the specific electrical power input (SPI) of CBi-systems from different studies

Reference	Period of investigation	Number of units in study	Specific electrical power input (SPI) in W/(m³/h)			
			state	average value	minimum value	maximum value
[8]	2007, 2008	6	n.a. [a]	0.59	0.30	1.03
[9]	2011	11	n.a. [a]	0.47	0.29	1.09
[6]	2019, 2020	6	as-found	0.39	0.26	0.51
			clean	0.35	0.22	0.44

a No details on state of filter and soiling of components recorded in this study

As a general rule, it can be stated that the SPI values have improved by about one third in the last 10 years.

The results in [6] show that in average a reduction of the SPI of 13% is reached by cleaning. This result includes an increase of the total airflow rate by 7% and a reduction of the electrical power input of 5%. Figure 13 compares the measured SPI with the product specification at the external reference pressure difference of 50 Pa, as it is required from the European ecodesign regulation [10]. Additionally the target value and the limit value of the Swiss standard SIA 382/1:2014 [11] are shown as bench mark.

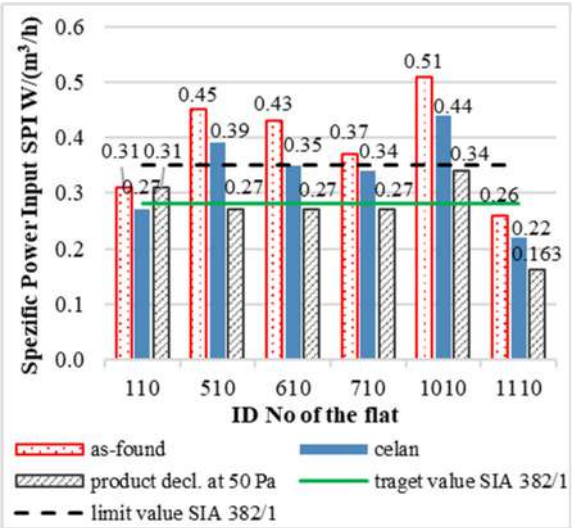

Fig. 13 – Specific electrical power input (SPI) of CBi systems measured in [6], as-found and in clean state. Comparison with target and limit values of SIA 382/1 and the product specifications at 50 Pa.

In [8] an important finding was that the internal pressure losses of the AHUs and the air duct network should be reduced to improve the SPI. The reduction of the SPI between the studies [8] and [6] of 41% for the average SPI in the cleaned state and of 57% for the maximum value suggests that such improvements took place in between. The difference between the average value to the minimum value of the SPI in the cleaned state (37%) and the encountered difference to the values stated by the product declaration at 50 Pa suggests that considerable improvements of the SPI are still possible.

4. Conclusion

With CBi systems, the air volume flow rates required by the Swiss standard were typically well achieved or exceeded in the supply air rooms and the entire flats. For the air volume flow rate of the flats, a tendency towards oversizing is observed, which mainly stems from the fact that supply air is blown in unnecessarily in living rooms that are located in the air transfer zone.

CUn systems did not achieve the air volume flow rates required by the standards in most cases. There is a tendency here to undersize. A major reason for this is probably that two OTD per room would typically be required for to meet the minimum value of the Swiss standard. However, for reasons of aesthetics, sound insulation, thermal comfort and possibly also costs, only one OTD is usually installed.

With DUVs, the required air flow rate in the rooms is slightly undercut on average. However, it should be noted that in 12 (with mainly newer designs) of the 16 units examined, on average only about half of the required supply air flow rate was available. The result that the mean value across all units is close to the standard value is due to the fact that the other 4 units (3 of which were old designs) delivered significantly higher air flow rates.

The ratio of the measured air flow rate in the found and in the clean state tells us how stable or robust the systems and ventilation units are in practical operation. Here the CBi systems obviously perform better than the other two systems. This can also be interpreted to mean that CUn systems (especially the OTDs) and DVUs should be maintained more frequently than CBi systems so that they have comparable stability.

Any imbalance reduces the energy benefit of the heat recovery and can lead to undesirable air flows in terms of building physics and hygiene. Here, too, the CBi systems perform significantly better than the other two. In particular, with the CBi systems the mean values, but also the extremes, are comparatively close to each other in the found and clean state, which again indicates a stable and robust operation. In the case of CUn systems and DVUs, it is astonishing to see the high imbalances that were determined in the found state, and how the imbalances increased due to the clogging.

5. Acknowledgment

The authors would like to thank the Conference of the Energy Offices of the Eastern Swiss Cantons for initiating the projects, the technical exchange, and the financial support.

6. References

[1] SIA 2023:2008 Lüftung in Wohnbauten. Schweizerischer Ingenieur und Architekten-verein, Zürich

[2] SIA 382/5:2021 Mechanische Lüftung in Wohn-gebäuden. Schweizerischer Ingenieur und Architektenverein, Zürich

[3] Gute Raumluft, Standardlüftungssysteme im Minergie-Wohnhaus. Minergie Schweiz, Basel, 2019

[4] Anwendungshilfe zu den Gebäudestandards

MINERGIE®/MINERGIE-P®/MINERGIE-A®, Version 2021.1. Minergie Schweiz, Basel

[5] Primas A., Huber H., Hauri C., Näf M. Abluftanlagen und Einzelraumlüftungen im Vollzug Energie. Hochschule Luzern, Horw, 2018

[6] Hauri C., Huber H., Primas A. Komfortlüftung im Vollzug Energie. Hochschule Luzern, Horw, 2021

[7] Roetzel W., Spang B. C1 Berechnung von Wärmeübertragern. In: VDI e. V. (eds) VDI-Wärmeatlas. VDI-Buch. Springer Vieweg, Berlin, Heidelberg. 2013

[8] Furter R., Casartelli E., Lang M. Reduktion des Elektrizitätsverbrauchs in Klein-Lüftungsanlagen. Hochschule Luzern, Horw, 2009

[9] Weber A. Qualitätskontrolle von Lüftungsanlagen in Minergie-Wohngebäuden. Beitrag am Energie-Praxis-Seminar 2/2011. Amstein + Walthert AG, Zürich, 2011

[10] Commission delegated regulation (EU) No 1254/2014 of 11 July 2014 supplementing Directive 2010/30/EU of the European Parliament and of the Council with regard to energy labelling of residential ventilation units

[11] SIA 382/1:2014 Lüftungs- und Klimaanlagen – Allgemeine Grundlagen und Anforderungen. Schweizerischer Ingenieur und Architektenverein, Zürich

The datasets analysed during the current study are available in [5] and [6]
https://www.endk.ch/de/dokumentation/studien

Office workers' health during the pandemic lockdown in the Netherlands

Marco Ortiz [a], Philomena Bluyssen [b]

[a] Chair Indoor Environment, Faculty of Architecture and the Built Environment, Delft University of Technology, the Netherlands, M.A.OrtizSanchez@tudelft.nl.

[b] Chair Indoor Environment, Faculty of Architecture and the Built Environment, Delft University of Technology, the Netherlands, P.M.Bluyssen@tudelft.nl.

Abstract. The worldwide spread of the Coronavirus disease 2019 forced governments to enact different measures to mitigate the infections. Employers and workers had to adjust by shifting a substantial number of jobs to a "work from home" configuration (WFH). On average, people used to spend around 90% of their time indoors, however, this number may have increased during the pandemic. This study aims to investigate the health status of office workers after nine months of a WFH format during the lockdown. A questionnaire was developed to assess the self-reported during the lockdown of office workers. A link to the questionnaire was sent to the employees of ten offices across the Netherlands, in November of 2020. A total of 502 employees responded to the questionnaire, which included diseases suffered during the last twelve months (i.e. asthma, wheezing, rhinitis, hay fever, anxiety, migraine, etc.). Data were analyzed by performing descriptive statistics of the general characteristics and the health status. The results show that during the lockdown and WFH, conditions such as eczema, depression and anxiety are higher than the average prevalence during non-lockdown situations. This may be due to lifestyle changes, such as reduced social interactions, increased distractions, and increased uncertainty.

Keywords. Health, working from home, lockdown, office workers, questionnaire.
DOI: https://doi.org/10.34641/clima.2022.428

1. Introduction

During the COVID-19 pandemic, the WHO advised governments to encourage employees who could to work from home. In the Netherlands, such measures started in March 2020. During non-lockdown situations, people used to spend around 90% of their time indoors, and 60% at home. These percentages may have increased drastically during the COVID pandemic, adding to the fact that people may stay only at home.

Although homes are meant to be healthy and comfortable indoor environments, they are not meant to be workplaces and should still maintain the occupants' wellbeing, even in lockdown situations. Therefore, even during a WFH or lockdown situations, a home should at least provide the right amount of social interaction, appropriate distraction, a healthy and comfortable indoor environmental quality, proper ergonomics, amongst many others. However, homes were not designed for this, which can lead to increased stress, lower productivity, and reduced mental and physical health. There is therefore a need to rethink the design of homes as hybrid living-working workspace and to encourage organizations to take actions to protect the health of their employees. Indeed, several factors such as specific occupants' particularities, environmental social, psychological, or physiological nature play a role in the health of people.

However, a majority of office workers are forced to reduce their social interactions with co-workers or other people, while also insecurities and stress may increase due to the situation itself. These factors seem to contribute to a detriment of the mental health of workers.

This study, therefore, aims at revealing whether certain health conditions were exacerbated during the lockdown in the Netherlands.

2. Methods

2.1 questionnaire

A total of ten companies agreed to distribute an online questionnaire to their employees (1). The companies included engineering firms, consultancies, and university faculties.

Copyright ©2022 by the authors. This conference paper is published under a CC-BY-4.0 license.

The online questionnaire was developed to assess seven characteristics of the respondents: demographics, lifestyle, IEQ preferences, psychosocial comfort preferences, IEQ comfort perception, control and satisfaction, and health, as seen in Table 1. The questionnaire was adapted from previously-validated questionnaires assessing similar constructs in other scenarios, such as homes, offices, and hospitals. The questionnaire was approved by the ethics committee of the TU Delft.

A first version was developed in English, which was then piloted, and adjusted based on the results of the test. The adjusted version was piloted again and then translated into Dutch. The Dutch version was also piloted, and the final version of the questionnaire was available to participants in the two languages.

To distribute the questionnaire, office workers first received an informative email from their company a week before the official distribution of the link. The participants were informed of the contents of the questionnaire, and that participation was voluntary, and that the data would remain anonymous and confidential and would only be used for the research.

The questionnaire was developed and distributed with the Qualtrics XM platform and employees were given two weeks to fill it out. A reminder was sent one week after the launch of the first invitation.

2.2 data analysis

After the closure of the questionnaire, the data was downloaded from the online platform and analyzed with IBM SPSS 27.

Because each organization had a single, designated anonymous link, each data for the individual organization was first downloaded. In order to make sure that the ten datasets could be pooled together, χ^2 and one-way ANOVA tests were conducted for categorical and numerical variables respectively, to ensure that no statistically significant differences existed between the companies. Once the tests were performed, and the results indicated that there were no differences, the datasets were merged.

To analyze the data of the employees, descriptive statistics were performed, including means, standard deviations, minimum and maximum values.

Tab. 1 – Questionnaire sections and subdivisions.

Section	Assessment
Demographics	Age, gender, education, mood
Lifestyle	Physical activity and consumption of alcohol or smoke
IEQ comfort preferences	Ventilation, temperature, lights, sounds, smells,
Psychosocial comfort preferences	Storage, hygiene, amenities, privacy, presence of others, size of the room
IEQ Comfort perception	Perception and rating of 19 items dealing with air quality, acoustical quality, thermal quality, and visual quality at the workspace
Control and satisfaction	Control of specific items in the workspace to adjust their comfort and satisfaction therewith
Health	Health status in the last year and symptoms in the workspace felt at least once in the last three weeks.

3. Results

3.1 general characteristics

A total of 1729 office workers received the invitation email with the link to the questionnaire, out of which 502 responded to it, representing a response rate of 29%. General characteristics are presented in Table 2.

About two-thirds of the respondents were male (63%), with a mean age of 42 years. In terms of lifestyle behaviors, around 36% of them reported to be smokers, 83% of them consume alcohol, and 85% of them report engaging in physical activity at least once during the week. In terms of the WFH situation, a total of 78% of respondents worked remotely as opposed to 22% who kept working in their office.

3.2 health status

In terms of health conditions, the least prevalent conditions were bronchitis (2%), diabetes and heart conditions (3%), respiratory problems (4%), and dermatitis (5%) (see Tab. 3.).

Conversely, the most prevalent conditions were hay fever (31%), rhinitis (28%), eczema (18%), and anxiety (17%). A total of 16% of the respondents reported having suffered from COVID-19.

Finally, conditions such as migraine, depression, and other psychiatric problems had prevalences of 13%; 10%, and 6% respectively.

Tab. 2 – Results of general characteristics.

Characteristics	Frequency (percentage)
gender	
Male	298 (63)
Female	166 (35)
Prefer not to answer	7 (2)
Age	
Mean (SD)	42 (12)
Min-max	20-68
Level of education	
Master, PHD, Specialization	224 (45)
University	154 (31)
Professional	57 (11)
Secondary School	31 (6)
Primary school	35 (7)
None	1 (0)
Smoking	178 (36)
Alcohol	416 (83)
Physical activity	396 (85)
Lockdown workspace	
Home	343 (78)
Office	94 (22)

Tab.3 - Health status.

Condition	Frequency (Percentage)
Asthma	22 (6)
Bronchitis	6 (2)
Wheezing of chest	22 (6)
Other respiratory problems	15 (4)
Hay fever	124 (31)
Rhinitis	113 (28)
Eczema	73 (18)
Dermatitis	18 (5)
Other skin conditions	47 12)
High lipids	33 (8)
Diabetes	11 (3)
High blood pressure	41 (10)
Other heart conditions	10 (3)
Migraine	54 (13)
Depression	41 (10)
Anxiety	68 (17)
Psychiatric problems	24 (6)
Other conditions	48 (12)
COVID-19	57 (16)

4. Discussion

Although the most prevalent conditions in this study were hay fever and rhinitis, they are actually within the average range for European countries and even lower than previously reported in the Netherlands.

Diseases that need to be paid attention to seem to be eczema, depression, and anxiety. In this study, 18% of the employees suffered from eczema. In a metanalysis review performed by Thyssen et al. (2010), it was reported that the average prevalence of eczema sufferers between 1964 and 2007 has steadily been 4% (2). In other professions, such as healthcare professionals, who need to sanitize their hands more often, in a Dutch study of 2013 it was reported that the prevalence was 12% while that of Dutch construction workers was 8%, a profession in which manual labor is high(3, 4). Indeed, several causes could be attributed to the high rate of eczema during the lockdown. The first reason can be due to the fact that people wash their hands more constantly and they use disinfecting gel more frequently than during non-COVID-19 times (5, 6). The second reason can be that lockdown and pandemic situations increase stress. When stress increases, the immune system can weaken, resulting in aggravation of skin diseases such as atopic dermatitis, including eczema (7-9).

17% of the people in this study claimed to have suffered from anxiety during the lockdown months. Some studies have suggested that the average rate for anxiety in the UK is 5% (10) while in the Netherlands, in a 2008 study, the rate was 6% (11).

In another study, it was found that anxiety, depression, and stress amongst university staff workers in Spain during at WFH formats was 21%, 34%, and 28% respectively (12). Which is comparable to the anxiety rate of this study but not to the depression rate of 10%. However, in previous studies conducted amongst hospital workers (13) and amongst office workers in the Netherlands (14) in pre-pandemic times, during non-WFH situations, the rates of depression were found to be 2% and 4% respectively, suggesting that depression may have also increased.

The increase in stress, depression, and anxiety due to a WFH format and the lockdown in general, may be due to several factors, such as less social interaction, decreased physical activity, work-life imbalance, imbalanced or changed rest and sleep patterns, poor working facilities (i.e. desks, chairs), poor ergonomics (15).

Another study proposed that the decreased mental health of people during the pandemic can be attributed to factors such as changes in nutrition, less communication with co-workers, increased distractions while WFH, presence of children, and indoor environmental quality (16).

5. Conclusion

The results of this questionnaire show that eczema, anxiety and depression have a higher prevalence than during non-lockdown or non-WFH situations. These increases may be due to increased stress and/or due to several factors that can range from distractions in the home office to reduce social interaction, sleep changes, or poorer nutrition. All of these situations can increase stress, which in its turn can exacerbate anxiety, depression, and eczema. In the case of eczema, besides increased stress, overzealous hand disinfection may also be a cause of its increase. The results show that employers and organizations need to take care of the mental health of their employees during WFH and lockdown situations and that the design of homes and the role of homes have to be rethought so that they can offer a healthy and comfortable hybrid working-living environment.

6. Acknowledgment

The authors would like to thank the following organizations and their employees for distributing and participating in this study: UNStudio, BBA-DGMR, Heijmans, Valstar-Simonis, Techniplan, ISSO, DGBC, IGG, ABE faculty TU Delft, and IDE faculty TU Delft.

7. References

[1] Ortiz M, Bluyssen P. Profiling office workers based on their self-reported preferences of indoor environmental quality and psychosocial comfort at their workplace during COVID-19. Building and Environment. *Under review.* 2022.

[2] Thyssen JP, Johansen JD, Linneberg A, Menné T. The epidemiology of hand eczema in the general population–prevalence and main findings. Contact dermatitis. 2010;62(2):75-87.

[3] van der Meer EW, Boot CR, van der Gulden JW, Jungbauer FH, Coenraads PJ, Anema JR. Hand eczema among healthcare professionals in the N etherlands: prevalence, absenteeism, and presenteeism. Contact dermatitis. 2013;69(3):164-71.

[4] Coenraads P, Nater J, Jansen H, Lantinga H. Prevalence of eczema and other dermatoses of the hands and forearms in construction workers in the Netherlands. Clinical and experimental dermatology. 1984;9(2):149-58.

[5] Patruno C, Fabbrocini G, Stingeni L, Napolitano M. The role of occupational dermatology in the COVID-19 outbreak. Contact dermatitis. 2020.

[6] Singh M, Pawar M, Bothra A, Choudhary N. Overzealous hand hygiene during the COVID 19 pandemic causing an increased incidence of hand eczema among general population. Journal of the American Academy of Dermatology. 2020;83(1):e37.

[7] Newaj R, editor Lockdown skin. The Specialist Forum; 2020: New Media.

[8] Böhm D, Stock Gissendanner S, Finkeldey F, John S, Werfel T, Diepgen T, et al. Severe occupational hand eczema, job stress and cumulative sickness absence. Occupational medicine. 2014;64(7):509-15.

[9] Garcovich S, Bersani F, Chiricozzi A, De Simone C. Mass quarantine measures in the time of COVID-19 pandemic: psychosocial implications for chronic skin conditions and a call for qualitative studies. Journal of the European Academy of Dermatology and Venereology. 2020.

[10] Smith LE, Amlot R, Lambert H, Oliver I, Robin C, Yardley L, et al. Factors associated with self-reported anxiety, depression, and general health during the UK lockdown; a cross-sectional survey. MedRxiv. 2020.

[11] Wit MA, Tuinebreijer WC, Dekker J, Beekman AJT, Gorissen WH, Schrier AC, et al. Depressive and anxiety disorders in different ethnic groups: a population based study among native Dutch, and Turkish, Moroccan and Surinamese migrants in Amsterdam. Social psychiatry and psychiatric epidemiology. 2008;43(11):905-12.

[12] Odriozola-González P, Planchuelo-Gómez Á, Irurtia MJ, de Luis-García R. Psychological effects of the COVID-19 outbreak and lockdown among students and workers of a Spanish university. Psychiatry research. 2020;290:113108.

[13] Eijkelenboom A, Kim DH, Bluyssen PM. First results of self-reported health and comfort of staff in outpatient areas of hospitals in the Netherlands. Building and Environment. 2020;177:106871.

[14] Kim DH, Bluyssen PM. Clustering of office workers from the OFFICAIR study in The Netherlands based on their self-reported health and comfort. Building and Environment. 2020;176:106860.

[15] Birimoglu Okuyan C, Begen MA. Working from home during the COVID-19 pandemic, its effects on health, and recommendations: The pandemic and beyond. Perspectives in Psychiatric Care.

[16] Xiao Y, Becerik-Gerber B, Lucas G, Roll SC. Impacts of working from home during COVID-19 pandemic on physical and mental well-being of office workstation users. Journal of Occupational and Environmental Medicine. 2021;63(3):181.

Data Statement

Due to the nature of this research, participants of this study did not agree for their data to be shared publicly, so supporting data is not available.

Kitchen ventilation system design and its effect on restaurant IAQ

Kamal Moumen [a], Nicolas Delporte [a]

[a] Halton Food Service, France, kamal.moumen@halton.com, nicolas.delporte@halton.com

Abstract. It is well established that exposure to high level of Particulate Matter (PM), especially smaller particles below 2,5 micron (PM2.5) has a negative impact on health. We also know that cooking is the major contributor to PM levels in dwellings (Jacobs et al, 2016). A recent field study in restaurants (Kulve et al, 2020) also showed elevated levels of PM exposure, exceeding those recommended by World Health Organization (WHO). It is obvious that ventilation systems do not meet the objective of providing good Indoor Air Quality (IAQ) in restaurants with high level of PM exposure. This presentation addresses ventilation system design and its effect on PM level in the commercial kitchen setting. The study was conducted in a ventilation laboratory setting using a charbroiler and gas fryers cooking hamburgers, and French fries. Two types of ventilation hoods were tested as well as two air distribution strategies: mixing and displacement ventilation. The study replicated elevated levels of PM2.5 concentrations with inadequate ventilation design and demonstrated that properly designed ventilation system can protect kitchen personnel from high PM exposure. The study also emphasized the importance of IAQ sensors in restaurants to guarantee adequate performance of ventilation systems.

Keywords. Indoor Air quality, Ventilation, Commercial Kitchen, PM2.5, Health, Thermal Comfort
DOI: https://doi.org/10.34641/clima.2022.74

1. Introduction

Indoor Environment Quality in commercial kitchens (IEQ) refers to the air quality within and around the working place of kitchen personnel. Commercial kitchen and cooking appliances are major contributors to pollutant releases in the indoor environment. Health effects from indoor air pollutants may be experienced soon after exposure or, possibly, years later (WHO).

It is well established that exposure to high level of Particulate Matter (PM), especially smaller particles below 2,5 micron (PM2.5) has a negative impact on health. It is known that cooking is the major contributor to PM levels in dwellings (Jacobs et al, 2016).

Recent field study in restaurants such as (M Loomans et al 2020) also showed elevated levels of PM exposure exceeding those recommended by World Health Organization (WHO). The study concluded that chefs in professional kitchens are exposed to PM2.5 concentrations well above the daily exposure limit of 25 µg/m^3 as defined by the WHO for the general public (average values ranging from 57-402 µg/m^3, with peaks >1 mg/m^3). The study showed also that cooking activities (such as baking) and the location of the chef (below or next to the hood) are important factors influencing the high values measured in the breathing zone

Known air quality issues related to cooking processes multiplied by the scale in professional kitchens lead to growing concerns about the employees and customers health.

The ventilation system plays a central role in the improvements of the IEQ.

The measurements are meant to evaluate the relative impact of the following parameters on the IEQ in professional kitchens: Exhaust airflow (with/without use of an air curtain system – see description in 2.1), the cooking type and appliance and the air supply method. This last parameter appears to be the least often considered, even if it has a considerable impact as will be shown later in this paper.

To compare the different scenarios, it has been decided that PM 2.5 quantities will be the variable to

Copyright ©2022 by the authors. This conference paper is published under a CC-BY-4.0 license.

be compared, as this is a well-known and often shared parameter. It's also common to use the PM2.5 in IEQ studies. Other measurements such us CO^2 and Volatile Organic Compounds (VOCs) have been measured and will be briefly discussed below.

2. Experimental set-up Description

2.1. *Cooking and Ventilation systems*

Extraction and supply

The Extraction hood used was a traditional hood used in the professional kitchen setting.

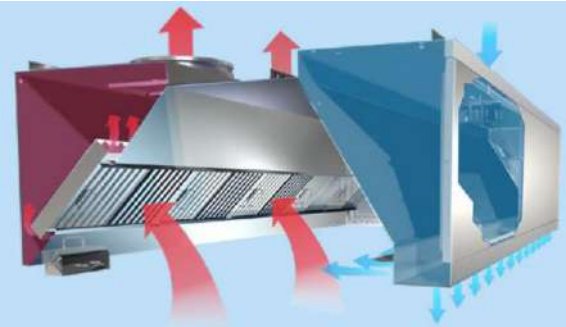

Fig. 1 - Schema of the extraction hood used for the tests

The hood was equipped with an air curtain system that consists of two sets of nozzles, one vertical and one horizontal. The horizontal nozzles push vapours back towards the filters. The vertical nozzles increase the containment volume and prevents vapours escaping from cooking areas. (See Fig.1 air curtain represented with blues arrows). The air curtain system could be enabled / disabled for the front and lateral sides of the hood, respectively and individually.

Two types of supply air systems were tested:

- One was provided by a wall mounted **air displacement unit.** This was done through two sets of grids of 2-OFF *H1900 x L520mm* with low velocity
- The other, using two **ceiling mixing units** that were mounted on the ceiling. they provided the same amount of airflow as the air displacement unit but with higher velocity through circular slots.

Fig 2 – Mixing and displacement units

Airflow Regimes

For each test, 3 airflow regimes were tested: **high, medium, and low**. The high corresponded to the Capture & Containment (**C&C) level** as measured in the laboratory according to the ASTM1704. The medium and low were both conducted at **75% of the C&C level, with (medium) and without (low) the air** curtain system, respectively.

Table 1 – Exhaust air flow regime $[m^3/h]$

Exhaust Regime	Broiler	Fryers
High	2000 + air curtain	1500 + air curtain
Medium	1500 + air curtain	1180 + air curtain
Low	1500 & no air curtain	1180 & no air curtain

Cooking Appliances

Two types of cooking appliances have been used: a gas charbroiler for burgers and 4 deep fryers for frozen French fries.

- **Broiler**: Charbroiler Vulcan (model 36) Griddle's installation at 900mm height

- **Fryers**: gas Electrolux L900xl800xH900

Fig. 3 - Cooking appliances - Fryers and Charbroiler

Cooking Procedure for Burgers

The tests started with a heating period. The griddles were turned on for approximately 30 minutes to reach 300°C. For each test, 5 series of 15 burgers each were cooked. The cooking of burgers was timed to be 3.5 minutes per face. A brushing and reheat to reach 300°C were done after each series.

Cooking procedure for French fries

Oil was pre-heated to 180°C. Each round was done using 2 baskets at the same time which represents around 1kg of French fries. Each batch of French fries were cooked for 10 minutes.

2.2. *Tests Layout*

All the measurements were done in an air-tight lab chamber of dimensions (l x w x h) 9m x 6m x 3.4m.

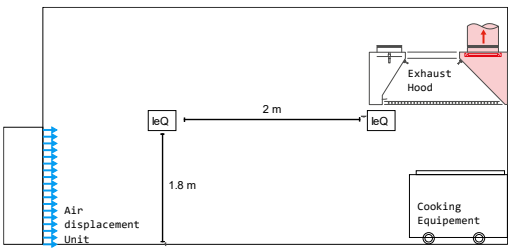

Fig. 4 - Ventilation, appliances, and sensors layout –

Displacement air units

IEQ sensors were installed in two positions:
1. **The breathing zone** of the chef under the hood,
2. **2m from the hood** at 1.80m from the floor.

PM 2.5 was measured using the following sensor: FS4408 (Transducer particulate matter / particles, active output (0-10V and 4-20mA)

Table 2 - PM sensor description

Measurement range PM2.5/PM10	0 µg/m^3 ... 1000 µg/m^3
Accuracy PM2.5/PM10	±5 ug/m^3 + max. ±4% FS (@ 20°C, 45% RH., 1013 mbar)
Temperature dependency	±1% FS / 10 K
Response time (t90)	< 10 s
Long term stability	±1% FS/year

3. Results

The results of the tests will be presented in the following order: Tests on the charbroiler and on the fryers with two different air supply modes (displacement and mixing).

PM2.5 levels will be shown under the hood and at 2m distance with 3 different airflow regimes: high, medium, and low.

The Low velocity displacement was installed on the opposite wall situated at 4.8 m from the front of the hood. Mixing air units were situated in the ceiling at 1.2 and 3.2 m from the front of the hood.

3.1. *The Charbroiler with Low Velocity Air Supply (displacement)*

It can be seen that, with C&C airflow level, the PM2.5 concentrations under the hood and in the room stay in average at 9 $\mu g/m^3$ and 4 $\mu g/m^3$ accordingly.

In case of Medium and Low airflow regimes (1500 m^3.h^{-1} with and without air curtain), the PM2.5 concentration are much higher. The tables below summarize the concentration levels.

Tab. 3 - PM2.5 in the breathing zone and in the room – Charbroiler - Displacement [µg/m^3]

	Breathing zone		**In the Room**	
Airflow	**Avg.**	**Max.**	**Avg.**	**Max.**
High	9	412	4	6
Medium	52	718	46	220
Low	118	289	280	636

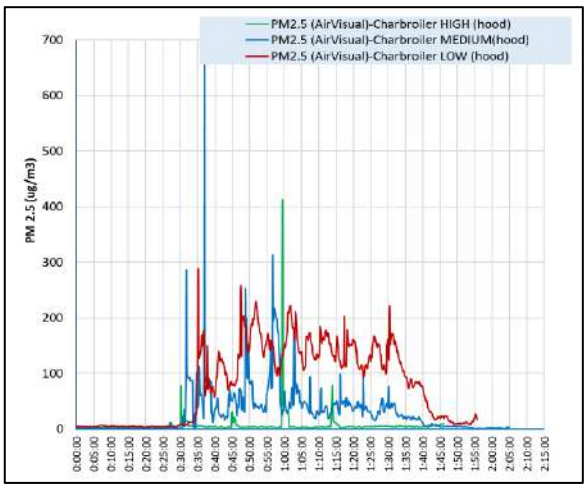

Fig. 5 - PM2.5 measurements **under the hood**, charbroiler with burgers with 3 air flow regimes and displacement air supply

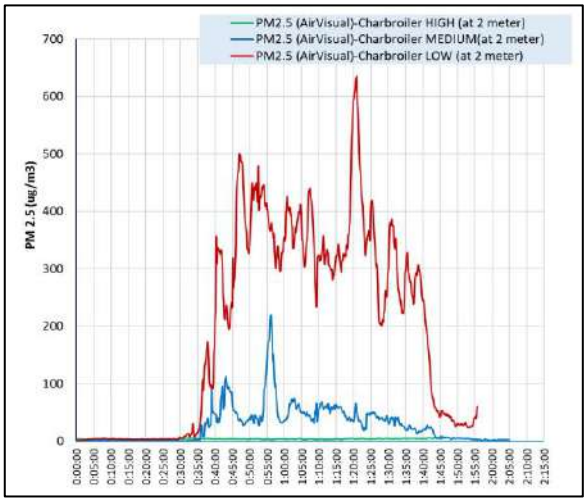

Fig. 6 - PM2.5 measurements at **2m from the hood**, charbroiler with burgers with 3 air flow regimes and displacement air supply

It can be seen that the concentrations in case of Medium and Low airflow regimes are higher than the WHO recommendation (25 $\mu g/m^3$). Levels in the absence of the air curtains were 6x higher in the room and 2x higher under the hood.

The measurements above shows that the air curtain helps to reduce the PM2.5 concentration levels in the room and therefore improve the IEQ in the kitchen (up to 6x times). This improvement is true in case of air supply with low velocity displacement in the room. Later in this paper it will be shown that this is not true for the case of mixing supply from the ceiling.

It was also seen that there were 4 PM2.5 peak events under the hood. That was due to the brushing and cleaning of the broiler. Indeed, after each round, the broiler was brushed with a metal comb to remove residue from the griddles.

3.2. *The Charbroiler with Mixing Air Supply (from the ceiling)*

The second round of test results were obtained following the same procedure as above but using a **mixing air supply from the ceiling.**

The method of supply air introduction was changed whilst all other parameters remained identical. The vertical air mixing supplies nearly the same airflow (90% of the supply) as the displacement method.

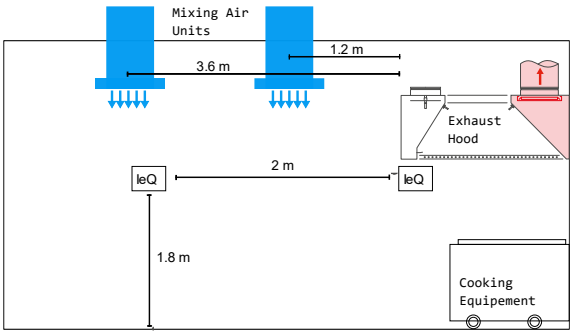

Figure 7 - Ventilation, appliances, and sensors layout – mixing air units

Firstly, it can be seen that there were higher concentrations during the mixing supply test compared to the displacement method test. During the "high" test regime, concentrations under the hood and in the room were on average 32 $\mu g/m^3$ and 17 $\mu g/m^3$, respectively.

Also, it can be seen that, in this case, there was no significant difference between the Medium and Low regimes. This shows that the air curtain doesn't have any impact on reduction of PM2.5 concentrations.

Tab. 4 - PM2.5 in the breathing zone and in the room – Charbroiler - mixing [µg/m^3]

	Breathing zone		In the Room	
Airflow	**Avg.**	**Max.**	**Avg.**	**Max.**
High	32	887	17	41
Medium	344	1001	254	782
High	397	1002	222	470

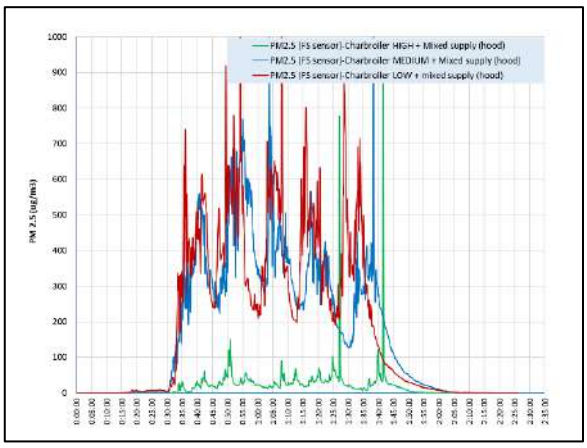

Fig. 8 - PM2.5 measurements under the hood, charbroiler with burgers with 3 air flow regimes and mixing air supply

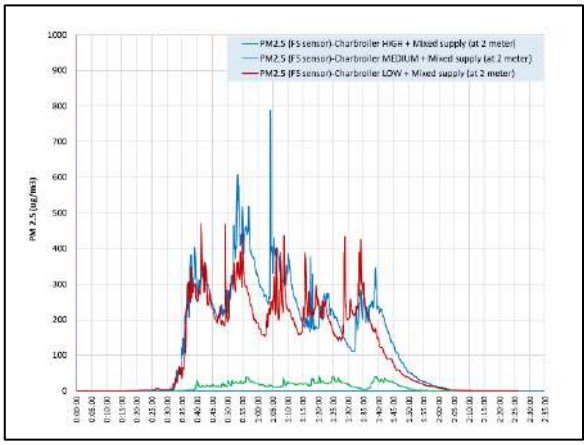

Fig. 9 - PM2.5 measurements at 2m from the hood, charbroiler with burgers with 3 air flow regimes and mixing air supply

3.3. *The Fryer with low velocity air supply (displacement)*

In this case, the max air flow was reduced to be at the appropriate C&C level: 1500 m^3/h.

Firstly, it can be seen that the concentrations were, on average, 10x lower than in the case of the broiler.

Tab. 5 - PM2.5 in the breathing zone and in the room – Fryers - Displacement [µg/m^3]

	Breathing zone		In the Room	
Airflow	**Avg.**	**Max.**	**Avg.**	**Max.**
High	0	1	0	1
Medium	1	3	1	4
Low	7.5	26	12	51

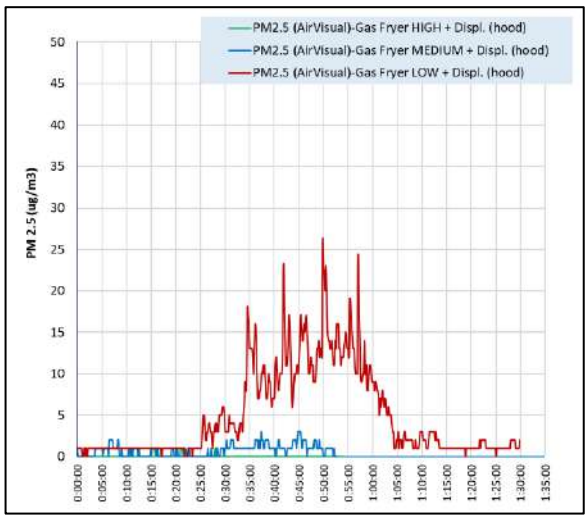

Fig. 10 - PM2.5 measurements under the hood, 2 fryer baskets with 3 air flow regimes and displacement air supply

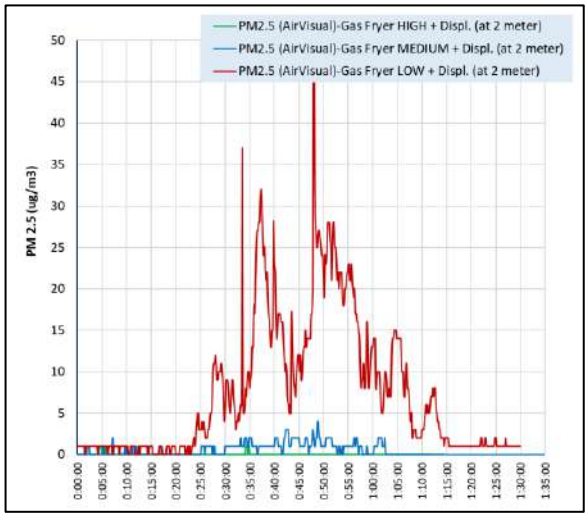

Fig. 11 - PM2.5 measurements 2m from the hood, 2 fryer baskets with 3 air flow regimes and displacement air supply

3.4. *The Fryer with Mixing Air Supply (from the ceiling)*

As per the charbroiler test, all variables apart from the method of supply air introduction remained constant between the different airflow regimes.

Tab. 6 - PM2.5 in the breathing zone and in the room – Fryers - Mixing [µg/m^3]

	Breathing zone		In the Room	
Airflow	**Avg.**	**Max.**	**Avg.**	**Max.**
High	0.2	0.3	0.2	0.4
Medium	1	2.5	1	2.5
Low	7.5	12	7.5	12

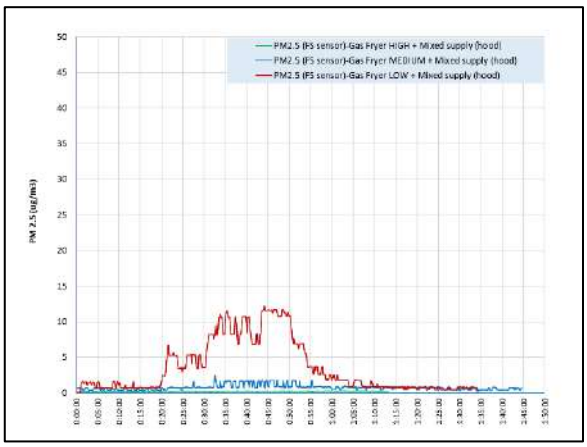

Fig. 12 - PM2.5 measurements under the hood, 2 fryer baskets with 3 air flow regimes and displacement air supply

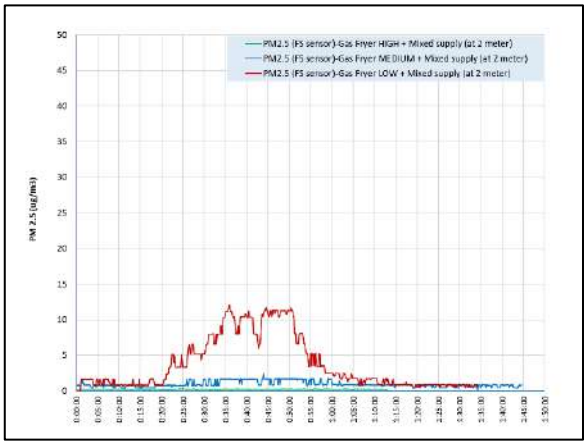

Fig. 13 - PM2.5 measurements 2m from the hood, 2 fryer baskets with 3 air flow regimes and displacement air supply

4. Discussion

4.1. Indoor Air Quality

the results above show that ventilation configuration (exhaust and supply) has a significant impact on the IEQ. The C&C level as determined by the ASTM1704 maximises the extraction efficiency of the hood. Although, frequently the C&C airflow cannot be adequately reached on live job sites. In this case, the IEQ could be heavily deteriorated.

In the case of broiler, we can see that the air curtain system helps improve the IEQ quality in case of air flow lower than C&C. this improvement could be 6x higher, but this could only be obtained by using the appropriate supply system. In our case, the displacement supply air method rather than the mixing air supply method. This could be explained by the turbulences created by the vertical supply. The air velocity in the supply slots is high and one of the supply slots is located close to the front end of the hood (1.2 m). The tables below sum up the results.

In the case of fryers, it was seen that there was no impact of the supply air system on the IEQ. This could be explained by the plume dynamic of the fryer

compared to the charbroiler. The fryer plume tends to follow the backwall due the Coandă effect. That means that the majority of the plume is situated toward the back of the hood; therefore, the wall curtain and supply air system have negligible impact on the plume dispersion.
On the other hand, the charbroiler tends to have a vertically ascending thermal plume and the total depth of the equipment is greater than that of the fryer. (900mm charbroiler depth vs 400mm fryer depth) Therefore, it is more susceptible to air dynamics in front of the hood, as the plume begins closer to the front lip of the hood.

4.2. *Thermal Comfort of the Chef*

Using these measurements, we can also explore the impact on thermal comfort of the chef. Indeed, the temperature at the breathing zone of the chef reached 40°C on average during the fryer tests. That means that even though the chef is protected by the natural rear plume dynamic of the fryers, it still can have a negative impact on the thermal comfort.

We compared temperatures and humidity at the breathing level of the chef with and without the curtain air system.

The following figures show the temperature (in blue) in Relative Humidity (in red) in the beathing zone of the chef. Fig 14. Gaz fryer at 75% of C&C with curtain air system and Fig 15. Is without the curtain air system.

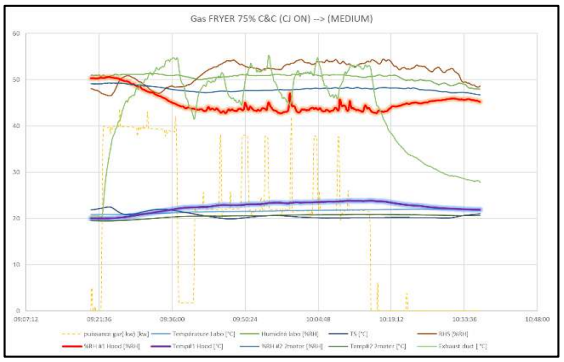

Fig. 14 - Temperature and humidity in the breathing zone with the air curtain system

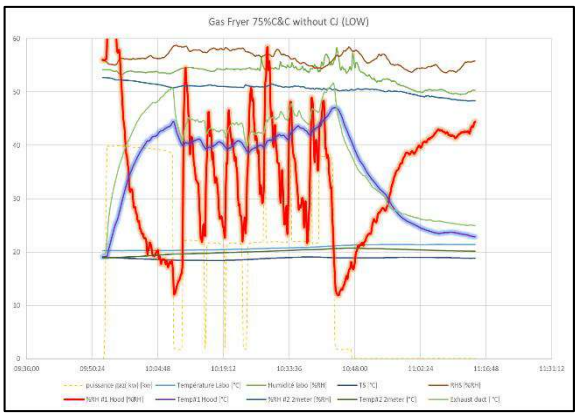

Fig. 15 - Temperature and humidity in the breathing zone without the air curtain system

It can be seen that in the absence of the air curtain system that the temperature is relatively high (average of more than 40°C). The relative humidity fluctuates between 20% and 50%. The fluctuations are correlated to frying series. The French fries are frozen before cooking and thus generate a significant amount of humidity.

When the air curtain is ON, temperature is, on average, equal to 21°C. The humidity is stable and, on average, equal to 45%RH. In this latter situation, the chef cooking is in a better thermal comfort environment.

5. Conclusions and next steps

The objective of this study was to study the impact of ventilation system design and its effect on PM level in commercial kitchens and therefore on the employees' health in these spaces.
3 main parameters have been studied: the cooking appliance type, the airflow settings, and the air supply method.
These three parameters have been found to have a substantial impact on the PM2.5 level in the kitchen and in the breathing zone of the chef.

<u>For cooking appliances:</u> cooking burgers on a broiler has been shown to generate a large effluent load compared to cooking fries with the fryer. At 75% of the C&C airflow without air curtain. The broilers generate up to 394 $\mu g/m^3$ compared to 8 $\mu g/m^3$ for fryers in the breathing zone of the chef.
These levels are 15 times higher than the WHO limit of 25 $\mu g/m^3$.

<u>For airflow settings:</u>
Three airflow regimes have been compared: C&C level, 75% of C&C both with and without air curtain system.
The C&C airflow ensures a good level of IEQ in the kitchen and in the breathing zone.
Degradation of the C&C to 75% deteriorates the IEQ: PM levels increase between 5-15x times dependant on the location, use of the air curtain system and the air supply method.

<u>For air supply method</u>:
Two methods were tested, mixing from ceiling and displacement from the wall. The former method increases the turbulences in front of the hood and reduces the extraction efficiency of the hood.
In the case of 75% of C&C airflow, the air curtain system plays a crucial rule in reducing the propagation of the PM (x6 times), when used with an air displacement unit. In the case of the mixing unit, the IEQ is degraded and the air curtain system has no impact on the reduction of the PM level.

In the case of the fryer, PM appears to be less of an issue because of the plume dynamic, tending to travel toward the back wall and is well captured by the hood. However, the use of the air curtain helps improve the thermal comfort of the chef by reducing temperature and the RH variations.

All of the above shows that the ventilation system is crucial in maintaining a healthy environment in the kitchen.

This study does not include the impact of human behaviour in the kitchen (i.e. hot food stored outside of hoods, doors kept open etc). We would expect that to have a significant impact on IEQ. More field studies will be needed to evaluate this parameter.

For the next studies in the lab, we'll be studying more appliances (Asian woks) and different types of hoods (proximity hood, canopy etc). That should help us to have a deeper understanding of the IEQ in commercial kitchens and how to improve it.

6. References

[Jacobs et al.] Jacobs P., Borsboom,W.A., Kemp R.E.J. PM2.5 in Dutch dwellings due to cooking. ASHRAE and AIVC Conference, 12-14 September 2016, Alexandria, VA, USA

[M Loomans et al. 2020] Loomans M,Te Kulve M, Atze Boerstra A. Particulate matter exposure of chefs in professional kitchens. International Society of Indoor Air Quality and Climate – ISLAQ - 2020

7. Appendices

Hood

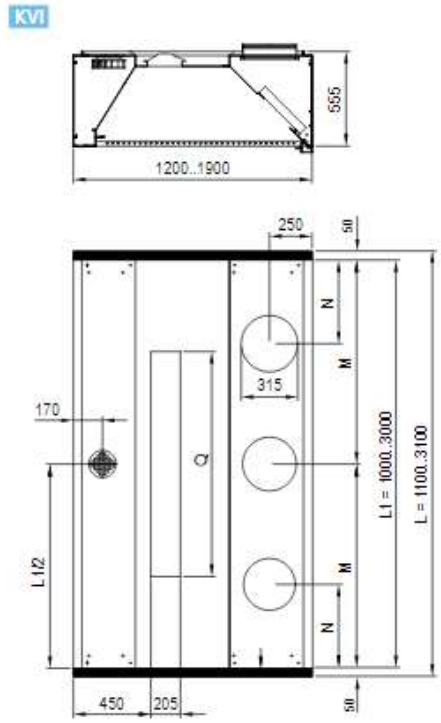

L	M	N
1600	L1/2	450

Mixing units dimensions

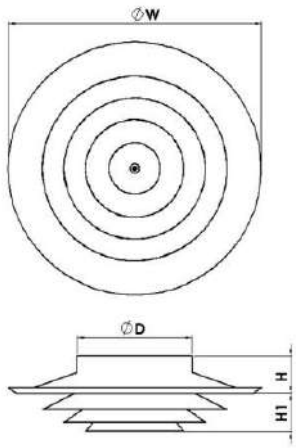

W 457 mm
H 80 – H1 75
D 199

Lab

The laboratory consists of 2 rooms, a test cell and a control command cell. The test cell is approximately 9m long by 6m large by 3.4m high. 2 doors allow installation of equipment and communication to the control command room. Once closed the test cell is airtight.

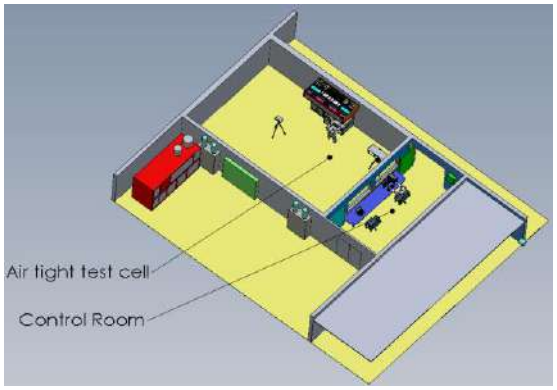

Exhaust (VFE) and Compensating Air Fans (VFS), with variable-speed drives, to allow for operation over a wide range of exhaust air flow rate from 200m3/h to 7000m3/h. Speed Inverters are controlled by the Datalogger in order to maintain a 0Pa or close to 0Pa pressure difference between outdoor and indoor. The ducting enables multiple configurations, from wall installation (this case) to island.

Air flow rate is measured by Laminar Flow Elements complying with ISO 5167 or equivalent, on ducting of exhaust and air supply.

Temperature and moisture content of exhaust and air supply are monitored, and air supply temperature is tempered by a Chilled or Heat Water system enabling to reach realistic and stable conditions inside the test cell.

Fig. 16 - lab layout – (with charbroiler)

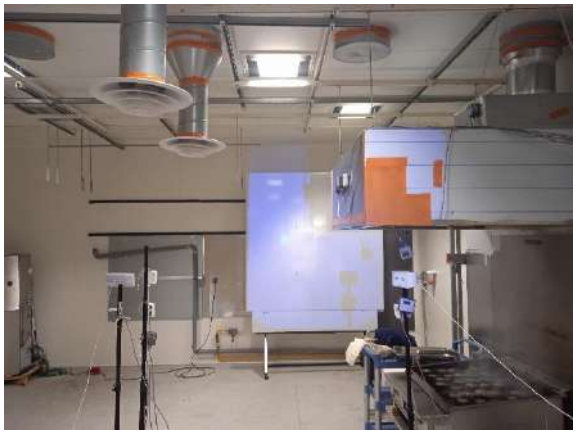

Fig. 17 - Burgers cooking

Fig. 18 - Stir-frying

Sensors

PM 2.5 FS4408 (Transducer particulate matter / particles, active output (0-10V and 4-20mA)

Measurement range PM2.5/PM10	0 µg/m^3 ... 1000 µg/m^3
Accuracy PM2.5/PM10	±5 ug/m^3 + max. ±4% FS (@ 20°C, 45% r.F., 1013 mbar)
Temperature dependency	±1% FS / 10 K
Response time (t90)	< 10 s
Long term stability	±1% FS/year

Self-reported health and comfort of outpatient workers in six hospitals

AnneMarie Eijkelenboom [a], *Philomena M. Bluyssen* [b]

[a] EGM architects, Dordrecht, annemarie.eijkelenboom@egm.nl

[b] Faculty of Architecture and the Built Environment, Delft University of Technology, Delft, the Netherlands, P.M. Bluyssen@tudelft.nl.

Abstract. As hospital workers are generally less satisfied with comfort than patients and limited information was available on health and comfort in outpatient areas, a PhD study was carried out on staff in outpatient areas. The study design, main conclusions and recommendations of this PhD study are discussed. To gain a more representative view of the occupants' perceptions, IEQ and social comfort were included. Social comfort was studied as a new construct, based on literature of privacy and crowding. A mixed methods approach was selected to justify the occupants' real-live experience of the physical environment. First, data were collected with building inspection of six hospitals and a questionnaire responded by 556 outpatient workers. Subsequently, a representative sample of them (17) was interviewed with photo elicitation. The survey was conducted before the COVID-19 pandemic, the interviews during the COVID-19 pandemic. Data were analysed with several techniques to describe comfort and health (descriptive statistics), determine associations of work and building-related aspects with comfort and health (regression analyses), to identify IEQ and social comfort profiles (Two-Step Cluster analysis) and to identify changes in preferences due to the COVID-19 pandemic (content analysis). The different analyses strengthened associations of contextual aspects, such as room types, with health and comfort. Also, the results indicate limited overlap of social comfort and IEQ. Therefore, it is recommended to include room types and social comfort aspects in future studies. Furthermore, as the results show differences in the occupants' preferences associated with differences in health (IEQ) and activities (social comfort) while their preferences can change in time, it is recommended to develop design strategies for an optimal fit beyond standardized solutions.

Keywords. comfort, hospitals, IEQ, COVID-19 pandemic, staff.
DOI: https://doi.org/10.34641/clima.2022.88

1. Introduction

Hospital workers spend most of their professional lives in hospitals, while patients stay relatively short in these buildings. Patients and their relatives are generally more satisfied with their comfort in hospitals than hospital workers [1-4], or occupants in office buildings [5]. For example, a study with 3811 hospital workers in Finland showed a higher percentage of occupants that was dissatisfied with the indoor air quality, noise, and glare than office workers [4]. Also, some building-related symptoms, such as irritated eyes or a dry skin, occurred more frequently among the hospital workers. While the pressure on hospital workers keeps growing [6], indoor environmental stressors, such as the presence of daylight, reverberation of noises, illumination, mould, and pollution from traffic, are related to work strain, health, and job satisfaction [7-11].

The characteristics of work in hospital departments, such as operating areas, inpatient, and outpatient areas, can vary largely. Due to differences in activities, needs for hygiene, and occupation hours, the perception of comfort may vary between hospital departments. Therefore, it is important to study hospital departments separately. Limited information was available on outpatient areas [3]. Taking these considerations into account, a PhD study was carried out on health and comfort of hospital workers in outpatient areas.

Within this study, comfort is approached as a multifactorial construct, including IEQ aspects (thermal, indoor air, acoustic, and visual) and social comfort aspects (privacy, interaction, crowding). The reason to include social comfort was because of the importance of both physical and social characteristics that can influence comfort. IEQ aspects as well as privacy and crowding can affect negative stress

Copyright ©2022 by the authors. This conference paper is published under a CC-BY-4.0 license.

reactions and dissatisfaction [12,13]. Also, personal aspects, such as age, sex, work strain, and diseases, may affect the perceptions of IEQ and building-related symptoms [14]. Building on previous studies that emphasized social and contextual aspects of comfort [15,16], the comfort perceptions and preferences of the occupants, as well as personal, work and building-related aspects, were included in this study to capture a broad view that justifies for the complexity of comfort perceptions and preferences of hospital workers.

To identify and explain relations of comfort and health of outpatient workers with personal, work, and building-related aspects, the following question was formulated: How are comfort and health in hospitals associated with personal, work, and building-related aspects? To answer this question, it was decomposed into four sub-questions: 1. How are the comfort and health of workers in outpatient areas of hospitals associated with work-related characteristics? 2. How do outpatient workers differ in their preferences and comfort perceptions? 3. How are dry eyes and headaches (the most prevalent building-related symptoms) associated with building-related aspects? 4. Which contextual aspects influence the preferences for comfort of outpatient workers?

To answer these questions a field study was conducted in two phases. The first phase was in the spring of 2019, before the COVID-19 pandemic, and the second phase in the autumn of 2020, during the COVID-19 pandemic. Contextual changes due to the pandemic were included in this study.

The main findings are presented and discussed in this paper.

2. Methods

2.1 study design

A mixed methods study was carried out to gain broad and in-depth insights into the occupants' perceptions and experiences. First, data were collected in a survey comprising a digital questionnaire for the outpatient workers, and a building inventory of the location, layout, building services, cleaning protocols and inspection of 127 rooms. The questionnaire comprised validated questions, based on OFFICAIR [17], a translated set of questions [12], and new questions. To test the new and translated questions, the questionnaire was piloted in a general hospital that did not participate in the final field study. The final questionnaire included questions on personal and work-related aspects, health, perceptions, and preferences for IEQ and social comfort.

Subsequently, the questions and sample for the follow-up phase were determined to build upon the results that needed more explanation. Therefore, data were collected with semi-structured interviews and photos. The interview guide comprised five main topics: work-related aspects, changes due to the COVID-19 pandemic, preferences for IEQ, preferences for social comfort, ranking of preferences. The interviews were tested with outpatient workers from hospitals that did not participate in the main study.

Before the interviews, the participants received instructions to take photos in their most frequently used rooms of IEQ and social comfort aspects that were important for them. They sent the photos before the interviews, digitally with e-mail, or prints by post. The interviews were conducted by telephone or videocalls, as the researcher could not visit the hospitals during the pandemic. All interviews were audio-taped with Microsoft Teams.

2.2 selection of the population and buildings

Only outpatient areas and workers were studied, because their comfort and health may vary from those in other hospital areas because of differences in duration of stay, activities, or building characteristics.

The hospitals varied in characteristics of the HVAC systems (e.g., type of heaters, type of heat recovery, replacement frequency of AHU filters, height of indoor air intake), individual control of the indoor environment, dimensions of building wings, possible outdoor pollutants, building year, cleaning protocol. Also, some building-related aspects varied within buildings, due to renovation period, room type or adjacency of the room to the façade.

2.3 ethical approval

Participation was voluntary. The participants could only participate after their approval of informed consent. The data were stored on a secured server. The study design was approved by the Ethics Committee of Delft University of Technology.

2.4 data analysis

Data from the questionnaire were imported from the Qualtrics XM platform to IBM SPSS Statistics 25. Data from building inspection were manually put into IBM SPSS Statistics 25. Building-related aspects were assigned to the respondents when the inspected variables were consistent. Consistency was identified with crosstabs of building-related aspects on different scale levels, such as organization, location, building-wing, room type, presence of a facade window, etc. The interviews were transcribed verbatim. Meaningful text fragments were manually put into Microsoft 365 Excel.

To answer the first sub-question descriptive statistics and logistic regression were used to identify differences in the perceptions of health and comfort between those in different room types (reception, consultation room, office, treatment room). The calculations were adjusted for personal aspects. Two-

Step Cluster analysis was used to identify profiles of outpatient workers, who differ in preferences and perceptions of comfort (sub-question 2). One set of six IEQ profiles and one set of three social comfort profiles were produced. To determine associations of headaches and dry eyes with building-related aspects, according to the third sub-question, multivariate logistic regression was used. Confounding variables were included. To answer the fourth sub-question, i.e., identification of changes in comfort due to the COVID-19 pandemic, inductive content analysis was carried out according to the steps defined by Gioia (2013) [18].

Detailed information on the study design and analysis can be found in [19-22].

3. Results and discussion

Three hospital organizations participated with two locations each. 556 outpatient workers responded to the questionnaire. Personal aspects, such as age or sex, did not vary between those working at the six locations.

3.1 IEQ and social comfort

Figure 1 shows (dis)satisfaction of the six IEQ aspects which the outpatient workers found most important. They selected three aspects from a list of 15. The figure represents the outpatient workers from the survey before the pandemic. The preferences of those who were dissatisfied vary from one of five (control of temperature) to one of two (sufficient daylight). The preferences of those who were satisfied vary from one of nine (no annoyance by noise) to one of two (control of temperature).

Figure 2 shows the (dis)satisfaction with the four most important social comfort preferences of the outpatient workers, that were selected from a list of 12 social comfort aspects. The preferences of those who were dissatisfied varied from four of ten (distraction by noise) to six of ten (contact with colleagues and patients and privacy of patients). The preferences of those who were satisfied varied from one of five (distraction by noise) to seven of ten (contact with colleagues and patients).

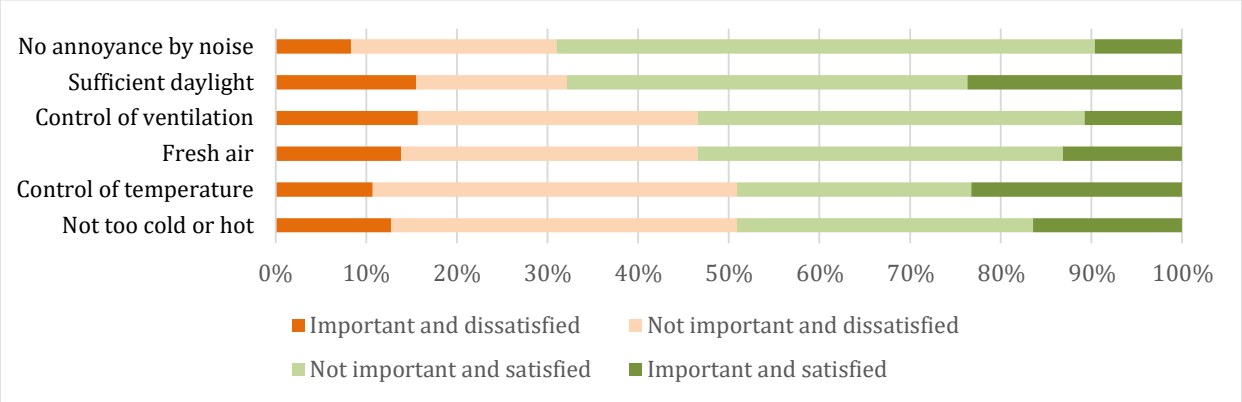

Fig. 1 – Importance and satisfaction of IEQ-aspects before the COVID-19 pandemic.

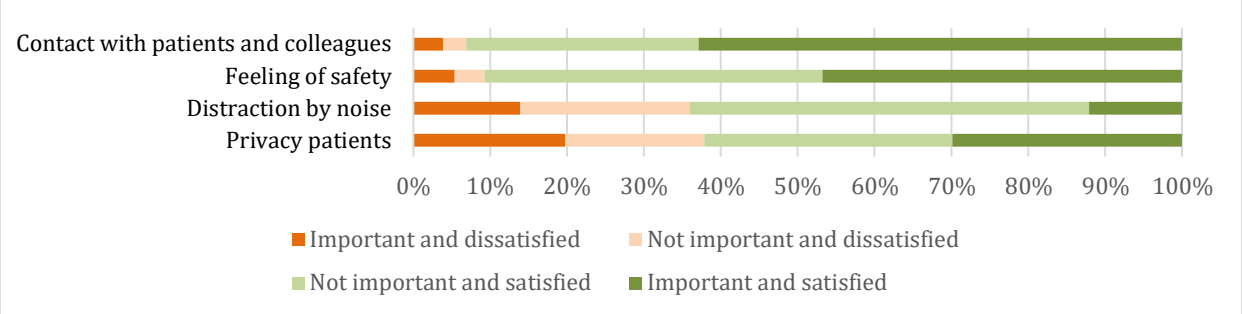

Fig. 2 – Importance and satisfaction of social comfort aspects before the COVID-19 pandemic.

The outpatient workers were more satisfied with social comfort aspects (Figure 1) than with IEQ-aspects before the pandemic (Figure 2). However, while only 7% of the outpatient workers was dissatisfied with contact with patients and colleagues, limited face-to-face contact with patients and colleagues was one of the main complaints during the pandemic [22]. The outpatient workers explained that interaction was important because it contributed highly to their work satisfaction and quality of care.

Satisfaction with IEQ was less likely to vary between those working in different room types than satisfaction with social comfort [19]. For example, only those who worked most frequently in consultation rooms were less likely to perceive dry

indoor air than those in treatment rooms or offices. While those in offices were more likely to be dissatisfied with privacy than those in consultation rooms and those in receptions more than those in offices, consultation, and treatment rooms.

To gain insights into differences in health, personal, work and building-related aspects between those with different preferences and satisfaction, six clusters for IEQ and three clusters for social comfort were found [20]. Both preferences and satisfaction were included, because there was no inter-collinearity between preferences and satisfaction. The preferences were stronger determinants for the profiles than satisfaction. The six main IEQ preferences (Fig. 1) and satisfaction with ten IEQ aspects, which were reduced with Principal Component Analysis (PCA), were included in the determination of IEQ clusters. The IEQ profiles, produced from comparisons between the IEQ clusters, were differentiated by the prevalence of building-related symptoms and sick leave. To determine the social comfort clusters the four main social comfort preferences (Fig. 2) and satisfaction with 11 social comfort aspects, also reduced with PCA, were included. The social comfort profiles were associated with activities. Both sets of profiles were associated with some personal, work, and building-related aspects. While over seventy comfort, personal, work or building-related aspects varied between the IEQ profiles or the social comfort profiles, only five aspects varied both between both the IEQ and social comfort profiles. These aspects were the preference for no annoyance by noise, dissatisfaction with natural light, room type, number of persons in the room, and the presence of a façade window.

Explanation of the profiles during the COVID-19 pandemic resulted in the finding that the main preferences can change and that the reason why IEQ and some social comfort aspects were important varied between the clusters [22]. While a comfort aspect, such as fresh indoor air, was for some related to dissatisfaction, others preferred it because of hedonic experiences, such as joy and feeling energized.

Tab. 1 – Associations of building-related aspects with profiles and building-related symptoms

Building-related aspect	Category	IEQ profiles	Social comfort profiles	Dry eyes	Headaches
Size outpatient area	<15.000m2 vs > 15.000m2		X		
Building year	1980-1999				
	2000-2009	X			
	2010-2018	X			
Façade window	Yes vs. no	X	X	X[a]	Y[a]
				X[b]	Y[b]
Corridor window	Yes vs. no	NA		X	Y
Control of heating	Manual vs. automatic	X			
Control of window view	Yes vs. no		X		
Direction of lighting	Direct vs. indirect + direct		X		
Cleaning protocol floors	Daily vs. weekly		X		
Cleaning protocol ventilation grills	Monthly vs. less frequent			Y	
Rotating heat exchanger	Yes vs. no			X	
Number of persons in the room[c]	1		X		
	(1 vs.) 2-4	X		X	Y
	1 (1 vs.) >4	X		X	Y
Room type[d]	Office		X		
	(Office vs.) reception	X			
	(Office vs.) consultation		X	X	X
	(Office vs.) treatment			Y	Y
Duration of stay	<4 hours vs. > 4 hours	X			

P-value of the clusters from Chi Square with Bonferroni correction
P-value of dry eyes and headaches from multivariate logistic regression
X=significant association (P-value<0.05)
Y= weak association (P-value<0.200)
NA= not applicable
[a] = façade window + corridor window
[b] = only façade window
[c] = changed during COVID-pandemic
[d] = varied also in satisfaction with IEQ and social comfort from univariate regression analysis including confounding variables

3.2 associations with building-related aspects

Table 1 shows associations of building-related aspects with the profiles and most prevalent building-related symptoms (dry eyes and headaches). The associations of the profiles were calculated with univariate analyses. The associations with dry eyes and headaches with multivariate analysis. The building-related aspects are part of the layout, HVAC systems, maintenance, and occupancy. Three building-related aspects are associated with both the profiles and building-related symptoms.

The absence of a façade window was a risk factor for dry eyes and headaches [21] and varied between the profiles [20]. Also, the number of persons in the room was a risk factor for dry eyes, a weak risk factor for headaches and differentiated between the profiles. During the COVID-19 pandemic the number of persons in the rooms were reduced [22]. Room types were associated with the profiles, building-related symptoms and satisfaction.

3.3 limitations

The sample size of this study was sufficient for multivariate regression analyses and Two-Step cluster analysis. The events per variable (EPV) were calculated to check the sample size for the regression analysis. Peduzzi et al. (1996) [23] recommended an EPV of at least 10. The EPV in the current study varied between 11 and 20. Dolniçar et al. (2014) [24] recommended at least 40 participants per included variable for cluster analysis. The IEQ clusters included 58 participants per variable, the social comfort cluster 108 per variable. Nevertheless, for the determination of associations of building-related aspects per cluster, a larger sample size is required.

Validation of the profiles was complex due to the COVID-19 pandemic. The outpatient workers experienced differences in comfort due to the contextual changes. These changes might have influenced the explanation of the preferences and the clusters. However, the study design in two phases enabled to gain insights into changes of comfort due to the unforeseen pandemic.

3.4 recommendations for research

It is complex to improve comfort of individuals with different preferences, also because most outpatient workers do not have a fixed room and they work generally in rooms with other occupants. Therefore, they need to negotiate frequently with others or adapt (to) the conditions of a room. As the participants used different strategies, such as manual control, use of other rooms, compensation during breaks, it is important to further study the conditions which affect adaptation strategies of the outpatient workers.

The study built on existing sets of questions and checklists while new variables, such as room types, were included. As the differences in satisfaction, preferences, and health between room types imply that comfort and health can be influenced by different situations, inclusion of room types in further studies might be considered. The set of questions for social comfort was based on previous literature. A validated set of questions was not available. More studies of social comfort with focus groups can contribute to further validate the set of questions. The questions can be included in studies of other hospital areas to improve the understanding of comfort.

As preferences during the COVID-19 pandemic changed, it is important to gain insights into the stability of preferences. In their study on changeability of preferences Hoeffler and Ariely (1999) [25] suggested that the stability can be influenced by the strength of an experience. Further study of the conditions which contribute to the formation of stable preferences and whether these vary between occupants, could contribute to further explanation of preferences, in order to improve comfort.

3.5 recommendations for practice

The profiles show that "one size does not fit all." Design strategies could be developed for design of an optimal fit with the specific function of rooms or areas, while the occupants' perceptions within a room or area can vary and change. To increase insights into differences between occupants and raise awareness during design processes the profiles are visualized into two foldable paper cubes. One cube for IEQ (figure 3) and one for social comfort (figure 4).
The cubes show the differences between the profiles of preferences, perceptions, personal, work, and building-related aspects from the survey in the spring of 2019. Each profile has its own colour. The size of a rectangle represents the proportion of outpatient workers for an aspect. For example, in IEQ cluster 1 the preference for control of ventilation is a square,

because all outpatient workers in cluster 1 found it important. On the top of the cubes are the numbers of the clusters. The lines help to navigate between satisfaction, preferences, personal, work, and building-related aspects.

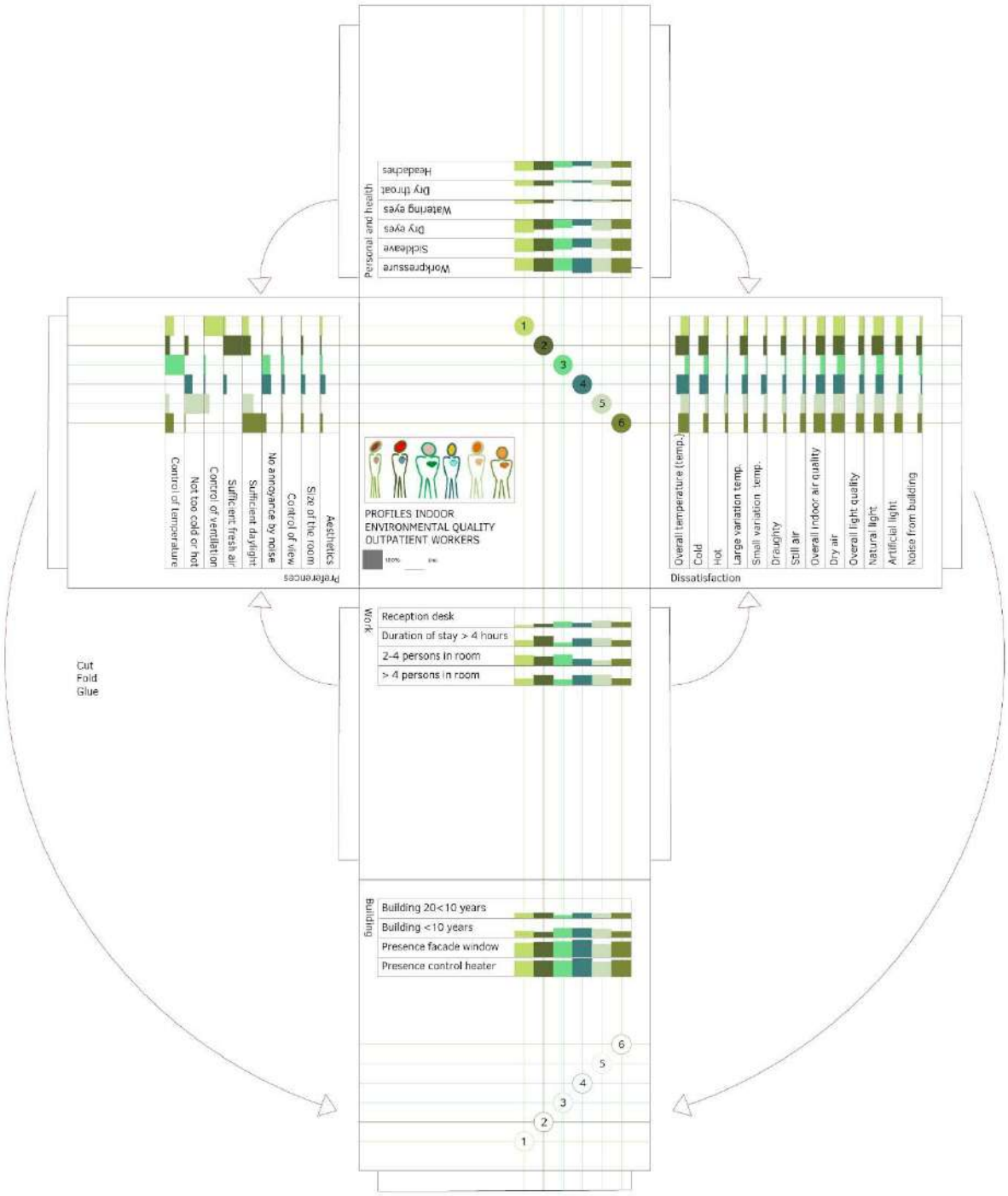

Fig. 3 – Cube of the IEQ profiles

The cubes show the differences between the profiles of preferences, perceptions, personal, work, and building-related aspects from the survey in the spring of 2019. Each profile has its own colour. The size of a rectangle represents the proportion of outpatient workers for an aspect. For example, in IEQ cluster 1 the preference for control of ventilation is a square, because all outpatient workers in cluster 1 found it important. On the top of the cubes are the numbers of the clusters. The lines help to navigate between satisfaction, preferences, personal, work, and building-related aspects.

4. Conclusion

This study shows relations of preferences and satisfaction of IEQ and social comfort of outpatient workers in hospitals with other aspects. Preferences for comfort can change due to contextual changes. The profiles suggest that those with different preferences can vary in health (IEQ) and activities (social comfort). As IEQ and social comfort have limited overlap, it might be useful to study both simultaneously in further studies. The broad type of building-related aspects that are associated with comfort and health show the importance of integrated design processes, including design of HVAC-systems, layout, façade and building maintenance.

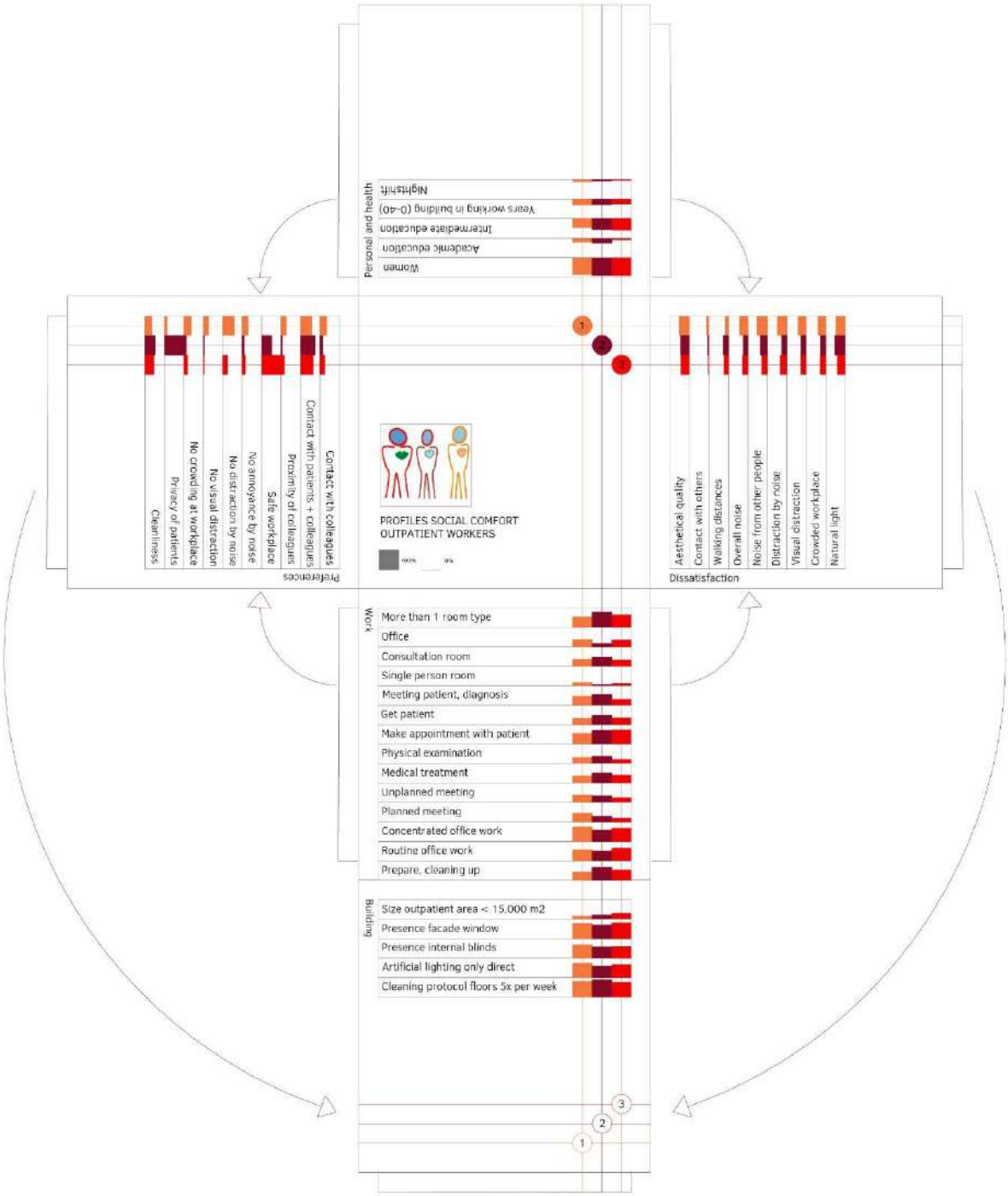

Fig. 4 – Cube of the social comfort profiles

5. Acknowledgement

This PhD study was supported by Daikin Netherlands and EGM architects and conducted at the Faculty of Architecture and the Built Environment at the Chair of Indoor Environment.

Data availability statement

The dataset is not publicely available because of personal information of the participants. The authors can be contacted for information.

6. References

[1] De Giuli V., Zecchin R., Salmaso L., Corain L., De Carli M., Measured and perceived indoor environmental quality: Padua Hospital case study. Build Environ. 2013; 59:211-226.

[2] Hashiguchi, N., Hirakawa M., Tochihara Y., Kaji Y., and Karaki C., Thermal environment and subjective responses of patients and staff in a hospital during winter. J Physiol Anthropol Appl Human. 2005; 24:111-115.

[3] Eijkelenboom, A., Bluyssen, P.M., Comfort and health of patients and staff, related to the physical environment of different departments in hospitals: a literature review. Intell. 2019.

[4] Eijkelenboom, A., Blok, G.A., Bluyssen, P.M., Comfort and satisfaction of patients, visitors and staff with patient rooms at inpatient wards, a pilot study, in CLIMA 2019. 2019, E3S Web Conf.: Bucharest, Romania [5]Hellgren U.-M., Reijula K., Indoor-air-related complaints and symptoms among hospital workers. SJWEH Supplements. 2006; 2(2): 47-49.

[6] Barker R., The future of medicine, avoiding a medical meltdown. Oxford University Press. 2011.

[7] Blomkvist V., Eriksen C.A., Theorell T., Ulrich R., Rasmanis G., Acoustics and psychosocial environment in intensieve coronary care. J. Occup. Environ Med. 2004;62: 8

[8] Alimoglu M.K., Donmez I, Daylight exposure and the other predictors of burnout among nurses in a University Hospital. Int. J. Nurs. Stud. 2005;42: 549-555.

[9] Hellgren U.M., Hyvärinen M., Holopainen R., Reijula K., Perceived indoor air quality, air-related symptoms and ventilation in Finnish hospitals. Int. J. Occup. Med. Environ. Health. 2011;24(1):48-56.

[10] Smedbold, H.T., Ahlen C., Unimed S., Nilsen A.M., Norbäck D., Hilt B., Relationships between Indoor Environments and Nasal Inflammation in Nursing Personnel. Arch. Environ. Health. 2002;57(2):155-161

[11] Zadeh, R.S., Shepley, M.M., Williams, G., Chung, S.S.E. The impact of windows and daylight on acute-care nurses' physiological, psychological, and behavioral health. HERD. 2014;7(4): p. 35-61.[12] Fisher J.D., Situation-specific variables as determinants of perceived environmental aesthetic quality and perceived crowdedness. J Res Pers. 1974;8(2):177-88.

[13] Bluyssen P.M.,Towards an integrated analysis of the indoor environmental factors and its effects on occupants. Intell. Build. Int. 2020;12(3):199-207

[14] Ghaffarianhoseini A., AlWaer H., Omrany H., Ghaffarianhoseini A., Alalouch C., Clements-Croome D., Tookey J., Sick building syndrome: are we doing enough? Archit. Sci. Rev. 2018;61(3):99-121.

[15] Chappells H., Shove E., Debating the future of comfort: environmental sustainability, energy consumption and the indoor environment, BRI. 2005; 33(10):32-40.

[16] Shin J., Toward a theory of environmental satisfaction and human comfort: A process-oriented and contextually sensitive theoretical framework. J. Environ. Psychol. 2016; 45:11-21.

[17] Bluyssen P.M., Roda C., Mandin C., Fossati S., Carrer P., de Kluizenaar Y., et al., Self-reported health and comfort in 'modern' office buildings: first results from the European OFFICAIR study. Indoor Air. 2016; 26:298-317.

[18] Gioia D.A., Corley K.G., Hamilton A.L., Seeking Qualitative Rigor in Inductive Research: Notes on the Gioia Methodology. Organ. Res. Methods. 2013;16(1):15-31.

[19] Eijkelenboom, A., Kim, D.H., Bluyssen, P.M. First results of self-reported health and comfort of staff in outpatient areas of hospitals in the Netherlands. Build and Environ. 2020; 177: p. 106871.

[20] Eijkelenboom, A., Bluyssen, P.M., Profiling outpatient staff based on their self-reported comfort and preferences of indoor environmental quality and social comfort in six hospitals. Build Environ. 2020; p. 107220.

[21] Eijkelenboom, A., Ortiz-Sanchez, M., Bluyssen, P.M., Building characteristics associated with self-reported dry eyes and headaches of outpatient workers in hospital buildings. Indoor Built Environ, 2021; p. 1420326X211023125 [22] Eijkelenboom, A., M.A. Ortiz, and P.M. Bluyssen, Preferences for indoor environmental and social comfort of outpatient staff during the COVID-19 pandemic, an explanatory study. International J Environ Public Health. 2021; 18(14): p. 7353

[23] Peduzzi P., Concato J., Kemper E., Holford T.R., Feinstein A.R., A simulation study of the number of events per variable in logistic regression analysis: J. Clin. Epidemiol. 1996; 49(12): 1373-1379.

[24] Dolnicar S., Grün B., Leisch F., Schmidt K., Required Sample Sizes for Data-Driven Market Segmentation Analyses in Tourism: J. Travel Res. 2014;53(3):296-306.

[25] Hoeffler S., Ariely D., Constructing Stable Preferences: A Look Into Dimensions of Experience and Their Impact on Preference Stability. J. Consum. Psychol, 1999; 8(2):13-139.

Experimental analysis of the ventilation rate in an amphitheater operating under the COVID-19 pandemic constraints

Luisa Dias Pereira [a], José Joaquim da Costa [b], Manuel Carlos Gameiro da Silva [c]

[a] ADAI, Department of Mechanical Engineering, University of Coimbra, Coimbra, Portugal, luisa.pereira@uc.pt.

[b] ADAI, Department of Mechanical Engineering, University of Coimbra, Coimbra, Portugal, jose.costa@dem.uc.pt.

[c] ADAI, Department of Mechanical Engineering, University of Coimbra, Coimbra, Portugal, manuel.gameiro@dem.uc.pt.

Abstract. In the context of the Covid-19 pandemic (officially declared by the WHO on March 11th, 2020), indoor air quality (IAQ) has resurged as a renewed paradigm, demanding enhanced attention, especially in spaces with high occupancy density, as is the case of school buildings. To minimize the risk of contamination indoors, it is needed to assure low concentrations of the biological pollutant load eventually resulting from the exhalation of the microorganism SARS-COV-2, through the dilution capacity of the ventilation systems. One way of checking the risk reduction is through the spatially comprehensive assessment of the air exchange rate (AER) in the indoor space. The present study was motivated by a request from the Faculty of Sciences and Technology of the University of Coimbra (FCTUC) in Portugal, whose spaces have been used under restrictive conditions derived from the recommendations on the operation of buildings during the pandemic. Two onsite experiments were carried out in an Amphitheater with only the exhaust component on, due to technical issues with the HVAC system in that period. The tests comprised measurements in ten different locations for representative monitoring of the occupied zone of the space. The estimation of the AER in the amphitheater in both tests was based on the analysis of the time evolution of the tracer gas (CO_2) concentration measured by each sensor/equipment. The results showed that the analyzed space presented an adequate rate of air renewal to ensure an effective dilution of indoor pollutants, and likewise of the biological pollutant load possibly resulting from the exhalation of microorganisms by an infected occupant.

Keywords. Ventilation rate, Fresh air flow rate, built environment, multisensory, Tracer Gas Method, COVID-19.
DOI: https://doi.org/10.34641/clima.2022.81

1. Introduction

In the context of the recent pandemic, Covid-19 (officially declared by the WHO on March 11th, 2020), indoor air quality (IAQ) has resurged as a renewed paradigm, demanding specific attention.

To minimize the risk of contamination indoors, it is needed to assure low concentrations of the biological pollutant load eventually resulting from the exhalation of the microorganism SARS-COV-2, through the dilution and exhaust capacity of the ventilation system. To assess the risk contamination reduction, the spatial broad value determination of the air exchange rate (AER) of an indoor space is one possibility.

In fact, Covid-19 has stressed the reprioritization of indoor air quality (IAQ) [1]. Concerning IAQ, the need to inspect HVAC systems before spaces return to their "normal" occupancy has been strongly advocated [2], starting from the early positioning of ASHRAE relating to SARS-COV-2 microorganism air transmission, in April 2020: "Transmission of SARS-CoV-2 through the air is sufficiently likely that airborne exposure to the virus should be controlled" [3].

The present study was motivated by a request from the Faculty of Sciences and Technology of the University of Coimbra (FCTUC) in Portugal, whose classrooms and amphitheaters have been used under restrictive conditions derived from the recommendations on the operation of buildings during the Covid-19 pandemic [4], namely reduced occupancy and all possible measures for ventilation enhancement. The methodology adopted is multiuse

Copyright ©2022 by the authors. This conference paper is published under a CC-BY-4.0 license.

and replicable to many other case studies such as concert halls, cinema rooms, or meetings rooms, for example.

To assess the current ventilation performance of the Amphitheater C.1 of the building of the Department of Physics of FCTUC, an experimental assessment of the air exchange rate (AER) was carried out. The amphitheater's fresh airflow rate (Q) was determined using the tracer gas method (TGM), in its concentration decay variant, as it is the best-suited one for a quick analysis. Besides the COVID-19 inherent restrictions – occupancy reduced to about one third, this amphitheater has presently a further limitation: its central heating, ventilation and air conditioning (HVAC) system cannot be fully operated because the air supply ducts are thermally insulated from the inside and the insulation material (rock wool) is degraded. Therefore, during the current academic activities, only the exhaust network of the HVAC system is active and the access doors (at the top level of this space) are kept frankly open. As stated in [5], "the prevention of indoor pollution is essential, especially considering the purpose of disease transmission resistance". The Amphitheater's current operation condition – just the extraction system is on – works also as a precaution manner against COVID-19 since no use of air recirculation is done [6], assuring one very important aspect: occupants' health [7].

In November 2020, two onsite experiments were carried out with the exhaust system on and: a) only the upper, main access doors open (at ground level); b) with all doors of the amphitheater open (i.e., two additional doors at the lower level). It should be remarked that this amphitheater is accessed through a big hall and a long corridor on the ground floor of the building, whose main entrance is kept open during the working day periods. As such, the ventilation air (infiltrated through the access doors) is not strictly outdoor fresh air; it is rather air transferred from the inner spaces of the building.

The tests comprised measurements in ten different locations for representative monitoring of the occupied space. The estimation of the AER in the amphitheater in both tests was based on the analysis of the time evolution of the tracer gas (CO_2) concentration measured by each sensor/equipment.

2. CO_2 concentration measurement in the indoor air

2.1 Method and object of study

The Amphitheater under study is located in the building of the Department of Physics of the University of Coimbra (b. 1969-75), in Portugal. Following the purpose of this study, the Amphitheater's fresh air flow rate (Q) was determined using the Tracer Gas Method (TGM), in its variant based on the concentration decay, as it is the one that best suited the aimed objective. This method consists essentially of the supply and homogenization of tracer gas in the compartment object of study and in the subsequent analysis of the time evolution (decay) of its concentration, by the action of the ventilation system operating in a steady-state regime.

Considering that this gas must be colorless, odorless, and tasteless, with a density close to that of air, and non-toxic, carbon dioxide (CO_2) was used as a tracer gas, since it is easily available and the respective monitoring sensors are nowadays affordable to be simultaneously used in multiple measuring locations. This gas is inherently present and associated with the human occupancy of indoor spaces (metabolic CO_2), but it can also be proposedly emitted through some equipment such as fire extinguishers (where the extinguishing agent is carbon dioxide, a liquefied gas stored under high pressure). The latter was the option in this study, since the amphitheater was not, nor had just been, occupied – only the authors were present. As such, after vigorous CO_2 spraying and a 5-minute homogenization period, using a movable long-range fan, the ventilation system (exhaust only) was turned on and the time evolutions of the CO_2 concentration measured at ten different locations were recorded for further analysis, aiming at the estimation of the AER λ [h^{-1}] in the amphitheater, in both tests.

Deriving from a steady-state mass balance, the time evolution of a pollutant concentration inside a uni-zone indoor space, during a period in which the emission rate of that pollutant and the fresh air flow rate remain constant, after a step variation of any of these parameters that can affect the concentration value, can be modeled by the exponential equation (1):

$$C(t) = C_{equi} + (C_0 - C_{equi}) \times e^{-\lambda t} \qquad (1)$$

where:
- $C(t)$ is the pollutant concentration at the instant t, [ppm] or [mg/m^3];
- C_{equi} is the asymptotic value of the concentration reached at equilibrium ($t \to \infty$);
- C_0 is the initial concentration value (t = 0), [ppm] or [mg/m^3];
- λ is the infiltration rate / AER in the compartment, [h^{-1}] or [n. º of air changes per hour].

Equation (1) can be written as follows:

$$C(t) - C_{equi} = (C_0 - C_{equi}) \times e^{-\lambda t} \qquad (2)$$

which suggests fitting to the experimental data an exponential function, in the form:

$$y = k \times e^{-\lambda x} \qquad (3)$$

To perform this type of adjustment (*e.g.*, using MS Excel), it is necessary to create the column of instantaneous values of y, corresponding to the difference $C(t)-C_{equi}$ (excess concentration), where $C(t)$ represents the measured values. In the case of

the CO_2 concentration decay in an indoor space, after the emission suppression from internal sources, the value of the equilibrium concentration C_{equi} usually corresponds to the CO_2 concentration of the ambient outdoor air (approximately 400 ppm, in a low-polluted area). To obtain the air exchange rate λ (number of air changes per hour, h^{-1}), the values of the independent variable (time instants t) must be expressed in hours, taking $t = 0$ as the instant corresponding to the initial concentration C_0.

As an example, **Fig. 1** shows the time evolution of the concentration values $C(t)$ measured with one of the sensors during one of the decay tests, and of the corresponding excess concentration, $C(t)-C_{equi}$, considering C_{equi} = 500 ppm [1]. The exponential regression fitted to the values of $C(t)-C_{equi}$ (dashed line) allows one to conclude that λ = 4.53 h^{-1}, *i.e.*, the ventilation rate would be 4.53 air changes per hour. The 1549 ppm value corresponds to the "fitted" estimate of the excess concentration C_0-C_{equi} at the beginning of the test.

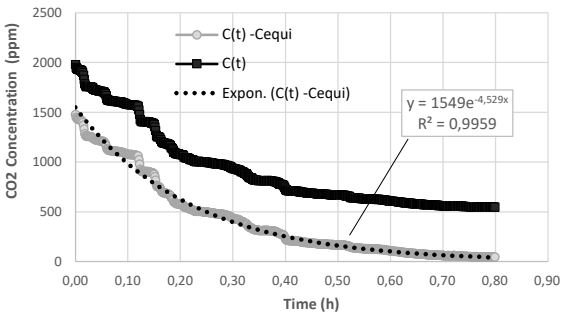

Fig. 1 - "Typical" time evolution of the CO_2 concentration $C(t)$ during a decay test. The AER λ corresponds to the symmetrical of the exponent coefficient of the fitting equation, Eq. (3).

2.2 The monitoring campaign

On November 9th, 2020 afternoon, for approximately three hours, two tests were carried out, under the following conditions: a) only the two upper doors open (just one of the two-door leaves); b) with all doors open (2).

The CO_2 concentration measurements were made simultaneously in ten different locations inside the amphitheater. **Fig. 2** shows the spatial distribution of the measurement points, over a plan drawing. **Fig. 3** also shows the interior of the amphitheater, with images of the spatial distribution of the various equipment and sensors. The sampling and measurement strategy is summarized in **Tab. 1**.

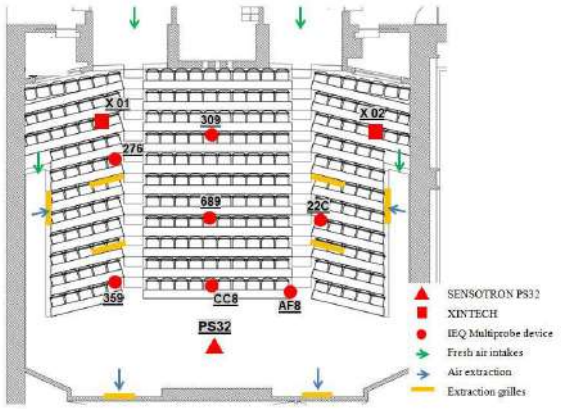

Fig. 2 - Amphitheater plan drawing with the location of the sensors, as well as the infiltration air intakes and the extraction grilles.

Tab. 1 - Sampling and measurement strategy.

Volume (m^3)	Nº points	Nº technologies	Nº tests
1200	10	3	2

Fig. 3 - Interior view of the amphitheater: images at various moments of the tests and of the spatial distribution of sensors and equipment.

2.3 Equipment

Information on the measurement equipment used and the respective metrological characteristics (accuracy and resolution) is shown in **Tab. 2**. The measurement methodology was the same in all devices (**Fig. 4**): non-dispersive infrared (NDIR) sensors and 5/10 s-time step data acquisition.

[1] This C_{equi} value is higher than the typical CO_2 concentration value in ambient air (~ 400 ppm) because, in this case, the ventilation intake air was not real outdoor air, but transferred air, from other spaces in the building (entrance hall and corridors).

[2] For the second test, two additional doors at the amphitheater's ground level were also opened. The upper two-leaf doors (at the building's ground level) are the usual access to the amphitheater; under the COVID-19 health security restrictions, these doors are kept frankly open (both leaves) before and during academic activities, while the occupancy capacity has been reduced from 206 to 64 (teacher included).

Tab. 2. Equipment used in measurements for the assessment of IAQ in the building and respective measurement methods

Pollutant	Equipment	Accuracy	Quantity	Sampling frequency
CO_2	SENSOTRON PS32	±10 + 3% rdg* ±50 ppm	1	10 s
	XINTEST data logger	±5% rdg ±50 ppm	2	
	IEQ Multiprobe device	±3% rdg ±30 ppm	7	5 s

**% rdg= % reading*

Fig. 4 - Monitoring equipment (*[8]).

2.4 Legal framework

The Portuguese legal framework, originally presented in M. C. Gameiro da Silva 2020, is cited as follows:

"In Portugal, the legal regime for indoor air quality in buildings is established by Decree-Law nº. 118/2013 of 20 August and other complementary and subsequent legislation (Decree-Law no. 68A / 2015, Decree-Law no. 194/2015, Decree-Law no. 251/2015, Decree-Law no. 28/2016, Decree-Law no. 52/2018 and Decree-Law no. 95/2019) and by Ordinance no. 349B / 2013 of 29 November, specifically for residential buildings and Ordinance No. 353-A / 2013 of 4 December and Law No. 52/2018 of 20 August for commerce and services buildings.

RECS [3] *establishes also the need to comply with minimum fresh air flow rates, to guarantee, under normal conditions, the dilution of contaminants to concentration values below the respective protection thresholds.*

For the calculation of the fresh air flow rate requirements, it is necessary to consider the pollutant load occupant-originated, two methods are proposed, both based on the CO_2 concentrations, inside the space in question, as this bio-effluent is most abundant and its evolution has a high correlation with occupancy rates:

- *The Analytical Method, in which the criterion to be verified is the average concentration of CO_2 during the occupancy period inside the space under analysis, is prescribed a protection threshold that should not be exceeded (2500 mg/m³ or 1250 ppm);*

- *The Prescriptive Method, in which the criterion is that the CO_2 equilibrium concentration does not exceed the prescribed value for the protection threshold (2500 mg/m³ or 1250 ppm). The values prescribed in the RECS resulted from the application of the expression*:

$$Q = G/(C_{equi} - C_{ext}) \quad (4)$$

Where:
- Q is the fresh air flow rate (m³/h);
- G is the generation of pollutants inside the room (mg/h);
- C_{equi} is the equilibrium concentration of the pollutant in the indoor air (mg/m³);
- C_{ext} is the concentration of the pollutant in the outside air (mg/m³).

In a simplified way, the required fresh air flow rates, per person, suggested by the prescriptive method in RECS (which takes into account human occupancy, can be calculated from the expression Q = 20 x M, where M represents the metabolic rate of occupants expected for the space/activity in question, expressed in the "met" unit defined in ISO 7730: 2015 [10]*".*

The studied Amphitheater has an approximate volume of 1200 m³. According to the terminology of the SCE [4], this building is considered a service

[3] RECS - Regulation of Energy Performance of Commercial and Service Buildings (In Portuguese, *Regulamento de Desempenho Energético dos Edifícios de Comércio e Serviços*).

[4] SCE - Building Energy Certification System (In Portuguese: *Sistema de Certificação Energética dos Edifícios*). Decree-Law no. 118/2013, of 20 August

building, therefore framed by the RECS [5].

In this context, according to Ordinance 353-A / 2013, *"the value of fresh air flow rate to be introduced into the spaces must be corrected by the efficiency of pollutant removal (...)."*, which defines that the minimum fresh air flow rates (Q) to be considered for a space can be determined using the two above-mentioned methods.

Herein, Q was determined through the *Prescriptive Method.* According to Ordinance No. 353-A / 2013, Table I.04, the metabolic rate (M) of the occupants in an amphitheater corresponds to 1 Met, prescribing 20 m^3/(hour. person). For this purpose, Q is estimated using the following expression:

$$Q = M_{med} \cdot Q_{1met} \quad \text{expressed in } m^3/(h.person). \quad (5)$$

As an example, in an amphitheater with a capacity for 100 people, Q = 2000 m^3/h would be necessary (4080 or 1280 m^3/h, in the cases of 204 or 64 occupants, respectively.

3. Results and Data analysis

3.1 Experimental data

As previously described, to determine the ventilation rates in the amphitheater under the COVID-19 restrictive conditions, two tests were carried out: a) first, only the two upper access doors were opened (only one leaf); b) afterward, all doors (upper and lower) open. In both tests, only the exhaust air part of the HVAC system was turned on.

The results of the measurements for all the sampling points considered (Figure 2) are shown in the following figures and tables.

As an example, in **Fig. 5**, the overall continuous monitoring of sensor SN_309 along the two tests is presented. The measurements by the other probes/equipment showed similar trends. Then, the CO_2 concentration decay periods were analyzed in the two tests (indicated in red in this figure).

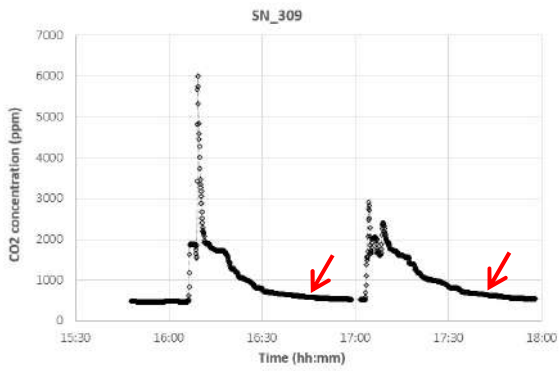

Fig. 5 - Graphical representation of CO_2 decay in the Amphitheater (measured in sensor SN_309). The red arrows indicate the analyzed decay periods.

The graphical representation of the decay period during the second test is shown in **Fig. 6**, showing the values measured with all the sensors/equipment. The interpretation of this graph can be followed by **Tab. 3**, regarding the first test. The results of the second test are shown in **Tab. 4**.

Based on the averages of the monitoring with the different sensors/equipment, in the different locations for representative distribution of the occupied zone of the space, the following average values of the air renewal rate and fresh air flow rate were obtained:

- 5.62 h^{-1} and 6744 m^3/h, first test;
- 4.77 h^{-1} and 5728 m^3/h, second test.

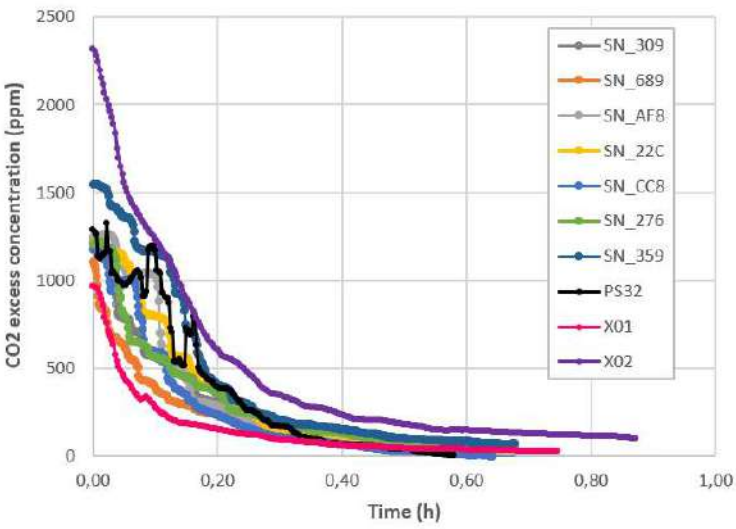

Fig. 6 - Graphical representation of CO_2 decay in Amphitheater C.1 during the second test (as in Fig.2).

[5] Ordinance No. 353-A / 2013 of 4 December.

Tab. 3. Results of the first test

Equipment	Sampling point reference	AER (λ, h^{-1})	Fresh Air Flow Rate ($Q = V \times \lambda$, m^3/h)
SENSOTRON	PS32	8.93	10716
XINTEST	X 01	4.69	5628
	X 02	3.46	4152
IEQ Multiprobe	SN_309	4.92	5904
	SN_689	5.13	6156
	SN_AF8	5.21	6252
	SN_22C	5.67	6804
	SN_CC8	7.95	9540
	SN_276	4.89	5868
	SN_359	5.35	6420

Tab. 4. Results of the second test

Equipment	Sampling point reference	AER (λ, h^{-1})	Fresh Air Flow Rate ($Q = V \times \lambda$, m^3/h)
SENSOTRON	PS32	7.58	9096
XINTEST	X 01	6.28	7536
	X 02	3.30	3960
IEQ Multiprobe	SN_309	4.53	5436
	SN_689	4.39	5268
	SN_AF8	4.27	5124
	SN_22C	4.92	5904
	SN_CC8	4.17	5004
	SN_276	4.48	5376
	SN_359	3.81	4572

Figure 7 shows the AER, λ (h^{-1}), values obtained in the two tests with each of the different sensors/equipment, together with the respective location in the amphitheater. This figure suggests the following essential conclusions:

1. There is no advantage in opening the lower-level doors in addition to the main access doors (2nd test). On the contrary, the air exchange rate is lower than keeping only the upper doors open (1st test).
2. With greater evidence in the 1st test, the flow of fresh air intaken through the two (upper) access doors tends to converge to the lower central zone, which presents a clearly higher ventilation rate than the average of the entire amphitheater.

3.2 Simulation results

Using a computational tool that allows modeling the time evolution of CO_2 concentration in an interior compartment [11], simulations were made for two different conditions of use of the studied amphitheater (see **Fig. s 8** and **9**). The current situation of the auditorium in the pandemic scenario was simulated, with the restriction of the total of 206 existing seats to a maximum of 64 occupied seats (63 students and 1 teacher).

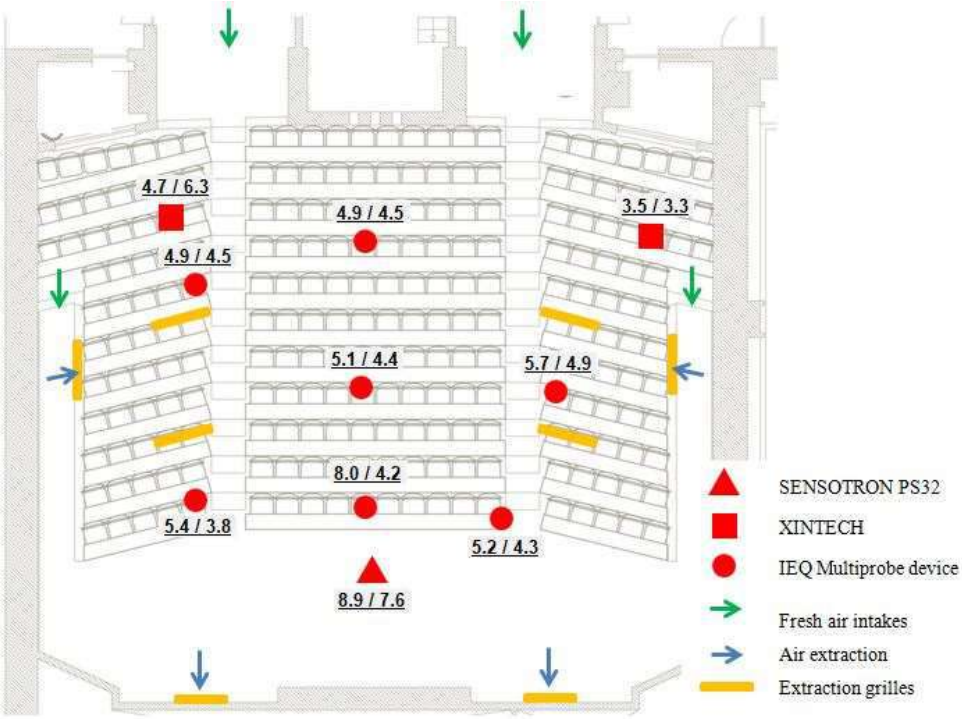

Fig. 7 - Air Exchange Rate values, λ (h^{-1}) obtained in the different locations in the two tests performed (1st / 2nd).

In this case, a typical value of 5.15 air changes per hour was considered, similar to what was determined in the experimental tests, which, for a room volume of 1200 m^3, indicates a total of 6080 m^3/h of fresh air, corresponding to 95 m^3/h per person.

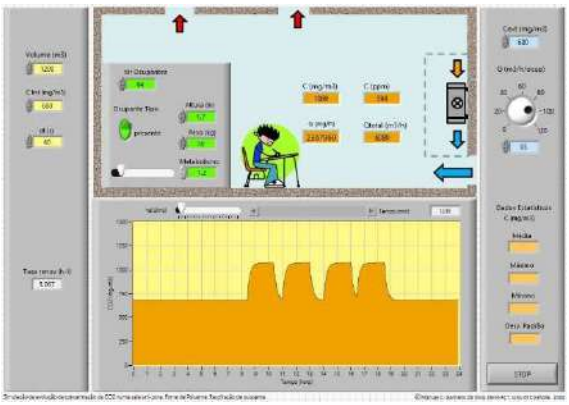

Fig. 8 - Simulation of the temporal evolution of CO_2 concentration in the Amphitheater in the current use (64 seated people).

In the simulation carried out, it was assumed that the Amphitheater would have 64 seats occupied, during a typical school day, comprising four 2h-classes. It was also considered that students would leave the space in the 15-min intervals between consecutive classes, as well as during the 1h-break for lunch. The value of the equilibrium/maximum CO_2 concentration reached during each of the classes, under the conditions mentioned above, is 1089 mg/m^3 (594 ppm), which indicates an excellent level of indoor air quality, particularly remarkable because the assumed value of ventilation rate (5.15 h^{-1}) is achieved by operating only the exhaust network of the HVAC system.

A second simulation was performed for the conditions that would certainly have been the design parameters of the ventilation system (maximum occupancy of the room with 206 people and a fresh air flow rate of 30 m^3/h/person). A room operation routine similar to the previous case was considered. A value of 1913 mg/m^3 (1063 ppm) was obtained for the CO_2 equilibrium concentrations, which shows to be frankly satisfactory.

Fig. 9 - Simulation of the time evolution of CO_2 concentration in the Amphitheater with the normal, pre-pandemic use (206 seated people).

4. Conclusions

The present study allows concluding that the analyzed space presents an adequate rate of air renewal to ensure that there is an effective dilution of the biological pollutant load that might result from the exhalation of this microorganism (SARS-COV-2) by an infected occupant. The values of fresh air flow rate guaranteed by the existing conditions, in this scenario of reducing the maximum number of occupied places from 206 to 64, are around 95 m^3/h

per occupant, which is more than thrice the values recommended by the national legislation and international standards for the pre-pandemic scenario.

However, considering that the "fresh air" is not directly intaken from the outdoors, but is rather transferred from interior spaces of the building itself – mainly from the access hall and the ground floor corridor –, it is important to ensure that the entrance door of the building remains open during operating hours, having all underlying health safety rules currently in effect at the UC, in the current COVID-19 pandemic context.

The proposed methodology that allows obtaining a spatial distribution of the air exchange rate in a large room is multiuse and replicable to other case studies such as concert halls, cinemas, or meeting rooms.

5. Acknowledgement

Authors thank Fernando Pedro Ortega de Oliveira Figueiredo, Assistant Professor and Vice-Director of FCTUC. This work was also carried out in the framework of Project UIDP/50022/2020 - LAETA - Laboratório Associado de Energia, Transportes e Aeronáutica, with the financial support of FCT/MCTES through national funds (PIDDAC).

6. References

[1] E. Scotford, Rethinking Clean Air: Air Quality Law and COVID-19, J. Environ. Law. (2020) 1–5. https://doi.org/10.1093/jel/eqaa027.

[2] J. Parker, C. Boles, N. Egnot, A. Sundermann, A. Fleeger, Return to normal operations: COVID-19 mitigation strategies for workplaces, Toxicol. Ind. Health. 36 (2020) 711–717. https://doi.org/10.1177/0748233720967525.

[3] ASHRAE (Society's Environmental Health, Committee Position Document), ASHRAE Position Document on Infectious Aerosols, Ashrae. (2020) 1–24.

[4] J. Ducharme, World Health Organization Declares COVID-19 a "Pandemic." Here's What That Means, Time. (2020). https://time.com/5791661/who-coronavirus-pandemic-declaration/ (accessed November 10, 2020).

[5] J. Ding, C.W. Yu, S.J. Cao, HVAC systems for environmental control to minimize the COVID-19 infection, Indoor Built Environ. 29 (2020) 1195–1201. https://doi.org/10.1177/1420326X20951968.

[6] M. Loomans, J. De Leeuw, G. Middendorf, P. V. Nielsen, COVID-19 and recirculation, REHVA J. 5 (2020) 5–9.

[7] M. Awada, B. Becerik-Gerber, S. Hoque, Z. O'Neill, G. Pedrielli, J. Wen, T. Wu, Ten questions concerning occupant health in buildings during normal operations and extreme events including the COVID-19 pandemic, Build. Environ. (2020). https://doi.org/10.1016/j.buildenv.2020.107480.

[8] M. Gameiro da Silva, L. Van Cappellen, E. Sanjuanello, Assessing and Communicating Indoor Environmental Quality, REHVA J. April (2019) 14–18.

[9] M.C. Gameiro da Silva, CAPÍTULO 5 - VENTILAÇÃO E QUALIDADE DO AR INTERIOR, in: E. Santos Júlio (Ed.), Guia FNRE. Fundo Nac. Reabil. Do Edif., FUNDIESTAM, Lisboa, 2020: pp. 73–82.

[10] International Organization for Standardization (ISO), ISO 7730: 2005. Ergonomics of the thermal environment. Analytical determination and interpretation of thermal comfort using calculation of the PMV and PPD indices and local thermal comfort criteria, 2005.

[11] M.C. Gameiro da Silva, Development of Indoor Climate Monitoring and Prediction Tools. Keynote speech at ROOMVENT2020 Virtual Conference, in: ROOMVENT2020, 2021. https://zenodo.org/record/4890596#.YkiaayjMK5e.

Data Statement

The datasets generated during and/or analysed during the current study are not available but the authors will make every reasonable effort to publish them in near future.

Spatiotemporal humidity variation in student housing

Cathrine Hafnor [a], Sverre Holøs [b], Tormod Aurlien [c], Kari Thunshelle [d]

[a] Norwegian University of Life Sciences, Ås, Norway

[b] SINTEF AS, Oslo, Norway, sverreb.holos@sintef.no

[c] Norwegian University of Life Sciences, Ås, Norway

[d] SINTEF AS, Oslo, Norway, kari.thunshelle@sintef.no

Abstract. Modern, urban apartments are space-efficient, have bathrooms with no windows, and require energy-efficient ventilation with heat recovery. The requirements for exhaust ventilation rates for the kitchen and bathrooms are independent of dwelling size. In some countries, it is required that the extract air can be increased on demand. There is a need for more knowledge on the effects of these requirements on the resulting moisture level in apartments, and whether these recommendations should be modified. Measurements were done in eight student apartments. Temperature and humidity were measured with 1-minute time resolution at 5 locations in each of the apartments. Median moisture excess was 0.9-1.4 g/m^3, indicating a small risk of interstitial condensation. 90th percentiles of relative humidity were 30-35 %, indicating an elevated risk of eye and airway symptoms due to low humidity. The moisture excess was lower in apartments with heat-recovery ventilation than mechanical extract ventilation. The median moisture excess was higher in the living rooms than in bathrooms, indicating that moisture from showering and personal hygiene had little impact on the overall indoor moisture conditions in the dwellings. The average number of showers per day per apartment varied between 0.6 and 3.1. High peak moisture excess values up to 20 g/m^3 were recorded in bathrooms, but for brief periods only. Consistently higher moisture peaks in extract vents than in bathroom air demonstrated that ventilation extract above the shower is effective in removing moist air from showering. Calculated moisture load in the extract air from a single shower was estimated to be 0.86 kg. Outdoor temperatures were negatively correlated with moisture excess, as predicted by EN -ISO 13788.

Keywords. Moisture excess, ventilation, dwellings
DOI: https://doi.org/10.34641/clima.2022.65

1. Introduction

Recommendations and regulations for residential ventilation aim at maintaining good indoor air quality by removing pollutants and moisture. In different countries, this may be reflected in requirements for overall air change rate, fresh supply airflow rate per floor area, as well as required extract flow rates from kitchens and bathrooms and supply rates for bedrooms. Important requirements in current Nordic regulations are summarized in Tab. 1.

Increasing ventilation rates beyond what is needed to avoid moisture damage risk and dilute pollutants to healthy and comfortable levels may contribute to uncomfortably or unhealthy low humidity levels. It also increases energy demand for fans, heating, and cooling, as well as space demand due to larger duct dimensions. The forced extract rates required in Norway and Finland also complicate the control of the ventilation system. Earlier studies from Nordic climates have indicated that the moisture excess generally is quite low in newer dwellings [1-4], also lower compared to older buildings[5]. An analysis of data from the Swedish building stock pointed out that smaller dwelling volumes, more recent construction, and higher ventilation rates were among factors associated with low indoor relative humidity [6]. Other countries with similar climatic conditions do not have this requirement. Since the motivation for the extract rates is moisture removal and not general air quality, it is of interest to examine if the extract rates are higher than needed for the removal of actual moisture sources. Most of the previous studies are done with limited temporal and spatial resolution, and mostly in somewhat larger dwellings.

Estimates of moisture loads from individual sources are available in the literature [7-9], but some of this information is relatively old, and may not reflect the current building usage. Short-term events like cooking or showering will typically cause highly variable moisture loads, and measurements with high time resolutioin at different locations within the dwelling would enable more precise risk evaluation than average values in one or two locations. Such datasets are scarce. As the discrepancy between

Copyright ©2022 by the authors. This conference paper is published under a CC-BY-4.0 license.

requirements due to extract air and general ventilation are most prominent in small dwellings, the present study examined student accommodation intended for couples or small families.

Tab. 1. Ventilation requirements in four Nordic countries. (Extract values are formally "pre-accepted suggestions" in Norwegian legislation)

		Denmark	Sweden	Finland	Norway
General ventilation requirement (m^3/h per m^2)		1.08	1.24	1.24	1.2
Supply rate bedroom (m^3/h)			14.4 / bed	29-43 / room	26 / bed
Extract bathroom	-normal (m^3/h)	-	54	36	54
	-forced (m^3/h)	54		40	108
Extract kitchen	-normal (m^3/h)	-	36	29	36
	-forced (m^3/h)	72	100-140	25	108

2. Methods

2.1 Apartments

Eight apartments in two student housing buildings were monitored for 14 days, either (I) February 25th – March 10th or (II) March 11th -24th, 2021.

The buildings are situated less than 100 m apart in the municipality of Ås, Norway. Characteristics of the buildings and their apartments are given in Tab. 2. Typical floorplans are shown in Appendix A.

Tab.2 Properties of the monitored apartments

	Palisaden	Pentagon
Construction year	2014, passive house standard	1975
Ventilation system	Balanced mechanical ventilation, supply and extract, heat recovery	Mechanical extract
Floor area per apartment (m^2)	28.0 -30.7	37.8 – 41.6
Extract airflow rates (m^3/h)	Bathroom: 50-59 Kitchen: 0 m^3/h (recycling hood, only)	Bathroom: 58-65 Kitchen: 0-37 Rangehood on: 83-85 m^3/h
Supply airflow rates (m^3/h)	48-53	Passive supply only

2.2 Measurement

Relative humidity (RH), CO_2, and temperature were measured in the kitchen/living rooms and the bedrooms using a Rotronics CP11 handheld instrument. The loggers were placed about 1.1 m above the floor (see Appendix A). RH and temperature were measured in the bathroom, the extract, and supply air ducts using smaller data loggers (EL-USB-2+ and Tinytag ULTRA 2-TGU-4500). All measurements were logged at 1-minute intervals. Measurements of outdoor temperature and relative humidity with 10 minute intervals from the meteorological station at Ås (NMBU) were downloaded and used for calculating moisture excess and assessing the outdoor dependency of indoor conditions. Parameters logged at the different locations in each apartment are summarized in Tab. 3. Airflow rates in air extract vents in bathrooms and kitchens were measured with a Swemaflow 125 air capture anemometer (Swema AB, Sweden) using the back-pressure method.

The inhabitants were asked to log a number of activities, including showers and window airing within each hour of the measurement period.

Tab.3 Monitored indoor parameters.

	Palisaden	Pentagon
Bedroom	T, RH, CO_2	T, RH, CO_2
Cooking/ living area	T, RH, CO_2	T, RH, CO_2
Bathroom	T, RH	T, RH
Extract hood (cooking area)	-	T, RH
Extract duct	T, RH	T, RH
Supply duct	T, RH	-

2.3 Analysis

Moisture excess Δv (g/m³) was calculated for each time i from indoor and outdoor absolute moisture content v_{ind} and v_{out} by:

$$\Delta v_i = v_{ind,i} - v_{out,i} \quad (1)$$

Where moisture content v is defined by

$$v = \phi_r \cdot \frac{\rho_{sat}}{461.4 \cdot \theta} \quad (2)$$

where ϕ_r = RH (%), ρ_{sat}= water saturation pressure (Pa) and θ is the temperature (K).

ρ_{sat} was calculated for different temperature intervals t as follows:

-30 °C ≤ t ≤ 0 °C: (3a)

$$p_{sat} = 611 \cdot \exp\big((82.9 \cdot 10^{-3} \cdot t) - (288.1 \cdot 10^{-6} \cdot t^2) + (4.403 \cdot 10^{-6} \cdot t^3)\big)$$

0 °C < t ≤ 40 °C: (3b)

$$p_{sat} = 611 \cdot \exp\big((72.5 \cdot 10^{-3} \cdot t) - (288.1 \cdot 10^{-6} \cdot t^2) + (0.79 \cdot 10^{-6} \cdot t^3)\big)$$

To identify the short-term events that generate moisture, we defined Δv(change) as the deviation from the 5-minute running mean of Δv as

$$\Delta v(change) = \Delta v_i - (\sum_{i-6}^{i-1} \Delta v_i)/5 \quad (4)$$

The starting point a of a short term event was determined by analyzing where the moisture excess Δv begins to rise above the humidity that already exists in the room. Pragmatically, $\Delta v(change) >$ 1,5 g/m ^{3}was selected as a criterion.

The endpoint b of an event was determined by analyzing where the moisture supplement again reaches the original moisture level, defined as $v_b < v_a$+0,2 g/m^3.

The total moistuire production G (g) was then estimating by summing 1 minute values according t eq. (5)

$$G = \dot{V} \cdot \sum_{i=a}^{b} (v_i - v_a) \quad (5)$$

where $\dot{V}$ is the measured extract airflow rate (m^3/min)

3. Results and discussion

3.1 Temperature, RH and moisture excess

Tab. 4 shows the outdoor conditions and Tab. 5 the indoor climatic parameters for all apartments in the two buildings. The median temperatures measured in all rooms in the apartments at Palisaden were generally slightly higher than Pentagon. Compared to a survey of 3195 Norwegian family dwellings from 2012 [10], the indoor temperatures in the student apartments in our study were notably higher, however, they were comparable to measured indoor temperature from high-performance residential buildings [11].

Tab. 4 Outdoor conditions during monitoring

Period	**Air temperature** (°C)	**Relative humidity** (%)
	median [min;max]	
I	*1.5* [-7.4;12.1]	*72.6* [28.1;100]
II	*2.5* [-4.6;11.6]	*75.6* [34.3;100]

Compared to previous studies on measurements of RH in dwellings [3, 4, 12], the RH measured in the apartments in our study is low (<30%) in both buildings. 90th percentiles of relative humidity for all rooms were between 30-35 %, indicating an elevated risk of eye and airway symptoms. Although humidification is generally not recommended, for buildings where humidification is installed, EN 16798-1:2019 [13] suggests the design relative humidity in category II for residential buildings to be set at 25 % RH, which is close to the median RH values in our study.

Tab. 5 Indoor parameters. Median [10th;90th percentile] of all measured values.

	Palisaden	**Pentagon**
	Kitchen/living rooms	
RH [%]	24.4 [19.8:29.9]	26.8 [20.9:34.7]
T [°C]	24.1 [23:25.4]	22.3 [21.3:24.2]
Δv [g/m^3]	1.3 [0.4:2.5]	1.4 [0.3:2.7]
	Bedrooms	
RH [%]	24.6 [18.5:31.3]	27.3 [20.5:35.4]
T [°C]	22.6 [20.4:24.6]	21.9 [20.6:23.7]
Δv [g/m^3]	0.9 [0:2]	1.2 [0.1:2.9]
	Bathrooms	
RH [%]	22 [17.1:29.5]	21.6 [16.9:28.8]
T [°C]	25.1 [23.6:25.8]	24.8 [23.7:25.7]
Δv [g/m^3]	1.1 [0.1:2.6]	1.0 [-0.1:2.3]

As shown in fig. 1-3, the moisture excess was also modest (<2 g/m^3) compared to previous studies [3, 5, 14, 15]. The highest median internal moisture excess was found in the kitchen/living rooms indicating that moisture from showering and personal hygiene had little impact on the overall indoor moisture conditions in the dwellings.

The moisture excess was generally lower in apartments with heat-recovery ventilation at Palisaden than at Pentagon (mechanical extract ventilation).

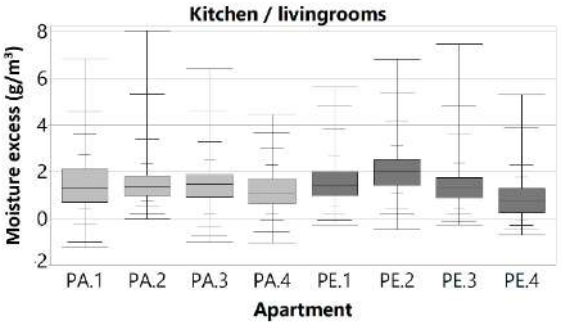

Fig. 1 Internal moisture excess in kitchen/living rooms measured during 14 days for each apartment at Palisaden (PA) and Pentagon (PE).

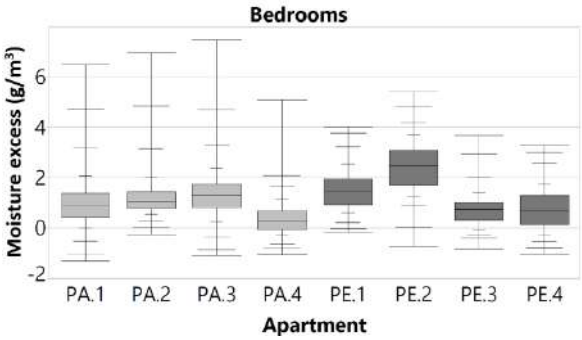

Fig. 2 Internal moisture excess in bedrooms measured during 14 days for each apartment at Palisaden (PA) and Pentagon (PE).

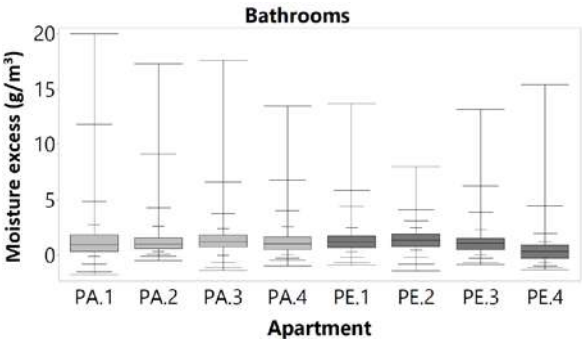

Fig. 3 Internal moisture excess in bathrooms measured during 14 days for each apartment at Palisaden (PA) and Pentagon (PE).

3.2 Outdoor temperature dependency

Previous studies have uncovered that the mean moisture excess levels tend to be higher with lower daily mean outdoor temperatures, an effect ascribed to more frequent opening of windows and doors at higher outdoor temperatures [16]. A common assumption is that this effect is present above a certain outdoor temperature, below which windows are kept closed and moisture excess is constant.

According to EN 13788, the moisture excess is reduced as outdoor temperature increases from 0 to 20°C. Based on the analysis of Finnish and Estonian dwellings, Ilomets et al. [12] suggested +5°C as a more suitable deflection point for an indoor humidity model.

Measurements for individual rooms and apartments were fitted to a linear model using the least sum of squares. The temperature coefficients are summarized in **Tab. *6***.

Tab. 6. Temperature coefficients of moisture excess (g/m^3 per °C). *Median* [minimum: maximum]

	Palisaden	Pentagon
Bedroom	*-0.04* [-0.08:0.08]	*-0.03* [-0.07:0.12]
Living room	*-0.05* [-0.19:0.03]	*-0.02* [-0.13:0.07]
Bathroom	*-0.14* [-0.70:0.95]	*-0.10* [-0.40:0.15]

In our study, we found an overall reduction of moisture excess with increasing temperatures. The strongest correlation between temperature and moisture excess was found for the bathrooms, and the temperature dependency was generally stronger at Palisaden than at Pentagon.

The daily mean outdoor temperatures during the study were below 0 °C for four days only, all occurring during the first monitoring period. Temperature coefficients for days where the outdoor mean temperature was < 0° C are given in **Tab. *7***. Any inferences from this small data set are highly uncertain, but it can be noted that the two apartments at Palisaden still show a negative correlation between moisture excess and outdoor temperature below 0°, while this is the case only for the bedrooms at Pentagon.

Tab. 7. Temperature coefficients of moisture excess (g/m^3 per °C) when daily outdoor temperatures were < 0°C. Values for individual apartments (N=4).

	Palisaden	Pentagon
Bedroom	-0.23/ -0.12	-0.18/ -0.26
Living room	-0.26/ -0.29	0.25/ 0.35
Bathroom	-0.48/ -0.15	0.26/ 0.24

According to the user logs, the inhabitants ventilate through windows even at the lowest temperatures, presumably to improve thermal comfort. The inhabitants are not billed for their individual heating costs and have little motivatation to reduce heat loss.

3.3 Moisture in bathrooms

Median relative humidity and moisture excess in the bathrooms were low, but with short periods of high humidity, as clearly visible in Fig. 3.

Moisture excess above running mean of previous 5 minutes ($\Delta v(change)$) higher that 1.5 g/m^3 effectively identified shower events reported by inhabitants, se example in Fig. 4, with a notable exception being one inhabitant reporting 2-3 repeated showers within one hour. These were not readily identified as separate events. In addition to 145 showers reported in the user logs, 8 further events with similar pattern were identified from measurement data. These were assumed to be showers as well. Average number of showers per day per apartment in the 14-day period ranged from 0.6 to 3.1.

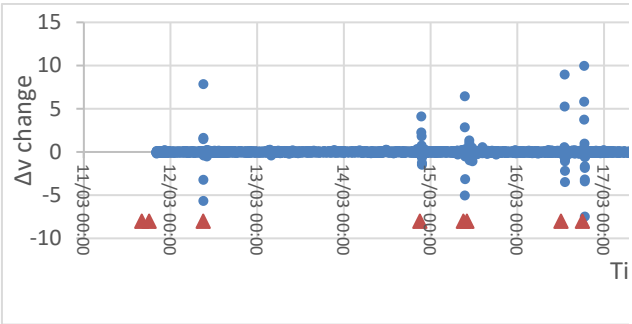

Fig. 4 Moisture excess change from 5-minute running mean (dots) and showers from user diaries (triangles)

3.4 Moisture loads

Moisture loads calculated from two representative shower events based on the ventilation rate and moisture excess above baseline were 0.75 and 0.86 kg when using data from the extract air duct, and 0.47 and 0.58 when using data from the room sensor. This is notably higher than values suggested by Johansson et al. [17] which were in the range of 0.20-0.38 kg per event.

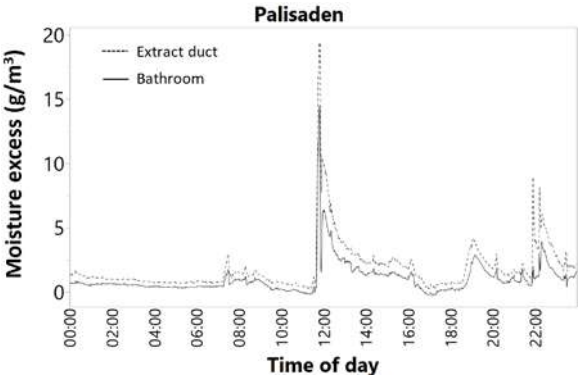

Fig. 5 One representative shower event in Palisaden showing the difference between moisture excess when using data from the extract duct and data from the room sensor.

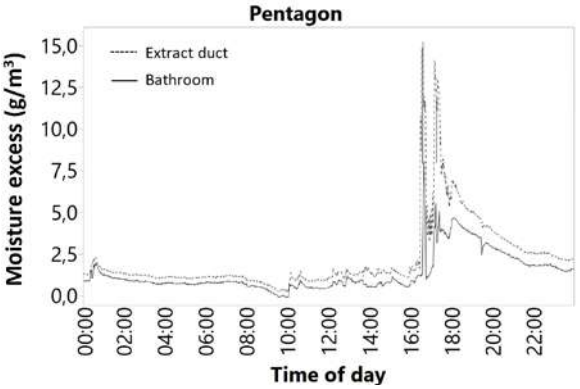

Fig. 6 Representative shower events in Pentagon (two showers during two hours) showing the difference between moisture excess when using data from the extract duct and data from the room sensor.

Fig. 7 shows the comparison of the time of day when showers are taken from our study with data from literature [17]. The data of showering is based on a survey of activity patterns for Californian residents in the period of 1987-1988.

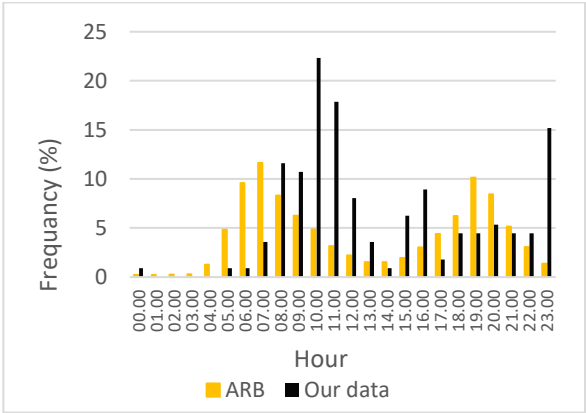

Fig.7 Relative frequency of showering in 1h intervals in our data, compared with data from California Air Research Board (ARB) *[17].*

The showering habits are likely affected by the monitoring taking place in a period of lockdown due to Covid-19 but are still plausible according to assumed student activities. Our findings support the results from analysis of domestic hot water loads that the diurnal patterns of showering in buildings may vary substantially between households [18]. The likelihood of several simultaneous showers may influence the function of the heat recovery units as well as the energy demand. Monitoring of humidity in dwellings can potentially add further insights into these patterns.

3.6 Risks

Indoor humidity can affect building users in several ways. In Nordic climate, the main concerns are possible negative effects on eyes, airways and skin due to low relative humidity [19, 20]. Risk of microbial growth due to condensation on surfaces or within the construction may be among consequences of high relative humidity. The mean relative humidities well below 30 % observed in this study are sufficiently low to cause some concern about possible negative effects of low humidity, in particular because the mean outdoor temperatures in the studied periods were higher than the local monthly normal mean temperature for January and February of -2.9 °C and -2.5 °C. Thus, even lower indoor humidity is probably common. The mean moisture excess, on the other hand, was well below the suggested design moisture excess [12]. Thus we regard that the low relative humidity as more likely to cause negative effects than any condensation due to indoor moisture excess.

4. Conclusion

The conditions in the apartments, and the bathromms in particular were mostly dry. The highest 90th percentile value for moisture excess and relative humidity in bathrooms in either of the eight apartments was 2.6 g/m^3 and 28.8 %, respectively. These low values, even in a period with low outdoor temperatures, and in apartments with up to 3 daily showers on average, indicate that the actual extract rates of 50-65 m^3/h may be sufficient to prevent moisture problems related to sources in the bathrooms, with no need for additional forced ventilation. However, the substantially higher moisture load estimated from showers when using measurements in the extract duct than in the room may not be representative for all ventilation configurations. Furthermore, moisture capture will be less efficient in situations where the supply air contains more moisture.

We recommend further studies of the factors affecting the efficacy of ventilation to remove moisture from sources, these include the location of air supply and extract relative to main moistur source (shower), the moisture content of supplied air, the moisture buffering and the effect of floor heating in bathrooms before making specific recommendations on extract ventilation rates in bathrooms.

5. Acknowledgements

This paper is based on the master thesis by Cathrine Hafnor as a part of the Urban Ventilation project. Urban Ventilation is funded by the Research Council of Norway, EnergiX program under Grant No. 308819 and the industry partner Røros Metall AS, BSH Husholdningsapparater AS, Miele A/S, Engebretsen AS, Mestergruppen Bolig AS, Obos BBL, Selvaag Bolig ASA and Flexit AS. Aileen Yang and two anonymous reviewers are thanked for helpful suggestions for improvemt of the manuscript.

6. Appendix A Floorplans

Fig. 8 Representative floorplan for apartment in Palisaden.

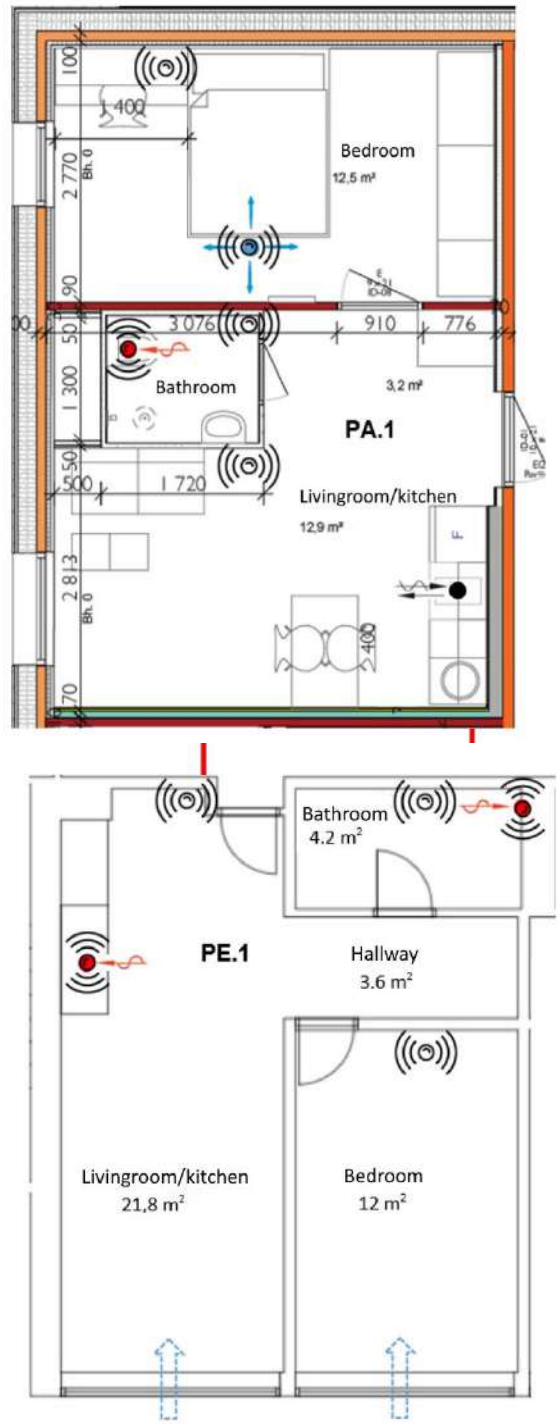

Fig. *9* Representative floorplan for apartments in Pentagon.

Tab. 8 Explanation of the symbols used in floor plans (Fig. 8 and Fig. 9)

Symbol	Explanation
	Extract valve
	Recycling kitchen hood
	Mechanical supply air
	Passive supply air
	Sensor

7. References

1. Kalamees T, Korpi M, Vinha J, Kurnitski J. The effects of ventilation systems and building fabric on the stability of indoor temperature and humidity in Finnish detached houses. Building and Environment. 2009:1643-50.
2. de Place Hansen EJ, Møller EB. Moisture supply in Danish single-family houses – the influence of building style. Energy Procedia. 2017;132:147-52.
3. Møller EB, de Place Hansen EJ. Moisture supply in Danish single-family houses – the influence of occupant behavior and type of room. Energy Procedia. 2017;132:141-6.
4. Vinha J, Salminen M, Salminen K, Kalamees T, Kurnitski J, Kiviste M. Internal moisture excess of residential buildings in Finland. J Build Phys. 2018;0(0):1744259117750369.
5. Geving S, Holme J. Mean and diurnal indoor air humidity loads in residential buildings. J Build Phys. 2012;35(4):392-421.
6. Psomas T, Teli D, Langer S, Wahlgren P, Wargocki P. Indoor humidity of dwellings and association with building characteristics, behaviors and health in a northern climate. Building and Environment. 2021;198:107885.
7. Rousseau MZ. Sources of moisture and its migration through the building enclosure. Standardization News. 1984;12(11):35-7.
8. IEA IEA. IEA Annex 14, Condensation and Energy: Volume 1, Sourcebook1991.
9. Yik FWH, Sat PSK, Niu JL. Moisture Generation through Chinese Household Activities. Indoor and Built Environment. 2004;13(2):115-31.
10. Halvorsen B, Dalen HM. Ta hjemmetempen. Oslo: Statistics Norway; 2013.
11. Berge M, Mathisen HM. Perceived and measured indoor climate conditions in high-performance residential buildings. Energy and Buildings. 2016;127:1057-73.
12. Ilomets S, Kalamees T, Vinha J. Indoor hygrothermal loads for the deterministic and stochastic design of the building envelope for dwellings in cold climates. J Build Phys. 2018;41(6):547-77.
13. STANDARDIZATION ECF. Energy performance of buildings - Ventilation for buildings - Part 1: Indoor environmental input parameters for design and assessment of energy performance of buildings addressing indoor air quality, thermal environment, lighting and acoustics (Module M1-6). 2019.
14. Geving S, Holme J, editors. Diurnal variations of indoor air humidity in Norwegian houses. Energy Efficiency and New Approaches - Proceedings of the 4th International Building Physics Conference; 2009: Istanbul Technical University.
15. Wang J, Engvall K, Smedje G, Nilsson H, Norbäck D. Current wheeze, asthma, respiratory infections, and rhinitis among adults in relation to inspection data and indoor measurements in single-family houses in Sweden—The BETSI study. Indoor Air. 2017;27(4):725-36.
16. Kalamees T, Vinha J, Kurnitski J. Indoor humidity loads and moisture production in lightweight timber-frame detached houses. J Build Phys. 2006;29(3):219-46.
17. Johansson P, Pallin S, Shahriari PDM. Risk Assessment Model Applied on Building Physics: Statistical Data Acquisition and Stochastic Modeling of Indoor Moisture Supply in Swedish Multi-family Dwellings2015.
18. Ivanko D, Taxt Walnum H, Lekang Sørensen Å, Nord N. Analysis of monthly and daily profiles of DHW use in apartment blocks in Norway. E3S Web Conf. 2020;172:12002.
19. Derby MM, Hamehkasi M, Eckels S, Hwang GM, Jones B, Maghirang R, et al. Update of the scientific evidence for specifying lower limit relative humidity levels for comfort, health, and indoor environmental quality in occupied spaces (RP-1630). Science and Technology for the Built Environment. 2017;23(1):30-45.
20. Wolkoff P. Indoor air humidity, air quality, and health - An overview. Int J Hyg Envir Heal. 2018.

Cooking habits and usage of kitchen hoods in Norwegian homes

Adele Helene Ninauve Jutulstad [a], Aileen Yang [b], Peter G. Schild [a], Arnab Chaudhuri [a], Kari Thunshelle[b]

[a] Department of Civil Engineering and Energy Technology, Oslo Metropolitan University, Oslo, Norway, adele.jutulstad@afry.com; peter.schild@oslomet.no; Arnab.chaudhuri@oslomet.no;

[b] Department of Architectural Engineering, SINTEF Community, SINTEF AS, Oslo, Norway; aileen.yang@sintef.no; kari.thushelle@sintef.no;

Abstract. Sustainable urban development results in more space and energy-efficient apartments. Open plan solutions are becoming more common, and the market is exploring new configurations and ventilation solutions for the kitchen in direction of the design and minimize space for ductwork. Cooking is an important aspect of human life and is considered one of the major sources of particle emissions. The cooking method, the type of cuisine, and the type of kitchen hood are some of the factors that will influence this. In Norway, the minimum requirement for general kitchen exhaust is 36 m^3/h, with a minimum additional forced ventilation by the kitchen hood of 108 m^3/h. However, these requirements might not be sufficient to mitigate the exposure from cooking. Electricity is the main heating source, traditionally with hot plate, today mainly induction or ceramic cooktop. In this work, we aim to investigate representative Norwegian cooking habits, typical meals and set up a procedure for cooking in the laboratory to perform intensive exposure studies. A survey has been performed to identify the type and usage of kitchen hoods in different living situations as well as typical Norwegian meals. A total of 336 people responded to the survey, of which 111 provided answers to a few additional questions. More than 60% of the respondents belonged in the age groups 30 – 60 years old and 92% owned their dwelling. Wall-mounted kitchen hoods were found in the majority of the homes, and almost 4% had downdraft. Only 12% of the homes had recirculating hoods. 76% of the respondents used the kitchen hood during cooking. The Norwegians mainly cook or fry their food, while deep-frying is not common. For the question related to what meal is most often cooked, the categories of food that were most mentioned were pasta dishes, taco, meat, fish, boiled potatoes, and chicken. Based on this we developed the cooking procedure for three different test meals suitable for exposure studies.

Keywords. kitchen hoods, cooking emissions, cooking activities
DOI: https://doi.org/10.34641/clima.2022.54

1. Introduction

Modern apartments in urban areas are built more energy and space-efficient, often resulting in open-plan kitchen solutions. We spend the majority of our time indoors and cooking activities can generate harmful air pollutants [1,2]. The open plan solution increases the risk of exposure if pollutants are not properly removed. The cooking method, the type of cuisine, and the type of kitchen hood are some of the factors that will influence the level of pollutants [3,4]. A kitchen hood can minimize the level of exposure to pollutants if they have a reasonable capture efficiency and are used during a cooking event [5].

As seen in Table 1, the requirements for kitchen extract airflow rates vary between countries. In Norway, the minimum requirement for the basic kitchen ventilation rate is 36 m^3/h, with a minimum additional forced ventilation by the kitchen hood of 108 m^3/h. However, these requirements might not be sufficient to mitigate the exposure from cooking.

The requirements are similarly low in other Scandinavian countries and are based on tests of volume range hoods done in the 1980s. At the same time, design and configuration for kitchen hood have progressed in the last decade, and the available maximum extract airflow for the offered products is often 400 -700 m^3/h, sometimes even higher. This results in a problem for makeup air, both in terms of under pressure in an airtight building, to be handled by the balanced ventilation system, as well as an

Copyright ©2022 by the authors. This conference paper is published under a CC-BY-4.0 license.

increased air change rate. Recirculating solutions are introduced as a measure, but with insufficient documentation on resulting exposure of cooking emissions and odor in the room, as well as not removing the moisture.

Tab. 1 – Kitchen ventilation requirements.

Country	Min. requirement (m^3/h)	Additional forced (m^3/h)
Sweden	36	140
Denmark		72
Finland	29	90
Norway	36	108
The Netherlands		72
UK		108

Cooking habits, kitchen configurations, usage of kitchen hoods among other things might vary geographically [6]. A major survey of everyday eating habits was conducted in the four Nordic countries in 1997 and 2012 [7]. The results indicate that meat and fish were the main ingredients in hot dinners in Norway, particularly minced meat. Almost a decade has passed since the survey, and thus it might be interesting to see whether there are any changes in Norwegian food habits.

This study is part of a larger research project, where one of the aims is to determine what principles and ventilation rates can be recommended for kitchens to avoid contamination risk, high energy use, and power load peaks, as well as maintain moisture control (hood configurations, the flow rate of range-hoods, types of cooking, installation position (wall/island). The purpose of the study reported in this paper is to identify typical cooking habits and usage of kitchen hoods in Norwegian homes, intending to set up a procedure for cooking in a laboratory kitchen.

2. Methods

A survey consisting of 15 questions with multiple answers was used. To gain as many answers as possible, the survey was shared on social media platforms such as Facebook and LinkedIn. The questions asked are given below:

- Do you rent or own your home?
- What type of housing do you live in?
- What age group are you in?
- How often do you cook in a week?
- How many do you cook for?
- What type of kitchen hood do you have?
- Do you have a recycling kitchen hood or with exhaust?
- How often do you wash the grease filter?
- If you have a recirculating fan, how often do you change the charcoal filter?
- How often do you use the kitchen hood when you cook?
- What setting do you usually have the kitchen hood on when it is in use?
- If you choose not to use a kitchen hood, what is the reason for it?
- Do you use the kitchen hood when you use the oven?
- What meal do you make most often?
- How long after cooking do you leave the kitchen hood on?

The responses were analyzed to determine the following parameters: (1) type of kitchen hood, (2) usage of kitchen hood and (3) typical Norwegian meals.

3. Results and discussion

3.1 Respondents

A total of 336 respondents answered the survey, of which 92% owned the dwelling. As shown in fig. 1, there is an even distribution of the various age groups, except the youngest age group. Almost 70% of the respondents live in houses, while 27% live in apartments. According to Statistics Norway, apartment blocks account for 25% of residential building types in Norway in 2021, while detached houses represent 49% and attached houses 12% [8]. The respondents are thus regarded representative of Norwegian households.

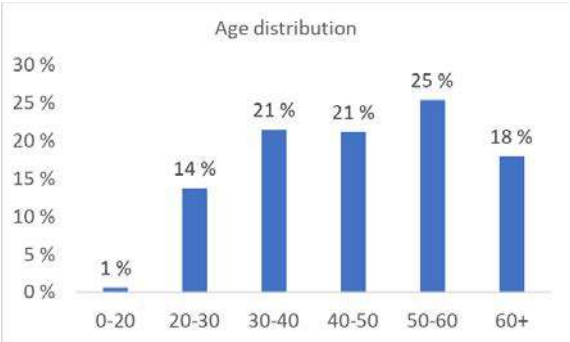

Fig. 1 – Age distribution of the respondents.

3.2 Types of kitchen hoods

Regardless of dwelling type, the majority of the kitchen hoods are wall-mounted. 13% of the homes have kitchen island with hood mounted on the roof, while close to 4% reported they have downdraft kitchen hoods. The majority of the kitchen hoods are ducted hoods (82%) where the air is exhausted outdoors, while 12 % are recirculating hoods.

Generally, kitchen hoods with an exhaust to open-air are the pre-accepted solution and regarded as a more safe and efficient solution for reducing cooking emissions than recirculating alternatives [9]. Fig. 2 shows the distribution of the different types of kitchen hoods and their ventilation solutions. Other kitchen hood types such as slimline and roof-mounted hoods are also reported by the respondents.

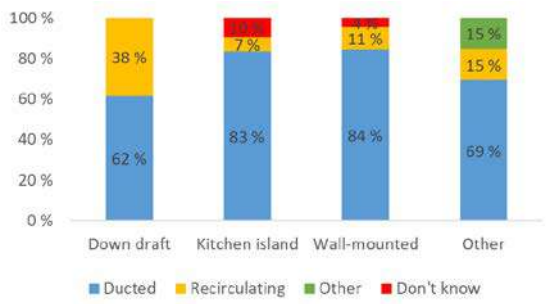

Fig. 2- Different types of kitchen hoods and the ventilation solution.

For those with recirculating hoods (N=40), more than 60% of the respondents reported that they rarely or never changed the charcoal filter, while 22.5% changed once a year. Charcoal filters are often used to removed gases and odors and might have less effect on particulate matter. A Dutch study on recirculating hoods showed that adding a carbon filter removed about 60% of the NO_2 concentrations and resulted in a reduction of about 30% for $PM_{2.5}$ [10]. However, the filter efficiency dropped substantially after only a few weeks of cooking, reducing the removal of NO_2 to 20%. Nevertheless, it is important to change it as the filter may lose its efficiency after a while. More documentation is needed for exposure risk by using recirculating solutions over time.

On the other hand, as shown in fig. 3, the grease filter was washed at least once a year by the majority of the respondents, where 32% washed it either once every 3 months or once a year. Only 16% washed it once a month. A few of the participants also responded that their kitchen hood had a notification function for when it was time to wash or change the charcoal filter and/or the grease filter.

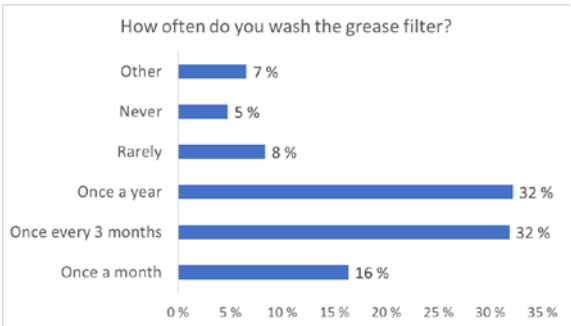

Fig. 3 - How often the grease filter is cleaned.

3.3 Usage of kitchen hoods

In terms of cooking habits, 74% of the respondents replied that they cook daily, while 16% cook five times a week. Also, the majority responded that they cook for 2 people (40%) or 3-5 people (46%). This is also reflected in the usage of the respective kitchen hood, the majority of the respondents reported daily use (76%) while cooking (see fig 4). The numbers reported in our study are much higher than the studies done in the US, where generally less than 40% reported the usage of the kitchen hood during cooking events [3,11].

When asked why the kitchen hood was not used, besides noise and having forgotten to turn the hood on, many respondents also mentioned that they did not see the necessity of turning on the kitchen hood when they only boiled food or cooked food that does not smell or generate fume. A survey done in the US indicated that noise is one of the causes of why the majority of people are not using the kitchen hood [12].

Fig. 4 – Overview of how often the kitchen hood is used.

How long time the kitchen hood is used as well as the flow rate will influence the exposure to cooking emissions. Regarding the operation setting chosen when the kitchen hood is used, as seen in fig. 5, the majority of the respondents replied the medium or max setting. The flow rates were not assessed in this survey, although one respondent did add that the kitchen hood had a capacity of 500 m^3/h.

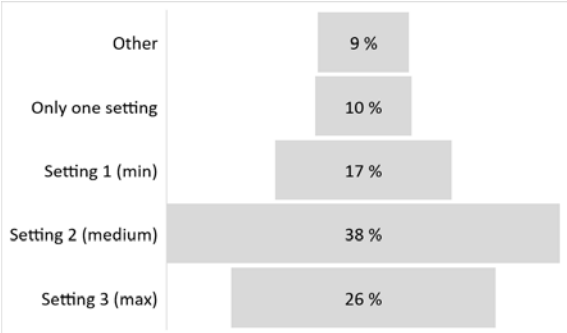

Fig. 5 – Operation setting when using the kitchen hood.

For newer apartments that often have balanced mechanical ventilation, the kitchen hood only has one setting, which is on and off. Some of the respondents that responded "Other" stated that they vary the operation setting depending on what is being cooked. This is also reflected in the question related to the usage of the kitchen hood when the oven is used, as close to 80% of the respondents replied "No" to this question. Some also commented that the oven was not placed nearby the cooktop.

Other habits such as leaving the kitchen hood on after cooking was finished were also questioned. It

can be seen from fig. 6 that more than half of the respondents (N=224) turn it off immediately after they finish cooking. For those who replied other, some had timers that can turn the hood off automatically after a certain amount of time, while the majority responded that they do leave the kitchen hood on for at least 5 – 10 minutes longer, depending on what they have cooked, and the amount of fume generated during cooking. One study in the US assessed the effect of running the kitchen fan continuously after cooking for various flow rates on pollutants but did not find significant reductions. They found that the flow rate and physical characteristics of the kitchen hood were more important factors affecting the exposure during cooking [13].

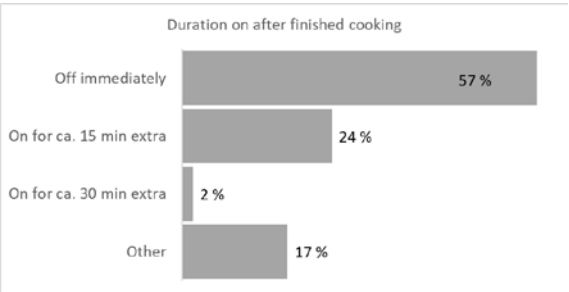

Fig. 6 – Duration of leaving the kitchen hood on after finishing cooking.

3.4 Typical Norwegian meals

With regards to the meal that is often cooked, we received a variety of answers. Since the majority of the respondents cook every day, several dishes are listed. Fig. 7 shows the meals that are most frequently mentioned. Fish, meat, and pasta dishes are the three mentioned the most often, followed by chicken and taco. Potato or rice was also mentioned as they are often boiled along with different types of proteins.

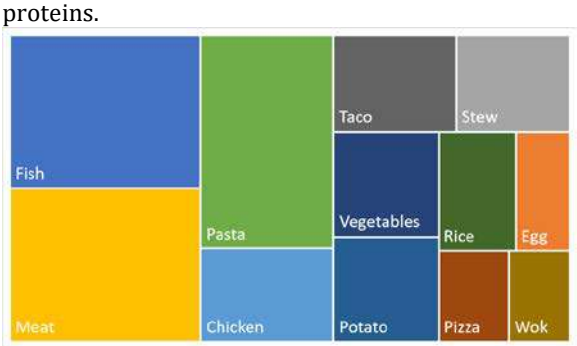

Fig. 7 - Illustration of the most common mentioned meals by the respondents.

Based on the results from the survey and test meals used in other studies, three different meals were chosen to be tested further in the kitchen lab. The chosen meals were taco (meal 1), vegetarian pasta Bolognese (meal 2), and fried salmon (meal 3). The vegetarian meal was added due to the increasing number of people choosing to eat a plant-based diet. According to a recent survey on "Trends in the Norwegian diet by the Norwegian Directorate of Health, more than 10% are substituting meat or other animal-derived foods for plant-based alternatives regularly [14]. Fish also ranked high as one of the most mentioned meals. We chose salmon filet, as it is very commonly used and a fatty fish, to address the issue of odor in open plan kitchen solutions. Fig. 8 shows the ingredients used in the different meals.

Fig. 8 - Ingredients for the three test meals.

3.5 Cooking procedures

In this section, we present the procedure for cooking typical Norwegian meals arising from the survey. These meals will be cooked in our laboratory kitchen to assess exposure from cooking emissions. To ensure the repeatability of the cooking procedure, the meals are simplified in such a way that, there is minimal possibility of variations in the content of the meals to perform exposure experiments. It was also decided to prepare a meal for two adults, considering that the kitchen lab is representative of a typical apartment with an open kitchen and living room. One portion size is assumed to be between 1400 kcal – 1600 kcal per meal.

An overview of the induction cooktop used in the study is shown in fig. 9. We chose to only use the front hot plates as previous studies have shown that the capture efficiency is lower compared to the backplate, resulting in higher exposure [5,15]. Two Teflon frying pans are used, with a diameter of 24 cm for fish at plate A, and 28 cm are used on plate D for minced meat, soya mince, and vegetable frying. A 36-liter aluminum pot was used for boiling pasta.

Table 2 – Table 4 show the detailed cooking procedure for each of the three test meals. All ingredients are prepared and measured in advance before the start of the cooking. Apart from ensuring the choice of the meals which represents the typical Norwegian meals, we also incorporated different ways of cooking (frying, boiling) the meals. Both meal 1 and meal 2 involved frying and boiling of ingredients, while meal 3 involves only frying. The cooking duration is 16 minutes for meal 1 and 13 minutes for meal 2 and meal 3.

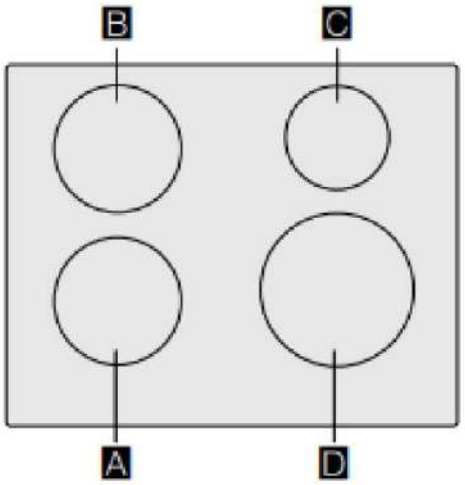

		9*	b*
A / B	Ø 18	1.800 W	3.100 W
C	Ø 14,5	1.400 W	2.200 W
D	Ø 21	2.200 W	3.700 W

* IEC 60335-2-6

Fig. 9 - Induction cooktop used in the study. 9* indicates the effect when the cooktop is used on setting 9, and b* for when the boost-mode is used.

Tab. 2 – Cooking procedure for test meal 1, taco.

Step	Description	Time mm:ss
1	Turn on burner D on setting 8, add 15 ml rapeseed oil	00:00
2	Add minced meat, fry	01:00
3	Flip the piece of meat	02:00
4	Chop the meat into pieces, fry without movement	02:30
5	Stir and chop up meat	04:00
6	Add spice mix, mix for 1 min	05:00
7	Add 1.5 dl of water, switch to setting 5, mix every 2 min for 10 minutes	06:00
8	Turn off, transfer to a serving plate, and move to dining area	16:00
9	Remove the pan from the room	17:00

Tab. 3 – Cooking procedure for test meal 2, vegetarian pasta Bolognese.

Step	Description	Time mm: ss
1	Turn on burner A, fill the pot with 2L of water and 10 g salt, turn on boost setting	00:00
2	Turn on burner D, setting 7, add rapeseed oil to the pan	01:00
3	Add soya mince, mix for a few seconds every minute for 7 minutes?	02:00
4	Add pasta to the pot, reduce to setting 8, boil for 7 min (without lid)	05:00
5	Add tomato sauce to the soya mince, mix well for 1 minute	09:00
6	Turn off burner A, drain pasta and add to pan	12:00
7	Turn off the cooktop, add pasta to a plate and transfer to dining area	13:00
8	Remove the pan from the room and leave the room.	14:00

Tab. 4 – Cooking procedure for test meal 3, fried salmon with wok vegetables and whole grain rice.

Step	Description	Time mm:ss
1	Season salmon filets with salt and pepper	
2	Turn on burner A to setting 9, add 15 ml rapeseed oil	00:00
3	Turn down to setting 7, add salmon filet skin side down	01:00
4	Press the salmon down with spatula for 5 seconds to get crispy skin, then let it fry for 5 mins	01:30
5	Change locations of the two salmon filets in the pan	03:00
6	Flip the salmon, fry for 30 seconds	06:00
7	Turn off burner A, remove the salmon from the pan, put it on a plate	06:30
8	Turn on burner D, setting 8, add oil	07:00
9	Add defrosted wok mix in the pan, stir every minute for 5 minutes	08:00
10	Turn off cooktop, transfer wok to the plate with salmon. Move the plate to the dining area	13:00
11	Remove the pan from the room and leave the room.	14:00

Different extract airflow rates will be assessed in addition to the Norwegian minimum requirement for basic kitchen ventilation rate (hood off, 36 m^3/h) and the minimum additional forced ventilation by the kitchen hood of 108 m^3/h. The developed cooking procedures and responses from the survey will provide the basis for further studies, these include: (1) comparing traditional wall-mounted ducted kitchen hoods with downdraft ducted solutions. (2) Ducted versus recirculation solutions, (3) Effect of filter for recirculating solutions, (4) different airflow rates and its relation to the type of kitchen hood.

4. Conclusions

A survey was conducted to identify the type and use of kitchen hoods as well as representative Norwegian cooking habits and typical meals. Based on the results, cooking procedures to be used in our lab kitchen are developed.

The ducted kitchen hood is still the main solution used, while recirculation is an emerging solution, especially the downdraft. A medium operation setting is a dominating choice, and cleaning of the grease filter is mainly done 1-4 times a year. Norwegian homes use electricity for cooking, mainly frying or boiling of a dinner meal. Frying different type of meat and fish is common, alongside boiling potato, rice, or pasta, and vegetarian alternatives are becoming popular.

Based on the results, procedures for three test meals were developed: taco-meal with minced meat, vegetarian pasta Bolognese and fried salmon with wok. The meals are regarded suitable for two persons and to have a reasonable nutritional content, as well as being simple enough for repeatability in cooking procedure and to be used in exposure studies.

5. Acknowledgments

This paper is based on the master thesis by Adele Jutulstad and was a part of the Urban Ventilation project. Urban Ventilation is funded by the Research Council of Norway EnergiX program under Grant number 308819 and the industry partner Røros Metall AS, BSH Husholdningsapparater AS, Miele A/S, Engebretsen AS, Mestergruppen Bolig AS, Obos BBL, Selvaag Bolig ASA and Flexit.

The datasets generated and analysed during the current study are not publicly available because they are in Norwegian and are part of an initial study but will be available by personal request.

References

[1] Q. Zhang, R.H. Gangupomu, D. Ramirez, Y. Zhu, Measurement of Ultrafine Particles and Other Air Pollutants Emitted by Cooking Activities, Int. J. Environ. Res. Public. Health. 7 (2010) 1744–1759. https://doi.org/10.3390/ijerph7041744.

[2] Y. Zhao, L. Liu, P. Tao, B. Zhang, C. Huan, X. Zhang, M. Wang, Review of Effluents and Health Effects of Cooking and the Performance of Kitchen Ventilation, Aerosol Air Qual. Res. 19 (2019) 1937–1959. https://doi.org/10.4209/aaqr.2019.04.0198.

[3] H. Zhao, W.R. Chan, W.W. Delp, H. Tang, I.S. Walker, B.C. Singer, Factors Impacting Range Hood Use in California Houses and Low-Income Apartments, Int. J. Environ. Res. Public. Health. 17 (2020). https://doi.org/10.3390/ijerph17238870.

[4] O. Han, A. Li, R. Kosonen, Hood performance and capture efficiency of kitchens: A review, Build. Environ. 161 (2019) 106221. https://doi.org/10.1016/j.buildenv.2019.106221.

[5] D. Rim, L. Wallace, S. Nabinger, A. Persily, Reduction of exposure to ultrafine particles by kitchen exhaust hoods: The effects of exhaust flow rates, particle size, and burner position, Sci. Total Environ. 432 (2012) 350–356. https://doi.org/10.1016/j.scitotenv.2012.06.015.

[6] M. Amouei Torkmahalleh, S. Gorjinezhad, H.S. Unluevcek, P.K. Hopke, Review of factors impacting emission/concentration of cooking generated particulate matter, Sci. Total Environ. 586 (2017) 1046–1056. https://doi.org/10.1016/j.scitotenv.2017.02.088.

[7] S. Bowen, Everyday Eating in Denmark, Finland, Norway, and Sweden: A Comparative Study of Meal Patterns 1997–2012, Contemp. Sociol. 50 (2021) 49–52. https://doi.org/10.1177/0094306120976390m.

[8] Statistics Norway, Dwellings, SSB. (n.d.). https://www.ssb.no/en/bygg-bolig-og-eiendom/bolig-og-boforhold/statistikk/boliger (accessed December 7, 2021).

[9] R.E. Militello-Hourigan, S.L. Miller, The impacts of cooking and an assessment of indoor air quality in Colorado passive and tightly constructed homes, Build. Environ. 144 (2018) 573–582. https://doi.org/10.1016/j.buildenv.2018.08.044.

[10] Jacobs, Piet, Cornelissen, Henricus J.M., Efficiency of recirculation hoods with regard to PM2.5 and NO2, in: Lublin, Poland, 2017: p. 7.

[11] W.R. Chan, Y.-S. Kim, B.D. Less, B.C. Singer, I.S. Walker, Ventilation and Indoor Air Quality in New California Homes with Gas Appliances and Mechanical Ventilation, Lawrence Berkeley National Lab. (LBNL), Berkeley, CA (United States), 2019. https://doi.org/10.2172/1509678.

[12] N.A. Mullen, Participant Assisted Data Collection Methods in the California Healthy Homes Indoor Air Quality Study of 2011-13, (2013).

https://escholarship.org/uc/item/4sd2k5nh (accessed December 7, 2021).
[13] N.A. Dobbin, L. Sun, L. Wallace, R. Kulka, H. You, T. Shin, D. Aubin, M. St-Jean, B.C. Singer, The benefit of kitchen exhaust fan use after cooking - An experimental assessment, Build. Environ. 135 (2018) 286–296. https://doi.org/10.1016/j.buildenv.2018.02.039.
[14] Norwegian Directorate of Health, Trends in the Norwegian Diet 2021, Helsedirektoratet. (2021). https://www.helsedirektoratet.no/rapporter/utviklingen-i-norsk-kosthold (accessed December 7, 2021).
[15] M.M. Lunden, W.W. Delp, B.C. Singer, Capture efficiency of cooking-related fine and ultrafine particles by residential exhaust hoods, Indoor Air. 25 (2015) 45–58. https://doi.org/10.1111/ina.12118.

Cooking emissions from typical Norwegian meals: basis for advanced exposure studies

Adele Jutulstad [a], Aileen Yang [b], Peter G. Schild [a], Arnab Chaudhuri [a], Kari Thunshelle [b]

[a] Department of Civil Engineering and Energy Technology, Oslo Metropolitan University, Oslo, Norway, adele.jutulstad@afry.com; peter.schild@oslomet.no; Arnab.chaudhuri@oslomet.no

[b] Department of Architectural Engineering, SINTEF Community, SINTEF AS, Oslo, Norway, aileen.yang@sintef.no; kari.thunshelle@sintef.no

Abstract. Sustainable urban dwellings are built space-efficient, and open-plan kitchens have increasingly become the norm. A study of newer building projects has shown that the kitchen space is in the inner area of the apartment with limited options for forced window airing, leaving the job of removing cooking emissions to the kitchen hood or general ventilation. One of the aims of our study is to measure exposure from actual cooking in modern apartments, as preparations for further advanced studies. To achieve this, particle number concentrations (>0.3 µm) are measured for three typical Norwegian meals with different ventilation rates at three locations in the kitchen lab. The kitchen setup is comparable to the EN 61591:2019 standard with an area of approximately 30 m^2 and a height of 2.7 m. The measurements show that the meals and cooking procedures developed are reasonably repeatable. Most of the particles are in the range 0.3-2.5 µm. The meal producing the lowest numbers of particles is the vegetarian pasta Bolognese, while taco and fried salmon which required both higher cooking temperature and contained more fat resulted in a much higher number of particles. The peak for particle number concentration was more than 40% lower for the vegetarian meal. Turning on the kitchen hood at medium setting (286 m^3/h) drastically reduced the particle number concentrations, however, the Norwegian requirement of 108 m^3/h (low) resulted in a 58% reduction for the taco meal.

Keywords. Kitchen ventilation, cooking emissions, indoor air quality, particulate matter, particle size distribution
DOI: https://doi.org/10.34641/clima.2022.52

1. Introduction

Indoor air quality (IAQ) is important to both personal health and well-being. During the Covid-19 pandemic, IAQ is of even greater significance as most people are spending a larger amount of their time at home. Moreover, urban dwellings are currently built more energy and space-efficient. This results in more compact and airtight apartments and open plan kitchen and living room solutions are becoming more common.

Cooking is considered one of the main sources of indoor pollutants. The magnitude of cooking emissions will vary depending on the type of food, cooking method, cooking temperature or the cooktop [1–3]. In Norway, electric cooktops dominate the market, either ceramics or induction, which, unlike gas stoves, do not generate emissions. Exposure to cooking fuels is less of an issue in developed countries, but studies have shown that cooking poses a significant health risk due to exposure to particulate matter (ultrafine, $PM_{2.5}$) and polycyclic aromatic hydrocarbons (PAH)[4–6]. The kitchen space is frequently placed in the inner area of the apartment with limited options for forced window airing, thus leaving the job of removing cooking emissions, odour and moisture to the kitchen hood or general ventilation.

The requirement for ventilation rates by the kitchen hood varies between countries. ASHRAE has a requirement of 180 m^3/h, while the extract rates by the kitchen hood in the European and Nordic countries range between 72-140 m^3/h. The minimum requirement for basic kitchen ventilation rate according to the Norwegian technical building regulations (TEK17) is 36 m^3/h, with a minimum additional forced extract rate of 108 m^3/h. Studies have shown that the TEK17 standard kitchen ventilation requirements in Norway may not be sufficient to reduce particle emissions generated by cooking [5,7].

Currently, there is a growing demand from the building industry in Norway for more knowledge about ventilation solutions for urban dwellings. Existing laboratory test standards for kitchen hoods

Copyright ©2022 by the authors. This conference paper is published under a CC-BY-4.0 license.

are rather simple and not representative of actual cooking routines in modern apartments. In this study, we aim to measure exposure from cooking typical Norwegian meals under controlled ventilation conditions to formulate the basis for more advanced exposure studies. In this paper, three typical Norwegian meals were cooked under different ventilation scenarios, and the exposure at different locations in the kitchen laboratory will be explored.

2. Materials and methods

2.1 Laboratory facilities

All experiments are performed under controlled ventilation conditions in a test room with a height of 2.7 m, a width of 6.2 m, a depth of 4.8 m and a total volume of 80.4 m^3. The kitchen lab, as shown in Fig.1, is larger than the test rooms mentioned in EN 61591:2019 standard for kitchen test facilities, but the kitchen setup is comparable to this standard.

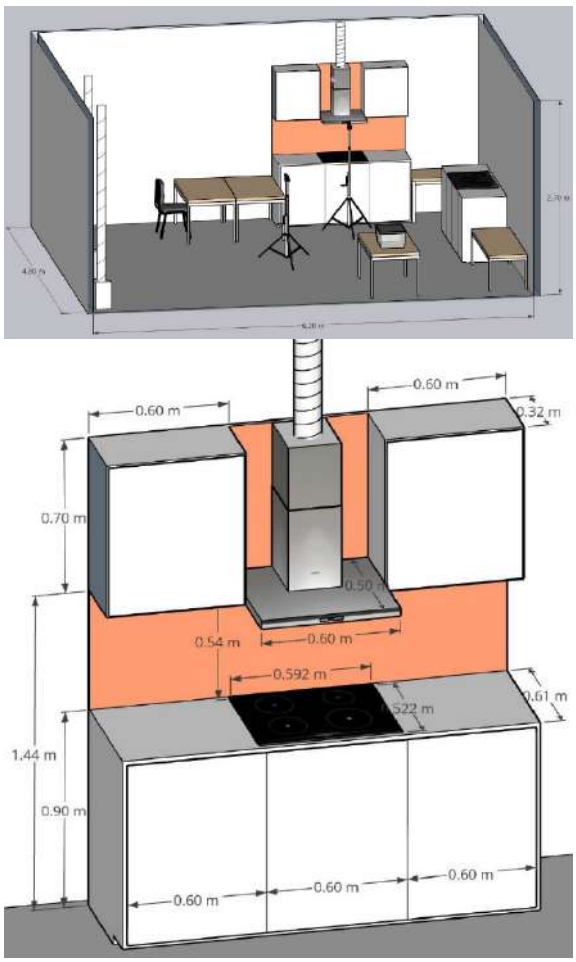

Fig. 1 - Upper: Kitchen lab dimensions and layout. Lower: Kitchen setup.

An individual balanced ventilation system for control of the supply and extract air was installed in the test room, and the supply air was filtered using a HEPA filter. The general exhaust was mounted in the ceiling and was regulated externally using a fan connected to the exhaust duct. The built-in hood fan can operate at four different airflow rates (183, 286, 362, 496 m^3/h) and could also be regulated externally. The flow rates were measured and recorded by an air handling controller DPT-CTRL 2500-D (HK instruments, Finland). Additionally, two different air diffusers were placed on the floor on each side of the entrance door to simulate a realistic apartment system with cascade ventilation and transfer of air from other rooms (e.g. bedroom).

2.2 Kitchen hood and cooktop

A Siemens induction cooktop with four cooking zones, of which two with Ø 18cm (left front and left back zone), one with Ø 14.5 cm (right back) and one with Ø 21 cm (right front). The cooktop has 9 main power levels and one boost function. A standard wall mounted kitchen hood from Siemens is used in the experiments which can operate at both exhaust and recirculation mode. In this study, only the exhaust mode was chosen. The kitchen hood is placed at 54 cm above the cooktop, at the same height as the cupboards.

2.3 Measurement instruments

Particle size distribution was measured using an AeroTrak Handheld particle counter 9303 (TSI Incorporated, USA), calibrated with NIST traceable PSL spheres. It measures particles in the size range of 0.3 – 25 µm and can report up to three channels simultaneously. The AeroTrak has a counting efficiency of 50% at 0.3 µm and 100% for particles >0.45 µm. The AeroTraks were placed in three locations in the kitchen lab (see Fig. 2). Location 1 is assumed to be at the breathing height of an average Norwegian person while cooking and is set to 154 cm above the floor (assuming the mouth is 20 cm lower than the total height), and 50 cm away from the cooktop. Measurement location 2 is chosen to be in the middle of the room and set to 125 cm above the floor. Measurement location 3 is assumed to be the dining location in the kitchen lab. The instrument is therefore placed at a height of 110 cm, which is assumed to be at the breathing height of a sitting person.

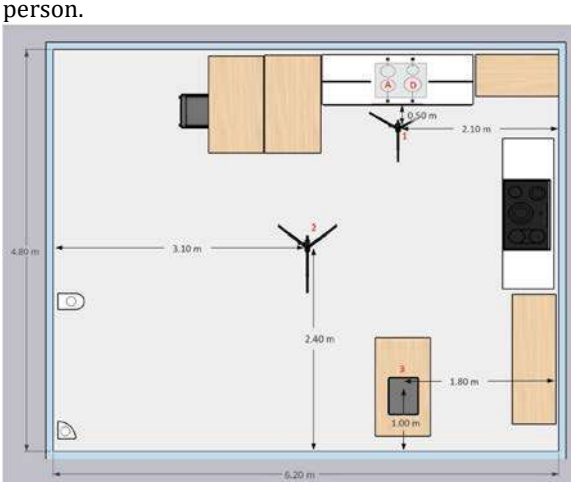

Fig. 2 - Measurement locations.

$PM_{2.5}$ mass concentration was also measured in location 2, using a GRIMM Portable dust monitor

1.108. It measures particles with diameters between 0.3-20 µm and classifies them into 15 size bins. The GRIMM has a reproducibility of ±3%. Measurements were logged at 1-minute intervals. Particle number concentration was converted to mass concentration for GRIMM, using the factory preset particle density of 1.65 kg/m^3 and a c- factor of 1 [8]. Whether this conversion is representative of the particles generated from cooking has not been investigated in this study. A further investigation considering the effect of this choice should be performed in future. Calibration factors have been provided for different meals by O'Leary et al. [9]. However, the kind/type of cooked meals and the equipment used for the preparation in our study are not directly comparable with their work.

Temperature and relative humidity in the kitchen lab were monitored every minute using a Rotronic CP 11 (Rotronic AG, Bassersdorf, Switzerland) with a declared accuracy of ±2.5%RH. In addition, a HIOKI data logger (Hioki EE corporation, Japan) also logged the temperature in the frying pan with thermocouple type K, and in the supply and exhaust air and the test hall next to the kitchen lab with thermocouple type T.

2.4 Test meals and cooking procedure

A review of potential test meals and cooking procedures were done, but relevant studies deviate from assumed typical Norwegian meals. Thus, a precursor survey of Norwegian cooking habits was performed to compose representative meals for this study. As the experiments need to be as reproducible as possible, the meals were simplified, and precise cooking procedures were developed. In short, both meal 1 involved frying and boiling, while meal 3 only frying. The detailed cooking procedure is available in [10]. The kitchen lab is assumed to be a living space for 2 adults. The portion sizes are therefore assumed to be for 2 adults and of relevant nutrition. A list of the meals selected for this study is given in table 1.

Table 1 Selected test meals.

Meal	Contains	Ingredients
1	Minced meat with taco spice 3 repetitions 16 minutes	• Minced meat, 400 g • Taco spice mix, 25 g • Rapeseed oil, 15 ml • Water, 150 ml
2	Vegetarian pasta Bolognese 3 repetitions 13 minutes	• Dried durum wheat spaghetti, 250 g • Pasta Bolognese sauce, 500g • Soya mince, 300 g • Rapeseed oil, 15 ml • Salt, 10 g • Water, 2 litres
3	Fried salmon with wok vegetables 3 repetitions 13 minutes	• Salmon, 400 g • Whole Grain Rice & Vegetable mix, 500 g • Rapeseed oil, 15 ml • Salt, 1 g • Pepper, 1 g

The nutritional value per 100 g for each of the meals is listed in table 2.

Table 2 Nutritional content of each test meal per 100g.

Nutritional value for each meal per 100 g	Minced meat with taco spice	Vegetarian pasta Bolognese	Fried salmon w/wok vegetables
Energy	866kJ/ 206kcal	623kJ/ 147kcal	656 kJ/ 157kcal
Fat (saturated), [g]	13.5 (5.9)	1.4 (0.2)	7.7 (1.4)
Carbohydrates (sugars), [g]	3.1 (0.9)	23.5 (4.7)	10.6 (1)
Fiber, [g]	0.01	3.04	1.44
Protein [g]	17.5	8.6	10.7
Salt [g]	2	0.8	0.4

2.5 Experimental setup

Table 3 shows an overview of all the experiments, the table is color coded to illustrate similar scenarios. Tests were performed for two ventilation scenarios: (1) with the kitchen hood off and a basic ventilation airflow rate of 72 m^3/h, (2) with the kitchen hood on setting 2 and thus achieving an airflow rate of 322 m^3/h (a basic ventilation airflow rate of 36 m^3/h plus kitchen hood extract of 286 m^3/h). Full mixing conditions were assumed. All experiments were repeated 3 times to ensure reproducibility and all experiments were logged for 1 hour.

Table 3 Overview of the experimental setup. Each experiment was repeated three times.

Exp. nr	Cooking duration (min)	Ventilation rate; Base+extract (m^3/h)	Duration of kitchen hood on (min)
Meal 1-1	16	72 + 0	0
Meal 1-2	16	36 + 286	60
Meal 1-3	16	36 + 286	16
Meal 1-4	16	36 + 286	55
Meal 1-5	16	36 + 108	60
Meal 2-1	13	72 + 0	0
Meal 2-2	13	36 + 286	60
Meal 3-1	13	72 + 0	0
Meal 3-2	13	36 + 286	60

The kitchen hood was turned on as the cooking started and kept on till the end of the measurement period. The results have been corrected for the difference in the basic ventilation rate when the kitchen hood is on (36 m^3/h) and off (72 m^3/h). The particle counts for the kitchen hood was off were multiplied by two to account for the different in the basic ventilation rate.

Three additional tests were also done to test different kitchen ventilation usage patterns. Due to time constraints, these tests were only done for meal 1 – taco. The purpose for these tests was to assess the effect of varying the duration of the use of the kitchen hood (1) by turning off the fan immediately after the cooking was done – exp. nr 1-3, (2) by turning on the fan 5 minutes after the cooking had started – exp. nr 1-4 and (3) the pollutant level at reduced extract rates using the minimum required kitchen ventilation in Norway (exp. nr 1-5; 36 + 108 m^3/h).

3. Results and discussion

3.1 Temperature and relative humidity

The room temperature in the kitchen lab during the experimental period was rather stable and varied between 21.4 - 23.9 °C. The relative humidity (RH) varied between the different test meals and fluctuated between 12.4 to 57.1%, particularly during meal 2 (vegetarian pasta bolognese) where boiling was involved, and the kitchen hood was turned off (RH>48.5%). An overview of the measured temperature and relative humidity in the kitchen lab during the different experiments is provided in Appendix A.

The temperature in the pan was measured with a thermocouple connected to a piece of aluminum. The calibration with only oil was very accurate to the actual temperature measured with the infrared thermometer. These preliminary experiments also revealed what power settings to use for stable pan temperature.

3.2 Instrument comparison

To ensure comparable result the particle number count of the GRIMM and Aerotrak was compared to see similarities in particle number count and the reproducibility of the repetitions for each test. Both the GRIMM and Aerotrak were placed in location 2. A comparison of the measured particle number concentrations over the entire size range (>0.3 µm) was done regardless of the differences in the cut-off diameter of the instruments. Fig. 3 shows the particle number concentrations of frying salmon with the kitchen hood off. Generally, the particle number concentrations obtained by Aerotrak are somewhat higher than the ones measured by the GRIMM. This is most likely due to the larger size range measured by the Aerotrak.

Scatterplot of each measurement series by the two instruments were plotted against each other and resulted in an average regression coefficient (R^2) of 0.84 when the kitchen hood was turned off indicating a good agreement of measured particle number concentrations by the two instruments.

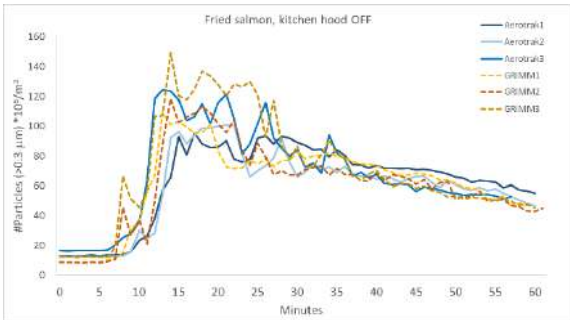

Fig. 3 - Particle counts as measured by GRIMM and AeroTrak at location 2 (middle of the room) cooking meal 3 – fried salmon when the kitchen hood was turned off.

A comparison of the three repetitions was also done and resulted in an average regression coefficient of 0.79 for GRIMM and 0.72 for Aerotrak. As seen in Fig. 3, there are variations in the magnitude of the particle number concentrations which could be due to insufficient airing in between each experiment. Moreover, due to time constraints, the experiments of the same test meal were not always done on the same day. However, the temporal trends are somewhat consistent. We simplified the cooking procedure to ensure the reproducibility of the outcome of the experiments. Each ingredient was also measured in advance, but cooking is a complicated process, and it is challenging to ensure that every movement is done the same way each time [1]. Between each experiment, the kitchen lab was ventilated well for 1.5h. Nevertheless, the three repetitions of making each meal are considered comparable enough, thus the remaining results are reported as an average of the three repetitions.

3.3 Effect of kitchen hood

For all meals, on average, more than 98% of the particles emitted were in the size fraction 0.3-2.5 µm, which is in agreement with previous research [2]. Figure 4 shows the average particle number concentrations for three different size distributions measured for 1h at the breathing height of the cook. The cooking duration is 16 minutes for meal 1 and 13 minutes for meal 2 and meal 3.

For meal 1 - taco and meal 3 – fried salmon, the number of particles increases rapidly in the beginning which corresponds to the rise of pan temperature. Both meals also yielded the highest peak particle number concentrations for all size fractions, resulting in the highest exposure for the cook when the kitchen hood is not turned on.

These two meals also have the highest content of saturated fat, confirming the positive correlations between fat content and emissions rates. This is in line with previous findings [3,11]. Also, high cooking

temperature results in increased emissions of particles, which is in line with our results as salmon were fried with the highest pan temperature out of all three meals.

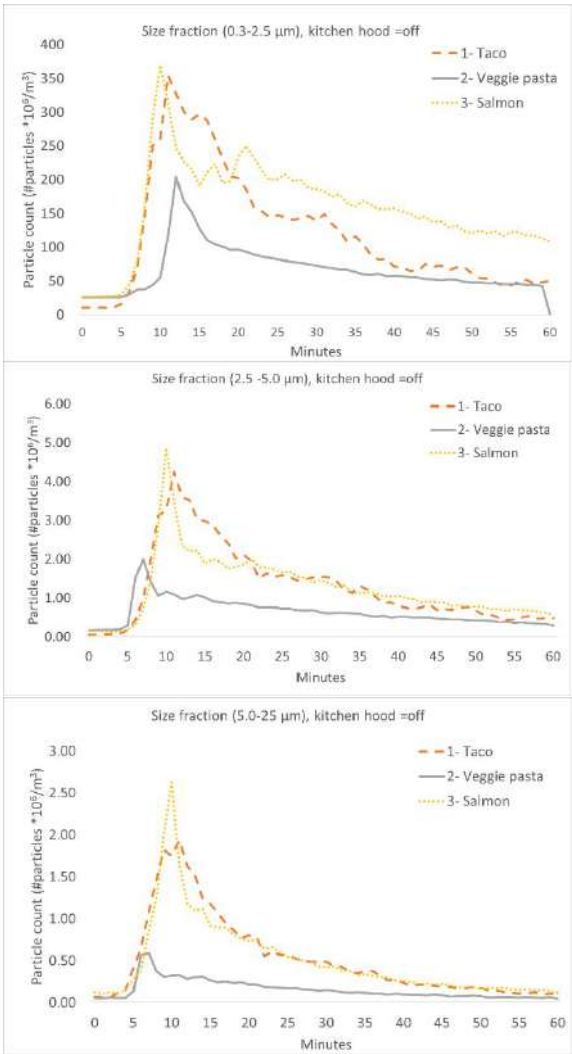

Fig. 4 - Particle counts for the three test meals with the kitchen hood off according to different size fractions. Measurement location=breathing height of the cook. Note the different scale on the y-axis.

In comparison, the peak particle number concentrations for vegetarian pasta Bolognese were much lower. Fig. 4 shows an initial increase of the larger size fractions due to the boiling of water. The increase of the smaller size fractions happens around 10 minutes when tomato sauce is added. For the other two meals, the increase in particle counts occurs simultaneously for all three size fractions. As seen in fig. 5, particles in the smaller size fractions do not decrease to the initial levels after one hour when the kitchen hood is turned off and with a base ventilation rate of 72 m^3/h.

Turning on the kitchen hood drastically reduced the particle number concentration for all three meals. Fig. 5 shows the particle number concentration for the smallest size fraction (0.3-2.5 µm) as most of the particles emitted are in that size fraction. Meal 1-taco resulted in the highest peak concentration ($16.6 \cdot 10^6/m^3$) followed by salmon ($15.7 \cdot 10^6/m^3$) and veggie pasta ($11.9 \cdot 10^6/m^3$), lowered from a level of above $360 \cdot 10^6/m^3$ for taco and salmon meals.

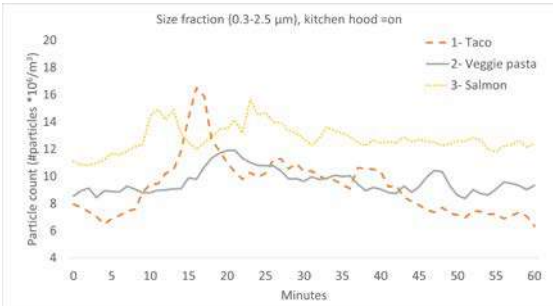

Fig. 5 - Particle counts for the smallest size fraction 0.3-2.5 µm (average values) for the three test meals with the kitchen hood on medium setting (36+286 m^3/h). Measurement location =breathing height of the cook.

Fig. 6 shows the average particle number concentrations for all size fractions (>0.3 µm) at different ventilation rates measured while cooking meal 1- taco. With the kitchen hood turned on using the minimum requirement for forced ventilation in Norway (108 m^3/h), the highest average peak particle number concentration was $152 \cdot 10^6/m^3$, resulting in a 58% peak reduction compared to when the kitchen hood was turned off. This indicates that the minimum requirement might not be sufficient to reduce the emissions from frying meat with taco spices and is also assumed to be the case for fried salmon.

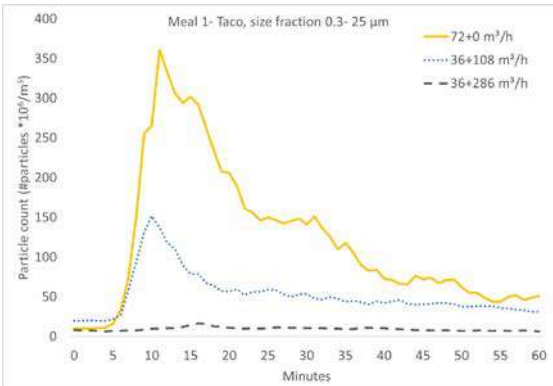

Fig. 6 - Particle counts for all size fractions 0.3-25 µm (averaged) for meal 1 - taco at different ventilation rates. Measurement location =breathing height of the cook. The cooking time is 16 minutes.

3.4 Exposure at different locations

Due to more open living room and kitchen solutions, we also assess exposure at different locations in the kitchen lab. Fig. 7 shows the particle number concentration for all size fractions for meal 1 - taco at the three measured locations with the kitchen. When the kitchen hood is off, the peak particle number concentration decreases with distance from the cooktop, a reduction of almost 50% from location 1 to location 3 (Table 4, exp 1-1, taco). The peak around 16 minutes at location 3 is when the dish was moved to the dining area.

When the kitchen hood is turned on, there are generally smaller differences in peak particle number concentrations and the 1h-averaged particle number concentrations at the different locations. For these experiments, the kitchen hood was on for the entire measurement duration of 1h.

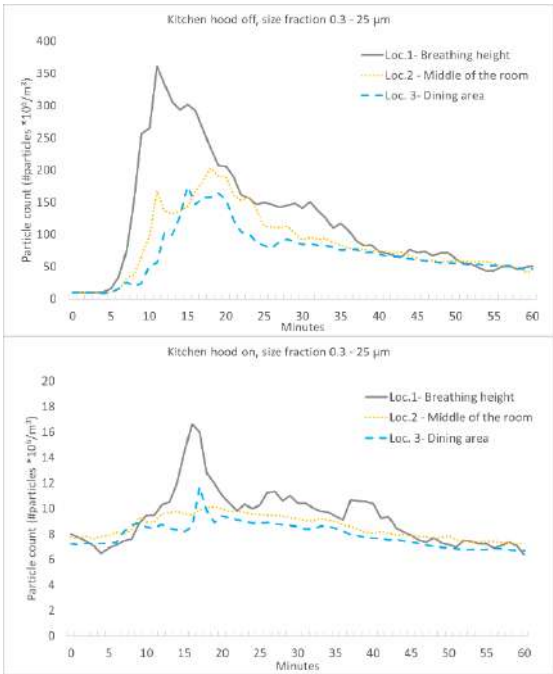

Fig. 7 - Particle number concentration (0.3-25 µm) for Meal 1-taco in all three locations (upper with the kitchen hood off, lower with the kitchen hood on).

Table 4 shows the peak particle number concentrations and average particle counts for the duration of 1h for all three meals.

Table 4 Peak particle number and 1-h average concentration of particle number for all size fractions for different test meals at three locations. Loc 1=breathing height, loc.2 =middle of the room, loc 3= dining area.

Exp.	Peak ($10^6/m^3$)			1-h average ($10^6/m^3$)		
	Loc. 1	Loc. 2	Loc.3	Loc. 1	Loc. 2	Loc.3
1-1	360.6	202.6	174.4	121.8	85.3	71.3
1-2	16.6	10.1	11.7	9.3	8.5	8.0
1-5	152	52	40	53	30	21
2-1	205.1	117.6	98.0	65.5	60.8	51.4
2-2	11.9	9.7	9.4	9.6	8.9	8.2
3-1	377.0	208.0	179.9	162.5	127.5	106.1
3-2	15.7	13.1	16.0	12.8	12.6	11.8

The trends for the other two meals (2-1, 3-1) are similar, with the highest exposure at the cooking area, and lower in the other areas in the kitchen lab when the kitchen hood is turned off. With the kitchen hood turned on (286 m^3/h), there are small differences in the particle number concentrations at the different locations in the kitchen lab. This indicates that cooking emissions are mitigated by the kitchen hood and does not influence the exposure in the rest of the room. An extract rate of 108 m^3/h (exp. 1-5) results in lower emissions, but not sufficiently compared to 286 m^3/h.

3.5 Hood usage pattern and emissions

A preliminary survey was performed to map the typical usage of the kitchen hood and other habits during cooking. It was found that more than 30% of the respondents did not always turn on the kitchen hood while cooking [10]. Noise and forgetting to turn it on were some of the reasons given, in addition, the usage of the kitchen hood was also depending on the type of food cooked or preparation method. Moreover, most people turn off the kitchen hood immediately after cooking. Based on these findings, we performed some additional experiments to assess the effect of kitchen hood usage patterns on particle emissions.

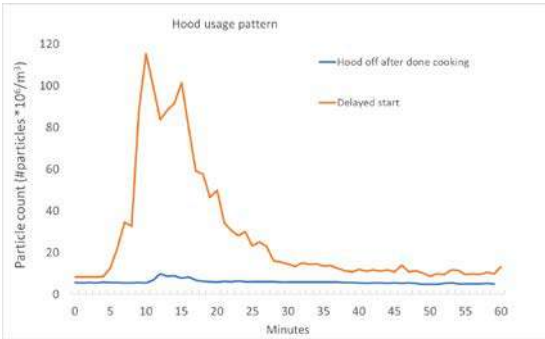

Fig. 8 - Particle counts for all size fractions for meal 1-taco with different hood usage patterns.

Fig. 8 shows that forgetting to turn on the kitchen hood when cooking by 5 minutes has a considerable effect on the number of emitted particles. Previous studies [10,13] have shown that some people might forget to turn on the kitchen fan or turn it off immediately due to the noise. In comparison, turning off the kitchen hood immediately after cooking versus leaving it on after cooking has little effect. This corresponds also with Fig. 6, showing that keeping the hood on for a long time after the cooking has ended does not make any difference in lowering the exposure level. This is in line also with the results from a study in the USA [12].

Our findings indicate that turning on the kitchen hood when the cooking starts or increasing the ventilation rate is a much better measure than leaving the kitchen hood on after the cooking has ended. Particles must be captured when generated.

3.6 Particle mass concentration

Particle mass concentration was only measured in the middle of the room (see Fig. 9), converted from the particle number concentrations measured by the GRIMM. When the kitchen hood is turned off, the highest $PM_{2.5}$ peak concentration was from meal 1-taco (84.9 $\mu g/m^3$), while the lowest was from meal 2 – vegetarian pasta bolognese (43.7 $\mu g/m^3$). When the kitchen hood was turned on, the measured $PM_{2.5}$

mass concentrations were lower than 2 µg/m³ for all three meals. The particle mass concentrations show similar trends as the particle counts.

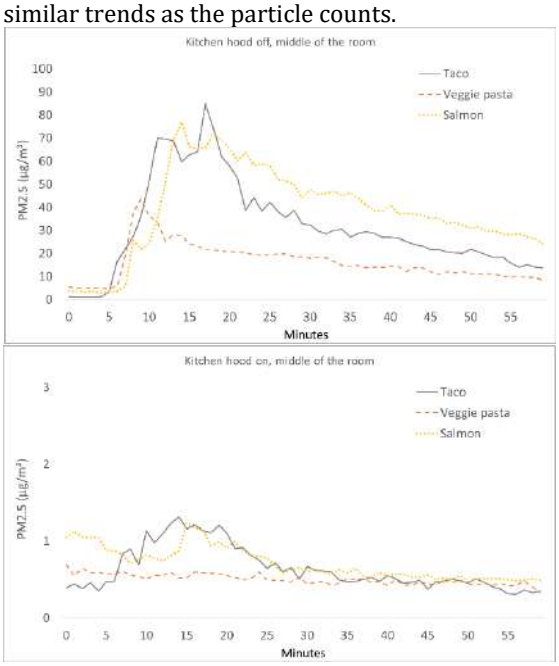

Fig. 9 - $PM_{2.5}$ mass concentrations measured in the middle of the room, for the three different meals. Upper: with kitchen hood off, and lower: with the kitchen hood on.

4. Conclusions

Particle number concentrations are measured for three typical Norwegian meals with different ventilation rates at three locations in the kitchen lab. The measurements show that the meals and cooking procedures developed are reasonable repeatable. Most of the particles are in the size range 0.3-2.5 µm.

The meal producing the lowest numbers of particles is the vegetarian pasta Bolognese, while the taco and fish meals which required both higher cooking temperature and contained more fat resulted in a much higher number of particles. The peak for particle number concentration was more than 40% lower for the vegetarian meal when the kitchen hood was turned off.

Turning on the kitchen hood at medium setting (286 m³/h) drastically reduced the particle number concentrations, however, the Norwegian requirement of 108 m³/h (low) reduced the number of particles at the breathing zone of the cook by only 58% for the taco meal.

Our experiments show that keeping the kitchen hood on after cooking has ended had minimal effect on the exposure, while a 5 min delay in turning on the kitchen hood resulted in an exposure level similar to the kitchen hood on a low setting. For open-plan kitchen solutions, the usage of the kitchen hood will impact the exposure of the occupants. Particles must be captured when generated.

5. Acknowledgements

This paper is based on the master thesis by Adele Jutulstad and was a part of the Urban Ventilation project. Urban Ventilation is funded by the Research Council of Norway EnergiX program under Grant No. 308819 and the industry partner Røros Metall AS, BSH Husholdningsapparater AS, Miele A/S, Engebretsen AS, Mestergruppen Bolig AS, Obos BBL, Selvaag Bolig ASA and Flexit.

The datasets generated and analysed during the current study are not publicly available because the datasets are in Norwegian and are part of an initial study but will be available by personal request.

Appendix A

Table A1 Measured average (minimum; maximum) relative humidity and temperature in the lab kitchen during the individual experiments. Measurement time=1h.

Test meal	Extract flowrate	Relative humidity (%)	Temperature (°C)
1-1	Off	27.2 (25.2; 30.5) 17.2 (15.2; 21.2) 17.4 (15; 21.7)	22.4 (22.2; 22.5) 21.5 (21.4; 21.6) 21.7 (21.6; 21.8)
1-2	On	12.7 (12.4; 13.2) 39.2 (37.5; 40.3) 37.1 (36.4; 37.8)	21.7 (21.4; 21.8) 22.6 (22.5; 22.7) 22.8 (22.7; 22.8)
1-3	On	39.7 (39.3; 40.2) 27.3 (26.5; 29.3) 20.9 (20; 21.9)	22.7 (22.6; 22.8) 22.4 (22.3; 22.4) 22.3 (22; 22.4)
1-4	On	40.1 (39.1; 40.6) 28.3 (26.7; 32.7) 27.6 (26.6; 30.1)	22.6 (22.5; 22.7) 23.8 (23.6; 23.9) 23.7 (23.6; 23.9)
1-5	On	40.4 (38.1; 42.9) 44.5 (43.6; 45.8) 43.9 (40.2; 48.2)	23.2 (23.1; 23.3) 23.3 (23.1; 23.4) 23.5 (23.4; 23.6)
2-1	Off	50.6 (39.5; 55.8) 52.7 (43.3; 57.1) 48.5 (43; 53.9)	23.2 (22.9; 23.3) 23.3 (23; 23.4) 23.4 (23.1; 23.6)
2-2	On	37.4 (37; 38) 36.6 (36.1; 37.5)	22.9 (22.8; 22.9) 23 (22.8; 23.1)

		36.9 (36.5; 38.1)	23.1 (23; 23.1)
3-1	Off	37.2 (36.3; 38.3)	23.1 (22.9; 23.3)
		36.8 (35.3; 37.9)	22.6 (22.2; 22.7)
		37.6 (36.8; 38.8)	22.4 (22; 22.6)
3-2	On	41.3 (40.8; 41.6)	23.3 (23.2; 23.3)
		42 (41.4; 42.7)	23.4 (23.3; 23.5)
		43 (42.7; 43.6)	23.5 (23.3; 23.6)

6. References

[1] K.L. Abdullahi, J.M. Delgado-Saborit, R.M. Harrison, Emissions and indoor concentrations of particulate matter and its specific chemical components from cooking: A review, Atmos. Environ. 71 (2013) 260–294. https://doi.org/10.1016/j.atmosenv.2013.01.061.

[2] Y. Zhao, L. Liu, P. Tao, B. Zhang, C. Huan, X. Zhang, M. Wang, Review of Effluents and Health Effects of Cooking and the Performance of Kitchen Ventilation, Aerosol Air Qual. Res. 19 (2019) 1937–1959. https://doi.org/10.4209/aaqr.2019.04.0198.

[3] M. Amouei Torkmahalleh, S. Gorjinezhad, H.S. Unluevcek, P.K. Hopke, Review of factors impacting emission/concentration of cooking generated particulate matter, Sci. Total Environ. 586 (2017) 1046–1056. https://doi.org/10.1016/j.scitotenv.2017.02.088.

[4] A.K. Sjaastad, K. Svendsen, Exposure to polycyclic aromatic hydrocarbons (PAHs), mutagenic aldehydes, and particulate matter in norwegian la carte restaurants, Ann. Occup. Hyg. 53 (2009) 723–729. https://doi.org/10.1093/annhyg/mep059.

[5] M.M. Lunden, W.W. Delp, B.C. Singer, Capture efficiency of cooking-related fine and ultrafine particles by residential exhaust hoods, Indoor Air. 25 (2015) 45–58. https://doi.org/10.1111/ina.12118.

[6] Gokhale, Maia, Salimifard, Parichehr, Cooking emissions, 2019.

[7] A.K. Sjaastad, K. Svendsen, Different types and settings of kitchen canopy hoods and particulate exposure conditions during Pan-frying of beefsteak, Indoor Built Environ. 19 (2010) 267–274. https://doi.org/10.1177/1420326X09347426.

[8] J. Burkart, G. Steiner, G. Reischl, H. Moshammer, M. Neuberger, R. Hitzenberger, Characterizing the performance of two optical particle counters (Grimm OPC1.108 and OPC1.109) under urban aerosol conditions, J. Aerosol Sci. 41 (2010) 953–962. https://doi.org/10.1016/j.jaerosci.2010.07.007.

[9] C. O'Leary, Y. de Kluizenaar, P. Jacobs, W. Borsboom, I. Hall, B. Jones, Investigating measurements of fine particle (PM2.5) emissions from the cooking of meals and mitigating exposure using a cooker hood, Indoor Air. 29 (2019) 423–438. https://doi.org/10.1111/ina.12542.

[10] A. Jutulstad, A. Yang, P.G. Schild, A. Chaudhuri, K. Thunshelle, Cooking habits and usage of kitchen hoods in Norwegian homes, in: TU Delft OPEN Publishing, Rotterdam, The Netherlands, 2022.

[11] G. Buonanno, L. Morawska, L. Stabile, Particle emission factors during cooking activities, Atmos. Environ. 43 (2009) 3235–3242. https://doi.org/10.1016/j.atmosenv.2009.03.044.

[12] N.A. Dobbin, L. Sun, L. Wallace, R. Kulka, H. You, T. Shin, D. Aubin, M. St-Jean, B.C. Singer, The benefit of kitchen exhaust fan use after cooking - An experimental assessment, Build. Environ. 135 (2018) 286–296. https://doi.org/10.1016/j.buildenv.2018.02.039.

[13] N.A. Mullen, Participant Assisted Data Collection Methods in the California Healthy Homes Indoor Air Quality Study of 2011-13, (2013). https://escholarship.org/uc/item/4sd2k5nh (accessed December 7, 2021).

TOWARDS ZERO ENERGY HOSPITAL BUILDINGS – ENERGY SAVING OPPORTUNITIES IN STEAM AND HUMIDIFICATION INSTALLATIONS

C.T. Ferreira Porto [a], W.H. Maassen [a,b], E. Swinkels [b], Perry van de Graaf [c], W. Zeiler [a]

[a] Building Physics and Services Department, Faculty of Architecture and the Built Environment, Eindhoven University of Technology, Eindhoven, the Netherlands.

[b] Royal HaskoningDHV, Postbus 1132, 3800 BC Amersfoort, the Netherlands, e-mail: wim.maassen@rhdhv.com.

[c] Utrecht Academic Medical Centre, Heidelberglaan 100, 3584 CX Utrecht, the Netherlands.

Abstract. The healthcare sector is highly energy intensive with circa 6% of the total global energy consumption. For this reason, hospitals strive to reduce their energy usage, especially of the most energy intensive systems like steam and humidification installations. Centralized steam plants are widely used by hospital complexes since many hospital functions rely on steam to properly fulfil its purpose (e.g. air humidification, sterilization, space and water heating, kitchen boilers). Central steam plants are not the most energy-efficient method to supply the consumers' demand due to the high energy and fossil fuel consumption for steam production and the consequent losses inherent to the extensive distribution installations. In general steam losses in steam system can represent over 30%. Total CO2 emissions for steam production can be over 20% of which humidification can represent over 50%. Therefore reducing the steam demand for humidification and implementing decentralized systems is of great importance for Hospital Buildings to fulfil for new buildings the nZEB requirements. In this paper the results of a literature study are presented and a method based on the so-called 5-step method [1] and the Kesselring method is used to select different systems based on their performances on different aspects. Solutions are presented that can save more than 50% of energy use and CO2 emissions used for the steam production.

Keywords. CO_2 emission reduction, Energy Savings, Hospitals, nZEB, Steam, Humidification, Sustainable Healthcare, Users Comfort, Infection Prevention.
DOI: https://doi.org/10.34641/clima.2022.51

1. Introduction

The need for (net) Zero Energy Buildings (nZEBs) is of increasing relevance due to climate change, rising energy prices and scarcity of fossil fuels. The built environment in the Netherlands is a great contributor to the overall energy consumption; according to IEA statistics, the sector has 46% of the total energy consumption share in 2016 [2]. The measures of the National Climate Agreement in the building sector aim to enhance energy efficiency by no longer enabling new buildings to be heated with natural gas and improving the existing building to fossil-free heating production.

The healthcare sector is highly energy intensive with circa 6% of the total global energy consumption. For this reason, hospitals strive to reduce their energy usage, especially of the most energy intensive systems like steam and humidification installations. In this context, the Dutch University Medical Centers (UMCs) consume approximately 64% of the healthcare demand [3].

The UMCs have a growing concern to fulfill the nZEBs requirements due to legislation. One of the many possibilities to decrease the energy consumption of hospitals is to re-evaluate the role steam plays in this environment. Steam use is a widespread method through many healthcare facilities. Since steam is considered a sterile medium, it can be used in hospitals for many different purposes, such as air moisturization, autoclaves, space and water heating, kitchen boilers and laundry. In hospitals, air humidification by steam has traditionally been used as part of the air treatment installation. The main arguments for this are the prevention of nosocomial infections, patient and staff comfort, safety

Copyright ©2022 by the authors. This conference paper is published under a CC-BY-4.0 license.

(electrostatic discharges) and maintaining equipment good functioning. Such a form of air humidification, however, is associated with high energy consumption. According to the TNO report [4], approximately 20-60% is used for air humidification. Moreover, thermal energy losses happen in flow distributing pipes where up to 30% of the total gas consumption of the steam boilers are lost.

The current study evaluates from a sustainability perspective, how to decrease energy consumption associated with steam in a building complex by using one of the Dutch UMC's as case study: The Utrecht Academic Medical Centre with ca. 400,000 m^2 buildings.

2. Methodology

The main objective of the research was to understand which are the main steam consumers of a hospital environment and, identify and recommend through functional analysis energy-efficient alternatives for the most significant consumer. Next a strategy was developed that can be applied in different hospital cases to identify energy reduction opportunities and measures that accelerate the path to nZEB hospital buildings and answer the main research question: Which measures can hospitals take for making the transition from centralized steam humidification to a more sustainable solution with less CO_2 emissions?

The literature research conducted for this study investigated the need for humidification and the ongoing debate that surrounds this topic. The research focuses on the influence of low relative humidity (RH) on health problems [5][1] and users' comfort. Furthermore, it provides an overview of all the other steam consumers within a hospital environment. Also, research was performed to give an overview of the possible alternatives for steam replacement in certain processes that could lead to energy reduction. In order to validate and assess the possible CO_2 emission reductions , data was gathered from the Utrecht Academic Medical Centre with actual measurements of steam used by each consumer and its energy consumption. A Pareto [6] energy analysis is applied to identify in the case study the main steam consumers and their overall energy share. The major energy consumers are identified on the campus level. In the development of the scenarios, the Pareto analysis is applied to the determined major consumer that can be improved and result in most energy reduction in comparison with the current situation (base case scenario).

The reduction of the energy demand is investigated through the evaluation and decision making supported by the Kesselring method [7]. This method consists of placing the possibilities in a morphological overview to generate different scenarios for energy consumption reduction. This morphological overview is used as a tool to structure the development process. The current scenario of the steam users is placed alongside the available alternatives for each function and humidification production method. This forms a matrix of possible solution combination scenarios. Scores are defined to rate the scenarios on multiple aspects, which are the criteria on which the possibilities should be evaluated.

The determined values are aggregated into a score for the overall rating of each alternative scenario and compared with the current base case scenario. The visualization technique, developed by Kesselring, allows different variants to be compared with each other. Within this method, the criteria for the requirements are separated into the categories for functionality and realization. The results of such evaluation can be seen in the so-called S-(Stärke) diagram [7]. Among the possible scenarios, the most viable options lie near the diagonal and have higher scores.

3. Case Study

As previously explained, the steam production is supplied to different functions. Each of these functions has different steam/energy demands. In order to statistically determine which of these different functions cause the most significant effect on energy demand, the Pareto Analysis technique is performed.

The Pareto Principle, explains that a small number of causes can be responsible for a large percentage of effects. This technique is particularly used to improve the decision-making process and efficiency.

The first step to applying such a technique is to identify and list all the causes (e.g. steam consumers) that may be leading to an issue (e.g. high energy consumption). Once all factors are known it was possible to identify the main contributors to the problem that needs to be solved.

There were no measuring sensors for quantifying the steam input for the air humidification of each separate building of the complex. This made the process of identifying inefficiencies and possible strategies more difficult. Therefore the assessment was based on the specifications of steam-equipment and its usage, feedwater metering and water-mass balance calculations (based on feedwater and condensate return metering). This resulted in the steam consumption share per steam consumer presented in Figure 1.

[1] The conclusions presented on this reference is that RH has little or no effect on reduction of infection risk, although the effect of RH on the susceptibility of the SARS-CoV-2 virus was not considered and will be further investigated.

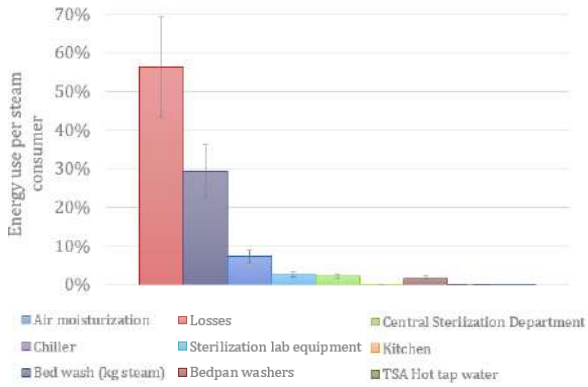

Fig. 1 - Steam consumption share per steam consumer

The steam energy consumption can then be divided into three main streams: air humidification, distribution losses, and other steam consumers. Data retrieved reinforces the information obtained on literature that steam losses represent a great disadvantage on buildings systems and that air moisturization is the largest consumer of steam in hospital applications. In the case study, the losses represent 29% (with ±23% of inaccuracy on the calculations, given the lack of precision of measuring sensors).

There is no sub-metering for the air humidification in each of the UMC buildings, however by making use of the typical functions area and their percentual area in each of the buildings it is possible to make an estimation of the energy consumption used for the humidification of each building and function. Figure 2 shows the functions that consume more energy on the UMC per net internal area (NIA). It reinforces the assumption that operation theatres/rooms (ORs) are the most energy demanding per m² in regard to their humidification systems.

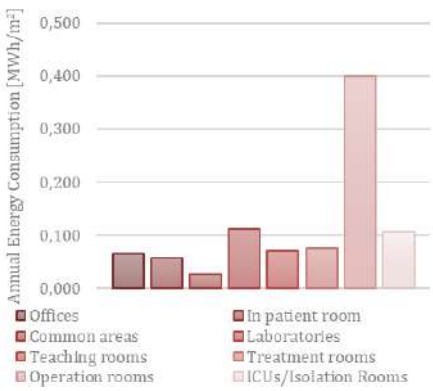

Fig. 2 - Annual energy consumption per NIA

Nevertheless, a Pareto analysis can also be used to determine which of the room functions are the major contributors in the overall UMC air humidification consumption. Figure 3 shows that despite the ORs requiring more energy for air humidification per area, offices and the common area are the major contributors to the overall consumption.

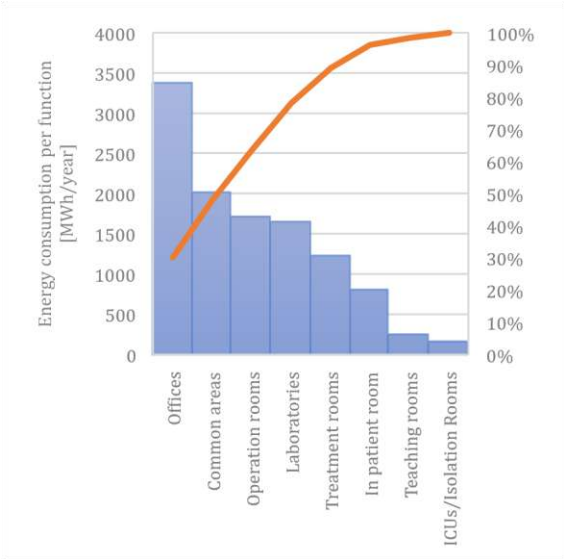

Fig. 3 - Pareto analysis of the room functions as contributors to the air humidification energy consumption

The analysed UMC has around 132,000 m² of offices and common areas that are daily humidified and herewith contributing 30% and 18%, respectively, the humidification energy consumption at this complex.

The results show which specific hospital functions are consuming large amounts of energy for their air humidification. It is necessary to discuss whether air humidification is really necessary and considerably contributing to the healing process to function properly and/or to significantly increase their building users' health and comfort.

4. Scenarios Evaluation

4.1 Kesselring Method

The functional aspects of air moisturization are very subjective and controversial. No exact values of each system's influence on users' health, comfort and ESD are given in the literature. Thus, this evaluation is only an estimation of the relation between these aspects, based on the opinion that was acquired by performing the literature study. The scores are given based mostly on the literature study. On the other hand, the realization aspects are measurable; thus, they represent the most significant difference in the comparison between the scenarios.

The functional criteria are based on:

• Health concerns: the highest score refers to the low impact on nosocomial infection threats, fungi growth and allergy symptoms, according to literature, assuming the implementation of the scenario.

• Electrostatic discharge prevention: scores high when the ESD possibility is the lowest when compared to other options.

• Users Comfort: scores high when the patients or staff comfort is believed to be improved, with the implementation of the scenario, according to the literature study.

The realization aspects are:

• Energy efficiency: the highest score refers to the highest energy saving potential of the scenario (≥75% than the baseline scenario).

• Carbon Emissions: scores high when the carbon emissions reduction potential of the scenario is very significant when compared with the baseline (≥75%).

• Operational costs: a high score means the scenario has low annual operation (energy + water treatment) costs when compared to the other scenarios.

• Investment costs: scores high when the estimated investment costs of the scenario are relatively low when balanced with its returns.

• Realization time: the highest scores are given when the scenario can be implemented in a short time span.

• Controllability: scores high when the scenario counts with a good RH-range control

4.1 Baseline scenario

In order to make a viable energy reduction comparison, a reference profile is needed. The energy consumption for air humidification in the whole campus for the year 2018 (≈12,945MWh) needs to be validated through calculations of a baseline scenario. Using calculation and formulas based on the Mollier diagram and internal setup points for the air treatment of the case study UMC, a baseline scenario matching the energy consumption data of 2018 was simulated. The resulting annual consumption for air humidification of the baseline is 12,274MWh, which represents 95% accuracy when compared to the gathered data.

The scenarios' energy calculations were based on the requirements for each typical hospital function (e.g. patient's rooms, operating rooms, offices, etc). The indoor temperature, RH levels range and air changes per hour (ACH) data were based on the UMC current or future requirements listed on its 2018 Masterplan. When the value in the masterplan is neither mentioned or required, recommended values from ASHRAE [8, 9, 10] or CBZ [11] are used.

The functions considered in the calculations represent the most important functions in a university hospital building and have relatively different air treatment requirements: offices, in patient, common areas, laboratories, teaching rooms, diagnostic and treatment, operating rooms and isolation room/ ICU.

1.1 Alternative scenarios

One of the goals of UMC's is to reduce the use of fossil fuels (e.g. natural gas) as its primary energy source. Thus, for the simulated scenarios, local electrical humidifier (isothermal) option to produce steam, adiabatic humidification process and use of energy wheel options are introduced.

Seven scenarios are analysed. These were created by combining alternatives from a Morphological Overview. The combinations are based upon different air humidification and energy efficiency concepts. Not every possible combination of the presented solutions, even with focus only on the air moisturization, is possible, since having different air treatment systems can lead to logistical problems in the hospital.

Scenario 1 – Reduced RH ranges

Scenario 1 is simulated considering the minimum RH levels for all rooms as recommended by ASHRAE [8, 9, 10]or the CBZ [11]. The humidification is maintained as isothermal, with the same steam production method, to be able to compare the benefits this scenario can bring when compared with the baseline. The total area to be humidified in this scenario is the same as the baseline scenario, 195,000m^2.

Scenario 2 – Reduced functions with air humidification

Scenario 2 is calculated according to the assumptions that not all rooms are supplied with moisturized air. Considering that air humidification is not a priority in all building's rooms, but only in the rooms that have stricter RH requirements, scenario 2 is simulated considering only the most crucial rooms for the patients' health: ORs and ICUs/isolation rooms. With the purpose of comparison with the baseline, the only change is on the building's functions, which are reduced; all the other parameters (e.g. RH levels, steam production method) are the same as the baseline.

The total area to be humidified is reduced to approximately 5,890 m^2, to be supplied with steam by the central energy plant.

Scenario 3 – ORs and ICU with electric humidification

This scenario is simulated as scenario 2; however, the difference is that this one assumes the local use of resistive humidifiers, instead of natural gas as a source for the steam production. The choice for this type of electrical humidifier was determined due to its advantages found during the literature study.

The total area to be humidified is reduced to approximately 5,890 m^2. The electrical humidifiers should be placed at a local level (in-duct).

Scenario 4 – Adiabatic in most building's functions

An alternative for steam in air humidification is the use of atomizing humidifiers, also known as adiabatic humidifiers. On this system, the water is vaporized in micron size droplets directly into the air. In the Netherlands, a report from TNO [12] describes the proper water treatment for being used in this type of system and states that adiabatic humidifiers types - without recirculation - are suitable to be used in healthcare facilities. Nevertheless, the report [12] recommends ORs and ICUs remaining with humidification being provided by steam.

Adiabatic humidification is the most likely future for humidification in large buildings since it is more energy-efficient than the isothermal type. In order to verify the energy efficiency of the proposed system, this scenario evaluates what would be the benefits of applying low-pressure adiabatic humidification to all rooms, except ORs and isolation rooms/ICUs, with the same RH levels as the baseline.

Moreover, scenario 4 considers that ORs and isolation rooms/ICUs have their humidification provided by locally produced steam electrical humidifiers. Thus, 188,800 m^2 are humidified by adiabatic technology; the adiabatic humidifiers should be placed at a central level (in approximately 100 AHUs). The remaining 5,890 m^2, or 226 rooms, are considered to be locally humidified by electrical (resistive) humidifiers.

Scenario 5 – Adiabatic for all rooms

A relatively new technology that has been applied in a few Dutch hospitals[2] is the hybrid adiabatic humidifier. This adiabatic humidifier hygiene has been tested, proven and confirmed by the award of the SGS-Fresenius Hygiene Certificate. Given the fact that this technology is already in use in the Netherlands and it has received a well-known hygiene certificate, its energy consumption and benefits to the case study are considered in this scenario. This technology has already been applied in one Dutch hospital with this type of humidifier applied to its ORs; therefore, this scenario takes this application into consideration for all building functions.

Scenario 6 – No humidification for most rooms + adiabatic

According to the research, humidification does not play a big role in many building areas. As previously stated, assuming a scenario wherein the Dutch hospitals do not use air moisturization in the majority of its buildings functions, is, therefore, a reasonable option.

However, for the middle-term, it is safer to consider that a few rooms will still need air humidification. In this scenario, humidification is considered in rooms that are focused on the most crucial patient treatment. This scenario assumes that only the AHUs which supply air to operating and isolation/ICU rooms of UMC to be equipped with the same adiabatic humidifier type of the previous scenario.

Scenario 7 – Energy recovery wheel

Heat and moisture recovery from mechanical ventilation air with energy wheels can be used if it is prevented that the possible suctioned contaminants are not returned to the supply channel. In regard to hospital environments, it is necessary to ensure there is no cross-contamination in specific treatment areas, such as intensive care and operation rooms. Therefore, this scenario considers the implementation of energy wheels for all the departments, except for the intensive care/isolation rooms and operating department. These are assumed to receive air moisturization via local use of resistive humidifiers (same as Scenario 3).

5. Results

5.1 Baseline

The baseline scenario considers that the air moisturization consumes 12,274 MWh/year, based on calculations regarding the isothermal air humidification process. The energy costs of the steam production for the baseline scenario consist of the costs for natural gas for steam production and the costs for the feedwater. The annual humidification load requires approximately 30,000m^3 of water per year.

Calculations are made for this per kWh and m^3 of input, considering:

- Natural gas rate ≈ € 0,0384/ kWh [13]
- Feedwater rate ≈ € 0,7211 / m^3
- Softened water treatment ≈ € 1,1012 / m^3

The annual energy costs and consequently CO_2 emissions for the total steam production of the baseline scenario can be seeing on Table 1.

5.1 Alternative scenarios

The results for the realization aspects to be evaluated are presented on Table 1.

[2] Examples are: Deventer ziekenhuis (in its operating rooms); Antonius ziekenhuis; Radboud UMC; ZGT ziekenhuisgroep Twente; VUMC

Tab. 1 - Summary of the Scenarios

Scenario	Energy Consumption [MWh/year]	Carbon Emissions [ton CO_2/year]	Energy Costs [€/year]
Baseline	12,274	2,250	525,300
1	4,200	770	167,300
2	3,000	350	130,100
3	3,000	1,040	273,900
4	11,780	3,730	1,264,100
5	9,650	3,280	1,106,800
6	300	100	99,300
7	2,200	750	205,000

Scenario	Operational Costs [€/year]	Investment Costs [€]
Baseline	2,626,500	-
1	836,500	-
2	650,500	-
3	1,369,500	>4,000,000
4	2,275,380	>7,000,000
5	1,992,240	>3,000,000
6	496,500	>1,040,000
7	1,025,000	>8,200,000

The scoring for functional and realization aspects was performed by assembling the aspects on matrixes of comparison (which aspect should carry a higher weighing factor) and evaluated on a grading system between 1 to 4 (e.g. 1 = scenario choice is the least recommended choice; 2 = scenario has some positive influence, however it is not very significant to the overall context; 3= scenario has a positive influence in large part of the case study; 4= is the most recommended choice). Each of the involved parties on this research has given their own score based upon knowledge acquired by literature study, professional experience and results from the calculations made for the realization aspects.

Figure 4 presents the summary of the scenarios' score for each of these aspects. The graphical result of the scoring is shown on the Kesselring diagram in Figure 5.

Air Moisturization								
	Max	Scenario 1	Scenario 2	Scenario 3	Scenario 4	Scenario 5	Scenario 6	Scenario 7
Function								
Health concerns	24	12	12	12	18	21	15	18
Eletrostatic discharge prevention	8	3	3	3	6	6	5	6
Users Comfort	8	3	3	4	7	7	4	6
Total	40	18	18	19	31	34	24	30
Percentage of whole	**100%**	**45%**	**45%**	**48%**	**78%**	**85%**	**60%**	**75%**
Realization								
Energy efficiency	24	15	21	21	6	9	24	21
Carbon Emissions	24	12	21	15	3	3	24	12
Operational costs	16	6	14	10	2	4	16	10
Investment costs	16	16	16	6	4	6	12	4
Realization time	8	8	8	5	2	3	5	2
Controllability	8	2	3	6	6	7	5	5
Total	96	59	83	63	23	32	86	54
Percentage of whole	**100%**	**61%**	**86%**	**66%**	**24%**	**32%**	**90%**	**56%**

Fig. 4 – Summary final scoring of scenarios

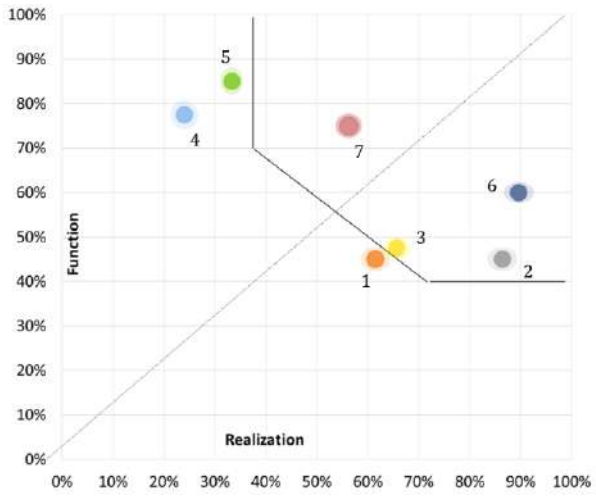

Fig. 5 - Kesselring Diagram final scoring of scenarios

As short-term solutions, maintaining steam as the humidification method, scenario 1 and scenario 2 represent energy consumption improvements. By decreasing the RH levels to the minimum recommended by ASHRAE (scenario 1) or reducing hospital areas that are humidified to only the ones that have more strict requirements regarding the RH levels (scenario 2), both are solutions that can be applied in a short time span with no investment costs. These are the solutions with the lowest financial costs since in the UMC case study there is already a power plant to supply the steam demand. However, both assume that the production of steam would still be made with natural gas, which is not the most sustainable solution, considering the long-term goal of reducing fossil fuel use. Additionally, even with the reduced demand of these scenarios, the steam losses are still implied in the overall system energy consumption.

Scenario 3 considers the same parameters as scenario 2; however, scenario 3 requires investment costs for the application of electrical humidifiers, whereas the latter does not require any initial investments. The electricity costs also make this an unattractive choice. Nonetheless, advantages of this system are not using natural gas as a primary energy source; also, once the main steam consumer has its demand locally supplied, the system losses are reduced as the centralized plant would no longer be required.

Scenario 4 and 5 scored the highest in the function aspects had poor scores on realization aspects. It can be assumed that it has received high scores in functional aspects because both scenarios consider humidified air being provided to all hospital areas, eliminating any health, electrostatic and discomfort risks for all users. Nonetheless, the implementation of adiabatic installations for all buildings would imply high investment costs, long realization time; moreover, the electricity consumption and carbon emissions would be higher than the current scenario, which can be assumed to be the reasons for the poor scores on realization aspects. For improving these scenarios scores in the realization aspects, the functions which are supplied with air humidification via adiabatic systems should be reduced, in order to reduce the investments and operational costs.

Scenarios 2, 3 and 6, that only consider a few hospital areas to be humidified, are the most promising ones, as the investment costs can be compensated in a few years, maintaining the areas which have more strict requirements humidified and having low energy consumption.

Scenario 6 is the most energy-efficient case in which only two types of hospital functions are considered and supplied with a highly efficient humidification system. Nonetheless, the investment costs are still very high and time for realization can be rather long.

Scenario 7 is the most beneficial for all hospital zones: with the energy wheels implementation in all building parts, humidity levels could be kept within the comfortable range, which could improve the perceived indoor air quality. Moreover, the functions with stricter requirements are considered to be supplied with steam via electrical local humidifier, to ensure no health risk to the patients. However, the investment costs and the realization time are very high in this scenario.

It can be assumed that a combination of alternatives, that would result in RH levels within the comfortable range for all hospital areas, would be the most optimal solution, such as scenario 7. With the use of energy recovery wheels in large part of the hospital, there would be no need of humidification being supplied via isothermal or adiabatic systems; this solution has a great reduction of costs and energy consumption when compared to the other scenarios; additionally, scenario 7 assumes the supply of air humidification via a sterile medium (steam) in the most strict areas of the hospital, thus guaranteeing a high score in all functionality aspects. However, this scenario could be improved if adiabatic systems were assumed instead of electric humidifiers: the electricity costs would be fewer and the overall energy efficiency would be improved.

The obtained values are an estimation of the energy, CO_2 emissions and costs savings of what the scenarios could represent if applied to the case study under these assumptions. There are many other variables which were not taken into account as the study case is a complex of several buildings each one with different characteristics and occupation profiles.

Investments' costs for the adiabatic and energy wheel systems are difficult to determine since adjustments are needed in the air handling units and ducts, particularly in the humidification sections. The existing steam system does not require any investment.

The complex heating and cooling demands would be affected by alternative systems choice. However, they are outside of the scope of this research. Their assessment would require extensive research focused on these systems alone. The focus is the air humidification, the recommended levels of air RH and possible alternatives for the steam demand. Research has shown that there are feasible paths to significantly reduce energy consumption in this system.

6. Conclusions

The main conclusion of this study and case evaluation is that hospitals have massive energy and CO_2 emission reduction possibilities by humidifying when necessary, or significantly beneficial, and applying alternatives for centralized steam plants.

The main starting point is the fact that many large hospitals have their own central plant to produce and distribute steam to its many consumers. This system, however, results in large amounts of CO_2 emissions and energy losses. In this study a strategy is developed that hospitals can apply to assess and evaluate alternative solutions for humidification and the central steam plant.

As an initial step of the aforementioned strategy an assessment of the hospital areas where humidification is not essential should be conducted, humidification demand reduced and investing on localized air humidification in crucial areas of the hospital. From a long-term perspective, investment on the adaptation of the whole hospitals' systems is required.

To ensure comfort in the majority of buildings' functions, energy-efficient energy wheels are the most optimal choice. The areas which may still need

air humidification to be supplied by other means could have local systems, either electrical steam humidifiers or adiabatic. By transitioning from centralized steam plants to localized solutions, the Dutch hospitals could guarantee energy savings, CO_2 emissions reductions and at the same time health, comfort, and safety.

The focus on air humidification was decided based on the performed Pareto analysis of all hospital steam consumers of the case study, as well as conclusions drawn from the literature study. According to the literature study and experts' opinions, no conclusive evidence was found that setting the humidification to off would increase infection spread risk to the user's health; however, for the thermal comfort of staff and long-stay patients, maintaining air relative humidity within determined range is advisable.

After the conducted research on the case study the recommendation is to verify for each building which AHUs supply treated air to critical healthcare functions as operating rooms, isolation rooms and intensive care units. On the buildings which do not have such functions, this study concludes that air humidification is not essential, and the determined ranges of RH could be achieved with alternative solutions.

In 4 out of 7 scenarios, the reduction in energy use and CO_2 emissions was over 75%, when compared to the current energy demand for humidification.

The 5-step method combined with a Pareto analysis to identify the main contributors to the overall CO_2 emissions and energy consumption and the Kesselring method to evaluate possible scenarios, were used to develop a generic strategy that can be applied in different hospital cases where humidification is applied with or without a central steam system, to achieve significant energy reductions and to accelerate the path to nZEB hospital buildings.

7. Acknowledgement

The present study was executed as a master graduation project [14] in cooperation of Eindhoven University of Technology , Royal HaskoningDHV and the Utrecht Academic Medical Centre. The study is part of a research program that was initiated by Royal HaskoningDHV in cooperation with the Eindhoven university of Technology and supported by TVVL and REHVA [1].

8. References

[1] Maassen W., "(nearly) Zero Energy Hospital Buildings," HaskoningDHV Nederland B.V., Rotterdam, NL, 2017.

[2] IEA. Available: https://www.iea.org/statistics/?country=NETHLAND&year=2016&category=Energy%20consumption&indicator=TFCShareBySector&mode=chart&dataTable=BALANCES . [Accessed July 2019].

[3] Dainese E., " Towards Zero Energy Hospitals – UMCU case study," 2018.

[4] TNO, "Routekaart Verduurzamin van het zorgvastgoed - Ziekenhuizen," 2019.

[5] Aganovic A., Bi Y., Cao G., Drangsholt F., Kurnitski J. & Wargocki P., "Estimating the impact of indoor relative humidity on SARS-CoV-2 airborne transmission risk using a new modification of the Wells-Riley model," Elsevier - Building and Environment, 2021.

[6] Dunford, R., Su, Q., Tamang, E., & Wintour, A. "The Pareto Principle", The Plymouth Student Scientist, 2014.

[7] Zeiler, W., Savanovic, P., & Quanjel, E., "Design decision support for the conceptual phase of the design process," in IASDR07 - International Association of Societies of Design Research, Hong Kong, 2007.

[8] ASHRAE, "ASHRAE Standard 62.1," 2016.

[9] ASHRAE, " ANSI/ASHRAE/ASHE Standard 170-2017, Ventilation of Health Care Facilities," 2017.

[10] ASHRAE, "ASHRAE Table 7.1 Design Parameters," Bureau of Architecture &ENgineering Review (BAER), 2017.

[11] CBZ, "Binnenmilieu en installatietechniek in de zorgsector. Utrecht: CBZ - College bouw ziekenhuisvoorzieningen," 2002.

[12] TNO, "Ontwikkeling van een beoordelingsmethode voor centrale luchtbevochtigingssystemen voor ziekenhuizen met het oog op de microbiologische veiligheid," 2009.

[13] Eurostat. Eurostat Statistics Explained - Electricity Prices Statistics. "Eurostat Statistics Explained - Electricity Prices Statistics," May 2019. Available: https://ec.europa.eu/eurostat/statistics-explained/index.php/Electricity_price_statistics#Electricity_prices_for_non-household_consumers . [Accessed October 2019].

[14] Ferreira Porto C.T. "Towards zero energy hospital buildings: Energy savings through central steam systems analysis and alternative humidification scenarios," 2020.

The datasets generated during and/or analysed during the current study are available in the TU/e repository, https://research.tue.nl/en/studentTheses/towards-zero-energy-hospital-buildings-2

Exploring futures of summer comfort in Dutch households

Lenneke Kuijer [a,b], Lada Hensen Centnerová [c]

[a] Future Everyday Group, Department of Industrial Design, Eindhoven University of Technology, Eindhoven, the Netherlands, s.c.kuijer@tue.nl.

[b] Eindhoven Institute for Renewable Energy Systems, Eindhoven University of Technology, Eindhoven, the Netherlands

[c] Building Performance Group, Department of the Built Environment, Eindhoven University of Technology, Eindhoven, the Netherlands, l.hensen@tue.nl.

Abstract. Due to climate change, the outdoor temperatures, frequencies, and durations of heatwaves and levels of solar gain in the Netherlands are expected to increase. Based on the European Energy Performance of Building Directive (EPBD) new standards are introduced. However, it is still uncertain how Dutch culture might adapt to this change in climate. The qualitative study underlying this paper addressed this question by focusing on the future of summer comfort in Dutch households. It comprised 21 interviews with diverse households and 10 expert interviews. Results show that while summer night ventilation and shading can prevent or reduce overheating through low-energy means, several cultural and practical barriers stand in the way of their full potential. Practices of shading and summer night ventilation require the active involvement of residents, but clash with their historically formed relation with the sun. A cultural shift is needed to better integrate these practices into household responses to hot weather. Moreover, the study identifies potential for technologies, policies and procedures to support acclimatisation of residents to higher temperatures. This could save energy as well as promote healthy living during hot weather.

Keywords. Summer comfort, Netherlands, cultural change, qualitative study, dwellings, energy.
DOI: https://doi.org/10.34641/clima.2022.388

1. Introduction

The climate in the Netherlands is getting warmer [1]. Due to climate change, the likeliness, severity, and duration of heatwaves is increasing. Dutch dwellings have long been built with a focus on keeping warm during winter, resulting in high levels of insulation and airtightness, which increases the risk of overheating. Other factors contributing to overheating issues are urbanisation and urban heat islands, and an ageing society.

Dutch households are beginning to experience the consequences of climate change in their everyday lives and starting to adjust their lives and homes to these new circumstances. For those who can afford it, mitigating discomforts and health risks of hot weather are within reach, but tend to require high amounts of energy. Essent, one of the main energy providers in the Netherlands reported a 30% increase in energy demand during the August 2020 heatwave [2]. This growth was attributed to the rising use of ventilators and air conditioners in households. While penetration rates for active cooling are relatively low in the Netherlands, this trend is worrying because it could jeopardize achieving national and international CO_2 reduction targets, and further contribute to climate change. Moreover, for those not able to take required measures, overheating is expected to pose increasingly severe health threats [3].

At this point in time, Dutch responses to global warming can still go in many directions, some of which are undesirable from health, inclusivity, and environmental points of view. This paper, which is based on a publicly available stakeholder report [4] presents a qualitative exploration of the future of domestic summer comfort in the Netherlands. By identifying and extrapolating current cultural, demographic and technological trends in domestic summer comfort, it identifies relevant questions, challenges, and points of friction.

While the focus of the study is on the Netherlands, its outcomes may be relevant beyond this context, particularly in countries where active cooling is currently on the rise due to global warming.

Copyright ©2022 by the authors. This conference paper is published under a CC-BY-4.0 license.

2. Background

The Dutch Meteorological Institute (KNMI) defines a heatwave as a period of at least five consecutive days with daily maximum temperatures exceeding 25°C, with at least three of the five days reaching maximum temperatures above 30°C. In the Dutch context, heatwaves of this kind are still considered extreme weather events; local governments put heat plans in action to protect vulnerable groups and people experience disruptions to their everyday lives such as more difficulty with sleeping, focusing and getting around. These heatwaves are expected to become longer, warmer, and more frequent [1].

The Netherlands is at a crossroad when it comes to summer comfort. Permanently adopting highly energy-intensive, cooling-dependent practices of summer comfort that exist in countries like Australia [5, 6] could still be prevented if well-informed decisions are taken today. 'Solving' overheating in dwellings with active cooling is not the only possible way forward; summer comfort in the Netherlands could still go in a variety of directions. Actions in the present regarding new building policies, proposing standards (e.g. the NTA 8800), designing infrastructure, building technologies, and passing on instructions have an effect on shaping futures of summer comfort in Dutch households. These actions, in turn, are informed by visions, assumptions and expectations of what futures are possible, desirable and likely to come about. Insight into these futures from a Dutch household perspective is so far limited.

This raises questions like: To what extent are mainstream Dutch households equipped and able to equip themselves to deal with longer, warmer, and more frequent heatwaves? Which strategies do households apply and aspire to achieve comfort in times of hot weather, and which currently not? What are possible consequences of these strategies for levels and patterns of energy demand, and general well-being? What are developments outside of these households that may affect these strategies?

Since they pertain to the future and therefore cannot be directly studied, these questions are challenging to answer. To come to answers, this study draws on theories and methods from social practice theory, which is a group of theories from sociology that approach everyday life as a collection of practices [7, 8]. Practice theories are useful for the challenge at hand because they are particularly good at studying larger scale societal changes while still considering the details of everyday life [9].

Summer comfort is a so-called dispersed practice [10], a practice that is part of many integrative practices. Examples of integrative practices are cooking, bathing, and sleeping. Part of the challenge is to identify the relevant integrative practices. Within social practice theory, the study builds on earlier work that explored dispersed practices (of winter comfort) historically [11]. What this earlier work highlighted, besides the importance of including a range of integrative practices, is the importance of including broader changes outside the household in the analysis: i.e. practices of domestic winter comfort co-evolve with changing indoor climate technologies and were affected by government policies such as the increased age of compulsory education and reduced work hours [11]. Inspired by Dahlgren et al. [12], these contextual trends were divided into three categories: (1) Climate changes, (2) Demographic changes, (3) Technological changes.

In line with current trends towards more 'smart', interactive technologies in the home, the study draws on the concept of co-performance. Co-performance is a modification of social practice theories that places automated technologies—such as thermostats—next to people as co-performers of practices [13]. The idea behind this shift is that automated technologies increasingly take over tasks from people. Sensors, processing power (matching sensor values to pre-set thresholds), connectivity (to weather predictions, mobile phones) and actuators (connected to power sources, usually the electricity network) allow these devices to act relatively independent of the inhabitants. Their 'behaviour', alongside that of humans, affects the development of everyday practices. For example, the actions of an automated sunscreen are based on a judgment—'*it is too sunny now, this sunshine should be prevented from entering the home, wind speeds are low enough: go down*'. As such, it, and by implication the designers who designed the judgment into the device, become performers of this judgment in everyday life. The actions of the sunscreen, reflecting judgments about 'good' and 'bad' sunshine, 'strong' and 'mild' winds, are experienced by inhabitants and passers-by who see and experience the action. This in turn influences their ideas of appropriate shading behaviour. A co-performance perspective therefore considers the combined behaviour of people and automated devices when considering practices and how they change.

These theoretic starting points: (1) summer comfort as a dispersed practice, (2) social change as a co-evolution of practices and contextual developments, and (3) automated technologies and their designers as co-performers of practices alongside people, form the basis for the methodology that was used to answer the main research question: where are Dutch households currently heading in terms of summer comfort?

3. Method

The study consisted of a set of interrelated research activities. These included a research visit to Australia, trade fair visits, internet scoping, expert interviews, household interviews, field observations, and a media analysis. Ethics approval for the studies involving human participants (household interviews and expert interviews) was obtained through the

Eindhoven University of Technology Ethics Board under reference ERB2020ID18 and ERB2020ID140 respectively.

To design the household interviews in a way that they would capture all relevant practices, background research was conducted to identify which practices are affected by and involved in summer comfort. Since dealing with hot weather is relatively new for the Netherlands, a research visit to Australia was used to gain more insight into living in hot weather. This resulted in the following list of seven focal integrative practices: (1) cooking and eating, (2) personal care and clothing, (3) laundering and cleaning, (4) home working, (5) free time, (6) sleeping, and (7) ventilating, shading and cooling.

While households are experts on their own current ways of dealing with hot weather, they are less able to predict their future options. Working from the range of everyday practices identified in the background research, a set of domain experts was consulted to gain an overview of near-future trends and developments related to these practices. These domains included HVAC, sleep, physiology, fashion, architecture, building standards, social housing and domestic shading. The ten expert interviews were conducted between March and December 2020. The expert interviews were tailored to the expertise of each interviewee and included preliminary results of the study where possible. The interviews lasted 30 minutes to 1,5 hours. All experts were offered the chance to read and comment on a concept version of the stakeholder report [4].

2030 and 2050 were taken as milestones for these futures. One nearer-future and one further-future. These are timeframes that are often mentioned in strategy documents by government and industries and are therefore expected to match decision-making practices among these important stakeholders.

Details on the data collected during household study – the core element of the research – are included below, followed by an overview of the data analysis approach and a discussion of the limitations of the data for the goals of the study.

3.1 Household study

The set-up for the household study consisted of a workbook and an interview. The workbook was designed to prime participants on the topics to be discussed in the interview and collected systematic data that is difficult to collect in an interview, such as the number of times the household does their grocery shopping or how often different categories of laundry are washed.

Interviews were semi-structured and conducted in the participating households. A flyer and application form were made to recruit participants. The recruitment message was spread through the social media accounts of the project partners, via Twitter, LinkedIn, and via email.

To recruit more participants from lower-income groups with practical education levels and migration backgrounds, a partnership was made with a social housing association in Rotterdam. This eventually resulted in the desired balance of owner and tenant participation.

While planning the study, it was uncertain whether there would be a heatwave. 'Luckily', a major heatwave occurred from 5 to 18 August 2020, well in-sync with the planned study. According to KNMI, August 2020 was the second warmest August since 1901. Exceptional to this heatwave was the high minimum temperature, with three tropical nights (minimum temperature above 20°C), which, on average have occurred less than once a year, and nine tropical days (max 30°C or above) which historically occur once a year on average.

Eventually, 15 of the 21 participating households completed the workbook and interview, while six were only interviewed. A total of 21 hours of interview material was collected, representing a total of 60 residents. The ages of interviewees varied from early 20s to early 70s. The study covered a variety of types of dwellings with buildings years ranging from 1909 to 2019 that roughly reflect the national figures, including both urban and rural locations.

3.2 Data analysis

Analysis of the household interview data used the following main steps:

a) Theoretic framework and approach to topic, also embedded in workbook and interview set-up, leads to initial coding frame (activities)
b) Coding I: Transcripts are all coded according to these nodes > additional nodes emerge from the first coding process, transcripts are scanned
c) Coding II: Nodes are analysed more in-depth and tables per participant are made that summarize subthemes per node, some additional coding is done, transcripts are read carefully
d) Counts are made where possible and relevant
e) Table overview is used to write aggregate text for each node/theme into report
f) Questions that arise are noted down
g) Additional information is gathered through literature, internet search, and expert interviews
h) Findings per practice are summarized in an overview table including current situation, prognosis and risks/opportunities.

This process is not fully linear. For example, in the case of cooking and eating, the report text was roughly written before the Coding II process and then gradually revised after Coding II and additional information gathering.

3.3 Limitations

No actual measurements of indoor temperatures were made, so conclusions regarding temperatures are based on self-reported values, which tend to be less reliable. The use of workbooks with daily exercises, which primed participants to notice their indoor temperature values in the week before the interview, partly compensated for this.

The interview focused on a selection of practices. Other possibly relevant practices that were not included specifically were pet care, parenting, and do-it-yourself activities.

The sample is not fully representative of the Dutch population. Relevant caveats are lower-income households, households with a migration background, and age groups above 70. These representation issues were addressed where possible through expert interviews and studies conducted by others.

4. Findings

This section brings together the findings and extrapolates trends and developments identified into speculations on probable futures of summer comfort in Dutch households. The detailed results of the data analysis with rich data on each practice can be found in [4].

Overall, the study confirms the expectation that the use of active cooling in Dutch dwellings is likely to increase in the future. This is reflected in growing sales figures of cooling systems, but also in actual and experienced overheating in dwellings and frictions with emerging practices of shading and ventilation. The latter, along with embodied acclimatisation, have potential to contribute to summer comfort in a low-energy manner. However, their establishment is hampered by existing infrastructures, and historically shaped cultural values and habits, as well as competition between practices. The sections below elaborate on these points.

4.1. Actual and experienced overheating

Overheating is already an issue in Dutch households. From the perspective of the NZEB (Net Zero Energy Buildings) standards, several dwellings in the study (all apartments) exceed the threshold of 450 WHOs (the Weighted Overheating Hours) above 27°C. Overall, reported indoor daytime temperatures during the heat wave ranged from 24°C to 45°C for dwellings without cooling. The dwellings that reported temperatures over 30°C in their main living areas were all rented city apartments.

Stories of residents confirm that these dwellings become practically unliveable during a heat wave. Moreover, most households in the study considered their dwelling to be overheated well below the formal overheating threshold. Indoor temperatures above 25°C were considered too high by all but four participants, particularly for working and sleeping. These higher temperatures inhibited their freedom of movement and capability to go about their daily business, such as focusing on work, sleeping well, and performing housework.

These issues were absent for households with active cooling, but they were inhibited in other ways, particularly, in being outdoors. The data indicated that households with active cooling have a stronger tendency to take the car instead of walk or cycle, because stepping outside from a cooled space felt like 'hitting a wall'. In other words, spending time in cooled spaces reduced their willingness and ability to tolerate the higher outdoor temperatures.

With climate change, these overheating issues are expected to grow. The next sections go deeper into the strategies that households currently apply and aspire to deal with these issues.

4.2 Acclimatizing

Participants that were able to enjoy or accept the heat and modify their daily schedules around it were most capable of getting through the heatwave without too much discomfort. For example, families that had their summer holidays during the heat wave or a student practicing mindfulness. However, the freedom to adjust one's daily schedule is not accessible for everyone, especially if heatwaves are to occur more often outside of summer holidays. Moreover, freedom to adjust one's schedule is not a guarantee for getting through the heatwave well, as illustrated by the participating retired couple. As known from physiological research, not all bodies are equally capable of dealing with heat and these capabilities decrease with age [14, 15].

However, the study shows that common knowledge among the general public on bodily responses to heat show a gap with state-of-the-art research, particularly regarding the role of sweat in dealing with heat (it is mostly seen as something negative) and the capability of bodies to adjust to higher temperatures over time. While research shows that people can adapt to heat by as much as 1°C per day as confirmed by the physiology expert, none of the participants referred to acclimatisation or related concepts of bodily adjustment to heat over time. This finding indicates that adjustments in knowledge, available products, skills, and attitudes to acclimatize could reduce people's experiences of being locked into their homes and bodies and contribute to well-being in a low-energy manner. Put more strongly, the adverse mental and physical effects of reduced physical activity in hot weather might be partly mitigated if people (are facilitated to) acclimatize.

4.3 Cultural frictions with shading, ventilation and cooling

Emerging practices often compete with existing

ones. As Shove et al. [8] explain, when practices change, new links must be made and old ones broken.

A seemingly embedded friction that arose from the interviews is the relationship that 'the Dutch' have with warm weather. Warm and sunny weather is associated with being outdoors and enjoying the light and warmth of the sun. In the spring, when days get longer and warmer, people open doors and windows to let fresh air in, extending their living spaces onto balconies and into gardens. Fluctuating temperatures mean that Dutch summers can have relatively cool spells that precede heatwaves. When temperatures go up, the sun is initially welcomed into the home. But when temperatures rise, this behaviour leads to overheating, which is then difficult to correct.

Proper, disciplined outdoor shading and summer night ventilation routines could reduce the extent to which indoor spaces heat up [16], but adopting these routines requires more than new equipment and behaviours. Viewing the sun as an 'enemy' instead of a 'friend' for part of the year requires a cultural shift. The Dutch friendship with the sun is deeply embedded in customs (opening doors, curtains and windows to enjoy light, views and fresh air), the built environment (ample, sun facing windows) and related professional practices such as architecture (disliking and sometimes prohibiting outdoor shading). For most of the year, the sun is and will remain a friend, helping to light and warm dwellings, and keep people healthy and cheerful. Learning to occasionally 'cool' this friendship may be difficult to achieve and implicitly seems to hamper the potential of shading and ventilation practices to develop.

Active cooling is more explicitly approached with reservation. Participants without active cooling are familiar with air conditioning, but find it too energy-consuming, noisy, expensive, and uncomfortable. However, even highly committed, knowledgeable residents in modern homes, equipped with the latest shading and ventilation technologies, had trouble maintaining a comfortable indoor climate without the use of active cooling. Many anticipated getting some form of active cooling in the future. Those who already had cooling were mostly content with their systems (except for mobile air conditioners). Although there are cultural and practical frictions to integrate active cooling into Dutch households, they seem easier to overcome than those related to shading and ventilating. Added to this lower barrier to uptake is the risk that active cooling creates a further threat for shading and ventilation practices to reach their potential because they compete.

4.4 Shading, ventilation and cooling compete

Shading and active cooling can complement each other in dwellings, but the study illustrates how they compete in the market. Both active cooling and outdoor shading require considerable investment. If households have an opportunity to only invest in one, then cooling has the better position in terms of low-effort comfort. This competition is also visible in the current NZEB requirements, where adding a form of active cooling eliminates incentives for other, low-energy measures against overheating such as shading.

Cooling and summer night ventilation compete directly in the dwelling. While the cooling system is on, windows and doors need to be closed to retain the microclimate. This effect is even stronger for mobile air conditioners, used in three participating households, because securing the hose in the window can further hamper the opening of windows when the device is not in use.

In general, active cooling, when properly designed and installed, can secure comfortable temperatures in the dwelling regardless of other measures such as shading or ventilation. Shading and ventilation require the active involvement of residents. With active cooling in place, the incentive to invest money, time, and effort in them is reduced. Mobile air conditioners have a particularly problematic position in this respect because of their relatively low threshold, and energy-efficiency. While they can be life-savers on the scale of individual users, in the broader picture these appliances form undesirable symptoms of overheating in Dutch dwellings that contribute to the problem of climate change and heat islands [17].

4.5 Entry points for active cooling

The attraction of active cooling is strong. The study shows that this temptation varies for different practices, rooms, dwelling types, and types of residents. Sleeping and working are practices that seem to be most receptive to air conditioning. Working occurs in different spaces in the home, but bedrooms form an appealing entry point. They can be cooled relatively efficiently and can be used for the two activities that require cooling most. The study did not find many bedroom/offices, but the architect consulted mentioned that they get frequent requests for workspaces in bedrooms because it is an efficient use of space.

When installed in living rooms first, work might move to the living room—although in multi-person households this is hampered by privacy issues. Sleeping then remains an issue, as people do not seem eager to sleep downstairs during heatwaves as a rule. This may stimulate installing multiple units in the living room and bedrooms.

Mobile air conditioners seem like an obvious solution to cover multiple activities, but on closer observation, they come with a range of challenges. Besides the issue of their relatively low efficiency, their capacity tends to be too small for most living rooms. When used in other rooms, they hamper ventilation practices, and their noise levels interfere with sleeping and working. Although mobile, they

cannot be easily moved up or down the stairs. As argued above though, they can play a role in a growing habituation of and appetite for active cooling at the cost of ventilation and shading.

The type of households that seem most receptive to air conditioning are higher income households that spend more time at home, for example, when habitually working from home, during a pandemic, or when in retirement. Active cooling can also spread between homes. Neighbours, friends, or family are more likely to get it installed after experiencing the cool escape during a heatwave.

These insights can be used to accelerate the spreading of active cooling, but also to design measures that might slow down or prevent Dutch households from becoming dependent on energy intensive cooling equipment that could hamper the development of other strategies to deal with a warming climate.

Automation can play a role here, when shading responds automatically to levels of solar gain, rain and wind, and ventilation to temperature and humidity differences inside and outside the dwelling. However, the role of residents cannot be ignored. Not only their autonomy in deciding whether to have these systems at all, but also in the ways they are used. The study revealed a wide array of circumstances in which people might disable automated shading, such as feeling locked-in, wanting more light, annoyance with repeated movement, wanting to open windows, etc. For ventilation systems, it became clear that their automated responses to CO_2 or humidity levels can conflict with summer comfort by drawing in hot outside air during the day, while summer night ventilation, in most homes, requires residents to open and close windows while they are sleeping.

4.6 Pathways for active cooling

So far, active cooling is discussed as one practice, but in fact, different forms of active cooling are currently developing in parallel. Main pathways are radiant cooling and air-conditioning. Radiant cooling, mainly in underfloor settings powered by heat pumps or district cooling are relatively slow systems that cool the building mass. Such systems are likely to run continuously during hot weather. An advantage of these systems is that for ground source heat pumps, cooling can be provided on low-energy demand, or even energy-positive manners when heat is stored for use in winter. Air-conditioners work more quickly by directly cooling the indoor air and are more likely to be used based on occupancy and direct demand. Spaces also heat up again relatively quickly when they are off. Mobile air-conditioners allow for even more directed, person-oriented, albeit fleeting forms of cooling. Apart from their efficiency, these different patterns of use are likely to affect their overall energy demand.

Moreover, levels of energy demand for active cooling do not only depend on the type of systems and when it is used, but also on the set-temperature. At present, the temperatures to which households will set their cooling systems has not been settled or stabilised, but it is likely that norms around acceptable and normal temperature ranges will develop in the coming years and decades. With heating, for example, Dutch households presently tend to set their thermostat somewhere between 18 and 22°C. This normalised temperature range has formed and changed over a long time period [21], and varies per cultural context [22] .

As illustrated in the introduction, building norms, standards and system design can play an important role in shaping these norms. Considering that technologies co-shape practices, it makes a huge difference for the way in which Dutch summer comfort practices will develop whether default settings, promotion materials, media and installer instructions for cooling systems recommend setting the system to 18°C or 27°C, introduce some other metric like a combined humidity/temperature value, or are designed to offer a variable temperature that moves with the outdoor temperature and slowly increases over time to support acclimatisation.

4.7 Cooling <> heating

When considering longer term consequences of a proliferation of active cooling in Dutch households, effects on heating practices should also be taken into account. Most cooling systems can also heat. Compared to the gas-fired, high-temperature central heating system still dominant in the Netherlands, air-conditioners are quicker and support more on-demand use patterns. Their proliferation might therefore lead to partial replacement of gas-fired central heating systems, which, next to electrification, could have a positive effect on overall household energy demand. Research has shown that on-demand forms of heating tend to be less energy-intensive than central heating [18, 19]. However, if air-conditioning is used in addition to—and not as a replacement of—central heating systems, then additional energy demand for indoor climate could arise. As shown in one of the participating households, air-conditioning is easy to use as a quick form of 'top-up heating' on cooler moments outside of the regular heating season. It might therefore replace existing, low-energy strategies for these moments such as sweaters. Further research is needed to investigate how these patterns may develop.

4.8 Additional effects of warming on everyday life

The use of active cooling in the home seems to lead to a dependence on cooled spaces that extends beyond the dwelling. The examples in the study indicate a trend towards spending more time indoors, and the car becoming preferred over other

means of transportation. Beside increases in CO_2 emissions and energy costs that accompany the increased use of most forms of active cooling, these trends indicate undesirable health effects resulting from lower activity levels and lower natural vitamin D intake.

Other areas in which increases in energy demand are likely to arise according to our finding are in increased capacity for cold food storage, showering and laundering. Several households reported that fruits and vegetables that are normally kept in dry storage are moved to refrigerators during hot weather, where they compete for space with more cooled drinks. This leads to an increased demand for (larger) fridges and freezers—appliances which, in turn, directly contribute to overheating in dwellings due to the heat they produce. The study also indicated that shower frequencies increase during hot spells. The main reason for more showers within the sample was not to cool down, but to rinse off sweat. This requires water, as well as energy to heat it. Finally, natural fluctuations in daily temperature patterns mean that morning time, as the coolest time of day, becomes populated with many activities: sports, work, cleaning, etc. This has consequences for energy demand for laundering. Hanging out laundry is physically intense. Doing it in the morning requires the washing machine to run during the night, which is out of sync with solar energy production. Moreover, a tendency to minimize physical activity may increase the use of dryers, which also generate heat inside the home. With a trend towards better insulated homes, these secondary effects could become significant.

4.9 Different consequences for different types of households and dwellings

While it is difficult to draw a strict line, some of the dwellings in the study were clearly overheated. These examples represent a larger group of households for which homes become unliveable for part of the year. Smaller, well-insulated dwellings, with higher window-to-content ratios, high sun exposure (e.g. in high-rise), little shading and ventilation opportunities, located in cities (heat islands) heat up quickly. Such dwellings are more likely to be occupied by lower-income households and are more often rented than owned. This might also mean that the potentially higher amount of time spent at home by the residents due to lower levels of employment could add to the overheating issues.

Also judging from recently introduced building standards in the Netherlands and elsewhere [20], overheating is slowly starting to be acknowledged as an issue, and social housing providers and landlords are beginning to contemplate on how to intervene. The study indicates that the costs of installing and maintaining outdoor shading on non-ground floor windows plays a role in hampering tenants and owners to act. Moreover, explicit demand for shading and cooling seems low among social housing tenants. This could have all kinds of causes such as other more pressing issues on the tenants' minds, a fear of unmanageable rises in rent, unfamiliarity with the effects of shading and ventilation on overheating, or better skills of acclimatizing. Despite various efforts to involve low-incomes households, they were only present indirectly in the study through stories of higher income tenants, experts and observations during fieldwork. More research is needed into the specific issues, wishes and strategies of this group.

5. Conclusions

This study set out to gain more in-depth insight into the ways in which Dutch households are likely to deal with the growing problem of overheating in their dwellings. Several opportunities were identified that might direct Dutch domestic practices of summer comfort onto more inclusive, healthy, and less energy-intensive pathways.

A range of opportunities present themselves around acclimatisation, i.e., modifying bodily relations with hot weather. There seems to be a gap between state-of-the-art physiological research on how bodies deal with heat and everyday knowledge among the households. The benefits of sweating (when combined with drinking enough water) as an effective way to deal with heat is not fully acknowledged. Moreover, none of the participants talked about bodily adjustment to heat over time, while research shows that this effect can be as strong as 1°C per day.

Outdoor shading during the day and ventilation during the night can reduce or prevent overheating. The study shows that barriers exist for these practices to develop to their full potential in Dutch households. Cooling might reduce residents' acceptance of the experienced downsides of shading (including the costs) and lowers incentives and opportunities to utilise cooler night air.

6. Acknowledgements

Thanks to the members of the User Committee and all experts and participants in the study. This research was funded by the Dutch Research Council (NWO) under grant number VENI17343.

7. References

1. Attema, J., et al., *Knmi'14: Climate change scenarios for the 21st century—A netherlands perspective.* KNMI: De Bilt, The Netherlands, 2014.
2. Veurman, M. *30 procent stijging energieverbruik tijdens hittegolf.* 2020 17 August 2020].
3. White-Newsome, J.L., et al., *Climate change and health: indoor heat exposure in vulnerable populations.* Environmental research, 2012. **112**: p. 20-27.
4. Kuijer, S. L. (2021). Exploring probable futures of summer comfort in Dutch households: Phase

1: Anticipating the role of smart technologies in the dynamics of everyday life. available from: https://research.tue.nl/en/publications/exploring-probable-futures-of-summer-comfort-in-dutch-households-
5. Strengers, Y. and C. Maller, *Integrating health, housing and energy policies: social practices of cooling.* Building Research & Information, 2011. **39**(2): p. 154-168.
6. Walker, G., E. Shove, and S. Brown, *How does air conditioning become 'needed'? A case study of routes, rationales and dynamics.* Energy Research & Social Science, 2014. **4**: p. 1-9.
7. Reckwitz, A., *Toward a Theory of Social Practices: A Development in Culturalist Theorizing.* European Journal of Social Theory, 2002. **5**(2): p. 243-263.
8. Shove, E., M. Pantzar, and M. Watson, *The Dynamics of Social Practice: Everyday Life and How it Changes*. 2012, London: Sage.
9. Kuijer, L., & Bakker, C. *Of chalk and cheese: behaviour change and practice theory in sustainable design*. International Journal of Sustainable Engineering, 2015. 8(3), 219-230.
10. Schatzki, T., *Social Practices: A Wittgensteinian Aproach to Human Activity and the Social*. 1996, Cambridge: Cambridge University Press.
11. Kuijer, L. and M. Watson, *'That's when we started using the living room': Lessons from a local history of domestic heating in the United Kingdom.* Energy Research & Social Science, 2017. **28**: p. 77-85.
12. Dahlgren, K., et al., *Digital energy futures: review of industry trends, visions and scenarios for the home.* 2020.
13. Kuijer, L., *Automated artefacts as co-performers of social practices: washing machines, laundering and design*, in *Social Practices and More-than-humans: Nature, materials and technologies*, C. Maller and Y. Strengers, Editors. 2019, Palgrave Macmillan.
14. Foster, K., et al., *Sweat responses in the aged.* Age and Ageing, 1976. **5**(2): p. 91-101.
15. Kenney, W.L. and P. Chiu, *Influence of age on thirst and fluid intake.* Medicine and science in sports and exercise, 2001. **33**(9): p. 1524-1532.
16. Alders, N., *Adaptive thermal comfort opportunities for dwellings: Providing thermal comfort only when and where needed in dwellings in the Netherlands.* A+ BE| Architecture and the Built Environment, 2016(13): p. 1-336.
17. Ohashi, Y., et al., *Influence of air-conditioning waste heat on air temperature in Tokyo during summer: Numerical experiments using an urban canopy model coupled with a building energy model.* Journal of Applied Meteorology and climatology, 2007. **46**(1): p. 66-81.
18. Nakagami, H., C. Murakoshi, and Y. Iwafune, *International Comparison of Household Energy Consumption and Its Indicator.* Proceedings of the 2008 ACEEE Summer Study on Energy Efficiency in Buildings, 2008: p. 214-224.
19. Kuijer, L. and A.d. Jong, *Identifying Design Opportunities for Reduced Household Resource Consumption: Exploring Practices of Thermal Comfort.* Journal of Design Research, 2012. **10**(1/2): p. 67-85.
20. Rahif, R., D. Amaripadath, and S. Attia, *Review on time-integrated overheating evaluation methods for residential buildings in temperate climates of Europe.* Energy and Buildings, 2021. **252**: p. 111463.
21. Van Overbeeke, P. (2001). *Kachels, geisers, en fornuizen: keuzeprocessen en energieverbruik in Nederlandse huishoudens, 1920-1975* (Vol. 10). Uitgeverij Verloren
22. Wilhite, H., Nakagami, H., Masuda, T., Yamaga, Y., & Haneda, H. (1996). A cross-cultural analysis of household energy use behaviour in Japan and Norway. *Energy policy*, *24*(9), 795-803.

Data Statement

The datasets generated and analysed during the current study are not publicly available because they are still in the process of preparation to be submitted to a database. They will be made available in a repository, probably DANS Easy.

Moreover, a detailed overview of the results of the study is available in the open access stakeholder report of the study through: https://research.tue.nl/en/publications/exploring-probable-futures-of-summer-comfort-in-dutch-households-

Impact of Spatial Distributions of Climate Condition on Building Overheating

Chang Shu[a,b], Abhishek Gaur[b], Liangzhu (Leon) Wang[a], Michal Bartko[b], Lili Ji[a,b], Abdelaziz Laouadi[b], Michael Lacasse[b]

[a] Department of Building, Civil and Environmental Engineering, Concordia University, Montreal, 1455 De Maisonneuve, H3G 1M8, Montreal, Quebec, Canada

[b] Construction Research Centre, National Research Council Canada 1200 Montreal Road, K1A 0R6, Ottawa, Ontario, Canada

Abstract. In this study, the spatial distribution of the urban climate is evaluated and its impact on indoor overheating conditions is assessed. This was done by modelling the near-field climate of Ottawa and Montreal at 1 km resolution for the summer of 2018 during which an extreme heat event occurred causing nearly 100 deaths in this area. The climate data obtained from Weather Research Forecasting simulations were used for assessing the extent of overheating within a prototype model of a single-detached home using EnergyPlus. The overheating conditions were evaluated using the mean temperature, the number of hours with the temperature above 28°C, and the number of hours cooling from a base temperature of 28°C. A workflow for selecting representative locations within the city for building overheating assessments was established by considering five (5) different quantiles, including 0%, 5%, 50%, 95%, and 100%, of the three calculated overheating metrics over the urban and the rural area. The degree of indoor overheating in homes was quantified and differences in overheating of homes in urban and rural settings as well as those arising within different urban areas (intra-urban) were determined. The most significant intra-urban indoor mean temperature differences of buildings at different locations were 1.8°C for Montreal and 1.6°C for Ottawa. For the number of hours with a temperature above 28°C, the intra-urban difference can be up to 829 hours for both cities. It was also found that the overheating conditions between different locations may be affected by the external air temperature and other variables, such as the local wind speed, which greatly varied the natural ventilation air change rate of buildings. The overheating conditions in buildings of different locations were also compared by analyzing the time-series variation in temperature. It was determined that there always exists a difference between the duration and intensity of indoor overheating in single-family homes of different locations.

Keywords. WRF, Overheating, Extreme heat event, Urban heat island, EnergyPlus
DOI: https://doi.org/10.34641/clima.2022.120.389

1. Introduction

As a consequence of global warming, the increased occurrence of extreme heat events leads to higher morbidity and mortality [1]. Overheating in buildings comes to be a major problem during the heatwaves which can impose fatal threats to the occupants' health [2]. The external climate is a significant driver of indoor building conditions. Taylor et al. [3] conducted multiple building simulations for six cities from different climate regions across the UK to justify the importance of the weather files in the assessment of building indoor overheating conditions. Amoako-Attah and B-Jahromi [4] examined the variation of the simulated indoor operative temperature of detached residential buildings in London by using different weather files, which also affirmed the importance of selecting weather files for building-related studies. Cumulative efforts have been invested in finding the most representative weather file from a long-term climate series for building simulations [5].

The traditional representative weather year data are normally selected from multiple years which cannot reflect the spatial variation of the climate conditions, while buildings may expose to very different overheating risks even in the same city due to the various surrounding conditions [6]. In 1999, a field monitoring campaign in London constructed a network of fixed temperature stations along eight transects of the city covering the whole urban and

Copyright ©2022 by the authors. This conference paper is published under a CC-BY-4.0 license.

suburban areas, which provided the air temperature data to be strong evidence of the urban heat island phenomenon [7]. The monitored data have been adopted by Kolokotroni et al. [8] to develop the London Site-Specific Air Temperature (LSSAT) model using an artificial neural network (ANN), which provides the localized weather data for a series of studies to discuss the urban heat island effect on buildings [9]. These studies used the climate data at the measured location across the Greater London Area, and a clear trend can be found that with the increase of the distance from the urban center the indoor temperature and cooling energy can be lower [10] in summer while the heating energy consumption in winter can be higher [11]. These studies compare the overheating in buildings using the climate conditions at limited locations with measuring stations, which can be hard to reflect the overall pattern for the whole city.

This study adopted the weather files extracted from a fine-resolution regional climate model, which permits the urban effect on climate. Multiple locations over the cities are sampled for building simulation to perform an overheating assessment. The results of this study quantify the intra-urban difference and the urban-rural difference in terms of building overheating.

2. Method

2.1 study area, model and data

This study focus on the analysis of two Canadian cities: Ottawa and Montreal. The five months (May 01 - September 30) are evaluated for the whole summer of 2018, because it covers a heatwave event that happened in the two cities from June 30 – to July 05, 2018, which caused approximately 100 deaths in the area. The high-resolution climate dataset has been simulated using the Weather Research and Forecast model at a grid resolution of 1 km. For the detailed configuration of the climate models please refer to [12,13].

2.3 urban and rural areas

In this study, the urban area is identified by the urban grid dominated by the urban and built-up land cover types around the centre of the city. The rural areas are identified by a polygon buffer surrounding the boundary of the urban region [14]. This study considered a buffer distance of 10km from the urban boundary for the rural area to avoid introducing other uncertainties caused by different climate conditions of father geospatial regions, which is also consistent with the implementation in existing studies [15]. The regions within 3km distance to the urban boundary are excluded because they might still be highly affected by the urban region [14]. We also excluded the water bodies and the terrains 50m higher than the highest elevation of the urban area, which might have a significant impact on the local temperature for the urban heat island intensity calculation [14,16].

The distribution of the land cover types and the shapes of the urban boundary, rural boundary and the excluded buffer region in between is specified in **Fig. 1**. The urban area of Montreal city is covered by 1184 1km grids which is double times the urban areas of Ottawa that are covered by 501 grids. The number of grids for the rural area of Montreal and Ottawa is 1316 and 1112.

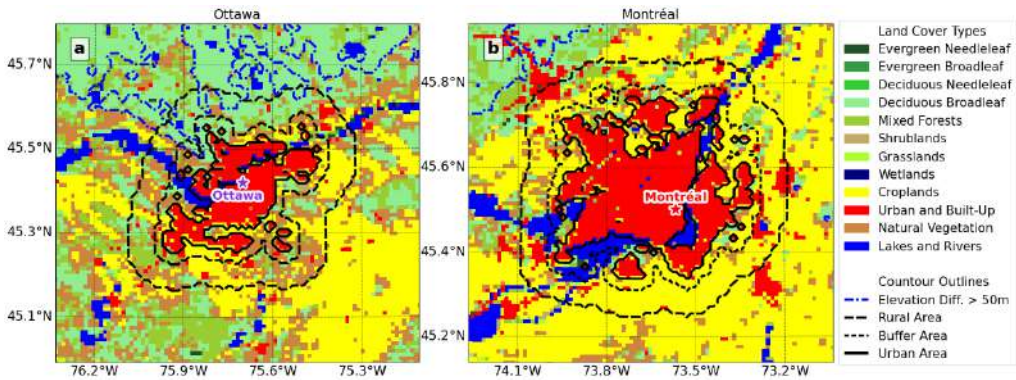

Fig. 1 - Land use and land cover with the outlines of urban and rural areas of a) Ottawa and b) Montreal cities

2.2 locations for building simulation

To specify the weather data to be used for the overheating assessment, multiple studies have been focused on developing a procedure for creating representative climate datasets from long-term climate datasets [17]. CIBSE [18] has developed a systematic approach to selecting the design summer year (DSY) by evaluations of several overheating metrics for the climate data from different years. A similar concept is adopted here in this study. Instead of selecting the climate data from multiple years, the evaluation of the climate data has been conducted over the different grids across the whole city to find the locations exposed to different levels of heat conditions.

For this study, the selection of the representative locations in the urban and rural areas adopted the temperature-based overheating assessment methods, which is the most straightforward for the comparisons of the indoor overheating conditions from different locations in the same city. The

locations are selected by the evaluation of three different aspects, including a) the time-averaged air temperature over the evaluated five months, b) the overheating hours above the fixed temperature threshold, c) and the cooling degree hours (CDH) with the base temperature of the fixed temperature threshold. The fixed temperature threshold in this study is 28°C for both the outdoor and the indoor conditions since it is the most used value in the literature and standards for overheating assessment in residential buildings [19] and the selection of extreme weather files [18]. It is defined to be an extremely hot condition when the temperature is higher than 28°C, so the number of hours above 28°C reflects the occurrence of overheating within the evaluated period. The cooling degree hour is defined as the cumulative number of overheating hours weighted by the magnitude of exceedance above the threshold temperature values, which evaluates both the temperature levels and the occurrence of overheating, the equation to calculate it is:

$$CDH = \sum_{T_{air}>28} (T_{air} - 28) \qquad (1)$$

After the three metrics are calculated, the locations with the five (5) different quantiles, 0%, 5%, 50%, 95%, and 100%, of the three evaluated metrics are considered to represent the general conditions in the city. The quantiles of 0% and 100% are selected for the locations of the extreme cases with the maximum and minimum potential of overheating in the city, and the quantiles of 5%, 50% and 95% help to conclude the most possible range of the overheating conditions in the city. The selection of the five locations using each of the metrics is conducted separately for the urban and rural regions to show the general difference in the climate conditions between the urban and rural areas. Therefore, 10 locations would be selected using each of the metrics for each city, and it is expected to have 30 locations selected in total for each city with the 3 metrics considered.

In **Fig. 2**, the selected locations are summarized with the distribution of the three metrics. The selected locations are indexed by the metrics for the selection (T for mean temperature, H for overheating hours, C for cooling degree hours) followed by its level of percentile of the evaluated metric hereafter. For example, T100 indicates the location with the maximum value in the urban/rural area in the city, H00 for the location with the minimum overheating hours in the urban/rural area in the city, and C50 means the cooling degree hour of the location is the median value of the whole urban/rural area of the city.

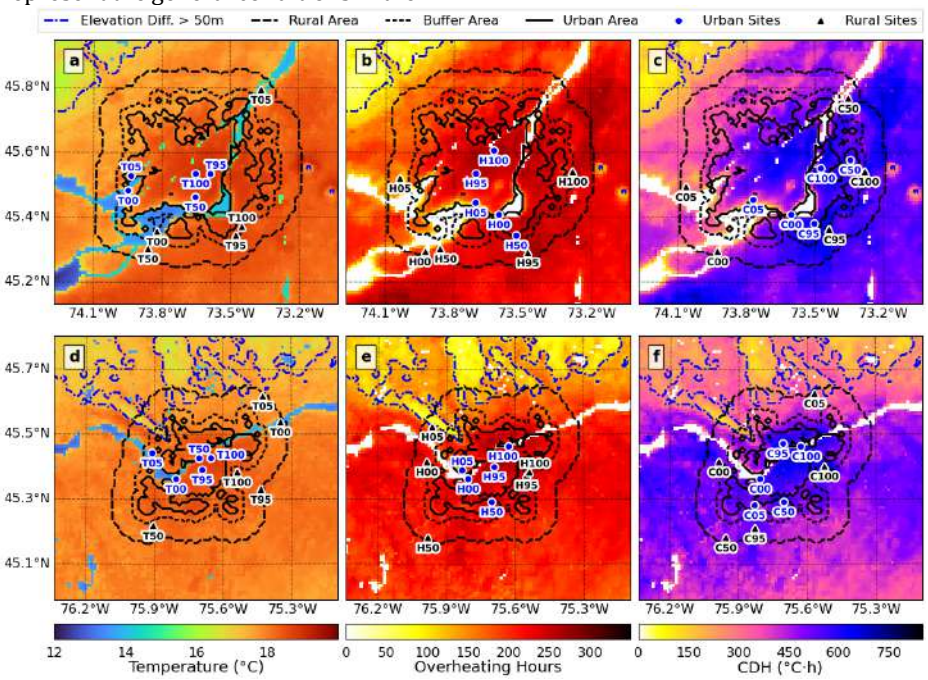

Fig. 2 - Site selection based on the three criteria of a, d) mean outdoor air temperature over the 5 months; b, e) the overheating hours above 28°C; and c, f) Cooling degree hours (CDH) with a base temperature of 28°C.

2.3 building model and overheating assessment method

To demonstrate the difference in indoor overheating at the different selected locations, a single-house archetype model is adopted for simulating the indoor thermal conditions in EnergyPlus. The configuration of the building model follows the National Building Code of Canada and National Energy Code of Canada for Buildings. To evaluate the overheating under a free-running condition, the building model in this study is naturally cross-ventilated using the Airflow Network Model in EnergyPlus. For a more detailed configuration of the building models please refer to [12]. The overheating of the buildings is identified by the number of hours with an indoor operative

temperature above 28 °C which is consistent with the location selection criteria in section 2.2.

3. Results

3.1 comparison of indoor overheating at selected locations

The indoor overheating conditions of the bedrooms in the single house buildings at different locations in the WRF model are summarized in **Fig. 3**. The buildings in rural areas may have lower values in the overheating metrics than the urban area in general, this is due to the cooler outdoor air temperature and higher wind speed in the rural area. For the locations with the 50 quantiles in Montreal, the overheating hours at the three locations in the urban area have an average of 104 hours higher than that of the three locations in a rural area. For Ottawa, the difference in the overheating hours between urban and rural is even larger.

A distinct difference can also be found in **Fig. 3** between locations in the urban area. For Montreal, location H100 has the maximum overheating hour of 862 hours, and T00 has the minimum of 33 hours, which identified a possible overheating hour difference of 829. For Ottawa, the maximum evaluated overheating hour difference is also 829 hours which is observed between T100 and T00. Notably, there exists a significant difference between locations with 00 quantiles and 05 quantiles, while the difference between locations with quantile 05 and quantile 100 is much smaller than that. This reminds us that only a small portion of the locations (grids) may fall into the evaluated range between locations with 00 quantiles and 05 quantiles, while most of the locations (grids) should be in the range of that between locations with quantile 05 and quantile 100. Therefore, when conducting the overheating analysis of the buildings in the city, people should avoid selecting these cool locations which cannot represent the overall overheating in the city.

Fig. 3 also exhibited the trend that, no matter for urban or rural areas, locations selected with the higher quantile of the overheating metrics for outdoor climate may have correspondingly more severe overheating indoors. However, exceptions can still be found that locations with higher quantiles may have lower mean operative temperature or overheating hours. For example, in Montreal, the urban C100 has a lower mean operative temperature and overheating hours than those from T, H, C95, T50 still has higher overheating hours than the three locations with 05 quantiles, but it has a lower mean operative temperature than that at T05. A similar outcome also happens in the urban area of Ottawa, the location H, C100 has both the mean operative temperature and overheating hours even lower than the buildings at T, H, C50 and H05, and location H05 may have a higher mean operative temperature than H, C50 though its overheating hour is still smaller than H, C50. This can be explained by the difference in the local wind speed which may lead to the different natural ventilation conditions of the building. The average air change rate of the rooms over the 5 months is therefore provided in **Fig. 4**. It can be found that, for the locations in Montreal urban area, C100 and T50 have much higher air change rates than the other sites, which indicates the natural ventilation at these two locations helped with the indoor temperature control. Among the locations in Ottawa, the air change rate in the buildings at H, C100 is much higher than the other sites, this significantly reduced the overheating in the buildings, while for H05, the air change rate is much lower than other sites apart from climate T, H, C00, which explains, why it may have comparable or even more severe overheating than locations with quantile 50. This suggests the importance to include the local wind condition for the whole building thermal simulation of naturally ventilated buildings.

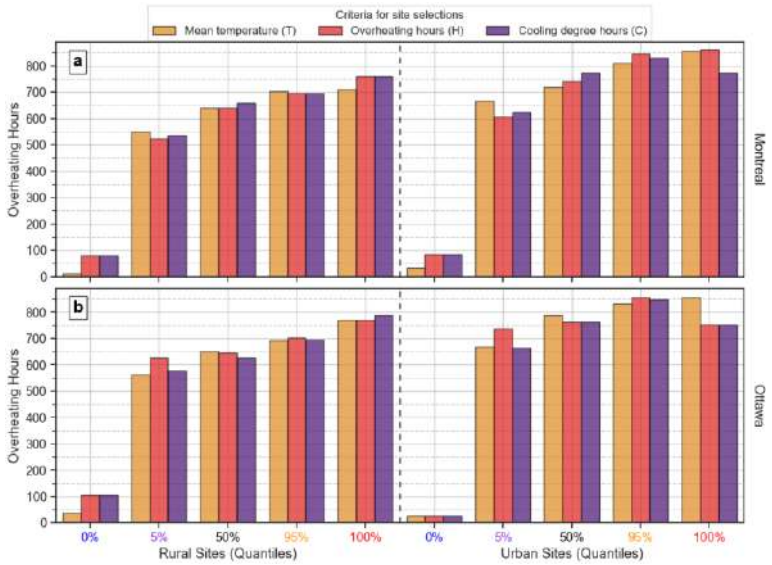

Fig. 3 - Comparison of the overheating hours above 28°C during the 5 months of summer (MJJAS) in the bedroom of single house buildings using the climate data from different selected locations in a) Montreal and b) Ottawa. (The colours of bars shown in the legend is to indicate the different criteria used for location selections)

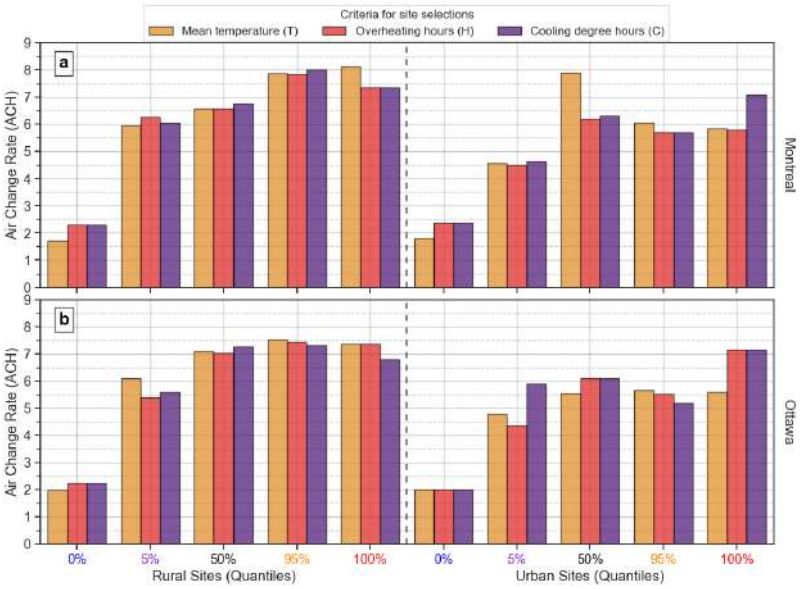

Fig. 4 - Comparison of the mean air change rate during the 5 months of summer (MJJAS) in the bedroom of single house buildings using the climate data from different selected locations in a) Montreal and b) Ottawa (The colours of bars shown in the legend is to indicate the different criteria used for location selections)

3.2 comparison of overheating in the urban area

The longer overheating exposure time can also impose a great threat to the health and safety of the occupants due to the cumulative water loss and the increased core temperature of the human body [20]. This requires a better estimate of the duration of the overheating, while the summarized overheating metrics of the overheating hours cannot fully reflect the detailed overheating information in the time series. The H95 and H05 locations in the urban area of Montreal are selected for the comparison of the whole time series between different locations. The hourly data of outdoor air temperature and the indoor operative temperature have been shown in the heatmap plot in **Fig. 5**. It clearly shows that the indoor operative temperature is higher than the outdoor air temperature in general, the temperatures indoors are elevated compared to that of the outdoors due to the indoor heat gain by the building utilities. For both the indoor and outdoor conditions, the simulation captured the higher temperature during the daytime than the nighttime and the more severe high temperature during the heatwave period than the rest of the days in the summer. The maximum indoor operative temperature at H95 during the heatwave can be 38.5°C, and 37.8°C at H05.

To better compare the difference in time series between the locations in the urban, the heatmap of the hourly temperature of H95 subtracted by that of H05 in Montreal is plotted in **Fig. 6** as an example. A greater temperature difference between the sites happens outdoors than indoor locations, while they still exist a great temperature difference indoors. The indoor operative temperature at H95 is higher than that at H05 for 75% of the hours during the five months, and the difference can be even higher in the hot hours during the heatwave period, which can be as great as 5.8°C. The indoor condition at both locations exhibits a longer time to be higher than 28°C compared to the outdoors, and the overheating conditions at H95 may normally have one or two hours longer on each of the days than that at H05, no matter for indoors or outdoors. In general, the increased overheating hours at a hotter location are normally distributed next to the existing overheating hours that can be found from a cooler location in the same city, this helps to better quantify the increased mortality risk at a location compared to another one in the city. And there are also exist several days that may have several hours of overheating above 28°C found in the building at H95, while none of such overheating can be observed in the building at H05. For example, there are 9 overheating hours at H95 on August 7, while no overheating hour is outlined at H05. A higher possibility is also observed for the building at H95 to have the condition of temperature above 28°C extends after 23:00, while for location H05, this overheating condition normally ends before 23:00. This means using the climate data at a cool location in the city, e.g., H05 may significantly underestimate the overheating during the night.

3.3 comparison between urban and rural locations

The overall difference in overheating conditions between urban and rural areas has been shown in **Fig. 3**. To better show the difference between locations in the urban and rural areas along with the time series, the locations with 50 percentiles (median) of the overheating metric are compared between urban and rural areas. For example, the urban T50 of Ottawa and rural T50 of Ottawa has been compared and their difference has been plotted

in **Fig. 7**. Although the location from the urban area has a higher mean temperature than the rural location as observed, a distinct lower temperature can still be observed in the morning than the location from the rural area for the outdoor condition. It can be identified as the urban cool island, which is consistent with existing findings [21]. While for the comparison of the indoor operative temperature, the building in an urban area does not show that many hours lower than those in a rural area, and the hours with the lower indoor operative temperature in an urban area would occur later than the cool hours in the outdoor.

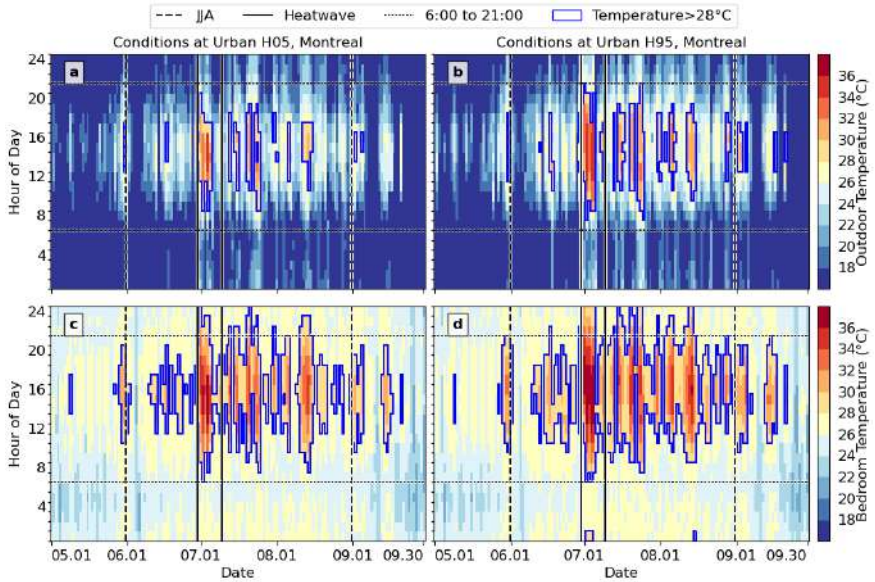

Fig. 5 - Time series heatmap of the a, b) outdoor air temperature, c, d) bedroom operative temperature at a, c, e) H05, and b, d, f) H95 locations in Montreal.

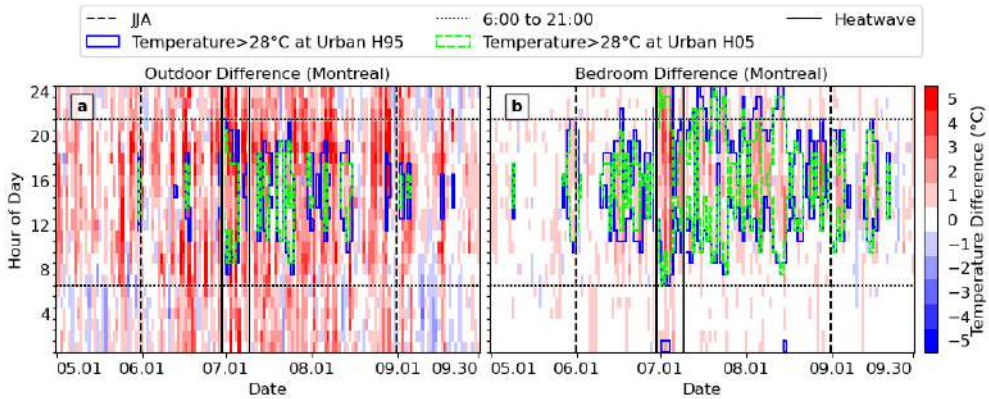

Fig. 6 – The difference of temperature at two urban locations, H95 and H05, of Montreal for a) outdoor air temperature and b) operative temperature in bedrooms

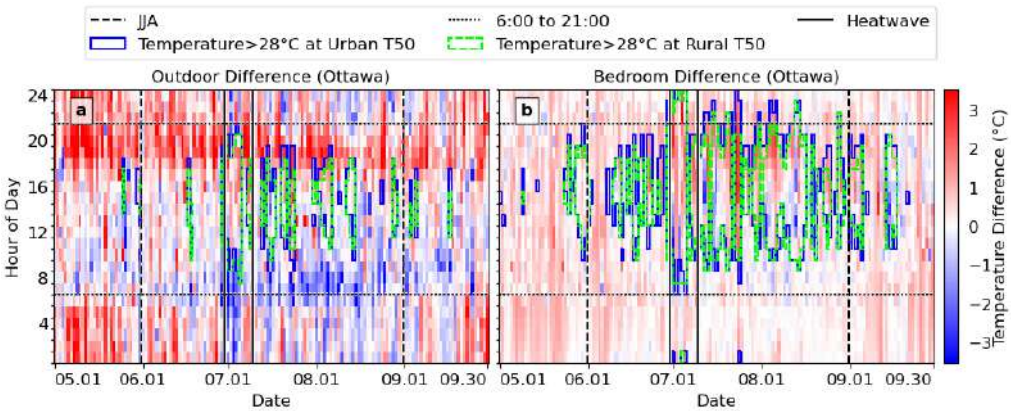

Fig. 7 - The difference of temperature between the T50 locations in urban and rural locations of Ottawa for a) outdoor air temperature and b) operative temperature in bedrooms

The absolute value of the temperature difference is also much smaller than that for the outdoor condition comparisons. For the example in **Fig. 7**, the building in the urban area has been exposed to the outdoor temperature with 40% of the hours lower than that in the rural area, and the greatest difference can be -7.2°C found during the heatwave, while for the indoor condition, the building in the urban area has 22% of the hours lower than that in the rural area, and the greatest difference can be -4.5°C. This exhibits that the urban cool island in the buildings is normally postponed for each of the days and with attenuated intensity due to the higher thermal capacity and the internal heat gain in the building enclosures, and the indoor overheating in an urban area is more severe than that in a rural area.

4. Conclusions

This study has been devoted to quantifying the effect of the spatial distribution of climate data at different locations for the building thermal analysis. A complete procedure of evaluating the overheating conditions of different locations in the city from the high-resolution climate data has been demonstrated by evaluating the distribution of the overheating metrics across the whole city followed by selecting the locations with different quantiles of the overheating metrics. The indoor simulation results of using the different climate data from different locations in the high-resolution are compared together with their local outdoor climate conditions to show the importance of using the climate data at a proper location even for the same city. Conclusions can be summarized in the following points:

- Great intra-urban overheating condition difference has been detected through a comparison of the locations with overheating metrics of the quantile of 00 and 100. The difference in the overheating hours between the locations can be 829 hours in both cities.

- In general, overheating is more severe in an urban area than in a rural area, although an urban cool island effect can be found in the morning when comparing the weather conditions between urban and rural.

- The duration of the overheating may normally have 2 hours difference between locations with overheating metrics of 95 and 05 quantiles. And even for different locations with similar mean indoor operative temperature and overheating hour values, the period of overheating occurrence can be quite different.

- Locations with higher temperature-based overheating metrics may have a more severe overheating condition in the buildings in general, while other climate variables may also affect indoor overheating conditions. In this study, the local wind speed is found very important for the overheating evaluation of the buildings with operable windows for natural ventilation in which the wind speed can markedly change the indoor overheating condition by variating the overall air change rate of the building.

The current study used an archetype single-house building model for the demonstration, which is the limitation of the current study, and in the future, the similar simulation can be performed for other building types to generalize the conclusions from this study.

5. Acknowledgement

The research described in this paper was supported by the Natural Sciences and Engineering Research Council (NSERC) of Canada through the Advancing Climate Change Science in Canada Program [#ACCPJ 535986–18] as well as funding from Infrastructure Canada by the means of Climate Resilient Buildings and Core Public Infrastructure project. This research was also made possible, in part, by Calcul Québec (www.calculquebec.ca) and Compute Canada (www.computecanada.ca).

6. References

[1] World Meteorological Organization (WMO), World Health Organization (WHO), Heatwaves and Health: Guidance on Warning-System Development, 2015.

[2] CIBSE, The limits of thermal comfort : avoiding overheating in European buildings, 2013. https://doi.org/10.1017/CBO9781107415324.004.

[3] J. Taylor, M. Davies, A. Mavrogianni, Z. Chalabi, P. Biddulph, E. Oikonomou, P. Das, B. Jones, The relative importance of input weather data for indoor overheating risk assessment in dwellings, Building and Environment. 76 (2014) 81–91. https://doi.org/10.1016/j.buildenv.2014.03.010.

[4] J. Amoako-Attah, A. B-Jahromi, The impact of different weather files on London detached residential building performance-deterministic, uncertainty, and sensitivity analysis on CIBSE TM48 and CIBSE TM49 future weather variables using CIBSE TM52 as overheating criteria, Sustainability (Switzerland). 8 (2016). https://doi.org/10.3390/su8111194.

[5] L. Guan, Preparation of future weather data to study the impact of climate change on buildings, Building and Environment. 44 (2009) 793–800. https://doi.org/10.1016/j.buildenv.2008.05.021.

[6] C.K. Uejio, O. V Wilhelmi, J.S. Golden, D.M.

Mills, S.P. Gulino, J.P. Samenow, Intra-urban societal vulnerability to extreme heat: The role of heat exposure and the built environment, socioeconomics, and neighborhood stability, Health and Place. 17 (2011) 498–507. https://doi.org/10.1016/j.healthplace.2010.12.005.

[7] M. Kolokotroni, I. Giannitsaris, R. Watkins, The effect of the London urban heat island on building summer cooling demand and night ventilation strategies, Solar Energy. 80 (2006) 383–392. https://doi.org/10.1016/j.solener.2005.03.010.

[8] M. Kolokotroni, Y. Zhang, R. Giridharan, Heating and cooling degree day prediction within the London urban heat island area, Building Services Engineering Research and Technology. 30 (2009) 183–202. https://doi.org/10.1177/0143624409104733.

[9] E. Oikonomou, M. Davies, A. Mavrogianni, P. Biddulph, P. Wilkinson, M. Kolokotroni, Modelling the relative importance of the urban heat island and the thermal quality of dwellings for overheating in London, Building and Environment. 57 (2012) 223–238. https://doi.org/10.1016/j.buildenv.2012.04.002.

[10] M. Kolokotroni, X. Ren, M. Davies, A. Mavrogianni, London's urban heat island: Impact on current and future energy consumption in office buildings, Energy and Buildings. 47 (2012) 302–311. https://doi.org/10.1016/j.enbuild.2011.12.019.

[11] M. Kolokotroni, M. Davies, B. Croxford, S. Bhuiyan, A. Mavrogianni, A validated methodology for the prediction of heating and cooling energy demand for buildings within the Urban Heat Island: Case-study of London, Solar Energy. 84 (2010) 2246–2255. https://doi.org/10.1016/j.solener.2010.08.002.

[12] C. Shu, A. Gaur, L. (Leon) Wang, M. Bartko, A. Laouadi, L. Ji, M. Lacasse, Added value of convection permitting climate modelling in urban overheating assessments, Building and Environment. 207 (2022) 108415. https://doi.org/10.1016/j.buildenv.2021.108415.

[13] A. Gaur, M. Lacasse, M. Armstrong, H. Lu, C. Shu, A. Fields, F.S. Palou, Y. Zhang, Effects of using different urban parametrization schemes and land-cover datasets on the accuracy of WRF model over the City of Ottawa, Urban Climate. 35 (2021) 100737. https://doi.org/10.1016/j.uclim.2020.100737.

[14] H. Li, Y. Zhou, X. Wang, X. Zhou, H. Zhang, S. Sodoudi, Quantifying urban heat island intensity and its physical mechanism using WRF/UCM, Science of the Total Environment. 650 (2019) 3110–3119. https://doi.org/10.1016/j.scitotenv.2018.10.025.

[15] K.B. Moffett, Y. Makido, V. Shandas, Urban-rural surface temperature deviation and intra-urban variations contained by an urban growth boundary, Remote Sensing. 11 (2019). https://doi.org/10.3390/rs11222683.

[16] D. Zhou, S. Zhao, S. Liu, L. Zhang, C. Zhu, Surface urban heat island in China's 32 major cities: Spatial patterns and drivers, Remote Sensing of Environment. 152 (2014) 51–61. https://doi.org/10.1016/j.rse.2014.05.017.

[17] A. Laouadi, A. Gaur, M.A. Lacasse, M. Bartko, M. Armstrong, Development of reference summer weather years for analysis of overheating risk in buildings, Journal of Building Performance Simulation. 13 (2020) 301–319. https://doi.org/10.1080/19401493.2020.1727954.

[18] CIBSE, Design Summer Years for London, Technical Memoranda 49. (2014) 1–29.

[19] CIBSE, Environmental design CIBSE: Guide A, 2011.

[20] A. Laouadi, M. Bartko, M.A. Lacasse, A new methodology of evaluation of overheating in buildings, Energy and Buildings. 226 (2020) 110360. https://doi.org/10.1016/j.enbuild.2020.110360.

[21] S. Duan, Z. Luo, X. Yang, Y. Li, The impact of building operations on urban heat/cool islands under urban densification: A comparison between naturally-ventilated and air-conditioned buildings, Applied Energy. 235 (2019) 129–138. https://doi.org/10.1016/j.apenergy.2018.10.108.

Aerosol transmission in rotary wheel heat exchangers

Heinrich Huber [a], Thomas Richter [b], Florian Brzezinski [a], Michael Riediker [c]

[a] Institute of Building Technology and Energy, Lucerne University of Applied Sciences and Arts, Horw, Switzerland, heinrich.huber@hslu.ch, florian.brzezinski@hslu.ch.

[b] Hoval Aktiengesellschaft, Vaduz, Lichtenstein, thomas.richter@hoval.com.

[c] SCOEH: Swiss Centre for Occupational and Environmental Health, Winterthur, Switzerland, michael.riediker@alumni.ethz.ch.

Abstract. Transmission by aerosols is considered the main route of COVID-19 infections indoors. Therefore, limiting air transfer between supply and extract air in ventilation systems is critical. Heat recovery components (HRCs) are used as standard in new ventilation systems. Rotary wheels are very efficient, but have a higher exhaust air transfer ratio (EATR) compared to other types. The fact that the surface of rotary wheels is touched by both supply and exhaust air allows humidity recovery, but also carries a risk of transferring undesirable substances. Aerosols can deposit on the surface if they come into contact with it. The characteristics of rotary wheels raise the question whether a relevant transfer of aerosols can take place and whether this is different from the EATR. Experimental investigations were carried out with two rotary wheels. The aerosol used was a water-glycol mixture whose properties compare well with human lung aerosols. Particle sensors were installed at all four duct connections of the HRC. In parallel, the EATR was determined with tracer gas. In 16 measurement series, the air velocity, rotor speed and air conditions were varied. The determined aerosol transfer ratio was typically 1 to 2 percentage points below the EATR. The results allow the conclusion that rotary wheels designed and operated according to current standards transfer only a non-relevant small amount of aerosols and thus do not pose an infection risk for COVID-19 in applications such as offices where the frequency of highly infectious individuals is low to moderate. However, aerosol transmission in hygienically relevant quantities is conceivable in poorly designed systems with incorrect pressure ratios and inadequate filters at the same time, but this does not only affect rotary wheels. Although first positive results are available, further investigations are planned. The understanding of aerosol absorption and HRCs surface's properties is to be deepened.

Keywords. Ventilation, aerosol transmission, heat recovery, rotary wheel
DOI: https://doi.org/10.34641/clima.2022.391

1 Introduction

Aerosols are considered a main cause of COVID-19 infections indoors. Therefore, limiting air transfer between supply and extract air in ventilation systems is critical.

In bidirectional ventilations systems, heat recovery is state of the art and is even required in the European regulation for ecodesign requirements for ventilation units [1]. Rotary heat exchangers (RHE) are an efficient and economically interesting solution and are therefore widely used. A disadvantage of RHE is that due to the physical principle and the mechanical implementation a higher exhaust air transfer ratio (EATR) can occur than with other common heat recovery categories such as plate heat exchangers or run around coil systems. Measures to minimise and evaluate the EATR of RHEs are well known and recommended e.g. in the REHVA COVID-19 Guide [2]. Special attention must be paid to the correct pressure ratios and purge sector. However, RHEs are not generally equipped with purge sectors, and in older AHUs the pressure ratios are not always optimal. Another aspect is the fact that the surface of an RHE is touched by both supply and extract air.

Copyright ©2022 by the authors. This conference paper is published under a CC-BY-4.0 license.

Although this enables humidity recovery, it also carries the risk of transferring undesirable substances. However, aerosols can adhere to the surface if they come into contact with it. Associated with adhesion are deposition and release [3].

The characteristics of RHEs raise the question of whether relevant aerosol transfer can take place and whether this differs from EATR. For hygienically demanding applications of RHEs, it is crucial to have more knowledge about the phenomenon of aerosol transfer. Additional knowledge is important for the acceptance of RHEs by both experts and occupants. Against this background, the industry is looking for answers.

On the initiative of a company, the University of Applied Sciences and Arts Lucerne (HSLU) together with the Swiss Centre for Occupational and Environmental Health (SCOEH) carried out first experimental investigations in January 2021 [4]. In the second half of 2021, the idea was supported by a manufacturer group under the administration of the association FGK Fachverband Gebäude-Klima e. V.. The investigations from the first project will be continued with further types of RHEs and conditions. The second project had not yet been completed at the time this paper was submitted. Therefore, only results from the first project are presented here.

Common to both projects was the use of an aerosol that behaves in the laboratory test system similar to human exhaled aerosols thus it had to be liquid, hygroscopic, moderately viscous and of similar size.

2 Research methods

The Building Technology Laboratory of the HSLU operates a test rig for heat recovery devices. In Figure 1 the scheme of the test rig is shown. In all four air streams temperature, humidity, air flow rate and tracer gas concentration can be measured. For the aerosol measurements, a particle generator was installed in the exhaust air inlet duct and additional measuring devices in all four air streams. In addition, the ambient conditions were measured.

Test objects were two RHEs with a free diameter of 1000 mm: a condensation rotor (aluminium) and a sorption rotor (aluminium with molecular sieve coating). With the diameter of 1000 mm the nominal airflow is between 1'400 to 4'199 m³/h for a face velocity of 1 – 3 m/s under standard conditions. On both sides air inlet temperatures were 20°C ± 1K and air inlet humidity 40% RH ± 10% RH.

The transfer of tracer gas and aerosols was measured by dosing up the exhaust air. In order to make a conclusion of the aerosol transmission, the EATR and the aerosol transfer ratio (ATR) were determined and compared. In this first round of experiments, the RHEs were installed in the test casing without a purge sector.

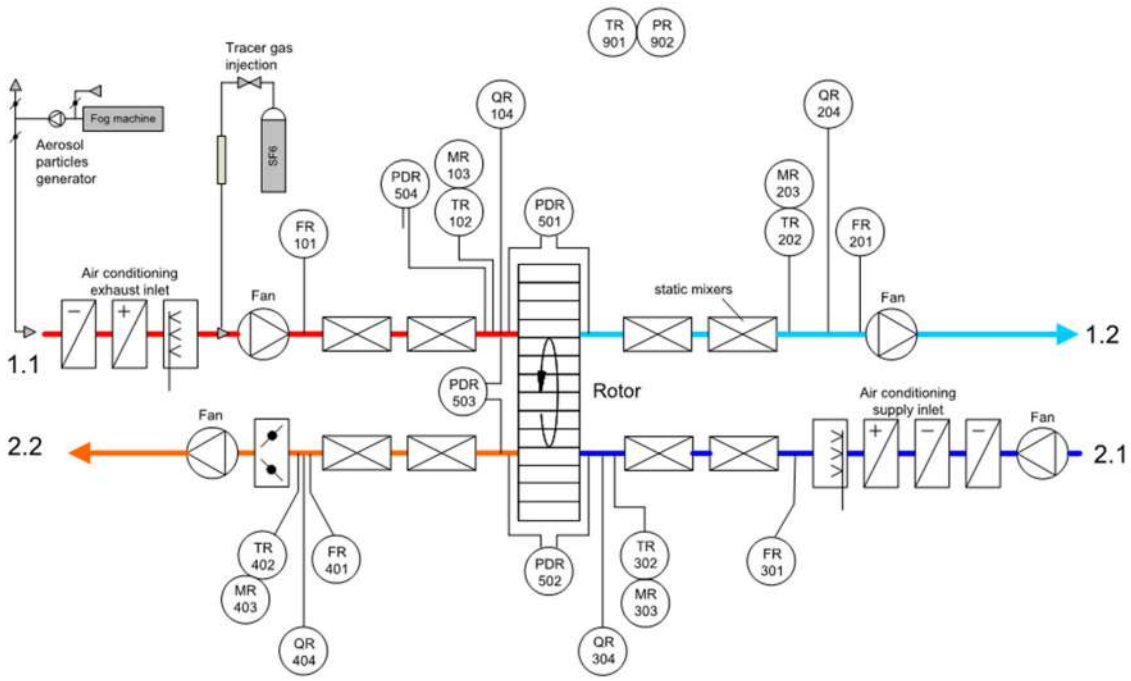

Fig. 1 - Scheme of the test rig for heat recovery devices. Symbols: **first letter** F air flow rate, P pressure, T temperature, M humidity, Q concentration; **subsequent letter** D difference; **auxiliary letter** R registration; **air flow type** 1.1 exhaust inlet, 1.2 exhaust outlet; 2.1 supply inlet, 2.2 supply outlet

2.1 *Exhaust Air Transfer Ratio (EATR)*

The EATR was measured based on EN 308:2021 [5] by injecting Sulphur Hexafluoride (SF_6) tracer gas in the duct of the exhaust air inlet. The SF_6 concentration was subsequently determined with a photoacoustic IR-gas monitor with a multipoint sampler in exhaust air inlet, supply air inlet and supply air outlet . The EATR can be calculated with the following formula:

$$EATR = \frac{a_{22}-a_{21}}{a_{11}-a_{21}} \times 100\ [\%] \qquad (1)$$

where

a_{11} is SF_6 concentration exhaust inlet [ppm],
a_{21} is SF_6 concentration supply inlet [ppm],
a_{22} is SF_6 concentration supply outlet [ppm].

In the given measurement range, a relative measurement uncertainty of the EATR between 3 and 5% is typical. In the sense of a rather conservative estimate, 5% relative is used in the evaluation.

2.2 *Aerosol Transfer Ratio (ATR)*

The test setup for the ATR measurements was done in the same way as for the EATR measurements. Two aerosol measuring devices were installed in each of the four air streams. The sensors count the particulate matter based on laser scattering in a size of 0.3 to 10 µm. To keep the aerosol concentration in the supply inlet air as low as possible, the installed filters of the class ISO ePM1 50% (F7) were replaced with HEPA filters H14. During the measurement, aerosol was applied in pulses in the duct of the exhaust inlet air. The aerosol used has an average diameter of just over one micrometer and is therefore comparable in size to exhaled aerosol [6]. The aerosol, like human exhaled aerosol, is liquid at normal ambient temperatures. It is produced by evaporation and condensation of a water-glycol mixture by a fog machine and is stable in air for a longer time [7]. The mixture used in the studies consists of triethylene glycol, monopropy-lene glycol and dipropylene glycol. The maximum peak heights at exhaust air inlet, supply air inlet and outlet were used for evaluation according following formula:

$$ATR = \frac{b_{22}-b_{21}}{b_{11}-b_{21}} \times 100\ [\%] \qquad (2)$$

where

b_{11} is peak PM10 exhaust inlet [P/cm³],
b_{21} is peak PM10 supply inlet [P/cm³],
b_{22} is peak PM10 supply outlet [P/cm³].

The measurement uncertainty was determined with the device-to-device variability after internal cross-correction for the test aerosol for the number of PM10. With this method, the relative measurement uncertainty for applications such as indoor measurements is given as 3%. For the new application in the test rig for heat recovery components, a relative measurement uncertainty of 10% is used as a conservative estimate in the evaluation.

3 Results

3.1 *Condensation rotary heat exchanger*

Table 1 shows the results of the condensation RHE. The measurements were conducted with three different air face velocities (v) of 1, 2 and 3 m/s. Rotor speed (n) was 20 rpm and pressure difference between supply outlet and exhaust inlet ($\Delta p_{22\text{-}11}$) 10 Pa. One additional measuring point with a difference of 250 Pa between supply outlet and exhaust inlet was conducted. In the project, additional measurements were made to determine the ATR without determining the EATR under the same conditions. These results are not presented.

Tab. 1 – Results EATR and ATR, condensation wheel

MP	v	n	$\Delta p_{22\text{-}11}$	EATR	ATR
-	m/s	rpm	Pa	%	%
1.1	1	20	10	10.4	7.5
1.2	2	20	10	4.7	3.8
1.3	3	20	10	3.3	2.4
1.4	3	20	250	2.6	1.6

Figure 2 shows that at all four measuring points (MP) the ATR value is below the EATR value. The difference is clearly higher than the measurement uncertainty.

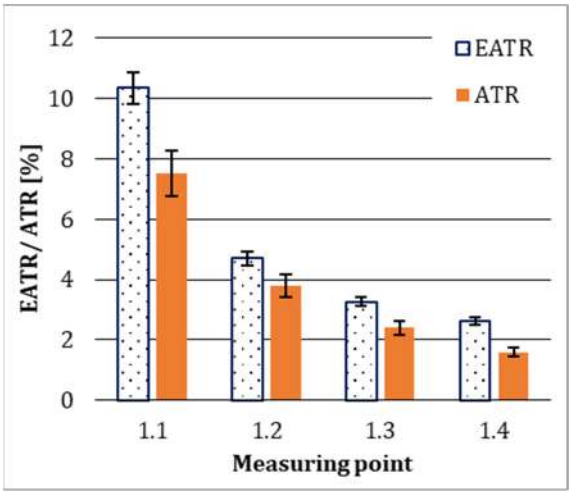

Fig. 2 - Results EATR and ATR, condensation wheel at isothermal condition 20°C, 40% RH

3.2 *Sorption rotary heat exchanger*

As with the condensation RHE, measurements with the sorption RHE were carried out at three different face air velocities. Pressure difference between supply outlet and exhaust inlet were 10 Pa. With the sorption RHE additional to the measurements with 20 rpm, measurements with 10 rpm rotor speed were conducted. Table 2 shows the results of the sorption RHE.

Tab. 2 – Results EATR and ATR, sorption wheel

MP	v	n	$\Delta p_{22\text{-}11}$	EATR	ATR
-	m/s	rpm	Pa	%	%
2.1	1	20	10	8.2	6.3
2.2	2	20	10	4.7	2.7
2.3	3	20	10	3.2	1.7
2.4	1	10	10	4.5	2.8
2.5	2	10	10	2.3	0.9
2.6	3	10	10	1.5	0.6

Comparable to the results of the condensation RHE Figure 3 shows that also with the sorption RHE at all six measuring points the ATR value is below the EATR value.

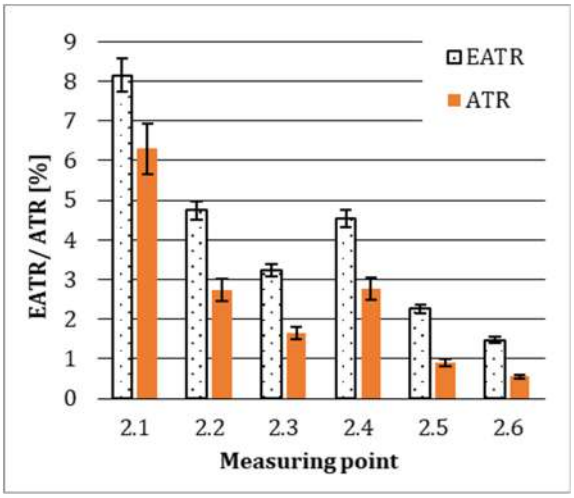

Fig. 3 - Results EATR and ATR, sorption wheel isothermal condition 20°C, 40% RH

4 Discussion

4.1 Significance of the results

AHUs that comply with the European Ecodesign Regulation [1] are typically designed for a face velocity (related to the inner cross-sectional area of the casing) of about 1.6 to 1.8 m/s at nominal air flow rate. Since the face area of the of the RHE is about 10 to 20% smaller than the cross-sectional area of the AHU, the nominal face velocity of a RHE is typical approx. 2 m/s. In applications such as office buildings and schools, face velocities in the range of about 1 m/s often occur in partial load operation mode. On the other hand, the REHVA COVID-19 guideline recommends not using partial load operation in pandemic situations. Therefore, the measured EATR and ATR at 2 m/s are considered for the infection risk assessment.

For condensation RHEs the rotor speed is in a range of 10 to 20 rpm, depending on design characteristics, e.g. foil thickness. For sorption RHEs 20 rpm can be seen as typical speed. Therefore, for the contamination risk assessment for both RHE types the measured values at 20 rpm are chosen and rounded up to the nearest integer percentage. This is to be understood as a rather conservative estimate for the two investigated RHEs. For the calculation of the contamination risk the following values are used:

- EATR for both RHE types 5%
- ATR for condensation RHE 4%
- ATR for sorption RHE 3%

It goes without saying that these data are valid only for the tested RHE when using this specific fog aerosol. They should not be taken as universally valid in the current state of knowledge. Nevertheless, the two RHEs examined are real products that are judged to be typical in a market comparison.

The draft revision of the European Ecodesign Regulation from [8] serves as a comparison. In this draft a maximum EATR at nominal flow and nominal pressure of 5% is required. With reference to this source, a maximum EATR of 5% can be considered state of the art.

However, for hygienically sensitive applications, such as public buildings, the authors recommend taking measures to achieve a lower EATR. For RHE with a purge sector, an EATR below 0.5% can be achieved.

4.2 State of the art in filters

In German speaking countries the VDI 6022-1 [9] is considered reflecting the state of the art. The minimum filter class for supply air is ISO ePM1 50%. The extract air before entering a RHE shall pass a filter of class ISO ePM10 50%. As general estimation for the separation efficiency of lung aerosols the gravimetric arrestance of the filters up to a particle size of PM10 can be used:

- For class ISO ePM1 50%: 85% [10]
- For class ISO ePM10 50%: 50% (by definition of the class)

A typical solution is that in the outdoor air (before entering the RHE) and in the extract air (before entering the RHE) an ISO ePM1 50% filter is placed. Thus, the potentially contaminated air passes through only one filter.

4.3 Estimation of the ATR including filter

The aerosol transfer ratio of an AHU ATR_{AHU} can be estimated as follow:

$$ATR_{AHU} = ATR_{RHE} \cdot (1 - f_{F,eta}) \cdot (1 - f_{F,sup}) \qquad (3)$$

where

ATR_{RHE} is the ATR of the RHE, acc. to Equation (2),

$f_{F,eta}$ is the separation efficiency of lung aerosols of an extract air filter (positioned before RHE),

$f_{F,sup}$ is the separation efficiency of lung aerosols of a supply air filter (positioned after RHE).

With the values shown in chapters 4.1 and 4.2, an ISO ePM1 50% filter in extract air and no additional filter in supply air, the result is an $APTR_{AHU}$ of approx. 0.005 to 0.006 or 0.5% to 0.6% respectively. This applies to RHEs without purge sectors. With purge sector, values 10 times lower can be achieved without problems. In addition, the ATR can be halved again if, for example, an ISO ePM10 50% filter is also used on the extract air side combined with an ISO ePM10 50% filter in supply air.

4.4 Estimation of the infection risk

The amount of virus released into the air can be done by combining the concentration of viruses in the lung lining liquid with the size-distribution of micro-droplets released during breathing and speaking and by taking into account the proportion that sediments rapidly [11]. To estimate the viral concentration at steady state in different situations, we used an indoor scenario simulator that is based on this emission concept [12]. In all the calculated scenarios, we assumed that a very contagious person (a so-called super-emitter) is in a room of 100 m³ volume and 3 air changes per hour. We then simulated a quiet office, a loud office (e.g. call centre) and a hospital situation with coughing COVID-19 patients. We further assumed that 1000 people are in this building with a ventilation flow rate of 30'000 m³/h. For the general population, a very high infection rate of 1% is assumed, for the hospital wing with COVID-19 patients a rate of 50% (50% patients, 50% staff). Table 3 summaries the simulated virus concentrations in these scenarios in the individual rooms and in the extract air of the building.

The concentrations indicate viral copies as assessed by RNA assays. For the Delta variant about 1 in 300 and for the Omicron variant about 1 in 100 of these copies was found to be able to infect cells [13]. Thus, doses above 300 or even only 100 virus-copies seems to be critical for viral infections. This is supported by simulation of super-spreading events where the virus dose (the amount taken up) was estimated in the range of a few thousand viruses.

Tab. 3 – Simulated virus concentrations (copies/m³) in individual rooms and in the extract air in different scenarios.

Scenario	*Infection rate*	*Steady state in room*	*Extract air*
	%	*Copies /m³*	*Copies /m³*
Quiet office	1	1200	1.2
Call centre	1	40'000	40
Hospital, COVID section	50	500'000	250'000

For the example of the call centre, it can be said that with the aerosol transfer ratio of an air handling unit of 0.6% shown in 4.1 and the virus concentrations in the extract air according to Table 3, the virus concentration in the supply air is 0.2 copies/m³. Even if the personnel directly inhale the supply air during an 8-hour shift (breathing air volume 0.6 m³/h), the amount of inhaled viruses is two orders of magnitude below the critical value for an infection risk. However, in a hospital situation with many highly emitting patients, the situation could rapidly become critical. Thus, the recommendation to use heat recovery systems without any risk of exhaust air transfer to supply air (e.g. tight plate heat exchanges or run around coil systems) [14] in such settings is well warranted.

Eurovent 6/15 - 2021 [15] deals comprehensively and in detail with the prevention of air leakage in air handling units. According to this, an elementary measure is to ensure correct pressure conditions in air handling units. This depends primarily on the fan positions. For hygienically sensitive applications, a purge sector is also recommended. AHUs operated with proper pressure conditions and well-designed purge sectors can achieve an EATR of practically zero.

It should be mentioned that the risk of exhaust air transfer also exists with other leakages in AHUs and ventilation systems that are not the subject of this paper.

5 Conclusion and outlook

The project investigated how aerosols, which behave similarly to human lung aerosols, are transferred in rotary heat exchangers without a purge sector under isothermal conditions. In the measurements on a condensation rotor, the exhaust air transfer ratio of the aerosols was around 1 percentage point lower than the exhaust air transfer ratio (EATR) of tracer gas. For a sorption rotor it was 2 percentage points lower. The results suggest that there is no risk of the used aerosols being transferred through the matrix with these rotary heat exchangers.

However, further investigations are needed to generalise the statement. In particular, we are interested in whether this also applies to different air conditions (temperature and humidity) and which transfer ratios result with purge section. For validation, measurements with additional products are also of interest. In the follow-up project further measurements were carried out, but these had not yet been completed when this paper was submitted. These results are expected to be available in spring 2022.

6 Acknowledgment

The authors would like to thank the company Hoval for initiating the project, the technical exchange, and the financial support.

7 References

[1] Commission Regulation (EU) No 1253/2014 of 7 July 2014 implementing Directive 2009/125/EC of the European Parliament and of the Council with regard to ecodesign requirements for ventilation units.

[2] Federation of European Heating, Ventilation and Air Conditioning Associations. RHEVA COVID-19 guidance document, version 4.1. Brussels. 2021-04-15.

[3] Wickman H.H. Deposition, Adhesion, and Release of Bioaerosols. In: Lighthart B., Mohr A.J. (eds) Atmospheric Microbial Aerosols. Springer, Boston, MA. 1994:99-165. ISBN 978-1-4684-6438-2_5.

[4] Prüfstelle Gebäudetechnik. Test Report No.: HP-202084 Measurements on two Rotary Heat Exchangers. University of Applied Sciences and Arts (HSLU), Horw. 2021-03-09.

[5] EN 308:2021 Heat exchangers - Test procedures for establishing performance of air to air heat recovery components. CEN, Brussels.

[6] Johnsona G.R., Morawskaan L., Ristovskia Z.D., Hargreavesa M., Mengersena K., Chaob C.Y.H., Wanb M.P., Lic Y., Xiecf X., Katoshevskid D., Corbett S. Modality of human expired aerosol size distributions. Journal of Aerosol Science 2011; 42.

[7] Maximoff S.N., Salehi A.A., Rostami A. Modality of human expired aerosol size distributions. Molecular dynamics simulations of homogeneous nucleation of liquid phase in highly supersaturated propylene glycol vapors; 2021.

[8] Draft Working Document on Ecodesign Requirements for Ventilation Units (Review EU1253/2014). European Commission, Brussels; 2021-03-01.

[9] VDI 6022 Blatt 1:2018-01 Ventilation and indoor-air quality - Hygiene requirements for ventilation and air-conditioning systems and units (VDI Ventilation Code of Practice). Verein Deutscher Ingenieure, Düsseldorf

[10] Brunner A. Filterrichtlinie SWKI VA101-01 und VDI 3803/4. 6. Schweizer Hygienetagung, 2021-09-10.

[11] Riediker, M., Tsai, D.-H.. Estimation of Viral Aerosol Emissions From Simulated Individuals With Asymptomatic to Moderate Coronavirus Disease 2019. JAMA Netw Open 2020; 3, e2013807.

[12] Riediker, M., Monn, C.. Simulation of SARS-CoV-2 Aerosol Emissions in the Infected Population and Resulting Airborne Exposures in Different Indoor Scenarios. Aerosol Air Qual. Res. 2021; 21, 200531.

[13] Riediker, M. et al. Higher viral load and infectivity increase risk of aerosol transmission for Delta and Omicron variants of SARS-CoV-2. Swiss Med Wkly. 2022;152:w30133

[14] SWKI VA105-01:2015 Raumlufttechnische Anlagen in medizinisch genutzten Räumen (Planung, Realisierung, Qualifizierung, Betrieb). Die Planer – SWKI, Urtenen-Schönbühl

[15] Eurovent 6/15 – 2021 Air Leakages in Air Handling Units: Guidelines for Improving Indoor Air Quality and Correcting Performance. First edition. Eurovent European Industry Association, Brussels

The data sets analyzed in this study are not publicly available because they are private measurements, but the authors can provide excerpts upon request if necessary.

Investigation of the group differences in indoor environmental quality

Zheng Li [1,2,3], Ongun Berk Kazanci [1], Qingwen Zhang [2,3], Bjarne W. Olesen [1]

[a] International Centre for Indoor Environment and Energy, Department of Environmental and Resource Engineering, Technical University of Denmark, Nils Koppels Allé, Building 402, 2800 Kgs. Lyngby, Denmark, hitlizheng@hotmail.com.

[b] Key Lab of Structures Dynamic Behavior and Control of the Ministry of Education, Harbin Institute of Technology, Harbin, 150090, China, hitlizheng@hotmail.com.

[c] Key Lab of Smart Prevention and Mitigation of Civil Engineering Disasters of the Ministry of Industry and Information Technology, Harbin Institute of Technology, Harbin, 150090, China, hitlizheng@hotmail.com.

Abstract. Based on the field measurements and questionnaires surveys carried out in 22 offices in Harbin, China, the group differences (gender, age, BMI, level of education, location groups) in human comfort for different levels of environmental parameters were investigated. It was found that males, elder subjects (above 25 years old) and the subjects with higher academic degrees have higher comfort votes than other groups. The group differences were larger in a warmer thermal environment and the differences in thermal comfort votes could be larger than 0.5 scale units on the comfort scale among gender, age and level of education groups when the temperature was higher than 26°C in summer or higher than 24°C in winter. For indoor air quality, the differences in comfort votes for air freshness were larger when the CO_2 concentration was less than 960 ppm and the difference in comfort votes for air pollution was larger when $PM_{2.5}$ concentration was higher than 25 μg/m^3. For sound comfort, it was found that the subjects near doors had higher sensitivity to the change in sound levels than the subjects at other locations. For light comfort, the higher illuminance could cause larger group differences. This study can be used to better develop comfort systems, especially personal comfort systems.

Keywords. Group difference, indoor environmental parameters, human comfort.
DOI: https://doi.org/10.34641/clima.2022.392

1. Introduction

Indoor environmental quality (IEQ) of buildings, including thermal, indoor air quality, acoustic and light environments, has significant effects on human comfort [1, 2]. In the previous studies, it has been reported that individual differences in human perceptions existed even when subjects were exposed to the same indoor environmental environment [3, 4]. It is necessary to explore group differences in human perceptions for indoor environmental parameters, which can be used to better decide the comfort systems.

For the gender groups, Lan [5] and Karjalainen [6] found that the thermal sensation values of females were lower than those of males. Nakano et al. [7] conducted a field study in an office in Tokyo and found significant gender differences in thermal comfort. Wang conducted a field study in winter in Harbin, China and found that the neutral temperature of females was 1°C higher than that of males [8]. In contrast, the studies of Peng [9], Choi et al. [10] and Becker et al. [11] found no statistically gender significant difference in thermal sensation votes [11]. For the age groups, Becker [11] and Indraganti [12] found no statistically significant differences in thermal sensation votes. But Peng [9] found that the range of the comfortable temperatures of the elderly subjects who were above 50 years old was narrower than that of the young subjects who were below 18 years old, and the same conclusion was given by Hwang [13]. For the BMI groups, Rupp [14] conducted a field study in offices and found that BMI had a significant impact on occupants' thermal sensation and clothing habits. Compared to the normal weight and underweight groups, the neutral temperature and mean clothing insulation of the overweight group were lower in the previous study [15]. The study of Kang found that subjects near windows had slightly lower thermal satisfaction than subjects at other locations [16]. The study of Yamtraipat et al. showed that people with higher educational degrees preferred lower air temperature [17]. The research on the effect of the level of education and subjects' location on thermal

Copyright ©2022 by the authors. This conference paper is published under a CC-BY-4.0 license.

comfort is still lacking.

Although the group differences in thermal responses have been studied in previous studies, the research on the group differences in other environmental factors was rare. It is necessary to explore the group differences in human comfort for all the environmental factors. Kang carried out 231 questionnaire surveys in 19 universities and analyzed the group differences in all indoor environmental factors [16]. This study showed that the elder subjects (24-35 years old) and the subjects near windows had higher mean light comfort votes than the younger subjects (below 24 years old). Also, The elder subjects were more sensitive and had lower acoustic satisfaction than the younger subjects. The subjects at other locations and the subjects near windows and doors were more satisfied with the air quality than the subjects at other locations.

In all the above studies, there was no study discussing the influence of the level of different indoor environmental parameters on group differences in human perceptions. It is necessary to study how big the group differences in human perceptions are when the environmental parameters are above or below the limits in the standard. Therefore, based on the field measurements and questionnaire surveys in open-plan offices in a severe cold region, this study investigated the group differences in human comfort (thermal, indoor air quality, light and sound comfort) for different levels of environmental parameters.

2. Methodology

2.1 Site and building information

In this study, 22 university open-plan offices, which are distributed on different floors (between the 2nd and 6th floors) of different orientations, were selected from four office buildings in Harbin Institute of Technology, which is located in a severe cold region in China. The central heating system was used in all buildings to provide space heating. The radiators were installed on the walls under the windows as the terminal unit, but the subjects cannot adjust the temperature of the radiators. The split-type air conditioner systems were installed in all buildings and the air conditioners can be adjusted by the subjects. The photos of the test sites and the physical characteristics of the offices can be seen in our other studies [18, 19].

2.2 Field measurements

The field study was conducted from August 10, 2018 to May 19, 2019. The outdoor temperature was monitored, and the 5-day average outdoor air temperatures are shown in the previous study [18]. According to QX/T 152-2012 [20], the sampling period was divided into summer, winter and transition seasons in Tab. 1. The point-in-time measurements were performed together with the questionnaire surveys every 3-4 weeks, and the recording interval for each parameter was 10s. The thermal physical parameters include indoor air temperature (°C), relative humidity (%), globe temperature (°C), and air velocity (m/s). For indoor air quality parameters, CO_2 concentration was measured by HOBO MX1102 and particulate matter ($PM_{2.5}$) was collected by GT-1000. The sound level was measured by a sound analyzer HS6288E, and TES1339P was used to measure the illuminance of each subject's location. The measurement of the illuminance of each subject's location lasted for more than 5 min, while the measurements of other parameters lasted for more than 1 hour. All the devices had self-recording functions and the measured range and the accuracy of all devices are shown in our previous study [19].

Tab. 1 - Division of seasons.

Seasons	Survey dates
Summer	11th August 2018 –25th August 2018
Winter	25th October 2018 –12th April 2019
Transition seasons (Autumn, Spring)	25th August 2018 – 24th October 2018 13th April 2019–19th May 2019

2.3 Questionnaire surveys

The questionnaire was designed based on ASHRAE 55 [21] and EN 16798-1 [22] and it was used to acquire human perceptions during the point-in-time measurement surveys. The survey begins with the individual information of subjects, including gender, age, level of education, body mass index (BMI), and subjects' location. The second section investigated human comfort for thermal, sound, indoor air quality (air freshness and air pollution) and light environments. Human comfort was investigated by the seven-point scale specified by Appendix E in ASHRAE-55, which is shown in Fig. 1, and the range of comfortable vote was from 4 to 7. Humans can be considered in a steady-state condition after a 30-45 min stay in a thermal environment, thus all the subjects filled out questionnaires after working in the offices for more than 30 min. The subjects were also required not to wear earphones or headphones for 10 min before filling in the questionnaires.

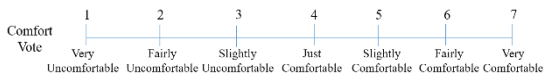

Fig. 1 - The scales of comfort vote [18].

3. Results

The result analysis focuses on the group differences in human comfort for different levels of parameters. The categories of the environmental parameters in EN16798-1 were used to divide the levels of the environmental parameters. Mann-Whitney U tests and Kruskal-Wallis H tests were applied for studying the group differences, and the result of the p-value below 0.05 reveals that a statistically significant

difference exists among groups.

3.1 Indoor environmental parameters

A total of 165 point-in-time measurements were carried out. The average values and standard deviations for the indoor thermal parameters during different seasons were shown in Tab. 2 [18]. According to Table 2, the mean air temperatures and globe temperatures in summer and winter were higher than those in transition seasons. In our previous study, it has also been found that during the sampling period, the mean outdoor air temperature in winter was -3.5°C, far lower than that in transition seasons (15.1°C). Thus, the difference between indoor and outdoor air temperatures was larger in winter than in transition seasons, which might cause uncomfortable feelings for subjects. The average values and the ranges for other parameters ($PM_{2.5}$ concentration, CO_2 concentration, A-weighted sound level and illuminance) during all seasons are shown in Tab. 3.

Tab. 2 – Average values for the thermal parameters [18].

Thermal parameters	Average value±SD		
	Summer	Winter	Transition seasons
Air temperature (°C)	26.7 ±1.6	25.5 ±2.0	23.8 ±2.0
Relative humidity (%)	53 ±2	19 ±6	29 ±8
Globe temperature (°C)	26.8 ±1.8	25.2 ±2.1	24.2 ±2.3
Air velocity (m/s)	0.07 ±0.03	0.03 ±0.02	0.04 ±0.02

Tab. 3 – Average values for other environmental parameters during all seasons [18].

Parameters	Average value±SD	Range
$PM_{2.5}$ concentration (μg/m^3)	28±19	3-83
CO_2 concentration (ppm)	897±215	493-1451
A-weighted sound level (dB(A))	50±4	40-61
Illuminance (lux)	433±293	39-1407

3.2 Profile of the sample

A total of 1352 valid questionnaires, filled in by 265 university researchers, were collected, with 227 for summer, 744 for winter, and 381 for transition seasons. The winter in Harbin lasted for almost 6 months, longer than the summer and transition seasons, thus we could obtain more questionnaires in winter. The questionnaires for all seasons covered different genders, ages, levels of education and BMI, and the subjects for different groups sat at different locations in the offices. The occupied zones within 1.5 m from the windows or doors were defined as the locations near windows or doors. The Pearson correlation coefficient between the age and level of education groups was calculated as 0.666 and the significant level p-value was less than 0.001 [18], which revealed that the age and level of education groups had a strong correlation. Due to the upper and lower quartiles for different levels of education, the occupants were divided into three age groups, which were the younger group (<23), the middle age group (23-25) and the elder group (>25). The sample sizes of different groups are listed in Tab. 4 [18]. It should be illustrated that the sample size of undergraduates in summer was only 3 and this small sample size might cause the low-test power for the analysis of group differences among the level of education groups in summer.

Tab. 4 – Sample sizes of different groups [18].

	Total number	Seasons		
		S	W	TS
Gender group				
Male	895	174	482	239
Female	457	53	262	142
Age group				
Younger<23	161	15	101	45
Middle age 23-25	711	144	378	189
Elder age>25	480	68	265	147
Level of education				
Undergraduate	107	3	71	33
Master student	539	106	286	147
Doctoral student	706	118	387	201
Location				
Near window	383	66	201	116
Near door	286	40	159	87
Other location	683	121	384	178
BMI				
<18.5	137	25	71	41
18.5-24.9	921	164	501	256
>24.9	294	38	172	84

3.3 Thermal comfort

For thermal comfort, the p-values and the mean thermal comfort votes among different groups during different seasons are shown in Tab. 5. It can be seen that statistically significant differences in thermal comfort votes occurred in more groups in summer and winter than in the transition seasons. In transition seasons, the statistically significant difference was only found in the BMI group (p-value=0.003).

The p-values below 0.05 were further studied. According to EN 16798-1 [22], the temperature range for heating seasons (winter) in the medium category in open-plan offices is from 20°C to 24°C and the range for cooling seasons (summer) is from 23°C to 26°C. The range of air temperatures in winter was from 20.5°C to 28.7°C, and the upper limit for winter (24°C) in EN 16798-1 was used to divide the temperatures into two categories, which were

respectively from 20°C to 24°C (comfortable range) and above 24°C (uncomfortable range). The range of air temperatures in summer was from 22.7°C to 29.1°C, and the upper limit for summer (26°C) was used to divide the temperature, which were respectively from 23°C to 26°C (comfortable range) and above 26°C (uncomfortable range). The range of transition seasons was from 20.4 to 28.3°C, and the upper limit temperatures for summer (26°C) and winter (24°C) were used to divide the temperatures into three categories.

Tab. 5 Mean thermal comfort votes during different seasons

	Thermal comfort vote		
	Summer	Winter	Transition seasons
Gender			
Male	4.8	4.4	5.2
Female	4.7	4.6	5.2
p-value	0.915	0.091	0.614
Age			
Younger<23	**5.0**	**4.9**	5.5
Middle age 23-25	**5.0**	**4.5**	5.2
Elder age>25	**4.3**	**4.3**	5.1
p-value	**0.016***	**0.003***	0.240
Level of education			
Undergraduate	5.3	**5.1**	5.7
Master student	4.9	**4.4**	5.2
Doctoral	4.7	**4.4**	5.1
p-value	0.717	**0.001***	0.240
Location			
Near window	**4.5**	**4.2**	5.1
Near door	**4.8**	**4.6**	5.3
Other location	**5.0**	**4.5**	5.2
p-value	**0.048***	**0.026***	0.494
BMI			
<18.5	**4.8**	**4.5**	**5.2**
18.5-24.9	**4.9**	**4.5**	**5.3**
>25	**4.3**	**4.2**	**4.8**
p-value	**0.042***	**0..021***	**0.003***

For the age groups, the distribution of thermal comfort votes for different categories of temperatures in summer and winter is shown in Fig. 2. It can be observed that statistically significant differences were found for the '>26°C' category in summer (p-value=0.027) and the '>24°C' category in winter (p- value=0.021). The thermal comfort votes for elder subjects were 4.1 for the '>26°C' category in summer and 4.2 for the '>24°C' category in winter, lower than other groups, and the differences in the mean thermal comfort votes among age groups for the higher temperature categories were larger than those for the lower temperature category.

For the level of education groups, the distribution of thermal comfort votes for different categories of temperatures in winter is shown in Fig. 3. It can be observed that statistically significant differences were found for the '>24°C' category. For both two categories, the mean thermal comfort votes for undergraduates were higher than those for the master and doctoral students, but the differences for the '>24' category were a bit larger than those for the '≤24°C' category. For the '>24°C' category, the mean thermal comfort vote for undergraduates was 4.9, 0.6 higher than those for master and doctoral students.

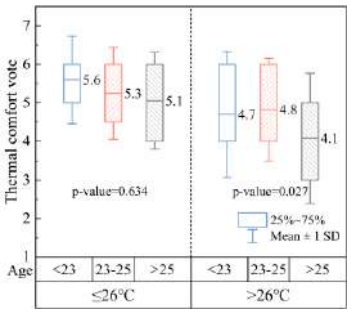

a) Summer

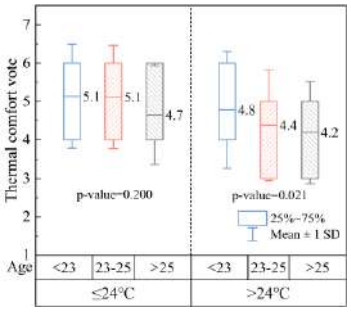

b) Winter

Fig. 2 - Distribution of thermal comfort votes for different categories of temperatures among age groups.

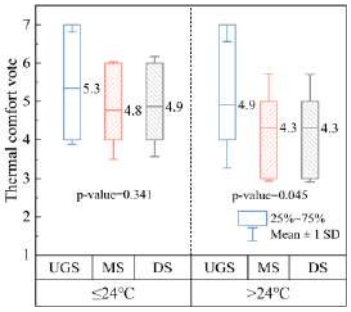

Fig. 3 - Distribution of thermal comfort votes for different categories of temperatures among the level of education groups in winter.
*UGS, MS and DS represent undergraduates, master students and doctoral students.

For the subjects' location groups, the distribution of thermal comfort votes for different categories of temperatures in summer is shown in Fig. 4. It can be observed that statistically significant differences were not found both for the '≤26°C' and '>26°C' categories, but the mean thermal comfort votes for subjects near windows were lower than the subjects near doors and at other locations for both two

categories.

For the BMI groups, the mean thermal comfort vote in winter was not larger than 0.5, thus it has not been further studied. The distributions of thermal comfort votes for different categories of temperatures in summer and transition seasons are shown in Fig. 5. In summer, the mean comfort vote for the overweight group was lower than for the underweight and normal-weight groups. However, in transition seasons, the normal-weight subjects had higher comfort votes than other groups for the '24-26°C' and '>26°C' categories.

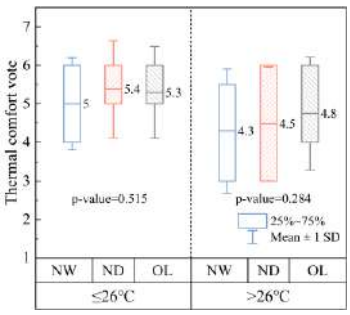

Fig. 4 - Distribution of thermal comfort votes for different categories of temperatures among subjects' location groups in winter.
*NW, ND and OL represent near windows, near doors and other locations.

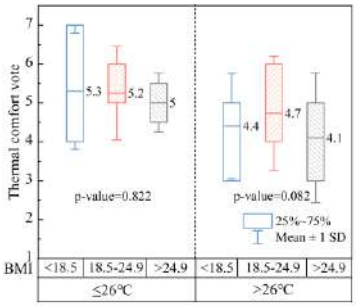

a) Summer

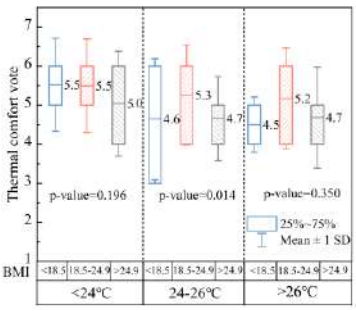

b) Transition seasons

Fig. 5 - Distribution of thermal comfort votes for different categories of temperatures among BMI groups.

3.4 Indoor air quality

For air freshness, statistically significant differences in comfort votes occurred in gender (p-value<0.001), age (p-value<0.001), level of education (p-value=0.019) groups. According to EN 16798-1 [22], when the indoor CO_2 concentration above outdoor was less than 550 ppm and 800 ppm, the air quality can be considered as high level and medium level. The annual atmospheric CO_2 concentrations in 2018 and 2019 were respectively 409ppm and 411 ppm, thus the outdoor CO_2 concentration was set as 410ppm in this study. Three categories of CO_2 concentrations were set as follows: <960 ppm, 960-1210 ppm and >1210 ppm. The group differences in comfort votes for air freshness for different CO_2 concentrations were calculated and given in Tab. 6. It can be observed that statistically significant differences in comfort votes for air freshness existed in all categories of CO_2 concentrations between male and female groups, but when the CO_2 concentration was less than 960ppm, the difference in comfort votes for males (4.3) and females (3.8) was larger than those for other categories. For the age and level of education groups, the differences in comfort votes among different groups were also largest when the CO_2 concentration was less than 960 ppm and the younger subjects and undergraduates had higher comfort votes than other groups.

Tab. 6 Mean comfort votes for air freshness for different CO_2 concentrations.

Group (Sample size)	Comfort vote for air freshness for different CO_2 concentrations (ppm)		
	<960	960-1210	>1210
Gender			
Male (895)	**4.3**	**4.0**	**3.8**
Female (457)	**3.8**	**3.6**	**3.5**
p-value	**<0.0**	**<0.0**	**0.001**
Age			
Younger<23 (161)	**4.6**	4.1	3.6
Middle age 23-25 (711)	**4.2**	4.0	3.9
Elder age>25 (480)	**3.9**	3.7	3.6
p-value	**<0.0**	0.251	0.446
Level of education			
Undergraduate (107)	**4.5**	4.3	**2.7**
Master student (539)	**4.2**	4.0	**3.8**
Doctoral student(706)	**4.1**	3.8	**3.8**
p-value	**0.02**	0.242	**0.028**
Location			
Near window (383)	4.3	3.9	3.8
Near door (286)	4.0	4.0	3.5
Other location (683)	4.2	3.9	3.8
p-value	0.07	0.848	0.618
BMI			
<18.5 (137)	4.2	3.9	3.6
18.5-24.9 (921)	4.2	3.9	3.7
>25 (294)	4.0	3.8	3.7
p-value	0.33	0.686	0.945

For comfort vote for air pollution, there were

statistically significant differences existed in gender (p-value<0.001), age (p-value<0.001), level of education (p-value=0.010) groups. EN 16798-1 [22] adopted the WHO guideline values for indoor and outdoor air pollutants, and the upper limit value for the 24-hour average $PM_{2.5}$ concentration is 25 μg/m³. Thus Tab. 7 shows the comfort vote for air pollution for two categories of $PM_{2.5}$ concentrations, which are <25 μg/m³ and ≥25 μg/m³. The comfort vote for air pollution for male subjects was 0.5 higher than that for female subjects for both two categories of $PM_{2.5}$ concentrations. For the age and level of education groups, the elder subjects and the doctoral students tended to have lower comfort votes for air pollution, and the difference was larger when the $PM_{2.5}$ concentration was larger than 25 μg/m³.

Tab. 7 Mean comfort votes for air pollution for different $PM_{2.5}$ concentrations.

Group (Sample size)	Comfort vote for air pollution for different $PM_{2.5}$ concentrations (μg/m³)	
	<25	≥25
Gender		
Male (895)	**4.6**	**4.0**
Female (457)	**4.1**	**3.5**
p-value	**<0.001**	**<0.001**
Age		
Younger<23 (161)	4.6	**4.1**
Middle age 23-25 (711)	4.5	**4.0**
Elder age>25 (480)	4.3	**3.5**
p-value	0.118	**<0.001**
Level of education		
Undergraduate (107)	4.5	**4.1**
Master student (539)	4.6	**4.0**
Doctoral student (706)	4.4	**3.7**
p-value	0.3	**0.006**
Location		
Near window (137)	4.5	3.9
Near door (921)	4.4	3.9
Other location (294)	4.4	3.8
p-value	0.788	0.539
BMI		
<18.5 (137)	4.2	3.9
18.5-24.9 (921)	4.5	3.8
>25 (294)	4.5	3.8
p-value	0.304	0.889

3.5 Sound comfort

For sound comfort vote, the statistically significant differences occurred in gender (p-value<0.001), age (p-value<0.001), level of education (p-value<0.001) and subjects' location groups (p-value=0.001). According to EN 16798-1 [22], the upper limit of the sound pressure level was 45 dB(A) in landscape offices, thus two categories of A-weighted sound levels (<45 dB(A) and ≥45 dB(A)) were set in this study. For both two categories, statistically significant differences in sound comfort votes occurred in gender and age groups, and the male and younger subjects had higher sound comfort votes than females and elder subjects. For the level of education group, the statistically significant difference was only found in the '≥45 dB(A)' category, but the differences among groups for both two categories were close and the doctoral students had the lowest sound comfort votes (4.9 for the '<45 dB(A)' category and 3.9 for the '≥45 dB(A)' category). For the subjects' location, the subjects near doors (5.7) had the highest sound comfort vote when the sound level was less than 45 dB(A), but when the sound level was higher than 45 dB(A), the subjects near doors had the lowest sound comfort vote (3.8).

Tab. 8 Mean sound comfort votes for different A-weighted sound levels.

Group (Sample size)	Sound comfort vote for different A-weighted sound levels (dB(A))	
	<45	≥45
Gender		
Male (895)	**5.5**	**4.3**
Female (457)	**4.5**	**3.7**
p-value	**<0.001**	**<0.001**
Age		
Younger<23 (161)	**5.3**	**4.3**
Middle age 23-25 (711)	**5.4**	**4.2**
Elder age>25 (480)	**4.6**	**3.9**
p-value	**0.002**	**<0.001**
Level of education		
Undergraduate (107)	5.5	**4.4**
Master student (539)	5.3	**4.2**
Doctoral student (706)	4.9	**3.9**
p-value	0.083	**0.001**
Location		
Near window (383)	5.1	**4.2**
Near door (286)	5.7	**3.8**
Other location (683)	4.9	**4.2**
p-value	0.071	**<0.001**
BMI		
<18.5 (137)	4.8	4.0
18.5-24.9 (921)	5.2	4.1
>25 (294)	4.9	4.0
p-value	0.304	0.504

3.6 Light comfort

For the light comfort, statistically significant differences occurred in gender (p-value<0.001) and level of education groups (p-value=0.006). EN 16798-1 [22] used the limit values of EN12464-1, and the illuminance level in offices should be higher than 500 lux, thus the illuminance levels were divided into two categories: '<500 lux' and '≥500 lux'. Tab. 9 shows the mean light comfort votes for different Illuminance levels. It can be observed that statistically significant differences existed in gender,

age and level of education groups when the illuminance is higher than 500 lux, but for the '<500 lux' category, the statistically significant difference only occurred in the gender group. For the mean light comfort votes among the gender, age and level of education groups, the differences were larger for the '≥500 lux' category than those for the '<500 lux' category. For example, the mean light comfort vote for male subjects (5.2) was 0.7 higher than that for female subjects (4.5) for the '≥500 lux' category, and that difference for the '<500 lux' category was 0.3.

Tab. 9 Mean Light comfort votes for different Illuminance levels.

Group (Sample size)	Light comfort vote for different Illuminance levels (lux)	
	<500	≥500
Gender		
Male (895)	**4.5**	**5.2**
Female (457)	**4.2**	**4.5**
p-value	**<0.001**	**<0.001**
Age		
Younger<23 (161)	4.6	**5.5**
Middle age 23-25 (711)	4.4	**5.1**
Elder age>25 (480)	4.3	**4.6**
p-value	0.059	**<0.001**
Level of education		
Undergraduate (107)	4.6	**5.6**
Master student (539)	4.4	**5.0**
Doctoral student (706)	4.4	**4.8**
p-value	0.355	**0.004**
Location		
Near window (383)	4.3	5.0
Near door (286)	4.4	5.1
Other location (683)	4.4	4.9
p-value	0.505	0.537
BMI		
<18.5 (137)	4.3	5.1
18.5-24.9 (921)	4.4	5.0
>25 (294)	4.3	4.9
p-value	0.243	0.841

4. Discussions

In this study, for all the environmental factors, males, elder age and subjects with high levels of education had higher comfort votes than other groups. The study of Hellwig [23] also showed that woman voted for 'extremely' and 'very important' compared to men. The significant level p-value for Pearson's correlation coefficient between the age and level of education groups was <0.001 [18], while for the Pearson's correlation coefficient between the other parameters, the p-values were all greater than 0.5. The result revealed that there was a strong correlation between the age and level of education groups. The range of age in this study was relatively narrow, but there were statistically significant differences in many human perceptions among age group, which might be caused by the statistically significant differences in human perceptions occurred among the level of education groups. The heavier stress of the master and doctoral students might cause them to have higher requirements for the environment than the undergraduates [18].

For thermal comfort, the mean indoor temperatures in summer and winter were higher than those in transition seasons, and according to our previous study, the differences between comfort temperatures and operative temperatures were 1.8°C in summer and 2.0°C in winter, higher than that in transition seasons (1.1°C), which illustrated that the subjects were not inclined to the warmer environment in summer and winter [18]. In section 3.3, it can be seen that the group differences occurred in more groups in summer and winter than in transition seasons, and the differences among groups were larger for the higher temperature categories, which revealed that individual differences could be magnified when people are in a warmer thermal environment.

For indoor air quality, the differences in comfort votes for air freshness among groups were larger when the air was relatively fresh (CO_2 concentration less than 960 ppm). In contrast, the differences in comfort votes for air pollution were larger when the $PM_{2.5}$ was above 25 μg/m^3, which means that serious air pollution could cause larger group differences. For sound comfort, the subjects near doors had the highest sound comfort vote than subjects at other locations when the sound level was less than 45 dB(A), and the opposite trend occurred when the sound level was higher than 45 dB(A), which revealed that the subjects near doors were more sensitive to the change in sound levels than subjects at other locations. For light comfort, the dim environment (<500 lux) caused the lower light comfort votes of subjects compared to the bright environment (≥500 lux), and the relatively bright environment caused larger group differences.

5. Conclusions

This study investigated the group differences in human comfort for different levels of environmental parameters, which can be used to better develop the comfort system, especially the personal comfort systems. For all the environmental factors, the higher comfort votes were found in male, elder age and higher levels of education groups. For thermal comfort, the differences were larger than 0.5 among gender, age and level of education groups for the higher temperature categories ('>26°C' in summer and '>24°C' in winter), and the group differences could be magnified in a warmer environment. For indoor air quality, the differences in comfort votes for air freshness among groups were larger when the CO_2 concentration was less than 960 ppm, and serious air pollution could cause larger group differences in the comfort votes for air pollution. For sound comfort, the subjects near doors were more sensitive to the change in sound levels than those at other locations. For light comfort, the higher

illuminance lever (≥500 lux) could cause larger group differences. One limitation of this study is that the environmental parameters at different locations were not monitored, which could be used to better analyze the effects of different locations of subjects on human perceptions. Although the numbers of the subjects for some groups (such as the undergraduate group in the summer) were relatively low in this study, the results could still be used as a practical reference to improve human comfort in offices.

6. Acknowledgment

This work was financially supported by the Chinese National Natural Science Fund Project (Grant No. 51978207, 51927813, 51508133) and the National natural science foundation of Heilongjiang Province (YQ2021E030). Zheng Li acknowledge financial support from China Scholarship Council (Grant No. 202006120330).

References

[1] Cheung T., Schiavon S., Graham L. T., Tham K. W. Occupant satisfaction with the indoor environment in seven commercial buildings in Singapore. Build. Environ. 2021;188:107443.
[2] Olesen B.W. The philosophy behind EN15251: Indoor environmental criteria for design and calculation of energy performance of buildings. Energy Build. 2007;39(7):740-749.
[3] Wang Z., Dear R. D., Luo M., Lin B., He Y., Ghahramani A., Zhu Y. Individual difference in thermal comfort: a literature review. Build. Environ. 2018; 138: 181-193.
[4] Wang Z., Zhang H., He Y., Luo M., Lin B. Revisiting individual and group differences in thermal comfort based on ASHRAE database. Energy Build. 2020;219:110017.
[5] Lan L. Mechanism and evaluation of the effects of indoor environmental quality on human productivity, Shanghai Jiao Tong University. Ph.D. thesis. 2010.
[6] Karjalainen S. Thermal comfort and gender: a literature review. Indoor Air. 2012;22:96-109.
[7] Nakano J., Tanabe S.I., Kimura K.I. Differences in perception of indoor environment between Japanese and non-Japanese workers. Energy Build. 2002;34(6):615-621.
[8] Wang Z. A field study of the thermal comfort in residential buildings in Harbin, Build. Environ. 41 (8) (2006) 1034-1039.
[9] Peng C. Survey of thermal comfort in residential buildings under natural conditions in hot humid and cold wet seasons in Nanjing. Front. Architect. Civ. Eng. China. 2010;4(4):503–511.
[10] Choi J., Aziz A., Loftness V. Investigation on the impacts of different genders and ages on satisfaction with thermal environments in office buildings. Build. Environ. 2010;45(6):1529-1535.
[11] Becker R., Paduk M., Thermal comfort in residential buildings – failure to predict by standard model. Build. Environ. 2009;44(5):948-960.
[12] Indraganti M., Rao K.D. Effect of age, gender, economic group and tenure on thermal comfort: a field study in residential buildings in hot and dry climate with seasonal variations. Energy Build. 2010;42(3):273-281.
[13] Hwang R.L., Chen C.P. Field study on behaviors and adaptation of elderly people and their thermal comfort requirements in residential environments. Indoor Air 2010;20(3):235-245.
[14] Rupp R.F., Vásquez N.G., Lamberts R. A review of human thermal comfort in the built environment. Energy Build. 2015;105:178-205.
[15] Dougherty K.A., Chow M., Larry Kenney W. Critical environmental limits for exercising heat-acclimated lean and obese boys. Eur. J. Appl. Physiol. 2010;108(4):779-789.
[16] Kang S., Ou D., Mak C.M. The impact of indoor environmental quality on work productivity in university open-plan research offices. Build. Environ. 2017;124:78-89.
[17]Yamtraipat N., Khedari J., Hirunlabh J. Thermal comfort standards for air conditioned buildings in hot and humid Thailand considering additional factors of acclimatization and education level. Sol Energy. 2005;78(4):504-567.
[18] Li Z., Zhang Q., Kazanci O.B., Fan F., Olesen B.W. A comprehensive comfort assessment method for indoor environmental quality in university open-plan offices in severe cold regions. Build. Environ. (Revised)
[19] Li Z., Zhang Q., Fan F., Shen S. A comprehensive comfort assessment method for indoor environmental quality in university open-plan offices in severe cold regions, Build. Environ. 197 (2021) 107845.
[20] QX/T 152-2012. China Standard, Division of climatic season, China Meteorological Administration. Beijing. 2010.
[21] ANSI/ASHRAE 55-2017. ASHRAE standard: Thermal Environmental Conditions for Human Occupancy, American Society of Heating, Refrigerating and Air-conditioning Engineers Inc. Atlanta (USA). 2017.
[22] EN 16798-1. Indoor Environmental Input Parameters for Design and Assessment of Energy Performance of Buildings Addressing Indoor Air Quality, Thermal Environment, Lighting and Acoustics. European Committee for Standardization. 2019.
[23] Hellwig R. T. Perceived importance of indoor environmental factors in different contexts. In: International PLEA Conference Passive Low Energy Architecture. Edinburgh. 2017

Data Statement

The datasets generated during and/or analyzed during the current study will be available with the permission of the first author upon reasonable request.

Performance evaluation of balanced heating and cooling with hydronic ceilings and floors

Peter Holzer [a], Georgios Gourlis [b], Philipp Stern [c]

[a] IBR&I Institute of Building Research & Innovation, Vienna, Austria, peter.holzer@building-research.at

[b] IPJ Ingenieurbüro P. Jung, Vienna, Austria, gourlis@jung-ingenieure.at

[c] IBR&I Institute of Building Research & Innovation, Vienna, Austria, philipp.stern@building-research.at

Abstract. Climate change increases the necessity of cooling demand in European housing. Systematic solutions in building planning and construction level are essential in order to avoid retrofit air conditioning units' installations. Implementation of Low Temperature Heating and High Temperature Cooling with embedded water-based systems is gaining ground in large scale residentials projects, being already a standardised practise in the tertiary building sector. In all related systems, heat dissipation and absorption at low temperature difference to room temperature, respectively surface systems, plays a central role. Economically motivated, the combination of cooling with underfloor-heating or also heating with ceiling-cooling systems is evident. This paper analyses challenges related to the capabilities and performance limitations of these applications, concerning thermal comfort limits, potential condensation risks, system energy efficiency and reliable control strategies. The outcomes of static and dynamic heat flux simulations are presented, accompanied with a literature review and conclusions from post occupancy performance evaluation surveys of realised projects. Arguments for utilising the ceiling surface for heating and cooling predominate those of the floor usage. Furthermore, there are convincing results in favour of laying the pipes close to the surface of thermally activated building systems (TABS). Control strategies of these systems in residential building should be very simple and robust. For cooling, best performance is obtained by TABS permanently operating with a constant water flow temperature of 21°C. For heating, very simple zone thermostats, without any features of nocturnal temperature reduction or weekly schedules are sufficient. This works also supports the argument of extending the applicability range of adaptive comfort to buildings with hydronic mass activation as a system cooling

Keywords. Hydronic radiant ceiling, hydronic radiant floor, thermal comfort, TABS
DOI: https://doi.org/10.34641/clima.2022.440

1. Introduction

Due to the rapidly evolving climate change, European housing is increasingly confronted with the necessity of cooling demand, additive to the heating demand. If individual retrofit installation of air conditioning units (ACU) is to be prevented, systematic solutions are essential in building level [1, 2].

Beyond comfort, the seasonally balanced supply of heating and cooling from environmental heat sources and heat sinks offers opportunities to make excess heat from cooling available as a resource for efficient heating. [3, 4]

As a result, developers of residential housing recently turn to a broad implementation of Low Temperature Heating and High Temperature Cooling with embedded water-based systems.

An especially promising technical solution is the combination of thermally activated building systems (TABS), ground heat exchangers and heat pumps in between both systems, widely addressed as GEOTAB-buildings [3].

Low Temperature Heating and High Temperature Cooling is a fully developed and well documented technology, so far dominantly implemented in newly built office and public buildings [5].

Recently the broad implementation of these technologies in the large-scale residential building sector gained momentum. There are some important issues arising at this point of mass application in a new building segment, which are still under discussion among designers, builders, producers and users.

Copyright ©2022 by the authors. This conference paper is published under a CC-BY-4.0 license.

The present paper discusses three key issues, related to the application of combined heating and cooling with embedded water-based systems in newly built multi-storey residential estates:

- Capacity limits of ceiling heating due to comfort aspects.
- Capacity limits of floor cooling due to comfort aspects and condensation risk.
- Energy efficiency and control issues of different types of TABS.

2. Research Methods

Results in the present paper are derived from the following sources:

Post occupancy performance evaluation and user surveys from eight Austrian GEOTABS housing estates: Size from 24 to 335 flats. Location in Vienna and Linz, both Austria. Heating/cooling-components either activated ceilings or floor-heating/cooling. Heat-generation/Heat-removal by monovalent HP/Freecooling or bivalent HP/district-heating/Freecooling. The estates analysed are in operation for 1 to 4 years and evaluations have been carried out by institutions of the authors.

Two-dimensional, static as well as dynamic, heat flux analysis of different types of activated ceilings and floors, embedded in a parametric study on the question of benefits and limitations of different positions of the hydronic pipe systems within the activated concrete ceiling. These calculations have been carried out with Antherm 2D DYN by the institutions of the authors.

Extensive literature review.

3. Capacity limits of ceiling heating due to comfort aspects

It is well known and validated that ceilings offer specific strengths for cooling, while floors offer specific strengths for heating. But for economic as well as technical reasons there's a strong wish to use one activated element for both services: Either (a) use the floor heating additionally for cooling, or (b) use the ceiling cooling additionally for heating.

The recent trend in multistorey residential buildings goes towards option (b), using thermally activated ceilings, both for cooling and for heating. However, this raises the question about the comfort and capacity limits of such heated ceilings.

It is well documented in scientific literature and international standards that ceiling cooling is significantly efficient and highly comfortable. Regarding capacity and efficiency ceiling cooling benefits from a high value of the total heat exchange coefficient in the range of 11 W/m^2K [6, 7]. Regarding comfort it benefits from mankind's evolutionary training living under the cold sky, which is the reason behind the low risk of dissatisfaction from temperature asymmetry beneath a cold ceiling [8].

On the contrary, the total heat exchange coefficient of ceiling heating is not higher than 6 W/m^2K. [6, 7] Furthermore, international comfort standards, namely ISO 7730, recommend limiting the temperature asymmetry to a level of $\Delta T_{rad} \leq 4$ K, when targeting a comfort level of category B [8].

The risk of local discomfort from asymmetry of radiant temperature is depicted **Fehler! Verweisquelle konnte nicht gefunden werden.**, according to [8].

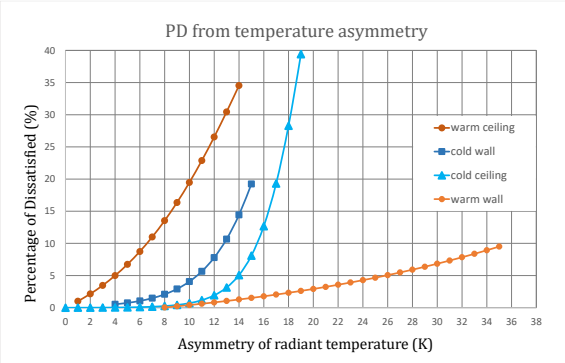

Fig. 1 Local discomfort from cold or warm ceilings & walls

It is this aspect of local discomfort that limits the capacity of heated ceilings. In practice though, observed in many real design processes, the comfort limit of $\Delta T_{rad} \leq 4$ K is repeatedly misunderstood as a limit of the temperature difference between the surface temperature of the ceiling and the room temperature, with again a varying interpretation of "room temperature". This interpretation leads to a mismatched leads to a limit of heating capacity of (6 W/m^2K * 4 K) = 24 W/m^2.

The correct definition of ΔT_{rad} is the difference between the plane radiant temperature of the two opposite sides of a small plane element, in case of the activated ceiling, of a horizontal plane element [5, 8, 9].

Fig. 2 illustrates qualities that influence the view factor of a ceiling, which are room dimensions, individual position in the room and room height.

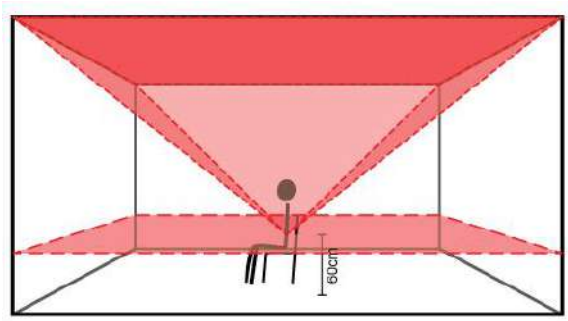

Fig. 2 View factor to an activated ceiling

Based on this correct definition and applied to a big and thus critical 5x6 m room with a height of 3 m, the maximum of the permissible surface temperature of a warm ceiling results in values of around 7 K above the room's operative temperature. This leads to a permissible heating design capacity of ceiling heating of slightly more than 40 W/m^2 [5].

This level of heating design capacity is sufficient for buildings with an up-to-date level of thermal insulation.

Based on qualitative interviews with the tenant service of eight multi-storey residential estates in Austria, complemented by ten further qualitative interviews with tenants, not a single complaint was reported regarding dissatisfaction due to the ceiling heating in general. However, in two flats on the ground floor, adjacent to the underground parking, complaints about thermal discomfort due to the cold floor have been reported. Thus, it is recommendation to backup ceiling heating in such special cases by additional floor heating.

4. Capacity limits of floor cooling due to comfort aspects and condensation risk

Namely in private residential houses, floor heating is still the preferred heating system. Therefore, together with climate change and together with reversible heat pumps, there's a strong tendency to use floor heating supplementary for cooling.

This raises the question about the capacity limits of floor cooling, in respect to comfort aspects as well as condensation risk.

Firstly, there is the risk of local discomfort arising from the thermal contact between the floor and the human body, i.e. the feet. The phenomenon is thoroughly described in the international comfort literature and standardisation [8, 10-12].

ISO 7330:2005 presents a correlation between the floor temperature and the predicted Percentage of Dissatisfied (PD), valid for people wearing light shoes. [8] Under these conditions, an acceptable level of comfort, with PD ≤ 5%, again targeting a comfort level of category B [8] is supported at floor surface temperatures between 19°C and 28°C. (See **Fig. 3**) Additionally, ISO/TS 13732-2:2001, based on original research from B. Olesen, 1977, presents comfortable floor temperature limits for people with bare feet or wearing light socks, for 1' and a 10' occupancy time, depending on the floor material, based on climate-chamber experiments. [11, 12] For the occupancy time of 10', the comfortable floor temperature range is given as 23°C to 28°C for wooden floors and as 26°C to 28,5°C for concrete floors.

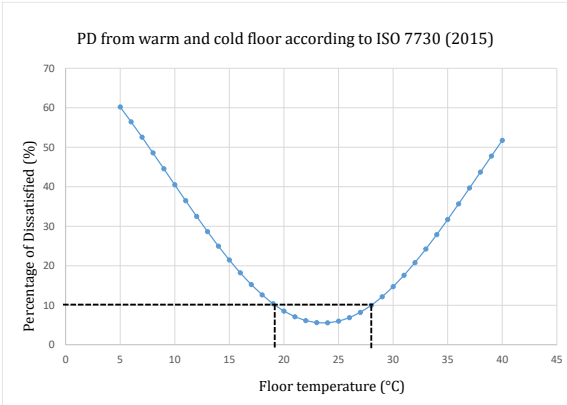

Fig. 3 acceptable range of floor temperature, for people wearing light shoes, according to ISO 7730:2005

Secondly, there is the risk of local discomfort arising from asymmetry of radiant temperature, caused by floor cooling. The influence of the floor's radiant temperature to the asymmetry of the radiant temperature is even more significant than it is from the ceiling, since the view factor from a seated or standing person to the floor is double as high as the view factor to the ceiling. [5] Based on the set of formulars and sources, which has already been discussed for ceiling heating, the surface temperature of a cold floor, again under the boundary conditions of a typical open-plan office, should not be more than 4 K lower than the room's operative temperature.

Thirdly, there is a condensation risk, when applying floor cooling in residential houses. Most flats are not equipped with ventilation systems, especially not with dehumidification systems. Therefore, there is little assurance against an uncontrolled rise of the absolute humidity and respectively of the dewpoint temperature, within the rooms. EN 1264-3 suggests a design dewpoint temperature of 18°C, what equals an absolute humidity of 13 g/kg. [14] Facing climate change, accompanied by longer heatwaves with less nocturnal cooling, the level of summerly humidity is expected to rise in most European cities. The dewpoint risk is exacerbated by the use of wooden floors, which are sensitive not only to condensate but also to mold growth, starting from persistent levels of >70% humidity. Finally, the condensation risk is not only relevant at the floor surface but is most

relevant at the boundary layer between the screed and the impact sound insulation: With floor cooling this is the coldest point of the system, exposed to the full level of indoor air vapour pressure.

In summary, floor cooling in residential buildings must be operated with utmost care, to avoid both comfort and condensation risks. As long as it is not supported by active dehumidification, it has to be generally avoided in warm and humid climates. [13] Even in climates with moderate humidity, below 15 g/kg, the water flow temperature should not be lower than 20°C. **Fig. 4** illustrates temperatures and heat flow for this safe setpoint, applied to an exemplary floor construction, made of 1 cm wooden floor on 6 cm of screed on 3 cm of impact sound insulation.

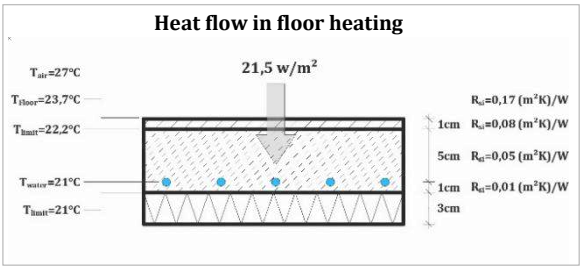

Fig. 4 Temperatures and heat flow in floor cooling and average water temperature of 21 ° C

Under these conditions, the cooling capacity of the floor cooling is limited to a value of approx. 20 W/m² at a room temperature of 27°C.

5. Energy efficiency, energy flexibility and control issues of different types of TABS in residential use

Low temperature heating and high temperature cooling in general, commonly addressed as Low Exergy Systems, TABS especially, are highly regarded as energy efficient. Which they are, in combination with heat generation by heat pumps and with heat extraction by chillers and/or free-cooling. Heat pump SCOPs as well as chiller SEERs benefit from the low temperature differences between process water and environmental heat sources/sinks. Thermal inertia of thermally activated building structures allows a temporal unbundling of heat generation and heat release, opening a wide field of energy flexible applications, maximizing the use of renewable environmental heat sources and heat sinks [15, 16].

The inertia of concrete core activation is a significant strength in terms of utilizing the potentials of energy efficiency and energy flexibility. But it is a challenge finding and applying the right control strategy for the operation of TABS. Again, there is a lot of literature available for the TABS application and control in office buildings, schools, and others.[16, 17] The field application in commercial housing is starting now, raising some new issues and already bringing some new learnings. Selected learnings from own studies and a post occupancy survey are presented here.

5.1 The position of the pipe layer, influencing energy efficiency and energy flexibility

In the application of TABS in residential buildings, the optimal position of the pipe layer within the concrete structure of the ceiling is a persistent point of discussion: The classical position, in the middle of the raw ceiling is claimed being optimal regarding activating the full thermal mass as well as being optimal for keeping the pipes save from later damage from drillers. But there is the strong argument for a pipe position adjacent to the ceiling surface, making repair of damage possible, what it is not the case with pipes between the reinforcement grids.

In own parametric studies, carried out with two-dimensional dynamic heat-flow analysis we investigated three different positions of the pipe layers and found even thermodynamically good reasons to prefer the position of the pipe layer close to the surface. **Fig. 5** illustrates this. It shows the heat distribution in steady operation of three variations of concrete core activated ceilings (CCAC). The variants differ from the position of the pipe layer. For comparison, also a typical floor heating was modelled.

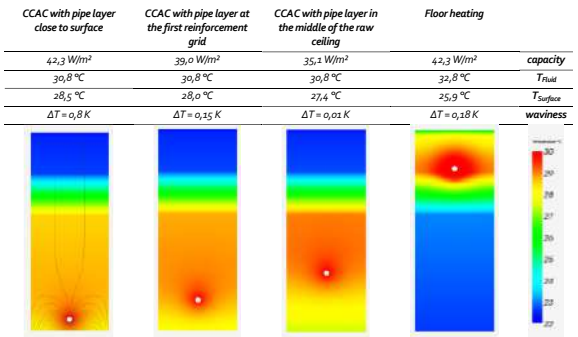

Fig. 5 Temperature distribution and performance indicators of three different variants of concrete core activation and a floor heating system

Learnings from the steady state operation are: Operated with a given flow temperature of 30,8°C and at a room temperature of 22°C, the variant with the pipes close to the surface reaches a surface temperature of 28,4°C and a heating capacity of 42 W/m². Both other variants, operated with the same flow temperature of 30,8°C, show losses in heating capacity up to 17% relative to the first variant. Quite surprising is the result from the floor heating: To reach the same heating capacity as the first variant of CCAC, the floor heating has to be supplied with a fluid temperature of already 32,8°C in stead of 30,8°C in case of the CCAC. This is the effect of the wooden floor, that even overcompensates the better heat flow coefficient of

the floor heating.

Further simulation runs investigate the dynamic performance of the CCAC variants. **Fig. 6** illustrates the temperature distribution on a timeline from the left to the right, at steps of 6 hours each. Starting from a constant temperature of 22°C. **Fig. 7** shows a diagram with the temporal development of the heating capacity for the three variants of CCAC in red, green and blue, and with the floor heating on violet. **Fig. 8** shows the corresponding diagram for switching off.

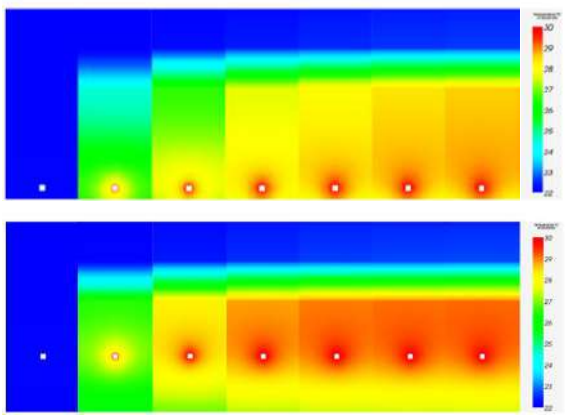

Fig. 6 Timeline of the temperature distribution in two variants of concrete core activated ceilings after switching on, in steps of 6 hours each.

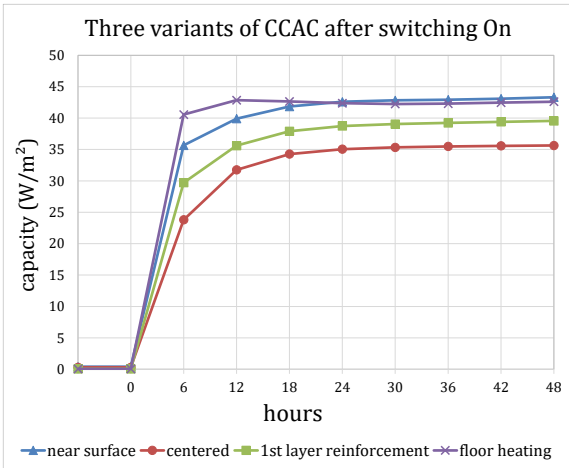

Fig. 7 Temporal development of the heating capacity after switching on: three variants of CCAC in red, green and blue, floor heating in violet.

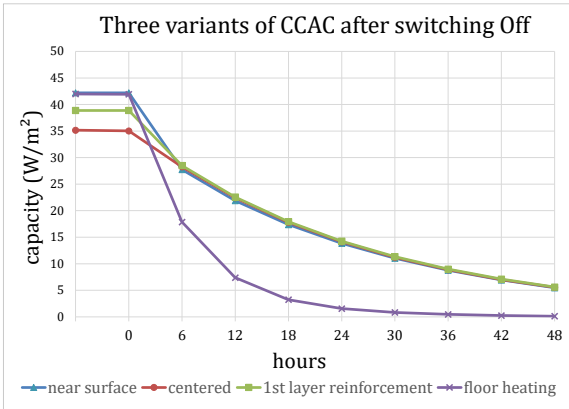

Fig. 8 temporal development of the heating capacity after switching off: three variants of CCAC in red, green and blue, floor heating in violet.

Learnings from the dynamic investigations are: Six hours after switching on, the CCAC variants reach between 70% and 83% of their maximum capacity. Slowest is the variant with the pipe layer in the middle of the raw ceiling. Six hours after switching off, the capacity of all three variants of CCAC drops to the value of 27 W/m² and drops further simultaneously. The mass activation happens for both surface-adjacent and deep position of the pipes.

Against the backdrop of these results, in multi-storey residential applications, we recommend concrete core activated ceilings with the pipe layer close to the ceiling's surface: The mass activation is still existent on a high level, what keeps the possibilities of energy flexibility. The fluid temperatures can be kept closer to the room's temperature, what is good for energy efficiency. And the chance of repair in case of damage is given.

5.2 control strategy

There is a lot of scientific literature dealing with optimized control algorithms for concrete core activated ceilings, including predictive control and others. Only a few of them give answers to the special needs of residential housing, being multiple users without a boss and certain time schedule. People of different needs, culture, age and educational background [17, 18].

Based on results from a post occupancy survey and monitoring in eight housing estates with thermally activated ceilings for both heating and cooling, we give the following recommendations regarding control strategies:

For cooling, full acceptable thermal comfort conditions are expected with permanently running the thermally activated structures through the full period between the heating season with a constant flow temperature of 21°C. This is a very robust strategy, with a good self-regulating effect: If a room's temperature drops, the temperature difference against the ceiling shrinks and cooling

stops. If a room's temperature rises, e.g. towards 27°C, the cooling capacity multiples, up to 40 W/m^2. Planners and contractors have learned, to never give guarantees for expected room temperatures. Yet, the survey revealed extraordinarily high levels of satisfaction with this system control strategy. However, complaints came concerning cooled bathrooms. We recommend therefore to exclude the bathroom circuit from cooling. It is thus important to shut down the water circuit in the ceiling of the bathroom during the cooling season.

Developers should indeed not promise certain temperature levels within the room. TABS are a strong improvement of summer comfort, they are though no air conditioning. Furthermore, landlords should not charge the cooling to the tenants. It would be bad for the seasonal efficiency of the system, if building residents started to block the cooling function.

For heating, a very flat heating curve is needed, controlling the flow temperature according to the outside temperature.

Residential spaces should be built in a way not to exceed a design heating load of 40 W/m^2. Zone thermostats proved being good enough. Manually regulating the flow in special circuits proved favourable. Finally, thermostats linked to TABS in residential buildings should be as simple as possible: There should be no options for night reduction and no weekly programs.

In case of heating with concrete core activated ceilings it has to be accepted that temporal, room-by-room temperature adjustment is impossible. In fact, this is no shortcoming, since it is the usual situation during all periods when the flats are in free running mode. Thus, the question arises whether buildings that are heated and cooled exclusively with embedded water-based surface heating and cooling systems may be evaluated according to the adaptive comfort requirements. According to the international standards, the application of the adaptive comfort theory is strictly restricted to buildings without active heating or cooling [20, 21]. In case of embedded water-based surface heating and cooling systems it night be argued that those buildings are perceived as free running buildings. The scientific discussion in this case is still going on [22].

6. Conclusions

Low temperature heating and high temperature cooling with embedded water based surface heating and cooling systems recently enters its broad application – newly – in residential buildings. Those systems enable highly efficient use of heatpumps and freecooling, not least in combination with geothermal environmental heat sources and sinks.

Available results from completed projects and accompanying scientific research confirm the functionality of these systems, also in commercial housing. First conclusions can be drawn, and first experiences and recommendations can be summarised as follows:

For commercial reasons it is necessary to decide either for ceiling heating and cooling or for floor heating and cooling. Both theoretically and practically substantiated, the arguments for using the ceiling predominate. In the discussion about the correct position of the pipes in the ceiling, there are convincing arguments in favour of laying the pipes close to the surface.

In view of the special usage situation in residential buildings, the control of the systems should be very simple and robust. For cooling, excellent experiences are made with permanently running the thermally activated structures with a constant flow temperature of 21°C. For heating, good results are obtained with very simple zone thermostats, without any features of nocturnal temperature reduction or weekly programs.

In practice, the conditioning of residential buildings that are heated and cooled exclusively with embedded water-based surface heating and cooling systems is satisfactory, though individual and room-by-room temperature adjustment is de facto impossible. Based on this, there's an ongoing scientific discussion, whether such buildings may be evaluated according to the adaptive comfort requirements. This would be in contradiction to the international standards, which restrict the application of the adaptive comfort theory to buildings without active heating or cooling. In case of embedded water-based surface heating and cooling systems it might be argued that those buildings are perceived as free running buildings. The scientific discussion in this case is still going on.

7. Acknowledgements

This research work is based on findings from the EBC Annex 80 Resilient Cooling of Buildings and has been partially funded by the Federal Ministry for Climate Action, Environment, Energy, Mobility, Innovation, and Technology. The authors want to express their gratitude to all involved parties.

8. References

[1] IEA. The Future of Cooling. IEA Paris; 2018. [cited 2022 March 4]. Available from: https://www.iea.org/reports/the-future-of-cooling

[2] Holzer P. et al. Annex Text Resilient Cooling of Buildings/ IEA EBC Annex 80; 2019. Available from: https://annex80.iea-ebc.org/.

[3] Bockelmann F, Plesser S, Soldaty H. et al. Advanced system design and operation of

GEOTABS buildings. REHVA Guidebook No. 20; 2013

[4] Holzer P. Ventilative Cooling and beyond: Dual use of surface heating/cooling. National Energy Efficiency Conference NEEC 2018 Australia, Sidney; 2018. Available from: https://www.eec.org.au/uploads/NEEC18/Presentations/HOLZER%20Peter.pdf

[5] Petráš D, Babiak J, Olesen B. Low temperature heating and high temperature cooling: embedded water based surface heating and cooling systems. REHVA Guidebook No. 07; 2007

[6] EN 1264-5:2021. Water based surface embedded heating and cooling systems Part 5: Determination of the thermal output for wall and ceiling heating and for floor, wall and ceiling cooling; 2021

[7] EN 15377:2008. (withdrawn) Heating systems in buildings - Design of embedded water based surface heating and cooling systems - Part 1: Determination of the design heating and cooling capacity; 2008

[8] EN 7730:2005. Moderate thermal environments - Determination of the PMV and PPD indices and specification of the conditions for thermal comfort; 2005

[9] EN 7726:2001. Thermal environments – Instruments and methods for measuring physical quantities; 2011

[10] ASHRAE standard 55-2020. Thermal Environmental Conditions for Human Occupancy. Atlanta. American Society of Heating, Refrigeration and Air-conditioning Engineers; 2020.

[11] ISO/TS, 13732-2:2001. Ergonomics of the thermal environment — Methods for the assessment of human responses to contact with surfaces — Part 2: Human contact with surfaces at moderate temperature. 2001.

[12] Olesen B. Thermal Comfort Requirements for Floors occupied by people with bare feet. ASHRAE Transactions 83:41-57; 1977. p. 41-57

[13] Chang-Ho J, Yeo M-S, Kim K-W. Feasibility of a Radiant Floor Cooling System for Residential Buildings with Massive Concrete Slab in a Hot and Humid Climate. International Journal of Concrete Structures and Materials; 2018. 10.1186/s40069-018-0314-z

[14] EN 1264-3:2021. Water based surface embedded heating and cooling systems — Part 3: Dimensioning; 2021

[15] IEA. EBC Annex 49: Low Exergy Systems for High Performance Buildings and Communities. Project Summary Report. Fraunhofer IBP; c2011. 10.18086/swc.2011.18.05

[16] Meggers F, Ritter V, Goffin P. Low exergy building systems implementation. Fuel and Energy Abstracts. Energy, Volume 41, Issue 1; 2012. p. 48-55. 10.1016/j.energy.2011.07.031

[17] Lehmann B, Dorer V, Koschenz M. Application range of thermally activated building systems tabs. Energy and Buildings Volume 39; 2007. p. 593-598. 10.1016/j.enbuild.2006.09.009

[18] Kreć K. Energiespeicher Beton. Ministry of Transport, Innovation and Technology. Vienna, Austria; 2016. Available from: https://www.zement.at/downloads/downloads_2016/energiespeicher_beton_krec_endbericht_1602.pdf

[19] Humphreys M, Nicol F, Roaf S. Adaptive Thermal Comfort: Foundations and Analysis. Abingdon: Routledge; 2016. 10.4324/9781315765815

[20] ASHRAE standard 55-2020. Thermal Environmental Conditions for Human Occupancy. Atlanta American Society of Heating Refrigeration and Air-conditioning Engineers; 2020

[21] EN standard 16798-1. Energy performance of buildings — Ventilation for buildings. Part 1: Indoor environmental input parameters for design and assessment of energy performance of buildings addressing indoor air quality, thermal environment lighting and Brussels. European Committee for Standardization; 2019

[22] Parkinson T, DeDear R, Brager G. Nudging the Adaptive Thermal Comfort Model. Energy and Buildings, Volume 206; 2020. 10.1016/j.enbuild.2019.109559

9. Data Access Statement

Data sharing not applicable to this article as no datasets were generated or analysed during the current study.

Thermal Comfort in Old Traditional Shophouses in Ho Chi Minh City, Vietnam

Hung Thanh Dang [a]

[a] Department of Architecture, Ho Chi Minh City University of Architecture, Ho Chi Minh City, Vietnam, hung.dangthanh@uah.edu.vn

Abstract. Cooling is the main requirement for occupant thermal satisfaction in buildings in warm to hot climates across much of the year. This is especially true in naturally ventilated housing, for example, in traditional houses of the tropics, which distinctive passive cooling design strategies including shading, natural ventilation, convective cooling, and light structure optimised to respond to the hot climate and retain the comfortable indoor environment. Thus, energy consumption can be reduced. Those effects are also found in traditional dwellings in Vietnam, in particular, traditional vernacular shophouses in Ho Chi Minh City (HCMC). However, due to the accumulative pressures of changing society, economy, and urban environment in the city, getting thermal comfort indoors has become difficult. The interplay between building, people, management, and comfort is usually complex in the towns preserving the values of the urban and architectural heritage of the city. The quality of traditional vernacular buildings has been degraded while local people desire comfortable living conditions and spatial expansion for the family extension. The paper aims to examine the building and urban characteristics of old traditional shophouses and their comfortable environment in Cho Lon town, HCMC, in which, a large number of traditional dwellings are reported. A case study built in the early 1900s on Trieu Quang Phuc street will be selected for analysing architectural features before and after renovation in 2007. Consequently, the indoor environmental impact due to the change of building features will be investigated. The problems of discomfort, renovation, and preservation will be explained. Then, some recommendations in design will be proposed to help designers/stakeholders renovate traditional shophouses toward achieving comfort, preserving vernacular architecture, saving energy, and getting occupant delight. The research techniques included field visits and numerical analyses to understand long-term environmental performances in such case studies and the effect of proposed design solutions.

Keywords: traditional shophouses, thermal comfort, indoor environment, Ho Chi Minh City.
DOI: https://doi.org/10.34641/clima.2022.394

1. Introduction

Over 300 years of history, Cho Lon town in the heart of district 5, HCMC has been a specially attractive land, which is mixed with multi-cultures including indigenous Vietnamese, Indian, Chinese, and French [1]. The development of Cho Lon has been attached to the whole history of Saigon (which is a former name of HCMC used before 1975). In 1679, the first Chinese people coming from southern China settled in Saigon and built up Minh Huong commune – the precursor of current Cho Lon. The contribution of Cho Lon and the Chinese community to the cultural and economic profile of the city is significant, in particular, architecture. An extravagant collection of diverse and distinct buildings is found around the town with various typologies (residence, retail, apartment, school, temple, and community house) and the interference of many architectural styles, such as Southern China, Chinese mixed with French, Indochina, and Vietnamese Tropical Modernism [2]. Amongst them, the number of old traditional shophouse dwellings and their values for the architectural system of Saigon are dominant (Fig. 1).

Fig 1 - Cho Lon in 1900 (a), Cho Lon in 1906 (b), Cho Lon in 1950 (c) (Source: Manh Hai, 2010)

As previously mentioned, under the increasing impacts of climate change, uncontrollable urbanisation, and population extension, the pleasant

Copyright ©2022 by the authors. This conference paper is published under a CC-BY-4.0 license.

environment inside old traditional shophouses has been highly vulnerable, which links to inhabitants' discomfort subsequently the need for renovation of their houses and installation of air-conditioners to retain thermal comfort. Additionally, less effective heritage management currently results in not only the loss of original architectural features of traditional buildings but unachievable comfort. The present study examines the environmental performance and the comfort level in the old traditional shophouses in HCMC, Vietnam through two typical housing cases found in Cho Lon including House No. 111 built on Trieu Quang Phuc Street in the 1920s and renovated in 2007. Some research steps were developed to achieve the aim. Firstly, the architectural characteristics of those dwellings before and after renovation were investigated by field observations. Especially, the responsive climatic design solutions applied to it were analysed. Secondly, the room thermal environment in the dwellings was evaluated by using computational analysis of the TAS software program. The comparison of environmental consequences between original and renovated houses was carried out. This action helps the author understand the influence of building envelop and less rational changes to it without concerns about vernacular architectural values on the low degree of comfort indoors. Finally, different cases of building improvement were proposed and tested with environmental impacts, and then, the analytical results were compared together in order to find out the best design option for the thermal satisfaction of occupants inside.

2. Location

The latitude and Azimuth of HCMC are 10.47°N and 106.4°E which highlights the tropical climate of southern Vietnam with two distinctive seasons: the dry season (December- April) and the rainy season (May-November) [3]. Its high level of average temperature and distinction of two seasons in a year significantly influence landscape and architecture. Because of the huge impacts of solar radiation, the temperature in HCMC is usually at a high level. The average temperature in HCMC is around 27°C and the average minimum temperature is over 20°C.

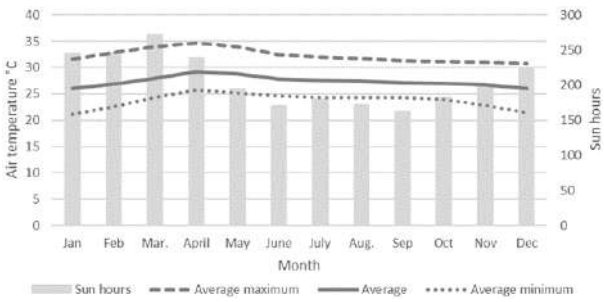

Fig 2 - The climatic characteristics in HCMC (Source: Science, 2009)

In the South of Vietnam, the highest temperature of the year occurs in the dry season from March to May. The annual average relative humidity is about 77%. Particularly in the rainy months, humidity is at 75 - 80% on many days and sometimes peaks at 100%, whilst the air might be drier in the first four months. HCMC is in a climatic zone that has a high annual average rainfall - about 1949mm per year, 90% of which is in the rainy season. Therefore, in architecture design, climatic responsive strategies are vital to allow benefits of natural conditions inside houses and to protect from harmful influences of climate.

3. Old traditional shophouse dwellings in Cho Lon

Shophouses are a popular residential style in Cho Lon with direct access to the street or alley. They are owned by individuals or rented by businessmen. Overall, their plot is a rectangle with a narrow width of 3 - 4 meters and a length of 18 - 20 meters [2].

Fig 3 - Shape of plots, street houses on Trieu Quang Phuc Street

The land is divided into a narrow plot to get as many street-front façades (for shops) as possible. Street (or sidewalk) and terrace play a role as communal spaces. Generally, most shophouses are two or three-storey terrace houses. At ground level, the front room is a commercial area, the kitchen and services are behind transverse walls, the stair is organised in the middle of the house. The family's living space is accommodated on the upper floors [2]. Most of these rooms are organized along a long corridor. It is very narrow and dark; its width is just enough for one person. In almost every Vietnamese household, the altar is a very sacred place where people worship their ancestors and a religious figure such as Buddha. The altar is often placed at a high point facing the

street or an alley on the highest floor. Another "Fortunate God" altar is normally positioned on the ground floor facing the main entrance. Since most families in Cho Lon are business owners, altars are very important not only to their religious beliefs but to their trade.

Figure 4 shows a typical spatial section of the traditional shophouse in Cho Lon. On the building envelope, elements such as openings (windows, doors, and wall apertures), overhangs, and louvres/shutters/screens are applied to protect interior spaces from direct sunlight and rainfall while maintaining natural ventilation and daylight.

Fig 4 - A typical section of the ancient shophouses in Cho Lon (A - Roof overhang, B - Outer wooden shutters, C - Above windows + lattice wood screen, D - Low partition walls)

4. Research methods

In this study, the application of different analytical tools helped researchers to understand the daylighting control and thermal comfort inside the house with individual architectural elements. Three methods are applied:

- Photos and drafts, initial observations of the luminous and ventilative environment in rooms were drawn. Moreover, the climatic responsive design of the house is explained more.

- Three-dimensional computer simulations such as Ecotect and Radiance are used to assume daylight distribution in the building. The simulation is tested in overcast sky conditions as the worst scenario.

- Assessment of thermal environment inside the house was conducted by Thermal Analysis Simulation (TAS) in conditions of hot humid tropical climate in Vietnam: no heating and use of natural ventilation. This quantitative analysis illustrates the thermal performance of each room tested in different cases. Finally, a range of architectural modifications will be applied to improve the current thermal environment.

The comfortable conditions indoor the case study through TAS were compared and assessed according to the national standard TCVN 9411:2012 for designing rowhouses in Vietnam. Referring to that, the limit of thermal comfort is from 22 to 28°C and its wider range between 20 and 29°C is acceptable [4].

5. Case studies

House No. 111 Trieu Quang Phuc Street was constructed in the 1920s and brings similarities in size and land shape, style of architecture and type of business among ancient houses in Cho Lon. The interior was renovated entirely in 2007 because of the need for family extension and improving living quality. The original facade is retained despite material alteration. This is a popular trend happening with the adjacent ancient shophouses on this street (Fig. 5). The height of some houses rises to four or five floors and buildings have a big volume. The appearance of the new modern houses in the ancient town affects the general appearance of architecture in this area.

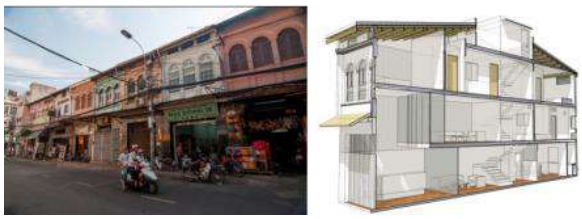

Fig 5 - Site plan, context and functionary section of house 111 Trieu Quang Phuc Street

5.1 Building layout

The interior of this house was rebuilt entirely. According to the owners, the original house of two floors was replaced by a house of two floors, a mezzanine and a terrace. The total floor area has a capacity of 7 people.

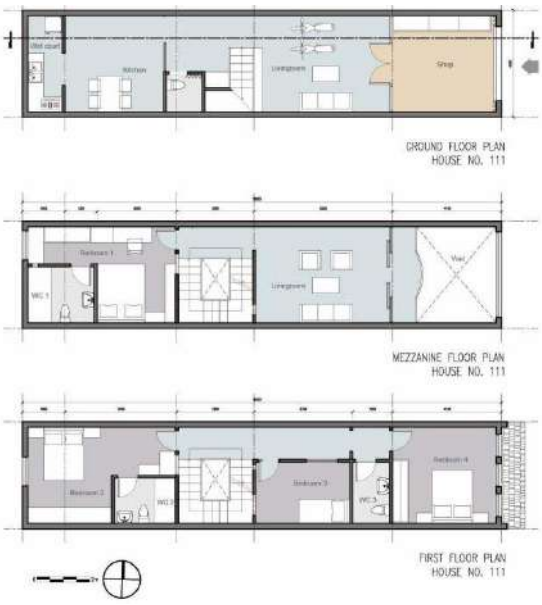

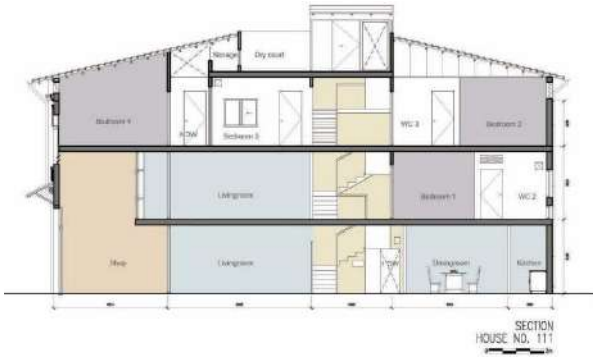

Fig 6 - Floor plans and section of House No.111

On the ground floor, the front room is a shop and the only entrance. The service rooms and stairs are positioned in the middle of the floor. A small living room is organised on this floor like a multi-function room - a public room, a place of motorbike parking at night and one of two altar rooms. The kitchen is minimised at the back of the house to leave a larger space for the dining room.

On the mezzanine, the layout is very simple with a large family room in the front and a master bedroom behind the staircase. The toilet is located at the end corner of the bedroom to leave space for a bed. On the second floor, due to the preservation of the ancient building envelope, the attic space was turned into three bedrooms. The front bedroom is also a mixed-use room: bedroom and altar. The bedrooms are connected by a narrow passageway. The expanded upper second floor is a terrace being used for storage and washing area and is being accessed by the iron stairs.

5.2 Environmental strategies

With most shophouses in Saigon, collecting outside daylight through side windows is very popular. However, the constraint of narrow frontage and a deep site plan is a reason for the glooming environment of middle rooms. The facade width and row housing typology also lead to few opportunities for side opening, even when the rooms are exposed to an open area of the neighbour. To increase light coming into the back of house 111, the envelope is pierced by windows casually in size, type and fenestration (Fig. 7).

Fig 7 - Windows on the back wall of bedrooms 1 and 2 of the house and on the facade looked from outside and inside of house 111

In the specific context of house 111, windows on the east façade are constrained. This also requires that the design of openings is attached to a design of shading elements. Unfortunately, the outer wooden shutters in the old house were also replaced by glass windows. The lighting penetration at 8:00 am is fine the sunlight in early mornings can reach all floors. At 10:00 am, the sunlight is cut off at the mezzanine and goes deep into the shop space. The roof overhang on the second floor starts to block out sunlight. This means that the direct light cannot penetrate inside the house after 10:00 am in all summer solstice, equinox and winter solstice except for shop. At noon, the sun is on the top. So, heat protection from the top is very important.

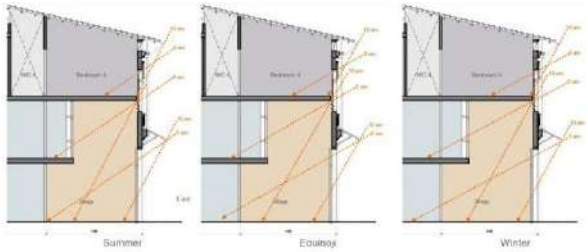

Fig 8 - Diagrams showing penetration and sun shading on facade hourly and seasonally

Through additional sunlight, the luminous environment of the lower spaces can be improved. The rooms on each floor towards the staircase open a sliding window to collect daylight in the courtyard. Thus, the luminous environment becomes better.

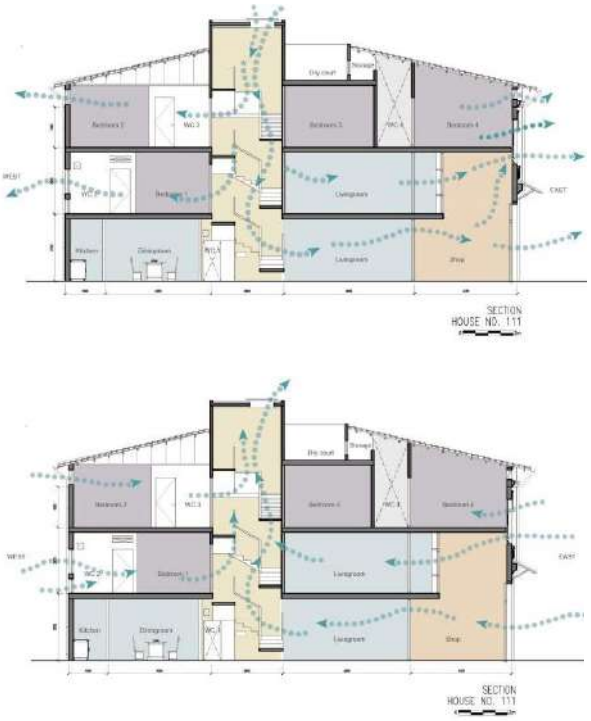

Fig 9 - Stack effect at daytime and night in house 111

In crowded urban development, the effectiveness of wind effects can meet difficulties. A solution to natural ventilation is the stack effect. If the stack effect can work, it can generate a moderate air exchange, but not a noticeable air velocity through the spaces [5]. In house 111, the use of stack ventilation and cross ventilation will control air movement better. The maintenance of moving air is

to provide a balance of moisture in the air and cause a cooling effect as heat is removed from the body by convection and evaporation, especially in the dry seasons.

The effect of natural ventilation by the staircase is different during the daytime and at night. During the diurnal time, the air near the ground is burned rapidly, so the temperature here is also much higher and the relative humidity is lower than in upper zones [6]. This means that the air on top of the court is cooler and the relative humidity here is also better. This can produce a downdraft. As a result, heat input in each room is dissipated [7].

In contrast, at night, the air moves the opposite direction. The warmer air by the staircase will rise and be replaced at the bottom of the stack by cooler outside air. Especially, at nighttime, preservation of the air exchange and air velocity inside the house and through spaces is that the fenestration of openings should be deliberated because of security, rainwater. In house 111, to maintain the cross ventilation between rooms and staircase, sliding windows, doors and louvres upper room doors are organized on sidewalls.

6. Indoor comfort

6.1 Daylighting performance

In this section, Ecotect Analysis 2011 and Radiance software will show the daylight level of each room. These results will be evaluated with the requirements of CIBSE Comfort (2006). The daylight environment of all rooms is investigated in the worst condition – 12:00 pm under a cloudy sky in the winter.

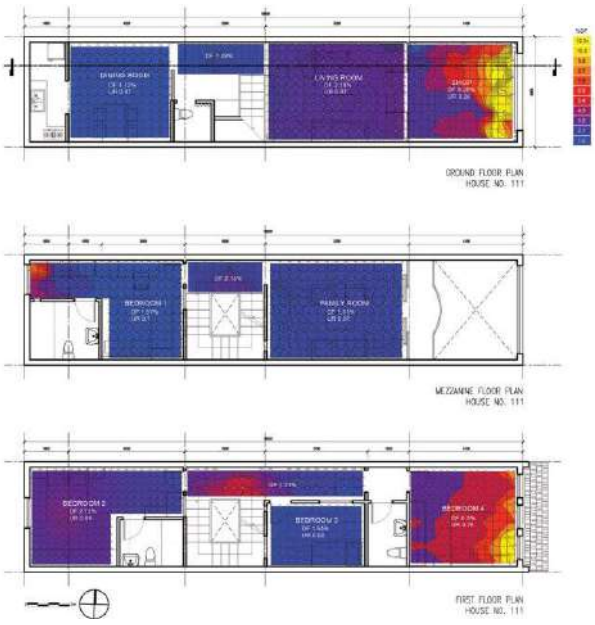

Fig 10 - Daylight distribution of all rooms in the existing house 111

Among the eight rooms, four have daylight factor is satisfied with a suggested minimum level of CIBSE Guide A (2006) – at least 1.5% for the bedroom and 2% for the living room. The daylight distribution of most rooms is even, whilst the luminous environment of bedroom 4 and shop is perceived as bright and over bright with DF of 6.3% and 9.08%. Although these rooms only welcome daylight during diurnal except in the early morning, the use of inappropriate finished materials and shading devices is the reason for excessive penetration of daylight. Over brightness means the number of heat absorbed by solar radiation is extreme.

In contrast, the light level of the kitchen, dining room and family room is the worst. The results for the two spaces are DF-1.12% for the kitchen and dining room and DF-1.83% for the family room. Artificial light is used regularly in the kitchen. Even if the full curtain wall in the front of the family room is designed to collect daylight as a secondary light adjacent space, this room still uses artificial light at certain times of the day.

6.2 Thermal performance

The thermal performance of the spaces is investigated by TAS simulations. The model was made based on the architectural forms, detailed construction, Ho Chi Minh weather condition and building aperture types of house 111 Trieu Quang Phuc Street. There are two cases - with and without natural ventilation which are examined to explain the impacts of the building envelope and natural ventilation on the internal thermal environment.

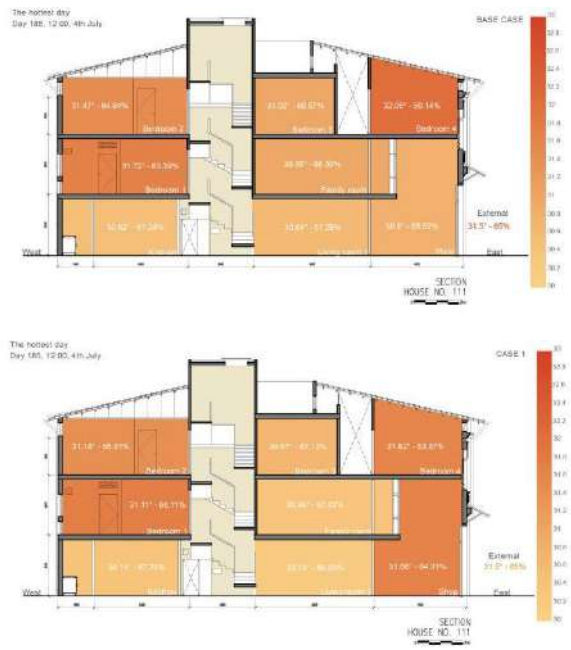

Fig 11 - Thermal performance in two cases - base case (above): without ventilation, case 1 (below): with ventilation

Both cases are tested on the hottest day: day 185 (4th of July), at 12:00 pm. The external condition on the

testing day is 31.5°C and 65% relative humidity. This condition is hot and out of the comfort zone. There are some same patterns of thermal performance in both cases. The rooms on the ground floor are cooler and the ones facing the roof directly are hotter. A concrete slab on the ground floor will provide a desirable heat sink for daytime rooms (living room, kitchen and dining room). Additionally, the impacts of the sun from the top are also prevented significantly in rooms in lower zones. So, indoor temperatures are close to the day's minimum [5].

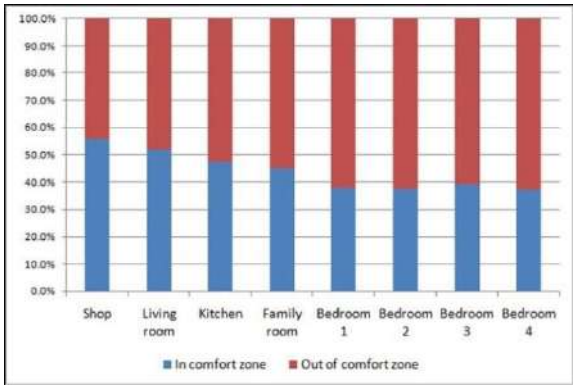

Fig 12 - Frequency of thermal comfort state of house No. 111– Base case

As observed from the above graph, in the base case, the conditions of the internal space are within comfort temperatures for about 40% of the time of the year. For the rooms on lower floors, total comfortable are greater (Fig. 12). In case 1, the thermal comfort is improved in all rooms. The frequency has stayed at 50%. Looking closer into the shop zone; the internal condition in case 1 is reduced slightly from the base case. Generally, natural ventilation shows a good strategy for expanding the thermal comfort zones of the internal spaces (Fig. 13).

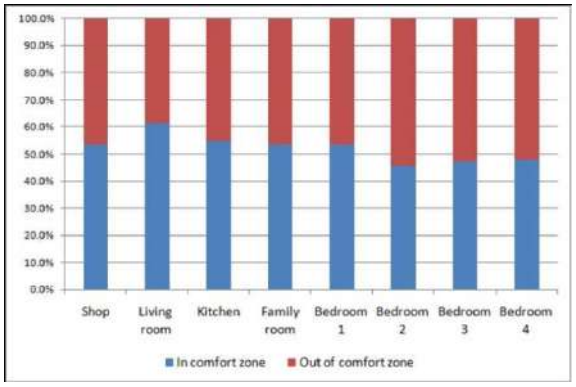

Fig 13 - Frequency of thermal comfort state of house No. 111– Case 1

7. Design proposal

From analyses of the advantages and disadvantages of house 111, seeking appropriate solutions to optimise the living condition in terms of environmental factors in the ancient street houses will be based on requirements of preservation of building envelope and budget. This means that the proposed ways of renovation will minimise demolition of the existing house but still ensure an increase of comfort for occupants.

For example, the renovation of the current house 111 is a typical scenario for ancient street houses in Cho Lon. To explain the results of each solution different case scenarios will be introduced:

Fig 14 – Base case

Base case: Indicates the current envelope: the window is a single-glazing aluminium frame, external/internal brick walls are 200mm and 100mm thick. The exterior doors/windows are closed (Fig. 14).

Case 1: Same as Base case, but the exteriors windows and entrance doors are opened on schedule. The result is that the thermal performance of the whole house may be changed. (Tested above) (Fig. 15).

Fig 15 – Case 1

Case 2: as in Case 1, additional internal insulation is applied to external walls which are exposed to the sun. In the climatic condition of HCMC, the amount of solar radiation by horizontal and vertical exposure is high. This way, the building envelope can protect from heat absorption and reduce the mean radiant temperature.

Case 3: as in Case 2, back to a traditional way, the glass windows on the east facade are replaced by wooden shutter windows for purposes of natural ventilation and prevention of burning by the sun. A narrow and long opening organised the door of bedroom 4 plays a role as an outlet on the leeward

side to increase air movement from the outside. Heat gain from the top down to this room is relieved better (Fig. 16).

Fig 16 – Case 3

Case 4: as in Case 3, in Vietnam, the sun's position is nearly at its peak and it radiates heat strongest in the middle of the day. The addition of overhead shading devices of rooflight not only ensures the effect of stack ventilation but also prevents direct sunlight partially. For this strategy, the height of shading bars needs to be considered to optimise the penetration of sunlight. The result is that the daylight and thermal environment is changed (Fig. 17).

Case 5: as Case 4: for the family room and bedroom 3, they are facing poor conditions of light and ventilation. The solid walls exposing the staircase are transferred by a full-height screen of wooden vertical louvres. One of two glazing curtain walls in the front of the mezzanine is taken out to bring tidiness to this room. The result is that the daylight and thermal environment of both rooms is changed (Fig. 18).

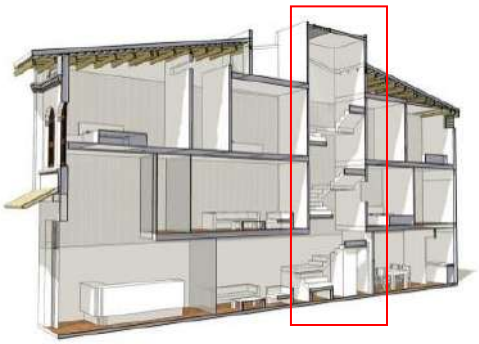

Fig 17 – Case 4

Fig 18 – Case 5

Case 6: as in Case 5: the layouts in the back of the house including kitchen and dining room, bedroom 1 and bedroom 2 is organised spatially: a void goes through from the ground floor to the roof; the windows of bedrooms and bathrooms are open to this void. The messy windows on the west wall are removed. A small nice green space is designed to bring spatial delight. The result is that the daylight and thermal environment of these rooms is changed (Fig. 19).

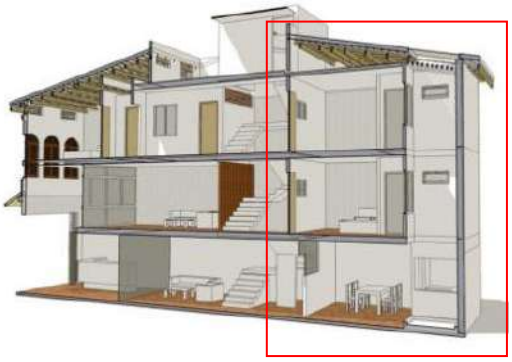

Fig 19 – Case 6

The step-by-step application of possible solutions shows an improvement of thermal comfort in house 111. Although there are some strategies which are only appropriate with some rooms, the achieved results are generally proved. In the above graph, the thermal performance in case 6 is the greatest in all cases with 4 solutions applied to increase internal living conditions. Particularly, the sixth step brings an impressive result for rooms at the back of the house: kitchen, bedroom 1 and bedroom 2. Their thermal condition increases more the 15% from the base case and more than 5% in Case 1. The appearance of another courtyard in the corner of the house introduces an opportunity to increase air convection and the effectiveness of both cross and stack ventilation, while categories of security and privacy are still ensured. In all cases 1-5, the annual total hours with comfort in the shop are stable. This best condition is achieved when the shop is closed and direct sunlight is kept out of the house while the low airflow is still preserved by an upper opening of the entrance door.

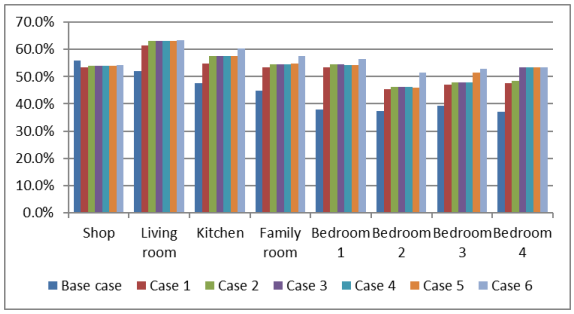

Fig 20 - Comparison in the percentage of thermally comfortable hours in different rooms between six cases

In the final scenario the internal daylight levels are numerically greater and the daylight distribution

more even by applying solutions 3 to 6. The luminous environment of all rooms is perceived as well-lit and meets the minimum requirement of CIBSE Guide A except for the shop.

In conclusion, the renovation of house 111 in 2007 has improved the house significantly in terms of living spaces and utilities, there are still some problems of privacy and security of the bedrooms. From an environmental point of view, the opening of the skylight at the staircase brings many benefits to occupants both in terms of daylight and thermal comfort which disappears in the existing ancient street houses on Trieu Quang Phuc Street. Through the proposed design solutions, the internal thermal condition is also improved gradually and the greatest result can be achieved in case 6. The solutions are deliberately chosen in for them, low budget and the required preservation of the ancient town.

Fig 21 - Climatic responsive design of house 111 in the renovated case in daytime

8. Conclusion

Trieu Quang Phuc Street is one of the central roads in Cho Lon in the past and present. This place has an important value of history, culture and architecture in Saigon. One of the architectural identities in this area is shopouses which are facing challenges of the free renovation, urbanisation, modernisation and lack of awareness of local people even when they wish to live and keep their values of lifestyle, architecture and local culture [2]. The turbulent renovation has started in 1975 and has become an obvious need due to family expansions, improvement of living quality and the poor existing construction of the ancient dwellings. The special context of the ancient town will require strict regulations for renovation in preservation and development. The design strategies used in these dwellings, balance explaining how the exterior environment affected the occupants living in hot-humid climatic regions without artificial conditions.

Generally, the renovation proposal needs to fulfil environmental strategies and also the requirements of preservation in an ancient town as well as the needs of occupants. As mentioned above, it is clear that thermal comfort is influenced by many factors including design strategies, materials, exterior environment, lifestyle, activities of occupants and personal aspects. The success of renovation and conservation will require simultaneous contribution from urban managers, architects, conservation experts and occupants.

References

[1] H. Nguyen, "Saigon Architecture," *Literature, Art and Architecture*, pp. 89-92, 2006.

[2] T. M. Nguyen, "Maintainance of diversity in architecture of Cho Lon Town, Saigon," HCMC University of Architecture, Ho Chi Minh, 2004.

[3] I. o. Science, Vietnam building code natural physical & Climatic data for construction, Hanoi: Construction Register, 2009.

[4] VIAP., TCXDVN 9411:2012 Rowhouses - Design Standards, Hanoi: Ministry of Construction, 2012.

[5] S. V. Szokolay, Introduction to architectural science: The basic of sustainable design, Oxford: Architectural Press, 2004.

[6] D. N. Pham, The solution for climatic architecture in Vietnam, Hanoi: Construction publisher, 1998.

[7] G. Brown and M. Dekay, Sun, light and wind: Architectural design strategies, New York: John Wiley & Sons, Inc, 2000.

[8] CIBSE, Comfort, London: Chartered Institution of BUilding Services Engineers, 2006.

[9] CIBSE, Environmental Design: CIBSE Guide A, London: Chartered Institution of Building Services Engineers, 2006.

Low-temperature radiant cooling panel for hot and humid climate

Gongsheng Huang[a], Nan Zhang[b], Yuying Liang[c]

[a] Department of Architecture and Civil Engineering, City University of Hong Kong, Kowloon, Hong Kong, email: gongsheng.huang@cityu.edu.hk

[b] Department of Architecture and Civil Engineering, City University of Hong Kong, Kowloon, Hong Kong, email: nzhang88-c@my.cityu.edu.hk

[c] Department of Architecture and Civil Engineering, City University of Hong Kong, Kowloon, Hong Kong, email: Yuying.Liang@my.cityu.edu.hk

Abstract. In this paper, the heat transfer and thermal environment of air-layer integrated radiant cooling panel (AiCRCP) was studied experimentally. AiCRCP was proposed in 1963, which was characterized by the use of an infrared-radiation transparent (IRT) membrane to separate the panel's radiant cooling surface from its external air-contact surface. Therefore, the panel's radiant cooling surface temperature can be reduced to increase the cooling capacity, while its external air-contact surface, due to the thermal resistance provided by the air layer and the IRT membrane, can be easily maintained at a high temperature to reduce condensation risks. The thermal performance of AiCRCP was investigated using a prototype. Several scenarios were tested to analyze the thermal performance of prototype, and the cooling capacity of the AiCRCP was also investigated according to the thermal performance of the prototype. The results demonstrated that this new type of radiant cooling systems could be more preferable to be implemented in hot and humid climates.

Keywords. Radiant cooling, air-layer integrated ceiling radiant cooling panel, IRT membrane, condensation, cooling capacity
DOI: https://doi.org/10.34641/clima.2022.395

1. Introduction

Radiant cooling has many benefits, such as its high thermal comfort, lower energy use, quiet operation, and smaller equipment footprint, compared with the methods of cooling air of indoor spaces through air circulation [1-2]. However, radiant cooling applications face great challenges in hot and humid climates from condensation and their limited cooling capacity [3]. In its cooling mechanisms, whether through panel cooling or slab cooling [4], the radiant surface is also the air-contact surface, as shown in Fig. (1a), where a conventional ceiling radiant-cooling panel (CRCP) is used. In this CRCP, the cooling capacity increases with the decrease of the radiant-cooling surface temperature, but this will increase the risk of condensation. This dilemma has inhibited the commercialization of radiant cooling in hot and humid climates [5], and explains why CRCPs should be used together with other air-cooling systems in practical applications to provide enough cooling for thermal comfort [6].

Many attempts have therefore been made to solve the condensation problem while increasing the cooling capacity [7, 8]. A typical method is to maintain a low relative humidity so low radiant temperature can be used [9, 10], but this dehumidification is costly and risks degrading the thermal comfort. By realizing that the radiant surface must be isolated from the air-contact surface to essentially solving this dilemma, Morse proposed a radiant-cooling panel covered with a sheet spaced several centimeters from it, filled with dry air, and sealed to prevent room air from contacting the cold radiant-cooling surface [11], referred to as an *air-layer-integrated radiant-cooing panel* (AiCRCP) and illustrated in Fig. (1b). Thus, the air-contact surface and radiant cooling surface in the AiCRCP are physically separated.

It should be noted that the cover sheet must be transparent to the energy radiated from a body at a temperature range of 29.4°C to 35°C, and thus titled as infrared transparent (IRT) membrane. It enables the panel to act as a radiation heat sink, and heat from occupants in the vicinity can radiate through the transparent cover to the cold plate behind. Teitelbaum et al. [12] revisited this design, investigating several manufactured materials, such as low/high density polyethylene and polypropylene, using Fourier transform infrared

Copyright ©2022 by the authors. This conference paper is published under a CC-BY-4.0 license.

(FTIR) spectroscopy to analyze its thermal performance. They also investigated the panel depth (spacing between the radiant-cooling panel and the membrane) to balance radiation, conduction, and convection when AiRCPs was applied to an outdoor environment.

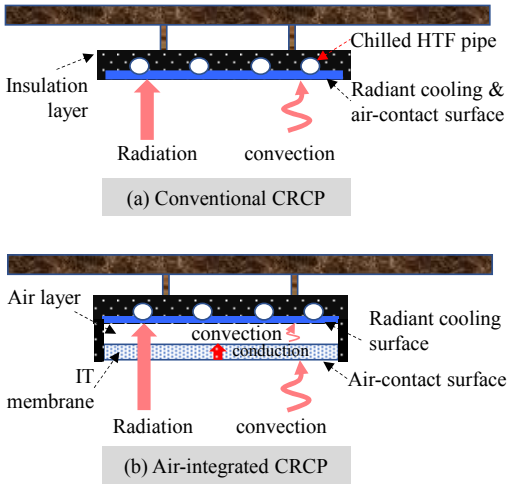

Fig 1. - Diagrams of (a) the conventional radiant cooling unit, (b) the air-integrated CRCP.

Teitelbaum et al.'s work motivated the studies on AiRCPs and AiCRCPs (here AiCRCP is used as the panel is installed on the ceiling for indoor cooling). Most of these studies, similar to Teitelbaum et al.'s work [12, 13], were focused on the thermal performance created by AiCRCPs. For example, Xing et al. [14] studied the influence of several factors, such as the flow regimes inside the air-layer, infrared transmissivity/emissivity of the IR-transparent membrane and relative humidity of indoor air, on the thermal performance of AiCRCPs. Sheppard [15] developed a heat balance model for AiRCPs to estimate their operational membrane temperature and cooling capacity. while Du et al. alalyzed the thermal performance of an AiCRCP with double-skin infrared-transparent membranes [16].

In our research group, Zhang et al. established a two-flux heat transfer model for the AiCRCP, to analyze the optical, physical and thermal properties of the IR-transparent membrane [17]. Liang et al. investigated the thermal environment and thermal comfort created by an AiCRCP with different low radiant temperatures (−2.3°C to 15°C) in a small thermal chamber using computational fluid dynamics simulations, and they demonstrated that both local and general thermal comfort indices, defined by ASHARE standards, could be satisfied even when the AiCRCP operated at a very low radiant temperature (e.g. −2.3°C) [18].

Previous literature has demonstrated that the enhanced cooling capacity and reduced condensation risk of AiCRCPs in addition to the thermal comfort they can maintain give them potential applications in hot and humid climates. However, most of the work reviewed above was based on simulation or numerical studies. In this paper, the cooling performance of an AiCRCP prototype and the thermal environment created by the AiCRCP were investigated using experiments, which showed that the AiCRCP could provide higher cooling capacity and better condensation prevetion.

2. Theoretical background

The heat transfer process of the AiCRCP is shown in Fig. 1(b), where the heat exchange between the AiCRCP and its thermal environment is mainly through two mechanims. One is radiation that occurs directly between the AiCRCP and its thermal environment; and other is the combination of convenction and conduction.

In the first mechanism, since the IRT membrane is assumed to have a poor ability to absorb infrared radiative heat flux and the air-layer is transparent to infrared radition, the radiative cooling power of the radiant cooling surface will not be much affected by the IRT membrane.

In the second mechanism, heat is firstly transfered to the IRT membrane from the air surrounding the AiCRCP through convection, and to the raidant cooling surface through the dyr air convenction (major) and conduction (minor). It should be noted that the IRT membreme is thin, its internal surface and exteral surface temperature could be consider as the same in the analysis of the thermal performance of AiCRCP.

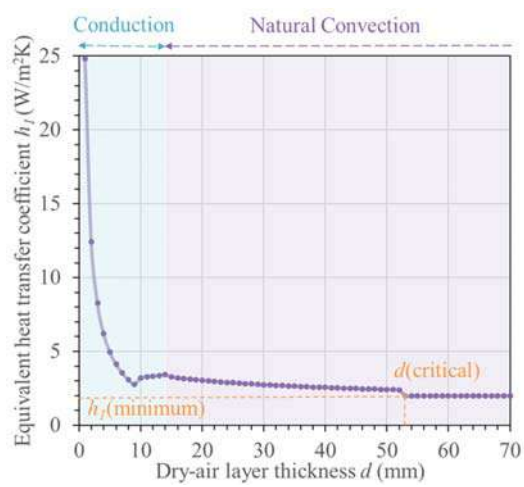

Fig. 2 - The heat transfer coefficient of an enclosed air layer [17].

Because the air layer has a large thermal resistance to both convection and conduction, as shown in Fig 2. [17], the IRT membrane can be maintained at a high temperature even if the radiant cooling temperature is low, for example 5°C (much lower than 17°C used in conventional CRCPs). Therefore, a low radiant cooling temperature can be used to

enhance the cooling capacity of the AiCRCP without increasing the condensation risk.

3. Experiment setup

3.1 Prototype of AiCRCP

Currently there is one prototype of AiCRCP in our laboratory with the dimension of 1 m × 1 m. This prototype uses a piece of aluminum plate: on one side high emissivity paint ($\varepsilon \approx 0.95$) was coated and used as cooling radiant surface, and on another side heat transfer fluid (HTF) pipes were attached and fixed using screws. The layout of the HTF pipes is shown in Fig. 3 (a). Thermal paste (grease) was used to increase the thermal conductivity between the HTF pipe and the aluminum plate, shown in the photo of Fig. 3 (b). This side was covered with a insulation layer (Nitrile rubber) to prevent cooling loss. A 20 μm thick low density *Polyethylene* (LDPE) was used as the IR-transparent membrane to seal a dry-air layer to separate the air-contact and radiant-cooling surfaces. A photo of the prototype is given in Fig. 3 (c). The prototype was connected with an air-cooled chiller that can provide heat transfer fluid with the temperature from −10°C to 20°C with the rated cooling capacity of 5.67 kW and coefficient of performance (COP) of 3.86. The membrane has a good IR transparency property as shown in Fig 3. (d), where the spectral transmittance was measured using FTIR (Spectrum Two, PerkinElmer).

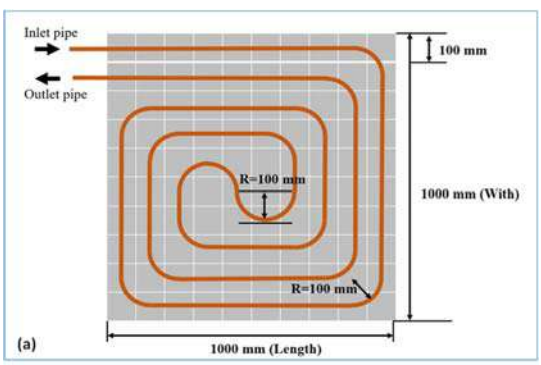

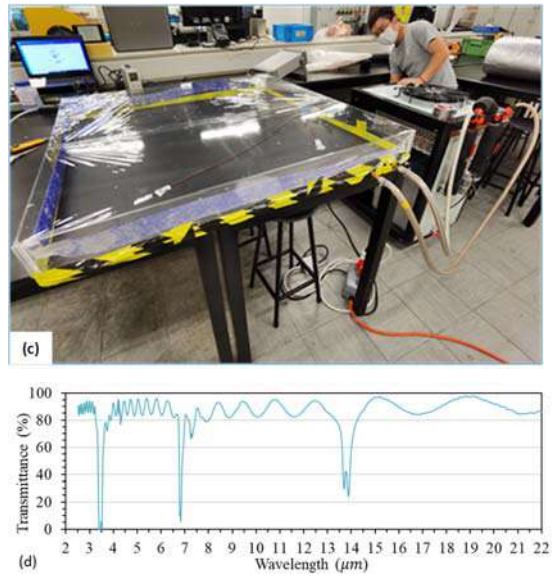

Fig. 3 - (a) HTF pipe layout on the radiant cooling panel; (b) The radiant cooling panel covered by an insulation layer; (c) LDPE membrane covering the panel and sealing a dry air layer; (d) IR spectral transmittance through LDPE membrane using FTIR.

3.2 Thermal chamber

The available thermal chamber is made of a wood layer, a metal layer, a thin insulation layer and an inner finish layer of mineral fiber. It is placed on a movable structure as shown in the photo of Fig. 4 (a). Fig. 4 (b) shows the internal view of the chamber. There is small window on the back with the dimension of 1.2 m×0.5 m.

A number of sensors/flow meters were installed to measure the temperature, flow and humidity. The measured qualities, number of sensors and sensor uncertainty were summarized in Table 1. Note that an FLIR infrared camera was also used to measure the radiant cooling surface temperature. All the measured data were collected using a data logger (SWEMA), connected to a computer for data analysis.

Tab. 1 - Measured quantities, number and uncertainty of sensors.

Measured Quantity	Sensor	Number	Uncertainty
HTF Fluid temperature	T-type Thermocouple	2	±0.5°C
Surface temperature	T-type Thermocouple	18	±0.5°C
Dry bulb air temperature	Swema 03+	1	±0.1°C
Indoor air velocity		1	±0.04m/s
Relative humidity	Swema HC2A-S	1	±0.8%RH
Globe temperatur	Swema 05	1	±0.1°C

e			
HTF flow rate	Turbine pulse flowmeter	2	±0.5%
Infrared temperature	FLIR infrared camera	1	±2%

Fig. 4 – (a) an external view of the thermal chamber and (b) an internal view of the chamber.

4. Experimental results and analysis

4.1 Testing scenarios

During the experiment, the thermal chamber was moved into a conditioned large hall, where the space temperature and humidity was maintained to be relatively stable in order to reduce the influence of the environmental disturbance from external weather conditions. Inside the thermal chamber, the cooling panel was installed horizontally on the ceiling, facing downward and working as ceiling cooling. In the test, the controlled variables were the indoor air temperature inside the thermal chamber and the radiant cooling temperature of the AiCRCP. The indoor air temperature was adjusted by several small heaters; the humidity was adjusted by a humidifier; while the radiant cooling temperature was controlled by the air-cooled chiller.

There were three testing scenarios, defined according to the total power of the heaters and listed in **Tab 2**. In scenario 1, the total power of the heater was the highest; while it was the lowest in scenario 2. In each scenario, the HTF supply temperature was varied in the range of -5~15°C, and the cooling panel radiant surface temperature had a gradient change between 1°C and 19°C. The RH of the indoor air temperature was controlled at 3 levels, i.e. 70%, 60% and 50%. When any variable was changed, the temperatures were measured 20 min after stability. No mechanical ventilation was used during the experiment.

Tab. 2 – Scenarios designed for the experiment.

Scenario	Total power of the heaters (W)	Cooling panel temperature (°C)
1	450 (RH=70%, 60%, 50%)	1~19
2	210 (RH=70%, 60%, 50%)	
3	0 (RH=70%, 60%, 50%)	

4.2 Temperature of the IRT membrane

Since the temperature of the IRT membrane surface (toward indoor air side) is an important variable that indicates the capability of the AiCRCP for condensation prevention, it was analysed at the beginning. Please note that it is required at least 1°C higher than the dew point of indoor air to avoid condensation risk [2].

Fig. 5 shows the average temperature of the IRT membrane under different radiant cooling panel temperature and different indoor air temperature and humidity. The dash lines are the dew point temperature of the indoor air. It can be seen that the dew point temperature decreased with the decrease of the cooling radiant temperature when the relative humidity was a constant. When the membrane temperature was equivalent to the dew point temperature, the cooling panel temperature was marked with a red circle in Fig. 5.

As shown in Fig. 5 (a) where RH was maintained at 70%, the cooling panel temperature should be higher than 13.5°C, 8.5 and 3 when the indoor air temperature was 28.9°C, 25 and 19.4°C, respectively. However, when RH=60%, the cooling panel temperature should be higher than 6°C when the environmental temperature was 29°C. When the indoor air was lower than 25°C, the condensation would not occur on the membrane even if the cooling surface temperature was reduced to below 2°C. When RH=50%, the results in Fig. 5 (c) showed that no condensation occurred on the membrane in these three different indoor air temperatures even the cooling panel temperature was reduced to 1°C.

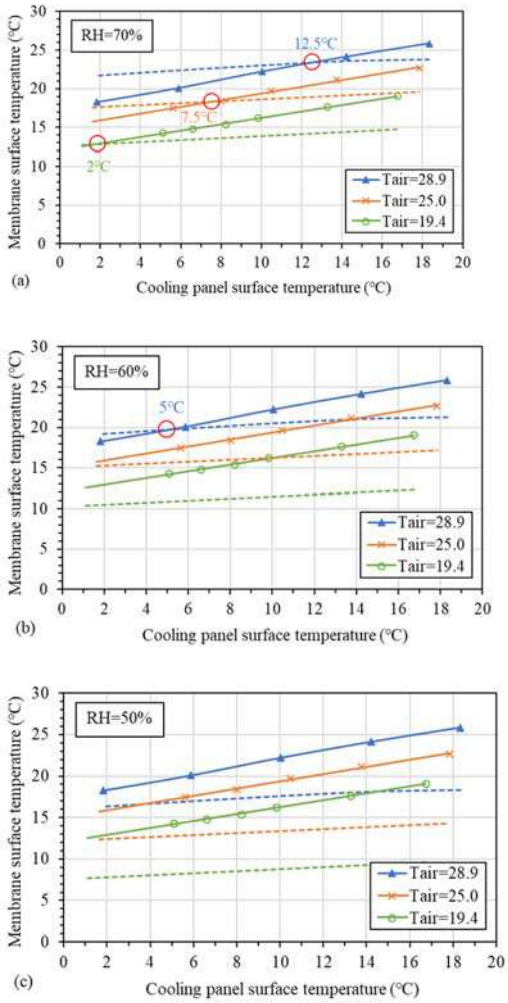

Fig. 5 – IRT membrane temperature in different indoor environments (a) RH = 70%, (b) RH = 60%, and (c) RH = 50%.

To further analyse the capability of the condensation prevention of the AiCRCP, the minimum allowable cooling panel temperature allowed was defined, which was the minimal temperature of the panel that can guarantee the IRT membrane temperature being 1°C higher than the dew point of the indoor air. The differences between the minimum allowable cooling panel temperature of the AiCRCP and the conventional ceiling radiant cooling panel were shown in Fig. 6 when RH=70% and RH=60%. The differences of the minimum cooling panel temperature was relatively constant when RH was same. For example, when RH=70% the minimum allowable temperature of the AiCRCP was around 10.8 lower than the conventional CRCP; and when RH=60%, the value was about 15°C. Therefore, the AiCRCP has a good performance in preventing condensation in hot and humid climates with lower radiant temperature.

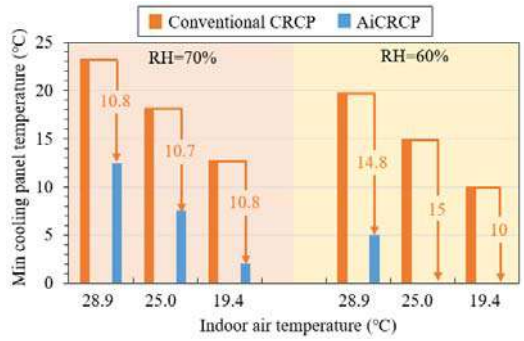

Fig. 6 – The minimum allowable cooling panel temperature of the AiCRCP and the conventional CRCP.

5. Cooling capacity of the AiCRCP

The cooling capacity of an AiCRCP depends on the thermal environment that is conditioned by the AiCRCP. Here we considered a room with the dimensions of 4 m× 4m ×3m. We assumed that the whole ceiling was used as AiCRCP. The walls and floors had the emissivity of 0.9. Referring to the Fig. (2d), the IRT transmittance of the membrane was assumed to be 80%. The temperature of the room air and the wall/floor surfaces were assumed to be 26°C.

The radiative heat transfer was calculated by Eqn. (1), where τ is the transmittance of the IRT membrane and Q'_{rad} is the radiation between surface 1 and 2 without membrane. In the calculation, view factors were considered and the equation matrix of all surfaces in the indoor environment was shown as Eq. (2), where ε is the emissivity, σ is the Boltzmann constant, J is the effective radiation, and $X_{i,j}$ is the view factor from surface i to j. The radiation heat flux between the cooling panel and other surfaces was calculated by Eq. (3), assuming the cooling panel being surface 1.

$$Q_{rad} = \tau \cdot Q'_{rad} \tag{1}$$

$$\left.\begin{array}{c} J_1\left(X_{1,1} - \frac{1}{1-\varepsilon_1}\right) + J_2X_{1,2} + J_3X_{1,3} + \cdots + J_nX_{1,n} = \frac{\varepsilon_1}{\varepsilon_1 - 1}\sigma T_1^4 \\ J_1X_{2,1} + J_2\left(X_{2,2} - \frac{1}{1-\varepsilon_2}\right) + J_3X_{2,3} + \cdots + J_nX_{2,n} = \frac{\varepsilon_2}{\varepsilon_2 - 1}\sigma T_2^4 \\ \cdots\cdots \\ J_1X_{n,1} + J_2X_{n,2} + \cdots + J_n(X_{n,n} - \frac{1}{1-\varepsilon_n}) = \frac{\varepsilon_n}{\varepsilon_n - 1}\sigma T_n^4 \end{array}\right\} \tag{2}$$

$$Q_{rad} = \tau \cdot \frac{\varepsilon_1}{1-\varepsilon_1} \cdot (\sigma T_1^4 - J_1) \tag{3}$$

The convective heat transfer was calculated according to the conservation of energy as shown in Eq. (4), where h_c and h_a were the heat transfer coefficients in the sealed air gap and room air side, T_c was the cooling panel temperature, T_m was the membrane temperautre and T_a was the indoor air temperature. Eq. (4) indicated that the heat transfer between the radiative cooling surface and

the IRT membrane should be equivalent to the amount between the IRT membrane and the room air.

$$Q_{conv} = h_c \cdot (T_m - T_c) = h_a \cdot (T_a - T_m) \quad (4)$$

In Eq. (4), the heat transfer coefficient h_c of the sealed air gap was calculated from Eqn. (5), where Gr is Grashof number, Pr is Prandtl number, λ is the thermal conductivity of dry air and d is the thickness of the air gap. Noted that Eq. (5) was also used to generate Fig. (2). Using the measurements of T_m , T_c and T_a in the experiments that were discussed in Section 4, h_a was approximated using a data fitting method.

$$h_c = \begin{cases} 0.059\frac{\lambda}{d}(Gr \cdot Pr)^{0.4}, 1700 < Gr \cdot Pr < 7000 \\ 0.212\frac{\lambda}{d}(Gr \cdot Pr)^{1/4}, 7000 < Gr \cdot Pr < 3.2 \cdot 10^5 \\ 0.061\frac{\lambda}{d}(Gr \cdot Pr)^{1/3}, Gr \cdot Pr > 3.2 \cdot 10^5 \end{cases} \quad (5)$$

The cooling capacity was the sum of radiative and convective heat fluxes. The cooling capacity of the AiCRCP was compared with that of the conventional CRCP in Fig. 7. When the RH was 70%, 60%, and 50%, the dew point temperatures of the room air were 20.12°C, 17.66°C and 14.81°C, respectively. Therefore, the cooling panel temperature of the conventional CRCP were set as 21°C, 19 °C and 16°C (approximated 1°C above the dew point). To maintain the IRT membrane temperature at 21°C, 19 °C and 16°C, the minimum allowable cooling panel temperatures of the AiCRCP were 13°C, 8°C and 2 °C respectively.

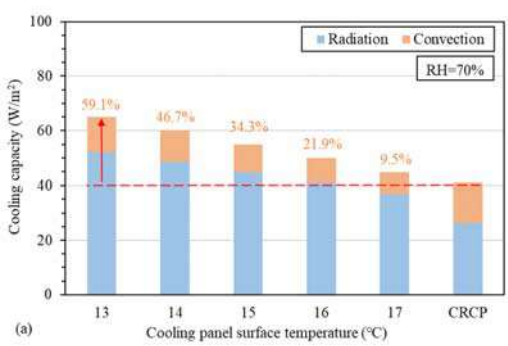

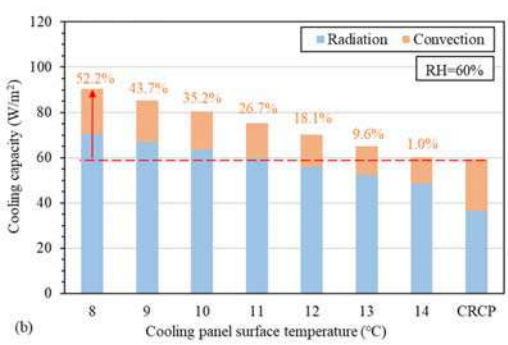

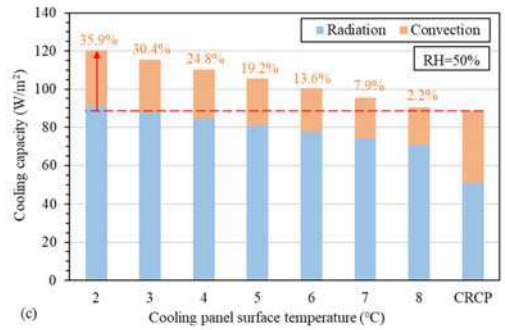

Fig. 7 – The cooling capacity of the AiCRCP and conventional CRCP.

Fig. 7 (a) showed the comparison when RH was 70%. The cooling capacity of the conventional CRCP was 40 W/m² using a radiant temperature of 21°C. 7.5% cooling capacity enhancement was achieved by the AiCRCP when its radiant cooling temperature was 17°C. Since the minimum allowable cooling panel temperature of the AiCRCP could be down to 13°C, the maximum cooling capacity of AiCRCP reached 63.63 W/m², improved by 59.1%.

Fig. 7 (b) showed the comparison when RH was 60%. At this condition, the cooling capacity of the conventional CRCP was 59 W/m² using a radiant temperature of 19°C. Similar cooling capacity was achieved by the AiCRCP when its radiant cooling temperature was 14°C. Since the minimum allowable cooling panel temperature of the AiCRCP could be down to 8°C, the maximum cooling capacity of AiCRCP was improved by 52.2%, reaching 90 W/m².

The comparison when RH was 50% was shown in Fig. 7 (c), where the cooling capacity of the conventional CRCP was 89 W/m² using a radiant temperature of 16°C. When the radiant cooling temperature of the AiCRCP was 8°C, 2.2% cooling capacity improvement was achieved. Similarly, when we considered the minimum allowable cooling panel temperature of the AiCRCP that could be down to 2°C, the maximum cooling capacity of AiCRCP reached 121 W/m², improved by 35.9%.

Fig. 7 also showed that due to a higher air contact surface temperature and a lower radiant surface temperature, the radiative heat flux of the AiCRCP was increased, while the convective flux was decreased when compared to the conventional CRCP. The radiative heat flux to the convective could be as high as 3.5:1. In the conventional CRCP, the ratio was typically 1.3 ~ 1. The enhanced radiative heat flux will benefit the heat exchange directly between heating sources (such as occupants) and the cooling panel.

6. Concluding remarks

This paper investigated the thermal performance of

a prototype of AiCRCP experimentally and then analysed its cooling capacity of AiCRCP in a simple room environment based on the thermal performance of the AiCRCP prototype. The results have shown that

- The AiCRCP has much enhanced capacity to prevent condensation even in hot and humid climates. Due to a large thermal resistance from the sealed air layer, the IRT membrane can be maintained at a high temperature even when the radiant temperature is controlled to a very low temperature.

- Due the possibility of using a low temperature, the cooling capacity of the AiCRCP can be enhanced significantly. At a higher humid environment, for example RH = 70%, the cooling capacity can be improved around 60%.

Thus, the thermal performance of the AiCRCP could make it more preferable when the technique of ceiling radiant cooling is adopted in hot and humid climates.

7. Acknowledgement

The research work presented in this paper was supported by a grant from the Research Grants Council of the Hong Kong Special Administrative Region, China (Project No. 11212919).

8. References

[1] Kim K.W., Olesen B.W., Radiant heating and cooling systems: Part 2, *ASHARE Journal* 2015; 57: 28-37.

[2] Rhee K.N., Kim K.W., A 50 year review of basic and applied research in radiant heating and cooling systems for the built environment, *Building and Environment* 2015; 91: 166-190.

[3] Mumma S.A., Ceiling panel cooling systems, ASHRAE Journal 2001; 43: 28-32.

[4] Rhee K.N., Olesen B.W., Kim K.W., Ten questions about radiant heating and cooling systems, *Building and Environment* 2017; 112: 367-381.

[5] Zhang L.Z., Niu J.L., Indoor humidity behaviors associated with decoupled cooling in hot and humid climates, *Building and Environment* 2003; 38: 99-107.

[6] Shin M.S., Rhee K.N., Park S.H., Yeo M.S., Kim K.W., Enhance of cooling capacity through open-type installation of cooling radiant ceiling panel systems, Building and Environment 2019; 148: 417-432.

[7] Ning B., Chen Y.M., Liu H., Zhang S., Cooling capacity improvement for a radiant ceiling panel with uniform surface temperature distribution, *Building and Environment* 2016; 102: 64-72.

[8] Zhong Z.W., Jiu J.L., Ma W., et al., An experimental study of condensation on an aluminum radiant ceiling panel surface with superhydrophobic treatment, *Energy and Buildings* 2021; 252: 111393.

[9] Hao X., Zhang G., Chen Y., Zou S., Moschandreas D.J., A combined system of chilled ceiling, displacement ventilation and desiccant dehumidification, *Building and Environment* 2007; 42: 3298-3308.

[10] Binghooth A.S., Zainal Z.A., Performance of desiccant dehumidification with hydronic radiant cooling system in hot humid climates, *Energy and Buildings* 2012; 51: 1-5.

[11] Morse R., Radiant cooling. *Architect. Sci. Rev.* 1963; 6: 50–53.

[12] Teitelbaum E., *et al.*, Revisiting radiant cooling: Condensation-free heat rejection using infrared-transparent enclosures of chilled panels. *Architect. Sci. Rev.* 2019; 62: 152–159.

[13] Teitelbauma E., Chen K.W., Dorit Aviv D. , et al., Membrane-assisted radiant cooling for expanding thermal comfort zones globally without air conditioning, *PNAS* 2020; 117: 21162–21169.

[14] Xing D.M, Li N.P., Cui H.J., Zhou L.X., Liu Q.Q., Theoretical study of infrared transparent cover preventing condensation on indoor radiant cooling surfaces, *Energy* 2020; 201: 117694.

[15] Sheppard D., Integrating membrane-assisted radiant cooling panels in building energy simulation, Master thesis, The University of British Columbia, Canada, December 2020.

[16] Du K., Wu H.J., Huang G.S., Xu X.H., Liu Y.C., Condensation-free radiant cooling with double-skin infrared-transparent membranes, *Building and Environment* 2021; 193: 107660.

[17] Zhang N., Liang Y., Wu H., Xu X., Du K., Shao Z., Zhou X., Huang G.S., Heat transfer modelling and analysis of air-layer integrated radiant cooling unit, *Applied Thermal Engineering*, 2021; 194: 117086.

[18] Liang Y.Y., Zhang N., Wu H.J., Xu X.H., Du K., Yang J.M., Sun Q., Dong K.J., Huang G.S., Investigation on the thermal comfort of the environment built by decoupled radiant cooling units with low radiant cooling temperatures, *Building and Environment* 2021;

206: 108342.

Data Statement

d. Data sharing not applicable to this article as no data sets were generated or analysed during the current study.

Monitoring the change of indoor environmental conditions of refurbished buildings in Milan.

Jacopo Vivian [a, b], Laura Carnieletto [a], Michele De Carli [a]

[a] Department of Industrial Engineering, University of Padua, Padua, Italy

[b] Urban Energy Systems Lab, EMPA Materials Science and Technology, Dübendorf, Switzerland.

Abstract. The energy performance gap, i.e. the difference between measured and predicted behaviour of buildings, is one of the main challenges for the building simulation community and it is highly relevant due to the increasing number of building renovations fostered by recent European Directives. In fact, occupants have a high influence on the building energy use for space heating and cooling, especially in refurbished buildings. The user behaviour may be indirectly investigated by monitoring the indoor environmental conditions before and after the refurbishment. However, in the literature there is a lack of monitoring studies that study the impact of user habits on the predicted energy savings for retrofitted buildings. This study contributes to filling this gap by analysing the air temperature and relative humidity monitored in twenty apartments in the city of Milan (Italy) during two consecutive years. Among them, eight were refurbished during the spring/summer period between the two monitored heating seasons. The analysis of the measured data shows that there is a slight increase in the average indoor air temperature of refurbished apartments. Moreover, the application of a simple hygrometric balance show that users are likely to increase air change rate in naturally ventilated buildings after their refurbishment. Finally, Energy Plus simulations of two monitored apartments showed that such changes in the indoor environmental conditions lead to significant variation in the energy needs for space heating.

Keywords. Building retrofit, indoor environment, energy performance gap, thermal comfort, monitoring.
DOI: https://doi.org/10.34641/clima.2022.396

1. Introduction

The Energy Performance of Building Directive [1] stated that buildings are responsible for 40% of the final energy use; among the different sectors, residential housing covers 60% to 85% of the national building stock within the European countries [2]. In the last decades, governments promoted building retrofit interventions to reduce energy use and CO_2 emissions associated with space heating and cooling.

However, buildings' renovation rates are meagre; thus the highest energy reduction can be achieved by a deep retrofit of the existing building stock [3] that belong to a large extent to the period after the World Wars. Ruggeri et al. [4] reviewed the crucial steps leading to energy retrofit planning, avoiding phenomena such as overheating or cooling or plant oversize. The energy use of buildings is supposed to decrease after refurbishment due to the reduction of transmission losses. Still, several cases show increased energy use compared to the expected one [5-6]. The resulting energy performance gap between the estimated and the real energy savings is linked to an increased demand for user comfort, also known in literature as *rebound effect*.

Galvin et al [7] recalled four different types of rebound effect previously defined as direct, indirect, economy-wide and transformational; the present paper focused only on the direct effect that is the increase of energy used by a retrofitted building, although it is supposed to have higher energy performance. An analysis of the Danish residential building stock based on energy performance certificates (EPC) investigated how the heat consumption can change due to energy improvements, finding a pseudo-rebound effect for a sample of 134.000 buildings with different characteristics [8]. However, even if data belonging to EPC can be used to describe the energy performance of a building stock, there may be data quality issues to be handled [9] when evaluating the potential energy saving. In fact, the available level of information is often not sufficient, thus requiring merging several sources and increasing the number of assumptions.

As demonstrated by Sunikka-Blank et al. [10] the rebound effect occurs when a fraction of the energy savings achievable after refurbishment is consumed

Copyright ©2022 by the authors. This conference paper is published under a CC-BY-4.0 license.

by additional energy use because the user expects more indoor comfort and changes his behaviour accordingly.
From a physical point of view, insulating the building should lead the users to accept a lower indoor air temperature due to the increase in temperature of the internal surfaces. However, calculating the performance of the upgraded building with the same thermal comfort can be misleading. Strictly related to the tendency of the user to increase the comfort level after an energy upgrade, the attitude of people that accept a poor indoor environment in poorly insulated buildings is named *prebound effect,* which is another variable responsible of the energy performance gap. Corrado et al. [11] pointed out that the rebound effect occurs when the users modify their behavior to obtain higher thermal comfort as a consequence of the renovation, increasing the energy demand by 35% to 55%.
Since national and international policies on building retrofit are based on the estimated energy savings after refurbishment actions, further research is needed to investigate the user behaviour and the related motivations and practices in households that could offset the estimated saving. Tackling behavioural change has a key role to develop effective strategies integrated to the improvement of thermal characteristics.
This paper used real data provided by a monitoring system installed in twenty apartments in two consecutive winter seasons, eight of which straddle a retrofit intervention on the building envelope. Data have been provided by TEICOS Group, as partner of the SPICA project to implement the study on living comfort and facilitate intelligent energy management through HEMS (Home Energy Management System). The aim of the SPICA project was to propose an innovative service for citizens to contain energy costs and to improve environmental comfort conditions. Therefore, the condominiums participating in the project have given the availability to install in some housing units, the "Valorizzami" monitoring kit consisting of a set of environmental sensors, native LoRaWAN class A. The objective of the analysis is to determine whether there is a change in indoor thermo-hygrometric conditions attributable to the intervention, and to estimate the impact of this possible change on the energy demand of the building. The influence of the user behaviour on energy savings has been investigated also by dynamic simulations carried out with EnergyPlus, simulating different combinations of envelope retrofit and indoor environmental conditions.

2. Case study

2.1 Monitoring program

The monitoring campaign was carried out in twenty apartments from 11 November 2018 to 31 December 2019. In this work, we aim to investigate the impact of building retrofit on user behaviour, whose habits can have a significant effect on the energy use of buildings as highlighted in the Introduction.
The monitored apartments are located in three apartment blocks in the suburbs of Milan, named M, B and F (Table 1). Eight apartments were monitored before and after refurbishment, while the other twelve did not undergo the retrofit in the same period. Two sensors were installed in each apartment, generally located in the living room, bedroom or entrance door.

Tab. 1 - Number of apartments per condominium

	M	B	F
Num. of apartments	10	142	47
Num. of monitored apartments	6	2	12

Sensors monitored indoor air temperature and pressure, relative humidity (RH), indoor illuminance and volatile organic compounds concentration (VOC) through the operation. Although measures were collected on an hourly basis, the percentages of non-available data range between 2.3% and 9.3% depending on the starting date of the monitoring campaign. Hourly profiles of dry-bulb temperature and relative humidity of the outdoor air were taken from the regional agency for environment protection (ARPA Lombardia) [12] and used to estimate the air change rates as explained in Section 3.1.

2.2 Simulated building

Dynamic simulations were performed with the software Energy Plus [13] to simulate the thermal behaviour of the building with the average indoor environmental conditions both ante and post retrofit. Weather data were simulated according to the .epw file of Milano Linate [14], which is the most similar to the weather conditions of the considered location. Information regarding the buildings were taken from the energy report required by the national standards according to the Decree of the 26/06/2015 [15-16]. The main characteristics of the three blocks M, B and F are summarized in Table 2.

Tab. 2 - Building retrofit interventions

	M	B	F
Retrofit actions on the building envelope (if any)	External wall and roof insulation	External wall insulation and blowing of insulating materials.	No actions on the envelope
HVAC system	Centralized heating system supplied by a heat pump	Centralized heating system supplied by a heat pump	Centralized heating system supplied by 3 condensing gas boiler
Emission system	High-temperature radiator	High-temperature radiator	Aluminium radiators
PV system	No	Yes	No

Block M had the most detailed information to perform a detailed energy model among the three

buildings. External and internal walls are made of solid bricks, while floors and ceilings have a traditional brick-concrete structure. The retrofit actions include 14 cm of rock wool panels for both envelope structures on the external side. The stratigraphy of the building envelope components are shown in Table 3.

Tab. 3 - Thermal properties of the building envelopes ante- (a) and post-retrofit (b)

(a)	Original structure	U value [W/(m² K)]
External wall	Internal plaster (2cm) Solid bricks (37.5 cm) External plaster (2 cm)	1.40
Internal wall	Internal plaster (1.5 cm) Solid bricks (12 cm) External plaster (1.5 cm)	1.43
Internal Floor/Ceiling (towards the basement)	Ceramic tiles (1.5 cm) Concrete screed (7 cm) Brick-concrete layer (20 cm) Internal plaster (1.5 cm)	1.39
Windows	Double-glazed	2.71
(b)	**Retrofitted structures**	**U value [W/(m² K)]**
External wall	Internal plaster (2cm) Solid bricks (37.5 cm) Rock wool panels (14 cm) External plaster (2 cm)	0.21
Internal Floor/Ceiling	Ceramic tiles (1.5 cm) Concrete screed (7 cm) Brick-concrete layer (20 cm) Rock wool panels (14 cm) Internal plaster (1.5 cm)	0.21

Two apartments were selected for the simulation considering representative configurations within the buildings investigated in terms of heated areas and surfaces bounded by the external environment, since the latter have a significant influence on the energy needs for space heating. Figure 1 (top) represents a typical small apartment of 66.8 m² (M5 bordered by the basement (yellow), other apartments on the top and two sides (pink), and has only two sides facing outside (blue).

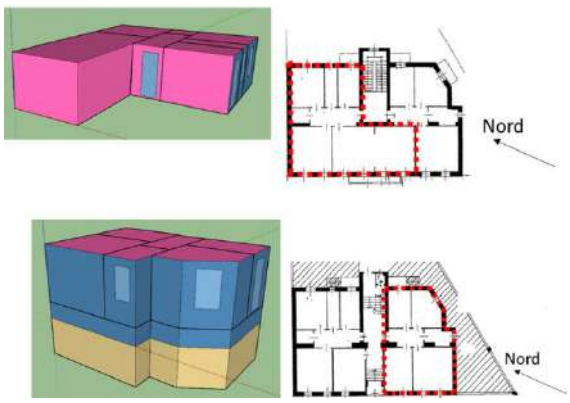

Figure 1 - 3D geometrical model and floor plan of the simulated apartments

The second configuration shown by Figure 1 (bottom), represents a typical large apartment (M2) of 98.5 m² with only one side facing the outdoor environment and the others adjacent to other heated apartments.

Since the main focus of the analysis is the real behaviour of the building, simulations used the net heated area, not considering the influence of thermal bridges. Internal loads and related schedules were estimated from BS ISO 18523 [17] for typical residential buildings, considering a family of 3 (M5) and 4 (M2) people, with a laptop, a TV and typical kitchen loads for a total peak load of 11.9 W/m² for M5 and 9.7 W/m² for M2. Schedule profiles are shown in Figure 2 for occupancy, lights and appliances.

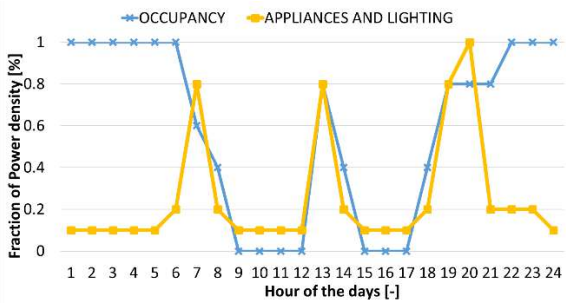

Figure 2 – Schedule profiles of internal loads.

3. Methods

This Section is divided into three parts. The first one describes the procedure to analyse the monitored data, including the estimation of the air change rates before and after the refurbishment. The second part outlines the main assumptions and scenarios for the energy simulations of the selected apartments. The third subsection describes the metrics used to assess indoor thermo-hygrometric conditions before and after the refurbishment based on both data and simulation results.

3.1 Analysis of the monitored data

The analysis of the monitored data was carried out on two subsets of the original dataset: one representing the situation before the refurbishment, and one after. In both periods, the analysis was conducted for 8 refurbished apartments and for 12 unrefurbished apartments separately. Periods of the same duration have been compared, with similar climatic conditions and similar expected activities in the daylife of the occupants. According to these criteria, two periods of five weeks before the Christmas holydays were identified as the most suitable ones, i.e. from 14/11/2018 to 21/12/2018 and from 14/11/2019 to 21/12/2019.

The weather conditions including outdoor air temperature, relative humidity (RH) and global solar irradiance (GHI) on the horizontal plane were collected from Lombardy's Regional Office for

Environmental Protection (ARPA) using data from Milan (Piazza Zavattari) weather station [12]. Table 4 shows a summary of weather conditions in the selected periods. It can be observed that in the monitored period after refurbishment the outdoor air was slightly warmer (+2.4°C on average) than in the previous period. In principle, this increase could affect user behaviour, thus introducing an external disturbance to the analysis. However, the air was also more humid and there was less solar radiation, thus partially compensating the feeling of cold during the post-retrofit period.

Tab. 4 – Summary of weather conditions in the selected periods

Scenario	Ante (2018)	Post (2019)
T_e	6.0±3.3°C	8.4±2.5°C
RH_e	81.6±13.5%	91.9±12.4%
GHI	1.36±0.57 kWh/(m² day)	0.83±0.59 kWh/(m² day)

Concerning indoor air conditions, hourly values of temperature and relative humidity were calculated by averaging measurements from all sensors. While the average internal humidity and the air change rate are calculated considering the full-day average (00:00-23:59), the indoor air temperature was calculated excluding night hours, i.e. only daytime. This operation allows to exclude the periods when the central gas boiler is off (22:00-7:00), i.e. when the occupants have no possibility to control their indoor temperature through the thermostatic valves.

Since the position and number of sensors changed from flat to flat and over time, no weighting factor was applied. Instead, data were filtered by considering only those days with a minimum number of hourly measurements. This lower acceptability threshold was set to 12 hours in the full-day data pre-processing, and 7 hours in the daytime data pre-processing.

The average ventilation rate was estimated for each apartment from the hygrothermal balance assuming a constant internal vapour generation of 0.375 kg_v/h, as shown in Eq. (1).

$$G_a = \frac{G_v}{x_i - x_e} \tag{1}$$

The air mass flow rate (kg_a/h) was then converted into air change rate (volumes per hour) by normalizing the data with respect to the building net heated volume, as shown in Eq. (2).

$$ACR = \frac{G_a}{\rho_a V} \tag{2}$$

The air change rate was then averaged over time to get daily values. In fact, the objective of this estimation is to compare ventilation rates before and after the refurbishment rather than calculating actual values, which would require either knowledge on the internal vapour generation or different monitoring methods. Outliers were filtered out using barrier functions to exclude negative air change rates or values higher than 2.0 h^{-1}.

3.2 Simulation scenarios

The analysis described in the previous Section allowed to determine the indoor environmental conditions before and after refurbishment. These conditions have been later used to simulate the buildings in the following three scenarios:

- Ante-Ante (AA): Both indoor environmental conditions and building envelope ante-intervention (i.e. before refurbishment).
- Ante-Post (AP): Retrofitted building envelope (i.e. after refurbishment) with the same indoor environmental conditions monitored ante-intervention.
- Post-Post (PP): Both indoor environmental conditions and building envelope post-intervention (i.e. after refurbishment).

3.3 Key Performance Indicators

The main objective of the present work was to determine whether the change in the buildings indoor environmental conditions is responsible for a significant change in the energy needs for space heating E_{SH} (kWh/m²) based on the monitoring campaign and on the results of the mentioned simulations. To this end, the energy needs were calculated using EnergyPlus for two reference housing units (M5 and M2), as explained above. The resulting operative temperature profile were used to calculate the thermal discomfort index TDI (°C h) as follows:

$$TDI = \begin{cases} \int (T_{i,min} - T_{op})\, dt\ , & T_{op} < T_{i,min} \\ \int (T_{op} - T_{i,max})\, dt\ , & T_{op} > T_{i,max} \end{cases} \tag{3}$$

Where $T_{i,min}$ and $T_{i,max}$ were assumed to be 20°C and 25°C, respectively. These values were chosen based on ISO 16798 [18] Standard.

Therefore, the expected key performance indicators for the refurbished buildings were calculated using the simulation results of AP scenario: $E_{SH,AP}$ and TDI_{AP}. The actual performance indicators –i.e. considering varied indoor environmental conditions were calculated, instead, using the simulation results of PP scenario: $E_{SH,PP}$ and TDI_{PP}. Usually, the Energy Performance Gap measures the difference between measured and predicted energy consumption. Here, the simulated energy performance gap EPG_{SH} (kWh/m²) was calculated as the relative difference between actual and expected energy performance:

$$EPG_{SH} = \frac{E_{SH,PP} - E_{SH,AP}}{E_{SH,AP}} \quad (4)$$

4. Results

Section 4.1 is focused on the difference between the indoor environmental conditions in the monitored apartments. The latter constitute the boundary conditions for the building simulations, whose results are reported in Section 4.2.

4.1 Analysis of the monitored data

Figure 3 shows the difference in the indoor air temperature before and after retrofit in one of the monitored apartments of condominium B. The profiles show that there is not a clear increase or decrease in the average temperature that lasts for the entire period. For instance, during 19-21/11/2019 the indoor air temperature was higher than that recorded in the same days of the previous year, while during 23/11/2019 the temperature was clearly below compared to the same day of 2018. This is most likely due to the diverse human activities, that are also affected by daily and weekly cycles. Predicting such occupant-related patterns is not among the objectives of the current work, that rather tries to discover significant year-to-year differences in the average indoor air measurements assuming to have similar internal heat and water vapour gains. A careful observation of the temperature profiles reveals that, on average, the daily oscillations are more pronounced during 2018, i.e. before building retrofit. Indeed, in the period considered, the difference between maximum and minimum indoor air temperature drops from 2.0°C to 1.4°C. The lower temperature decrease occurring in 2019 is likely caused by the higher thermal insulation of the building envelope.

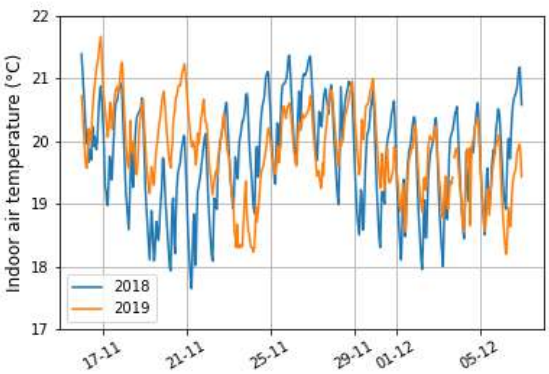

Figure 3 - Example of average indoor air temperature profiles over three weeks ante and post retrofit.

Table 5 and Table 6 report the average indoor thermos-hygrometric conditions in the refurbished and unrefurbished apartments, respectively. One may see that in the refurbished flats there is a clear increase in the indoor air temperature (+0.4°C) during daytime, that goes from 21.3°C to 21.7°C. The same increase does not occur in the unrefurbished flats. However, a reduced increase in temperature (+0.2°C) is still present. This means that the temperature increase after building retrofit should not be entirely explained with the rebound effect, but is likely due to individual preferences/activities of the occupants that cannot be considered as a general trend. Indeed, a more careful analysis of the data reveals that only four apartments out of eight experience an increase in the indoor temperature (+0.97°C on average) while the other four show a limited yet significant reduction (-0.19°C), as shown in Figure 4(a). These discrepancies may also be due to other factors, such as a different size and orientation of the external walls and windows. Repeating the same analysis on a bigger sample of apartments could provide more statistically significant, representative trends.

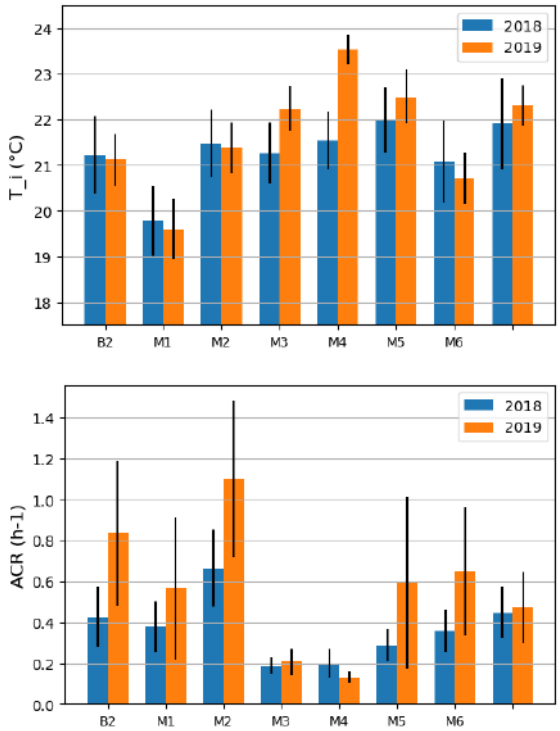

Figure 4 – Indoor environmental conditions ante and post retrofit in the refurbished apartments: average air temperature (top) and air change rate (bottom).

The daily air change rates show a notable increase after building retrofit. In fact, they go from 0.37 to 0.57 volumes/hour (+55%). Such variation is also confirmed by the fact that 7 apartments out of 8 have the same increasing trend, as shown in Figure 4(b). However, differently from the indoor temperature, the air change could not be measured directly. Therefore, these values should only be interpreted as an estimation of the relative change in the ventilation rates after the retrofit. This result relies on the assumption that internal water vapour generation was the same in the monitored periods. Although being a strong assumption, it is deemed as reasonable due to the duration of the periods considered (five weeks). In the flats of block F, the increase in the air change rates was less pronounced,

going from 0.53 to 0.64 volumes/hour (+21%). Here, 8 flats out of 12 experience an increase. The analysis therefore shows that the increase in the air change rates cannot be explained simply with a change in the user behaviour linked to the request of a more comfortable indoor environment. Instead, it is more likely that this change is, at least in part, due to the different weather conditions in the periods compared. This hypothesis is confirmed by the fact that in the five weeks of 2019, there was a higher external air temperature. This could have been a driver to increase ventilation for both refurbished and non-refurbished buildings.

A similar consideration holds true for the internal relative humidity, that increases from 48% in 2018 to 53% in 2019 despite the higher indoor air temperature and increased estimated air change rates. These trends can be physically explained with the inflow of warmer and more humid outdoor air occurring during the five weeks of 2019.

Tab. 5 – Summary of indoor thermo-hygrometric conditions ante and post retrofit.

Scenario	Ante (2018)	Post (2019)
$T_{i,avg}$	21.3±0.8°C	21.7±0.5°C
$RH_{i,avg}$	47.9±5.6%	53.2±4.9%
ACR	0.37±0.11 hr^{-1}	0.57±0.26 hr^{-1}

Tab. 6 – Summary of indoor thermo-hygrometric conditions in non-refurbished buildings.

Scenario	2018	2019
$T_{i,avg}$	21.2±0.7°C	21.4±0.7°C
$RH_{i,avg}$	48.1±5.8%	55.4±5.2%
ACR	0.53±0.16 hr^{-1}	0.64±0.24 hr^{-1}

4.2 Simulated buildings

Simulations belonging to scenario AP, that simulated the refurbished apartments maintaining the previous thermo-hygrometric indoor conditions, should highlight the expected energy demand for space heating, i.e. the energy demand without a change in the user behaviour. Scenario PP, instead, simulated the refurbished apartments with the changed user behaviour, thus shading light on the effect of user behaviour on the final energy demand of the buildings. The degree-hours of thermal discomfort were also calculated for the same scenarios in order to quantify the possible gain in thermal comfort linked to the rebound effect. For each scenario, both the energy demand and thermal discomfort index were calculated for both simulated apartments (M2 and M5), thus finding the ranges shown in Table 7.
Results of scenario AP showed that the energy saving obtainable with the retrofit goes from 50% (M2) to 58% (M5) in the monitored period, and are even higher if the same indoor conditions are considered for the whole heating season (53-61%).

The difference between scenario AP and PP is consistent, confirming the existence of a rebound effect. Indeed, the energy savings drop to 32-40% considering the monitored period only, and to 33-43% considering the whole heating season.
As a consequence, the energy performance gap EPG_{SH} calculated from the simulation outputs was found to be 36-41% in the monitored period and 42-47% assuming the same user behavior holds true for the entire season. These values are very high and reflect the importance of user behavior in achieving the desired energy savings after a technical intervention on the building envelope. However, they must not be interpreted as actual gaps but rather as an upper limit to the rebound effect. In fact, they are based on simulations that rely on several assumptions reported in the Methods Section. The main assumption is that occupancy and human activities do not change after retrofit and that the effect of a different weather does not influence indoor conditions significantly.

Looking at thermal comfort, the increase in energy use after retrofit is strictly related to the need of the user for a higher indoor comfort, which corresponds to a lower amount of time where with an operative temperature lower than 20°C (TDI low). The lower indoor temperatures are not entirely linked to user preferences, but also to physical constraints such as the inertia required to heat up the apartments before the building refurbishment. The higher ACR obtained from the hygrometric balance led to lower overheating, with few periods with operative temperatures higher than 25°C (TDI high).

Tab. 7 – Comparison on energy need and thermal discomfort obtained with building simulations.

Scenario		AA	AP	PP
		M2-M5	M2-M5	M2-M5
Seasonal E_{SH} (kWh/m^2)		85.1-97.5	40.3-38.1	57.1-56.0
Monitored period E_{SH} (kWh/m^2)		20.6-23.4	10.4-9.9	14.1-14.0
TDI (°C h)	Low	532.3-760.8	19.3-16.8	17.6-18.1
	High	0-0	44.9-66.3	0-1.4

5. Conclusions

The present work investigated a dataset reporting temperature and humidity profiles recorded in twenty apartments in Milan in two consecutive winter seasons, eight of which were refurbished during the summer in between. The research

question was whether there is a significant change in the indoor conditions that could be linked with the so-called rebound effect, i.e. a demand for increased comfort that typically occurs after energy efficiency measures such as the thermal insulation of residential buildings.

The study shows that, on average, a slight increase (+0.4°C) in the indoor temperature that occurs as a result of a significant increase in half of the refurbished flats. This change must not be attributed entirely to a behavioural change, since a slight increase (+0.2°C) occurs also in non-retrofitted buildings. Therefore, the increase could be more likely linked to lower transmission losses at night and different weather conditions in the monitored periods. An hygrothermal balance based on measurements of indoor and outdoor humidity reveals that the air change rates increase significantly after the intervention (+55%). The same increase is lower in non-refurbished apartments (+21%), thus confirming the hypothesis of the behavioural cause to increased ventilation.

Overall, a rebound effect seems to occur and to be due to higher ventilation requirements rather than to higher indoor temperatures. In absence of measured energy consumption data, simulations of two representative apartments were carried out to estimate the energy performance gap linked to this behavioural change. The latter ranged from +36% to +47% depending on the simulated apartment and on the duration of the period considered.

The small number of the analysed sample hinders the generalization of the results. However, the analysis points out that a rebound effect occurs. Therefore, estimating the energy-saving potential based only on improved thermal characteristics can lead to a significant overestimation of the heat saving potential in residential buildings and more attention should be put on the behaviour of the final users. Future work will try to extend these findings using a larger dataset.

6. Acknowledgement

The authors would like to show their gratitude to TEICOS Group as holder of the collected data provided for the analyses. The database was collected within the SPICA project funded under the FESR 2014-2020 Regional Operational Program.

References

[1] The European Parliament and the Council of the European Union, Directive (EU) 2018/844 of 30 May 2018 amending Directive 2010/31/EU on the energy performance of buildings and Directive 2012/27/EU on energy efficiency

[2] https://ec.europa.eu/energy/eu-buildings-factsheets_en (Last seen: 04/01/2022)

[3] Visscher, H., Dascalaki, E., Sartori, I. Towards an energy efficient European housing stock: Monitoring, mapping and modelling retrofitting processes. Energy and Buildings. 2016; 132: 1–154.

[4] Ruggeril, A., Gabrielli, L., Scarpa, M. Energy Retrofit in European Building Portfolios: A Review of Five Key Aspects. Sustainability. 2020; 12.

[5] Haas, R., Biermayr, P. The rebound effect for space heating Empirical evidence from Austria. Energy policy. 2000; 28 (6-7): 403-410.

[6] Ben, H., Steemers, K. Energy retrofit and occupant behaviour in protected housing: A case study of the Brunswick Centre in London. Energy and Buildings. 2014; 80: 120-130.

[7] Galvin, R., Sunikka-Blank, M. Quantification of (p)rebound effects in retrofit policies – Why does it matter?. Energy. 2016; 95

[8] Brøgger, M.; Bacher, P.; Madsen, H.; Wittchen, K.B. Estimating the influence of rebound effects on the energy-saving potential in building stocks. Energy and Buildings. 2018; 181: 62–74.

[9] Mangold, M.; Österbring, M.; Wallbaum, H. Handling data uncertainties when using Swedish energy performance certificate data to describe energy usage in the building stock. Energy and Buildings. 2015. 102: 328–336.

[10] Sunikka-Blank, M., Galvin, R. Introducing the prebound effect: The gap between performance and actual energy consumption, Building Research and Information. 2012, 40(3):260-273.

[11] Corrado, V., Ballarini, I., Paduos, S., Primo, E. The Rebound Effect after the Energy Refurbishment of Residential Buildings towards High Performances. 4th International High Performance Building Conference, Purdue, July 11-14, 2016

[12]https://www.arpalombardia.it/Pages/Meteorologia/Richiesta-dati-misurati.aspx (last seen: November 2021)

[13] "EnergyPlus | EnergyPlus." [Online]. Available: https://energyplus.net/. [Accessed: 20-Feb-2020].

[14]https://energyplus.net/weather-location/europe_wmo_region_6/ITA/ITA_Milano-Linate.160800_IGDG [Last seen: Jan2022]

[15] Presidente della Repubblica Italiana, Decreto interministeriale 26 giugno 2015 - Adeguamento linee guida nazionali per la certificazione energetica degli edifici, Rome, Italy, 2015.

[16] Presidente della Repubblica Italiana, Decreto interministeriale 26 giugno 2015 - Applicazione delle metodologie di calcolo delle prestazioni energetiche e definizione delle prescrizioni e dei requisiti minimi degli edifici, Rome, Italy, 2015.

[17] International Standard Organisation - ISO, ISO 18523-2:2016 Energy performance of buildings — Schedule and condition of building, zone and space usage for energy calculation, 2016.

[18] European Committee for Standardization-CEN, "BS EN 16798 - Energy performance of buildings - Ventilation for buildings - Part 1: Indoor environmental input parameters for design and assessment of energy performance of buildings addressing indoor air quality, thermal environment, lighting and acoustics", Brussels, Belgium, 2019.

Data Statement

The datasets generated during and/or analysed during the current study are not available because of privacy agreements but the authors will make every reasonable effort to publish them in near future.

Experiment on Indoor Pollutants Reduction from Duct System Applied with TiO_2 Photocatalyst

Seong Eun Kim [a], Yong Woo Song [b], Jin Chul Park [c]

[a] Graduate School, Chung-Ang University, Seoul, the Republic of Korea, asteria03@naver.com

[b] School of Architecture & Building Science, Chung-Ang University, Seoul, the Republic of Korea, yongma0930@naver.com

[c] Professor, School of Architecture & Building Science, Chung-Ang University, Seoul, the Republic of Korea, jincpark@cau.ac.kr

Abstract. This study analyzed the indoor pollutants (toluene, formaldehyde) reduction performance of a ventilation duct system using a titanium dioxide photocatalyst(TiO_2) to improve indoor air quality. The ventilation duct system has a loop-type closed circuit structure with a diameter of 100 mm and a length of 6.6 m that includes a reaction section to which UV lamps and photocatalysts are applied. The length of the reaction section was 0.6 m, and 0.18 m2 of the photocatalyst was applied. Toluene and formaldehyde were each injected at a concentration of 1 ppm, and the average airflow velocity inside the duct was set to 1 m/s and the experiment was performed. As a result of the experiment, toluene showed 0 ppm in 14 minutes and formaldehyde showed 0 ppm in 12 minutes after the photochemical reaction had started. Therefore, it was confirmed that the indoor pollutant concentration could be reduced when the TiO_2 photocatalyst is applied to the ventilation duct system.

Keywords. Titanium Dioxide Photocatalyst, Ventilation Duct System, Toluene, Formaldehyde, Ultraviolet, Photochemical Reaction, Reduction Test
DOI: https://doi.org/10.34641/clima.2022.49

1. Introduction

Korea has continuously strengthened standards related to improving the energy performance of buildings to reduce national greenhouse gases, and insulation and airtightness performance have improved significantly with the goal of zero energy buildings.[1] However, the decrease in ventilation rate due to improved airtight performance, the concentration of pollutants such as carbon dioxide, formaldehyde, and volatile organic compounds generated indoors may increase.[2,3] To solve this problem, Korea is required to install a total heat exchange ventilation system in all new apartments. [4]

As a method for removing indoor pollutants, there is a method of using a photocatalyst having air purification performance in addition to ventilation.[5] Photocatalyst is a compound word of light and catalyst that promotes a chemical reaction by receiving light. Examples of the photocatalytic material include titanium dioxide (TiO_2), zinc oxide (ZnO), cadmium sulfide (CdS), tin oxide (SnO_2), vanadium oxide (V_2O_3), iron oxide (Fe_2O_3), zirconium oxide (ZrO_2), tungsten oxide (WO_3), and the like. Among them, TiO_2 is representative and is used in various places such as coating materials, concrete panels, paints, and road paving materials. TiO_2 can be used semi-permanently because its properties do not change even when it receives light, and it is widely used because it has the advantage of decomposing into water (H_2O) and carbon dioxide (CO_2) that are not harmful to the human body. [6,7]

That is, when the TiO2 photocatalyst reacts with ultraviolet rays as shown in Figure 1, electrons (e-) and electron holes are generated on the surface of the material, which again reacts with oxygen in the air to generate hydroxyl radicals (•OH) and superoxide anion radicals ($O_2^{\cdot-}$).[8] The generated ions react with toluene and formaldehyde (HCHO), which are indoor pollutants that cause sick building syndrome, and finally decompose into H_2O and CO_2.

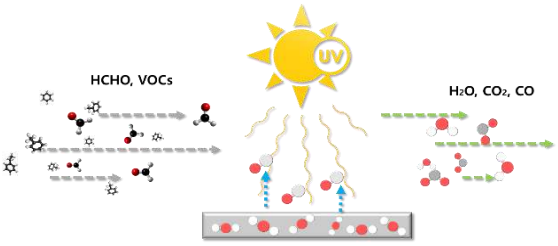

Fig. 1 - Photocatalytic reaction conceptual.

Therefore, this study is a basic research stage for the development of a mechanical ventilation system with indoor pollutant removal performance, and the

Copyright ©2022 by the authors. This conference paper is published under a CC-BY-4.0 license.

photocatalytic coating material was applied to the ventilation duct system and the removal performance of toluene and formaldehyde (HCHO) was confirmed through an experiment.

2. Experiments

2.1 Experiment overview

In order to confirm the performance of removing indoor pollutants for the ventilation duct system to which the TiO_2 photocatalyst is applied, a small-scale model was produced and an experiment was performed. Currently, there is no test method for the ventilation duct system to which a photocatalyst is applied, so the conditions(UV source, light intensity, temperature, humidity, air velocity, etc.) were determined by referring to ISO 22197, an international standard photocatalyst test method. [9,10]

As shown in Table 1, the experiment was conducted with two types of representative indoor pollutants, toluene and HCHO. The light source used for the photocatalytic reaction was a UV-A lamp, and the irradiance was 10 W/m^2. The starting concentration of the pollutant gas is 1 ppm each. In the experiment, after stabilizing for 60 minutes after injecting the gas concentration, a UV-A lamp was turned on to perform a photoreaction, and the change in concentration was measured using the equipment shown in Table 2.

Tab. 1 - Experiment conditions.

Type of pollutants	Toluene, HCHO
Gas concentration	1 ppm each
Light source and irradiance	UV-A, 10 W/m^2
Air velocity	1 m/s
Temperature	25±2.5℃
Relative humidity	RH 50%

Tab. 2 - Measuring Equipment.

Name of equipment	Airwell plus gas analyzer
Measurement material	Toluene, HCHO
Measurement range	0~10 ppm
Resolution	0.02 ppm
Measurement flow rate	1.5 L/min

2.2 Configuration of experimental device

Figure 2 shows the diagram of the small-scale photocatalytic ventilation duct system for the experiment. The total size was width 2,300.0 mm, lenght 1,060.0 mm, and height 101.8 mm. The material of the duct was made of stainless steel with low adsorption to pollutants.

Also, it consists of closed-circuit ducts and consists of photo-catalyst reaction section and non-response section. The reaction section is applied with a TiO_2 photocatalyst coating inside the duct, and the UV-A lamp is installed as shown in Figure 3. The applied coating is about 30 g, and the area of that is about 0.18 m^2. Figure 4 is a photo of the experimental system.

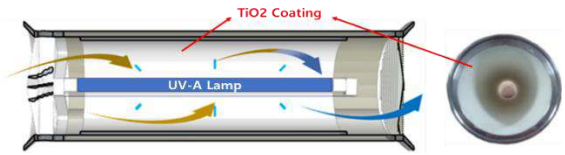

Fig. 3 - Internal composition of the photocatalyst reaction section.

Fig. 4 - System of the duct system applied with TiO_2.

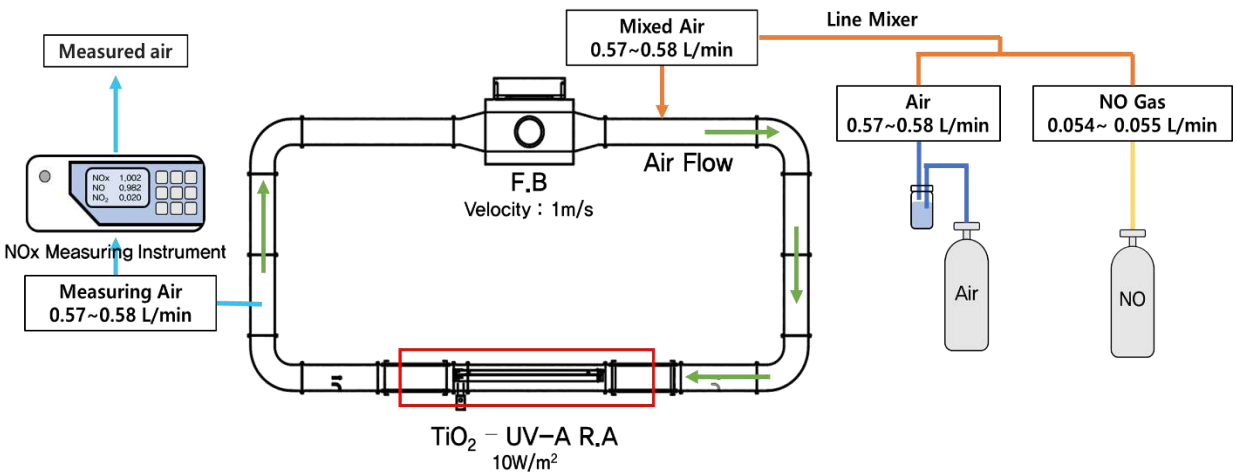

Fig. 2 - Experiment diagram of model reduction of photocatalyst ventilation duct system.

3. Results

3.1 Toluene reduction result

As a result of examining the toluene reduction performance through the experiment, Figure 5 and Table 3 are shown. After the concentration inside the ventilation duct reached 1 ppm, the UV-A lamp was turned on and the light reaction was performed, and as a result, it reached 0 ppm in 14 minutes. The removal efficiency was 100 %, and the reduction rate was 0.07 ppm/min.

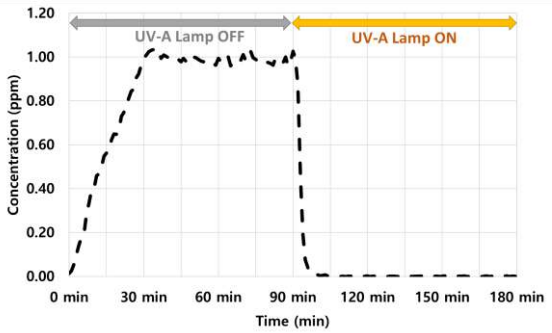

Fig. 5 - Toluene reduction graph.

Tab. 3 - Toluene reduction result.

Contents	Time	Concentration
Reaction Start	90 min	1 ppm
Reaction End	104 min	0 ppm
Reaction Time	14 min	
Reduction Rate	0.07 ppm/min	

3.2 HCHO reduction result

The results of examining the HCHO reduction performance are shown in Figure 6 and Table 4. The concentration inside the ventilation duct dropped from 1 ppm to 0 ppm in 12 minutes after the start of the photoreaction. Therefore, like toluene, the removal efficiency is 100%, and the reduction rate is 0.08 ppm/min.

4. Conclusions

This study is an experimental study to review the removal performance of indoor pollutants (Toluene, HCHO) when photocatalysts are applied to ventilation duct systems, and the results are as follows. In the case of toluene, the concentration dropped from 1 ppm to 0 ppm 14 minutes after the photocatalytic reaction decreased to 100%. In the case of HCHO, it was reduced by 100% after 12 minutes.

Therefore, through this study, it was possible to verify the indoor pollutant removal performance of the ventilation duct system using TiO_2 photocatalysts, and it is considered to be effective when combined with mechanical ventilation systems such as apartments and multi-used facilities. In the future, it is necessary to install a photocatalytic ventilation duct system for actual apartments and check the effectiveness of the actual environment through field experiments.

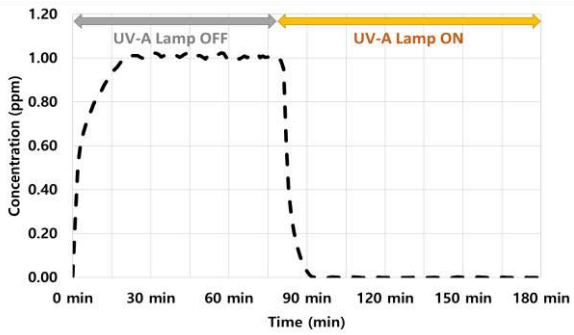

Fig. 6 - HCHO result graph.

Tab. 4 - HCHO reduction result.

Contents	Time	Concentration
Reaction Start	80 min	1 ppm
Reaction End	92 min	0 ppm
Reaction Time	12 min	
Reduction Rate	0.08 ppm/min	

5. References

[1] Kim Y., Yu K. H. Study on the Certification Policy of Zero-Energy Buildings in Korea. Sustainability. 2020;12(12):5172.

[2] Howieson S. G., Sharpe T., Farren P. Building tight – ventilating right? How are new air tightness standards affecting indoor air quality in dwellings?. Building Services Engineering Research and Technology. 2013;35(5):475-487.

[3] Park J. H., Lee S. H., Kim H. K. Effect of Mechanical Ventilation System on Improvement of Indoor Air Quality in A Newly Built Apartment and B Department Store. Journal of Korean Society of Occupational and Environmental Hygiene. 2014;24(1):38-45.

[4] Ministry of Land, Infrastructure and Transport of Korea, Rules on facility standards of buildings, MOLIT ordinance No. 23, 2013. 9. 2

[5] Song Y. W., Kim M. Y., Chung M. H., Yang Y. K., Park J. C. NOx-Reduction Performance Test for TiO2 Paint. Molecules. 2020;25(18):4087.

[6] Shayegan Z., Lee C. S., Haghighat F. TiO2 photocatalyst for removal of volatile organic

compounds in gas phase–A review. Chemical Engineering Journal. 2018;334:2408-2439.

[7] Fujishima A., Zhang X., Tryk D. A. TiO2 photocatalysis and related surface phenomena. Surface Science Reports. 2008;63(12):515-582.

[8] Ballari M. M., Hunger M., Hüsken G., Brouwers H. J. H., Modelling and experimental study of the NOx photocatalytic degradation employing concrete pavement with titanium dioxide. Catalysis Today. 2010;151(1-2):71-76.

[9] DIN German Institute for Standardization, Fine Ceramics, Test Method for Air-Purification Performance of Semiconducting Photocatalytic Materials, ISO-22197-3.

[10] DIN German Institute for Standardization, Fine Ceramics, Test Method for Air-Purification Performance of Semiconducting Photocatalytic Materials, ISO-22197-4.

Acknowledgements

This research was supported by a grant (22SCIP-C146254-05) from the Infrastructure and Transportation Technology Promotion Research Program funded by the Ministry of Land, Infrastructure and Transport of the Korean government.

Energy and comfort in spaces equipped with ascendant airflow

Eusébio Conceição [a], João Gomes [b], M. Inês Conceição [c], M. Manuela Lúcio [a], Hazim Awbi [d]

[a] Faculdade de Ciências e Tecnologia, Universidade do Algarve, Faro, Portugal, econcei@ualg.pt; maria.manuela.lucio@gmail.com.

[b] CINTAL, Universidade do Algarve, Faro, Portugal, jgomes@ualg.pt.

[c] Instituto Superior Técnico, Universidade de Lisboa, Lisboa, Portugal; ines.conceicao@tecnico.ulisboa.pt.

[d] School of Built Environment, University of Reading, Reading, United Kingdom; h.b.awbi@reading.ac.uk.

Abstract. This article presents a numerical study on an impinging jet ventilation system applied in a virtual office with the aim of improving indoor air quality (IAQ) and thermal comfort conditions for its occupants. The study was carried out for winter conditions, also evaluating the thermal energy consumption obtained in the acclimatized space by the proposed ventilation system. The numerical model used is based on the coupling of two numerical models, the Computational Fluid Dynamics to simulate the heat and mass turbulent flow, and the Human Thermal Modelling to evaluate the human and clothing thermal response. A third numerical model, the Building Thermal Modelling, was used to provide some input data required for the two aforementioned models. The evaluation of the thermal comfort is done by the Predicted Percentage of Dissatisfied (PPD) people index. The evaluation of the IAQ is done by the dioxide carbon (CO_2) concentration in the breathing zone of occupants. The evaluation of the impinging jet ventilation system is done by the Air Distribution Index (ADI). This study was done in a virtual chamber occupied by four virtual manikins seated around a table. The impinging jet ventilation system has an inlet system based on four ducts located in the corners of the chamber, whose air terminal devices are 0.25 m from the floor, and an outlet system, whose air terminal device is located close to the ceiling central area. This numerical study considered different values of the airflow rate for the impinging jet ventilation system. When the airflow rate increases, the level of IAQ, the level of thermal comfort and the ADI improve. Moreover, results obtained for PPD and CO_2 show values within acceptable limits accordingly to the international standards.

Keywords. ADI, Indoor Air Quality, Thermal Comfort; Virtual Thermal Manikin.
DOI: https://doi.org/10.34641/clima.2022.378

1. Introduction

In this study it is applied a ventilation system based on impinging jets with downward supply (near the floor) and upward exhaust (ceiling). The principle of operation of this ventilation system is described in the study of Ye et al. [1]. This kind of ventilation system has the advantages of mixing and displacement ventilation systems in the occupied area [2], and lower energy consumption than mixed ventilation systems [1]. The ventilation performance of impinging jet ventilation systems was assessed, e.g., in works of Karimipanah et al. [3], Ye et al. [4] and Chen et al. [5]. Factors as the shape of the air supply device, the discharge height, the supply airflow rate, the supply air temperature and the thermal load in space influence the performance of these systems [6]. Staveckis and Borodinecs [7] concluded that impinging jet ventilation systems can improve the thermal comfort and Indoor Air Quality (IAQ) in indoor occupied spaces due higher ventilation effectiveness.

Therefore, in order to assess the performance of these types of ventilation systems, it is important to use methodologies for assessing thermal comfort and IAQ.

In order to evaluate the thermal comfort in occupied spaces provided by Heating, Ventilation and Air Conditioning (HVAC) systems, Fanger developed through experimental tests two comfort indexes, PMV (Predicted Mean Vote) and PPD (Predicted Percentage of Dissatisfied) [8]. These indexes were adopted by the international standard ISO 7730 to define three acceptable thermal comfort categories [9].

Copyright ©2022 by the authors. This conference paper is published under a CC-BY-4.0 license.

The carbon dioxide (CO_2) concentration can be used as reference to evaluate the IAQ level in occupied spaces [10,11]. The international standard ASHRAE 62.1 [12] defines a concentration of CO_2 released in the occupant breathing process of 1800 mg/m^3 as the acceptable limit for IAQ in occupied spaces. The CO_2 concentration depends on the airflow rate used by the ventilation system [13,14].

In this work the numerical models used, developed by the authors over the years, are based on the Building Thermal Response [15], and a coupling between two numerical models, namely, a numerical model that simulates the turbulent flow of heat and mass using Computer Fluid Dynamics [16], and a numerical model that simulates the thermal response of the human body and respective clothing, named Human Thermal Response [17]. Results obtained by the Building Thermal Response are used as input data in the coupling numerical models.

The Air Distribution Index (ADI) is used to evaluate the HVAC system performance [18]. The thermal comfort level, IAQ level, effectiveness for heat removal and effectiveness for contaminant removal are parameters considering by ADI. The ADI depends of the thermal comfort number and the air quality number. The thermal comfort number depends of the coefficient between the effectiveness for heat removal and the PPD due the thermal comfort level. The air quality number depends of the coefficient between the effectiveness for contaminant removal and the Percentage of Dissatisfied people due to IAQ level. The application of ADI is shown, e.g., in the works of Almesri et al. [19] and Conceição and Awbi [20].

The objective of this numerical work is to present the influence of an impingement jet ventilation system on the IAQ and thermal comfort levels of the occupants of a space with dimensions similar to a small office. This virtual office is occupied by four occupants seated on chairs around one table. The impingement jet ventilation system is constituted by an inlet system located in the four corners of the office and one outlet system located at the central area of the chamber close to the ceiling. The study, carried out in steady state regime, was done for five different air inlet velocities considering external winter conditions.

2. Methodology

The numerical simulation was carried out for a virtual chamber (Fig. 1), with the dimensions 2.7×2.45×2.4 m^3. The virtual chamber, simulating a small office, is occupied by four people sitting in chairs around a table, and is equipped with an inlet and outlet airflow systems, based on impinging jet ventilation. Each occupant, represented by a virtual manikin, is 1.70 m tall and 70 kg in weight.

The impinging jet ventilation consists of:

- An exhaust system equipped with an exhaust fan, installed 1.8 m from the floor, connected to the central ceiling area;
- An inlet system, based on four vertical ducts, of 0.125 m diameter, located in the walls corners. Each duct is equipped with a fan. The inlet airflow, with downward airflow, is located 0.25 m from the floor.

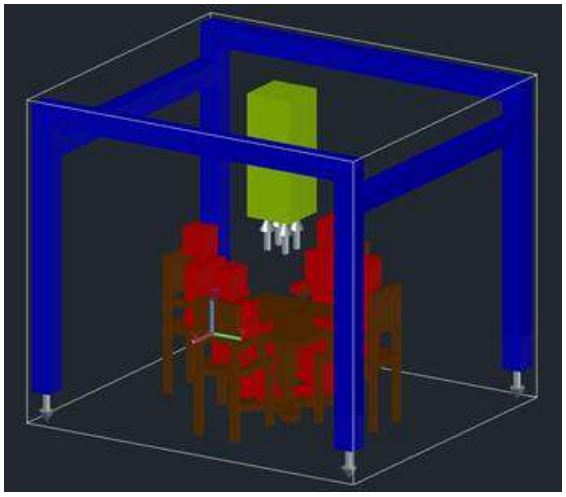

Fig. 1 – Scheme of the virtual chamber used in the numerical simulation. The inlet system is represented in blue and the outlet system in green. Arrows indicate the direction of airflow.

The numerical simulation was done considering winter conditions. The external inlet air temperature is 0°C. The inlet CO_2 concentration is 500 mg/m^3. The inlet turbulent intensity is 2.5%.

It was considered that the occupants have an activity level of 1.2 met [9], and are considered to be dressed at a clothing insulation level of 1.0 clo [9], a typical value for winter conditions.

This numerical simulation was done for five different Cases characterized by the inlet air velocities and inlet air temperatures present in Tab. 1.

Tab. 1 – Cases considered in the numerical simulation.

Case	Air inlet velocity (m/s)	Air inlet temperature (°C)
A	0.43	13.0
B	0.86	16.5
C	1.29	17.7
D	1.72	18.3
E	2.15	18.6

The air introduced into the virtual office comes from outside and is heated by the HVAC system in order to reach a temperature that guarantees thermal comfort conditions for the occupants. The inlet air velocity is varied to ensure that the air quality in the occupants'

breathing zone is acceptable.

The occupants' thermal comfort level is evaluated by the PPD index, which in turn depends on the PMV index [8]. The PMV index depends on four indoor environmental parameters, air temperature, relative air humidity, air velocity and Mean Radiant Temperature, and two personal parameters, clothing and occupant activity [8,9].

The assessment of the IAQ is done through the concentration of CO_2 released in the breathing zone of the occupants [12].

The performance of the ventilation system is measured using the ADI index. The ADI depends on the thermal comfort number and the air quality number [18]. The thermal comfort number depends of the coefficient between the effectiveness for heat removal and the PPD due the thermal comfort level [18]. The air quality number depends of the coefficient between the effectiveness for contaminant removal and the Percentage of Dissatisfied people due to IAQ level [18].

3. Results and discussion

This section presents the results obtained from PPD (Fig. 2), CO_2 concentration (Fig. 3), effectiveness for heat removal and effectiveness for contaminant removal (Fig. 4), thermal comfort number and air quality number (Fig. 5), and ADI (Fig. 6) for the five Cases defined in Table 1. The values of the results presented refer to the average of the values obtained in each occupant.

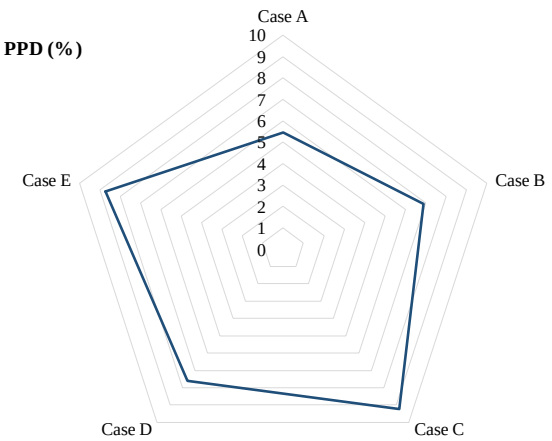

Fig. 2 – Results obtained from PPD for the five Cases simulated.

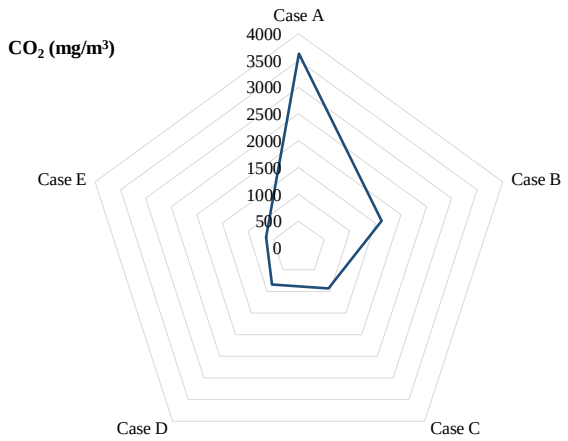

Fig. 3 – Results obtained from CO_2 concentration for the five Cases simulated.

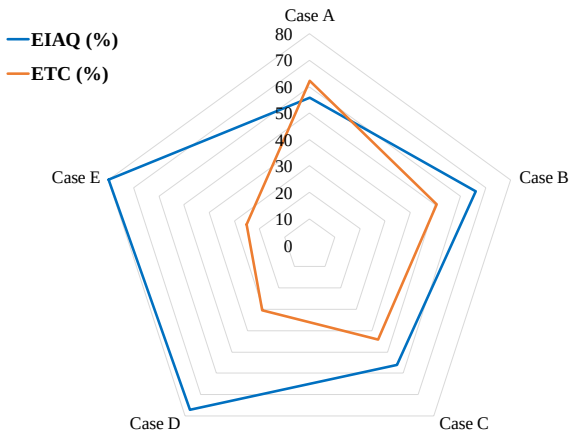

Fig. 4 – Results obtained from effectiveness for heat removal (ETC) and effectiveness for contaminant removal (EIAQ) for the five Cases simulated.

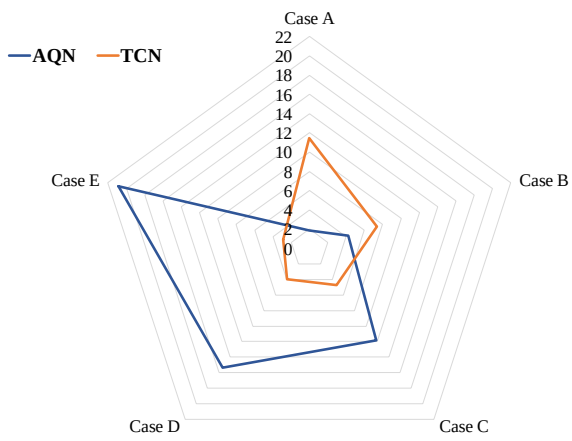

Fig. 5 – Results obtained from thermal comfort number (TCN) and air quality number (AQN) for the five Cases simulated.

Fig. 6 – Results obtained from ADI for the five Cases simulated.

The results show that when the air velocity increases the PPD value increases. The average increase rate between Cases is about 14.4%. However, for all cases, the PPD values obtained show acceptable levels of thermal comfort according to the ISO 7730 standard [9].

The CO_2 concentration decreases as the air velocity increases. The decrease between Cases is significant. The value of the CO_2 concentration in Case E is around 18% of the value of the CO_2 concentration obtained in Case A. Analysing Case by Case, it appears that the level of air quality in the occupants' breathing zone does not is acceptable according to ASHRAE 62.1 [12] only for the air velocity used in Case A. The air velocities used in Cases C to E allow obtaining CO_2 concentration levels significantly below the acceptable limit of 1800 mg/m^3 recommended by ASHRAE 62.1 [12].

The effectiveness for heat removal decreases with increasing air velocity. The value obtained for the effectiveness for heat removal for Case E is about 40% of the value obtained for Case A, so it can be said that when the air velocity increases, the effectiveness for heat removal worsens.

The effectiveness for contaminant removal increases with increasing air velocity. The value obtained for effectiveness for contaminant removal for Case E is about 143% of the value obtained for Case A, so it can be said that when the air velocity increases, effectiveness for contaminant removal improves.

The thermal comfort number decreases with increasing air velocity. The value obtained for the thermal comfort number for Case E is about 25% of the value obtained for Case A, so it can be concluded that when the air velocity increases, the thermal comfort number gets worse.

The air quality number increases with increasing air velocity. The value obtained for the thermal comfort number for Case E is about 112% of the value obtained for Case A, so it can be concluded that when the air velocity increases, the air quality number improves.

The ADI increases with increasing air velocity. The value obtained from the ADI for Case E is about 168% of the value obtained for Case A, so it can be concluded that when the air velocity increases, the performance of the HVAC system, given by the ADI value, improves.

In general, the results show that IAQ and ADI improve with increasing air velocity, despite the decrease in thermal comfort level, but managing to maintain PPD values within the recommended acceptable values [9].

The values obtained for the heating power for the five Cases are shown in Tab. 2. The heating power was calculated from the integral of the energy over the time required to heat the air transferred from the outside to the interior of the room. The results show that the heating power increases with the increase in air velocity. Note that increasing the inlet air temperature from Case to Case (see Tab. 1) shows that the heating power must increase.

Tab. 2 – Heating power obtained for each of the Cases simulated.

Case	Power (W)
A	546.9
B	1388.2
C	2233.7
D	3079.3
E	3912.2

4. Conclusions

In this paper it was applied an impinging jet ventilation system with downward supply (near the floor) and upward exhaust (next to the ceiling). The performance of this system was evaluated for five different values of air velocity through the average value of the ADI obtained for each of these air velocities. Simultaneously, for each of these air velocities, the level of thermal comfort was evaluated, through the average values of the PPD obtained, and the level of IAQ in the breathing zone of the occupants was evaluated, through the average values of the concentration of CO_2 obtained.

When the air velocity increases, the results obtained allow us to conclude the following:

- As a positive contribution, the decrease in CO_2 concentration, the increase in effectiveness for contaminants removal, in the air quality number and in the ADI;
- From a less significant perspective, the decrease in PPD, effectiveness for heat

removal and thermal comfort number.

However, the thermal comfort level is acceptable, according to ISO 7730 [9], for all simulated air velocities. On the other hand, the IAQ level is acceptable, according to ASHRAE 62.1 [12], for the air velocities used in Cases B to E.

As the air velocity increases, the performance of the ventilation system improves, mainly due to the improvement of IAQ conditions close to the occupants' breathing zone.

5. Acknowledgement

The authors acknowledge to the project (SAICT-ALG/39586/2018) from Algarve Regional Operational Program (CRESC Algarve 2020), under the PORTUGAL 2020 Partnership Agreement, through the European Regional Development Fund (ERDF) and the National Science and Technology Foundation (FCT). The authors acknowledge also to the project (70156-Safeair) from Algarve Regional Operational Program (CRESC Algarve 2020), under the PORTUGAL 2020 Partnership Agreement, through the European Regional Development Fund (ERDF).

6. References

[1] Ye, X., Zhu, H., Kang, Y., Zhong, K. Heating energy consumption of impinging jet ventilation and mixing ventilation in large-height spaces: A comparison study. Energy and Buildings. 2016; 130:697-708.

[2] Karimipanah, T., Awbi, H. Theoretical and experimental investigation of impinging jet ventilation and comparison with wall displacement ventilation. Building and Environment. 2002; 37:1329-1342.

[3] Karimipanah, T., Awbi, H., Moshfegh, B. The Air Distribution Index as an indicator for energy consumption and performance of ventilation systems. Journal of the Human-Environment System. 2008; 11(2):77-84.

[4] Ye, X., Zhu, H., Kang, Y., Zhong, K. Study of factors affecting warm air spreading distance in impinging jet ventilation rooms using multiple regression analysis. Building and Environment. 2017; 120:1-12.

[5] Chen, H., Moshfegh, B., Cehlin, M. Investigation on the flow and thermal behavior of impinging jet ventilation systems in an office with different heat loads. Building and Environment. 2013; 59:127-144.

[6] Chen, H., Moshfegh, B., Cehlin, M. Computational investigation on the factors influencing thermal comfort for impinging jet ventilation. Building and Environment. 2013; 66:29-41.

[7] Stavecki, A., Borodinecs, A. Impact of impinging jet ventilation on thermal comfort and indoor air quality in office buildings. Energy and Buildings. 2021; 235:110738.

[8] Fanger, P. Thermal Comfort: Analysis and Applications in Environmental Engineering. Danish Technical Press: Copenhagen, Denmark. 1970.

[9] ISO 7730. Ergonomics of the Thermal Environments – Analytical Determination and Interpretation of Thermal Comfort Using Calculation of the PMV and PPD Indices and Local Thermal Comfort Criteria. International Standard Organization: Geneva, Switzerland. 2005.

[10] Conceição, E., Lúcio, M. Air quality inside a school building: Air exchange monitoring, evolution of carbon dioxide and assessment of ventilation strategies. International Journal of Ventilation. 2006; 5(2):259-279.

[11] Asif, A., Zeeshan, M., Jahanzaib, M. Indoor temperature, relative humidity and CO2 levels assessment in academic buildings with different heating, ventilation and air-conditioning systems. Building and Environment. 2018; 133:83-90.

[12] ANSI/ASHRAE Standard 62-1. Ventilation for Acceptable Indoor Air Quality. American Society of Heating, Refrigerating and Air-Conditioning Engineers: Atlanta, GA, USA. 2016.

[13] Conceição, E., Silva, M., Viegas, D. Air quality inside the passenger compartment of a bus. Journal of Exposure Analysis and Environmental Epidemiology. 1997; 7(4):521-534.

[14] Conceição, E., Silva, M., Viegas, D. Airflow around a passenger seated in a bus. Journal of Exposure HVACR Research. 1997; 3(4):311-323.

[15] Conceição, E., Lúcio, M. Numerical study of the influence of opaque external trees with pyramidal shape in the thermal behaviour of a school building in summer conditions. Indoor and Built Environment. 2010; 19(6):657-667.

[16] Conceição, E., Farinho, J., Lúcio, M. Evaluation of indoor air quality in classrooms equipped with cross-flow ventilation. International Journal of Ventilation. 2012; 11(1):53-67.

[17] Conceição, E., Santiago, C., Lúcio, M., Awbi, H. Predicting the air quality, thermal comfort and draught risk for a virtual classroom with desk-type personalized ventilation systems. Buildings. 2018; 8(2):35.

[18] Awbi, H. Ventilation of buildings. Routledge:

London, UK. 2004.

[19] Almesri, I., Awbi, H., Foda, E., Sirén, K. An air distribution index for assessing the thermal comfort and air quality in uniform and non-uniform thermal environments. Indoor and Built Environment. 2013; 22:618-639.

[20] Conceição, E., Awbi, H. Evaluation of integral effect of thermal comfort, air quality and draught risk for desks equipped with personalized ventilation systems. Energies. 2021; 14(11):3235.

Impact of Ventilation Air Supply Type on Indoor/Outdoor PM: In-Situ Measurements

Kevin Verniers [a], Frederik Losfeld [a], Ivan Pollet [a], Jelle Laverge [b]

[a] R&D Digital Innovation, Renson Ventilation NV, Waregem, Belgium, kevin.verniers@renson.be

[b] Department of Architecture and Urban Planning, Ghent University, Ghent, Belgium

Abstract. Indoor comfort has been given significant attention to satisfy the occupants' needs, yet the Covid-19 pandemic accelerated awareness for creating also a healthy atmosphere. Besides infectious aerosols, Particulate Matter (PM) and Volatile Organic Compounds (VOCs) can induce health issues on the short and long term. Commercial ventilation systems are increasingly based on providing a good indoor comfort by monitoring CO_2, RH, and/or VOCs while targeting a low as possible energy consumption. Indoor PM is determined by various indoor and outdoor sources ranging from cooking and household activities to outdoor PM transported or infiltrating into the building. Consequently, the indoor PM level varies and potentially affects human health. This research contains in-situ measurements with Renson Senses quantifying indoor and outdoor PM in and near one single dwelling for examining the impact of commercial ventilation systems (Mechanical Extract Ventilation (MEV) and Mechanical Ventilation with Heat Recovery (MVHR)) on indoor PM1, 2.5, 4 and 10. The measurements encompassed four system configurations either without filter (natural or mechanical supply) or mechanical supply equipped with ISO Coarse >90% or ISO ePM1 50% filters to assess the filter efficiency in practice. The extraction flow rate was kept constant and identical to avoid the impact of different air exchange rates on indoor PM. Each configuration was active during two weeks resulting in a two months period (May-June, 2021) during which occupancy and indoor polluting activities were rare, allowing to assess the ventilation and filter impact on indoor PM. The analysis revealed that indoor PM levels are about half the outdoor PM levels without filtering on the air supply, when there was no occupation or activities. Using an ISO Coarse >90% filter showed no clear effect with a similar performance as an MEV system. Next to this, a MVHR system equipped with an ISO ePM1 50% filter significantly impacts the transport of outdoor PM to indoors, with an efficiency, expressed as the Indoor/Outdoor ratio, of about half the laboratory efficiency. Supposing that PM originates 50/50 from indoors and outdoors, the actual fine filter efficiency influencing indoor PM is about 15-25% of the measured lab efficiency.

Keywords. Indoor/Outdoor Particulate Matter, In-Situ Measurements, Mechanical Extract Ventilation, Mechanical Ventilation Heat Recovery, Filter Efficiencies.
DOI: https://doi.org/10.34641/clima.2022.78

1. Introduction

The percentage of time that humans spend indoors at places like homes or offices is on average 87% [1]. Next to this, the Covid-19 pandemic demonstrated the importance of creating a healthy indoor climate by preventing the spread of diseases via infectious aerosols [2]. As a result, people are becoming aware of the quality of the air that we breathe in at each time of day, outdoors as well as indoors. Besides infectious aerosols, other pollutants like Volatile Organic Compounds (VOCs) and Particulate Matter (PM) are also present in the air and can impose severe health issues [3,4]. Recently constructed dwellings compared to older ones have an improved airtightness resulting in a reduced uncontrolled ventilation rate that depends on the cracks and crevices in the building envelope. Consequently, the concentration of pollutants generated indoors in modern dwellings can increase over time leading to a deteriorated indoor air quality. For this reason, a controlled ventilation system is applied to provide an adequate ventilation rate in the building to guarantee the indoor air quality [5]. An outcome of the AIVC project "Ventilation & Health" ranked PM in the indoor residential environment the highest priority concerning chronic health issues [3,4]. PM is classified based on particle diameter and typical PM fractions are PM1 (<1 μm), PM2.5 (<2.5 μm, fine), and PM10 (<10 μm, coarse). PM with a smaller particle diameter penetrates deeper into the human body imposing a higher

Copyright ©2022 by the authors. This conference paper is published under a CC-BY-4.0 license.

health hazard. The indoor PM level is determined on the one hand by indoor activities like cooking, smoking, and walking; while on the other hand outdoor PM infiltrates the dwelling through leakages in the building envelope, via open windows, and the ventilation system [6]. The fraction of outdoor PM contributing to the indoor PM level is estimated to be up to 56% [3,4].

Over the years, outdoor PM levels have significantly improved in continents like Europe with a reduction of about 50% over 20 years, although PM peaks causing significant problems can still occur. Therefore, the Out2In study assessed with outdoor air the real-life performance of filters applied in a simple lab-constructed mechanical ventilation system and concluded that fine filters (class F7 or F9) improved the indoor air quality in contrast to the typically used coarse filters (class G3 or G4) [7,8]. This conclusion is supported by a simulation study that considered a Mechanical Ventilation with Heat Recovery (MVHR) system with filter types ranging from coarse to fine. That simulation study also encompassed a comparison between a Mechanical Extract Ventilation (MEV) system and a MVHR where the latter achieved a 50% reduction of indoor PM2.5 when compared to the former [9,10]. A field study examined in a classroom located near a highway the impact on indoor PM when a commercial MVHR is equipped once with and once without a F8 filter. The use of the filter reduced the indoor PM2.5 and PM10 by 30% and 34%, respectively, which are clearly lower than the theoretical filter values, despite no or limited indoor PM sources [11]. Similarly, the effect on outdoor PM2.5 transported to indoors when mechanical or mixed mode ventilation with eventual filtering is applied was examined in 37 offices in four countries. The field study concluded that indoor PM2.5 was generally lower than outdoor PM2.5 and the highest reduction was obtained when mechanical ventilation combined with a high efficiency filter was deployed [12]. Another field study analysed the influence of ventilation (natural versus unbalanced or balanced mechanical) on indoor PM in 15 homes selected from three sites and came to the same conclusions as the aforementioned work [13]. Next to this, also the variation of PM1, PM2.5, and PM10 was investigated in 40 inhabited houses in Germany. The main conclusion was an elevated indoor PM10 compared to outdoor PM10 due to indoor activities, whereas indoor PM10 significantly decreases or even reaches zero during the absence of activity [14].

The amount of transported outdoor PM to indoors due to the applied ventilation system has been extensively investigated over the years. Many studies focused on MVHR with filters, however, there is also a large share of houses equipped with MEV instead of MVHR, a system that was considered in the simulation study of Rojas [9,10]. In addition, the field studies encompassed a large variety of building functions ranging from residential housing to offices and classrooms, each exhibiting a specific occupancy profile and associated activities. Consequently, the indoor PM measurements were accompanied with periods of indoor generated PM, making it rather difficult to quantify the amount of transported outdoor PM via the ventilation system. Another aspect is the construction of both the building envelope and the ventilation system affecting the infiltration and transportation, respectively, of outdoor PM to indoors. For clarification, a study observed the PM transport from outdoors to indoors for two identically constructed houses each equipped with the exact same type of mechanical ventilation system. The amount of transported PM from outdoors to indoors differed up to 20% despite the fact that both houses should provide the same circumstances [15]. In this paper, the transport of outdoor PM to indoors between MVHR and MEV is assessed by means of in-situ measurements in several rooms of a dwelling. Both ventilation systems are present in the same dwelling providing identical test conditions for the following aspects: the exhaust framework, the set exhaust ventilation rate, and the house layout and interior. The outdoor PM concentration was the most variable parameter during the study. Moreover, the residence is typically unoccupied indicating the absence of indoor PM generating activities like cooking and smoking; while only a few people visited the house during the measurement campaign and therefore is the resuspension of indoor particles considered to be limited.

2. Research methodology

2.1 House and ventilation systems description

The in-situ measurements were conducted in the unoccupied Renson Concept Home that was completed in 2019 and is located in a low urban district of Waregem (Belgium). The building is an uninhabited furnished single-family detached house consisting of two bedrooms, a bathroom, a living room with open kitchen, and a technical room; the building layout is shown in Fig. 1. The residence has a total surface area of 184 m^2, a leakage rate of 2.20 $m^3/(h.m^2)$ at 50 Pa, and a Belgian energy performance score of E13 which corresponds with an A label. The house is equipped with two commercial ventilation systems: the smart Healthbox 3.0 and the Endura Delta [16,17]. The first system is MEV while the second is balanced MVHR that can be equipped with coarse or fine filters.

2.2 Measurement approach and schedule

Tab. 1 shows the timing schedule of the activated ventilation systems during the PM measurements. A total of four configurations were considered and each was in operation for two weeks at a fixed exhaust flow rate of 300 m^3/h. MEV was the first examined configuration where supply air is provided through trickle vents in the dry rooms, while mechanical extraction takes place in the wet rooms as well as in the bedrooms. The remaining configurations were MVHR where supply air in dry

Fig. 1 – The building layout: left is ground floor, right is upper floor. The location of the PM measuring devices in and near the house are marked in colours.

rooms and return air in wet rooms are both mechanically driven. The difference between the three MVHR configurations was the utilized filter type, i.e.: no filter, a ISO Coarse >90% (≈ G4), and a ISO ePM1 50% (≈ F7) filter. This allowed to assess the impact of the filter on the amount of transported outdoor PM to indoors. The filters were brand new.

The PM levels were measured by means of Renson Senses at five indoor and two outdoor locations near the dwelling which are indicated in Fig. 1. The Sense at garden front was placed near the streetside whereas the one at garden back was positioned further away. In this manner, the impact of combustion particles caused by traffic can be examined as a function of the distance. Both outdoor devices were placed on the ground under a small roof to protect them from rain. The devices present indoors provide insight about the distribution of indoor PM throughout the building. These apparatus were at floor (living), night stand (bedrooms), or desk height (kitchen, bathroom). The use of identical devices allows a relative comparison of the results. The Sense is a connected autonomous device measuring parameters like PM, CO_2, humidity, temperature, VOC, and so on [18]. Concerning PM, the SPS30 optical PM sensor is integrated in the Renson Sense and measures PM1, PM2.5, PM4, and PM10 each minute [19]. From this data, the instantaneous Indoor/Outdoor ratio (IO ratio) of each considered room relative to the outdoor Senses was calculated and afterwards averaged to provide a general impression about the amount of transported outdoor PM into the building [1]. This was analysed for each of the ventilation systems listed in Tab. 1 and the aggregate data was used afterwards to compare the impact of the ventilation system and filter on the amount of transported outdoor PM to indoors.

Tab. 1: Considered ventilation systems, description, and measurement period.

Ventilation system (exhaust flow rate = 300 m^3/h)	Description	Measurement period (DD/MM/YYYY)
MEV	Natural supply in dry rooms, mechanical extraction in wet spaces as well as in bedrooms	28/04/2021 – 12/05/2021
MVHR without filter	Mechanical supply and extraction in dry and wet rooms, respectively	12/05/2021 – 26/05/2021
MWHR with ISO Coarse >90% filter (≈ G4)	Mechanical supply and extraction in dry and wet rooms, respectively	26/05/2021 – 09/06/2021
MVHR with ISO ePM1 50% filter (≈ F7)	Mechanical supply and extraction in dry and wet rooms, respectively	09/06/2021 – 23/06/2021

3. Results and discussion

3.1 Ventilation systems

Fig. 2 depicts the average IO ratio of the four PM fractions for each considered room relative to both outdoor locations (garden back and front) when MEV was the activated ventilation system. The average IO ratios in Fig. 2 lie in the range of about 40% up to 50% indicating that the indoor PM level is about half that of outdoors. Considering that there is no presence or indoor activities like cooking and smoking which can generate significant PM indoors, one concludes that about half of the outdoor PM transported into the building via the ventilation system (and also infiltration via leakages although this is small because of a good airtightness).This observation is in line with the literature where the fraction of outdoor PM contributing to the indoor PM level can be up to 56% according to the results of AIVC's "Ventilation & Health" project [3,4]. The average IO ratios related to the PM measurements at garden front are slightly lower than those referred to the garden back PM measurements. The small difference is due to the fact that the device at garden front was located near the street in contrast to the one at garden back. Consequently, the combustion particles emitted by traffic were more numerous present there, resulting in a larger denominator value for the IO ratio calculation, while the numerator representing the indoor PM level did not change. The average IO ratios of all considered rooms are quite similar except in case of bedroom front which are at least 5% higher. This room is located on the street side where the infiltration of combustion particles due to traffic through the trickle vents is more pronounced than in the other rooms, resulting in a slightly higher indoor PM level and therefore an increased IO ratio. The IO ratios of PM1 towards PM10 show a slight decrease which indicates that large diameter particles are less likely to be transported from outdoors into the building.

Tab. 2 gives an example of the measured PM mass concentrations at one sampling moment, similar observations would be drawn if another sampling moment was selected. Supposing that the PM sensor measures accurately the several PM fractions, the following results were found. A small difference is observed between the PM fractions when measured outdoors, whereas there is no difference among PM2.5 up to PM10 for indoors. Zhao et al [14] observed that the absence of indoor activities leads to almost no additional mass concentration for coarse particles (range 2.5 µm – 10 µm) in the indoor environment of dwellings with a good airtightness, which can explain the observation in Tab. 2. Next to this, the indoor PM concentrations in Tab. 2 are small compared to other studies like Zhao et al. [14] due to no human presence and therefore no activities in the house. Moreover, Tab. 2 demonstrates also that small particle sizes are dominant in both indoor and outdoor environments as expected from literature [7,9].

Tab. 2: Example of measured PM mass concentrations when the MEV system was activated.

	Concentrations of PM fractions [µg/m^3]			
Location	PM1	PM2.5	PM4	PM10
Garden back	7.27	7.73	7.77	7.80
Garden front	6.31	6.77	6.85	6.86
Kitchen	2.98	3.15	3.15	3.15
Living	2.37	2.51	2.52	2.53
Bedroom front	3.72	3.94	3.94	3.94
Bedroom back	3.48	3.55	3.55	3.55
Bathroom	2.71	2.76	2.76	2.76

Fig. 3 displays the average IO ratios when MVHR without a filter was deployed. All the IO ratios are similar, even that of bedroom front indicating that this air supply type realizes an evenly distributed transportation of outdoor PM into the entire building in contrast to the air supply type (trickle vents) of MEV. The central air intake by the MVHR system in contrast to the decentral air intake by the MEV system, could explain this difference. The average IO ratios based on the one hand by the outdoor PM measurements at garden front and those on the other hand at garden back, exhibit an analogous trend as in the case of MEV, therefore the same explanation is valid. The average IO ratios achieved with the MVHR without filter are about 10% higher than those of MEV, with the exception of bedroom front where it is rather unchanged. When considering no indoor PM generating activities like cooking and smoking, one concludes that MVHR without filter leads to slightly higher transport of outdoor PM into the building, as also found by Rojas [9]. Possible reasons are: a higher supply of outdoor PM when mechanically done, higher air turbulence and eventual resuspension due to mechanical instead of natural air supply, as well as the position of the measuring devices in the room may contribute also to the increased indoor PM levels.

Fig. 4 shows the average IO ratios when the MVHR was equipped with an ISO Coarse >90% (≈ G4, coarse) filter in the air supply path before the heat exchanger. This filter type is typically used in MVHR to protect the heat exchanger from fouling [10]. The average IO ratios except that of bedroom front drop about 5-6% when compared to those of MVHR without filter, thus less outdoor PM transports into the building because of the presence of the coarse filter. The average IO ratios are about 3-4% higher with respect to MEV, so MVHR equipped with a coarse filter does not outperform MEV, which agrees with the simulation study in literature [9]. The average IO ratios determined by the PM

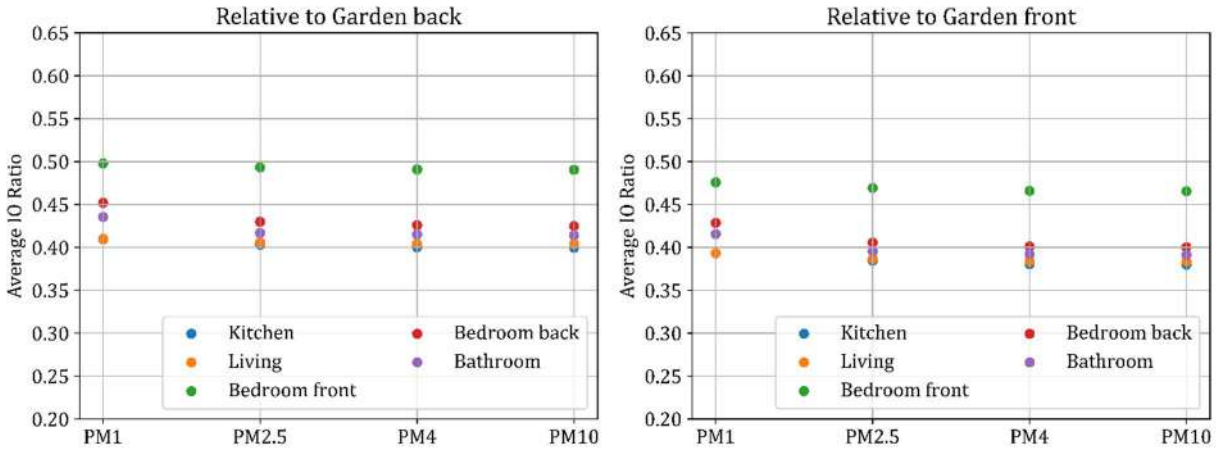

Fig. 2 – Average IO ratios of the PM fractions: PM1, PM2.5, PM4, and PM10 in the considered rooms of the building when MEV was activated (left: relative to garden back sensor; right: relative to garden front sensor).

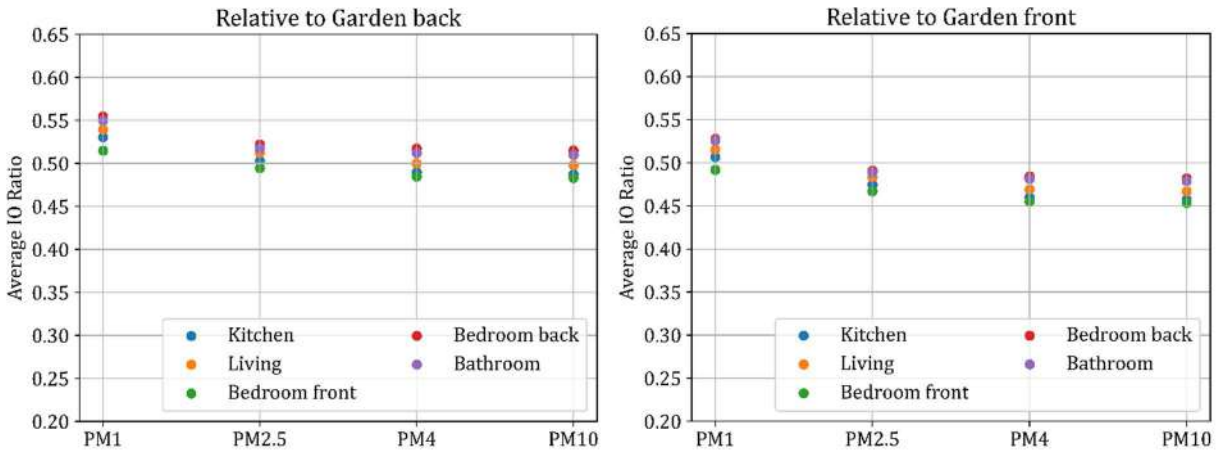

Fig. 3 – Average IO ratios of the PM fractions: PM1, PM2.5, PM4, and PM10 in the considered rooms of the building when MVHR without filter was activated (left: relative to garden back sensor; right: relative to garden front sensor).

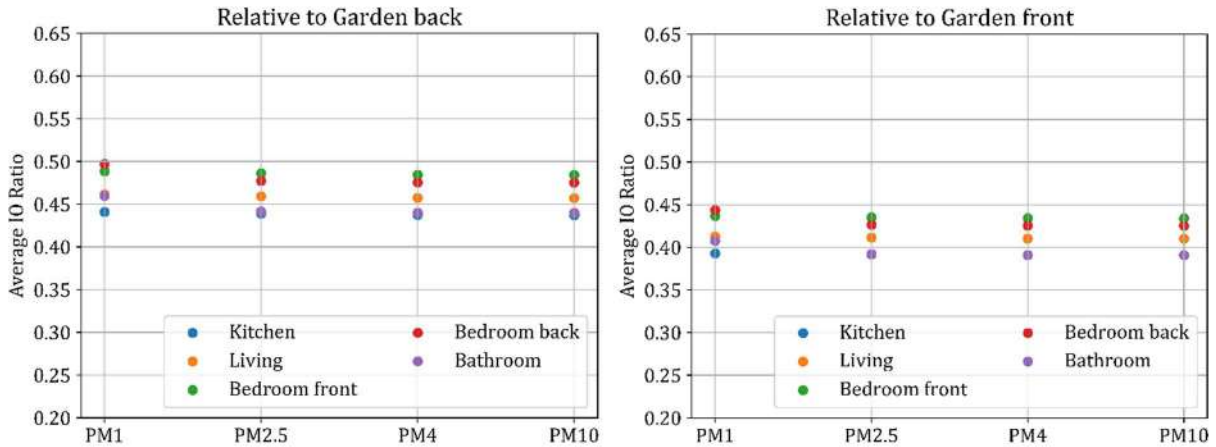

Fig. 4 – Average IO ratios of the PM fractions: PM1, PM2.5, PM4, and PM10 in the considered rooms of the building when MVHR with ISO Coarse > 90% (≈ G4) filter was activated (left: relative to garden back sensor; right: relative to garden front sensor).

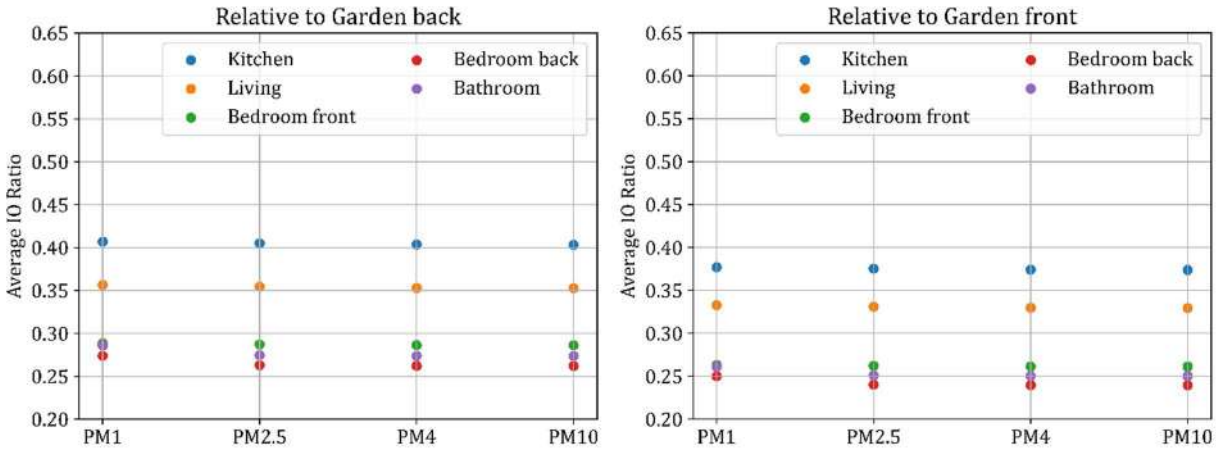

Fig. 5 – Average IO ratios of the PM fractions: PM1, PM2.5, PM4, and PM10 in the considered rooms of the building when MVHR with ISO ePM1 50% (≈ F7) filter was activated (left: relative to garden back sensor; right: relative to garden front sensor).

measurements of either garden front or back demonstrate comparable trends as in the cases of MVHR without filter and MEV, thus the same explanation applies again. A slightly wider spread of the average IO ratios is observed between the rooms which can be due to the weather conditions, temporary occupancy in the house, and so on. Yet, the values lie within the range of IO ratios in literature.

Fig. 5 presents the average IO ratios when the coarse filter was upgraded to an ISO ePM1 50% (≈ F7, fine) filter. The impact of this filter type on the average IO ratios is apparent for the rooms: bedroom front, bedroom back, and bathroom; while the effect is less pronounced for the living room and kitchen. This can be due to the location of the measuring devices in both the kitchen and living room, while temporary occupancies of the ground floor of the dwelling may contribute to a momentary elevated indoor PM level in those spaces. In general, more differences in IO ratio between the rooms are observed with higher filter efficiencies in case of a central MVHR system. Compared to MVHR without filter, the application of an ISO ePM1 50% filter reduces the average IO ratio from about 50% up to about 25-40%, thus the relative reduction in IO ratio is 20-50%. Similar results were obtained in the field study of the classroom (with minimal indoor PM sources) located near the highway where the MVHR was equipped once with and once without a F8 filter (≈ ISO ePM1 65%). The relative reduction in the IO ratio during teaching hours was 30% and 34% for PM2.5 and PM10, respectively. During non-teaching hours, the relative reduction in IO ratio was 42% for PM2.5 and 48% for PM10 [11]. Analogous to the conclusions made in literature, Figs. 4 and 5 point out that IO ratios improve from about 45% to 25-40% when applying a fine instead of coarse filter. Thus, the relative reduction in IO ratio is about 11-44%. The same finding is made when the average IO ratios of Fig. 5 are compared to those of Fig. 2 representing the MEV case. Also the simulation study by Rojas [9] pointed out that MVHR with F7 filter (≈ ISO ePM1 50%) achieves roughly a higher 50% reduction of exposure to outdoor PM2.5 relative to the case of MEV. Concerning the amount of transported outdoor PM to indoors, the results of Fig. 5 (neglecting kitchen) indicate a value up to about 30% when considering the absence of indoor PM generating activities like cooking or smoking. This value is in line with the in literature reported 67% reduction of indoor exposure to transported outdoor PM to indoors [10].

3.2 Room level filter efficiencies

The room level efficiency of the filters utilized in the MVHR are assessed at PM2.5 by calculating the percentual relative difference between the obtained IO ratios relative to those of MVHR without a filter, a method already reported in literature [11]. The measured IO ratios at PM2.5 for the considered MVHR configurations are given in Tab. 3, while the calculated room level filter efficiencies are listed in Tab. 4. According to the filter specifications, the PM2.5 filtration efficiency of the ISO Coarse >90% (≈ G4, coarse) filter is unspecified, whereas that of the ISO ePM1 50% filter (≈ F7, fine) ranges from 65-80% [20]. The room level filter efficiencies vary between the rooms due to small differences among the PM2.5 average IO ratios (see Tab. 3). The impact of the fine filter is clearly demonstrated, yet its room level filtration efficiency is lower than the specified in-lab values of 65-80%. On average, the room level filter efficiency is roughly about half, i.e., 30-50%, for outdoor-originated particles. Simulations performed by Rojas [9] showed a slightly improved reduction of the exposure to outdoor originated PM2.5 of about 55% when using a F7 filter. A similar observation is drawn from the classroom field study with limited indoor PM sources and a F8 filter on the air supply, where a 30% indoor PM2.5 reduction was observed compared to the filter efficiency of >80% [11,20]. The deviation between the room level and specified filter efficiency results from the change in testing of the filter performance. The room level filter efficiency was obtained for a practical scenario with natural outdoor particles, actual housing, ventilation

system, and ductwork while the measuring devices were located at room level. The specified filter efficiency is evaluated in a laboratory environment with artificial PM where measuring probes are applied just before and after the filter to accurately quantify its performance [21]. Consequently, the observations suggest that the fine filter efficiency measured in-situ is roughly 30-50% of the specified lab value. Suppose that the indoor PM level consists of 50% indoor generated PM [3,4] and 50% transported outdoor PM, then the overall estimated fine filter efficiency on room level based on the indoor PM level is reduced once again by 50% resulting in an indoor PM fine filter efficiency of around 15-25% of the in-lab determined efficiency. A reduction of about 35% was estimated by Rojas [9] probably due to a lower supposed fraction of indoor generated PM.

Tab. 3: PM2.5 average IO ratios relative to the PM measurements at garden back for the considered MVHR configurations.

	PM2.5: average IO ratio relative to PM measurements at garden back		
Location	MVHR without filter	MVHR with ISO Coarse >90% filter	MVHR with ISO ePM1 50% filter
Bedroom front	0.49	0.48	0.29
Bedroom back	0.52	0.47	0.26
Living	0.51	0.46	0.35

Tab. 4: Room level filter efficiencies for PM2.5 of the MVHR systems equipped with either the ISO coarse >90% or ISO ePM1 50% filter.

	Room level filter efficiency [%] at PM2.5 (relative to MVHR without filter)	
Location	ISO Coarse >90%	ISO ePM1 50%
Bedroom front	2.04	40.82
Bedroom back	9.62	50.00
Living	9.80	31.37

4. Conclusions

For each indoor measurement location, no significant difference occurred between the indoor PM fractions at that location (≤1 µm up to ≤10 µm) which is probably due to the absence of indoor PM sources. The average IO ratios demonstrated that the indoor PM level in all rooms is clearly lower than outdoors, which is consistent with values reported in literature for unoccupied conditions. MVHR without a filter exhibited the worst IO ratio ranging between 50-55%. A slight reduction was obtained when equipping MVHR with an ISO Coarse >90% filter (≈ G4, coarse) where the IO ratio varied between 45-50%. Note that this MVHR configuration is commonly deployed and the single purpose of the filter is to protect the heat exchanger from fouling. A slightly better performance was achieved with MEV, although the position of the air inlet with respect to outdoor PM sources like traffic turned out to be important. The IO ratio was between 40-45% over all rooms, except for the room located near the street side where the value was about 50%. MVHR equipped with an ISO ePM1 50% filter (≈ F7, fine) realized the lowest IO ratio of about 27% on average. Compared to MVHR without filter, the fine filter achieved on average an indoor PM2.5 filtration efficiency on room level in the range of 30-50% which is approximately half of the in laboratory specified filter efficiency. Moreover, when indoor activities are present and assuming that a 50/50 contribution on the total indoor PM level exists between indoor generated PM and transported outdoor PM, then the actual filter efficiency on room level is further halved, leading to an achieved fine filter efficiency on room level of about 15-25% of the in laboratory determined efficiency. A continuation of this research could be the examination of the impact on the I/O PM ratio when the location of the indoor measuring devices is different compared with the locations adopted in this paper.

5. References

[1] Klepeis NE, Nelson WC, Ott WR, Robinson JP, Tsang AM, Switzer P, et al. The National Human activity Pattern Survey (NHAPS): a resource for assessing exposure to environmental pollutants. Journal of exposure science & environmental epidemiology [Internet]. 2001 [cited 2022 Mar 2]; 11(2001):231-252. Available from: https://www.nature.com/articles/7500165.pdf

[2] REHVA. REHVA COVID19 Guidance. Guidance no.: 4.1. [Internet]. Elsene (BE) :REHVA; 2021 Apr 15 [cited 2021 Oct 28]. Available from: https://www.rehva.eu/fileadmin/user_upload/REHVA_COVID-19_guidance_document_V4.1_15042021.pdf

[3] Coggins M, Jones S. Ventilation Information Paper n° 43: Residential ventilation and health. [Internet]. Sint-Stevens-Woluwe: INIVE EEIG; 2021 Jul. Available from: https://www.aivc.org/sites/default/files/VIP43.pdf

[4] Borsboom W, De Gids W, Logue J, Sherman M, Wargocki P. Technical note AIVC 68 residential ventilation and health. [Internet] Sint-Stevens-Woluwe: INIVE EEIG; 2016 Feb. Available from: https://www.aivc.org/sites/default/files/TN68_Heath&Ventilation.pdf

[5] Liu S, Song R, Zhang T. Residential building ventilation in situations with outdoor PM2.5 pollution. Building and Environment [Internet]. 2021 June 9 [cited 2021 Oct 28];202(September 2021):1-14. Available from:

https://www.sciencedirect.com/science/article/abs/pii/S036013232100442X
doi:10.1016/j.buildenv.2021.108040

[6] Jacobs P, Hoes ECM, Vijlbrief O, Kornaat W. Openbaar eindrapport TKI Be Aware Bewustwording van binnenluchtkwaliteit in woningen: bronnen en effectieve energie-efficiënte interventie strategieën. [Internet]. Delft (NL) :TNO; 2020 Apr 20 [cited 2021 Oct 28]. Available from: https://www.bouwwereld.nl/wp-content/uploads/2020/10/TNO-2020-R10627.pdf

[7] Van Herreweghe J, Caillou S, Haerinck T, Van Dessel J. Out2In: impact of filtration and air purification on the penetration of outdoor air pollutants into the indoor environment by ventilation. Paper presented at: 40th AIVC Conference; 2019 Oct 15-16; Ghent, Belgium.

[8] Van Herreweghe J, Caillou S, Haerinck T, Van Dessel J. Real-life ventilation filter performance in a city environment. REHVA Journal. 2020 Apr;57(2):4-7

[9] Rojas G. Ambient air filter efficiency in airtight, highly energy efficient dwellings – A simulation study to evaluate benefits and associated energy costs. Paper presented at: 40th AIVC Conference; 2019 Oct 15-16; Ghent, Belgium.

[10] Rojas G. Particle filtration in energy efficient housing with MVHR. REHVA Journal. 2020 Apr;57(2):8-11

[11] van der Zee SC, Strak M, Dijkema MBA, Brunekreef B, Janssen NAH. The impact of particle filtration on indoor air quality in a classroom near a highway. Indoor Air [Internet]. 2016 May 4 [cited 2021 Oct 28];27(2):291-302. Available from: https://onlinelibrary.wiley.com/doi/full/10.1111/ina.12308. doi:10.1111/ina.12308

[12] Jones ER, Laurent JGC, Young AS, MacNaughton P, Coull BA, Spengler JD, Allen JG. The effect of ventilation and filtration on indoor PM2.5 in office buildings in four countries. Building and Environment [Internet]. 2021 May 19 [cited 2021 Oct 28];200(August 2021):1-11. Available from: https://www.sciencedirect.com/science/article/pii/S0360132321003796.
doi:10.1016/j.buildenv.2021.107975

[13] Park JS, Jee NY, Jeong JW. Effects of types of ventilation systems on indoor particle concentrations in residential buildings. Indoor Air [Internet]. 2014 Apr 17 [cited 2021 Oct 28];24(6):629-638. Available from: https://onlinelibrary.wiley.com/doi/10.1111/ina.12117. doi:10.1111/ina.12117

[14] Zhao J, Birmili W, Wehner B, Daniels A, Weinhold K, Wang L, et al. Particle Mass Concentrations and Number Size Distributions in 40 Homes in Germany: Indoor-to-outdoor Relationships, Diurnal and Seasonal Variation. Aerosol and Air Quality Research [Internet]. 2020 Mar [cited 2021 Oct 28];20(3):576-589. Available from: https://helda.helsinki.fi/handle/10138/325011.
doi:10.4209/aaqr.2019.09.0444

[15] Wallis SL, Hernandez G, Poyner D, Birchmore R, Berry T. Particulate matter in residential buildings in New Zealand: Part I. Variability of particle transport into unoccupied spaces with mechanical ventilation. Atmospheric Environment [Internet]. 2019 Mar 11 [cited 2021 Oct 28]; X(2):1-9. Available from: https://www.sciencedirect.com/science/article/pii/S2590162119300292.
doi:10.1016/j.aeaoa.2019.100026

[16] Renson, Healthbox 3.0 [Internet]. Waregem (BE): Renson; 2021 Sep 27 [cited 2021 Oct 28]. Available from: https://cdn.renson.eu/Public_Publications/6855/Healthbox-3-0?encoding=UTF-8

[17] Renson, Endura Delta [Internet]. Waregem (BE): Renson; 2019 Sep 9 [cited 2021 Oct 28]. Available from: https://cdn.renson.eu/Public_Publications/5710/?encoding=UTF-8

[18] Renson, Sense [Internet]. Waregem (BE): Renson; 2021 [cited 2021 Oct 28]. Available from: https://www.renson.eu/gd-gb/producten-zoeken/ventilatie/mechanische-ventilatie/units/sense

[19] SPS30 Optical PM Sensor [Internet]. Switzerland: Sensirion AG; 2021 [cited 2021 Oct 28]. Available from: https://sensirion.com/products/catalog/SPS30/

[20] Trane Belgium, From EN779 to ISO 16890 Norm [Internet]. Oudergem (BE): Trane Belgium; 2016 Feb 12 [cited 2021 Oct 28]. Available from: https://www.tranebelgium.com/files/product-doc/364/fr/Norme-ISO-16890.pdf

[21] ISO 16890: Air Filters for General Ventilation. Geneva (Switzerland): ISO; 2016.

Data Statement

The datasets generated during and/or analysed during the current study are/will be available upon reasonable request from the corresponding author.

Using HAIEQ methodology for holistic analysis of IEQ in modern family houses

Zuzana Veverkova [a], Karel Kabele [b], Pavla Dvorakova [c]

[a] Faculty of Civil Engineering, Czech Technical University in Prague, Czech Republic, zuzana.veverkova@fsv.cvut.cz.

[b] Faculty of Civil Engineering, Czech Technical University in Prague, Czech Republic, kabele@fsv.cvut.cz.

[c] Faculty of Civil Engineering, Czech Technical University in Prague, Czech Republic, pavla.dvorakova@fsv.cvut.cz.

Abstract. The indoor environment of buildings consists of a set of physical, chemical, and social reactions between users and the building, including phenomena that affect the technical, natural, and medical sciences. To describe and quantify the parameters of the indoor environment of buildings, we commonly use a simplified model, describing and evaluating the individual components of the environment separately - thermal comfort, air quality, acoustics, lighting, electromagnetic and other fields that co-create the final state of the environment. Presented methodology is based on a holistic approach to the integration of information about the building-technical design and interior, heating, cooling, ventilation, lighting, acoustics and electromagnetic, ionic, -static fields, and ionizing radiation, information about the real operation of the evaluated building, based on data from measurements, mathematical model, and questionnaire survey. The output is a set of information expressing whether the object under assessment, in terms of each criterion, is solved at the level of the current state of knowledge or has the potential to improve the quality of the indoor environment, or whether there are significant deficiencies in terms of the quality of the indoor environment. The methodology is applied here to the assessment of two similar modern family houses. The output shows not only the evaluation of IEQ in both houses, but also the potential to improve IEQ in these houses with identification of causes of the potential problems and ways of possible solutions. The case study points out, among other things, interesting differences in the perception of the indoor environment by individual occupants and shows user behaviour in connection with ensuring the indoor environment of their homes.

Keywords. Indoor Environmental Quality (IEQ), Holistic IEQ Assessment, IEQ Assessment Method, etc.
DOI: https://doi.org/10.34641/clima.2022.384

1. Introduction

Current design, implementation, and operation of buildings based on energy savings have an impact on the quality of the indoor environment. The primary emphasis on energy savings leads to such a building design where energy savings in most cases minimize the natural interaction of the indoor and outdoor environment. Many building functions that previously took place without human intervention are eliminated in modern low-energy buildings and replaced by technical systems with high energy efficiency but negative impact on the quality of the indoor environment. (1). Examples are systems to ensure thermal comfort. The mass and shape proportions of the building, optimized by millennia of development, are being replaced in today's modern fully glazed buildings by the installation of cooling and heating equipment. Natural air exchange by window infiltration is replaced by controlled ventilation in buildings with a perfectly sealed envelope. Daylight is replaced by artificial lighting in extended rooms.

There are sophisticated and well-established tools and methods for the determination and assessment of energy performance (energy performance certification, building certification, etc.). Quantification of IEQ is more difficult, and tools and methods are being developed only.

2. HAIEQ (Holistic Assessment of Indoor Environment Quality) assessment methodology

The aim of this methodology is to create a complex holistic view of the assessed object in terms of all

Copyright ©2022 by the authors. This conference paper is published under a CC-BY-4.0 license.

factors of the indoor environment.

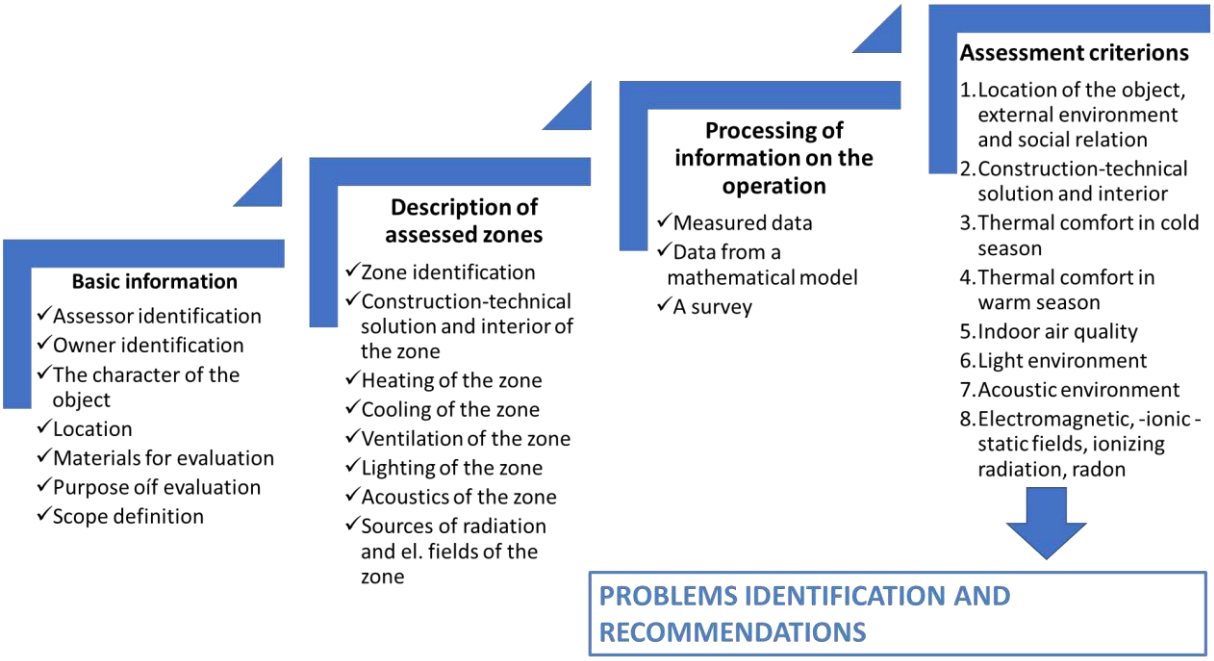

Fig. 1 HAIEQ assessment methodologv.

The HAIEQ methodology is based on a holistic approach to the integration of information about the building-technical design and interior, heating, cooling, ventilation, lighting, acoustics and electromagnetic, -ionic, -static fields and ionizing radiation, information about the real operation of the assessed building, based on data from measurements, mathematical model, and questionnaire survey [2]. The output is a set of information expressing whether the object under assessment, in terms of each criterion, is solved at the level of the current state of knowledge or has the potential to improve the quality of the indoor environment, or whether there are significant deficiencies in terms of the quality of the indoor environment. The advantage of the methodology is the assessed method, which is intended not only to classify IEQ in buildings, but primarily to indicate bottlenecks. In addition, a holistic approach helps to identify the causes of the problems and to better find ways to possible remedies. The information obtained can also be used to evaluate the SRI (Smart Readiness Indicator [3]).

The HAIEQ methodology [2] contains four basic parts, which are described in **Fig. 1.** The fourth final part contains an assessment of the state described above of the building solution in terms of the eight criteria, **Tab. 1**. Each of the eight criteria contains 3-10 subcriteria, each of which is scored with grade 1 to 3 or N (not evaluated). The grades are awarded based on the subjective assessment of the assessor, who has information about the object, measured data, and, if possible, the result of a questionnaire survey. The evaluation expresses the state of the assessed criterion. If there are not enough data for the assessment of the given criterion or if its assessment is not relevant for the given object, it is evaluated as '0'. If there are sufficient data to assess the criterion and the analysis of the criterion, considering user feedback, does not provide any recommendations to improve the current situation, it is evaluated as '1'. If the assessor suggests a measure that leads to an improvement in the indoor environment, he evaluates the criterion '2' or '3'. A rating of '3' indicates a serious problem in a given criterion that must be addressed immediately (eg, violation of binding regulations, emergency state, malfunction, or malfunctioning equipment). A rating of '2' indicates a condition that is acceptable but can be improved, and it is desirable to do so. The proposed measure must be feasible for the given object and substantiated by justification (e.g., technical-economic analysis, expression of the benefit of the given measure, etc.).

Tab. 1 Criteria for assessment

LS	Locality and place of the object in terms of the external environment and social relations
STI	Building structures and technical solution and interior of the evaluated zone (STI)
TCW	Thermal comfort in the cold season
TCS	Thermal comfort in the warm season
IAQ	Indoor air quality
LC	Light comfort
AC	Acoustical comfort
EC	Electro-magnetic, -ionic, - static fields, ionizing radiation

3. Case study

IEQ assessment using the HAIEQ methodology is

based on the assessment of data describing architectural and construction design, the design of technical systems and the operation. The evaluated buildings are two similar family houses built in 2019-2020. These are single-storey brick houses with hipped roofs with five living rooms, inhabited by two adults and two children. All windows have outdoor blinds. One of these houses (FM1) is equipped with a controlled ventilation system with heat recovery and climatization, windows are not used for ventilation. The main heating system is electric underfloor heating foils controlled by room controllers with a thermostat, located on the walls of the rooms, and with the possibility of communication with the central AHU unit. Thermostats are not used by the user; the required temperature of 22.5 ° C is set in all rooms for heating. The sources used for artificial interior lighting are LEDs with the possibility of adjusting the light intensity at the discretion of the users. The other house (FM2) has a natural ventilation system combined with negative pressure ventilation of the kitchen and the sanitary facilities, and main heating system is underfloor hot water heating with the possibility of control by room thermostats located on the walls of the rooms. The heat source is an electric boiler with equithermal regulation. The sources used for artificial interior lighting are LEDs with the possibility of adjusting the intensity and colour of light at the discretion of users.

The assessment of both buildings was based on project documentation, detailed local investigation, measurements of the state health institute immediately after the construction of the houses, own measurements and questionnaire survey. The case study of selected zones of two family houses shows the use of the methodology not only for the evaluation of IEQ, but also for the diagnostic and identification of problems related to indoor environment quality in buildings with low energy consumption, [4].

3.1 Measurement

An important source of information is the measurement of selected IEQ parameters. The monitoring process started with one-off indicative measurements of selected parameters (VOC, CO2, formaldehyde, negative ions, measurements of illuminance, electromagnetic fields) to get an overall picture of the state of the environment. The installation of long-term online monitoring of air temperature, relative humidity, CO_2 concentration, sound, and barometric pressure levels followed. Several sensors have been placed in characteristic locations of selected zones of the building (mainly habitable rooms and bathrooms). Data were evaluated using the VISIEQ method developed within the 'CTU Methodology' [2], **Fig. 2**. This allows an integrated view of measured data and allows time identification of problem situations.

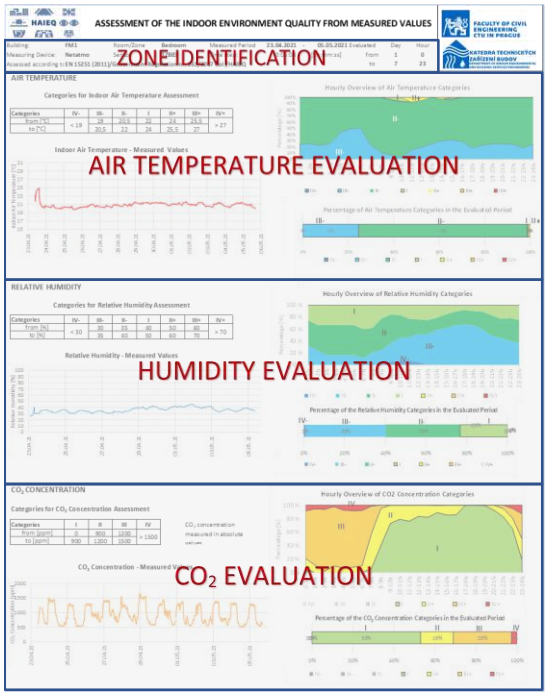

Fig. 2 Evaluation concept of measured values in the VISIEQ format.

3.2 Questionnaire

To determine how users subjectively perceive the environment, a questionnaire focused on individual components of the indoor environment and their perception by users was elaborated.

All the data obtained formed a picture of the object, which was assessed and evaluated in the next step.

3.3 Assessment

Based on all data (local survey, available documentation, monitoring of selected parameters of the indoor environment, questionnaire), an IEQ assessment of both family houses was prepared according to the HAIEQ methodology in eight criteria. The evaluation result is quantified by the grades according to **Tab. 2**.

Tab. 2 Table of grades for criteria evaluation.

Grade	Meaning
N	Not evaluated - e.g. lack of data, not relevant for the zone, other reasons (the reason must be stated)
1	No comments – without a draft measure, optimal condition, suitable solution
2	Proposed measure - Comments, shortcomings
3	Serious deficiency - failure to comply with legislation, emergency state, equipment malfunction, and, in the case of comments and serious deficiencies, their specification for comment.

The principle of the HAIEQ methodology, based on a rating of N / 1 / 2 / 3 of a total of 48 subcriteria grouped into eight areas, provides a holistic view of indoor environmental quality. The following tables (**Tab. 3** to **Tab. 10**) summarise the results of the evaluation of each criterion and comment on the criteria rated 2 or 3 for both houses; first house is marked 'FM1', the second 'FM2'.

Evaluation of the first criterion Locality and place of the object in terms of the external environment and social relations ´LS´ is in the **Tab. 3**, where LS2 for FM2 is rated as '2' based on an open windy landscape.

The second criterion Building structures and technical solution and interior of the evaluated zone 'STI' is in the **Tab. 4**. STI4 for FM1 is rated as '2' based on low daylight when the blinds are lowered (not closed). STI5 for FM1 is rated grade '2' due to automatic control of all blinds at once. STI3 for FM2 - is rated as '2'; it is a new building with new materials and furniture and measurements revealed traces of formaldehyde which, although not exceeding the permissible limits, can be removed. STI4 for FM2 is rated as '2'; there are poor light conditions during a day due to lowered blinds, curtains, and smaller windows. STI5 for FM2 is rated grade ´2"; there is an application available for electrically powered blinds installed in the building that are not used.

Tab. 3 Evaluation of the locality and the location of an object in terms of the external environment and social relations (LS).

Criterion		FM1	FM2
LS1	Air quality (pollution)	1	1
LS2	Wind region	1	2
LS3	Noise from the surroundings	1	1
LS4	Orientation to cardinal points	1	1
LS5	Influence of heat island	1	1
LS6	Psychic perception of surroundings, interpersonal relationships	1	1
LS7	Risk of energy poverty	1	1
LS	**Average of non-zero values LS1 to LS7**	**1,000**	**1,143**

Tab. 4 Evaluation of building structures and technical solution and interior of the evaluated zone (STI).

Criterion		FM1	FM2
STI1	Use of hazardous materials in building structures (asbestos, etc.)	1	1
STI2	Risk of water vapor condensation on structures (thermal bridges)	1	1
STI3	Use of hazardous materials for equipment (formaldehyde, etc.)	1	2
STI4	Use of daylight	2	2
STI5	Active shielding and its control	2	2
STI6	Greenery in the interior	1	1
STI7	Visible defects and disorders (mold, leakage, cracks, poor surfaces, etc.)	1	1
STI8	Color space solution	1	1
STI9	Layout solution, occupancy of the zone	1	1
STI10	Maintenance	1	1
ST	**Average of non-zero values STI1 to STI10**	**1,200**	**1,300**

Tab. 5 Evaluation of thermal comfort (TC) in the cold season (TCW).

Criterion		FM1	FM2
TCW1	Choice and operation of the heating system	2	1
TCW2	The ability of the heating system to adapt its operating mode in response to the users' needs with due regard to user-friendliness, maintaining a healthy indoor environment – e.g. individual temperature control, user feedback – subjective environmental quality assessment	2	2
TCW3	The ability of the heating system to report energy usage to the user	2	2
TCW4	The ability of the heating system to report the quality of the indoor environment in terms of thermal comfort in cold to the user	1	2
TCW5	Summary of TC assessment results for the cold season from the measurement/simulation (e.g. risk of overheating of the zone in cold due to heat gains, underheating, etc.)	2	N
TCW6	Summary of TC assessment results for the cold season from the questionnaire survey (if performed)	1	1
TCW	**Average of non-zero values TCW1 to TCW6**	**1,667**	**1,600**

The third criterion Evaluation of thermal comfort in the cold season ´TCW" is in **Tab. 5**. TCW1 for FM1 is rated grade ´2´– Choice and operation of the heating system are comfortable, but it has a high energy consumption, which can have a secondary impact on the quality of the environment. TCW2 for FM1 is rated grade ´2´ - the heating system allows the function, but the user does not take full advantage of the control options; temperature is set to a fixed value of 22.5 ° C. TCW3 for FM1 is rated grade ´2´ – the secondary electricity meter is not installed. TCW5 for FM1 is rated grade ´2´ - there is low relative humidity in the building. TCW2 for FM2 is rated grade ´2´ – Heat source - The electric hot water boiler is a common source for heating and hot water and its output is incorrectly controlled based on heating demand only. To ensure sufficient hot water, the heating system must be set so that the boiler is not switched off when the required room temperature is reached. The user has solved this by setting the room thermostats in each room to 26°C, thus de facto taking them out of operation in winter. The installed underfloor heating never reaches this temperature when operating with equithermal control, so the heat source is not switched off. TCW3 for FM2 is rated grade ´2´ – the secondary electricity meter is not installed. TCW4 for FM2 is rated grade ´2´ – only the air temperature report is available. TCW5 for FM2 is not rated (´N´) due to the lack of data for the evaluation of TC in the cold season.

The fourth criterion Evaluation of thermal comfort in the warm season ´TCS´ is in **Tab. 6**. TCS3 for FM1 is rated grade ´2´ – the control system is sophisticated, but the information is not used by users. TCS2 for FM2 is rated grade ´2´- adapting ability is not available. TCS3 for FM2 is not rated (´N´) only shielding elements are used in the building; there is no cooling system. TCS4 for FM2 is rated grade ´2´ – only the air temperature report is available. TCS5 for FM2 is not rated (´N´) due to the lack of data to evaluate TC in the warm season.

Tab. 6 Evalation of thermal comfort (TC) in the warm season (TCS).

Criterion		FM1	FM2
TCS1	Choice of the cooling system	1	1
TCS2	The ability of the cooling system to adapt its operating mode in response to the users' needs with due regard to user-friendliness, maintaining a healthy indoor environment – e.g. individual temperature control, user feedback – subjective environmental quality assessment	1	2
TCS3	The ability of the cooling system to report energy usage to the user	2	N
TCS4	The ability of the cooling system to report the quality of the indoor environment in terms of thermal comfort in warm season to the user	1	2
TCS5	Summary of TC assessment results for the warm season from measurement/simulation (e.g. risk of overheating of the zone in cold due to heat gains, under-heating, etc.) (if performed)	N	N
TCS6	Summary of TC assessment results for the warm season from the questionnaire survey (if performed)	1	1
TCS	**Average of non-zero values TCS1 to TCS6**	**1,278**	**1,500**

Tab. 7 Evaluation of indoor air quality (IAQ).

Criterion		FM1	FM2
IAQ1	Choice of the ventilation system	2	3
IAQ2	The ability of the ventilation system to adapt its operating mode in response to the users' needs with due regard to user-friendliness, maintaining a healthy indoor environment – e.g. user feedback – subjective environmental quality assessment	2	1
IAQ3	The ability of the ventilation system to report energy use to the user	2	2
IAQ4	The ability of the ventilation system to report the quality of the indoor environment in terms of indoor air quality	1	2
IAQ5	Summary of IAQ assessment results from measurement/simulation (if performed)	2	2
IAQ6	Summary of IAQ results from the questionnaire survey (if performed)	1	1
IAQ	**Average of non-zero values IAQ1 to IAQ6**	**1,667**	**1,833**

The fifth criterion Evaluation of indoor air quality ´IAQ´ is in Tab. 7. IAQ1 for FM1 is rated grade ´2" – the entire building is ventilated as one zone regardless of the stay of the persons. IAQ2 for FM1 is rated grade ´2´ – the system is able to adapt, but requires the intervention of the user, who uses this option only to reduce air flow in the building at night, which is an unsuitable solution for sleeping rooms. IAQ3 for FM1 is rated grade ´2´ – the system cannot do this. IAQ5 for FM1 is rated grade ´2´ – high concentrations of CO2 in the bedroom were measured at night.

IAQ1 for FM2 is rated grade ´3´ – natural ventilation is conditioned by high user cooperation and without IAQ indication it cannot ensure air quality. IAQ3 for FM2 is rated grade ´2´ – there is no information on heat consumption for heating the ventilation air. IAQ4 for FM2 is rated grade ´2´ - information not available. IAQ5 for FM2 is rated grade ´2´ – high concentrations of CO2 were measured in the bedroom at night and higher but below the limit values of the formaldehyde concentration were measured during the control measurement.

The sixth criterion Evaluation of light comfort ´LC´ is in Tab. 8. LC3 and LC4 for FM1 is rated grade ´2´ – the system cannot do this. LC5 for FM1 is rated grade ´2´ – low daylight when the blinds are lowered (not closed). LC3 and LC4 for FM2 is rated grade ´2´ – the system cannot do this. LC5 for FM2 is rated grade ´2´ – bad light conditions during a day due to lowered blinds, curtains and smaller windows.

Tab. 8 Evaluation of light comfort (LC)

Criterion		FM1	FM2
LC1	Choice of the lighting system	1	1
LC2	The ability of the lighting system to adapt its operating mode in response to the users' needs with due regard to user-friendliness, maintaining a healthy indoor environment – e.g. regulation of intensity and spectrum of light sources in the workplace, user feedback – subjective environmental quality assessment	1	1
LC3	The ability of the lighting system to report energy usage to the user	2	2
LC4	The ability of the lighting system to report the quality of the indoor environment in terms of light comfort	2	2
LC5	Summary of light comfort assessment results from measurement/simulation (if performed)	2	2
LC6	Summary of light comfort assessment results from the questionnaire survey (if performed)	1	1
LC	Average of non-zero values LC1 to LC6	**1,500**	**1,500**

Tab. 9 Evaluation of acoustic comfort (AC).

Criterion		FM1	FM2
AC1	Sources of noise and measures to eliminate them	2	1
AC2	The ability of the system to report the quality of the indoor environment in terms of acoustic comfort	2	2
AC3	Summary of acoustic comfort assessment results from measurement/simulation (if performed)	2	1
AC4	Summary of acoustic comfort assessment results from the questionnaire survey (if performed)	2	1
AC	**Average of non-zero values AC1 to AC4**	**2,000**	**1,250**

Tab. 10 Evaluation of electro-magnetic, -ionic,- static fields, ionizing radiation (EC).

Criterion		FM1	FM2
EC1	Sources of Electro-magnetic, -ionic,- static fields, ionizing radiation and measures to eliminate their negative effects	1	1
EC2	Summary of assessment results from measurement/simulation (if performed)	2	1
EC3	Summary of assessment results from the questionnaire survey (if performed)	1	1
EC	**Average of non-zero values EC1 to EC3**	**1,333**	**1,000**

Zone:			FM1		FM2	
Evaluation criteria			Evaluation	Potential for improvement	Evaluation	Potential for improvement
	LS	Locality and place of the object in terms of the external environment and social	1,000	0%	1,143	7%
	STI	Building - construction and technical solution and interior of the evaluated	1,200	10%	1,300	15%
	TCW	Thermal comfort for the cold period	1,667	33%	1,600	30%
	TCS	Thermal comfort for the warm period	1,278	14%	1,500	25%
	IAQ	Indoor air quality	1,667	33%	1,833 !	42%
	LC	Light comfort	1,500	25%	1,500	25%
	AC	Acoustic comfort	2,000	50%	1,250	13%
	EC	Electro-magnetic, -ionic,- static fields, ionizing radiation	1,333	17%	1,000	0%

Fig. 3 Summary evaluation and potential for improvement

The seventh criterion Evaluation of acoustic comfort ´AC´ is in Tab. 9. AC1 for FM1 is rated grade ´2´ – the source of noise is the air handling unit. There is a spread of noise through the open space of the house layout (unrealized door between the living area and the hallway) and the openings under the door. AC2 for FM1 is rated grade ´2´ – the system cannot do this. AC3 for FM1 is rated grade ´2´ – the measurement shows the probability that the air handling unit in the technical room affects the sound pressure level of the surrounding rooms. These values may be higher after increasing the ventilation intensity to ensure comfort at night. AC4 for FM1 is rated grade ´2´ – users are bothered by noise from the technical room. AC2 for FM2 is rated grade ´2´ – the system cannot do this.

The eighth criterion Evaluation of electro-magnetic, -ionic,- static fields, ionizing radiation ´EC´ is in Tab. 10. EC2 for FM1 is rated grade ´2´ – in the interior of the bedroom, the values of negative ions are lower than the recommended optimum and sometimes lower than the recommended minimum.

3.4 Results

An overview of partial evaluations of individual criteria is given in **Fig. 3** for both evaluated objects. The evaluation of the criterion can take values from 1, which expresses the state without comments, to a value of 3, which points out a serious problem of the entire evaluated criterion. The occurrence of the classification ´3´ (marked ´!´) in the criterion indicates that there is a serious problem in one or more parameters of the criterion.

Based on the evaluation, the potential for improving the indoor environmental quality is determined, expressed as a percentage from 0% to 100%.

Overall, family house FM1 does not show any serious problems and all criteria are classified as level 1 or 2. The greatest potential for improvement is in the field of acoustics (AC), where the air conditioning unit is a source of noise. This is noise that does not exceed hygienic limits, however, it is perceived by the user as annoying and indirectly affects the air quality (IAQ), because the performance of the air handling unit is reduced for the user at night. This will reduce the sound pressure level, but at the same time worsen the air quality, which will be reflected in higher (though not dangerous) CO_2 concentrations in the bedroom. A possible measure would be to zone the ventilation system and control according to the CO_2 concentration in the individual rooms. The air conditioning control system is sophisticated; however, its control requires the involvement of the user. The area of thermal comfort in the cold season (TCW) has the potential to improve, especially in the concept of heating solutions and its control. Electric underfloor heating in direct heating mode is one of the most energy intensive (from the point of view of primary energy from non-renewable sources). High energy intensity is reflected in the higher price, and in the case of unfavorable development of the user's economy, it can lead to energy poverty. It would be appropriate to supplement the heating system with a system that provides the user with feedback on the state of thermal comfort and at the same time on energy consumption with possible optimization of the operating mode with a self-learning function. The field of lighting (LC) has potential mainly in the absence of information on the amount of electricity used for artificial lighting and its regulation. The criterion of electromagnetic fields (EC), including the amount of negative ions, draws attention to the fact that during measurements in the bedroom interior, the values of the concentration of negative ions were lower than the recommended optimum and sometimes lower than the recommended minimum. This is not a critical condition; however, if users experience heavy air, this is a possible cause, and we recommend installing an air ionizer commonly available on the market, for example, in some air purifiers.

Overall, family house FM2 does not have any serious problems and all criteria are classified as level 1, 2 and in one case 3. These are the air quality criterion

(IAQ) and the choice of ventilation concept, which is based on natural ventilation. This system requires a high level of user cooperation and, without any indication of air quality indicators, cannot ensure the required air quality while maintaining operating economy. This fact was reflected in the CO_2 concentration course in the bedroom at night, which regularly exceeded 2000 ppm. At the same time, measurable formaldehyde concentrations were measured during a single measurement, which contributes to the assumption that sufficient air exchange is not ensured when the windows are closed. A possible low-cost measure is to equip the building with a CO_2 indication system, which alerts the user to the increasing concentration of harmful substances in the air, which can react by opening a window. There is a higher potential for improvement in the area of heating and its regulation, where the user is looking for the optimal setting of the system so that he has enough hot water and heat for heating at the same time. Currently, the heating operation does not use the possibility of individual regulation, the entire system is switched to equithermal mode. Likewise, information on heating energy consumption would help optimize plant operation. The thermal comfort in the summer is ensured by the building itself with a large construction, active shading and the size of the windows, and based on user feedback, the thermal comfort is subjectively ensured. Sensitive automation of blind settings and monitoring of internal temperatures would contribute to its increase. The absence of controlled ventilation can also be expected in the summer. The field of lighting (LC) has potential mainly in the absence of information on the amount of electricity used for artificial lighting.

4. Conclusion and summary

Many questions arise with the assessment of the quality of the indoor environment, but they do not and cannot have a clear-cut answer. The aim of this methodology is to obtain a detailed analysis of the state of the indoor environment of a building in context and the resulting proposals for measures to improve or eliminate risk factors, even though all the building's structures and technical systems have been designed according to valid standards and knowledge of current technology. This analysis is the basis for decision making on changes in maintenance, operation, or the need for refurbishment leading to increased building resilience.

HAIEQ methodology does not compete with evaluation tools such as BREEAM, WELL, LEADS etc., which are primarily intended for the comprehensive evaluation of buildings. These instruments assess IEQ only as part of the overall assessment and have different weightings [5].

The case study of two family houses shows the use of methodology not only for IEQ evaluation, but also for diagnostics and identification of problems related to indoor environment quality in buildings with low energy consumption. The aim of this study is also to show the potential for improving the indoor environment quality in the building.

5. Acknowledgement

This project was implemented with financial support from the state budget of the Czech Republic through the Ministry of Industry and Trade in the TRIO-FV40183 programme.

6. References

[1] Kabele, K.; Urban, M.; Veverková, Z., 2016.Indoor Environmental Quality and Building Performance Assessment in nZEB, In: Slovak Society of Environmental Engineering, Indoor climate of buildings 2016 - environmentally friendly and energy efficient buildings. Štrbské Pleso, Slovakia, 28. 12. – 30.12. 2016: pp. 137-146. ISBN 978-80-89878-04-8.

[2] Kabele K., Veverková Z., Urban M. Methodology of IEQ assessment in energy efficient buildings. Windsor 2020 Resilient Comfort. 2020-04-16/2020-04-19. Witney: Ecohouse Initiative Ltd., 2020: p. 861-876. ISBN 978-1-9161876-3-4. Available from: https://windsorconference.com/proceedings/

[3] Verbeke S., Waide P., Bettgenhäuser K., Uslar M.; Bogaert S. Et al. Support for setting up a Smart Readiness Indicator for buildings and related impact assessment - final report; August 2018; Brussels.

[4] Kabele, K., Veverková, Z., Urban, M. Methodology for assessing the indoor environmental quality in low energy buildings in the Czechia. 10th IAQVEC 2019 Conference on Indoor Air Quality, Ventilation and Energy Conservation in Buildings, Italy, Bari 5 – 7.9.2019 available on-line https://iopscience.iop.org/article/10.1088/1757-899X/609/4/042103

[5] Mattoni B., Guattari C., Guattari C., Evangelisti L., Asdrubali F. Critical review and methodological approach to evaluate the differences among international green building rating tools. Renewable and Sustainable Energy Reviews 2017 091105: 82:950-96

Data sets analysed during the current study are not available as they are sensitive to the privacy of the owners of the objects under study.

Thermal conditions and occupant satisfaction in energy retrofitted buildings in Finland

Virpi Leivo [a], Ulla Haverinen-Shaughnessy [b]

[a] Unit of Civil Engineering, Tampere University, Tampere, Finland, virpi.leivo@tuni.fi.

[b] Faculty of Technology, University of Oulu, Oulu, Finland, Ulla.Haverinen-Shaughnessy@oulu.fi.

Abstract. In this paper different factors effecting into thermal comfort are compared with results of housing diaries. The data was collected in a project which object was to demonstrate the effects of energy retrofits on IEQ and occupant health. Data from existing 46 multi-family buildings (218 apartments) were collected both before and (usually about one year) after energy retrofits, including various thermal condition and indoor air quality (IAQ) measurements combined with occupant surveys. Measurements were performed during two winter months. The relatively high indoor temperatures observed in apartments before the retrofits indicated overheating. After the retrofits, the average temperatures remained unchanged. The temperature even in the coldest spot, i.e. place where coldest inner surface temperature was detected by thermographic camera or IR-thermometer (usually by the balcony door) was quite high, about +20,3 °C. According to 2-week diaries, considering perceived housing satisfaction, the occupants were quite satisfied with the IAQ. In 11-point scale considering daily perceived disturbance, (0 "not at all" and 10 "intolerably") the average was less than 1 considering indoor temperature, humidity, draught and stuffiness/ poor IAQ. The differences before and after were not statistically significant, except considering stuffiness/ poor IAQ, which was reported less disturbing after the retrofits (Mann-Whitney U-test, p=0.001). The indoor thermal conditions were quite good and occupant satisfaction were relatively high even before the energy retrofits and remained about the same after the retrofits.

Keywords. IEQ, occupant satisfaction, thermal comfort
DOI: https://doi.org/10.34641/clima.2022.345

1. Introduction

The Energy Performance of Buildings Directive 2010/31/EU (EPBD) and the Energy Efficiency Directive 2012/27/EU promote policies that will help achieve a highly energy efficient and decarbonised building stock by 2050. In October 2020, the Commission presented its renovation wave strategy, as part of the European Green Deal. Its objective is to at least double the annual energy renovation rate of buildings by 2030 and to foster deep renovation [1]. Most of the residential buildings (about 70% of the building area) in the EU-27 countries have been constructed before 1980, in Finland about 65% [2]. Therefore, there is an important energy saving potential in old multi-family buildings, which are also in need of renovation as many construction parts have reached their expected service life.

Thermal comfort is commonly defined as "condition of mind which expresses satisfaction with the thermal environment" [3].

This paper is focused on assessing impacts of energy retrofits on indoor thermal conditions (temperature (T) and relative humidity (RH)) and comparing the results with housing diaries, collected from the occupants. Measurements following the same protocol were performed in multifamily buildings before and after retrofits in Finland and Lithuania (two countries located in Northern Europe). This paper presents results from Finland. The purpose of the whole project (INSULAtE) was to demonstrate impacts of energy retrofits on indoor environmental quality (IEQ) and occupant satisfaction, and to develop a common assessment method of these impacts on building and national levels [4].

2. Case studies

2.1 Case study buildings

Case study buildings were selected from

Copyright ©2022 by the authors. This conference paper is published under a CC-BY-4.0 license.

volunteering multi-family buildings that were planned to be retrofitted during the project, and where about five apartments per building were willing to participate in the measurements before (Pre) and after the retrofit (Post). Also some buildings, which were not retrofitted during the project, were included as control buildings. Retrofitted buildings were divided into two groups: focused energy retrofit buildings (FER), where only one retrofit action was performed, and deep energy retrofit buildings (DER), where several retrofit actions addressing multiple building components were performed. Majority of the case study buildings were built in 1960-1980 and typical outer wall was prefabricated concrete element where thermal insulation is between concrete slabs. A total of 46 multi-family buildings (218 apartments) were included: 39 retrofitted (30 FER and 9 DER) cases, as well as seven control buildings. The most common retrofit action was changing new windows (U-value of old windows 2,1 W (m-2 K-1) and new 1,0 W (m-2 K-1)) and/or installing heat recovery system to exhaust ventilation system, which then became mechanical ventilation with heat recovery (MVHR) (Figure 1). Deep energy retrofits were performed only in 11% of the case buildings.

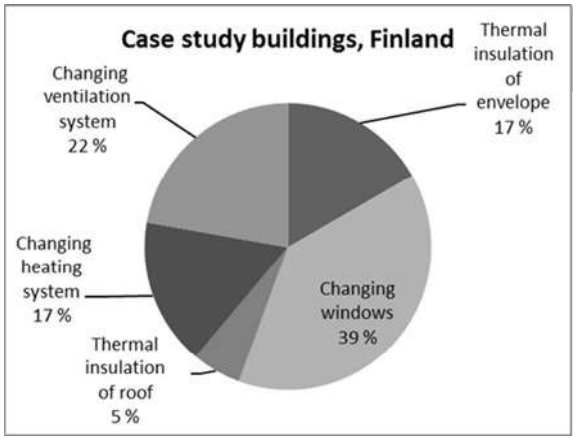

Fig. 1 – Performed energy retrofits.

Most typical U-values of the structures of case buildings were: outer walls U= 0.40 ... 0.28 W(m-2 K-1), roof 0.40 ... 0.36 W(m-2 K-1), floors 0.40 ... 0.29 W(m-2 K-1), windows 2.1 W(m-2 K-1) [5].

2.2 Measurement methods

Two rounds of measurements were performed: before and after the retrofits. Both rounds were performed in the same season, usually during heating season. The measurements took place between November and April, excluding Christmas holidays.

Two months continuous monitoring of temperature (T) and relative humidity (RH). Two loggers (T range -40 -+ 70 °C, accuracy ± 1 °C; RH range 3 - 100%, accuracy ± 3%) per apartment were placed. The data were logged once per hour. One logger was placed in the occupied zone, e.g., middle of the living room (height of 1.2-1.5 m above ground, i.e. human breathing zone as seated), presented as Tw and RHw. The other logger was placed to the coldest spot, i.e. place where coldest inner surface temperature was detected by thermographic camera or IR-thermometer (usually by the balcony door) (Figure 2), presented as Tc and RHc.

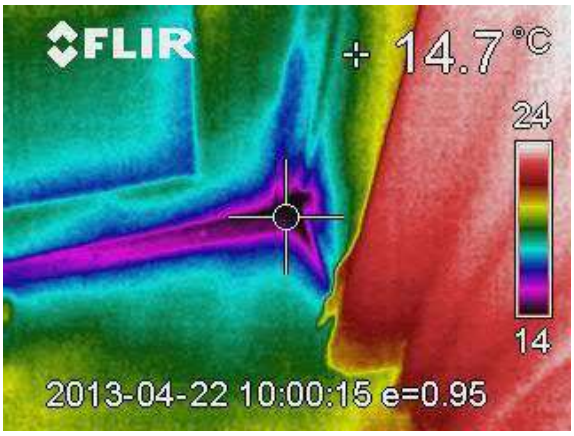

Fig. 2 – Thermographic camera picture, coldest spot on the right (corner), near balcony door.

Occupant surveys were used to collect information concerning occupant perceived housing satisfaction, including thermal comfort, satisfaction with IAQ, lighting, and noise disturbance. All adults living in the apartment were asked to fill in a diary once a day during a two-week period. The diary consisted of two-sided one-page form, including questions concerning symptoms, time consumption, and activities. Fig. 3 shows the question considering perceived housing satisfaction. The issues bothering the occupants at home were assessed in using a 11-point scale, i.e., from 0 to 10, where 0 was the “not at all” and 10 was “intolerably”.

4. On a scale from 0 to 10, indicate how much you felt the following things bothered you in your home during the past 24 hours?

	0 - Not at all					↔				Intolerably - 1
Air pollution, exhaust gas, etc.	0	1	2	3	4	5	6	7	8	9	10
Noise outside your dwelling	0	1	2	3	4	5	6	7	8	9	10
Odours outside your dwelling	0	1	2	3	4	5	6	7	8	9	10
Odours inside your dwelling	0	1	2	3	4	5	6	7	8	9	10
Stuffiness/poor quality of indoor air	0	1	2	3	4	5	6	7	8	9	10
Dust or dirtiness	0	1	2	3	4	5	6	7	8	9	10
Too high an inside temperature	0	1	2	3	4	5	6	7	8	9	10
Too low an inside temperature	0	1	2	3	4	5	6	7	8	9	10
Too high humidity (“moist air”)	0	1	2	3	4	5	6	7	8	9	10
Too low humidity (“dry air”)	0	1	2	3	4	5	6	7	8	9	10
Draught	0	1	2	3	4	5	6	7	8	9	10
Other*	0	1	2	3	4	5	6	7	8	9	10

* Other, please specify:_____

Fig. 3 – Question in dairy considering housing satisfaction.

3. Results and discussion

3.1 Thermal conditions (indoor average) versus thermal comfort

The average indoor temperatures and relative humidity have been reported earlier [6]. As a summary, average indoor Tw during heating season was relatively high in all measurements among both

groups, before retrofits 22.8 °C in FER and 22.7 °C in DER and after retrofits 22.7 °C and 22.7 °C, respectively. The average RHw was low, before retrofits 28.8 RH% in FER and 29.2 RH% in DER and after retrofits 30.5 RH% and 28.2 RH%, respectively. Therefore, overheating was common in the studied apartments.

Table 1 presents results of perceived occupant satisfaction concerning indoor temperature and humidity. Typically, occupant reported "not at all" or slightly disturbance "1" considering temperature and humidity, average was less than 1. The differences between Pre and Post were not statistically significant.

Tab. 1 – Results of perceived occupant satisfaction, temperature and humidity.

Pre or post		Too high tempe-rature	Too low tempe-rature	Too humid	Too dry
Pre	Mean	.6	.6	.2	.9
	Median	.0	.1	.0	.0
	Std. Dev.	1.2	1.2	.7	1.6
	N	159	160	158	162
Post	Mean	.7	.6	.2	.8
	Median	.0	.0	.0	.0
	Std. Dev.	1.6	1.2	.4	1.7
	N	105	105	105	106
Total	Mean	.6	.6	.2	.9
	Median	.0	.0	.0	.0
	Std. Dev.	1.4	1.2	.6	1.7
	N	264	265	263	268

Before the retrofits, occupants reported slightly more "too low temperature" than after the retrofits, but the difference was not statistically significant. Also, reporting of "too dry" indoor air was more common than "too humid", which could be expected during the heating season.

3.3 Thermal conditions (coldest spot) versus thermal comfort (draught)

The average indoor temperatures and relative humidity near the coldest spot of building envelope have been presented in Fig. 4 and 5. Table 2 presents medians, standard deviations, and 95th percentiles for indoor temperature and relative humidity. The outdoor temperature was a higher after retrofits, the median temperature before retrofits in FER buildings was 1.85 °C and after retrofits 2.03 °C. In DER buildings the outdoor temperature was 7,66 °C and 8.30 °C, respectively.

The indoor temperature near the coldest spot of building envelope was higher after retrofits in buildings with deep retrofits (DER), as expected since the thermal insulation of the envelope was commonly improved. Also, the outdoor temperature after retrofits was higher, which could also be influenced to the indoor temperatures.

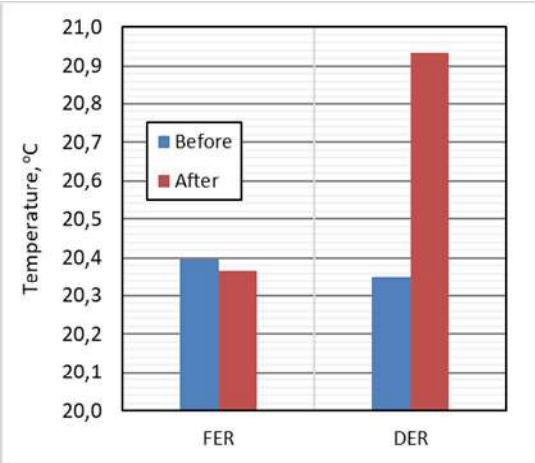

Fig. 4 – Temperature (coldest spot) before and after retrofits.

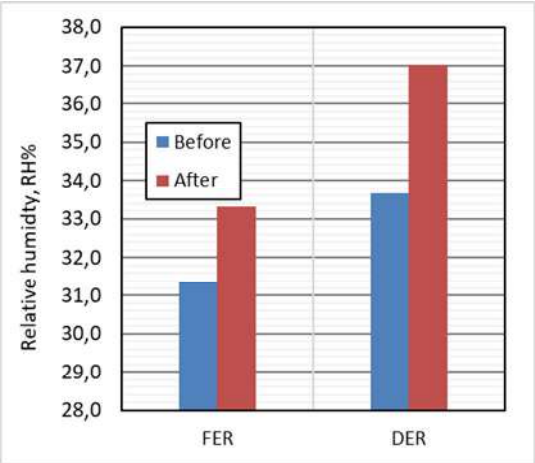

Fig. 5 – Relative humidity, RH (coldest spot) before and after retrofits.

Tab. 2 – Temperature and relative humidity near coldest spot.

T	Pre		Post	
ºC	FER	DER	FER	DER
Median	20.73	20.32	20.79	20.60
Std.dev.	1.63	1.61	1.69	2.44
95th	22.83	22.40	22.58	24.48
N	147	23	103	21
RH	Pre		Post	
%	FER	DER	FER	DER
Median	30.41	34.27	32.24	35.21
Std.dev.	7.99	6.73	7.71	4.70
95th	45.58	42.79	48.19	45.38
N	147	23	103	21

Table 3 presents results of perceived occupant satisfaction concerning stuffiness/ poor IAQ and draught. Occupant reported not at all or slight disturbance considering stuffiness or draught, with an average less than 1. There was no statistically significant difference considering draught between Pre and Post retrofit. However, there was a significant difference (p=0.001) concerning stuffiness / poor IAQ, which was reported less disturbing after the retrofits (Fig. 6).

Tab. 3 – Results of perceived occupant satisfaction, IAQ and draught.

Pre or post		Stuffiness / poor IAQ	Draught
Pre	Mean	1.0	1.0
	Median	.4	.2
	Std. Dev.	1.4	1.8
	N	163	162
Post	Mean	.6	.7
	Median	.0	.1
	Std. Dev.	1.1	1.3
	N	105	105
Total	Mean	.8	.9
	Median	.2	.1
	Std. Dev.	1.3	1.6
	N	268	267

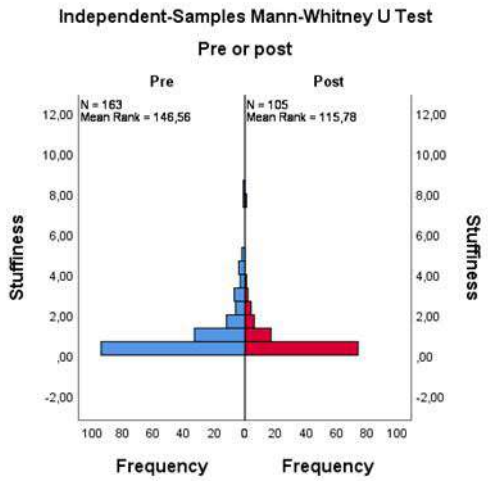

Fig. 6 – Mann-Whitney U-test, perceived stuffiness / poor IAQ.

4. Acknowledgement

Insulate project was co-financed by EU Life+ programme (LIFE09 ENV/FI/000573), the Housing Finance and Development Centre of Finland, and Finnish Energy Industries. The data collection was coordinated by Environmental Health Unit, National Institute for Health and Welfare, Finland.

5. References

[1] European Commission, "Energy performance of buildings directive". [Online]. Available: https://ec.europa.eu/energy/topics/energy-efficiency/energy-efficient-buildings/energy-performance-buildings-directive_en. [Accessed: 19-Oct-2021].

[2] Finnish official statistics (SVT). Buildings and holiday houses, network publication. (In Finnish) Statistics Finland. ISSN=1798-677X. Helsinki.

[3] "ASHRAE Standard 55-2020. Thermal environmental conditions for human occupancy.," Atlanta, 2020.

[4] L. Du, T. Prasauskas, V. Leivo, M. Turunen, M. Pekkonen, M. Kiviste, A. Aaltonen, D. Martuzevicius, and U. Haverinen-Shaughnessy, "Assessment of indoor environmental quality in existing multi-family buildings in North-East Europe," Environ. Int., vol. 79, pp. 74–84, 2015.

[5] Ministry of the Environment, Guidance for Energy Certificate 2013. Appendix: typical original design values of existing buildings (in Finnish). 2013.

[6] V. Leivo, T. Prasauskas L. Du,, M. Turunen, M. Kiviste, A. Aaltonen, D. Martuzevicius, and U. Haverinen-Shaughnessy, "Indoor thermal environment, air exchange rates, and carbon dioxide concentrations before and after energy retro fits in Finnish and Lithuanian multi-family buildings," Science of The Total Environment 621:398-406. 2017.

Data Statement

The datasets generated and analysed during the study are not available but the authors will make every reasonable effort to publish them in near future.

Predicting indoor air temperatures by calibrating building thermal model with coupled airflow networks

Lili Ji[a,b], Chang Shu[a,b], Danlin Hou[a], Abdelaziz Laouadi[b], Liangzhu (Leon) Wang[a], Michael Lacasse[b]

[a] Department of Building, Civil and Environmental Engineering, Concordia University, Montreal, Canada.

[b] Construction Research Center, National Research Council Canada, Ottawa, Canada.

Abstract. Building models that can accurately predict hourly indoor air temperatures in free-running situations are key to understanding overheating conditions and the resilience of passive cooling strategies under a changing climate. To accurately predict indoor temperatures it is necessary to properly model pressure-driven infiltration and natural ventilation. This can be achieved by coupling a building thermal model to an airflow network model. In this paper, the development of coupled building thermal and airflow network models is described to calibrate building models using field measurements of indoor air temperature. Building models of three types of buildings were configured: long-term care building, primary school and multi-unit social housing. The building models were developed in Design Builder™ and exported for use in an EnergyPlus simulation package. From information obtained from building surveys, site visits and architecture drawings, building parameters and operation schedules were collected. The unknown parameters, which included envelope thermal properties, shading devices, internal heat gains, envelope air leakage, window and door openings, were then calibrated based on measured values of indoor temperature. Reasonable ranges in value of the unknown parameters were first retrieved from applicable building construction practice documents and building energy standards. Two rounds of calibration were conducted through parametric simulations using the Monte-Carlo sampling method. A sensitivity analysis was also conducted for ranking the importance of all building parameters. The values for indoor air temperature as obtained through simulation were compared with measurements and the RMSE (root mean square error) was calculated for all values. The parameter value combinations corresponding to the minimum RMSE were adopted for the building models. The calibration process ended when the value for RMSE was <1.5°C. Results showed that the detailed building model was capable of predicting room air temperatures with minimum error levels (0.56°C ≤ RMSE ≤ 1.50 °C) within the limits of applicable building model calibration standards (MBE±10%, CVRMSE<20%).

Keywords. Indoor air temperature, building thermal model, airflow network, calibration, field measurement
DOI: https://doi.org/10.34641/clima.2022.340

1. Introduction

Predicting indoor temperature accurately through building performance simulation is important to analyse the overheating situation of buildings in current and future projected climates. Previous studies mainly focused on the calibration of building energy performance [1]. A generalized and easily applied method is still needed to calibrate the indoor thermal performance. Before the calibration stage, the pre-modelling of buildings with proper consideration of natural ventilation and pressure-driven infiltration also significantly affect the accuracy of prediction results. Airflow networks [2], therefore, can be coupled to the building models to calculate air flows through cracks, doors, windows ducts, and other flow paths between zones.

In this study, three types of buildings are modelled through coupling with airflow network models and then calibrated based on the field measurements of indoor hourly air temperature. A framework of building calibration and validation is proposed, which can be applied to other building thermal simulation models.

2. Methodology

2.1 Workflow overview

Fig. 1 shows the procedure of building modelling and calibration. Through building survey, site visit and architecture plan, building parameters, operation

Copyright ©2022 by the authors. This conference paper is published under a CC-BY-4.0 license.

schedules, and HVAC systems information are collected. Airflow network (AFN) is applied to the building models. There are unknown parameters to be calibrated based on the measured indoor hourly temperature. The subsections below will introduce the procedure in detail with three measured and modelled buildings.

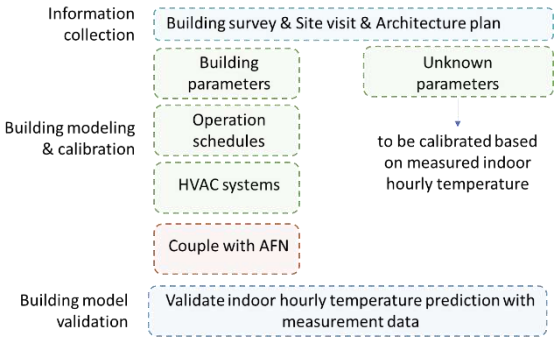

Fig. 1 - Workflow overview

2.2 Building measurement campaign

A building measurement campaign was conducted to monitor the indoor and outdoor thermal conditions of different types of buildings in Montreal, Canada [3]. The indoor temperature and relative humidity (RH) in selected spaces on different floors and orientations of 13 buildings (three primary schools, three hospitals and four residential buildings) were monitored continuously over the summer seasons from 2020 to 2021. On-site weather stations were placed on the roofs of buildings to gather local weather data, including air temperature, relative humidity, solar radiation, wind speed and direction, and precipitation. With the monitored indoor and outdoor conditions, the overheating issues of these buildings can be assessed during the monitored period. However, with climate change, the overheating conditions in future climate projections need to be predicted and possible mitigation strategies need to be investigated using calibrated building models.

2.3 Building modelling

Among the monitored buildings, three buildings including a long-term care building (LTCB), a primary school (PS), and a multi-unit social housing (SH) are modelled in Design Builder™ and exported for use in an EnergyPlus simulation package.

The monitored LTCB is an L-shaped building facing the northwest direction and is composed of five floors above the ground and below-grade basement floor. The total length and width of the building are 44m and 42m, respectively. The size of a typical private patient room in the building is 5.4m x 3.6m. The building was constructed in 1980 with exterior walls made of concrete and solid brick veneer cladding. There were no central cooling systems in the building. As for the mechanical ventilation system, five lounge spaces used a central system to provide fresh air.

The PS building is a 3+1 story building originally built in 1930. The building was partially retrofitted six times including the extension in 1955, adding boiler room in 2008, masonry in 2009, plumbing in 2014, and new roof in 2015, sanitary blocks and foundations in 2019. The building can accommodate 396 students and 24 teaching staff. The total length and width of the building are 53m and 46m, respectively. The size of a typical private classroom in the building is 9.4m x 8.1m. The building was constructed with exterior walls made of concrete panels and solid brick veneer claddings. There were no cooling systems or mechanical ventilation system in the buildings. The classrooms were cooled by natural ventilation by opening windows and portable fans (in some classrooms).

The SH building is a three-story building built in 2008 and mainly occupied by older people. The total length and width of the building are 105m and 18.5m, respectively. The size of a typical unit in the building is 9.2m x 8.2m. The building is composed of 54 suites (dwelling units) with one bedroom. Each unit was occupied by one or two people. There were no cooling and mechanical ventilation system in the dwelling units. An activity room on the first floor is cooled by a rooftop unit.

Indoor sensors were installed in selected rooms in the above buildings to monitor the air temperature and relative humidity. In each building, all the sensors were installed in the same locations in each room, about 1.7-meter height near the corner. Outdoor weather stations were installed on the roof of the buildings to monitor the air temperature, relative humidity, wind speed, and solar radiation. The monitored data were collected during the summer 2020.

According to the information collected through building surveys, site visits and onsite measurement, the original building models were developed. The 3D models of the three buildings are shown in **Fig. 2**.

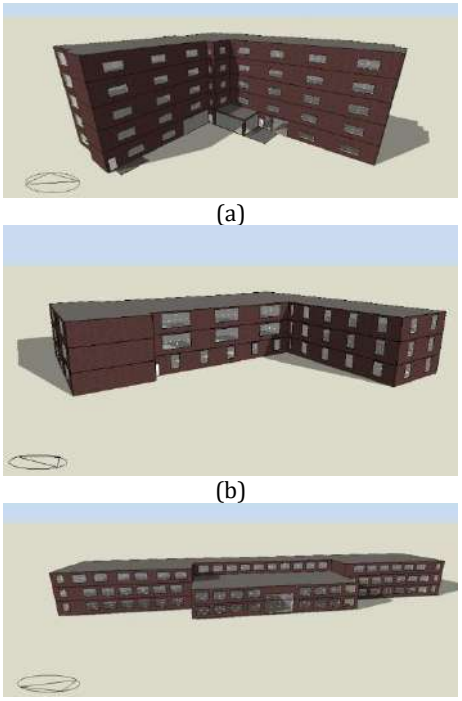

(a)

(b)

(c)

Fig. 2 - 3-D view of the as-simulated building models

The unknown building parameter values were calculated through building model calibration using the monitored temperature data. The ranges of the unknown parameter values were taken from related published literature and the national building code of Canada. **Tab. 1** summarizes the ranges of the unknown building parameters for building calibration of the LTCB. Unknown parameters and ranges of the primary school and social housing are also analysed in a similar way, the tables of which are not listed here due to the page's limitation.

Tab. 1 - Unknown parameters and ranges of the Long-term care building

Building Parameter		Range	Unit	References
Wall	U-Value	0.25-0.62	W/m^2K	RDH (2017)
	Thermal mass	150-350	W/m^2K	
Roof	U-Value	0.15-0.39	KJ/km^2	
	Thermal mass	150-350	KJ/km^2	
Window	U-Value	2.38-3.31	W/m^2K	Double glazing with aluminum frame
	SHGC	0.3-0.7	/	
Shading	Slat angle	5-175	Deg	Blind shading parameter
	Solar reflectance	0.4-0.9	/	
Internal heat gain	Lighting power density	6.6-11.3	W/m^2	NECB2017
	Equipment power density	2.5-10	W/m^2	NECB2017
Infiltration	Air mass flow coefficient at reference crack condition	Walls: 0-0.0040 Roof: 0-0.0045	kg/s	RDH (2017)
Natural ventilation	Natural ventilation temperature set point	22-26	°C	Comfort range
	Window opening factor	0-0.1	/	Site visit
	Room door opening factor	0-1		
	Exterior doors opening factor	0.025	/	

2.4 Airflow network (AFN)

The airflow network models are applied to the building models. The buildings are treated as a collection of nodes representing thermal zones in the building and flow elements representing cracks, doors, ducts, and other flow paths between the zones. Conservation of mass flows between the zones generates simultaneous nonlinear equations, which can be solved to determine the resultant flow through the building.

Using an airflow network model to predict ventilation rates in a building allows the inclusion of external weather data in the calculation. The natural variability of the ventilation drivers such as wind speed and direction and thermal effects can be incorporated into the calculation, providing more realistic ventilation predictions than using a fixed ventilation rate based on open window area alone.

The airflow through each leakage component is assumed to follow the leakage relationship of a crack flow, which is characterized by the air mass flow coefficient (C) and exponent (n) as in **Eq. 1**.

$$\dot{m}_a = \dot{V}_a \times A \times \rho = C \cdot \Delta P^n \quad (1)$$

Where $\dot{m}_a$ is the maximum mass flow rate of each surface (kg/s), $\dot{V}_a$ is the maximum volume flow rate per area ($m^3/s/m^2$), A is the component surface area (m^2), ρ is air density (kg/m^3), ΔP pressure differential across the leakage component (Pa), n is the leakage exponent coefficient, defaulted to 0.65.

In the pre-modelling stage, the design infiltration rate for good airtightness of 0.4 ACH [4] for the whole building is set, and the DesignBuilder software automatically creates the leakage data of each exterior and interior surface. However, the infiltration rate is dynamic, affected by wind pressure and surface leakage characteristics. For old buildings (1980), the maximum leakage rate for the entire similar buildings was found to be 0.72 CFM/SF@75Pa = 3.66L/s/m2@75Pa, according to RDH (2017) [5]. For retrofit or new buildings, referring to ASHARE 90.1 [6], ABAA and NECB [4], the maximum air leakage for the entire building built after 2005 is 2.0L/s·m2@75Pa. Therefore, to make the leakage data closer to the actual situation, calculations of the maximum air mass flow coefficient for the exterior surfaces of the monitored rooms, assuming a uniform distribution over exterior building surfaces, are shown in **Tab. 2**.

Tab. 2 - Calculated air leakage data of the monitored natural ventilated rooms (using the Long-term care building as an example)

Surface	Air leakage limit @75Pa ($L/s/m^2$)	Area (m2)	Air density (Reference condition) (kg/L)	n	C (max)
Roof	3.66	20.297	0.0012	0.7	0.0043
Wall_North	3.66	13.095	0.0012	0.7	0.0028
Wall_West	3.66	2.987	0.0012	0.7	0.00063
Wall_South	3.66	18.893	0.0012	0.7	0.0040

In the airflow model, the exterior windows are opened when the indoor temperature is higher than the outdoor temperature and a given set point temperature (the natural ventilation setpoint

temperature will be calibrated based on the monitored data). The thermal and ventilation conditions in the zones are affected by the window and door operations (the opening area percentage will be calibrated based on the monitored data), infiltration through the crack of roofs, walls, and partitions, as well as the air released through exhaust fans. The airflow path through the large horizontal openings is applied to the vertical stairway and elevator thermal zones.

2.5 Building calibration and validation

The building calibration process is composed of five steps: parametric simulation with all variables, the first-round calibration, sensitivity analysis, parametric simulation with the most important four variables, second round calibration, as shown in **Fig. 2.**

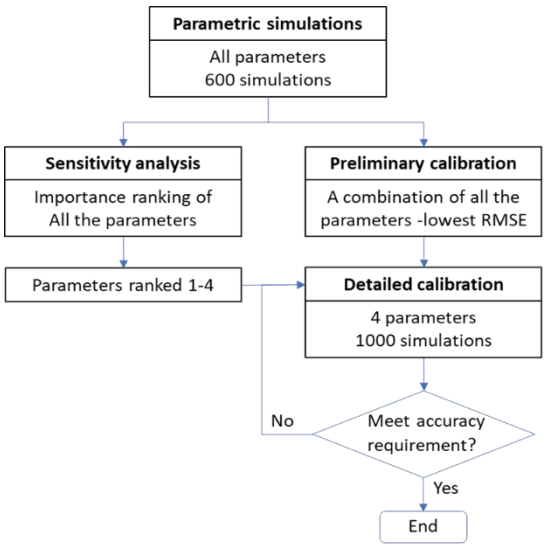

Fig. 3 - Building calibration procedure

In the first step, the unknown model parameters with their practical ranges are defined. The Hamiltonian Monte-Carlo (HMC) sampling method is used for 600 random samplings within each parameter range. HMC is a random sampling algorithm applicable when the model parameters are continuous rather than discrete and able to suppress random walk behaviour through a clever auxiliary variable scheme that transforms the problem of sampling from a target distribution into the problem of simulating Hamiltonian dynamics [7]. So 600 combinations of all the defined parameters are obtained, and then 600 parametric simulations are performed. The parametric simulations are realized with an R package named "eplusr", which enables to use EnergyPlus directly in the R language. The input-output dataset can be used to do sensitivity analysis to identify the most important parameters of the building thermal model, as explained in the next paragraphs. The input-output dataset can also be used to do the first round calibration of all the defined parameters. In this round calibration, the simulated indoor air temperatures are compared with measurements, and the RMSE (root mean square error, **Eq. 2**) is calculated. The parameter combination corresponding to the minimum RMSE is adopted for the building model. In the second step, the most important four parameters (obtained from the sensitivity analysis) are further calibrated. HMC is again used for 1000 random samplings within each parameter range, resulting in 1000 combinations of all the defined parameters, and then 1000 parametric simulations are performed. The simulated indoor air temperature is compared with measurements, and the RMSEs are calculated. The parameter combination corresponding to the minimum RMSE is adopted for the building model. The calibration process stops when the RMSE reaches its low-level value of below 1.5°C. This low-level value is taken from the study of [8] about the error of predicting air temperatures in a naturally ventilated building. After calibration, validation is then done with the other set of measured data during the different periods for the calibration stage. All the above steps are realized and automated using a script developed in the R programing language.

$$RMSE = \sqrt{\frac{\sum_{i=1}^{n}(y_i - \hat{y}_i)^2}{n}} \quad (2)$$

Where y_i and $\hat{y}_i$ are the simulated and measured hourly temperatures, respectively, and n is the number of hours.

Typical building calibration metrics in existing standards [9] include: the coefficient of variance root mean square error (CVRMSE) and the mean bias error (MBE), as calculated in **Eq. 3** and **Eq. 4**, are used to evaluate the calibration and validation results, to check if the result errors meet the standard requirements. **Eq. 4** indicates that the positive value of MBE means the simulated data are in general higher than the measured data; the negative value of MBE means the simulated data are in general lower than the measured data. The threshold limits of the two metrics for hourly calibration are shown in **Tab. 1**.

$$CVRMSE(\%) = \frac{RMSE}{\sum_{i=1}^{n}\hat{y}_i/n} \times 100\% \quad (3)$$

$$MBE\ (\%) = \frac{\sum_{i=1}^{n}(y_i - \hat{y}_i)}{\sum_{i=1}^{n}\hat{y}_i} \times 100\% \quad (4)$$

Tab. 3 - Threshold limits of building calibration metrics in compliance with ASHRAE (2002), IPMVP (2003) and FEMP (2008)

Metrics	ASHRAE	IPMVP	FEMP
MBE [%]	±10	±5	±10
Cv(RMSE) [%]	30	20	30

Typically, there are six steps for implementing sensitivity analysis in building performance analysis: determine input variations; create building energy models; run energy models; collect simulation results; run sensitivity analysis; presentation of sensitivity analysis results. The first four steps have been finished after the first round of parametric simulation. So that the input-output dataset from the first round parametric simulations is collected to feed the sensitivity analysis to identify the most important parameters.

In this study, three different approaches are utilized to offer robust analysis results: SRC, t-value, and random forest variable importance. High SRC means more important of the variable. The t-value is the statistic used to test whether the coefficient of the corresponding variable is zero. The higher the absolute value of t, the more important is the corresponding variable. The conditional variable importance from the random forest applies to correlated inputs. If there is a large variation of the outputs unexplained (i.e., non-linear effects in the model), the conditional variable importance from the random forest can be used. The three approaches are integrated into one index called Sensitivity Value Index (SVI) [13] to avoid the potential inconsistency.

After calibration, the building models are validated with measured indoor temperature data (over different periods of time). For the LTCB, the monitored data were collected from July 14, 2020 to August 13, 2020. Therefore, the data from July 14 to July 28 were selected for model calibration so that all the parameters to be calibrated have significant effects on indoor temperature, and the data from July 29 to August 13 were selected for model validation. For the PS, the monitored data were collected from August 04, 2020 to September 30, 2020. Therefore, the data from August 26 to September 13 (school occupied) were used for the calibration and the data from September 14 to 30 were used for validation. For the SH, the monitored data were collected from May 01 to 26, 2021. However, from May 01 to 13, the outdoor temperature was from 5℃ to 20℃ and the simulated indoor temperature was lower than 22℃, which made natural ventilation not activated. Therefore, the data from May 14 to 20 were used for the calibration and the data from May 21-26 were used for the validation.

3. Results

3.1 Evaluation of calibration and validation results

Tab. 4(a) shows the evaluation criteria (RMSE, CvRMSE and MBE) of the calibration and validation results for each room and their spatial averages in LTCB. At a room level, the RMSE of the calibration and validation are from 0.56℃ to1.09℃, which are less than the 1.5℃ requirement (O'Donovan et al. 2019). The MBE is within ±1.2% and the CvRMSE is less than 3.65%, which are well within the requirement of standards (±5% and 20% as listed in **Tab. 3**). At a building level (calculated by averaging the data of the three rooms), the validation results show that the RMSE is 0.54℃, the MBE is 0.58% and the CvRMSE is 1.85%, which are all within the error limit requirements. **Tab. 4(b)** shows the evaluation criteria results of PS. At room level, the RMSE of the calibration and validation are from 0.63℃ to 0.78℃. The MBE is within ±1.39% and the CvRMSE is less than 3.19%. At the building level (calculated by average data of the two rooms), validation results show that the RMSE is 0.67℃, the MBE is -0.12% and the CvRMSE is 2.78%. The errors are all within the error limit requirements. **Tab. 4(c)** shows the evaluation criteria results of SH. At room level, the RMSE of the calibration and validation are from 0.56℃ to1.50℃. The MBE is within ±4.9% and the CvRMSE is less than 5.28. In building level (calculated by average data of the four rooms), validation results show that the RMSE is 0.71℃, the MBE is 0.47% and the CvRMSE is 2.55%, which are all within the error limit requirements. The positive MBE value means the simulated data are in general slightly higher than the measured data. The negative MBE value means the simulated data are in general slightly lower than the measured data.

Tab. 4 - Error metrics for the predictions of the hourly indoor air temperatures of monitored rooms in (a) LTCB (b) PS and (c) SH

(a)

Error metrics	Room 1		Room 2		Room 3		Room Average	
	Cal.	Val.	Cal.	Val.	Cal.	Val.	Cal.	Val.
RMSE (°C)	0.56	0.66	0.57	0.55	1.09	1.08	0.46	0.54
MBE (%)	0.25	0.90	-0.70	0.57	1.182	0.285	0.244	0.58
CvRMSE (%)	1.93	2.31	1.89	2.02	3.63	3.61	1.54	1.85

(b)

Error metrics	Room 1		Room 2		Room Average	
	Cal.	Val.	Cal.	Val.	Cal.	Val.
RMSE (°C)	0.73	0.7	0.63	0.78	0.63	0.67
MBE(%)	-0.82	1.17	-0.90	-1.39	-0.86	-0.12
CvRMSE(%)	2.57	3.12	2.22	3.19	2.21	2.78

(c)

Error metrics	Bedroom 1		Livroom 1		Bedroom 2		Livroom 2		Room average	
	Cal	Val	Cal	Val	Cal	Val	Cal	Val	Cal	Val
RMSE (°C)	0.63	1.05	0.56	0.91	1.49	0.77	1.21	1.50	0.59	0.71
MBE (%)	1.19	1.08	1.25	0.52	-4.90	-0.67	-3.72	0.99	-1.65	0.47
CvRMSE (%)	2.44	3.86	2.16	3.33	5.28	2.71	4.35	5.51	2.18	2.55

3.2 Comparison of the measured and simulated indoor temperature

Fig. 4 compares the measured and simulated indoor temperature (average values of the three monitored rooms of LTCB) after applying the calibrated parameter values during the calibration and validation periods. To analyse whether the simulated data can capture the peak indoor temperatures, the distribution of the measured and simulated hourly temperatures during the validation period are shown in **Fig. 5**. During the validation period, there are 11 hours when the measured temperature is above 30.4℃ (the last bin in **Fig. 5(a)**), and 8 hours when the simulated temperature is above 30.4℃ (the last bin in **Fig. 5(b)**). Therefore, the simulated data can capture 73% of the peak temperatures. Comparing the three bins of 29.8℃ to 30.4℃, the

simulations overestimate the hours between 29.8℃ to 30.4℃ by 85 hours, but underestimate the temperature in the bins of 28.4℃ to 29.4℃ by 87 hours. This deviation might be because of occupant behaviour in adjusting window and door openings under different weather conditions to control nature ventilation, whereas in the simulation the opening factors of windows and doors are kept constant during the simulation period.

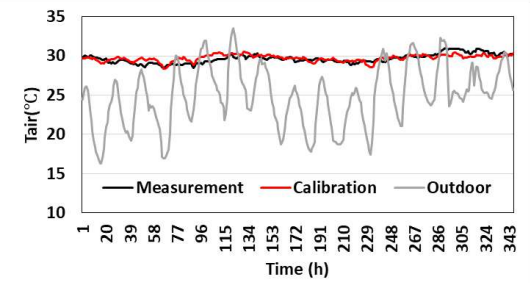

(a)

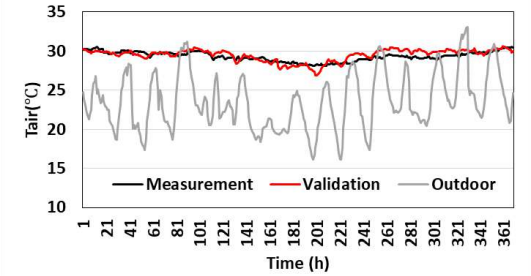

(b)

Fig. 4 - Comparison of the measured and simulated data (room averages of LTCB) during (a) calibration period and (b) validation period

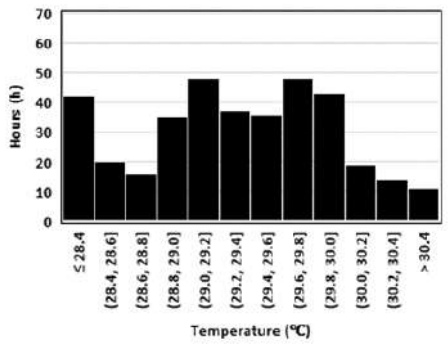

(a)

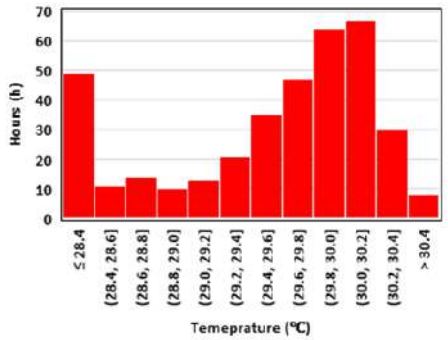

(b)

Fig. 5 - Distribution of average room data of LTCB during the validation period: (a) measured and (b) simulated temperatures

Fig. 6 shows a comparison between the measured and simulated data (average data of the two rooms in PS) after applying the calibrated parameter values, and the distribution of the measured and simulated hourly temperatures during the validation period is shown in **Fig. 7**. There are 26 hours when the measured temperature is above 31.2℃, and 42 hours when the simulated temperature is above 31.2℃. Therefore, the simulated data can capture 100% of the peak temperatures with a slight overestimation. The hours of the measured and simulated temperature above 28℃ are as well comparable: 514 hours versus 522 hours, respectively.

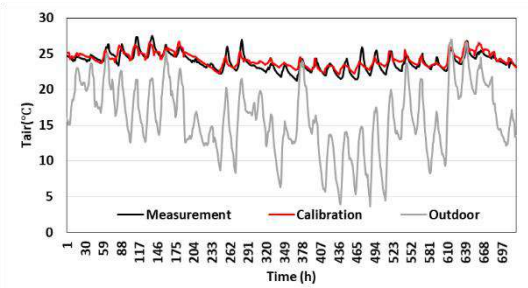

(a)

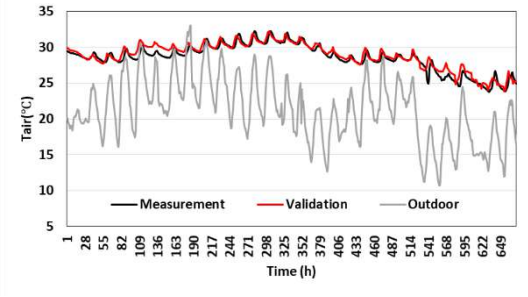

(b)

Fig. 6 - Comparison of the measured and simulated data (room averages of PS) during (a) calibration period and (b) validation period

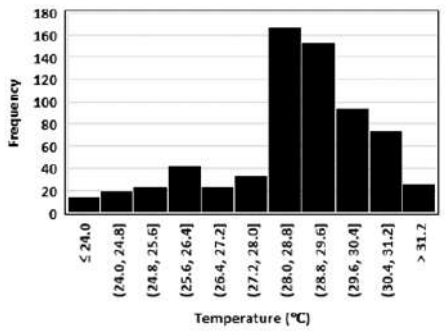

(a)

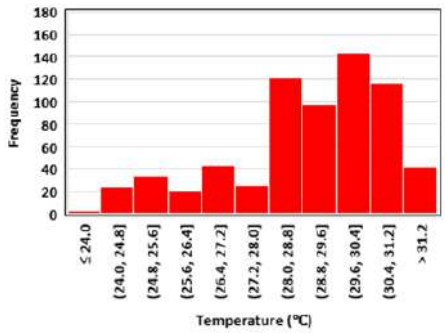

(b)

Fig. 7 - Distribution of average room data of PS during the validation period: (a) measured and (b) simulated temperatures

Fig. 8 shows the comparison of the measured and simulated data (average data of the four rooms in SH) after applying the calibrated parameters. The distribution of the measured and simulated hourly temperatures during the validation period is shown in Fig. 9. There are 10 hours when the measured temperature is above 30.0°C, and 8 hours when the simulated temperature is above 30.0°C. Therefore, the simulated data can capture 80% of the peak temperatures. The hours of the measured and simulated temperatures above 29°C are comparable: 36 hours versus 41 hours, respectively.

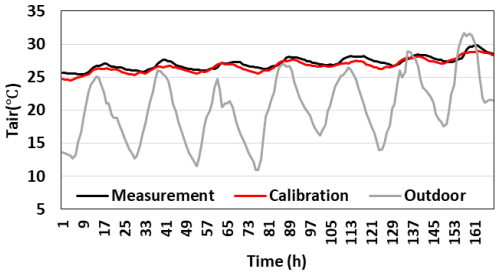

(a)

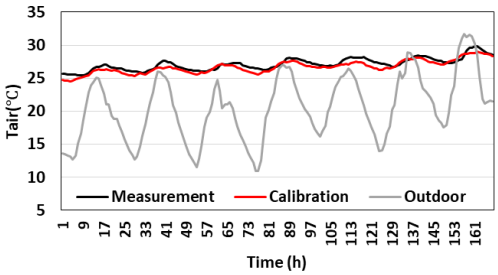

(b)

Fig. 8 - Comparison of the measured and simulated data (room averages of SH) during (a) calibration period and (b) validation period

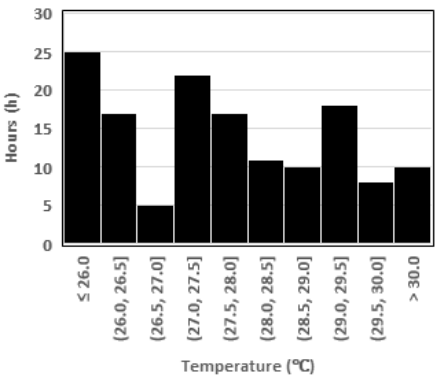

(a)

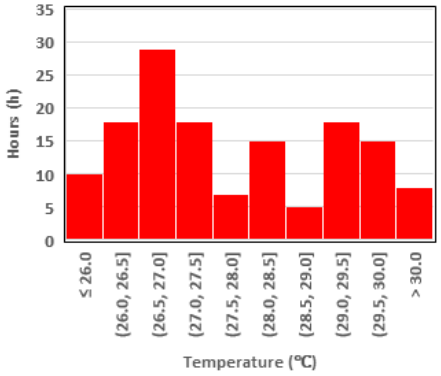

(b)

Fig. 9 - Distribution of average room data of SH during the validation period: (a) measured and (b) simulated temperatures

3.3 Calibrated building parameter values

The calibrated values of the unknown parameters of the LTCB model are shown in **Tab. 5**. The tables for PS and SH are not listed here due to the pages limitation.

Tab. 5 Calibrated parameter values of LTCB

Object	Parameter	Unit	Final value
Wall	Wall U-Value	W/m^2K	**0.3**
Roof	Roof U-Value	W/m^2K	**0.25**
Wall	Wall thermal mass	KJ/km^2	**220**
Roof	roof thermal mass	KJ/km^2	**335**
Window	Window U-Value	W/m^2K	**2.72**
Window	Window SHGC	-	**0.37**
Interior blinds	Slat angle	Deg	**59**
	Solar reflectance		**0.6**
Equipment	Equipment power density	W/m^2	**2.93**
Lighting	Lighting power density	W/m^2	**9.94**
Air mass flow through cracks	Air mass flow coefficient at reference crack condition of walls and roof surfaces	kg/m·s	**0.0025**
		kg/m·s	**0.0012**
Natural ventilation control	Natural ventilation set point	°C	**26**
Interior room door opening factor	Width factor for door opening	%	**47**
Room window opening factor		%	**10**

4. Discussion

The mechanical ventilation systems are not considered in the three building models in this study. The calibration method is only demonstrated in the naturally ventilated buildings. Future studies can be conducted to apply the method to building models with mechanical cooling or ventilation systems.

5. Conclusion

This study developed building performance simulation models coupled with airflow networks. A two-round calibration framework was proposed to

calibrate the building models based on measured hourly temperature data. The results showed that the detailed building model was capable of predicting room air temperatures with minimum error levels (0.56℃ ≤ RMSE ≤ 1.50 °C) within the limits of applicable building model calibration standards (MBE±10%, CVRMSE<20%). As a future work, the calibrated building models will be used to implement and evaluate strategies to reduce overheating risk arising from extreme heat events of current and projected climates.

6. Acknowledgement

The research was supported by the Natural Sciences and Engineering Research Council of Canada (NSERC) through the Discovery Grants Program [#RGPIN-2018-06734] and the "Advancing Climate Change Science in Canada" program the Advancing Climate Change Science in Canada Program [#ACCPJ 535986-18], and the Construction Research Centre of the National Research Council of Canada through funding from Infrastructure Canada in support of the Pan Canadian Framework on Clean Growth and Climate Change.

7. References

[1] P. Raftery, M. Keane, A. Costa, Calibrating whole building energy models: Detailed case study using hourly measured data, Energy Build. 43 (2011) 3666–3679.

[2] A.S. Ancrossed D Signelković, I. Mujan, S. Dakić, Experimental validation of a EnergyPlus model: Application of a multi-storey naturally ventilated double skin façade, Energy Build. 118 (2016) 27–36.

[3] C. Shu, L. Ji, L. Wang, X. Bai, M. Lacasse, H. Ge, R. Zmeureanu, L. (Leon) Wang, Field Survey on Indoor Overheating in School and Hospital Buildings in Montréal, 2nd Int. Conf. New Horizons Green Civ. Eng. (NHICE-02), Victoria, BC, Canada, April 29 – May 01, 2020. (2020) 2–5.

[4] NRC, National Energy Code of Canada for Buildings, Can. Comm. Build. Fire Codes. (2017).

[5] RDH, Deep Building Enclosure Energy Retrofit Study, Multi-Unit Residential Building Deep Energy Retrofit Study-Enclosure Retrofit, 2017.

[6] ASHRAE Standards Committee, Addendum to Standard 90.1-2001. Energy Standardfor BuildingsExcept Low-RiseResidential Buildings, 8400 (2004).

[7] Hoffman, The No-U-Turn Sampler: Adaptively Setting Path Lengths in Hamiltonian Monte Carlo, 15 (2014) 1593–1623.

[8] A. O' Donovan, P.D. O' Sullivan, M.D. Murphy, Predicting air temperatures in a naturally ventilated nearly zero energy building: Calibration, validation, analysis and approaches, Appl. Energy. 250 (2019) 991–1010.

[9] E. Fabrizio, V. Monetti, Methodologies and advancements in the calibration of building energy models, Energies. 8 (2015) 2548–2574.

[10] ASHRAE, ASHRAE Guideline 14-2002: Measurement of Energy Demand and Savings; American Society of Heating, (2002).

[11] IPMVP, International Performance Measurement & Verification Protocol: Concepts and Option for Determining Energy Savings in New Construction, (2003).

[12] FEMP, M&V Guidelines: Measurement and Verification for Federal Energy Projects Version 3.0, (2008).

[13] H. Lim, Z.J. Zhai, Comprehensive evaluation of the influence of meta-models on Bayesian calibration, Energy Build. 155 (2017) 66–75.

Importance and design of ventilation for an improved sleep quality

Nur Çobanoğlu [a], Ziya Haktan Karadeniz [b], Sait Cemil Sofuoğlu [c], Macit Toksoy [d]

[a] Graduate School of Natural and Applied Sciences, İzmir Kâtip Çelebi University, İzmir, Turkey, ncobanoglu93.phd@gmail.com.

[b] Department of Energy Systems Engineering, İzmir Institute of Technology, İzmir, Turkey, haktankaradeniz@iyte.edu.tr.

[c] Department of Environmental Engineering, Izmir Institute of Technology, İzmir, Turkey, cemilsofuoglu@iyte.edu.tr.

[d] RD&PM, macittoksoy@gmail.com.

Abstract. Sleep quality, which significantly affects daily life, is also affected by indoor air quality as well as comfort aspects such as noise, temperature, and relative humidity in the sleeping environment. Carbon dioxide concentration is commonly considered as an indicator of indoor air quality, and it has been observed that increasing concentrations increase the number of awakenings resulting in lower sleep quality. In this study, ventilation flow rate is investigated specifically for bedroom and dormitory room dimensions as recommended by different countries to ensure that the carbon dioxide concentration in sleeping spaces is below an upper limit value (1000 ppm). The ventilation flow rate is evaluated by comparison to the methods recommended in ASHRAE standards (Ventilation Rate Procedure–VRP, Indoor Air Quality Procedure–IAQP and Natural Ventilation Procedure–NVP). Although VRP is widely used because a constant flow rate is recommended, which is an advantage due to design simplicity, it has been found to be insufficient for smaller sleeping space volumes and it gives higher values for larger volumes compared to the needed ventilation flow rates recommended by IAQP. Moreover, the fact that the flow rates calculated with VRP and IAQP overlap in a very narrow area shows that the use of VRP values for effective designs is limited. Consequently, we suggest that the system design should be operated with the IAQP and with demand-controlled ventilation, and an approach is offered to designers for direct use in practice.

Keywords. Sleep quality, indoor air quality, ventilation rate
DOI: https://doi.org/10.34641/clima.2022.335

1. Introduction

Today, people spend most of the day indoors and spend approximately a third of this time sleeping. Sleep quality, which has a significant effect on daily activities, is highly dependent on environmental factors and physical and mental functions of people. A high-quality sleep environment in terms of noise, room temperature, and relative humidity is necessary for good sleep quality [1,2]. CO_2 concentration is considered as an indicator of the ventilation efficiency of the environment and thus the indoor air quality. Higher ventilation rates and so lower CO_2 concentrations provide a reduction in the number of awakenings [2–4] and higher sleep quality [4–6].

Ventilation standards for bedrooms show that countries have different design approaches regarding the fresh air flow that should be provided in bedrooms [7]. These approaches can be classified as (i) consideration of the air flow rates predicted for the unit area and the number of people; (ii) consideration of the air flow rates predicted for the number of people; (iii) consideration of certain values of air change per hour per unit area; (iv) consideration of certain values of air change per hour at the prescribed volume; (v) considering that the CO_2 concentration does not exceed an average value during the sleep period, and (vi) consideration of an upper limit value of the CO_2 concentration in the design.

ASHRAE standards propose three different procedures to determine the ventilation rate: Ventilation Rate Procedure (VRP), Indoor Air Quality Procedure (IAQP), and Natural Ventilation Procedure–(NVP) [8]. As VRP, ASHRAE 62.1-2019 standard [8] provides a calculation of a ventilation rate for any dwelling unit while the total required fresh air flow rate for whole dwelling can be calculated by ASHRAE 62.2-

Copyright ©2022 by the authors. This conference paper is published under a CC-BY-4.0 license.

2019 standard [9].

Pollution concentration is related to volume and dependent on the architectural codes and traditions of the countries, and their social and economic development. Therefore, determining the fresh air flow rate by constant values according to the floor area and/or the number of people, or volume for ventilation (the first four approaches) cannot guarantee that the CO_2 concentration in the bedrooms during the sleeping period will exceed the value that affects the sleep quality, which has negative physical and mental effects. Although VRP is widely used to determine ventilation rate due to providing ease of calculation independent of the intended use of the space, it is not considered appropriate in ventilation design.

On the other hand, NVP should be considered as an auxiliary system by architects and mechanical installation engineers in all building designs, rather than being the main solution. Because natural ventilation can reduce the load of mechanical systems and improve energy savings. However, these systems cannot provide 100% of ventilation safety.

In IAQP, which is the recommended procedure for ventilation design, the required reliable ventilation flow is determined by using the safe pollution level, the volume of the living space, and the anthropometric characteristics of the people using the space as in this study. Monitoring the CO_2 concentration by demand-controlled ventilation provides an adaptation to changes related to volume functions and a possibility to use the advantages of natural ventilation. Although keeping CO_2 concentration below a constant value could be possible in demand-controlled ventilation systems designed by IAQP, it is practically not possible to ensure that the CO_2 concentration during sleep is below an average value considering the parameters affecting the sleep duration. Therefore, the fifth design approach is not considered as appropriate for ventilation design. The proposed design approach is the sixth approach: The ventilation system of the sleeping space should be a demand-controlled system that can provide fresh air at the air flow rate determined according to the maximum number of people and keep the CO_2 concentration in the sleeping space below an upper limit value.

In this study, it is recommended to use IAQP to determine the ventilation flow rate to ensure that the CO_2 concentration in the bedroom is below an upper limit value. Considering the difficulty with using this method which is the lack of a designer-friendly and approved calculation tool, this study aims to present an approach that designers can use directly for application by explaining the IAQP specific to bedrooms and dormitories.

2. Research Methods

2.1 CO_2 concentration as a control parameter in IAQP

CO_2 concentration is used as a control parameter which should be below an upper limit for determining ventilation rate by IAQP. The reason behind using the CO_2 concentration is that the source of this pollution is people in an indoor environment, and it is also an indicator of increasing pollutant concentrations since the accumulation of emitted chemicals from other sources occurs along with CO_2 from people in limited-ventilation indoor environments.

A tentative relationship between CO_2 concentration and sleep quality, which needs to be verified, is presented in a comparative study of the ventilation standards in bedrooms by Sekhar et al. [7]. Although the CO_2 concentrations below 750 ppm did not disturb the sleep quality, the range between 750-1150 ppm results in possibly disturbed sleep quality. In addition to disturbing sleep quality in the range of 1150-2600 ppm, reduced next-day cognitive performance was also observed for the concentrations higher than 2600 ppm. Additionally, the CO_2 concentration (higher than the average value of 800-1000 ppm) in the sleeping space shows the following effects [10]: (1) sleep efficiency, (2) waking frequency during the sleep phase, (3) sleep stages, and finally (4) mental performance the next day. Although the range of CO_2 concentration does not disturb sleep quality was given as < 750 ppm in the study [7], this study [10] expressed the range as <800 ppm. Moreover, the CO_2 concentration of 800 ppm is the standard upper limit for bedroom ventilation in Denmark [11].

To date, the upper limit value is 1000 ppm or 700 ppm above the outdoor CO_2 concentration (+700 ppm difference) as given in the “Informative Annex-D” in ASHRAE 62.2-2016. However, discussions continue on the suitability of these values for acceptable indoor air quality and mitigation of impact on human health and performance. Although these values were not given as mandatory upper limits that should be provided by ventilation in the relevant ASHRAE standards (62, 62.1, and 62.2), they were perceived as mandatory limits in practice and ventilation flow rates were used in the design to ensure that these values were not exceeded by the IAQP [12]. It is stated that the reference value of 1000 ppm is not included in ASHRAE 62.1-1999 [13]. Additionally, it was emphasized that the +700 ppm difference value, which is stated as a limit value that people find 80% acceptable in terms of odor quality in ASHRAE 62.1-2016 "Informative Annex-D", is not a limit value, and therefore this information is not included in ASHRAE 62.1-2019 [13].

Considering the mathematical model given in ASHRAE 62.1-2016 "Informative Annex-D", a CO_2 concentration difference limit value varies with each of the ventilation rates per person recommended for the VRP in the ASHRAE 62.1 standards (7.5 l/s of

ventilation rate corresponds to the parameters of 1.2 MET of metabolic rate, 0.31 l/s-person of bio-CO_2 emission, +700 ppm difference value for ~350 ppm outdoor CO_2 concentration). However, the +difference values obtained with this mathematical model depend on metabolic rate and anthropometric values as well as ventilation rate. In this case, the results could create a chaotic structure in terms of health safety. Using 1000 ppm of upper limit value instead of 700 ppm above the outdoor CO_2 concentration results in more effective ventilation and thus prevention of indoor accumulation of the various air pollutants and their concentration reaching relatively high levels in indoor air.

Within the scope of these discussions, 1000 ppm of CO_2 concentration value is assumed as an upper limit value to define the ventilation rate in sleeping spaces by IAQP in this study.

2.2 CO_2 emissions for the design of ventilation systems in sleeping spaces

The main source of CO_2 emissions in sleeping spaces (residential bedrooms, dormitories, hotel rooms, etc.) is emissions from sleeping people. The CO_2 emission of people depends on their metabolic rate (MR), anthropometric characteristics, respiratory coefficients depending on their dietary habits (carbohydrate, fat, protein), temperature and altitude. Therefore, it would be appropriate to take the maximum possible values of the CO_2 emissions of the people who sleep in these spaces to design a system providing adequate service within the physical life of the space. Here, the 95-percentile values were used for the weight (W) and height (H) of the men and women staying in the sleeping spaces [14]. The respiratory coefficient (RC) which is defined by average dietary habits and the MR are assumed as 0.83 and 1 MET, respectively. Since it is inversely proportional to temperature, the lowest value of temperature (18 °C) was used as the design temperature of the sleeping space. Tab. 1 presents the calculated CO_2 emission values by the model of Kalema and Viot [15] as a function of these parameters. The values given in Tab. 1 are used to calculate the total CO_2 emissions for different sleeping spaces, as indicated in Tab. 2.

Tab. 1 - CO_2 emission rates in terms of the safe design of ventilation systems in sleeping spaces.

	95-percentile		MR (MET)	RC	CO_2 emission rate (g/s)
	W (kg)	H (m)			
Woman	95.3	1.7985	1	0.83	0.0093
Man	96.8	1.7740			0.0095

Tab. 2 – The total emission values in sleeping spaces.

Sleeping Space	CO_2 emission rate (g/s)
Residential bedroom - Double	0.0188 (=0.0095+0.0093)
Residential bedroom - Single	0.0095
Dormitory rooms	Number of beds × 0.0095
Hotel room - Single	0.0095
Hotel room - Double	0.0188 (=0.0095+0.0093)
Hotel room - Multiple	Number of beds × 0.0095

2.3 Sleeping spaces

Within the scope of indoor air quality, the pollutant concentration is related to the volume of the sleeping space which depends on the countries' architectural codes, traditions, socio-economic status. Tab. 3 presents the minimum sizes of bedrooms and dormitory rooms. Most of the dimensions in the Tab. 3 indicate the general practice instead of the minimum requirement. Although the ceiling height is also an important parameter for ventilation, some of the sources only gave a value of area per person. Tab. 3 shows that the minimum volume per person in dormitory rooms all over the world is 10 m^3/person. The highest value is calculated as 21.6 m^3/person corresponding to the area of 9 m^2/person given by TS 11498 for single-person dormitories [16–18].

Tab. 3 – The total emission values in sleeping spaces.

Country	Area (m^2/person) / Volume (m^3/person)	Dormitories	Ref.
Turkey	**9** / 21.6	Single-room Min. Ceiling height = 2.4 m	[16–18]
	5 / 12.5	Multiple-room Min. Ceiling height = 2.4 m	
	8 / 19.2	Single-room Min. Ceiling height = 2.4 m	[19]
	4.17 / 10	Multiple-room (3-6 people) Min. Ceiling height = 2.4 m Min. Volume = 10 m^3/person	
	6 / 13.2	Single-room Min. Ceiling height = 2.2 m	
	4.55 / 10	Multiple-room	

		Min. Ceiling height = 2.2 m Min. Volume = 10 m³/person	
	2.98 / -	8-people Room floor area = 23.8 m²	[18]
USA	12.1 / -	[20]	
	8.6 / -	[21]	
	4.6 / -	[22]	
China	4.5 / 12.5 3.73 / 10	4-people Ceiling height = 2.8 m 6-people Ceiling height = 2.8 m	[23]
Australia	10-12 / -	[24]	
	20 / -		
Country	**Area (m²/person) / Volume (m³/person)**	**Bedrooms**	**Ref.**
Turkey	**9** / 21.6 – 2.34	Ceiling height = 2.4 – 2.6 m	[25]
UK	8 / -	Single-room	[26]
	6 / -	Double-room	
	7.5 / -	Single-room Min. ceiling height = 2.3 m	[27]
	5.75 / -	Double-room Min. ceiling height = 2.3 m	
	16-25 / -	[28]	

3. CO_2 Concentration in Sleeping Environments

In many countries, the variation of the CO_2 concentration in sleeping spaces (bedrooms) in buildings with different purposes (residential, residence, dormitory, etc.) has been measured in different seasons and the effect of this variation on sleep quality has been tried to be determined by objective or subjective methods. Most of these studies show that the CO_2 concentration increases during sleep and in some cases reaches serious values (7500 ppm) for the absence of ventilation in the sleeping spaces and the conditions of the open window and/or door during the measurements.

3.1 CO_2 balance in sleeping environments

The CO_2 balance in any sleeping space (bedroom, dormitory, etc.) is expressed considering the amount of CO_2 produced in the volume, entering and leaving the volume if there is no other CO_2 source in the volume (Fig. 1). Components entering the sleeping space are the CO_2 rates emissions of sleeping people in the volume, entering by ventilation and infiltration. The outputs are the CO_2 rates which release through infiltration and ventilation. Considering these values, the CO_2 rate in the sleeping volume is given in equation (1). The parameters in equation (1) are explained in Tab. 4.

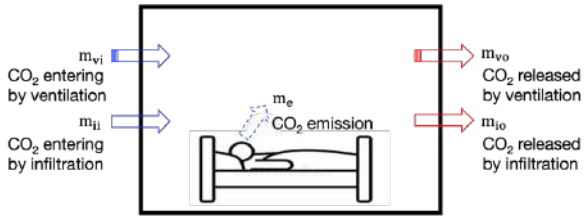

Fig. 1 – CO_2 balance in the sleeping space

$$\frac{dm(t)}{dt} = M_e + m_{vi} + m_{ii} - m_{vo} - m_{io} \quad (1)$$

Tab. 4 – Parameters of the CO_2 balance in the sleeping space

$m(t) = VC(t)$	The amount of CO_2 in the sleeping volume (mg)
V	Sleeping volume (m³)
t	Time (h)
$M_e = N_b m_e$	Time-dependent CO_2 concentration in the sleeping volume (mg/m³)
N_b	Number of people in the sleeping space (-)
m_e	CO_2 emission of the sleeping person (mg/s)
$m_{ii} = Q_i C_d$	CO_2 concentration entering the volume by infiltration (mg/s)
Q_i	Infiltration rate (m³/s)
C_d	Outdoor CO_2 concentration (mg/m³)
$m_{io} = Q_i C(t)$	CO_2 concentration released by infiltration (mg/s)
$m_{vi} = Q_v C_d$	CO_2 concentration entering the volume by ventilation (mg/s)
Q_v	Ventilation rate (m³/s)
$m_{vo} = Q_v C(t)$	CO_2 concentration released by ventilation (mg/s)

By substituting the terms given in equation (1) and Tab. 4, the time-dependent change in CO_2 concentration is:

$$\frac{dC(t)}{dt} = \frac{N_b m_e}{V} + \frac{Q_v + Q_i}{V}[C_d - C(t)] \quad (2)$$

3.2 Minimum sleeping volume without ventilation and infiltration

Since the highest CO_2 concentration value should be in the case where ventilation and infiltration are not

taken into account, equation (2) is written as:

$$\frac{dC(t)}{dt} = \frac{N_b m_e}{V} \tag{3}$$

When the boundary conditions for $C(0)=C_d$ at $t=0$ and $C=C(t)$ at $t=t$ are employed in equation (3), the equation required to define the maximum CO_2 concentration value is obtained as

$$C_{\max}(t) = \mathrm{C_d} + \frac{N_b m_e}{V} t \tag{4}$$

The maximum CO_2 concentration in equation (4) is rewritten in ppm unit instead of mg/m³ by equation (5).

$$C_{\max}(t) = \mathrm{C_d} + \frac{N_b m_e}{V} t \left[\left(\frac{\mathrm{V_m}}{\mathrm{M_{CO_2}}}\right)\left(\frac{273+T}{273}\right)\left(\frac{1013}{P}\right)\right] \tag{5}$$

Here, the molecular weight of CO_2 is M_{CO2} = 44.01 g/mol, and the molar volume of air is V_m = 24.47 l/mol. T and P are the temperature [°C] and pressure [hPa] of the air.

The required time to reach the 1000 ppm value defined as the upper limit for any volume of CO_2 concentration is expressed by

$$t = \frac{(1000-\mathrm{C_d})V}{\left(\frac{\mathrm{V_m}}{\mathrm{M_{CO_2}}}\right) M_e \phi_T \phi_P} \tag{6}$$

where $\phi_T = \frac{273+T}{273}$ and $\phi_P = \frac{1013}{P}$.

Additionally, the volume in which ventilation is not required during sleep is given as a function of time in equation (7).

$$V_f = \frac{N_b m_e}{C(t)-\mathrm{C_d}} t \tag{7}$$

The National Sleep Foundation (NSF) recommends between 7 and 9 hours of sleep for adults aged 18-25 years [29,30]. The V_f was found to be 311.4 m³/person if the CO_2 concentration in the room did not exceed the C(t)=1000 ppm value after 9 hours of sleep. The variation of this value according to sleep duration is presented in Fig. 2. The V_f values obtained for the 7-9 hours of sleeping period recommended for an adult human are inaccessible for conventional sleeping spaces, therefore it should be noted as a necessity to ventilate any sleeping space smaller than the V_f value.

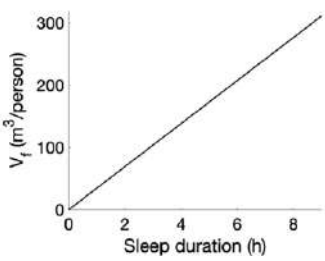

Fig. 2 – The variation of smallest sleeping space volume which does not require ventilation with the sleeping duration ($(C(t))_{max}$=1000 ppm).

Fig. 3 shows the time-dependent variation of CO_2 concentration for different volumes per person. Since the sleeping volume changes in the range of 10-21.6 m³/person in dormitories (Tab. 3), the minimum value of the sleeping volume is defined as 10 m³/person in this study. As expected, the increasing slope of the CO_2 concentration decreases for higher volumes, and the time to reach the 1000 ppm of CO_2 concentration also increases as the volume increases.

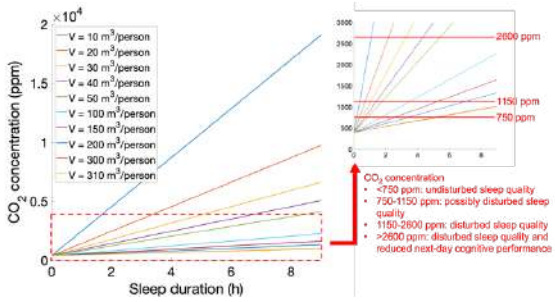

Fig. 3 – The time-dependent variation of CO_2 concentration for different volumes and the typical effects of CO_2 concentration on people [7].

3.3 Safe ventilation rates for sleeping environments

In order not to affect sleep quality in any sleeping place, the differential solution of the equation (2) is required to define CO_2 concentration in the sleeping space sourced by sleeping people's emissions. The equation (2) is rearranged by neglecting the infiltration as

$$\frac{dC(t)}{dt} = \frac{N_b m_e}{V} + \frac{Q_v}{V}[\mathrm{C_d} - C(t)] \tag{8}$$

Equation (8) is a first-order linear ordinary differential equation, and its solution is given by

$$C(t) = c_1 e^{-\frac{tQ_v}{V}} + \mathrm{C_d} + \frac{N_b m_e}{Q_v} \tag{9}$$

When the boundary conditions for $C(0)=C_d$ at $t=0$ and $C=C(t)$ at $t=t$ are employed in equation (9), the equation (9) is re-written as

$$C(t) = \mathrm{C_d} + \frac{N_b m_e}{Q_v}\left(1 - e^{-\frac{tQ_v}{V}}\right) \tag{10}$$

The equation (10) allows calculating the safe ventilation rate (Q_v) in the sleeping space for the volume per person by applying the upper limit value of $(C(t))_{max}$=1000 ppm. The variation of the safe ventilation rate with the volume per person is presented in Fig. 4 for 9 hours of sleep duration, and the ventilation rate decreases as the volume per person increases. However, this reduction in the ventilation rate, which is obtained from the volume of 100 m³/person, has no implications in real-life conditions. Because the sleeping volume ranges

between 10 and 25 m³/person in real life, and the ventilation flow rate remains almost constant (9.60 l/s-person) in this volume range.

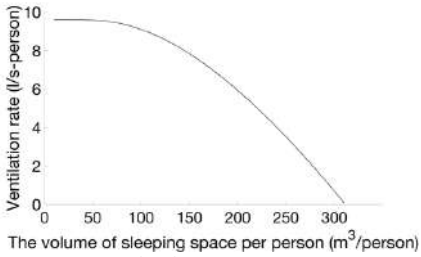

Fig. 4 – The change of safe ventilation rate with sleeping volume per person (C(9 h)=1000 ppm).

Although the need for ventilation decreases as the volume of the sleeping area increases, Fig. 5 shows the necessity of ventilation for the volumes of 10-30 m³/person from the first hour of the sleep period in case of the CO_2 concentration to not exceed the upper limit of 1000 ppm.

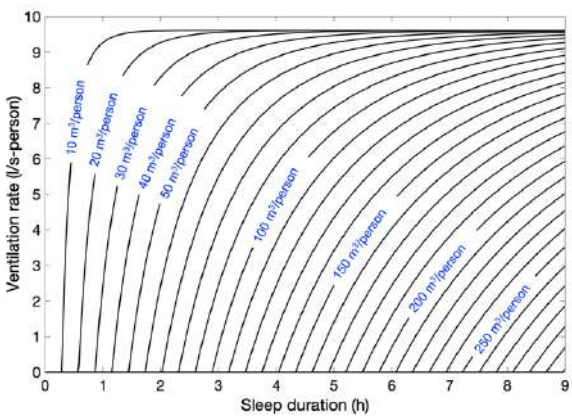

Fig. 5 – The variation of the ventilation rate with sleep duration for different sleeping volumes per person.

3.4 Comparison of IAQP and VRP in determining the safe flow rate to be used in the design of ventilation

Sekhar et al. [7] investigated the ventilation rate standards of 15 countries, from the USA to China for bedrooms. In the table they presented to compile all standards of different countries, specific ventilation design flow rates for bedrooms are defined in the European Union and in five countries, and in some of 9 countries, separate values are given for kitchens and bathrooms, and the same design flow rates are recommended for all remaining residential spaces. This study aims to investigate the effect of these recommended flow rates on the CO_2 concentration in the sleeping space and the difference from the values recommended by IAQP. The proposed design flow rates within the scope of VRP and the models given in ASHRAE Standard 62.1 and 62.2 to be used in the comparison of IAQP and VRP are presented in Tab. 5. In ASHRAE Standard 62.2, A_{floor} is the residential floor area (m²) and N_{br} is the number of bedrooms (N_{br}>1) in the residential. N_b represents the number of people in the bedroom and A_b represents the area of the bedroom (m²) in ASHRAE Standard 62.1.

Tab. 5 – The ventilation rates obtained from [7] and proposed by VRP.

Country	Flow rates
ASHRAE 62.2	$Q_{total} = 0.15A_{floor} + 3.5(N_{br} + 1)$ (l/s)
Belgium	1 (l/s m²)
Sweden	0.35 (l/s m²)
Netherlands	0.90 (l/s m²)
UK	0.30 (l/s m²)
Country	**Flow rates**
ASHRAE 62.1	$Q_b = 2.5N_b + 0.3A_b$ (l/s)
CEN – Category 1	2.90 (h⁻¹)
CEN – Category 2	2.00 (h⁻¹)
CEN – Category 3	1.20 (h⁻¹)
Norway	7.20 (l/s person)
Denmark	0.30 (l/s m²)
China	1.00 (h⁻¹)
India	3.00 (h⁻¹)

The effect of the ventilation rates for the bedroom determined by VRP on the CO_2 concentration in the sleeping space is shown in Fig. 6 for 9 hours of sleep duration. The volume of the sleeping space was calculated considering the minimum ceiling height as 2.4 m corresponding to the minimum volume value in the standard TS 11498 [16–18]. It is observed that the ventilation rates calculated by VRP for the bedroom decrease the CO_2 concentration below 1000 ppm as the volume of sleeping space per person increases. In addition, the CO_2 concentration for 10 m³/person, which is the lowest volume of sleeping space in the standards, is above 1000 ppm for the values recommended in all standards.

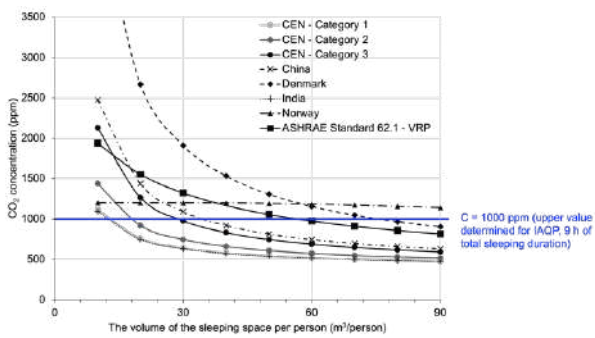

Fig. 6 – The effect of ventilation rates calculated by VRP on the CO_2 concentration for different volumes of sleeping space per person.

Fig. 7 shows the variation of ventilation rates with the volume per person after 9 hours of the sleep. In

the calculations, the minimum residential floor area is assumed as 28.5 m² and the lowest area that the sleeping space was defined as 9 m² [25]. The ventilation flow rates for the whole dwelling were calculated as the ratio of the sleeping space area to the total floor area of the dwelling (0.32).

Although the flow rates calculated by VRP for low volumes of sleeping spaces are insufficient, the flow rates calculated by VRP exceed the safe ventilation flow rate calculated with IAQP for higher volumes. Intersecting the ventilation rates defined by VRP and IAQP in a narrow area limits the utilization of the VRP. In the cases where VRP values are insufficient or too high, it is recommended to demand-controlled ventilation by IAQP considering the system design.

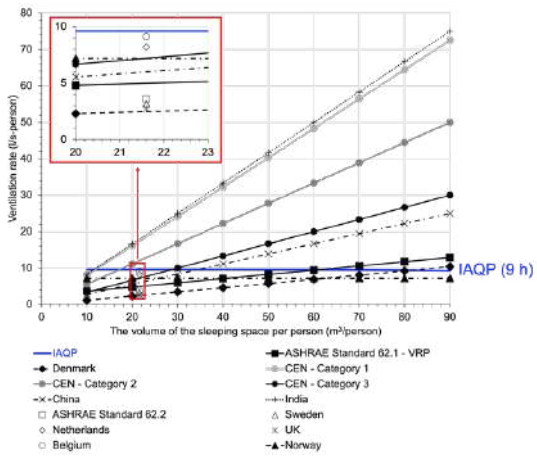

Fig. 7 – The ventilation rates calculated by VRP and IAQP for different volumes of sleeping space per person.

4. Conclusions

Within the scope of different approaches for the required ventilation rate for sleeping spaces, the applicability of these procedures proposed by ASHRAE standards has been evaluated in this study. In order to ensure that the CO_2 concentration in the sleeping space is below an upper limit value (1000 ppm), the proposed IAQP is explained specifically for bedrooms and dormitory rooms, and an approach that designers can use directly for implementation is presented. Ventilation rate diagrams have been proposed for different sleeping space volumes and sleep times by assuming the upper limit value of the CO_2 concentration as 1000 ppm. In addition, the model in which the upper limit value of CO_2 concentration, space volume, and sleep duration are variable has been developed to calculate a reliable ventilation flow.

While the mathematical model given in ASHRAE 62.1-2016 "Informative Annex-D" indicates the appropriateness of 7.5 l/s person ventilation flow per person to reach a safe 1000 ppm value, the safe ventilation rate recommended by the IAQP method, which accepts the upper limit of the CO_2 concentration as 1000 ppm, has been calculated as 9.60 l/s person, up to a sleeping area volume of approximately 70 m³/person.

The proposed design criteria for sleeping spaces within the scope of this study can be summarized as follows:

- Upper limit value of CO_2 concentration: 1000 ppm
- The procedure for calculating ventilation rate should be IAQP
- The number of people in the bedroom:
  - Main bedroom: 2
  - Other bedrooms: 1 or 2 depending on the size of the room
  - Dormitory rooms: possible maximum number of people
- Maximum CO_2 emission per sleeping person: 9.5 mg/s
- System control: Demand-controlled ventilation

5. References

[1] Ohayon M, Wickwire EM, Hirshkowitz M, Albert SM, Avidan A, Daly FJ, et al. National Sleep Foundation's sleep quality recommendations: first report. Sleep health. 2017;3(1):6–19.

[2] Liao C, Delghust M, Wargocki P, Laverge J. Effects of window opening on the bedroom environment and resulting sleep quality. Science and Technology for the Built Environment. 2021;1–21.

[3] Laverge J, Janssens A. Analysis of the influence of ventilation rate on sleep pattern. In: Indoor Air 2011. ISIAQ; 2011.

[4] Mishra AK, Van Ruitenbeek AM, Loomans M, Kort HSM. Window/door opening-mediated bedroom ventilation and its impact on sleep quality of healthy, young adults. Indoor Air. 2018;28(2):339–51.

[5] Lan L, Sun Y, Wyon DP, Wargocki P. Pilot study of the effects of ventilation and ventilation noise on sleep quality in the young and elderly. Indoor air. 2021;

[6] Strøm-Tejsen P, Zukowska D, Wargocki P, Wyon DP. The effects of bedroom air quality on sleep and next-day performance. Indoor air. 2016;26(5):679–86.

[7] Sekhar C, Akimoto M, Fan X, Bivolarova M, Liao C, Lan L, et al. Bedroom ventilation: Review of existing evidence and current standards. Building and Environment. 2020;107229.

[8] ANSI/ASHRAE. Standard 62.1-2019: Ventilation for Acceptable Indoor Air Quality. ASHRAE. Atlanta, Georgia;

[9] ANSI/ASHRAE. Standard 62.2-2019: Ventilation and acceptable indoor air quality in residential buildings. ASHRAE. Atlanta, Georgia;

[10] Akimoto M, Sekhar C, Bivolarova MP, Liao C, Fan X, Laverge J, et al. Reviewing how bedroom ventilation affects IAQ and sleep quality. ASHRAE Journal. 2021;63(4):56–60.

[11] Braun G-J, Zeiler W. The CO2 conditions within the baby cots of day care centres. In EDP Sciences; 2019. p. 02045.

[12] Herrmann DC. Understanding CO2 and ASHRAE 62: A technical note. Energy engineering. 2002;99(1):50–3.

[13] Persily AK. Don't Blame Standard 62.1 for 1,000 ppm CO2. ASHRAE Journal. 2021;63(2).

[14] Güleç E, Akın G, Sağır M, Koca B, Gültekin T, Bektaş Y. Anadolu insanının antropometrik boyutları: 2005 yılı Türkiye antropometri anketi genel sonuçları. Ankara Üniversitesi Dil ve Tarih-Coğrafya Fakültesi Dergisi. 2017;49(2).

[15] Kalema T, Viot M. Methods to reduce the CO 2 concentration of educational buildings utilizing internal ventilation by transferred air. Indoor air. 2014;24(1):71–80.

[16] Öztürk SM, Dincer AE. An Investigation on the Design Principles of Dormitory Buildings in Karabük. Journal of Design+ Theory. 2020;16(30):61–76.

[17] Yıldırım K, Uzun O. The effects of space quality of dormitory rooms on functional and perceptual performance of users: Zübeyde Hanım Sorority. Gazi University Journal of Science. 2010;23(4):519–30.

[18] Çağatay K, Yalçın M, Yıldırım K. Öğrenci Yurdu Odalarının Mekân Kalitesinin Kullanıcıların Fonksiyonel ve Algısal Performansı Üzerine Etkisi; Tahsin Banguoğlu Örneği. Tasarım+ Kuram. 2014;10(18):53–72.

[19] MEB Özel Öğrenci Barinma Hizmeti Kurumlarinin Standartlari İle Çalişma Usul Ve Esaslari Hakkinda Yönerge [Internet]. 2018 [cited 2022 Jan 8]. Available from: https://ookgm.meb.gov.tr/meb_iys_dosyalar/2018_04/11120321_Yzel_YYrenci_BarYnma_Hizmeti_KurumlarYnYn_StandartlarY_ile_YalYYma_Usul_ve_EsaslarY_HakkYnda_YYnerge.pdf

[20] 2020 Yale University Dorm Tours and Info [Internet]. [cited 2022 Jan 8]. Available from: https://www.campusreel.org/colleges/yale-university/dorms

[21] Freshman Challenge: a Virtually Decorated Dorm Room [Internet]. [cited 2022 Jan 8]. Available from: https://www.wsj.com/articles/SB10000872396390444042704577587662345274568

[22] Minimum Dorm Room Size [Internet]. [cited 2022 Jan 8]. Available from: https://www.thebuildingcodeforum.com/forum/threads/minimum-dorm-room-size.29006/

[23] Lei Z, Liu C, Wang L, Li N. Effect of natural ventilation on indoor air quality and thermal comfort in dormitory during winter. Building and Environment [Internet]. 2017 Nov 15;125:240–7.

[24] Living on Campus Questions - What's the size of my bedroom? [Internet]. [cited 2022 Jan 8]. Available from: https://accommodation.unsw.edu.au/faq/living-campus/what's-size-my-bedroom

[25] İzmir Büyükşehir Belediyesi İmar Yönetmeliği [Internet]. 2021 [cited 2022 Jan 8]. Available from: https://www.resmigazete.gov.tr/eskiler/2021/06/20210603-11.htm

[26] London Housing Design Guide [Internet]. [cited 2022 Jan 8]. Available from: https://www.london.gov.uk/sites/default/files/interim_london_housing_design_guide.pdf

[27] Technical housing standards – nationally described space standard [Internet]. 2015 [cited 2022 Jan 8]. Available from: https://assets.publishing.service.gov.uk/government/uploads/system/uploads/attachment_data/file/1012976/160519_Nationally_Described_Space_Standard.pdf

[28] Morgan M, Cruickshank H. Quantifying the extent of space shortages: English dwellings. null [Internet]. 2014 Nov 2;42(6):710–24.

[29] Hirshkowitz M, Whiton K, Albert SM, Alessi C, Bruni O, DonCarlos L, et al. National Sleep Foundation's sleep time duration recommendations: methodology and results summary. Sleep health. 2015 Mar;1(1):40–3.

[30] National Sleep Foundation. How Much Sleep Do You Really Need? [Internet]. 2020 [cited 2022 Jan 8]. Available from: https://www.thensf.org/how-many-hours-of-sleep-do-you-really-need/

Data Statement

The datasets generated during and/or analysed during the current study are not publicly available because they are to be the subject of further studies but will be available from the corresponding author on reasonable request.

Development of a human body thermo-physiological model considering the effect of gravity on blood

Hiroya Azemachi [a], Hideaki Nagano [b], Atsushi Ooi [c], Riku Emoto [d], Suguru Shiratori [e], Kenjiro Shimano [f]

[a] Department of Mechanical Systems Engineering, Tokyo City University, g1812003@tcu.ac.jp

[b] Department of Mechanical Systems Engineering, Tokyo City University, hnagano@tcu.ac.jp

[c] Department of Mechanical Systems Engineering, Tokyo City University, 1712019@tcu.ac.jp

[d] Graduate School of Integrative Science and Engineering, Tokyo City University, g2081007@tcu.ac.jp

[e] Department of Mechanical Systems Engineering, Tokyo City University, sshrator@tcu.ac.jp

[f] Department of Mechanical Systems Engineering, Tokyo City University, kshimano@tcu.ac.jp

In general, blood flow in the human body is significantly impacted by gravity; thereby resulting in thermo-physiological effect. In the present study, we modeled and formulated the effect of gravity on blood flow for each body part, depending on the body posture. We added the gravity term to the segmented two-node model; whereby skin temperature was calculated. This value agrees well with the results of the human subject experiment.

Keywords: postural changes, thermal comfort, blood flow, gravity, thermo-physiological model
DOI: https://doi.org/10.34641/clima.2022.323

1. Introduction

Conventional comfort assessment has considered six elements of the thermal environment: air temperature, radiant temperature, airflow, humidity, amount of clothing and metabolic rate.[1] However, considering that the rate of blood flow changes as the posture of the human body changes, there exists a possible need to consider "posture" as the seventh element of the thermal environment. Therefore, we hypothesized that the gravitational effect caused by posture change may also affect the skin temperature. The purpose of this study is to verify this hypothesis through experiments, to formulate the blood flow change owing to gravity, and finally to develop a simulator that can evaluate thermal comfort considering the effect of gravity.

2. Computational theory

2.1 Development of 2-node blood pressure model (2NBPM)

The conventional two-node model (2 NM) developed by Gagge[2] as a thermal comfort evaluation method does not consider the effect of gravity. Thus, we developed a new 2NBPM based on 2 NM that can consider the effects of gravity and blood pressure. This model considers that the positional relationship between both the core layer and skin layer changes with posture and defines it as the "posture angle". The posture angle is the position of the skin layer when viewed from the core layer, where counterclockwise is positive($0° \leqq \theta \leqq 360°$). The deep layer and the skin layer are considered to be connected by blood vessels, as in 2 NM. This blood vessel is defined as a "virtual blood vessel," which is a single conduit that includes all arterioles and capillaries in the real human body. Fig. 1 demonstrates the developed 2NBPM and the definition of posture angleθ.

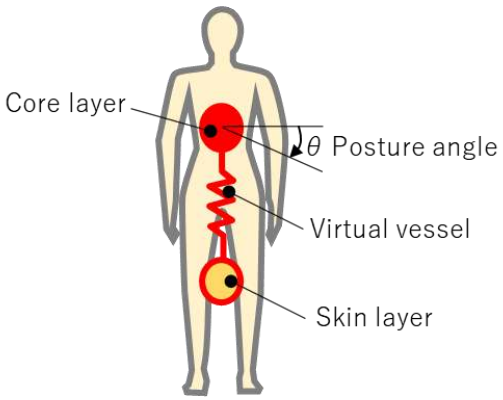

Figure. 1- Definition of posture angle θ in the 2NBPM

2.2 Development of a Segmented Two-node Blood Pressure Model

The segmented two-node model developed by Kohri et al[3] and Okabe et al. [4] divides the human body into 22 parts, and the model calculates skin temperature by solving the heat balance between the common core layer and the skin layer of each part. In this

Copyright ©2022 by the authors. This conference paper is published under a CC-BY-4.0 license.

study, we introduce the gravitational effect described in the previous section into the segmented two-node model and further introduce the concept of "standard posture". Many existing thermo-physiological models and thermal environment indices assume sitting posture or standing posture. In this study, all existing models were considered to be taking the standard posture. Therefore, the blood flow rate between the core and skin layers during standard posture is consistent with the conventional 2 NM and segmented two-node models. Fig. 2 illustrates the definitions of the standard posture angle and site height.

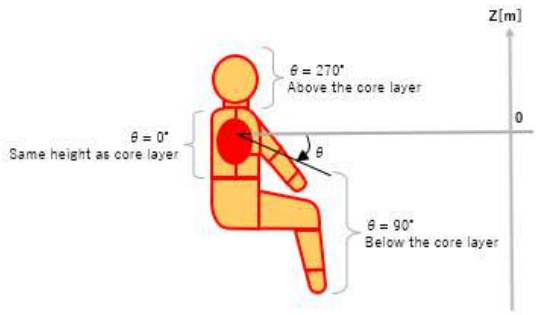

Figure. 2-Definition of Standard Posture angle θ and seating height z

The force applied to the blood flowing through the virtual blood vessel is called the total driving force(F_i), and the ratio to the total driving force $F_{g,i}$ in the standard posture is defined as the change rate of blood flow $r_{b,l,i}$. i indicates the number of each body part. The total driving force and the rate of change in blood flow are expressed by the following equations:

$$F_i = \left(p_0 + \frac{1}{2}\rho v^2\right) \cdot \pi r^2 + m_i g sin\theta_i - \rho g z_i \cdot \pi r^2 \quad (1)$$

$$F_{g,i} = \left(p_0 + \frac{1}{2}\rho v^2\right) \cdot \pi r^2 + m_i g sin\theta_{g,i} - \rho g z_{g,i} \cdot \pi r^2 \quad (2)$$

$$r_{bl,i} = \frac{F_{g,i}}{F_i} \quad (3)$$

m_i is the weight of blood flowing to each site, z_i is the site height with respect to the heart during standard posture and $z_{g,i}$ is the site height with respect to the heart during posture change. p_0 is the blood pressure in the heart, v is the virtual blood flow velocity, and r is the virtual vessel diameter. In the model, we adopted a mean blood pressure of 13.3 kPa, a blood flow velocity of 0.6 m/s in the ascending aorta, and a vessel diameter of 0.035 m in a man[5]. The first term on the right-hand side of equations (1) and (2) is the force that pumps blood from the depth to each part of the body, the second term on the right-hand side is the gravity on the blood, and the third term on the right-hand side is the hydrostatic pressure with respect to the depth. In addition, in the conventional segmented two-node model, each human body part is directly connected to the core layer, but in this model, each part is connected in series from the core layer. For example, when you raise your hand, blood flow is assumed to be in the order of the upper arm, forearm, and hand. Therefore, by multiplying the rate of change in blood flow at the upstream site by the rate of change in blood flow at the downstream site, the blood flow rate changes more significantly at the downstream site. If the rate of change in blood flow at the upstream site is $r_{bl,i}$ and the rate of change in blood flow at the downstream site is $r_{bl,j}$, the rate of change in blood flow at the downstream site can be expressed by the following equation:

$$r^*_{bl,j} = r_{bl,i} \times r_{bl,j} \quad (4)$$

$r^*_{bl,j}$ is the rate of change in blood flow at the downstream site after serialization. In the conventional segmented two-node model, the constant D_{bl} that distributes the blood flow to each site is defined experimentally. In the segmented two-node blood pressure model, the rate of change in blood flow is multiplied by this distribution rate to achieve the change in blood flow in each region.

$$D'_{bl,i} = r^*_{bl,j} \times D_{bl,i} \quad (5)$$

However, because the distribution rate D_{bl} is defined by the body surface area ratio of each body part, the calculation in the above equation is not consistent. Therefore, we redefined the blood flow distribution ratio by normalizing it to the body surface area ratio.

$$D''_{bl,i} = D'_{bl,i} \times \frac{\sum D_{bl,i}}{\sum D'_{bl,i}} \quad (6)$$

Therefore, the blood volume can be changed by multiplying the redefined distribution rate by the blood flow rate at each site.

$$V'_{bl,i} = D''_{bl,i} \times V_{bl,i} \quad (7)$$

In this way, the effects of attitude angle and gravity can be considered for the conventional segmented two-node model by calculating the blood flow.

3. Validation

3.1 Examination (1) Comparison of fingertip skin temperature when the upper arm is raised

We conducted a simple subject experiment with four subjects to validate the developed variance two-node blood pressure model. The experimental conditions are presented in Table 1.

Tab. 1-Experimental condition

Environment	Air temperature	24.5 °C
	Radiant temperature	24.5 °C
	Airflow velocity	0.1 m/s
	Relative humidity	50 %
Human	Metabolic rate	1 met as standing
	Amount of clothing	0.7 clo

In the experiment, thermocouples were attached to the fingertips of the right and left hands to measure the skin temperature. Fig. 3 shows the skin temperature differences at the fingertips of the four subjects and their averages.

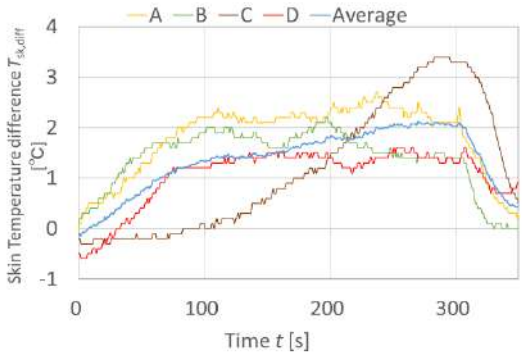

Fig. 3-Skin-temperature difference between left and right fingertips in four subjects

Figure 3 shows the 300 seconds after the right hand is raised. Focusing on the difference in skin temperature between the left and right sides of the body when 300 s elapsed after the right hand was raised. The largest difference in skin temperature between the left and right was 3.4 °C for subject C. The smallest difference in skin temperature was 1.3 °C for subject D. We confirmed that skin temperature changes owing to the effect of gravity, although it varied from subject to subject. Next, we illustrate a comparison of the results of simulations under the same conditions as the experiments using the developed two-node blood pressure model in Fig. 4. Figure 4 shows the 300 seconds after the right hand is raised. In the initial state, there was no difference in skin temperature between the left and right hands, but immediately after the right hand was raised, the temperature of the left hand increased, and at the 300-second elapsed time, the temperature difference between the left and right hands reached 2.1 °C. This agrees with the average value of 2.0 °C for the four subjects. The temperature of the left hand was higher than that of the right hand immediately after the right hand was raised.

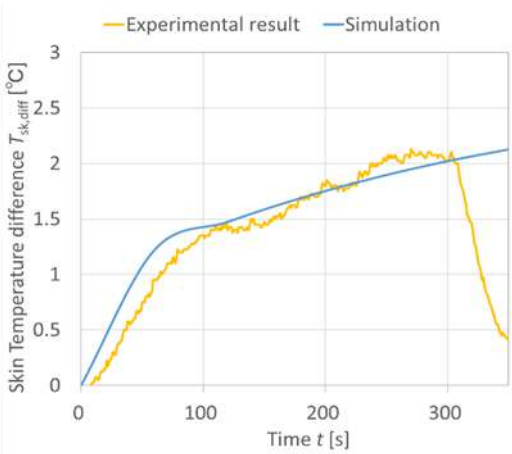

Fig. 4-Comparison of average experimental results with simulation results

3.2 Examination (2) Examination of the effects of whole body posture changes

Next, we conducted experiments and simulations in the upraised posture (Case 1) and supine posture (Case 2) to compare skin temperature changes and analyze the effects on blood flow changes and SET* in the simulations. In the experiment, seven subjects engaged in a sitting position for 30 min and then maintained the changed posture for 10 min, and their skin temperatures before and after the change were compared. The skin temperature was measured on the left palm. Table 2 summarises the posture angles and site heights in Case1 and Case2.

3.2.1 Blood flow and skin surface temperature

Fig. 5 illustrates the changes in blood flow and skin temperature in the upper arm, forearm, and hand in Case 1, and Fig. 6 illustrates the changes in blood flow and skin temperature in each body part in Case 2. In the simulation of Case 1, the blood flow decreased in the upper arm, forearm, and hand; the skin temperature decreased by 0.31 °C in the upper arm and 0.12 °C in the forearm. The skin temperature of the hand in the subject experiment decreased by 1.0 °C, whereas in the simulation, it decreased by 0.17 °C. Case 2 confirmed that blood flow in the upper body, especially in the head, increased in the simulation, while blood flow in the lower body decreased. The skin temperature decreased by a maximum of 0.54 °C in the feet. The simulation shows a decrease of about 0.086 °C in the hands and 0.54 °C in the feet, compared with a decrease of about 0.55 °C in the hands and 0.4 °C in the feet in the subject experiments.

Tab. 2- Posture angle and site height in Case1 and Case2

Part	Case 1		Case 2	
	Posture angle θ [deg]	Height of part z [m]	Posture angle θ [deg]	Height of part z [m]
Head	270	0.52	0	0
Neck	270	0.282	0	0
Chest	0	0	270	0
Back	0	0	90	0
Abdomen	90	0	270	0
Waist	90	-0.24	0	0
Upper arm (L / R)	270	0.521	0	0
Forearm (L / R)	270	0.772	0	0
Hand (L / R)	270	0.962	0	0
Thigh_Fr (L / R)	90	-0.716	0	0
Thigh_Bk (L / R)	90	-0.716	0	0
Leg_Fr (L / R)	90	-1.111	0	0
Leg_Bk (L / R)	90	-1.111	0	0
Foot (L / R)	90	-1.194	0	0

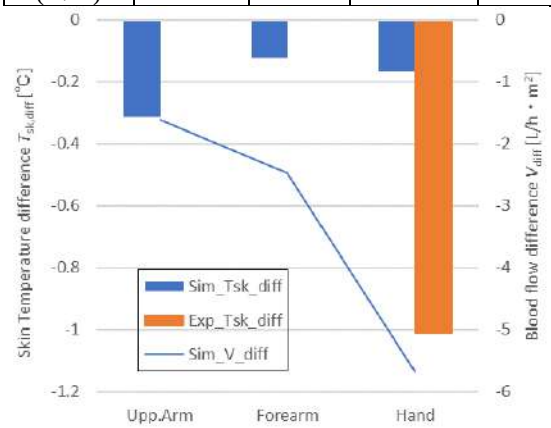

Fig. 5- Amount of change in blood flow and skin temperature in Case1

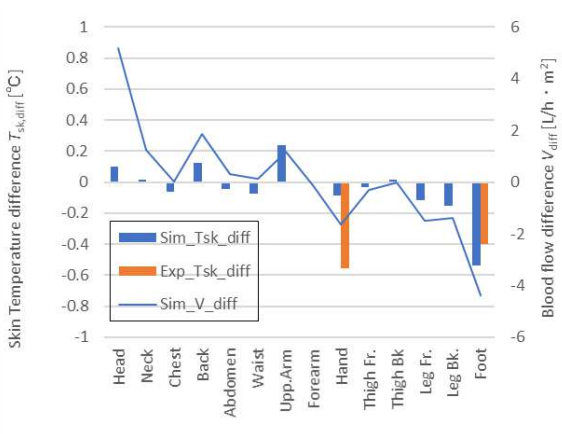

Fig. 6- Amount of change in blood flow and skin temperature in Case2

By introducing the rate of change in blood flow into the model, the skin temperature decreased in the area where blood flow decreased in the simulation. Compared with the experiment, the amount of change in the model was different for the reproduction of the skin temperature change by changing the posture angle; therefore, further improvement is necessary.

3.2.2 Blood flow response rate

Figs. 7 and 9 illustrate the rate of change of blood flow in the hand between simulation and experiment in Cases 1 and 2. In Case 1, when comparing the speed of response of blood flow changes between simulation and experiment, the experimental results illustrate a faster increase. Therefore, we extended the calculation time of the simulation, and the result is illustrated in Fig. 8. Fig. 8 illustrates that the blood flow rate changed at about 1800 seconds after the postural change. In Case 2, when comparing the speed of response of blood flow changes between simulation and experiment, the experimental results increased faster, as in Case 1.

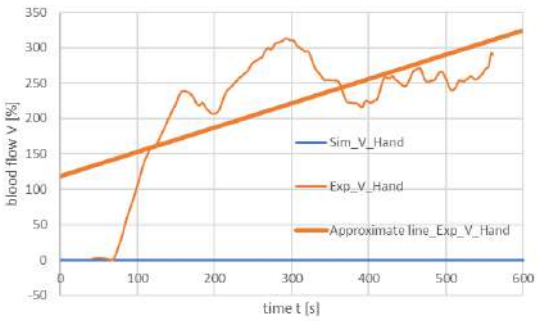

Fig.7- Blood flow changes in the hand in Csae1

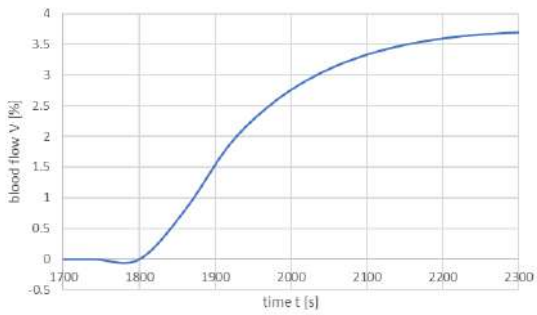

Fig.8- Simulation results of blood flow changes in the hand in Case1

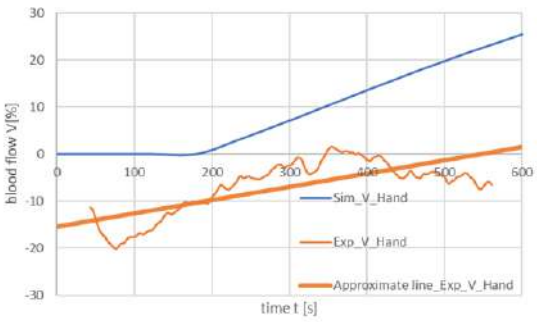

Fig.9- Blood flow changes in the hand in Case2

The simulation illustrates a slower response time to blood flow changes than the experiment. Therefore, future improvements are needed.

3.2.3 Change in SET from standard posture*

Fig. 10 and 11 illustrate the change in SET* from the standard posture in Cases 1 and 2. In addition to the aforementioned difference in skin temperature, a slight difference in SET* was observed owing to the effect of posture. In particular, a difference of 0.25 °C was observed for the upper arm in Case 1, and a difference of 0.68 °C was observed for the head in Case 2. This difference is considered to be perceived by the human body. Therefore, the gravitational effect owing to the difference in posture is considered to affect the warm and cold sensations of the human body.

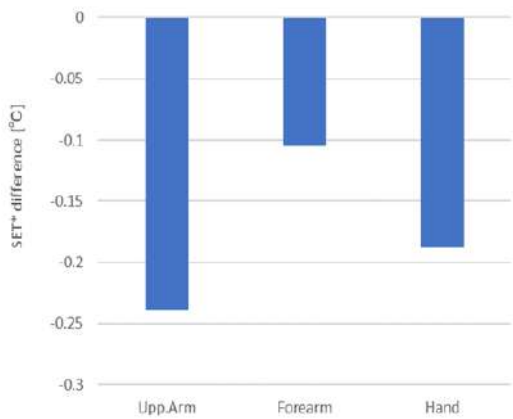

Fig. 10- Amount of change in SET* in Case1

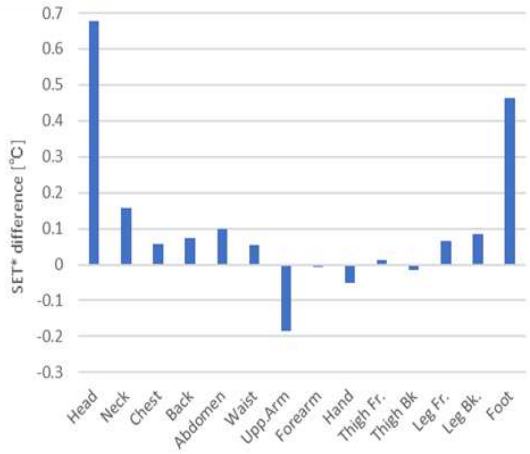

Fig. 11- Amount of change in SET* in Case2

4. Conclusion

In this study, we developed a thermos-physiological model of the human body to consider the effect of gravity on blood flow on thermal comfort. The effects of posture on blood flow, skin temperature, and SET* were clarified through experiments and numerical simulations with subjects in different postures.

1) By treating the core skin as a one-dimensional blood vessel and considering the total driving force acting on the blood, the blood flow rate determined by the conventional thermal regulation was formulated to be affected by gravity.
2) A model that incorporates a blood pressure model into a segmented two-node model with partitions and changes the direction of gravity action was developed.
3) In the experiment with subjects, the difference between the skin temperature of the raised fingertips of the right hand and that of the lowered fingertips of the left hand ranged from 1.3 °C to 3.4 °C, depending on the subject, and we confirmed that the skin temperature could change owing to gravity. This result agrees with the simulation results of the proposed model.
4) When both hands were raised, the skin temperature of the upper arms decreased by 0.31 °C, and the SET* decreased by 0.24 °C. In the supine position, skin temperature decreased by 0.54 °C in the feet, and SET* increased by 0.68 °C in the head and 0.46 °C in the feet.

In the future, we will increase the number of subjects in the experiment and measure the skin temperature and blood flow at 22 body parts. We will also increase the number of studies under different posture conditions and compare the experimental and simulation results to improve the accuracy of the model.

5 References

[1] ASHRAE chapter8 thermal comfort, 2001

[2] Gagge et al, An Effective Temperature Scale Based on a Simple Model of Human Physiological Regulatiry Response, 1972

[3] Ituhei Kohri et al: Prediction of local skin temperature using a distributed two-layer model, Proceedings of the of the Society of Air-Conditioning and Sanitary Engineers, 2003

[4] Rikiya Okabe et al: Calculation of the Human-body Thermo-Physiological Exergy Balance Model for the Evaluation of Thermal Sensation, 2019

[5] Yoshiaki Masuda et al: Measurement of flow by MRI, Journal of Japanese Society of Biorheology (B&R), Vol. 7, No. 4, 1993

Data sharing not applicable to this article as no datasets were generated or analysed during the current study.

A Comparison of Indoor Pollution using Different Ventilation Methods: A Case Study

Salam Al-Samman [a], Mahroo Eftekhari [a], Vanda Dimitriou [a], Daniel Coakley [b], Charalampos Angelopoulos[b]

[a] School of Architecture Building and Civil Engineering, Loughborough University, Loughborough United Kingdom.

[b] Mitsubishi Electric R&D Centre Europe BV (MERCE), Livingston, United Kingdom.

Abstract. One of the essential aspects of healthy buildings is the air quality that people breathe indoors, as it directly impacts their comfort, health, and well-being. Achieving an acceptable indoor air quality (IAQ) has become an essential design objective for newly constructed and renovated buildings as well as for the operational system in existing buildings. The COVID-19 pandemic, which began in 2019, highlighted the need for better IAQ. The quality of indoor air space is not only affected by ambient or external pollution but also by indoor sources and inadequate ventilation. For instance, the build-up of pollutants may differ for the same space due to the ventilation method. This paper uses a case study of an open-plan office in Loughborough, UK, simulated under two ventilation schemes, mechanical ventilation (MV) and natural ventilation (NV), for the same weather file to diagnose and examine the difference in the IAQ. The results of the simulations were compared with monitored data using an IAQ sensor located in the centre of the open-plan office. The air parameters measured were indoor temperature (Ta), relative humidity (RH), carbon dioxide (CO_2), formaldehyde (CH_2O) and particulate matter ($PM_{2.5}$). It was found that the average CO_2 levels were better by 10% under MV than in NV because higher ventilation rates were achieved during occupied hours. The average $PM_{2.5}$ was twofold better under NV than MV, as well as CH_2O was also better under NV than MV by 26% in the simulated scenarios. The open-plan office was ventilated at all times under NV; unlike in MV, the air handling unit was only operating during the occupied hours, which contributed to better IAQ. The simulation results for this study revealed that both mechanical and natural ventilation could achieve acceptable IAQ for this specific case study and location. The ventilation control strategy is the manipulator of jeopardising the IAQ in the space.

Keywords. IAQ, mechanical ventilation, natural ventilation, IAQ monitoring, open-plan work environments
DOI: https://doi.org/10.34641/clima.2022.315

1. Introduction

The quality of the air people breathe indoors directly impacts their health [1], well-being and productivity [2] and constitutes one of the most important aspects of healthy buildings. The usual way of diluting and controlling indoor air pollution is via ventilation. The purpose of ventilation is to supply fresh air as well as meeting the heating/cooling requirements and air quality of occupants within an indoor environment [3]. Ventilation could be introduced to the indoors either naturally or mechanically. The adjective "natural" differentiates the driving force causing the air movement compared to a "mechanical" means.

Indoor pollutants are derived from both outdoor and indoor sources. These sources impose different requirements on the ventilation control strategies needed to secure good health and comfort conditions. It is essential to know the outdoor pollution to limit its entry to the indoor space via the ventilation system and openings [4], while also knowing the spatial distribution during the day. Understanding the outdoor pollution and observing its trend may be used to control the ventilation system and limit the entry of pollutants at peak levels. On the other hand, indoor pollutants are present due to many sources found in the building, both chemical and biological. Sources such as building materials, cleaning products, furnishings and fabric, equipment and electrical appliances, and pollutants resulting from occupants' presence or activities, etc [5]. The actual pollutants and pollutant

Copyright ©2022 by the authors. This conference paper is published under a CC-BY-4.0 license.

sources present in a building will largely be determined by the type of building and its usage. For example, residential buildings are likely to have greater diversity (and certainly a different range) of pollutants and pollutant sources than in a typical office.

One of MV's advantages over NV is that it can filter and trap particles and gaseous pollutants [6]. Consequently, better IAQ is better achieved through MV than NV [7]. The scope for filtering or treating the supply of exhaust air is very limited with NV. This is because the flow-inducing pressures involved are low, so any increase in resistance to flow, for example, imposed by filters, would substantially reduce the effectiveness of NV [8]. However, in the last few years, the air in many megacities has become so heavily polluted with gaseous substances and particles that it is no longer advisable to ventilate interior spaces with unfiltered outside air [9]. Therefore, NV is limited in heavily polluted environments, and MV is almost independent of weather conditions. However, both ventilation approaches have the potential to increase concentrations of outdoor pollutants into the indoor space [10,11].

One of the critical needs associated with controlling air pollution (generally indoors and outdoors) is continuous air pollution monitoring. With the increased attention to the importance of air quality, especially indoors, the continual development of low-cost sensor technology for monitoring purposes made it much more feasible to use in different indoor sectors [12-15]. The selection of the air quality sensor is based on reliability, accuracy, resolution, autonomy, and response time [12]. Continuously monitoring regularly occupied spaces using accredited monitors such as those referred by RESET Air [16] has become a necessity for any building to be rated as a healthy environment.

Offices are a typical building type that is operationally amenable to both ventilation types, MV and NV [11]. A design question would be encountered by the building services engineer, would NV work for a proposed building given activities therein, its form, shape, construction method and material used in the proposed location[5]? To assess the impact of these different modes of ventilation on IAQ, the current paper uses an open-plan office in Loughborough UK and simulate it under the two ventilation systems, MV and NV, using IAQ and a ventilation analysis computer program. The open-plan office is originally mechanically ventilated and includes an IAQ sensor located in the centre of the office and measures indoor temperature (Ta), relative humidity (RH), carbon dioxide (CO_2), formaldehyde (CH_2O) and particulate matter ($PM_{2.5}$). The results of the simulations were compared and analysed to determine if acceptable levels of IAQ can be achieved by NV. The results of the simulations of the MV were compared with the real-time measured data. The real-time measured data were analysed to allow more informed decision-making about the indoor pollution found in the office for each ventilation mode and propose an appropriate control strategy accordingly.

2. Methodology

2.1 Case Study

The open-plan office is located on the ground floor of a two-story building oriented southwest (with a degree angle of 208° relative to the north) in Loughborough, UK. The area and the volume of the office are 148.5m^2 and 445.5m^3, respectively. The external façade of the office includes six windows of the same shape, type, and dimension. The office can accommodate up to 19 occupants. The occupancy hours are from 08:00 to 18:00 Monday to Friday but also open at the weekends. The type of activity work is sedentary office work. The open-plan office is mechanically ventilated with the supply and extract diffusers at ceiling level (mixing ventilation), as shown in Fig.1. The open-plan office includes an EnLink IAQ sensor [17] located in the middle of the room at a height of 1.1 meters [18]. An overview of the accuracy of the measurements using the EnLink IAQ sensor is available in the appendices.

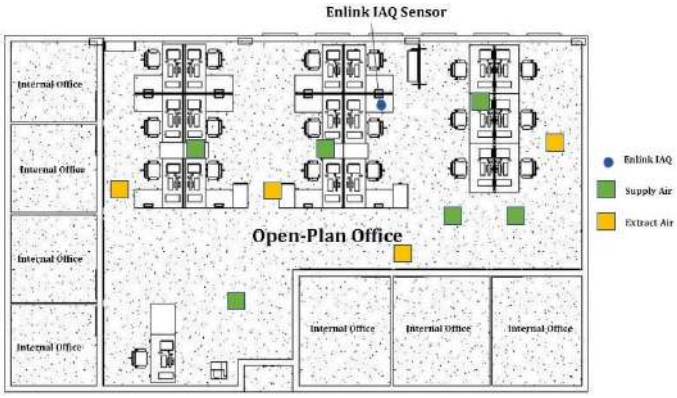

Fig. 1 - Examined open-plan office layout, including the occupant workplaces, IAQ sensor location, and supply and extract air diffusers at the ceiling level.

2.2 Simulation Setup

The simulations were carried out using CONTAM [19], a multizone building airflow and contaminant transport computer program often used for ventilation and IAQ analysis. It was developed at the National Institute of Standards and Technology (NIST) in the USA. It helps determine airflows, contaminant concentrations and personal exposure.

The simulation method for the airflows and contaminants was set to be transient to obtain time histories of airflow rates, pressure differentials and contaminant concentrations under changing ventilation systems. The simulation period and time were set from 25th of May 00:00 to 31st of May 23:59. The monitored period was the same as the simulated period.

The interior leakage was assumed to be uniformly distributed. It does not account for the leakage pathways associated with interstitial spaces that almost always exist within buildings. The effective leakage areas and wind pressure coefficient for the external wall (Cp=0.6) were taken from the library manager of CONTAM [19]. To verify that the defined building surface areas and the associated leakage rates are correct, a simulated building pressurisation test was performed and compared against CIBSE Guide TM23.

2.3 Comfort Criteria

The recommended comfort criteria for the open-plan office are summarised in Tab.1[5]. The outdoor air rate was based on the floor area of the space as the number of occupancies was unknown for the monitored period. The outdoor air requirement for the office with full occupancy was found to be 383.05 L/s. For every occupant in the simulation, a CO_2 generation rate was defined (0.0052L/s), and a prescribed removal rate of 10 L/s/person was added as recommended by guidelines. The prescribed outdoor air supply rates are based on the metabolic pollutants of occupants according to their activity or to the size of the space. For sedentary office work, the minimum ventilation rate is 10 L/s per person for an office. The outdoor air supply per m^2 was set to 1.3 L/s [8]. Thus, the rates at which the main air handler unit delivers outdoor air are proportional to the floor area in the MV scenario. No windows were opened in the MV scenario, and no filters were added.

For the NV scenario, the office was ventilated by using windows. The area of each opening required to give a ventilation rate for a specified height value was calculated using the CIBSE ventilation tool [20]. The approximate opening area required for each window in the office to supply the sufficient ventilation rate was found to be 0.28 m^2.

Tab. 1 – Air parameters and key pollutants in offices.

Air parameter	Impact	Comfort range	Evaluated
Ta	Working in hot conditions can cause heat stress, discomfort, and heat exhaustion. Also, it can lead to reduced performance, more mistakes and, depending on the extremities, several disorders. [3]	22-25°C [5]	Yes
RH	Low RH levels can give rise to respiratory discomfort and nuisance from electrostatic effects [8,22]. High RH levels incurs the risk of condensation and mould growth on surfaces that have temperatures that fall below the dewpoint temperature of the air [8,22].	40-60% [5]	Yes
Metabolic CO_2	Indoor CO_2 can significantly impact productivity and decision-making capabilities [23]. Indoor CO_2 levels <1000-1500 ppm contribute to symptoms such as headache, dizziness, tiredness, and difficulties concentrating [23-25]. Indoor CO_2 levels above < 2,500 ppm contribute to unsatisfactory performance by occupants and loss of concentration [23] , especially when exposed for 2.5 hours or more [24].	Acceptable 1000 ppm [24] Not to exceed 1500 ppm [25] Dangerous 5000 ppm [26]	Yes
CH_2O * Very volatile organic compound (VVOC)	When formaldehyde is present in the air at levels exceeding 0.3 -3.2 ppm for 35 minutes, individuals may experience throat irritation, an increase in the eye-blinking rate, eye irritation, nose irritation, and a desire to leave the room [27].	Acceptable 1000 ug/m³ [27, 28] Not to exceed 2500 ug/m³ ≈2 ppm [26]	Yes
$PM_{2.5}$	Particles in the $PM_{2.5}$ size range can travel deeply into the respiratory tract, down into the lungs' deepest (alveolar) portions, where gas exchange occurs between the air and the bloodstream [29]. The alveolar portion of the lungs has no efficient means of removing PM2.5 [30]. Exposure to fine particles can cause short-term health effects such as eye, nose, throat and lung irritation and coughing, sneezing, runny nose, and shortness of breath.	Acceptable < 35 μg/m³ [31] High performance $PM_{2.5}$ < 12 μg/m³ [31]	Yes

	Particulates within the lungs may cause lung disease, emphysema, and/or lung cancer [29].	
O_3	Found in offices in the presence of photocopiers, laser printers, or any electrical appliances that are poorly maintained.	No
Dust, dirt and moisture	Present especially if the open-plan office contains communal area spaces.	N/A
Odour	generated as part of metabolism and emitted from furnishings and fabrics and bioeffluents.	N/A

[a]15 minutes average
[b]The threshold is met for a project located where the annual average ambient $PM_{2.5}$ level is 35 μg/m³ or higher.

Tab. 2 – CONTAM input data.

Contaminant	Initial concentration	Generation rate	Schedule
CO_2	400 ppm	0.0052 L/s	8:00 - 18:00
CH_2O	0	1.0×10-9 kg/s	Always
$PM_{2.5}$[a]	0	0.1 1/h	Always
		1.7 mg/h	8:00 - 18:00

[a] The default value of $PM_{2.5}$ was set to zero as observed from the monitored data. Two models were defined, a decomposition rate of 1/h and a constant coefficient model of 1.7mg/h for printing.

2.3 Contaminants

The air quality at Loughborough UK is categorised as 'fair', meaning that the air quality is generally acceptable for most individuals. However, sensitive groups may experience minor to moderate symptoms from long-term exposure [32].

As for the IAQ in offices, the indoor sources of air pollution are usually carpets, furniture, HVAC and people. Some of the key pollutants found in offices are listed in Tab. 1, including their source and impact on health.

The air parameters and pollutants measured and assessed in this study were T_a, RH, CO_2, CH_2O and $PM_{2.5}$. As for the simulated scenarios, the pollutants defined were CO_2, CH_2O and $PM_{2.5}$. The 'threshold limit value' (TLV) of each pollutant assessed in this study are listed in Tab. 1. Also, the input requirements of each pollutant in the simulations are defined in Tab. 2.

3. Results and Discussion

The simulation results show that the average CO_2 levels in the MV were better than NV by only 10%. That is because higher ventilation rates were achieved in MV than in NV. In both scenarios, the CO_2 levels did not exceed 610 ppm. Comparing the CO_2 simulated results with the real-time measurements, the maximum CO_2 level reached was 530 ppm. The average $PM_{2.5}$ was twofold better under NV than MV, as well as CH_2O was also better under NV than MV by 26% in the simulated scenarios.

The CO_2 and CH_2O levels did not exceed or even reach the TLV in the MV scenario due to the ventilation rate associated with the presence of the occupants. However, $PM_{2.5}$ levels reached 55 μg/m³ in the MV scenario as subject to the office equipment schedule and were above the acceptable limit for all working hours (50 hours, which is the working hours at the open-plan office per week). In the real-time measurements, the $PM_{2.5}$ reached 43 μg/m³ and exceeded the acceptable level by only 4 hours for the entire week.

CH_2O and $PM_{2.5}$ levels were better in NV because the vents were open all day long, whereas, in the MV, the air handling unit was operating during the occupied hours only. An additional scenario was performed, including a control schedule for the windows in the NV scenario. The windows were scheduled to open only during occupied hours. As a result, CO_2 and $PM_{2.5}$ levels took more time to dilute and drop to the default concentrations. However, the CH_2O levels increased significantly by 14 times due to the defined constant generation rate of 1.0 $\times 10^{-9}$ kg/(m₂·s). Therefore, the trend in the simulated data for CO_2 and $PM_{2.5}$ varied according to the defined occupancy schedule. Unlike CH_2O, which was defined to be generated at a constant rate based on the office area for all times. Besides, lower ventilation rates were achieved in the NV scenarios as the wind direction was not towards the office openings for that week.

Comparing the real-time measurements and the MV-base case simulation results, the CO_2 levels appeared to be better by 1.4% in the simulation scenario. However, the average $PM_{2.5}$ levels from the real-time measurements were better than the simulated scenario by 39%. Also, when comparing the ambient levels of $PM_{2.5}$ with the simulated results, the ambient levels of $PM_{2.5}$ were better by 48%. The ambient $PM_{2.5}$ were also better than the real-time measurements by 41%. However, the real-time measurements and the ambient $PM_{2.5}$ levels appear to be highly correlated with R^2= 0.34. As for the CH_2O levels, the measured values were much higher than the MV base-case scenario. The measured data exceeded the TLV [26] by 16 hours during the working hours.

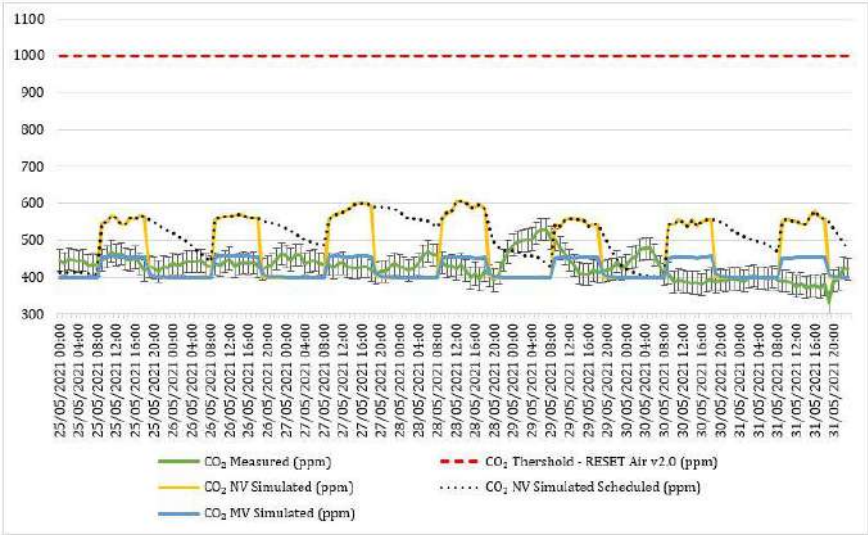

Fig. 2 - Measured and simulated CO_2 in the open-plan office and the acceptable threshold.

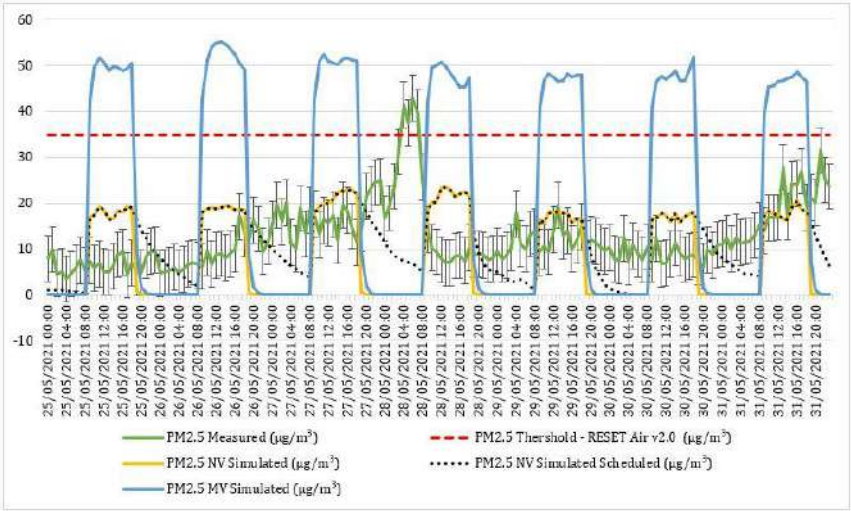

Fig. 3 – Measured and simulated $PM_{2.5}$ in the open-plan office and the acceptable threshold.

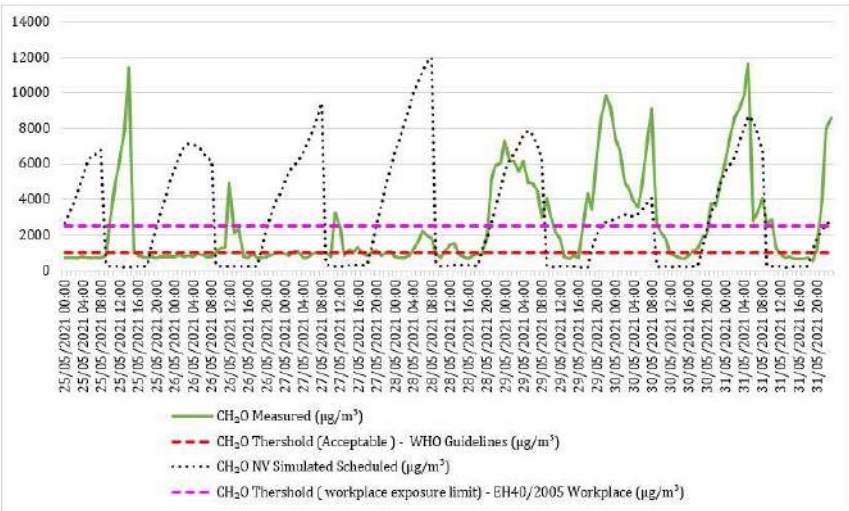

Fig. 4 - Measured and simulated CH2O (NV scheduled scenario) in the open-plan office and the acceptable threshold.

The simulation results of the MV scenario for CO_2 and the real-time measurements reveal that the office was overly ventilated. Although the open-plan office was simulated for full occupancy for the simulation scenarios, and during the measuring period, the occupancy rate was unknown. The office was never at full capacity during the measuring period due to the COVID-19 safety measures taken in the office. Due to the relatively small difference between the simulation results and the real-time measurements, it could be anticipated that if the open-plan office was fully occupied and all office equipment was operating in the real scenario, the CO_2 levels would have been higher than what the simulation results revealed. It is fair to assume that the current ventilation rate in the office is not suitable for full occupancy.

Also, the simulated results for $PM_{2.5}$ levels concluded that in the real case scenario, when the office is fully occupied, and all office equipment is operating, the $PM_{2.5}$ will exceed the TLV for all times as appeared in the MV simulation results. Again, the measured $PM_{2.5}$ has exceeded the TLV only by four hours. However, the office was not fully occupied, and the equipment was not in full use. It is fair to assume that the density of occupants and their operating accompanying office equipment is not suitable for the office area.

As for the CH_2O levels, the measured data shows that the defined generation rate in the simulations was minimal. The trend in the measured confirms that CH_2O levels do increase with the presence of occupants and operating office equipment.

Both the field measurements and simulation results prove that diagnosing and classifying the IAQ of enclosed space based on the analysis of one pollutant is not enough. For instance, the real-time measured data ranks the ventilation and IAQ standard in the open-plan office as 'high' in terms of CO_2, referring to Table 4.1 in CIBSE Guide A, Chapter 4 [5]. Also, the measured data of CO_2 and simulation results reveal that the open-plan office is overly ventilated in terms of CO_2. However, the real-measured data and simulation results indicate that the open-plan office is marginally under-ventilated in terms of CH_2O and $PM_{2.5}$. Measurements of CO_2 levels in indoor spaces effectively identify poor ventilation in high occupancy spaces. However, in low occupancy or large volume spaces, low levels of CO_2 do not necessarily indicate good ventilation.

As for the other comfort conditions in the open-plan office, the measured indoor Ta and RH office were in the comfort range.

4. Conclusion

This study provides results from field measurements compared with simulation results that assess the IAQ under MV and NV ventilation systems of an open-plan office. Overall, this study's results demonstrate the need to diagnose the IAQ of open-plan offices by assessing different pollutants that are likely to be found in the environment. The pollutants measured and assessed in this study were all dominant in the open-plan office. The real-time measured data revealed that the open-plan office is overly ventilated in terms of CO_2 but marginally under-ventilated in terms of CH_2O and $PM_{2.5}$.

Besides, the simulation results for this study revealed that both MV and NV could achieve acceptable IAQ for this specific case study and location (with the existing location of the supply and extract and layout of the office). However, the ventilation control strategy is the manipulator of jeopardising the IAQ in the space. The study confirmed that it is important for the open-plan office to remain ventilated during unoccupied hours under a reasonable control schedule to dilute any pollutants reaching the TLV and control other sources of pollutants, e.g., CH_2O and $PM_{2.5}$ from furniture and electrical equipment. Yet, a trade-off between the IAQ, thermal comfort and energy consumption should be achieved, especially during wintertime, to avoid creating an uncomfortable thermal environment and resulting in higher energy consumption.

It is important to diagnose the indoor air of an enclosed environment to understand the behaviour and trend of the indoor air throughout the seasons and identify the causes of failure of the HVAC system in the building. It is also important to have the number of occupancies known during the evaluation period to assess the indoor pollution associated with the occupancy presence and their activities to indicate the indoor climate quality more accurately. In this study, the measured data provided an understanding of the current ventilation operational status verifying the need to adjust the setpoints as higher ventilation is required for full occupancy for the real case scenario. As in the established guidelines to control COVID-19 indoors, such as in the '*CIBSE COVID-19 Ventilation Guide*' [33], a higher ventilation rate with 100% fresh air is necessary at all times.

Ventilation is the foundation of a healthy building and the most appropriate means of control to replace and dilute the heat, moisture, and gaseous and particulate pollutants that eventually build up indoors. For future studies, a more detailed IAQ analysis will be required. It is recommended that CFD is to be used instead of multizonal analysis (which is based on the well-mixed assumption) to give a detailed pollution profile across the office and demonstrate the movement of pollutants and viruses throughout enclosed spaces. Also, energy analysis is recommended to compare the energy consumption in a building to the corresponding indoor climate comfort conditions. The results can be used to understand the trade-offs of energy and indoor air pollution.

5. Appendices

Tab.3 – An overview of the accuracy of the measurements using the EnLink IAQ sensor

Type	Accuracy	
RF Transmit power Up to +18dBm	Ta	Accuracy: ±0.2°C
	RH	Accuracy: ±2%
	CO_2	Accuracy: ± (30, +3%) ppm
	CH_2O	± 15%
	$PM_{2.5}$	0 μg/m³ to 100 μg/m³ ± 10 μg/m³ 100 μg/m³ to 1000 μg/m³ ±10 % m.v.

6. References

[1] The World Health Report 2000: Health Systems: Improving Performance. Geneva: World Health Organization, 2000. Available from: https://www.who.int/whr/2000/en/whr00_en .pdf

[2] Wyon, D.P. (2004), The effects of indoor air quality on performance and productivity. Indoor Air, 14: 92-101. https://doi.org/10.1111/j.16000668.2004.00278.x

[3] Yuanhui Zhang. Indoor air quality engineering [Internet]. [cited: 2022 Mar 25]. Available from: https://doi.org/10.1201/b12485.

[4] 2009. Indoor Air Quality Guide: Best Practices for Design, Construction, and Commissioning. Atlanta: American Society of Heating, Refrigerating and Air-Conditioning Engineers, Inc.

[5] Nicol, F. and Nikolopoulou, M., 2015. CIBSE Guide A: Environmental design. 8th ed. London: Chartered Institution of Building Services Engineers.

[6] 2020. CIBSE TM64: Operational performance - indoor air quality - emissions sources and mitigation measures. London: Chartered Institution of Building Services Engineers.

[7] Montgomery JF, Storey S, Bartlett K. Comparison of the indoor air quality in an office operating with natural or mechanical ventilation using short-term intensive pollutant monitoring. Indoor Built Environ. 2015;24(6):777–87.

[8] British Standards Institution. BS 5925:1991: Ventilation principles and designing for natural ventilation [internet]. London: BSI; [cited 2020 Nov5]. Available from: https://www.bsigroup.com.

[9] Baklanov A, Molina LT, Gauss M. Megacities, air quality and climate. Atmos Environ [Internet]. 2016;126:235–49. Available from: http://dx.doi.org/10.1016/j.atmosenv.2015.11.059

[10] Dutton SM, Banks D, Brunswick SL, Fisk WJ. Health and economic implications of natural ventilation in California offices. Build Environ [Internet]. 2013;67(2013):34–45. Available from: http://dx.doi.org/10.1016/j.buildenv.2013.05.002

[11] Ben-David T, Waring MS. Impact of natural versus mechanical ventilation on simulated indoor air quality and energy consumption in offices in fourteen US cities. Build Environ [Internet]. 2016; 104:320–36. Available from: http://dx.doi.org/10.1016/j.buildenv.2016.05.007

[12] Kumar P, Skouloudis AN, Bell M, Viana M, Carotta MC, Biskos G, et al. Real-time sensors for indoor air monitoring and challenges ahead in deploying them to urban buildings. Sci Total Environ [Internet]. 2016;560–561(April):150–9. Available from: http://dx.doi.org/10.1016/j.scitotenv.2016.04.032

[13] Morawska L, Thai PK, Liu X, Asumadu-Sakyi A, Ayoko G, Bartonova A, et al. Applications of low-cost sensing technologies for air quality monitoring and exposure assessment: How far have they gone? Environ Int. 2018;116(April):286–99.

[14] Schieweck A, Uhde E, Salthammer T, Salthammer LC, Morawska L, Mazaheri M, et al. Smart homes and the control of indoor air quality. Renew Sustain Energy Rev [Internet]. 2018;94(May):705–18. Available from: https://doi.org/10.1016/j.rser.2018.05.057

[15] Marques G, Pitarma R. A cost-effective air quality supervision solution for enhanced living environments through the internet of things. Electron. 2019;8(2).

[16] RESET® Standard [Internet]. Reset.build. 2018 [cited 5 November 2021]. Available from: https://www.reset.build/directory/monitors/type/indoor

[17] enLink Air [Internet]. Synetica. 2021 [cited 5 November 2021]. Available from: https://synetica.net/enlink-air/

[18] ANSI/ASHRAE Standard 55-2017 . Thermal environmental conditions for human occupancy. Atlanta, GA: American Society of Heating, Refrigeration and Air Conditioning Engineers, Inc., 2017.

[19] CONTAM [Internet]. NIST. 2021 [cited 5

November 2021]. Available from: https://www.nist.gov/services-resources/software/contam

[20] Persily A, Ivy E. Input Data for Multizone Airflow and IAQ Analysis. NISTIR 6585. Gaithersburg, Maryland: National Institute of Standards and Technology;2001.

[21] CIBSE - Digital Tools - CIBSE Symbols [Internet]. Cibse.org. 2021 [cited 5 November 2021]. Available from: https://www.cibse.org/Knowledge/Design-Tool-for-IAQ-Analysis

[22] 2016 ASHRAE Handbook—HVAC Systems and Equipment. SI ed. HUMIDIFIERS. Atlanta, Ga.: American Society of Heating, Refrigerating and Air-Conditioning Engineers; 2016.

[23] Satish U, Mendell MJ, Shekhar K, Hotchi T, Sullivan D. Concentrations on Human Decision-Making Performance. Environ Health Perspect. 2012;120(12):1671–8.

[24] Myhrvold AN, Olsen E, Lauridsen O. Indoor environment in schools–pupils health and performance in regard to CO2 concentrations. Vol. 94, Proceedings of the 7th International Conference on Indoor Air Quality and Climate. 1996. p. 369–71.

[25] Bierwirth P. Carbon dioxide toxicity and climate change: a major unapprehended risk for human health. Res Gate Work Pap. 2021;(March):1–25.

[26] Executive H and S. EH40 / 2005 Workplace exposure limits: limits for use with the Control of Substances (Fourth Edition 2020). Tso [Internet]. 2020;2002:61. Available from: https://www.hse.gov.uk/pubns/books/eh40.htm

[27] Golden R. Identifying an indoor air exposure limit for formaldehyde considering both irritation and cancer hazards. Crit Rev Toxicol. 2011;41(8):672–721.

[28] World Health Organization. WHO GUIDELINES FOR INDOOR AIR QUALITY. Copenhagen, Denmark: WHO Regional Office for Europe 2010. [cited 2021 Nov 5]. Available from: https://www.euro.who.int/__data/assets/pdf_file /0009/128169/e94535.pdf

[29] Xing YF, Xu YH, Shi MH, Lian YX. The impact of PM2.5 on the human respiratory system. J Thorac Dis. 2016;8(1): E69–74.

[30] Dylosproducts.com. 2021. Understanding Particulate Matter, Air Quality, Particle Pollution. [online] Available at: <http://www.dylosproducts.com/whispama.html> [accessed 5 November 2021].

[31] U.S. Environmental Protection Agency. National Ambient Air Quality Standards. https://www.epa.gov/pm-pollution/table-historical-particulate-matter-pm-national-ambient-airquality-standards-naaqs

[32] AccuWeather.CurrentAirQuality [Internet]. [cited 2022 Feb 24]Available from:https://www.accuweather.com/en/gb/loughborough/le11-5/air-quality-index/324590

[33] 2020. CIBSE COVID-19 Ventilation Guide. The Chartered Institution of Building Services Engineers.

Cooling effects on fatigue recovery during summer sleep

Noriko Umemiya [a] and Mitsunori Suzuki [a]

[a] Department of Architecture and Building Engineering, Graduate school of Engineering, Osaka City University, Osaka, Japan. umemiyanor@osaka-cu.ac.jp.

Abstract. Sleep quality has been difficult to maintain recently, particularly for urban residents. This study investigates effects of cooling use on fatigue recovery during sleep for dwellings and residents with various attributes. Measurements of sleeping room thermal environments and questionnaire surveys were conducted for 188 Osaka apartment residents on 765 nights during four summers. Each resident recorded bedside air temperature and humidity and kept a diary reporting occupation of sleeping rooms, sleep, and cooling use at intervals of 30 min for seven days. Subjective sleep quality by the OSA sleep inventory was recorded every morning. Residents evaluated their dwelling environment and constitution and consciousness. Sunshine, sunlight glare, heating efficiency, outside air clearness in items of dwelling environment and heat tolerance, cold tolerance, circulation and stress in items of constitution were related directly to sleep quality. Data were divided into two categories for each item. The mean outdoor temperature during sleep was higher and lower for over and under 27.3°C, which was the median value. Results indicate the following for dwellings with high thermal insulation: a) when outdoor temperatures were higher, fatigue recovery scores were higher for 'not sunny', 'not cooling efficient' and 'not clear outside air' dwellings, with 'low heat tolerance' residents using cooling and higher scores for 'sunny' dwellings and 'good circulation' residents without cooling; b) when outdoor temperatures were lower, fatigue recovery scores were higher for 'cooling efficient' dwellings and 'low stress' residents without cooling. For dwellings with less thermal insulation, results showed the following: a) when outdoor temperatures were higher, fatigue recovery scores were higher for 'poor circulation' residents using cooling and were higher for 'high cold tolerance' residents without cooling; b) when outdoor temperatures were lower, fatigue recovery scores were higher for 'not sunny' dwellings without cooling.

Keywords. Sleep, cooling use, fatigue recovery
DOI: https://doi.org/10.34641/clima.2022.312

1. Introduction

Tropical nights with minimum temperatures higher than 25°C in Osaka, Japan were fewer than twenty days in the 1960s, but they became greater than 40 days on a regular basis in the 2010s (1). Good sleep quality has become difficult to maintain, especially in urban areas during summer. Kusaka et al. (2) predicted from simulation results that almost every August night in Osaka will be a tropical night in the 2070s. Okamoto-Mizuno et al. (3) investigated humid heat exposure effects on sleep and showed that air temperature 35°C/relative humidity 75% conditions caused more wakefulness and lower sleep efficiency than 29°C/50% or 29°C/75%; moreover, rapid eye movement stage and stage 3 sleep occurred less than at 29°C/50% or 35°C/50%. Horne et al. (4) clarified that sleep-related vehicle accidents accounted for 16% of all accidents on major roads in southwest England, and for over 20% of those on midland motorways. Air conditioner use is necessary, but the conditions for their use remain unclear. Nakayama et al. (5) analyzed responses to a questionnaire survey of 256 apartment residents in Osaka, which investigated effects of cooling use on the relation between residence thermal performance and sleep quality. Results demonstrated that a 'Fatigue recovery' score in OSA sleep inventory using subjective scales (6) was better for evaluation of residential heating and showed that cooling

Copyright ©2022 by the authors. This conference paper is published under a CC-BY-4.0 license.

performance was better for residents with frequent cooling use. However, it was not related to the evaluation of residential heating and cooling performance for residents without frequent cooling use. Nakayama et al. described that the 'Fatigue recovery' score was unrelated to evaluation of solar heat annoyance from windows, irrespective of the cooling use. This study surveys the actual status of cooling use during sleep of Osaka apartments residents for four summers and over 700 nights, with analyses of cooling effects on fatigue recovery during sleep. The results clarify conditions for cooling use.

2. Research Methods

2.1 Measurement of sleeping room thermal environments

Residents of 6–15-floor concrete buildings with family-type apartments in an urban area of Osaka recorded air temperature and relative humidity in sleeping rooms for seven successive days in summer. Air temperatures were recorded every ten minutes automatically using a button-shaped thermo-logger. Humidity was recorded by residents before and after sleeping. Residents themselves set sensors at their bedside according to instructions. **Fig.1** presents a view of sensors set near a sleeping mattress (futon). Because residents might decline participation in the survey because they disliked strangers entering their private sleeping rooms, sensors and questionnaire sheets were delivered and returned by mail. A manual instructed respondents to avoid several places as sensor positions: places with higher air movement of electric fans or air conditioners, places with direct sunlight, places near heating devices such as television sets or artificial lighting, and places at the back of a shelf. Layouts were drawn of the sleeping rooms, showing positions of the sleeping mattress, the sensors, air conditioner, electric fan, and windows. The acquired data were examined carefully. If the sensor position was presumed to be inadequate to measure the room air temperature, then those data were not used for analyses. Inadequate sensor positions were also recognized from recorded temperatures. Outdoor weather data measured at 10 min intervals were acquired from an Osaka weather observatory in central Osaka city, about 10 km north of the surveyed apartments.

2.2 Questionnaire survey

Residents recorded a 'cooling use diary' with the times of sleep beginning and end, occupation of the sleeping room, cooling and electric fan use, and opening and closing windows of sleeping rooms at intervals of 30 min. **Fig.2** depicts an example.

Every morning, respondents also evaluated sleep quality and thermal sensations of the prior night. If diary data clearly differed from recorded temperature changes, then data of that night were deleted. Data from sleep with children under two years old, and data showing extreme night owl sleep habits were not used.

Fig.1 Sensors and futon in sleeping room

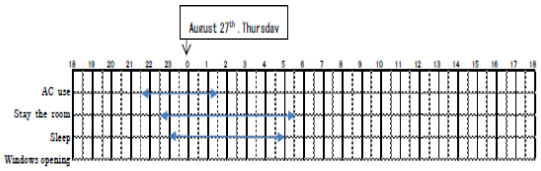

Fig.2 Example of 'Cooling use diary'

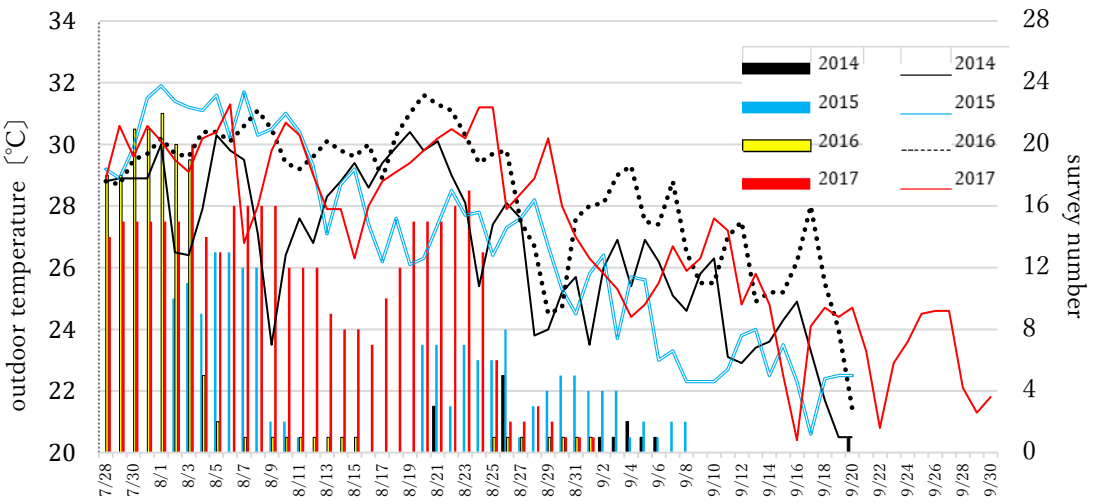

Fig.3 Daily survey number and mean outdoor temperature for four summers

Finally, records of 765 nights at 188 apartments during four summers were accumulated. **Fig.3** shows the numbers of daily measurements and daily mean outdoor temperatures for those periods.

The sleep evaluation scale OSA-MA inventory measures five factors of sleep: 1) drowsiness when waking, 2) falling asleep and maintaining sleep, 3) dreaming, 4) fatigue recovery, and 5) sleep duration, in addition to a profile of sleep using 16 bipolar four-point scales. The present study used this prevailing sleep scale produced by Oguri, Shirakawa and Azumi [6], with successive category method on the bases of 634 healthy students with regular lifestyles in Japan and revised by Yamamoto et al. [7] for middle-aged people with data from 580 middle-aged respondents.

The scales for Factor I are 'I have the power of concentration', 'I feel a sense of liberation', and 'I feel clear-headed'. Those for Factor II are 'I was able to sleep soundly', 'I dozed off until I finally fell asleep', 'I got to sleep easily', 'I often woke up from sleep', and 'The sleep was shallow'. Those for Factor III are 'I had many nightmares' and 'I had many dreams'. Those for Factor IV are 'Fatigue persists after waking up', 'I feel languorous', and 'I feel unwell'. Those for Factor V are 'I have a generally good appetite' and 'The sleep duration was long'. 'I can answer the questions in a crisp manner' was not used for considering the cases for which respondents could not answer immediately after they awakened. Fifteen scales were used for the present study.

Each question response was given on a four-response scale: very good, somewhat good, somewhat poor, and very poor. These questions yield standard scores of five factors, the averages of which are 50 and standard deviations are 10. Averaged standard scores of five factors are defined as the OSA score. Higher scores indicate higher the sleep quality.

Data of numbers and basic attributes of people sharing the sleeping room, air conditioner setting temperature, and sleep clothing every night were obtained. Sunshine, circulation, outdoor air clarity, view, outdoor noise, cooling efficiency, heating efficiency, mold presence, insect presence, muffled moisture and smell, and dwelling security were asked. Basic attributes were also found from other questionnaire sheets: air conditioner attributes and health state, heat tolerance, cold tolerance, poor circulation, perspiration occurrence, and recent mental stress and mood states of the respondents.

3. Attributes of dwellings and respondents

3.1 Dwelling attributes

Fig.4 portrays a frequency distribution of living areas: 60–69 m^2 were 36.7%, 70–79 m^2 were 22.7% and 50–59% were 21.1 m^2. The average living area was 59.4 m^2. Residences with three bedrooms, a living room, a dining room, and kitchen were 32.5%, which was the most frequent plan. The building 5th floor residents were 12.0%, 6th were 11.3%, and 7th and 8th were 7.3%. The average building floor was 5.8. South, North, East and West oriented sleeping room were 48.2%, 19.6%, 19.6% and 17.0%.

Energy conservation laws, which prescribed insulation amounts, were enacted in 1979 and were amended greatly in 1991 and in 1999. Thermal insulation levels were estimated by the year of apartment building construction. As **Fig.5** shows, those before 1991 were 35.8%, 1992–1998 were 33.1%, and those after 1999 were 34.1%. Frequencies of the three classes were almost equal.

Fig.6 presents the sleeping room environment evaluation. About 60% evaluated circulation and sunshine as good. Almost 70% evaluated the outdoor air as normal. Of respondents, 53.2% evaluated heating efficiency as good; 38.1% evaluated it as normal. Also, 43.7% of respondents evaluated cooling efficiency as good; 46.5% evaluated it as normal. Cooling efficiency of sleeping rooms was evaluated as lower than the heating efficiency. Of respondents, 24.7% reported that condensation occurred often in sleeping rooms, 11.9% often found mold, and 14.5% felt moisture and smells were muffled. In addition, 19.6% felt that the solar heat was annoying, whereas 25.0% felt the indoor solar glare to be annoying. Also, 25.2% evaluated the outdoors as noisy. Poor security of the sleeping room was reported by 38.5% of respondents.

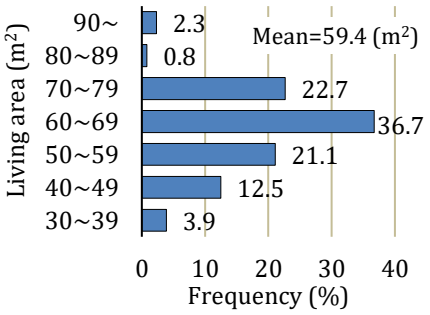

Fig.4 Frequency distribution of living area

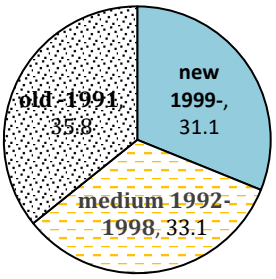

Fig.5 Frequency distribution of thermal insulation level

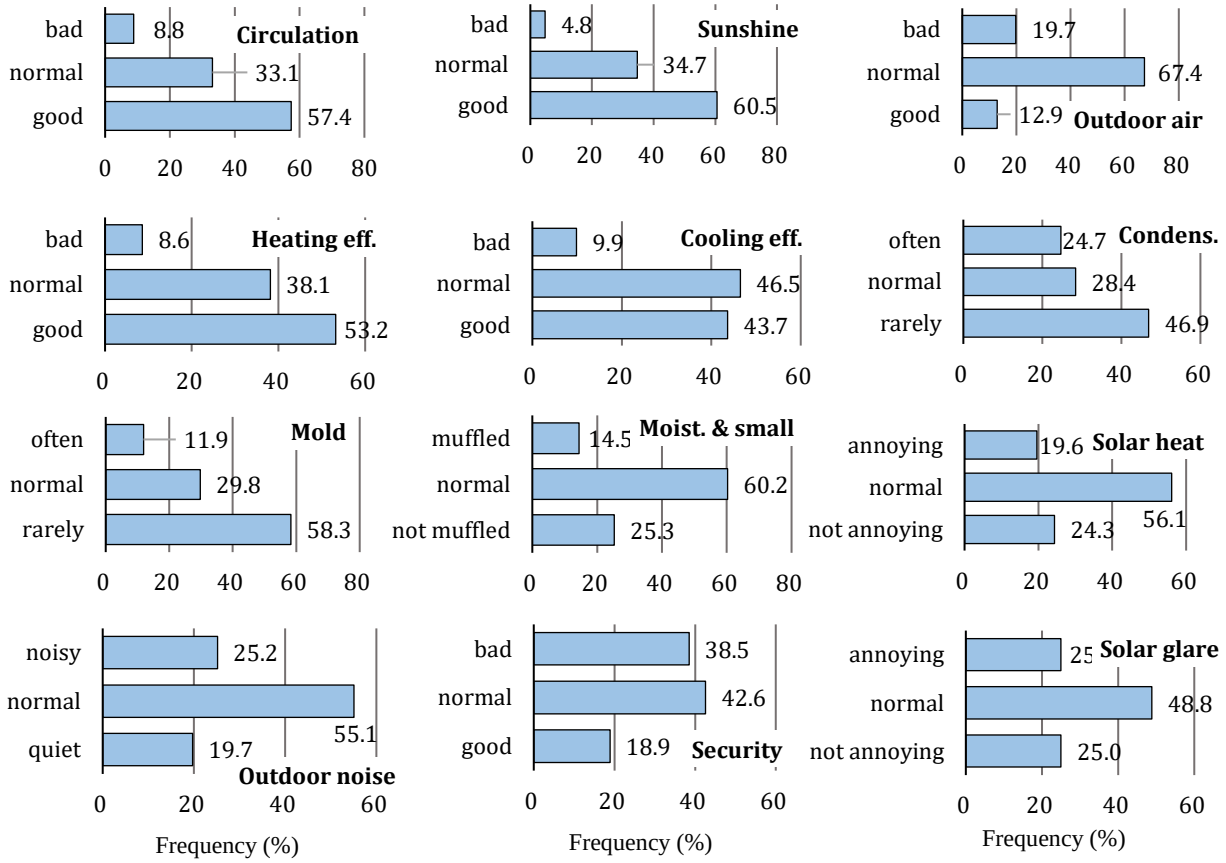

Fig.6 Frequency distribution of sleeping room environment evaluation

3.2 Resident attributes

Women were 61.2% of all respondents. Of respondents, those 50–55 were 16.3%, 65–70 were 11.6%, 40–45 were 10.9%; the average respondent was 52.9 years old. Residents reported as very healthy were 15.6%, healthy were 40.2%, and those of normal health were 36.1%. Those who were self-reported as vulnerable to heat stress were 19.5%, whereas those with little vulnerability were 17.9%. Those self-reported as weak against cold stress were 30.5%; those who were strong against it were 22.2%. Much mental stress was reported by 3.2%. Some stress was reported by 23.7%. A little stress was reported by 45.2%, but 25.8% reported no stress. **Fig.7** portrays the distribution of mental stress and poor circulation. Little perspiration and slight perspiration were 23.2%. Frequent poor circulation was reported by 21.1% of respondents. Often, sometimes, and none were each 23.2%.

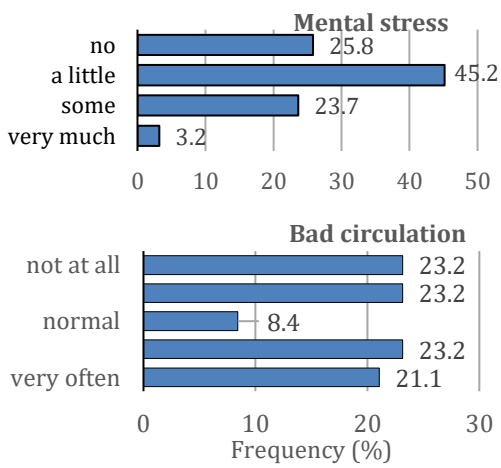

Fig.7 Frequency distribution of respondent attributes

4. Thermal environment, sleep quality and thermal sensation

Fig.8 portrays a distribution of mean outdoor and indoor temperature during sleep. **Fig.9** shows the distribution of mean difference (outdoor–indoor). Mean outdoor and indoor temperatures were 27.2°C and 27.9°C. The mean difference was -0.73 K and 0, -1 and -2 K were dominant. The mean and standard deviations of relative humidity were 71.2±6.1% and 65.1±8.2% for outdoor and indoor.

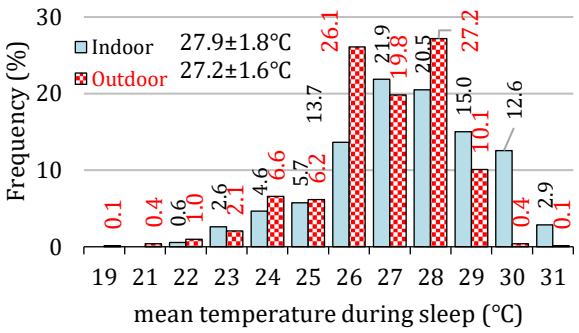

Fig.8 Mean indoor and outdoor temperature during sleep

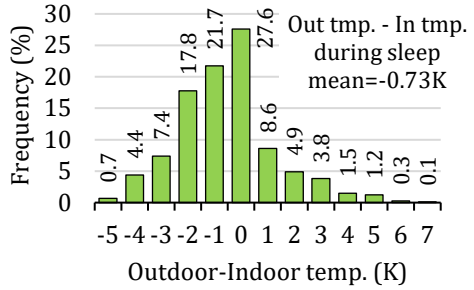

Fig.9 Distribution of outdoor-indoor temperature difference during sleep

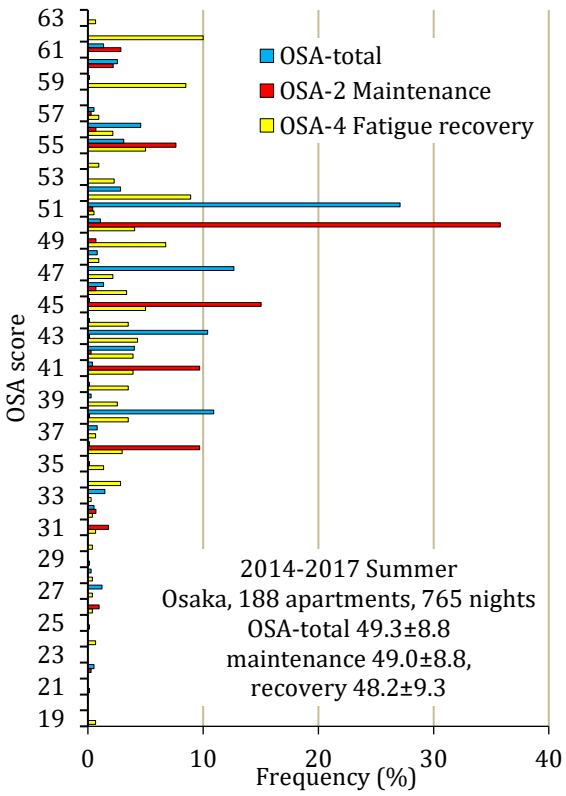

Fig.10 Distribution of OSA sleep quality scores

Fig.10 depicts the distribution of OSA scores. The OSA-total score was 49.3±8.8. The most frequent score was 51. The OSA-total and OSA-2 (sleep maintenance) scores were distributed around 50.0, but OSA-4 (fatigue recovery) was distributed rather uniformly. **Fig.11** shows a distribution of thermal sensation. Neutral was 26.3%: the most frequent.

5. Dwelling insulation and Fatigue recovery

Sunshine, indoor solar glare, heating efficiency, and outdoor air in sleeping room evaluation items were related directly to OSA scores. Data were divided into two categories by each item to mitigate the direct effects by these items. Data were also divided into two by outdoor temperature 27.3°C, median of the mean outdoor temperature during sleep and by cooling use nights (64.5%) and non-use nights (35.5%).

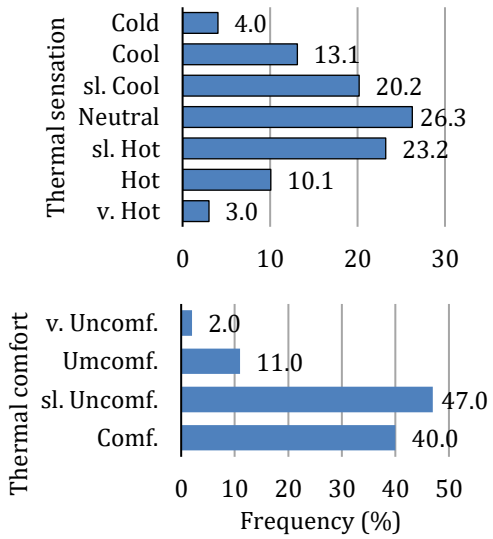

Fig.11 Distribution of thermal sensation during sleep

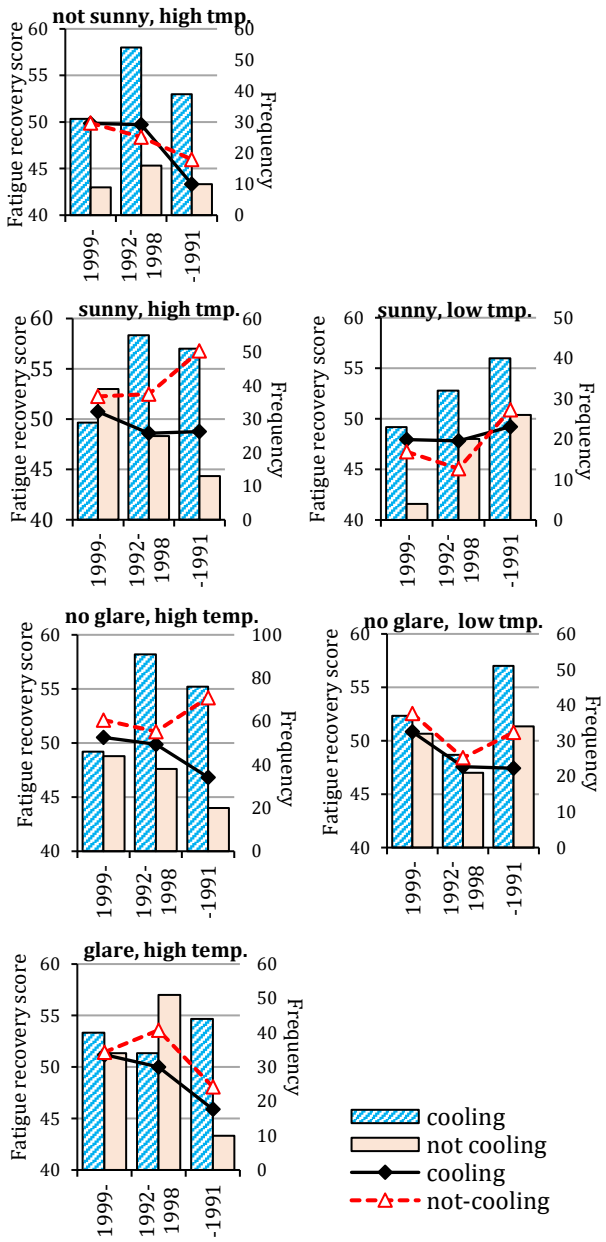

Fig.12 Fatigue revovery score for different outdoor temp., sleeping room environment, and insulation level

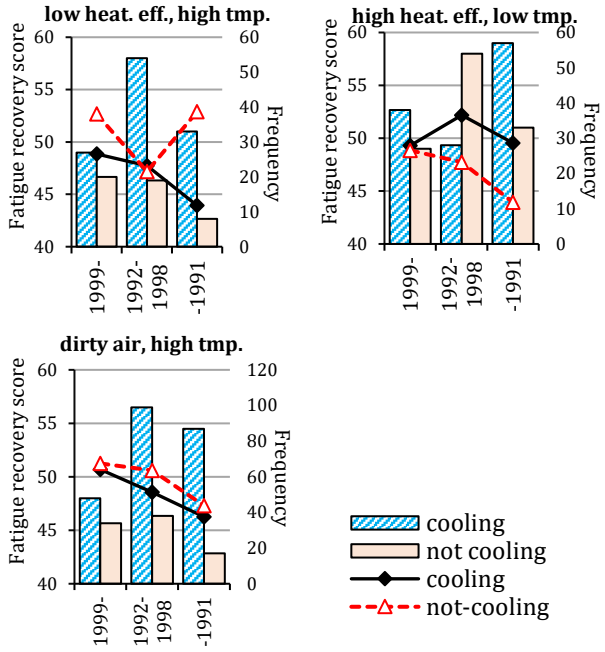

Fig.12 Fatigue revovery score for different outdoor temp., sleeping room environment, and insulation level (continued)

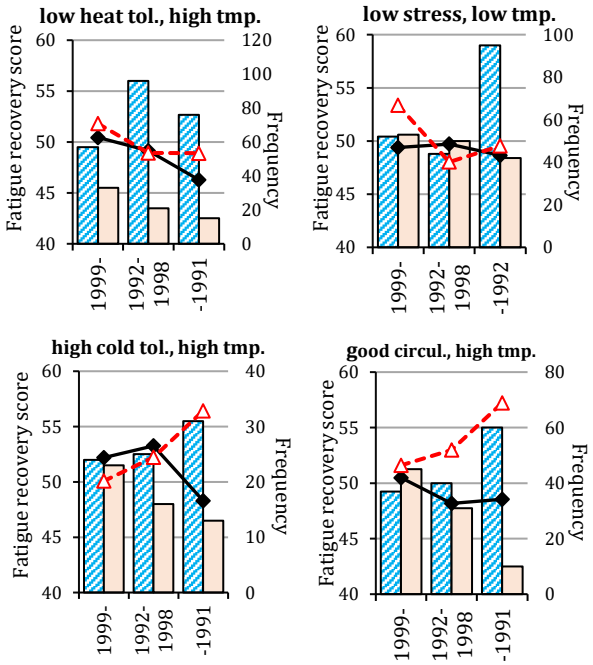

Fig.13 Fatigue recovery score for different outdoor temp., sleeping room environment, and insulation level

Fig.12 shows the relation between the insulation level and the fatigue recovery score. Lines show the score. Bars show the number of nights. The solid line and left colored bar are for cooling use nights and dotted line. The white bars are for nights with no cooling use. Higher and lower respectively mean over and under 27.3°C, which is the median of the mean outdoor temperatures during sleep.
Fatigue recovery score was better for highly insulated dwellings under the following conditions: 1) Outdoor temperatures were higher; cooling was not used in sleeping rooms with good sunshine. 2) Cooling was used in sleeping rooms with indoor solar glare, irrespective of the outdoor temperature. 3) Outdoor temperatures were lower; cooling was not used in sleeping rooms with high cooling efficiency. 4) Outdoor temperatures were higher; cooling was used in sleeping rooms with poor outdoor air quality.

6. Respondent attributes and Fatigue recovery

Heat tolerance, cold tolerance, poor circulation, mental stress, cooling cost anxiety, and mood states in respondent attributes were found to be related directly to OSA scores. Data were divided into two categories by these six items.

Fig.13 portrays the relation between the insulation level and the fatigue recovery score. Fatigue recovery score was better for highly insulated dwellings under the following conditions: 1) Outdoor temperatures were high; cooling was used for respondents with low tolerance to heat. 2) Outdoor temperatures were low; cooling was not used for respondents with low mental stress.

Fatigue recovery score was better for less-insulated dwellings under the following conditions: 1) Outdoor temperatures were high; cooling was not used for respondents with high tolerance against cold. 2) Outdoor temperatures were high; cooling was used for respondents without poor circulation.

7. Conclusions

Sleeping room measurements and data from a questionnaire survey of 188 Osaka apartment residents for 765 nights during four summers clarified the following points about cooling effects on fatigue recovery during summer sleep. For residences with higher amounts of insulation, the following findings were obtained: 1) Cooling use is recommended for higher outdoor temperature nights for cases of a) poor sunshine, b) sunlight glare, c) low cooling efficiency, d) poor outdoor air dwellings, and e) residents with low heat tolerance. 2) Cooling use is not recommended for higher outdoor temperature nights for cases of a) good sunshine dwellings and b) good circulation residents. 3) Cooling use is not recommended for lower outdoor temperature nights for cases of a) dwellings with high cooling efficiency and b) residents with little mental stress. For residences with less insulation, the following findings were obtained. 4) Cooling use is recommended for higher outdoor temperature nights for residents reporting better circulation. 5) Cooling use is not recommended for higher outdoor temperature nights for residents with higher cold tolerance. 6) Cooling use is not recommended for lower outdoor temperature nights, for dwellings with poor sunshine.

8. References

[1] Japan Meteorological Agency
https://www.jma.go.jp/

[2] Kusaka H., Iijima N., Ihara T., Hara M., Takane Y., Iizuka S. Future projection of heat stroke and sleep disturbance for 2070's August in Tokyo, Nagoya and Osaka. J. Environ. Eng., AIJ. Nov. 2013; Vol.78, No.693: 873-881.

[3] Okamoto-Mizuno K., Mizuno K, Michie S, Maeda A,. Iizuka S. Effects of humid heat exposure on human sleep stages and body temperature. Sleep. 1999; 22(6):767-773.

[4] Horne J. A., Reyner L. A. Sleep related vehicle accidents. BMJ. March 1995; 310:565.

[5] Nakayama Y., Umemiya N., Sakane T., Arai J., Kobayashi T. and Tachibana Y. Questionnaire survey of air-conditioner effects on sleep quality in summer -Analyses of falling asleep, maintaining sleep factor and fatigue recovery factor. Proceedings of the 6th International Building Physics Conference. June 2015; No.862: 1-6.

[6] Oguri Y., Shirakawa S., Azumi K. Development of OSA sleep inventory. Clinical Psychiatry. July 1985; 27(7):791-799. in Japanese.

[7] Yamamoto Y., Tanaka H., Takase M., Yamazaki K., Azumi K., Shirakawa S.. Standardization of revised version of OSA sleep inventory for middle age and aged. Brain Science and Mental Disorders. 1999; 10(4): 401-409. in Japanese.

The datasets generated during and/or analysed during the current study are not available because the university repository is under construction, but the authors will make every reasonable effort to publish them in near future.

Mostly dry: current ventilation practice efficiently limits moisture excess in mechanically ventilated apartments

Salih Berkay Coskuntuna [a], Dimitrios Kraniotis [b], Siavash Barnoshian [c], Sverre Holøs [d], Kari Thunshelle [e]

[a] Dep. of Civil Engineering and Energy Technology, Oslo Metropolitan University, Oslo, Norway, berkaycoskuntuna@gmail.com
[b] Dep. of Civil Engineering and Energy Technology, Oslo Metropolitan University, Oslo, Norway, dimkra@oslomet.no.
[c] Dep. of Civil Engineering and Energy Technology, Oslo Metropolitan University, Oslo, Norway, siavashbarnoshian@gmail.com
[d] Dep. of Architectural Engineering, SINTEF Community, Oslo, Norway, sverreb.holos@sintef.no.
[e] Dep. of Architectural Engineering, SINTEF Community, Oslo, Norway, kari.thunshelle@sintef.no.

Abstract. The current Norwegian building code (TEK 17) requires the new residential buildings to have balanced ventilation with heat recovery, in addition to the strict regulations regarding thermal performance and airtightness of the fabric. During the cold winters in the South-East part of the country, the moisture content in the air outdoors is very low and results in a dry climate indoors as well. This study investigates in-situ the moisture excess indoors (Δv) in a series of urban residential apartments that have been built according to TEK 17. In particular, air temperature and relative humidity have been measured in six locations/rooms in each of the monitored apartments. Variations in moisture production as well as in ventilation rates have resulted in different moisture excess levels. The findings reveal that the current practice limits moisture excess and have led to an overall reduction of Δv compared to results found in similar studies performed two decades ago. 90th percentiles of Δv have been calculated as below 2 g/m^3 in all types of rooms, while in bathrooms it has been 2.6 g/m^3. The relative humidity (RH) has been respectively below 30%, with bathrooms being the only exception with RH just over this level. The results from a survey among the occupants showed that most of them complain about fatigue, difficulty in concentrating and a head that feels heavy. In addition, dust and too high air temperature have been identified as the main problems of the indoor environment.

Keywords. indoor moisture excess, relative humidity, residential buildings, mechanical ventilation, Nordic climate.
DOI: https://doi.org/10.34641/clima.2022.293

1. Introduction

The low or high humidity indoors is closely related to many health problems and it is also linked to energy consumption and durability of construction. Therefore, it is essential to control the relative humidity in order to achieve a healthy and comfortable indoor environment [1]. During the cold and dry winter periods in Nordic climates, the relative humidity can drop down to 10% [2]. The studies revealed correlations between low humidity and health problems such as discomfort in the skin, eye and nose [3]. Besides, the Norwegian Institute of Public Health recommends relative humidity to be over 20% due to the fact that low humidity has an effect on respiratory health [4]. Moreover, in the Norwegian standards, the lower limit of relative humidity in residential apartments was recommended to be at 25% and the upper limit at 60% when humidification and dehumidification systems are installed [5].

With the recent Norwegian building code (TEK 17), residential buildings started to contain balanced ventilation with heat recovery, in addition to the strict regulations regarding airtightness and thermal performance. Despite the very positive results from the energy efficiency point of view, this might cause problems in the indoor environment in Nordic countries, e.g., too low relative humidity. Since the new regulations applied, there are limited studies that have researched the humidity levels in residential buildings. The objective of this study was to determine the indoor environment of modern Norwegian residential buildings in relation to moisture-related parameters.

2. Methods

2.1 Experimental site

The field measurements were conducted in 10 modern dwellings in Oslo, Norway where the large majority of the apartments were located in the

Copyright ©2022 by the authors. This conference paper is published under a CC-BY-4.0 license.

project building in the city district Bjerke. In order to utilize the climatic data near the tested apartments, the weather station at Blindern in Oslo was selected as a resource for outdoor climate data such as temperature, RH and pressure.

As this study has a focus on modern Norwegian urban homes, the selection of apartments was done according to the following criteria: the buildings were built/renovated after 2012 and apartments have BRA ≤ 115 m². Summary of building characteristics shown in Tab. 1.

During the field experiments, measurement and monitoring of the time-varying relative humidity (RH), air temperature (T), pressure values and CO_2 levels indoors were monitored and measured utilizing two different sensor types, i.e., Airthings wave mini and Airthings wave plus at 5 minutes interval over a period of 7 days. In order to conduct measurements of each apartment, one set of Airthings sensors, which contains 4 pcs of Wave Mini, 2 pcs of Wave Plus and one Airthings Hub (for the wireless transfer of data) were used. In each testing apartment, placement of the sensors was following; wave plus sensors to the living room and master bedroom, wave mini sensors to bathroom, kitchen, secondary bedroom and entrance.

Each device was wall-mounted 150-170 cm above the floor level and as a minimum 1 meter / 3 feet away from air supply/exhaust, exterior walls, windows, doors, mechanical fans, heaters or any other noteworthy source of heat gain or loss [7].

Moreover, measurement of the air flow supply rates and mechanical exhaust ventilation air flows were conducted by utilizing two different equipment sets where first set was consisted of Kimo K35 measuring funnel and Velocicalc® Air Velocity Meter 9545 anemometer with hot wire and the second one was consisted of Swemaflow 125 air flow hood. For the measurements of the ventilation airflow rates, one sample apartment from each project area was selected and the measured values were used as a reference for all tested apartments in the same project areas. Apart from Apartment #1, all other tested apartments were located in the same project area which includes 4 buildings with similar characteristics. Thus, Apartment #1 and Apartment #2 were selected as sample apartments for the ventilation airflow rates measurements.

Furthermore, the calibration processes of the devices called Airthings Wave Plus and Wave Mini were performed in SINTEF Community laboratory by utilizing a climate chamber called Termarks KB 8400 F/L.

2.3 From experiment to data

The hourly averaged absolute humidity levels were calculated from logged data of indoor temperature, relative humidity and pressure along with the outdoor temperature, relative humidity and pressure data collected from the nearest meteorological station. The indoor moisture excess levels were calculated using the equation (2).

$$\Delta v = v_i - v_e \; [g/m^3] \tag{2}$$

Tab. 1 - Summary of building characteristics of the 11 apartments included in the research

Apartment	#1	#2A	#2B	#3	#5	#7	#8	#10	#11	#12	#20
Area (m²)	30	60		N/A	45	60	87	90	85	115	67
Number of Occupants	2	3		1	1	1	1	2	4	4	3

2.4 Questionnaire

The online questionnaire consists of 26 questions related to occupancy level, moisture sources, characteristics of the apartment, occupant behaviours and health symptoms related to indoor environment. A multiple-choice, yes-no and scaled choices as "Never, Sometimes and Often" were used to record the responses to the questions. All responses to the questionnaires were stored anonymously. Moreover, a permission from Norwegian centre for research data [8] were granted to perform the surveys.

3. Results

3.1 Measurement period and overall climate

The defined experiment period for this study was February 14, 2021 – April 22, 2021. During the experiment period, the average outdoor temperature was 1.87 °C; this was 0.08°C cooler than the 30-year average of 1.95°C recorded at the Oslo Blindern weather station for the period of February to April 1990-2021.

3.2 Participating households

In this study a total number of 10 households was participated. The detailed characteristics of participating households are shown in Table 2 [6]. It must be noted that Apartment #2 was tested two times in different time periods and presented as Apartment #2A and #2B, where A stands for the period of the measurements without a humidifier, B stands for the period of the measurements with a humidifier. Since, it was the same households, to avoid confusion the details of the Apartment #2B

was not counted in the mean value calculations except for the row showing the owning humidifier(s).

Tab. 2 - The characteristics of participating households

		Mean values (Range)
Total household members		2.4 (1-4)
Age of household members		41.73 (26-60)
Rooms in home		3.2 (2-5)
Floors in building		6.5 (6-7)
BRA (m^2)		72.6364 (30-115)
Can turn heat on and off		
	Yes	10 (%100)
	No	0 (%0)
Own humidifier(s)		
	Yes	2 (%18.2)
	No	9 (%81.8)

Note. Adapted from [6]

3.3 Ventilation air flow rates

The measured air supply and air extraction rates in aforementioned apartments and a comparison with the design values recommended in TEK 17 [9] are shown in Tab. 3 [6]. It is obvious that the obtained values differ from the recommended values.

3.4 Relative humidity, temperature and indoor moisture excess

The air temperature and relative humidity values in the bathroom, kitchen, master bedroom, living room and secondary bedroom of each apartment which were measured over a period of 5-13 days are presented as boxplot graphs according to room types, respectively, in Fig. 4, Fig. 5, Fig. 6, Fig. 7. In boxplot graphs, the top of the box (upper quartile) represents 90th percentile while the bottom (lower quartile) stands for 10th percentile.

Relative humidity

For each type of apartments without a humidifier, 90% of the measured values of RH levels indoors were below 32% while the mean values were lower than 23% (25% is the lowest limit for "Category II" according to the NS-EN 16798-1:2019 [5]). While, 10% of the RH levels indoors measurement results were even lower than 15%. Although, the mean values of the RH indoors for the apartments with humidifier was between 32-43%. Additionally, RH peaks were lower in Apartment #10 and #12 compared to other apartments. The highest measured RH indoors was observed in Apartment #11, nevertheless some attention-grabbing high values were also observed in Apartments #1, #2B and #7. Moreover, the measured highest RH levels were observed in bathrooms and bedrooms of the apartments regardless of owning humidifier(s). Besides, the RH levels in the bathrooms of Apartments #1, #2B, and #11 display larger interquartile ranges which comprise higher RH values than the others. However, the median RH value in the bathroom of Apartment #11 was still between 15-25%, likewise all apartments excluding Apartments #1 and #2B.

Tab. 3 – The ventilation rates measured in Apartments #1 and #2 and design targets from TEK 17 [9]

Room Type	Apartment #1		Apart-ment #2		Design Targets	
	S* [m^3/h]	Ext* [m^3/h]	S* [m^3/h]	Ext* [m^3/h]	S* [m^3/h]	Ext* [m^3/h]
Bathroom	-	25		100	-	54
Master Bedroom	37	-	18	-	26	-
Living room	37	-	25	21	-	36
Kitchen						
Small Bedroom	-	-	11.5	-	26	
Total (Apartment #1)	**74**	**25**			**36**	**54**
Total (Apartment #2)			**54.5**	**121**	**72**	**90**

Abbreviations: S*, Supply; Ext*, Extract.
Note. Adapted from [6]

The maximum measured RH levels in master bedrooms were observed in Apartment #1 and followed by Apartment #2. However, this only observed for one time roughly 20 minutes about 15:20 during one monitoring day, correspondingly an increase was observed in RH levels every day roughly around 15:20. Moreover, some findings were also observed in Apartment #11, even though the median RH value of Apartment #11' master bedroom was observed as 21.49%, it was exposed to higher levels of RH as far as 38% and after some days of the measurement period, it was reduced till 15% levels while at the same time there was a decrease observed in its CO_2 levels.

The minimum mean RH value was monitored in living rooms. Except for Apartment #2, the median RH values were observed as below 25% in all other apartments' living rooms.

The maximum RH level measured in kitchens was observed as 43.53%, however 90% of the monitored RH levels were down below 29.66%. Moreover, comparing to the others, the highest number of weekly cooking events were observed in apartments

#2 and #11, according to the survey data.

Temperature

The mean indoor temperature values of the monitored apartments were observed as between 21-27 °C. It was found that 10% of the monitored indoor temperature values were above 23 °C, which considered as higher than the recommended value in TEK 17 and required value in NS-EN 16798-1:2019 [5,9].

The lowest mean temperature value was observed in master bedrooms. While the mean temperature in the bedrooms of most of the monitored apartments was between 20-23 °C except for three apartments (#8, #10 and #12) where higher values were observed.

The maximum mean temperature value was observed in bathrooms as 38.99 °C in Apartment #20. Moreover, when compared to others, significantly lower temperatures were observed in Apartment #3 and #12' bathrooms.

Although the maximum reached temperature in kitchens was 29.01 °C, 90% of the measurement results were below 25.9 °C. In addition, the findings show that the temperatures measured from the kitchens were considerably higher ($p < 0.05$) compared to the monitored living rooms and bedrooms, without making discrimination of with or without humidifier(s) [6].

Furthermore, considering the effect of outdoor temperature on indoor temperature, as shown in Fig. 1, the correlations were only observed in Apartment #1 and #10 which shows an increase in indoor temperature together with the outdoor temperature.

Absolute Humidity

The hourly average absolute humidity values from kitchen and living rooms were at their maximum in the evenings (approximately 3 pm – 10 pm) when the majority of the people from Norway are generally at home. Also, 80% of the hourly average absolute humidity values from bedrooms were at their maximum between evening and night hours (approximately 6 pm – 3 am). Moreover, as shown in Fig. 2, outdoor absolute humidity levels were generally low during the whole experiment period with an exception for Apartment #1 and #2A' period of measurement.

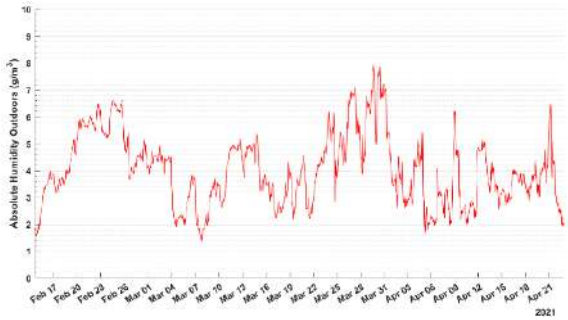

Fig. 2 - Absolute humidity outdoors expressed in g/m3, during the experiment period [6].

Moisture Excess

The maximum mean internal moisture excess value was observed as 1.3565 g/m³ in bathrooms of the apartments without humidifiers. And this was followed by kitchens as 0.896 g/m³. As for the apartments with humidifier(s), the maximum mean internal moisture excess value was observed in the secondary bedroom as 5.44 g/m³ and it was followed by bathroom as 4.77 g/m³.

For the apartments without humidifier(s), the minimum mean Δv has been calculated as 0.59 g/m³ in bedrooms and followed by living rooms as 0.69 g/m³. Besides, 90th percentiles of Δv have been calculated as below 2 g/m³ for all types of rooms of the apartments without humidifier(s) except for bathrooms which were calculated as 2.6 g/m³.

As concerns the highest hourly average values in bedrooms, 50% of them were observed through the night-time whereas the rest were observed afternoon and evenings (around 12 pm – 7 pm).

Regarding kitchens, 90% of the estimated Δv values were below 1.862 g/m³ and the highest estimated Δv was 4.33 g/m³. While the mean estimated Δv from kitchens of the apartments which did not own humidifier(s) was 0.896 g/m³. Furthermore, the

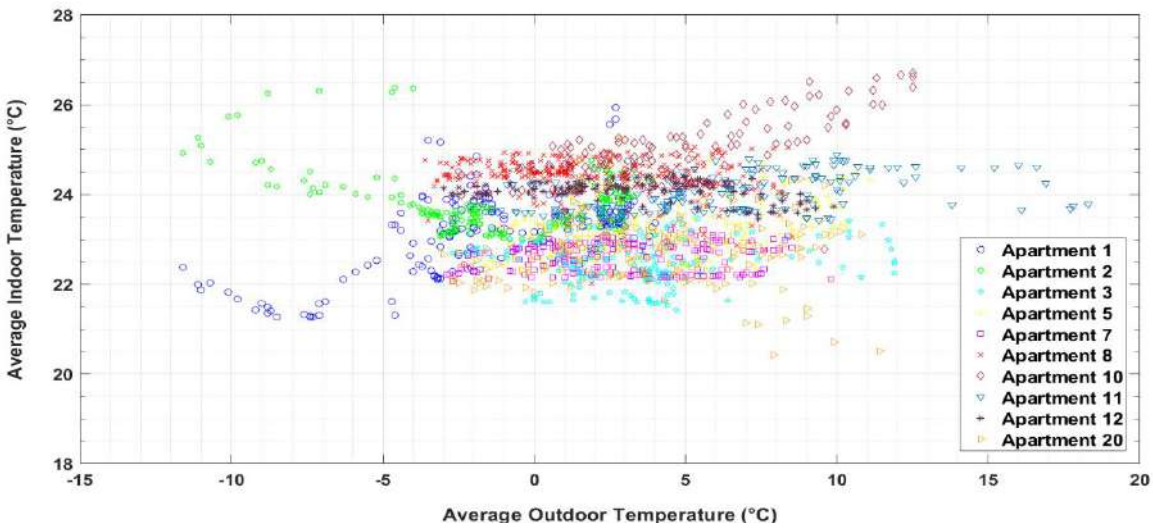

Fig. 1 - The correlation between indoor and outdoor temperatures, average values per house [6].

apartments (2,7,10,11,12 and 20) with more occupancy levels and claimed to have more dinner activities compared to others, had generally higher internal moisture excess from their kitchen.

As to bathrooms, the minimum mean moisture excess in bathrooms was observed as 0.36 g/m³ in Apartment #3. However, the median Δv values for seven of eleven measurements (Aparments 5,7,8,10,11,12 and 20) were between 0.8 – 2 g/m³. Furthermore, the maximum Δv have been calculated as 9.13 g/m³ was from bathrooms of the apartmens without humidifier(s).

3.4 Survey results

The survey responses to some health problems were shown in Tab. 4. The occupants have reported little but some issues with health problems for instance headache, fatigue, difficulty in concentrating and dizziness. As shown in Table 4, "often" was used only once as a response to a dizziness by Apartment #7. Besides, majority of the occupants responded as "sometimes" to difficulty in concentrating, fatigue and heavy in the head.

Tab. 4 – The survey responses to some health problems

Apart-ment	1	2 A	2 B	5	7	8	10	11	12	20
Dizzi-ness	N	S	S	N	O	N	N	N	N	S
Head-ache	S	S	S	N	N	N	N	N	S	S
Fatigue	S	S	S	S	N	N	N	S	S	N
Diffi-culty in concen-trating	S	S	S	S	S	N	N	S	S	N
Heavy in the head	S	S	S	S	S	N	S	N	S	N

Note. Adapted from [6].

Further, Fig. 3 shows the survey responses related to the thermal environment. As shown in Figure 3, 90% of the households responded that they never felt too low room temperature, while only 10% responded that they felt sometimes too low room temperature which was in phase with the field measurement results that showed indoor temperatures being often high and rarely being too low. However, 30% of the participants reported often too high room temperatures and 40% reported sometimes too high room temperatures. As to varying room temperature, 30% of the participants responded as "sometimes" and 70% of the participants never felt any varying room temperature.

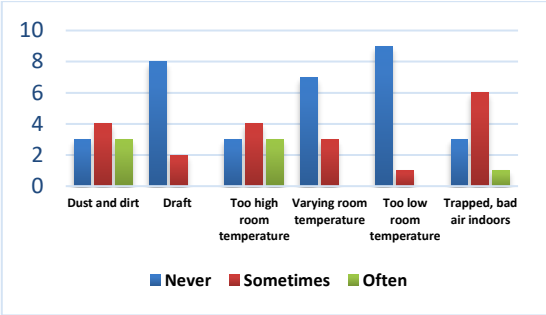

Fig. 3 - Survey responses correlated with the thermal environment [6].

As concerns humidity related problems, except for the occupants of the apartments with humidifier(s), all other participants responded that the perceived indoor air was dry. The majority of the participants were responded as "often" to questions about an irritated, stuffy or runny nose. As to hoarseness / dry throat, 60% of the participants responded as "Sometimes" and 20% as "Often" and the rest as "Never". While each participant reported at least one humidity related problem, the participant from Apartment #8 responded as "Never" to all questions even though he/she expressed the perceived air as dry.

4. Discussion

4.1 Ventilation airflow rates

The air supply and extraction rates monitored in apartments were far away from the recommended values of TEK 17 [9]. The measured air supply rate in Apartment #1 was higher than its extraction rate resulting in under pressurisation, while the exact opposite situation was occurred in Apartment #2 resulting in over pressurisation. It must be noted that the aforementioned rates were only measured once for a small period of the measurement periods in each mentioned apartment, therefore, no certainty can be provided that the data obtained during the small period of the measurement remains unvaried throughout the entire measurement.

4.1 Relative humidity, temperature, and indoor moisture excess

The low RH levels might occur mostly during winter period, due to various factors such as high indoors temperatures, excess air conditioning, high ventilation exhaust air rates, and so on. The low levels of RH peaks in the Apartments #10 and #12 were presumed to be due to higher ventilation rates, since these two apartments had the largest BRAs. The high monitored levels of RH in Apartment #1' bathroom, is assumed to be because of under ventilation.

In the majority group of bedrooms, the RH levels were usually lower through the period between morning and evening-time while these periods also low CO_2 levels (approx. 400 ppm) were observed. However, higher levels of RH were observed in the

Tab. 5 – The survey responses to humidity related problems.

Apartment	Is the indoor air perceived as dry, humid?	Itchy burning/ irritation in the eyes	Irritated, stuffy, or runny nose	Hoarseness / dry throat	Dry or red skin on the face	Cough	Dandruff/ itching of the scalp/ears	Dry, irritated/ red skin on the hands
1	Dry	Sometimes	Often	Sometimes	Often	Never	Never	Often
2A	Dry	Sometimes	Often	Often	Never	Sometimes	Never	Never
2B	Humid	Never	Sometimes	Sometimes	Never	Never	Never	Never
5	Dry	Sometimes	Never	Never	Never	Never	Sometimes	Sometimes
7	Humid	Often	Often	Often	Often	Often	Often	Never
8	Dry	Never	Never	Never	Never	Never	Never	Never
10	Dry	Never	Often	Sometimes	Never	Sometimes	Never	Sometimes
11	Dry	Never	Often	Sometimes	Sometimes	Never	Never	Sometimes
12	Dry	Never	Never	Sometimes	Sometimes	Sometimes	Never	Sometimes
20	Dry	Sometimes	Often	Sometimes	Never	Sometimes	Sometimes	Often

Note. Adapted from [6].

night-times, meanwhile high levels of CO_2 (above 700 ppm) have occurred. Based on these observations, it was concluded that the occupancy rate and/or window opening and closing activities in the bedrooms from morning to evening caused low relative humidity rates. It has also been hypothesized that the peaks of RH levels and indoor moisture excess in bedrooms during the daytime were due to short-term use of bedrooms, i.e., children's nap time and/or usage of the bedroom as a home office.

Furthermore, it was assumed that the higher RH levels and temperatures observations from the living rooms and kitchens were due to higher occupancy rate leading more cooking events and/or less window opening activities, taking into consideration that all monitored apartments had an open kitchen design. Besides, the observed low air temperatures in the kitchens and/or living rooms were assumed as due to small BRA of the apartments, low occupancy rates leading to low numbers of cooking activities. The low air temperature in bedrooms were assumed due to window opening activities and/or low occupancy rates through the day time.

In addition, it was presumed that the higher peak temperature values in bathrooms (apartments #1, #2 and #5) have occurred due to hot and long showering events while, as to apartment #20, it was assumed to be high-temperature settings of floor heating in-line with the dryer usage whereas low levels of RH were observed meanwhile air temperatures were in their peaks. Also, the small interquartile ranges indicate the occurrence of stable temperature values in the bathrooms. And it was assumed that the stable temperatures were due to the normal showering temperatures and keeping the bathroom door closed.

As concerns correlations between indoor and outdoor temperatures, as shown in Fig. 1, it gave the impression that changes in indoor temperature were not a result of outdoor temperature.

The outdoor absolute humidity's effect on indoor moisture loads were noteworthy. The low absolute humidity outdoors together with high temperatures indoors were assumed to be a cause of the dry indoor environment. However, as for indoor moisture excess, many factors play a role, such as occupancy rates, dinner activities, occupant behaviours, BRA, ventilation rates and so forth. The higher ventilation rates compared to total supply rates, low RH levels, overheating and large BRA, which minimise the effect of moisture-generating activities in the environment, was assumed to be a reason for the low median moisture excess values as well as negative moisture loads. Moreover, without making discrimination of with or without humidifier(s), it was assumed that the cause of the observed peak Δv values in bathrooms were due to warmer temperatures together with high RH levels which resulted by showering events. However, the minimum Δv values observed in Apartment #3' bathroom were result of low temperature and RH levels which might be caused by several factors such as short-cold showering, keeping the door open most of the time, which were supported by the logged data showing an air exchange between bathroom and corridor after showers.

The ventilation exhaust air rate was probably effective in drawing polluted air such as CO_2 and humid air out of the apartments. The higher CO_2 concentrations in bedrooms compared to kitchen/livingroom and bathrooms were assumed to caused due to bedrooms not having an outlet. While, not enough fresh air inlet might be a cause for some of the health related problems which participants claimed to have. Moreover, gradually varying temperatures could explain why the participants were not feeling varying temperatures but rather high temperatures.

5. Conclusion

The indoor climate conditions in 10 selected apartments from modern Norwegian residential buildings were assessed considering the following parameters; temperature, RH, outdoor air supply/extract, CO_2 concentration, indoor moisture excess. The research indicated that monitored ventilation rates deviated from the required values in Norwegian building regulations (TEK 17) [9].

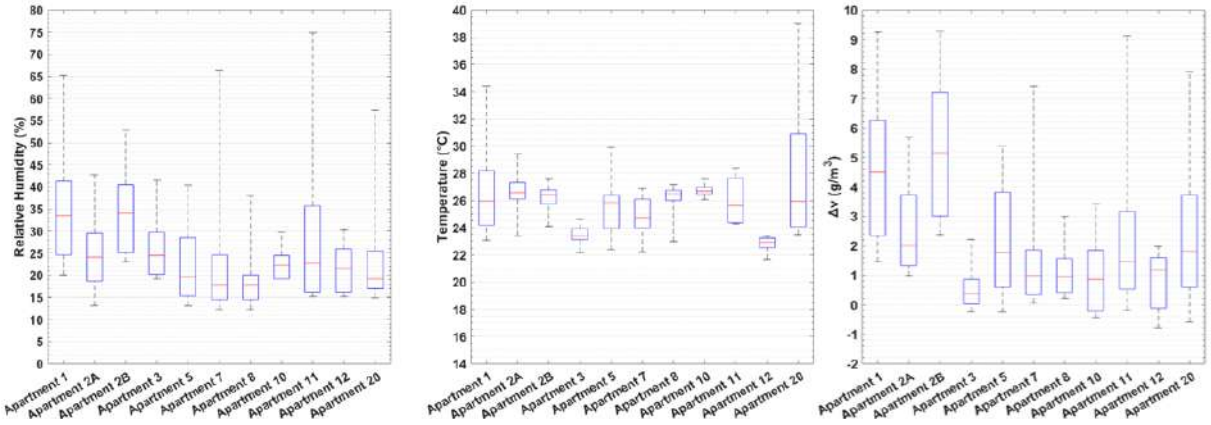

Fig. 4 - Measurements of RH, air temperature and Δv values from the bathroom of each tested apartment.

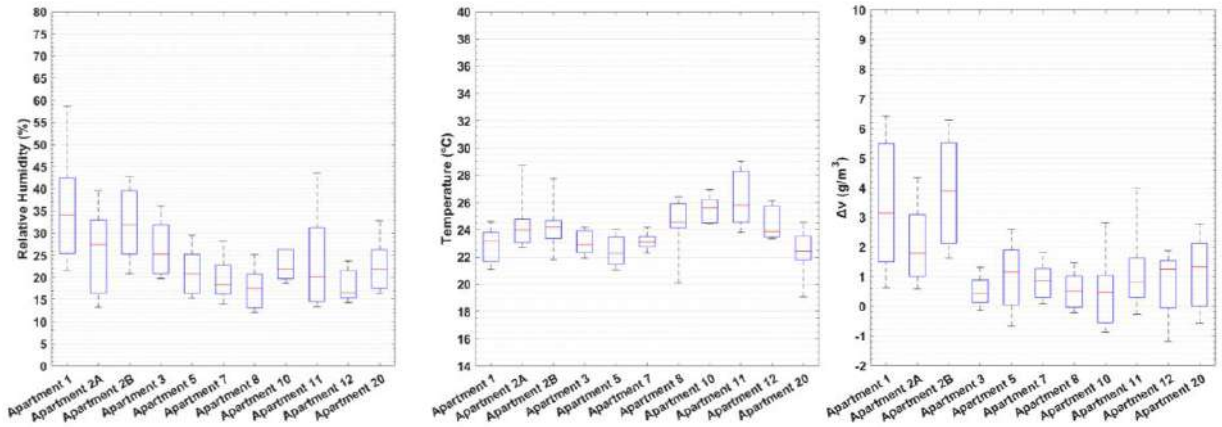

Fig. 5 - Measurements of RH, air temperature and Δv values from the kitchen of each tested apartment.

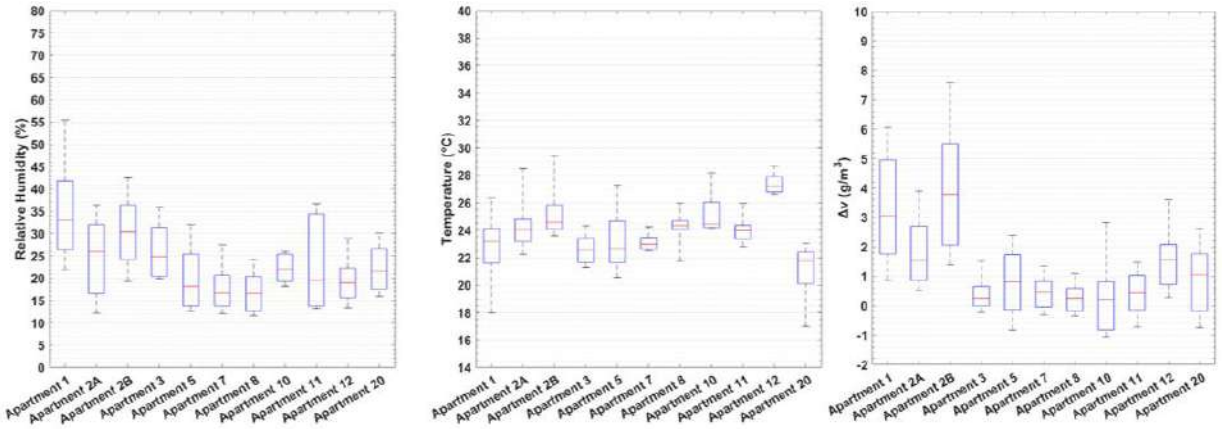

Fig. 6 - Measurements of RH, air temperature and Δv values from the living room of each tested apartment.

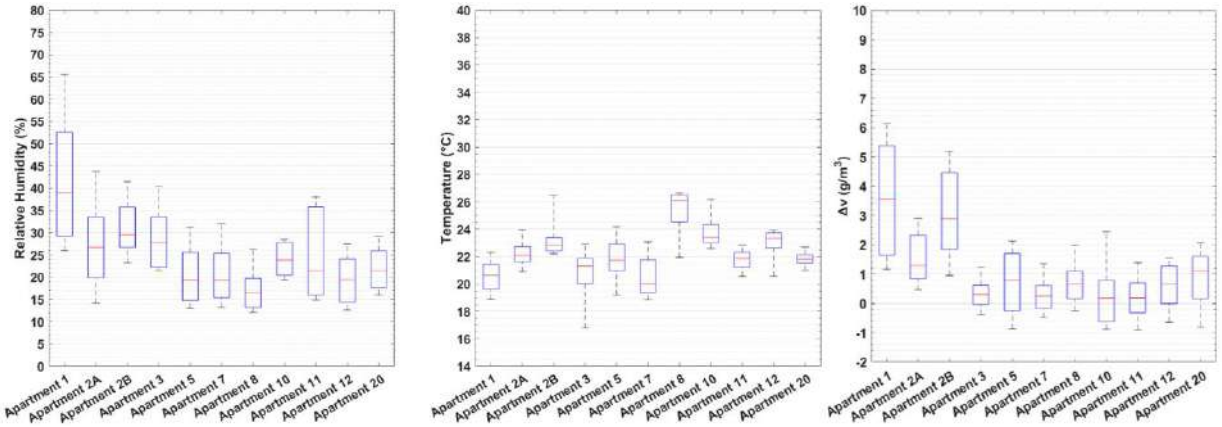

Fig. 7 – Measurements of RH, air temperature and Δv values from the master bedroom of each tested apartment.

Generally, the causes of low moisture excess were presumed to be high ventilation rates, low absolute humidity and low internal moisture supply. Also, the findings reveal that there is an overall reduction of Δv compared to the results found in similar studies [10–14].

The monitoring period is also noteworthy for assessing moisture conditions indoors. The study showed that the low outdoor absolute humidity during the monitoring of the majority group of apartments caused low moisture levels indoors when combined with high indoor temperatures. Moreover, the findings revealed that indoor temperatures were very often exceed 20 °C which is the temperature value assumed for simulating moisture conditions.

Furthermore, the survey findings indicated that majority of the participants perceived air as dry. Substantial number of participants complain about fatigue, difficulty in concentrating and a head that feels heavy. Besides, 70% of the participants claimed to expose to high indoor temperatures and 60% of the participants reported feeling of bad, trapped air indoors.

6. Acknowledgement

This paper is based on the master thesis by S. Berkay Coskuntuna & Siavash Barnoshian and was a part of the Urban Ventilation project. Urban Ventilation is funded by the Research Council of Norway EnergiX program under Grant No. 308819 and the industry partner Røros Metall AS, BSH Husholdningsapparater AS, Miele A/S, Engebretsen AS, Mestergruppen Bolig AS, Obos BBL, Selvaag Bolig ASA and Flexit AS.

7. References

[1] Zhang H, Yoshino H. Analysis of indoor humidity environment in Chinese residential buildings. Build Environ 2010;45:2132–40. https://doi.org/10.1016/j.buildenv.2010.03.011.

[2] Lind M, Holøs SB, Thunshelle K, Yang A, Mysen M. How Does Low Relative Humidity Affect Perceived Air Quality, Thermal Comfort and Symptoms in Modern Office Buildings in Cold Climates? 2019.

[3] Derby MM, Hamehkasi M, Eckels S, Hwang GM, Jones B, Maghirang R, et al. Update of the scientific evidence for specifying lower limit relative humidity levels for comfort, health, and indoor environmental quality in occupied spaces (RP-1630). Sci Technol Built Environ 2017;23:30–45.

[4] Folkehelseinstitutt. Anbefalte faglige normer for inneklima. Revisjon av kunnskapsgrunnlag og normer – 2015. 2015.

[5] Standard Norge. Energy performance of buildings - Ventilation for buildings - Part 1: Indoor environmental input parameters for design and assessment of energy performance of buildings addressing indoor air quality, thermal environment, lighting and acoustics (Module M1-6) (NS-EN Standard No. 17772-1:2017) 2019.

[6] Coskuntuna SB, Barnoshian S. Indoor environment in modern Norwegian buildings in connection with moisture-related parameters. Oslo Metropolitan University, 2021.

[7] ASA A. Airthings for Business | Improve Productivity, Save Time & Money n.d. https://www.airthings.com/en/business (accessed December 26, 2021).

[8] NSD. Norwegian Centre for Research Data. NSD n.d. https://nsd.no/en (accessed January 7, 2022).

[9] Direktoratet for byggkvalitet (TEK 17). Byggteknisk forskrift (TEK17) 2017.

[10] Bagge H, Johansson D, Lindstrii L. Measured indoor hygrothermal conditions and occupancy levels in an arctic Swedish multi-family building. HVACR Res 2014;20:376–83. https://doi.org/10.1080/10789669.2014.888367.

[11] Geving S, Holme J. Mean and diurnal indoor air humidity loads in residential buildings. J Build Phys - J BUILD PHYS 2012;35:392–421. https://doi.org/10.1177/1744259111423084.

[12] Ilomets S, Kalamees T, Vinha J. Indoor hygrothermal loads for the deterministic and stochastic design of the building envelope for dwellings in cold climates. J Build Phys 2017;41:547–77. https://doi.org/10.1177/1744259117718442.

[13] Kalamees T, Vinha J, Kurnitski J. Indoor Humidity Loads and Moisture Production in Lightweight Timber-frame Detached Houses. J Build Phys 2006;29:219–46. https://doi.org/10.1177/1744259106060439.

[14] Geving S, Holme J, Jenssen J. Indoor air humidity in Norwegian houses, Citeseer; 2008, p. 16–8.

Numerical Analysis of Age of Air and Suspended Particle Distribution in Ventilated Operating Room

Riou Yamada [a], Hideaki Nagano [b], Hidehiro Asami [c], U Yanagi [d], Shinsuke Kato [e]

[a] Graduate School of Integrative Science and Engineering, Tokyo City University, Tokyo, Japan, g2181054@tcu.ac.jp

[b] School of Science and Engineering, Tokyo City University, Tokyo, Japan, hnagano@tcu.ac.jp

[c] School of Science and Engineering, Tokyo City University, Tokyo, Japan, g1812002@tcu.ac.jp

[d] School of Architecture, Kogakuin University, Tokyo, Japan, yanagi@cc.kogakuin.ac.jp,

[e] Office of Senior Professor, the University of Tokyo, Tokyo, Japan, kato@iis.u-tokyo.ac.jp

Abstract. This paper evaluates the indoor-air contamination caused by surgical smoke in the operating room and verifies the improvement caused by installing hanging walls suspended from the ceiling. A Computational Fluid Dynamics (CFD) analysis was performed to analyze the gas contaminant in the operating room with and without the installation of hanging walls suspended from the ceiling. The analysis showed how the downward air-conditioned flow blown from the ceiling surface and the upward flow caused by the hot surgical smoke interacted to form a complex flow field. Due to the close proximity of the source of smoke to the breathing zone, there was a steep gradient in the concentration of particles near the operating field.

Keywords. Operating room, Surgical smoke, Breathing air quality, CFD
DOI: https://doi.org/10.34641/clima.2022.47

1. Introduction

In recent years, various electrosurgical tools, including laser scalpels and ultrasonic surgical generators are available for surgery. These tools work by burning biological tissue, creating large quantities of vapor and droplets in the air, especially when there is a lot of moisture. This is called surgical smoke, and its composition includes not only water vapor, but also substances harmful to medical staff and patients, including toxic gases such as benzene, toluene, and xylene, as well as bacteria and viruses [1-3]. In this case, the generation of contaminants in the operating room cannot be avoided. Therefore, to ensure breathing air quality, it is necessary to ensure that the contaminants that are generated are quickly exhausted before they reach the breathing zone of the medical staff.

Hence, the purpose of this study is to determine the diffusion characteristics of contaminants from surgical smoke by numerical analysis and to verify the effect of installing hanging walls to improve the quality of the air that is breathed by the medical staff.

2. Outline of simulation

A computational fluid dynamics simulation was conducted to evaluate the contaminant concentration distribution in the operating room and the effect of installing hanging walls to improve the simulated air chamber. The target space is an actual operation room with the highest level of cleanliness—class 100, based on US. Federal Standard 209 E—in the pulmonology ward of a university hospital in Shanghai, China [4-5]. The operation was a thoracotomy for the purpose of removing a tumor from the right lung of a patient. Table 1 shows the calculation conditions and Table 2 shows the boundary conditions. The computational model features an operating table in the center of the room with the air conditioning system blowing downward from the ceiling, just as in the actual operating room (Fig. 1). The analysis treated that all the particles were scalar transport and followed the airflow perfectly. The steady-state concentration distribution in space was analysed by solving the transport equation for the scalar quantity generated from the operating field at a constant rate. The simulated medical staff at the operating table were given an opening corresponding to the mouth, and their breathing was simulated by way of constant suction. Three heat sources were configured: the electrocautery used in the operating field, the human-generated metabolic heat, and the surgical light. To improve the quality of the air that is breathed by the medical staff, it is necessary for the air conditioned flow from the ceiling to reach the level of the breathing zone without diffusing. Therefore, several different hanging wall configurations

Copyright ©2022 by the authors. This conference paper is published under a CC-BY-4.0 license.

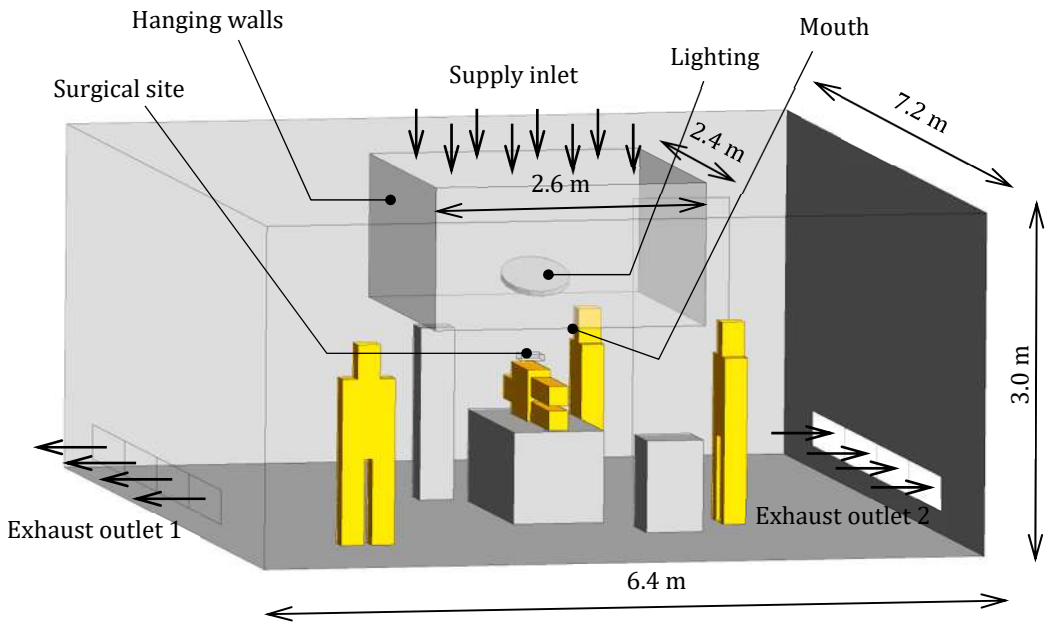

Fig.1 - Computational model of OR

Tab. 1 - Calculation condition.

Mesh type	Prism on human surface Tetra for space
Mesh number	3 million
Min. mesh height	5 mm
Governing equation	Continuity, RANS, Average heat transfer, Scalar transport
Time marching	Steady state
Turbulent model	SST *k-ω* model
Differential scheme	2nd order upwind
Pressure coupling	SIMPLE
Buoyancy	Incompressible ideal gas
Heat radiation	View factor

Tab. 2 - Calculation condition.

Inlet	Velocity	0.25 m/s
	(Air change rate	40 h^{-1})
	Turbulent intensity	5 %
	Turbulent viscosity ratio	10
	Temperature	21 °C
Outlet	Zero pressure	
Wall	No-slip / Adiabatic	
Respiration of medical staff	Continuous inhalation 0.71 m/s (14.4 L/min)	
Metabolic rate	86 W	
Electrocautery	300 W	
Surgical light	80 W	

Tab. 3 - Case condition.

	Case 1	Case 2	Case 3	Case 4
Height of hanging wall	N/A	1.25 m	0.25 m	1.25 m
Area of hanging wall region	N/A	2.6 x 2.4 m		0.88 x 0.8 m

were investigated to see if they would prevent the air conditioning airflow from mixing with the room air. The condition with no hanging wall was designated as Case 1. Cases 2 to 4 corresponded to the installation of pairs of hanging walls of different heights and enclosing different surface areas. The case conditions are shown in Table 3.

3. Results and discussion

3.1 Flow field

Fig. 2 shows the distribution of the flow velocity vectors. In all cases, the air conditioning airflow blown down from the ceiling vents is blocked by the surgical light and then diverted to the left and right exhaust outlets. In the upper corners of the room, vortices are formed where the flow velocity is low; hence, the air in that section is believed to remain in the same place for longer.

In the operating field, the surgical smoke generates an upward flow of heat with a velocity of about 0.30 m/s. Because the air conditioning airflow from the ceiling is blocked by the surgical light, an upward flow develops and is amplified by the metabolic heat generated by the medical staff. This, combined with the effect of inspiration by the medical staff, causes the surgical smoke to reach the level of the breathing zone, where it is inhaled by the medical staff. In Case 1, since there is no hanging wall, the air conditioning airflow is slowed by the shear stress caused by the velocity gradient with surrounding low-velocity airflow. However, in Case 2, which features hanging walls, the air conditioned flow appears to reach the bottom of the hanging walls without mixing or diffusing, allowing it to be delivered to the level of the breathing zone with its purity intact. Case 3 produces a similar effect, but because the hanging walls are shorter, the air mixes below it, and the improvement is not as significant. In Case 4, the hanging walls are

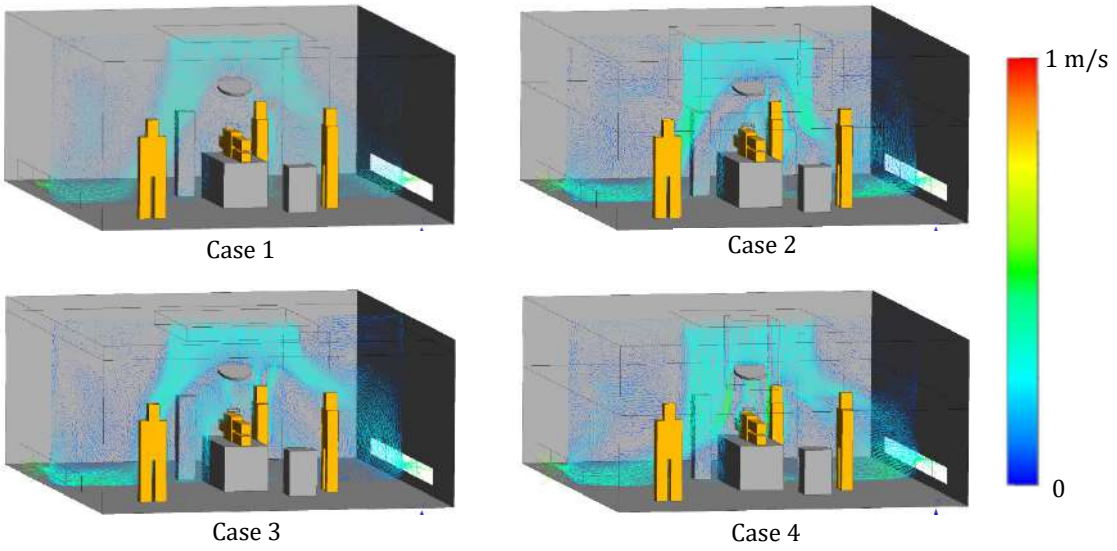

Fig. 2 - Airflow distribution

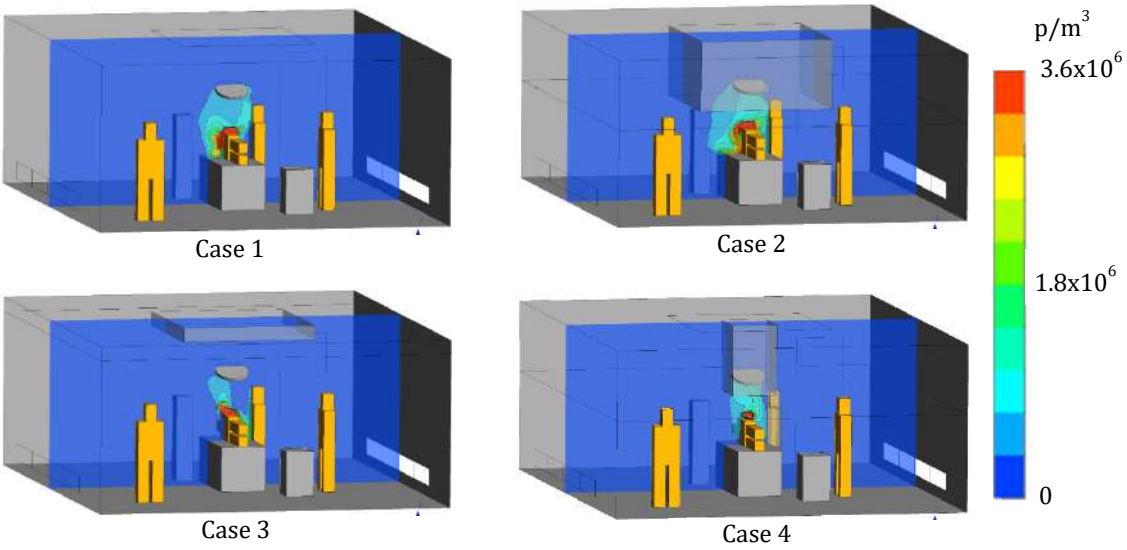

Fig. 3 - Concentration distribution

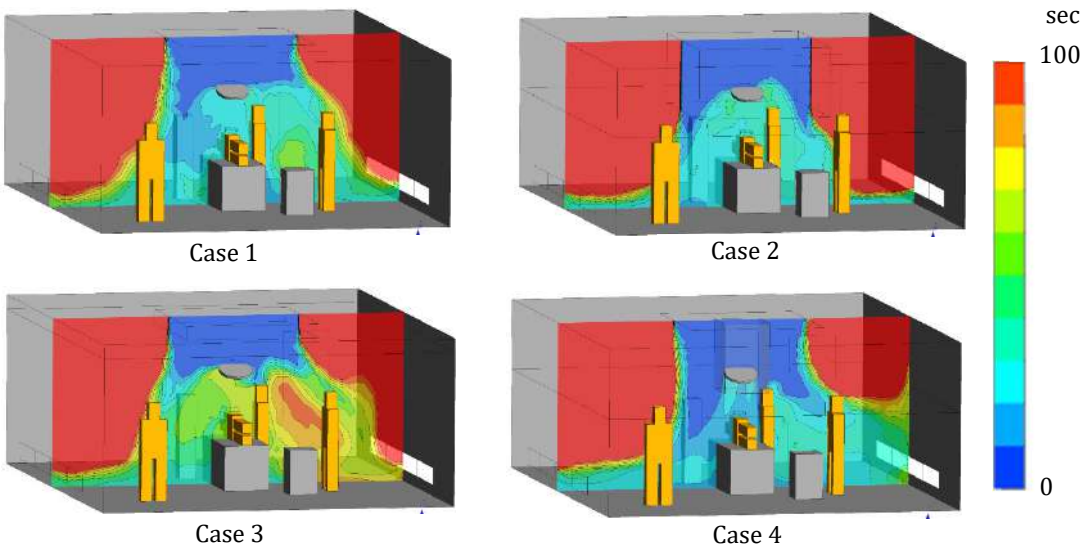

Fig. 4 – Age of air distribution

closer together, defining a narrower region with almost the same surface area as the surgical light. In this case, the air conditioning airflow passes both through and around the region defined by the hanging walls. This allows the air in the hanging wall area to reach the level of the breathing zone without any mixing at all.

3.2 Concentration distribution

Fig. 3 shows the concentration distribution. The numeric concentration levels (converted to number of particles) shown in the figure were calculated based on the measured number of particles at the outlets and the intensity computed in the CFD simulation [4-5]. In all four cases, the concentration gradient is steep in the vicinity of the breathing zone because the medical staff are positioned close to the source of the particles. In order to ensure the quality of the air in the breathing zone, it is important that the clean air blown from the ceiling reaches the breathing zone while remaining uncontaminated. In Case 4, however, the surgical smoke rises due to buoyancy, but the hanging walls prevent its diffusion. In the resulting flow field, the breathing zone is now directly downstream of the source of smoke; thus, the smoke ends up reaching the vicinity of the breathing zone.

3.3 Age of air distribution

The air age distribution is shown in Fig. 4. The figure shows that in all four cases, the blowout airflow from the ceiling has the youngest air age, with values of 10 seconds or less in the area between the ceiling and the surgical light. On the other hand, in the regions near the ceiling away from the air vents, areas of stagnation form with an air age of more than 100 seconds as the air stays in the place. The older age of the air in the operating field in the vicinity of the operating table is likely due to the complex flow field formed by the collision of the clean air blowing down from the ceiling against the upward flow of heat generated by the electrocautery and the human bodies. The upward flow entrains the ambient air from the floor and mixes it with the clean air, reducing its quality. In Case 3, the hanging walls allow the air to reach the breathing zone without mixing, which is an advantage. In Case 4, the effect of the hanging walls was even greater, and the air in the breathing zone was the youngest of all the cases. However, it is important to note that relatively younger air compared to other cases can still mean that the particle concentration is high if there is particle generation from a point source such as surgical smoke, as can be seen from the concentration distribution in the previous section.

4. Conclusions

This paper addressed the problem of contaminant generated by the use of electrocautery in the operating field. The contaminant concentration distribution was analysed by numerical analysis during surgery. It showed that the airflow from the ceiling was blocked by the surgical light, preventing clean air from reaching the operating field. The use of electrocautery produced an upward flow of heat that was amplified by the metabolic heat generated by the medical staff and affected the flow field in the breathing zone. Specifically, the breathing zone was characterized by steep gradient in the concentration of particles. The simulation also showed that the installation of hanging walls around the ceiling vent had a significant impact on the number of particles inhaled by the medical staff. Analysis of the distribution of the air age showed that under normal conditions without hanging walls, the blowout airflow is immediately mixed with the room air, but the installation of hanging walls was effective in suppressing the mixing and quickly bringing clean air to the operating field and the level of the breathing zone.

The pollutant source such as electrocautery analysed in this paper is in the vicinity of the breathing zone of the medical staff. In such a case, the fresh airflow through filtration from the air-conditioning system does not assure the breathing air quality. Not only the thermal plume caused by the electrocautery but also the surgical light prevent the downflow from reaching the breathing zone of the medical staff. The air-age distribution in the micro-environment around the surgical site needs to be analysed in order to locate the source on the upstream of the breathing zone.

5. References

[1] Centers for Disease Control and Prevention (Cdc), Health and Safety Practices Survey of Healthcare Workers, 2020. https://www.cdc.gov/niosh/topics/healthcarehsps/smoke.html. (Accessed 25 September 2021). accessed

[2] B.King, J. McCullough, Health Hazard Evaluation Report No. 2001-0066-3019 (CDC), 2006. https://www.cdc.gov/niosh/hhe/reports/pdfs/2001-0066-3019.pdf

[3] I.V. Limchantra, Y. Fong, K.A. Melstrom, Surgical smoke exposure in operating room personnel A review, JAMA Surgery 154 (No.10) (2019) 960-967, https://doi.org/10.1001/jamasurg.2019.2515

[4] Akane Odagiri, U Yanagi. The characteristic of particle spread in during open chest surgery in hospital operating room and the analysis of air flow, Roomvent 2020, ID277

[5] Akane Odagiri, U Yanagi, Shinsuke Kato, Comparison of Generation of Particles and Bacteria in Endoscopic Surgery and Thoracotomy. Building and Environment, 193 (2021) 107664. https://doi.org/10.1016/j.buildenv.2021.107664

Data Statement

Data sharing not applicable to this article as no datasets were generated or analysed during the current study.

Field study of diffuse ceiling ventilation performance under high air change rate

Gael Tougne [a], Christian A. Hviid [b]

[a] aereNmore, Saint-Gobain Denmark, Copenhagen, gael.tougne@saint-gobain.com

[b] Dept. of Civil and Mechanical Engineering, Technical University of Denmark, Kgs. Lyngby, Denmark, cahv@dtu.dk

Abstract. Diffuse ceiling ventilation utilizes the entire ceiling surface to distribute airflow to rooms. The air seeps via perforations, often present in acoustic ceilings, from the pressurized plenum to the occupied zone below. In the literature, this concept has proven superior in terms of draught, even for quite high airflow rates and sub-temperatures. However, documentation of practical installations followed by measurements campaigns and in-depth analyses of the concept, are rare. Consequently, we present a study to showcase the performance of the installation under rather extreme conditions: air change rate of 20 h^{-1} and supply temperature 3-4°C below room temperature. The corresponding cooling was 56-74 W//m^2.

The investigated room was 165m^2 and 2.75m high. Numerous computers and TV screens caused significant heat loads, as well as the large windows on 3 facades of the room (West, North, East). The ventilation, equipped with a cooling coil, supplied 9200 m^3/h to maintain the temperature in the room. The airspeeds and temperatures were measured at 7 different heights (from 0.1m to 2.4m) in 26 positions.

The results showed an even distribution of the temperature in the room with measurements between 23 and 26˚C and an average temperature gradient of 0.33˚C/m (max 0.8˚C/m) while in the plenum the difference of temperature was 1.5˚C between the inlet and the opposite corner. The airspeeds were on average between 0.11 m/s and 0.17 m/s with the highest values at the ankle level. Half of the logged points had Draught Rate (DR) below 10% and all positions were below 20% except one. The airspeed exceeded 0.2m/s in less than 9% of the measurements.

For comparison, we discuss the implications of using ceiling swirl diffusers or displacement ventilation in the same context.

Keywords. Diffuse ceiling ventilation, indoor comfort, air speed, office, high air change, vertical temperature gradient, draught, Draught Rate.
DOI: https://doi.org/10.34641/clima.2022.270

1. Introduction

The performance of diffuse ventilation was assessed multiple times under different conditions in the scientific literature. The performance was evaluated using benchmarks in standards and codes [1-3] and by comparing the solution with other ventilation solutions [4-5] in terms of draught. Often the studies are made in laboratories and limited to air change rates (ACR) and temperatures that are relevant in office or school settings. Zukowska-Tejsen [6] presented results from live ventilation operation in an office setting with ACRs in the range of 1.2, 11.5 and 17.9 h^{-1} and temperatures differences between extract and supply of 5.5 and 10.6K. The results indicated low risk of draught even at cooling load of 116 W/m^2.

This study was aimed at mapping the performance of DCV in an office setting with cooling load of 56-74 W/m^2, and ACR of 20 h^{-1} (0.015 m3/s per m^2). In this setting, high-impulse mixing would most probably cause elevated risk of draught [5, 7]. In this study, the temperatures and airspeeds were rigorously mapped and compared to standards to verify the refurbished indoor climate.

2. Methods

2.1 Facility

The room is used for the control of the metro traffic and the safety in the stations. There are always a least 5 employees in the room at the same time and the room is used 24 hours a day as the metro traffic never stops. Each employee has many computer towers and screens on his desk causing significant heat loads. There is also a wall of screens displaying the security cameras in the stations. The façade is entirely made of windows except for the wall facing South-West. The overall heat loads in the room are important. The total volume of the room is 453 m^3 (11 m x 15 m x 2.75 m).

In order to improve the indoor conditions, the room was refurbished with a new high-capacity air-

Copyright ©2022 by the authors. This conference paper is published under a CC-BY-4.0 license.

handling unit and acoustic ceiling tiles from Ecophon. The new ventilation system consists of the existing air-handling unit that provides 1200 m^3/h of fresh air at any time and a new air-handling unit, equipped with a cooling coil, that provides 8000 m^3/h of recirculated air to maintain an indoor temperature (actually extract) of 23°C. The cold air is supplied in the plenum above the acoustic ceiling tiles in different places for diffuse ceiling ventilation. There are 10 extraction outlets in the room to remove the polluted air and the heat. The new ventilation unit is placed on the roof top and reaches the supply and extraction ducts through 10 holes in the slab represented in Fig. 1 with red and blue circles. The extraction ducts act as obstructions in the plenum, and as a consequence, in the perimeter area between the duct and the wall, the supplied air might not mix as easily as in the rest of the plenum. The cooling system is capable of 21 kW in normal conditions and up to 26 kW for short periods of time. It is therefore capable of handling 130 W/m^2 and maintain the indoor temperature at 23°C.

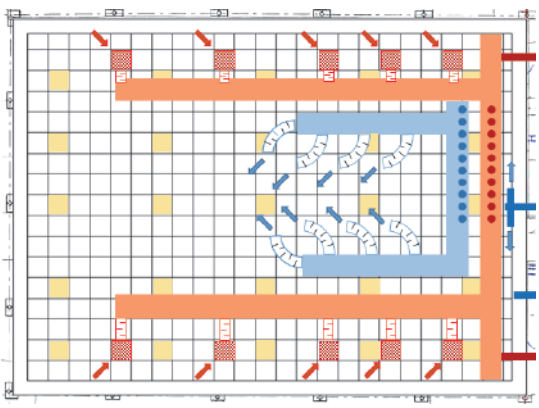

Fig. 1 - Ventilation system in the plenum. Air was distributed using pieces of flexible duct in the plenum. Extract trough ducted grilles in ceiling. Room dimensions: 11 x 15 x 2.75 m

The two air-handling units were programmed to maintain a total constant airflow of 9200 m^3/h in the room. The conditions of the test were very steady. The measurements were conducted on Friday the 2nd of July 2021 from 12:30 until 2:30 pm. There were between 6 and 8 users at the same time in the room during the measurements. As seen in Fig. 4, the temperature outside was warm and stayed between 21-24.2°C.

2.2 Measurements

The indoor comfort in the room was investigated in terms of temperature distribution and draught risks. Anemometers AirDistSys5000 from Sensor-Electronic were used to measure simultaneously the air temperature and air speeds. These devices have a high measurement accuracy and sensitivity of 0.05 m/s. Measurements were performed in 26 different positions in the room, distributed evenly except around the occupants where additional measurements were performed. For each position, 7 anemometers were mounted vertically at the heights 0.1 m, 0.3 m, 0.6 m, 1.1 m, 1.7 m, 2.0 m and 2.4 m. The data was recorded for 5 minutes with a logging interval of 2 seconds. The first and second minute were used to achieve a steady state and the reported results represent average values of the last three minutes.

The plenum temperature and relative humidity were measured in 2 different places (S1 and S2 in Fig. 2), next to the inlet and in the opposite corner where the temperature difference is believed to be the warmest in the plenum. Also two room sensors (S3 and S4) measured room air temperature and relative humidity at height 75 cm. A sensor (S5) was placed outside to keep track on the external conditions during the investigation. Sensors S1-S5 were battery-driven Hobo loggers from Onset. A thermal camera (FLIR C2) was used to take pictures of the ceiling in order to identify potential temperature differences and radiant discomfort.

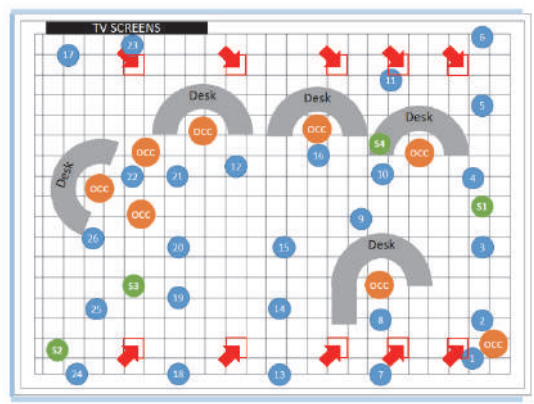

Fig. 2- Position of sensors, occupants and extractions

Fig. 2 depicts the floor plan of the room. The grey shapes represent the desks, the red arrows show the extraction outlets and the black rectangle is the wall of TV screens.

2.3 Evaluation

The results were compared to the indoor comfort criteria of EN ISO 7730 [8], which are summarized in Tab. 1.

Tab. 1 - Comfort categories as in ISO 7730

Cat.	Draught rate (DR)	Vertical temperature gradient	Vertical temp. difference, head-ankles
A	< 10 %	< 3 K/m	< 2K
B	< 20 %	< 5 K/m	< 3K
C	< 30 %	< 10 K/m	< 4K

The draught rate (DR) is calculated according to equation (1). It defines the expected percentage of people feeling uncomfortable because of the draught in the room. T_a is air temperature (°C), V_0 is mean air speed (m/s) and I_0 is the turbulence intensity (-).

$$DR = (34 - T_a)(V_0 - 0.05)^{0.62}(37.\, I_0\, V_0 + 3.14) \quad (1)$$

The air diffusion performance index ADPI was formulated to rate the indoor environment in rooms as a result of the air diffusion performance of the installed diffusers. It is described in ASHRAE Standard 113, 2005 [9]. The ADPI is defined as the percent of test points in the room where the effective draft temperature, θ and mean velocity, V_m, meet the criteria: -1.7 °C < θ < 1.1 °C and V_m < 0.35 m/s. These criteria are defined under the assumption that sedentary occupants will be comfortable. The effective temperature θ is defined in equation (2):

$$\theta = T - T_{ar} - 8(V_m - 0.15) \quad (2)$$

where T is the temperature at the measurement point and T_{ar} is the average room air temperature (°C).

Finally, the results were compared to literature by means of a q-T design chart.

3. Results and discussions

This section presents the results in the following order: plenum temperatures, vertical temperature gradient and radiant temperatures and then mapping of airspeeds, temperatures and draught rates in the room and in the proximity of the occupants.

3.1 Plenum temperature and relative humidity

The plenum is around 165 m² and substantial pre-heating of the ventilation air is expected in the plenum [2]. This pre-heating allows to supply colder air in the plenum without creating discomfort in the room. The supplied air increases its temperature by absorbing heat transferred from the room. Fig. 3 depicts the evolution of the temperature across the plenum; over the whole experiment, there was an average of 1.5 °C difference between the 2 sensors placed in the plenum. Given the airflow rate, the ventilation air absorbs approx. 28 W/m² through the ceiling or approx. 50% of the total cooling supply.

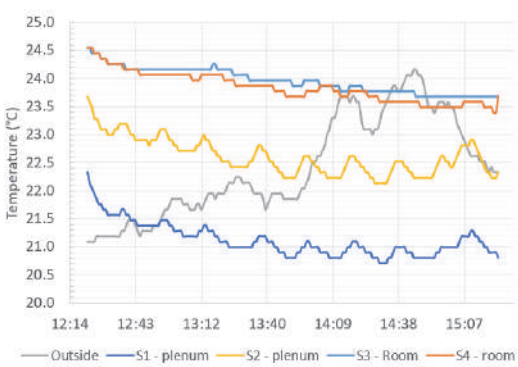

Fig. 3 - Temperature outside and in the plenum during test day

While the surface temperature is even in most of the room, the corners above position 1 and 6 are significantly colder as illustrated by the thermos-photos in Fig. 4, but this is probably due to the impinging jets of the old ventilation system in the plenum. From Fig. 1 it is clear, that the dynamic pressure of these jets are converted to high static pressure in the corners causing higher airflow in the corners.

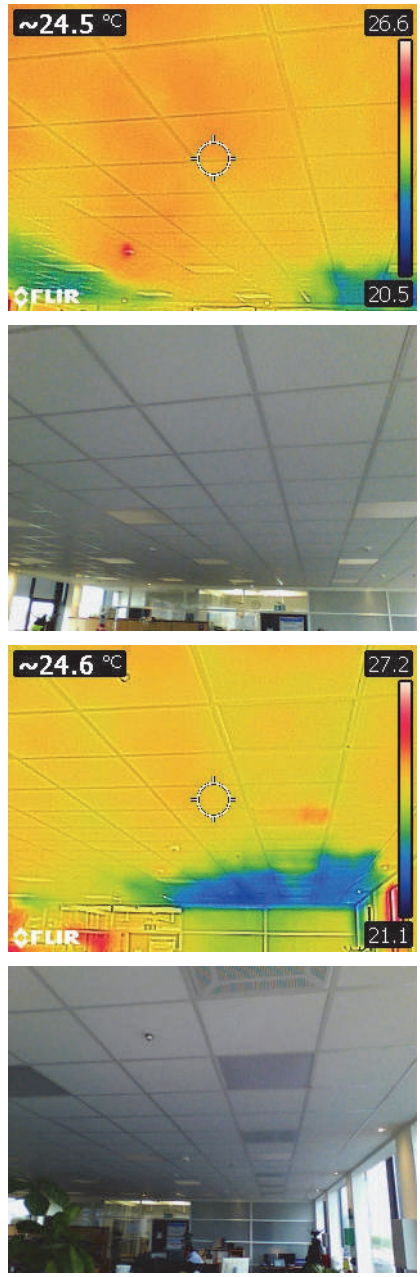

Fig. 4 - Thermal pictures of the ceiling

The relative humidity in the plenum is very stable with a 5% difference between the measurement at the inlet and the measurement at the opposite corner of the plenum. There does not seem to be any condensation or humidity rise in the plenum due to the dehumidification of the recirculation air in the cooling coil.

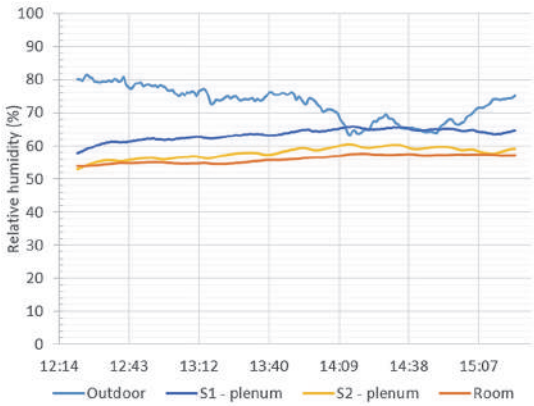

Fig. 5 - Relative humidity during the experiment

3.2 Vertical temperature gradient

The average temperatures for all the measurements are presented in Fig. 6. The temperature in the room is very even during the time of the measurements. The standard deviation is lower than 0.7 ˚C at every height and the temperature gradient per meter is below 0.8 ˚C everywhere in the control room and 0.34 ˚C on average.

Except for three positions, the temperatures are between 23 ˚C and 25 ˚C in the room. The differences come mainly from the different heights of measurements. It is also noticeable that the largest temperature difference (2 ˚C) occurs at the highest point of measurement (measured at 2.4 m in a room of 2.75 m height, so very close to the ceiling).

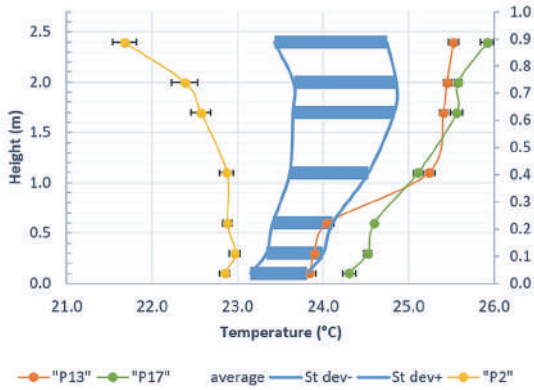

Fig. 6 - Vertical temperature gradient. The blue area represents the average temperature ± standard deviation

The three most extreme positions are still within the reasonable range of temperature. Position 17, placed next to the screen wall in the room, reaches slightly higher temperatures at the highest point, but still below 26 ˚C. The results in position 2 are the coldest. This is probably due to impinging jets of the old ventilation system in the plenum. Position 13 is located next to the windows and an extraction.

3.3 Air speed

The airspeed measured were on average between 0.10 and 0.17 m/s. Fig. 8 maps the airspeeds at four different heights. The figure illustrates that the highest airspeeds were below the ceiling and at ankle height. It also shows the high airspeeds below point 2. On a general level, 0.2 m/s is usually regarded as the threshold for draught and in this case, the airspeed exceeded 0.2 m/s in less than 9 % of the measurements.

The research literature shows that with diffuse ceiling ventilation, the dominant flow is created by the heat loads and that their power and distribution have an impact on the draught [4]. Considering the location of heat sources and the distribution of airspeeds at ankle height, a room size counter-clockwise vortex is probably mixing the air. Consequently, it is very important to measure the airspeeds in the proximity of the occupants. The results showed that the airspeeds were between 0.1 and 0.2 m/s from floor to ceiling, which is very slow considering the air change rate in the room. Another parameter that influences the draught in the room is the height. In the facility, the height was under 3 m and therefore was not problematic [10].

3.4 Draught rate

Fig. 7 below shows the draught rate around the occupants. The highest air speed observed was at the ankle level as a result of the room-size vortex.

Almost all the measurements have a DR below 20% and 71% of them have a DR below 10%. The lowest DR are usually found between 0.6 m and 1.7 m. As observed previously, the highest airspeeds are around ankle level and above the comfort zone. According to ISO 7730, the comfort level regarding the Draught Rate is Class B since it is below 20% everywhere (Tab. 2).

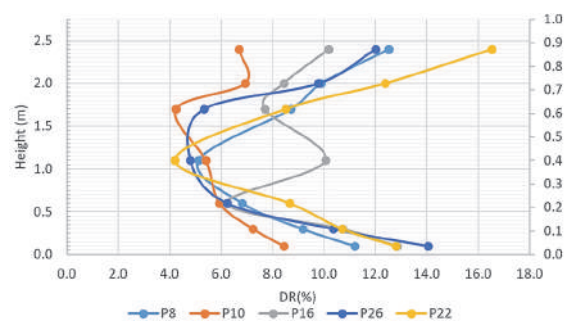

Fig. 7 - Draught rate in the proximity of the occupants

Tab. 2 - Overall results of the draught rates

Measurement points	Total: 182	%
DR < 20%	179	98.3%
DR < 10%	130	71.4%

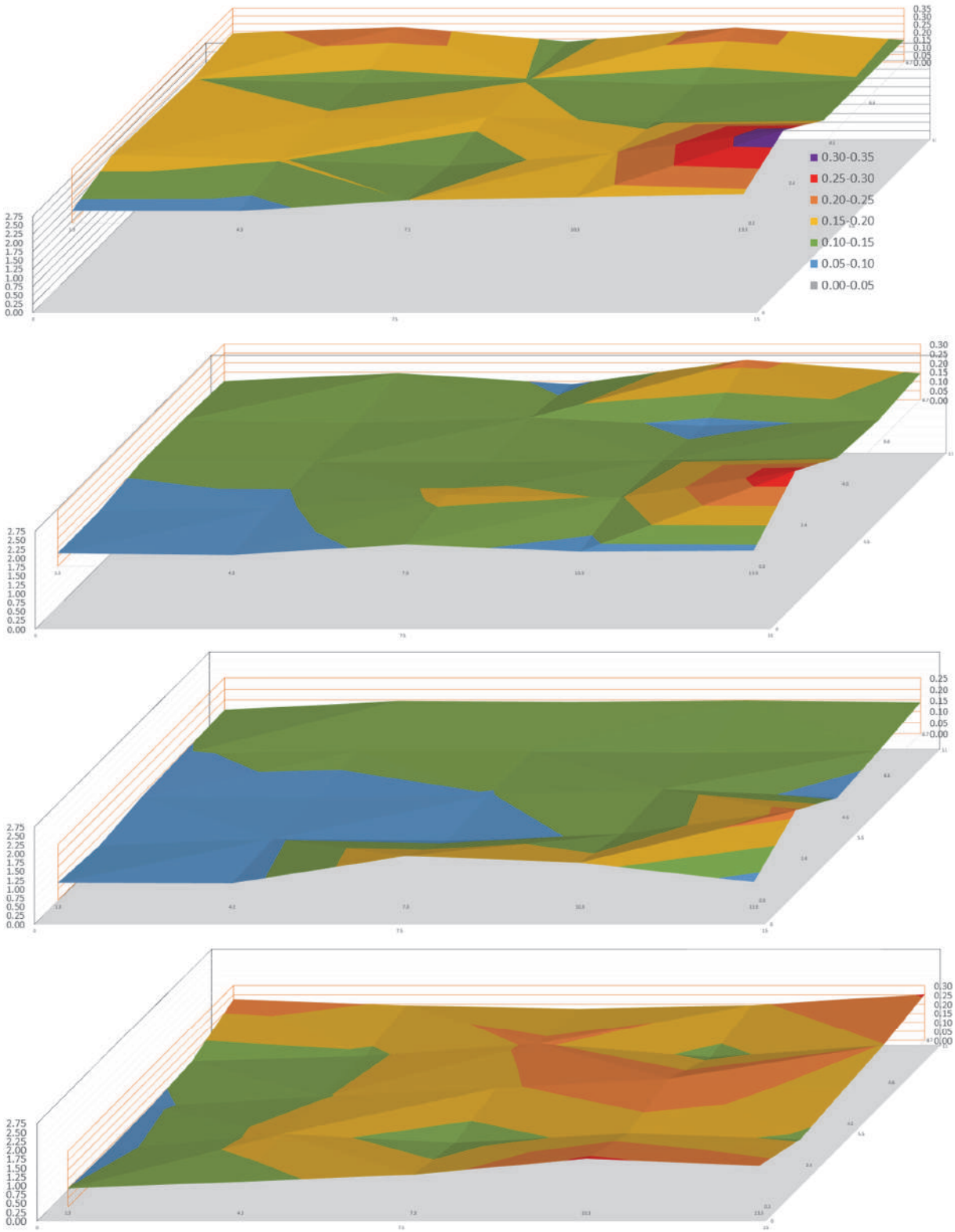

Fig. 8 - Air speeds at four different heights (2.4m, 1.7m, 0.6m, 0.1m). The map shows that airspeeds are highest below the ceiling (2.4 m) and at ankle height (0.1 m)

3.5 Air diffusion performance

In general, high ADPI is desired as it indicates a high level of comfort and good air mixing. The air diffusion performance index was 84% (Tab. 3), which is on par with many alternative overhead air diffusers at cooling load of 50 W/m2 [11]. The field mapping of velocities and temperatures was made with horizontal and vertical resolution as high as was practically possible, however, the ADPI index should be used carefully, because it may be influenced by furniture layout, location of heat sources and pollution sources.

Tab. 3 - Overall results of the draught rates

Measurement points	Total: 182	%
-1.7 °C $< \theta <$ 1.1 °C	153	84.1%
$V_m < 0.35$ m/s	182	

3.6 Occupant satisfaction

We did not conduct a formal survey as the number of users in the room is quite small, on an anecdotal basis, the occupants were very satisfied with the solution mainly because there were no high temperatures in the room any more as there used to be before the renovation. The occupants *were* asked if they could feel any draught and none of them reported any discomfort of any kind. The noise from the ventilation was audible next to the entrance, just below the inlet in the plenum but the level was reasonable and it was not close to the working places.

3.7 Other air supply options

There are many ways to supply ventilation air to the space. Rehva Guidebook 01 [7] provides some guidelines for the options: mixing and displacement. Using these guidelines on the airflow rate per floor area and the needed cooling capacity per floor area, displacement ventilation is recommended.

Displacement ventilation creates thermal stratification which can be exploited to reduce the airflow rate, because heat and pollution is concentrated in the upper zone. Assuming 20% lower airflow rate, divided between four corner diffuser units, Rehva Guidebook 01 recommends a unit of 1.2 m high with an adjacent zone length of 8 meters. With expected under temperature of 3K the system provides approximately the needed cooling. But it is clear from the room dimensions in Fig. 2 that adjacent zones would be difficult to keep free of occupancy in the office space and that the risk of draught therefore is high. Alternatively, radial ceiling diffusers could be an option. Each diffuser supplies 575 m3/h, which means 16 diffusers are necessary in a 4x4 pattern. Each diffuser has a throw length of approx. 3-4 m from the datasheet. Considering the throw length and the risk of jets colliding and being diverted into the occupied zone, it is very difficult to fit 16 diffusers into the space without creating a high risk of draught.

These results match the literature. Fig. 9 depicts a q-T design chart adapted from Nielsen [5] and Zukowska-Tejsen [6] that relates displacement diffusers and radial ceiling diffusers with diffuse ceiling ventilation. The result of this study is marked with an X and supports the dashed extrapolation on diffuse ventilation that Zukowska-Tejsen suggested.

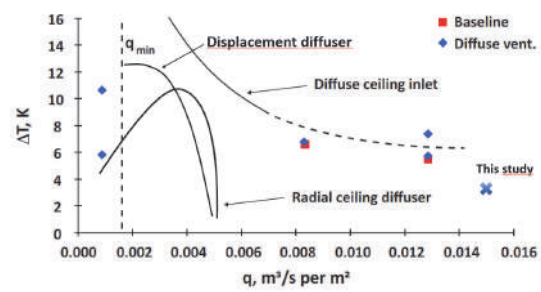

Fig. 9 – Design chart. Adapted from [5, 6].

4. Conclusion

In the plenum the difference of temperature was 1.5 ˚C between the inlet (supposedly the coolest point) and the opposite corner (supposedly the warmest point). The measurements showed an even distribution of the temperature everywhere in the room with measurements between 23 and 26 ˚C and an average vertical temperature gradient of 0.34 ˚C/m (max 0.8 ˚C/m). The infrared camera did not disclose significant radiant discomfort in the room.

The hygrometry in the plenum was also even and not close to the dew point so there was no risk of condensation that could cause damages to the ceiling tiles for instance.

The airspeeds were on average between 0.10 m/s and 0.17 m/s with the highest values at the ankle level as previously shown in different studies on diffuse ceiling ventilation. 71% of the logged points had Draught Rates (DR) below 10% and all positions were below 20% except one (position 2). The airspeed exceeded 0.2 m/s in less than 9 % of the measurements. The ADPI index showed performance on par with other overhead air diffusers.

As concluding remarks, the field mapping did not disclose zones with problematic high airspeeds and it was possible to keep a comfortable level, despite the high air change rate of 20 h^{-1}. Delivering the same amount of ventilation with displacement or swirl diffusers would have restricted the occupiable space significantly.

Data statement

The datasets generated during and/or analysed during the current study are not publicly available because the detailed data is owned by the client but will be available upon request.

5. References

[1] Zhang, C., Heiselberg, P., Nielsen, P.V. Diffuse Ceiling Ventilation – A Review, International Journal of Ventilation, 2014:13(1):49-64 10.1080/14733315.2014.11684036

[2] Hviid, C.A., Svendsen S. Experimental study of perforated suspended ceilings as diffuse ventilation air inlets. Energy and Buildings 2013:56:160-168

[3] Fan, J., Hviid, C. A., & Yang, H. Performance analysis of a new design of office diffuse ceiling ventilation system. Energy and Buildings. 2013:59:73-81. 10.1016/j.enbuild.2013.01.001

[4] Lestinen S., Kilpeläinen S., Kosonen R., Jokisalo J., Koskela H. Experimental study on airflow characteristics with asymmetrical heat load distribution and low-momentum diffuse ceiling ventilation, Building and Environment 2018:134:168-180 10.1016/j.buildenv.2018.02.029

[5] Nielsen, P.V. Analysis and Design of Room Air Distribution Systems, HVAC&R Research, 2007:13(6):987-997 10.1080/10789669.2007.10391466

[6] Zukowska-Tejsen, D., Wolsing, M., Grysbæk, M. & Hviid, C. A. Field Study of Diffuse Ceiling Ventilation Performance in a Landscape Office. In: CLIMA 2016, ID478, Aalborg, May 22-25

[7] Rehva Guidebook No 01. Displacement Ventilation in Non-industrial premises. Federation of European Heating and Air-conditioning Associations, 2002

[8] EN ISO 7730. Ergonomics of thermal environment. European Committee for Standardization, 2005

[9] ASHRAE Standard 113. Method of Testing for Room Air Diffusion, 2013. American Society of Heating, Refrigeration and Air-Conditioning Engineers

[10] Nielsen, P. V., Vilsbøll, R. W., Liu, L., & Jensen, R. L. Diffuse Ceiling Ventilation and the Influence of Room Height and Heat Load Distribution. In: Healthy Buildings 2015, ID413, International Society of Indoor Air Quality and Climate

[11] Liu, S., Clark, J., Novoselac, A. Air diffusion performance index (ADPI) of overhead-air-distribution at low cooling loads. Energy and Buildings 2016:134. 10.1016/j.enbuild.2016.10.055

The experimental study of the indoor climate with the micro-environment systems

Weixin Zhao [a], Risto Kosonen [a, b], Simo Kilpeläinen [a], Sami Lestinen [a]

[a] Department of Mechanical Engineering, Aalto University, Espoo, Finland

[b] College of Urban Construction, Nanjing Tech University, China

Abstract. One of the major challenges in modern buildings is to guarantee healthy indoor air quality and excellent thermal comfort in an energy efficient manner. In this study, the performance of two micro-environment systems combined radiant panel and convective flow was designed. In one of micro-environment system of personalized ventilation and radiant panel (PVRP), two local personal air terminal devices supplied clean air directly to occupants. In the other micro-environment system, low velocity unit was installed just over the radiant panels (LVRP) and the air was supplied through those panels. The radiant panels were used to satisfy the required cooling load. The results show that that it is possible to enhance system performance with micro-environment control systems, where users are able to control their own set points for room air temperature and indoor air quality, the satisfaction on indoor climate conditions increased significantly. Furthermore, the air temperature near the workstation can be maintained at designed value with the micro-environment systems. In particularly, the vertical temperature difference did not cause thermal discomfort with the micro-environment systems near the workstation.

Keywords. Micro-environment, Personalized ventilation, Radiant cooling, Thermal comfort, Airflow pattern
DOI: https://doi.org/10.34641/clima.2022.190

1. Introduction

Building sector accounts for about one-third of the global greenhouse gas emissions and at the same time uses about 40% of the world's energy [1]. A considerable fraction of this energy use is utilized for achieving desirable indoor climate in buildings [2]. According to the European Commission, improved energy efficiency of buildings means maintaining good indoor air quality and thermal comfort levels with less energy use than before [3]. In the European Union, policies have been stricter according to the EU 2030 goals on energy efficiency demands in buildings to meet EU's long- term 2050 greenhouse gas reductions target, which is -30% in 2030 and -80% in 2050 compared the reference year of 1990 [4].

In many cases, a good indoor environment and energy efficiency are often seen as conflicting requirements. Therefore, novel Heating, Ventilating and Air-Conditioning (HVAC) systems are required to achieve simultaneously indoor climate and energy efficiency requirements. For that reason, more concerns have been focused on the novel solutions e.g., micro-environment of occupants to optimize energy usage and trade-off energy conservation and indoor comfort, where the main challenge is to supply clean air to the breathing zone and maintain thermal conditions.

To maintain indoor air quality, international standards or design criteria, for example, [5, 6] typically require a ventilation rate of 4–10 L/s per person of outdoor air supply to office spaces. The air inhaled by each occupant is only 0.1 L/s [7]. Thus, this inhaled air is only 1% of the supplied air. However, the required supply airflow rate is typically much higher when the ventilation is used for cooling.

In general, there is a need for a paradigm shift from uniform indoor environment to non-uniform indoor environment accommodating various individual preferences [8]. The target should be only to control local conditions when a person is at the workplace. There should be also a need to introduce more advanced systems where users can influence their own local micro-environment. An individually controlled micro-environment by providing local heating/cooling of the body and body parts has a potential to satisfy a greater number of occupants in

Copyright ©2022 by the authors. This conference paper is published under a CC-BY-4.0 license.

a space compared to a centrally controlled total volume environment [9-13].

The novelty of this paper is to introduce and analyse the performance of new ventilation and cooling systems where local micro-environment is created by using personalized ventilation or low velocity unit in a double office layout. In one of micro-environment system of personalized ventilation and radiant panel (PVRP), two local personal air terminal devices supplied clean air directly to occupants. In the other micro-environment system, low velocity unit was installed just over the radiant panels (LVRP) and the air was supplied through those panels. The radiant panels were used to satisfy the required cooling load.

2. Methods

The experimental measurements were performed in the steady-state laboratory condition. The measurements were carried out in a test chamber with internal dimensions of 5.50 m (length), 3.84 m (width) and 3.20 m height from the floor up to diffuse ceiling panels. The floor area was around 21 m2. The test chamber was located inside a laboratory hall such that the outer environment was stable.

In one of the studied personalized system, a PV (personalized ventilation) air terminal device (ATD) was installed on the desk at a distance of 40 cm from the dummy to supply fresh air directly to the breathing zone [14]. In the other personalized system, low velocity unit was installed just over the radiant panels and the air was supplied through those panels [15], as shown in Figure 1. Diffuse ceiling ventilation was used to provide background ventilation outside the occupied zone.

The all studied systems were measured at 60 and 80 W/m2 heat gain levels. The supplied total airflow rate was kept the same (42 l/s) with two micro-environment systems. The local airflow rates were 10 l/s and 15 l/s with the personalized ventilation or low velocity unit and the rest of the airflow rate required is released from background ventilation (DVC system) as shown in Table 1.

Tab. 1 - Two tested airflow modes supplied to each workstation with two micro-environment systems.

	Normal mode	Boost mode
Airflow rate of PV/ low velocity unit terminal (l/s)	10*2	15*2
Airflow rate at unoccupied zone (DCV) (l/s)	22	12
Total airflow rate (l/s)	42	42

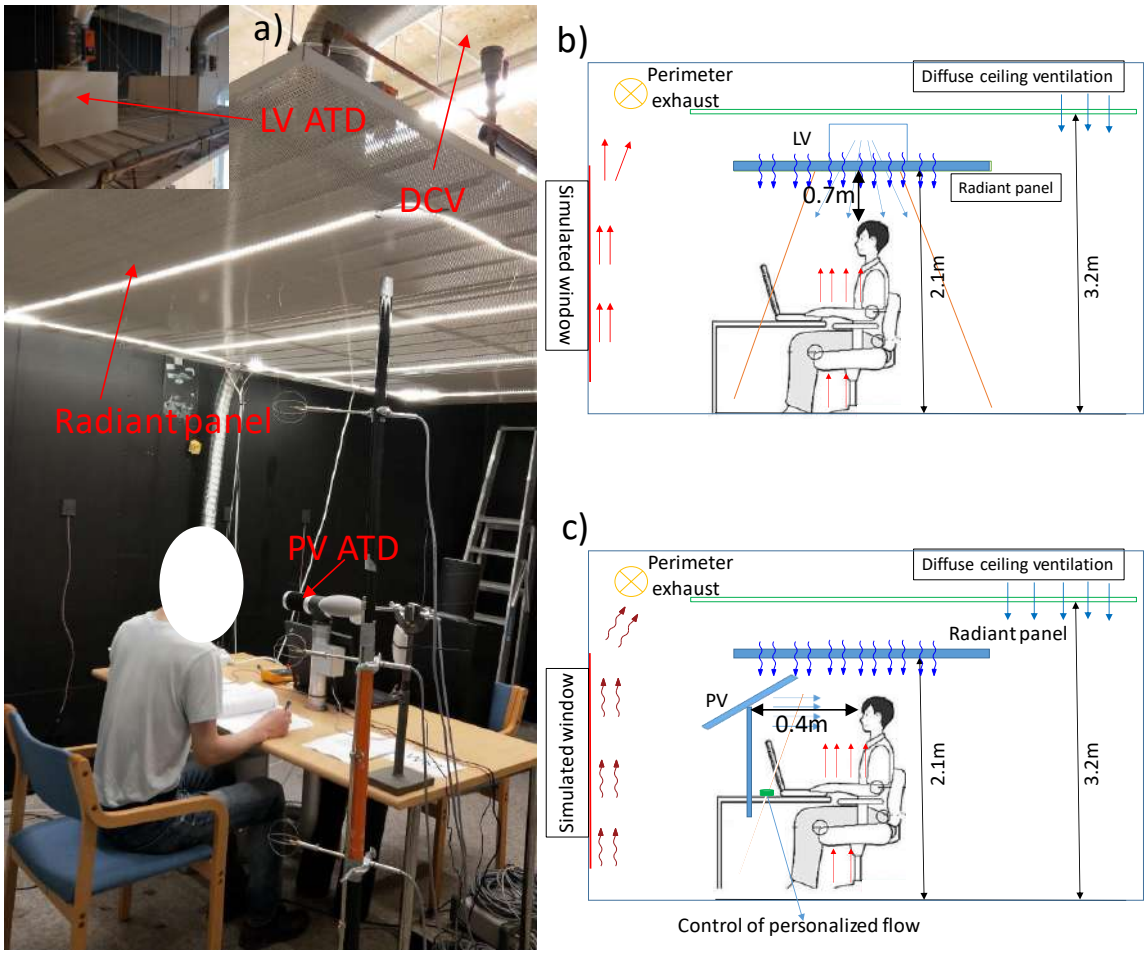

Fig. 1 - a) The set-up of low velocity unit and PV ATD at workstation. Two studied personalized systems, b) low velocity

unit and radiant panel (LVRP) and c) personalized ventilation unit and radiant panel (PVRP).

3. Results

3.1 smoke visualization of air distribution

Figure 2 shows the air movement with a 10 l/s local air flow rate over the workstation. Smoke visualization indicates that the momentum flux of the jet was not strong enough to reach the dummy. When the local airflow rate was increased to 15 l/s, the airflow from the low velocity unit was just strong enough to reach the level of the top of the dummy. This smoke visualization confirmed that the airflow rate of 15 l/s could be used for local micro-environment control without increasing significantly the draught risk.

The airflow structure of the PV around the workstation was visualized by the maker smoke to assess the airflow pattern of the personalized system (Figure 3). When the personalized airflow rate was 10 l/s, the air jet turned slightly upward because of the combined buoyancy flow of the computers and dummy. However, the jet still reached the breathing zone. The momentum flux of the jet overcame the effect of the buoyancy effect, and the jet was able to approach the dummy when the personalized airflow rate was increased to 15 l/s. The central axis of the jet was aligned with the level of the subject's chest and after the jet collided with the dummy, it turned both downwards and upwards along the body. Hence, the personalized airflow entrained the convective boundary layer existing the human body and cooled down the upper body.

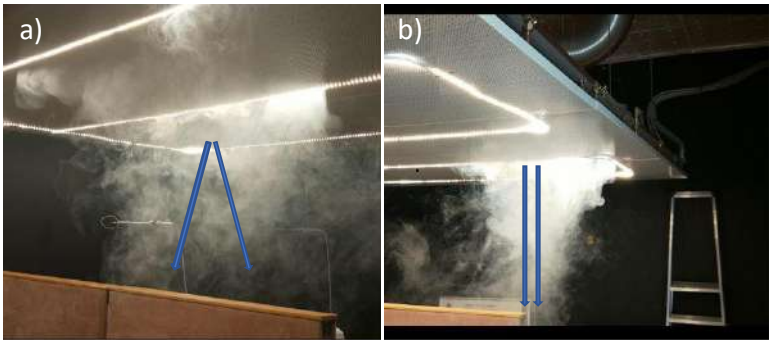

Fig. 2 - The smoke visualization of the low velocity system (LVRP) a) the local air distribution with the airflow rate of 10 l/s and b) the local air distribution with the airflow rate of 15 l/s. The blue arrows show the direction of the local airflow.

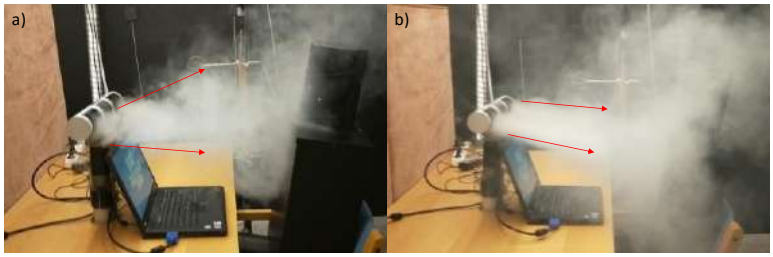

Fig. 3 - Smoke visualization of the personalized airflow pattern with PVRP system a) 10 l/s and b) 15 l/s. The red arrows mean the main direction of the air jet.

3.2 temperature profile

The temperature at the reference location as well as the exhaust air temperature with the two micro-environment systems were summarized in Table 2. Air temperature, operative temperature and mean radiant temperature all decreased with the increasing local airflow rate. The average temperature difference between the exhaust air and room air at the reference point was rather significant (from 0.7°C to 1.9°C), especially with a higher local airflow rate. Also, this difference was bigger with a higher heat gain level. Therefore, better thermal comfort can also be achieved in the micro-environment near the workstation at the higher heat gain level.

Tab. 2 - The average thermal conditions in different test cases.

Measurement results at occupied zone	LVRP 60 W/m² 10 L/s	LVRP 60 W/m² 15 L/s	LVRP 80 W/m² 10 L/s	LVRP 80 W/m² 15 L/s	PVRP 60 W/m² 10 L/s	PVRP 60 W/m² 15 L/s	PVRP 80 W/m² 10 L/s	PVRP 80 W/m² 15 L/s
Air temperature (°C)	25.9	25.9	26.1	25.9	25.9	25.6	26.5	25.9
Exhaust temperature (°C)	26.3	26.9	26.9	27.4	26.1	25.9	26.2	25.9
Operative temperature (°C)	26	25.8	26	25.8	26.3	25.9	26.2	26
Mean radiant temperature (°C)	26.1	25.9	26	25.9	26.1	25.9	26.7	26.5
Average difference between room air at the reference point and operative temperature (°C)	-0.07	0.08	0.1	0.11	-0.17	0.06	0.05	-0.13
Average difference between exhaust-room air temperature at the reference point (°C)	0.99	1.63	1.22	1.92	0.24	0.31	0.25	0.57

3.3 Draught risk

Figure 4 shows the vertical distribution of draught rate of all studied systems in the occupied zone with 80 W/m². With the LVRP system, the draught risk was quite small, less than 10%. With PVRP system, the draught risk (DR) was relatively low. The highest DR happened at the heights of 0.6 – 1.1 m. With the lower personalized airflow rate, DR was below 10% with PVRP system. When the personalized flow rate was increased to 15 l/s, the draught risk increased to18 % at the 1.1 m level at 80W/m2.

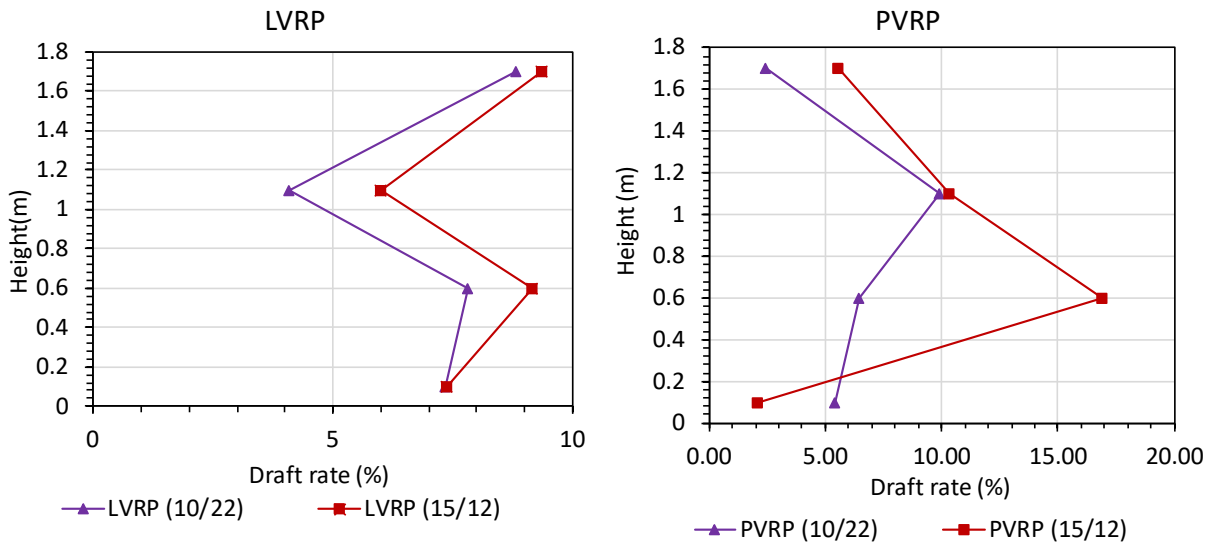

Fig. 4 - The vertical distribution of draught rate in the occupied zone with heat gains of 80 W/m2.

4. Conclusion

This study analysed the performance of the micro-environment control systems by experimental studies. The study shows that that it is possible to enhance system performance with micro-environment control systems, where users are able to control their own set points for room air temperature and indoor air quality, the satisfaction on indoor climate conditions increased significantly. The smoke visualization showed that the PV or low velocity unit supplied the fresh air directly to the occupants and created a micro-environment around the dummy. The mean temperature in the micro-environment at the workstation can keep at design 26°C. Also, the draught rate was between 5-20 % in most of the cases. With a higher local airflow rate, the draught risk at 0.1 m can remain at a reasonable value without discomfort.

5. Acknowledgement

The author wishes to acknowledge the funder of Aalto scholarship.

6. References

[1]. ETP International Agency. IEA Energy Technology Perspectives 2008 – Scenarios and Strategies to 2050. International Energy Agency, Paris, 2008.

[2]. Pérez-Lombard L, Ortiz J and Pout C. A review on buildings energy consumption information. Energy and buildings 2008; 40(3): 394-398.

[3]. European Commission. Energy efficiency in the European Union. https://ec.europa.eu/energy/en/topics/energy-efficiency 2016 (accessed 12 July 2019).

[4]. Council of the European Union, European Council. EUCO 169/14 Conclusions. European

[5]. BS EN15251: 2012. Indoor environmental input parameters for design and assessment of energy performance of buildings addressing indoor air quality, thermal environment, lighting and acoustics. London: British Standard Institution (BSI), 2007.

[6]. CEN CR 1752:1998. Ventilation for Buildings: Design Criteria for the Indoor Environment. European Committee for Standardization, Brussels, Belgium 1988.

[7]. Fanger PO. Indoor air quality in the 21st century: search for excellence. Indoor air 2000; 10(2): 68-73.Council, Brussels, Belgium, 24 October 2014.

[8]. Melikov AK. Advanced air distribution: improving health and comfort while reducing energy use. Indoor Air 2016; 26(1): 112-124.

[9]. Melikov AK, Langkilde G and Rasmussen LW. Human response to local heating for use in connection with low enthalpy ventilation. In Mundt E, Malmstrom T-G, In the Proceedings of RoomVent'98, 6th International Conference on Air Distribution in Rooms, Stockholm, Sweden, 14 -17 June, 1998, Vol. 98, pp. 315-321.

[10]. Tsuzuki K, Arens E, Bauman F and Wyon D. Individual thermal comfort control with desk-mounted and floor-mounted task/ambient conditioning (TAC) systems, In Indoor Air 1999: Proceedings of the 8th International Conference on Indoor Air Quality and Climate, Edinburgh, Scotland, 8-13 August, 1999, London: Construction Research Communications, pp. 368-373.

[11]. Akimoto TAT, Lee SLS, Iesaki NIN, Yokota TYT, Hayashi JHJ, Tanabe STS and Akimoto T. Impact of non-isothermal task conditioning system on thermal comfort. In: Healthy Buildings 2003 - Proceedings 7th International Conference, 7-11 December 2003, National University of Singapore, Singapore, Vol. 1, pp. 776-782.

[12]. Watanabe S, Shimomura T and Miyazaki H. Thermal evaluation of a chair with fans as an individually controlled system. Building and Environment 2009; 44(7): 1392-1398.

[13]. Bauman F, Carter T and Baughman A. Field study of the impact of a desktop task/ambient conditioning system in office buildings. ASHRAE Trans 199; 104(Part 1): SF-98-11-2.

[14]. Zhao W, Kilpeläinen S, Kosonen R, Jokisalo J, Lestinen S, Mustakallio P. Thermal environment and ventilation efficiency in a simulated office room with personalized micro-environment and fully mixed ventilation systems. Building and Environment. 2021 Jan 15;188:107445.

[15]. Zhao W, Kilpeläinen S, Kosonen R, Jokisalo J. Experimental comparison of local low velocity unit combined with radiant panel and diffuse ceiling ventilation systems. Indoor and Built Environment. 2020 Jul;29(6):895-914.

Assessment of the Indoor Environment Quality in UM6P Classrooms

Houda Er-retby [a], Abdelkader El kounni [a], Bouthayna Idrissi Gartoumi [a], Hicham Mastouri [a], Brahim Benhamou [a,b], Hassan Radoine [a], Manuel Carlos Gameiro da Silva [c]

[a] School of architecture planning & design, Mohammed VI Polytechnic University, BenGuerir, Morocco, houda.er-retby@um6p.ma, abdelkader.elkounni@um6p.ma, bouthayna.idrissigartoumi@um6p.ma, hicham.mastouri@um6p.ma, hassan.radoine@um6p.ma.

[b] ProcEDE, Cadi Ayyad University, Marrakech, Morocco, BBenhamou@uca.ac.ma.

[c] University of Coimbra, Coimbra, Portugal, manuel.gameiro@dem.uc.pt.

Abstract. The present study is the result of a global study conducted by the students of the Master Program "*Green Building Engineering and Energy Efficiency*" at the School of Architecture Design and Planning (SAP+D) of Mohammed VI Polytechnic University (UM6P) in Benguerir, Morocco. The study is a hands-on experience that allows the master's students to learn by doing about the concepts of the indoor environment quality, in addition to the classroom training. The objective of the study is to assess the indoor environment quality of selected classrooms in different buildings of the UM6P campus. To this end, seven classrooms were monitored by means of sensors that measure all the IEQ parameters including thermal, acoustic, and lighting. In addition, the occupants of these classrooms were asked to fill out a survey based on a questionnaire. In this paper, we report a sample of the results of this study relative to one classroom. The analysis of these results reveals that students' thermal perceptions differed because they were divided into three vote categories: neutral, feeling slightly hot, and feeling slightly cold. Based on the survey analysis, the percentage of each category varied during each session. The obtained results were later compared with the thermal comfort model, and the two approaches showed a good match in terms of describing the overall satisfaction of the occupants.

Keywords. Learning, Education, University Classroom, IEQ, Survey, Monitoring.
DOI: https://doi.org/10.34641/clima.2022.272

1. Introduction

Observational studies of indoor climate in classrooms have generally been justified by highlighting the negative effects of conditions such as warm temperatures and poor ventilation on student comfort and academic performance [1-2]. According to adaptive comfort theory, occupants are considered to be an agent in creating "ideal" indoor thermal conditions by adjusting behavior or changing the surrounding environment [3]. A classroom occupied by students and a teacher represents a good environment for studying indoor comfort because the occupant's activities are known and their metabolic rate can be estimated and the schedules of occupancy allow us to determine the periods when occupants/indoor environment interaction is significant; the periods of non-occupancy were used only to get an idea of the initial state when the classroom is empty.

The most difficult challenge for architects and building engineers today is to maintain a comfortable indoor environment passively throughout the year. In a hot semi-arid climate similar to the one of the city of Benguerir, Morocco [4], occupants are exposed to relatively high temperatures with possible high fluctuations inside a naturally ventilated building, causing the occupant to perceive dissatisfaction with the surroundings. Other factors such as humidity and air velocity, lighting, etc. can contribute to this discomfort [5].

In this study, we report on a hands-on experience that allowed the master's students at UM6P university (Benguerir, Morocco) to learn by doing about the concepts of indoor environment quality. This hands-on experience was conducted in the frame of the course 'Indoor Comfort' of the Master Program "*Green Building Engineering and Energy Efficiency*" (G*reenBEEE*) at the School of Architecture Design and Planning (SAP+D) of UM6P. The objective is mainly to show how the students of G*reenBEEE*, conducted a survey and measurement campaigns to assess the IEQ in the university classrooms during the COVID-19 pandemic. This is education-oriented research for "learning by doing". The results presented in this paper are a sample of

Copyright ©2022 by the authors. This conference paper is published under a CC-BY-4.0 license.

those obtained by the 21 students of *GreenBEEE* in the Spring 2021 semester. These students, gathered in 7 groups, monitored 7 classrooms and conducted a field survey of the occupants. Due to the pandemic situation and the time limitation of the study, it was not possible to extend the monitoring beyond 2.5 days per classroom.

2. Study methodology

This work is part of a larger study that includes various aspects of comfort, namely acoustic comfort, visual comfort, air quality, and thermal comfort. The primary focus of this paper will be on thermal comfort.

The study was conducted by means of monitoring several indoor parameters inside the selected classroom during a relatively long period which includes occupation (class hours) or no occupation (off course). In addition, the occupants of these classrooms were asked to fill out a survey based on a questionnaire. The monitoring system enables to calculate the mean PMV of the occupants based on the Fanger model considering the mean values of the clothes insulation (CLO parameter) as well as the metabolism rate (MET parameter) of the occupants. Moreover, the PMV of each occupant was calculated at the beginning and the end of each class, based on the survey. Due to COVID-19 pandemic restrictions, the classroom ventilation system was turned off during the period of this study.

2.1. Climate conditions of the case study

The study location is in the city of Benguerir, which is in southwest Morocco with a hot semi-arid climate, cold in winter, and hot in summer. The typical average temperature throughout the year is 19°C, and the average wind speed does not exceed 7m/s. The humidity level remains moderate throughout the year, with an average rate of 45% [4].

The study was conducted in May 2021, at the end of the spring season, given the rise in the outdoor air temperature as well as changes in the level of air humidity, which becomes almost dry during this period in mid-day, while it is still high at the beginning of the day due to the low outdoor air temperature. Figures 1 show the meteo data recorded during the period of the study which lasts from May 24 to May 26, 2021.

2.2. Indoor measurements

Measuring the building's physical conditions is often one of the most challenging tasks to achieve. In the case of a school classroom, it is advisable to use the smallest size and amount of equipment possible. The recording data loggers are suitable options, as they record time-based information and can measure different parameters simultaneously. Our study was carried out with a system called BAPPU-Evo which allows measuring air temperature, humidity, and air velocity as well as lighting, acoustic and CO2 levels, and globe temperature [6]. All these parameters were recorded every 5 minutes during the whole period of the study including the off-class period (24h monitoring per day). The sensors of the BAPPU-Evo system were placed on one of the classroom's tables in the middle of the classroom. The globe temperature sensor was at the mean level of the heads of the seated occupants. The technical characteristics of these sensors are given in Table 1.

In addition to monitoring the IEQ parameters of the classroom, the occupants were asked to fill out a questionnaire to indicate their sensations regarding thermal comfort, acoustics, and lighting. The occupants needed to fill out two questionnaires, one 30 min after the beginning of the class and the second one at the end. A specific questionnaire is dedicated to the teacher, who was also asked to report about the light operation and windows and doors opening. The questionnaires are given in Annex.

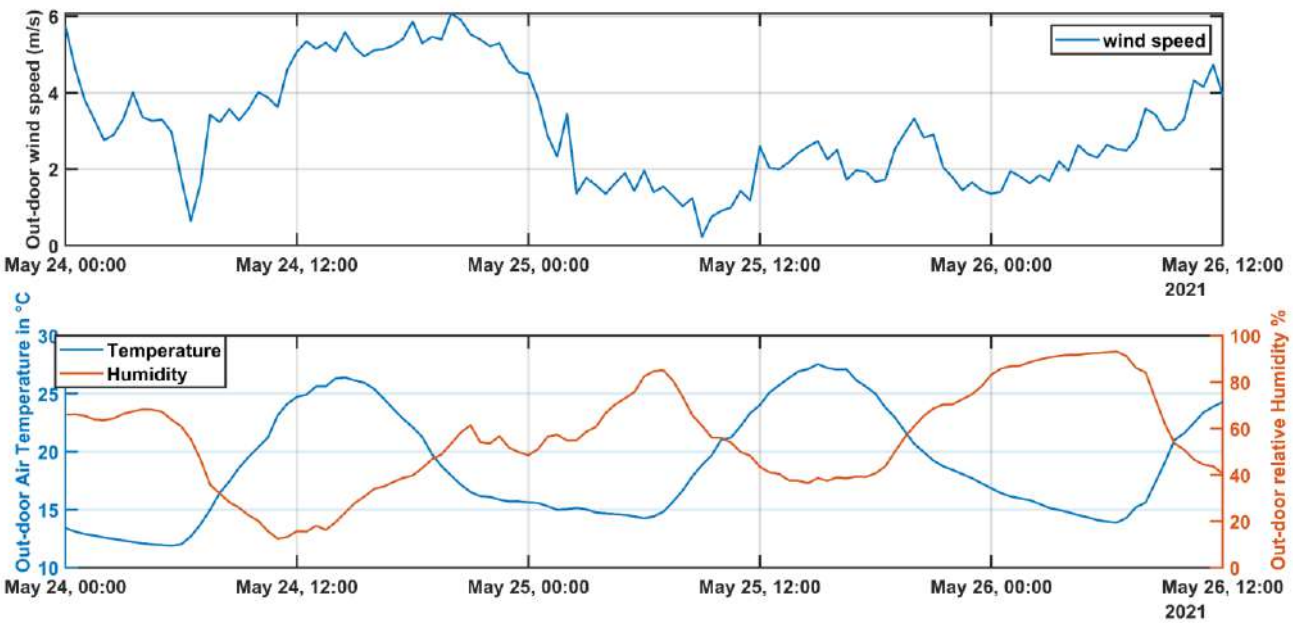

Fig.1 – Meteo data recorded by a local weather station

Table.1 – Technical details of the monitoring system

Technical Details BAPPU-evo			
measured physical characteristics	Measurement Range	Tolerance	Sensor
Air temperature	-20....50°C	+/-0.5°C	PT 1000 Sensor
Globe temperature	0...70°C	+/-0.5°C	Integrated temperature
Relative humidity	10...90%	+/-4% r.H	Capacitive humidity sensor
Air speed	0.0...5m/see	+/-10%f.MV,+/-3 Digit	Thermo-anemometer
Noise level	30...100dB(A)	+/-1.0dB(A) (at 1 kHz)	Precision electret
Illuminance level	50...30000Lux	V-Lambda adjustment 7.5% Cos-accurate evaluation 4% linearity 3%	Silicon photo element with adapted spectral sensitivity
CO_2(Carbone dioxide)	0...10 000ppm	+/- 75ppm +/-5%f.MV. (at 0...2 000ppm)	Non-dispersive infrared

2.3. Classroom Characteristics

The monitored classroom is located on the main campus of UM6P. It was occupied by the 2nd year students at EMINES School of Industrial Management. Fig. 2 shows the architecture plan of this classroom and Tables 2-3 show additional information about the classroom. The electrical switches as well as the windows were identified to allow for easy identification of their on/off and open/close operation that has been reported to us by the teacher in a specific survey (see the Annex). During the monitoring period, the number of occupants varied each day the given results in the following section are representative of the group of students who attended the class.

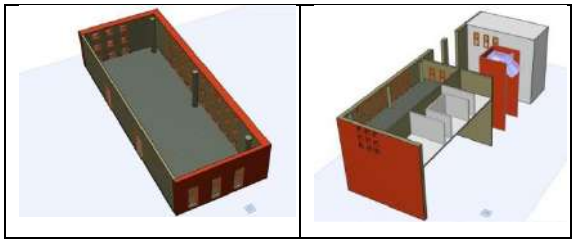

Fig.2 - The architecture of the studied classroom

Table.2 – Building specifications

Locatin	Oriontation	Surface	Occupancy
Ben Guerir	South-Eeast	107,6 m^2	50

Table.3 – Information about the monitored classroom

Occupants	Students and Professors
Number of occupants	50
Switches	4
Windows Glazing	3 (0,98m x 0,75m) 39 (0,6m x 0,6m)
Doors	2 (2m x 1m)
Ventilation Cooling system	Centralized system (Not activated)

3. Results of the surveys

Fieldwork and post-occupancy studies are generally complex. Therefore, it is vital to gather all the necessary information while on-site then the planning stage is often laborious due to the type and number of parameters that could be measured to study thermal comfort. Our state required a study of several factors that make the link between the studied entourage and the occupants. These parameters can vary according to the model chosen for the assessment process. The survey was constructed for the professor and students based on the model of ASHRAE 55. It is composed of three sections. The first section considers the physiological parameters the second section corresponds to the clothing insulation and the activity level. The clothing insulation and activity level are expressed in terms of Clo and Mets units, respectively, according to ISO 7730 and ASHRAE standard 55 [7]. In the third section, the questionnaire considers the climate control device in use. The fourth section included subjective information such as the thermal sensation vote TSV, the thermal preference or acceptability in the lighting, and the noise level [1][7].

To follow the thermal perception of the group of students and not disturb the teaching process the survey was distributed twice at the beginning and the end of the session and filled after 30 mins to ensure thermal equilibrium.

Table.4 – Duration and numbers of occupants per session

Date	Time	Total observation	Female	Male	Total
24/05/2021	08:30 10:30	2	8	17	25
25/05/2021	09:00 12:00 14:00 16:30	2 2	9 10	12 18	21 28
26/05/2021	11:00 12:30	2 2	2 2	5 5	7 7

Table.5 – Voting scale for indoor comfort

Scale	Thermal sensation	Lighting	Acoustic
-3	Too cold	-	-
-2	Cold	Very poor	-
-1	Slightly cold	poor	poor
0	Neutral	Neutral	Neutral
1	Slightly warm	Intense	Intense
2	warm	very intense	-
3	Hot	-	-

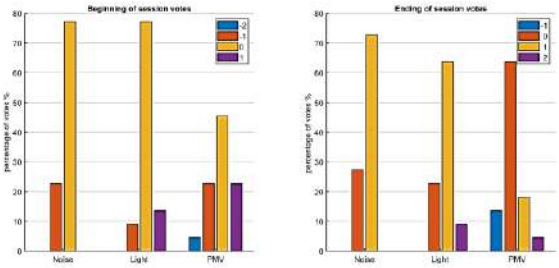

Fig.3 - Survey data first day of the assessment

At the beginning of the session, 45% of the students were showing satisfaction with the indoor environment the rest were unsatisfied, figure 3 shows that the votes were varying from a hot perception to cold and slightly cold. At the end of the sessions, the students' votes showed more tendency toward a neutral sensation as the percentage reaches 60% of satisfaction, but still, a group of students was voting hot and slightly hot, 12% also were feeling cold.

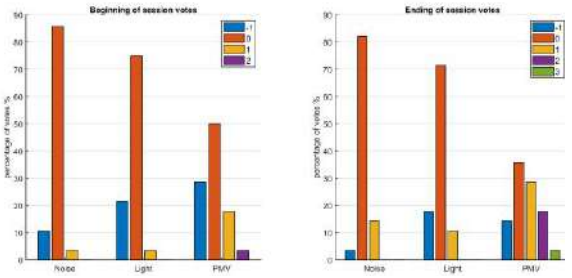

(a): Morning session

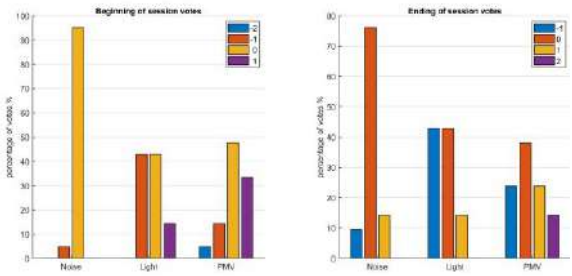

(b): Afternoon session

Fig.4 - Survey data second day of the assessment

On the second day at the morning session (figure 4. a), 50% of the students were satisfied but the rest were voting that they were unsatisfied with indoor conditions, it goes for both the beginning and end of the session, also we remark that the percentage of satisfied people has dropped which cause an encasement in the dissatisfaction of the group of students. In the second session (figure 4. b) we observe that almost 50% of the students were voting neutral and the rest were voting slightly hot, with the same variation at the end of the session. Some variation in the votes might be caused by the clo of the students, sex, and metabolic rate.

The first session of the third day (figure (5. a) shows that the slightly cold sensation was dominated with a percentage of 43% and the rest vote were divided equally between neutral and slightly warm. But, at the end of the session, most of the students were feeling cold, approximately 43% of the votes had a cold sensation, and 15% of the votes had a sightly cold sensation. Unlike the percentage of neutral vote stay the same.

The last session of the monitoring (figure 5. b) shows an increase in the neutral sensation between the beginning and the end of the session, unlike the slightly cold sensation decrease, but the warm sensation stays the same.

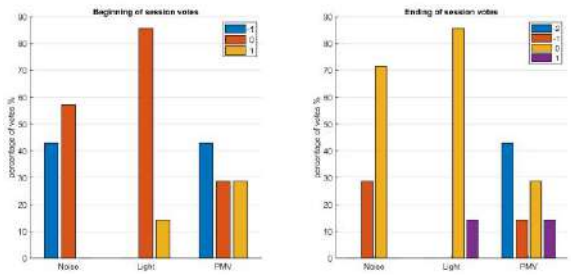

(a): First session

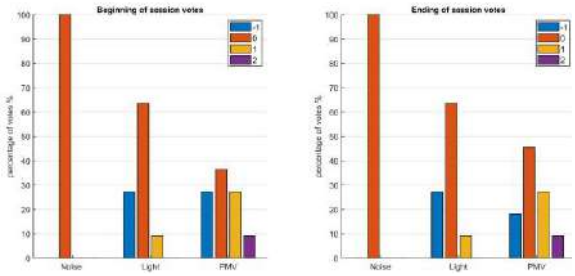

(b): Second session

Fig.5 - Survey data third day of the assessment

After analyzing the survey's results during the three days of the monitoring, we can conclude that the classroom offers different categories of comfort to the occupants. In the next session, we will analyze the temperature variation during the period of occupancy, and it relates to the thermal sensation perceived by the students and professor.

4. IEQ Monitoring results

The results of the monitoring are presented in Fig. 6 for the considered parameters in this paper.

4.1. Indoor air temperature

The mean operative temperature recorded (figure6) for the 3 days is around the value of 23.7°C. This value causes the occupants to feel discomfort usually in the morning, the occupants were perceiving cold thermal sensation in the interval of 8:00 AM to 10:30 AM, where the temperature was ranging from 20°C to 24°C and this is caused by the average Clo of the

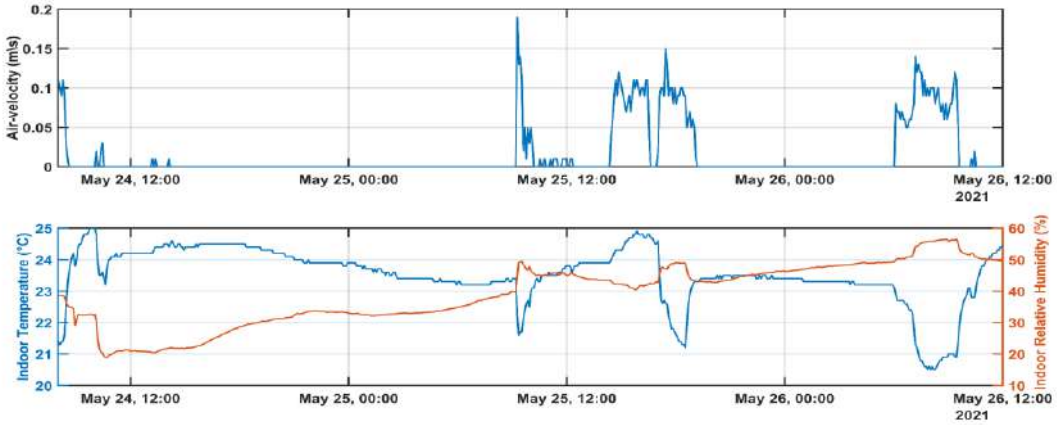

Fig.6 - Measured average indoor parameters

class was 0.58 clo which is close to the summer average Clo value. For the activity, only the professor who was in standing mode the rest of the class were all sitting.

For the interval of time 11:00 AM to 16:30 PM, the operative temperature was ranging from 23°C to 25.3°C, in this range, the occupant was feeling slightly hot even if the average clo value remains the same. Concluding that the students were feeling discomfort in this range would not be convening if we base our analyses only on temperature there is other parameters intervening in the thermal perception of the student that will be analyzed in the next session, these factors are humidity and air velocity.

4.2. Indoor air velocity

The average air velocity recording for the 3 days was ranging from 0.0009m/s to 0.076m/s. In some periods the air velocity peaks because of doors and windows opening, for 25th and 26th may the velocity was fluctuating around the value of 0.1m/s. According to Edward Arens et al [8] if the operative temperature is ranging from 22.9◦ C to 24.24◦ C and the airspeed is in the interval of 0 m/s to 0.2 m/s the occupant perceived a cold sensation. For the other periods where people were perceiving a slightly hot sensation, the temperature ranged from 23◦ C to 25◦ C and the air velocity was ranging from 0 to 0.2 m/s.

During the 3 days of the monitoring, the average value of humidity was ranging from 24.44% to 54.7%. The influence of relative humidity on physiology and thermal sensation has been conducted both under steady state [9,10] and under transient conditions [11]. In modest environments, the effect of humidity on thermal sensation could be ignored when the air temperature is in the comfort range. In warm environments, discomfort may be caused by too much moisture on the skin by high humidity levels [12].

4.3. Predicted Mean Vote (PMV) and Predicted Percentage of Dissatisfied (PPD)

Using the air temperature, the mean radiant temperature, the air velocity, the relative humidity, the average metabolic rate, and the average of the students' clothing, a representative instantaneous PMV is calculated for each time step of the data; this PMV progression over the three days, particularly during the occupation hours, assists us in evaluating comfort based on an analytic approach to be compared with the experimentation findings.

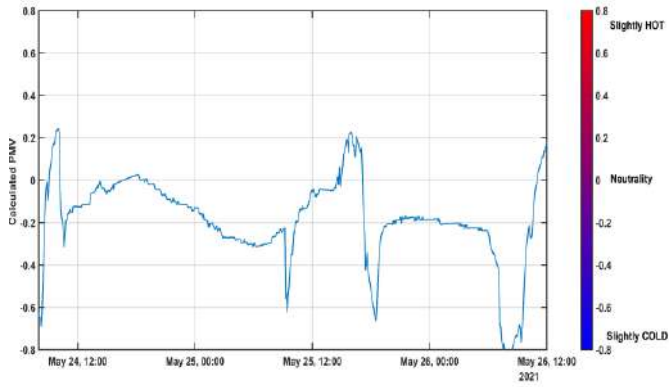

Fig.7 – Predicted Mean Mote calculated by the BAPPU system

Figure 7 shows that during the occupation hours, the PMV ranges between -0.2 and 0.2, as shown by the graph, thermal neutrality was obtained at specific points in small time intervals (the curve crosses the neutrality line PMV=0). The calculated PMV results agree with the experiment's findings. Because the obtained PMV values ranged from slightly hot to slightly cold, this demonstrates the neutral TSV's dominance, for the rest of the votes were always ranging from -1 to 1; however, in a few cases, a minority of students voted outside of this range.

The percentage of dissatisfaction based on the PMV can be used to determine the abundance of satisfaction among students; however, in this experiment, only the calculated PPD values associated with the occupancy hours were considered. Because the night periods are

characterized by a negative PMV, including the entire data set in this process would result in misleading results because the number of samples with high PPD would increase.

Figure 8 depicts two plots. The first is a histogram of the calculated PPD, which shows the number of samples and the ranges of dissatisfaction. In this study, the PPD ranged from 5% to 18%. In this observation, we found approximately more than 140 samples with a PPD of less than 6.5 percent. This demonstrates why more than half of the students were pleased with the temperature of the indoor environment.

The second plot illustrates the average PPD of each session; as we can see, the calculated PPD on the first and second days was less than 7%, which explains why the satisfaction perception was more prominent. In contrast, the PPD increased to 8% on the last day, which explains why the number of satisfied students was less than 50% on this day.

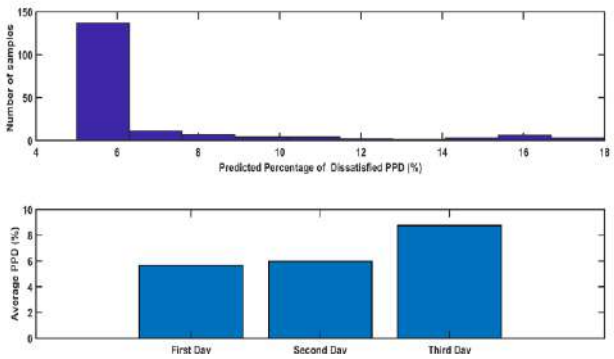

Fig.8 – The average Predicted percentage of dissatisfaction (PPD) each day

4.4. Operative temperature

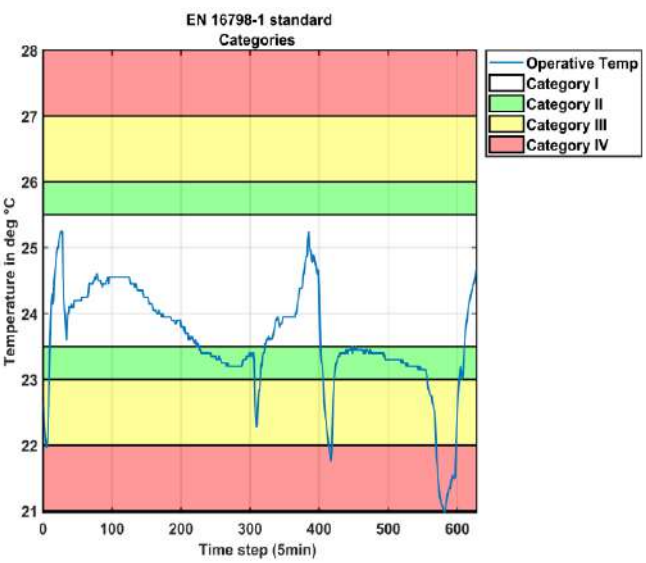

Fig.9 – Time evolution of operative temperature according to EN16798-1 comfort categories

According to a work done by professor Gameiro da silva [14], a similar methodology was adapted to evaluate the operative temperature according to the EN16798-1.

As we can see in our instance, the extreme values of the operating temperature reach down to 21°C, which was obtained in the early morning of the last day, for most of the time manly day one and two the operative temperature is in the category 1 during the occupancy.

4.5. Thermal neutrality temperature

The neutrality temperature is the operative temperature at which the occupant feels in equilibrium with the environment in other words the heat gains are equal to heat losses [13]. It is also the operative temperature value associated with TSV that is equal to zero. To determine the neutrality temperature, we had to calculate the average TSV for each session and associate it with the operative temperature perceived at the same time when students were voting. The results, presented in Table 5, show that the neutrality temperature is 24.2°C. After the elimination of some aberrant values of the mean TSV, the results enable to get a linear regression from Fig 10 according to equation 1

$$TSV = 0.143 \times T_{op} - 3.41 \qquad (1)$$

Table.5 – Average calculated temperature and average TSV base in the survey

TSV	0	0.13	0.28	0.09	0.60	-0.03	0.10	0.27	-0.14	-0.85
T_{op}	24.2	23.9	24.8	24.13	23.4	22.2	23.2	24.5	21.2	23.0

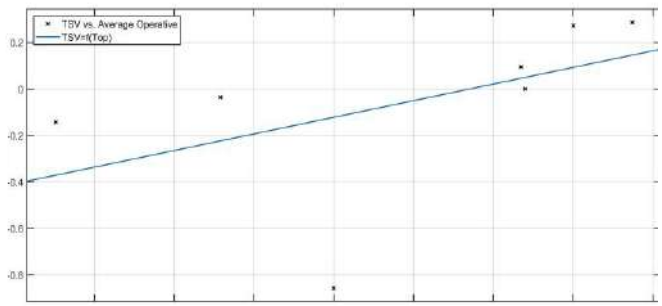

Fig.10 - Regression model plot of TSV as a function of operative temperature

Regression analysis is considered more appropriate for cooling mode's data. On the other hand, Griffith's method is more useful in estimating the comfort temperature with a small number of samples. We utilize the following expression (Eq. (2)) to calculate the comfort temperature of Griffiths [13]:

$$Tcmf = Top + \frac{(0 - TSV)}{\alpha} \qquad (2)$$

Using this model, we were able to calculate the comfort

temperature for the entire session, and the average values were ranging from 23.98 to 24.11 which still confirms that the obtained comfort temperature is reflecting the real case, the chosen value of alpha is 0.5 according to Talukdar et al[13].

5. Conclusion

This study was conducted in the frame of the GreenBEEE Master students project for the purpose of learning by doing. Its objective was to assess the Indoor Environment Quality (IEQ) in selected university classrooms. The study was conducted either by means of IEQ parameters monitoring aspect and by surveying the occupants of the classroom. A sample of results, that corresponds to three days of monitoring in May 2021, are presented and analyzed in terms of thermal comfort. The meteo data was also recorded by means of a weather station located not far from the monitored classrooms. Due to COVID-19 pandemic restrictions, the air conditioning system of the classrooms was deactivated by the administration. This allowed assessing the IEQ in a free-running mode.

Overall, the results showed that the majority of students were satisfied by the indoor thermal comfort, due to the comfortable outdoor conditions. The mean calculated percentage of dissatisfaction based on the surveys was less than 6%. However, this percentage increased slightly to around 9%, during the last day due to low outdoor air and students' clothing which seemed not adapted to this situation.

This first experience which suffered from the pandemic situation is going to be repeated next April by the next cohort of the GreenBEEE Master students. The lessons learned from this first study at the UM6P level will be of good guidance to perform better monitoring and survey.

Acknowledgment

The authors would like to express their gratitude to all the UM6P students who contributed to the survey, as well as the administrative staff of UM6P for making the monitoring process easier. GreenBEEE master students of cohort 2 are thanked for their contribution to the monitoring and survey material preparation.

References

[1] Mishra, Asit Kumar, and Maddali Ramgopal. "A thermal comfort field study of naturally ventilated classrooms in Kharagpur, India." Building and Environment 92 (2015): 396-406.

[2] Puteh, M., Ibrahim, M. H., Adnan, M., Che'Ahmad, C. N., & Noh, N. M. (2012). Thermal comfort in classroom: constraints and issues. Procedia-Social and Behavioral Sciences, 46, 1834-1838.

[3] KIM, Jungsoo et DE DEAR, Richard. Thermal comfort expectations and adaptive behavioral characteristics of primary and secondary school students. Building and Environment, 2018, vol. 127, p. 13-22.

[4] BORN, Kai, CHRISTOPH, Michael, FINK, A. H., et al. Moroccan climate in the present and future: combined view from observational data and regional climate scenarios. In: Climatic changes and water resources in the Middle East and North Africa. Springer, Berlin, Heidelberg, 2008. p. 29-45.

[5] López-Pérez, L. A., Flores-Prieto, J. J., Et Ríos-Rojas, C. Adaptive thermal comfort model for educational buildings in a hot-humid climate. Building and Environment, 2019, vol. 150, p. 181-194.

[6] BAPPU-EVO, https://www.bappu.de/en/

[7] Olesen, Bjarne W. "Guidelines for comfort." Ashrae Journal 42.8 (2000): 41-47.

[8] ARENS, Edward, TURNER, Stephen, ZHANG, Hui, et al. Moving air for comfort. 2009.

[9] AlpinKöknelYener. (2011) "Daylight analysis in classrooms with solar control. "Architectural Science Review 45.4 (2011): 311-316.

[10] Eduardo L. Kruger and Adriano Lucio Dorigo. (2008) "Daylighting analysis in a public school in Curitiba, Brazil. "Renewable Energy33.7 (2008): 1695–1702.

[11] X. Yo and Y. Su. "Daylight availability assessment and its potential energy-saving estimation –A literature review." Renewable and Sustainable Energy Reviews 52 (2015): 494-503.

[12] Jing, Shenglan, et al. "Impact of relative humidity on thermal comfort in a warm environment." Indoor and Built Environment 22.4 (2013): 598-607.

[13] Talukdar, Md Sarwar Jahan, et al. "Status of thermal comfort in naturally ventilated university classrooms of Bangladesh in hot and humid summer season." Journal of Building Engineering 32 (2020): 101700.

[14] M. Gameiro da Silva, L. W. van Cappellen, and E. Sanjuanello, "Assessing and Communicating Indoor Environmental Quality," vol. Rehva Journal, Volume 56, pp. 14–18, Apr. 2019.

[15] Stefano Paolo Corgnati, Manuel Gameiro da Silva (Editors). Indoor Climate Quality Assessment. Finland, Forssa Print 2011: ISBN 978-2-930521-05-3

ANNEX: Questionnaires used in the survey

Questionnaire : Etudiant

Date(jr/m/an):
heure(hr:mn):

1. Quel est votre numéro de table ? ☐
2. Sexe
   Femme ☐ Homme ☐
3. Age ☐
4. Taille ☐
5. Poids ☐
6. A quel moment êtes-vous entré dans la classe ? ☐
7. Cochez la totalité de ce que vous portiez avant d'entrer en classe (Aller sur Image 1)
8. Si vous avez enlevé un vêtement pendant le cours, veuillez indiquer lequel/lesquels ? (Aller sur Image 2)
9. Quelle est votre activité à cet instant?
   Assis (e) ☐ Debout ☐
10. Quel est votre ressenti thermique à cet instant?

Très froid	froid	frais	neutre	Légèrement chaud	chaud	très chaud
-3	-2	-1	0	1	2	3

11. Comment jugez-vous l'éclairage de la salle?

Très faible	faible	neutre	intense	très intense
-2	-1	0	1	2

12. Comment jugez-vous le son de la salle?

faible	neutre	forte
-1	0	1

(reportez votre numéro de table svp) ☐

Image 1 (question 7) :

Image 2 (question 8) :

Questionnaire : Professeur

Date(jr/m/an):
heure(hr:mn):

1. Sexe
   Femme ☐ Homme ☐
2. Age ☐
3. Taille ☐
4. Poids ☐
5. A quel moment êtes-vous entré dans la classe ? ☐
6. Cochez la totalité de ce que vous portiez avant d'entrer en classe (Aller sur Image 1)
7. Si vous avez enlevé un vêtement pendant le cours, veuillez indiquer lequel/lesquels ? (Aller sur Image 2)
8. Quelle est votre activité?
   Assis (e) ☐ Debout ☐
9. Quelle est la fenêtre ouverte à cet instant ?
   1 ☐ 2 ☐ 3 ☐ 4 ☐ 5 ☐ 6 ☐ aucune ☐
10. Quelle est la Porte ouverte à cet instant ?
    1 ☐ 2 ☐ aucune ☐
11. Le système de chauffage ou de climatisation est-il allumé ?
    Oui ☐ Non ☐
    Si oui à quelle valeur :
12. Le DATASHOW (vidéo projecteur) est-il allumé ?
    Oui ☐ Non ☐
13. Quel (s) est ? interrupteur(s) allumé?
    1 ☐ 2 ☐ 3 ☐ 4 ☐ 5 ☐ 6 ☐ aucun ☐
14. Quel est votre ressenti thermique? (encercler la valeur)

Très froid	froid	frais	neutre	Légèrement chaud	chaud	très chaud
-3	-2	-1	0	1	2	3

15. Sinon que préfériez-vous ressentir? (encercler la valeur)

Très froid	froid	frais	neutre	Légèrement chaud	chaud	très chaud
-3	-2	-1	0	1	2	3

16. Quelle est votre niveau d'acceptation thermique?(encercler la valeur)

Très faible	faible	neutre	intense	très intense
-2	-1	0	1	2

17. Comment jugez vous l'éclairage de la salle?(encercler la valeur)

Très faible	faible	neutre	intense	très intense
-2	-1	0	1	2

18. Comment jugez vous le son de la salle?(encercler le numéro choisi)

faible	neutre	forte
-1	0	1

Image 1 (question 7) :

Image 2 (question 8) :

Machine Learning Models for Indoor $PM_{2.5}$ Concentrations in Residential Architecture in Taiwan

Yu Chen, Lin [a], Yaw Shyan Tsay [b], Chien Chen Jung [c]

[a] Department of Architecture, National Cheng Kung University, Tainan, Taiwan, e74036085@gs.ncku.edu.tw

[b] Department of Architecture, National Cheng Kung University, Tainan, Taiwan, tsayys@mail.ncku.edu.tw

[c] Department of Public Health Assistant, China Medical University, Taichung, Taiwan, ccjung@mail.cmu.edu.tw

Abstract. People typically spend 80-90% of their time indoors. Therefore, establishing prediction models to estimate particulate matter ($PM_{2.5}$) concentration in indoor environments is of great importance, especially in residential households, in order to allow for accurate assessments of exposure in epidemiological studies. However, installing monitoring instruments to collect indoor $PM_{2.5}$ data is both labor and budget-intensive. Therefore, indoor $PM_{2.5}$ concentration prediction models have become critical issues. This study aimed to develop a predictive model for hourly household $PM_{2.5}$ concentration based on the artificial neural network (ANN) method. From January 2019 to April 2020, $PM_{2.5}$ concentration and related parameters (e.g., occupants' behavior information and ventilation settings) were collected in a total of 62 houses and apartments in Tainan, Taiwan (tropical and subtropical region). Overall, 2136 pairs of data and 9 possible variables were used to establish the model. Meteorological data were primarily used to establish the model. Meanwhile, occupants' behavior and building characteristics were generalized as effective opening areas to describe the importance of ventilation in subtropical areas. We performed five-fold cross-validation to assess prediction model performance. The prediction model achieved promising predictive accuracy, with a coefficient of determination (R^2) value of 0.88 and a root mean square error value of 3.35 ($\mu g/m^3$), respectively. Outdoor $PM_{2.5}$ concentrations were the most important predictor variable, followed in descending order by temperature, outdoor carbon dioxide concentration, outdoor relative humidity, and opening effective areas. In summary, we developed a prediction model of hourly indoor $PM_{2.5}$ concentrations and suggest that outdoor meteorological data, building characteristics, and human behavior can be powerful predictors. The results also confirm that the model can be used to predict indoor $PM_{2.5}$ concentrations across seasons.

Keywords: Artificial neural network, Indoor air quality, Subtropical
DOI: https://doi.org/10.34641/clima.2022.247

1. Introduction

Fine particle matter (PM) has been recognized as a key air pollutant that influences occupants' health [1]. Recently, the monitoring methods for $PM_{2.5}$ have primarily been through direct field measurement, which is labor-intensive and costly. Moreover, this method is primarily suitable for outdoor measurements and is difficult to widely use in indoor environments. Since most people spend 85%-90% of their life indoors [2], assessing indoor particle pollution is important for understanding the impact of particle pollution and can avoid exposing occupants to harmful levels of pollution.

In addition to indoor sources like cooking and smoking, outdoor pollution particles are major contributor to indoor concentrations. A previous study observed that outdoor air has more critical influences on indoor air in tropical and subtropical areas than in cold and temperate zones [3]. Using ventilation systems and natural moving winds, outdoor particles can be transported indoors. Furthermore, infiltration from leaks in the building envelopes is another dominant source [4]. Consequently, indoor particle concentration fluctuates according to such mixed factors as climates, seasons, human behaviors, and building characteristics, thus demonstrating the importance of research on local data.

As mentioned, the spatiotemporal distribution of indoor $PM_{2.5}$ concentrations involves complex natural and anthropogenic sources, thus making the

Copyright ©2022 by the authors. This conference paper is published under a CC-BY-4.0 license.

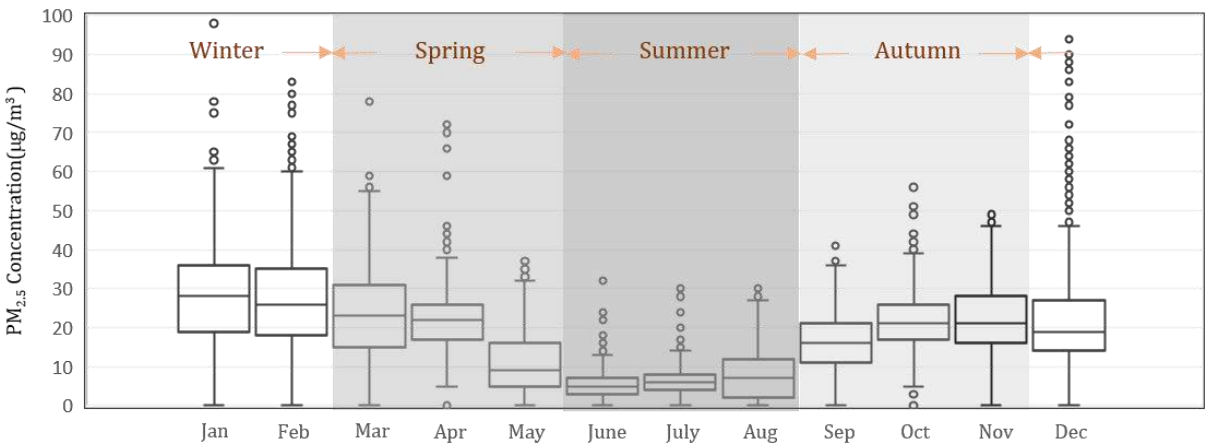

Fig. 1 - Historical plots of the outdoor PM2.5 concentrations at Tainan station (120'12'E; 22'59'N).

control and accurate prediction of $PM_{2.5}$ a challenging task.

In recent years, with the development of machine learning, such algorithms as random forest [5], gradient boosting regression [6], and artificial neural networks [7] have been used to overcome the above drawbacks of linear models with multiple parameters.

The purpose of this study is to explore the features of pollution sources and establish a prediction model for indoor concentration based on the long-term datasets collected from residential buildings in southern Taiwan. The results of this study can provide occupants with valuable information, including air quality control strategies and their risks to human health.

2. Dataset analysis

2.1 wide area data

The target city was Tainan, which is the sixth-largest city in Taiwan. Tainan is located between tropical and subtropical regions, and the annual temperature and relative humidity are 24.3 ℃ and 77.2%, respectively. **Fig. 1** shows the historical distribution of outdoor $PM_{2.5}$ concentrations from 2018 to 2020. Measurement $PM_{2.5}$ data were downloaded from the Tainan air quality monitoring network, which is an officially organized open-source website.

Fig. 1 illustrates the monthly temporal variation of the outdoor $PM_{2.5}$ concentrations. This figure indicates that the $PM_{2.5}$ concentration reached a peak during winter, dropped gradually through spring and summer, and started to increase again during autumn. The reason being that starting from September, the prevailing wind (northeast monsoon) affects the island, thereby easily dispersing and diluting air pollutants, as well as bringing pollutants from nearby China. Furthermore, the subtropical high pressure over the Pacific Ocean in the summer causes high convection of air mass, which leads to the vertical dispersion of pollutants [8].

2.2 survey objects

From Oct 2019 to Jan 2020, hourly data were

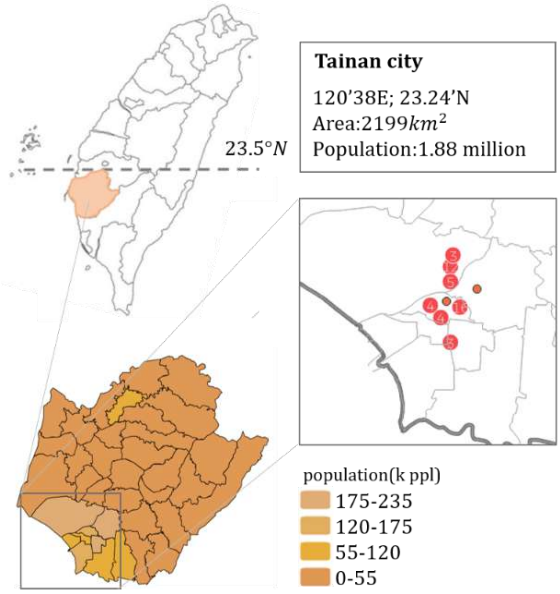

Fig. 2 - Location of the survey object

collected from 62 houses in Tainan using real-time devices (TSI Q-TRAK and TSI DUST-TRAK) over a day (**Fig. 3**). Occupants' behavior and building characteristics were also recorded through questionnaires filled out by family members. Two out of three of the surveyed objects were located in the city center, and the rest of them sat in the nearby suburban An-nan district. The processes and specifications are shown in **Fig. 3**.

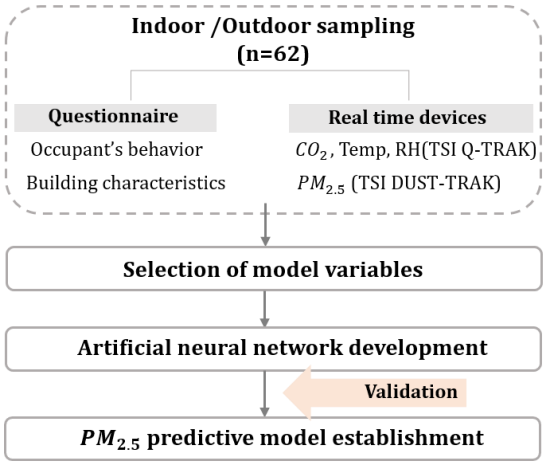

Fig. 3 - Research workflow

Tab. 1 - Summary of building characteristics and human activities of surveyed households

Variables	Description	Results(n,%)	Variables	Description	Results(%)
Building characteristics (n=62 houses)			human activities (t=2135 hrs)		
building types	Townhouse Apartment	42(67.7%) 20(32.3%)	electric devices(computer, printer)	YES	9%
Building age	<20 years 20-40 years >40 years	29(46.8%) 30(48.4%) 3(4.8%)	cooking(oven, microwave)	YES	0.7%
Building floor level	1-5 floors 6-10 floors >10 floors	62(83.9%) 6(9.7%) 4(6.5%)	intense burning	YES	10%
Number of openings	1 2 3	54(87.1%) 6(9.7%) 2(3.2%)	smoking	YES	0%
Near main road(<8m)	YES	12(19.4%)	Airpurifier	YES	15%

2.3 building characteristics and human activities

The vast majority (67.7%) of the objects were two to five-story houses, which is the most common residential type in southern Taiwan. Most buildings were 20-40 years old and were located away from the main road. All of the measured spaces were rooms with more than one opening.

As presented in **Tab. 1,** 9%, 0.7%, 0% and 10% of the time occupants indulged in using the computer, cooking, smoking and intense burning. Furthermore, air purifiers were turned on for more than 15% of the observed time.

2.4 correlation analysis of indoor and outdoor $PM_{2.5}$ concentration

I/O ratio simply describes the relationship between indoor and outdoor particle concentrations according to equation (1):

$$\text{I/O ratio} = \frac{C_{in}}{C_{out}} \quad (1)$$

Where C_{in} and C_{out} are the indoor and outdoor particle concentrations (μg/m^3), respectively. The summary of the measured objects shows a mean value of 0.8 and varies within the range of 0.14-2.37, as shown in **Tab. 2**. The low I/O ratio is strongly related to the presence of few indoor sources, window opening behavior, and the use of filtration systems, such as 0.71 for $PM_{2.5}$ with few indoor sources as also found by Clayton et al. [9].

2.5 data analysis

Among the observed objects, indoor pollution sources were seldom recorded, which indicates that meteorological parameters and building characteristics were the main factors to influence indoor $PM_{2.5}$ concentrations. Previous studies also pointed out that outdoor $PM_{2.5}$ was a major variable in $PM_{2.5}$ prediction models [10]. In particular, opening windows is a universal behavior for adapting to Taiwan's hot and humid climate [11]. Therefore, outdoor $PM_{2.5}$ concentration plays an important role in predicting indoor $PM_{2.5}$ concentrations.

3. Machine learning models

3.1 artificial neural networks

Artificial neural network (ANN) has been proven to be a powerful tool to deal with nonlinear and noisy environmental data when traditional models have failed to predict [12].

A typical ANN model contains interconnected input, hidden, and output layers. The information processed by the hidden layer is assigned weights and is then adjusted by an activation function that determines how they transmit data to the next layer. The output layer predicts a value and compares it with the ground truth to assess the error according to the loss function (generally by minimizing the error).

3.2 selection of variables

Outdoor $PM_{2.5}$ concentrations were matched to indoor $PM_{2.5}$ concentration and meteorological data (temperature, CO_2, and humidity) on an hourly basis. Since building types and stories generally do not differ, the information was excluded. Furthermore, household appliances were only activated a small fraction of time, so those variables were also discarded in the training datasets.

In contrast, window opening behavior was of great importance, as described in the previous section. Its influence because of natural ventilation was considered using the "opening effective area" parameter, which was defined as the product of area of the main openings and the occupants' behavior(True(1) or False(0)). Considering the

Tab. 2 - Descriptive statistics of the variables

n=1316	Symbol	Mean±STD	Min	Max	Median
Meteorological data					
Outdoor $PM_{2.5}$ concentration(μg/m^3)	C_{out}_$PM_{2.5}$	21.3±14.0	0.9	115.2	17.5
Outdoor CO_2 concentration(ppm)	C_{out}_CO_2	385.6±65.9	253..9	766.5	377.5
Outdoor temperature(°C)	$Temp_{out}$	26.0±5.1	15.1	44.0	26.0
Outdoor relative humidity(%)	RH_{out}	66.5±7.5	26.8	91.1	66.6
Indoor $PM_{2.5}$ concentration(μg/m^3)	C_{in}_$PM_{2.5}$	15.3±9.7	0.8	78.5	13.1
Indoor CO_2 concentration(ppm)	C_{in}_CO_2	490.5±189.3	308.0	1967.8	430
Indoor temperature(°C)	$Temp_{in}$	26.4±3.1	19.0	33.8	26.4
Indoor relative humidity(%)	RH_{in}	65.6±6.7	43.7	82.5	66.4
IO Ratio		0.8±1.2	0.14	2.37	0.7
Building characteristics					
Opening effective area(m^3)	A	0.9±1.7	0	13.1	0
Space volume	V	71.0±38.8	14.9	213.3	62.6

uncontrolled flow of air through cracks and leaks in the building envelope, the space volume was also included as a building information variable.

The statistics for all variables are described in **Tab. 2**. The measured indoor $PM_{2.5}$ concentrations were 15.3±9.7 μg/m^3 at 62 houses, and the outdoor $PM_{2.5}$ concentrations ranged between 0.9 and 115.2 μg/m^3, with a mean value of about 21.3 μg/m^3.

3.3 variables correlation

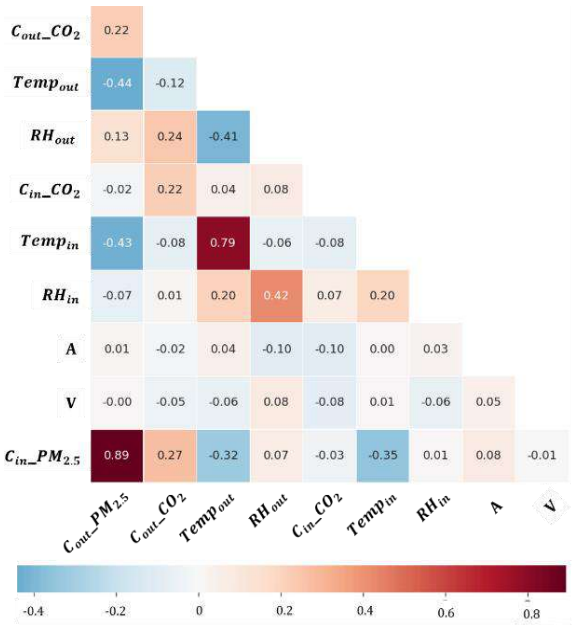

Fig. 4 - Variables correlation matrix

A correlation matrix (**Fig. 4**) illustrates the correlation between the indoor $PM_{2.5}$ and other variables using Pearson correlation coefficients. Of the nine outdoor predictor variables (including outdoor $PM_{2.5}$ concentration, CO_2 concentration, temperature, humidity, effective opening area, and space volume), all predictors were found to be correlated to indoor $PM_{2.5}$. The largest correlation coefficient was 0.89 between the indoor and outdoor $PM_{2.5}$ concentrations. The indoor $PM_{2.5}$ concentration showed a positive correlation with outdoor CO_2 concentrations (0.29), outdoor humidity (0.09), and effective opening area (0.08). Furthermore, a negative correlation was observed with the temperature factors, (-0.33) and (-0.35), respectively.

3.4 model development

This research adopted the Google Colaboratory platform with python language to generate the ANN model for prediction. First, the collected data was proven to be normalized before training to achieve better performance [13]. The missing pairs of data were then dropped to create a robust model. The total training sets were consequently composed of 1316 pairs of data and were then divided into training, validation, and testing datasets with a ratio of 6:2:2. The hyperparameters for the ANN training algorithms are shown in **Tab. 3**.
In total, nine variables served as potential input parameters, and the objective output was the indoor $PM_{2.5}$ concentrations. The structure of the proposed basic model was set up using nine neurons in the input layer for the nine input parameters and single neurons in the output layer for the output variables. The model has three hidden layers, and each layer has 30 neurons, which we tested and verified to be the best performing network.

Tab. 3 - Summary of the ANN model settings

Hyperparameter	Model
Neurons	[30,30,30]
Optimizer(learning rate)	Adam(0.001)
Batch size	20

4. Results

Prediction model performance was assessed using the coefficient of determination (R^2) and root mean square error (RMSE). We used five-fold cross-validation to confirm model reliability. The R^2 of the cross validation ranged between 0.85-0.90, with an average of 0.88.

Fig. 5 displays a plot of the test set target values against the measured values from the ANN-based regression model implemented in this work. The RMSE was about 3 (μg /m^3) in all validation cases, indicating significant prediction performance; since the measured indoor $PM_{2.5}$ ranged between 0.8 to 78.5 μg /m^3, the error was relatively small.

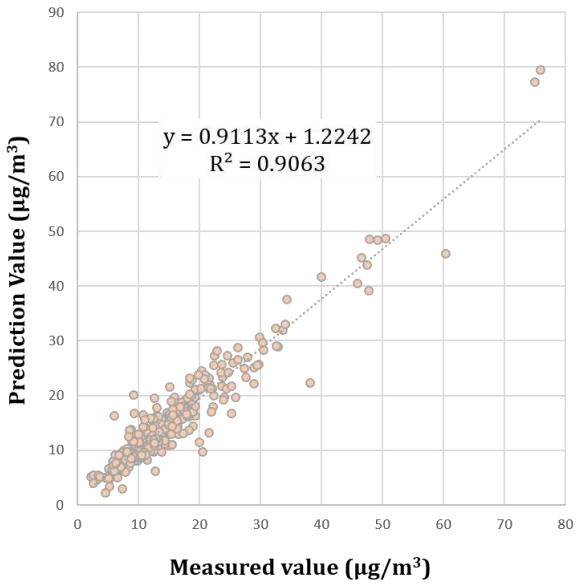

Fig. 5 - Relationship between predicted and measured hourly average indoor $PM_{2.5}$ concentration

5. Conclusions and discussions

In this study, we established a prediction model for hourly average indoor $PM_{2.5}$ concentrations conducting the ANN method. The collected data revealed that outdoor $PM_{2.5}$ was the key predictor, which was consistent with the findings of previous studies [3][5][10]. Furthermore, ventilation and building characteristics alongside human activities were comprehensively included by the effective opening area as a highly relative variable in the model. The results indicated that controlling the window opening behavior is beneficial for reducing indoor $PM_{2.5}$ concentrations. This prediction model can also be adopted in future research for automated ventilation systems in smart buildings.

In this study, about half of the buildings were aged 20-40 years, and over 80% of them were classified as two- to five-story townhouses. According to the official statistical data, they represent the typical building type and age distributions of the area [14]. These data reflected that the prediction model can be applied throughout Taiwan.

Studies in the past have indicated that indoor occasion human activities, especially smoking and incense stick burning, can be influential factors in $PM_{2.5}$ concentrations [15]. However, the above behavior was seldom recorded in our field measurements, which minimized their impact on indoor pollution. For further research, object selections and detailed records could be included and tested as variables to enhance the prediction model.

This Taiwan-based prediction model differs from those of other climate regions, where infiltration can be the primary pathway entering the building. Occupants who embrace natural ventilation should be warned about outdoor air quality levels. The established ANN model using outdoor environmental data and simple building factors has advantages over the classic multiple linear regression model with higher R^2 and lower RMSE [10], which can be used for rapid pollution regulation.

6.References

[1] Huang, Y. L., Chen, H. W., Han, B. C., Liu, C. W., Chuang, H. C., Lin, L. Y., & Chuang, K. J. Personal exposure to household particulate matter, household activities and heart rate variability among housewives. PloS one, 9(3), e89969.

[2] N.E. Klepeis, W.C. Nelson, W.R. Ott, J.P. Robinson, A.M. Tsang, P. Switzer, J.V. Behar, S.C. Hern, W.H. Engelmann. The National Human Activity Pattern Survey (NHAPS): a resource for assessing exposure to environmental pollutants, J. Expo. Sci. Environ. Epidemiol., 11 (3) (2001), p. 231

[3] Chien-Cheng Jung, Nai-Yun Hsu, Huey-Jen Su. Temporal and spatial variations in IAQ and its association with building characteristics and human activities in tropical and subtropical areas, Building and Environment, Volume 163,2019,106249.

[4] Chun Chen, Bin Zhao. Review of relationship between indoor and outdoor particles: I/O ratio, infiltration factor and penetration factor, Atmospheric Environment, Volume 45, Issue 2,2011,Pages 275-288.

[5] XuXu, D., Liu, Z., Li, Y., Li, N., Chartier, R., Chang, J., Wang, Q., Wu, Y., & Li, N.C. Estimating hourly average indoor PM2.5 using the random forest approach in two megacities, China. Building and Environment.

[6] Doreswamy, Harishkumar K S, Yogesh KM, Ibrahim Gad. Forecasting Air Pollution Particulate Matter (PM2.5) Using Machine Learning Regression Models, Procedia Computer Science, Volume 171, 2020, Pages 2057-2066,

[7] Gholamreza GoudarziK. Hopke, Mohsen YazdaniPhilip. Forecasting PM2.5 concentration using artificial neural network and its health effects in Ahvaz, Iran, chemosphere.2021.131285.

[8] Lee, M., Lin, L., Chen, CY. et al. Forecasting Air Quality in Taiwan by Using Machine Learning. Sci Rep 10, 4153

[9] C A ClaytonL Perritt, E D Pellizzari, K W Thomas, R W Whitmore, L A Wallace, H Ozkaynak, J D SpenglerR. Particle Total Exposure Assessment Methodology (PTEAM) study: distributions of aerosol and elemental concentrations in personal, indoor, and outdoor air samples in a southern California community. J Expo Anal Environ Epidemiol. 1993 Apr-Jun;3(2): 227-250

[10] Jung, C.-C.; Lin, W.-Y.; Hsu, N.-Y.; Wu, C.-D.; Chang, H.-T.; Su, H.-J. Development of Hourly Indoor PM2.5 Concentration Prediction Model: The Role of Outdoor Air, Ventilation, Building Characteristic, and Human Activity. Int. J. Environ. Res. Public Health 2020, 17, 5906.

[11] Lu, H.-Y.; Lin, S.-L.; Mwangi, J.K.; Wang, L.-C.; Lin, H.-Y. Characteristics and source apportionment of atmospheric PM2.5 at a coastal city in southern Taiwan. Aerosol Air Qual. Res. 2016, 16, 1022–1034.

[12] Kukkonen, J., Partanen, L., Karppinen, A., Ruuskanen, J., Junninen, H., Kolehmainen, M., ... & Cawley, G. Extensive evaluation of neural network models for the prediction of NO2 and PM10 concentrations, compared with a deterministic modelling system and measurements in central Helsinki. Atmospheric Environment, 37(32), 4539-4550.

[13] JoJun-Mo. (2019). Effectiveness of Normalization Pre-Processing of Big Data. Journal of the KIECS: 547-552.

[14] Interior of the Ministry. (2018). Statistical Report of Ministry of the Interior. Taipei, Taiwan.

[15] Gurung, G.; Bradley, J.; Delgado-Saborit, J.M. Effects of shisha smoking on carbon monoxide and PM2.5 concentrations in the indoor and outdoor microenvironment of shisha premises. Sci. Total Environ. 2016, 548, 340–346

Data Statement

The datasets generated during and/or analysed during the current study are not available because the findings of this study are available on request from the corresponding author, but the authors will make every reasonable effort to publish them in near future.

Effects of humidification process on the thermal behavior of floor heating systems

Tianying Li [a,b], Abdelatif Merabtine [a,b], Mohammed Lachi [a], Rachid Bennacer [c]

[a] MATIM, Université de Reims Champagne-Ardenne, Reims, France, mohammed.lachi@univ-reims.fr

[b] EPF Campus de Troyes, Troyes, France, tianying.li@etudiant.univ-reims.fr, abdelatif.merabtine@epf.fr

[c] LMT/ENS-Paris-Saclay/CNRS/Université Paris Saclay, Gif-sur-Yvette, France, rachid.bennacer@ens-paris-saclay.fr

Abstract. Since the outbreak of the Covid-19 pandemic, working from home has become the norm for millions of workers in the world. Indoor humidification and heating are essential for health and comfort in a dry and cold climate. In order to investigate the interaction between humidification process using a cool mist humidifier and the heating process using a floor heating system, a total of 4 experimental tests were carried out, which included three experimental groups with humidification process in the conditions of three relative humidity setpoints (45%, 55%, 65%), and one control group without humidification process. In the process of experiments, indoor relative humidity of the control group basically maintained around 30%. Therefore, the heated room would be dehumidified to about 30% before each experiment started. The indoor temperature was maintained at 25 ℃ by the floor heating system. Obtained results showed the floor heating system was stimulated to reheat the room due to the cooling effect of the humidifier and a new balance was established in the process of competition between the evaporative cooling and floor heating. When humidifying air to over 45%, it would lead to floor overheating. Furthermore, the humidification process improves the non uniformity of air temperature distribution, but at the same time brings more uneven RH distribution. Besides, the energy consumption increases following with the rising of setpoints of RH, and the growth rate is 60%, 87% and 100% respectively for RH 45%, 55% and 65%. In conclusion, the optimal setpoint of the humidifier is RH 45% based on a comprehensive consideration of health, thermal comfort and energy consumption.

Keywords. Humidification, Floor heating system, Thermal comfort, Energy consumption, Experiments
DOI: https://doi.org/10.34641/clima.2022.246

1. Introduction

Since the beginning of its history, man has been preoccupied with protecting oneself against environment assaults and always tries to create a safe and comfortable indoor environment. Currently, people spend most of their time indoors especially since the outbreak of the Covid-19 pandemic and working from home becomes the norm for millions of workers in the world. In this case, a safe, clean and comfortable indoor environment is particularly important.

Indoor temperature and humidity are two important parameters that could affect thermal comfort in buildings. The effects of humidity on the thermal sensation is rather limited compared to air temperature based on the ISO 7730 [1], while low relative humidity probably causes dryness of the eyes and skin, and even exacerbates symptoms in the upper and lower airways [2,3]. Jin et al [4] carried out a field study and found that a minimum humidity of 41% could be predicted to avoid dry skin for elderly people in care homes, if the room temperature is maintained at 21 ℃. Cold and dry environments also facilitate the survival and spread of viral diseases, and some studies observed air humidity negatively correlated with Covid-19 morbidity and mortality [5,6].

Some studies on the indoor environment of buildings located in Greenland [7], Beijing [8] and New York [9] cities have shown that the heating systems of residential buildings in winter generate dry indoor environments where the indoor humidity remains below 30%. However, it remains to be noted that the recommended humidity comfort range is 40-70% based on CIBSE Guide A [10]. Clearly, it's quite necessary to increase indoor humidity in the heating season of these regions.

Copyright ©2022 by the authors. This conference paper is published under a CC-BY-4.0 license.

Portable humidifiers humidifying air directly may induce greater impacts than humidification systems installed in ventilation ducts with heat recovery on indoor thermal and humid environment. Feng et al [11] studied the impact of the humidification process on the indoor environment in a reference chamber using a portable ultrasonic humidifier generating steam and water droplets. The results showed that the evaporation of water droplets as a "constant enthalpy process" led to an increase in humidity and a decrease in temperature.

Portable humidifiers generally fall into three categories: ultrasonic, cool mist, and warm mist [12]. Of them, the cool mist humidifier has a 50% of high market penetration [12]. In a cool mist humidifier, air is forced through a water-saturated filter by an in-built ventilator and absorbs the evaporated moisture. The total enthalpy of the air flow is considered as constant in this process [13,14].

Therefore, when a cool mist humidifier, subjected to constant enthalpy humidification, is used in a heated room, in which air temperature is controlled around a comfort setpoint by heating systems, the reduction of air temperature in this humidification process may induce the room to be reheated. In this situation, when it happens in a building with a floor heating system (FHS) of high thermal inertia [15], the regulation system would have a time lag in response to the sudden change in indoor temperature, further leading to a larger deviation of air temperature from setpoint, which will cause FHS to deliver more hot water to the pipes embedded in the floor. Besides, since the constant enthalpy humidification enhanced indoor air cooling process, hot water supply would be also more frequent. Therefore, the competition between the humidification and the heating process probably leads to the overheating of the floor surface and have an influence on the indoor thermal comfort and on the energy consumption of the FHS as well.

Up to now, for the best knowledge in comportment or regulation of this combined systems, there is no available studies combining a cool mist humidifier with a floor heating system to investigate their interactions. In this paper we present a study on a full-scale experiment in order to be able to provide some measurement-based answers to the following questions: (1) how does the underfloor heating system behave when a humidification process is used? (2) In this situation, how does the thermal comfort is impacted? (3) What is the impact on the energy consumption of such heating systems when combined to the humidification process?

2. Research methods

The experiments were performed in a full-scale test cell with an available space of 11 m² of area and 2.1 m of height, located at EPF School of Engineering in City of Troyes (France) as shown in Fig. 1. The test cell is composed of two adjacent well-insulated rooms. The first one is equipped with a floor heating system as the heated room, and the other one is as a cold room with an air conditioner to simulate outdoor conditions in winter. In this study, the cold room was fixed at 5 ℃ as the outdoor condition of the heated room, which was relatively close to the average temperature in winter season in City of Troyes.

The FHS is a hydronic system that circulates hot water in a spiral layout of crosslinked polyethylene tube to provide heat to the room through the floor surface. The tube is embedded in the bottom of a 5 cm thick of anhydrite screed slab and the top of a 6 cm thick of insulation layer. The length of tube is 51m and the inner and outer diameters are 13 mm and 16 mm, respectively. Hot water is supplied by an air source heat pump. In this study, the inlet water temperature was set to 35 ℃. The volume flow rate of supply water is controlled by means of a thermostatic valve to keep the indoor air temperature within a setpoint value.

The time-dependent air temperature, relative humidity, floor surface temperature, inlet and outlet water temperature in the tube, and water flow rate values were measured in the experimental tests. Figure 2 presents the position of the humidifier and the arrangement of measuring points. The humidifier was placed below the sensor at control point 1 (1.78 m in height along Z axis) that connected the control system and provided measured air temperature and relative humidity to be compared with the setpoint. Besides, the sensors located at points 2 and 3 were 1.1 m and 0.1 m above the floor respectively and were also used to measure the air temperature and relative humidity. According to their locations, the temperature and relative humidity gradients in vertical direction would be acquired. All measurements would be collected to process and analyze the changes occurred on the indoor environment. The characteristics of measuring instruments are given in Tab. 1.

Figure 3(a) shows the schematic diagram of the humidifier (P=18W) used in this study, which is a cool mist humidifier. Indoor air is forced through water-saturated anti-bacterial filter cartridges by an in-built ventilator. In this process, water absorbs heat from air and releases vapor to humidify the air. It is considered as an approximate constant enthalpy humidification process as shown in Fig. 3(b). The humidifier used tap water in each experiment. The tap water temperature varied from 10 ℃ to 20 ℃. A total of 4 experimental tests were carried out in the heated room, which included three experimental groups with humidification process in the conditions of three relative humidity setpoints (45%, 55%, 65%), and one control group without humidification process. Each experiment was repeated three times. The indoor temperature was maintained at 25℃ by the FHS. The setpoints of RH were selected according to CIBSE Guide A [15]

and the recommended humidity comfort range is 40%-70%. When air temperature of the heated room reached the setpoint and followed an equilibrium state, the humidifier was started to humidify air and keep the relative humidity at 45%, 55% and 65%, respectively. In the process of experiments, indoor relative humidity of the control group basically maintained around 30%. Therefore, the heated room would be dehumidified to about 30% before each experiment started.

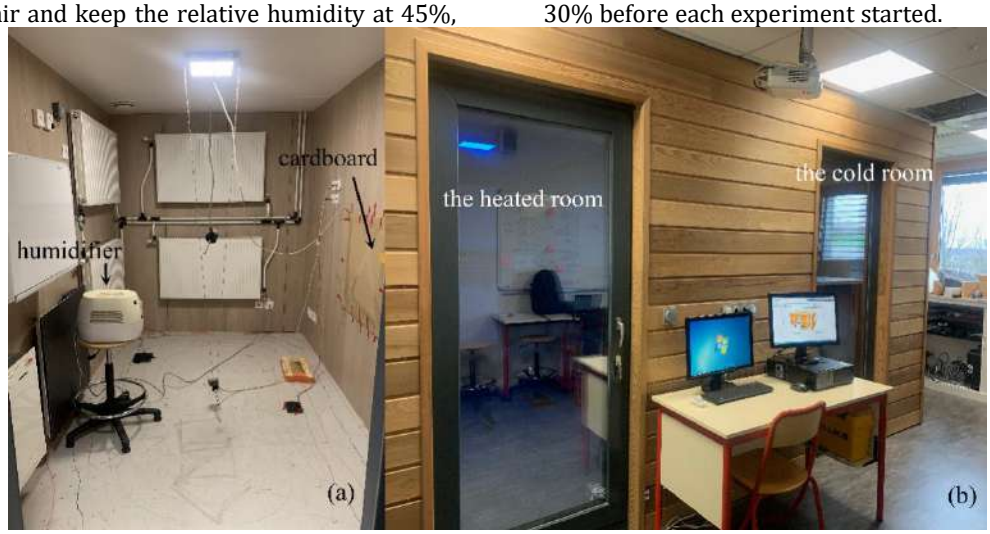

Fig. 1 - Full-scale test cell (a) Inside view of the heated room. (b) Outside view.

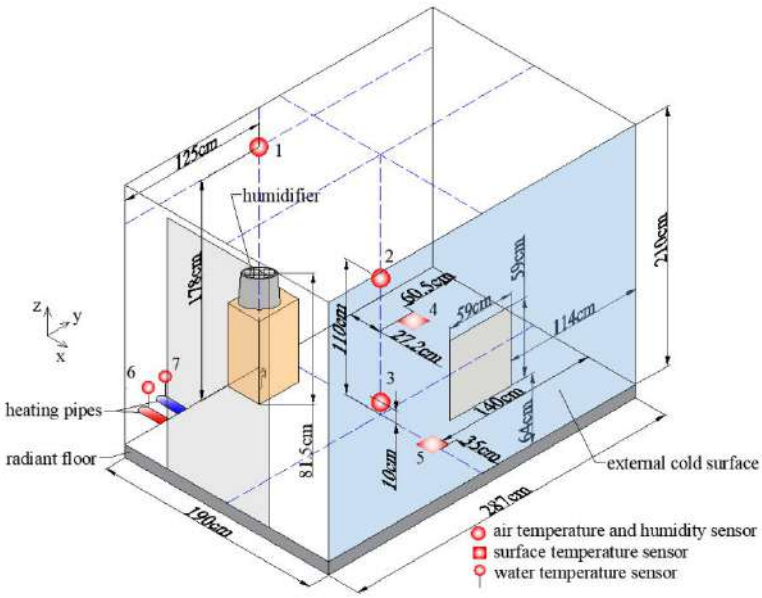

Fig. 2 - Arrangement of the measuring points in the heated room.

Tab. 1 - Measuring instruments characteristics.

Instrument	Number	Measuring points	Measuring range	Accuracy
Air RH and temperature sensor (KLH 100)	1	1	[-50, 50]°C [0, 100]%	±0.5°C at 25°C ±2% at 25°C
Air RH and temperature sensor (KLK100)	2	2, 3	[-50, 50]°C [0, 100]%	±0.5°C at 25°C ±3% at 25°C
Temperature sensor (PT 1000)	2	4, 5	[-20, 100]°C	±0.3°C at 0°C
Surface temperature sensor (TEPK PT1000)	2	6, 7	[-20, 80]°C	±0.3°C at 0°C

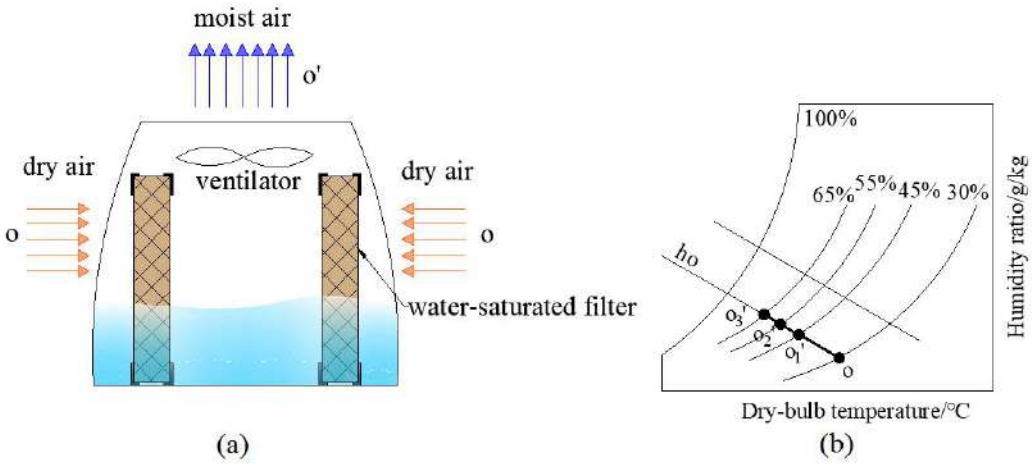

Fig. 3 - (a) Schematic diagram of the humidifier. (b) Change of state points in psychrometric chart.

3. Results and discussion

3.1 Impact of humidification process on the thermal performance of the FHS

Figure 4 illustrates the changes of average floor surface temperature, hot water volume flow rate, air temperature and RH at the control point with different setpoints of RH during the humidification process. For the control group of RH 30%, indoor thermal environment is in a dynamic equilibrium under the regulation of FHS. When the air temperature is below the setpoint, the hot water is supplied to heat the floor and the floor then transfers heat to the air through thermal convection and radiation. In this process, the volume flow rate of hot water is constant approximately around 1.8L/min. Then, when the air temperature reaches the setpoint, the inlet valve is closed. Due to the high thermal mass of the floor, there is a time delay to get the thermal response of the floor surface after hot water supplied. Therefore, the air and floor surface temperature continue to increase after the valve closed. Finally, the variations of indoor temperatures form stable fluctuating curves.

For the experimental groups, the humidification process disrupts the equilibrium described above. At the beginning, when the humidifier is turned on, the air temperature drops firstly due to the evaporative cooling effect of the humidifier and at the same time, the floor heating system is reactivated to reheat the room with a volume flow rate of more than 2L/min.

The higher is the design value of RH, the longer the cooling duration and so the air temperature is harder to return the setpoint and further more, the system feeds more hot water to heat the floor. Consequently, the maximum floor surface temperatures have exceeded 30℃ obviously, which are over the maximum limit value of 29 ℃ recommended by ASHRAE [16] in occupied-spaces for comfort reasons in terms of overheating. Ultimately, a new balance is established in the process of competition between the evaporative cooling and floor heating. The cool mist humidifier enhances the cooling of indoor environment, and therefore it could be found that in the steady state, the FHS works more frequently by supplying more hot water in the experimental groups compared to that in the control group. The floor surface temperature is obviously higher than that before humidifying. After indoor RH reaching 45% and 55%, the humidifier operates intermittently to keep the RH within a gap of ±1%. However, RH 65% is difficult to attain due to the appearance of water condensation, as a result, the humidifier is kept working.

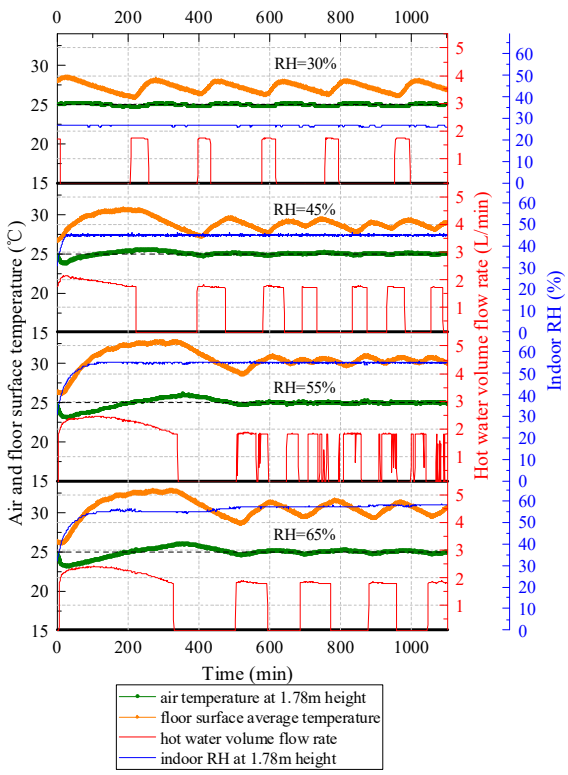

Fig. 4 - Changes of indoor environment parameters with time during the humidification process at different setpoints of RH.

3.2 Thermal comfort evaluation

This study aims to evaluate the indoor thermal comfort and energy consumption during a daytime and/or a nighttime over the humidification process in a cold and dry climate. The data for the first 12 hours was selected for analysis.

Figure 5 shows the average value of floor surface temperatures during 12 hours for different setpoints of RH. It could be found that the floor surface temperature increases following with increasing the setpoint of RH. The higher the design value of RH, the longer the cooling duration and so the system inputs more hot water to heat the floor in order to keep air temperature around the setpoint. When humidifying air to over 45%, it would lead to floor overheating based on ASHRAE [16], which gives a limit value of 29℃ marked with a black dash dot line. Therefore, floor overheating problem should be taken into account while meeting humidification needs at air temperatures of 25℃ or higher.

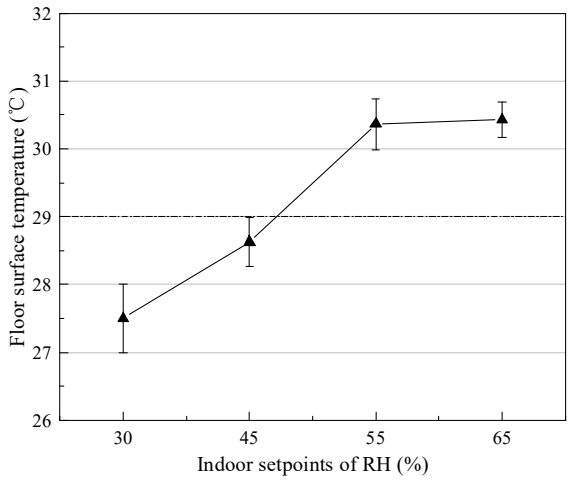

Fig. 5 - Average floor surface temperature varying with different setpoints of RH.

In this study, air temperatures and RH were measured at three different heights of 1.78m, 1.1m and 0.1m from the floor surface respectively. The average values of air temperatures and RH at the three heights were used to evaluate overall indoor temperature and RH. The non uniformities of indoor air temperature and RH distribution are amounted with the standard deviation (SD) [17] defined by equation (1). The larger SD value, the worse the uniformity of indoor air temperature or RH, and vice versa.

$$SD = \sqrt{\frac{\sum_{i=1}^{n}\left(y_i - \overline{y}\right)^2}{n}} \quad (1)$$

Where y_i is the air temperature or RH at the measuring point, $\overline{y}$ is the average air temperature or RH, n is the number of measuring points.

Figure 6(a) displays the average indoor air temperature and its non uniformity varying with different setpoints of RH. The results show that the average air temperature slightly increases with the RH increasing. The FHS regulates the air temperature based on the control point namely the measuring point at 1.78m, and thus the air temperatures at other locations away from the humidifier would be mainly influenced by the floor surface temperature. As a result, the overall indoor air temperature rises with the floor surface temperature under the influence of humidification. It ' s worth noting that the non uniformity of air temperature has significantly reduced in the experimental groups and slightly decreases with the RH set value. During the humidification process, the humidifier sucks dry air and injects the humid air into the room, which facilitates air flow and avoids air stratification so as to make air temperature distribution more uniform. Figure 6(b) shows the average indoor RH and its non uniformity varying with different setpoints of RH. The non uniformities of RH distributions for the experimental groups are larger than that of the control group and slightly increases with the RH set value. The uniformity of RH in the room during humidification process is limited by the spatial position of the humidifier. As a result, the humidification process improves the non uniformity of air temperature distribution, but at the same time brings more uneven RH distribution.

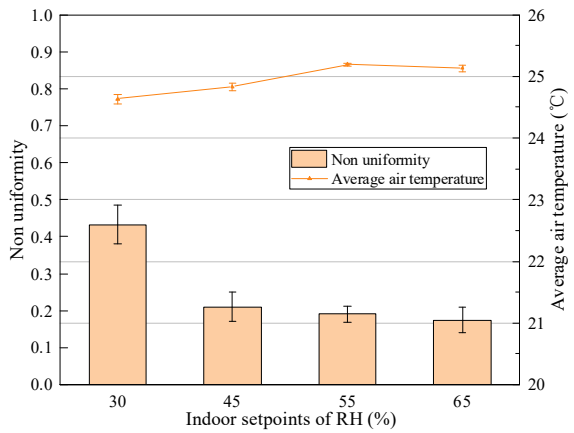

(a)

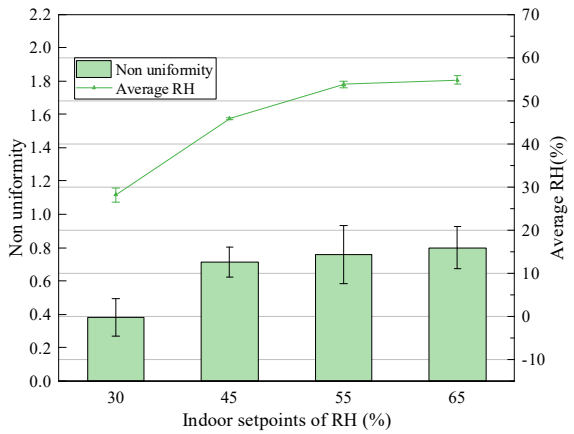

(b)

Fig. 6 - (a) Average indoor air temperature and its non uniformity varying with different setpoints of RH. (b)

Average indoor RH and its non uniformity varying with different setpoints of RH.

3.3 Energy consumption analysis

In humidification process, the energy consumption of floor heating system was evaluated by heat energy circulating hot water released. Based on the experimental data, the energy consumption was amounted by integration as shown in equations (2) and (3). The calculation range was the first 12 hours considering the daytime and/or the nighttime people used humidifiers.

$$Q = c\int_{\Delta t} \dot{m}(T_{inlet} - T_{outlet})dt \quad (2)$$

$$\dot{Q} = \frac{Q}{\Delta t} \quad (3)$$

Where Q is the released heat energy (J) and $\dot{Q}$ is the power (W), c is the specific heat of water (4.18 kJ/kg·°C), $\dot{m}$ is the mass flow rate (kg/s), T_{inlet} is the inlet water temperature (°C), T_{outlet} is the outlet water temperature (°C), and Δt is the calculation range (s).

The obtained results are shown in Fig. 7. It can be seen that the energy consumption increases following with the rising of setpoints of RH. The power consumption of control group is 146W and the power consumption of the experimental groups are 234W, 273W and 292W respectively for RH 45%, 55% and 65%. The growth rate is 60%, 87% and 100% respectively for RH 45%, 55% and 65%. Due to the cooling effect of the humidifier, the heating load of the FHS is increased in the process of humidifying the room. This effect becomes greater as the RH setpoint increases.

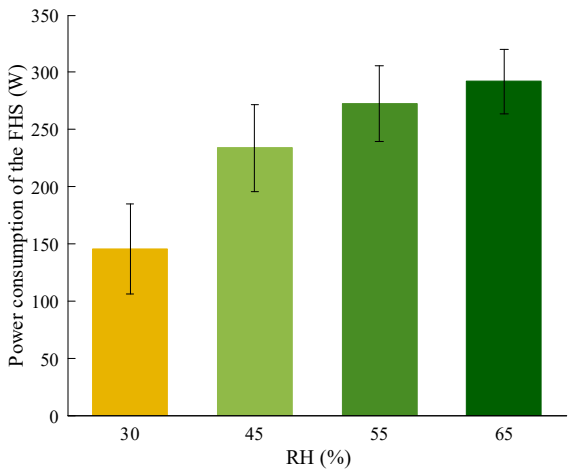

Fig. 7 - Power consumption of the floor heating system under different setpoints of RH.

4. Conclusions

This study mainly investigates the interaction between humidification process using a cool mist humidifier and the heating process using a floor heating system. The main findings are as follows:

1. The floor heating system is stimulated to reheat the room when the air temperature drops due to the evaporative cooling effect of the humidifier. The higher the design value of RH, the longer the cooling duration and so the system feeds more hot water to heat the floor. Eventually, a new balance is established in the process of competition between the evaporative cooling and floor heating.

2. The floor surface temperature increases following with the increase of RH setpoint. When indoor air temperature is 25 ℃, humidifying air to over 45% would lead to floor overheating. Therefore, floor overheating problem should be underlined while meeting humidification needs at air temperatures of 25 ℃ or higher. The non uniformity of air temperature decreases with the rising of RH setpoint, but at the same time the non uniformity of RH rises accordingly.

3. The energy consumption increases with the rising of RH setpoint. The growth rate is 60%, 87% and 100% respectively for RH 45%, 55% and 65%.

In summary, when working with a FHS at 25 ℃ air temperature setpoint, the optimal setpoint of the humidifier is RH 45%, which observably improves the non uniformity of air temperature distribution and there is no much difference even compared with 55% and 65%. Meanwhile, the non uniformity of RH and energy consumption are also lowest.

5. Acknowledgement

The authors gratefully acknowledge financial support from China Scholarship Council (No.201908120112), Grand-Est Region, Troyes Champagne Métropole, European Regional Development Fund, and EPF Foundation.

6. References

[1] ISO 7730:2005(E) [Internet]. Switzerland: ISO (the International Organization for Standardization); 2005. Annex F Humidity; [updated 2015; cited 2021]. Available from: https://www.iso.org/standard/39155.html.

[2] Sunwoo Y, Chou C, Takeshita J, et al. Physiological and subjective responses to low relative humidity in young and elderly men. J Physiol Anthropol. 2006 May;25(3):229-38.

[3] Lukcso D, Guidotti TL, Franklin DE, et al. Indoor environmental and air quality characteristics, building-related health symptoms, and worker productivity in a federal government building complex. Arch Environ Occup Health. 2016;71(2):85-101.

[4] Jin Y, Wang F, Carpenter M, et al. The effect of

indoor thermal and humidity condition on the oldest-old people's comfort and skin condition in winter. Build Environ. 2020 May;174:106790.

[5] Ma Y, Zhao Y, Liu J, et al. Effects of temperature variation and humidity on the death of COVID-19 in Wuhan, China. Sci Total Environ. 2020 Jul 1;724:138226.

[6] Biktasheva IV. Role of a habitat's air humidity in Covid-19 mortality. Sci Total Environ. 2020 Sep 20;736:138763.

[7] Kotol M, Rode C, Clausen G, et al. Indoor environment in bedrooms in 79 Greenlandic households. Build Environ. 2014 Nov;81:29–36.

[8] Fan G, Xie J, Liu J, Yoshino H. Investigation of indoor environmental quality in urban dwellings with schoolchildren in Beijing, China. Indoor Built Environ. 2017;26(5):694-716.

[9] Quinn A, Shaman J. Indoor temperature and humidity in New York City apartments during winter. Sci Total Environ. 2017 Apr 1;583:29-35.

[10] Guide A Environmental design [Internet]. London: CIBSE (the Chartered Institution of Building Services Engineers); 2015. Humidity; [updated 2019 May; cited 2021]. Available from: http://www.cibse.org/GuideA.

[11] Feng Z, Zhou X, Xu S, et al. Impacts of humidification process on indoor thermal comfort and air quality using portable ultrasonic humidifier. Build Environ. 2018 Apr;133:62–72.

[12] United States Environmental Protection Agency. ENERGY STAR Market & Industry Scoping Report Residential Humidifiers. Washington: EPA; 2012 Oct. 21 p.

[13] Ghazikhani M, Khazaee I, Vahidifar S. Exergy analysis of two humidification process methods in air-conditioning systems. Energy Build.. 2016 Jul 15;124:129-140.

[14] Trane air conditioning manual. 75th ed. La Crosse, Wisconsin: Trane Company; 2007.

[15] Rhee K-N, Olesen BW, Kim KW. Ten questions about radiant heating and cooling systems. Build Environ. 2017;112:367-381.

[16] 2016 ASHRAE Handbook – HVAC Systems and Equipment. ASHRAE; 2016.

[17] Pu L, Li Y, Xiao F, et al. Effects of different inlet vent positions on the uniformity of humidity inside a building chamber. Energy Build.. 2014 Jan 1;76:565-571.

Data Statement

The datasets generated and analysed during the current study are not available because authors need the approval of the funders and faculty staff, but the authors will make every reasonable effort to publish them in near future.

Creating health and resilience by a dynamic indoor climate

Wouter van Marken Lichtenbelt [a], Hannah Pallubinsky [a,b], Rick Kramer [c]

[a] Dept. Of Nutrition and Movement Sciences, NUTRIM School of Nutrition and Translational Research in Metabolism, Maastricht University, NL
[b] Institute of Occupational, Social and Environmental Medicine, Medical Faculty, RWTH Aachen, D
[c] Department of the Built Environment, Eindhoven University of Technology, Eindhoven, NL

Abstract. Even today, comfort and health are still considered as synonyms in the design of the indoor climate. On top of that there is a strong focus on average-person comfort which has resulted in tightly controlled indoor air temperatures. Our studies show that regular exposure to temperatures outside the thermal neutral zone may result in significant health benefits. Exposure to cold, but also to heat, positively affects our metabolism, the cardiovascular system, and, in addition, 'trains' our resilience to extreme temperatures (heat waves and cold spells). Importantly, it is not necessary to be exposed to extreme temperatures: mild cold and mild warm environments can already elicit beneficial health effects. Translating these insights to the built environment leads to the concept of dynamic indoor conditions. Here, we show that a dynamic indoor climate is acceptable or even pleasant and will contribute to a healthy indoor environment and, because of less strict climate control, will result in lower building energy consumption.

Keywords. health, comfort, resilience, energy. **DOI:** https://doi.org/10.34641/clima.2022.232

1. Introduction

Our indoor climate generally is strictly controlled around a presumed average-person comfort level. However, there is a growing amount of evidence indicating that regular exposure to temperatures outside the thermal neutral zone may result in significant metabolic health benefits. Exposure to cold, but also to heat, positively affects our metabolism, the cardiovascular system, and, in addition, 'trains' our resilience to extreme temperatures (heat waves or cold spells). Importantly, it is not necessary to be exposed to extreme temperatures: mild cold and mild warm environments can already elicit beneficial health effects.

It is important to realise that it is not necessary to be exposed to extreme heat or cold. Firstly, medium-term (days-weeks) temporal excursions outside the thermal comfort zone result in acclimatization, which in turn results in increased comfort ratings. Secondly, short-term (minutes-hours) exposure to low or high temperatures in a dynamic thermal environment may be perceived as acceptable or even pleasant (evoking so-called thermal alliesthesia). Additionally, another positive result is that allowing indoor temperatures to drift within an extended range and applying seasonal adjustments to this range can substantially reduce energy consumption in the built environment.

Accordingly, the study of dynamic thermal conditions is advocated, to assess the effects of thermal dynamics in actual living conditions as well as link and integrate short-term dynamic thermal changes (additional to seasonal differences) to the adaptive comfort model. This information is needed to support the design of healthy, comfortable, and energy-friendly buildings for a sustainable future. Therefore, we conducted and are conducting controlled laboratory tests, studying the effects of dynamic indoor conditions on thermophysiology, health, and subjective comfort parameters. An overview of the results of these and ongoing studies will be presented.

2. Research Methods

In the course of the last decennia we have conducted many laboratory studies to reveal physiological and metabolic health effects of mild excursions outside the thermal neutral zone (see below) and the thermal comfort zone. This begun with exploring the effects of mild cold on human energy metabolism and metabolic health, thus the effect of a cold environment without shivering. The so-called non-shivering thermogenesis was studied in detail and led to the discovery of brown adipose tissue in adult humans [1]. Later we started studying mild heat exposure and the effect on energy metabolism, the cardiovascular system and metabolic health. Critical to the success of our studies were the measurements in the respiration/climate chambers.

Copyright ©2022 by the authors. This conference paper is published under a CC-BY-4.0 license.

2.1 Respiration chambers at Maastricht University

All of our twenty laboratory-rooms are flexible in climate settings, but five of them are specially designed climate-controlled respiration chambers (a kind of room calorimeters). These airtight chambers enable studying human energy expenditure and substrate oxidation by measuring O_2-consumption and CO_2-production under standardized conditions over a period of 12 h up to 7 days. This means that humans can be measured under relatively normal living conditions. Though confined to the room, the subjects can engage in normal daily activities such as sleeping, eating, office work, etc. The rooms (18 m^3) can be equipped with a desk with computer, TV and DVD player, a bed, sink, and toilet. Depending on the study, the room can be used as a bed room, living room or an office. The chambers are equipped with a deep-freeze toilet for collecting faeces; urine is collected separately in bottles. Three air locks provide passage for the exchange of food, collection of urine, and for sampling of blood. Physical activity of the subjects can be performed by using a cycle ergometer, a treadmill or a stepping platform. All in all, the energetics, metabolic aspects, and subjective experiences of human volunteers can be studied in great detail.

The climate is constantly controlled and monitored by an automated information system. The temperature range can be controlled from 10˚C to 45°C and the relative humidity from 20% RH to 80% RH. The rooms are equipped with a Philips SkyRibbon LED light system. The latter allows for tunable white light with correlated colour temperatures ranging from 2000 K to 10000 K, offering a maximum intensity of 1600 lux (under 4000 K). Both temperature and light conditions can also be modified by the participants within pre-set ranges. Air is re-circulated through the air conditioning unit within the enclosed compartment. This allows a circulation rate in the range of 200 – 800 m^3/h. The air can be supplied in two different ways, through mixing or displacement ventilation. For full description of the respiration chamber including technical information, see references [2, 3].

2.2 Physiology and thermal experience

Different sensors are used to assess a variety of physiological parameters during our respiration chamber studies. Core temperature is measured using telemetric pills (VitalSense, EquivitalTM, UK, or CoreTemp, HT150002; HQ, Inc. Palmetto, FL, USA). Skin temperatures are measured by means of wireless iButton dataloggers (DS-1922 L, Maxim, USA). Physical activity is measured using a three-axial accelerometer attached to predefined skin sites (MOX, Maastricht Instruments, NL or Actigraph, wGT3X-BT, USA). Depending on the study, several cardiovascular parameters are collected such as heart rate (HR) by the Polar H10 chest belt (Polar, USA) and blood pressure (Omron M6 Comfort IT, Omron Healthcare, JPN). In addition, often sweat rate is measured by Qsweat (WR medical Maplewood, USA), and skin blood perfusion by laser doppler flowmetry (PeriFlux System 5000, Perimed, SE). Muscle biopsies and blood samples are often used to reveal additional cellular and metabolic parameters.

For thermal experiences, participants fill in questionnaires: Subjective thermal sensation is evaluated using the standard 7-point ASHRAE thermal scale and a continuous visual analogue scale (VAS) is used to indicate thermal comfort. Other regularly used questionnaires are Subjective thermal preference and local thermal sensation by ASHREA 7-point scale.

Results

3.1 Thermal neutral zone

There are limited studies that link thermal comfort to thermophysiology. A classical physiological indicator for the thermal comfort range is the thermal neutral zone (TNZ) [4]. In physiology, the TNZ is defined by the thermo-physiological parameters metabolic rate and sweat production. Below the TNZ metabolic rate increases by non-shivering and shivering thermogenesis to provide extra heat to the body, and above this zone sweat production takes place to cool the body down. The TNZ determines to a large extent thermal comfort and shows considerable overlap with the thermal comfort zone, although individual variation is large [5].

3.2 Physiology and mild temperature conditions

With respect to *cold exposure* just beyond the TNZ, we have repeatedly shown, in line with some older studies [6], that body heat production increases by non-shivering thermogenesis (NST) e.g. [7, 8]. That means that in mild cold conditions the human energy balance can be influenced without noticeable shivering and without appreciable discomfort. Indeed, in both young adults and elderly we have shown experimentally that gradual temperature variations are accepted without significant discomfort [9, 10]. We also tested mild *cold acclimation*, revealing after ten days of regular cold exposure a significant increase of NST, a significant decrease in thermal discomfort and the desire to change temperature, combined with significant improvement of insulin sensitivity [11]. Our results also show a significant individual variation in NST and a variation between groups: blunted in obese and reduced in elderly [8, 12]. In general, our results clearly show metabolic and cardiovascular adaptations of our body to (mild) cold and regular cold exposure and an improved resilience to cold.

Just as some classic, active and extreme (exercise-induced) heat acclimation protocols, also passive and mild *heat acclimation* induces typical physiological adaptation [13]. Thermal acclimation is a fine-tuned process, which is why in the passive and mild heat acclimation studies, we observed typical acclimation effects to heat, but to a lesser extent as in the active

heat acclimation studies. Indeed, mild heat acclimation shows improved sweat production, improved skin blood perfusion, lowering of heart rate and blood pressure and also a lowering of the core body temperature. All these are indicators of improved heat resilience. On top of that, in line with the cold studies, we found that sugar metabolism is improved: lower blood sugar levels and improved insulin sensitivity were observed after passive mild heat acclimation [14]. Although mechanisms seem to be different, both regular exposure to cold *and* to heat reveal improved metabolic health and increased resilience to temperature extremes.

3.3 Towards dynamic indoor climates for the built environment

These results show that, due to the application of the traditional standards and the resulting small variation of the indoor climate, the human thermoregulatory system is much less challenged. This affects our metabolism and makes occupants vulnerable to temperature extremes. More frequent exposure to heat and cold has a positive effect on metabolic health and may create more resilience to these deviant temperature conditions. As described in the adaptive comfort model [15, 16], which nowadays is included in the ASHRAE standard 55, field studies show that people adapt to climatological, seasonal and daily variations in temperature and tolerate a much wider range of temperatures than prescribed by the predicted mean vote model [17] .

Integrating this adaptive model into buildings' indoor climate control results in a more dynamic indoor climate and also leads to lower energy consumption and costs for heating and cooling. However, physiological parameters and health aspects are not specifically included in the adaptive model, which underpins the need for further development of modern indoor climate standards.

Moreover, although the adaptive comfort model has changed the paradigm from maintaining a constant indoor climate to seasonal changes in temperature control, the adaptive comfort model has been designed and validated for so-called Naturally Ventilated Buildings only.

In the DYNKA research project we focus on dynamic indoor temperature conditions for offices with HVAC systems to elicit health benefits combined with energy savings. Building energy simulations have been performed to demonstrate the energy saving potential on a building level by relaxing the ambient indoor temperature requirements to NEN-EN16798 categories III and IV. The permissible operative indoor temperatures were determined based on the Running Mean Outdoor Temperature (RMOT). In this standard, the setpoints are, however, only stipulated for the Winter (RMOT<10˚C) and Summer scenario's (RMOT>15˚C). Hence, the settings for 10˚C<RMOT<15˚C were determined via interpolation. In this way, temperature ranges were constructed for HVAC-buildings analogue to the adaptive comfort model for NV buildings. To increase thermal comfort levels, a daily temperature drifting was introduced, as well as night ventilation, starting cooler and warming up gradually during the day. The building simulation models comprise office buildings of approximately 5,000 m2 and with three floors with three different years of construction: 2012, 1990 and 1970. The building simulation results were compared to reference models, with conventional thermostat setpoints of 21°C for heating and 23°C for cooling. The results showed that for category III, savings in energy demand up to 45% are possible in a climate region like the Netherlands, depending on the year of construction. For category IV the energy demand savings are up to 62%.

By aligning the indoor climate control with the dynamic thermal needs of humans and applying them in the built environment, health and thermal resilience can be improved and at the same time the energy demand of buildings can be greatly reduced, but more research is needed on balancing comfort, health and energy efficiency.

3.4 Personal control

Finally, as we described above, there are significant differences in thermal responses and thermal experiences between individuals and groups of people. It is also well known that if individuals have enough time to adapt and, secondly, have some control of their living environment, they accept larger ranges of temperatures to be exposed to. Therefore, rooms and offices may need controllable thermostats, preferably windows that can be opened, and personal control systems. Recently we have shown that a dynamic climate with 8°C variation over the day can lead to acceptable comfort, and with a PCS, this comfort was even improved. Importantly, the PCS was designed to locally affect the body temperature, without compromising the health effects of the dynamic indoor climate [18].

3. Discussion

Our results over the years clearly highlight the advantages of a dynamic indoor environment for health, resilience and for building energy savings.

For application of this knowledge, building users need to be convinced to apply this new concept. For office environments, more knowledge is needed on how alertness and productivity are affected by the dynamic climate. There are indications that productivity may be enlarged compared to a fixed indoor climate. This topic will be a next step in our study series.

Conclusions

Our studies reveal that a dynamic indoor climate can be acceptable and can contribute to a healthy indoor environment. Secondly, a dynamic indoor climate needs less strict control and therefore will result in lower building energy consumption.

4. Acknowledgements

We thank Loes Visser, Pascal Rense and Wei Luo for their contribution for collecting and interpreting data. This work was supported by EU FP7 project DIABAT (HEALTH-F2-2011-278373), Netherlands Organization for Scientific Research (NWO) (TOP 91209037), Dutch TKI Urban Energy project DYNKA (TEUE117G3L6U), and Netherlands Organization for Health Research and Development (ZonMW)/Dutch Diabetes Research Foundation (95105007).

Data sharing not applicable to this article as no datasets were generated or analysed during the current study.

5. References

[1] van Marken Lichtenbelt WD, Vanhommerig JW, Smulders NM, Drossaerts MAFL, Kemerink GJ, Bouvy ND, et al. Cold-activated brown adipose tissue in healthy adult men. New Engl J Med. 2009;360(15):1500-8.

[2] Schoffelen PFM, Westerterp KR, Saris WHM, Hoor Ft. A dual-respiration chamber system with automated calibration. J Appl Physiol. 1997;83:2064-72.

[3] Schoffelen PFM, Plasqui G. Classical experiments in whole-body metabolism: open-circuit respirometry-diluted flow chamber, hood, or facemask systems. Eur J Appl Physiol. 2018;118(1):33-49.

[4] Kingma B, Frijns A, van Marken Lichtenbelt W. The thermoneutral zone: implications for metabolic studies. Front Biosci (Elite Ed). 2012;4:1975-85.

[5] Kingma B, Marken Lichtenbelt WDv. Energy consumption in buildings and female thermal demand. Nature Climate Change. 2015;5(12):1054-6.

[6] Dauncey MJ. Influence of mild cold on 24 h energy expenditure, resting metabolism and diet-induced thermogenesis. Brit J Nutr. 1981;45(2):257-67.

[7] Claessens-van Ooijen AM, Westerterp KR, Wouters L, Schoffelen PF, van Steenhoven AA, van Marken Lichtenbelt WD. Heat production and body temperature during cooling and rewarming in overweight and lean men. Obesity (Silver Spring). 2006;14(11):1914-20.

[8] Wijers SL, Saris W, van Marken Lichtenbelt WD. Cold Induced Adaptive Thermogenesis in Lean and Obese. Obesity. 2010;18:1092-9.

[9] Schellen L, van Marken Lichtenbelt WD, Loomans MG, Toftum J, de Wit MH. Differences between young adults and elderly in thermal comfort, productivity, and thermal physiology in response to a moderate temperature drift and a steady-state condition. Indoor air. 2010;20(4):273-83.

[10] Ivanova YM, Pallubinsky H, Kramer R, van Marken Lichtenbelt W. The influence of a moderate temperature drift on thermal physiology and perception. Physiology & behavior. 2021;229:113257.

[11] Hanssen MJ, Hoeks J, Brans B, van der Lans AA, Schaart G, van den Driessche JJ, et al. Short-term cold acclimation improves insulin sensitivity in patients with type 2 diabetes mellitus. Nat Med. 2015;21(8):863-5.

[12] Kingma BR, Frijns AJ, Saris WH, van Steenhoven AA, van Marken Lichtenbelt WD. Increased systolic blood pressure after mild cold and rewarming: relation to cold-induced thermogenesis and age. Acta Physiol. 2011;203(4):419-27.

[13] Pallubinsky H, Schellen L, Kingma BRM, Dautzenberg B, van Baak MA, van Marken Lichtenbelt WD. Thermophysiological adaptations to passive mild heat acclimation. Temperature (Austin). 2017;4(2):176-86.

[14] Pallubinsky H, Phielix E, Dautzenberg B, Schaart G, Connell NJ, de Wit-Verheggen V, et al. Passive exposure to heat improves glucose metabolism in overweight humans. Acta physiologica (Oxford, England). 2020.

[15] Nicol JF, Humphreys MA. Adaptive thermal comfort and sustainable thermalstandards for buildings. Energy and Buildings. 2002;34:563-72.

[16] de Dear RJ, Brager GS. Developing an adaptive model of thermal comfort and preference. ASHRAE Transactions. 1998;104(1a):145-67.

[17] Fanger PO. Thermal comfort. New York: Danish Technical University; 1970.

[18] Luo W, Kramer R, Kort Yd, Rense P, van MLWD. The effects of a novel personal comfort system on thermal comfort, physiology and perceived indoor environmental quality, and its health implications -Stimulating human thermoregulation without compromising thermal comfort. 2021;Indoor Air.

Productivity prediction via human physiological signals for an optimum thermal environment

Dongwoo (Jason) Yeom [a], Taegeun Kim [b], Sung-Guk Yoon [c]

[a] Architecture, The Design School, Arizona State University, Tempe, Arizona, USA, d.yeom@asu.edu

[b] Department of Electrical Engineering, Soongsil University, Seoul, Korea, taegeun1520@soongsil.ac.kr

[c] Department of Electrical Engineering, Soongsil University, Seoul, Korea, sgyoon@ssu.ac.kr

Abstract. This study aims to understand the relationship between indoor temperature, physiological signals, thermal sensation, and productivity and to estimate the occupant's productivity. A series of human experiments were conducted with 48 participants, and local skin temperatures, heart rate, and thermal sensation data were collected in 6 temperature conditions. OSPAN (Operation Span Task) was used to measure the occupant's productivity and the LightGBM algorithm was used to generate a predictive model. The result verified that there is a significant correlation between certain local body skin temperatures and the occupant's productivity, and the overall thermal sensation between high and low performing groups was significantly different by gender and BMI groups. The result suggested gender, BMI, and two local skin temperatures as effective factors to predict the occupant's productivity.

Keywords. Thermal comfort, Productivity, OSPAN, Physiological signal, LightGBM
DOI: https://doi.org/10.34641/clima.2022.233

1. Introduction

People spend most of their time indoors these days which were extended further due to the ongoing pandemic [1], and the indoor environment quality became more critical for the occupant's health and productivity in the buildings. Many studies demonstrated that the thermal environment has a strong impact on the occupant's emotions, behaviors, and productivity [2], and a comfortable indoor thermal environment showed a positive relationship with the occupant's given task [3,4].

Currently, predefined models, such as PMV, are used to control the thermal environment of the buildings. However, it doesn't consider individual occupant's characteristics and preferences, thus it has shown limitations to satisfy each occupant's preference and improve their productivity [5]. Considering thermal environment control, human physiological signal, such as local body skin temperature, heart rate, and EEG, has a significant impact on the occupant's thermal sensation [6] and it was also verified as an effective factor to predict the occupant's thermal sensation and comfort [7–9]. However, only a few studies dealt with the human physiological signals, thermal sensation, and the occupant's productivity under limited experiment conditions, thus further studies are required. Therefore, the purpose of this study is to investigate a relationship between indoor temperature, human physiological signals, thermal sensation, and productivity and to establish a productivity prediction model as a function of the occupant's physiological signals.

2. Methodology

2.1 Experiment equipment

The list of the sensors and their specifications are described in Table 1. A dry-bulb temperature and relative humidity were recorded by HOBO sensors, and a wire-type surface temperature sensor was used to measure the participant's skin temperature. A chest band type sensor was used to monitor the heart rate. The collected data was recorded on the laptop.

Tab. 1 – Specifications for data collection devices.

Device	Model	Specification
Dry bulb temp.	U12-012	Accuracy: ± 0.35°C (from 0 to 50°C, Resolution: 0.03°C
RH	U12-012	Accuracy: ± 2.5% (from 10 to 90%, Resolution: 0.05%)
Skin temp.	SBS-BTA	Accuracy: ± 0.5°C, Resolution: 0.03°C
HR	HER-BTA	Transmission frequency: 5kHz ±10%

Copyright ©2022 by the authors. This conference paper is published under a CC-BY-4.0 license.

2.2 Experiment room

The experiment room was located at Lawrence Technological University (LTU) in Michigan, USA. The size was 3 m (W) × 5 m (D) × 3 m (H) and there was one south-east facing window. The central HVAC system was disabled during the experiment, and the room temperature was controlled by the independent heating and cooling system with two nozzles. Each nozzle was placed at the opposite corner to prevent direct airflow to the participant, and a general office chair and desk were provided in the room (Figure 1). The Venetian blind covered the window to minimize the impact of the daylight.

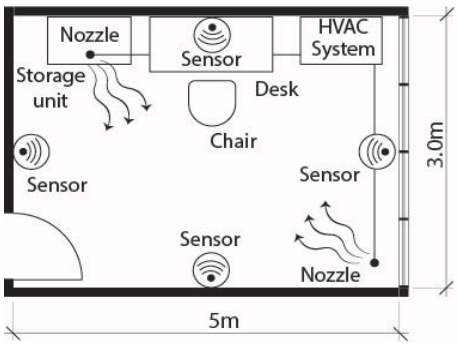

Fig. 1 – Experiment room plan.

2.3 Productivity test

Operation Span Task (OSPAN) was used to measure the participant's working memory capacity as a productivity measurement. Working memory supports temporary storage and manipulation of the information for comprehensive cognitive tasks in daily works [10], which is critical to understanding productivity. In the OSPAN, the participant needs to answer a simple math question by selecting 'Yes' or 'No' (e.g. 1+1=3, Yes or No?) and then needs to read and memorize a random letter (e.g. A or T). After a random series of math questions and letters (Maximum 6), the participant needs to select the letter (s) in chronological order. This set was repeated 20 times.

2.4 Experiment procedure

A series of human experiments were conducted that was approved by the Institutional Review Board at LTU (IRB #01418). Every participant was asked to wear basic clothes (Clo level 0.55 or 0.59; Long-sleeve tee or shirts, long pants, socks, underwear, bra). The participant was assigned to 6 experiment conditions randomly (18°C, 20°C, 22°C, 24°C, 26°C, and 28°C). The temperature was controlled the same during the experiment, and every data was recorded every minute.

Once arrived, the participant waited 20 minutes in the designated area to neutralize their physical status, while taking the survey and signing the IRB consent form. Once entered the room, the participant sat on the chair and attached the required sensors to their body spots. This study used a total of 8 local body spots (Forehead, neck, chest, arm, wrist (in), wrist (back), and belly) and heart rate as a physiological signal. When they were ready, the participant took the first survey about overall thermal sensation. The Likert 7-point scale question from the ASHRAE PMV was used (Table 2). Then, the participant took the OSPAN task and one more thermal sensation survey.

Tab. 2 – Thermal sensation questionnaire

-3	-2	-1	0	1	2	3
Cold	Cool	Slightly cool	Neutral	Slightly warm	Warm	Hot

2.5 Data analysis and predictive model

The collected data were analysed by multiple statistical methods, including T-test, correlation analysis, etc. Minitab and Microsoft Excel were used as initial analysis tools. Based on the analysis, LightGBM (Light Gradient Boosting Machine) was used to generate a predictive model. LightGBM is an improved version of the GBM model which was designed for faster training speed and high efficiency, accuracy, and to support GPU learning [11]. The boosting algorithm is an ensemble method that combines several sequential models to improve the performance of prediction or classification. The gradient boosting method is one way to adapt boosting algorithm that focuses on the important weights. LightGBM algorithm is a gradient boosting framework that uses leaf-wise tree growth algorithms. This study adapted the LightGBM classifier model to predict OSPAN performance as a function of the participants' physiological signals. The proposed model was trained in Python 3.8, TensorFlow-2.5.0 environment, and two Intel Zeon Silver 4215R CPUs, Nvidia GeForce 3090, 128G RAM Workstation were used.

3. Results and discussions

3.1 Physiological signals and thermal environment

50 participants' data were collected and 48 datasets were analysed due to the recording errors. Demographic information including age, height, and weight was surveyed and no one reported a specific health issue. Most of the participants were students in their 20s (Avg. age: 23.1). Figure 2 and 3

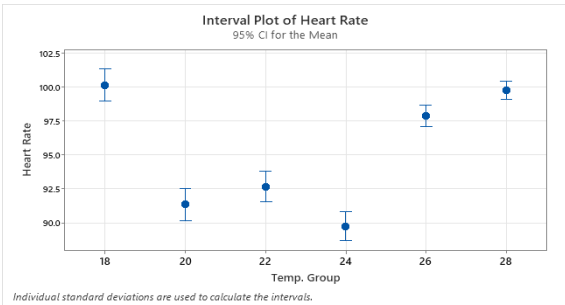

Fig. 2 – Interval plot of heart rate by the temp. group.

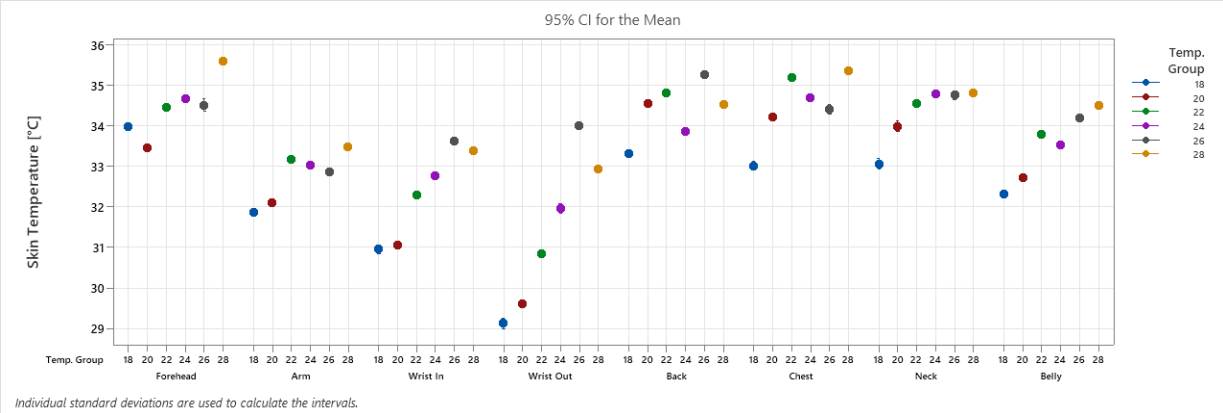

Fig. 3 – Interval plot of local body skin temperature by the temperature group.

demonstrate the interval plot of local skin temperature and heart rate by the temperature group. It shows that local body skin temperatures and heart rate increased as the indoor temperature increased mostly. The correlation analysis showed (Table 3) that all physiological signals were correlated with the indoor temperature positively ($p<0.001$). Wrist (Out) and wrist (In) showed a relatively strong correlation than the others, while heart rate showed an insignificant correlation, due to relatively high heart rate in the temp. group 18.

Tab. 3 – Correlation between temperature groups and physiological signals.

Fore head	Arm	Wrist (in)	Wrist (Out)	Heart rate
0.333	0.399	0.539	0.590	0.04
Back	Chest	Neck	Belly	
0.227	0.309	0.255	0.425	

The correlation analysis between overall thermal sensation (OTS) and physiological signals is shown in Table 4. Although it does not demonstrate general tendency, wrist (In) and wrist (Out) showed a significantly positive correlation with the OTS, demonstrating potential as an effective factor to predict thermal sensation and productivity.

Tab. 4 – Correlation between OTS groups and physiological signals.

Fore head	Arm	Wrist (in)	Wrist (Out)	Heart rate
-0.016	0.266	0.476	0.544	-0.029
Back	Chest	Neck	Belly	
0.043	0.166	-0.094	0.115	

3.2 OSPAN result

The average of the OSPAN appeared 88.5 out of 100, ranging from 55 to 100. Figure 4 demonstrates that the score is higher when the temperature is

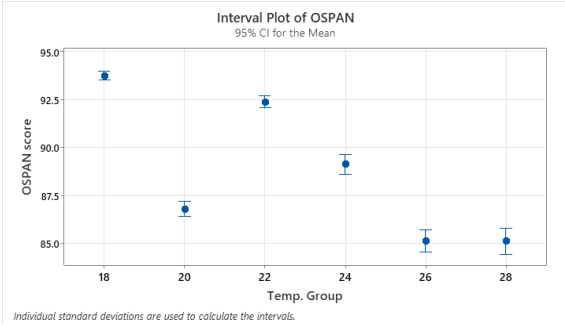

Fig. 4 – Interval plot of OSPAN score by the temperature group.

relatively low, and the correlation results verified its negative relationship (Pearson R: -0.225, $P < 0.001$). The relationship between OSPAN and OTS appeared similar which demonstrates that indoor temperature and thermal sensation are negatively correlated with the occupant's productivity.

Considering thermal comfort in the built environment, gender and BMI have a significant impact on the occupant's thermal sensation. Figure 5 shows the OSPAN score by the OTS and gender group. Both male and female groups showed higher performance when their OTS was lower, and both groups' correlations appeared negative (Pearson R – Female: -0.207, Male: -0.278).

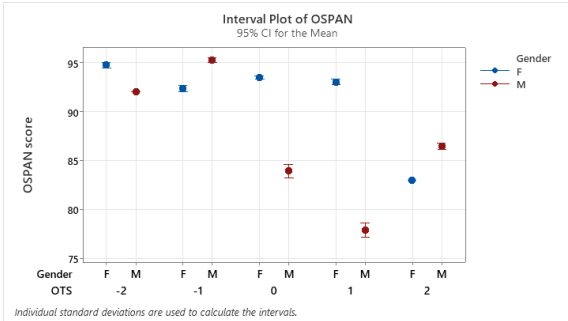

Fig. 5 – Interval plot of OSPAN score by the OTS and Gender group.

Figure 6 demonstrates the OSPAN score by the OTS and BMI groups. Both groups showed higher scores when the participants felt cool or slightly cool, and both groups' OTS were negatively correlated with the OSPAN score (Group 1: -0.269, Group 2: -0.395).

Considering the analysis result, it is clear that some human physiological signals are correlated with the occupants' thermal perception. Also, both gender and BMI affect occupant's thermal sensation, which has a significant impact on their performance on the given tasks. This demonstrates the potential of the human physiological signal as a factor to predict the occupant's thermal comfort and productivity.

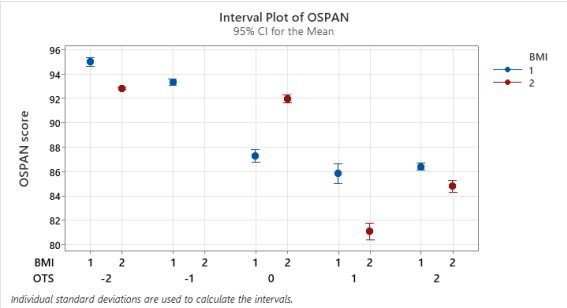

Fig. 6 – Interval plot of OSPAN score by the OTS and BMI group (1: Healthy or underweight, 2: Overweight or beyond).

3.3 Predictive model

Based on the analysis, selective datasets were used to generate a predictive model for the occupant's productivity as a function of human physiological signals. Original datasets included gender, BMI, local body skin temperatures, and heart rate as well as thermal sensation survey results. Considering that the wrist showed a relatively high correlation, as well as the practicality of the monitoring system (smartwatch and thermographic camera), wrist (Out), forehead, and heart rate was selected as input components. Also, the OSPAN score was divided into two groups, high and low performing groups, based on the average score.

Table 5 shows the components of each dataset for the LightGBM classifier. Gender and BMI were the default component in each dataset, and the other components were randomly assigned. Total 7 datasets were generated and tested to compare the predictive performance for high-performing and low-performing groups. The number of rows in the dataset was 10,075, and the number of each OSPAN group was 7,219 (High-performing) and 2,856 (Low-performing) respectively. The data was split into the training set (66%) and the test set (33%). The number of the rows in the training set's OSPAN group was 4,835 (High-performing) and 1,915 (Low-performing), and the number of the rows in the test set's OSPAN group was 2,384 (High-performing) and 941 (Low-performing) respectively.

Tab. 5 – Dataset component.

Dataset	Component	Target
Data 1	Gender, BMI, Wrist (Out)	OSPAN High / Low
Data 2	Gender, BMI, Forehead	
Data 3	Gender, BMI, Heart rate	
Data 4	Gender, BMI, Wrist (Out), Forehead	
Data 5	Gender, BMI, Wrist (Out), Heart rate	
Data 6	Gender, BMI, Forehead, Heart rate	
Data 7	Gender, BMI, Wrist (Out), Forehead, Heart rate	

Tab. 6 – Trained model accuracy.

Dataset	Accuracy (%)	Dataset	Accuracy (%)
Data 1	92.87	Data 5	95.30
Data 2	93.17	Data 6	97.14
Data 3	81.2	Data 7	99.63
Data 4	99.48		

Each dataset was used to train each model using the LightGBM algorithm. Table 6 shows the accuracy of each trained model. Overall models demonstrated relatively high predictive performance over 91% accuracy, except the model that the data 3 was used. The heart rate showed the lowest correlation to the OSPAN score in the prior analysis, thus, the accuracy appeared relatively lower than the others (81.2%). When every component was used, the accuracy was the highest at 99.63% respectively and for one component, data 2 demonstrated the highest accuracy at 93.17% respectively, among data 1 - 3. This result verifies that there is a significant relationship between certain human physiological signals and the occupant's productivity, and its

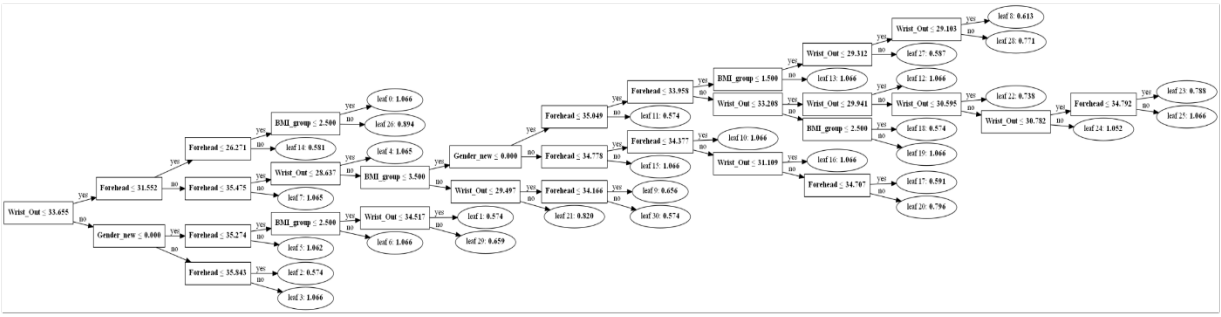

Fig. 7 – Decision tree of the dataset 4.

potential as a control factor for building's thermal environment. Considering the practicality of using a thermographic camera and smartwatch, data 4 showed the highest accuracy at 99.48% which is similar to the one from data 7. Figure 7 indicates the generated decision tree model based on dataset 4. This decision tree can be applied to the smart indoor temperature control system which can predict the occupant's productivity and provide a personalized thermal environment for the occupant's high productivity.

4. Conclusions

This study aimed to understand the relationship between indoor temperature, human physiological signals, thermal sensation, and productivity and to develop a productivity prediction model as a function of the occupant's physiological signals.

The result verified that there is a negative correlation between certain local body skin temperatures and the occupant's productivity, and the overall thermal sensation between high and low performing groups was significantly different by gender and BMI groups. The result suggested gender, BMI, and two local skin temperatures, wrist (out) and forehead, as effective factors to predict the occupant's productivity by using the LightGBM algorithm. The findings of this study can be implemented in the smart thermal environment control system to provide optimum temperature conditions for the occupants' high productivity.

As a future study, various participant groups with larger sample sizes are required for other human factors, such as age and race, to increase the validity and accuracy of the results. Also, subjective factors, such as personal thermal preferences, cultural preferences, may affect thermal perception and productivity, so these factors should be studied in the future.

5. Acknowledgement

This work was partially supported by Institute for Information & Communication Technology Planning & evaluation (IITP) grant funded by the Korea government (MSIT, No. 2021-0-01525-001). The author wants to express the gratitude to Dr. Franco Delogu for the contributions on OSPAN test.

6. References

[1] Parker K, Horowitz J, Minkin R, Arditi T. How the Coronavirus Outbreak Has-and Hasn't-Changed the Way Americans Work FOR MEDIA OR OTHER INQUIRIES. 2021;(December). Available from: www.pewresearch.org.

[2] Lan L, Lian Z, Pan L. The effects of air temperature on office workers' well-being, workload and productivity-evaluated with subjective ratings. Appl Ergon [Internet]. 2010;42(1):29–36.

[3] Sun C, Han Y, Luo L, Sun H. Effects of air temperature on cognitive work performance of acclimatized people in severely cold region in China. Indoor Built Environ. 2020;0(66):1–22.

[4] Tanabe S ichi, Haneda M, Nishihara N. Workplace productivity and individual thermal satisfaction. Build Environ [Internet]. 2015;91:42–50.

[5] Yeom DJ, Delogu F. Local body skin temperature-driven thermal sensation predictive model for the occupant's optimum productivity. Build Environ [Internet]. 2021;204(August):108196.

[6] Choi J, Loftness V, Aziz A. Post-occupancy evaluation of 20 office buildings as basis for future IEQ standards and guidelines. Energy Build. 2012 Mar;46(null):167–75.

[7] Choi J-H, Yeom D. Investigation of the relationships between thermal sensations of local body areas and the whole body in an indoor built environment. Energy Build. 2017;149.

[8] Wu Y, Liu H, Li B, Kosonen R, Wei S, Jokisalo J, et al. Individual thermal comfort prediction using classification tree model based on physiological parameters and thermal history in winter. Build Simul. 2021;

[9] Salehi B, Ghanbaran AH, Maerefat M. Intelligent models to predict the indoor thermal sensation and thermal demand in steady state based on occupants' skin temperature. Build Environ [Internet]. 2020;169(September 2019):106579.

[10] Baddeley A. Working Memory. Science (80-). 1992;255(5044):556–9.

[11] Ke G, Meng Q, Finley T, Wang T, Chen W, Ma W, et al. LightGBM: A highly efficient gradient boosting decision tree. Adv Neural Inf Process Syst. 2017;2017-Decem(Nips):3147–55.

7. Data Access Statement

The datasets analysed during the current study are not available because the extended studies are currently ongoing but the authors will make every reasonable effort to publish them in near future.

Understanding effects of ventilation on airborne microorganisms in build environments: A perspective

So Fujiyoshi [a,b], Mateja Dovjak [a,c], Janja Vaupotič [d], Fumito Maruyama [a,b]

[a] Office of Research and Academia-Government-Community Collaboration, Hiroshima University, Hiroshima, Japan.

[b] Center for Holobiome and Built environment (CHOBE), Hiroshima University, Hiroshima, Japan.

[c] Faculty of Civil and Geodetic Engineering, University of Ljubljana, Ljubljana, Slovenia.

[d] Department of Environmental Sciences, Jožef Stefan Institute, Ljubljana, Slovenia.

Corresponding email: fujiyoshi.so.62w@kyoto-u.jp

Abstract. The indoor air quality is associated with occupant productivity and a host of chronic health problems, including allergies, asthma, and depression. Ventilation is one of the solutions to improve air quality. Qualitative and quantitative characteristics of different ventilation systems, i.e., natural, mechanical and hybrid systems, might have an influence on several aspects of indoor environmental quality. As potential indoor pollutants, there are a great variety of components such as chemical substances and microbes, but our knowledge about the relationship between ventilation and microbes inhabiting the built environment is limited, including SARS-CoV-2. This limitation may partly be caused by the facts that i) methods, especially sampling of low concentration microbes from the air, for investigating indoor microbial community have not yet been established, ii) microbes in the built environment are greatly influenced by the surrounding environment and human lifestyle and behavior, and iii) different ventilation methods also affect the microbial community. The purpose of this study is to summarize the importance of airborne microorganisms in the built environment, focus on very different built environments with natural and mechanical ventilation, respectively, from a microbiological view, and attempt to find the characteristics of microbial communities in each environment. As a result, the possibilities and limitations of the current ventilation systems are highlighted, as well as tools and methods useful for analyzing airborne microbial communities, with preliminary results from our new-generation sequencer.

Keywords. Ventilation, public health, microbiome, airborne microorganism, bioaerosol.
DOI: https://doi.org/10.34641/clima.2022.60

1. Introduction

Humans spend most of their time in indoor environments, and in recent years, infections and allergic diseases caused by inhalation of indoor bioaerosols have become a problem. Deteriorated indoor air quality (IAQ) presents one of the most critical health risk factors in living and working environments, where inadequate air quality parameters (i.e., qualitative, and quantitative) might affect the health, comfort, and productivity of building occupants [1,2,3]. Several research works over the world found the strongest association of health issues with IAQ among many quality factors such as thermal comfort, noise and acoustics, and daylight in indoor environment [4]. The engineering measures and environmental health activities have to be directed toward attaining the optimal IAQ, which is an essential precondition for protecting users' health. That results in saved healthy life years [5] and decreased number of deaths, and significant economic savings [2,3]. According to the report by WHO in 2016 [5], 4.3 million people's death per year globally can be decreased if we prevent their exposure to household air pollution. Recent cost-benefit analysis has shown that costs of the poor indoor environment for the employer, the building owner, and society are often considerably higher than the cost of the energy used in the same building. Ventilation plays one of the essential roles to solve this problem. The general purpose of ventilation in buildings is to provide healthy air for breathing by both diluting the pollutants originating in the building and removing the pollutants from it [6]. Regarding selected pollutants guideline, WHO published another guideline in 2010 that considered the following substances: benzene, carbon monoxide, formaldehyde, naphthalene, nitrogen dioxide, polycyclic aromatic hydrocarbons (especially benzo[a]pyrene), radon, trichloroethylene, and

Copyright ©2022 by the authors. This conference paper is published under a CC-BY-4.0 license.

tetrachloroethylene [1]. Each pollutant was described on general description, indoor sources, pathways of exposure, indoor concentrations, indoor-outdoor relationship, kinetics and metabolism, health effects, health risk evaluation. However, there is a lack of ventilation studies, especially in the area of synergistic interactions of chemical pollutants and microbes. Therefore, we summarized the importance of airborne microorganisms in the built environment, focusing different built environments with natural and mechanical ventilation, respectively.

2. Airborne microorganisms in built environments

Microorganisms are tiny organisms (ranging from 0.002 to 100 μm in size), often single celled and invisible to the naked eye. In this perspective, when we talk about airborne microorganisms, it contains the conditions such as airborne (≤ 5 μm), droplet, and falling.

2.1 importance of airborne microorganisms

Biological agents affect building materials and the built environment as well as human health. They are widely heterogeneous, ranging from pollen and spores of plants (mainly from outdoors) to bacteria, bacterial endotoxins, archaea, fungi, algae, and some protozoa emitted outdoor and indoors. Some of the airborne algae, moulds, lichens, and mosses that grow on walls can cause the soiling of building surfaces [7] and sometimes even cause concrete degradation [8].

The air inhaled by a human typically contains 10^6 airborne microorganisms/day [9]. Among the one to ten million species of microorganisms on the earth, scientists estimate that less than one percent cause disease [10]. The rest may contribute to the ecosystem, including humans. Their mechanisms are not yet clearly understood, however, recently diversity of microbial exposure has been associated with a reduced risk of asthma, atopic dermatitis and allergic sensitization in population studies [11,12]. For example, the human gut contains microbes that are essential for digestion and to produce vitamins, antimicrobials, and neurotransmitters [13,14]. On the other hand, some fungi such as *Aspergillus versicolor*, *A. alternata*, *A. niger*, and *Penicillium* positively related to allergic diseases and asthma [15]. Also, other airborne pathogenic bacteria like *Legionella pneumophila*, *Mycobacterium*, *Micrococcus luteus*, *Staphylococcus aureus*, and the component of the exterior cell-wall of Gram-negative bacteria (endotoxins) could perform infectivity and allergenicity [16]. Influenza-infected patients generate < 20 influenza virus RNA particles per minute just by breathing [17], and it is known that each sneeze releases about 200 million virus particles [18]. A single sneeze produces about 4,600 – 40,000 microbe-filled particles at a velocity of 360 km/h, and a single cough generates about 3,000 droplets [19,20]. Just by taking these things into consideration, the quality and quantities of the airborne microorganisms in a built environment are closely related to human health both in a positive and negative way.

2.2 source of airborne microorganisms

Like our bodies, the buildings we live in are filled with microbes. Occupants, water, building materials, and ventilation are important sources of microbes in the built environment [21,22,23]. When a resident moves to a new home, it may take only a few days for his or her unique microbiome to rebuild in the new location [24]. The number of occupants (including pets and plants), gender and room specifications for activity areas (bathrooms, kitchens, etc.) affect the bacterial communities [21,25]. Scientists also found that water significantly impacts building damage and microbial growth. The number of culturable fungi was about 20 times higher in homes with moderate/heavily water damage than in homes with mildly water damage, and mould, endotoxins, and fungal glucans were detected in the environment at concentrations that could cause health effects [26]. The impact of flooding on the microbiome continued even after the relative humidity had returned to baseline and residents had removed flood-damaged items and renovated damaged rooms [27]. Ventilation is also known as one of the major sources of the indoor microbiome. Within offices, the source of ventilation air had the greatest effect on bacterial community structure [28], and at high outdoor air ventilation rates, the bacterial community in the indoor air tended to be closer to the bacterial community in the outdoor air [29,30]. Another study indicates that indoor fungal communities were originally come from outdoors [31].

3. The impact of ventilation on indoor airborne microbial communities and their concentration

3.1 microbes in a completely mechanically ventilated built environment

Theoretical analysis of housing types suggests that reduced ventilation has potential health effects, including the transmission of infectious diseases. Studies have also shown that building design affects the indoor microbial community, that mechanically ventilated buildings have lower microbial diversity than naturally ventilated buildings, and that the microbes present in mechanically ventilated buildings have a high percentage of taxa closely related to potential pathogens and a very low presence of environmental taxa [32,33]. We chose the internal space station (ISS) as a case study of an airtight built environment because there is no air outside the ISS, and outdoor sources are negligible. Mechanical ventilation is controlled to remove the target particle size range inside the ISS: the ISS filters

media, called a bacteria filter element (BFE), has a 99.97% efficiency rating in removing particles of 0.3 μm diameter. It means this filter removes bacteria and larger particles from the air before flowing into the ISS air reclamation system for reuse [34]. Of six references on microbial community analysis of the ISS, two were using swabs [35,36], one was using the contents of a vacuum cleaner bag (ISS-debris in the paper) [37], and the remaining three were using aerosol filters or HEPA filters [34,38,39]. As a result, two fungal genera, *Aspergillus* and *Penicillium*, were commonly found in all studies, both by culture methods and by using culture-independent methods with a new generation sequencer (NGS). While, in the case of bacteria, no genus was found to be common to all the study by culture method, and two genera, *Staphylococcus* and *Streptococcus*, were found to be common by NGS analysis (Tab. 1). All those four genera are ubiquitous microorganisms in built environments. *Aspergillus-Penicillium* type spores are known to be the most prevalent in the indoor air of residential properties [40]. Regarding the bacteria, these two genera have been detected as originating from humans, supporting previous research [15,16,17]. They are almost ubiquitously found in the nasal cavity for *Staphylococcus* and in the oral cavity for *Streptococcus*, suggesting that these bacteria were released from humans, especially through nasal and oral respiration. Another potentially major source of airborne microorganisms, faecal-derived species such as *Escherichia*, have not appeared as common genera. It is probably because most of these bacteria do not have desiccation tolerance, unlike *Staphylococcus* and *Streptococcus*.

Tab. 1- Commonly found fungal and bacterial genera in selected studies. Only genus-level in taxonomy data were compared.

Fungi		Bacteria	
Culture	Sequencing	Culture	Sequencing
Aspergillus	*Aspergillus*	-[a]	*Staphylococcus*
Penicillium	*Penicillium*		*Streptococcus*

a. No common bacterial genus was found in all the studies.

3.2 microbes in a highly naturally ventilated built environment

Recently, a few studies suggest that opening windows itself does not have a significant impact on the indoor airborne microbial community. This may be due to the fact that the studies were performed at homes without envelope airtightness. While it is well known that opening windows and ventilating a room primarily through outside air results in higher bacterial diversity than those with the windows are closed, and the room is ventilated using an HVAC system [28]. Also, in buildings with a large amount of outdoor air, such as traditional houses and houses in a rural area (Fig. 1), the bacterial community in the indoor air tends to be closer to the bacterial community in the outdoor air [21,41,42]. As mentioned above, the bacterial genus of *Staphylococcus* and *Streptococcus*, and the fungal genus of *Aspergillus* and *Penicillium* are common and abundant in the built environment with mechanically ventilated. It is also shown that indoor air contains significantly more potentially harmful bacteria than outdoor air [43]. While in the built environment with naturally ventilated, *Microcystis*, *Prochlorococcus*, and *Methylocella* are common bacterial genus [20]. Other studies have shown that the bacterial genera *Rhodanobacter*, *Gemmatimonas*, and *Reyranella* are more common in rural buildings [44], and *Hymenobacter* and *Solirubrobacter* are the indicator bacteria in rural areas [45].

Studies have shown associations between increased ventilation rates and improved health outcomes, including reduced incidence of influenza and asthma, and allergy symptoms [46,47]. In outdoors, the fine particles that we cannot see are almost always quickly dispersed, and when viruses released into the air are rapidly diluted, carried by wind currents, and spread over seemingly infinite space. Sunlight also inactivates the virus [48]. Exposure to certain microbes is especially important at an early age when the immune system is still developing. For example, it is known that children living in homes with pets such as dogs and cats are less likely to develop asthma and allergies than those without pets [12,49]. Unlike pathogens, there is little evidence of which microorganisms are good for health. It could be a combination of several species rather than a specific substance or microbes. In the future, if the relationship between natural ventilation and health is elucidated, we may be able to design a human- and eco-friendly ventilation system.

Fig. 1- Traditional Japanese house with a thatched roof. In summer, windows and partitions are opened, and in winter, windows are closed with the use of a wood stove.

3.3 impact of ventilation rate and types on indoor airborne microbial concentrations

There are controversial reports regarding the effect of ventilation on the airborne microorganisms. Some studies show that the effect of outdoor air ventilation rate on the concentration of bacteria and fungi in indoor air is not significant [43, 50]. On the other hand, previous studies have shown that hospital areas with natural ventilation have bioaerosol concentrations as 10 times higher than those with conventional mechanical ventilation systems [51].

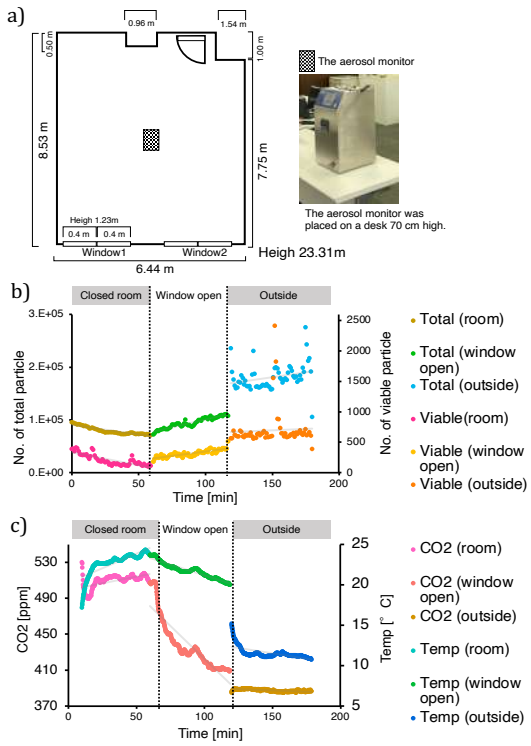

Fig. 2- a) Numbers of total particles and viable microorganisms was monitored using a real-time viable particle counter (BioTrak, TSI Inc., Shoreview, MN, USA) in a room. The room size is approximately 1,280 m^3 and there were 5 people in it. The counter was placed in the center of the room, and on a desk 70 cm high. There were two windows and one door. The area of the open window is 0.49 m^2. b) For the first 1 hour, windows and the door were closed and mechanically ventilated; for the next 1 hour, window1 and the door were opened. For the last 1 hour, the counter was placed outside and monitored. c) Temperature and CO_2 concentrations were measured using sensors RTR-576 (T&D Corp., Nagano, Japan).

Our unpublished observation also showed the ventilation from a window had an impact not only on the number of total particulate matter but also on the number of viable microorganisms. During natural ventilation with open windows for one hour, when the number of particles in the outdoor air was higher than that in the indoor air, the number of particles in the indoor air increased (Fig. 2a, b). While, both CO_2 concentration and air temperature were lower outside, and both became lower inside when windows were opened (Fig. 2c). These results indicate that particles from the outdoor air entered the room and may influence the indoor microbial concentration as well as the community composition.

4. Useful tools/methods for airborne microbial community analysis

Culture-independent methods have been developed such as fluorescent microscopy, quantitative polymerase chain reaction (qPCR), digital PCR, and metagenomic approaches targeting small subunit ribosomal RNA gene with new generation sequencer. A growing number of studies have been conducted with these new techniques, in which the concentration of bioaerosol is up to 1,000 times higher than those with conventional culture methods [52]. Furthermore, culturable bacteria account for only 1-20% of the total bacterial diversity [53]. Aerosol sampling methods are quite complicated, including impaction, impingement, filtration, gravity sampling, electrostatic precipitation, cyclone methods, thermal precipitator, and condensation technique [54]. The sampling method used for studying airborne microorganisms is important because the concentration of biomass in samples is generally low, and the yield obtained depends on the collection device, sample matrix (dry/liquid, type of medium, filter, and buffer with/without DNA/RNA later, etc.), sampling time, and speed. Although there are standard operating procedures for marine and soil environmental samples, the development of standardized protocols for bioaerosol research is still in its beginning stages. In addition, it is worth noting that the efficiency of the DNA extraction method and the purity of the obtained DNA need to be improved. The following section shows our unpublished example of the effect of different DNA extraction methods on the microbial community structure.

4.1 air sampling

Air samples were collected on the roof of the three-story building of the Faculty of Science, the University of Toyama (36°41′54″N, 137°11′13″E, 23 m above mean sea level, AMSL) in August 2017 using a Teflon membrane filter (PTFE membrane, 46.2 mm

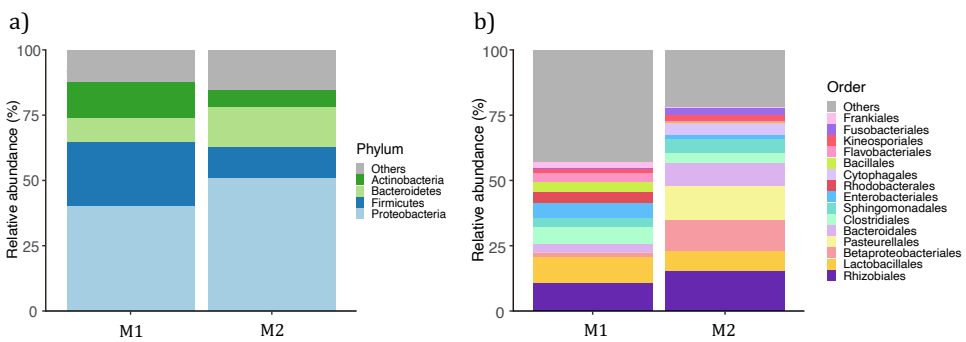

Fig. 3- Differences in DNA extraction methods and bacterial community. At the phylum level, the bacterial community was almost the same in both M1 and M2 extraction methods (a), while there was a difference in the bacterial community at the order level (b).

diameter, 2 μm pore size, GVS Japan KK, Tokyo, Japan) and slit jet air sampler (MCAS-SJ, Murata Keisokuki Service Co., Ltd., Kanagawa, Japan) at a flow rate of 30 L/min for 23 h. A total volume of 42 m^3 of air was collected. After sampling, the filter was immediately carried to the laboratory and cut in half with sterile scissors under a laminar flow cabinet.

4.2 DNA extraction

Method 1 (M1): a half-cut filter was directly placed in a bead tube of a DNeasy PowerBiofilm Kit (QIAGEN, Germantown, MD, USA) under a laminar flow cabinet, and DNA was extracted as described previously [55].

Method 2 (M2): the other part of the filter was directly placed in a bead tube of a FastDNA SPIN Kit for Soil (MP Biomedicals, Santa Ana, CA, USA) under a laminar flow cabinet, and DNA was extracted according to the manufacturer's protocol.

Each DNA sample was quantified using a DS-11FX+ Spectro/Fluorometer (DeNovix, Wilmington, USA) and a QuantiFluor™ dsDNA System (Promega, Madison, USA), and stored at −30°C until sequencing.

4.3 sequence and data analysis

PCR conditions, sequencing library constructions, sequencing using MiSeq (Illumina, San Diego, CA, USA) and a Miseq reagent kit V3 600 cycles (Illumina), taxonomic assignment with DADA2 v.1.14.1 [56] on SSU Ref tree of SILVA release v.132, data analysis with phyloseq v.1.38.0 [57] and vegan v.2.5.7 were performed as described in Yarimizu et al., 2021 [58].

4.4 DNA extraction methods result in different microbial community and diversity

In our study, the same filter sample was cut in half and DNA was extracted using different methods (M1 and M2), resulting in the different microbial community: the microbial community was similar at the phylum and class levels (Fig. 3a), but the one at the order level in taxonomy was different (Fig. 3b). Furthermore, the number of operational taxonomic units (OTUs) detected and alpha-diversity using the Shannon index, which is an index of microbial diversity based on the species richness and its evenness, differed depending on the extraction method (Fig. 4a, b). Currently, molecular biological and immunological detection methods and culture methods are mainly used for the detection of microorganisms, including pathogens [59]. Like other physicochemical metrics such as CO_2, Volatile Organic Compounds (VOC), Particulate Matter (PM), radon, temperature, and relative humidity, the ability to monitor the species and quantity of airborne microorganisms, including pathogens in real-time would facilitate rapid assessment of potential airborne microbial contamination and help improve the management and maintenance of indoor air quality.

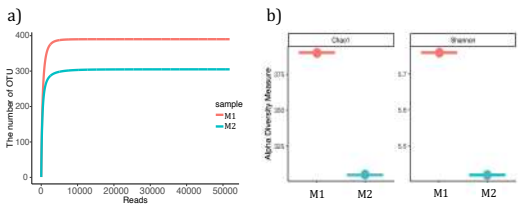

Fig. 4- Differences in the diversity of microbial community structure by DNA extraction method. Both at the OTU level (a) and in Shannon diversity (b), extraction method M1 has a higher microbial diversity than that of M2.

5. Conclusion

This study systematically reviewed recent papers to elucidate the impact of mechanical/natural ventilation on the type and concentration of indoor airborne microorganisms. The fact that a mechanically ventilated-only built environment does not differ significantly from the microbes that appear in a typical built environment suggests mechanical ventilation works well to maintain airborne microorganisms in some parts. Recently, energy-efficient buildings with high building airtightness and minimal ventilation are increasingly being used as eco-friendly homes. Regarding the effect of ventilation on the airborne microbial community, there are controversial reports to maintain the microbial diversity in such high airtightness-built environments. Through our reviewing the conflicting reports, we measured the concentration of indoor airborne microorganisms, resulting in that natural ventilation affects indoor microbial concentrations. In addition, the composition of the microbial species varied greatly depending on the DNA extraction method, indicating that methodological standardization is a first essential step for indoor airborne microbiological analysis. Qualitative and quantitative monitoring of airborne microorganisms in the built environment is important from the perspective of public health, and the first priority should be to establish systems that allow constant monitoring of microbial concentrations in airborne particle counts like physicochemical factors such as CO_2, temperature, relative humidity, daylight, radon, etc., and periodically (e.g., seasonally or annually) analyse the dynamics of airborne microbial communities including pathogens. The built environment, which is said to be good for human health, may not be a closed system. In order to understand the fluctuations of airborne microbial communities in the built environment, comprehensive research is needed on the dynamics of suspended particles, human behaviour, living space, neighbourhoods, and architectural design as a "meta-community" [60] that considers the entire community as an ecosystem. We are currently working on expanding the local and global bioaerosol research network through CHOBE (Center for Holobiome and Built Environment) [61] and BioskyNet [62]. In the future, further development of glocal (global + local) aerosol research and the definition of a "healthy" indoor and outdoor microbiome will open the window to a more comfortable and healthier living environment.

6. Acknowledgement

This work was supported by the Japanese Society for the Promotion of Science under Grants-in-Aid for Scientific Research (KAKENHI) (grant number 20K18903 to S.F.), the Japanese Agency for Medical Research and Development (grant number 20wm0225012h0001/21fk0108129h0502 awarded grants to F.M.), 2021 Japan Prize Foundation Heisei Memorial Research Grant Program, and 2021 RIKEN-Hiroshima Univ. Science & Technology Hub Collaboration Program. The authors also acknowledge the financial support from the Slovenian Research Agency (research core funding No. P2-0158, Structural engineering and building physics; No. P1-0143, Cycling of substances in the environment, mass balances, modelling of environmental processes and risk assessment).

7. References

[1] WHO. Guidelines for Indoor Air Quality. 2010. Retrieved October 10, 2018; http://www.euro.who.int/__data/assets/pdf_file/0009/128169/e94535.pdf.

[2] Wargocki P. The effects of ventilation in homes on health. Int. J. Ventilation 12. 2013;12:101–18.

[3] Wyon DP., Wargocki P. Effects of indoor environment on performance. ASHRAE Journal. 2013;46–50.

[4] Dovjak M., Kukec A. Creating healthy and sustainable buildings: an assessment of health risk factors. Cham: Springer; 2019.

[5] WHO. Household air pollution and health. 2016. Retrieved October 10, 2018; http://www.who.int/mediacentre/factsheets/fs292/en/.

[6] Awbi, HB. Ventilation of buildings. 2nd ed. New York: Taylor & Francis; 2003.

[7] Nakajima M., Masueda D., Hokoi S., Matsushita T. Airborne algal growth on roofs on membrane-structured residences in cold area of Japan. J. Building Physics. 2021;45(2):113–47.

[8] Kiledal EA., Keffer JL., Maresca JA. Bacterial communities in concrete reflect its composite nature and change with weathering. mSystems. 2021;6(3):e01153–20.

[9] Mandal J., Brandl H. Bioaerosols in indoor environment-a review with special reference to residential and occupational locations. Open Environ. Biol. Monit. J. 2011;4:83–96.

[10] Microbiology by numbers. Nat. Rev. Microbiol. 2011;9:628.

[11] Ege MJ, Mayer M, Normand AC, Genuneit J, Cookson WO, Braun-Fahrländer C, Heederik D, Piarroux R, von Mutius E; GABRIELA Transregio 22 Study Group. Exposure to environmental microorganisms and childhood asthma. N. Engl. J. Med. 2011;364(8):701–9

[12] von Mutius E., Vercelli D. Farm living: effects on childhood asthma and allergy. Nat Rev Immunol. 2010;10(12):861–8.

[13] LeBlanc JG., Milani C., de Giori GS., Sesma F., van Sinderen D., Ventura M. Bacteria as vitamin suppliers to their host: a gut microbiota perspective. Curr. Opin. Biotechnol. 2013;24(2):160–8.

[14] Lyte M. Microbial endocrinology in the microbiome-gut-brain axis: how bacterial production and utilization of neurochemicals influence behavior. PLoS Pathog. 2013;9(11):e1003726.

[15] van Tilburg Bernardes E., Gutierrez MW., Arrieta MC. The fungal microbiome and asthma. Front. Cell. Infect. Microbiol. 2020;10:583418.

[16] Song L., Zhou J., Wang C., Meng G., Li Y., Jarin M., Wu Z., Xie X. Airborne pathogenic microorganisms and air cleaning technology development: A review. J. Hazard Mater. 2022;424(Pt B):127429.

[17] Fabian P., McDevitt JJ., DeHaan WH., Fung ROP., Cowling BJ., Chan KH., Leung GM., Milton DK. Influenza Virus in Human Exhaled Breath: An Observational Study. Plos One. 2008;3(7):e2691.

[18] Lindsley WG., Pearce TA., Hudnall JB., Davis KA., Davis SM., Fisher MA., Khakoo R., Palmer JE., Clark KE., Celik I., Coffey CC., Blachere FM., Beezhold DH. Quantity and size distribution of cough-generated aerosol particles produced by influenza patients during and after illness. J. Occup. Environ. Hyg. 2012;9(7):443–9.

[19] Gralton J., Tovey E., McLaws ML., Rawlinson WD. The role of particle size in aerosolised pathogen transmission: a review. J. Infect. 2011;62(1):1–13.

[20] Wei J., Li Y. Airborne spread of infectious agents in the indoor environment. Am. J. Infect. Control. 2016;44(9)S102–8.

[21] Prussin AJ., Marr LC. Sources of airborne microorganisms in the built environment. Microbiome. 2015;3:78.

[22] Adams RI., Bhangar S., Dannemiller KC., Eisen JA., Fierer N., Gilbert JA., Green JL., Marr LC., Miller SL., Siegel JA., Stephens B., Waring MS., Bibby K. Ten questions concerning the microbiomes of buildings. Build. Environ. 2016;109(Suppl. C), 224–34.

[23] Fujiyoshi S., Tanaka D., Maruyama F. Transmission of airborne bacteria across built

environments and its measurement standards: A review. Front Microbiol. 2017;8:2336.

[24] Lax S., Smith DP., Hampton-Marcell J., Owens SM., Handley KM., Scott NM., et al. Longitudinal analysis of microbial interaction between humans and the indoor environment. Science. 2014;345:1048–52.

[25] Luongo JC., Barberán A., Hacker-Cary R., Morgan EE., Miller SL., Fierer N. Microbial analyses of airborne dust collected from dormitory rooms predict the sex of occupants. Indoor Air. 2017;27(2):338–344.

[26] Rao CY., Riggs MA., Chew GL., Muilenberg ML., Thorne PS., Van Sickle D., Dunn KH., Brown C. Characterization of airborne molds, endotoxins, and glucans in homes in New Orleans after Hurricanes Katrina and Rita. Appl Environ Microbiol. 2007;73(5):1630–4.

[27] Emerson JB., Keady PB., Brewer TE., Clements N., Morgan EE., Awerbuch J., Miller SL., Fierer N. Impacts of flood damage on airborne bacteria and fungi in homes after the 2013 Colorado Front Range flood. Environ. Sci. Technol. 2015;49(5):2675–84.

[28] Kembel SW., Meadow JF., O'Connor TK., Mhuireach G., Northcutt D., Kline J., Moriyama M., Brown GZ., Bohannan BJM., Green JL. Architectural design drives the biogeography of indoor bacterial communities. PLoS One. 2014;9:e87093.

[29] Meadow JF., Altrichter AE., Kembel SW., Kline J., Mhuireach G., Moriyama M., Northcutt D., O'Connor TK., Womack AM., Brown GZ., Green JL., Bohannan BJ. Indoor airborne bacterial communities are influenced by ventilation, occupancy, and outdoor air source. Indoor Air. 2014;24:41–8.

[30] Adams RI., Bhangar S., Pasut W., Arens EA., Taylor JW., Lindow SE., Nazaroff WW., Bruns TD. Chamber bioaerosol study: outdoor air and human occupants as sources of indoor airborne microbes. PLoS One. 2015;10:e0128022.

[31] Adams RI., Miletto M., Taylor JW., Bruns TD. Dispersal in microbes: fungi in indoor air are dominated by outdoor air and show dispersal limitation at short distances. ISME J. 2013;7(7):1262–73.

[32] Skelley ST., Gilbert JA. Studying the microbiology of the indoor environment. Genome Biol. 2013;14:202.

[33] Kembel SW., Jones E., Kline J., Northcutt D., Stenson J., Womack AM., Bohannan BJ., Brown GZ., Green JL. Architectural design influences the diversity and structure of the built environment microbiome. ISME J. 2012;6(8):1469-79.

[34] Haines SR., Bope A., Horack JM., Meyer ME., Dannemiller KC. Quantitative evaluation of bioaerosols in different particle size fractions in dust collected on the International Space Station (ISS). Appl. Microbiol. Biotechnol. 2019;103(18):7767-82.

[35] Checinska Sielaff A., Urbaniak C., Mohan GBM., Stepanov VG., Tran Q, Wood JM., Minich J., McDonald D., Mayer T., Knight R., Karouia F., Fox GE., Venkateswaran K. Characterization of the total and viable bacterial and fungal communities associated with the International Space Station surfaces. Microbiome. 2019;7(1):50.

[36] Stahl-Rommel S., Jain M., Nguyen HN., Arnold RR., Aunon-Chancellor SM., Sharp GM., Castro CL., John KK., Juul S, Turner DJ., Stoddart D., Paten B., Akeson M., Burton AS., Castro-Wallace SL. Real-time culture-independent microbial profiling onboard the International Space Station using Nanopore sequencing. Genes (Basel). 2021;12(1):106.

[37] Venkateswaran K., Vaishampayan P., Cisneros J., Pierson DL., Rogers SO., Perry J. International Space Station environmental microbiome - microbial inventories of ISS filter debris. Appl. Microbiol. Biotechnol. 2014;98(14):6453-66.

[38] Novikova N., De Boever P., Poddubko S., Deshevaya E., Polikarpov N., Rakova N., Coninx I., Mergeay M. Survey of environmental biocontamination on board the International Space Station. Res. Microbiol. 2006;157(1):5-12.

[39] Checinska A., Probst AJ., Vaishampayan P., White JR., Kumar D., Stepanov VG., Fox GE., Nilsson HR., Pierson DL., Perry J., Venkateswaran K. Microbiomes of the dust particles collected from the International Space Station and Spacecraft Assembly Facilities. Microbiome. 2015;3:50.

[40] Fairs A., Wardlaw AJ., Thompson Jr, Pashley CH. Guidelines on ambient intramural airborne fungal spores. J. Investig. Allergol. Clin. Immunol. 2010;20(6):490-8.

[41] McCall LI., Callewaert C., Zhu Q., Song SJ., Bouslimani A., Minich JJ., Ernst M., Ruiz-Calderon JF., Cavallin H., Pereira HS., Novoselac A., Hernandez J., Rios R., Branch OH., Blaser MJ., Paulino LC., Dorrestein PC., Knight R., Dominguez-Bello MG. Home chemical and microbial transitions across urbanization. Nat Microbiol. 2020;5(1):108–15.

[42] Kokubo M., Fujiyoshi S., Ogura D., Nakajima M., Fujieda A., Noda J., Maruyama F. Relationship between the microbiome and indoor temperature/humidity in a traditional Japanese house with a thatched roof in Kyoto, Japan. Diversity. 2021;13:475.

[43] Núñez A., Gracía M. Effect of the passive natural ventilation on the bioaerosol in a small room. Build. Environ. 2022;207(B):108438.

[44] Shan Y., Guo J., Fan W., Li H., Wu H., Song Y., Jalleh G., Wu W., Zhang G. Modern urbanization has reshaped the bacterial microbiome profiles of house dust in domestic environments. World Allergy Organ. J. 2020;13(8):100452.

[45] Parajuli A., Grönroos M., Siter N., Puhakka R., Vari HK., Roslund MI., Jumpponen A., Nurminen N., Laitinen OH., Hyöty H., Rajaniemi J., Sinkkonen A. Urbanization reduces transfer of diverse environmental microbiota indoors. Front. Microbiol. 2018;9:84.

[46] Seppänen OA., Fisk WJ. Summary of human responses to ventilation. Indoor Air. 2004;14:102–18.

[47] Sundell J., Levin H., Nazaroff WW., Cain WS., Fisk WJ., Grimsrud DT., Gyntelberg F., Li Y., Persily AK., Pickering AC., Samet JM., Spengler JD., Taylor ST., Weschler CJ. Ventilation rates and health: multidisciplinary review of the scientific literature. Indoor Air. 2011;21(3):191–204.

[48] Schuit M., Ratnesar-Shumate S., Yolitz J., Williams G., Weaver W., Green B., Miller D., Krause M., Beck K., Wood S., Holland B., Bohannon J., Freeburger D., Hooper I., Biryukov J., Altamura LA., Wahl V., Hevey M., Dabisch P. Airborne SARS-CoV-2 is rapidly inactivated by simulated sunlight. J. Infect. Dis. 2020;222(4):564–71.

[49] Ownby DR., Johnson CC., Peterson EL. Exposure to dogs and cats in the first year of life and risk of allergic sensitization at 6 to 7 years of age. JAMA. 2002;288(8):963–72.

[50] Kwan SE., Shaughnessy R., Haverinen-Shaughnessy U., Kwan TA., Peccia J. The impact of ventilation rate on the fungal and bacterial ecology of home indoor air. Build. Environ. 2020;177:106800.

[51] Stockwell RE., Ballard EL., O'Rourke P., Knibbs LD., Morawska L., Bell SC. Indoor hospital air and the impact of ventilation bioaerosols: a systematic review. 2019;103(2):175–84.

[52] Duquenne P. On the identification of culturable microorganisms for the assessment of biodiversity in bioaerosols. Annals of Work Exposures and Health. 2018;62(2):139–46.

[53] Ruiz-Gil T., Acuña JJ., Fujiyoshi S., Tanaka D., Noda J., Maruyama F., Jorquera MA. Airborne bacterial communities of outdoor environments and their associated influencing factors. Environ. Int. 2020;145:106156.

[54] Ghosh B., Lal H., Srivastava A. Review of bioaerosols in indoor environment with special reference to sampling, analysis and control mechanisms. Environ. Int. 2015;85:254–72.

[55] Fujiyoshi S., Nishiuchi Y., Maruyama F. Structure of bacterial communities in Japanese-style bathrooms: Comparative sequencing of bacteria in shower water and showerhead biofilms using a portable nanopore sequencer. bioRxiv. 2021.07.14.452346. doi:10.1101/2021.07.14.452346

[56] Callahan BJ., McMurdie PJ., Rosen MJ., Han AW., Johnson AJ., Holmes SP. DADA2: High-resolution sample inference from Illumina amplicon data. Nat. Methods. 2016;13(7):581–3.

[57] McMurdie PJ., Holmes S. phyloseq: an R package for reproducible interactive analysis and graphics of microbiome census data. PLoS One. 2013;8(4):e61217.

[58] Yarimizu K., Fujiyoshi S., Kawai M., Acuña JJ., Rilling JI., Campos M., Vilugrón J., Cameron H., Vergara K., Gajardo G., Espinoza-González O., Guzmán L., Nagai S., Riquelme C., Jorquera MA., Maruyama F. A standardized procedure for monitoring harmful algal blooms in Chile by metabarcoding analysis. J. Vis. Exp. 2021;174:e62967. doi:10.3791/62967

[59] Li M., Wang L., Qi W., Liu Y., Lin J. Challenges and perspectives for biosensing of bioaerosol containing pathogenic microorganisms. Micromachines. 2021;12(7):798.

[60] Lymperopoulou DS., Adams RI., Lindow SE. Contribution of vegetation to the microbial composition of nearby outdoor air. Appl. Environ. Microbiol. 2016;82(13):3822–33.

[61] Hiroshima University, Center for holobiome and built environment (CHOBE) (2020). Available: https://chobe.hiroshima-u.ac.jp/en/ Accessed: 2022.03.29

[62] UK Research and Innovation (2022). Available: https://gtr.ukri.org/projects?ref=NE%2FV008293%2F1 Accessed: 2022.03.29

Data access statement

The datasets generated during and/or analysed during the current study are available in the DDBJ repository, under the accession number DRA012566.

Monitoring the indoor environment for older people with dementia: a lesson learned

Chuan Ma [a,], Olivia Guerra-Santin [a], Anne Grave [a], Masi Mohammadi [a]*

[a] Smart Architectural Technologies, Department of the Built Environment, Eindhoven University of Technology, the Netherlands.

Email address: c.ma@tue.nl (C. Ma), o.guerra.santin@tue.nl (O. Guerra-Santin), a.j.j.grave@tue.nl (A. Grave), m.mohammadi@tue.nl (M. Mohammadi)

Abstract. Dementia is a syndrome that progressively affects cognitive, behavioural and psychological functions. People with dementia may have difficulties in sensing and expressing indoor environmental changes. Sensor technologies, such as environmental sensors, can be used to evaluate indoor environmental quality by accurately detecting the indicators, including air temperature, relative humidity, illuminance, noise level, CO_2, TVOC, and particulate matter. Monitoring these indicators for older people with dementia helps maintain their health and comfort. Moreover, some clues of behaviours and symptoms of older people with dementia could also be shown in the sensor data. This study used a mixed-method approach to find the links between indoor parameter variations and residents' activities. In a care home in the Netherlands, we collected quantitative environmental data through a sensor network deployed in bedrooms and central living rooms, and the care professionals filled qualitative data by diaries. Ten residents and two care professionals were recruited to take part in observation and diary recording. During two months monitoring campaign, care professionals selected one week that recorded five-category information on residents' daily lives: 1) building facility operation; 2) external factors; 3) details in daily lives; 4) problem behaviours or symptoms; 5) indoor comforts. By comparing the two types of data obtained, residents' wandering and sleeping problems have been found that coincide with the data fluctuations to some extent. The timing and process of these behaviours can be presented through data analysis. But more underlying factors in behavioural changes of people with dementia still require long-term observation and validation of future research.

Keywords. people with dementia, care home, indoor environmental quality, sensor, problem behaviour.
DOI: https://doi.org/10.34641/clima.2022.277

1. Introduction

In 2019, over 50 million people lived with dementia globally, and this number is steadily increasing [1]. In the Netherlands, the population diagnosed with dementia was 270,000 in 2017, and the number will rise to 520,000 in 2040 [2]. Dementia is a progressive syndrome that leads to a change in cognitive, behavioural and psychological functions [3]. Appropriate indoor environmental conditions could have positive impacts on helping delay the dementia progression and reducing problem behaviours [4]. Some studies have explored the effects of indoor environmental indicators on people with dementia. For instance, controlling the indoor air temperature in an appropriate range can alleviate agitation; long-term exposure to a dark environment could disrupt biological rhythms; overexposure to noise can cause confusion, illusions, and sleep disorders; and poor indoor air quality can accelerate the spreading of airborne diseases in care facilities [5-8]. However, the suitable ranges of these indicators and the thresholds that could trigger symptoms and problem behaviours still need to be validated.

The development of smart technologies could support older people's daily activities and monitor their safety, health, and living environment [9,10]. As the data gathering part of smart systems, sensors have a broad range of potential applications in dementia care [11]. Although indoor environmental quality is important, the majority of sensor applications are focused on monitoring the health indicators, locations, and activities of people with dementia. Moreover, the devices with cameras are not welcomed, so gathering data on older people with dementia's daily lives normally requires a relatively sophisticated sensor network, including passive infrared sensors (PIR), contact sensors, power usage sensors, pressure sensors, wearable

Copyright ©2022 by the authors. This conference paper is published under a CC-BY-4.0 license.

sensors, environmental sensors, etc. [12].

In a review study on the research that used IoT devices and sensor technologies for elderly care in the last decade, Stavropoulos et al. found that only five of them used environmental sensors in a total of fifty-three studies [13]. Directly detecting people with dementia's physical conditions, positions, and activities is essential to maintaining their health and safety. However, the impacts of indoor environmental quality cannot be ignored, which could be precipitating factors of problem behaviours and symptoms. For instance, Cremers's research showed that the restless behaviour of people with dementia coincided with peaks in the bedroom CO_2 level above 800 ppm. And this behaviour will disappear after the room has been ventilated for thirty to forty-five minutes [14]. In most cases, sensor data is only used to evaluate indoor environmental quality in a given space, and a few studies have explored the extent of indoor environmental parameter variations influencing occupants' health and well-being.

This paper describes a preliminary method to gain more insight into people with dementia's actual living conditions. We collect quantitative and qualitative data from the participants' daily lives and living environments. The study aims to find underlying factors behind these data that link indoor environmental parameters with residents' circumstances. Section 2 introduces the research methods of the case study, including data collection and analysis. Section 3 shows the findings by elaborating on two samples. Section 4 contains the discussion and conclusion.

2. Research Methods

The case study was conducted in a small-scale care facility in the Netherlands for older people with dementia. Each floor of this two-storey building consists of sixteen bedrooms, two lounges, a central living room, and a nurse station. A spacious green courtyard locates on the ground floor, and a semi-opened terrace is on the first floor. Each bedroom is equipped with a private bathroom, and the ventilation outlet is inside. The mechanical ventilation inlet is on the top of the bedroom entrance. The floor heating system supplies hot water in heating seasons or cold water in summer to cool down the indoor temperature.

Residents can furnish the interior according to personal preference, and with their own belongings, so the layouts of bedrooms were slightly different. Sensors were placed on the top of wardrobes or shelves and away from heat and light sources (Figure 1). The receiver side of sensors was toward beds, where some residents with severe dementia spend most time every day. This study collected indoor environmental data from the main activity areas of residents.

Fig. 1 - Sensors in bedrooms.

The monitoring campaign was continuously in June and July that measured indoor environmental data in ten bedrooms and two central living rooms. Table 1 shows the sensor specifications of light intensity, relative humidity, air temperature, particle matter (PM), CO_2, and total volatile organic compound (TVOC). 10 of 32 residents living in the care home participated in this study. Two care professionals were invited to record participants' information by using a designed checklist template (see Appendix), including: 1) building facility operation (curtain, light, ventilation system, window, floor-heating, and electronic devices); 2) external factors (weather and visitor number); 3) details in daily lives (mood, status, vitality, clothes, and activities); 4) problem behaviours or symptoms (agitation, depression, wandering, aggression, restless sleep, screaming, hallucinations, dry eyes, cough, chest tightness, etc.); 5) indoor comforts (thermal comfort, visual comfort, and air quality). For simplifying the tasks, icons were used instead of long texts for describing the scenarios. Care professionals could tick the proper selection or make a cross if the description was not correct. They also can write down comments or remarks if they have other findings.

Tab. 1 – Sensor specifications.

Parameter	Range	Accuracy	Resolution
Humidity	0 – 100 %	± 3 %	0.01 %
Temperature	0 - 60 °C	± 0.4 °C	0.01 °C
CO_2	400 – 2000 ppm		
TVOC	0– 600 μg/m^3		
Light	0.01 - 83k Lux		
$PM_{2.5}$	0 – 500 μg/m^3		1 μg/m^3

The diary recording started from the 19th to the 25th of June, 2021, for one week and followed the ward round schedule three times a day (8:00 to 10:00 in the morning, 14:00 to 16:00 in the afternoon, and 20:00 to 22:00 at night). Each time care professionals asked participants about their indoor comforts and observed the other required information by the checklist. The diary records were analysed by SPSS Statistics associated with environmental sensor data and local weather data (from The Royal Netherlands

Meteorological Institute) to find the links between data deviations and participants' circumstances.

3. Results

We received 184 valid records that involved ten bedrooms for approximately six days and selected one-day data of two residents living in adjacent bedrooms to show the analysis method and results. We use Resident A, B and Room A, B to refer to these two participants and their bedrooms.

By comparing the sensor data with ASHRAE Standard 55, CIBSE Guide A, and WHO air quality guidelines [15-17], the indoor environmental parameters in the care home were in the suggested ranges most of the time. The indoor air temperature was between 22 to 27 degrees Celsius, and the relative humidity was in the range of 40 to 70%. $PM_{2.5}$ was kept at a low level, and the mean value was less than 3 μg/m³. The CO_2 and TVOC concentrations and the indoor illuminance varied significantly among rooms and changing followed the time. Furthermore, the weather had obvious influences on the indoor light environment. The maximum illuminance in bedrooms was between 150 to 300 lux and matched the moderate light intensity level [18,19]. But the mean indoor illuminance value of a windy day (June 20th) was 43.2 lux, and the mean value of a rainy day was only 18.5 lux (June 21st).

Figures 2 and 3 show the data of Residents A and B and their bedrooms on the 20th of June. Both sensor and diary data were integrated into these figures. According to the diary records, Resident A had no sleeping problems but had other symptoms such as depression, cough, and bad mood since the 19th. The main activities were sitting on the sofa and watching TV in the following days. Resident A felt cold at night due to the outdoor temperature dropping from 23 to 16 degrees Celsius since the 20th. Care professionals opened the curtain and window at the first ward round in the morning for natural ventilation and light. The bedroom started getting brighter and fresher around 9 am (Figure 2). Because the window in Room A kept open from 19th to 20th, the data clearly shows the air quality parameters were low while the relative humidity and temperature had fluctuations. After the window closed on the 20th night, both CO_2 and TVOC concentrations increased significantly, but relative humidity and temperature fluctuations tended to be a straight line. This figure shows regular indoor environmental parameter changes of a room from ventilated to confined.

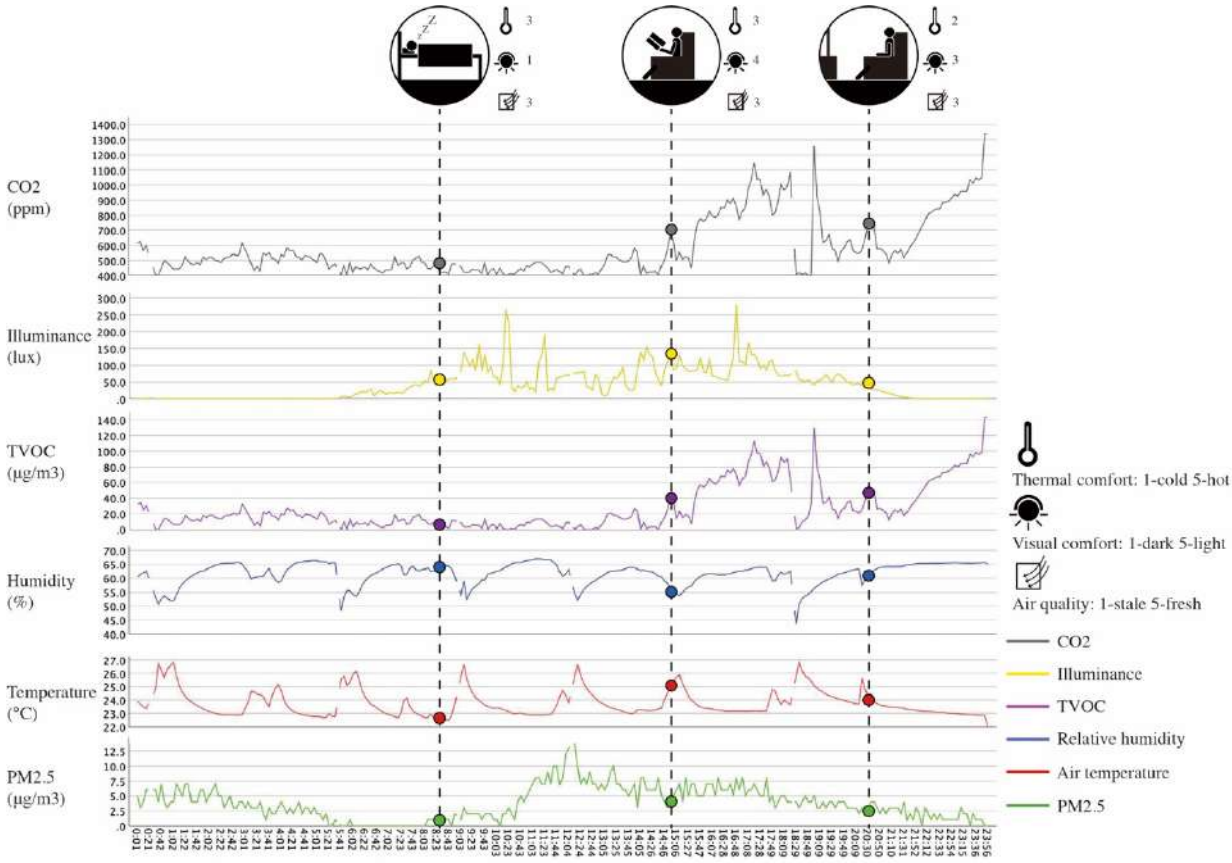

Fig. 2 - Room A and Resident A data on the 20th of June.

Resident B had sleeping problems, wandering behaviour, and joint pain. During the diary logging period, Resident B was found wandering in the care home several times when care professionals checked the room. Figure 3 shows the data of Room B on the 20th of June when the wandering behaviour of Resident B was reported. The first air quality parameter fluctuations were captured around 1:00 to 3:00 am. The CO_2 and TVOC concentration significantly increased to 2000 ppm and 280 μg/m³. Then the data decreased to 750 ppm and 50 μg/m³ from 3:00 to 6:00, while the rest parameters were stable. The second air quality parameter fluctuations

were between 7:00 to 9:00 am. The CO_2 and TVOC variation ranges were from 850 to 2350 ppm and 70 to 230 μg/m³. Resident B was found in the corridor at 8:30 and brought back to the bedroom. Then the care professional opened window and curtain that the illuminance data increased to 150 lux, and the CO_2 and TVOC concentrations dropped from 1900 ppm and 230 μg/m³ to 450 ppm and 10 μg/m³. Because the door was not closed after the last ward round on the 20th, Room B was continuously ventilated via the corridor. Air quality parameters were at low levels, and the rest parameters were stable at night. This figure shows a very different indoor variation trend than Room A.

Data and diary logging were recorded simultaneously to capture the real-life conditions of the participants and to determine the actual living scenarios. All participants living in similar indoor environments and having similar daily routines was an advantage since we could find similarities and differences by comprehensive analysis and comparison. For example, we could find different ventilation habits by comparing the data of the central living room on the same floor. We can speculate the time when Resident B was wandering into the corridor on the early morning of June 20th. The sensor data show the CO_2 level decreased significantly from 2000 ppm to 750 ppm since 2:30, and this value was close to the data (700 ppm)

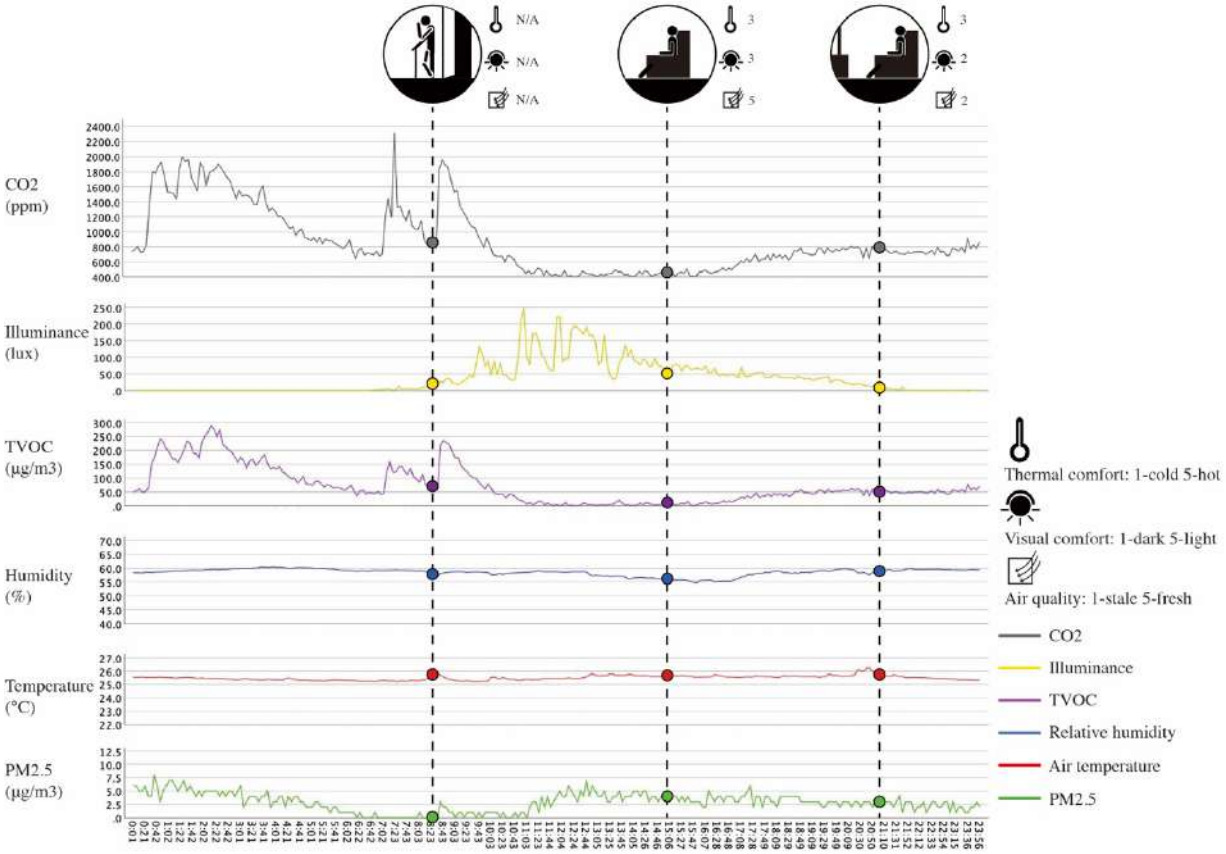

Fig. 3 - Room B and Resident B data on the 20th of June.

4. Discussion and Conclusion

Using environmental sensors to monitor people with dementia's living environments could contribute to dementia care. The proposition explored in this study was the method used to find the relationship between the circumstances of people with dementia with indoor environmental parameter changes. We assumed that the environmental data could reveal some health impacts, problem behaviours, or living details that could improve the quality and efficiency of dementia care. Therefore, this study used a mixed-method approach to continuously collect the indoor air temperature, relative humidity, illuminance, CO_2, TVOC, and particulate matter data in different rooms and capture the details of residents' living conditions at specific moments to verify the hypothesis.

monitored in the central living room at that time. Room B was ventilated via the corridor. The temperature, humidity, and illuminance had tiny fluctuations because these data were similar in the care home. Of the 16 reported sleeping problems and wandering behaviours of all participants, 11 cases happened in poorly ventilated spaces as a similar trend in Figure 3. Moreover, collecting outdoor environmental data could also benefit the study. For example, natural ventilation plays an essential role in indoor air quality. We assume that Room A kept the window open all day until the night of June 20th because its CO_2 concentration was around 450 ppm (near the outdoor level [20]). We still need to confirm our assumption by comparing indoor and outdoor data. From the diary records, we found that residents prefer to close curtains or window shades for protecting their privacy and prevent glare. If a bedroom was kept less than 50 lux on a sunny day, it could more likely indicate the resident was staying in

the room with the curtains closed. Thus, outdoor lighting data could help identify residents' occupancy.

Many limitations remained in this study due to the heavy workload of the care professionals, limited access to the residents, and the small research sample. Data from more participants filling in the diary logging, as well as a monitoring campaign across different seasons, could provide more insightful results. Evaluating residents' indoor comfort only by asking them might not be accurate if they were impatient with answering repeated questions. The diary recording frequency of each room is also open to debate. The air quality in bedrooms was usually getting worse during the night. One ward round during midnight could have improved the quality of the data. In addition, we found that many of the diaries filled in by the care professionals were not completely filled in. In 45% of them (83/184), the information regarding the dementia problem behaviours or symptoms was not completed. Most of the mood selections were neutral and happy, which seems less relevant to the indoor environmental quality. These lead us to conclude that either the care professionals did not have enough time to fill in this part due to their busy schedules or the right questions were not included in the diary. Further research is suggested to use less time-consuming data collection methods that reduce participants' workload.

Sensor placement was also a challenge for measuring the living environment of people with dementia. Data loss due to devices offline was a limitation in this study. Older people with dementia might fiddle with sensors if they are placed reachable, such as on bedside tables. The sensors used in this study were Wi-Fi-based and connected with the local Wi-Fi network. Because the routers were in central living rooms located in the middle of the building, signals in bedrooms at the end of corridors were too weak for data transmission. In this case, adding routers or using other protocol sensors, such as Zigbee, could improve the sensor network. Sensor selection and installation are suggested to consider the building layouts.

Objectively understanding the living conditions of people with dementia requires taking into account all the possibilities of data variations. For example, indoor air temperature fluctuations could be caused by heating, cooling, building insulation, or weather changes. If the temperature deviation is shown to be minor for a long time, it could mean the excellent building insulation but could also indicate the lack of natural ventilation in the room. Normally, air temperature fluctuates with air quality parameters and relative humidity in a reasonable range in a ventilated room. The behavioural habits of residents living in familiar environments usually show regular variations in environmental data. Occasional fluctuations in data are likely linked to behavioural changes. However, the connections from the diary records, such as cough, dizziness, and shivering to indoor environmental parameters still require more data and long-term observation.

Overall, the care home provided good living conditions for residents since indoor environmental parameters were basically within suggested ranges. This study provides a preliminary method to collect data from older people with dementia. By comparing and verifying the environmental sensor data with the diary records, the occurrence of some problem behaviours, such as wandering, can be revealed. With more solid evidence linking sensor data with health indicators and building environments, using sensors to monitor people with dementia's living environments could be more efficient and non-intrusive to maintain their comfort and well-being.

5. Appendices

Date and time: _____ Weather:

Room number: _____ Visitor number: _____

Building facilities and electronic devices (✓: open/on; X: closed/off)

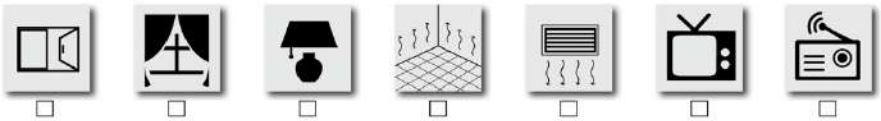

What is he/she wearing?

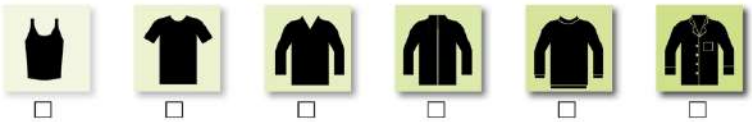

What is he/she doing?

What is his/her mood?

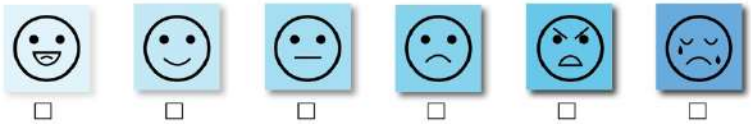

Any symptoms?

Any problem behaviours?

Agitation ☐ Aggression ☐ Restless ☐ Screaming ☐ Depression ☐ Wondering ☐ Hallucinations ☐

Additional remarks

_____

_____

_____

_____

_____

_____

_____

What is his/her thermal comfort?

Hot ☐ ☐ ☐ ☐ ☐ Cold

Neutral

What is his/her preference of the light environment?

Dark ☐ ☐ ☐ ☐ ☐ Light

Neutral

How is the indoor air quality?

Bad ☐ ☐ ☐ ☐ ☐ Good

Neutral

Other comments

_____

_____

_____

_____

_____

_____

Appendix - Diary recording template.

6. References

[1] World Alzheimer Report. World Alzheimer Report 2019, Attitudes to dementia. Alzheimer's Dis Int London [Internet]. 2019;1–15. Available from: https://www.alz.co.uk/research/world-report-2019

[2] Alzheimer Nederland. Factsheet. Cijfers en feiten over dementie. [Internet]. [Factsheet. Numbers and facts on dementia]. 2020. Available from: https://www.alzheimer-nederland.nl/%0Afactsheet-cijfers-en-feiten-over-dementietie

[3] Fadil H, Borazanci A, Ait Ben Haddou E, Yahyaoui M, Korniychuk E, Jaffe SL, et al. Chapter 13 Early Onset Dementia [Internet]. 1st ed. Vol. 84, International Review of Neurobiology. Elsevier Inc.; 2009. 245–262 p. Available from: http://dx.doi.org/10.1016/S0074-7742(09)00413-9

[4] Wong JKW, Skitmore M, Buys L, Wang K. The effects of the indoor environment of residential care homes on dementia suffers in Hong Kong: A critical incident technique approach. Build Environ [Internet]. 2014; 73:32–9. Available from: http://dx.doi.org/10.1016/j.buildenv.2013.12.001

[5] Ellis EV, Gonzalez EW, McEachron DL. Chronobioengineering indoor lighting to enhance facilities for ageing and Alzheimer's disorder. Intell Build Int. 2013;5(SUPPL1):48–60.

[6] Hayne MJ, Fleming R. Acoustic design guidelines for dementia care facilities. INTERNOISE 2014 - 43rd Int Congr Noise Control Eng Improv World Through Noise Control. 2014;1–10.

[7] Kulve M, Loomans M, Huisman E, Kort H. Indoor air in long term care facilities and spread of infectious diseases. Indoor Air 2014 - 13th Int Conf Indoor Air Qual Clim. 2014;(July):579–87.

[8] Tartarini F. Impact of temperature and indoor environmental quality in nursing homes on thermal comfort of occupants and agitation of residents with dementia. 2017;

[9] Ma C, Guerra-Santin O, Mohammadi M. Smart home modification design strategies for ageing in place: a systematic review. J Hous Built Environ [Internet]. 2021;(0123456789). Available from: https://doi.org/10.1007/s10901-021-09888-z

[10] Kwok J, Wong W, Leung JKL. Modelling factors influencing the adoption of smart-home technologies. 2016;

[11] Husebo BS, Heintz HL, Berge LI, Owoyemi P, Rahman AT, Vahia I V. Sensing technology to facilitate behavioral and psychological symptoms and to monitor treatment response in people with dementia: A systematic review. Front Pharmacol. 2020;10(February):1–13.

[12] Lotfi A, Langensiepen C, Mahmoud SM, Akhlaghinia MJ. Smart homes for the elderly dementia sufferers: Identification and prediction of abnormal behaviour. J Ambient Intell Humaniz Comput. 2012;3(3):205–18.

[13] Stavropoulos TG, Papastergiou A, Mpaltadoros L, Nikolopoulos S, Kompatsiaris I. Iot wearable sensors and devices in elderly care: A literature review. Sensors (Switzerland). 2020;20(10).

[14] Cremers B. Effect of CO on restlessness of an Alzheimer patient. 2015;(October):41–4.

[15] ANSI/ASHRAE. ANSI/ASHRAE Standard 55-2017: Thermal Environmental Conditions for Human Occupancy. ASHRAE Inc. 2017; 2017:66.

[16] CIBSE. CIBSE Guide A: Environment Design. 2008.

[17] WHO. WHO Air quality guidelines for particulate matter, ozone, nitrogen dioxide and sulfur dioxide. 2006;

[18] De Lepeleire J, Bouwen A, De Coninck L, Buntinx F. Insufficient Lighting in Nursing Homes. J Am Med Dir Assoc. 2007;8(5):314–7.

[19] Goudriaan I, van Boekel LC, Verbiest MEA, van Hoof J, Luijkx KG. Dementia enlightened?! a systematic literature review of the influence of indoor environmental light on the health of older persons with dementia in long-term care facilities. Clin Interv Aging. 2021; 16:909–37.

[20] EN 16798-2 TR. Energy performance of buildings - Indoor environmental Quality - part 2: Guideline for using indoor environmental input parameters for the design and assessment of energy performance of buildings. 2014; 2014:71.

Development of the TAIL rating scheme for indoor environmental quality in schools

Minh-Tien Tran [a,b], Wenjuan Wei [a], Claire Dassonville [a], Corinne Mandin [a], Pawel Wargocki [c,], Valérie Hequet [b]*

[a] Health and Comfort Department, Scientific and Technical Center for Building (CSTB), Marne-la-Vallée, France.

[b] IMT Atlantique, CNRS, GEPEA, UMR 6144, Nantes, France.

[c] Department of Civil Engineering Indoor Environment, Technical University of Denmark.

*Corresponding author: paw@byg.dtu.dk

Abstract. The TAIL rating scheme was developed to assess indoor environmental quality (IEQ) in offices and hotels undergoing deep renovation and was recently extended by the PredicTAIL method allowing prediction of IEQ through modeling. TAIL provides the methodology for rating the quality of the thermal, acoustic, and luminous environments, the indoor air quality, and the overall quality of the indoor environment. The present work is an extension of the use of TAIL rating scheme for school classrooms to provide necessary information for effective actions and mitigation measures to improve classroom IEQ. The TAIL was invented by examining the literature and certification schemes to identify the parameters that characterize IEQ in offices and hotels; 12 parameters were selected. A similarly pragmatic approach is followed when developing the TAIL for schools. The literature published after 2010 was surveyed to identify papers presenting measurements of IEQ in classrooms in Europe, the USA, and Australia; 75 papers were identified. Besides the 12 parameters already included in TAIL, the studies also used other parameters to characterize classroom IEQ. These parameters will be evaluated for their importance for the teaching, learning, and well-being of pupils, as well as measuring complexity, among others. Based on this assessment, the relevant parameters will be selected for inclusion in the TAIL rating for schools. The selection will be assisted using the measurements from the extensive campaign organized by the Indoor Air Quality Observatory in 308 schools and 602 classrooms in France; some of these data will be used to assess the efficacy of the TAIL for schools indicator. The relationships between the newly developed TAIL for schools, the teacher's perceptions of indoor environmental quality, and detailed building characteristics will be studied.

Keywords. Indoor environmental quality, school, classrooms, rating scheme, TAIL
DOI: https://doi.org/10.34641/clima.2022.244

1. Introduction

Four major indoor components, i.e., thermal environment, acoustics, indoor air quality (IAQ), and lighting, characterize the indoor environmental quality (IEQ); they can be associated with occupants' perception of an environment [1,2]. It has been shown that poor IEQ impacts children's comfort, health, cognitive function, and academic achievement [3,4]. These effects can be more pronounced than for adults because children's bodies and organs are under development resulting in increased sensitivity and susceptibility [5,6]. It is therefore important to secure high IEQ in schools where children spent a substantial part of their time. To date, no standard rating system has been developed to evaluate the overall IEQ in schools based on the numerous parameters measured to assess IEQ. This leads among others to the incapability to compare different measurements and make justified decisions. There is therefore an obvious need to develop a scheme for rating IEQ in schools. Recently a rating scheme for IEQ was developed for offices and hotels; it is called TAIL [7]. The TAIL scheme is a product of the European project ALDREN (ALliance for Deep RENovation in buildings, November 2017 – October 2020, https://aldren.eu/). TAIL is an abbreviation of the

Copyright ©2022 by the authors. This conference paper is published under a CC-BY-4.0 license.

four major IEQ components: Thermal, Acoustic, Indoor air quality, Lighting. The scheme allows evaluation of the quality of the components of IEQ and the overall IEQ and was shown to perform well when applied in real buildings [8]. Since TAIL is functional, it seems reasonable to investigate whether it can be also applied to evaluate IEQ in schools. This may however require modifications to account for IEQ parameters that are relevant in schools. This paper presents the first step towards adapting the TAIL scheme for assessing IEQ in schools. It presents a literature review to identify the relevant IEQ parameters to be included in the TAIL scheme for schools.

2. Materials and methods

A two-step review was performed. The first step consisted of a review of all parameters characterizing IEQ that have been measured in schools to analyse the measurement protocols to find the most effective way of measuring an IEQ parameter, taking into account the reliability, cost, and difficulty of measurement. The literature search was performed in Scopus on 24/03/2021, with the following keywords: [("indoor environmental quality" OR "IEQ" OR "thermal" OR "acoustic" OR "indoor air quality" OR "IAQ" OR "luminous" OR "visual" OR "lighting") AND ("school" OR "daycare center") AND ("Measurement")]. As there are studies that focused on only one or many components of IEQ at a time, a combination of keywords as presented here ensured that all studies of IEQ in schools and classrooms had been identified. Only studies from Europe, the United States, and Australia were selected. Only studies published in the last decade (from 2010) were considered to include the most updated measurement technologies. After removing non-relevant and duplicate articles, 75 publications on IEQ measurements in school/classroom were used for analysis.

The second step examined the relations between measured parameters and health symptoms, cognitive performance, and/or comfort. The literature search was performed in Scopus on 24/03/2021, with the following keywords: [("cognitive performance" OR "health") AND "indoor environmental quality" AND "review")]. A total of 20 publications were obtained for further analysis.

3. Results and discussion

The review shows a total of 25 IEQ parameters measured in the studies identified through the literature review. Figure 1 presents these 25 indoor parameters with their occurrence out of the 70 analysed articles. In order to be selected into the rating scheme, the parameters must have a fool-proof, simple, and deployable measurement protocol, and observed relations with health symptoms, cognitive performance, and/or comfort of occupants.

3.1 Thermal environment

Thermal comfort has an impact on children's academic performance, mental concentration, and perception [9–11]. Thermal comfort has 6 measured parameters based on the literature searches Thermal environment can be evaluated by air temperature measurement or by subjective evaluations based on questionnaires [9,11–13]. Perceived mean vote (PMV) and predicted percentage of dissatisfied (PPD) are derivative parameters that depend on air temperature, relative humidity, air velocity, mean radiant temperature, and occupant's feedback on their thermal perception, preference, metabolic rate, and clothing information. While thermal perception and preference are complex concepts to explain to children, there are studies with an innovative way of illustrating the question for children [9]. Besides, PMV and PPD being a developed model in controlled climate conditions, making results less distinctive in narrow temperature ranges [14], it is not a viable technic in extreme climate conditions [15]. This leads to the choice of thermal parameters to air temperature and relative humidity, with an example of children's learning progress enhanced with adapted thermal comfort level [16]. Air temperature and relative humidity can be measured simultaneously and continuously using a hygrometer-thermometer, preferably in 1 month and in 2 seasons (heating and non-heating season).

3.2 Acoustics

Noise in a school classroom is of concern due to its impact on children's learning and performance [17]. Studies have pointed out that acoustic quality in school is vital, as chronic exposure to high noise levels can severely hinder children's reading ability [17]; various classroom tasks involving cognitive function can also be affected [17,18]. One characteristic of a classroom is a speaking teacher and capacity of hearing and understanding of the speech of children with different physical characteristics, thus speech intelligibility is an important parameter. Children under development might find it hard to concentrate and capture every word until hearing capacity is fully matured at the age of 13-15 [19]. A bad acoustic and bad speech intelligibility can also affect teachers' vocal capacity when they tried to speak up to compensate for the bad quality [20]. There are 6 measured parameters: background noise equivalent level (dB), reverberation time (s), clarity index 50 (dB), speech transmission index (STI) (%), definition index (%) and early decay time (s). While early decay time is derived from the reverberation time, the speech transmission index parameter is dependent on reverberation time [21], so a measurement of reverberation time will not be necessary. The existing state-of-the-art instruments are capable of measuring speech intelligibility, with either an intrusive or a non-intrusive method. The intrusive method measures the receiving sound signal emitted from a source at the goal location; the result is the speech transmission index in percentage. The non-

intrusive method results in the clarity index [22], which measures the response energy level within 50 m of the emitted sound. STI can be measured with a handheld device, equipped with a test sound generator and a capture microphone. Besides STI, sound pressure level (dBa) can also be measured using a sound meter, or with sophisticated instruments such as a symphony system of speaker set up around the room with various measured microphones. Sound pressure level can be measured in the occupation period of a school week, directly in the classroom.

3.3 Indoor air quality

IAQ has 7 frequently measured parameters or group of parameters: ventilation rate, concentrations of carbon dioxide, volatile organic compounds (VOC), semi-volatile organic compounds (SVOC), particulate matter, and radon, and visual mold inspection. A high CO_2 concentration, with ventilation rate as a similar indicator, is associated with children's cognitive performance [23]. Formaldehyde and benzene are the most measured VOCs; formaldehyde can trigger acute respiratory symptoms and irritation [24], and benzene is a carcinogenic compound [25]. Many VOCs can be measured through passive sampling using a porous polymer resin to capture the compound in the air followed by laboratory analyses. SVOC measurement is mostly performed through active sampling. Particles have different size ranges: the smaller the size of particles, the more harmful they are for the respiratory system [26]. $PM_{2.5}$ represents nowadays the consensus PM indicator to measure since their health effects have been largely described. They are measured preferably by gravimetric sampling (standardized method), or by an optical counter. Radon is carcinogenic [27], and can be measured using a dosimeter exposed for two months. Indoor mold can damage the respiratory system, is an asthma-induced and exacerbations factor [16]; sick building syndrome can be also related to mold exposure [35]. Bio-contaminants can be measured by many factors, with visible mold area inspection the simplest form of characterization in a studied room and in places with high relative humidity, other than deploying a specific sampling. Another aspect to consider is the sampling locations in a school, other than the classroom for some type of school. One example is nurseries, where children spend time in the dormitory, often characterized by low ventilation and high occupancy. It is a commonplace for virus spreading [28].

3.4 Lighting quality

Lighting can cause eye strain and discomfort, or a problem of glare [29,30]. Lighting measurements in literature consist of 4 parameters: artificial illuminance, natural illuminance, daylight factor, color rendering index. The color rendering index is complex to measure and its effects on occupants' perception cannot be directly observed. The daylight factor is assessed by simulation and can provide interesting information about glare and discomfort in the classroom. In the four analysed studies, there is only one [31] with a distinction between illuminance sources. In the presence of windows blinds, they can be closed to reduce glare [32]. In this study, four measurements per spot under four lighting conditions are carried out: (a) lights on, blinds open, (b) lights off, blinds open, (c) lights on, blinds closed, (d) lights off, blinds closed. Leaving out daylight factor as a simulated parameter, and just by measuring natural light and artificial light in different locations of the room, the illuminance quality of the classroom can be assessed. Another interesting point is to look at the difference of occupant's comfort level with different types of lighting (fluorescent lamps, LED, etc.), as different types of lighting can have a different interaction with occupant's eyesight.

4. Conclusion and perspectives

Based on the literature review of 25 measured IEQ parameters in school and their impact on children's health and comfort, a proposal of 13 IEQ parameters to be included in TAIL for school are summarized in Table 1, along with the measurement protocol. The next step will be a feasibility test using measurement data from the national school survey carried out in France in 2013-2017 in 308 schools/602 classrooms. Besides the measurements of IEQ indicators, building characteristics and perception were also documented. The relations between the scores from the rating scheme and the corresponding building characteristics first, and occupants' perception secondly, will be studied. This will fully complete TAIL as an IEQ rating scheme in school and classroom. Although relatively crude, it is expected that TAIL for schools will be implemented in practice as a standard tool.

5. Figures

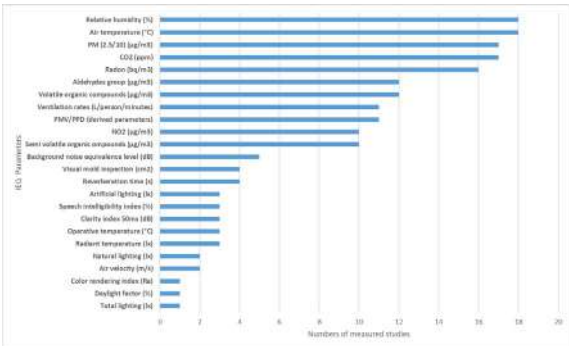

Fig. 1 – IEQ measured parameters in schools in literature.

6. Tables

Tab. 1 – Proposed list of parameters defining TAIL for schools.

Indicators	Measurement protocol (with standards)	Some documented effects on children's health, comfort and learning
Thermal environment		
Air temperature (°C)	Active measurement, 1 month duration, 1-10 minutes time interval, 0.5 °C accuracy, measurement to follow EN16798-1 standard.	Children's learning progress, mental concentration (13), occupant's thermal perception.
Air relative humidity (%)	Active measurement, 1 month duration preferably, if not Monday to Friday measurement, time interval of 1-10 minutes, calibrated sensor at 5% accuracy, comply with the EN 16798-1 standard	
Acoustic environment		
Sound pressure level (dB(A))	Active measurement, Monday to Friday, 1 min time interval, 1 db(A) accuracy, measurement to follow EN16798-1 standard.	Children's learning progress, Cognitive performance [17,33]
Speech intelligibility index (%)	Active measurement in different location in the classroom, and to follow IEC 60268-16:2020 standard	Children's learning progress, Cognitive performance [17,33]
Indoor air quality		
Ventilation rate (l/s/person)	Spot measurement at the mechanical system's supply/exhaust. Flow hood measurement to follow EN 16798-1 standard	Children's learning progress, cognitive performance [23,34]
Carbon dioxide concentration (ppm)	Active measurement using calibrated Fourier transform infrared sensor, Monday to Friday, 1-10 minutes time interval, ±50 ppm accuracy	Children's learning progress, cognitive performance [23,34]
Formaldehyde concentration (μg/m^3)	Passive measurement, Monday to Friday, a suggestion of measure in 2 critical outdoor period, measurement to be comply with ISO 16000-4:2011	Cough, asthma and allergy induced [35,36]
Benzene concentration (μg/m^3)	Passive measurement, Monday to Friday, a suggestion of measure in 2 critical outdoor period, measurement to be comply with ISO 16017-2:2003	Carcinogenic compound [25,37]
Particle (PM2.5) concentration (μg/m^3)	Preferably with gravimetric method, if not possible optical counter, Monday to Friday, suggestion of measure in 2 critical outdoor period, measurement to be comply with CEN – EN 12341:2014	Respiratory tract damage [26,38]
Radon concentration (Bq/m^3)	Passive measurement with 2 dosimeters in ground floor, 2 months duration in winter, ISO 11665-8:2013	Carcinogenic compound [27]
Visible mold area (cm^2)	Visual observation in measured room, and directly adjacent location based on relative humidity.	Asthma and asthma exacerbations [39]
Luminous environment		
Natural Illuminance (lux)	Spot measurement on 3 occasions, at morning, midday and afternoon, 5 points of measurements, 1 in the middle of the room and in the 4 corners. Sensor calibrated at ± 3lx, measurement to be comply with the EN 16798-1 standard	Headache, eyestrain, glare [29,32]
Artificial Illuminance (lux)	Spot measurement with windows blinds closed, 5 points of measurements, 1 in the middle of the room and in the 4 corners. Sensor calibrated at ± 3lx, measurement to be comply with the EN 16798-1 standard	Headache, eyestrain, glare [29,32]

7. References

1. Lee MC, Mui KW, Wong LT, Chan WY, Lee EWM, Cheung CT. Student learning performance and indoor environmental quality (IEQ) in air-conditioned university teaching rooms. Build Environ [Internet]. 2012;49(1):238–44.

2. Campano-Laborda MÁ, Domínguez-Amarillo S, Fernández-Agüera J, Acosta I. Indoor comfort and symptomatology in non-university educational buildings: Occupants' perception. Atmosphere (Basel). 2020;11(4).

3. Wu H, Wu Y, Sun X, Liu J. Combined effects of acoustic, thermal, and illumination on human perception and performance: A review. Build Environ [Internet]. 2020;169(August 2019):106593.

4. Sá JP, Branco PTBS, Alvim-Ferraz MCM, Martins FG, Sousa SIV. Children's exposure to indoor air in schools: Impact on wheezing. WIT Trans Ecol Environ. 2019;236:205–12.

5. Landrigan PJ, Kimmel CA, Correa A, Eskenazi B. Children's health and the environment: Public health issues and challenges for risk assessment. Environ Health Perspect. 2004;112(2):257–65.

6. Simoni M, Annesi-Maesano I, Sigsgaard T, Norback D, Wieslander G, Nystad W, et al. School air quality related to dry cough, rhinitis and nasal patency in children. Eur Respir J. 2010;35(4):742–9.

7. Wargocki P, Mandin C, Wei W, Espigares C, Bendzalova J, Greslou O, et al. Assessment of indoor environmental quality (IEQ) in offices and hotels undergoing deep energy renovation. REHVA J. 2019;(August):49–53.

8. Wargocki P, Wei W, Bendžalová J, Espigares-Correa C, Gerard C, Greslou O, et al. TAIL, a new scheme for rating indoor environmental quality in offices and hotels undergoing deep energy renovation (EU ALDREN project). Energy Build. 2021;244.

9. Fabbri K. Thermal comfort evaluation in kindergarten: PMV and PPD measurement through datalogger and questionnaire. Build Environ [Internet]. 2013;68:202–14.

10. Balbis-Morejón M, Rey-Hernández JM, Amaris-Castilla C, Velasco-Gómez E, San José-Alonso JF, Rey-Martínez FJ. Experimental study and analysis of thermal comfort in a university campus building in tropical climate. Sustain. 2020;12(21):1–18.

11. Papadopoulos G, Panaras G, Tolis E. Thermal comfort and Indoor Air Quality assessment in university classrooms. IOP Conf Ser Earth Environ Sci. 2020;410(1).

12. Vilcekova S, Meciarova L, Burdova EK, Katunska J, Kosicanova D, Doroudiani S. Indoor environmental quality of classrooms and occupants' comfort in a special education school in Slovak Republic. Build Environ [Internet]. 2017;120:29–40.

13. Papazoglou E, Moustris KP, Nikas KSP, Nastos PT,

Statharas JC. Assessment of human thermal comfort perception in a non-air-conditioned school building in Athens, Greece. Energy Procedia [Internet]. 2019;157(2018):1343–52.

14. Arens E, Humphreys MA, de Dear R, Zhang H. Are "class A" temperature requirements realistic or desirable? Build Environ [Internet]. 2010;45(1):4–10.

15. Hamzah B, Ishak MT, Beddu S, Osman MY. Thermal comfort analyses of naturally ventilated university classrooms. Struct Surv. 2016;34(4–5):427–45.

16. Barrett P, Davies F, Zhang Y, Barrett L. The impact of classroom design on pupils' learning: Final results ofaholistic, multi-level analysis. Build Environ [Internet]. 2015;89:118–33.

17. Shield BM, Dockrell JE. The effects of noise on children at school: A review. Build Acoust. 2003;10(2):97–116.

18. Clark C, Martin R, Van Kempen E, Alfred T, Head J, Davies HW, et al. Exposure-effect relations between aircraft and road traffic noise exposure at school and reading comprehension: The RANCH project. Am J Epidemiol. 2006;163(1):27–37.

19. Russo D, Ruggiero A. Choice of the optimal acoustic design of a school classroom and experimental verification. Appl Acoust [Internet]. 2019;146:280–7.

20. Vilkman E. Occupational safety and health aspects of voice and speech professions. Folia Phoniatr Logop. 2004;56(4):220–53.

21. Weismer G. Speech Intelligibility. Handb Clin Linguist. 2009;568–82.

22. Suzumura GGR, Moisan L, Suyama R. A Non Intrusive Audio Clarity Index (NIAC) and its Application to Blind Source Separation. 2021;

23. Wargocki P, Porras-Salazar JA, Contreras-Espinoza S, Bahnfleth W. The relationships between classroom air quality and children's performance in school. Build Environ [Internet]. 2020;173(December 2019):106749.

24. Daisey JM, Angell WJ, Apte MG. Indoor air quality, ventilation and health symptoms in schools: An analysis of existing information. Indoor Air. 2003;13(1):53–64.

25. Becerra JA, Lizana J, Gil M, Barrios-Padura A, Blondeau P, Chacartegui R. Identification of potential indoor air pollutants in schools. J Clean Prod. 2020;242.

26. Heal MR, Kumar P, Harrison RM. Particles, air quality, policy and health. Chem Soc Rev. 2012;41(19):6606–30.

27. Al-Zoughool M, Krewski D. Health effects of radon: A review of the literature. Int J Radiat Biol. 2009;85(1):57–69.

28. Yang F, Sun Y, Wang P, Weschler LB, Sundell J. Spread of respiratory infections in student dormitories in China. Sci Total Environ [Internet]. 2021;777:145983.

29. Vetter C, Pattison PM, Houser K, Herf M, Phillips AJK, Wright KP, et al. A Review of Human Physiological Responses to Light: Implications for the Development of Integrative Lighting Solutions. LEUKOS - J Illum Eng Soc North Am [Internet]. 2021;00(00):1–28.

30. Baloch RM, Maesano CN, Christoffersen J, Banerjee S, Gabriel M, Csobod É, et al. Indoor air pollution, physical and comfort parameters related to schoolchildren's health: Data from the European SINPHONIE study. Sci Total Environ. 2020;739.

31. Winterbottom M, Wilkins A. Lighting and discomfort in the classroom. J Environ Psychol [Internet]. 2009;29(1):63–75.

32. Osterhaus WKE. Discomfort glare assessment and prevention for daylight applications in office environments. Sol Energy. 2005;79(2):140–58.

33. Zhang D, Tenpierik M, Bluyssen PM. Individual control as a new way to improve classroom acoustics: A simulation-based study. Appl Acoust [Internet]. 2021;179:108066.

34. Simanic B, Nordquist B, Bagge H, Johansson D. Indoor air temperatures, CO2 concentrations and ventilation rates: Long-term measurements in newly built low-energy schools in Sweden. J Build Eng [Internet]. 2019;25(March):100827.

35. Lam J, Koustas E, Sutton P, Padula AM, Cabana MD, Vesterinen H, et al. Exposure to formaldehyde and asthma outcomes: A systematic review, meta-analysis, and economic assessment [Internet]. Vol. 16, PLoS ONE. 2021. 1–44 p.

36. Yao Y, Liang W, Zhu L, Duan Y, Jin Y, He L. Relationship between the concentration of formaldehyde in the air and asthma in children: A meta-analysis. Int J Clin Exp Med. 2015;8(6):8358–62.

37. Camacho-Montano SC, Wagner A, Erhorn-Kluttig H, Mumovic D, Summerfield A. Clearing the air on EU guidance projects for school buildings. Build Res Inf [Internet]. 2019;47(5):624–34.

38. Morawska L, Ayoko GA, Bae GN, Buonanno G, Chao CYH, Clifford S, et al. Airborne particles in indoor environment of homes, schools, offices and aged care facilities: The main routes of exposure. Environ Int. 2017;108(April):75–83.

39. Oluwole O, Kirychuk SP, Lawson JA, Karunanayake C, Cockcroft DW, Willson PJ, et al. Indoor mold levels and current asthma among school-aged children in Saskatchewan, Canada. Indoor Air. 2017;27(2):311–9.

Evaluation of students' perceptions and thermal comfort in London

Junpeng Lyu[a]
[a] The Bartlett School of Sustainable Construction, University College London (UCL), London, United Kingdom, j.lyu@ucl.ac.uk

Abstract. A thermal comfort field study was conducted in a lecture room involving 44 participants to investigate occupant perception and thermal comfort, as well as compare it with other 37 lecturer theatres. All buildings are located in a temperature climate region of the UK. Additionally, objective measurements including dry-bulb air temperature, relative humidity, and subjective responses concerning thermal sensation, thermal preference, and air velocity were additionally collected. Through Hobo measurement and a questionnaire survey in the site lecture room, we present the association linking thermal comfort and seating location. A similar tendency can be found through the comparison between the AMV values of all lecture theatres and PMV ones, which could be explained by the fact that occupants have a very limited physical adaption to their surroundings in the lecture room. Furthermore, the level of thermal comfort of the occupant sitting in the back (higher seats) is lower than that of the occupant sitting in the front row (lower seats).Through a statistical contrast of the level of thermal comfort among individuals seated at the back and front in all lecture theatres, it was illustrated that the occupants at the back were warmer compared to those at the front, and the decreased level of thermal comfort of occupants could be found in many lecture theatres. Overall, in the relationship between thermal comfort and seat position, thermal comfort has a close association with the front seat, which comprises greater comfort in contrast to the rear seat.

Keywords. Thermal comfort, seat position, indoor air temperature, PMV, AMV
DOI: https://doi.org/10.34641/clima.2022.118

1. Introduction

Due to increased occupant density inside classrooms and the detrimental impact that an insufficient thermal setting may have on students' performance and learning, providing comfortable conditions for educational buildings has always been critical [1]. This study focuses on the thermal environment in conjunction with certain connected factors such as indoor air quality and movement. In modern countries, more than 90% of people spend their time inside [2]. Students spend more daytime at school than in any other building other than their homes, emphasising the need to provide acceptable interior temperature conditions inside these institutions. As a consequence, lecture theatres' interior thermal comfort is critical, as it has a significant influence on the degree of thermal comfort experienced by students, especially those situated at the back due to the buoyancy effect [3].

The purpose of this research is to examine the thermal comfort levels of naturally ventilated lecture rooms. To accomplish this goal, numerous effective strategies, such as objective methodologies and subjective analyses, are required for the physics A1/3 lecture room, and further verification is accomplished through comparison with the other 37 lecture theatres. First, a questionnaire survey was conducted to assess the student's thermal perception, while physical parameters including air temperature and relative humidity were monitored and recorded using HOBO loggers. Students are required to mark their specific seat position, and two HOBO loggers are situated at the front and back of the lecture theatre, respectively. Following that, the predicted mean value (PMV) is calculated using physical data and the Fanger model, and then compared to the actual mean vote (AMV) obtained by surveys.

2. Literature review

Thermal comfort can be described as a state of mind or satisfaction that is impacted by human behavioural, psychological, physiological, and a large number of other factors [4]. Thermal perceptions are different among individuals even though they are exposed to the same environment. Developing knowledge of thermal comfort plays an important role in providing a satisfactory indoor environment for people, suggesting or improving standards [5] as well as reducing energy consumption of buildings [6]. According to a previous survey, compared with visual and auditory comfort, occupants focus more on thermal comfort and indoor

Copyright ©2022 by the authors. This conference paper is published under a CC-BY-4.0 license.

air quality [7]. Furthermore, according to a research [8], building energy consumption accounts for around 40% of global energy consumption and over 30% of carbon emissions, with a substantial part of this being used to achieve thermal comfort. Consequently, the optimal use of energy should strictly conform to the requirements for thermal comfort, and it is essential to carry out a comprehensive assessment of the thermal comfort factors.

2.1 thermal comfort approaches

Heat balancing and adaptive models are the two main methods for thermal comfort. Heat balance employs data from climate chamber experiments, which is best characterised by the Fanger model, while the adaptive models are primarily based on data from field research of occupants in buildings.

The heat balancing method was developed by Fanger using a steady-state heat transfer model in a climate chamber with controlled climatic parameters [9]. The closing insulation and metabolic rate of participants are determined and standardised in these studies when they are exposed to different thermal environments. Participants use the ASHRAE seven-point scale of thermal sensation to report how hot or cold they feel under the indicated thermal condition (-3 cold, -2 cool, -1 slightly cool, 0 neutral, +1 slightly warm, +2 warm, and +3 hot). Fanger's model states that the human body's thermoregulatory system is able to respond physiologically, such as sweating and shivering, to any thermal imbalance with the surrounding environment. This heat balance can make people maintain constant internal body temperature and achieve a neutral thermal sensation [10].

Fanger developed the Predicted Mean Vote (PMV) index to evaluate whether a certain environment could be accepted by a large group of people [11]. Over one thousand subjects in the climate chambers are required to give their thermal perception based on the seven-point scale sensation in ASHRAE. The mean of all subjects' responses is found to give a mean vote under the given thermal condition. Fanger combined PMV with the thermal physiological properties of humans at a given activity level and their thermal balance with the specified environment [12]. The PMV equation is complicated and, to be brief, it is a function of two personal parameters (activity level M in W/m^2 and clothing level I_{cl} in clo) as well as four environmental parameters (air temperature ta in °C, mean radiant temperature t_{mrt} in °C, air velocity v in m/s and relative humidity/vapor pressure pa in kPa). Therefore,

$$PMV = \int(M, I_{cl}, t_a, t_{mrt}, v, pa) \quad (1)$$

Some researchers developed a method for calculating thermal comfort indices based on six parameters in accordance with ASHRAE Standard 55-2013 [13]. Predicted Percentage Dissatisfied (PPD) is another index that predicts the percentage of people who responded ±2 and ±3 on the seven point sensation scale using the PMV. It was noted based on a study that those who answered ±1 and 0 were considered to be comfortable [11].

Previous studies assessed the accuracy of comfort theories based on Fanger's model through a few field studies and demostrate that, in naturally ventilated buildings, the calculated PMV consistently underestimates the actual mean vote (AMV) [14-18]. According to a research, the application of the heat balance model led to an inaccurate assessment of thermal comfort because it failed to account for human thermal adaptation ability, including physiological and behavioural variation and psychological effects [17].

2.2 Influence factors of thermal comfort

The effect of air temperature on human thermal comfort and performance has been extensively studied. It is generally agreed that too high or too low temperatures can have a negative impact on occupants' performance [19-20], but for the comfortable range of the inside temperature, there are some different opinions. Some research insisted that the range should be within the comfort zone [21-22], whereas others contended that improved thermal comfort could be obtained by the air temperature being outside the comfort zone dependent on specific performance tasks and environmental conditions. Some researchers put forward a correlation between them that a 2% decrease in thermal comfort could be caused by 1 ℃ increase in temperature [23-24]. In addition, indoor air temperature has an indirect impact on air quality, and the lower the temperature, the better the air quality is perceived [25]. Indoor air quality is primarily described by the CO2 concentration.

Indoor air velocity is another factor influencing occupants' thermal comfort. The research confirmed that thermal comfort levels with elevated air velocity are equal to or greater at warmer temperatures than those without it at cooler temperatures [26]. Furthermore, some research has proposed that elevated air speed has a positive impact on the perceived air quality in spaces with high temperature [27-28]. Based on a research, high temperature and high concentration of pollution may be mitigated by increasing air flow toward the face [29]. Consequently, the strategy of supplying room air with high speed and keeping a high indoor temperature with less supply of outdoor air can be energy efficient during the heating period without reducing the indoor thermal comfort and air quality [29]. However, it is challenging to achieve this strategy in a lecture theatre with various breathing levels and high occupancy density.

3. Methodology

3.1 Object of the study

Through literature surveys, research documents relevant to the assessment of students' thermal adaption to the lecture theatres with special architectural geometry have not received much attention. In the lecture theatres, the seats are placed on a slope, and non-uniform environmental conditions

can result from the different height levels. The purpose

Figure 1. Physics A1/3 lecture theatre in UCL

of this research is to obtain a better understanding of the varying levels of thermal comfort in lecture theatres, taking into account the occupants' sensation. This is to be achieved through a combination of objective and subjective approaches.

The main object of study is the Physics A1/3 Lecture Theatre (Figure 1), with comparison to the results of the other 37 lecture theatres in UCL for further verification. Physics A1/3 is a small-sized lecture theatre with increasing seat height. It is located on the fourth floor of the building and surrounded by several adjacent rooms. The main features of the lecture theatre are summarised in Figure 2.

All lecture theatres were studied during the lesson time from October 28th to November 24th, 2019 and indoor thermal comfort was investigated during the winter period in this report. The lecture theatres are located in central London. According to the CIBSE Guide A, London has a temperate maritime climate which is mild and humid all year round. The annual average temperature is over 11 °C, and the temperatures in winter are equal to or exceed -3 °C for 99.6% of the year.

Number of seats	53
Floor area (m^2)	76
Space height (m)	3.5
Volume (m^3)	266
Number of windows	4

Figure 2. Main features of the case study

3.2 Subjective approach

A total of 44 questionnaires were conducted in the classroom during the lecture break, which was one hour after the lecture began, in order to allow students to adjust to the environment. Students in Physics A1/3 are unable to change their environmental conditions through accessible control systems, which are driven by centrally controlled mechanical systems. Students have to sit at their desks with a certain degree of limitation on adjusting their activity or clothing level during the lecture time, but their physical actions are free during the break. The adaptive actions of occupants were not considered during the field campaign, but they could act before the start of the questionnaire survey.

The questionnaire content used in the research topic can be divided into four main categories: - General information: individual seat position, gender, clothing level - Thermal comfort: thermal vote based on Fanger seven-point scale and thermal preference - Indoor air movement/quality - Concentration level The actual mean vote (AMV), thermal preference as well as the correlation between all of these results are deeply investigated in this research.

3.3 Objective approach

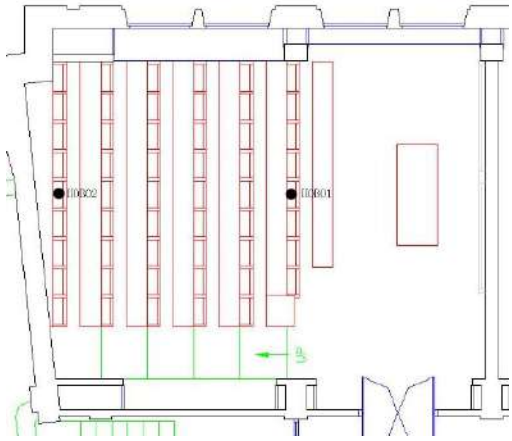

Figure 3. The location of two HOBOs

Two HOBOs in the occupied zone monitored thermal-hygrometric parameters in the space to ensure an accurate assessment of human exposure to thermal comfort (Figure 3). One HOBO was located in the middle of the first row (one of the lowest seats) and the other one was in the middle of the last row (one of the highest seats). The HOBOs were launched half an hour ahead of measuring, with the consideration of their response time and the HOBO specifications being:

- Dry-bulb air temperature: measure range from -20° to 70°C, accuracy ± 0.35°C from 0° to 50°C

- Relative humidity: measure range from 5% to 95% RH, accuracy ±2.5% from 10% to 90% RH

Subsequently, a mean value for clothing insulation level was obtained from all surveys, which resulted in average values for temperature and humidity in the indoor environment. All seated students have a metabolic rate of 1.0 MET. The PMV comfort zone's still air conditions (0.2 m/s) are closely matched by the indoor air velocity in many situations. Through the use of the CBS Thermal Comfort Tool, the PMV comfort index was calculated.

4. Results and analysis

4.1 Descriptive results

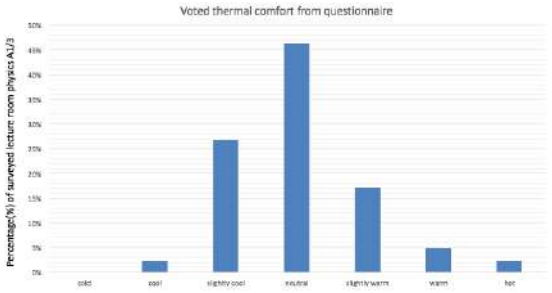

Figure 4. Voted thermal comfort percentage in Physics A1/3 Lecture Theatre

Figure 4 and Figure 5 illustrate the difference in thermal comfort between students in physics A1/3 and all lecture theatres. Thermal comfort was rated using a questionnaire. According to Fanger's definition of thermal comfort, -1 to 1 is the satisfaction range of indoor thermal environment; consequently, satisfaction with thermal comfort accounts for 90% of the total, with an average indoor temperature of 21.95°C and an average air humidity of 65.625 %, in line with ASHRAE Standard 55-2013. The predicted percentage of dissatisfied (PPD) has a proportion of 10%, which is remarkably similar to the estimated number in Figure 4. When comparing the physics A/13 lecture theatre (Figure 4) to the other lecture theatres (Figure 5), it becomes clear that the residents of physics A1/3 prefer a colder environment. Additionally, the discontent rate for all lecture theatres was 20%, which is higher than the dissatisfaction rate for the physics A1/3 lecture room.

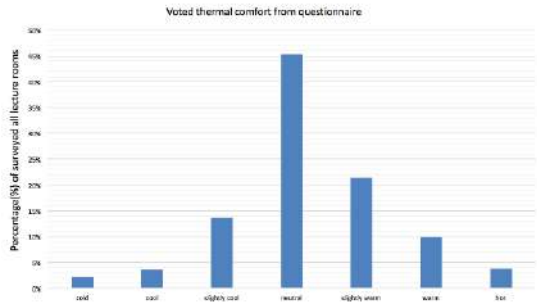

Figure 5. Voted thermal comfort percentage for all Lecture Theatres

4.2 Comparison between PMV and AMV

The Fanger PMV is a widely used indicator for evaluating occupant thermal comfort that has been used in international standards such as ISO 7730 [30], ASHRAE 55 [31], EN 15215 [32], and Chinese Standard [33]. It is based on the steady state heat balance principle and predicts the mean value of a large group of people's votes on the 7-point thermal sensation scale (cold (-3), cool (-2), slightly cool (-1), neutral (0), slightly warm (+1), warm (+2), hot (+3)) based on six inputs (air temperature, mean radiant temperature, air speed, humidity, metabolic rate, and clothing insulation) [9]. Figure 6 shows the relationship between PMV and AMV , where the black line indicates a benchmark based on Fanger's research in the environmental chamber, each dot in the figure represents the mean value of PMV and AMV of each lecture rooms. The results showed that the PMV and AMV of all lecture theatres reveal little fluctuation when compared with the benchmark. PMV can be calculated based on the calculation procedure showed in ISO 7730. AMV can be calculated by value obtained from the questionnaires. London features a temperate oceanic climate, located in the United Kingdom (51°30 N, 0°39 W), generally featuring mild summers and cool but not cold winters, with a relatively narrow annual temperature range and few extremes of temperature [34]. Therefore, this minimal fluctuation can be regareded as the thermal adaptation generated by the past thermal experience of a long time spent living in a specific region with a stable thermal comfort environment. Additionally, for students who prefer to be cooler or warmer, the PMV has several pitfalls that must be presumed to have a similar metabolic level. Appropriate cooling or heating of the room is acceptable throughout the winter or summer, which enables buildings to save massive amounts of energy.

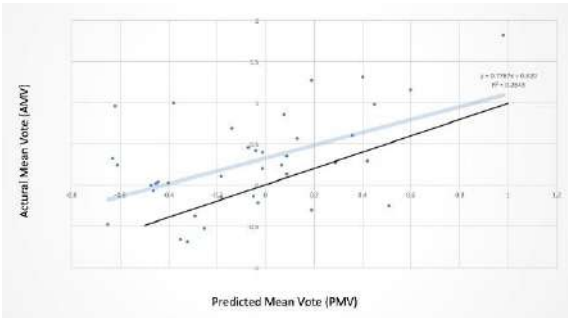

Figure 6. Comparison between PMV and AMV of all surveyed lecture theatres

4.3 Air movement difference between seat positions with various height levels

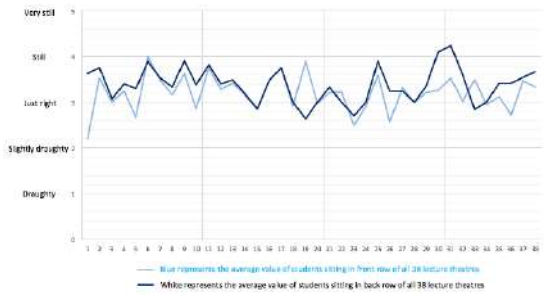

Figure 7. Voted about air movement satisfaction from students sit at the front and back respectively

Figure 7 showed all 38 lecture theatres, with students

seated in the front demonstrating more air movement and satisfaction than those seated in the back, with the exception of a few classes due to the following causes: 1. The interior structure of the house - as a consequence of the internal construction of the house, which includes windows at the back of the class, the back air velocity is fast, resulting in a higher level of satisfaction for students in the rear compared to the front. 2. Gender differences in air movement; women perceive it as higher, while men perceive it as more frail, and when completing the questionnaire, the women seated in the back are comparatively many, which explains why certain rooms have a higher level of satisfaction in the back than in the front. However, the common consensus is that students placed in the front enjoy better ventilation, which results in higher thermal comfort than students seated in the back row in theatres.

4.4 Thermal comfort difference between seat positions with various height levels

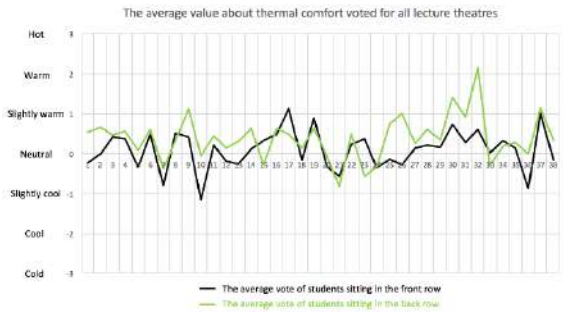

Figure 8. All lecture rooms average thermal comfort evaluation of different position

Figure 8 showed each classroom has a unique code, and the black line represents the thermal comfort trend for students situated in the first row of the 38 lecture theatres, while the green line represents the tendency of students placed in the rear. The line's substantial volatility reflects the decreased thermal comfort shown in the figure closer to the average. Overall, the black line is more stable than the green line, indicating that students situated in the front row experience more thermal comfort than those seated in the rear row. Unexpectedly, 13 lecture theatres demonstrate that students situated in the rear are more comfortable than those seated in the front, owing mostly to the back's lower temperature in comparison to the front, which might be attributed to the open system of natural ventilation.

5. Conclusion and limitation

Through a statistical comparison of thermal comfort levels between students situated in the back and front of all lecture theatres, it was determined that those seated in the rear were warmer than those in the front and had reduced thermal comfort in the majority of lecture theatres. In times, as a consequence of the significantly reduced temperature, thermal comfort may be compromised at the front. Thus, seat position and thermal comfort are strongly related to the front seat, which provides more comfort than the back seat. The back seat comfort, on the other hand, may be improved. Increasing the ventilation at the rear might be an effective strategy, since thermal comfort and air velocity are inextricably linked, and an adequate amount of interior ventilation can improve students' focus by enhancing their comfort. Additionally, when comparing PMV and AMV to Fanger's benchmark, it can be observed that the two have similar tendencies with little variation. This is mostly attributed to London's temperate oceanic climate, which has relatively stable temperature conditions. This will result in occupant thermal adaptation, generated by long-term thermal experience in a particular location with a consistent thermal comfort environment, which is in line with Fanger's experiment condition.

The purpose of the study was to examine the relationship between thermal comfort and seat position employing statistical analysis. This study excludes gender issues, since the male to female ratio is 3:1, and preferably, the male to female ratio should be 1:1 to get more precise data result. The relationship between sitting position and thermal comfort seems to be quite close in average, and the relationship between thermal comfort and seating position is evaluated using three variables: indoor air quality, indoor air velocity, and indoor air temperature. Additionally, the AMV values for all lecture rooms were compared to the PMV values and found to have similar tendencies, since the students in the lecture theatres had significantly limited physical adaptation to their environment. Nonetheless, an average absolute error exists between the two sets of numbers, which might be the consequence of an imperfect method of estimating the amount of clothing and a greater variation in individual opinion. Thus, it is suggested that 13 scale values be used to precisely scale the PMV to 0.5 increments.

6. References

[1] Zomorodian Z S, Tahsildoost M, Hafezi M. Thermal comfort in educational buildings: A review article[J]. Renewable and sustainable energy reviews, 2016, 59: 895-906.

[2] de Blas M, Navazo M, Alonso L, et al. Simultaneous indoor and outdoor on-line hourly monitoring of atmospheric volatile organic compounds in an urban building. The role of inside and outside sources[J]. Science of the total environment, 2012, 426: 327-335.

[3] Cheng Y, Niu J, Gao N. Stratified air distribution systems in a large lecture theatre: A numerical method to optimize thermal comfort and maximize energy saving[J]. Energy and Buildings, 2012, 55: 515-525.

[4] Yao R, Li B, Liu J. A theoretical adaptive model of thermal comfort–Adaptive Predicted Mean Vote (aPMV)[J]. Building and environment, 2009, 44(10): 2089-2096.

[5] Nikolopoulou M, Lykoudis S. Thermal comfort in outdoor urban spaces: analysis across different European countries[J]. Building and environment, 2006, 41(11): 1455-1470.

[6] Santos R S, Matias J C O, Abreu A, et al. Evolutionary algorithms on reducing energy consumption in buildings: An approach to provide smart and efficiency choices, considering the rebound effect[J]. Computers & Industrial Engineering, 2018, 126: 729-755.

[7] Huang L, Zhu Y, Ouyang Q, et al. A study on the effects of thermal, luminous, and acoustic environments on indoor environmental comfort in offices[J]. Building and Environment, 2012, 49: 304-309.

[8] Yang L, Yan H, Lam J C. Thermal comfort and building energy consumption implications–a review[J]. Applied energy, 2014, 115: 164-173.

[9] Fanger P O. Thermal comfort. Analysis and applications in environmental engineering[J]. Thermal comfort. Analysis and applications in environmental engineering., 1970.

[10] Djongyang N, Tchinda R, Njomo D. Thermal comfort: A review paper[J]. Renewable and sustainable energy reviews, 2010, 14(9): 2626-2640.

[11] Fanger P O. Thermal comfort, analysis and application in environmental engineering[J]. 1972.

[12] Lin Z, Deng S. A study on the thermal comfort in sleeping environments in the subtropics—developing a thermal comfort model for sleeping environments[J]. Building and environment, 2008, 43(1): 70-81.

[13] Hoyt T, Schiavon S, Piccioli A, et al. CBE thermal comfort tool[J]. Center for the Built Environment, University of California Berkeley, 2013, 40.

[14] Humphreys M. An adaptive approach to thermal comfort criteria[J]. Naturally Ventilated Buildings: Buildings for the senses, the economy and society, 1997: 129-139.

[15] Humphreys M A. Field studies and climate chamber experiments in thermal comfort research[J]. Standard for Thermal Comfort, 1994.

[16] Humphreys M A. Thermal Comfort Requirements, Climate and Energy, World Renewable Energy Congress[J]. Reading, England, 1992.

[17] Humphreys M A, Nicol J F. The validity of ISO-PMV for predicting comfort votes in every-day thermal environments[J]. Energy and buildings, 2002, 34(6): 667-684.

[18] Nicol J F, Humphreys M. Understanding the adaptive approach to thermal comfort[J]. ASHRAE transactions, 1998, 104(1): 991-1004.

[19] Lorsch H G, Abdou O A. The impact of the building indoor environment on occupant productivity--part 1: recent studies, measures, and costs[J]. ASHRAE Transactions-American Society of Heating Refrigerating Airconditioning Engin, 1994, 100(2): 741-749.

[20] Parsons K C. Environmental ergonomics: a review of principles, methods and models[J]. Applied ergonomics, 2000, 31(6): 581-594.

[21] Hancock P A, Vasmatzidis I. Effects of heat stress on cognitive performance: the current state of knowledge[J]. International Journal of Hyperthermia, 2003, 19(3): 355-372.

[22] Federspiel C C, Liu G, Lahiff M, et al. Worker performance and ventilation: Analyses of individual data for call-center workers[R]. Lawrence Berkeley National Lab.(LBNL), Berkeley, CA (United States), 2002.

[23] Cui W, Cao G, Park J H, et al. Influence of indoor air temperature on human thermal comfort, motivation and performance[J]. Building and environment, 2013, 68: 114-122.

[24] Seppanen O, Fisk W J, Faulkner D. Cost benefit analysis of the night-time ventilative cooling in office building[J]. 2003.

[25] Toftum J, Jørgensen A S, Fanger P O. Upper limits of air humidity for preventing warm respiratory discomfort[J]. Energy and Buildings, 1998, 28(1): 15-23.

[26] Rohles F H, Konz S A, Jones B W. eiIin Fans Extenders of the Summer Comfort Envelope[J]. ASHRAE Trans, 1983, 89: 245-263.

[27] Melikov A K, Kaczmarczyk J, Sliva D. Impact of air movement on perceived air quality at different level of relative humidity[C]//11th International Conference on Indoor Air Quality and Climate. 2008.

[28] Zhang H, Arens E, Kim D E, et al. Comfort, perceived air quality, and work performance in a low-power task–ambient conditioning system[J]. Building and Environment, 2010, 45(1): 29-39.

[29] Melikov A K, Kaczmarczyk J. Air movement and

perceived air quality[J]. Building and Environment, 2012, 47: 400-409.

[30] ISO I S O. 7730: Ergonomics of the thermal environment Analytical determination and interpretation of thermal comfort using calculation of the PMV and PPD indices and local thermal comfort criteria[J]. Management, 2005, 3(605): e615.

[31] Refrigerating, Air-Conditioning Engineers, American National Standards Institute. Thermal environmental conditions for human occupancy[M]. American Society of Heating, Refrigerating and Air-Conditioning Engineers, 2004.

[32] Comite'Europe'en de Normalisation C E N. Indoor environmental input parameters for design and assessment of energy performance of buildings addressing indoor air quality, thermal environment, lighting and acoustics[J]. EN 15251, 2007.

[33] GB/T 50785-2012. Evaluation standard for indoor thermal environment in civil buildings[J]. 2012.

[34] Athamena K. Microclimatic coupling to assess the impact of crossing urban form on outdoor thermal comfort in temperate oceanic climate[J]. Urban Climate, 2022, 42: 101093.

Data access statement:

Data sharing not applicable to this article as no datasets were generated or analysed during the current study.

Crossed effects of visual factors on human thermal response

Roberta Jacoby Cureau [a], Mateus V. Bavaresco [b], Ilaria Pigliautile [a,c], Claudia Fabiani [a,c], Anna Laura Pisello [a,c]

[a] CIRIAF, Interuniversity Research Center on Pollution and Environment Mauro Felli, University of Perugia, Italy.

[b] Laboratory of Energy Efficiency in Buildings, Department of Civil Engineering, Federal University of Santa Catarina, Brazil.

[c] Department of Engineering, University of Perugia, Italy.

Abstract. Recently, the approach for studying human comfort indoors has been changing for a multi-domain framework once some studies have reported crossed effects between different comfort domains (i.e., thermal, visual, acoustic, and air quality). An example of crossed effects between comfort domains is the hue-heat hypothesis (HHH), referring to the possible association between lighting and the human thermal response. This paper presents a new investigation to verify the validity of the HHH. Several experiments were conducted in a test room under a fully controlled setting, combining two thermal (slightly cold and slightly hot) and three lighting conditions (blue, red, and white lights with nearly the same illuminance level). The experiments were divided into two parts, each one dedicated to a thermal setting. After acclimatisation, the participants were submitted to each colour of light for seven minutes under a constant air temperature. A total of 39 people participated twice in the experiment, each time in a different thermal condition, and before changing the colour of light, they answered a survey about their thermal sensation, thermal comfort, visual comfort, overall comfort, and perceived level of productivity. Answers were compared using statistical methods. The results did not allow to confirm the HHH, since no statistically significant differences were observed for thermal comfort and thermal sensation for the different colours of light. The only significant difference observed was for visual comfort in the slightly cold thermal condition, between red and white lights. In fact, the survey responses for visual comfort indicate that people preferred the white light. White light was also associated with better overall comfort assessment and perceived productivity in both thermal conditions, but the differences were not statistically significant. Further investigations should be performed under more thermally stressful environments and should also evaluate the physiological factors of participants as a thermal response instead of only subjective outcomes.

Keywords. Thermal comfort, multi-domain comfort, coloured lights, hue-heat hypothesis.
DOI: https://doi.org/10.34641/clima.2022.276

1. Introduction

Indoor environmental quality can significantly influence the health, well-being, comfort, and productivity of building occupants [1]. Humans are simultaneously exposed to environmental stimuli associated with different domains, namely thermal, visual, acoustic, and air quality. Recently, the assessment of human comfort in indoor environments has been changing for the multi-domain approach since some studies identified combined and crossed effects between these domains [2]. Light, for instance, influences thermal comfort and other non-visual responses, like mood and alertness [3]. An example of the interaction between visual and thermal domains is the hue-heat-hypothesis (HHH) [4], which suggests that colours affect people's subjective thermal perception. In detail, light frequencies toward the red end of the visible spectrum are perceived as thermally warmer, while blue frequencies lead to a perception of a cooler environment.

Some studies tested the HHH, investigating the effects of lighting (coloured or with different correlated colour temperature (CCT)) on thermal responses, and confirmed this assumption [5,6]. Other researchers found significant differences only

Copyright ©2022 by the authors. This conference paper is published under a CC-BY-4.0 license.

under specific thermal conditions [7,8] or during a particular season of the year [9], while some papers reported no significant associations between the lighting colours or CCT and the thermal perception [10,11]. Therefore, the reported results about the HHH are still unclear.

The ambiguity related to the results of the HHH testing supports the importance of further exploring this topic once the confirmation of the HHH would allow an enlargement of the temperature range found comfortable by occupants through the control of the lighting [7]. Considering that heating, ventilation, and air conditioning systems represent about 50% of building energy use [12], visual factors could be used to trigger varied thermal sensations in an energy-saving perspective.

In this context, the aim of this paper is to assess the influence of the colour of light on human thermal sensation and comfort. The HHH was tested, verifying if reddish lights could induce a hotter thermal sensation, and bluish lights could stimulate a colder thermal sensation. Then, 39 subjects participated in an experiment conducted in a fully controlled test room, being submitted to two thermal conditions (slightly cold and slightly hot) and three colours of light (blue, red, and white). The illuminance level for the three lighting conditions is nearly the same, then the only visual factor being altered during the experiments was the colour of light. Participants answered a survey about thermal sensation, thermal, visual, and overall comfort, and perceived level of productivity in each environmental condition, and the responses were compared through statistical techniques.

2. Research Methods

This article reports a multi-domain (thermal and visual) comfort investigation, aiming to identify whether the colour of light affects the human thermal perception. For this, it was planned an experiment associating different thermal settings and colours of light.

2.1 Experimental campaign

The experiments were conducted in a test room under a fully controlled setting, in October and November 2021. The test room [13] is located at the Engineering campus of Perugia (Italy) belonging to the Cfa climate class according to Köppen Geiger [14]. The internal layout was specifically designed and built for reproducing an office environment (Figure 1). Inside this space, several environmental parameters, such as temperature, relative humidity, air velocity, surface temperatures, illuminance, and CO_2 concentration are continuously monitored every 30 seconds. The participants stayed seated during the whole procedure to simulate office activities.

Fig. 1 – Interior of the test room used in the experiments.

The tests combined two air temperatures, representing slightly cold and slightly hot conditions (i.e., 20 °C and 25 °C, respectively, since we were approaching the winter season [15]), and three colours of light (white (~540 lx), red (~587 lx), and blue (~563 lx)). The only source of light considered in the experiments was artificial (no daylight). The tests were separated into two parts, each one with a fixed thermal setting and varying colours of light. This approach was conceived because light colour is quickly adjusted indoors, easing the experiment procedure. The test room was pre-conditioned to guarantee a thermal equilibrium between the air and surface temperatures. Therefore, the air temperature was assumed equal to the mean radiant temperature, and so to the operative temperature, during the test.

Each part of the experiment lasted 41 minutes in total, and the thermal conditions were kept constant during this period. Figure 2 presents the experiment procedure.

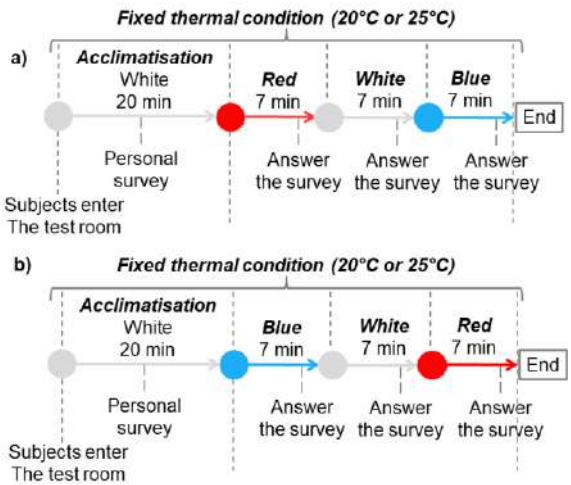

Fig. 2 – Experiment procedure when starting with red light (a) and blue light (b).

The first 20 minutes were dedicated to acclimatisation, with white light. During this stage, participants answered a personal survey (age, gender, height, weight, worn garments, and profession). The following 21 minutes were divided

into three phases of 7 minutes, each one corresponding to a specific colour of light. In the last two minutes of every lighting condition, the participants answered a survey about their thermal sensation, thermal, visual and overall comfort, and perceived level of productivity. All questions were answered in a 5-point Likert scale.

A total of 39 subjects took part in the experiment and every person participated twice, each time dedicated to a thermal condition (at 20°C and 25°C). Aiming to minimise the bias of colours order, half of participants started the test with the red light, while the other half started with blue light. The order of the colours of light was unchanged in the two tests for the same participant.

As the test room where the experiments were performed simulates an office environment, the selection of participants were made considering people who usually stay in this kind of space in their daily life. The 39 subjects who participated in the experiment are students and young professionals who perform typical office tasks.

2.2 Statistical Analysis

The first step of the analysis was the characterisation of the sample of participants. Data collected through the personal survey were used to describe the sample composition using descriptive statistics methods. The quantitative variables were evaluated by their mean, standard deviation, median, mode, skewness, kurtosis, minimum and maximum values, and 25, 50, and 75 percentiles. The qualitative variables were characterised in terms of percentage distribution.

In the end of the experiment, 234 answers (39 participants times two thermal conditions times three colours of light) related to thermal sensation and comfort, visual comfort, overall comfort, and perceived productivity were obtained. These responses were compared using the Friedman test [16], a non-parametric statistical test used to compare more than two paired samples. A non-parametric method was chosen because the survey's answers are ordinal variables. The significance level adopted in this study was 5%.

The aim of the study is to verify the crossed effects of colour of light on thermal perception, that is, the hypothesis tested is that people perceive the thermal environment differently when changing the colour of light and keeping the thermal condition constant. Therefore, responses were grouped by temperature, also to verify if the effects of colour of light on thermal perception are altered under different thermal settings. Then, the test was applied twice (two thermal conditions), each time comparing three samples related to the subjects' answers to the survey in every colour of light.

3. Results

3.1 Sample Composition

The sample was characterised in terms of age, height, weight, body mass index (weight divided by the square of height), clothing insulation (calculated according to the guidelines of the ISO 7730:2005 [15], determined from the responses related to worn garments), gender, and profession. Table 1 presents the distribution characteristics regarding the quantitative variables. The distribution of clothing insulation involves the values of the two tests in which the subjects participated.

Tab. 1 - Descriptive statistics analysis of quantitative variables.

		Age	Height (m)	Weight (kg)	Body mass index (kg/m^2)	Clothing insulation (clo)
N		39	39	39	39	78
Mean		22.44	1.73	66.66	22.29	0.83
Median		23	1.73	65	21.67	0.85
Mode		23	1.70	60	25.13	0.85
Std. deviation		1.93	0.09	11.41	3.01	0.06
Skewness		-0.22	-0.53	0.30	0.42	-1.77
Kurtosis		1.81	-0.20	-0.60	-0.31	1.58
Minimum		18	1.50	44	16.56	0.70
Maximum		28	1.85	90	29.30	0.90
Interval		10	0.35	46	12.74	0.20
Percentiles	25	22	1.65	60	20.46	0.85
	50	23	1.73	65	21.67	0.85
	75	23	1.80	75	24.47	0.85

Height and clothing insulation are less dispersed in relation to the mean (low standard deviations), while weight and body mass index samples have more spread-out values. Age is also concentrated around mean, which is expected since this was a criterion for the choice of the subjects. Height, weight, and body mass index were considered as approximately normally distributed because the skewness and kurtosis values between −1 and +1.

Gender and profession are qualitative variables, so they were described in terms of percentage distribution, as shown in Figure 3.

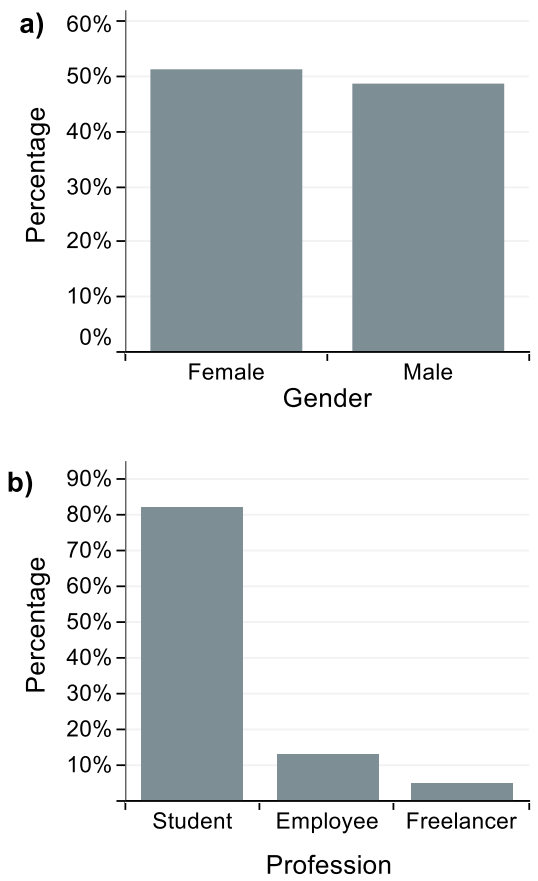

Fig. 3 – Sample description in terms of percentage for gender (a) and profession (b).

Participants are equally distributed among gender, following the same distribution as the local population [17]. Concerning the profession, as mentioned in Section 2.1, participants were selected according to their daily life activities. They are mainly students because this is the principal activity practiced by local people of this age [18].

3.2 Survey responses

During the experiments, participants were asked about their thermal sensation; thermal, visual, and overall comfort; and perceived level of productivity, for each colour of light. No differences in answers were observed between genders for these questions.

Figure 4 presents the votes regarding thermal sensation separated by colour of light and thermal condition. At 20°C, the "hot" sensation is mainly associated with the red light. However, in this environmental condition, the same percentage of votes is observed for "cold" sensation, which contradicts the hypothesis tested that reddish lights induce a hotter sensation. Blue and white lights in this case represent the larger amount of "neutral" sensation. At 25°C, small differences are observed between red and blue lights on votes for "hot" and "very hot" sensation, which again goes on the opposite of the initial hypothesis that bluish lights provoke colder sensation.

Concerning thermal comfort, no differences in votes for blue and red lights were observed at 25°C, while at 20°C more votes associated to "comfortable" or "very comfortable" were reported in blue light. The white light is the one associated with the highest part of positive thermal comfort votes under the two thermal conditions. The same is observed for the answers related to overall comfort and perceived level of productivity: the highest number of "very comfortable" and "very productive" votes are related to the white light.

For visual comfort, it is important to highlight that even though the negative votes represent a small amount of the total, they are mainly associated to blue and red lights, while the highest part of "very comfortable" votes are associated with the white light.

3.3 Statistical Tests

The survey responses were compared using the Friedman test to check if there is a difference statistically significant in their answers for different colours of light. Table 2 presents the *p* values obtained when applying the statistical test, for the two thermal conditions.

Tab. 2 – *p* values for the Friedman test.

Question	Thermal condition	
	20°C	25°C
Thermal sensation	0.389	0.090
Thermal comfort	0.128	0.153
Visual comfort	0.004	0.107
Overall comfort	0.123	0.708
Productivity	0.289	0.208

For a significance level of 5%, it was observed no statistically significant difference in answers for different colours of light, except for visual comfort at 20°C. For this case, a post hoc test (Nemenyi test) was applied, and it was verified that the difference is statistically significant only between white and red lights ($p = 0.010$).

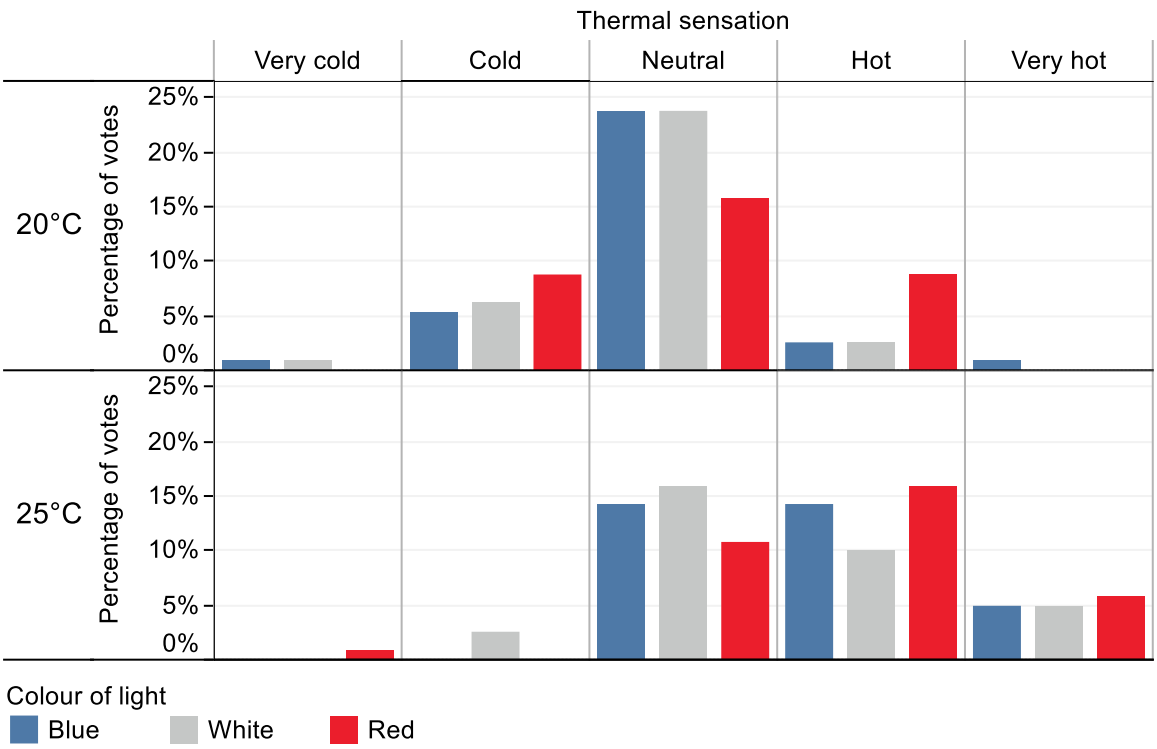

Fig. 4 – Survey answers regarding thermal sensation according to each thermal condition and colour of light.

Through this analysis, it was concluded that this specific segment of the population (young adults in their 20s) does not have their thermal sensation and comfort changed when modifying the colour of light and keeping the air temperature constant. Therefore, the initial hypothesis that a reddish light induces a hotter sensation, and a bluish light causes a colder sensation was not confirmed with this experiment. In fact, some participants reported a "cold" or "very cold" sensation even with red light (Figure 4). Moreover, changing the colour of light did not affect significantly the overall comfort and the perceived level of productivity of the participants for both thermal conditions.

The only aspect that presented some significant variation when changing the colour of the light was visual comfort, which is directly related to light. However, this was noted only for a specific thermal setting, slightly cold, that is close to the neutrality and thus without significant thermal disturbances, theoretically. In this thermally comfortable space, the coloured light could be more noticed by the subjects who could consider it a source of discomfort.

4. Conclusions

This paper presents an experiment that tested if colour of light could induce different thermal perceptions under fixed thermal settings in office environments. The sample of participants was formed by young adults that usually perform office tasks in their routines, and their perceptions were assessed through surveys.

No statistically significant differences were observed in thermal sensation and comfort reported by the subjects, opposing the initial assumption that red lights could induce a hotter sensation, and blue lights could provoke a colder sensation. Therefore, this study was not able to confirm the HHH, considering the specific group of the population under investigation. Furthermore, the negative votes for visual comfort are associated mainly with the red and blue lights, indicating that this group prefer the white light in this kind of environment. The variation is significantly different only in the slightly cold thermal condition.

The seven-minute exposure to each colour of light allowed carrying out the within-subjects experiment with a larger number of participants in a limited time. However, this interval could be considered short in view of people's long exposure to artificial lights during the day. The effect of long exposures should also be explored, taking into account a possible visual adaptation that could influence the thermal response of participants. Furthermore, the time of the day when the experiment was conducted should be explored, since some studies already reported significant differences in thermal perception with the time of the day [22].

Further investigations should be done in more uncomfortable thermal environments (too hot and too cold settings) to evaluate if colour of light could reduce the thermal stress under these conditions, and should involve other age groups. They could also include the investigation of physiological parameters of subjects as a thermal response.

Moreover, the productivity could be additionally assessed with psychological tests developed to evaluate specific cognitive functions like attention, concentration, and reaction time, that could be associated to productivity. Some examples are the Stroop test [19], the d2 test [20], and the Continuous Performance test [21].

5. Acknowledgement

The authors thank Andrea Silei for his support in conducting the monitoring activity and engaging participants. R.J. Cureau's acknowledgements are due to the PhD school in Energy and Sustainable Development from the University of Perugia (Italy). M.V. Bavaresco's acknowledgements are due to the Coordenação de Aperfeiçoamento de Pessoal de Nível Superior - Brasil (CAPES) - Finance Code 001. I. Pigliautile, C. Fabiani, and A.L. Pisello thank the Italian Ministry of Research for supporting NEXT.COM (Towards the NEXT generation of multiphysics and multidomain environmental COMfort) project (Prin 2017–20172FSCH4). I. Pigliautile further acknowledges the PON project (D.M. 1062 PON Ricerca e Innovazione) entitled "Red-To-Green". C. Fabiani's acknowledgments are also due to the European Union's Horizon 2020 program under grant agreement No. 792210 (GEOFIT). A.L. Pisello also acknowledges the Horizon Europe ERC Grant HELIOS (GA 101041255).

6. References

[1] Al Horr Y, Arif M, Kaushik A, Mazroei A, Katafygiotou M, Elsarrag E. Occupant productivity and office indoor environment quality: A review of the literature. Build Environ. 2016 Aug 15;105:369–89.

[2] Schweiker M, Ampatzi E, Andargie MS, Andersen RK, Azar E, Barthelmes VM, et al. Review of multi-domain approaches to indoor environmental perception and behaviour. Build Environ. 2020 Jun 1;176.

[3] te Kulve M, Schellen L, Schlangen LJM, van Marken Lichtenbelt WD. The influence of light on thermal responses. Acta Physiol. 2016 Feb 1;216(2):163–85.

[4] Bennett CA, Rey P. What's So Hot about Red? Hum Factors. 1972 Apr 1;14(2):149–54.

[5] Winzen J, Albers F, Marggraf-Micheel C. The influence of coloured light in the aircraft cabin on passenger thermal comfort. Light Res Technol. 2013 Jun 13;46(4):465–75.

[6] Chinazzo G, Wienold J, Andersen M. Combined effects of daylight transmitted through coloured glazing and indoor temperature on thermal responses and overall comfort. Build Environ. 2018 Oct 15;144:583–97.

[7] Toftum J, Thorseth A, Markvart J, Logadóttir Á. Occupant response to different correlated colour temperatures of white LED lighting. Build Environ. 2018 Oct 1;143:258–68.

[8] Brambilla A, Hu W, Samangouei R, Cadorin R, Davis W. How correlated colour temperature manipulates human thermal perception and comfort. Build Environ. 2020 Jun 15;177:106929.

[9] Bellia L, d'Ambrosio Alfano FR, Fragliasso F, Palella BI, Riccio G. On the interaction between lighting and thermal comfort: An integrated approach to IEQ. Energy Build. 2021 Jan 15;231.

[10] Baniya RR, Tetri E, Virtanen J, Halonen L. The effect of correlated colour temperature of lighting on thermal sensation and thermal comfort in a simulated indoor workplace. Indoor Built Environ. 2016 Oct 6;27(3):308–16.

[11] Toftum J, Thorseth A, Logadóttir Á, Markvart J, Stoffer S. Will correlated colour temperature affect peoples' thermal sensation outside the laboratory? J Phys Conf Ser. 2021;2069(1):12238.

[12] te Kulve M, Schlangen L, van Marken Lichtenbelt W. Interactions between the perception of light and temperature. Indoor Air. 2018 Nov 1;28(6):881–91.

[13] Vittori F, Chiatti C, Pigliautile I, Pisello AL. The NEXT.ROOM: Design principles and systems trials of a novel test room aimed at deepening our knowledge on human comfort. Build Environ. 2022 Jan 4 [cited 2022 Jan 13];108744.

[14] Kottek M, Grieser J, Beck C, Rudolf B, Rubel F. World Map of the Köppen-Geiger climate classification updated. Meteorol Zeitschrift. 2006;15(3):259–63.

[15] International Organization for Standardization. ISO 7730:2005 Ergonomics of the thermal environment — Analytical determination and interpretation of thermal comfort using calculation of the PMV and PPD indices and local thermal comfort criteria. Geneva: ISO; 2005.

[16] Corder GW, Foreman DI. Nonparametric Statistics for Non-Statisticians: A Step-by-Step Approach. Nonparametric Statistics for Non-Statisticians: A Step-by-Step Approach. 2011. 1–536 p.

[17] Istituto Nazionale di Statistica. Geo demo - Population estimates [Internet]. 2021 [cited 2021 Dec 10]. Available from:

https://demo.istat.it/ricostruzione/index.php?lingua=eng

[18] Istituto Nazionale di Statistica. Censimento permanente della popolazione e delle abitazioni - Condizione professionale per età [Internet]. [cited 2021 Dec 10]. Available from: https://esploradati.censimentopopolazione.istat.it/databrowser/#/it/censtest/dashboards

[19] Scarpina F, Tagini S. The Stroop Color and Word Test. Front Psychol. 2017;8.

[20] Bates ME, Lemay EP. The d2 Test of Attention: Construct validity and extensions in scoring techniques. J Int Neuropsychol Soc. 2004/05/01. 2004;10(3):392–400.

[21] Shalev L, Ben-Simon A, Mevorach C, Cohen Y, Tsal Y. Conjunctive Continuous Performance Task (CCPT)—A pure measure of sustained attention. Neuropsychologia. 2011 Jul 1;49(9):2584–91.

[22] Vellei M, Chinazzo G, Zitting K-M, Hubbard J. Human thermal perception and time of day: A review. Temperature. 2021;8(4):320-341.

Data Statement

The datasets generated during and/or analysed during the current study are not available because this is an ongoing project, but the authors will make every reasonable effort to publish them in near future.

Using ASHRAE Standard 55 Adaptive Comfort Method for Practical Applications

Peter Simmonds
Building Systems and Analytics, Los Angeles, and Bergen (The Netherlands)

Abstract. The question of comfort under a natural conditioning scheme when governed by ASHRAE Standard 55, which describes the use of the adaptive comfort standard, including the elevated speed option, and compares this model to other comfort indices. The analysis requires a combined dynamic heat transfer and bulk airflow analysis method that delivers simultaneous output of expected indoor temperatures and indoor ventilation rates.
To determine if the space is compliant, the designer must demonstrate that the indoor operative temperature conditions stay within the prescribed range during occupied hours. Typically, dynamic thermal simulation software capable of modelling natural ventilation schemes is used to simulate the cooling effects of the natural ventilation airflows and the radiant impacts of the room surface temperatures.
This paper shows a Standard 55 compliance analysis and how the results are presented in an understandable manner.

Keywords. Natural Ventilation, Occupant Comfort, Ventilation
DOI: https://doi.org/10.34641/clima.2022.83

1. Introduction

In 2021 ASHRAE published the Design Guide for Natural Ventilation 2021b) which provided information and clarification on designing and operating Natural Ventilation systems for buildings. The acceptable comfort zone is prescribed by the American Society of Heating, Refrigerating, and Air Conditioning Engineers (ASHRAE) Standard 55, Thermal Environmental Conditions for Human Occupancy (ASHRAE 2020b). Comfort is defined as the conditions under which eighty percent or more of the building occupants will find an area thermally acceptable in still air and shade conditions.

The ASHRAE Design Guide for Natural Ventilation is meant to assist owners, architects, engineers, facilities personnel, and building design professionals to explore the feasibility of natural ventilation for their project during the early phases of design. Many in the industry can see the appeal of natural ventilation for environmental stewardship concerns, however, there appears to exist some reticence in application and confusion over the interpretation of the current standards. This may be since there is not an ASHRAE-endorsed methodology that establishes a rigorous analytical path, and the inputs and equations necessary to complete even a feasibility analysis are in disparate standards and guidance documents. This guide attempts to consolidate and organize the key information necessary to perform a feasibility analysis by excerpting content when approved by the originating authors or by reference to information in the public domain.

The progress of a design team from conception to fruition for a natural ventilation scheme is one of collaborative review of critical analysis results. Natural ventilation is reliant on a variable source of air movement and cooling capacity. Owners and tenants must be aware not only of the average expected results, but also the frequency of the extreme conditions for the current day and in a future climate-changed condition. Natural ventilation as a comfort-conditioning method will always be compared to HVAC schemes that are easier to control from a predictability perspective. Thus, the social acceptability of a natural ventilation scheme is as important to its success as its technical feasibility. This guide is intended to normalize expectations regarding the minimum steps and analyses necessary to facilitate key decision-making conversations with the stakeholders.

When natural ventilation and natural conditioning are pursued, it is important to ensure that the minimum outside air requirements are achievable under all conditions, inclusive of those hours when the back-up mechanical ventilation system is operational. This is a requirement of ASHRAE Standard 62.1 (ASHRAE 2020a) clause 6.1.3 and Section 6.4. Complying with the natural ventilation requirements does not imply any likelihood of compliance with the comfort standard. At high outdoor air temperatures, the amount of air necessary to provide a heat-absorption function is

Copyright ©2022 by the authors. This conference paper is published under a CC-BY-4.0 license.

far higher than the amount of air required to meet the minimum ventilation requirements. The design team should never assume that complying with ASHRAE 62.1 (ASHRAE 2016b) will result in a comfortable space.

2. NATURAL VENTILATION STRATEGY

The I City Project is in Moscow, Russia, and lies just to the northeast of Moscow City, the new high-rise district in Moscow. The Design Brief provided by the MR Group requests a Class A office development with a total above grade area of 175,100m2 (excluding Podium Parking and Mechanical). The project is to have 2 towers: Tower 1 has a height limit of 126.9 m, and Tower 2 is to be designed to fulfil the outstanding buildable area with a desired height in the range of 236 m. The location of the two towers was generally established by an Insolation Study which positioned the tall tower at the northern end of the site and the lower tower at the site's southern half.

The two towers are naturally ventilated through the façade. The typical façade module is 2.8 meters wide and consists of a 2100 mm fixed glass panel and a 700 mm hinged window panel. The fixed glass panel is double-glazed and features high-performance and heat-reflecting properties. The narrow operable window features an exterior perforated, stainless-steel panel that provides protection from the sun, wind, and rain. This panel also contains soundproofing elements to minimize the noise from the surrounding highway and ring road. The interior side of the hinged window consists of a translucent printed screen pattern applied to heat-insulating double glazing.

The BMS controls both the natural ventilation openings and the mechanical conditioning system. Based upon outdoor conditions the BMS decides what conditioning system to operate, the mechanical system of the natural ventilation system.

The control strategy aims at enhancing individual thermal comfort of tenants in the towers. As previously mentioned, the narrow-hinged windows of the façade can be opened or closed individually to allow occupants direct control over their environment. The operation of these windows can also be controlled automatically by the central BMS to offer night-time ventilation during the hot season.

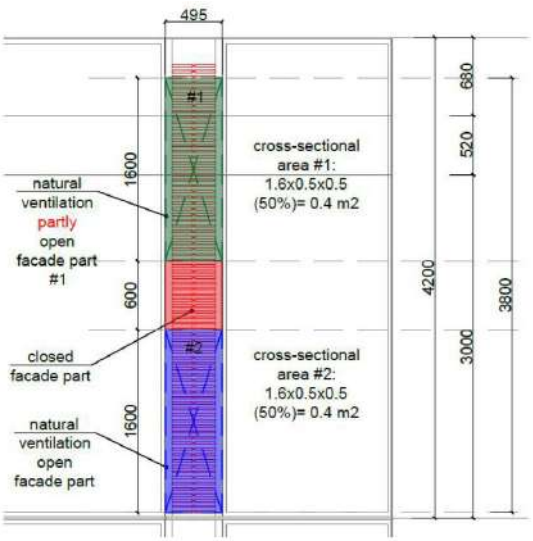

Figure 1 shows the Natural Ventilation openings integrated in the facade

The equation for estimating airflow rate, Q, through two openings of areas A_1 and A_2 on one wall as given in CIBSE Guide A (2015), where h is the total height of the single opening and $A=2A_0$. In the last step $2\sqrt{2}$ has been approximated by 3. This is the equation given in for airflow rate due to temperature difference only for a single opening. So, to simulate a single opening, we equate the single and two opening equations which gives

$h_a = 4/9 * h$

Where: h_a is the height between the two openings

i.e., A single opening may be represented by two equal size openings of half the area of the single opening with a distance between their centers of 4/9 of the total height of the single opening. To represent a single 0.7 m wide by 3.9 m high opening we have modeled a low-level opening is 0.7 m wide by 1.6m high, covered with a 50% perforated stainless-steel plate. The high-level opening is 0.7 m wide by 1.6m high, covered with a 50% perforated stainless-steel plate. The distance between the two openings is 1.73 m.

In total there are 60 openings around the perimeter of a typical floor.

The side-hinged windows can be electronically opened inward on each floor to provide individually controlled natural ventilation. When the windows are open, fresh air is drawn into the offices through the fixed perforated panels. A control panel in each office can be used to individually control lighting, ventilation, temperature, and the operability of the windows and blinds. At night, the building management system (BMS) can electronically open the hinged windows to provide night cooling and modulate temperature fluctuations within the building.

3. ASHRAE STANDARD 55 Adaptive Comfort Compliance

It is the design team's responsibility to ensure that they are using the correct based on the known and predicted conditions of the space and the representative occupants within the space.

There will be times of the year when a natural conditioning system could operate under outside air conditions that allow the space to be compliant with the simplified Graphical Method or the computer based prescriptive Analytical Method. Under warm conditions, however, most naturally conditioned spaces rely on the elevated air speed of both the Elevated Air Speed Method and the Adaptive Method, along with possibly the extended allowable comfort range under the Adaptive Method. It is important to note that the methods are means of showing compliance with comfort under a very narrowly defined set of parameters. Each path has constraints on applicability for each of the available comfort paths in ASHRAE Standard 55 (ASHRAE 2017a), primarily surrounding variables such as clo, met, and air speed.

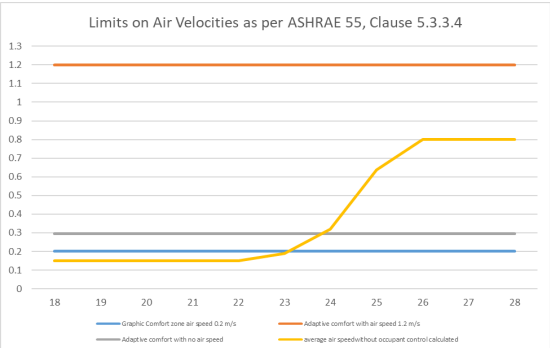

Figure 2 shows a comparison of maximum air velocities from ASHRAE Standard 55 (ASHRAE 2020)

Under the Elevated Air Speed Comfort Zone method, the following limits on air velocity apply as extracted and reordered from ASHRAE Standard 55 (2020b) clause 5.3.3.4:

- Air speed should be greater than 0.2 m/s.
- For operative temperatures (t_o) below 23.0°C.
- For operative temperatures (t_o) between 22.5°C and 25.5°C, the upper limit to average air speed (v_a) it is acceptable to approximate the curve in I-P and SI units by the following equation:
- v_a = 50.49 – 4.4047 to + 0.096425(to)2 (m/s, °C)
- For operative temperatures (t_o) above 25.5°C, the upper limit to average air speed (v_a) should be 0.8 m/s.

This upper limit for the Elevated Speed method is appropriate for most offices and commercial spaces, an air speed of 0.8 m/sec because it corresponds to the point at which loose paper, hair and other light objects may be blown about. It should be noted that when the occupants have control, there is no upper limit so long as one of the following control mechanisms is available (as excerpted from ASHRAE 2021a p.12):

a) "One means of control exists for every six occupants or fewer.

b) One means of control exists for every 84 m2 or less.

c) In multioccupant spaces where groups gather for shared activities, such as classrooms and conference rooms, at least one control shall be provided for each space, regardless of size. Multioccupant spaces that are subdivided by movable walls shall have one control for each space sub-division."

In the case of natural conditioning, the air velocity can rise to 1.2 m/s as per Table 5.4.2.4 in ASHRAE Standard 55 (ASHRAE 2020b). This table is replicated in the excerpts provided in Appendix A6.1 for ease of reference. The Adaptive Method, or Occupant Controlled Naturally Conditioned Spaces Method, also requires that occupants have control over the window openings. Although there are no regulations on control mechanism layout or rules on sharing cohort size for this path, the rules of the Elevated Air Speed Method may serve as a useful starting point, with expansion to more openings or more distribution of openings depending on the results of the dynamic thermal analysis and bulk air flow modelling exercise.

4. LIMITATIONS ON THE USE OF THE ADAPTIVE COMFORT METHOD

Appendix J of ASHRAE Standard 55 (ASHRAE 2020b) advises:

"For the purposes of ASHRAE Standard 55 Section 5.4, occupant-controlled naturally conditioned spaces are those spaces where the thermal conditions of the space are regulated primarily by the occupants through opening and closing of openings in the building envelope. Field experiments have shown that occupants' thermal responses in such spaces depend in part on the outdoor climate and may differ from thermal responses in buildings with centralized HVAC systems primarily because of the different thermal experiences, changes in clothing, availability of control, and shifts in occupant expectations. This optional method is intended for such spaces.

"The space in question must be equipped with operable openings to the outdoors and can be readily opened and adjusted by the occupants of the space."

5. CONSTRAINTS ON OUTDOOR AIR TEMPERATURES

Clause 5.4.1 states "The prevailing mean outdoor temperature is greater than 10°C and less than 33.5°C." This criterion establishes the allowable outdoor air temperatures that are likely to ensure acceptable indoor temperatures with occupant control over windows and openings. When temperatures expand outside this range on the low end, heating systems are likely to exceed allowable heat outputs as regulated by the applicable energy code and thus, occupants will feel overcooled. When temperatures extend outside the range on the upper end, the outdoor air temperature is essentially above the 33°C mean skin temperature of a resting human in comfortable surroundings (as per equation 85 in Chapter 9 of 2021 ASHRAE Handbook Fundamentals (ASHRAE 2021), and thus the outdoor air loses its ability to cool a body during the time when air temperature is this high. The actual outdoor air temperatures are likely to fail in compliance for indoor conditions at temperatures lower than the upper limit on prevailing mean as noted in this limitation.

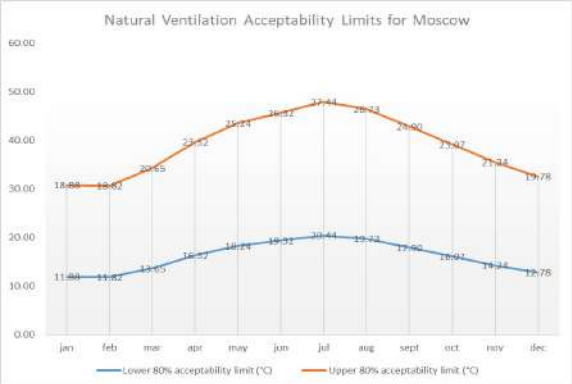

Figure 3 shows the monthly 80% upper and lower temperature limits for Natural Ventilation compliance for Moscow using the Flat Mean approach.

6. APPLYING THE ADAPTIVE COMFORT ZONE METHOD

The Standard 55 User's Manual (ASHRAE 2013) provides a worked example of the application of the Adaptive Comfort Method. This is replicated in Appendix A6.5 for ease of reference. It should be noted that this example used a Flat mean approach for the analysis proposed, which was applicable in older versions of the Standard. The new approach using a prevailing running mean is discussed in a section below.

The procedural steps followed in that example include:

1. Evaluate the applicability of the design against the requirement for operable elements and the four constraints noted above.

2. Calculate the Comfort Zone Thresholds for Compliance

3. Determine Comfort using a dynamic thermal simulation

4. Resolve Comfort Conditions if space is found to be non-compliant.

7. ACCEPTABILITY LIMITS

The acceptability limits for this comfort zone method originated as a graphical representation of empirical data (noted as Figure 5.4.2 in the standard), but the information has since been resolved into the equations noted in Section 5.4.2.2:

- Upper 80% acceptability limit (°C) = 0.31 tpma(out) + 21.3

- Lower 80% acceptability limit (°C) = 0.31 tpma(out) + 14.3

As noted in the Standard 55 User's Manual (ASHRAE 2013):

"It is important to note that only the 80% acceptability limit is used when a user is to show compliance with the Adaptive Method. The 90% acceptability limits are for illustrative purposes only but can be used on a voluntary basis if a designer or building owner chooses to provide higher level of acceptability. For any jurisdictions requiring compliance with Standard 55 though, compliance is only required at the 80% acceptability limits."

8. METHOD

When the design team must demonstrate the compliance of a proposed scheme with the Standard's requirements, it is typical that a bulk airflow and dynamic thermal simulation model will be required at a minimum to understand the complexities of how a space performs under natural ventilation and natural conditioning.

Bulk airflow analytical modelling involves solving simple (linear) equations by hand (or spread sheet) to give more detail about aspects of the ventilation flow, e.g., stack pressure at a certain height or likely stratification height. This type of modelling alone will address natural ventilation flows under limited simple conditions as noted in Chapter 5 but is not sufficiently sophisticated to address natural ventilation.

9. POST-PROCESSING OF RESULTS FROM SIMULATION MODELING

Space dry bulb and operative temperatures as well as air flow through the space are calculated by a simulation program (or manually). The temperatures and air flow are calculated for each hour of the month. The results from a bulk air analysis are fed into a spreadsheet for post-processing.

The results data is sorted into workdays and hours of occupancy and then evaluated for compliance with the comfort thresholds.

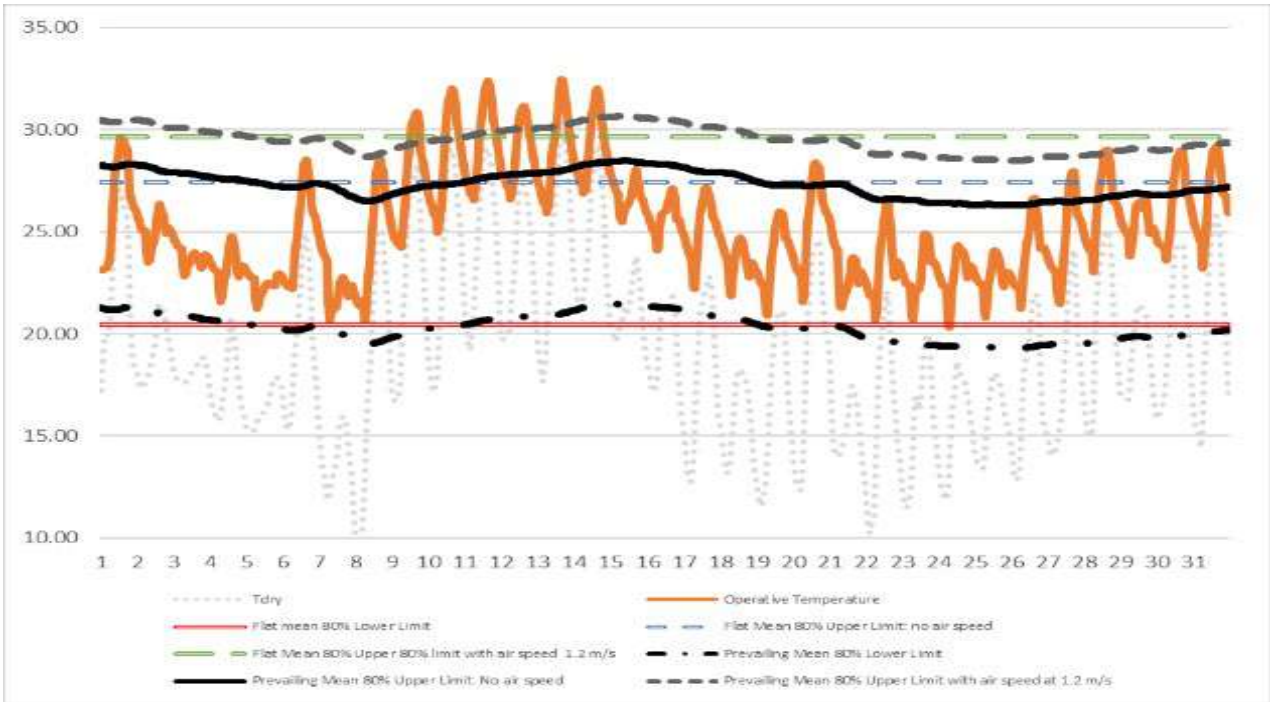

Figure 4 ASHRAE 55 Adaptive Comfort Comparison of Indoor Operative Temperature to Flat Mean and Prevailing Mean Criteria: Buoyancy driven for Moscow in the Month of July, alpha = 0.7 for prevailing mean

Adaptive Comfort Compliance Status July	
Flat mean TOO COLD	0
Flat mean No Speed GOOD	129
Flat Mean with Speed GOOD	177
Flat Mean TOO HOT	21
Prevailing Mean TOO COLD	0
Prevailing Mean No Speed GOOD	127
Prevailing Mean with Speed GOOD	177
Prevailing Mean TOO HOT	21

For the analyses performed for this paper, the assumed external dry bulb used to seed the start of the prevailing mean calculation used the first 24 hours of the outside air-dry bulb.

10. "FLAT" MEAN VERSUS PREVAILING MEAN TO SET TEMPERATURE LIMITS

Section 5.4.2.1.3 of ASHRAE Standard 55 (ASHRAE 2020b) requires that the compliance analysis use a prevailing mean daily temperature within the acceptability equations in 5.4.2.2 as noted above. According to ASHRAE Standard 55 (ASHRAE 2020b) Appendix J, this requirement "represents the broader external climatic environment to which building occupants have become physiologically, behaviourally, and psychologically adapted."

When a design team is testing the quick feasibility of a scheme, it may be easier to obtain and calculate the Flat mean temperatures to see if the scheme is in the realm of gross compliance.

For Moscow, the Flat mean temperature is calculated to set the full month's 80% acceptability limits as noted in the figure below.

Taking the data, the results below show the comparison between the Flat mean and Prevailing running mean methods for a month's worth of data. As noted in the graph below, the prevailing mean fluctuates in response to the outdoor air temperatures, and it runs sometimes lower and sometimes higher than the Flat mean.

11. DEMONSTRATING COMPLIANCE WITH THE ASHRAE STANDARD 55 ADAPTIVE COMFORT METHOD

A further post-processing bins the Flat and Prevailing Mean results to show how many hours in the month meet the comfort standard, with and without elevated air speed, for the model's current

configuration of openings. The primary observation shown in the two figures below is that there is less than a 5% difference in the estimate of the hours falling into the compliance zone, whether without elevated speed or with it. The greatest percent differential is in the TOO HOT category, but as the total number of non-compliant hours is so low, this represents a total of 17 hours difference in the variability of using the Flat mean instead of the Prevailing mean.

There remain several hours in the TOO HOT category, which would fall into the definition of exceedance hours. Per the definitions in Section 3 of ASHRAE Standard 55 (ASHRAE 2020b), these are "the number of occupied hours within a defined time period in which the environmental conditions in an occupied space are outside of the comfort zone." The designer can either perform iterations to increase opening sizes to comply with the Adaptive Comfort Method for 100% of occupied hours.

Alternatively, one could discuss with the Owner and the Authority having Jurisdiction what the acceptable number of exceedance hours can be. If one looks for parallels with mechanical comfort conditioning systems, ASHRAE Standard 90.1 (ASHRAE 2019) clauses 11.5.2.i and G3.1.2.3 require that unmet load hours not exceed 300 in terms of equipment sizing and performance within the energy model showing compliance for energy efficiency.

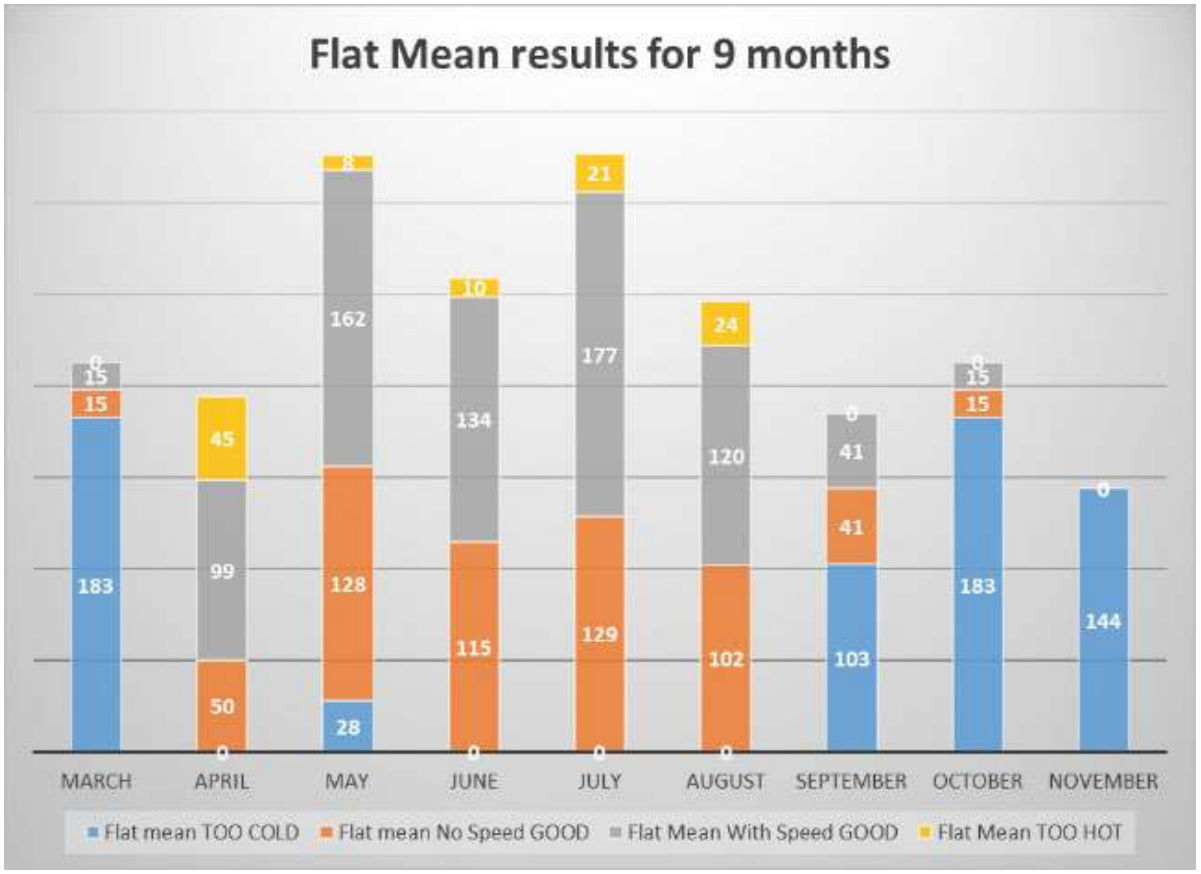

Figure 5 Shows the ASHRAE 55 Flat Mean Natural Conditioning Compliance Hours for a typical floor of the Moscow project due to Buoyancy Driven ventilation for 9 months of the year.

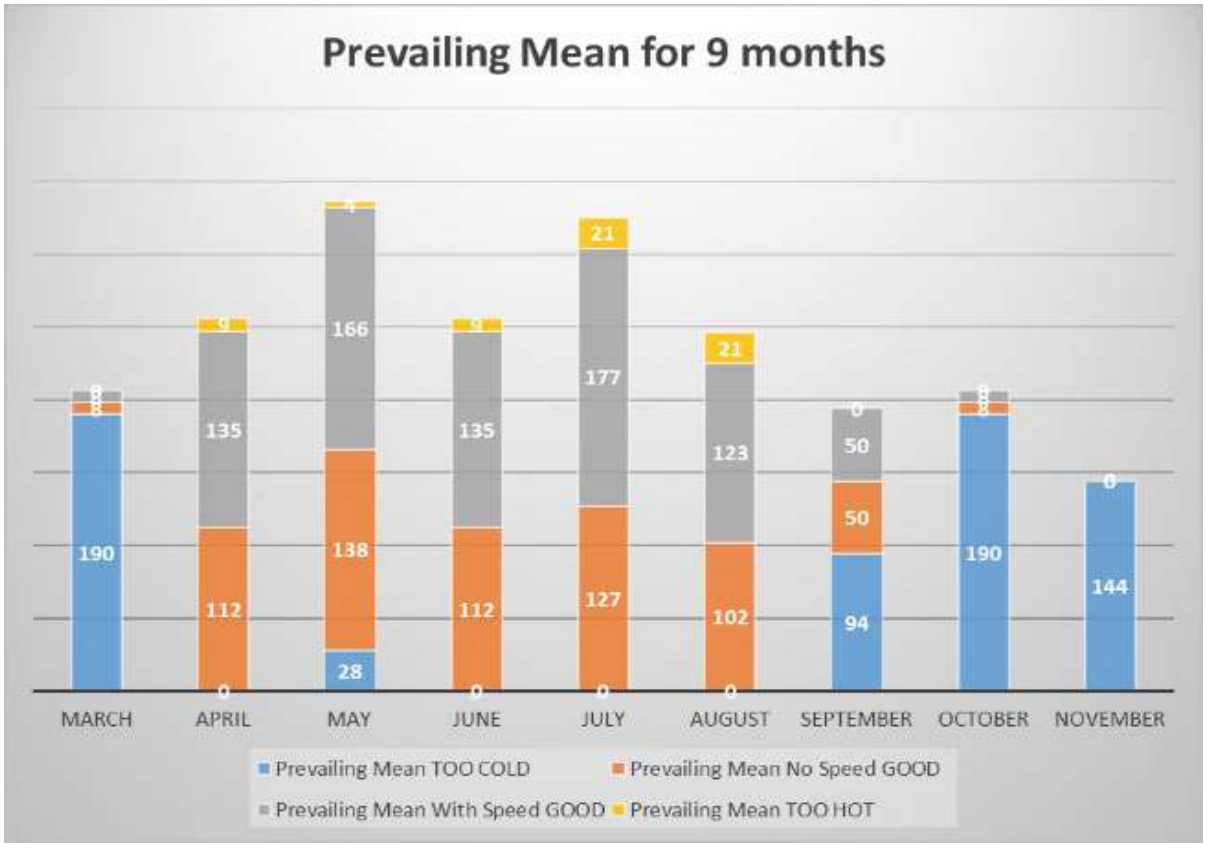

Figure 6 Shows the ASHRAE 55 Prevailing Mean Natural Conditioning Compliance Hours for a typical floor of the Moscow project due to Buoyancy Driven ventilation for 9 months of the year

From Figures 5 and 6 we can see that months March, October and November have most hours which are "too cold" and therefore Natural Ventilation should not be considered during these months as well as December, January, and February. September has more than 100 hours when it is "too cold" and we would not recommend utilizing Natural Ventilation during this month.

From Figure 5 we can see that months March, October and November have most hours which are "too cold" and therefore Natural Ventilation should not be considered during these months as well as December, January, and February. September has more than 90 hours when it is "too cold" and we would not recommend utilizing Natural Ventilation during this month.

12. Conclusions

The adaptive comfort method does provide a clear method of showing compliance for naturally ventilated spaces. However, there is some disparity when using the compliance method from ASHRAE Standard 55 (2020b) as the limits required for compliance are based upon steady state conditions. The results shown in the paper are based upon results from a dynamic simulation program. When using a post processor, the results can be simply shown as good or no good, which greatly assists the design process.

Most compliance hours during warm weather come from the assumption that spaces will have controllable ceiling fans.
This study is unique in that it simulates and reports comfort simultaneously to energy savings for each of the studied climate zones. This direct comparative reporting from simulation models can be applied at the single building level to provide credible trade-off information to help with decision making on the energy versus comfort question after many of the other risks have already been deemed manageable.
The true energy savings from utilizing natural ventilation options are integrated with dynamic simulation programs.

Acknowledgement

The author would like to acknowledge Erin McConahey who was co-author of the ASHRAE Design Guide for Natural Ventilation (2021).

Data Access

The datasets generated during or analysed during the current study are not publicly available because they are owned by the client.

References

Alliance for Sustainable Energy, LLC. Undated. Open Studio®. This software can be obtained at

https://www.openstudio.net as of August 24, 2019.

ASHRAE. 2019 ANSI/ASHRAE Standard 90.1-2019. Energy Standard for Buildings Except Low-Rise Residential Buildings (I-P Edition). Atlanta: ASHRAE.

ASHRAE. 2020a. ANSI/ASHRAE Standard 62.1-2020. Ventilation for Acceptable Indoor Air Quality. Atlanta: ASHRAE.

ASHRAE. 2013. Standard 55 User's Manual Based on ANSI/ASHRAE Standard 55-2013 Thermal Environmental Conditions for Human Occupancy. Atlanta: ASHRAE.

ASHRAE. 2020b ANSI/ASHRAE Standard 55-2020. Thermal Environmental Conditions for Human Occupancy. Atlanta: ASHRAE.

ASHRAE. 2021a ASHRAE® Handbook, Fundamentals, SI Version. Atlanta: ASHRAE.

ASHRAE 2021b Design Guide for Natural Ventilation, Atlanta: ASHRAE

Belding H., and Hatch, T. 1955. Index for evaluating heat stress in terms of the resulting physiological strains. *Heating, Piping and Air Conditioning*. 27 (8):129-136.

Brotherhood, J. 2008. Heat stress and strain in exercise and sport. Journal of Science and Medicine in Sport (2008) 11: 6-19.

CIBSE Guide A, Environmental Design, 2015, The Chartered Institution of Building Services Engineers (CIBSE)

DesignBuilder Software Ltd. Undated. Design Builder Software Packages. Accessed on August 24, 2019 at https://designbuilder.co.uk/software/product-overview.

Digital Alchemy Inc. Undated. Simergy™. Digital Alchemy, Inc. This software can be obtained at https://d-alchemy.com/products/simergy as of August 24, 2019.

Havenith, G., K. Kuklane, J. Fan, S. Hodder, Y. Ouzzahra, K. Lundgren, Y. Au, and D. Loveday. 2015. A database of static clothing thermal insulation and vapor permeability values of non-Western ensembles for use in ASHRAE Standard 55, ISO 7730, and ISO 9920. ASHRAE Transactions 121(1).

Hoyt, T., Schiavon, S., Piccioli, A., Cheung, T., Moon, D., and Steinfeld, K. 2017. CBE Thermal Comfort Tool. Center for the Built Environment, University of California Berkeley, http://comfort.cbe.berkeley.edu/

Humphreys, M., and J.F. Nicol. 1998. Understanding the adaptive approach to thermal comfort. ASHRAE Technical Data Bulletin 14(1):1-14.

ICC. 2014. 2015 International Mechanical Code®. International Code Council, Inc. Country Club Hills, IL.

IES. Undated-b. IES Virtual Environment (IESVE). Integrated Environmental Solutions Limited. This software can be obtained at https://www.iesve.com/software as of August 24, 2019.

McConahey, E. 2008. Finding the Right Mix. ASHRAE Journal 50(9): 36-48.

McCullough, E., and B.W. Jones. 1984. A comprehensive data base for estimating clothing insulation. IER Technical Report 84-01, Institute for Environmental Research, Kansas State University, Manhattan. ASHRAE Research Project RP-411, Final Report.

McCullough, E., B.W. Jones, and T. Tamura. 1989. A data base for determining the evaporative resistance of clothing. ASHRAE Transactions 95(2).

NIST. Undated. CONTAM. National Institute of Standards and Technology. This software can be obtained at https://www.nist.gov/services-resources/software/contam as of August 24, 2019.

Oasys Ltd. Undated. UNIPAC Software for Students and Institutions. This software can be obtained at https://www.oasys-software.com/education/ as of August 24, 2019.

Trimble Inc. Undated. Sefaira: Early stage analysis for designers who care about building performance. This software can be obtained at https://sefaira.com/ as of August 24, 2019.

UW Madison. Undated. A Transient Systems Simulation Program. The University of Wisconsin, Madison. This software can be obtained at https://sel.me.wisc.edu/trnsys/ as of August 24, 2019.

Investigation of PECS on the basis of a virtual building controller

Katharina Boudier [a], *Sabine Hoffmann* [b]

[a] Chair of Built environment, Faculty of Civil Engineering, Technical University of Kaiserslautern, Kaiserslautern, Germany, katharina.boudier@bauing.uni-kl.de.

[b] Chair of Built environment, Faculty of Civil Engineering, Technical University of Kaiserslautern, Kaiserslautern, Germany, sabine.hoffmann@bauing.uni-kl.de.

Abstract. Thermal comfort is one of the key parameters for occupant satisfaction and, accordingly, for the energy performance of buildings. In recent years, decentralized heating and cooling systems, so called personal environmental comfort systems (PECS) are gaining more interest for research and the market. PECS include, for example, office chairs with heating and cooling functions, thermoelectric heating and cooling walls, or even desk fans. Studies have shown that these systems can reduce the heating and cooling demand of the central HVAC systems by improving comfort.

This paper presents a newly developed adaptive building controller that uses a holistic approach in the consideration of central HVAC systems and a heated and cooled office chair, within the framework of the building simulation software Esp-r. The presented building controller can adapt the setpoint temperatures of the central heating and cooling system and also regulate the usage of the office chair's climate function based on the thermal sensation and comfort values of a virtual thermal manikin with the help of PhySCo a transient "Physiology, Sensation and Comfort Model". This approach can be used for an analysis of the potential of PECS.

In this context, the virtual adaptive building controller with a wide deadband and adaptive setpoints between 18 to 26 °C is compared to a basic controller with a fixed and narrow setpoint range between 21 to 24 °C. The simulations were performed for temperate climate (Mannheim, Germany) that is classified as Cfb climate according to the Köppen-Geiger classification.

The results showed that the newly developed adaptive controller with the PECS kept the comfort values at the same level as the basic controller. An office chair with heating/cooling function had been added to the controller and helped to keep comfort while reducing the heating demand (13 % in winter, 4 % in spring) and the cooling demand (10.3 % in spring, 2.6 % in summer).

Keywords. decentralized heating and cooling systems, PECS, office chair with heating and cooling function, virtual building controller, thermal comfort.
DOI: https://doi.org/10.34641/clima.2022.191

1. Introduction

The building sector has a high influence on greenhouse gas emission. Buildings together with the buildings construction sector are responsible for over one-third of the global end energy consumption and almost 40 % of the direct and indirect CO2 emissions [1]. New solutions are required to reduce the global warming compared to the pre-industrial era and to achieve near climate neutrality [2]. The European EPBD (Energy Performance of building directive) supports buildings which will be offer new control devices for monitoring and controlling the indoor air quality (IAQ) [3]. As the energy balance of buildings is highly driven by the thermal comfort satisfaction of building occupants and by occupant behaviour (e.g., window opening, heating and cooling periods/time and heating/cooling setpoints) [4][5] further solutions are required.

Office buildings are often maintained with a tight, so called deadband, with setpoints around 21 °C to 24 °C, in order to sustain a thermally comfortable state. In reality building occupants prefer a more adaptive deadband and room temperatures which are not predefined in a strict range [6]. In addition, maintaining a tight deadband consumes a higher amount of energy to satisfy the temperature range[7].

Copyright ©2022 by the authors. This conference paper is published under a CC-BY-4.0 license.

To reduce the energy demand of office buildings, the usage of decentralized heating and cooling systems, or so called "Personal Environmental Comfort Systems" (PECS) seems a promising approach. During a few years an increasing interest of these systems can be seen in research and the market. They influence the direct environment of building occupants by heating or cooling local body parts or supply fresh air. From a thermal comfort aspect individual body parts should get more consideration, as the discomfort of individual body parts can drive overall discomfort [8].

Thermal comfort is affected by personal factors of the activity level (metabolic rate), the clothing insulation (e.g., winter/summer clothing) but also from environmental conditions as air temperature, radiant temperature, air velocity relative humidity and direct solar influence. Aside from the above mentioned the cultural background has an impact on thermal comfort [9] and the thermal history of people, as considered in the "Adaptive Comfort Model", implemented in the ASHRAE Standard 55. Moreover, particular body parts indicate different sensitivities to heat or cool effects. While the head is susceptible to heat and might lead to a general feeling of discomfort, the feet are more sensitive to cold stimuli. The total overall comfort is determined by a few strong body parts with a high influence on overall comfort like chest, back, pelvis [8].

Liu et al. found that building occupants alter their working environment in reaction to discomfort [10, 11], and that the ability to control the direct environmental conditions around a person can improve their satisfaction [11], which support the usage of PECS. Various studies have demonstrated the energy-saving effects of PECS by increasing the comfortable deadband [12]. Office chairs with heating and cooling functions could reduce the setpoint temperatures of the central HVAC system to 18 °C or even 16 °C [13]. Few studies are available for even lower room temperatures, as mentioned in the review paper from Rawal et al. [14].

For this reason, the application of decentralized heating and cooling systems in office buildings seems promising, as they have the ability to directly change the occupant's immediate environment and consider individual body parts. Also, the individual needs can get considered. Decentralized heating and cooling systems or PECS like office chairs [13, 15, 16], fans [18, 19], and thermo-electric cooling walls [28–30] have been researched for their cooling properties. Foot warmers [20], office chairs [16, 17, 21] and further solutions, such as localized floor heating mentioned by Rawal et al. [14] can be used for heating purpose. Fig.1 shows a few of the used systems in the "Living lab smart office" space in Kaiserslautern.

Some of these systems are already available on the market but proper planning tools for architects, facility manager, etc. are missing for an estimation, whether it is worthwhile for the operation and acquisition of these systems.

Fig. 1 – Decentralized heating and cooling systems in the Living lab smart office space: an office chair with heating and cooling function, a foot warmer and a desk-fan.

The aim of this paper is to present the developed virtual building controller which consider the office chair with heating and cooling function. All the previous mentioned environmental influences must be included in the planning phase of the building and plant systems in order to account for the energy demand of buildings. For the planning stage building simulation software can get used. For the controlling of PECS, the calculation of detailed local sensation and comfort values is fundamental. For this the coupled "Physiology, Sensation and Comfort" model PhySCo was used [21–25]. PhySCo is based on the work of the 65-Node model of Tanabe [26], Huizenga [27], Hoffmann [28]. The "Sensation and Comfort Model" is based on the equations of Zhang et al. [8, 29, 30] and Zhao [31]. PhySCo can be used as a standalone version or coupled with the building simulation software Esp-r [22].

To calculate detailed sensation and comfort values, it is mandatory to gather detailed MRT-values for the Physiology model. This happens with the approach of "(Wo)Man in Cube" [24]. This solution gathers detailed view-factors for long time building simulations. The view-factors are used for the comprehensive MRT calculations for different body parts. The approach is based on a precalculated view-factor set for different manikin positions like sitting/standing. The manikin can be moved in the building zone and allows the consideration of asymmetric and transient conditions.

This presented work will contribute to an approach that allows an analysis of the potential of decentralized heating and cooling systems in terms of occupant comfort and possible energy savings using a building simulation tool. The study shows how to regulate decentralized heating and cooling systems as well as the central heating and cooling system using a virtual adaptive building controller that takes specific thermal comfort values of a manikin into account.

2. The virtual building controller

2.1 General information

PhySCo is coupled with the building simulation software ESP-r [21, 32]. The Physiology model calculates 16 skin and core temperatures based on the environmental conditions like dry bulb temperature, relative humidity, mean radiant temperature, air velocity and solar influence. Furthermore, personal parameters like the clothing insulation and the metabolic rate are considered. For the) calculation the physiology model takes thermoregulation processes as sweating, shivering, vasodilatation and vasoconstriction of the blood vessels into account. With the 16 skin and core temperatures the local sensation S_l is calculated.

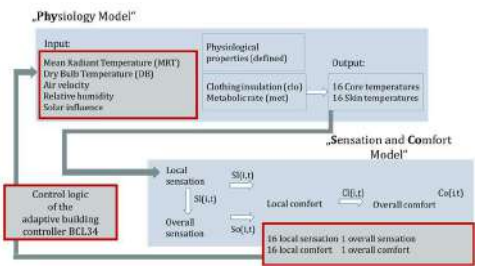

Fig. 2 – Coupling of PhySCo within the virtual adaptive building controller BCL34 to maintain thermally comfortable conditions.

Based on the (S_l), overall sensation (S_o) is calculated and in combination with the latter local comfort (C_l) can get determined. Overall comfort (C_o) is based on the local comfort (C_l) values.

2.2 The adaptive building controller

The virtual adaptive building controller is based on an ideal basic controller (BCL00) in ESP-r. BCL00 considers the area-weighted mean radiation fraction. In addition, the indoor air temperature Q_a is included as a convective component. The percentage ratio (C) between air temperature and the mean radiant temperatures Q_r can be set separately for the sensor and the actuator. The mixed sensed temperature Q_s is calculated as following:

$$Q_s = \frac{Q_a * C}{100} + \frac{Q_r * (100 - C)}{100} \quad (1)$$

If the sensed temperature Q_s exceeds the upper setpoint TU, heat energy is dissipated in the next time step (equation 2). $\dot{Q}$ represents the heating and cooling demand of the next timestep. If the temperature falls below the lower setpoint TL, heat energy is supplied in the next timestep (equation 3).

$$Q_s > \text{TU} \quad \dot{Q}^* = -Q \quad (2)$$

$$Q_s < TL \quad \dot{Q}^* = +Q \quad (3)$$

Changes have been made for the setpoints (TU, TL) of the controller, which are controlled based on sensation and comfort values of a virtual manikin instead of fixed setpoint-temperatures. The sensation and comfort values can be shown with an extended ASHRAE-7-point scale based on Zhang's et al. publication [29]. For sensation a 9-point scale is used, which ranges from very cold (-4) over neutral (0) to very hot (+4). For thermal comfort a 6-point scale, without a neutral point, is used. A person feels either comfortable or uncomfortable. The range is from very uncomfortable (-3) to very comfortable (+3). Fig. 3 shows a one-day simulation in summer with the adaptive building controller.

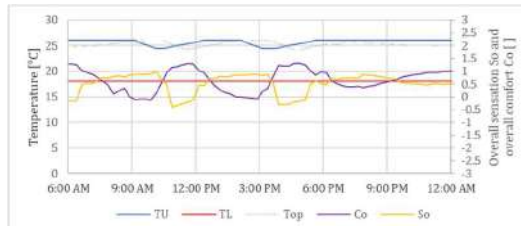

Fig. 3 – One day simulation in summer with the adaptive building controller based on thermal sensation and comfort.

In Fig. 3 the cooling setpoint TU was relevant and have been adapted according to a negative comfort value Co (< 0). If Co is negative, the overall sensation (So) level of the manikin decides about raising or reducing the setpoint. In the above shown case, So was in a warm direction (> 0). Accordingly, the controller lowers the cooling setpoint (TU) unless a positive comfort level is reached. If Co is between 0.5 to 1.0 the setpoints of the HVAC system are slowly set back to the initial setpoints (TU = 26°).

2.3 The adaptive building controller in combination with the office chair with heating and cooling function

To increase the comfort of the adaptive building controller further and subsequently reduce the energy demand of the central HVAC system, a decentralized heating and cooling system was added to the building controller. The office chair with heating and cooling function (Fig. 4) already on the market, was modelled and used in the controller.

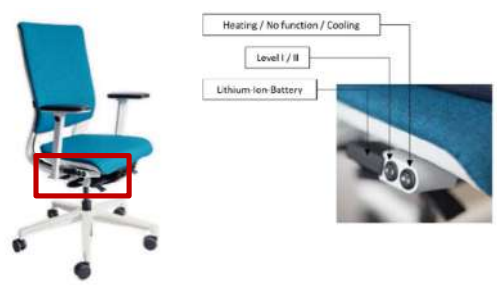

Fig. 4 – Office chair with heating and cooling function and control panel (climate functions, power level).

<u>Modelling the usage of climate functions</u>

The climate changes for the chair directly affect the exposed body parts as back, pelvis and thighs, in the physiology model. For this purpose, equation 4 (proposed by Madsen et al. [33]) of the equivalent temperature $t_{eq,i}$ is relevant. This equation is calculated for each of the 16 body parts (i). It

considers the influence of the zone air temperature t_a, the mean radiant temperature of the single body parts $\bar{t}_{r,i}$, the air velocity at the single body parts $v_{a,i}$ and the clothing insulation $I_{cl,i}$ of the specific body parts.

$$t_{eq,i} = \left(0.55t_a + 0.45\bar{t}_{r,i} + \frac{0.24-0.75\sqrt{v_{a,i}}}{1+I_{cl,i}}(36.5 - t_a)\right) \quad (4)$$

Based on the control logic of the adaptive controller (Fig. 5), the chair temperature is changed for no use, cooling (-4 K) or heating (+4 K). The temperature difference is assumed based on a subjective experiment in the "living lab smart office space" in Kaiserslautern.

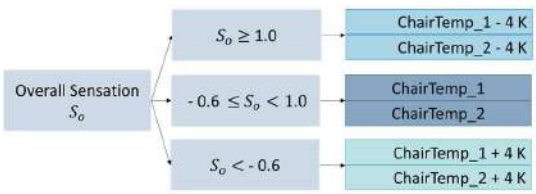

Fig. 5 – Decision of the control logic of the adaptive building controller for the office chair with heating and cooling function, based on overall sensation S_o. ChairTemp_1 represents the backrest, ChairTemp_2 represents the seat.

In the case of a negative S_o value, the control logic decides for the use of the chairs heating function (ChairTemp + 4 K) on the basis of the equation 5. Accordingly, the cooling function will be used for a positive S_o value higher than 1.0 on the sensation scale (equation 6).

Heating function:

$$t_{eq} = \left(0.55t_a + 0.45\bar{t_r} + \frac{0.24-0.75\sqrt{v_a}}{1+I_{cl}}(36.5 - t_a)\right) + 4\ K \quad (5)$$

Cooling function:

$$t_{eq} = \left(0.55t_a + 0.45\bar{t_r} + \frac{0.24-0.75\sqrt{v_a}}{1+I_{cl}}(36.5 - t_a)\right) - 4\ K \quad (6)$$

2.4 Use of the adaptive building controller in combination with the office chair with heating and cooling function

The following figures show the use of the adaptive building controller with the chair for a one-day simulation in summer and the local sensation and comfort values for the back. The left y-axis shows the chair temperature; ChairTemp_1 for the backrest and ChairTemp_2 for the seat, DB represents the dry bulb temperature for the comparison and for the case no climate function is used. The secondary y-axis represents the overall sensation (So), which is responsible for the controlling of the chair temperature.

The following graph shows the usage of the cooling and the heating function. First the cooling function is used (visible due to the 4 K decrease compared to DB). Around noon the heating function is used, as S_o dropped below the sensation setpoint for cooling of -0.6 on the sensation scale. The black lines show the S_o setpoints (SP) at -0.6 and +1.0. If S_o is within the SP, the temperature function of the chair is not used. The upper SP of 1.0 is exceeded at 9:00 AM, at 9:30 AM as well as at 13:30 AM, so the cooling function is used. Once S_o falls below the lower SP value of -0.6, the heating function is used.

Fig. 6b shows a clear effect of the office chair with heating and cooling function in local thermal sensation (S_l), which results in a change in local thermal comfort (C_l). After using the cooling function of the office chair there is an increase for the back (C_{l_back}). After using the heating function of the office chair, there is an increase in the S_l with an initial increase in C_l until it decreases later on. After using the cooling function at 1:30 pm (**Fig. 6**), there is once again an increase in C_l.

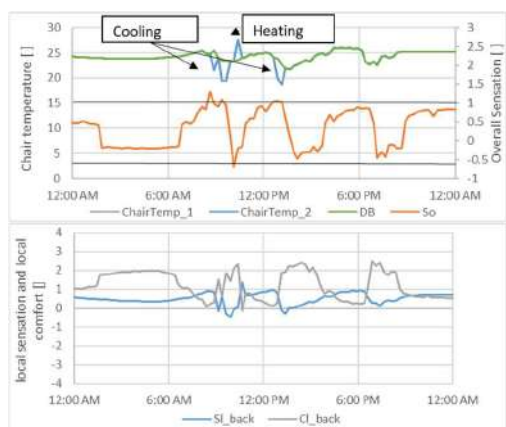

Fig. 6 - One day simulation in August with the adaptive controller with chair. a) use of the cooling and heating function, based on overall sensation, b) local sensation S_l and local comfort C_l for the back

3. Simulation study

3.1 Simulation model and parameter

To show the influences on thermal comfort and on a possible reduction of the energy demand, the newly developed adaptive controller (BCL34) with variable setpoints is compared with a basic controller (BCL00) with fixed setpoints. A simulation study has been conducted with a shoebox model, consisting of one zone, with the dimensions of 5m length x 3m width x 2.7m height.

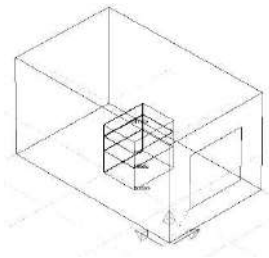

Fig. 7 – One zone shoebox-model with "(Wo)Man in Cube", window-to-wall ratio 30 %

Tab. **1** shows the heating and cooling capacity of the basic controller BCL00 with a tight deadband and fixed setpoints and the adaptive controller BCL34 with a wide deadband and variable setpoints.

Tab. 1 - Heating and cooling capacity, heating (TL) and cooling setpoint (TU) of the basic controller BCL00 and the adaptive controller BCL34.

	BCL00	BCL34
Max. heating capacity [W]	2000	2000
Max. cooling capacity [W]	2000	2000
Heating setpoint TL [°C]	21	18
Cooling setpoint TU [°C]	24	26

Table 2 shows the different simulation periods regarding of the used clothing insulation values. The activity level (met) is always constant with 1.0 met. Simulation timesteps (TS) are chosen with 4 TS per hour; the number of TS are shown for each period.

Tab.2 - Simulation periods based on clothing insulation.

Simulation periods	Clothing [clo]	Activity [met]	timesteps [n]
15th October to 15th March	1.0	1.0	14496
15th March to 15th May	0.7	1.0	5856
15th May to 15th October	0.5	1.0	14688

3.2 Simulation results

Figure 9a shows the frequency of comfort values for BCL00, BCL34 and BCL34_Chair during the winter period (15th October to 15th March). It can be seen, that BCL00 reaches the highest frequency in the area from 0.4 to 0.8 on the comfort scale, whereas in the area of 1 to 2 the three controllers perform similar. The adaptive variants with BCL34/BCL34_Chair show a higher frequency in the area from -0.2 to 0.2 on the comfort scale. However, when comparing the heating and cooling demand for the building zone (Tab. **3**) for the winter period it is clear that the variant with chair has a 13.5% lower heat demand compared to the basic controller (BCL00). The proportion of the cooling demand is small during the winter period and can be neglected.

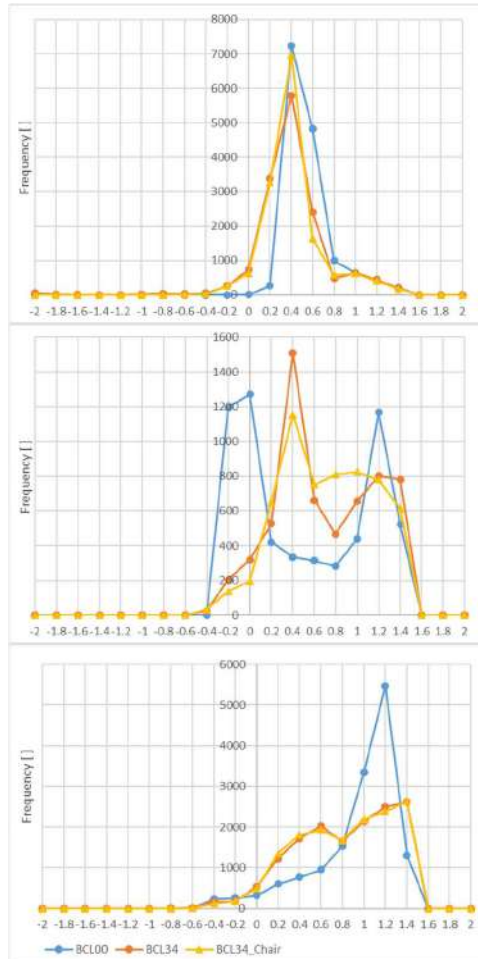

Fig. 8 - Frequency of the comfort values for the period from a) 15th October to 15th March, b) 15th March to 15th May, c) 15th May to 15th October for the different controllers: Basic controller BCL00, adaptive controller BCL34, adaptive controller with office chair with heating and cooling function BCL34_Chair

Tab. 3 - Heating demand (HD) and Cooling demand (CD) of the three periods (winter, spring, summer) and an annual comparison between BCL00 and BCL34_Chair

Comparison BCL00 und BCL34_Chair								
Time period	Winter		Spring		Summer		Annual	
Controller	**BCL00**	**BCL34_ Chair**	**BCL00**	**BCL34_ Chair**	**BCL00**	**BCL34_ Chair**	**BCL00**	**BCL34_ Chair**
Heating demand HD [kWh/m²]	54	47	5	5	0	0	60	52
Cooling demand CD [kWh/m²]	1	0	7	6	43	42	51	48
Reduction HD [kWh/m²]	13.50% (7.3)		3.60% (0.2)		--		12.70% (7.6)	
Reduction CD [kWh/m²]	--		10.30% (0.7)		2.60% (1.1)		5.40% (2.8)	
Chair power [kWhel]	--	39	--	9	--	4	--	52
Chair power [kWhel/m²]	--	2.6	--	0.6	--	0.3	--	3.4

The results for spring show an interesting distribution of the comfort values. BCL00 presents two frequency peaks in the area of -0.4 to 0 and in the area of 1 to 1.2, whereas the adaptive variants show a distribution in the area of 0.4 to 1. BCL34_Chair has less frequency in the area of 0.2 to 0.6 but a higher frequency in the area of 0.6 to 1 compared to BCL34.

Higher frequency can get reached with the adaptive variants for comfort values of 1.6. During the spring period, both the heating demand and the cooling demand can get reduced with BCL34_Chair. The variant saves 3.6% of heating demand and 10.3% of cooling demand compared to the BCL00.

For the summer months, the adaptive variants indicate a peak in the area of 0 to 0.6 and again for a comfort value of 1.4 compared to BCL00. BCL00 present a high frequency of comfort values in the area of 1 to 1.2. During the summer period, the controller with chair shows a 2.6 % lower cooling demand compared to the basic controller BCL00.

Compared to BCL00 for the adaptive controller with chair a reduction of the annual heating and cooling demand is evident. The heating demand was 12.7% lower compared to BCL00. The cooling demand was reduced by 5.4 % compared to BCL00.

4. Discussion

The simulations clarify that the comfort level can be mostly maintained in a positive range or even increased with the help of the chair with heating and cooling function simultaneously reducing the heating and cooling demand.
The usage of the office chair with heating and cooling function can be recommended for all season with regard to the thermal comfort level as well as the reduction of the energy demand.
Nevertheless, the reduction for the cooling demand of the central HVAC system is not as high as expected. For higher room temperatures above 28°C, the additional usage of a desk fan is recommended, as the heat sensitive head has a high influence on overall comfort. The supporting effect of an office chair with heating and cooling function regarding thermal comfort, which have been studied in various field and laboratory experiments, have been showed in the simulation study.

5. Outlook

The presented adaptive controller with chair can get used for a potential analysis for other decentralized systems like a thermoelectric cooling wall, fans or combinations of the systems. In the future, further systems should get implemented and the systems will be modelled as separate heating and cooling systems within the plant technology to allow a more detailed analysis.
The PhySCo model predicts detailed comfort values through annual simulations, which will support the planning process of the decentralized and the central HVAC system. The shown approach offers a promising solution for a base to analyses the potential of decentralized heating and cooling devices as they are coming more and more to the market.

6. References

Literatur

[1] International Energy Agency: Buildings. A source of enormous untapped efficiency potential. https://www.iea.org/topics/buildings.

[2] Bundesministerium für Wirtschaft und Energie (BMWi): Klimaschutz. Abkommen von Paris. https://www.bmwi.de/Redaktion/DE/Artikel/Industrie/klimaschutz-abkommen-von-paris.html (Abruf: 31.01.2022).

[3] European Commission: Questions and Answers on the Revision of the Energy Performance of Buildings Directive. https://ec.europa.eu/commission/presscorner/detail/en/QANDA_21_6686 (Abruf: 05.01.2022).

[4] IEA-EBC Annex 66: Energy in Buildings and Communities Programme. Definition and Simulation of Occupant Behavior in Buildings. https://www.annex66.org/?q=Introduction (Abruf: 18.01.2018).

[5] IEA EBC - Annex 79: IEA EBC - Annex 79 - Occupant-Centric Building Design and Operation. https://annex79.iea-ebc.org/ (Abruf: 04.01.2022).

[6] Luo, M.; Zhang, H.; Arens, E.; Ghahramani, A.; Wang, Z.; Jin, L.; He, Y.: Heating and cooling the human body with energy-efficient personal comfort systems (PCS). Indoor Enviornmental Quality (IEQ). In: The 15th Conference of the International Society of Indoor Air Quality & Climate (ISIAQ), 2018.

[7] Ghahramani, A.; Zhang, K.; Dutta, K.; Yang, Z.; Becerik-Gerber, B.: Energy savings from temperature setpoints and deadband: Quantifying the influence of building and system properties on savings. Applied Energy 165 (2016), S. 930–942.

[8] Zhang, H.; Arens, E.; Huizenga, C.; Han, T.: Thermal sensation and comfort models for non-uniform and transient environments, part III: Whole-body sensation and comfort. 1st International Symposium on Sustainable Healthy Buildings 45 (2010), Heft 2, S. 399–410.

[9] Mahdavi Adeli, M.; Farahat, S.; Sarhaddi, F.: Increasing thermal comfort of a net-zero energy building inhabitant by optimization of energy consumption. International Journal of Environmental Science and Technology 17 (2020), Heft 5, S. 2819–2834.

[10] Liu, J.; Yao, R.; McCloy, R.: An investigation of thermal comfort adaptation behaviour in office buildings in the UK. Indoor and Built Environment 23 (2013), Heft 5, S. 675–691.

[11] Lee, S. Y.; Brand, J. L.: Effects of control over office workspace on perceptions of the work environment and work outcomes. Journal of Environmental Psychology 25 (2005), Heft 3, S. 323–333.

[12] Hoyt, T.; Arens, E.; Zhang, H.: Extending air temperature setpoints. Simulated energy savings

and design considerations for new and retrofit buildings. Building and Environment 88 (2015), S. 89–96.

[13] Pasut, W.; Zhang, H.; Arens, E.; Kaam, S.; Zhai, Y.: Effect of a heated and cooled office chair on thermal comfort. HVAC&R Research 19 (2013), Heft 5, S. 574–583.

[14] Rawal, R.; Schweiker, M.; Kazanci, O. B.; Vardhan, V.; Jin, Q.; Duanmu, L.: Personal comfort systems: A review on comfort, energy, and economics. Special Issue on Thermal Comfort Standards 214 (2020), S. 109858.

[15] Hoffmann, S.; Boudier, K.: A new approach to provide thermal comfort in office buildings: A field study with heated and cooled chairs.". In: Proceedings of Indoor Air Quality Ventilation & Energy Conservation in Buildings (IAQVEC), Incheon Songdo, Republic of Korea, October 2016, 2016.

[16] Boudier, K.; Hoffmann, S.: Heated and cooled chairs for office use. In: conference proceedings ICHES2016 Nagoya; October/November 2016, 2016.

[17] Rissetto, R.; Schweiker, M.; Wagner, A.: Personalized ceiling fans: Effects of air motion, air direction and personal control on thermal comfort. Special Issue on Thermal Comfort Standards 235 (2021), S. 110721.

[18] Habchi, C.; Chakroun, W.; Alotaibi, S.; Ghali, K.; Ghaddar, N.: Effect of shifts from occupant design position on performance of ceiling personalized ventilation assisted with desk fan or chair fans. Special Issue on Thermal Comfort Standards 117 (2016), S. 20–32.

[19] Zhang, H.; Arens, E.; Taub, M.; Dickerhoff, D.; Bauman, F.; Fountain, M.; Pasut, W.; Fannon, D.; Zhai, Y.; Pigman, M.: Using footwarmers in offices for thermal comfort and energy savings. Special Issue on Thermal Comfort Standards 104 (2015), S. 233–243.

[20] Boudier, K.; Hoffmann, S.: Komforterhöhung und Energieeinsparung im Büroumfeld durch Klimastühle. In: Tagungsband Bauphysiktage: Bauphysik in Forschung und Praxis, Kaiserslautern, Germany, Oktober 2015, 2015.

[21] Boudier, K.: Modellierung der Interaktion von Gebäudenutzer*innen und Gebäudetechnik. Dissertation, Technische Universität Kaiserslautern, 2021.

[22] Boudier, K.; Hoffman, S.: Modeling decentralized systems for energy savings based on detailed local thermal comfort calculations. In: Proceedings of IBPSA Italy Rome 2019. Rome, Italy, 2019.

[23] Ganji Kheybari, A.; Boudier, K.; Hoffmann, S.: Using a “MRT Manikin” To Assess Local and Overall Thermal Sensation and Comfort. In: Proceedings of BauSIM 2018, 2018.

[24] Boudier, K.; Fiorentini, M.; Hoffmann, S.; Kalyanam, R.; Kokogiannakis, G.: Coupling a thermal comfort model with building simulation for user comfort and energy efficiency. In: Proceedings of the Central European Symposium on Building Physics (CESBP) and BauSIM, Dresden, Germany, September 2016, S. 481–487, 2016.

[25] Boudier, K.; Hoffmann, S.: Analysis of the Potential of Decentralized Heating and Cooling Systems to Improve Thermal Comfort and Reduce Energy Consumption through an Adaptive Building Controller. Energies 15 (2022), Heft 3, S. 1100.

[26] Tanabe, S.; Kobayashi, K.; Nakano, J.; Ozeki, Y.; Konishi, M.: Evaluation of thermal comfort using combined multi-node thermoregulation (65MN) and radiation models and computational fluid dynamics (CFD). Special Issue on Thermal Comfort Standards 34 (2002), Heft 6, S. 637–646.

[27] Huizenga, C.; Zhang; Hui; Arens, E.: A model of human physiology and comfort for assessing complex thermal environments. Building and Environmental Performance Simulation:Current State and Future Issues. Building and Environment 36 (2001), Heft 6, S. 691–699.

[28] Hoffmann, S.; Jedek, C.; Arens, E.: Assessing thermal comfort near glass facades with new tools, BEST 3 Building Enclosure Science, UC Berkeley, Center for the Built Environment, 2012.

[29] Zhang, H.; Arens, E.; Huizenga, C.; Han, T.: Thermal sensation and comfort models for non-uniform and transient environments: Part I: Local sensation of individual body parts. 1st International Symposium on Sustainable Healthy Buildings 45 (2010), Heft 2, S. 380–388.

[30] Zhang, H.; Arens, E.; Huizenga, C.; Han, T.: Thermal sensation and comfort models for non-uniform and transient environments, part II: Local comfort of individual body parts. 1st International Symposium on Sustainable Healthy Buildings 45 (2010), Heft 2, S. 389–398.

[31] Zhao, Y.; Zhang, H.; Arens, E. A.; Zhao, Q.: Thermal sensation and comfort models for non-uniform and transient environments, part IV. Adaptive neutral setpoints and smoothed whole-body sensation model. Fifty Year Anniversary for Building and Environment 72 (2014), S. 300–308.

[32] ESRU: ESP-r. https://github.com/ESP-rCommunity/ESP-rSource (Abruf: 14.12.2018).

[33] Madsen, T. L.; Olesen, B. W.; Kristensen, N. K.: Comparison between operative and equivalent temperature under typical indoor conditions. (Paper presented at) ASHRAE meeting, Atlanta, Ga. 1984. Lyngby. Danmarks tekniske højskole, Laboratoriet for varmeisolering. Meddelelse, Heft 160. Lyngby 1984, 1984.

ENERGY

From Diesel to Eletric to NZEB, an Energy Performance Contract in a Hotel

João Raposo [a], Daniel Silva [a], António Mortal [b], João Lopes [b]

[a] Âmago-Energia Inteligente, Lda, Portimão, Portugal, amago@amago.pt

[b] Instituto Superior de Engenharia, Universidade do Algarve, Faro, Portugal, info@ualg.pt

Abstract.
How could a 1975 4* 220# bedroom beach hotel evolve from an old system with Diesel Boiler and cooling only chiller to become a NZEB building. An Energy Performance Contract, funded by Innovation funds, an hotel in south Portugal obtained 60% Energy reduction, a new Chiller and integrated Heat Recoveries results on eliminating diesel consumption with almost free Sanitary Hot Water in the summer and next steps to achieve a NZEB Building. Energy Performance Certificate came from D to B which is already considered NZEB in Portugal.

Keywords: Energy efficiency, Energy Performance Contract, Heat Recovery, ESCO, NZEB, Hotel, BMS
DOI: https://doi.org/10.34641/clima.2022.28

1. Introduction

From first Energy Audit to implementation commissioning, post-work improvements, installation conduction, energy management and maintenance management a story on how an old idyllic 220-bedroom hotel by the beach can become a modern NZEB building. This is the PESTANA VIKING RESORT in *Sra. Da Rocha* beach, near Porches, Algarve, PortugalLessons learned and what remains to be done

2. Methodology

2.1. Motivation and procedure

In 2013 "*FAI-Fundo de Apoio à Inovação*" (Innovation support Fund in Portugal) launched a national challenge for Energy Performance Contracts in Portuguese Hotels.

Main objectives were to promote awareness of this business model as an effective way to achieve Energy Efficiency so needed in this Industry and in Portugal in general.

In a first stage several hotels concurred and the one with most expected savings was selected.

Savings were diagnosed via an Energy Audit included in the Energy Performance Certificate according to the EPBD Directive. This hotel was was the one with more potential savings.

In a second stage several ESCO companies applied to implement the Energy Efficiency Contract. Among 9 companies that presented a proposal the best two were pre-selected and allowed to run a final Energy Audit and present a final proposal.

The same candidate had the first place in both situations. The prize consisted of financing the investment needed without interests with one year of payment absence to allow implementation and three years of monthly payments according to a M&V report.

This loan was secured by a bank first demand guarantee.

The juridic discussion to reach an agreement between FAI and the Bank (which is also state owned) took over 8 months.

The final contract between the ESCO company and the Hotel is five years long despite paying the loan in three years

2.2. Existing situation

The Viking Hotel met particularly advantageous conditions for reduction of Energy Costs. It is a building from the 70's, it did functional and cosmetic renovations over the years, but maintaining most of the original Air Conditioning Systems.

A major renovation in 2005/2006 created an indoor pool with a dehumidifying machine, but pool heating was made still with boilers.

The construction is entirely in concrete, there are no bricks, only concrete and glass, which makes it thermically inefficient and very dependent on active air conditioning to maintain the comfort of customers.

An original cold water/water chiller with cooling tower produces the hotel comfort cooling.

Copyright ©2022 by the authors. This conference paper is published under a CC-BY-4.0 license.

Existing Chiller had EER~1

Fig. 1- Old Chiller and Cooling Tower

Chiller circulating pumps were fixed speed.Fan-coils and AHUs had three-way valves with no hydraulic balancing.

Two diesel boilers produced all the Ambient Heating in winter and all the SHW- Sanitary Hot Water and all Pool Heating during all the year.

Heating Diesel in Portugal is almost at the price of Road Diesel, making it an expensive energy.

2.3. Energy Audit

A thorough Investment Grade Energy Audit was carried out under the mandatory Energy Performance Certificate for this application.

A detailed Thermal Simulation of the building was carried out making a 3D model in REVIT exported to IES/VE thermal simulation Software.

A high degree of calibration of the building was achieved, allowing for an accurate study of improvement measures and simulation if interaction between measures.

The response of future Air Conditioning equipment was studied in detail by calculating an EER-Energy Efficiency Ratio and COP-Coeficient of Performance for all hours of the year for various reversible chillers considering the thermal load required in each hour obtained from the building thermal simulation and the Average Outside Temperature for that hour obtained from an average statistic of last three years.

This study allowed to approach specific SEER-Seasonal EER and SCOP- Seasonal COP of this Building for each chiller analysed which led to a more fundamented decision.

The building consumed 1.4 MWh in Electricity and 1.1 MWh in Diesel per year in which HVAC-Heating, Ventilation and Air Conditioning including SHW accounted for about 42% and Illumination about 19%.

The analysis of hydraulic schematics of existing installation showed something very old and obsolete, in view of new technologies and new ways of connecting equipment.

Realizing how the facility worked by listening to the maintenance people who knew how to operate, problems and complaints of the various users, such as the Kitchen, Restaurant, Reception, Rooms, and Swimming Pools were very important to know the current state and think about the future.

A big problem created in the 2005 remodulation were ten Condensing Refrigeration groups from the freezing and cooling modules located in a closed basement with minimal mechanical ventilation and an AHU-Air Handling Unit cooling the technical room in summer when chiller was on. That space overheated frequently creating breakdowns on the refrigerating machines

Fig. 2- Refrigerating Condensers

2.4. Results of Energy Audit

Disaggregation of consumptions are below

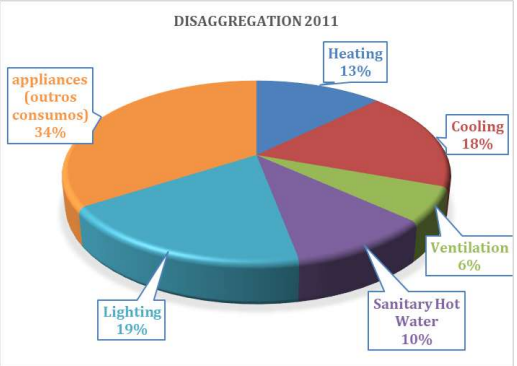

Fig. 3- Energy disaggregation 2011

Wall thermal insulation and Windows replacing would result in many years of Return On investment. Most Promising Energy Conservation Measures are about remodelling hvac system and lighting

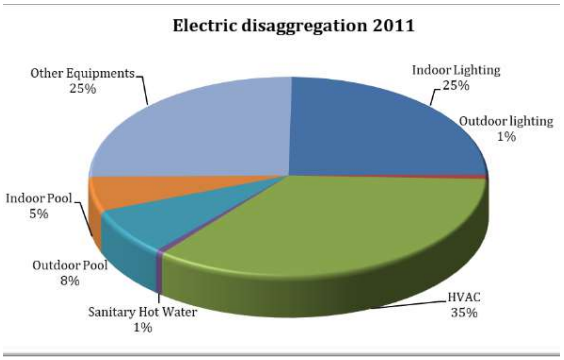

Fig. 4- Eletric Consumption disaggregation

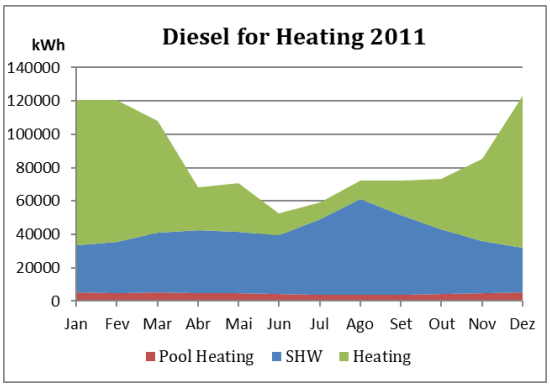

Fig. 5- Diesel Monthly consumption

3. Measurement & Verification Plan

The path between EIM-Energy Improvement Measures stated in a report, how to really obtain them and how to invoice them is an iterative road, with both financial, hvac engineering, statistical and juridic discussion of work and contract.

Each time we go to the building we discover new things and get deeper insights until we format the final solution

A M&V – Measurement & Verification Plan was developed according to EVO IPMVP protocol Option C. [1]

This option includes overall building consumptions and is based on the actual Electricity and Diesel invoices paid by the Hotel.

Baselines formulas were provided for Electricity and Diesel consumptions. After dozens of tests, we agreed with the client on the formulas below obtained wit statistical regression methods made in advanced Excel.

according to IPMVP protocol an accordance of at least 75% should be obtained as enough precision to make it agreeable between both parties. Above 90% the dependency of the Y variable is very well explained by the independent variables.

The data set used was the latest 24 months, including monthly real occupation of hotel, real historic consumptions and daily temperatures obtained by the nearest official weather station, as no historical temperatures measurements existed at the hotel.

This was a laborious and iterative investigation process till find options both could agree on.

Baseline Eletricity

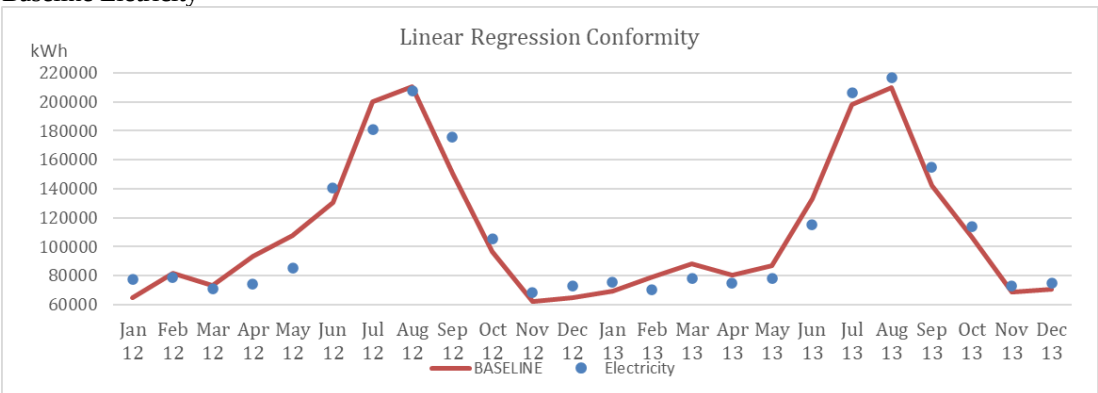

Fig. 6 – deviation between data and Electricity Baseline

$$E = a + b\,NC + c\,DDheating + d\,DDcooling$$

Where:

E= monthly Electricity kWh	DDheating = Heating monthly Degree Days in base 18ºC
NC = Number of monthly clients	DDcooling = Cooling monthly Degree Days in base 24ºC
a,b,c are constants	$R^2 = 94.4\%$

Baseline diesel

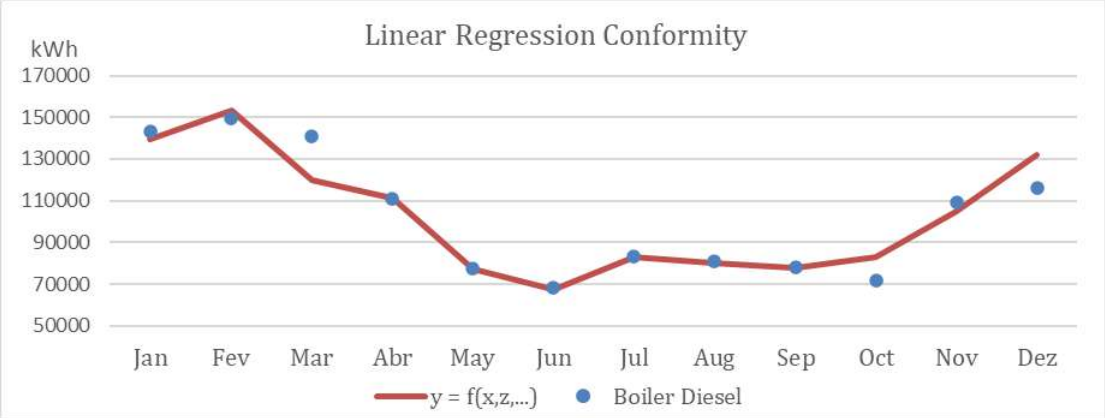

Fig. 7 – deviation between real data and baseline Diesel

$F = d + e\,NC + f\,DDheating - g\,Texternal$

Monthly data used is an average of 2012 and 2013, a typified year for 24 months

L= monthly diesel kWh	DDheating = Heating monthly Degree Days in base 18ºC
NC = Number of monthly clients	Texternal = average outdoor monthly temperature
d,e,f,g are constants	$R^2 = 91.2\%$

Please notice the negative ***"g"*** coefficient on diesel expression, as diesel was all year long for SHW production and winter heating.

4. Initially Implemented measures

The call was released 2013, implementation only started in2016 due to a lot of legal contracting delays.

Main works were done in spring of 2016, including new chiller and boiler remodulation

The hotel closed for other renovations from November 2016 to February 2017, allowing for works inside rooms to be done without constraints.

Fig. 8 – New Reversible 2 pipe Chiller 300 kW cooling

The great revolution consists of altering the Centralized Hydraulic schematics. We now have a chiller with Variable Speed in the Primary Circuit, Partial Heat Recovery at high temperature using desuperheater with high Delta T on the heat recovery water. Heat production in counter current with the consumption of SHW and an auxiliary Heat Pump.

Installation of a Reversible Chiller produces all Cooling, Heating and most of the need for Sanitary Hot Water. We chose the one that had the best Values of EER and COP in Eurovent and in our study, but also the one that could achieve the desired Heat Recovery values.

Fig. 9 – Heat Pump recovering heat from refrigeration Condensers and producing SHW, 15kW thermal at 60ºC.

Building Management system was designed in partnership between a BMS contractor and the ESCO company became the only way to commission and explore the entire installation automatically to obtain the best results, controlling the entire thermal power plant and AHU-Air Handling Units.

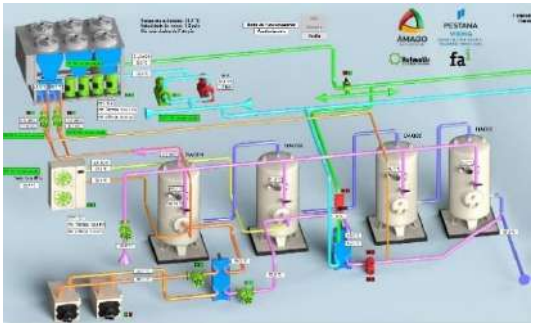

Fig. 10 – BMS synoptics

It took roughly one year to optimize the BMS system, we had to see it working and tweak it one winter and one summer to achieve the desired results

BMS works together with an Energy Monitoring System producing automatic alarms detecting early anomalies and inefficiencies as a complement to daily remote visits to the system by an engineer that makes a close installation follow up, daily decisions on setpoint temperatures, etc.

Review of all energy-consuming equipment connected to HVAC, Swimming Pools and Kitchen considering the daily control and operation trying to improve some energy-saving behaviours.

Recommissioning has been done for the AHUs and Pool dehumidifier, measuring air and water flows on the machines and balancing Air diffusers.

Pressure Independent Control Valves for AHUs and room's Fan Coils, combined with Variable Speed Circulation Pumps have been installed. This guaranteed proper balance of hydraulic circuits.

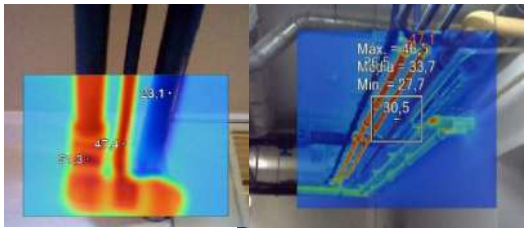

Fig. 11 – Infrared thermography on SHW pipes

Low flow showers were installed

As original condition had many flaws, thermal insulation of the entire distribution network of Sanitary Hot Water and Recirculation with 30mm thickness insulation was applied, which is operating 24hours/day and responsible for 12 to 15 kW of constant heat losses on the building. Even with proper insulation Sanitary Hot Water pipes accounts for 20% to 30% of total heat necessary for Hot Water. There is still room for a lot of improvement here.

Installation of a hot water disinfection system by Chlorine Dioxide to avoid frequent thermal shocks and reduce or nullify the risk of Legionella; This system proved effective on disinfection but also very corrosive for all kinds of plastic piping, accessories in brass and bronze. It was decommissioned late 2018 due to piping bursts.

Illumination retrofit for LED lamps was already ongoing by hotel Maintenance, including bedrooms, except service areas, so all Tubular Fluorescent lamps were replaced in common and service areas, like kitchen, reception, corridors, technical rooms, etc.

4.1. Commissioning and First Results

Commissioning and optimizing the new installation are an ongoing process since months since February 2017 till the end of 2018

Results improved a lot since early 2017, but still spending too much diesel till June 2017, as the objective is to have zero diesel consumption

Till July of 2017 diesel consumption remain high due to:

- Compressor in Dehumidifier was burned, and all pool heating was provided from the boiler;
- Condensing Heat from the chiller was not being properly recovered due to lack of stability on circulating pumps, controls need improvement.
- These problems were solved during 2017 leading to much better results and achieving the proposed goals
- Other improvements opportunities were detected meanwhile.

4.2. After commissioning investments

Indoor Pool Air Treatment Dehumidifier Ventilator was a centrifugal belt driven with 5.5 kW electric motor replaced by an EC plug fan of

2.2kW running at half speed at night time with 0.8kW power.

Around 2k€ Investment for 1k€/year energy savings, two years Return on Investment, we still had four years to go, so was a easy decision.

Fig. 12 – Old belt Ventilator and new EC Fan

Also, the Extraction Fan for the main Hood in the Kitchen needed replaced for Fire Safety purposes, we analysed the possibilities and replaced an old 4 kW centrifugal and belt ventilator, for a direct coupling plug fan 400ºC/2h ventilator

Fig. 13 – New Kitchen Fan

Heat Recovery form the two large refrigerating condensers was made directly to heat Indoor Pool Water through an Heat Exchanger, which accounted for almost all pool water heating needs in summer and dismissing other need for the boiler.

An hydromassage tub exists on the Indoor Pool space and was heated by electric immersion heaters. A Pool heating Heat Pump was installed inside the kitchen providing cooling for the kitchen and simultaneously heating the tub. small 9m2 room is used as a refrigerated wine cellar including two refrigerators for soft drinks and white wines while red wines were left at room temperature. An Air Conditioning split type Unit worked inside to cool the premisses. We were able to remove the condensers for the room and install another small heat pump producing SHW while cooling the wines. In this way both sides of the compressor are useful, cooling and heating.

5. Results for 2018 and 2019

All the implemented measures resulted on a highly efficient operation.

The graphs in Fig. 13 to Fig.16 allow several conclusions:

- Peak Electricity consumptions on summer due to high cooling needs remain, but are now at much lower level
- There is no Diesel utilization in summer and mid seasons, therefore all Sanitary Hot Water and Pool heating is being made with Chiller, Heat Recovery and Heat Pumps.
- Electrical consumption in Winter, from December to February, is almost the same as it was before, but with no Diesel spending, meaning other ECM-Energy Conservation Measures were able to reduce electricity use in Winter, like lighting, ventilation fans and better control on climatization by BMS
- A Photovoltaic system would be the ideal complement to this building, has almost all use is electric energy. The conditions on the call were not interesting for Photovoltaic, so it as not integrated on the first investment.
- Most Energy Consumption is about appliances, not traditional hvac, lighting and other regulated uses.

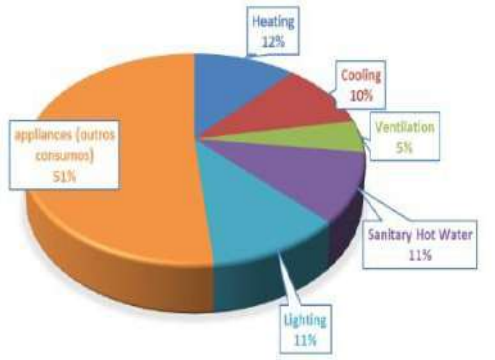

Fig. 14 Energy Disaggregation 2019

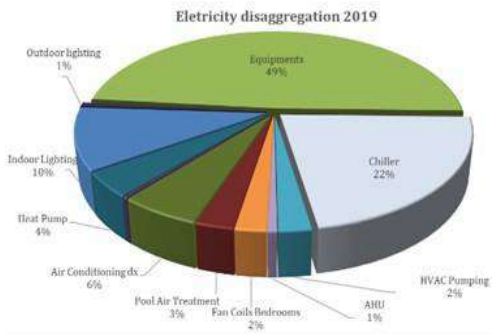

Fig. 15 Electricity Disaggregation 2019

In March 2020 a general lockdown was declared in Portugal as most of Europe and the World. Hotel opened only from 06/07/2020 till 12/09/2020 and reopened in July 2021 to close again in September 2021. No more full years of operation are available.

No further investments were made

As life is expected to normalize in 2022 so will hotel exploration and investments.

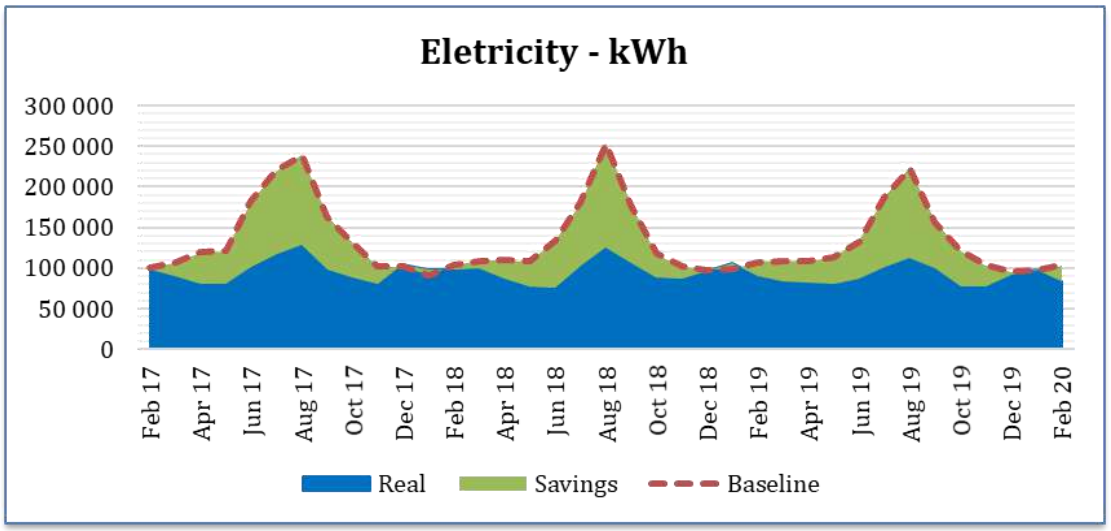

Fig. 16 – Electricity savings between Feb 2017 and Feb2020

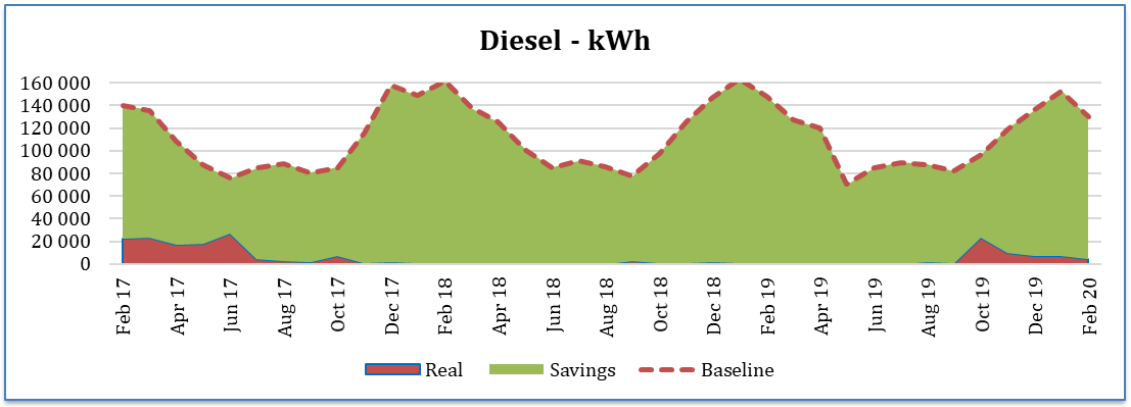

Fig. 17 – diesel savings from Feb2017 to Feb2020

The Diesel used in October 2019 was due to a Heat Pump malfunction

6. Conclusions and steps to NZEB

According to Portuguese Energy Performance Certificates for 2021, this building is already considered to NZEB, as it reaches Class B minimum on 2021 classification for commercial and Service Buildings

Fig. 18 – Energy Rating in Portugal in 2021

But the REHVA definition of a NZEB building [2], [3], [4] has a wider scope, and in a very short version can be defined as the balance between imported and exported energy throughout an year tending to zero, reducing internal consumptions, complementing with self-consumption renewables, a building could sell energy some hours of the day and buy at other hours.

Table 1 resumes energy consumption on three phases of the building being able to achieve NZEB status since 2011, on 2019 and with future implementation of a PV system.

More work will be done to improve the building exploring new improvements. Reducing electric consumption on kitchen, restaurant, bar appliances and bedrooms, will be of utmost

importance. Adhering the final client to this sustainability challenge is another task, involving him on saving energy water, residues, laundry, etc.

Available space in roofs allow a Photovoltaic installation of 120kWp with an expected yearly production of 243 MWh allowing hotel to become a NZEB building.

Example of measures to study are [5]:

- Heat Recovery from refrigerating condensers
- EC fans on refrigeration devices
- Advanced Room Management to reduce equipment, lighting and hvac consumptions with and without client presence.
- Occupancy detection on corridor lightings
- Fan Coils with EC fan motors
- Develop a energy monitoring plan allowing early detection of deviations
- Hydric efficiency, with low flow lavatories and toilets
- Thermal insulation on walls. Walls are concrete, applying ETICS would result on greater comfort. ROI is above 50 years, but with incentive financing would be viable.
- Window replacing from single pane to double pane. ROI is more than 50 years, but with expected financing would be viable
- Replacing old AHUs with new EC fan motors and Heat Recovery.
- Make achieving energy goals part of staff evaluation and bonus

Tab. 1 – Hotel Evolution from inefficient to ZEB

			Class B	Class A
		2 011	2 019	2 023
	Class	**C**	**B**	**A**
Specific Energy	$kWh_{EP}/m^2/year$	295	198	157
	$kWh_{EP}/room$	114	51	41
	$kWh_{EP}/client$	50	23	18
CO2	Ton/year	753	430	342
Total Energy use	$kWh_{EP}/year$	4 395 149	2 952 579	2 952 579
Delivered Energy	kWh	4 395 149	2 952 579	2 343 082
Exported Energy	kWh	0	0	0
Self-Renewables	kWh	0	0	243 799
Disaggregation	$kWh_{EP}/m^2/year$			
Heating		37	23	23
Cooling		53	21	21
Ventilation		18	10	10
Sanitary Hot Water		30	21	21
Lighting		56	21	21
appliances		101	102	102

7. Reference List

[1] IPMVP Core Concepts, 2016, IPMVP Core Concepts Addendum 2018

[2] Kurnitski J., RHEVA Journal May 2013 – Technical definition for nearly zero energy buildings.

[3] Buso T., Corgnat S., Kurnitski J., Litiu A., Derjanecz A. RHEVA Journal January 2014 – Nearly Zero Energy Hotel

[4] Buso T., Corgnat S., Kurnitski J., RHEVA Journal May 2014 – An Existing Best Practice nearly Zero Energy Hotel

[5] Styles D., Schönberger H., Martos J., Best Environmental Management Practices in the Tourism Sector. 2013.

Innovative heating and cooling systems based on caloric effects: A review

Hicham Johra [a], *Christian Bahl* [b]

[a] Department of the Built Environment, Aalborg University, Aalborg, Denmark, hj@build.aau.dk.

[b] Department of Energy Conversion and Storage, Technical University of Denmark, Lyngby, Denmark, chrb@dtu.dk.

Abstract. Heat pumps (HPs) are an excellent solution to supply heating and cooling for indoor space conditioning and domestic hot water (DHW) production. Conventional HPs are typically electrically driven and operate with a vapour-compression thermodynamic cycle of refrigerant fluid to transfer heat from a cold source to a warmer sink. This mature technology is cost-effective and achieves appreciable coefficients of performance (COP). The HP market demand is driven up by the urge to improve the energy efficiency of building heating systems coupled with the increase of global cooling needs for air-conditioning. Unfortunately, the refrigerants used in current conventional HPs can have large greenhouse or ozone-depletion effect. Alternative gaseous refrigerants have been identified but they present some issues regarding toxicity, flammability, explosivity, low energy efficiency or high cost. However, several non-vapour-compression HP technologies have been invented and could be promising alternatives to conventional systems, with potential for higher COP and without the aforementioned refrigerant drawbacks. Among those, the systems based on the so-called "caloric effects" of solid-state refrigerants are gaining a lot of attention. The caloric effects are large entropy and adiabatic temperature changes caused by the application or removal of an external field in certain specific solid materials. There are 4 main caloric effects: magnetocaloric, elastocaloric, electrocaloric and barocaloric. Each of them is characterized by the nature of the field and the response that induces the entropy and adiabatic temperature change: variation of the magnetic field, uniaxial mechanical stress, electrical field or hydrostatic pressure, respectively. A HP cycle can be based on these caloric effects and several heating/cooling prototypes were developed and tested over the last few decades. Although not mature technologies yet, some of these caloric systems are well suited to become new efficient and sustainable solutions for indoor space conditioning and DHW production. This paper aims to raise awareness in the building community about these innovative caloric systems. It sheds some light on the recent progress in that field and compares the performance of caloric systems with that of conventional vapour-compression HPs for building applications.

Keywords. Innovative heat pump, caloric effects, magnetocaloric, elastocaloric, barocaloric, electrocaloric, non-vapour-compression heat pump alternatives.
DOI: https://doi.org/10.34641/clima.2022.275

1. Introduction

Current and future social, environmental and economic challenges call for the different energy sectors to take a sharp turn and accelerate their decarbonization and sustainability optimization. In that context, the building sector is a key target as it accounts for most of the energy end-use in industrialized countries. Moreover, most of the energy used in buildings is dedicated to indoor space conditioning (space heating and space cooling) and the production of domestic hot water (DHW) [1]. The tightening of energy regulations and renovation campaigns tend to decrease the space heating needs of buildings and allow for low-temperature heat emitters. However, the energy share for DHW production, which requires higher temperatures (50-65°C) to avoid legionella problems, is increasing. In addition, because of global warming, higher thermal comfort standards, purchasing power increase and population growth, especially in warm countries, cooling air conditioners (ACs) are more and more common. It is estimated that 2/3 of the world's households may end up being equipped with ACs (half of them being in China, India and Indonesia). Cooling demand is also increasing significantly in temperate and cold climates during summer, especially for office buildings. Indoor space

Copyright ©2022 by the authors. This conference paper is published under a CC-BY-4.0 license.

cooling is thus the largest contributor to the growth of global building electricity demand [2].

In that context, heat pumps (HPs) have been proven to be a very efficient and flexible solution for space heating/cooling and DHW production. They are the most cost-efficient supply of heat for individual buildings outside of urban areas. In cities, large industrial HPs can be used for heat generation at district heating network plants or can be installed in buildings as decentralized booster HPs for low-temperature district heating networks. Consequently, the market demand for HPs has sustained significant growth over the last years. Vapour-compression systems are dominating the HP industry for building applications. Unfortunately, the refrigerants used in these conventional systems have a large greenhouse effect when released into the atmosphere. Several gaseous refrigerant alternatives have been identified, but they present other disadvantages such as toxicity, flammability, explosivity, low energy efficiency or high cost [3].

Non-vapour-compression alternative systems are also possible. Several of these non-conventional and innovative HP technologies have been identified as particularly promising, without the aforementioned drawbacks and with the potential for a larger coefficient of performance (COP) than that of conventional vapour-compression heat pumps (VCHPs). Among these alternatives, a particular interest has developed over the last few years for systems based on the so-called caloric effects of solid-state refrigerants to create a thermodynamic HP cycle. Although not mature technologies yet, some of these caloric systems are well suited to become new efficient and sustainable solutions for indoor space conditioning and DHW production [3].

This paper aims to raise awareness in the building community about these innovative caloric systems. Firstly, the different caloric effects are presented together with a brief history and the recent developments of these non-conventional heat pump technologies. The performances of the different caloric systems are then reviewed and compared with that of VCHPs for building applications. Finally, the article closes with some outlook on the future of caloric systems and conclusions.

2. Caloric effects for innovative heat pump systems

Conventional HPs are typically electrically driven and operate with a vapour-compression thermodynamic cycle of refrigerant fluid to transfer heat from a cold source to a warmer sink. Although capable of a similar heat transfer with COP > 1, the caloric HPs operate with a different thermodynamic cycle based on the so-called “caloric effects”.

The caloric effect is large entropy and adiabatic temperature changes caused by the application or removal of an external field in certain specific solid materials: the caloric materials. When the external field is increased in the material, its entropy decreases and its temperature increases. Reciprocally, the external field in the material is reduced the entropy increases and its temperature decreases. This phenomenon can be employed to create a HP cooling/heating thermodynamic cycle. Because of the in-principle reversible nature of this caloric effect, it opens up the possibility for heat pump systems with COPs higher than that of conventional VCHPs [4].

There are 4 main caloric effects. Each of them is characterized by the nature of the field and the response that induces the entropy and adiabatic temperature change:

- Magnetocaloric effect: Adiabatic temperature change induced by a variation of the magnetic field (magnetization/demagnetization).
- Elastocaloric effect (a.k.a. thermoelastic): Adiabatic temperature change induced by a variation of the uniaxial mechanical stress (stretching/squeezing).
- Electrocaloric effect: Adiabatic temperature change induced by a variation of the electrical field (polarization/depolarization).
- Barocaloric effect: Adiabatic temperature change induced by a variation of the hydrostatic pressure (compression/decompression).

A detailed description of the different caloric effects and their heating/cooling applications can be found in Kitanovski et al., 2015a [4] (caloric effects), Kitanovski et al., 2015b [5] and Smith et al., 2012 [6] (magnetocaloric effect), Tušek et al., 2015 [7] and Kabirifar et al., 2019 [8] (elastocaloric effect), Torelló & Defay, 2022 [9] (electrocaloric effect), Aprea et al., 2020 [10] (barocaloric effect).

The basic operation principle of most caloric HP systems is similar for all 4 caloric effects. The caloric material is used as a solid refrigerant. It is contained as a porous media inside a regenerator casing that allows bi-directional circulation of the coolant fluid through the porous caloric material to transfer (by convection) the thermal energy from the cold side (heat source) to the warm side (heat sink) of the device [11].

The porous caloric material can be arranged in different configurations: irregular crushed particles, parallel plate matrices, packed sphere beds, circular or rectangular micro-channel matrices, packed screen beds or other mesh geometries [12]. The geometries of the porous solid refrigerant and the regenerator casing should be optimized to maximize the heat transfer (convection) between coolant fluid in the entire volume of caloric material, and minimize the pressure losses (pumping work) of the system.

The coolant fluid is usually a harmless and environmental-friendly water-based brine. Air can also be employed for direct usage in a ventilation

system with an active regenerator. Coolants made of metallic fluids or nanofluids (fluids with dispersed solid nanoparticles) have also been tested for their high thermal conductivity to enhance the heat transfer in the porous refrigerant [5].

The sole adiabatic temperature change of the caloric effects (e.g., typically 0.5-4 K for the magnetocaloric effect) is usually too small for any useful direct applications in buildings or industries. Timing the oscilating fluid flow with the changing applied field, the caloric effect is employed to create an active caloric regenerative thermodynamic cycle that can generate an adequate temperature span for HP operations (5-60 K) [4, 6].

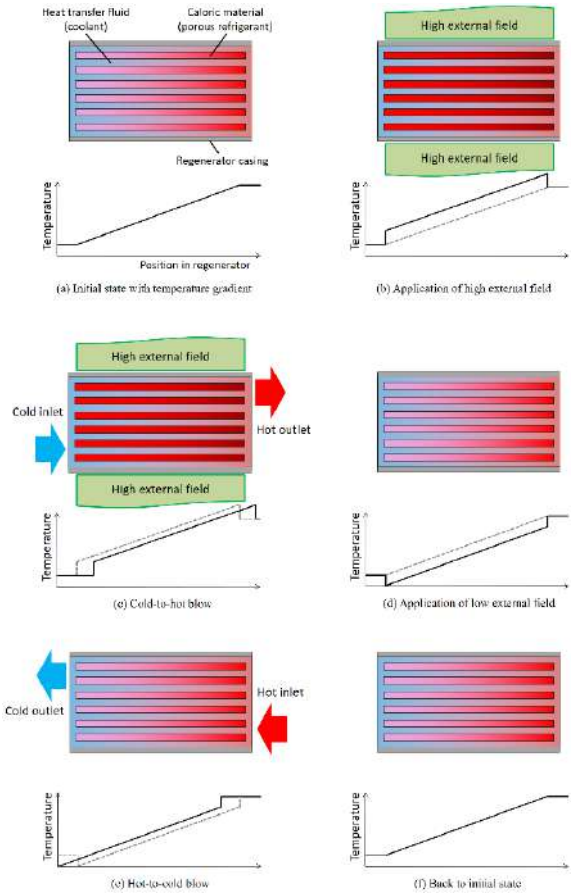

Fig. 1 – The different phases of the active caloric regenerative cycle for the operation of a generic caloric HP system (adapted from [11]).

One can see in **Fig. 1** the 4 processes that form the active caloric regenerative thermodynamic cycle of a generic caloric HP to transfer heat from a cold source to a warmer heat sink. **Fig. 1 (a)**: The regenerator presents an initial temperature gradient over its length and zero external field is applied to the refrigerant caloric material. **Fig. 1 (b)**: The cycle starts with the application of a large external field to the caloric material (e.g., magnetization, stretching, polarization or compression) leading to a temperature increase over the length of the regenerator (shown as uniform for simplicity). **Fig. 1 (c)**: The coolant fluid is then pushed from the cold side (heat source) to the hot side (heat sink) of the regenerator (cold-to-hot blow). The warmer fluid rejects the heat into the heat sink and the regenerator is cooled down under a constant large external field. **Fig. 1 (d)**: The external field is removed (e.g., demagnetization, squeezing, depolarization or decompression) leading to a temperature decrease over the length of the regenerator (again shown as uniform for simplicity). **Fig. 1 (e)**: To complete the cycle, the coolant fluid is pushed back from the hot side to the cold side of the regenerator (hot-to-cold blow) under a zero external field, which re-heats the bulk of the regenerator caloric material (heat regeneration process and heat extraction from the cold source). **Fig. 1 (f)**: The coolant fluid and the caloric material reach local thermal equilibrium and the temperature distribution across the regenerator length is the same as at the initial stage of the cycle.

The active regenerator cycle described above (**Fig. 1**) can also be represented in a Temperature-Entropy diagram as a (caloric) Brayton thermodynamic cycle (see **Fig. 2**). This caloric Brayton active regenerative cycle is the most commonly used one for caloric HP systems. It is very similar to the Erikson cycle. Other (sometimes, more efficient) thermodynamic cycles can also be employed for caloric systems [4].

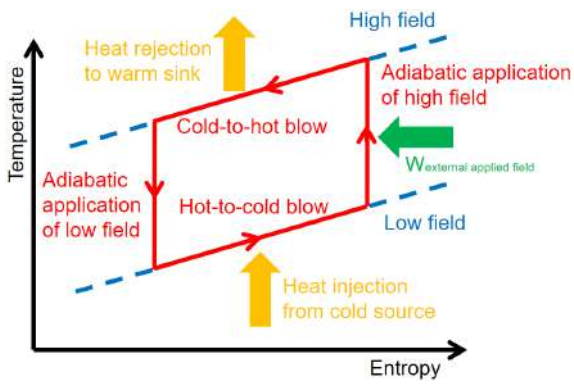

Fig. 2 - The caloric Brayton cycle: a common active caloric regenerative cycle for caloric HPs.

Certain materials can combine several types of caloric effects at the same time: multicaloric effects observed in, e.g., certain multiferroic materials. It is thus possible to conceive systems that exploit multiple-coupled caloric effects within the same refrigerant materials. This could increase the overall adiabatic temperature change and improve the system's efficiency and temperature span. Some researchers are thus developing devices combining, e.g., the magnetocaloric effect with the electrocaloric effect or the elastocaloric effect [4, 13].

The field of caloric systems is relatively young. The number of international research groups working on the topic is still limited compared to other energy conversion technologies. However, signifficant progress has been made within the last 10-20 years: multiple theoretical, numerical and experimental studies have been conducted on the different caloric effects, new caloric materials have been discovered and manufactured, general guidelines and models

have been developed for both generic caloric systems and specific ones, and a number of very peculiar engineering challenges has been addressed to improve the energy efficiency and cost affordability of the magnetocaloric [14], elastocaloric, electrocaloric and barocaloric HP prototypes. The growing enthusiasm for caloric systems is mainly driven by their theoretically high COP because of the in-principle reversible nature of the caloric effects. In addition, they have the potential for quiet and low vibration level operation, miniaturization and compactness, efficient part-load control, no use of toxic, flammable, explosive, ozone-destructive or greenhouse gases, environmental friendliness, and the possibility for recycling the caloric materials. However, the development of the different caloric technologies is very unequal. Historically, the magnetocaloric effect was the first one to be observed and studied. Consequently, the magnetocaloric technology is the most mature. In recent years, however, elastocaloric systems have seen a rapid increase in activity among the scientific community, while the electrocaloric and barocaloric technologies are still in their infancy.

2.1 Magnetocaloric heat pumps

The history of magnetocaloric technology starts in 1918 when Weiss and Piccard discovered the magnetocaloric effect. In 1976, Brown demonstrated that gadolinium (Gd) could be used for room-temperature magnetocaloric heat pumps (MCHP) and since then Gd has been the reference material for magnetocaloric applications at room temperature. A major breakthrough came in 1982 when Barclay and Steyert patented the active magnetic regenerator cycle (magnetocaloric version of the caloric Brayton active regenerative cycle presented in **Fig. 1** and **Fig. 2**). This operation design is one of the most thermodynamically efficient for MCHPs. It allowed a tremendous improvement of the energy efficiency and useful temperature of magnetocaloric systems. It has therefore been the founding principle of most following MCHPs, but also for HPs based on other caloric effects [5, 15]. From that point, magnetic heating/cooling technology gained popularity and several research groups built their prototypes. A large variety of design and engineering options have been tested to improve the overall COP, cooling/heating power and temperature span between the heat source and sink. Notable design explorations were: assembly of permanent magnets, superconducting magnets, oscillatory translating regenerator or magnet, rotating magnets or rotating regenerators, vertical or horizontal rotation. Currently, the most advanced prototypes are now rotary systems with a permanent magnet assembly rotor and a fixed regenerator (see **Fig. 3**). Static regenerators simplify the implementation and operation of the fluid distribution system (valves) [15, 16].

In the last 30 years, around 100 different prototypes have been tested and reported [16, 18]. Over the years, the performance of these MCHPs has been slowly rising with a tradeoff between COP (usually ranging from 0.1 to 4), temperature span (usually ranging from 0 to 25 K) and useful heating/cooling power (usually ranging from 10 W to 2000 W) [15, 18]. An extensive review of the different MCHP prototypes was made by Greco et al. [18].

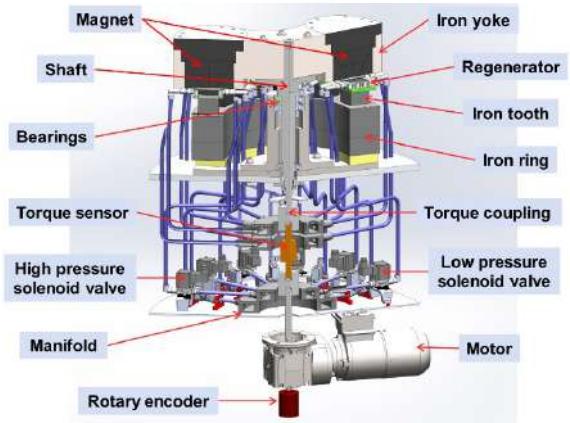

Fig. 3 – View cut of the rotary MCHP prototype "MagQueen" [15].

As aforementioned, magnetocaloric technology is the most mature of all caloric-based systems. Current MCHP prototypes can now operate near commercially relevant cooling loads and temperature spans with appreciable COPs. For instance, one of the latest MCHP studies by Dall'Olio et al. has reported impressive performances with a heating power of 340 W over a 10.3 K temperature span with a COP of 6.7, and heating power of 950 W over a 5.6 K temperature span with a COP of 7 [16]. In 2022, Masche et al. have reported heating power of 265 W over a 14.8 K temperature span with a COP of 3.97, and a heating power of 445 W over a 7.3 K temperature span with a COP of 15.9 [17]. The best MCHPs are therefore suitable for low-temperature lift cooling/heating applications in low-energy dwellings [11]. This is being explored in the H2020 project RES4BUILD [res4build.eu] Numerical studies also indicate that higher temperature lift for DHW production can be achieved by cascading magnetocaloric regenerators in series [19].

2.2 Elastocaloric heat pumps

One of the main cost limitations of MCHPs is the rare-earth-based magnet material creating the magnetic field. In recent years, some researchers working on MCHPs are thus also developing new HPs exploiting the other caloric effects. Among them, the elastocaloric effect is particularly encouraging as certain non-rare earth materials (e.g., Ni-Ti-, Cu- and Fe-based superelastic shape-memory alloys with austenitic–martensitic phase transformation; shape-memory polymers) present an elastocaloric adiabatic temperature change that is significantly larger (10-25 K) than that of the magnetocaloric effects reachable with permanent magnets (0.5-4 K). In 2014, the U.S. Dept. of Energy actually designated the elastocaloric heat pump (ElastHP) as the most

promising alternative to VCHPs [3]. However, the first demonstrator of this emergent technology was only presented in 2012 [18]. The design of the first ElastHPs was largely influenced by the work on MCHPs. The refrigerant (usually in the form of thin plates, tubes or wires) is alternatively loaded (stretched) and deloaded (unstretched) inducing a large adiabatic temperature increase and decrease, respectively, to generate a regenerative elastocaloric Brayton cycle (see **Fig. 1** and **Fig. 2**).

The heat transfer from the elastocaloric refrigerant to the heat source and sink can be performed in different ways: by convection with an oscillatory by-directional flow of water-based brine (similar to MCHPs) or air, displacement of the refrigerant from a cold air stream (heat source) to a warmer air stream (heat sink), or solid-to-solid direct contact heat transfer by displacement of the refrigerant to be alternatively touching the solid heat source and heat sink. The main actuator (driver) solutions to load and deload the elastocaloric material are as follows: hydraulic, pneumatic, piezo or magnetostriction linear actuators, or rotary system with a cam track and a cam follower. One notable rotary ElastHP prototype for direct active heat recovery and extraction in a ventilation system has been developed by Kirsch et al. [20]. It shows promising simulation results with a COP of 9.5 for a 250 W thermal power over a 10 K temperature span.

The very large temperature response of elastocaloric materials allows to significantly increase the coolant mass flow rate through the regenerator without destroying the internal temperature gradient, which is not the case for MCHPs. In addition, it is possible to recover part of the loading mechanical work by coupling regenerators two by two (one is loading while the other one is unloading). A flywheel could also be a solution to retrieve, store and re-inject the kinetic energy of the unloading process. The temperature span of ElastHPs can also be improved by cascading several regenerators in series.

The first results show that ElastHP has the potential to outperform MCHPs in terms of temperature span, COP and costs. Elastocaloric devices can be much more compact than MCHPs. For the same thermal power output, it can require up to 20-times less mass than for MCHP. This opens the possibility for high-COP miniaturized cooling devices. However, this technology is at the beginning of its R&D phase and far from commercialisation. The current ElastHPs are restricted to very small-size prototypes with limited heating/cooling power below 100 W. Moreover, the ElastHP technology faces a few challenges: the durability/fatigue lifetime and functional stability/reliability of the elastocaloric materials over millions of cyclical loading, and the implementation of efficient actuators able to deliver large forces needed to induce the elastocarolic effect. A detailed review of the different ElastHP prototypes and their operation can be found in Greco et al., 2019 [18] and Kabirifar et al., 2019 [8].

2.3 Electrocaloric heat pumps

The electrocaloric technology is in its infancy and some way from any commercial applications. It is only very recently that the first few electrocaloric heat pump (ElecHP) proof of concepts were developed. The electrocaloric effect was discovered in 1930 by Kobeko & Kurtschatov. However, it was only in 1979 that the first ElecHP was developed. The electrocaloric effect is very analogous to the magnetocaloric one. The development of the latter thus largely influenced the design of ElecHPs. In 1989, Sinyavsky et al. created the first implementation of an active regenerative electrocaloric Brayton cycle (see **Fig. 1** and **Fig. 2**). The use of thermal diodes is also a possible ElecHP alternative to the active electrocaloric regenerator configuration. Until now, only about 20 small-scale ElecHP prototypes have been built and reported. They all produce very small heating/cooling power outputs with a temperature lift below 10 K.

The electrocaloric materials suitable for ElecHPs are usually dielectric Pb-based PZT or PST ceramics, or ferroelectric polymers. When implemented as thin polymer film or thin ceramic film regenerators (instead of bulk elements) it is possible to generate a high electric field with relatively low voltages and induce an appreciable electrocaloric temperature response. Compared to the magnetocaloric ones, these electrocaloric refrigerants could be cheaper and can operate over a much broader temperature range. However, the electrocaloric regenerator can be a complex assembly, which drives the manufacturing costs up.

The ElecHP does not require any moving elements apart from the pumping system of the coolant fluid, which is a great asset compared to other caloric systems and VCHPs. It is also possible to add an energy recovery system to lower the energy use for refrigerant polarisation. This solution can recover 65% of the work. Similarly to ElastHPs, electrocaloric technology has a great potential for miniaturized cooling solutions with minimum moving parts and no need for auxiliary coolant fluid.

Recent encouraging experimental results should be emphasized: In 2017, Ma et al. [21] made a miniature ElecHP with electrostatic actuation to rapidly oscillate a flexible electrocaloric polymer thin film that alternatively gets in direct contact with the heat source and sink. The prototype produces 0.64 W of cooling power for a 1.4 K temperature span with a COP of 13. In 2020, this prototype was cascaded in 4 layers by Meng et al. This cascade ElecHP also has a charge recovery circuit and can reach 8.7 K temperature with no load, or a 0.785 W cooling power for a 2.7 K temperature span with a COP of 9. A comprehensive review of the ElecHP technology and prototypes can be found in Torelló & Defay, 2022 [9], Greco et al., 2019 [18] and Greco & Masselli, 2020 [22].

2.4 Barocaloric heat pumps

The R&D of barocaloric technology is at an embryonic stage [18]. There is currently no reported experimental results of any functional barocaloric heat pump (BCHP) prototypes. One can only find some design ideas of BCHPs operating with an active barocaloric regenerative Brayton cycle (see **Fig. 1** and **Fig. 2**) and a handful of numerical simulation-based performance studies for BCHPs. The scientific literature mostly comprises characterizations of barocaloric effect in materials such as elastomers (e.g., natural rubber), plastic crystals (Neopentyl glycol), shape-memory alloys and other materials already presenting caloric effects (especially magnetocaloric and elastocaloric materials). Because of this last point, barocaloric technology has a good potential to be employed in multicaloric systems, e.g., barocarolic-assisted magnetocaloric heat pumps. Although the barocaloric effect can be observed in a wide range of materials, its practical applicability has yet to be proven.

3. Performances overview of caloric heat pumps

This section gives a performance overview of the different caloric heat pump systems and put them in perspective with that of conventional VCHPs for building applications. This overview is built upon experimental and numerical data collected from around 140 scientific publications. Because of space limitation in this paper, all references from which the data has been collected and additional performance overview figures can be found in a dedicated technical report (https://vbn.aau.dk/en/publications/performance-overview-of-caloric-heat-pumps-magnetocaloric-elastoc) [23]. Numerical and experimental data for MCHPs is relatively abundant. Such data also exists for ElastHPs, although much more scarce and recent (less than 10 years old). For ElecHPs, there is very little performance experimental data. The achieved temperature span is reported but the COP is rarely documented. Concerning BCHPs, only a handful of simulation-based studies could be found.

One can see in **Fig. 4** that VCHPs typically have a Carnot efficiency between 40% and 60% for temperature spans compatible with building applications. The performances of most caloric HP prototypes are modest in comparison: often below 20% Carnot efficiency and with a maximum temperature span of 30 K. However, for temperature lifts around 20-25 K (minimum limit for low-temperature space heating with high-temperature heat sources such as ground source boreholes), the best MCHP prototypes have a COP that is similar or higher than VCHPs. Simulation data suggests that MCHPs could maintain a 60% Carnot efficiency for higher temperature spans of 50-60 K. All data points for ElastHPs are below the 30 K temperature lift. The best ElastHP prototypes have a Carnot efficiency of around 20%. 2 ElastHP prototypes reach around 40% Carnot efficiency for temperature lifts of 10-16 K. The maximum temperature span that has been reported for an ElecHP prototype is 8.7 K with a very small heating/cooling power. The best ElectHP

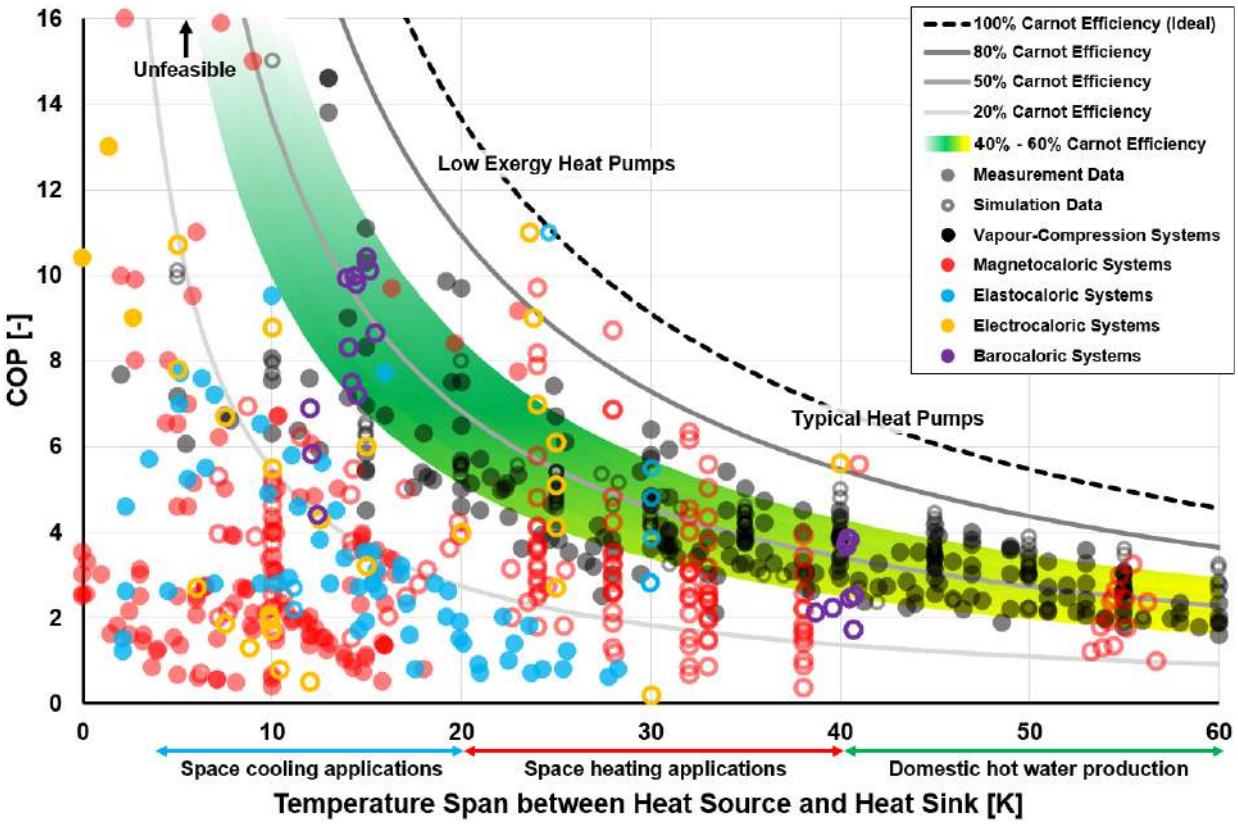

Fig. 4 – Performance overview of different heat pump systems: COP as a function of temperature span.

prototypes show promising COPs of 9-14 but for temperature lifts and effective power that insufficient for building applications. However, theoretical data suggests that an adequate temperature span for space heating and cooling can be reached with ElecHPs. Finally, there is no available experimental data for BCHPs, but simulation data suggests that such technology could sustain a 40-60% Carnot efficiency for temperature lifts up to 40 K.

One can see in **Fig. 5** and **Fig. 6** that, currently, only MCHP prototypes can reach a heating/cooling power output that is sufficient for building applications. Apart from 1 device, all existing ElastHP and ElecHP prototypes are limited to power output lower than 10 W. However, simulation studies indicate a good potential for a significant increase of the heating/cooling power output and temperature span with appreciable COP. It should, however, be noted, that modelling studies often neglect some of the system losses, leading to more optimistic performance predictions.

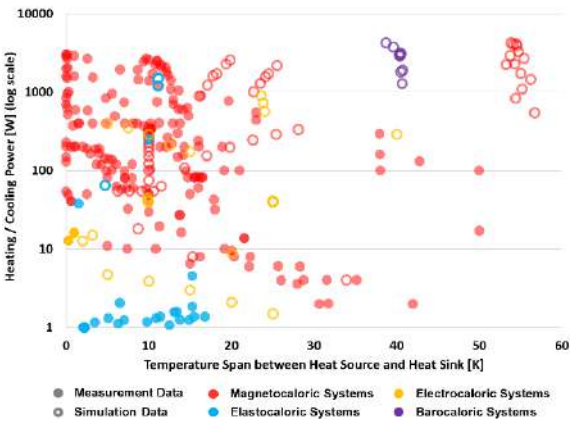

Fig. 5 – Performance of caloric HPs: heating/cooling power as a function of temperature span.

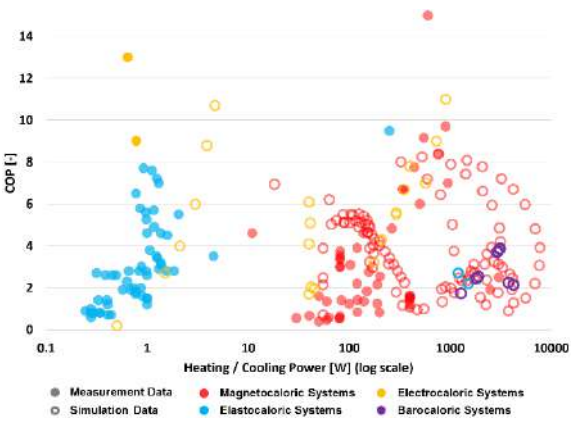

Fig. 6 – Performance of caloric HPs: COP as a function of heating/cooling power.

4. Conclusions and perspectives on the future of caloric heat pumps

Solid-state caloric refrigeration and HP technologies have made a tremendous leap forward in the last decade, and the first large-scale implementations show technical performances that are similar or superior to conventional VCHPs. The research on caloric systems has produced nice pieces of engineering with very promising capacities. However, caloric HPs have yet to prove their cost competitiveness and sustainability superiority against the mature vapour-compression systems.

At the moment, only magnetocaloric systems (the most mature caloric technology) have been experimentally proven suitable for high-COP low-temperature space heating and cooling in buildings. Elastocaloric and electrocaloric systems are still at an early R&D stage: their COPs are very promising but their power output and temperature span are rather limited for now. Since no working barocaloric HP system has been built until now, this emergent caloric technology has yet to demonstrate its feasibility and practical usefulness. However, simulation and theoretical studies tend to show that all 4 caloric effects presented in this paper could be employed for energy-efficient space heating, cooling and DHW production in buildings, and compete with conventional VCHPs because of potential lower vibration and noise level operation, compactness, efficient part-load control, no use of toxic, flammable, explosive, ozone-destructive or greenhouse gases, and better overall sustainability and environmental impact.

The expansion of caloric HPs faces a number of challenges that researchers endeavour to tackle. The main one probably resides in the development of caloric materials with larger adiabatic temperature changes and long-term durability. The creation of non-Pb electrocaloric materials (for health consideration) and non-rare-earth caloric materials (especially for magnetocaloric systems) is crucial. The durability issue is particularly problematic for elastocaloric and electrocaloric materials that are subjected to large electrical voltages and high stretching strains in HP devices. Good caloric refrigerants should keep stable caloric properties and structural integrity when exposed to coolant fluid for a long time. They should withstand the long term fatigue induced by hundreds of millions of (de)magnetization/(un)stretching/(de)polarization /(de)compression cycles. Currently, there is a lack of study on the long-term durability of caloric materials and the impact of hysteresis in caloric refrigerants. Moreover, new manufacturing processes have to be invented to inexpensively fabricate and shape these caloric materials into useable forms for regenerators (spheres, wires, foils, plates, etc) without degrading mechanical stability or weakening the strength of the external field applied to the caloric refrigerant.

The performance of active regenerators should be improved by decreasing the pumping pressure losses and enhancing heat transfer between the refrigerant and the auxiliary heat transfer fluid. Tuning the Curie temperature of caloric materials for optimum layered active regenerators can also improve performance. The use of nanofluids as a coolant in

caloric regenerators should be explored further. For elastocaloric regenerators, different geometries (plates with various shapes, wires, tubes, cascaded tube bundles, foams, thin films) should be tested with different loading techniques (tension, compression, bending or twisting). For MCHPs, new and affordable permanent magnet assembly with optimum magnetic field distribution in the regenerator and minimum eddy current and counter-torque should be developed. Joule heating effect should be curtailed electrocaloric refrigerant. To increase the caloric systems' capacity, the fluid flow rate through the regenerator should be increased while maintaining a high heat transfer efficiency (NTU) and a stable temperature gradient inside the regenerator. Parasitic heat losses in regenerators and hydraulic systems should be minimized. Caloric systems are often implemented with auxiliary systems (motors, valves, pipes and pumps) that have been designed for other purposes but have not necessarily the most optimum specifications for caloric HPs. Customized hydraulic elements might be necessary to achieve accurate coolant flow control.

The synergy of coupling multiple caloric effects within the same system should be explored further and implemented in a prototype. Finally, cascading regenerators in series is probably the most promising solution to increase the temperature span of all caloric systems.

5. References

[1] Cao X., Dai X., Liu J. Building energy-consumption status worldwide and the state-of-the-art technologies for zero-energy buildings during the past decade. Energy and Buildings 2016;128:198-213.

[2] International Energy Agency. The future of cooling: Opportunities for energy-efficient air conditioning. 2018.

[3] Goetzler W., Zogg R., Young J., Johnson C. Energy savings potential and RD&D opportunities for non-vapor-compression HVAC technologies. U.S. Department of Energy 2014.

[4] Kitanovski A., Plaznik U., Tomc U., Poredoš A. Present and future caloric refrigeration and heat-pump technologies. International Journal of Refrigeration 2015;57:288-298.

[5] Kitanovski A., et al. Magnetocaloric Energy Conversion: From Theory to Applications. New York: Springer International Publisher 2015.

[6] Smith A., et al. Materials Challenges for High Performance Magnetocaloric Refrigeration Devices. Advanced Energy Materials 2012;2:1288-1318.

[7] Tušek J., et al. The Elastocaloric Effect: A Way to Cool Efficiently. Advanced Energy Materials 2015;5:1500361.

[8] Kabirifar P., et al. Elastocaloric Cooling: State-of-the-art and Future Challenges in Designing Regenerative Elastocaloric Devices. Strojniški Vestn. – J. Mech. Eng. 2019;65:615-630.

[9] Torelló A., Defay E. Electrocaloric coolers: A review. Advanced Electronic Materials 2022;2101031.

[10] Aprea C., et al. The use of barocaloric effect for energy saving in a domestic refrigerator with ethylene-glycol based nanofluids: A numerical analysis and a comparison with a vapor compression cooler. Energy 2020;190:116404.

[11] Johra H., et al. Integration of a magnetocaloric heat pump in a low-energy residential building. Building Simulation 2018;11:753-763.

[12] Lei T., et al. Study of geometries of active magnetic regenerators for room temperature magnetocaloric refrigeration. Applied Thermal Engineering 2017;111:1232-1243.

[13] Moya X., et al. Multicalorics. Journal of Applied Physics 2020;128:240401.

[14] Zimm C., et al. The evolution of magnetocaloric heat-pump devices. Materials Research Society Bulletin 2018;43:274-279.

[15] Johra H., et al. Integration of a magnetocaloric heat pump in an energy flexible residential building. Renewable Energy 2019;136:115-126.

[16] Dall'Olio S., et al. Novel design of a high efficiency multi-bed active magnetic regenerator heat pump. International Journal of Refrigeration 2021;132:243-254.

[17] Masche M., et al. Performance assessment of a rotary active magnetic regenerator prototype using gadolinium. Applied Thermal Engineering 2021;204:117947.

[18] Greco A., et al. A review of the state of the art of solid-state caloric cooling processes at room-temperature before 2019. International Journal of Refrigeration 2019;106:66-88.

[19] Johra H., et al. Numerical Simulation of a Magnetocaloric Heat Pump for Domestic Hot Water Production in Residential Buildings. Proceedings of Building Simulation 2019: 16th Conference of IBPSA 2019:1948-1955.

[20] Kirsch S.M., et al. NiTi-Based elastocaloric cooling on the Macroscale: from basic concepts to realization. Energy Tech. 2018;6:1567-1587.

[21] Ma R., et al. Highly efficient electrocaloric cooling with electrostatic actuation. Science 2017;357:1130-1134.

[22] Greco A., Masselli C. Electrocaloric Cooling: A Review of the Thermodynamic Cycles, Materials, Models, and Devices. Magnetochemistry 2020;6:67.

[23] Johra H. Performance overview of caloric heat pumps: magnetocaloric, elastocaloric, electrocaloric and barocaloric systems. DCE Technical Reports No. 301. Department of the Built Environment, Aalborg University 2022.

Heat Pump Solutions in Renovations of Multi-Storey Buildings

Georgios Dermentzis[a], Mara Magni[a], Fabian Ochs[a], William Monteleone[a], Benjamin Schaffer[b]

[a] Unit of Energy Efficient Buildings, University of Innsbruck, Austria, Technikerstrasse 13, Innsbruck, 6020

[b] TBH Ingenieure GmbH, Austria, Reininghausstraße 78, Graz, 8020

Abstract. EU set the target for deep renovation and for phasing out gas or oil-based heating systems to reach the ambitious climate goals. Although technical solutions for the renovation of multi-story residential buildings (i.e. window replacement, thermal insulation) and boiler replacement in central energy supply concepts already exist since several years, the renovation rate has been stagnating at a low level for years (well below 1% of the stock). This means that the ambitious climate protection goals in the building sector cannot be nearly achieved. Heat pump is a key technology also for building renovations to get rid of fossil fuel based technologies such as oil and gas boilers. In this study, a method is proposed targeting serial renovations of multi-apartment buildings. Simulations are performed deriving a guide to support decision-making considering both active and passive measures. Three energy renovation levels are applied in a building, located in Innsbruck, and several heating variants are implemented, which are categorised in central (one system per building), decentral (one system per apartment) and mixed. The calculated electricity consumption of the system to supply space heating and domestic hot water as well as the auxiliaries is used to rank the different solutions, resulting in a range between 19.7 kWh/(m² a) and 44.8 kWh/(m² a).

Keywords. Heat pumps, renovation, multi-storey buildings, thermal losses.
DOI: https://doi.org/10.34641/clima.2022.71

1 Introduction

The European Union is aiming at reducing the CO_2 emission by at least 55% by 2030 in order to reach the goal of climate neutrality by 2050 [1]. To accomplish these ambitious targets, the national renovation rate has to be increased and financial strategies have to be developed to drastically reduce the energy demand. The building sector is responsible for 35% of the global final energy consumption, in particular, 22% is covered by the residential sector [1].

Within this framework, a research project explores innovative approaches for highly energy-efficient renovation strategies for apartment buildings in Austria, aiming to develop a new service model (one-stop-shop) for property managers, housing and owner associations through a targeted, novel mix of technical and non-technical measures. The technical measures are focused on modular and scalable building technology systems, multifunctional building components and standardization in industrial prefabrication that assure minimal disruption during the renovation process.

Due to the overall limited availability of renewable electricity and district heating on the Austrian level and the increasing demand, the thermal renovation of buildings is indispensable for achieving the climate goals. Switching from fossil heating systems to heat pumps is (often) only technically feasible in combination with an appropriate thermal renovation. To achieve a significantly higher renovation rate and phase-out of fossil-based heating systems, new minimal invasive and adaptive renovation processes are required, which merge construction and building systems with energy conversion based on renewable energy sources. Standardization and industrial prefabrication enable a reduction in costs and expenditure of time for the construction while the quality of the renovation is increased.

More than 250.000 combinations of building types were analyzed, ages, climate zones, building envelope efficiency levels and HVAC system configurations in Europe, also considering economic feasibility [2]. Besides, various renovation packages were also analyzed concerning their economic feasibility and environmental impact [3]. In Ref. [4], a comprehensive simulation study for a new housing

Copyright ©2022 by the authors. This conference paper is published under a CC-BY-4.0 license.

development was carried out to develop a decision-making support tool regarding the choice of the heating system, the degree of centralization of the heating system, the heat distribution system and the corresponding degree of pipe insulation. In Ref. [5], guidelines for the deep renovation of buildings based on the experience with demo buildings are provided.

This contribution highlights the potential of serial renovations with different heat pump solutions. These solutions are categorised in central (one system per building), decentral (flat-wise) or mixed heating systems, aiming to be the basis for serial, adaptive and industrialized renovations with heat pump solutions. In a reference multi-story building, these solutions are investigated through simulations calculating the final electricity i.e. the electricity consumption to supply space heating, domestic hot water (DHW) and auxiliaries.

2 Methodology

2.1 Proposed method

This work aim at proposing a methodology tailored to support the planner to select the most suitable solution for each specific renovation case study. A simplified scheme of the proposed method can be seen in **Fig. 1**. The first step of this scheme, which supports the whole process, is the collection of all the relevant information. A checklist of required inputs regarding both technical and non-technical aspects is provided. In the second step, the collected data are used to select a bundle of possible solutions regarding the envelope and the system with the help of the decision tree developed within the research project. The set of solutions are then analysed within an iterative process in which the generation, distribution and emission systems have to be sized and the minimum requirements for the envelope quality have to be assessed excluding unfeasible solutions (e.g. compact heat pump system with air heating in combination with a non-insulated envelope have to be excluded). The number of feasible solutions, as an outcome of this step, should be reduced and for the remaining solutions, a calculation of the energy balance is performed considering the integration of renewables. At this point, it is possible to evaluate the life cycle cost and investment cost of each selected combination and from here based on technical and non-technical aspects, the "best" solution can be selected.

This simulation study focuses mainly on step 2, aiming to set a basis to support decision-making. In step 1, after the collection of the required data for the building, some decisions were made such us that new radiators have to be installed. The simulation results for step 2 include three renovation levels from the building envelope point of view, and several variants of centralised, decentralised of mixed heating systems. Finally, the required electricity for various distribution and emission systems combined with heat pumps is calculated.

The used simulation model is based on Matlab using the Carnot toolbox presented in [4].

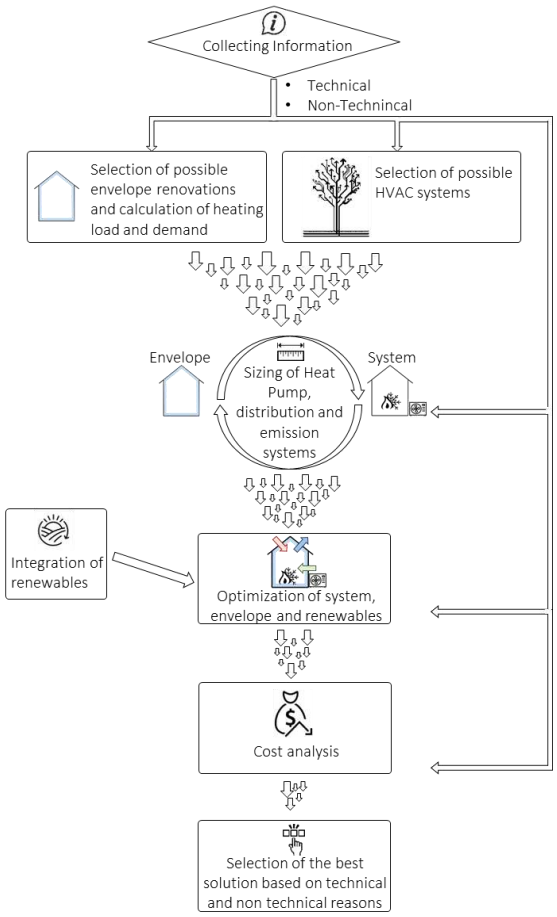

Fig. 1 – Scheme of the proposed method

2.2 Building and climate

The modelled building that is located in Innsbruck and a floor plan including the four flats are shown **Fig. 2**.

Fig. 2 – Outside view of the multi-family building and a floor plan (NHT, Innsbruck).

The main characteristics of the building are summarised in **Tab. 1**.

Tab. 1 - Building characteristics.

Description	Quantity
Treated area [m²]	1296
Foot print area [m²]	449
Storeys	4
Flats per storey	4
Area of the flats [m²]	73/98/98/109
Persons per flat	3

Innsbruck has relative cold winters and mild summers. Thus, cooling demand is almost negligible at the moment, however, is increasing over the years due to comfort reasons. The related climate data of i.e. monthly global radiation and ambient temperature are depicted in **Fig. 3**.

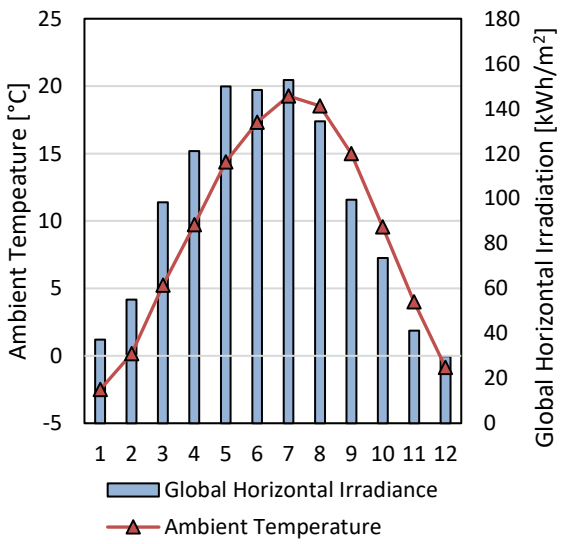

Fig. 3 – Monthly global radiation and outside temperature in Innsbruck

Three renovation levels are applied to the building, as shown in **Tab. 2**, which summarizes the corresponding requirements for space heating and domestic hot water. The HD25 is based on EnerPHit standard [6], the HD45 is similar to EnerPHit but the mechanical ventilation is without heat recovery, and the HD60 is based on the Austrian standards [7].

Tab. 2 – The space heating and DHW demand for the three renovation levels.

	HD25	HD45	HD60
Space heating [kWh/(m²a)]	25	45	60
Building energy Standards	EnerPHit [6]	EnerPHit without heat recovery [6]	Austrian standards [7]
DHW [kWh/(m²a)]		19.8	

Remark: mechanical ventilation with heat recovery is considered in HD25 and not in HD45 and HD60

2.3 Heat pump, distribution and emission systems

A selection of central, decentral and mixed hydraulic solutions is analysed and compared in order to evaluate the influence of heat pump performance, distribution losses and auxiliary energy on the final energy consumption of the systems. The overall efficiency depends in particular on the temperature level of the system: On the one hand, the heat losses increase with a higher temperature level, on the other hand, especially in heat pump systems, the temperature level has a major influence on the efficiency of heat generation.

Air-source heat pumps are used with COP of 3.7 at 2 °C outdoor temperature and 35 °C flow temperature and COP of 2.4 at 7 °C outdoor temperature and 55 °C flow temperature. The flow temperature is varied within the heating period based on the ambient temperature i.e. a so-called heating curve is implemented. In simulations, the COP is calculated dynamically for the given source and sink temperature. The investigated emission systems are mainly radiators or air heating in case of deep energy renovation i.e. low space heating demand.

In order to achieve the goal of a minimally invasive renovation, several different heat pump solutions are analysed:

1. Central solution: A central heat pump should supply the entire building with both space heating and domestic hot water. To guarantee a minimally invasive renovation, the distribution can take place via the old central distribution system or, if this can no longer be used, by laying cables in the staircase or in the facade.

2. With the mixed solution, decentralized systems are used for the preparation of domestic hot water, while

a central heat pump provides the space heating, which can be significantly smaller than the heat pump of the previous category.

3. In the case of decentralized solutions, both the DHW preparation and the space heating of each flat is prepared individually. This solution can be implemented with various technologies such as compact heat pumps or separate components for hot water preparation, heating and ventilation.

The modelled systems are presented in **Tab. 3**. Additionally, the hydraulic scheme of each system is presented in **Fig. 4** for central ones, in **Fig. 5** for mixed ones and in **Fig. 6** for decentral ones.

Tab. 3 – Investigated systems-variants

	Description	Abbreviation
Centralised	four-pipe system with circulation	4P-C
	four-pipe system with fresh water station	4P-FWS
	two-pipe system with fresh water station	2P-FWS
	two-pipe system with charging window	2P-CW
Mixed	two-pipe system with e-boilers	2P-EB
	two-pipe system with e-boilers and shower-drain water heat recovery	2P-EB& DWHR
	two-pipe system with DHW heat pumps	2P-DHW_HP
Decentralised	split units and e-boilers	SU&EB
	split units and DHW heat pumps	SU&DHW_HP

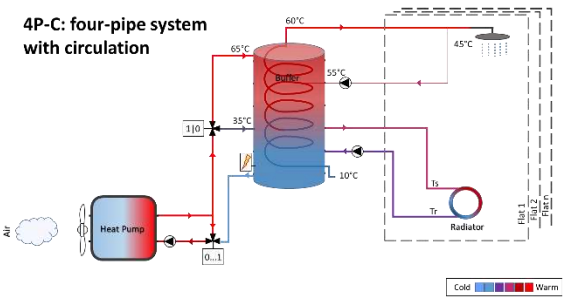

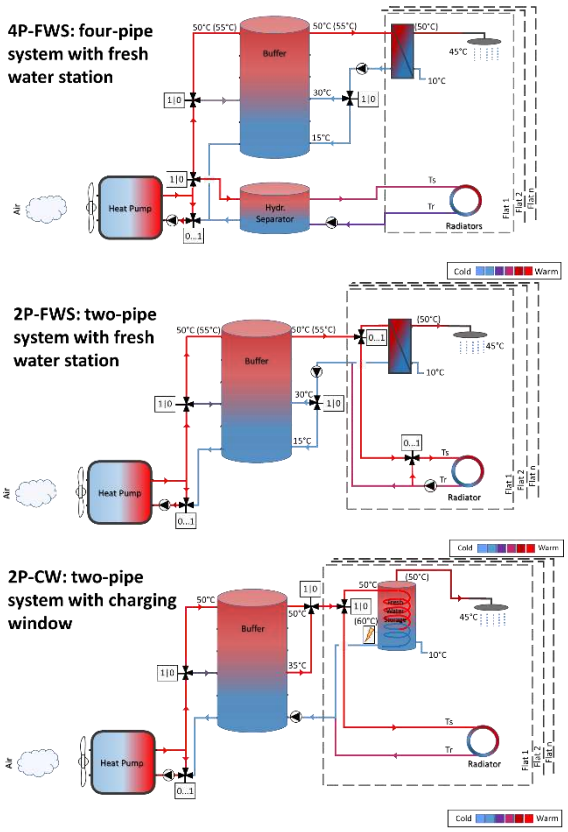

Fig. 4 – Hydraulic schemes of the variants with centralised solutions

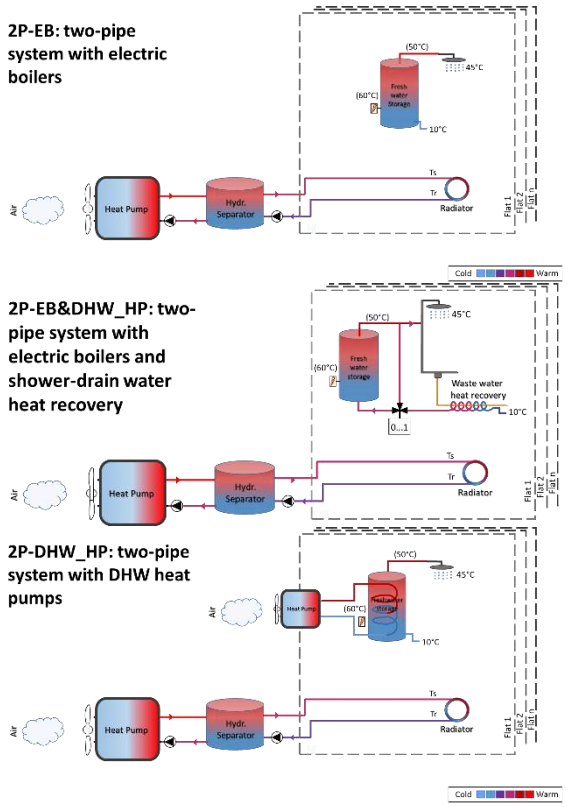

Fig. 5 – Hydraulic schemes of the variants with mixed solutions i.e., centralised for SH and decentralised for DHW

The pipe-distribution systems are designed according to Austrian/European standards [8,9], and the size of the pipes vary based on the heating

demand levels and the corresponding flow and return temperature (see **Tab. 4**).

Tab. 4 – Flow and return temperature for space heating (SH), and .DHW temperature based on three renovation levels

	HD25	HD45	HD60
Flow temperature for SH [°C]	40	45	55
Return temperature for SH [°C]	30	35	40
DHW temperature [°C]	55 (except:2P- or 4P-FWS with 50 °C and 4P-C with 60 °C)		

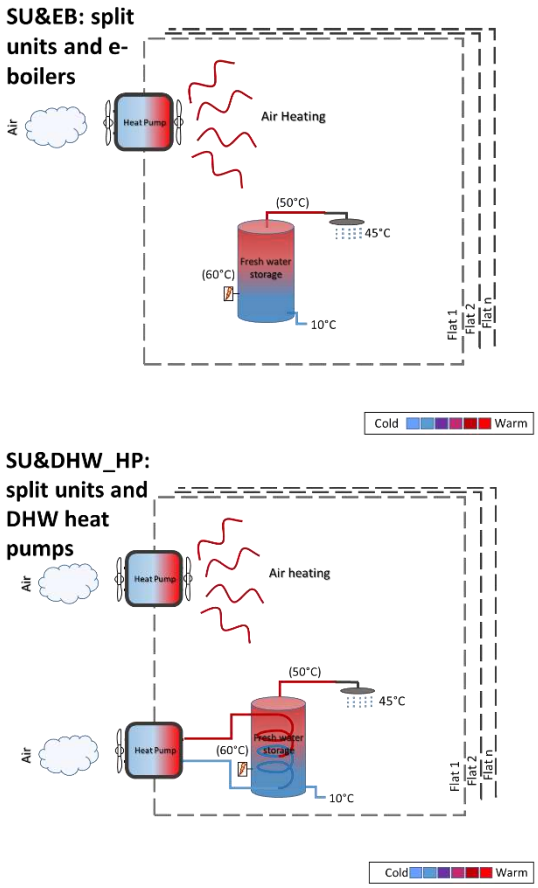

Fig. 6 – Hydraulic schemes of the variants with decentralised solutions

3 Results and discussion

Fig. 8 presents the electricity consumption of all the simulated systems in the three renovation levels. These results can be used to support decision-making process finding the optimum combination of envelope quality and HVAC system configuration. For example, it can be observed that electric boilers should be avoided since even in HD25 with low space heating demand the systems with electric boilers require more electricity than the other systems in HD45 or similar level to other systems in HD60. The installation of shower-drain water heat recovery combined with an electric boiler reduces the consumption significantly by 4.5 kWh/(m² a), however, it is not enough to change the order in the ranking of the systems. It must be noted that the required thermal comfort level is reached in all variants.

Comparing the different solutions in each renovation level, the central system 4P-FWS is the optimal one with the lowest electricity consumption in all renovation levels. In HD25, the mixed system 2P-DHW_HP, and the decentral system SU&DHW_HP result in similar electricity consumption. The central systems 2P-FWS and 2P-CW have slightly higher consumption compared to 4P-FWS. In addition, the later has the advantage that it can also supply cooling compared to other 2-pipe central systems that cannot.

4P-C in HD25 consumes more than other systems in HD45 such as 4P-FWS and 2P-DHW_HP, therefore, it cannot be suggested.

Fig. 7 presents the electricity consumption of the investigated systems for the HD25, which is separated in the electricity dedicated to space heating, DHW and auxiliaries. As can be seen, the requirement for space heating does not vary significantly between the different systems mainly due to high heat pump performance because of low flow temperature. However, the requirement for DHW varies significantly between the systems. For example, the consumption in case of DHW_HP is 9.6 kWh/(m² a) and in case of 4P-C is 14.4 kWh/(m² a). The reasons for that differences are the choice of a heat pump or an electric boiler, the use of central or decentral DHW system (with or without distribution losses), and the different required DHW temperature (**Tab. 4**) that influences significantly the performance of the heat pump and the distribution losses.

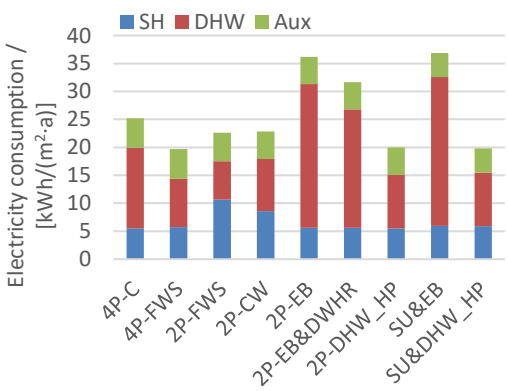

Fig. 7 – Required electricity for SH, DHW and Aux for the different variants applied in renovation level HD25. Remark: distribution losses in 2P-FWS and 2P-CW are dedicated in SH, however, are for both SH and DHW.

In **Fig. 9**, the overview of the energy flows for the central 4P-FWS system are shown in a Sankey diagram. The distribution losses are 7.8 kWh/(m² a) from which the 2.6 kWh/(m² a) can be used as gains in heating period. In addition, the mechanical ventilation with heat recovery reduces the heating demand by 15 kWh/(m² a). In such a renovation level, the demand of DHW and space heating are in the similar range.

As mentioned in the proposed method, the final choice of the system depends on the challenges and the costs for implementing these measures. Usually, when a central system can be an option is less expensive than the use of decentral ones. However, often that is difficult to realise. Besides, space limits and sound emissions should be considered in the decision-making process.

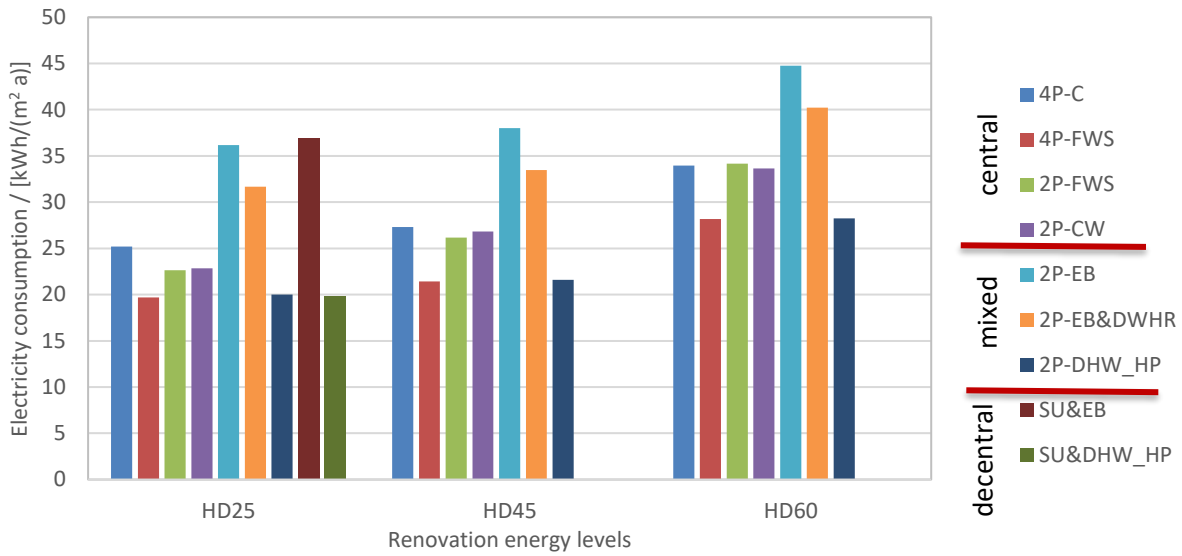

Fig. 8 – Final energy (electricity) required by the heat pump and auxiliaries (including mechanical ventilation) in the three renovation levels (25, 45 or 60 kWh / (m2 a)). Remark: Decentralized systems not simulated for HD45 and HD60 (not recommended).

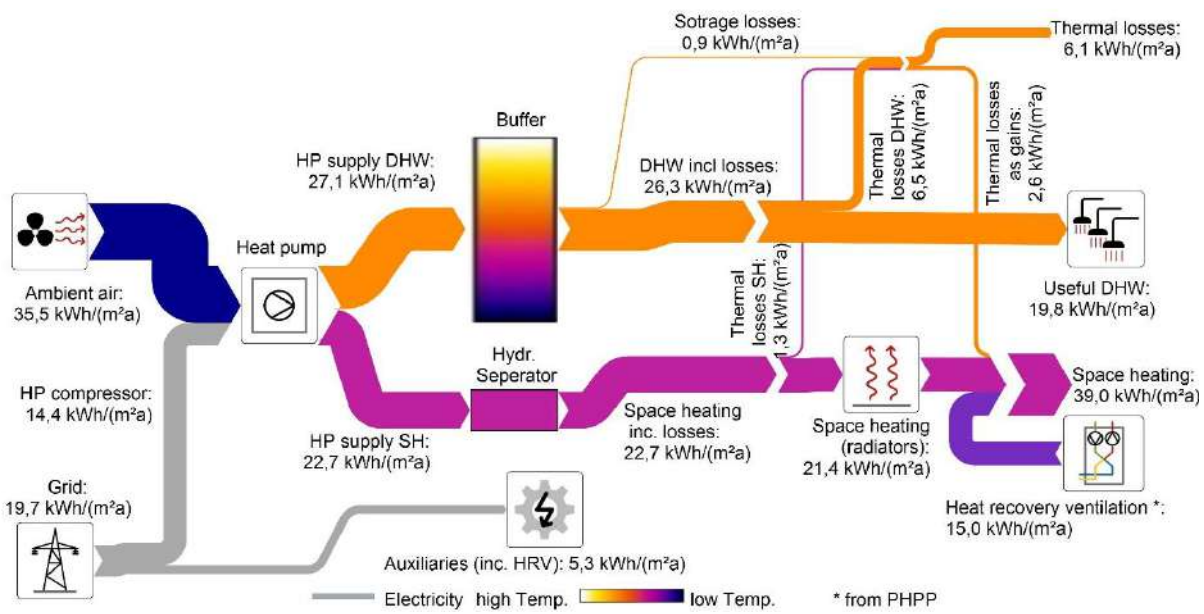

Fig. 9 – Sankey diagram of the centralised 4-pipe distribution system with fresh water station (4P-FWS) implemented in renovation level HD25 (i.e. 25 kWh/(m² a))

4 Conclusions

A method is proposed targeting serial renovations for multi-apartment buildings. Aiming to support decision-making, simulations are performed considering three renovation levels from the thermal envelope point of view and several heat production, heat distribution and emission systems categorised in central (one prebuilding), decentral (one per flat) or mixed solutions.

The electricity consumption for the different solution varies significantly from 19.7 kWh/(m^2 a) up to 44.8 kWh/(m^2 a). The energy optimal solutions in each renovation level (thermal envelope), are the central system 4P-FWS and the mixed one 2P-DHW_HP. In addition, the decentral SU&DHW_HP has similar performance, however, it is suggested to be used in HD25 with low heating load in which air heating can be an option due to comfort reasons. Besides, the central 2P-FWS and 2P-CW have slightly higher consumption than the optimal systems in HD25, thus, the decision can be made considering also other criteria such as non-technical or economic ones.

The not recommendable solutions from the energy point of view are those with circulation for DHW (4L-C) and those with electric boilers, even if deep renovation is applied.

Finally, the final decision depends on a combination of energetic and economic evaluation, and non-technical criteria such as resilience, possibility of cooling, space issues, etc. In a future work, economic calculations including investment, operation and maintenance costs should be performed.

5 Acknowledgement

This work was performed within the framework of the Austrian research project RENEWnow (FFG 879432). Financial support was provided by the Austrian Ministry for Transport, Innovation and Technology and the Austrian Research Promotion Agency (FFG).

6 References

[1] United Nations Environment Programme (2020), Global Status Report for Buildings and Construction: Towards a Zero-emission, Efficient and Resilient Buildings and Construction Sector. Nairobi, 2020.

[2] C. Dipasquale, R. Fedrizzi, A. Bellini, M. Gustafsson, F. Ochs, C. Bales, Database of energy, environmental and economic indicators of renovation packages for European residential buildings, Energy and Buildings. 203 (2019) 109427. https://doi.org/10.1016/j.enbuild.2019.109427.

[3] M. Gustafsson, C. Dipasquale, S. Poppi, A. Bellini, R. Fedrizzi, C. Bales, F. Ochs, M. Sié, S. Holmberg, Economic and environmental analysis of energy renovation packages for European office buildings, Energy and Buildings. 148 (2017) 155–165. https://doi.org/10.1016/j.enbuild.2017.04.079.

[4] G. Dermentzis, F. Ochs, A. Thuer, W. Streicher, Supporting decision-making for heating and distribution systems in a new residential district - An Austrian case study, Energy. 224 (2021) 120141. https://doi.org/10.1016/j.energy.2021.120141.

[5] F. Ochs, R. Fedrizzi, C. Bales, G. Dermentzis, D6.7 - Guidelines on Systemic Approach and Checklist. EC FP7 project iNSPiRe Grant agreement no. 314461, 2016. http://inspirefp7.eu/wp-content/uploads/2017/01/WP6_D6.7_20160931_P1_Guidelines-on-Systemic-Approach-and-Checklist.pdf.

[6] B. Zeno, W. Feist, EnerPHit Planerhandbuch - Altbauten mit Passivhaus Komponenten fit für die Zukunft machen, Darmstadt, Germany, 2012.

[7] OIB, OIB-Richtlinie 6. Energieeinsparung und Wärmeschutz (Austrian energy building code), 2015.

[8] ÖNORM EN 806 Dimensioning of piping for DHW systems, n.d.

[9] ÖNORM EN 12828:2014 Planning of heating systems, n.d.

Room-side and Plenum-side Cooling Prediction of Suspended Radiant Ceiling Panels

Jun Shinoda [a,], Ongun B. Kazanci [a], Shin-ichi Tanabe [b], Katsuaki Hidari [c], Hiroki Watanabe [c], Yoshimi Takahashi [c]*

[a] International Centre for Indoor Environment and Energy, Department of Environmental and Resource Engineering, Technical University of Denmark, Koppels Allé, Building 402, 2800 Kgs. Lyngby, Denmark (* junshi@dtu.dk).

[b] Department of Architecture, Waseda University, 3-4-1 Okubo, Shinjuku-ku, Tokyo, 169-8555, Japan.

[c] Takenaka Corporation, 1-1-1 Shinsuna, Koto-ku, Tokyo, 136-0075, Japan.

Abstract. Hydronic radiant ceiling panels use a chilled surface to cool a room, and their cooling capacity is normally measured in a certified test chamber. However, current measurement standards calculate the cooling capacity of a panel based on the heat carried by the circulating water, which is the sum of the heat extraction from the room and plenum. Thus, sizing the radiant system based on the cooling capacity of the panels may result in an undersized system. In this study, a series of test chamber measurements and field measurements were conducted to quantify and empirically predict the proportion of the heat extracted from the room-side to the total heat extracted by the radiant panel. The cooling capacity of suspended radiant ceiling panels was first measured in a certified test chamber, with the temperature difference between the room and plenum as the main parameter. Within the tested temperature range (plenum temperature of 24 – 28 °C, room temperature of 26 °C), the heat extracted from the room side was 77 – 92 % when the panels were insulated and decreased to 46 – 71% when they were not insulated. A simplified, empirical approach for estimating the heat extraction at both sides of the panel was proposed based on the obtained results. A field measurement was then conducted to examine the validity of the proposed methodology. Measurements were conducted in an office building located in Japan, which was equipped with radiant ceiling panels of the same type as the ones tested in the chamber measurements. Heat flux sensors were placed at both the room and plenum sides of a single radiant panel to obtain the proportion of heat extraction from the room-side. The measured room and plenum temperatures were used as input for the prediction of the room-side heat extraction ratio, and the average error of the predicted heat flux was 6%, confirming the validity of the proposed methodology.

Keywords. Radiant Ceiling Panel, Chilled Ceiling, Cooling Capacity, Radiant Cooling, Plenum
DOI: https://doi.org/10.34641/clima.2022.137

1. Introduction

Prefabricated radiant ceiling panels are a common form of radiant heating and cooling systems. As opposed to embedded systems, which often requires on-site construction and therefore a numerical estimation of its cooling performance, prefabricated panels can have their cooling capacity measured in a test chamber. However, current measurement standards such as EN 14240 [1] calculate the cooling capacity based on the heat carried by the circulating water, which is the total heat extracted from the room and plenum. Field measurements conducted by Li et al. [2] showed that about 30 – 40% of the heat extraction by the water circuit of suspended radiant ceiling panels was from the plenum. Ito et al. [3] conducted tracer gas measurements to quantify the air exchange between the room and plenum, and developed a numerical model for cooling capacity predictions. Further simulations with the developed model was performed by Ojima et al. [4], and it was concluded that sizing a radiant panel system based on the manufacturer-stated cooling capacity may result in an under sizing of the system.

2. Methodology

The purpose of the current study was to present possible improvements to the cooling capacity measurement procedure of suspended radiant ceiling panels. Test chamber measurements were conducted following the same setup and procedure

Copyright ©2022 by the authors. This conference paper is published under a CC-BY-4.0 license.

as stated in the standards [1, 5] but with different plenum temperatures to quantify its effect on the cooling capacity and proportion of heat extraction from the room and plenum. A simple, empirical model to predict the room-side heat extraction was then developed. Finally, the proposed model was validated with dataset obtained in the field.

2.1 Chamber measurements

The radiant panel selected for this study was composed of capillary pipes. Table 1 lists the physical properties of the panels. The cooling capacity was measured according to the ARCH 2017 CHTRS standard [5], a Japanese standard derived from the EN14240 [1]. The nominal cooling capacity is the measured heat extraction from the panel circuit with 8 K difference between the mean water temperature and the room temperature. The panel comes with an optional insulation layer, and the nominal cooling capacity is slightly lower when the panel is insulated.

Table 1 – Physical properties of the measured panels.

Properties	Units	Description
Dimensions	mm	584 × 1184 × 8
Nominal Cooling capacity	W/m²	61 (non-insulated); 58 (insulated)
Panel Material	-	Aluminium
Pipe material	-	Polypropylene
Inner/Outer Pipe Diameter	mm	2.3 / 3.4
Insulation (optional)	-	32 kg/m³ glass wool, 40 mm, 0.036 W/(m·K)

Fig. 1 shows the dimensions of the chamber. Eight suspended radiant ceiling panels were installed as one circuit, without any intentional gaps. The remaining ceiling surface was covered with insulation. The numbers on the panels denote their order in the panel circuit. The chamber had dimensions of 2.664 m × 2.920 m × 2.385 m. The chamber complied with the EN14240 and ARCH 2017 CHTRS standards [1, 5], and the measurement procedures followed those specified in these standards, except for the cooling loads that were added to the plenum for the purpose of the study.

The room reference temperature was measured by a black globe thermometer positioned in the center of the room at a height of 1.1 m. The plenum reference temperature was substituted by the average of the air temperature and uncooled/surrounding surface temperatures (area-weighted). Surface and air temperatures were measured with thermocouples with accuracies of ±0.5 K. All the sensors were calibrated against a Pt100 temperature sensor with an expanded uncertainty of 0.02 K.

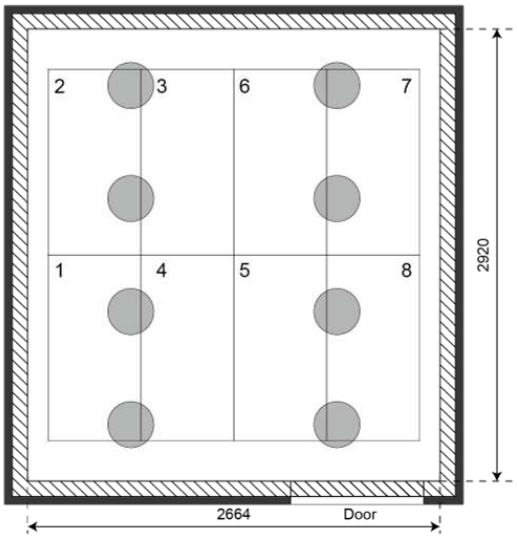

(a) Plan

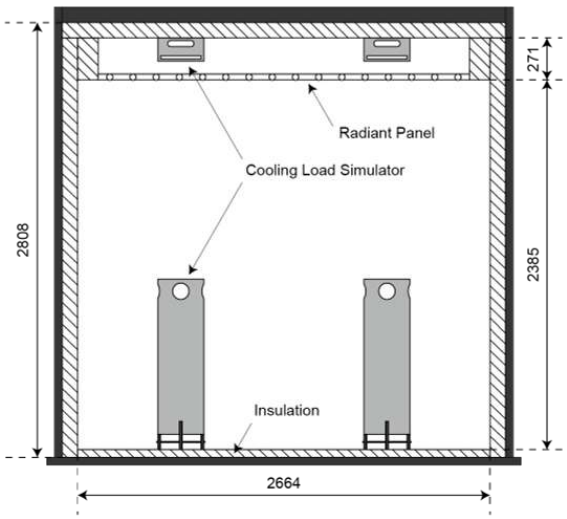

(b) Section

Fig. 1 – Dimensions of the test chamber (units: mm).

For both the room and the plenum, eight cooling load simulators were each installed to enable temperature control of both spaces. For each measurement case, the room and plenum temperatures were controlled by adjusting the electrical input to the cooling load simulators and the supply water temperature to the panel circuit. The supply water flow rate was fixed to 3.33 L/min. The surrounding wall and floor temperatures were maintained at a temperature as close as possible to the room temperature by the hydronic pipes embedded behind each surface. All the surfaces except for the radiant panels were covered with insulation at the inner side of the chamber.

Table 2 lists the measurement cases. For each case, the room reference temperature was maintained at 25.7 ± 0.1 °C. The temperature differences between the room reference and mean water temperature of

6, 8, and 10 K were tested. In addition, for each temperature difference, the plenum temperature was adjusted to approximately 24, 26, and 28 °C (corresponding to ± 2 K from the room reference temperature). Nine tests were conducted for non-insulated panels and three for the insulated panels. Each measurement case was conducted for 15 min with a logging interval of 30 s under steady state conditions. Electrical inputs to the cooling load simulators of the room and plenum were assumed to be the heat extracted from each space. The cooling capacity of the panels and the extracted heat from each space were compared and used for analysis.

Table 2 – Measurement cases.

Case name	Room reference temp. [° C]	Plenum reference temp. [° C]	Room reference – mean water temp. [° C]
Non-insulated Panels			
N_6_-2	25.7	23.8	6.0
N_6_0	25.8	25.6	5.9
N_6_+2	25.8	27.5	5.9
N_8_-2	25.7	23.7	7.8
N_8_0	25.7	25.7	7.7
N_8_+2	25.7	27.5	7.5
N_10_-2	25.7	23.5	9.5
N_10_0	25.7	25.5	9.4
N_10_+2	25.7	27.6	9.2
Insulated Panels			
I_8_-2	25.6	23.8	7.9
I_8_0	25.8	26.1	7.9
I_8_+2	25.7	27.9	7.8

2.2 Model Development

ISO 11855-2 [6] provides an equation to calculate the downward heat loss of an embedded floor heating system. In this study, the same equation was used for the plenum-side heat extraction for the radiant ceiling panels, as shown in equation (1).

$$q_p = \frac{U_{w,p}}{U_{w,r}} q_r + U_{w,p} \cdot (t_p - t_r) \tag{1}$$

Where:

- q_p : plenum-side heat flux (W/m²)
- q_r : room-side heat flux (W/m²)
- t_p : plenum reference temperature (°C)
- t_r : room reference temperature (°C)
- $U_{w,p}$: heat transfer coefficient between water and plenum (W/(m² · K))
- $U_{w,r}$: heat transfer coefficient between water and room (W/(m² · K))

If the two spaces have the same temperature ($t_p = t_r$), the equation could be further simplified in the form of equation (2), and the ratio of the room-side heat flux to the total heat extraction can be expressed as equation (3).

$$q_p = \frac{U_{w,p}}{U_{w,r}} q_r \tag{2}$$

$$\frac{q_r}{q_r + q_p} = \frac{\Delta t_{w,r}}{\Delta t_{w,r} + \frac{U_{w,p}}{U_{w,r}} \cdot \Delta t_{w,p}} \tag{3}$$

Where:

- $\Delta t_{w,p}$: difference between mean water and plenum temperatures (K)
- $\Delta t_{w,r}$: difference between mean water and room temperatures (K)

In this study, the heat transfer coefficients ($U_{w,p}$, $U_{w,r}$) were substituted with an empirically obtained coefficient that is dependent on the temperature difference between the room and plenum so that equations (2, 3) could be used even when the room and plenum temperatures are not the same ($t_p \neq t_r$). A linear regression of the results obtained from the test chamber measurements were used to obtain the empirical heat transfer coefficients.

2.3 Field measurements

To validate the empirical prediction method described in section 2.2, dataset obtained from a field measurement was used. The case study building was a newly constructed office in the Greater Tokyo Area of Japan. The radiant panels installed in the building was the same type (product) as those tested in the test chamber measurements. The radiant ceiling panels covered 58% of the ceiling surface. The ceiling height was 2.8 m, and the plenum height was 1.08 m.

Fig. 2 shows the typical floor plan of the building. The office floor had dimensions of 56.4 × 56.4 m, and the office area (open plan layout) was positioned along the north, west, and south sides. The remaining area are the building core and meeting rooms.

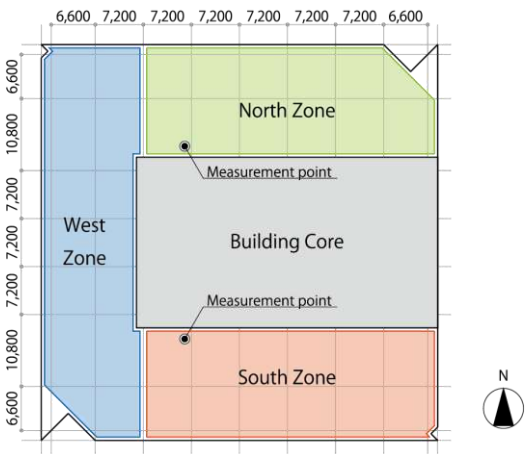

Fig. 2 – Floor plan of case stud building (units: mm).

Field measurements were conducted continuously in the summer of 2020, between 18 – 25th of August, in the north and south zones. In each zone, heat flux sensors and thermocouples were placed on the room- and plenum-sides of a single panel, and they were logged in 1 min intervals. The air and globe temperatures of the plenum was measured above the selected panels with a 5 min logging interval. The room temperature was obtained from the Building Management System (BMS), which was logging at a 1 min interval.

The building was at its first year of operation, and therefore in the phase of tuning the operation and control of the systems. During the measurement period, the room temperature setpoint was adjusted between 24.5 and 25.5 °C, which allowed the measurements to be conducted under different temperature conditions.

3. Results and Discussion

3.1 Room and plenum cooling loads in the test chamber

Fig. 3 shows the cooling load in the room and plenum for the 12 measurement cases. The cooling load was divided by the installation area of the panels (5.76 m^2). The room-side load ratio was calculated by the ratio of the room-side load to the sum of the room and plenum loads. The results were grouped in sets of three cases, according to the difference between the mean water and room reference temperature (6, 8, 10 K) and insulation type (N: non-insulated, I: insulated). Within each group, the plenum temperatures were set to 2 K lower than room temperature, equivalent to room temperature, and 2 K higher than the room temperature (-2, 0, 2 K).

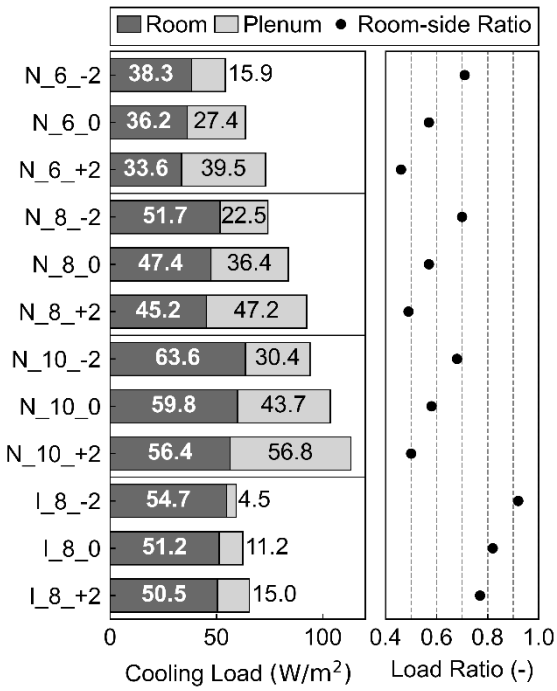

Fig. 3 – Cooling load in the room and plenum

The results show that the increase in plenum temperature increases the total cooling capacity (i.e., total heat extraction from the room and plenum) but decreases the proportion of the room-side heat extraction. When the plenum temperature was 2 K higher than the room temperature, about half of the cooling was from the plenum-side for non-insulated panels. Insulated panels were able to decrease the amount of cooling to the plenum, but the room-side ratio dropped to 0.77 when the plenum temperature was 2 K higher than the room temperature, which is non-negligible. In the observed scenarios, the room-side ratio of non-insulated panels ranged between 0.46 and 0.71, and the ratio of insulated panels ranged between 0.77 and 0.92.

3.2 Empirical adjustment of heat transfer coefficients

Fig. 4 shows the empirical heat transfer coefficient between the water and room/plenum in relation to the temperature difference between the two spaces. The heat transfer coefficient was calculated by dividing the loads in Fig. 3 by the mean water and room/plenum reference temperature differences. Note that these values are different from the actual HTC ($U_{w,p}$, $U_{w,r}$) in equations (2), (3). For both the insulated and non-insulated panels, the obtained coefficients showed a linear relationship with the temperature difference between the room and plenum. Therefore, the empirical heat transfer coefficients to be used in equation (3) can be calculated with equation (4).

$$U = X \cdot (t_p - t_r) + Y \tag{4}$$

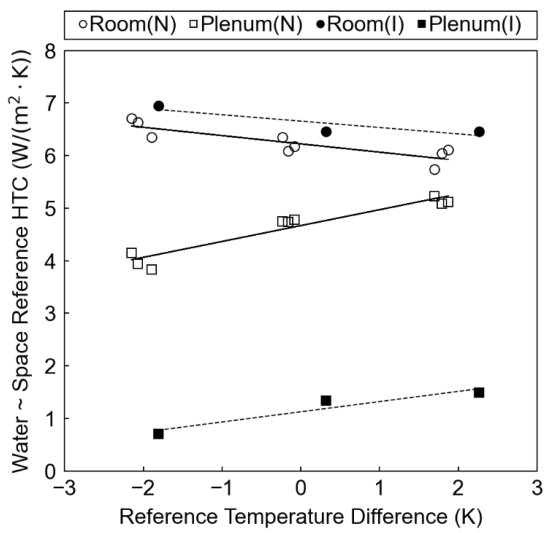

Fig. 4 – Empirical heat transfer coefficients (HTC: heat transfer coefficient, N: non-insulated panels, I: insulated panels)

The slope (X) and intercept (Y) for the non-insulated panels are listed in Table 3. The slope is negative for the room-side and positive for the plenum-side, as the cooling rate at the room-side will decrease, and

increase at the plenum-side when the plenum temperature is higher than the room temperature. These empirical values are unique to each panel type, and therefore the same measurement procedures have to be followed to obtain corresponding values for each product.

Table 3 – Slope and intercept of heat transfer coefficient adjustment (non-insulated panels)

Constants	Corresponding Space	
	Room ($U_{w,r}$)	Plenum ($U_{w,p}$)
Slope (X)	-0.158	0.302
Intercept (Y)	6.224	4.669

3.3 Validation of prediction model in the field

The plenum globe and room temperature from the field measurement was used to predict the room-side heat extraction ratio of the panel, with equations (3) and (4), and the values in Table 3. The predicted value was compared against the ratio of the room-side heat flux to the sum of heat flux at both sides of the measured panel.

Fig. 5 shows the heat flux and room-side ratio of a representative day in the south zone. The symbol of the heat fluxes was reversed (positive: cooling, negative: heating). The heat fluxes are shown as a stacked value. The bypass signals of the panel circuits could not be obtained from the BMS, and thus the exact time in which cooling water was supplied to a specific panel could not be obtained. Therefore the ratio was assumed to be zero when the main pump of the panel circuits was turned off or when the ratio exceeded 1 (i.e., when one side was heating and the other was cooling).

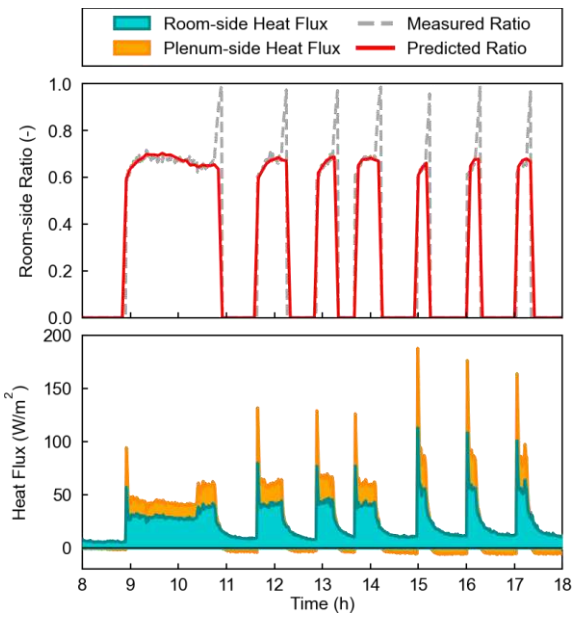

Fig. 5 – Heat flux and flux ratio of a representative day (South zone; Monday, 24. August 2020)

The results show that the room- and plenum-side heat flux varied at different times of the day, and with a different operation interval. This is mainly due to the variation of the supply water temperature to the panels in response to the tuning of the whole system operation. However, the room-side ratio was maintained at around 0.6 to 0.7, which was similar to those reported in previous studies [2]. The predicted room-side ratio and its time response was in good agreement with the measured ratio. The measured ratio deviated from the predicted value when the heat flux of the panel decreased, presumably when water supply was bypassed from the panel being measured.

Fig. 6 shows the comparison of the measured and predicted room-side heat flux ratio throughout the whole measurement period (but limited to occupied hours). As the results from Fig. 5 showed that the prediction model is applicable when there is water circulation to the panels, the plots were further filtered. Only the measurements that meet the criteria of a room-side heat flux higher than 22 W/m² and a plenum-side heat flux higher than 14 W/m² were considered to be instances when the panels were turned on. The criteria corresponds approximately to a 2 K temperature difference between the active surface and the reference temperature in the room/plenum [7].

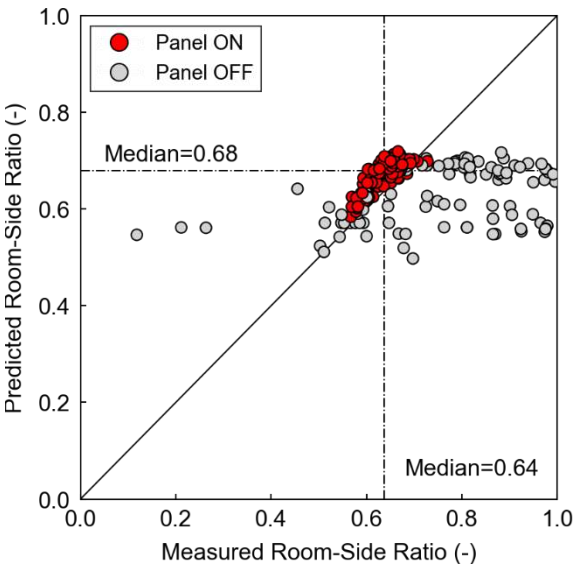

Fig. 6 – Measured and Predicted Room-side heat flux ratio (all measurement period)

The comparison of the measured and predicted ratio over the whole measurement period shows a good agreement between them. The difference between the measured and predicted ratio ranged from -0.02 to 0.08, with an average of 0.04. This corresponded to an average error of 6% (with a standard deviation of 3%) for the room-side heat flux. The validity of the proposed methodology was thus confirmed.

4. Overall Discussion

The results from the test chamber measurement showed that the plenum temperature has a considerable effect on the cooling capacity and proportion of the room-side cooling. It is highly recommended that radiant panels be insulated to prevent unnecessary cooling of the plenum. However, in the tested conditions for the insulated panels, when the plenum temperature was equal to or higher than the room temperature, about 20% of the cooling was dedicated to the plenum, which cannot be dismissed. Therefore, regardless of the panel insulation, cooling capacity measurements should be conducted with different temperature differences between the room and plenum. The calculation of the heat balance within the plenum is critical, especially for cases in which larger loads are to be expected in the plenum e.g., in a top floor where the ceiling slab is exposed to solar radiation, or when waste heat from lighting armatures may be present.

When evaluating a single zone of a building, cooling of the plenum would be an excess use of energy. In a multi-story building, a cooled plenum may provide additional cooling to the floor above, or provide cooling to the room with a time delay. Whether or not the cooling of the plenum would be beneficial for the entire cooling system would depend on multiple factors, such as building construction, control and operation. This would require further studies.

5. Conclusion

A series of test chamber measurements and field measurements were conducted to provide improvements to the cooling capacity measurement of suspended radiant ceiling panels. The conclusions were as follows.

- Test chamber measurements were conducted to quantify the effect of plenum temperature on the cooling capacity and the proportion of cooling to the room and plenum. With a plenum temperature 2 K lower to 2 K higher than the room temperature, heat extraction from the room-side was 46 – 71% for non-insulated panels and 77 – 92% for insulated panels.
- Based on the equation presented in ISO 11855-2 [6], an empirical equation to predict the room-side heat extraction ratio was developed. The necessary values for this calculation may be obtained by repeating the measurement procedure of this study.
- Data from field measurements were used to validate the developed model. The case study building had the same type of radiant panel as those tested in the test chamber measurements. Heat flux at both sides of a selected panel was compared against the predicted values. The model was able to predict the room-side heat flux with an average error of 6% when water was being supplied to the panels. The validity of the proposed methodology was thus confirmed.

6. Acknowledgements

This work was supported by the Waseda University Research Institute for Science and Engineering (WISE) Project Research and Japan Society for the Promotion of Science (JSPS KAKENHI Grant Number JP 19J14856). The authors would like to thank Satoshi Yamakita and Hiroki Iwata for their support in planning and carrying out the test chamber measurements.

7. Data Access Statement

The datasets generated during and/or analyzed during the current study are not available because of a non-disclosure agreement but the authors will make every reasonable effort to publish them in near future.

8. References

[1] EN14240: Ventilation for buildings – Chilled ceilings – Testing and rating. European Committee for Standardization. 2004.

[2] Li, R., Yoshidomi, T., Ooka, R., Olesen, B. W. Field evaluation of performance of radiant heating/ cooling ceiling panel system. Energy and Buildings. 2015;86:58-65.

[3] Ito, S., Akashi, Y., Lim, J., Miura, N., Kawamura, A. Performance prediction method for ceiling radiant cooling panel. Journal of Environmental Engineering (Japan). 2018;83:737-747.

[4] Ojima, K., Ito, S., Lim, J., Akashi, Y. Designing a ceiling radiant cooling system for different installation conditions. IOP Conference Series: Earth and Environmental Science. 2019;238.

[5] ARCH: Cooling and Heating – Testing and Rating Standard (CHTRS) Ver. 1.1. The Association of Radiant Cooling and Heating systems of Japan. 2017.

[6] ISO 11855-2: Building environment design – Design, dimensioning, installation and control of embedded radiant heating and cooling systems – Part 2: Determination of the design heating and cooling capacity. International Organization For Standardization. 2012.

[7] Shinoda, J., Kazanci, O.B., Tanabe, S., Olesen, B.W. A review of the surface heat transfer coefficients of radiant heating and cooling systems. Building and Environment. 2019;159:106156.

[8] Shinoda, J., Kazanci, O.B., Hidari, K., Watanabe, H., Takahashi, Y., Tanabe, S. Improvements to the cooling capacity of suspended radiant ceiling panels to prevent under-sizing. Journal of Building Engineering. 2022; 51:104242.

Hardware-in-the-loop heat pump model validation for flexibility evaluations

Maarten Evens [a, b], *Alessia Arteconi* [a, b, c]

[a] Department of Mechanical Engineering, KU Leuven, 3000, Leuven, Belgium, maarten.evens@kuleuven.be, alessia.arteconi@kuleuven.be

[b] EnergyVille, 3600, Genk, Belgium

[c] Dipartimento di Ingegneria Industriale e Scienze Matematiche, Università Politecnica delle Marche, 60131, Ancona, Italy

Abstract. Heat pumps play a paramount role in carbon emission reductions as they allow the use of sustainable energy. As heat pumps mainly use electricity to provide thermal services, they also enable the provision of energy flexibility services. In this context, new heat pump control strategies are investigated. Though, the comparison of smart and traditional control strategies requires an accurate knowledge of the real heat pump behaviour, both in short- and long-term. Firstly, this paper presents a hardware-in-the-loop set-up which allows a real heat pump behaviour analysis, while the required communication is also shown. Secondly, the test bench was used to validate and further develop a water/water heat pump model. Hence, artificial test cycles were used to distinct and validate the internal control strategies of the heat pump, with the focus on both the short-term behaviour and energy consumption. As the heat pump model started from the manufacturer documentation, comparing the experimental results to the simulations revealed deviated behaviour due to a different modelling approach of the heat pump internal control strategies. Hence, the heat pump model was improved by changing and adding control strategies such as a compressor modulation controller, timing constraints and condenser and evaporator pump control. Although the improved heat pump model reached better profile agreement, deviations remained and indicated a calibration work necessity. Analysis also showed that the real heat pump was not able to quickly recover for the combination of high space heating temperatures and low thermal loads, while increasing the supply temperature for energy flexibility services is common. To conclude, results proved that only using heat pump manufacturer documentation is not sufficient for real heat pump behaviour representation.

Keywords. Heat pump, model validation, hardware-in-the-loop, energy flexibility.
DOI: https://doi.org/10.34641/clima.2022.242

1. Introduction

Heat pumps (HP) can play a paramount role to reach the required carbon emission reductions for several reasons. Indeed, electric driven HP ease the use of renewable electricity production and can thus exclude the use of fossil-based energy resources for heating purposes. When smartly controlled, HP also enable the provision of energy flexibility services. In this context, new HP control strategies are investigated [1,2]. Though, to fairly compare smart and traditional control strategies, an accurate HP model is required. Several authors already indicated the necessity to precisely represent the real HP behaviour. In their research, Evens and Arteconi [3], investigated the effects of neglecting/incorporating the internal control strategies of HP such as timing constraints, compressor control, pump control, back-up heater (BUH) control etc. By gradually increasing the HP modelling complexity, the authors showed a changing operational behaviour which was caused by different control blocks. With most effects visible in the short-term, the authors also showed an affected energy flexibility. Moreover, Clauß and Georges [4] investigated the modelling complexity of HP and showed that for short-term analysis, such as demand response, a precise HP model is required.

Though, an accurate short-term behaviour HP model is novel and requires manufacturer information about internal control strategies. To better understand and represent its real behaviour, HP models should be validated and calibrated against experimental results. As field trials require a physical

Copyright ©2022 by the authors. This conference paper is published under a CC-BY-4.0 license.

building and are hard to compare due to changing boundary conditions, hardware-in-the-loop (HIL) experiments enable the optimal use of both software and hardware. The building and its heat emission system can be kept in simulations, while a real HP can be coupled to an experimental test bench. Within this framework, several studies already proved the added value of HIL experiments. In their study, Blervaque et al. [5] compared four different modelling approaches for air/air HP and showed modelling difficulties due to the amount of parameters when calibrating. In [6], El-Baz et al. investigated the energy performance of brine/water HP and developed a Modelica model to represent the dynamic HP behaviour which showed deviations up to 3 % and 4 % for the produced heat and electricity consumption, respectively.

In addition, Ruiz-Calvo et al. [7] developed TRNSYS models to represent a Mediterranean building equipped with a water/water HP and for which they also compared HP models to field measurements. Furthermore, Conti et al. [8] compared the energy performance of an air/water HP in a HIL experiment to simulations based on manufacturer datasheets. They concluded that the transient behaviour of the real HP reduced its energy performance. Moreover, Péan et al. [9] experimentally investigated Model Predictive Control (MPC) strategies for HP and clearly showed practical bottlenecks when coupling the steady-state MPC controller to the real HP. They concluded that the dynamic HP operation differed from the scheduled plan of the MPC controller and proposed solutions to overcome these difficulties.

Insights in these modelling approaches and HIL experiments indicated that internal HP control strategies are mainly neglected or simplified. It could be seen that the pump control is generally replaced by constant flow rate provision or that on/off pump control was used. In addition, compressor control, timing constraints and BUH control are generally simplified. Furthermore, in some cases, the HP control decisions were used as inputs in simulation environments, e.g. using the measured compressor frequency as a model input. Although that such an approach is useful to predict the actual performance/status of the real HP, it cannot be used in a full simulation environment. Indeed, in those cases, the HP model should be complete by itself and it should well represent the operational behaviour.

The goal of this paper is twofold. In a first part, an experimental set-up will be presented, including the required measurements and communication set-up. In a second part, the HIL set-up was used to validate and to further improve a dynamic HP model, able to represent the operational behaviour of the HP. The validation work includes an analysis of both the energy consumption and short-term behaviour.

2. Research methods

This sections starts with a description of the HIL set-up and the required communication. As the test bench is used to validate a water/water HP model, the HP model parameters are shown and are based on a detailed analysis of the HP documentation. Hence, the HP model should well replicate the real HP behaviour. This section also presents HP model validation cycles. As results will show, deviations between the experiments and simulation model occurred and led to HP model improvements as will be further discussed within the Results section.

2.1 Hardware-in-the-loop set-up description

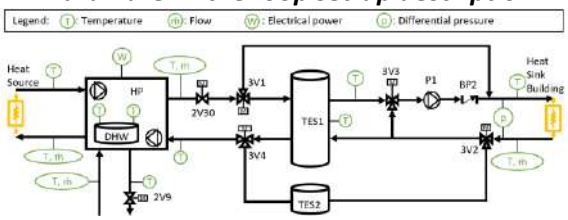

Fig. 1 – Hydraulic lay-out

Fig. 1 shows a hydraulic scheme of the HIL set-up with a reversible water/water HP, including corresponding measurements. The HP in place is a Daikin type EGSAX06DA9W with a nominal thermal power of 7.98 kW at B0/W35 according EN 14511 [10]. The HP also has a 180 l integrated domestic hot water (DHW) tank and is equipped with a 3 kW BUH. Tab. 1 provides more specifications of the measuring devices and the relative error at nominal conditions for the coefficient of performance (COP) is 1.661 %.

Tab. 1 – Specifications of measuring devices

Measurement	Specifications and accuracy
Temperature	Four-wire PT100 : 1/10 DIN Class B, except two DIN Class A sensors within the DHW TES
Flow	Electromagnetic: ± 0.2171 %
Differential pressure	± 0.055 % for a measuring span of 100 kPa
Electrical power	EN 50470-3 Class B: ± 1 %

Both the heat source and building load are emulated by heat exchangers for which a supply water setpoint can be set. The setpoint is reached by mixing cold and hot water from the laboratory with 3-way valves. Valve 2V9 emulates DHW draw-offs, while cold water is supplied by the community water grid. For space heating/space cooling (SH/SC), different hydraulic configurations can be realised, by either bypassing thermal energy storage (TES) TES1 via TES2 or by using TES1 in parallel or even partially bypassing TES1. Three-way valves and back-pressure valves (BP) enable the remote change of the hydraulic set-up. For TES1, a 200 l or 750 l storage can be tested, while TES2 is sized at 25 l to reach a minimum water volume for sufficient thermal inertia in case of directly coupling the HP to the virtual building as required by the manufacturer. Thermal stratification in TES1 is measured by 2 or 4 temperature sensors for the 200 l or 750 l TES, respectively. When TES1 is

used between the HP and virtual building, the flow rate of pump P1 can be set via an analogue input signal. For this paper, TES2 was used, while TES1 was bypassed. The HP is also equipped with both an evaporator and condenser pump which are internally controlled by the HP. Valve 2V30 can be used to throttle the internal condenser pump as its flow rate cannot be controlled by the user. Finally, the set-up allows to change the measured outdoor temperature by the HP as its outdoor temperature sensor was replaced by a potentiometer.

2.2 Hardware-in-the-loop communication

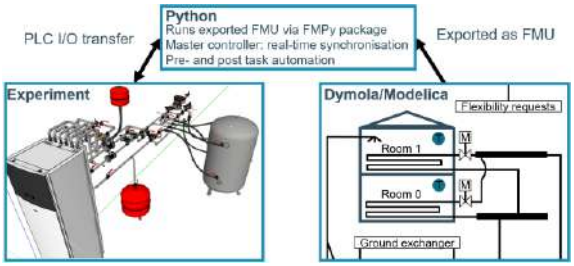

Fig. 2 – Communication set-up of the HIL-experiment

Fig. 2 shows the communication set-up between the simulation and experiment. A PLC is used to retrieve measurements from and send setpoints to the experiment at time steps of 15 seconds. The communication interval should be small enough to correctly represent the real HP behaviour and to provide correct inputs for both the experimental and simulation environment [11,12]. Furthermore, A Modelica model is translated into a FMU-file (Functional Mock-up Unit) and imported in Python via the FMPy package [13]. Python acts as a master controller to maintain the real-time synchronisation.

The HP is also equipped with a Modbus-interface to remotely communicate both the setpoints and measurements within the HP system. The Modbus interface allows the setting of the condenser leaving water temperature in both SH and SC mode, the DHW reheating temperature and the (de)activation of SH, SC, DHW, DHW booster and quiet working mode. Internal HP measurements are temperatures at the condenser inlet and outlet, temperature after the back-up heater, DHW tank temperature, liquified refrigerant temperature and condenser pump flow rate. In addition, fault codes and the status of the compressor, circulation pump, legionella protection service, booster, three-way valve and operational mode can be read out. Though, it should be noted that the accuracy of the measurements within the HP itself is not known due to a lack of documentation. Hence, measurements outside the HP are preferred.

The HP also has energy flexibility interfaces such as a preferred kWh contact, a SG-ready interface [14] and digital inputs to limit its power consumption.

2.2 Heat pump model

Modelling the HP internal control strategies requires manufacturer information and is not error prone. A preliminary work [3] investigated the modelling approaches for short- and long-term HP behaviour. The HP model in the current paper starts from the most accurate model in the preliminary work. The modelling parameters are based on the HP manufacturer documentation and provide the best estimate. The model includes performance data for both part- and full-load conditions, minimum compressor on/off-times, minimum compressor modulation, DHW timing constraints, anti-legionella cycles for the DHW disinfection, BUH control, proportional-integral (PI) condenser pump control. Tab. 2 summarises the HP model start parameters.

Tab. 2 – Overview heat pump modelling data

Start parameter	Value
Minimum compressor speed	Condenser outlet temperature dependent
Performance data	Tables with thermal and electrical power at 30 %, 50 %, 70 %, 90 % and 100 %
Compressor off-temperature	Setpoint + 2 °C
Compressor on-temperature	Setpoint – 2 °C
Compressor cycles	Maximum 6 per hour
BUH control	Discrete steps of 1 kW and only activated after compressor switch-off at a 53 °C DHW TES temperature during anti-legionella cycles
DHW on-time	Minimum one minute, while the maximum time is weather dependent, unless a fixed maximum time of 125' for anti-legionella cycles
DHW off-time	Minimum 30 minutes
DHW control	Cycle starts if the DHW TES temperature drops below 42 °C and cycle stops at 47 °C
Anti-legionella cycle control	Keep DHW temperature at 60 °C for at least 40 minutes with a maximum anti-legionella cycle duration of 4 hours before forcing an error if not accomplished
Condenser pump control	PI-controlled to maintain a 5 °C temperature difference between HP outlet and inlet, with a minimum flow rate of 12 l/min, with pump curves
Evaporator pump control	Continuous fixed speed operation with pump curves

2.3 Model validation with predefined cycles

Comparing the short-term behaviour of a real HP

system and a HP simulation model by directly coupling it to a building heat emission system can cause validation issues. Indeed, the mutual influence of the HP and building prevent an easy distinction of the different modelling parameters of the HP model. In addition, the dynamic behaviour of heat emission systems such as underfloor heating systems complicate a model validation and possibly require post-corrective measures. Therefore, it was chosen to validate the HP model according to a predefined load profile which was artificially constructed, both for SH and DHW provision. During all cycles, the evaporator inlet temperature setpoint was fixed at 15 °C. The minimum return temperature from the SH load was set to 20 °C to prevent unlimited SH load extraction during DHW mode. Indeed, during DHW charging cycles, the HP is not providing SH services.

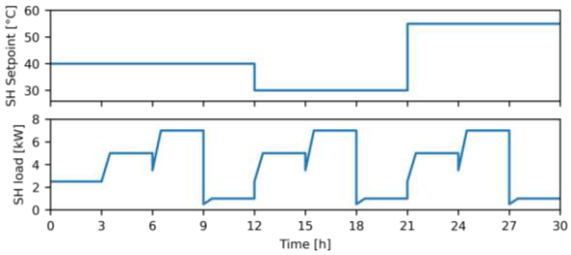

Fig. 3 – SH Cycle 1 with three hours of preconditioning

For SH purposes, three different supply water temperature setpoints were used, namely 30 °C, 40 °C and 55 °C. For each of those temperature setpoints, three thermal loads were tested and set at 1 kW, 5 kW and 7 kW. Fig. 3 shows the SH load profile in which a preconditioning period of three hours was foreseen to start the system. Each setpoint was maintained for three hours in which the SH load linearly increased from 50 % to 100 % of the required load in the first 30 minutes to assure a stable operation of the experimental facility and HP. Except for the preconditioning period, this SH cycle was executed two times to provide sufficient data for each setpoint as DHW provision was also activated and influenced the operational behaviour. This cycle was mainly used to validate the controller stability for the compressor and circulation pumps.

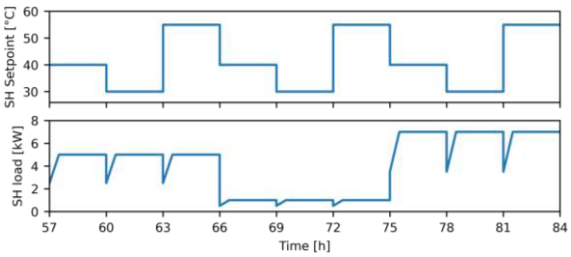

Fig. 4 – SH Cycle 2

A second cycle, as shown in Fig. 4, focusses on the HP dynamics during changing SH temperature setpoints and loads. This cycle was executed only once, but shows similarity to the first SH cycle. The two cycles only differ in the order of firstly changing the SH thermal load and SH temperature setpoint afterwards for Cycle 1 and firstly changing the SH temperature setpoint and then the load for Cycle 2.

A DHW draw-off profile was derived from a profile generation tool of Jordan et al. [15]. Four different flow rates of 5 l/min, 7 l/min, 8 l/min and 12 l/min were used for fixed time slots of 1', 1', 5' and 10', respectively. Combining the extracted flow rates, an average daily draw-off volume of 242 l was reached. The experiment also included an anti-legionella cycle, which enabled the BUH controller validation. Lastly, to validate the weather-dependency of the DHW timing constraints, tests were performed for two outdoor temperatures, namely 0 °C and 8 °C.

3. Results

This section presents the HP model validation and contains HP model improvements. Prior to the model validation, the pressure losses and water content of the experimental facility were implemented in the simulation model. On the level of the evaporator, a maximum flow rate of 32.4 l/min was reached, while 18 l/min was measured for the condenser water flow rate during SH mode. By using the HP manufacturer pump curves, pressure losses were implemented. Due to insufficient technical data, the pressure losses of the DHW heating spiral could not be determined in advance and were thus kept at a default value.

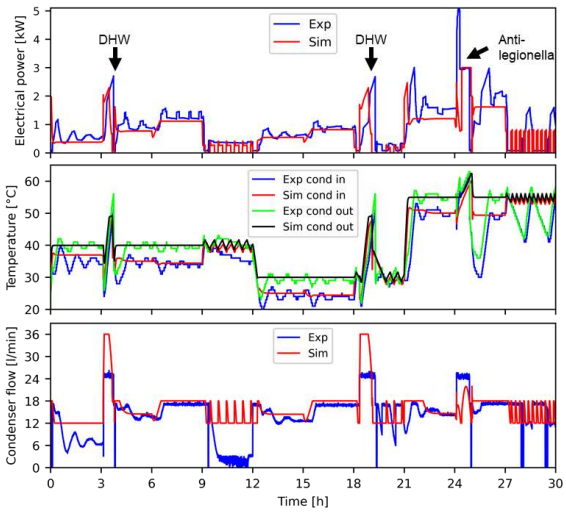

Fig. 5 – SH Cycle 1: electrical power, condenser water temperatures and water flow rate - original

Fig. 5 compares the experimental (Exp) and simulated (Sim) results of the original HP model for the electrical power, condenser water inlet (cond in) and outlet (cond out) temperatures and the condenser water flow rate during SH Cycle 1. It shows reasonable agreements when considering the condenser inlet and outlet temperatures, while the condenser water flow rate and the overall HP power consumption show higher variations. In addition, analysing the short-term behaviour, the experiments showed more variability around the temperature setpoint, while the simulation results showed a more stable behaviour. The simulated HP model was also able to faster reach the temperature setpoint.

The aforementioned differences can be explained by the HP modelling approach. Firstly, the modelled compressor was not equipped with a proportional

integral derivative (PID) controller, but the model used a modulation controller with the performance curves to determine the required compressor speed. Such an approach causes the compressor to take an immediate action as soon as a difference between the measured and required setpoint is measured. In addition, the minimum thermal capacity of the experimental HP was also lower compared to the HP model. This can be seen in Fig. 5 from hour 9 till hour 12 in which the real HP was able to remain activated, while the HP model performed cycling behaviour.

Secondly, the condenser pump control is also different. The modelled minimum condenser flow rate of 12 l/min was only required in space cooling mode and not during space heating. Further experimental analysis showed a minimum flow rate of 2.8 – 3.2 l/min. In addition, the condenser pump control in SH mode differed from DHW mode, while the HP model assumed a control approach which tries to keep 5 °C temperature difference between HP inlet and outlet water, both for SH and DHW mode. Such an approach was correct for SH mode, while the HP maintained a fixed water flow rate of 25 l/min during DHW mode. Comparison with experimental results also showed the inability of the modelled controller to quickly react on temperature changes.

Thirdly, the simulated electricity consumption is mainly lower than the experimental results. This is due to the use of the performance maps. These maps should already incorporate the consumption of additional equipment such as the evaporator pump, condenser pump and control logic, though for only a small part. Indeed, the additional consumption due to head losses and control logic should only refer to the losses caused by the device itself [16]. Hence, measurements according EN 14511 [17] neglect the head losses of ground loops and SH circuits.

Fourthly, the HP cycles during too low compressor modulation speeds are different. While the HP model used a hysteresis of +2/-2 °C around the setpoint temperature, the real controller uses both the supply and return temperature in an AND-function to determine the compressor off-signal. Analysis showed that the compressor remained on as long as the supply temperature did not increase 3 °C above the temperature setpoint and as long as the return temperature did not reach the supply temperature setpoint. An exception is made for when the supply temperature reaches a temperature 5 °C higher than the setpoint temperature. In those cases, the return temperature is not incorporated due to safety constraints. Such an approach allows a more stabilised compressor operation and prevents excessive compressor cycles as both the supply and return temperature should reach a certain threshold. The lower hysteresis limit of a supply temperature 2 °C below the supply temperature setpoint was still correctly modelled. Moreover, the compressor off-time was also 2' shorter compared to the HP model.
Differences could also be seen during anti-legionella cycles. According the operation ranges of the BUH and compressor, the BUH only works at DHW temperatures above 53 °C. During the experiments, it could be seen that within anti-legionella cycles, the BUH can simultaneously work with the compressor. Both elements are initially activated, while the compressor turned off at a DHW temperature of 53 °C. The simultaneous operation of the compressor and BUH caused a faster anti-legionella cycle, but also decreased the efficiency due to the lower efficiency of the electrical resistance. In addition, the BUH power was not exactly 3 kW but slightly lower, even if measuring errors were considered.

The HP model also showed dependency on the measuring height of the DHW TES temperature sensor, the position of the heating spiral and the insulation thickness. With a ten layer-stratified DHW TES model, it was concluded that positioning the sensor in the third layer with a hot water spiral ranging from a height of 10 % – 75 % and a smaller insulation thickness showed better agreement with the experimental results. In contrast with the simulations, the experimental DHW temperature has a resolution of 1 °C due to the HP Modbus module.

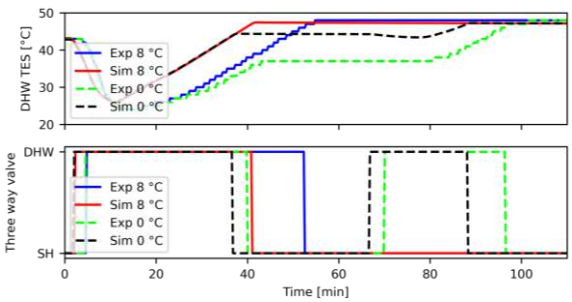

Fig. 6 – Maximum DHW cycle time weather dependency

Fig. 6 shows the comparison of a DHW charging cycle for two different outdoor temperatures, namely 0 °C and 8 °C. It can be seen that the DHW TES was not completely charged within the maximum DHW cycle time at an outdoor temperature of 0 °C. Hence, a second DHW cycle was necessary after the minimum DHW off-time. In contrast, the maximum DHW cycle time was not reached for an outdoor temperature of 8 °C. Results also showed that the maximum time for anti-legionella cycles was not weather-dependent.

In addition, during DHW cycles, the measured supply temperature differed from the simulation results. Within the model, it was assumed that the condenser supply temperature was limited to 55 °C as stated by the HP manufacturer. Experiments indicated that the compressor was able to provide condenser temperatures until 60 °C. Furthermore, the HP model showed a decreasing modulation speed towards the DHW charging cycle end, while the experimental HP remained close to full-load conditions. This can be explained by the HP model in which a supply water setpoint of 2 °C higher than the DHW temperature setpoint was modelled, while it is assumed that the experimental HP has a fixed compressor setpoint temperature of 60 °C to fasten the DHW cycles.

Fig. 7 shows an improved similarity between the

experimental and simulated results after model improvement of the aforementioned differences. Although a better profile agreement, differences still exist. Indeed, larger variations between experiment and model occurred during SH temperature setpoints of 55 °C, for which Fig. 8 shows more details. During the shown time slot, the SH supply setpoint increased from 40 °C to 55 °C, while SH load variations are also indicated within the figure. The shown temperatures are the temperatures within the HP system and thus dependent on the provision of SH or DHW services. Moreover, it can be seen that an anti-legionella cycle occurred from hour 24 to hour 25. A reasonable good match can be seen for SH loads above the minimum thermal capacity.

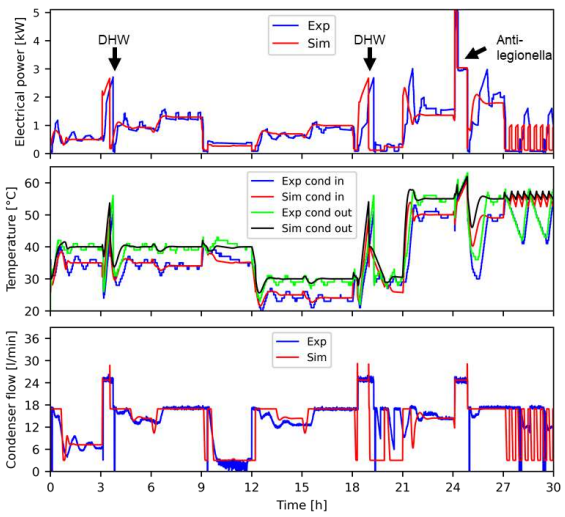

Fig. 7 – SH Cycle 1: electrical power, condenser water temperatures and water flow rate – adapted

Though, for low SH loads, the real HP was not able to closely follow the temperature setpoint. Indeed, when the compressor off-trigger signal is reached, the real HP remains off for a long time, while the simulated HP was able to remain close to the requested SH temperature. Such a behaviour only appeared during low SH loads accompanied by high temperature setpoints. Further experimental tests at other, but also high SH temperature setpoints, showed equal behaviour. As shown in Fig. 8, the compressor was only reactivated as soon as the return temperature dropped below 45 °C and it could be seen that this remained independent from the supply temperature setpoint. This control approach is also in contrast with the approach for lower SH temperature setpoints as already showed. It could be explained by a possible internal control strategy from the HP manufacturer to limit the number of compressor cycles during low SH loads at high SH supply temperatures. Further experimental tests will determine the exact point for which the internal control strategy is changed. Fig. 8 also indicates a compressor switch-off after a 2' on-time, while the setpoint was not reached. Analysis showed that during those moments, the liquified refrigerant temperature was not equal to or above the return temperature at the condenser side and caused the compressor to switch off. In those cases, the HP controller assumed that the compressor was not heating up, but cooling down the condenser. Hence, it switched off the compressor, while for those cases, it could also be seen that the minimum compressor off-time was reduced from 6' to 4.5'. Finally, as the HP model is based on performance maps, including a refrigerant temperature-dependency is difficult.

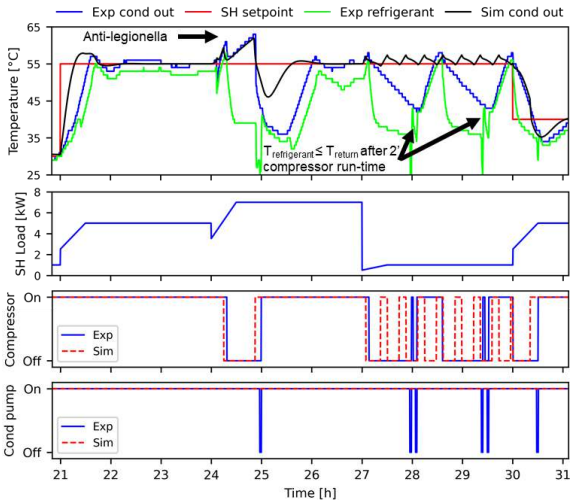

Fig. 8 – Cycling behaviour at 55 °C SH supply setpoints

Analysis of DHW cycles also showed a consistent compressor switch-off after a DHW cycle, even with a SH setpoint of 55 °C. As HP mainly provide low SH temperatures to e.g. an underfloor heating system, the switch-off signal can be caused by a HP safety control strategy. Indeed, such a strategy prevents too high supply temperatures fed into the SH system.

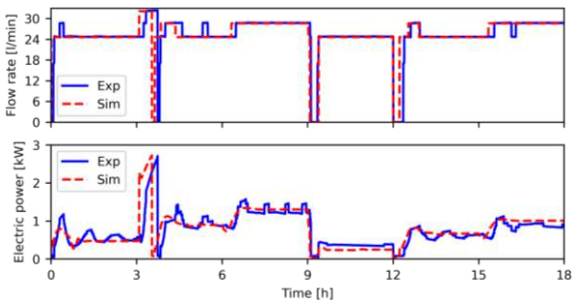

Fig. 9 – Evaporator pump control

The condenser pump control also differed, while a continuous operation was expected due the HP settings in place. If the compressor activation was triggered and if the condenser outlet was more than three degrees higher than the liquified refrigerant temperature, then the pump switched off for two minutes. Afterwards, both the pump and compressor were simultaneously activated. At the level of the evaporator, the evaporator pump went off along with compressor, while it switched on two minutes prior to the compressor activation. Four evaporator flow rates were detected and showed a dependency on the compressor speed. Pump speeds of 76 %, 89 % and 100 % were found for compressor speeds below 45 %, 45 – 75 % and 75 – 100 %, respectively. When the evaporator pump started two minutes in advance to the compressor, the pump speed was 53 %. While such a hypothesis should be further verified with more experiments, Fig. 9 shows similarities between

the hypothesis and experiment. It should be noticed that the compressor speed was estimated from the HP model as it was not possible to read out the compressor speed from the real HP.

Tab. 3 – Full cycle duration analysis (84 hours) after model improvement at an outdoor temperature of 8 °C

Overall indicator	HIL	Simulation
Evaporator energy (kWh)	382.2	300.9 (- 21.3 %)
SH energy (kWh)	327.7	329.3 (+ 0.5 %)
DHW thermal energy (kWh)	26.9	31.1 (+ 15.6 %)
Electrical energy (kWh)	77.5	76.9 (- 0.8 %)
Total DHW draw-off volume (l)	829.5	799.7 (- 3.6 %)
Compressor cycles	39	41 (+ 5.1 %)
DHW cycles	6	6 (0 %)

Tab. 3 shows performance indicators for comparing the simulated to the experimental results over a full cycle duration of 84 hours at an outdoor temperature of 8 °C. While small variations exist for the majority of the indicators, larger deviations were found at the evaporator level and DHW provision. Differences within DHW provision can be explained by the time delay and PI-control of the experimental DHW draw-off valve. Before reaching a stable flow rate within +/- 10 % of the setpoint required on average 30 – 45 seconds. Results also showed larger deviations for small flow rates up to two times the required flow rate due to the controller overshoot and also, due to the pressure difference over the DHW valve. Hence, the extraction of small flow rates for short time slots can be found as the main reason for those differences. Hence, for future experimental testing, a DHW flow accumulator will be tested to close the valve when the required draw-off volume is reached. The experimental DHW inlet temperature was also mainly warmer compared to a modelled temperature of 10 °C. Indeed, during periods without DHW draw-offs, the temperature of the piping materials and water converged to the environmental temperature of 22 °C, while during draw-off periods of several minutes, a temperature of 10 °C was measured. Using the experimental inlet temperature within the simulation, decreased the DHW thermal energy from 31.1 kWh to 25.5 kWh, which is closer to the experimentally measured DHW energy of 26.9 kWh.

At the evaporator level, two main differences were seen. While the condenser heat exchanger followed the required temperature setpoint within +/- 0.25 °C, the evaporator heat exchanger showed larger variations of mainly +/- 0.75 °C. Reasons can be found in the modulation control of the real HP which increased stepwise. These steps caused sudden temperature drops in the evaporator return temperature for which the heat exchanger could not directly react due to its system inertia. Moreover, the off-state of the evaporator pump within the HP caused the PI controller of the heat exchanger to saturate as it did not detect a change of the measured temperature. Hence, the heat exchanger temperature went to one of the two supply temperatures of the laboratory. Though, analysis showed that including these temperature variations within the simulations did not cause major improvements as the HP model mainly extracted less evaporator power which caused a smaller simulated temperature difference between evaporator inlet and outlet. As the HP model is based on performance maps with the thermal condenser (*Qcond*) and electrical power (*Pelec*), reasons can be found in the determination of the evaporator power (*Qevap*) as shown in equation (1).

$$Qevap = Qcond - Pelec \quad (1)$$

Such an approach assumes an ideal conversion of all electrical energy into useful thermal energy, while a part is also preserved for supplying the control logic and for both the evaporator and condenser pump. Therefore, a recalculation factor within the HP model should separate the electrical power from the performance maps into two parts, namely (1) a compressor power which is converted into thermal energy and (2) an auxiliary power supply. While such an approach should be further verified, it remains unlikely to completely solve the evaporator energy difference. Indeed, the energy difference is 81.3 kWh, while the overall electricity consumption within the experiment was only 77.5 kWh. Hence, it can be stated that performance maps do not allow an accurate determination of the extracted evaporator power. Further experiments will also evaluate the evaporator power extraction on both the primary and secondary side of the heat exchangers.

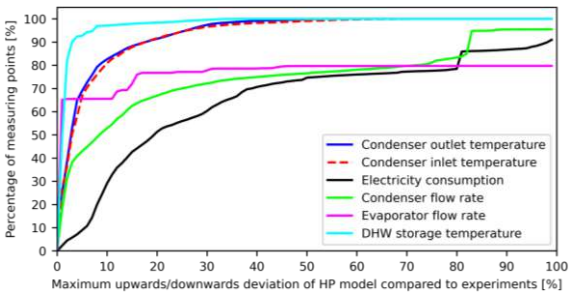

Fig. 10 – HP model agreement to experimental results

Finally, Fig. 10 shows the agreement of several HP model variables to the experimental results. The curves can be interpreted as duration curves which contain all data points with time steps of 15 seconds. For a certain percentage of the measured points on the vertical axis, the horizontal axis provides the maximum deviation percentage of the HP model, e.g. a maximum deviation of +/- 10 % for 83 % of the data points of the condenser outlet temperature. It can be seen that DHW and condenser temperatures show good agreement, while the pump control and especially the electricity consumption show the necessity for a future calibration work with more experimental data as previously explained.

4. Conclusions

This paper presented a hardware-in-the-loop test bench to develop new control strategies for energy flexibility provision with water/water heat pumps. It showed a thorough presentation of the set-up, the communication requirements, the possible hydraulic configurations and a description of the measuring equipment, for which a relative measuring error of 1.661 % on the coefficient of performance was determined. In a second part, the test bench was used to validate a water/water heat pump model. As the model not only includes the performance maps, but also the internal control strategies such as timing constraints, compressor control and pump control, both the overall energy consumption and short-term behaviour were analysed. An overall energy analysis showed that direct usage of the performance maps underrated the energy consumption due to the neglection of the heat pump auxiliary equipment. Inclusion of those elements, showed a closer match, while deviations remained for the evaporator energy, electricity consumption and domestic hot water. A short-term behaviour analysis also showed the necessity for heat pump model improvements as the experimental results differed from the modelling assumptions, which were derived from the heat pump documentation. Model improvements by using new timing constraints and modulation controllers showed better agreement. Though, the experiments showed unexpected behaviour for the combination of low space heating loads and high temperatures for which the heat pump was not able to closely follow the temperature setpoint. Hence, it was shown that an accurate heat pump model is required to represent the real heat pump behaviour, especially when analysing energy flexibility. It was shown that modelling the real heat pump behaviour only based on heat pump manufacturer documentation is not sufficient. A future work will present a calibrated heat pump model and the development of control strategies for energy flexibility with heat pumps.

5. Acknowledgement

This research work was funded by the Internal Funds KU Leuven. We thank Daikin for providing part-load data for the heat pump EGSAX06D9W.

6. References

[1] Hogeling J, Corgnati S, Dziergwa A, Ceyhan I. The REHVA European HVAC Journal. Vol 54, Issue 2. 2021;58(4):76.

[2] Arteconi A, Hewitt NJ, Polonara F. Domestic demand-side management (DSM): Role of heat pumps and thermal energy storage (TES) systems. Appl Therm Eng. 2013;51(1–2):155–65.

[3] Evens M, Arteconi A. Influence of Internal Control Simplifications in Heat Pump System Modelling for Energy Flexibility Evaluations. In: Proceedings of Building Simulation 2021: 17th Conference of IBPSA. IBPSA; 2021.

[4] Clauß J, Georges L. Model complexity of heat pump systems to investigate the building energy flexibility and guidelines for model implementation. Appl Energy. 2019;255(May):113847.

[5] Blervaque H, Stabat P, Filfli S, Schumann M, Marchio D. Variable-speed air-to-air heat pump modelling approaches for building energy simulation and comparison with experimental data. J Build Perform Simul. 2016;9(2):210–25.

[6] El-Baz W, Tzscheutschler P, Wagner U. Experimental study and modeling of ground-source heat pumps with combi-storage in buildings. Energies. 2018;11(5).

[7] Ruiz-Calvo F, Montagud C, Cazorla-Marín A, Corberán JM. Development and experimental validation of a TRNSYS dynamic tool for design and energy optimization of ground source heat pump systems. Energies. 2017;10(10).

[8] Conti P, Bartoli C, Franco A, Testi D. Experimental analysis of an air heat pump for heating service using a "hardware-in-the-loop" system. Energies. 2020;13(17).

[9] Pean T, Costa-Castello R, Fuentes E, Salom J. Experimental Testing of Variable Speed Heat Pump Control Strategies for Enhancing Energy Flexibility in Buildings. IEEE Access. 2019;7:37071–87.

[10] Technical Data EGSAH/X series Daikin. Oostende; 2020.

[11] Zottl A, Nordman R, Coevoet M, Riviere P, Benou A, Riederer P. D4.1/D2.3 Guideline for heat pump field measurements for hydronic heating systems. 2011;1–33.

[12] Haller MY, Haberl R, Persson T, Bales C, Kovacs P, Chèze D, et al. Dynamic whole system testing of combined renewable heating systems - The current state of the art. Energy Build. 2013;66:667–77.

[13] FMPy. Dassault Systèmes.

[14] Bundesverband Wärmepumpe e.V. (bwp). SG Ready-label.

[15] Jordan U, Vajen K, Braas H. DHWcalc: Tool for the Generation of Domestic Hot Water Profiles on a Statistical Basis (version 2.02b). 2017;10(March):1–14.

[16] Klein B. Independent testing of heat pumps is needed for reliable COP. REHVA J. 2012;(October):15–8.

[17] EN 14511-3:2018 - Air conditioners, liquid chilling packages and heat pumps for space heating and cooling and process chillers, with electrically driven compressors - Part 3: Test methods. 2018.

Data Statement

The datasets generated during and/or analysed during the current study are available in the Clima2022 repository, . https://github.com/Maaeve/Clima2022.

Design of Renewable Energy Production in District Heating System

Martina Mudrá [a], Ján Takács [b]

[a] Faculty of Civil Engineering, Department of Building Services, Slovak University of Technology in Bratislava, Bratislava, Slovak Republic, email address: martina.mudra@stuba.sk

[b] Faculty of Civil Engineering, Department of Building Services, Slovak University of Technology in Bratislava, Bratislava, Slovak Republic, email address: jan.takacs@stuba.sk

Abstract. One way to decarbonise the heat supply in buildings by using environmentally friendly and highly energy-efficient equipment and technologies that save primary energy is through existing district heating systems (DHS´s) that supply several buildings at once. Many heat sources and equipment on the heat production and distribution side of these DHS´s are beyond their service life or use fossil fuels as an energy source. It is therefore necessary to modernize such systems through highly efficient and renewable energy sources (RES´s). As the Slovak Republic has a number of DHS´s, we have designed streamlining the existing heat source operation for the DHS of the West housing estate in the town of Brezno through a cogeneration unit (CU) and water - to - water heat pumps (HP´s). The existing heat source consists of three hot water boilers burning natural gas. In addition to the existing equipment, we designed a CU and HP´s, which would be used to prepare hot water. The flow of the heating heat transfer medium passes first through the HP´s and then through the CU. If the temperature of the working medium is not sufficient, the flow of heat transfer medium will also pass through the boilers. The operation of the CU and HP´s is designed in island mode, i. e. without external connection to the electricity grid. The proposal is based on real operational data provided to us by heat supplier for the period 2016 - 2018. We have assessed the proposal from the point of view of energy and economics. From the point of view of energy, we focused on energy consumption before the design of new equipment and the expected energy consumption after the design of new equipment. From the point of view of economics, we examined the return on investment. The aim of the proposal is to point out the importance of modernizing DHS´s, as they are an ideal place for the application of high-efficiency technological equipment and equipment using renewable energy.

Keywords. District heating system, cogeneration unit, heat pump, hot water.
DOI: https://doi.org/10.34641/clima.2022.39

1. Introduction

The depletion of fossil fuels, climate change, and the consequences of human activity that result in rising levels of atmospheric CO_2 concentration force society to consider using alternative or renewable energy sources (RES´s) [1]. In buildings, more than 80% of energy is used in the form of heat, cold or electricity to ensure the comfort of their users through energy systems such as heating, ventilation and air conditioning, domestic hot water, and electrical installations [2]. Therefore, the European Union (EU) is issuing strategy papers aimed at increasing the use of renewable energy sources and reducing the energy intensity of heating, ventilation, and air conditioning systems [2].

Point 35 of Directive 2012/27/EU of the European Parliament and of the Council of 25 October 2012 on energy efficiency states that high-efficiency cogeneration and district heating offer significant potential for primary energy savings [3].

2. Operation of the Existing Heat Source

2.1 Description of the Site

Combined heat and power through a cogeneration unit (CU) and heat pumps (HP´s) will be designed for the West housing estate located in the town of Brezno, Slovakia. The existing hot water boiler plant is situated near the Hron River in the residential

Copyright ©2022 by the authors. This conference paper is published under a CC-BY-4.0 license.

area of the Ladislav Novomeský District. The proximity of a watercourse creates preconditions for an excess of groundwater in the surrounding subsoil – a source of low-temperature energy. This energy will be transformed to a higher temperature level by water-to-water HP´s [4].

2.2 Condition of the Boiler Plant

During heating season, there is uninterrupted 24-hour operation. In summer, the boiler plant is in operation from 4:00 am to 11:00 pm. The heat transfer medium is hot water with the original design temperature gradient of 90/70 °C. The heat source is represented by three hot water boilers with a total output of 6.76 MW. A flue gas heat exchanger is installed after each of these boilers. Hot water preparation is realized through plate heat exchangers connected in series as pre-heating and water heating with the circulation of these exchangers leading to better cooling of the return water to the boilers [4].

Fig. 1 shows the interior view of the existing boiler plant.

Fig. 1 – Interior view of the existing boiler plant [4].

3. Design Model for the Application of New Devices

3.1 Operation of the New Heat Source

A CU and HP´s shall be installed instead of the existing heat source - hot water boilers. The energy source for driving the CU will be natural gas. The energy source for driving the HP´s will be the electricity produced by the CU. The CU and HP´s will be used to prepare hot water in an accumulative way. The storage tank will be located behind the CU and HP´s and, at a time when the demand for hot water consumption is reduced, the heated hot water will accumulate in it. The accumulated heat will be supplied to the grid at the time of increased demand. The essence of the design is ensuring a continuous operation of the equipment so that it works as long as possible and with a minimum of starts [4].

3.2 Power of the Cogeneration Unit and Heat Pumps

The average hourly heat demand for domestic hot water preparation in 2016 was 275 kW, in 2017 it was 280 kW, and in 2018 it was 267 kW. By comparing the data for the period 2016 - 2018, the heat output of the CU and two HP´s was set to 270 kW [4].

The CU and HP´s will be located in front of the boilers in the direction of the return heating water flow. The heat transfer medium - heating water has a temperature of 45 °C. The aim is to produce a heat-transfer working substance - heating water with a temperature of 60 °C. The temperature drop in the hot water system is therefore 60/45 °C, which means that the temperature difference ($\Delta\theta$) is 15 K. A very important parameter in the design of thermal outputs of the equipment is also the volume flow that will flow through the system. The volume flow that enters the system must be equal to the volume flow that leaves it. The volume flow at a heat output of 270 kW and a temperature difference of 15 K is 15.48 m^3/h [4].

The HP´s operate with a primary gradient of 5/1 °C - this means that a low-temperature heat source enters the HP´s (groundwater from wells) and is transformed in the HP´s to a higher temperature, transferred to the secondary heating system circuit. The underground water flow is high enough to supply the energy that is used. Return heating water with a temperature of 45 °C enters the HP and is heated up by 10 K, which means that the water temperature at the outlet of the HP will be 55 °C. This time the temperature difference ($\Delta\theta$) is known to be 10 K and the volume flow (M) through both HP´s is 15.48 m^3/h. The output of both HP´s was calculated to be 180 kW. It follows from the above that the heat output of the CU will be 90 kW [4].

The CU works with a temperature gradient ($\Delta\theta$) of 20 K as standard. This means that if water with a temperature of 55 °C enters the CU, the CU will heat the water to 75 °C at the outlet of the CU. We know determine the volume flow rate that the CU must take to reach 60 °C at the outlet of the unit and before entering the hot water storage tank. The volume flow through the CU to reach 60 °C at the outlet of the unit and before entering the hot water storage tank is 3.87 m^3/h [4].

For better controllability of the system, two identical two-stage water-water HP´s are proposed. Through a detailed recalculation, the design of two identical HP´s was determined, while the heat output of one was 89.6 kW [4].

Fig. 2 shows a schematic diagram of the CU and HP´s.

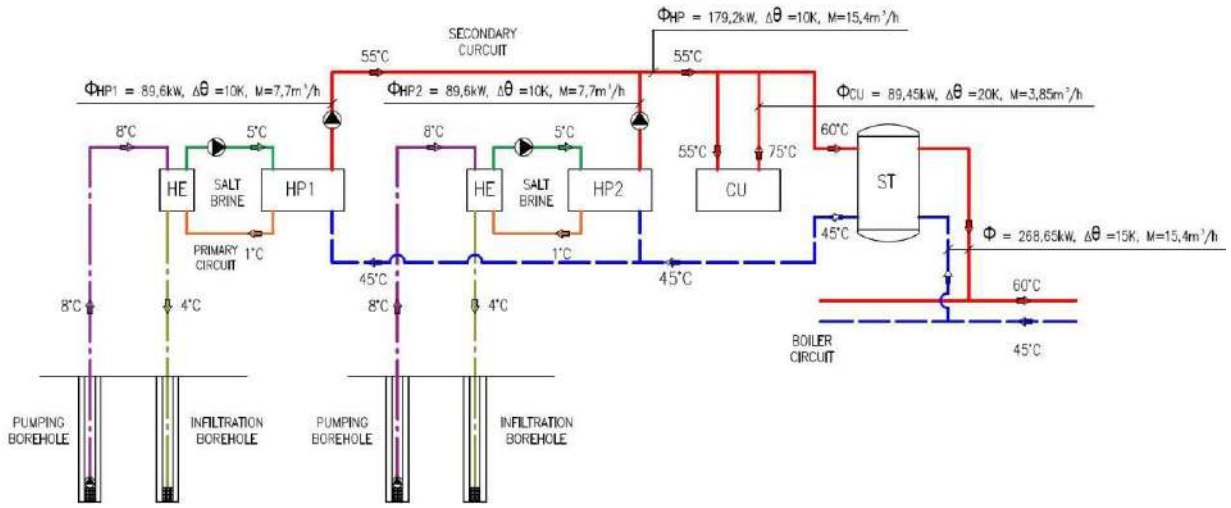

Fig. 2 - Schematic diagram of the cogeneration unit and heat pumps [4].
HE – heat exchanger, HP – heat pump, CU – cogeneration unit, ST – storage tank

4. Results – Energy Aspects

4.1 Natural Gas Consumption

To be able to assess the proposed design from an economic point of view, it is important to determine how much natural gas is saved by installing new technological equipment, a CU and HP´s, as compared to the original condition. The equipment was designed based on the operation and average energy consumption in 2016 - 2018. The average natural gas consumption was 598,740 m³/year and the average heat produced by the heat source was 6,066,354 kWh/year for the period 2016 – 2018 [4].

The number of days in individual periods, the number of operating hours during the day, and the expected hourly outputs of the set are given in **Tab. 1**. Using these data, the amount of thermal energy produced per year can be determined. In real operation, however, there may be moments when the equipment breaks down or there is a planned shut down due to its maintenance, which is taken into account by reducing the produced thermal energy by 5% [4]. For clarity, the data are shown in **Tab. 1**.

The thermal energy produced by boilers is 3,817,305 MWh. A very important data is the consumption of natural gas by the CU. The producer of the CU declares that the maximum hourly consumption of natural gas is approximately 24 nm³/h at a calorific value of natural gas of 35.5 MJ/m³ [6].

The consumption of natural gas for the CU in individual periods and throughout the year is shown in **Tab. 2**. The total natural gas consumption by the CU throughout the year is 189,240 m³. The value of the total heat in natural gas is obtained as the product of the total consumption of natural gas by the CU and the average calorific value of the fuel (9.701 kWh / m³), which is 1,835,817 kWh [4].

Tab. 1 - Use of cogeneration unit and heat pumps throughout the year [4].

Season	Months	Days	Operating hours	Operating hours in the season (h)	Hourly power of equipment (kW)	Produced thermal energy reduced by 5% (kWh)
Winter	7	212	24	5,088	300	1,450,080
Transition	2	61	24	1,464	270	375,516
Summer	3	92	19	1,748	255	423,453
Σ CU +HP	12	365	-	8,300	-	2,249,049

Tab. 2 - Natural gas consumed by the cogeneration unit [4].

Season	Hourly natural gas consumption by cogeneration unit (nm³/h)	Operating hours in the season (h)	Final consumption of natural gas by the cogeneration unit reduced by 5% (m³)
Winter	24	5,088	116,006
Transition	24	1,464	33,379
Summer	24	1,748	39,854
Σ	-	8,300	189,240

These findings show that 1,835,817 kWh of energy consumed in natural gas is needed to produce 2,249,049 kWh of heat energy per year by the CU and HP´s [4].

To determine the total consumption of natural gas at a heat source, we need to know the consumption of natural gas by gas boilers. The consumption of natural gas by boilers was calculated to 401,527 m^3. It follows from the above that the estimated total consumption of natural gas at the heat source is 590,767 m^3 [4].

If we look at the average natural gas consumption before the installation of the unit, which is 598,740 m^3/year and the expected natural gas consumption after the installation of the unit, which is 590,767 m^3/year, it is seen that applying a CU and HP´s should save 7,973 m^3 of natural gas as compared to the existing operation of gas boilers [4].

At the time when the application was being addressed, the purchase price of natural gas per 1 kWh was 0.04234 euros [5]. By multiplying the saved amount of natural gas by the average value of combustion heat (10.754 kWh/m^3) and the purchase price of natural gas, an annual saving of 3,631 euros is determined [4].

4.2 Electricity Consumed

A CU is a device for the combined production of heat and electricity [7]. A part of the generated electricity is used for its consumption, the predominant part is used to drive the HP´s. It will also power submersible pumps in pumping wells and circulating pumps on the primary and secondary side [4].

The surcharge for electricity is 34.55 euros/MWh [4].

To find the prices of revenues for high-efficiency cogeneration, we must determine how much electricity is produced by the CU each month and throughout the year. The obtained data are shown in **Tab. 3**.

The electricity produced during the annual operation of the facility will be 567,302 kWh per year, which represents 567.302 MWh per year. This value is again reduced by 5% due to a fault or maintenance on the equipment [4].

As we know the surcharge for electricity and the amount of electricity produced, we can use the product of these items to find out what the revenues for high-efficiency cogeneration will be. Annual revenues for high-efficiency cogeneration amount to 19,600 euros [4].

Tab. 3 - Amount of electricity produced by the cogeneration unit [4].

Season	Months	Days	Operating hours	Operating hours in the season (h)	Hourly electricity production (kWe)	Electricity produced reduced by 5% (kWh)
Winter	7	212	24	5,088	73	352,853
Transition	2	61	24	1,464	73	101,528
Summer	3	92	19	1,748	68	112,921
Σ CU +HP	12	365	-	8,300	-	567,302

5. Results – Economic Aspects

The total investment costs for the implementation of the work amount to 502,820 euros [6].

5.1 Cogeneration Unit Maintenance Costs

For the CU, we consider the costs of maintenance service of the CU, including work and transport within Slovakia. The average cost per operating hour of a CU, including all the costs mentioned above, is 1.54 euros/Mth [6].

The number of year-round operating hours of the CU was estimated to 8,300. Due to possible failures or repairs on the equipment, we will reduce the operating hours by 5 %. The resulting number of operating hours is 7,885. If this figure is multiplied by the average cost per 1 operating hour, the resulting annual maintenance costs of the CU amounts to 12,143 euros [4].

5.2 Heat Pumps Maintenance Costs

The maintenance is considered to take place once a year. Maintenance costs include routine maintenance, refrigerant inspection, transport from Bratislava to Brezno and back [4].

The annual maintenance costs for both HP´s are 1,206 euros. The work of a service technician is already included in this final price [4].

5.3 Profitability Based on Cash Flow

Since the streamlining of the operation of the heat source is solved in the boiler plant, which is managed by the energy company, we can claim a legitimate claim from depreciation in the price of heat. We must divide the individual equipment and works into depreciation groups and write off the relevant amount each year. This written-off amount represents cash income through the price of heat (quasi-profit item without the need for taxation).

Subsequently, in the individual years, we apply the saved finances on natural gas and revenues for high-efficiency cogeneration. During these years, we also must think about the maintenance of the CU equipment and HP´s, which represent negative items. With the sum of profit and loss items in individual years, we work towards the overall benefit from the operation of the facility [4]. Results are visualized in the form of accumulated cash flow as shown in **Fig. 3**.

Fig. 3 shows that the revenue from depreciation, financial savings on natural gas and revenues for high-efficiency cogeneration will return the investment in 6 years from the installation of the equipment [4].

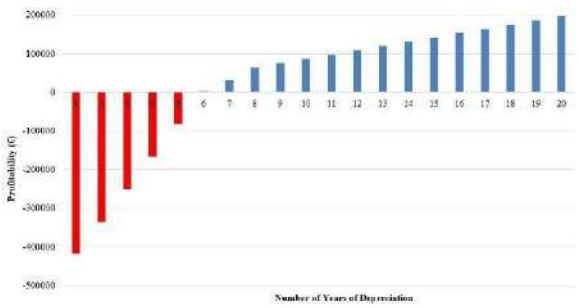

Fig. 3 - Cumulated cash flow [4].

6. Discussion

The reason to apply the CU and HP´s in the given operation was the fact that DHS´s have the potential for high efficiency combined heat and power generation and efficient use of environmental energy through HP´s. These devices can be installed separately, but as mentioned in the article, there is also a presumption of the interaction of both devices.

The CU could also supply electricity to the public electricity network, but at the time of this optimization study, there was a ban on connecting new larger sources of electricity to the public electricity network.

The application of a CU and HP´s to the existing operation of hot water gas boilers saves fossil fuel - natural gas, the reserves of which are gradually running out. The energy of the environment - groundwater - is used instead. From an energy point of view, the same or more heat energy is produced but less fuel is consumed.

7. Conclusion

To ensure energy efficiency, the original technologies are gradually being replaced by modern equipment. First, it is important to determine the area of operation of these facilities, which is also affected by the determination of performance. A CU and HP´s were used to produce the heat needed to prepare hot water in an accumulative way, especially in the summer. During the heating season, the additional heat produced will not accumulate but will be supplied to the heating network.

8. Acknowledgement

This work was supported by the Ministry of Education, Science, Research and Sport of the Slovak Republic through the grants VEGA 1/0303/21, VEGA 1/0304/21 and KEGA 005/STU-4/2021.

9. References

[1] Kassai, M. (2019), Heat Pump Heating System Development of Educational Building based on Energy Economical and Environmental Impacts, Periodica Polytechnica Mechanical Engineering, 2019, Volume 63(3), ISSN 324-6051, pp. 207-213.

[2] PETRÁŠ, D. - LULKOVIČOVÁ, O. - TAKÁCS, J. - FÜRI, B. Renewable energy sources for low temperature systems. Bratislava: Jaga Group, 2009. ISBN 978-80- 8076-075-5. 223 p.

[3] Directive 2012/27/EU of the European Parliament and of the Council of 25 October 2012 on energy efficiency. From: https://eur-lex.europa.eu/legal-content/EN/TXT/HTML/?uri=CELEX:32012L0027&from=SK (online)

[4] MUDRÁ, M. Streamlining the operation of heat source TP5 for the housing estate Západ in Brezno [diploma thesis]. Bratislava: Slovak University of Technology in Bratislava, Faculty of Civil Engineering, Department of Building Services, 2019. 106 p.

[5] Veolia Energia Brezno a.s. From: https://vesr.sk/sk/veolia-energia-brezno (online)

[6] Engul,s.r.o. From: https://www.engul.sk/kontakt/ (online)

[7] PASTOR, P. – HORÁK, M. - HORNÍK, Š. Efficient use of energy in the operation of equipment and buildings. Bratislava: Jaga group, 2000. ISBN 80-88905-33-8. 159 p.

Data Statement

The datasets analysed during the current study are not publicly available, because the heat source operator has not approved their publication but will be available on individual request.

Cooling Performance Evaluation of an Independent Modular Air Containment with Row-based Cooling System for Data Centers

Jinkyun Cho [a], Beungyong Park [b], Seungmin Jang [c]

[a] Professor, Department of Building and Plant Engineering, Hanbat National University, Daejeon, Republic of Korea, jinkyun.cho@hanbat.ac.kr

[b] Professor, Department of Building and Plant Engineering, Hanbat National University, Daejeon, Republic of Korea, bypark@hanbat.ac.kr

[c] Researcher, Department of Building and Plant Engineering, Hanbat National University, Daejeon, Republic of Korea, rainbow9704@naver.com

Abstract. Owing to the rapid growth of information technology services over the past decade, data centers have become the core infrastructure for Industry 4.0. Meanwhile, the energy use of data centers has increased rapidly. In this study, a prototype of an independent module containment system that applied the row-level cooling system of a high-density data center was developed to overcome the limitations of the existing room-based cooling system and satisfy the demand for energy efficiency. The main purpose is to evaluate the cooling performance of a new in-row cooling unit package with multiple heat-transfer medium, which is a sequentially water-refrigerant-air heat exchange system in independent row-based air containment. Based on in-situ measurements, the applicability and cooling efficiency of the row-level cooling system were evaluated. While complying with the standard test method and procedure for cooling unit, the cooling performance and efficiency of the row-based cooling system was derived in connection with the actual operation situation of the data center, and the partial energy contribution was analyzed. The row-based cooling system with the multiple heat exchange in-row cooling package was found to be the better efficient in removing heat output of IT equipment based on the observations and experimental results.

Keywords. Data center; Row-based cooling; Air containment system; Cooling performance; PUE
DOI: https://doi.org/10.34641/clima.2022.97

1. Introduction

As of 2018, global data center energy consumption is estimated to be 205 TWh, accounting for about 1.0% of global electricity consumption [1]. User behaviour increases data center energy needs 353 TWh in 2030 [2]. As entering the era of the 4th industrial revolution, data is rapidly emerging as a key growth engine for future development, and discussions about its importance and revitalization are active. Recently, as a large amount of data is generated due to the expansion of new businesses such as cloud, big data, AI, and IoT, the importance of data centers to process them is increasing. At the global level, hyper-scale data centers are proliferating. Hyper-scale data centers are massive business-critical facilities designed to efficiently support robust, scalable applications and are associated with big data-producing companies [3]. Data centers are energy-intensive facilities, with typical power densities of 540-2200 W/m^2 [4]. In the current data center, when a rack server that consumes an average of 10 kW or more is configured, it is considered high density [5]. The basic function of data center cooling is to effectively remove heat from IT equipment by supplying and distributing cold air to each rack server. As shown in **Fig. 1**, the design approach is divided into room-based and rack-based cooling according to the basically configured rack density to efficiently perform these functions [6].

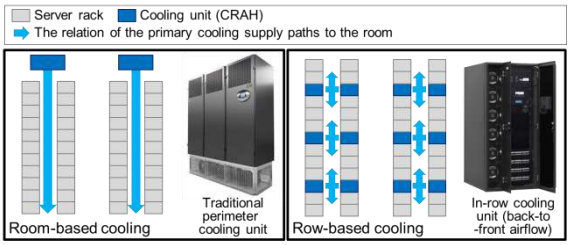

Fig. 1 - Floor plans showing the basic concept of room- and row-based cooling.

Copyright ©2022 by the authors. This conference paper is published under a CC-BY-4.0 license.

In the hyper-scale data center environment, the average density of IT equipment increases, so cooling strategies that can respond to changes in the IT industry are required. A traditional cooling strategy, room-based cooling, may no longer be effective or ineffective. For new data centers, it needs to consider row-based cooling when applying high-density IT loads (10 kW/rack or more). In row-based cooling, in-row computer room air handling (CRAH) units should be placed between rack servers to provide efficient cooling closer to the IT equipment without heat loss. This is because the air distribution path is shorter and simpler compared to room-based cooling. In addition, the airflow is predictable and can operate close to the maximum rated capacity of the CRAH unit to serve the higher IT power density. The row-based cooling can provide higher IT power density and is suitable for independent modular air containment (MAC) pods. For high-density IT power in excess of 10 kW/rack, row-based cooling can be implemented without a raised floor [7].

In this study, in order to improve the cooling efficiency of high-density data centers, a prototype of independent MAC applying a row-based cooling has been developed. The main purpose of this experimental study is to evaluate the applicability and cooling performance of the independent MAC with row-based cooling that can overcome the limitations of the existing room-based cooling and meet the recent requirements for IT environment and energy efficiency. The field application test of new in-row CRAH unit package with multiple heat-transfer medium, which is a sequentially water-refrigerant-air heat exchange system, has been conducted.

2. The MAC with row-based cooling

In order to maximize the advantages of the row-based cooling, the developed independent MAC focused on minimizing the heat loss by shortening in the cold air distribution path. In addition, to prevent the air re-circulation and air by-pass phenomenon, a complete containment structure has been implemented that shields both the cold aisle and the hot aisle. The row-based cooling system should be installed inevitably in the white space where the CRAHs are installed between rack servers operating at higher power density to cool IT equipment efficiently. the reason that it is difficult to apply a central chilled water type CRAH unit is that the supplied chilled water pipe passes through the white space, so if a problem occurs in the pipe, it directly affects the IT equipment. An important detail to consider when installing a CRAH unit in the white space is the condensate drains. The movement of the drain pipe inside the white space must be also avoiding. Although row-based cooling was superior to the existing room-based cooling method in terms of air distribution and could improve much inefficiency, it could not be universally applied due to the aforementioned limitations. In order to overcome this limitation, an in-row CRAH has been constructed to include a water-refrigerant primary cycle and a refrigerant-air secondary cycle so that the primary chilled water pipe does not directly pass through the white space. Because the secondary refrigerant liquid pipe in the white space uses only sensible heat without causing a phase change, condensate drain isn't necessary. The features of row-based cooling system constituting this independent MAC are the efficient cooling distribution in each IT equipment and the development of a new in-row CRAH package with multiple heat-transfer medium, which is a sequentially water-refrigerant-air heat exchange system for improving cooling efficiency and safety. Therefore, it is a row-based cooling system that is optimized to operate the refrigerant liquid at a temperature that does not cause condensate drain. **Fig. 2** shows a row-based cooling system in the MAC prototype.

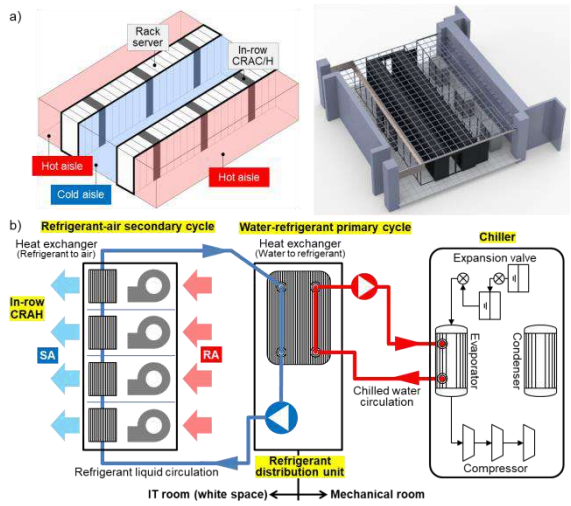

Fig. 2 - a) An independent modular air containment prototype and b) A new in-row CRAH package with sequentially water-refrigerant-air heat exchange system.

3. Methodology

In-situ measurement of the row-based cooling system in the independent MAC, the cooling performance evaluation of the sequentially multiple heat exchange system is the main technical factor. This is because it is the most important part of predicting the target PUE of the data center. Since PUE, which is the data center energy efficiency, is based on annual cumulative power usage, how to use short-term field test results for predicting PUE is the key. Among them, the first step, the performance evaluation of the row-based cooling, must be preceded by ensuring the reliability of the results by the standard testing method. Therefore, the field testing method has been divided into the performance test of the CRAH unit itself and the energy efficiency evaluation of the row-based cooling system of the independent MAC.

3.1 Method of testing for rating of CRAHs

In general, IT room maintain constant air

temperature and humidity to keep an appropriate operation condition for protecting IT equipment. All IT equipment must operate within recommended equipment environmental specifications for air cooling. **Tab. 1** shows the equipment environmental specification of data center according to the IT environmental classes presented by ASHRAE TC9.9 [8]. Since most of high-density data centers fall under A1 and it is important to maintain the IT environment according to the recommended guideline, it is essential to comply with this standard for performance evaluation of CRAH units.

Tab. 1 – Thermal guidelines for IT environment.

A1 Class	Dry-bulb temp.	Humidity range (non-condensing)	Maximum dew-point
Recommended	18~27°C	-9~15°C (DP) and 60% (RH)	-
Allowable	15~32°C	-12~17°C (DP) and 8~80% (RH)	17°C

For testing methods of data center cooling system, those standards have been well formulated to evaluate the performance rating of CRAH considering the IT environment. The application scope of ANSI/ASHRAE Standard 127 [9] is a representative standard for evaluating the performance rating CRAH, which includes chilled water units, air-cooled, evaporative and glycol-cooled units. **Tab. 2** shows the testing conditions for rated cooling of the CRAH unit. Class 1-4 classifies application conditions of CRAH, which are presented step by step to be able to respond in various air flowrate. Another performance testing standard, AHRI Standard 1361 [10] is similar to that of ANSI/ASHRAE Standard 127. However, the CRAH units have been classified by mounting location and the return air temperature control conditions have been detailed in consideration of the air supply direction.

Tab. 2 – Standard rating conditions of CRAHs.

Cooling		Application classes	Rated cooling
Air temperature surrounding indoor part of unit (control is on return temperature)	Return dry-bulb temp.	Class 1	23.9°C
		Class 2	29.4°C
		Class 3	35.0°C
		Class 4	40.5°C
	Return dew-point temp.		11.1°C
Chilled-water CRAH units	Entering water temp.		10.0°C
	Leaving water temp.		16.7°C
Reheating			Base Rating
All units	Return dry-bulb temp.		23.9°C

3.2. In-situ measurement procedures

An independent MAC prototype with row-based cooling system was installed in a reference data center (**Fig. 3**). Cooling performance was evaluated before the rack servers were mounted in consideration of the safety of IT room during operation.

Fig. 3 - A test mock-up system of row-based cooling: sequentially multiple heat exchange system.

Considering the high-density IT environment conditions, testing methods and procedures of the cooling performance were confirmed, and the in-situ measurement of the in-row cooling package consisting of six indoor units and two refrigerant distribution units was conducted in actual operation conditions in the reference data center. The field test measured the cooling performance of the CRAH units and the refrigerant distribution units at the same time. Each measurement item was simultaneously measured in real time, such as air temperature and relative humidity of the supply air (SA) and return air (RA), air flowrate, chilled water temperatures, water flowrate, and power consumption. To simulate the test environment reflecting the IT operating conditions, total 180 kW of heat load banks were installed to realize the power load of IT equipment (about 5.0 kW/rack). As shown in **Fig. 4a**, cooling capacity of the air-side can be expressed as the amount of heat that can be removed from the IT equipment when CRAH units are operated. An in-row CRAH unit is composed of four secondary refrigerant-air micro-pin-fin heat exchangers and four EC fans. The air temperature and humidity were measured eight points at SA and RA side of CRAH. The air-side cooling capacity of a CRAH was based on the only sensible heat because there is no source of latent heat, and calculated according to **Equation (1)** determined in cold aisle. The water-side cooling capacity of a refrigerant distribution unit can be calculated as in **Equation (2)** as the amount of heat supplied through chilled water.

$$q_a^S = \frac{C_{\rho a} \times Q_a \times (t_{ai} - t_{ao})}{v_n \times (1 + x_n)} \quad (1)$$

$$q_w = C_{\rho w} \times Q_w \times (t_{wi} - t_{wo}) \quad (2)$$

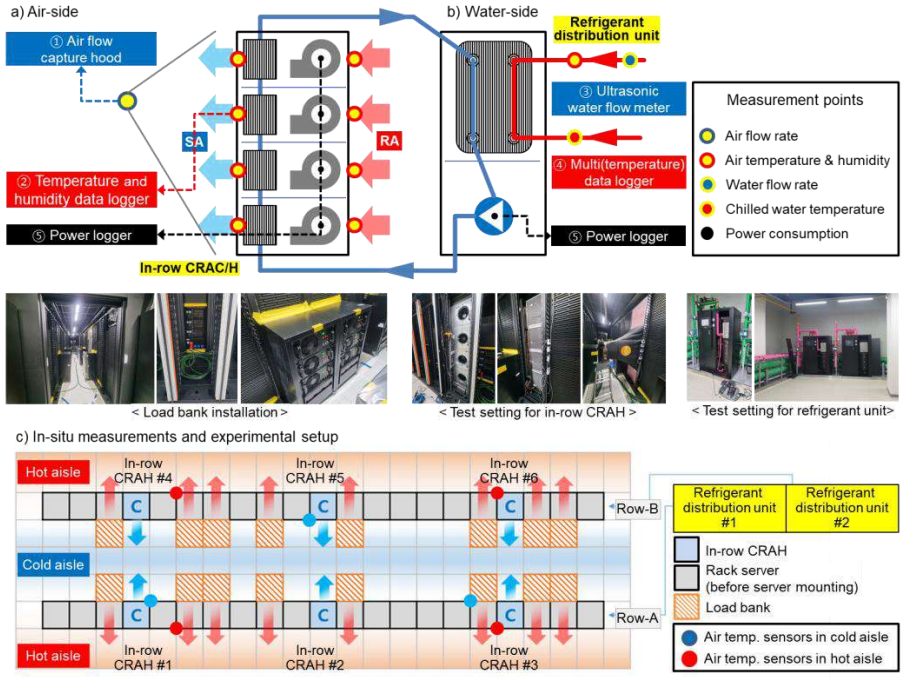

Fig. 4 - In-situ measurements and experimental setup (measuring instruments and sensors installation).

As shown in **Fig. 4b**, a refrigerant distribution unit consists of one primary water to refrigerant heat exchanger and one refrigerant liquid pump. The water temperature and flowrate were measured at the chilled water supply and return points. The final evaluation item is the total energy efficiency ratio (EER). The performance evaluation of the row-based cooling system was basically performed in accordance with the standard testing procedures. All testing procedures were officially carried out in the presence of a third party organization. **Fig. 4c** shows the experimental setup for row-based cooling system in the MAC pod to measure input power, air temperature in hot/cold aisle, air flowrate of CRAH, and the supply chilled water flowrate and temperature difference of the refrigerant distribution unit for the evaluation of the cooling performance described above. As shown in **Tab. 3**, the base testing conditions were on operating the system to keep air temperature in the cold aisle below 25.0°C, and the inlet supply chilled water temperature was 8.0°C.

Tab. 3 – Test condition of cooling performance for the row-based cooling system.

Test condition of (Equipment)		Capacity [kW]	Qty. [EA]	Total Capacity [kW]
IT operations	Load bank	11.25	16	180
Row-based cooling	CRAH unit	45	6	270
	RDU unit	135	2	270

4. Experimental measurements

4.1 Measurement condition-setting

The experimental investigations were divided into the measurements of the cooling capacity for each component unit and evaluation of overall cooling performance for the row-based cooling system. As shown in **Fig 4**, a row-based cooling system that three in-row CRAH units and one refrigerant distribution unit for row-A were evaluated. And at the same time, the cooling capacity test was performed on only an in-row CRAH (#2) and a refrigerant distribution unit (#1) among this component system. A preliminary test was performed for about 120 minutes to secure the operation stability of the IT environments and cooling system. After trial-run, the main test was continuously measured every one-minute for 75 minutes. As the standard of the accredited test for cooling performance is to measure three times at 10-minute intervals in principle [11], real-time continuous measurement during 75 minutes satisfied the relevant conditions and there was no problem in data acquisition. **Fig. 5** shows that the air temperature in the cold and hot aisles of row-A during the measurement period, and the supply and return temperatures of the chilled water for the refrigerant distribution unit (#1) are kept very constant. It can be seen that the experiment was performed in the stabilization stage.

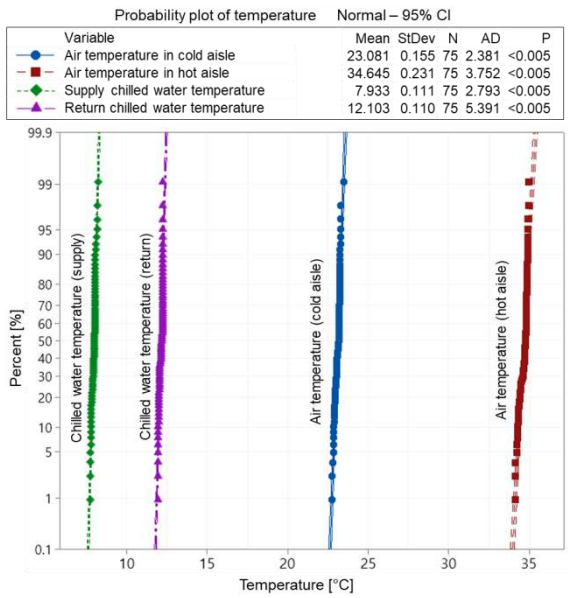

Fig. 5 - Stabilization conditions of IT environment (cold/hot aisle) and chilled water supply during the measurements.

Tab. 4 – Results of cooling performance test for component units.

	Test conditions	Application	Cooling units	Items	Results
Water-side	Entering water temperature [°C]	7.0±1.0	In-row CRAH #2 (surrounding indoor part of unit)	Cooling capacity [W]	12,083
	Due to reference central cooling system condition CHW supply temp.	10.0→ 8.0°C		Electrical energy [W]	100.51
				Air flow rate [m3/h]	2,052
Air-side	Return dry-bulb temp. [°C]	35±1.0		Return dry-bulb temp. [°C]	34.21
	Return wet-bulb temp. [°C]	17.4±1.0		Return wet-bulb temp. [°C]	17.57
	Due to CHW supply temperature condition	WB 19.8°C→ WB 17.4°C		Supply dry-bulb temp. [°C]	16.67
				Supply wet-bulb temp. [°C]	10.92
System setting	Fan speed [%]	35	Refrigerant distribution unit #1 (heat rejection & cooling fluid)	Cooling capacity [W]	59,248
	Refrigerant pump [Hz]	28		Electrical energy [W]	633.44
IT load	IT load in row-A [kW]	65		Water flow rate [liter/min]	161.4
	Assigned IT load for CRAH #2 [kW]	Approx. 13		Entering water temp. [°C]	7.83
	Assigned IT load for RD #1 [kW]	Approx. 60		Leaving water temp. [°C]	12.61

4.2. Cooling capacity for each component unit

Rating test for air-side cooling performance of an in-row CRAH unit and water-side cooling performance of a refrigerant distribution unit was based on ASHRAE [9]. **Tab. 4** shows the measurement results of the individual cooling capacity of the CRAH unit (#2) and refrigerant distribution unit (#1). However, since the chilled water supply condition of the central chiller system installed in the reference data center to be tested is already in cooling operation in connection with other IT rooms, the test was conducted under a fixed condition around 8.0°C. In addition, according to the chilled water temperature testing condition, the return air dry-bulb temperature of the CRAH unit could be realized as 35°C, but the dew-point temperature was inevitably adjusted downward, and the return air wet-bulb temperature condition was also slightly adjusted. The IT power supplied to the independent MAC was about total 130 kW (72% of total heat bank capacity) and the IT load assigned to the row-A is expected to be about 65 kW (heat load bank). The IT load assigned to the in-row CRAH unit (#2), which again controls the 55% of supply air flowrate considering the fan speed, was expected to be about 13 kW. In addition, the IT load allocated to the refrigerant distribution unit (#1) was set to 60 kW in consideration of the rated cooling capacity of the actual CRAH unit. As a result of the individual cooling rating test of the equipment, the In-row cooling package showed the output of the cooling performance corresponding to the assigned IT load, and the refrigerant distribution unit also implemented cooling capacity and performance to remove IT heat through the chilled water to refrigerant heat exchanger.

4.3. Total cooling performance

First, in-row cooling package is very important to maintain the thermal equilibrium between the primary and secondary heat exchange cycle. As shown in **Fig. 6** and **Tab. 5** as a result of evaluating the cooling performance of a row-based cooling system based on one zone (row-A), it was possible to supply cooling exceeded the given IT load (heat load). The water-side cooling capacity of heat removal may differ depending on the chilled water temperature, but it has maintained thermal balance between the water to refrigerant primary cycle and the refrigerant to air secondary cycle. In addition, it was analyzed that the cold aisle in row-A satisfies the ASHRAE thermal guideline by converging air temperature to 23.1°C based on the supply chilled water temperature of 7.9°C under the IT load of 61.1

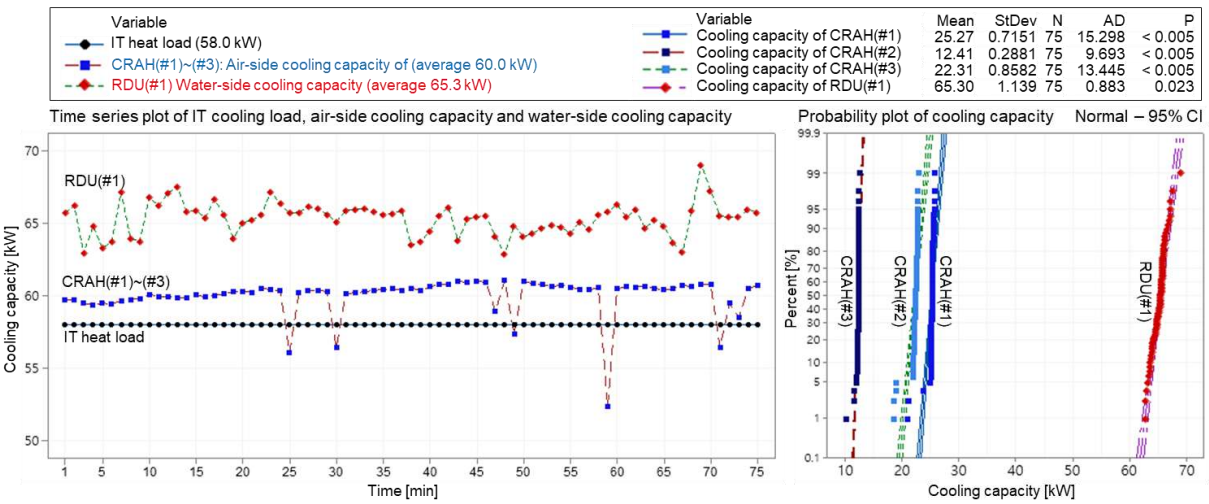

Fig. 6 – Results of cooling performance evaluation for row-based cooling system (at row-A).

kW. Where, IT cooling load was assumed to be 95% of IT load (power). It is expected that the cooling performance will decrease when the supply chilled water temperature increases, but it is determined that there is no problem in maintaining the proper air temperature in the cold aisle up to 25°C. The net power consumption of CRAH fans and refrigerant liquid pump is average of 1.17 kW based on the IT power of 61.1 kW, excluding energy of the central chilled water system such as the chiller plant and chilled water circulation pump.

Tab. 6 - Descriptive statistics of cooling performance; row-A with an in-row cooling package.

Variable (row-A results)	N	Mean	StDev
Air temp. in cold aisle [°C]	75	23.081	0.155
Air temp. in hot aisle [°C]	75	34.645	0.231
CRAH (#1) SA temp. [°C]	75	19.663	0.110
CRAH (#2) SA temp. [°C]	75	19.596	0.144
CRAH (#3) SA temp. [°C]	75	20.626	0.117
CRAH (#1) RA temp. [°C]	75	36.495	0.165
CRAH (#2) RA temp. [°C]	75	34.713	0.237
CRAH (#3) RA temp. [°C]	75	35.552	0.239
RDU (#1) CWS temp. [°C]	75	7.9330	0.1106
RDU (#1) CWR temp. [°C]	75	12.103	0.110
CRAH (#1) fan power [kW]	75	0.1946	0.000320
CRAH (#2) fan power [kW]	75	0.1044	0.000195
CRAH (#1) fan power [kW]	75	0.1914	0.000253
RDU (#1) pump power [kW]	75	0.6828	0.00214
CRAH (#1) cooling capacity [kW]	75	25.272	0.715
CRAH (#2) cooling capacity [kW]	75	12.408	0.288
CRAH (#1) cooling capacity [kW]	75	22.309	0.858
RDU (#1) cooling capacity [kW]	75	65.302	1.139
IT Power [kW]	75	61.050	-
IT cooling load [kW]	75	57.998	-
Cooling power [kW]	75	1.1732	0.00222
pPUE	75	0.0192	0.000036

$$pPUE_{Cooling} = \frac{Cooling\ power}{IT\ power + Cooling\ power} \quad (3)$$

The effect of the calculated cooling partial PUE ($pPUE_{Cooling}$), can be calculated as in **Equation (3)**, is almost insignificant with an average of 0.019 (19.22 W/IT-kW). It was analyzed that the in-row cooling package with primary-secondary heat exchange system overcomes the biggest limitation of the existing chilled water type in-row cooling system, where the row-based cooling system has to take the risk of connecting the chilled water pipe to white space of IT room, and also does not have a significant effect on energy.

5. Conclusion

In order to cope with the new data center according to the IT technologies and characteristics centered on operation and service and to secure sustainable cooling strategy for those IT environments, it is necessary to propose a new cooling system. Following the previous numerical optimization work, this experimental study has developed a prototype of an independent MAC that overcomes the limitations of the existing room-based cooling system and applied a row-based cooling system for a high-density data center that can meet the requirements for energy efficiency. While complying with the standard CRAH test method and procedures, it has derived the objective cooling performance through real-time in-situ measurement in connection with the actual operation situation of the reference data center, and analyzed the practical PUE contribution. The results can be summarized as follows:

- In order to prevent air recirculation and bypass, which are chronic problems in data centers, it has presented a complete air containment prototype that shields both cold and hot aisles, minimizing hot air mixing and heat loss, and maximizing airtightness.
- It has made row-based cooling of an independent MAC efficient, developed a new in-row cooling package with multiple heat-transfer medium, which is a sequentially water to refrigerant to air heat exchange system for improving cooling efficiency and safety.
- In order to fundamentally prevent water damage in IT rooms, the in-row cooling package has been constructed to include a water-refrigerant primary cycle and refrigerant-air secondary cycle so that the primary chilled water pipe does not directly pass through the IT room.
- As a result of the rating test of cooling capacity for each component unit, the In-row cooling package showed the output of the cooling capacity corresponding to the assigned IT heat load.
- As a result of total cooling performance of the in-row cooling package, thermal balance was maintained between the water to refrigerant primary cycle and the refrigerant to air secondary cycle. The row-based cooling system was analyzed that the cold aisle satisfies the thermal guideline.
- The effect of the calculated cooling partial PUE is almost insignificant with an average of 0.019 (19.22 W/IT-kW).

Through this experimental study and previous our numerical study, the new in-row cooling package was able to secure both IT operational safety and economical energy efficiency. Therefore, it is considered that it is necessary to expand the application as a cooling solution for new high-density data centers.

Nomenclature

q	: Cooling capacity [W]
Q	: (A measured value of) air flowrate [m³/h] or water flowrate [liter/min]
t	: (A measured value of) temperature [°C]
x	: Absolute humidity of air [kg/kg']
u	: Specific volume of air [m³/kg]
C_p	: Specific heat [Wh/kg°C]

Superscripts and superscripts

S : Sensible heat

L : Latent heat

Subscripts and superscripts

a : air (air-side)

w : chilled water (water-side)

i : inlet to unit (return)

o : outlet from unit (supply)

n : The nth measurement point

6. Acknowledgement

This work was supported by the National Research Foundation of Korea (NRF) grant funded by the Korea government (MSIT) (2020R1F1A104949812).

7. References

[1] Masanet, E., Shehabi, A., Lei, N., Smith, S., Koomey, J. Recalibrating global data center energy-use estimates. Science. 2020;367(6481): 984-986.

[2] Koot, M., Wijnhoven, F. Usage impact on data center electricity needs: A system dynamic forecasting model. Appl. Energy. 2021;291: 116798.

[3] Cisco. Cisco global cloud index: forecast and methodology 2016-2021, Cisco white paper 1513879861264127. Cisco and/or its affiliates; 2018.

[4] Beaty, D.L. Internal IT Load profile variability. ASHRAE J. 2013;55(2):72-74.

[5] Cho, J., Kim, Y. Development of modular air containment system: thermal performance optimization of row-based cooling for high-density data centers. Energy. 2021;231:120838.

[6] Dunlap, K., Rasmussen, N. Choosing between room, row, and rack-based cooling for data centers, APC white paper 130 rev02. Schneider Electric-Data Center Science Center; 2012.

[7] Abbas, A.M., Huzayyin, A.S., Mouneer, T.A., Nada, S.A. Thermal management and performance enhancement of data centers architectures using aligned/staggered in-row cooling arrangements. Case Stud Therm Eng. 2021;24:100884.

[8] ASHRAE TC 9.9. Thermal guideline for data processing environments. American Society of Heating Refrigerating and Air-Conditioning Engineers, Inc. 2015.

[9] ASHRAE. ANSI/ASHRAE standard 127-2012; method of testing for rating computer and data processing room unitary air conditioners. American Society of Heating, Refrigerating and Air-Conditioning Engineers, Inc. 2012.

[10] AHRI. AHRI standard 1361-2017; performance rating of computer and data processing room air conditioners. Air-Conditioning Heating and Refrigeration Institute; 2017.

[11] ISO. ISO/IEC Guide 98-3:2008, uncertainty of measurement - Part 3: guide to the expression of uncertainty in measurement (GUM:1995). International Organization for Standardization; 2008.

TEWI and energy assessment of integrated CO2 refrigeration, heating and cooling technology

Nishant Karve [a], Kris Van de Velde [b], Stefan Vandaele [c]

[a] Daikin Europe N.V., Oostende, Belgium, karve.n@daikineurope.com

[b] Daikin Europe N.V., Oostende, Belgium, vandevelde.k@daikineurope.com

[c] Daikin Europe N.V., Oostende, Belgium, vandaele.s@daikineurope.com

Abstract. In order to meet with the regulations proposed by the Intergovernmental Panel of Climate Change to control emissions from fluorinated gases, an EU funded project (LIFE) has been engaged in. Through this project, the reduction of CO2 emissions by using an integrated refrigeration, heating and cooling system, in real shops across Europe and the impact of the raw materials used will be investigated. In a theoretical evaluation, the Seasonal Energy Performance Ratio and Total Equivalent Warming Impact of the unit is compared to an R-410A unit using test measurements. Although the CO2 unit has a lower Seasonal Energy Performance Ratio, the Total Equivalent Warming Impact was calculated to be lower in comparison to the R-410A unit over a period of 10 years. These measurements were also used to discuss the importance of heat recovery by comparing the unit to a non-integrated refrigeration, heating and cooling system. The energy assessment of the unit at a real installation in a supermarket in Europe has been presented on a monthly basis. This assessment involves the use of a compressor curve method to estimate mass flow and as a result, the delivered energies in the absence of expensive flow meters. The precision of such a method has been discussed. To conclude, challenges concerning the technology and important results and conclusions have been discussed.

Keywords. CO2 emissions, heat recovery, refrigeration, energy efficiency, TEWI.
DOI: https://doi.org/10.34641/clima.2022.193

1. Introduction

1.1 LIFE Project

A LIFE project has been engaged in, in line with the F-gas regulations proposed by the IPCC [1]. This project aims at presenting an integrated refrigeration, space heating and cooling solution to the commercial market with a natural refrigerant i.e. CO2. The main objectives of this project are to demonstrate the unit in supermarkets across various countries in the EU, develop a CO2 cassette indoor unit, investigate the integration of a thermal storage, improving safety standards and energy efficiency regulations, training of service engineers, installers, designers and dissemination of information. This paper discusses the theoretical climate impact of the unit as compared to an R-410A unit through TEWI calculations and the impact of heat recovery on the SEPR. Real site data from one of the installations also presents an energy assessment of the unit, with an introduction to a mass flow estimation method to calculate the delivered energies. Feedback and comments received on a previous paper have been taken into account and applied wherever applicable in this follow-up paper.

1.2 Combined Refrigeration, Heating and Cooling unit

The CO2 unit under consideration is an integrated refrigeration, heating and cooling system with CO2 as a refrigerant, with the possibility of heat recovery from the refrigeration cabinets for indoor space heating. The unit also has the ability to operate as a heat pump in case of additional space heating demand. This can be achieved by two independent low-stage swing compressors; one for refrigeration and the other for air conditioning or heating, with a common high-stage compressor. The indoor units can switch between cooling or heating depending on the demand with the help of solenoid valves. The indoor units are either ducted or in a cassette form. The schematic of the CO2 unit is shown in figure [1].

Copyright ©2022 by the authors. This conference paper is published under a CC-BY-4.0 license.

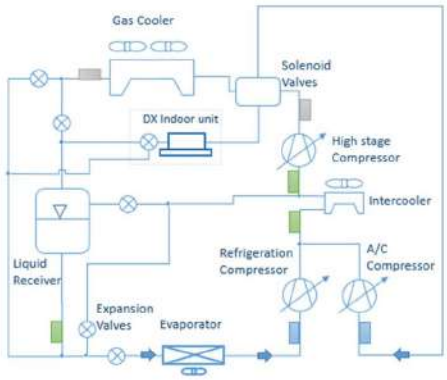

Fig. 1 – Schematic of integrated CO2 unit

2. Methods

2.1 TEWI Analysis

The climate impact of the unit was studied using a theoretical evaluation of the TEWI in comparison with a R-410A unit. The equation used for this is as shown in Equation (1).

$$TEWI = (GWP \cdot L_{annual} \cdot n) + GWP \cdot m \cdot \left(1 - \alpha_{recovery}\right) + (E_{annual} \cdot \beta \cdot n) \quad (1)$$

This equation comprises direct and indirect emissions of the technology over the lifetime considered. The first two terms in the equation show the direct emissions caused as a result of the Global Warming Potential of the refrigerant, the annual leakage rate, refrigerant charge and the recovery rate of the system. The last term represents the indirect emissions as a result of the annual energy consumption and emission factor based on the energy mix of the region. The values used for the parameters in the equation are given below in table [1].

Tab. 1 – Parameters for TEWI calculation

Parameter	R410A	R744	Unit
GWP	2088[3]	1	
L_{annual}	2 %	2 %	
n	10	10	years
m	20	30	kg
$\alpha_{recovery}$	50 %	50 %	
E_{annual}	23062	24119	kWh/year

2.2 Impact of HR on SEPR

As described in the previous section, the integrated system delivers refrigeration, cooling and heating with one outdoor unit with the possibility of heat recovery. A non-integrated system, on the other hand, needs independent outdoor units to perform the same functions. Figure [2] shows the difference in configuration of the two systems. This analysis compares the Seasonal Energy Performance Ratio of both systems and evaluates the impact of heat recovery in integrated systems. The SEPR was calculated based on temperature bins from EN13215 and EN14825 [4][5]. The capacity and COP values from test rooms were used at various condition points to calculate the SEPR.

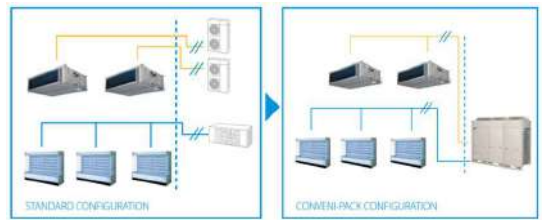

Fig. 2 – Difference between non-integrated (left) and integrated (right) systems

Figure [3] and Figure [4] show the P-design points used for these calculations. In order to account for heat recovery in an integrated unit, a common P-design point at 5 was chosen instead of 7C or 2C, as seen for heating in a non-integrated system.

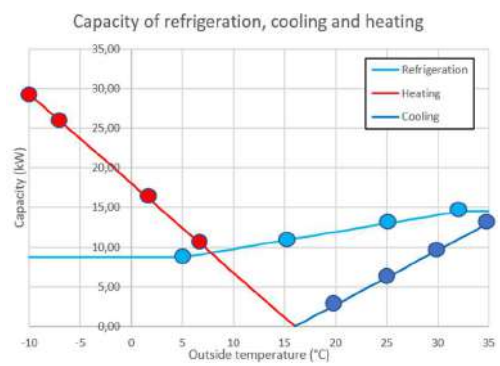

Fig. 3 – P-design points for non-integrated system

Similarly, for cooling, a common P-design point at 32C was chosen. This was done to accommodate for the lack of a methodology to calculate the SEPR of such combined refrigeration, heating and cooling equipment.

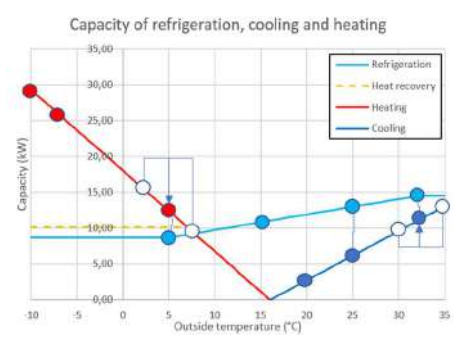

Fig. 4 – P-design points for integrated system

2.3 Compressor Curve method

As mentioned in the introduction to the project, it is the aim to demonstrate the technology in various sites across EU. Along with the demonstration, it was also the objective to monitor the operational data of the units to evaluate the delivered energies, i.e. refrigeration, heating and cooling; and consumed energies. While the consumed energies were measured using energy meters, the delivered energies were calculated using the product of enthalpies and estimated mass flows as shown in the succeeding section. The mass flows were estimated based on the compressor speed, the density of the refrigerant at the suction side and a constant representing the swept volume of the compressor. As the CO2 Coreolis mass flow meters were expensive, they were only installed at two local sites to validate the method. Separate constants were derived for refrigeration, heating and cooling respectively. The precision of the method will be discussed in the results section for each function.

2.4 Energy assessment

As mentioned in the previous section, delivered energies were calculated using operational data from each site, site 1 situated in Czechia and site 2 in Germany. This, along with the measured consumed energy was used to calculate the operational COP of the units. Following are the formulae used to calculate delivered refrigeration, cooling and heating energies. The refrigeration capacity was calculated as the product of the estimated refrigerant mass flow through the cabinets and the difference in the enthalpy between the outlet and inlet of the cabinets respectively, as shown in equation (2). The inlet enthalpy, $h_{ref,in}$, was calculated using the receiver pressure and the liquid temperature of the refrigerant. The outlet enthalpy, $h_{ref,out}$, was calculated using the suction pressure and temperature.

$$Ref_{cap} = m_{ref} \cdot \left(h_{ref,out} - h_{ref,in}\right) \quad (2)$$

The heating capacity was calculated as shown in equation (3). The inlet heating enthalpy, $h_{heat,in}$, was calculated using the discharge pressure and temperature of the refrigerant after the high stage compressor. The outlet enthalpy, $h_{heat,out}$, was calculated using the discharge pressure and the liquid outlet temperature after passing through the indoor units.

$$Heat_{cap} = m_{ac} \cdot \left(h_{heat,in} - h_{heat,out}\right) \quad (3)$$

Similarly, the cooling capacity delivered was calculated using receiver pressure and the liquid refrigerant temperature for the enthalpy on the inlet side and the suction pressure and temperature for the enthalpy on the outlet side of the indoor units. This is shown in equation (4).

$$Cool_{cap} = m_{ac} \cdot \left(h_{ac,in} - h_{ac,out}\right) \quad (4)$$

3. Results

3.1 TEWI Analysis

The TEWI analysis was performed using the parameters mentioned in Table 1. As can be seen in figure (5), contributions as a result of direct and indirect emissions have been shown with a stacked bar graph for both refrigerants, R410A and R744. From the table, it could be seen that the annual energy consumption of the R744 system is higher than that of the R410A system, thus, resulting in slightly higher indirect emissions from the former. But this is offset by the negligible direct emissions from the R744 system, owing to a GWP of 1 as compared to significantly higher direct emissions from the R410A unit owing to a GWP of 2088. The total difference in the emissions results in the R744 unit emitting 37% less as compared to the R410A unit.

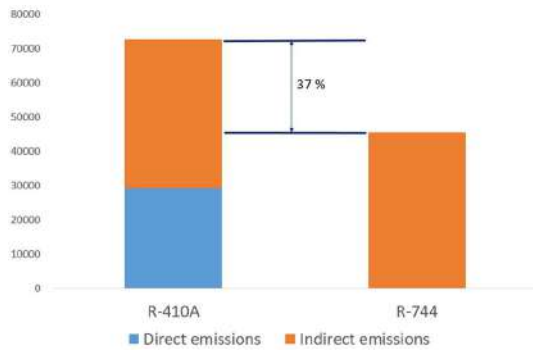

Fig. 5 – TEWI comparison between R-410A & R-744

Although product specifications indicate an annual leakage rate of about 1 % for both systems, a leakage rate of 2 % was chosen for the analysis to conform wih existing research literature [6]. It was observed that with a leakage rate of 1%, the R744 system emitted about 34 % lower as compared to the R410A unit over their lifetime. This clearly indicates that the R744 unit becomes more attractive as the leakage rate is increased.

3.2 Impact of HR on SEPR

Based on the methodology described in section 2.2, the distribution of consumed energy was plotted as a function of ambient temperature, as shown in figure (6) and figure (7) for a non-integrated and integrated system respectively. It can be observed that the total energy consumption for the non-integrated system shows a peak between ambient temperatures of 0°C and 5°C due to the high heating demand which needs to be supplied by the independent heating system. This peak can be observed to be shaved off in the integrated unit, as the heat demand during this range was satisfied by the heat recovered from the refrigeration cabinets. This results in a 43% increase in the SEPR for the integrated unit as can be seen from table [2].

Tab. 2 – SEPR values

	Non-integrated system	Integrated system
SEPR	3,4	4,9

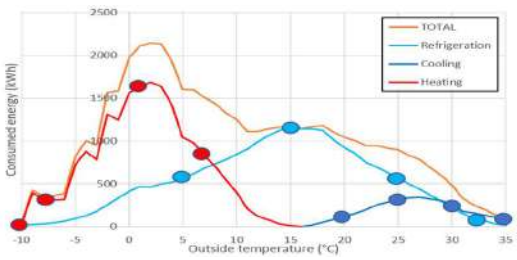

Fig. 6 – Consumed energy distribution for non-integrated CO2 system

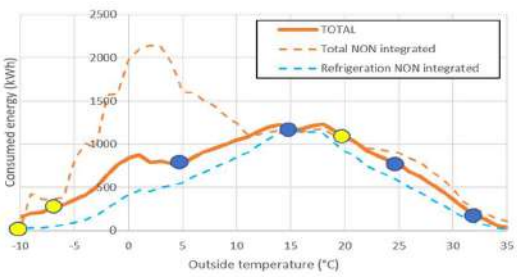

Fig. 7 – Consumed energy distribution for integrated CO2 unit

3.3 Precision of Compressor Curve method

This section discusses the precision of the compressor curve method for each function i.e. refrigeration, cooling and heating respectively. For each function, the precision has been described on an hourly and daily basis respectively. The x-axis on the below graphs indicates the deviation of the calculated capacity from the capacity measured using flow meters. Thus, a value of -10 indicates that the capacity calculated using the CC method is lower than the measured capacity by 5 to 10 %. The Y-axis indicates the occurrence of the deviation. In figure (8), the precision of the refrigeration capacity on an hourly basis is described by the blue line and on a daily basis by the red line. For both resolutions, it can be observed that majority of the datapoints occur within +-5% of the measured values, about 70% on an hourly resolution and more than 80% on a daily resolution.

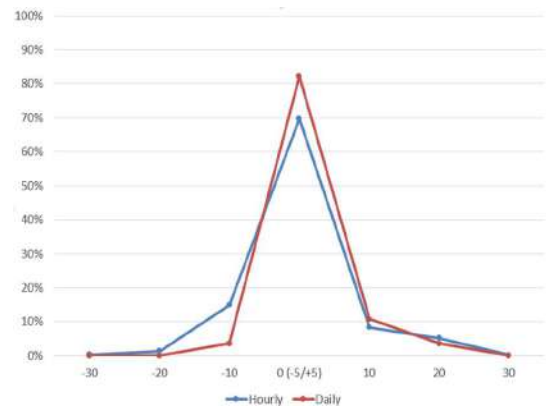

Fig. 8 – Precision of CC method for refrigeration

The following graph in figure (9) describes the deviation of the heating capacity from the measured values. It can be observed that the calculated heating capacity is more deviant from the measured capacity than what was observed for refrigeration and, as will be seen below, for cooling. This can be attributed to the complexity arising due to the presence of four different heating operation modes in the unit. These include two heat recovery modes and two heat pump modes with or without refrigeration. A large part of the deviation arises from the heat recovery mode, wherein not all of the refrigerant mass flow coming from the refrigeration cabinets is delivered to the indoor units after the second stage compressor. Thus, without flow meters, it was not suitable to assign a constant purely based on compressor speed.

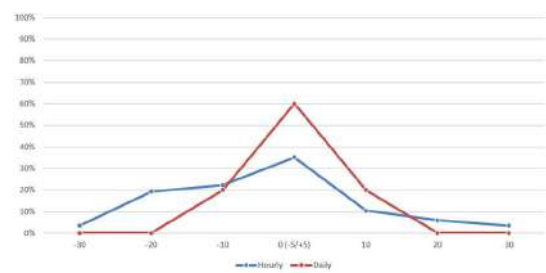

Fig. 9 – Precision of CC method for heating

For cooling capacity, although the percentage of values occurring within 5% of the measured values is lower, it can be observed from figure (10) that the majority of the deviation is either less than or equal to the measured value. On an hourly basis, a deviation of 0 to -10% occurs more than 80% of the duration and this occurrence reaches 100% when a daily resolution is considered. This shows that the compressor curve method has been adapted to under-estimate the capacities rather than over-estimate them.

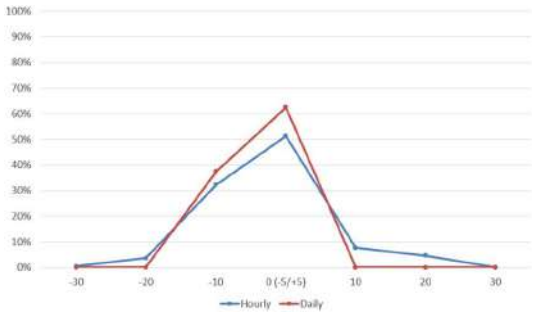

Fig. 10 – Precision of CC method for cooling

3.4 Energy Assessment

In this section, a monthly energy overview is presented for two independent sites. In the following graphs, the delivered refrigeration, heating energy through heat pump operation, heating energy through heat recovery and cooling energy is shown for both sites. From figure (11), it can be observed that there was a high demand for heating throughout the year. This demand was to a large extent satisfied using heat recovered from the refrigeration cabinets. Besides the bars labelled as 'HR Energy' in the graphs, a large portion of the 'HP Energy' delivered was also recovered from the cabinets in addition to the heat extracted from the ambient. Site 2, in comparison, was observed to have a lower heating demand as compared to site 1 as shown in figure (12). A large amount of cooling energy was also delivered in this site during the summer. This was due to a low indoor setpoint temperature of 17°C.

Fig. 11 – Energy overview of LIFE project site 1

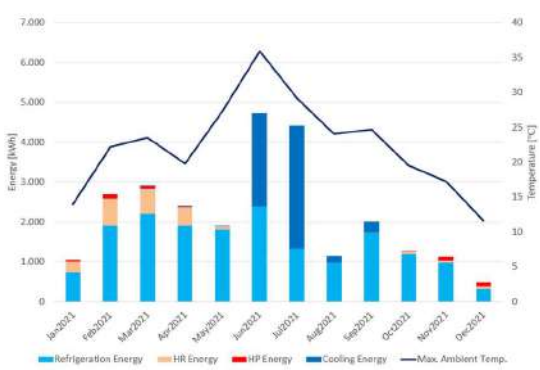

Fig. 12 – Energy overview of LIFE project site 2

As opposed to site 2, site 1 showed no cooling demand even during the summer when the ambient temperature reached a maximum of about 39 °C. This has been highlighted using figure (13), where a distribution of the operation modes of the unit at site 1 during the summer months of June, July, August and September has been shown. It can be seen that the unit ran as a heat pump for about 27% of the duration, besides the 67% of heat recovery operation observed. This was because of the layout of the store and the type of refrigeration cabinets used. While site 2 had almost entirely closed door cabinets, site 1 was installed with open cabinets. To add to that, the total area of the store was only 100 m^2, thus the indoor units were required to heat up the space which was being cooled by the open cabinets. This shows how important a role the layout, store design and selection of equipment play in efficient performance of commercial units.

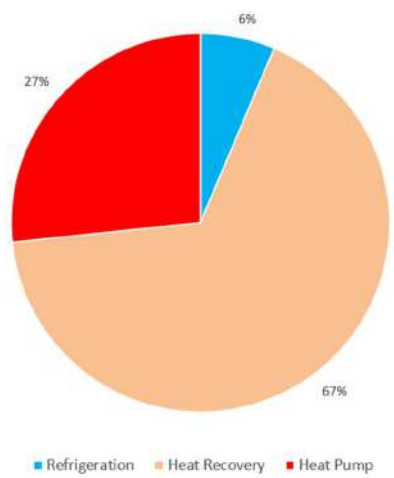

Fig. 13 – Operation mode distribution of site 1 during summer

The SEPR for site 1 was calculated to be about 7% lower than that of site 2. This can be attributed to the large amount of heat pump operation observed in site 1. Additionally, both sites showed a large occurrence of operation in a heat recovery mode. It was observed that there was a significant difference in power consumption during this operation mode.

4. Challenges

Due to the low critical temperature and high operating pressures of CO2, implementing such solutions for cooling in regions with a warm climate is a challenge and an important obstacle in facilitating the spread of this technology further. To counter this, propositions such as an adiabatic cooling system for the gas cooler and thermal storage are currently being tested. The difficulty in the selection and availability of components such as valves, suitable refrigeration cabinets for the

operating pressures also needs to be addressed. As mentioned in sections 2.2 and 3.2, no methodology currently exists in calculating SEPR of such combined refrigeration, space heating and cooling systems with the appropriate consideration of heat recovery. Efforts are being taken currently to establish such a methodology with a third-party research institution and validation from experts and scholars within the field. It is the aim to propose this methodology for inclusion in future standards concerning similar technologies. Monitoring and recording real operational data is invaluable and equally challenging from the point of view of logistics, economics and maintenance. The CC method, as discussed in the previous sections, has been proposed as one solution to tackle this challenge, by eliminating the need for installation of expensive and often intrusive CO2 Coreolis flow meters. Although it has been observed to have a high precision for lower resolutions, a more sophisticated algorithm would be needed for a higher precision at higher resolutions to account for the dynamic operation of the unit and the error between multiple sources of data. As the data is currently being recorded every 15" at every site, handling such large amounts of data has also been found to be an important aspect in implementing such projects. Finally, with the growth in CO2 technologies in the market, there is a constant need for a knowledge transfer between engineers, technicians, installers and researchers. It is the aim of this project to share as much information as possible to improve the state of the art and help in further development.

5. Conclusions

Through a theoretical analysis of the technology, it was observed that the R744 unit has a significantly lower TEWI than that of a R410A unit over a lifetime of 10 years. It was also seen that this difference increases with an increase in the annual leakage rate, owing to the large difference in GWP of the two refrigerants. The presence of heat recovery was found to have a positive impact on the SEPR of a combined refrigeration, heating and cooling unit as compared to a system with independent units for the same. The compressor curve method, devised to estimate the mass flow of the refrigerant in the absence of expensive flow meters, was found to improve in precision as the resolution of the data was lowered. This was found to be positive for the calculation of SEPR of such systems, wherein the calculated values were found to be within 5% of the measured values and adapted to under-estimate rather than over-estimate delivered capacities. Based on the assessment of the real site data from the two sites, the importance of store layout, selection of equipment and indoor setpoint can be noted. At site 1, even at a high ambient temperature of 39 °C, a need for heat pump operation was observed due to the presence of open refrigeration cabinets and a small store area. On the other hand, site 2 showed a high cooling demand during the summer due to a low setpoint of 17 °C indoors. Site 1 showed a lower SEPR than site 2 due to higher operating pressures during the heat recovery modes and a large occurrence of heat pump operation throughout the year.

6. Acknowledgement

The contribution and support of the European Commission in the project would like to be sincerely acknowledged.

7. References

[1] European Commission. Refulation (EU) No 517/2014 of the European Parilament and of the Council of 16 April 2014 on fluorinated greenhouse gases and repealing Regulation (EC) No 842/2006. Official Journal of the European Union. 2014.

[2] European Commission. EN 378:2017; AR4: Fourth Assessment Report of the IPCC. 2017.

[3] Technical Committee CEN/TC 113 "Heat pumps and air conditioning units", "European Standard EN 14825," European Committee for Standardization, 2018

[4] Technical Committee CEN/TC 113 "Heat pumps and air conditioning units", "European Standards EN 13215," European Committee for Standardization, 2016.

[5] Llopis R., Calleja-Anta D., Maiorino A., Nebot-Andres L., Sanchez D., Cabello R. TEWI analysis of a stand-alone refrigeration system using low-GWP fluids with leakage ratio consideration. International Journal of Refrigeration. June, 2020.

Development of occupancy-based multi-scale building archetypes

Divyanshu Sood [a], Ibrahim Alhindawi [b], Usman Ali [a], James McGrath [b], Miriam Byrne [b], James O'Donnell [a]

[a] School of Mechanical and Materials Engineering and Energy Institute, University College Dublin, Dublin, Ireland, divyanshu.sood@ucdconnect.ie, usman.ali@ucd.ie, james.odonnell@ucd.ie

[b] School of Physics & Ryan Institute's Centre for Climate and Air Pollution Studies, National University of Ireland Galway, Ireland, i.alhindawi1@nuigalway.ie, james.a.mcgrath@nuigalway.ie, miriam.byrne@nuigalway.ie

Abstract. In the context of the European building stock, more than 50 % of buildings were built before 1960, and it has been estimated that 75 % of the current building stock will still exist in 2050. A typical approach to estimate energy consumption at multiple scales is by using archetypes which are the cohort of representative buildings with similar characteristics. Typically, archetypes are classified based on year of construction, type of dwelling and type of heating system. Since, this classification does not account for the stochastic nature of occupancy, a typical occupant presence pattern from the literature is considered. This study develops a methodology to generate stochastic occupancy profiles using the UK Time Use Survey (TUS) 2014-15 data. The occupancy profiles take into account the affect of the day of the week, the month of the year, the number of residents in the household and the type of dwelling. To test the methodology, we used the Irish residential building archetypes and 5-8% variations in energy use intensity are observed using the developed occupancy profiles for an apartment archetype having one and two occupants. The generated occupancy profiles facilitate the pathway to develop robust archetypes for reliable energy prediction at an urban scale. Furthermore, robust archetypes allow policymakers and urban planners to recommend appropriate energy efficiency measures for the sustainable development of residential building sector.

Keywords. Urban building energy modelling, Stochastic occupant behaviour, Building archetypes
DOI: https://doi.org/10.34641/clima.2022.243

1. Introduction

Urbanization has put more stress on the environment, and therefore, more than ever, sustainability needs to be considered in the construction sector for energy-efficient urban planning. Energy in Buildings is a trending topic as part of the wider climate change agenda. Buildings as a sector are the largest energy consumer with 36 % and 39 % of CO_2 emissions in the European Union and the United States, respectively. The European Union (EU) has set the target to reduce greenhouse gas emissions by 40 % before 2030 when compared to 1990 levels [1].

Cities contain thousands of buildings, and energy estimation of each building at such a larger scale is a tedious task. However, energy estimation at district, city, regional or national scale is required to allow policymakers and building energy experts to formulate energy policies for sustainable urban planning. In addition, the energy estimation helps evaluate the scope for energy retrofitting to make the existing buildings energy efficient and reduce associated carbon emissions. Hence, archetypes are developed to simplify the analysis and represent a more extensive building stock. Reinhart et al. [2] defines archetypes as a representative set of buildings that share similar geometric and non-geometric characteristics. Normally, archetype characterisation uses national average values of occupancy schedules and U-values. However, the national average values are invalid while estimating energy at district or city, or regional scale [3].

Instead of using average values to fill the gap in data, researchers use data-driven approaches to improve the quality of the data to develop an effective methodology for archetype development [4]. Machine learning techniques such as segmentation can be used on large datasets including EPC and TABULA to identify archetypes and corresponding input parameters. Ali et al. [5] developed archetypes at multiple scales to predict the energy demand at various levels by segmenting archetypes based on construction year and type of dwelling. The values during characterisation were the average values according to the scale of analysis. Fewer studies

Copyright ©2022 by the authors. This conference paper is published under a CC-BY-4.0 license.

focused on integrating occupancy behaviour into archetypes. Buttitta et al. [6] developed occupancy integrated archetypes, segmented based on various occupancy schedules developed using Time Use Survey (TUS) data and considered occupancy pattern as active or non-active. Although, this does not capture the logic behind occupants' active and non-active status in the buildings. Moreover, using archetypes with fixed occupancy patterns have led to unrealistic peak heat demand at high temporal resolutions [7]. The deviation in energy estimation could be up to 30 % when fixed occupancy profiles are considered with archetypes rather than occupancy integrated archetypes[6].

The energy consumption patterns for dwellings are highly stochastic and vary considerably between different customers. Yao et al. [8] categorised energy consumption determinants in two categories: physical and behavioural, to generate load profiles. Widen et al. [9] used time-use data to interpret occupants' usage patterns along with appliance ratings to produce the energy consumption profiles. The load profiles generated using meter data can be hourly/weekly/monthly or 15 minutes, depending on the data availability. Sensors help capture the load variations in a building and based on these variations, occupancy schedules can be developed by using a Markov Chain model [10], [11]. These deterministic models are easy to implement and can be represented as fractions with values in the range [0,1]. Chong et al. [12] used spatial occupancy data and applied the Bayesian calibration approach to reduce occupancy prediction errors from 37% to 24%. The IEA-EBC Annex 66 project focused on setting up a platform to standardise a simulation methodology to incorporate occupancy and occupant behaviour into building energy modelling. Several publications were produced under Annex 66 [13], [14]. The majority focused on developing occupancy models based on data collected from sensors and energy meters to track the presence and absence of occupants based on load profiles. The aforementioned studies do not explain the behavioural changes among occupants and their variations in daily activities due to the type of dwelling they live in and the number of occupants residing in the dwelling. It is crucial to realistically develop the profiles of the occupants in a household to understand the logic behind variations in energy use.

Previous studies link occupancy to building energy modelling and minimal information is available on developing occupancy models for UBEM and evaluating their effect on energy consumption. The major issue is the use of typical occupant presence profiles from the literature or is based on priorknowledge that leads to large discrepancies in the predicted energy. As occupants significantly influence the energy consumption in buildings, energy usage is highly dependent on the number of occupants, their behaviour and type of dwelling they livein. Due to highly stochastic occupant behaviour, a fixed pattern could lead to substantial differencesin energy estimation of similar dwellings. It is crucial to consider the realistic interaction of occupants with the building while quantifying archetypes to estimate energy consumption at an urban level. Therefore, archetypes classification should also consider the number of occupants so that their behavioural patterns can be linked within archetypes.

The novelty of this paper lies in formulating a methodology to develop stochastic occupancy profiles and integrating them into building archetypes to reliably predict the energy consumption of building stock. This study classifies the building archetypes based on the number of occupants along with considered year of construction and type of dwelling. This classification allows us to investigate the influence of occupants and their activities on energy consumption at different geographical scales such as postcode, county and national.

The paper consists of the following sections: Section 2 defines the methodology used to develop occupancy profiles and occupancy-based archetypes. Section 3 introduces a case study to implement the devised methodology. This section also includes the analysis of results and discussion. Section 4 describes the conclusions from the study.

2. Methodology

This paper assesses the impact of stochastic occupancy behaviour on energy consumption of multi-scale archetypes. To develop the occupancy profiles, UK Time Use Survey (TUS) 2014-15 data are used. The data represents various activities performed by occupants on a daily basis.

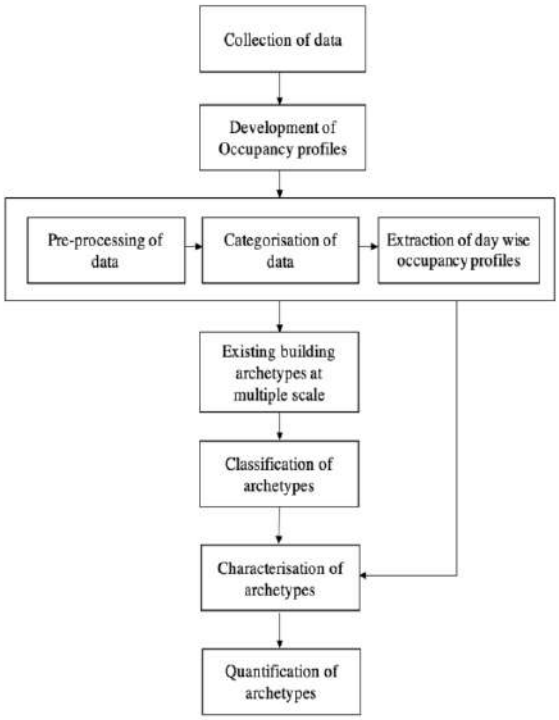

Fig. 1 - Overarching methodology to study the impact of occupancy on multi-scale archetypes

Fig 1 illustrates the overarching methodology used in this study to develop and evaluate occupancy enabled archetypes. This study used the mixed-method approach as the data used to develop occupancy profiles are qualitative data which is further used to quantify energy consumption. The mixed-method approach uses both qualitative and quantitative techniques for data collection and analysis [15]. The TUS data are qualitative and were recorded through interviews and by updating activity diaries.

2.1 Collection of data

The TUS data can be directly linked with the user's behaviour to generate occupancy profiles. The data consists of an activity diary that records occupants' activities such as sleeping, cooking, eating, bathing and so on at 10-minute intervals. For 4460 households data, 11460 interviews were recorded in a diary for two consecutive days by a different household member. The diary also consists of other information related to the type of housing, the number of adults & children in the house, the month of the year and the day of the week on which the diary was filled. The data were recorded in such a way that for day of the week, 1 represents Sunday, 2 represents Monday followed by other days of the week in a similar pattern. The diary assigned a unique serial number to every house that helped identify the total number of respondents from the household.

2.2 Pre-processing of data

Originally, the data were recorded in a numeric format and every number represents the activity performed by the occupants. To start with, the numeric entries were replaced with the corresponding activities as given in the dictionary provided with the data. The occupancy data are usually collected through surveys that are prone to data irregularities such as incomplete data and missing data. It is important to remove these inconsistencies in order to make the data usable. TUS data contains few entries that do not have all the information related to the occupancy activities. Therefore, rows with incomplete or non-applicable entries were removed from the dataset for data consistency throughout the analysis. The data has more than 110 various activities performed by different individuals. To reduce the number of activities and make data useful for further processing, activities that fall under similar category were combined. For instance, admin work, office work and shopping were named as "Outdoor Activities (OA)" to understand the data better and to remove the unnecessary variables. The data were recorded in 2014-15, therefore office work is considered as an "Outdoor Activities (OA)". More details are provided in Tab 1.

Tab. 1: Details on grouping of activities

Activity group name	Activities
Fitness (FT)	Exercise Gym Fitness
Outdoor Activities (OA)	Office work Admin work Travel Shopping Office break
Socialising (Soc)	Cinema Movie Concert

2.3 Categorisation of data

Firstly, the data are grouped based on the type of accommodation, and we assumed that apartments shared similar characteristics as flats or maisonettes. Therefore, the occupancy profiles developed for flat or maisonette is also used for the various apartment types (see Fig. 2). Similarly, occupancy profiles for other dwellings such as semi-detached houses, detached houses, and terraced houses used profiles developed for the houses or bungalows (see Fig. 2).

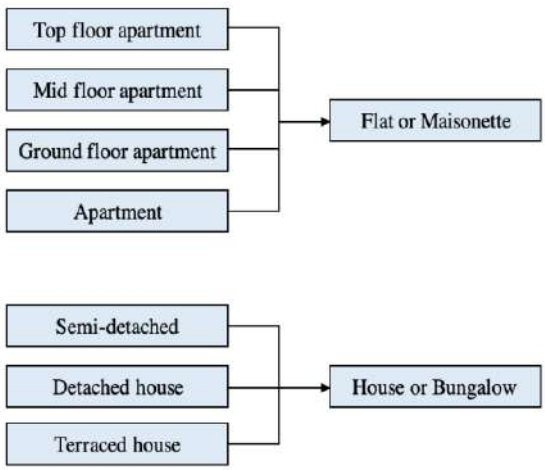

Fig. 2 - Assumptions to use the occupancy profiles for various building archetypes

The occupancy profiles are based on the day of the week, the month of the year, the number of occupants and the type of dwelling, see Algorithm 1. The total number of occupants in a household is determined by adding the total number of adults and children. This enables us to group the data based on the number of occupants living in a household. This allows us to visibly understand the variations in occupancy behaviour. To further capture the effect of monthly and daily variations in occupancy activities, data were sorted into different months followed by days of the week. The above-mentioned steps for categorisation enable us to capture the effect of various parameters on occupancy behaviour.

Algorithm 1 Categorisation of TUS data to develop occupancy profiles

```
i = HouseorBungalow, FlatorMaisonette
for TypeOfAccomodation = i do
    for OccuNum = 1,2 do
        for Month = 1,2,3...12 do
            for DayOfWeek = 1,2,3...7 do
                DayOfWeek.mode()
            end for
        end for
    end for
end for
```

2.4 Extraction of occupancy profiles

Once the data categorisation is completed, the next step is to extract the profiles. For categorical data or qualitative data, a mode is the best way to identify the frequently occurring data point in a given dataset[16]. Statistics.mode() was used to measure the central tendency in each time slot to extract the most frequently performed activities. Mode provides the activity that appears most often in each time slot, leading to a full day activity profile. The data were divided into 10-minute intervals; therefore, we have 144-time slots per day. The developed methodology also supports statistics.multimode(), i.e. bimodal or multimodal, to consider the second, third or further modes, if they exist. However, this study only used the profiles based on the first mode to balance the computational load, time and complexity.

2.5 Modelling and quantification of archetypes

Archetypes are helpful to estimate the energy demand at various geographical scales when insufficient building stock data is available. This study utilised the previously developed archetypes and further classified them based on the number of occupants in a dwelling to incorporate the stochastic nature of occupants. The archetypes are modelled in Design Builder and the 7/12 activity schedule is considered to incorporate the developed day wise occupancy schedule and simulated using EnergyPlus software, which is the most used software for BEPS. EnergyPlus is considered a reliable software for simulating residential buildings by carefully selecting and defining input parameters. The equipment schedule has also been modified as per the occupancy presence or absence and the activity schedule. The input data such as multi-scale U-values required for the energy simulations were taken from Ali et al. [5] except for the occupancy related data. The occupancy profiles developed in this study are linked with the archetypes and using jEPlus Macros, parametric simulations were performed.

3. Results and discussion

There was an 85 % growth in apartments between 2002 and 2016 in Ireland [17]; therefore this study focuses on evaluating the impact of occupancy on the energy consumption of an apartment built after 2006 using multi-scale archetypes. A case study of the Irish apartment archetype is chosen to establish the relationship between occupancy and multi-scale building archetypes. In this study, we used archetypes at three geographical scales namely, postcode (Dublin 1), county (Dublin county), and national (Ireland).

3.1 Overview of the TUS data

The initial impression of the TUS data provides an insight into the diverse range of activities performed by occupants in a household. In TUS data, 16,550 diary days were completed by respondents selected for interviews. Fig. 3 represents the value count of the various activities recorded in the data by the respondents. It is evident from the Fig. 3 that occupants undertake various activities on a daily basis and sleeping has the highest value count in the data followed by TV Watching, Office work and so on.

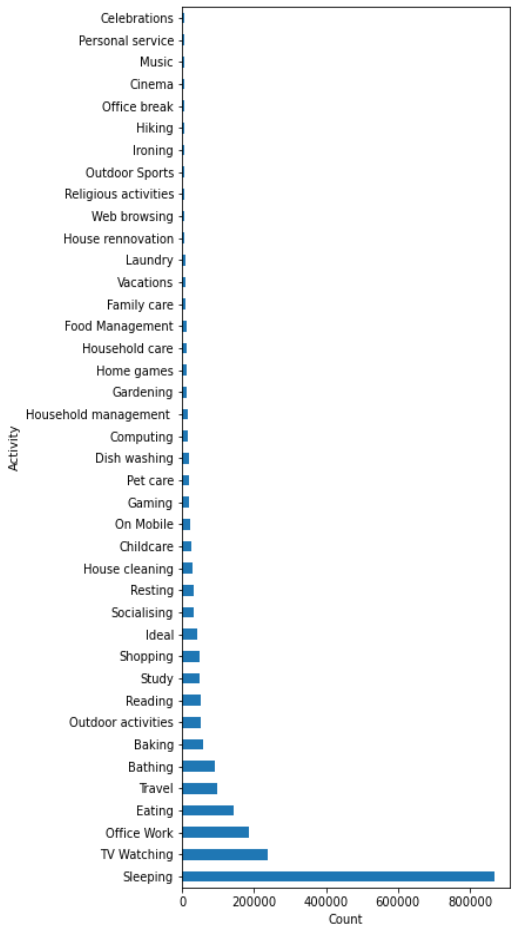

Fig. 3 - Different activities and their value count in the TUS data at 10-minute intervals

There are approximately 40 various activities mentioned in the TUS data recorded by the

occupants. The TUS data are an effective way to record occupant activities that enable us to understand on how people spend their time on a daily basis.

3.2 Stochastic occupancy profiles

In this study, we developed stochastic occupancy profiles using activity diary data that consists of actual occupancy patterns updated at 10-minutes intervals. The profiles represent the various activities performed by occupants on a daily basis.

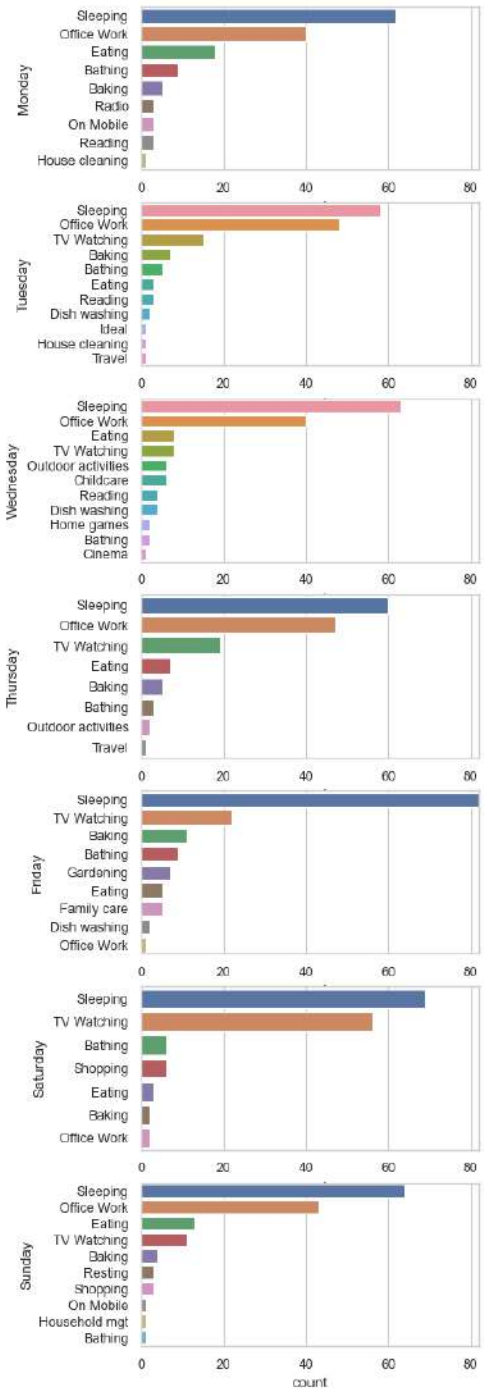

Fig. 4 - Value count of activities performed in a week in the month of January to represent the variations in occupancy behaviour in a one occupant household

A month has seven profiles representing seven days of the week. For instance, for January, the occupancy profile for Monday is representative of all the Mondays in January. In total, 168 profiles were developed for an apartment with one occupant and two occupants. Fig 4 represents the value count of activities performed in a one occupant apartment. From Fig 4, we can see that each day is different in terms of activities performed and duration of the activities. For instance, the sleeping count for Monday is over 60, and for Tuesday, the count falls below 60. Similarly, for Friday, the sleeping count is more than 80, 10-15 counts more than Saturday and Sunday, respectively. Similarly, TV watching time, bathing time, eating and cooking time varies significantly each day. This shows the merits of having realistic profiles for building energy modelling as these enable us to closely understand the occupancy behaviour within the building. These variations are usually ignored and assumed constant to reduce the complexity of analysis.

Fig 5 represents the variation in activities performed by occupants on Monday in a one and two occupant apartment. Apart from the value count, the kind of activities performed by occupants is different in both cases. Based on the value count and kind of activities performed, it can be comprehended that using fixed profiles for energy simulations can lead to significant discrepancies in predicted energy.

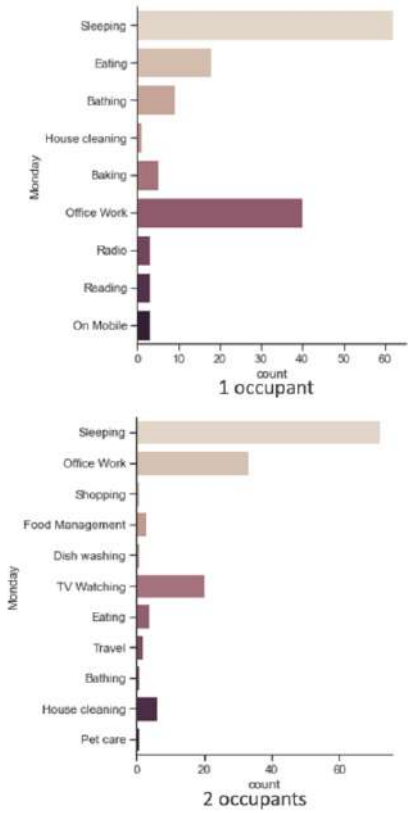

Fig. 5 - Variations in activities on Monday in a one and two occupant apartment

3.3 Multi-scale U-Values

The multi-scale U-values for apartment archetypes are taken from [5]. It is evident from Fig 6 that U-values for different building elements such as wall, roof, window, floor, and door varies at different geographical scales.

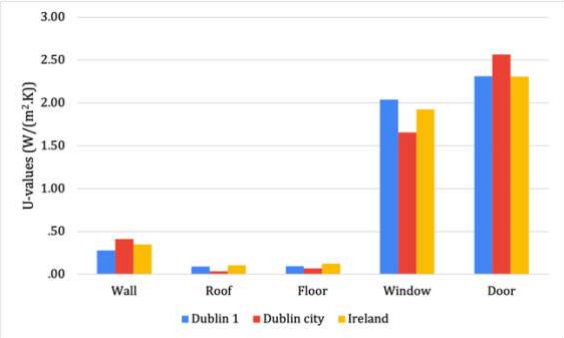

Fig. 6 - U-values for an Apartment built after 2006 over multiple scales (W/(m²-K))

For instance, U-values for apartment windows are 2.04, 1.66, and 1.93 ($W/(m^2K)$) for Dublin 1, Dublin county and Ireland, respectively. U-values significantly affect the building energy estimation and should be carefully chosen for the multi-scale analysis. For multi scale archetypes, assuming national average U-values for other geographical scales such as postcode and county remain invalid as these values lead to substantial discrepancies in energy output.

3.4 Building energy performance simulation

This section represents the effect of the number of occupants and their behaviour on multi-scale apartment archetypes. The multi-scale apartment archetypes with typical occupancy profiles and state-of-the-art developed stochastic occupancy profiles are compared in terms of EUI. We used the EUI results from a study carried out by Ali et al. [5] as a base case that used typical occupancy profiles provided by the Design Builder software irrespective of the number of occupants and type of dwelling.

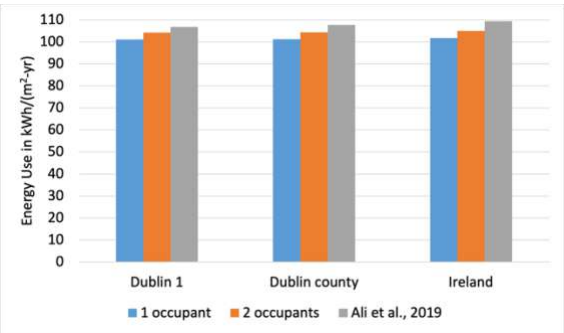

Fig. 7- Comparison of apartment archetype energy use with 1 occupant profile and the base case (kWh/(m²-yr)

Fig 7 compared the base case with one occupancy and two occupancy household. It is evident from the Fig 7 that energy consumption using conventional profiles is different from the results obtained using profiles based on one and two occupants. There is approximately 5-8 % variation in EUI when the base case is compared with different occupancy households using archetypes at multiple scales. The absolute differences in EUI were found to be 3.14 $kWh/(m^2yr)$ when one occupancy household is compared with two occupancy households at the national level. As can be observed from the Fig 7, fixed occupancy profiles used in the base case overestimate the EUI which increases the pre-bound effect, i.e. actual energy consumption is lower than the calculated energy. For instance, occupants' activity schedules can be completely different when a comparison is made based on the number of occupants. This concludes the importance of using dynamic occupancy profiles to reliably estimate the energy consumption of archetypes.

4. Conclusions and Future work

Using typical compact occupancy profiles from the literature leads to over or under estimation of energy demand. The variations in occupancy behaviour are inherently uncertain, and assuming typical profiles does nothing but increase the uncertainty. For UBEM, archetypes are used to estimate energy consumption at multiple scales. Conventionally, archetypes are classified in such a way that they do not incorporate occupancy. This study focuses on understanding how the number of occupants and their stochastic nature impacts energy assessment using archetypes. The methodology evaluated the effect of occupancy on multi-scale archetypes. The developed occupancy profiles are based on the type of dwelling, the number of occupants, months of the year and days of the week. Based on Fig 4, it is evident that no day is same in terms of activities performed by occupants. Therefore, using fixed occupancy profiles lead to large discrepancies in predicted energy consumption. The results showed that there is approximately 5-8 % variations in EUI when base case is compared with one and two persons household for an apartment archetype. The variations are due to the number of occupants and their distinct activities. The relative difference of 5-8% is observed at an archetype level when fixed & compact occupancy schedule is substituted with stochastic & yearly schedule. This variation does not seem significant at an archetype level. However, when archetypes' results are extrapolated to various geographical scales, this 5-8% variation can be significant compared to measured energy values at a particular scale. A conventional means of archetypes' classification does not consider the number of occupants and their associated stochastic nature, which is essential as archetypes' result is extrapolated to

various geographical scales by using the total number of existing buildings corresponding to that particular archetype. This extrapolation is usually based on determining a factor of multiplication which is typically the number of different types of dwellings. This energy difference can result in inappropriate identification of the inefficient energy areas and lead to unsatisfactory policy recommendations.

The developed occupancy profiles enable us to understand the stochastic nature of occupants and push the researchers to focus on collecting more occupancy data for better energy modelling results. The methodology will help in developing various occupancy profiles and integrate them within archetypes to improve the building energy modelling results. Occupancy integrated archetypes allow us to reduce the gap between estimated and measured values at the building stock level. Measured values refer to the cumulative energy consumption of building stock at various geographical scales such as postcode, county and national. These archetypes improve the reliability of the results at the building stock level and help policy makers, local authoritiesand urban planners to modify, update and implement energy recommendations for the better and sustainable growth of residential building sector.

The present work is limited to an apartment archetype having up to 2 occupants. This study only used the first mode to develop occupancy profiles, however, the research could be extended to take advantage of the second or third mode and develop more detailed occupancy profiles that further enhance the results by providing a range of values. Furthermore, the work could be extended for different types of archetypes for a comprehensive evaluation of the effect of occupancy on multi-scale residential building archetypes. Moreover, IEQ is greatly influenced by the number of occupants and significantly affect energy consumption. Apart from the energy analysis, these realistic occupancy schedules allow us to determine the overheating scenario and various indoor air quality parameters to appropriately evaluate the performance of energy efficiency measures.

5. Acknowledgement

This publication has emanated from research supported in part by a research grant from Sustainable Energy Authority of Ireland (SEAI) Grant number 19/RDD/537. The opinions, findings and conclusions or recommendations expressed in this material are those of the author(s) and do not necessarily reflect the views of the Sustainable Energy Authority of Ireland.

6. Data access statement

The datasets generated during and/or analysed during the current study are not publicly available due to ethical, legal or commercial restrictions.

7. References

[1] A. Malhotra *et al.*, "Information modelling for urban building energy simulation—A taxonomic review," *Build. Environ.*, p. 108552, Nov. 2021, doi: 10.1016/J.BUILDENV.2021.108552.

[2] C. F. Reinhart and C. C. Davila, "Urban building energy modeling--A review of a nascent field," *Build. Environ.*, vol. 97, pp. 196–202, 2016.

[3] C. Cerezo, J. Sokol, S. AlKhaled, C. Reinhart, A. Al-Mumin, and A. Hajiah, "Comparison of four building archetype characterization methods in urban building energy modeling (UBEM): A residential case study in Kuwait City," *Energy Build.*, vol. 154, pp. 321–334, 2017.

[4] G. Tardioli, A. Narayan, R. Kerrigan, M. Oates, J. O'Donnell, and D. P. Finn, "A methodology for calibration of building energy models at district scale using clustering and surrogate techniques," *Energy Build.*, vol. 226, p. 110309, 2020.

[5] U. Ali, M. Haris, C. Hoare, E. Mangina, and J. O. Donnell, "Energy & Buildings A data-driven approach for multi-scale building archetypes development," vol. 202, 2019, doi: 10.1016/j.enbuild.2019.109364.

[6] G. Buttitta, W. J. N. Turner, O. Neu, and D. P. Finn, "Development of occupancy-integrated archetypes: Use of data mining clustering techniques to embed occupant behaviour profiles in archetypes," *Energy Build.*, vol. 198, pp. 84–99, Sep. 2019, doi: 10.1016/j.enbuild.2019.05.056.

[7] L. Diao, Y. Sun, Z. Chen, and J. Chen, "Modeling energy consumption in residential buildings: A bottom-up analysis based on occupant behavior pattern clustering and stochastic simulation," *Energy Build.*, vol. 147, pp. 47–66, 2017.

[8] R. Yao and K. Steemers, "A method of formulating energy load profile for domestic buildings in the UK," *Energy Build.*, vol. 37, no. 6, pp. 663–671, 2005.

[9] J. Widén and E. Wäckelgård, "A high-resolution stochastic model of domestic activity patterns and electricity demand," *Appl. Energy*, vol. 87, no. 6, pp. 1880–1892, 2010.

[10] K. U. Ahn, D. W. Kim, C. S. Park, and P. de Wilde, "Predictability of occupant presence and performance gap in building energy simulation," *Appl. Energy*, vol. 208, pp. 1639–1652, Dec. 2017, doi: 10.1016/J.APENERGY.2017.04.083.

[11] J. Parker, A. Hardy, D. Glew, and C. Gorse, "A methodology for creating building energy model occupancy schedules using personal location metadata," *Energy Build.*, vol. 150, pp. 211–223, Sep. 2017, doi: 10.1016/J.ENBUILD.2017.06.014.

[12] A. Chong, G. Augenbroe, and D. Yan, "Occupancy data at different spatial resolutions: Building energy performance and model calibration," *Appl. Energy*, vol. 286, p. 116492, Mar. 2021, doi: 10.1016/J.APENERGY.2021.116492.

[13] S. Pan *et al.*, "Cluster analysis for occupant-behavior based electricity load patterns in buildings: A case study in Shanghai residences," *Build. Simul. 2017 106*, vol. 10, no. 6, pp. 889–898, May 2017, doi: 10.1007/S12273-017-0377-9.

[14] S. Yilmaz, S. K. Firth, and D. Allinson, "Occupant behaviour modelling in domestic buildings: the case of household electrical appliances," *https://doi.org/10.1080/19401493.2017.1287775*, vol. 10, no. 5–6, pp. 582–600, Nov. 2017, doi: 10.1080/19401493.2017.1287775.

[15] J. W. Creswell, "Mixed-method research: Introduction and application," in *Handbook of educational policy*, Elsevier, 1999, pp. 455–472.

[16] M. Allen, "The SAGE Encyclopedia of Communication Research Methods," *SAGE Encycl. Commun. Res. Methods*, Jul. 2017, doi: 10.4135/9781483381411.

[17] CSO, "'Occupied Dwellings - CSO - Central Statistics Office.'" 2016, [Online]. Available: https://www.cso.ie/en/releasesandpublications/ep/p-cp1hii/cp1hii/od/.

Potential assessment of coupling PV electricity with district heating supply of building

Paul Seidel [a], Martin Altenburger [b], Joachim Seifert [c], Marta Sophia Potyka [d]

[a] Chair of Building Energy Systems and Heat Supply, Institute of Power Engineering, Faculty of Mechanical Science and Engineering, Technical University of Dresden, Dresden, Germany, paul.seidel@tu-dresden.de.

[b] Chair of Building Energy Systems and Heat Supply, Institute of Power Engineering, Faculty of Mechanical Science and Engineering, Technical University of Dresden, Dresden, Germany, martin.altenburger@tu-dresden.de.

[c] Chair of Building Energy Systems and Heat Supply, Institute of Power Engineering, Faculty of Mechanical Science and Engineering, Technical University of Dresden, Dresden, Germany, joachim.seifert@tu-dresden.de.

[d] Institute of Electrical Power Systems and High Voltage, Faculty of Electrical and Computer Engineering. Technical University of Dresden, Dresden, Germany, marta_sophia.potyka@tu-dresden.de

Abstract. The energy transition in Germany is leading to an increasing decentralized generation of electrical energy. In Fact, the feed-in of electrical surplus of PV systems causes a higher load on the electrical grid. Increased local use prevents this. Significant potential for the integration of produced electrical power of PV plants for this purpose exists in the heat supply. This paper describes the development and evaluation of a system solution from the cross-sectoral use of surpluses from PV plants and district heating. The latter is often used to supply urban apartment buildings. According to research on the market situation, independently controlled heating rods are available for converting electrical power of PV plants into heat. However, a coordinated operation of these heating rods with district heating is not possible so far. In this paper different approaches for combining these two heat sources with various hydraulic concepts and system controllers will be developed and evaluated. As a potential assessment, a parameter study on influencing factors (e.g. user behaviour, power size of the components, building characteristics) was carried out by numerical simulations. As one result, the highest potentials arise from the use of a forecast-based charging control of a combi-storage tank. The charging control can be realised with different techniques, either through simple if-then decisions or a model predictive control. This can only use slightly more produced electrical power of PV plants, as it is limited due to the time lag between PV surpluses and heat demand. Predictions of future energy flows are necessary for both approaches but these have relatively high errors for individual consumers and PV systems. The results of the paper shows, that more complex forecast approaches (demanding large data sets) do not perform significantly better than simple forecast approaches (which can deal with smaller data sets). Model predictive control requires a higher forecast resolution and is therefore also more error-prone, thus it is not recommended. The desired relief of the electrical grids can be achieved through local consumption. In addition, the economic implementation and the carbon footprint of such a concept are analysed under local and global (whole energy-system) aspects.

Keywords. district heating, sector coupling, photovoltaic, renewable energies, carbon footprint, model predictive control, residential building forecasts, operation of HVAC-systems
DOI: https://doi.org/10.34641/clima.2022.258

1. Introduction and boundary conditions

The local use of electrical energy from renewable energy systems is the focus of the implementation of the energy transition due to the limited capacities of the electrical distribution network. This is based on the premise of the decentralization of the energy supply to use if possible the resources locally. Only surpluses (produced power of the PV plant minus household electricity demand) are to be exchanged via an energy network. In the heat supply there is great potential for the local integration of produced electrical power of PV plants, since a large proportion of the final energy requirement is implemented, especially in residential buildings [1]. In the following, an approach for converting PV surpluses into thermal energy to supply heat to an apartment building (fig. 1) is described and analysed with regard to its technical, economic and ecological potential. The investigation builds on the analysis by Altenburger [2]. The parameters of the building, composed of four apartments, are shown in tab. 1. The model building represents a newer building with an energy rating of 44 kWh/m^{2}a.

Copyright ©2022 by the authors. This conference paper is published under a CC-BY-4.0 license.

Tab. 1 – key facts of the building

	value
cross building area	905 m^2
number of apartments	4
heated area per apartment	110 m^2
specific heating energy value	44 kWh/m^2
installed PV power	22 kW
total heating demand per year	19.347 kWh/a
total domestic hot water demand	6.027–8.378 kWh/a
total building electricity consumption per year	11.350-15.800 kWh/a

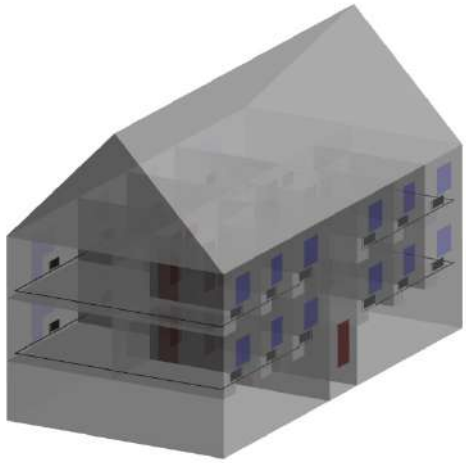

Fig. 1 – apartment building

The aim is to use the PV surpluses as much as possible locally. A district heating supply with central drinking water heating was assumed. Based on the initial analysis and potential assessment of the approach, a heating rod in a storage tank is used to convert the electrical energy. Fig. 2 shows the analysed hydraulic scheme.

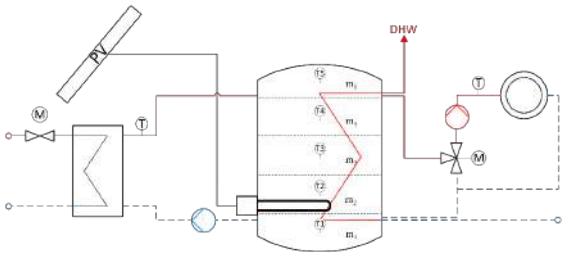

Fig. 2 – analysed hydraulic scheme of this investigation

2. Methodology

To estimate the potential, simulations were carried out with the numerical simulation program TRNSYS-TUD [3]. The model represents a characteristic multi-family house with a PV system, which is installed on the roof, the hydraulic scheme of fig.2 and typical requirement profiles in terms of domestic hot water and household electricity consumption. Variations were made with regard to the orientation of the building and the size of the PV system. As weather data, the test reference year 04, with the reference location of Potsdam [4], was used. An idealized forecast was used to forecast the heat demand. The numerical analyses were carried out with a time step size of τ = 60 s.

3. Control concepts

The integration of PV surpluses in the heat supply requires the implementation of various subtasks in the control. As part of the investigation, the focus was on regulating the heat supply from a district heating station and a heating rod. The flow temperature in the heating circuit is regulated according to the outside temperature. The electronic regulation of the heating element is able to implement the required output immediately. The control concepts to be considered are described below.

3.1 Independent ad-hoc control

At the beginning, a market analysis of the existing systems was carried out. This showed that systems that work independently from each other are available on the market. Based on this knowledge, the approach of the independent ad-hoc controlling system was developed. To do this, it is necessary to set loading limits for the thermal storage tank in relation to minimum and maximum temperatures. These are defined as the maximum temperature of the storage tank and as the minimum flow temperature. If the minimum flow temperature at the storage tank is not reached and the heat supply is restricted, the district heating is used to charge the storage tank (water tank). The charging process ends when the minimum flow temperature is reached at the bottom of the tank (fully charged tank). Regardless of this, the heating rod converts the PV surplus that occurs up to its nominal output into heat. The heating rod is switched off when the maximum storage tank temperature is reached, in addition to a switching hysteresis of $\Delta\vartheta = 3$ K. The control takes place without the use of a forecast.

3.2 Forecast-based ad-hoc control

A further development of the approach described above is the forecast-based ad-hoc control. The aim is to reduce the use of district heating to load the storage tank in order to be able to convert a higher proportion of the PV surplus into heat and to use it. For this purpose, with sufficient forecasted PV power, the switch-off limit for district heating operation is changed so that the charging process is stopped when the minimum flow temperature is reached at a higher temperature sensor. In this consideration, a thermal storage tank with five sensors (see fig. 2) was used. The top sensor

corresponds to the flow temperature and the second highest sensor is used as an alternative sensor for the switch-off point, in this example. Therefore, the storage tank is only charged to approximately 20 % by district heating. As a limit for the adjustment of the charge limits, the ratio between the forecast PV surplus and the heat demand is used. The criterion is defined as $\varphi_{\mathrm{PV\,sur\,lim}} = 0{,}1$.
If $\varphi_{\mathrm{PV\,sur}} > 0{,}1$. The load is adjusted, otherwise the procedure is analogous to the independent ad-hoc control. For the described regulation, forecasts with only daily resolution are sufficient, whereby the regulation is tolerant of incorrect prognoses due to its use as a limit value. A completely combined control with the integration of an optimization is not possible with this approach.

3.3 Model-predictive control

A common approach to regulate systems with temporally variable influences and target values is the use of a model-based predictive control (MPC). With this, it is possible to optimize the schedule within a prediction horizon based on the current system status and the predicted requirements as well as the predicted produced power of the PV plant. The aim of the analysis is to minimize the district heating consumption, as this allows the maximum proportion of the PV surplus to be used. The control concept and the creation of schedules is based on approaches for CHP systems and heat pump systems [5], [6]. The creation of the schedule is carried out on a rolling basis for each time step of the entire prediction horizon. The first time step is always implemented in a subordinate control system, so that after this time step the new (then current) system status can flow in the calculation again. Due to possible forecast deviations, a condition monitoring of the storage tank has to be integrated in the continuous implementation, which ensures the use of the storage within its temperature limits.

4. System assessment

The system assessment shows the technical potential of the different control concepts, presents an ecological and economic evaluation and considers the effects of the system solution on upstream energy systems.

4.1 Comparison of the controller concepts

Overall, different variants for user behaviour (domestic hot water and electricity consumption) were analysed. The evaluation is based on the mean value and the fluctuation range of the results of a selected variant. More information is documented in [2]. The aim of the investigation is to maximize the locally used proportion of electricity (share of self-consumption) as well as the proportion of heat demand generated by PV surpluses. It is also important to analyse what proportion of the PV surplus can be integrated into thermal use. This is in addition to the self-consumption proportion, which also includes the produced power of the PV plant used as household electricity consumption. The results are shown in tab. 2. The values in brackets represents the fluctuation range of the analysed variants in relation to thermal and electrical consumption of the building (Tab. 1).

Tab. 2 – Results of the controller comparison (mean value and range)

concept	PV - quantity of heat in %	el. self-con-sumption quantity in %	usable quantity of PV surpluses in %
independent ad-hoc control	22,8 (20,1 – 25,6)	69,4 (61,7 – 77,6)	58,0 (51,7 – 65,4)
forecast ad-hoc control	24,9 (21,7 – 28,5)	73,0 (66,2 – 80,8)	63,1 (57,4 – 70,3)
model-predictive control	25,8 (22,2 – 29,5)	75,0 (68,3 – 82,4)	65,7 (59,9 – 72,6)
theoretical limit	26,5 (22,2 – 30,9)	75,9 (62,5 – 92,2)	67,0 (60,2 – 82,0)

The MPC concept achieves the most efficient local use of the PV surplus. However, the increase compared to the two simpler concepts is small. This is due to the problem of the time difference between the highest PV generation in summer and the highest heat consumption in winter. The concept with the forecast-based ad-hoc control is therefore to be preferred due to the lower complexity.

In order to determine a reference, a theoretical limit case was defined. This describes a daily balance analysis in which the PV surpluses can be used up to the level of the heat demand. The district heating provides the missing energy in the daily heat balance. If the PV surpluses exceed the heat demand, they are fed into the electrical grid. It can be seen that the mpc concept is close to the defined limit case. The deviations are justified by restrictions in the storage tank temperatures, the output of the heating rod or by the use of daily amounts in the theoretical limit. The fig. 3 shows the course of a year and the temporal offset of the heat demand, the PV generation and the PV surpluses. It can be seen that a large part of the PV surplus cannot be used in summer.

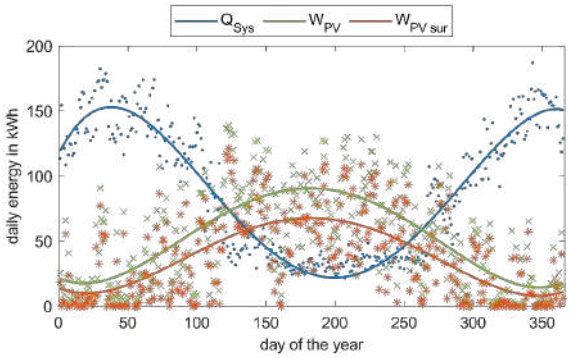

Fig. 3 – annual profile of daily key values

4.2 Carbon footprint / Economic valuation

In the following, the system with forecast-based ad-hoc control is analysed according to its carbon footprint. For a holistic view, the carbon emissions from district heating, the purchase of electrical energy and the PV output were determined. In addition, for the greenhouse gas emissions in the life cycle of the PV system, a credit was used for the feed-in of electrical energy compared to the displacement electricity mix. The boundary conditions for the CO_2 emissions are [7], [8], [9]:

- District heating: 253,2 g/kWh
- PV electricity: 67,0 g/kWh
- Electricity from the grid: 401,0 g/kWh
- Displacement mix: 860,0 g/kWh

The displacement mix refers to the factual displacement of amounts of conventional electricity by renewable energies. This is primary the generation of hard coal and lignite power plants in condensation mode. In relation to the reference variant, there was an average increase in global CO_2 emissions of approx. 150 %. It means that from an environmental point of view, a local use of the PV surpluses in the heat supply is not recommended. This is a contradiction to the goal of decentralizing the energy supply from the necessity of relieving the load on the electrical grid. The reason for this result is the assumption of a significantly higher reduction in CO_2 emissions when feeding into the electrical grid compared to district heating. In the future, a decrease in CO_2 emissions from the displacement electricity mix is to be expected. However, these static assumptions do not cover situations with an oversupply of renewable energy systems, in which these energy sources must also be regulated. This means that if too much EEG electricity is currently being fed into the electrical network, these systems will be switched off. This leads to an improvement in the ecological balance, which was not considered here.

In addition to the technical potential and the ecological consideration, the economic profitability is decisive for the use of such a system. There are various costs for the energy supply of the building, the costs of district heating (energy price), the credit for the feed-in of PV electricity have a special influence. It should also be noted that the system solution creates additional installation costs of around 116 – 200 € per year (annual cost of installation in 15 years of operation). Fig. 4 shows the previous development of the feed-in compensation and the district heating energy prices since 2010. Furthermore, a forecast based on the development since 2014 is assumed for the next few years. For the district heating energy price, the development with rising costs for greenhouse gas emissions is also shown [10].

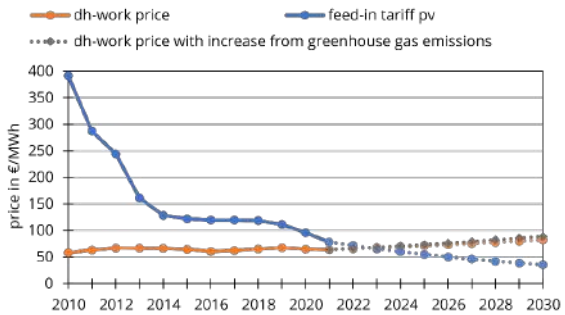

Fig. 4 – previous and forecast of PV and district heating (dh) prices

In order to clarify the knowledge of the necessary relationship between the district heating energy price and the feed-in price, a sensitivity analysis was carried out. The scenarios are shown in tab. 3 and tab. 4.

Tab. 3 – scenarios of district heating energy price.

scenario	energy price in €/MWh	description
current	64,03	mean current price
current + 10 %	70,43	increase of 10 %
current + 25 %	80,04	increase of 25 %

Tab. 4 – scenarios of PV feed-in energy price.

scenario	energy price in ct/kWh	description
1	9,45	status 02.2020
2	7,41	status 02.2021
3	6,63	10 % reduction
4	5,46	25 % reduction
5	3,51	50 % reduction

The result of the sensitivity analysis is shown in fig. 5. In this, the area of the amortization costs of the additional system costs is coloured green. It becomes clear that the system solution will be economical in

the next few years with rising district heating prices and falling feed-in compensations. With the current conditions, a positive economic balance is not possible.

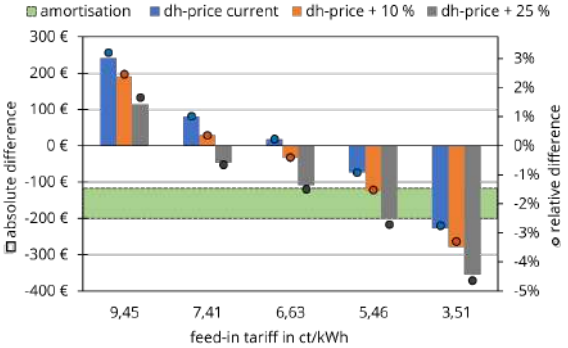

Fig. 5 – relative additional costs in comparison to the reference

But in the next few years, the point of district heating parity will be reached. From this point, the local use of PV electricity to replace district heating is preferred. Based on the relative costs, it can be seen that the resulting saving potential is rather in the low range in relation to the total energy costs.

4.3 Impact on the upstream energy systems

The use of the system solution has effects on the upstream district heating and electricity grid. These are also to be assessed. The investigation relates to the comparison with the reference system based on the consumption or generation profiles.

District heating

With this solution, the total of the annual district heating purchases is reduced by approx. 25 %, as this proportion is covered by the produced power of the PV plant. But the reduction is not evenly distributed. On days with no PV generation, the entire heat requirement must still be covered by district heating. In contrast to this, in summer the district heating requirement is almost completely covered by the PV surplus, which is shown in fig. 6. This results in a higher output fluctuation for district heating between summer and winter.

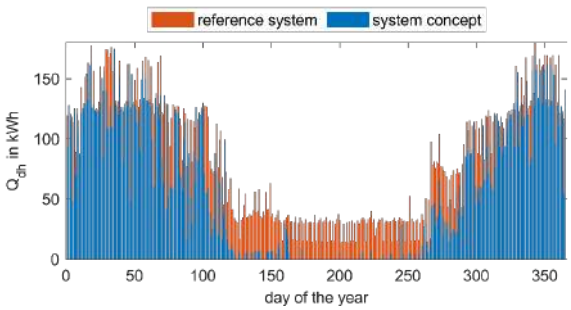

Fig. 6 – comparison of district heating consumption

This reduction leads to a decreasing income of a district heating operator, which creates economic pressure. At the same time, the already existing problem of summer heat surpluses from CHP systems and the competitive situation between various renewable energy sources are exacerbated by the falling district heating sales.

Another point is that the adjusted charge control of the storage tank unit leads to a decrease of the return temperatures in the district heating. This is shown in fig. 7 and results from the shorter charging processes and the reduced consumption of district heating in summer.

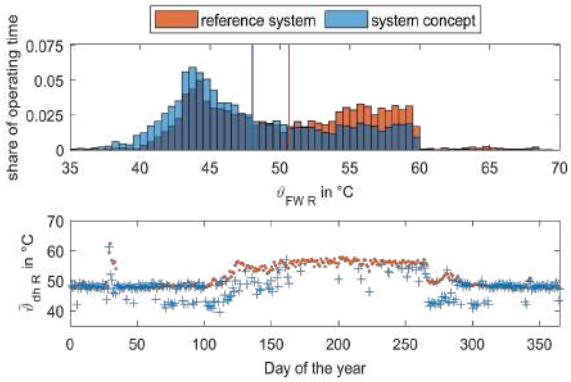

Fig. 7 – effects to the return temperature of the district heating

The figure shows the frequency distribution of the values for the district heating return temperature in 15 minute intervals and their mean values (vertical lines). The annual profile is also shown. The reduction occurs mainly in areas with PV generation. Outside of these times there is no difference in the regulation between the reference system and the system solution. The reduction in return temperatures is positive for the district heating, as the efficiency of energy conversion and energy transport is increased (Lower return temperatures lead to more efficient energy conversion during energy supply).

Electrical grid

There are also effects on the electrical grid. A significant reduction in feed-in can be achieved here through local consumption. This is desired to relieve the distribution in the grid. At the same time, the pre-set system control does not enable a reduction in the feed-in peaks, since local use is only possible with sufficient storage capacity. A time-shifted loading process could solve this problem, but is not implemented in this analysis. Fig. 8 shows the frequency distribution of fed energy in an interval of 15 minutes. The distribution in the annual profile shows that PV surpluses are fed into the grid, especially in summer. In winter, almost the entire PV yield can be used locally.

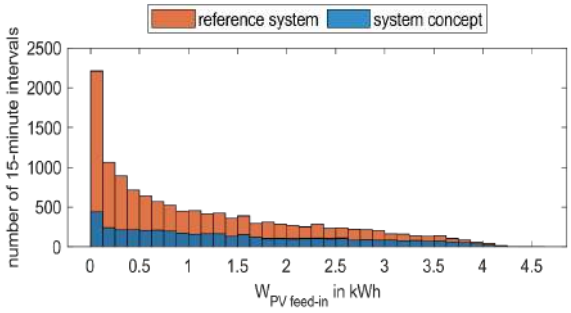

Fig. 8 – Frequency distribution of fed PV energy

As it can be seen, there is a significant reduction in the area of low feed-in of electrical power. This can be explained by the good integration of the PV surpluses in the heat supply in times of high heat demand, if the PV generation tends to be rather low. Nevertheless, the analysis of the feed-in profiles shows that it is possible to reduce the load on the grid.

5. Conclusion

With the combination of a district heating supply using the PV surplus locally and thermally, a cross-sectoral solution for the decentralization of the energy supply and the relief of the electrical grids was analysed. Basically, a model of a representative apartment building was developed, which was implemented in the simulation environment TRNSYS-TUD. From the view of regulation and control, three different approaches were considered. In the case of the modelled apartment building, the use of this control concept only makes sense from a certain installed PV power. Because in the case of low PV generation, an independent charge control of the thermal storage tank for the use of high produced power of the PV plant also generates a very high proportion of self-consumption.

A comparative ecological assessment showed that the current CO_2 balance of the system solution is worse than that of a reference variant with full feed-in of the PV surpluses. The reason for this is the significantly lower saving potential of PV electricity when substituting district heating compared to the displacement electricity mix of the grid. It should be noted that the balance does not include any dynamic processes in the event of limitation of renewable energy systems due to grid overloads.

Furthermore, the economic assessment produces a negative balance, as the feed-in compensations is currently still higher than the district heating energy prices. This will change in the future, so that an economical use of the system solution then seems possible.

Regarding to the upstream energy systems, it could be shown that with a simple technical implementation, the self-consumption ratio of the model building can be increased to approx. 73 % and thus the power feed-in can be significantly reduced. This results in a relevant reduction in the load on the grid. For the district heating, the reduction in demand with a constant maximum heating requirement in winter creates new challenges, for example additional excess heat in summer.

6. Acknowledgement

This publication is based on a research project, called TEK-EKG [11, 12], which was supported by the german federal ministry for economic affairs and climate action under the code 03ET1478A/B.

7. Symbols and abbreviations

dh	district heating
DHW	Domestic hot water
$\Delta\vartheta$	switching hysteresis
M	actuator
MPC	model-based predictive control
m_{i}	mass
PV	photovoltaic
$\varphi_{\mathrm{PV\ sur}}$	ratio forecast PV surplus
Q_{dh}	thermal energy from district heating
Q_{Sys}	thermal energy demand
T	temperature sensor
τ	time step
$\bar{\vartheta}_{\mathrm{dh\ R}}$	return temperature district heating
W_{PV}	electrical power – PV generation
$W_{\mathrm{PV\ sur}}$	electrical power – PV surplus
$W_{\mathrm{PV\ feed-in}}$	electrical power – PV feed-in

8. References

[1] S. Wilke, Energieverbrauch privater Haushalte, [Online]. Available: https://www.umweltbundesamt.de/daten/private-haushalte-konsum/wohnen/energieverbrauch-privater-haushalte.

[2] M. Altenburger, Potenzialabschätzung eines Systemreglers zur Einkopplung von PV-Strom in ein Fernwärmeversorgungskonzept für Mietwohn-gebäude, Diploma Thesis, TU Dresden, 2021.

[3] A. Perschk, „Gebäude- und Anlagensimulation - Ein "Dresdner Modell"," gi Gesundheits-Ingenieur - Haustechnik - Bauphysik - Umwelttechnik, Nr. Jg. 131 Nr. 4, 2010.

[4] M. Webs, T. Deutschländer und J. Christoffer, „Testreferenzjahre von Deutschland für mittlere und extreme Witterungsverhältnisse TRY," in Klimastatusbericht 2004, 2004.

[5] P. Seidel, „Ein Beitrag zur energetischen Analyse von vernetzten Energiesystemen am Beispiel von Klein-KWK-Anlagen (virtueller Verbund)," Dissertation, 2019.

[6] D. Lödige, B. Thomas und C. Widmann, Stromoptimierter Betrieb von KWK-Anlagen durch intelligentes Wärmespeicher-management: Forschungsbericht BWPLUS, Förderkennzeichen BWE 13002
[7] Länderarbeitskreis Energiebilanzen, Spezifische CO2-Emissionen der Strom- und Wärmeerzeugung – Länderarbeitskreis Energiebilanzen, 2019.
[8] H. Wirth, „Aktuelle Fakten zur Photovoltaik in Deutschland," 2 2021. [Online]. Available: https://www.ise.fraunhofer.de/content/dam/ise/de/documents/publications/studies/aktuelle-fakten-zur-photovoltaik-in-deutschland.pdf
[9] P. Icha und G. Kuhs, „Entwicklung der spez. Kohlendioxid-Emissionen des deutschen Strommix in den Jahren 1990 -2019," Dessau-Roßlau, 2020.
[10] K. Pittel, H. Cordt, S. Gschnaller, M. Mier and V. Azarova, "Kurz zum Klima: Die Coronakrise und ihre Auswirkungen auf den Europäischen Emissionshandel," ifo Schnelldienst, vol. 73, p. 67–71, 2020.
[11] J. Seifert, P. Seidel, K. Wolffgang, M. Potyka et. al., "Thermisch, Elektrisches Anlagen-EKG von Gebäuden und Quartieren" - Zwischenbericht, TU Dresden, 2022.
[12] P. Seidel, J. Seifert, K. Wolffgang, „Thermal-electrical Measurement System – a modular, expandable Concept for short-term energy recordings in Buildings " HVAC2021, Tallin, 2021.

Data Statement

The datasets generated during the current study are not publicly available but will be available in the final research paper of the project "TEK-EKG: Thermal-electrical Measurement System for Buildings and districts" in the end of 2022.

Nearly zero energy buildings with air-source heat pumps across Europe

László Zsolt Gergely [a], Zsuzsa Szalay [b], Tamás Csoknyai [a]

[a] Faculty of Mechanical Engineering, Department of Building Services and Process Engineering, Budapest University of Technology and Economics, Hungary, email address: gergely.laszlo@gpk.bme.hu

[b] Faculty of Civil Engineering, Department of Construction Materials and Technologies, Budapest University of Technology and Economics, Hungary

Abstract. Buildings are one of the most significant energy consumers and carbon emitters. As a result, their energy efficiency is a focal subject of European legislation, including the regulation of nearly zero energy building (NZEB) constructions. NZEB definition, however, differs significantly when it comes to the national level. Consequently, residential NZEBs can be characterised with altering building physical characteristics and various energy demands, according to the location of the buildings. More than that, not only the construction, but also heating, ventilation and air conditioning (HVAC) systems can be highly dependent on the geographic, especially weather conditions. With the help of dynamic building energy performance simulation (BEPS), this study reveals how the location of a single-family house affects the operational energy consumption of heating and cooling, once from the perspective of the different national NZEB regulations and also as a result of diverse climatic conditions influencing the performance of the technical building system. For the latter, we focus on one of the most expanding heat supply solution, the air-source heat pumps. To adequately address the reduction of the environmental impacts of the building sector, besides energy consumption the study analyses operational carbon emissions as well. Results highlight that though there are differences in the requirements of the specific NZEBs, some remain to produce similar indicators in all aspects, while other Member States (MS) are appealing from certain indicators, yet much worse in carbon emission. Conclusions of the paper can be considered to improve operational energy or emission management through the legislation of the building stock, MS specifically.

Keywords. nearly zero energy building, energy consumption, carbon emission, regulation, thermal transmittance, building energy performance simulation, TRNSYS, heat pump
DOI: https://doi.org/10.34641/clima.2022.48

1. Introduction

Buildings contribute a major part of global energy consumption and carbon emission. Residential buildings account for an approximate of 22% of final energy consumption, and 17% of the CO_2 emission [1]. As the European Union targeted minimizing its environmental impact on these fields, the recast of the Energy Performance of Buildings Directive (EPBD) made it mandatory for new residential buildings to fulfil the criteria of Nearly Zero Energy Building (NZEB) level, from 2021 [2]. Though, the definition is to provide energy performance requirements and renewable measures to be implemented, the specific requirements are to be defined by the Member States (MS) [3]. Hence on one hand, MSs regulate different performance indicators to form their definition of NZEB and on the other hand, even the same indicators have various limits depending on the MS. Consequently, under the same definition of NZEB, buildings could appear on a wide range of energy consumption or carbon emission.

Certain researchers have aimed to investigate the problem. Simson et al. contrasted the same residential buildings for Denmark, Estonia and Finland with the specific climatic conditions and legislations regarding the energy-related calculations [4]. The report of Garzia et al. compared the primary energy demand of NZEBs in Austria, Germany, France, Italy and Sweden with the help of the Passive House Planning Package tool [5]. It is also worth mentioning that Guillén-Lambea et al., highlighted that differences in the energy demand could appear within a single country as well [6].

A conclusion of the mentioned studies and the regulation trend is that there is a lack of research that reflects the difference of energy consumption and

Copyright ©2022 by the authors. This conference paper is published under a CC-BY-4.0 license.

carbon emission emerging from the varying measures and altering climatic conditions of the Member States, while eliminating certain limitations. Most often these are using steady state calculations, considering the same level of insulation for a building in different countries, neglecting weather change effects on the efficiency of the technical building system or using country-specific suggestions when calculating the energy demand.

The goal of this paper, therefore, is comparing the energy consumption and carbon emission of a case study residential building in different MSs of the EU highlighting the effect of altering climatic conditions and country specific regulations on the building physical parameters while applying the same calculation principles. The paper is organized as follows: Research Methods provides the method of the calculation, explaining how the limits are resolved or minimized. Section 3 presents the results of the calculation, while conclusions are drawn in Section 4.

2. Research Methods

The method of the study was developed to minimize the limitations found in other studies. The main pillars that had to be considered were the selection of:

- the countries to examine,
- the building to study,
- the technical building system to approach and
- the method of the calculation.

2.1 countries and requirements

Specifying the thermal insulation level of the studied building is challenging when examining under different conditions. However, as more and more countries implement requirements on the thermal transmittance (U-value) of the specific building structures, using the minimum values that fulfil the criteria eases comparison. For this consideration, some of the countries were selected that have published threshold levels of building structure U-values, namely Belgium, Cyprus, Hungary, Ireland, Italy, Poland, Slovakia and Slovenia [7].

It is notable, that countries from various climate are included in the further calculations. The tendencies of thermal transmittance values of the building structures of the specific countries somewhat align with the climatic characteristics. Generally, colder climate countries appear with lower U-value limits, while warmer climate Member States have higher values. Consequently, Cyprus is the most permissive, with 2.25 W/m²K regarding the openings, and 0.4 W/m²K for the other structures [8]. The strictest is Slovakia with a maximum of 0.6 W/m²K for glazed openings, 0.15 W/m²K for external walls and 0.1 W/m²K for both the ground and roof slabs [9]. Other transmittance values are represented in **Tab. 1**.

Italy is separated for many climate zones depending on the number of heating degree days. In the calculations, zone E is considered later.

Tab. 1 – Thermal transmittance requirements of the specific building structures in the selected countries.

U-values [W/m²K]	BEL [10]	CYP [8]	HUN [11]	IRL [12]
External wall	0.24	0.40	0.24	0.21
Glazed opening	1.50	2.25	1.15	1.60
Ground slab	0.24	0.40	0.26	0.21
Roof slab	0.24	0.40	0.17	0.16
U-values [W/m²K]	ITA_E [13]	POL [14]	SVK [9]	SLO [15]
External wall	0.24	0.20	0.15	0.20
Glazed opening	1.40	0.90	0.60	1.00
Ground slab	0.26	0.30	0.10	0.18
Roof slab	0.22	0.15	0.10	0.18

2.2 reference building

The reference building for the analysis was selected with the assumption of a geometry that could be realistic for all the countries of the study. The case study single-family house (SFH) can be characterised with standard design, without particular energy awareness concept of compactness or glazed surface ratio. The net floor area of the building is 98 m², heated volume of 283 m³, thermal envelope surface of 337 m² and a glazed opening area of 36 m². The geometry of the SFH was modelled with SketchUp software.

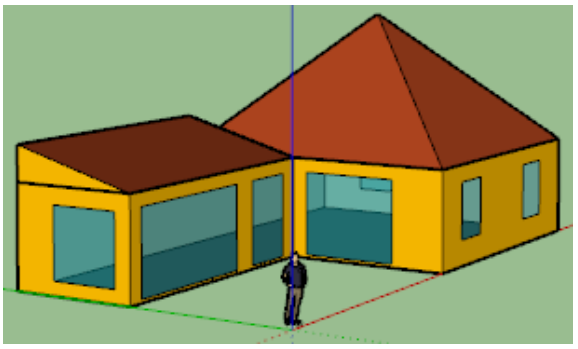

Fig. 1 – SketchUp model of the reference building.

An air-to-water heat pump was considered as heat supplier, because it meets the requirements of a highly efficient, renewable source system and is likely to spread in most of the countries NZE buildings [3]. As heat emitter floor heating and slab cooling were considered. In the calculations we focused only on heating and cooling, although such a system is capable of covering domestic hot water needs as well. As the objective was to highlight the differences of the space heating and cooling energy performance indicators as a result of various climatic conditions and regulations, domestic hot water production was excluded from the calculations.

2.3 calculation specifications

The modelled geometry was imported to TRNBuild, where the layers, thermal bridges, infiltration and ventilation and internal gains were specified.

The thermal transmittance of the building structures was adjusted to exactly the threshold value of each country, with only modifying the insulation thickness, no other elements of the layer order. Similarly, glazed elements were selected to meet the exact value of the national requirements.

Regarding the internal gains, 5 W/m² was considered in the calculations. Ventilation and infiltration were considered as a minimum of 0.5 1/h. This was increased at warm nights to reduce net energy need for cooling: in case when the mean temperature of a day exceeded 23 °C, windows were opened for a night-time period of 10 pm to 6 am, providing a more intensive ventilation, 9 1/h for the night period [11].

2.4 loads and demands

The parameters specified in TRNBuild were imported into TRNSYS v18 dynamic building energy performance simulation (BEPS) tool. Both loads and demand were calculated with a 5 minute timestep, external weather data of each locations, and a heating setpoint of 20°C and cooling setpoint of 26°C [16].

2.5 system specifications

As the heat pump is considered in a monovalent use, heating and cooling performance of the unit are sized to meet the loads during the coldest and warmest periods. Regarding the efficiency of the heat pump, TRNSYS component Type941 air-to-water heat pump performance map was used, that accounts the ambient temperature and humidity ratio. Both floor heating and slab cooling were assumed with a temperature difference of 5°C between the supply and return water temperature. Circulating pumps were sized to meet the exact heating and cooling loads with this temperature difference under the most extreme conditions. The overall pump efficiencies are considered as 0.7.

3. Results

3.1 heating and cooling load

Heating and cooling loads of the reference building are represented on **Fig. 2** in a plot, with the associated external temperatures. Heat loads appear to be proportional to external design temperature for most of the countries. Exception to this are Slovakia and Ireland. Both appear to be the effect of their relatively strict regulations, as temperature data fits in the range of the other cases. From **Tab. 1** this is more obvious for Slovakia, though comparing Ireland's requirements with the much colder Poland, threshold levels of structural thermal transmittance values are relatively strict for Ireland as well.

The heating load of Poland and Cyprus quite fit the trend of the remaining countries, though it can be highlighted that the minimum temperatures and loads alter significantly, resulting in the highest heating load, 5.2 kW for the former, and the lowest, 3.3 kW for Cyprus.

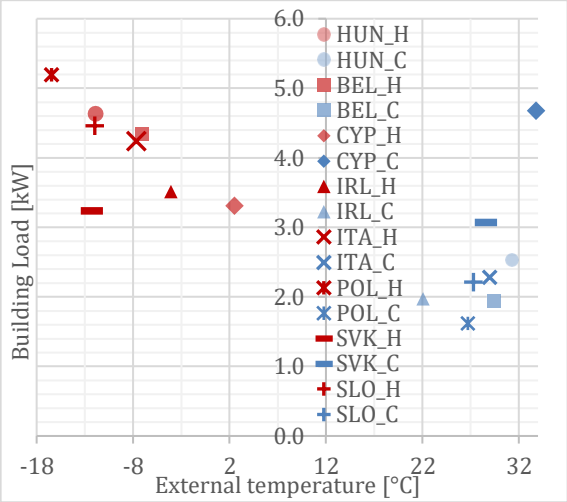

Fig. 2 – Net energy demands and loads of the reference building in different Member States.

In case of the cooling load, it is hard to find any regularities. Cyprus, with by far the highest temperature and solar radiation loads, scores the highest cooling load, even higher than its heating load as anticipated. Surprisingly, the second highest cooling load appears in case of Slovakia. A possible explanation can be that high insulation level enhances the risk of overheating [17].

3.2 net energy demands

Results of the net energy demands are resembling to the loads as **Fig. 4** reveals. Hungary, Italy and Slovenia represent similar net energy demands for the SFH with their certain conditions. Despite the lower heating load, net energy demand for heating in Ireland is close to these countries, which is the result of longer heating season (**Fig. 3**).

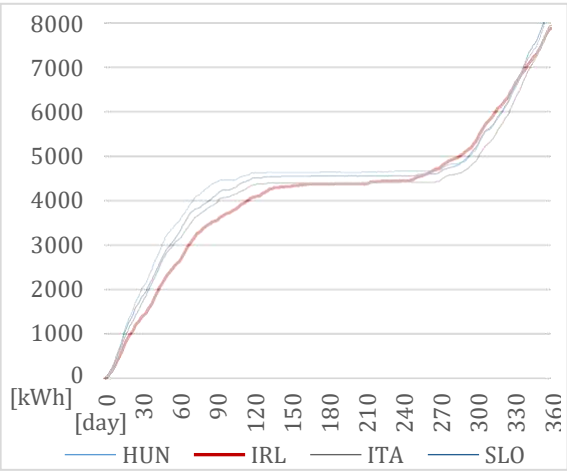

Fig. 3 – Accumulated heat loads of the countries with similar heating demand.

Belgium at first might seem a bit off these countries, however, its 9,434 kWh/year demand is just 12% higher than the average of the above-noted four countries.

Opposingly, MSs highlighted for their mismatching loads are dissimilar in this comparison again. The SFH has by far the lowest net energy demand, 5,171 kWh/year in Cyprus, which is 40% less than the average demand of the above-mentioned five countries (8,634 kWh/year). Furthermore, unsurprisingly, Cyprus is the only country that has a higher share of net energy needed for cooling than heating.

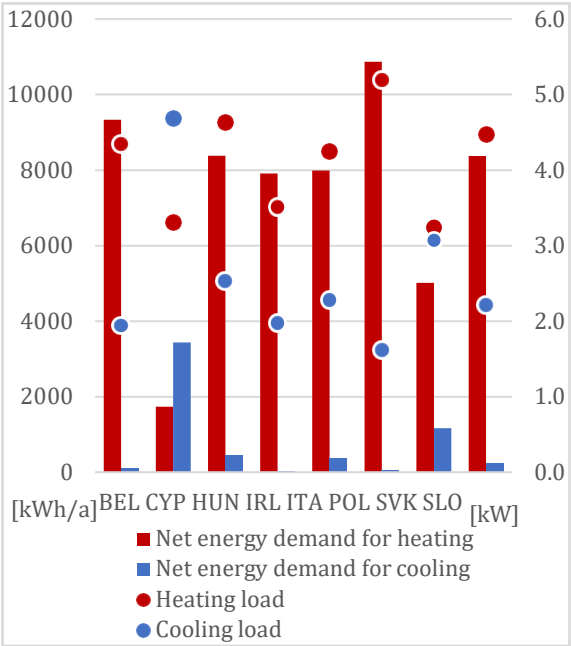

Fig. 4 – Net energy demands of the reference house for the test reference year of each countries.

Slovakia has not only the lowest heating load, but strictest U-value criteria also provides the second lowest net energy demand for heating 5,014 kWh/year and the second lowest sum of net energy need, 6,178 kWh/year. Relatively high share of the energy demand for cooling presumably appears for the previously (section 3.1) mentioned reasons.

When adapting the Polish weather conditions and requirements, the demand is more than the double of the Cyprus case, namely 10,938 kWh/year. This suggests that despite the rather strict regulation, extremely low temperatures (compared to the other countries) not only result in the highest demand but also the highest, 27% higher net energy demand than the average of Belgium, Hungary, Ireland, Italy and Slovenia.

Though the simulations result in cooling needs in all of the cases, in many countries this seems to be logically avoidable and therefore excluded in the further analysis.

3.3 operational energy consumption

Besides the differences caused by altering climates and regulations, efficiencies of the heating and cooling systems also affect energy consumption. This is especially true in case of appliances highly relying on external weather parameters, just like air-to-water heat pumps.

In case of the present study, Seasonal Performance Factor of Heating (SPFH) and Seasonal Performance Factor of Cooling (SPFC) values (including the energy consumption of the circulating pumps) show 30% and 11%, difference, respectively, among the countries. As expected, SPFH is the lowest in case of the coldest climate (Poland) and SPFC is the lowest in the warmest Member State (Cyprus). This implicitly widens the gap of indicators based on operational energy consumptions of the technical building system, like primary energy consumption or carbon emission.

Furthermore, other factors, such as the poor control due to the high thermal inertia and the slowly reacting system could cause losses and increase the energy consumption.

Fig.5represents the operational energy consumption of the analysed SFH in the different MSs. It is clearly notable, that while net energy need of the SFH in Ireland was close to the Hungarian, or the Italian cases, the much better SPFH results in a significantly lower operational energy consumption in Ireland.

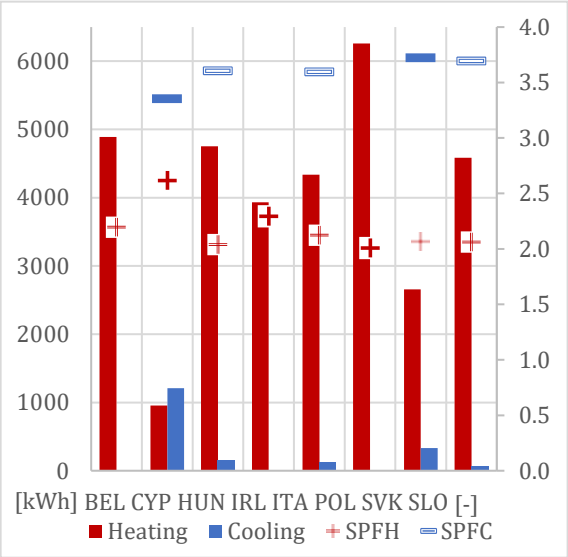

Fig. 5 – Seasonal performance factors of heating and cooling and energy consumptions

For the same reason, the SFH in Poland is even more energy consuming, having the worst SPFH of all the presented examples.

It is to mention that SPFs were calculated with on-off heat pumps as momentarily, no inverter-driven option is available in TRNSYS, though the trend of the SPF values of these appliances is similar as a function of external weather parameters [18].

3.4 operational carbon emission

Though one of the most significant indicators of NZEBs is the primary energy consumption of the building, conversion factors could mislead the results when comparing the countries, as they are also at the discretion of the MSs [19]. To avoid this effect, operational carbon emission of the SFHs are represented in the study. An advantage of this approach is that carbon intensity factors are not declared by the MSs but calculated, usually, based on life cycle assessment.

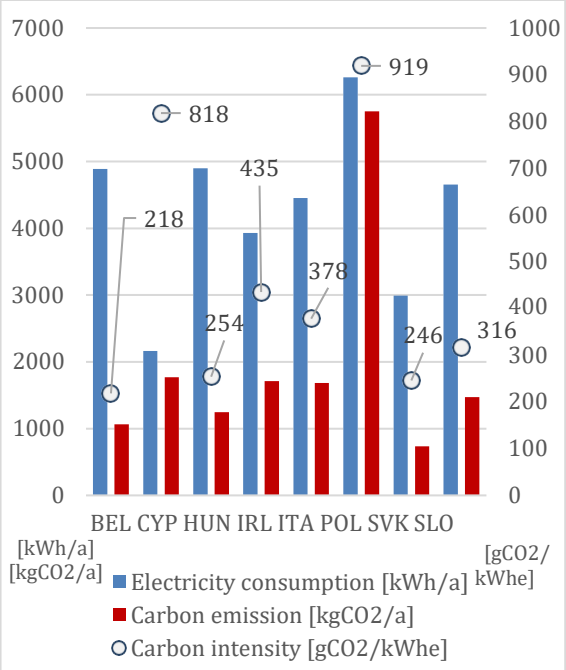

Fig. 6 – Annual carbon emission of the heating and cooling system of the reference building in different Member States

The deviation of the carbon intensity factors of the studied Member States though is significant [20]. On the top of that, Poland, consuming the most electricity for heating and cooling has way the worst carbon intensity factor, 919 g/kWh$_e$ which is almost 4 times of the second least consuming Slovakia's 246 g/kWh$_e$. This obviously widens the gap amongst the environmental impact of the SFH in these countries. The reference building located in Slovakia only emits 13% of the Polish extremely high level of 5,753 kgCO$_2$eq/year.

In case of Cyprus, similarly, the high carbon intensity factor boosts the emissions of the SFH and as a result, the least consuming location is the same time the second most emitting however it is to note that with 1,768 kgCO$_2$eq/year it is still only 31% of the Polish carbon emission level.

Interestingly, countries that were highlighted for their similar net energy needs, carbon intensity factor represents a decisive factor from the perspective of greenhouse gas emissions. In the end, among of those the Belgian case has the lowest annual emission, 1066, as a result of the lowest carbon intensity factor, while Ireland has the highest, 1710 kgCO$_2$eq/year, with the highest carbon intensity factor of the focused countries.

4. Conclusion

Residential buildings have a lot to offer in climate change mitigation for their huge share of energy consumption and carbon emission. The European Union aimed to have impact this sector with the mandatory implementation of Nearly Zero Energy Building definition, nevertheless the development of the requirements are to be determined by the Member States individually.

This is a source of not only various indicators for NZEB characterization, but also leaves room for different threshold levels on the same ones, like in case of the thermal transmittance regulation of specific building structures. Comparing eight Member States have revealed that the maximum of thermal transmittance values vary between 0.90-2.25 W/m^{2}K for the glazed openings, 0.15-0.40 W/m^{2}K for external walls and 0.10–0.40 W/m^{2}K for the ground and roof slabs.

Building energy performance simulation of a reference single family house has shown that despite these alternating values, heating loads are consistent compared with the minimum temperatures of each country. An exception to this is the Slovakian heating load, which appears to be significantly lower than the others. Regarding the cooling load, there are no general trends, nevertheless it is interesting that Slovakia scores the second highest cooling load, which is attributed to the risk of overheating as a result of the combined effect of hight level insulation and high thermal inertia.

Net energy needs appear as anticipated by the heat loads. The case of Ireland well represents the importance of climatic conditions. Despite the much lower heating load, net energy needed for heating is approximately the same in Ireland as in Italy, Hungary or Slovakia, as a consequence of longer heating season. Unsurprisingly, Poland has by far the highest net energy need for heating and Slovakia has the second lowest (after Cyprus).

When served with a modern, renewable energy source-based technical building system, such as air-to-water heat pump with surface heating, altering seasonal performances of the appliance have a visible impact on energy consumption. In case of Poland, the high net energy need for heating is further enhanced with the lowest seasonal performance factor for heating. On the contrary, Irelands second highest SPFH reduces its energy consumption notably, compared to the other countries.

What Ireland gains on high efficiency, loses it on high carbon intensity factor. An indicator to highlight is the operational carbon emission, in which aspect

Ireland worsens its relatively good position of energy-based indicators. Slovakia, opposingly, is even more appealing in the context of operational carbon emission, with far the lowest 735 $kgCO_2eq$/year due to the low electricity-consumption and the second least carbon intensity factor of 246 g/kWh_e. On the other end comes Poland, with an extremely high 5,753 $kgCO_2eq$/year, a combined result of worst energy consumption and carbon intensity factor.

Consequently, nearly zero energy buildings are the most similar in their heating load trends. Energy-consumption related indicators of the reference building differ a lot depending on its location for the specific climatic conditions. This is a bit controversial as this leads to the same naming, NZEB, meaning "nearly zero" to largely different extents. Seeing the results, it is advised to either perform similar investigations that could properly suggest thermal transmittance requirement values, balancing the specific target indicators (like net energy needs), or to highlight in communication that NZEB indicators could have huge variations depending on the exact location. For the latter it could be added that for further harmonization of the indicators, some Member States would need to invest disproportionately much money.

It is also suggested that operational carbon emission indicators shall appear in the definition as a flagship of environmental awareness. This would also provide room in differentiating the support schemes of renewable energy sources.

4.1 limitations and future work

Recently, more and more countries announce requirements on the specific thermal transmittance of the specific building structures. As the present study is limited to eight Member States, it is planned to expand scope with other countries. Furthermore, other building types must be included to clarify the extent the reference building selection influenced the results.

5. Acknowledgement

The work has been carried out within the research projects entitled "Large Scale Smart Meter Data Assessment for Energy Benchmarking and Occupant Behavior Profile Development of Building Clusters". The project (no. K 128199) and "Optimisation of buildings and building elements from life cycle and building physics perspective based on complex numeric modelling" (FK 128663) have been implemented with the support provided from the National Research, Development and Innovation Fund of Hungary, financed under the K_18 and FK_18 funding scheme. The research has also been supported by the NRDI Fund (TKP2020 NC, Grant No. BME-NCS) based on the charter of bolster issued by the NRDI Office under the auspices of the Ministry for Innovation and Technology.

6. Appendices

For the weather specifications Test Reference Year weather files of Brussels, Larnaca, Budapest, Dublin, Milan, Warsaw, Bratislava and Ljubljana were used. For shading, default settings of TRNBuid were applied.

Complete result tables of the mentioned indicators are presented in further tables. For more information see the link below.

Tab. 2 - Simulation results of the reference building for the eight specified locations

	Heating load [kW]	temp. [°C]	Cooling load [kW]	temp. [°C]
BEL	4.341	-7.08	1.940	29.38
CYP	3.312	2.53	4.682	33.79
HUN	4.632	-11.88	2.534	31.30
IRL	3.513	-4.08	1.974	22.08
ITA	4.244	-7.66	2.281	28.98
POL	5.194	-16.48	1.618	26.71
SVK	3.238	-12.28	3.071	28.59
SLO	4.465	-11.98	2.212	27.28
Net energy	Heating [kWh]	Cooling [kWh]	Sum [kWh]	
BEL	9331	103	9434	
CYP	1735	3436	5171	
HUN	8379	458	8837	
IRL	7910	27	7936	
ITA	7986	375	8361	
POL	10871	68	10938	
SVK	5014	1163	6178	
SLO	8374	229	8603	
HVAC	SCOP [-]	SPFH [-]	SEER [-]	SPFC [-]
BEL	2.85	2.20		
CYP	3.37	2.62	4.57	3.35
HUN	2.65	2.04	4.95	3.61
IRL	2.98	2.29		
ITA	2.76	2.12	4.93	3.60
POL	2.61	2.01		
SVK	2.71	2.07	5.17	3.72
SLO	2.68	2.06	5.09	3.70
Elect-ricity	Heating [kWh_e]	Cooling [kWh_e]	Sum [kWh_e]	CO_2 [kg/a]
BEL	4890		4890	1066
CYP	955	1207	2162	1768
HUN	4753	148	4901	1244
IRL	3931		3931	1710
ITA	4334	119	4454	1684
POL	6260		6260	5763
SVK	2657	334	2991	736
SLO	4584	70	4654	1471

The datasets generated during and/or analysed during the current study are not available because at the moment of publishing but the authors will make every reasonable effort to publish them at https://epget.bme.hu/oktatoi_oldal.php?lepes=4&oid=151 in near future.

7. References

[1] International Energy Agency, "2019 Global Status report for Buildings and Construction," 2019.

[2] EPBD, Directive 2018/844 of the European Parliament and of the Council of 30 May 2018 amending Directive 2010/31/EU on the energy performance of buildings and Directive 2012/27/EU on energy efficiency. 2018.

[3] D. D'Agostino, S. T. Tzeiranaki, P. Zangheri, and P. Bertoldi, "Assessing Nearly Zero Energy Buildings (NZEBs) development in Europe," Energy Strateg. Rev., vol. 36, no. July, p. 100680, 2021, doi: 10.1016/j.esr.2021.100680.

[4] R. Simson, K. E. Thomsen, K. B. Wittchen, and J. Kurnitski, "A Comparative Analysis of NZEB Energy Performance Requirements for Residential Buildings in Denmark, Estonia and Finland," E3S Web Conf., vol. 246, no. April, 2021, doi: 10.1051/e3sconf/202124614001.

[5] F. Garzia et al., "Report on EU implementation of nZEBs," 2018. [Online]. Available: http://www.cravezero.eu/wp-content/uploads/2018/07/CRAVEzero_D21_Report-of-EU-implementation-of-nZEBs.pdf.

[6] S. Guillén-Lambea, B. Rodríguez-Soria, and J. M. Marín, "Comfort settings and energy demand for residential nZEB in warm climates," Appl. Energy, vol. 202, pp. 471–486, 2017, doi: 10.1016/j.apenergy.2017.05.163.

[7] Concentrated Action, "Energy Performance of Buildings Database." https://epbd-ca.eu/database-of-outputs.

[8] C. Ministry of Commerce Industry and Energy Tourism, "2nd National plan fo increasing the number of Nearly Zero-Energy Buildings (NZEBs)," Press Inf. Off., 2017.

[9] Z. Sternova and J. Magyar, "EPBD implementation in the Slovak Republic," 2018. [Online]. Available: https://epbd-ca.eu/wp-content/uploads/2018/08/CA-EPBD-IV-Slovak-Republic-2018.pdf.

[10] M. De Meulenaer and T. Kristien, "Belgium Flemish 2016 - Implementing the Energy Performance of Buildings Directive 2018," 2018. [Online]. Available: https://epbd-ca.eu/wp-content/uploads/2018/08/CA-EPBD-IV-Belgium-Flemish-Region-2018.pdf.

[11] Ministry Without Portfolio of Hungary, "Regulation 7/2006 determining the energy performance of buildings," 2020. https://net.jogtar.hu/jogszabaly?docid=a0600007.tnm (accessed Jun. 17, 2021).

[12] I. Department of Housing, Local Government and Heritage, Building Regulations - Technical Guidance Document L- Conservation of Fuel and Energy – Buildings other than Dwellings. 2021, pp. 1–100.

[13] C. Ezilda, A. Federici, A. Martino, M. Antinucci, and G. Varalda, "EPBD implementation in Italy," 2018. [Online]. Available: https://www.buildup.eu/sites/default/files/content/ca-epbd-iv-italy-2018.pdf.

[14] D. Bekierski, R. Geryło, and D. Kaczorek, "EPBD implementation in Poland - status 2016," 2018. [Online]. Available: https://www.buildup.eu/sites/default/files/content/ca-epbd-iv-poland-2018.pdf.

[15] M. Š. Zavrl, M. Tomšič, A. Rakušček, and E. Potočar, "EPBD Implementation in Slovenia," 2018. [Online]. Available: https://epbd-ca.eu/wp-content/uploads/2018/08/CA-EPBD-IV-Slovenia-2018.pdf.

[16] E. C. for S. CEN, EN 15251 (2012) - Indoor environmental input parameters for design and assessment of energy performance of buildingsaddressing indoor air quality, thermal environment, lighting and acoustics, vol. 44. 2012, pp. 0–9.

[17] S. Verbeke and A. Audenaert, "Thermal inertia in buildings: A review of impacts across climate and building use," Renew. Sustain. Energy Rev., vol. 82, no. August 2017, pp. 2300–2318, 2018, doi: 10.1016/j.rser.2017.08.083.

[18] G. Bagarella, R. Lazzarin, and M. Noro, "Sizing strategy of on-off and modulating heat pump systems based on annual energy analysis," Int. J. Refrig., vol. 65, pp. 183–193, 2016, doi: 10.1016/j.ijrefrig.2016.02.015.

[19] R. Hitchin, K. E. Thomsen, and K. B. Wittchen, "Primary Energy Factors and Members States Energy Regulations - Primary factors and the EPBD," no. 692447, p. 4, 2018, [Online]. Available: https://www.epbd-ca.eu/wp-content/uploads/2018/04/05-CCT1-Factsheet-PEF.pdf.

[20] European Joint Research Centre, "Reporting guidelines," Covenant of Mayors for Climate and Energy, 2020. https://data.jrc.ec.europa.eu/dataset/919df040-0252-4e4e-ad82-c054896e1641.

Textile-based heat exchanger for humidity recovery between spatially separated air flows

Hannes Rosenbaum [a], Christian Friebe [a]

[a] Air-conditioning Department, Main Department Ventilation and Air Conditioning, Institut für Luft- und Kältetechnik gemeinnützige GmbH, Dresden, 01309, Germany, klima@ilkdresden.de

Abstract. Both, sensible heat recovery and the combined heat and humidity recovery are state of the art. Of particular importance is humidity recovery in winter season. The transfer of water vapour from the humidity-laden extract air to the very dry outdoor air is very important for a good room air quality. Enthalpy exchangers potentially reduce the energy requirements of any subsequent air humidification on the supply air side considerably. In the planning phase, the possibility of enthalpy recovery is therefore often used as a weighty argument for dispensing with humidification systems.
However, all systems established on the market require a coupling of supply air and extract air by means of recuperation (e.g. plate heat exchanger) or direct regeneration (rotating storage mass). Nevertheless, enthalpy recovery systems for HVAC-Systems with spatially separated supply air and extract air are not available on the market.
In order to close this gap in the market, ILK Dresden has developed textile-based heat exchangers, which - integrated in closed loop systems - can transfer humidity as well as sensitive heat between spatially separated air flows (e.g. between supply air and exhaust air). The functional principle is based on a liquid sorption process via semipermeable membranes. This is regardless of whether it is a 2-fluid system (air, brine), in which the heat-transferring fluid and the mass-transferring fluid is the same fluid and only one circuit is utilised, or a 3-fluid system (air, brine, water), in which the fluids involved flow in separated circuits. In general, the developed system can be used all year round - thus also for air dehumidification or indirect evaporative cooling processes.
The current state of development is presented. In addition, an outlook is given for which applications the textile heat exchangers could be further developed and which application potentials are offered.

Keywords. Semipermeable membrane, liquid sorption, humidity recovery, enthalpy recovery, HVAC, textile heat exchangers, hygiene, energy efficiency, evaporative cooling, closed-loop-system.
DOI: https://doi.org/10.34641/clima.2022.256

1. Introduction

Research and development on the field of heat transfer applications with membranes lies within the scope of ILK Dresden for more than twelve years. The initial idea was to eliminate or improve air conditioning processes in HVAC systems, with direct contact between water and air, in order to improve hygienic conditions. The reason for this is that - whether air humidification or air dehumidification by condensation - the availability of water is a precondition for any undesired organic growth.

The second objective is the application of renewable energy sources or available waste heat as energy source for air humidification or dehumidification in order to increase both the energy efficiency and the sustainability of air conditioning.

Initial investigations showed that both liquid sorption-based air humidification and dehumidification using semi-permeable membranes work quite well [1, 2]. Contrary to sorption processes with direct contact between brine and air, corrosion damage can also be avoided [3, 4]. In the course of the development process several technical issues were solved e.g. how to fix the membranes in the air flow or how to implement them in a sufficiently pressure-stable construction [5].

In addition, an ongoing research project focuses on improved applications with long-term stable materials. Using the example of humidity recovery between spatially separated air flows, this paper gives an overview of the current state of development of membrane heat exchangers as well as its application potential in future air conditioning technology.

Copyright ©2022 by the authors. This conference paper is published under a CC-BY-4.0 license.

2. Development emphases

2.1 Pre-discussion on humidification

The air-conditioning industry is becoming increasingly aware of the importance of relative humidity for health-related well-being [6]. Complaints such as dry eyes or dry mucous membranes in the mouth, nose and throat can be caused by excessively dry indoor air. According to [6, 7, 8, 9], in general, the risk of spreading viral infections or bacterial diseases is lowest in the range between 40 and 60 % RH, which is perceived as thermally comfortable. Excessively dry air (< 30 % RH), on the other hand, increases the risk of respiratory infections [10]. From a health/medical point of view and due to the current corona virus pandemic, the argumentation pro air humidification systems or even pro establishing a minimum air humidity of 40 % is considerably supported.

The most important counter-argument against the use of humidification systems is the energy requirement. Due to the high specific evaporation enthalpy of water (approx. 2260 kJ/kg), an isothermal humidification of a fixed air volume by Δx = 4.0 g/kg requires a heat input of 9.04 kJ/kg dry air. With the same energy input, however, the same air volume could also be warmed up by 9.0 K without changing the moisture content. This is considerable and shows the conflict between energy saving vs. medically based advises.

2.2 Humidity recovery between spatially separated air streams

Heat recovery systems with humidity transfer between the outside air and exhaust air cannot completely resolve the discussion about the pros and cons of air humidification. They can only "recover" a proportion of the humidity mass (water vapour) previously introduced into the balance scope from a humidity source. The humidity input by people is by far not sufficient to realise room air humidity ≥ 40 % RH permanently (i.e. also in winter) [11]. Nevertheless, so-called enthalpy exchangers have established themselves on the market. They supplement humidity conditioning by humidifiers and, in this constellation, they significantly reduce the energy requirement of air humidification.

However, all heat recovery systems with built-in humidity recovery require that the supply and extract air streams cross within the unit (plate heat exchanger) or that a rotating mass storage is moved through both air streams while both airstreams mounted in a directly adjacent arrangement.

Enthalpy recovery systems for system concepts with spatially separation of supply and extract air - for example in the form of closed-loop systems - are not yet available on the market. Closing this gap in the market is interesting for all ventilation and air-conditioning tasks (office, work, residential buildings) up to process air technology. Centralised or decentralised air handling concepts with separated supply and extract air units or air handling systems with contaminated extract air (workshops, laboratories,...) would benefit particularly.

2.3 Liquid desiccant process using membranes

In a R&D project, the ILK Dresden has developed textile heat and mass transfer units equipped with semi-permeable membranes, which - integrated into a circulation system - are flowed through by a liquid desiccant and thus enable mass transfer between spatially separated air flows (**Fig. 1**):

While the liquid desiccant binds water vapour from the air on the exhaust side (absorption) according to the driving forces in the liquid desiccant process (water vapour partial pressure differences), it releases the water vapour to the dry outdoor air flow (desorption). At the same time, the sorbent absorbs sensible heat on the exhaust air side and releases it on the outside air side.

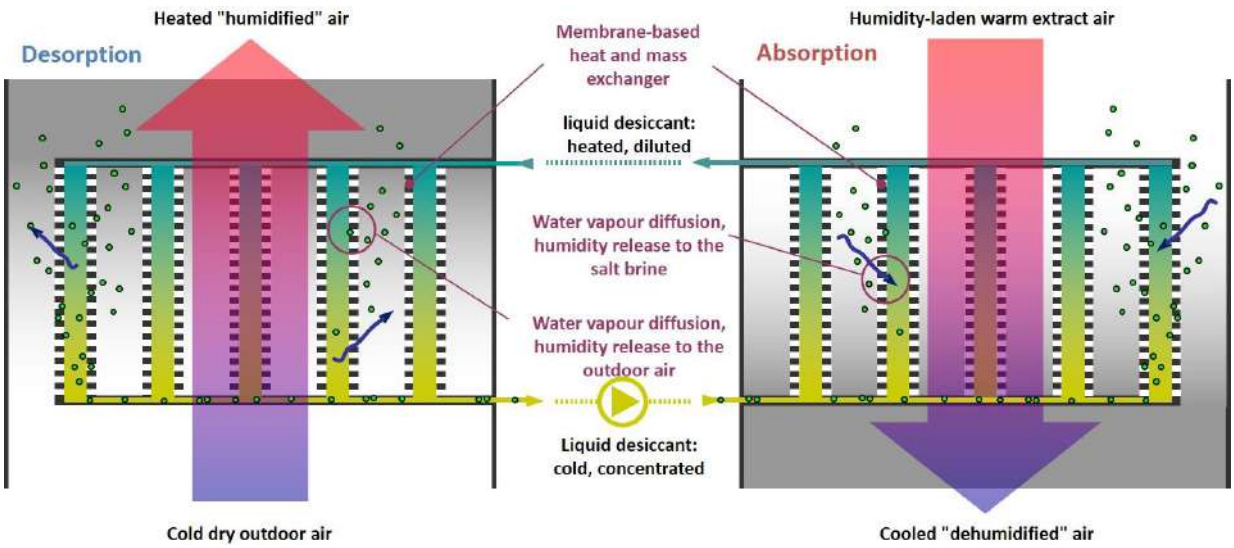

Fig. 1 - Schematic of enthalpy recovery using two membrane heat exchangers and a liquid sorption circuit.

2.4 Membrane-based textile laminates

The development and composition of the basic textile structure (multi-layer laminates comprising membrane, backing structure and flow-throughable spacer textile) were realised in cooperation with the Sächsisches Textilforschungsinstitut, Germany (STFI). Based on a huge number of test series, the most suitable material and processing parameters for the technical and physical requirements were worked out. The following properties were considered (the achieved target values of the laminate are listed in brackets): Water vapour permeability (> 5000 g/m^{2}d), pressure stability (> 1.0 bar gauge pressure), flow resistance (< 100 mbar/m), free volume (< 0.5 l/m^2), adhesive strength, adhesive quantity, adhesive type, application method (hotmelt), textile face structure and membrane material (ePTFE/PU).

2.5 Technical design of the membrane-based heat and mass exchanger

The development of the technical design of the textile heat exchangers is based on the experience the ILK Dresden has accumulated in the field of liquid sorption via membranes over a period of more than 10 years. Water vapour permeable membranes and non-woven fabric layers are laminated onto the cover surfaces of multi-dimensional spacer textiles (material thickness < 1.0 mm). Cut-to-size multilayer laminates with sealed edges and fluid connections are used to create membrane elements. Several membrane elements are assembled in parallel to form a simple (2-fluid) membrane heat exchanger. (**Fig. 2**)

Construction designs in which heat and humidity recovery are functionally separated from each other by adding exclusively water-flowed heat exchanging surfaces (3-fluid heat exchangers) were also developed and analysed. This includes, for example, the use of capillary tube mats or spacer textiles with integrated thin tubes. (**Fig. 3** and **Fig. 4**)

If the membrane-based textile heat exchanger is to operate on the counter flow principle, one of the greatest challenges is the uniform supply of the liquid desiccant to the membrane elements, which are stacked at close intervals of ≤ 4 mm. In the absence of available precision-fit micro manifolds which allows an incident flow of 50 membrane elements with a centre-to-centre spacing of 4.0 mm, these had to be developed. As a result, the single fluid connections of the membrane elements can be integrated into their edge seal.

Textile-physical material characteristics of the membrane-based textile laminates as well as air-sided flow properties are the basis for the dimensioning of the textile membrane heat exchangers.

2.6 Experimental setup

For the measurement analyses of the heat and humidity recovery, one membrane heat exchanger at the outside air side and one membrane heat exchanger at the extract air side were connected to each other on the liquid side. According to the design of the respective pair of membrane heat exchangers, both a 2-fluid and a 3-fluid heat and humidity recovery system were created. The configurations are shown in **Tab. 1**. The 3-fluid system is depicted in **Fig. 5** and **Fig. 6**.

In addition to the flow rates of each fluid flowing through each heat and mass exchanger, the most important measured variables were the following parameters on each inlet and outlet side: Air temperature and humidity, desiccant temperature and conductivity (mass concentration) as well as water temperatures and the mass flows of the respective fluids. Flow resistances had been recorded too.

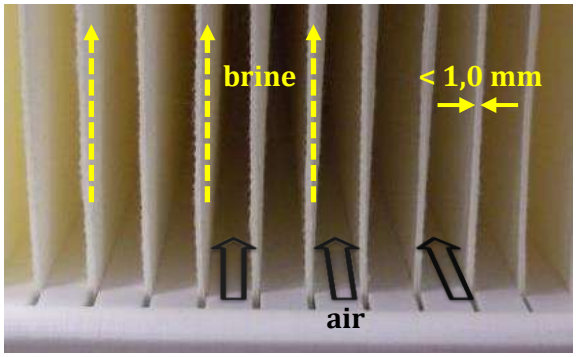

Fig. 2 – Stack of membrane elements with brine flowed through them (thickness < 1.0 mm each) assembled as a cross-flow heat exchanger (2-fluid)

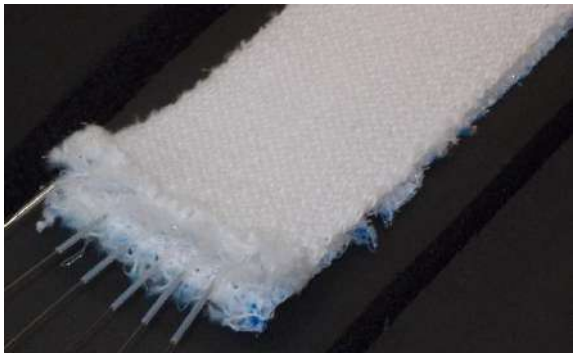

Fig. 3 – Flow-throughable spacer fabric (brine-side) with mechanically incorporated capillary tubes (waterside) for 3-fluid heat exchangers

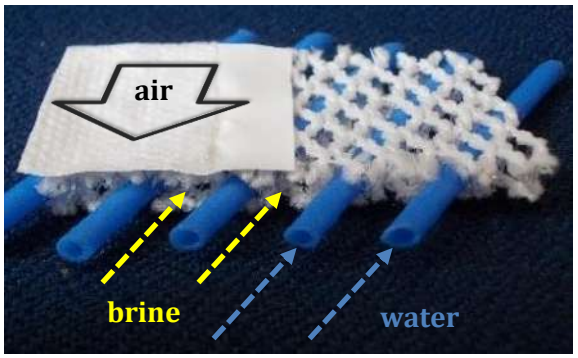

Fig. 4 – View of a sample conducted as a 3-fluid membrane element

Tab. 1 – Membrane-based heat and mass exchanger

one exchanger in each air stream	2-fluid crossflow	3-fluid counterflow
System design	1…2 people	3…4 people
Airflow	50 m^3/h	100 m^3/h
Duct size	20 x 30 cm	20 x 44 cm
Active surface (tex. Multilayer)	15 m^2 (7.5 m^2)	20 m^2 (10 m^2)
Membrane-elements	50	50
Initial brine concentration	25…35 %	25…35 %
Water mass flow	-	25…30 kg/h
Desiccant mass flow	20…65 kg/h	30…40 kg/h
Membrane material	ePTFE/PU	ePTFE/PU

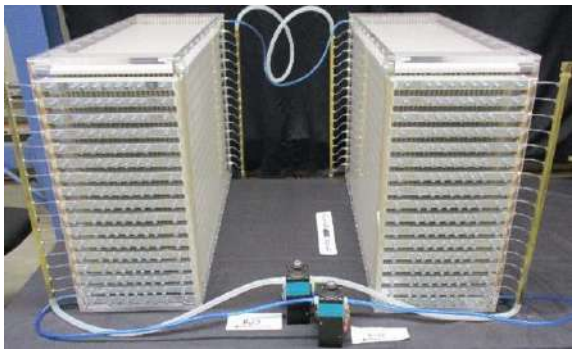

Fig. 5 – 3-fluid membrane-based heat exchanger before mounting into the experimental setup

Fig. 6 – experimental setup of the 3-fluid closed-loop system for temperature and humidity recovery

3. Measurements

3.1 enthalpy recovery rates

In a first measurement session on the 2-fluid system, the enthalpy, humidity and the sensible heat recovery rates were determined (**Fig. 7**). This was done at fixed air conditions but variable desiccant flow rates. (t_{ODA} = 8.0 ± 0.5 °C; x_{ODA} = 3.0...4.5 g/kg; t_{ETA} = 27 ± 0.5 °C; x_{ETA} = 15...17.5 g/kg)

The results confirm a significant heat and mass transfer between the spatially separated air flows. With a desiccant/air heat capacity flow ratio of 1.1, the sensible heat recovery rate (relation of the temperature differences SUP-ODA and ETA-ODA) is just about 0.5. To increase the heat recovery rate to 0.6, it is necessary to double the desiccant flow rate.

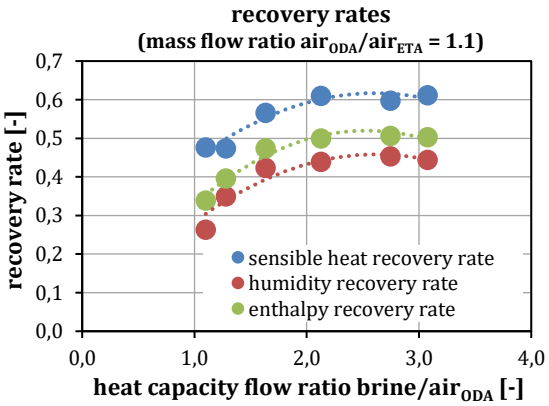

Fig. 7 – Recovery rates depending on heat capacity flow ratio

3.2 long-time monitoring

A further measurement session on the 2-fluid system with statically defined inlet parameters was provided in order to analyse the performance of the recovery rates at different temperatures but constant humidity differences between the outdoor air and the extract air. The measurement results show that the sensible heat recovery rate decreases with decreasing temperature difference, while the humidity recovery rate increases at the same time. If both air streams have the same temperature, the highest level of humidity recovery is measured with η_x = 0.60. On the other hand, the enthalpy recovery rate constantly remains at η_h = 0.51 ± 0.02 independently of temperature.

The liquid sorption process always wants to reach a sorption equilibrium. Depending on the driving forces (temperature differences and water vapour partial pressure difference between air and desiccant), the brine concentration level mainly depends on the weather but hardly on room air conditions. Due to the transport of water molecules between the outdoor air and the extract air this concentration level varies slightly by one to two percentage points.

For a long-term measurement of the dynamic operating performance of the new two-fluid heat and humidity recovery system (two membrane-based heat exchangers in a circulating system), the air flow rate of 50 m^3/h each and the heat capacity flow ratio between desiccant and air of 2.0 were kept constant, while the inlet conditions on the air side changed dynamically.

The measurement results, illustrated in **Fig. 8**, show a permanently constant enthalpy recovery (η_h = 0.55), the inverse trend in the temperature and humidity recovery depending on the temperature difference between the extract air and the outdoor air, and the weather-dependent variation in the concentration level of the desiccant (28...33 %). Drier outdoor air conditions characterised by temperature peaks cause an increase in concentration level, while more humid days cause a decrease in the concentration level.

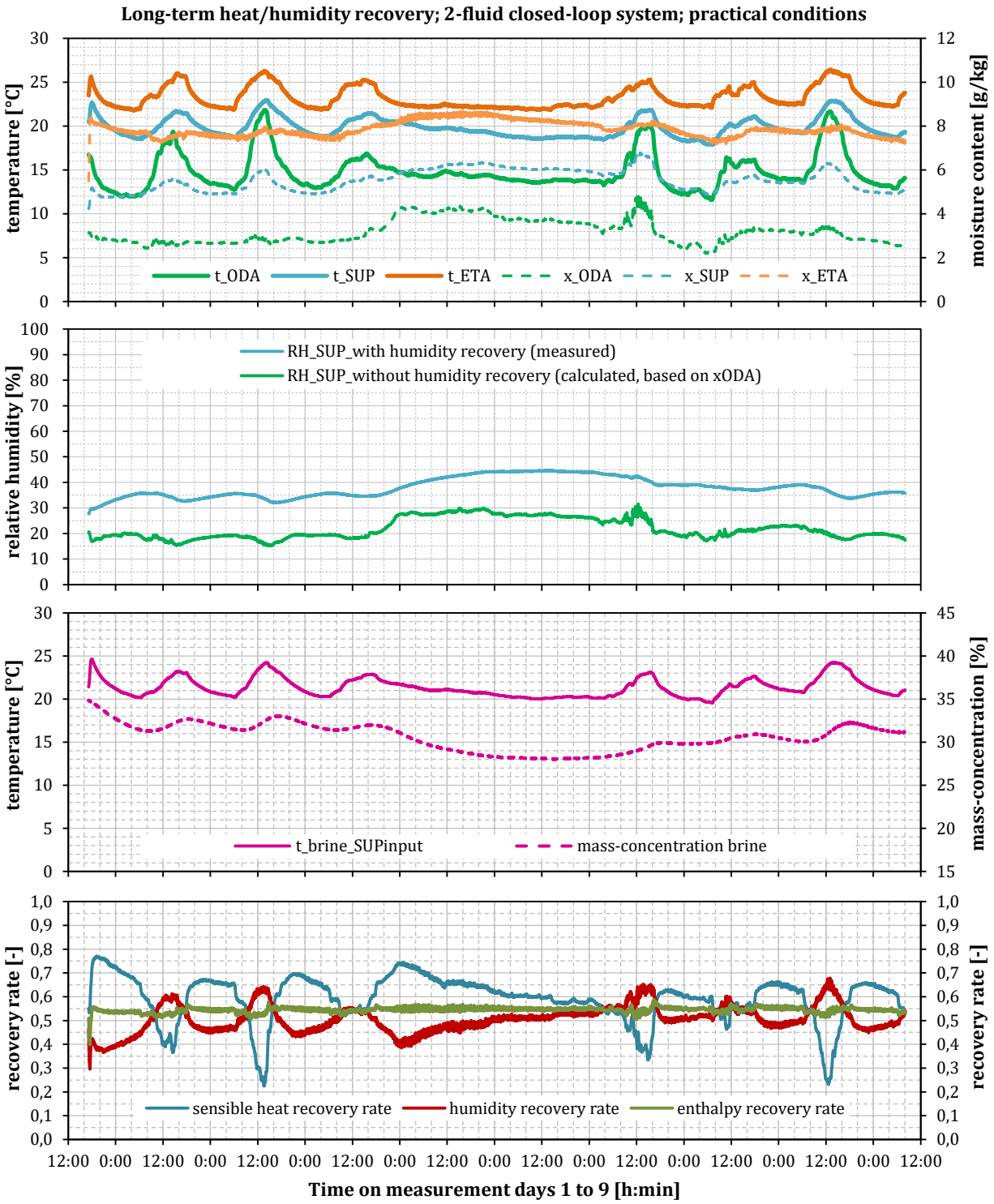

Fig. 8 – long-term measurement of the dynamic operating performance of the 2-fluid heat and humidity recovery system

3.3 Additional thermal functions

The particular advantage of closed-loop systems in general is the possibility of coupling heat into or out from the heat transfer fluid. In this way, the outdoor air flow can already be tempered to the setpoint of the supply air temperature via the heat exchangers of the closed-loop system.

To test this multi-functional utilisation on the innovative 2-fluid system with humidity recovery via textile heat exchangers, desiccant-sided a plate heat exchanger was installed directly upstream to the outdoor air membrane heat exchanger. A heating water circuit with a speed-controlled metering pump and a motor-controlled 3-way valve regulate the heat input into the desiccant circuit and consequently the temperature of the supply air.

With the aim of testing the automatic supply air temperature control by coupling heat into the desiccant circuit, another long-term measurement was performed. In terms of practice-related test conditions, temperature variations between 5 and 20 °C (without regulation of the humidity) were simulated at the outdoor air side. On the extract air side, temperature variations of the environment around the experimental setup (21...27 °C) were used and the moisture content was set to approx. 8.0 g/kg. The supply air temperature setpoint of 23.0 °C and the volume flow rates (50 m^3/h air, 32 l/h desiccant) were part of the fixed specifications. The control parameters of the valve drive were adjusted for optimisation purposes during the measurement period.

According to the measurement results, heat and humidity recovery with simultaneous supply air temperature control is possible. In contrast to closed-circuit systems without humidity recovery, the membrane-based 2-fluid system can transfer so much humidity from the extract air, even at a controlled supply air temperature, that the supply air humidity is usually above 30 %. Therefore, the risk of the room air being perceived as too dry would decrease.

4. Results

4.1 Optimisation potential

Measurements of the thermal inertia of the system indicate a correlation of the outdoor and supply air temperature trends, whereby the temporal shift roughly corresponds to the circulation rate of the desiccant. The circulation rate itself is significantly influenced by the filling volume of the desiccant circuit (heat exchangers, tubes, tanks) and the desiccant volume flow rate. Reducing the thermal inertia of the system (about 45 min in the above measurements) requires the minimising of the volume of the desiccant circuit to be flowed through.

Operating scenarios with very warm, humidity-laden extract air and very cold outdoor air cause a local condensation risk inside of the 2-fluid cross-flow heat exchanger especially near the intersection areas of outdoor air and desiccant inlet (ODA-SUP part of the heat exchanger) or extract air and desiccant inlet (ETA-EHA part of the heat exchanger). Membrane-based heat exchangers with countercurrent air and liquid flows could minimize this risk. A risk of crystallization of the liquid desiccant during enthalpy recovery in the 2-fluid system is not expected whilst the mass concentrations of the liquid desiccant is between 25 to 32 %. To play it safe, the liquid desiccant circuit shall be emptied into a system-integrated tank when it is not in use.

There is still an optimisation potential concerning the sensible heat recovery rate. Nonetheless to the already achieved heat recovery rates of more than 50 % higher recovery rates are expected. According to ErP Guidelines (2018) this should be more than 68 % [12, 13].

It is also preferred that the recovery of sensible heat and humidity can be regulated independently from each other. In the two-fluid system, this option is highly limited.

Some of the optimisation approaches have already been implemented in the 3-fluid system.

4.2 Results of the three-fluid system

The measurement results of the 3-fluid system confirm the expected higher enthalpy recovery rate compared to the 2-fluid system. The sensible heat recovery rate increase slightly whereas the humidity recovery rate is a little lower (**Tab. 2**). In both systems, the air-side pressure loss of 5 or 10 Pa is very low.

Tab. 2 – Recovery rates of the closed-loop systems during long-term measurements cf. Tab. 1

twice in each system	2-fluid crossflow	3-fluid counterflow
Enthalpy recovery rate	0.50…0.55	0.57…0.61
Sensible heat recovery rate	0.25…0.70	0.71…0.77
Humidity recovery rate	0.40…0.65	0.38…0.41
air-side pressure loss	5 Pa	12 Pa

5. Conclusions

The functionality of the heat and humidity recovery with textile heat exchangers in a 2-fluid, liquid desiccant closed-loop system was successfully demonstrated. This also applies to the coupling of heat for the supply air temperature control. The

thermodynamic and fluidic parameters achieved can also be assessed positively. They can certainly be compared with current normative requirements, e.g. DIN EN 13053.

As a result of the endurance tests under practical conditions, the recovery rates - especially the humidity recovery rate - almost permanently caused relative humidities of the supply air to exceed 30 % RH. In the context of the discussion about the pros and cons of air humidification systems mentioned at the beginning, the membrane heat exchangers developed for humidity recovery between spatially separated air flows make a substantial contribution to energy saving. Without humidity recovery, drier air conditions would have been measured in more than 60% of the measurement period. Maintaining specified humidity standards (>30 % RH) would have required the usage of active humidification and therefore a significant energy demand.

With the application of further thermal functions, especially 3-fluid textile heat and mass exchangers in corresponding closed-loop systems can be expanded into a multifunctional component. Potentially, in addition to heat and humidity recovery, all thermal state changes (heating, cooling, dehumidification, and humidification) can then be realised independently of each other at the outdoor air side as well as at the extract air side. Indirect evaporative cooling can also be realised. Temperature and humidity control can operate independently of each other. Conventional reheating or cooling coils can be omitted.

Potentially, the liquid desiccant process - i.e. sorptive and condensate-free air dehumidification - can also be used for dehumidification [11, 14, 15, 16, 17, 18, 19]. This enables the use of synergy effects all around the year and supports the use of renewable energies and works in a resource-saving and energy-efficient way. That is sustainable.

Back to the pre-discussion: The basis of closing the gap in the market for heat and humidity recovery between spatially separated air flows has been founded. In order to enable economic operation in the long term and to be able to establish itself on the market, the design, manufacture and production must be improved. Particularly necessary are issues regarding the long-term stability of the materials and automated production methods as well as assembly lines for membrane elements, media connections and entire membrane-based heat exchangers.

6. Acknowledgement

This work has been supported by the Federal Ministry for Economic Affairs and Energy of the Federal Republic of Germany under Contracts no. MF 180112.

Supported by:

Federal Ministry for Economic Affairs and Energy

on the basis of a decision by the German Bundestag

The datasets generated and analyzed as part of this study are not publicly available, but can be made available for specific purposes upon request from the authors.

7. Appendix

Tab. 3 – Symbols and indices, used in this paper

t	Temperature
x	Moisture content
h	Enthalpy
η	Recovery rate
ODA	Outdoor air
SUP	Supply air
ETA	Extract air
RH	Relative humidity

8. References

[1] Franzke U, Friebe C, Rosenbaum H. Air Conditioning with liquid sorption solution. 9th IIR Gustav Lorentzen Conference, Sydney 2010.

[2] Rosenbaum H. Der Grundstein ist gelegt… Erhebliches Einsparpotential durch Membranbasierte Raumklimatisierung. Sanitär+Heizungstechnik 7/2011; 34-37.

[3] Rosenbaum H. Membranbasierte Raumklimatisierung. Die KÄLTE + Klimatechnik 12/2011; 48-51.

[4] Rosenbaum H. Membranbasierte Raumklimatisierung – dezentrale sorptionsgestützte Klimatisierung. KI Kälte Luft Klimatechnik 04/2012; 19-21.

[5] Rosenbaum H, Herfert H. Prima Klima ohne Haevy-Metal-Technik – Textile Verbundsysteme mit Abstandstextilien für die Raumklimatisierung. Kettenwirk-Praxis Textilinformationen, Karl Mayer, 01/2013; 27-29.

[6] Nienaber F, Rewitz K, Seiwert P, Müller D. Einfluss der Luftfeuchte auf den Menschen und seine Gesundheit. RWTH-EBC 2021-001.

[7] Sterling E M, Arundel A, Sterling T D. Criteria for human exposure to humidity in occupied buildings. ASHRAE transactions 1985; 91.1: 611–622.

[8] Arundel A V, Sterling E M, Biggin J H, Sterling T D. Indirect health effects of relative humidity in indoor environments. Environmental Health Perspectives, 1986; 65:351–361.

[9] Wolkoff P. Indoor air humidity, air quality, and health - An overview. International journal of hygiene and environmental health, 2018; 221(3):376–390.

[10] Noti J D, Blachere F M, McMillen C M, Lindsley W G, Kashon M L, Slaughter D R, Beezhold D H. High humidity leads to loss of infectious influenza virus from simulated coughs. PloS one, 2013; 8(2):e57485,.

[11] Rosenbaum H. Hygrisch aktiver Lufterhitzer – hygienische und energieeffiziente Luftbefeuchtung über Membranen. Deutsche Kälte- und Klima Tagung, Dresden 2015.

[12] EU Commission Regulation 1253/2014 from 7-7-2014 for the implementation of the Directive 2009/125/EG of the European Parliament and of the Council regarding the requirements for the eco-design of ventilation systems. Published on 11-25-2014.

[13] Beuth-Verlag. DIN EN 13053:2020-05. Lüftung von Gebäuden - Zentrale raumlufttechnische Geräte – Leistungskenndaten für Geräte, Komponenten und Baueinheiten; Deutsche Fassung EN 13053:2019.

[14] Simader, Rakos. Klimatisierung, Kühlung und Klimaschutz: Technologien, Wirtschaftlichkeit und CO2-Reduktionspotentiale. Materialband Austrian Energy Agency. Wien 2005; 74.

[15] Hauer, Lävemann. Möglichkeiten offener Sorptionsspeicher zum Heizen, Klimatisieren und Entfeuchten. Veröffentlichung des ZAE Bayern zum Thema Thermochemische Speicher. BINE-Informationsdienst 2006.

[16] Lävemann, Peltzer. Offenes Sorptionssystem zur solaren Klimatisierung eines Gebäudes in Singapur. ZAE-Bayern, L-DCS Technology GmbH; IHK-Arbeitskreis Energieeffizienz; Garching 2006.

[17] Rosenbaum H. Membran-Kühldecke mit kondensatfreier Luftentfeuchtung – Messtechnische Analyse einer ersten Pilotanwendung dezentraler Flüssigsorptionsprozesse. KI Kälte Luft Klimatechnik, 03/2014; 26-30.

[18] Rosenbaum H. Flüssigsorption mit Membran-Kühldecke – Voraussetzungen, Einsatzpotential und –grenzen. tab – Das Fachmedium der TGA-Branche, 05/2014; 62-65.

[19] Rosenbaum H. Einsatz textiler Materialien zum Feuchtetransport – Luftreinhaltung bei der thermischen Luftbehandlung nach dem Filter. 12. Dresdner Kolloquium zur Luftreinhaltung; Dresden 2019.

Data-driven statiscal and machine learning modelling of real building stock energy use

Matthias Van Hove[1], Jelle Laverge[1], Arnold Janssens[1], Marc Delghust[1]

[1]Department of Architecture and Urban Planning, Ghent University, Belgium, matthias.vanhove@ugent.be

Abstract. One of today's major challenges is to become climate neutral by 2050. Large potential for energy reduction is found in the building sector (which accounts for 40% of Europe's total primary energy use). To compare energy reduction strategies, Building-Stock Energy Models are vital instruments. Yet, the regulatory energy performance calculation (which is currently used by EU policy makers) poorly predicts the real building energy use in residential buildings and largely overestimates the potential energy savings. Promising data-driven black-box models are gaining considerable traction in a wide range of applications. This paper evaluates whether data-driven linear regression and gradient boosting machine models provide better predictions of the real total building energy use at large scale as compared to the current regulatory white-box building energy calculation method. Compared to the performance of the regulatory method, both the linear regression models and the gradient boosting regression trees perform better (gradient boosting regression trees slightly worse than multiple linear regression). Yet, a large part of the variance in the linear regression models is left unexplained and also for the gradient boosting trees, there is room for improvement. At individual building level, it is clear that both the linear regression model performance and the gradient boosting regression tree performance is too poor for inference. At stock level, however, both types of models seem promising and can be a useful tool to inform big housing owners (*e.g.*, financial institutions, governments, housing companies *etc.*) or for policy making.

Keywords. Data-driven modelling, Linear regression, Gradient boosting trees, Building stock energy use
DOI: https://doi.org/10.34641/clima.2022.379

1. Introduction

One of today's major challenges is to become climate neutral by 2050. Large potential for energy reduction is found in the building sector, which accounts for 40% of Europe's total primary energy use and 36% of the CO_2-emissions (EU, 2020). To compare competing energy reduction strategies, Building-Stock Energy Models (BSEMs) are vital instruments. Yet, the current regulatory energy performance calculation (which is currently used by EU policy makers) poorly predicts the real building energy use in residential buildings and consequently poorly informs current and future home owners and tenants about their energy use, largely overestimates the potential energy savings and therefore undermines policy making (Van Hove *et al.*, 2021).

Since the introduction of the regulatory energy performance calculation methods in 2009 (*i.e.*, specified by the Energy Performance of Buildings Directive (EPBD)), national building energy registries have emerged and vastly increased ever since. These data registries consist of aggregated building characteristic data which are used for the regulatory energy performance calculation (white-box) (EPC, 2015). With this data being available and the fact that the regulatory methods only poorly estimate the real building energy use (Macjen *et al.*, 2013; Van Hove *et al.*, 2021), the question rises whether data-driven statistical models and/or machine learning models can replace the regulatory methods for predicting the real annual building energy use.

Statistical models on the one hand, such as the Ordinary Least Squares (OLS) linear regression (Zdaniuk, 2014), have been around for a couple of

Copyright ©2022 by the authors. This conference paper is published under a CC-BY-4.0 license.

decades and have already been tested in other EU-countries, though not for Flanders and often not including socio-demographic variables. Machine learning models on the other hand, such as gradient boosting regression trees (de Queiroz *et al.*, 2016), are gaining considerable traction in a wide range of applications and have only been scarcely used for predicting the annual building energy use (also not for Flanders).

In this paper, we aim to study the predictive performance of data-driven linear regression models and data-driven gradient boosting regression trees for predicting the real annual total building energy use. Then, the results are being compared to the predictive performance of the regulatory calculation methods and there is being evaluated wether these data-driven black-box models can potentially replace the current regulatory white-box models for predicting the annual building energy use at individual building level as well as at stock level.

2. Research Methods

2.1. Data set

The data analysed for this paper were collected from a former study together with Flemish Energy and Climate Agency (Van Hove *et al.*, 2021). In total, it comprises 122,680 cases from the Flemish EPC registry (*i.e.*, one centralised database with data from the regulatory energy performance certificates of all registered existing buildings constructed before 2006). The data provide information about the building characteristics, technical systems and some detailed building geometry data. Also, there are annual real meter data available from the Belgian distribution system operator Fluvius and there are some socio-demographic and climate variables as well. After data cleansing, filtering and coupling, 56,930 cases were excluded from the sample based on the following five criteria:

(i) Coupling of data from various databases (*e.g.*, Fluvius real energy use data and data from the energy performance database).
(ii) Inconsistencies in the PV-data.
(iii) Doubt about the reliability of the real energy consumption data.
(iv) Single-family houses with energy sources other than natural gas and electricity for space heating (SH) and/or domestic hot water (DHW).

Hence, the total sample size was 69,870 cases which formed the basis for all the analyses carried out in this paper.

2.2. (In)dependent variables

The dependent variable in all analyses, the OLS regression models and the gradient boosting regression tree models is the annual real primary total energy use [kWh/y]. An overview of the independent variables (or predictors) is given in *Table 1* and *Table 2*. *Table 1* shows the general building variables used and their frequencies or summary statistics (M means Mean, SD means standard deviation for the continuous variables). *Table 2* shows descriptive information for the socio-demographic and weather variables.

Tab. 1 - Overview of general building variables and their frequencies (bold = reference category).

Variable	Categories (N)
Energy score	n/a (cont.: M=363kWh/m²·y, SD=173)
Construction year	n/a (cont.: M=1966, SD=28)
Latitude	n/a (cont.: M=51.05, SD=0.17)
Longitude	n/a (cont.: M=4.17, SD=0.72)
Usable floor space	n/a (cont.: M=169.6m², SD=61.7m²)
Building volume	n/a (cont.: M=512.1m³, SD=193.9m³)
Dwelling type	Detached (39.8%), **semi-detached (31.2%)**, terraced (29.0%)
Number of floors	n/a (cont.: M=2.3, SD=1.6)
Basement?	Yes (43.4%), **no (56.6%)**
Roof insulation?	Yes (25.4%), **no (74.6%)**
Floor insulation?	Yes (18.9%), **no (81.1%)**
Wall insulation?	Yes (38.4%), **no (61.6%)**
DHW on gas? (no=elec)	Yes (78.4%), **no (21.6%)**
SH on gas? (no=elec)	Yes (93.4%), **no (6.6%)**
Ventilation system	**A (96.8%)**, B (0.2%), C (2.1%), D (0.9%)
Condensing boiler?	Yes (49.4%), **no (50.6%)**
DHW storage vessel?	Yes (30.6%), **no (69.4%)**
SH Floor heating?	Yes (3.6%), **no (96.4%)**
SH Radiator/ Convector?	Yes (20.9%), **no (79.1%)**
SH Air heating?	Yes (1.1%), **no (98.9%)**
PV-panels?	Yes (3.6%), **no (96.4%)**
Heat pump?	Yes (0.3%), **no (99.7%)**
Solar collector?	Yes (1.5%), **no (98.5%)**
Space cooling?	Yes (1.5%), **no (98.5%)**
Social housing?	Yes (5.8%), **no (94.2%)**

Tab. 2 - Overview of socio-demographic and weather variables and their frequencies (bold = reference category).

Variable	Categories (N)
Number of occupants	n/a (cont.: M=2.63, SD=1.33)
Children 00-04yr?	Yes (28.4%), **no (71.6%)**
Children 05-12yr?	Yes (25.1%), **no (74.9%)**
Children 13-18yr?	Yes (14.4%), **no (85.6%)**
Adults 19-29yr?	Yes (26.8%), **no (73.2%)**
Adults 30-44yr?	Yes (53.0%), **no (47.0%)**
Adults 45-64yr?	Yes (38.0%), **no (62.0%)**
Adults 65+yr?	Yes (16.1%), **no (83.9%)**
Number of 65+-adults	n/a (cont.: M=0.21, SD=0.53)
Number of Children	n/a (cont.: M=0.95, SD=1.12)
Number of adults	n/a (cont.: M=1.92, SD=0.72)
HH composition	1Ad, 0Ch (17.3%), 1Ad, 1Ch (2.5%), 2Ad, 0Ch (24.1%), 2Ad, 1Ch (15.1%), 2Ad, 2Ch (18.2%), 2Ad, 3Ch (5.2%), 3Ad, 0Ch (4.7%), 3Ad, 1Ch (2.2%)
Length residency	n/a (cont.: M=7.19y, SD=10.4y)

weighted annual average temperature (Δ_Tav)	n/a (cont.: M=0.04°C, SD=0.19°C)
weighted annual DegreeDays (Δ_DD)	n/a (cont.: M=-26.0, SD=42.9)
weighted annual Global Horizontal Irradiance (Δ_GHI)	n/a (cont.: M=-1.16W/m^2, SD=17.56W/m^2)
weighted annual SolarHours (Δ_SH)	n/a (cont.: M=226.4, SD=73.3)

2.3. OLS linear regression

Statistical modelling with the data are all conducted in Python with the statistical packages 'scikit-learn' (Pedregosa *et al.*, 2011) and 'statsmodels' (Skipper *et al.*, 2010) in combination with the data analysis and visualisation package 'pandas' (McKinney, 2010). Initially, a linear ordinary least squares (OLS) regression model (Zdaniuk, 2014) has been built for both a set of 'general building variables' and a set of 'socio-demographic and weather variables'. Given the suspected issue of multicollinearity, the variance inflation factors (VIF) have been inspected. VIF indicates how much the variance of an estimated regression coefficient increases if the explanatory variables are correlated. If uncorrelated, VIF=1. In this paper a threshold of 5 has been used, as suggested in literature (Roberts *et al.*, 2009; Chan *et al.*, 2012). If VIFs greater than 5 are found in the OLS regression, then one (or more) of those correlated variables are excluded one-by-one stepwise depending on the regression coefficient and the individual VIF until a model is obtained with no collinearity issues.

Further, all *p*-values and bootstrapped 95% confidence intervals (CI) of the predictors are checked for irregularities. Only the predictors for which the *p*-values are <.05 and the confidence intervals do not include nil are significant and thus kept in the model. The exclusion of explanatory variables from the model is once more done one by one stepwise. After building the individual models (*i.e.,* 'general building variables' and 'socio-demographic and weather variables'), the models are combined until resulting in a final model encompassing all explanatory variables, tested and adjusted for multicollinearity and significant regression coefficients. As all model input variables are normalised, the magnitude of the regression coefficients gives an indication of the parameters relative importance in the regression model.

In order to fulfil the necessary assumptions for linear regression models, the model input variables are checked for linearity, autocorrelation and multicollinearity; the residuals are checked for independency, homoscedasticity and normality.

2.4. Gradient boosNng regression trees

The gradient boosting machine (GBM) is part of a class of powerful ensemble machine learning algorithms based on the concept that a "strong learner" (de Queiroz *et al.*, 2016), having high prediction accuracy, can be obtained by iteratively combining several less complex models, called "weak learners". Such ensembles are constructed from decision tree models. Trees are added one at a time to the ensemble and fit to correct the prediction errors made by prior models. This is a type of ensemble machine learning model referred to as boosting. Models are fit using any arbitrary differentiable loss function and gradient descent optimisation algorithm. This gives the technique its name, "gradient boosting", as the loss gradient is minimised as the model is fit, much like a neural network. Gradient boosting is an effective machine learning algorithm and is often the main, or one of the main, algorithms used to win machine learning competitions (like Kaggle) on tabular and similar structured datasets, which is why we test its performance in this paper.

The algorithm provides hyperparameters that must be tuned for a specific dataset. Such parameters include the number of trees or estimators in the model, the learning rate of the model, the maximum tree depth, the minimum tree weight *etc.* The gradient boosting implementation that we are using in this paper is XGBoost (Extreme Gradient Boosting) with the Python package 'xgboost' (Chen *et al.*, 2016). First a baseline model is made with a 80%-20% training-set split without hyper parameter tuning. Then hyper parameter tuning is performed with the Bayesian optimisation algorithm (HYPEROPT) (*N.B.*, see *Table 3* for the used hyperparameter space) (Bergstra *et al.*, 2015), with 80%-20% training-set split and a 5-fold cross-validation. Similar to the OLS regression models, first initial models are built for a set of 'general building variables' and a set of 'socio-demographic and weather variables'. Then models are combined until resulting in a final model encompassing all explanatory variables.

Tab. 3 - List of hyperparameters of the GBM models and tuning range.

name	tuning range
learning rate	[0.001, 0.1]
hessian regularisation	[1, 10]
loss regularisation	[1, 12]
column sampling by tree	[0.5, 1]
column sampling by level	[0.5, 1]
maximum depth	[3, 25]
number of iterations	[100, 1800] (with early stopping at 50)

We further use SHAP (Shapley Additive exPlanations) values to interpret the outputs (Lundberg *et al.*, 2017)(Fig. 1). The x-axis of a SHAP summary plot shows the impact off features on the outcomes, based on the SHAP values. Features are sorted based on their impact, thus the variable at the top has the highest impact. The color represents the feature values, with red for high values and blue for low values. The vertical dispersion for each feature corresponds to the data

points with the same SHAP values. If red points are mostly present on the positive side of SHAP values, it means by increasing the value of the independent variable, the dependent variable increases as well.

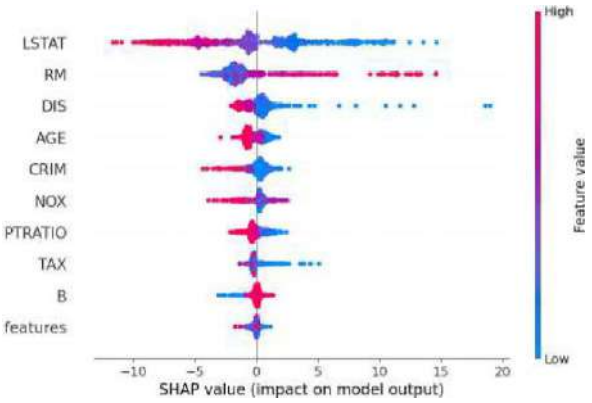

Fig. 1 - SHAP reference graph.

3. Results

3.1. General building characterisNcs OLS model

General building variables explained (adjusted) R^2=38.1% of the variability in the real total energy use. Two variable showed VIF values above the chosen threshold criterion so some of those had to be excluded one-by-one stepwise (*i.e.*, building volume). Further, five variables had confidence intervals including nil and a *p*-value >.05 meaning that some of those had to be excluded one-by-one stepwise as well (*i.e.*, type of ventilation system, construction year, roof insulation?, number of floors and SH energy carrier). After exclusion of those variables, an OLS regression rerun on the remaining variables resulted in a model that explained R^2=41.3% of the variability in the real total energy use. *Table 5* shows the coefficients of the reduced OLS model (*i.e.*, standardised coefficients β_{OLS}, 95% confidence intervals of the standardised coefficients β_{OLS} and the p-values of the standardised coefficients β_{OLS}). Five variables are significant: A larger dwelling size is associated with higher total energy use, the presence of renewable systems (*i.e.*, PV-panels, heat pump and solar collector) is associated with using less total energy use, floor and air heating is associated with more total energy use compared to radiator space heating, having space cooling is associated with having higher total energy use and detached houses are associated with having higher total energy use compared to semi-detached houses while terraced houses are associated with having less total energy use compared to semi-detached houses.

3.2. Socio-demographic & weather OLS model

The socio-demographic and weather model explained (adjusted) R^2=11.7% of the variability in the real total energy use. Six variables showed VIF values above the chosen threshold criterion so some of those had to be excluded one-by-one stepwise (*i.e.*, the number of children, average age of HH, HH with children, the number of 65+ per HH). Further, six variables had confidence intervals including nil and a *p*-value >.05 meaning that some of those had to be excluded one-by-one stepwise as well (*i.e.*, HH with children 5-12 and 13-18, HH with adults 30-44 and 65+, HH composition 2Ad 1Child and weighted annual GHI). After exclusion of those variables, an OLS regression rerun on the remaining variables resulted in a model that explained R^2=13.6% of the variability in the real total energy use. *Table 6* shows the coefficients of the reduced OLS model. Three variables are significant: A larger household size and a larger number of adults is associated with higher total energy use, singles are associated with less total energy use and a more annual heating degree days at the dwelling's location are associated with higher total energy use.

3.3. Combined OLS model

In the next step, the two different individual models are combined together for increments in explanatory power through adding additional variables. For the building and socio-demographic and weather model, only the variables that had remained after VIF- and CI-checks have been included. The combined 'general building and socio-demographic and weather' model explained (adjusted) R^2=46.6% of the variability in real total energy use. No variables showed VIF values above the chosen threshold criterion and no variables had confidence intervals including nil. An OLS regression rerun on the remaining variables was thus not necessary. This 5.3% increase in R^2 compared to the model with general building characteristic variables only is significant (p<.01). Also in comparison to the socio-demographic and weather OLS model, the increase in R^2 is significant (p<.01). *Table 7* summarises the coefficients for all variables that remained after VIF- and CI-checks.

Table 4 shows the adjusted R^2 of the individual OLS models and the combined OLS model as well as results for the Mean Absolute Error (MAE) and Root Mean Squared Error (RMSE) metrics. As expected, building characteristic variables explain by far the most of the variability in real total energy use, on their own, and also when added to building and socio-demographic and weather variables. Socio-demographic variables play a lesser but still significant role in explaining real total energy use. Extra detailed building variables don't add much information to the model to predict more of the variability in the real total energy use. Therefore, in explaining more of the variability (and avoiding collinearity problems), the modeller can better gather more different types of variables (*i.e.*, building characteristics, socio-demographics, incomes, weather, appliance ownerships *etc.*) rather than more detailed variables within the same type of variables (*e.g.*, extra detailed variables related to

building characteristics). Further, as a model with general building characteristics (*i.e.*, building features that inhabitants can easily fill in themselves) performs equally well compared to a model including detailed building characteristics and intermediate results from the regulatory calculation, the final model can be used (*e.g.*, in an online tool) as a primary model to inform inhabitants, tenants and home owners about their energy use, without needing extra inputs from the EPC-registry to improve performance.

Tab. 4 - Adjusted R^2, MAE and RMSE for the two individual models and the combined model.

model	gen_build	socio	final
(adj) R^2	41.3%	13.6%	46.6%
MAE	5227 kWh/y	6211 kWh/y	5011 kWh/y
RMSE	6469 kWh/y	7832 kWh/y	6214 kWh/y

Tab. 5 - Coefficients of OLS regression model, general building variables.

Predictor	β_{OLS}	95% CI_{OLS}	p_{OLS}
(constant)	22694.2	[22526.9, 24373.3]	<.001
Energy score	1698.9	[1549.1, 1927.9]	<.001
Latitude	193.0	[20.4, 342.7]	<.013
Longitude	695.6	[550.6, 876.8]	<.001
Usable floor space	5034.9	[4854.8, 5212.1]	<.001
Detached?	2214.8	[1834.0, 2443.4]	<.001
Terraced?	-1800.9	[-2096.4, -1579.6]	<.001
Basement?	745.6	[506.5, 967.8]	<.001
Floor insulation?	-553.3	[-850.4, -247.2]	<.002
Wall insulation?	-517.2	[-772.3, -228.3]	<.001
DHW on gas?	717.4	[306.3, 1018.2]	<.001
Condensing boiler?	-1404.5	[-1611.4, -1098.0]	<.001
DHW storage vessel?	1719.0	[1525.3, 2085.8]	<.001
SH Floor heating?	3928.5	[3244.1, 4740.9]	<.001
SH Radiator?	2145.3	[1884.9, 2687.9]	<.001
SH Air heating?	3589.5	[2581.5, 4933.7]	<.001
PV-panels?	-3475.2	[-3991.1, -3080.9]	<.001
Heat pump?	-4613.1	[-6561.9, -813.4]	<.003
Solar collector?	-1865.6	[-2488.6, -752.7]	<.001
Space cooling?	2236.3	[1374.4, 2679.9]	<.002
Social housing?	1154.5	[775.8, 1399.9]	<.001

Tab. 6 - Coefficients of OLS regression model, socio-demographic variables.

Predictor	β_{OLS}	95% CI_{OLS}	p_{OLS}
(constant)	24760.7	[24326.2, 25237.3]	<.001
Number of occupants	1247.5	[1027.9,1606.9]	<.001
Number of adults	1397.5	[1045.1,1703.2]	<.001
Children 00-04yr?	-1028.6	[-1398.4,-630.6]	<.001
Adults 19-29yr?	-1143.6	[-1463.4,-809.2]	<.001
Adults 45-64yr?	870.8	[517.1,1099.1]	<.001
Length residency	158.2	[127.2,186.3]	<.001
HH: 1Ad, 0Child	-3133.4	[-3789.8,-2416.8]	<.001
HH: 1Ad, 1Child	-1227.0	[-2282.9,-505.5]	<.001
HH: 2Ad, 0Child	-1190.3	[-1688.9,-720.7]	<.001
HH: 2Ad, 2Child	1238.4	[701.7,1464.8]	<.001
weigh. ann. Tav	703.2	[326.9,1028.9]	<.001
weigh. DegreeDays	1413.0	[981.2,1783.4]	<.001
weigh. SolarHours	-659.7	[-825.1,-490.8]	<.001

Tab. 7 - OLS coefficients for the final combined regression model.

Predictor	β_{OLS}	95% CI_{OLS}	p_{OLS}
(constant)	11427.4	[21995.9, 23892.4]	<.001
Energy score	1619.9	[1483.9, 1852.8]	<.001
Usable floor space	3780.8	[3199.2, 4138.1]	<.003
Detached?	2334.4	[1967.6, 2544.4]	<.001
Terraced?	-1846.7	[-2111.1, -1619.2]	<.001
Basement?	659.4	[435.4, 894.8]	<.001
Floor insulation?	-399.9	[-698.8, -98.6]	<.001
Wall insulation?	-451.8	[-669.5, -198.2]	<.001
DHW on gas?	546.2	[169.9, 857.1]	<.001
Condensing boiler?	-1168.1	[-1387.5, -883.1]	<.001
DHW storage vessel?	1607.6	[1435.4, 2009.9]	<.001
SH Floor heating?	4010.4	[3448.2, 4875.4]	<.001
SH Radiator?	2024.9	[1767.9, 2508.9]	<.001
SH Air heating?	3546.6	[2499.6, 4855.8]	<.001
PV-panels?	-3913.3	[-4436.5, -3477.3]	<.017
Heat pump?	-4981.3	[-6854.2, -1449.2]	<.011
Solar collector?	-1553.6	[-2321.5, -465.6]	<.002
Space cooling?	2237.1	[1427.8, 2752.5]	<.001
Social housing?	527.2	[199.2, 830.8]	<.001
Children 00-04yr?	-642.3	[-829.8, -89.3]	<.001
Children 05-12yr?	654.2	[207.2, 1007.5]	<.001
Children 13-18yr?	701.2	[393.1, 1218.1]	<.001
Adults 45-64yr?	454.9	[265.9, 773.9]	<.001
Number of occupants	1177.8	[842.0, 1401.1]	<.001
Number of adults	840.2	[548.9, 1048.2]	<.001
Length residency	78.8	[62.2, 112.7]	<.001
HH: Average Age	841.2	[492.8, 1049.8]	<.001
HH: 1Ad, 0Child	-1660.9	[-2218.1, -1069.6]	<.001
HH: 2Ad, 0Child	-1132.6	[-1408.9, -560.5]	<.001
weigh. ann. Tav	564.8	[302.3, 851.8]	<.001
weigh. DegreeDays	720.3	[471.6, 1123.4]	<.001
weigh. SolarHours	-201.1	[-319.5, -42.3]	<.001

3.4. General building characterisNcs XGB model

For a XGB baseline model with general building variables, we obtained a MAE and RMSE of respectively 6041 kWh/y and 7856 kWh/y. After hyperparameter tuning with 5-fold cross-validation, a XGB rerun resulted in a model with a MAE and RMSE of respectively 6020 kWh/y and 7828 kWh/y (learning rate = 0.0118, n estimators = 1450, colsample bytree = 0.510, gamma = 0.451, min child weight = 1, max depth = 3, colsample bylevel = 0.563). *Fig. 2* shows the SHAP summary plot for predicting the real total energy use based on general building variables. The most important general building variables are the usable floor space, the building volume, the dwelling type and the calculated energy performance score.

3.5. Socio-demographic & weather XGB model

A XGB baseline model with socio-demographic and weather variables resulted in a MAE and RMSE

of respectively 6993 kWh/y and 9088 kWh/y. After hyperparameter tuning, a XGB rerun resulted in a model with a MAE and RMSE of respectively 6990 kWh/y and 9100 kWh/y (learning rate = 0.0468, n estimators = 370, colsample bytree = 0.817, gamma = 0.352, min child weight = 9, max depth = 4, colsample bylevel = 0.563). *Fig. 3* shows the SHAP summary plot for predicting the real total energy use based on socio demographic and weather variables. The most important socio-demographic and weather variables are the number of occupants, the number of adults, the length of residency and the normalised number of solar hours and degree days.

3.6. Combined XGB model

For the combined 'general building and socio-demographic and weather' XGB baseline model, we obtained a MAE and RMSE of respectively 5747 kWh/y and 7499 kWh/y. After hyperparameter tuning, a XGB rerun resulted in a model with a MAE and RMSE of respectively 5740 kWh/y and 7505 kWh/y (learning rate = 0.0290, n estimators = 1360, colsample bytree = 0.507, gamma = 0.966, min child weight = 8, max depth = 3, colsample bylevel = 0.501). *Fig. 4* shows the SHAP summary plot for predicting the real total energy use for the final combined XGB model. The most important variables are the dwelling type, the usable floor space, the building volume and the number of occupants.

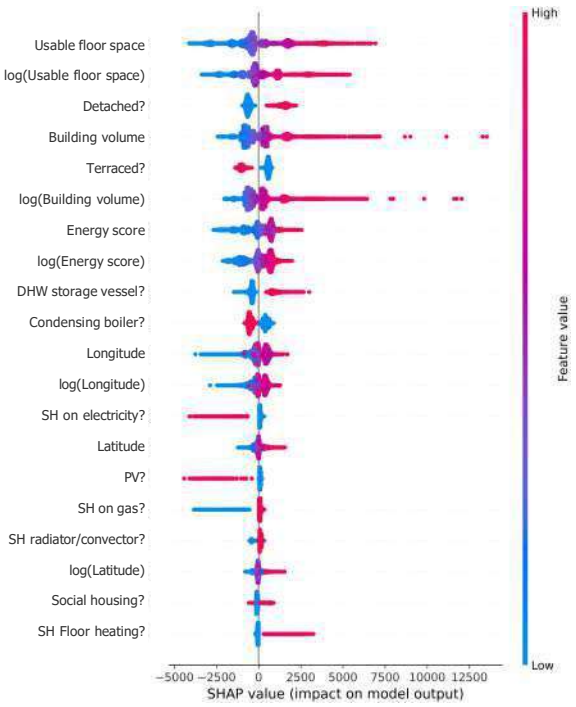

Fig. 2 - Contribution of the 20 most important features in the 'general building variables model'.

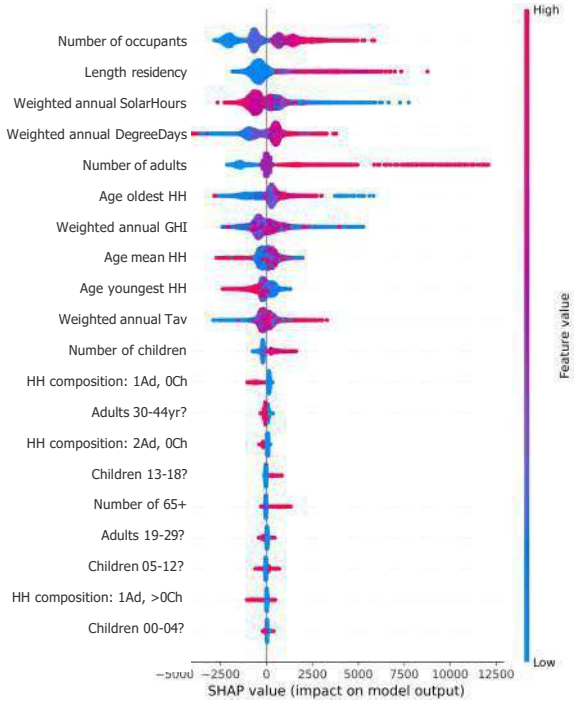

Fig. 3 - Contribution of the 20 most important features in the 'socio demographic and weather variables model'.

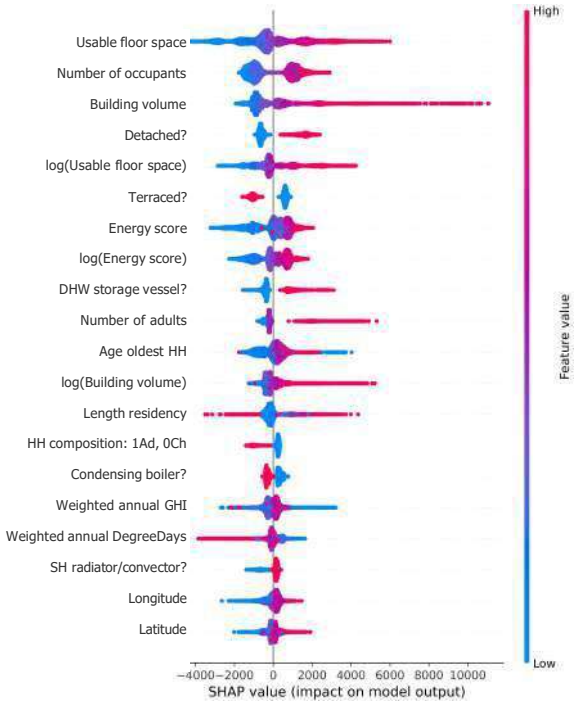

Fig. 4 - Contribution of the 20 most important features in the 'combined model'.

3.7. Regulatory calculaNon method

Fig. 5 shows a scatter plot of the real and regulatory calculated total energy use [kWh/y]. In an ideal scenario, a linear function should closely describe the relationship between both parameters. As expected, an ideal relation is not obtained. In fact, a negative R^2 (R^2=-15%) between both (*N.B.*, R-Squared can be negative only when the chosen model does not follow the trend of the

data, so fits worse than a horizontal line (Hastie *et al.*, 2009; James *et al.*, 2013) indicates that the average real total energy use of the stock is, on average, a better prediction of the real total energy use of an arbitrary single-family house than the annual regulatory calculated total energy use. Furthermore, the RMSE and MAE between both variables are respectively 45808 kWh/y and 35325 kWh/y. When considering that the average real total energy use of the studied sample is 27286 kWh/y, the MAE and RMSE results are 1.29 to 1.68 times larger.

Compared to the performance of the regulatory method, both the linear regression models and the gradient boosting regression trees perform better with results for the MAE respectively 6.05 and 5.15 times better (smaller) and the results for the RMSE respectively 6.37 times and 5.10 times better. Gradient boosting regression trees perform slightly worse than multiple linear regression.

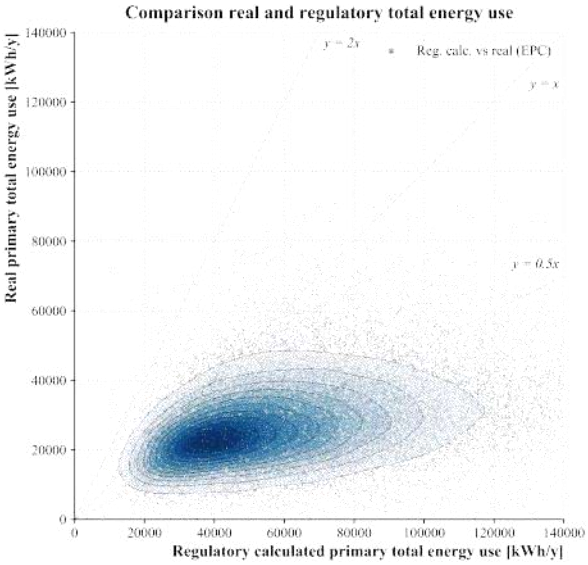

Fig. 5 - Scatter plot of the real and regulatory calculated annual total primary energy use in Flemish single-family houses.

4. Conclusions

This study investigated the predictive performance of data-driven linear regression models and data-driven gradient boosting regression trees for predicting the real annual total building energy use. Also, the results are being compared with the predictive performance of the regulatory calculation methods and there is being evaluated wether these data-driven black-box models can potentially replace the current regulatory white-box models for predicting the annual building energy use at individual building level as well as at stock level.

A total of 46.6% of the variability in total energy use is explained by the final linear regression model based on a combined set of predictors (general building variables, socio-demographic and weather variables) and we obtained MAE and RMSE results of respectively 5011 kWh/y and 6214 kWh/y. For a final XGB model with hyperparameter tuning, based on a combined set of predictors (general building variables, socio-demographic and weather variables), we obtained MAE and RMSE results of respectively 5432 kWh/y and 6543 kWh/y.

Compared to the performance of the regulatory method, both the linear regression models and the gradient boosting regression trees perform better (gradient boosting regression trees slightly worse than multiple linear regression). Yet, a large part of the variance in the linear regression models is left unexplained and also for the gradient boosting trees, there is room for improvement. This means that a large portion of evidence/information has to be attributed either to parameters that are not listed among the variables of the EPB registry (*e.g.*, occupant behaviour, appliance ownership, income) or that the values of the parameters listed are inaccurate (*e.g.*, inaccurate default values).

At individual building level, it is clear that both the linear regression model performance and the gradient boosting regression tree performance is too poor for inference. At stock level, however, both types of models seem promising and can be a useful tool to inform big housing owners (*e.g.*, financial institutions, governments, housing companies *etc.*) or for policy making.

5. Acknowledgements

The authors want to thank the Flemish Energy and Climate Agency (VEKA) and the Belgian grid operator Fluvius for data collection and helpful feedback during the course of the study.

6. Funding

This study and the work by the first author were supported by the VEKA and by a PhD scholarship granted by Ghent University (BOF).

7. References

(1) EU. (2020). Energy performance of buildings directive. European Commission Department of Energy.

(2) Van Hove, M., Delghust, M., Janssens, A. (2021). Analyse naar de haalbaarheid van statistische modellen die energiegebruik in woningen kunnen voorspellen op basis van gebouwparameters. https://www.energiesparen.be/marktonderzoek

(3) EPC Formulestructuur. (2015). Flemish Energy and Climate Agency.

(4) Majcen, D., Itard, L. C. M., & Visscher, H. (2013). Theoretical vs.actual energy use of labelled dwellings in the Netherlands: Discrepancies and policy implications. *Energy Policy*, 54, 125-136.

(5) Van Hove, M., Deurinck, M., Lameire, W., M., Janssens, A., Delghust, M. (2021). Data-driven statistical modelling of real energy use for spatial heating and DHW in modern Flemish single-family houses: a feasibility study. *Proceedings of the 17th International Conference of IBPSA (BS2021)*, Brugge, Belgium.

(6) Zdaniuk, B. (2014). Ordinary Least-Squares (OLS) Model. In: Michalos A.C. (eds) *Encyclopedia of Quality of Life and Well-Being Research.* Springer, Dordrecht.

(7) de Queiroz, G., Vaidyanathan, R. (2016). useR! Machine Learning Tutorial. https://github.com/ledell/useR-machine-learning-tutorial/blob/master/gradient-boosting-machines.Rmd

(8) Hastie ,T., Tibshirani, R., Friedman, J. (2009). *The Elements of Statistical Learning: Data Mining, Inference, and Prediction.* Springer, New York.

(9) James, G., Witten, D., Hastie, T., Tibshirani, R. (2013). An Introduction to Statistical Learning: with Applications in R. Springer, New York.

(10) Pedregosa *et al.* (2011). Scikit-learn: Machine Learning in Python. *JMLR.* 12, 2825-2830.

(11) Skipper, Seabold, Perktold, J. (2010). Statsmodel: Econometric and statistical modeling with python. *Proceedings of the 9th Python in Science Conference*.

(12) McKinney (2010). Data structures for statistical computing in python. *Proceedings of the 9th Python in Science Conference*. 445.

(13) Roberts, N., Thatcher, J.B. (2009). Conceptualising and testing formative constructs: tutorial and annotated example. *Data Base for Advances in Information Systems*, 40, 9-39.

(14) Chan, S.H., Chen, J.H. Li, Y.H., Tsai, L.M. (2012). Gly1057Asp polymorphism of insulin receptor substrate-2 is associated with coronary artery disease in the Taiwanese population. *Journal of Biomedical Science*, 19, 1-8.

(15) Chen, T., & Guestrin, C. (2016). XGBoost: A Scalable Tree Boosting System. In Proceedings of the 22nd ACM SIGKDD International Conference on Knowledge Discovery and Data Mining (pp. 785–794). New York, NY, USA: ACM.

(16) Bergstra, J., Komer, B., Eliasmith, C., Yamins, D., Cox, D. (2015). Hyperopt: a Python library for model selection and hyperparameter optimization. *Computational Science and Discovery*, 8(1), 014008.

(17) Lundberg, S.M., Lee, S.-I. (2017). A Unified Approach to Interpreting Model Predictions. *Advances in Neural Information Processing Systems*, 30.

Design of highly compact indirect evaporative coolers

Francisco Comino [a], Jesús Castillo-González [b], Francisco J. Navas-Martos [b], Pablo E. Romero [a], Manuel Ruiz de Adana [c]

[a] Departamento de Mecánica, Escuela Politécnica Superior, Universidad de Córdoba, Campus de Rabanales, Antigua Carretera Nacional IV, km 396, 14071 Córdoba, España, email address: francisco.comino@uco.es; p62rocap@uco.es.

[b] Centro Tecnologico del Plastico Andaltec, Pol. Ind. Cañada de la Fuente, Calle Vílches, s/n, 23600, Martos, Jaén, España, email address: jesus.castillo@andaltec.org; francisco-javier.navas@andaltec.org.

[c] Departamento de Química-Física y Termodinámica Aplicada, Escuela Politécnica Superior, Universidad de Córdoba, Campus de Rabanales, Antigua Carretera Nacional IV, km 396, 14071 Córdoba, España, email address: manuel.ruiz@uco.es.

Abstract. Evaporative cooling units are an effective alternative to conventional air conditioning technologies, due to their high efficiency and reduced primary energy consumption. There are two main types of evaporative cooling systems: the direct evaporative cooling (DEC) system, and the indirect evaporative cooling (IEC) system. DEC is based on direct contact between air and water, while IEC is based on heat and mass transfer between two flows of air, separated by a heat transfer surface with a dry side, where only air is cooled, and a wet side, where water is evaporated into air. The main objective of the present work was to design and manufacture a highly compact indirect evaporative cooler. Firstly, a mathematical model based on ε-NTU numerical method to determine the optimal geometrical and operating parameters of an IEC system was developed. The mathematical model allowed to obtain the temperature, enthalpy and humidity distributions of the air inside the exchanger. Then, the air-cooling system was manufactured. The device consisted of a compact heat and mass exchanger, a water distributing system and an outer casing. Finally, the IEC system was studied experimentally. An experimental facility was designed to study these air-cooling systems. The cooling unit performance indicators were the cooling capacity per unit volume and per unit airflow rate. The experimental results showed that the cooling capacity per unit volume of the device was 177 kW/m^3, and the cooling capacity per unit airflow rate was 10.9 kW/(m^3/s). These results suggested that highly compact indirect evaporative coolers can achieve air-cooling processes with a low energy consumption and a low environmental impact.

Keywords. air-cooling system, heat and mass exchanger, evaporative cooler, cooling capacity, manufacturing.
DOI: https://doi.org/10.34641/clima.2022.182

1. Introduction

European Union directives reinforced the objective of reducing primary energy consumption and the integration of renewable energies in buildings, instead of using fossil fuels [1]. A large percentage of current energy consumption and CO2 emissions are due to heating, ventilating and air conditioning, HVAC, systems.

A traditional method widely used in air cooling is that of conventional HVAC systems based on direct expansion units [2]. However, direct expansion systems typically use refrigerant gases, which could emit polluting gases into the atmosphere, and in addition, they depend mainly on electrical energy.

Another air-cooling technology is evaporative cooling. The evaporative cooling units are based on heat and mass transfer between air and cool water [3]. There are two main types of evaporative cooling systems: the direct evaporative cooling, DEC, system and the indirect evaporative cooling, IEC, system. DEC is based on direct contact between air and water, while IEC is based on heat and mass transfer between two flows of air, separated by a heat transfer surface with a dry side, where only air is cooling, and a wet side, where water is evaporated into air [4]. In addition, there are different types of IEC [4]: conventional IEC, which supply air between the dry bulb temperature and the wet bulb temperature; dew-point evaporative cooler (DIEC), including single-stage counter-flow, and finally, Maisotsenko-cycle (MIEC), including multi-stage

Copyright ©2022 by the authors. This conference paper is published under a CC-BY-4.0 license.

cross-flow. The last two supply air between the dry bulb temperature and the dew point temperature.

One of the most effective indirect evaporative cooling solutions are the dew-point counter-flow cycles, DIEC, [5]. The DIEC systems have been studied for many applications [6]. A DIEC with a direct expansion system applied to a residential building in China showed high potential for energy savings [7], up to 39% compared to a direct expansion system. DIEC systems were combined with desiccant systems [8–10], managing to control temperature and humidity independently.

IEC systems have been widely analysed by many authors in the available literature [11,12], in particular focusing on the analysis of influential parameters on outlet air conditions, such as inlet air temperature, inlet air humidity. The coefficient of performance of IEC systems was analysed for different operating conditions, evaluating the effect of variable inlet air velocities [13]. The amount of water flow rate was also analysed [14], which has a significant effect on system performance. The influence of the exchanger material was studied in other works [15].

The design of IEC systems was also analysed in recent works to improve their thermal behaviour. The cooling power of a DIEC system with different number of perforations between the dry and wet channels was analysed [16]. The results showed that the configuration with a single air passage increased the cooling power compared to configurations with four air passages. In another work, a mathematical model of DIEC was developed with different numbers of air passages. [17]. Two DIEC systems with cross flow configuration, one with fins and one without fins, were developed and analysed under different inlet air conditions [18]. The DIEC system with fins improved thermal performance up to 40% compared to the same system without fins. An optimization study of a DIEC unit with counter-flow configuration was developed [19]. The goal of the study was to increase the performance of the system by varying the air speed, the flow rate and the length and height of the channels. A DIEC with counter-flow configuration was manufactured from the results obtained of an optimal design with a mathematical model [20]. The energy performance of this system increased up to 19 %.

Therefore, managing air with an efficient air-cooling unit, such as IEC systems, which does not depend mainly on electrical energy and does not use any refrigerant, could be an interesting alternative to conventional air-cooling units based on vapor-compression cycles. The main advantages of evaporative coolers are their constructive simplicity and high efficiency.

The main objective of the present work was to design and manufacture a highly compact indirect evaporative cooler. The cooling unit performance indicators were the cooling capacity per unit volume and per unit airflow rate. Firstly, a mathematical model based on modified ε-NTU numerical method to determine the operating parameters and optimal geometrical of an IEC was developed. Then, the air-cooling system was manufactured.

2. Materials and methods

The steps followed to develop the IEC system were as follows: (i) an IEC design was carried out and the ε-NTU mathematical model was applied to the IEC design; (ii). the numerical results were analysed; and (iii) the IEC system was manufactured.

2.1 Description of the indirect evaporative cooler

In the present work was designed an IEC system to handle air in small spaces. The air-cooling device consisted of a compact heat and mass exchanger, a water distributing system and an outer casing.

The heat and mass exchanger was designed with a counter-flow configuration. The air handling process consisted of an inlet air flow, which circulates through dry channels, exchanging heat with the attached channels, see Fig. 1. The inlet air stream was divided into two air streams at the end of the device, one air stream was recirculated in the inverse direction through wet channels, exchanging heat and mass between air and water, and another stream was supplied, see Fig. 1. Water only enters wet channels, so the supply air stream was cooled without varying its moisture content.

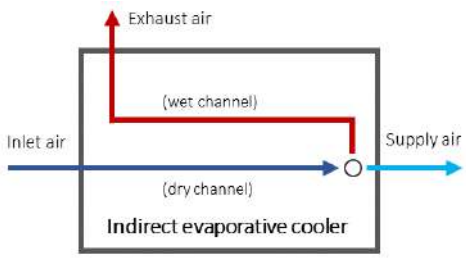

Fig. 1 - Diagram of the air flows of an IEC system.

2.2 Mathematical model of the indirect evaporative cooler

A mathematical model of IEC systems was developed to study the energy performance of an IEC system. This model was based on ε-NTU numerical method. The main equations of the model are expressed by (1)-(3).

$$NTU = U^{*}dA/C_{min,i} \tag{1}$$

$$U^{*}dA = \left(a\left[\frac{1}{\alpha_{d,i}} + \frac{\delta}{K} + \frac{\delta_w}{K_w}\right] + \frac{1}{\beta_i}\right)^{-1} N_{ch}Wdx \tag{2}$$

$$\varepsilon = f(NTU, C_{r,i}) \quad (3)$$

Where NTU is number of transfer units; U is overall heat transfer coefficient [W m^{-2} K^{-1}]; A is area [m^2]; C is heat capacity rate [kg s^{-1}]; a is slope of the temperature-enthalpy saturation line [kJ kg^{-1} K^{-1}]; δ is thickness of plates [m]; δ_w is thickness of water film [m]; $\alpha_{d,i}$ is ; K is thermal conductivity of wall [W m^{-1} K^{-1}]; K_w is thermal conductivity of water film [W m^{-1} K^{-1}]; β_i is mass transfer coefficient for water vapor [kg s^{-1} m^{-2}]; N_{ch} is number of channels; W is width of the exchanger [m]; x is distance of sub-heat exchanger [m]; ε is effectiveness.

The IEC mathematical model developed allows to determine the optimal geometrical and operating parameters. The IEC mathematical model was implemented in *Engineering Equation Solver* (EES) software.

2.3 Manufacturing of the indirect evaporative cooler

The heat and mass exchanger of the IEC system was manufactured by using 3D printing techniques. 3D printing can be used to manufacture complex design prototypes at a low economical cost. However, the main limitation of this manufacturing technique could be the size of the prototypes.

A design of the manufactured IEC system is shown in Fig. 2. It can be observed the heat and mass exchanger, a reservoir for water and adapter parts for testing the IEC system. The water distribution was carried out through perforations in the upper part of the device. The driven water came from the network. The exchanger was made up of 12 dry channels and 11 wet channels. The dimensions of the exchanger were 130 mm high, 140 mm long and 116 mm wide, and the material used to make the exchanger was resin [21].

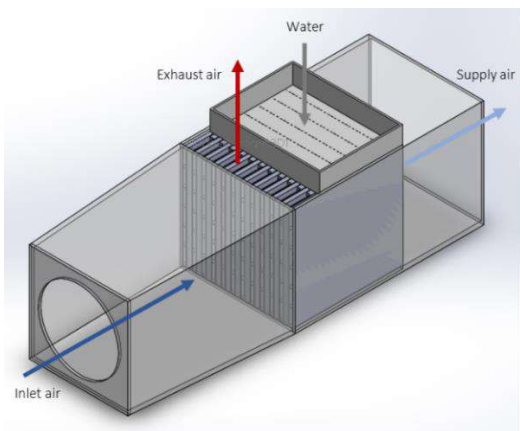

Fig. 2 - Design of the IEC system.

The design of a dry channel of the IEC system is shown in Fig. 3.

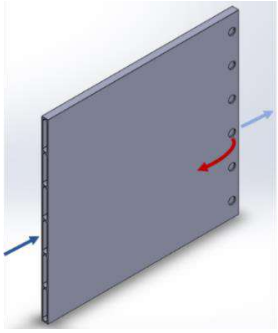

Fig. 3 - Design of the dry channels.

The thickness of the walls was 0.9 mm. These channels were composed of 6 perforations with a diameter of 5 mm. In addition, the wet channels were covered with a thin layer of cotton in order to retain the maximum amount of water.

2.4 Evaluation indexes of the indirect evaporative cooler

The performance of the IEC system designed was evaluated under the following ratios:

- Cooling capacity per unit volume of the IEC system, see Eq. (4).

$$C_V = Q_{cooling}/Volume \quad (4)$$

- Cooling capacity per unit airflow rate of the IEC system, see Eq. (5).

$$C_R = Q_{cooling}/\dot{V}_{supply} \quad (5)$$

Where $Q_{cooling}$ was computed with energy balance on the dry-side fluid, see Eq. (6).

$$Q_{cooling} = \dot{m} \cdot (h_{out} - h_{in}) \quad (5)$$

Some commercial IEC systems obtained values of C_V and C_R of 5.1 kW/m^3 and 23.5 kW/(m^3/s), respectively [22].

A test facility was used to analyse the experimental performance of the IEC system under different inlet air temperatures, from 27 °C to 46 °C, and different inlet air flow rate, from 100 m^3/h to 190 m^3/h. The supply air flow rates were 75 m^3/h for the inlet air flow rate of 100 m^3/h and 115 m^3/h for the inlet air flow rate of 190 m^3/h. The value of inlet humidity ratio remained constant, 10 g/kg.

All the experimental tests were carried out under steady-state conditions. The sampling time was 3 seconds, and the values are averaged every 30 min. The accuracy of the measuring devices used was ±0.12 °C for the temperature sensors, ±0.15 °C for the dew-point temperature sensors and ±0.5 % for the differential pressure transmitters.

The energy consumption of a fan to overcome the pressure losses of the heat exchanger was calculated with the values of friction losses and minor losses.

3. Results

The numerical and experimental results of the manufactured IEC system are shown in this section.

3.1 Results of numerical modelling

The mathematical model can be individually applied to *n* sub-heat exchangers of an IEC system. For the present work, 60 sub-heat exchangers were considered. As an example, the air conditions of the dry and wet air streams for each computational element of the exchanger are shown in Fig. 4. This model allowed to obtain the temperature, enthalpy, and humidity distributions of the air inside the exchanger. Moreover, this mathematical model could be used to obtain the length of the heat and mass exchanger from pre-established inlet and outlet air conditions.

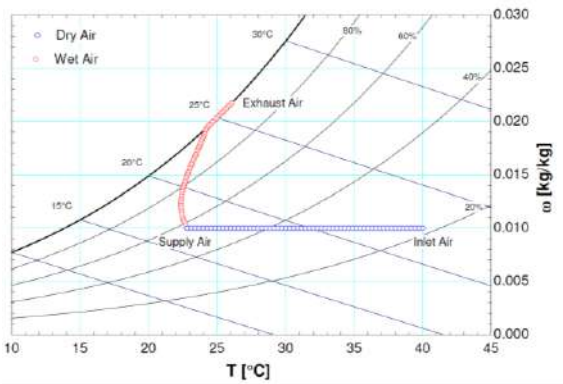

Fig. 4 – Psychrometric chart with the dry and wet air streams for each computational element.

3.2 Experimental results

The result of the manufacture of the heat and mass exchanger of the IEC system is shown in Fig. 5. It can be observed that the exchanger was stacked using dry and wet channels. The wet channels were covered with a thin layer of cotton in order to retain water, which was supplied from the top.

Fig. 5 – Heat and mass exchanger of the IEC system.

The experimental results of C_V and C_R for each case study are shown in Fig. 6 and Fig. 7. It can be observed than the C_V values increased when the inlet air temperature was raised, see Fig. 6. The IEC system also improved the C_V value when the inlet air flow rate increased from 100 m³/h to 190 m³/h, as shown in Fig. 6. The maximum C_V value was 177 kW/m³ for an inlet air temperature of 46 °C and an inlet air flow rate of 190 m³/h. However, the minimum C_V value was 45 kW/m³ for an inlet air temperature of 27 °C and an inlet air flow rate of 100 m³/h. Therefore, the air-cooling device increased its cooling capacity for hot inlet air conditions and higher air flow rate.

The C_V values obtained in the present work were significantly higher than those obtained by commercial IEC systems, shown in section 2.4. Therefore, the device was designed and manufactured with high compactness.

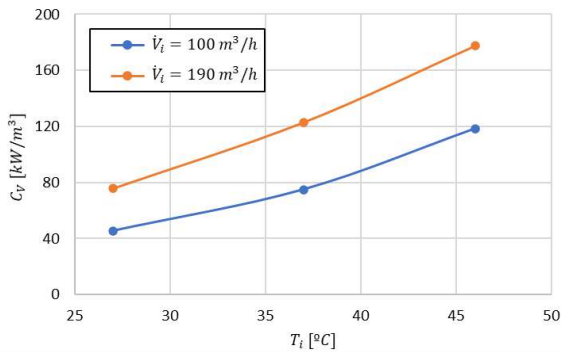

Fig. 6 – Results of cooling capacity per unit volume of the IEC system.

Regarding C_R, similar trends to those obtained for C_V were found when the inlet air temperature increased. That is, the higher the air temperature, the higher the C_R value, as shown in Fig. 7. However, C_R decreased when the inlet air flow rate increased. The maximum C_R value was 14.51 kW/(m³/s) for an inlet air temperature of 46 °C and an inlet air flow rate of 100 m³/h, and the minimum C_R value was 5 kW/(m³/s) for an inlet air temperature of 27 °C and an inlet air flow rate of 190 m³/h. For this ratio, the C_R values obtained in the present work were lower than those obtained by commercial IEC systems, shown in section 2.4. Therefore, the device needed to supply less flow to cool air.

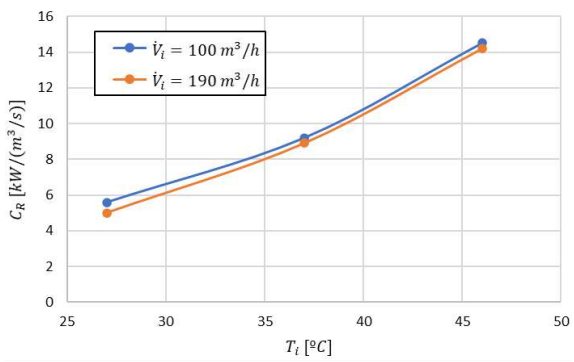

Fig. 7 – Results of cooling capacity per unit airflow rate of the IEC system.

4. Conclusions

In the present work, the geometric design and manufacture of an indirect evaporative cooling (IEC) system was carried out.

The design of the IEC system was achieved from numerical results obtained with a mathematical model based on ε-NTU numerical method. Moreover, this model allowed to obtain the temperature, enthalpy, and humidity distributions of the air inside the IEC system.

The experimental performance of the air-cooling device was evaluated under two ratios: cooling capacity per unit volume (C_V) and cooling capacity per unit airflow rate (C_R). The results showed high C_V values, up to 177 kW/m^3, mainly for high inlet air temperatures and inlet air flow rates. The C_R results were higher for high inlet air temperatures and low inlet air flow rates, with a maximum value of 10.9 kW/(m^3/s).

These results suggested that highly compact indirect evaporative coolers can achieve air-cooling processes with a low energy consumption and a low environmental impact.

Acknowledgement

The authors acknowledge the financial support received by the European Regional Development Fund and the Andalusian Economy, Knowledge, Enterprise and University Council, Spain, through the research project HICOOL, reference 1263034, and by European Union's Horizon 2020 research and innovation programme, through the research project WEDISTRICT, reference H2020-WIDESPREAD2018-03-857801. The present work has also been conducted as a part of the CLIMASEE project 12020113 funded by Diputación Provincial de Jaén.

Data Statement

The datasets generated during and/or analysed during the current study are not available because the authors continue to investigate the air-cooling system, but the authors will make every reasonable effort to publish them in near future.

5. References

[1] European Parliament, European Directive 2010/31/EU on the Energy Performance of Buildings, 2010. doi:doi:10.3000/17252555.L_2010.153.eng.

[2] P. Sun, J.Y. Wu, R.Z. Wang, Y.X. Xu, Analysis of indoor environmental conditions and heat pump energy supply systems in indoor swimming pools, Energy Build. 43 (2011) 1071–1080. doi:10.1016/j.enbuild.2010.08.004.

[3] B. Porumb, P. Ungureşan, L.F. Tutunaru, A. Şerban, M. BĂlan, A Review of Indirect Evaporative Cooling Operating Conditions and Performances, Energy Procedia. 85 (2016) 452–460. doi:10.1016/j.egypro.2015.12.226.

[4] B. Porumb, P. Ungureşan, L.F. Tutunaru, A. Şerban, M. BĂlan, A Review of Indirect Evaporative Cooling Technology, Energy Procedia. 85 (2016) 461–471. doi:10.1016/j.egypro.2015.12.228.

[5] H. Sadighi Dizaji, E.J. Hu, L. Chen, A comprehensive review of the Maisotsenko-cycle based air conditioning systems, Energy. 156 (2018) 725–749. doi:10.1016/j.energy.2018.05.086.

[6] M.H. Mahmood, M. Sultan, T. Miyazaki, S. Koyama, V.S. Maisotsenko, Overview of the Maisotsenko cycle – A way towards dew point evaporative cooling, Renew. Sustain. Energy Rev. 66 (2016) 537–555. doi:10.1016/j.rser.2016.08.022.

[7] Z. Duan, X. Zhao, J. Liu, Q. Zhang, Dynamic simulation of a hybrid dew point evaporative cooler and vapour compression refrigerated system for a building using EnergyPlus, J. Build. Eng. 21 (2019) 287–301. doi:10.1016/j.jobe.2018.10.028.

[8] S. Delfani, M. Karami, Transient simulation of solar desiccant/M-Cycle cooling systems in three different climatic conditions, J. Build. Eng. 29 (2020) 101152. doi:10.1016/j.jobe.2019.101152.

[9] F. Comino, J. Castillo González, F.J. Navas-Martos, M. Ruiz de Adana, Experimental energy performance assessment of a solar desiccant cooling system in Southern Europe climates, Appl. Therm. Eng. 165 (2020) 114579. doi:10.1016/j.applthermaleng.2019.114579.

[10] F. Comino, M. Ruiz de Adana, F. Peci, Energy saving potential of a hybrid HVAC system with a desiccant wheel activated at low temperatures and an indirect evaporative cooler in handling air in buildings with high latent loads, Appl. Therm. Eng. 131 (2018) 412–427. doi:10.1016/j.applthermaleng.2017.12.004.

[11] D. Pandelidis, S. Anisimov, P. Drag, Performance comparison between selected evaporative air coolers, Energies. 10 (2017) 1–20. doi:10.3390/en10040577.

[12] F. Comino, S. Milani, S. De Antonellis, C.M. Joppolo, M. Ruiz de Adana, Simplified performance correlation of an indirect evaporative cooling system: development and validation, Int. J. Refrig. 88 (2018) 307–317. doi:10.1016/j.ijrefrig.2018.02.002.

[13] A. Ahmad, S. Rehman, L.M. Al-Hadhrami, Performance evaluation of an indirect evaporative cooler under controlled environmental conditions, Energy Build. 62 (2013) 278–285. doi:10.1016/j.enbuild.2013.03.013.

[14] S. De Antonellis, C.M. Joppolo, P. Liberati, S. Milani, L. Molinaroli, Experimental analysis of a cross flow indirect evaporative cooling system, Energy Build. 121 (2016) 130–138. doi:10.1016/j.enbuild.2016.03.076.

[15] A. Tejero-González, M. Andrés-Chicote, E. Velasco-Gómez, F.J. Rey-Martínez, Influence of constructive parameters on the performance of two indirect evaporative cooler prototypes, Appl. Therm. Eng. 51 (2013) 1017–1025. doi:10.1016/j.applthermaleng.2012.10.054.

[16] S.J. Oh, M.W. Shahzad, M. Burhan, W. Chun, C. Kian Jon, M. KumJa, K.C. Ng, Approaches to energy efficiency in air conditioning: A comparative study on purge configurations for indirect evaporative cooling, Energy. 168 (2019) 505–515. doi:10.1016/j.energy.2018.11.077.

[17] H. Sadighi Dizaji, E.J. Hu, L. Chen, S. Pourhedayat, Development and validation of an analytical model for perforated (multi-stage) regenerative M-cycle air cooler, Appl. Energy. 228 (2018) 2176–2194. doi:10.1016/j.apenergy.2018.07.018.

[18] M. Ali, W. Ahmad, N.A. Sheikh, H. Ali, R. Kousar, T. ur Rashid, Performance enhancement of a cross flow dew point indirect evaporative cooler with circular finned channel geometry, J. Build. Eng. (2020) 101980. doi:10.1016/j.jobe.2020.101980.

[19] J. Lin, R. Wang, C. Li, S. Wang, J. Long, K.J. Chua, Towards a thermodynamically favorable dew point evaporative cooler via optimization, Energy Convers. Manag. 203 (2020) 112224. doi:10.1016/j.enconman.2019.112224.

[20] Z. Duan, X. Zhao, J. Li, Design, fabrication and performance evaluation of a compact regenerative evaporative cooler: Towards low energy cooling for buildings, Energy. 140 (2017) 506–519. doi:10.1016/j.energy.2017.08.110.

[21] Formlabs, https://formlabs.com/materials/, (Accessed 10.12.21). (2021).

[22] Climate Wizard by Seeley International, Indirect Evaporative Air Conditioning, (2021).

Extension of the Air Distribution Network Design Optimization algorithm: implementation of fittings

Sandy Jorens [a], Zakarya Kabbara [a], Ehsan Ahmadian[a], Ivan Verhaert [a]

[a] Research Group BEASt (Built Environment Assessing Sustainability), Faculty of Applied Engineering: Electromechanics, University of Antwerp, Antwerp, Belgium, sandy.jorens@uantwerpen.be.

Abstract. The number of requirements that heating, ventilation, and air conditioning (HVAC) systems in buildings have to fulfill continues to rise. Design engineers are being challenged to design HVAC systems with high standards of performance considering, comfort and energy efficiency. These conflicting objectives have to be achieved within a limited budget and time. Presently, considerable reliance is still placed on rules of thumb and the designer's experience, which often results in sub-optimal designs. More than ever, there is a need for practically usable design tools. Especially in the field of centralized air distribution system design, user-friendly tools are needed to support the design engineer. In previous research, an air distribution network design (ADND) optimization algorithm was developed. The ADND algorithm is a heuristic optimization algorithm that automatically generates numerous different air distribution system configurations (i.e., ductwork layout and sizing) for non-residential buildings while minimizing the material costs. Although the ADND algorithm shows promising results, some additions are still required before the algorithm can be used in practice. Currently, the objective function is limited to the minimization of material costs. However, other objectives, e.g., minimization of energy costs or noise levels, are not yet considered. Moreover, the generated configurations are based on the aeraulic performance of only circular and rectangular ducts. Fittings and other ventilation components (e.g. silencers and diffusers) are not yet included. In this research, the ADND optimization algorithm was improved by implementing fittings (i.e., bends, reducers, tees, and cross fittings) in the optimization algorithm. A practical test case demonstrates the extended ADND optimization algorithm.

Keywords. Air distribution system design, layout optimization, fittings, zeta values, heuristics, test case.
DOI: https://doi.org/10.34641/clima.2022.99

1. Introduction

1.1 Design of centralized air distribution systems

Nowadays, design engineers are being challenged to design HVAC systems with high standards of performance considering, comfort, and energy efficiency, while time and budget are limited. To achieve these (conflicting) objectives, the design engineer is left with numerous difficult decisions.

When designing centralized air distribution systems in non-residential buildings, a major part of these decisions is related to the air distribution system's configuration, i.e., the ductwork layout and duct and fan sizing. The complexity of this design problem is determined not only by its conflicting objectives, but also by numerous linear and non-linear constraints to which the decisions are subjected (e.g., limitations on space, duct sizes, and fan pressure)[1]. Therefore, a simulation-based tool for informed decision-making could benefit design engineers to achieve superior ventilation systems with optimal performance.

Although both the ductwork layout and ducts and fan sizing, have a significant impact on the performance and the total cost of the air distribution system, most design methods are limited to the ducts and fan sizing [2-5]. The layout itself is predetermined using rules of thumb and the designer's experience, which results in workable designs, but not necessarily optimal designs. Even when, for example, drawing tools are used that partly automate the drawing of the layout, a comparison of different layouts in terms of costs and other performance parameters is still lacking.

To overcome this shortcoming, Jorens et. al. (2018)

Copyright ©2022 by the authors. This conference paper is published under a CC-BY-4.0 license.

introduced a novel optimization problem, i.e., the air distribution network design (ADND) optimization problem [1]. In this problem, the optimal ductwork layout is determined jointly with the duct and fan sizes, while minimizing the total cost of the system. The authors also laid the basic strategy to solve this novel optimization problem by developing a novel heuristic algorithm, i.e., the ADND algorithm [6]. The ADND optimization algorithm can generate different air distribution system configurations for buildings with varying characteristics while minimizing material costs.

1.2 ADND algorithm

The ADND algorithm starts from a building's floor plan where all demand nodes (= diffusers) with the corresponding design airflow rates are indicated, as well as all the potential duct and fan locations.

Graph theory [7] is used to represent this floor plan as a rooted undirected weighted graph G(N, E), with E being the set of edges representing potential air ducts and N the set of nodes or vertices representing potential supply nodes (fans), demand nodes (terminal units or diffusers), and junctions (fittings). Additionally, several constraints are specified and given as input to the ADND algorithm, e.g., maximum duct heights, maximum air velocities, and maximum fan pressure. These constraints depend on local standards, the customer's preferences, and the building's restrictions. For example, when the ductwork has to run above a suspended ceiling, the available building space is limited, which impacts the maximum allowable duct height. Figure 4 and appendix 1 give an example of the algorithm's input data (see section 3 Test case).

The ADND algorithm consists of two major phases, i.e., a construction phase and a local search phase. In the first phase, complete air distribution system configurations are generated from scratch and evaluated for feasibility. A feasible layout can be seen as a directed tree, without loops, that connects the root node (i.e., fan) to all demand nodes (i.e., diffusers) in the graph (e.g., figure 5 gives an example of a feasible layout). To generate numerous feasible layouts, an adapted randomized version of Prim's algorithm is applied [6,7]. Adapted in the sense that a layout generation starts from a predefined root node instead of a random node and that the ending solution does not need to be a spanning tree. The stopping criterion is achieved when all demand nodes are part of the tree. Instead of growing the tree by adding the edge with minimal weight each time, this edge is chosen randomly to increase the variety of the generated layouts. After generating the layouts, the ADND algorithm continues with an initial sizing of the ductwork using average velocities [5]. All resulting configurations are subjected to a feasibility check to evaluate if each configuration meets the predefined constraints (e.g., maximum duct height constraints [6]). The second phase of the ADND algorithm, i.e., the local search phase, optimizes the duct sizes of every feasible layout in terms of material costs. A steepest descent-mildest ascent strategy is chosen as a move strategy. This means that every move results in the best possible improvement or the least possible deterioration. Specific for the ADND optimization problem, duct sizes are decreased one by one (starting with the biggest ducts first) until a predefined maximum pressure constraint is exceeded. Next, duct sizes are increased again one by one (starting with the smallest ducts first), until the maximum pressure constraint is satisfied again.

The result of the ADND algorithm is a list of feasible ADN configurations, sorted by material price. Although the objective function is defined as a single objective function, the ADND optimization algorithm does allow the user to make a tradeoff between the material costs and energy use. For every feasible configuration that is generated, the following data is calculated: ductwork costs, pressure loss in every path of the network, theoretical fan power, and the pressure difference between the critical path and the path with the lowest pressure loss.

1.3 ADND algorithm: shortcomings

Before the algorithm can be used in practice, some features still need to be added. Besides the ductwork, other ventilation components still have to be integrated into the algorithm, e.g., fittings, silencers, filters, diffusers, and dampers. Moreover, the objective function should include not only the material costs but also other costs, such as maintenance, installation, and energy costs.

In this paper, the ADND algorithm is extended by implementing both circular and rectangular fittings in the algorithm. Specifically, the following fittings were integrated: bends, tees, cross fittings, and reducers. Section 2, first discusses which models are used to calculate the pressure losses of all fittings. Secondly, we discuss how the ADND algorithm automatically detects all fittings (location and type) in an ADN configuration.

2. Fittings

2.1 Fittings modeling

The pressure drop due to a bend or reducer is calculated with the following equation:

$$\Delta p = \xi * \frac{\rho * v^2}{2} \tag{1}$$

Where:

- Δp = pressure drop (Pa),
- ξ = local loss coefficient (/),
- ρ = density (kg/m^3),
- v = velocity (m/s).

The pressure drops due to tees and cross fittings (figure 1) are calculated with equations 2 and 3.

$$\Delta p = \xi_{c,s} * \frac{\rho * {v_c}^2}{2} \quad (2)$$

and

$$\Delta p = \xi_{c,b} * \frac{\rho * {v_c}^2}{2} \quad (3)$$

Where:

- $\xi_{c,s}$ = loss coefficient straight path S (/)
- $\xi_{c,b}$ = loss coefficient branch path B (/)
- v_c = air velocity in the common duct C (m/s).

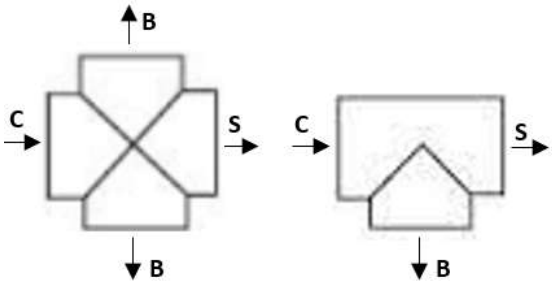

Fig. 1 – A cross (left) and a tee (right)

Depending on the fitting type, the local loss coefficient ξ depends on different parameters (e.g., cross-sectional area or the ratio of inlet area over the outlet area). The required ξ value can be looked up in tables. In this research, the duct fitting database of ASHRAE [2] was implemented in the ADND algorithm to calculate the local loss coefficients. Appendix 2 gives an overview of the different fitting types that are implemented in the ADND algorithm. It should be noted that the algorithm applies linear interpolation when the input values of the models are between index values of the rows and columns of the ASHRAE tables.

2.2 Automatic fitting detection

The detection of the fittings takes place at the end of the construction phase, i.e., after the initial sizing of the feasible layouts. The flowchart in figure 2 gives an overview of the different steps that the algorithm has to go through to determine all junction types of an air distribution network layout.

To clarify the detection process, a simplified example is used. Assume that figure 3 represents a feasible layout that consists of four ducts: [0,1], [1,2], [1,3] and [2,4]. Node 0 is the fan, nodes 3 and 4 are demand nodes, and nodes 1 and 2 are junctions.

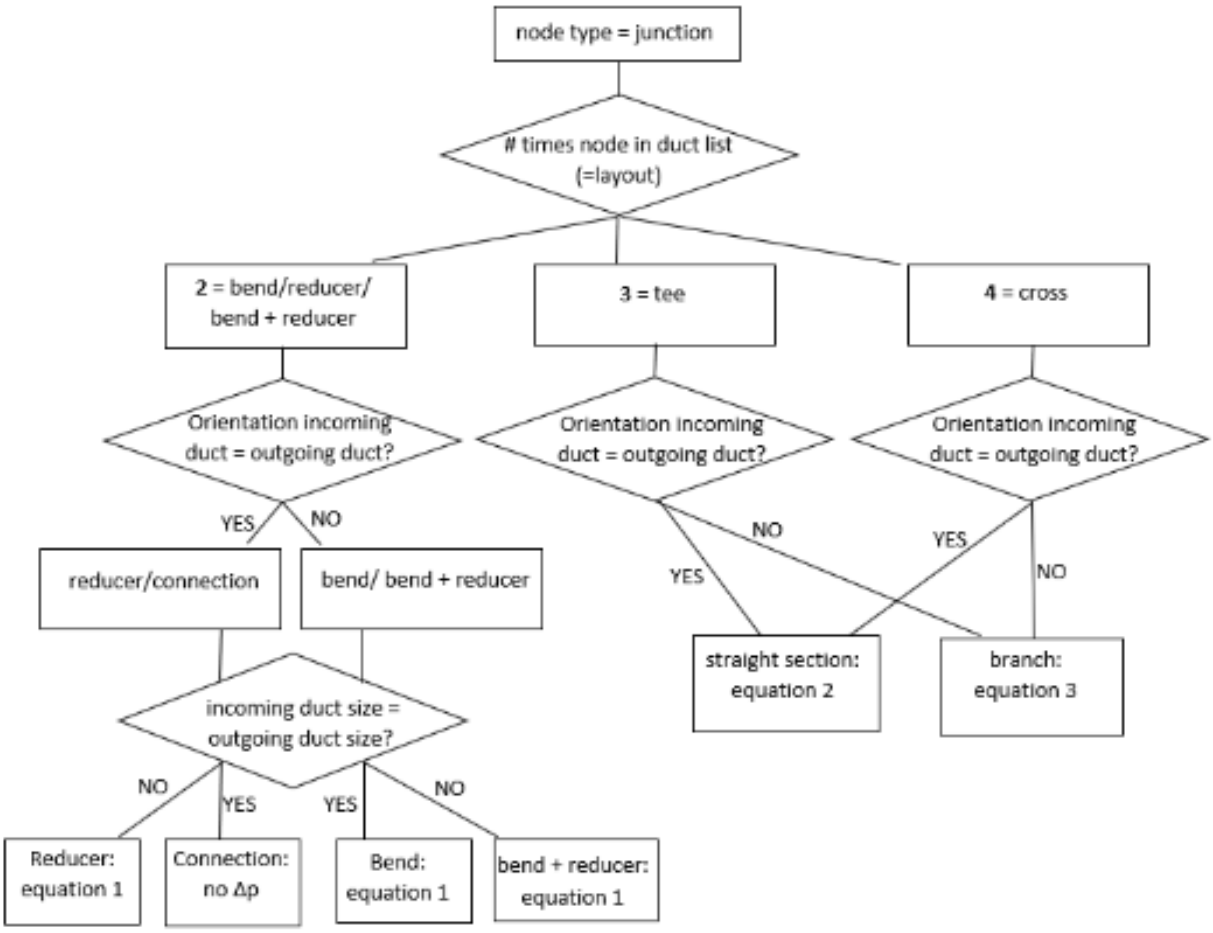

Fig. 2 – Flow chart: automatic fitting detection

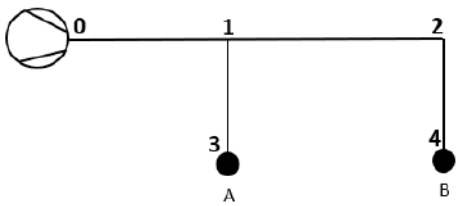

Fig. 3 – A simple air distribution network

According to the flowchart (figure 2), the first step is to count the number of times a junction occurs in the duct list. In this case, there are 2 junctions, i.e., node 1 and node 2. Node 2 occurs two times in the duct list (i.e., one time as an end node in duct [1,2] and one time as a start node in duct [2,4]). This means that node 2 is either a bend, a combination of a bend and a reducer, or a reducer. Next, the algorithm determines if both the incoming [1,2] and outgoing ducts [2,4] have the same or different orientations to specify the node type. For the algorithm to be able to identify a duct orientation (i.e. straight or branch), coordinates have to be first introduced. Until now, a node was characterized solely by a node name and a type. Now, coordinates are added as additional parameters for every node. This means that every node is not only characterized by its name and type, but also by an x and y coordinate. To compare the orientation of two adjacent ducts, the x and y coordinates of the first duct's start node are compared with the x and y coordinates of the second duct's end node. If both coordinates are different, the orientation of the ducts is not the same. If either the x coordinates or the y coordinates are equal, the ducts have the same orientation (i.e., straight).

In the example layout, duct [1,2] has a different orientation than duct [2,4]. Consequently, node 2 is a bend or a combination of a bend and a reducer. If the dimensions of the incoming and outgoing duct are equal, node 2 can be defined as a bend. If not, node 2 is a combination of a bend and a reducer. Similar to this example, the ADND algorithm can identify the other fitting types as well.

3. Test Case

In this section, a simplified, but realistic test case demonstrates some of the capabilities of the extended ADND algorithm.

3.1 Input data

Figure 4 shows one floor of a small office building. The location of all demand nodes and the associated airflow rates (in m^3/h) are indicated on the floor plan (x), as well as all potential duct locations (black lines) and potential junctions (black dots). In total, there are 37 nodes, i.e., one root node (i.e., fan), 13 demand nodes, and 23 junctions. The fan is located in the technical room on the top floor of the building. An overview of the input data for the ducts can be found in appendix 1 as well. All potential ducts that can be installed in the building are listed, where each duct is characterized by a start and end node (i.e., red numbers in figure 4), and a length. Additionally, all ducts must comply with the maximum height and velocity restrictions that have been set (i.e., H_{max} and v_{max}).

3.2 Results

In this paper, two scenarios are simulated. In the first case, the maximum pressure constraint of the critical path is set at 30 Pa, and in the second case at 50 Pa. The best (i.e., cheapest) resulting configurations are displayed graphically in figure 5. Additionally, table 1 compares the two solutions in terms of several evaluation parameters.

As can be seen, the ADND algorithm calculates the total volumetric flow rate (m^3/h), ductwork costs (€), the total pressure loss of the critical path (Pa), and the theoretical fan power (W) for every solution. Since a direct relation exists between the fan power and the energy use, this evaluation parameter gives more insight into the energy use of a solution. Last, the ADND algorithm calculates the pressure difference between the critical path and the path of minimum pressure loss (Pa). According to the pressure balancing constraint, this parameter should be as low as possible [6].

Tab. 1 – Test case results

	Solution 1 (max 30Pa)	**Solution 2 (max 50 Pa)**
Flow rate (m^3/h)	3420	3420
Duct costs (€)	1220	1179
Δp critical (Pa)	29.96	49.56
Theoretical fan power (W)	28.46	47.08
Δp_{max} - Δp_{min} (Pa)	13.05	34.17

It should be noted that the following assumptions were made for the pressure and price calculations.

- Constant air density (1.2 kg/m^3).
- Ductwork material: galvanized steel (roughness e = $0.15*10^{-3}$ m).
- Fully developed airflow in all ducts and fittings.
- The total pressure loss of the critical path includes the pressure losses of both the ductwork and the fittings. The material cost, however, solely includes the ductwork costs and is based on the price list of manufacturer Lindab [8].

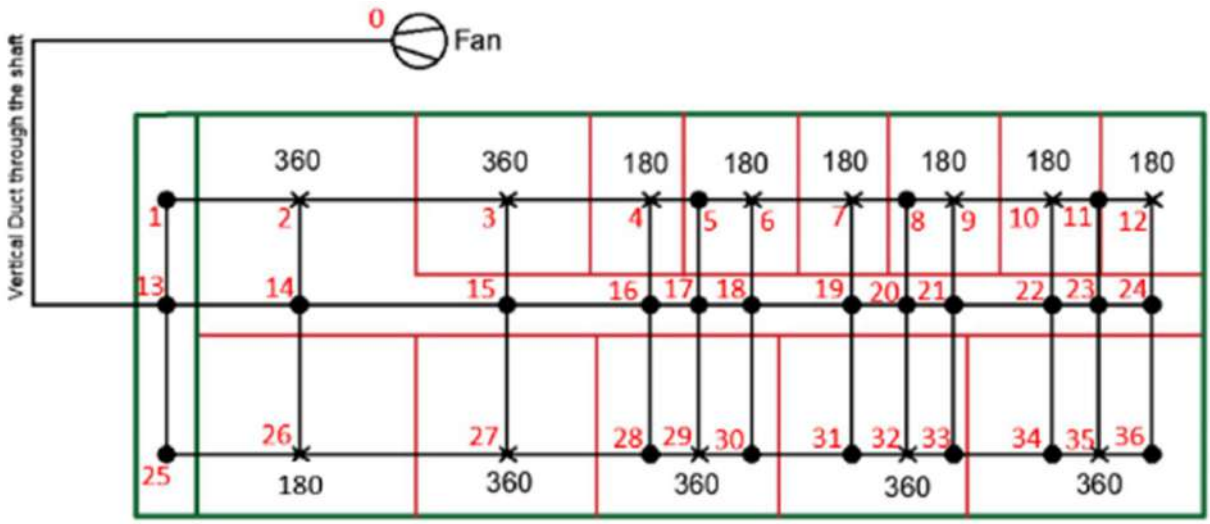

Fig. 4 – Floor plan of one floor in an office building (= input graph ADND algorithm), where all demand nodes with corresponding flow rates in m³/h (x), root node (fan), potential ducts (black lines), and potential junctions (black dots) are indicated

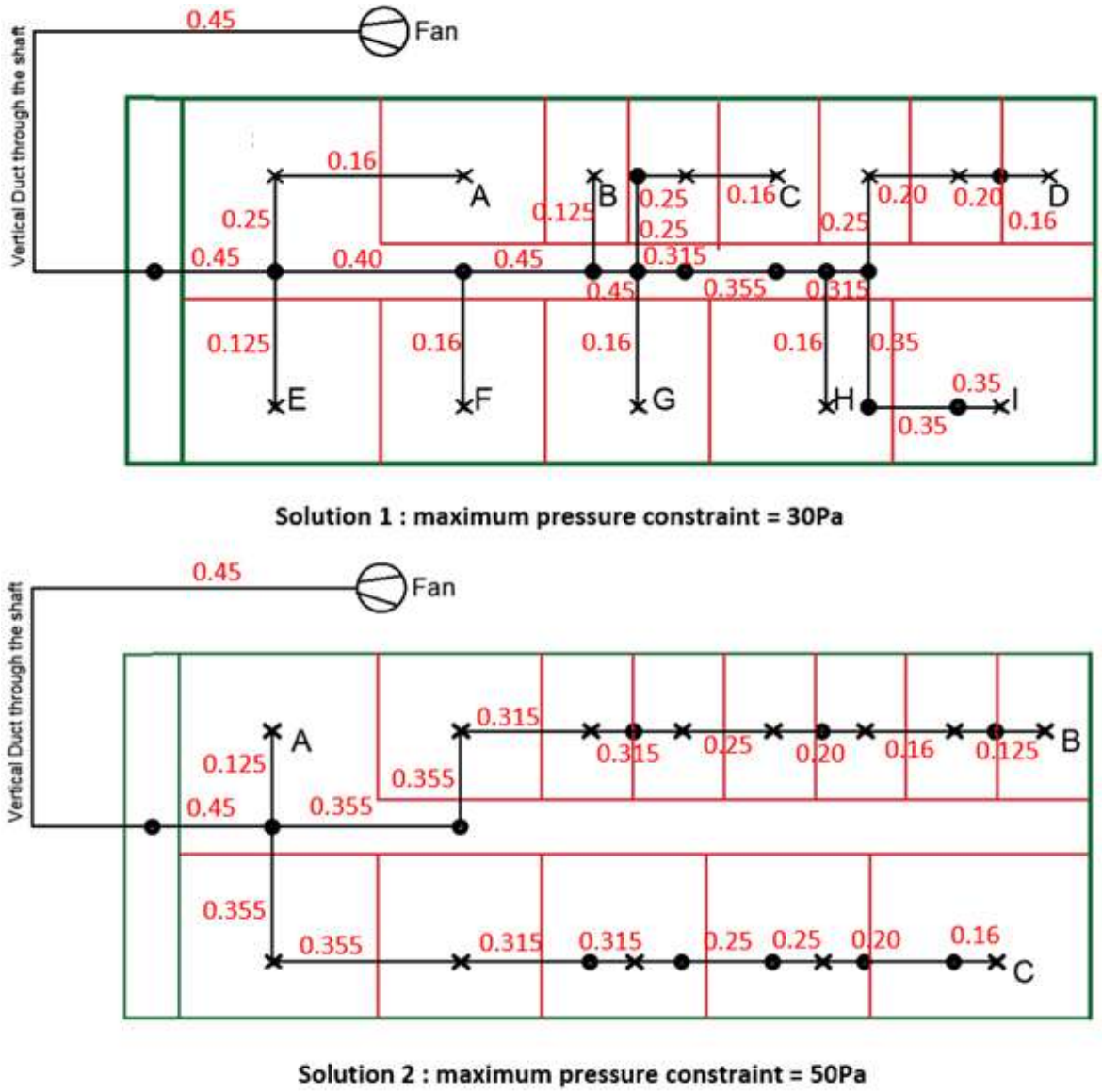

Fig. 5 – The two best resulting ADN configurations, generated with the ADND algorithm (duct dimensions in m)

3.3 Discussion

As can be observed in table 1, there is a relatively small price difference between solutions 1 and 2. Solution 2 is 3.4% cheaper than solution 1. The difference in fan power, however, is very significant. The fan power of solution 2 is not less than 65% higher than the fan power of solution 1.

This can be explained using the graphs presented in figures 6 and 7. Figure 6 presents the pressure drop (Pa) in a duct as a function of the air velocity (m/s). The pressure loss in a duct grows exponentially with increasing air velocity. Figure 7, on the other hand, shows the relation between the pressure loss in the branch part of a tee (Pa) and the inlet air velocity (m/s). As can be observed, the pressure loss rises substantially once the air velocity exceeds 4 m/s.

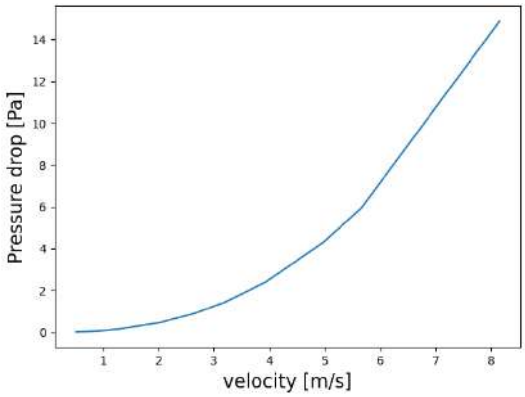

Fig. 6 – Pressure drop (Pa) in a 2m galvanized steel duct vs the velocity (m/s)

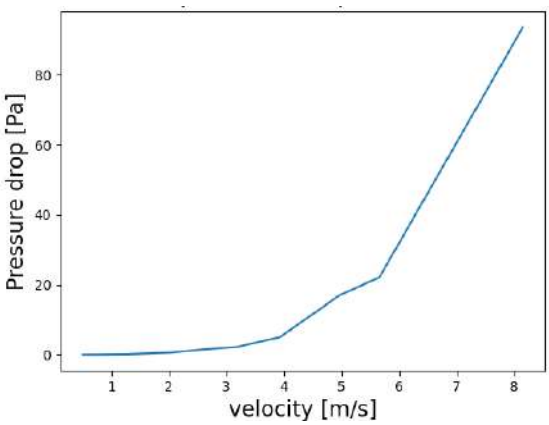

Fig. 7 – Pressure drop (Pa) in the branch part of a circular tee vs velocity (m/s) in the common duct

The pressure drop constraint of 30 Pa (i.e., solution 1) has resulted in a solution with larger duct sizes and consequently lower to medium air velocities. When the pressure limitations are increased to 50Pa, the algorithm starts reducing duct dimensions until the critical path achieves a pressure loss of 50Pa. However, because of the reduction of the duct sizes, the velocities rise (> 4 m/s) and thus the pressure losses increase substantially (see figures 6 and 7). As a result, the maximum allowable pressure drop is already reached after reducing only a few duct diameters, thus limiting the price savings.

On the other hand, if the pressure constraint would be reduced below 30Pa (e.g., 20 pa), then this pressure reduction would correspond to a significant cost increase. Since a duct enlargement (i.e., velocity decrease) now leads to a relatively smaller pressure drop (see Fig. 6 and 7), many more ducts have to be enlarged before the pressure drop in the critical path is less than 20 Pa. Consequently, the ductwork costs will increase significantly.

This example demonstrates the need for a tool that supports the design engineer in informed decision-making to achieve superior air distribution systems with optimal design and performance. The development of the ADND algorithm is a fundamental first step in launching such a tool.

4. Conclusion and future research

In this research, the usability of the ADND optimization algorithm is increased by implementing both circular and rectangular fittings. For every feasible layout, generated with the ADND algorithm, the algorithm can detect automatically the location and type (i.e., bend, reducer, tee, or cross) of every fitting in the air distribution network. The pressure losses due to the fittings are calculated using the duct fitting database of ASHRAE.

The importance of a design algorithm, such as the ADND algorithm, that supports the design engineer in its decision-making, is demonstrated using a test case. It is clear that the design choices (e.g., duct sizes and layout) have a major impact on both the cost and performance of the air distribution network.

Although the ADND algorithm shows promising results, several features can still be added to increase its flexibility and usability in practice, e.g.:

- The extension of the objective function with other objectives, e.g., minimization of the energy costs, maintenance costs, and installation costs.
- The implementation of additional components, e.g., silencers, filters, and diffusers.
- The implementation of CAVs and VAVs, so that optimal demand controlled ventilation systems can be designed and evaluated.
- Models that can evaluate the generated designs in terms of air quality, comfort, and acoustics.
- After all component models have been implemented in the ADND algorithm, a validation on system level has to be conducted.

The implementation of these features in the ADND algorithm is part of future research.

5. Acknowledgement

This work has been supported by the Flemish Agency for Innovation and Entrepreneurship (VLAIO) in the Flux50 project Smart Ventilation (HBC.2020.2520).

6. Appendices

Appendix 1- Input data test case

Start node duct	End node duct	Length (m)	H_{max} (m)	V_{max} (m/s)
1	2	3.2	0.45	5
1	13	2.5	0.5	8
2	3	4.9	0.45	5
2	14	2.5	0.35	5
3	4	3.4	0.45	5
3	15	2.5	0.35	5
4	5	1.1	0.45	5
4	16	2.5	0.35	5
5	6	1.3	0.45	5
5	17	2.5	0.35	5
6	7	2.4	0.4	5
6	18	2.5	0.35	5
7	8	1.3	04	5
7	19	2.5	0.35	5
8	9	1.1	0.4	5
8	20	2.5	0.35	5
9	10	2.3	0.4	5
9	21	2.5	0.35	5
10	11	1.1	0.35	5
10	22	2.5	0.35	5
11	12	1.25	0.35	5
11	23	2.5	0.35	5
12	24	2.5	0.35	5
13	14	3.2	0.5	8
13	25	2.5	0.45	8
14	15	4.9	0.5	5
14	26	2.5	0.45	5
15	16	3.4	0.5	5
15	27	2.5	0.45	5
16	17	1.1	0.45	5
16	28	2.5	0.35	5
17	18	1.3	0.45	5
17	29	2.5	0.35	5
18	19	2.4	0.45	5
18	30	2.5	0.35	5
19	20	1.3	0.45	5
19	31	2.5	0.35	5
20	21	1.1	0.4	5
20	32	2.5	0.35	5
21	22	2.3	0.4	5
21	33	2.5	0.35	5
22	23	1.1	0.4	5
22	34	2.5	0.35	5
23	24	1.25	0.35	5
23	35	2.5	0.35	5
24	36	2.5	0.35	5
25	26	3.2	0.45	5
26	27	4.9	0.45	5
27	28	3.4	0.45	5
28	29	1.1	0.4	5
29	30	1.3	0.4	5
30	31	2.4	0.4	5
31	32	1.3	0.4	5
32	33	1.1	0.4	5
33	34	2.3	0.35	5
34	35	1.1	0.35	5
35	35	1.25	0.35	5
0	13	4	0.5	8

Appendix 2 - Fittings ASHRAE [2]

Component	Component ID	Input parameters
Rectangular bend 90°	ASHRAE CR3-1	Height h, width w, r/w is assumed to be 0.75
Circular bend 90°	ASHRAE CD3-1	Diameter D r/D is assumed to be 1.5
Rectangular reducer	ASHRAE SR4-1	Ratio of inlet area over the outlet area, reduction angle θ
Rectangular to circular reducer	ASHRAE SD4-2	Inlet and outlet diameter, reduction angle θ_2
Circular to circular reducer	ASHRAE SD4-1	Inlet and outlet area, angle of the transition θ (i.e., 15° by default)
Rectangular tee (180° outlets)	ASHRAE SR5-15	Ratio of inlet area over the outlet area, ratio of inlet volumetric flow rate over the outlet flow rate
Rectangular to circular tee (90° and straight outlets)	ASHRAE SR5-11	Ratio of inlet area over the outlet area, ratio of inlet volumetric flow rate over the outlet flow rate
Circular tee (90° and straight outlets)	ASHRAE SD5-9	Ratio of inlet area over the outlet area, ratio of inlet volumetric flow rate over the outlet flow rate
Cross (90° and straight)	ASHRAE SD5-24	Ratio of inlet area over the outlet area, ratio of inlet volumetric flow rate over the outlet flow rate

7. References

[1] Jorens S., Verhaert I., Sörensen K. Design optimization of air distribution systems in non-residential buildings. Elsevier. 2018; 175:48-56.

[2] ASHRAE. ASHRAE Handbook – Fundamentals. Chapter 21: Duct Design, pages 21.1-21.67. 2009.

[3] Asiedu Y., Besant R.W., Gu P. HVAC duct system design using genetic algorithms. HVACR research. 2000; 6: 149-173.

[4] Kim T., Spitler J.D., Delahoussaye R.D. Optimum duct design for variable air volume systems – part 1: problem domain analysis of vav duct systems and part 2: optimization of vav duct systems. ASHRAE Transactions. 2002; 108: 96-127.

[5] Mitchel J.W., Braun J.E. Principles of heating, ventilation and air conditioning in buildings. Wiley. 2012.

[6] Jorens S., Verhaert I., Sörensen K. Design optimization of air distribution systems in nonresidential buildings. Antwerp: University of Antwerp; 2021.

[7] Marcus D.A. Graph theory. A problem oriented approach. United States: Mathematical Association of America.

[8] https://www.lindab.com.

The datasets generated and/or analyzed during the current study are not fully available yet, because they are part of a larger research, which will be published in the near future.

Experimental assessment of thermal effectiveness of a regenerative indirect evaporative cooler

María Jesús Romero-Lara [a], Francisco Comino [b], Manuel Ruiz de Adana [a]

[a] Departamento de Química-Física y Termodinámica Aplicada, Escuela Politécnica Superior, Universidad de Córdoba, Campus de Rabanales, Antigua Carretera Nacional IV, km 396, 14071 Córdoba, España, p42rolam@uco.es; manuel.ruiz@uco.es

[b] Departamento de Mecánica, Escuela Politécnica Superior, Universidad de Córdoba, Campus de Rabanales, Antigua Carretera Nacional IV, km 396, 14071 Córdoba, España, francisco.comino@uco.es.

Abstract. Heating, ventilation and air-conditioning, HVAC, systems represent a significant energy use in Europe, around 50% of total energy use in buildings. Conventional HVAC systems are mainly based on direct expansion units, whose use of 100% outdoor air leads to high energy use. Then, different innovative and efficient air-cooling systems could be an interesting alternative to approach Nearly Zero Energy Buildings, nZEB. One of these efficient solutions is the technology of indirect evaporative cooling. This work was based on the experimental evaluation of a regenerative indirect evaporative cooler, RIEC. Several empirical tests were carried out under different inlet conditions: inlet air temperature values between 29 °C and 43 °C, T_{OA}, and inlet air humidity ratio values between 9 g/kg and 13 g/kg, ω_{OA}, were considered. A constant inlet air stream, $\dot{V}_{OA}$, and a constant supply air stream, $\dot{V}_{SA}$, were adjusted during these tests for a steady-state period of thirty minutes each. The response variables which evaluated the thermal behaviour of this RIEC system were: (i) dew point effectiveness, ε_{dp}; (ii) wet bulb effectiveness, ε_{wb}. High values of ε_{dp} and ε_{wb} were reached when the inlet air humidity ratio was 9 g/kg, around 0.87 and 0.92, respectively. However, low values of dew point effectiveness, 0.71, and wet bulb effectiveness, 0.78, were showed when the inlet air temperature was 29 °C and the inlet air humidity ratio was 13 g/kg. According to the results that this study showed, the RIEC system could be an interesting alternative in spaces where improved indoor air quality is required by using 100% outdoor air. This type of systems could achieve high values of thermal performance, specially under hot-dry climatic conditions.

Keywords. Regenerative indirect evaporative cooling, effectiveness, air-cooling system.
DOI: https://doi.org/10.34641/clima.2022.145

1. Introduction

Heating, ventilation and air-conditioning, HVAC, systems account for 50% of the total final energy use in buildings [1]. Nowadays, conventional air-cooling systems based on direct expansion units dominate the air-conditioning market, whose the highest values of coefficient of performance, COP, are 4 [2].

However, Directive 2010/31/EU established "to promote an improvement in the energy performance of buildings" as the main objective of the Energy Performance of Buildings Directive (EPBD) [3]. According to the target of the energy use reduction, different solutions such as the modification of the building's thermal envelope, the use of efficient air-cooling systems and the use of renewable energies are proposed. In this way, the achievement of nearly Zero Energy Buildings, nZEB, mainly in the climatic zones of Southern Europe, will be closer.

Efficient evaporative cooling systems can contribute to achieve nZEB. There are two main categories for evaporative cooling systems: direct and indirect. In the first case, the water is evaporated by direct contact with the air stream. Therefore, the dry bulb air temperature is lowered, and the air humidity is increased. In the second case, the heat from the primary air stream is removed by a secondary air stream. It takes place through a heat exchanger. The main components in direct evaporative coolers are water pump, fan motor and a cooling pad which can be made of different materials.

Previous research works on evaporative coolers have been developed by several authors. Most of

Copyright ©2022 by the authors. This conference paper is published under a CC-BY-4.0 license.

them were focused on the study of energy performance of different efficient air-cooling systems [4]. An experimental investigation of a direct evaporative cooler, DEC, and an indirect evaporative cooler, IEC, was carried out for buildings under different climatic conditions [5]. Different outdoor conditions and different types of pad material were considered. The results showed that the performance of the DEC system was between 85% and 93%. The IEC-DEC combination presented a higher efficiency value, in the range of 95-110%. Comparative works carried out experimental investigations related to novel organic materials in DEC [6,7]. Eucalyptus fibres and ceramic pipes showed maximum effectiveness values of 72% and 68%, respectively [6]. Other material with high level of porosity was studied with the goal of solving the water stagnation. In this study, the cooling pad and the pump were replaced by the vermicompost material. An energy saving of 21.7% was showed compared to a conventional air-cooling system [7].

There are several works in the literature that studied the thermal behaviour of different types of IEC [8–10]. A study done with the original ε-NTU model compared a traditional heat recovery exchanger with an IEC. The main finding was the counter-flow indirect evaporative cooler was suitable for temperate climates [8]. In addition, in contrast to conventional heat recovery units, this type of IEC allowed to increase the temperature difference during the process of the heat recovery. Regression and numerical models were developed to predict the outlet temperature of a dew point evaporative cooling system. There was a variation between 4% and 10% between these values and the experimental results [9]. In other research work, a novel dew point cooler was investigated as part of a building energy model. The most favourable values of coefficient of performance, COP, were recorded between the months of June and September. The peak of this index, 51.1, was reached in July in the climate of Riyadh, Saudi Arabia [10].

Several hybrid systems composed of IEC and other technology were also analysed in literature [11,12]. A comparative analysis between three different air-cooling systems were carried out in terms of thermal comfort, air quality and energy use in different climates of Mediterranean area [11]. One of these systems was a desiccant regenerative indirect evaporative cooler, DRIEC, composed by an IEC and a desiccant wheel, DW. Results of this study shows that high values of thermal comfort were reached by DRIEC significantly reducing the energy use, four times lower than a direct expansion unit system, DX. The energy use of a hybrid system composed by an IEC and an air handling unit, AHU, was evaluated in other work [12]. In this way, the outdoor air was pre-cooled and pre-dehumidified before supplying it to the room. The reached value of COP in this research study was 14.2.

Regarding the IEC technology, different methods have been used to develop mathematical models of them. Neural network (NN), multiple polynomial regression (MPR) and design of experiments (DOE) are the most used mathematical methods. A prediction of hourly COP and the energy use saving of a dew point cooler, DPC, were studied by the NN method [13,14]. The most important conclusions were that the hourly COP prediction of the optimized IEC was better than the design one [13] and the annual energy use is reduced by up to 49.4% [14]. Other studies developed statistical models of a DPC with the aim of getting different performance indices [15,16]. The regression models developed in these works provided a well solution of forecasting the energy performance of DPCs. In addition, a simplified model of an IEC was developed by the DOE method and a detailed model of this air-cooling system was based on heat and mass transfer equations [16]. The low value of the wet bulb effectiveness deviation in each case, 3.4% and 2.1% respectively, showed they could an interesting tool in simulation works.

The main objective of this study was to evaluate experimentally the dew point effectiveness, ε_{dp}, and wet bulb effectiveness, ε_{wb}, of a regenerative indirect evaporative cooler, RIEC, under different inlet air conditions. This system worked with a single inlet air stream, 100% outdoor air, which was divided into two air streams, exhaust air and supply air.

2. Research Methods

2.1 Description of the RIEC system

An innovative air-cooling system based on a regenerative indirect evaporative cooler, RIEC, was studied in this research work. The modelled efficient equipment was composed by the following elements, see Fig. 1:

- A process fan, where a constant inlet air stream of 3700 m^3/h entered.
- A gross 60% filter placed before the heat exchanger.
- The regenerative indirect evaporative cooler based on a counter flow heat exchanger core.
- An ePM1 65% filter, or fine filter, after the RIEC system to improve the supply air quality.
- Several sensors located in the experimental setup:
    - Three air temperature sensors for the outside air stream, OA, the supply air stream, SA, and the exhaust air stream, EA.
    - Three air relative humidity sensors for the three different air streams above.
    - A pressure sensor in the supply air flow damper.
    - A volumetric water flow rate sensor to control the supplied water to the RIEC.
    - An energy consumption sensor in the process fan of this air-cooling system.

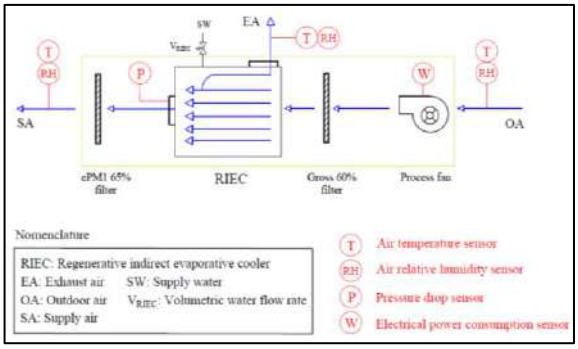

Fig. 1 – Experimental setup of the RIEC system.

In this research study, the RIEC unit consisted of alternative wet and dry channels separated by thin plates. The supplied air and the outdoor air were the main air streams, primary and secondary, respectively. The last one was cooled by water evaporation in the wet channels, and it was exhausted as humid air. The first one was supplied after being cooled, without moisture added. The main characteristics of this RIEC system are shown in Tab. 1.

Tab. 1 – Main characteristics of the RIEC system.

Parameter	Value	Unit
Nominal cooling capacity	18	kW
Nominal supply air flow rate	2880	m³/h
Inlet air flow rate in tests	3700	m³/h
Supply air flow rate in tests	1850	m³/h
Maximum water consumption	44	l/h

2.2 Experimental tests

An experimental test rig was built to study the dew point effectiveness and the wet bulb effectiveness of a RIEC under different working conditions. Inlet air temperature and inlet air humidity ratio were considered as input variables. Inlet air temperature values were varied between 29 °C and 43 °C during the experimental tests. Inlet air humidity ratio was set between 9 g/kg and 13 g/kg in these. A constant inlet air stream of 3700 m³/h was considered for this experimental study. The supply air stream of 1850 m³/h was also constant during all tests by maintaining a constant pressure of 120 Pa at the supply air flow damper.

The output variables analysed to evaluate the thermal behaviour of this RIEC system were: (i) dew point effectiveness, ε_{dp}; (ii) wet bulb effectiveness, ε_{wb}. Temperature, relative humidity and pressure sensors were used to control the experimental conditions. The type of each sensor and the accuracy of them are shown in Tab. 2.

Tab. 2 – Accuracy of the input variables sensors

Input variable	Sensor	Accuracy
Temperature (T)	PT100	±0.2 °C
Relative humidity (RH)	Capacitive	±3 %
Pressure drop (P)	Piezo-resistive	±0.05 hPa
Electrical power consumption (W)	3-phase	±1% measurement (kW)

A pressure drop sensor was located in the supply gate of RIEC to adjust the constant supply air volumetric flow rate to 1850 m³/h. The measurement frequency of the different variables was 30 seconds. Data measurements, in steady state conditions, were recorded in a data cloud monitoring system for each tested condition. The design of experiments technique, DOE, was used to develop the RIEC system study. This work was based on the Box-Behnken design. It showed the results of the most representative five experimental tests. They consisted in tests under different working conditions of the single inlet air stream temperature and humidity ratio, see Tab. 3. The values of the inlet air temperature, T_{OA}, were between 29 °C and 43 °C. The inlet air humidity ratio values, ω_{OA}, were between 9 g/kg and 13 g/kg. The combination of tests was developed to study the thermal effectiveness of the RIEC system. In this way, performance indexes could be studied under conditions of the same temperature and different humidity ratio, and vice versa. A total of four experimental tests were performed.

Tab. 3 – Experimental tests conditions for studying the RIEC system.

Test	T_{OA} [°C]	ω_{OA} [g/kg]	$\dot{V}_{OA}$ [m³/h]	$\dot{V}_{SA}$ [m³/h]
1	29	13	3700	1850
2	43	13	3700	1850
3	43	9	3700	1850
4	29	9	3700	1850

The thermal assessment of this regenerative indirect evaporative cooler was carried out by the analysis of the output parameters. The outlet air temperature value, T_{SA}, the outlet humidity ratio value, ω_{SA}, and the energy use value in RIEC in each case were the variables which were collected.

Polynomial equations of second order to study the relationship between output and input parameters were obtained with this DOE methodology. These initial tests conditions are represented in the

following Fig. 2.

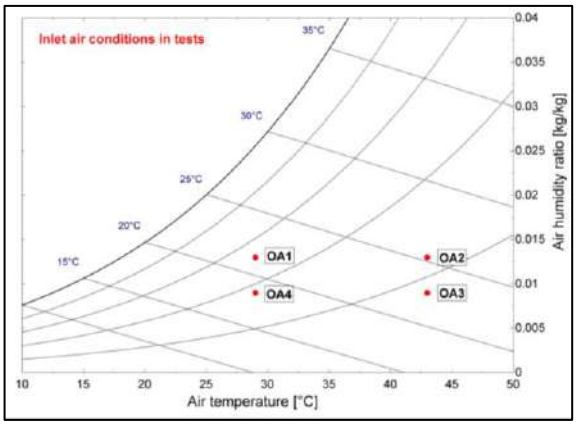

Fig. 2 – Psychrometric chart with the inlet air conditions of experimental tests in RIEC.

2.3 RIEC system evaluation indexes

This innovative and efficient RIEC system was evaluated in terms of dew point effectiveness, ε_{dp}, and wet bulb effectiveness, ε_{wb}. The values of the response variables described above, T_{SA} and ω_{SA}, were treated to develop the study of these indexes.

Dew point effectiveness and wet bulb effectiveness were calculated according to the equations (1) and (2), respectively.

$$\varepsilon_{dp} = \frac{T_{OA} - T_{SA}}{T_{OA} - T_{SA,dp}} \quad (1)$$

$$\varepsilon_{wb} = \frac{T_{OA} - T_{SA}}{T_{OA} - T_{SA,wb}} \quad (2)$$

Where $T_{SA,dp}$ is the outlet dew point temperature and $T_{SA,wb}$ is the outlet wet bulb temperature in each experimental test. The outlet air temperature and outlet air humidity ratio values were necessary to calculate these. The energy use in each test was also saved in this research work.

3. Results and Discussion

A summary of the values of outlet air temperature, outlet air humidity ratio, dew point temperature and wet bulb temperature in each experimental test is shown in Tab. 4. It should be noted that the results of the energy use in RIEC did not change, since the inlet air flow and supply air flow were constant during all experimental tests. The experimental analysis was divided into two parts: first, the influence of the inlet air temperature on the dew point effectiveness and the wet bulb effectiveness was analysed; and then, the influence of the inlet humidity ratio on both efficiencies was studied.

Tab. 4 – Dew point and wet bulb temperatures in each outlet air condition in RIEC testing.

Test	T_{SA} [°C]	ω_{SA} [g/kg]	$T_{SA,dp}$ [C]	$T_{SA,wb}$ [C]
1	21.3	13	18.1	19.1
2	23.4	13	18.1	19.8
3	16.6	9	12.5	14.1
4	14.6	9	12.5	13.3

The tests 1-4 and 2-3 showed the influence of the inlet air humidity ratio on the supply air temperature while the inlet air temperature was constant, 29°C and 43°C, respectively. Test 3 and test 4 showed the influence of the inlet temperature on the supply air temperature while the inlet humidity was constant, 9 g/kg. Test 1 and test 2 showed the influence of the inlet temperature on the supply air temperature while the inlet humidity was constant, 13 g/kg.

3.1 Effect of inlet air humidity ratio on supply air temperature

The experimental tests 1 and 4 were used to study the variation of the supply or outlet air temperature regarding the inlet air humidity ratio level. This research was developed when the inlet air temperature was constant in 29 °C, see Fig. 3.

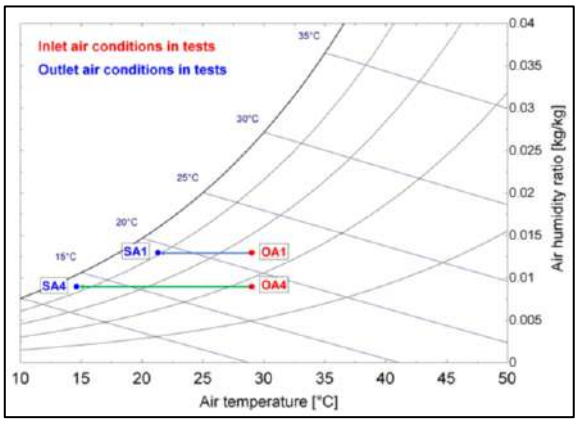

Fig. 3 – Inlet and outlet air conditions in tests 1 and 4.

The experimental tests 2 and 3 were compared to analyse the influence of the inlet air humidity ratio value on the outlet air temperature. In this case, the inlet air humidity ratio difference between tests also was 4 g/kg. However, the inlet air temperature was maintained constant at 43 °C, see Fig. 4.

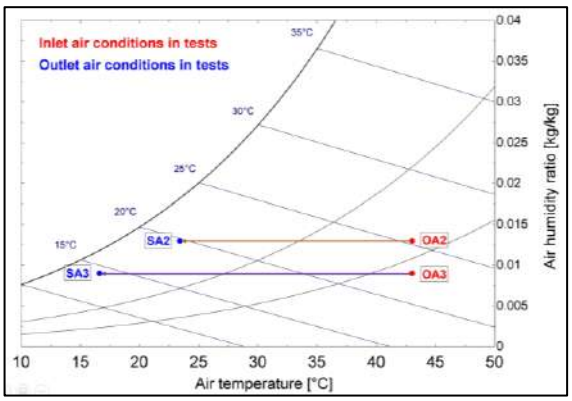

Fig. 4 – Inlet and outlet air conditions in tests 2 and 3.

It can be observed that the impact of inlet air humidity ratio on outlet air temperature was significant. An increase of 4 g/kg in ω_{OA} represented an increase in the outlet air temperature of 6.8 °C. This trend was obtained both in the tests 1-4, with a constant T_{OA} of 29 °C (points OA1 and OA4 in Fig. 3), and in the tests 2-3, with a constant T_{OA} of 43 °C (points OA2 and OA3 in Fig. 4).

3.2 Effect of inlet air temperature on supply air temperature

The experimental tests 3 and 4 were used to analyse the influence of the inlet air temperature on the supply air temperature when the inlet air humidity ratio was constant in 9 g/kg, see Fig. 5. Tests 1 and 2, described in Tab. 3, were also used to analyse the variation on the supply air temperature when the inlet air humidity ratio was 13 g/kg in both tests, see Fig. 6. For this case study, the inlet air temperature variation was 14 °C in the tests 3-4 and 1-2.

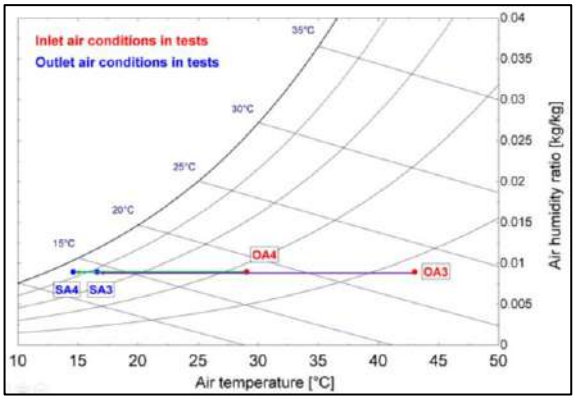

Fig. 5 – Inlet and outlet air conditions in tests 3 and 4.

Regarding tests 3 and 4, an increase in the outdoor air temperature of 14 °C led to an increase in the supply air temperature of 2.0 °C. The inlet air conditions in tests 1 and 2 showed the same variation in terms of temperature. The humidity ratio value of the inlet air in these cases was 13 g/kg. A increase in supply air temperature of 2.1 °C could be observed in this pair of tests. Therefore, it should be noted the similar trend in both case studies, see Tab. 4.

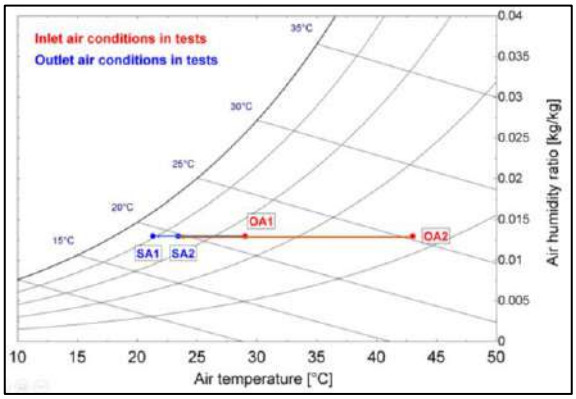

Fig. 6 – Inlet and outlet air conditions in tests 1 and 2.

This last response variable, T_{SA}, increased by a maximum of 2.1 °C when T_{OA} increased 14 °C, in contrast to the previous increase of 6.8 °C, when the difference in ω_{OA} was 4 g/kg (section 3.1).

Fig. 7 show a gradient plot which summarize the influence of the inlet air temperature, T_{OA}, and the inlet air humidity ratio, ω_{OA}, on the outlet air temperature, T_{SA}. These results were obtained for constant values of inlet air flow rate and supply air flow rate. It should be noted that the highest values of T_{SA} were shown when ω_{OA} increased to 13 g/kg. On the contrary, low T_{SA} values could be seen, between 14.6 °C and 17 °C, when the inlet air humidity ratio was 9 g/kg.

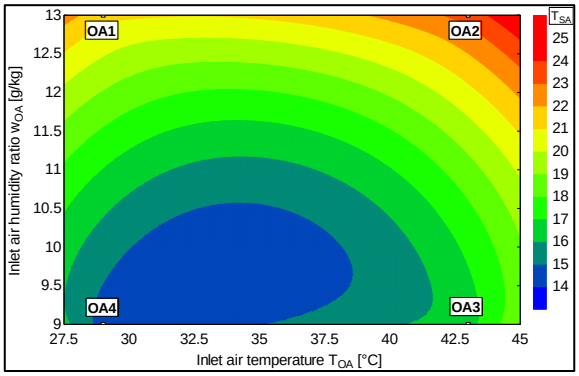

Fig. 7 – Gradient plot of inlet air temperature and inlet air humidity ratio influence on outlet air temperature.

The T_{SA} value varied between 14 °C and 22 °C when T_{OA} was 29 °C and ω_{OA} varied between 9 g/kg and 13 g/kg. T_{SA} ranged between 16 °C and 24 °C when T_{OA} was 43 °C and ω_{OA} was between 9 and 13 g/kg. That is, an increase of 1 g/kg in inlet air humidity resulted in an increase of 2 °C in T_{SA}. However, to decrease the supply air temperature by 2 °C, keeping the humidity constant, a reduction of 14 °C in the inlet air temperature was necessary.

3.3 Analysis of dew point and wet bulb effectiveness

The influences between the input variables, T_{OA} and

ω_{OA}, and the T_{SA} output variable were reflected in the results of ε_{dp} and ε_{wb}. According to equations (1) and (2), dew point effectiveness and wet bulb effectiveness were determined for each experimental test. The results of these response variables are shown in Tab. 5.

Tab. 5 – Evaluation indexes values of the studied RIEC.

Test	T_{OA} [°C]	ω_{OA} [g/kg]	ε_{dp} [-]	ε_{wb} [-]
1	29	13	0.71	0.78
2	43	13	0.79	0.85
3	43	9	0.86	0.91
4	29	9	0.87	0.92

High dew point and wet bulb efficiency values, ε_{dp} and ε_{wb}, were reached when the inlet air humidity ratio was reduced by around 9 g/kg, as shown in Tab. 5. According to the values shown, it should be noted that the greatest difference in the dew point effectiveness was found in tests 1 and 4. ε_{dp} increased by 16.5% when the inlet temperature was constant at 29 °C and the inlet humidity was reduced by 4 g/kg. However, the pair of tests 3-4 showed similar values of dew point effectiveness with the same inlet air humidity, 9 g/kg, and 14 °C difference in inlet air temperature. The influence of the inlet air conditions, T_{OA} and ω_{OA}, on the dew point effectiveness and the wet bulb effectiveness are shown in Fig. 8a and Fig. 8b, respectively.

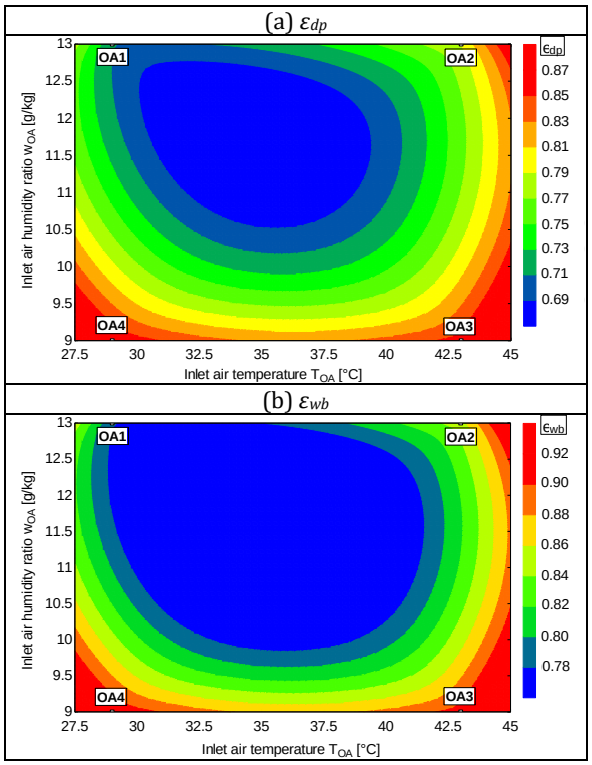

Fig. 8 – Gradient plot of inlet air temperature and inlet air humidity ratio influence on: (a) dew point effectiveness and (b) wet bulb effectiveness.

ε_{dp} increased 0.6% when the inlet air humidity ratio was kept at 9 g/kg and the inlet air temperature was reduced by 14 °C. In the tests 2-3 and 1-2, the difference in this dew point effectiveness was very similar, around 8% between the corresponding points. It can be observed that ε_{wb} showed a similar trend to ε_{dp}, The maximum ε_{wb} values were obtained for the tests 3 and 4, 0.91 and 0.92, respectively, when the inlet air humidity ratio was 9 g/kg and the inlet air temperature was 43 °C and 29 °C, respectively. The maximum values of ε_{dp} were shown in these same tests, 0.86 and 0.87, respectively.

4. Conclusions

An experimental analysis of a regenerative indirect evaporative cooling system, RIEC, was carried out in this work. This efficient air-cooling system was tested under different working conditions, regarding the inlet air temperature and the inlet air humidity ratio. The DOE methodology was used to determine the influence of the inlet air conditions on the thermal effectiveness. Dew point and wet bulb effectiveness were analysed for these different experimental tests.

Based on the results, the RIEC system showed high values of the dew point effectiveness and the wet bulb effectiveness, up to 0.87 and 0.92, respectively, when the inlet air temperature and the inlet air humidity ratio were 29 °C and 9 g/kg, respectively. However, at this same inlet temperature and an inlet humidity of 13 g/kg, the effectiveness of the dew point was reduced to 0.71 and the wet bulb effectiveness was also reduced to 0.78. Then, a increase in the inlet air humidity ratio of 4 g/kg led to a reduction in the dew point effectiveness of 16.5%. The same trend was obtained in the wet bulb effectiveness index, but the variation in this case was 13.8%. The lowest values of dew point effectiveness and wet bulb effectiveness were obtained with an inlet air temperature of 43 °C and an inlet air humidity ratio of 13 g/kg, below 0.79 and 0.85, respectively. Therefore, the RIEC system could be an interesting alternative to conventional HVAC systems. RIEC system allows achieving a good thermal performance, specially under hot-dry climatic conditions, by using 100% outdoor air.

Acknowledgement

The authors acknowledge the financial support received by the European Regional Development Fund and the Andalusian Economy, Knowledge, Enterprise and University Council, Spain, through the research project HICOOL, reference 1263034, and by European Union's Horizon 2020 research and innovation programme, through the research project WEDISTRICT, reference H2020-WIDESPREAD2018-03-857801.

Data Statement

The datasets generated during and analysed during the current study are available in the ZENODO repository, doi.org/10.5281/zenodo.6327341.

References

[1] Z. Duan et al. Indirect evaporative cooling: Past, present and future potentials. Renew. Sustain. Energy Rev. 2012;16(9):6823-6850.

[2] U. Sajjad et al. A review of recent advances in indirect evaporative cooling technology. Int. Commun. Heat Mass Transf. 2021;122 (January).

[3] Directive 2010/31/EU. European parliament and of the council of 19 May 2010 on the energy performance of buildings (recast). Off J Eur Union 2010. pp. 13–35.

[4] H. Yang, W. Shi, Y. Chen, and Y. Min. Research development of indirect evaporative cooling technology: An updated review. Renew. Sustain. Energy Rev. 2021;145(March):111082.

[5] A. Al-Mogbel, S. Hussain, M. Z. Rafique, and M. Almeshaal. Experimental investigations of evaporative cooling system for buildings under hot and dry environmental conditions. Heat Transf. Res. 2020;51(9):825-835.

[6] P. A. Doğramacı and D. Aydın. Comparative experimental investigation of novel organic materials for direct evaporative cooling applications in hot-dry climate. J. Build. Eng. 2020;30(January):101240.

[7] S. Abaranji, K. Panchabikesan, and V. Ramalingam. Experimental study on the direct evaporative air-cooling system with vermicompost material as the water storage medium. Sustain. Cities Soc. 2021;71(August):102991.

[8] D. Pandelidis, A. Cichoń, A. Pacak, S. Anisimov, and P. Drąg. Counter-flow indirect evaporative cooler for heat recovery in the temperate climate. Energy. 2018;165:877-894.

[9] A. Pakari and S. Ghani. Regression models for performance prediction of counter flow dew point evaporative cooling systems. Energy Convers. Manag. 2019;185(February):562-573.

[10] A. Badiei, Y. G. Akhlaghi, X. Zhao, J. Li, F. Yi, and Z. Wang. Can whole building energy models outperform numerical models, when forecasting performance of indirect evaporative cooling systems? Energy Convers. Manag. 2020;213(April).

[11] M. J. Romero-Lara, F. Comino, and M. Ruiz de Adana. Seasonal Analysis Comparison of Three Air-Cooling Systems in Terms of Thermal Comfort, Air Quality and Energy Consumption for School Buildings in Mediterranean Climates. Energies. 2021;14(15):4436.

[12] X. Cui, M. R. Islam, and K. J. Chua. An experimental and analytical study of a hybrid air-conditioning system in buildings residing in tropics. Energy Build. 2019;201:216-226.

[13] Y. Golizadeh Akhlaghi et al. Hourly performance forecast of a dew point cooler using explainable Artificial Intelligence and evolutionary optimisations by 2050. Appl. Energy. 2021;281(October):116062.

[14] Y. Golizadeh Akhlaghi et al. A constraint multi-objective evolutionary optimization of a state-of-the-art dew point cooler using digital twins. Energy Convers. Manag. 2020;211(February):112772.

[15] Y. G. Akhlaghi, X. Ma, X. Zhao, S. Shittu, and J. Li. A statistical model for dew point air cooler based on the multiple polynomial regression approach. Energy. 2019;181:868-881.

[16] F. Comino, S. Milani, S. De Antonellis, C. M. Joppolo, and M. Ruiz de Adana. Simplified performance correlation of an indirect evaporative cooling system: Development and validation. Int. J. Refrig. 2018;88:307-317.

Experimental Investigation of PCM System Improved with Nighttime Ventilation for Enhanced Solidification

Eva Zavrl [a,b], Mohamed El Mankibi [c], Mateja Dovjak [d], Uroš Stritih [a]

[a] Faculty of Mechanical Engineering, University of Ljubljana, Ljubljana, Slovenia, eva.zavrl@fs.uni-lj.si and uros.stritih@fs.uni-lj.si

[b] Institute for Innovation and Development of University of Ljubljana, Ljubljana, Slovenia, eva.zavrl@iri.uni-lj.si

[c] National School of State Public Works (ENTPE), Vaulx-en-Velin, France, mohamed.elmankibi@entpe.fr

[d] Faculty of Civil and Geodetic Engineering, University of Ljubljana, Ljubljana, Slovenia, mateja.dovjak@fgg.uni-lj.si

Abstract. It is predicted that in EU-buildings by 2030, the energy used for cooling will increase by 72%. Simultaneously, the energy needed for heating will drop by 30%. Thermally well-insulated lightweight framed buildings prevent heat losses through their envelope and reduce the energy demand over the heating season. However, the heat capacity of the lightweight wall is relatively low, and in summer, the building lacks thermal stability and overheats. Phase change materials (PCM) are broadly investigated for their well-known benefits of improving indoor thermal comfort by decreasing indoor temperatures while reducing the energy needed for space cooling when melting. One of the possible application methods is to encapsulate the material and place it in the 'building's building assemblies, such as walls and ceilings. However, due to a low material density (insulation effect) and high indoor temperatures on summer nights, the material does not completely solidify in the night cycle, and does not fully perform (melt) in the day-cycle. Thus, the nighttime outdoor air ventilation has to accelerate the solidification. The system is investigated in an experimental chamber divided into two units (reference and PCM modified). Each unit represents an office located in a South-Eastern Europe region with an above-average sun hours. Both units are equipped with a ventilation inlet (on the bottom of the wall) and outlet (in the middle of the ceiling). The internal wall and ceiling are entirely covered by macro-encapsulated PCM plates (SP24E) placed in the wooden frame. The original wall and ceiling are forming the airtight ventilation gap. In the nighttime cycle, the plates are being solidified with the linear diffuser (placed at the bottom of the wall), distributing the airflow behind the plates upwards (direction wall-ceiling). The results show that under the current configuration, the active-passive system decreases the indoor cell air temperatures in the hottest daily scenario up to 5 °C. Also, the complete PCM plates solidification may be accomplished within the nighttime cycle (12 h), when the air-gap is ventilated, average inlet air temperatures of 15 °C and 16 °C at a flowrate of 500 m^3/h.

Keywords. Phase Change Materials, Cooling Application, Nighttime Ventilation, Passive system, Enhanced Solidification
DOI: https://doi.org/10.34641/clima.2022.249

1. Introduction

For heating and cooling of the building sector, 40 % of final energy is used. This sector is one of the largest energy consumers in Europe, and it is responsible for more than one-third of the EU's emissions [1]. Due to global warming, the outdoor air temperatures in the summertime are increasing and with it the energy demand for cooling [2], [3]. In Europe over the last decade, the number of heating days in buildings decreased by 13 %, while by 2030, 72% increase in energy cooling demand is predicted [4]. Lightweight prefabricated buildings are popular structural concept. They have a skeleton structure with low-density thermal insulation as the prevailing material in wall composition. Often, they are designed with large window areas. Event thought in the heating season, the indoor building spaces are kept warm. In the cooling season, lightweight buildings easily overheat due to low thermal accumulation, which results in instant cooling demand to establish healthy and comfortable indoor conditions [5]–[7]. Besides bioclimatic architectural design, the buildings can be heated or also cooled by passive or active systems.

Copyright ©2022 by the authors. This conference paper is published under a CC-BY-4.0 license.

Passive building systems do not require a drive power, moving parts and controls for their function and demand little maintenance. In contrast, active building systems include mechanical systems for heating, cooling and ventilation (HVAC), illumination and are managed by control systems [8]. Such passive solutions are also Phase Change Materials (PCMs) integrated into building component such as roof, ceiling, internal and external walls and floor. However, many studies showed that PCM integrated into building components did not completely solidified over the nighttime cycle due to heat discharge indoors which results in deteriorated daily performance.

For example, in numerical investigation, Prabhakar et al. used the natural ventilation for enhancing the nighttime solidification of macro-encapsulated PCM plates (Rubitherm RT24 - 15 mm thick) and showed that in temperate climate nighttime ventilation increased the PCM performance from 3.32% to 25.62% [9]. Furthermore, Memarian et al. in Teheran summer and autumn studied DuPont Energain (5 mm thick PCM panel) experimentally and BioPCM (21 °C, 23 °C, 25 °C, 27 °C and 29 °C) numerically [10]. Several NV rates were tested (0 ACH, 1 ACH, 3 ACH, 5 ACH, 7 ACH and 10 ACH), and the combination of NaV at 5 ACH and BioPCM with melting point temperature (MP) at 29 °C provided 15% reduction in yearly energy consumption. In addition, the cooling effect of nighttime ventilation coupled with 5 mm thick PCM celling (MP: 26 °C, 28 °C, 30 °C and 32 °C) was simulated in six different cities in Kazakhstan (Nur Sultan, Karaganda, Kokshetau, Almaty, Aktobe and Atyrau; extremely hot to cold) by Adilkhanova et al. [11]. The natural ventilation was set to 8 ACH operating when indoor temperatures are 2 °C or higher from the outdoor. In Almaty and Aktobe with PCM MP 28 °C and natural ventilation, the maximum operative temperature was reduced up to cca. 5 °C. Similarly, the application of a 0.02 m thick layer of BioPCM25 to the ceiling and/or wall of the rooms was investigated under the Melbourne (Australia) climate conditions by Jamil et al. [12]. When the nighttime outdoor air temperatures dropped to 22 °C or lower the windows were opened for 20% which successfully contributed to the maximum daily temperature of 2 °C and more. Under the summer conditions in Lativa, Sinka et al. experimentally tested the performance of two PCMs (DuPont Energain and BioPCMQ25M51) applied in five materially diverse test buildings coupled with various HVAC systems. During the night, nighttime mechanical ventilation rate was set to 0.76 ACH and by additionally opening the windows, the BioPCM completely solidified, which resulted in 2 °C lower daily indoor temperatures.

However, PCM may also be cooled by applying the air locally. Many studies reported beneficial effects on solidification by ventilating the PCM enriched building components.

For instance, in Tianjin (China), Hou et al. and Li et al. experimentally investigated the thermal performance of a composite phase change ventilated roof [13], [14]. The melting temperature of the outer PCM layer was 32.55 °C and inner 24.12 °C. 1. Among the studied cases, the system reduced the indoor air temperatures by 34.4–47.0% (3.74–8.2 °C). Additionally, Alizadeh and Sandrameli measured the indoor thermal parameters of a PCM-based storage system with MP of 27 °C integrated with ceiling fan ventilation for enhanced nighttime solidification [15]. During summer period in Teheran (Iran), the peak indoor temperatures is decreased by 2.5 °C. Similarly, Weinläder et al. introduced a ventilated PCM (MP: 24 °C) ceiling for cooling application and monitored it over the summer in Munich (Germany) [16]. The ceiling air-gap was free ventilated (300 m3/h) in the nighttime, which corresponded to daily indoor operative temperature drop of 2 K (to 28 °C). Moreover, Jiao and Xu used EnergyPlus energy simulation software to simulate a simplified ventilated PCM ceiling (MP: 26 °C, 27 °C and 28 °C) at various night ventilation rates (5–20 ACH) combined with several window opening ventilation rates (3-8 ACH) [17]. The most effective PCM was with the melting temperature of 27 °C, which could keep the indoor temperatures within the recommended summer indoor thermal comfort range. Nevertheless, Evola et al. evaluated the performance of nighttime ventilated air gap in contact with PCM placed on the internal wall using Energy Plus located in Catania (Italy) [18]. The presence of the ventilated air-gap improved the daily PCM storage efficiency from 42.4% to 78.2%.

The present research introduces an active-passive system for cooling application (APS) combining the PCM plates on the internal wall and ceiling coupled with a locally ventilated air gap for improved heat transfer during the nighttime cycle. The cooling potential of the APS in the daily cycle is assessed by measuring the indoor air temperatures in test cells and the required PCM 'plates' solidification time during the nighttime cycle is determined by measuring the PCM surface temperatures. The results show that the APS decreases the daily indoor temperatures. With the proposed configuration and sufficiently low inlet temperatures, the PCM plates may be completely solidified over the night.

2. Method

2.1 Operation principle

The proposed diurnal APS system for cooling application consists out of a passive and active operation cycle. The left side of **Fig. 1** represents the passive daily operation cycle when PCM plates are melting and cooling the indoor space by accumulating heat from the space. The right side of the figure shows the active nighttime operation, where the air gap is ventilated and the PCM plates are solidified by the cool outdoor air (arrows: blue – cool outdoor air, yellow – slightly heated air and red – air fully heated by the plates and exhausted outdoors).

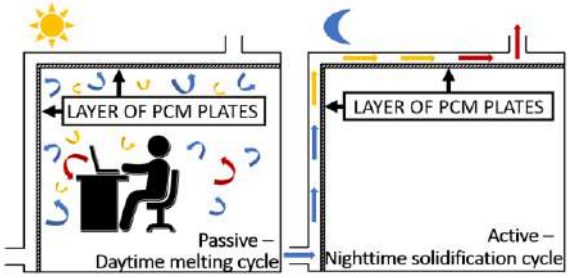

Fig. 1 – Principle of the APS for cooling operation

2.2 Experimental configuration

The APS system is located in the test facility named Hybcell at National School of State Public Works (ENTPE) in Lyon, France. Two identical test cells were monitored, cell A (PCM modified) and cell B (reference). **Fig. 2** shows the PCM modified cell.

Fig. 2 – Experimental facility (PCM modified cell)

The metal PCM plates are framed in the wooden substructure and form an airtight air-gap with the original wall (29 plates) and ceiling (38 plates) of the cell. The air-gap is nocturnally ventilated by the white linear diffuser inlet on the bottom of the wall. **Fig. 3** shows the main elements and dimensions of the PCM modified cell. The blue crosses in the figure represent the air temperature measuring points. The blue cross outlined with red represents the air thermometer positioned in the centre of the room (located in cell A and in cell B).

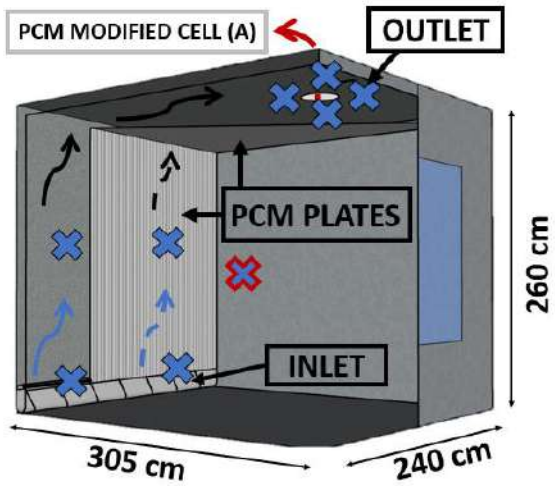

Fig. 3 – Sketch with elements of the PCM modified cell

The PCM plates are encapsulated in CSM aluminium cases (dimensions: 40x30x15 mm and weight: 2 kg) and filled with salt-hydrate SP24E (Rubitherm) [19]. The peak melting temperature is reached at 24 °C with storage capacity of 180 kJ/kg. The solidification occurs at 22 °C and 23 °C with storage capacity of 118 kJ/kg and 42 kJ/kg, respectively. The density of solid and liquid material is 1.5 kg/l and 1.4 kg/l, respectively with heat conductivity ~0.5 W/(mK). The melting point of the material is selected according to the thermal characteristics proposed for thermal comfort in hot summer periods in cooling season [20].

2.3 Experimental mechanical features and measuring equipment

Fig. 4 shows the schematic sketch of the

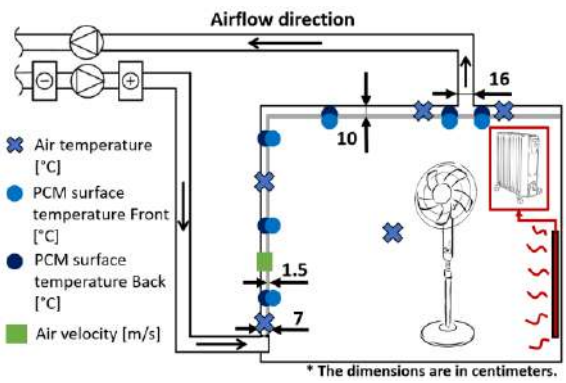

Fig. 4 - Experimental features and measuring points

experimental mechanical features for the establishment of the experimental conditions and locations of the air temperature, PCM surface temperature on the front (room side) and back (air-gap side) of the plates and velocity sensors. The air-gap was ventilated with conditioned and mechanically supplied air. The required air temperatures for nighttime solidification of the PCM were lower than indoor temperatures in test facilities, so the air had to be cooled and thermally stabilised by the air chiller located in the duct before the inlet fan. Two axial fans (300-3000 m³/h, 1500

Pa, 50/60 Hz) were located on the inlet and outlet duct, operating simultaneously. The cooled air was additionally conditioned with the spiral heating coil located after the inlet fan. The linear inlet diffusor was made by establishing a 1 cm thick opening along the entire 2 m long oval 5 cm wide duct component. It distributed the air along the air-gap separated into 5 channels.

The air temperature was measured in the air-gap determining inlet temperature, mid-air-gap temperature, outlet temperature using PT 100 sensor (DeltaOHM HD_35EDWH data accusation) in two points per height and in the centre of cell A and B with DeltaOHM HD_35EDG_1NB (acc.: ± 0.2 °C, range: 0…+60 °C) on 1.1 m height. The plates were monitored by measuring the front (cell side) and back (air-gap side) surface temperature in three points per height protected by aluminium tape to avoid the effect of radiation. The velocity was sampled at 1.3 m height in each channel and in the middle of the gap (average value of the channels is 0.9 m/s) with DeltaOHM HD403TS and DeltaOHM HD2903TO1 anemometers (acc.: ± 0.05 °C, range: 0.05…25 m/s). The volume flow rate was estimated to 500 m^3/h. Both cells were equipped with 2000 W heaters for simulation of the summer conditions and room fans for the establishment of the sufficient mixing of the air the cell.

2.4 Experimental protocol

The study presents two different sets of experimental results. The first set is purposed to show the cooling effect of the plates during the daily cycle when the PCM is melted. The heater in cell B was navigated to maintain the required set point cell temperature based on the air temperature measured in the centre of the room. The exact same amount of power was provided by the heater in cell A. The temperature difference between the measured values of air temperature in cell A and B was the cooling effect of the PCM plates. Three different set point temperatures were tested 26 °C, 30 °C and 35 °. Prior to the experimental case, the plates were cooled to 20 °C, to ensure the complete PCM solidification. The case was completed when the cell air temperature in cell A reached the cell air temperature in cell B. The room fans in cell A and B were switched ON during the entire test.

The second set of experiments aims to reveal the PCM solidification time required during the nighttime cycle. Prior to the experimental case, the plates were heated to 28 °C to ensure the completely melted PCM material and obtain the predicted indoor temperatures in summer. Afterwards, the plates were cooled with the average inlet air of 15 °C, 16 °C and 17 °C. The indoor temperatures were selected based on the Central European outdoor temperatures in summer (cooling season). The case was finalised, when the average PCM surface temperatures on the front and on the back of PCM plates' surface dropped to 18 °C or lower.

3. Results and Discussion

The results present daily operation of the APS during the PCM melting cycles and its nighttime operation during the application of the ventilation for enhanced PCM solidification.

3.1 Daily PCM melting cycle performance

The cooling effect of the APS system is determined based on the cell air temperature drop measured in cell A (PCM modified cell) in comparison to the cell air temperatures measured cell B (reference cell without PCM). **Fig. 5** shows the cell air temperature fluctuations (T_a) depending on the time during three different investigated cases (set point temperature in cell B 26 °C – light grey line, 30 °C – dark grey line and 35 °C - black line) where temperatures obtained in cell A are marked with dashed line and in cell B with solid line.

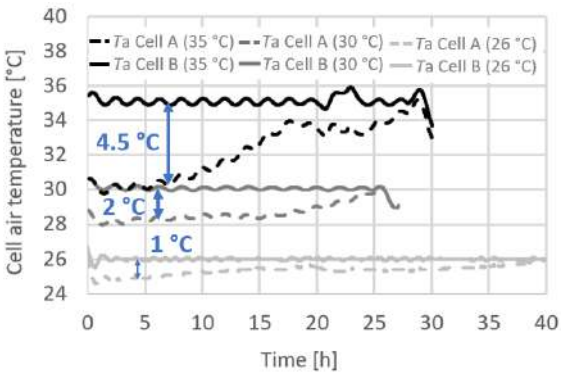

Fig. 5 – Cell air temperatures obtained during the daytime melting cycle in cell A and cell B

The results showed, that in all investigated cases, APS system with PCM plates decreased the daily cell air temperatures. The cooling effect of the plates is the strongest during the first hours of the experiment.

In the simulation case where air in cell B was heated to 26 °C ($T_{a\ CELL\ B\ 26\ °C}$), the cell air temperatures in cell A ($T_{a\ CELL\ A\ 26\ °C}$) dropped for 1.5 °C in first 3 h, for 1 °C between 3-10 h and later gradually increased from 1 to 0 °C in the last 10-40 h of the test. Since the heat added to the space is relatively little compared to the other cases, the $T_{a\ CELL\ A\ 26\ °C}$ are kept at cca. 25 °C during the entire time which is within recommended summer indoor air temperatures for thermal comfort (between 22 and 26 °C). Therefore, no additional space cooling systems need to be applied.

In the simulation case where air in cell B was heated to 30 °C ($T_{a\ CELL\ B\ 30\ °C}$), the cell air temperatures in cell A ($T_{a\ CELL\ A\ 30\ °C}$) compared to the reference cell differed for 2 °C in first 15 h and for 1.5 °C to 0 °C in 15-25 h. During the first 12 h, the $T_{a\ CELL\ A\ 30\ °C}$ were kept at 28 °C.

In the simulation case where air in cell B was heated to 35 °C ($T_{a\ CELL\ B\ 35\ °C}$), the cell air temperatures in cell A ($T_{a\ CELL\ A\ 35\ °C}$) dropped for 5 °C in first 5 h, from 5 to 2 °C in 5-15 h and later on increased from 2 -0 °C in

15-30 h. In this case, the cooling effect is the highest among all investigated cases. The indoor air temperatures $T_{a\ CELL\ A\ 35\ °C}$ are kept between 30 °C and 31 °C during the first 12 h.

Since the cell air temperatures ($T_{a\ CELL\ A\ 30\ °C}$ and $T_{a\ CELL\ A\ 35\ °C}$) are higher from the recommended summer values for indoor thermal comfort, additional cooling devices such as air-conditioning device are required to decrease the indoor air temperatures. In cases with set point temperature in cell B fixed to 26 °C and 30 °C, the $T_{a\ CELL\ A\ 26\ °C}$ and $T_{a\ CELL\ A\ 30\ °C}$ are kept at constant decreased value where the melting cycle lasts more than 12 h. These results indicate, that the amount of PCM plates could be decreased for. However, the decreased amount of PCM plates could negatively affect the $T_{a\ CELL\ A\ 35\ °C}$, which is kept at 30 °C in first 5 h and later starts to increase to 32 °C by the end of the daytime cycle at 12 h.

These results are in agreement with the results obtained from the other studies. For example, Weinläder et al. [16] used salt-hydrate with MP of 24°C attached only to the ceiling of the room and decreased the daily indoor tempeartures for 2 °C (to 28 °C), which corresponds to tempertures $T_{a\ CELL\ A\ 30\ °C}$ obtained in cell A. Hou et al. and Li et al. used two PCM layers in the ventilated roof (MP external: 32 °C and MP internal: 24 °C) and thus, reached higher drop in indoor tempeartures [13,14]. Prabhkar et al. specified, that by adding the nighttime ventilation to PCM with MP of 24 °C, the daily indoor temperatures droppedfrom 3.3% to 25.6 % [9].

3.2 Nighttime PCM solidification cycle performance

The duration of the nighttime solidification is presented in **Fig. 6 –8**. The figures show average surface temperatures measured on the front (cell side) surface of the PCM plate (solid line), average surface temperatures measured on the back (air-gap side) surface of the PCM plate (dashed line) and inlet air temperature (dotted line) measured in the inlet of the air-gap depending on the time. The results are presented in separated figures during three different cases with average inlet air temperatures of 15 °C (light grey), 16 °C (dark grey) and 17 °C (black). The selected PCM material transfers to sensible phase at 21 °C. During the solidification cycles, a non-uniform temperature distribution along the PCM wall and ceiling in size of 1 °C was observed. Therefore, the blue dashed line designates the end time of the solidification cycle determined at 20.5 °C In all investigated cases, average surface temperatures measured on the front of the PCM plates strongly correspond to the average surface temperatures measured on the back, which indicates that the phase change quickly overcame the thickness of the plate.

Fig. 6 shows the average surface temperature on the front and backside of the PCM plates during the solidification with inlet air temperatures of 15 °C. The results show that under stable inlet temperatures the PCM was fully solidified already in first 5 h of the case, which is the shortest period among all investigated cases. In this case, the energy consumed for the fan operation could be decreased by reducing its power and volume air flowrate.

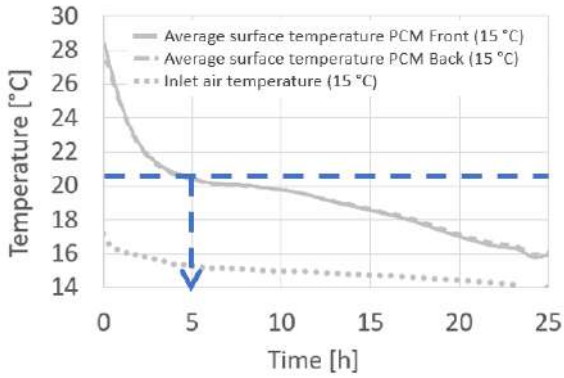

Fig. 6 – The average PCM surface temperatures and inlet air temperatures obtained during the case solidified with average inlet air of 15 °C

Fig. 7 shows that the average surface temperature on the front and back side of the PCM plates during the solidification with average inlet air temperatures of 16 °C. The complete PCM solidification was obtained after 14 h, which is 2 h longer than the nighttime solidification cycle. However, it must be noted, that due to the experimental conditions, in the first 10 h the inlet temperatures was higher than 16 °C (18 °C – 16 °C, on average 17 °C) which notably affects the solidification time in first 12 h. Based on this note, the inlet air with temperatures of 16 °C is conditionally sufficient for the complete nighttime PCM solidification.

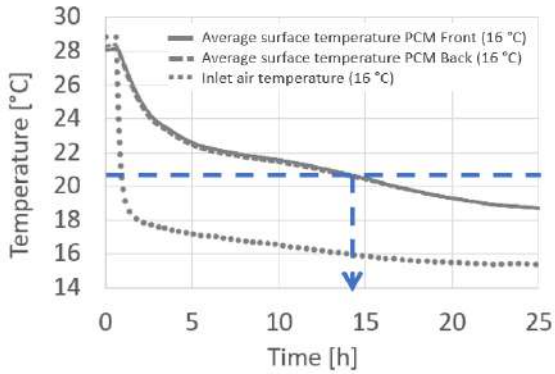

Fig. 7 - The average PCM surface temperatures and inlet air temperatures obtained during the case solidified with average inlet air of 16 °C

Fig. 8 shows that the average surface temperature on the front and back side of the PCM plates during the solidification with average inlet air temperatures of 17 °C. The results show, that the solidification is completed after 16 h of the experiment. Compared to the other two cases, the initial plate temperature was higher (30 °C instead of 28 °C) and thus, slightly affecting the total solidification time. Similarly, also in this case, the average inlet temperatures needed 5 h to completely stabilise from 18 °C to 17 °C, which may also affect the time needed for solidification.

Considering these two anomalies, it is expected that the total solidification time would decrease. However, it is expected that the solidification time would still exceed the nighttime solidification cycle for 12 h. Therefore, at current conditions, the average inlet air temperatures of 17 °C is insufficient (too high) to completely solidify the PCM plates. Nevertheless, the solidification time may be improved by increasing the air flow rate in the air-gap, although compared to the airflow size used by Weinlader et al. (300 m^3/h), the amount of air supplied in present stuy is rather high [16].

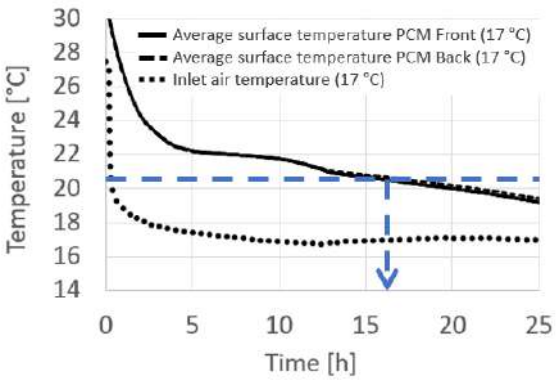

Fig. 8 - The average PCM surface temperatures and inlet air temperatures obtained during the case solidified with average inlet air of 17 °C

4. Conclusions

The research investigates the active-passive system (APS) for cooling application of buildings. It shows that the system indeed provides cooling to the indoor space during the daily cycle with the melting of the PCM plates. At cooler investigated indoor conditions (reference cell air temperature of 26 °C) no additional mechanical cooling systems are required. However, at warmer tested indoor conditions (reference cell air temperature of 30 °C and 35 °C) the system alone cannot sufficiently cool the indoor space and thus, requires additional cooling sources. The additional cooling provided by active mechanical systems increases the daily cooling energy demand. In such case, the expediency of APS system application could be questionable. Also, the electrical energy consumed by the fans for the nighttime air-gap ventilation 'shouldn't be exceed the total energy needed for the daily operation of active cooling systems. The investigated cases showed, that with the air-gap flow rate of 500 m^3/h and average inlet temperatures of 15 °C and 16 °C, the PCM plates may be solidified in the predicted nightime cycle (12 h).

In the future, such system should be tested for lower amount of PCM plates, different air-gap flowrates and temperatures and optimise them, transient conditions for different climate types, determine the energy removed from the space by APS and the energy needed for additional cooling of the plates. The APS system should be investigated in combination with daytime ventilation for IAQ and nighttime natural ventilation for improved solidification from the cell-side.

5. Acknowledgement

The authors acknowledge the financial support from the Slovenian Research Agency (research core funding No. P2-0158, Structural engineering and building physics and No. P2-0223, Heat and Mass Transfer) and Région Auvergne-Rhône-Alpes. The authors would also like to thank EU Comission for its financial contributions in the framework of Horizon 2020 project named Driving decarbonization of the EU building stock by enhancing a consumer centred and locally based circular renovation process (DRIVE0) with Grant agreement ID: 841850.

6. References

[1] European Commission, Renovation wave. 2021. [Online]. Available: https://ec.europa.eu/energy/topics/energy-efficiency/energy-efficient-buildings/renovation-wave_en. [Accessed: 01-Feb-2021].
[2] Eurostat, Share of Population Living in a Dwelling Not Comfortably Cool during Summer Time by Income Quintile and Degree of Urbanization. 2012. [Online]. Available: https://ec.europa.eu/eurostat/data/database?node_code=ilc_hcmp03. [Accessed: 04-Apr-2019].
[3] Intergovernmental Panel on Climate Change, Global Warming of 1.5 °C. 2018.
[4] Stazi F., Bonfigli C., Tomassoni E., Di Perna C. and Munafò P. The effect of high thermal insulation on high thermal mass: Is the dynamic behaviour of traditional envelopes in Mediterranean climates still possible?. Energy Build. 2015;88:367–383.
[5] Liu C., Kershaw T., Fosas D., Ramallo Gonzalez A. P., Natarajan S. and Coley D. A. High resolution mapping of overheating and mortality risk. Build. Environ. 2017;122:1–14.
[6] Lomas K. J. and Porritt S. M. Overheating in buildings: lessons from research. Build. Res. Inf. 2017;45(1–2):1–18.
[7] Bundle N., O'Connell E., O'Connor N. and Bone A. A public health needs assessment for domestic indoor overheating. Public Health;2018:9–15
[8] Blumenfeld A., Thumm W. T. and Phelps H. Passive Building Systems vs. Active Building Systems and the Return On Investment. Building Innovation Conference and Expo.2014. [Online]. Available: https://cdn.ymaws.com/www.nibs.org/resource/resmgr/Conference2014/BI20140109_BETEC_Thumm_Blume.pdf. [Accessed: 13-Nov-2020].
[9] Prabhakar M., Saffari M., de Gracia A. and Cabeza L. F. Improving the energy efficiency of passive PCM system using controlled natural ventilation. Energy Build. 2020;228(110483)
[10] Memarian S., Kari B. M., Fayaz R. and Asadi S. Single and combined phase change materials: Their effect on seasonal transition period. Energy Build. 2018;169:453–472.
[11] Adilkhanova I., Memon S. A., Kim J. and Sheriyev A. A novel approach to investigate the thermal

comfort of the lightweight relocatable building integrated with PCM in different climates of Kazakhstan during summertime. Energy. 2021;217(119390).
[12] Jamil H., Alam M., Sanjayan J. and Wilson J. Investigation of PCM as retrofitting option to enhance occupant thermal comfort in a modern residential building. Energy Build. 2016;133:217–229.
[13] Hou M., Kong X., Li H., Yang H. and Chen W. Experimental study on the thermal performance of composite phase change ventilated roof. J. Energy Storage. 2021;33(102060).
[14] Li H., Li J., Xi C., Chen W. and Kong X. Experimental and numerical study on the thermal performance of ventilated roof composed with multiple phase change material (VR-MPCM"). Energy Convers. Manag. 2020;213(112836).
[15] Alizadeh M. and Sadrameli S. M. Indoor thermal comfort assessment using PCM based storage system integrated with ceiling fan ventilation: Experimental design and response surface approach. Energy Build. 2019;188–189:297–313.
[16] Weinläder H., Körner W. and Strieder B. A ventilated cooling ceiling with integrated latent heat storage - Monitoring results. Energy Build. 2014;82:65–72
[17] Jiao F. and Xu P. Simulation and Feasibility Analysis of PCM Based Passive Cooling Technique in Residential House. Procedia Engineering. 2015;121:1969–1976.
[18] Evola G., Marletta L. and Sicurella F. Simulation of a ventilated cavity to enhance the effectiveness of PCM wallboards for summer thermal comfort in buildings. Energy Build. 2014;70:480–489.
[19] Rubitherm. Data Sheet Rubitherm SP24E. 2020. [Online]. Available: https://www.rubitherm.eu/media/products/datasheets/Techdata_-SP24E_EN_09112020.PDF. [Accessed: 24-Nov-2021].
[20] EN 15251:2007:E. Indoor environmental input parameters for design and assessment of energy performance of buildings addressing indoor air quality, thermal environment, lighting and acoustics. 2007.

Design and optimal integration of seasonal borehole thermal energy storage in district heating and cooling networks

Massimo Fiorentini [a], Jacopo Vivian [a], Philipp Heer [a], Luca Baldini [b]

[a] Urban Energy Systems Laboratory, Empa - Swiss Federal Laboratories for Materials Science and Technology, 8600 Dübendorf, Switzerland.

[b] Centre for Building Technologies and Processes, ZHAW Zurich University of Applied Sciences, 8401 Winterthur, Switzerland.

Abstract. Technologies that can close the seasonal gap between summer renewable generation and winter heating demand are crucial in reducing CO_2 emissions of energy systems. Borehole thermal energy storage (BTES) systems offer an attractive solution, and their correct sizing is important for their techno-economic success. Most of the BTES design studies either employ detailed modelling and simulation techniques, which are not suitable for numerical optimization, or use significantly simplified models that do not consider the effects of operational variables. This paper proposes a BTES modelling approach and a mixed-integer bilinear programming formulation that can consider the influence of the seasonal BTES temperature swing on its capacity, thermal losses, maximum heat transfer rate and on the efficiency of connected heat pumps or chillers. This enables an accurate assessment of its integration performance in different district heating and cooling networks operated at different temperatures and with different operating modes (e.g. direct discharge of the BTES or via a heat pump). Considering a case study utilizing air sourced heat pumps under seasonally varying CO_2 intensity of the electricity, the optimal design and operation of an energy system integrating a BTES and solar thermal collectors were studied. The optimization, aiming at minimizing the annual cost and CO_2 emissions of the energy system, was applied to two heating network temperatures and five representative carbon prices. Results show that the optimal BTES design changed in terms of both size and operational conditions, and reductions in emissions up to 43% could be achieved compared to a standard air-source heat pumps based system.

Keywords. Renewable heating and cooling, seasonal thermal storage, borehole thermal energy storage (BTES), district heating/cooling networks, design optimization, optimal management.
DOI: https://doi.org/10.34641/clima.2022.64

1. Introduction

In the frame of the United Nations' climate conferences (COPs) and the declared target of limiting the atmospheric temperature, there is a strong need for fast decarbonization of our economies. This involves a substitution of fossil fuels with renewables, which due to their non-dispatchable nature, require a significant increase in storage capacity build-up in the energy system. Electric, thermal and chemical storages play a crucial role and all converge in their effect as the sectoral coupling is strengthened. In this context, coupling electric heat pumps with large scale seasonal thermal energy storage is essential for decarbonising heat and cold supply for buildings. Seasonal load shifting through thermal energy storage enables a strict minimization of total CO_2 emissions and thus supports moving away from the so far common *energy* efficiency perspective. Leveraging that, Borehole Thermal Energy Storage systems are an attractive solution. Historically, BTES systems were designed to support centralized solar plants and were designed to operate at high temperatures, such as the implementation in Drake Landing in Canada [1]. These installations show a BTES efficiency generally lower than expected at the design stage. This is one of the reasons that led modern systems to generally operate BTES at lower temperatures, reducing thermal losses but also enabling integration of waste heat sources at relatively low temperatures.

To this end, finding optimal combined design and operational strategies for these technologies is

Copyright ©2022 by the authors. This conference paper is published under a CC-BY-4.0 license.

important to ensure they achieve their techno-economical objectives.

BTESs are generally modelled in detail using software tools such as TRNSYS [2] at both district [3] and residential scales [4], but this approach does not allow the application of numerical optimization methods, requiring iterative processes to optimize the system configuration. The energy-hub approach, which is based on numerical optimization methods and employed in district heating and cooling system design, can help with this task. Nevertheless, only a few studies included seasonal thermal energy storage within their framework, particularly considering a BTES [5–7]. To formulate the system design optimization as a Mixed-Integer Linear Programming (MILP) problem, these studies do not model the dynamical behaviour of the thermal storage (temperature evolution, heat transfer mechanisms) influencing the storage properties and the efficiency of the connected equipment. The performance of a BTES is highly dependent on how it is used in relation to defined boundary conditions, as highlighted in [8]. Potential alternative approaches were proposed in [9], employing genetic algorithms to optimize non-linear models. An alternative approach, based on a mixed-integer bilinear optimization framework, is also proposed in a manuscript by some of the authors currently under review [10], and extended in this study. The bilinear problem formulation, a particular subcategory of non-linear problems, enables finding a guaranteed optimal solution using modern solvers such as Gurobi [11].

The proposed method, outlined in [10] and extended in this study, can consider: i) the influence of operational variables such as the initial temperature of the BTES and the storage temperature swing (seasonal sinusoidal fluctuation of the average BTES temperature) on the total capacity of the storage and thermal losses of the storage, ii) the relationship between the volume of the BTES and its maximum heat transfer rate and iii) the impact of boundary conditions such as the availability of solar thermal generation, the CO_2 intensity of the grid electricity consumed on the optimal design of the storage and energy system.

In particular, this paper studies an electricity-based heating and cooling system coupled with a BTES and investigates its optimal design considering the effect of different BTES parameters such as its size, its integration in networks operating at different temperatures and the possibility to discharge it either directly or through a heat-pump on the overall system performance and operational carbon dioxide emissions. The proposed optimization framework is employed to identify optimal system design (sizing and operation), including BTES, heat pumps, chillers and solar collectors, leading to optimal trade-offs between operational CO_2 emissions and levelized cost.

2. Energy system layout

In this paper, we study a generic district heating and cooling system with a centralized design, which has the possibility to integrate a BTES to store thermal energy seasonally. It is assumed that the BTES is cylindrical, with uniformly distributed boreholes and a parallel plumbing configuration. In line with the requirement of avoiding the use of fossil fuels for heat generation, it is assumed that the district's cooling demand can be met by two chillers, one that rejects the waste heat in a BTES and a second one that uses the ambient air as a sink. Similarly, the heating demand can be met by two heat pumps, also using the BTES and the ambient air as sources, together with the possibility to directly discharge the BTES when its temperature is higher than the district heating supply temperature. As the heating demand of the site might differ significantly from the cooling one, an additional solar thermal heat source can be considered in the design optimization of the system. The solar thermal system is assumed to be able to provide heat either directly to the district heating system, or store it in the BTES. It is also assumed that the solar thermal collectors are coupled with a buffer tank large enough to absorb daily fluctuations in energy generation. A schematic of the system is presented in Fig. 1.

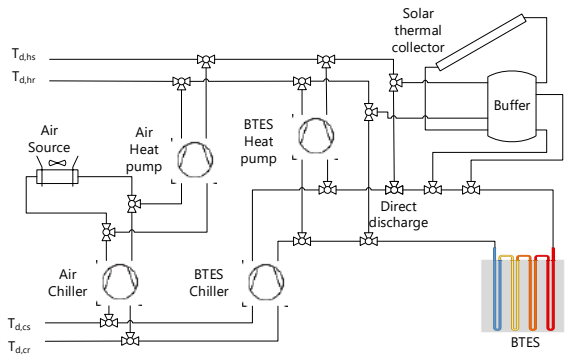

Fig. 1 - Case study centralized district heating and cooling system layout.

3. Methods

This Section presents the main inputs (3.1) and assumptions (3.4) used and a description of the optimization model, including the constraints (3.2) and the objective function (3.3).

3.1 Inputs and optimization framework

The optimization framework uses weather conditions (solar radiation I_t and ambient temperature T_a), a CO_2 intensity profile (I_{CO2}), and heating ($P_{load,heat}$) and cooling demand profiles ($P_{load,cool}$) as inputs. It returns the optimal system design in terms of technology sizing and operational conditions, listed below. The input data are provided with a daily resolution for a year, and they are assumed not to change along the lifetime of the system. It is assumed that the system must strictly meet the defined heating and cooling demand. The

decision variables include:

- The optimal equipment sizing, including the heat pump and chillers heating and cooling capacity (S_{hp_BT},S_{ch_BT},S_{hp_a},S_{ch_a}), solar thermal collectors area (S_{sol}), and the size (ground volume) of the BTES (discretized, V_j).
- The optimal initial temperature of the BTES ($T_{BT,init}$).
- The fraction of heating and cooling demand provided, by the solar generation (P_{th,sol_used}), by the direct discharge of the BTES (P_{th,BT_direct}), by the heat pump and chiller connected to the BTES (P_{th,hp_BT}, P_{th,ch_BT}) or by the air-source heat pump and chiller (P_{th,hp_a}, P_{th,ch_a}) at each time step *k*,
- The fraction of solar generation stored in the BTES (P_{th,sol_tr}) at each time step *k*.

The electrical power consumption of each heat pump ($P_{el,hp_{BT}}$, P_{el,hp_a}) and chiller ($P_{el,ch_{BT}}$, P_{el,ch_a}) is calculated at each time step *k* to derive the total energy system ($P_{el,tot}$), used to estimate the operational costs and CO_2 emissions to be included in the optimization objective function. Consumption of circulation pumps is considered negligible in this study, as the pumping energy difference among cases is small and not affected by operational conditions and temperatures as much as heat pumps and chillers.

3.2 Models and constraints

BTES

In this optimization framework, BTES sizing was discretized as the properties of the storage change with the storage volume, such as the thermal losses and the maximum heat transfer rate. The BTES is modelled as a single capacitance with losses calculated with the steady-state equation proposed by Hellström [12] as a function of the storage depth, storage aspect ratio and ground thermal conductivity. This model is considered valid as it is assumed that the BTES is cylindrical, with uniformly distributed boreholes, and employing an in-parallel plumbing setup. The top insulation, of area A_i and a U-value U_i, contributes to the losses. A number of n_j storage sizes are considered, each corresponding to a storage volume V_j. As it is assumed that the storage keeps the same aspect ratio (diameter equal to depth) when scaled, the heat loss factor h is the same for each size considered. The equation proposed by Hellström can also be employed to model storages with a parallelepipedal shape. Other shapes can be used in this optimization framework, as long as the temperature dynamics are described by a linear time-invariant model. The storage temperature evolution for the *j-th* size is presented in Eq. 1:

$$T_{BT}(k+1) = T_{BT}(k) + \frac{\Delta t}{\rho_g c_{p,g} V_j}\left(\left(P_{\mathrm{th,ch_{BT}}} + P_{\mathrm{el,ch_{BT}}}\right) + P_{\mathrm{th,sol_{tr}}} - \left(P_{\mathrm{th,hp_{BT}}} - P_{\mathrm{el,hp_{BT}}}\right) - P_{\mathrm{th,dir_{BT}}} - U_i A_{i,j}\left(T_{BT}(k) - T_a(k)\right) - k_g h \frac{D_j}{2}\left(T_{BT}(k) - T_g(k)\right)\right) \quad (1)$$

where T_{BT} is the temperature of the storage, T_a the ambient temperature, T_{sol} is the supply temperature of the solar system and T_g is the undisturbed ground temperature. ρ_g and $c_{p,g}$ are the density and specific heat capacity of the ground respectively. As direct charge and discharge with the heat pump must not occur simultaneously, a Boolean variable δ_m is introduced with (2) and (3) to define which operating mode is being used (in this case δ_m is equal to 1 when the heat pump is used) and constraining to zero the heat provided in the other mode. Furthermore, if the temperature of the storage T_{BT} is lower or equal to the network heating supply temperature $T_{d,hs}$, the BTES cannot be discharged directly (i.e. δ_m = 1). The supply temperature of the thermal network is not considered as a decision variable, but as a constant parameter. An equivalent UA_j coefficient is used to linearly represent the heat exchange in the boreholes and is calculated for each BTES size, assuming a uniform borehole wall temperature that is equal to the overall BTES temperature. In this study, the value of this UA coefficient was identified as presented in [8]. The heat transfer is constrained in each storage size by the total UA value (UA_j) of the ground heat exchangers and the temperature difference between heat transfer fluid and storage (ΔT_{eq}, T_{sol} - T_{BT}). An example of this constraint for rejection of heat from cooling operations is shown in Eq. 2:

$$P_{th_ch_{BT}} \leq \delta_m (UA_j \Delta T_{eq} - P_{el_{ch_{BT}}}) \quad (2)$$

A similar constraint is applied to the direct discharge of the BTES as well, which is expressed as in Eq. 3.

$$P_{th_dir_{BT}} \leq (1-\delta_m) UA_j \left(T_{BT} - T_{d,hr}\right) \quad (3)$$

The BTES cost (J_{BT}) in each scaling option is obtained from the total drilling length, calculated as the product of the number of ground heat exchangers ($n_{GHX,j}$) and their depth (D_j), multiplied by a drilling price per meter (λ_{GHX}) and an annuity factor (ω_{BT}), as presented in Eq. 4:

$$J_{BT} = D_j n_{GHX,j} \lambda_{GHX} \omega_{BT} \quad (4)$$

Several constraints are introduced in the optimization problem, which are not listed explicitly for conciseness. These ensure that: i) only one size of storage can be selected at a time, ii) that the storage temperature and the storage initial temperature are within predefined temperature boundaries, iii) that the storage temperature at the beginning and end of the year is the same.

Heat pumps and chillers

To enable the optimization to choose the best source between the BTES and the air sources for providing heating and cooling, the sizing and the operation of the two heat pumps and chillers are considered as optimization variables. The heating and cooling capacity of each energy conversion equipment is constrained between zero and the maximum heating demand of the plant. For instance, the heat pump

using the BTES as a source is presented in Eq. 5.

$$0 \leq S_{hp_BT} \leq P_{th,load_heat}^{max} \quad (5)$$

The COP of the air-source heat pump and chiller, as it is not a function of a state of the system and can be pre-computed before the optimization is performed. Indeed, the temperatures of district heating and cooling networks are constant, as explained in the BTES model subsection. An example for the air-source heat pump supplying heat to the district network at temperature $T_{d,hs}$ is calculated as in Eq. 6.

$$COP_{hp_air}(k) = 0.5 \frac{T_{d,hs}}{T_{d,hs}-(T_a-\Delta T_{eq})} \quad (6)$$

As the COP of the heat pump and chiller connected to the BTES are a function of a state of the system (i.e. the temperature of the BTES), the following linearized relationship of the inverse of the COP was employed to calculate the electrical consumption of the equipment, as presented in Eq. 7.

$$COP_{hp_{BT}}^{-1}(k) = a_{hp}\left(T_{BT}(k) - \Delta T_{eq}\right) + b_{hp} \quad (7)$$

Solar collectors

To support the optimization with a daily resolution, it is assumed that the solar panels are coupled with a buffer tank capable of shifting part of the daily generation to the night. The collectors are also assumed to operate at a constant efficiency η_{sol}. The heat generation of the solar panels $P_{th,sol}$ can be calculated at each time step as in Eq. 8:

$$P_{th_sol}(k) = \eta_{sol} I_{sol}(k) S_{sol} \quad (8)$$

where I_{sol} is the solar radiation and S_{sol} the solar array area. A constraint on the maximum size of the array is also added. The buffer tank is size S_{STTS} is designed to shift half of the maximum daily solar generation:

$$S_{STTS}(k) = \eta_{sol} I_{sol}^{max} S_{sol} \Delta t/2 \quad (9)$$

The solar energy can be either used directly for heating operations ($P_{th_sol,used}$) or transferred to charge the BTES ($P_{th_sol,transf}$), provided that the sum of these two elements, at each time step, does not exceed the total heat production $P_{th,sol}$.

Plant thermal balance

Thermal energy loads must be met at each time step, using the available energy resources. The heating load can be provided by the solar system directly, by the direct discharge of the BTES, as well as by the air-source and BTES heat pumps (Eq. 10).

$$P_{load,heat}(k) = P_{th_hp_{BT}}(k) + P_{th_hp_a}(k) + P_{th_dir_{BT}}(k) + P_{th_sol,used}(k) \quad (10)$$

Similarly, the cooling demand can be satisfied by the air source and BTES chillers (Eq. 11).

$$P_{load,cool}(k) = P_{th_ch_{BT}}(k) + P_{th_ch_a}(k) \quad (11)$$

3.3 Objective function

The objective of the optimization is to minimize the annual cost of the energy system, which comprises of three elements: i) a capital component (J_c), ii) an operational component associated with the electricity consumption ($J_{o,e}$) and iii) an operational component associated with the cost of CO_2 emissions ($J_{o,CO2}$). These are shown in Eq. 12, Eq. 13 and Eq. 14 respectively.

$$J_c = \omega_{eq}(\lambda_{hp}(S_{hp_{BT}} + S_{hp_a}) + \lambda_{ch}(S_{ch_{BT}} + S_{ch_a}) + \lambda_{sol} S_{sol} + \lambda_{STTS} S_{STTS} \quad (12)$$

$$J_{o,e} = \sum_{k=1}^{N} (P_{el,tot}(k)) v_{el} \Delta t \quad (13)$$

$$J_{o,CO2} = \sum_{k=1}^{N} (I_{CO2}(k) P_{el,tot}(k)) v_{CO2} \Delta t \quad (14)$$

Maintenance costs are neglected in this formulation.

3.4 Implementation

The optimization problem was formulated in Matlab R2020b, using the YALMIP toolbox [13] and Gurobi v9.1 as a solver [11]. A maximum MIPGap 0f 0.1% was considered as a stopping criterion for each optimization run.

Heating and cooling demand

The heating and cooling demand data were collected from the operational history of the Empa campus in Dübendorf, Switzerland, which includes 35 buildings of different use (e.g. office, laboratory, etc.) thus requiring energy both for process and space heating and cooling. The thermal energy, currently generated with a natural gas boiler and a chiller, is distributed to the buildings using two separate thermal grids. The resulting net demand of the campus was calculated from an hourly dataset and averaged over each day, thus obtaining the daily load profiles shown in Fig. 2.

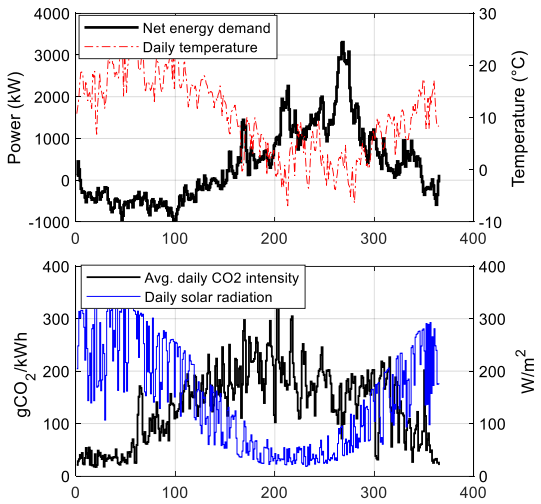

Fig. 2. Boundary conditions for the optimization: energy demand and outdoor temperature (top); CO_2

intensity and solar irradiation (bottom).

The peak heat demand was approximately 3.3 MW and the maximum cooling demand approximately 1 MW. The climate data were taken from the Dübendorf TMYx weather file [14]. The CO_2 equivalent intensity profile for Switzerland was sourced from [15].

Assumptions on techno-economic parameters

The size of the borehole thermal energy storage was selected among five volumes, all with the same cylindrical shape and aspect ratio (equal depth and diameter). Therefore, increasing the volume V of the storage results in an increase in both depth and diameter (D) and number of the boreholes (n_b), as shown in Table 1. The optimization can also choose not to include the BTES if this option minimizes the objective function shown in Section 3.3.

Tab. 1 – BTES design options.

Opt.	D (m)	V (10^3 m^3)	UA (kW/K)	n_b (-)
1	53.4	119.2	22.5	158
2	61.2	179.6	33.8	207
3	70.0	269.4	50.6	271
4	80.1	404.1	76.0	355
5	91.7	606.1	113.9	466
6	No BTES			

The undisturbed ground temperature and the thermal conductivity of the ground were assumed to be 12°C and 2.4 W/(m*K), respectively. The annual cost of the BTES was calculated assuming a lifetime of 60 years, and a borehole cost of 66 €/m [16]. This study does not consider the initial transient to reach a stable temperature swing, which can be problematic at a high initial storage temperature $T_{BT,0}$. Therefore, an upper limit on the initial BTES temperature was set to 30°C to avoid financially infeasible solutions caused by a too long initial transient. A fixed temperature difference ΔT_{eq}= 10 K was set between the heat transfer fluid and heat source/sink for heat pump/chiller COP calculation of Eqs. 6 and 7. Table 2 shows the specific costs assumed for the heat generation systems.

Tab. 2 – Capital cost and maximum size considered for solar collectors, heat pumps and chillers.

Parameter	λ	Max. size
Solar collectors	500 €/m^2	10^4 m^2
Heat pumps	576 €/kW$_t$	3300 kW$_t$
Chillers	576 €/kW$_t$	975 kW$_t$

Two supply temperature levels were considered for the district heating network: 65°C and 40°C. The latter implies that all heat emission systems in the campus are replaced by low-temperature ones (e.g. low-temperature radiators and radiant floors), but the heating demand remains unchanged. The cooling network operates with a supply temperature of 6°C.

Assessment of the optimal solutions

A range of CO_2 prices from 50 €/t to 450 €/t was tested. As a reference, the lower limit is approximately the current EU carbon price [17], while direct extraction of CO_2 from the atmosphere is estimated to cost between 110€/t and 280€/t [18]. Both the environmental and economic parts of the objective function, i.e. annual CO_2 emissions and costs, were compared to a Baseline setup. This baseline setup consisted of a thermal network with an air-source heat pump for heating and an air-source chiller for cooling (no BTES, heat pump and chiller connected to it, or solar thermal collectors).

4. Results

Fig. 3 shows optimal design parameters, such as the volume of the BTES, the nominal heating and cooling capacity of the ground-source and air-source heat pumps and chillers (summed), and the area of the solar thermal collectors. The graphs show how different CO_2 prices influence the optimal design of the system for the two temperature levels of the district heating network. While, as expected, the size of the heat pumps and chillers does not change with the temperature levels of the district heating network (only adding solar generation can reduce the peak heating demand), the BTES volume and the surface area of the solar collectors do. It can be noted that both the BTES and the solar field increase their size with increasing CO_2 price, and that a higher-temperature network generally requires a higher BTES volume to operate optimally. This choice is linked to the optimal operation of the system, which will be discussed later in this Section. The case study is the Empa campus in Switzerland, which features a heating-dominated climate.

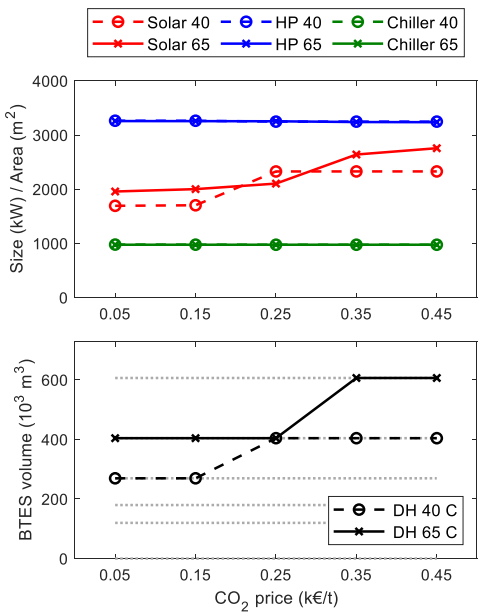

Fig. 3 - Effect of CO_2 price on key design parameters.

Therefore, the solar collectors contribute to filling the mismatch between the heat extracted from the ground during the heating season and the heat rejected into the ground during the cooling season, as shown in Fig. 4 (top) for the 65°C thermal network. The air source heat pump compensates for the remainder of the missing energy that BTES cannot provide in winter. The lower plot in Fig. 4 shows that the contribution of the air source heat pump is more significant (26%) at low CO_2 prices compared to higher ones (11%), which is clearly due to the smaller size of the seasonal thermal storage (see Fig. 3).

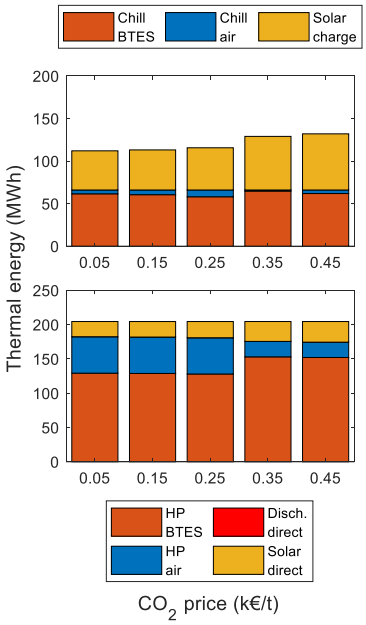

Fig. 4 - Effect of CO_2 price on the annual heating and cooling supply mix in the 65°C temperature network. Cooling operation (top), heating operation (bottom).

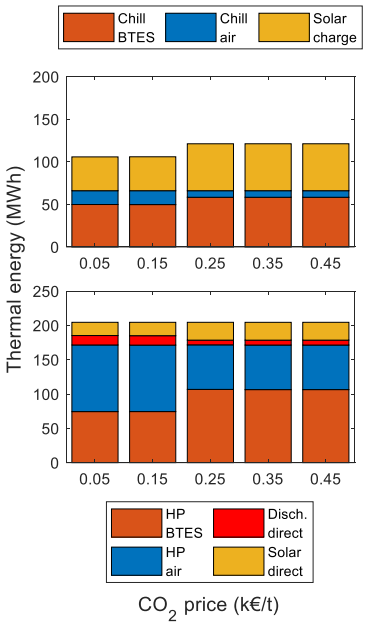

Fig. 5 - Effect of CO_2 price on the annual heating and cooling supply mix in the 40°C temperature network. Cooling operation (top), heating operation (bottom).

When the heat is supplied at 40°C in the district heating network, the relative contribution of the air source heat pump during the heating season is more significant, and ranges from 32% to 47% of the heating demand depending on the CO_2 price. Similarly to the previous higher-temperature network case, this range is due to the different optimal sizes of the BTES at the different CO_2 prices. In this case, the BTES is charged at a temperature high enough to allow a direct discharge of the heat (i.e. without a heat pump) from the BTES in Autumn, as shown by the red portions of the bars in Fig. 5 and in the upper temporal plot in Fig. 6.

Fig. 6 shows the optimal operation of the system at both temperature levels –by way of example of the identified optimal solution at a CO_2 price of 0.15 k€/t. In the upper chart, it can be seen that the average BTES temperature profile exceeds the network supply temperature (40°C), thus allowing part of the heating demand to be covered by direct BTES discharge in Autumn, which cannot occur in the high-temperature case. In the bottom chart in Fig. 6 the peak temperature barely reaches 40°C. This is not a trivial result because the optimizer could also opt for different decisions, such as a higher temperature swing of the seasonal thermal storage. The maximum temperature is a combination of the initial storage temperature and of the seasonal temperature swing. The first decision variable always reaches the upper bound, which was set at 30°C to limit the duration of the initial transient to heat the BTES (not considered in this study). The peak storage temperature in summer increases with decreasing CO_2 price, driven by the low BTES volume, but is always lower than 42.3°C. This occurs because the maximum thermal energy that can be extracted from the BTES during the heating season is constrained by its maximum heat transfer rate, which in turn depends on the volume of the storage. Therefore, the same amount of heat exchanged with a smaller BTES does not necessarily lead to a higher temperature swing. The absence of fossil-fuelled backup generators forces the air source heat pump to cover most of the remaining heating demand, including the peaks occurring in the coldest part of the winter, when the efficiency is lower and heating demand larger. In the low-temperature network, part of the heating demand is supplied by directly discharging the BTES. However, this occurs in Autumn only, when the thermal storage is almost fully charged and the heat demand is rather low (red area). In this period the CO_2 intensity is also relatively low and the outdoor air temperature mild, i.e. when the air source heat pump would have the lowest economic and environmental impact. However, the only way to increase the share of heat directly supplied from the BTES would be either to have an even lower network supply temperature or to increase the solar collector area. Therefore, the limited amount of direct storage discharge can be interpreted as an optimal trade-off between the increased investment cost needed to increase the size of the solar collector field and the reduced running costs due to avoided heat pump operation.

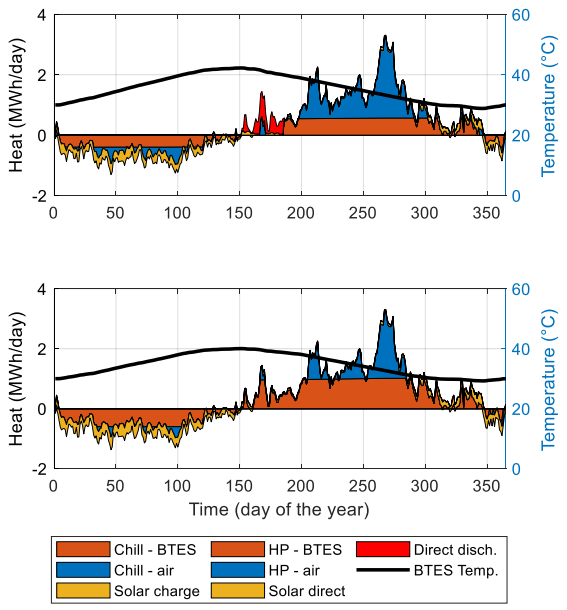

Fig. 6 - Optimal operation of the system for 40°C (top) and 65°C thermal networks (bottom).

As far as the comparison between the two district heating temperature levels is concerned, Fig. 7 shows that the solutions with the low-temperature network (black square dots) are always better than those with the high-temperature network (red squared dots), both from economic and environmental standpoints. This is mainly due to the higher COP of both the ground and air-source heat pumps in the low-temperature network, which reduces the electricity consumption to meet the same heating demand, thereby improving both indicators. The optimal solutions led to a reduction in CO_2 emissions compared to the baseline system in the range between 33.0-43.1% and a change in costs, excluding those related to CO_2 emissions, of approximately 3.2% less to 0.4% more, depending on CO_2 tariff and heating supply temperature.

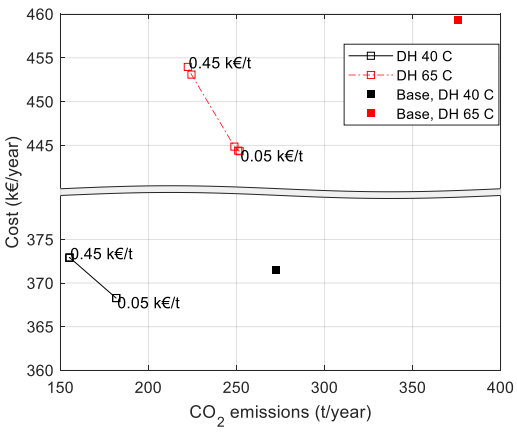

Fig. 7 – Economic vs environmental cost of the optimal solutions.

Including the cost of the CO_2 emissions as well, the optimal design of the energy system at 40°C could achieve a reduction in the range from 2% (in the case of the lowest CO_2 price) to 10.4% (in the case of the highest CO_2 price). The optimal design of the energy system at 65°C could achieve a slightly larger reduction compared to the baseline system, ranging from 4.4% to 11.8%

5. Conclusions

This paper presented a design optimization methodology for a district heating and cooling energy system integrating a Borehole Thermal Energy Storage (BTES) that considers the temperature-dependent operational implication of the BTES in conjunction with the rest of the energy system. In particular, the implications of a lower or higher heating network temperature on the optimal system design and its possibility to directly discharge the storage were studied. This methodology was applied to a case study district heating and cooling system, located in a heating-dominated climate. It was assumed that the district heating and cooling demand could be met either by an air-source heat pump and chiller, or by a BTES-connected heat pump and chiller, enabling seasonal storage of the waste heat. Solar thermal generation could also be integrated to compensate for the unbalance between cooling and heating demands. Two heating network temperatures (40 and 65°C) were studied. The optimization results showed that, for the case study system considered: i) it is always beneficial to have seasonal storage with integrated solar thermal generation, increasing in size with an increase in CO_2 price, ii) the BTES was operated at the highest initial temperature allowed, to increase heat pump efficiency during discharge and reduce CO_2 emission when the CO_2 intensity is the highest and iii) direct discharge was employed with the lower heating network temperature, but in a limited amount. This outcome is particularly interesting, as the BTES can only be discharged at the beginning of the heating season, when the BTES temperature is the highest but the CO_2 intensity not as much. Furthermore, the highest point of the BTES temperature swing is limited by the limited maximum heat transfer rate associated with the BTES size, as the borehole density is assumed to remain constant with the different BTES sizes considered.

6. Acknowledgement

The authors would like to acknowledge the financial support of the Swiss Federal Office of Energy SFOE through the SWEET DeCarbCH program and of the Swiss National Science Foundation SNSF through the Sinergia SOTES project.

7. References

[1] Sibbitt B, McClenahan D, Djebbar R, Thornton J, Wong B, Carriere J, et al. The Performance of a High Solar Fraction Seasonal Storage District Heating System – Five Years of Operation. Energy Procedia 2012;30:856–65. https://doi.org/10.1016/J.EGYPRO.2012.11.097.

[2] Laboratory U of W--MSE, Klein SA. TRNSYS, a transient system simulation program. Solar Energy Laborataory, University of Wisconsin--Madison; 1979.

[3] Shah SK, Aye L, Rismanchi B. Seasonal thermal energy storage system for cold climate zones: A review of recent developments. Renew Sustain Energy Rev 2018;97:38–49. https://doi.org/10.1016/j.rser.2018.08.025.

[4] Antoniadis CN, Martinopoulos G. Optimization of a building integrated solar thermal system with seasonal storage using TRNSYS. Renew Energy 2019;137:56–66. https://doi.org/10.1016/j.renene.2018.03.074.

[5] Prasanna A, Dorer V, Vetterli N. Optimisation of a district energy system with a low temperature network. Energy 2017;137:632–48. https://doi.org/10.1016/j.energy.2017.03.137.

[6] Gabrielli P, Gazzani M, Martelli E, Mazzotti M. Optimal design of multi-energy systems with seasonal storage. Appl Energy 2018;219:408–24. https://doi.org/https://doi.org/10.1016/j.apenergy.2017.07.142.

[7] Wirtz M, Kivilip L, Remmen P, Müller D. 5th Generation District Heating: A novel design approach based on mathematical optimization. Appl Energy 2020;260:114158. https://doi.org/10.1016/j.apenergy.2019.114158.

[8] Fiorentini M, Baldini L. Control-oriented modelling and operational optimization of a borehole thermal energy storage. Appl Therm Eng 2021:117518. https://doi.org/10.1016/J.APPLTHERMALENG.2021.117518.

[9] Miglani S, Orehounig K, Carmeliet J. Integrating a thermal model of ground source heat pumps and solar regeneration within building energy system optimization. Appl Energy 2018;218:78–94. https://doi.org/10.1016/J.APENERGY.2018.02.173.

[10] Fiorentini M, Heer P, Baldini L. Design optimization of a borehole seasonal thermal energy storage in a district heating and cooling system. Manuscript submitted for publication.

[11] Gurobi. Gurobi Solver. https://www.gurobi.com/products/gurobi-optimizer/ (accessed November 10, 2020).

[12] Hellström G. Ground heat storage: Thermal analyses of duct storage systems. Lund Univ 1991:310.

[13] Lofberg J. YALMIP : a toolbox for modeling and optimization in MATLAB. 2004 IEEE Int. Conf. Robot. Autom. (IEEE Cat. No.04CH37508), 2004, p. 284–9. https://doi.org/10.1109/CACSD.2004.1393890.

[14] Lawrie L, Drury C. Development of Global Typical Meteorological Years (TMYx) 2019. http://climate.onebuilding.org (accessed June 3, 2021).

[15] electricitymap https://www.electricitymap.org/map (accessed November 2, 2020).

[16] Luo J, Rohn J, Bayer M, Priess A. Thermal performance and economic evaluation of double U-tube borehole heat exchanger with three different borehole diameters. Energy Build 2013;67:217–24. https://doi.org/10.1016/j.enbuild.2013.08.030.

[17] EMBER Daily EU ETS carbon price n.d. https://ember-climate.org/data/carbon-price-viewer/ (accessed April 30, 2021).

[18] IEA. Levelised cost of CO2 capture by sector and initial CO2 concentration 2019. https://www.iea.org/data-and-statistics/charts/levelised-cost-of-co2-capture-by-sector-and-initial-co2-concentration-2019.

Heath Recovery from Waste Recreational Pools Water of Thermal Baths and Medical Sanatoriums

Anna Predajnianska [a], *Ján Takács* [a]

[a] Slovak University of Technology in Bratislava, Faculty of Civil Engineering, Department of Building Services, Slovakia

Abstract. In Slovakia we can find 35 thermal baths and 28 thermal healing sanatoriums that use geothermal or thermal healing water for their operation. After the use of water in these facilities, waste pool water with relatively high temperature is drained out of these facilities. This wastewater has considerable energy potential, which is used in any way. There are number of buildings in the premises of recreational and medical facilities, which are used for various purposes. Whether it is a building used by the staff of the recreational facility or by visitors. We have two options for using the energy potential of wastewater. The first option in the summer is to use waste heat to preheat cold water, which is used together with geothermal water to fill and operate of pools. The second option in the winter is to use waste heat to defrost the sidewalks within the recreational facility or use this heat in the system of active thermal protection of buildings that are part of the complex. The aim of the paper is to present more ways of using the energy potential of waste pool water, which is produced by thermal baths and medical sanatoriums and calculation results of geothermal water volume decreasing.

Keywords. Geothermal energy, thermal baths, wastewater, heat recovery.
DOI: https://doi.org/10.34641/clima.2022.146

1. Introduction

Geothermal energy is one of the renewable energy sources. Its advantage is that it does not depend on weather conditions or the alternation of day and night. Geothermal sources in Slovakia provide thermal water with a temperature from 30 °C to °30 °C. The possibility of using depends on the temperature of the thermal water. Thermal water with a temperature 110 °C can be used to generate electricity. We do not currently have any thermal power plant in Slovakia, while there are 72 registered in the world. Thermal wells that provide water with a temperature below 100 °C can be used for direct utilization.

"From 114 wells at 74 sites, geothermal energy is used for heating production. Following a long tradition of using geothermal waters, begun in medieval times, the recreation sector remains the predominant use for geothermal waters in Slovakia [4]." World surveys, which are based on information from Slovak experts, show that geothermal energy in Slovakia is widely used in recreational facilities [5].

The most widely used method of direct utilization of thermal water in Slovakia are thermal baths. According to data from the Ministry of Health of the Slovak Republic, we have 213 registered artificial swimming pools in Slovakia with a total of 658 pools. Of these, 461 are filled with non-thermal water and 197 pools are filled with thermal water. It is the recreational and leisure pools that use thermal water with a temperature of up to 40°C for their operation that have the greatest potential for this work. The work is focused on the system of heat recovery from wastewater produced by thermal baths.

1.1 Pool types used in recreational facilities

The following chapter will introduce two basic types of swimming pools that are used in recreational facilities. In both cases, it is possible to use a heat recovery system from the waste pool water. In general, two basic types of pools are used in thermal baths. The first is a flow system that is relatively resource intensive. It is a simple system, where thermal water is fed directly into the pool, if it has the required temperature and a suitable mineralisation. If this is not possible, thermal water must be mixed with cold water to ensure the required pool water parameters. Wastewater flows out of the frow pool without further use. The second type is the circulation pool system, which has a significantly lower composition of thermal water. It is a more technologically demanding system, which is more advantageous and therefore more used. Wastewater does not immediately drain from the circulation pool. Pool water circulates in the system again. The multiplicity of the water exchange on which the volume of water added to the system

Copyright ©2022 by the authors. This conference paper is published under a CC-BY-4.0 license.

depends is determined by the body of the hygienic service. From the pool, the pool water flows into a buffer tank, in which thermal water is mixed with cold water. Only after the buffer tank is overfilled does wastewater flow out of the system.

In both cases, the waste pool water, which has a temperature of up to 40 °C, flows out of the pool system. Wastewater with such a high temperature represents a large energy potential that is not used. Another problem with recreational facilities is that the maximum temperature of wastewater that can be discharged into a water recipient is prescribed by the laws and regulations described in the following chapter.

1.2 Legislative requirements

An important factor is the maximum temperature of the waste pool water that can be discharged into the recipient. According to the Regulation of the Government of the Slovak Republic no. 269/2010 of 25 May 2010 laying down requirements for achieving good water status and pursuant to Law No. 364/2004 on waters and on the amendment of the Act of the Slovak National Council No. 372/1990 Coll. on offenses, known as the Water Law, the maximum temperature of waste pool water that can be discharged into the recipient without demanding the environment is set at 26 °C [1, 2]. In most cases this temperature is exceeded. Therefore, the aim of this article is to present the heat recovery system as possibility of cooling the wastewater to a suitable temperature. The heat recovery system has several positive aspects. One of the advantages is the cooling of the waste pool water to a temperature at which is safe to discharge it into the recipient without environmental pollution.

2. Heat recovery system

The wastewater from the pools reaches a temperature of 40 °C. Water with such a high temperature has an energy potential that is not used. Thermal and non-thermal swimming pools use cooling ponds or canals to cool wastewater. It is one of the solutions, but it is necessary to realize that in this way the wastewater is aimlessly cooled, and the energy potential is not used. The heat recovery from the waste pool water is based on a recuperative heat exchanger, which is inserted into the wastewater circuit. Waste pool water flows through the heat exchanger, which transfers its heat to the cold water. This principle is illustrated in the Fig. 5. Preheated cold water can be used in several ways:

- preheating of cold water used to operate swimming pools (yearly),
- preheating of cold water for the domestic hot water preparation (yearly),
- absorption cooling (summer operation),
- snow melting system (winter operation),
- active thermal protection of the buildings.

There are two ways to install a heat exchanger. The first is to install a heat exchanger in the pool engine room. The second option is to install a heat exchanger in the cooling pond or canal. Both options will be described in the following subsections.

2.1 Heat exchanger in the engine room

Each pool has its own engine room, which in most cases is located near to the pool. In the engine room is located the technological equipment needed to operate the pool, such as a buffer tank, sand filter and circulating pump. In the case of using a heat recovery system, where the heat exchanger will be in the engine room, it is necessary to consider the space which is available. The design of the heat exchanger is based especially on this.

The analysis of the suitability of different types of heat exchanger in this system showed that the most positive is the use of a plate recuperative heat exchanger, which can be seen in Fig. 1. Construction of the plate heat exchanger consists of back and front stand between which the plates are places. The plates form the heat exchanger surface where heat is exchanged between heat transfer fluids. Plate heat exchanger advantages are mainly relatively small size and high performance. This system is suitable for preheating cold water, which is used directly in the engine room for mixing with thermal water. Scheme of the flow pool system with heat recovery system is show in Fig. 2 and scheme of the circulation pool system with heat recovery system is show in Fig. 3.

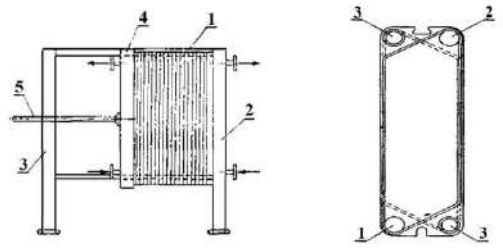

Fig. 1 – Scheme of the flow pool system with heat recovery system. 1 – plate heat exchanger, 2 – back stand, 3 – front stand, 4 – pressure plate, 5 – tightening plate [3]

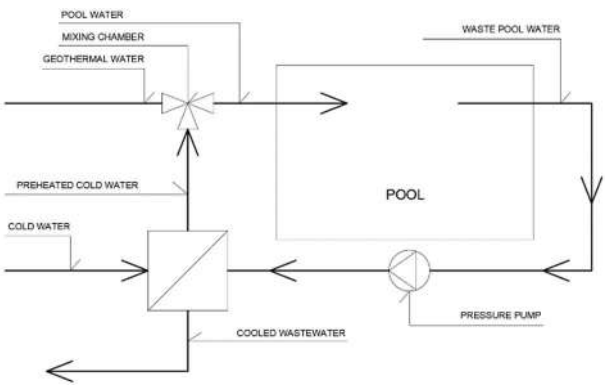

Fig. 2 – Scheme of the flow pool system with heat recovery system.

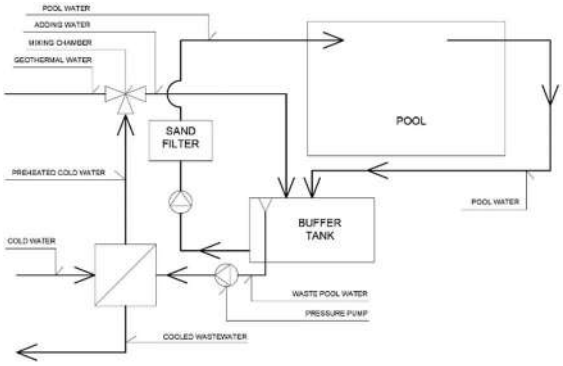

Fig. 3 – Scheme of the circulation pool system with heat recovery system.

The most suitable types of heat exchangers that suit this applications, material, shape, and quality of heat transfer are plate heat exchangers. The heat exchange surface of the plate heat exchangers is formed by parallel, most often vertical plates placed in a rack so that slot channels 3 to 10 mm wide are formed in the interpolate space. Two liquids, ideally in counter current, flow alternately through these slots. The most important element of these heat exchangers is the worktop, which is pressed from thick sheet metal, today most often from stainless steel or titanium. The plates allow the assembly of heat exchangers with a total heat exchange area of up to 600 m^2. Due to the relatively high heat transfer coefficient, they need a relatively small area per unit to output. The operating temperature range is from -10 °C to 200 °C. The advantage of this type of heat exchanger is the good maintenance and accessibility of the work surface due to the possibility of rapid disassembly of the plate bundle for visual inspection [3].

2.2 Heat exchanger in the cooling canal

In principle, this system also consists in the inclusion of a heat exchanger in the wastewater circuit, however, a cooling canal or pond is used. A tubular heat exchanger is installed in the cooling canal, through which cold water flows. Waste pool water with higher temperature flows around the oven, transferring its heat to the cold water. The design of a tubular heat exchanger depends on the properties of the cooling canal, such as its cross-section and water depth. The scheme of the installation of the tubular heat exchanger in the cooling canal is show in Fig. 4.

3. Calculation methodology

One of the advantages of a heat recovery system is the use of waste heat to preheat the cold water which the thermal water is mixed to ensure the required pool water parameters. Because the thermal water is mixed with preheated cold water, a smaller volume of thermal water is needed to ensure the same pool water parameters. This fact was verified by calculation methods.

For the calculation was chosen the pool with parameters based on real data. A recreational pool was chosen, working on a flow pool system. The water area is 295,0 m^2. The depth of the pool is 1,25m and volume is 368,0 m^3. The geothermal well provides water with a temperature of 70 °C, which is mixed with cold water with a considered average temperature of 15 °C, to desire pool water temperature of 38 °C. In this calculation, we considered only the summer operation of the pool, which lasted 70 days. The pool was out of order for 7 days, during which it was drained and refilled.

The calculation must be made separately for the filling and operation of the pool. The reason is that it is not possible to use a heat recovery system during filling, because no wastewater flows out of the pool. The heat recovery system can be used during the operation of the pool, when the waste pool water flows in the recipient.

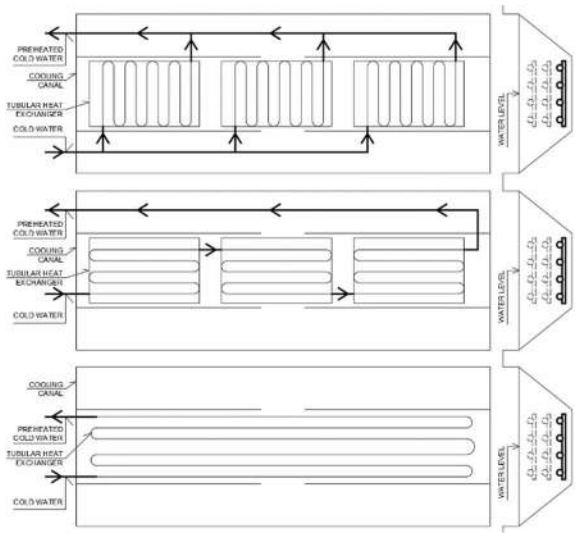

Fig. 4 – Scheme of the installation of the tubular heat exchanger in the cooling canal.

4. Results

The calculation is based on the transfer of heat from the waste pool water through the heat exchanger surface. This process is illustrated in Fig. 4. It is clear from the Fig. 5 that cold water with a temperature of 15 °C and wastewater with a temperature of 38 °C are fed to the heat exchanger. The wastewater transfers heat to the cold water, which is preheated to 27 °C.

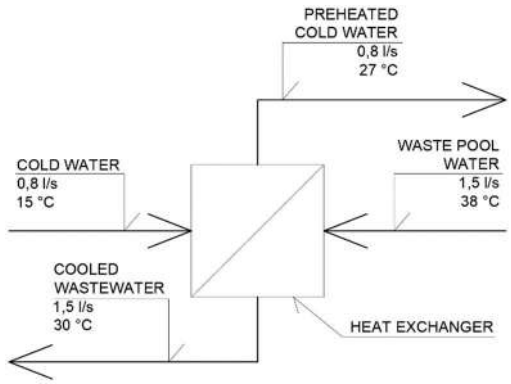

Fig. 5 – Heat transfer scheme in a plate heat exchanger.

The necessary volume of cold and geothermal water to achieve the required parameters of pool water was also calculated. The calculation was made separately for the filling and operation of the pool. The calculation was made for the system without and with heat recovery system.

4.1 Pool without heat recovery system

The results of the calculation without heat recovery showed that a pool water flow of 11,4 l/s is required to fill the pool. Pool water is mixed from geothermal water with flow of 4,7 l/s (57% of total pool water flow) and cold water with flow of 6,6 l/s (43% of total pool water flow). During the summer season, which lasted 70 days, the pool will be filled seven times. A total of 2 962,4 m³ is needed to fill the pool during the summer operation. 57% (1 238,8 m³) of the total volume will be cold water, the remaining 43% (1 723,6 m³) geothermal water. The results of the calculation are summarized in Graph 1.

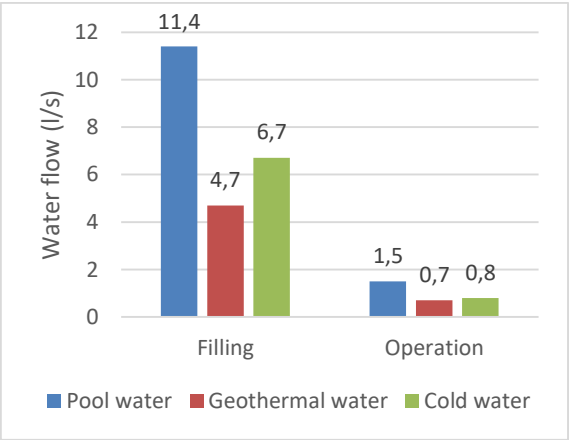

Graph 1 – The results of the calculation of the pool without heat recovery system during filling and operation.

4.2 Pool with heat recovery system

The next step is to calculate the same pool system, but after installing the heat recovery system into the wastewater circuit. The aim of the calculation is to prove that the use of this system brings several advantages. The results of the installation of the heat exchanger, the required flow and the volume of geothermal water needed for the same operation of the pool are reduced. This phenomenon is due to the increased use of cold preheated water that has been preheated using wastewater energy potential. The total pool water flow remains unchanged. The ratio of geothermal and cold-water use is changing. After installing a heat recovery system, the flow of geothermal water decreases and, conversely, the flow of cold water, which is preheated to a higher temperature, increases. In the solved example, the use of cold preheated water increased by 13%. 11,4 l/s of pool water are still needed to fill the pool. The mixing ratio of geothermal and cold water varies. 3,8 l/s (33% of total pool water flow) of geothermal water and 7,6 l/s (67% of total pool water flow) of cold water is needed to achieve the required pool water parameters. The results of the calculation of the pool with heat recovery system during filling and operation are showed in Graph 2. In the solved example, the waste pool water was cooled to 30 °C. The maximum temperature of the wastewater that can be discharged into the recipient is set at 26 °C. If the required wastewater temperature is reached, the use of wastewater energy potential will be even more advantageous.

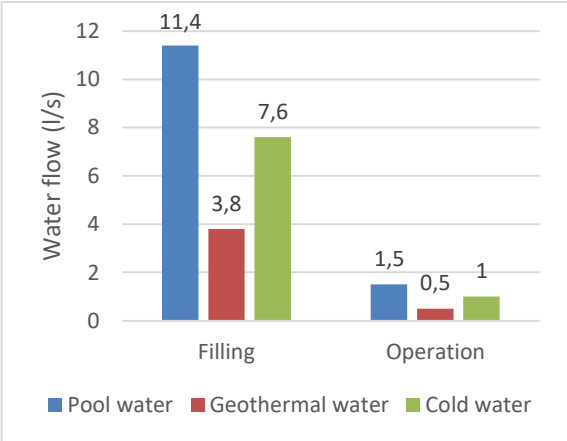

Graph 2 – The results of the calculation of the pool with heat recovery system during filling and operation.

A comparison of the volume of pool, geothermal and cold water is shown in Graph 3 and Graph 4. It is clear from the graph that after the application of the heat recovery system, the consumption of geothermal water decreased during operation of the pool, and the consumption of cold preheated water increased. During the filling, the values are constant because no wastewater flows out of the pool during filling and the heat recovery system is not active.

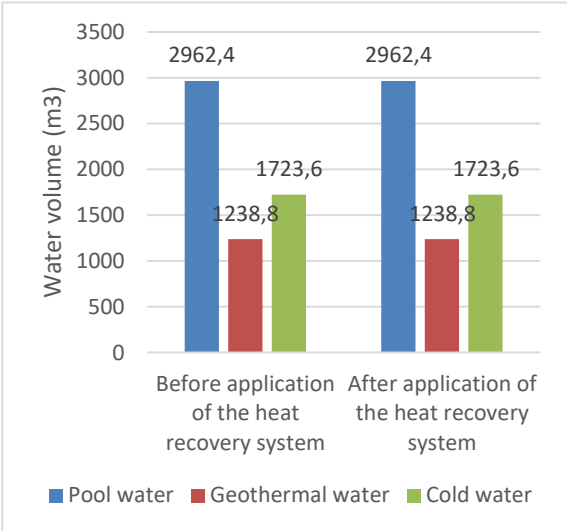

Graph 3 – The comparison of the volume of pool, geothermal and cold-water during filling of the pool before and after application of heat recovery system.

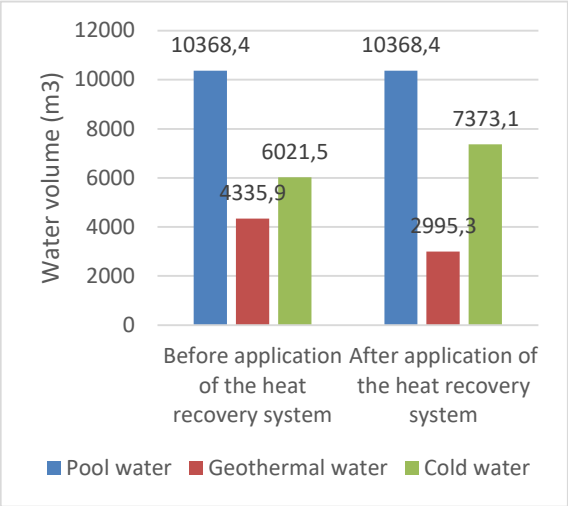

Graph 4 – The comparison of the volume of pool, geothermal and cold-water during operation of the pool before and after application of heat recovery system.

5. Discussion

The aim of the heat recovery system is to reduce the temperature of the wastewater to a value at which it will not be necessary to face sanctions for environmental pollution. With the help of a heat recovery system using a plate or tube heat exchanger, it is possible to reach a temperature of 26 °C, which is given by laws. The use of a heat exchanger in a heat recovery system can be considered as a one-stage cooling of wastewater. The zero level of water exergy is 15 °C. In the case of the inclusion of the second stage of wastewater cooling in the form of heat pumps, it would be possible to reach this temperature and use the full energy potential of the water [6, 7]. However, it is necessary to consider whether the law provides not only a maximum but also a minimum temperature of wastewater that can be discharged into the recipient. Legislation in Slovakia does not prescribe a minimum temperature of wastewater that can be discharged to the recipient. Another aspect that needs to be considered is the economic aspect. In this case, it is necessary to compare the investment costs for heat pumps, the return on such a system and the fact whether it is necessary from an economic point of view to include the second stage of wastewater cooling.

The significance of this work lies in the use of energy potential, which is considered waste. The idea of heat recovery from waste pool water is not used in any swimming pool in Slovakia. This study is currently under development. The following procedures will also include energy saving potential and resources saving potential, which are not assessed in the current article and have not been the aim of this work. The aim of the work was to prove numerically that thanks to the heat recovery system it is possible to reduce the volume of thermal water needed to operate the pool what is clearly shown in Graph 4.

6. Conclusion

Waste pool water which is largely produced by thermal as well as non-thermal swimming pools, has a great energy potential, which is not used in any way. There are several possibilities of heat recovery from waste pool water. The article focused on the use of waste heat in the cold-water preheating system, which is used in pool management to achieve the required parameters of pool water. Due to the preheating of cold water to a higher temperature, it is possible to achieve a reduction in the required volume of geothermal water, which is needed for the operation of pool management by 13 %. This can be achieved by means of an energy-saving measures as application of a recuperative heat exchanger into the wastewater circuit, or by applying a second stage of wastewater cooling by means of heat pumps. The aim of this system of heat recovery from waste pool water is the possibility to reduce the temperature of waste pool water to a value at which it is safe to discharge it into the recipient without damaging the surrounding environment. In the calculation given in the paper, the temperature of the waste pool water was reduced to 30 °C. By using a heat exchanger with a higher power, it is possible to reach the temperature required by laws. In Another aspect is the reduction in the volume of geothermal water pumped from the geothermal well, which will extend the lifetime of the geothermal source. Finally, it will be possible to reduce sanction for environmental pollution, which depend on the temperature of the wastewater discharged into the recipient.

7. Acknowledgement

This article was supported by the Ministry of Education, Science, Research and Sports of Slovak Republic through a grant VEGA 1/0303/21, VEGA 1/0304/21 and KEGA No. 005STU-4/2021.

8. References

[1] Regulation of the Government of the Slovak Republic No. 269/2010 of 25 May 2010 laying down requirements for achieving good water status.

[2] Law No. 364/2004 on waters and on the amendment of the Law of the Slovak National Council No. 372/1990 Coll. on offenses (Water Law).

[3] Jelemenský, K. (2021). Heat exchangers – principles, advantages, and disadvantages, iDB Journal, No. 2/2021, ISSN 1338-3337, pp. 34–36.

[4] Lund, J. W., & Toth, A. N. (2021). Direct utilization of geothermal energy 2020 worldwide review. Geothermics, 90. https://doi.org/10.1016/j.geothermics.2020.101915.

[5] Fričovský, B., Černák, R., Marcin, D. et. al. (2020). Geothermal Energy Use, Country Update for Slovakia, European Geothermal Congress 2020, Reykjavik, Iceland, 11-14 June 2019, p. 19.

[6] Nyers, J. (2016), COP and Economic Analysis of the Heat Recovery from Waste Water using Heat Pumps, Acta Polytechnica Hungarica, 2016, Volume 13(5), ISSN 1785-8860, pp. 135-154.

[7] Kassai, M. (2019), Heat Pump Heating System Development of Educational Building based on Energy Economical and Environmental Impacts, Periodica Polytechnica Mechanical Engineering, 2019, Volume 63(3), ISSN 324-6051, pp. 207-213.

Data Statement

The data used in the calculation are provided by the operator of the thermal swimming pool in Slovakia. The calculations are based on real data of the recreational facility.

Acknowledgement

This work was supported by the Ministry of Education, Science, Research and Sports of the Slovak Republic through a grant VEGA 1/0303/21, VEGA 1/0304/21 and KEGA 005STU-4/2021.

Performance Evaluation of Passive Cooling in a Multi-Zone Apartment Building Based on Natural Ventilation

Essam Elnagar [a], Alanis Zeoli [a], Vincent Lemort [a]

[a] Thermodynamics Laboratory, Aerospace and Mechanical Engineering Department, Faculty of Applied Sciences, Université de Liège, Belgium, essam.elnagar@uliege.be

Abstract. In moderate climates, using natural ventilation systems could allow to save up to 60 % of the end energy for ventilation and air conditioning. Natural ventilation systems depend on pressure differences to move fresh air into buildings by wind effect and pressure effect. Night cooling can be achieved either by an increased air change rate. The higher air change rate can be realized by ventilators/ mechanical ventilation systems or by free convection. The main objective of this paper is to reduce the internal summer cooling load by increasing the natural cross ventilation between different zones in apartment buildings. The performance of natural ventilation is highly dependent on the external outdoor temperature. Over the last years, an increase in the outdoor temperature has been noticed and predicted to rise by the end of this century according to IPCC which puts into consideration the uncertainty of the climate. This paper investigates the performance of natural ventilation using building energy simulation tool 'DesignBuilder" to simulate a multi-zone apartment building in Belgium. The indoor thermal comfort is enhanced by determining an optimum set of input parameters such as the setpoint temperatures, the discharge coefficient of the night ventilation, and the opening areas in the building. Those parameters are optimized using current and future weather data to evaluate the evolution of natural ventilation system performance and indoor thermal comfort. The results show that proper use of natural ventilation can significantly reduce the overheating risk during a typical year and that the benefits of natural ventilation are not expected to vanish with global warming. It can be seen that, without natural ventilation, thermal comfort could be reached on average 53.7% of the time, while it could reach 66.2% of the time using single-sided ventilation and 78.8% with cross ventilation. However, during heatwaves, natural ventilation becomes inefficient and cannot guarantee the thermal comfort of the occupants all the time as the thermal comfort of occupants can only be achieved 51% of the time during heatwaves.

Keywords. natural ventilation, passive cooling, cooling demand, thermal comfort, heatwaves
DOI: https://doi.org/10.34641/clima.2022.263

1. Introduction

The energy demand for space cooling is growing fast in the next decades and will be tripled by 2050, the increase in the cooling demand led to a significant increase in the sales of air-conditioning systems between 1990 and 2016 [1]. Therefore, there is an attention to the passive cooling techniques that reduce the need for air-conditioning systems by improving the internal environmental conditions with low or no energy consumption [2].

There is a growing interest in passive cooling techniques due to the energy and indoor air quality problems associated with mechanically ventilated systems. Natural Ventilation (NV) is one of the most promising passive cooling techniques used in buildings in different climates. NV helps to create healthy indoor environments for occupants and meet the EU targets to reduce CO_2 emissions by 2050.

Several studies analyzed the performance of NV in different climates. In the temperate climate, NV has a good potential for thermal comfort improvement that varies between 8% and 56% [3]. In the Mediterranean climate, it was predicted that cross NV during day and night resulted in up to 7 K temperature decrease in apartments [4]. In different climate zones in Australia, NV was investigated for a single-storey building, the results showed in hot humid summer, warm winter zone, the annual NV hours is 4728, while the least NV hours is in cool temperate zone [5].

However, the performance of NV under the climate change scenarios including the disruptive events of

Copyright ©2022 by the authors. This conference paper is published under a CC-BY-4.0 license.

heatwaves is not appropriately addressed. This study focuses on the NV strategies performance under different future climate change scenarios in Belgium including summer heatwaves.

2. Methodology

The conceptual framework of the study is presented in Fig. 1. The first part of the framework introduces the literature review that has been conducted to identify the natural ventilation strategies and specify the performance indicators and the comfort models. The second part presents the case study as well as the weather data used in the framework.

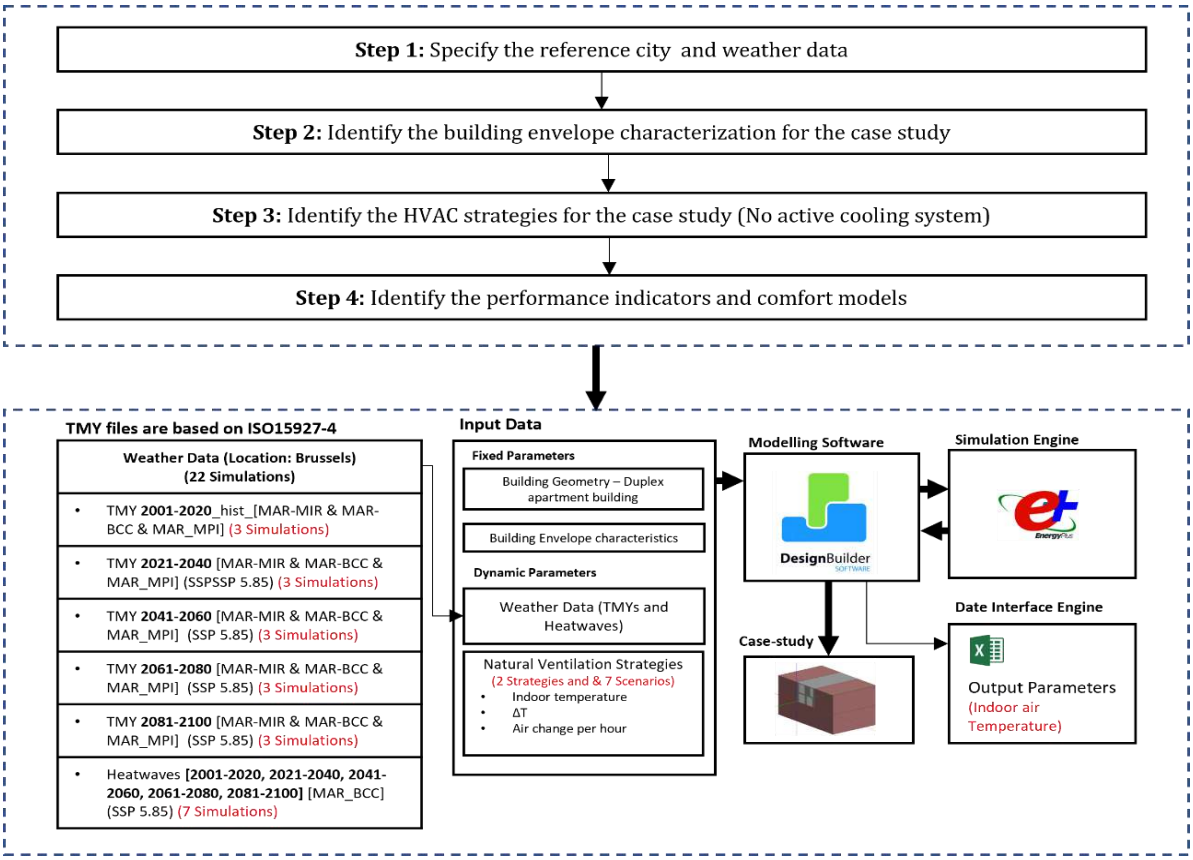

Fig. 1 – Conceptual framework of the study.

2.1 Building Model

This section gives the most important information about the geometry, envelope characteristics and operation features of the studied dwelling (see Tab. 1). Fig. 2 is an upper view of the studied duplex. The building has a North-South orientation and a large window-to-wall ratio (0.6) on the South façade. The dwelling has been divided into seven thermal zones, which have been defined depending on the zone usage, temperature setpoint and orientation.

The EPBD imposes energy performance standards for buildings. The building walls are compliant with the EPBD 2020 [6]. The glazing has been defined in the EPB file of the building as triple-glazing. The frame of the window, made of wood and aluminum, has a U-value of 0.9 W/m^2·K, resulting in a net U-value of 0.6 W/m^2·K, in compliance with the EPBD. The duplex is equipped with a balanced mechanical ventilation system with a heat recovery module of 85% efficiency and a by-pass system. The heating system is traditional with water radiators fed by a gas boiler. There is no mechanical cooling system.

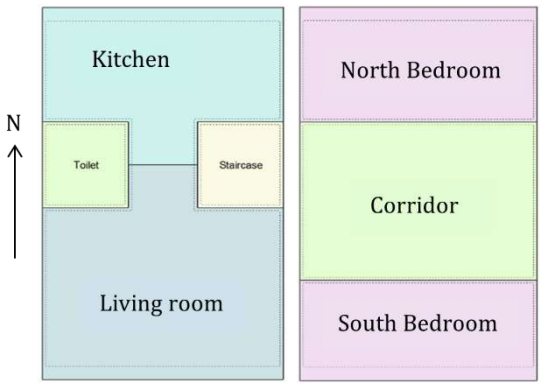

Fig. 2 – Upper view of the duplex.

Regarding the operation of the building, it is assumed that the occupants are four adults each emitting 100 W. For lighting, it is good practice to consider a consumption of 6 W/m^2, according to norm NBN EN 15193 [7]. The energy consumption linked to electric appliances is assumed to be 3 W/m^2. Some operation/occupancy schedules can be applied to that energy consumption. They can be found in standard ISO 17772 [8].

Tab. 1 – General characteristics of the case study.

General information		Envelope	
Building location	Liège, BE (50°37'57" N 5°34'47"E)	Walls	
Building type	Residential	U-value [W/m²]	
Nb storeys	9	External wall	0.152
Case study	4-person family duplex	Internal wall	0.452
Floor	8-9	Adjacent wall	0.198
Orientation	South	Roofing	0.081
Surface	173 m²	Floor/ceiling	0.132
WWR	0.6	Windows	
Infiltration rate	0.6 ach at 50 Pa	U-value [W/m²]	0.6
Ventilation rate	3.6 m³/h/m²	Solar factor [-]	0.5

2.2 Weather Data

This study uses MAR regional atmospheric model, MAR is a three-dimensional atmospheric model coupled to a one-dimensional transfer scheme between the surface, vegetation, and atmosphere [9]. Since MAR is a regional model, it must be forced at its lateral boundaries (temperature, wind, and specific humidity) by a global model by the reanalysis of the ERA5 which represents the closest climate to reality, and then by 3 Earth System Models (ESMs) from CMIP6 database namely BCC-CSM2-MR (MAR-BCC), MPIESM.1.2 (MAR-MPI), and MIROC6 (MAR-MIR) [10].

These ESMs forced MAR simulations can be used to anticipate future periods. MAR simulations are able to represent the current climate and its interannual variability with success, except MAR-MIR which significantly overestimates temperature and solar radiation in summer. MAR-MPI can be considered as the coldest MAR simulation and MAR-BCC is the ensemble mean of all the MAR simulations [10]. MAR Model runs at 5 km spatial resolution over the Belgian territory as shown in Fig. 3.

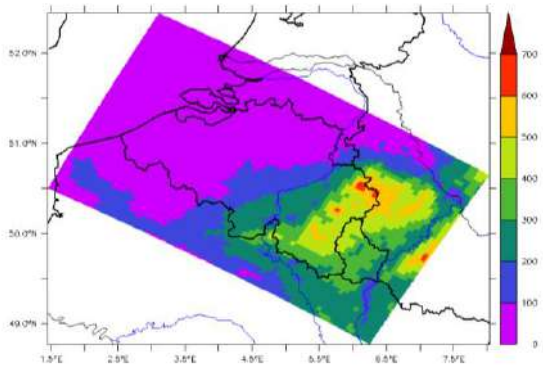

Fig. 3 – Topography (in meters above sea level) of the MAR domain representing Belgian territory [11].

In the framework of this study, data sets of the Typical Meteorological Years (TMY) are used for the 3 MAR-Simulations for the Shared Socioeconomic Pathway (SSP5.85) [12]. There are 3 main scenarios, SSP2-4.5, SSP3-7.0, and SSP5-8.5, which are respectively increasingly warming for 2100, this study used SSP5.85. In addition to that, TMY for historical scenarios based on MAR-BCC simulation is used as a reference TMY for the period (2001-2020).

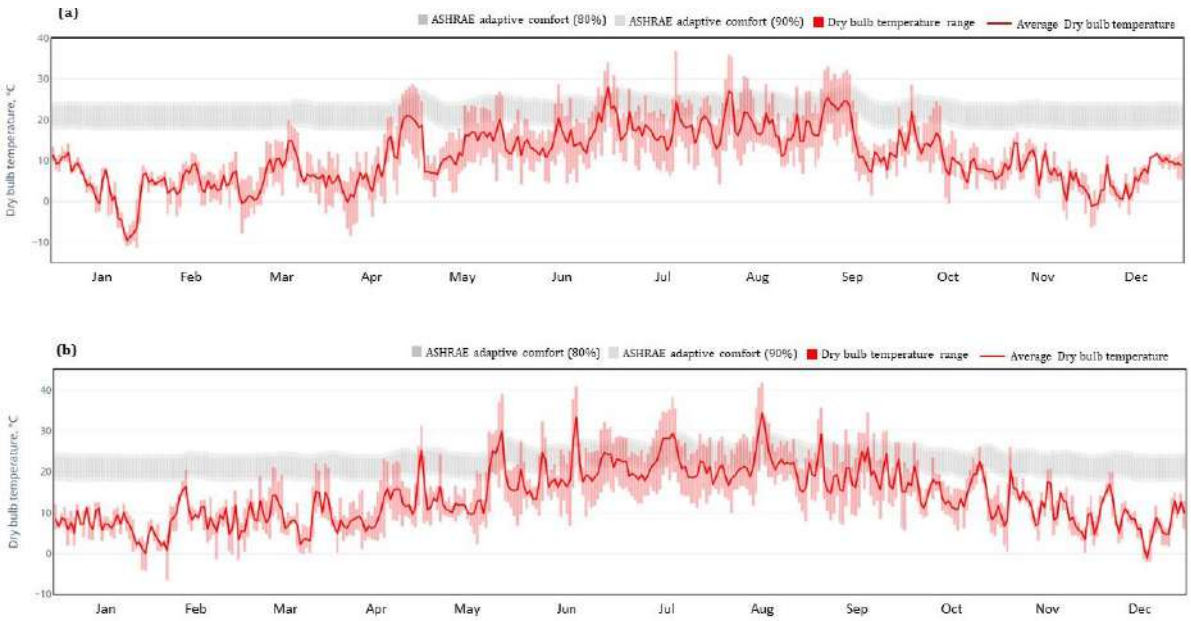

Fig. 4 – Evolution of monthly outdoor temperature with the adaptive comfort model for two periods (a) TMY 2001-2020 and (b) TMY 2081-2100.

Fig. 4 shows the evolution of the monthly outdoor temperature between the reference period and the period 2081-2100. It can be seen that, there is a significant increase in the temperature range during the periods, especially in the summer months by 3.4 K.

In addition to the TMYs, this paper also studies the performance of natural ventilation during heatwaves in the summer period. Belgium has two definitions for the heatwaves, the retrospective heatwave is defined according to the Royal Meteorological Institute as a period of 5 consecutive days with a maximum daily temperature of 25°C or more (summer days) and with a 3 day period of 30°C or higher [13], while the prospective heatwave is defined as a period of 3 consecutive days with a minimum temperature of 18.2°C or higher (average for the 3 days) and a maximum temperature of 29.6°C or higher [14].

However, this paper followed a different definition of heatwaves which is considering the local climate of each region, based on the statistical definition of a heatwave by Ouzeau et al. [15], they defined the heatwave events and classified them according to three criteria of the heatwave (the duration, the highest temperature and the intensity).

- The duration is specified according to the duration of the heatwave which is calculated by the number of consecutive days of the heatwave.
- The highest temperature is detected based on the maximal daily mean temperature reached during the period of the heatwave event.
- The intensity is calculated by the cumulative difference between the outdoor temperature and the temperature threshold (Sdeb) of 23°C for the whole duration of the event, divided by the difference between Sdeb and Spic (26°C).

2.3 Passive Cooling Concept

A passive cooling concept based on natural ventilation is applied to cool the apartment. A series of cooling simulations were conducted using DesignBuilder simulation tool to investigate the impact of climate change on the potential of natural ventilation in Belgium.

The control strategy of the natural ventilation in this study is based on the minimum indoor temperature, the temperature difference between the indoor and outdoor temperature (ΔT) and the occupancy schedule in the different scenarios. Single-sided ventilation and cross ventilation strategies are studied using the TMYs for the different MAR simulations in the kitchen zone. Single-sided ventilation occurs when the fresh air exits the room in the same direction it had entered. Cross-ventilation occurs when there are pressure differences between one side of the building and the other, the airflow path goes from one side of the building and exits from the other side after rotating around the openings and windows [16]. The airflow path for single-sided ventilation and cross ventilation is illustrated in Fig. 5. Natural ventilation is assumed to be triggered by the opening of the windows and there is no obstacle to cross-ventilation as there is no physical separation between the kitchen and the living room.

During heatwaves, different scenarios have been conducted by adapting the parameters of the natural ventilation control strategy. The maximum admissible airflow rate has also been changed. The characteristics of the considered scenarios are described in Tab. 3.

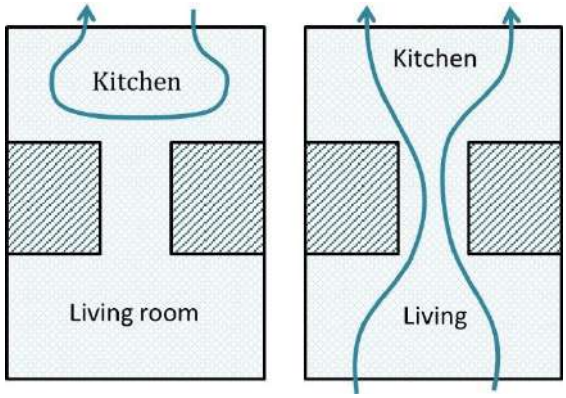

Fig. 5 – Illustration of the single-sided and cross-ventilation strategies in the studied building.

The minimum indoor temperature corresponds to the indoor temperature above which windows can be open. ΔT is the temperature difference between the indoor and the outdoor temperature. The windows can only be open if $T_{in} - T_{out} > \Delta T$. The schedule defines the periods during which the windows can be open. In the end, the windows are open only if all the previous conditions are satisfied.

Due to the unavailability of monitoring data, the performance evaluation of the different NV strategies and the different scenarios are analyzed in a comparative method.

2.4 Comfort Evaluation

In this study, the adaptive comfort model is used to determine the overheating risk in the dwelling and the efficiency of passive cooling. The adaptive comfort theory states that the comfort temperature range can be broadened because the occupants can adapt their behavior depending on the outdoor conditions. The adaptive comfort model is described in norm EN 15251 [17]. In a naturally ventilated building without any air-conditioning, the occupants feel more connected to the outdoor environment and can bear higher temperatures in summer. The maximum comfort temperature adaptive can be expressed by a relationship depending on the mean outdoor temperature:

$$T_{confort,max} = 0.33\, T_{rm} + 21.8$$

where T_{rm} is the running mean outdoor temperature during the previous seven days. For the adaptive comfort theory to be applicable, there should be neither a heating nor a cooling system in operation and window opening and closing should be of primary importance as a means of regulating thermal conditions in the space. They should also be able to adapt their clothing to indoor and outdoor conditions.

3. Results

The results of the simulations are shown in Fig. 6. The most interesting room to study regarding natural ventilation is the kitchen. The graph shows the evolution of time during which thermal comfort is reached in the kitchen with global warming. By the end of the century, the average indoor temperature is expected to increase by 3 to 3.7 K depending on the considered MAR simulation, which results in thermal comfort degradation.

The percentage of time during which the indoor temperature remains below the maximum comfort temperature drops from 53% to 43.6% over the century. Single-sided ventilation results in an average indoor temperature decrease by 2.5 K and an increase of 12.5% in thermal comfort achievement. Cross ventilation allows for a further reduction of 1.8 K on average and a 12% increase in thermal comfort achievement.

The 3 different heatwaves are studied: The most intense heatwave (HI), the maximum temperature (HT) and the longest duration (LD) of the heatwave. The characteristics of the studied heatwaves are shown in Tab. 2. As expected, by 2100, heatwaves will last longer (around 20 days vs 5 nowadays) with a significant temperature increase (15% of time above 40°C in the period 2081-2100 vs 0% in the period 2001-2020).

Fig. 7 shows the temperature profile of an average day during heatwaves throughout the century. Some natural ventilation strategies are studied and compared in Fig. 8 for a heatwave between 19/06/2015 and 24/06/2015. It can be directly seen that natural ventilation has a positive impact on indoor temperature. In particular, the use of natural ventilation also during the night allows for a reduction of 6 K.

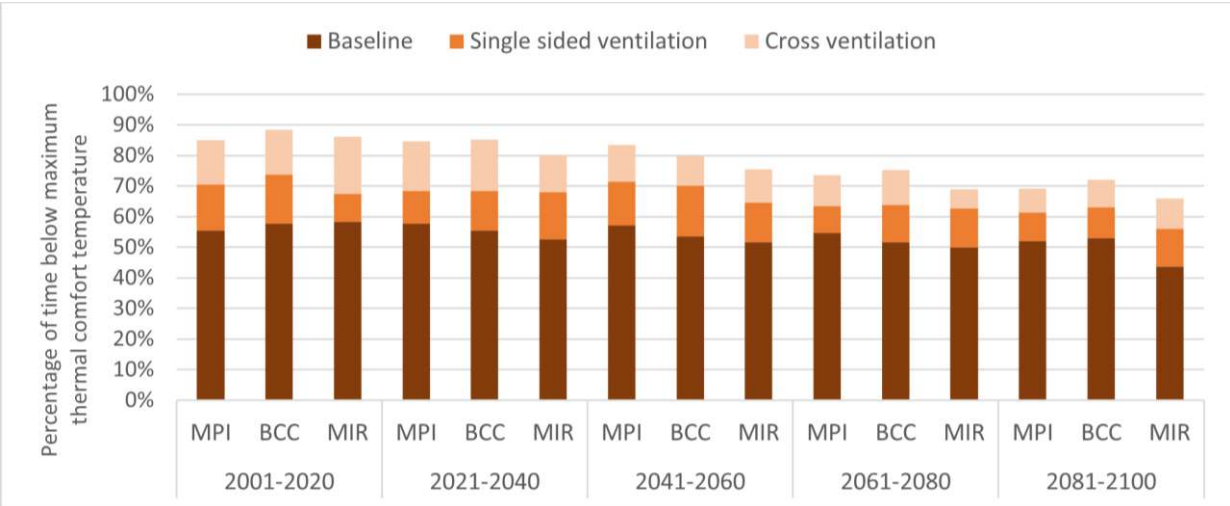

Fig. 6 – Percentage of thermal comfort time during the cooling period depending on the climate scenario and the adopted natural ventilation strategy.

Tab. 2 – Main characteristics of the studied heatwaves.

Period **Type of heatwave**	**2001-20** **HI**	**2021-40** **HI & HT**	**2021-40** **LD**	**2040-60** **HI**	**2061-80** **HI**	**2081-100** **HI**
Number of days of the heatwave	5	7	8	26	21	19
Percentage of time above						
25°C	83%	70%	60%	60%	76%	80%
30°C	57%	50%	34%	34%	47%	55%
35°C	29%	21%	13%	8%	19%	30%
40°C	0%	9%	0%	0%	1%	14%
Maximum temperature	39.8	43.6	37.4	38.0	41.6	44.4
Minimum temperature	14.9	14.1	14.9	14.8	15.4	17.1

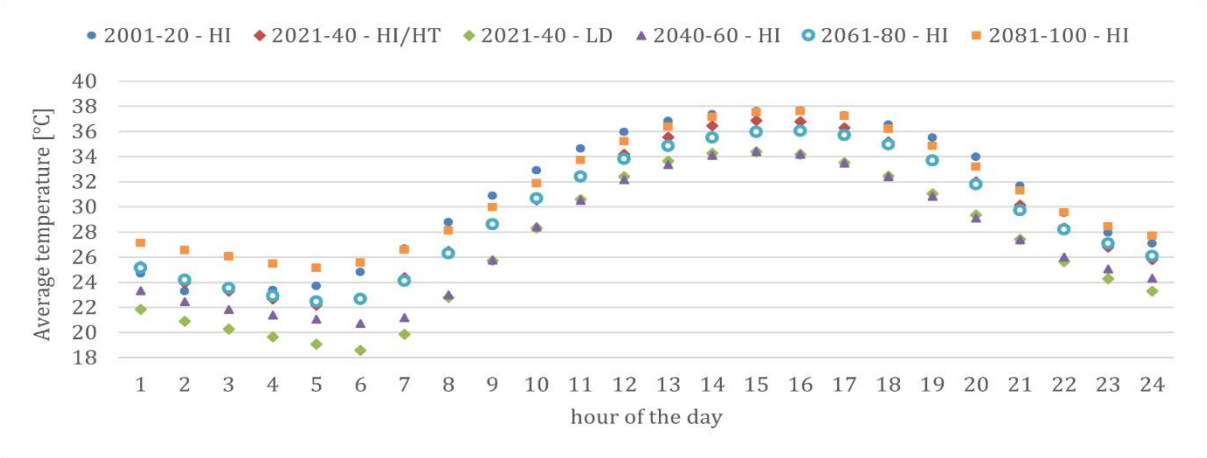

Fig. 7 – Evolution with global warming of an average day during the different heatwaves.

The enhancement of the ventilation flow rate during the night also has a positive effect on the indoor temperature. During the night, the temperature can even fall to 25°C. However, during the day, it is impossible to reach an indoor temperature below 30°C. Tab. 3 also shows the percentage of time during which thermal comfort is reached. The minimal thermal comfort temperature has been calculated with the adaptive comfort theory. When the airflow rate is at its highest, thermal comfort is reached only half of the time, and mostly during the night.

Tab. 3 – Description of the parameters used for the natural ventilation strategies and calculation of the percentage of time during the heatwaves during which thermal comfort is reached.

	Min T_{in}	ΔT	Schedule	Max airflow rate (ach)	Thermal comfort
Scenario 1	23	2	Day	5	0%
Scenario 2	23	2	Night	5	2.5%
Scenario 3	23	2	24/7	5	5.0%
Scenario 4	23	0	24/7	5	5.0%
Scenario 5	23	0	24/7	10	21.7%
Scenario 6	23	0	24/7	20	44.2%
Scenario 7	23	0	24/7	40	51.7%

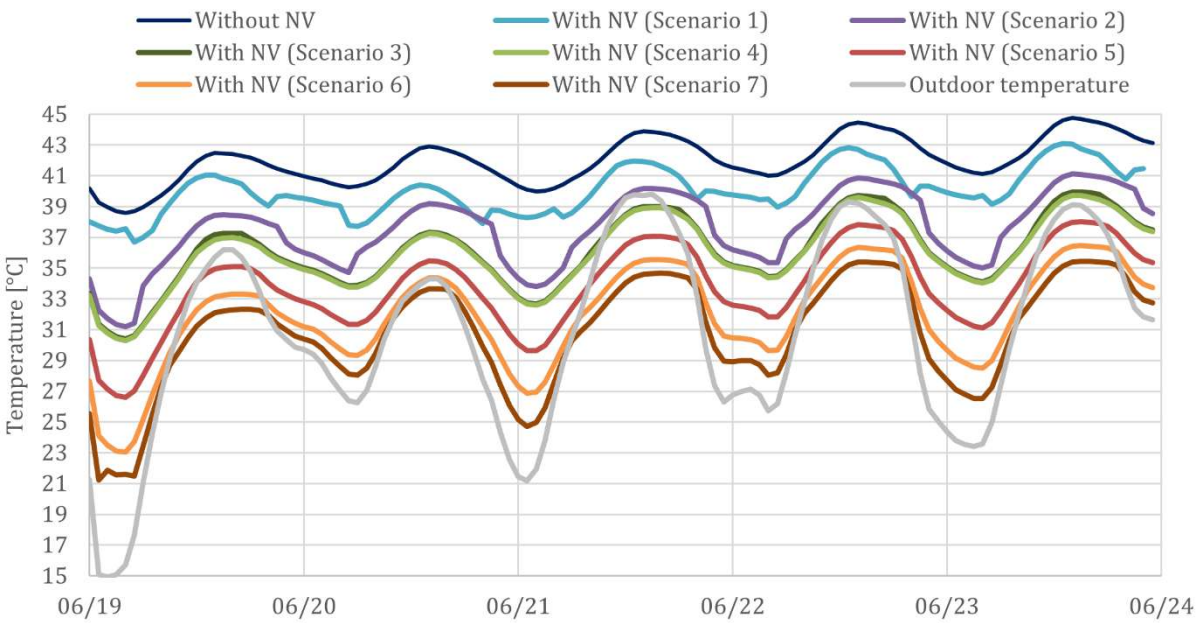

Fig. 8 – Evolution of the indoor temperature in the living room during a heatwave depending on the different natural ventilation strategies.

4. Discussion

Two natural ventilation strategies have been studied. The graph of Fig. 6 highlights the indoor temperature decrease due to the natural ventilation strategy. Those two strategies are well-known in the field of natural ventilation: single-sided ventilation and cross ventilation. Cross ventilation is the most efficient technique regarding natural ventilation, especially if the building is oriented according to the main wind direction. From this graph, it can be deduced that, for the whole cooling period, the potential of natural ventilation is not expected to vanish with global warming.

It is also interesting to study the evolution of the potential of natural ventilation during heatwaves. With global warming, heatwaves in Europe are expected to become more frequent, more intense and to last longer. Some present and future heatwaves have also been analyzed using MAR-BCC simulation. Globally the temperature profile is similar for all heatwaves (Fig. 7) but by 2100, the temperature decrease during the night will be lower, threatening the benefits of night ventilation. The main principle of night ventilation is to take advantage of the cooler outdoor air during the night to release the heat stored all day long within the walls, "resetting" the thermal inertia of the building. With global warming, it is thus expected that the potential of night ventilation will be reduced due to warmer nights. The potential of natural ventilation is also jeopardized by the longer duration of the heatwaves.

Natural ventilation on its own is thus not sufficient to reach thermal comfort in the living room. Aflaki et al. [18] suggested that natural ventilation should always be coupled to heat avoidance complementary techniques to increase its potential. The orientation of the building is also of primary importance. Eastern and western windows receive twice as much irradiation as north-south elevation. However, it is also recommended that the building should be oriented according to the prevailing wind direction, which could lead to a contradiction.

It also possible to study the evolution of the prevailing wind direction to see if the building design should also take climate change into consideration. Fig. 9 shows that the wind direction profile of Brussels remains similar all along the century. Wind mainly has a South orientation which matches the recommendations linked to solar gain avoidance. In Belgium, new constructions should preferably have a north-south orientation.

5. Conclusion

This paper studied the potential of natural ventilation in Belgium to reduce the internal cooling loads during summer period through different natural ventilation strategies (single-sided ventilation and cross ventilation). The simulations are conducted by DesignBuilder and using MAR regional atmospheric model. The results compared between the two aforementioned natural ventilation strategies and the impact on the indoor air temperature. The results show that without natural ventilation thermal comfort could be reached on average 53.7% of the time, while it could reach 66.2% of time using single-sided ventilation and 78.8% with cross ventilation. The paper also discussed the effect of adapting the operating schedule and airflow rate during heatwaves on the indoor temperature in the different scenarios. The ventilation strategies proved that natural ventilation only is not sufficient to satisfy the thermal comfort of occupants for more than 51% of the time during heatwaves.

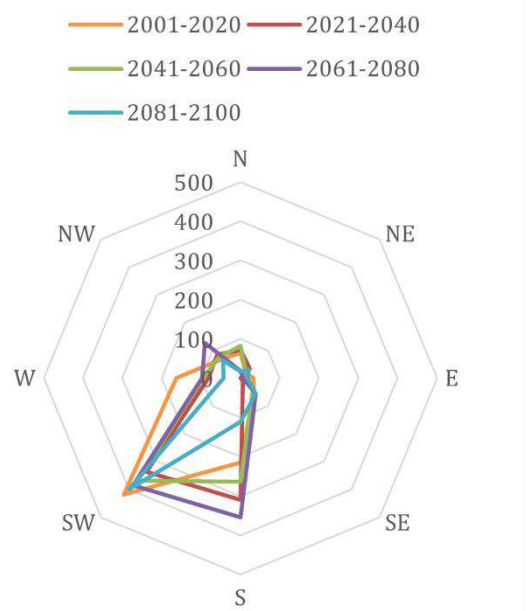

Fig. 9 – Wind diagram showing the number of hours during which wind blows in each direction at a speed higher than 3.5m/s. The number of hours is counted only during the cooling period to emphasize the potential of natural ventilation.

6. Acknowledgment

This research was partially funded by the Walloon Region under the call 'Actions de Recherche Concertées 2019 (ARC)' and the project OCCuPANt, on the Impacts Of Climate Change on the indoor environmental and energy PerformAnce of buildiNgs in Belgium during summer. The authors would like to gratefully acknowledge the Walloon Region and Liege University for funding. This study is a part of the International Energy Agency Annex 80 project activities to define resilient cooling in residential buildings.

7. References

[1] IEA- International Energy Agency. The Future of Cooling- Opportunities for energy efficient air conditioning. 2018.

[2] O' Donovan A, Murphy MD, O'Sullivan PD.

Passive control strategies for cooling a non-residential nearly zero energy office: Simulated comfort resilience now and in the future. Energy and Buildings 2021;231:110607. https://doi.org/10.1016/j.enbuild.2020.110607.
[3] Haase M, Amato A. An investigation of the potential for natural ventilation and building orientation to achieve thermal comfort in warm and humid climates. Solar Energy 2009;83:389–99. https://doi.org/10.1016/j.solener.2008.08.015.
[4] Spentzou E, Cook MJ, Emmitt S. Natural ventilation strategies for indoor thermal comfort in Mediterranean apartments. Build Simul 2018;11:175–91. https://doi.org/10.1007/s12273-017-0380-1.
[5] Tan Z, Deng X. Assessment of Natural Ventilation Potential for Residential Buildings across Different Climate Zones in Australia. Atmosphere 2017;8:177. https://doi.org/10.3390/atmos8090177.
[6] Exigences PEB du 1er juillet 2019 au 31 décembre 2020. Site énergie du Service public de Wallonie n.d. https://energie.wallonie.be/fr/exigences-peb-du-1er-juillet-2019-au-31-decembre-2020.html?IDD=136456&IDC=7224 (accessed November 4, 2021).
[7] The Bureau for Standardisation in Belgium. Standard NBN EN 15193-1:2017 - Energy performance of buildings - Energy requirements for lighting 2021. https://www.nbn.be/shop/en/standard/nbn-en-15193-1-2017-a1-2021_104645/ (accessed December 27, 2021).
[8] International Organization for Standardization. ISO 17772-1:2017 - Energy performance of buildings — Indoor environmental quality. ISO n.d. https://www.iso.org/cms/render/live/en/sites/isoorg/contents/data/standard/06/04/60498.html (accessed December 28, 2021).
[9] Ridder KD, Gallée H. Land Surface–Induced Regional Climate Change in Southern Israel. Journal of Applied Meteorology and Climatology 1998;37:1470–85. https://doi.org/10.1175/1520-0450(1998)037<1470:LSIRCC>2.0.CO;2.
[10] Sebastien D, Fettweis X, Rahif R, Elnagar E, S. Pourkiaei M, Amaripadath D, et al. Historical and Future Weather Data for Dynamic Building Simulations in Belgium using the MAR model: Typical & Extreme Meteorological Year and Heatwaves 2022.
[11] Elnagar E, Doutreloup S, Lemort V. Modeling the Impact of Climate Change on the Future Heating Demand in Different Types of Buildings in the Belgian Residential Building Stock. Proceeding of the International Building Simulation Conference, KU Leuven; 2021.
[12] Doutreloup, Sébastien, Fettweis, Xavier. Typical & Extreme Meteorological Year and Heatwaves for Dynamic Building Simulations in Belgium based on MAR model Simulations 2021. https://doi.org/10.5281/ZENODO.5606983.
[13] Royal Meteorological Institute of Belgium,. Rapport climatique 2020 de l'information aux services climatiques. Brussels Belgium: 2020.
[14] FPS Public Health, Food Chain Safety and Environment of Belgium. Hittegolf en Ozonpiekenplan. 2008.
[15] Ouzeau G, Soubeyroux J-M, Schneider M, Vautard R, Planton S. Heat waves analysis over France in present and future climate: Application of a new method on the EURO-CORDEX ensemble. Climate Services 2016;4:1–12. https://doi.org/10.1016/j.cliser.2016.09.002.
[16] Daemei AB, Limaki AK, Safari H. Opening Performance Simulation in Natural Ventilation Using Design Builder (Case Study: A Residential Home in Rasht). Energy Procedia 2016;100:412–22. https://doi.org/10.1016/j.egypro.2016.10.196.
[17] The Bureau for Standardisation in Belgium. Standard NBN EN 15251:2007 - Indoor environmental input parameters for design and assessment of energy performance of buildings addressing indoor air quality, thermal environment, lighting and acoustics 2007. https://www.nbn.be/shop/en/standard/nbn-en-15251-2007_12248/ (accessed December 29, 2021).
[18] Aflaki A, Mahyuddin N, Al-Cheikh Mahmoud Z, Baharum MR. A review on natural ventilation applications through building façade components and ventilation openings in tropical climates. Energy and Buildings 2015;101:153–62. https://doi.org/10.1016/j.enbuild.2015.04.033.

Development of Heat Recovery Radiant Heating System using Dynamic Insulation

Jaeung Hwang[a], *Sihwan Lee*[b]

[a] Graduate School of Science and Technology, Shinshu University, Japan, 21W5037G@shinshu-u.ac.jp.

[b] Graduate School of Environmental Studies, Nagoya University, Japan, shany@nuac.nagoya-u.ac.jp.

Abstract. From various studies, it is said that floor heating is a more hygienic and comfortable heating system than air-conditioning heating. However, floor radiant heating does not use all of the energy used for indoor heating, and some of it causes heat loss to the underfloor space. This research proposes a heat recovery type radiant heating system that can recover heat radiation under the floor by applying dynamic insulation to the underfloor space. The purpose of this study is to examine the heat recovery effect and the risk for condensation by using the actual measurement and CFD simulation of the experiment module. To achieve this goal, using 2 m × 5 m × 2.5 m experiment module measurement with and without dynamic insulation during the heating period, the heat load, ventilation rate, and thermal environment were measured. Previously, according to the results of model measurements on a 1/3 scale of the experiment module, when the temperature difference between indoors and outdoors was 20 °C, a dynamic insulated floor radiant heating system was used to reduce the heat load by 23.8%.
And, as the real-scale CFD simulation results, the heat load was reduced by up to 49% using the heat recovery radiant heating system. In order to confirm the risk of condensation during the cooling period, the relative humidity of the underfloor space was measured. When air is taken into the room from under the floor, there is a high possibility that condensation will occur during the cooling period. To reduce the risk of condensation, it is necessary to take air out of the room from under floor during the cooling period.

Keywords. Floor Heating, Dynamic Insulation, CFD simulation
DOI: https://doi.org/10.34641/clima.2022.197

1. Introduction

From various studies, floor radiant heating is said to be a more hygienic and comfortable heating system than convection heating. When floor radiant heating is performed, the vertical temperature in the room is constant. Floor radiant heating produces less noise, draft, and dust than convection heating.[1)] However, floor radiant heating does not use all of the energy used for indoor heating, and some of it causes heat loss to the underfloor space. Shimizu[2)] reported that up to 47.9% of the heat from floor heating emits below the floor. The reason is that the floor surface is heated at a temperature higher than that of the outside air and the ground surface, so that heat is transferred under the floor. According to ASHRAE Standard 55[3)], a floor temperature range of 19˚C to 29˚C is recommended range in the occupied zone for rooms with sedentary or standing occupants wearing normal shoes. In the japan standard, 25 ˚C to 29˚C is recommended range in the occupied zone for rooms. Therefore, when considering energy saving, it is necessary to reduce the heat loss to the floor.

This study is to propose a heat recovery type radiant heating system that can recover heat radiation under the floor by applying dynamic insulation[4)] to the underfloor space, and to measurement the heat recovery effect. This system recovers the heat that escapes from the ground and takes heat into the room to improve the insulation performance of the floor (Fig.1). Since the heat recovery system provides a ventilation path in the underfloor space, it is possible to secure a ventilation rate of 0.5 times/h or more as stipulated by Japanese law. At the same time, it recovers the heat loss that escapes to the ground and sends it indoors, so it can be expected as an efficient energy-saving system. It is also expected to be effective in preventing dew condensation in the underfloor space by changing the ventilation direction depending on the season. Therefore, in this study, the heat recovery effect of the heat recovery type radiant heating system will be quantitatively examined by measurement and CFD simulation.

Copyright ©2022 by the authors. This conference paper is published under a CC-BY-4.0 license.

2. Examination of heat recovery effect by model measurement

2.1 Measurement methods

In order to examine the heat loss reduction effect of the proposed heat recovery system, we will actually measure the model. The model is a conventional dirt floor heating system model (Fig. 2 (a)). Heat recovery is a model that introduces outside air by providing a ventilation layer in the space under the dirt floor. (Fig. 2 (b)). The model is shown in Fig.3. The dimensions of the model are 910 x 910 mm for the concrete floor. The indoor space is 910 x 910 x 800 mm for the soil floor model and 1,000 x 910 x 800 mm for the heat recovery floor model. The wall of the model is 100 mm styrofoam. The dirt floor is a 100 mm concrete block, and the heat recovery model is provided with a ventilation layer of 30 mm. Ventilation uses a small sirocco fan and a variable resistance of 15.7 m^3/h. However, with a ventilation volume of 0.24 m^3/h, it is difficult to maintain a uniform flow velocity in the ventilation layer. Therefore, it is uniform in the ventilation layer. A large air volume is given to confirm the flow velocity. For heating, a PTC (positive temperature coefficient) heat ray is embedded between two aluminum plates in a sandwich manner and installed on the concrete in order to uniformly apply heat to the model. The output of the PTC heat ray is 20 W/m. A maximum of 600 W of heat can be applied by using 30 m per model. A thermostat (temperature controller) is installed at the indoor ventilation and exhaust port to keep the temperature inside the model constant. On-off control is performed at the set temperature of 20.0 °C (± 0.1 °C). In addition, in order to clarify the heat recovery effect of the proposed system, the change in underground temperature and the amount of energy used for PTC are measured in the actual measurement of this model. Table.1 shows the actual measurement conditions.

2.2 Measurement Result

Figure 4 shows the cumulative values of the internal temperature, outside temperature, and power consumption of the model. The room temperature of the Dirt floor model could be maintained from 19.0 °C to 20.3 °C. The room temperature of the Heat recovery model fluctuated from 20.8 °C to 21.0 °C, both of which were found to be stable near 20 °C. During the actual measurement period, the power consumption of the PTC heat ray was 122 kWh for the Dirt floor model and 65 kWh for the Heat recovery model. The Heat recovery model reduces power consumption by 42% compared to the Dirt floor model. From this actual measurement, it was found that the heating load can be reduced by applying this system. However, in this measurement, the ventilation volume is large, so it cannot be said that the heat recovery effect is accurate. Therefore, the heat recovery effect of this system will be quantitatively examined using CFD simulation.

(a) Concept (b) Detail view

Fig.1 - Heat recovery radiation system

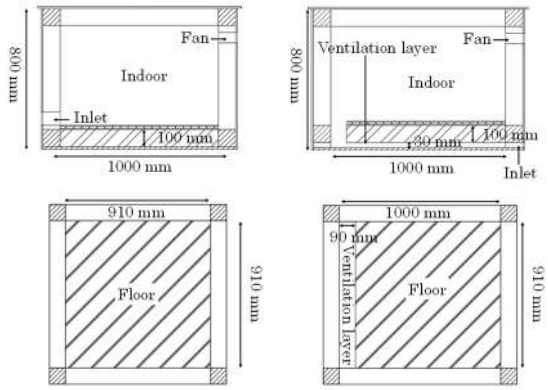

(a) Dirt floor model (b) Heat recovery model

Fig.2 - Model sectional view

(a) Model in production (b) measurement model

Fig.3 - Model photo

Tab.1 - measurement conditions

Item	contents
Period	2020.02.13~02.28 (16 Day)
Model scale	Heat recovery: 1.00 (x) × 0.91 (y) × 0.8 (z) [m] Dirt floor: 0.91 (x) × 0.91 (y) × 0.8 (z) [m]
Model indoor temperature	20.0 °C (±0.1 °C), On-off control
Heating capability	600 W
Measurement location	4-17-1 Wakasato, Nagano City, Nagano, Japan
Ventilation rate	15.7 [m3/h]

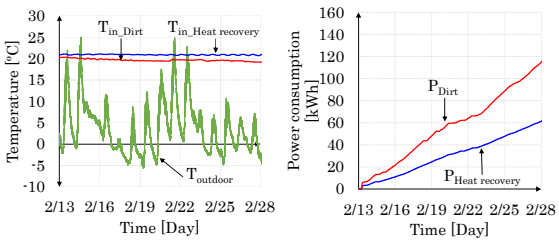

(a) T_{in} and T_{out} (b) P_{Dirt} and $P_{Heat\ recovery}$

Fig.4 - Measurement result

3. Examination of consistency of CFD simulation model

3.1 Simulation methods

To quantify the energy saving effect of this system, it is necessary to clarify the heat loss toward the ground. The underground temperature distribution constantly changes depending on the solar radiation, wind speed, temperature, and the presence or absence of a building. Therefore, in this study, we will create an underground CFD simulation model and compare it with the measurement in time series to examine the consistency. The temperature distribution in the ground is measured by the method shown in Fig.5. Figure 6 (a) shows the outline of the simulation model. The simulation area is 4.0 (x) x 4.0 (y) x 3.0 (z) m, and the soil part is 4.0 (x) x 4.0 (y) x 1.5 (z) m. A model with an atmospheric region of 4.0 (x) x 4.0 (y) x 1.5 (z) m was assumed. For the external wind speed, the speed change in the height direction of the model is taken into consideration by using the wind speed profile by Hargreaves et al.[5]. The wind speed data is from Nagano Meteorological Observatory, every 10 minutes on March 17, 2021 (Fig. 7 (b)). The standard height in the wind speed profile is 19.0 m for the anemometer of the Nagano Meteorological Agency. Shows the wind speed profile used in Fig. 6 (b). The total amount of solar radiation obtained by actual measurement is used for the simulation (Fig. 7 (a)). Therefore, the total amount of solar radiation is separated into direct solar radiation and scattered solar radiation. For direct insolation, the direct insolation method by Udagawa et al.[6] is used in consideration of the convenience of being able to estimate the amount of direct and scattered insolation only from the horizontal total amount of solar radiation.

3.2 Simulation result

Figure 8 shows a comparison between the measured values of the underground temperature and the simulation results. On the ground surface (0 mm) affected by convection, the simulation value was higher than the measured value after 18:00, and the result was about 3 °C higher at 0 o'clock. It is considered that this is because the wind speed higher than the data of the AMeDAS was generated due to the influence of obstacles (trees, buildings, etc.) around the measured site, or the uneven state of the ground surface caused the turbulence of the air flow and increased the convection transmission rate. On the other hand, at depths of 200 mm and 600 mm other than the ground surface, the measured and analyzed values were similar, so it is considered that the consistency of the CFD simulation model was ensured. Table.2 shows the simulation conditions. In order to analyze the heat transfer coefficient near the ground with high accuracy, the Abe-Kondo-Nagano low Reynolds k-ε model is applied as the turbulence model in this simulation.

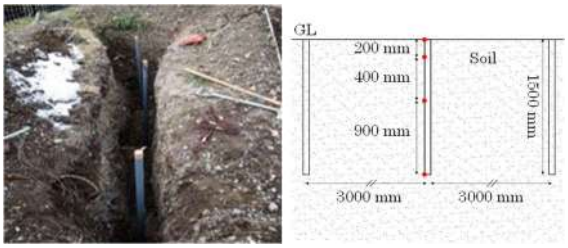

(a) Picture (b) Detail view

Fig.5 - Measurement summary

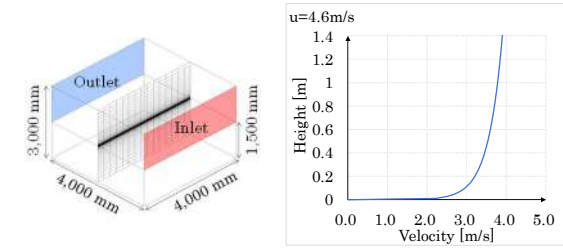

(a) Mesh (b) Wind profile

Fig.6 - Simulation summary

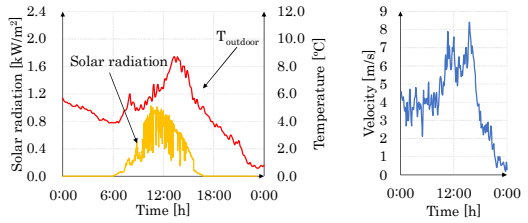

(a) Solar radiation and temperature (b) Wind velocity

Fig.7 - Observed values

Tab.2 - Simulation condition

Item	contents
Number of mesh	100,000 ea
Simulation area	Soil: 4.0 (x)×4.0 (y)×1.5 (z) [m] Air: 4.0 (x)×4.0 (y)×1.5 (z) [m]
Turbulent model	Abe-Kondo-Nagano low Re number k-ε model
Radiation model	Surface to surface
Temperature conditions	Observed values , Fig. 7
Wind velocity and direction	AMeDAS (automated meteorological data acquiaition system, Japan), Fig. 7
Solar radiation	Observed values , Fig. 7
Physical property (Soil)	Density ： 1,350 [kg/m³] Specific heat ： 500 [J/(kg·K)]

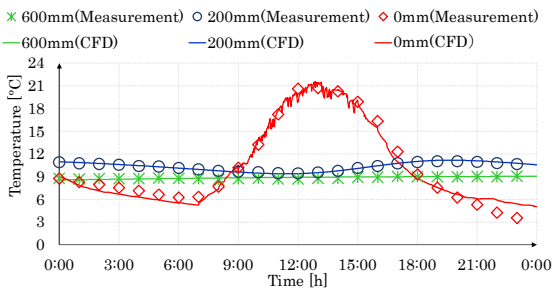

Fig.8 - Simulation result

4. Examination of heat recovery effect on a full-scale scale by CFD simulation

4.1 Simulation methods

A full-scale heat and air transfer simulation is performed using a CFD simulation model to evaluate the heat recovery effect of the proposed system. Figure 9 shows the simulation model. The interior space will be 8.0 (x) x 8.0 (y) x 2.5 (z) m by simplifying the one-story house. Figure 10 shows a cross-sectional view of the study case. (a) In the Dirt floor, the concrete floor is 180 mm, the insulation is 30 mm, and the foundation height is 210 mm. (b) Heat recovery (Dirt floor) is a case where a heat recovery type system is applied to the soil. A 65 mm ventilation layer is provided between the concrete soil and the heat insulating material to introduce the outside air from the outside to the room. In addition, a heat reduction sheet is attached to the concrete surface in contact with the ventilation layer in order to reduce the radiant heat generated from the concrete. (c) The double floor consists of concrete 150 mm, heat insulation 30 mm, air layer 65 mm, mortar 70 mm, particle board 20 mm, and foundation height 335 mm. (d) Heat recovery (Double floor) is a structure that introduces outside air into the room by using an air supply port in the air layer of the buried double floor.

Table.3 show the CFD conditions and the physical property values of the materials. A 24-hour unsteady calculation is performed to take into account changes in the heating load due to the heat storage effect of concrete and soil. In order to simplify the calculation, the simulation is performed assuming that the heating method is floor heating by directly applying 100 W/m^2 to concrete and mortar. In addition, in this calculation, except for the solar radiation calculation of the indoor space, the temperature change of the soil gave the measured temperature to the ground. The emissivity is 0.1 on the surface to which the heat reduction sheet is attached. Where it is not attached is set to 0.8.

4.1 Simulation result

Figure 11 shows the simulation results. The amount of energy required to maintain the room at 20 °C is 242 MJ for the dirt floor, 184.2 MJ for the heat recovery floor (dirt), 192.1 MJ for the buried double floor, and 151.9 MJ for the heat recovery floor (double). The heat loss that escaped under the floor was 54.7 MJ for the dirt floor, 19.3 MJ for the heat recovery floor (dirt), 2.9 MJ for the buried double floor, and -4.7 MJ for the heat recovery type floor (double floor). Figure 12 shows the heat balance of each case. (a) Of the 242 MJ on the dirt floor, 54.7 MJ was transferred into the ground, 112.8 MJ was transferred indoors, and 3.6 MJ was transferred to the outside, and 70.7 MJ was stored in the soil. (b) In

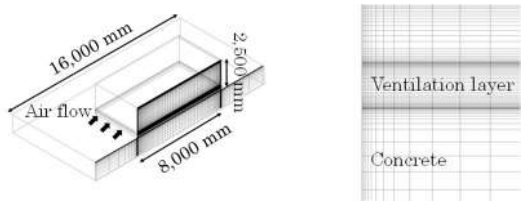

(a) Calculation model (b) Meshes

Fig.9 - Calculation model and meshes

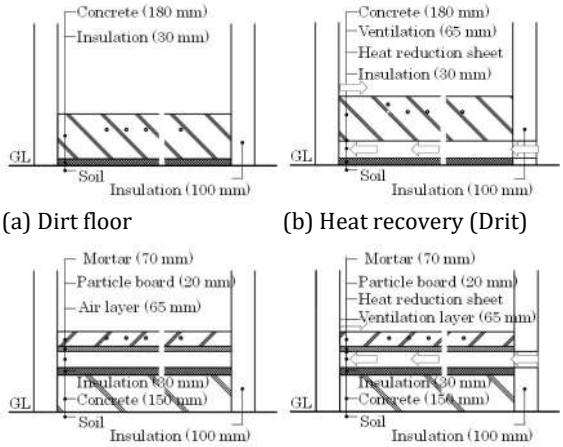

(a) Dirt floor (b) Heat recovery (Drit)

(c) Double floor (d) Heat recovery (Double)

Fig.10 - Simulation model

Tab.3 - Simulation condition

Item	contents
Number of mesh	1,100,000 ea
Simulation area	Soil: 16.0(x) × 16.0(y) × 1.5(z) m Indoor: 8.0(x) × 8.0(y) × 2.5(z) m
Turbulent model	Abe-Kondo-Nagano low Re number k-ε model
Radiation model	Surface to surface
Scheme	SIMPLE
Indoor temperature	20 °C
Heating capacity	100 W/m^2
Simulation time	24 h
Ventilation rate	80 m^3/h
Physical property (Air)	Density: 1.20 kg/m^3 (20 °C, Boussinesq approximation)
Physical property (Thermal conductivity)	Concrete: 1.6 W/(m·K) Insulation: 0.04 W/(m·K) Particle board: 0.12 W/(m·K) Mortar: 1.5 W/(m·K)
Physical property (Emissivity)	Heat reduction sheet: 0.1 Without heat reduction sheet: 0.8

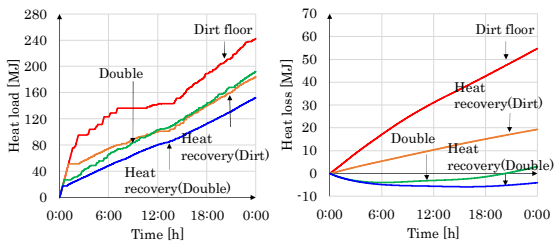

(a) Heat load (b) Heat loss

Fig.11 - Simulation result (Cumulative value)

the heat recovery floor (dirt), of the energy of 184.2 MJ, 19.3 MJ in the ground, 70.8 MJ indoors, 35.8 MJ heat recovery, 3.6 MJ energy moves to the outside, and 54.9 MJ stores heat in the soil. Heat recovery is the energy recovered by this system and goes indoors. By applying this system, it was possible to reduce the heat escaping to the ground by 64% and the amount of energy by 23.8% on the dirt floor. (c) In the buried double floor, energy of 2.9 MJ in the ground, 110.9 MJ indoors, and 3.7 MJ outside was transferred in 192.1 MJ, and 74.3 MJ was stored. (d) In the heat recovery floor (double floor), out of 151.9 MJ of energy, -4.7 MJ in the ground, 73.6 MJ in the room, 35.8 MJ in heat recovery, 3.3 MJ of energy moves to the outside, and 46.5 MJ. The heat was stored. By applying this system, the amount of energy in the buried double floor was reduced by 20.9%. In the (c) and (d), there is foundation concrete under the floor, and it is considered that the heat loss is small because the foundation concrete stores heat toward the underfloor. In particular, (d) recovers the heat stored in the foundation concrete indoors by this system, so the temperature of the foundation becomes lower than the temperature of the ground, and the heat that takes heat from the ground and escapes to the ground. Shows a negative value.

5. Examination of heat recovery effect on a full-scale scale by CFD simulation

5.1 Simulation method

This system can reduce heat loss in winter. On the other hand, there is a high risk of dew condensation in the underfloor space in summer. In summer, the hot and humid outside air is taken into the room from under the floor, so the underfloor surface cooled by cooling contact with the outside air, causing reverse dew condensation. In this study, we propose an operation system that changes the ventilation direction depending on the season (Fig.13). In this chapter, the presence or absence of dew condensation under the floor depending on the ventilation direction will be examined by CFD simulation. The simulation model targets the interior space of a detached house-shaped living room proposed by the Building Environment and Energy Conservation Organization (IBEC). The outline of the model is shown in Fig.15. A variable fan for introducing and discharging air into the room is placed in the center with a size of 200 x 120 mm. The structure and physical properties of the underfloor space are shown in Fig. 15 and Table.4. The case is for taking in air, and the room temperature is 26 °C (case 1-1), 24 °C (case 1-2), and the humidity is 60%. When taking out indoor air, the room temperature is 26 °C (case 2) and the humidity is 60%. The data for the weather on August 11, 2020 (sunny) in Tokyo (Fig. 16) will be used for the simulation. The ventilation volume shall be 29.06 m^3/h, which is 0.5 times ventilation of the target space. The simulation interval is calculated every 10 minutes for 24 hours.

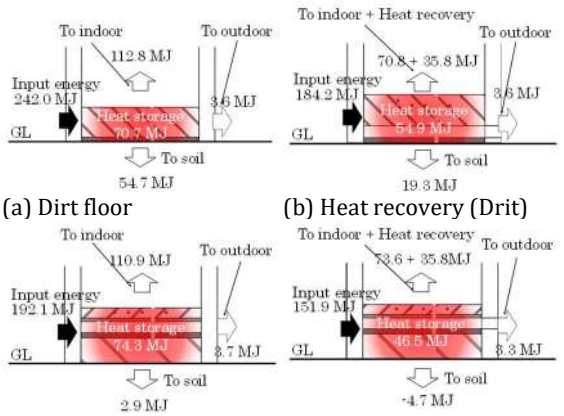

(a) Dirt floor (b) Heat recovery (Drit)

(c) Double floor (d) Heat recovery (Double)

Fig.12 - Energy balance

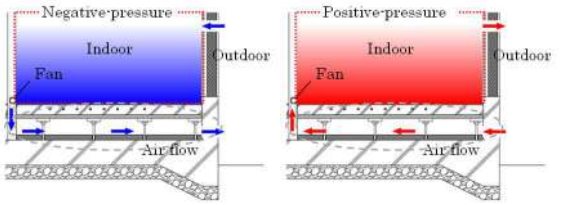

(a) In winter (b) In summer

Fig.13 - Variable ventilation system

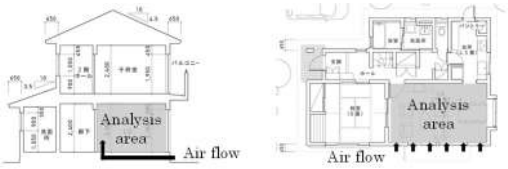

(a) Cross view (b) Plan view

Fig.14 - Simulation area

Tab.4 - Simulation condition

Item	contents
Number of mesh	500,000 ea
Simulation area	3.640(x) × 8.915(y) × 0.330(z) m
Radiation model	Surface to surface
Simulation time	24 h
physical property (Thermal conductivity)	Concrete : 1.60 [W/(m·K)] Insulation : 0.04 [W/(m·K)] Particle board : 0.12 [W/(m·K)] Mortar : 1.50 [W/(m·K)]

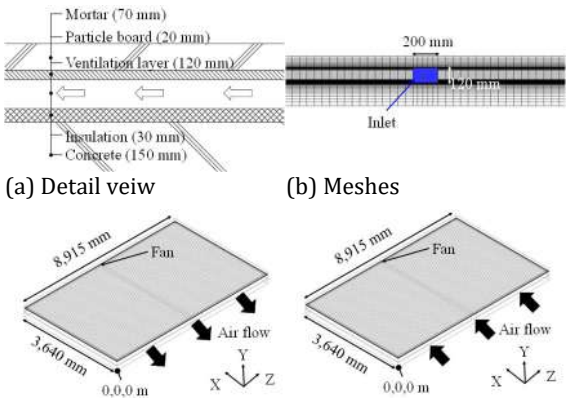

(a) Detail veiw (b) Meshes

(c) Case 1-1,2 (d) Case 2

Fig.15 - Simulation model

5.2 Simulation result

Fig. 17 shows the maximum and average relative humidity of the floor surface at 24:00, and (c) shows the humidity contour of the floor surface at 12 o'clock. In Case 1-1, the relative humidity exceeded 90% for 24 hours, and in Case 1-2, dew condensation occurred for 24 hours. In Case 2, the relative humidity of 60% was maintained and the occurrence of dew condensation could be suppressed.

6. Conclusions

In this research, we propose a heat recovery type radiant heating system that uses ventilation driving force to recover heat loss generated in the ground by utilizing the underfloor space of floor heating as a ventilation path and examine it by model measurement and CFD simulation. The following findings were obtained from the examination results.

(1) Heat Recovery Radiant Heating System using a model, we examined the power consumption of electric floor heating by this system. The Dirt floor model generated 122 kWh in 2 weeks, and the Heat recovery model consumed 65 kWh, which was a 42% reduction in power consumption compared to the Dirt floor mode.

(2) In the CFD simulation on a full-scale scale, the input energy for maintaining the room at 20 °C for 24 hours is 242 MJ for the dirt floor, 184.2 MJ for the heat recovery floor (dirt floor), 192.1 MJ for the buried double floor, and heat recovery floor (double floor) generated 151.9 MJ, and by applying this system, it was possible to reduce energy by 23.8% in the full-scale model of dirt floor and 20.9% in the buried double floor model. This clearly confirmed the heat recovery effect of this system.

(3) The structure of this system was embodied, and the reverse dew condensation in the summer was examined by CFD simulation. When the outside air was taken into the room on a representative day of summer, when the room was cooled at a room temperature of 26 °C, dew condensation occurred 6 times in 24 hours, and the relative humidity was maintained at 90% or higher throughout the day. Then, when the cooling temperature was set to 24 °C. under the same conditions, almost dew condensation occurred. On the other hand, when the air in the room was taken out, the underfloor space was the same environment as the room because no backflow occurred, and there was no risk of dew condensation.

(4) In the future, we will study the heat insulation performance and heat recovery effect of this system by measuring it on a full-scale scale by designing it for actual housing and using the experimental building. We also plan to study the energy-saving effect of applying this optimized system to actual houses.

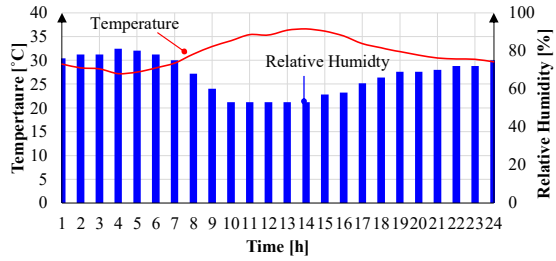

Fig.16 - Outdoor air conditions

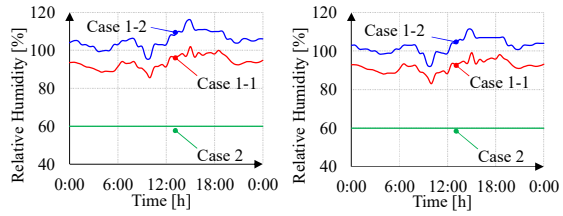

(a) In 24h max RH (b) In 24h average RH

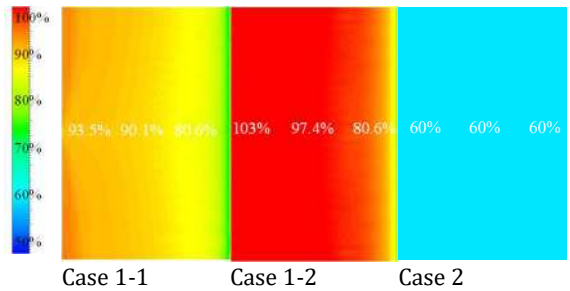

(c) At 12:00 RH contour

Fig.17 - Simulation result

7. References

[1] Kazunori Matsumae, Evaluation of Thermal Comfort for Various Heating Systems Part 3, The Society of Heating, Air-Conditioning Sanitary Engineers of Japan, 2007; 457-460.

[2] Norio Shimizu, Study on Thermal Output of Floor Heating System, J. Archit. Plan. Ecviron. Eng., AIJ, 1999; No. 516: 61-68.

[3] ASHRE, ASHRE Standard 55-2017, 2017; Chapter 5 :p42.

[4] Arvid Dalehaug, Dynamic Insulation in a wall, Japan Architectural Society Hokkaido Branch Research Report Collection,1993;No.66.

[5] David Hargreaves., Nigel George Wright: On the use of the k-ε model in commercial CFD software to model the neutral atmospheric boundary layer. Journal of Wind Engineering and Industrial Aerodynamics,2006;95(5):355-369.

[6] Mitsuhiro Udagawa, Kenichi Kimura:Estimation of direct solar radiation from horizontal solar radiation observations. The Architectural Institute of Japan's journal of Environmental Engineering, 1978;267:83-90.

Insights of the DYDAS Project: The Use Case Energy

Ilaria Abbà [a], Cristina Becchio [b], Stefano Paolo Corgnati [c], Paolo Pasquali [d], Maria Cristina Pinto [e], Elena Roglia [f], Sara Viazzo [g]

[a] TEBE-IEEM Research Group, Energy Department, Politecnico di Torino, Torino, Italy, ilaria.abba@polito.it.

[b] TEBE-IEEM Research Group, Energy Department, Politecnico di Torino, Torino, Italy, cristina.becchio@polito.it.

[c] TEBE-IEEM Research Group, Energy Department, Politecnico di Torino, Torino, Italy, stefano.corgnati@polito.it.

[d] LINKS Foundation, Torino, Italy, paolo.pasquali@linksfoundation.com.

[e] TEBE-IEEM Research Group, Interuniversity Department of Regional and Urban Studies and Planning, Politecnico di Torino, Torino, Italy, mariacristina.pinto@polito.it.

[f] SDG11lab, Interuniversity Department of Regional and Urban Studies and Planning, Politecnico di Torino, Torino, Italy, elena.roglia@polito.it.

[g] TEBE-IEEM Research Group, Energy Department, Politecnico di Torino, Torino, Italy, sara.viazzo@polito.it

Abstract. In the current energy transition, Renewable Energy Sources are identified as key enablers for the achievement of the ambitious European target of climate neutrality by 2050; among them, solar and wind energy play a crucial role. The evolution of production, storage and end users' technologies goes hand in hand with the rapid development of the information sector, where High Performance Computing (HPC) infrastructures allow the exploitation of Internet of Things devices and Artificial Intelligence techniques. The use of HPCs in the energy field enables the use, processing and sharing of large volumes of energy data. The funded by the CEF TELECOM 2018 DYDAS (Dynamic Data Analytics Services) Project is carried out in the above-mentioned framework, aiming to create a collaborative platform, called DYDAS, that, using high-performing computers, will offer data, algorithms and data analysis services to a wide range of final users, both private and public. More specifically the paper will focus on the Use Case Energy, whose objective is to test and validate the DYDAS platform, by exploiting meteorological forecast techniques and using satellite information to facilitate and boost up the assessment of both energy demand and power production. Considering the strong dependency on resource availability, the localization of the resources and the related infrastructure is essential for an efficient and strategic energy planning. Therefore, the mix of traditional algorithms, climatic variables and remote sensing techniques represents an added value for supporting decision-makers in the energy planning processes at local and national scales, taking advantage of the geomatics instruments to visualize and monitor decision strategies. Given the role of electricity in the energy transition, the current paper deepens the Use Case Energy focusing on power generation from photovoltaic plants and on-shore and off-shore wind farms located in Italy. The aim of the use case is to estimate the potential local power production, by collecting information about technical features and geo-localization of real plants, and integrating them with georeferenced climatic variables, which can influence the electricity production (e.g., air temperature, solar irradiance, etc.).

Keywords. Renewable Energy Sources, High Performance Computing, remote sensing techniques, databases, geospatial data.
DOI: https://doi.org/10.34641/clima.2022.124

1. Introduction

In order to effectively tackle climate changes and speed up the energy transition process towards the 1.5°C goal as a limit for global temperature rising [1],[2], strong effort must be devoted to the efficient deployment of Renewable Energy Sources (RES). In particular, among the proposed solutions to achieve the target of a net zero energy system by 2050 [3], more than 90% concerns renewable energy [4]. Therefore, how to develop a strategic and efficient renewable planning process becomes a crucial step. According to this, the exploitation of geo-referenced data to assess geo-informed interventions plays an essential role, considering that different areas can do things differently, and thus understanding that the

Copyright ©2022 by the authors. This conference paper is published under a CC-BY-4.0 license.

energy transition is a geographically-constituted process [5]. To this end, the integration of different instruments able to combine a large volume of heterogeneous data and to extract valuable information can be exploited; in particular, using advanced Internet of Things (IoT) devices and Artificial Intelligence (AI) techniques. In this context, the DYDAS European project comes out to combine these aspects. In detail, DYDAS is a project funded by the CEF Telecom 2018 work program with the aim of contributing to the European data infrastructure by offering data, algorithms, processing and analysis services to different public and private user communities. The project is carried out by a consortium led by K2 Business partnering with ENEA, LINKS Foundation, Gmatics and ANCI Lazio. The platform DYDAS has been conceived as a marketplace platform that enables transactions for accessing data and services powered by High Performance Computing (HPC) and based on Big Data technologies, Machine Learning (ML), Artificial Intelligence and advanced data analytics. The platform consists of three main components: (i) data from different sources, algorithms and service providers; (ii) a supercomputing centre and the services it offers; (iii) various end-users from the public and private sectors. The adoption of a Geospatial Data Model and the use of interoperability rules enable large dataset integration and processing capabilities; this allows using geospatial information of different types and sources with data that are not intrinsically geo-referenced. Data are stored in a data lake defined by a Geospatial Data Architecture (GDA); the handling of all the datasets in a common geospatial fashion, through GDA, enables the application of HPC-AI-based services. To test the platform three Use Cases are developed: Maritime, Mobility and Energy.

Aiming to focus on the energy transition challenges and opportunities, especially with respect to the RES deployment, the Use Case Energy is suitable for this purpose and the current work will focus on its main features. Following the need of building up geo-informed solutions, it is mainly based on the use of meteorological forecast techniques and satellite information as a way to facilitate and boost up the assessment of both energy demand and renewable power production. In particular, being the renewable potential intrinsically based on geographical constraints, the strategic use of geo-referenced data, though the exploitation of Remote Sensing techniques and climate variables, as input for traditional algorithms and advanced data-processing systems, can support the energy planning processes, from a local to a national scale. The DYDAS Platform will provide access to a data domain able to offer an interesting mix of production and demand, in particular with respect to photovoltaic (PV) plants and on-shore and off-shore Wind Farms (WF) located in Italy. Specifically, it will allow the use of a data domain of interest, through its download and processing, and also of user-friendly visualization tools. In particular, (i) the data domain, (ii) the analysis domain and (iii) the communication domain are at the basis of an adequate geo-informed infrastructure [6]. As stressed by Fremouw et al. [7], in order to elaborate ad-hoc tools and support informed decisions combining physical-spatial problems with energy-environmental ones, the access to geo-referenced datasets is essential; improving their availability and quality is a crucial step towards their effective exploitation. Offering a structured spatial visualization of energy data means to support appropriate strategies and geo-informed interventions, then to identify priorities in energy planning, also through the selection of the most suitable locations [7]. The DYDAS Project, though the Use Case Energy, aims to address all the aforementioned challenges, making use of several instruments that, if correctly and efficiently combined, will allow to positively influence the energy transition process, paving the way for a more strategic allocation of RES. Specifically, being aware of the large volume of data involved in this type of analyses, the DYDAS platform makes use of HPC to deliver products that, through the integration of heterogeneous instruments and information, are able to share knowledge and to support decisions.

In this framework, the present paper aims to track and deepen the main steps leading to the elaboration of the hourly production profiles with respect to PV and wind technologies, in order to obtain geo-referenced data for renewable electricity generation to be matched with the local energy demand. Section 2 is dedicated to the main algorithms needed to obtain the production profiles; these algorithms, concerning respectively solar PV plants and wind farms, require certain data domains which are deepened in section 3. Section 4 reports some results of the work, and finally, section 5 summarizes the main outcomes and future perspectives of the project.

2. Research Methods

Wind and solar power are the most promising and widespread renewable sources in the world, being recognised as necessary and sustainable solutions to deal with the energy transition needs. Despite the high potentialities, the unpredictability of these sources represents a challenge for their integration in the energy system [8]. Therefore, to guarantee the correct operation of the power system and the correct demand-supply match, a prediction of wind farm and photovoltaic plant production is required. Akhter et al. [9] review the principal forecasting techniques for solar power previsions, classifying them according to the used method (physical, statistical or hybrid), forecasting horizon (intra-hour, intra-day or day ahead) and time step (minutes or hour according to the objective of the analysis). Considering that the objective of the current research is to provide at least a day ahead forecast, a physical model was used, since it performs better for short-/medium-term provisions, despite its high computational cost [10] (that in this case is mitigated

by the use of HPC), and an hourly time step was selected.
Both solar and wind sources are highly dependent on external weather conditions such as air temperature, solar radiation, wind velocity, as well as on local morphology of the ground. To consider all these aspects, the adopted methodology consists in the following steps: (i) identification of influencing climatic parameters; (ii) selection of proper algorithms from literature, able to take into account climatic and ground dependencies; (iii) identification of inputs and selection of relevant and complete databases for data collection; (iv) implementation of algorithms in a language suitable to be included and managed by the DYDAS platform.
In the following sub-sections, the main algorithms for the estimation of power production from wind farms and PV plants will be listed, while in Appendix A all the equations with the relative parameters involved in the calculation are reported.

2.1 Wind farms power production

Starting from wind farms, the assumption was that only horizontal axis wind turbines are used. In order to estimate the electric power output, it is necessary to calculate the mechanical power (P_{mech}) in W, generated by the turbine as in Eq.1 [11].

$$P_{mech} = \frac{1}{2} * c_p * \rho_{air}(h) * \pi * \frac{D^2}{4} * u^3(h, z_0) \quad (1)$$

Where c_p is the Power Coefficient and comes from producers' data (it must be lower than 16/27), h is the hub height. Then, as a rule of thumb, the height of the tower is almost 1.5 times the diameter of the rotor [12]. Therefore, since the height hub is a known parameter for each WF, the rotor diameter can be calculated as D=h/1.5. u and z_0 represent the wind speed [m/s] at the hub height and the roughness length of the soil [m], respectively.

If real data are not available, supposing air as a perfect gas, the following equations can be used to estimate the air density at the hub height. Equations expressing air pressure, temperature and density in function of the hub height are listed in Appendix A, according to [12],[13]. Moreover, there is a strong dependency also between wind speed (u), the height of the hub and the roughness of the ground (z_0), it can be expressed by Eq.2 [14].

$$u(h, z_0) = u_{ref} \frac{\ln\left(\frac{h}{z_0}\right)}{\ln\left(\frac{h_{ref}}{z_0}\right)} \quad (2)$$

It is well known that the wind turbine cannot exploit all the wind speeds, but there are some constrains, that are:

- Cut-in speed (u_c = 3-6 m/s), the wind turbine is not able to produce power until the wind reaches the cut-in speed [15];
- Rated speed (u_r = 12-15 m/s), before the rated speed the wind turbine tries to optimize the power output, while after this speed the regulation control starts to limit the power in order not to damage the turbine. Wind turbines are designed to deliver the maximum power at a speed of 12-15 m/s. Therefore, when the wind speed is higher, the power must be dissipated [15];
- Cut-off speed (u_f = 25 m/s), if the wind speed is higher than the cut of speed, the so-called thrust limit has been reached and the regulation control of the turbine shut-down the machine in order not to damage it [15].

According to this, the real mechanical power curve (P_{curve} in W) in function of wind speed follows Eq.3.

$$P_{curve} = P_r * \begin{cases} 0, & u < u_c \ or \ u > u_f \\ P_{asc,} & u_c < u < u_r \\ 1, & u_r < u < u_f \end{cases} \quad (3)$$

Where:
P_r is the rated power output [W], while $P_{asc} = P_{mech}/P_r$ is the turbine output as a percentage of P_{mech}. Finally, to convert the actual mechanical power (P_{curve}) into electric power (P_{el}), an efficiency of 40-45 % [14] must be used.

2.2 Photovoltaic plants power production

Moving to photovoltaic plants, the first step to calculate power production is the computation of solar radiation that arrives on the tilted plan of the panel (G_T). Solar radiation intensity depends not only on a set of meteorological parameters, but it is strictly influenced also by geometric features (e.g., solar angles, panel slope, tilt angle, etc.). All equations needed to compute the parameters involved in (G_T) are listed in Appendix A [16],[17],[18]. Moreover, Eq.4 allows to compute G_T for each hour of the year and for every location around the world.

$$G_T = G_{bn} * \cos(\theta) + G_{dh} * F_{c-s} + \rho * G_{th} * (1 - F_{c-s}) \quad (4)$$

$G_{bn,}$ G_{dh} and G_{th} represent the beam normal radiation, the diffuse horizontal radiation, and the total horizontal radiation [W/m^2], respectively. θ is the angle of incidence [°] of beam solar radiation on a surface whatever oriented and tilted; F_{c-s} is the collector-sky view factor, while ρ represents the albedo (or reflection coefficient) and are both dimensionless. Then, once knowing the total irradiance, the output DC power of the plant (P_{out_DC}) can be calculated, integrating equations [19] with technical data coming from PV panel datasheets.

$$P_{peak,plant} = \frac{G_T}{1000} * P_{N,plant} \quad (5)$$

$$T_c = T_a + \frac{[T_{c,NOCT} - T_{a,NOCT}]}{G_{NOCT}} * \frac{G_T}{1000} \quad (6)$$

$$P_{out_DC} = P_{peak,plant} - (\alpha_p * P_{peak,plant}) * (T_c - T_{c,STC}) \quad (7)$$

$P_{peak,plant}$ and $P_{N,plant}$ are the PV system peak power [kW] and the nominal power [kW]. T_c and $T_{c,STC}$ mean

the cell temperatures [°C] in operation and in Standard Test Condition (STC). T_a is the air temperature [°C], while $T_{c,NOCT}$, $T_{a,NOCT}$ and G_{NOCT} represent constant and predefined values concerning the panel cell temperature, the air temperature and the radiation on tilted surface in Nominal Operating Cell Temperature (NOCT) conditions. In particular, $T_{c,NOCT}$=45°C, $T_{a,NOCT}$=20°C and G_{NOCT}=800 W/m^2. Indeed, α_p is a correction factor, namely the temperature coefficient of maximum power of the solar cell.

2.2.1 Machine learning techniques for a proper detection of PV panels

Machine learning techniques were exploited for the purpose of using accurate datasets as input for the algorithms. Specifically, a trained model and high-resolution aerial images were used. Every time a new set of images is available the job can be run to update the census of active plants and estimate the power production over time. In particular, the accurate detection and delineation of PV panels was carried out by means of two similar deep learning approaches, namely Semantic Segmentation and Instance Segmentation. The former consists of classifying the whole image, pixel by pixel, in a predefined number of categories. The latter, after providing a detection box for every single panel, segments its contents to delineate the entity inside it, regardless of the category.

3. Applications

The Use Case Energy is applied to the Italian country, but the proposed methodology can be generalised and, in presence of consistent databases, can be implemented for any area of the World.

The Italian use case exploits data from different sources. In detail, climatic data, in the form of real time-products from the Atmospheric Model high-resolution 10-day forecast, come from European Centre for Medium-Range Weather Forecasts (ECMWF) [20] and Aeronautica Militare. Data are provided in GRIB format and 4 forecast runs per day (00:00; 06:00; 12:00; and 18.00) are performed with hourly steps to step 90 for all four runs. On the other hand, the spatial resolution is a 0.1° x 0.1° (almost 11.1 km) latitude/longitude grid, covering the whole Italian territory. The RES (wind farms and PV panels) location and features were collected from Gestore dei Servizi Energetici (GSE) datasets [21], while machine learning techniques were developed by LINKS Foundation (and then applied on CGR Spa Very High Resolution (VHR) Imagery [22].

The DYDAS platform adopts Apache Spark as processing engine [23]; all Spark jobs are written in Python as well as custom jobs submitted by remote users. Users can interact with the Platform exploiting a web interface running in Docker containers [24] in order to guarantee security and isolation by accessing only allowed resources and libraries.

In order to develop the Use Case Energy, a function is in charge to: (i) download the climate data from ECMWF [20]; (ii) calculate the required parameters from that data with an hourly time-step; and then (iii) assign the obtained spatial- and temporal-related values to each RES site to perform the energy production estimate.

Concerning the solar panel detection through machine learning techniques, a dataset of very high-resolution (VHR) images over two large areas of Piedmont, provided by CGR [22], was used. Over the same regions, LINKS Foundation also provided accurate manual annotations for more than 2000. To generate the input for the models, a pre-processing step was carried out independently for both modalities, with further tiling and filtering away every patch not containing useful information.

4. Results and discussion

Since the DYDAS project is currently ongoing, the platform is not yet implemented in its final and completed version; due to this, its potentiality cannot be fully exploited to extract valuable outputs, as it will be at the end of the project. In line with the above, this section is devoted to deepening some results of the process of solar panel delineation through aerial imagery. Using Semantic Segmentation, a class label was assigned to every pixel in the image according to three classes: (i) Background, for each object which does not represent a solar panel; (ii) Polycrystalline panels and (iii) Monocrystalline panels.

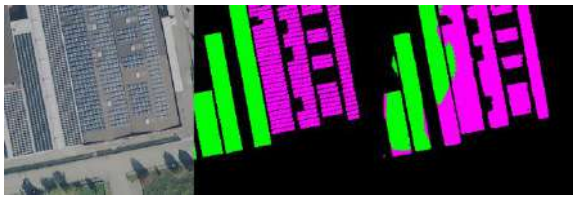

Fig. 1 - Example of Semantic Segmentation prediction.

Fig. 1 offers a visual output of Semantic Segmentation prediction. Specifically, from left to right a snapshot of Aerial image (RGB input), ground truth and, model prediction is shown, where green and magenta colors refer to Monocrystalline and Polycrystalline panels, respectively.

Concerning performances, the metric used to evaluate the accuracy of the Segmentation procedure was the Intersection over Union (IoU). This metric, varying between 0 and 1, is calculated as the ratio between the area of overlap (between the predicted bounding box and the ground-truth bounding box) and the area of union (the area encompassed by the predicted and the ground-truth bounding boxes). Therefore, the greater the overlapping area, the greater the accuracy is. According to this definition, the Background class, which is by far the most represented, performs very well, reaching an IoU = 0.9777. The second most accurate category is the Polycrystalline one (IoU =

0.9174), due to more frequent examples and its pattern was easier to notice from above. On the other hand, concerning Monocrystalline panels, their lower representation in terms of samples and the consequent more challenging detection, results in a lower performance of Monocrystalline (IoU = 0.7525). Generally speaking, the model performs very well on large solar plants, also thanks to a large panel surface, less background noise and simply a larger number of samples. Regarding the Instance Segmentation technique, considering the Average Precision with IoU at least of 0.5 the model can achieve a IoU of 0.8. Lower scores are typically associated with the extreme situation of solar plants that are very small or extremely large: smaller panels are more difficult to be delineated with precision, while larger panels cover a large portion of the image, making the detection step inherently more challenging. Therefore, in both cases (i.e., Semantic and Instance Segmentation), performances reach an IoU higher than 0.75 (considering Monocrystalline and Polycrystalline panels). Translating this score in percentage values, it means that at least 75% of the detections agree with human annotations, and the value can increase up to 88% in case of good conditions, especially for Polycrystalline panels. Therefore, it can be said that the outcomes of IoU calculation justify the use of Semantic Segmentation and Instance Segmentation techniques as a support tool for the identification of solar panels. Moreover, the final score can be negatively affected by the possible human error conflicting with the rightful detection of the model.

Concerning the power production by wind farms, the application of the algorithms presented in section 2.1 allowed to obtain the evolution of the electric power produced for the desired time horizon. In **Fig. 2** the forecast of the electric power output (P_{el}) of a wind farm located in Golfo di Manfredonia (Puglia, Italy) for the 2nd of March 2022 is shown through an hourly timestep; it is evident how the evolution of P_{el} follows the one of the wind speed along the day.

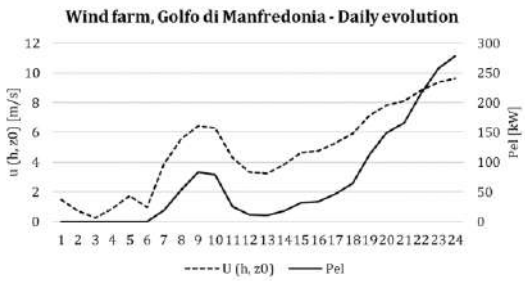

Fig. 2 - Example of daily evolution of wind speed and related electric power output for a wind farm.

Moreover, in **Fig. 3** the power production as a function of wind speed is reported. It highlights the cubic proportionality of the electric power output in the "usable range" of wind speed before the rated speed (as said in Eq. 3), and clearly shows that before the cut-in speed (3 m/s) the power output is zero since the wind speed is too low to produce power.

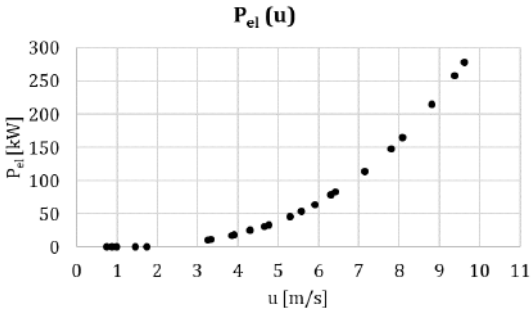

Fig. 3 - Daily wind power production as a function of wind speed.

5. Conclusions

Dealing with the opportunities and challenges of the energy transition requires strong efforts concerning the use of the appropriate instruments and datasets, specifically for an efficient deployment of RES. The DYDAS project, through the Use Case Energy, aims to create a marketplace enabling transactions for accessing data and services powered by HPC, to support geo-informed interventions for RES allocation. The integration of IoT devices and AI techniques makes the platform able to exploit advanced datasets, to optimize data processing and to deliver user-friendly outputs, supporting decisions and sharing knowledge. Focusing on the potentiality of the platform with respect to the prediction of renewable production, this paper introduced the appropriate algorithms for wind farm and PV plant production, to guarantee the correct operation of the power system and the correct demand-supply match. Specifically, the Use Case Energy is applied to the Italian territory, through the exploitation of different data sources and datasets. In addition, to deepen the integration of machine learning techniques in the platform structure, two deep learning approaches were investigated to obtain a more accurate detection of solar panels. These advanced models allow to improve the quality of input data used in the algorithms, obtaining a better accuracy.
Since the project is still ongoing, further work will be devoted to the validation of the production profiles and the implementation of user-friendly visualization tools to share geo-informed solutions. Moreover, future development of the DYDAS project will address the coupling of renewable production and electricity demand coming from residential and office buildings.

6. Acknowledgements

DYDAS is a project co-financed by the Connecting Europe Facility of the European Union, in particular by the CEF Telecom 2018 work program.

We thank the Italian "Servizio Meteorologico dell'Aeronautica Militare" for its collaboration in the provision of data.

The PhD research work of Ilaria Abbà and Maria Cristina Pinto has been financed by the Research Fund for the Italian Electrical System under the Contract Agreement between RSE S.p.A. and the Ministry of Economic Development - General Directorate for the Electricity Market, Renewable Energy and Energy Efficiency, Nuclear Energy in compliance with the Decree of April 16th, 2018.

7. Data access statement

The datasets generated during and/or analysed during the current study are not available because the DYDAS project is still ongoing, but the authors will make every reasonable effort to publish them in near future.

8. References

[1] UNFCCC. 2015. Key aspects of the Paris Agreement. https://unfccc.int/process-and-meetings/the-paris-agreement/the-paris-agreement/key-aspects-of-the-paris-agreement

[2] UN Climate Change Conference. 2021. COP 26 Glasgow Climate Pact. https://ukcop26.org/wp-content/uploads/2021/11/COP26-Presidency-Outcomes-The-Climate-Pact.pdf

[3] IEA. 2021. Net Zero by 2050, IEA, Paris https://www.iea.org/reports/net-zero-by-2050

[4] IRENA. 2021. World Energy Transitions Outlook. 1.5°C Pathway. https://irena.org/publications/2021/Jun/World-Energy-Transitions-Outlook

[5] Bridge G., Bouzarovski S., Bradshaw M., Eyred N. Geographies of energy transition: Space, place and the low carbon economy. Energy Policy. 2013;53:331-340.

[6] Calvert K., Pearce J. M., Mabee W. E. Toward renewable energy geo-information infrastructures: Applications of GIScience and remote sensing that build institutional capacity. Renewable and Sustainable Energy Reviews. 2013;18:416-429.

[7] Fremouw M., Bagaini A., De Pascali P. Energy Potential Mapping: Open data in support of Urban Transition Planning. energies. 2020;13(5):1264.

[8] Sun M., Feng C., Zhang J. Probabilistic solar power forecasting based on weather scenario generation. Applied Energy. 2020;266, 114823.

[9] Akhter M. N., Mekhilef S., Mokhlis H., Shah, N. M. Review on forecasting of photovoltaic power generation based on machine learning and metaheuristic techniques. IET Renewable Power Generation. 2019; 13(7):1009-1023.

[10] Feng C., Cui M., Hodge B. M., Zhang J. A data-driven multi-model methodology with deep feature selection for short-term wind forecasting. Applied Energy. 2017;190, 1245-1257.

[11] Mirzaei M., Göçmen T., Giebel G., Sorensen P., Poulsen N. Estimation of the possible power of a wind farm. IFAC Proceedings Volumes (IFAC-PapersOnline). 2014;19, 6782-6787.

[12] Manwell J.F., McGowan J.G., Rogers A.L. Wind Energy Explained: Theory, Design and Application. Wiley. 2010.

[13] Negash T., Möllerström E. Ottermo F. An Assessment of Wind Energy Potential for the Three Topographic Regions of Eritrea. Energies. 2020; 13(7), 1846.

[14] Wind Energy Department of Risø National Laboratory, Det Norske Veritas: Guidelines for Design of Wind Turbines. 2002.

[15] Chen K., Song M., He Z., Zhang X. Wind turbine positioning optimization of wind farm using greedy algorithm. Journal of Renewable and Sustainable Energy. 2013.

[16] Karafil A., Ozbay H., Kesler M., Parmaksiz H. Calculation of Optimum Fixed Tilt Angle of PV Panels Depending on Solar Angles and Comparison of the Results with Experimental Study Conducted in Summer in Bilecik, Turkey. 9th International Conference on Electrical and Electronics Engineering (ELECO), IEEE. 2015.

[17] Duffie J. A., Beckman W. A. Solar Engineering of Thermal Process. Fourth Edition. Wiley & Sons, Inc. 2013.

[18] Bottaccioli L., Patti E., Macii E., Acquaviva A. GIS-Based Software Infrastructure to Model PV Generation in Fine-Grained Spatio-Temporal Domain. IEEE Systems Journal. 2018; 12(3), 2832–2841.

[19] Mar A., Pereira P., Martins J. Energy Community Flexibility Solutions to Improve Users' Wellbeing. Energies. 2021;14(12), 3403.

[20] European Centre for Medium-Range Weather Forecasts (ECMWF).

https://www.ecmwf.int/en/about

[21] ATLAIMPIANTI. Gestore Servizi Energetici (GSE). https://www.gse.it/dati-e-scenari/atlaimpianti

[22] CGR SpA (Compagnia Generale Ripreseaeree) Very High Resolution (VHR) Imagery. https://www.cgrspa.com

[23] Apache Sparks. https://spark.apache.org

[24] Docker: Empowering App Development for Developers. https://www.docker.com/

Appendix A

This section lists all equation needed to compute power production Equations (reported in Section 2) for PV and WF plants, with a detailed description of each parameter involved.

Photovoltaic Plants

$$\delta = 23.45 * \sin\left(360 * \frac{284+n}{365}\right) \quad (8)$$

$$C = (n-1) * \frac{360}{365} \quad (9)$$

$$E = 229.2 * (0.00075 + 0.001868 * \cos(C) - 0.032077 * \sin(C) - 0.014645 * \cos(2C) - 0.04089 * \sin(2C)) \quad (10)$$

$$t_{solar} = t_{standard} - \frac{(L_{loc} - L_{ref})}{15} + \frac{E}{60} - DST \quad (11)$$

$$\omega = 15 * (t_{solar} - 12) \quad (12)$$

$$\cos(\theta_z) = \cos(\phi) * \cos(\delta) * \cos(\omega) + \sin(\phi) * \sin(\delta) \quad (13)$$

$$\cos(\gamma_s) = \frac{\cos(\theta_z) * \sin(\phi) - \sin(\delta)}{\sin(\theta_z) * \cos(\Phi)} \quad (14)$$

The slope of the panel changes daily, according to the following equation:

$$\beta = |\phi - \delta| \quad (15)$$

$$F_{c-s} = \frac{1+\cos(\beta)}{2} \quad (16)$$

$$\cos(\theta) = \cos(\theta_z) * \cos(\beta) + \sin\theta_z * \sin(\beta) * \cos(\gamma_s - \gamma) \quad (17)$$

Tab. 1 – Variables for PV production estimation.

Variables	Definition	Source	Dependencies
δ [°]	Solar declination. Positive towards North	Eq.8 – Cooper Formula [16]	Day of the year
n [day]	Ordinal day of the year	From 1 to 365	Day of the year
C [°]	Parameter for the calculation of E	Eq. 9	Day of the year
E [min]	Equation of time	Eq. 10	Day of the year
t_{solar} [h]	Time based on the apparent angular rotation of the Sun across the sky, assuming Solar time = 12 at Noon	Eq. 11	Hour of the day and location
$t_{standard}$ [h]	Time given by the local clock	Meteo-rological data	Hour of the day
L_{loc} [°]	Local longitude	GIS/ Meteorological data	Location
L_{ref} [°]	Longitude of the reference meridian for the local time zone	$L_{ref} = -15°$	Constant value for Italy
DST [-]	Daylight Saving Time ("ora legale")	DST = 1 when "ora legale" DST = 0 when "ora solare"	Day of the year
ϕ [°]	Latitude. Positive towards North	GIS/ Meteo-rological data	Location
ω [°]	Hour angle. Positive towards West	Eq.12 [16]	Hour of the day and location
θ_z [°]	Zenith angle	Eq.13 [17]	Hour of the day and location
γ_s [°]	Azimuth angle. Positive towards West	Eq.14 [16]	Hour of the day and location

β [°]	Tilt angle	Eq.15 [16]	Day of the year and Location
γ [°]	Surface azimuth	Assumed γ = 0° [16]	Constant
ρ [-]	Reflection coefficient, albedo	Assumed ρ = 0.23.	Constant
F_{c-s} [-]	Collector-sky view factor	Eq. 16 [17]	Day of the year and Location
θ [°]	Angle of incidence of beam solar radiation on a surface whatever oriented and tilted	Eq. 17 [17]	Hour of the day and location
G_{bn} [W/m²]	Beam normal radiation	Meteo-rological data	Hour of the day and location
G_{dh} [W/m²]	Diffuse horizontal radiation	Meteo-rological data	Hour of the day and location
G_{th} [W/m²]	Total horizontal radiation	Meteo-rological data	Hour of the day and location
G_T [W/m²]	Total radiation on the tilted surface	Eq.1 [18]	Hour of the day and location

Wind Farms

First of all, pressure and temperature in function of the hub height (h) must be calculated, through Eq.18 [12],[13] and Eq.19 [12], respectively.

$$Pressure_{air}\,(h) = 101.29 - (0.011837) * h + (4.793 * 10^{-7}) * h^2 \quad (18)$$

$$T_{air}\,(h) = T_{air} - 0.0066 * h \quad (19)$$

Then, using perfect gas equation density at the hub height can be computed (Eq. 20) [12],[13].

$$\rho_{air}(h) = 3.4837 * \frac{Pressure_{air}\,(h)}{T_{air}\,(h)} \quad (20)$$

Tab. 2 – Variables for WF production estimation.

Variables	Definition	Source	Dependencies
P_{mech} [W]	Mechanical power output	Eq.1 [11]	Hour of the day and location
$Pressure_{air}(h$ [Pa]	Pressure of the air at the hub height	Eq. 18 [12][13]	Hour of the day and location
T_{air} [°C]	Air temperature at ground level	Meteo-rological data	Hour of the day and location
$T_{air}\,(h)$ [°C]	Air temperature at hub height	Eq. 19 [12]	Hour of the day and location
$\rho_{air}(h)$ [kg/m³]	Air density at the hub height	Eq.20 [12][13]	Hour of the day and location
c_p [-]	Power coefficient	Producer data or assumption	Constant
u [m/s]	Wind speed at the hub height	Eq.5 [14]	Hour of the day and location
D [m]	Diameter of the rotor blade	Eq. 6 [12]	Location
h [m]	Height of the hub	Elaborations	Location
z_0 [m]	Roughness length of the soil	Producer data or assumption	Constant
u_{ref} [m/s]	Wind speed at the reference height	Meteo-rological data	Hour of the day and location
h_{ref} [m]	Reference height	10 m [14]	Constant

Heat recovery potential from ventilated passive and active facades: A numerical study

Mohammad Rahiminejad, Dolaana Khovalyg

Ecole Polytechnique Fdérale de Lausanne (EPFL), Laboratory of Integrated Comfort Engineering (ICE), CH-1700 Fribourg, Switzerland, mohammad.rahiminejad@epfl.ch.

Abstract. A ventilated air-space behind external claddings can potentially affect the thermal performance of the entire building structure. In particular, in the Building Integrated Photovoltaic (BIPV) facades, ventilated cavities are typically present between the PV panels and the walls of the building. The airflow in the cavity can remove the generated heat behind the active external cladding, which could be eventually used as an additional source for heat recovery. In this study, the heat recovery from a ventilated air-space behind passive (wood) and active (BIPV) facades are investigated using transient simulations.
The numerical model used in this study is validated against experimental measurements carried out in a building prototype located in the Smart Living Lab in Fribourg (Switzerland). The original façade is made of wooden cladding that is separated from the wall core incorporating a ventilated cavity. To study the impact of façade type on the results, the external cladding is virtually replaced with typical polycrystalline PV panels. The analyses are performed for representative days in the winter and summer of 2021 using recorded weather data on the test building. The results are examined in terms of the temperature distribution of the layers in the wall assembly, heat flux through the indoor space, airspeed in the cavity, and heat flow in the air gap. The potentials for heat recovery per day of interest are also calculated and compared. It was shown that the heat recovery from the cavity behind the BIPV façade could become equal to 5341 kWh on a representative summer day, which is considerably higher compared to the value obtained for a passive cladding. The results highlight the potential for harvesting heat from the ventilated air gaps behind passive and active facades. The outcome of this study highlights the need for the integrated vision for energy-savings at the building scale.

Keywords. Passive cladding, BIPV façade, Ventilated cavity, Heat recovery
DOI: https://doi.org/10.34641/clima.2022.147

1. Introduction

The introduction of wall designs that incorporates air-spaces behind claddings can reduce energy use in buildings by impacting the thermal performance of the entire wall structure [1-5]. The thermal resistance caused by the ventilated air-space depends on multiple parameters, and it can be measured to evaluate the contribution of the air-space to the total R-value of the assembly [6-8]. In North America, the air cavity is used to eliminate capillary flow between the cladding and sheathing and provide ventilation to remove moisture [9]. In the European community, the ventilated façade is usually used in refurbishment projects to reduce the heat loss through the building envelope and improve the thermal resistance of the wall [10]. Traditionally, ventilated façade systems have been predominantly used in colder climates of Europe and North America to reduce the load on the heating systems by warming the airflow in the cavity caused by the Sun. More recently, the ventilation of the warm air due to the stack effect of natural air circulation inside the cavity has begun to be used in warmer climates such as Australia to benefit from the reduced solar heat gain of the building; and consequently, reducing the load on the cooling systems [11].

In addition to the aforementioned advantages, the ventilated air gaps behind external claddings can be considered as a possible source for heat recovery. The wasted heat from the air cavity can be harvested and utilized for the HVAC system in the building, which can eventually reduce the operational energy of the building [12].

The ventilated cavity can be incorporated in both passive (traditional) and active Building Integrated PV (BIPV) facades. Particularly in the latter type, the heat flow removed from the ventilated air-space can reduce the temperature of the PV modules and enhance the electrical efficiency of the BIPV system

Copyright ©2022 by the authors. This conference paper is published under a CC-BY-4.0 license.

[13]. Despite the prevalence of studies on the heat removal from the air gap behind the traditional claddings [14, 15] and BIPV facades [16-19], research works that compare the heat recovery from the ventilated air-spaces behind passive (traditional) and active (BIPV) claddings in a real-scale building are still lacking. Most of the previous works have only focused on the heat recovery potential behind external claddings in a small scale wall structure. In the present study, a numerical transient 2-D model is employed to investigate the heat recovery of the naturally ventilated air-space behind passive (wood) and active (BIPV) facades implemented in a full-scale building prototype. The original façade of the test building is made of wooden cladding, and it is virtually replaced with typical polycrystalline PV modules to study the impact of the façade type on the results. The analyses are performed for two representative days, one in the winter and one in the summer of 2021, using weather data monitored on the test building.

2. Methodology

2.1 Case Study: CELLS

The test building that is used for the simulations is a shared research facility CELLS (Controlled Environment for Living Lab Studies), in the Smart Living Lablocated in Fribourg, Switzerland (Figure 1). The test building is composed of two identical rooms with different thermal inertia walls. The low inertia room is east-oriented, and the high inertia room is west-oriented. The wooden cladding of the wall assembly is separated from the wall core with an air-space behind the façade. The cavity is naturally ventilated by the airflow that can freely move through the bottom and top openings. In this study, the heat flow removal from the ventilated cavity behind the west-oriented wall is investigated.

Fig. 1 – Façade of the building prototype CELLS (Fribourg, Switzerland).

2.2 Numerical model of the wall structure

To model the transient heat transfer mechanisms through the entire structure, a 2-D finite-difference method is employed. The system is divided into multiple control volumes, and a two-dimensional nodal network with 5 nodes along with the height and 3 nodes through the depth of each layer in the geometry is created. The model is elaborated in detail by Rahiminejad & Khovalyg [20] and has been validated for wall structures with both passive and active facades using experimental measurements. Figure 2 shows a schematic of the ventilated wall assembly. The wind effect and stack effect are mechanisms that naturally drive airflow in the cavity and cause a temperature difference between the top and bottom openings [21]. The heat flow through the air gap per area of the cavity (equation (1)) is a function of the density and specific heat capacity of the airflow, airspeed in the cavity and its temperature gradient from top to bottom:

$$q_{cav} = \rho V_{cav} c_p \left(T_t - T_b\right) \qquad (1)$$

The heat flow removed from the cavity can also affect the heat flux through the interior surface of the wall (equation (2)), which is a function of the heat transfer coefficient and the temperature difference between the interior surface and indoor space:

$$q_{int} = h_{int}\left(T_{s,int} - T_{ind}\right) \qquad (2)$$

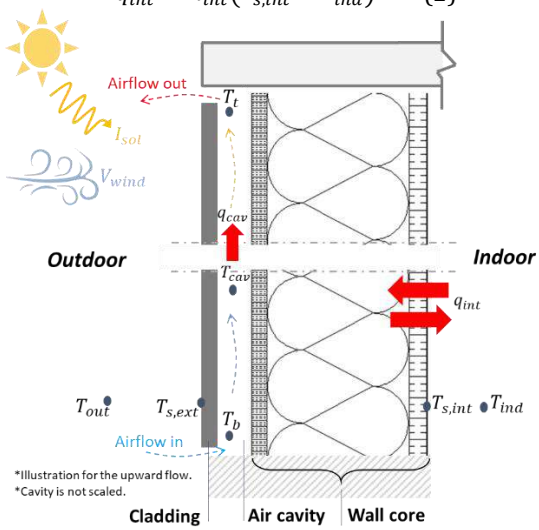

Fig. 2 - Schematic representation of a ventilated wall.

In total, four simulations are performed considering representative days in winter and summer of 2021; 2 for wall structures with original passive cladding (wood) of the building prototype, and 2 for a similar wall assembly but with the external cladding entirely replaced with polycrystalline PV modules. As shown in Figure 3, the PV module consists of tempered glass, photovoltaic cells encapsulated between ethyl vinyl acetate (EVA) layers, and a polymer back sheet. The thermo-physical properties of the layers used in the simulation are summarized in Table 1.

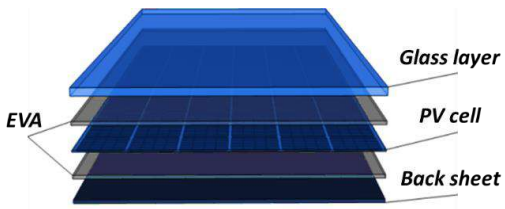

Fig. 3 – Layers used in the PV module.

The simulations are performed using the data of 8 hours in advance of the chosen day to ensure convergence of the simulations prior to the day of interest. Assumptions made in the calculation process are: (i) fully developed flow across the width of the air cavity, (ii) no airflow infiltration between

the photovoltaic modules along with the height of the wall, and (iii) negligible effects of thermal bridges.

Tab. 1 - Thermo-physical properties of the test wall*.

Material (exterior to interior)	d (m)	k (W/m·K)	ρ (kg/m³)	c_p (J/kg·K)
Passive facade				
Wood	0.024	0.10	450	1800
Active façade				
Tempered glass	0.0036	1.8	3000	500
EVA	0.0004	0.35	960	2090
PV cell	0.0004	148	2330	700
Back sheet	0.0004	0.13	1450	1650
Wall core				
Insulation	0.180	0.03	15	1404
Timber hardwood	0.140	0.13	471	1600
Earth brick	0.050	0.79	1900	1100
Jute coating	0.015	0.80	1600	1450
Air-space	0.070	varies	varies	varies

**Only selected properties are mentioned. See [20] for more details.*

2.3 Weather Data

The weather data of two representative days in Fribourg, Switzerland, in winter (March 02nd) and summer (July 29th) of 2021 are used as the outdoor conditions. The diurnal variations of outdoor air temperature, vertical solar radiation [22], and wind speed are shown in Figure 3. The data are collected using a weather station installed on the facade of the test building (Figure 1). The weather station includes an air temperature sensor (S-THB-M002, Onset), Davis® wind speed and direction sensor (S-WCF-M003, Onset), and silicon pyranometer for global horizontal irradiance (S-LIB-M003, Onset).

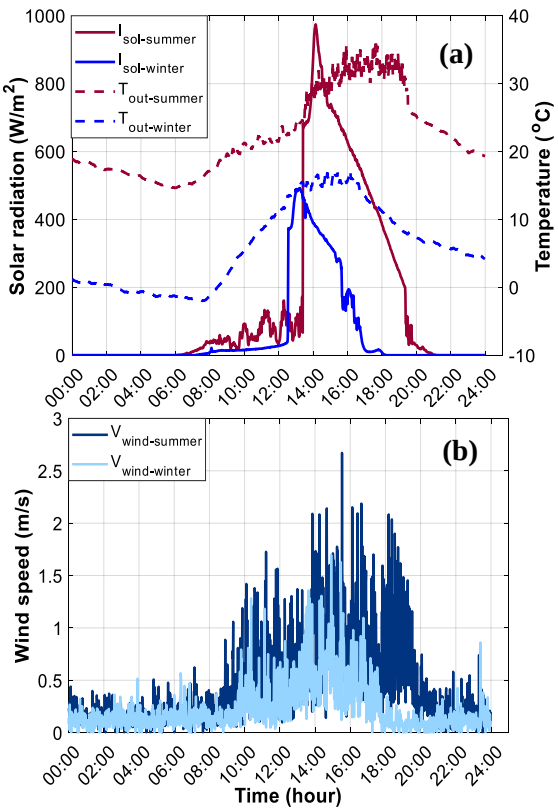

Fig. 3 – (a) Outdoor air temperature and vertical solar radiation, (b) Wind speed for representative days in winter (March 02nd) and summer (July 29th) of 2021.

The sensors in the weather station are connected to a micro station data logger (H21-USB, Onset) to record data at 1-minute intervals. Indoor air temperatures are assumed to be equal to 21°C in winter and 26°C in summer [23].

3. Results

In this section, the results of the simulations are presented in terms of temperature distribution through the wall structures, heat flux through the interior surface, airspeed in the cavity, and heat flow in the air-space. The results shown in the following subsections, unless it is indicated, are averaged for 5 nodes along with the height of the wall assembly.

3.1 Temperature distribution on the surfaces

The daily evolution of temperature on the exterior surface of cladding with both passive and active facades is presented in Figure 4(a). According to the results, the surface temperature of the passive façade reaches up to 38°C in winter and 62°C in summer. The corresponding values for the active façade are 54°C and 98°C, respectively, which are 16°C and 36°C higher compared to the passive cladding. The high rear surface temperature of the active façade in summer is due to the assumption of a closed-joint BIPV façade (i.e., the connections between the PV panels are with no air infiltration). Similar values are reported in other works [24-25], which would strongly affect the efficiency of the panels. The difference between the maximum surface temperature of passive cladding with the maximum outdoor temperature is equal to 20°C in winter and 27°C in summer. In the case of using an active façade, the values become 36°C in winter and 63°C in summer. These differences imply the impact of solar radiation on the surface temperature of the external cladding. Comparing the plots in Figure 4(a) with the weather data shown in Figure 3 reveal that the surface temperature of the external cladding with passive façade generally follows the diurnal outdoor temperature, while the variation in solar radiation during a day has a predominant impact on the surface temperature of the external cladding with active façade. This could be attributed to the difference in the thermal properties of the layers used in the passive and active façades. In particular, the high thermal transmittance and solar absorptivity of the glass layer in the BIPV façade exposed to outdoor could result in a more pronounced effect of solar radiation on the surface temperature of the active façade. Moreover, it can be seen from the plots in Figure 4(a) that the difference in the thermal mass of the external claddings, defined as volumetric heat capacity × volume of the material, has caused a time delay of up to 3 hours in winter and 4 hours in summer in the maximum surface temperature between the passive and active façades.

The temperature of the interior surface of the jute coating that is adjacent to the indoor space is shown in Figure 4(b). According to the results, the difference between the temperatures of the interior surfaces in wall structures with passive and active

façades reaches up to 0.1°C in winter and 0.4°C in summer. The higher value in the latter is due to the higher difference between the surface temperature of the two claddings in summer, which has been propagated through the entire wall structure. Moreover, the results indicate that the maximum deviation of the interior surface temperature from the fixed indoor temperatures in winter and summer is equal to 0.4°C. The plots in Figure 4(b) show that the interior surface temperature of the wall structure with both passive and active façades is almost always lower than the fixed indoor temperature in winter, which is due to the temperature gradient through the wall assembly caused by the lower outdoor temperature compared to the fixed indoor temperature. In summer, however, the temperature on the interior surface of the wall with passive cladding is lower than the indoor temperature, while it becomes higher (from 1:00 to 6:00, and from 17:00 to 24:00) in case of using an active façade. This is mainly due to the higher surface temperature of the external cladding in the latter. Furthermore, the impact of the thermal mass of the external cladding is noticeable in the diurnal behavior of the interior surface temperature. In other words, the amplitude of the interior surface temperature is higher in the wall structure with the active façade compared to the wall assembly with passive cladding, which is due to the lower thermal inertia of the former one.

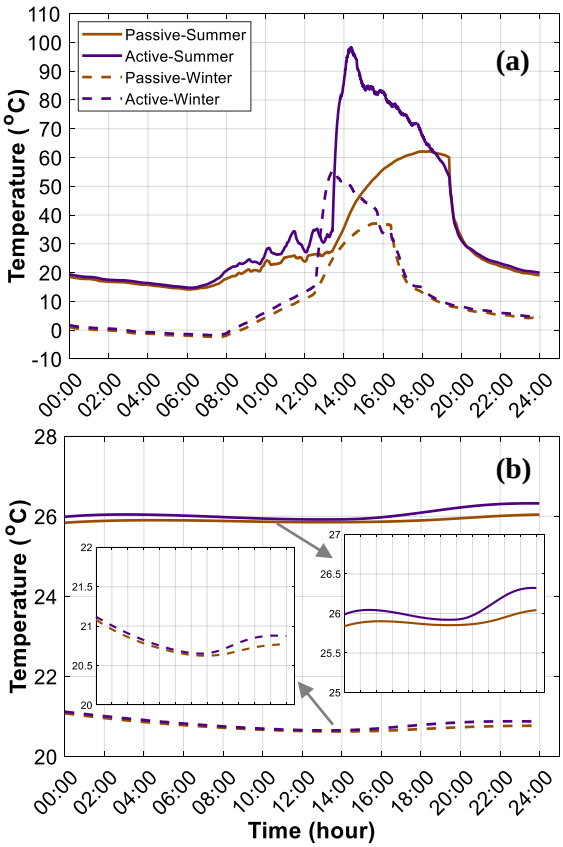

Fig. 4 – Temperature distribution averaged along with the height of the wall (a) Exterior surface of cladding, (b) Interior surface of jute coating.

The evolutions of the airflow temperature in the cavity at the middle height and top opening are shown in Figure 5. The airflow temperature at the bottom opening in each time step is assumed to be equal to the outdoor temperature and is not shown here. According to the results in Figure 5(a), the airflow temperature in the middle of the cavity behind the passive cladding reaches up to 20°C in winter and 40°C in summer. In case of using the BIPV façade, the values are 20°C and 30°C higher compared to the passive façade. The results in Figure 5(b) indicate that the airflow temperature at the top opening is higher compared to the middle of the air-space. The difference is 8°C for passive cladding in winter and summer conditions. By replacing the original cladding of the test building with PV panels, the difference between the airflow temperature at the top opening and in the middle of the cavity becomes 18°C in winter and 30°C in summer. The wind effect and stack effect are more pronounced in summer compared to winter. The airflow in the air-space becomes warm at the time when the wall structure is exposed to the Sun. Consequently, the temperature of the airflow becomes higher at top points compared to the lower points in the cavity. This phenomenon is more noticeable in the cavity behind the active façade, which is due to the lower thickness and higher thermal conductivity of the PV panel compare to the wood.

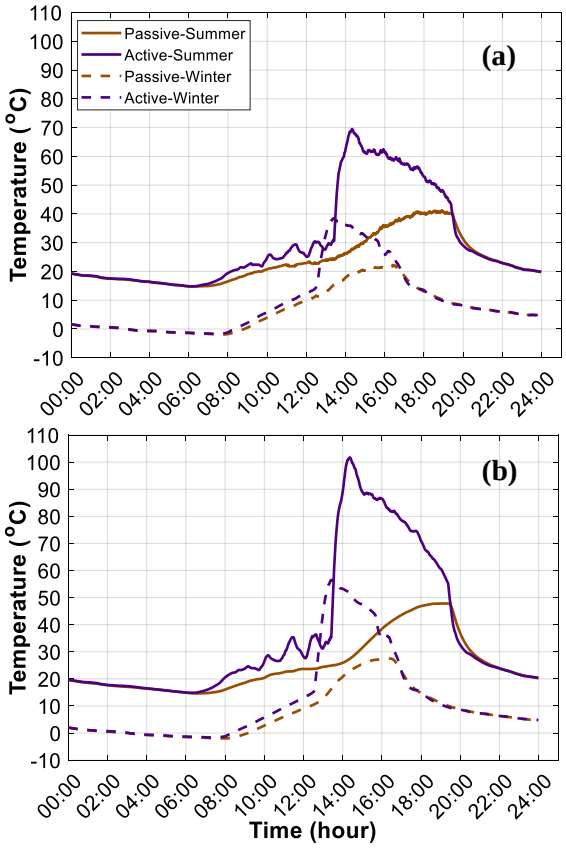

Fig. 5 - Temperature distribution of the airflow in the ventilated cavity (a) middle height, (b) top opening.

3.2 Heat flux through the interior surface

The heat flux through the interior surface of the wall assembly with both passive and active façades in winter and summer is presented in Figure 6. The negative values in the plots indicate that heat leaves the indoor space. According to the results, the heat

flux leaves the room in winter considering wall structure with both cladding types, which was expected due to the higher indoor temperature compared to the outdoor temperature. In summer, however, the heat flux most of the time (except after 22:00) leaves the indoor space of the wall assembly with the passive cladding, which is due to the lower interior surface temperature compared to the indoor temperature. By replacing the external cladding with an active façade, the wall structure may lose or gain heat, depending on the time of the day and the diurnal variation of the interior surface temperature, as it was discussed in section 3.1. The maximum difference in the heat loss of the wall with passive and active façades reaches up to 0.5 W/m² in winter and 1.5 W/m² in summer.

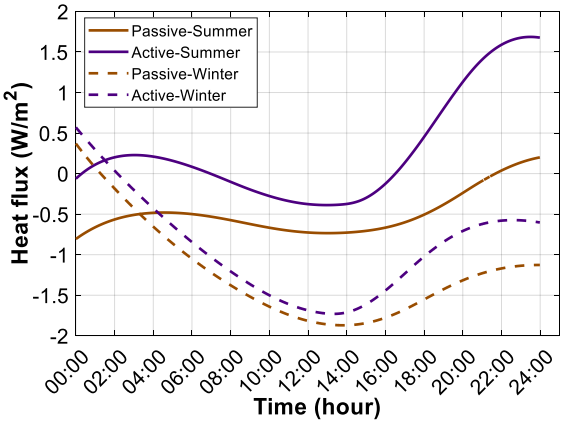

Fig. 6 – Heat flux through the interior surface.

3.3 Airspeed in the cavity

The profiles of the speed of airflow moving in the ventilated air-space are shown in Figure 7. Based on the results, the airspeed in the air gap behind the active façade is most of the time higher compared to the passive cladding. This is due to the higher gradient in the airflow temperature in the cavity behind the active façade caused by the stack effect that is more pronounced during the daytime. The maximum difference between the airspeed in the cavity behind passive and active façades reaches 0.3 m/s in winter and 0.5 m/s in summer. Comparing the results for each cladding type in winter and summer reveals that the airspeed in the ventilated cavity is most of the time higher in the latter, which can be attributed to the higher wind speed (i.e., wind effect) and solar flux (i.e., stack effect) in summer (Figure 3).

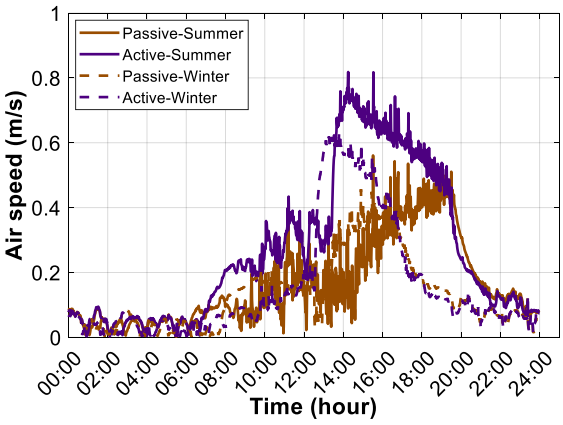

Fig. 7 – Airspeed in the ventilated cavity.

3.4 Heat flow in the cavity

The profiles of the heat flow removed from the air-space are shown in Figure 8. The plots clearly show the higher heat flow passing through the ventilated cavity behind the active façade compared to passive cladding. Interestingly, the cavity behind the BIPV system generates more heat in winter compared to the cavity behind the original cladding of the test building in summer. The maximum heat flow that is removed from the air gap of the wall structure with PV modules reaches 30 kW/m² in winter and 60 kW/m² in summer. The values are much lower in the case of the wooden cladding and do not exceed 10 kW/m². The total amount of heat flow through the cavity behind passive cladding is equal to 16.7 kW/m² on a typical winter day and 33.2 kW/m² on a typical summer day. The corresponding values for the wall assembly with active façade are 77.8 kW/m² and 211.9 kW/m². The results show promising potential for heat recovery behind both cladding types, but more significant in BIPV façade. This aspect is further addressed in the next section.

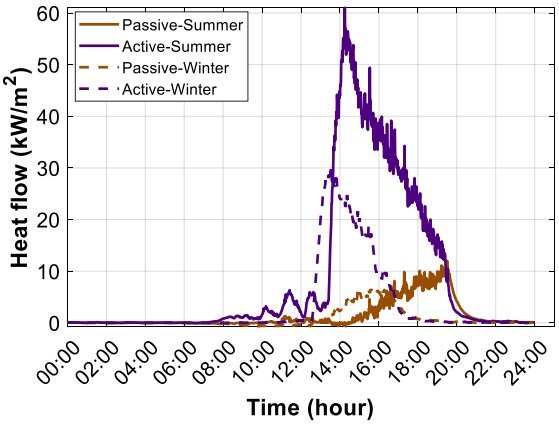

Fig. 8 – Heat flow in the ventilated cavity.

3.5 Heat recovery in the cavity

The heat recovery (i.e., HR in kWh) from the ventilated air-space is calculated using the absolute sum of heat flow through the cavity that could be hourly harvested, considering the area of the cavity with the thickness of 0.07 m and the width of 6.00 m (equation (3)) [26]. It is assumed that the heat flow is uniformly distributed throughout the entire width of the wall.

$$HR = \sum (q_{cav})_{hourly} \times d_{cav} \times w_{cav}/1000 \qquad (3)$$

The results are provided in Figure 9 for representative days in winter and summer. As it is shown, the HR from the ventilated cavity behind the active façade in winter is almost 3 times and in summer 6 times higher than the passive cladding. The HRP in summer is 1.6 times higher than in winter for the cavity behind the passive cladding, while the corresponding value is 2.7 times for the active façade.

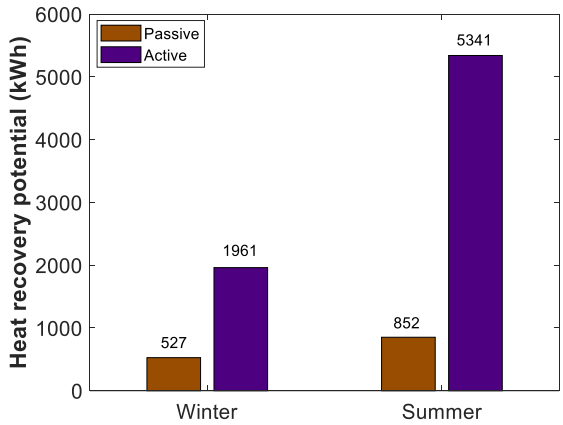

Fig. 9 – Heat recovery in the ventilated cavity.

The results confirm the advantage of replacing passive claddings with active BIPV façades to benefit from the electricity generated by the PV panels and also to achieve the higher potential of the heat flow recovered from the ventilated air cavity. Further analysis is needed to assess the applicability of the heat flow collected from the back of external claddings. The harvested heat from the air gap may have enough thermal energy, which eventually can be used in the subsequent system in the building section. In other words, the preheated air extracted from the air cavity can be used as an additional source to provide ventilation for the room space, reduce the heating load provided by the HVAC system, and increase the water temperature in the hot water supply system. Furthermore, since the airflow in the ventilated cavity has a major impact on the heat recovered, it is necessary to increase the airspeed in the air gap to boost the amount of thermal energy harvested. This could encourage practitioners to take advantage of using a fan system and control the air flow rate in the air gap.

4. Conclusion

The impact of the presence of a ventilated air-space behind a passive wooden cladding and an active BIPV façade on the thermal performance of the wall structure was examined in this study. A transient 2D model was employed, and the simulations were performed for a case study of a building prototype in Fribourg, Switzerland. Two representative days in the winter and summer of 2021 were selected, and the measured weather data was used to numerically investigate the performance of the wall structures assuming fixed standardized indoor temperatures in winter and summer. The results were presented and compared in terms of the temperature distribution through the wall assembly, heat flux through the interior surface of the wall, airspeed in the ventilated air gap, and heat flow passing through the cavity. The heat recovery from the air-space behind both passive and active façades was also evaluated and the possible applications of the harvested heat flow in the building were addressed.

According to the results, the temperature of the active façade becomes higher compared to the passive cladding due to the difference in the thermo-physical properties of materials. The results showed that the thermal mass of the external cladding affects the diurnal variation of the temperature profiles. Moreover, it was revealed that the stack effect has a considerable impact on the air temperature gradient along with the height of the cavity. The results indicated that the heat flux through the interior surface alters between the loss and gains in summer, while the heat always leaves the indoor space in winter. It was shown that the airflow in the cavity driven by the wind-induced and stack effects has a higher speed in the air gap behind the active façade compared to the passive cladding. Consequently, the heat flow within the air-space became higher in the former. Analyzing the heat flow from the ventilated cavity showed that there is a noticeable potential of recovery of the heat energy from the air-spaces, particularly, for the active BIPV façade system in summer.

This study was performed to highlight the possibility of harvesting heat flow from the ventilated air-spaces behind passive and BIPV façade systems. The results confirmed that instead of wasting the potential heat energy of the airflow in the cavity, it could be recovered and further utilized as an additional heat source for the building. The results of this study are provided assuming a wall structure completely covered with the PV modules, while the presence of small air passages between the panels should be considered in future works, which could affect the hydrodynamic behavior of the airflow in the air-space, and consequently, the heat recovery potential. Moreover, the analysis was carried out assuming a uniform distribution of heat flow within the entire width of the wall. Therefore, 3D simulations are recommended to be done in future studies to investigate the impact of non-uniformity of the airflow on the results.

Nomenclature

Symbol	Definition [Unit]
c_p	Specific heat capacity [J/kg K]
d	Thickness of the material [m]
h	Heat transfer coefficient [W/m^2 K]
H	Height [m]
I	Solar radiation [W/m^2]
k	Thermal conductivity [W/m K]
m	Mass flow rate [kg/s]
q	Heat flux [W/m^2]
T	Temperature [°C]
V	Speed [m/s]
w	Width [m]

Subscripts

Symbol	Definition
b	bottom
cav	cavity
ext	exterior
ind	indoor
int	interior
out	outdoor
s	surface
t	top

5. References

1. Aelenei LE. Thermal performance of naturally ventialted cavity walls. Ph.D. dissertation. 2006.
2. Rahiminejad M, Khovalyg D. Impact of the Ventilated Cavity on the Thermal Performance of Traditional Wall Structures. ASHRAE Trans. 2021;127:187-195.
3. Rahiminejad M, Berquand C, Khovalyg D. Transient thermal response of opaque building envelope elements: EPFL campus case study. J Phys Conf Ser. 2021;2042(1):012080.
4. Rahiminejad M, Khovalyg D. In-situ measurements of the U-value of a ventilated wall assembly. J Phys Conf Ser. 2021;2069: 012212.
5. Schindelholz R, Rahiminejad M, Chatterjee A, Khovalyg D. Assessment of thermal and electrical performance of BIPV façades using simplified simulations. J Phys Conf Ser. 2021;2042(1):012081.
6. Rahiminejad M, Khovalyg D. Thermal resistance of ventilated air-spaces behind external claddings; definitions and challenges (ASHRAE 1759-RP). Sci Technol Built Environ. 2021;27(6):788-805.
7. Rahiminejad M, Khovalyg D. Thermal resistance of the ventilated air-spaces behind external claddings; theoretical definition and a parametric study. J Phys Conf Ser. 2021;2069: 012197.
8. Rahiminejad M, Khovalyg D. Measuring the effective thermal resistance of ventilated air-spaces behind common wall assemblies: theoretical uncertainty analysis and recommendations for the hot box method modifications (ASHRAE 1759-RP). Sci Technol Built Environ. 2022;in press.
9. Straube J, Finch G. Report 0906: Ventilated wall claddings: review, field performance, and hygrothermal modeling. Test. 2009:25. www.buildingscience.com.
10. Bikas D, Tsikaloudaki K, Kontoleon KJ, Giarma C, Tsoka S, Tsirigoti D. Ventilated Facades: Requirements and Specifications Across Europe. Procedia Environ Sci. 2017;38:148-154.
11. Straube JF, Straaten R van. Field Studies of Ventilation Drying. 2004;47(11-12):387-406.
12. Zogou O, Stapountzis H. Flow and heat transfer inside a PV/T collector for building application. Appl Energy. 2012;91(1):103-115.
13. Rahiminejad M, Khovalyg D. Dynamic Thermal Performance of the BIPV Facades. ASHRAE Trans. 2021;127:170-178.
14. Richman RC, Pressnail KD. A more sustainable curtain wall system: Analytical modeling of the solar dynamic buffer zone (SDBZ) curtain wall. Build Environ. 2009;44(1):1-10.
15. Diallo TMO, Zhao X, Dugue A, et al. Numerical investigation of the energy performance of an Opaque Ventilated Façade system employing a smart modular heat recovery unit and a latent heat thermal energy system. Appl Energy. 2017;205:130-152.
16. Rounis ED, Bigaila E, Luk P, Athienitis A, Stathopoulos T. Multiple-inlet BIPV/T modeling: Wind effects and fan induced suction. Energy Procedia. 2015;78:1950-1955.
17. Hailu G, Dash P, Fung AS. Performance evaluation of an air source heat pump coupled with a building-integrated photovoltaic/thermal (BIPV/T) System under cold climatic conditions. Energy Procedia. 2015;78:1913-1918.
18. Dehra H. An investigation on energy performance assessment of a photovoltaic solar wall under buoyancy-induced and fan-assisted ventilation system. Appl Energy. 2017;191:55-74.
19. Ahmed-Dahmane M, Malek A, Zitoun T. Design and analysis of a BIPV/T system with two applications controlled by an air handling unit. Energy Convers Manag. 2018;175:49-66.
20. Rahiminejad M, Paris A, Ge H, Khovalyg D. Performance of lightweight and heavyweight building walls with naturally ventilated passive and active facades. Energy Build. 2022;256:111751.
21. Rahiminejad M, Khovalyg D. Review on ventilation rates in the ventilated air-spaces behind common wall assemblies with external cladding. Build Environ. 2021;190:107538.
22. Finch G. The Performance of Rainscreen Walls in Coastal British Columbia. Univ Waterloo. 2007.
23. SIA (2015). Standardized data for building energy modeling (SIA 2024:2015). Zurich, Switzerland.
24. Agathokleous R. Thermal Analysis of naturally ventilated BIPV systems. Ph.D. dissertation. 2017.
25. Gan G. Numerical determination of adequate air gaps for building-integrated photovoltaics. Sol Energy. 2009;83:1253-1273.
26. Girma GM, Tariku F. Experimental investigation of cavity air gap depth for enhanced thermal performance of ventilated rain-screen walls. Build Environ. 2021;194:107710.

Data Statement

The datasets generated during and/or analyzed during the current study are not publicly available because of ensuring privacy policies but are/will be available upon request under particular circumstances and agreements·

Identification of dynamic U-values for supply-air double windows based on experiments

Yujian Huang[a], Mohamed El Mankibi[b], Richard Cantin[c]

a LTDS, ENTPE, University of Lyon, Vaulx-en-Velin, France, Yujian.HUANG@entpe.fr

b LTDS, ENTPE, University of Lyon, Vaulx-en-Velin, France, Mohamed.ELMANKIBI@entpe.fr

c ENTPE, University of Lyon, Vaulx-en-Velin, France, Richard.CANTIN@entpe.fr

Abstract. The double windows with supply-air are recommended for both new and retrofitted buildings where preheating fresh air is needed especially when dealing with historical and protected buildings. To evaluate their energy saving potentials in buildings and optimize their performance, building energy simulations are necessary. In building energy simulation tools, the thermal transmittance (i.e., *U*-value) is one of the most important input parameters. The conventional *U*-value is a static indicator and a number of numerical studies have been proposed to identify *U*-value with varying window parameters. However, there is still a lack of laboratory experimental studies to get accurate *U*-value and evaluate numerical modelling results. Moreover, the performances of supply-air windows are related with environmental parameters and thus the use of conventional *U*-value might lead to a significant deviation between the simulated building energy and the real one. The purpose of this study is to provide dynamic *U*-values which could be varied according to environmental conditions. Firstly, an adapted guarded hot box is set up and it is calibrated by controlling air velocities and air temperatures in both cold and hot sides. Secondly, the *U*-values of supply-air windows are measured with varying environmental parameters and window parameters. Thirdly, the regression analysis is applied to describe the correlation between *U*-values and the influential factors, and thus one can easily evaluate *U*-value under different environment conditions. A future work is to integrate the regression correlation with energy simulation tools to have a comprehensive exploration of supply-air windows in different climate regions.

Keywords. Supply-air double windows; *U*-values; Guarded hot box method; Experiment
DOI: https://doi.org/10.34641/clima.2022.265

1. Introduction

Utilizing supply-air double windows is an effective way to reduce heating demand in winters for both new built and existing buildings [1–4]. Supply-air windows have several advantages. First, they can provide fresh air to improve indoor air quality. Second, they can preheat fresh air before air enters into the room and thus reduce the ventilation heating load. Third, they can be retrofitted by putting an additional window inside or outside of the existing window, without damaging the building structure. Fourth, using them do not affect the view to the outside.

U-value is an important indicator in characterizing window thermal performance and analysing building energy consumption. The *U*-value defined in ISO 15099 [5] represents the heat transferred through the window per square meter under one degree of the air temperature difference between indoor and outdoor environment. Different from conventional windows, the heat loss through the interior glazing of supply-air double windows could be partly recovered by the flowing air. This is not considered in the conventional *U*-value, and thus additional *U*-values, including U_{loss}-value, U_{use}-value and U_e-value, were proposed for supply-air double windows [6,7]. The detailed description of U_{loss}-value, U_{use}-value and U_e-value could refer to [7].

Most of the existing studies on *U*-values of supply-air windows are based on simulations or in-situ experiments.

Wright [6] performed simulations to get U_e-value based on 2D analytical solutions. In their study, eleven supply-air windows with different inner and outer glazing were simulated with and without ventilation. The air flow channel was 15 mm. They found that attributed to the ventilation, the U_e-value could be reduced by 30%-50%.

Copyright ©2022 by the authors. This conference paper is published under a CC-BY-4.0 license.

Baker and Mcevoy [8] measured air temperature within the gap between two panes to calculate the U_e -value. They concluded that the U_e -value are dependent on the ventilation rate.

Mcevoy et al. [9] conducted in-situ experiments in the PASSYS test cell and they directly placed a heat transfer mat in the middle of the outer window to deduce the U_e-value, using shading screen. Test were performed with 10, 20, 30 mm air flow channels and 6, 10, 13 l/s flow rates. They concluded that, regardless of the width of air flow channel, increasing the ventilation rate results in a decrease in the U_e-value. In particular, as the ventilation rate increased from 5.6 l/s to 14 l/s, the U_e-value of the window with 30 mm gap was decreased from 1.12 to 0.67 W/m^2 K. Moreover, they found that placing the Low-E coating in the surface facing the air flow channel could reduce the U_e -value by approximately 50%. They also established an ESP-r model and simulated U_e-value. Based on the simulation result, it was found that the higher U_e -value is coinciding with higher exterior air temperature.

Southall and Mcevoy [10] investigated the effect of window size on the U_e-value based on experiments and CFD model. They found that the aspect ratio had very little effect on the U_e-value when the window aera was the same. In addition, the U_e-value could be larger for the larger window size. They also established a correlation between U_e -value and window size.

Carlos et al. [7] investigated *U*-values based on experiments and numerical analysis. They found that compared to the supply-air double window with an inner single-glazed unit, the window with an inner double-glazed unit had a lower U_{loss}-value, a lower U_{use}-value and a lower U_e-value. When the air flow rate increased, the U_{loss} -value and U_{use} -value increased, while the U_e -value decreased. They also found that when the air temperature difference between cold and hot sides increased, the U_{loss}-value and U_{use} -value increased, while the U_e -value decreased.

Mcevoy and Southall [11] performed CFD to simulate the U_e-value and also compared the simulated value with measured value. The comparison results showed that the simulated value agreed with the measured one when the temperature difference between cold and hot sides was 44 °C, while a large deviation between the simulated value and measured one could be observed when the temperature difference was 33 °C.

There is still a lack of laboratory experiments to identify *U*-values of supply-air windows. In this study, we conducted experiments in an adapted guarded hot box to measure the *U*-values with varying the air flow rate and air temperature difference between cold and hot sides. Moreover, dynamic U-values, which could be varied according to environmental conditions, were proposed based on the regression analysis.

2. Definition of *U*-values

The *U*-value defined in ISO 15099 [5] can be expressed by the following equation,

$$U = \frac{q}{\Delta T} \tag{1}$$

Where q is the heat flux through the tested sample per square meter (W/m^2), without incident solar radiation; ΔT is the air temperature difference between the indoor and outdoor environment (K).

The U_{loss}-value represents the heat loss through the interior window per square meter under one degree of air temperature difference between the indoor and outdoor environment [7]:

$$U_{loss} = \frac{q_1}{\Delta T} \tag{2}$$

Where q_1 is the heat flux through the interior window per square meter (W/m^2), without incident solar radiation.

The proposed U_{use} -value could represent the capability of supply-air double windows in recovering the heat loss through the interior glazing. It can be calculated as Eq. (3) [7]:

$$U_{use} = \frac{c\dot{m}(T_{ol} - T_{il})}{A \cdot \Delta T} \tag{3}$$

Where A is the window area, m^2; c is the heat capacity of air, J/kg °C; $\dot{m}$ is the air mass flow rate, kg/s; T_{ol} is the outlet air temperature and T_{il} is the inlet air temperature, °C.

The U_e -value is the heat loss through the exterior window per square meter under one degree of air temperature difference between the indoor and outdoor environment. It can be calcualted based on U_{loss}-value and U_{use}-value [7]:

$$U_e = U_{loss} - U_{use} \tag{4}$$

3. Methods

3.1 Apparatus and sensors

(1) Guarded hot box

The guarded hot box (GHB) in LTDS/ENTPE laboratory (as shown in Fig.1) is used to measure the *U*-values of supply-air double windows. It comprises a metering box, a guard box, a cold box and a sample frame between metering box and cold box to hold samples.

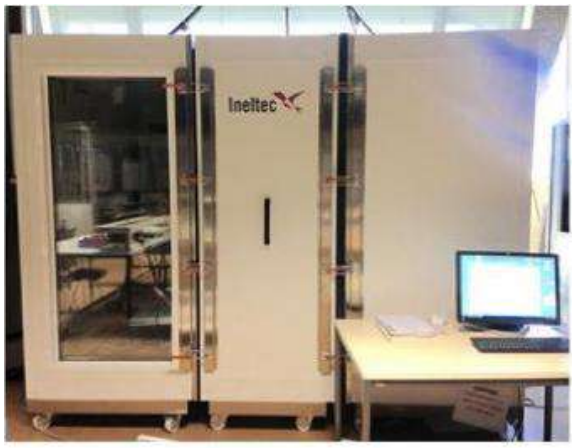

Fig.1 - GHB in LTDS/ENTPE laboratory

Inside the metering box, there are four resistance heaters to maintain the air temperatures at desired values. In addition, a wooden Baffle painted black was placed in the metering box, and three DC powered axial flow fans were installed on the top of baffle to achieve uniform air circulation between the baffle and surface of the tested sample. The input voltage to the heaters and fans was controlled using LABVIEW. It should be mentioned that, under steady state conditions, the input power of the fans was considered to be fully converted into heat.

The function of the guard box is to minimize the heat loss through the walls of metering box. There are four heaters in the guard box to maintain the air temperature of the guarded box the same as that of metering box.

In the cold box, there is a glycol cooling system. Similar to the measuring box, a baffle and three DC powered axial flow fans were installed in the cold box.

(2) Adapted GHB

As mentioned in [12], to prevent insufficient air mixing and to achieve an even temperature distribution in metering box, the flowing air was returned to the cold box through a tube instead of entering the metering box. The tube was installed as shown in Fig.2.

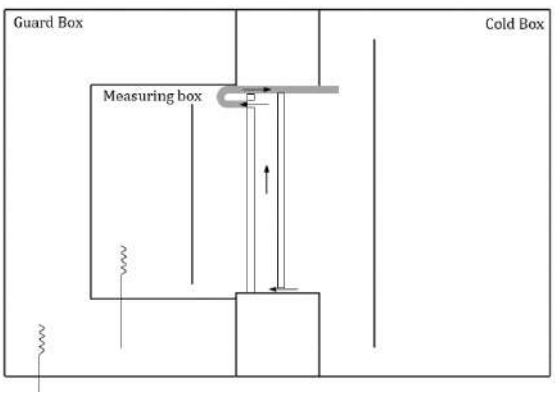

Fig.2 - Schematic of the adapted GHB

(3) Sensors

According to the standard ISO 8990 [13], fourteen air temperature sensors were installed in metering box, guard box and cold box to measure air temperatures. In addition, eighteen surface temperature sensors were placed on the baffle surfaces. Three hot wire anemometers were applied to measure the inlet air velocity, the air velocity in cold side and that in hot sides. Two air temperature sensors were utilized to measure the inlet and outlet air temperature. The energy input to the heaters and fans were measured by energy meters. Also, heat flux meters were put at the middle of each side of the tested sample to measure the heat flow rate. The sensor positions are shown in Fig.3 and the sensor accuracy is shown in Table 1

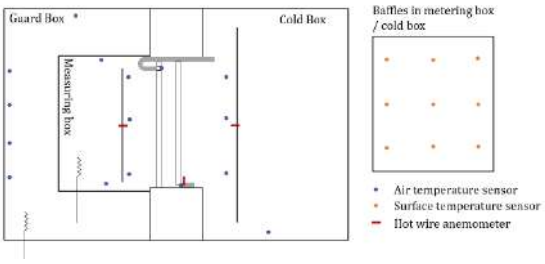

Fig.3 – Positions of sensors

Table. 1 Sensors for experiments

Sensors	*Accuracy of sensor*
PT100 temperature sensor	±0.1 °C
Energy meter	±1%
Heat flux meter	±3%
Hot wire anemometer	±3%

3.2 Calibration of guarded hot box

The metering box wall loss and flanking loss need to be calibrated before testing the supply-air double window. The sum of metering box wall loss and flanking loss can be calculated as

$$Q_{loss} = Q_{in} - Q_{XPS} \quad (5)$$

Where Q_{loss} is the sum of metering box wall loss and flanking loss, W; Q_{in} is the heat input into metering box; Q_{XPS} is the measured heat flow through the XPS plate placed in the sample frame.

The calibration tests were performed under four conditions, as shown in Table. 2. The velocity in hot side was kept at 0.1m/s and that in cold side was kept at 1.5 m/s. The air temperatures of metering box and guard box were set at 30 °C and that of cold box was varied from 1 to 15 °C.

Table. 2 Test conditions in calibration tests

No.	*Ta*-CB (°C)	*Ta*-MB (°C)	*Ta*-GB (°C)	*v*-MB (m/s)	*v*-CB (m/s)
1	1	30	30	0.1	1.5
2	5	30	30	0.1	1.5
3	10	30	30	0.1	1.5
4	15	30	30	0.1	1.5

(*Ta*-MB: air temperature in measuring box, °C; *Ta*-GB: air temperature in guard box, °C; *Ta*-CB: air temperature in cold box, °C; *v*-MB: air velocity in hot side, m/s; *v*-CB: air velocity in cold side, m/s)

The controllers shall keep air temperature fluctuations within 1% of the air temperature difference between cold and hot sides. Calculations of heat loss were done after all of the air temperatures were stabilized. Fig. 4 shows the correlation between the measured heat loss and air temperatrue difference.

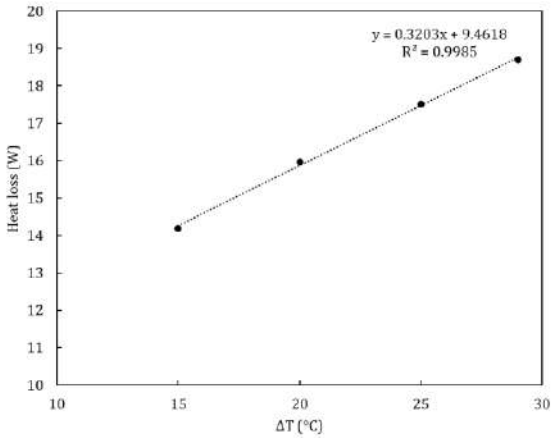

Fig.4 – Heat loss against temperature difference betwen cold and hot sides

As shown in Fig.4, the heat loss of guarded hot box has a positive linear correlation with the air temperature difference between cold and hot sides. This can be explained by the fact that the heat flow from metering box to cold box increases with increasing air temperature difference, leading to an increased heat loss.

3.3 Test configurations and test conditions

The tested window configuration is shown in Fig.5. It is composed of an inner single-glazed window (located in hot side) and an outer single-glazed window (located in cold side). The window frame is made of wood and the glazing is 4 mm clear glass. The air flow channel is 95 mm. The ventilation inlet is on the bottom of the outer window and the outlet is on the top of the inner window.

Fig.5 - Picture of the test configuration

Tests were carried out for the supply-air double window with different air flow rates and air temperature differences. As shown in Table 3, tests were performed under eleven test conditions. Calculations of *U*-values were done after all the air temperatures were stabilized.

Table. 3 Test conditions for the supply-air double window

No.	*Ta*-CB (°C)	*Ta*-MB (°C)	*Ta*-GB (°C)	$\dot{V}$ (l/s)	*v*-MB (m/s)	*v*-CB (m/s)
1	1	30	30	3	0.1	1.5
2	1	30	30	6	0.1	1.5
3	5	30	30	3	0.1	1.5
4	5	30	30	6	0.1	1.5
5	5	30	30	9	0.1	1.5
6	10	30	30	3	0.1	1.5
7	10	30	30	6	0.1	1.5
8	10	30	30	9	0.1	1.5
9	15	30	30	3	0.1	1.5
10	15	30	30	6	0.1	1.5
11	15	30	30	9	0.1	1.5

($\dot{V}$: air flow rate, l/s)

4. Results

In this section, the effects of air flow rate and air temperature difference on *U*-values of the tested supply-air double window are analysed. Also, the multi-linear linear regression model is used to learn the correlations between the *U*-values and influential factors (i.e., air flow rate and air temperature difference), and the expressions of dynamic *U*-values are given in this section.

(1) Effect of air flow rates on *U*-values

As shown in Fig.6, the trends of *U*-values against the air flow rate are the same under different air temperature differences (i.e., 15, 20 and 25 °C). In particular, the U_{loss} -value and U_{use} -value always increase with increasing the air flow rate from 3 l/s to 9 l/s. This is consistent with the fact that the heat transfer between the window surfaces and the

flowing air is enhanced when the air flow rate increases.

For the U_e-value, it also increases when the air flow rate increases from 3 l/s to 9 l/s, which indicates the increase rate of U_{loss}-value is higher that that of U_{use}-value.

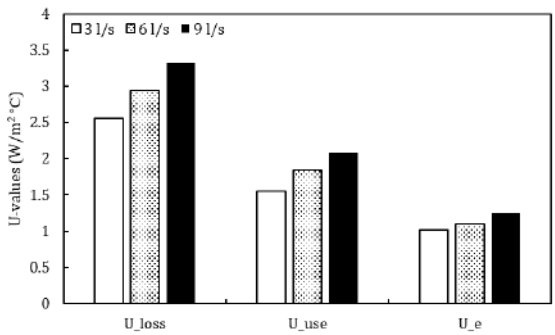

(a) ΔT= 15 °C

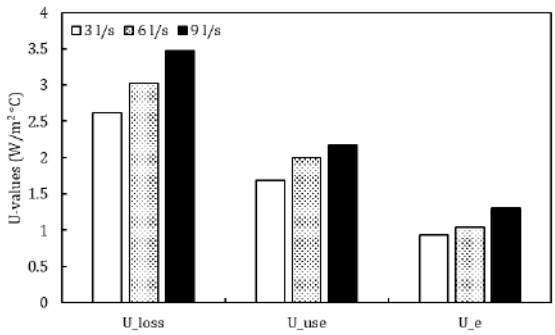

(b) ΔT= 20 °C

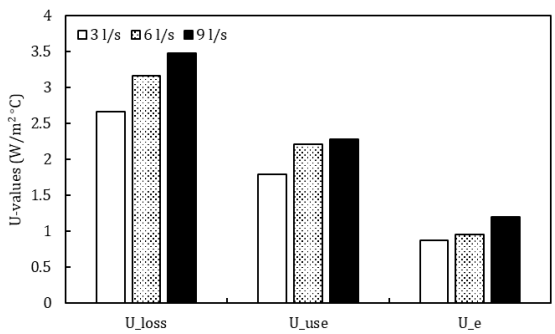

(c) ΔT= 25 °C

Fig.6 - *U*-values against air flow rates

(2) Effect of temperature difference on *U*-values

The U-values measured under different air temperature difference between cold and hot sides are shown in Fig.7. It can be observed that the effect of temperature difference on U-values is less significant than the effect of air flow rates on U-values. For the U_{use}-value, it increases by increasing the tempeatrue from 15 to 25 °C. A further increase in the U_{use}-value could be observed in the case with 6 l/s air flow rate when the air temperature difference further increases from 25 to 29 °C.

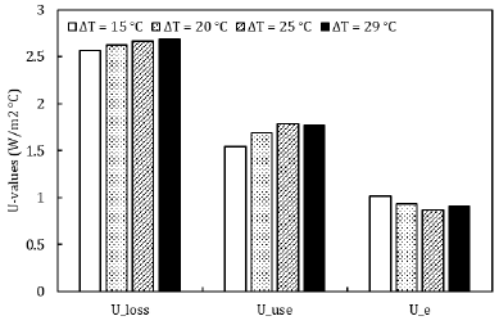

(a) $\dot{V}$ = 3 l/s

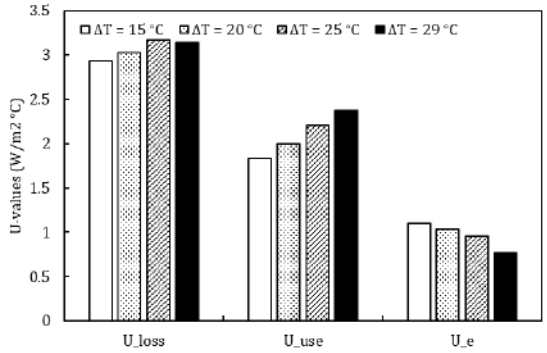

(b) $\dot{V}$ = 6 l/s

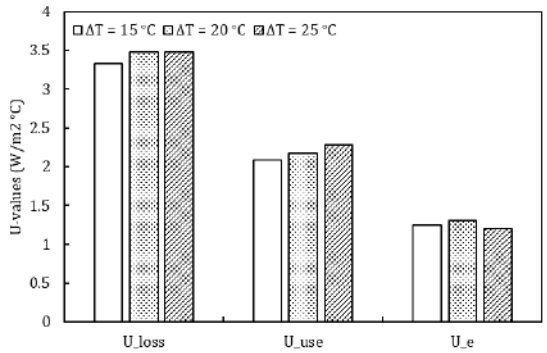

(c) $\dot{V}$ = 9 l/s

Fig.7 - *U*-values against air temperature difference between cold and hot sides

(3) Dynamic *U*-values

The multi-linear regression model [14] was adopted to get dynamic *U*-values. The expression of multi-linear regression equation is shown in Eq. (6), and the goal is to determine values of β coefficients.

$$U_i = \beta_{i,0} + \beta_{i,1}\dot{V} + \beta_{i,2}\Delta T \quad (6)$$

The equations of U_{loss}-value, U_{use}-value and U_e-value are shown in Eq. (7)-(9).

$$U_{loss} = 1.93116 + 0.13793\dot{V} + 0.01329\Delta T \quad (7)$$

$$U_{use} = 0.84398 + 0.09244\dot{V} + 0.02786\Delta T \quad (8)$$

$$U_e = 1.08719 + 0.0455\dot{V} - 0.01458\Delta T \quad (9)$$

5. Conclusions

In this study, experiments were performed in an adapted guarded hot box to measure U-values of supply-air windows.

From experimental results, it could be concluded that U-values are dependent on the air flow rate and air temperature difference between cold and hot sides. In particular, the U_{loss}-value, U_{use}-value and U_e-value are all increased when the air flow rate increases from 3 l/s to 9 l/s. The trends of U-values against the temperature difference are related with air flow rate. Furthermore, dynamic U-values are given in this study by using multi-linear regression model to learn the correlation betwen U-values and influential factors. Based on the given dynamic U-values, one can easily calculate window heat loss and recovered ventilation heat in real applications according to corresponding environment.

Acknowledgements

The authors would like to thank the Région Auvergne-Rhône-Alpes for its financial contributions. In addition, the authors would like to thank the CSC (China Scholarship Council) to provide financial support for the study in France.

References

[1] Coillot M, El Mankibi M, Cantin R. Heating, ventilating and cooling impacts of double windows on historic buildings in Mediterranean area. Energy Procedia. 2017;133:28–41.

[2] Carlos JS, Corvacho H, Silva PD, Castro-Gomes JP. Real climate experimental study of two double window systems with preheating of ventilation air. Energy and Buildings. 2010;42(6):928–34.

[3] Carlos JS, Corvacho H, Silva PD, Castro-Gomes JP. Heat recovery versus solar collection in a ventilated double window. Applied Thermal Engineering. 2012;37:258–66.

[4] Carlos JS, Corvacho H. Ventilated Double Window for the Preheating of the Ventilation Air Comparison of Its Performance in a Northern and a Southern European Climate. Journal of Renewable Energy. 2013;2013:1–11.

[5] International Standard. ISO 15099: Thermal performance of windows, doors and shading devices – Detailed calculations. 2003.

[6] Wright JL. Effective U-values and shading coefficients of preheat/supply air glazing systems. solar energy society of Canada. 1986;219–24.

[7] Carlos JS, Corvacho H. Evaluation of the performance indices of a ventilated double window through experimental and analytical procedures: Uw-values. Energy and Buildings. 2014;86:886–97.

[8] Baker PH, Mcevoy M. Test cell analysis of the use of a supply air window as a passive solar component. Solar Energy. 2000;69(2):113–30.

[9] Mcevoy M, Southall RG, Baker PH. Test cell evaluation of supply air windows to characterise their optimum performance and its verification by the use of modelling techniques. Energy and Buildings. 2003;35(10):1009–20.

[10] Southall RG, Mcevoy M. Investigations into the functioning of a supply air window in relation to solar energy as determined by experiment and simulation. Solar Energy. 2006;80(5):512–23.

[11] Mcevoy M, Southall R. Validation of a computational fluid dynamics simulation of a supply air'ventilated'window. CISBE Conference. 2000;

[12] Appelfeld D, Svendsen S. Experimental analysis of energy performance of a ventilated window for heat recovery under controlled conditions. Energy and Buildings. 2011;43(11):3200–7.

[13] International Standard. ISO 8990: Thermal insulation - determination of steady-state thermal transmission properties - calibrated and guarded hot box. 1994.

[14] Coillot M. Caractérisations numérique et expérimentale du comportement thermo-aéraulique d'une double-fenêtre active. Doctoral dissertation,Université de Lyon. 2019;

Data Statement

The datasets generated during and/or analysed during the current study are not available because they are proprietary and confidential in nature but the authors will make every reasonable effort to publish them in near future.

Sizing a collective heat pump system in an apartment building: impact of occupancy profiles

Matthias Criel [a], Maarten Sourbron [b], Hilde Breesch [c]

[a] Thermiek cvba, Wijgmaal, Belgium & Building Physics and Sustainable Design, Department of Civil Engineering, Ghent Technology Campus, KU Leuven, Ghent, Belgium, m.m.f.criel@student.tudelft.nl

[b] Thermiek cvba, Wijgmaal, Belgium, maarten@thermiek.be

[c] Building Physics and Sustainable Design, Department of Civil Engineering, Ghent Technology Campus, KU Leuven, Ghent, Belgium, hilde.breesch@kuleuven.be

Abstract.
Current sizing of collective heating systems utilizes conservative methods to size the capacity of the heat production unit, which results in an over sizing of the system. When collective heat pumps (CHP) are considered, an exact sizing would increase their competitiveness on the market. Residential user patterns are often not considered in the sizing strategy, neither is the simultaneity between central heating and domestic hot water (DHW) demand. This paper aims to identify the impact of occupancy patterns on sizing of a collective heat pump in an apartment building. The use of an occupancy-based heat and DHW demand model opens the possibility to reach a more appropriate sizing of the collective heat pump. This occupancy-driven model includes time dependant occupancy, temperature set points and DHW consumption. The impact of the occupancy patterns is analysed by building energy simulations (BES) in Open Studio for a case study apartment building in Belgium. A collective heat pump (CHP) system is considered where the link between consumption (building) and production (CHP) is made through a buffer tank. The production of DHW is individually supported by booster heat pumps heating up a small buffer tank. The simulation results illustrate that only 42% of the summed design capacity for heating and DHW is required to cope with the heat demand. It can be concluded that there is a significant impact of the occupancy profiles on the sizing of the collective heat pump system in this case study.

Keywords. Collective heat pump system, occupancy patterns, sizing
DOI: https://doi.org/10.34641/clima.2022.269

1. Introduction

The European Green Deal focuses on 7 different topics to create a closed carbon cycle and utilizing the potential of increasing energy efficiency. One topic focusses on a reduction of the energy demand of buildings in order to reach net zero greenhouse gas (GHG) emissions in 2050 [1]. The implementation of collective heat pump (CHP) systems can contribute to reach this goal. A CHP produces heat for a collective low temperature heating system supplying central heating (CH) for several units, e.g., flats in an apartment building. Individual domestic hot water (DHW) can be produced by so-called booster heat pumps (BHP) in the apartments. These BHPs use the low-temperature heating system as a heat source to produce high-temperature hot water in a storage tank. This type of system is considered in this paper and is schematically presented in Figure 2. This system layout avoids high-temperature distribution circuits throughout the building to supply the hot water demand, and the subsequent distribution losses. However, it comes with an increased investment cost due to the individual booster heat pumps. Therefore, a better sizing of the central heat demand in apartment buildings is essential to reduce this increased investment cost and make the system competitive on the market. Second, an exact heat demand determination implies a better sized central heat pump, which will result in a smoother operation (less on-off behaviour). This on its turn results in an increased energy efficient heat pump operation.

In the sizing procedure, DHW is more and more important as this capacity is no longer small compared to the required heating capacity. After all, the latter has decreased significantly during recent years because of stricter insulation requirements. Currently, there are 3 demand sizing methods that

Copyright ©2022 by the authors. This conference paper is published under a CC-BY-4.0 license.

take CH and DHW into account: (1) the total summation, (2) the maximum method, and (3) 3 hybrid solutions. The first method, i.e., full summation, is defined as the total sum of the total CH capacity and total DHW capacity. Second, the maximum method takes the maximum of the total CH capacity and total DHW capacity into account. An extra 20% is added in actual sizing when using this method because of a fear of under sizing the system [2].

Moreover, the hybrid solutions are divided based on the type of individual DHW system per apartment with the CHP as its source. For a plate heat exchanger, a summation of both capacities is applied and a diversity factor (f_{sub}) should be added on the total DHW capacity. This diversity factor describes the ratio of the maximum CHP demand to the coincident maximum CHP demand of the whole system. For collective substations, the maximum method is used but for the CH: an extra 1 kW per apartment is added and an extra 5% is applied to the total CH capacity. For the DHW, a diversity factor (f_{sub}) is applied based on the total number of substations. For both cases, the diversity factor (in decimals) decreases with increasing number of apartments.

The methods mentioned in the previous paragraph cannot integrate developments and new insights for CH and DHW determination in their calculation. The DeltaQ method [2] is based on 2 standards: DIN4708 and EN12831 [3] and uses a combination of the full summation and the maximum method. As long the DHW capacity is larger than the CH capacity, only the DHW is considered. If the number of apartments increases and the CH capacity exceeds the DHW's, a full summation is implemented. The same problem of oversizing occurs when the number of apartments increases [2]. Verhaert [2] suggested a method called "the maximum sum of parts" to be used. The collective capacity is a function of the CH- and DHW-function, which results in a sizing in between the full summation and the maximum method. The total collective capacity lies around 20% above the maximum method. This should limit the oversizing of the system. Van Minnebruggen [4] worked on this problem and tried to verify this method.

These current sizing methods do not consider the residential user patterns, which define at which time CH and DHW is demanded and how CH and DHW demand contributes to the collective demanded capacity. By neglecting this, it is unknown whether the sized capacity would be sufficient for a certain building by which a safety factor is often introduced to avoid undersized systems. These user patterns give the opportunity to avoid over and under sizing.

This paper aims to identify the impact of occupancy patterns on sizing of a collective heat pump in an apartment building. This is based on the master thesis of Criel [5] and is structured as follows.

Section 2 describes the most important definitions used in this paper. Section 3 gives a description of the case study building and collective system. Section 4 describes the different steps taken for creating a feasible sizing method for a CHP. This is divided in 3 parts: building and system modelling, the usage profiles and interpretation of the results. Section 5 discusses the results of the simulations and ends with the feasible sizing method of the collective heat pump in the case study apartment building, which is followed by conclusions in Section 6.

2. Definitions

Collective heat pump (CHP) system: This is a collective low temperature heating system supplying central heating using a central heat pump.

Booster heat pump: small heat pump connected to a hot water storage tank in one housing, located in the separate apartments. The heat source is the central heating system.

Diversity factor: ratio of the maximum central peak demand to the sum of individual peak loads.

Residential user patterns/profile: defines the times at which the user demands DHW and/ or CH.

Occupancy profile: the times at which a user is active, inactive or absent. Based on this profile, residential user patterns are extracted.

3. Case study of building and system

The studied case (Figure 1) is a newly built apartment building in Ghent (Belgium). The building contains 4 floors with a total of 31 three persons apartments with each a floor area of about 80m^2.

Table 1 shows the heat transfer coefficient of the walls. The shared floors and walls describe the boundaries between apartments. The window to wall ratio equals 0.19 and the airtightness (v_{50}) equals 5 m^3/h.m^2.

A balanced mechanical ventilation system is implemented. The total airflow per apartment is equal to 175 m^3/h, which is distributed over the different zones in an apartment.

The examined system of the apartment building is presented in Figure 2. In the building, the CHP extracts heat from the ground. It produces water at low temperature to a buffer tank (not shown in Figure 2 however) from where the different distribution circuits leave to provide heat to the underfloor heating of the different apartments. The DHW is provided by a booster heat pump, which uses the heating system as its heat source. This produced DHW is collected in a 180l storage tank for every apartment. The advantages of this CHP system are the lower distribution losses (no high temperature distribution for the DHW is required).

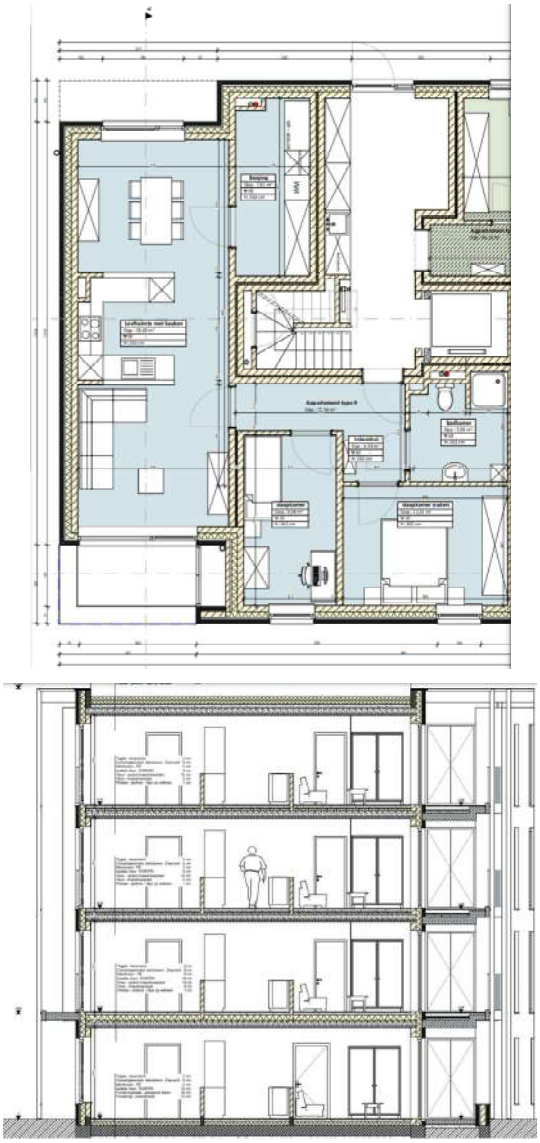

Figure 1: Floor plan of 1 apartment (above) and cross section of the building (below)

Table 1: Heat transfer coefficients U of the walls of the apartment building

Wall type	U (W/m^2K)
External walls	0.14
Floor	0.16
Shared floors	0.53
Roof	0.15
Shared walls	0.4
Internal walls	1.4
Internal doors	2.3
Windows	1.12

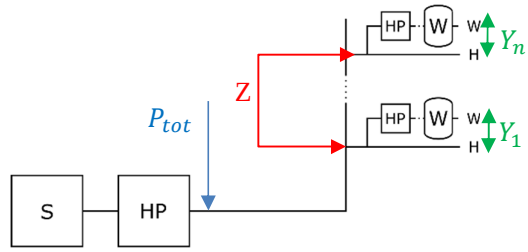

Figure 2: Schematic drawing of the CHP-system

The schematic drawing in Figure 2 presents the CHP-system where every apartment has underfloor heating (H) and a booster heat pump with storage tank (HP+W). S is the environmental heat source (ground in this case), HP in the bottom is the CHP. Z and Y indicate the two locations in the system where simultaneity is considered: between heating and DHW demand (Y_i), and between the demand of the individual apartments (Z) (and therefore influenced by the occupancy profiles. P_{tot} is the calculated total capacity.

It is important to notice that this paper investigates how the total capacity P_{tot} is influenced by the user occupancy profiles. Therefore, the CHP, nor its buffer tank is considered in the rest of this paper.

The CHP provides water at 35°C (low temperature level) for CH and in the booster heat pump the hot water is produced at 65°C. The booster heat pump provides this transition from 35°C (heating circuit) to 65 °C with an assumed COP of 5.

The heat loss of 1 apartment is calculated according to the standard NBN EN12831:2003 and the user guide of BBRI [6]. The steady state heat capacity is equal to 2032W and if the heating up capacity is considered, the required heat is equal to 4000W. For the entire building, a steady state heat capacity of 63 kW and a capacity of 124 kW is considered if temperature drops are considered.

For the capacity of DHW, 2000W is assumed, corresponding to the designed capacity in this project. This is the capacity the booster heat pump can deliver (see Figure 2). A COP of 5 is assumed, which results in 1600 W that is supplied by the CHP and the rest is supplied by electricity. The temperature of the produced water equals 65 °C and is stored in the tank.

4. Method

4.1 Building and system modelling

Building energy simulations (BES) are executed in OpenStudio [7] , which uses Energy+ as calculation software, to determine the impact of occupancy on the capacity of the collective heat pump system.

In the following paragraphs, different modelling assumptions are made. Only 1 apartment is modelled and extrapolated afterwards, as the difference in CH requirements between apartments is negligible

because the apartments are similar in size. Second, strict insulation and airtightness requirements causes that differences between DHW and CH demand per apartment only depends on the user profile (demand). A conservative approach is chosen by considering an apartment on the ground floor (larger heat loss compared to second and third floor) with 3 external walls (see Figure 1).

In Figure 3, the apartment is split up in 3 different thermal zones depending on the use and temperature set point: a day-time zone, a night-time zone, and the bathroom. The characteristics of these zones are described in Table 2. These zones are connected to each other via designed ventilation system that includes supply in the day and night-time zone and extract in the bathroom and day-time zone. The temperature set points in Table 2 are based on NBN EN12383-1:2017 [8].

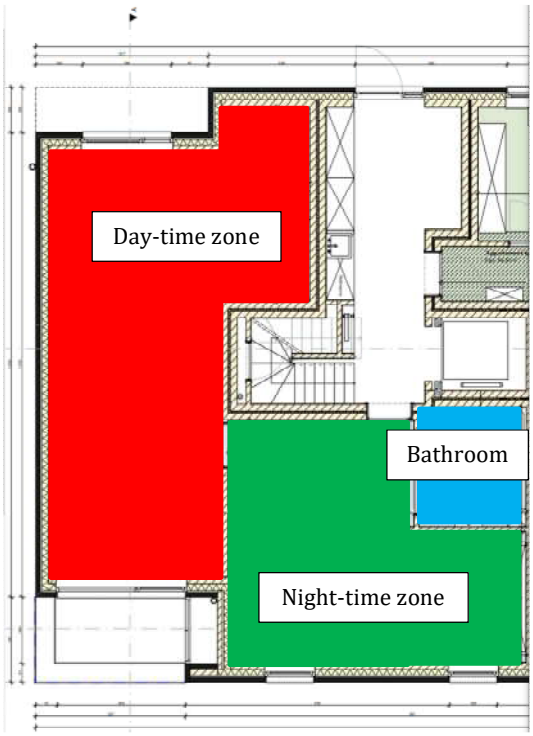

Figure 3: Thermal zoning of the apartment

Table 2: Characteristics of thermal zones

	Zones		
	Day-time zone	Night-time zone	Bathroom
Floor area (m^2)	41	27	6
Temperature (°C)	20	18	22
Ventilation airflow (m^3/h)	75	50	50

4.2. Usage profiles

The implementation of usage profiles, an outside temperature profile and solar irradiation gives the model its dynamic properties by which it differentiates itself from static calculations [6].

When implementing usage profiles, it is required to envelop the entire population. To incorporate the population, the occupancy profiles are based on the models of Buttitta et al. [9]. From these occupancy profiles, the usage profiles can be defined. Buttitta et al. [9] created a model dividing the households in the UK into 5 standard cases describing the hours of the day that the residential users are absent, active, or not active, as shown on Figure 4. For example, occupancy profile 1 has an "absent character" while occupancy profile 4 and 5 have an "active character". The fractional division of the households into these profiles is shown in Table 3.

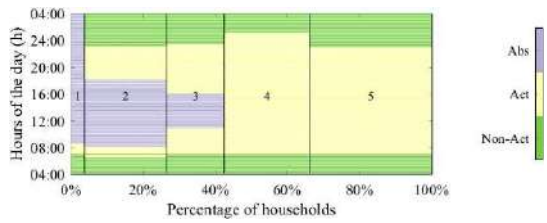

Figure 4: The division in 5 occupancy profiles. Abs means absent, Act means active and Non-Act means not active [9]

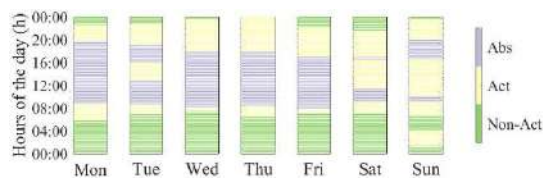

Figure 5: Refined occupancy profile n°2. Abs means absent, Act means active and Non-Act means non-active [10]

This division is used to determine the usage profiles of the 31 flats in the apartment building in Table 3 in 3 different ways. The first division of occupancy profiles over the various flats is based on the fractions proposed by Buttitta et al. [9] and is referred as (N) in this work: 11 flats have an occupancy profile n°5, while only 1 flat has the occupancy profile n°1. The 2 other divisions are extreme distributions, characterised by users with an extreme absent (i.e., only user profile n°1 and 2) (L) or extreme active character (i.e., only occupancy profile n°4 and 5) (Z).

Buttitta et al. [10] refined these profiles to weekly occupancy profiles, as shown in Figure 5 for occupancy profile n°2.

Table 3: Division of the different users over the 31 apartments for the 3 different occupancy distributions. Each type of user gets assigned a certain amount of apartments described by the table

Type of user profile	Fractional division of the population	Division for Buttitta et all. [9] [N]	Division with absent character [L]	Division with active character [Z]
USER1	3.7%	1	4	-
USER2	22.9%	7	27	-
USER3	15.9%	5	-	-
USER4	23.7%	7	-	13
USER5	33.8%	11	-	18

Based on these occupancy profiles, 5 different usage profiles are made for the 3 different thermal zones as follows. During the time that the user is active (Act), the day-time zone is heated up to its set point (see Table 2). Based on the SHW peak consumptions described by Fuentes et al. [11], the bathroom is heated between 6h-9h and 18h-21h for all users unless users are absent (Abs). If users are non-active (Non-Act), the night-time zone is heated up to the set point. When the users are absent (Abs), the set point in all zones is set to 16 °C.

The DHW profile of Fuentes et al. [11] is implemented in this model. The average use of DHW is 45 l/day/person of which 70% is attributed to the bathroom zone. The DHW tapped in bathroom area is fixed at 40 °C while the rest of the consumption in de day-time zone is fixed at 60 °C. The occupancy profile is than matched with the DHW profile, where no DHW is consumed if the users are Abs.

The result is a unique CH and SHW profile for the 5 standard users. An example of the CHP profile for user profile n°2 on Wednesday is shown in Figure 6. These combined profiles are for further reference defined as "usage profiles".

4.3. Determination of the equivalent diversity factor

Figure 2 defines diversity factors Y and Z. Diversity factor Z (%) represents the difference in energy demand between the different apartments, which originates from different types of users in a building. Second, per apartment the CH- and DHW- energy demand do not coincide for the different timesteps, which is represented by factor Y (%). A difference in time occurs when a user demands CH or DHW.

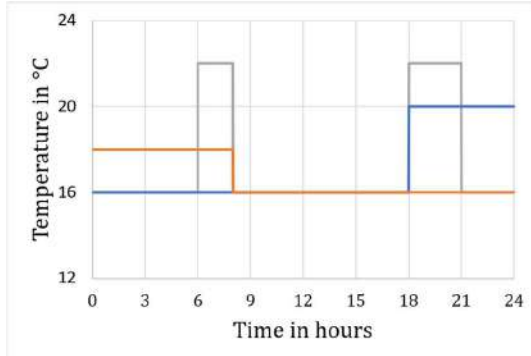

Figure 6: The requested temperature profile (CH) of n°2 on Wednesday. The grey line represents the bathroom profile, the orange line represents the night-time profile and the blue line represents the day-time profile.

The total capacity (P_{total}) is the minimal capacity that must be delivered by the CHP to provide the different apartments with their individual CH and DHW demands. The sizing problem is than translated to a mathematical expression, which is used to calculate the P_{total}:

$$P_{total} = (\sum_{i}^{N} (P_{CH_i} + P_{DHW_i}) \times Y_i) \times Z \,;\, 0 \leq Y_i, Z \leq 1;$$

Where P_{Chi} and P_{DHWi} are the CH and DHW capacity per apartment respectively and N is the total amount of apartments. Y is the diversity factor between CH and DHW per apartment and Z is the diversity factor between the different apartments.

A simplification of the formula is possible if Y, Z are replaced by an equivalent diversity factor X:

$$P_{total} = (\sum_{i}^{N} (P_{CH_i} + P_{DHW_i})) \times X \,;\, 0 \leq X \leq 1$$

If the value of X is calculated, a solution for the problem has been found and the capacity of the CHP is determined.

The result of these simulations is the capacity of the CHP system as a function of time. Based on this dynamic behaviour, it is assumed to size the system on 97.5% of the maximum value. After this point, the rise in sizing capacity is not justified compared to the rise in time the requested capacity is met. Based on this 97.5%, the value of the equivalent diversity factor X is determined.

5. Results

5.1. Capacity curves of CHP

Figure 7 shows the delivered capacity of the collective system over 1 week in January for occupancy distribution N. In function of time, a central capacity is deliverd by the CHP.

When assuming the occupancy distribution N according to Buttitta [10], the total delivered capacity is almost always different from zero (only during 12 hours, no heat is supplied during the week in Figure 7). The delivered capacity with a maximum value of 150 kW, is always smaller than a total sumation sizing method, i.e; 173.6 kW. Second, only during 16h of the year more than 80% of this summation is required. Furthermore, the maximum of 174 kW is never requested. This can be found in

Table 4. If usage profiles L and Z are implemented, similar results are reached. For L, a peaked trend is observed: 72h of the year more than 80% of a total summation is required and only during 3h a total summation is required. For Z, the trend lies between N and L where during 37h more than 80% is delivered and only 11h the maximum of 173.6 kW is requested.

Table 4: The first row descibes the number of hours where 80% of the maximum capacity is exceeded for the different occupancy distributions. The second row describes the number of hours where the maximum capacity is required.

	Occupancy distribution		
Time capacity is	N	L	Z
> 0.8 × 174 kW	16h	72h	37h
= 174 kW	0h	3h	11h

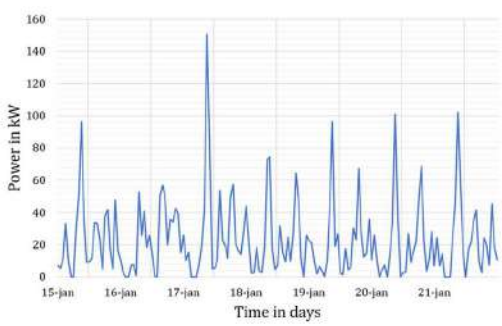

Figure 7: Delivered capacity (in kW) of collective systems for the 3rd week of January with N as occupancy distribution

A comparison to the heat loss calculation (NBN EN 12831:2003) is possible if the total capacity is seperated in a SHW- and CH-part (see Figure 8). During this week, only during 2 hours the steady state heat loss calculation capacity (2032W per apartment) is exceeded and the heating up capacity (4000W per apartment) is not reached during this week.

An annual analysis has also been made. The hours when the steady state heat capacity (required capacity in absence of temperature drop [6]) is exceeded or the heating up capacity (required capacity with including temperature drop [6]) is reached, are shown in Table 5. For the occupancy distribution N, there is a negligible number of hours observed where the heating up capacity is reached. Altough the steady state heat capacity is exceeded several times, the value reamains small compared to the other occupancy distributions. Occupancy distribution L has the most extreme profile because during 432h the steady state loss is exceeded, but even here the absolute maximum is not reached on a regular basis.

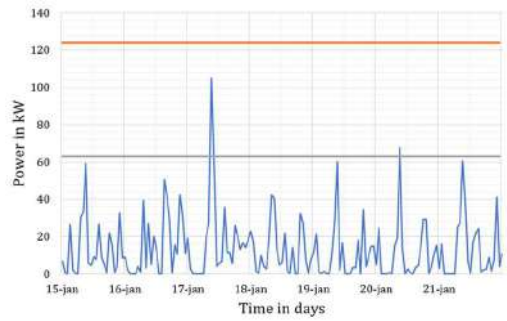

Figure 8: Comparison heat loss calculation and deliverd CH capacity by CHP for the 3rd week of January with N as occupancy distribution. The orange line represents the heat loss calculation including the heating up loss. The grey line represents the steady state heat loss.

A similar type of analysis is done for the DHW. The hours when the full sanitairy capacity is reached, is described in Table 5. The duration that the maximum capacity is supplied for occupancy distribution N is 50% smaller than L and 83% smaller than Z. This implies that distribution N supplies a negligible amount of times the full sanitairy capacity. In this case, occupancy distribution Z is the most extreme due to the residents being present in the apartment for large fractions of the day. Nevertheless, 154 h is still a small fraction of the entire year.

Table 5: The number of hours the steady state heat loss capacity is exceeded (required capacity exclusion of temperature drop) and the number of hours the heating up capacity is reached (required capacity including of temperature drop)

	Occupancy distribution		
	N	L	Z
Steady state heat capacity	89h	432h	221h
Heating up capacity	1h	18h	15h
Sanitary capacity	26h	52h	154h

5.2. Diversity factors

Figure 9 shows the cumulative distribution of the capacity as a functon of the diversity factor for all three occupancy distributions. These functions describe the frequency that a capacity equal or smaller than a chosen delivered capacity occurs. For example, 52 kW of the central capacity (diversity factor of 30 percent), satisfies demand during 94 % of the time for N, 87,4 % for L and 90.4 % for Z.

The different distributions are fairly similar, which would imply the diversity factors are similar in size. Nevertheless, large differences occur at the upper part of the different graphs (above 90 % occurrence for the different occupancy distributions). To obtain energy security throughout the year, the capacity of the CHP should be able to supply the requested heat almost all the time. Occupancy distribution N reaches around 90% coverage at 43 kW (diversity factor of 0.25), while 69 kW (diversity factor of 0.4) is required for L to obtain the same coverage. This means the occupancy distribution has a large influence on the final result (diversity factor) and occupancy profile L is less stable and hard to size the CHP on.

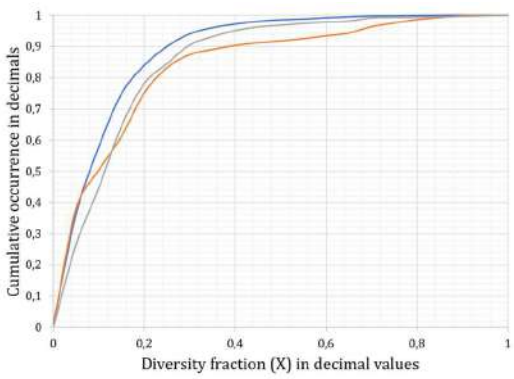

Figure 9: Cumulative distribution of the total capacity output of CHP for different occupancy distributions during 1 year. The blue lines describes the distribution for N, the grey line describes the distribution for L and the grey line describes the distribution for Z.

Based on section 4.3, the diversity factor is determined for the various occupancy distributions as shown in Table 6. As explained before, the diversity factor of N is based on the study of Buttitta et al. [10] and describes the presumed reality, while the other two profiles describe extreme cases. Second, the occupancy distribution N locates itself in an optimum. When a deviation occurs from the presumed reality to users with a more active charater, the diversity factor should rise for the same coverage. The same trend occurs for users with an absent character.

As already mentioned, it is observed that the sizing for occupancy distribution N finds itself in an optimum. A difference of 58.6 kW is observed with L (rise of 78%) and a difference of 25.3 kW with Z (rise of 34%).

This implies an increase in diversity factor occurs to cope with the peaked profile. Occupancy distribution Z has a profile that is more extreme than N but remains quite average. An increase in diversity factor should occur but this increase should be limited compared to the occupancy distribution L.

Table 6: Resulting diversity factors X for different occupancy distributions at 97,5% coverage

	Occupancy distribution		
	N	L	Z
Diversity factor (%)	42	74.9	56.2

5.3. Comparison with existing methods

If a comparison of the diversity factor method is made with the current sizing methods, the differences are noticed to be signficant as shown on Figure 10. If the current sizing methods are compared to the a diversity fraction of 42% (N), the following results are noticed: a reduction of 98.7 kW (56.9%) occurs compared to the total summation, a reduction of 49.1 kW (39.6%) occurs compared to the maximum method and a reduction of 87.9 kW (54%) occurs compared to the hybrid solution.

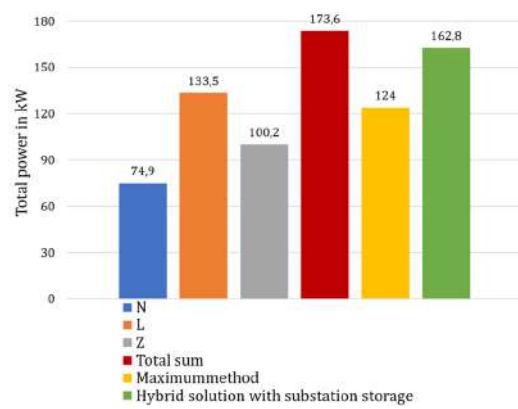

Figure 10: Comparison of total capacity of CHP sizing

6. Conclusions

This paper aimed to identify the impact of occupancy patterns on sizing of a collective heat pump in an apartment building.

To solve the formula described in section 4.3, 3 different occupancy distributions were created where every user in an apartment had its own type of CH and DHW consumption. These occupancy distributions were applied to an actual case in Ghent.

A diversity factor of 42 % (N) is chosen to be the result of the formula from section 4.3, because it is the only occupancy distribution with a theoretical background is from Buttatti et al. [10]. The rest are extreme cases which describe deviations where the diversity factor could evolve to. This implies that the main limitation of the result is the size of the apartment building. It should be large enough (greater than 24 apartments) to apply a diversity factor of 42 %. In this way, every type of user gets

assigned at least 1 apartment. Moreover, different usage profiles and occupancy distributions give specific results. More research is required to develop better general applicable and accepted profiles and distributions.

From the BES simulations in a case study apartment building, it can be concluded that the occupancy distributions have a large effect on the required capacity (diversity factor). This can be noticed if the differences between N and L/ Z are observed. A difference of 25.3 kW (33,8 %) occurs compared to Z or 58.6 kW (78,2 %) occurs compared to L could occur compared to the optimal value.

If the different methods on the market are compared to the diversity factor of 42 %, they seem too conservative. This implies new methods should give more specific results.

Data access statement

The datasets generated during and analysed during the current study are not available but the authors will make every reasonable effort to publish them in near future.

References

[1] European Union, "Going climate-neutral by 2050," 16 07 2019. [Online]. Available: https://op.europa.eu/en/publication-detail/-/publication/92f6d5bc-76bc-11e9-9f05-01aa75ed71a1. [Accessed 2021 12 14].

[2] I. Verhaert, "Design methodology for combined production and distribution," *E3S Web of Conferences,* vol. 111, 2019.

[3] Vlaamse overheid, "Transmissie referentiedocument," *Belgische staatsblad,* pp. 1-88, 29 Oktober 2007.

[4] S. Van Minnebruggen, "Analyse meetdata combilus: Validatie van een dimensioneringsmethode," Universiteit Antwerpen, Antwerpen, 2020.

[5] M. Criel, M. Sourbron, H. Breesch and B. Merema, "Dimensionering van een collective warmtepompinstallatie in een appartementsgebouw: Impact van gebruikersgedrag," Catholic University of Leuven, Sint-Katelijne-Waver, 2021.

[6] WTCB, "Warmtebelasting van gebouwen," WTCB, 25 August 2021. [Online]. Available: https://www.wtcb.be/expertise-ondersteuning/wtcb-tools/warmtebelasting-van-gebouwen/.

[7] Alliance for Sustainable Energy, "OpenStudio," National Laboratory of the US, 05 11 2021. [Online]. Available: https://openstudio.net/.

[8] European Committee for Standardization, "Energy performance of buildings - Method for calculation of the design heat load - Part 1: Space heating load, Module M3-3," European Committee for Standarization, Brussels, 2017.

[9] G. Buttitta, W. J. Turner, O. Neu and D. P. Finn, "Development of occupancy-integrated archetypes: Use of data mining clustering techniques to embed occupant behaviour profiles in archetypes," *Energy and Buildings,* vol. 198, pp. 84-99, 2019.

[10] G. Buttitta and D. P. Finn, "A high-temporal resolution residential building occupancy model to generate high-temporal resolution heating load profiles of occupancy-integrated archetypes," *Energy and Building,* vol. 206, no. 109577, 2020.

[11] E. Fuentes, L. Arce and J. Salom, "A review of domestic hot water consumption profiles for application insystems and buildings energy performance analysis," *Renewable and Sustainable Energy Reviews,* vol. 81, pp. 1530-1547, 2018.

[12] Koninklijke vereniging van de verwarmingsventilatie- en klimaatbeheersingstechniek, «Praktijkgids voor de berekening van de warmteverliezen van gebouwen,» 04 08 2016.

[13] Wienerberger, «Thermobrick 15N,» Wienerberger, 2020. [Online]. Available: https://www.wienerberger.be/Binnenmuur/productzoeker/thermobrick-15n.html.

[14] WTCB, «Luchtdichtheid van gebouwen,» *TECHNISCHE VOORLICHTING,* vol. 255, pp. 19-24, 2015.

[15] Itho Daalderop, "Booster warmtepomp 2 kW W/W WP tapwater," 1 4 2021. [Online]. Available: https://www.ithodaalderop.nl/nl-NL/professional/product/576-0020#downloads. [Accessed 1 4 2021].

Impact of integration of electric and gas heat pumps on the final energy consumption of Belgian residential building stock

Essam Elnagar [a], Camila Davila [a], Vincent Lemort [a]

[a] Thermodynamics Laboratory, Aerospace and Mechanical Engineering Department, Faculty of Applied Sciences, Université de Liège, Belgium, essam.elnagar@uliege.be

Abstract. The paper investigates the evolution of electricity-driven and gas-driven heat pumps technologies used for heating in the residential building stock in Belgium in the market. A base and predictive scenarios are considered. The base scenario includes the current share of the existing heat pumps in the Belgian market while the predictive scenario considers the increased share of the studied heating systems based on the evolution of the buildings envelope over the period 2020-2050. Two different types of heat pumps are considered, one driven by electricity which performance indicators are based on the literature, while experimental data is used for natural gas-driven heat pumps. The latter is modeled in an empirical way based on the system operating conditions and weather data. This paper presents the entire housing stock in Belgium which is divided in 752 cases. A tree structure model defining Belgian housing typology was created, characterizing Belgian residential building stock in terms of various parameters like building age, scale, level of insulation and energy vectors. A weighting factor to represent their occurrence in the existing Belgian building stock is associated to each building type. To study the impact on the load profile and the final energy consumption, the penetration of the selected heat pumps is calculated through the base and predictive scenarios. The penetration rates obtained of 67.6% and 42.7% for electricity and gas-driven HPs respectively, will allow to carry out some production planning for energy suppliers, manufacturers, and policymakers. Finally, the evolution of the sizing criteria in the future will have an impact on the penetration rates of the studied systems and must not be neglected.

Keywords. energy consumption, heating demand, heat pumps, residential buildings
DOI: https://doi.org/10.34641/clima.2022.102

1. Introduction

Buildings in the EU account for 40% of our energy consumption and 36% of our greenhouse gas emissions [1]. European countries are developing strategies to reduce energy consumption in buildings and the associated CO_2 emissions [2]. In long-term scenarios, energy use is very important to be taken into account, particularly in the residential sector, by looking at energy end uses, which gives a better understanding of the evolution of energy use and the possible impacts and adaptation of climate change on energy use. In most European countries, the amount of energy required for heating is greater by far than the energy used for space cooling [3]. Climate change has drawn great attention in recent years because of its large impact on many aspects of building energy use [4,5]. In Belgium, the residential energy needs for space heating and domestic hot water are mainly met by fuel oil, gas or electricity supplied by the grid. The present research aims at assessing the impact of contrasting penetration scenarios of technologies such as heat pumps.

In Belgium, gas boilers have been for years the most common heating device used due to an extensive gas network available and the relatively low gas prices. Year after year, the European Energy Performance of Buildings Directive (EPBD) imposes more demanding targets, increasing heat pumps installations since it has become more and more difficult to achieve the requirements without using renewable technologies [6].

The benefits associated with these technologies are not only energetic but also environmental. A study by Famiglietti, et al. [7] shows that the impact over the entire life cycle of a Gas Absorption Heat Pump (GAHP) offers a lower environmental impact compared to a traditional boiler mainly because of the lower amount of natural gas (NG) needed in the use phase, representing an average reduction of 27% of $CO_{2\,eq}$ and a reduction of 25% of fossil resource consumption.

Even if the heat pump market share in Belgium remains low (around 10% in 2014), this group of

Copyright ©2022 by the authors. This conference paper is published under a CC-BY-4.0 license.

technologies has been growing steadily since 2013. Just in 2018, the market increased by almost 10% compared to 2017 [8], a trend that would continue in the coming years. Even though most of the statistics point to electric heat pumps, the high electricity prices are opening the market to alternative technologies such as thermally driven heat pumps, making them well suited not only for new buildings but also for the existing ones since they can heat water to high temperatures in a very efficient way offering substantial cost and energy savings thanks to the involved technologies [9].

The aim of this paper is to assess the impact of heat pumps evolution in different scenarios (Electricity-driven heat pumps) and (Gas-driven heat pumps) on the annual consumptions of the residential building stock as well as the impact on the CO_2 emissions. In addition to that, A business-as-Usual Scenario (BAU) is investigated up to the horizons 2030 and 2050 by considering the construction, demolition and renovation rates of the buildings. The Energy simulations are conducted with MATLAB.

2. Methodology

The methodology used in this paper is based on the modeling of the energy end-use consumptions. This study uses a forward method for building energy use with a physical description of various parameters (e.g., building geometry, location, characteristics and operating schedules). According to ASHRAE, the forward method is more suited for improvements due to it higher level of details, compared to the data-driven method [10].
This paper also used an updated model of the tree structure model representing the Belgian residential building stock developed by Gendebien et. al [11].

2.1 Building Stock (Base Scenario-up to 2012)

The Belgian building stock tree structure is based on a hybrid approach (mix between typical and representative approaches). In the typical approach, a set of typical buildings closely related to the existing buildings are chosen, while a set of fictional buildings based on average values are selected in the representative approach. As shown in Fig. 1, the final tree structure of the base scenario is based on different parameters:

1. Building type (freestanding, semi-detached, terraced and apartment).
2. Year of construction (<1945, 1946-1970, 1971-1990, 1991-2007 and 2008-2012)
3. Insulation level for the building envelope (wall, window, roof and floor).
4. Space heating "SH" (fuel oil, NG, electricity and others (coal, wood,…)).
5. Heating production system (centralized, decentralized).
6. Domestic Hot Water "DHW" (fuel oil, NG, electricity and others (coal, wood,…)).

The final tree structure presents 752 cases representing the whole Belgian building stock till 2012, each case is characterized by the aforementioned parameters.

The simplified building model of a zone is based on the simple hourly method described in ISO13790-2007 [12]. The method is based on the thermal-electrical analogy between the analyzed thermal zone and the equivalent 5R-1C (5 resistances and 1 capacity). The thermal-electrical network is characterized by temperature nodes (θ), thermal resistances (1/H), heat fluxes (Φ) and a capacity (C_m) [13]. The 5 resistances in the network are used to describe the heat transfers coefficients, while the thermal mass is represented by a single thermal capacity C_m.

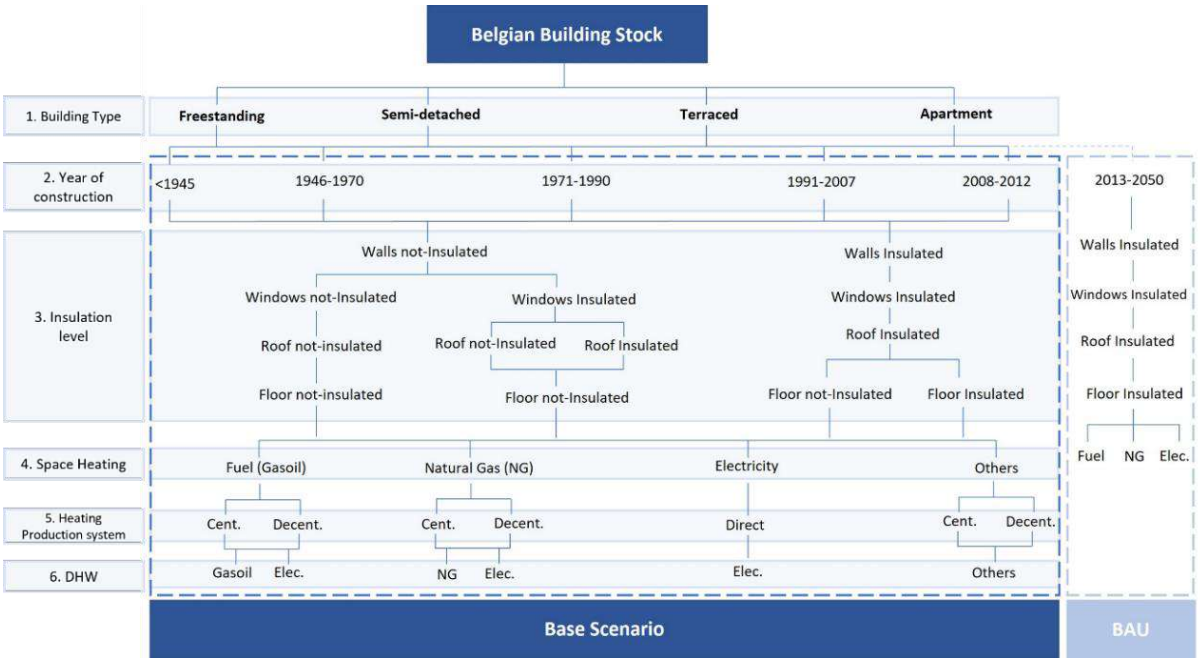

Fig. 1 - Belgian building stock tree structure

Fig. 2 (a) shows the distribution of Belgian dwelling types for the base scenario, it can be seen that the freestanding houses have the highest share by 29.2%. Fig. 2 (b) also presents the energy mix of the different energy sources used for SH; the SH energy needs are mainly met by NG and liquid fuels for boilers by 50.14% and 40.02% respectively, while the electricity and other energy sources represent the lowest distribution.

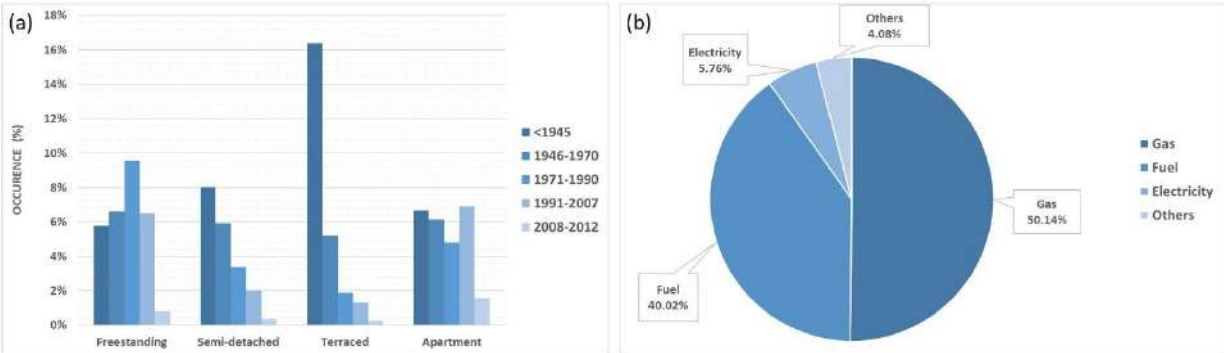

Fig. 2 - Base scenario (up to 2012) (a) Distribution of the Belgian dwelling types differentiating the five construction periods (b) Distribution of energy sources used for SH.

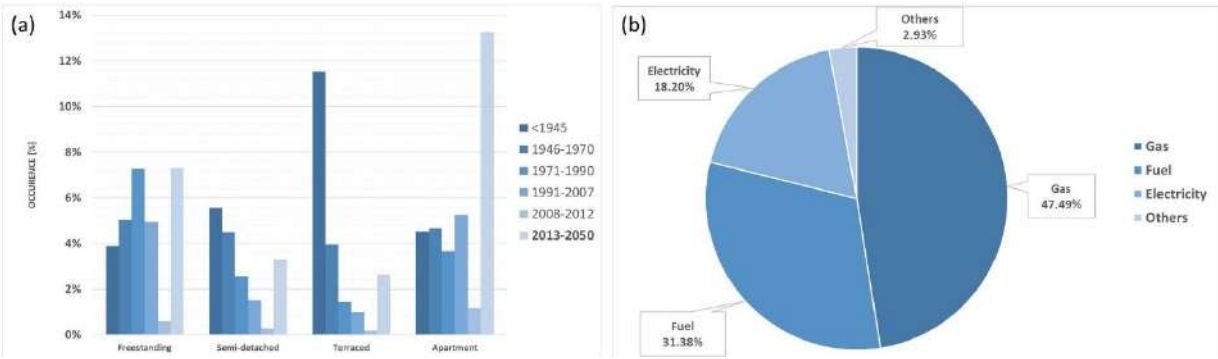

Fig. 3 - BAU scenario (up to 2050) (a) Distribution of the Belgian dwelling types differentiating the six construction periods (b) Distribution of energy sources used for SH.

2.2 Weather Data

The recent decades have seen a major concern about global warming and climate change. This study also aims to upscale the impact of climate change on future heating consumption and to evaluate the minimum indoor temperature used for sizing the heat pumps in Belgium.

The regional climate model used in this study is the "Modèle Atmosphérique Régional" model (hereafter called "MAR") [14]. Since MAR is a regional model, it must be forced by a global model. Therefore, the atmospheric conditions from a general circulation model (GCM) must be directly forced to the boundaries of the MAR domain every 6 hours. MAR Model runs at 5 km spatial resolution over the Belgian territory as shown in Fig. 4. In this study MAR is forced by the global model BCC-CSM2-MR (called BCC hereafter) [15] with both scenarios historical (1960-2014) and ssp585 (2015-2100) from the CMIP6 project [16]. MAR-BCC is the ensemble mean of all the MAR simulations, compared to MAR-MPI (the coldest) and MAR-MIR (the warmest) [14]. In this study MAR-BCC model is used for the SSP585.

2.3 Future Scenarios

In the future scenarios, the tree structure is then extended for the period 2013–2050 as shown in Fig. 1. The new dwellings that are constructed in this period are fully insulated. In addition to that, two scenarios are assessed to calculate the maximum penetration rate of electricity-driven and gas-driven heat pumps in the building stock and their impact on the overall building stock energy use.

The performance of electricity-driven heat pumps is based on the performance map provided by different manufacturers, while the gas-driven heat pump performance is based on laboratory tests.

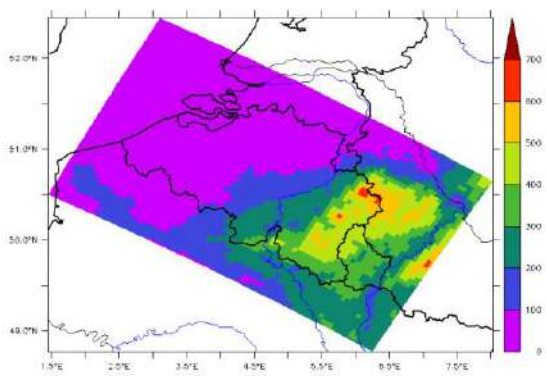

Fig. 4 - Topography (in meters above sea level) of the MAR domain representing Belgian territory [13].

- ***Business-as-Usual (BAU-up to 2050)***

The BAU scenario is the first step to update the building stock for the new dwellings, insulation characteristics and the energy sources used for SH and DHW for the period 2013-2050. Based on the Long term renovation strategies of Wallonia and Flanders in Belgium, an average annual construction and demolition rates are set respectively to 0.8% and 0.075%. In addition to that, a total of 1.3% per year renovation rate is counted to renovate the different buildings. The priority was given first to the older non-insulated and after to the partially insulated buildings.

Fig. 3 (a) shows the expected distribution of the newly constructed dwellings between 2013-2050, the number of dwellings for the reference year 2012 was 4,675,433 buildings which increased by 0.348% in 2050 to reach 6,152,311 dwellings. Fig. 3 (b) represents the distribution of energy sources used for SH in 2050. It can be seen that the electricity share is 18.20% compared to 5.76% in the base scenario because of the policies and regulations to increase the share of electricity and to ban the use of oil boilers for the newly constructed buildings and NG connections for the large apartments as well [17]. The share of NG and fuel is also reduced compared to the base scenario in 2012.

- ***Electricity-Driven Heat Pump Scenario***

The electricity-driven heat pump scenario is characterized by the maximum penetration rate of air-source heat pumps used for SH and DHW production. The heat pumps are modeled using polynomial laws to fit with the performance maps provided by the manufacturers for the different machines.
The model gives the heating capacity at full load and the COP at full load (COP_{FL}) as a function of two variables; the outside air temperature ($T_{air,out}$) and the temperature of the heating fluid at the outlet of the condenser (T_w).

This polynomial model gives accurate results when the working conditions are close to the full load conditions, in order to predict the performance of a heat pump better, a third order low has been chosen. The model has been calibrated with an air-to-water heat pump Viessmann Vitocal 300-A.

The energy input ratio at full load ($EIRFT$) is calculated as a function of ΔT as shown in equation (1) and the capacity at full load ($CAPFT$) is also calculated as a function of ΔT as shown in equation (3).

$$EIRFT = \frac{\mathrm{COP}_n}{\mathrm{COP}_{fl}} = Co + C1 * \Delta T + C2 * \Delta T^2 + C3 * \Delta T^3 \quad (1)$$

$$\Delta T = \frac{T_{air,out}}{T_w} - \left(\frac{T_{air,out}}{T_w}\right) n \quad (2)$$

$$CAPFT = \frac{\dot{Q}_{FL}}{\dot{Q}_n} = Do + D1 * (T_{air,out} - T_{air,out,n}) + D2 * (T_w - T_{w,n}) \quad (3)$$

At part load, the energy input ratio is also calculated ($EIRFPLR$) to give the performance at part load as shown in equation (4).

$$EIRFT = \frac{\dot{W}_{PL}}{\dot{W}_{FL}} = K1 + (K2 - K1) * PLR + (1 - K2) * PLR^2 \quad (4)$$

$$PLR = \frac{\dot{Q}_{PL}}{\dot{Q}_{FL}} \quad (5)$$

Where:
C0 = 1.01283
C1 = -9.6421
C2 = 65.2973
C3 = 359.06
D0 = 0.973861827
D1 = 0.025752873
D2 = -0.00340588
K1= 0
K2= -0.82

In this scenario, the priority of the production is given to the DHW as the backup is used for SH (if there is a backup system in the building) and for SH and DHW simultaneously if there is no backup system in the building.
Three different types of heat pumps were considered for the sizing depending on the overall U-value of the building as shown in Tab. 1, Low temperature heat pumps are selected when the average U-value is below 0.3 W/m^{2}K which is related to the EPB legislation in Belgium, high-temperature HPs are selected for U-value higher than 0.8 W/m^{2}K and medium temperature for U-value between 0.3 and 0.8 W/m^{2}K.

Tab. 1 – Electricity-driven HP selection and sizing.

U-value [W/m^2]	HP Type	Heating power [kW] ($\dot{Q}_{in}$)
U_{avg} <0.3	Low T HP (Air 7°C/ Water 35°C)	4.4 to 16
0.3 < U_{avg} > 0.8	Medium T HP (Air 7°C/ Water 45°C)	11 to 16
U_{avg} > 0.8	High T HP (Air 7°C/ Water 65°C)	11 to 16

The criteria for determining whether or not a heat pump may be placed in a given building is based on a stationary balance that takes into account the building SH and DHW loads, by considering a maximum rating power of 8.6 kW at -10°C, and 80% of the loads at these conditions. Currently, the minimum outdoor temperature used in sizing in the heating seasoni s -10°C according to the ecodesign requirements [18].

- ***Gas-Driven Heat Pump Scenario***

In order to expand the energy sources used for the same technology, a gas-driven absorption heat pump (GAHP) is proposed as a second scenario. Designed for SH and DHW production for residential applications, the appliance has been tested and the results obtained are used to develop a model compatible with that of buildings. The GAHP has a nominal heating capacity of 18.9 kW and its main features are shown in Tab. 2.

Tab. 2 - Main characteristics of the selected GAHP.

Heating power	Air 7°C / Water 50°C 17.6 kW Air 7°C / Water 35°C 18.9 kW
GUE efficiency (relative to LCV)*	Air 7°C / Water 50°C 157% Air 7°C / Water 35°C 169%
Elec. Power absorption	0.35 kW
Heating capacity	11.4 kW (nominal, relative to LCV, 1013 mbar – 15°C) 11.2 kW (real)

** Gas utilization efficiency; efficiency index of gas heat pumps, equal to the ratio between the thermal energy produced and the energy of fuel used (relative to low calorific value).*

The system is based on the Water-Ammonia absorption cycle using outdoor air as the low-temperature heat source and NG combustion as high-temperature heat source; the delivered hot water is the medium-temperature heat sink. The working principle of the system is represented in the diagram shown in Fig. 5.

To reduce its pressure, the refrigerant leaving the COND is throttled by means of a restrictor valve and cooled down inside the Pipe-in-Pipe heat exchanger (PiPHx); then, by means of a second restrictor valve, is brought to the ideal pressure and temperature conditions before entering the Evaporator (EVAP) where the liquid refrigerant is evaporated by taking heat from the surrounding air. Then, the low-pressure vapor ammonia is overheated in the PiPHx before being sent to the Solution Cooled Absorber (SCA), where it meets the poor refrigerant solution coming from the GEN. The pressure of the incoming solution is reduced by a third restrictor valve.

Since the absorption process is an exothermic reaction, the solution is sent to the Water Cooled Absorber (WCA) where a considerable amount of thermal energy is transferred to the water of the heating circuit. Once the absorption is completed, the solution is pumped back to the GEN using a Solution Pump (SP).

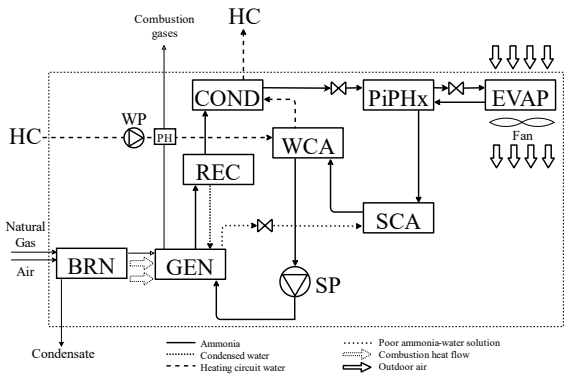

Fig. 5 - Gas absorption heat pump schematic.

The system is installed and tested in a climatic chamber to vary and control the temperature and humidity conditions. From the performance map and the tests conducted in the laboratory, a simple model based on an ordinary least squares linear regression is developed.
The model should give the Heating Capacity at full load ($\dot{Q}_{HC,FL}$) as a function of outdoor temperature (T_{out}), delivery water temperature ($T_{delivery}$) and specific humidity (ω), as shown in Equation (6) The COP at full load (COP_{FL}) depends on the same variables as shown in Equation (7).

$$Q_{HC,FL} = f(T_{air,out}, T_w, W_{out}) \quad (6)$$
$$COP_{FL} = g(T_{air,out}, T_w, W_{out}) \quad (7)$$

The part load ratio (PLR) is the ratio of the heating capacity at part load ($\dot{Q}_{HC,PL}$) to the heating capacity at full load as expressed in Equation (8). This ratio is an input and must be a number between 0 and 1 since the heating capacity varies proportionally with the modulation of the system.

$$PLR = \frac{\dot{Q}_{HC,PL}}{\dot{Q}_{HC,FL}} \quad (8)$$

The same approach is used to model the inputs to the system, in this case, the gas heat input and electrical input (consumption of fans and electronics) are defined as $\dot{Q}_{gas}$ and $\dot{W}_{in}$ in Equations (9) and (10). The gas heat input varies according to the water delivery temperature and outdoor temperature, in addition to the modulation of the system; the electrical consumption depends on the modulation of the system thus it is modeled as a function of the part load ratio and represented as a linear proportion.

$$\dot{Q}_{gas} = h(T_{out}, T_{delivery}, PLR) \quad (9)$$
$$\dot{W}_{in} = i(PLR) \quad (10)$$

The obtained coefficients for the linear model are such that the residual sum of squares between the observed targets in the dataset and the targets predicted by the linear approximation is minimized. The results are shown in Equations (11), (12), (13) and (14). The R^2 of each formula is defined as $1 - (u/v)$, where u is the residual sum of squares and v is the total sum of squares; the best possible score for

R^2 is 1.

$$\dot{Q}_{HC,FL} = 0.0958\, T_{out} - 0.1809\, T_{delivery} + 146.192\, \omega + 25.0752 \quad R^2 = 0.89 \quad (11)$$

$$COP_{FL} = 0.0059\, T_{out} - 0.0118\, T_{delivery} + 15.1612\, \omega + 1.6759 \quad R^2 = 0.86 \quad (12)$$

$$\dot{Q}_{gas} = -0.00287 T_{out} - 0.0164\, T_{delivery} + 11.9143 PLR + 2.9169 \quad R^2 = 0.89 \quad (13)$$

$$\dot{W}_{in} = 0.2762\, PLR + 0.0540 \quad R^2 = 0.91 \quad (14)$$

The obtained formulas are evaluated for the experimental conditions from which the performance map is obtained. The results are within the order of magnitude and show the same trends and behavior observed during the experimental tests performed with small variations explained by the R^2 value of each formula.

In this scenario, the same criteria has been used to determine if a heat pump can be installed or not by considering a maximum rating power of 16.9 kW at -10°C, based on the manufacturer data. In addition to that the same sizing criteria is also used to size the GAHP according to the overall U-value of the building.

3. Results and Discussion

The results of the base scenario are shown in Fig. 6, comparing the total SH and DHW energy consumption in 3 different periods. It can be seen at Fig. 6 (a) that there is a slight change in the distribution of energy sources used for SH and DHW as there was no change in the building stock, while there is a significant decrease in the total SH and DHW consumption. In the base scenario with a reference year using TMY (2001-2020), the total SH and DHW consumption was 102184 GWh and it decreased to 81320 GWh and 77825 GWh in (2041-2060) and (2081-2100) respectively.

Fig. 6 (b) also shows the average consumption per dwelling in the 3 periods for the base scenario. It decreased from 21.86 MWh in (2001-2020) to 17.40 MWh in (2041-2060) and 16.65 MWh in (2081-2100). It can also be seen that the CO_2 emissions decreased for an average dwelling from 5.10 ton CO_2 to 3.88 ton CO_2. The emission factors for electricity, gas, fuel and others in Belgium are 0.160 kg/kWh, 0.202 kg/kWh, 0.267 kg/kWh and 0.342 respectively [19,20].

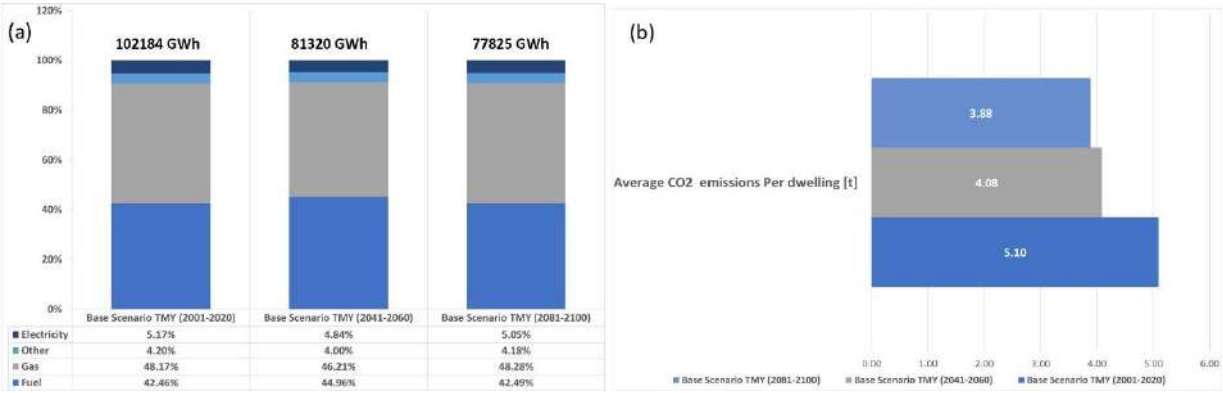

Fig. 6 - Comparison between the SH and DHW energy consumption in the Base Scenario in different years (a) Total SH and DHW energy consumption (b) average CO2 emissions per dwelling.

For the BAU Scenario, the building stock has been updated as shown before in Fig. 3. The new distribution of the buildings has been used to simulate the electricity-driven heat pumps scenario and to calculate the maximum penetration rate of both heat pumps in the building stock and their impact on the overall building stock energy use.

Fig. 7 shows the maximum penetration rate of the electricity-driven heat pumps. Based on the criteria mentioned before, 67.6% is the maximum possible penetration rate of the electricity-driven HPs in 2050 Horizon. It can also be seen that in the electricity-driven HPs scenario, the NG and fuel share amongst the whole building stock decreased to 15.5% and 15% respectively compared to their share in the BAU scenario as shown in Fig. 3.

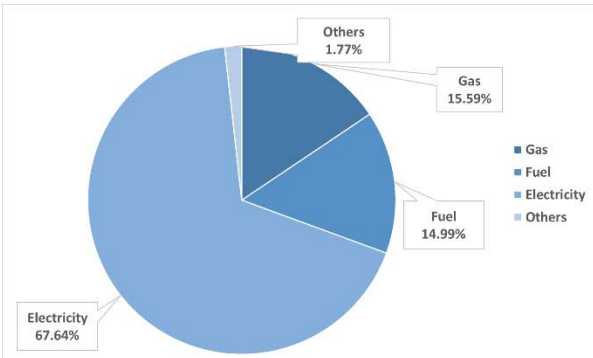

Fig. 7 – Electricity-driven HP scenario - distribution of energy sources used for SH.

The increase of the electricity share has also an impact on the total SH and DHW energy consumption of the building stock as shown in Fig. 8.
It can be seen that electricity represents 45.4% of the total SH and DHW energy consumption in the

electricity-driven HPs scenario compared to 13.64% in the BAU scenario.
The total SH and DHW energy consumption decreased by 3.23% in the electricity-driven HPs scenario compared to the BAU scenario and the consumption per average dwelling decreased from 15.6 MWh in the BAU scenario to 15.1 MWh in the electricity-driven HPs scenario.

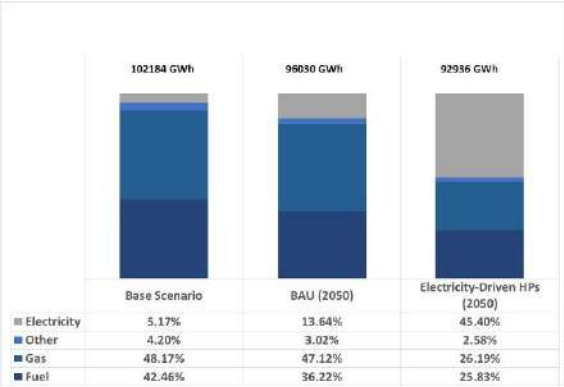

Fig. 8 - Comparison between the total heating energy consumption in the Base scenario, BAU scenario and electricity-driven HPs scenario.

For the gas-driven HPs scenario, based on the same criteria of installing a GAHP with a maximum power of 16.9 kW at -10°C. The maximum penetration rate of GAHP is 42.7% by 2050, compared to the distribution of NG source in BAU scenario in 2050 which is 47.5% as shown in Fig. 3(b). The share of the GAHP represents 89.92% of the total number of buildings that use NG for SH and DHW purposes as shown in Fig. 9.

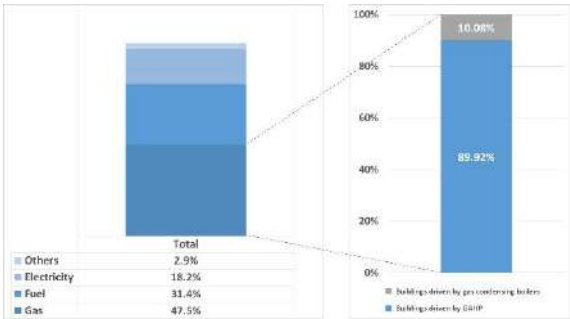

Fig. 9 – Gas-driven HP scenario – share of GAHP amongst the buildings that use NG for SH and DHW.

Fig. 10 compares between the total heating energy consumption in the gas-driven HP scenarios, BAU scenario as well as the base scenario. The total heating consumption for SH and DHW in the gas-driven HP scenario is 4.5% lower than the BAU scenario.

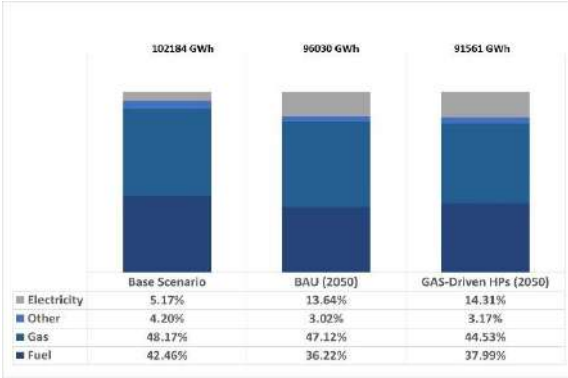

Fig. 10 - Comparison between the total heating energy consumption in the Base scenario, BAU scenario and gas-driven HPs scenario.

The results also show that the minimum outdoor temperature is increasing in the coming years. Compared to the reference year TMY(2001-2020), there are 26 hours when the Temperature is below -10°C, while in the period (2081-2100), the minimum outdoor temperature is -5°C for 3 hours. Based on those results, the minimum outdoor temperature used in the criteria to determine the maximum penetration rate of HPs is updated to -5°C. The change in the maximum penetration rate is not significant, it has been found that the electricity-driven heat pumps penetration rate increases from 67.6% to 68.9% and the gas-driven heat pumps penetration rate will increase from 42.7% to 43.5%.

4. Conclusion

In this paper, a bottom-up approach has been updated to describe the Belgian building stock with the base scenario and BAU scenario. The results show that, climate change has a significant impact on the energy use of buildings, by 2100 the SH and DHW energy consumption for the whole building stock decreased by 23.8%.

In the second step, the evolution of the building stock till 2050 has been updated while taking into consideration the construction, demolition and renovation rates in the BAU 2050 scenario. The distribution of energy sources used for SH and DHW has been changed compared to the base scenario.

The paper also investigates two different scenarios to calculate the maximum penetration rate of heat pump technologies used for SH and DHW in the residential buildings in Belgium. In the first scenario, the maximum penetration rate of electricity-driven HPs is 67.6%, while the maximum penetration rate of GAHP is 42.7%.

The evolution of temperatures in the coming years showed that increasing the minimum indoor temperature used in the sizing criteria for the HPs to -5°C instead of -10°C, will also have an impact on the maximum penetration rate of both HPs.

5. Acknowledgment

This research was partially funded by the Walloon Region under the call 'Actions de Recherche Concertées 2019 (ARC)' and the project OCCuPANt, on the Impacts Of Climate Change on the indoor environmental and energy PerformAnce of buildiNgs in Belgium during summer. The authors would like to gratefully acknowledge the Walloon Region and Liege University for funding.

6. References

[1] European Commission. Directorate General for Energy. Good practice in energy efficiency :for a sustainable, safer and more competitive Europe. LU: Publications Office; 2017.

[2] Nishimwe AMR, Reiter S. Building heat consumption and heat demand assessment, characterization, and mapping on a regional scale: A case study of the Walloon building stock in Belgium. Renewable and Sustainable Energy Reviews 2021;135:110170. https://doi.org/10.1016/j.rser.2020.110170.

[3] Ürge-Vorsatz D, Cabeza LF, Serrano S, Barreneche C, Petrichenko K. Heating and cooling energy trends and drivers in buildings. Renewable and Sustainable Energy Reviews 2015;41:85–98. https://doi.org/10.1016/j.rser.2014.08.039.

[4] Wang H, Chen Q. Impact of climate change heating and cooling energy use in buildings in the United States. Energy and Buildings 2014;82:428–36. https://doi.org/10.1016/j.enbuild.2014.07.034.

[5] Radhi H. Evaluating the potential impact of global warming on the UAE residential buildings – A contribution to reduce the CO2 emissions. Building and Environment 2009;44:2451–62. https://doi.org/10.1016/j.buildenv.2009.04.006.

[6] European heat pump association. European Heat Pump Market and Statistics Report 2014. 2014.

[7] Famiglietti J, Toppi T, Pistocchini L, Scoccia R, Motta M. A comparative environmental life cycle assessment between a condensing boiler and a gas driven absorption heat pump. Science of The Total Environment 2021;762:144392. https://doi.org/10.1016/j.scitotenv.2020.144392.

[8] Association of the European heating industry. Heating Market Report 2020. 2020.

[9] Keinath CM, Garimella S. An energy and cost comparison of residential water heating technologies. Energy 2017;128:626–33. https://doi.org/10.1016/j.energy.2017.03.055.

[10] Ashrae handbook: Fundamentals. Atlanta: Ashrae; 2013.

[11] Gendebien S, Georges E, Bertagnolio S, Lemort V. Methodology to characterize a residential building stock using a bottom-up approach: a case study applied to Belgium. International Journal of Sustainable Energy Planning and Management 2015:71-88 Pages. https://doi.org/10.5278/IJSEPM.2014.4.7.

[12] International Standard Organization. Energy performance of buildings. Calculation of energy use for space heating and cooling: BSI British Standards; 2007. https://doi.org/10.3403/30133624.

[13] El Nagar E, Doutreloup S, Lemort V. Modeling the Impact of Climate Change on the Future Heating Demand in Different Types of Buildings in the Belgian Residential Building Stock 2021.

[14] Sebastien D, Fettweis X, Rahif R, Elnagar E, S. Pourkiaei M, Amaripadath D, et al. Historical and Future Weather Data for Dynamic Building Simulations in Belgium using the MAR model: Typical & Extreme Meteorological Year and Heatwaves 2022.

[15] Wu T, Yu R, Lu Y, Jie W, Fang Y, Zhang J, et al. BCC-CSM2-HR: A High-Resolution Version of the Beijing Climate Center Climate System Model. Climate and Earth system modeling; 2020. https://doi.org/10.5194/gmd-2020-284.

[16] O'Neill BC, Tebaldi C, van Vuuren DP, Eyring V, Friedlingstein P, Hurtt G, et al. The Scenario Model Intercomparison Project (ScenarioMIP) for CMIP6. Geosci Model Dev 2016;9:3461–82. https://doi.org/10.5194/gmd-9-3461-2016.

[17] Government of Flanders. LONG-TERM STRATEGY FOR THE RENOVATION OF FLEMISH BUILDINGS. n.d.

[18] Commission Regulation (EU). Commission Regulation (EU) No 206/2012 of 6 March 2012 implementing Directive 2009/125/EC of the European Parliament and of the Council with regard to ecodesign requirements for air conditioners and comfort fans Text with EEA relevance. 2012.

[19] International Energy Agency (IEA). Data & Statistics. IEA n.d. https://www.iea.org/data-and-statistics/data-browser (accessed March 31, 2022).

[20] Koffi B, Cerutti A, Duerr M, Iancu A, Kona A, Janssens-Maenhout G. Covenant of Mayors for Climate and Energy: Default emission factors for local emission inventories – Version 2017. JRC Publications Repository 2017. https://doi.org/10.2760/290197.

Repeated solar regeneration of a medium-term heat storage for a heat pump

Annemarie Lauffer, Christian Schweigler

CENERGIE - Center for Energy-Efficient Buildings and Districts, HM Hochschule München University of Applied Sciences, Munich, Germany, annemarie.lauffer@hm.edu.

Abstract. This paper deals with a heat pump system with two heat sources, a medium-term ground collector heat storage and a façade-integrated massive solar-thermal collector. Aiming at affordable system cost, a medium-term heat storage is applied instead of a seasonal heat storage. During milder phases of the heating period, the heat storage is regenerated by the solar absorber to be used as ambient heat source under frosty weather conditions. Preparing for the design of heat pump systems with multiple heat sources, the energy balance of a medium-term underground heat storage has been investigated, based on physical component models. Yearly and seasonal analyses for different absorber sizes from 7.5 to 37.8 m² lead to the following statements. In general, even for small absorber sizes solar yields during winter are sufficient for continuous operation of the heating system, with increasing average temperature of the storage for larger sizes of the solar system. Higher ground temperatures result in higher seasonal coefficients of performance of the heat pump, and in higher annual heat losses of the storage. The medium-term character of the storage is shown by the in-season heat gain contributed by the solar absorber. Finally, to assure frost-free operation of the storage the absorber size must be at least 15% of the ground collector size.

Keywords. Heat pump systems, medium-term storage, underground heat storage, solar absorber, regeneration
DOI: https://doi.org/10.34641/clima.2022.151

1. Introduction

In Germany in 2020, 53 % of the newly built houses have been equipped with a heat pump as the heating device [1]. About 79 % of them use air as ambient heat source [1], motivated by the simple installation and low investment cost. The setback of air source heat pumps is the low efficiency at low outdoor temperatures. In comparison the source temperatures of ground collectors, such as geothermal probes or ground water, are higher in winter months, when most heating power is needed. Higher source temperatures result in higher COP (Coefficient of Performance) and therefore in lower electric power demand. Günther et al. researched the efficiencies of heat pumps in the field [2]. High energetic efficiency is essential for the energy transition towards a completely regenerative energy supply.

Depending on the ground structure and local regulations, the use of geothermal probes or ground water may be restricted in a region or in individual cases. Horizontal earth collectors need large surface areas to collect sufficient heat input for the heat pump. Due to urban redensification and smaller building sites there is often not enough space for an earth collector for the heat supply of a building.

Another approach is to use heat storages to store solar energy for subsequent use. Seasonal heat storages are used, due to the lack of sufficient solar energy in winter. Since a seasonal storage contains the heat for the whole heating season, the construction has a high investment cost. Thus, with one storage cycle per year the amortisation is often too long to be considered profitable as reviewed by Amaya et al. [3].

Regenerating the storage during the heating season allows the reduction of the storage size and its investment cost. The solar yield necessary to regenerate a medium-term storage, serving as ambient heat source for a heat pump system, is investigated in this paper. The storage is regenerated by a façade-integrated massive solar-thermal collector, similar as described by Tanzer et al. [4]. This paper presents a pre-investigation of the models for later validation by the monitoring data of a pilot plant with the goal to design further heat pump

Copyright ©2022 by the authors. This conference paper is published under a CC-BY-4.0 license.

system with multiple heat sources. Comparison between different absorber sizes is made to describe the characteristic of the thermal behaviour of the storage and find an optimal absorber size.

This work is organised as follows: After describing the mathematical models of the ground collector storage, the façade-integrated massive solar-thermal collector, and the building, the models are combined in a system simulation. Yearly simulations of the ground collector temperatures, solar yield, and geothermal energies for systems with different absorber sizes lead to the solar fraction of the heat supply during the heating season. The necessity for frost-free operation results in a minimum required absorber size. For this absorber the prerequisites for a frost-free storage are analysed by the energy balance at the top of the storage.

2. Research Methods

The analysis is made with the mathematical software tool EES (Engineering Equation Solver). In the following chapter two models are described, representing the components ground collector storage and solar massive façade absorber. The two models are then combined to represent a heat pump heating system for a residential building.

2.1 ground collector storage

The ground collector storage is modelled by a set of parallel horizontal tubes serving for thermal activation of a cuboid ground volume underneath the building. The collectors size equals the rectangular footprint of the building and is positioned directly underneath the insulation of the base plate of the building. For heat input and output an aqueous brine is circulated through the pipes. A thermal insulation is inserted between the base plate of the building and the storage volume, which is considered ideal. There is no thermal insulation of the storage volume to the surrounding ground.

The heat transport $\dot{Q}_{\mathrm{T}}$ from the brine through the tube wall to the earth outside the tube is described by the heat transfer through a cylinder. Starting from the ground outside the tube, heat is transported deeper into the ground. To describe the heat flow in the ground without a FEM (finite element method) approach using a fine geometric mesh a simplification is made. The depth – 10 m – of the underground collector storage is divided into 40 blocks. The temperatures in each block are calculated with the differentiation method.

A geometric approach based on the from factor, described in the VDI Wärmeatlas (engl.: heat atlas) [5] is chosen to describe the heat flow from the cylindrical outer surface of the tube to the first horizontal block of the storage volume underneath the building. Equation (1) describes the heat flow $\dot{Q}$ transmitted through the earth. λ is the thermal conductivity of the earth, S_{l} the form factor calculated by equation (2), l the length of the tube, $T[1]$ is the temperature of the first block and T_{T} the surface temperature of the tube. d is the distance from tube to the centre layer of the first block, δ is half the tube spacing between two horizontal tubes of the collector and r the tube radius. The ground material is "clay/silt, water-saturated" as defined in the VDI 4640 part 1 [6].

$$\dot{Q} = \lambda \cdot S_l \cdot l \cdot (T[1] - T_{\mathrm{T}}) \qquad (1)$$

$$S_l = \frac{2\pi}{\frac{\pi d}{\delta} + \ln\left(\frac{\delta}{\pi r}\right)} \qquad \text{for: } r \ll d, \delta \qquad (2)$$

In the course of the year, the uninfluenced ground changes its temperatures according to the ambient air temperature and solar yields at the surface. Yet, in 10 m depth a rather constant ground temperature with only marginal seasonal swing around a 10 °C average is found. Therefore, the storage is regarded as 10 m deep with an undisturbed ground temperature of constant 10 °C at its bottom layer. A storage charged with higher temperatures loses heat to the ground underneath the storage. When the storage is cooled to lower temperatures a heat flow towards the storage volume occurs. Heat losses to the sides of the storage are not considered.

2.2 façade-integrated massive solar-thermal collector

The solar massive façade absorber is integrated in the south facing outer wall of a building as a low-tech heat source providing temporarily stable low-grade heat to the heat pump. It consists of a vertical sandwich structure with an outer concrete layer, which includes a tube meander serving as thermal collector. Brine is pumped through the tube to absorb energy from the collector. The back of the absorber is insulated, which eliminates heat transfer to the inside of the building, as an idealistic approximation within the model.

The thermal behaviour of the massive solar absorber is modelled according to equation (3). Heat fluxes conveyed by long $\dot{q}_{\mathrm{rad,lw}}$ and short-wave $\dot{q}_{\mathrm{rad,sw}}$ solar radiation hit the outer concrete surface and heat the bulk of the massive absorber. The heat losses of the absorber to the surroundings consist of long wave radiation $\dot{q}_{\mathrm{loss,lw}}$ and convective losses $\dot{q}_{\mathrm{loss,conv}}$. The heat transfer fluid heats up while flowing through the collector tubes $\dot{q}_{\mathrm{htf}}$ and serves for heat transfer to the thermal storage. Surplus heat stays in the concrete volume $\dot{q}_{\mathrm{MA,stored}}$ of the massive absorber, resulting in a temperature rise of the wall element with increasing heat content. In operation, the temperature of the brine lies in between the temperatures of the massive absorber and the underground thermal storage, governed by the respective heat transfer characteristics of the absorber and the storage.

$$\dot{q}_{\mathrm{rad,lw}} + \dot{q}_{\mathrm{rad,sw}} - \dot{q}_{\mathrm{loss,lw}} - \dot{q}_{\mathrm{loss,conv}} = \dot{q}_{\mathrm{htf}} + \dot{q}_{\mathrm{MA,stored}} \qquad (3)$$

For the weather conditions, ambient temperature, solar radiation, and wind speed are specified by the TRY (test reference year) for Potsdam, Germany.

Condensation of air humidity at the absorber surface occurs when the absorber temperature falls below dew temperature. Although condensation provides additional energy for the absorber, it is not considered in the calculations, because the growth of moss and the formation of frost could damage the surface of the absorber. Further information about the use of solar massive absorbers can be found in Tanzer et. al [4].

As a preliminary investigation, figure 1 shows the potential heat output of a solar massive absorber on the left ordinate. Monthly sums for the specific solar yield $\dot{Q}_{\mathrm{MA}}$ are displayed for six different brine inlet temperatures T_{in} from -5 to 20 °C, kept constant throughout the year.

2.3 building

A heat pump uses the underground thermal storage as heat source for the heat supply of a building. The hourly heating demand of the building is determined by the ambient weather conditions, given by the TRY. The building is a single storey building with the same ground area as the ground collector storage. The insulation standard of the building is KfW40 – i.e., the heating demand is limited to 40 % of a standard newly built dwelling – according to EnEV standard (Energieeinsparverordnung – engl.: Energy Saving Ordinance). The single-storey model building with a footprint of 150 m^2 has an annual heat demand of 5100 kWh with a peak heat load of 4 kW at minimum ambient temperature of -13.4 °C.

The heat pump extracts heat from the earth collector storage. The heat flow to the evaporator of the heat pump is estimated by the COP, according to performance data provided by the manufacturer. Monthly values of the heat source energy $\dot{Q}_{\mathrm{source}}$ are shown in figure 1 on the right ordinate.

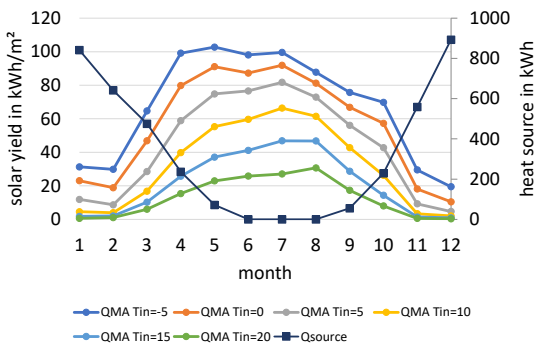

Fig. 1 – solar yield Q_{MA} in dependency of the inlet temperature T_{in}; heat source $\dot{Q}_{\mathrm{source}}$.

2.4 storage regeneration

The EES models of the ground collector storage, the massive façade absorber and the building are combined for representation of the entire heating system. The heat pump extracts heat from the storage or the solar absorber according to the heat demand of the building. Surplus heat generated by the solar massive absorber is used for regeneration of the storage whenever possible.

In figure 2 a schematic description of the combined model is given, comprising the three components: solar massive absorber, ground collector storage, and building. $\dot{Q}_{\mathrm{source}}$ is the heat source for the heat pump. The heat is extracted from the ground collector. $\dot{Q}_{\mathrm{MA}}$ is the collected energy provided by the massive absorber, $\dot{Q}_{\mathrm{net}}$ the net heat flow transferred to the heat storage via the ground collector. The heat flows $\dot{Q}[\mathrm{i}]$ with $\mathrm{i} = 1 \ldots 41$ denote the change of the heat content in the respective storage blocks. This results in a change of the related temperatures $T[\mathrm{i}]$ of the round layers. The bottom layer is assumed to stay at constant temperature $T[41] = 10$ °C throughout the year. Depending on the temperature profile of the lower cells of the storage, heat loss or heat gain $\dot{Q}_{\mathrm{geo}}$ is exchanged with the undisturbed ground underneath the ground heat storage.

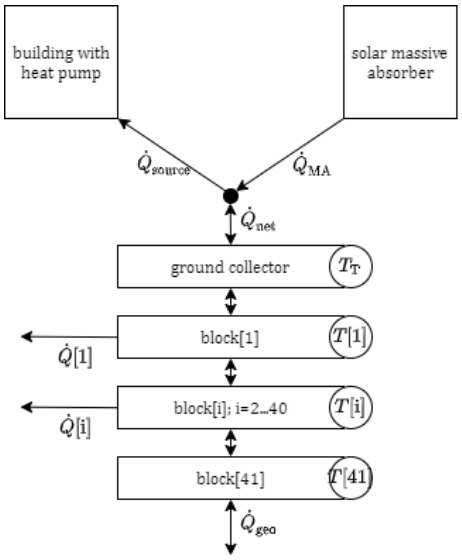

Fig. 2 – EES model of the heating system, comprising the three components: solar massive absorber, ground collector storage, and building.

3. Performance of the heating system

This chapter deals with the analysis of the operation of the described heating system. The system's efficiency and usability are characterised by the temperature curve of the ground storage over a year. Together with the storage temperature the heat transfer fluid's temperature is determined, which is a decisive parameter for the efficiency of the heat pump system. For the system to be financially viable, the seasonal coefficient of performance (SCOP) must be high, resulting in low electrical power consumption and savings in the operating costs.

The following scenario is considered for the analysis. A given one-storey building with a building area of

150 m², as described in section 2.3, is heated by a brine/water heat pump. The COP of the heat pump is taken from nominal design point specified by the manufacturer and is considered constant for a conservative approximation, even though higher source temperatures would result in higher COP values. With this, the required heat input to the heat pump which is to be covered by the heat source is set for the hourly simulation of the heating system. The ground area of the building is identical with the area of the ground collector storage, i.e., the complete footprint of the building is thermally activated by the ground collector. The absorber size is the single variable to influence the performance and usability of the heating system.

The solar massive absorber is varied in size to find the optimal system design for the given situation, defined by the underground heat storage and the building. The size varies from 7.5 m² to 37.8 m² (37.8 m² is the size of a pilot plant, which is not part of this paper). The different solar absorbers equal 5% to 25.2% in relation to the ground collector size.

To obtain a realistic initial state for the modelling of the entire year, the annual calculations have been repeated 10 times until a stable state is reached.

3.1 ground collector storage temperatures

The course of the ground collector storage temperature during the heating period is characteristic for the efficiency of the heating system. The annual temperature profiles of the underground storage are analysed for different absorber sizes. Since the storage is considered a medium-term heat storage, regeneration during the heating season is necessary. A cooled down storage allows for solar yield at low heat transfer fluid temperatures, which enables regeneration during the heating period.

The temperature in the storage is a result of the heat extraction by the heat pump and the regeneration by the solar absorber. The temperature of the first block from the top $T[1]$ changes first depending on the input or output of energy. The temperature difference between two adjacent blocks causes the heat to spread between the blocks. While charging the storage, heat is transferred deeper into the storage. During discharging, lower temperatures at the top cause the heat to travel upward.

Figure 3 shows selected temperatures of blocks in different depths of the storage regenerated by a massive solar absorber with the size of 37.8 m² for one year, starting on January 1st. During the heating period the temperature $T[1]$ is decreasing due to the heat extraction by the heat pump. When the storage is regenerated, $T[1]$ is rising. The temperatures of the deeper blocks follow this trend with a temporal delay as a result from the high thermal capacity of the storage material – earth. The temperature $T[41]$ in 10 m depth is constant since it is defined fixed at 10 °C. If the adjacent block (No. 40) has a higher temperature, the energy exchange between these two blocks is lost to the deep ground. If the temperature of the second last block is lower, heat is gained from the ground underneath the storage volume.

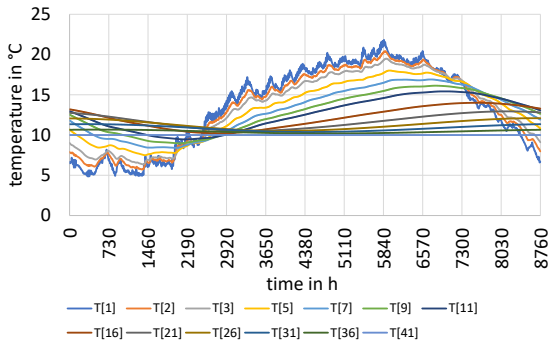

Fig. 3 – temperatures $T[i]$ in different depth of the storage for an absorber size of 37.8 m².

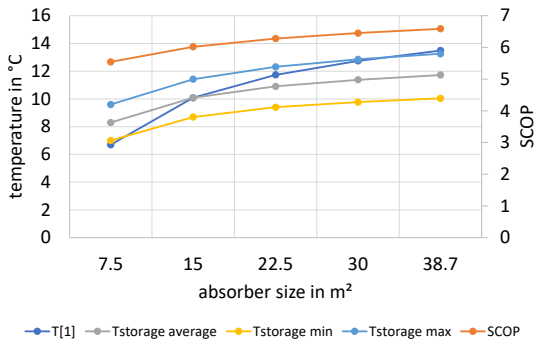

Fig. 4 – yearly average, minimal and maximal temperatures $T_{storage}$ and $T[1]$ (left ord.); SCOP (right ord.) for different absorber sizes.

Regeneration is possible in winter, even if the solar radiation is low. In figure 3 different phases of the operation of the storage can be identified. In fall the temperature in the first block decreases. On a mild day with high ambient temperature and low or no heat extraction this decrease flattens. On a sunny day with more solar yield than heat extraction the temperature is increasing. In addition, the storage temperatures in the upper layers show relaxation. Heat from the lower blocks of the storage flows towards the upper blocks depending on the temperature difference. On days with no heat extraction and no solar yield the temperature in the first block is rising to converge to the temperature of the second block. In winter the temperature decrease of the first block slows down even during high heat extraction and low solar yields, because of the heat flow from the depth of the storage. A ten day long regenerating period until the end of January (500 to 730 h) is shown in figure 3. In this phase, the solar yield surpasses the heat extraction and the temperature in the storage is increasing. The behaviour of the underground heat storage with solar regeneration during the winter months is analysed further in chapter 4. In spring and summer, the solar yield surpasses the heat extraction. Consequently, the temperature in the first block

stays above the temperature in the second block. Heat flows from the first block to the depth of the storage and regenerates it.

When the absorber size is decreased, a lower annual mean temperature T_{storage} of the ground storage is found. The minimal, maximal as well as the average temperature as a function of the absorber size is shown in figure 4. Since the ground temperature is decisive for the performance of the heat pump, – primarily the average temperature of the first block $T[1]$ – the value of SCOP is lower for smaller solar massive absorbers and corresponding lower temperatures of the ground collector.

3.2 solar yield and storage regeneration

As shown in the last section, different absorber sizes result in different storage temperatures. In return, the storage temperature is decisive for the solar yield of the absorbers. This interdependency is analysed regarding the energy balance for different absorber sizes. The resulting regeneration behaviour of the underground heat storage is shown in the following section based on the solar yield.

The yearly solar yield of the massive absorbers Q_{MA} is quantified in figure 5. Larger absorbers allow both, higher storage temperatures and increased solar yield, although the demand for heat from the source Q_{source} by the heat pump is set constant. For an absorber size of 7.5 m^2 the solar yield cannot fulfil that heat demand. Additional energy is required to meet the heat demand, which is provided by heat from the depth of the storage Q_{geo}. The solar yield of an absorber with 15 m^2 surface area fulfils the heat demand. For absorber sizes greater than 15 m^2 the heat gain exceeds the heat demand. The surplus heat balances the energy lost in the depth of the storage. These heat losses are higher for higher storage temperatures. Further analysis of the heat losses and gains is made in subsection 3.3.

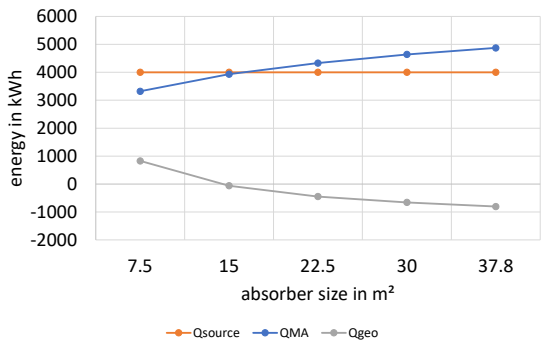

Fig. 5 – annual solar yield Q_{MA}, heat source Q_{source}, and geothermal energy Q_{geo} for different absorber sizes.

For all absorber sizes equation (4) is valid. The source heat flow supplied to the evaporator of the heat pump is covered by the solar yield and the geothermal energy exchanged with the deep ground.

$$Q_{\text{source}} = Q_{\text{MA}} + Q_{\text{geo}} \qquad (4)$$

Since the yearly solar yield shows variance for the different absorber sizes, a more detailed analysis is made in monthly intervals, to determine the temporal profile of the solar yield. The monthly solar yield for the absorbers is shown in figure 6. In winter months (November to February – month 11 to 2) the absorbed energy is the same for all absorber sizes. Although the larger absorbers have more absorber surface area to collect the solar energy, their solar yield is the same as for the smaller absorbers. This is due to the higher temperature of the underground heat storage which is achieved by the larger sizing of the solar system. The resulting higher inlet temperatures in the absorber reduce the specific solar yield. During the rest of the year larger absorber sizes result in higher solar yields, due to the larger surface of the solar absorber. Although the highest solar radiation occurs in summer, for larger absorber sizes the maximum solar yield appears already in spring (month 4 and 5). When a large absorber is used, in spring the storage temperature increases at a higher rate, resulting in higher inlet temperatures in the absorber and consequently decreasing solar yields.

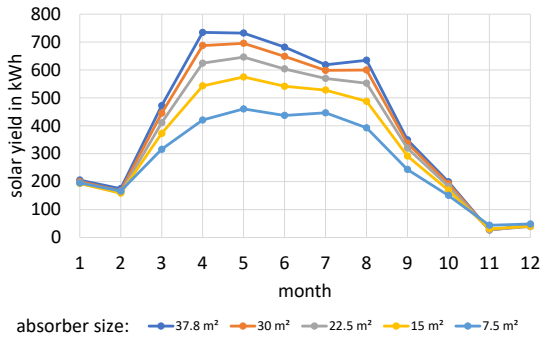

Fig. 6 – monthly solar yield Q_{MA} for different absorber sizes.

3.3 geothermal balance of the storage

Larger absorbers have higher solar yields and allow for higher storage temperatures, resulting in higher efficiencies for the heat pump heating system. Higher storage temperatures also result in higher heat losses to the deep ground underneath the storage volume. The yearly geothermal losses and gains are shown in figure 5. The data are based on a consolidated cyclic situation, which is reached after several years of operation with an identical annual profile to be repeated year by year. To determine the energy balance of the underground heat storage during the year the geothermal energy is investigated in the following section.

The energy balance Q_{balance} of the heat storage, i.e., the change of the heat content of the storage is found by summation of the geothermal energy Q_{geo}, the demand for heat from the source Q_{source} by the heat pump, and the solar yield Q_{MA}, as given in equation (5).

$$Q_{\text{balance}} = Q_{\text{geo}} + Q_{\text{source}} + Q_{\text{MA}} \qquad (5)$$

During the year the energy balance is alternating, as

shown in figure 7 for the heat pump heating system with solar absorber sizes from 7.5 to 37.8 m^2. The storage is charged in summer and discharged in winter, resulting in an increasing and decreasing storage balance. For comparison of the heat content of the storage for different absorber sizes, the start is normalised to a heat content of 0 kWh at the beginning of the year. The differences in the graphs are due to the losses and gains of geothermal energy in the depth of the storage.

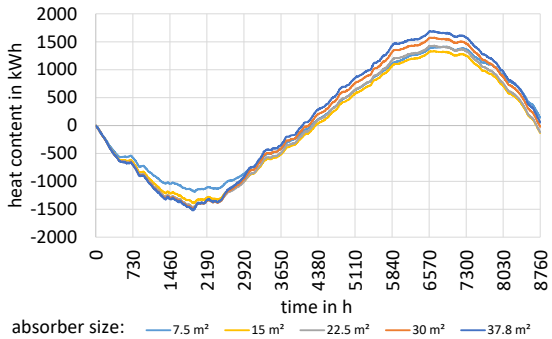

Fig. 7 – heat content of a storage for different absorber sizes over one year.

The geothermal energy is determined by the heat flow from the 40th to the 41st block, as described in equation (6). The 41st block stays at constant temperature of 10 °C throughout the year. When the 40th blocks temperature is above this temperature, energy is lost. Vice versa, energy is gained. The geothermal heat flow depends on the heat transfer coefficient of earth λ, is the thickness of a block d, and the ground collector area A.

$$Q_{\text{geo}} = (T[41] - T[40]) \cdot \frac{\lambda \cdot A}{d} \qquad (6)$$

The geothermal energy is dependent on the temperature profile of the bottom blocks of the storage. Since the temperature of the storage is alternating according to the seasons, the geothermal energy is also fluctuating. Although, the storage temperature is highest in summer, the heat losses and lowest heat gains are found in winter. Energy, which is stored in the summer, heats up the first blocks at the top of the storage. The heat is distributed through the storage and flows into the deeper blocks. The maximum of the temperature of the first block reaches the last block five months later.

Figure 8 shows the summation of the geothermal energy $Q_{\text{geo,sum}}$ during a year for different collector sizes. For smaller solar absorber (7.5 m^2) the annual balance is positive. For all other configurations, a heat loss to the deep ground is found. Larger absorbers result in higher losses, due to higher average storage temperatures. When the minimum temperature of the last block is reached in summer the heat losses are the lowest, as can be seen in figure 9 at about 4380 h. For smaller absorber sizes the temperature falls below 10 °C and heat is gained, causing the summation curve to rise. Since the average temperature of the smallest absorber is below 10 °C, there are continuous heat gains throughout the year for this absorber size.

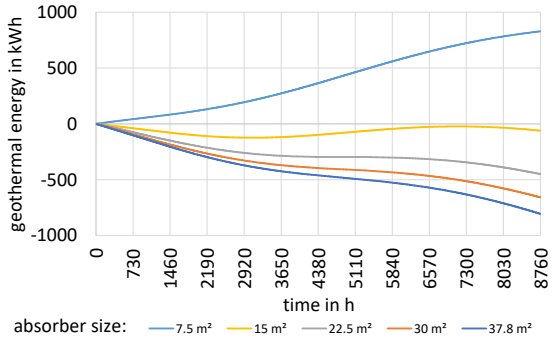

Fig. 8 – summation of the geothermal energy $Q_{\text{geo,sum}}$ for different collector sizes over one year.

3.4 regeneration during the heating season

To reach affordable system cost, a heat storage of limited size shall be sufficient for reliable operation of the heating system. Thus, the storage shall act as a medium-term storage with repeated regeneration within the heating season and not as a seasonal heat storage providing a full seasonal time shift from summer to winter. The additional in-season energy input in the storage is needed to meet the heat demand of the building. In this section the energy input, output, and balance of the storage is analysed for the time period of the heating season. As an example, figure 9 shows these energies for an absorber size of 22.5 m^2.

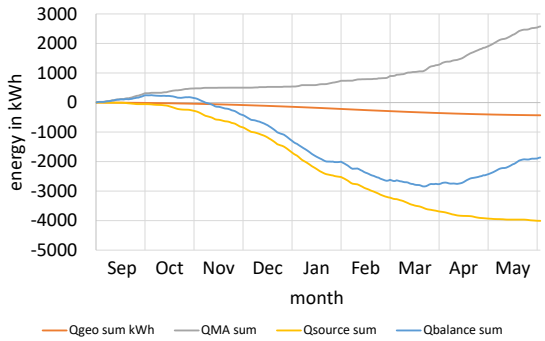

Fig. 9 – summation of the solar yield Q_{MA}, the geothermal energy Q_{geo}, heat source Q_{source}, and energy balance Q_{balance} over the heating season for an absorber size of 22.5 m^2.

The heating season starts in September, when the heat demand Q_{source} is low and solar radiation still allows for a positive energy balance Q_{balance} of the storage, i.e., heat content. In mid-winter the solar yield Q_{MA} is low, while the heat demand is at its highest, resulting in a decreasing energy balance. The storage temperature decreases and allows for solar yield at low temperatures of the heat transfer fluid in the second half of the heating season. In March the solar yield exceeds the heat demand, and the energy balance increases. At the end of the heating season in May, the energy balance of the storage is still negative. Further regeneration in the summer month is required to fully regenerate the storage reaching a

neutral balance of the storage at the beginning of the next heating period in September.

As shown in the example for an absorber size of 22.5 m², the regeneration during the winter covers most of the heat demand by the heat pump. The absolute and relative values of the solar contribution for the different absorber sizes are shown in figure 10. With increasing size if the solar absorber, the annual solar yield increases from 3,200 to 4,900 kWh. When considering coverage rate, two ratios are of interest. The first is the rate of solar yield during winter to the total annual solar yield ($Q_{\mathrm{MA}}\mathrm{HS}/Q_{\mathrm{MA}}$). The second is the rate of solar yield during winter to the evaporator heat demand ($Q_{\mathrm{MA}}\mathrm{HS}/Q_{\mathrm{source}}$). The in-season share of the solar yield ($Q_{\mathrm{MA}}\mathrm{HS}/Q_{\mathrm{MA}}$) is about 60% for all absorber sizes. The second rate ($Q_{\mathrm{MA}}\mathrm{HS}/Q_{\mathrm{source}}$) rises with the absorber size, expressing a 51% to 73% coverage of the heat demand. These rates are implicitly influenced by the storage temperatures and geothermal heat. In general, the values found for both rates point out the medium-term character of the storage.

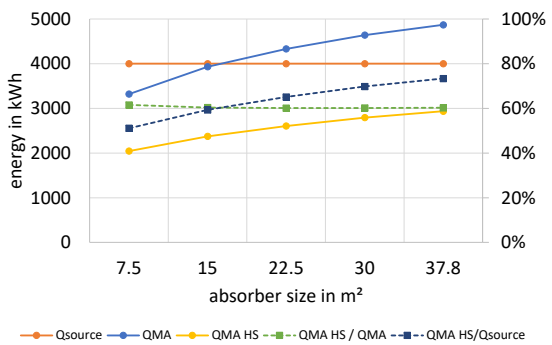

Fig. 10 – solar yield during the heating season $Q_{\mathrm{MA}}\mathrm{HS}$ and total Q_{MA}, heat source Q_{source} (left ord.); solar rates $Q_{\mathrm{MA}}\mathrm{HS}/Q_{\mathrm{source}}$ and $Q_{\mathrm{MA}}\mathrm{HS}/Q_{\mathrm{MA}}$ (right ord.).

3.5 optimal absorber size

As mentioned earlier, frost in the ground collector storage should be avoided. Therefore, the temperature outside the ground collector tube must stay above 0 °C. Temperatures of the heat transfer fluid slightly below 0 °C are acceptable at the inlet of the ground collector if there is no phase change on the outside of the tube. For this purpose, the heat carrier temperature, and the temperature of the ground in contact with the underground collector has been investigated. Figure 14 shows the minimum values of the fluid inlet temperature T_{in}min and of the temperature of the outer tube wall of the collector T_{T}min occurring in the course of the heating season for different sizes of the solar system. As shown in figure 14 the minimal temperature outside the tube is about 1 K higher than the minimal inlet temperature, independently from the size of the solar absorber. For practical application it must be assessed how often situations with formation of frost occur within the course of the heating season. For a limited duration, such situation can be bridged using an electrical heater. Yet, regarding the desired high energetic efficiency, the use of the electric heater should be avoided.

The grey line in figure 11 shows the annual occurrence of situations with potential formation of frost (T_{T}<0 °C, in hours per year). According to the result of the system analysis, a size of the massive solar absorber of 7.5 m² is insufficient for an efficient operation of the heating system. The solar collector should have a surface area of about 20 m² or larger. Therefore, in the following section an absorber size of 22.5 m² is chosen.

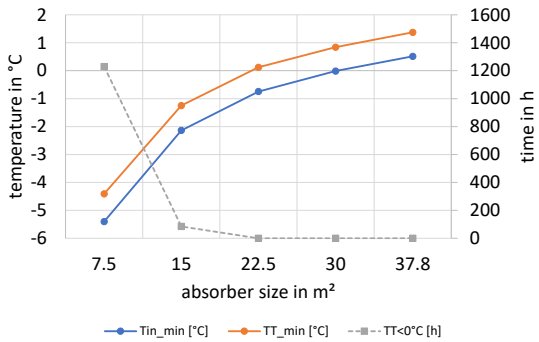

Fig. 11 – minimal temperature at the inlet T_{in}min and outside the tube T_{T}min (left ord.); frost occurrence (right ord.).

4. Balance of the storage in winter

For the selected absorber size frost is avoided in the modelled system configuration. However, this might only be true for the given weather condition of the TRY. In this chapter the characteristics of the storage in the middle of the winter are investigated further, to acquire knowledge about the general prerequisite for a frost-free operation of the storage. The critical time is in January and February during the lowest ground temperatures.

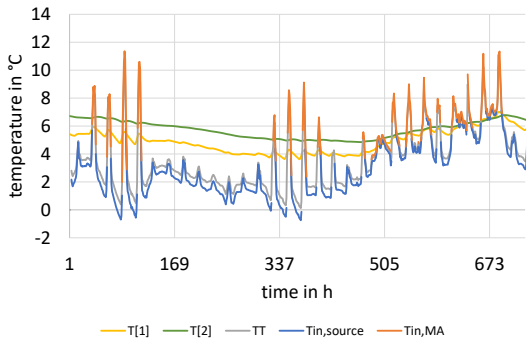

Fig. 12 – temperature in the first $T[1]$ and second $T[2]$ storage block, temperature around the tube T_{T}, inlet temperatures in the storage from the heat pump $T_{\mathrm{in,source}}$ and the massive absorber $T_{\mathrm{in,MA}}$ in January.

Frost occurs when water around the ground collector tube cools below 0 °C and freezes. To avoid frost, the earth around the collector tube must stay above freezing temperature. This temperature is influenced by heat extraction from the heat pump, regeneration by the solar massive absorber, and relaxation from the storage below the collector tubes. The influencing inlet temperatures of the heat transfer fluid ($T_{\mathrm{in,source}}$ for heat extraction, $T_{\mathrm{in,MA}}$ for heat input into the storage) are shown in figure 12.

For relaxation, heat is exchanged between the storage blocks as well as between the first block and the earth around the tube T_T, governed by the respective temperature differences. When no heat is extracted or regenerated, the storage relaxes and the temperature around the tube converges to the temperature of the first storage block.

The daily energy balance in the top of the storage is analysed to quantify the energy flows. The temperature around the tube is fluctuating based on the alternating weather condition during the daily cycles. The net energy flow Q_{net} from or to the heat transfer fluid is calculated by equation (7). The daily energy sums of the heat transfer fluid for January and February are shown in figure 13. Although there is solar yield on 41 out of 60 days, the net energy is positive only for 12 days.

$$Q_{\text{net}} = Q_{\text{source}} + Q_{\text{MA}} \tag{7}$$

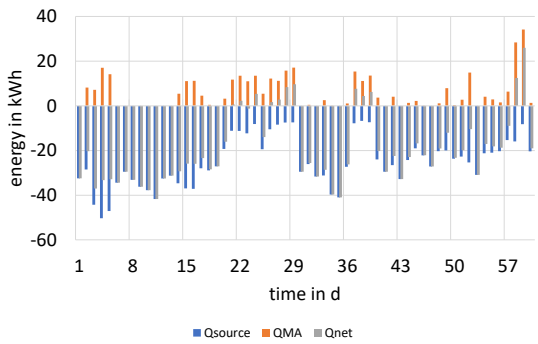

Fig. 13 – solar yield Q_{MA}, heat source Q_{source}, and energy balance Q_{net} in January and February.

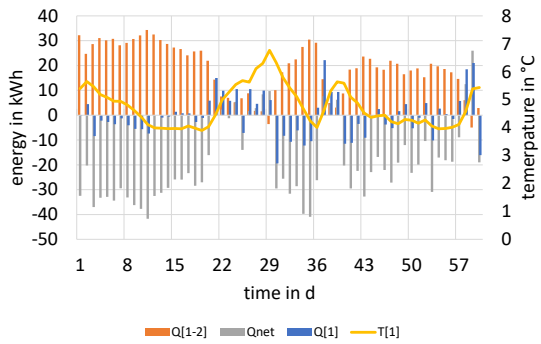

Fig. 14 – daily net energy Q_{net}, heat transfer between the first and second block $Q[1\ 2]$, and energy balance of the first block $Q[1]$ (left ord.); daily average temperature in the first block $T[1]$ (right ord.) in January and February.

Whenever the net energy is negative, the temperature around the tube decreases and heat from the storage flows towards the tube to level out the temperature difference. Therefore, the temperature of the first block is analysed by calculating the energy balance in the first block $Q[1]$ in equation (8). The heat $Q[1]$ supplied to block 1 is obtained by summation of the net energy flow Q_{net} exchanged via the heat collector and the heat transfer between the first and the second block $Q[1\ 2]$, calculated in equation (9), analogously to equation (6). Since the heat flow $Q[1]$ adds or subtracts to the heat content of the first block, the temperature alternates accordingly. The analysis demonstrates that the energy balance of the first block is alternating, but balanced over the two winter months, as expressed by the temperature of block $T[1]$ displayed in figure 14.

$$Q[1] = Q_{\text{net}} + Q[1\ 2] \tag{8}$$

$$Q[1\ 2] = (T[2] - T[1]) \cdot \frac{\lambda}{d} \cdot A \tag{9}$$

5. Conclusion and outlook

In this paper a heat pump system with two building-integrated low-tech heat sources, a massive solar-thermal collector regenerating a medium-term ground collector storage, is analysed theoretically. It is shown that the heat storage can be effectively recharged during the heating season, allowing for reduced size and cost of the storage. It is found that an absorber size equal to 15% of the ground collector is required to operate the heating system, avoiding freezing of the underground heat storage. A small absorber size will allow for minimal investment cost. Whereas larger absorbers result in higher storage temperatures and consequently in higher efficiency of the heat pump heating system.

The medium-term character of the storage is pointed out. The critical months in winter are evaluated regarding the risk of frost and the energy balance at the top of the storage.

Further investigations will include different ground collector storage configurations and the use of ambient air as an additional heat source.

6. References

[1] Bundesverband Wärmepumpe. www.waerme-pumpe.de/presse/zahlen-daten/. 1.6.2021

[2] Günther D., Wapler J., Langner R., Helmling S., Miara M., Fischer D., Zimmermann D., Wolf T., Wille-Hausmann B. WPsmart im Bestand – Feld-untersuchung optimal abgestimmter Wärme-pumpenheizungssysteme in Bestandsgebäuden beim Betrieb im konventionellen sowie im intelligenten Stromnetz (Smart Grid). 2020

[3] Novo A., Bayon J., Castro-Fresno D., Rodriguez-Hernandez J. Review of seasonal heat storage in large basins: Water tanks and gravel–water pits. 2010

[4] Tanzer B., Schweigler C., Eberherr H., Laumer R. Abschlussbericht des Forschungsvorhabens: Solarwärmesystem für die Beheizung von Industriehallen mit Massivabsorber und Saisonwärmespeicher. 2017

[5] Gesellschaft Verfahrenstechnik und Chemieing-enieurwesen. VDI-Wärmeatlas. 2013; 11: 718

[6] Verein Deutscher Ingenieure. Thermal use of the underground. Fundamentals, approvals, environ-mental aspects. VDI 4640 part 1. 2010.

Data Statement

The dataset generated is available on demand through direct contact to the author.

Impact of the Weather Forecast Quality on a MPC-driven Heat Pump Heating System

Sebastian Hummel, Christina Betzold, Arno Dentel

Energy Efficient Building Systems, Institute of Energy and Building (ieg), Technische Hochschule Nürnberg Georg Simon Ohm, Germany, sebastian.hummel@th-nuernberg.de.

Abstract. Electrically driven heat pumps offer in combination with thermal energy storage systems the potential to response to fluctuating renewable energy sources, e.g. photovoltaics. To fully exploit this flexibility and financial potential, smart predictive control strategies such as Model Predictive Control (MPC) are needed. For such a controller, weather forecast data are mandatory to perform the optimization. Several sources of weather forecast data are available with variable forecasting quality. In this study, the impact of the weather forecast quality on a realistic heat pump heating system is investigated in experiments and simulations. Therefore, the operation of a MPC strategy is carried out for a perfect forecast compared to two imperfect forecast scenarios over a consecutive period of 4 days on a Hardware-in-the-Loop test bench with a geothermal heat pump and a thermal energy storage system. In order to evaluate the benefits in real operation compared to rule-based controllers, a heat-controlled (HC) and a PV self-consumption optimized controller (PVC) are also operated on the test bench. In addition and as a validation process, all scenarios are simulated and compared to the measurement results. Compared to a standard rule-based HC strategy the PV self-consumption can be increased by using a PVC and MPC strategy by 6.2 % and 38.9 %, respectively. The accurately the weather forecasting quality is in general the higher the performance of the HP heating system. Thus, the PV self-consumption is reduced for high-quality and low-quality weather forecasts by 4.6 % and 11.1 %, respectively, compared to a perfect MPC. Even a MPC with low-quality weather forecast data can achieve higher system performance as a simple rule-based HC strategy. For achieving higher system performance by using a MPC instead of a rule-based control strategy like PVC the, forecasting quality has to be as accurate as possible.

Keywords. model predictive control, weather forecast, self-consumption, experimental study
DOI: https://doi.org/10.34641/clima.2022.152

1. Introduction

The demand-side flexibility of residential buildings is becoming more and more relevant to operate and stabilise the power grid properly. The heating (and cooling) demand of such a building can be regarded as flexible in terms of shifting and storing electrical energy in both battery and thermal energy storage systems. Electrically driven heat pumps offer in combination with thermal energy storage systems the potential to response to fluctuating renewable energy sources, e.g. photovoltaics. To fully exploit this flexibility and financial potential, smart predictive control strategies, such as Model Predictive Control (MPC), are mandatory.

A MPC strategy rely basically on solving an optimization problem periodically, by considering weather forecast data, e.g. the solar irradiance and the ambient temperature, in combination with a system model to optimize the subsequent control sequence. Its accuracy is occasionally based on the model complexity and, if applicable, the weather forecast quality. MPC strategies have shown a major interest in recent research [1, 2], as they provide advantages in terms of operational cost savings, system performance, indoor comfort and energy flexibility. Operational cost savings for a MPC strategy of up to 11 % and 16 % for constant and flexible electricity prices, respectively, were determined by Fischer et al. [3] in comparison to a standard rule-based controller. For a similar comparison, Bechtel et al. [4] exhibited cost savings of up to 24 % for a single-family house and flexible electricity prices. Pichler et al. [5] carried out an annual simulation study on an MPC-driven heat pump heating system. They determined an increase of the photovoltaic self-consumption of up to 30 % in a single-family household.

The literature on MPC strategies, which investigates

Copyright ©2022 by the authors. This conference paper is published under a CC-BY-4.0 license.

the weather forecast in general, utilizes keywords such as "perfect", "idealized" or "optimal" MPC to refer to operating conditions exhibit an agreement between the weather forecast and the measured ("real") weather conditions. Such kind of conditions can only be met in simulations, where the forecast data is well known. Thus, a perfect MPC can be considered as a benchmark for other control strategies, e.g. rule-based strategies or MPC strategies with lower forecast quality, to determine the upper limits of the benefits under optimal forecasting conditions. In general, it is not applicable to field test operation. Such a benchmark study was carried out by Mendoza-Serrano and Chmielewski [6]. The authors compared a MPC-driven heating, ventilation, and air conditioning (HVAC) system provided with perfect and "zero" forecast information. Compared to their reference situation, they exhibited cost reductions for the perfect and the "zero" forecasts of up to 31 % and 27 %, respectively. The authors emphasizes the strong influence of the forecast information on the system performance. Allen et al. [7] determined cost savings of up to 13.1 % with a perfect forecast and 11.1 % with a non-ideal forecast. A reduction of the overall system energy consumption of the heating system in a single family house of up to 15 % was simulated by Rolando et al. [8] by means of TRNSYS simulations. The authors implemented a predictive rule-based controller, to which the perfect solar irradiance forecast was applied to over the whole heating season. Lazos et al. [9] reviewed the potential of energy and cost savings in commercial buildings by implementing an optimized energy management algorithm. The authors highlighted the strong influence of high quality weather forecast data on the accuracy of predicting the evolution of the building load or energy generation. However, they stated possible savings from 15 % up to 30 %, by using rather weather predictive than non-weather sensitive control strategies. Löhr and Mönnigmann [10] compared a "yesterday-based" prediction, which utilizes the previous day weather data as prediction for the subsequent day, to a controller with a perfect forecast. Both controllers performed well. They concluded, that the system performance decreases only slightly by using historical / yesterday weather data as the tomorrow's forecast. Péan et al. [11] carried out an experimental study to evaluate the weather forecast quality on the performance of a MPC controlled air-to-water heat pump in cooling mode in a residential building. Within a three day testing profile, they compared a perfect weather forecast to a (imperfect) forecast from a commercial service. The setup with imperfect forecast resulted in an increase of the total electrical energy demand and the operational costs of 5.8 % and 11.2 %, respectively.

Our literature review reveals, that commonly a perfect MPC strategy is compared to both a rule-based algorithm and a MPC strategy with no weather forecast data. Nowadays, more and more devices / controllers are connected with the internet or can be equipped with receiving aerials and thus, have access to historical or forecast weather data. Especially the quality of the weather forecast services, which rely basically on the forecast horizon and the used forecasting model, and their influence on a heat pump heating system have to be investigated. Furthermore, most of the reviewed articles are based on simulative investigations and did not consider the operation in a realistic heat pump heating system. In a previous simulative study, Betzold et al. [12] compared different control strategies of a geothermal heat pump heating system. The authors emphasized cost savings of 3 % to 10 % by utilizing a MPC controller instead of a rule-based control strategy. An experimental verification of the cost savings potential is of particular importance in a realistic operation environment due to the low differences achieved in the simulations.

In this study, the impact of the weather forecast quality on a realistic heat pump heating system is investigated. Therefore, the operation of a MPC strategy is carried out for a perfect forecast compared to two imperfect forecast scenarios over a consecutive period of 4 days on a Hardware-in-the-Loop test bench with a geothermal heat pump and a thermal energy storage system. In order to evaluate the benefits in real operation compared to rule-based controllers, a heat-controlled (HC) and a PV self-consumption optimized controller (PVC) are also operated on the test bench. In addition, as kind of a benchmark or validation process, a preliminary simulative study of the above mentioned MPC, HC and PVC strategies is carried out and is compared with the measurement results.

2. Research Methods

In order to implement MPC strategies, knowledge about the expected thermal behaviour of the building (heating and domestic hot water demand), the moment and the amount of renewably generated energy gain as well as the operating behaviour of the technical building equipment is necessary. Additionally, for weather-based MPC strategies weather forecasting services or historical weather data have to be implemented.

2.1 Weather data

The basic requirement for a weather-dependent MPC strategy is weather forecast data in good quality, to achieve the best possible benefits in terms of cost savings or increase of system performance. For this study, three different sources of weather data are utilized, to create a profile of five consecutive days: measured / real weather data and two types of forecasting services.

All sources provide the solar irradiance G and the ambient temperature T_a in 15 minutes intervals for the location of the suburban district "Herzo Base" of the city of Herzogenaurach (Germany) for the 7th until the 11th of March, 2021, as can be seen in Figure 1. The measured weather data (abbr. and index MEAS), which were recorded with appropriate sensors on

the roof a single-family house at the mentioned location, is used as the perfect weather forecast in the experiments and simulations. Furthermore, an internet-based Weather Forecast Service (WFS) and an installed Weather Forecast Centre (WFC) provide forecast data at the given location and period of time. The latter represents a long wave receiver, which receives its data from a commercial service.

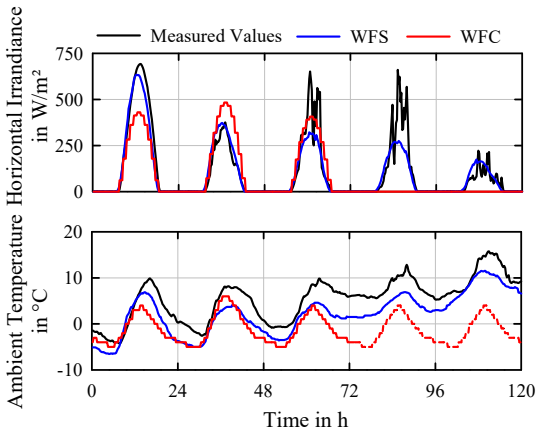

Fig. 1 – Horizontal irradiance and ambient temperature profiles of the three different weather data sources for five consecutive days from for the 7th until the 11th of March, 2021.

It is worth noted, that the WFC does not provide any valid weather data starting off 1 am of the 4th day of the selected period of time. The received data shows constant values of $G = 0$ W m^{-2} and no data for T_a, which indicate communication faults. An inspection of the received data of 2021 shows that communication faults occur regularly and frequently. At 25.6 % of the time no or faulty data was received. In addition, the transmission is normally interrupted in longer consecutive time intervals. Thus, the selected interval of time for this evaluation represents the typical data availability for this weather forecasting service. For any further evaluation, the values of the irradiance are set as received, whereas the ambient temperature is set to values recorded 24 h earlier. Thus, the 4th and 5th day of the WFC profile is almost equal to the 3rd day, as can be seen as the dotted red line in Figure 1.

Qualitatively the three profiles resemble each other in temporal progression, but exhibit some major differences in their absolute or integral values. The horizontal irradiation for the whole five days aggregates to 13.3 kWh m^{-2}, 11.7 kWh m^{-2} and 9.3 kWh m^{-2} for the measured, the WFS and the WFC profile, respectively. The maximum deviations can be identified between the measured and the WFC profile on the 1st day, with a difference of 1.7 kWh m^{-2}. The mean ambient temperature can be calculated to 5.4 °C, 2.2 °C and – 1.2 °C for the measured, the WFS and the WFC profile, respectively. Without regarding the non-valid ambient temperatures of the WFC profile, a maximum difference of up to 10 K can be reported at the end of the 3rd day (72 h) between the measured values and WFC profile. Whereas the temporal progression of the temperature only influences the heating demand of the simulated building, the solar irradiance influences both the building simulation (internal solar gains) and the PV generation.

The WFC profile features the highest deviation to the measured (perfect) weather data in all aspects. Thus, this weather data set is referred to as "low-quality" in terms of the forecasting quality. In contrast, the WFS profile performs significantly better and is referred to as "high-quality".

2.2 Building simulation

By means of TRNSYS building simulations the profiles of the space heating load of a single family house (SFH) is simulated on the basis of the three given weather data sets. As a basic system and building concept the SFH and heating system, described in the IEA SHC TASK32 by Heimrath and Haller [13], are used. They defined a SFH with three types of building standards in terms of their annual area-related heating demand, namely SFH30, SFH60 and SFH100. E.g. the building SFH60 exhibits an annual heating demand of approximately 60 kWh m^{-2}. Each building type have a heated gross area of 140 m^2. Some minor changes were made on the pre-defined standard values of the simulation, to adapt the simulated heating system to our test bench, e.g. the volume of the thermal energy storage. For this investigation the building standard SFH60 and no domestic hot water demand are considered. This building standard is quite similar to the buildings at the suburban district "Herzo Base".

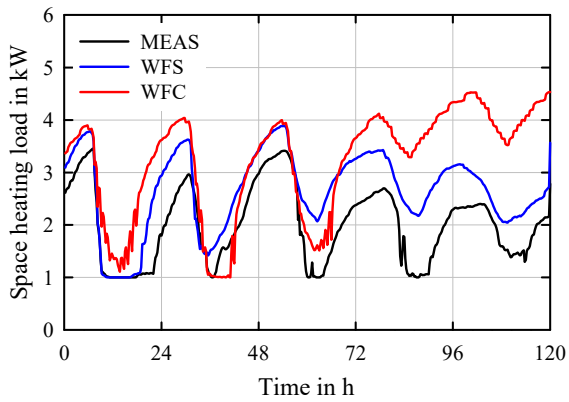

Fig. 2 – Space heating load profiles for the building standard SFH60 and the three considered weather data sets. Due to limitations in terms of its controllability of the used test bench, the space heating load is increased by 1 kW at each time step.

The profiles of the space heating load for the building standard SFH60 and the three considered weather data sets can be seen in Figure 2. As the measured weather data shows the highest irradiation and mean ambient temperature, the heating loads and the heating demand is accordingly low. Due to the partially non-valid weather data of the WFC profile the space heating load rises gradually after 72 h and lead to a significantly increased heating demand.

Tab. 1 – Total heating demand of the defined building standards by Heimrath and Haller [13] and the three considered weather data sets. Only SFH60 is considered in any further investigations.

Building standard	MEAS in kWh	WFS in kWh	WFC in kWh
SFH30	152.2	202.4	252.1
SFH60	**240.6**	**318.1**	**387.5**
SFH100	350.5	454.6	544.9

In total, an amount for the space heating demand of 240.6 kWh, 318.1 kWh and 387.5 kWh can be calculated for the measured, WFS and WFC weather profile, respectively (see Table 1). The test bench used possesses a limitation in terms of its controllability of the requested heating load. Values of the heating load lower than 1 kW can result in control deviations between the set and actual value, which normally results in higher heating demands as expected. To overcome this limitation, the simulated space heating load profiles are raised by 1 kW at each time step, as can be seen in Figure 2.

2.3 Photovoltaic generation profile

For each weather data set the photovoltaic (PV) generation profile is simulated in advance to the experimental study. The PV load is calculated in accordance with an isotropic sky model by Shukla et al. [14] on the basis of the horizontal irradiance, the PV area (40 m²), the inclination angle (60°, c.f. the slope of the roof of the reference building) and the efficiency of the PV modules (17.89 %) and inverter (95 %).

The resulting PV generation profiles can be seen in Figure 3 with maximum values of up to 5.2 kW. The total amount of PV generation within the period of five days is 93.1 kWh, 78.5 kWh and 66.4 kWh for the measured, the WFS and the WFC weather data profile, respectively.

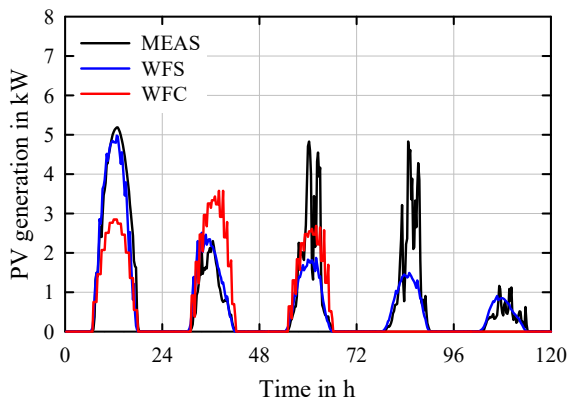

Fig. 3 – Photovoltaic generation profiles for the three considered weather data sets.

2.4 Residential load profile

Both for the preliminary simulations as well as the experimental study a residential load profile is mandatory. In combination with the PV generation a surplus in the electrical energy of the building can occur. This enables the controller to operate the heat pump in a flexible and dynamic way. Combined with the electrical load of the heat pump, the residential load is responsible for the total electrical energy consumption of the building. The residential load profile is based on measured data of one of the buildings, on which the measured weather profile was performed. The time span is identical to that of the weather profiles.

The residential load profile and the PV generation profile for the measured weather data set can be seen in Figure 4. Thus it appears that residential and PV peak loads rarely occur simultaneously. Normally PV peak loads result from high solar irradiance at noon, whereas the residential peak loads rather appear in the evening hours. The total residential energy consumption is 48.1 kWh with a baseload of approximately 0.2 kW.

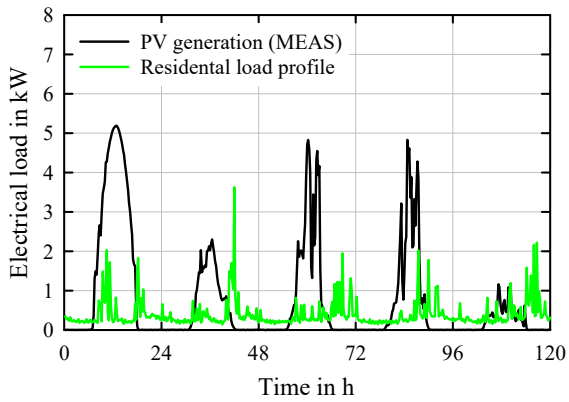

Fig. 4 – Residential load and PV generation profile.

2.5 Hardware-in-the-Loop test bench

The comparative experimental study is carried out on a Hardware-in-the-Loop (HiL) test bench, which combines several heat generation units and a variety of thermal energy storage systems (TES). The heating demand, the domestic hot water demand and the source temperature of the heat pump are emulated. The HiL concept ensures a flexible, dynamic and realistic investigation of one single component or the whole heating system.

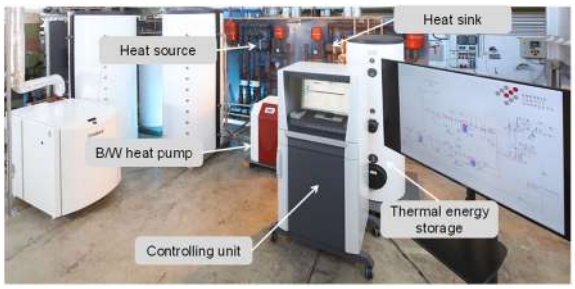

Fig. 5 – Hardware-in-the-Loop test bench for innovative heating systems at TH Nürnberg.

In this study, a brine/water heat pump (HP) is utilized in combination with a 500 litres TES. The HP exhibits a standard heating power of 10.9 kW and an electrical power of 2.2 kW at its operating point B0/W35. A Coefficient Of Performance (COP) of 4.9 is

obtained. The test bench and its main components used for this contribution can be seen in Figure 5. A hydraulic scheme and the installed sensors are presented in Figure 6.

Throughout the experimental study, standard manufacturers' settings for the HP internal controller are set. However, operationally relevant settings were changed, e.g. the monoenergetic or the return line temperature set point related operational mode. To ensure, that the external control strategy (MPC, PVC or HC) can switch on/off the HP properly, without being omitted by the internal HP controller, the return line temperature set point is set to 55 °C. The evaporator of the HP is provided with almost constant temperatures $T_{evap,FL}$ of 10 °C.

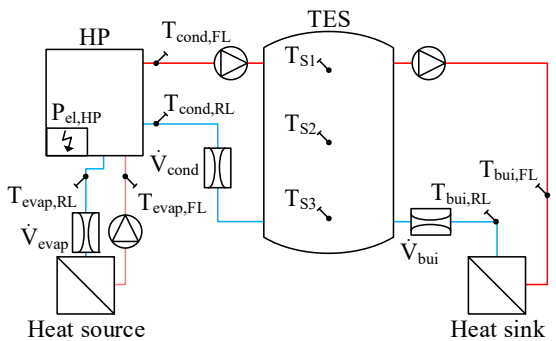

Fig. 6 – Hydraulic and sensor schema of the Hardware-in-the-Loop test bench at TH Nürnberg.

Appropriate sensors are installed in the HiL test bench for a detailed evaluation of the thermal behaviour of the HP heating system, as can be seen in Figure 6. The outgoing heating demand of as well as the delivered heating load to the TES can be assessed separately. The electrical power of the HP is measured by an energy meter. In addition, three temperature probes are installed equally spaced over the height inside the TES, to estimate the State Of Charge (SOC) or the storage stratification.

2.6 Simplified system simulation model

For the described control strategies (MPC, PVC and HC) a simulation model of the HP heating system is mandatory, to evaluate the SOC of the TES. The SOC is a main feature of each control strategy, to regulate the HP operation. As described by Hummel et al. [15] and Betzold and Dentel [16], a simplified system model is sufficiently accurate at frequently update intervals of the control strategy.

In accordance with Betzold et al. [12], the TES is assumed to be fully mixed, as it is represented as one single temperature node T_S in the simplified system model. As the TES is stated as the main storage component in the heating system its energy balance

$$C_S \frac{dT_S(t)}{dt} = \dot{Q}_{HP}(t) - \dot{Q}_{Load}(t) - \dot{Q}_{S,loss}(t) \qquad (1)$$

can be calculated as a function of the heat pump heating power $\dot{Q}_{HP}$, the space heating load $\dot{Q}_{Load}$ and the storage ambient heat losses $\dot{Q}_{S,loss}$.

The storage capacity C_S is equal to the product of the storage volume V_S = 500 litres, the fluid density ρ_W = 1000 kg m^{-3} and the fluid specific heat capacity $c_{p,W}$ = 4.18 kJ kg^{-1} K^{-1} (both for water). The heating power $\dot{Q}_{HP}$ is assumed to be constant and is set to a typical mean operating point, which occurs during the simulations and experiments (B10/W40). Based on heat pump efficiency measurements on the test bench, the heating power and the electrical power is set to constant values of $\dot{Q}_{HP}$ = 12.94 kW and $P_{el,HP}$ = 2.45 kW, respectively, in operation of the heat pump. Likewise, the ambient heat losses are assumed to be constant with $\dot{Q}_{S,loss}$ = 0.043 kW. The building thermal load $\dot{Q}_{Load}$ can be calculated from an energy balance between the TES and the heat sink. However, the space heating load profiles are predetermined by the building simulation (see Figure 2).

2.7 Model Predictive Control

In this research, a mixed-integer linear programming (MILP) optimization algorithm is used, as described by Betzold et al. [12], which is based on the simplified system simulation model. The MPC is realized in MATLAB [17]. The operating limits are defined by a minimal and maximal storage temperature of 25 °C and 45 °C, respectively, as well as by the complete cover of the thermal and electrical load. The cost function is based on operating costs for the residential load, the heat pump electrical power and the PV generation separated in grid feed-in, grid consumption or PV self-consumption. The assumed prices for each type of electricity are listed in Table 2. The price for PV self-consumption includes taxes and insurance.

Tab. 2 – Electricity prices used for the MPC cost function.

Type of electricity	Price in €/kWh
Grid consumption	0.34
PV self-consumption	0.0883
PV / Grid feed-in	0.11

The optimization horizon is set to 24 h with an optimization time step and optimization interval of 15 minutes both. Thus, every 15 minutes the MPC is restarted with new initial boundary conditions to generate the subsequent control sequence. As the optimization horizon is set to 24 h and the weather profiles provide a five day period of data, the experiments and simulations can only last four consecutive days (96 h).

2.8 Evaluation metrics

A robust evaluation of the experiments or simulations in terms of operational costs or cost savings is only possible, if the total runtime of the heat pump is similar in each scenario. Differences in the operational costs then exclusively occur due to the point in time, when the heat pump is switched on beneficially, thus at high PV generation and at most no grid consumption. But in the experimental study the overall runtimes exhibit differences in each scenario. Mainly

caused by a non-documented variable compressor after-run time, a difference of 0.2 h is accumulated over the 4 day period between two scenarios, even if the amount of start-up events are equally. This amount of time corresponds to an increase of electrical energy of about 0.5 kWh and causes an increase in operational cost of up to 0.16 € (c.f. Table 2). In contrast, both the absolute operational costs and the operational cost differences between the examined scenarios are such low, that the influence of the weather forecast quality cannot be evaluated in terms of operational costs. Thus, we define other system parameters to assess the experiments and simulations properly.

PV self-consumption: The fraction of PV generation, which is consumed directly within the building (residential or heat pump electricity) is referred to as the PV self-consumption.

Self-sufficiency: The fraction of the total building energy demand (residential plus heat pump electricity), which can be covered by the PV generation is referred to as the self-sufficiency of the building.

Mean State Of Charge (SOC): The mean SOC value of the thermal energy storage is calculated over the measurement or simulation period of 96 h. This value can be referred to as its mean thermal workload within the operating limits of 25 °C (0 %) and 45 °C (100 %) of the storage temperature.

3. Preliminary simulation study

As a validation process, a preliminary simulative study is carried out in MATLAB and is compared with the measurement results. This investigation focuses primarily on the influence of different types of control strategies on a HP heating system. The main objective is the validation of the functionality of the HiL test bench as well as the confirmation of the results presented by Betzold et al. [12]. Beside the MPC, a PV self-consumption optimized Control (PVC) and a Heat Controlled (HC) strategy is implemented. Further details of this rule-based algorithms are presented by Betzold et al. [12]. On the basis of the measured weather data set and for each of the control strategies (MPC, PVC and HC), the HP heating system is examined experimentally on the test bench and via simulations in MATLAB.

In general, the metrics of the simulations agree well with the experimental measurements in a qualitative perspective, as can be seen in Figure 7. The measured PV self-consumption exhibits a high accordance with the simulation results. The differences between the measured and the simulated values for the MPC and PVC control strategy amount to 0.1 and 0.2 percentage points, respectively. The difference for the HC strategy is slightly higher and can be calculated to 1.7 percentage points. A similar high accuracy can be evaluated for the mean SOC value. Differences up to 2.3 (MPC) and 0.4 (HC) percentage points can be identified. The measured values of the PVC strategy do not exhibit any deviation. The measured values of the self-sufficiency of the HP heating system possess an increase by a mean value of 4 percentage points compared to the simulation.

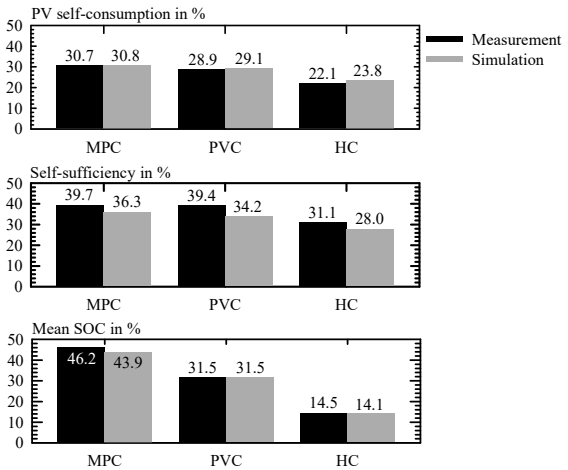

Fig. 7 – Comparison of the considered system evaluation metrics between measured and simulated data for each control strategy (MPC, PVC and HC) on the basis of the measured weather data set.

The influence of the control strategy on the system performance can be investigated as well by the considered evaluation metrics. Obviously the MPC strategy offers the highest system metrics / performance in all considered aspects. The PV self-consumption of the test bench experimental run possesses for the MPC, the PVC and the HC strategy values of 30.7 %, 28.9 % and 22.1 %, respectively. Thus, a reduction of 5.9 % (PVC) and 28.0 % (HC) compared with the MPC strategy is determined. Similarly, a reduction of the measured self-sufficiency of 0.7 % (PVC) and 21.7 % (HC) to the MPC strategy is identified. The storage capacity of the TES is used more beneficial, if a (perfect) MPC is implemented instead of a rule-based algorithm. The mean SOC value increases significantly from 14.5 % (HC) to 46.2 % (MPC).

4. Comparison of the weather forecast quality

Three experimental measurements on the HiL test bench are carried out to investigate the influence of the weather forecast quality on the MPC strategy and thus, on the HP heating system performance. The deployed MPC algorithm, which is utilized in each experiment, uses the space heating load profiles, the residential load profiles and the PV generation profiles resulting from either the perfect weather data set (MEAS), the high-quality WFS profile and the low-quality WFC profile (cf. section 2.1). Again, the measurements last a period of four days.

Highest values in all considered aspects can be determined for the perfect MPC. Thus, a clear progression is obviously visible for all evaluation metrics, as can be seen in Figure 8. The PV self-consumption of the perfect MPC achieves maximum values of 30.7 %, whereas the values of the WFS and WFC data set slightly decrease. With the high-quality WFS profiles

and the low-quality WFC profiles the PV self-consumption amounts to 29.3 % and 27.3 %, respectively. This reduction is equal to a decrease of 4.6 % (WFS) and 11.1 % (WFC) compared to the perfect MPC strategy. Similar reductions can be determined for the self-sufficiency, at which the perfect MPC obtained values up to 39.7 %. Compared to the perfect MPC the self-sufficiency is reduced for the WFS profiles and WFC profiles by 2.5 % and 8.8 %, respectively.

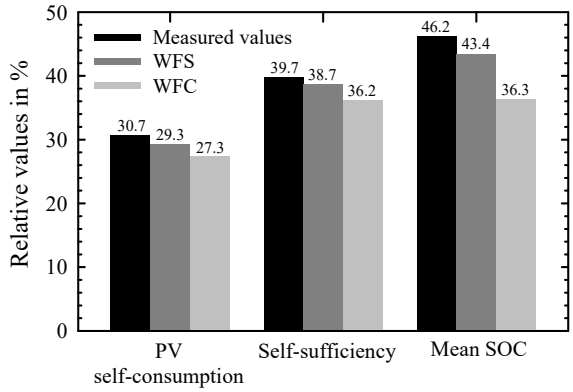

Fig. 8 – Considered system evaluation metrics for each weather data set (MEAS, WFS and WFC) in comparison.

The thermal capacity of the TES is used in the most efficient and beneficial way for the perfect MPC and achieves mean SOC values of 46.2 %. This is equal to a useful energy of about 5.4 kWh. A significant decrease of 9.9 percentage points (-21.4 %) can be calculated for the mean SOC between a perfect MPC and a MPC with low-quality weather forecast. It is worth noted, that the TES, driven by low-quality WFC profiles, fall below the minimum storage temperature of 25 °C, whereby the space heating demand cannot be covered. Negative SOC values down to -1.7 % can be determined.

5. Conclusions

The functionality of the HiL test bench is validated by means of system simulations compared to measurements with equal boundary conditions. The considered metrics of the simulations agree well with the experimental measurements. In regard to the PV self-consumption and the mean SOC a high accuracy with low deviations between simulations and measurement can be achieved. Significantly higher differences are determined for the self-sufficiency. Due to significantly higher HP runtimes in the simulations, the electrical energy demand is increased, which increases the total building energy demand as well. As a result, the self-sufficiency of the building is negatively influenced. The longer HP runtimes in the simulations can be caused by the simplifications in the HP model of the simplified system model.

The influence of the control strategy on the system performance is investigated for a MPC, PVC and HC strategy on the test bench. In contrast to a rule-based control strategy (e.g. PVC and HC), a MPC offers the highest system performance in all considered aspects. The HC strategy operated the HP heating system in a non-optimized manner. The main objective of this strategy is to cover the space heating demand at any time. Due to the fact that the highest space heating demands occur at night-time, the heat pump is predominantly operated at this time. The storage temperature as well as the SOC is kept as low as possible. However, the PV generation is contracyclical to the space heating demand. Furthermore, the HC has no built-in option to operate the HP in more efficient periods of time. Thus, the grid consumption is increased and PV self-consumption or building self-sufficiency is accordingly lower. Compared to a MPC, the PVC strategy performs quite well. It offers the possibility to operate the HP in a PV optimized manner. The considered evaluation metrics are marginally lower, compared to the MPC. The significant increase in the mean SOC value of 7.1 percentage points compared to the HC strategy reveals a charging of the TES, if high PV generation is available. This strategy enables the ability to react to the fluctuating renewable energy source. We conclude, that a MPC significantly offers a more beneficial operating strategy compared to rule-based controllers. The space heating load and PV generation profiles, resulting from either the perfect (measured) weather data set (MEAS), the high-quality WFS profile and the low-quality WFC profile, are utilized by means of three experimental measurements on the HiL test bench, to investigate the influence of the weather forecast quality on the system performance. In general, the perfect MPC offers the highest system performance. A perfect weather forecast, which is in this study equivalent to measured data and thus corresponds to the real ambient conditions, can only be met in simulations. The considered high-quality forecast (WFS) is rather applicable to field test installations. However, a clear trend can obviously be determined: the accurately the weather forecasting quality is in general the higher the performance of the HP heating system. E.g. the low-quality weather data set reduces the PV self-consumption and the self-sufficiency of up to 11.1 % and 8.8 %, respectively. Primarily the non-valid weather data given at the 4th and 5th day of the profile lower the ability of the MPC to generate the subsequent control sequence in the most beneficial way. The HP is operated in more unfavourable periods of time in terms of electricity prices and PV generation.

Tab. 3 – Combination of the results from the comparison of different control strategies (PVC and HC) from Figure 7 and different qualities of weather forecast data profiles (MEAS, WFS and WFC) from Figure 8.

Metrics in %	MEAS	WFS	WFC	PVC	HC
PV self-consumption	30.7	29.3	27.3	28.9	22.1
Self-sufficiency	39.7	38.7	36.2	39.4	31.1
Mean SOC	46.2	43.4	36.3	31.5	14.5

Table 3 combines the measurement results of the preliminary study (PVC and HC strategy) and those of the weather forecast quality comparison (MPC

with MEAS, WFS and WFC profiles). The results of the MPC with high-quality WFS profiles are comparable to those of the rule-based PVC strategy. Merely the usage of the TES capacity is more favourable at the MPC. Even a MPC with low-quality weather forecast data (WFC) can achieve higher system performance as a simple rule-based HC strategy. For achieving higher system performance by using a MPC instead of a rule-based control strategy like PVC the forecasting quality has to be as accurate as possible.

6. Acknowledgement

This paper presents results from the projects "Herzo Base - Energy storage houses - An energy flexible building and energy concept of tomorrow" (FKZ 03ET1364A) and "Herzo Opt - Monitoring of the building envelope, thermal room comfort and energy system with operational optimization" (FKZ 03ET1641A). The project is funded by the German Federal Ministry for Economic Affairs and Climate Action based on a resolution of the German Bundestag.

7. References

[1] Péan T., Salom J., Costa-Castelló R. Review of control strategies for improving the energy flexibility provided by heat pump systems in buildings. Journal of Process Control. 2019;74:35–49.

[2] Thieblemont H., Haghighat F., Ooka F., Moreau A. Predictive control strategies based on weather forecast in buildings with energy storage system: A review of the state-of-the art. Energy and Building. 2017;153:485–500.

[3] Fischer D., Bernhardt J., Madani H., Wittwer C. Comparison of control approaches for variable speed air source heat pumps considering time variable electricity prices and PV. Applied Energy. 2017;204:93–105.

[4] Bechtel S., Rafii-Tabrizi S., Scholzen F., Hadji-Minaglou J.-R., Maas S. Influence of thermal energy storage and heat pump parametrization for demand-side-management in a nearly-zero-energy-building using model predictive control. Energy and Building. 2020;226.

[5] Pichler M., Heinz A., Rieberer R. Model predictive heat pump- and building control to maximize PV-power on site use. 12th IEA Heat Pump Conference, Rotterdam, Netherlands. 2017.

[6] Mendoza-Serrano D. I., Chmielewski D. J. Smart grid coordination in building HVAC systems: EMPC and the impact of forecasting. Journal of Process Control. 2014;24:1301–1310.

[7] Allen J., Halberstadt A., Powers J., El-Farra N. H. Supervisory Model Predictive Control of Flexible Building Loads with On-site Solar Generation. Proceedings of the Annual American Control Conference, Milwaukee, USA. 2018;4622–4627.

[8] Rolando D., Madani H., Braida G., Tomasetig R. Heat pump system control: the potential improvement based on perfect prediction of weather forecast and user occupancy. 12th IEA Heat Pump Conference, Rotterdam, Netherlands. 2017.

[9] Lazos D., Sproul A. B., Kay M. Optimisation of energy management in commercial buildings with weather forecasting inputs: A review. Renewable and Sustainable Energy Reviews. 2014;39:587–603.

[10] Löhr Y., Mönnigmann M. Receding horizon heat flow control in domestic buildings- Yesterday-based disturbance predictions. Proceedings of the European Control Conference (ECC), Limassol, Cyprus. 2018;404–409.

[11] Péan T., Bellanco I., Salom J. Impact of the weather forecast on a predictive controller performance: experimental studies with a residential heat pump for space cooling. 13th IEA Heat Pump Conference, Jeju, Korea. 2020, May;11-14.

[12] Betzold C., Bordin S., Dentel A., Harhausen G. Control strategies for modulating heat pumps in a plus energy building. 13th IEA Heat Pump Conference, Jeju, Korea. 2020, May;11-14.

[13] Heimrath R., Haller M. Project Report A2 of Subtask A: The Reference Heating System, the Template Solar System. Task 32, Solar Heating and Cooling Programme, International Energy Agency (IEA). 2007.

[14] Shukla K., Rangnekar S., Sudhakar K. Comparative study of isotropic and anisotropic sky models to estimate solar radiation incident on tilted surface: A case study for Bhopal, India. Energy Reports. 2015;1:96-103.

[15] Hummel S., Betzold C., Kandasamy K., Bordin S., Dentel A. Experimentelle Validierung von Simulationsmodellen an einem Hardware-in-the-loop Wärmepumpenprüfstand. The 8th Conference of IBPSA Germany and Austria, Graz, Austria. 2020. (in german)

[16] Betzold C., Dentel A. Evaluation and test operation of different model predictive control approaches for an energy system. The 17th International Conference of IBPSA - Building Simulation, Bruges, Belgium. 2021.

[17] MathWorks. MATLAB. Version R2020a. 2020.

8. Data access statement

The datasets generated during and/or analysed during the current study are not publicly available because of privacy of the residents but will be available on request with privacy agreement.

From collective to individual decision-making: barriers and opportunities to improve the success rate of the energy retrofits in the Dutch owner-occupied sector

Shima Ebrahimigharehbaghi [a], *Queena K. Qian* [b], *Gerdien de Vries* [c], *Henk J. Visscher* [d]

[a] Faculty of Architecture and the Built Environment, Delft University of Technology, Delft, the Netherlands, s.ebrahimigharehbaghi@tudelft.nl

[b] Faculty of Architecture and the Built Environment, Delft University of Technology, Delft, the Netherlands, k.qian@tudelft.nl.

[c] Faculty of Technology, Policy, and Management, Delft University of Technology, Delft, the Netherlands, G.deVries-2@tudelft.nl.

[d] Faculty of Architecture and the Built Environment, Delft University of Technology, Delft, the Netherlands, H.J.Visscher@tudelft.nl.

Abstract. The building sector can contribute considerably to reducing global greenhouse gas (GHG) emissions. In the Netherlands, the GHG emissions must be mitigated by 95% by 2050 relative to the 1990 baseline. Various factors, such as low renovation rates cause uncertainties in reaching these targets. The current study aims for investigating the barriers and opportunities regarding the energy efficiency renovations (EER) and programs offered by the cities in the Netherlands. Homeowners encounter individually and collectively different forms of barriers during their journeys of EERs. By collective decision-making, we mean when an individual homeowner cannot make the final decision on EER by themselves. Homeowners may have to decide together with other homeowners or even tenants in case of living in a multi-family dwelling. The local authorities sometimes offer the energy efficiency programs at neighbourhood levels and the agreement of most households is essential for the continuation of the energy efficiency programs. The literature review, semi-structured interviews and focus groups are conducted with experts from the largest cities in the Netherlands. The focus groups and interviews are used to examine the barriers and opportunities especially at neighbourhood and street levels. Our main initial findings include the barriers of (a) Individual homeowners: difficulties in making them interested to conduct EER, lack of knowledge for the starting point of renovation, additional barriers of following many steps in conducting EERs for the old dwellings; (b) Homeowner associations: difficulties in reaching agreement by 70% of homeowners, time-consuming process for agreement, and not well-organised meetings by all the homeowners' associations; (c) Neighbourhood level: cultural diversities, difficulties in finding solutions for different groups of people, etc.

Keywords. Energy efficiency renovation, Individual homeowners, Homeowner association, Decision-making, Behavioural factors, Transaction cost barriers, Neighbourhood approach.
DOI: https://doi.org/10.34641/clima.2022.330

1. Introduction

The building sector accounts for 25% of global greenhouse gas (GHG) emissions. The United Nations has announced a global action to reduce GHG emissions. In the Paris climate agreement, 200 countries agreed to limit global warming to no more than 2°C above pre-industrial levels. The Netherlands has set a target to stop using natural gas for heating and cooking by 2050. Most homes in the Netherlands are owner-occupied. The proportion of newly built homes is also low. Considering these two factors, renovating owner-occupied homes can contribute significantly to achieving the energy efficiency targets in this country.

The Netherlands, following the European Commission's policy, focuses on neighbourhood or district approaches. Recently, local authorities promoted energy retrofits through various support. They provide financial support, communicate with homeowners about collective solutions such as district heating, and offer cost-efficient and sustainable renovations for specific buildings and households. In implementing these approaches, municipalities also face many challenges. The local authority provides the whole package of technical and financial support. However, some homeowner associations did not participate in the programs. As a result, other factors may hinder the adoption of the energy efficiency technologies offered by the communities. The local authorities need to figure out how to change household behaviour by identifying the key motivations and barriers to sustainable

Copyright ©2022 by the authors. This conference paper is published under a CC-BY-4.0 license.

renovations.

The behavioural factors and the transaction cost barriers significantly influence the homeowners' decisions to conduct energy retrofits based on the literature review [1]–[6]. Behavioural factors contain contextual (e.g., building characteristics), motivational (e.g., comfort improvement), and personal (e.g., awareness of energy use) factors [1], [2]. Transaction cost means any hidden costs incurred by a transaction with an external source, such as finding a reliable contractor [7]–[9]. However, few studies have examined the impact of behavioural factors and transaction cost barriers on the individual homeowner's decision to make energy retrofits. The number of studies on these influencing factors for condominium associations is even more restricted. This study aims to fill the gap in the literature by examining behavioural factors and transaction cost barriers for individual homeowners, homeowner associations.

This study aims to answer the research question: how can the success rate of the current practices on energy efficiency renovations be improved in the owner-occupied sector? We investigate the current energy efficiency programmes focusing on the owner-occupied housing sector at different levels: individual homeowners, condominium associations in the three largest cities in the Netherlands, i.e., Amsterdam, Rotterdam, and The Hague. We conduct a literature review, semi-structured interviews, and focus groups to investigate the research problem of this study. First, we examine the initial barriers through semi-structured interviews with the experts of three municipalities on energy efficiency programs. Then, we collect a group perspective through focus group sessions on the initial hindrances and drivers of homeowners' energy retrofits. The purpose of focus group meetings is to evaluate the best practices in the largest cities in the Netherlands.

2. Review of earlier studies on the barriers and opportunities towards energy retrofit

2.1 Individual homeowners' decision-making process

The homeowners experience different stages in their journeys of energy retrofits. Homeowners need to fulfil the pre-conditions to start the customer journey, such as perceived needs and social norms by homeowners [10]. In addition, these people have specific thoughts, experiences, and social networks before and during their journeys that considerably determine their decisions. The energy retrofit journey consists of different stages/moments: (1) the homeowner becomes aware of energy retrofit; (2) the homeowner becomes acquainted with the potential options for their dwellings, delay, or resistance against the energy retrofit options. (3) the homeowner may choose to continue for the renovation; (4) the energy retrofit/s may be implemented if the homeowner decides to continue the process; (5) after implementing the energy retrofits, the homeowner experiences the benefits/disadvantages of new technologies. This homeowner may also share the experiences with other neighbours/social networks [1], [8], [11]. The behaviour influencing factors and transaction cost barriers determine the renovation decision. The behavioural factors influence the behaviour before the decision stages, and the transaction cost barriers influence after the decision stages.

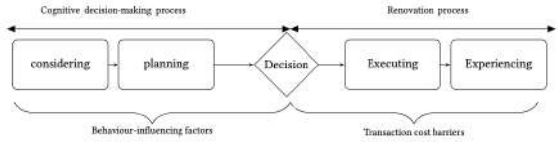

Fig. 1 – Stages of a renovation process of an individual homeowner using the literature review.

(1) Awareness of energy retrofits. Becoming aware of energy retrofits depends on the homeowners' cognitive capability. The behavioural factors of household characteristics, attitudes, and beliefs towards energy retrofit determine the homeowner awareness. Also, the complexity of processing information hinders homeowner awareness. The building is also an important factor since the renovation needs to be implemented based on the dwellings' characteristics. Becoming fully aware of energy retrofits is not easy. Homeowners encounter many barriers even at the first stage. The homeowners may have difficulties processing the information provided by external parties when the information is not clear, concise, and convincing [8], [12]. For instance, many homeowners are not interested to read the letters provided by public authorities. These letters are usually too long and not appealing to people. Homeowners may be uncertain if they live in the current dwellings for the future. This type of uncertainty may hold back the homeowners' willingness to invest in energy retrofits [13].

(2) Positive/negative attitudes towards energy retrofits. After becoming aware of the importance of energy retrofits, homeowners make a positive/negative attitude towards the energy retrofits. This stage is also part of the decision-making process. Therefore, cognitive awareness and biases are the main determinants of this stage. In addition, homeowners' experiences and social networks have critical roles in making positive/negative attitudes towards energy retrofits. The perceived attributes of energy retrofits, such as cost-saving, are one of the main determinants of positive/negative attitudes to retrofits.

    Homeowners may perceive the hassle, mess, and nuisance during the execution phase. They may also experience technical restrictions in the dwellings and low energy prices [2], [8], [13]. These are examples of transaction cost barriers that originated from external sources.

(3) Finalising decision to stop/continue the energy retrofits. Homeowners need to find specific information on the appropriate types of energy retrofits and reliable contractors to install the energy retrofits. Therefore, homeowners must interact with external parties to find reliable information and contractor. These external parties are, for instance, contractors, energy experts, energy efficiency technologies suppliers, banking

systems for financial sources, and homeowner associations. Homeowners may also need to interact with their neighbours if an agreement with neighbours is essential. From this stage onward, the transaction cost barriers significantly influence the final decision and implementation of energy retrofits.

Homeowners may have difficulties in finding reliable information and contractor. They may spend much time finding all the essential sources of a reliable expert or subsidies for the renovation. The planning time may also slow down the process. Uncertainties of the benefits, negative experiences, and complexity of regulations by public authorities are other sources of transaction cost barriers for homeowners [9], [14]-[16].

(4) Implementation of the energy retrofits (implementation phase). At this stage, homeowners live in a dwelling where a contractor executes the energy retrofits [3], [11]. Many factors can facilitate this process for homeowners, such as experiences and skills of previous renovations, confidence while implementing, and particularly supports from family, friends, and acquaintance [2], [17]. Homeowners need to find the energy retrofit activities in which they should supervise. They also must examine how much hassle and mess the renovation may bring. Furthermore, complexity in doing renovation and lack of trust between the contractor and homeowners may delay/stop the implementation of the energy retrofits [15], [16], [18].

(5) Experience of the energy retrofits. homeowners evaluate the effect of the installation of energy retrofit and form a positive/negative attitude toward it. Homeowners may disseminate their experiences through their social network since other homeowners, who have not completed the entire customer journey, can learn from these experiences. Homeowners may also think about the next steps of renovations, for instance, whether homeowners need to conduct other renovations for the better performance of the current energy retrofits [3], [11], [13].

2.2 Homeowners association decision-making process

Promoting energy retrofits is challenging for condominium associations. Previous research has identified six steps when condominium associations perform sustainable renovations. Condominium associations begin the renovation process for different reasons, including a long-term building maintenance plan, a proposal from a member of the condominium association, or a sustainable renovation grant programme offered by a government agency. The second step is for the homeowner's association members to evaluate the possible sustainable renovation options. The third step is to consider various options and decide. The fourth step is for the condominium associations to collect votes for the feasibility study of the different renovation measures. A feasibility study is essential in this step as it significantly influences member decisions. If homeowners vote for a renovation, the responsible members solicit bids and prepare a business case. The condominium association votes for the second time if the board finds the business case profitable. After this step, the condominium association implement the energy retrofit if most members approve the plan.

The main influencing factors are like individual decision-making processes, such as the availability of financial sources for implementing retrofit. The financial support can be provided by the financial savings of the condominium associations or condominium association members or by the financial support of the public sector. Condominium associations may also be motivated by the payback period or expected cost savings of energy conservation measures. The presence of a professional party providing technical assistance at various stages can speed up the decision-making processes of condominium associations. On the other hand, the absence of trusted professional support or contractor is a transaction cost barrier that hinders the decision-making process of the condominium association. In addition, group dynamics influence the decision-making processes of condominium associations. For example, conflicts of interest among condominium association members prolong the renovation process. Communicating the benefits of an appropriate energy conservation measure among residents can stimulate the energy retrofit and facilitate agreements among members. The knowledge and characteristics of the members also determine the decision to make sustainable renovations. In some apartments, both tenants and owners live in the same buildings. In this case, the decision-making process for sustainable renovations becomes even more complicated as it requires the agreement of both parties [19-22].

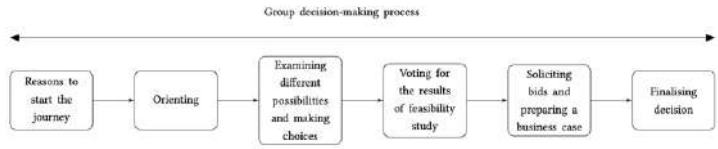

Fig. 2– Stages of group decision-making process of homeowner condominium using the literature review.

3. Research methods

The semi-structured interviews and focus group sessions are conducted to collect the data.

3.1 The Semi structured interviews

We collected information about the barriers and opportunities of energy retrofits in the owner-occupied housing sector. We asked similar questions in all interviews and defined new questions based on the previous interviews. The duration was approximately 1-1.30 hours. 12 semi-structured interviews were conducted.

The interviews contain general information about the interviewees, aims and the target groups of the initiatives at the municipalities and barriers of energy

retrofits. The interviewees are the experts who are active in the energy transition programme in the Netherlands.

3.2 Focus group sessions

The focus group sessions aimed to investigate the obstacles and opportunities for individual and collective actions towards energy retrofits from group perspectives. We investigated the decision-making process, the barriers, the right message, the right messengers promoting sustainability. We examined these factors for the individual homeowners, homeowner associations and social housing corporations. Two focus group sessions (8 and 6 experts, respectively) are conducted to collect the data on the barriers and motivations to energy retrofits.

4. Results

The main identified barriers for individual homeowners and homeowner associations are as follow:

4.1 Individual homeowners' barriers to energy retrofits

Lack of technical knowledge on the appropriate types of energy retrofits during the planning phase. During the first focus group meeting, an expert explained that it is always a big challenge for homeowners to figure out the most appropriate type of energy retrofit for their home. The energy advisor of the municipality provides technical information on the possible energy retrofit measures for the buildings. The final decision on the most appropriate energy retrofit requires more specific technical advice for the dwellings providing information on the feasibility of the energy retrofit and the phases that the homeowners need to follow.

Lack of technical knowledge during the implementation phase. In one programme, an expert only provides the necessary information about the types of energy-efficient measures. The target group for this program has a positive attitude towards energy-efficient retrofits. Two groups of households are identified. The homeowners who are well motivated. This group is proceeding with the implementation. The other group is also interested, but their main obstacle is the lack of knowledge on how and where to begin energy retrofit. This program does not yet consider the obstacles in the implementation phase.

Complexity and hassle factors during the implementation phase. The owners of old buildings specified the reason for not continuing with energy renovations. The main obstacle is the complexity and effort involved in the energy retrofitting of old buildings. Homeowners must follow many steps which were not provided within the programme offered by the local authority. Therefore, homeowners must apply to other programmes to receive technical, informational, and financial assistance.

Time and effort in finding reliable experts, reliable information, and financial sources. In the homeowner association grant programme, homeowners invest a long time to get an estimate from a contractor and financial assistance. The homeowners receive different financial advice. They ask about the reliability of the financial advisor. The municipality cannot provide information on the reliability of financial advisors. During the implementation phase, Homeowners also face the challenge of finding a reliable contractor. It is also a challenge for the municipality to help homeowners identify a reliable contractor. In some local authorities, an external party gives neutral advice on the reliability of professional contractors.

Lack of interest in reading the letters from public authorities. Residents are reluctant to respond to letters from the authorities. The reason could be that people receive so many letters to pay their bills that they are unwilling to respond to more letters. In another experiment, the energy expert spoke to people in a neighbourhood. In the end, people responded and acted on their conversation with the energy expert.

High costs for deep renovations and uncertainties about the benefits of energy refurbishments. According to the experts' observations, people prefer to start with small energy retrofits and avoid investing high capital costs in energy retrofits due to other necessary living expenses. In addition, the project manager of the condominium association grant programme explained that owners of multifamily buildings must pay various types of costs for their buildings, such as the elevator. Individual owners may not see the value in paying additional costs for energy retrofits with uncertain benefits. A project manager of incentive programmes for larger condominium associations emphasised that the cost of energy retrofits is the key factor in the final decision, regardless of the condominium owners' willingness and interest in energy retrofits. The energy retrofits must also provide short-term benefits. Otherwise, homeowners will not invest in something that does not pay for itself within five years, given other expenses and financial investments.

The complexity of the process of application for accessing financial resources by public authorities. Homeowners interested in energy retrofits regularly ask for assistance in applying for grants/loans, although there are numerous programmes and online platforms for grants, loans, and aid. As homeowners found out where they could access funding sources. They also wanted to know if those funding sources were still available long before they made their final decision. All kinds of uncertainties also hinder the process, such as the likelihood of getting the grants/loans/grants, the impact of changes in political parties on financial support for energy retrofits, and the right time to invest.

Homeowner uncertainties regarding the policies, such as removing the natural gas from the heating system. Homeowners must recognise the need and urgency for energy retrofits to act. Most people are reluctant to act until they are less uncertain, and those actions become the social norm. For example, homeowners need to know exactly how to remove natural gas from their heating systems. Currently, residents are very unsure about removing natural gas, so it is difficult to motivate them to begin the process. There could be an explanation for this, such as miscommunication by officials regarding energy retrofit programmes and public-private initiatives. For example, the city government promises to plan for the

elimination of natural gas in the heating system. However, the planning for individual districts is not entirely clear.

4.2 Homeowner associations' barriers to energy retrofits

Homeowners' associations also use voting to make the final decision. In the Netherlands, the positive vote of 70% of the individual homeowners is crucial for the renovation to proceed. The lack of approval can have several reasons, such as differences in groups of people (e.g. young vs. old generation, low vs. middle income), lack of financial savings, such as a low budget for energy renovations, or lack of knowledge of members of housing associations about the benefits of energy renovations.

Lack of financial savings by homeowners' associations. From the condominium association grant programme, it was found that owners are interested in renovating and maintaining the buildings. However, condominium associations usually have difficulty in having sufficient sources of funds for capital expenditures. In addition, community fund managers only provide the loans if the condominium associations can demonstrate that they can repay the total costs.

Conflicts of interest among homeowner associations' members. In smaller condominium associations, people are more likely to perceive their blocks of buildings as individual houses compared to larger condominium associations. For example, if a flat building consists of four houses, the units on the top and ground floors benefit more from the roof and floor insulation than the houses on the second and third floors. Therefore, these two units may not see the direct benefit of energy retrofits to the floor and roof insulation and resist the decision. To overcome this obstacle, the multi-annual maintenance plan can be used as the right time to combine with the energy retrofit. During this process, the benefits of energy savings can be highlighted to gain the approval of other homeowners who may not directly benefit from the energy retrofit.

In larger condominium associations, energy retrofits that benefit most homeowners from their installations, such as façade insulation, have a higher chance of acceptance by residents. The municipality of The Hague offers packages of energy retrofits for condominium associations where most residents can benefit from the energy retrofits. In the municipality's experience, condominium associations usually opt for the package with the highest financial benefits, i.e. with low investments and high energy savings. However, the benefits of the energy package may not be evenly distributed in the end.

Among residents of condominium associations, there are people who can finance energy retrofits more easily than others. As a result, it is much more difficult for these individuals to vote for expensive energy retrofits, such as solar panels. In addition, many condominium associations do not have access to government grants. Given the lack of savings and financial assistance, this is a barrier to members who cannot afford to spend the money on energy retrofits.

Complexities in making agreements among the members of housing associations and long delay in making the decision. This barrier is identified during the implementation of a project called 'sustainable broker' and 'homeowners associations funding program'. The first project provides the complete packages of financial and technical supports from the municipalities and only financial support by the second project. The project leaders explained that despite these full supports, homeowners' associations and social housing corporations did not succeed to get the majority of votes of all the tenants or homeowners in conducting renovations or energy retrofits. These neighbourhoods also contain a mix of social and homeowner dwellings in one building block which amplifies the complexities of making agreements of renovation from both associations.

Mismanagement by homeowners' associations, e.g., lack of organised meetings by homeowner associations. Collective action requires the agreement of all the participants. In the case of a programme, it is easier since the smaller homeowners' associations have been targeted. However, even for smaller ones, the homeowner associations act differently. For instance, some of them have an organised meeting which might not be the case. Therefore, uncertainties exist in achieving the targets of this project due to this reason.

4.3 Message effects

Homeowners may be at different phases of energy retrofits. Some of them are not even thinking about energy retrofits yet. Some are thinking about different types of energy retrofits, and others are already doing energy retrofits. They have different characteristics and needs for their houses. In the semi-structured interviews and the focus group session, the question was asked what messages the experts use to motivate households to carry out energy retrofits. The general answer to this question was that it depends on the context and the intermediary delivering these messages. For example, improving the quality of life is important for people who can repay the cost of energy retrofits. Similarly, the availability of financial support from national and local authorities may be more influential for people who cannot afford the cost. In addition, a combination of messages is used to motivate households to undertake energy efficiency retrofits. The main messages are described below:

Improving the quality of life. In almost all programmes, experts mentioned that using the word sustainability does not lead to the implementation of energy retrofits. Most people are motivated to renovate their homes if they feel it is necessary or perceives an improvement in their quality of life. For example, in a programme implemented by the municipality of Rotterdam, improving comfort by insulating the floor was the most attractive message for the residents of the North Region of Rotterdam, as people in this region struggle with cold floors.

Essential maintenance of the house. The necessary maintenance of the building was mentioned in all programmes as well as in the focus group meetings as the most important moment to motivate households to

participate in energy retrofits. For example, if the roof needs to be renewed, this maintenance can be combined with the insulation of the roof. The municipalities of Rotterdam and The Hague offer subsidies and financial options that oblige to use a part of the budget for energy renovation and the rest for maintenance of the building. This type of incentive seems to be very effective for the implementation of energy retrofits. This message applies to both individual homeowners and condominium associations.

In one of the regions in the southeast of Amsterdam, the households own very old buildings that need renovation. It would be impossible to ask people to bear the extra costs of energy renovations. However, if the expert can convince people that they will have a more comfortable home in the future, they may consider energy renovation.

Condominium associations: through the multi-year maintenance plans (MJOP). This message is only valid for condominium associations. Every homeowner association (VvE) is required by law to maintain a healthy reserve that can cover the costs of maintaining the property contained in the homeowners' association. The best way to ensure a realistic source of funds is to have a multi-year maintenance plan. The project manager of the condominium association grant program explains that this is the best time to motivate households to make energy improvements. In addition, condominium associations are most likely planning to fund the maintenance of the building and additional costs for energy retrofits need to be reconsidered. In this case, the financial support from the national and local governments can compensate for the budget deficit of the condominium associations.

Expected cost saving. If people have a clear idea of the expected cost savings from an energy retrofit, they will certainly consider it. For example, owners of buildings with the lowest energy labels, such as F and G, must pay hundreds of euros per month for energy costs. There were cases in the Southeast Amsterdam where the owners had to pay 4000 euros per year for energy costs. The Energy Ambassador explained to the building owners the benefits of energy renovation in terms of cost savings per year. In this way, the owner was convinced to carry out the energy refurbishments.

4.4 Messenger effects

The first moment of communication is critical to make homeowners interested and engaged in the energy retrofit programs. The local authorities realised that official communication through letters and municipalities ambassadors does not influence the households' energy retrofit decisions. Then, who should transfer the message to homeowners to motivate them in energy retrofits?

A trusted neighbour/person. It emerges from the focus group meetings that a building ambassador can also help to motivate people to make energy-efficient renovations. Government, local authority programme managers or housing associations are seen as third parties. Households may feel pressured by these bodies and resist the measures they propose to improve the sustainability of buildings. If a household is interested in energy retrofits, it would be much easier to motivate other households through this household than through external third parties. One expert said that if you have trust and some relationship with a person, you can convince them to do something. This can be a trusted neighbour or caretaker, and, in most cases, it is neither an expert nor someone from the municipality.

An expert hired by homeowners. If the homeowners are already positive about an energy retrofit and have gone through the consideration phase, an expert hired by the homeowners can effectively communicate the benefits and convince the homeowners to go through with the energy retrofit. For example, if someone wants to install a heat pump, the first action is to find a reliable expert who can provide them with information and services for installing the heat pump specifically for their building.

Energy ambassador. In the southeast of Amsterdam, it is more expensive to rent a house than to buy one with a mortgage from the banks. In this region, the lowest income households usually own a house. The owners of these houses perceive the condominium associations as their landlords. Any expenses that condominium associations demand is seen by them as additional costs. The homeowners may resist these costs, for example, to improve the energy efficiency of the buildings. Shared events and creating local networks, such as cooking together or playing sports, can be a safe environment to talk to homeowners about sustainability. The Energy Ambassador can combine these events into activities to put sustainability into practice. In this case, an event using visualisations or different languages of the region to communicate the benefits of a more comfortable home equipped with energy efficiency measures can also be helpful.

A front runner. In the focus group sessions, the experts mentioned that people may not even be thinking about energy retrofit. Moreover, most people wait for one person to implement the measure first, and if the results are satisfactory, they may follow that person. The environmentally conscious group of households could be an example of the front runners, as this group is actively looking for ways to live more sustainably. After this phase, if households decide to undertake energy retrofits, they may contact an expert they have hired themselves or who has been hired by the municipality to get information or other services, such as financial support, to continue the process. So it also depends on the stage of the energy retrofit. An expert hired by the homeowners can also effectively communicate the benefits and convince the homeowners to undertake the energy retrofit. In addition, experts hired by local governments often offer free services. So in this respect, homeowners can also benefit from these services.

5. Conclusions

The aim of this study was to examine current energy policy and public-private initiatives in the Netherlands. It investigated which messages and ambassadors are effective in promoting sustainability. In addition, the main identified barriers to energy retrofits were examined from the perspective of policymakers and practitioners. The data collection methods are semi-structured interviews and focus group meetings.

Promoting sustainable retrofits. The results of this study show that (a) the word sustainability does not persuade homeowners to make energy-efficient retrofits. The quality-of-life improvements expected cost savings, and integration of energy efficiency retrofits with basic home maintenance may convince individual homeowners to make the energy efficiency retrofits. (b) Municipal project managers have cited letters and surveys from government agencies as ineffective means of promoting energy retrofits. (c) Trustworthiness and familiarity of the energy ambassador with households are the most important attributes to increase the effectiveness of energy programmes or household adoption of energy retrofit by households.

Barriers to sustainable retrofits. Even people who are interested and motivated in energy retrofits consider them to be a complex process. Households want a straightforward process, both technically and financially. Moreover, people expect the authorities to provide this step-by-step process for a hassle-free energy retrofit for households. Based on expert opinions, people asked questions about the cost, energy savings, loans/subsidies, type of energy retrofit, reliable contractors, and facilitation of the energy retrofit process in the decision-making phase.

The data suggest that municipal project managers and practitioners are aware of key transaction cost barriers. The main transaction cost barriers identified in energy retrofit programmes were (a) a lot of time and effort to find reliable information, (b) expensive energy-saving measures, and (c) the complexity of implementing energy-saving measures, e.g., due to structural reasons or living in an old building. In addition, they reported new transaction cost barriers, such as homeowners' uncertainty about national energy policies, e.g., the elimination of natural gas heating.

6. Acknowledgement

This project is financially supported by the MMIP 3-4 scheme of the Ministry of Economic Affairs & Climate and the Ministry of the Interior & Kingdom Relations (In Dutch: Dit project wordt uitgevoerd met ondersteuning vanuit de MMIP 3-4 regeling van het Ministerie van Economische Zaken & Klimaat en het Ministerie van Binnenlandse Zaken & Koninkrijksrelaties.).

7. References

[1] C. Wilson, H. Pettifor, and G. Chryssochoidis, "Quantitative modelling of why and how homeowners decide to renovate energy efficiently," *Applied Energy*, vol. 212, pp. 1333–1344, Feb. 2018, doi: https://doi.org/10.1016/j.apenergy.2017.11.099.

[2] C. Wilson, L. Crane, and G. Chryssochoidis, "Why do homeowners renovate energy efficiently? Contrasting perspectives and implications for policy," *Energy Research and Social Science*, vol. 7, pp. 12–22, 2015, doi: 10.1016/j.erss.2015.03.002.

[3] S. Ebrahimigharehbaghi, Q. K. Qian, F. M. Meijer, and H. J. Visscher, "Transaction costs as a barrier in the renovation decision-making process: A study of homeowners in the Netherlands," *Energy and Buildings*, vol. 215, p. 109849, May 2020, doi: 10.1016/J.ENBUILD.2020.109849.

[4] S. Ebrahimigharehbaghi, Q. K. Qian, F. M. Meijer, and H. J. Visscher, "Unravelling Dutch homeowners' behaviour towards energy efficiency renovations: What drives and hinders their decision-making?," *Energy Policy*, vol. 129, pp. 546–561, Jun. 2019, doi: 10.1016/J.ENPOL.2019.02.046.

[5] S. Ebrahimigharehbaghi, F. Filippidou, P. van den Brom, Q. Qian, and H. J. Visscher, "Analysing the Energy Efficiency Renovation Rates in the Dutch Residential Sector," in *Clima2019*, 2019, no. May, pp. 1–7.

[6] L. Mundaca, M. Samahita, J. Sonnenschein, and R. Seidl, "Behavioural economics for energy and climate change policies and the transition to a sustainable energy use—A Scandinavian perspective," *Energy and Behaviour: Towards a Low Carbon Future*, pp. 45–87, Jan. 2020, doi: 10.1016/B978-0-12-818567-4.00004-1.

[7] L. Mundaca, "Transaction costs of energy efficiency policy instruments," 2007. Accessed: May 18, 2018. [Online]. Available: http://portal.research.lu.se/ws/files/5765055 /Contents.pdf

[8] G. de Vries, M. Rietkerk, and R. Kooger, "The Hassle Factor as a Psychological Barrier to a Green Home," *Journal of Consumer Policy*, vol. 43, no. 2, pp. 345–352, Jun. 2020, doi: 10.1007/S10603-019-09410-7/TABLES/1.

[9] G. de Vries, M. Rietkerk, and R. Kooger, "The Hassle Factor as a Psychological Barrier to a Green Home," *Journal of Consumer Policy*, pp. 1–8, Feb. 2019, doi: 10.1007/s10603-019-09410-7.

[10] C. Wilson and H. Dowlatabadi, "Models of Decision Making and Residential Energy Use," *Annual Review of Environment and Resources*, vol. 32, no. 1, pp. 169–203, Nov. 2007, doi: 10.1146/annurev.energy.32.053006.141137.

[11] "Drijfveren en barrières richting aardgasvrij wonen in kaart | TNO." https://www.tno.nl/nl/aandachtsgebieden/energietransitie/roadmaps/systeemtransitie/succesvolle-wijkaanpak-motiveer-bewoners/drijfveren-en-barrieres-aardgasvrij-wonen-in-kaart/ (accessed Jan. 13, 2022).

[12] L. Zhang and G. Reniers, "A Game-Theoretical Model to Improve Process Plant Protection from Terrorist Attacks," *Risk Analysis*, vol. 36, no. 12, 2016, doi: 10.1111/risa.12569.

[13] W. M. H. Broers, V. Vasseur, R. Kemp, N. Abujidi, and Z. A. E. P. Vroon, "Decided or divided? An empirical analysis of the decision-making process of Dutch homeowners for energy renovation measures," *Energy Research & Social Science*, vol. 58, p. 101284, Dec. 2019, doi: 10.1016/J.ERSS.2019.101284.

[14] C. A. Klockner and A. Nayum, "Specific barriers and drivers in different stages of decision-making about energy efficiency upgrades in private homes," *Frontiers in Psychology*, vol. 7, no. SEP, pp. 1–14, 2016, doi: 10.3389/fpsyg.2016.01362.

[15] I. Stieß and E. Dunkelberg, "Objectives, barriers and occasions for energy efficient refurbishment by private homeowners," in *Journal of Cleaner Production*, Jun. 2013, vol. 48, pp. 250–259. doi: 10.1016/j.jclepro.2012.09.041.

[16] S. R. Jansma, J. F. Gosselt, and M. D. T. de Jong, "Kissing natural gas goodbye? Homeowner versus tenant perceptions of the transition towards sustainable heat in the Netherlands," *Energy Research & Social Science*, vol. 69, p. 101694, Nov. 2020, doi: 10.1016/J.ERSS.2020.101694.

[17] R. Baumhof, T. Decker, H. Röder, K. M.-S. cities and society, and undefined 2018, "Which factors determine the extent of house owners' energy-related refurbishment projects? A Motivation-Opportunity-Ability Approach," *Elsevier*, Accessed: Jan. 13, 2022. [Online]. Available: https://www.sciencedirect.com/science/article/pii/S2210670717308272?casa_token=ztetwLFChEoAAAAA:Bxh86qLaa4lvp8RlMJRhX_SRgNcT34LCeW37k7ddr_0eSdo-ONZ_G4KcSfmoIfYdqKTrL4L4_A

[18] J. P. Baginski and C. Weber, "A Consumer Decision-Making Process? Unfolding Energy Efficiency Decisions of German Owner-Occupiers," *HEMF Working Paper*, vol. 08, Aug. 2017, Accessed: Oct. 23, 2017. [Online]. Available: https://papers.ssrn.com/sol3/papers.cfm?abstract_id=3023997

[19] Paradies, G., Beekman, L., Ooms, M., De Koning, N., Mulder, G., Van Baar, M., … _Van Winden, J. 2017. De Duurzame VvE

[20] Buessler, S., Badariotti, D., & Weber, C. Evaluating the complex governance arrangements surrounding energy retrofitting programs: The case of collective ownership buildings in France. *Energy Research and Social Science*, *32,* 2017.

[21] ACE Retrofitting. *Financial Solutions for Condominium Retrofitting*. Maastricht, 2018.

[22] Van Bentum, E., Cremers, R., de Koning, N., Kwant, J., van Winden, J., Brester, CH., De Duurzame VvE: samenvatting, 2017

Development and characterization of thermal insulation materials based on rice straw and natural binder

Yaping Zhou [a], Abdelkrim Trabelsi[b], Mohamed El Mankibi [c]

[a] Univ Lyon, LTDS, ENTPE, UMR5513, 69120 Vaulx-en-Velin, France, yaping.zhou@entpe.fr.

[b] Univ Lyon, UCBL, INSA Lyon, CNRS, CETHIL, UMR5008, 69622 Villeurbanne, France, abdelkrim.trabelsi@univ-lyon1.fr.

[c] Univ Lyon, LTDS, ENTPE, UMR5513, 69120 Vaulx-en-Velin, France, mohamed.elmankibi@entpe.fr.

Abstract. Thermal insulation is an essential factor to reduce energy demand during the stage of building operation. Nowadays, thermal insulation materials are however commonly produced from petrochemicals, causing high energy consumption and detrimental environment impact during production and arising the reuse and recycle issues. Insulation materials derived from local agricultural straws are becoming more attractive due to their availability, cost effectiveness, sustainability and low carbon footprint. Rice straw has the advantage of low density and low thermal conductivity due to its hollow internal structure. Also, the utilization of rice straw in buildings prevents the negative environmental impact of burning straw or mixing them with soil. The aim of this study is to develop an innovative composite insulation material from rice straw. A biobased binder, i.e., sodium alginate, derived from brown algae is used as binder. A modified method is developed to solve the water solubility issue of the composite material. The final product is rigid, lightweight and fully eco-friendly. The effect of fiber size and binder ratio (i.e., 8%, 16% and 24%) on the density, thermal conductivity and water vapor permeability are studied. The composite materials are insulating with thermal conductivity values in the range of 0.039-0.045 W/(m·K) for an average density in the range of 100 to 200 kg/m^3.

Keywords. Rice straw, sodium alginate, insulation material, water solubility, thermal conductivity.
DOI: https://doi.org/10.34641/clima.2022.332

1. Introduction

Nowadays, green buildings are increasing in demand to meet higher and more complex standards on energy efficiency, sustainability and comfort. To achieve this objective, an effective strategy is enhancing the insulation properties of the building envelop as well as using environment friendly materials in their lifetime. In this context, there is an increasing interest in production of thermal insulators from agricultural straw wastes. Agricultural straws (e.g., wheat, rice, barley, oats and rape straws) are available locally in any country in huge amounts [1]. They also exhibit the advantage of low density and low thermal conductivity due to its hollow internal structure [2].

A large quantity of 3.9 million tons rice straw is produced each year in Europe [3] . Burning straw in the field is one of the oldest practices in Europe and worldwide. It has negative effects, such as the greenhouse gases emission, pollution and toxicity to human health, which is banned in EU countries according EC regulation 1259/1999. Mixing rice straw with soil is another management option. This approach generates methane during the straw's anaerobic decomposition, leading to a higher global warming potential compared to burning straw [4]. Application of rice straw waste in building insulation material is a cost-effective alternative to solve these issues. Zhao et al [5] reported that agricultural straw waste insulation material has a life cycle cost of 150 RMB/m^2 for 25 years span, which is lower than the municipal solid waste, industrial solid waste and traditional insulation materials (e.g., XPS, EPS, rock wool and glass wool).

Nowadays, straw composites are produced by bonding straw fibers with inorganic cementing materials [6, 7] and organic resins [8]. These

Copyright ©2022 by the authors. This conference paper is published under a CC-BY-4.0 license.

binders, however, can increase the embodied energy and prevent the degradability of the final insulation products. The use of natural binders, e.g., starch, alginate and chitosan, can be an alternative to solve this issue. Mati-Baouche et al. [9] have developed biobased insulating composites from sunflower's stalk particles and chitosan with thermal conductivity values of 0.056-0.058 W/(m·K) for density of 150-200 kg/m^3. Lacostea et al. [10] have developed wood fibers/recycled cotton fibers composites using sodium alginate as binder. The thermal conductivity values were ranging from 0.078 W/(m·K) to 0.089 W/(m·K) for density of 308-333 kg/m^3. Palumbo et al. [11] have developed insulation panels from three crop wastes, i.e., barley straw, corn pith and rice husk and three binders, i.e., corn starch, sodium alginate and casein. The results showed that the alginate-based composites had lower densities and thus presented lower thermal conductivity values. The lowest thermal conductivity of 0.052 W/(m·K) was obtained for the composite from corn pith and alginate with the density of 80 kg/m^3.

Sodium alginate is a natural polysaccharide which is derived mainly from brown seaweeds. It can dissolve in water and then form a gel at room temperature without a heating and cooling cycle. The properties of sodium alginate such as being nontoxic, adhesive, biocompatible, biodegradable with low cost make it appealing as a binder for biobased materials. But it should be noted that composites with sodium alginate as binder can have poor water resistance, and even be destroyed when they are contacted with water due to the solubility of sodium alginate in water. Water-insoluble property can be developed by adding multivalent cation [12].

The aim of this study is to develop a lightweight insulating composite from rice straw and sodium alginate. A modified procedure is developed to prepare insoluble alginate-based composite through inducing cross-link with ionic calcium. The effect of fiber size and binder ratio on the physical, thermal conductivity and water vapor permeability of the composites are also investigated.

2. Materials and methods

2.1 Raw Material

Two types of rice straw fibers i.e., RS1 and RS2 were provided by FBT isolation (Dagneux, France). The fiber size distribution of RS1 and RS2 was investigated by mechanical sieving [13]. First, a sample of 60 g rice straw fibers was manually homogenized and divided into four similar parts by a non-cutting blade. Then the three samples (approximately 15 g) were separated by applying a series of sieves (i.e., 0.5, 1, 2, 4, 8, 16, 32 mm). The mechanical sieving was done by a mechanical sieve shaker for 30 minutes. The mass fraction retained on each sieve was obtained by weighing each sieve with and without fibers.

Fig. 1 compares the fiber size distribution of the RS1 and RS2. Both the RS1 and RS2 contains the fibers between 0 and 32 mm. It could be clearly seen that the RS1 contained more fibers below 2 mm.

A commercial sodium alginate, purchased from Algaia™ under the trademark Algogel® 6021, was used to bind straw fibers in this study. It is composed of a fine water-soluble powder (<200 μm). It has a viscosity of 150-300 cps and a pH of 6-8.5 in a 1% aqueous solution. Calcium sulphate ($CaSO_4$), calcium chloride ($CaCl_2$) and sodium citrate were purchased from Glentham Life Sciences (UK).

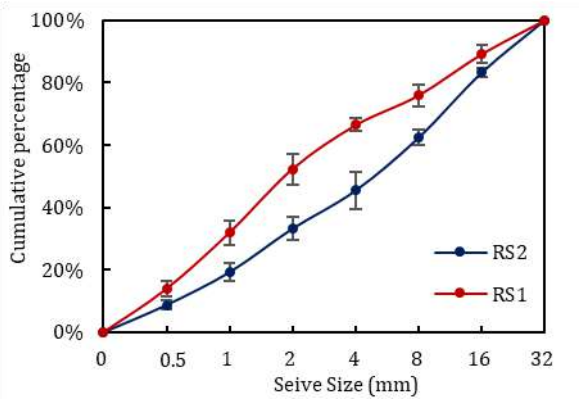

Fig. 1 – Fiber size distribution of RS1 and RS2

2.2 Sample preparation

The sodium alginate solution was firstly prepared by slowly adding sodium alginate power to distilled water under continuous stirring at 250 rpm for 30 min. The fibers were then mixed with the sodium alginate solution by using a force-action rotary paddle at 20 rpm for 2 min. The mixture was put into a polystyrene mold of dimensions 30×30×4 cm^3 and compacted using a weight of 10kg for 4 hours. Note that the aforementioned steps were done at ambient condition. The whole was then placed in an oven at 50 °C for 48 hours to accelerate the drying process. This method is referred as M0 to distinguish with other two modified procedures.

Modified procedures were prepared based on two different methods of calcium ion cross-linking [10, 14]. In the first modified method (M1), a content of 83 wt.% sodium alginate, 15 wt.% CaSO4 and 2 wt.% sodium citrates instead of pure sodium alginate for M0 was dissolved in distilled water to prepared the binder solution. In the second modified method (M2), the composite samples obtained from M0 was immersed in $CaCl_2$ solution at concentration of 4% (m/v) for 5 min. The process for obtaining bio-based composites from rice straw fibers and sodium alginate is shown in Fig. 2. After the immersion, the samples were drained for 10 min and then further oven-dried. In addition, different binder ratio (e.g., 0.08, 0.16 and 0.24) was investigated. Table 1 shows the different formulations.

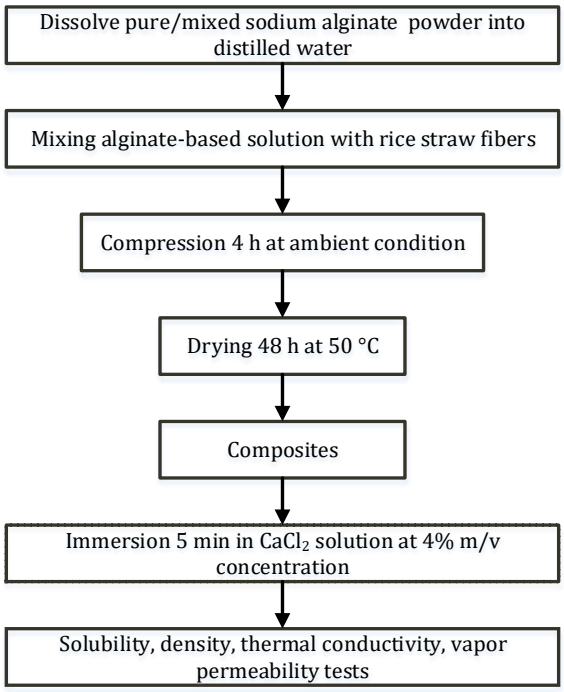

Fig. 2 – Manufacture process of composite samples from rice straw fibers and sodium alginate

Tab. 1 – Board formulation

Sample	Modification method	Straw type	Binder/straw ratio
1	M0	RS2	0.16
2	M1	RS2	0.16
3	M2	RS1	0.08
4	M2	RS1	0.16
5	M2	RS1	0.24
6	M2	RS2	0.08
7	M2	RS2	0.16
8	M2	RS2	0.24

3. Methods for materials characterization

3.1 Density

Three composite samples for each formulation with dimensions of 10×10×d cm^3 were used for density measurements. First, the samples were dried in an oven at 50 °C until a constant weight and then the volume was calculated after measuring the size by a vernier caliper. Density was determined by the gravimetric method that relates the mass and the volume of the composite samples.

3.2 Thermal conductivity

Thermal conductivity was measured by a hot wire apparatus. This technique allows for a quick measurement on small samples. First, the samples were dried in an oven at 50 ºC until a constant weight and then the samples were placed in desiccator to decrease their temperature to ambient temperature. Three pairs of samples (i.e., 1&2, 1&3, 2&3) with dimensions of 10×10×4 cm^3 were measured for each formulation.

3.3 Water vapor permeability

Water vapor permeability was measured by wet cup according to EN12572:2001 [15]. Prior to measurement, the composite samples were stored at 23±5ºC and 50±5% RH for a period long enough for their weight to stabilize (the difference in mass between the two measurements within 24 h is less than 5%). A thin layer of silicone was then applied to seal the samples on Plexiglas cups containing a saturated aqueous solution of potassium sulphate (97% RH). A vapor-tight aluminum tape was used to seal the sides of the sample with the side of the cup. The air layer, i.e., the space between the salt solution and the bottom of the composite sample was set to 20 mm. The whole cup was then put in a box containing a saturated aqueous solution of magnesium nitrate (53% RH). The box was placed in a room with temperature controlled at 20 ºC. The whole cup was weighed periodically until the change of the mass was constant (five successive determinations of change in mass within 24 h intervals is less than 5%).

Due to the partial water vapor pressure between the interior space of the cup and the box, a water vapor flow through the sample partial water vapor is generated, leading to the mass variation of the cup. The water vapor flow is calculated as follows:

$$G = \frac{\Delta m}{\Delta t}$$

$$\delta_p = \frac{G \cdot d}{A \cdot p_s(RH_1 - RH_2)}$$

$$\mu = \frac{\delta_a}{\delta_p}$$

Where m is the mass of sample and cup assembly, t is time, G is the water vapor flow rate through sample, A is the exposed area (m^2), p_s is saturated vapor pressure (Pa), RH_1 is the relative humidity inside the cup (%RH), RH_2 is the relative humidity in the box (%RH), d is the thickness of sample (m), δ_a is the water vapor permeability of air (kg/(s·m^2·Pa)), δ_p is the water vapor permeability of sample (kg/(s·m^2·Pa)), μ is the water vapor resistance factor of sample.

4. Results and discussion

4.1 Water solubility

Fig. 3 shows the revolution of the composite samples after immersed in water. The composite samples are sample 1, 2 and 7 from the left to right. It can be observed from Fig. 3 (b) that the thickness of the sample 1 and 2 were increased while that of the sample 7 remained unchanged after immersion in water for 1 hour. It can be seen from Fig. 3 (c) that the water color was red for the sample 1 and 2, while the color was light yellow for sample 7. This result indicated that the alginate was partly dissolved in water for the samples manufactured by M0 and M1. It can also be seen from Fig. 3 (d) that the sample 1 and 2 were destroyed, while the sample 7 kept complete after immersion in water for 24 hours.

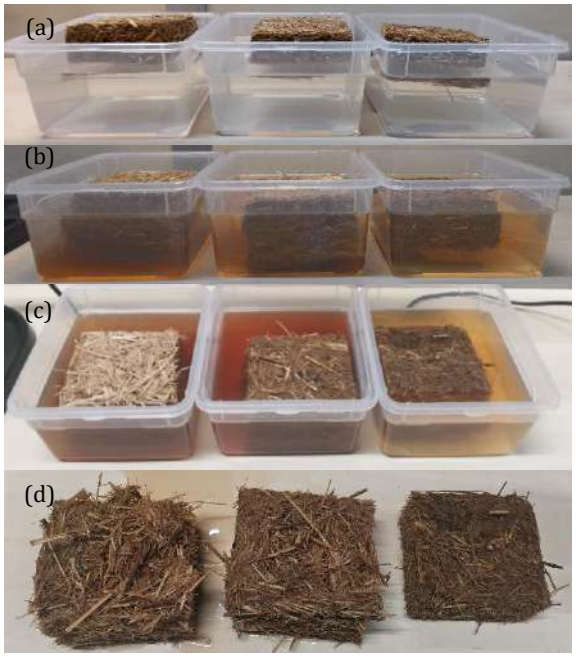

Fig. 3 - From left to right: sample 1, 2 and 7 immersed in water for (a) 1 min; (b) 1 h; (c) 24 h and (d) after 24h.

4.2 Density

Fig. 4 shows the average density with standard deviation of the composite samples by M2 with different types of rice straw fibers and binder ratio. All the composite samples have densities ranging from 100 to 200 kg/m³. It can be seen that the composite samples with RS1 have the larger density than the composite samples with RS1. Also, the density increases as the binder ratio increases.

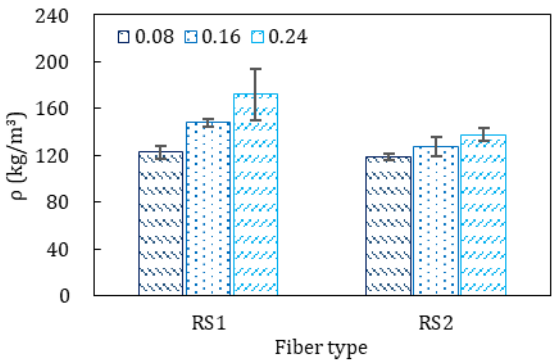

Fig. 4 - Density of the composite samples by M2 with different types of fibers and binder ratio.

4.3 Thermal conductivity

Fig. 5 shows the thermal conductivity of the composite samples by M2 with different types of rice straw fibers and binder ratio. All the composite samples are insulating with their thermal conductivity values from 0.039 to 0.045 W/(m·K). It can be seen that the composite samples with RS2 have the lower thermal conductivity than the composite samples with RS1. For example, the average thermal conductivity of the sample 3 was 0.044 W/(m·K), whereas that of the sample 6 was 0.039 W/(m·K). This can be attributed to the fact that the porosity of the composite samples increases by using the larger fibers, leading to the decrease of their thermal conductivity as air has a lower thermal conductivity. The binder ratio seems to have a minor effect on the thermal conductivity. This might because the binder content is low for all the composite samples.

Thermal conductivity values of straw insulating materials in the present study and literature are plotted versus their density, as shown in Fig. 6. Straw bale [16] and straw composites using starch [17, 18], liquid glass[19, 20], lime [21] and clay [22] as adhesive have been added for comparison. It can be seen from Fig. 6 that for density of around 150 kg/m³, the thermal conductivity values were 0.044 W/(m·K) in present study and 0.058 W/(m·K). The thermal conductivity of the composite samples is generally increased with their density. However, a weak correlation was observed in the present study, which can be attributed to the small variation in composites' densities.

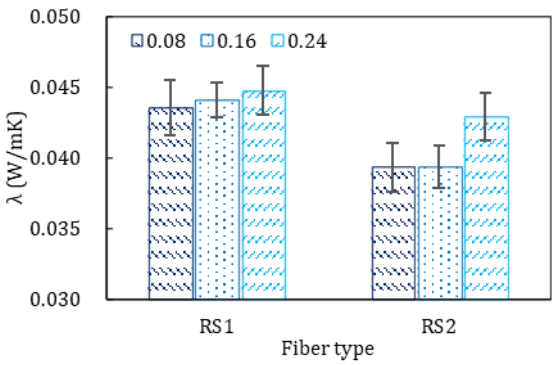

Fig. 5 – Thermal conductivity of the composite samples by M2 with different types of fibers and binder ratio.

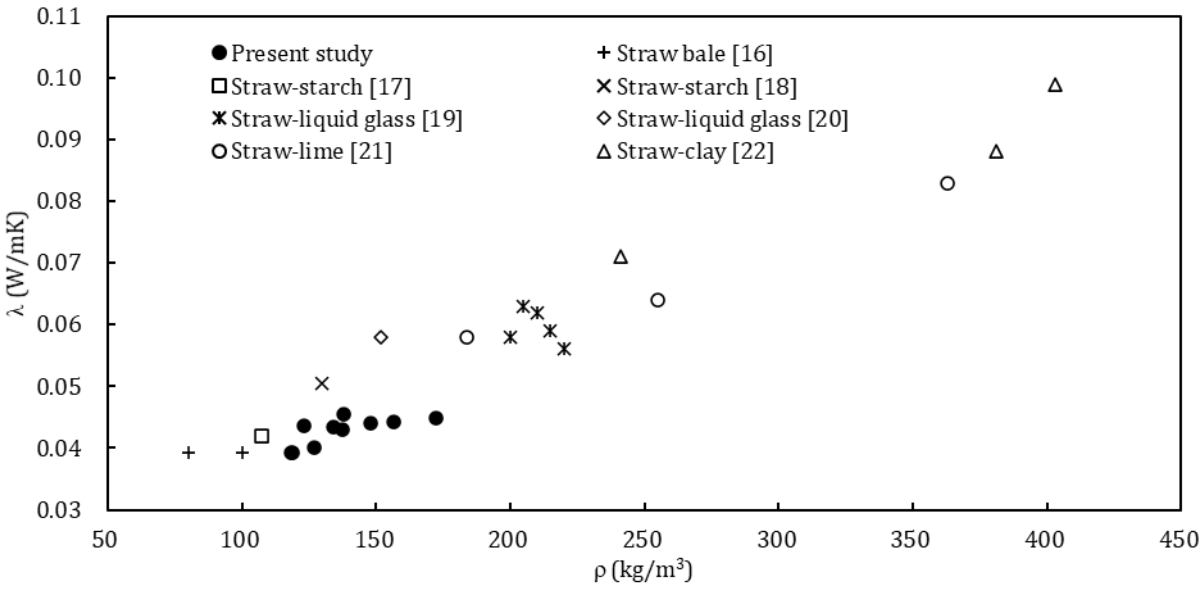

Fig. 6 - Density versus thermal conductivity in present study and in literature

4.4 Water vapor permeability

Fig. 7 shows the water vapor resistance factor of the composite samples by M2. It is clear that the fiber size and binder ratio have an effect on water vapor resistance factor of the composite samples by M2. Decreasing binder ratio from 0.24 to 0.08 decreased the μ-value by approximately 38% and 22% for RS1 and RS2, respectively. Compared to the composites from RS1, the composites from RS2 decreased the μ-value by 6%, 9% and 21% for binder ratios of 0.08, 0.16 and 0.24, respectively.

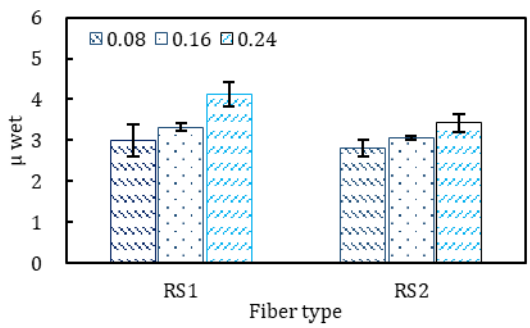

Fig. 7 – Water vapor resistance factor of the composite samples by M2 with different types of fibers and binder ratio.

5. Conclusions

Rice straw fibers with a biobased binder, sodium alginate, was developed for composite insulation materials in buildings. In order to solve the solubility issue, a modified procedure was developed to prepare insoluble alginate-based composite through inducing cross-link with ionic calcium. The water solubility of the composite samples with and without cross-link were investigated. The effect of fiber size and binder ratio on the density, thermal conductivity and water vapor resistance factor of the resulting composites were also studied.

Immersion the composite sample in $CaCl_2$ solution for a short time can solve the water solubility issue. All the composite samples can be considered as insulators for building applications. The larger fiber size leads to a lower density, thermal conductivity and water vapor resistance factor. The binder ratio seems to have a minor effect on the thermal conductivity.

6. Acknowledgement

The authors would like to thank the Région Auvergne-Rhône-Alpes for its financial contributions. In addition, the authors would like to thank the CSC (China Scholarship Council) to provide financial support for the study in France.

7. References

[1] A. Korjenic, V. Petránek, J. Zach, J. Hroudová, Development and performance evaluation of natural thermal-insulation materials composed of renewable resources, Energy and Buildings 43(9) (2011) 2518-2523.

[2] K. Strømdahl, Water sorption in wood and plant fibres, Technical University of Denmark. Danmarks Tekniske Universitet, Department of Structural Engineering and Materials Institut for Bærende Konstruktioner og Materialer (2000).

[3] M. Kapoor, D. Panwar, G. Kaira, Bioprocesses for enzyme production using agro-industrial wastes: technical challenges and commercialization potential, Agro-Industrial Wastes as Feedstock for Enzyme Production, Elsevier2016, pp. 61-93.

[4] A. Quintana-Gallardo, J.R. Clausell, I. Guillén-Guillamón, F.A. Mendiguchia, Waste valorization of rice straw as a building material in Valencia and its implications for local and global ecosystems, Journal of Cleaner Production 318

(2021) 128507.
[5] J. Zhao, S. Li, Life cycle cost assessment and multi-criteria decision analysis of environment-friendly building insulation materials-A review, Energy and Buildings (2021) 111582.
[6] Y. Zuo, J. Xiao, J. Wang, W. Liu, X. Li, Y. Wu, Preparation and characterization of fire retardant straw/magnesium cement composites with an organic-inorganic network structure, Construction and Building Materials 171 (2018) 404-413.
[7] M.R. Ahmad, B. Chen, M.A. Haque, S.F.A. Shah, Development of a sustainable and innovant hygrothermal bio-composite featuring the enhanced mechanical properties, Journal of Cleaner Production 229 (2019) 128-143.
[8] K. Wei, C. Lv, M. Chen, X. Zhou, Z. Dai, D. Shen, Development and performance evaluation of a new thermal insulation material from rice straw using high frequency hot-pressing, Energy and Buildings 87 (2015) 116-122.
[9] N. Mati-Baouche, H. De Baynast, A. Lebert, S. Sun, C.J.S. Lopez-Mingo, P. Leclaire, P. Michaud, Mechanical, thermal and acoustical characterizations of an insulating bio-based composite made from sunflower stalks particles and chitosan, Industrial Crops and Products 58 (2014) 244-250.
[10] C. Lacoste, R. El Hage, A. Bergeret, S. Corn, P. Lacroix, Sodium alginate adhesives as binders in wood fibers/textile waste fibers biocomposites for building insulation, Carbohydrate polymers 184 (2018) 1-8.
[11] P. Mariana, N. Antonia, A. Jaume, A.M. Lacasta, Characterization of thermal insulation materials developed with crop wastes and natural binders, WSB 14 Barcelona Sustainable Building, 2014, pp. 188-1-188-10.
[12] M.S. Hasnain, E. Jameel, B. Mohanta, A.K. Dhara, S. Alkahtani, A.K. Nayak, Alginates: sources, structure, and properties, Alginates in Drug Delivery, Elsevier2020, pp. 1-17.
[13] M. Viel, F. Collet, C. Lanos, Chemical and multi-physical characterization of agro-resources' by-product as a possible raw building material, Industrial Crops and Products 120 (2018) 214-237.
[14] J.-W. Rhim, Physical and mechanical properties of water resistant sodium alginate films, LWT-Food science and technology 37(3) (2004) 323-330.
[15] E.I. 12572, Hygrothermal performance of building materials and products-Determination of water vapour transmission properties-Cup method, British Standard, 2016.
[16] B. Marques, A. Tadeu, J. Almeida, J. António, J. de Brito, Characterization of sustainable building walls made from rice straw bales, Journal of Building Engineering (2019) 101041.
[17] M. Palumbo, A.M. Lacasta, N. Holcroft, A. Shea, P. Walker, Determination of hygrothermal parameters of experimental and commercial bio-based insulation materials, Construction and Building Materials 124 (2016) 269-275.
[18] M. Ali, A. Alabdulkarem, A. Nuhait, K. Al-Salem, G. Iannace, R. Almuzaiqer, A. Al-turki, F. Al-Ajlan, Y. Al-Mosabi, A. Al-Sulaimi, Thermal and acoustic characteristics of novel thermal insulating materials made of Eucalyptus Globulus leaves and wheat straw fibers, Journal of Building Engineering 32 (2020) 101452.
[19] A. Bakatovich, N. Davydenko, F. Gaspar, Thermal insulating plates produced on the basis of vegetable agricultural waste, Energy and Buildings 180 (2018) 72-82.
[20] S. Liuzzi, C. Rubino, F. Martellotta, P. Stefanizzi, C. Casavola, G. Pappalettera, Characterization of biomass-based materials for building applications: The case of straw and olive tree waste, Industrial Crops and Products 147 (2020) 112229.
[21] N. Belayachi, D. Hoxha, M. Slaimia, Impact of accelerated climatic aging on the behavior of gypsum plaster-straw material for building thermal insulation, Construction and Building Materials 125 (2016) 912-918.
[22] M. Labat, C. Magniont, N. Oudhof, J.-E. Aubert, From the experimental characterization of the hygrothermal properties of straw-clay mixtures to the numerical assessment of their buffering potential, Building and Environment 97 (2016) 69-81.

Data Statement

c. The datasets generated during and/or analysed during the current study are not available because they are proprietary and confidential in nature but the authors will make every reasonable effort to publish them in near future.

Performance of a mixed-use ground source heat pump system in Stockholm

Jeffrey D. Spitler [a], *Signhild E. A. Gehlin* [b]

[a] School of Mechanical and Aerospace Engineering, Oklahoma State University, Stillwater, Oklahoma, spitler@okstate.edu

[b] The Swedish Geoenergy Center, Lund, Sweden, signhild.gehlin@geoenergicentrum.se

Abstract. The 6300 m^2 two-story Studenthuset building at Stockholm University in Stockholm, completed in 2013, was thoroughly instrumented. Space heating and hot water are provided by a ground source heat pump (GSHP) system consisting of five 40 kW off-the-shelf water-to-water heat pumps connected to 20 boreholes of 200 m depth in hard rock. Space cooling is provided by direct cooling from the boreholes. This system has now been monitored for five years. This paper presents the results in the form of a range of performance indicators that describe the short-term and long-term system performance. Performance factors are computed for several boundaries defined by the IEA HPT Annex 52 boundary schema. Seasonal, monthly, daily, and binned performance factors for both heating and cooling operation are presented and discussed. Contrary to expectations based on thermodynamic theory, the performance is better correlated to the quantity of heating or cooling provided than it is to the exiting fluid temperatures from the ground heat exchanger. Despite being in Stockholm, the building rejects about 30% more than it extracts, leading to a minimal temperature increase over the five measured years. The analysis indicates that if operated as is, the GHE will not exceed its temperature constraints for many decades. The five-year seasonal performance factor (SPF) for combined heating and cooling is 5.2±0.2 considering only the heat pump and source-side circulating pump. However, the load-side distribution system and Legionella protection systems result in a significant decrease in the 5-year combined heating and cooling SPF at the outer boundary to 1.8±0.3.

Keywords. GSHP, system performance, monitoring, SPF, Annex 52
DOI: https://doi.org/10.34641/clima.2022.126

1. Introduction

The energy consumption of building heating and cooling systems often exceeds design expectations. This difference is often referred to as the "building energy performance gap." [1-4] Reasons for the gap include errors in design and installation, as well as non-optimal operating and control settings. Problems that don't lead to occupant discomfort may neither be detected nor mitigated for months or years unless performance measurements are made. Despite the need for such measurements, published results from long-term performance monitoring of building energy systems are scarce.

Gleeson and Lowe [5] reviewed field measurements of heat pump systems for residential buildings, mainly single-family buildings, comprising 600 heat pump systems in six European countries. For larger non-residential ground-source heat pump (GSHP) systems. Spitler and Gehlin [6] give an overview of published long-term (> 1 year) measured SPF and COP values reported in the literature for 55 systems worldwide. Such systems are necessarily more complex than GSHP systems for small residential buildings, and often include both heating and cooling as well as supplementary heating and cooling sources and heat recovery.

In 2018 a four-year international collaboration project IEA HPT Annex 52, *Long-term performance measurement of GSHP systems for commercial, institutional and multi-family buildings* [7] was initiated with the aim to monitor and analyze the long-term performance of a large number of GSHP systems in several countries. The emphasis in the project was on heat pump and system performance, e.g. determining coefficients of performance, seasonal performance factors and other system efficiency indicators. The project closed at the end of 2021, with performance measurement results from 30 large GSHP systems in seven countries. At the time of writing, the Annex has yielded a number of case study reports as well as guidelines for instrumentation [8] and uncertainty analysis [9].

Copyright ©2022 by the authors. This conference paper is published under a CC-BY-4.0 license.

One of the monitoring projects within IEA HPT Annex 52 is the GSHP system at the student union building Studenthuset at Stockholm University in Sweden. "Studenthuset" literally translates as "The Student Building", and so will be referred to simply as "Studenthuset" in this paper. Analysed performance data for one year of operation (April 2016-March 2017) were presented by Gehlin et al. [10] and Spitler and Gehlin [6], including seasonal performance factors and monthly, daily, and binned average values of coefficients of performance. Spitler and Gehlin [6] also include a detailed uncertainty analysis. Spitler and Gehlin [11] present an extended analysis of performance data from Studenthuset, including three years of analysed data and a discussion about the correlation between performance factors and heating and cooling load. The authors conclude that the system performance is strongly related to the load. With increasing load, the system performance also increases, and the system has relatively poor performance at times when the heating and cooling loads are low.

In this paper an extended analysis of 60 months of monitoring (January 2016 - December 2020) from the Studenthuset GSHP system is presented. Performance factors for multiple system boundaries and time frames as well as additional performance indicators and their correlation to load are analysed and discussed.

2. Studenthuset GSHP system

The student union building Studenthuset, located within the Stockholm University campus in central Stockholm, Sweden, is a 6300 m² four-story building completed in the fall of 2013. It contains office area, meeting rooms, study-booths for students and a café. The building services are thoroughly instrumented and maintained by highly skilled staff. The building services and GSHP system are described in references [6] and [11].

2.1 Building heating and cooling

The building's heating, cooling and domestic hot water (DHW) loads are met by the GSHP system. No auxiliary heating or cooling is installed, except for an electric resistance heater that boosts the hot water temperature to protect against Legionella. Heat distribution is provided by radiators with extra-large surface areas at a distribution temperature of 40°C instead of 55°C, which is the more common distribution temperature in Sweden. The cooling distribution system is a combination of VAV (variable air volume) and CAV (constant air volume) with chilled beams for ventilation and cooling.

2.2 GSHP system

Space heating and DHW are provided by the GSHP system which consists of five 40 kW off-the-shelf water-to-water heat pumps connected to a borehole field with 20 groundwater-filled boreholes in hard rock. The boreholes are 200 m deep and are fitted with single u-tubes filled with an ethanol/water mixture. The bore field is located below a landscaped courtyard and the boreholes are drilled at an angle so that they reach under the surrounding building (Figure 1). Space cooling is provided by direct cooling from the boreholes, with the fluid temperature leaving the boreholes at maximum 16°C.

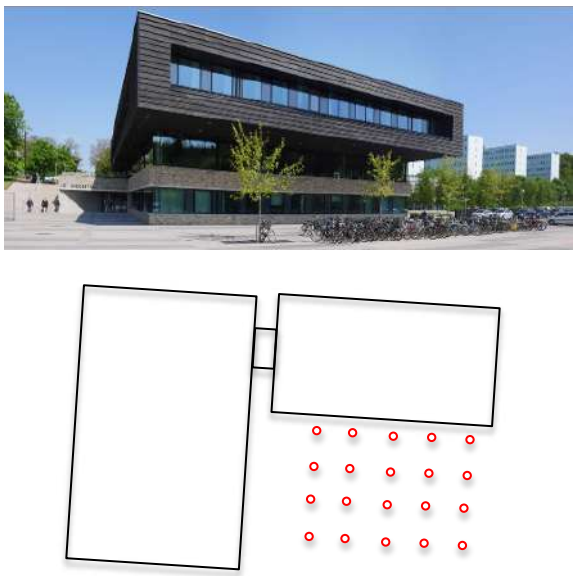

Fig. 1 - Studenthuset in Stockholm, front view (upper) and top view with borehole field (lower). Photo: JD Spitler.

2.3 System schematic and boundaries

Figure 2 shows a simplified schematic layout of the Studenthuset GSHP system. Six levels of system boundaries (0-5) are defined in the figure, for the evaluation of performance indicators.

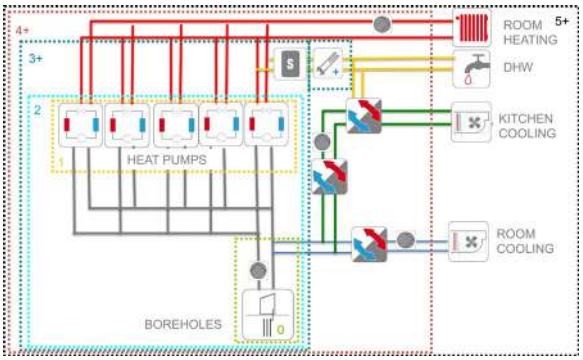

Fig. 2 - Schematic and Annex 52 system boundaries for Studenthuset. Pictograms in drawing used with permission from TU Braunschweig IGS

The six system boundary levels were developed within the IEA HPT Annex 52 project and represent an extension of the widely used system boundary schema developed within the EU project SEPEMO [12] in 2012. While the SEPEMO boundary schema was aimed at small monovalent or bivalent heat pump systems, the Annex 52 schema allows for a higher degree of system complexity such as in larger

GSHP systems like Studenthuset. The Annex 52 system boundary schema with six boundary levels and an indicator for use of supplemental heating or cooling is one of the outcomes from the IEA HPT Annex 52 project and is described in more detail in [13]. It is used in this paper and [11] for the analysis of the Studenthuset operation and performance, while the SEPEMO schema was used in [6] and [10].

The measured data for Studenthuset allows for calculation of heating performance at boundary levels H2, H3+ and H5+* and cooling performance at boundary levels C2 and C3(which are the same for this system). Performance factors may also be estimated for boundary levels H1* and C5*, with some approximations; the asterisk is used to indicate that the measured performance factor does not exactly correspond to the Annex 52 definition.

Specifically, the electrical measurements of the heat pumps include internal circulating pumps and control boards in the heat pumps. We therefore denote the boundary level as H1*, including the internal heat pump electricity use, with an asterisk. Level C5 includes the cooling provided by the ventilation air, but there are no measurements available for the airflow rate, and therefore we designate the boundary level as C5*.

2.4 Instrumentation and uncertainty analysis

A full description of the instrumentation is given in [6]. While most data points are collected with individual meters, the electricity use for the five heat pumps and the electricity consumed by the Legionella protection system are measured by one electricity meter. To estimate the electrical energy consumed by the heat pumps for boundary H2, the energy consumed by the Legionella protection system (LPS) is subtracted. The LPS electrical energy is estimated based on measured DHW flow rates and temperature rise, along with a nearly constant 3kW usage for recirculation pumps and heat losses from the piping to the space.

Measurements of the electrical energy consumed by the source-side circulation pump, fans used for ventilation and cooling, circulation pumps on the load side (distribution), and circulation pumps on the source side (boreholes), as well as electricity used for running the rotary exhaust air heat exchangers in the kitchen and building were measured with a single meter. A separate set of measurements over a two-week period was made to allow estimation of the electricity used by the source-side circulation pump as a function of flow rate. The electricity used for pumps respectively during the many hours of operation when both heating and cooling are being provided by the system, was allocated based on the amount of heating and cooling provided at each hour.

A detailed uncertainty analysis of the Studenthuset measurement is described in [6]. The same analysis is used here to determine uncertainty, as represented by error bars in the figures.

3. Energy loads

A common way to characterize the building space heating and cooling loads is the energy signature, shown in Fig. 3 for Studenthuset. To be clear, domestic hot water heating and kitchen refrigeration are not included. Surprisingly, the building uses a modest amount of cooling even down to low outdoor air temperatures. Presumably, this is due to chilled water being circulated and casually gaining heat from the space.

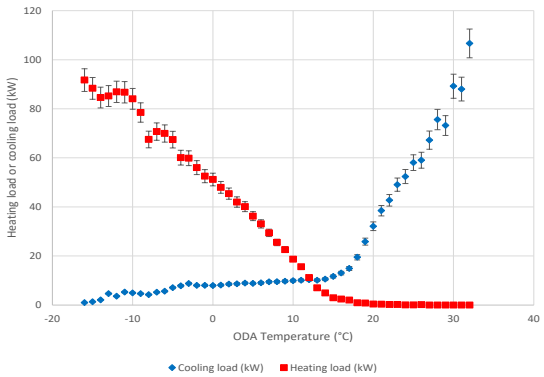

Fig. 3 – Energy signature showing building heating and cooling loads.

3.1 Annual balance

For ground-source heat pump systems, the balance between annual heat rejection and heat extraction is an important parameter. The instrumentation did not include an energy meter on the ground heat exchanger. Furthermore, the ground heat exchanger (GHE) flow rate was controlled to a minimum flow of 8 L/s, leading to low temperature differences, making it impossible to accurately measure the heat transferred to/from the ground. Therefore, annual loads on the ground were estimated as shown in Figure 4, with positive values representing heat extraction and negative values representing heat rejection or reductions in heat extraction. E.g. the heating provided to the building (red), of which the portion provided by the compressors (yellow) reduces the amount of heat extraction. If the annual heat transfer were perfectly balanced, the positive and negative portions in Figure 4 would have the same magnitude. It is notable that the load-side circulating pumps and fans (LSCPF) consume more energy than the heat pump compressors, while the source side circulation pumps (SSCP) use a very small amount of energy. As a result of the LSCPF energy consumption, even though the building heating loads are higher than the building cooling loads, the system rejects more heat than it extracts. In addition, some kitchen refrigeration also rejects heat to the ground, and further adds to the net imbalance, leading to the system rejecting about 30% more heat than it extracts. Uncertainty of these approximations have not been estimated, but the

building heating and cooling loads have uncertainties on the order of 5-6%.

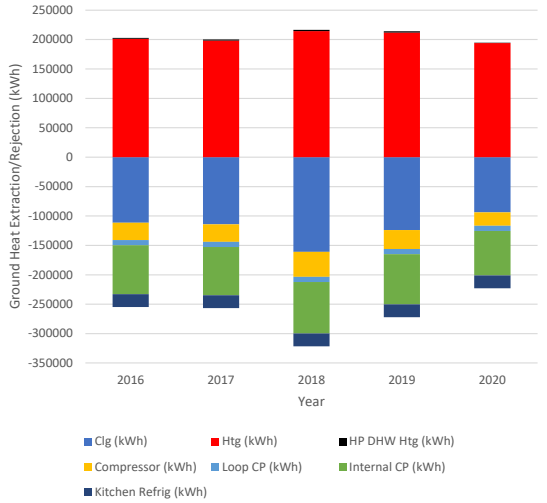

Fig. 4 – Estimated energy rejection and extraction components (to/from ground)

3.2 Ground heat exchanger performance

Ground-source heat pump systems usually have more favorable source temperatures than air-source heat pump systems. Figure 5 illustrates this, showing both the hourly outdoor air temperature and hourly exiting fluid temperature from the GHE. Not shown in the plot, if a trendline is fitted to the ground heat exchanger exiting fluid temperature (GHE ExFT), it shows a very slight (0.2°C) rise over the five-year period of operation. This is consistent with the annual heat rejection being higher than the annual heat extraction.

The cooling system was designed to operate with a maximum temperature of 16°C coming back from the boreholes. To date, the highest return temperature was 14.1°C during the unusually hot summer of 2018. This suggests that if the system continues operating as it does now, and if summers don't get hotter, the system will operate for many years before peak temperatures hit 16°C. That is, there is plenty of time to adjust system operation to mitigate this slight temperature rise.

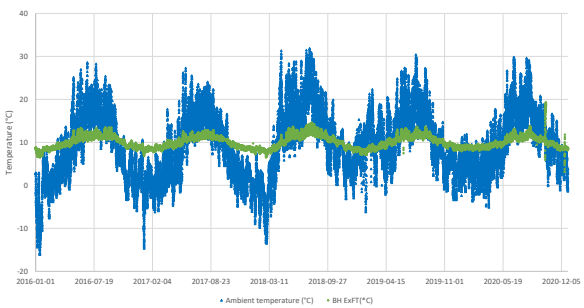

Fig. 5 – Ground heat exchanger entering fluid temperature and ambient temperature over the five years of measurement (2016-2020).

Figure 6 shows the relationship between the GHE ExFT and the outdoor air temperature, for 0.5°C bins. On average, the relationship is close to being linear – with hotter outside conditions corresponding to maximum cooling loads and accordingly warmer return temperatures from the ground.

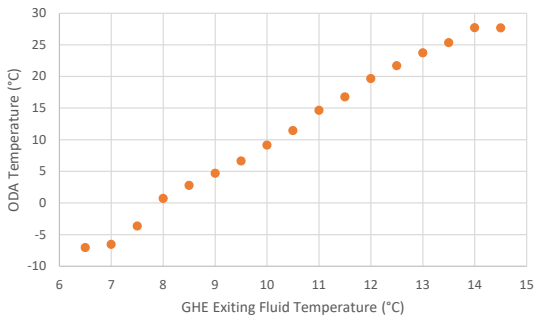

Fig. 6 – Binned ODA (Outdoor air) temperature vs. ground heat exchanger exiting fluid temperature .

4. Results

4.1 Energy consumption

The electrical energy consumption for each of the measured five years is summarized for heating (Fig. 7) and cooling (Fig. 8). The electrical energy for the load-side circulating pumps and fans (LSCPF) and the source-side circulating pump (SSCP) are allocated proportionally to the amount of heating and cooling provided. It's notable that the energy used for distributing heating (LSCPF) is similar to that used by the heat pumps for heating. This has a deleterious impact on the system performance. For cooling, the electrical energy used to distribute the cooling inside the building is about seven times the energy used to pump the heat carrier fluid through the ground heat exchanger. More careful analysis of the load-side distribution energy is needed to determine if the operation could be adjusted to reduce the energy consumption, but this has not been part of our study.

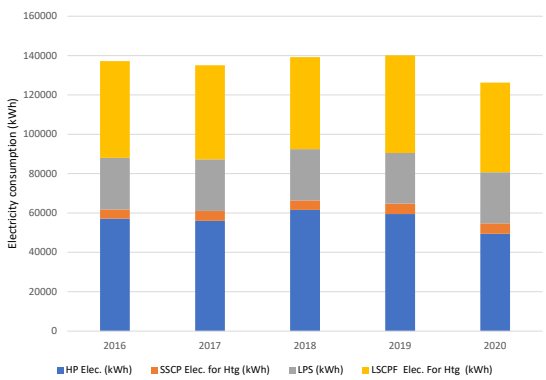

Fig. 7 – Electricity use breakdown for heating (2016-2020).

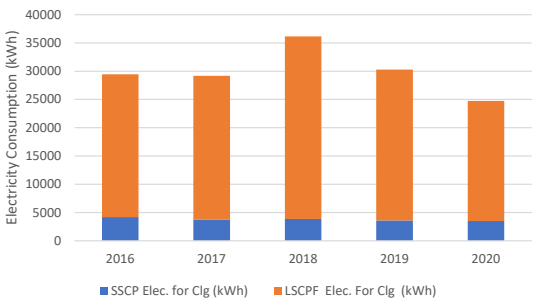

Fig. 8 – Electricity use breakdown - cooling (2016-2020).

4.2 Heating Performance

Seasonal performance factors for heating are computed for each year, grouped by the Annex 52 boundaries defined in Fig. 2, with deviations indicated with asterisks as discussed in Section 2. For each boundary, minor year-to-year fluctuations can be observed. From boundary 1* to 2, the SPF decreases due to the source-side circulating pump (SSCP). A further drop from boundary 2 to boundary 3+ is caused by the Legionella protection system (LPS), which consists of electric resistance heating to raise the hot water temperature to 60°C from the 55°C water provided by the heat pumps, and recirculation pumps that maintain high water temperatures throughout the piping network. Finally, from boundary 3+ to 5+*, the load-side circulation pumps and fans consume more electrical energy than the heat pump compressors and consequently reduce the seasonal performance factor (SPF) by more than 40% to approximately 1.5. The design and operation of the load-side pumping and piping was not part of our study, but it seems likely that there is significant room for improvement.

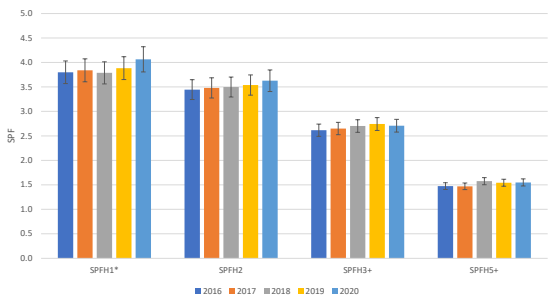

Fig. 9 – Heating SPF (2016-2020).

4.3 Cooling Performance

SPFs for the cooling system are given in Figure 10 for boundaries 2 and 5*. (Note the difference in scale.) Boundary 2 shows very high SPF values, as the only electrical energy accounted for is the source-side circulating pump. However, when accounting for the load-side circulating pumps and fans, with boundary 5*, the system performance is not so great. Meaningful comparisons can be difficult to make, but Southard, et al. [14] reported cooling SPFC5 (including fan energy) of a distributed GSHP system with much higher ground temperatures of 4.2±0.6. The distributed GSHP system did not have "free cooling" yet was able to provide cooling to the space significantly more efficiently than the Studenthuset system.

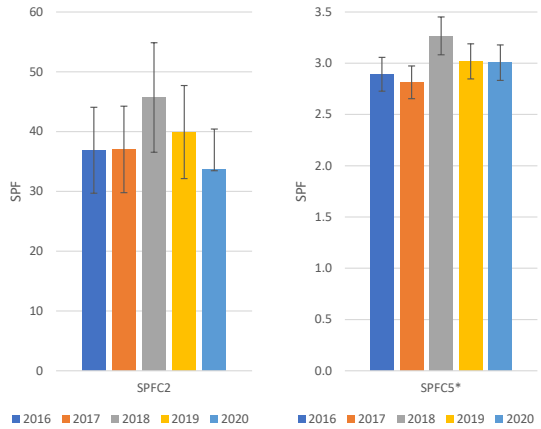

Fig. 10 – Cooling SPF (2016-2020).

4.4 Overall Performance

The performance factors shown above rely on allocation of the energy consumed by circulating pumps and fans between cooling and heating. An alternative approach is to calculate an overall performance factor for heating and cooling, as shown in Tab. 1. The impact of the internal heating and cooling distribution energy is still substantial, decreasing the 5-year SPF from 5.2 at boundary HC2 to 1.8 at boundary HC5+*.

Tab. 1 – Overall Seasonal performance factors

Year	SPF_{HC2}	SPF_{HC5+*}
2016	5.0±0.2	1.8±0.3
2017	5.1±0.2	1.7±0.3
2018	5.6±0.2	2.0±0.3
2019	5.2±0.2	1.8±0.3
2020	5.1±0.2	1.8±0.4
2016-2020	5.2±0.2	1.8±0.3

4.5 Monthly Heating and Cooling Performance

Monthly performance factors (MPF) for heating and cooling are shown in Fig. 11 and 12, respectively. Perhaps contrary to thermodynamic expectations, even MPFH1* is higher in the winter and lower in the summer, when the ground heat exchanger return temperatures are more favorable. As previously observed for this system and other

systems – parasitic losses (e.g. control boards and energized solenoid valves) and cycling losses decrease the performance of GSHP under low-load conditions.

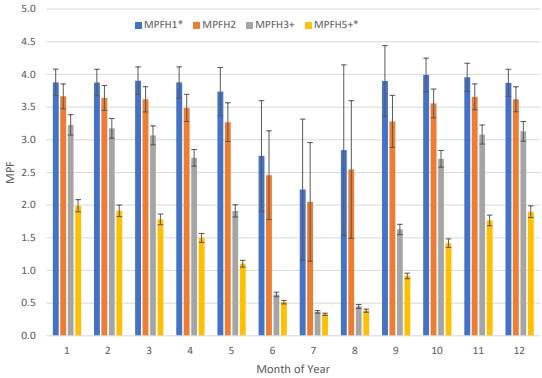

Fig. 11 –Heating monthly performance factors (2016-2020)

For cooling, MPF are higher during the winter months, when return fluid temperatures from the ground are lower. This is as expected, but the trend is also due to the allocation of pumping energy between heating and cooling, as will be shown in the next section.

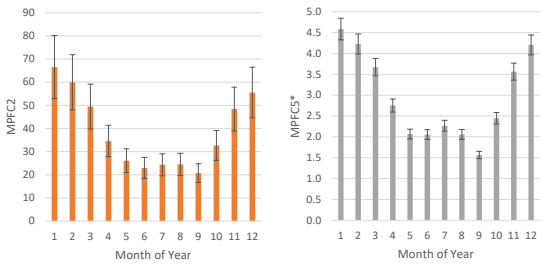

Fig. 12 – Binned monthly performance factors for cooling for each month in 2016-2020, with error bars.

4.6 Effect of source temperature

From a thermodynamic perspective, heat pump performance is expected to increase as source temperatures become more favorable. Binned performance factors have been calculated for heating and cooling, as shown in Figs. 13 and 14. Each symbol or bar in these figures represents performance for all hours in a certain bin. E.g., the symbol at a GHE exiting fluid temperature of 8°C represents all hours with temperatures between 7.75 and 8.25°C. The gray bars represent the number of hours in each bin.

Opposite to thermodynamic expectations for heating with heat pumps, the performance for every boundary trends downward with increasing entering fluid temperature to the heat pump. The decrease in performance is more dramatic for the boundaries H3+ and H5+*. The highest GHE ExFT occur in the summer period, which is a period with low use of Studenthuset and when the need for heating is mainly for DHW and Legionella protection. Energy use for circulation pumps and LPS will then be high compared to delivered energy, hence the low performance factors.

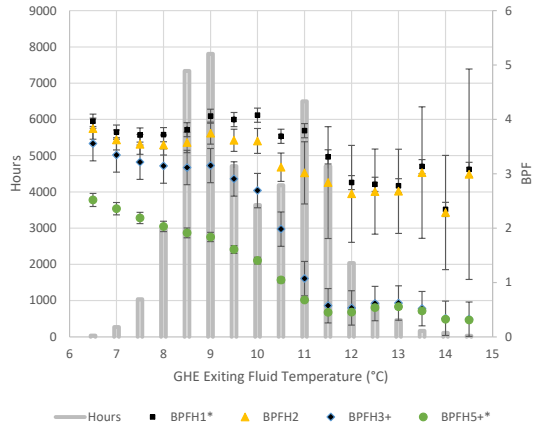

Fig. 13 – Binned performance factors for heating vs ground heat exchanger exiting fluid temperature.

For cooling, the performance factors show a V-shaped trend – highest at low or high temperatures, lowest at the middle point. For space reasons only boundary 5* is shown here, but the trend is the same for boundary 2. At low temperatures, where cooling is being provided simultaneously with heating, the amount of pump energy allocated to cooling is small, leading to high BPF. This is shown by calculating the BPF assuming that all of the pump and fan energy is allocated to cooling –shown as the orange triangles in Fig. 14. In this case the performance increases with increasing fluid temperature. This is also contrary to expectations – for any given amount of pump and fan energy, one would expect to see a decrease in performance factor for cooling, as the GHE ExFT increases. However, the temperatures are highest during periods of high loads, which is also when the amount of energy used for circulation pumps and fans are lowest compared to delivered cooling.

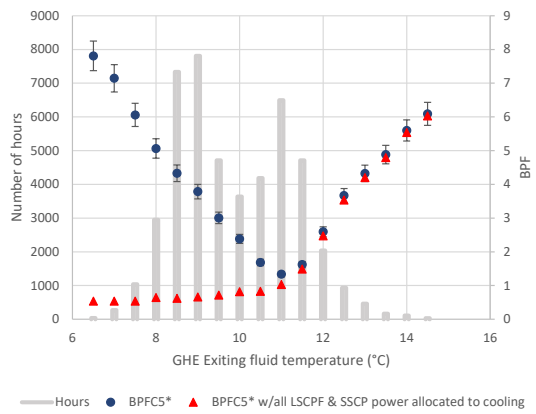

Fig. 14 – Binned performance factors for cooling vs ground heat exchanger exiting fluid temperature.

4.7 Effect of total heating and cooling

As may be inferred from the above results, the amount of heating and cooling being provided has a significant impact on the overall system

performance, reducing the proportion of electrical energy used for pumping, blowing, and "parasitic" uses like control boards and solenoid valves.

Figure 15 shows binned daily system performance factors (boundary HC5+*) for heating and cooling combined, vs. the total amount of heating and cooling being provided. The performance factors are divided into days that are "mainly cooling", "mixed", and "mainly heating", based on the ratio of heating provided to total heating and cooling providing being less than 0.25, between 0.25 and 0.67, and greater than 0.67, respectively. The general trend for all categories is increasing performance with increasing total load. The mainly cooling days give relatively high performance as the better performance of the free cooling system becomes dominant with higher loads. The character of the "mixed" days follows the trend of the "mainly heating" days, although in the lower load and performance factor region. The "mixed" days (in the spring and fall shoulder seasons) show two bands of performance. The higher band occurs when there is low DHW consumption, correlated to low occupancy. Almost all of these days in the higher performance band are either weekend days or occurred in 2020 after the pandemic began and the university closed.

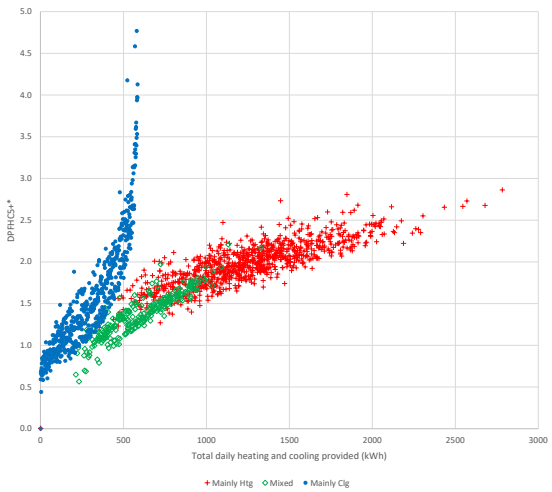

Fig. 15 – Binned daily total performance factors vs total heating and cooling provided at boundary 5+*.

5. Conclusions

In this paper, five years of data from the Studenthuset ground-source heat pump system have been analyzed from a system performance perspective. The GSHP system has previously been analyzed with data from one year [6, 10] and three years [11] and the general trends observed in those papers remain valid for the five-year period. Studenthuset was built in 2013 and the measured data for the period 2016-2020 show that the ground heat rejection exceeds the ground heat extraction by about 30%, leading to a minimal temperature increase over the five measured years. The analysis indicates that if operated as is, the GHE will not exceed its temperature constraints for many decades.

The five-year data analysis shows that the performance factors increase with increasing heating and cooling load. This confirms the results from the previously analyzed shorter data series.

The dominant factor for the overall system performance is the amount of heating and cooling provided by the GSHP system. The reason is that the proportion of electrical energy used for circulation pumps, fans and "parasitic" uses such as control boards and solenoid valves decrease when energy provided increases. The Studenthuset GSHP system performance factors are highest when the building is used heavily, and the lowest performance factors appear during those periods when students are off campus and the building is little used. During those periods standby circulation, DHW and Legionella protection are dominant.

The Studenthuset study pinpoints the deleterious effect of the load side distribution (piping, pumping, fans) and Legionella protection on the system performance factors. The distribution system and Legionella protection systems result in the 5-year combined heating and cooling SPF decreasing from 5.2 at boundary HC2 to 1.8 at boundary HC5+*. While it is important to maintain proper Legionella protection, the LPS operation ought to be optimized so that it does not use more energy than necessary. There is room for further system improvement and component development to minimize the energy use for load side distribution.

From a European perspective, where centralized heat pump systems are most common, it is tempting to argue that the load side distribution losses should not be taken into account, since they would be the same regardless of the heating and cooling source used, e.g. gas or district heating apart from heat pumps. Hence only system boundary 2, which includes the source side circulation pumps and the heat pumps, should be considered. However, in many countries, e.g. the USA, distributed heat pump systems are common. In such systems multiple smaller heat pump units are distributed in the buildings that they serve, and the main distribution losses appear on the source side of the heat pump. There are to our knowledge no systematic comparisons of the efficiency of centralized versus distributed heat pump systems, and to do that it is necessary to consider the load side system boundaries as well. Comparisons to a distributed GSHP system [14] in the USA suggest that the load-side system distribution energy in Studenthuset is excessive. It is our belief that additional comparative studies between centralized and distributed GSHP systems would be useful in shedding further light on the usage of energy for distribution of heating and cooling in heat pump systems.

6. Acknowledgements

Thanks to Anders Larsson at Akademiska Hus for his help and support, and for providing measurement data and information about the monitored building. Permission to make the data publicly accessible was kindly granted by Akademiska Hus. The support from the authors' employers and the Swedish Energy Agency (TERMO research program Grant 45979-1) is gratefully acknowledged. This work is part of the IEA HPT Annex 52, *Long-term performance measurement of GSHP systems serving commercial, institutional and multi-family buildings.* [7].

7. Data Access Statement

The datasets generated and analyzed during the current study are available in the ShareOK repository at: https://doi.org/10.22488/okstate.22.000005

8. References

[1] de Wilde P. The gap between predicted and measured energy performance of buildings: a framework for investigation. Automation in Construction. 2014;41:40-9.

[2] Scofield JH. Do LEED-certified buildings save energy? Not really. Energy Build. 2009;41(12):1386-90.

[3] Geng Y, Ji W, Wang Z, Lin B, Zhu Y. A review of operating performance in green buildings: Energy use, indoor environmental quality and occupant satisfaction. Energy Build. 2019;183:500-14.

[4] Spitler JD. Addressing the building energy performance gap with measurements. Science and Technology for the Built Environment. 2020;26(3):283-4.

[5] Gleeson CP, Lowe R. Meta-analysis of European heat pump field trial efficiencies. Energy Build. 2013;66(0):637-47.

[6] Spitler JD, Gehlin S. Measured Performance of a Mixed-Use Commercial-Building Ground Source Heat Pump System in Sweden. Energies. 2019;12(10):2020.

[7] IEA HPC.: Annex 52 - Long term performance measurement of GSHP Systems serving commercial, institutional and multi-family buildings. 2019 https://heatpumpingtechnologies.org/annex52/

[8] Davis JM, Martinkauppi I, Witte H, Berglöf K, Vallin S. IEA HPT Annex 52 - Long-term performance monitoring of GSHP systems for commercial, institutional, and multifamily buildings Guidelines for Instrumentation and Data. 2021. DOI.: 10.23697/tgr4-qn89.

[9] Spitler JD, Berglöf K, Mazzotti Pallard W, Witte H. EA HPT Annex 52 - Long-term performance monitoring of GSHP systems for commercial, institutional and multi-family buildings. Guidelines for Calculation of Uncertainties. 2021. DOI.: 10.23697/m2em-xq83.

[10] Gehlin, S., Spitler, J.D., Larsson, A. & Annsberg, Å.: Measured performance of the University of Stockholm Studenthuset ground source heat pump system. 14th International Conference on Energy Storage-EnerSTOCK2018, Adana, Turkey. 2018.

[11] Spitler, J.D. and Gehlin, S.: Three Years' Performance Monitoring of a Mixed-Use Ground Source Heat Pump System in Stockholm. Proceedings of the 13th IEA Heat Pump Conference, April 26-29, 2021, Jeju, Korea. 2021.

[12] Nordman, R.: Seasonal performance factor and monitoring for heat pump systems in the building sector, SEPEMO-Build, Final Report. Intelligent Energy Europe 2012.

[13] Gehlin, S. and Spitler, J.D.: Half-term Results from IEA HPT Annex 52 - Long-term Performance Monitoring of Large GSHP Systems. Proceedings of the 13th IEA Heat Pump Conference, April 26-29, 2021, Jeju, Korea. 2021.

[14] Southard, LE., X. Liu and J. D. Spitler. 2014. Performance of HVAC Systems at ASHRAE HQ – Part 2. ASHRAE Journal 56(12): 12-23.

STUDY ON REPRODUCIBILITY OF EXHAUST DIFFUSION PROPERTIES OF GAS WATER HEATERS

Saki Nakano [a], Takashi Kurabuchi [b], Jeongil Kim [c]

[a] Department of Architecture, Graduate School of Engineering, Tokyo University of science, Tokyo, Japan, mbcaj.10.fk27do30@gmail.com.

[b] Department of Architecture, Graduate School of Engineering, Tokyo University of science, Tokyo, Japan, kura@rs.tus.ac.jp.

[c] Department of Architecture, Graduate School of Engineering, Tokyo University of science, Tokyo, Japan, jeongil.kim@rs.tus.ac.jp.

Abstract. When installing a gas water heater in a common corridor, the common way of the installation in Japan, there are restrictions on the installation location and the shape of the corridor in order to avoid the exhaust gas stagnating in the corridor and flowing into the rooms through the vent. Therefore, the standards limit the building planning and require more relaxation. We had been conducting experiments by using full-scale models over the past years, however, as there are many shapes of common corridor, it is difficult to examine all the possibilities. It is necessary to reproduce the exhaust properties on computational fluid dynamics (CFD) so that the examination of reference relaxation can be performed by simulation using CFD. We needed to collect target data to confirm reproducibility by actual measurement. It was ejected without any obstacles to the jet flow, and we measured the velocity, temperature, CO2 concentration, etc.
We estimated that the model of the interface on a gas water heater and setting boundary conditions can be the factors to improve the reproducibility.

Keywords. heater, corridor, exhaustion, prediction
DOI: https://doi.org/10.34641/clima.2022.336

1. Introduction

In Japan, we have a bath culture and home water heater are popular. There are two types of air supply and exhaust, we usually use Roof Top Flue gas water heater in a common corridor of apartments.

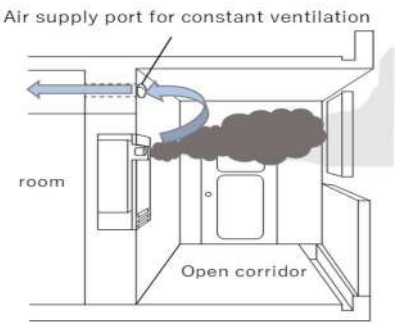

Figure1. Installation status of gas water heaters in Japan

In such cases, installation standards have been established to prevent exhaust gases from stagnating in the corridor and flowing into the rooms through the vents. Installation standards restrict the location of water heaters and vents, and the shape of corridors.

Since the current standards are a constraint on architectural planning, we have been conducting various experiments using full-scale models in order to relax the standards as much as possible. However, in recent years, heaters and architectural styles have diversified, and it is difficult to study all cases by experiment.

Therefore, we are trying to establish a method to reproduce the exhaust gas in CFD to enable us to decide whether or not to install the water heater by simulation analysis. If we can examine the possibility of installation using CFD, it will be easier to determine the installation of various shapes, which will expand the range of design.

2. Measurement of exhaust jet

An image of a gas water heater and an air supply port installed in an open corridor is shown below.

Copyright ©2022 by the authors. This conference paper is published under a CC-BY-4.0 license.

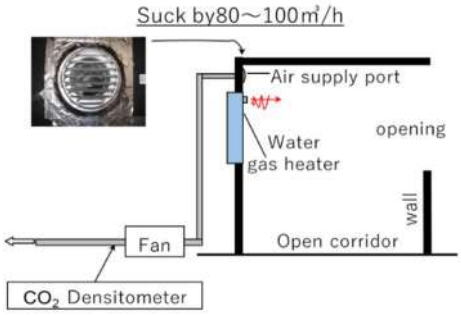

Figure2. a gas water heater and an air supply port installed in an open corridor

We have attempted to reproduce the exhaust in previous studies, but adequate methods have not yet been established. We believe the reason for that is that they were using the CO2 concentration in the vents to check for consistency. In this study, we operated the water heater in a space where there was nothing that could affect the exhaust air, and measured the temperature, CO2 concentration, and other exhaust air properties. The results will be used to check the consistency with the analysis results to improve reproducibility.

2.1 Measurement Summary

We measured the velocity, temperature, and concentration at the exhaust port as shown in the figure3.

For the measurement of exhaust distribution, a mesh with 56 thermocouples uniformly arranged so as not to interfere with the exhaust air is used. By changing the mesh height in two steps, we measure the temperature at all 98 points within 0.8 m above and 0.4 m below the exhaust port height. A tube is placed at 18 of these points to measure the CO_2 concentration. By moving the above mesh parallel to the gas appliances, the diffusion of exhaust gas at points 1m, 2m, and so on away from the appliances was measured.

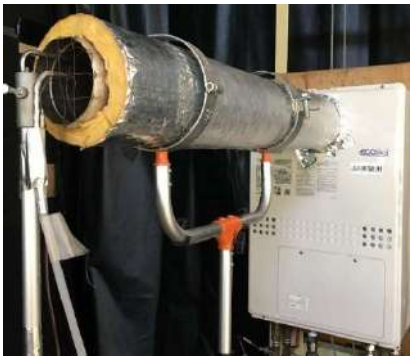

Figure3. Experimental method for blowout condition of Exhaust port

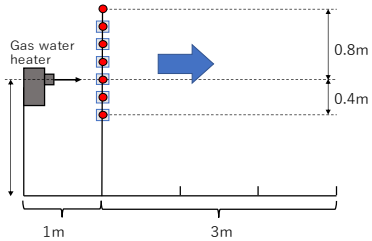

Figure4. Experimental method for exhaust distribution

In addition, we conducted visualization experiments to confirm the trajectory of the vertical cross section in the blowing direction.

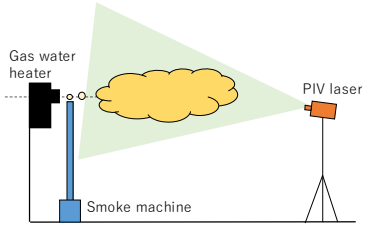

Figure5. Experimental method for visualization of exhaust

2.2 Measurement results

We focused on two different operating conditions: "maximum combustion" and "heating only. The case of maximum output in heating and hot water supply is called "maximum combustion", and the state in which only heating is operated is called "heating only". The exhaust measurement results for each condition are shown below.

Table1. The exhaust measurement results

	Maximum combustion	Heating only
Velocity[m/s]	4.81	3.08
Temperature[K]	341.3	324.8
Concentration[ppm]	65005	12751

Depending on the output, we found differences in temperature, CO2 concentration and ascent rate, as well as left and right deflections.

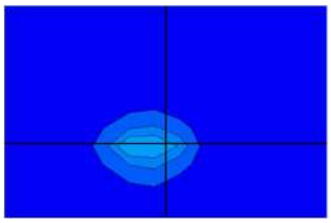

at *1.0m* from the equipment

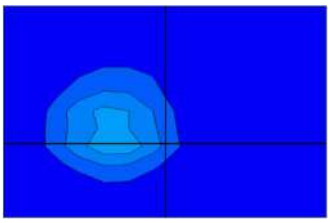

at *2.0m* from the equipment

Figure6. "*Maximum combustion*" the temperature distribution

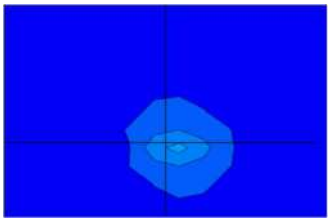

at *1.0m* from the equipment

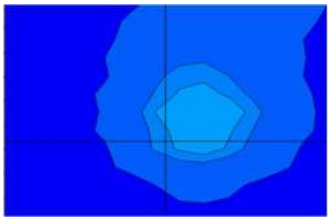

at *2.0m* from the equipment

Figure7. "heating only" the temperature distribution

The internal shape of the exhaust outlet was checked, and it was found that the outlet surface was divided between heating and hot water supply, causing deflections to be created.

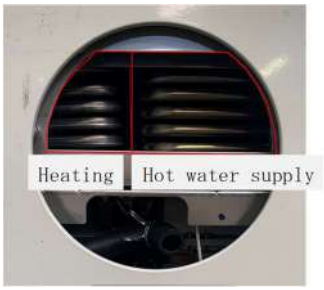

Figure8.interal shape of the exhaust outlet

3. CFD summary

We set up an analysis area of 16 m wide, 10 m deep, and 10 m high was set up. And we installed an exhaust outlet at a height of 2.2 m to reproduce the experimental conditions. As mentioned earlier, it was found that the exhaust air blowing surface is divided between the heating system and the hot water supply system, so an adapter shape that reproduces the actual situation is used. At First, we tried to reproduce the trajectory without separating the air outlets (Model A). Then, to further improve the accuracy, we used a separated boundary outlet (Model B).

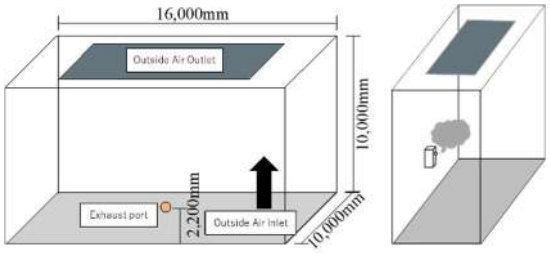

Figure9. Analysis area model

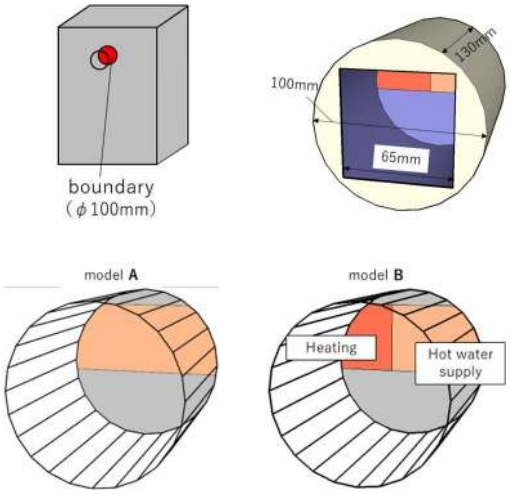

Figure10. Exhaust outlet model

The analysis model and outside air inflow conditions are shown below.

Table2. Analysis conditions

Analysis conditions		
Analytical method		steady-state analysis
Turbulence model		64989
Analysis area		12m × 16m × 10m
Boundary condition	outlet	Wind speed, temperature, CO2 concentration based on actual measurement
	Outside air outflow surface	Pressure outlet
Difference scheme		Secondary accuracy upwind

Table3. boundary conditions (outside air inflow surface)

Boundary condition		
Outside air inflow surface	Velocity[m/s]	0.05
	Temperature[K]	287.69
	Concentration[ppm]	480

4. Considerations for Improving Reproducibility

4.1 Comparison of the two kinds of velocity

Compare the analysis results using two speeds. One(1) is the velocity calculated with measured CO2 concentration and gas consumption, and the other(2) is the numerical value measured by an anemometer inside the exhaust port.

Table4. boundary conditions

Boundary condition	(1)Calculated by gas consumption	(2)measured
Velocity[m/s]	8.50	8.76
Temperature[K]	338.49	
Concentration[ppm]	64989	

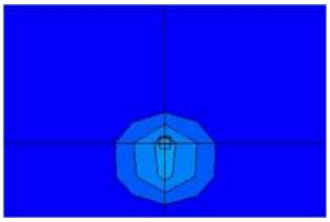

(1) 1.0m from the equipment

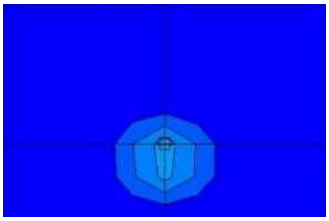

(2) 1.0m from the equipment

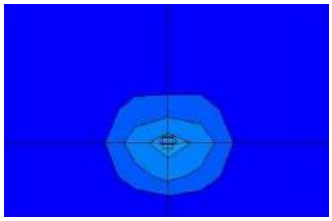

(1) 2.0m from the equipment

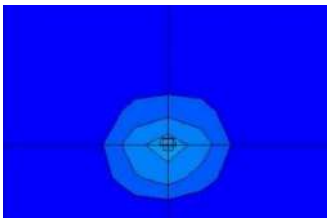

(2) 1.0m from the equipment

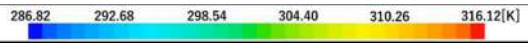

Figure11. "Comparison of the two kinds of velocity"
the temperature distribution

Comparing the results of the analysis, there was little difference in terms of distribution. In terms of core temperature, the diffusivity in (1) was close to the actual measurement results, especially after 2.0 m. Therefore, the wind speed obtained from CO2 is used from now on.

3.2 Correction of orbit centre position

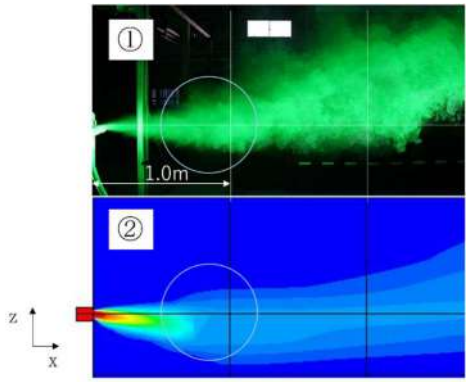

Figure 12. difference in center height of the exhaust orbit(①: results of visualization experiments, ②: analysis results)

From the figure14, it can be seen that there is a shift in the center height of the exhaust track. Both the visualization and analysis results show a gradual rise after sinking downward immediately after exhaust. However, the analysis results showed a stronger downward trend than actual. As for the cause of the downward trend, we found that the exhaust jet is hitting the wall above the model.

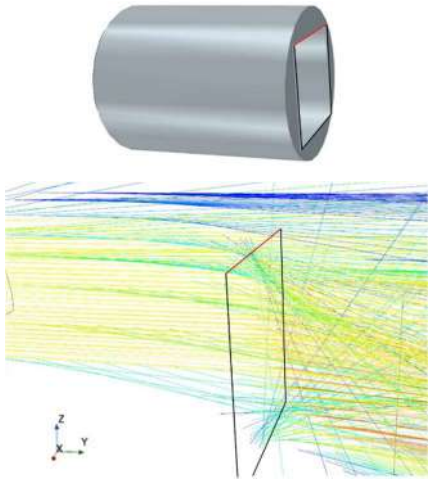

Figure13. Velocity vector diagram near exhaust model

As an improvement measure, apply a correction of 15% of the main jet velocity upward to the boundary surface.

Table5. boundary conditions

Boundary condition	
Velocity(x,y,z)[m/s]	8.50 , 0 , -1.275
Temperature[K]	338.49
Concentration[ppm]	64989

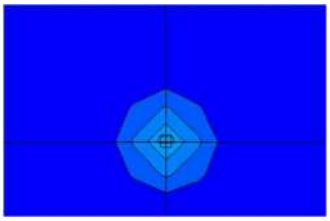

At 1.0m from the equipment

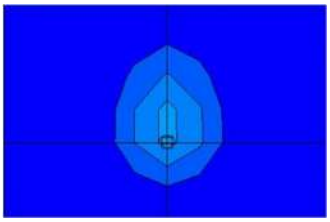

At 2.0m from the equipment

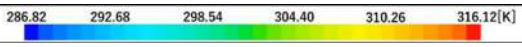

Figure14. "Correction of orbit centre position" the temperature distribution

At 1.0m from the equipment, the orbit height of the exhaust was close to the actual measurement results. And at 2.0m, the results showed the same rise as in reality. It found that adding z-direction correction to the boundary surface is effective in adjusting the orbit height.

3.3 reproducing of deflection

Reproduce the inside of a device (Figure9), and set the conditions by systematically dividing the blowing boundary surface. For each blowing condition, we used the temperature and CO2 concentration proportional to the gas consumption, assuming the same speed.

Table6.heating and hot water supply

Boundary condition	Hot water supply	heating
Velocity[m/s]	8.50	
Temperature[K]	342.05	332.03
Concentration[ppm]	69260	57235

No deflection appeared as in the actual measurement results by dividing boundary surface, and the exhaust went straight.

So, to reproduce the deflection, we applied a correction of 15% of the velocity towards the weaker output (from hot water supply to heating) and got the following results.

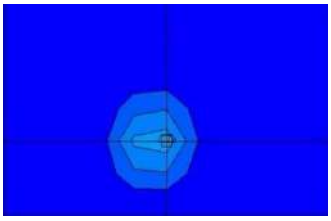

At 1.0m from the equipment

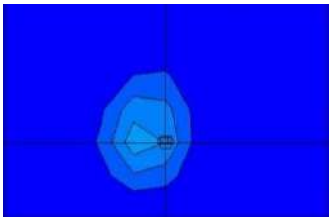

At 2.0m from the equipment

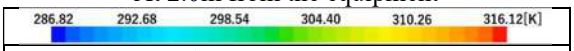

Figure15. "Reproducing of deflection" the temperature distribution

The distribution is now closer to the actual orbit.

5. Conclusion

In the Free-flowing state, deflections to the left or right were observed due to the difference in power output, which may be attributed to the blowing shape inside the device.

Four types of boundary condition setting methods were examined. At the results, we found that using the velocity calculated from the gas consumption is more suitable for reproducing the diffusion state close to the actual measurement. In addition, adding a correction of 15% of the velocity in the +Z and +Y directions is effective in adjusting the orbit position.

6. References

1)Nishizawa et al., Study on installation of ventilation opening in common corridor apartment houses where gas heaters are installed, ROOMVENT conference 2020

The datasets generated during and/or analysed during the current study are not available because it is currently in preparation, but the authors will make every reasonable effort to publish them in near future.

Upgrade of ice storage system in congress centre

Urška Mlakar [a], Uroš Stritih [a]

[a] Faculty of Mechanical Engineering, University of Ljubljana, Ljubljana, Slovenia, urska.mlakar@fs.uni-lj.si

Abstract. Storage of various forms of energy is a relevant topic in last decades. The ability to store energy that is produced at a time when we have a surplus of a particular source and use it at a time when energy needs are greater is crucial. We can store energy as electricity or as thermal energy (heat and cold). In this paper, we will take a closer look at latent cold storage with ice bank technology. Ice bank technology exploits latent heat in the liquid-solid phase change of water. Of all the cold storage technologies available, ice storage is the most popular in recent decades due to its high latent heat, especially when available space is limited. Cold in ice banks is produced at night, when electricity is cheaper, and is used to cover cooling needs especially at peak hours during the day.
In Slovenia, the technology of ice banks has already been applied several times. Among other buildings, this technology is also used in buildings such as the Opera and Ballet, the Crystal Palace, and the Congress centre Cankarjev dom. This Congress centre has a system with nine ice banks with a total nominal capacity of 405 kWh per ice bank, for its cooling needs. The transition to ice bank technology has allowed them to cut by 41 % the power of their refrigeration units, while saving money is achieved since ice is produced at night time with lower prices. The article presents the three phases of the system: Energy for cooling of a system without ice banks, a system with ice banks and saved energy with this technology and an analysis of the upgrade of this system with PV modules. The simulations were done with the Trnsys program. Indicative savings with the application of ice banks and additional upgrades with PV modules are presented. The payback periods are also analysed.

Keywords. energy storage, ice storage, case study, economic analysis, upgrade analysis.
DOI: https://doi.org/10.34641/clima.2022.235

1. Introduction

According to the storage mechanism, thermal energy storage (TES) is divided into three types: sensible, latent, and thermo-chemical storage. Among them, energy storage occurs in sensible storage with a change in temperature and latent storage with a change in aggregate state (1).

Cold storage technology is an effective way of shifting maximum electrical loads as part of an energy management strategy in buildings. Such systems can help electrical devices to reduce peak loads and increase loads during off-peak periods, which could improve the utilization of base load generation equipment and thus reduce dependence on peak units with higher operating costs (2).

The use of spherical capsules for PCM encapsulation in air conditioners has been studied by various researchers. Fang et al. (3) experimentally studied the characteristics of the operation of refrigeration air conditioning systems with spherical capsule filling. Spherical capsules with an outer diameter of 100 mm and a wall thickness of 1 mm were filled with water. Experimental results have shown that refrigerated air conditioners with spherical capsules have better performance and can operate during charging and discharging; and have a COP system variation of 4.1 to 2.1 during the latent heat storage period.

The term ice storage is used as a general name for heat storage, which uses the enthalpy of water as part of its storage capacity to change its physical state from liquid to solid. By freezing water, a high amount of heat can be removed: 333 kJ (0.093 kWh) are released per kilogram of water during this process (4).

We know different ice storage technologies (5); Ice Harvesting, Ice on coil, encapsulated ice (6) and others. Key benefits of ice bank technologies (7):

- Reduced final power requirements (kW) for pumps and fans - Designs that use cooler liquids and larger temperature changes reduce the need for air and water flow, so component sizes, including the size of the electric motor, may be smaller. The first savings in equipment and work can be significant.

Copyright ©2022 by the authors. This conference paper is published under a CC-BY-4.0 license.

- Reduced electrical distribution - smaller components such as refrigeration units, fans and pump motors reduce connected power and thus save on electricity distribution costs from the building's main transformer to the starting panels. Reduced connection power can also reduce the size of emergency generation equipment that may be required.

- Space savings in the building - smaller supply and return channels require less floor space. Smaller air ducts reduce the height of the ceiling, allowing for shorter floor-to-ceiling dimensions. The result is lower construction costs and more usable/rental floor space.

- Operation at 100 % capacity - Refrigeration units will always operate at or near 100 % capacity while filling the storage system, and usually have a higher capacity factor compared to a conventional chilled water system. This shortens the time when the refrigeration units operate in low load conditions as well as on / off at refrigeration loads. When refrigeration units operate at near full capacity most of the time, they require less maintenance. Any fluctuations in the cooling load will be covered by an ice storage tank.

- Adaptation to cooling peaks - Process operations often have short but high cooling peaks. Refrigeration units are not designed to adapt quickly to these peaks. The ice storage tank can respond quickly and efficiently to variations in load fluctuations and can follow rapid cooling peaks.

- Adapting to changes in the schedule of energy use - Periods of use of electric peaks vary greatly. The demand period can be 8-10 hours or a series of shorter sections 2-3 hours. Ice storage is very efficient at any service demand schedule and can be easily changed if periods change in the future.

An example of a successful application of the use of ice bank technologies is the University of Arizona campus presented by Tarcola (8). The ice storage system is powered by a Combined Heat and Power [CHP] system located at the Arizona Health Sciences Centre (AHSC) plant, that supplies electricity to three ice chillers. These chillers make ice at 3,2 MW and 0.783 kilowatts per ton. They freeze water in the 156 storage tanks that are discharged on demand. They are so satisfied with the operation of the system that they decided to upgrade the system with an additional 49 ice storage tanks and a 4.4 MW refrigeration unit.

Examples of the use of ice bank technologies in Slovenia are the Crystal Palace (9), Ljubljana Castle (10) and Cankarjev dom which example is presented below.

2. Research methods

2.1 System presentation

Cankarjev dom has decided to modernize and improve its air conditioning systems, as the appropriate comfort in the premises where various events, performances, conferences and other events take place is very important for the satisfaction of guests.

Until the replacement, two water-cooled liquid coolers were intended for cooling in Cankarjev dom, each with a cooling capacity of 1021 kW, which prepared cooled water with a temperature range of 11/6 ° C. When they were replaced, they were replaced by two new ones with a lower cooling capacity of 595 kW. To one of the refrigerant units was added a system of latent cold storage - an ice bank. The system has nine 340-liter latent storage tanks with a total rated capacity of 405 kWh (1 ice bank) (11). **Fig. *1*** shows the system of nine ice banks in Cankarjev dom.

Their system allows them different modes of operation. Night operation - filling the latent cold storage tank; daily operation - preferably mechanical cooling with a liquid cooler and additional emptying of the cold storage tank, and daily operation - preferably cooling by emptying the cold storage tank and supplementary mechanical cooling with another liquid cooler.

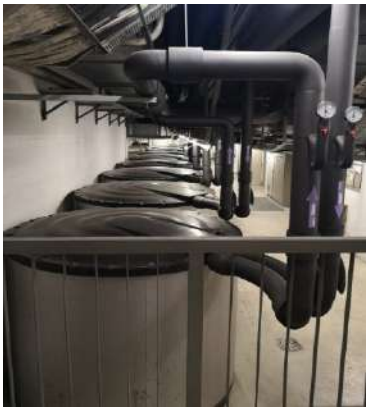

Fig. 1: System of nine ice banks in Cankarjev dom

2.2 Building

The building of the Cankarjev dom congress centre is interesting to consider because part of this building is underground. The building has eleven floors, of which seven are above ground and four below ground. Under the ground are Kosovel's, Linhart's, Štih's, Gallus's hall (ground floor) and ten conference halls. Above the ground is only part of the Gallus Hall (balconies), the Duše Počkaj Hall and the Lili Novy Glass Hall. Below the second lobby are a few more floors that provide storage and preparation of the program in the technical field, e.g., storage of acoustic shell and other props, shelters, technical rooms, etc. The total area of Cankarjev dom is 36,000 m^2. On the south side, the envelope of the building is lined with marble slabs, while in the western part we have mostly brick and in the higher floors concrete, and at the same time about 80 % of the western part is glazed. **Fig. *2*** shows a view of the envelope of

Cankarjev dom from the Southwest. The northern part of the building envelope is partly covered with marble slabs, and partly has copper foil on the envelope as an outer layer. In the eastern part of the envelope, we have marble slabs, but also a lot of glass surfaces.

Fig. 2: Cankarjev dom from the Southwest

The interior of the building is covered in the simulation model with 40 zones, which have no further division with the interior walls. The building is divided into so many zones that we were able to define it as relevantly as possible. Through all these zones, we were also able to define the parameters that affect the internal heat gains, which are especially important in the zones where the congress halls are located. The building has a lot of glass surfaces, through which we get quite a few external heat gains from the sun, and at the same time we have heat losses in the winter. We also defined ventilation in the building, which is tied to a system with latent cold storage. In most zones the temperature is set to 20 ° C.

2.3 Photovoltaic module

To be able to use the real values of the photovoltaic panel surfaces in the simulations, we first inspected all the roof surfaces of Cankarjev dom on site. The most suitable areas were found to be in the southern and south-eastern part of the building, as illustrated in **Fig.** ***3***.

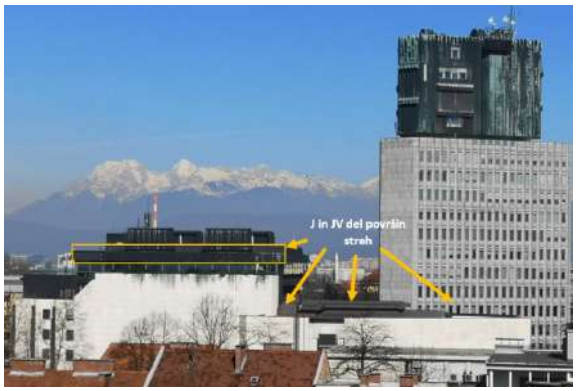

Fig. 3: Roof surfaces of Cankarjev dom taken into account for the installation of PV panels

In the simulations, we used a value of 430 m^2 and the inclination of the panels at an angle of 45 °.

2.4 Numerical simulations

The scheme of the system without latent cold storage consists of the following sets; weather data, building, soil temperature and display and storage of results. The Cankarjev dom module is crucial, as it contains all the information about the building, its construction, heat gains, cooling with a refrigeration unit, etc. The weather data module contains a file with weather data for Ljubljana and, in combination with the radiation module, contributes the necessary data to take into account solar radiation on the building. The ground temperature module allows this temperature to be considered as a boundary condition for parts of the building envelope elements that are in contact with the ground (we have 4 basements under the ground). The Q_cooling module sums up the output data of the building, which illustrates the use of cooling energy for each zone in the building (we have 40 zones). The results display module allows us to monitor the results in the form of a graphical display. The results module generates an external txt file in which the hourly data of the calculations are stored. The lines and arrows between the individual modules show the connections between them. The output of an individual module is the input for another module. Cooling is switched on at 24 ° C.

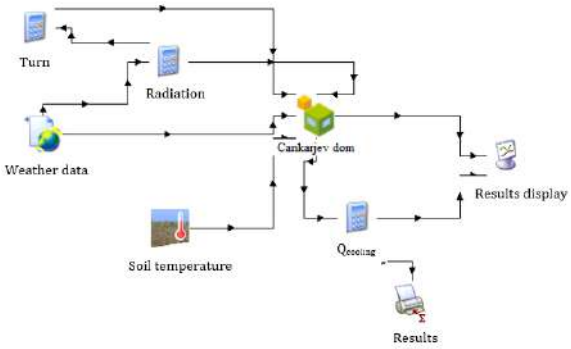

Fig. 4: Schematic of a system without latent cold storage in the Trnsys software environment

Due to the complexity of the system, we did not perform a dynamic calculation of ice bank charging in Trnsys, but a static calculation in Excel, which was as follows. The latent capacity of ice banks was calculated by the equation **1**:

$$Q_{\text{lat}} = m_{water} \cdot q_{fus} \qquad \textbf{(Eq. 1)}$$

A value of 333 kJ / kg was taken into account for the heat of fusion. The mass of water in one latent storage tank is 3677.9 kg. The monthly value of stored energy of ice banks was calculated according to the equation **2**:

$$Q_{\text{january}} = Q_{\text{lat}} \cdot n_{\text{bank}} \cdot n_{days} \qquad \textbf{(Eq. 2)}$$

Tab. 1 shows how we obtained the results of stored energy in 9 ice banks on an annual basis. We assumed the number of days in the month when the ice banks are fully filled and the number of days when they are

half full charged (the use of cold did not completely empty the ice banks, for example, in the winter months days energy needs for cold are smaller compared to summer days, therefore withstands cold in ice banks for several days). In the months from June to August, ice banks are certainly filled every day, but it is not necessary that ice banks are completely emptied every day. The results are presented in the subchapter 3.2.

Tab. 1: Number of days in the month when the ice banks are fully charged and the number of days when they are half charged

Month	Number of days - full charge [days]	Number of days of half charge [days]
January	5	0
February	6	1
March	8	7
April	11	9
May	15	10
June	19	11
July	25	5
August	20	11
September	16	11
October	12	8
November	8	5
December	6	2
Sum	151	79

Using a separate model, we calculated how much electricity we produce with a 51.6 kW photovoltaic power plant, which is presented in more detail in the economic analysis section. ***Fig. 5*** shows the scheme in the Trnsys program, through which we calculated the energy production potential of photovoltaic panels.

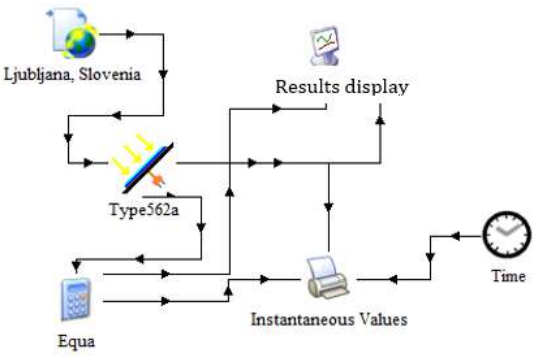

Fig. 5: Scheme for calculating the production potential of a PV power plant

3. Results

3.1 System without latent cold storage

In the case of a building without the use of latent cold storage, the simulation time was one year. For each simulation, we showed the energy consumption for cooling by months for a period of one year. The location of the simulations was Ljubljana, where the Cankarjev dom building also stands. In the simulations, the building is supposed to turn on cooling at 24 °C. Cooling is provided to ensure suitable conditions in rooms where the presence of people, devices (e.g., computers) and lighting generates internal heat gains. The premises of the building that are exposed to solar radiation also have external benefits due to the sun. Without cooling, all the above heat gains would lead to overheating of the premises.

In the case of a system that does not use latent cold storage, the total energy required for cooling or. it produces air conditioning with refrigeration units (leading and reserve refrigeration unit). **Tab. *2*** shows the monthly energy consumption for cooling of Cankarjev dom without latent cold storage tanks. Simulations were performed on an hourly basis (8760 hours = 1 year) and then the values were summed to give monthly values. When the temperature in the individual room to be cooled or air-conditioned exceeded 24 °C, the cooling was switched on and the program recorded the energy required for cooling on an hourly basis.

Tab. 2: Monthly values of energy use for cooling of Cankarjev dom without the use of latent cold storage tanks

Month	$E_{c_without}$ [MWh]
January	18,89
February	20,97
March	36,02
April	59,38
May	98,12
June	138,76
July	180,68
August	167,52
September	112,67
October	72,70
November	35,44
December	21,45
Annually	962,60

Tab. *2* shows that the use of energy for cooling is highest in the summer months, as we have higher use due to external heat gains. Cooling energy is also needed in the winter to ensure the basic conditions of the indoor environment in the premises, especially in the halls, where people and lighting contribute to greater internal heat gains. Most of the halls are underground, so interior comfort is even more

important.

3.2 System with latent cold storage

In the case of the system using latent cold storage, the simulation time was one year. For each simulation, we showed the stored energy by months for a period of one year. In the analysis of the system with latent storage tanks, we simulated and calculated the stored energy in latent cold storage tanks on an annual basis. **Tab. *3*** collects the monthly values of energy stored in latent cold storage tanks and the column with the energy required to cool a building in a system without latent cold storage tanks.

Due to the complexity of the system in Cankarjev dom, which uses 52 air conditioners for the purpose of air conditioning the building, we were not able to "dynamically" model this scheme in the Trnsys program. We decided to use all the data on the system and its operation, which we obtained during the acquaintance with the system, to make a "static" calculation or energy estimate, which is provided with the help of nine ice banks.

Tab. 3: Monthly values of estimated energy stored in latent cold storage tanks and required energy for cooling in a system without latent storage tanks

Month	$E_{c,\,bank}$ [MWh]	$E_{c_without}$ [MWh]
January	15,31	18,89
February	19,90	20,97
March	35,21	36,02
April	47,46	59,38
May	61,24	98,12
June	75,02	138,76
July	84,20	180,68
August	78,08	167,52
September	65,83	112,67
October	48,99	72,70
November	32,15	35,44
December	21,43	21,45
Annually	583,29	962,60

According to equation **3** , proportion of cooling energy stored in latent cold storage tanks can be calculated.

$$E_{c,bank,\text{ann.},\%} = \frac{E_{c,\text{bank,ann.}} * 100}{E_{c,without,ann}} \qquad \textbf{(Eq. 3)}$$

The share of energy stored in latent cold storage tanks is 60.6 %. The rationale for using latent cold storage tanks is evident from the result, as this share of energy is produced at a time when electricity is cheaper.

Then we calculated how much more energy could be stored in latent cold storage tanks in case we would charge them every day from May to September, when the energy needs for cooling or air conditioning are maximum (in the remaining months we cover all the necessary energy). If we subtract the values of required energy and lack of energy, we get 733.33. The maximum stored energy was calculated as the product of the ice bank capacity, the number of ice banks and the number of days in each month. The result of the calculation of the largest share of stored energy in latent cold storage tanks for the case of the Cankarjev dom building is 76,2 %, calculated by equation **4** :

$$E_{\text{bank,ann,max,\%}} = \frac{E_{bank,may-sept} * 100}{E_{c,without,ann}} \qquad \textbf{(Eq. 4)}$$

3.3 Upgraded system with latent cold storage

Considering that Cankarjev dom still has a higher use of electricity most of the year at a time when electricity is more expensive, we thought it would make sense to include in the system the production of electricity from solar energy, which would allow additional reducing the required electricity from the grid.

In this part, a simulation of electricity production of a 51.6 kW photovoltaic power plant on monthly basis was performed. The area of the power plant was 430 m2. The results of the simulation of electricity production of the 51.6 kW photovoltaic power plant on monthly basis are summarized in **Tab. *4***.

Tab. 4: Electricity production of 51.6 kW PV power plant on monthly basis in MWh for Ljubljana

Month	E_{PV} [MWh]
January	1,23
February	1,86
March	3,40
April	4,42
May	5,80
June	6,08
July	6,68
August	5,67
September	3,78
October	2,34
November	1,12
December	0,75
Annually	43,1

From the extended energy audit of Cankarjev dom (12), which was carried out in 2016, we obtained data on the estimate of electricity consumption of the refrigeration unit, which amounts to 213 MWh per year.

By calculating the electricity production of a 51.6 kW

photovoltaic power plant on monthly basis for Ljubljana and having data on the energy consumption of the refrigeration unit, we can calculate what share of energy consumption for the refrigeration unit can be covered by a photovoltaic power plant. The calculation is made according to equation **5**:

$$E_{\text{refrig. unit,\%}} = \frac{E_{\text{PV,ann}} * 100}{E_{\text{refrig. unit, ann}}} \qquad \textbf{(Eq. 5)}$$

20 % of energy needs for refrigeration unit can be covered by photovoltaic power plant.

3.4 Economic analysis

The first part of the analysis presents the calculation of the return-on-investment costs in the upgrade of the system with ice banks and the reconstruction of the old system. **Tab. *5*** shows some of the costs that make up the entire investment.

Tab. 5: Ice bank price data, documentation and total investment

Data	Cost [EUR]
The price of an ice bank - CALMAC 1098A	11000 -15000
Price of reconstruction documentation	9998,56
The cost of the entire investment in the reconstruction of the system	482.736,53

The price of the entire investment includes all elements of the system from 9 ice banks, 2 refrigeration units with a cooling capacity of 595 kW, installation prices, the price of distribution elements, insulation, etc. The representative of CALMAC in Slovenia is VALMOR, where we also received information on the price of the ice bank, which at the time of purchase also depends on the cost of transport from America.

The savings were calculated as the difference between the price of the high and low tariff multiplied by the energy stored in the ice banks throughout the year. We got savings of 22.835,72 EUR/year.

The savings are such because all the energy stored in latent storage tanks is produced at the time of the lower tariff. The price difference between high and low tariff is 50 %. With such savings, our investment pays off in 21 years. If we take a loan with a 2 % interest rate, the investment will be repaid in 28 years, and at a 3 % interest rate in 35 years. If we had invested in only 9 ice banks, our investment would have paid off in 6 years.

The following is a calculation of the return-on-investment costs in a photovoltaic power plant. All calculations were performed in Excel. **Tab. *6*** collects basic data on the photovoltaic power plant, such as different efficiencies and the mean density of solar radiation on the Earth's surface.

Tab. 6: Data on photovoltaic power plant

Data	Unit	Value
Average density of solar radiation on the Earth's surface	W/m^2	1000
Efficiency of PV panels	%	12
Relative efficiency	%	86
Efficiency of inverters	%	95

Tab. *7* contains data and calculations on the area, rated power of the photovoltaic power plant, annual electricity produced and operating time at nominal power.

Tab. 7: Data and calculations on the size and nominal power of the power plant

Data	Unit	Value
PV power plant surface	m^2	430,00
Nominal power of a PV power plant	kW	51,60
Annual electricity produced	kWh/a	47.469
Operating time with nominal power	h/a	1021,8

The repayment period is calculated by dividing the total investment costs by the annual savings. **Tab. *8*** contains basic economic data and calculations on the photovoltaic power plant.

Tab. 8: Basic economic data and calculations on PV power plant

Data	Unit	Value
Total investment costs	EUR	50.000
Amortisation period	let	15
Amortisation costs	EUR/a	3.333
Savings due to own electricity production	EUR/a	3.377
payback period	years	15

We calculated average monthly values of daily sums of incident solar energy and electricity production monthly. Calculations of average monthly values were made from data obtained from the website meteo.si (13) for the location Ljubljana. The data are made for a typical meteorological year, which consists of data from 2001 to 2015. The electricity produced for each month was obtained by multiplying the average monthly values of the daily sums of the incident solar energy and the number of days in the month.

Based on the data and calculations collected in **Tab. *6*-Tab. *8*** and the calculations of electricity produced monthly, calculations were made for two variations. In the first variation, own funds are used for the investment, and in the second, credit is taken to pay the price of the investment.

When using own funds for the investment, it is repaid within 15 years. If we take a loan, the investment will be repaid in 18 years (2 % interest rate) or in 20 years (3 % interest rate). In the case of obtaining an Eco Fund subsidy, the repayment periods may be even shorter.

4. Conclusions

Energy storage is one of the key areas in which more attention and projects will need to be focused to better address the challenges of energy efficiency and the integration of renewable energy sources into heat storage systems in the future. Storing cold in latent heat accumulators or. in this case, the technology of ice banks can help solve various problems such as: overloading the electrical network, reducing the rated power of refrigeration units, reducing operating costs, etc. The building of the Cankarjev dom congress centre was interesting to consider because part of this building is underground. The building has eleven floors, of which seven are above ground and four below ground. The premises are intended for different types of activities, which had to be considered when modelling the building zones. As part of the work, we performed the following steps and came to the following conclusions:

1) In TRNBuild, we assembled and defined the Cankarjev dom building, which covers 40 zones. The building was then included in the simulations of the operation of the cooling and air conditioning system, through which we were able to determine the energy required for air conditioning.

2) We designed the original cooling system in Cankarjev dom, before the ice banks were installed, in the Trnsys software environment. In this system, refrigeration units were used for cooling. We have calculated that they need 963 MWh of energy for air conditioning on an annual basis.

3) The original system was upgraded to a system with ice banks, which enables the production and storage of cooling energy at times of lower electricity prices to cover the need for cooling during peak cooling loads, when electricity is more expensive. We have shown that ice banks in Cankarjev dom cover 61 % of all energy needs for cooling. In the case of continuous recharging of ice banks (every night from May to September), ice banks could cover a maximum of 76 % of the annual energy required.

4) The system with ice banks was upgraded with photovoltaic modules to produce a share of electricity from renewable energy sources, and at the same time the refrigeration unit could be supplied with the produced electricity. The obtained results showed that a solar power plant could produce 20 % of electricity for a refrigeration unit. To increase the share of electricity produced from photovoltaics, we would increase the area of the solar power plant, as we still have some suitable space compared to the roof area of Cankarjev dom.

5) We found that for an investment in a 51.6 kW photovoltaic power plant, it would be repaid within 15 years if own funds were used. If we had taken out a loan with a 2 % interest rate for an investment in a photovoltaic power plant, the investment would have been repaid in 18 years, and at a 3 % interest rate in 20 years.

6) We found that given the savings that an investment in an ice bank system brings, we need 21 years to recoup the investment when we use our own funds. If we took out a loan with an interest rate of 2% for the investment, it would be repaid in 28 years, and at a 3% interest rate in 35 years. If we had invested in only 9 ice banks, our investment would have paid off in 6 years.

7) Given the amount of investment for the reconstruction of the system, it will pay off faster if we successfully apply for a tender for grants or subsidies. This would be an additional incentive to integrate energy storage technologies.

5. References

1. Feng PH, Zhao BC, Wang RZ. Thermophysical heat storage for cooling, heating, and power generation: A review. Appl Therm Eng [Internet]. 2020;166:114728. Available from: http://www.sciencedirect.com/science/article/pii/S135943111935567X

2. Oró E, de Gracia A, Castell A, Farid MM, Cabeza LF. Review on phase change materials (PCMs) for cold thermal energy storage applications. Appl Energy. 2012;99:513–33.

3. Fang G, Wu S, Liu X. Experimental study on cool storage air-conditioning system with spherical capsules packed bed. Energy Build. 2010;42(7):1056–62.

4. Philippen D, Carbonell D, Zenhäusern D, Granzotto M, Haller M, Brunold S. High-Ice System development for high solar thermal gains with ice storage and heat pump - Final report. 2015.

5. Araner. Thermal energy storage technologies & applications. 2017. 1–24 p.

6. Kalaiselvam S, Parameshwaran R. Latent Thermal Energy Storage. In: Thermal Energy Storage Technologies for Sustainability. 2014. p. 83–126.

7. Evapco. Thermal ice storage: Application & Design guide [Internet]. p. 1-68 (Dostopano 6. marec 2021). Available from: https://www.evapco.eu/sites/evapco.eu/files/2017-03/Thermal Ice Storage Application %26 Design Guide.pdf

8. Tarcola A. Fire and ice. Distrib energy - J energy Effic Reliab. 2009;Marec/apri:1–3.

9. Celarc d.o.o. BTC d.d. – Stolpnica II - Strojne instalacije - vročevod, toplotna postaja, ogrevanje, hlajenje - PZI. 2009.

10. Hočevar B. V Ljubljani zagnali novo banko. Finance, št 133 [Internet]. 2016 Jul 12;18 (Dostopano 12. julij 2020). Available from: http://www.bankaledu.si/Finance 20160712 - Banka ledu.pdf

11. Medvešek B. Preureditev hladilne strojnice - Načrt strojnih inštalacij in strojne opreme. Ljubljana; 2009.

12. Dolinšek S, Burkeljca A, Vetršek J. Razširjeni Energetski Pregled_ Končno poročilo. Ljubljana; 2016.

13. Ministrstvo za okolje in prostor, ARSO ,Značilno meteorološko leto [Internet]. [cited 2021 May 22]. Available from: https://meteo.arso.gov.si/met/sl/climate/tables/test_ref_year/

The datasets generated during and/or analysed during the current study are available in the RUL repository (Repozitorij Univerze v Ljubljani), https://repozitorij.uni-lj.si/IzpisGradiva.php?id=129124&lang=slv ·

Comparison and implementation of MPC and simple predictive control into a heat pump system

Christina Betzold [a], *Arno Dentel* [b]

[a] Energy efficient building systems, Technische Hochschule Nuernberg Georg Simon Ohm, Germany, christina.betzold@th-nuernberg.de.

[b] Energy efficient building systems, Technische Hochschule Nuernberg Georg Simon Ohm, Germany, arno.dentel@th-nuernberg.de.

Abstract. Heat pumps in combination with thermal energy storage systems offer the potential to response to fluctuating renewable energy sources, e.g. photovoltaics. To fully exploit this flexibility and financial potential, predictive control strategies are needed. Since an additional effort due to detailed knowledge and programming skills is required to create the model predictive control (MPC) strategies, a fast and easy implementation is prevented. Therefore, a second model-based approach is developed with a predictive but rule-based control. This simplified approach uses predictive models as well but energy balancing to determine the heat pump operation and the state of charge of thermal storage units throughout the day. In this paper, two predictive approaches were compared with two rule-based controls and evaluated for their potential for PV self-consumption and cost savings in annual simulations. In addition, one rule-based PV optimized control (PVC) and the predictive approaches, MPC and the simple predictive control (SPC), are implemented in the real operation in a plus energy building. In simulation, the best result is achieved by the MPC with a cost saving of 8.3 % due to a high PV energy consumption but mainly to the best efficiency with a SPF of 4.5. Despite the predictive approach of SPC, SPC and PVC achieve very similar results with cost savings of 2.5 % and 0.8 %. Since the costs of PV include taxes, these moderate cost savings are achieved. Excluding these taxes, there are significantly higher cost savings of up to 34 % for MPC. In real operation, differences between simulation results and measured data become apparent. This gap between the set point output of the simulation and the set point input of the real components poses a challenge to the implementation of efficient and cost-effective control like the MPC.

Keywords. MPC, simple predictive control, PV self-consumption, operating costs
DOI: https://doi.org/10.34641/clima.2022.154

1. Introduction

Heat pumps in combination with thermal energy storage systems offer the potential to response to fluctuating renewable energy sources, e.g. photovoltaics. To fully exploit this flexibility and financial potential, predictive control strategies are needed. Model-based control approaches range from simple calculations to very complex and detailed models with long computation times. The modelling effort can therefore be very high, so that the implementation in a real plant is inhibited. Simplified predictive approaches can reduce these inhibitions. However, the question is which predictive approaches lead to good operation and results.

In previous research work, several studies examined MPC strategies to reach operating costs savings in a range of 10 % to 30 % and an increase of PV direct consumption of up to 30 %. Fischer et al. [1] shows cost savings of 6 % to 11 % for constant electricity prices and up to 16 % for variable electricity prices in comparison to a default rule-based controller. Likewise, the application of MPC can favorably influence Photovoltaics (PV) self-consumption. Pichler, M. et al. [2] shows in an annual simulation that the targeted MPC control of a heat pump can increase the PV direct consumption in a single-family house by 30 %. In addition, Salpakari and Lund [3] find that when MPC is applied to heat pumps, PV systems are beneficial because the amount of PV electricity fed into the grid is reduced by up to 88 %. Self-consumption of PV electricity can be profitable when electricity prices are higher than the feed-in tariff. The study also targets an energy cost reduction of 25 % in the case of flexible market electricity prices in Finland compared to a rule-based controller. A publication by Bechtel et al [4] shows

Copyright ©2022 by the authors. This conference paper is published under a CC-BY-4.0 license.

cost savings of a maximum of 24 % for a single-family house in Luxembourg when variable electricity prices based on the electricity market are applied. In some cases, field tests of model predictive control strategies are realized in residential and office buildings. De Coninck et al. [5] implemented a MPC control with non-linear models in an office building and showed that the MPC provides a similar or better thermal comfort than the reference control while reducing the energy costs by more than 30 %.

In contrast to the complex modelling and programming of an MPC, advanced system control strategies with a predictive approach can reduce the programming effort and still achieve good results. Few works on simple predictive controls in the building sector are provided in the literature. Rolando and Madani [6] present a control algorithm developed in a Swedish research project that shows annual energy savings of 10 % by predicting solar energy gains in single-family homes.

The mentioned research works on advanced system control strategies with a predictive approach show a similar potential of cost saving to MPC. Therefore, in the following work, an MPC and a simple predictive control approach will be compared in simulation and in a real energy system of terraced houses in Germany. The real heat pump system, which supplies eight terraced houses, is to be operated in such a way that it optimally uses the PV power of the shared PV system. The heat pump system consists of two central modulating heat pumps (MWPs) and eight decentral on/off heat pumps (boosters) for providing domestic hot water (DHW). In addition, the energy system of the terraced houses consists of a shared PV and battery system.

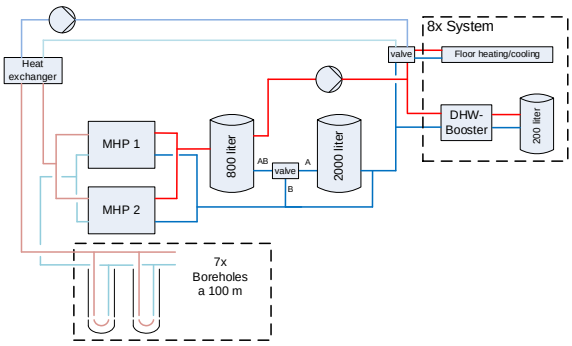

Fig. 1 – Heat pump system of eight terraced houses.

Besides two rule-based controls, two Model Predictive Control (MPC) strategies are implemented, which are based on different system and forecast models as well as different optimization algorithms. Since an additional effort due to detailed knowledge and programming skills is required to create the MPC strategies, a fast and easy implementation is prevented. Therefore, a second model-based approach is developed with a predictive but rule-based control. This simplified approach uses predictive models as well but energy balancing to determine the heat pump operation and the state of charge of thermal storage units throughout the day.

2. Research Methods

To determine and compare the potential and differences of the two predictive control approaches, they are first compared in an annual simulation. In a second step, the real operation of the MPC and SPC will be implemented in the energy system of the terraced houses and tested over several weeks.

In the annual simulation, the results of the control approaches (set points) are entered into the energy system model. The forecast horizon is 48 h in a 15 minute time step, whereby only the first 24 hours are transferred to the system model as setpoints. This results in 366 simulation runs in year 2020. In addition, the two control approaches were compared with two rule-based control approaches to evaluate the predictive approaches. The rule-based approaches include a heat-guided (HC) and a PV-optimized (PVC) control. The process of the annual simulation is shown in Fig. 2.

For offering an overview of the potential of the different control strategies monitoring data from the terraced houses for a period of 12 months from January 2020 until December 2020 is chosen. The measured PV power as well as measured thermal and electrical load are used as ideal prediction for the MPC and SPC. For the simulation of the energy system, controlled by the outputs of HC, PVC, SPC and MPC, the measured data serve as actual PV production and loads. The operation and comparison are implemented in MATLAB [7]. Boundary and start conditions are the same in the four cases.

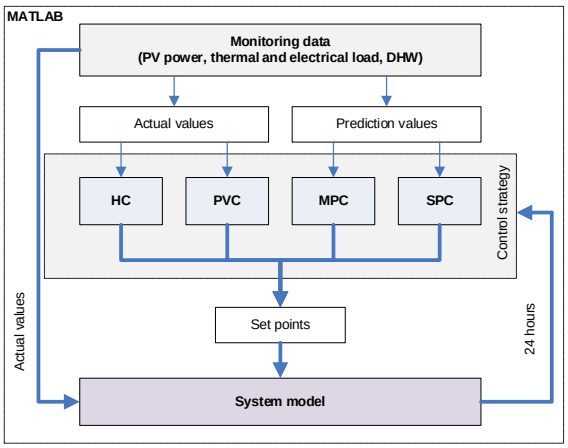

Fig. 2 – Process of annual simulation

First, the system model is described, which serves as the basis for all modelling of the controls. In this model, the energy system is represented, which is controlled by the outputs of the different controls.

2.1 System model

In general, the system models base on energy flows coupled in an energy node. The model of the thermal storage is an energy node of incoming and outgoing thermal power with constant thermal losses and presented in equation (1). The MHPs are represented by a polynomial for B5 °C/W35 °C with a variable modulation speed.

$$\sum_{n=1}^{2} \dot{Q}_{MHP,n}(t) + \dot{Q}_{cap}(t) = \dot{Q}_{loss}(t) + \dot{Q}_{th}(t) \quad (1)$$

Depending on the operation plan (set points) of the control strategy, the MHPs adapt their thermal power either to the thermal building load or to the available PV power. Equation (2) shows thermal adaption where Q_{MHP} the thermal power of one MHP is. Equation (3) shows electrical power, where P_{MHP} the electrical power of one MHP is.

$$P_{MHP} = p1 * \dot{Q}_{MHP}{}^{4} + p2 * \dot{Q}_{MHP}{}^{3} \ldots + p3 * \dot{Q}_{MHP}{}^{2} + p4 * \dot{Q}_{MHP} + p5 \quad (2)$$

$$Q_{MHP} = q1 * P_{MHP}{}^{6} + q2 * P_{MHP}{}^{5} \ldots + q3 * P_{MHP}{}^{4} + q4 * P_{MHP}{}^{3} \ldots + q5 * P_{MHP}{}^{2} + q6 * P_{MHP} + q7 \quad (3)$$

The model of the DHW storage is an energy node of incoming and outgoing thermal power with a constant thermal loss. Each boosters is represented by one operation point at 25 °C/55 °C with a thermal power of 3 kW and COP of 4.3.

As well, the battery model is an energy balance of incoming and outgoing electrical power with inverter efficiency and calculated by equation (4). The battery is not controlled and serves a passive component that is charged and discharged by the electrical energy balance of PV power (P_{PV}), electrical consumption of MHPs (P_{MHP}) and boosters (P_b).

$$P_{PV}(t) * n_{loss} + C_{bat,cap} = \cdots \sum_{n=1}^{2} P_{MHP,n}(t) + \sum_{n=1}^{8} P_{b,n}(t) \quad (4)$$

The validation of models with energy balancing showed moderate but sufficient accuracy in the real energy system [8] and in a hardware-in-the-loop test bench [9].

2.2 Prediction models

For the use of predictive controls, MPC and SPC, forecasting models are used to generate the thermal and electrical load forecast.

Artificial neural networks (ANN) in Python with the library Tensorflow (Apache, 2019) determine the prediction of thermal building load and household electricity. Both ANN are recurrent, trained with measured data of 15 months from the energy monitoring of the terraced houses and deliver prediction data for 24 hours in a 15 minutes timestep. Inputs are date information (month, day, hour), ambient temperature and horizontal global solar radiation. In addition, the ANN of the household electricity has inputs of historic values of one day and one week ago. During a long-time operation of the MPC in April 2020, the ANN of thermal building load receive values of RMSE of 3.7 kW and NRMSE of 19 %, the household electricity values of RMSE of 1.6 kW and NRMSE of 14 %.

2.3 MPC

In this paper, the MPC approach is realized by a mixed-integer linear programming (MILP). As the system model, all energy models base on energy flows coupled in an energy node in order to receive linear models (see equation (1)). The characteristics of the MHPs differ, as they are represented by fixed operation points at B5 °C/W35 °C between which the MILP can interpolate. The interpolation is enabled by the additional software GUROBI [10], for using the Special Ordered Set (SOS) option and is integrated in MATLAB.

The cost function (J) bases on operating costs (c) for the consumed electricity, including household electricity, the MHPs and the DHW-HPs depending on the consumption of grid ($E_{el,grid}$), PV ($E_{el,PV}$) or battery ($E_{el,Bat}$) as well as a bonus for grid feed-in ($E_{el,\mathrm{feedin}}$). The PV costs include costs for insurance (0.0243 €/kWh) and national taxes for renewable energies (0.064 €/kWh). Battery costs consists of PV costs and losses of 20 %. In this context, the battery price results from PV price multiplied by a factor of 1.2. The energy prices are shown in Tab. 1.

Tab. 1 - Electricity prices.

Energy prices	Price
Grid electricity	0.34 €/kWh
PV electricity	0.0883 €/kWh
Battery electricity	0.0883 €/kWh *1.2
PV feed-in electricity	0.11 €/kWh

The results of this MPC approach provides an SOC determining the set value for the MHPs. The SOC is divided into 8 areas, respectively allocated to a set value of 32 °C to 46 °C in a 2 K step. The boosters

receive the set temperature of the storage tank as set value when they are to be on (60 ° C) or off (45 ° C). The minimum value of 45 °C ensures the comfort limits of the habitants. A detailed description of the MILP MPC can be found in [11].

2.4 SPC

The SPC is based on a modification of the electrical operation of the MHPs, which results from the thermal building load forecast. As balancing of the loads is performed on electrical loads the thermal building load forecast is converted into an electrical load with a constant COP, which should reflect the operation of the heat pumps. Electrical operation loads that occur after PV production are shifted forward to times with PV production. The modified electrical operation results in set point for the MHPs. Therefore, the electrical operation is converted back to a thermal building load using the polynomial in equation (2) that reflect the characteristic curve of the heat pump at B5 °C/W35 °C. The shifting of the loads is limited up to the maximum storage level, which is 46 °C. Without PV production the set point is 32 °C, while with PV production the set point results from the shifted loads. Fig. 3 (above) shows electrical operation of the MHPs from the thermal building load forecast, the modified electrical operation and the PV power forecast. Below in Fig. 3 is the set temperature, which results from the modified electrical operation. The same procedure is repeated for the boosters, but with a constant COP of 4.3.

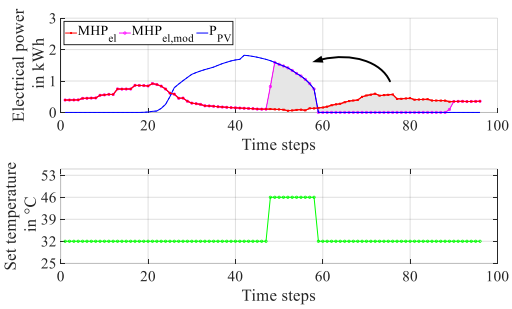

Fig. 3– Modification of electrical operation of MHPs (above) and resulting set temperature (below)

2.5 Rule-based controls

For comparing the MPC and SPC to standard heat pump operation, two common rule-based controls are introduced. The PV control (PVC) aims to increase the PV self-consumption by operating the heat pumps during PV surplus and charge the thermal storage to its maximum. PV surplus means the available PV power after satisfying the household electricity. In this case, the MHPs adapt to PV power, using equation (3). During grid and battery operation, the MHPs adapt to the thermal building load using equation (2). As well, the boosters charge to maximum storage capacity while PV surplus after MHPs or charge to minimal storage capacity while grid and battery consumption.

The heat control (HC) only operates the MHPs in adaption to the thermal building load (equation (2)) and the boosters to charge the minimal storage capacity.

2.6 Simulation

For the comparison of the control strategies, measured data of the energy system of the terraced houses is used. The process of the annual simulation is shown in Fig. 2. The energy consumption and production for the period of 12 months are shown in Tab. 2.

The results of the simulation for the 12 months period show low differences for the energy shares, but differences for operating costs. The results of the PV self-consumption and the self-sufficiency of the comparison are shown in Fig. 4. In general, the results do not vary significantly between the different control strategies. HC shows less PV direct consumption and highest grid consumption.

Tab. 2 – Energy consumption in 2020

Energy consumption	
Thermal load	36.56 MWh
DHW load	26.66 MWh
Electrical load	30.85 MWh
PV production	85.88 MWh

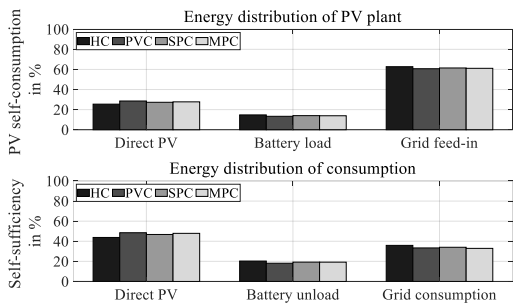

Fig. 4 – Energy shares regarding PV self-consumption and self-sufficiency

Fig. 5 gives an overview of operating costs and total energy consumption in comparison to the HC, which serves as standard control. In total, the operating costs under HC operation are 3,172 € for the energy consumption including household electricity, heating, DHW and bonus from grid feed-in. The MPC achieves most of the cost savings as well as less energy consumption. Even PVC and SPC have slightly higher energy consumption, the operating costs are less. The MPC cost saving of about 10 % confirms the results of Fischer et al. [1] when German energy prices are applied. Taxes for renewable energies reduce the potential savings from increased PV use. Without the taxes for renewable energies, that means PV costs of 0.0243 €/kWh, a much higher cost saving can be achieved. The PVC achieves cost

savings of 13 %, the SPC of 15 % and the MPC of 34 %. These cost savings of the MPC are in a range of EU-wide simulation studies, such as Salpakari and Lund [3] and Bechtel et al [4]. Although the differences between PVC und SPC are small, favourable results are shown for the predictive approach.

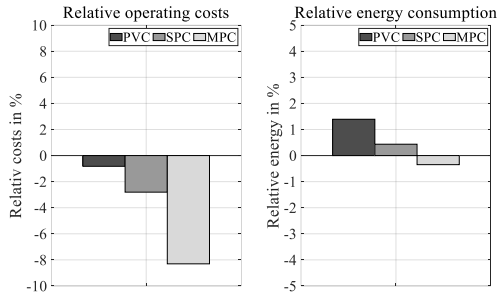

Fig. 5 – Operating costs and total energy consumption

The differences of the energy consumption results from different values of Seasonal Performance Factors (SPF) for the MHPs and consequently for the system. The SPF values of the control strategies are shown in Tab. 3. High modulation speed during PV adaption lowers the SPF.

Tab. 3 – Seasonal Performance factors of control strategies

	SPF_{MHPs}	SPF_{system}
HC	4.46	4.43
PVC	4.23	4.27
SPC	4.38	4.38
MPC	4.51	4.46

The simulation study was repeated with the measurement data from the year 2019 and very similar results are obtained for the four control strategies. Regarding the results of years 2019 and 2020 the PVC has an energy consumption from 1.4 % to 1.7 %, the SPC from 0.2 % to 0.4 % and the MPC from – 0.3 % to – 0.6 %, compared to HC. The potential of cost saving is for the PVC in a range of 0.2 % - 0.8 %, for the SPC in a range of 2.8 % - 4.6 % and for the MPC in a range of 8.3 % - 9.6 % under PV costs with taxes for renewable energies.

3. Real-life implementation

To test the control strategies in real operation, the MPC and SPC are implemented in the real energy system of the terraced houses. Since October 2018, the energy system has been operated with the PVC installed in an energy management software which controls the heat pumps. In contrast, the MPC and SPC will run on the software MATLAB and the set points will be transferred to the energy management system via an SQL database and set to the heat pumps from there.

Fig. 6 shows the process of the control strategies. When operating the predictive controls, the MPC or SPC are started at a certain time T. The MPC starts every hour, the SPC only once a day at 6 am. The created operation plan is passed on to the Set/Check Loop. The Set/Check sets the set values into the SQL database and checks the operation of the system for disturbances and deviations of the operation plan, and if necessary, sets set values for switch on or off. This ensures the operation reliability during time slot of next set values. In this paper this process is called online simulation.

In previous work [11] the MPC flow process was successfully tested and SPC was also successfully integrated into the process in this work. The energy management software includes communication with the controllable components of the energy system, the logging of measurement data and functions for setting up a rule-based control strategy. The PCV was implemented in the energy management software, which operates the plant independently of MATLAB and most of the time. In addition, the energy management software can pass values from the SQL database to the energy system. The structure makes it possible to implement many control strategies for a reliable operation.

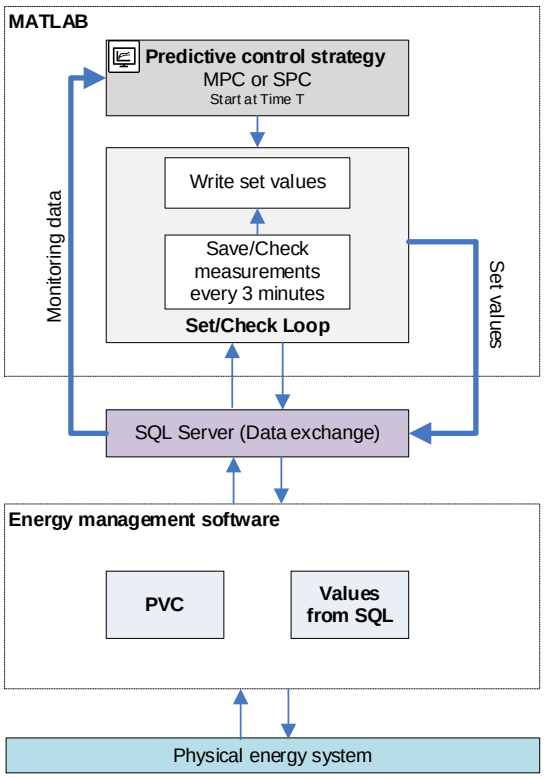

Fig. 6 – Process of control strategies

For the evaluation of the PVC, long operating times from October 2018 until now are available. However, the MPC and SPC were only operated over several weeks, so that a direct comparison is not possible due to the short period of time and the different boundary conditions (e.g. weather, user behaviour, etc.). In order to give an impression of the control

strategy, characteristic values from the target specification (online simulation) and from measured values from the real operation of the MPC and SPC are compared. In addition, the measured results of the PVC are presented over the period from year 2019 as no additional control strategy was tested in this year.

3.1 Real operation of PVC

The standard operation in the energy system of the terraced houses is PVC. In order to not only obtain an overview of the characteristic values of the PVC in real operation for the year 2019, the offline simulation results of the PVC for the year 2019 from the upper chapter are also presented. In the simulation model, however, other boundary conditions are partly applied. The temperature limit of the thermal storage in the model is 46 °C, in the implemented PVC it is 39 °C in 2019.

Tab. 4 – Comparison of offline simulation and measured data of PVC in year 2019

	Simulation	Measurement
PV production	85.1 MWh	85.1 MWh
Energy consumption	49.3 MWh	47.9 MWh
PV self-consumption/ incl. Battery	28 % / 42 %	26 %/ 36 %
PV self-sufficiency/ incl. Battery	49 % / 67 %	45 %/ 62 %
Operating costs	2,843 €	3,430 €
SPF_{MHP}	4.2	4.8

The comparison of offline simulation and measurement in Tab. 4 clearly shows differences, which reflect the different boundary conditions for the maximum storage level. In particular, the lower PV self-consumption and PV self-sufficiency lead to higher operating costs of 17 %. In contrast, the SPF of the MHP is better. This could be due to an efficient modulation level throughout the year and a lower supply temperature below 35 °C. Since the characteristic curve of the MHP in the model (see equation (2) and (3)) is only dependent on modulation level and has its best operation in the modulation range of 30 % to 40 %, it can be assumed that high or low modulation levels are selected more often in offline simulation.

3.2 Real operation of MPC

Compared to PVC the operation of MPC was operated for several weeks in February and April 2021. During the operation in February 2021 adaptions to the model were identified and implemented. The comparison of online simulation and measured data is from 22.03.2021 until 03.05.2021 and is shown in Tab. 5. Although the values of the PV self-consumption and the PV self-sufficiency are very similar, the operating costs show a clear difference. However, since about 27 % more PV was produced in the measurement than in the PV forecast of the online simulation, there is a higher feed-in in absolute values. The same is shown in the energy consumption, but the relative (13 %) and absolute grid consumption is not significantly higher in the measurement. The low operating costs of the measurement arise mainly from the significantly higher profit from the PV feed-in tariff. The SPF is significantly worse in the measurement, although there is the same heating and DHW consumption. This shows that the targeted compressor control from the online simulation cannot be implemented in real operation at the MHPs.

Tab. 5 – Comparison of online simulation and measured data of MPC

	Simulation	Measurement
PV production	10.0 MWh	12.7 MWh
Energy consumption	5.2 MWh	6.0 MWh
PV self-consumption/ incl. Battery	30 % / 38 %	29 %/ 40 %
PV self-sufficiency/ incl. Battery	58 % / 78 %	59 %/ 79 %
Operating costs	118 €	42 €
SPF_{MHP}	4.8	4.2

3.3 Real operation of SPC

Similar to the MPC, the SPC has only been in operation for a few weeks. The SPC was in operation from 13.01.2022 to 22.01.2022 as well as from 04.02.2022 to 13.02.2022. The results from both operation periods are presented in Tab. 6.

The load forecasts receive very good results for thermal building load with an NRMSE of 16 % / 15 % and household electricity with an NRMSE of 15 % / 14 %. But nevertheless, the PV production and energy consumption are higher than in the online simulation, as already seen in the MPC operation. The load forecasts tend to lower results.

The operating costs are 20 % higher in the measurement, which results from a higher consumption, especially of the grid consumption. In addition, the PV self-consumption is lower. Due to the absolute lower feed-in, the bonus from feed-in is not relevant for the amount of the operating costs.

The SPF, although slightly lower, is quite well in line. Due to the low PV production, the MHPs were only occasionally operated in the high temperature range, so that the characteristic curve from the simulation was reproduced well.

Tab. 6 – Comparison of online simulation and measured data of SPC

	Simulation	Measurement
PV production	1.2 MWh	1.4 MWh
Energy consumption	2.9 MWh	3.3 MWh
PV self-consumption/ incl. Battery	70 % / 92 %	56 %/ 84 %
PV self-sufficiency/ incl. Battery	30 % / 40 %	25 %/ 34 %
Operating costs	679 €	818 €
SPF_{MHP}	4.6	4.4

4. Discussion

In the simulation, the MPC achieves the best results in energy consumption and cost savings, although it does not have the highest PV self-consumption. These results come from the high SPF resulting from the better operation strategy of the MPC. Unlike the other control strategies, the MPC specifically takes advantage of the better efficiency of the MHP in partial load operation. Not only during PV, but also during grid consumption, the thermal storage is charged to operate the heat pump at the optimal operating point continuously. Therefore, the lowest grid consumption results, which is weighted the most by the energy prices.

In contrast, the control of HC, PVC and SPC adapts the MHPs in case of grid consumption to the thermal load and operates them, depending on the load, also in less efficient operating points. This predictive operation with a focus on efficient partial load operation out of PV periods has not been implemented in SPC and should therefore be integrated in further work. This could improve the results compared to the PVC.

In real operation, PVC, MPC and SPC were implemented in the energy system of the terraced houses. MPC and SPC were implemented in MATLAB and coupled with an SQL interface to the energy management software. The PVC runs directly in the energy management software. During the operation phases the controls were shown to be reliable and to cover the thermal loads of the building.

When comparing online and offline simulation and measured data, the main differences are in the SPF and consequently in the energy consumption. The differences come from the MHPs characteristic curve and additionally for the MPC and SPC by the load forecasts. The simple MHP characteristic curve in the simulation does not correctly reflect the SPF in operation. Especially the annual comparison of the PVC shows clear differences between measured data and simulation. Due to the higher storage temperatures, the characteristic curve in the simulation should be set at higher temperatures, e.g.: B5 °C/W 40 °C or be created with another variable, which reflects the storage tank level. In this way, the results from the measurement could be better reflected in simulation.

Real operation control by SPC was well implemented and it shows secure operation and full cover of loads.

Finally, it is shown that not only the full utilization of the storage in PV phases reduces the operating costs, but also the efficient operation of the MHPs. This efficient operation is achieved by operating points in the range of 30 % to 40 % of the maximum thermal power. In PV phases, the thermal storage should be charged over a longer time period in efficient operation points. In grid operation, it is more advantageous to use the thermal storage also as a buffer to operate the MHPs continuously in efficient mode instead of adapting to the thermal building load. In real operation, targeted compressor control cannot be implemented due to the manufacturer's specifications of these MHPs. This gap between the set point output of the simulation and the set point input of the real components poses a challenge to the implementation of efficient and cost-effective control like the MPC. However, at the same time, the advantage is that poor control implementation, incorrect load forecasts or unpredictable events can be compensated by the internal heat pump control.

5. Conclusion

In this paper, a PV optimized control, an MPC approach and a simple predictive control approach are investigated in simulation and real operation.

The annual simulation was performed with measured data from 2019 and 2020. Both annual simulations achieve very similar results. In the annual simulations, the two predictive approaches were compared with two rule-based controls and evaluated for their potential for PV self-consumption and cost savings. The two rule-based controls are heat controlled (HC) default operation and a PV controlled (PVC) operation with temperature rise in case of PV surplus.

Compared to the HC in the annual simulation from 2020, the PV self-consumption can only be increased to a few absolute percentage points (2 % - 3 %). Despite the predictive approach of SPC, SPC and PVC achieve very similar results. The relative cost saving

of the SPC is 2.8 % and thus only slightly better than that of the PVC. The best result is achieved by the MPC with a cost saving of 8.3 %. The energy prices used are those of the year 2019 for the terraced houses and include taxes for PV direct consumption. Excluding these taxes, there are significantly higher cost savings of up to 34 % for MPC. The good results of the MPC are due to a high PV energy consumption but mainly to the best efficiency with a SPF of 4.5.

PCV, MPC and SPC were operated in the real energy system of the terraced houses. During the operation phases, the controls were shown to be reliable and to cover the thermal loads of the building. In real operation, differences between offline/online simulation results and measured data become apparent. Since the set point specifications from the simulation can only be transferred to the real MHPs in the form of set point temperatures, the operating plan cannot be fully implemented. In the case of PVC this is advantageous, since better results have been obtained in the measurement than in the offline/online simulation. In the case of MPC and SPC, however, worse results are obtained in real operation.

6. Acknowledgement

This paper presents results from the projects "Herzo Base - Energy storage houses - An energy flexible building and energy concept of tomorrow" (FKZ 03ET1364A) and "Herzo Opt - Monitoring of the building envelope, thermal room comfort and energy system with operational optimization" (FKZ 03ET1641A). The project is funded by the German Federal Ministry for Economic Affairs and Energy based on a resolution of the German Bundestag.

7. References

[1] Fischer, D.; Bernhardt, J.; Madani, H.; Wittwer, C. Comparison of control approaches for variable speed air source heat pumps considering time variable electricity prices and PV. Appl. Energy 2017, 204, 93–105.

[2] Pichler, M., Heinz, A., Rieberer, R., 2017. Model predictive heat pump- and building control to maximize PV-power on site use. 12th IEA Heat Pump Conference 2017.

[3] Salpakari, J.; Lund, P. Optimal and rule-based control strategies for energy flexibility in buildings with PV. Appl. Energy 2016, 161, 425–436.

[4] Bechtel, S.; Rafii-Tabrizi, S.; Scholzen, F.; Hadji-Minaglou, J.-R.; Maas, S. Influence of thermal energy storage and heat pump parametrization for demand-side-management in a nearly-zero-energy-building using model predictive control. Energy Build. 2020, 226, 110364.

[5] De Coninck, R. and Helsen, L. (2016). Practical implementation and evaluation of model predictive control for an office building in Brussels. Energy & Buildings, Volume 111, Pages 290-298.

[6] Rolando, D. and Madani H.; A heat pump system control based on solar gain prediction. HPT MAGAZINE 3/2020, Vol. 39, 18–21.

[7] MathWorks. 2020. MATLAB. Version R2020a

[8] Betzold, C., Dentel, A. and Bordin, S. (2020). Entwicklung und Implementierung von Betriebsführungsstrategien in einem Plusenergiegebäude. The 8th Conference of IBPSA Germany and Austria, Graz, Österreich.

[9] Hummel, S., Betzold, C., Kandasamy, K., Bordin, S., and Dentel, A. (2020). Experimentelle Validierung von Simulationsmodellen an einem Hardware-in-the-loop Wärmepumpenprüfstand. The 8th Conference of IBPSA Germany and Austria, Graz, Österreich.

[10] Gurobi Optimization, LLC., 2019, Gurobi Version 8

[11] Betzold, C., Dentel, A. (2021). Evaluation and test operation of different model predictive control approaches for an energy system. The 17th International Conference of IBPSA - Building Simulation 2021, Bruges, Belgium.

8. Data access statement

The datasets generated during and/or analysed during the current study are not publicly available because of privacy of the residents but are/will be available on request with privacy agreement

Measurement and statistical evaluation of hot water tapping profiles in (non-)residential buildings

Jonas Keuler, Paul Mühlenweg, Semiramez Mende, Sven-Yannik Schuba, Daniel Eggert, Peter Pärisch

Institute for Solar Energy Research Hamelin, Emmerthal, Germany, info@isfh.

Abstract. For a good design of water heaters, an exact knowledge of the hot water demand and its temporal distribution is required. According to DIN EN 12831-3, cumulative demand profiles must be determined that represent the daily tapping behavior in the building. In addition, knowledge of the simultaneity of tapping events and thus of the maximum tapping capacity is crucial for the use of central instantaneous water heaters (IWH), which offer advantages for the integration of regenerative heat generators. The following article presents the results of two measurement campaigns to record the domestic hot water demand in residential and non-residential buildings. In 19 water heaters of multi-family houses and 10 water heaters of non-residential buildings, data on temperature and volume of the domestic hot water and, if available, of the circulation are determined. The applied measurement technology for this purpose is presented. The recorded data is analyzed with the help of a Python tool. At first the focus is put on the necessary measuring period and the measuring interval. It is recommended to measure for at least four weeks and with a measurement interval of 5 s or less to be able to make reliable statements about load peaks for the design of IWH. Furthermore, cumulative demand profiles for multi-family houses and hotels are presented, showing that the profiles in the hotel depend on the change of guests checking in to checking out. In addition, the simultaneity of tapping events in non-residential buildings is considered and a good match with formulas for residential buildings from VDI 2072 is achieved.

Keywords. EN 12831-3, instantaneous water heater, measured tapping profiles, simultaneity.
DOI: https://doi.org/10.34641/clima.2022.73

1. Introduction

In Germany, heating of domestic hot water (DHW) requires about 91.6 TWh primary energy per year [1]. Obstacles to its decarbonization, especially in large-scale systems by using heat pumps and solar thermal collectors, are the current hygiene rules [2,3] for planning and operating DHW heaters. Based on these requirements instantaneous water heaters compared to conventional storage water heaters offer the following two advantages. First, because of their much smaller volume, water exchange is improved and the residence time of the water in the system is reduced. Any filters in the circulation system have to filter significantly less water. The extent to which the hot water temperature can be lowered directly is the subject of ongoing research [1,4,5]. The potential for a reduction of 5 K is 15.8 TWh per year for Germany [1]. Second, regenerative heat generators can be efficiently integrated in the buffer storage at lower temperature levels, e.g. for preheating [6]. The potential of this advantage amounts to up to 100 % of CO_2 emissions, as only CO_2 neutral energy sources can be used.

However, the design of heat supply systems with IWH is more complex due to their limited thermal transfer capacity. The capacity limit is defined by the heat exchanger and the maximum primary flow rate. If the tapping capacity exceeds this capacity limit for a short time, the outlet temperature drops and comfort problems may occur at the tapping point. The same applies in the event that the required storage temperature is undershot, which in turn can have a variety of reasons. Ideally, the design of the DHW heating system should be based on a dynamic system simulation with an object-specific, high temporal resolution tapping profile. Since this is not always possible, simple design recommendations are derived in the research projects FeBOp-MFH (FKZ: 03ET1573) and TA-DTE-XL (FKZ: 03EN1025) based on measurement campaigns in residential and non-residential buildings. On the one hand, these projects enable to measure the cumulative demand profiles and the total daily demand, which are required for a design of the storage tank and the heat generator according to DIN EN 12831-3 [7] or the solar thermal according to VDI 6002-1 [8]. On the other hand, these studies provide information about the simultaneity

Copyright ©2022 by the authors. This conference paper is published under a CC-BY-4.0 license.

of use and thus the maximum required output of the IWH. By knowing the exact demand variables, it is possible to prevent oversizing of the systems and thus to install a system that is optimized both energetically and economically.

2. State of the art

Based on the above reasoning, a distinction between maximum capacity or simultaneity and cumulative demand profile and daily demands is made in the sections below.

2.1 Maximum capacity

In buildings with many taps, simultaneous tapping at all taps never occurs. For residential buildings, if the tapping capacity of the residential units $\dot{Q}_{RU}$ is the same, the total capacity can be determined using the simultaneity factor φ (shown in Fig. 1) and the number n of residential units according to equation (1) and equation (2) (e.g. VDI 2072 [9]).

$$\dot{Q} = \varphi \cdot n \cdot \dot{Q}_{RU} \quad (1)$$

$$\varphi = 0.03 + \frac{0.5}{\sqrt{n}} + 0.47 \cdot \frac{1}{n} \quad (2)$$

A comparison of this relationship with current measured values is given in chapter 4.2.

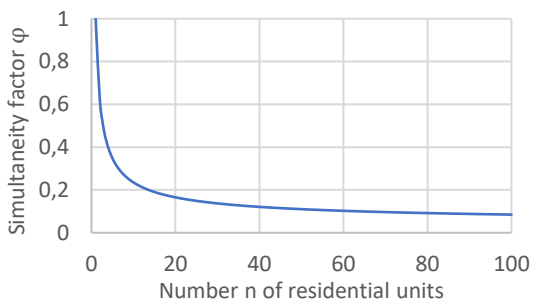

Fig. 1 - Simultaneity factors according to VDI 2072 [9]

An important focus of this work is set on the measurement interval used. In many measurement campaigns (listed in [10]) logging intervals of 1 minute and longer are used. Also the DIN EN 12831-3 requires logging at every minute if possible [7]. However, the authors [10] conclude based of their measurements, that a resolution of seconds is essential. In chapter 4.1 we investigate the influence of temporal resolution on different statistical indicators together with recorded secondary data.

2.2 Cumulative demand profiles and daily values

For the design of DHW heaters according to DIN EN 12831-3, a cumulative demand profile (CDP) must be used. According to DIN EN 12831-3 two way are applicable to determine this object-specific CDP:

1. Measurement of the DHW flow rate on a minute basis, considering the temperature of the hot and cold water – only for retrofit

2. Calculation by multiplying normalized CDP (e.g. Annex B of DIN EN 12831-3) with daily demands, based on statistical analyses – both for new and existing buildings

The determination based on measured values has the highest accuracy for an existing object. [7] For new buildings, there is still a lack of normalized CDP.

3. Measurement campaign

The measurement concept of the DHW profiles for this study is shown in Fig. 2. Independent of the building type and water heating system, both heat flows, tapping capacity and circulation load (if available), can be measured with high temporal resolution.

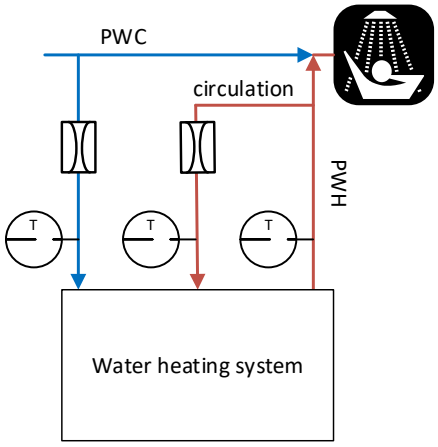

Fig. 2 - Scheme of measuring points used in this study.

In Germany, the building stock is dominated by one- and two-family houses (see Fig. 3). However, buildings that have three or more units, which account for 18 % of Germany's building stock (see Fig. 3), represent approximately 54 % of all residential units in Germany. [11]

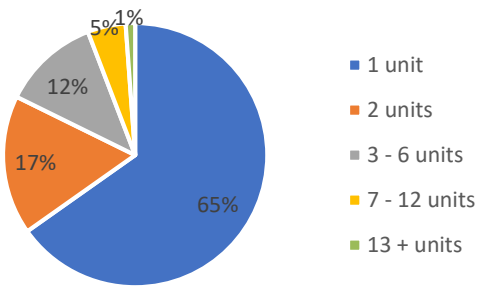

Fig. 3 - Units per building in Germany, data [11]

Therefore, multi-family houses are a relevant sector to make the production of DHW sustainable. The number of multi-family houses and the number of

residential units in these houses considered in this study is shown in Fig. 4. The monitoring system is designed for the long term; a continuous period of six weeks outside the vacations is selected for the present analysis.

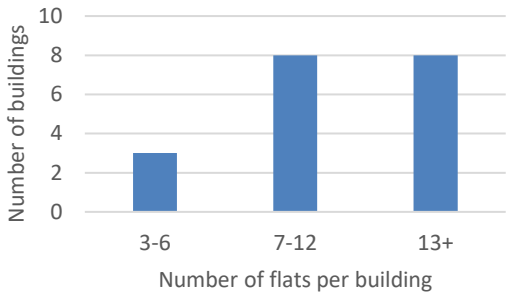

Fig. 4 – Number of units in the residential buildings considered in the study

The measurement results of the non-residential buildings taken as a base in this study are determined in 2 hotels with 5 water heaters as well as in 4 campsites with 5 water heaters. The minimum evaluated period is at least 4 full weeks, whereby at least a part of the measurement period for the campsites is measured during the vacation season.

Due to the specific focus, the two projects use different sensors that allow for different evaluations. These are described in the following chapters.

3.1 Measurement system for residential buildings

Over a period of two years, 19 residential buildings with central hot water supply are equipped with a monitoring system to optimize the system performance. During this time span, the monitoring system is further developed (lessons-learned), so that it varies between different buildings. The basic measurement principle is based on a data logger that reads the flow rate of a calibrated cold water flow sensor as well as the temperatures of drinking cold water, drinking hot water and circulation in minute intervals and transfers them to a server. In some installations, the flow rate of the circulation line is also measured. Flows are either read as instantaneous value or as cumulative volume since installation, the latter will be used in the following.

In the beginning, OneWire contact temperature sensors are coupled directly or via an additional arithmetic unit. Later, PT1000 contact temperature sensors (class A, 2L) are used. The flow rates are measured with commercially available ultrasonic water meters approved for heat meters according to MID 2014/32/EU.

3.2 Measurement system for non-residential buildings

The measuring system (see Fig. 5) consists of a router for data transmission, a data logger, a heat meter, 2 *Keyence FD-Q* clamp-on ultrasonic sensors and 3 contact temperature sensors P1000 (class A, 2L). The measurement period is at least 4 full weeks and the data is logged every second.

Fig. 5 - Measurement system for non-residential buildings

Different *FD-Q* series sensors are used depending on the pipe material and diameter. On a test facility at *ISFH* with a Coriolis reference sensor (accuracy 0.1 %), a calibration factor is determined to correct for systematic errors as shown in Fig. 6 for a specific pipe material, pipe diameter and fluid temperature. These factors can be found in [12]. By calibrating the sensors, a measurement accuracy of ± 2 % is achieved for flow velocity above 0.5 m/s.

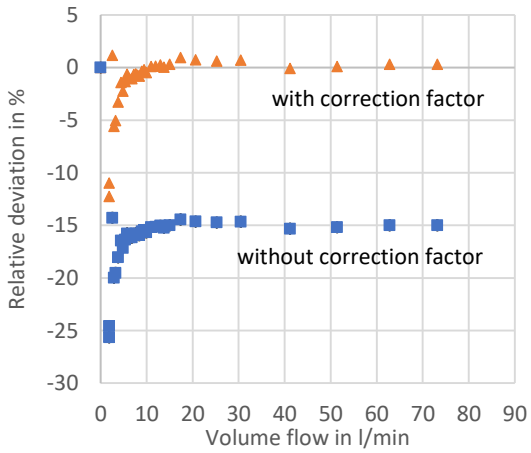

Fig. 6 - Influence of correction factors on the measurement accuracy of *Keyence FD-Q* sensors using the example of the *FD-Q 32C* with a 35mm CU pipe and 55°C water temperature [12]

4. Statistical evaluation

A *Python* tool was developed at *ISFH* for the statistical evaluation of the measured data, which is briefly described below. Subsequently, with the help of this tool, evaluations of the peak load, the

necessary logging interval and determined CDP are presented.

The tool uses the *Pandas* package (version 1.3.3 [13]) for the calculation. With the help of the tool the measurement data of an object are read. Data gaps of one measuring point are closed by interpolation with the previous and next measured value. The *Pandas interpolate* function with the *time* method [13] is used for this purpose. In case of larger gaps, the measured values of this time step are not filled and the user is informed about the gap. Therefore, larger gaps in the non-residential measurement data may result in reduced cumulative values.

4.1 General analyses

Measuring period

The measured peak load is not only a function of the temporal resolution, but also of the duration and period of the measurement. Based on estimated information from the operator, the measurement period is chosen to cover the expected maximum utilization period.

According to DIN EN 12831-3 [7], minute-by-minute data is used for the design of water heating systems and the duration of the measurement period is not specified. With the tapping data measured in the non-residential buildings, it has to be checked whether the minute-by-minute recording of measured data is suitable for the design of various systems for domestic hot water heating. In Fig. 7 the peak load measured in the period up to the respective day is plotted over the measurement period of 28 days. It shows that in 9 out of 10 water heaters the maximum peak load occurred within the first 14 days, in the last case the measured peak load increased by another 2.5 % by extending the measurement period.

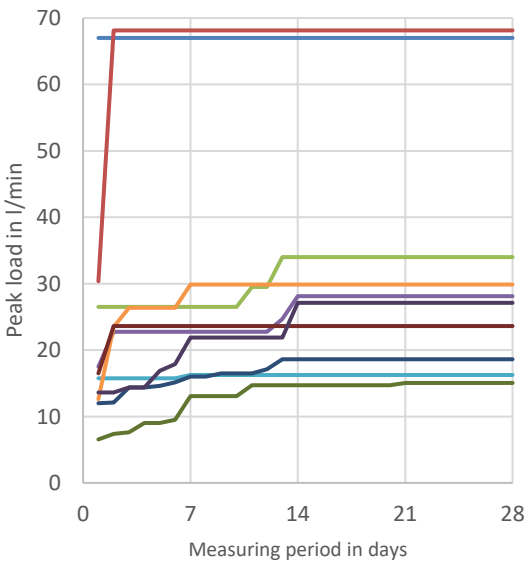

Fig. 7 - peak load measured up to the respective day over the measurement period for 10 examined non-residential water heaters

Logging interval

To investigate the influence of the logging interval, the data are calculated using the method *resample(f'{interval}s').mean()* from the *Pandas* package [13]. Here, we artificially decrease the temporal resolution of data, by calculating the mean value of the measured data in set intervals. This represents a standard cumulative water meter that is read according to the logging interval. The logging intervals chosen for the study are $t_m = 5$ s, $t_m = 10$ s, $t_m = 30$ s, $t_m = 60$ s, $t_m = 120$ s and $t_m = 300$ s. In the case of data gaps, the function fills in empty values. All further calculations are then performed with these averaged values.

For the calculation of the peak load, the time interval with the highest measured value was determined for the respective period under consideration. Fig. 8 shows the normalized peak loads determined for 4 water heaters in hotels relative to the peak load per second over the logging interval. The plot shows that the determined peak values decrease with increasing logging interval, in some cases significantly.

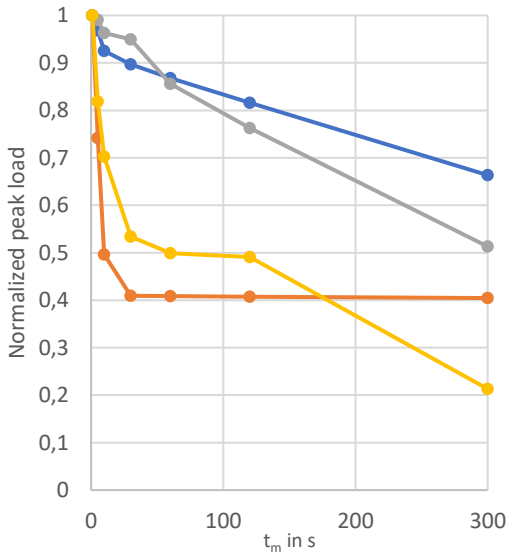

Fig. 8 - Dependence of the measured, normalized peak load over the logging interval for 4 water heaters in hotels

To examine this issue in more detail, the influence on the maximum tapping volume flow during the measurement period is considered for all 10 water heaters mentioned in section 3.2. For $t_m = 5$ s it is obvious that the peak load is underestimated by 6.6 % on average (0-26 %). For $t_m = 60$ s, the peak loads are underestimated by 27.7 % on average (15-59 %). In both cases, as already expected from Fig. 8 there is a wide spread deviation (compare Fig. 9), which is related to different durations of the maximum tapping. For the 10 non-residential water heaters the normalized 1-minute peak load is up to 60 % smaller than the 1-second peak, whereas the 5 s peak is practically as large as the second peak in half of the cases.

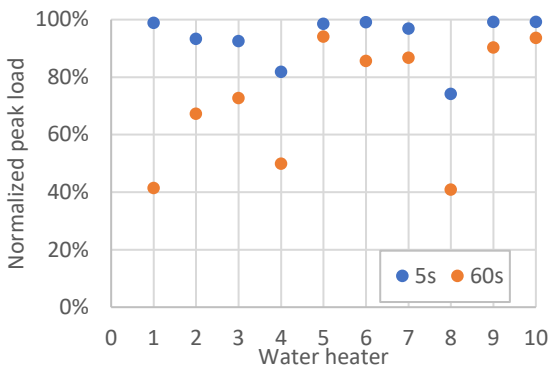

Fig. 9 - Deviations of the normalized peak load due to logging interval for 10 non-residential water heaters.

To increase the data base of the sample, the daily peak loads were also evaluated. A total of 310 measurement days are considered for the 10 non-residential water heaters and the results are listed in the Tab. 1.

Tab. 1 - Deviation of the normalized peak load due to the logging interval for 310 days

t_m in s	5	60
Mean	4.8 %	26.6 %
Min	0 %	3 %
Max	32 %	69 %

4.2 Object-specific analyses

Residential buildings

In the following, we investigated how the average daily tapping demand (temperature differences normalized to 10 °C cold water heated to 60 °C hot water) per residential unit behaves in different buildings. The results are shown in Fig. 10.

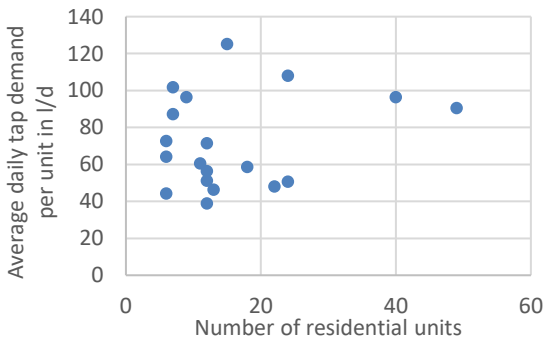

Fig. 10 – Average normalized daily tapping demand (@10/60 °C) per residential unit

The average daily amount of water tapped per residential unit fluctuates between 39 l/d and 125 l/d; this fluctuation is independent of the total number of residential units in the building. According to [14], the results are within a range that can be expected, but no information is available for the buildings on the number of persons or occupant structure of the buildings, so no further correlation between tapped water and residents can be investigated.

Furthermore, the CDP of the daily tappings are examined. The cumulative energy demands Q_{ti} and hot water demands V_{ti} are formed from the individual values by means of cumulative totals based on the *Pandas* function *cumsum* [13].

$$Q_{ti} = \sum_{t0}^{ti}(\dot{Q}_i \cdot \Delta t) \quad (3)$$

$$V_{ti} = \sum_{t0}^{ti}(\dot{V}_i \cdot \Delta t) \quad (4)$$

For each time t_i of the day, the cumulative energy demand Q_{ti} or the hot water demand V_{ti} is calculated from the sum of the individual quantities. The individual quantities result from the instantaneous flow $\dot{Q}_i$ rep. $\dot{V}_i$ and the duration Δt of a time step. These are then normalized to the daily total demand to provide for comparability.

Based on the days with the highest DHW demand, a CDP was calculated for each property, although one property with 3 - 6 and one property with 13 + residential units could not be included due to data gaps. Thus, for the three classes of residential buildings (compare Fig. 3), a mean CDP is formed for each class. These graphs are shown in Fig. 11. In addition, an average, a minimum and a maximum CDP is determined, averaged over all buildings.

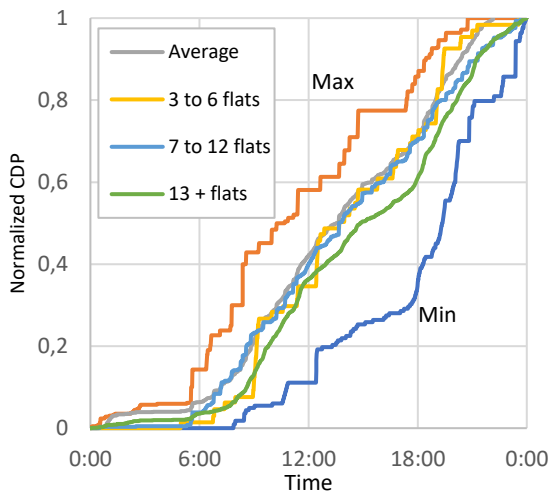

Fig. 11 - Cumulative demand profiles of the residential buildings

Non-residential buildings

The non-residential buildings surveyed are 5 central water heaters in hotels, where one is only supplying showers and washbasins for a swimming pool. Two other water heaters are supplying 1 and 3 kitchens in addition to their assigned guest rooms. Furthermore, 5 shower houses at campsites are measured. In the following, exemplary evaluations of these water heaters are discussed.

Fig. 12 shows the daily peak load over the number of guests for a hotel object. A distinction is made between the number of guests recorded after check-in on the previous day and the number recorded after check-in on the day of measurement. The plot shows that the peak load correlates significantly better with the number of guests on the previous day

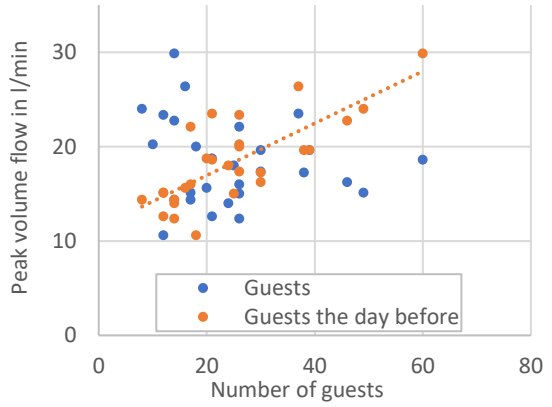

Fig. 12 - Maximum daily volume flow depending on the number of guests present

Furthermore, the results show that with a similar number of guests on the previous day, the maximum load can vary by more than 30 % (compare Fig. 12). This is related to user behavior and only with a measurement over a longer period of time, the possible simultaneity can be accurately represented even at constant load.

An explanation why the peak load correlates better with the guests of the previous day becomes obvious when looking at the cumulative demand profiles (compare Fig. 13). Here, there is a clear peak load in the morning. The guests recorded the day before the measurement have to be responsible for this peak, assuming no guest is checking in during the early morning hours from 00:00 h to 08:00 h.

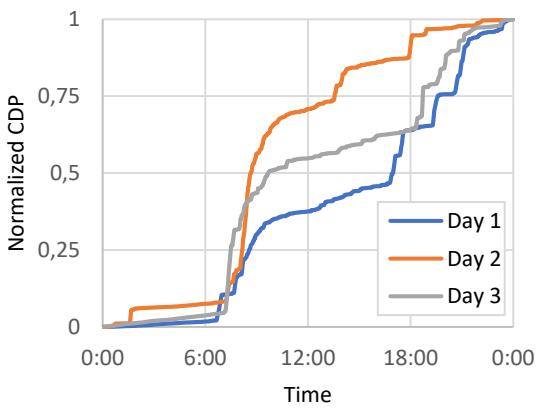

Fig. 13 - Daily cumulative demand profiles of a hotel

The guests present have an influence on the expression of the CDPs. To illustrate this, the guests for an exemplary period are listed in Tab. 2. The CDP of day 1 and day 2 show very clearly that more than half of the daily tapping is accounted for by the morning hours and thus the guests from the previous day have to be responsible for that tapping. However, if there are more guests in the evening than on the previous day, it is also possible that the main load will shift to the afternoon as on day 1.

Tab. 2 - Example data of a hotel

Day	Number of guests	Peak load in l/min	Sum in l
0	30	19.6	918
1	46	16.3	1074
2	14	22.8	896
3	24	14	574

This also becomes clear when looking at all measured daily CDP of the object, which are shown in Fig. 14. The green lines show the days when the number of guests is increased by more than 10, and the red lines show when the number of guests is decreased by more than 10 compared to the previous day. All other days are marked in blue. It is noticeable that on days with an increase of more than 10 people, the proportion of tappings up to 12:00 h at noon is mostly below average. In other cases, well over 75 % of the daily total is tapped until 12:00 h at noon on days with a decrease in number of guests more than 10.

Therefore, it should be considered whether the measurement period for the evaluation of lodging establishments should be daily from 0:00 h to 23:59 h or whether it would be appropriate to start the evaluation between the check-out and check-in time of a hotel (e.g. 13:00 h to 12:59 h). In this case, the housekeeping should be counted for the previous day.

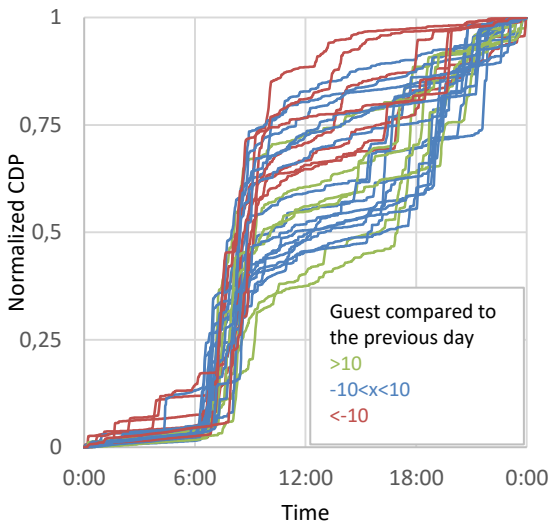

Fig. 14 – Normalized CDP of a hotel depending on the difference of guests checking in to out

The back-calculation of measured data to simultaneity factors is not possible without further ado. This requires precise knowledge of all the taps used, the pressure losses in the system and other variables. In order to be able to give an estimate of the simultaneity of tappings, the approach shown in Fig. 15 was chosen. Here, the measured maximum tapping capacity $\dot{Q}_{max,n}$ per installed shower is plotted on the first y-axis over the number n of installed showers. The heat demand $\dot{Q}$ was determined for this purpose according to equation (5).

$$\dot{Q} = \dot{m} \cdot c_{p,m} \cdot (\vartheta_{out} - \vartheta_{in}) \quad (5)$$

Here, for simplicity, a fixed mean specific heat capacity $c_{p,m}$ = 4,179 kJ/(kg·K) is assumed.

The trend line is calculated from the measured values with *Excel*. It shows a theoretical performance of a shower $\dot{Q}_{max,1}$ of about 27 kW. Since $\dot{Q}_{max,1}$ corresponds to the power of a shower, the second Y-axis, which gives the simultaneity factor over the number of showers installed, is normalized so that $\dot{Q}_{max,1}$ corresponds to 1. According to equation (2), the simultaneity factor for residential units from VDI 2072 [9] is plotted in blue. The number of showers installed is used for n. By this approach it is possible to give an estimation for the simultaneity without exact knowledge of other boundary conditions like for example the installed taps. The determined trend line of the non-residential buildings agrees well with the simultaneity factors for residential buildings. However, deviations of more than 100 % are found for individual objects.

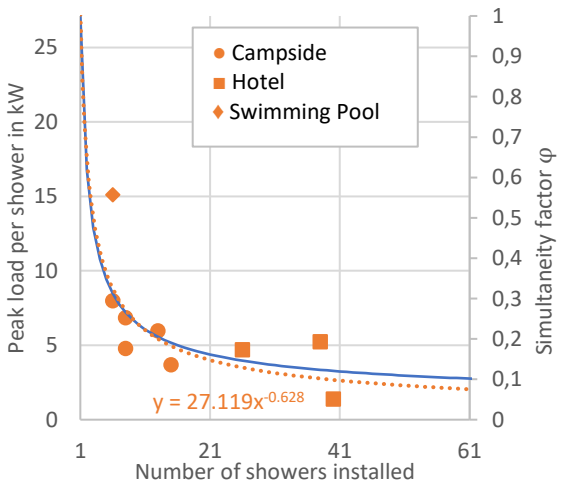

Fig. 15 – Comparison of determined simultaneity factors in non-residential buildings with the curve from VDI 2072 (blue)

5. Conclusion

In this paper, two measurement campaigns in residential and non-residential buildings with different methods for recording DHW consumption are presented. In the residential buildings, commercial heat and water meters are used to measure temperatures and total volumes in minute-by-minute resolution. In the non-residential buildings, clamp-on ultrasonic sensors and temperature sensors are used to measure the instantaneous volume flows in second-by-second resolution.

In the following, the evaluation is presented by means of a *Python* tool. First, the required measurement period and the measurement interval are examined for load peaks and daily CDPs. We have shown that the length of the selected measurement period of 4 weeks is sufficient for the evaluation. Since the peak loads depend on the user behavior even at the same utilization and can differ significantly, it is advisable to measure over a period of several days even at full utilization.

Furthermore, it can be noted that a minute-by-minute recording of measured values, as required in DIN 12831-3, is suitable for the determination of cumulative demand profiles and daily demands. However, for a statement about a short-term peak load, e.g. for the design of an IWH, these data are not suitable. For this purpose, tapping profiles should be measured with a logging interval of at least 5 seconds. A reliable extrapolation based on minute data is not possible. In this case, a prudent planner should apply at least a 60 % increase in the minute peak for the selection of an appropriate IWH.

Additionally, measured data from 19 residential buildings are considered. They show that information on the facilities and occupancy of residential units are necessary for a good design.

In the case of non-residential buildings, 10 water heaters are investigated, these are 5 in hotels and 5 at camping sites in total. An example of a hotel shows how the daily peak load correlates with the number of guests the previous day. The CDPs show that in most cases more than 50 % of the daily energy is used before 12:00 h at noon. Here, a shift in the CDP can be seen depending on the ratio of guests checking in to guests checking out. If significantly more guests check in, the load tends to be distributed more evenly throughout the day. If, on the other hand, significantly more guests check out, the load is strongly focused on the morning.

If we look at the load peak per shower installed, the trend line determined is a good approximation to the simultaneity factors according to VDI 2072, even if this standard is actually only established for residential buildings.

6. Outlook

In the course of the current research project TA-DTE-XL, many more non-residential buildings are going to be measured. With the help of these data, the authors want to confirm the findings on the dependence of the simultaneity factors on the installed showers in

hotels, at campsites and to an extent in indoor sports facilities. This way, more precise design recommendations for instantaneous water heaters should be made. For this purpose, it should also be investigated to what extent a short-term exceeding of the design capacity of the IWH can be tolerated. In this way, it may be possible to reduce the proposed safety buffer during design.

7. Acknowledgement

The presented work is part of the research projects "TA-DTE-XL" (grand no. 03EN1025A) and "FeBOp-MFH" (grand no. 03ET1573).
TA-DTE-XL is a joint project with Viega GmbH & Co. KG, while in FeBOp ISFH is collaborating with Klimaschutz- und Energieagentur Niedersachsen (KEAN), proKlima – der enercity Fonds and Corona Solar GmbH.
The authors are grateful for the support of the State of Lower Saxony and the Federal Ministry for Economic Affairs and Climate Action (BMWK). The authors are responsible for the content and would also like to thank PAW GmbH & Co. KG, Oventrop GmbH & Co. KG, Solvis GmbH, Malotech GmbH, cbb software GmbH, Taconova GmbH, Reich + Hölscher, Varmeco GmbH & Co.KG, Bosch Solarthermie GmbH, Vaillant GmbH for their support.

8. References

[1] Rühling K, Rothmann R, Haupt L, Hoppe S, Löser J, Schreiber C. EnEff: Wärme - Verbundvorhaben Energieeffizienz und Hygiene in der Trinkwasser-Installation im Kontext: DHC Annex TS1 "Low Temperature District Heating for Future Energy Systems" : Akronym: EE+HYG@TWI : koordinierter Schlussbericht zu 03ET1234 A bis D. 30042018th ed. [Dresden]: [Technische Universität Dresden, Fakultät Maschinenwesen, Institut für Energietechnik, Professur für Gebäudeenergietechnik und Wärmeversorgung]; 2018.

[2] DIN 1988-200:2012-05: Technische Regeln für Trinkwasser-Installationen_- Teil_200: Installation Typ_A (geschlossenes System)_- Planung, Bauteile, Apparate, Werkstoffe; Technische Regel des DVGW. Berlin: Beuth Verlag GmbH; 2012.

[3] DVGW e.V. Trinkwassererwärmungs- und Trinkwasserleitungsanlagen; Technische Maßnahmen zur Verminderung des Legionellenwachstums; Planung, Errichtung, Betrieb und Sanierung von Trinkwasser-Installationen. Bonn; 2004.

[4] DVGW Deutscher Verein des Gas- und Wasserfaches e.V. - Technisch-wissenschaftlicher Verein. EnOB: ULTRA-F: Ultrafiltration als Element der Energieeffizienz in der Trinkwasserhygiene [Internet]. c2018 [cited 2021 Nov 29]. Available from: https://www.enargus.de/pub/bscw.cgi/?op=enargus.eps2&q=ultrafiltration&m=1&v=10&s=10&id=1011673.

[5] Institut für Solarenergieforschung Hameln. Analyse und Erarbeitung notwendiger Maßnahmen zur Absenkung der Trinkwarmwassertemperatur in Niedertemperatur-Versorgungssystemen: Trans2NT-TWW [Internet]. c2021 [cited 2021 Nov 29]. Available from: https://isfh.de/forschung/solare-systeme/projekte/trans2nt-tww/.

[6] Pärisch P, Büttner C, Keuler J, Lampe C, Giovannetti F. Parameter study of four different instantaneous water heaters in a solar assisted multi-family-house with TRNSYS. In: International Solar Energy Society, editor. EuroSun 2020 Proceedings; 2020b.

[7] Energetische Bewertung von Gebäuden – Verfahren zur Berechnung der Norm-Heizlast: Teil 3: Trinkwassererwärmungsanlagen, Heizlast und Bedarfsbestimmung, Module M8-2, M8-3;, 91.140.10; 91.140.65: Beuth; 2017.

[8] VDI. VDI 6002 - 1. Berlin: Beuth Verlag GmbH; 2014.

[9] Verein deutscher Ingenieure. Wärmeübergabestation mit Wasser-Wasser-Wärmeübertrager für Durchfluss-Trinkwassererwärmung/ Raumwärmeversorgung: VDI 2072, Vol 91.140.65: Beuth; 00.2019.

[10] Marszal-Pomianowska A, Jensen RL, Pomianowski M, Larsen OK, Jørgensen JS, Knudsen SS. Comfort of Domestic Water in Residential Buildings: Flow, Temperature and Energy in Draw-Off Points: Field Study in Two Danish Detached Houses. Energies 2021;14:3314.

[11] Statistische Ämter des Bundes und der Länder. Zensus 2011: Gebäude und Wohnungen [Internet]. c28.05.2014 [cited 2021 Nov 25]. Available from: https://www.zensus2011.de/DE/Home/Aktuelles/DemografischeGrunddaten.html?nn=559100.

[12] Harms H. Kalibrierung von Clamp-On Ultraschallsensoren zur Ermittlung von Summenlinien zur Auslegung von zentralen Durchfluss-Trinkwassererwärmern. Bachelorarbeit. Hannover; 2021.

[13] Wes McKinney and the Pandas Development Team. pandas: powerful Python data analysis toolkit: Release 1.3.3 2021.

[14] Albers K-J, editor. Taschenbuch für Heizung und Klimatechnik: Einschließlich Trinkwasser- und Kältetechnik sowie Energiekonzepte. 80th ed. Kleinaitingen: ITM InnoTech Medien GmbH; 2020.

The data sets generated and analyzed during the current study are not available because more data will be collected and then published, but the authors will make every reasonable effort to publish them in the near future.

Analysis of Internal Leakages of Residential Ventilation Units by various test methods

Marie-Teres Moser [a], Anneli Halfvardsson [b], Jaroslav Chlup [c], Heinrich Huber [d]

[a] Department of Engineering and Architecture, Lucerne University of Applied Science and Arts, Lucerne, Switzerland, marie-teres.moser@hslu.ch.

[b] Flexit AS, Ørje, Norway, anneli.halfvardsson@flexit.no.

[c] Research Department, 2VV s.r.o., Pardubice-Staré Hradiště, Czech Republic, jaroslav.chlup@2vv.cz.

[d] Department of Engineering and Architecture, Lucerne University of Applied Science and Arts, Lucerne, Switzerland, heinrich.huber@hslu.ch.

Abstract. Internal leakages of bidirectional residential ventilation units (RVU) have a negative impact on hygiene and energy efficiency. Therefore, internal leakages are an essential part of the European standards and should be a requirement and part of the energy labelling in the revision of Regulation EU 1253/2014. The current test standard defines a static pressure method intended for RVUs with plate heat exchangers. In addition, there is an in-duct method and a chamber method, using tracer gas, for air handling units (AHU) with rotary heat exchangers. The Eurovent Product Group Residential Air Handling Units launched a project to analyse these methods. The project was also supported by the Swiss Federal Office of Energy and GebäudeKlima Schweiz. Two AHUs, one with plate heat exchangers and the other with rotary heat exchanger, were tested with all three methods. The finding was that the results of the different methods were not comparable. A Master's study confirmed this with a third RVU. Hence, a new method was introduced, the so-called Advanced Pressure Method (APM). This approach allows testing without tracer gas, but with comparable results to the in-duct method. The APM is based on a node model of the flow paths within the RVU. All in all, the APM is a reliable approach to determine the internal leakage, even though the measurement uncertainty is higher than with the in-duct method. The accuracy is limited due to the sensitivity of the mathematical model. Therefore, the APM has been proposed for the use of the APM in manufacturers' laboratories. Furthermore, in the EN 13142 standard, the internal leakage is used to correct the temperature efficiency. The current test standard leads to results that depend not only on the quality of an RVU, but also on the test method. In addition, test conditions that are not clearly defined, e.g. rotary speed, have an effect. The project is intended to open the discussion on the three mentioned test standards and their influence on energy labelling.

Keywords. Residential Ventilation Unit, Leakage, Test Method, Tracer gas measurement.
DOI: https://doi.org/10.34641/clima.2022.337

1. Introduction

Before a bidirectional Residential Ventilation Unit (RVU) hits the market, it will get tested not only for the temperature efficiency, but also for its external and internal leakage. These are mandatory product information according to the European ecodesign requirements [1]. The testing standard for ducted bidirectional RVUs EN 13141-7:2021 [2] defines three different test methods for the determination of internal leakages of RVUs, but it is a common understanding among experts that, with the current knowledge, the results cannot be directly compared or converted. The resulting leakage will be considered to calculate the corrected temperature ratio. The leakage rates vary within the different methods and thus some exchangers get rated better or worse than others. In general, the higher the internal and external leakage of the unit, the lower the efficiency of it. This is taken into account when correcting the temperature ratio with Table 2 in standard EN 13142:2021 [3].

Against this background, the Eurovent Product Group Residential Ventilation Units (PG RAHU) has launched a project to compare existing test methods for internal leakage of ducted bidirectional RVUs. The first target was to sort out the existing test methods and investigate if there is any relation between them. Next, try to work out a base for a

Copyright ©2022 by the authors. This conference paper is published under a CC-BY-4.0 license.

unified test method for all types of exchangers. This could open the possibility for developing a common and standardized test method for RVUs with all categories of heat recovery [4].

2. Object and method

First, two standard RVUs were measured using the three existing test methods to get results that can be compared.

2.1 Existing standard test methods

In the European standard EN 13141-7:2021, Annex B.2 and Annex C.3, three different methods for the determination of the internal leakage of ducted bidirectional RVUs are defined [2].

Pressure method (see **Fig. 1**): Adjustable fans are connected on each side of the unit, but the unit itself is switched off. The fan connected to the supply air side is used to set a pressure difference of 0 Pa towards the ambient pressure. The fan on the exhaust air side can then be used to vary the over or under pressure on the exhaust air side. In addition, a gas meter or volumetric flow meter is installed on the supply air side, to measure the air flowing from the side set to over pressure or under pressure to the one set zero to ambient. The measured air volume flow is then set in relation to the reference air volume flow and thus results in the leakage rate. According to EN 13141-7:2021 the pressure method applies for plate heat exchangers.

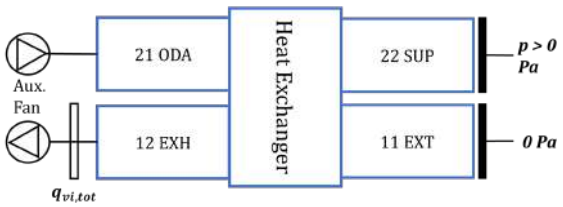

Fig. 1 – Test setup for Pressure Method

In-duct method (see **Fig. 2**): The In-duct method applies to Rotary RVU when it is known that the external leakage of the unit is not higher than three percent. The unit is connected to all four air ducts and runs on reference conditions described in the standard EN 13141-7:2021. The tracer gas itself is introduced into the extract air. The concentration in all four duct connections is measured. The transfer ratio R_s of recirculated air in the supply air stream is calculated with equation (1):

$$R_s = \frac{c_{22}-c_{21}}{c_{11}-c_{21}} \quad (1)$$

where c_{11} is the tracer gas concentration in the extract air, c_{21} in the outdoor air and c_{22} in the supply air. The transfer ratio of recirculated air in the exhaust air stream is calculated analogously.

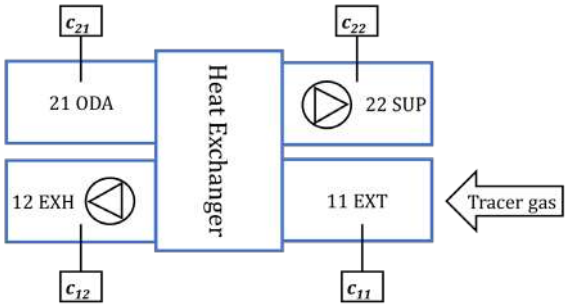

Fig. 2 – Test setup for In-duct Method

Chamber method (see **Fig. 3**): In the Chamber method the RVU is placed in a chamber, where a high dosage of tracer gas is dispensed. The tracer gas is mixed well with the air. The connections of outdoor air and supply air are led into a low concentrated chamber, while the exhaust and extract air connections end open into the high-dosage chamber. The unit will be running at reference conditions, too. Since, with the Chamber method, the sum of the internal transfer and external transfer are determined, the result is defined in EN 13141-7:2021 as: $R_{s,tot}$ total transfer ratio in supply air.

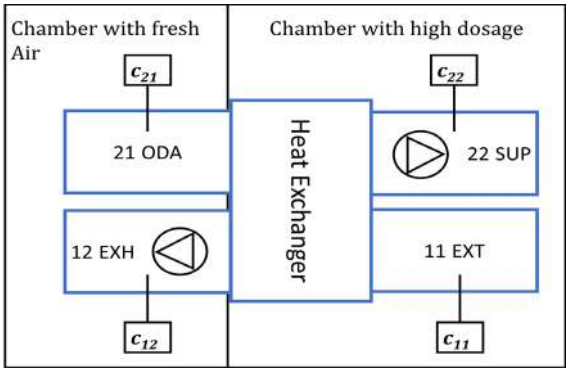

Fig. 3 – Test setup for Chamber Method

2.2 Test Procedure

Two ducted bidirectional RVUs have been delivered by the PG RAHU to the HVAC testing laboratory of the Hochschule Luzern (HSLU):

- a RVU with a **rotary heat exchanger** (in the following called Rotary RVU) and

- a RVU with a counterflow **plate heat exchanger** (in the following called Plate RVU)

The maximum flow rate of the RVUs is 400 m³/h (± 6 %) and the reference flow rate is 280 m³/h (± 6 %). The configuration of the RVUs include both fans (supply and exhaust) located downstream the heat exchanger. Both units, regardless of the heat exchanger category, have been tested by all three test methods for internal leakage of EN 13141-7:2021:

- Internal leakage with pressure method (**Pressure method**)

- Internal leakage with tracer gas with in-duct method (**In-duct method**)

- Total leakage with tracer gas with chamber method (**Chamber method**). In the project the concentration

was measured in all four ducts as well as in each chamber.

Before the internal leakage tests, the external leakage was measured with static over and under pressure according to EN 13141-7:2014, Annex B.1 (in the following called external leakage test). The intention of the external leakage test was to confirm the external tightness of the units. During the In-duct method and the Chamber method the internal leakage of the Rotary RVU was measured with different rotor speed (0, 4, 8 and 12 rpm) to determine the carryover leakage and the pressure leakage separately. Both RVUs have been equipped with additional tabs for pressure measurement to acquire additional information about the pressure ratios and distribution during the leakage tests and in regular operational conditions.

3. Results of the test methods

3.1 Leakage rates and classification

Tab. 1 summarizes the different test results. Detailed test results can be found in the test reports of the Rotary RVU [5] and Plate RVU [6]. The results of the Rotary RVU are shown by the different settings of the rotor speed.

Tab. 1 – Results of the leakage tests according to EN 13141-7:2021 of the measured RVUs.

	Ext. leakage	Int. leakage	Total leakage	Int. leakage
		Pressure	Chamber	In-duct
Plate RVU	1.0 %	1.8%	1.1 %	0.6 %
Rotary RVU 0 rpm	0.6 %	3.4 %	1.7 %	0.9 %
Rotary RVU 4 rpm	0.6 %	n.a.	2.9 %	2.1 %
Rotary RVU 8 rpm	0.6 %	3.8 %	4.1 %	3.3 %
Rotary RVU 12 rpm	0.6 %	n.a.	5.4 %	4.6 %

Accordingly, for the measured leakages the classification of the units according to EN 13141-7:2021 are shown in **Tab. 2**.

Tab. 2 – Leakage classification of the measured RVUs.

	Pressure	Chamber	In-duct
Plate RVU	Class A1	Class B2	Class C2
Rotary RVU 0 rpm	Class A2	Class B2	Class C2
Rotary RVU 4 rpm	n.a.	Class B3	Class C3
Rotary RVU 8 rpm	Class A2	Class B3	Class C3
Rotary RVU 12 rpm	n.a.	Class B3	Not classified

The leakage at the speed of 4 rpm and 12 rpm with the pressure method couldn`t be measured since the programmed speed control wasn't available at the time.

3.2 Conclusions on the standard methods

Overall, the tested RVUs were very tight and the measured leakages of the two units comply well with the product information of the manufacturers. The classification and leakage ratios for each of the two units with the different methods could not be compared or converted.

The internal leakage of the Rotary RVU depends not only on the tightness of the casing and sealing, but also on the rotor speed. The final report of the project [7] shows the dependency of the internal leakage on the rotor speed, determined with the In-duct method and the Chamber method. Roughly estimated, the In-duct leakage is the subtraction of the external leakage from the chamber leakage. For the exhaust air leakage it is reversed, the in-duct leakage is the sum of external leakage and chamber leakage. Accordingly, the total leakage consists of the leakage caused by constant pressure, which can be determined in the static state of the rotor, and the leakage caused by the carry over.

For the examined RVUs, the values of the internal leakage are lower with the In-duct method than for the Pressure method. This can't be seen as a general conclusion. The test results and the assertion can be different for other constructions, fan positions, components (e. g. pressure loss) and position of the leaks. Further work and analyses are necessary for a differentiated statement. Nevertheless, the result shows that the pressure method is pointing in the right direction. Furthermore, interesting results of these comparison tests were the additional pressure measurements for the pressure distribution inside the RVUs. This additional information seems a promising option to refine the pressure method, which is dealt in the next chapter.

4. Advanced Pressure Method

The Advanced Pressure Method (APM) is a proposal to obtain all the relevant information for the calculation of the internal leakage without tracer gas. The RVU model used for this is shown in **Fig. 4**.

4.1 Model

The APM is based on a node-resistance model of the RVU, analogously to an electrical network.

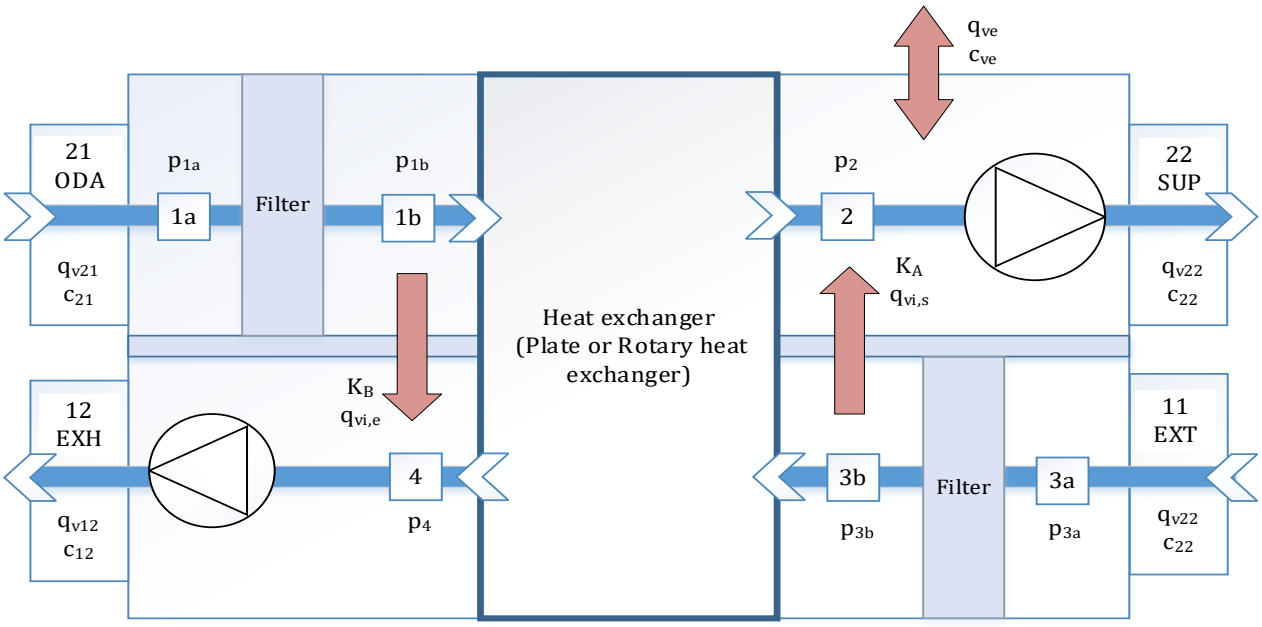

Fig. 4 – RVU model used for the APM

Physically correct would be a model with power functions to describe the relationship between the pressure difference and the air flow rate between the nodes. The comparison of the numerical tests with linear and power functions showed no significant difference in the results. Therefore, to keep the model simple and easier to understand at this stage, it was decided to use linear simplification.

It is assumed that the relevant internal leakages occur between the points 1b – 4 and 3b – 2 shown in **Fig. 1**. **Tab. 3** explains the symbols used to picture the APM.

Tab. 3 – Symbols for APM.

Symbol	Unit	Designation
p	Pa	Pressure
c	ppm	Tracer gas concentration
q_v	m³/h	Air volume flow
K	Pa/(m³/h)	Resistance

In addition, the indices for the symbols used with the APM are listed below in **Tab. 4**.

Tab. 4 – Indices for the APM.

Index	Designation
11/EXT	Extract air at the duct connection of the RVU
12/EXH	Exhaust air at the duct connection of the RVU
21/ODA	Outdoor air at the duct connection of the RVU
22/SUP	Supply air at the duct connection of the RVU
1a ,1b ,2	Nodes of pressure tabs on supply air side
3a, 3b, 4	Nodes of pressure tabs on exhaust air side
A	Relating to the leak between nodes 3b – 2
B	Relating to the leak between nodes 1b – 4
e	Exhaust air side, or external
i	internal
int	Relating to internal leakage
s	Supply air side

The flow resistances in these paths are called K_A for the supply air side and K_B for the exhaust air side. The reciprocal value of K_A is the leakage coefficient C_A and the reciprocal value of K_B is the leakage coefficient C_B. The complex model of the RVU in **Fig. 1** is abstracted and reduced to the elements that are necessary for the calculation, see **Fig. 5**.

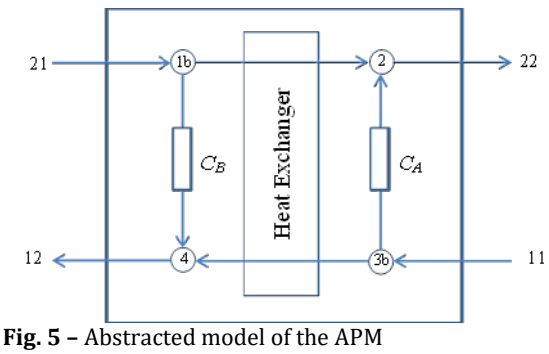

Fig. 5 – Abstracted model of the APM

For testing purposes one of the duct connections is sealed. At the second duct connection on the same main air path (either 11 – 12 or 21 – 22) the total of the internal leakage flow rate $q_{vi,tot}$ through the leakage paths C_A and C_B is measured. The values of C_A and C_B are unknown and thus have to be determined with two equations, which represent two independent measurements.

Values from measurement series No. 1 are from here on marked with index 1 and those from measurement series No. 2 with index 2. These indices are listed after the indices of Table 4. With two measurements, equations for $q_{vi,tot1}$ and $q_{vi,tot2}$ are built up with equation (2) and (3).

$$q_{vi,tot1} = \Delta p_{A1} \cdot C_A + \Delta p_{B1} \cdot C_B \quad (2)$$

$$q_{vi,tot2} = \Delta p_{A2} \cdot C_A + \Delta p_{B2} \cdot C_B \quad (3)$$

The relevant pressure differences can be calculated with equations (4) – (7):

$$\Delta p_{A1} = p_{2,1} - p_{3b,1} \quad (4)$$

$$\Delta p_{B1} = p_{1b,1} - p_{4,1} \quad (5)$$

$$\Delta p_{A2} = p_{2,2} - p_{3b,2} \quad (6)$$

$$\Delta p_{B2} = p_{1b,2} - p_{4,2} \quad (7)$$

With the measured values of Δp_{A1}, Δp_{B1}, Δp_{A2}, Δp_{B2}, $q_{vi,tot1}$ and $q_{vi,tot2}$ the leakage factors C_A and C_B can be calculated.

If the two measurements are finished, the transfer ratio of the supply side R_s can be calculated. For that calculation, firstly the pressure differences $\Delta p_{A,ref}$ and $\Delta p_{B,ref}$ at reference conditions are determined. These pressures can e. g. be measured at the test set-up for thermal tests. Then the supply leakage air flow rate at reference conditions is determined by equation (8):

$$q_{vi,s} = \Delta p_{A,ref} \cdot C_A \quad (8)$$

Finally, the transfer ratio of recirculated air in the supply air stream for RVUs with plate heat exchangers is expressed by equation (9):

$$R_s = \frac{q_{vi,s}}{q_{v,ref}} \quad (9)$$

This should be equal to the internal leakage as determined with the In-duct method.

For rotors the carry over of air volumes in wheel and the rotor speed is not included in equation (9). Therefore, the transfer of this effect has to be added. This total ratio with recirculated air for RVUs with rotor is defined by equation (10):

$$R_s = \frac{q_{vi,s} + q_{v,co}}{q_{v,ref}} \quad (10)$$

where $q_{v,co}$ is the transferred air by carry over. The calculation can be found in literature or manufacturer information e.g. [8].

4.2 Test setup and procedure

The APM is performed with one fan of the RVU switched on and the other one switched off. The measurement setup is pictured in **Fig. 6**.

The airflow side where the fan is switched off is treated as with the pressure method. That is, the pressure difference between this airflow side and the environment is 0 Pa. This is achieved by an adjustable auxiliary fan connected to the unit. The supplied air corresponds to the internal leakage air flow and is measured. On the airflow side with the fan switched on, the settings are varied. It is recommended to start with the reference air flow and a unit pressure of 50 Pa (distributed 1/3 and 2/3 on exhaust and extract air as described for the In-duct method).

For the other test points, the setting of the pressure ratios and thus the leakage airflows should be varied so that the ratios of the pressure differences 1b - 4 and 3b - 2 are clearly different between the test points.

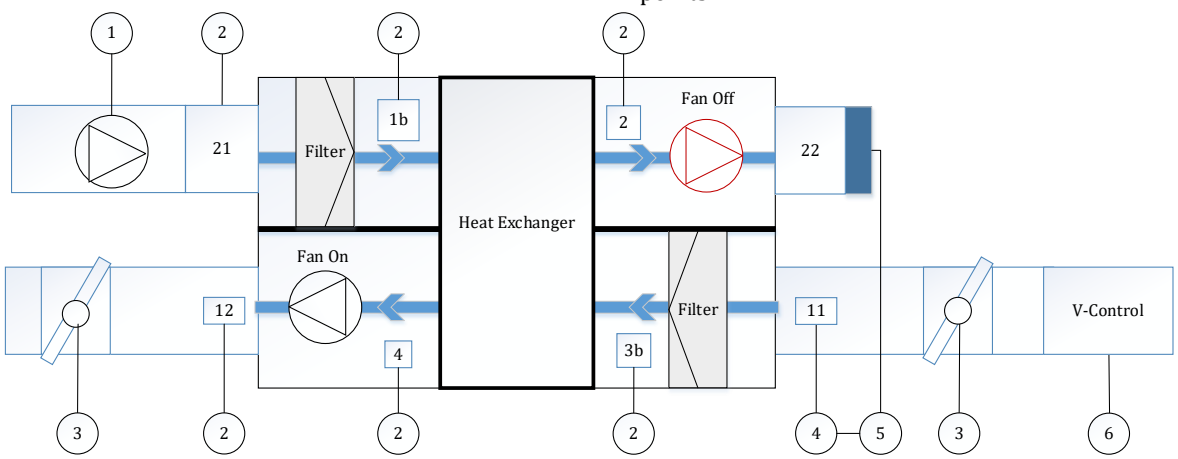

Legend for exhaust fan on:
1) Adjustable fan and rotary displacement meter
2) Pressure gauge connection to ambient
3) Iris diaphragm (or alike) for adjusting the pressure
4) Differential pressure gauge connection 22-11
5) Differential pressure gauge connection 22-ambient
6) Air flow measuring equipment

11 = Extract Air
12 = Exhaust Air
21 = Outdoor Air
22 = Supply Air (sealed)

Fig. 6 – Test setup APM

This can be achieved by varying the setting of throttle valves installed at the duct connections.

For measurements the reference air flow was kept constant and only the pressures were varied.

Even though the model only requires data from two test points, it is recommended to perform at least five points. Some of the test points can be obtained by changing the two airflow sides.

4.3 Measurements and test results

Examples of measurement results of the APM for the Plate RVU are shown in **Tab. 5**. The measured value of the In-duct method with the given pressures was R_s = 0.6 % as described in **Tab. 1**.

Tab. 5 – Examples of four Measurement Points (MP); Plate RVU with APM

	MP 1	MP2	MP3	MP4
Δp_{A1}	-58	-58	-50	-50
Δp_{B1}	-106	-106	-99	-99
Δp_{A2}	-50	-79	-79	-140
Δp_{B2}	-99	-123	-123	-190
q_{v1}	-2.3	-2.3	-2.1	-2.1
q_{v2}	-2.1	-2.9	-2.9	-4.1
C_A	0.013	0.021	0.019	0.002
C_B	0.014	0.010	0.012	0.020

The mean value of the four measurements is C_A = 0.013 and leads to the calculated R_s = 0.38 %.

The measurements carried out for the Rotary RVU are shown in **Tab. 6**. In these measurements the wheel switched off (0 rpm).

The measured value of the In-duct method with the given pressures was R_s = 0.9 % (0 rpm) as described in **Tab. 1**.

Tab. 6 – Four realistic Measurement Points (MP); Rotary RVU with APM

	MP 1	MP2	MP3	MP4
Δp_{A1}	-109	-109	-118	-147
Δp_{B1}	-194	-194	-205	-233
Δp_{A2}	-147	-99	-147	-99
Δp_{B2}	-233	-186	-223	-186
q_{v1}	-13.9	-13.9	-14.5	-16.7
q_{v2}	-16.7	-13.2	-16.7	-13.2
C_A	0.003	0.016	0.017	0.007
C_B	0.070	0.063	0.061	0.068

The mean value of the four measurements is C_A = 0.016 and leads to the calculated R_s = 0.34 %.

It is worth mentioning that in the example of this Rotary RVU, the additional air transfer ratio due to carry over is 2.5 % at the nominal wheel speed of 8 rpm. This puts the difference between the APM and In-duct method (with 0 rpm) into perspective.

4.4 Measurement Uncertainty

The measurement results were evaluated hence their measurement uncertainty, see **Tab. 7**. The declared measurement uncertainties of the single quantities are higher than the measurement uncertainty of the used measurement instruments. The reasons are effects as fluctuation and not ideal position of probes. Nonetheless, the result shows this influence is not crucial. The extended measurement uncertainty of the pressure difference is relatively high, because besides the uncertainty of the pressure probes, the setting of the pressure tabs is difficult (and will presumably differ in testing by different laboratories). The calculations were carried out with the software GUM Workbench [9].

Tab. 7 – Comparison of measurement uncertainties

C_A [(m³/h)/Pa]	In-duct	APM
Plate RVU	0.020 ± 0.002	0.012 ± 0.019
Rotary RVU	0.045 ± 0.004	0.017 ± 0.034

For the internal leakage of the Plate RVU, the high relative uncertainty of the APM is not crucial. An internal leakage of R_s = 0.4 ± 0.4 % still confirms, that this RVU is in Class C2, even if for the classification the measurement uncertainty would be added to the probable value.

Also, for the Rotary RVU a result of R_s = 0.9 ± 0.4 % (rotor speed 0 rpm) has no big impact on the classification, especially if it is considered that the carry over at nominal wheel sped has a much higher influence.

4.5 Conclusions of the APM results

In conclusion, the relative uncertainty in these examples is high, but the absolute uncertainty is in an acceptable range, at least for a first application example of the APM. It is expected that a similar absolute uncertainty would be achieved for RVUs with higher internal leakage rates which then means a lower relative uncertainty.

In a master student's project [10], some of the previous findings could be taken into account. Furthermore, an additional RVU with a different positioning of the fans was investigated. In summary, it can be said that a smaller absolute measurement uncertainty could be achieved and the APM worked with a different fan configuration.

5. Discussion

Both tested RVU's have a good tightness and thus a low internal leakage rate. In this respect, the results of the APM are promising that low leakage rates could be confirmed. Also, the results are in the range of the In-duct method. Even, the relative measurement uncertainty has been high, it has had no impact on the classification of the two investigated RVU's. Nevertheless, the APM needs some further development to reduce the measurement uncertainty. For example, testing points with supply air fan switched off (and extract air fan running) and additionally testing points with extract air fan switched of (and supply air fan running). Thus, increasing of the number of the testing points (to a total of about 10).

Also, a model with power functions for leakage air flow could be evaluated. In this project, numerical test calculations were carried out to compare the linear with an exponential function. For the performed measurements in this project the impact on the result of $\boldsymbol{R_s}$ and the measurement uncertainty was marginal.

An open question is whether all types of RVU are suitable for APM. The pressure differences during the APM could deform a sealing differently than under reference conditions. If a leakage factor is not constant, then the APM will not work.

6. Conclusion

For laboratories with tracer gas equipment, the APM will not lead to easier and faster testing; on the contrary, the In-duct method will remain more efficient. However, there are only a few accredited laboratories in Europe that have RVU testing with tracer gas in their scope. In comparison, there are dozens (if not hundreds) of manufacturers' laboratories and also independent testing bodies that do not have tracer gas equipment or do not use it in the accredited area. However, these laboratories are well qualified for pressure and air flow measurements, which are required for the APM. The main advantage of the APM is that these laboratories can achieve comparable results to the in-duct method without tracer gas measurement. In addition, the APM provides a good understanding of an RVU, as it provides information about leakage on the supply air side, leakage on the exhaust air side and the pressure distribution in the RVU.

All in all, the APM is a good first approach to determine the leakage of an RVU without tracer gas and gives the opportunity to compare the different unit types with each other. Nevertheless, more work for the further development of the test procedure and more experience is needed.

7. Acknowledgement

The HSLU and the authors would like to thank the EUROVENT Product Group Residential Ventilation Units for initiating the project, the technical exchange, and the financial support. We also thank the Swiss Federal Office of Energy (SFOE) and GebäudeKlima Schweiz (GKS) for the straightforward exchange and the financial support of an R&D project with international partners.

8. References

[1] Commission Regulation (EU) No 1253/2014 of 7 July 2014 implementing Directive 2009/125/EC of the European Parliament and of the Council with regard to ecodesign requirements for ventilation units.

[2] EN 13141-7:2021-04 Ventilation for buildings — Performance testing of components/products for residential ventilation — Part 7: Performance testing of ducted mechanical supply and exhaust ventilation units (including heat recovery). CEN, Brussels (BEL).

[3] EN 13142:2021-04 Ventilation for buildings — Components/products for residential ventilation - Required and optional performance characteristics. CEN, Brussels (BEL).

[4] Eurovent Product Group Residential Air Handling Units. Request for quotation for comparative test and analysis of internal leakages in bidirectional RVU by various test methods. Brussels. 2020.

[5] Hochschule Luzern. Prüfstelle Gebäudetechnik. Test report Nr. HP-202040-R V2. Horw (CH). 2020.

[6] Hochschule Luzern. Prüfstelle Gebäudetechnik. Test report Nr. HP-202040-P V3. Horw (CH). 2020.

[7] Huber H., Moser M. Final report Comparative test and analysis of internal leakages in bidirectional RVU by various test methods. Hochschule Luzern, Horw (CH). 2021.

[8] Richter T. Carryover in heat wheels. 2020. Available from: https://www.hoval-8energyrecovery.com/en/blog/enventus-1/carryover

[9] Metrodata GmbH. (2010). GUM Workbench Professional Version (2.4). Danish Technological Institute. Available from: http://www.metrodata.de/ver24.html

[10] Moser M. Internal Leakage in Residential Ventilation Units - Modelling and Experimental Methods. Hochschule Luzern, Horw (CH). 2021.

Data Statement

The datasets generated during the study are not

publicly available because they are still used in a research project that will be continued but the data can be obtained by a request to the authors.

Renewable energy sources used for a low energy University building

Popescu Razvan[a], Popescu Lelia[a], Catalina Tiberiu[a], Lungu Catalin[a]

[a] Technical University of Civil Engineering, Faculty of Building Services Bucharest, razvan22@yahoo.com

Abstract. Nowadays, the renewable energy sources have to be implemented in every new building. This paper describes the case study, and related simulations, of a university building in Romania, that has to become zero energy. Ground source heat pumps (GSHP) are ideal to be implemented in new buildings, being able to produce either heating and cooling. A good insulation is important too, to reduce the cooling and heating energetic needs. Asides active cooling, the passive cooling should be taken into account because it can lower the cooling consumption. For the domestic hot water (DHW), solar panels are taken into consideration to reduce at least 60-70% of the energy consumption, for DHW only. To be able to accomplish the goal of a near zero energy building, photovoltaic solar panels are taken into consideration, placed on the terrace of the building, the system being off-grid type. For all the dynamic simulations Designbuilder software was used, a powerful simulation tool which is able to model all renewable energy sources above mentioned. Also very detailed yearly energetic consumption is presented for all types of consumers from the building: heating, cooling, lighting, ventilation, heating, cooling and domestic hot water. Concerning ventilation, a recovery heat exchanger is used in simulations, having a 80% efficiency, also to reduce the energy consumption. The energy between building and heat pump is using fan coils in all the occupied areas,. Finally, regarding the results of the simulations, after a good insulation of the building and the implementation of the geothermal heat pump, heat recovery unit, solar thermal and solar photovoltaic solar panels, a zero energy building has been obtained. The simulated building had initially a poor energy efficiency, without proper insulation but also with old heating and cooling systems. For the characteristics of the soil measurements with thermal response test (TRT) method from Bucharest were used. Dynamical simulation is one of the best methods to simulate as accurate as possible energy consumption for several case studies, varying insulation type and thickness and different heating/cooling systems.

Keywords: Building simulation, Designbuilder, dynamic models, passive building, renewable sources
DOI: https://doi.org/10.34641/clima.2022.103

1. Introduction

Because of outdoor pollution and greenhouse gasses that are increasing continuously, major concern is in all the world for improvements in the building sector.

A major sector concerning energy consumption the building one, either residential or the tertiary one. Some buildings are old with poor energy efficiency, other newly constructed and better from the energetically point of view. There are many studies nowadays to improve energy efficiency, in many countries from EU [1].

Copyright ©2022 by the authors. This conference paper is published under a CC-BY-4.0 license.

In Romania for new buildings only NZEB (Nearly Zero Energy Buildings) are accepted by the authorities, since the beginning of 2021, being a novelty in the construction sector. This is the reason why studies are very important to find out optimal measures to achieve this goal. In the European Union the building sector is a very important energy consumer, having around 40% of the total energy consumption, therefore the huge interest in this area to improve energy efficiency. There are studies that show how many buildings in EU should be improved soon, to lower the energy consumption [2].

Because of the increasingly prices of fossil fuels in the last halt year, the transition to clean energy sources should be taken into consideration soon, EU would like to achieve 32% till the year of 2030 [3].

Romania is trying to achieve EU goals concerning energy efficiency by implementing NZEB in every sector of the building sector. Studies, especially dynamic simulation should show how this goal can be achieved. Renewable energy sources like geothermal heat pump, solar energy either thermal or electric ones, heat recovery units, are very important to be simulated and optimised [4-6]. Another important result that should be accomplished after building rehabilitation is to reduce CO_2 emission, being an important condition to achieve NZEB building [7]. As known, one of the most efficient type of building is the passive house [8], and maybe in the future this should be built more frequently because of its benefits. There are only some few passive buildings in Romania, in the Faculty of Building Services from Bucharest there are two passive buildings, that have been simulated in Romania as well as other climates [9]. Therefore dynamic simulation software are very important to present final or primary energy as well as renewable energy production [10].

2. Description of the case study

This paper presents dynamical simulations for a tertiary building which is located in Bucharest, capital of Romania. The activity inside the building is mainly of student activity with laboratories and offices of the teachers. A short description of the building is presented as follows:

- total surface 501 m^2;
- height regime: underground, ground floor, and 1_{st} floor;
- the building is poorly insulated not being according to the present regulations;
- the heating is produced with an old boiler and the Domestic Hot Water (DHW) with an electric accumulator;
- the cooling is produced using split type devices;
- destination: educational building with 10 permanent persons;
- Height of the building: 8m

The purpose of this research is to be able to find which are the measures to achieve a passive house using the following equipments:

- ground source heat pump (GSHP) for heating;
- passive and active cooling to obtain a low cooling load;
- photovoltaic panels to cover the electrical consumption;
- solar thermal collectors to produce DHW;
- heat recovery unit for fresh air intake.

Case study 1- initial case building

As presented briefly the building envelope need major improvement concerning energy efficiency. That's the reason why this study is very important to reduce as much as possible the energy costs after major renovation.

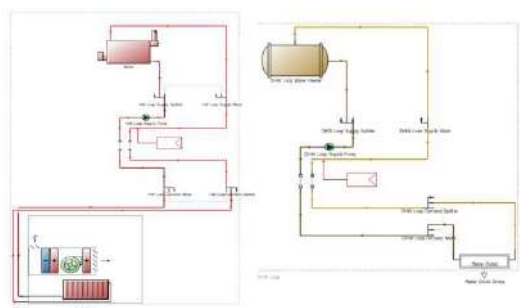

Fig. 1- Initial case with classic heating system and electric DHW

In Fig.1 the initial case from Designbuilder software is presented with an old gas fired boiler with low efficiency and radiators, and DHW production with an electric accumulator.

Case study 2- rehabilitated building using renewable sources of energy (RSE)

The building is rehabilitated by improving its envelope, implementing 30cm of insulating material (polystyrene having a thermal conductivity of 0.04 W/m K) and new windows. Also the source of energy production, cooling and heating ones are modern, GSHP type. There are two systems used in simulations for interior thermal energy distribution:

heated/cooled floor and fan coil units (FCU), the latter working when the first system can't deliver enough energy. So, passive cooling is working most of the time, with low energy consumption, and only when there are hot days (high outdoor temperature such asa 32-35°C) the active system is turned on, to achieve 26°C setup temperature inside the building during summertime (Fig.2).

For winter time, the conventional outdoor temperature is -15°C and the indoor setup temperature considered is 20°C.

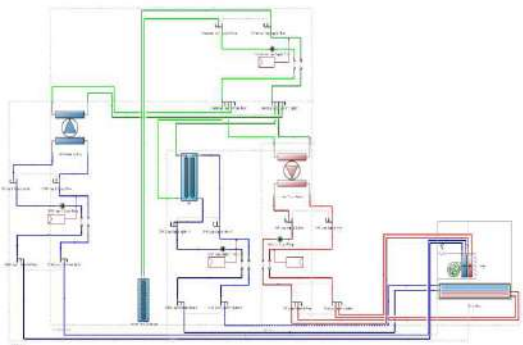

Fig. 2- Ground source heat pump with active and passive cooling

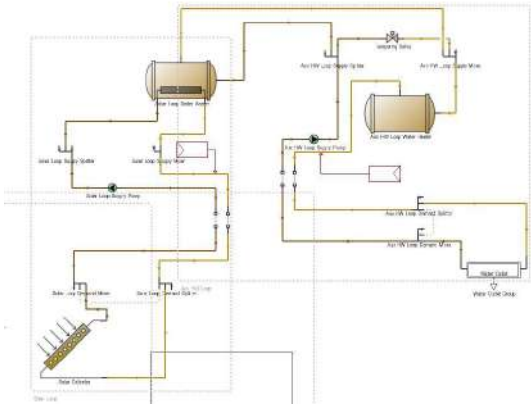

Fig. 3- Solar heating system for DHW production

In Fig. 2 we can find the representation in Designbuilder software for the active and passive cooling as well as the heating system. In Fig. 3 the representation of the solar heating system is presented, with a 3m² vacuum panel.

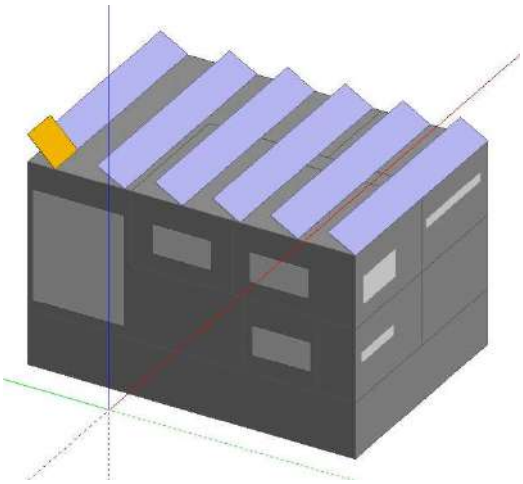

Fig. 4- Representation of the building with solar thermal and photovoltaic panels

In Fig. 4 the representation of the simulated building after rehabilitation is presented. In orange colour is the solar thermal panel, having 45° angle from horizontal plane, and photovoltaic collectors in blue colour, having 35° angle, also from horizontal plane, to achieve maximum energy production, either thermal or electrical. The photovoltaic installed power is 24,1 kW_p with monocrystalline collectors (the electric load of the building is 29209 kWh/year). To reduce fresh air heating and cooling loads, for the rehabilitated building, a heat recovery unit is implemented, with 92% efficiency, compared to the initial case that has important infiltrations, due to old windows mounted in its envelope.

The building has separate thermal zones for each office or chamber inside, with different glazing surface (a total glazing of 103 m²) and indoor temperatures. The basement is also a distinct zone, without heating or cooling for this area.

The boreholes connected to the heat pump, and simulated in Designbuilder are double U type, of 100m depth. The number of borehole needed is estimated at 7, estimation that is confirmed by Groundloop design software that is dedicated only to this kind of estimation. Also, very important parameters introduced in Designbuilder concern the soil thermal properties:

Tab. 1. Soil thermal properties [5]

Thermal properties	Value	Unit
Soil characteristics		
Conductivity	2.1	W/mK
Heat capacity	2.3	MJ/m3K
Ground temperature	10.5	°C
Ground conductivity	1.7	W/m2
Coolant properties		

Conductivity	0.36	W/mK
Heat capacity	4028	J/kgK
Density	960	kg/m3
Freezing point	-25	°C

The ground temperature is a mean value in the borehole. Designbuilder software has a library with such data.

The thermal properties of the building, are presented, for the two case studies:

Tab. 2 - Building thermal properties of the building, thermal resistance, [m² K/W]

Envelope/ R, m² K/W	Case study 1	Case study 2
Exteriour walls	0.61	10.4
Ceiling	0.81	9.6
Floor	4.23	10.2
Windows	0.5	1.2

3. Results

The results obtained by means of dynamic simulation software use are shortly presented in Tab. 3. The energy consumptions are presented in as final energy types, but also converted in primary energy consumptions, as a function of fuel type. Also the CO_2 emissions were calculated.

Tab. 3 -Energy consumption and CO_2 emissions.

	Case study 1	Case study 2
Thermal energy consumption [kWh/m² year] (1)	357.6	0
Electrical energy consumption [kWh/m² year] (2)	65.4	42.1
Conversion to primary energy Natural gas fuel (1) [kWh/ m² year]	418.4	0
Conversion to primary energy Electric energy (2) [kWh/ m² year]	171.3	110.2
Yearly primary energy consumption Total (1)+(2) [kWh/ m² year]	589.7	110.2
Primary energy economy compared to initial case [%]	-	81%
Specific CO_2 emission [kg CO_2/m² year]	79.2	3.8
CO_2 emission decrease [%]	-	95%

For the proposed scenario, the building is only using electrical energy as energy type. The results present a primary energy economy between the initial case and the final case of 81%. The carbon dioxide specific emissions were also reduced by 95%. For the final case, the photovoltaic system provides 100% annual coverage of the electric consumption. According to Romanian legislation [11], the initial case of the studied building has a "D" label for total energy consumption. After the retrofit, the building will be labelled with a total energy class "A".

An investment of 272k euro was taken into account for building's envelope and building's services rehabilitation. In Romania, starting with the 2020 year the energy market shifted from a regulated one to a liberalized one. Due to this fact, but also as worldwide energy prices incensement, the price of the kWh of thermal or electrical energy exploded. For example, the natural gas kWh price increased 4 times during the 2021 year, and higher prices are to be expected for the 2022 one. In the view of this facts, the transit from conventional energy use to renewable ones will be faster than expected. The payback time of 10 years was calculated according to Romania legislation [11], less than their life time, but this period will be significantly reduced as the energy price market is in continously increasment.

Tab. 4 - Comparison with the passive house requirements.

	Case study 2	Passive house
Yearly space heat energy demand [kWh/m² year]	12.7	15
Yearly space cooling energy demand [kWh/m² year]	6.9	15
Renewable primary energy demand [kWh/m² year]	42.1	60
Air tightness [changes/hour]	0.5	0.6
Heat recovery system, with efficiency of at least 75%	yes	yes
Mean heat transfer coefficient of windows [W/m²K]	1.11	0.80
Mean heat transfer coefficient of all opaque building components [W/m²K]	0.16	0.15
Absence of thermal bridges	yes	yes

4. Conclusions

The initial case for the studied building was poorly thermally insulated (thermal properties of the building are presented in Tab.2) and provided with high energy consumption equipments, only from fossil fuels. The total energy class of the building in accordance with the Romanian legislation for

buildings' energy efficiency [11] was label "D" for the initial case and "A" after the retrofit. Our aim was to obtain a passive building, so the passive house' requirements were considered and accomplished, as proved in Tab.4. A primary energy reduction of 81% was obtained. The final energy reduction between the initial case and the retrofit scenario was 90% and the CO_2 emissions decreased by 95%. The photovoltaic system ensure 100% of the building's electric energy consumption. So, by means of dynamical simulation an existing building was converted in a passive one provided only with "green energy".

Very important is to calculate the payback time for every investment, so also in this case. Not only energy savings are important but also economic aspect. Using the Romanian legislation [11] for building's energy performance, a payback time of 10 years was calculated. Considering that energy costs are increasing continuously, it is expected that this period of time to decrease in the future.

5. References

[1] LL. Popescu, R.S. Popescu, T. Catalina, Improving the energy efficiency of an existing building by dynamic numerical simulation, Applied Sciences Journal, 2021, 11(24), 12150;

[2] Directive of the European Parliament and of the Council COM (2016) 765 amending Directive 2010/31/EU on the energy performance of buildings, EUROPEAN COMMISSION, 2016

[3] Directive (EU) 2018/2002 of the European Parliament and of the Council of 11 December 2018 amending Directive 2012/27/EU on energy efficiency, Official Journal of the European Union, 2018

[4] LL. Popescu, R.S. Popescu, A. Damian, A. Serban, Renewable energy sources used for a low energy building rehabilitation, CIEM International Conferfence, 2021

[5] R.S. Popescu, LL. Popescu, A. Preda, K. Limam, Using a geothermal heat pump for an office building with low energy consumption, Baltica Journal, 2020, 33 (5)

[6] Marco Molinari, Alberto Lazzarotto, Folke Bjork The application of the parametric analysis for improved energy design of a ground source heat pump for residential buildings, Elsevier magazine, Vol. 63, 2013

[7] Buildings' energy efficiency measures effect on CO2 emissions in combined heating, cooling and electricity production, Petri Pylsy, Kimmo Lylykangas, Jarek Kurnitski, Renewable and Sustainable Energy Reviews, Volume 134, December 2020, 110299

[8] Passive house requirements https://passiv.de/en/02_informations/02_passive-house-requirements/02_passive-house-requirements.htm (last visited oct.2021)

[9] Passive solar house from Bucharest, https://efden.org/ (last visited oct.2021)

[10] Designbuilder software, https://designbuilder.co.uk/ (last visited oct.2021)

[11] The Law concerning the Buildings Energy Performance, no.372/2005 re-casted by the Law 101/2020, published in the Romanian Official Monitor Part I, nr.868/23.09.2020

A decision-making methodology of decarbonization for a dwelling stock in France

Tianrui Ouyang, Richard Cantin, Mohamed Elmankibi, Pierre Michel

Ecole nationale des travaux publics de l'état (ENTPE), Vaulx-en-Velin, France, tianrui.ouyang@entpe.fr, richard.cantin@entpe.fr, mohamed.elmankibi@entpe.fr, pierre.michel@entpe.fr.

Abstract. Decarbonization is a hot topic in the building sector. In response to the national ambition of carbon neutrality in 2050, a social housing company that manages about 100,000 housings in France, wants to know how to decarbonize its dwellings. This dwelling stock form a heterogeneous dynamic group with new constructions and demolitions every year. Carbon emission is mainly caused by fossil energy consumption in the building exploitation phase, especially in space heating and hot water. There are many instructions to reduce energy consumption in building exploitation phase, like the thermal insulation of building envelope, the update of equipment, the energy transition, and the sobriety of energy...But how to organize these methods to find out an optimum with the restrictions of resources? How to take the initiative in an ever-changing political and technical environment? Inspired by the discipline of "System Dynamics", we propose a methodology to represent and simulate the intricate system of the dwelling stock, to have a better insight into how the outside impacts, like the changes in policy and technological innovation, influence the inside system of the dwelling stock, and how the inside elements interact. This methodology is composed of two aspects: The typologies of housing type and the simulation of the dwelling stock. The 100,000 housing has been classed several times independently, which is quite distinct from the traditional classification method. The simulation part is carried out in the software "Vensim" and is based on the calculation method 3CL DPE. For each scenario of outside political-technical environment, we test several options to propose a suitable integration of concrete methods to decarbonize the whole dwelling stock.

Keywords. Decarbonization, dwelling stock, energy retrofit, system dynamics, typology
DOI: https://doi.org/10.34641/clima.2022.156

1. Introduction

"To achieve carbon neutrality by 2050" is an objective introduced by the July 2017 France climate plan and is enshrined in French law. The National Low Carbon Strategy (SNBC for Stratégie Nationale Bas-Carbone) [1] describes a roadmap and provides guidelines for France to enable the transition to zero net emissions. It sets out objectives for reducing greenhouse gas emissions in the short and medium term in all sectors of activity in France. For the building sector, the strategy put the "Energy Efficiency" in the first place, which implies a radical thermal renovation for the existing national housing stock, from the improvement in the performance of building's envelope to that of equipment and installation. It is also important to rely on carbon-free energy sources in the building sector and have a much greater reliance on less carbonized construction materials.

This paper focuses only on the energy efficiency, the first and the most urgent aspect in the national strategy. This translates to an acceleration of renovation in the building sector to arrive at a level in line with Low Consumption Building standards (BBC in French) [2] across the whole stock by 2050. From the aspect of Life Cycle Assessment (LCA), only the exploitation phase of dwellings is researched in this study, which means not including the embodied energy and emission in building materials.

Among all types of buildings, the social dwellings are pioneers of renovation. According to the French

Copyright ©2022 by the authors. This conference paper is published under a CC-BY-4.0 license.

climate and resilience law, it is programmed to carry out progressively the ban on the rental of high energy-consuming dwellings. In France, when selling or renting a dwelling, a Diagnostic of Energy Performance (DPE, "Diagnostic de Performance Energétique" in French) must be presented to inform the tenant of the dwelling's annual energy consumption and greenhouse gas emission. All the social dwellings are therefore classed from A to G, according to their performance grades: label A for dwellings that have the highest energy efficiency and lowest carbon emission, and label G is the worst that consumes the most energy and have the worst impacts on environment. The French climate and resilience law is translated for social housing companies to retrofit all their dwellings of label G by 2025, of label F by 2028, and of label E by 2034 [3].

A social housing company who manages about 100,000 dwellings in Paris and the parisian region, is responsive to the strategies defined in SNBC leading to carbon neutrality in 2050. The SNBC has clearly indicated the renovation objective for the whole building sector, but there is still a gap between the sectoral strategies and that for corporations. The social housing company wants to know how to do exactly to be in line with the sectoral decarbonization ambition. A decision-making tool is proposed to assist the social housing company to set guidelines to renovate their dwellings. A stock-level model is built to simulate the evolution of the dwelling stock in terms of carbon emission. It enables the policymakers to test different scenarios in terms of construction, renovation, and demolition, in order to have a better insight into the relationship between the company's strategies and that of the building sector. To subdivide and adapt the renovation strategy to different dwelling types, a dwelling-level model is proposed to complete the stock-level model. This dwelling-level sub model can calculate the carbon emission of each dwelling type defined in this study and is able to simulate different concrete retrofit scenarios, which provide, in the end, retrofit suggestions for the dwelling type given.

This study references the work of the European project TABULA EPISCOPE. The first part of this European project is to establish the TABULA concept for developing national building typologies representing the residential building stock of each country partner [4]. A calculation method focusing only on the energy use for space heating and domestic hot water is developed during the TABULA project. The follow-up EPISCOPE project aims to make energy-saving processes in the European housing sector more transparent and effective by developing targeted monitoring approaches, combined with scenario analyses and building typologies. As part of the EPISCOPE project, 40 types of buildings are proposed in France [5], each represented by an example building. For each example building, the energy performance is calculated, and two energy efficiency improvement plans of different grades are proposed. The social dwelling stock of OPHM (Office Public de l'Habitat Montreuillois) is selected to set up a pilot process in France to apply the EPISCOPE methodology [6]. The typology has been adapted to fit in the specifies of the OPHM social dwelling stock. Assumptions have been made on the rate of demolition and construction, and on the evolution of the carbon content per kWh of energy consumed. Three refurbishment scenarios have been proposed with different renovation rates to compare with the national objectives. The refurbishment scenarios proposed in OPHM study are established only from a view of the whole dwelling stock. The fact that the dwellings of different types have not been distinguished stops this study from going further to have a more detailed strategies for each dwelling type.

In response to this argument, the authors come up with this two-level model to combine the strategies for the whole stock and that for each dwelling type.

The remaining part of the paper is structured as follows. Section 2 presents the two principal aspects of the research method. Section 3 and 4 then describe in detail the two-level model, while Section 5 summarises and concludes the paper.

2. Research Methods

2.1 System Dynamics approach

System Dynamics (SD) is a computer-aided approach for strategy design, it helps people to make better decisions when confronted with complex, dynamic systems. System Dynamics aims to gain a better understanding of the structural causes of a system's behaviour, which implies an increased knowledge of the role of each element by assessing how different actions on different parts of the system influence its behavioural tendencies [7].

To model the complexity involved in housing energy and carbon emissions, the SD is an appropriate approach [8] [9]. SD approach is capable of managing processes by involving changes over time and

allowing the transmission of information to build feedbacks. SD models are able to capture multiple interdependencies.

The two-level model is carried out by the system dynamics software Vensim, which provides an effective platform for implementing SD simulations. Vensim offers 4 types of variable expressions for SD models: 1) Level variables, representing the accumulation over time of a given quantity; 2) Rate variables, the flow of quantity, representing the amount of the variation of level variables each time step; 3) Auxiliary variables, assisting the transformation of the system which can also be an indicator variable for later analyses; 4) Constant variables, which remain the same value over time.

Vensim proposes a subscription language to represent arrayed variables, it is a way to simplify the repeated parts of a model and can also make the model structure more comprehensible. Two types of simulation are used to analyse the model: "SyntheSim", running simulations on each movement of sliders, and "Sensitivity Simulations" simulating by varying parameters. The details of the simulations part will be discussed in section 3.

The construction of a SD model starts from a causal diagram which helps to represent the key elements of the system and the relationships between them [10]. For the stock-level model, the causal diagram is inspired by the real evolutional pattern of the social dwelling stock given, and for the dwelling-level model, the causal diagram is based on the French calculation method 3CL DPE [11].

2.2 Typologies

Building stock modelling usually deploys representative archetypes from building typology to obtain reliable results of energy consumption. It is found that in the French residential sector, different levels of energy consumption are related to socio-economic, dwelling, and regional characteristics [12]. The dwellings of this social dwelling stock have the same regional characteristics and the households of these stock have almost the same socio-economic characteristics. Therefore, only the characteristics related to dwelling, combined with the energy carriers type in considering the liaison between the energy consumption and the GES emission, will be considered in this paper to define the building archetypes. Previous TABULA studies define archetypes by the physical characteristics of buildings. These archetypes, however, have not been integrated into the building stock modelling and have no direct relationship with the stock's energy and GES emission result. The new classing method is proposed here to help in connecting the GES emission of the entire dwelling stock and that of a dwelling type under different retrofit scenarios.

Tab. 1 – Four categories defined in stock-level sub model

Categories name for short	Corresponding DPE labels	Carbon emission range (Kg CO2eq/m2.an)	Current company policies
AB	A and B	x <=11	Not to have efficiency retrofit for the dwellings of label A and B before 2050
CD	C and D	11< x <=50	-
E	E	50< x <=70	Refurbish all the dwellings of label E by 2030
FG	F and G	x > 70	Refurbish all the dwellings of label F and G by 2025

In the stock-level sub model, the dwelling stock has been classed into four categories (shown in **Tab.1**), according to their energy-environment label (DPE), to integrate the current national energy-environmental policies. The latest version of DPE, which has been implemented since the 1st July 2021, is applied in this research. The potential rescaling of DPE labels due to the future legislation is not considered in this study.

And in the dwelling-level sub model, all the dwellings have been firstly classed by their envelope performance and then classed by their type of system and equipment. With the basic information of a building's envelope, the heat loss can be measured by applying a simplified 3CL method. A threshold is set to identify the high-performance envelope and that which need to be retrofitted. The two categories defined according to the performance of building's

envelope in the dwelling-level sub model is showed in **Tab.2**.

Tab. 2 – Two categories defined by the performance of envelope in the dwelling-level sub model

Nb. of category	Explication of categories
1	The envelopes of dwellings are not suggested to be retrofitted by 2050.
2	The envelopes of dwellings are suggested to be retrofitted.

Meanwhile, the dwellings are classed by their types of energy carrier and that of system and equipment for space heating and domestic hot water. According to the database of this social housing company,13 categories have been found in this stock. They are listed in the **Tab. 3**.

Tab. 3 -Thirteen categories of the system aspect in the dwelling-level sub model.

Nb. of category	Space heating	Domestic hot water
1	Urban heat, collective	Urban heat, collective
2	Urban heat, collective	Electricity, individual
3	Urban heat, collective	Natural gas, individual
4	Natural gas, collective	Natural gas, collective
5	Natural gas, collective	Natural gas, individual
6	Natural gas, individual	Natural gas, individual
7	Natural gas, collective	Electricity, individual
8	Natural gas, individual	Electricity, individual
9	Electricity, collective	Electricity, collective
10	Electricity, collective	Electricity, individual
11	Electricity, individual	Electricity, collective
12	Electricity, individual	Electricity, individual
13	Electricity, individual	Natural gas, individual

3. Stock-level sub model

The stock-level model gives a general orientation and the overall goal for the dwelling stock renovation. The objective of this sub-model is to find out how to manage and renovate the different type of dwellings, from A to G, to be in line with the BBC standards, which is indicated in SNBC. The model calculates the total emission of all types of dwellings under different scenarios, and to come up with renovation suggestions for each type.

3.1 from the causal diagram to model

The model construction starts from the causal diagram. **Fig. 1** shows the causal diagram of the stock-level sub model. The social dwelling stock is divided into two parts: the existing dwellings built before 2020 and the new dwellings built after 2020. The existing dwellings which have been refurbished are distinguished from those to be refurbished on account of the dwellings' performance improvement. In addition to the process of refurbishment, the dynamic of the existing dwelling stock is influenced by the acquisition, the demolition, and the selling. The total carbon emission of this stock depends both on existing dwellings and new dwellings.

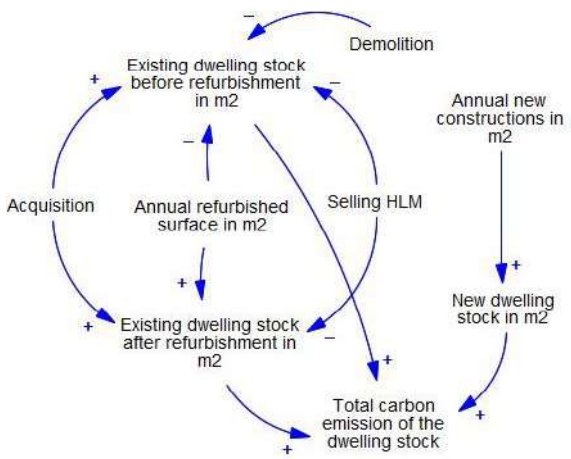

Fig. 1 – causal diagram of stock-level sub model

3.2 The stock-level model and variables

The diagram is then enriched by integrating the typology of dwellings to build a stock-flow model. The time of the model is set from the year 2020 to

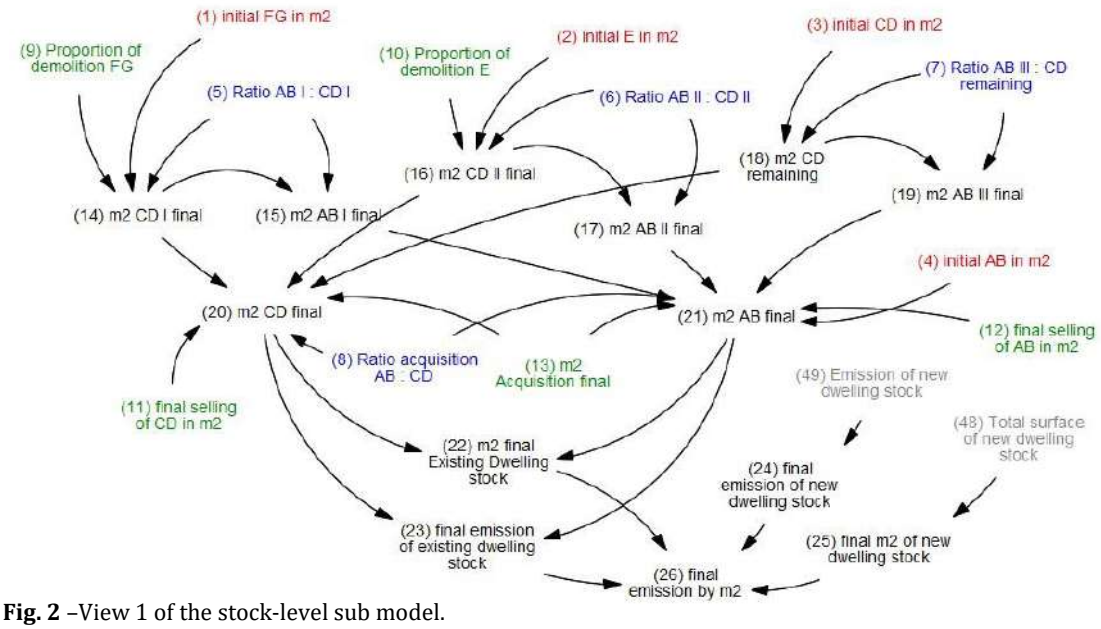

Fig. 2 –View 1 of the stock-level sub model.

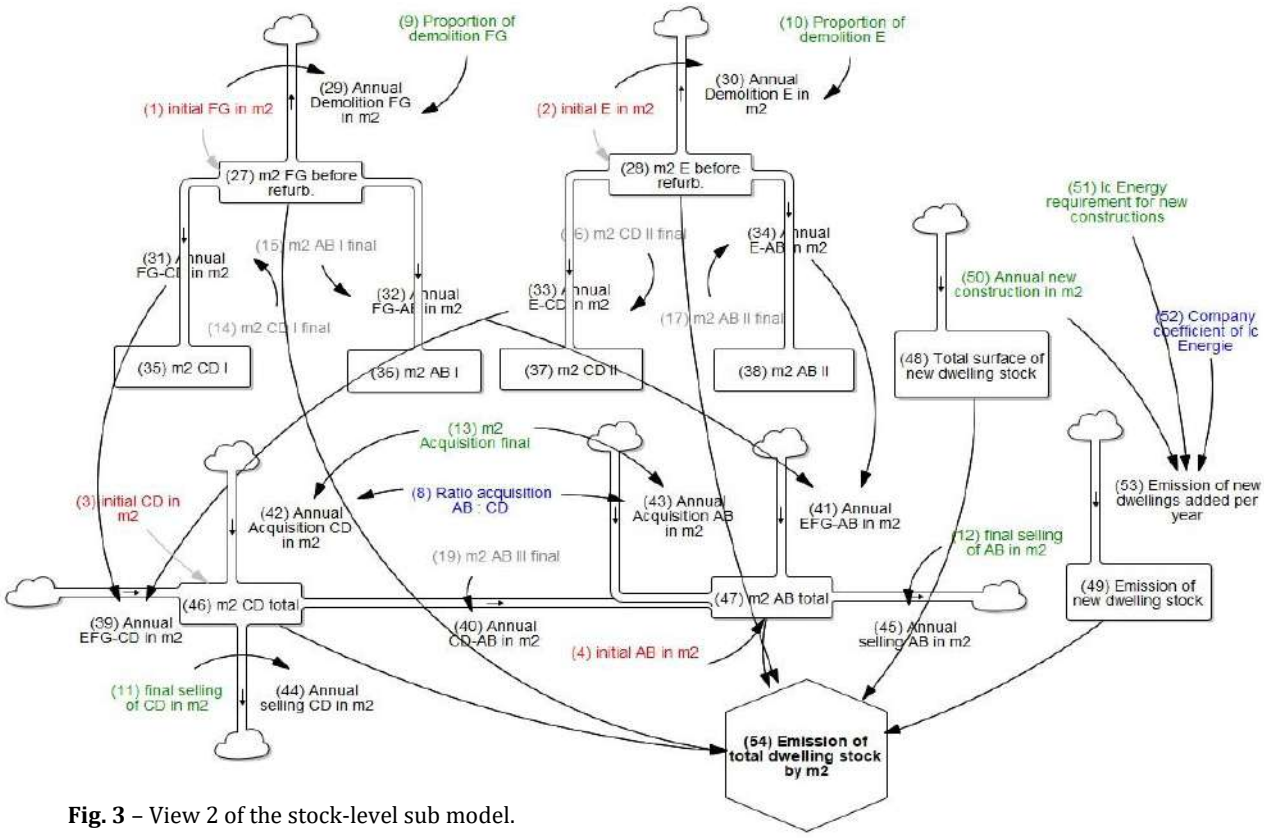

Fig. 3 – View 2 of the stock-level sub model.

2050. This model is made up of two views: The view 1(shown in the **Fig. 2**) describes the final projected state of the dynamic dwelling system in 2050, while the view 2 (shown in the **Fig. 3**) displays a constantly changing system from the year 2020 to 2050. These two views are connected by the duplicate variables, which are black in one view and turn to grey in the other view. The variables in red are input data, they are unchangeable constants whose values do not change over time. The variables in green and blue are also constant variables, but their values can be modulated according to different political scenarios. The blue variables depend only on the company's internal decisions, while the green variables can be influenced by external policies as well.

The variables (1)(2)(3)(4) represent respectively the initial dwelling surface of category FG, E, CD and AB. The data is available in the company's database.

The variables (9) and (10) are in the form of percentage, they represent the proportions of demolition in the categories FG and E.

The variables (14)-(19) are the final dwelling surface of each type refurbished by 2050. They are distinguished by their initial performance category and also by their final category after refurbishment.

The variable (20) represents the final dwelling surface that enters in CD category after retrofit by 2050, and (21) is the final dwelling surface that enters in AB category after retrofit by 2050.

The variables (11)(12)(13) represent the final acquisition and selling surface of the stock by 2050.

The variables (5)(6)(7)(8) represent the ratio of AB dwellings' surface to that of CD dwellings. The sliders are created for these variables to generate different internal political scenarios. For example, the increase of (5) can reflect the increase of FG dwellings entered in AB category after retrofit, which means the company has a greater ambition in the FG dwellings' performance improvement. And for the variable (8), its increase results in the increase of the AB acquisitions, which means the company tries to get more AB dwellings from outside.

The variable (50) is the annual new construction surface from 2020 to 2050, which can be influenced by external sectorial politics and companys' internal decisions. The variable (48) is the integral of (50), it represents the total surface of all the new dwellings built after 2020.

The variable (51) is the environmental requirement settled for new constructions by the national legislations. Scenarios can be generated to test the varies tendencies of future requirements. The variable (52) is an internal coefficient depending on the company's decision. It is the ratio between the company's internal carbon requirement for new buildings and that of the national requirement. The added carbon emission to the new dwelling stock per year (53) is then calculated by (53) = (50)x(51)x(52).

3.3 Scenario analysis and simulations

The variable (52) is chosen to demonstrate the first step of the model analysis. The value range of this variable is set from 0.1 to 1. When the value is equal to 1, the company's internal carbon requirement has the same maximum threshold as the national requirement. And when the coefficient (52) is set to 0.1, the threshold defined by the company is one-tenth of that defined in national strategies. Three different values (0,3 0,5 and 0,7) have been tested for the coefficient (52) in the displayed simulations. Three different curves are then generated to show the variation of the variable (54) due to the three values of (52). The variable (54) is an observation object in this model.

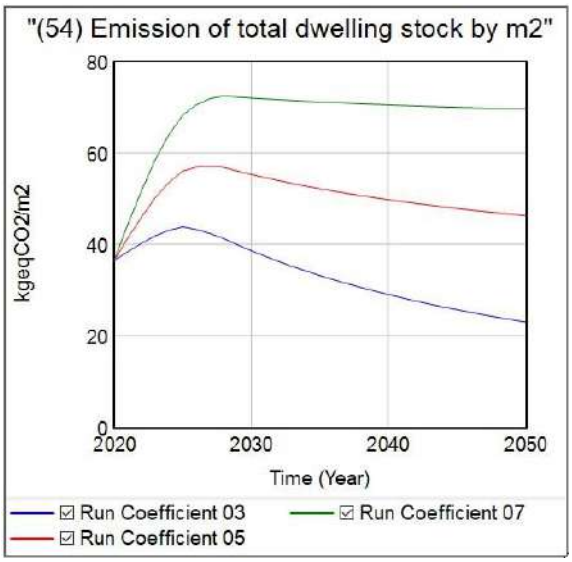

Fig. 4 – Three simulations of different coefficient values

Fig. 4 shows the three simulations**.** It is observed that the coefficient (52) is influential to the target variable (54), and a great difference of the stock emission in 2050 can be observed when the coefficient changes from 0.3 to 0.7.

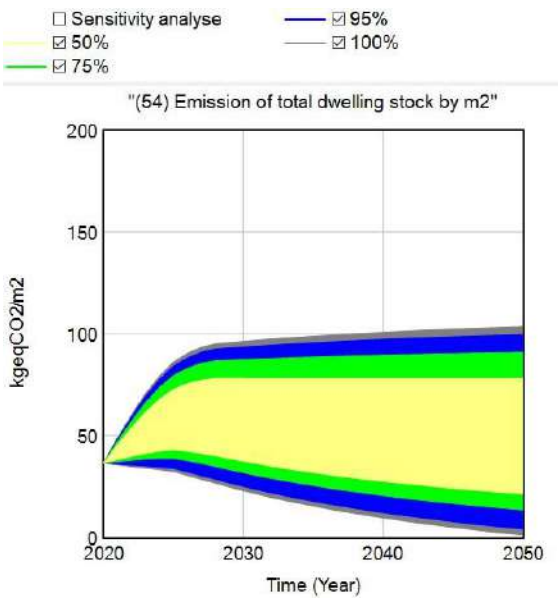

Fig. 5 - Sensitivity analysis.

A sensitivity analysis was then lanced to find out the value range of the target emission (54) when the coefficient (52) varies between 0.1 and 1. The value range of (54) from the year 2020 to 2050 is shown in the **Fig.5**.

It is found that the emission of dwelling stock is sensitive to the coefficient (52). For the further research, it is suggested to reduce the interval of scenarios to test more values between 0.1 and 1.

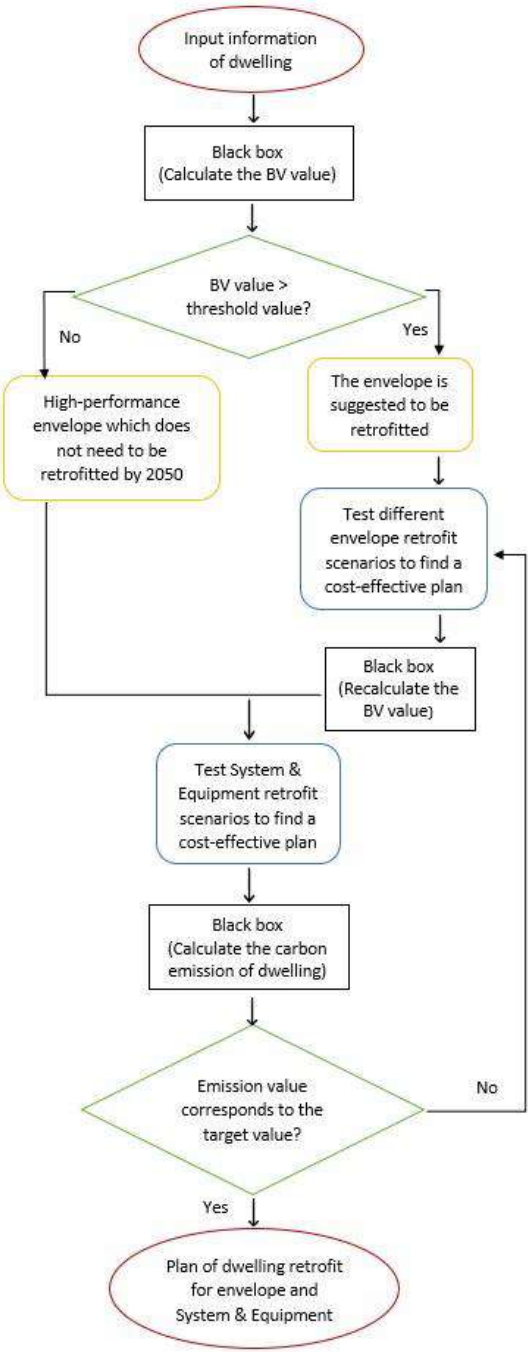

Fig. 6 – Using steps of the dwelling level decision-making tool

4. Dwelling-level sub model

The dwelling-level sub-model gives retrofit suggestions for a dwelling. For example, if the stock-level sub-model suggested refurbishing all the E dwellings into AB dwellings, the dwelling-level sub-model will indicate how to retrofit from E to AB for each dwelling type (in terms of envelope and equipment).

This sub model, which is based on the 3CL method, can be seen as a calculation engine, but more than a calculation engine. It also provides a functioning to test the options of retrofit methods to find the best solution.

Many hypotheses have been made to simplify and adapt the 3CL method to different type of dwellings. To justify theses hypotheses and to calibrate this model, the calculation results of the model is compared to the carbon emission value indicated in the DPE label.

The flow chart **Fig.6** demonstrates the steps of using this decision-making tool. The first step is to collect the dwelling data from the aspect of envelope and that of system and equipment. These data are then input into the model to calculate the BV value. BV is an intermediate variable defined by the 3CL method. It represents the monthly home heating requirement of a dwelling and can reflect the performance of building's envelope. The obtained BV value is then compared with a predefined threshold value to see if the envelope needs to be retrofitted or not. If yes, different envelope retrofit scenarios can be tested to find out an appropriate envelope retrofit plan. And meanwhile, the BV values of different scenarios have been recalculated. The same process is for the system and equipment aspect. The two scenario tests can be repeated to find out an appropriate retrofit plan, for a given dwelling type, to meet the target emission value.

5. Conclusions

This paper presents a new decision-making tool to help a social housing company make strategies in response to the national emission ambition. The model tool is built by using the system dynamic approach, which helps to represent, simulate, and analyse the carbon emission of the social dwelling stock in France. A new class method is proposed not only to distinguish different types of dwellings by their characteristics but also to match with the

current sectoral politics. The model tool is composed of two parts: the stock-level sub-model for a big scale and the dwelling-level sub-model for a dwelling-scope simulation. The two sub-models cooperate to offer a more comprehensive analysis of the dwelling stock. The next stage of the research is to generate appropriates scenarios of renovation for the scale of the stock and for each concrete dwelling type. After the identification of theses scenarios, the process of analysis can be conducted by comparing the simulation results of each scenario, to propose suggestions for the renovation strategies.

6. Acknowledgement

The authors would like to express their gratitude to the funding agency ANRT (for "Association Nationale Recherche Technologie" in French) and the Région Auvergne-Rhône-Alpes for their financial contributions to this CIFRE project. The authors would also thank their cooperative partner, the social housing company, who proposes the experimental subject along with abundant data to this project and contributes to the research funds.

References

[1] National low carbon strategy. Ministère de la transition écologique [on line]. March 2020. Update May 5th, 2021. Available at: https://www.ecologie.gouv.fr/strategie-nationale-bas-carbone-snbc

[2] Règles Techniques des bâtiments rénovés – BBC effinergie Rénovation® et effinergie Rénovation®. October 1st, 2021.

[3] Loi climat et résilience : l'écologie dans nos vies. Ministère de la transition écologique [on line]. July 20th, 2021. Available at: https://www.ecologie.gouv.fr/loi-climat-resilience

[4] Loga T., Stein B., Diefenbach N. TABULA building typologies in 20 European countries—Making energy-related features of residential building stocks comparable. Energy and Buildings. 2016 ; 132:4-12

[5] Rochard U., Shanthirablan S., Brejon C., Château le bras M. Bâtiment résidentiels – Typologie du parc existant et solutions exemplaires pour la rénovation énergétique en France. 2015.

[6] Rochard U., Shanthirablan S. National report on pilot actions. November 2015.

[7] Garcia J. Theory and practical exercises of system dynamics: cases and basic examples in industry, environment, business and research. May 2020. ISBN: B08BDK5431

[8] Oladokun M., Aigbavboa C. 2018. Simulation-based analysis of energy and carbon emissions in the housing sector: a system dynamic approach. Switzerland: Springer International Publishing AG part of Springer Nature. ISBN 978-3-319-75345-4

[9] Oladokun M., Motawa I., Banfill P. 2012. Modelling techniques for capturing the socio-technical aspects of sustainability in post-occupancy stage of buildings. Retrofit Academic Conference 2012 Project: Socio-technical systems of household energy.

[10] Bala B., Arshad F., Noh K. 2017. System dynamics: modelling and simulation. Singapore : Springer Nature. ISBN 978-981-10-2043-8

[11] Arrêté du 8 octobre 2021 modifiant la méthode de calcul et les modalités d'établissement du diagnostic de performance énergétique – annexe 1 méthode de calcul 3CL-DPE 2021 (Logements existants). Légifrance – Le service public de la diffusion du droit [on line]. October 2021. Available at: https://www.legifrance.gouv.fr/jorf/id/JORFTEXT000044202205

[12] Hache E., Leboullenger D., Mignon V. Beyond average energy consumption in the French residential housing market: A household classification approach. Energy Policy. 2017; 107:82-95

Data Statement

The datasets analysed during the current study are not available because of the confidentiality agreement with the social housing company, but the authors will make reasonable effort to publish part of them in near future.

Characterization of a Constant Air Volume (CAV) Box Based on Measurements

Zakarya Kabbara [a], Sandy Jorens [a], Bert Belmans [b], Ivan Verhaert [a]

[a] Faculty of Applied Engineering, Department of Electromechanics, University of Antwerp, Belgium, Zakarya.kabbara@uantwerpen.be

[b] Faculty of Applied Engineering, Department of Civil Engineering Technology, University of Antwerp, Belgium

Abstract. HVAC engineers are frequently challenged to design and operate ventilation systems with a high standard of performance considering comfort, energy efficiency, and indoor air quality. However, currently, most design, commissioning and control processes of ventilation systems rely on rules of thumb and engineers' experience. A simulation-based framework for informed decision-making could be an effective tool to achieve ventilation systems with optimal design and performance. To develop such a framework, the integration of solid component models that provide insight into the system's aeraulic behavior is vital. In previous research, a simulation framework known as Air Distribution Network Design (ADND) optimization algorithm was developed. The ADND algorithm provides a basic strategy to design centralized air distribution networks. However, the method is missing some features before it can be used in practice. Currently, the method is limited to generating layout by accounting for the ductwork only. Some ventilation system components (e.g., CAV control box) are not yet integrated. This paper presents the development of a new CAV control box model that is typically used in nonresidential buildings, viz., a mechanically controlled damper that maintains airflow to a predefined fixed airflow level. The model aims to predict the aeraulic performance of the control box at any given inlet volumetric flow rate and set airflow rate (i.e., the airflow index at which the CAV box is commissioned to maintain the flow) for diameters between 125 and 250 mm. First, lab setups were built to measure pressure drops for different CAV diameters by varying the inlet airflow rates and set airflow rates. Next, the measurement data was used to develop a model of the CAV control box by training a regression model. Finally, the model was tested and validated on experimental data that was not used in the training set. The accuracy of the CAV box model justifies its integration into the ADND algorithm and also its potential to be integrated into common building simulation frameworks. Once integrated, it can be exploited in many applications, including evaluating the performance of designs, automating the iterative balancing process, and optimizing the control strategy of ventilation systems.

Keywords. Mechanical Ventilation, Constant Air Volume (CAV) box, CAV systems, Simulation Framework, Design optimization
DOI: https://doi.org/10.34641/clima.2022.157

1. Introduction

1.1 Overview

Nowadays, HVAC engineers are challenged to design and operate ventilation systems with a high standard of performance concerning comfort, energy efficiency and indoor air quality (IAQ) at minimal expenses (i.e., material, installation and maintenance costs). However, most of these features contradict; for example, achieving the desired IAQ, i.e., CO2 levels, is usually reached by increasing the supply and/or extract airflow rates, which concurrently increases the energy usage and sound levels. This illustrates that achieving an optimal design and system operation can be complex. Consequently, design and operation decisions still often rely on rules of thumb [1,2]. Therefore, a method supporting and guiding engineers in designing, commissioning, and controlling ventilation systems would be desirable.

Previous research developed an optimization method for Air Distribution Network Design (ADND) [1,3]. This method can quickly generate numerous different air distribution system configurations (i.e., ductwork layout and duct sizes). The method provides a basic strategy to generate optimized air distribution network designs for nonresidential buildings. Although the ADND optimization method

Copyright ©2022 by the authors. This conference paper is published under a CC-BY-4.0 license.

results in promising outcomes, some additional features are required before it can be used in practice. Currently, the method is limited to generating layouts by accounting for ductwork only. Ventilation system components (i.e., diffusers, silencers and volume flow controllers) are not yet included in the ADND method [1,2]. Implementing all existing ventilation components to the ADND algorithm devotes the potential for further design optimization.

To integrate the missing components in the ADND algorithm, it is essential to have aeraulic models for every component that may exist in the ductwork. These component models should predict the pressure drop as a function of airflow rate by allowing input for all the parameters that may affect the aeraulic performance of the component (e.g., inlet and outlet dimensions in case of a transition or bend angle in case of a bend). Most of these component models exist in literature, design standards, building simulation frameworks or are provided by the manufacturer [4,5]. However, some component models solely exist at a high abstraction level, while others do not exist at all. Therefore, they cannot be integrated into the ADND optimization algorithm as they cause performance inaccuracies. One of these components is the Constant Air Volume (CAV) box.

Several CAV box types are used in practice. Some of them are inserted inside the ducts Fig 1-B. These types of CAV boxes are often used in residential buildings as they are only suitable for low velocities and small sizes. However, the ADND algorithm is still limited to designing air distribution systems in nonresidential buildings. The CAV box that is typically used in nonresidential buildings is the one having a blade and control mechanism presented in Figs 1-A and 1-E. It is inserted at both sides into a round duct for easier installation and maintenance. This CAV box can have several control settings depending on the manufacturer (Figs 1-C and 1-D), but always the same controller structure and function (i.e., blade type and spring connection). This paper focuses on developing a CAV box that is often used in nonresidential buildings.

1.2 CAV Mechanism

A CAV control box ideally maintains the passing volumetric flow rate at a predefined fixed level, independently of the pressure variation upstream or downstream in the air distribution network. In practice, this can be achieved to a certain extent by respecting the minimum and maximum pressure difference over the CAV box. The CAV box is a mechanically self-powered unit that controls airflow by setting an external controller assembly mounted on the CAV (Fig 1-C-D). The control assembly provides an index for the range of airflow rates (i.e., Qsets) that the CAV box can maintain to achieve the demand flow. The desired flow rate is usually set while commissioning the air distribution system.

In a random hydraulic component, the flow rate is directly proportional to the square root of the pressure drop. Thus, the flow rate increases with the pressure drop and vice versa. To achieve a fixed flow rate for a range of pressure variations over the inlet and outlet of the CAV box, the blade inside the CAV box should close when the inlet pressure is high and vice versa. This is achieved by the blade shape presented in Fig 1-F. Due to the bend shape of the blade, the blade is dragged to a more closed position at higher inlet pressure, reducing the opening area and flow rate. A spring provides a counterforce to regulate the opening position according to certain inlet pressure. At lower pressures, the spring pushes the blade back to a more open position.

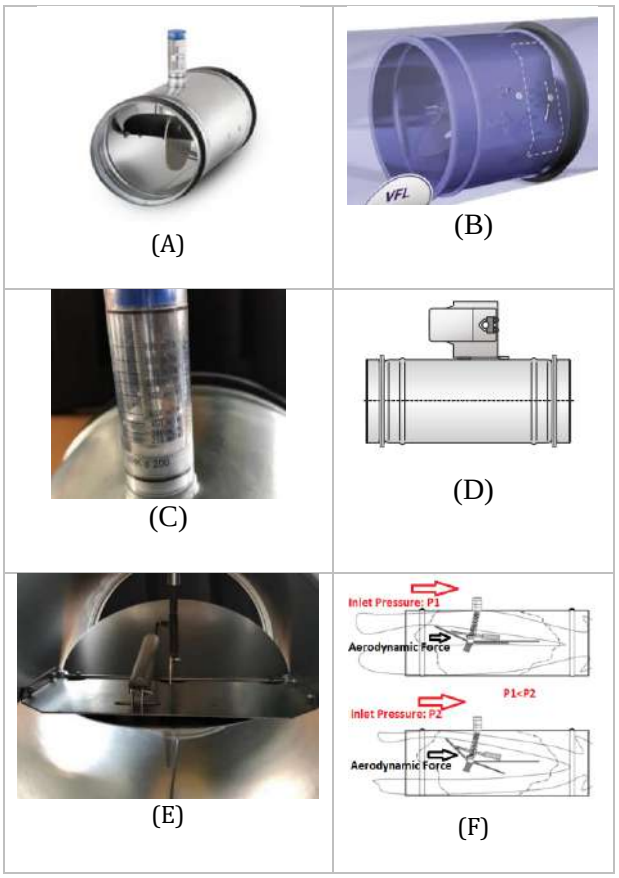

Fig. 1 - : (A): Nonresidential CAV box (B): Residential CAV box (C-D): Two different CAV Controller Assemblies (E): CAV blade with a spring attached; (F): Aerodynamic force sketch [6].

Considering physical limitations, in general, the CAV has three working areas. At low inlet pressure, the CAV is almost fully open, and the flow rate is directly linked to the available pressure drop. At very high inlet pressure (typically beyond the operational limit), uncertain behavior of the airflow vs. the pressure drop occur due to the developed vortices (more explanation in section 3.2). In between these limits, the maintaining phase occurs where the airflow rate is ideally fixed.

1.3 State of the Art

Some ventilation components' manufacturers

provide the CAV box's aeraulic curve models (i.e., airflow rate vs pressure drop curve) [7]. However, those curves describe the CAV box's performance only when the box is operating at the maintaining phase. Nevertheless, the transition phase (the phase at low-pressure drops before the maintaining phase) is not included in the curves. Furthermore, the curves are averaged for several diameters for every Qset. This leads to imprecisions when determining which pressure drop is required to maintain a particular airflow rate (Fig 2). The imprecisions of averaging the curves were proven by experimental measurement (graphically presented in sections 2 and 3); while changing the diameter of the CAV box and commissioning it at the same Qset, the pressure required to maintain the airflow rate is different for every diameter. For example, considering a Qset=250 m^3/h, the airflow is maintained for a CAV box diameter of 160mm when the pressure drop is 50 Pa. On the other hand, for a diameter of 200mm, the airflow is not maintained until reaching a pressure drop of 75 Pa. Consequently, this will affect the aeraulic performance assessment of the ADND algorithm and, therefore, the design decisions.

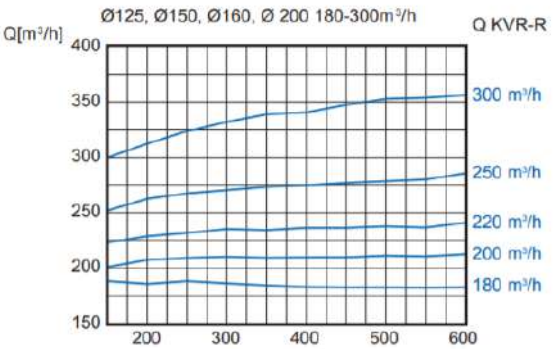

Fig. 2 - Airflow rate vs pressure drops for diameters 125, 150, 160, 200 and airflows between 180 and 300 m^3/h [7].

CAV boxes are often used in CAV ventilation systems, where the system supplies a constant airflow rate at variable temperatures [8]. Therefore, a CAV damper that maintains the airflow at a specified airflow rate is implemented in common building simulation frameworks (i.e., EnergyPlus [9]). However, the damper models do not allow to exceed their maximum set airflow rate (i.e., Qset) [9]. Ideally, this is how CAV boxes are meant to perform. Therefore, the common simulation frameworks assume ideal CAV box performance. However, manufacturers declare that there might be an airflow rate deviation of $\pm 10\%$ in the stable control range (i.e., maintenance range) [10,11].

Furthermore, CAV boxes can also operate with partial load behavior in practice. For example, during the daytime, the building is fully occupied; thus, the system operates at full load; nevertheless, at night, the building is almost unoccupied; thus, the system operates at partial load. Such a system is still a CAV system with two operating modes (i.e., day and night modes). Moreover, CAV boxes are also used in variable air volume (VAV) systems, where partial airflow behavior or demand-controlled ventilation occurs (i.e., Building Z – UAntwerpen, Belgium). In the same VAV air distribution system, there might be rooms with a VAV box as a volume flow controller and other rooms with a CAV box volume flow controller. For example, considering a VAV system, VAV boxes (i.e., automatically adjusted dampers) are installed to control the airflow in rooms with unstable occupancy behavior (e.g., meeting rooms) by controlling the damper position and the AHU fan. On the other hand, the CAV boxes are installed in the system for rooms with a stable demand profile (i.e., storage rooms), as they are much cheaper than the VAV boxes. Nonetheless, the CAV box model developed in the common simulation framework cannot operate in partial load behavior or a VAV system. For instance, in EnergyPlus, the CAV box, which is categorized under the terminal components (i.e., Air:Terminal:SingleDuct:ConstantVolume:NoReheat), is not allowed to be implemented in a system with a variable airflow fan [9]. However, an alternative for a CAV box in a VAV system used by design developers is a VAV box with a constant flow control signal to maintain the airflow rate. Although the alternative is meant to control airflow rate, it does not have the same aeraulic performance because CAV and VAV boxes have different mechanisms. Therefore, integrating the CAV box model of the common simulation frameworks or its alternative during partial load behavior in the ADND algorithm leads to an inaccurate aeraulic performance and defect in the design optimization potentials. The desired CAV model to be integrated into the ADND algorithm should estimate the aeraulic performance (i.e., pressure drop vs. airflow rate) for all available sizes and Qsets within the operational limit, i.e., low-pressure phase and intermediate pressure phase or maintaining phase.

1.4 Aims and Objectives

Since no CAV box model is compatible with the ADND algorithm, a CAV box model that can mimic the aeraulic performance of a real CAV box is needed mainly to be integrated into the ADND algorithm for further optimization. This model will also be useful for integration into common simulation frameworks to make better aeraulic performance predictions than with existing models.

In this paper, a model for the CAV box that is typically used in nonresidential buildings is developed to determine its aeraulic performance for any given Qset of the CAV box diameters between 125 and 250mm. Lab setups for three CAV boxes with three different diameters (i.e., 125, 160, and 200 mm) were constructed at the HVAC Lab – University of Antwerp. First, pressure drop and airflow rate measurements were collected, as discussed in section 2.1. Next, airflow rate vs. total pressure drop curves for the three CAV boxes at every airflow rate index (i.e., Qset) were fitted to the collected measurements, as discussed in section 2.2. Curves fitting was only applied to the collected measurements for the three

tested diameters (results are presented in section 3.1). However, it allowed the generation of enough data to train an artificial neural network (ANN) regression model that can predict the aeraulic performance (i.e., total pressure drop vs. airflow rate and vice versa) of any existing CAV box with a particular diameter and Qset range. An ANN regression model was used due to uncertainty on the CAV box aeraulic performance. Simply interpolating and extrapolating between the fitted curves proved to be less accurate than the ANN predictions, especially when extrapolating to a CAV box with a different diameter. Further explanation of why ANN was the chosen approach to develop the CAV model is presented in section 3.2. The results, validation, and discussion on the application potential are included in section 3.3.

2. Methodology

2.1 Experimental Measurements

The American Society of Heating, Refrigerating and Air-Conditioning (ASHRAE) standard [12] is used to measure the pressure drop of the CAV box and the volumetric flow rate in the branch with the CAV box. The performed setups for the three CAV box diameters follow the description of duct mounted fitting test setup [12,13] where,

- The distance before the fitting is at least 4.6m to achieve a fully developed flow. For the CAV setups, the distance before the CAV box was at least 6 m.
- The total pressure drop is measured at a distance of $(1.5 \pm 0.5)D$ upstream (i.e., before the CAV box) and $11D$ downstream (i.e., after the CAV box), where $D = diamter\ of\ the\ inlet\ duct = diameter\ of\ the\ outlet\ duct$. The pressure difference upstream and downstream is the sum of the total pressure drops from the CAV box and the duct parts between the upstream and downstream measuring points.
- The air velocity measurement plane is at least 7.5 diameters downstream. Fig 3 represents the measurements locations per diameter. A volume flow hood was placed at the terminal of each test setup to ensure the velocity measurements. Therefore, the velocity and the airflow rate measurements are expected to match.

The measuring instruments and their accuracy are presented in Tab. 1.

Tab. 1- List of Instruments

Type-of measurements	Instrument	Error	Serial Number
Multi-function measuring instrument, which was used for pressure and velocity measurements		± (0.3Pa + 1%)	0563 4800
Pressure		Follows the multi-function measuring instrument	0635 2045
Velocity		± (0.2m/s + 1%)	0635 9542
Volume flow rate		± 3%	0563 4200

2.2 Data Augmentation

Experimental setups were created on three CAV boxes with 125, 160, and 200mm diameters to develop an empirical CAV model that can predict its aeraulic performance at any given diameter and Qset. For each diameter, 7 to 8 Qsets were tested. For each Qset, at least eight airflow rates and total pressure drop measurements must be taken, according to ANSI/ASHRAE standard 120-2017 [12].

After measuring the data, one way to develop the CAV model would be by interpolating and extrapolating the available measured data to determine the aeraulic performance at any given diameter and Qset. Several input parameters may affect the aeraulic performance of the CAV box (i.e., airflow rate, pressure, diameter, Qset). Interpolation and extrapolation can be performed to estimate the aeraulic performance by following the existing trend of measured data. Interpolation and extrapolation can only be valid to know the aeraulic performance between two measured points having the same diameter and Qset. However, interpolating and/or extrapolation between points having different diameters and/or Qsets results in an inaccurate output due to the CAV box uncertainty in the aeraulic performance. For example, the CAV box of 200mm with Qset= 300 m^3/h had eight measured points (airflow vs. pressure drop); interpolating between

the eight measured points to determine the airflow vs. the pressure drop can give an accurate result. However, extrapolating to an unmeasured diameter (i.e., 250mm) to determine aeraulic performance results in inaccurate outputs due to the CAV box uncertainty. Section 3.2 presents the CAV box's aeraulic performance uncertainties and justifies why interpolating and extrapolating between the measured data is inaccurate. To overcome the uncertainties, curves are first fitted to the measured data to generate enough data to train a regression model. The fitted curves are shown in Figs 4, 5, and 6. An accurate correlation that can describe the equation of the measured data is equation 1.

$$Q = A + (B \times PD) - Ce^{-D \times PD} \qquad \textit{Equation 1}$$

Where Q is the airflow rate [m^3/h], PD is the pressure drop [Pa], A, B, C, and D are coefficients that are estimated for each curve using the curve_fit function from the SciPy library on Python [14]. The R squared value for every fit is estimated to indicate how well the curve fits the measured data. The closer the R squared value to 1, the more accurately the curve is fitted to the data. Although the R squared function can also be imported from the scikit-learn library [15] in Python, its correlation is presented in equation 2.

$$R^2 = \frac{\Delta mean - \Delta fitted\ curve}{\Delta mean} \qquad \textit{Equation 2}$$

Where $\Delta mean$ is the variation around the mean, which is the sum of the square differences between the actual measured values and the mean. $\Delta fitted\ curve$ is the sum of the square differences between the actual measured value and the predicted ones from the fitted curve.

After fitting the curves to the measured data, enough data can be generated by implementing parameters into equation 1. The generated data is used to train an ANN model to predict the aeraulic performance of the CAV box, given its diameter and Qset. The model prediction is expected to be accurate even when inputting different diameters (e.g., 250mm) and Qsets than those used for training. The diameters and Qsets that were used for training are presented in Table 2.

2.3 The ANN Model

ANN has been an attractive tool for solving nonlinear problems [16], making it suitable to describe the nonlinear performance of the CAV box. ANN learns from the data provided, i.e., training dataset. The training dataset for the CAV box model is the measured data (section 2.1) and the expanded data (section 2.2). The input parameters for training the ANN regression model are the diameter of the CAV box, Qset, and the total pressure drop. The output of the model is the airflow rate. Besides, ANN can deal with uncertainties, which are discussed in section3.2.

3. Results

This section presents the outcomes of the curve fitting of the measured data in section 3.1. Then, the fitted curves are used to generate more data (as discussed in section 2.2) to train an ANN regression model, i.e., the CAV box model that predicts the aeraulic performance given at any given diameter and the Qset of the intended CAV box. Before reporting the model results, some measurement observations and the reason for using the ANN regression model is used are presented in section 3.2. Finally, the trained CAV model results and the model validation are presented in section 3.3.

Fig. 3 - Experimental setup – UAntwerpen HVAC Lab

3.1 Curve Fitting

The minimum and maximum R squared of the fitted curves are presented in table 2.

Tab. 2 - R squared outputs for the fitted curves

CAV Diameter (mm)	Qset [m³/h]	R squared
125	125, 150, 175, 200, 225, 250, 280	Min = 0.9926 Max = 0.9989
160	180, 200, 250, 300, 350, 450, 500	Min = 0.9935 Max = 0.9996
200	250, 300, 350, 400, 500, 600, 700, 800	Min = 0.9889 Max = 0.9996

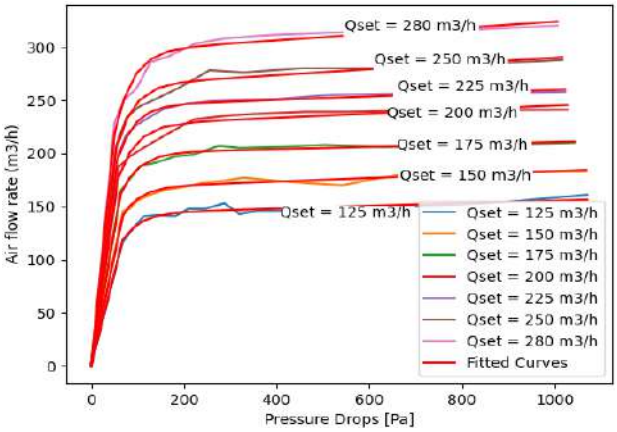

Fig. 4 - Airflow rate vs total pressure drop for 125 mm CAV box

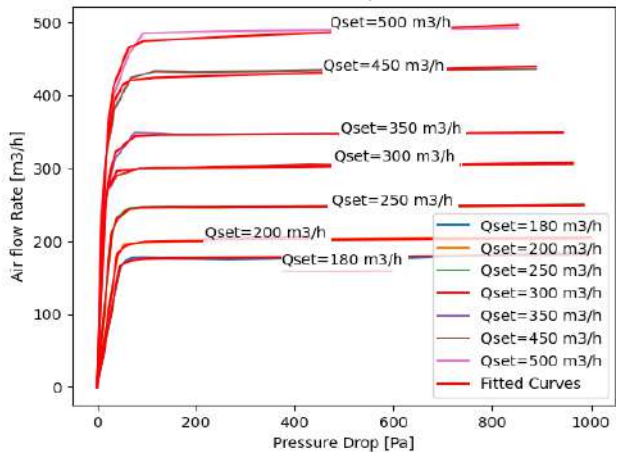

Fig. 5 - Airflow rate vs total pressure drop for 160mm CAV box

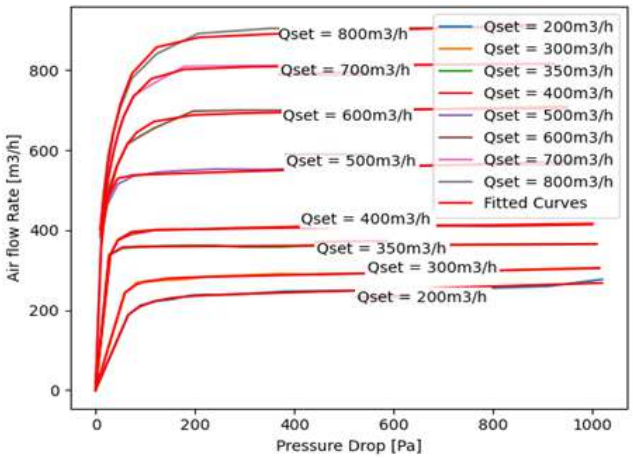

Fig. 6 - Airflow rate vs total pressure drop for 200mm CAV Box

From the fitted curves, 2100 data sets (i.e., Pressure Drop, CAV diameter, Qset, actual airflow rate) were generated to train an artificial neural network (ANN) regression model that predicts the airflow rate given the pressure drop at any given CAV diameter and its Qset.

3.2 Curves Behaviour

From Figs 4, 5, and 6, it can be observed that to reach the constant airflow rate; the fan must supply enough pressure to overcome the first part of the curve, i.e., where the pressure drop from the CAV box is usually between 0 and approximately 75 Pa. The second part of the curve is where the CAV is desired to function, i.e., where the airflow rate barely changes with the increase of the fan pressure. In this latter part, the CAV blade closes to drop enough pressure, thus maintaining the airflow rate. The last part of the curves is presented in Fig 7. Although this region is reached at a high-pressure inlet of the CAV box (>600 Pa), in practice, this part is unlikely to be reached as it requires too much power from the fan and produces too much noise along the ductwork. Besides, the pressure in this part of the curve is often higher than the operating range of the CAV box. The high inlet pressure results in unstable behavior of the curve, where the airflow rate starts to fluctuate around the stable airflow rate. The fluctuation is due to the vortices developed after the CAV box. These vortices can result in forces opposite or the same counterforce direction discussed in section 1.2. Therefore, these vortices can help open or close the CAV blade, leading to an increase or decrease in the airflow rate. However, while fitting the curves, the average airflow of these fluctuations is considered.

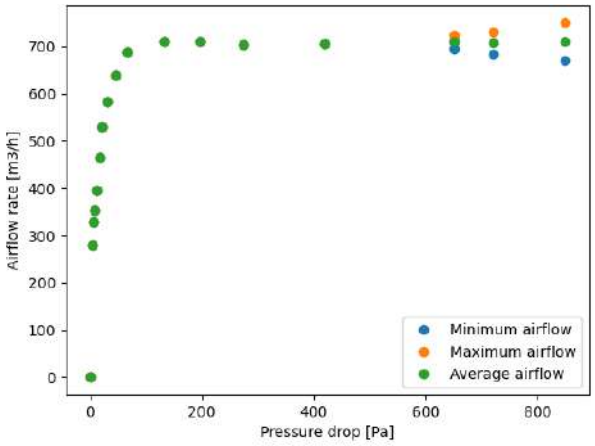

Fig. 7 - Airflow rate vs. total pressure drop for 200mm CAV box (Qset =600 m³/h)

Although Qset is the index where the airflow rate is supposed to be maintained, it can be observed from Figs 4, 5, and 6 that in most of the curves, the airflow rates are maintained at a slightly different airflow. For example, in Fig 6, when Qset =600 m³/h, the airflow rate is not maintained until around 650m³/h. The manufacturers declare that this difference in airflow rate can arise in the maintaining range, and it is often quantified as 10% airflow control accuracy [10,11]. This means that in order to maintain the airflow rate at 600 m³/h, the airflow index should be commissioned somewhere between Qset=500 m³/h and Qset=600 m³/h.

For a CAV box model, which can predict the aeraulic performance at any given CAV box diameter and its Qset, interpolation and extrapolation are inaccurate techniques in predicting the aeraulic performance. This is due to the uncertainties of the CAV aeraulic performance. To be more specific, typically, Qset is the index where the airflow is maintained. By observing Fig 4, where the diameter of the CAV box is 125mm, the airflows are maintained at a value slightly higher than their Qsets. On the other hand, for a CAV box diameter of 160mm, the airflows are maintained at a slightly lower value than their Qsets (Fig 5). By extrapolating between these 125mm and 160mm to predict the aeraulic performance of a 200mm CAV box, the airflow rates are expected to be maintained at a lower value than their Qsets. However, the measured data proved that this is not the case. From Fig 5, it can be observed that the measured airflow rates are most of the times maintained at a value slightly higher than the Qset (i.e., Qsets = 350, 400, 500, 600, 700, and 800 m³/h) but maintained once at an airflow rate lower than the Qset (i.e., Qset = 300 m³/h). Since ANN learns from the training dataset without requiring prior knowledge of the relationships between process parameters [16], it is expected to deal with the uncertainties properly. Furthermore, the collected measurements proved that the Qset is just an index to demonstrate a roughly maintained airflow rate. However, by commissioning the same Qset on different diameters, the airflows are not maintained at the same airflow. For example, considering Qset = 350 m³/h for CAV box diameter of 160 and 200mm (Figs 5 and 6), the airflows are maintained at 330 m³/h and 375 m³/h, respectively. Although the difference seems to remain small (±10% from the Qset), it accumulates with several CAV boxes in an air distribution system. This leads to a less energy-efficient system because the CAV boxes are not well commissioned. As the developed model should predict the airflow rate vs. the total pressure drop at any given Qset and diameter of the CAV box, it is vital to determine the best position to set the index (i.e., Qset), i.e., where the desired airflow is maintained. This will be automated while integrating the CAV model into the ADND algorithm.

3.3 The Model

The developed empirical model of the CAV box is a BlackBox model that predicts the aeraulic performance (i.e., airflow vs. pressure drop) for any given diameter and Qset of the CAV considering the chosen CAV type that is typically used in nonresidential buildings. The model trains the data collected from the fitted curves in sections 2.1 and 2.2 on the ANN regression model. The model has four hidden layers with a total of 40 units.

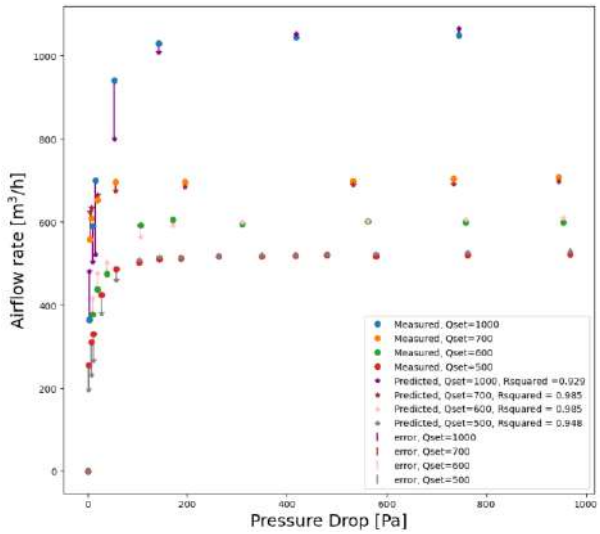

Fig. 8 - Predicted and measured airflow rate as a function of pressure drop for 250mm CAV box

Two validation methods were undertaken to validate the developed CAV box model. First, while training the model, 20% of the collected dataset was randomly taken to test the outputs of the trained ANN model. The test dataset included data for CAV diameters of 125, 160, and 200mm at different Qsets. The R squared value of the test set is approximately 0.98.

The other validation method was performed on CAV boxes with diameters that were not included in the training process. Therefore, these CAV boxes' experimental setup was also built by committing to the measurements standard in section 2.2 to collect pressure drop and airflow rate for some of their Qsets. Fig. 8 represents the measurements and the

predicted outputs from the trained model for the CAV box of 250mm diameter and Qset of 500, 600, 700, and 1000 m^3/h. It can be observed that the trained model predicts accurate outcomes in the maintaining phase (i.e., accuracy of at least 93%). However, less accuracy occurs in the transition phase (the phase at low-pressure drops before the maintaining phase). This is because the data from the transition phase accounts for less than 10% (0 up to 100 Pa) of the entire range of each curve (0 up to 1000 Pa); the rest of the data (more than 90% of the data) are in the maintaining phase. Still, the prediction accuracy in the transition phase did not fall below 75%.

4. Conclusion

To conclude, an empirical CAV box model for typical CAV boxes used in nonresidential buildings was developed using experimental lab measurements. The measured data were fitted into curves. These curves allowed the expansion of the measured data to acquire enough data to train the ANN regression model. The ANN regression model is the CAV empirical model that can mimic the aeraulic performance of the CAV box at any given Qset for diameters between 125 and 250mm. To achieve the model that can mimic the aeraulic performance at any given CAV box diameter, data from experimental measurements for diameters smaller than 125 mm and higher than 250 mm can be included in the ANN training dataset.

The predicted outcomes from the developed model matched the experimental dataset of the CAV control box with an accuracy of at least 75% during the transition phase and 93% during the maintaining phase. Therefore, the model's outcomes endorse integrating it into the ADND algorithm to optimize air distribution systems further (i.e., design, commissioning, and control optimization). Moreover, it can be integrated into the common simulation frameworks, where less accurate CAV box models are used.

5. Acknowledgment

This work has been supported by the Flemish Agency for Innovation and Entrepreneurship (VLAIO) in the Flux50 project Smart Ventilation (HBC.2020.2520).

6. Reference

[1] Jorens S, Verhaert I, Sörensen K. Design optimization of air distribution systems in non-residential buildings. University of Antwerp; 2021.

[2] Jorens S, Sörensen K, Verhaert I, De Corte A. Air distribution system design optimization in non-residential buildings: Problem formulation and generation of test networks. J Build Eng [Internet]. 2017;12(May 2017):60–7. Available from: http://dx.doi.org/10.1016/j.jobe.2017.05.006

[3] Jorens S, Verhaert I, Sörensen K. Design optimization of air distribution systems in non-residential buildings. Vol. 175, Energy and Buildings. 2018. 48–56 p.

[4] Smith S. Determination of K-Factors f HVAC system components using measurement and CFD modelling. University of Nottingham; 1998.

[5] ASHRAE. ASHRAE Handbook of Fundamentals. Vol. 30329. 2009. 926 p.

[6] Halton RMC. Airflow management damper (CAV) [Internet]. Available from: https://www.halton.com/products/mechanical-cav-damper-rmc-en_gb/#:~:text=Constant airflow damper Halton RMC, system balancing is not needed.

[7] Cairox. KVR-R • Adjustable constant air volume dampers [Internet]. Available from: https://www.cairox.be/EN/documentation/B02.010.1BIS-KVR-R-Adjustable-constant-air-volume-dampers/?cf=721543641184212748f816

[8] Yan Y, Luh PB, Pattipati KR. Fault diagnosis of HVAC: Air delivery and terminal systems. IEEE Int Conf Autom Sci Eng. 2017;2017-Augus(2):882–7.

[9] Engineering Reference; U.S. Department of Energy. EnergyPlus [Internet]. EnergyPlus v.9.6.0; 2021. Available from: https://energyplus.net/

[10] Aerotechnik. Volume flow controller [Internet]. Vol. 49. 2019. Available from: https://www.aerotechnik.de/fileadmin/downloads/en/prospekte/Best-Nr_233.pdf

[11] Trox. CAV controllers Type VFC [Internet]. 2017. Available from: https://www.trox.de/en/cav-controller /vfc-20c13b1afbcbd54d

[12] ANSI/ASHRAE Standard 120-2017. Method of Testing to Determine Flow Resistance of HVAC Ducts and Fittings. 2017. Atlanta, GA: ASHRAE

[13] ANSI/ASHRAE Standard 41.2-2018. Standard Methods For Air Velocity And Airflow Measurement. 2018.

[14] Virtanen P, Gommers R, Oliphant TE, Haberland M, Reddy T, Walt SJ Van Der, et al. SciPy 1.0: fundamental algorithms for scientific computing in Python. 2020;17(March).

[15] Raschka S, Mirjalili V. Python Machine Learning. Third Edit. 2019.

[16] Živković Ž, Mihajlović I, Nikolić Đ. Artificial neural network method applied on the nonlinear multivariate problems. Serbian J Manag. 2009;4(2):143–55.

Data Statement

The dataset generated during and/or analyzed during the current study are available in the data.zip repository.

Study of bioclimatic shading strategies in Seville: Habitability in open public spaces

Teresa Rocío Palomo Amores [a], María del Carmen Guerrero Delgado [a], Daniel Castro Medina [a], Alberto Cerezo Narváez [a], José Sánchez Ramos [a], Servando Álvarez Domínguez [a]

[a] Higher School of Engineering, University of Seville, Seville, Spain. tpalomo@us.es

Abstract. It is necessary to adapt urban areas to climate change through solutions that combine tradition with innovation. This need is more pronounced due to climate change and the heat island effect. This work aims to design a mitigation technique that allows recovery life on the street through an adaptive solar control solution combined with vegetation. This technique will be designed and implemented in a square in the centre of Seville (Spain). The solution is defined as a green structure where the trees are the key part. However, the trees are planted small and are grow-slowly. Urban designs based on tree growth are estimated to reach design conditions 30 years after these trees are planted. That is why an innovative urban solar control prosthesis is required that adapts between winter and summer and that allows modifying its geometry according to the growth of the trees. The design of this solution has been made by studying in detail a real case with real problems. These problems have been characterized by temperature measurements, thermographies, transects for the evaluation of the heat island, level of incident irradiation, and actual use of space. Different alternatives for the rehabilitation of the urban fabric have been studied using computational fluid dynamics (CFD) simulations in ENVI-met. The optimal solution will reduce air temperature by 1ºC and surface temperatures by up to 12ºC, increasing the number of trees reaching close to 100% of the area covered to make them the natural mitigation solution in the future. The coverage developed in this work appears as a temporary solution until the trees reach a reasonable size that generates adequate shade to allow the use of the space during the summer months. The aim is to improve the habitability of cities and regain the prominence of people in them.

Keywords. Solar control system, greenery, habitability, open spaces.
DOI: https://doi.org/10.34641/clima.2022.158

1. Introduction

The rapid growth of urban areas, coupled with the current health situation caused by COVID-19, highlights the need to use open spaces in daily life. Open spaces in urban environments provide benefits to pedestrians [1], however, the increase in heat waves puts people's health at risk, being of particular importance in pandemic outbreaks such as COVID-19 [2]. Most of the world's population will live in urban environments of low-quality environments by the middle of the century [3]. Therefore, it is necessary to act on open spaces through mitigation techniques to create sustainable and fresh spaces within cities, improving their habitability. These techniques include the reduction of air and surface temperatures, as well as the reduction of solar radiation. This study will focus on the review and analysis of solar control techniques.

Solar control techniques, based on the use of coverings, can differentiate between natural coverings through vegetation and artificial ones. The use of green infrastructure in the urban environment remains one of the most effective measures to cool the urban heat island [2], reducing air and surface temperature [4], as well as humidity and wind speed [5]. Artificial coverings, traditionally used as a shading strategy in the streets [6], behave in a similar way to the previous one in terms of improved comfort. The benefits of the natural technique will depend on the type of vegetation, height, and percentage of area covered, while its counterpart will depend on the optical properties, color, spatial distribution, arrangement, or size. Within this context, numerous authors have evaluated its impact on the urban microclimate. Thus, authors such as E. Chatzinikolaou et al. [7] study different bioclimatic scenarios of the vegetation plan through the ENVI-met numerical model, in Athens, highlighting the improvement in exterior comfort due to the inclusion of vegetation on the roadside, achieving a reduction of 5 in the PMV scale. Amiraslan Darvish et al. [6] study the

Copyright ©2022 by the authors. This conference paper is published under a CC-BY-4.0 license.

impact of the configuration of trees and their species, comparing a real case with and without trees located in Iran, through simulations carried out with ENVI-met and DesignBuilder. They conclude that the case with trees manages to reduce the average monthly air temperature by 1.6ºC in July, while the average temperature in the cold months manages to remain 0.9ºC higher than the case without trees. Dalia Elgheznawy et al. [8] studies the effect of using artificial shading in the courtyard of a teaching center in Egypt. Through simulations in ENVI-met and Rayman 1.2, the results obtained show that adding 60% or more of sun protection, reduces the average air temperature by 1ºC, and the average radiant temperature by 24%. I. Lee et al. [9] compare both types, concluding that plant shading achieves better results than artificial shading in terms of temperatures and comfort level evaluated with the COMFA model.

As can be seen, the most used technique is the natural coverings, however, all studies evaluate the impact of the vegetation when the trees are mature, a phenomenon that only occurs when a high number of years have passed since its planting in the treated area. That is why it is necessary to use adaptive solutions to the growth of trees to achieve the objectives from the moment of planting, hence the interest of this study.

2. Case study

The area analyzed in this study corresponds to a square located in the urban center of Seville, with a surface area of 612 m^2 mostly covered by pavement. It is a consequence of the intersection of 3 streets, with high traffic density, that separate it from medium-sized buildings.

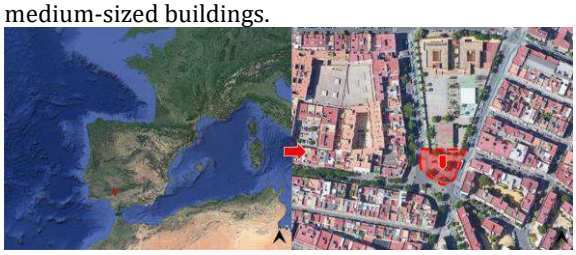

Fig.1 – Location

Seville is characterized by a warm climate, ranking within the Köppen-Geiger climate classification, as Csa, with hot and dry summers [10]. The average daily temperature of Seville in 2021 does not fall below 4ºC in cold months, being between 25-30ºC in the summer period, with maximum hourly temperatures of 43.7ºC in August. Therefore, the quality of the environment in the summer months is poor in the city center.

The current vegetation is scarce, made up of 8 small trees, which means that the square is in the sun almost all of the time. In order to know the current use of the square, a measurement campaign is carried out for 3 months through 2 cameras placed in the vicinity of the square. The results show that the use of the place at present is not high, serving as a passage area instead of a stay area. The area with the greatest influx is in the upper west part, corresponding to the entrance to the adjoining school. On the other hand, in order to know the current climatic situation, a monitoring campaign is carried out during the months of April to June 2021. Two fixed temperature and humidity sensors are installed with sampling periods of 5 minutes, for which a protective cover is designed to protect from rain and radiation.

Fig.2 – Fixed monitoring

Fig.3 shows the temperature results for a week in May. It can be observed as the temperatures are between 15 and 35ºC, exceeding this temperature in several days. It shows again how in the intermediate months the temperatures remain high.

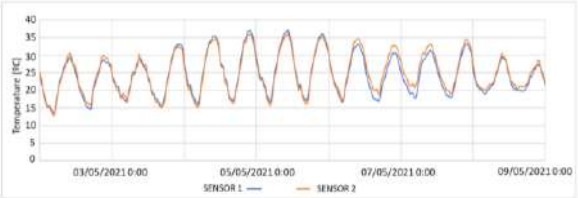

Fig.3 – Air temperature for a week in May

In addition to air temperature, surface overheating has a negative impact on human comfort [11], so knowing surface temperatures is an essential part of the city's sustainable design.

To find out the surface temperatures, measurements are carried out with the thermographic camera Testo 875-i during several days at different times of the day.

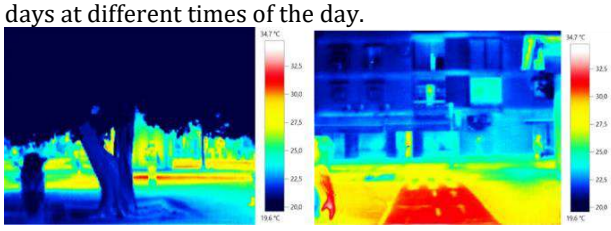

Fig.4- Thermographies of the square

Qualitatively, the temperature gradient between the sun and shade surfaces can be observed thanks to the existence of trees, demonstrating the need for them.

3. Intervention description

The intervention in this square aims to create a space within the city that enhances the relationship of the inhabitants with nature, in addition to achieving a natural coverage, lasting over time and with clear benefits in the environment, finally

improving the habitability of the area. To do this, the aim is to generate a green cover made up entirely of vegetation, increasing the number of trees in the square by 500%, adding 5 new species to create a “green roof”. However, the trees are planted in their early growing season, so in the first years after the performance, there will not be the necessary shade to improve the exterior comfort of the area. The tree species used in the study are in their entirety of rapid growth, therefore estimating an average of years until reaching the adult size of 25-35 years. In the present study, the trees will be planted in the square with an average age of 5 years, so the average estimated time to reach adult size from their planting in the plaza is 30 years.

For this reason, as long as the trees reach the necessary size to provide the space with shade, it is proposed to create an "artificial green roof", defined as a green-structure, union of the existing vegetation, the new one of small size and an adaptative artificial cover. The artificial cover must be adaptable to the growth of trees and to the seasons of the year so that it provides shade in summer and lets in the sun in winter. According to the growth of trees, the intervention can be divided over time into 4 different scenarios:

1-Current scenario: The number of planted trees is small, without any additional shade element.
2-Green-structure scenario: The square has all the new trees planted, but with small dimensions. Artificial coverage appears.
3-Medium scenario: The trees have grown to medium dimensions, which allows the cover to be partially replaced.
4-Final scenario: The trees have reached maturity and their size is capable of shading the entire square. In this scenario, the role of the green-structure is no longer required.

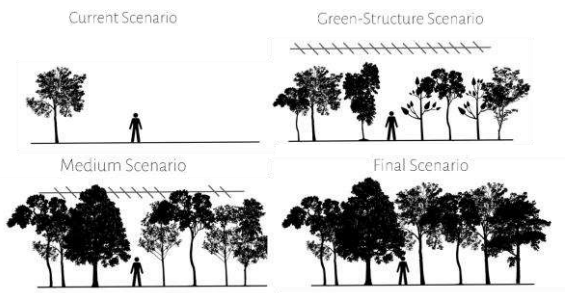

Fig.5 – Proposed scenarios

3.1 Adaptative cover design

The roof is made up of individual structures assembled. The design of each structure seeks to resemble trees in shape and size, however, to facilitate assembly and connection between them, they are designed in the shape of hexagons, formed in turn by six equilateral triangles independent of each other, with a height of 5 meters.

Fig.6 – Green-Structure

One of its main characteristics is the possibility of modifying its geometry in the short and long term. In the short term, it is possible to partially eliminate the triangular modules in winter months, allowing the increase in solar radiation, if necessary. In the long term, solar coverage allows adaptation to the growth of trees, permanently eliminating the necessary triangular modules when the tree reaches the required dimensions to cover that space. The modules eliminated in this case may be used occasionally in other parts of the city.

Each triangular module that forms the green-structure must allow radiation to pass in the winter months and block it in summer months. For this, slats are used as the structural system of the roof. To obtain the optimum geometry that achieves this objective, a sensitivity analysis of the different variables is carried out during summer days. Thus the distribution of slats is defined with an orientation (α) south-east, inclination (β) of -55º, width (w) of 0.1m and separation between them (s) of 0.1m (Fig. 7).

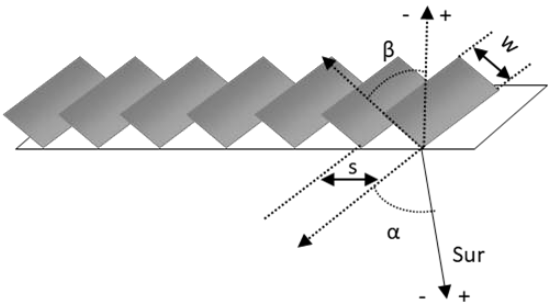

Fig.7 – Slat scheme

Therefore, it is achieved that, through adaptive artificial coverage, direct solar radiation decreases to a great extent, which will cause a reduction in surface and air temperatures, improving thermal comfort and habitability of the space allowing to recover life on the street.

3.2 Solution integration

For the vegetative shading strategy to achieve the expected cooling benefits, the correct location and arrangement of the trees is essential [8]. The mass

of trees has both deciduous species that favor the entry of radiation in winter, and evergreen species, which guarantee shade in the summer period. It will be arranged in such a position that, given the solar path in the summer months, the entire square is shaded once the trees reach adult size (Fig. 8). In turn, the roof will be located in the western area marked by its predominant use.

Fig.8.- Square design

4. Impact assessment

4.1 Simulation

The different scenarios studied will be simulated following the ENVI-met microscale numerical model. The results obtained through ENVI-met simulations have been validated by real measurements in numerous studies [3], [12], [13], so in this document the climatic data of the tool will be used to evaluate the impact of the proposed intervention. The days selected for the simulation are April 16, and July 15, 2021, the latter being one of the hottest of that year. The initial values of the simulation, for each time of the year are shown in Table 1.

Tab.1 – Initial meteorogical conditions

Variable	Summer	Spring
Wind speed measured in 10 m height (m/s)	3	2.5
Wind direction (deg)	225	225
Min. temperature of atmosphere (ºC)	12	5
Max. temperature of atmosphere (ºC)	27	14
Min. relative humidity in 2m (%)	30	50
Max. relative humidity in 2m (%)	69	70

The vegetation will be modeled through ENVI-met database (Albero), modifying the dimensions of the species depending on the evaluated scenario. The albedo and transmittance values used are shown in Table 2.

Tab.2 – Vegetation propierties

Species	Albedo	Transmittance
Citrus x Aurantium	0.4	0.3
Platanus x Acerofilia	0.18	0.3
Ficus Benjamina	0.18	0.3
Celtis Australis	0.18	0.3
Coco plumoso	0.18	0.3
Paulownia	0.60	0.3
Cercis Siliquastrum	0.60	0.3
Albizia Julibrissin	0.60	0.3

Following the arrangement of the vegetation and taking into account its dimensions, as well as the location of the roof in those scenarios in which it is in use, the geometric modelling is carried out, presented in Fig. 9. The resolution of the grid is 1 metre per square cell, reaching a grid model of 60x70x40 meters.

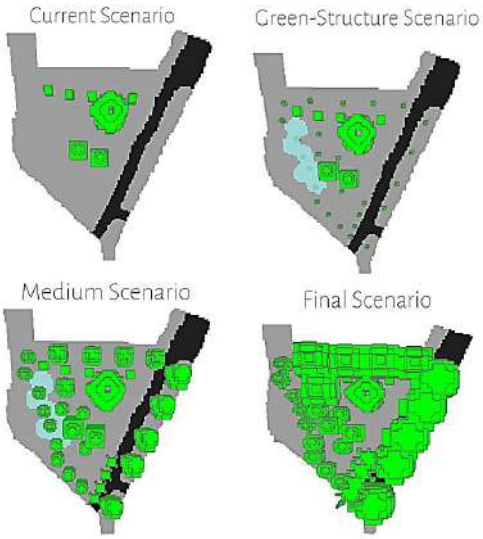

Fig.9 – Simulations models in ENVI-met

5. Results

In the first place, it is worth highlighting the final result of the plaza made through visual models that allow us to know the scale of the intervention.

Fig.10- Final realistc model of the square

On the other hand, the results obtained can be differentiated between results related to environmental changes in terms of air temperature, radiation incident on the square and surface temperatures and the consequent changes in thermal comfort.

5.1 Enviromentals variables

After the simulation carried out, the air temperature in the square at 1.5 meters from the ground is obtained, to know the conditions at an average height of the pedestrians both in summer and in spring at different times of the day.

As can be seen in Fig. 11.a, referring to the air temperature in the square for the four scenarios on July 15 at noon, the inclusion of the vegetation reduces the temperature by around 1ºC in the area with the highest concentration of vegetation for extreme cases. It also manages to reduce the negative effect of hot surfaces such as the asphalt that surrounds the square. The effect is similar to 6:00 p.m. on the same day (Fig. 11.b), where the temperature of the place is higher due to the accumulation of heat during the day, achieving temperatures close to 35ºC in the surrounding areas. Inside the plaza, the temperature reduction in extreme scenarios is 0.5ºC.

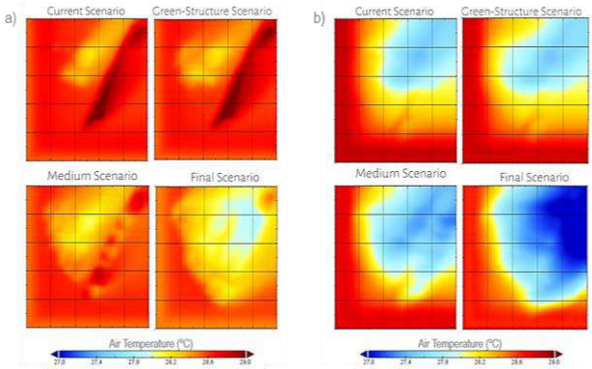

Fig.11 – a) Air temperature in the 4 scenarios for July 15 at 12:00h. b) Air temperature in the 4 scenarios for July 15 at 6:00 p.m.

For April 16 at noon, a reduction in air temperature of up to 1ºC is achieved again in extreme scenarios. The reduction of air temperature in the Green-Structure Scenario, where the vegetation still has a very reduced size and only the artificial cover appears, is reduced, showing the clear importance of the vegetation in the reduction of temperature. However, it is notable in both seasons of the year, as the artificial structure manages to slightly improve the thermal conditions.

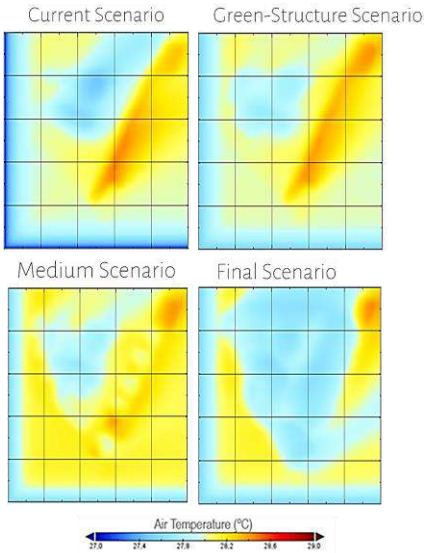

Fig.12 – Air temperature in the 4 scenarios for April 16 at 12:00h

Regarding the surface temperatures, the differences obtained are significant. On July 15 at noon, the surface temperatures are reduced by around 9ºC in the areas where vegetation is added. It is worth highlighting the improvement obtained in the asphalt area with a reduction of 12ºC thanks to the effect of the vegetation. During the afternoon, again, temperature differences of the order of 10ºC are achieved with a maximum of 12ºC. The effect of the artificial cover, in this case, supposes a reduction in temperatures of 6ºC, below that achieved through the vegetation.

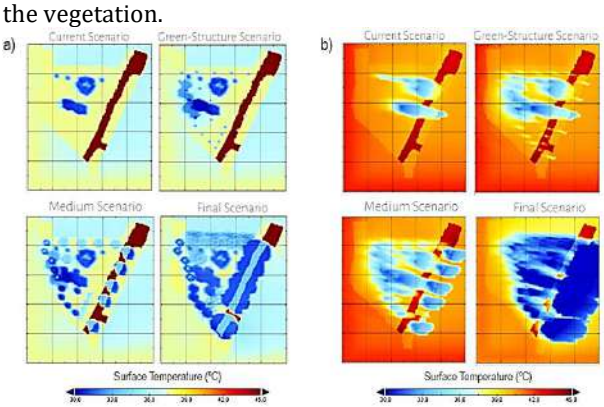

Fig.13 – a) Surface temperatures in the 4 scenarios for July 15 at 12:00. b) Surface temperatures in the 4 scenarios for July 15 at 6:00 p.m.

The variation in surface temperature on April 16 at noon, again, achieves a reduction in extreme scenarios of the order of 10ºC, with a maximum of 12ºC in the case of the asphalt area. For the intermediate season, the effect of the artificial cover is closer to the effect produced by the vegetation.

Finally, the effect of the intervention on incident radiation is remarkable. Thus, Fig. 14 shows the simulation results obtained for July 15 at noon, where the incident radiation on the square changes

from 1000 W/m² until it is practically nullified in extreme scenarios. The use of artificial cover allows creating a meeting space where radiation is 60% lower, before the total growth of vegetation, improving the habitability of the area from the beginning of the intervention.

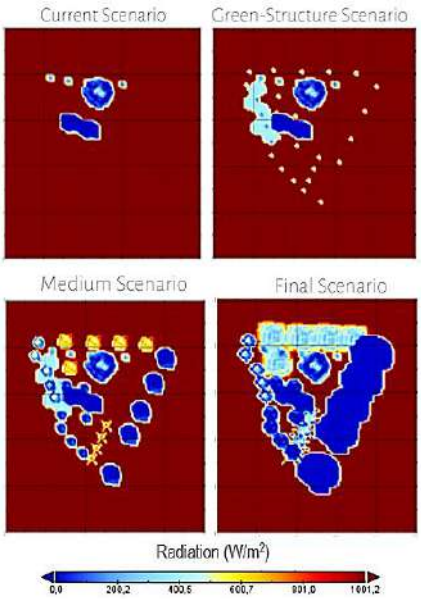

Fig.14 – Radiation in the 4 scenarios on July 15 12: 00h.

For this same time in the intermediate period, the results are very similar, managing to reduce almost all the radiation.

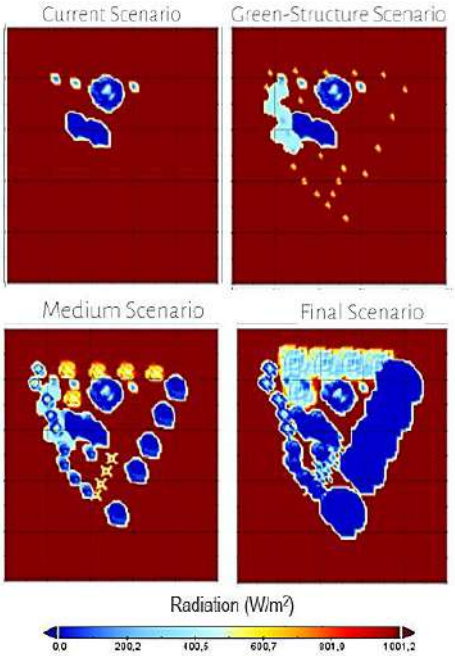

Fig.15 – Radiation in the 4 scenarios on April 16 12: 00h.

6. Conclusions

The innovative solution study has been carried out in a square in the center of Seville (Spain). The intervention based on the innovative integration of adaptive solar control solution combined with vegetation as a bridge between the current situation and the growth of the trees, achieves a place within the city throughout the year where climatic conditions improve considerably, thus improving the habitability of the area. A green and pleasant space is generated. It is possible to reduce the air temperature by up to 1ºC in the final situation, as well as up to 12ºC in the surface temperatures. On the other hand, the initiating radiation, the main cause of discomfort outdoors, manages to be reduced to almost its elimination. It is possible to highlight the necessary use of artificial cover as an intermediate step between the planting of the vegetation and its final growth, being an innovative solution that manages to improve the climatic situation of the square from the beginning of the intervention.

7. Acknowledgment

This research has been funded by the European LifeWatercool project (LIFE18 CCA / ES / 001122 Water efficient systemic concept for the climate change adaptation in urban areas)

8. References

[1] D. Lai, W. Liu, T. Gan, K. Liu, and Q. Chen, “A review of mitigating strategies to improve the thermal environment and thermal comfort in urban outdoor spaces,” *Sci. Total Environ.*, vol. 661, pp. 337–353, 2019, doi: 10.1016/j.scitotenv.2019.01.062.

[2] K. Degirmenci, K. C. Desouza, W. Fieuw, R. T. Watson, and T. Yigitcanlar, “Understanding policy and technology responses in mitigating urban heat islands: A literature review and directions for future research,” *Sustain. Cities Soc.*, vol. 70, no. March, p. 102873, 2021, doi: 10.1016/j.scs.2021.102873.

[3] S. Garshasbi *et al.*, “Urban mitigation and building adaptation to minimize the future cooling energy needs,” *Sol. Energy*, vol. 204, no. May, pp. 708–719, 2020, doi: 10.1016/j.solener.2020.04.089.

[4] M. Fahmy, M. Mahdy, S. Mahmoud, M. Abdelalim, S. Ezzeldin, and S. Attia, “Influence of urban canopy green coverage and future climate change scenarios on energy consumption of new sub-urban residential developments using coupled simulation techniques: A case study in Alexandria, Egypt,” *Energy Reports*, vol. 6, pp. 638–645, 2020, doi: 10.1016/j.egyr.2019.09.042.

[5] N. Meili, J. A. Acero, N. Peleg, G. Manoli, P. Burlando, and S. Fatichi, “Vegetation cover and plant-trait effects on outdoor thermal comfort in a tropical city,” *Build. Environ.*, vol. 195, no. September 2020, p. 107733, 2021, doi:

10.1016/j.buildenv.2021.107733.
[6] A. Darvish, G. Eghbali, and S. R. Eghbali, "Tree-configuration and species effects on the indoor and outdoor thermal condition and energy performance of courtyard buildings," *Urban Clim.*, vol. 37, no. March, p. 100861, 2021, doi: 10.1016/j.uclim.2021.100861.
[7] E. Chatzinikolaou, C. Chalkias, and E. Dimopoulou, "Urban microclimate improvement using ENVI-MET climate model," *Int. Arch. Photogramm. Remote Sens. Spat. Inf. Sci. - ISPRS Arch.*, vol. 42, no. 4, pp. 69–76, 2018, doi: 10.5194/isprs-archives-XLII-4-69-2018.
[8] D. Elgheznawy and S. Eltarabily, *The impact of sun sail-shading strategy on the thermal comfort in school courtyards*, vol. 202. Elsevier Ltd, 2021.
[9] I. Lee, J. A. Voogt, and T. J. Gillespie, "Analysis and comparison of shading strategies to increase human thermal comfort in urban areas," *Atmosphere (Basel).*, vol. 9, no. 3, 2018, doi: 10.3390/atmos9030091.
[10] M. C. Peel, B. L. Finlayson, and T. A. McMahon, "Updated world map of the Köppen-Geiger climate classification," *Hydrol. Earth Syst. Sci.*, vol. 11, no. 5, pp. 1633–1644, 2007, doi: 10.5194/hess-11-1633-2007.
[11] E. Garcia-Nevado, B. Beckers, and H. Coch, "Assessing the Cooling Effect of Urban Textile Shading Devices Through Time-Lapse Thermography," *Sustain. Cities Soc.*, vol. 63, no. August, p. 102458, 2020, doi: 10.1016/j.scs.2020.102458.
[12] D. Pearlmutter, D. Jiao, and Y. Garb, "The relationship between bioclimatic thermal stress and subjective thermal sensation in pedestrian spaces," *Int. J. Biometeorol.*, vol. 58, no. 10, pp. 2111–2127, 2014, doi: 10.1007/s00484-014-0812-x.
[13] D. Du Bois and E. F. Du Bois, "A formula to estimate the approximate surface area if height and weight be known. 1916.," *Nutrition*, vol. 5, no. 5, p. 303, 1989.

Energy efficiency and indoor climate benefits of demand-based ventilation in simulated office rooms

Vili Kohtaniemi [a], Panu Mustakallio [b]

[a] Halton Oy, Haltonintie 1-3, 47400 Kausala, Finland, vili.kohtaniemi@halton.com

[b] Halton Oy, Haltonintie 1-3, 47400 Kausala, Finland, panu.mustakallio@halton.com

Abstract. The demand for high energy efficiency of office buildings with an increasing focus on safety and good indoor air climate has increased the use of demand-based HVAC systems. The varying occupancy of office spaces can lead to unnecessarily high ventilation airflow rates and cooling of the room when there are no occupants. To achieve the same level of indoor climate with a more traditional ventilation system causes high energy consumption and inefficient operation of the HVAC system. A comparison of three active chilled beam systems was made with energy simulation software for finding the best performing room configuration in realistic operating conditions. Office room and meeting room cases) were simulated with 1) traditional CAV (Constant Air Volume) ventilation system, 2) BCV (Boost Controlled Ventilation) system with 2 automatic operating modes and 3) DCV (Demand-Controlled Ventilation) system with 3 automatic operating modes. For BCV and DCV systems same active chilled beam unit was used for office and meeting room cases to highlight the possibility of office layout changes without additional modifications to the ventilation system. CAV ventilation system required change between two different chilled beam units for office and meeting room cases to maintain the same level of indoor climate. Energy consumption, indoor climate conditions, and cooling system operation were simulated. The office building was located in a middle European temperate climate and had generic building materials and energy-efficient window characteristics Operation of demand-based ventilation system control logic for controlling airflow rates was studied between CO2 control and CO2 control with added presence control. The most energy-efficient solution was DCV system having 3 operating modes as the energy savings based on the ventilation airflow rates required at minimum operating mode is large compared to normal or maximum operating mode. With BCV active chilled beam ventilation system having 2 operating modes, energy efficiency can be increased notably compared to CAV active chilled beam ventilation system. BCV ventilation system could have performed with lower energy consumption for office room case if the active chilled beam was designed to be used for only office room operation, and not for meeting room operation as well.

Keywords. Demand-based ventilation, chilled beam, energy efficiency, office building
DOI: https://doi.org/10.34641/clima.2022.296

1. Introduction

The demand for high energy efficiency of office buildings with an increasing focus on safety and good indoor air climate has increased the use of demand-controlled ventilation (DCV) systems [1,2]. Demand-based ventilation systems' energy saving potential for offices is highly dependent on occupancy, which can vary between 15% to 80% for average day time office [3,4]. This paper presents an energy simulation study between three different active chilled beam (ACB) systems for simplified office and meeting room cases. It compares cooling load, HVAC energy consumption, and indoor environmental quality (CO_2, air age, and temperature) for finding a safe and most energy-efficient system.

2. Methods

2.1 Simulation model

IDA Indoor Climate and Energy 4.8 (IDA-ICE) simulation tool was used in the study for assessment of indoor climate and energy performance.

Copyright ©2022 by the authors. This conference paper is published under a CC-BY-4.0 license.

Performance of three different active chilled beam systems was compared: 1) Traditional CAV (constant air volume) ventilation system manually adjusted and designed to office or meeting room situation 2) BCV (boost-controlled ventilation) system with two operating modes where boost airflow rate is automatically controlled based on room CO_2-level and temperature 3) DCV (demand-controlled ventilation) system with three operating modes automatically controlled based on occupancy, room CO_2-level and temperature.

The simulation model in the study consisted of a single room used as a two-person office room (10.9 m^2/person) or as an eight-person meeting room (2.7 m^2/person). The model had one external wall with two windows that was directed to south, and all other surfaces were internal. The net heat transmission through internal surfaces was ignored. The office building located in middle European temperate climate and had generic building materials and energy-efficient window characteristics with solar shading. The geometry of the simulated room is presented in Fig. 1. Energy performance and indoor climate conditions were studied during the cooling season from May to September. The building construction data used in different simulation cases are presented in Table 1.

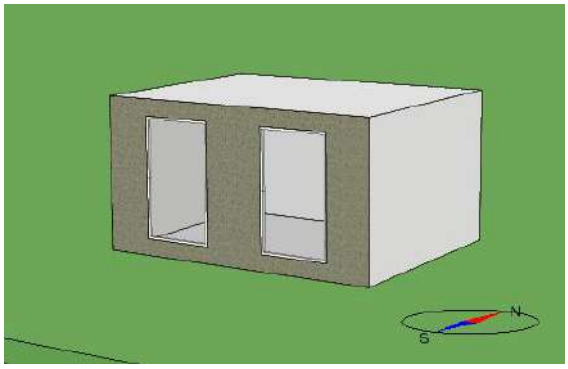

Fig. 1 – Geometry of simulated room

Tab. 1 – Building construction details

Building construction details	
Main building data	Paris weather data, 1 office room with orientation to south
Room data	5.3 m wide, 4.1 m long, floor area 21.7 m^2, 2.8 m high, one external wall (other internal)
Window size	two 1.3 m wide, 2.2 m high windows located 0.3 m from the floor (38.5 % of external wall area)
Window performance	U=1.1 W/(m^2, K), g=0.37, T_{vis}=0.7 Frame with U=2.0 W/(m^2, K)
Solar shading	Blind between panes, multipliers for U=0.87, g=0.39, T=0.12
External wall heat conductivity and material layers from inside	0.54 W/(K, m^2), render 0.01 m, concrete 0.25 m, render 0.01 m
Internal wall conductivity and material layers from inside	0.62 W/(K, m^2), gypsum 0.026 m, air gap 0.032 m, light insulation 0.03 m, air gap 0.032 m, gypsum 0.026 m
Internal floor material layers from inside	coating 0.005 m, concrete 0.25 m
Infiltration	Wind-driven 0.5 ACH at 50 Pa

Internal heat loads during office hours consisted of occupants, equipment, and lighting. Heat loads were simulated for office and meeting room cases based on the number of occupants. The occupancy schedule for office and meeting room cases was based on EN16798-1 standard's occupancy schedules for energy calculation [5]. Smoothing of ± 12 minutes was used for all schedules. Operating data used in different cases for internal heat loads and occupancy schedules are presented in Table 2.

Tab. 2 – Operating data of internal heat loads

	Office	Meeting room
Occupancy schedule during office hours Mo-Fri 6.00-20.00	Weekdays: 6-9 0.0 9-13 1.0, 13-14 0.0, 14-17 1.0 17-20 0.0	Weekdays: 6-9 0.0 9-10 0.5, 10-11 0.8, 11-12 0.9, 12-13 0.8, 13-14 0.0, 14-15 0.7, 15-17 0.8, 17-18 0.7 18-20 0.0
Heat loads	Number of occupants 2 (1.0 MET)	Number of occupants 8 (1.0 MET)
	Equipment load 13.8 W/m^2 (during occupancy)	Equipment load 27.6-49.8 W/m^2 (based on occupancy load)
	Lighting load 9.2 W/m^2 (during occupancy)	Lighting load 9.2 W/m^2 (during occupancy)

2.2 Active chilled beam systems

Modern active chilled beam systems with mixing ventilation were designed with manufacturer's

design tool into office and meeting room cases with realistic performance data [6,7]. Traditional CAV ventilation system was designed with two different active chilled beam units for office room and meeting room cases to achieve good indoor climate conditions. For this ventilation system airflow rate was controlled based on AHU (air handling unit) operating schedule, maintaining designed office room and meeting room airflow rates.

BCV system with two operating modes was designed with a single chilled beam unit for both office and meeting room cases. The additional boost airflow controlled based on room CO_2-level and temperature was introduced for this system without boost airflow passing through the active chilled beam cooling coil. With the boost airflow, additional boost air cooling could be utilized when airflow rates were increased above normal operation. Airflow rates for BCV system was operated in two operating modes: 1) Normal airflow rate operation based on AHU operating schedule if room CO_2-level or temperature isn't above set limits 2) If room temperature with water cooling fully in use, or CO_2-level is above set limits, airflow rate is increased between normal and maximum airflow rate to maintain the desired room temperature and CO_2-levels.

DCV system with three operating modes was designed with a single chilled beam unit for both office and meeting room cases. For this system the additional air was introduced with supply air increasing room airflow circulation through the active chilled beam cooling coil, leading that water cooling is increased with additional air cooling. Airflow rates were controlled in three operating modes: 1) When no occupancy is detected in the room, airflow rate is decreased to the minimum level and room temperature setpoint is increased by 1°C 2) If occupancy is detected in the room and the room CO_2-level or temperature isn't above set limits, airflow rate is increased to normal operation 3) If temperature with water cooling fully in use, or CO_2-levels increase above set limits air flow rate is increased between normal and maximum airflow rates to maintain the desired room temperature and CO_2-levels.

Ventilation airflow rates for different simulation cases fulfilled airflow rate requirements in standard EN-16798-1 category 2 for low-polluting building. Due to SARS-CoV-2 recommendations room CO_2-levels were maintained at lower level than required in the standard [1]. Maximum room CO_2-level was limited to 800 ppm with studied occupancy schedule, and outdoor air CO_2-level of 400 ppm was used in simulation cases. With studied occupancy schedule this corresponds to maximum airflow rates of 1.4 l/s, m^2_{floor} for office room case and 3.7 l/s, m^2_{floor} for meeting room case. The operating parameters and cooling design of different HVAC systems are presented in Table 3.

Tab. 3 – Operating parameters and cooling design of HVAC system in office (O) and meeting room (M) cases

	Active chilled beam (CAV)	**Active chilled beam (BCV)**	**Active chilled beam (DCV)**
Cooling set-point (room air temperature)	25 °C		Occupied 25 °C Unoccupied 26 °C
Operating data of ventilation system (AHU)	Weekdays 6-20, 16 °C supply air		
Cooling water circulation	Only during AHU operating hours		
Supply air sensible cooling in design operation	(O) 15.1 W/m^2_{floor} (M) 40.6 W/m^2_{floor}	(O) 15.2 W/m^2_{floor} (M) 40.5 W/m^2_{floor}	*6.2 W/m^2_{floor} (O) 15.2 W/m^2_{floor} (M) 41.7 W/m^2_{floor}
Water coil cooling capacity in design operation	(O) 43.4 W/m^2_{floor} (M) 57.1 W/m^2_{floor}	53.2 W/m^2_{floor}	*28.1 W/m^2_{floor} (O) 43.1 W/m^2_{floor} (M) 58.9 W/m^2_{floor}

*DCV system minimum airflow operation.

3. Results

Energy performances of different ACB systems during cooling season (May to September) for office and meeting room cases are presented in table 4. DCV system showed the lowest energy consumption, most stable temperature conditions, and highest utilization of room water cooling (zone cooling).

AHU fan energy consumption in the office room case for the DCV system was 25% lower compared to the CAV ventilation system and 28% lower compared to the BCV system. BCV system had higher fan energy consumption than CAV system for office room case because airflow rates were increased during office hours briefly above normal operation to maintain the room temperature and CO_2-levels at setpoint values.

AHU fan energy consumption in meeting room case for DCV system was 53% lower compared to CAV ventilation system and 7% lower compared to BCV system. CAV system had noticeably higher energy consumption for meeting room case compared to BCV and DCV systems because airflow rates were at a constant maximum level compared to BCV and DCV systems which were able to decrease the airflow rates during unoccupied hours.

Differences for pump energy consumptions in office and meeting room cases were minor. DCV system

had the lowest pump energy consumption for office room and meeting room cases.

Tab. 4 – Energy performances for different ACB systems in office (O) and meeting room (M) cases

	Active chilled beam (CAV)	**Active chilled beam (BCV)**	**Active chilled beam (DCV)**
Fan energy O	37.1 kWh	38.4 kWh	27.7 kWh
Fan energy M	201.2 kWh	101.6 kWh	94.3 kWh
Pump energy O	1.3 kWh	1.3 kWh	1.1 kWh
Pump energy M	3.4 kWh	3.1 kWh	3.0 kWh
*Electric cooling energy O	166.7 kWh	169.3 kWh	152.8 kWh
*Electric cooling energy M	434.8 kWh	429.9 kWh	424.2 kWh
Total electric energy O	205.1 kWh (100 %)	209 kWh (102 %)	181.6 kWh (89 %)
Total electric energy M	639.4 kWh (100 %)	534.6 kWh (84 %)	521.5 kWh (82 %)
Cooling energy (sensible and latent) O	Zone cooling: 102.4 kWh	Zone cooling: 95.6 kWh	Zone cooling: 149.0 kWh
	AHU cooling: 397.8 kWh	AHU cooling: 412.3 kWh	AHU cooling: 309.5 kWh
Cooling energy (sensible and latent) M	Zone cooling: 247.0 kWh	Zone cooling: 562.1 kWh	Zone cooling: 611.4 kWh
	AHU cooling: 1057.4 kWh	AHU cooling: 727.6 kWh	AHU cooling: 661.3 kWh

*COP (Coefficient of Performance) value of 3 was used.

Room air temperature stability curves for cooling season during office hours for different ACB systems in office room cases are presented in fig. 2 and for meeting room cases in fig. 3. X-axis in the fig. 2 and fig. 3 represents hours when the office is in use (office hours). Temperature didn't exceed the 25 °C room temperature setpoint in any ACB systems during office hours, in exception of DCV system which was controlled so that temperature could rise by 1 °C during office hours in unoccupied periods. DCV system showed the best temperature stability for office and meeting room cases. In the office room case DCV system temperature was below 25 °C setpoint for 400 h, compared to CAV and BCV systems which were below 25 °C setpoint for 600 h. In the office room case, CAV and BCV systems had similar temperature stability curves as the airflow rates during unoccupied hours were higher in both systems, leading to unnecessary cooling of the room.

The CAV ventilation system in the meeting room case had a temperature below 25 °C setpoint for 500 h, compared to the BCV system with 250 h and the DCV system with 150 h. In the meeting room case, BCV system performed better than in the office room case with a more stable temperature curve due to the possibility of airflow rate variation between normal and maximum airflow rates.

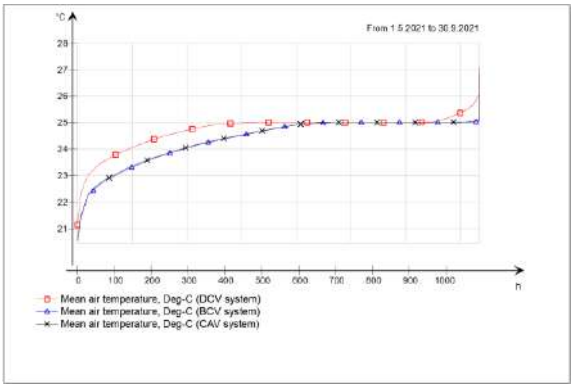

Fig. 2 – Temperature stability curves between different ACB systems during office hours for office room case

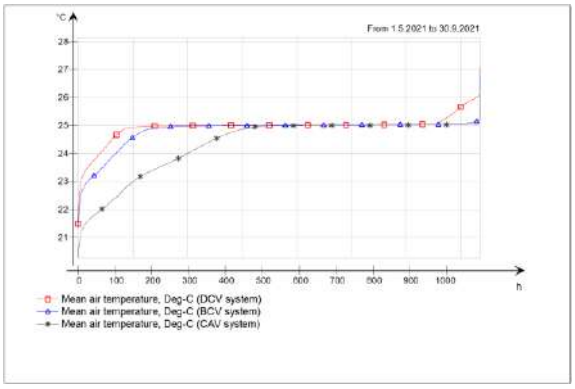

Fig. 3 – Temperature stability curves between different ACB systems during office hours for meeting room case

Ventilation airflow rates during design day for different ACB systems for office room cases are presented in fig 4. and for meeting room cases in fig 5. Ventilation airflow rates in office room cases show the minimum airflow rate operation for DCV system during unoccupied periods when both CAV and BCV systems stay on higher airflow rates. In the meeting room case, airflow rate trends for DCV and BCV systems are closer to each other, compared to the CAV ventilation system which has a constant maximum airflow rate. For meeting room case difference between DCV and BCV can be seen during unoccupied hours and after people leave the office, as the ventilation airflow rates can be

lower in the DCV system.

CO_2-level setpoint for BCV and DCV systems in office and meeting room cases was 800 ppm. In all office and meeting room cases, CO_2-levels were maintained at setpoint levels. For office room cases CO_2-levels in all cases were at a maximum of 700 ppm, and for meeting room cases at a maximum of 800 ppm. For the DCV system morning flush operation was used where air flow rate was increased to normal operation for 2 h when AHU started to maintain better indoor air quality and lower age of room air. CAV ventilation system and BCV system showed similar air age for office room cases. CAV ventilation system had the lowest air age for meeting room case which was close to 0 h when occupants entered the room. DCV system had the highest air age for meeting room case which was close to 1 h when occupants entered the room.

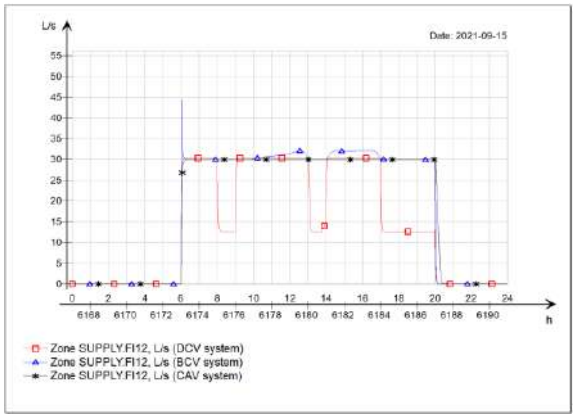

Fig. 4 – Ventilation air flows between different ACB systems during design day for office room case

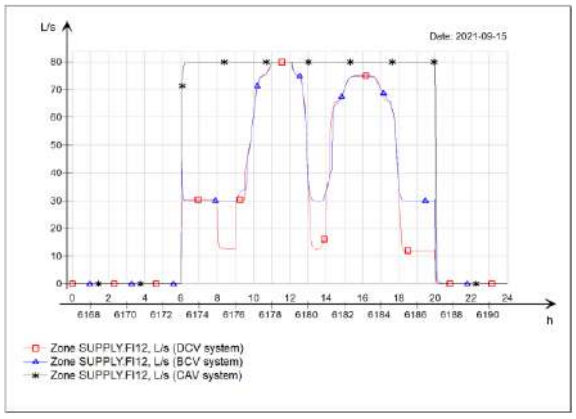

Fig. 5 – Ventilation air flows between different ACB systems during design day for meeting room case

4. Conclusions

The demand-controlled ventilation (DCV) system showed the best energy performance while maintaining good indoor climate conditions. Boost-controlled ventilation (BCV) system had similar fan energy consumption than CAV ventilation system for office room case but had only 7% higher energy consumption than DCV system for meeting room case. BCV system could have performed better in office room case if the ACB design was made only for office room operation, so the maximum (boosted) air flow rate would be the office room airflow rate. This highlights additional benefits of the 3 operating modes in the DCV system compared to the BCV system when the DCV system could operate with the lowest energy consumption in both cases while maintaining good indoor climate conditions. Constant air volume (CAV) ventilation system had highest fan energy consumption in meeting room case with 53% higher energy consumption than in DCV system and 50% higher than in BCV system.

Additional benefits of the DCV and BCV systems in the study were the use of the same chilled beam unit for both cases when the CAV ventilation system required different chilled beam units for office and meeting room cases. This highlights the adaptability of chilled beams for possible room layout changes without making additional adjustments to the active chilled beams or ventilation system. For CAV ventilation system chilled beams would require manual work to adjust the chilled beam to operate in either office room operation or meeting room operation and this could also pose problems with too low-pressure level for required airflow rate in meeting room operation.

The benefits of the DCV system could be realized better with real-life occupancy profiles of office spaces. In the study, occupancy profiles were based on occupancy schedules for energy calculation presented in EN16798-1 standard, where the occupancy profile is the same for all workdays. With a high occupancy rate, the energy-saving benefits of the DCV systems are lower but with low or highly varying occupancy rates the energy-saving benefits of the system can be utilized the most. With the increase of remote work in offices due to SARS-CoV-2 occupancy rates can vary highly and energy benefits of the DCV system could be utilized, by also maintaining a safe indoor environment.

5. Acknowledgment

The study was supported by Business Finland.

6. References

[1] REHVA. COVID-19 guidance: How to operate HVAC and other building service systems to prevent the spread of the coronavirus (SARS-CoV-2) disease (COVID-19) in workplaces. Version 4.1. 2021.

[2] Kosonen R., Penttinen J., Mustakallio P. The effect of free-cooling and demand-based ventilation on energy consumption of self-regulating and traditional chilled beam systems in cold climate.

[3] Kaiser A., Kurnitski J., Sormunen P. Demand controlled ventilation indoor climate and energy performance in a high performance building with air flow rate controlled chilled beams. Energy and Buildings. 2015;109:115-126

[4] Yau Y.H., Tam J.H. A Comparison study for active chilled beam and variable air volume systems for an office building. Energy Procedia. 2018;152:378-383

[5] SFS-EN 16798-1:2019. Energy performance of buildings – Ventilation for buildings – Part 1: Indoor environmental input parameters for design and assessment of energy performance of buildings addressing indoor air quality, thermal environment, lighting and acoustics.

[6] Halton HIT Design product selection tool, 2019, Halton Oy, Finland.

[7] Halton workplace solution description. 2021. Halton Oy. Finland.

DATA ACCESS STATEMENT

The datasets generated during and/or analysed during the current study are not available due to the simulation file sizes but the authors will make every reasonable effort to publish them in near future.

Design and integration of innovative rehabilitation technique: Improving habitability in social housing

Teresa Rocío Palomo Amores [a], María del Carmen Guerrero Delgado [a], Daniel Castro Medina [a], José Luis Molina Félix [a], José Sánchez Ramos [a], Servando Álvarez Domínguez [a]

[a] Higher School of Engineering, University of Seville, Seville, Spain. tpalomo@us.es

Abstract. The current commitments proposed by the European Union to mitigate the effects of climate change lead to the necessary action on the building sector. Acting on the existing building stock, improving energy efficiency becomes a key point on the road to 2030, where the role of air conditioning will change completely. Unsatisfied basic needs for energy supply characterize the energy-poor social housing districts in Spain. The energy inefficiencies of the dwellings worsen this situation. This situation is aggravated in the south of Spain, presenting a severe overheating problem in cooling, making residents outside the comfort limits a high number of hours. In these cases, conventional strategies to improve the performance of the building envelope are not enough. In this work, an innovative active roof solution of more than 2000m2 is designed and integrated in a district of social housing blocks. Said roof reduces the energy demand for conditioning through the exploitation of thermal inertia and the integration of environmental sinks, enhancing its effect with direct evaporative cooling systems through water micronization. It stands out for being a climate-adaptive design, intelligently controlled based on climate predictions and with different operating modes, which allows it to adapt to the needs of the building. The assessment of the impact of this innovative solution has been analyzed both in the pre-design phase and after the completion of the intervention, thus allowing us to know the actual improvement of the dwellings. Serving as an example of the integration of high-tech components, its objective has been to improve the energy efficiency of the housing stock, allowing it to reduce energy demand, as well as increase comfort levels for residents.

Keywords. Adaptative cover, habitability, innovative rehabilitation.
DOI: https://doi.org/10.34641/clima.2022.159

1. Introduction

The Sustainable Development Agenda adopted by all UN Member States in 2015 to mitigate the effects of climate change leads to the necessary action on the building sector. This situation is aggravated in areas where the low energy efficiency of homes can cause a state of continued discomfort and with it serious consequences for the health of the occupants [1]. In Spain, between 3.5 and 8 million people are in a situation of energy poverty, not being able to maintain appropriate temperatures in both summer and winter [2]. This situation is aggravated within the social housing districts in southern Spain where the situation worsens due to the progressive increase in overheating in the cooling months [3]. The rehabilitation of social housing districts includes measures such as improving the transmittance of enclosures by incorporating thermal insulation in them, replacing existing carpentry, improving thermal bridges and increasing watertightness [4]. Said conventional strategies achieve a considerable reduction in the demand for heating [5,6], however, they are not sufficient under cooling conditions in dominant summer climatic zones, as is the case in southern Spain. Along these lines, the interest in the use of passive cooling techniques in buildings stands out, which are based on the use of solar and thermal control techniques, amortization and heat dissipation [7].

The roof is one of the critical elements of the cooling demand due to its extension, exposure to solar radiation and because it is free of obstacles or solar protection elements. Double skin construction are one of the passive heat dissipation technology solutions for energy saving and climate adaptation [8]. These elements have been widely developed and used for passive heating purposes, however, the study and development of these elements for passive cooling purposes is currently very limited [9]. There is a need to re-design ventilated roof solutions to integrate natural heat sinks and achieve

Copyright ©2022 by the authors. This conference paper is published under a CC-BY-4.0 license.

an optimal implementation that makes them viable according to the established rules for defining rehabilitation projects [10].

Therefore, this work integrates an innovative solution in more than 2000m2 of active roof in a district of block social housing located in Morón de la Frontera, Seville, serving as an example of integration of high-tech components. It allows reducing the energy demand for conditioning through the exploitation of thermal inertia, being intelligently controlled based on climate predictions and having different operating modes, which allows it to adapt to the needs of the building. This solution also allows the integration of natural heat sinks such as evaporative cooling. In line with these objectives, the document has been structured according to the methodology used. In the first place, the case study is presented and analyzed, justifying the need for action in relation to interior temperatures and thermal comfort. Subsequently, the set of improvement measures and the choice of the optimal solution are described. Finally, the ventilated roof solution necessary to achieve the comfort objectives is defined. Finally, the evaluation of the energy impact in the district under study is shown.

2. Case study

As an object of study, two residential complex to the East of Morón de la Frontera have been analysed, divided into phase 3 and phase 4, formed by 11 and 6 blocks respectively (Fig. 1). It is a group of social housing promoted by the Junta de Andalucía, which houses families with a low socio-economic level. Most of the blocks have between 3 and 4 floors, whose floors consist of an entrance, kitchen, living room and 2 or 3 bedrooms. The houses were built in 1981 (phase 3) and 1983 (phase 4).

Fig.1 – Localitation

Figure 2 shows the variance of the average daily temperature in the location in 2019. In it is observed that the daily average maximum temperature is generally above 30ºC in the summer months and generally below 10ºC in the winter months.

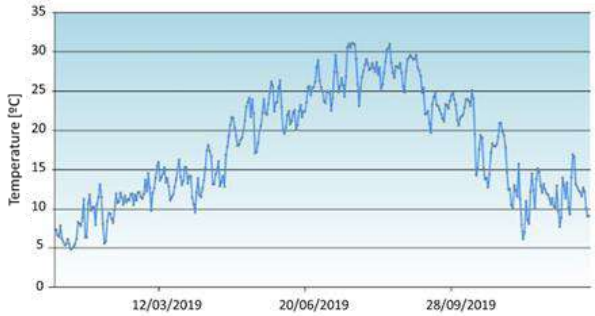

Fig.2 – Outdoor temperature (2019)

To evaluate the initial conditions of the houses, a monitoring campaign is carried out. Of all the houses of phases 3 and 4, several were chosen to be monitored, whose owners volunteered for the study. Air temperature and humidity sensors are installed in two of the rooms. After data collection for 4 months, the data was analyzed to select only those dwellings with a set of valid measures. Fig. 3 shows the selection of homes, distinguishing between those homes whose monitoring had failed and therefore there were no measures (owners who requested the uninstallation of the sensors, disconnected emitters, etc.), those that presented failures or periods without data, those whose data were acceptable and those where there was also consumption data.

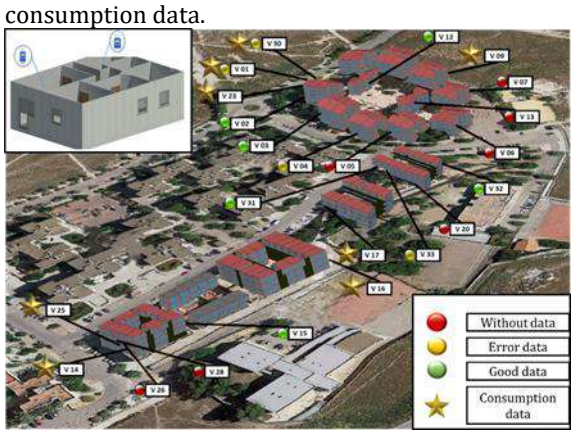

Fig.3 – Representation of the monitored dwellings

As can be seen, of the totality of dwellings, 6 of them are validated for their study, differentiating between dwellings under roof and dwellings on intermediate floors. The experimental measurements on the six monitored dwellings (Fig. 4) reveal substantial differences between them in the periods of heating and cooling and how, especially in the cooling regime, the interior temperatures of the dwellings are very far from the comfort conditions. This highlights the difference between the houses undercover and the houses with intermediate floors with differences of up to 7ºC.

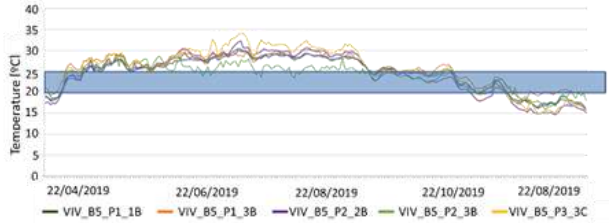

Fig.4 – Average daily temperatures measured (2019)

See how house B5_P2_3B presents an operation of the air conditioning during the cooling period. Likewise, house B5_P3_3C has the highest average daily temperatures. A daily average of almost 35ºC on some of its days means excessively high hourly temperatures. It also stands out in heating, where daily measured temperatures reach minimums below 15ºC, which shows the lack of comfort in the homes themselves.

2.1 Effect of covers

As previously observed, dwellings undercover present higher interior air temperatures than the houses on intermediate floors.

Through these temperature measurements, the thermal comfort of the dwellings is evaluated. Fig.5 shows, first and to the left, a table with 10 temperature ranges (interior) from values below 20 to above 40 with a step of 2.5ºC that will facilitate the subsequent calculation of comfort. The graphical results are presented for a dwelling located on the middle floor and a dwelling located on the upper floor based on the resulting indoor temperature data. Thus, for each range defined in the table, the number of hours that each of them is within it for the month of July is shown, as well as the weighted hour degrees out of comfort. The indicator of degrees-hours weighted outside comfort [ºC · h · ppi] not only takes into account the number of hours that the home is out of comfort but also considers the importance of the temperature difference over the comfort.

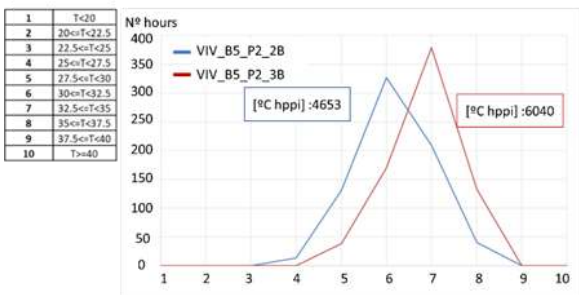

Fig.5 – Effect of roof on indoor temperatures and degrees-hours weighted out of comfort [ºChppi]

As can be seen, the upper floor dwelling (red) presents a greater number of hours within the higher temperature ranges (air temperatures above 32.5ºC). Furthermore, as is to be expected, depending on the frequency of temperatures obtained, the degree hours weighted out of comfort present a value 30% higher in the house undercover, this being due solely to the effect of the cover.

The same typology of results discussed in the previous figure has been obtained for the different months associated with the cooling regime (June, July, August, and September) and for 2 additional groups of dwellings (Group 2: B5-P1-1B (intermediate floor), B5-P1-3B (upper floor); Group 3: B5-P3-1C (intermediate floor), B5-P3-3C (upper floor)). Table 1 shows the average results for the 6 dwellings in the 4 months. As can be seen, the average contribution is 43% for the month of June, reaching 50% in the B5-P3-3C dwelling. In the hottest months, the difference caused by the contribution of the roof is less due to the high temperatures that are reached in both dwellings.

Tab.1 – Average roof contribution to improve thermal discomfort

Month	Roof Contribution average[ºC h ppi] (%)
June	43
July	20
August	20
September	30

3. Improvement measures

3.1 Retrofit

The objective of improving habitability in social housing districts is the use of passive improvement strategies adapted to the reality of the tenants, a population with limited resources. In order to solve the situation presented above, various passive improvement strategies are proposed whose objective is to reduce the demand for heating and cooling. For this, it is proposed to improve the transmittances of the enclosures through the incorporation of thermal insulation in them, improvement of the carpentry, thermal bridges, and reduction of infiltrations by improving the air tightness. These improvements have different levels of efficiency, therefore, a set of alternatives is generated with a total of 450 possible combinations of improvement. Each one is associated with a decrease in energy demand in buildings, as well as a cost of its integration. To find the optimal rehabilitation solution from the defined catalog, the optimal cost methodology proposed in the European regulation [11] is followed, seeking to achieve the minimum consumption of primary energy (PEC) and LCC. To do this, the life cycle cost (LCC) is plotted against the total primary energy consumption (Fig.6). Said indicator is required by Spanish regulations [12] and for its calculation the reference system also defined therein is used. The initial situation of the district is shown in red. The selection of the optimal case, in the case of not being subject to regulatory restrictions, would be that combination defined by that energy saving achieved with less LCC. However, the choice of the optimal case is subject to country regulatory restrictions

associated with energy demand and consumption for the climatic zone in question [12]. Of the set of combinations defined, figure 6 shows the set of combinations that meet the demand indicators established by the regulations (points marked in dark green). Finally, in addition to the restrictions on demand, restrictions on consumption are applied. The figure shows the consumption limit established by means of a blue line. The combination to be implemented is the one that meets the restrictions on demand and consumption and has a lower LCC (marked in black).

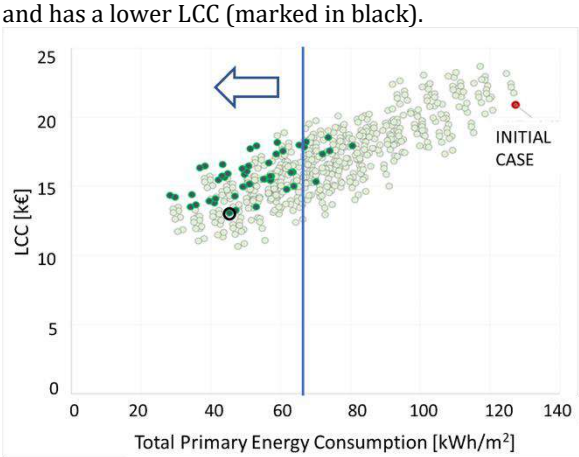

Fig.6 – Total primary energy consumption-LCC

The optimal case selected corresponds to the combination of parameters defined in Table 2.

Tab.2 – Selected rehabilitation measure

	Select combination	
Heating reduction alternative	Walls [W/m2K]	0.28
	Roof [W/m2K]	0.22
	Floor [W/m2K]	0.32
	Windows [W/m2K]	2.0
	Linear transmittance of Thermal Bridges	75%reduction
	Infiltrations + Ventilation	3
Cooling reduction alternative	Solar control (g-value of Windows in summer)	Base
	Night ventilation [1/h]	4

In the optimal case selected, the installation of an external thermal insulation system (SATE) is carried out, which is arranged on the exterior face of the building's façade; the carpentry is replaced by break of thermal bridge windows and thermoacoustic glass 5 + 15 + 6b; transmittance of walls, ceiling, floor, and windows is 0.28, 0.22, 0.32, and 2 W/m^{2}K respectively, with a 75% reduction in thermal bridges and a n50 level of 3 as alternatives for reducing heating. In the case of cooling reduction, 4 h-1 of night ventilation is contemplated, keeping the g-value of Windows in summer as the base case.

3.2 Passive cooling

As mentioned, the roof contributes significantly to the thermal discomfort of the building under cooling conditions and therefore the interest in its intervention. In view of this, the present study also carried out the integration of a ventilated roof solution.

The active roof is made up of a 5 cm high air chamber between the existing roof and the exterior wall, in such a way that it resembles a conventional ventilated façade (Fig.7) . The exterior wall is insulated in the form of an EPS "sandwich", with a total thickness of 8 cm, providing a great insulation capacity as well as lightness and thus helping to reduce the temperature transfer achieved in the chamber towards the outside. The inner sheet is located in the lower part, with one of its surfaces bordering the interior of the building. This element is where the cold that will be directed to the interior of the building is stored. Therefore, it is desirable that it has a high thermal mass and at the same time be a good conductor of heat. In the case under study, the inner sheet corresponds to the existing roof, which has 25 cm of concrete with a density of 1330 kg/m3.

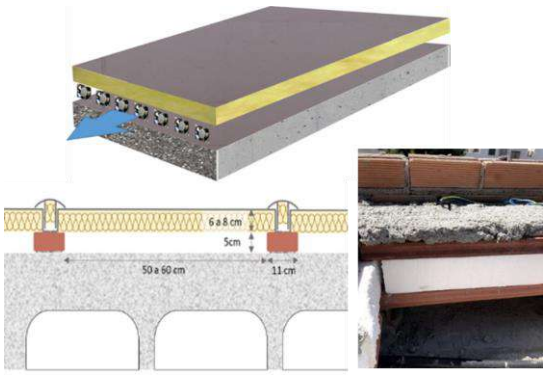

Fig.7 – Description of the innovative solution

The designed cover stands out for being an adaptive design to the climate. Therefore, this solution has two modes of operation:

In the cooling mode of operation, during the day, the air circulation is stopped. The insulated outer blade repels most of the heat while preventing the cold stored overnight on the inner blade from escaping to the outside. During the night, when the outside temperature is low enough, the air circulation is activated and dissipates heat from the inner sheet of the cover which consequently cools down. However, in case the minimum nighttime temperatures do not drop enough, an evaporative cooling system is included to achieve a further reduction in air temperature.

During the heating regime, the air chamber remains watertight and due to the high insulation of its outer sheet, high performance in the heating regime is guaranteed.

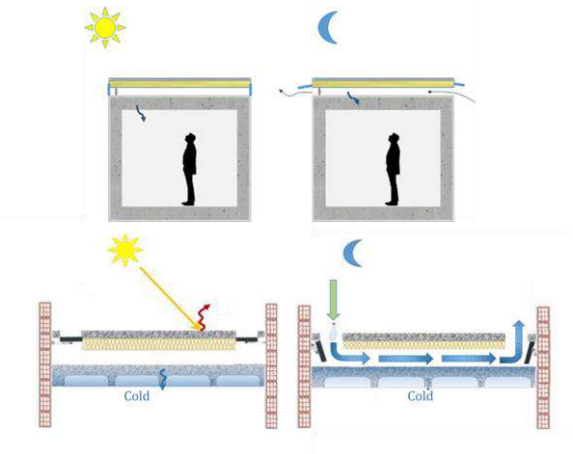

Fig.8 – Operation of the active roof

For its implementation, 3 types of modules were designed using CFD techniques with ANSYS software (Fig.8). Each module has different dimensions and geometry. The designed distribution must guarantee a uniform flow throughout the roof from a centralized air inlet and outlet of the module. Hot or cold spots must be avoided. Figure 9 shows the integration of the modules in the district blocks.

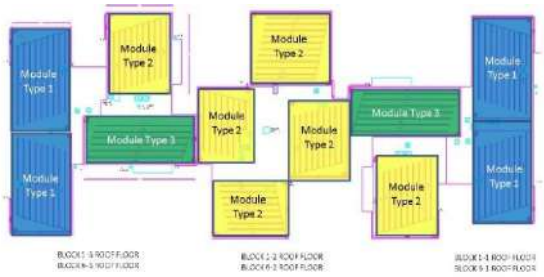

Fig. 9- Distribution of modules

The air extraction is carried out using fans, which must be capable of generating an air flow in the chamber such that the speed is approximately 1 m / s in order to avoid high-pressure losses. Finally, the water spray system must generate droplets with a size smaller than 20 micrometers and with a total water flow greater than 2.5 l/h for each meter of width of the roof. The sprinkler nozzles must be located inside the air chamber, near the inlet, downstream of the inlet hatch, and arranged in such a way as to favor the evaporation of the water in the air stream and at the same time avoid, as much as possible, surfaces to get wet.

The Figure 10 shows the assembly of the cover and its construction details.

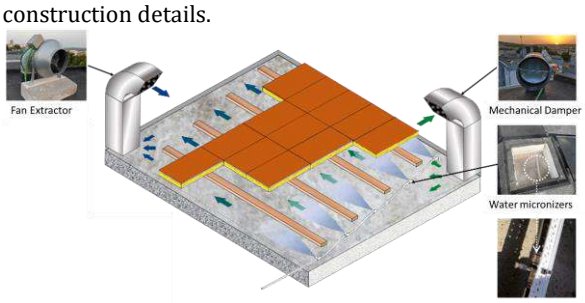

Fig. 10- Assembly of cover

4. Results

The change after the retrofit in the district is visually remarkable as shown in Fig. 11.

Fig. 11- Current state of the district

On the other hand, the cover has become a flat cover that can be fully used, with fans and extractors for air entry and exit (Fig.12).

Fig. 12- Current state of floor

Regarding the energy impact, this being the most important thing, the thermal evaluation of the buildings is carried out under the same climatic conditions as previously with the aim of subsequent comparison. For this purpose, the LIDER-CALENER Unified tool (HULC for its acronym in Spanish) is used, the official energy certification tool for buildings in Spain [13] and used by numerous studies in the recent literature [14,15]. The effect of different operating operations for one of the houses under cover in a cooling regime is analyzed. The operating operations analyzed are: ventilation operation during 8 hours at night, ventilation operation and evaporative cooling during 8 hours at night, and ventilation operation and evaporative cooling throughout the day.

Tab.3 – Evaluation of diferent operations

Type of operation	Cooling needs (kwh/m^2 year)	% Improvement
Initial case	24.7	-
Conventional rehabilitation	21.5	-
Conventional rehabilitation + vent 8h	15.56	**28**
Conventional	13.19	**39**

rehabilitation + vent-evap 8h		
Conventional rehabilitation + vent-evap 24h	7.66	**65**

As can be seen in Table 3, the operation of the ventilated roof in cooling mode increases the percentage of reduction in cooling demand from a minimum of 28% when it operates only at night in ventilation mode, to 65% when operates in ventilation and evaporative cooling mode 24 hours a day. The solution studied in the present work highlights that it is capable of achieving the maximum percentage of reduction of the load expected in the literature without causing an increase in the heating load.

In addition to the results on demand, the impact on the interior temperature of the house is evaluated, and therefore, the improvement of thermal comfort achieved after the implementation and operation of the ventilated roof. For a house under cover, the interior temperature of the house can drop up to 4 degrees compared to the non-operation of the cover when it works in ventilation and evaporative cooling mode throughout the day.

Finally, the impact is evaluated in terms of thermal comfort (Tab. 4). The results show that the operation of the active cover in ventilation mode at night reduces thermal discomfort by up to 9% compared to the conventional improvement situation (the ventilated cover does not operate). The use of the evaporative cooling system considerably increases the improvement of thermal comfort, being 36% when the operation of the same occurs only at night but reaches 80% if the use of said system occurs (ventilation and evaporative) throughout the day.

Tab.4 – Thermal comfort results

	RETROFIT			RETROFIT + VENT 8H			RETROFIT + VENT-EVAP 8H			RETROFIT + VENT-EVAP 24H		
JUNE	[ºC h]	[ºC h ppl]	[h]	[ºC h]	[ºC h ppl]	[h]	[ºC h]	[ºC h ppl]	[h]	[ºC h]	[ºC h ppl]	[h]
	667	292	323	573	233	280	458	152	259	166	29	162
JULY	RETROFIT			RETROFIT + VENT 8H			RETROFIT + VENT-EVAP 8H			RETROFIT + VENT-EVAP 24H		
	[ºC h]	[ºC h ppl]	[h]	[ºC h]	[ºC h ppl]	[h]	[ºC h]	[ºC h ppl]	[h]	[ºC h]	[ºC h ppl]	[h]
	1883	1213	640	1730	1102	617	1405	795	574	688	273	364
AUGUST	RETROFIT			RETROFIT + VENT 8H			RETROFIT + VENT-EVAP 8H			RETROFIT + VENT-EVAP 24H		
	[ºC h]	[ºC h ppl]	[h]	[ºC h]	[ºC h ppl]	[h]	[ºC h]	[ºC h ppl]	[h]	[ºC h]	[ºC h ppl]	[h]
	2157	1392	682	2042	1289	672	1673	893	650	848	282	495
SEPTEMBER	RETROFIT			RETROFIT + VENT 8H			RETROFIT + VENT-EVAP 8H			RETROFIT + VENT-EVAP 24H		
	[ºC h]	[ºC h ppl]	[h]	[ºC h]	[ºC h ppl]	[h]	[ºC h]	[ºC h ppl]	[h]	[ºC h]	[ºC h ppl]	[h]
	1201	707	502	1096	662	460	881	465	400	475	165	254
COOLING	5908	3604	2147	5441	3286	2029	4417	2305	1883	2177	749	1275
%IMPROVEMENT				**8**	**9**	**5**	**25**	**36**	**12**	**63**	**79**	**41**

The results obtained show not only the importance of integrating the ventilated roofing solution but also the optimal operating mode, which will clearly depend on the climatic zone where said system is located.

5. Conclusions

The social housing districts of southern Spain are subject to energy poverty and buildings overheating. In order to mitigate this problem in a set of real houses located in Morón de la Frontera, Seville, in the present work the design and integration of a reinforced comprehensive retrofit solution has been carried out through the use of a ventilated roof solution as a passive cooling technique. The proposed roof design allows the integration of two environmental heat sinks: cold night air and evaporative cooling. The results of the evaluation of the energy impact of the solution show that the integration of the roof solution as a passive cooling technique can achieve a reduction of the cooling load of 65% without penalizing the heating regime. The present study also highlights the real integration of the proposed solution in more than 2000 m2 and being one of the first real experiences in the world of such magnitude.

6. Acknowledgement

This research has been co-financed by the Andalusian Housing and Rehabilitation Agency under the contract "Analysis and Monitoring of the Energy Efficiency Intervention of 150 Homes in Mengíbar, in the Province of Jaén (JA-0910)" and by the European project "Mediterranean University as Catalyst for Eco-Sustainable Renovation (Med-EcoSuRe) (Grant agreement A_B.4.3_0218). Both under the support of the European Regional Development Fund ERDF.

7. References

[1] Zhang Z, Shu H, Yi H, Wang X. Household multidimensional energy poverty and its impacts on physical and mental health. Energy Policy 2021;156:112381. https://doi.org/10.1016/j.enpol.2021.112381.

[2] DCLG (Department for Communities and Local Government). Investigation into Overheating in Homes: Literature Review. 2012.

[3] Rodrigues E, Fernandes MS. Overheating risk in Mediterranean residential buildings: Comparison of current and future climate scenarios. Appl Energy 2020;259:114110. https://doi.org/10.1016/j.apenergy.2019.114110.

[4] Serrano-Lanzarote B, Ortega-Madrigal L, García-Prieto-Ruiz A, Soto-Francés L, Soto-Francés VM. Strategy for the energy renovation of the housing stock in Comunitat Valenciana (Spain). Energy Build 2016;132:117–29. https://doi.org/10.1016/j.enbuild.2016.06.087.

[5] Eskander MM, Sandoval-Reyes M, Silva CA, Vieira SM, Sousa JMC. Assessment of energy efficiency measures using multi-objective optimization in Portuguese households. Sustain Cities Soc 2017;35:764–73. https://doi.org/10.1016/j.scs.2017.09.032

.
[6] Brandão De Vasconcelos A, Pinheiro MD, Manso A, Cabaço A. EPBD cost-optimal methodology: Application to the thermal rehabilitation of the building envelope of a Portuguese residential reference building. Energy Build 2016;111:12–25. https://doi.org/10.1016/j.enbuild.2015.11.006.
[7] Santamouris M, Pavlou K, Synnefa A, Niachou K, Kolokotsa D. Recent progress on passive cooling techniques: Advanced technological developments to improve survivability levels in low-income households. Energy Build 2007;39:859–66. https://doi.org/10.1016/J.ENBUILD.2007.02.008.
[8] Ascione F, Bianco N, Iovane T, Mastellone M, Mauro GM. The evolution of building energy retrofit via double-skin and responsive façades: A review. Sol Energy 2021;224:703–17. https://doi.org/10.1016/j.solener.2021.06.035.
[9] Bhamare DK, Rathod MK, Banerjee J. Passive cooling techniques for building and their applicability in different climatic zones—The state of art. Energy Build 2019;198:467–90. https://doi.org/10.1016/j.enbuild.2019.06.023.
[10] Lissen JMS, Escudero CIJ, De La Flor FJS, Escudero MN, Karlessi T, Assimakopoulos MN. Optimal renovation strategies through life-cycle analysis in a pilot building located in a mild mediterranean climate. Appl Sci 2021;11:1–25. https://doi.org/10.3390/app11041423.
[11] EU. Directive 2010/31/EU of the European Parliament and of the Council of 19 May 2010 on the energy performance of buildings (recast). Off J Eur Union 2010:13–35. https://doi.org/doi:10.3000/17252555.L_2010.153.eng.
[12] Ministerio de Fomento. Documento Básico HE Ahorro de Energía 2019. Código Técnico La Edif 2019:1–129.
[13] Ministry of Development. Unified LIDER-CALENER software Tool (HULC); 2019. n.d.
[14] Gallego Sánchez-Torija J, Fernández Nieto MA, Gómez Serrano PJ. The merits of making energy costs visible: The sustainability benefits of monetizing energy efficiency certificates in Spanish rental homes. Energy Res Soc Sci 2021;79:102169. https://doi.org/10.1016/j.erss.2021.102169.
[15] Las-heras-casas J, Olasolo-alonso P, Luis ML, Luis ML. Towards nearly zero-energy buildings in Mediterranean countries : Fifteen years of implementing the Energy Performance of Buildings Directive in Spain (2006 – 2020) 2021;44. https://doi.org/10.1016/j.jobe.2021.102962.

Evaluation of Building Retrofitting Alternatives Towards Zero Energy School Building in Turkey

Ayşe Özlem Dal [a,c], *Touraj Ashrafian* [b,c]

[a] Graduate School of Engineering and Science, Özyeğin University, İstanbul, Turkey, ozlem.dal@ozu.edu.tr.

[b] Faculty of Architecture and Design, Özyeğin University, İstanbul, Turkey, touraj.ashrafian@ozyegin.edu.tr.

[c] Building Materials and Physics Laboratory, Özyeğin University, İstanbul, Turkey.

Abstract. The building sector plays a vital role in coping with current worldwide challenges: climate change, urbanization, and environmental pollution. Building performance analysis is essential from the energy consumption, comfort, and carbon emission point of view. Different paradigms have been studied for many years, like bioclimatic architecture, sustainable architecture, green architecture, and carbon-neutral architecture. The regenerative paradigm has been a critical topic since 2016 to look toward positive impact architecture for going beyond the neutral impact. The research aims to examine the existing condition of a school building in İstanbul, Turkey, to investigate a strategy for achieving energy-efficient school building towards zero energy. The research method is based on preparing the energy model of the school and making simulations by using Design Builder software and Energy Plus software. The validated simulation is used to examine the retrofit packages for the efficiency of the school building and discuss the alternatives that are categorized as two alternatives for the insulation layer, three types of glazing alternatives, two types of the lighting system, and five alternatives for the HVAC system. By the combination of the alternatives, 111 retrofit packages are analysed. According to the comparison of the packages, the P102 scenario has the lowest results for the primary energy for electricity (P.E.E), primary energy for natural gas (P.E.N.), and the total primary energy (T.P.E) as 1.84 kWh/m^2, 1.51 kWh/m^2, and 3.35 kWh/m^2 thanks the integration of renewable energy systems; while the existing condition of the case study school building has 29.99 kWh/m^2, 63.05 kWh/m^2, and 93.05 kWh/m^2 respectively. Therefore, towards zero energy school building, the retrofit scenarios are significant to reduce the negative impact of a building on the environment by highlighting the combination of the renewable energy system and advanced HVAC system and with the integration of proper insulation thickness, efficient glazing, and lighting type. The alternatives and aspects of the research can provide a strategy for further study steps and related studies to improve the building stock towards zero energy in school buildings.

Keywords. Building Energy Efficiency, School Building, Regenerative Architecture, Primary Energy.
DOI: https://doi.org/10.34641/clima.2022.160

1. Introduction

In the world, buildings and construction sectors are responsible for almost %40 of total energy consumption and 36% of CO2 emissions [1,2,3,5]. Energy Performance Building Directive aims to decrease greenhouse gas emissions by at least 40% by 2030 compared with 1990, as mentioned in the latest version [4]. All these targets are to decrease the negative impacts of the building sector like increasing carbon emissions, climate change, scarcity of resources, depletion of fossil fuels, population growth, and urbanization [5]. From the 20th to 21st century in the field of architecture and urbanization, to enhance a sustainable build environment, seven phases of sustainable paradigms [6] can be categorized as bioclimatic architecture [7], environmental architecture, energy-conscious architecture, sustainable architecture [8], green architecture [9], carbon-neutral architecture [10], and regenerative architecture which is mainly focused on after 2016 about providing the positive ecological built environment for both building and urban level by going beyond neutrality [11,5].

The education sector has an essential part of the world's building sector since it is stated that more than 40% of the existing schools are insufficient for providing Indoor Air Quality in the world [12]. Thus, it causes the usage of additional heating, cooling, and air-conditioning systems, which account for 60% and 70% of the total energy used in non-industrial buildings like educational facilities [13]. In Europe, 64 million students and nearly 4.5 million teachers spend their time in pre-primary

Copyright ©2022 by the authors. This conference paper is published under a CC-BY-4.0 license.

schools and elementary schools [12]. In 2018, Eurostat data stated that by 2050 annual student population growth rate will increase 3 percent, which means a need for 40.000 new classrooms [14]. Thus, school buildings are a significant part of the building sector not only for the environment and economy by saving energy and being positive and neutral approaches but also to have a healthy and comfortable learning environment for children and teachers since students spend 30% percent of their time in schools [12].

There are several actions worldwide toward going beyond net-zero energy building requirements. In the USA, there are 117,007 schools and nearly 73 million students. Educational facilities are responsible for 80% of energy consumption for lighting, ventilation, heating, and cooling energy consumption and they pay more than $ 6 billion per year to encounter their energy costs [15]. Therefore, *the "green school"* concept is developed for saving energy, resources, and the economy without compromising the need of students and teachers as a healthy environment [15]. In Belgium, education facilities are responsible for 1.5 percent of greenhouse gas emissions; nearly 3 million students attend 6000 schools every day. They set a target for 2021 to be carbon neutral and usage of renewable sources in educational facilities [14]. *Nearly Zero Energy Schools* program is managed to reduce energy use from 0.7 to 0 in academic buildings in Dutch by 2050; there will be an 80% reduction in primary energy consumption compared to 1990 [12]. With the aim of climate-neutral new buildings in Germany [16], there are 15.446 schools with a total consumption of 270,000 MWh [15]. Therefore, the application of "*Passive House Standards in School Buildings"* is to provide solutions to achieving *NZEB* standards in schools with the basis of the directive [17]. Providing Net Zero Energy schools strategies are mentioned as the further improvement of passive schools [18]. More than 60% of school buildings were built in Italy without energy-related regulation; 30% of them were measured as poor energy performance. Thus, the average energy use of the school's buildings is almost 290 kWh/m2/year [15]. A deep energy renovation study was conducted in Italy by achieving a %60 reduction in heating consumption and electricity neutrality regarding upgrading the performance of the envelope by including an insulation layer on the roof and floor, adding external shading devices to protect new windows, redesigning the heating system, conducting a roof PV plant [19]. The other related projects in Europe to raise awareness for sustainable strategies in schools both for new and existing ones *"School of The Future"* [20,19], *"ZEMeds"* [21], *"Educa-RUE (Rational Use of Energy)"* [22], *"Renew Schools", "Veryschool", "Teenergy Schools" and "Check It Out"* [13]. Education facilities which are a part of the non-residential building sector, seem a vital topic to saving energy, resources and having a positive impact on the three main components of sustainability in the world.

Turkey, a candidate of being a European country, shares the same significant problems and is in the adaptation process for European Union, needs to take the responsibility of decreasing the negative impacts of building stock. About the existing building stock, as it is mentioned by the European Commission, nearly half of the dwellings are over 50 years [23]. There is a meager percentage of refurbishment rate between 0.4 and 1.2 % per year; therefore, renovation of existing buildings is critical to 2050 as a long-term target [24]. Educational facilities are essential to consider both for new and existing buildings. According to the nation's non-residential energy needs, % 15 of total energy consumption is accounted for from the non-residential sector, including educational buildings. According to national statistics for 2015 and 2016 [25], 99,156 school buildings serve 23 million students and 1.290 million teachers. It means that most of the population spends more time in schools [26]. There needs to act toward regenerative architecture and positive impact architecture on educational facilities from this moment. It is necessary not only to reduce energy consumption as an economical feature by directing renewable sources but also for the environment to cope with the 21st-century environmental problems and encourage society to be more sustainable since it is proved that just by changing the behavior in school buildings, energy consumption can be sustained between %5 to 15% in a school [27]. There can be achieved %60 of primary energy savings and CO2 emission reductions; % 42 of global cost-saving in a maximum of 7 years by implementing energy-efficient retrofit scenarios on school buildings [28].

The study aims to conduct research by focusing on retrofitting an existing school building based on the alternatives of envelope measures, lighting measures, and HVAC measures. The combination of the alternatives enables the retrofit scenarios after validating the energy modeling. The comparison demonstrates the optimum scenario of retrofitting strategies toward zero-energy school buildings.

2. Methodology

For the evaluation of envelope, lighting, and HVAC measures, a school building in İstanbul, Beykoz is decided. The total building area of the school is 2044 m^2. The school building has five floors, including the basement and attic floor. There are fifty-nine different zones like classroom, library, kindergarten, and corridor. The HVAC system of the case study is based on radiator heating, boiler hot water, and natural ventilation. All the zones, excluding elevator, kitchen, staircase, fire stair, windbreak, and WCs are heated by the same mechanical system. The HVAC system is combined with packaged thermal air conditioner for the zones of "teacher room 1" and "director room 3". Design Builder 4.7 software was used for energy modelling by indicating 2D drawing of the school from the AutoCAD programme. Figure 1 shows the Design

Builder model of the school building. Figure 2 indicates the summary of the progress.

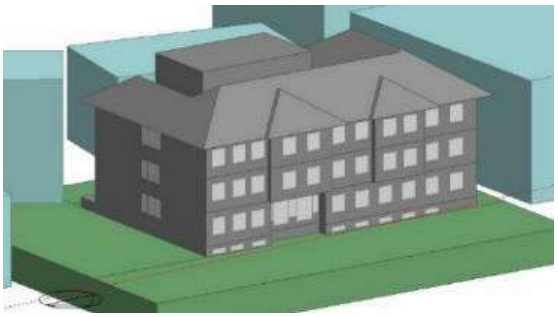

Fig. 1 – Design Builder model of the school building.

To reflect the existing condition of the school, the data about density, equipment, and lighting of the zones were indicated according to the site analysis. The occupancy schedules related to the daily usage of the zones are indicated. The data is taken from the school administration. The schedule of the zones for occupancy, lighting, and equipment is organized based on class and breaking times. The schedule of lessons identifies the usage pattern of the corridors, storages, and WCs. The school is mainly available between 09.00 am and 16.00 pm. Still, some of the zone's schedules can differ, like the heating centre available during weekends between 08.00 am and 12.00 pm. Table 1 shows the primary occupancy management of the school building.

Tab. 1 – Schedule the organisation of the case study.

Main Zones	Weekdays	Weekends	Holidays
Classroom	09.00-16.30	Off	Off
Classroom 2	09.00-13.10	Off	Off
Kindergarten	09.00-14.00	Off	Off
Kitchen	08.00-16.30		Off
Administration and teachers	08.00-15.35	Off	Off
Heating centre	07.00-16.00	08.00-12.00	Off

The usage of the zones identifies the type of metabolism. Standing/ walking is for circulation areas. Reading seated is for classrooms, kindergarten, administration, and teacher rooms. Light manual work is for the engine room and kitchen and eating/drinking is for the canteen. Also, target illuminance is managed as 400 lux.

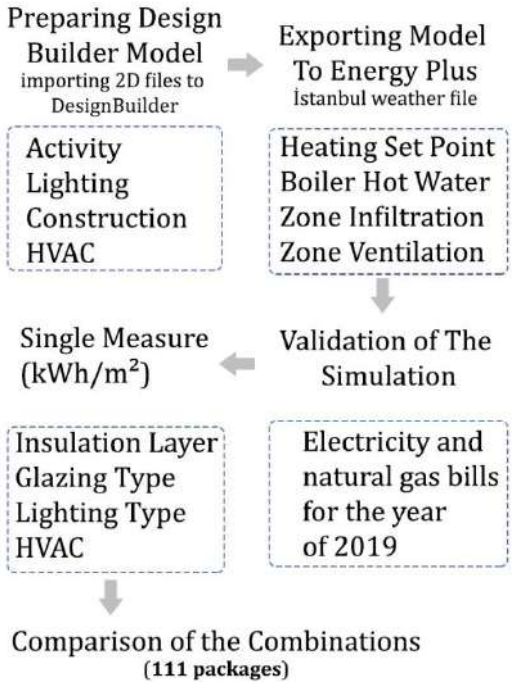

Fig. 2 – Summary of the progress.

The construction materials of the case study are indicated according to technical drawings. The materials for external walls, underground walls, roofs, internal partitions, ground floor, basement floor, and internal floors were obtained. The U value (W/m^2-K) results are compared with TS 825 Standard for İstanbul [29]. A detailed explanation is in Table 2. The comparison of the existing situation of the school with the standard shows that the U value (W/m^2-K) results of the external floor, flat roof, and glazing system exceed the standardized number. Also, the result for the basement floor can be reduced. Therefore, the retrofit scenarios are categorized as an insulation layer, lighting type, glazing type, and heating system improvements. The scenarios are compared according to equation (1), which is the primary energy calculation [28].

Total Primary Energy= (Total End Uses Electricity(kwh) x 2,36) +Total End Uses Natural Gas(kwh) (1)

After the modeling process, the validation of the simulation is conducted based on the bills of electricity (kWh) and natural gas (kWh) for 2019. Energy Plus software is used for this stage of the research. In the software, the heating setpoint is conducted as 24, and the nominal thermal efficiency of the boiler is taken as 0.75. About zone infiltration, for the zones that have an external wall, air changes per hour unit is indicated as 0,6 1/hr. 0,2 1/hr is for the zones of the basement floor. The rate is obtained as zero for the zones that do not have an external wall. About zone ventilation, the air changes per hour unit is indicated as 3 for the zones in the south. The zoned in the north, the value is obtained as 2. For the zones that do not have windows, the rate is indicated as 0.

Tab. 2 – The properties of the construction.

Construction	Properties (meters)	U value (W/m^2-K)	Maximum U value in TS825
External wall	Plaster (0,03), XPS (0,03), Plaster (0,02), Brick (0,30), Plaster (0,02)	0.617	0.57
Below grade walls	Brick (0,09), Plaster (0,02), XPS (0,03), Insulating Plaster (0,02), Reinforced Concreate (0,3), Plaster (0,04)	0.645	No value
Flat roof	Gravel (0,07), Roofing Felt (0,01), XPS (0,05), Mortar (0,05), Cast Concreate (0,2), Plaster (0,03)	0.462	0.38
Pitched roof (occupied)	Clay (0,04), Air Gap (0,02), Wood (0,1)	2.214	No value
Internal partitions	Plaster (0,01), Masonry (0,15), Plaster (0,01)	0.946	No value
Ground floor	Plaster (0,02), Cast Concreate (0,3), Floor Screed (0,03), Marble (0,03)	1.622	No value
Basement floor	Cast Concreate (0,3), Screed (0,03), XPS (0,03), Floor Screed (0,05), Plaster (0,03), Ceramic (0,02)	0.386	0.57
Internal Floor	Plaster (0,02), Cast Concreate (0,3), Floor Screed (0,03), Marble (0,03)	1,499	No value
Opening	Double Clear Glazing (6mm/13mm air)	2.708	1.8

Tab. 3 – Validated simulation results.

Months	Actual Electricity (kwh)	Sim. Electricity (kwh)	Actual Natural Gas (kwh)	Sim. Natural Gas (kwh)
1	2,412.50	2,666.00	37,867.76	30,356.25
2	2,131.27	2,507.00	37,420.88	26,414.65
3	2,630.65	2,879.00	25,408.32	24,629.03
4	2,676.10	2,726.00	26,004.16	16,323.91
5	2,404.92	2,879.00	1,936.4	2,399.42
6	1,324.57	1,791.00	566.05	566.05
7	725.35	56.60	354.66	354.66
8	725.35	56.60	354.66	354.66
9	725.35	1,943.00	354.66	354.66
10	1,881.37	2,843.00	1,010.8	1,010.80
11	1,856.62	2,788.00	13,448.96	14,252.69
12	2,482.87	2,831.00	24,759.28	28,516.17
Total	21,976.9	25,966.5	169,486.67	145,532.95

According to the ASHRAE standard [30], the simulation is validated for the difference of 15% yearly and 5% monthly. The yearly electricity result is 25,966.53 kWh in the simulation, the existing situation of the school is 21,976.92 kWh. The annual result of the electricity is proper at 15%.

Tab. 4 – Single Measures.

	Single Measure	P.E.E.	P.E.N.	T.P.E.
	Existing Condition	**29.99**	**63.05**	**93.05**
Insulation Layer	**I1** 6;10;6	29.99	55.78	85.77
	I2 9:15;9	29.99	52.18	82.17
Glazing	**G1** Dbl LoE Clr	28.37	59.39	87.77
	G2 Triple Clr	28.35	57.97	86.33
	G3 Trp LoE	28.51	57.42	85.93
Lighting	**L1** CFL	27.33	63.7	91.04
	L2 LED	27.03	63.7	90.83
HVAC	**H1** PV Panel (10kW=11750kWh)	16.43	63.05	79.98
	H2 PV Panel (20 kW= 23500kWh)	2.86	63.05	65.91
	H3 PV Panel (30 kW=32250 kWh)	-10.69	63.05	52.36
	H4 Heat Pump	48.05	1.13	49.19
	H5 %95 efficient Condensing Boiler	29.99	46.1	76.1

According to monthly results, except for three months, the results are between 5%. The yearly result for natural gas is 145,532.95 kWh in the simulation, while the existing situation is 169,486.67 kWh. The simulation result of natural gas is in the suitable difference of 15%. Also, the monthly results are in between the proper percentage of 5% excepting January, February, and April. Table 3 displays the detail of validated simulation results.

For the existing condition of the school building, the primary energy for electricity is 29.99 kWh/m^2; the primary energy for natural gas is 63.05 kWh/m^2; the total primary energy is 93.05 kWh/m^2. There are four main retrofit alternatives: increasing the thickness of the insulation layer, changing the glazing type, changing the lighting type, and suggesting different HVAC systems. There are two alternatives for improving the insulation: two times of existing condition and three times for external wall, flat roof, and basement floor, respectively. Three alternatives of the glazing type are Dbl LoE (e=1) Clr 6mm/13mm Air, Triple Clr 3mm/13mm Air, and Triple LoE (e2=e5=1) Clr 3mm/13mm Air. Fluorescent compact (CFL) and LED are the lighting alternatives. For the HVAC system, the main ones are photovoltaic (PV) panel, heat pump, and condensing boiler with 95% efficiency. The potential of generating electricity from PV panel implementation has three alternatives as 10Kw, 20kW, and 30Kw, respectively. Table 4 indicates the detailed explanation of single alternatives with the calculations of primary energy. In the table, P.E.E. is the abbreviation of primary energy for electricity (kWh/m^2); P.E.N. is the abbreviation of primary energy for natural gas (kWh/m^2), and T.P.E. is the abbreviation of total primary energy (kWh/m^2).

The efficiency rate of CFL is between 62% and 80% [31,32]. The average of the numbers is 76%, calculated in the alternative scenario. The efficiency rate of LED is between 75% and 93% [33]. Thus, the average of the numbers is 85% indicated in the scenario. Also, the generated electricity number thanks to PV panels is identified according to the radiation received by Turkey as 10kW solar panel generates electricity between 11.000 kWh and 12.500 kWh per year [34]. Thus, the average is 11.750 is considered in the research.

3. Results and Discussion

According to combinations of four single alternatives, 111 retrofit packages have been organized by including two alternatives for insulation thickness, three types of glazing, two types of lighting, and five alternatives for HVAC systems. Also, the HVAC alternatives of H1 and H5 are combined with H1, H2, and H3. The results of the 111 packages in terms of P.E.E., P.E.N, and T.P.E. are indicated in Figure 3.

The packages between P1 and P12 are the combinations of the 10kW PV panel. The minimum result for the primary energy for electricity is in P10 with 17.71 kWh/m^2. In contrast, the minimum value for the primary energy for natural gas is 62.69 kWh/m^2 in P6. P12 has the minimum value for total primary energy with 80.49 kWh/m^2 thanks to I2, G3, and L2 combinations.

The packages between P13 and P24 integrate a 20kW PV panel. Package 20 has the lowest primary energy of electricity at -0.47 kWh/m^2. P24 has the lowest primary energy for natural gas and total primary energy at 62.77 kWh/m^2 and 62.32 kWh/m^2, respectively.

For the 30 kW PV panel combinations that are between the packages P25 and P36, the minimum result for the P.E.E. is in the scenario of P32 as -14.01 kWh/m^2. P.E.N and T.P.E, P36 has the minimum result of 62.77 kWh/m^2, and 48.77 kWh/m^2, respectively. The main finding for the packages between P1 and P36 which is the combinations of PV panel scenarios is that although the P.E.E. results are remarkably decreased especially by combining 30 kW PV panel and G3 type glazing alternative, the P.E.N. results are close to the existing condition of the school which is 63.05 kWh/m^2.

The heat pump alternatives and their scenarios are between P37 and P48. The combinations of heat pumps have a considerable decrease for the results of P.E.N. as 1.51 kWh/m^2. However, the minimum values of P.E.E. and T.P.E are 51.75 kWh/m^2 and 53.26 kWh/m^2, respectively, in the P48 scenario.

The 95% efficient condensing boiler combinations are between P49 and P60. The packages of P55 and P56 has the minimum results for P.E.E with 35.89 kWh/m^2, while the minimum result for P.E.N. is 45.80 kWh/m^2 in the scenario of P54. According to the T.P.E., P60 has a minimum result of 81.77 kWh/m^2. To exemplify the impact of PV panel alternatives by the combination of a 95% efficient boiler, the packages between P61 and P96 were analyzed. P86 has a -14.18 kWh/m^2 P.E.E result which is the least number for P.E.E in the 111 scenarios. P.E.N is 47.61 kWh/m^2, and T.P.E. is 31.86 kWh/m^2, which is approximately one-third of the existing condition of the school building.

The packages between P97 and P111 combine scenarios by integrating both heat pump and PV panel alternatives. The results of the related packages show that a combination of heat pump and PV panel enables a significant decrease for the P.E.E. by comparing with the results of offering a 95% efficient condensing boiler and PV panel. Suggesting only a heat pump, PV panel, and the efficient condensing boiler is not enough to achieve the aims of zero energy school building. The combination of heat pump and PV panel implementation verifies the statement.

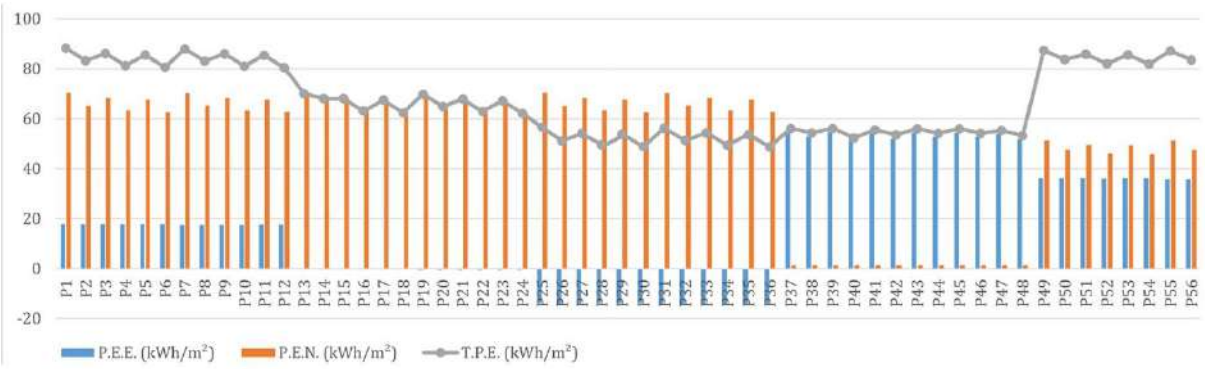

(continued)

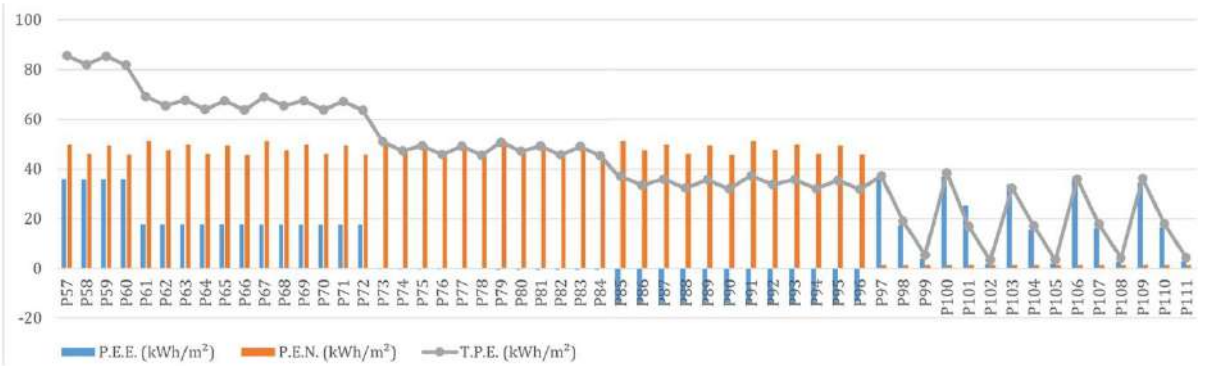

Fig. 3 – Simulation results for 111 packages.

P102 is the best scenario in the 111 packages with the results of P.E.E, P.E.N, and T.P.E as 1.84 kWh/m^2, 1.51 kWh/m^2, and 3.54 kWh/m^2 respectively. The scenario includes the alternatives of I2. G3, and L2. Table 5 shows the lowest results for P.E.E., P.E.N., and T.P.E by the packages with different HVAC alternative combinations. All the scenarios include I2 alternative as the maximum thickness of the insulation layer. Most of them are combined with G3 as the Triple LoE glazing alternatives and L2 as the LED lighting type. Therefore, these three alternatives can be mentioned as the efficient single alternatives of the retrofit packages.

4. Conclusion

Energy efficiency for educational buildings is critical since a significant part of the population as students and teachers spend most of their time in schools. Therefore, the research focuses on increasing the energy efficiency of a school building in İstanbul, Turkey, towards zero energy.

111 retrofit packages were examined in the study with the combination of the two different thicknesses for insulation layer, three types of glazing system, two alternatives for lighting types as CFL and LED, also five alternatives for the HVAC system. The results are compared according to primary energy for electricity, primary energy for natural gas, and total primary energy. The package of P102 has the lowest results for P.E.E, P.E.N., and

Tab. 5 – Packages with minimum primary energy for electricity (kWh/m^2), natural gas (kWh/m^2), and total primary energy (kWh/m^2).

Package	P.E.E.	P.E.N	T.P.E
P6: I2, G3, L1, H1	17.96	62.69	80.65
P10: I2, G2, L2, H1	17.71	63.42	81.13
P12: I2, G3, L2, H1	17.72	62.77	80.49
P20: I2, G1, L2, H2	-0.47	65.37	64.90
P24: I2, G3, L2, H2	-0.45	62.77	62.32
P26: I2, G1, L1, H3	-14.18	65.29	51.10
P32: I2, G1, L2, H3	-14.01	65.37	51.35
P36: I2, G3, L2, H3	-13.99	62.77	48.77
P40: I2, G2, L1, H4	52.81	1.51	54.32
P48: I2, G3, L2, H4	51.75	1.51	53.26
P54: I2, G3, L1, H5	36.14	45.80	81.94
P60: I2, G3, L2, H5	35.91	45.86	81.77
P70: I2, G2, L2, H1+H5	17.71	46.11	63.82
P78: I2, G3, L1, H2+H5	-0.22	45.80	45.58
P80: I2, G1, L2, H2+H5	-0.47	47.68	47.21
P86: I2, G1, L1, H3+H5	-14.18	47.61	33.43
P96: I2, G3, L2, H3+H5	-13.39	45.86	31.86
P102:I2, G3, L2, H3+H4	1.84	1.51	3.35
P105:I2, G3, L1, H3+H4	2.03	1.51	3.54

T.P.E. as 1.84 kWh/m^2, 1.51 kWh/m^2, and 3.35 kWh/m^2; while the existing condition of the case study school building has 29.99 kWh/m^2, 63.05 kWh/m^2, and 93.05 kWh/m^2 respectively. P102 combines a 30 kW PV panel and heat pump with I2, G3, and L2 alternatives for insulation layer, glazing, and lighting. The result of the retrofit scenarios can provide a basis towards zero energy school building level by highlighting the importance of renewable energy integration for the alternatives of advanced HVAC system types can make a remarkable decrease for the results of primary energy for electricity, natural gas, and total primary energy results.

The regenerative paradigm toward positive impact architecture is an essential research area in recent years to decrease the negative impacts of the building sector. As a further step of the research, by taking as a base the P102 scenario, the different alternatives, and renewable energy solutions can be examined toward positive impact on a school building, since the result of the retrofit scenarios displays those single combinations are not enough to achieve the efficiency level of the building towards regenerative and positive impact architecture. These can be critical for further studies related to the topic. Since a major part of schools in Turkey use natural ventilation as a basis, retrofitting scenarios do not include mechanical ventilation. The research does not include the integration of comfort, system, and cost. Further studies can also consider the results and aspects of the scenarios in their research and analysis.

5. Acknowledgement

There is a need to express gratitude to the case study school building of this research which is Necip Fazıl Kısakürek Primary-Secondary School in İstanbul, Beykoz.

6. References

[1] Abergel T, Delmastro C, Lane K. Tracking Buildings 2020 [Internet]. Paris: International Energy Agency; [updated 2020; cited2022 Jan2]. Available from: https://www.iea.org/reports/tracking-buildings-2020.

[2] Directive 2002/91/EC of the European Parliament and of the Council of 16 December 2002 on the Energy Performance of Buildings. Off J Eur Union. 2003; 1:65-71.

[3] EPBD recast. Directive 2010/31/EU of the European Parliament and of council of 19 May 2010 on the energy performance of buildings (recast). Off J Eur Union. 2010: 13-35.

[4] Directive (EU) 2018/844 of the European Parliament of the Council of 30 May 2018 amending Directive 2010/31/EU on the energy performance of buildings and Directive 2012/ 27/ EU on energy efficiency. Off J Eur Union. 2018: 75-91.

[5] Attia S. Regenerative and positive impact architecture: learning from case studies. Springer International Publishing; 2018.

[6] Attia S. Towards regenerative and positive impact architecture: a comparison of two net zero energy buildings. Sustainable Cities and Society. 2016; 26: 393-406.

[7] Sala M, Gallo C, Sayigh A. Architecture- Comfort and Energy. Elsevier; 1999.

[8] Lechner N. Heating, cooling, lighting: sustainable design methods for architects. John Wiley & Son; 2014.

[9] Bauer M, Mösle P, Schwards M. Green building: guidebook for sustainable architecture. Springer Science & Business Media; 2009.

[10] La Roche P. Carbon-neutral architectural design. CRC Press; 2017.

[11] Shandiz SC, Rismanchi B, Foliente G. Energy master planning for net-zero emission communities: state of the art and research challenges. Renewable and Sustainable Energy Reviews. 2021; 137(110600):110600.

[12] Golshan M, Thoen H, Zeiler W. Dutch sustainable schools towards energy positive. Journal of Building Engineering. 2018; 19:161-171.

[13] Gil-Baez M, Barrios-Pudara A, Molina-Huelva M, et al. Natural ventilation systems in 21st centuary for near zero energy school buildings. Energy. 2017; 137:1186-1200.

[14] Attia S, Shadmanfar N, Ricci F. Developing two benchmark model for nearly zero energy schools. Applied Energy. 2020; 263:114614.

[15] AlFaris F, Juaidi A, Manzano-Agugliaro F. Improvement of efficiency through an energy management program as a sustainable practice in schools. Journal of Clear Production. 2016; 138:794-805.

[16] Ascione F, Bianco N, De Masi R.F, Mauro G.M, et al. Energy retrofit of educational buildings: transient energy simulations, model calibration and multi-objective optimization towards nearly zero-energy performance. Energy and Buildings. 2017; 144:303-319.

[17] Wang Y, Du J, Kuckelkorn A, et al. Identifying the feasibility of establishing a passive house school in central Europe: an energy performance

and carbon emissions monitoring study in Germany. Renewable and Sustainable Energy Reviews. 2019; 113:109256.

[18] Zeiler W, Boxem G. Net-zero energy building schools. Renewable Energy; 49:282-286.

[19] Zinzi M, Battistini G, Ragazzini V. Energy and environmental monitoring of a school building deep energy renovation in Italy. Energy Procedia. 2015; 79:3318-3323.

[20] Morck O, Thomsen K.E, Jorgensen B.E. School of the future: deep energy renovation of the Hedegaards School in Denmark. Energy Procedia. 2015; 78:3324-3329.

[21] Dalla Mora T, Righi A, Peron F, et al. Cost-optimal measures for renovation of existing school building towards Nzeb. Energy Procedia. 2017; 140:288-302.

[22] Desideri U, Leonardi D, Arcioni L, et al. European projects Educa-RUE: an example of energy efficiency paths in educational buildings. Applied Energy. 2012; 97:384-395.

[23] Sekki T, Airaksinen M, Saari A. Effect of energy measures on the values of energy efficiency indicators in Finnish daycare and school buildings. Energy and Buildings. 2017; 139:124-132.

[24] Assimakopoulos M, De Masi R.F, Fotopoulou A, et al. Holistic approach for energy retrofit with volumetric add-ons toward nzeb target: case study of a dormitory in Athens. Energy and Buildings. 2020; 207:109630.

[25] Turkish Ministry of National Education. National education statistics-formal education-2015-2016. Ankara: National Education Strategy Development Presidency; 2015.

[26] Ashrafian T, Moazzen N. The impact of glazing ratio and window configuration on occupants' comfort and energy demand: the case study of a school building in Eskisehir, Turkey. Sustainable Cities and Society. 2019; 47:101483.

[27] Salleh M.N.M, Kandar M.Z, Sakip S.R.M, et al. User's perception of energy efficiency in school design. Procedia-Social and Behavioral Sciences. 2014; 170: 155-164.

[28] Moazzen N, Ashrafian T, Yılmaz Z, et al. A multi-criteria approach to affordable energy-efficient retrofit of primary school buildings. Applied Energy. 2020; 268:115046.

[29] Turkish Standardization Institute. TS825: Thermal insulation requirements for buildings. TSE; 2013.

[30] American Society of Heating, Refrigerating and Air-Conditioning Engineers (ASHRAE). ASHRAE Guideline 14: Measurement of Energy, Demand, and Water Saving. Atlanta, US; 2014. ISSN: 1049-894X.

[31] Soori P.K, Alzubaidi S. Study on improving the efficiency of office building's lighting system design. IEE GCC Conference and Exhibition. 2011:585-588.

[32] Mills B, Schleich J. Household transitions to energy efficient light. Energy Economics. 2014; 46:151-60.

[33] Perdahçı C, Hanlı U. Verimli aydınlatma Yöntemleri. EVK 2009. 2009:323-7.

[34] My Energy Solar. 10 kW Güneş Enerjisi Kurulum Maliyeti 2020 [Internet]. [place unknown]: [publisher unknown]; 2020 [cited 2022 Jan 6]. Available from: https://www.myenerjisolar.com/10-kw-gunes-enerjisi-kurulum-maliyeti-2020/

Data sharing not applicable to this article as no datasets were generated or analysed during the current study.

Design under uncertainty of solar hot water systems for hospitals

Antonio Atienza-Márquez, Fernando Domínguez Muñoz, Francisco Fernández Hernández, José Manuel Cejudo López

Energy Research Group (GEUMA), Department of mechanical, thermal and Fluids Engineering, Universidad de Málaga. C/Doctor Pedro Ortiz Ramos s/n, 29013 Málaga, Spain. E-mail: atienza-marquez@uma.es

Abstract. Failed designs are often behind underperforming solar hot water systems and excessive fossil fuel consumption in backup units. This paper proposed a reliable and robust method to design a solar thermal system combined with boilers for hot water preparation in a medium size-hospital hospital building with an average daily demand of 8.69 m^3. To start with, the conventional deterministic design, which assumes business-as-usual parameter values and overlooks their uncertainties, gives a required solar caption area of 223.0 m^2 to achieve an annual solar fraction of 70%. However, if the uncertainties of input parameters are considered, the reliability of this design solution is barely 22% regarding the solar fraction target set, and a solar caption area of 326 m^2 would be required to achieve a reliability of 90%. This work proposes a revised design solution which such high level of trustworthiness but with a lower solar caption area and, therefore, more attractive from an economic perspective. The strategy consists of narrowing the uncertainty bounds of those controllable parameters causing major variance on the system performance. A sensitivity analysis showed that the most significant uncertainties concerning the variance of the solar fraction are the following (in decreasing order of importance): variation of the hot water supplying set-point, insulation defects in the hot water distribution loop, wrong adjustment of thermostatic valves and dust deposition on collectors. According to the improved design proposed rooted in the revision of uncertainties through the installation of high-quality measurement and control equipment and effective maintenance, a design with a solar caption area of 257.3 m^2 would be enough to reduce the probability of failure below 10%.

Keywords. Domestic hot water, uncertainty, hospital building, solar thermal system, robust design.
DOI: https://doi.org/10.34641/clima.2022.161

1. Introduction

The integration of solar thermal systems in hospitals is a widespread solution to mitigate the carbon footprint of domestic hot water (DHW) production systems. Indeed, the minimum solar contribution required in such kind of large hot water consumer buildings is usually set from regulations, and thereby installations are designed accordingly.

In early design stages of these renewable energy systems, engineers use simulation programs that require various input parameters. However, these parameters are generally set with limited accuracy since they have a certain degree of tolerance. For instance, the random nature of the weather [1] or variables that depend on habits of users or the type of day, such as the hourly distribution of the hot water demand, are significant sources of uncertainty with a dramatic impact on the system performance.

The previous expertise on similar installations or the monitoring of key input data enhances the accuracy of simulation results, but uncertainties are never eradicated. The degradation of components (e.g., insulation materials) or modifications during the project execution are also significant sources of deviations between the expected system performance and the actual one. These factors can lead to weak designs with significant dependency on conventional backup systems like boilers. Numerous authors have applied uncertainty analysis to study the design of energy systems at buildings [2]. For instance, Ekström et al. [3] predicted the energy performance of a multi-family building using such kind of analysis. Li and Wang [4] proposed a robust design method for net-zero energy buildings using uncertainty analysis. A previous study [5] tackled the design under uncertainty of solar systems for hot water preparation in dwellings. Nevertheless, this issue is understudied in buildings with intensive domestic hot water demand such as hospitals.

Copyright ©2022 by the authors. This conference paper is published under a CC-BY-4.0 license.

This paper investigates a more robust and reliable design strategy of a solar thermal system for hot water preparation in hospital buildings. The reliability of the conventional design is evaluated through Monte Carlo stochastic simulations and then an improved design is proposed by narrowing the uncertainty bounds of those design parameters with major influence on the system performance.

2. Case-study hospital

2.1 Description and operation

Figure 1 shows the schematic layout of the DHW preparation system in a medium-size hospital, which is based on the "Hospital Comarcal de la Axarquía" with 193 beds and located Vélez-Málaga (36.75ºN, 4.09ºW), Spain. Basically, the installation is divided into (1) the solar thermal system, (2) the auxiliary system, and (3) the distribution network. The auxiliary system consists of gas-fired boilers and a pasteurizer that prevent legionella growth and supplies DHW at the specified set-point. Regarding the DHW distribution network, the system operation is continuous (i.e., 24 hours per day) with a constant recirculation flow rate. Therefore, there is always hot water available at the consumption points with low waiting times.

The system operates as follows. The water leaving the solar field (stream S1) flows through the hot side of heat exchanger HE-1, heating the cold water coming from the bottom of the stratified solar storage tank. The fluid leaving the hot side of the heat exchanger HE-1 is still at high temperature and is used in the heat exchanger HE-2 to preheat the incoming consumption water coming from the water reservoir. This preheated water leaving the heat exchanger HE-2 (stream W2) enters the service tank, where it is mixed with the recirculated flow (stream W7) and the water stream W3 that has absorbed the heat from the solar storage circuit through the heat exchanger HE-3. If the water temperature at the top of the service tank is below the supplying set-point, the water stream W5 enters the pasteurizer. As shown in Figure 2, this unit is fed with the hot water produced in the gas boilers. Afterward, the water stream W6 is distributed through the DHW pipeline network up to the consumption points distributed throughout the building.

The control system plays a key role in the energy management of the installation. The following control algorithm is applied to the different pumps of the system:

- Pump P1 (solar primary circuit) is activated when the radiation level on the caption plane is above a pre-set value or turned off if the radiation falls below a pre-fixed limit. Additionally, the controller of the pump P1 is equipped with an inverter to control proportionally the pumping capacity between 100% to 50% in function of the temperature of the stream S1.

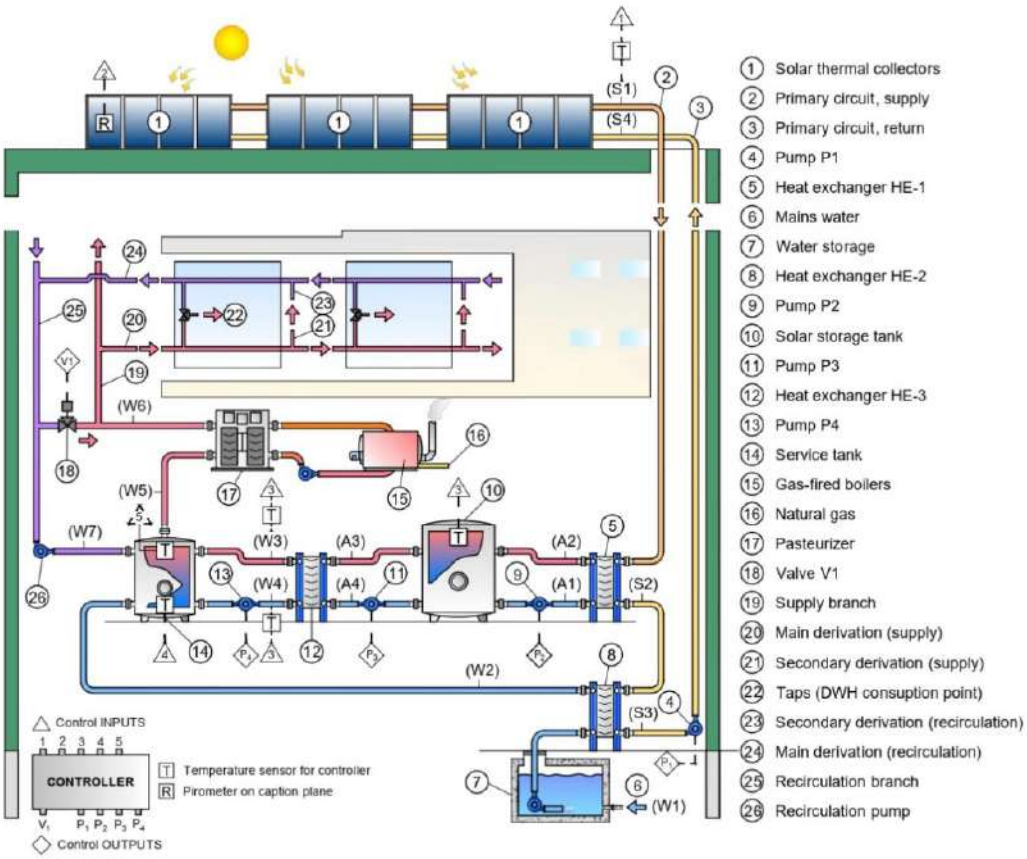

Fig. 1 – Schematic layout of the domestic hot water preparation system in the case-study hospital building.

- Pump P2 (solar storage, i.e., secondary circuit) is activated whether the temperature of the stream S1 leaving the solar collectors is a pre-set quantity higher than the temperature at the upper level of the solar storage tank. Pump P2 is a constant flow pump.

- Pump P3 (discharge of the solar storage tank) is activated when the temperature at the top of the solar storage tank is a pre-set quantity higher than the temperature at the bottom of the service tank.

- Pump P4 follows the same control logic as pump P3. Nonetheless, the inverter controller of pump P4 regulates proportionally the flow rate between 50% to 100% in function of the temperature difference between streams W3 and W4 (heat exchanger HE-3).

- Pump P5 (recirculation) is always activated.

The function of the thermostatic two-way valve V1 installed in the recirculation manifold is to avoid supplying temperatures above the DHW set point.

2.3 Mathematical modelling

The system was modelled using TRNSYS 18 [6]. The simulation time-step was set to 5 minutes. The global steady-state energy balance of the system (Figure 1) is written as follows:

$$Q_S + Q_P - D = 0 \quad (1)$$

where ΔU denotes the variation of internal energy in pipes (modelled with Type 31) and service tank (modelled with Type 158). Both the thermal losses through the primary circuit and the solar storage circuit are implicitly included in the solar production (Q_S) term, which is calculated from the energy balance in the heat exchangers HE-2 and HE-3 (modelled with Type 91):

$$Q_S = Q_{HE\text{-}2} + Q_{HE\text{-}3} = m_{W1} \times Cp \times (T_{W2} - T_{W1}) + m_{W3} \times Cp \times (T_{W3} - T_{W4}) \quad (2)$$

where m and Cp are the mass flow rate and specific heat of water streams, respectively. The solar collectors are modelled using TRNSYS Type 1. The net solar caption area of a single collector is 8.578 m^2 with a connection pattern of two in series.

The DHW demand (D, in kW) includes thermal losses throughout the distribution pipes and in the service tank and is calculated as follows:

$$D = m_{W1} \times Cp \times (T_{W6} - T_{W1}) + m_{W7} \times Cp \times (T_{W6} - T_{W7}) + Q_{L,\,\text{servicetank}} \quad (3)$$

The baseline monthly average temperatures of the tap water reservoir (T_{W1}) from January to December are the following (in °C): 16.5, 17.4, 18.0, 18.3, 20.2, 21.5, 22.7, 23.0, 21.9, 20.1, 18.8, 16.6. The hourly DHW demand (V_{DHW}, in L/h) is calculated as:

$$V_{DHW} = \Omega \times \alpha \times V_{av,DHW} \quad (4)$$

where $V_{av,DHW}$ is average daily DHW demand. On the other hand, the parameters α and Ω represent the DHW hourly demand ratio (Figure 2) and the baseline daily dimensionless demand (Figure 3, together with other two profiles that will be use in the uncertainty analysis), respectively. Both parameters have been developed from the statistical analysis of the data gathered from the monitoring of the hospital in which the case-study presented in this paper is based on.

The thermal energy supplied to the DHW stream in the pasteurizer (Q_P) is calculated as follows:

$$Q_P = m_{W5} \times Cp \times (T_{W6} - T_{W5}) \quad (5)$$

The total thermal losses through the DHW distribution pipelines (Q_L) are calculated as the sum of the thermal losses through each i-pipe section:

$$Q_L = \sum UA_i \times \Delta T_{m,i} \quad (6)$$

As shown in Table 1, the pipes are classified into these three categories: main branches, main derivations, and connections with taps.

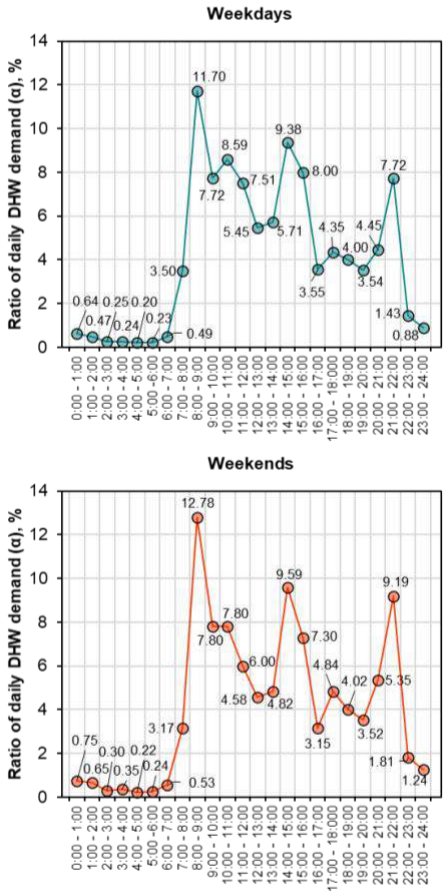

Fig. 2 – Hourly domestic hot water demand ratio for weekdays and weekends.

Tab. 1 – Number and dimensions (outer and inner diameters, length, and thermal insulation thickness) of the domestic hot water pipeline distribution categories [7,8]. Thermal conductivity of pipes and insulation: 0.24 and 0.04 W/(m·K).

Pipe	Supply					Recirculation				
	No.	o.d./i.d., mm	Ins., mm-thick	*U*-value, W/(m²·K)	Total length, m	No.	o.d./i.d., mm	Ins., mm-thick	*U*-value, W/(m²·K)	Total length, m
Branches	9	40.0/29.0	30	2.84	135.0	9	20.0/14.4	25	4.25	135.0
Main derivations	27	32/23.2	25	3.45	270.0	27	16.0/11.6	25	4.69	270.0
Connections with taps	135	20/14.4	25	4.25	337.5	135	16.0/11.6	25	3.09	337.5

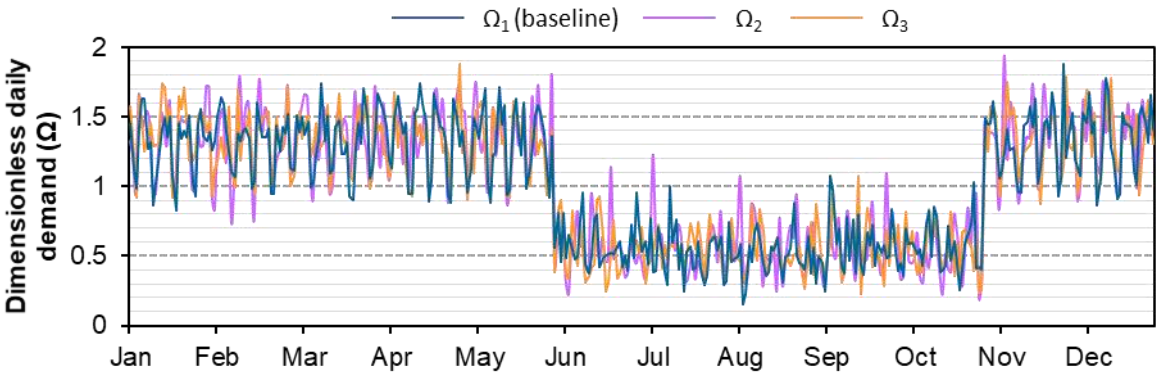

Fig. 3 – Baseline dimensionless daily domestic hot water demand.

The log-mean temperature difference of each pipe section (ΔT_m) is calculated from the following expression:

$$\Delta T_{m,i} = (\Delta T_{1,i} - \Delta T_{2,i})/\ln(\Delta T_{1,i} \times \Delta T_{2,i}^{-1}) \quad (7)$$

where $\Delta T_{1,i} = T_{W,in,i} - T_{amb}$, and $\Delta T_{2,i} = T_{W,out,i} - T_{amb}$. The term T_{amb} is the temperature of the surrounding air, and it is assumed that the whole DHW distribution pipeline layout is inside the building. The overall heat transfer coefficient for each pipeline category (UA_i) is approximated as follows:

$$1/UA_i = \ln[(d_{o,i} + 2\times\delta_i)/d_{o,i}] \times (2\,\pi\, k\, L_i)^{-1} \quad (8)$$

where d_o, k and δ represent the outer pipe diameters and thermal conductivity and thickness of the insulation material, respectively. The parameter L is the total length of each pipeline type. Note that the same strategy is followed to calculate the thermal losses through the primary circuit pipelines and through both the solar and service tank, whose baseline insulation thickness is estimated accordingly with the Spanish standard for thermal systems at buildings [7].

The annual solar fraction (SF) and utilization factor (UF) of the system is defined as follows:

$$SF = \int Q_S \cdot \mathrm{dt} \,/\, \int D \cdot \mathrm{dt} \times 100\% \quad (9)$$

$$UF = \int Q_S \cdot \mathrm{dt} \,/\, \int A \cdot I_T \cdot \mathrm{dt} \times 100\% \quad (10)$$

where A is the net caption area of the solar installation and I_T is the solar radiation on the caption plane.

2.3 Identification and quantification of uncertainties

Table 2 depicts the base-case values and the distributions proposed to model the uncertainties of the input parameters involved in the design of the system. The column "base values" contains a reasonable combination of inputs that any designer could have chosen to solve the problem in a deterministic fashion. The column "distributions" defines the probability density function associated with each factor. These distributions have been proposed based on literature recommendations, theoretical considerations or educated guesses [5].

The Monte Carlo method is used to propagate the uncertainty of the different input parameters given in Table 2 and generate a sample of 1,500 simulations. Finally, the reliability (R) of the deterministic design is calculated from the following expression:

$$R = N_{feasible}/N_{runs} \times 100\% \quad (11)$$

where $N_{feasible}$ is the number of simulation runs that achieved the minimum solar fraction of 70%, and N_{runs} is the total number of simulation runs conducted.

Tab. 2 – Baseline values and uncertainty range of the input parameters of the environment. Sources: [5,8,9].

Factor X	Description	Base values	Distribution
1	Hourly weather data: Total horizontal radiation ($G_{t,i}$), kWh/m^2, and outdoor ambient temperature ($T_{o,i}$), ^{o}C.	Contemporary	UD [Contemporary, RCP2.6, RCP4.5, RCP8.5]
2	Monthly average mains water temperature, ^{o}C.	$T_{W1,i}$	$T_{W1,i}$ + U [0, 3]
3	Tilted surface radiation model.	Isotropic	UD [Isotropic, Hay, Reindl, Perez]
4	Angular height of remote obstacles, deg (^{o})	10	UD [8, 12]
5	Ground reflectivity.	0.25	U [0.15, 0.55]
6	Dusting effect on collector transmissivity.	1	U [0.9, 1]
7	Weighting factor (*wf*) between outdoor ambient (T_o) and temperature of conditioned zones (T_r, interior spaces such as wall cavities or plenums inside where pipes run through): $T_{amb} = wf \times T_o + (1-wf) \times T_r$	0.5	U [0.2, 0.8]
8	Weighting factor between outdoor ambient and temperature of conditioned zones (basement): $T_{amb,\ basement} = wf \times T_o + (1-wf) \times T_{r,\ basement}$	0.8	U [0.3, 0.9]
9	Average daily DHW demand ($V_{av,DHW}$), m^3/day.	8.66	$V_{av,DHW}$ × U [-0.8, 1.2]
10	Daily dimensionless DHW demand (Ω).	Ω_1	UD [$\Omega_{1...3}$] (Fig. 3)
11	Hourly ratio of daily DHW demand (α).	α	- (Fig. 2)
12	No. of solar collectors.	N_c	-
13	Collectors' slope, deg (^{o}).	45	-
14	Collectors' azimuth, deg (^{o}).	0	-
15	Intercept collector efficiency at normal incidence, $F_R(\tau\alpha)_n$.	0.795	N [0.795, 0.00494]
16	Slope of collector efficiency ($F_R U_L$), W/(m^2·K).	4.177	N [4.177, 0.11934]
17	First order incidence angle modifier.	0.14	N [0.14, 0.0014]
18	Flow rate through each solar collector, L/(h·m^2).	70	LN [70, 35; 30, 210]
19	Ethylene-glycol concentration (primary circuit), %.	20	U [0, 30]
20	Effectiveness of heat exchangers (ε).	0.82	U [0.60,0.82]
21	*U*-value of the primary circuit pipes, based on the inside pipe surface area, W/(m^2·K).	1.83	1.83 × T [1.0, 2.0, 1.0]
22	Total length of primary circuit pipelines, m.	50	30×U [0.9 1.1]
23	Storage volume of the solar tank, L/m^2.	75	-
24	*U*-value of the solar tank, based on the inside surface area, W/(m^2·K).	0.50	0.50 × T [1.0, 2.0, 1.0]
25	Pump P2 flow rate (V_{P2}), L/h.	V_{P1}	V_{P1}×N [1,0.20]
26	Pump P3 flow rate (V_{P3}), L/h.	V_{P1}	V_{P1}×N [1,0.20]
27	Pump P4 flow rate (V_{P4}), L/h.	V_{P1}	V_{P1}×N [1,0.20]
28	*U*-value of the service tank, based on the inside surface area, W/(m^2·K).	0.50	0.50 × T [1.0, 2.0, 1.0]
29	Storage volume of the service tank, L/m^2.	40	-
30	Total length of distribution pipelines ($L_{tot,\ design}$), m.	$L_{tot,\ design}$	$L_{tot,\ design}$ × U [0.9, 1.1]
31	*U*-value of DHW pipes (supply and recirculation), based on the inside pipe surface area, W/(m^2·K).	*U*-value (Tab. 1)	*U*-value × T [1.0, 2.0, 1.0]
32	Recirculation flow rate (V_{rec}), L/h.	V_{rec} = max (250×No. branches, Q_L/3.48)	V_{rec} × N [1, 0.20]

Tab. 2 (cont.) – Baseline values and uncertainty range of the input parameters of the environment. Sources: [5,8,9].

Factor X	Description	Base values	Distribution
33	DHW supply set-point temperature ($T_{sp,DHW}$), ºC.	60	T [55,65,60]
34	Maximum solar tank temperature, ºC.	90	T [88, 90, 92]
35	Maximum service tank temperature, ºC.	90	T [88, 90, 92]
36	Radiation level for activation of Pump P1, W/m².	185	T [185, 190, 180]
37	Lower radiation limit to keep pump P1 switched on, W/m².	160	T [160, 165, 155]
38	Pump P1's frequency shifter temperature set-point (T_{S1}) for 100% capacity, ºC.	85	U [80, 90]
39	Pump P1's frequency shifter temperature set-point (T_{S1}) for 50% capacity, ºC.	15	U [10, 20]
40	Upper ΔT (T_{S1}-T_{A3}) to switch on pump P2, ºC.	1.5	T [1.0, 2.0, 1.5]
41	Lower ΔT (T_{S1}-T_{A3}) to switch off pump P2, ºC.	0.5	T [0.0, 1.0, 0.5]
42	Upper ΔT (T_{A3}-T_{A4}) to switch on Pumps P3 and P4, ºC.	5.0	T [3.0, 7.0, 5.0]
43	Lower ΔT (T_{A3}-T_{A4}) to switch off Pumps P3 and P4, ºC.	1.0	T [0.0, 2.0, 1.0]
44	Upper ΔT (T_{W3}-T_{W4}) to set the frequency shifter of P4 at 50 Hz (i.e., 100% of its pumping capacity), ºC.	5.0	U [4.0, 6.0]
45	Lower ΔT (T_{W3}-T_{W4}) to set the frequency shifter of P4 at 25 Hz (i.e., 50% of its pumping capacity), ºC.	1.0	U [0.0, 2.0]
46	Adjustment of valve V1 concerning the hot water supply set-point temperature (factor X-33).	1.0	N [1,0.05]

Nomenclature of distributions. U [a, b]: Uniform distribution between a and b; UD [a, b]: Uniform discrete distribution between a and b; LN [λ, ξ; a, b]: Truncated lognormal with mean value λ, and standard deviation ξ truncated between a and b; T [a, b, c]: Triangular distribution with minimum value a, maximum value b and likeliest value c; N [μ, σ]: Normal is a normal distribution with mean value μ and standard deviation σ.

3. Results and discussion

2.1 Reliability of the deterministic design

Table 3 shows the deterministic or base results obtained running the TRNSYS model for different caption areas (i.e., ranging between 32 to 52 solar collectors) using the baseline parameters given in Table 2. The reliability of achieving a minimum solar fraction of 70% (required by the Spanish energy code for buildings for the specified location and its corresponding climatic zone [10]) is also provided for each design-case.

According to the deterministic results, which overlooks the uncertainty of the different input parameters involved in the design, a solution with 26 solar collectors (i.e., net caption area of 223.0 m²) would be required. In such case, the solar fraction and utilization factors calculated are 70.7% and 41.7%, respectively. However, the Monte Carlo results depicted in Figure 4 show that the possible outcomes of the model spread across a large region when it is considered the effect of the uncertainties on this deterministic solution. In fact, the reliability of the deterministic design barely achieves 22%. Therefore, deviations in operating conditions and system characteristics could lead into a failed design, so the solar fraction of the installation once executed is likely to underperform concerning the target.

2.2 Design improvement

The trivial solution to enhance the reliability of the system consists solely of oversizing the solar field. As shown in Table 3, a design solution with 38 solar collectors (326.0 m²) would achieve the minimum annual solar fraction with a reliability beyond 90%. Nevertheless, this solution is far from ideal because a huge capital investment would be required. Besides, the system will more likely suffer from long harmful stagnation periods in the summertime [5].

An effective strategy to improve the reliability of the design is based on identifying those sources of uncertainty with major impact on the system performance through a sensitivity analysis. Afterwards, the objective will be focused on narrowing the allowed range of variation of these parameters, but only whether they are somehow controllable.

Tab. 3 – Solar fraction, utilization factor and reliability of the design for different number of solar collectors considered.

No. of solar collectors	Net caption area, m²	*SF*, %	*UF*, %	Design reliability, %
24	205.9	67.6	43.0	9.7
26	223.0	70.7	41.7	22.4
28	240.2	73.6	40.4	36.9
30	257.3	76.3	39.2	46.7
32	274.5	78.8	38.1	60.9
34	291.7	81.1	37.1	74.1
36	308.8	83.3	36.1	83.3
38	326.0	85.2	35.1	90.0

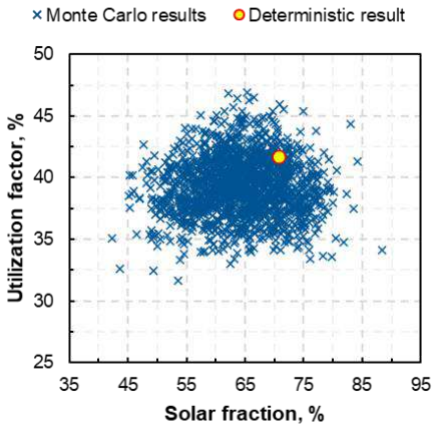

Fig. 4 – Solar fraction and utilization factor of the deterministic design (26 collectors, 223.0 m²).

Figure 5 shows the Standardized Regression Coefficients (SRCs) obtained from the sensitivity analysis using Monte Carlo sampling. The numbering of the design parameters corresponds to the given in Table 2. Since the system modelling varies linearly and is additive (R-square 0.95), the SRC coefficients obtained can be considered meaningfulness. The sign of these coefficients indicates if the output increases (positive) or decreases (negative) as the corresponding input factor increases. According to the results obtained, the following design parameters explains most of the variance of the solar fraction reported by the modelling:

1. *U*-value of the DHW distribution pipes (factor X-31, SCR = -0.54).

2. Hot water supply set-point temperature (factor X-33, SRC = -0.49).

3. Deviation of valve V1 (factor X-46, SCR = -0.31).

4. Average daily demand (factor X-9, SCR=-0.30).

5. Dust on solar collectors (factor X-6, SRC = 0.28).

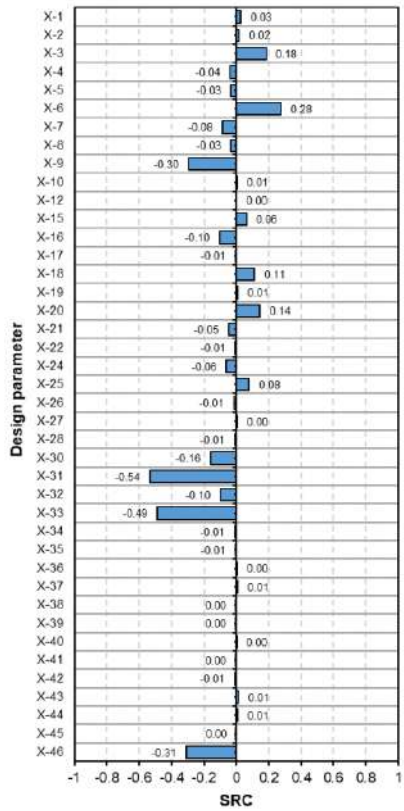

Fig. 5 – Standardized sensitivity coefficients for each input parameter involved in the design (Table 2).

An effective thermal insulation of hot water pipes is central to avoid excessive thermal losses along lengthy DHW distribution networks of medium/large buildings. Regarding the DHW supplying set-point temperature and wrong adjustment of the valve V1, higher temperatures require higher natural gas consumption (because boilers must switch on more often) and involves higher thermal losses both through the distribution pipelines and in the service tank. Consequently, the lower is the hot water supplying temperature, the higher solar fraction for a given caption area. Nevertheless, the temperature of the hot water at taps and through recirculation loops must be above 50°C due legionella issues. Thus, because of thermal losses through the distribution circuit, there is little chance to supplying the hot water below 60°C. Nonetheless, the uncertainty ranges around the set-point can be narrowed, for example, by installing top quality valves and measurement and control devices.

On the other hand, an effective maintenance of the system is crucial to avoid the worsening of the solar fraction because of dust deposition on collectors or concerning the early detection of insulation defects that set off thermal losses. However, there are parameters with a significant impact of the performance of the system but whose uncertainty are uncontrollable, for example, the average daily domestic hot water demand.

But regarding an improved design, what should be the *target reliability*? Ultimately, this is a decision for

the engineer designing the system. In this paper, the authors assume a minimum target of 90%. As an example, it is proposed an improved design with the following revised uncertainties: deviation of the baseline *U*-value of the DHW distribution pipes (factor X-31) T [1.0, 2.0, 1.0]; hot water supplying set point (factor X-33) T[58, 62, 60]; deviation of thermostatic valve V1 (factor X-46) N[1, 0.01]; and dusting effect on collector transmissivity (factor X-6) U[0.98, 1]. The rest of uncertainty distributions remains as given in Table 2. Figure 6 shows the Monte Carlo simulation results for this revised and improved design and for the case of 30 solar collectors installed. As a result, the reliability fairly enhances concerning the original design for such number of collectors (i.e., from 70.7% to 90.3%).

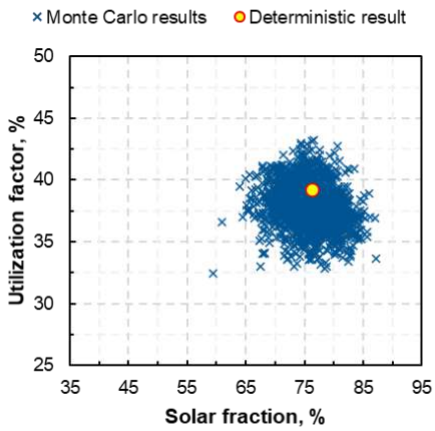

Fig. 6 – Solar fraction and utilization factor of the revised design (30 collectors installed, 257.3 m^2).

4. Conclusions

In this paper, the authors explored the improved design of a solar thermal system for domestic hot water preparation in a medium-size hospital.

It was found that the uncertainty of the following factors introduced a dramatic variance of the solar fraction: the hot water supplying set-point, lack or defect in thermal insulations, wrong adjustment of valves, as well as factors requiring an intensive maintenance such as the periodic cleaning of solar collectors. While the reliability of the original design (22%) which overlooks the uncertainty of input parameters could be enhanced up to 90% just by expanding the solar field from 26 to 38 solar collectors (i.e., from 223.0 to 326.0 m^2), the revised design proposed in this paper requires only 30 solar collectors (257.3 m^2). The strategy followed is more attractive from an economic perspective and it was rooted in narrowing the uncertainties of those controllable input parameters with major impact on the system performance. Despite a lacking fixed rule to reduce the uncertainty of design parameters beyond expertise, the use of high-quality measurement and control equipment as well as an effective maintenance are both vital to reduce the probability of failed designs down to acceptable risks.

In a future work, the authors will study the trade-off between increasing the reliability of the design of the energy system presented in this paper and its economic performance throughout its lifetime.

5. Acknowledgement

The authors acknowledge the Universidad de Málaga and "*Programa Operativo FEDER Andalucía 2014-2020*" the financial support of the contract UMA18-FEDERJA-247, and Mr. Pedro Quintero Jiménez for providing data and helpful information.

6. References

[1] Lan B., Tian Z., Wu X. A simplified method of generating sequential meteorological parameters for uncertainty-based energy system design, Energy Build, 2021;237:110780.

[2] Mavromatidis G., Orehounig K., Carmeliet J. A review of uncertainty characterisation approaches for the optimal design of distributed energy systems, Renew Sustain Energy Rev, 2018;88:258–277.

[3] Ekström T., Burke S., Wiktorsson M., Hassanie S., Harderup L.E., Arfvidsson J. Evaluating the impact of data quality on the accuracy of the predicted energy performance for a fixed building design using probabilistic energy performance simulations and uncertainty analysis, Energy Build, 2021;249:111205.

[4] Li H., Wang S. Coordinated robust optimal design of building envelope and energy systems for zero/low energy buildings considering uncertainties, Energy Build, 2020;265:114779.

[5] Domínguez-Muñoz F., Cejudo J.M., Carrillo-Andrés A., Ruivo C.R. Design of solar thermal systems under uncertainty, Energy Build, 2012;47: 474–484.

[6] TRNSYS 18, https://sel.me.wisc.edu/trnsys/features/features.html (Accessed 13/01/2022).

[7] Reglamento de Instalaciones Térmicas en los edificios (RITE), 2013.

[8] Documento Básico HS-4 Suministro de agua, https://www.codigotecnico.org/pdf/Documentos/HS/DBHS.pdf (Accessed 12/01/2022).

[9] Meteonorm (2021). https://meteonorm.com (Accessed 13/01/2022).

[10] Código Técnico de la Edificación, Sección HE-4: Contribución solar mínima de agua caliente sanitaria.

Integration of an innovative dual day-night technique for air conditioning of public spaces

Daniel Castro Medina [a], María del Carmen Guerrero Delgado [a], Teresa Rocío Palomo Amores [a], Rocío González Falcón [a], José Sánchez Ramos [a], Servando Álvarez Domínguez [a]

[a] Escuela Técnica Superior de Ingeniería, University of Seville, Seville, Spain, dcastro@us.es.

Abstract. The citizen has lost his place in the streets. Also, streets have become hostile and unlivable due to climate change and unsustainable urbanization. CartujaQanat project was born to mitigate the problems discussed. CartujaQanat is an innovative urban transformation project through which the use of the street as a social activator will be promoted, improving it and involving the city's entire ecosystem in this transformation. This new model of urban governance will serve as a facilitator for introducing these models in their expansion throughout the city to gradually change the appearance and functionality of the street concept and its future evolution in the next 15 years. So, this paper shows a set of solution for climatic control of outdoor conditions for two open public spaces in Seville. These techniques guarantee thermal comfort by the implementation of passive and adaptive bioclimatic solutions. The natural element of thermal dissipation is water, which will allow the air conditioning of spaces by cooling the air. One of the keys to the project is the cooling of water using the natural technique "falling-film". The water is driven from accumulation volumes by fan nozzles on the photovoltaic panels arranged on the installation roof, forming a falling film on them. This innovative technique allows the water to be cooled through a convective-radiant effect during the night thanks to the low temperature of the sky, obtaining promising results of thermal dissipation, whose dissipation heat varies depending on the flow width and length of the film travel. The duality of the system allows the cooling of water at night and the production of electricity during the day in order to guarantee a zero-energy balance in the installation.

Keywords. Falling-film, energy, natural techniques; thermal dissipation.
DOI: https://doi.org/10.34641/clima.2022.104

1. Introduction

Global warming has caused the rapid growth of hot days and extreme weather, significantly increasing the demand for refrigeration [1]. This situation promotes the need to develop and use natural cooling techniques that reduce energy consumption, support the environment and the ecosystem and provide a satisfactory degree of comfort.

The CartujaQanat project is an innovative urban transformation project through which the use of the street as a social catalyst will be promoted, improved and involving the entire ecosystem of the city (public, private and citizen agents) in this transformation. This project is a continuation of the works started by Servando Álvarez Domínguez et al. [2] at the Universal Exhibition in the city of Seville in 1992, in which it seeks to innovate, improve and above all be able to integrate it into real projects and buildings.

This new urban governance model will serve as a facilitator for introducing these models in their expansion throughout the city to gradually change the appearance and functionality of the street concept and its future evolution in the next 15 years. A set of actions and elements will be developed that, integrated, act as social dynamizes. All this is to improve universal accessibility and ensure that superficial interventions on existing urbanization manage to reconfigure the urban planning. It is, therefore, an innovative urban design experience that will improve environmental comfort, promote social exchange and promote sustainable models of urban growth. The initiative is part of the Seville strategy in the fight against climate change, which has two main lines of action: developing strategies to adapt to climate change at the local level and recognizing the essential nature of the artery of the streets and neighbourhoods [3].

The execution of the project takes place on Thomas Alva Edison Avenue. This avenue is located in the city of Seville, specifically on the island of La Cartuja,

Copyright ©2022 by the authors. This conference paper is published under a CC-BY-4.0 license.

where the 1992 universal exhibition took place. Buildings and open spaces were built for the universal exhibition. After the end of the event, some pavilions were dismantled by the exhibition participants, but the vast majority remain today. At present, the island of La Cartuja encompasses part of the infrastructure of the University of Seville, as well as numerous companies or institutions with a scientific - innovative nature.

Over the years, the Cartuja Science and Technology Park has grown, taking advantage of most of the buildings found on the island. However, the main objective continues to be to achieve a higher percentage of occupancy, which is why the growth margin of the said park continues to be enormous. The Expo left an architectural framework for business settlement and numerous public spaces surrounded by dense vegetation that, together with innovative and pioneering natural cooling techniques in the world, fought the extreme temperatures registered in the city of Seville during the summer season. The expensive maintenance of public spaces and the lack of funds caused them to be abandoned, so the vegetation and urban furniture have deteriorated over the years, completely disused by the inhabitants of the city of Seville.

The CartujaQanat project aims to rehabilitate, recover, and thermal condition an existing amphitheatre inherited from Expo 92 and create a new space called Zoco. Both spaces aim to guarantee the thermal comfort of their occupants through innovative natural conditioning techniques and the management of said energy through the use of thermal storage, where the star concept of the project stands out, which are the so-called "qanats."

This work focuses on corroborating that the falling film technology developed by Servando Álvarez Domínguez et al. [4] - [6] can be adapted to photovoltaic panels using a comprehensive opening fan nozzle solution, showing that the performance is identical, with the addition of solving the details of its implementation in the CartujaQanat project. This natural cooling technique, a falling film, uses water as a heat transfer fluid. Water is propelled from some volumes of accumulation by fan nozzles on the photovoltaic panels arranged on the installation roof, forming a falling water film on them. This innovative technique allows the water to be cooled through a convective-radiant effect during the night thanks to the low temperature of the sky, obtaining promising results of thermal dissipation, whose dissipation power varies depending on the flow width and length of the water film travel. The duality of the system allows the cooling of water at night and the production of electricity during the day to guarantee a zero-energy balance in the installation.

2. Methodology

The present study aims to show the design and evaluation of the integration of the falling film nocturnal dissipation system on photovoltaic panels [6]. The innovative character of this technology requires the development of a simplified model of energy characterization of the system that allows the evaluation of the system's potential under different operating conditions quickly and easily. In the particular case of the Cartuja Qanat project mentioned above, the simplified energy characterization model is required to evaluate the design and cooling potential of the natural cooling water stored in the accumulation volumes (qanats). Finally, about the system's design, the evaluation of the typology and arrangement of the nozzles is required to guarantee the optimal development of the falling film. In line with the previous objectives, this study first shows the description of the experimental prototype of the system under investigation. Second, given the integration of nozzles, the study of these is required, distinguishing the parameters of interest for their research. Third, the fundamentals of the simplified model developed are shown. Finally, the results show the simplified model obtained and the experimental tests associated with the integration of the falling film forming nozzles.

Fig. 1 – Recreation of the souk. Dual day-night technique on top.

3. Experimental prototype

To obtain the model's parameters, an experimental prototype of the falling film system is carried out based on the work of Guerrero et al. [6]. The experimental prototype said, shown in figure X, is described below:

1. Tank: storage tank for the volume of water to be cooled.

2. Water transport: The impulsion pipe conveys the water towards the impulsion nozzle; therefore, a circulation pump is necessary for this section. The return pipe gets the water from the collection gutter back to the storage tank. In this case, a pumping system is not required since the water circulates naturally towards the said reservoir.

3. Nozzle in charge of the impulsion: large opening fan nozzle located on the upper end of the drop panel. The large opening of the nozzle allows the water driven from the tank to bathe the panel thoroughly, forming a homogeneous water film.

4. Photovoltaic panel for lowering the water: a flat surface whose material has adequate characteristics for cooling by night radiation (low reflectivity and transmittance in the atmospheric window, which is equivalent to a high emissivity (approximately 0.90)).

5. Water collection gutter: gutter connected to the bottom of the drop panel. Said element is connected to the water return pipe to the tank.

Fig. 2 - Experimental prototype of the falling-film system.

4. Study of nozzles

To determine which nozzle is adapted to the project's needs, a set of these are evaluated. The ideal nozzle for the application in the CartujaQanat project on photovoltaic panels must meet a series of characteristics that guarantee quality and formation of the complete falling water film, low operating pressure, which translates into energy savings on the part of the pressure equipment and a flow rate that optimizes the thermal dissipation of the falling film system. Another point to study and no less important is the arrangement of the nozzle for the photovoltaic panel, which must correspond to the most significant possible travel of the water film developed on the panel and low losses caused by the large opening of the nozzle or direct impact of the jet with the panel.

For this reason, for evaluating each of the nozzles, they are subjected to the following parameters to study:

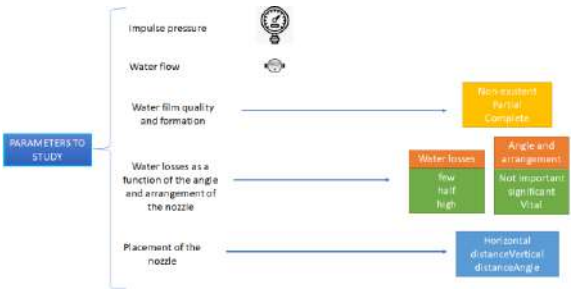

Fig. 3 - Nozzles study parameters.

5. Simplified model

The simplified model used is based on Guerrero et al. [4] - [7], which details the fundamentals of the model summarized here for calculating the water temperature in a solar collector. This simplified model performs a standard treatment of the convective-evaporative transfer, formulating the power dissipated in a falling film system according to equation 1.

$$P_d = Q_{cv-evap} + Q_{rad} \qquad \text{(eq.1)}$$

Where P_d is the total dissipation power of the falling water film system $\left(\frac{W}{m^2}\right)$, $Q_{cv-evap}$ the nocturnal cooling power referring to the heat loss due to convection and evaporation and Q_{rad} the nocturnal cooling power refers to the thermal losses by radiation with the sky.

The cooling power referred to the convective and evaporative thermal losses is formulated according to equation 2.

$$Q_{cv-evap} = h_{cv-evap} \cdot (T_w - T_{wb}) \qquad \text{(eq.2)}$$

Where $h_{cv-evap}$ is the convective-evaporative transfer coefficient of the water film $\left(\frac{W}{m^2 °C}\right)$, T_w is the water temperature (°C) and T_{wb} wet bulb temperature (°C).

The formulation associated with the radiation heat transfer between the water film, the surroundings and the sky is formulated according to equation 3. Since the form factor between the falling film system and the sky is practically unity, they are neglected radiant effects with the surroundings and given that the temperature difference between the water and the sky is less than 100K, it is possible to linearize the formulation developed in equation two so that the cooling power referred to the thermal losses by radiation. The sky is formulated according to equation 4.

$$Q_{rad}\left(\frac{W}{m^2}\right) = h_{rad} \cdot (T_w - T_{sky}) \qquad \text{(eq.3)}$$

$$h_{rad} = 4 \cdot \sigma \cdot \varepsilon \cdot \left(\frac{T_w + T_{sky}}{2}\right)^3 \qquad \text{(eq.4)}$$

Where h_{rad} is the radiant transfer coefficient of the water film $\left(\frac{W}{m^2 °C}\right)$, T_w is the water temperature (°C)

and T_{sky} is the temperature of the sky(°C).

6. Results and discussion

The experimental results obtained in the elaborated works [4] [6] show that the cooling of the water throughout the night presents a change of behaviour characterized by the variation of the thermal conditions of the water and the air. This evolution can be described in two sections:

- Section 1 characterizes the thermal dissipation of the system when the thermal conditions of the air and water cause evaporative cooling phenomena to occur, that is, when the air is not saturated.

- Section 2 characterizes the dissipation of the system given the radiant exchange with the sky once the air saturation has been reached. In this section, the convective transfer of water with saturated air can even counteract heat dissipation from the sky. The slope of the water cooling in said section is more attenuated.

Therefore, given the clear distinction of water cooling trends, the simplified characterization model parameters are obtained ($h_{cv-evap}$ and h_{rad}) in both sections. The proposed sectional model is shown below and the results of its experimental validation (Table 1). The values of the parameters obtained are valid for a dissipation area of 2.4 m^2 and a water circulation flow for cooling it of 1440 l/h.

Tab. 1 - Proposed simplified model (reference operating conditions) [4]

Section 1: Unsaturated air (Radiation+Convection+Evaporation)	Section 2: Saturated air (Radiation+Convection)
$P_d = 33.11 \cdot (T_w - T_{wb}) + 5 \cdot (T_w - T_{sky})$	$P_d = 3.44 \cdot (T_w - T_{wb}) + 5 \cdot (T_w - T_{sky})$
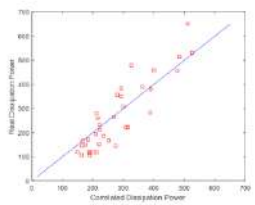	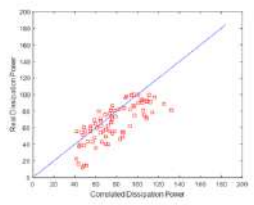

Given the definition h_{rad} according to equation 4, said radiant transfer coefficient varies with the temperature of the water and sky. According to the experiments' results, the values of h_{rad} obtained vary between 4.8 y 5.3 $\frac{W}{m^2 °C}$, so that the value of h_{rad} obtained from the experimental adjustment in both sections is within the expected range. In addition, the proposal made in detailed studies of the combined effect of heat and mass transfer has been revised. The proposed convective-evaporative heat transfer coefficient takes a value of 33.11 $\frac{W}{m^2 °C}$. This value, as discussed in the previous section, is understood as the net effect of the sum of convection and evaporation with the air. So if the approximation of the convective coefficient [7] is taken in the range of wind speeds measured between 0 and 2, we have a value that can range between 3-5 $\frac{W}{m^2 °C}$. In turn, the execution of the correlations [4] returns a value of the evaporative transfer coefficient between 18 and 45 $\frac{W}{m^2 °C}$. Therefore, the value of 33.11 can be considered within the expected range, and it is even proved that evaporation dominates the heat transfer with the surrounding air.

As mentioned above, the parameters' values are valid for a dissipation area of 2.4 m^2 and a water circulation flow for cooling of 1440 L/h. To analyze the variation in night-time dissipation power when modifying these operating conditions, its evolution is experimentally analyzed by varying the L/h·m^2 of system operation. Figure 3 shows the results obtained where an asymptotic behavior of the increase in night dissipation power can be observed from approximately 600 L/h·m^2

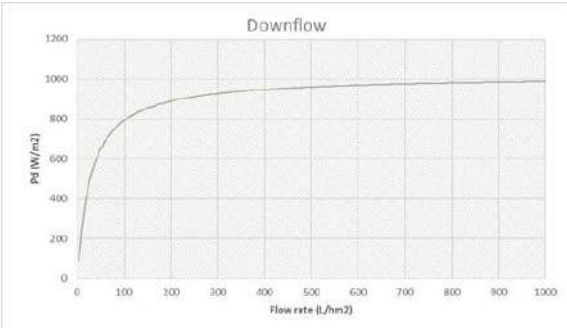

Fig. 4 - Variation of dissipation power as a function of operating conditions [4]

Taking as a reference the test conditions of the experimental prototype (600 L/h·m^2), the variation of the correction factor as a function of the operating conditions is shown in Figure 4.

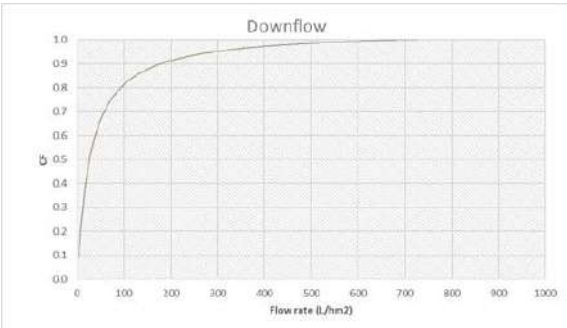

Fig. 5 - Correction factor for dissipation power as a function of operating conditions [4]

Therefore, the estimated night-time dissipation power corrected for the variation of the operating conditions of the reference system is formulated according to equation 5:

$$P_{d_c} = P_d \cdot CF \qquad \text{(eq.5)}$$

Where P_d is the estimated night-time dissipation power for the reference system operating conditions as shown in table 1 and CF is the corrective factor associated with the variation in operating conditions $(\frac{L}{h \cdot m^2})$.

The correction factor associated with the variation in operating conditions is formulated according to equation 6:

$$F = 1 - a \cdot \exp\left(-b \cdot Flow\ rate\ \left(\frac{L}{\mathrm{h \cdot m^2}}\right)^c\right) \qquad \text{(eq.6)}$$

The data graphed in figure 4 allow to identify the model presented in eq. 6. From this identification an almost perfect fit is obtained (correlation coefficients above 0.99, with a maximum relative error of less than 1%) with the values of the coefficients shown in table 2.

Tab. 2 - Coefficients of the correction factor calculation model CF=f (L/h· m²) [6].

Correction factor coefficients CF (ver eq. 8)	Best value	95% Confidence bounds
a	1.273	(1.237, 1.308)
b	0.1647	(0.1527, 0.1768)
c	0.5312	(0.5187, 0.5437)

After multiple experimental checks, it is determined that the following configuration is optimal, minimizing water losses due to side-impact and obtaining the best possible use of the panel surface:

Fig. 6 - Optimal nozzle arrangement.

As seen in the image, the optimal configuration places the nozzle 8 cm away from the panel (axes shown) and at the height of 5 cm up to the head of the nozzle used. Regarding the angle, an inclination of 60º for the horizontal is estimated, guaranteeing that all the water is poured onto the panel and avoiding more significant losses due to the flight of the flow directly to the outside.

From the different tests carried out, the conclusion is drawn that the optimal nozzle to perform the desired function on the photovoltaic panels placed on the roof of a house must present the following technical data and placement on the panel:

Tab. 3 - Technical data of the selected nozzle

Nozzle	Pressure	Flow	Water film	Loss	Optimal Layout		
CW04	0.7 bar	16 l/min	Full	Low	8 cm horizontal	5 cm height	60° angle

- This placement of the nozzle allows that for lower pressures (up to 0.5 bar) it is guaranteed that the water is deposited on the panel in the same way, only varying the beginning of a fully developed falling water film.

- The lateral leak "only" is important in the panels placed on the sides on the roof of the souk since in consecutive panels, the water hits and jumps to the adjacent panel without generating losses. It is important to install lateral gutters to collect this water and avoid possible leaks between panels. For safety, implement channels under the photovoltaic to redirect potential losses to the central gutter.

- Regarding the panel used, it is proposed that these do not have a frame to avoid problems in the transition of the water film between consecutive panels, guaranteeing the continuity of the film as if it were a single panel.

7. Conclusions

The studies carried out at a theoretical and practical level allow natural cooling to implement a falling water film using wide-opening fan nozzles for their impulsion on the photovoltaic panels as thermal dissipation technology in the Cartuja Qanat project.

As demonstrated experimentally, the falling water film technique has a high cooling potential due to convective, radiant and evaporative transfer. Together with this, the low consumption of necessary water stands out, which is 7 and 8 times less than in the conventional evaporative cooling system. Therefore, the enormous interest of said technology in the project is demonstrated.

The results obtained on photovoltaic panels are similar to the enormous cooling potential of this nighttime natural dissipation technology, proposed by Guerrero et al. [5], which corroborates the integration of innovative dual technology, day-night, which combines electricity production during the day for the energy supply of the installation and the

enormous thermal dissipation capacity of the falling film on the panels during the night.

8. Acknowledgement

The European Commission funded this study under the projects UIA03-301-CartujaQanat of Urban Innovative Action (UIA). It has been co-financed by the European Regional Development Funds (ERDF).

9. References

[1] M. Santamouris, "Innovating to zero the building sector in Europe: Minimising the energy consumption, eradication of the energy poverty and mitigating the local climate change," Sol. Energy, vol. 128, pp. 61–94, 2016, doi: 10.1016/j.solener.2016.01.021.

[2]"SISIUS: Ficha personal: Servando Álvarez Domínguez." https://investigacion.us.es/sisius/sis_showpub.php?idpers=3126 (accessed Nov. 20, 2020).

[3] "Inicio|CartujaQanat." https://cartujaqanat.com/#proyecto (accessed Oct. 19, 2020).

[4] Mc. C. Guerrero Delgado, J. Sánchez Ramos, J. A. Tenorio Ríos, and S. Álvarez Domínguez, "Falling-film as natural cooling technique: Modelling and energy impact assessment," Energy Convers. Manag., vol. 221, Oct. 2020, doi: 10.1016/j.enconman.2020.113168.

[5] Mc. C. Guerrero Delgado, J. Sánchez Ramos, and S. Álvarez Domínguez, "Using the sky as heat sink: Climatic applicability of night-sky based natural cooling techniques in Europe," Energy Convers. Manag., vol. 225, Dec. 2020, doi: 10.1016/j.enconman.2020.113424.

[6] Mc. C. Guerrero Delgado, J. Sánchez Ramos, Mc. C. Pavón Moreno, J. A. Tenorio Ríos, and S. Álvarez Domínguez, "Experimental analysis of atmospheric heat sinks as heat dissipators," Energy Convers. Manag., vol. 207, no. January, p. 112550, 2020, doi: 10.1016/j.enconman.2020.112550.

[7] M. del Carmen Guerrero Delgado Directores and S. Álvarez Domínguez José Sánchez Ramos, "Tesis Doctoral Doctorado Ingeniería Energética, Química y Ambiental."

Analysis of heat storage using Phase change material

Petar Nusev, Matija Špegel, Uroš Stritih

Faculty of Mechanical Engineering, University of Ljubljana, Ljubljana, Slovenia, email: uros.stritih@fs.uni-lj.si

Abstract. In many cases heat released from some of the renewable energy sources, cannot be directly used at the time of its generation. Therefore, facilities for thermal-energy storage (TES) which would allow delayed use of the harvested heat are very important for increase of the total process efficiency. An approach to thermal-energy storage is based on the use of the latent heat of phase-change materials (PCMs). The use of PCMs as thermal storage has a theoretical advantage over the sensible one because of their high latent heat that is released or accumulated during the phase-change process.

The advantage of PCM in thermal energy storage is in applications that needs narrow temperature range of supplying and storing thermal energy. The focus of the paper is on the analysis of thermal energy storage devices based on macroencapsulated PCM. The aim of this paper is to design a latent heat storage (LHS) system with spherical modules filled with PCM. Several measurements were performed on the experimental system under constant input conditions which shows that PCMs improve the release of heat from thermal storage and can supply heat or cold at a desired temperature level for longer time periods. With the help of the computer simulation program TRNSYS, a validation of the simulation model of the latent heat storage system Type 840 was carried out with the initial and boundary conditions of the experimental system. Finally, a parameter analysis for different diameters of the spherical modules was carried out using the simulation model.

Keywords. Energy storage, Latent heat storage, Phase change materials, Optimization, Parametric analysis.
DOI: https://doi.org/10.34641/clima.2022.76

1. Introduction

Nowadays, as global warming is becoming one of the most urgent problems in the world, we need to find a better way to utilize energy: not only in the field of energy production, transmission, distribution, and consumption, but also in the area of energy storage (1).

Current energy production in the EU comes from five different sources, namely oil and petroleum products (36%), natural gas (8,5%), solid fossil fuels (15%), nuclear energy (32%) and renewables (15%) (2,3). Of this, the household, together with services, consumes 40% of the total energy produced, of which 80% energy is used for heating and cooling (4).

Buildings' CO_2 operational emissions account for 30% of the total energy-related carbon emissions (2,3). Indeed, the decarbonization of the building sector plays a central role in the action against climate change. To reduce greenhouse gas emissions by at least 40% (Paris Agreement), the EU has introduced a new directive (2010/31 / EU) as one of the ways to increase the energy efficiency of buildings, for which it has invested heavily in their renovation (5, 6). The EU's goal is to become carbon neutral by 2050. The process of decarbonization of greenhouse gases is primarily part of the building sector in the fight against global warming. Reducing carbon emissions in the building sector goes through improving energy efficiency and the use of renewable energy sources (7).

In order to achieve better energy efficiency of buildings, new ways need to be explored energy storage and efficiency. The focus of the paper is on the analysis of thermal energy storage devices based

Copyright ©2022 by the authors. This conference paper is published under a CC-BY-4.0 license.

on macroencapsulated PCM (4,8). The aim is to design a latent heat storage (LHS) system with spherical modules filled with PCM. Several measurements were performed on the experimental system under constant input conditions which shows that PCMs improve the release of heat from thermal storage and can supply heat or cold at a desired temperature level for longer time periods. With the help of the computer simulation program TRNSYS, a validation of the simulation model of the latent heat storage system Type 840 was carried out with the initial and boundary conditions of the experimental system. Finally, a parameter analysis for different diameters of the spherical modules was carried out using the simulation model.

2. Thermal energy storage

Thermal energy storage (TES) is a technology that accumulates thermal energy by heating or cooling a storage medium so that the stored energy can be used at a later time for heating and cooling applications or power generation. TES systems can help balance energy demand and supply on a daily, weekly and even seasonal basis. They can also reduce peak demand of energy, energy consumption, CO2 emissions and costs, and increase overall efficiency of the system(10).

There are three different types of TES systems, namely:

a. *Sensible heat storage* – technology based on storing thermal energy by heating or cooling mostly a liquid or solid storage medium (e.g. water, sand, molten salts, rocks), where water is the cheapest option;

b. *Latent heat storage* using phase change materials (PCM) e,g from a solid state into a liquid state, and;

c. *Thermo-chemical storage* using chemical reactions to store and release thermal energy.

The well-known consequence is an increase in temperature (sensible heating) or change of phase (latent heating) is shown in **Error! Reference source not found.** . Starting with an initial solid state at point A, heat addition to the substance first causes sensible heating of the solid (region A–B) followed by a solid–solid phase change by crystalline structure change (region B–C), again sensible heating of the solid (region C–D), solid–liquid phase change (region D–E), sensible heating of the liquid (region E–F), liquid–gas phase change (region F–G) and sensible heating of the gas (region G–H).

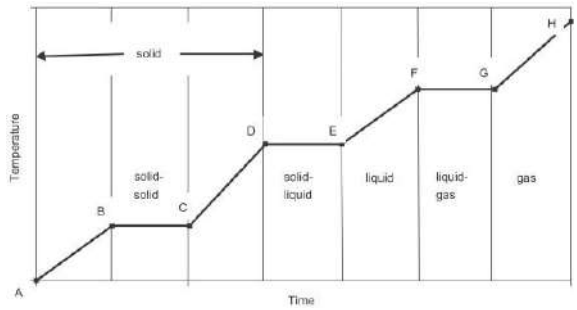

Fig. 1: Temperature-time diagram for the heating of substance*(9).*

The total amount of energy stored can be written as:

$$Q = m\left[\int_{Ta}^{Td} Cps(T)dT + L_p + L + \int_{Te}^{Tf} Cpl(T)dT + L_g + \int_{Tg}^{Th} Cpg(T)dT\right] \quad \textbf{(Eq. 1)}$$

where m is the mass of material, Cps specific heat of material in solid phase, Cpl specific heat of material in liquid phase, Cpg specific heat of material in gas phase, Lp is latent heat of solid–solid phase change, L is latent heat of solid–liquid phase change and Lg is the latent heat of liquid–gas phase change(9)..

2.1 Sensible thermal energy storage

In sensible heat storage (SHS), thermal energy is stored by raising the temperature of a material, typically a solid or liquid. SHS system depends on the heat capacity and the change in temperature of the material during the process of charging and discharging heat. The amount of heat stored depends on the specific heat capacity of the medium, temperature change and the amount of storage material. Heat transferred to the storage medium leads to a temperature increase of the storage medium. A sensor can detect this temperature increase and the heat stored is than called sensible heat. The amount of heat stored in or released form a material can be described as:

$$Q = m\int_{T_i}^{T_f} c_p dT \quad \textbf{(Eq. 2)}$$

where Q [J] is the amount of thermal energy stored or released in form of sensible heat, Ti is the initial temperature of medium, Tf is the final temperature of medium, m [kg], is the mass of material used to store thermal energy, and cp [J/kgK] is the specific heat capacity of material used to store thermal energy [3]. SHS is often used with solids like stone or brick, or liquids like water, as storage material(11).

2.2 Latent thermal energy storage

In case of latent thermal energy storage, thermal energy is stored through phase change of storage medium. During phase change of medium thermal energy can be released at nearly constant temperature. Materials used in latent thermal stages are known as phase change materials (PCMs).

The storage capacity of the material depends on both its specific heat and latent heat values. Thus, it is desirable for the storage medium to have high specific heat capacity and latent heat value. Latent heat storage may be classified on the basis of the phase change process as solid–solid, solid–liquid, solid–gas and liquid–gas.

Latent heat storage (LHS) is based on the heat absorption or release when a storage material undergoes a phase change from solid to liquid or liquid to gas or vice versa. The storage capacity of the LHS system with a PCM medium is:

$$Q = m\left[\int_{T_i}^{T_m} c_{p,s}dT + a_m \Delta h_m + \int_{T_m}^{T_f} c_{p,l}dT\right] \quad \textbf{(Eq. 3)}$$

where T_m is the melting temperature, $c_{p,s}$ [J/kg K] is the specific heat capacity of solid PCM, $c_{p,l}$ [J/kg K] is the specific heat capacity of liquid PCM, a_m is the fraction of PCM melted [-] and Δh_m [J/kg] is the heat of fusion per mass unit. Note that c_p has different values fort he solid state ($T_i < T < T_m$) and the liqud state($T_m < T < T_f$), which is denoted by the indices s and l.

2.3 Materials for latent heat thermal energy storage LH

Materials that are used for LHTES should have a large latent heat and high thermal conductivity. These materials are expected to fulfil some requirements, such as:

- A melting temperature lying in the practical range of operation,
- Melt congruent with minimum sub-cooling,
- To be chemically stable,
- Low cost,
- Nontoxic and noncorrosive

Materials that have been studied during the last 40 years are hydrated salts, paraffin waxes, fatty acids and eutectics of organic and non-organic compounds. The idea to use PCMs for the purpose of storing thermal energy is to make use of the latent heat of a phase change, usually between the solid and the liquid state, to store a high quantity of energy. Since a phase change involves a small temperature changes, PCMs are used for temperature stabilization and for storing heat with large energy densities in combination with rather small temperature changes(13).

Error! Reference source not found. compares the achievable storage capacity at given temperature difference for a storage medium
with sensible heat storage and with latent heat storage.

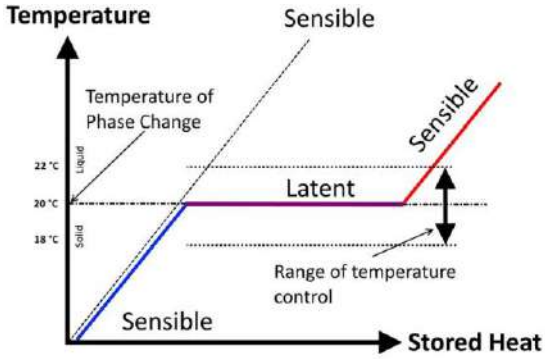

Fig. 2: Heat storage as latent heat for the case of solid-liquid phase change*(12).*

Because one of the goals of LHTES is to achieve a high storage density in a relatively small volume, expected thermal characteristics for PCMs are a high melting enthalpy [J/kg] and a high density [kg/m^3], i.e. a high volumetric melting enthalpy [J/m^3].

3. Experimental investigation

The purpose of this experiment was to investigate improvement in increased energy density for thermal energy storage by integrating PCM modules in water storage tank. The influence of integrated modules on time of providing heat demand and the maximum heat output ha also been studied.

3.1 Experimental system

The experimental system was designed according the standard *VID 2146 – PCM energy storage systems in building services.* With experimental system we have an opportunity to make measurements of charging, discharging and standby of energy storage under different initial conditions.

The storage tank of volume 0,1 m^3 was used. A large part of time has been dedicated to selection of the right shape of the modules. There are different forms in which PCMs can be inserted into the storage tang, e.g. pack, panels, balls (spherical modules), cylindrical shape etc. According to the standard parameters, the spherical modules *FSS PCM HS24* were used in our system, as shown in **Fig. 3.**

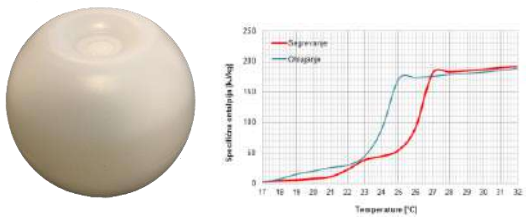

Fig. 2: Spherical modules filled with PCM and enthalpy-temperature function of PCM of FSS PCM HS24.

The temperature was measured with thermocouples, which were arranged along the height of the system and at the inlet and outlet of storage tank. For charging and getting propriate inlet temperate we used 4 kW electric heater. For discharging of storage tank was used the Omega air TAE 031 water cooler.

The scheme of the experimental system is shown in Fig.***4***, with the charging process being shown in red, with blue colour shows the process discharging system. On the diagram are presented all the hydraulic connections and locations of temperature sensors, shut-off valves and circulation pump for each circle.

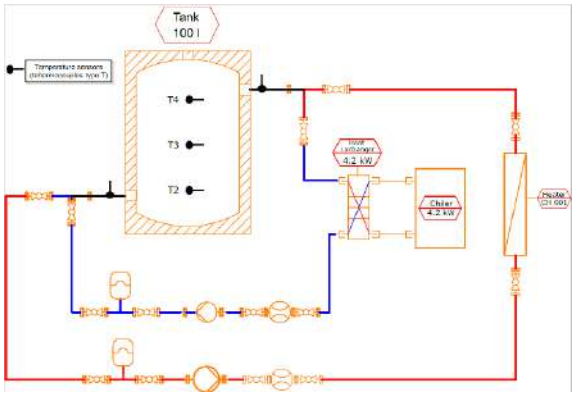

Fig. 4: Scheme of experimental setup.

3.2 Measurements

Two sets of measurements were performed, charging process with temperature of inlet water of 35 and 45°C and discharge process with temperature of inlet water of 16°C.

On the **Fig. 5** and **Fig. 6** can be seen that with higher inlet temperature we need shorter time of changing storage tank. In our case we can see that for inlet temperature of 35° C time of phase changing is $\Delta t = 164\ min$ and $\Delta t = 118\ min$ for inlet temperature of 45° C. From here we can make a concussion that inlet temperature has significant affect to the operation of the LHS.

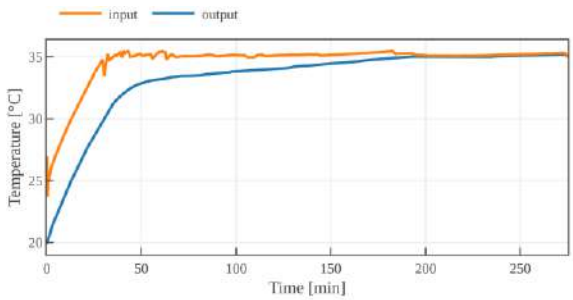

Fig. 5 Charging of LTS with inlet temperature of 35° C.

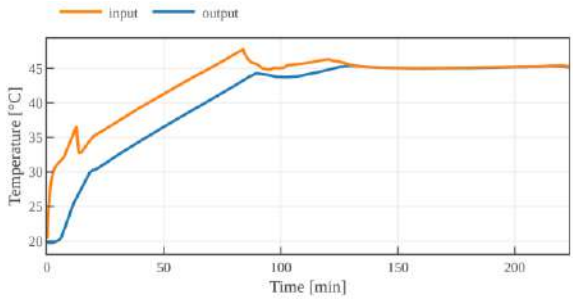

Fig. 6: Charging of LTS with inlet temperature of 455° C.

On the ***Fig.7***, shows changing of absorbed energy during different inlet parameters. We can noted that absorption of energy depends exponentially of temperature. Due to larger temperature difference, the maximum accumulated energy is 4kWh. For reaching this energy we need approximately 130min. on the other side, maximum accumulate energy for inlet temperature of 35° C is 2.5kWh for 200min.

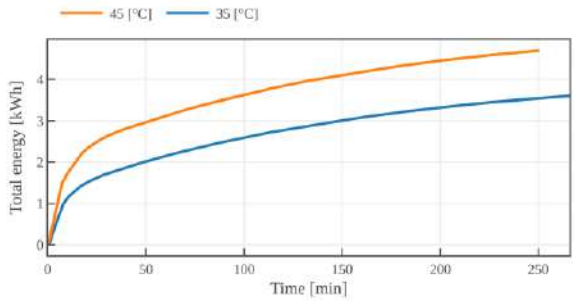

Fig. 7. Storage energy in different charging temperature of 35 and 45 ° C.

During the discharging process were made the same measurements with max. flow rate of the water of $q_v = 490\ {}^{kg}/_{h}$. On **Fig. 8** is shows that time that we need for discharging all system was 135 min.

And from the **Fig. 9** is shown energy released during the time of discharging of LTS. From the fig. we can say that the in the period of 250 min we released 4,7 kWh of energy. This amount of energy was released when the LHS was charge with inlet temperature of 45°C.

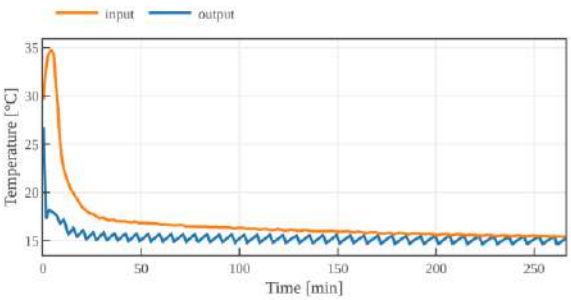

Fig. 8. Discharging of LTS with inlet temperature.

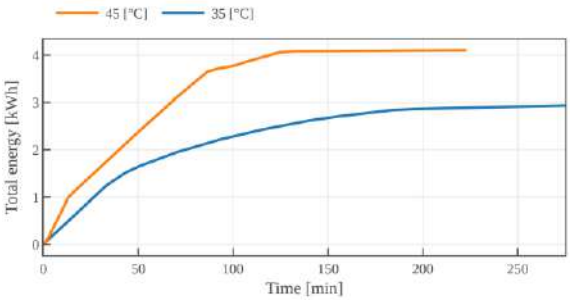

Fig. 9. Heat released during discharging of LHS.

4. Results and discussion

With the help of the computer simulation program TRNSYS, a validation of the simulation model of the latent heat storage system Type 840 was carried out with the initial and boundary conditions of the experimental system.

On the **Fig.10** shows the schematic of TYPE 840 simulation model that was built by team from TU Graz. The scheme consists of the following sets: latent storage tank, a module for the implementation of experimental data and a module for plotting graphs and printouts of the results of a numerical model. A comparison of the temperatures inside the heat accumulator and the outlet temperatures between the simulation and the experiment was made during the melting process as well as during the solidification process of the FSS.

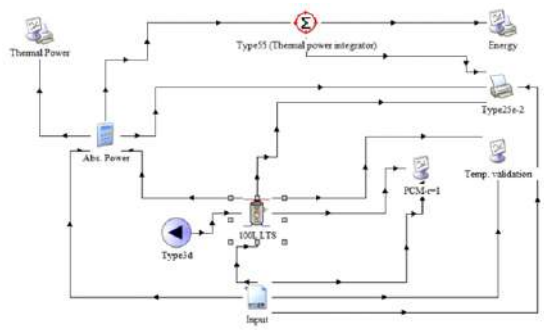

Fig. 10: Schematic of simulation system TYPE 840 in the Trnsys software environment.

For validation of our model, we made comparation of measuring and simulated temperatures data. Validation was made regarding to relative error on the outlet temperature and the temperature inside the storage tank. On **Fig.11** and **Fig.12** are shows relative errors between outlet temperature and temperature inside storage tank during process of charging and discharging of the system.

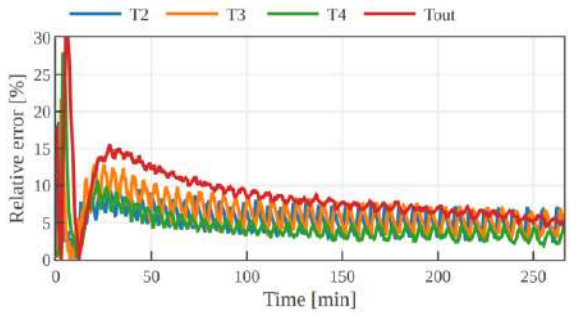

Fig. 10: Relative errors between simulation and measuring results during the process of discarding.

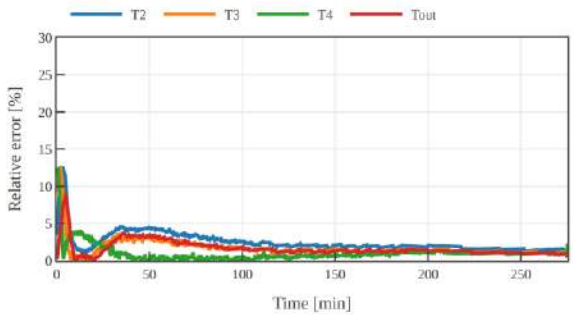

Fig. 10: Relative errors between simulation and measuring results during the process of charging with inlet temperature of 35^{0}C.

The most important parameter is outlet temperature. According to the relative errors shows in the **Fig.11** and **Fig.12,** we can say that the numerical model during charging is presenting results with relative error of 3% and 5% during discharging the system.

One of the reasons why the relative error is higher is due to the placement of thermocouples inside the LHS. The thermocouples were attached to a tube inserted in the middle of the tank. To prevent contact between the thermocouples and the pipe wall, the thermocouples were moved a few centimetres' away from the pipe. In addition to the basic reasons, deviation is also greatly influenced by the inaccuracy of temperature measurements within the modules, which would give us an accurate start data. The results show that the smallest difference is in the middle of the tank, and the largest at the top. Similar to the outlet temperature, the numerical model better describes the processes during the charging than in discharging of the system.

Finally, a parameter analysis was made for different diameters of the spherical modules was carried out using the simulation model. For analysis we use

different diameters PCM $D = [50, 75, 100, 120]mm$. Number of the PCM modules (N) can be determined by following equation:

$$N = \frac{6V}{D^3\pi} \qquad \textbf{(Eq. 2)}$$

Where V is a volume of the tank and D represent the dimeter of the module.

We made 2 different simulation, charging the system with flow rate of $q_v = 350\,{}^{kg}/_{h}$ and discharging with flow rate of $q_v = 490\,{}^{kg}/_{h}$.

On the **Fig.13** shows that the temperature inside the tank is changing proportional to the size of the modules. Time required for to equalizing to the inlet temperature of 35⁰C is $\Delta = 190min$ for the FSS diameter of 50 mm, and for diameter 120 mm $\Delta = 437min$.

On the **Fig.14** showing variation of outlet temperature in time. From the chart we can see that we have logarithmic temperature scale in time.

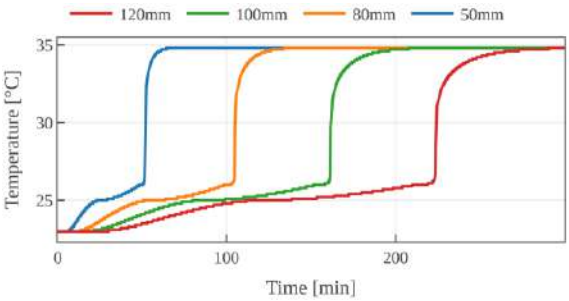

Fig. 13: Temperature inside the storage tank in time during the process of charging.

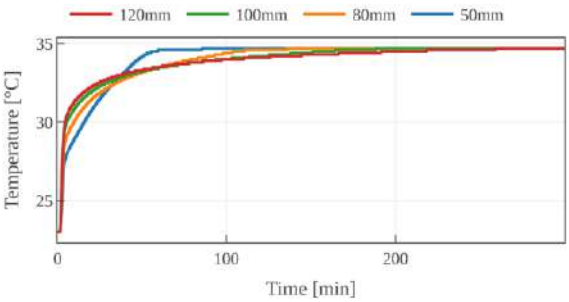

Fig. 14: Outlet temperature during the process of charging.

In the next two charts **Fig.15** and **Fig.16** are showed changing the temperature in time during the process of discharging. From the **Fig.15** we can see that we required time for to equalizing inside temperature with to the inlet temperature of 16⁰C is $\Delta = 120min$ for the FSS diameter of 50 mm, and for diameter 120 mm $\Delta = 324min$.

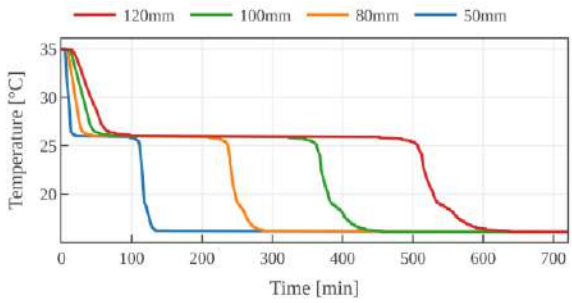

Fig. 15: Temperature inside the storage tank in time during the process of discharging.

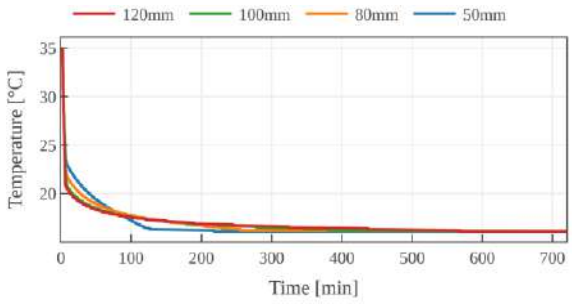

Fig. 16: Outlet temperature during the process of discharging.

5. Conclusions

Energy storage is one of the key areas in which more attention and projects will need to be focused to better address the challenges of energy efficiency and the integration of renewable energy sources into heat storage systems in the future.

The paper focused on improvement of latent energy storage with PCMs where its main advantages have been reviewed and researched. One of the advantages of using PCMs for energy storage is there low thermal conductivity, which has a direct effect at the time of charging and discharging the storage tank. As part of the work, we performed the following steps and came to the following conclusions:

1. When we charge the storage tank with an inlet water temperature of 45 ⁰C, we were able to accumulate energy of 4 kWh and it took 130 min. When we were performing a discharge of system we were able to relesed maximum energy in the amount of 4.7 kWh for 250 min.

2. With used TRANSYS software as a tool where the numerical model LHT Type 840 was adjusted to the initial and boundary conditions of the experimental system and validated with the measurement results. Validation of the numerical model was performed on the basis of calculated relative errors between measured and simulation results. From the obtained results we can say that the numerical model

better describes the process of charging LHS for both temperatures (35^{0}C and 45^{0}C) and the relative error is less than 3%. In the process of charging with 45°C, the relative error is lower than 5%, while in the case of discharging the LHS it is less than 35° C, the relative error is between 5% and 10%.

3. Based on a validated numerical model, we performed a parametric analysis of LHS with different boundary conditions. The analysis was performed at the maximum number of modules that can be inserted into the storage tank, at different diameters $D = [50, 75, 100, 120]mm$. From the results we can see that in the case of melting and solidification of FSS the outlet temperature changes logarithmically in time for different size of modules. The inlet temperature significantly affects the melting time of the PCMs when using larger modules. However, in the process of emptying the LHS, the temperature inside the storage tank does not significantly affect the required solidification time of the PCMs.

4. To summarize the results obtained, the Type 840 simulation model is an excellent tool for performing various analyses for the LHT area of operation. In order to achieve the minimum charging and discharging time of the system, it makes sense to use a smaller diameter PCMs modules.

This work was supported by EU Research and Innovation programme Horizon 2020 trough project number 768921 – HEART.

6. References

1. S. Cao, "State of the art thermal energy storage solutions for high performance buildings", master.degre, Department of physics, University of Jyv¨askyl¨a, Finland,, 2010.

2. Eurostat, Energy statistics - an overview, https://ec.europa.eu/eurostat/statistics-explained/index.php/Energy statistics - an overview#Primary energy production, accessed: 2020-08-12.

3. S. Kalaiselvam in R. Parameshwaran, Thermal energy storage technologies for sustainability: systems design, assessment and applications. Elsevier, 2014..

4. E. Zavrl in U. Stritih, "Improved thermal energy storage for nearly zero energy buildings with pcm integration," Solar Energy, let. 190, str. 420–426, 2019

5. E. Recast, "Directive 2010/31/eu of the european parliament and of the council of 19 may 2010 on the energy performance of buildings (recast)," Official Journal of the European Union, let. 18, ˇst. 06, str. 2010, 2010.

6. E. Commission, "Communication from the commission to the european parliament, the council, the european economic and social committee and the committee of the regions youth opportunities initiative," 2011.

7. Eurostat, Transition to Sustainable Buildings Strategies and Opportunities to 2050,https://www.iea.org/reports/transition-to-sustainable-buildings, accessed: 2020- 08-12.

8. A. Heinz in W. Streicher, "Application of phase change materials and pcm-slurries for thermal energy storage," v 10th International Conference on Thermal Energy Storage, 2006.

9. A. F. Regin, S. Solanki in J. Saini, "Heat transfer characteristics of thermal energy storage system using pcm capsules: a review," Renewable and Sustainable Energy Reviews, let. 12, ˇst. 9, page. 2438–2458, 2008

10. H. Mehling in L. F. Cabeza, Heat and cold storage with PCM. Springer, 2008, year. 308.

11. T. L. Bergman, F. P. Incropera, D. P. DeWitt in A. S. Lavine, Fundamentals of heat and mass transfer. John Wiley & Sons, 2011

12. Heat and cold storage with PCM: an up to date introduction into basic applications. Mehling, Harald Cabeza, Luisa F., edited by D. Mewes, F. Mayinger; chapter: Basic thermodynamics of termal energy storage.

13. Farid Mohammed M., Khudhair Amar M., Razack Siddique Ali K., and Al-Hallaj Said,"A Review on Phase Change Energy Storage: Materials and Applications'', Energy Conversion and Management, Vol. 45, pp. 1597–1615, 2004

A Practical Application of DC Droop Control with IoT capabilities

Damiën Zuidervliet[a], Holly Engelbrecht[b], Christiaan Nagy[c], Diëgo Zuidervliet[d], Peter van Duijsen[e]

a The Hague University of Applied Sciences Delft, The Netherlands 18088015@student.hhs.nl
b The Hague University of Applied Sciences Delft, The Netherlands 18162533@student.hhs.nl
c The Hague University of Applied Sciences Delft, The Netherlands 18118062 @student.hhs.nl
d The Hague University of Applied Sciences Delft, The Netherlands D.C.Zuidervliet@hhs.nl
e The Hague University of Applied Sciences Delft, The Netherlands P.J.vanDuijsen@hhs.nl

Abstract. The application of DC grids is gaining more attention in office applications. Especially since powering an office desk would not require a high power connection to the main AC grid but could be made sustainable using solar power and battery storage. This would result in fewer converters and further advanced grid utilization. In this paper, a sustainable desk power application is described that can be used for powering typical office appliances such as computers, lighting, and telephones. The desk will be powered by a solar panel and has a battery for energy storage.
The applied DC grid includes droop control for power management and can either operate stand-alone or connected to other DC-desks to create a meshed-grid system.
A dynamic DC nano-grid is made using multiple self-developed half-bridge circuit boards controlled by microcontrollers. This grid is monitored and controlled using a lightweight network protocol, allowing for online integration. Droop control is used to create dynamic power management, allowing automated control for power consumption and production. Digital control is used to regulate the power flow, and drive other applications, including batteries and solar panels. The practical demonstrative setup is a small-sized desktop with applications built into it, such as a lamp, wireless charging pad, and laptop charge point for devices up to 45W. User control is added in the form of an interactive remote wireless touch panel and power consumption is monitored and stored in the cloud. The paper includes a description of technical implementation as well as power consumption measurements.

Keywords. *DC grid, power management, sustainable, solar, battery, office desk, droop control, digital control, IoT.*
DOI: https://doi.org/10.34641/clima.2022.162

1. Introduction

Power consumption in an office was until recently not problematic, as consumption was low compared to energy use for cooling or heating. However, reducing the carbon footprint in the office is becoming a trend for companies to increase their sustainability. Reducing power consumption by optimizing the lighting at the office is discussed in [1]. If the lighting in an office is optimized in the areas where light is required, less power is consumed. In [2] the trend in consumption is analyzed. To optimize the use of energy, an algorithm is used to control all components. This requires extra communication with all components. Using the DC droop control as is done in this work, the same goal can be reached without the extra external control. And in [3] the power consumption at an office is discussed. To know where the power consumption can be optimized, the consumption profiles need to be known. Based on these profiles, the droop control can be specified.

DC power [4] is independent of frequency and phase, and could therefore be utilized to make full use of renewable energy sources without needing complicated AC synchronizing mechanisms. Furthermore, most appliances in offices are already DC-powered, so there is no need for an AC grid. Secondly, power congestion management is easier to implement in a DC grid[5][6]. For controlling power in a DC nano-grid[7] new techniques are being developed, one such technique being droop control [8]. This requires measuring the voltage on the main power grid, and changing power consumption accordingly, which dynamically assists in keeping the power grid in good health and keeping critical applications from failing. In [9][10][11] the method and application of droop control in DC grids is discussed. From the experimental work done on low voltage DC grids at [12], an experimental setup was created [13][14], including power electronics educational training laboratory exercises [15][16]. In [17] a DC grid manager with training software [18] is presented. In this paper, a DC nano-grid specific for an office desk is proposed. The main idea is to have a sustainable DC nano-grid inside each office desk. Not to increase efficiency, but to have full control of the

Copyright ©2022 by the authors. This conference paper is published under a CC-BY-4.0 license.

self-regulating system. If a solar panel and battery are connected to the office desk, the office desk can operate independently from the national grid. And additionally, It can also share electric power with neighboring DC desks, creating a larger nano-grid. The choice for DC is made as there is no need for AC, since all sources, e.g. the battery and solar cell, as well as the loads, LED, laptop, and phone chargers are DC. As well that DC has more capability to regulate the power flow by using DC droop control compared to AC.

The sections in this paper contain the following information. In section 2 an overview of the implementation methods is presented. The developed converter to build the DC-powered desk is presented in section 3. The benefit of a DC-powered desk, DC droop control, is outlined by an example in section 4. In section 5 the system control is further elaborated, along with measured response times of the system. In section 6 the monitoring method along with network features are discussed and in section 7 the safety regulations and protection aspects of a DC installation. In section 8 the demonstrative setup is presented followed by the conclusion in section 9. Ending with the references in section 10.

2. Implementation methods

The DC-powered desk is subdivide into three distinct parts: the DC nano-grid, a demonstrative setup, and IoT capabilities. Each elaborated below:

2.1 DC nano-grid

This part includes the used circuits, and the software driving them. It's responsible for regulating the grid and managing the applications connected to the grid. The power electronic circuits in the DC grid enable the following functions:

- Voltage control for a specific voltage;
- Current control for a specific current;
- Implement a dynamic droop curve;
- Charging a battery with charge algorithm;
- Maximize generated PV power using MPPT.

With these functions, it's possible to create a DC nano-grid structure and drive a large variety of different applications. If the DC bus is connected to another DC nano-grid, power can be exchanged. The appliances in the external connected DC nano-grid can be either a consuming load or a producing source. As the power flow can be bidirectional, these appliances are called prosumers, being the combination of either producing or consuming electric power.

The maximum power the office desk can deliver is limited by the State of Charge [SoC] of its battery. However, two connected office desks can deliver twice the amount of power to a third DC nano-grid. The maximum current that can be supplied to the loads is limited by the rating of the DC cable and connectors, which in the case of the office desk is calculated on 10 Ampere.

2.2 Demonstrative Setup

A demonstrative DC nano grid setup is built. A desk is modified to contain all kinds of office appliances, such as phone and laptop chargers, a desk lamp, and USB charge sockets. The desk will function as an off-grid DC platform, able to function on solar and battery energy. Figure 1, gives an overview of the desk. The desk will be able to connect along with other desks, creating one larger meshed grid [19]. This meshed grid can manage electricity among each connected smart-desk and autonomously keep the grid healthy on a local scale. This means that each desk has a battery and a solar source. when insufficient energy is available in one prosumer, the energy sources of other grids can manage the miss-match. This becomes possible by using DC droop control, where the power flow is regulated, to maintain a stable grid.

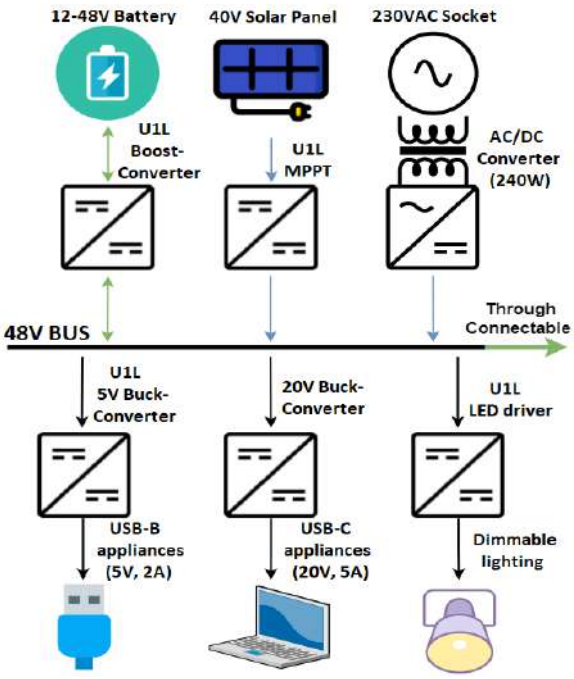

Fig. 1 – Overview of the DC-powered desk.

2.3 IoT capabilities

Internet of Things [IoT] capabilities to measure and exchange data are added to this system. The network protocol MQTT *(Message Queuing Telemetry Transport)* is used, due to its simple structure to send and receive telemetry data through different interfaces. A Raspberry Pi is used as a server and logs all received data. This data can be plotted in time graphs to get a visual understanding of produced and consumed energy. Each driver in the DC desk has an integrated Arduino Nano 33 IoT. The Arduino sends all measured data to the server. The Arduino can also receive data from the server which is easily accessible through the user-friendly interface. The server-UI is realized with Home Assistant, which any smart device can connect to. The UI allows the user to easily control the system with features like On/Off toggles and changing the voltage/current

parameters. Figure 2 shows an overview of the implementation of the IoT system.

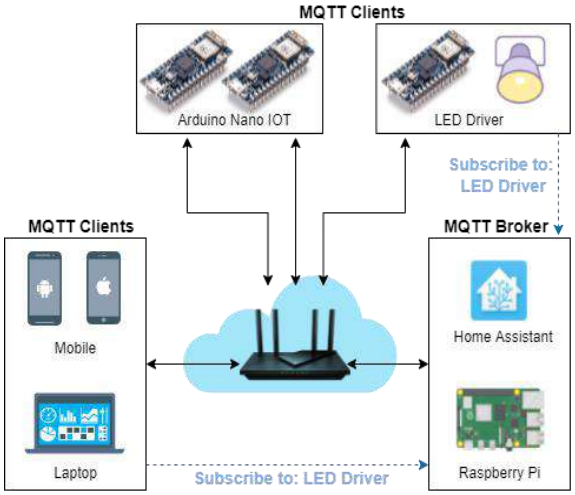

Fig. 2 – MQTT overview of the IoT DC-powered desk.

3. Powering the DC nano-grid

To power this DC nano-grid, a Universal One Leg[16] (U1L) is used. This circuit is based on a half-bridge topology[20], developed by The DC-LAB[12]. The U1L functions as educational hardware to help students better understand power electronics. An Arduino Nano socket is available on each of the U1L. As seen in Figure 3, the Arduino Nano can be programmed to measure voltage and current signals and adjust the output accordingly by changing its PWM. The input ranges from 15V up to 60Vdc and the output ranges from 0 to Vin. The U1L can function as both voltage or current controller by adjusting the halve bridge PWM ratios to keep a reliable output. This way it becomes possible to regulate the amount of consumed energy, based on the available energy.

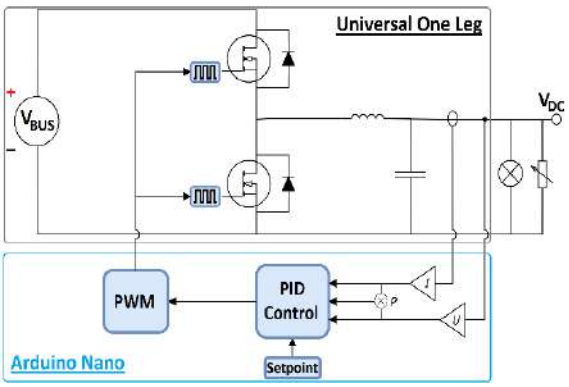

Fig. 3 – Schematic interaction U1L and Arduino Nano.

The U1L can switch as a buck- or boost-converter depending on which terminal is used as input or output. The Vbus (in) terminal and Vdc (out) terminal can be changed, depending on connecting a source or a load to these terminals. The half-bridge topology enables these possibilities.

4. DC Droop Control

In AC systems, switches can be used to regulate energy consumption. This is done by looking at the grid frequency and adding or removing loads based on the available energy. The disadvantage is that AC regulation is limited to passively enabling or disabling systems to adjust the energy consumption. In a DC grid, regulation using power electronics is possible, which allows power congestion management via droop control. This is because DC droop control is not only available to add or remove loads, but also to adjust the amount of energy that is used in loads. This is important for power management. With the increase of daily electricity consumption to compensate for electric cars and electric heating, more advanced technology will be required to manage the grid[19]. To demonstrate the difference between using an AC grid with a constant voltage level, and a DC grid where droop control is implemented, an illustrative simulation is made. In this scenario, an electricity grid typical for an office environment is pictured with three active components, Figure 4.

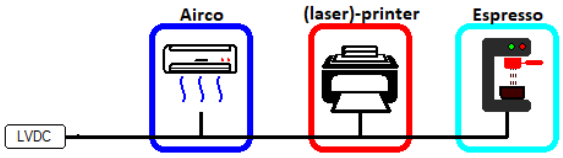

Fig. 4 – CASPOC Simulation model of an LVDC branch with three common components as active loads.

Figures 5 and 6 display the power consumption, of the active loads with corresponding colors, in an electricity branch. The purple line indicates a maximum allowed power of 3.5 kW and the green line indicates the total consumed power. The first figure demonstrates the scenario with a constant voltage AC grid supply. The amount of current used by the appliances is simply the sum of each appliance at full power. Therefore it is a simple addition of all currents. When all components are turned on at the same time, the electrical branch will exceed its maximum power and a fuse will blow, shutting down the entire branch. Since all components consume maximum power, the total power is simply the summation of all individual powers, exceeding the 3,5kW branch fuse, as indicated in figure 5.

When the components are implemented in a DC grid, the amount of power available is indicated by the voltage level in the DC grid. If the voltage level is high, there is enough energy in the DC grid and the components can consume maximum power. If the voltage level is reduced, the power consumption has to be lowered. If the total power consumption is increasing, the voltage level is decreasing accordingly. Due to the lower voltage level, each component is then reducing the power consumption until the final total power consumption is below the maximum power level of 3.5kW. The air conditioning is programmed to reduce its power consumption accordingly, allowing the espresso and printer to

fully operate. Once the espresso completed its task, the air conditioning continues with its nominal power, and the branch is never shut down. This way components in a branch can each be tasked with different priorities. This way important components, such as lighting, will maintain full functionality while lower priority components can reduce the power they consume.

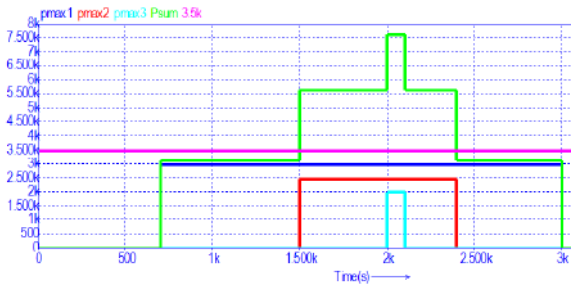

Fig. 5 – AC system, the maximum power (pink) is exceeded as the total power (Green) increases. Fuse breaks.

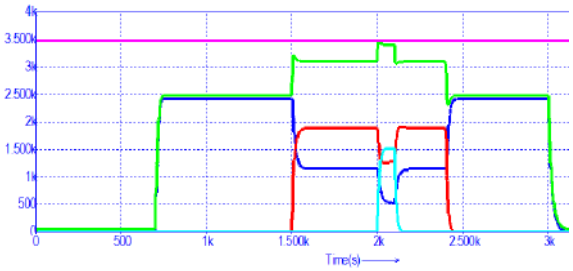

Fig. 6 – DC system, total energy consumption is regulated automatically. No fuse is broken

5. Controlling The System

To actively drive the halve bridge for a stable output voltage, a feedback loop is used. This feedback loop acts as a PI controller, taking the measurement from the output and comparing it to the input, altering the output PWM accordingly. This core system is used for every application that the software can do, along with minor adjustments. For example, the code regulating a normal output voltage is identical to the code charging a battery, the only difference being the parameters of the feedback loop and a few physical header changes.

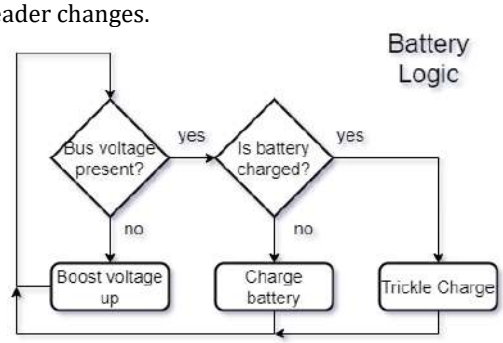

Fig. 7 – Flowchart Battery management.

Software is not only designed for the PI feedback loop. It also includes being able to switch between different operation modes, perform calibrated measurements, and understand the state of other parts of the system. For example, as shown in figure 7, the battery is only allowed to charge itself if a steady external voltage is present on the Vbus. If this voltage is not present, the battery is in charge of creating it. Likewise in figure 8, the U1L which generates the Vbus voltage from an external 24 V DC source needs to keep its feedback cycle in check whenever the battery is delivering power.

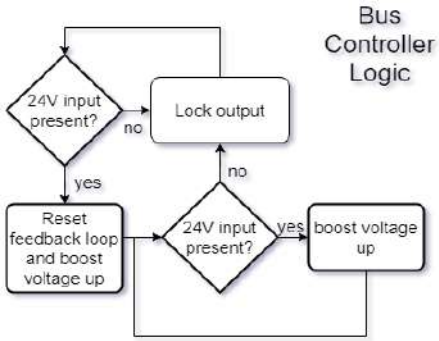

Fig. 8 - Flowchart Vbus management.

To stabilize the system further, extra functions are included to aid the current controller add-on. The function is built to detect whether the current controller is functioning correctly, and use the start-up function if it is not. This ensures that it does not lose control of its output during unforeseen events, locking up the feedback loop.

5.1 Feedback Loop

The feedback loop programmed in the Arduino for this system contains the following equation(1). It is needed to ensure reaching the desired value.

$$PWM[n] += \frac{V_{out}[n] - V_{goal} * 0{,}2}{V_{Bus}} + \frac{\sum(V_{out}[n] - V_{out}) * 0{,}02}{V_{Bus}} \quad (1)$$

It continually takes the previous PWM value, adding an error to bring it closer to the desired value. The amount of error that's added is based on the difference between where the output is and where it needs to be, scaled appropriately in perspective to the bus voltage (since the amount of change in the output due to change in PWM is scaled by the strength of the bus voltage). It also includes a small integral value, to add a marginal amount of extra aggression for large-error cases, ensuring that the voltage rise is as fast as possible in all parts of the curve.

This technology is used in the demonstrative setup to actively adjust the flow of energy. As the source voltage level exceeds or drops below certain critical points, the system will adjust its output behavior accordingly. This way the consumer can use the desk unhindered. Figure 9 visualizes this in the practical setting. As the source voltage (red) changes, the power output (blue) will differ accordingly. With this feature, the available electricity can be used optimally. Charging the battery only when the source is healthy and disabling low-priority components when the available energy is lower.

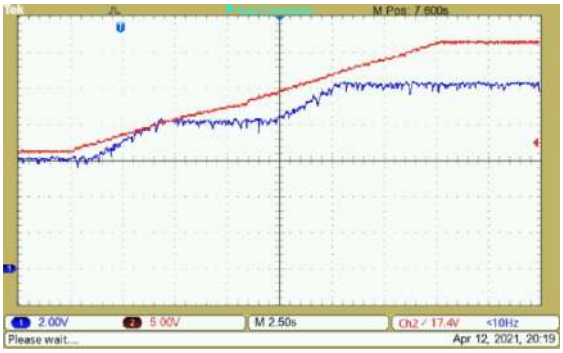

Fig. 9 – A droop curve measured with an oscilloscope. As Vbus (red) changes, Voltage out (blue) dynamically changes along.

5.2 Response time

The feedback loops in this system were calibrated and have acceptable performance. The rise-time of 305 ms, from 0 V to 10 V at the output, can be considered acceptable. Figure 10 demonstrates this rise-time. If looked closely, the individual correction cycles of the Arduino are visible. Completing a cycle of code takes about 30 ms and increases the output according to equation*(1)*.

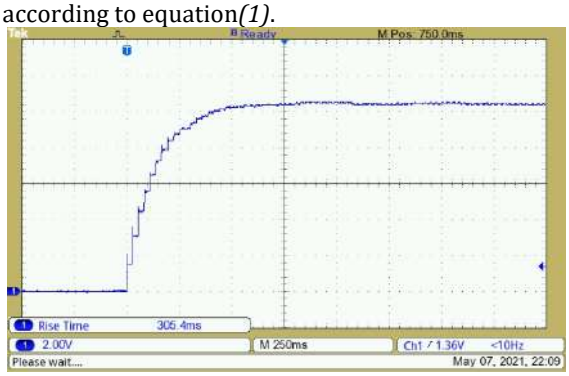

Fig. 10 – Rise-time and Feedback-cycle time to reach 10 V SteadyState output.

5.3 SteadyState accuracy

Once the SteadyState is reached on the output, a noise of 50 mV is experienced on the output line. This is an acceptable error compared to a general laptop charger. Typical usb 5volt chargers are known to experience a 200 mV deviation from the mean voltage and in the USB-PD specification, transients are allowed up to 5% from the mean plus/minus an extra 0.5 volt. Figure 11, demonstrates the SteadyState noise.

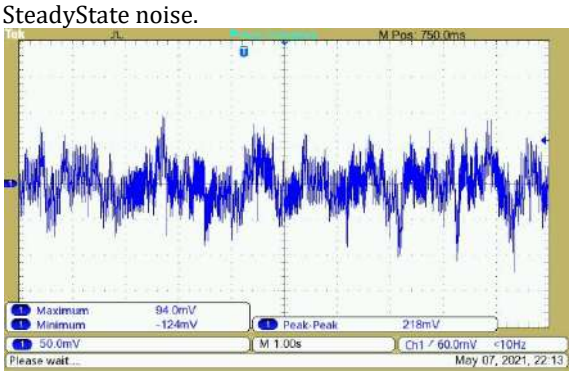

Fig. 11 – AC measurement of the SteadyState performance during active feedback loop. Common deviation of 50 mV with occasional peaks up to 100mV.

6. IoT and grid monitoring

To monitor and control the nano-grid, Home-Assistant is used for the online User Interface [21]. Home Assistant has the capabilities to display and monitor all kinds of data. The collected data is visualized in a simple overview making it ideal to read the grid status from any smart device. The accessibility can be made as simple as needed, depending on the end-user.

6.1 MQTT Protocol

The MQTT allows devices to publish and subscribe to self-made channels, allowing simple to set up telemetry communication. The central broker, the Raspberry Pi, receives published messages, forwarding them to any subscribed client. This allows many clients to log data, and allows any client to access the data that is considered relevant to them. This makes MQTT ideal for sharing information within this particular network. This helps to get all communication to one location in the network and add multiple U1L converters to the Office environment.

6.2 Communicating with the U1L

The communication with the U1L boards can be split into two groups: telemetry and control. The telemetry part sends all measured data to Home-Assistant for display purposes. Each U1L sends two voltage and two current measurements, for the bus and output3 terminal. For the control part, bi-directional communication can be possible. The user can change parameters on the U1L from Home-Assistant, as shown in Figure 12. This includes the operation mode of the U1L, the output voltage, the droop control curves, battery characteristics, and a toggle switch, allowing the system to be shut down remotely.

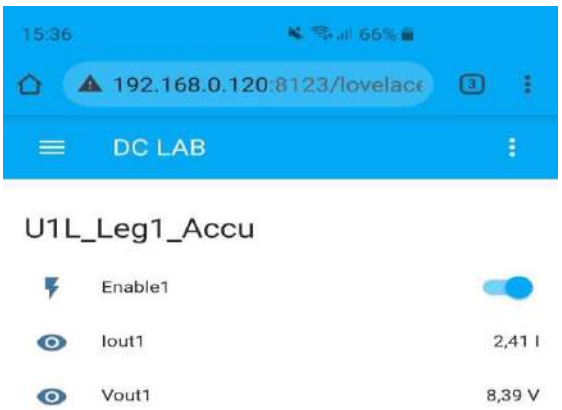

Fig. 12 – Simple Home Assistant User Interface (PC).

6.3 Data Visualization

Once logged into the Home Assistant server the visuals can be extended according to preference, as shown in Figure 12. This enables the data to be observed in a visually pleasing way. All data is also stored on the internal SD card of the Raspberry Pi, also allowing a historical view of all measured data.

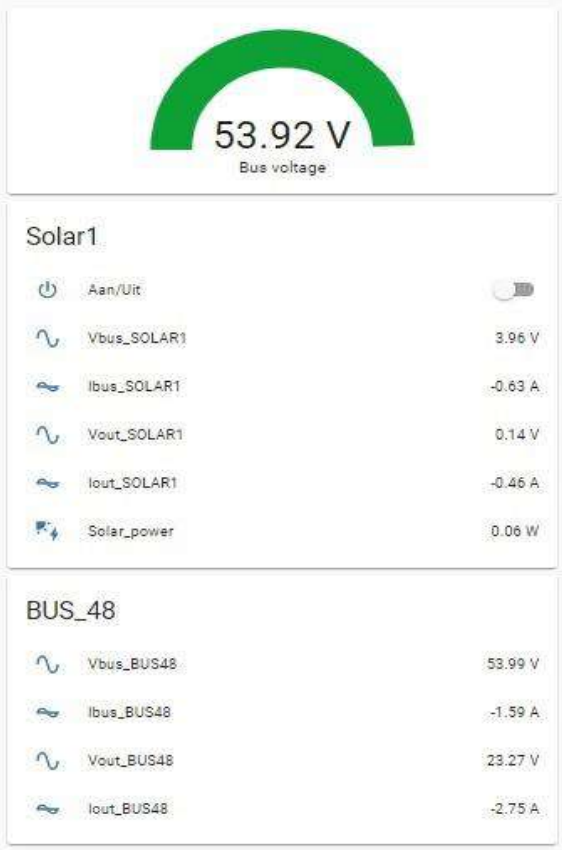

Fig. 12 – More advanced layout for Home Assist User Interface (Smartphone).

Additionally, it is possible to run custom scripts inside Home assistant. This enables endless possibilities for the user to manage its system. One of these scripts is seen in figure 13. Multiple sources of data such as the bus voltage, outputs, and battery levels are plotted on a single time graph. This visualization creates a better understanding of the energy flows within the demonstrative setup.

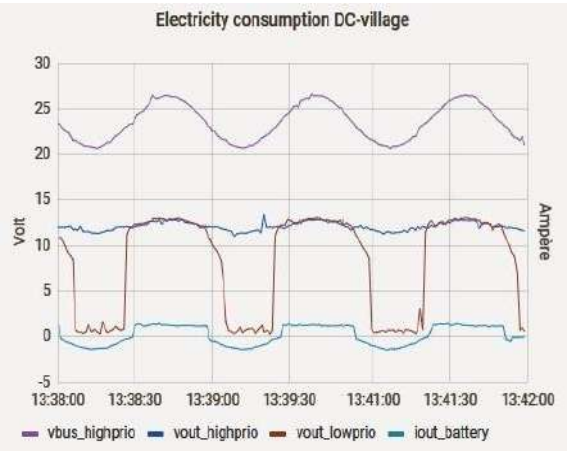

Fig. 13 – Plotting multiple sources on a time graph for an easy understanding of the energy flow in this setup.

As shown in figure 13, the purple line indicates a grid voltage, which swings between 20~26 V. When the grid voltage gets below a certain point, the low priority loads(red) are disabled, while the high priority loads(blue) stay operational for a healthy grid.

7. Protection

The demonstrative setup is designed to be placed in the office environment as a single-person work desk. The goal is to practically experience the pros and cons when using a DC-grid instead of the usual AC-grid. The NPR9090[22] for Dutch practical guidelines explains how DC power sources need to be safely protected. This document divides all kinds of LVDC-installations into 5 separate zones, each indicating how they should be protected to keep the environment safe, Figure 14. In this list, the most dangerous zone is in zone-0. This zone categorizes Solar parks, Battery plants, and the public grid. The important properties of these components are that they are capable to deliver huge currents on demand, acting as an infinite current source. The safest zone is in zone-4. This zone contains all connectable devices below 60 V, the Low Voltage Direct Current (LVDC) level, and below 1000 W. The short-circuit current for devices in zone-4 is very limited as these devices are unidirectional and below the human hazard voltage. The U1L-hardware powering the applications is protected against electrical surges and other hazards. Fuses and RVS diodes are used to shut down the system directly once a malfunction is detected. Devices connected to this side of the source are safe for touch and are not able to harm people.

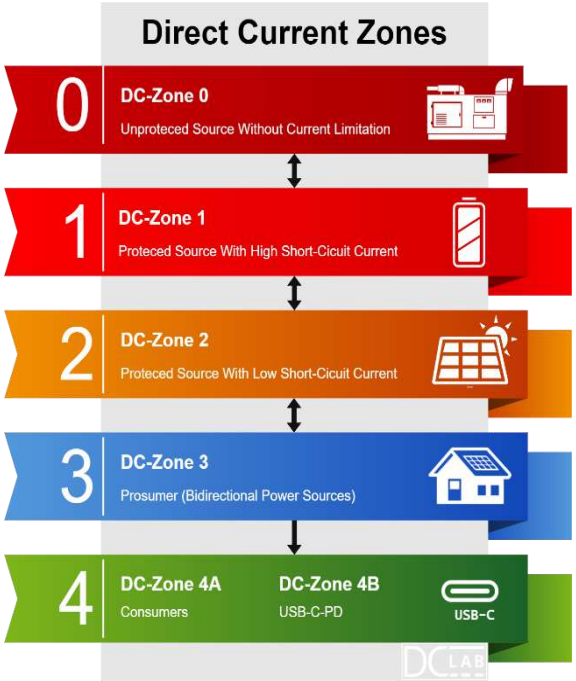

Fig. 14 – DC-zones stated by the NPR9090[22]. Each zone is defined with criteria to connect the devices.

In the demonstrative setup, two zones are represented. As the product will contain a lot of human interaction, the entire desk itself is only equipped with a zone-4 installation, for the lighting and charge sockets. The energy sources powering the system are identified as a zone-3 installation. These sources are applied to the table in a concealed way. Those who use the table as an office desk will be out of direct reach of these components.

8. Demonstration setup

The demonstration setup contains a 74x74 cm Scandinavian homemade table redesigned with multiple appliances connected to all the U1L converters, Figure 15. There are four U1L converters able to power four types of appliances. The bus voltage is realized by connecting a 48Vdc lead acid battery to the Vbus.

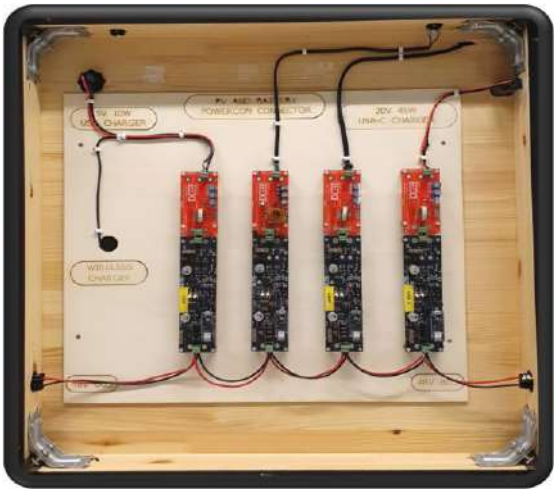

Fig. 15 – Bottom-view demonstrative setup. All devices powered by U1L circuits are mounted underneath the table.

To power this system, three different methods are available:

- A 48V is applied on the Vbus line;
- A 24-48V battery is applied on the battery line;
- A 24-48V Solar panel is applied on the PV line;
- A mixture of these sources is applied.

With sufficient power, each of these options can operate the table. Once powered, the devices will automatically boot up within 10 seconds.
During this time each U1L will upload their operation mode and create each of their desired voltages. Each U1L connected to a load will function as a buck converter and those connected to a power source will function as a boost converter. As the devices in the table turn on, all measured data is published through Wi-Fi. The broker will gather this information once connected in the same network space as the table.

<u>The four U1L's installed in the table are specified as:</u>

1. The 5Vdc line for all portable appliances that need USB power through a typical USB-B port. In this office table, it is a 10W wireless charger and 10W USB-B charge port.
2. A 12Vdc line as a LED-Driver, this line can go in current-control mode to drive LED lights, up to 100W.
3. A 20Vdc USB-C socket with power delivery, capabilities to charge laptops with 45W.
4. A ranged input for PV with a maximum power point algorithm, up to 100W. Or a ranged input for external batteries to boost the bus voltage. This battery acts as a backup for the 48Vdc line.

Fig. 16 – DC-powered table placed in the living lab in the auditorium of THUAS, fed by a 48V battery. While charging the laptop and Phone with LEDs [23]

Figure 16, shows the final result. The table can fully function as an off-grid system. By connecting multiple tables on the same Vbus line, a meshed grid can be created. This meshed grid can communicate grid statuses among each consumer and act accordingly if certain events occur. For example, each table can be connected with a PV panel and battery. If half of the tables are barely used, excessive solar energy can be used to power neighboring batteries. This way each table becomes a prosumer, using dynamic droop control curves to contribute to a healthy state of the grid.

9. Conclusion

In a DC grid, power management can be performed using droop control. To demonstrate the use of power management by droop control, in an office environment, a demonstration desk including a DC nano grid is developed. The DC nano grid includes energy storage, has a photovoltaic connection with a maximum power point tracker, and is remotely configurable and monitored. The desk can be connected to other desks to form a larger DC grid for the exchange of energy.
Since the desk can be configured and monitored remotely it is flexible in use, especially in an office building.

10. References

[1] M. Hajjaj, M. Miki and K. Shimohara, "The Effect of Using the Intelligent Lighting System to Deduct the Power Consumption at the Office," 2019 IEEE 7th Conference on Systems, Process and Control (ICSPC), 2019, pp. 65-69, doi: 10.1109/ICSPC47137.2019.9068078.

[2] F. Gong, N. Han, D. Li and S. Tian, "Trend Analysis of Building Power Consumption Based on Prophet Algorithm," 2020 Asia Energy and Electrical Engineering Symposium (AEEES), 2020, pp. 1002-1006, doi: 10.1109/AEEES48850.2020.9121548.

[3] Hu Hu, Lihong Han, Xin Tian and Guangping Wu, "Concerning with standby power consumption and creating low carbon life —Trailing and studying the standby power consumption of office equipment in Kunming," 2011 Second International Conference on Mechanic Automation and Control Engineering, 2011, pp. 2049-2051, doi: 10.1109/MACE.2011.5987375.

[4] L. E. Zubieta, Are Microgrids the Future of Energy? DC Microgrids from Concept to Demonstration to Deployment, IEEE Electrification Magazine, vol. 4, no. 2, pp. 37 - 44, 2016.

[5] Spaans, Alexander and Zuidervliet, Diëgo and van Duijsen, Peter, Droop Control in DC Grids using the Universal Four Leg as Laboratory Setup (July 26, 2021). AIUE Proceedings of the 2nd Energy and Human Habitat Conference 2021, Available: http://dx.doi.org/10.2139/ssrn.3899714

[6] H. T. Engelbrecht, D. C. Zuidervliet and P. J. van Duijsen, "Educational Droop Control Laboratory Setup," 2021 International Conference on Electrical, Computer, Communications and Mechatronics Engineering (ICECCME), 2021, pp. 1-6, doi: 10.1109/ICECCME52200.2021.9591123.

[7] Laurens Mackay, Nils H. van der Blij, Laura Ramirez-Elizondo & Pavol Bauer (2017) Toward the Universal DC Distribution System, Electric Power Components and Systems, 45:10, 1032-1042, DOI: 10.1080/15325008.2017.1318977

[8] S. E. Mhankale and A. R. Thorat, Droop Control Strategies of DC Microgrid: A Review, 2018 International Conference on Current Trends towards Converging Technologies (ICCTCT), 2018, pp. 372-376, *https://doi.org/10.1109/ICCTCT.2018.8550854*

[9] A. Abhishek, A. Ranjan, S. Devassy, B. Kumar Verma, S.K. Ram and A.K. Dhakar, Review of hierarchical control strategies for DC microgrid. IET Renewable Power Generation, 14: 1631-1640. https://doi.org/10.1049/iet-rpg.2019.1136

[10] R. Kumar and M.K. Pathak, Distributed droop control of dc microgrid for improved voltage regulation and current sharing. IET Renew. Power Gener., 14: 2499-2506. https://doi.org/10.1049/iet-rpg.2019.0983

[11] K. Rouzbehi, A. Miranian, A. Luna and P. Rodriguez, A generalized voltage droop strategy for control of multi-terminal DC grids, 2013 IEEE Energy Conversion Congress and Exposition, 2013, pp. 59-64, doi: 10.1109/TIA.2014.2332814

[12] DC-LAB, Educational Hardware Design. [Online] Available: http://www.dc-lab.org/

[13] P.J. van Duijsen, J. Woudstra and P. van Willigenburg, DC grid laboratory experimental setup, 2018 International Conference on the Domestic Use of Energy (DUE), 2018, pp. 1-6, https://doi.org/10.23919/DUE.2018.8384397

[14] P.J. van Duijsen, D.C. Zuidervliet and J.B. Woudstra, Electronic Learning Experience Setup : Power Electronics and Electrical Drive Education, 2020 43rd International Convention on Information, Communication and Electronic Technology (MIPRO), 2020, pp. 1549-1554, https://doi.org/10.23919/MIPRO48935.2020.9245230

[15] J.B Woudstra, P.J. van Duijsen, P. van Willigenburg, P.M. Witte, DC Educational Development, Improving understanding of DC to DC / DC to AC conversion, SEFI Conference 2018, ISBN 978-2-87352-016-8, [online] Available: https://www.sefi.be/conference/copenhagen2018/

[16] P. J. van Duijsen, D. C. Zuidervliet and C.F.M. Dirksen, Enhancing Laboratory Learning Experience: A New Experimental Setup For Power Electronics And Electrical Drive Education, SEFI Conference 2019, ISBN 978-2-87352-018-2, [online] Available: https://www.sefi.be/conference/2019-budapest-isbn-978-2-87352-018-2/

[17] P.J. van Duijsen and D.C. Zuidervliet, Structuring, Controlling and Protecting the DC Grid, International Symposium on Electronics and Telecommunications (ISETC), 2020, pp. 1-4, doi: 10.1109/ISETC50328.2020.9301065.

[18] Simulation Research, Caspoc Simulation and Animation. 2021 [Online] Available: https://www.caspoc.com/

[19] P. van Duijsen, J. Woudstra and D. Zuidervliet, Requirements on Power Electronics for converting Kitchen Appliances from AC to DC, 2019 International Conference on the Domestic Use of Energy (DUE), 2019, pp. 190-197.

[20] S. Ang, A Oliva, Power-Switching Converters 3rd Edition, CRC Press; 3rd edition, 2010, ISBN:978-1439815335

[21] Home Assistant [Online], Available: *https://www.home-assistant.io/*

[22] NPR9090, Nederlandse Praktijk Richtlijn, Online Available: https://www.nen.nl/en/npr-9090-2018-nl-250370

[23] Stichting-gelijkspanning YouTube Channel. Interview and Demonstration DC Powered Office Table. Video: Webinar, het DC lab van de Haagse Hogeschool Available: *https://youtu.be/GUqeGBunwwU?t=2030 (timestamp 33:50)*

Experimental assessment of radiant panel for thermal conditioning of open spaces

Daniel Castro Medina [a], María del Carmen Guerrero Delgado [a], Teresa Rocío Palomo Amores [a], Alberto Cerezo Narváez [b], José Sánchez Ramos [a], Servando Álvarez Domínguez [a]

[a] Escuela Técnica Superior de Ingeniería, University of Seville, Seville, Spain, dcastro@us.es.

[b] Escuela Superior de Ingeniería, University of Cádiz, Spain.

Abstract. Climate change resulting from the high emission of greenhouse gases has caused a continuous increase in the Earth's temperature, leading to an increase in the demand for refrigeration in the residential sector. Added to this is the heat island effect that generates even worse microclimatic conditions. Based on this idea, the CartujaQanat project was born, which seeks to recover life on the street by providing up-to-date solutions to combine the knowledge obtained from experience, tradition, innovation, and research. These solutions include reducing solar radiation, lowering the temperature of surrounding surfaces, and lowering the air temperature. Furthermore, this study explores a new concept of radiant solution adapted to outdoor spaces to improve thermal comfort and determine the radiant effect it provides since only radiant heat flux is relevant in open spaces with a low level of confinement of air. For this, the proposed solution is evaluated in a test cell to obtain its thermal behaviour under different operating conditions. Thanks to the experimentation carried out, it has been possible to obtain an inverse model to analyze the thermal behaviour of the solution. The inverse model obtained achieves high precision in its estimates and the possibility of fractioning the radiant and convective heat flux rate, allowing to evaluate the system's different operating conditions and know the solution's impact in open spaces. Thanks to this control of surface temperatures, an increase in thermal comfort by 40% is guaranteed. In addition, it prolongs the time of use of the open space, allowing attendees to be in comfort conditions for a longer period.

Keywords. thermal comfort, radiant system, open spaces, thermal adaptation.
DOI: https://doi.org/10.34641/clima.2022.105

1. Introduction

The original concept of EXPO'92 [1] had as its main purpose that open spaces were the differential and cohesion component between the different pavilions of the venue. The function of the open spaces was not limited to a simple transition between the various pavilions. Still, they were spaces with their personality that favoured their use as outdoor leisure places where numerous activities were carried out. For this, it was necessary to develop innovative climate control techniques [2] to combat the high temperatures in the city of Seville in the summer, allowing those attending the venue to stay outside of the pavilions and carry out numerous activities in a situation of thermal comfort.

The climate control strategies developed depending on numerous factors and on the different characteristics of each outdoor space and its function. The longer the stay, the greater the intensity of conditioning. Actions that included confinement, solar control, surface cooling and air cooling were progressively used in many ways, including the later popularized micronization systems.

To recover the spirit of the climate conditioning works developed for EXPO'92, the CartujaQanat project was born. New technologies, materials, and modern and innovative design tools are introduced. From the social point of view, the project aims to be a catalyst, allowing citizens to enjoy open spaces during the warm months. High temperatures make practically any activity impossible.

The project takes place on Avenida Thomas Alba Edison, on Isla de la Cartuja (Seville). A new semi-confined space is being built, and an existing one is being rehabilitated, an amphitheatre located on the avenue itself and dating from the EXPO' 92. The new space is known as the souk. The amphitheatre will be naturally conditioned to offer comfort conditions during the hottest months, obtaining a thermal jump of up to 10 ° C less than the outside temperature than the conditioned open spaces. As heat transfer fluid,

Copyright ©2022 by the authors. This conference paper is published under a CC-BY-4.0 license.

water will be used, stored in two Qanat and cooled during the night thanks to the nocturnal use of environmental sinks [3]. During the day, this water is used to cool the air to be introduced in both spaces [4].

This work deals in detail with the characterization and applicability of a radiant panel. To do this, experimentally the results obtained from numerous experiments are analyzed and a simplified model is proposed, which allows determining the total heat flux absorbed from a series of input data.

In addition, the different modes of operation existing in the CartujaQanat project that allow the conditioning of the two rooms mentioned above are explained.

2. System description

2.1 System

The radiant solution of this study is a modular solution, which facilitates the coupling of successive modules in parallel (figure 1). A module consists of meanders made by machine from multilayer composite pipe placed on a metal structure attached to the ceiling. Each module has dimensions of 1.6 m long by 0.33 m wide. The configuration adopted for the experiments presents 10 steps the tube for each module. The linear length of a 10-tube module is approximately 18 m with an outer diameter of 16 mm and 2 mm thick.

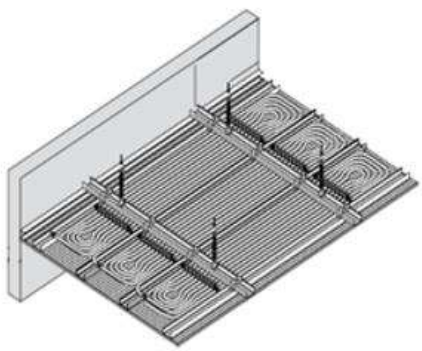

Fig. 1 – Three module coupling.

2.2 Experimental facility

The experimental prototype to test the radiant solution deals with a modular solution, which facilitates the coupling of successive modules in parallel. It takes place in a test cell, located at the Eduardo Torroja Institute of Construction Sciences in the city of Madrid, Spain.

The proposed experimental prototype consists mainly of the radiant solution, a heat pump to cool or heat the water accumulated in the buffer tank and a pump in charge of driving the water from the buffer tank to the radiant solution through a collector of supply and return of the two available circuits.

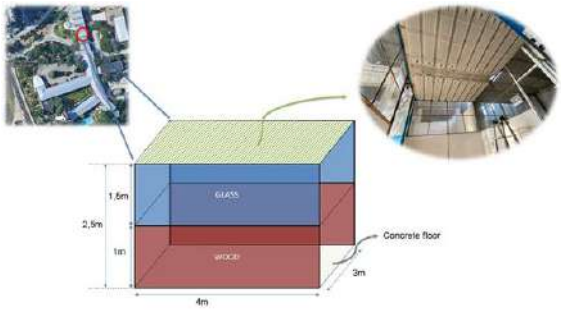

Fig. 2 - Layout.

The described System is fully monitored by multiple calibrated sensors coupled to a DAQ.

3. Methods: characterisation model

3.1 Theoretical basis

The theoretical basis of the radiant system described are based on an energy balance. If the energy balance is carried out in an active roof system, wholly isolated from the top, the variation in water-energy refers to the thermal gains due to convection and radiation with the conditioned space ($Q_{cv} + Q_{rad}$).

Therefore, the energy variation of the water that circulates through the radiant cover is formulated according to equation 1:

$$m_w \cdot \rho_w \cdot Cp_w \cdot \frac{dT_w}{dt} = Q_{cv} + Q_{rad} \qquad \text{(eq.1)}$$

Where m_w is the flow of water that circulates through the radiant cover, ρ_w the density of water, Cp_w the specific heat of the water, $\frac{dT_w}{dt}$ the difference in temperature between the inlet and outlet of the water of the radiant system, Q_{cv} is the convective heat flux between the surface and the surrounding air, Q_{rad} is the radiant heat flux between the surface and the rest of surface.

3.1 Model

To predict the convective and radiant heat flux for the tested system, a model is formulated that allows determining the heat flux as a function of the discharge temperature, the projected air of the radiant roof based on the number of modules and the impulsion flow. Among the parameters to highlight of the model:

- The heat flux referred to as the radiant thermal gains are linearized, so the hypothesis is made that the representative temperature difference is less than 100K. Therefore, the error made when linearizing the radiation heat flux is acceptable [5].

- The convective heat coefficient is modelled based on the Morgan correlation for a long horizontal cylinder [6]:

$$h_{cv} = \mathrm{k} \cdot LMTD_{cv}{}^{\mathrm{n}} \qquad \text{(eq.2)}$$

Where the coefficients K and n are the parameters to be determined based on the data obtained from the experimentation of the experimental prototype.

4. Results

6.3 Identification of parameters and validation

The experiments have been carried out for different water flow rates. As a first result, the variation of absorbed heat flux is obtained as a function of the water flow.

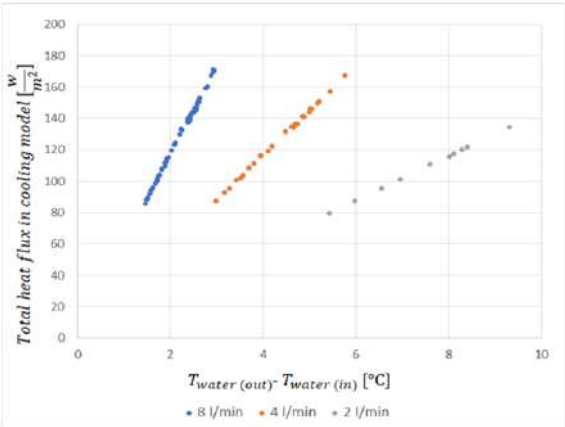

Fig. 3 - Total heat flux.

As this flow increases, the thermal jump between the water inlet and outlet is less.

To determine the absorbed radiant heat flux it is necessary to know the emissivity of the material. The manufacturer's data indicates that the emissivity is 0.85.

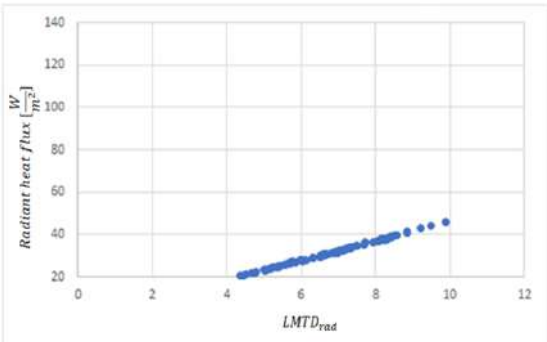

Fig. 4 - Radiant heat flux.

To determine the absorbed radiant heat flux it is necessary to know the emissivity of the material. The manufacturer's data indicates that the emissivity is 0.85. The absorbed radiant heat flux results vary linearly with the LMTD, which implies that the radiant transfer coefficient has a constant near value of 4.6 $\frac{W}{m^2 \cdot °C}$.

The following figure shows the results of the evolution of heat transfer by convection.

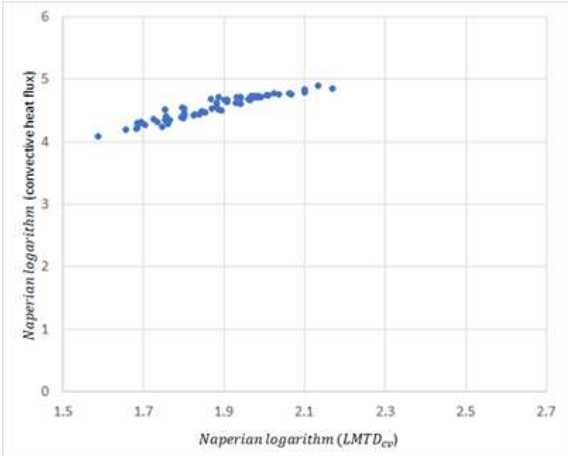

Fig. 5 - Obtaining model parameters.

It is possible to adjust the expression (eq. 2) using data from figure 5. Experimental data is divided into two groups: group 1 identifies the coefficients (40% of the experimental data) and group 2 validates the expressions (60% of the data). The coefficients for the cooling mode are

$$h_{cv} = e^{1.8127} \cdot LMTD_{cv}{}^{0.4596} \qquad \text{(eq.3)}$$

To verify that the expression obtained is valid, the model is run with a series of input data. The data obtained from the model are the water outlet temperature and the total heat flux absorbed. These are compared with experimental data to confirm the quality of the model obtained.

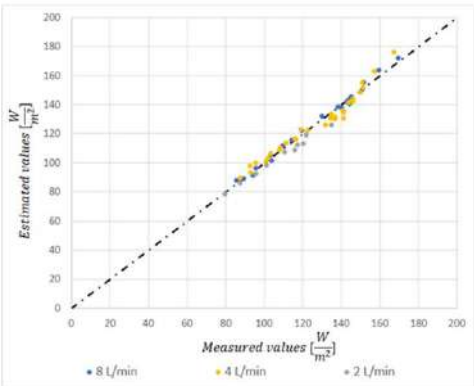

Fig. 6 - Estimated vs measured values – Heat flux

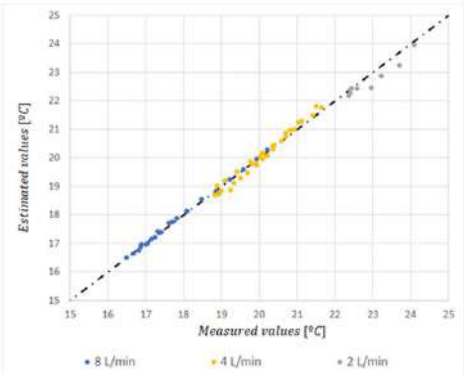

Fig. 7 - Estimated vs measured values – Water outlet temperature

Both the estimated total heat flux and the temperature of the water at the outlet show errors not exceeding 2% with respect to the experimental data. Therefore, the quality of the model is confirmed.

5. Applicability

Thanks to the previously exposed model, it is possible to estimate the thermal performance of the radiant panel in any operating condition. In the case of the souk, a newly built room in the CartujaQanat project, it is possible to determine the number of modules needed to install and size the cold-water production system. Figure 8 shows the souk and the installation site of the experienced radiant panel.

Since the radiant panel system studied has been assimilated its operation to that of a heat exchanger, the use of the NTU efficiency method is proposed for the applicability of the model. The results shown below have been calculated using a mean air temperature of 25 ° C, a mean radiant temperature of 24 ° C and an inlet water temperature of 15 ° C.

Fig. 8 - Design of climatic outdoor conditioning system by radiant surface in the souk.

In the first place, the efficiency of the system is evaluated for the three water flows studied based on the number of modules installed. If the water flow is the minimum, the maximum length per m2 of active surface is required to achieve the same efficiency as the other cases. This result allows deciding if it is more interesting a low operation cost (pumping cost) or a high initial cost.

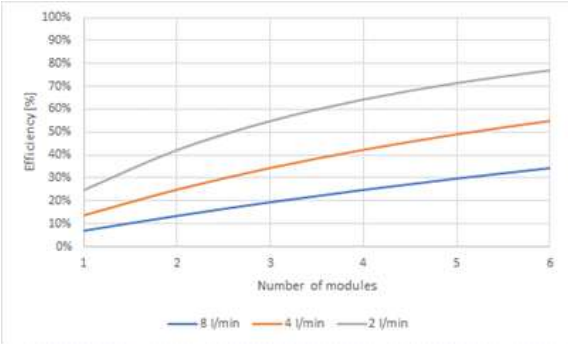

Fig. 9 - Efficiency vs number of modules.

The following result shows the variation of the efficiency as a function of the NTU

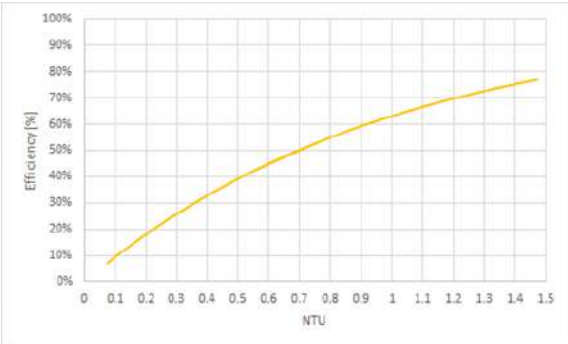

Fig. 10 - Efficiency vs NTU.

It follows that a higher NTU implies a greater linear length of tubes through which a low flow circulates.

In addition to the results before, ε-NTU procedure allows evaluating the results for a known solution (108 m of radiant exchanger and water flow of 2 $\frac{l}{min}$). The total absorbed heat flux is represented for different given radiant LMTD as a function of the convective LMTD.

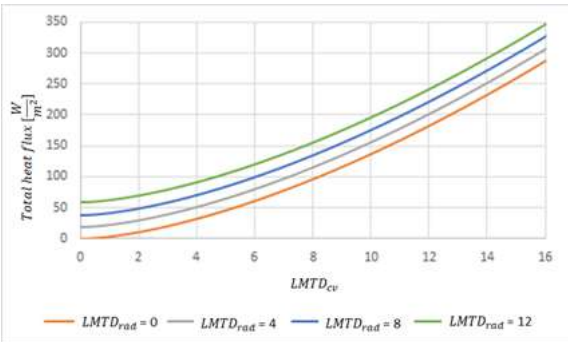

Fig. 11 - Total heat flux based on different DTLMs.

Thanks to this result, a pre-design of the radiant panel and the necessary auxiliary equipment is possible.

6. CartujaQanat operating modes

The operating modes of the installation for the natural conditioning of the rooms are:

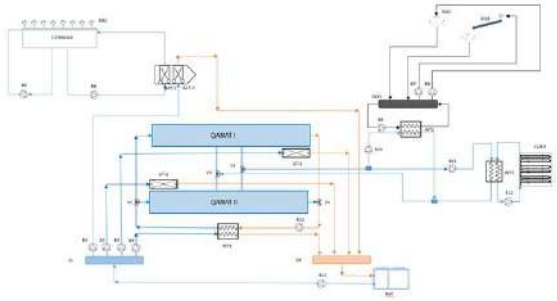

Fig. 12 - CartujaQanat hydraulic diagram

Mode 1. Nocturnal cooling of the water of the Qanats: The CartujaQanat project stands out for the use of natural thermal dissipation, thanks to the use of environmental heat sinks. For this, there are two dissipation systems, one placed on the aqueduct, which is made up of numerous nozzles placed along it in charge of cooling the water through the evaporative effect. On the other hand, there is a dual and innovative system such as the falling film on photovoltaic panels, in charge of producing the electrical energy of the installation during the day, which consists of throwing the water on the surface of these, obtaining a great evaporative cooling - radiant by using the sky as a heat sink.

Mode 2. Buried ducts: The new Qanat concept integrates buried ducts specially designed for cooling air during the day. The ground in the ducts is regenerated overnight using mode 5. The air from the buried ducts is strategically blown into the souk. In the event that the cooling is not sufficient, a water-fed terminal unit from the Qanats is available (mode 6).

Mode 3. Submerged ducts: The Qanats accumulation volume has 4 submerged ducts at two levels of depth. The air introduced through the upper ducts circulates from left to right, while through the lower ones it does so from right to left. With this, a better distribution of the blown air is achieved in the conditioned space.

Mode 4. Radiant roof: Installed in the souk, it aims to keep the roof temperature practically constant over 26-27 °C, thus guaranteeing the thermal comfort of the attendees.

Mode 5. Regeneration of the buried ducts: The air coming from outside at night is at a lower temperature than the ground, so its journey through the ducts gives the ground heat, cooling it. If the outside temperature is not low enough to cool the ground, a regenerative system is available by Qanat which performs an evaporative pre-cooling of the air to be introduced.

Mode 6. Terminal cooling: At the outlet of the buried conduits there is a battery powered by water from the Qanats.

Mode 7. AHU amphitheater: The conditioning of the amphitheater is given by the impulsion of cooled air through the air handling unit. The batteries receive the water from the cooled pond by means of mode 8, cooling the air as it passes and distributed in the amphitheater evenly from the front.

Mode 8. Pond dissipation system: The pond dissipation system consists of a set of nozzles on the surface of the pond at a certain height, which drive the water at high pressure, thus achieving the evaporation of part of the drop and therefore, cooling pond water.

At the technology level, the qanats stand out. The reinterpretation of the Qanat made for this project as a cold-water storage element and cold air production. The Qanats used are 40m long and are thermally insulated from the outside using low conductivity fillings and a vegetated surface treatment. 140 $m3$ of water (70m3 per Qanat) is naturally cooled every night from 25ºC to 19°C. This water is used to: cool 48600 $m3$/h of air using buried and submerged ducts (mode 2 and 3); and cool the bottom surface of the souk using high density non-inertial radiant panels type Thermatop mode 4).

7. Conclusions

Obtaining a simplified model has allowed the development and evaluation of the radiant solution proposed for the CartujaQanat project. Results show that the radiant effect accounts for 40% of the system's energy consumption in summer conditions. On the other hand, it is possible to maintain the temperature of the surface practically homogeneous, guaranteeing the exchange of heat with the assistants.

The experimental facility has allowed thermal characterisation by a simplified model. Validation results confirm the high quality and precision of its estimations. The developed model allows obtaining the exchanged heat flow and the return temperature of the water as a function of the environmental conditions surrounding that active surface and the design and operation parameters of that solution.

The experimental results have tested the proposed system's efficiency and have allowed knowing the convective and radiant effects in detail. In addition, the proposed model provides the thermal response of the solution to variations in its design or operating conditions. So, different examples have been

described in the discussion section. Furthermore, this application includes the usefulness of the model for decision-making in design phases or even optimal management of such solutions. Finally, it is possible to design the integration of the radiant system into a new space using the model developed.

8. Acknowledgement

The European Commission funded this study under the projects UIA03-301-CartujaQanat of Urban Innovative Action (UIA). It has been co-financed by the European Regional Development Funds (ERDF).

The materials for the experimental prototype carried out to test the radiant solution furnished by radiant flooring industry leader Uponor is gratefully acknowledged.

9. References

[1] Guerra Macho J, Cejudo López JM, Molina Félix JL, Álvarez Domínguez S, Velázquez Vila R. Control climático en espacios abiertos: Evaluación del proyecto EXPO'92, Sevilla. Sevilla, Spain: 1994.

[2] Velazquez R, Alvarez S, Guerra J [Seville U (Spain)]. Climatic control of outdoor spaces in EXPO 92 1992.

[3] Alvarez S, Maestre IR, Velazquez R. Design methodology and cooling potential of the environmental heat sinks. Int J Sol Energy 1997;19:179–97. doi:10.1080/01425919708914336.

[4] Guerrero Delgado McC, Sánchez Ramos J, Pavón Moreno McC, Tenorio Ríos JA, Álvarez Domínguez S. Experimental analysis of atmospheric heat sinks as heat dissipators. Energy Convers Manag 2020;207:112550. doi:10.1016/j.enconman.2020.112550.

[5] Incropera, F.P. Fundamentals of heat and mass transfer; Vol. 16; ISBN 9780471457282.

[6] Doulos, L.; Santamouris, M.; Livada, I. Passive cooling of outdoor urban spaces. The role of materials. Sol. Energy 2004, 77, 231–249, doi:10.1016/j.solener.2004.04.005.

Are bedroom air temperatures affected by temperature boosts in adjacent rooms?

Louise Christensen, Thea Hauge Broholt, Steffen Petersen

Department of Civil and Architectural Engineering, Section for Design and Construction, Aarhus University, Aarhus, Denmark, lch@cae.au.dk

Abstract. Recent research has indicated that economic model predictive control (E-MPC) of residential space heating can be a significant demand response (DR) asset in district heating systems. Typical E-MPC formulation for this purpose relies on acceptance of occasionally increased indoor temperatures and the DR potential is thus limited by thermal comfort constraints. This paper reports on a field experiment on whether bedroom air temperatures are affected by temperature boosts in adjacent rooms in three case buildings. The measured bedroom air temperature was increased slightly but interviews with the residents indicate that they did not notice the increase. E-MPC in rooms adjacent to the bedroom in these or similar houses can therefore be utilised for providing DR to district heating systems.

Keywords. Occupant thermal comfort, physical measurements, semi-structured interview.
DOI: https://doi.org/10.34641/clima.2022.38

1. Introduction

Energy flexibility of various temporal resolution is increasingly considered to be an important asset in the management of thermal energy systems with a high penetration of intermittent renewable energy sources. The thermal mass of residential buildings can for instance be utilised as short-term heat storage [1-2] for demand response using model predictive control (MPC) of heating systems triggered by price-based demand response programs resulting in so-called economic MPC (E-MPC), see e.g. [3-5] to mention a few, or in combination with signals on CO_2 emissions [6]. The demand response potential of the individual building in absolute terms is relatively small [7] but current simulation-based studies have demonstrated that the aggregated demand response potential of MPC of residential space heating systems can be an asset to operational challenges in urban district heating systems [8-11].

A typical formulation of E-MPC is to minimize heating costs constrained by thermal comfort criteria. A thermal comfort criterion often used is that occupants are assumed comfortable if temperatures are within a predefined comfort band, e.g. defined by a preferred temperature and an acceptable deviation from it. In addition, limitation on the steepness of ramping the temperature up or down are also applied [3]. The common behaviour of this MPC formulation for residential space heating is that the MPC boost the indoor temperature to a user-defined upper comfort limit during low-price periods - thus storing heat energy in the thermal mass of the building - so that the indoor temperature can drift in free float back to a lower comfort limit during the subsequent high-price period. The MPC is therefore tracking either the upper or the lower boundary of the comfort band, meaning that the air temperature is rarely the preferred temperature of occupants (i.e. somewhere between the upper and lower comfort limit). Alternative strategies taking offset in tracking a preferred temperature during normal operation and then provide demand response by either boosting up to the upper limit or drifting down to a lower limit have therefore been proposed [12,13]. However, neither the typical formulation of thermal comfort criteria nor the mentioned alternative is applicable for all functions of a residential building. Especially ramping up from a preferred indoor temperature – denounced *temperature boost* henceforth – to an upper comfort limit may be problematic for some function, e.g. the bedroom; here, the preferred temperature might be the upper comfort limit.

There seems to be a tendency that residents in Northern European countries with temperate climate prefer a bedroom temperature either on par or lower than the preferred temperature in the remaining rooms of the home – also during the heating season. This is e.g. evident in the results from a questionnaire study involving residents in 28 Norwegian low-energy buildings where no one felt 'hot', ~10% felt warm, ~40% felt slightly warm, ~45% found the temperature appropriate, and ~5% felt slightly cool [14], and in another Norwegian study interviewing 38 residents in low-energy homes where the residents in general prefer a bedroom temperature that is lower than what they are experiencing [15]. Madsen and Gram-Hanssen [16] derive from 17 interviews with residents of 14

Copyright ©2022 by the authors. This conference paper is published under a CC-BY-4.0 license.

Danish single-family houses built between 1969-2013 that *"the interviews reflected a cool bedroom as comfortable in contrast to the warmth of the living room*". A similar conclusion can be drawn from the study by Larsen and Johra [17] investigating user engagement with smart home technology for enabling building energy flexibility in 12 apartments and four terrased houses in the greater Copenhagen area built between 2004-2017. However, a study by Mlecnik et al. [18] on 88 responses from a questionnaire on end-user experiences in nearly-zero energy houses in the Nederlands did not indicate the same level of dissatisfaction as the previously mentioned study; here, only 1% and 8% were very dissatisfied or dissatisfied, respectively, with the indoor climate in the bedroom during winter time. Strøm-Tejsen et al. [19] found in a study involving 20 residents of identical dorm rooms that the sleep quality of residents was affected negatively when the bedroom air temperature was increased by 2 K above their preferred bedroom air temperature (mean: 22 ˚C, SD: 1.3 ˚C). Additional data from the experiment indicate that sleep quality was not affected if the bedroom air temperature decreased approx. 1.4 ˚C below their preference [20]. The study also indicated that it is probably not a low room temperature that residents desire but the notion of fresh indoor air that comes with cool air.

The above-referenced studies indicate that it is difficult to pinpoint the preferred temperature in bedrooms, but a common denominator seems to be that the temperature in the bedroom should not be increased above the preferred temperature – in many cases it should in fact be lowered. This comfort criterion means that radiators in bedrooms should not be controlled by E-MPC schedules that allows temperature boosts – let alone be affected by temperature boosts in adjacent zones. The latter issue is a concern raised in simulation-based studies by Clauβ et al. [21] and Johnsen et al. [22]. Here it was found that bedroom temperatures were not strongly dependent on the heating control strategies applied in the other rooms. However, to the knowledge of the authors of this paper, there has been no reports on field measurement of the phenomenom. This paper therefore present data from field measurements of bedroom air temperatures in three different Danish single-family houses during an investigation on the effect of night-time temperature boosts in the kitchen, living room, and hallway.

2. Method

The data presented in this paper origins from a field experiment first reported in Christensen et al. [23] where focus was on evaluating how residents experience leaving the bedroom and enter zones of the house with air temperatures elevated 1 or 2 ˚C above their normal temperature. The elevated temperature was the result of a temperature boost schedule designed to mimic the behaviour of an E-MPC attempting to store heat energy in the thermal mass of the building to avoid using heat for space heating during the morning peak energy use of the local district heating system. There was no attempt to analyse the effect of the temperature boosts on the bedroom air temperature in [23]; this effect is presented in this paper.

The following sections recap the case buildings and their installed experimental equipment as well as the experimental design.

2.1 Case buildings

Three houses with the layout shown in Fig. 1 was featured in the experiment. The houses are in Aalborg, Denmark, which has a temperate climate. The three houses, henceforth named House 1, 2 and 3, are low-energy houses built in 2018 on the foundations of old houses from the 1960s. Inner walls are of light weight concrete with an R-value of 0.12 m^2K/W, which is a common construction in Denmark for buildings from this period. House 1 and 3 are single-family houses, and House 2 is part of a two-family house. House 1 was occupied by an elderly retired couple (male and female), the residents of House 2 were a young couple (male and female) attending their higher studies, and House 3 was occupied by a male adult and a female child.

The houses were equipped with sensors from Lansen measuring air temperature (±0.2 °C), relative humidity (±2 %), and CO_2 concentration (±50 ppm) every five minutes. Window and door opening state was also monitored with sensors. Radiators were equipped with Danfoss ECO thermostats that enables wireless remote control of temperature setpoints. The thermostat has an imbedded PID controller using an internal temperature sensor as control variable. Location of sensors and thermostats are shown in Fig. 1.

2.2 Experimental design

Three temperature schedules designed to mimic the behaviour of a boosting E-MPC as described in the introduction was created, see the last three graphs in Fig. 2. The schedules varied in temperature boost as well as duration. The weekly experimental schedule shown in Table 1 was executed three times

Fig. 1 – Floor plan layout and location of experimental equipment (from paper [23]).

during what is usually considered the coldest month of the heating season in Denmark (Feb 8th to Feb 28th 2021). The boosts were always ended at 7:00 am.

The occupants provided feedback on thermal comfort using "right-here-right-now" questionnaires during the experiment and they were interviewed at the end of the experiment; see paper [23] for further details about the design of the questionnaires and interviews.

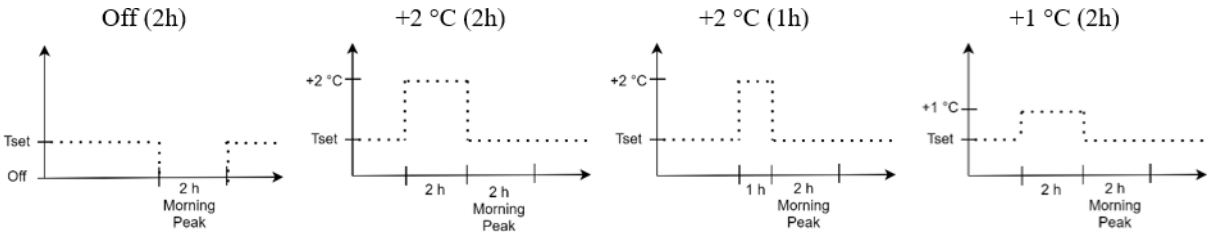

Fig. 2 – Temperature boost schedules (from paper [23])

Tab. 1 – Weekly schedule for the experiment (from paper [23]).

Week	Mon	Tue	Wed	Thu	Fri-Sun
1	-	-	-	-	-
2	Off (2h)	+2 °C (2h)	+1 °C (2h)	+2 °C (1h)	-
3	+2 °C (2h)	+1 °C (2h)	+2 °C (1h)	Off (2h)	-
4	+2 °C (1h)	Off (2h)	+2 °C (2h)	+1 °C (2h)	-

3. Results

Fig. 3 illustrates the trajectory of the air temperature in the bedrooms (first column of graphs) alongside the trajectory of the air temperature in the adjacent room (second column of graphs) in the three houses during the temperature boost schedule *+2 ˚C (2h)*. The residents in House 3 were only present in week 2 of the experiment which is why there is only a graph for week 2 for this house. The schedule *+2 ˚C (2h)* was potentially 'worst case' in terms of effect on the bedroom air temperatures. Data from these experiments exemplifies the trajectory of the temperature in the different rooms across the entire experiment but the magnitude of effect on the bedroom air temperature were somewhat different.

The bedroom of House 1 was in close connection to the living room and the hallway where the temperature boosts were executed (see Fig. 1). It is unknown whether the bedroom door was open during the temperature boosts. The air temperature in the bedroom was increased by 1, 0.9 and 0.6 ˚C during the *+2 ˚C (2h)* schedule, 0.7, 0.7, and 0.6 ˚C during the *+2 ˚C (1h)* schedule, and 0.8, 0.4, and 0.5 ˚C during the *+1 ˚C (2h)* schedule in week 2, 3 and 4, respectively. It is noted that the setpoint of the thermostat in the bedroom was 6 ˚C (i.e., the radiator was not heating the room).

In House 2, there is a small hallway without a radiator between the bedroom and the living room where the temperature boosts were executed (see Fig. 1), and the bedroom door was partly open during the temperature boosts. The air temperature in the bedroom was increased 0.3, 0.2 and 0.2 ˚C during the *+2 ˚C (2h)* schedule, 0.1, 0.2 and 0.1 ˚C during the *+2 ˚C (1h)* schedule, and 0.2, 0.1 and 0.1 ˚C during the *+1 ˚C (2h)* schedule in week 2, 3 and 4, respectively. It is noted that the setpoint of the thermostat in the bedroom was between 21-23.5 ˚C during the three weeks.

The bedroom in House 3 was adjacent to a small hallway in open connection to the living room (see Fig. 1), and the bedroom door was closed during the temperature boosts. Temperature boosts were executed in both the hallway and the living room. The air temperature in the bedroom was increased 0.67 during the *+2 ˚C (2h)* schedule, 0.31 ˚C during the *+2 ˚C (1h)* schedule, and 0.35 ˚C during the *+1 ˚C (2h)* schedule in week 2. It is noted that the setpoint of the thermostat in the bedroom was 6 ˚C (i.e. the radiator was not heating the room).

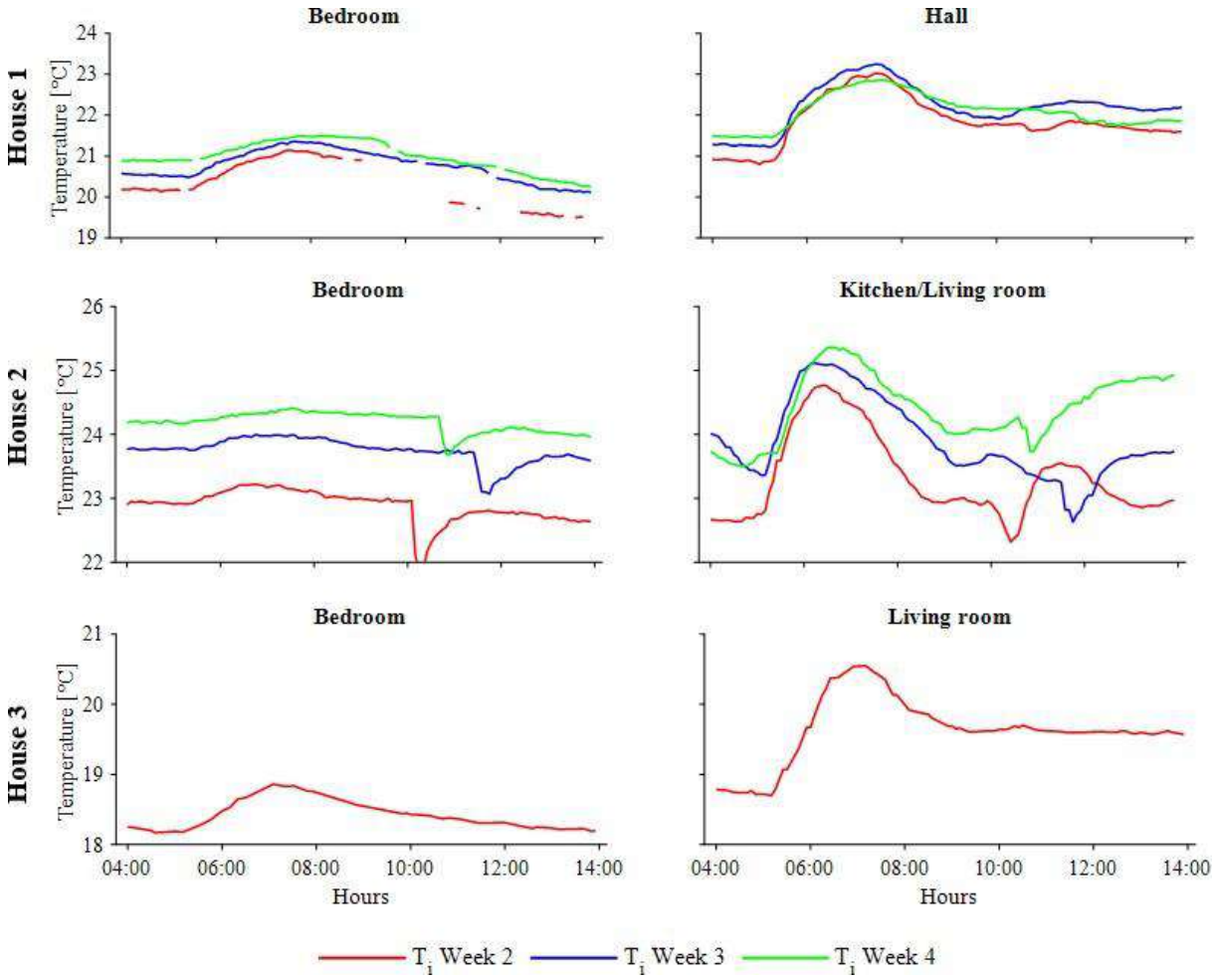

Fig. 3 – Air temperature (T_i) in the bedrooms and adjacent rooms with temperature boosts during the schedule *+2˚C (2h)*.

There was no solar radiation during the temperature boosts as the sun had not yet risen, and the ambient temperature was -1.66 °C ± 6.3 °C. It was therefore not expected that the ambient conditions caused any variation in the bedroom temperatures.

Data from the interviews with the residents after week 4 of the experiment indicate that they did not notice the increased bedroom air temperatures.

4. Discussion

The data from the experiments indicate that the bedroom air was slightly affected by the temperature boosts in other rooms of the house. Data suggest that the magnitude of the increase depends on how close the bedroom is to the rooms where temperature boosts were executed, and whether the residents want the bedroom air temperature to be lower or on par with the room temperature of the remaining house. There is no indication in data on whether open or closed bedroom door affected the bedroom temperature. Results for the individual houses are further discussed in the following.

The bedroom air temperature of House 1 had the highest increase of bedroom air temperature; 0.6-1 ˚C during the *+2 ˚C (2h)* schedule. This was probably due to a combination of the bedroom being in close connection to the rooms with temperature boost while the radiator in the bedroom was also turned off – most likely due to a desire for a lower temperature than in the rest of the house.

Data from House 3 also indicates a desire for a lower temperature in the bedroom compared to the rest of the house but the effect of the temperature boosts on bedroom air temperature were less pronounced than in House 1 probably because of less connection between the bedroom and the rooms with temperature boosts.

The bedroom air temperature in House 2 was not affected significantly by the temperature boosts. The situation in House 2 is somewhat different for House 1 and 3 as the residents seemed to desire a bedroom air temperature close to the temperature of the remaining house. Furthermore, there was a passively heated hallway between the bedroom and the room with temperature boost that probably worked as a thermal buffer between the two rooms.

5. Conclusion

This paper reported on field measurements on the effect of air temperature boosts in rooms adjacent to the bedroom in the three different case buildings. The measured bedroom air temperature was increased slightly but interviews with the residents indicate that they did not notice the increase. A slightly increased bedroom air temperature in these houses is therefore not a hindrance for utilising the remaining house for employing MPC formulation for residential space heating that boost the indoor temperature to store heat energy in the thermal mass of the building for demand response purposes.

It is noted that no general conclusions can be made based on these three case studies. The case studies represent a rather common building type in Denmark, but the identified tendencies might be different in other layouts or type of buildings with better or worse energy-efficiency of building enclosures and systems.

6. Acknowledgement

The research was conducted as part of the project, FED (Jour. No. 8090-00069B) and HEAT 4.0 (Jour. No. 8090-00046B) financed by Innovations Fund Denmark. The authors would like to thank Himmerlands Boligforening and their tenants for participating in the experiment.

7. References

[1] Le Dréau J., Heiselberg P. Energy flexibility of residential buildings using short term heat storage in the thermal mass. Energy 2016;111:991-1002.

[2] Reynders G., Diriken J., Saelens D. Generic characterization method for energy flexibility: Applied to structural thermal storage in residential buildings. Applied Energy 2017;198:192-202.

[3] Pedersen, TH., Hedegaard RE., Petersen S. Space heating demand response potential of retrofitted residential apartment blocks. Energy and Buildings 2016:141;158-166.

[4] Awadelrahman, AM., Zong Y., Li H., Agert, C. Economic Model Predictive Control for Hot Water Based Heating Systems in Smart Buildings. Energy and Power Engineering 2017;9:112-119.

[5] Finck C., Li, R., Zeiler W. Economic model predictive control for demand flexibility of a residential building. Energy 2019;176:365-379.

[6] Knudsen MD., Petersen S. Demand response potential of model predictive control of space heating based on price and carbon dioxide intensity signal. Energy and Buildings;125 2016:196-204.

[7] Knudsen MD., Georges L., Skeie KS., Petersen S. Experimental test of a black-box economic model predictive control for residential space heating. Applied Energy 2021;298:117227

[8] Dominković DF., Gianniou P., Münster M., Heller A., Rode C. Utilizing thermal building mass for storage in district heating systems: Combined building level simulations and system level optimization. Energy 2018;153:949-966.

[9] Cai H., Ziras C., You S., Li R., Honoré K., Bindner HW. Demand side management in urban district heating networks. Applied Energy 2018;230:506-518.

[10] Hedegaard RE., Kristensen MH., Pedersen TH., Brun A., and Petersen S. Bottom-up modelling methodology for urban-scale analysis of residential space heating demand response. Applied Energy 2019;242:181-204.

[11] Hedegaard RE., Friedrichsen L., Tougaard J., Mølbak T., Petersen S. Building energy flexibility as an asset in system-wide district heating optimization models. In: uSIM2020 - Building to Buildings: Urban and Community Energy Modelling. Proceedings of the 2nd IBPSA-Scotland Conference on Urban-scale Simulation. 2020 Nov 12; Edinburgh, Scotland. In press.

[12] Pedersen TH., Knudsen MD., Hedegaard RE., Petersen S. Handling thermal comfort in economic model predictive control schemes for demand response. Energy Procedia 2017;122:985-990.

[13] Hedegaard RE., Pedersen TH., Petersen, S. Multi-market demand response using economic model predictive control of space heating in residential buildings. Energy and Buildings 2017;150:253-261.

[14] Berge M., Thomsen J., Mathisen HM. The need for temperature zoning in high-performance residential buildings. Journal of Housing and the Built Environment 2017;32:211-230.

[15] Thomsen J., Gullbrekken L., Grynning S., Holme J. Evaluering av boliger med lavt energibehov (EBLE) (Evaluation of housing with low energy needs). Oslo (Norway): SINTEF; 2017. 145 p. Report no: SINTEF Fag 43.

[16] Madsen LV., Gram-Hanssen K. Understanding comfort and senses in social practice theory: Insights from a Danish field study. Energy Research & Social Science 2017;29:86-94.

[17] Larsen SP., Johra H. User engagement with smart home technology for enabling building energy flexibility in a district heating system. IOP Conference Series: Earth Environmental Science 2021;352:012002.

[18] Mlecnik E., Schütze T., Jansen SJT., de Vries G., Visscher HJ., van Hal A. End-user experiences in nearly zero-energy houses. Energy and Buildings 2012;49:471-478.

[19] Strøm-Tejsen P., Mathiasen S., Bach M., Petersen S. The effects of increased bedroom air temperature on sleep and next-day mental performance. In: Van Kenhove E, Laverge J, Delghust M, De Vlieger P, editors. The 14th international conference of indoor air quality and climate : conference proceedings. Ghent; 2016.

[20] Mathiasen S., Bach M. The Effect of Deviations from Personal Room Temperature Preference on Sleep and Performance [master's thesis]. Aarhus (Denmark): Aarhus University; 2015.

[21] Clauß J., Stinner S., Sartori I., Georges L. Predictive rule-based control to activate the energy flexibility of Norwegian residential buildings: Case of an air-source heat pump and direct electric heating. Applied Energy 2019;237:500-518.

[22] Johnsen T., Taksdal K., Clauß J., Xingji Y., Georges L. Influence of thermal zoning and electric radiator control on the energy flexibility potential of Norwegian detached houses. In: Tanabe SI, Zhang H, Kurnitski J, Gameiro da Silva MC, Nastase I, Wargocki P, Cao G, Mazzarela L, Inard C, editors. CLIMA 2019. Proceedings of the 13th REHVA World Congress World Congress. 2019 May 26-29, 2019. Bucharest, Romania. E3S Web of Conferences; 2019. p. 06030.

[23] Christensen LRL., Broholt TH., Barthelmes VM., Khovalyg D., Petersen S. A mixed-methods study on resident thermal comfort and attitude towards peak shifting of space heating. Energy Research & Social Science [submitted].

Solar Cooling Integrated Façades: Main Challenges in Product Development for Widespread Application

Hamza Hamida [a], Thaleia Konstantinou [b], Alejandro Prieto [c], Tillmann Klein [d], Ulrich Knaack [e]

[a] Faculty of Architecture and the Built Environment, Delft University of Technology, Julianalaan 134, 2628BL Delft, The Netherlands, H.B.Hamida@tudelft.nl

[b] Faculty of Architecture and the Built Environment, Delft University of Technology, Julianalaan 134, 2628BL Delft, The Netherlands, T.Konstantinou@tudelft.nl

[c] School of Architecture, Diego Portales University, República Av. 180, 8370074 Santiago, Chile, alejandro.prieto@udp.cl

[d] Faculty of Architecture and the Built Environment, Delft University of Technology, Julianalaan 134, 2628BL Delft, The Netherlands, T.Klein@tudelft.nl

[e] Faculty of Architecture and the Built Environment, Delft University of Technology, Julianalaan 134, 2628BL Delft, The Netherlands, U.Knaack@tudelft.nl

Abstract. The global attention to solar cooling systems has increased during the last years as a result of the expected growth in the world cooling demand. Such systems encompass the use of renewable energy as the main driver for mitigating indoor temperatures. Currently, some of these technologies are mature enough for their commercial application in buildings. Building facades present high potential for the integration of such technologies. This is because of their direct effect on the indoor comfort of buildings, and also their ability to provide external surfaces exposed to the sun radiation. However, there are different challenges affecting the widespread application of solar cooling integrated façades. This paper aims to identify and categorize these challenges through conducting a comprehensive literature review. A literature review was conducted on scientific papers published in conference proceeding and scientific journals, through considering two databases, namely Scopus and Web of Science. Then the study suggested three main potential dimensions that should be tackled and integrated when supporting the widespread application of the façade integration a particular solar cooling technology. The dimensions include technical, financial, as well as process and stakeholder related aspects. Such proposed dimensions represent an initial step for identifying important aspects to be considered for supporting the product widespread application in the built environment.

Keywords. Solar cooling, façade, challenges, widespread, product development
DOI: https://doi.org/10.34641/clima.2022.353

1. Introduction

The global need for space cooling in buildings is expected to increase in the coming future for various factors, such as climate change and the associated temperature increase (1,2). Other factors comprise the population and economic growth with the subsequent increase in the quality of life, and the affordability of air-conditioning units (2,3). It has been demonstrated that the global energy demand for the building space cooling may increase by 50% in 2030 if no considerable improvements take place in efficiency of cooling equipment (4).This is particularly true in cooling dominated areas such as the Gulf region, where the building cooling demands in countries such as Saudi Arabia and the United Arab Emirates, account for 70% of their annual energy consumption (5). Hence, this necessitates the use of environmentally-friendly cooling systems to meet the expected increase in the demand for space cooling and energy consumption.

There are different cooling approaches considered in building design that are intended to meet cooling demands in the built environment. The passive cooling approach involves the removal of indoor heat without energy consumption (6). It employs cooling strategies such as the window-to-wall ratio, insulation and shading devices (7,8). The potential impact for implementing such strategies has been found to be relevant in different climate contexts, with a considerable impact in warm-dry regions compared to the warm-humid areas. However, applying them alone does not guarantee relevant reductions in the energy consumption, since their effectiveness is influenced by the climatic harshness and other various building parameters (8). Furthermore, their potential is expected to decrease

Copyright ©2022 by the authors. This conference paper is published under a CC-BY-4.0 license.

due to the increase in ambient temperatures resulted from the global warming (2).

Therefore, active cooling, representing a secondary approach, is still needed in many conditions, especially in warm regions such as hot and humid climates (3,9). Such approach employs complementary mechanical cooling systems to meet required cooling demands in buildings (6). According to Neyer *et al* (10), the estimated total global room air-conditioning units sold in 2016 exceeded 100 million unit. The increase in the use of such active cooling systems depends on electricity consumption, which therefore affects peak energy demand negatively due to their dependency on power plants (2).

The production of cooling effect through sunlight tends to be one of the promising options intended to address such an environmental challenge. The peak cooling demands are proportional to the solar intensities due to maximum sunlight hours (11,12). The potential main advantages of solar cooling technologies include saving the primary and conventional sources of electricity, reducing peak demand of energy for cost saving, and friendly to the environment and have no ozone depletion effects (12). The concept of solar cooling technologies, which started in the seventies, is based on generating conditioned air or chilled water from solar energy (13). The technologies can be in a form of producing hot water through Solar Thermal Collectors (STC) or producing electricity through Photovoltaic (PV) panels (14). This represents two principal pathways for energy conversion to be used to produce cooling from solar radiation, namely thermally-driven processes or electrically-driven processes (10,13–17). Some of these technologies are mature enough for building application, such as the solar absorption cooling technologies (15,18).

Building facades present high potential for the integration of solar cooling technologies. This is because of their direct effect on the indoor comfort of buildings, and also ability to provide external surfaces exposed to solar radiation (19). They are moving toward being multifunctional components that are actively involved in the building energy system through integrating technologies that contribute to energy savings and building occupants' comfort (20–22). It should be noted that such integration represent an inclusion of extra functions into the façade as a next step when other measures, such as thermal insulations and shading systems cannot sufficiently meet the indoor requirements (22,23). The integration can be achieved through two different design approaches, namely integral or modular paths (**Figure 1**)(23). The functions and components associated integral products are mapped based on a many-to-one approach. In addition to that, they have coupled interfaces, which means that making a change in one component (in the case of having a coupled interface of two components), a change is required to be carried out on the other interface. On the other hand, the functions and components associated with modular products are mapped based on a one-to-one approach. The connection of components is based on using modular interfaces, which allows changing the interfaces separately (24).

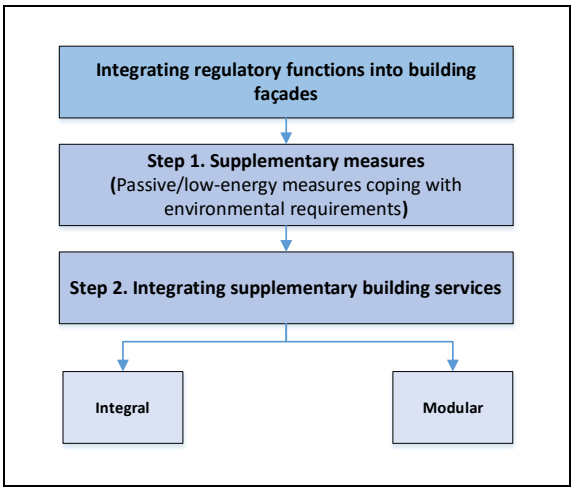

Fig. 1 – Decision-making process for integrating regulatory functions into building façades (23)

When having an insight into the consideration of solar cooling technologies, solar cooling integrated façades have been previously defined as *"façade systems which comprise all necessary equipment to self-sufficiently provide solar driven cooling to a particular indoor environment"*, which indicates that the necessary equipment needed at least for cooling generation and distribution should be integrated by façade systems (23). **Figure 2** indicates different examples of solar cooling integrated façades concepts. However, there are various challenges affecting the widespread application of integrating solar cooling technologies into building facades. This paper aims to identify and categorize those challenges through conducting a comprehensive literature review in order to propose main potential dimensions that should be tackled and integrated for supporting the product widespread application of solar cooling integrated façades.

2. Research Approach and Methods

A literature review was conducted on scientific papers published in conference proceeding and scientific journals. The review includes a literature search, using the concepts indicated in **Table 1**, through considering two databases, namely Scopus and Web of Science. The assessment of a particular article's relevance involved different criteria, that include the scope of the journal and the article novelty (from 2015 to 2021). Such criteria were set in order to narrow down the amount of documents to be reviewed and also ensure relative modernity of information obtained from the reviewed papers. Different journals were found to provide relevant articles, namely Journal of Façade Design and Engineering, Renewable and Sustainable Energy Reviews, and Journal of Cleaner Production. In

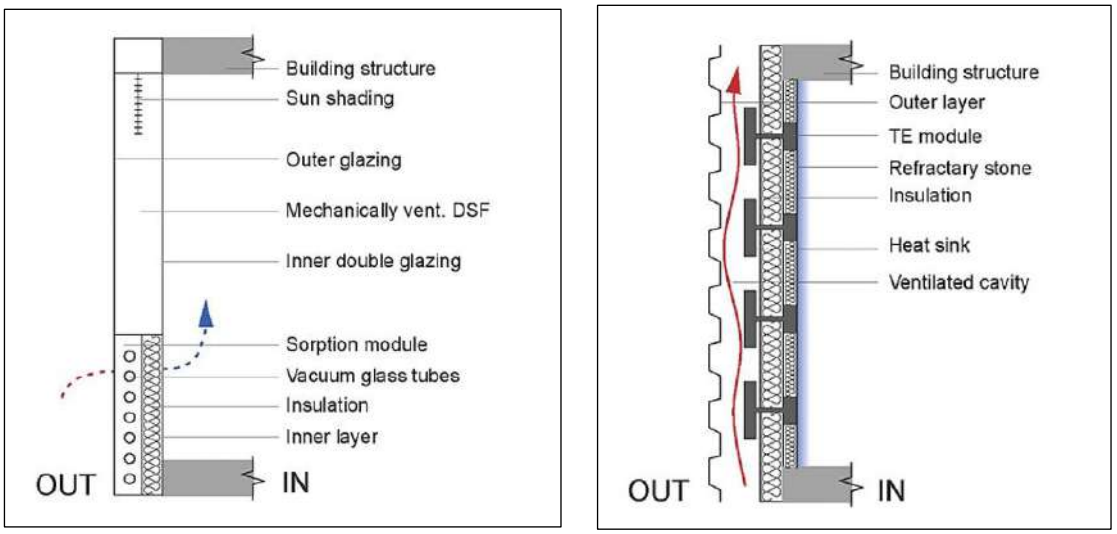

(a) Solar-thermal sorption cooling façade (b) Solar solid-based cooling thermoelectric facades

Fig. 2 – Concepts of solar cooling integrated facades (23)

addition to that, various conference papers were considered in the review process.

It should be noted that there were different initial trials that were carried out before finalizing **Table 1**. For instance, one of the most relevant trails included only the first four concepts. This combination provided irrelevant papers that did not provide information related to the challenges affecting product widespread application. Some of these articles were related conducting experiments or preforming numerical analysis on thermal storage tanks to be used for building heating. Accordingly, the consideration of the fifth concept assisted in narrowing the outcomes and providing more relevant articles. Besides, various articles were excluded during the search process when considering such concepts. The excluded articles are the ones were found to provide no information regarding the issues affecting the widespread of solar technologies in the built environment. Based on that, total of thirteen relevant references were found to be provide reliable information regarding the main challenges affecting the widespread of solar cooling integrated façades. All of the information obtained from the 13 articles are presented and discussed in section 3.

3. Results and Discussion

The results obtained from the literature search revealed that there are various forms of challenges stated by different scholars. Therefore, an appropriate way to differentiate and simplify such variation is needed to facilitate the ability of having an insight to them. Hence, the challenges were divided into two main forms, which are as follows:

- Challenges associated with the integration of solar technologies into building façades in general, regardless the technology type.
- Specific product-related challenges precisely linked to different solar cooling technologies, which varies from one technology to another.

Regarding the general challenges, a categorization to them was adapted from (25). It includes total of six main groups, namely financial, product-related, knowledge, information, processes, and interest. **Table 2** summarizes the general challenges and their categories. Regarding the product-related challenges precisely linked to different solar cooling technologies, the literature pointed out that such barriers vary from one technology to another. This variation is due to the fact that various solar cooling

Tab. 1 - Concepts included in the literature search

	Concepts No. (Combined with AND)				
	1	2	3	4	5
Synonyms and Related Terms (Combined with OR)	challenges	solar	cooling	façade	widespread
	barriers	renewable	air-conditioning	building integrated	application
	obstacles	photovoltaic	-	integration	implementation
	-	collector	-	envelop	-

technologies have different barriers and attributes related to the performance and sizes. These product-related challenges associated with different solar cooling technologies were analysed by Prieto *et al.* (9).

Tab. 2 - Challenges affecting product development and widespread application of solar technologies integrated façades.

Category	Issues related to the such challenges	References
Product-Related Challenges	Performance and efficiency	(25–31)
	Technical considerations (complexities, space availability, and interrupting other building services)	(25,27,28,32)
	Availability of products appropriate for quality integration	(25)
	Maintenance and Durability	(25,26,33)
	Aesthetics	(25,26,28)
Financial Challenges	High Costs (Initial, operation, and maintenance)	(25,27,28,30,32–35)
	Long payback period	(25,28,34)
	Current energy prices are low	(25)
	Lack of incentives/subsidies to execute such technologies	(18,25,30,32)
Challenges Related to the Knowledge	Lack of technical knowledge and experience of architects/engineers about technical aspects related to solar technologies	(25,28)
	End users' lack of knowledge associated with operating the systems	(25,35)
	Required workforce experience for installing the products	(25,32,35)

Tab. 2 - Challenges affecting product development and widespread application of solar technologies integrated façades (cont.).

Category	Issues related to the such challenges	References
Challenges Related to the Information	Need for documenting the properties of technologies appropriately	(25)
	Lack of standards/guidelines related to the technology, such as the ones related to building integration	(25,28)
	Uncertainties associated with changes in legal legislations	(28)
Challenges Related to the Design and Construction Processes	Need to consider integration during early stages of the project (considering close collaboration among various disciplines)	(25,28)
	Need for design-oriented tools so that (A/E)s are involved in technical issues during early design stages	(25)
	Ability to provide varieties forms of products for attracting customers	(28)
Challenges Related to the Interest	Lack of interest in the field of solar designs by designers, developers, and clients	(25)

Having such various forms of challenges illustrates the complexity for supporting the widespread application of solar cooling integrated façades in the construction market. Narrowing the challenges as a first step can assist in simplifying the problem, so that particular dimensions can be tackled for supporting the widespread application of a particular technology. Accordingly, to minimize the problem complexity, the study suggested three main potential dimensions that should be tackled and integrated when supporting the widespread application of the façade integration a particular solar cooling technology (**Figure 3**). The dimensions include technical, financial, as well as process and stakeholder related aspects. Such proposed dimensions represent an initial step for identifying important aspects to be considered for supporting

the product widespread application in the built environment.

3.1 Technical Aspects

The development of an appropriate building product with the required technical attributes, such as product shape, performance, and sizes, is a primary step supporting its penetration to the construction market. Technical challenges related to current products, such as technical complexities and aesthetics, result in challenges related to the interest as well as financial aspects. The resulted challenges include the lack of incentives to execute such technologies. Accordingly, the lack of such incentives leads to challenges related to the knowledge and information in the building industry, such as the lack of technical knowledge and experience of architects/engineers about technical aspects related to solar technologies. Consequently, this can have a direct influence on the design and construction processes in a way that there is lack of considering the integration during early design stages of buildings.

Accordingly, technical developments of building products needs to go hand in hand with the financial as well as stakeholders and process related aspects. Tackling technical aspects associated with façade integration of a solar cooling technology requires an understanding the specific aspects related to selected cooling technology (9). This is due to the fact that such aspects varies from one technology to another. In addition to that, understanding the definition of products and how it is linked to building façades is needed for tackling such aspects. Products can be defined as tangible and quantifiable goods that are produced for customers, which can be end items in themselves or component items (36,37). Additionally, they do have a scope that indicate their features and functions (37). Based on that, building façades represent a form of products that serve the different customers' needs, such as building occupants. In addition, they do have a scope of various functions, such as providing an appropriate insulation with respect to noise, heat, and cold (38). Since products can be end items in themselves or component items (37), façades have been identified to have different product levels that ranges from the material (base ingredients) to the building (24). Therefore, it essential to have a well-defined product scope of functionalities and level for an integration of particular solar cooling technology into the building façade.

3.2 Financial Aspects

High initial costs of solar cooling systems and the low energy prices can result in challenges related to the interest, namely the lack of interest in the field of solar designs by designers, developers, and clients. This illustrates that achieving cost-effective solutions is needed to increase the attention of various stakeholders to adopt the technology in market. It should be noted that not only the initial cost is the only parameter to be considered. Other parameters are should be included, which may include the maintenance cost as well as potentials for energy savings. Accordingly, considering the life cycle cost can aid in investigating cost-effectiveness for an integration of particular solar cooling technology into the building façade.

3.3 Process and Stakeholder Related Aspects

Products are developed through having a process consisting of a sequential set of activities aiming to cause particular end results (37). Having an insight into façade products, they were traditionally identified to have various processes contributing their design and development in built environment, which start from the system design till the assembly, use, and end of life. Moreover, the role of different stakeholders have been identified in façade processes, which include suppliers, façade builders, general contractors, architects, consultants, and clients (24). For instance, façade builders represent one of the important stakeholders in the architecture, engineering, and construction (AEC) industry. They are usually involved in the translation of architectural design into an achievable construction and assure the overall façade performance. They also work on integrating various subcomponents which require putting efforts on planning and logistical arrangements. Such stakeholder take into account the necessity of establishing relationships with architects and general contractors.

Therefore, it is essential to shed the light on processes and stakeholders, when considering an integration of particular solar cooling technology into the building façade. Tackling such dimension can consider identifying the potential integrated roles and responsibilities of various stakeholders during the product life cycle. Such identification can contribute to address issues affecting the interest and provide stakeholders with required knowledge of information supporting the product development and use.

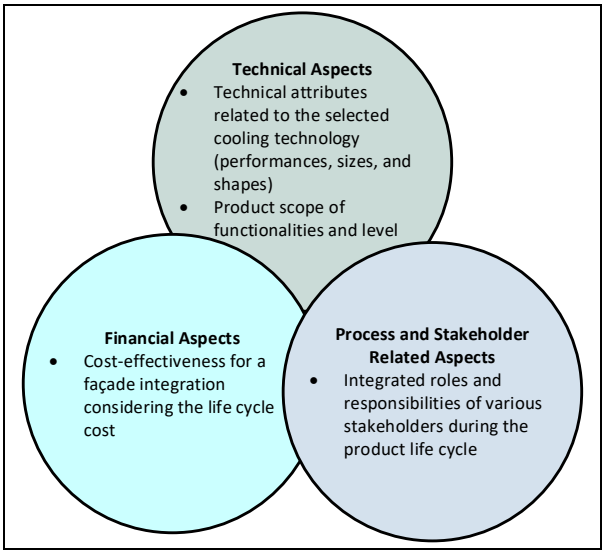

Fig. 3 – Proposed main potential dimensions to be tackled for supporting the application of a façade integration of solar cooling technologies

4. Conclusion

This paper presents a comprehensive literature review conducted to identify and categorize challenges affecting the widespread application of façade integration of solar cooling technologies in the built environment. The results obtained from the literature search revealed that there are various forms of challenges that were divided into two main forms. The first form includes challenges associated with the integration of solar technologies into building façades, regardless the type of technology. The second from covered specific product-related challenges precisely linked to different solar cooling technologies, which varies from one technology to another. Taken into account that having various forms of challenges illustrate the complexity for supporting the widespread application in the construction market, the paper suggested three main potential dimensions to be tackled. The dimensions include technical, financial, as well as process and stakeholder related aspects. Such proposed dimensions represent an initial step for identifying important aspects to be considered for supporting the product widespread application in the built environment. Based on the identified three main dimensions to be tacked, future work should consider investigating a further breakdown of the aspects to a more specific opportunities and bottlenecks in order to develop a framework for supporting product widespread application of solar cooling integrated façades as building products in the construction market. Such framework would tackle and combine the three main aspects.

5. Acknowledgement

This paper is part of an ongoing Ph.D. research project entitled "Solar Cooling as Building Product: A framework to support product widespread application of solar cooling integrated façades". The project is developed within the Architectural Facades and Products research group in the Department of Architectural Engineering + Technology, Faculty of Architecture and the Built Environment, Delft University of Technology, the Netherlands.

6. References

1. Sahin G, Ayyildiz FV. Chapter 14: Climate Change and Energy Policies: European Union-Scale Approach to a Global Problem. In: Qudrat-Ullah H, Asif M, editors. Dynamics of Energy, Environment and Economy: A Sustainability Perspective. Springer Nature Switzerland AG; 2020. p. 295 – 320.

2. Santamouris M. Cooling the buildings – past, present and future. Energy Build. 2016;128:617–38.

3. Enteria N, Sawachi T. Air Conditioning and Ventilation Systems in Hot and Humid Regions. In: Enteria N, Awbi H, Santamouris M, editors. Building in Hot and Humid Regions: Historical Perspective and Technological Advances. Springer Nature Singapore Pte Ltd.; 2020. p. 205–19.

4. IEA. Cooling [Internet]. International Energy Agency. 2020 [cited 2021 Oct 27]. Available from: https://www.iea.org/reports/cooling

5. Rashid M, Ara D. Tectonics in the Gulf Architecture: 'Modernity of Tradition' in Buildings. In: Enteria N, Awbi H, Santamouris M, editors. Building in Hot and Humid Regions: Historical Perspective and Technological Advances. Springer Nature Singapore Pte Ltd.; 2020. p. 137–50.

6. Konstantinou T, Prieto A. Environmental Design Principles for the Building Envelope and More _: Passive and Active Measures. In: Konstantinou T, Ćuković N, Zbašnik M, editors. Reviews of Sustainability and Resilience of the Built Environment for Education, Research and Design. TU Delft Open; 2018. p. 147–80.

7. Ching FDK. Building Construction Illustrated. 5th ed. New Jersey: John Wiley & Sons; 2014.

8. Prieto A, Knaack U, Auer T, Klein T. Passive cooling & climate responsive façade design exploring the limits of passive cooling strategies to improve the performance of commercial buildings in warm climates. Energy Build. 2018;175:30–47.

9. Prieto A, Knaack U, Auer T, Klein T. COOLFACADE: State-of-the-art review and evaluation of solar cooling technologies on their potential for façade integration. Renew Sustain Energy Rev. 2019;101:395–414.

10. Neyer D, Mugnier D, Thür A, Fedrizzi R, Vicente Quiles PG. Solar Heating and Cooling & Solar Air-Conditioning. IEA Solar Heating and Cooling Technology Collaboration Programme; 2018.

11. Otanicar T, Taylor RA, Phelan PE. Prospects for solar cooling – An economic and environmental assessment. Sol Energy. 2012;86(5):1287–99.

12. Tiwari GN, Tiwari A, Shyam. Solar Cooling. In: Handbook of Solar Energy Energy Systems in Electrical Engineering. Springer, Singapore; 2016. p. 471–87.

13. He W, Zhang X, Zhang X. Solar Heating, Cooling and Power Generation—Current Profiles and Future Potentials. In: Zhao X, Ma X, editors. Advanced Energy Efficiency Technologies for Solar Heating, Cooling and Power Generation. Springer Nature Switzerland AG; 2019. p. 31–78.

14. Sarbu I, Sebarchievici C. Solar Heating and Cooling Systems: Fundamentals, Experiments and Applications. Academic Press; 2016.

15. Alahmer A, Ajib S. Solar cooling technologies: State of art and perspectives. Energy Convers Manag. 2020;214:112896.

16. Alsagri AS, Alrobaian AA, Almohaimeed SA. Concentrating solar collectors in absorption and adsorption cooling cycles : An overview. Energy Convers Manag. 2020;223:113420.

17. Karellas S, Roumpedakis TC, Tzouganatos N, Braimakis K. Solar Cooling Technologies. CRC Press; 2019.

18. Kalair AR, Dilshad S, Abas N, Seyedmahmoudian M, Stojcevski A. Application of Business Model Canvas for Solar Thermal Air Conditioners. Front Energy Res. 2021;9:1–23.

19. Prieto A, Knaack U, Auer T, Klein T. Feasibility study of self-sufficient solar cooling fa ade applications in different warm regions. Energies. 2018;11(6):121693718.

20. Ibraheem Y, Piroozfar P, Farr ERP. Integrated Façade System for Office Buildings in Hot and Arid Climates: A Comparative Analysis. In: Dastbaz M, Gorse C, Moncaster A, editors. Building Information Modelling, Building Performance, Design and Smart Construction. Springer, Cham; 2017. p. 273–88.

21. Bonato P, D'Antoni M, Fedrizzi R. Modelling and simulation-based analysis of a façade-integrated decentralized ventilation unit. J Build Eng. 2020;29:101183.

22. Prieto A, Klein T, Knaack U, Auer T. Main perceived barriers for the development of building service integrated facades: Results from an exploratory expert survey. J Build Eng. 2017;13:96–106.

23. Prieto A, Knaack U, Auer T, Klein T. Solar Coolfacades: Framework for the Integration of Solar Cooling Technologies in the Building Envelope. Energy. 2017;137:353–68.

24. Klein T. Integral Facade Construction: Towards a new product architecture for curtain walls. Delft University of Technology; 2013.

25. Prieto A, Knaack U, Auer T, Klein T. Solar façades – Main barriers for widespread façade integration of solar technologies. J Facade Des Eng. 2017;5(1):51–62.

26. Visa I, Moldovan M, Comsit M, Neagoe M, Duta A. Facades integrated solar-thermal collectors – challenges and solutions. Energy Procedia. 2017;112:176–85.

27. Visa I, Duta A. Innovative Solutions for Solar Thermal Systems Implemented in Buildings. Energy Procedia. 2016;85:594–602.

28. Klysner NF, Lenau TA, Lakhtakia A. Building-integrated photo-voltaics: Market challenges and bioinspired solutions. In: SPIE 11586, Bioinspiration, Biomimetics, and Bioreplication XI. 2021.

29. Curpek J, Cekon M. Climate response of a BiPV façade system enhanced with latent PCM-based thermal energy storage. Renew Energy. 2020;152:368–84.

30. Liu Z, Zhang Y, Yuan X, Liu Y, Xu J, Zhang S, et al. A comprehensive study of feasibility and applicability of building integrated photovoltaic (BIPV) systems in regions with high solar irradiance. J Clean Prod. 2021;307:127240.

31. Ghosh A. Potential of building integrated and attached/applied photovoltaic (BIPV/BAPV) for adaptive less energy-hungry building ' s skin: A comprehensive review. J Clean Prod. 2020;276:123343.

32. Kalogirou SA. Building integration of solar renewable energy systems towards zero or nearly zero energy buildings. Int J ofLow-Carbon Technol. 2015;10:379–85.

33. Irshad K, Habib K, Saidur R, Kareem MW, Saha BB. Study of thermoelectric and photovoltaic facade system for energy efficient building development: A review. J Clean Prod. 2019;209:1376–95.

34. Montagnino FM. Solar cooling technologies. Design , application and performance of existing projects. Sol Energy. 2017;154:144–57.

35. Blackman C, Bales C. Experimental evaluation of a novel absorption heat pump module for solar cooling applications Experimental evaluation of a novel absorption heat pump module for solar cooling applications. Sci andTechnology Built Environ. 2015;21:323–31.

36. Foster ST. Managing Quality: Integrating Supply Chain. 6th ed. Pearson Education Limited; 2017.

37. PMI. A guide to the project management body of knowledge (PMBOK guide). 6th ed. Newtown Square, Pennsylvania: Project Management Institute (PMI); 2017.

38. Knaack U, Klein T, Bilow M, Auer T. Façades: Principles of Construction. 2nd ed. Birkhäuser; 2014.

Data Statement

Data sharing not applicable to this article as no datasets were generated or analysed during the current study.

Adaptive Envelopes for Better Energy Efficiency and Enhanced Indoor Thermal Comfort

André Badura[a], Ivo Martinac[b], Birgit Müller[c]

[a] KTH Royal Institute of Technology ABE Division of Sustainable Buildings, Stockholm, Schweden, abadura@kth.se

[b] KTH Royal Institute of Technology ABE Division of Sustainable Buildings, Stockholm, Schweden, im@kth.se

[c] HTW Berlin – University of Applied Sciences Building energy technology, Berlin, Germany, birgit.mueller@htw-berlin.de

Abstract. The increased use of renewable energy in the built environment is a key objective for sustainable development. While being a key priority for the future of energy use, renewable power generation is affected by local resource fluctuations, such as the amount of incoming solar radiation. Energy storage and increased energy efficiency will continue to gain importance in this context.

In cold and moderate climates, heating has traditionally accounted for the predominant part of energy use in buildings. In many parts of the world, heating remains fossil-fuel based to a significant extent. Due to a number of issues, including climate change, the proportion of heating energy has been steadily decreasing, while cooling loads have been on the rise. The use of electricity for heating and cooling has been increasing, partly related to an increased use of different types of heat pump technologies. Growing electricity use for cooling is increasingly seen in highly-insulated, low-infiltration, high energy-performance buildings, but also in other parts of the building stock.

High levels of insulation efficiently decrease heat losses during the heating season, but they also impair the removal of excess heat. This study explores how adaptive envelopes can be used to optimize the use of solar radiation during the heating season and enhance the removal of excess heat during the warm part of the year, depending on parameters including outdoor and indoor temperatures and the desired levels of thermal comfort. The IDA-ICE energy and indoor-climate simulation tool is used for exploring different adaptive envelope scenarios. It allows the calculation of heat flows through the walls, currently however without considering the impact of radiation on external walls. To compensate for this, a new approach is presented to simulating heat flows through different types of adaptive envelopes and wall constructions. This allows for a more detailed understanding of how adaptive envelopes allow incoming solar radiation in summer to be stored before it is transmitted to the main wall structure. Conversely, a more detailed analysis becomes possible of how accumulated heat can be released during the night by removing insulating layers of the wall, thus cooling the indoor environment.

Keywords. Adaptive building envelope, Building energy simulation
DOI: https://doi.org/10.34641/clima.2022.355

1. Introduction

The (European) building sector uses 43 % of the European primary energy, out of which 66 % for space heating [1]. At 70%, the energy use for space heating in Germany is slightly higher [2]. To reach the goals of the European Climate Law to achieve net-zero greenhouse gas emissions (GHG) in the EU by 2050 [3], it is necessary to substantially reduce the energy use in building sector.

National frameworks such as the German Gebäude-Energien-Gesetz (GEG) and international frameworks such as the Energy Performance of Buildings Directive (EPBD) define criteria for the primary energy requirement of buildings and the permissible heat transmission through building envelopes for residential and non-residential buildings [4].

Copyright ©2022 by the authors. This conference paper is published under a CC-BY-4.0 license.

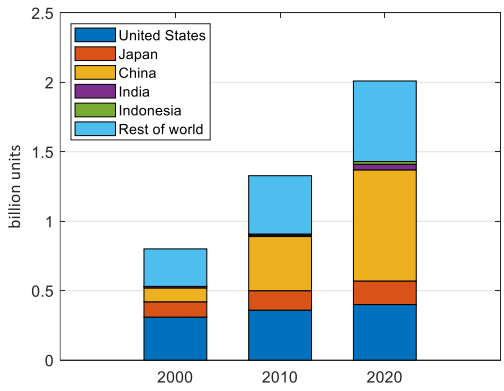

Figure 1 – Increase in the use of air conditioning units during 2000-2020 [5].

Adding to the challenge of efficient energy use, the cooling demand in buildings has been on the rise over the past two decades. This has been reflected by a commensurate increase in the number of air conditioning unit installed [5]. Figure 1 illustrates the world-wide growth in the use of air conditioning units.

The heating energy savings achieved in recent years in many parts of the world are being overshadowed by the an increasing use of cooling energy.

Parallel to stringent limitations on the amounts of energy used, strict requirements are setting the stage for an increased use of clean and renewable energies, as well as a rapid decrease and, eventually, avoidance of GHG emissions. Germany has decreed to no longer use nuclear power [6], emphasizing the need for an accelerated development and deployment of renewable energy technologies.

This study analyses the possibilities of managing variable heat loads in a residential building in Stuttgart by using adaptive building envelopes. The energy simulations were carried out with the IDA ICE software.

2. State of the art

2.1 Key previous research

A number of studies of adaptive building envelopes have been conducted [7], documenting different approaches to achieving variable thermal resistance to building envelopes.

Two main approaches can be distinguished, as shown in Figure 2, Switchable Insulation Systems (SIS) and Dynamic Insulation Materials (DIM) [8]. The difference between the two methods is that in SIS-systems, insulation may be used or removed to modify thermal resistance. The insulation layer can be made of one material or may be formed by air-gaps separated by thin materials. DIM-systems consist of a mixture of different materials, allowing them to dynamically adjust their insulating properties. Variable heat transfer resistance is used to manage heat flow, based on outdoor conditions and conditions in a room, a zone, or an entire building.

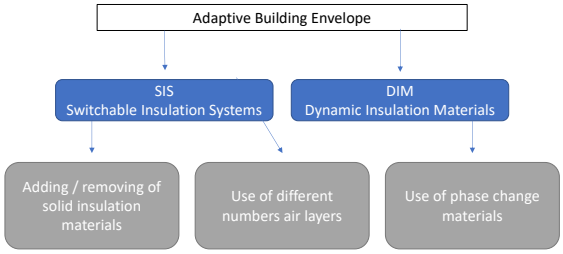

Figure 2 – Overview of adaptive building envelope systems.

That leads to the advantage of reducing heat loss in the cold season and the combination reducing heat input or provide heat loss to the outside in the warm season.

One example where SIS were simulated shown in [9]. Initially using a zone of a non-residential building, with an uninsulated and insulated building envelope, simulated with IDA-ICE. With Matlab the results were combined and differentiated according to various variables. Dependeing on the conditions in the zone, the building envelope was adapted. A reduction of the total energy demand up to 15 % was determined compared to the use of insulation throughout. In [10] switchable insulation was applied using several film layers. By using d different number of layers, the thermal resistance value is changed. The results show a reduction of 29 % of the total energy demand for heating and cooling.

In [11] a SIS was applied to a zone in a residential building. By removing and adding insulation layers, two different thermal resistance values were achieved for the wall. The study was carried out as a simulation for case studies in Sweden and Germany, with the overall result that the total energy demand could be deceased compared to using static insulated building envelopes.

2.2 Physical background

A detailed investigation of the transmission heat losses from buildings requires an analysis of the heat transfer through the individual layers of the building envelope, including conduction, radiation and convection. In buildings, heat transfer typically occurs through air change (mechanical or natural ventilation) and heat transmission through the building envelope. In the simulation described here, the heat transfer through air change is assumed to be constant. The heat conduction is described locally by the heat flux density $\dot{q}$, which depends on the temperature (T) gradient:

$$\dot{q} = -\lambda \, grad \, T \tag{1.1}$$

Here, λ represents the local value of the thermal conductivity. Assuming constant thermal conductivity λ_l and a constant temperature gradient for a temperature difference ΔT, the heat flow along the x-direction perpendicular through a wall (or a layer of thickness Δx for the one-dimensional case), can be expressed as:

$$\dot{q}_l = -\lambda_l \frac{\Delta T}{\Delta x} \tag{1.2}$$

Multiplying equation (1.2) by the area A, leads to (Fourier's law):

$$\dot{Q}_l = -\lambda_l A \frac{\Delta T}{\Delta x} \tag{1.3}$$

where $\dot{Q}_l$ is the the heat [W] transmitted through a solid wall or layer with thickness Δx, across which a temperature difference ΔT exists for the period of time under consideration. The thermal conductivity and temperature gradient are considered to be constant over time and across the wall or layer thickness [12].

The convective heat transfer (Figure 3) from a wall or a solid layer to a convective layer is also described by a heat flux density $\dot{q}_{l,n}$. It depends on the difference ΔT_n between the temperature of the solid surface $T_{s,n}$ and the temperature of the fluid T_n as well as on the heat transfer coefficient. Equation (1.4) describes the relationship:

$$\dot{q}_{l,n} = -\alpha \left(T_{s,n} - T_n \right) = -\alpha \, \Delta T \tag{1.4}$$

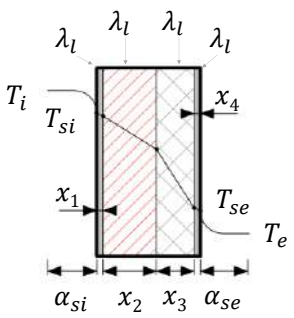

Figure 3 – Schematic representation of the temperature profile in a wall from the inside to the outside through different material layers. The layers of convective heat transfer are represented by their heat transfer coefficients $\boldsymbol{\alpha_{si}}$ and $\boldsymbol{\alpha_{se}}$, respectively.

If one looks again at an area A of the wall or a solid layer, then multiplying equation (1.4) by A results in a relationship (1.5) between the transferred power per unit area A from wall or solid layer to the fluid, non-stationary medium:

$$\dot{Q}_{l,n} = -\alpha A \left(T_{s,n} - T_n \right) = -\alpha A \Delta T_n \tag{1.5}$$

The direction of the fluid flow must be taken into account for the heat transfer coefficient. For this reason, a distinction is made for the building envelope between the heat transfer coefficient α_{si} for inside and α_{se} for outside. In the case $T_i > T_e$, there is a falling fluid flow on the inside, while an ascending fluid flow is present on the outside. In the case $T_i < T_e$ there is an ascending fluid flow in the zone (inside) and a falling fluid flow on the outside [12]. For this reason, a fixed value, e.g. according to DIN 4108-2, can be used for stationary calculations. The current convective heat transfer value is continuously calculated for simulations. The entire heat flow through the wall is ultimately made up of several heat flows as per above. The temperature for the individual wall layers is unknown. These can be eliminated. By repositioning a heat transfer coefficient k for example for a complex overall strucutre according to equation (1.6) can be derived [13, 14].

$$k = \frac{1}{\alpha_{si} + \sum_{j=1}^{N} \frac{\Delta x_j}{\lambda_j} + \alpha_{se}} \tag{1.6}$$

The wall structure consists of N directly connected solid layers and is covered with a fluid layer (air) on the outside and inside. When using IDA ICE, the wall layer thicknesses Δx_j are used in the simulation as fixed parameters. They cannot be changed during the simulation. Changing the heat transfer coefficient to the value 0 is not possible and leads to a numerical error. For this reason, in the version of IDA ICE used, the heat transfer coefficient cannot be changed during the simulation which poses a shortcoming.

3. Modelling Approach

3.1 Model properties

For the research, a zone model of a residential building is used. The construction period of the building is between 1950 and 1960. For this period, a typical thermal resistance value for the building envelope is $k = 1.4\ W/m^2K$ [15]. A typical thermal resistance value for windows with double glazing is assumed as $k = 2.7\ W/m^2K$. As a part of an energy renovation, the use of insulation results in a lower thermal resistance value of $k = 0.20\ W/m^2K$. Furthermore, the windows are replaced with better windows with a thermal resistance value of $k = 1.3\ W/m^2K$. The new values of the building envelope and the window meet the requirements of the Building Energy Act [3]. Additionally, for the window an external blind is used after the energy renovation. A summary of the details of the building envelope and the window are shown in Table 1.

Table 1 – Summary details of the IDA ICE Zone model.

Name	Value	Unit
Wall surface	14.5	m^2
Window surface	2.50	m^2
Wall k-Value	0.20	W/m^2K
Window k-Value	1.30	W/m^2K

The schedule for heating and cooling setpoints is set to reflect conditions in a residential building (Table 2). During the daytime a lower setpoint is used. From the evening to morning and for the weekend, a higher setpoint is used. Occupancy (two persons) is scheduled as shown in Table 3. On weekends, the occupants are assumed to be present all day. The air exchange rate is assumed as 0.4 h-1, a ventilation system is not used. No schedule is considered for window opening.

Table 2 – Daily schedule details of the IDA ICE zone model for heating and cooling.

	Value	Unit
Heating setpoint:		
06:00 a.m. – 06:00 p.m.	18	°C
06:00 p.m. – 06:00 a.m.	21	°C
Cooling setpoint:		
06:00 a.m. – 06:00 p.m.	27	°C
06:00 p.m. – 06:00 a.m.	25	°C

For the annual simulation in IDA-ICE, internal loads are considered, as shown in Table 3 and Table 4. The tables account for occupants (internal loads 1) and other devices (internal loads 2).

Table 3 – Internal loads (1) of the IDA ICE zone model.

	Value
Zone occupancy	(Monday – Friday)
Person 1 (75W)	00:00 a.m. – 07:00 a.m
	03:00 p.m. – 12:00 a.m.
Person 2 (75W)	00:00 a.m. – 07:00 a.m.
	05:00 p.m. – 12:00 a.m.
	(Saturday – Sunday)
Both persons	00:00 a.m. – 12:00 a.m.

Table 4 shows the operating schedules for lighting and other equipment.

Table 4 - Internal loads (2) of the IDA ICE zone model.

	Value
Zone lighting	(mon. – sun.) 50 W
	06:00 a.m. – 08:00 a.m.
	15:00 p.m. – 23:00 p.m.
Zone equipment	(mon. – fri.) 150 W
	06:00 a.m. – 08:00 a.m.
	15:00 p.m. – 23:00 p.m.
	(sat. – sun.) 150 W
	08:00 a.m. – 11:00 a.m.
	14:00 p.m. – 23:00 p.m.

3.2 Control strategy

In this simulation study, the control strategy is based on the temperatures shown in Figure 4. These include the air temperature in the zone T_i, the surface temperature of the external wall T_{se}, as well as the outdoor air temperature of the air otuside T_e. Whetever an insulated wall is used depends on different boundary conditions, see below. Is any of the two conditions described below TRUE, the temperature T_{se} is transferred to position T'_{se} (Figure 4). Is none of the conditions TRUE, no temperature transfer is applied. In that case, a temperature between $T_{l,2}$ and $T_{l,3}$ will occur at position T'_{se}.

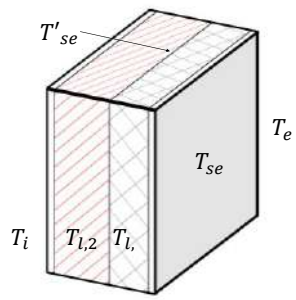

Figure 4 – Schematic representation of the wall structure showing the temperatures on which the control strategy is based.

If air exchange and lighting are neglected, the following control strategy conditions can be set for heating/cooling:

$$con_1 = \begin{Bmatrix} 1;\ T_e \leq 15, T_{se} \geq 22 \\ 0;\ T_i > 22 \end{Bmatrix}$$

$$con_2 = \begin{Bmatrix} 1; T_{se} \leq 24, T_i > 24 \\ 0;\ T_i < 20 \end{Bmatrix}$$

Condition 1 (con_1) leads to heating. The outside temperature will be set to T_e 15 °C. If the outside temperature is lower than the setpoint, the heating of the zone is allowed. In Germany, 15 °C is often used

as heating limit temperature. If the outside surface temperature $T_{s,e}$ is higher than 22°C, a heat flow into the zone will occur. In order to prevent overheating of the zone, at an inside temperature $T_{i\,a}$ above 22 °C the condition 1 goes to FALSE and heating is stopped.

Condition 2 (con_2) leads to cooling. If the indoor temperature T_i is greater than 24 °C and at the same time the wall surface temperature T_{se} less than 24 °C, a heat flow from the zone to the outside will occur. If either or both conditions (con_1) or (con_2) are TRUE, an enhanced insulation of the building envelope is not necessary. Through an extension in IDA-ICE, the insulation command will be bypassed. If none of the conditions is TRUE, the control stops functioning, the and the heat flow is allowed to pass through the temperature control layer.

3.3 Model validation

A multiple-step simulation model was developed using a temperature layer where the temperature T'_{se} is controlled, see Figure 4. The individual steps are shown in Figure 5. In the first step a standard model (level 0) was built in IDA-ICE. In the second step (level 1) the model was converted into an advanced level model, were the individual modulescould be changed. Thus, the temperature layer consists of a space heating element, becoming separate from the heating and cooling supply elements. At the second level, the temperature calculation is developed for the case "without control", followed by a temperature calculation "with control" at the third level. At the last level, level 4, the control is actively used throughout the simulation.

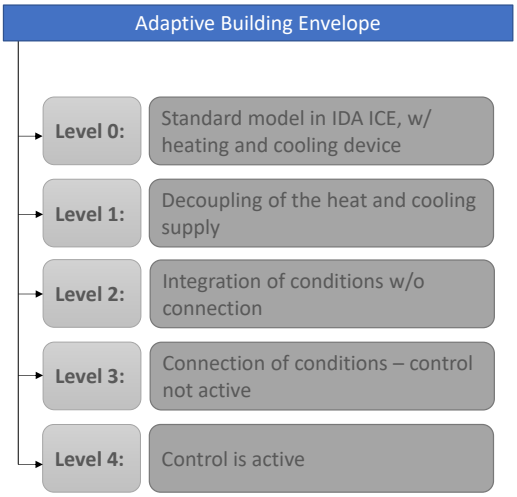

Figure 5 – Overview of the model development.

After completing every individual level, a test simulation was performed. The results of each test simulation, shown in Table 5, were evaluated for plausibility. The calculated energy demands are shown in Table 5 indicating fluctuations between the different simulation levels. Between level 0 and level 1, changes in the hydraulic system were made, and slight variations in the calculated values are understandable. Differences in water volumes can lead to additional result variations.

Table 5 – Energy demand of IDA ICE zone model for different extension levels.

Extension Level	Heating [kWh]	Cooling [kWh]
Level 0	54	520
Level 1	58	510
Level 2	54	521
Level 3	60	484
Level 4	64	91

Between level 1 and level 2 only calculations were inserted, the resulting variations are difficult to explain. The same results as in level 1 would be expected. Since the deviation is less than 10 % (for heating 7 %, for cooling 2 %), the model will continue to be used further.

Between level 2 und level 3, the comparison and calculation algorithm are linked to the model. The differences in calculated energy demand can be attributed in part to transitional phases when the condition of the control system changed. These transitional phases are shown in Figure 6.

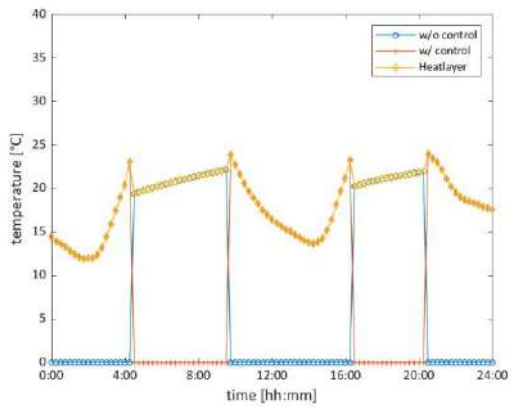

Figure 6 – Heat layer temperature (yellow), for the simulation cases with (red) and without (blue) control.

Figure 6 illustrates the temperature variation of the temperature layer T'_{se} as affected by control. Control was either active (w/ control) or not active (w/o control). The model was designed such that transition phases occurred during the simulation when the control mode was switched between the mode (w/ control) and the mode (w/o control). The change between the control modes was implemented through a dedicated additional algorithm which generated the output signal. As shown in Figure 6, the transition phases were completed within 30 min. The output interval for the simulation was therefore set to 30 min.

4. Results

4.1 Building energy demand

Figure 7 shows the simulated annual building heating and cooling energy demand. It shows a typical energy use for a building with an optimized building envelope for a low heating energy requirement. Due to the insulation, there is a short period in which the building needs to be heated (dec-feb) and another short period in the transition period in which there is only slight heating or cooling demand (mar, oct-nov). During the rest of the year there is a need for cooling (apr-sep). According to Table 6, the modelled zone has a heating energy demand of 60 kWh and a cooling energy demand of 484 kWh.

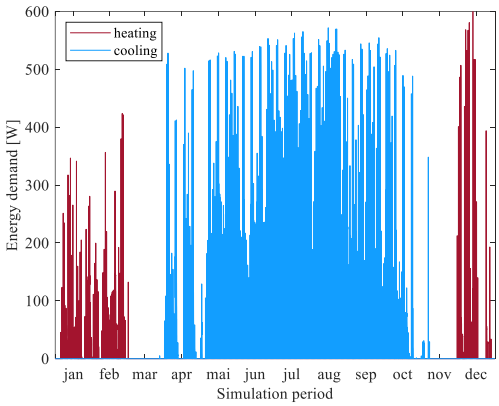

Figure 7 – Annual energy demand for heating and cooling without adaptive building envelope.

Table 6 – Overview of annual energy demand for heating and cooling with and without adaptive building envelope (abe). Cooling energy demand assuming COP=3.0.

	Heating [kWh]	Cooling [kWh]	Cooling^{COP} [kWh]
w/ abe	64.4	91.0	30.3
w/o abe	60.0	484.0	161.0

Figure 8 shows the annual heating and cooling energy demand building energy demand with active use of the adaptive building envelope. No significant change in the heating energy demand was found compared with when no ABE is used. According to Table 6, the heating energy demand without ABE increased by only 7 %, from 60 kWh to 64.4 kWh. However, a significant reduction in cooling energy demand for cooling could be observed when ABE is used. The period in which the zone needs to be cooled could be reduced by around 3 months. According to Table 6, the cooling energy demand with ABE decreased by 81 %, from 484 kWh to 91 kWh.

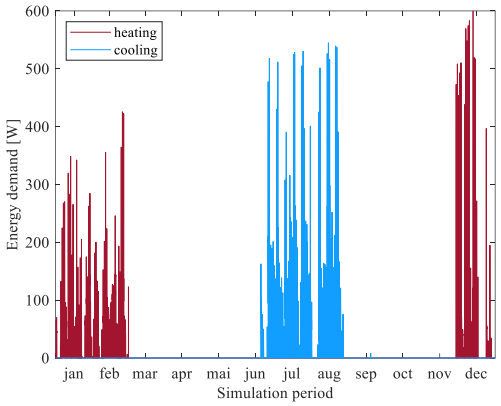

Figure 8 – Annual Energy Demand for Heating and cooling with adaptive building envelope (ABE).

For the total energy demand for heating and cooling of the modelled zone, the result shows a reduction from 544 kWh to 155.4 kWh with ABE, corresponding to 71 %.

4.2 Frequency of application of the adaptive building envelope

Figure 9 shows the frequency of condition (con_1) and condition (con_2), see section 3. The logging of the Simulation results were logged in 30-min intervals resulting in a total of 1.752 x 10^4 values on which the data in Figure 9 are based. Data are presented separately for the time intervals 7:00 a.m. to 7:00 p.m. and 7:00 p.m. to 7:00 a.m.

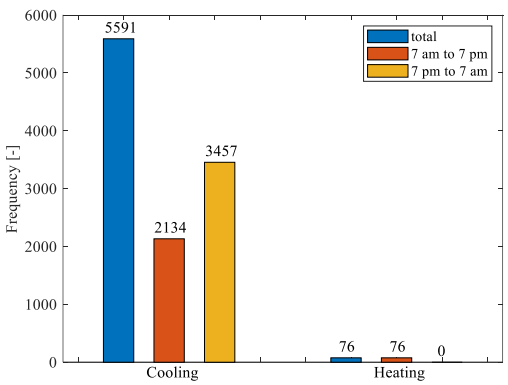

Figure 9 – Annual frequency of adaptive building envelope use, during the day (orange), the night (yellow) and overall (blue).

It is remarkable that the adaptive building envelope for heating only needs to be used for 36 hours per year. The time range is only during the day, which is plausible because only during the day there is the possibility of increasing the surface temperature of the building envelope through solar radiation.

In the cooling mode, the control of the adaptive building envelope is active for 2796 hours. At 61.8 % of total time, the ABE is mainly used during the night. Thus, the key goal of cooling the building through

night cooling, is achieved. In addition, the natural cooling of the building can be used during 1067 daytime hours.

4.3 Indoor thermal comfort

The thermal comfort is determined for time intervals when occupants are present in the zone. The duration (number of hours) of occupant dissatisfaction is shown for the simulation time of 8760 hours. The change is examined using three simulation scenarios.

- (1) Zone without cooling,
- (2) Zone with cooling, without adaptive building envelope,
- (3) Zone with cooling and with adaptive building envelope.

Table 7 shows the results of the three simulation scenarios. Scenario 1 shows the longest duration of occupant dissatisfaction due to the high temperatures in the zone.

Table 7 – Comparison of hours of occupant dissatisfaction depending on the scenario used.

Scenario	Heating [kWh]	Cooling [kWh]	Hours of dis-satisfaction [h]
(1)	51.0	0	6735
(2)	60.0	484.0	1129
(3)	64.4	91.0	871

In scenario 2, the number of hours of dissatisfaction can be reduced by 83 % by using the cooling device, but an additional cooling demand of the zone of 484.0 kWh is required. In scenario 3, the number of hours of dissatisfied occupants is reduced by a further 4 % compared to scenario 2, with a reduction of cooling enegery demang by 81%. A positive effect of ABE use was thus also obtained on simulated perceived thermal comfort.

5. Conclusions

In this study, the application of an adaptive building envelope as a switchable insulation system (SIS) was investigated by simulating a zone in Stuttgart with IDA-ICE software. For the simulation, an outer wall of an existing residential building, from the construction period between 1950-1960, underwent an energy refurbishment in order to implement current national requirements as defined in German Gebäude-Energie-Gesetz (GEG).

The effects of the adaptive building envelope were analysed for two alternatives: the building envelope is either considered to be uninsulated, having an overall wall k-value of 1.40 W/m^2K, or insulated with a k-value of 0.20 W/m^2K. This switch cannot be achieved with the current BDF-wall model in IDA-ICE. A temperature change was therefore assumed between the outer surface of the outer wall and the surface between the insulation and the load-bearing masonry. Thus, the insulation's influence on simulated heat flow can be bypassed. The simulation results showed a reduction in cooling energy demand of 81 % by applying ABE. The heating energy demand was found to increase by approximately 7 %. The calculated increase in annual heating energy (7 %) is caused by computational aspects of the control strategy simulation, where a temperature spread in the order of +0.25 K to -0.25 K needed to be introduced to avoid numerical errors.

Overall, ABE use reduced the energy demand for heating and cooling of the zone by 71 % compared to using static insulation. This indicates the significant potential of using ABE toward achieving substantial energy savings in the building sector.

In energy-refurbished buildings there remains a risk of zone overheating. Cooling devices can, of course, be used to prevent overheating and reduce the incidence and duration of occupant dissatisfaction. However, active cooling energy use increases the overall energy use. Instead, ABEs can be used to reduce occupant dissatisfaction while using significantly less energy.

Buildings are usually built for a period of use longer than 50 years. An adaptive building envelope shell is not permanently connected to the building (glued to the supporting structure) but is attached in front of it in a moveable way. Therefore, it has the advantage of being easier to recycle when the building is dismantled. There is no need for a complex separation. Furthermore, national and international requirements for the thermal permeability of the building envelope are currently changing at a significantly shorter interval than the usage time. An adaptive building envelope can be replaced more easily than a fixed insulation connected to the structure contributing to a sustainable development.

6. References

[1] Energy efficiency trends in buildings in the EU. URL: https://www.odyssee-mure.eu/publications/policy-brief/buildings-energy-efficiency-trends.pdf, p. 1, Accessed dec 2021

[2] DENA-Gebäudereport kompakt 2019. URL: https://www.dena.de/fileadmin/dena/Publikationen/PDFs/2019/dena-GEBAEUDEREPORT_KOMPAKT_2019.pdf, p. 19, Accessed dec 2021

[3] United Nations Sustainable Development Solutions Network,

https://www.unsdsn.org/european-commission-launches-proposals-to-reach-55-emissions-reduction-by-2030, Accessed dec 2021

[4] GEG:08-2020 *Gesetz zur Einsparung von Energie und zur nutzung erneuerbarer Energien zur Wärme- und Kälteerzeugung in Gebäuden*. p. 57-59 (2020)

[5] IEA (2021), Cooling, IEA, Paris https://www.iea.org/reports/cooling, Accessed dec 2021

[6] BMU: *Atomkraftwerke in Deutschland – Abschaltung ... gemäß Atomgesetz*. URL: https://www.bmu.de/media/atomkraftwerke-in-deutschland-abschaltung-der-noch-betriebenen-reaktoren-gemaess-atomgesetz-atg, Accessed dec 2021

[7] Z. Zeng, G. Augenbroe, J. Chen, *Realization of bi-level optimization of adaptive building envelope with a finite-difference model featuring short execution time and versatility*. Energy, **154**, pp. (2021)

[8] R. Carlier, M. Dabbagh, M. Krarti, *Impact of Wall Constructions on Energy Performance of Switchable Insulation Systems*. Energies, **13**, p. 6068, 22 (2020)

[9] A. Badura, I. Martinac, B. Mueller, *Managing climate-change-induced overheating in non-residential buildings*. In: E3S Web of Conferences. EDP Sciences, 2020. S. 02009.

[10] T. Pflug, B. Bueno, M. Siroux, T. E. Kuhn, *Potenial analysis of a new removable insulation system*. Energy and Buildings, **154**, pp. (2017)

[11] A. Badura, I. Martinac, B. Mueller, *Managing overheating in buildings induced by climate change*. In: IOP Conference Series: Earth and Environmental Science. IOP Publishing, 2020. S. 052016.

[12] W. Polifke, J. Kopitz, *Wärmeübertragung*, **1**, 39-47 (2005)

[13] S. Baumgarth, B. Hörner, J. Reeker, *Handbuch der Klimatechnik*, **5**, 109-110 (2011)

[14] H. Recknagel, E. Sprenger, K.-J. Albers, *Taschenbuch Heizung- und Klimatechnik*, **79**, p. 180 (2019)

[15] DIN/TS 12831-1:04-2020 *Method for calculation of the room heat load – Part 1: National addition to DIN EN 12831-1*. p. 61,62 (2020)

Laboratory test of commercial smart radiator thermostats when used for load shifting

Virginia Amato [a], Thea Hauge Broholt [a], Louise Rævdal Lund Christensen [a], Rasmus Elbæk Hedegaard [a], Michael Dahl Knudsen [a], Steffen Petersen [a]

[a] Department of Civil and Architectural Engineering, Aarhus University, Aarhus C, Denmark, viam@cae.au.dk

Abstract. The recent development of smart radiator thermostats has made it possible to integrate them in demand response programs. Advanced control strategies for demand response such as Model Predictive control (MPC) can be combined with radiator thermostats in a hierarchical way for the regulation of space heating systems: the MPC controller calculates the optimal set-point temperature to be tracked by the PID controller of the thermostat. Coupling MPC and thermostat-based control gives the possibility to regulate independently each radiator flow and therefore has the advantage of an efficient room temperature control. Currently, several smart thermostats available on the market are programmable, can be controlled remotely and allow to implement advanced control algorithms. In addition, the thermostats used for load shifting should be reliable, fast responding to changes in settings and precise in tracking a room temperature set-point. The purpose of this study was to compare the performance of different commercial smart radiator thermostats by performing laboratory experiments and to evaluate whether they are appropriate for load shifting purposes. The thermostats tested were Danfoss Eco 2, Eurotronic Spirit Z-Wave Plus and MClimate Vicki. The experiments were carried out in a room where the temperatures in strategic locations were measured. The experiments were designed to evaluate how the thermostats reacted to a changed set-point and if they were able to maintain the desired room temperature. Additionally, the experiments assessed how an increasing temperature set-point affected the flow, the radiator cooling and the thermal comfort in proximity to the radiator. The results obtained so far show that the three tested thermostats had different behaviours in terms of temperature control reliability and accuracy. The three products had different advantages and drawbacks and they all require adjustments for successful integration in an MPC system.

Keywords. Smart thermostats, thermostat performance, load shifting, Model Predictive Control.
DOI: https://doi.org/10.34641/clima.2022.163

1. Introduction

Demand response has a crucial role for reaching the increasingly ambitious targets of energy efficiency and penetration of renewable energy sources. Many studies have demonstrated that exploiting the building thermal mass can have a substantial demand response potential for heating supply systems such as district heating (1–4). Advanced control strategies of space heating of rooms in residential buildings such as Model Predictive Control (MPC) are frequently proposed in current literature as a mean to realise this potential, see e.g. (5). This type of MPC typically modulate the thermal power of room heaters throughout the day constrained by considerations on thermal comfort to obtain demand response purposes and therefore use this thermal power as control input for room heaters. This is easy to implement if space heating is based on direct electrical heaters, but it is not directly implementable for hydronic radiator systems where the thermal power is a function of temperature and flow of the fluid in the heater as well as the room air temperature. The thermal output from radiators is often determined by a manually set position of a thermostatic radiator valve (TRV) controlling the water flow through the radiator with e.g. a wax motor. In recent years, TRVs that use electronic sensing of temperatures and PID controllers to mechanically adjust the valve position to maintain a desired temperature set point have become commercially available. Some of these TRVs can also

Copyright ©2022 by the authors. This conference paper is published under a CC-BY-4.0 license.

be remotely controlled which in principle makes them applicable for MPC as these thermostats are able to receive and track a continuously updated variable set-point schedule modulating the flow in order to achieve the desired demand response. Very few studies have been reported using TRVs for this purpose (6). Overall, there is a lack of knowledge on how commercially available electronic TRVs for hydronic systems reacts when prompted the fluctuating temperature set-point schedules of an MPC.

The study reported in this paper investigated the ability of three different commercial smart thermostats to realise the heating set-point schedule of typical demand response control strategies. The following sections provide a description of the equipment and test room used and of the design of the experiments, followed by an overview and a discussion of the results obtained, and ending with concluding remarks.

2. Research methods

2.1 Experimental setup

The objective of the study was to evaluate and compare how three commercial smart thermostats – Danfoss Eco 2, Eurotronic Spirit Z-Wave, and MClimate Vicki – behave when subject to changes in set-point temperature.

A series of experiments (see section 2.2 for details) were performed in a 15 m^2 test room with a room height of 2.8 m and one insulated wall with a window facing outdoors to the south (Figure 1). The window glass was covered with non-transparent tape on the outside to avoid solar heat gains disturbing the experiment. All other wall surfaces were insulated and faced other heated rooms, and the highly insulated floor faced an unheated basement. The entrance door was on the internal wall opposite the window. The room had one radiator supplied by district heating located at one of the internal walls. The only piece of furniture present was a table placed at the internal wall opposite to the radiator and a chair in front of the radiator.

The specifications of the used sensors, data loggers, and the measured variables are summarized in Table 1. The air temperature sensor of the brand *Lansen Lan-Wmbus–G* was placed on the table in a distance of two meters from the radiator and the height is one meter above floor. The data from the sensor was assumed to be a measure of the general air temperature in the room. In addition, an air temperature data logger of the brand *TinyTag Ultra 2* was placed 0.6 m from the centre of the radiator at a height of 0.5 m to enable evaluation of air temperature near the radiator. An ultrasound flow meter of the brand *Katronic Katflow 230* measured the flow and water temperature of the inlet and outlet radiator pipes. All three thermostats had an internal temperature sensor measuring a temperature used as control variable; this data was also logged. Figure 1 shows the location of all equipment, and Figure 2 is a picture of the setup at the radiator.

The experiments were performed by controlling the thermostats remotely. The Danfoss and Vicki thermostats were controlled through a Bluetooth and LoRawan gateway, respectively. The Eurotronic thermostat was included in a Z-wave network and was controlled through a Raspberry Pi. Unlike the Danfoss thermostat, the thermostats by Eurotronic and Vicki allowed the customization of many settings. The Eurotronic thermostat allowed adapting the set-point temperature offset as well as direct control of the valve opening, and the Vicki thermostat allowed modification of the PI controller parameters. In this study, the three thermostats were compared using their default settings.

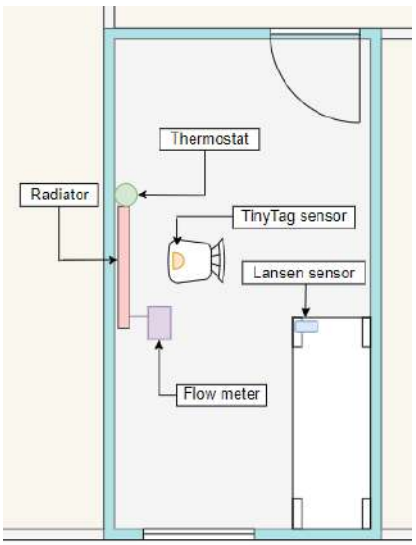

Fig. 1 – Layout of the test room and position of equipment.

Fig. 2 – Radiator, TinyTag data loggers and flow meter

Tab. 1 – Measured entities by different pieces of equipment, temporal resolution and accuracy

Product name	Measured entity	Data logging frequency	Reading resolution
TinyTag Ultra 2	Air temperature in front of the radiator at a distance of 60 cm and height 50 cm	1 minute	0.01 °C
Katronic Katflow 230	• Flow through the radiator • Inlet and outlet water temperature in the radiator	1 minute	• Volume flow: 0.001 l/h • Temperature: 0.01 °C
Lansen Lan-Wmbus-G	Air temperature at a distance of 2 meters from the radiator, at a height of 1 meter	5 minutes	< 0.01 °C
Danfoss Eco 2	Room air temperature	15 minutes	0.5 °C
Eurotronic Spirit Z-Wave Plus	Room air temperature	1 minute	0.1 °C
Vicki MClimate	Room air temperature	5 minutes	0.1 °C

2.2 Experiments

Three experiments were designed to explore the behaviour of the thermostats during step changes in temperature set-point – which is often prompted by an MPC to provide demand response – as well as their behaviour during set-point tracking. The behaviour was evaluated in terms how fast the internal temperature sensor in the thermostats reached a new set-point, the flow control strategy to realize the set-point, how the internal thermostat sensor compares to the other sensors, and the consequential cooling (difference between supply and return temperature) and the air temperatures measured by the two room sensors.

Experiment 1 had the purpose of evaluating how the thermostat reacts to a sharp increase in set-point. The experiment was conducted by changing the temperature set-point to the maximum value (28°C) and keeping it for five hours before returning to the initial set-point.

Experiment 2 was designed to evaluate how the thermostats tracks a set-point after an increased set-point was reached. The experiment was performed by increasing the set-point by 3 °C above a current (initial) temperature measured by the thermostat. The increased set-point was kept for ten hours before changing it back to the initial value.

In Experiment 3, the temperature set-point was increased gradually by setting the set-point 1 °C higher than the temperature measured by the thermostat every 15 minute. This step increase was stopped and the set-point changed back to the initial value after the temperature measured by the thermostat had reached 26°C, or when the temperature increase became too small (lower than 0.5°C increase in 8 hours).

Each of the three experiments were performed using a starting set-point of 18°C prior to the experiment (i.e. starting the experiment with radiators turned off) and with a starting set-point of 22.5°C (starting the experiment with radiators already on, or having been on a short time before), respectively. The reason for the relatively high starting set-point temperature in the latter experiment was to ensure that the radiators were on as the temperature in the test room never dropped below 20-21°C without heating.

3. Results

The data measured during the experiments are shown in Figure 3-8. The plots in the top show the set-point temperature and the temperatures measured by the thermostat as well as two meters and 0.6 m from the radiator, respectively. The plots in the middle report the inlet and outlet radiator pipe temperature and the plots in the bottom show the water flow to the radiator.

The results of Experiment 1 with a starting temperature of 18°C and 22.5°C are shown in Figure 3 and 4, respectively. Once the temperature set-point was changed to 28°C, the flow controlled by the Danfoss ECO increased to a maximum level andstayed there until the set-point was reduced again. This behaviour was as expected, as the internal temperature sensor (the control variable of their PI controller) never reached the setpoint. The temperature 0.6 m from the radiator was significantly higher than the temperature measured by the internal sensor. The sensor placed two meters from the radiator displayed a temperature somewhat lower than the internal sensor.The Eurotronic Spirit showed a similar behaviour in terms of flow compared to Danfoss ECO, but in the experiment displayed in Figure 4 the heating was continued even after the set-point was decreased, as a result of the integral action of the PI control. The temperature 0.6 m from the radiator was significantly higher than the temperature measured by the internal sensor, as observed with the Danfoss

ECO. The sensor placed two meters from the radiator, however, displayed a temperature slightly higher than the internal sensor. The flow control strategy of the M-Climate Vicki was different compared to the two others as it fluctuated around approx. 50% of the maximum flow but it also had a district supply temperature which was 10 °C higher than in the experiments featuring the other two thermostats. Furthermore, the internal sensor in the M-Climate Vicki reached the set-point before the set-point was reduced again, the temperature 0.6 m from the radiator was on par with the internal temperature sensor throughout the experiment, while the temperature two meters from the radiator was a couple of degrees lower than measured with the internal sensor. The cooling was minimal for Danfoss ECO and Eurotronic Spirit due to the large flow and somewhat higher for the M-Climate Vicki due to a higher supply temperature.

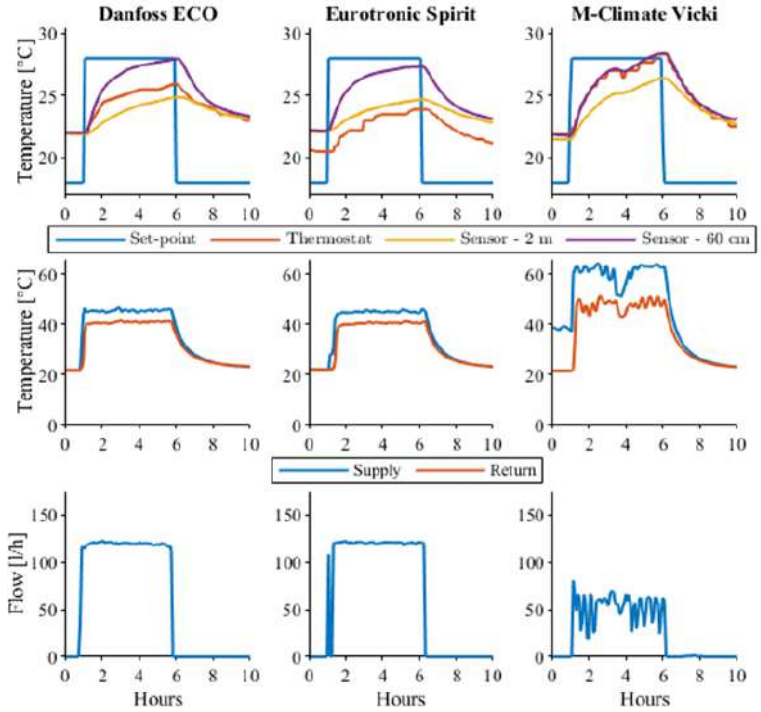

Fig. 3 – Results from Experiment 1 – starting temperature at 18°C

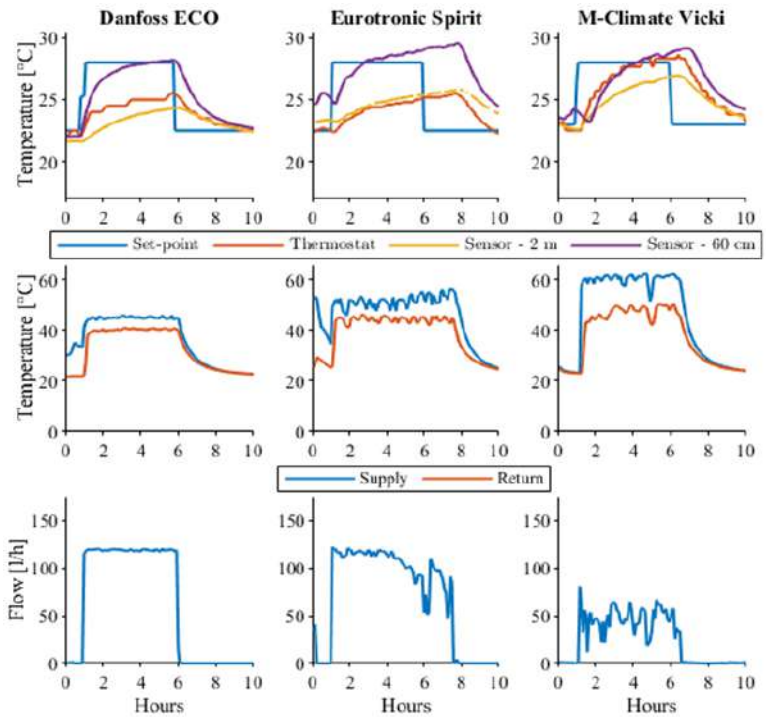

Fig. 4 - Results from the first experiment – starting temperature at 22.5°C

Figure 5 and 6 show a clear difference in behaviour among the thermostats during Experiment 2. The internal temperature sensor of the Danfoss ECO reached the set-point after a period of utilising the maximum flow available resulting in a low cooling, and then tracked the set-point rather precise by minor adjustments of a lower constant flow – and consequently a higher cooling. However, after few hours the flow went to zero for unknown reasons, and the temperatures consequently dropped more than 1°C below the set-point. This behaviour was also observed when the experiment was repeated several times. The temperature 0.6 m from the radiator was in general higher than the temperature of the internal sensor while the sensor placed two meters from the radiator displayed a temperature somewhat lower than the internal sensor – which was also observed in Experiment 1. The Eurotronic Spirit displayed the same initial behaviour as Danfoss ECO but once the temperature of the internal sensor had reached the set point, the temperature oscillated somewhat around the set-point using an on/off control of the flow. The temperature measured by the room sensors were shifted the same way as in Experiment 1. The M-Climate Vicki did not start out with utilising the maximum flow available to reach the set point as the two other thermostats. Instead, a relatively low flow was used to overshoot the set-point temperature before entering a set-point tracking with significant oscillations employing an on/off flow control. The temperature 0.6 m from the radiator was on par with the temperature of the internal sensor, while the sensor placed two meters from the radiator displayed a temperature significantly lower than the internal sensor – which was also observed in Experiment 1. As in Experiment 1, the cooling was somewhat higher due to a higher supply temperature.

The results obtained from Experiments 3 are shown in Figure 7 and 8. The length of the time axis differ among the three thermostats because of the different speeds at which the thermostat temperature increased. Using the Danfoss ECO, the flow did not initially go to the maximum available flow as in Experiment 2 but increased gradually as the set-point rose. This was also the case for Eurotronic Spirit but the flow oscillated much at the beginning of the experiment until it stabilized at a constant value instead of using an on/off control as in Experiment 2. It is noted that the temperature measured by the internal sensor in Danfoss ECO and Eurotronic Spirit never reached the set-point as in Experiment 2 an therefore the flow was almost always at the maximum value. The M-Climate Vicki required a shorter amount of time to reach the set-point temperature as its internal temperature measurement increased faster than in the other thermostats. The room temperatures and cooling displayed the same behaviour as in Experiment 1 and 2 for all three thermostats.

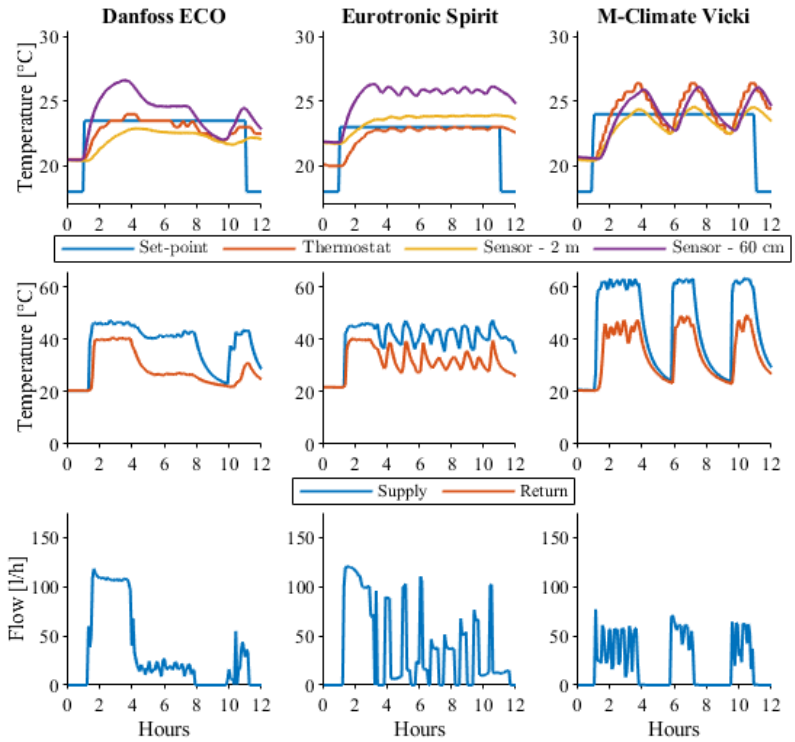

Fig. 5 - Results from the second experiment – starting temperature at 18°C

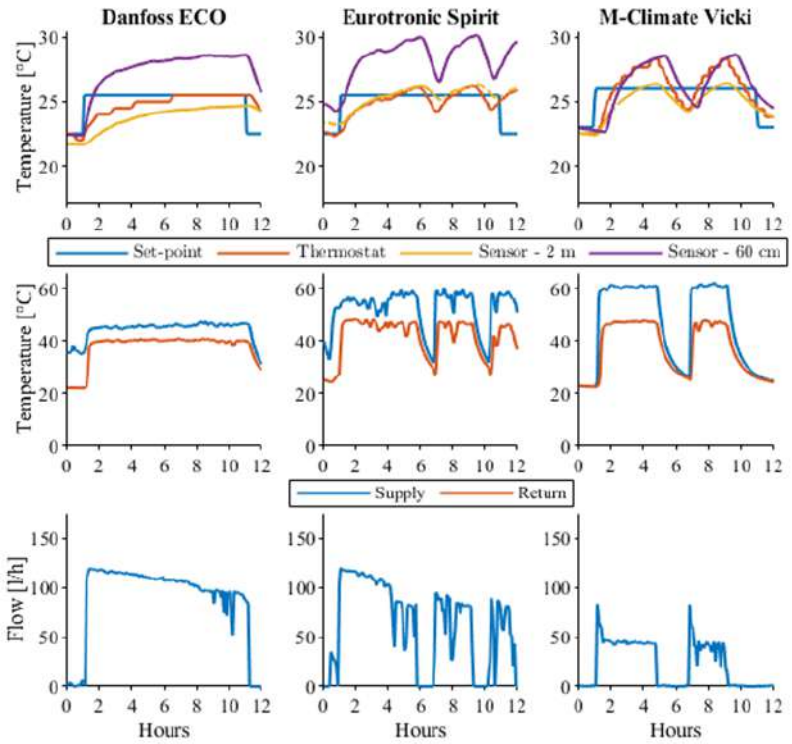

Fig. 6 - Results from the second experiment – starting temperature at 22.5°C

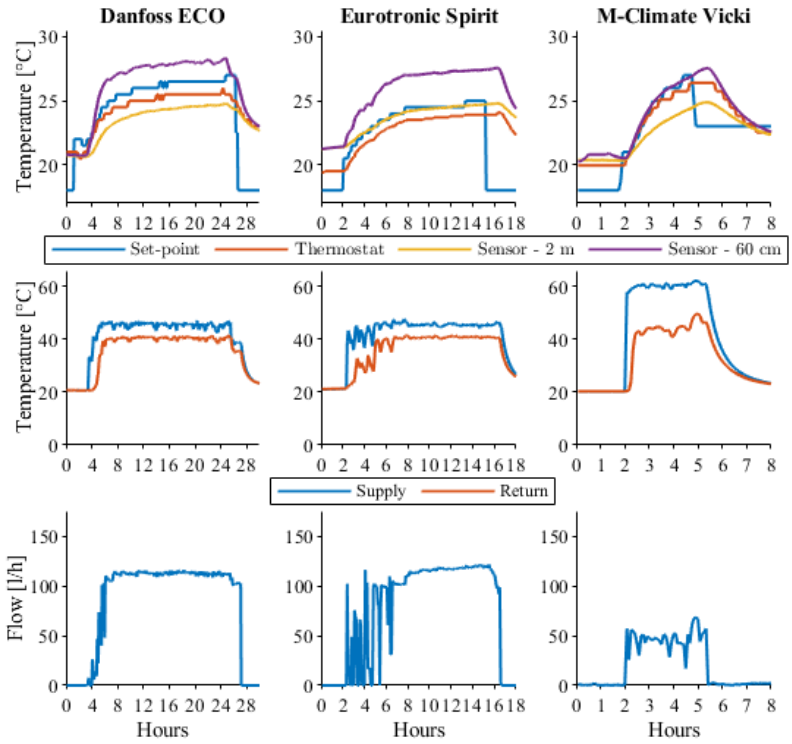

Fig. 7 - Results from the third experiment – starting temperature at 18°C

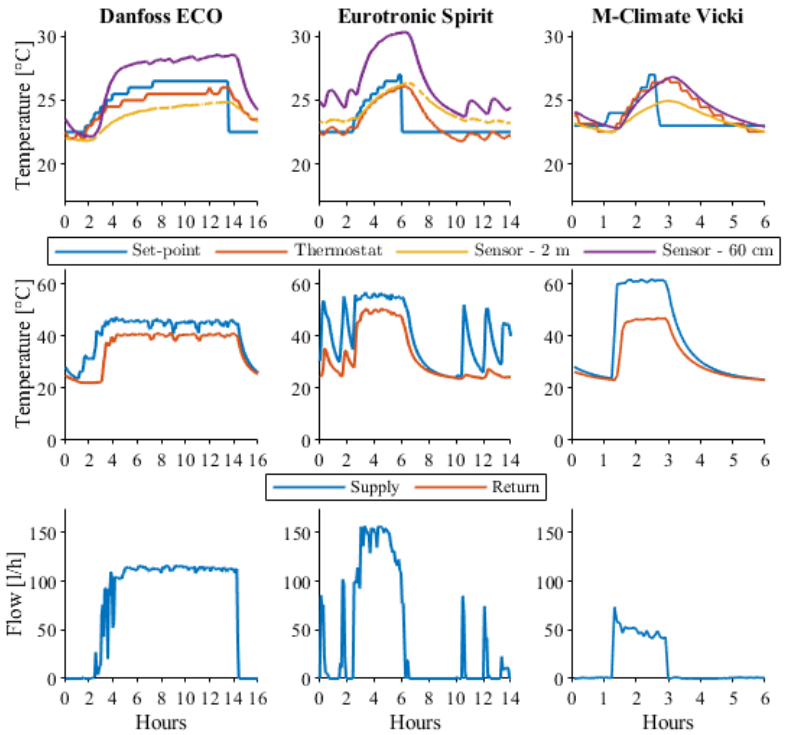

Fig. 8 - Results from the third experiment – starting temperature at 22.5°C

4. Discussion

The experiments gave many different insights about how different thermostats react to a changing set-point as well as their strategy to track a set-point. Below is a list of general observations deemed important to be aware of then using the thermostat for MPC:

- Common for all thermostats was that it was possible to make them follow a variable set-point schedule and that the thermostats reacted to changing set-points within few minutes.
- There were significant differences in the way the thermostats control the flow to track the set-point temperature.
- The two different ways of changing the set-point in Experiment 1 (one instant step change) and Experiment 3 (gradual change) resulted in significantly different flow patterns at the start of the experiment. However, when the set-point in Experiment 3 reached a certain level, the behaviour was similar to Experiment 1.
- The internal temperature sensor in the thermostats used as control variable seems to aim at representing different room temperatures. Danfoss ECO and Eurotronic Spirit is most similar to a room temperature far away from the radiator (absolute difference not higher than 1°C), whereas M-Climate Vicki is quite similar to the temperature close to the radiator.
- The data obtained about cooling of the radiator water are not always directly comparable across the experiments because of supply temperatures. What can be observed is that the radiator cooling tended to decrease between 5°C and 15°C depending on the case when increasing the set-point, and that the cooling followed the oscillations in flow (as expected). A higher cooling was obtained when the set-point during the gradual change of set-point (up to 24°C) of Experiment 3 but ended at the same level as the other experiments.
- The experiments had to start over several times because the thermostats lost their wireless connection and were therefore not able to receive set-points.

A general challenge for all three thermostats was to ensure a stable wireless connection. This is critical if they are employed for MPC where new set points are sent to the thermostat regularly to obtain demand response. Making the connection more reliable and ensuring that the thermostat keeps tracking a desired set-point if the connection is lost is important future work.

The different thermostats have different behaviour with pros and cons, and it is therefore difficult to pinpoint whether one thermostat is better for MPC than the others. One important issue to consider across the different thermostats is how their control strategy impact the room temperature near as well as far from the radiator – locations where people are present and where temperature is a proxy for their

thermal comfort. The internal sensor in the thermostats used as control variable was not an expression of the temperature in the room for any of the thermostats (except for the M-Climate Vicki that closely expressed the temperature close to the radiator) and it might therefore be relevant to use one of the room temperature sensors as control variable to ensure thermal comfort.

It is noted that the thermostats were tested using their default settings and future studies could therefore investigate if customisable settings of the thermostats can be tuned for optimal performance in an MPC scheme. For example, it is possible to regulate the temperature offset or to control directly the valve opening of the Eurotronic Spirit, and to tune the PI control parameters of the M-Climate Vicki. It is not possible to customise the Danfoss ECO.

Limitations of this study could also be explored in future research. For example, the experimental results are all things being equal affected by the physical circumstances of the test room; repeating the thermostats in rooms with a different geometry and heat loss to surroundings is likely to lead to different results.

5. Conclusions

The paper reports on a study on how three wireless remotely controlled thermostats for a hydronic radiator behave following a variable set-point schedule typical to MPC schemes. The study shows that there are different issues that needs to be dealt with before the thermostats are expedient for MPC. As such, the study points at different focus areas for future product development of wireless remotely controlled thermostats useful for realisation of demand response through MPC of hydronic radiator systems in buildings.

6. Acknowledgements

This study was conducted as a part of the project PreHeat (Jour. No. 64019-0127) funded by EUDP, and Flexible Energy Denmark (Jour. No. 8090-00069B) and Heat 4.0 (Jour. No. 8090-00046B) funded by Innovation Fund Denmark.

The datasets analyzed during the current study are not publicly available because of practical reasons but are available on request from the corresponding author Virginia Amato (viam@cae.au.dk).

7. References

1. Hedegaard R.E., Kristensen M.H., Pedersen T.H., Brun A., Petersen S. Bottom-up modelling methodology for urban-scale analysis of residential space heating demand response. Applied Energy [Internet]. 2019;242(March):181–204. Available from: https://doi.org/10.1016/j.apenergy.2019.03.063
2. Le Dréau J., Heiselberg P. Energy flexibility of residential buildings using short term heat storage in the thermal mass. Energy. 2016 Sep 15;111:991–1002.
3. Dominković D.F., Gianniou P., Münster M., Heller A., Rode C.. Utilizing thermal building mass for storage in district heating systems: Combined building level simulations and system level optimization. Energy. 2018 Jun 15;153:949–66.
4. Cai H., Ziras C., You S., Li R., Honoré K., Bindner H.W.. Demand side management in urban district heating networks. Applied Energy [Internet]. 2018 Nov 15 [cited 2020 Sep 2];230:506–18. Available from: https://doi.org/10.1016/j.apenergy.2018.08.105
5. Knudsen M.D., Petersen S. Demand response potential of model predictive control of space heating based on price and carbon dioxide intensity signals. Energy and Buildings [Internet]. 2016;125:196–204. Available from: http://dx.doi.org/10.1016/j.enbuild.2016.04.053
6. Knudsen M.D., Georges L., Skeie K.S., Petersen S. Experimental test of a black-box economic model predictive control for residential space heating. Applied Energy [Internet]. 2021;298(May):117227. Available from: https://doi.org/10.1016/j.apenergy.2021.117227

Individual EV load profiling and smart charging to flatten total electrical demand

Ward Somers [a], Waqas Khan [a], Kevin de Bont [b], Wim Zeiler [a, b]

[a] Faculty of Architecture and the Built Environment, Eindhoven University of Technology, Eindhoven, the Netherlands, w.p.a.somers@student.tue.nl, w.khan@tue.nl, W.Zeiler@tue.nl.

[b] Kropman Installatietechniek B.V., Nijmegen, the Netherlands, kevin.de.bont@kropman.nl.

Abstract. The rapid growth of electric vehicles (EVs) is stimulating their integration into the existing power grid to reduce power peaks and avoid grid congestion using smart charging strategies. Specifically, at commercial buildings, most EVs charge simultaneously in the morning resulting in large power peaks. This uncoordinated EV charging is changing the existing building load profile, which already fluctuates due to HVAC operations and PV fluctuations, significantly with their dominant charging load by amplifying power peaks. The changed building load profile of a single building does not influence the grid significantly, but the cumulative power peaks at commercial buildings can cause grid congestion. Smart charging can solve this problem by regulating power rates of charging sessions to anticipate the electrical building load. Therefore, this research aims to evaluate individual EV charging load profiles, based on real-world data, and the smart charging potential to flatten the total electrical load of a case study. Daily charging load profiles are constituted with k-means data clustering techniques to obtain the general charging profiles of individual EVs for deploying smart charging strategies. Additionally, the HVAC load flexibility potential is explored to complement smart charging with load flattening. The smart charging potential showed promising results with individual power peak reductions up to 37.8% and an average power peak reduction of the total EV load of approximately 60%.

Keywords. Electric vehicles, EV load profiling, smart charging, demand side management, load flexibility.
DOI: https://doi.org/10.34641/clima.2022.164

1. Introduction

Electric vehicles (EVs) are increasingly adopted as an alternative for internal combustion engine vehicles (ICEVs) to comply with the Paris Agreement on climate change aiming to reduce CO_2 emissions. It is expected that the Dutch EV fleet will increase from 0.21 million in 2021 to approximately 4-5 million in 2035 [1-3]. Besides the rapid growth, EVs often charge at their maximum power rate until the battery is fully charged, which can be characterized as uncoordinated charging. The growing EV fleet in combination with uncoordinated charging, result in an increasing power demand, power peaks and demand variability. For grid operators, it becomes more difficult to accurately predict the required load, which endangers the reliability and quality of the power supply [4,5]. Specifically, at commercial buildings, EVs can create a problem since typical occupancy patterns are noticeable, where employees arrive in the morning and depart late in the afternoon [6]. The occupancy pattern in combination with uncoordinated charging results in power peaks in the morning and long idle times in the afternoon. This uncoordinated EV charging is changing the existing building load profile, which already fluctuates due to HVAC operations and PV fluctuations, significantly with their dominant charging load by amplifying power peaks. However, EVs can offer significant load flexibility with smart charging and thereby regulate the voltage frequency of the grid or on a smaller scale the voltage frequency of a building [7,8]. The generally long idle times of EVs at commercial buildings enable load shifting by scheduling the load over the entire workday to flatten power peaks. Complementary to smart charging strategies, HVAC systems can assist with grid balancing by throttling the power rate without affecting occupants' comfort [9,10]. Therefore, it is of major importance to gain knowledge about the individual EV charging behaviour and the potential load flexibility of HVAC systems to accomplish smart charging strategies.

2. Literature review

This section describes some approaches that have been used for load profiling of EVs, smart charging scenario and the underlying assumptions that have been adopted.

Real-world EV charging datasets are scarce,

Copyright ©2022 by the authors. This conference paper is published under a CC-BY-4.0 license.

resulting in research [11,12] that use travel patterns of conventional cars – often retrieved from national surveys – in combination with EV characteristics assumptions to constitute EV charging load profiles. Therefore, these studies could only rely on the parameter parking duration. and assumed other parameters, such as charging power, idle time and battery capacity. The assumptions of EV charging behaviour in these studies cause significant uncertainties. Fortunately, real-world data becomes widely available due to the increasing growth of EV adaptation. Researchers [13-17] have used historical data of EV charging events to constitute EV charging load profiles. The most important parameter found in the literature to constitute proper EV charging load profiles is the average charging power per time interval of maximum 15 minutes. Other parameters, such as connection duration, charging time, idle time and energy consumption, can be obtained with the charging power per time interval. Moreover, the initial and final state of charge (SoC) are valuable parameters found in the literature [15-17]. These parameters are useful to schedule charging events and to determine the charging sequence with smart charging strategies. However, it should be noted that the availability of SoC values depends on the charging protocols. DC-chargers – used for fast chargers – can obtain SoC values, where AC-chargers cannot obtain SoC values with the current widely applied IEC 61851-1 protocol. Fortunately, SoC values could be available for AC-chargers with the new ISO-15118-20 protocol and the cooperation of original equipment manufacturers (OEMs) in the near future [18]. In the existing literature, the generation of general EV load profiles are based on averages of large datasets and EV fleets. This paper distinguishes itself by collecting and evaluating the individual load profiles of EVs at a commercial building per weekday.

After investigating the EV charging behaviour, smart charging scenarios can be constituted. Flattening power peaks to secure the reliability of the grid is the most important objective of smart charging. Ref. [4] investigated the impact of smart charging on the transmission and distribution lines of Great-Britain. The smart charging focused on unidirectional charging with a maximum of 7 kW, an efficiency of 90% and charging based on SoC values and the electricity price. According to this strategy, EVs charge at off-peak hours when the electricity price is low. At peak hours when the prices are higher, EVs with a low SoC still charge at a higher rate, while EVs with a higher SoC does not charge or charge at a low rate. This smart charging strategy can reduce network intervention from 28% to 9%. Ref. [8] investigated peak shaving and valley filling of a university building with an EV parking lot. The study focused on a tool to monitor the occupancy at the parking lot by registering the arrival and departure times of conventional cars. By knowing the required energy for the next trip, based on user preference, and assuming that EVs have a battery capacity of 24 kWh and charge/discharge slowly, power peaks could be reduced by approximately 20%. In addition to Ref. [8], Ref. [19] investigated the peak shaving and valley filling of the same university, but this time with PV panels. In the most ideal situation of this scenario, the power peak could be reduced by approximately 25%. Ref. [20] developed a smart charging/discharging schedule algorithm aiming to peak shave and valley fill the power load profile of the grid. This study considers several constraints related to EVs. First, charging and discharging rates must be within maximum and minimum values to avoid battery degradation. Second, batteries must be charged up to a maximum limit and discharged to a set depth of discharge (DOD). These limits can be set by the EV owner. In Ref. [21] a smart charging strategy is compared with uncontrolled charging. The smart charging strategy uses price signals and the SoC of the EVs as input to determine the charging power output, assuming an initial SoC of 20% and a charging rate of 6.6 kW.

Most studies [7,19-21] use SoC values to constitute smart charging strategies, however, this paper purely focuses on historical EV charging rates and the interaction with the electrical building load. The historical charging rates are used to constitute EV charging load profiles, which are valuable to obtain a better understanding of the individual and aggregated charging behaviour, such as charging power, charging time, idle time and presence, without compromising the privacy and convenience of the EV owner. Not using SoC values is more representative to reality, since SoC values are currently not available with AC/DC charging due to a lack of protocols. Therefore, this paper distinguishes itself by investigating load profiles of individual and aggregated EVs, flattening the power demand using smart charging and by evaluating the energy flexibility capability of the HVAC system at a case study. To that end, the main contributions of this work can be summarized with the following research questions:

- What are important parameters to constitute appropriate EV charging load profiles?
- What are the characteristics of the individual and total EV charging loads at the case study?
- How large is the smart charging potential of the case study?

The rest of the paper is organized as follows: Section 3 describes the case study, methodology of load profiling and determination of the smart charging potential. The results of the smart charging potential and the HVAC flexibility are presented in Section 4. The discussion about the obtained results is presented in Section 5. Finally, conclusions are drawn, and recommendations are provided in Section 6.

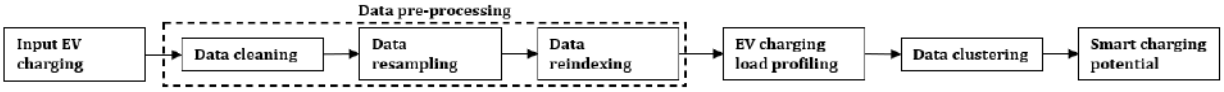

Fig. 1 – Stepwise process of the research.

3. Methodology

In this section, the process and used methods in this study are explained in detail. The sequence of the process is illustrated in Figure 1.

3.1 Case study

The office building of Kropman Breda is used as case study and can be characterized as a traditional Dutch office building. The HVAC system consists of a gas-fired boiler and an air handling unit (AHU) which controls the ventilation, cooling and humidification demand. Additionally, a photovoltaic (PV) system is installed in combination with a battery energy storage system (BESS) to increase self-consumption. Moreover, the case study contains two EV chargers each with two charging sockets. Both EV chargers are 3 phase 32 A and connected to a voltage of 230 V. Therefore, a single charger has a maximum power output of 22 kW (3 * 32 A * 230 V = 22,080 W = 22 kW). When an EV plugs in, it communicates with the Electric Vehicle Supply Equipment (EVSE), EV charger, according to the IEC 61851 protocol. This protocol only supports unidirectional energy exchange, thus, EVs can only charge their battery. The EV charger communicates its maximum power output to the EV and the EV communicates its maximum charging rate to the EV charger. Then the actual charging rate is determined by the lowest maximum charging rate. Data of the charging event is transferred from the EV charger to the charge point operator (CPO) where the data is collected. In addition, the CPO can set charging profiles for individual EVs via the Open Charge Point Protocol (OCPP).

3.2 Data acquisition

The used datasets are obtained from the EV chargers of the investigated office building and contain approximately six months of data (November 2020 – May 2021) from five EVs in total. The datasets only consist of unidirectional charging events, since discharging with bidirectional charging events is currently not supported by most EVs. The datasets are log data and contain a lot of parameters, but only data about datetime, charging rate (kW) cumulative energy consumption of the charging session (kWh) and ID number are relevant. The ID numbers are necessary to differentiate data from individual EVs in the pre-processing phase, whereas the charging rate is used to constitute load profiles and energy consumption is used to obtain some general insights, such as average charging time.

3.3 Data pre-processing

The first step is to clean the data by filtering valuable information. The second step involved the resampling of the data. The datasets are down sampled to 15 minutes time intervals to replace the irregular time intervals from the log data, since regular time intervals are necessary for the constitution of representative EV charging load profiles. Finally, the datasets are reindexed to create similar time series.

3.4 Constitution of load profiles

K-means data clustering is used to extract clusters which represent common daily load profiles. The number of clusters are validated with two different methods. The first method is the silhouette score. The silhouette value is a measure of how well an object fits in its own cluster in comparison to other clusters. The silhouette score can vary between +1 and -1. A value close to +1 indicates a good match, a value close to 0 indicates overlap between the clusters and a value of -1 indicates a mismatch of clusters. The second method is the elbow method. This method calculates the Within-Cluster Sum of Square (WCSS) for different amounts of 'k' clusters. WCSS is the sum of squared distance between each point and the centroid in a cluster. With an increasing amount of 'k' clusters, the WCSS decreases. The optimal number of clusters can be determined by plotting the WCSS of all clusters. The optimal number of clusters according to the elbow method can be recognized when the graph bends and the decrease of WCSS stagnates.

3.5 Smart charging scenario

Based on knowledge about the electrical building load, a smart charging scenario is proposed to determine the smart charging potential of the case study. The scenario aims to flatten the EV charging load, since the electrical building load is already flattened due to operations of the photovoltaic (PV) system in combination with the battery energy storage system (BESS). Multiple assumptions are made to simplify the scenario:

- A default charging threshold of 7 kW is set for the individual cars, based on assumptions from earlier research [4].
- The maximum charging power is limited to 14 kW, which corresponds to two EVs charging simultaneously at the default charging rate.
- Only 'morning' clusters of the EVs are evaluated. The morning clusters seem most realistic because earlier research [6] indicates that most

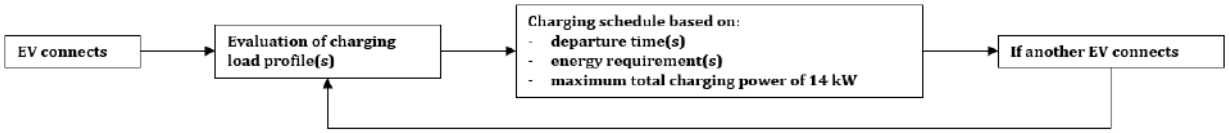

Fig. 2 – Smart charging scheduling.

power peaks occur in the morning.

- The energy requirements of an EV are determined with the integral of the investigated cluster according to the equation (1):

$$E_{e;d} = \int_{0}^{48} P(t)\, dt \qquad (1)$$

$E_{e;d}$ = energy consumption of a specific EV (e) at a specific weekday (d) [kWh]
P(t) = average power demand in 15 minutes time interval [kW]
t = time [1/4 h]

- The number of charging events throughout a week is assumed to be worst-case, meaning that an EV charges at all workdays on which it has charged previously.

The charging sequence is based on priority by continuously monitoring the presence and energy requirements of EVs as illustrated in Figure 2.

4. Results

4.1 Exploratory data analysis

Initially, the pre-processed dataset is explored to obtain an indication of the individual EV charging load profiles. A boxplot of the charging power and energy consumption provides valuable insights about the general charging power, energy consumption and charging duration. From the charging power distribution in Figure 3, it is noticeable that EV 1-3 have overlapping quartiles, indicating uncoordinated charging patterns at maximum power rate (11 kW). Contrary, wider ranges for charging rates are noticeable for EV 4 and 5, indicating some kind of 'manual smart charging'. Moreover, the average energy consumption varies between 25 – 30 kWh approximately according to Figure 3. The charging power and energy consumption combined, roughly indicates an average charging duration between 2.5 – 4 hours.

4.2 EVs load profiles

The exploratory analysis shows valuable insights. However, important daily and quarter hourly information is missing, thus, daily load profiles based on quarter hourly data are necessary for more detailed information. In general, it is noticeable that all EVs have quite similar clusters. Most EVs have two clusters, where one cluster starts charging in the morning, stops charging after several hours and has a relatively long idle time. The other cluster, which is not considered in this study, starts charging later in the morning or in the afternoon and has almost no idle time.

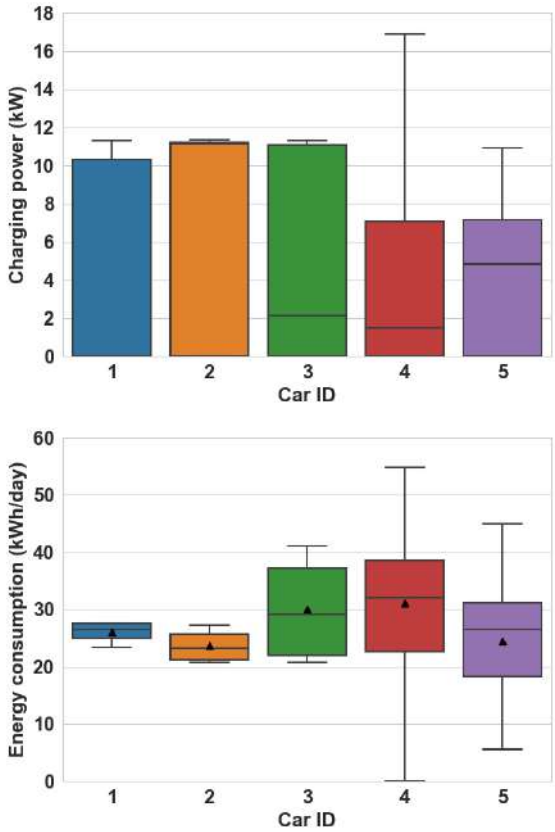

Fig. 3 – Charging power distribution of individual EVs (top) and energy consumption distribution (bottom).

4.3 Comparison between building load and total EV load

The total EV load contains four clusters of which three clusters can be characterized as 'morning cluster', one cluster as 'afternoon cluster' as illustrated in Figure 4. The outcome is comparable with earlier research [6] and empowers our assumption to focus on morning clusters. Moreover, it is noticeable that the power peaks of the total EV load are occasionally larger than the electrical building load of the case study, depending on the buildings' cluster and the EV's cluster, which emphasizes the importance of smart charging. In addition, quick ramp ups and downs of the EV load are noticeable during office hours (07:30-17:30 h) due to arriving, departing employees and fully charged batteries, whereas the building load has only one quick ramp up before the office hours and one quick ramp down before the end of the office hours.

4.4 Smart charging potential

The smart charging potential at the case study is evaluated by comparing EV charging loads

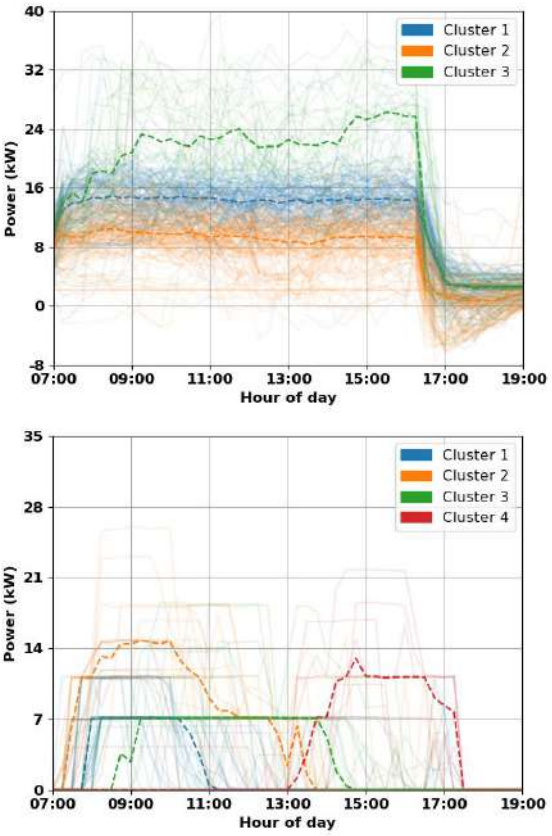

Fig. 4 – Comparison between electrical building load (top) and total EV charging load (bottom).

according to uncoordinated and coordinated charging sessions, using real-world data. The proposed smart charging scenario aims to flatten the EV load since the electrical building load is already flattened. Overall, it is possible to reduce the power peaks in the morning by spreading the EV load over the day. Load shifting is arranged by limiting the charging power and delaying the charging sessions on individual level, where its applicability depends on the connection time and required energy. The smart charging potential is evaluated per weekday during a typical week as illustrated in Figure 5. The average individual power peak reductions vary from a slight decrease of 2.83% up to 37.8%, where the average power peak reduction of the total EV load equals 59.6% as shown in Table 1.

4.5 Potential HVAC flexibility

In addition to the load flexibility of smart charging, the load flexibility of HVAC systems is considered. Especially at critical days when a lot of EVs charge simultaneous with inevitably large power peaks, complementary load flexibility from the HVAC system could be desirable. Earlier research [9,10] investigated the load flexibility potential of the ventilation fan, chiller and humidifier at our case study. They found a significant potential to reduce the power demand by adjusting the active operation, without affecting indoor comfort and human health, as shown in Table 2.

Tab. 2 – Characteristics of HVAC load flexibility.

Criteria	Ventilation	Chiller	Humidifier
Response time [min.]	0.5 – 5	5	5
Availability duration [min.]	120	20	60
Power reduction [kW]	4	7	14
Energy reduction [kWh]	8	2.3	14

The load flexibilities of the ventilation fan and humidifier are suitable for complementary power reductions, since the response time is fast, the availability duration is long and the power demand is arranged with proportional integration derivative (PID) controllers. In contrast, the chiller is less suitable for complementary load flexibility since the power demand is controlled per stage and the availability duration is short. The HVAC load flexibilities are currently not incorporated in our smart charging strategy, because further research is necessary to investigate the controllability of HVAC components within smart charging strategies.

Tab. 1 – Numerical overview of smart charging results ('-' indicates absence).

EV load	Monday	Tuesday	Wednesday	Thursday	Friday	Average
EV 1	–	–37.7%	–37.8%	–	–	–37.8%
EV 2	–	–	–37.7%	–23.9%	–11.0%	–24.3%
EV 3	–	–37.7%	–	–	–22.2%	–30.0%
EV 4	–24.4%	+0.24%	–37.1%	–1.19%	–37.1%	–19.9%
EV 5	–2.45%	–3.06%	–2.89%	–2.80%	–2.94%	–2.83%
Total	–57.4%	-61.5%	–63.4%	–63.1%	–52.4%	–59.6%

5. Discussion

The results of the smart charging potential are very promising. However, the smart charging potential is accompanied by certain uncertainties and limitations which will be described in this section.

First, the used datasets have a limited number of charging events. Only 122 charging sessions are registered since the operation of the EV chargers. A larger dataset would increase the reliability of the clustered charging profiles.

Second, in most cases it is unknown how much energy an EV needs to charge, since SoC values are often not available due to a lack of open protocols. Therefore, this study determined the energy requirement of an EV at a specific weekday by the integral of the obtained cluster.

Finally, assuming that EVs charge at all weekdays on which it has previously charged, probably results in a significant overestimation of the charging load, since it is unlikely that an EV always charges when present. The presence of a single EV is investigated and compared with charging sessions from the datasets. This particular EV only charges 52% of the time. Therefore, it is plausible that this presence-charging ratio is also applicable to other EVs. Unfortunately, it was not possible to investigate the presence of other EVs due to privacy issues.

6. Conclusions and recommendations

6.1 Conclusions

Motivated by a lack of research regarding individual EV load profiling and smart charging, this research aims to evaluate individual EV charging load profiles to flatten the total power demand of a commercial building. Conclusions of this study are drawn by answering the defined research questions from section 2.

What are important parameters to constitute appropriate EV charging load profiles?

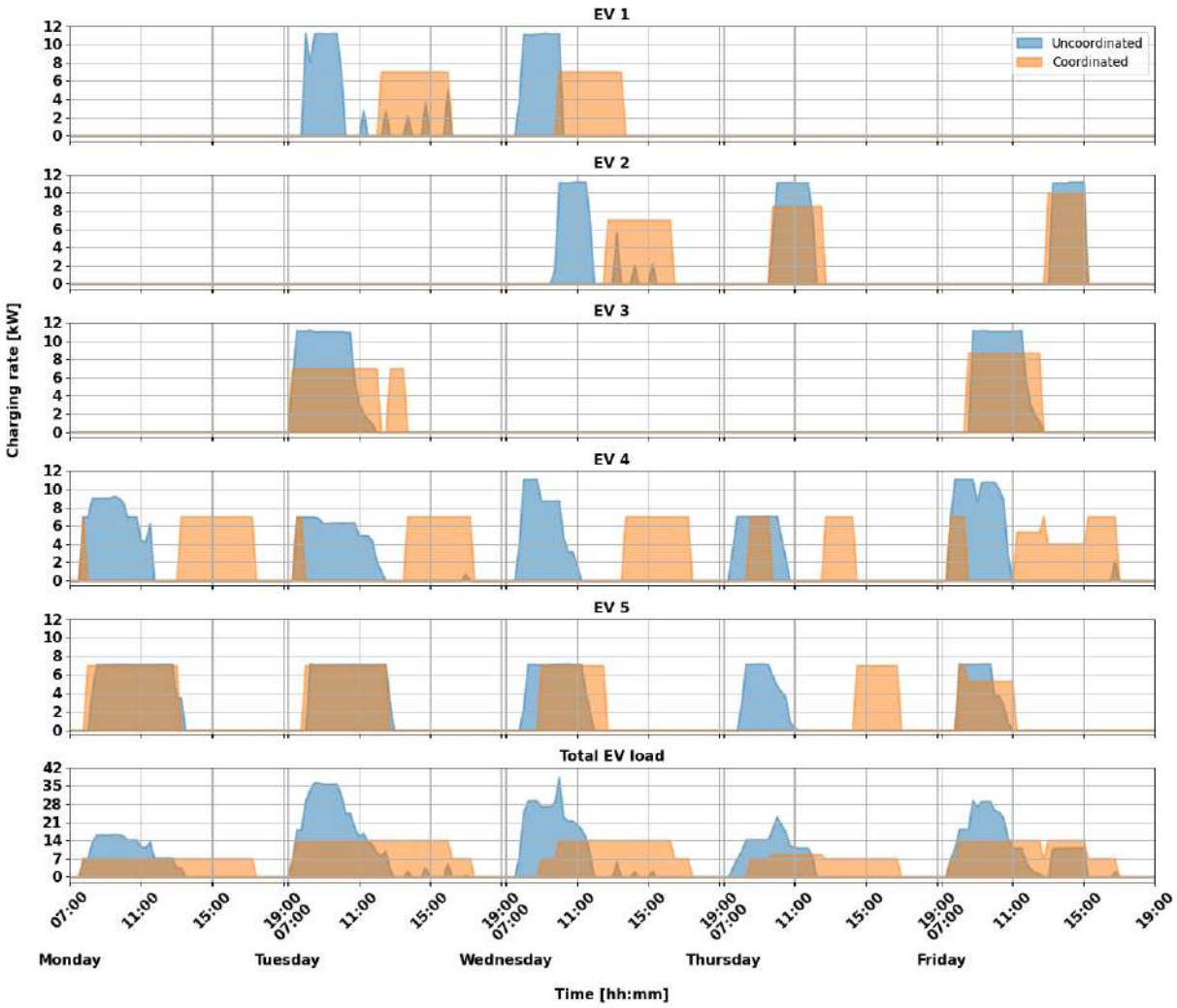

Fig. 5 – Visual overview smart charging potential.

It can be concluded that charging power per time interval is the most important parameters for the constitution of EV charging load profiles since other parameters can be retraced with the charging power. Additionally, initial and final SoC are key parameters for optimizing smart charging. Unfortunately, SoC values are often not available due to a lack of open protocols.

What are the characteristics of the individual and total EV charging loads at a commercial building?

Generally, it is noticeable that EVs often have two clusters, a morning and afternoon cluster, which are quite similar for all EVs at the case study. The morning cluster starts charging in the morning, stops charging after several hours and has a relatively long idle time. The afternoon cluster starts charging later in the morning or in the afternoon and has almost no idle time. Especially, the morning cluster enables smart charging by shifting loads to the afternoon to reduce power peaks. This holds for EVs with just a few charging sessions, but also for the EVs with relatively a lot of charging sessions. Moreover, the total EV charging load has four clusters and can also be distinguished in morning and afternoon clusters. three from the four clusters are morning clusters, which emphasizes the occurrence of power peaks in the morning.

How large is the smart charging potential of a commercial building?

To quantify the smart charging potential at a commercial building, power peaks of uncoordinated charging profiles are compared with coordinated charging profiles. Power peak reductions of individual and total EV load per weekday (Monday-Friday) are evaluated. Overall, it is possible to reduce the power peaks in the morning by spreading the EV load over the day. The average individual power peak varies from a slight increase of 0.24% to a decrease of 37.8% and the average power peak reduction of the total EV load equals 59.6%. Therefore, the smart charging potential of this scenario shows very promising results.

6.2 Recommendations

This exploratory research on individual EV load profiling and smart charging is the basis for more sophisticated research on smart charging. Therefore, this section provides the following suggestions for further research:

- In this study, data about EV charging and presence is limited. For further research, it is recommended to collect more data.
- Only one scenario is investigated in this research. However, there are more interesting scenarios to investigate. For example, a scenario without BESS since most commercial buildings do not have a BESS. Without BESS, the building load differs since energy storage is not possible. In this scenario, the scheduling of the charging load would mainly depend on the electricity production of the PV system to increase self-consumption.
- It would be interesting to implement the complementary load flexibility of the ventilation fan and humidifier into smart charging scenarios.
- The next step would be to create forecast models to predict the EV charging load a day-ahead. The forecast models would increase the accuracy and possibilities for smart charging strategies. It would be interesting to create two types of forecasting models: a forecast model to predict individual EV loads with detailed data and a model to predict the aggregated EV load of a larger population with limited data.
- After constituting a forecast model, optimization techniques could be used to find optimal smart charging scenarios and charging power rates. In this study, a default power rate of 7 kW was assumed, but with the application of optimization techniques, optimal power rates can be determined, which are based on the forecast of the building load and the presence of EVs.

7. References

[1] 2021-10 - Statistics Electric Vehicles and Charging in The Netherlands up to and including October 2021.pdf [Internet]. [cited 2022 Mar 4]. Available from: https://www.rvo.nl/sites/default/files/2021/11/2021-10%20-%20Statistics%20Electric%20Vehicles%20and%20Charging%20in%20The%20Netherlands%20up%20to%20and%20including%20October%202021.pdf

[2] 2021-10 – Statistics Electric Vehicles and Charging in The Netherlands up to and including October 2021.pdf [Internet]. [cited 2022 Mar 4]. Available from: https://www.elaad.nl/uploads/files/2021Q3_Elaad_Outlook_Personenautos_2050.pdf

[3] Rietmann N, Hügler B, Lieven T. Forecasting the trajectory of electric vehicle sales and the consequences for worldwide CO2 emissions. Journal of Cleaner Production. 2020 Jul 10;261.

[4] Crozier C, Morstyn T, McCulloch M. The opportunity for smart charging to mitigate the impact of electric vehicles on transmission and distribution systems. Applied Energy. 2020 Jun 15;268.

[5] Jovanovic R, Bayhan S, Bayram IS. A multiobjective analysis of the potential of scheduling electrical vehicle charging for flattening the duck curve. Journal of Computational Science. 2021 Jan 1;48.

[6] Sadeghianpourhamami N, Refa N, Strobbe M, Develder C. Quantitive analysis of electric vehicle flexibility: A data-driven approach. International Journal of Electrical Power & Energy Systems. 2018 Feb 1;95:451–62.

[7] Sharifi P, Banerjee A, Feizollahi MJ. Leveraging owners' flexibility in smart charge/discharge scheduling of electric vehicles to support renewable energy integration. Computers & Industrial Engineering. 2020 Nov 1;149.

[8] Loakimidis CS, Thomas D, Rycerski P, Genikomsakis KN. Peak shaving and valley filling of power consumption profile in non-residential buildings using an electric vehicle parking lot. Energy. 2018 Apr 1;148:148–58.

[9] Aduda KO, Labeodan T, Zeiler W, Boxem G, Zhao Y. Demand side flexibility: Potentials and building performance implications. Sustainable Cities and Society. 2016 Apr 1;22:146–63.

[10] Aduda K, Zeiler W, Boxem G, de Bont K. On the Use of Electrical Humidifiers in Office Buildings as a Demand Side Resource. Procedia Computer Science. 2014 Dec 31;32:723–30.

[11] Pareschi G, Küng L, Georges G, Boulouchos K. Are travel surveys a good basis for EV models? Validation of simulated charging profiles against empirical data. Applied Energy. 2020 oktober;275.

[12] Zhang J, Yan J, Liu Y, Zhang H, Lv G. Daily electric vehicle charging load profiles considering demographics of vehicle users. Applied Energy. 2020 Sep 15;274.

[13] Xydas E, Marmaras C, Cipcigan LM, Jenkins N, Carroll S, Barker M. A data-driven approach for characterising the charging demand of electric vehicles: A UK case study. Applied Energy. 2016 Jan 15;162:763–71.

[14] Brady J, O'Mahony M. Modelling charging profiles of electric vehicles based on real-world electric vehicle charging data. Sustainable Cities and Society. 2016 oktober;26:203–16.

[15] Schäuble J, Kaschub T, Ensslen A, Jochem P, Fichtner W. Generating electric vehicle load profiles from empirical data of three EV fleets in Southwest Germany. Journal of Cleaner Production. 2017 mei;150:253–66.

[16] Quirós-Tortós J, Espinosa AN-, Ochoa LF, Butler T. Statistical Representation of EV Charging: Real Data Analysis and Applications. In: 2018 Power Systems Computation Conference (PSCC). 2018:1–7.

[17] Flammini MG, Prettico G, Julea A, Fulli G, Mazza A, Chicco G. Statistical characterisation of the real transaction data gathered from electric vehicle charging stations. Electric Power Systems Research. 2019 Jan 1;166:136–50.

[18] Gonzalez Venegas F, Petit M, Perez Y. Active integration of electric vehicles into distribution grids: Barriers and frameworks for flexibility services. Renewable and Sustainable Energy Reviews. 2021 Jul 1;145.

[19] Genikomsakis KN, Bocquier B, Lopez S, Ioakimidis CS. Utilizing plug-in electric vehicles for peak shaving and valley filling in non-residential buildings with solar photovoltaic systems. In: 2016 5th International Conference on Smart Cities and Green ICT Systems (SMARTGREENS). 2016: 1–10.

[20] Ramadan H, Ali A, Nour M, Farkas C. Smart Charging and Discharging of Plug-in Electric Vehicles for Peak Shaving and Valley Filling of the Grid Power. In: 2018 Twentieth International Middle East Power Systems Conference (MEPCON). 2018:735–9.

[21] Nour M, Said SM, Ali A, Farkas C. Smart Charging of Electric Vehicles According to Electricity Price. In: 2019 International Conference on Innovative Trends in Computer Engineering (ITCE). 2019:432–7.

Data Statement

The datasets generated and analysed during the current study are not publicly available because of privacy issues.

Identifying promising use cases for a novel heat battery in Dutch residential buildings

Shuwei Wang [a], Pieter-Jan Hoes [a], Jan L.M. Hensen [a], Olaf C.G. Adan [b, c, d], Pim A.J. Donkers [d]

[a] Department of the Built Environment, Eindhoven University of Technology, Eindhoven, the Netherlands. s.wang5@tue.nl.

[b] Department of Applied Physics, Eindhoven University of Technology, Eindhoven, The Netherlands.

[c] TNO Materials Solutions, High Tech Campus 25, Eindhoven, the Netherlands.

[d] Cellcius BV, Horsten 1, Eindhoven, the Netherlands.

Abstract. Owing to the recent breakthrough in thermochemical storage technology, a novel closed-loop thermal energy storage (TES) system, the heat battery (HB), has been introduced. With higher energy density and no storage loss, this system is believed to have a greater potential of helping the energy transition in the built environment compared to other conventional TES systems. To identify the most promising use case of the HB, this research proposes a simulation approach to predict and assess how the HB will influence the performance of Dutch residential buildings. Based on a literature review and discussions with developers of the HB, a list of potential use cases is defined and the most important stakeholders are identified (homeowner, distribution system operator, and district heating system operator). Next, the simulation approach was conducted. The results show that the HB has the potential of both reducing the operational energy cost for the homeowner and reducing the peak heating load from the building to the district heating system.

Keywords. Thermochemical storage, building simulation, demand-side management.
DOI: https://doi.org/10.34641/clima.2022.165

1. Introduction

Energy storage in buildings has attracted many research efforts because of the growing challenge of both managing the building energy demand and the fluctuating production of renewable energy sources. Various energy storage technologies are used in buildings, such as electrical batteries (chemical storage) [1], [2], water tanks (sensible heat storage), PCMs (latent heat storage) [3]. Thermochemical heat storage is another promising type of energy storage as it shows high energy densities, high round-trip efficiencies, and high flexibility of charging/discharging temperatures [4], [5], [6]. However, the technological readiness level [7] of solutions based on thermochemical heat storage is still between conceptual development and industrial application.

The heat battery is a novel thermochemical heat storage solution. It absorbs/releases heat from/to the heating system in the building based on the dehydration/hydration reactions of potassium carbonate (K_2CO_3), as can be seen in Fig. 1 [8]. It employs an electricity-based circulating system to maintain continuous charging/discharging powers of heat.

To support the further development of the heat battery (HB), this paper investigates which use cases of the HB are promising for Dutch residential buildings. The section 2 of this paper explains the simulation-based approach adopted by this study. In Section 3, the investigated use cases are described. The predicted performance of the use cases are analyzed in Section 4, and Section 5 concludes this paper with a discussion and conclusion.

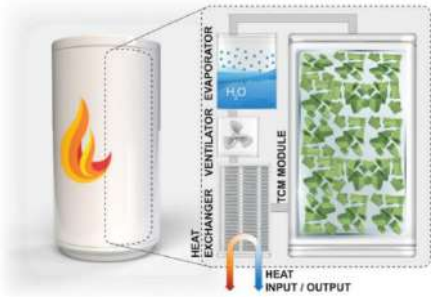

Fig. 1 – Schematic diagram of the HB [8].

2. Methodology

2.1 Defining potential use cases

This study defines the potential use cases of the HB based on the following five use case elements: WHO

Copyright ©2022 by the authors. This conference paper is published under a CC-BY-4.0 license.

– WHY – WHERE – HOW – WHEN. For the HB, this means that we need to identify the main stakeholders (WHO) and their main purpose of using the HB (WHY). Moreover, we need to specify various design options of buildings (WHERE) and their energy systems including several relevant operational strategies (HOW) and certain scenarios (WHEN), e.g., for the building occupants and the electricity price. This research firstly includes a review of previous literature to define the proper options of these five aspects, then combines suitable ones according to the practice of Dutch residential buildings to form diverse use cases.

2.2 Modeling and simulation approach

The second part of this methodology is a simulation approach for the performance prediction of the HB in each use case. As shown in Fig. 2, this approach firstly includes modeling the building based on the design options and occupant's scenarios selected in each use case, then the heat consumption for space heating, domestic hot water (DHW) usage, and other electricity consumptions (e.g., lighting, plug-in appliances, etc.) of the building will be simulated in EnergyPlus. The simulation employed the weather file of a typical reference year in Amsterdam [9], and generated the time series (with a 15-minute timestep) of the heat demand and other electricity demand for a whole calendar year.

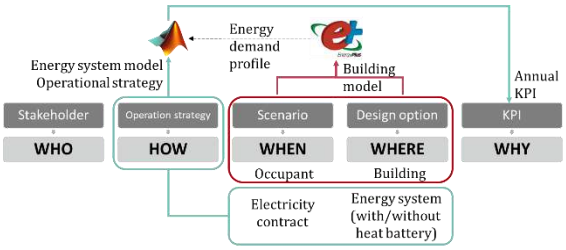

Fig. 2 – Workflow of the simulation approach.

With the predicted energy demand profiles, the energy systems and their operational strategies are then modeled and simulated in MATLAB to calculate the annual key performance indicators (KPIs) based on the energy contracts chosen in the use case. Many performance indicators related to the building's operational energy performance, e.g., the operational energy cost or peak load, can be estimated based on a model with a conceptual complexity level [10]. An example of the conceptual model is to represent a heat pump system with its coefficient of performance or heating seasonal performance factor. This modeling approach can avoid unnecessary long simulation time. Therefore, both the heat supply systems and the HB are modeled at this complexity level. If the defined performance indicators require a more detailed model, then the complexity can be increased accordingly [11].

Appendix A lists the conceptual level models used for possible heat supply systems in this study.

The heat balance of the HB is calculated by:

$$Q_{HB}(t)=Q_{HB}(t-\Delta t)+q_c(t)\cdot\Delta t-q_d(t)\cdot\Delta t \qquad (1).$$

Here, Q_{HB} is the heat stored inside the HB, kWh. q_c and q_d are the thermal charging and discharging powers, kW. The t is the time and Δt is the timestep of simulation (=15 minutes).

The HB is assumed to be loss-free of storage but still needs electricity to drive the circulation of the closed air loop. Its electricity consumption is calculated by:

$$E_{HB}(t)=q_c(t)\cdot\Delta t\cdot COP_c+q_d(t)\cdot\Delta t\cdot COP_d \qquad (2).$$

In Eq. (2), E_{HB} means the electricity consumed by the HB, kWh, while the COP_c or COP_d is equal to the charged or discharged heat divided by the electricity consumed by the HB itself. The charge and discharge powers are related to the storage capacity of the HB and the operational strategy defined in each specific use case.

3. Definition of use cases

Based on discussions with developers of the HB and a literature study ([3], [12], [13], [14]), the scope of use cases are defined as follows (see also Fig. 3). Three stakeholders are considered: the homeowner, the electricity distribution system operator (DSO), and the district heating (DH) system operator. Moreover, six operational strategies are defined (S1~S6, see Fig. 3).

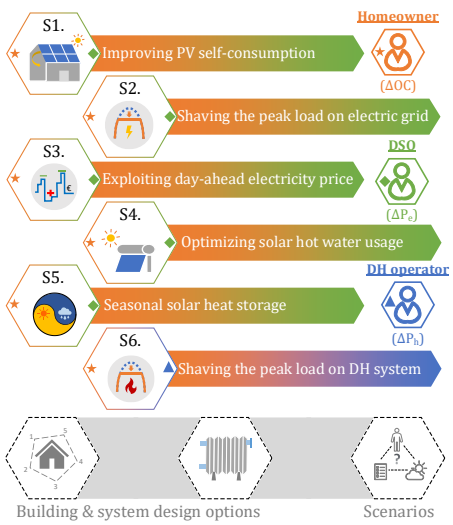

Fig. 3 – Scope of use cases in this research.

3.1 The homeowner

The homeowner is assumed to use the HB mainly for reducing operational energy costs. For those buildings unconnected to the local DH system, it is expected that in the future these costs will mostly come from electricity consumption as the residential sector in the Netherlands is moving towards electrification [15]. Therefore, the operational energy cost is calculated as follows:

$$OC = E_{im} \cdot p_{im} + \sum_{m=1}^{12} E_{p,m} \cdot p_p - (E_{ex} \cdot p_{ex} + E_{self} \cdot p_{self}) \quad (3).$$

Here, OC is the annual operational electricity cost of the building without HB, €. E_{im} is the electricity imported from the grid, kWh, and E_{ex} is the electricity exported to the grid, kWh. Their basic prices are assumed to be p_{im} and p_{ex}, €/kWh. Especially, OC includes an extra peak load cost [16] and an extra PV-self-consumption incentive. The extra peak load cost is calculated by the electricity consumed with an electric load above 2.5kW (E_p, kWh) every month (m) and its related price (p_p, €/kWh/kW). The OC also includes an extra PV-self-consumption incentive calculated by the locally consumed electricity from PV (E_{self}, kWh) and its incentive rate(p_{self}, €/kWh).

Based on (3), the HB's reduction on OC can be calculated by:

$$\Delta OC_{HB} = OC - OC_{HB} \quad (4).$$

Here, OC_{HB} denotes the operational electricity costs of buildings with HBs, it uses the same algorithm as OC and has a unit of €. The ΔOC_{HB} is exactly how much annual electricity cost the HB will reduce for the building.

To reduce OC, the homeowner can use the HB under five different strategies (S1~S5) as mentioned in Fig. 3. The first three strategies (S1~S3) require an air-to-water heat pump and S1 needs PV modules, while the other two strategies (S4~S5) use solar thermal collector as the main heat source with an electric water heater as a backup. In addition, three different scenarios of electricity contracts (both importing and exporting) are considered, as shown in Tab. 1.

Tab. 1 – Scenarios of different electricity contracts.

No.	Importing		No.	Exporting	
	p_{im}, €/kWh	p_p, €/(kW·kWh)		p_{ex}, €/kWh	p_{self}, €/kWh
1	0.25	0.00	1	0.25	0.00
2	Day-ahead [17]	0.00	2	0.06	0.00
3	0.20	0.08	3	0.00	0.06

According to the current situation in the Netherlands, various building design options (building type, and insulations' values) and occupant scenarios (occupancy patterns, heating setpoints, etc.) are defined. Details can be found in Appendix A.

3.2 The electricity Distribution System Operator (DSO)

The second stakeholder is the electricity DSO. Different from the homeowner, DSO normally will not directly install the HB in its system. It will adjust its pricing strategy to encourage the demand side to manage the peak load by itself. In this way, the DSO is assumed to encourage the homeowners to use the HB to reduce the peak load of importing and exporting electricity from the grid ($P_{e,im}$, kW and $P_{e,ex}$, kW). The reduction can be described as:

$$\Delta P_{elec,im,HB} = P_{elec,im} - P_{elec,im,HB} \quad (5).$$

The $P_{elec,im}$ is the peak load of importing electricity from the grid in the building without HB, kW. It is the maximum value in the annual time series with a 15 minutes timestep. $P_{elec,im,HB}$ is the peak load in building with HB, kW, so $\Delta P_{elec,im,HB}$ is the reduction, kW.

3.3 The district heating system operator

The third stakeholder is the operator of the DH system. It is assumed to directly use the HB to reduce the peak heat load on its system, as described in [18]. In this study, the HB is assumed to be installed in a DH system serving a residential neighborhood consisting of 50 houses, and all the houses in one neighborhood are assumed to have the same building designs and occupant scenarios as mentioned in Appendix B. The KPI for the operator is the reduction of the peak load of supplying heat from the DH system to the 50 houses, and it can be calculated by:

$$\Delta P_{heat,im,HB} = P_{heat,im} - P_{heat,im,HB} \quad (6).$$

Here, The $P_{heat,im}$ is the peak load of supplying heat from the DH system without HB to the 50 houses, kW. It is the maximum value in the annual time series with a 15 minutes timestep and includes a coincidence factor of 0.3 [19]. $P_{heat,im,HB}$ is the peak load in the DH system with HB, kW, and $\Delta P_{heat,im,HB}$ is the reduction, kW.

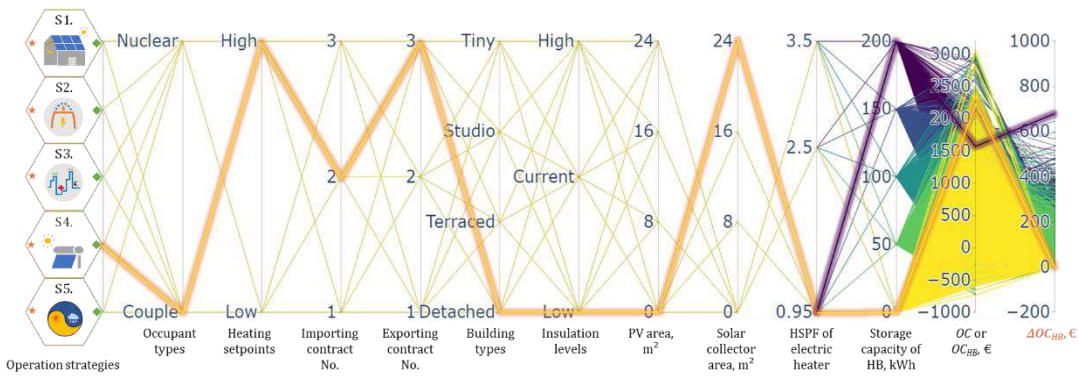

Fig. 4 – Parallel coordinate plot of the annual operational electricity cost (OC and OC_{HB}) and the reductions (ΔOC_{HB}) in all use cases with strategies S1 to S5. The highlighted pair of lines denotes the highest reduction.

4. Performance prediction of use cases

4.1 Predicted performance of use cases for homeowner and DSO

Fig. 4 shows the predicted performance of all considered use cases (more than 28,000 combinations) where the homeowner is the main stakeholder. The colors of the lines distinguish the storage capacity of the HB in each case, and lines (in yellow) connected to zero capacity represent the reference cases without HB. The highlighted lines show the use case with the highest reduction by the HB, where the 200kWh HB can reduce the annual electricity cost approximately from 2100 euros to 1500 euros. Generally, the HB has the potential of reducing the annual electricity cost by 0~400 euros, and this value can be more than 600 euros in some extreme cases.

To further compare the potential of different operational strategies, the predicted annual operational electricity cost with HB (OC_{HB}) and the reduction by HB (ΔOC_{HB}) are then grouped as shown in Fig. 5. Compared with other strategies, S1 and S4 can reach larger values of ΔOC_{HB}, while S1 tends to result in lower values of OC_{HB}. Therefore, use cases with S1 and S4 are selected for further screening of design options.

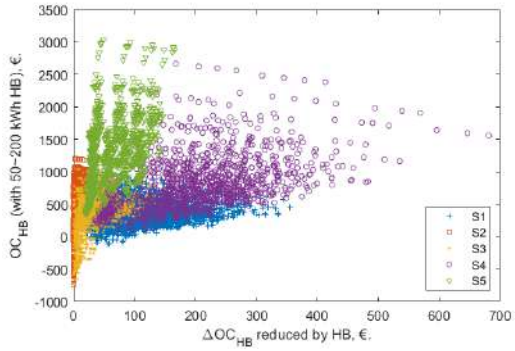

Fig. 5 – Scatter plot of annual operational electricity costs of houses with HBs (OC_{HB}) and reductions by HB (ΔOC_{HB}) grouped by different operational strategies **(the 'HOW').**

Fig. 6 shows how different design options will influence the ΔOC_{HB} in use cases with S1 or S4. Each box in Fig. 6 contains all the use cases with specified design options and operational strategies.

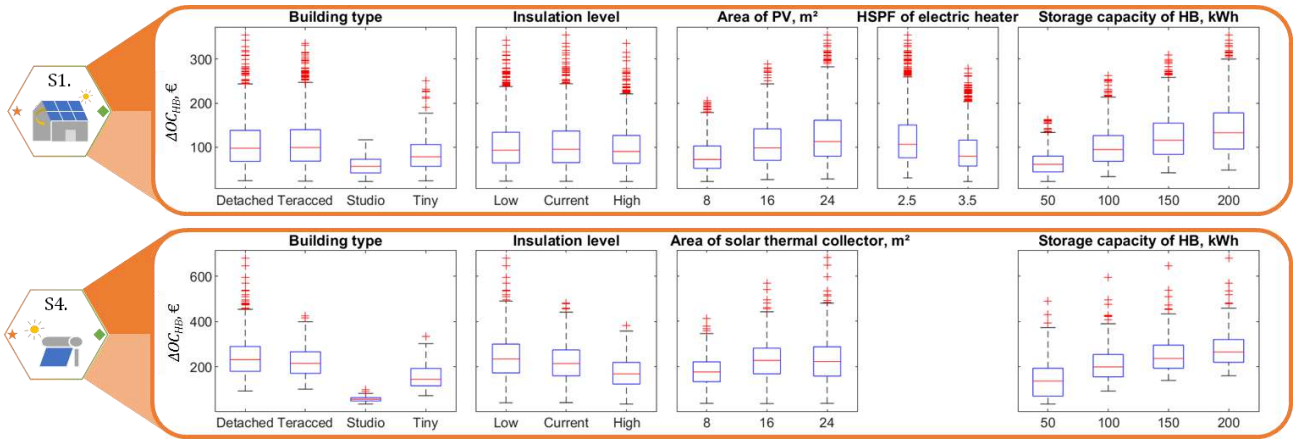

Fig. 6 – Boxplots of the reduction of electricity costs by HBs (ΔOC_{HB}) with different design options **(the 'WHERE')** in use cases with S1 and S4.

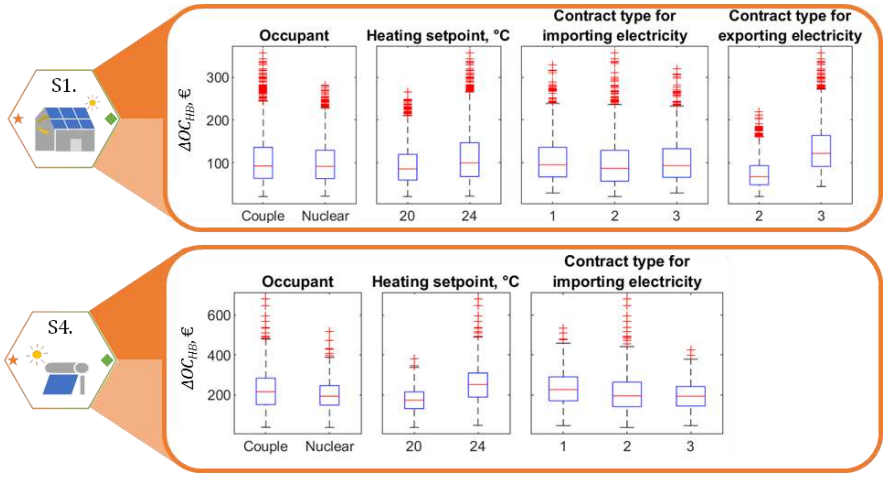

Fig. 7 – Boxplots of the reduction of electricity costs by HBs (ΔOC_{HB}) with different scenarios **(the 'WHEN')** in use cases with S1 and S4.

For use cases with S1, all design options do not change the lower boundary of the ΔOC obviously, but the building type, area of PV, HSPF of the heater, and the storage capacity of HB will shape the upper boundary in different ways. With S1, the HB may reduce more electricity costs when used in larger buildings with more PV modules and heat pumps with lower HSPF.

For use cases with S4, the type of building and HB storage capacity will influence both the upper and lower boundaries of ΔOC_{HB}, while the other two design options change just the upper one. So it would be more interesting for the homeowner to use the HB in buildings with higher heating demand. Additionally, the larger the storage capacity of HB, the more OC it can reduce.

Fig. 7 shows how different scenarios of occupants' behavior and energy contracts can alter the ΔOC. Exporting contract type 1 is not included in use cases with S1 because it does not make sense to store heat from PV electricity if the prices of importing and exporting it are the equal. Use cases with S4 do not include PV modules in their energy system so exporting contracts are not considered. For use cases with S1 or S4, types of occupants and contract of importing electricity will not influence the ΔOC as much as the heating setpoint. Especially for S1, the ΔOC is very sensitive to the contract of exporting electricity.

In addition to the homeowner, use cases with S1 to S5 may also interest the DSO because of the interaction between their electric heat sources and the electric grid. Therefore, the 15-min averaged electricity peak load $P_{elec,im,HB}$ and $\Delta P_{elec,im,HB}$ were also calculated and grouped as shown in Fig. 8.

Due to the mismatch between the historical data of the day-ahead prices and the predicted electric demand of building models, the HB will even increase the $P_{elec,im,HB}$ in some use cases with S3. This exactly reveals the risk of applying this pricing strategy for DSO, because the low price might lead to unpredictable peak load. In use cases with S1 and S4, the HB could reduce the P_e more or less despite that the ΔP_e would be less than 0.3 kW. In use cases with S2, where the HB is specially used for shaving electric peak load, the HB brought a better performance of peak shaving (nearly 35% peak load reduction).

Specially, the homeowners can use the HB to reduce the peak load of importing heat from the DH system if they are connected. Based on the same design options mentioned in Appendix B and the operational strategy S6, the $P_{heat,im,HB}$ and $\Delta P_{heat,im,HB}$ were calculated.

Fig. 9 shows how the HB can influence the peak heat load if it is installed in a single house and operated upon S6. It can be seen that the HB can reduce the 15-min averaged electricity peak load $P_{heat,im,HB}$ by more than 1.5kW (because the maximum discharging power of the HB is 1.5kW) and make it less than 2kW in some extreme cases, although the reduction would be less than 0.5kW in some other cases. Hence, if the DH system operator adopts a pricing strategy that can stimulate the homeowner to manage the peak heat load, it will also be a valuable way for the homeowner to use the heat battery.

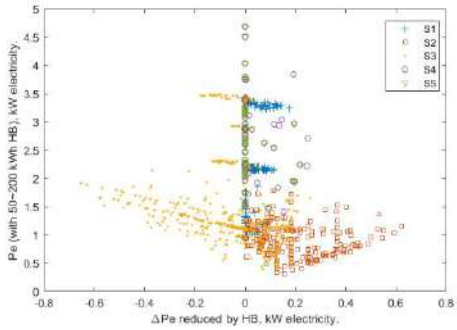

Fig. 8 - Scatter plot of the peak loads of importing electricity to houses with HBs ($P_{elec,im,HB}$) and the peak load reductions ($\Delta P_{elec,im,HB}$). The colors and shapes of dots distinguish the operational strategies from S1 to S5 **(the 'HOW').**

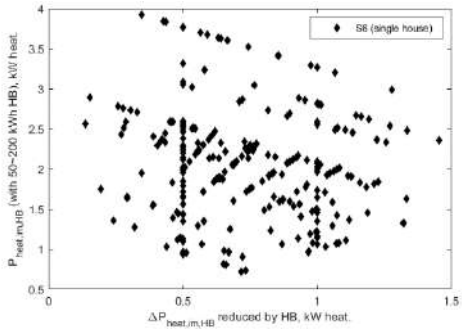

Fig. 9 - Scatter plot of the peak loads of importing heat from the DH system to a single house with HB ($P_{heat,im,HB}$) and the peak load reduction ($\Delta P_{heat,im,HB}$) in use cases with S6 **(the 'HOW').**

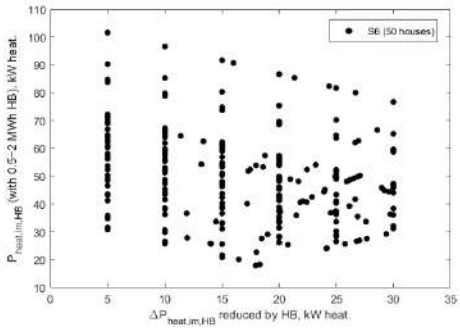

Fig. 10 - Scatter plot of the peak loads of supplying heat from the DH system with HB to 50 houses ($P_{heat,im,HB}$) and the peak load reduction ($\Delta P_{heat,im,HB}$) in use cases with S6 **(the 'HOW')**.

4.2 Predicted performance of use cases for DH system operator

Other than the decentralized heating systems mentioned above, the DH system operator is assumed to install the HB in their centralized heating system to reduce the peak load of supplying heat to

50 houses (assumed to have the same design). Based on a coincidence factor of 0.3, $P_{heat,im,HB}$ and $\Delta P_{heat,im,HB}$ were predicted.

Fig. 11 shows the predicted values of all use cases for the DH system operator. In this figure, some dots are clustered on specific values of $\Delta P_{heat,im,HB}$ (5kW, 10kW, 15kW, etc.) which are consistent with the values of the maximum discharging powers of different HB models. This reveals the importance of HB design parameters. Therefore, the values of $\Delta P_{heat,im,HB}$ should be grouped by the design options of both buildings and HBs for further analysis.

As shown in Fig. 11, studios and detached houses imply the higher potential of peak load reduction, and the box of terraced houses contains the highest value of $\Delta P_{heat,im,HB}$, as well. Althought the tiny houses do not reach the top boundary as the other building types, it still allows a peak reduction up to 25kW. But different from building type, the insulation level does not show any obvious impact on $\Delta P_{heat,im,HB}$.

As for the design of the HB, it can be seen from Fig. 11 that larger storage capacity can lead to larger $\Delta P_{heat,im,HB}$., especially from 1MWh to 2MWh. But the maximum discharging power of HB, however, shows different trends. In the boxplot of maximum discharging power, it can be seen that the values of $\Delta P_{heat,im,HB}$ cannot exceed the maximum limit of discharging power.

5. Discussion and conclusion

5.1 Promising use cases

This research defined three stakeholders in the use cases of the HB: the homeowner, DSO, and DH system operator. The homeowner and DH system operator can directly deploy the HB in their systems for performance improvement (reducing operational energy cost or shaving the peak heat load) while the DSO will pay attention to its influence on the peak electric load of the building.

Based on the proposed simulation approach, this research found that solar-related operational strategies (S1 and S4) will be more interesting than those for demand-side management (S2, S3) if the homeowner wants to use the HB to reduce the energy cost. And the reduction will be more obvious where the building has a higher heating demand and larger areas of PV or solar thermal collector. However, the potential of S1 will be limited when the contract of exporting electricity does not provide enough motivation for the self-consumption of PV-generated electricity (as is the case for all types of batteries). The HB also shows the ability to reduce the peak electric load when coupled with an electric heater (electric boiler or heat pump) in some cases, but it may also lead to a higher electric peak load when used with S3 if the fluctuation of the electricity price differs a lot with the electric demand profile of the building.

When using the HB for reducing the peak heat load, the DH system operator can expect a higher reduction by using HB in the neighborhood consisted of larger houses while apartments containing studios may also be interesting. In addition, the value of peak load reduction is sensitive to the maximum discharging power and the storage capacity of HB, so it would be necessary to optimize these two parameters during the design phase of the whole integration.

5.2 Limitation and future work

This research developed a screening approach in order to perform a fast screeing of all the potential use cases. The approach is able to analyze thousands of use cases in several minutes, however it also brings some limits and drawbacks. Firstly, the conceptual models of the energy system and the HB reduce the resolution of the simulation and may lead to distortion of the results. In addition, some detailed practical boundaries, e.g., indoor thermal comfort limits, were not considered in the models, because no data was fed back from the energy system model to the building model.

The promising use cases as identified by the screening approach will be studied in more detail in the future. This requires a more detailed HB model which will be implemented in the building performance simulation tool. In addition, the six operational strategies (S1-S6) will be refined and combined according to the specific design option and future scenario to explore a higher performance improvement by the HB.

6. Acknowledgment

This research has been supported by the project 9.4: development of closed-loop TCM system, which is part of the program 'Integrale Energietransitie Bestaande Bouw' (IEBB).

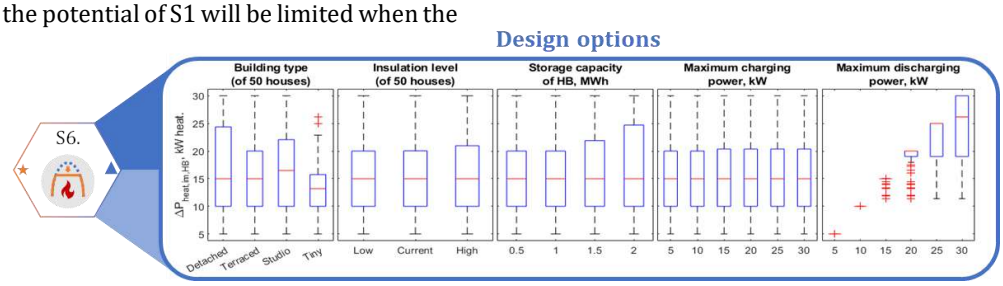

Fig. 11 - Boxplots of peak heat load reduction ($\Delta P_{heat,im,HB}$) with different design options **(the 'WHERE')** in all use cases with S6.

7. Appendices

Appendix A – Design options of energy system and related models.

Energy system designs		Input variables	Models	Output variables
Possible electricity source	Photovoltaic	Solar irradiance, kW/m^2; Area, m^2.	Module conversion efficiency; DC to AC conversion efficiency.	Electric power, kW.
	Electric grid	-	–	Electric power, kW.
Possible heat source	Solar thermal collector	Solar irradiance, kW/m^2; Outdoor air temperature, °c; Inlet temperature, °c; Area, m^2.	ISO efficiency equation [20].	Thermal power, kW.
	Electric boiler	Electric power, kW.	Heating seasonal performance factor (HSPF).	Thermal power, kW.
	Air-to-water heat pump	Electric power, kW.	HPSF.	Thermal power, kW.
	District heating system	-	-	Thermal power, kW.

Appendix B – Design options and occupant scenarios of building models.

Building designs	Possible options			
Building type (gross floor area, m^2)	Detached house (240) [21]	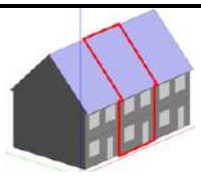 Mid-terraced house (135) [21]	Apartment studio(55) [21]	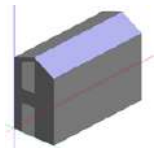 Tiny house (39) [22]
Insulation level (Rc value, K·m^2/W)	Low (Rc- roof = 2.5 Rc - wall = 2.5 Rc- ground floor = 2.5)	Current (Rc- roof = 6 Rc - wall = 4.5 Rc- ground floor = 3.5)	High (Rc- roof = 10 Rc - wall = 8.5 Rc- ground floor = 6)	
Occupancy pattern [23]	Working couple		Nuclear family	
Heating setpoints, °C	20°C		24°C	
DHW [24]	40L/person/day			

8. References

[1] Salpakari J, Lund P. Optimal and rule-based control strategies for energy flexibility in buildings with PV. Applied Energy 2016;161:425–36. https://doi.org/10.1016/j.apenergy.2015.10.036.

[2] Mohammadi Z, Hoes PJ, Hensen JLM. Simulation-based design optimization of houses with low grid dependency. Renewable Energy 2020;157:1185–202. https://doi.org/10.1016/j.renene.2020.04.157.

[3] Borri E, Zsembinszki G, Cabeza LF. Recent developments of thermal energy storage applications in the built environment: A bibliometric analysis and systematic review. Applied Thermal Engineering 2021;189:116666. https://doi.org/10.1016/j.applthermaleng.2021.116666.

[4] Lizana J, Chacartegui R, Barrios-Padura A, Valverde JM. Advances in thermal energy storage materials and their applications towards zero energy buildings: A critical review. Applied Energy 2017;203:219–39. https://doi.org/10.1016/j.apenergy.2017.06.008.

[5] Aydin D, Casey SP, Riffat S. The latest advancements on thermochemical heat storage systems. Renewable and Sustainable Energy Reviews 2015;41:356–67. https://doi.org/10.1016/j.rser.2014.08.054.

[6] Wu S, Zhou C, Doroodchi E, Moghtaderi B. Techno-economic analysis of an integrated liquid air and thermochemical energy storage system. Energy Conversion and Management 2020;205:112341. https://doi.org/10.1016/j.enconman.2019.112341.

[7] Hensen JLM, Loonen RCGM, Archontiki M, Kanellis M. Using building simulation for moving innovations across the “Valley of Death.” REHVA Journal 2015;52:58–62.

[8] Heat-Insyde. Heat battery introduction n.d. https://www.heat-insyde.eu/project/technologies/ (accessed October 19, 2021).

[9] EnergyPlus Weather Data by Country, All Regions - Europe (WMO Region 6) - Netherlands n.d. https://energyplus.net/weather-region/europe_wmo_region_6/NLD (accessed October 16, 2021).

[10] Hensen J. Application of modelling and simulation to HVAC systems. 1996:1–6.

[11] Xu L. Design Optimization of Seasonal Thermal Energy Storage Integrated District Heating and Cooling System. 2021.

[12] Finck C, Li R, Kramer R, Zeiler W. Quantifying demand flexibility of power-to-heat and thermal energy storage in the control of building heating systems. Applied Energy 2018;209:409–25. https://doi.org/10.1016/j.apenergy.2017.11.036.

[13] Papadopoulos V, Knockaert J, Develder C, Desmet J. Peak shaving through battery storage for low-voltage enterprises with peak demand pricing. Energies 2020;13:1–17. https://doi.org/10.3390/en13051183.

[14] Xu L, Torrens JI, Guo F, Yang X, Hensen JLM. Application of large underground seasonal thermal energy storage in district heating system: A model-based energy performance assessment of a pilot system in Chifeng, China. Applied Thermal Engineering 2018;137:319–28. https://doi.org/10.1016/j.applthermaleng.2018.03.047.

[15] González JM, Mulder M. Electrification of heating and transport; a scenario analysis for the Netherlands up to 2050. Centre for Energy Economics Research (CEER) Policy Papers 2, University of Groningen, The Netherlands 2018:1–3.

[16] From 2022, our electricity bill will be calculated differently: those who cause a power peak will pay more n.d. https://www.vrt.be/vrtnws/nl/2020/08/15/stroompiek-veroorzaken-meer-betalen/ (accessed October 19, 2021).

[17] Noord Pool day-ahead price n.d. https://www.nordpoolgroup.com/Market-data1/Dayahead/Area-Prices/nl/hourly/?view=table (accessed October 19, 2021).

[18] Hutty TD, Patel N, Dong S, Brown S. Can thermal storage assist with the electrification of heat through peak shaving? Energy Reports 2020;6:124–31. https://doi.org/10.1016/j.egyr.2020.03.006.

[19] Knoben RJW. Design optimization of the heating solution of a neighbourhood in Brainport Smart District – A simulation study using high-resolution occupant behaviour data. 2020.

[20] SRCC certification n.d. https://secure.solar-rating.org/Certification/Ratings/RatingsReport.aspx?device=7656&units=METRICS.

[21] BENG Reference Buildings n.d. https://www.rvo.nl/onderwerpen/duurzaam-ondernemen/gebouwen/wetten-en-regels/nieuwbouw/energieprestatie-beng/beng-gebouwtype/referentiegebouwen (accessed October 16, 2021).

[22] Heijmans-ONE n.d. https://www.heijmans.nl/nl/producten-diensten/woningbouw/woonproducten/heijmans-one/ (accessed October 16, 2021).

[23] Guerra-Santin O, Silvester S. Development of Dutch occupancy and heating profiles for building simulation. Building Research and Information 2017;45:396–413. https://doi.org/10.1080/09613218.2016.1160563.

[24] Kotireddy R, Hoes PJ, Hensen JLM. Towards Robust Low-Energy Houses -A Computational Approach for Performance Robustness Assessment using Scenario Analysis. vol. 212. 2018.

Experimental investigation of the contaminated volume around a person in a clean room

Julia Lange [a], Yunus Cetin [a], Martin Kriegel [a]

[a] Hermann-Rietschel-Institut, Chair of Energie, Comfort and Health in Buildings, Technische Universität Berlin, Germany, julia.lange@tu-berlin.de

Abstract. To monitor the particle concentration in a clean room, the measuring position is usually chosen based on a risk analysis and a monitoring plan. The demand zone is the area on the table, where the product is placed and where very clean air must be assured. Measuring the particle concentration in this working area is often difficult, as the measuring probe may obstruct the work flow. A situation that frequently occurs in a clean room is that of a person working at a work table. In this experimental investigation, the radial spread of particles, emitted by a dummy, is investigated. Particles are emitted from the proximity of the mouth region, with a source strength that is much higher than the normal particle emission of a human being when speaking. The aerosol distribution is measured with a laser particle counter at varying measuring positions. In the present case, the demand zone is defined as the area above the table in front of which the dummy is standing, 250 mm deep and 500 mm wide. Hot-wire anemometers are used to measure the velocity profile in the close-up range of the dummy. The influence of the distance between table and wall on the velocity and particle field is investigated, at varying inlet airflow velocities between 0.25 - 0.45 m/s. The results show that the table positioning has an influence on the flow velocities in the demand zone and that the table should be positioned in the room if possible.

Keywords: cleanroom, monitoring, unidirectional airflow, particle, anemometer.
DOI: https://doi.org/10.34641/clima.2022.204

1. Introduction

People create a buoyancy current in the area of which particles can be stirred up. The supply air velocity in the cleanroom must ensure that the buoyancy current is effectively prevented, as particles can spread in this area. The particles are representative of contaminants of various origins that are emitted by people, either through their clothing, skin or when they speak.

Starting from the person, a volume of contaminated air is created, which depends on the activity and clothing of the person, as well as on the positioning of the person in the room, the inflow speed and possibly other obstacles in the room for the air flow, such as a table. A model for calculating the radius of contaminated air around a cylindrical particle source can be found in [1]. At an inflow velocity of 0.25 m/s, the maximum radius of contaminated air is $R_{\max} = 750$ mm, at an inflow velocity of 0.45 m/s, it is $R_{\max} = 400$ mm. According to an experimental study by [2], the buoyant flow of people in rooms with vertical piston flow can be effectively suppressed from a supply air velocity of 0.25 m/s.

The human particle emission rate was investigated by several authors. According to [3], the human particle emission rate, is $PM_{5.0} \approx 66$ particles/sec, when speaking at normal volume, and it could be up to 570 particles/sec when speaking loudly [4].

The heat output of humans is 100 W when standing and performing light laboratory work. Activity increases the heat output and thus the buoyancy flow along the person. In order to safely prevent the human buoyancy current, cleanrooms are usually operated with a supply air velocity of 0.45 m/s. The aim of this study is to investigate the particle and velocity distribution around a dummy for different boundary conditions.

There are specific recommendations for the table height of workstations, but not for the specific positioning of tables in the cleanroom. The height of a standard work table should be between 650 - 850 mm if mainly sedentary activities are performed and the height can be extended up to 1250 mm if standing activities are still performed [5]. According to DIN EN 14644-4, a table in a clean room should not be placed directly against the wall, but at a certain distance from it. [6] However, the decision on the

Copyright ©2022 by the authors. This conference paper is published under a CC-BY-4.0 license.

selected distance lies with the operator. The recommentation according to the European Good Manufacturing Practice (GMP) is also very general, recommending "to ventilate production areas effectively with ventilation systems that are appropriate for the products handled there, the operations performed, and the external environment." [7] Therefore, two concrete table positions are to be investigated and their influence on the particle concentration in the requirement zone.

Cleanrooms with unidirectional airflow guarantee a very short residence time of airborne contamination. They are accompanied by a high air exchange rate and thus high energy consumption, but also meet the highest requirements for air quality. Concrete application cases for a person working at a table in a clean room with unidirectional airflow are packaging steps in the pharmaceutical industry or manual product inspections. The ventilation system assures a clean area in the demand zone on the table. Understanding the dynamic airflow distribution in this area helps to identify possible energy saving measures.

2. Research Methods

2.1 Experimental set-up

The experiments were performed in a cleanroom with vertical, unidirectional airflow, where the air change rate can be set of up to 540 times per hour. 16 Filter Fan Units (FFU) with terminal ultraclean U13 filters are mounted on the ceiling. A laminating mesh below the outlet ensures a very even flow. The air leaves the room through a perforated double floor, is filtered and fed back to the supply air. The floor space of the clean room is 4.8 x 4.8 m, the height is 3 m. A sketch of the test set-up is shown from above in **Fig. 1** and from aside in Fig. 2(a). The dummy was heated with an electrical power input of 100 W.

In the present case, the demand zone is defined as the area above the table in front of which the dummy is standing, 250 mm deep and 500 mm wide. The influence of the following aspects was investigated:

1. Table position: distance of the table from the wall
2. Supply air velocity

1. Table position

The table used was a common work table with a length of 1560 mm, a width of 780 mm and a height of 772 mm. There were two 2 options chosen for varying the distance Δx between the wall and the table:

(a) $\Delta x_1 = 15$ mm
(b) $\Delta x_2 = 900$ mm

First, the table was placed very close to the wall. And then a little further away, whereby the table was positioned at the 2nd position so that the dummy was centrally below a Filter Fan Unit (FFU) outlet. Both table positions are shown in **Fig. 1**. The dummy was positioned centrally below the FFU outlet.

2. Supply air velocity

The supply air velocity v_0 and the corresponding air change rate ACR were varied as follows:

v_0 (m/s) = 0.25 – 0.30 – 0.35 – 0.40 – 0.45
ACR (1/h) = 300 – 360 – 420 – 480 – 540

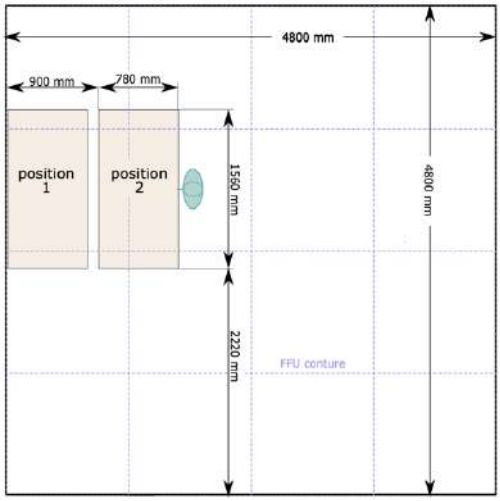

Fig. 1 - View from above: Test stand with a person standing at the table, for 2 different table positions.

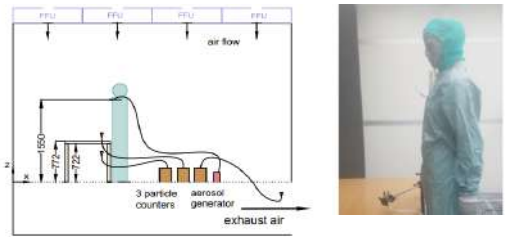

a) b)

Fig. 2 - a) View from aside: test stand with a dummy standing at the table, with the table-wall distance Δx_2=900 mm. b) Photo of the dummy.

2.2 Velocity measurements

In a first step, velocity measurements were carried out. Therefore, omnidirectional hot wire anemometers were used (type Schiltknecht ThermoAir 6). The measuring principle of this anemometer is based on a Negative Temperature Coefficient (NTC) resistance. The hot wire is heated to a constant excess temperature to ambient and the power required to maintain this temperature is measured. It measures the magnitude of the velocity in a range 0.01 – 1 m/s with an accuracy of $\pm$1,5% from the measured value at a room temperature of 22°C.

The supply air velocity was measured continuously centered below a FFU, 250 mm below the ceiling. The velocities around the dummy were measured at a height of 150 mm above the table, i.e. 922 mm from

the raised floor. The results of the velocity measurements were evaluated in Python, with the Tricontour function.

2.3 Particle countings

To investigate the distribution of particles, emitted by a dummy, Di-Ethyl-Hexyl-Sebacat (DEHS) particles were artificially generated using an aerosol generator (type Topas ATM 225). The aerosol outlet was positioned close to the breathing zone, 778 mm above the table surface. The aerosol outlet was located 60 mm from the dummy. The distance between the dummy and the table was 40 mm, and the aerosol was introduced at a horizontal distance of 20 mm from the edge of the table. The flow rate of the aerosol generator was 0.150 m³/h. The generated particles have a particle size distribution as shown in **Fig. 3**, with most particles generated at a size of 0.23 µm.

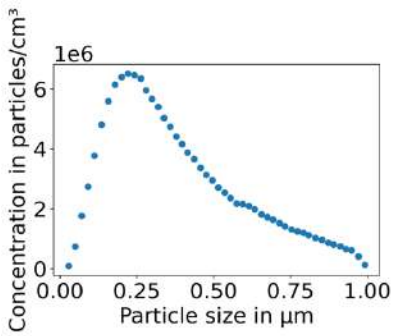

Fig. 3 – Generated particle size distribution [8]

The particle counts were performed with 3 mobile laser particle counters (type LDCP 5-10P0 from kmOptoelektronik).

There were two measuring points which were measured continuously, a position below the table and the concentration in the exhaust air. And there was a third measuring probe, whose position was varied at a height of 150 mm above the table. There were different distances to the aerosol outlet chosen, to detect the radial particle range as shown in **Fig. 4**.

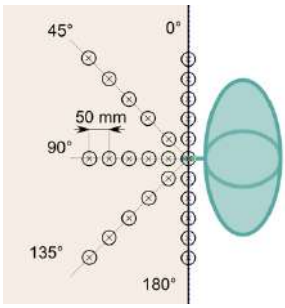

Fig. 4 - View from above: Scattered measuring positions for the particle countings above the table.

3. Results

3.1 Velocity measurements

The velocity field was measured at several points around the dummy at a height of 150 mm above the table, as shown in **Fig. 5**. In a) and b), the velocity fields are shown for the incoming velocities of 0.35 and 0.45 m/s at a table-wall distance of Δx_1= 15 mm. And in c) and d), the velocities are plotted for a distance of Δx_1= 900 mm. It can be seen in all 4 cases that the flow velocities decrease significantly towards the centre of the table. There, a stagnation area forms, where the flow velocity is about 1/3 of the inflow flow velocity and thus significantly lower. This is particularly clear frontally to the dummy. At the same time, there is an acceleration in the lateral direction of the dummy, along the edge of the table. The velocity gradient is stronger at the higher velocity of 0.45 m/s than at the lower velocity of 0.35 m/s. When the table is positioned more closely to the wall (Δx_1= 15 mm), the velocities are also lower in the immediate vicinity of the dummy and the velocity gradient to the side is more distinctive.

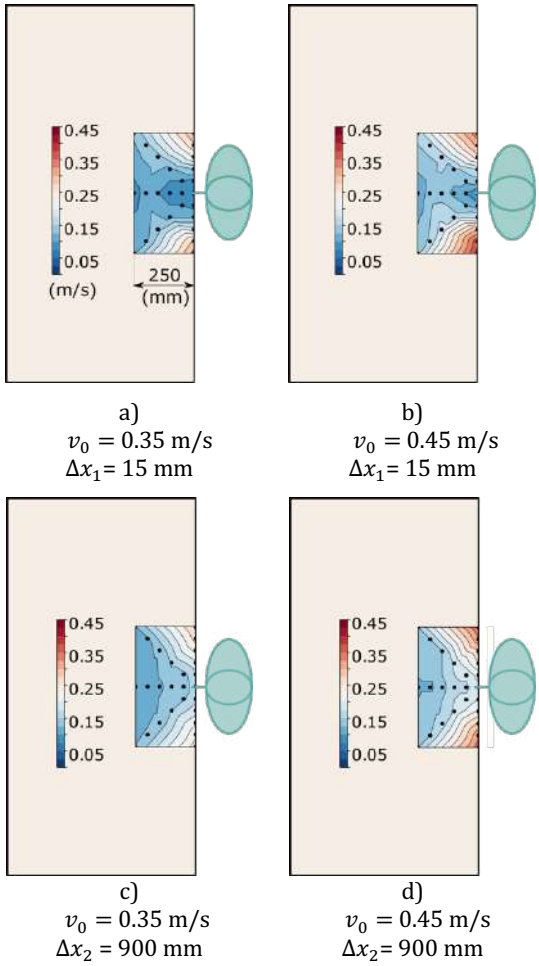

Fig. 5 - Flow velocities (in m/s) around the seated dummy at an incident flow velocity of a) v_0 = 0.35 m/s and b) v_0 = 0.45 m/s at a table-wall distance of Δx_1= 15 mm and c) v_0 = 0.35 m/s and d) v_0 = 0.45 m/s at a table-wall distance of Δx_2= 900 mm.

3.2 Particle countings

The particle counts examined how they spread radially from the aerosol outlet. The results are shown in **Fig. 6**. The following cases were investigated:

(a) grey: table close to wall ($\Delta x_1 = 15$ mm)
(b) orange: table inside room ($\Delta x_2 = 900$ mm)

The different colour gradations indicate the different velocities. The dots in the plot show the mean particle concentration as a function of the radial, horizontal distance of the measuring probe to the position of the aerosol outlet. The lower the incident flow velocity, the higher the concentration close to the dummy. This applies to both cases, whether the table is close to the dummy or it is positioned in the middle of the room.

If the table is close to the wall, the black markers, at the speed of 0.45 m/s the concentration is also very low even close to the dummy. This striking influence of the flow velocity is less pronounced when the table is positioned in the room, the orange markers. Here the concentration close to the dummy is in a similar range for all air velocities. With increasing distance from the aerosol outlet, the velocity decreases, especially strongly at the high air velocity of 0.45 m/s.

For this study, particle counts were conducted at various intervals between 70 mm - 450 mm. The results of the particle counting were grouped as follows: they are grouped into the 4 quantiles of the distance from the aerosol outlet. At the 1st point at approx. 150 mm, the mean value of the measured values of the 1st quantile (<=25%) is thus plotted. At the 2nd point, at 255 mm the mean values of the 2nd quantile (<= 50%) are plotted. At the 3rd point, at 357 mm radial distance the mean values of the 3rd quantile (> 50% and <= 75%) are plotted and at the last point at 426 mm distance the results of the 4th quantile (> 75% and <= 100%) are plotted.

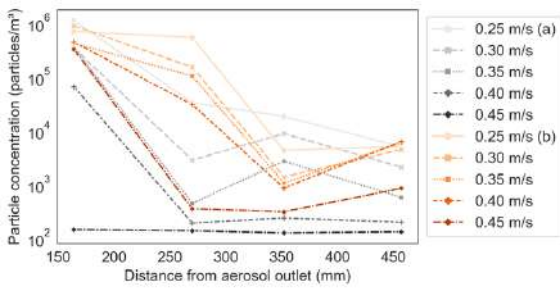

Fig. 6 - Measured mean particle concentrations at different distances between the measuring position and the aerosol outlet. The grey markers indicate that the table was positioned close to the wall (a), $\Delta x = 15$ mm, the orange markers indicate a wider distance (b), $\Delta x = 900$ mm.

2. Discussion

The measurements of the air velocity show that there is a stagnation area of the flow above the table. The air velocity decreases significantly towards the centre of the table and this occurs already a few centimetres from the edge of the table. When the flow velocity is increased from 0.35 m/s to 0.45 m/s, this stagnation area is weaker, as the air velocity in the requirement zone is higher overall.

There are several reasons for this. First of all, there are two currents which act in opposite directions. The buoyant flow, caused by heat near the dummy and the desired downward flow, caused by the FFU. At the higher speed of 0.45 m/s, the buoyant flow is clearly prevented and there is a smaller area where the flow is impaired.

Second, there is a loss of momentum in the vertical direction, when the supply air propagates to the surface of the table. This is expected to happen earlier at lower supply air velocities and we measure lower velocity magnitudes over the table at 0.35 m/s compared to 0.45 m/s.

If the table is positioned in the middle of the room instead of directly against the wall, the stagnation area is also smaller. This could be due to the fact that there is better air exchange to all sides of the table. The vertical air movement downwards is thus not additionally impaired by the vertical room wall.

In the radial dispersion of the particles, it can be seen that at low air velocities (0.25 - 0.30 m/s) the particles disperse in high concentrations, up to a distance of about 275 mm. After that, the concentration up to a distance of 450 mm is about 1/100 of the value in the close-up area around the aerosol outlet.

When positioning the table on the wall (black markers), it was noticeable that the measured particle concentration at the speed of 0.45 m/s was very low for all distances. For lower speeds, the overall particle concentration decreases less with increasing distance from the aerosol outlet. This is consistent with the velocity measurements, as here too the stagnation area is more pronounced than when the table is positioned in the room.

When the table was positioned in the centre of the room, the concentration in the vicinity of the aerosol outlet was quite as high as at the lower air velocities, but then dropped more sharply to 1/1000 of the initial concentration, from a distance of approximately 350 mm on.

3. Conclusions

Overall, the results show that the stagnation area is more pronounced when the table is positioned against the wall. It is therefore recommended to position the table with some distance to the wall in the cleanroom. This way, the buoyancy volume flow of the human is better suppressed and the particle concentration in the requirement zone is lower. The

flow velocity should be at least 0.35 m/s so that the emitted particles only reach the requirement zone in low concentration. It can therefore be seen that a very small distance between the table and the wall of 15 mm is not sufficient to prevent a backflow of the flow above the table. the selected minimum distance between the table and the wall, according to the recommendation of DIN EN 14644-4, should therefore be significantly greater and better in the range of 900 mm.

4. Acknowledgements

We would like to thank the Federal Ministry for Economic Affairs and Energy for supporting this study (funding code 03ET1604).

5. References

[1] Valeria Hofer. Zum kontaminierten Raumvolumen von Partikel-und Wärmequellen in laminarer Verdrängungsströmung. PhD-Thesis, Technische Universität Berlin, 2019, doi: 10.14279/depositonce-8642.

[2] Peter V. Nielsen. Control of airborne infectious diseases in ventilated spaces. Journal of the Royal society interface. 2009; 6: 747–755. doi: 10.1098/rsif.2009.0228.focus.

[3] D. Mürbe and M. Kriegel and J. Lange *et al*. Aerosol emission in professional singing of classical music. Sci Rep 11, 14861 (2021). doi: 10.1038/s41598-021-93281-x

[4] M. Alsved and A. Matamis and R. Bohlin *et al*. Exhaled respiratory particles during singing and talking. Aerosol Science and Technology 54, 11 (2020). doi: 10.1080/02786826.2020.1812502

[5] DIN EN 527-1: 2011. Office furniture - Work tables and desks - Part 1: Dimensions; German version EN 527-1:2011.

[6] DIN EN ISO 14644-4. Cleanrooms and associated controlled environments - Part 4: Design, construction and start up; German version EN ISO 14644-4:2001.

[7] European Comission, EU Guidelines for Good Manufacturing Practice for Medicinal Products for Human and Veterinary Use. Part 1. Chapter 3: Premises and Equipment, 3.12, url: https://ec.europa.eu/health/sites/default/files/files/eudralex/vol-4/chapter_3.pdf

[8] Topas GmbH. Manual: Atomizer aerosol generator ATM 226. 2015. URL: https://www.topas-gmbh.de/en/produkte/atm-226/

a.The datasets generated during and/or analysed during the current study are available in the DepositOnce repository, http://dx.doi.org/10.14279/depositonce-15371

Designed vs. Actual Occupant Behaviour in Buildings – A Historical Perspective

Zsófia Deme Bélafi [a]

[a] Department of Building Services and Process Engineering, Faculty of Mechanical Engineering, Budapest University of Technology and Economics, Budapest, Hungary, deme@epgep.bme.hu

Abstract. Energy efficiency and actual energy use in buildings depend on various factors. As building technology, construction quality, climate representation, advanced design tools and other non-human-related aspects are under scientific investigation and development for many decades, energy consumption in buildings started to decrease and reached a certain level. However, the desired net zero or even net positive energy consumption levels are far from reality yet in many cases. It was found that there is an essential component which is still underestimated and little researched: humans. Without understanding and appropriately representing building occupants and their needs in the design process, it seems impossible to estimate real, in-use energy consumption levels. In the 2nd half of the 20th century, occupant needs and behaviour were in the centre of many design cases. For example, prefabricated concrete block apartment buildings that were mass-produced in the Soviet era in Eastern Europe. These residential units were designed to fit the era's occupants in all aspects. The purpose of the rigorous design process was to make sure that the mass-produced buildings will fit well the families moving in. Somewhat differently, today our goal in occupant-centric design is to improve energy efficiency and to make sure that occupants have a comfortable and easy-to-use space to live or work. However, the results and methods applied by our ancestors should be examined and from many aspects their rigorous occupant-investigations can teach us a lot and can improve our practices today. This paper analyses the process of module-design of the 50-60's and their resulting apartment and occupant type "templates" using documents of the era and interviews with designers and other participants of that process and highlights the parts that are adaptable to today's design practices.

Keywords. Occupant behaviour, occupant-centric design, personas, history of design
DOI: https://doi.org/10.34641/clima.2022.57

1. Introduction and literature review

It is now accepted in the research community that occupant behavior can play an important role in building performance and it should be considered when designing a building and developing simulations [1]. Occupant behavior needs to be investigated and appropriately represented in research on the building life cycle as it is critical in achieving the goal of low or nearly zero energy (nZEB) buildings [2].

This paper contains the findings of a research focusing on three different aspects of occupant behaviour research: occupant types (personas), occupant-centric design methods and the influence of occupant behaviour in a specific historical era (1945-1960) in Hungary. In later sections, these concepts are introduced and then historical findings are presented which may be relevant to today's experts of the area of occupant behaviour in buildings.

1.1 personas

There is a new method applied in occupant-centric design projects where instead of using one single "standard" occupant (and its presence, needs and behaviour) developed by designers or relying on standards and guidelines, designers build up types of occupants or personas to represent different groups of occupants during simulations and design decision-making [3]. Occupants can be grouped together based on various aspects depending on the actual design context and level of detail.

A study [4] determined categories based on indoor environmental quality (IEQ) perceptions and attitudes: the ones who are satisfied with their indoor environments, the ones who complain about indoor noise, and the ones who are bothered by indoor air and temperature. Hong et al. used personality traits linked to occupant actions to determine 6 types of patterns: average, reserved,

Copyright ©2022 by the authors. This conference paper is published under a CC-BY-4.0 license.

environmentally friendly, role model, self-centered, and mechanist [5].

Ortiz et al. has built up residential archetypes: Restrained Conventionals, Incautious Realists, Positive Savers, Sensitive Wasters, and Vulnerable Pessimists. Their attitudes could be connected to energy use behaviour [6].

Czétány et al. analysed residential smart meter data using clustering to examine daily electricity use profiles of household types. 3 different clusters were built: 1 is even throughout the days, 2 have morning and evening peaks in different types and magnitude. Also, settlement types were investigated and they had some influence on the daily user profiles. Village-meters showed an earlier afternoon peak and highest morning peak compared to those in towns and cities. However, the consumption data do not support the belief that people would rise significantly earlier in villages compared to towns and cities. Regarding building types (condominiums, old and new single-family houses), no significant differences were found in daily consumption profiles [7].

Another study has created lighting preference profiles: users can be profiled based on their control behaviour, regarding characteristics as activeness, dominance, lighting tolerance, and dimming level preference [8].

The use of personas can be beneficial in many phases of the life cycle of a building. Starting at the early conceptual design phases, where architects are supported by more specific needs and occupant scenarios when deciding on spatial distribution. Then, during detailed design, comfort and performance models and simulations can be made more precise with the additional information on user diversity. Also, in the post-occupancy phase, they can be used for in-use model calibration and for fine-tuning building automation systems.

The main question of the application of personas is the data availability and the methods of building up these occupant types. It is often an obstacle that future occupants are unknown or there is a lack of data available on them. However, it is not always necessary to build up large databases and creating "new" archetypes of occupants. This paper introduces occupant types used in the past showing that it might be beneficial to look back and search for earlier "personas" to enrich our today's knowledgebase.

1.2 occupant-centric design methods

There is a new tendency in the research area of building design methods that argues that a more occupant-centric design approach is needed. [9] Not only the physical needs and presence of a human should be considered during the course of design but they should be captured in whole, as a coherent part of a physical and a social environment.

Horayangkura states that this movement for a more social and environmental approach in building design dates back to 1969 to a meeting of the Environmental Design Research Association. Back then a more technical approach was accepted in the early design phases [10]. Eversince an enormous body of research was conducted both in human sciences and environmental design. Social design practitioners have played vital roles in matching behaviour, spatial design and other building settings to improve the habitability of the built environment. In 1997, the idea of the "social cushion" emerged which argues that every individual exists in a social context of a given culture and the physical environment is "lost" as a separate reality [10]. Although the social cushioning effect sounds to be only an abstract idea, but it is certain that individuals in a building should be considered during the life-cycle of a building not only with physical factors but also with psychological, social and contextual variables.

Some research studies have been already conducted to capture the extent of the match, how a designer managed to match the real essence and needs of its future occupant. Azar et al. found many studies using space-use efficiency metrics to describe if a designed space is used as intended in reality [9]. These metrics can be an appropriate indicator whether the designer managed to find the ideal space-distribution for future occupants. These metrics mentioned in the study cited above are mostly used for the office context but in the future they could be extended for residential settings as well.

In the framework of this research, early examples are introduced from Hungary where designers tried to abstract and capture their future occupants not only in a traditional way but using unusual techniques such as wardrobe element counting or detailed household type picturing. Later, residents of the earliest experimental housing estates reflected on their success which may serve with lessons learnt for today's scientists and designers as well.

1.3 influencing occupant behaviour

In many cases, scientific evidence shows that actual residential energy use may significantly differ from modelled assumptions [11] [12]. Byrne argues that everyday practices of occupants should be considered when residential energy use variations are investigated [13]. It has been demonstrated that changing occupant behaviour alone can achieve significant energy savings [14] [12].

As scientists and designers have acknowledged the potential in residential behaviour change, many approaches were developed to do so. Modifying occupant practices and everyday life is an approach to influencing household energy demand. This approach posits that energy use is mainly affected by practice or by how a certain activity is carried out. Practices in turn are the result of habits, knowledge

(skills, competence), motivations (image, meaning) and technology (stuff, material)[15] [16] [17].

Another approach to affect behaviour has been through influencing attitudes [18], providing information and social norms and delivering feedback [13]. However, such top-down approaches were heavily criticised arguing that intrinsic motivation and needs should be always taken into consideration to have significant impact on someone's behaviour [19]. Another approach for providing feedback for behaviour change is when technologies such as smart metering and in-home are used to deliver feedback to households and make them more aware of their own energy use [20] [21]. However, this is claimed to have only short-term effects in most cases [19] [22].

It can be seen that changing and influencing an occupant's behaviour in a building has been a hot topic recently. It raises not only ethical, cultural and psychological questions but there are doubts about the efficiency of these measures also.

This paper introduces the idea of a top-down behaviour change attempt in the post-war era of Hungary when the state initiated the change and "improvement" of occupants' apartment use and the overall way of living of the people. Later some evidence of the failure of this approach are introduced.

1.4 historical context

In 1946, Gádoros has evaluated the post-war number and condition of residential rooms in Budapest [23]. The SUM of rooms was 481 280 out of which 5.4% was destroyed, 18.4% was damaged but restorable. He calculated that with the current average 3-year apartment building rate (110 000/3 yrs), it is impossible to supply citizens with an appropriate number of apartments (destroyed or severely damaged and new needs: 230 000/3 yrs). He concludes that a completely new housing strategy is needed with "optimized" needs and argues that the pre-war upper-class large apartments do not suit the needs of modern residents. He and Kismarty-Lechner were contracted by two architect members of the Communist Party to work out a concept for reforming housing in Hungary. Their concept is introduced in section 3 in detail.

They formulate their goal as follows: "It is the task of our era to equalize and eliminate class differences in society" [24]. "We fully drew the case of new apartment building under common care, direction and control" [24] Kismarty-Lechner sets the foundations of the ideal apartment design and distribution system in Hungary in 1947. He states (representing architects of the era) that income levels should never decide the type and size of apartments of anyone. Rather occupant number, habits and profession should be the determining factors.

At the beginning of the 50s, the first 5-year economic plan was announced in Hungary stating that residents will be provided with +50% raise in the standard of living country-wide compared to the era before world war II [25]. In 1954, the 2-year programme of apartment type development was launched by the Ministry of Construction [26]. This was the first step of the period where the layouts of mass-produced concrete apartment block buildings were designed.

In 1955, Csordás states that class-differences in society should be gradually eliminated. Bigger and better apartments should not be the privilege of upper classes. [26] The only factors influencing the type of apartment of a household should be the number of people living in the apartment, user habits and profession of occupants (resembling the ideas of 1947 above).

Reischl wrote a chapter in Fórizs's book about the ideal solution for the apartment supply crisis in 1958 [27]. At that time, 237 persons were living in 100 rooms in Budapest on average and 267 outside of it in Hungary. He compared this situation to 1955 levels which was 170 persons in Hungary and 73 in Switzerland, 120 in the Federal Republic of Germany. Therefore, he draws attention to the urgency of the housing problem in the country as well and reinforces the socialism's principle: "if the needs of the working population were fulfilled entirely, also the production levels of the country will rise".

1.5 aim of research

The historical context explains the specific problem of the era. From it, it can be seen how eager the era's designers might have been to find optimal solutions fitting the needs of residents as urgently as possible. The aim of this research is to find out what we can learn from this historic era, from our ancestors which can support today's occupant-centric design and occupant behaviour research professionals.

2. Methodology

1945-1958 literature was scanned focusing on the design, construction and post-occupancy evaluation of the first soviet-type mass-produced apartment buildings in Hungary. Architectural journal archives are available in an online collection called Arcanum [28]. Relevant books and ministry-issued publications could be found in Széchenyi National Library in Hungary. Transcripts of interviews with designers of the era and also with residents of the first experimental housing estate were available in the Oral History Archive of the 1956 Institute in Hungary [29].

The literature review focused on personas, occupant-centric design methods and influence on occupant behaviour in the post-war architectural discussions and the process of the apartment-types development of the new mass-produced housing estates (later on

constructed from 1958 to 1986). This was followed by interviews with experts of the field of societal history of the era and prefabricated concrete block building construction and energy-related behaviour.

3. Results

The very first concept for formulating the apartment types fitting all households was introduced in 1947. Kismarty-Lechner determined 5 apartment types based on the initial idealistic set of requirements: [24]

A. 1 person – 1 room + cooking chamber
B. 2 persons – 1-2 rooms + cooking chamber + dining area
C. 2 persons – 1-2 rooms + kitchen with storage+ dining chamber + bathroom
D. 4 persons – 2 rooms + kitchen with storage + dining room + bathroom
E. 6 persons – 3 rooms + kitchen with storage + dining room + bathroom

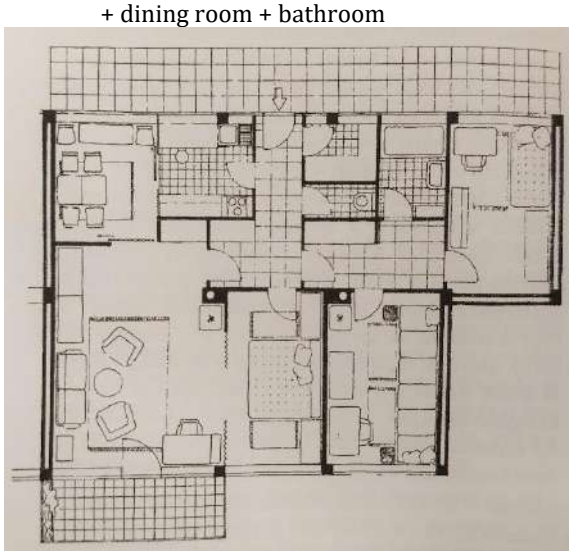

Fig. 1 – Template apartment design for 6 persons. [24]

(Families with more than 4 children should move to a single family house.) Apartment types A and B were to assign to young either single persons or freshly married but in any case they should be separated into different buildings from families with children to avoid conflicts. It is also mentioned that there is a tendency that only a few wives have in-home assistance, therefore designers should support their work in the kitchen and dining area with more efficient kitchen layout design and furniture prototypes.

3.1 personas

Later apartment type concepts put more focus on the specific types of residents based on profession and everyday habits. Csordás states that there are 5 types of professions where separate characteristics and living needs can be determined in the following aspects: wives working or not; children at home or in children's institutions; number of staying at home and night-shift working household members; furniture possession and needs; food purchasing and storing habits; heating options; intellectual work at home; social life needs and habits; culture of living: [26]

UNSKILLED WORKERS: low salary, workers who are traditionally used to village-life;

MINERS: occurring in very specific regions, also used to traditional village housing culture;

INDUSTRIAL and TRANSPORTATION WORKERS: mainly living in housing estates in larger towns, cities and in Budapest;

STATE ADMINISTRATION, COMMERCE EMPLOYEES; INTELLECTUALS.

He argues that the other determining factor of assigning a given apartment type to a family is the total number of people in the household. [26]

Reischl established 4 specific types of personas based on the profession of the head of the family in 1958: [27]

FARMER: entire family works, rests, eats at the same time; work place is around the house; self-sustaining household; low fuel stock; local traditions are important; usually lives in villages with no electricity, water or sewage utility service.

MINER: family works in different shifts; eats, rests at different times; wants to spend as much time outdoors as possible; gardening, backyard poultry; high level of fuel stock (as a benefit from coal mines); miner towns equipped with electricity and water service but not sewage; more salary earned by hard work therefore can afford enjoy miner town benefits (childcare, minerclubs).

INDUSTRIAL WORKER: "each family member (even women) demand the conditions of an independent life"; women work and earn, housework is shared; everyone eat outside at the factory or school; homes are equipped with electricity, water and sewage utility services, sometimes even natural gas for central heating and hot water; family enjoys "city-life services".

INTELLECTUAL: very similar to category industrial worker but family members work at home as well.

Tab. 1 – Apartment design needs of profession-based personas in 1958.

	Farmer	Miner	Industrial worker	Intellectual
Rooms	1-2, not separat	Separated[1]	Separated[2]	Separate

[1] Heating can be controlled in each room if occupied at different times.

[2] Equipped with bed, wardrobe and a reading area as a minimum.

	ed			d[3]
Kitchen	In room	Yes, large	Yes, small	Yes, small
Bathroom	No[4]	Yes[5]	Yes, with washing machine	Yes, with washing machine
Storage	8-14 m^2	coal storage + 4-5 m^2	1 m^2 [6]	1 m^2 [7]
Work room	No	No	No	Yes, for every working family member

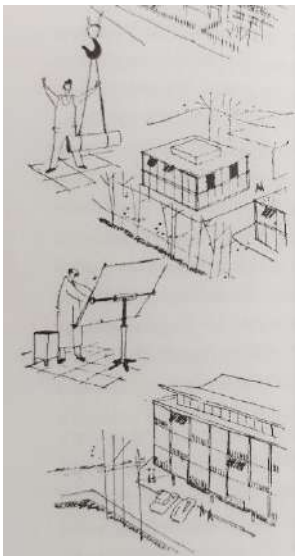

Fig. 1 – Vision for ideal living conditions for different occupantions. [27]

3.2 occupant-centric design methods

Kaesz states in the foreword of Gádoros's book from 1946 that "today's architect should be the organizer of measures and sizes where the human body should be the base" [23]. He refers to Adolf G. Schneck and Ernst Neufert who established the size and measure system for building and furniture design between the two world wars. However, he states that it needs to be supervised and actual minimum space needs should be determined based on an "average resident with average needs" and amount of belongings.
Gádoros made an exhaustive list of belongings of a man (34 types of clothing items – e.g. 2 winter and 2 summer suits, 4 pijamas, 12 shirts, etc.; 14 types of other items – e.g. 2 hats, 2 black shoes, 2 brown shoes, 6 towels, etc.), a woman, a 3-6 and a 6-12 years old child and for an infant. He collected the items of a kitchen as well and then produced exact sizes for kitchen cabinets and wardrobes and all other furniture based on the size of these average people and their belongings.
Reischl states in 1958 [27] that all apartments should fulfil the general needs of the family members (protection[8], bathing, visitors, cooking). Then a given template apartment design should reflect the profession and family structure of the residents. Architects are suggested design layouts and furniture of the template apartments to follow the personas developed by the author and introduced in section 3.1 of this paper.
The results and overall acceptance of this "space minimization" program can be seen in the interviews with residents of the first Experimental housing Estate in Óbuda, Budapest (built in 1958) [30]. Residents complain that everything in the apartments are extremely small and narrow, especially bathrooms and kitchen. The idealistic kitchen cabinets were not deep enough to fit the era's standard cooking pot.

3.3 influencing occupant behaviour

In the post-war socialist housing concept, the theory was that to achieve an "ideal society", "ideal apartments" should be provided which were designed based on "good and correct" (approved by the state) principles. [31] Also, the primary intention was to "determine, improve and reform" the residents' way of living, habits and overall use of their apartments especially from 1945-1950 and from 1955. [31]

Several examples were found in the framework of this research where either the Ministry of Health, or other government-hired architects formulate recommendations on the use of the apartments and behaviour and lifestyles of residents.

The Ministry of Health issued two publications in 1951 which contained several detailed recommendations on the healthy use of an apartment and tried to prescribe the use of an apartment and occupants' behaviour: [25][32]

- **External surfaces and heating:** low conductivity, waterproof, soundproof, no moisture inside. Assimetric radiant temperatures should be avoided (cold, wet walls and hot stoves) to avoid sicknesses. [25] External wall and floor surfaces should be kept at room temperature, a maximum of 2-3^{0}C air temperature difference is allowed between a person's head and the floor. Stove surface temperature should be below 70-80^{0}C to avoid burning house dust on surface. Heating should be controlled easily and working efficiently. It is important to find the best location of the stove in the apartment. Central heating systems are the best solutions but still mostly unavailable

[3] Equipped with bed, wardrobe and a reading area as a minimum.
[4] Until no water and sewage utility service is available.
[5] WC separately
[6] Family does daily shopping in the city.
[7] Family does daily shopping in the city.
[8] Also referring to heat and sound insulation and heat storage capacity of building structures.

and expensive [25]. Indoor air temperature should be between 18-20^{0}C during winter [32].

- **Artificial lighting:** electric bulbs are suggested (not candles or gas-fired lights to avoid air contamination [32]) with even distribution, no glare and with blue/yellow white colour [25].
- **Ventilation:** intermittent cross-ventilation: either door+opposite window opened for 3 minutes or opposite windows opened for 5 minutes 3 times a day and windows should be opened any time an odour can be smelled [25]. Another publication proposes 5-10 minutes window opening per day for winter period and 20-30 minutes for summer [32]. Also stating that extra humidity should not be released in living- or bedrooms from washing, drying or cooking.

Reischl states in 1958 that an apartment is a place where a resident rests, studies, meets culture and starts a new family [27]. He argues that the housing condition of wide social classes determines the "level of culture of the population". Seemingly, architects of the era were committed that with providing modern and "better" apartments for a large percentage of people, they can influence their everyday life habits and the affinity to culture.

At the time of the first apartment template design efforts, literature on how to use "appropriately" a small apartment started to appear. In Gyarmati's book, clear guidance is given how to use a small place for different purposes in different times (e.g. a room for rest, visitors, dining) with practical furniture and room separation tricks (sliding doors, curtains). [33]

Pataki gives specific recommendations about heating setpoint temperatures and heating methods for working women in 1956. [34] Desired heating setpoint of an apartment should be 18-20^{0}C, not lower during the nights and not higher to avoid sicknesses. Halls, other ancillary rooms should be kept at 15-16^{0}C, whereas bathrooms should have a temperature of 20-22^{0}C. Right before the chapters on clothes moths and indoor flowers, a very detailed typology and user manual is given on iron stoves, co-fired boilers with 1 or 2 chambers and filling holes. Pataki also argues that "the ancestors' standpoint on women' role in the household should be eliminated" thus suggesting a lifestyle change and promoting the equal share of housework at home.

In the interviews with residents of the first Experimental housing Estate in Óbuda, Budapest (built in 1958), also some feedback can be found on the apartment-use recommendations of the era [30]. For example even though central heating was built in most of the apartments, residents tend to disconnect from it as usually a landlord was responsible to heat it up manually many times during the day and it usually happened only once or twice a day which made it extremely uncomfortable. Many interviewees mentioned the semi-permanent tricks of taking out built-in furniture or reorganizing spaces because they could not use the apartments "as intended". Many times, residents moved in the apartments with much more furniture that could be placed in the new apartment comfortably. Some residents managed to get a washing machine which was a rarity in that era and put it in the middle of the bathroom as nowhere else could fit and lived their life tiptoeing around it for decades.

4. Discussion and Conclusions

Based on the findings of this research regarding residential personas, it was interesting to see what were the parameters which determined a given occupant type's characteristics. Nowadays, in occupant-centric and environmental design processes, experts categorize occupants based on IEQ perceptions, attitudes, environmental control usage, settlement or building types. Whereas back in the post-war era of Hungary, designers established occupant categories based on household size, profession, home occupancy, lifestyle and culture of living aspects. The question here really is which parameters describe the best an occupant's characteristics and expected behaviour in which context and phase of a building's life-cycle. To answer this question, more research has to be done to connect social, cultural, psychological parameters to indoor comfort and energy-use behaviour.

Based on the results of the occupant-centric design investigations of the era, two issues can be further concluded. Firstly, that the previously developed space-use efficiency metrics could be interpreted for a residential setting in the future as in the framework of this historical experiments, evidence was shown that in many design cases post-occupancy feedback is available on space-use as well. And it can provide a valuable "feedback loop" for original designers improving their design practices for the future.

Weakness of the template design methodologies introduced in this paper lies in the lack of references to the methods applied to collect information on the actual layers and state of demographical layers in the country. According to conference transcripts of the era and interviews with experts of this period, it seems that architects were considered to have enough experience and expertise about these issues based on their multiple design projects and life experience. This is of course a very strange concept with today's eyes but supposedly no one questioned their authority on this matter. There is some literature on the idea of architects being the engineers of the society. [35][36] This of course raises the question of the role of an architect in the design process but this is outside of the scope of this paper. However, it explains why this research has not found any kind of record of involvement of social scientists or other experts into the template apartment design process of this era.

It has to be noted that even though some apartments were designed and built following the principles developed in the era introduced, in many cases the

occupant selection and the apartment-assignment process was not working ideally. These apartments were assigned to applicants based on a credit system by housing committees. Late post-occupancy interviews (after regime change) revealed some irregularities of the system. Therefore, when an occupant states that the apartment design did not fit his/her actual needs, it does not necessarily imply that the design itself was poor but sometimes it was the lack of consistency of the system (e.g. miners moving into apartments designed for intellectuals or villagers moved into small housing estate studios). At the same time, the most important question arising from this very specific design case remains what metrics and parameters could be used to evaluate the post-occupancy "goodness" and usability of a building's design which might teach a lesson for designers for the future.

Also, Keller states that often architects and designers developing template apartments had to represent the state's principles to some extent [30]. Applying these template designs were obligatory for state-financed or co-financed new housing estates which made up a significant share (40-50% between 1950-60) of all new apartment buildings in Hungary. This significant influence coming from the state shows that the template designs were predestined to unfit future occupants to a certain level shown in the post-occupancy interviews by residents.

Regarding the intention to change residents' way of living, the post-occupancy interviews also show that the theoretical methods did not work out well in practise. Current research also suggests the weakness of such top-down approaches. Interestingly, the recommendations by the Ministry of Health introduced above contained information on thermal comfort and indoor environmental quality which implies that the state's primary intention with changing behaviour was not only using the new apartment types with minimized floor areas efficiently but also to improve comfort levels of the occupants.

This paper introduced historical findings from one specific era and country focusing on three aspects of the occupant behaviour research area. In the future, it would be beneficial to do the same exercise focusing on different periods of time, different regions and also different design problems in different geo-political contexts. Author believes that such future research projects using a historical approach might add to our current knowledgebase on the role of occupants in building design.

5. Acknowledgement

This paper was supported by the János Bolyai Research Scholarship of the Hungarian Academy of Sciences.

Data access statement: data sharing not applicable to this article as no datasets were generated or analysed during the current study.

6. References

[1] S. D'Oca, T. Hong, J. Langevin, The human dimensions of energy use in buildings: A review, Renew. Sustain. Energy Rev. 81 (2018) 731–742. doi:10.1016/j.rser.2017.08.019.

[2] H. Chandra, T. Hong, C. Andrews, An ontology to represent synthetic building occupant characteristics and behavior, Autom. Constr. 125 (2021) 103621. doi:10.1016/j.autcon.2021.103621.

[3] P. Agee, X. Gao, F. Paige, A.P. Mccoy, B.M. Kleiner, A human-centred approach to smart housing, Build. Res. Inf. 49 (2021) 84–99.

[4] D. Hyun, D.H. Kim, P.M. Bluyssen, Clustering of office workers from the OFFICAIR study in The Netherlands based on their self-reported health and comfort, Build. Environ. 176 (2020) 106860. doi:10.1016/j.buildenv.2020.106860.

[5] T. Hong, C. Chen, Z. Wang, X. Xu, Linking Human-Building Interactions in Shared Offices with Personality Traits, Build. Environ. 170 (2020) 106602. doi:10.1016/j.buildenv.2019.106602.

[6] M.A. Ortiz, D.H. Kim, P.M. Bluyssen, Substantiation of home occupant archetypes with the use of generative techniques : analysis and results of focus groups, Intell. Build. Int. https://do (2020). doi:10.1080/17508975.2020.1747381.

[7] L. Czétány, V. Vámos, M. Horváth, Z. Szalay, A. Mota-babiloni, Development of electricity consumption profiles of residential buildings based on smart meter data clustering, Energy Build. 252 (2021). doi:10.1016/j.enbuild.2021.111376.

[8] M. Despenic, S. Chraibi, T. Lashina, A. Rosemann, Lighting preference profiles of users in an open office environment, Build. Environ. 116 (2021) 89–107. doi:10.1016/j.buildenv.2017.01.033.

[9] E. Azar, W.O. Brien, S. Carlucci, T. Hong, A. Sonta, J. Kim, M.S. Andargie, T. Abuimara, M. El, R.K. Jain, M.M. Ouf, Simulation-aided occupant-centric building design : A critical review of tools , methods , and applications, Energy Build. 224 (2020) 110292. doi:10.1016/j.enbuild.2020.110292.

[10] V. Horayangkura, Incorporating Environment-Behavior Knowledge into the Design Process : An Elusive Challenge for Architects in the 21st Century, Procedia - Soc. Behav. Sci. 50 (2012) 30–41. doi:10.1016/j.sbspro.2012.08.013.

[11] O. Guerra Santin, L. Itard, H. Visscher, The effect of occupancy and building characteristics on energy use for space and water heating in Dutch residential stock, Energy Build. 41 (2009) 1223–1232. doi:10.1016/j.enbuild.2009.07.002.

[12] M. Ambrose, M. James, A. Law, P. Osman, S. White, The Evaluation of the 5-Star Energy Efficiency Standard for Residential Buildings (CSIRO Final Report), 2013.

[13] J. Byrne, The influence of design and everyday practices on individual heating and cooling behaviour in residential homes, (2018) 273–293. doi:10.1007/s12053-017-9563-y.

[14] M.A.R. Lopes, C.H. Antunes, R. Martins, Energy behaviours as promoters of energy efficiency: A 21st century review, Renew. Sustain. Energy Rev. 16 (2012) 4095–4104.

[15] K. Gram-Hanssen, New needs for better understanding of household's energy consumption—behaviour, lifestyle or practices? Architectural, Archit. Eng. Des. Manag. 10 (2014) 91–107.

[16] K. Scott, C. Bakker, J. Quist, Designing change by living change, Des. Stud. 33 (2012) 279–297.

[17] E. Shove, M. Pantzar, M. Watson, The dynamics of social practice: everyday life and how it changes, Sage Publications, 2012.

[18] I. Ajzen, The Theory of Planned Behavior, Organ. Behav. Hum. Decis. Process. 50 (1991) 179–211. doi:10.1922/CDH_2120VandenBroucke08.

[19] H. Brynjarsdóttir, M. Håkansson, J. Pierce, E.P.S. Baumer, C. DiSalvo, Sustainably unpersuaded: how persua- sion narrows our vision of sustainability, in: SIGCHI Conf. Hum. Factors Comput. Syst., Austin, TX, 2012.

[20] G. Peschiera, J.E. Taylor, J.A. Siegel, Response–relapse patterns ofbuilding occupant electricity consumption following exposure to personal, contextualized and occupant peer network utilization data, Energy Build. 42 (2010) 1329–1336.

[21] I. Vassileva, M. Odlare, F. Wallin, E. Dahlquist, The impact of consumers' feedback preferences on domestic electricity consumption, Appl. Energy. 93 (2012) 575–582.

[22] D. Lockton, Design with intent and the field ofdesign for sustainable behaviour, in: D. V. Keyson, O. Guerr. D. Lockt. (Eds.), Living Labs Des. Assess. Sustain. Living. Berlin Springer, 2017.

[23] L. Gádoros, Space needs and equipment of a modern apartment (A korszerű lakás térszükséglete és berendezése), Móricz Ny., Orsz. Építésügyi Kormányb., Budapest, 1946.

[24] J. Kismarty-Lechner, Urban apartment types (Városi lakástípusok), Móricz Ny., Orsz.Építésügyi Kormányb., Budapest, 1947.

[25] Ministry of Health, Requirements of a healthy apartment (Az egészséges lakás követelményei), (1951) 12.

[26] T. Csordás, Design quesitons of mass-apartment building (A tömeges lakásépítés tervezési kérdései), Magy. Építőművészet. 9–10 (1955) 257–272.

[27] A. Reischl, A human and its apartment (Az ember és lakása), in: M. Fórizs (Ed.), Apartm. (A Lakás), Kossuth Ny, Közgazd. és Jogi Kiadó, Budapest, 1958: p. 277.

[28] Arcanum: Digital Science Collection (Hungary), (n.d.). https://adt.arcanum.com/hu/.

[29] 1956 Institute, Oral History Archive, (n.d.). http://www.rev.hu/en.

[30] M. Branczik, M. Keller, Modern Apartment, 1960 - the experiment in Óbuda (Korszerű lakás, 1960 - az óbudai kísérlet), Budapesti Történeti Múzeum, 1956-os Magyar Forradalom Történetének Dokumentációs és Kutatóintézete Közalapítvány, Budapest, 2011.

[31] M. Keller, Socialist housing? - The housing problem in the 1950s in Hungary (Szocialista lakhatás? - A lakáskérdés az 1950-es években Magyarországon), Országos Széchenyi Könyvtár, L'Harmattan Kiadó, Budapest, 2017.

[32] Ministry of Health, Let's make our homes healthier! (Tegyük egészségesebbé lakóházunkat!), (1951) 10.

[33] I. Gyarmati, Small apartment, nice home (Kis lakásból szép otthon), Terv ny., Kisipari Szöv. Kiadó, Budapest, 1957.

[34] M. Pataki, The household of a working woman (A dolgozó nő háztartása), Szikra Ny., Közgazd. és Jogi Kiadó, Budapest, 1956.

[35] D. Kuchenbuch, Orderly community: Architects as Social Engineers (Geordnete Gemeinschaft: Architekten als Socialingenieure), Transcript Verlag, 2010.

[36] J.M. Diefendorf, In the Wake of War. The Reconstruction of German Cities after World War II, Oxford University Press, New York, 1993.

Experiment-based testing routine to characterize building energy flexibility for potential aggregators

Vojtěch Zavřel [a, b], Jakub Šimek [a], Tomáš Bäumelt [b], Vladislav Martínek [b] Artem Mishukov [c], Martin Barták [a]

[a] Czech Technical University in Prague, Faculty of Mechanical Engineering, Department of Environmental Engineering, Technická 4, 166 07 Prague 6, Czech Republic

[b] Czech Technical University in Prague, University Centre for Energy Efficient Buildings, Třinecká 1024, 273 43 Buštěhrad, Czech Republic

[c] Elpramo s.r.o., Nademlejnská 600/1, 198 00 Praha 9 – Hloubětín

Abstract. The ultimate goal is to introduce a standardized routine to characterize flexibility of a given building for the purpose of potential flexibility aggregators. The routine should provide the characteristic demand response of the building under various smart-grid control signals (e.g. time-of-use (stage) pricing, real-time pricing etc.). The scope of this paper is limited to the experimental part, that demonstrates measured demand response provoked by testing sequences. The testing sequences were applied via cloud-based service to the building management system (BMS) of a mid-size office building in Prague. The evaluation is not limited only to power metering but also includes indoor environment quality (in terms of room air temperatures and CO_2 concentrations), HVAC system and local meteorological data monitoring. The air handling unit (AHU) and cooling system response were investigated using 'step' and 'modular' testing sequences. The real-life experiments revealed authentic demand response allowing to characterize building flexibility in full details. The key findings are, that the operation of the HVAC system components can be blocked for relatively long period of time (2 to 5 hours in studied case) without any critical consequences to the indoor environment quality. Approximately 30 % of the total power load per the testing event can be considered as flexible. The quality of the power profile was found highly irregular. Due to the power profile fluctuation the ramping/modulation at the single building level was found ineffective. In contrary to the modular control, the multi-stage control led to more detectable power reduction. The stage type of control provoked more observable, reliable, and easier-to-predict demand response.

Keywords: Building energy flexibility, flexibility characterization, aggregation support, experimental testing, HVAC system
DOI: https://doi.org/10.34641/clima.2022.356

1 Introduction

Energy sector in the European union has been undergoing transformation towards carbon neutrality, which is the key objective for 2050 stated by European Green Deal [1]. Increasing penetration of the intermittent renewable energy sources into the transmission and distribution electrical systems requires higher storage capability and/or flexibility at the demand-side. Building sector (both residential and commercial buildings) represents major electricity consumption in the Europe counting around 54 % of the total delivered electricity into the grid[2]. Attempting the closer integration of these sectors via smart-grid technologies seems like a logical step, that may accelerate the ongoing transformation.

Building energy flexibility was generally defined by IEA as "the ability to manage demand and generation according to local climate conditions, user needs and energy networks requirements". More detailed characteristics at building level, possible stakeholders and flexibility indicators have been collected in the framework of the IEA EBC project Annex 67 which is followed up by the Annex 82 [3]. The further research area investigated by the ongoing Annex 82 are: scaling from single buildings

Copyright ©2022 by the authors. This conference paper is published under a CC-BY-4.0 license.

to clusters of buildings (aggregation); energy flexibility and resilience in multi-carrier energy systems (electricity, district heating/cooling and gas); acceptance/engagement of the stakeholders; and new business models. From the perspective of transmission and distribution system operators (TSOs and DSOs), two types of demand-side flexibility are recognized as explicit and implicit [4].

Explicit flexibility is committed, dispatchable flexibility supporting balancing services, such as frequency restoration reserves, traded on whole-sales, balancing, or system support and reserves markets. These balancing services have been already well specified in the codes of TSOs or DSOs, that require very high service reliability (e.g. sub-minute monitoring, 5 to 15 minutes ramping, high power quality etc.). The balancing services must be fast, accurate and activated on demand (randomly), which can hardly be provided by buildings. Explicit flexibility is commonly provided by vendors with industrial size of energy plants, that has sufficient volume and power capacity (e.g. minimum quantity 1MW) to enter the market, though they still may use flexibility aggregator to maximize their profit.

Implicit flexibility is the consumer's reaction to retail price or other grid signals. The end-user (e.g. building owner/operator) has the possibility to choose retail tariffs corresponding to supplier needs, variability on the market, and ultimately the network balance as common goal for all stakeholders. The role of so-called 'business' flexibility aggregator is crucial here to compile the sufficient size of the building's portfolio in order to reach minimum volume of the bids allowing to enter the wholes-sale or spot (day-ahead) energy markets. Since the spot-market trading is usually based on hourly (rarely 15 minutes) interval and the bids are specified in volume blocks, the requirements for demand response reliability and quality are significantly lower, than in previous type. The building flexibility may be effectively accommodated as implicit flexibility services; however, such services have not been yet fully developed [5].

Scaling from a single building to building clusters is a key aspect for the building flexibility as a viable service. As stated in [6], the building demand response still needs to be defined as a product for further flexibility aggregation, that will be recognized by the aggregators, market operators, TSOs or DSOs. The main barriers, that were also identified in the report are: lack of requirements for smart customer assets, low observability in low-voltage grids (complicating the settlement) and inadequate load and generation forecasting at distribution level.

The building energy flexibility characterization needs to be expanded to support the reliable prediction (with sub-hourly resolution) of total building demand under various type of the smart grid (SG) 'activation' signals. The current research proposes an approach combining series of experiment- and simulation-based tests improving the building flexibility characterization in terms of flexible capacity and power profile quality for potential aggregators. The ultimate goal is to introduce a standardized routine to characterize the building flexibility of a given building. The routine should report flexibility characteristic and support creating or refining a model of aggregated building portfolio. The scope of this paper is limited to the experiment-based part demonstrating measured demand response. This response is provoked by the testing sequences applied via newly developed cloud-based service to the building management system (BMS) of the demonstration office building in Prague.

2 Testing routine to characterize building energy flexibility

Focusing on the single building level, where the testing sequences are realized, major part of the energy in buildings (around 60 %) is consumed by HVAC systems [7]. Moreover, according to the EU roadmap, HVAC systems supposed to be massively electrified in the near future (i.e. support of heat pumps, electric boilers, etc.) [8]. For that reason, the presented method specifically aims at these systems. The SG solution is built on premise, that any modern devices or BMS will be able to receive commands from the SG (i.e. based on aggregator needs). Based on these commands the building demand will be shifted or shed accordingly, while partially blocking system functionality and utilizing available electrical or thermal storage capacity (i.e. batteries, storage tanks, piping thermal capacity, envelope capacity etc.). Since each building system is usually unique, the demand response is very case-dependent. The testing routine is proposed to characterize flexibility capacity, quality of output power response as well as impact to the indoor environment quality (IEQ) of a given building prior adding it into the possible aggregator's portfolio. The testing routine schematically depicted in Fig. 1 links three stakeholders: aggregator, building operator and occupants.

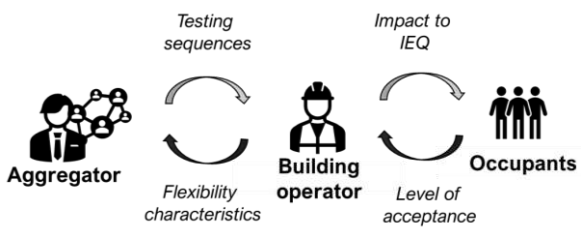

Fig. 1 Stakeholders involved in testing routine

Hereunder the testing routine is further explained in following steps.

2.1 HVAC system and BMS audit

In this step, a given HVAC system and/or BMS is inspected based on available documentation. Nominal loads of individual devices and expected part load (based on data from regular operation) are

reported. The audits should also include critical levels related with allowable range of indoor environment variation. In this research IEQ is represented by thermal comfort limits and Indoor air quality (IAQ) in terms of indoor CO2 concentration

2.2 Monitoring and actuation report available for flexibility activation

In this step, the capability of BMS system is investigated to ensure the aggregator, that all required sensors and actuators supporting flexibility services are available. If missing sensors or actuators are found, the BMS system is extended.

2.3 Verification of aggregator's support service connectivity

In this step, the connectivity with aggregator's service providing the grid signal (e.g. current tariffs, price prediction etc.) is verified. During the verification activity, the actuators do not listen to smart-grid commands/settings. Only the capability to receive the signal by the BMS is checked.

2.4 Experiment-based testing sequences for building flexibility characterization

Once the (supervisory) aggregator's service communicates correctly with the BMS (or individual devices), the service is used for execution of testing routine, that provoke the flexibility event. During this testing activity, the actuators follow the testing commands. The quantity of shifted or shed load and overall quality of the power profile are analyzed for the given test. The testing sequences are designed to test the response under a) step change, b) modular change of the testing signal. The testing sequences aim to reveal the authentic characteristic behavior of the building demand response for a current boundary condition (weather condition, occupancy etc.). The experiment-based assessment may serve underlying data for modelling and calibration purpose, if necessary.

2.5 Simulation-based assessment of for building flexibility characterization

As the final step, the testing sequences are repetitively tested on the numerical model developed either in building energy simulation tools or data-driven models to observe the demand response capability for typical conditions during the entire year to address weather-dependency or different occupation. Simulation also enables to generate a baseline profile and quantify typical flexibility indicators. To recall, the simulation-based assessment is out of scope of this paper.

3 Case-study description

3.1 Building and its HVAC description

A case-study building is a commercial administrative building located in Prague (see Fig. 2). A building envelope is made of iron-concrete with additional extruded polystyrene insulation. The building itself consists of three interconnected smaller blocks with a total usable area of 3568 m^2 . The building HVAC system, a scheme of which is in Fig. 2, consists of the following devices. Cooling is delivered by the roof-top chiller with nominal electric power of 65 kW. There are also two cold storage tanks with the total volume of two cubic meters.

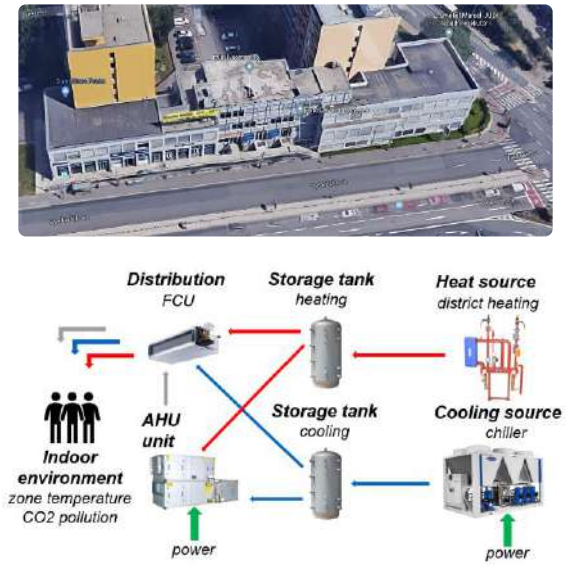

Fig. 2 Scheme of demo office building and HVAC system

Heating of the building is primarily provided by the district heating. The heat supply with the nominal heating capacity of 303 kW is then controlled using the weather-dependent control curve. The chiller is capable to operate in the heat-pump mode as back up source, however it is not practically used in this regime. As in the case of cooling, the heating system also comprises two cubic storage tanks.

Local zone temperatures and IAQ are controlled locally by FCUs with ventilation, cooling and heating capability. The fresh air is supplied by two AHUs equipped with heat recovery. The two AHUs have nominal air flow 5100 m^3/h and 8000 m^3/h. The nominal electric power of ventilation fans in both units is 6.7 kW.

3.2 Flexible control and its architecture

Control and monitoring are realized on the building level via multiple PLCs governed by BMS. The data collection is executed with a 10-minute period by the BMS interface called 'Thingsboard'. This system is also equipped with a secured API which allows to communicate with remote control systems. This feature is crucial and was utilized by the newly developed supervisory control which runs at university cloud service representing the aggregator's support service. This service translates the SG signals to commands, that can be accepted by the local BMS. The cloud service scheme as well as the local building control is depicted in Fig. 3. Regarding the cloud service there are several data sources which are needed: a) current status or prediction of the *SG* signal (e.g. time-of-use or real-time pricing tariff) from aggregators or other providers. b) source of the weather forecast. c) the actual state of the building, especially current

conditions of the IAQ.

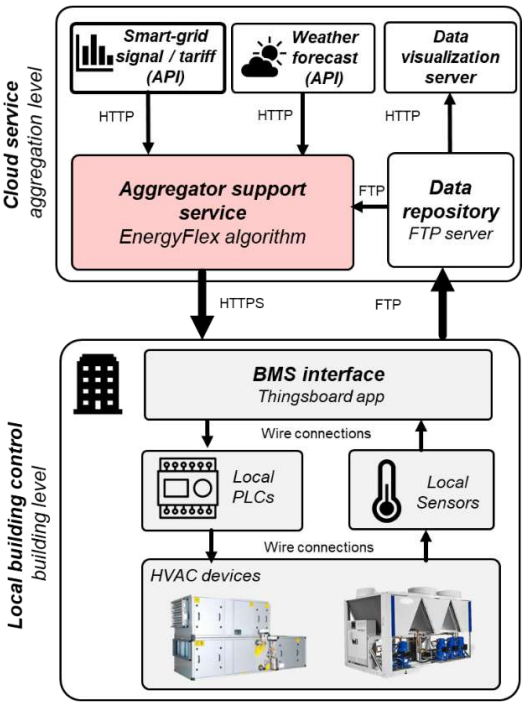

Fig. 3 Control architecture supporting building flexibility aggregation

The flexible control algorithm (called '*EnergyFlex*') communicates through HTTPS requests with the 'Thingsboard' interface on regular basis, thus forming a superior control loop of the building HVAC system. Thermal load metering of HVAC covers the heating and cooling demand measured at hydraulic distributor per each floor and building section. Further, active electric power of the following is measured: the total building active power (all three phases), chiller power and air handling unit (AHU) power. Regarding the IAQ, besides common zone temperature measurement, there are several IEQ sensors placed in the building which purvey information about not only temperature but also CO_2 concentration, relative humidity etc.

The 'EnergyFlex' service is also used to execute the testing sequence on the HVAC. The superior control algorithm takes control by sending "alive" commands to the BMS interface. The internet connection is secured by so-called 'watchdog' service in the 'Thingsboard'. The 'watchdog' signalizes to the BMS whenever the connection is lost enabeling fluent shift to the default control settings. Otherwise, the building HVAC is ready to be controlled from the cloud service when the testing sequence can be generated.

4 Testing sequence results

4.1 AHU demand response – response to step testing sequence

This test (see Fig. 4a) represents AHU demand response activated by the discontinuous (ON-OFF) control sequence. This particular test was executed during regular occupancy regime with feedback from CO2 monitoring. The CO_2 concentration was selected as constraint for the AHU flexibility events.

During the testing sequence, the AHU fan speed (setting of fan's frequency convertors) was set at following stages 0,70,25,80 and 0 % The 70 % stage represents regular operation. The drop to the 25 % stage represents the flexibility event activation. The 80% stage represents maximal fan speed in order to eliminate violation of the hygienic standards.

To satisfy the national hygienic standards (allowable limit of 1500 ppm, recommended 1000 ppm), the safety measure was introduced. When the CO_2 concentration reached 1300 ppm, the maximal possible fan speed (80% in this case) was automatically set.

As can be seen in Fig. 4, the power response to the control sequence was prompt and corresponds to the setpoint variation. The AHU power load was decreased about 4.9 kW till the CO_2 concentration level in the zone reached the safety margin, approx. 5 hours. Then the power load was increased about 6.6 kW during the rebound effect.

4.2 AHU demand response – response to modulated testing sequence

During this test (represented on Fig. 4b), the AHU demand response was activated by modular testing sequence. The AHUs were gradually modulated from 70 to 0 % and back to 70 % of their nominal capacity.

This test was executed out of working hours without occupancy to avoid hygienic standards violation during the test. Thus, the measured CO_2 concentration of indoor air, followed the concentration of the outdoor air.

The AHU power response followed immediately the modular control signal. The AHU power was gradually modulated in range from 6.84 kW to 0 kW.

4.3 Chiller demand response – response to step testing sequence

Testing sequence used during this test (Fig. 5 a) was conducted to characterize the chiller demand response to discontinuous control setting. The operation of the chiller was controlled indirectly by manipulating the chilled water temperature setpoint (leaving water temperature) by the predefined testing sequence. To provoke chiller to switch off, the temperature setpoint was suddenly increased from 9 to 20 °C for a predefined time period with consecutive decrease back to 9 °C.

The sudden temperature setpoint change resulted in approx. 5.5 h of chiller inactivity in the first case and approx. 4.5 h in the second case, before reaching the 20 °C chilled water setpoint and starting to cool again. The switching off the chiller was followed by almost immediate decrease of chiller power input. In our case by 11.1 kW in the first case and by 10.8 kW in the second case, resulting in steady total building power load profile without significant cycling caused by chiller operation. After decreasing the setpoint

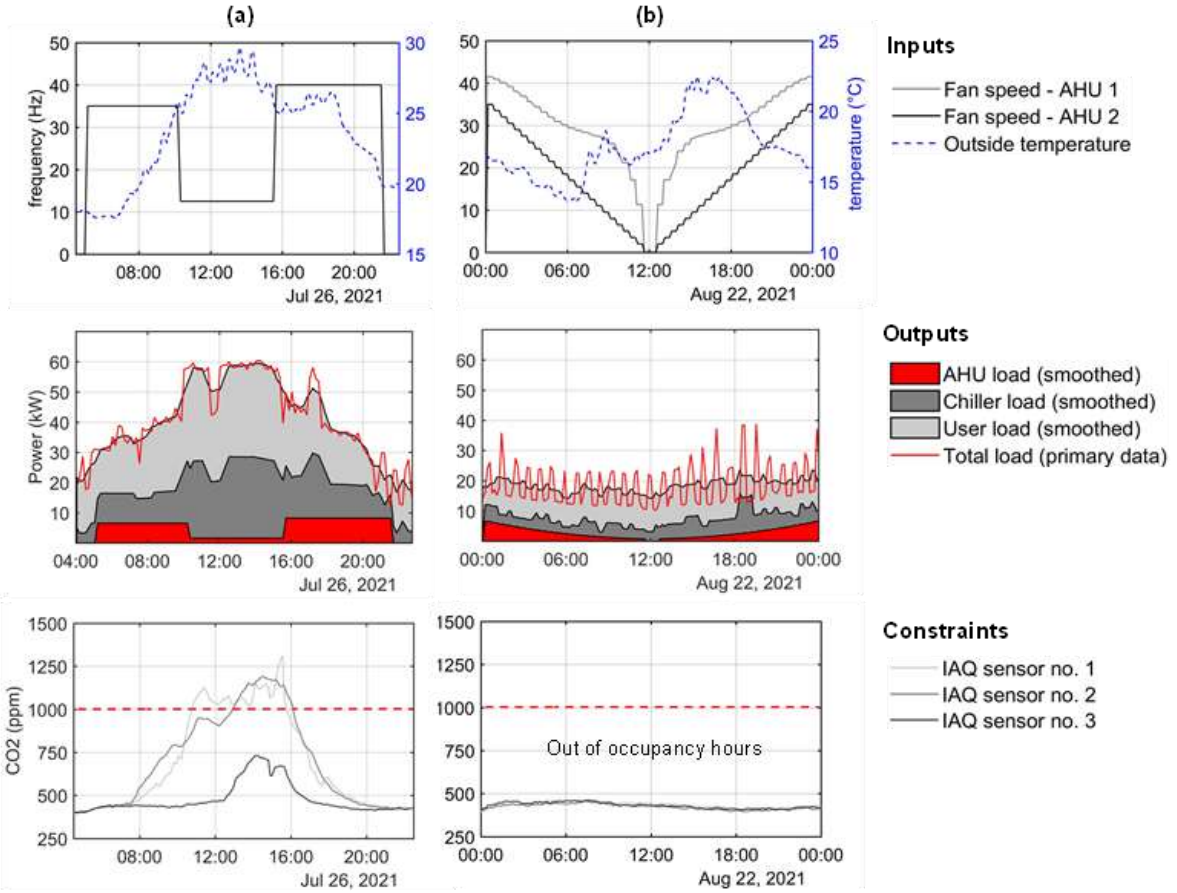

Fig. 4 Testing sequences provoking AHU's demand response

back to 9 °C. The significant increase of the power load at 28.4 kW can be observed, when the setpoints was set back to the original setting. The cooling water temperature followed the setpoints with minimal delay approx. 15 min.

The constrain for the chiller modulation was the indoor temperature and thermal comfort of the occupants. During these tests which were conducted during hot summer days, there was no violation of the indoor temperature in the zone with 25 °C zone temperature setpoint (setpoint no. 1). In case of the zone with temperature setpoint at 22 °C (setpoint no. 2), the indoor temperature exceeded the required temperature by 1 K during the chiller inactivity in first case (after 5.5 h) and by 1.4 K in second case (after 4.5 h).

4.4 Chiller demand response – response to modulated testing sequence

The conducted test presented in Fig. 5b shows the building response to modular control (modular testing sequence) of the chiller. Modular control was realized by gradual modulation of the chilled water temperature setpoint from 6 to 16 C during two summer weekend days based on the predefined testing sequence.

As can be seen in figure, the chilled water temperature was in line with the desired temperature setpoint and was modulated gradually. As can be also observed, the higher temperature setpoint correlates to chiller end electricity power consumption decrease during certain time period and otherwise. From the perspective of the power load reliability or predictability, despite the modular control of a chilled water temperature there can be observed significant fluctuation in the total building load profiles. These irregularities, with fluctuation in the range of 10 kW are given by the dual compressor construction of the studied chiller, specifically due to the cycling between operational stages. As observed, the given chiller is not able to provide modular demand response. The modulation is limited to the stages 0, 50, 100 % of its nominal capacity.

4.5 Chiller demand response – expected response to the real-time pricing

The final test presented in Fig. 6, was the most complex test, which tested building response to synthetic real time pricing profile during few weeks pilot operation, instead of short testing sequence. The modulation of the chiller as a dominant HVAC (and overall building) device was chosen for this test. During the test chilled water temperature setpoint was modulated based on the demand response rule-based algorithm, which was applied as a supervisory control. Based on the current energy price, the chiller temperature setpoint was modulated in a range of 6 to 16°C.

As can be seen from the figure, total building load increases and decreases in opposite to the course of a price signal due to demand-response operation of

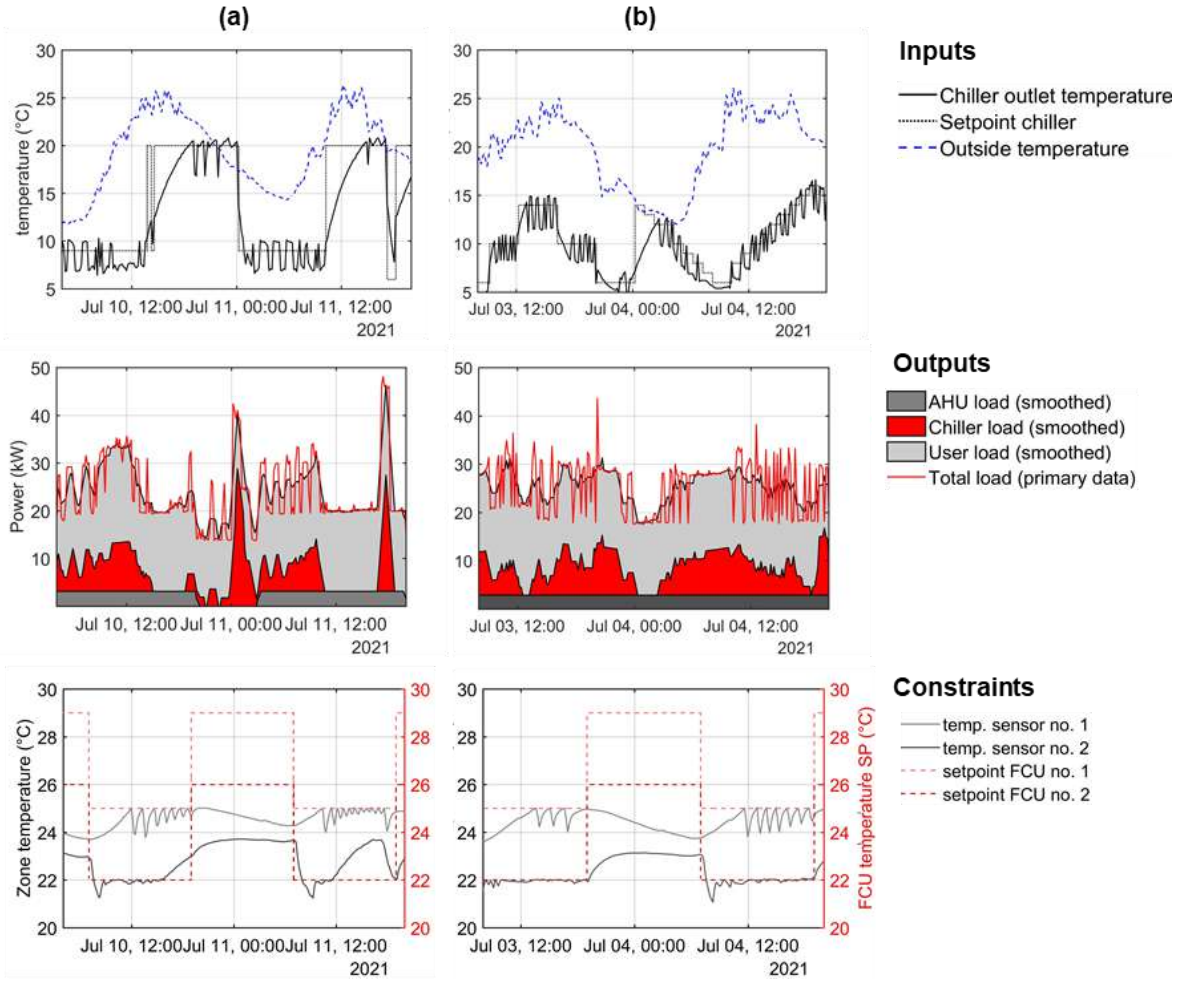

Fig. 5 Testing sequences provoking chiller's demand response

the chiller. However, due to chiller cycling, the peak power load often reaches the same values regardless of the value of a price signal or chilled water temperature setpoint, respectively.

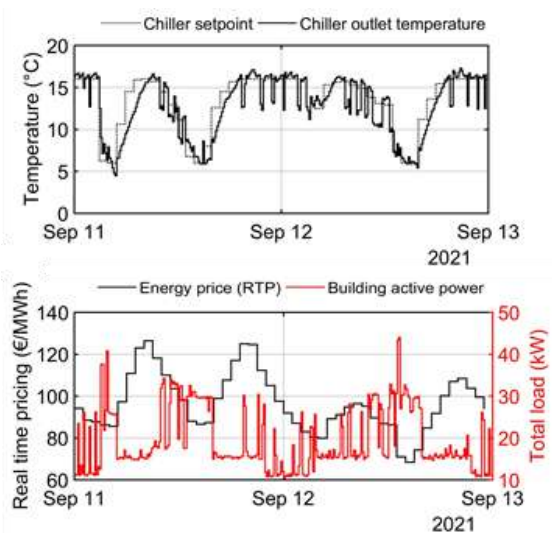

Fig. 6 Chiller demand response to real-time pricing signal

The internal temperature during this test (not plotted) was not significantly affected and followed the desired temperature with acceptable deviation. The rises of the chilled water temperature were sufficiently compensated by the existing thermal capacity of the storage tanks, the piping system and envelope.

5 Discussion

In the previous section, series of testing sequences were assessed to investigate the authentic demand response of the specific building. Although the results of these experiments cannot be entirely generalized, they indicate some important characteristics of the building flexibility, that might be shared with similar type of buildings and HVAC systems. The results are further discussed with respect of the proposed testing routine.

In terms of impact to IEQ and level of occupant's acceptance, the testing sequences did not cause significant disturbances to the thermal comfort and IAQ. The demand of the HVAC systems was reduced in the range of 2-5 hours with acceptable disturbance to the indoor environment. The demand shift is accounted mainly to thermal inertia of the water storage tanks, volume of piping system and building construction mass. The indoor environment satisfied relevant standard (e.g. EN-16798) during the presented tests. It should be noted, that in extreme

weather conditions or at maximum occupancy, the impact of the SG adaptation may increase the overheating risk or air quality discomfort. The IEQ feedback to the aggregator support service or overrule function at local control is recommended, to enable consideration of the occupant's comfort. It can be generally stated, that, the level of acceptance is relatively high, unless the change in the indoor environment is not rapid (e.g. FCU demand control). Our experience is that, the building demand response could be realized in synergy with occupant's requirements.

To recall, the presented routine mainly consists of 'step' and 'modular' testing sequences acting at AHUs and chiller. The experiments revealed the building capability to shed the AHU system's load about 4.9 kW (6.8 kW, if unit is completely switched off) for 5 hours, while still satisfying IEQ standards. Similarly for chiller, the capability to shed the load was found around 10 kW for period in range of 4.5 to 5.5 hours depending on the type of experiment. The resulted flexible energy can be estimated in range of 72 to 84 kWh per event. These numbers correspond to previous research [10] done for family houses in Belgium, where median flexible capacity trigged by changing zone setpoints over a 2h period differ from 13 to 18 kWh.

While the quantity of the flexible energy is in line with the previous research, the quality of the responded power profile (as characteristic) is rarely discussed. The total building demand, provoked by either 'step' or 'modular' testing sequence, was found very irregular. The fluctuation is mainly driven by the chiller with two-compressor configuration. Partially it is also generated by user's and auxiliary (e.g. lighting) building demand. The quality of the power demand is questionable, especially if the building flexibility should have provided reliable and predictable ramping of the profile. The modulation of the power profile has certain limits which are discussed hereunder.

Although the AHU power demand (itself) can respond fairly well to the modular testing sequence, the quality of the overall building profile is minimally affected. Moreover, utilizing only part of the nominal flow rate may disturb the pressure settings in the ventilation system. For part-load fan speed settings, the supply air in the ventilation system may be distributed unevenly to the supply elements (FCUs). The part-load operation may introduce risk of IAQ discomfort or even lead to exceeding hygiene criteria locally in some zones.

This specific type of chiller due to the previously mentioned construction issue is not capable to provide reasonable ramping respond to the modular testing sequence. Better respond could be expected from modern chillers with inverter compressor technology. However, the commonly embedded controller of these devices may still lead to the stage control accompanying by the cycling between stages as presented in this study (especially when the cascade of chillers is present). Other issue to state is relatively large weather-dependence of chiller's power demand, that makes the modulation even more challenging. To summarize, the profile modulation at the building level does not seem to be effective, reliable and easy-to-predict, unless the device and its control would be specifically optimized for that purpose.

The 'step' testing sequence led always to switching off the devices for a certain period of time. From the perspective of aggregator, this type of activation may offer more reliable and predictable outcome within the given time resolution of day-a-head markets (15 to 60 min). In addition, the 'step' testing sequence mostly provoke the maximal possible power reduction (about 16 kW for 5 hours) representing 29 % of the total peak load (assuming peak load at 55 kW). This amount is measurable by common power meters. Thus, the observability of the activated load and further settlement between aggregator and building operator/owner may be improved by using stage control.

In any case, the single building demand represents very minor part of the minimum tradable volume, that is typically 1 MW. The aggregation is absolutely necessary to enter the wholesale or short-term energy market with building energy simulation. Based on the studied case, the aggregated building cluster should reach size in terms of hundreds similar buildings.

The main limitation of this experimental flexibility characterization is case dependency on given system and also testing period with various weather conditions and level of occupancy. The presented experimental results represent rather nominal value neglecting the whole-year operation. Moreover, the calculation of most of the flexibility metric in experimental studies is complicated due to difficulty in estimating baseline definition at the single building level. Therefore, the building energy simulation tool are currently being exploited. The testing routine will be executed on the validated model to complete the characterization of the flexibility.

6 Conclusion

This paper introduced experimental testing routine to characterize building energy flexibility. The routine addressed a possible procedure to be done prior adding a given building to a larger aggregated portfolio. The procedure aimed to align requirements and expectations of main actors: building flexibility aggregators, building owner/operators and occupants via several audits and tests. The procedure was mainly built on testing sequences, specifically 'step' and 'modular' testing sequences were utilized and demonstrated on the real mid-size office building in Prague. The testing control sequences were sent to the BMS via newly developed cloud-based service supporting the building aggregation. The testing sequences provoked authentic demand response measured and stored for the flexibility characterization. The

monitoring was not only limited to power metering but includes also IEQ, HVAC system and meteorological monitoring. The tests were successfully executed on AHUs and the chiller and their flexibility potential was evaluated.

To conclude the key findings, 1) the operation of the HVAC system can be blocked or limited for relatively long period of time, (range of 2 to 5 hours in the studied cases) without any critical consequences to indoor environment quality. 2) approximately 30 % of the total power per testing event can be considered as flexible, however the long-term flexibility potential must be further investigated using simulation tools. 3) The quality of the power profile was found highly irregular. Due to the power profile fluctuation the ramping/modulation at the single building level was not found effective. The multi-stage control causing detectable power reduction can be recommended. This type of control provoked more observable, reliable, and easy-to-predict demand response.

The flexibility characterization will be extended for the whole-year performance in the following research, where the building energy simulation tools are being exploited. The testing sequences will be applied again to the validated simulation model.

7 Abbreviations

AHU	Air Handling Unit
API	Application Programming Interface
BMS	Building Management System
DSO	Distribution System Operator
HVAC	Heating, Ventilation, Air-Conditioning
IAQ	Indoor Air Quality
IEQ	Indoor Environment Quality
PLC	Programmable Logic Controller
SG	Smart Grid
TSO	Transmission System Operator

8 Acknowledgment

This research is co-financed from the state budget by the Technology Agency of the Czech Republic within the THETA programme, project no. TK02010164.

The authors participate in IAE EBC Annex 82 - Energy Flexible Buildings Towards Resilient Low Carbon Energy Systems.

9 Reference

[1] European Commission, "The European Green Deal - COM(2019) 640 final," Brussels, 2019.

[2] IEA, "IEA sankey." [Online]. Available: https://www.iea.org/sankey/.

[3] I. Pernetti Roberta and D. Søren Østergaard Jensen, "Characterization of Energy Flexibility in Buildings Energy in Buildings and Communities Programme Annex 67 Energy flexible buildings," 2019.

[4] SmartEn, "SEDC Position Paper: Explicit and Implicit Demand-Side Flexibility - September 2016 - smartEn," 2016.

[5] D. Shah and S. Chatterjee, "A comprehensive review on day-ahead electricity market and important features of world's major electric power exchanges," *Int. Trans. Electr. Energy Syst.*, vol. 30, no. 7, Jul. 2020.

[6] SGTF EG3, "Demand Side Flexibility Perceived barriers and proposed recommendations European Smart Grids Task Force Expert Group 3," 2019.

[7] Eurostat, "Energy consumption in households - Statistics Explained," 2021. [Online]. Available: https://ec.europa.eu/eurostat/statistics-explained/index.php?title=Energy_consumption_in_households. [Accessed: 12-Jan-2022].

[8] European Climate Foundation, "Roadmap 2050: A practical guide to a prosperous low-carbon Europe," 2010.

[9] H. Li, Z. Wang, T. Hong, and M. A. Piette, "Energy flexibility of residential buildings: A systematic review of characterization and quantification methods and applications," *Adv. Appl. Energy*, vol. 3, p. 100054, Aug. 2021.

[10] J. Le Dréau and P. Heiselberg, "Energy flexibility of residential buildings using short term heat storage in the thermal mass," *Energy*, vol. 111, pp. 991–1002, 2016.

Adjusting the design of a radiant heating system for office retrofit

Barbora Junasová [a], Ondřej Šikula [b], Michal Krajčík [c], Müslüm Arıcı [d], Martin Šimko [e]

[a] Faculty of Civil Engineering, Slovak University of Technology in Bratislava, Slovakia, barbora.junasova@stuba [b] Faculty of Civil Engineering, Brno University of Technology, Czech Republic, sikula.o@vutbr.cz

[c] Faculty of Civil Engineering, Slovak University of Technology in Bratislava, Slovakia, michal.krajcik@stuba.sk [d] Mechanical Engineering Department, Engineering Faculty, Kocaeli University, Turkey, muslumarici@gmail.com [e] Faculty of Civil Engineering, Slovak University of Technology in Bratislava, Slovakia, martin.simko@stuba

Abstract. Installation of low-exergy water-based radiant systems can help alleviate the negative effects of increased energy consumption due to their suitability for combination with low-grade renewable energy sources. Radiant heating and cooling installations in buildings are common, but their application in existing buildings as part of retrofit is relatively rare. The present study investigated some of the aspects of the installation of radiant heating systems in existing buildings. Wall and ceiling systems with pipe underneath the surface were considered because of various potential benefits. These include the possibility of operating as cooling in summer and heating in winter, easy installation in existing buildings, minor space requirements, and no or little need to reduce the height of the storey, especially in the case of walls. It was found that with a thermally conductive core, only a thin insulation layer of 1 cm may suffice if the temperature difference between rooms is relatively small. For an insulating core, no insulation may be needed even at higher temperature differences between rooms. Reducing the pipe spacing to about 5 cm was found to be efficient in terms of increased thermal output per 1 cm of spacing. The location of the insulation had a small effect on the thermal losses, but the output was higher for insulation placed on the outer side of the wall due to a more uniform temperature distribution in the structure. This configuration also allows for considerably higher heat storage capacity.

Keywords. Radiant heating, retrofit, thermal performance, ceiling heating, wall heating.
DOI: https://doi.org/10.34641/clima.2022.205

1. Introduction

Radiant heating and cooling are commonly used in newly constructed buildings in situations where they can provide benefits compared to convective systems such as fan coils, radiators, air terminals and beams [1, 2, 3, 4]. The benefits of radiant systems involve the suitability for combination with renewable energy sources due to the water temperature close to room temperature [5, 6, 7, 8], comfortable thermal environment [9, 10, 11] and use of thermal mass for peak load shifting [12, 13, 14]. These favorable characteristics could make radiant systems a suitable heating and cooling solution for building retrofitting. To achieve this, the construction of the radiant systems needs to be adapted to the retrofitted room, minimize negative impacts such as reduction of the room height or a need for destruction of existing structures, while providing the desired thermal behavior.

In building retrofitting, placing pipes directly on the existing ceiling or wall structure can be practical because it is easy to do and leads to a relatively high thermal output and low thermal losses [15]. Its thermal characteristics depend on the conductivity of the thermal core and the spacing of the pipe. Using an insulating thermal core results in a fast thermal response, whereas a conductive core slows the thermal response but provides a potential for thermal storage [16, 17].

This study aims to provide conceptual recommendations on the construction of radiant heating and cooling systems in existing rooms. Two radiant systems that are potentially suitable for building retrofitting were selected. These systems are ceiling with pipes attached to the bearing structure (**Fig. 1**) and pipes attached to an existing wall (**Fig. 2**). The systems were studied in the heating operation mode, but the results are also applicable to cooling conditions, provided that the temperature

Copyright ©2022 by the authors. This conference paper is published under a CC-BY-4.0 license.

difference between water and room temperature is similar to that in heating cases. The parameters considered in this study included the placement of thermal insulation on the inner/outer surface of the thermal core, pipe spacing, wall thickness, and thermal conductivity of the core. The effect of these parameters on the thermal output and losses and on the homogeneity of the surface temperature was studied. To accomplish this, a simulation model was created in a verified software tool. The results are recommendations for the design of radiant heating systems that can be applied to existing buildings.

2. Description of the radiant systems and boundary conditions

Only radiant heating and cooling systems with pipes underneath the inner surface were considered. The two selected radiant systems comprise a radiant ceiling with pipes attached to the supporting structure (**Fig. 1**) and pipes attached to an existing wall (**Fig. 2**). Such systems are efficient in terms of heat transfer between the pipe and the room and should be able to provide reasonable variability of design solutions and thermal behaviors. Both systems are well suited both for heating and cooling operation, meaning that they can be operated all year round, provided that they are connected to a corresponding energy source, e.g. a heat pump. The thermal conductivity of the material layers is shown in **Tab. 1**. In the analysis, the thermophysical properties of the materials were considered isotropic, temperature independent and constant in time.

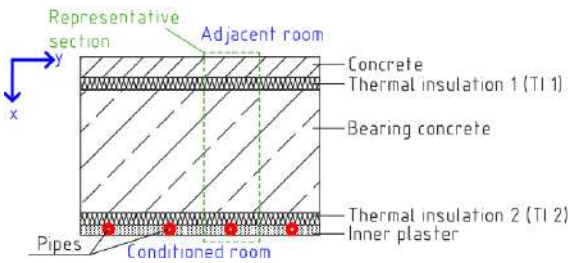

Fig. 1 – Radiant ceiling.

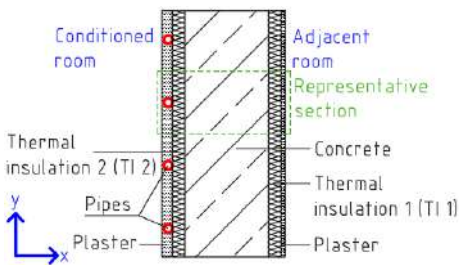

Fig. 2 – Radiant wall.

Representative sections of the radiant systems were used for the calculation. The room temperature (T_i) was 20°C. The mean water temperature was 35°C, which is representative of relatively demanding winter climatic conditions in Central Europe to cover a critical situation. For the wall system, this water temperature ensures that the surface temperature is well below the maximum limit for wall systems of approximately 40°C. For the ceiling system, the water temperature is relatively high, and depending on the resulting surface temperature and room geometry, it could lead to a risk of discomfort due to radiant temperature asymmetry. Therefore, in practical situations, care must be taken to verify if the comfort limits are met and adjust the water temperature as needed.

The temperature difference between the conditioned room and the adjacent room (T_i - $T_{i,adj}$) was 5 K, except for the case of C-3 and W-3, where the temperature difference (T_i - $T_{i,adj}$) was 15 K. The 5 K represented a conditioned adjacent room. This temperature difference may seem small, but it was the relative difference between the cases and the loss in W/m² per 1 K temperature difference that was most relevant for the analysis. The 15 K represented an unheated adjacent room. The total heat transfer coefficient on the thermo-active surface was 6.5 W/(m².K) for the ceiling system and 8 W/(m².K) for the wall system. The heat transfer coefficient on adjacent surfaces that were not thermally active was 6 W/(m².K). The heat transfer coefficient between the pipe and water was determined to be 1274 W/(m².K). This value is realistic, and further increasing or decreasing this value by several hundreds of W/(m².K) has negligible effect on the results [17].

Tab. 1 - Thermophysical properties of materials.

Material	Thermal conductivity λ (W/(m·K))	Thickness d (m)
1 – Simple concrete	0.6	0.05
2 – Reinforced concrete (RC)	1.58	0.2 (wall) or 0.3 (ceiling)
3 – Aerated concrete (AC)	0.15	
4 – Thermal insulation	0.035	0.01
5 – Pipe PE-Xa*	0.35	-
6 – Inner plaster	0.49	0.025

* outer diameter 10.1 mm, wall thickness 1.1 mm

The two systems were considered to be located in a corner room with two partition walls dividing the conditioned room from adjacent rooms (**Fig. 3**). In the present study, the room was designated as an office room, but the results are also applicable to other room types with similar boundary conditions. Another adjacent room was located above the conditioned room. This means that in the present study, the ceiling or walls that contained pipes were not exposed to weather conditions.

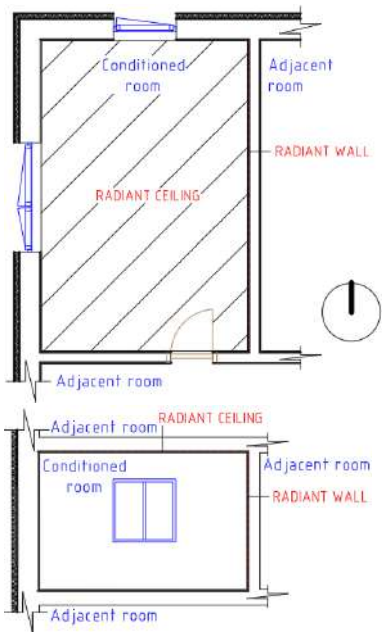

Fig. 3 – Location of office room and radiant systems.

3. Principle of heat transfer calculation

The numerical model was created and solved using CalA software [18] developed to calculate two-dimensional heat transfer in building structures. The software was verified following the procedure in ISO 11855 [19], Part 2 (Annex D). The verification can be found in the supplementary material to Ref. [16]. The governing equation described the problem as two-dimensional transient heat conduction as follows:

$$\frac{\partial T}{\partial \tau} = \alpha \left(\frac{\partial^2 T}{\partial x^2} + \frac{\partial^2 T}{\partial y^2} \right) \quad (1)$$

where T, τ and α represent the temperature (K), time (s) and thermal diffusivity (m²/s), respectively. Thermal diffusivity is the ratio of the thermal conductivity of a substance to the product of its density and its specific heat capacity. The boundary conditions defining the specific heat flux on the surface of a computational domain were calculated according to Newton's law of cooling, assuming adiabatic wall boundaries. The boundary condition on the surface of the computational domain was:

$$-\lambda \left(\frac{\partial T}{\partial n} \right)_w = h\left(T_w - T_f\right) \quad (2)$$

where h is the total heat transfer coefficient (convective and radiative) between the radiant surface and the environment (W/(m².K)); T_w is the temperature of wall surface (K), T_f is the temperature of the surrounding fluid (K), n is index denoting a line perpendicular to the surface.

The boundary condition on the adiabatic wall boundary was as follows:

$$-\lambda \left(\frac{\partial T}{\partial n} \right)_w = 0 \quad (3)$$

In **Eq. 2**, w denotes the surface of the computational domain through which heat transfer occurs between the wall or ceiling structure and the rooms. In **Eq. 3**, w denotes the adiabatic boundary between two wall sections along the horizontal (wall) or vertical (ceiling) symmetry plane. The calculation was converged when the sum of the normalized heat flux residues met the convergence criterion:

$$\frac{\sum_{i=1}^{k} q_{,i}}{\sum_{i=1}^{k} |q_{,i}|} \leq 10^{-6} \quad (4)$$

where q_i is the heat flux entering and leaving the control volume.

4. Cases studied

The ceiling system (C) can be easily constructed by adding a thermally active layer to the bearing structure (**Fig. 1**). The default thickness of the bearing structure and the spacing of the pipes used in the calculations were 30 and 10 cm, respectively. The construction factors considered that can affect the thermal performance of the ceiling were the presence of thermal insulation in the floor of an adjacent room, the presence of insulation between the thermoactive layer and the thermal core, and the thermal conductivity of the bearing concrete (reinforced concrete - RC, aerated concrete - AC). The five cases of ceilings in **Tab. 2** were planned to study the effect of these factors. The parameter of interest in each case is written in bold in the table. The cases that are compared together are explained as follows:

- C-1 and C-2 – effect of the presence of original insulation in the floor of an unheated adjacent room on thermal losses to the room,
- C-1 and C-4 – effect of thermal conductivity of the concrete core in case of no thermal insulation,
- C-3 and C-4 – effect of thermal conductivity of the concrete core and low temperature in the adjacent room in case of no thermal insulation (T_i - $T_{i,adj}$) is 15 K,
- C-1 and C-5 – effect of adding insulation layer between the thermoactive layer and the thermal core.

A wall system (W) with pipes in plaster can be built by embedding the pipes in a newly created plaster attached to an existing wall (**Fig. 2**). The default thermal core thickness was 20 cm as compared to the 30 cm used for the ceiling. The default pipe spacing was 10 cm. The design factors considered that can affect the thermal performance were the conductivity of the thermal core (reinforced concrete - RC or aerated concrete - AC), pipe spacing, and the presence of insulation between the thermoactive layer and the core. The seven cases of walls studied are listed in **Tab. 2**, where the parameters of interest are written in bold. The cases are compared with each other as follows:

- W-1 and W-2 – effect of adding insulation layer on the outer side of the concrete core.

- W-1 and W-4 – effect of thermal conductivity of the concrete core in case of no thermal insulation,
- W-3 and W-4 – effect of thermal conductivity of the concrete core and low temperature in the adjacent room in case of no thermal insulation (T_i - $T_{i,adj}$) is 15 K,
- W-1 and W-5 – effect of adding insulation layer between the thermoactive layer and the thermal core,
- W-5, W-6 and W7 – effect of pipe spacing.

The insulation thickness on the outer side (TI 1) and inner side (TI 2) of the concrete core in **Tab. 2** is defined in **Fig. 1** and **Fig 2**.

Tab. 2 - Cases studied.

Case	TI 1	TI 2	Pipe spacing (cm)	Core material
CEILING SYSTEM:				
C-1	no	no	10	RC
C-2	**yes**	no	10	RC
C-3*	no	no	10	**AC**
C-4	no	no	10	**AC**
C-5	no	**yes**	10	RC
WALL SYSTEM:				
W-1	no	no	10	RC
W-2	**yes**	no	10	RC
W-3*	no	no	10	**AC**
W-4	no	no	10	**AC**
W-5	no	**yes**	10	RC
W-6	no	yes	**5**	RC
W-7	no	yes	**15**	RC

(T_i - $T_{i,adj}$) = 15 K instead of 5 K

5. Results and discussion

The results for the representative sections of the radiant heating systems are shown in **Figs. 4** to **10**. **Figs. 4, 5,** and **6** illustrate the temperature distribution in the structure for selected cases. The thermal output (q_i) and losses (q_e) are shown in **Fig. 7** for the ceiling and **Fig. 8** for the wall. All heat flux values presented refer to square meter of wall (ceiling) surface area. The average temperature ($T_{suf,i}$) and the difference between the maximum and minimum surface temperature ($T_{surf,max}$ - $T_{surf,min}$) are shown in **Fig. 9** for the ceiling and **Fig. 10** for the wall.

Comparing C-1 and C-2 where in the case of C-2 the original insulating layer was preserved in the floor showed that the presence of just 1 cm insulation reduced the heat loss by 37% (**Fig. 7**). The losses were similar when insulation was placed on the inner side of the ceiling between the thermo-active plaster and the concrete core (C-1 vs. C-5). However, the output and storage capacity were different depending on the location of the insulation. In C-2 (insulation on the outer side), the output was 10% higher compared to C-5 (insulation on inner side) due to the more homogeneous surface temperature distribution, as illustrated in **Fig. 4**. Besides, in C-5 the thermal storage capacity is very low compared to C-2, resulting in a very fast thermal response. The same principles were valid for the wall system (**Fig. 8**), but the effect of adding thermal insulation was even more important because of the lower thickness of the concrete core. Additional calculations showed that adding insulation up to about 3 cm was sensible. A further increase in insulation thickness reduced the losses, but the reduction per 1 cm of insulation became relatively small.

A comparison of C-1 and C-4 illustrates the effect of the thermal conductivity of the concrete core if there is no thermal insulation. The effect is tremendous. Thermal losses were lower by 80% when the concrete core was made of a thermally insulating material (AC) compared to conductive concrete (RC), assuming no additional thermal insulation (**Fig. 7**). Increasing the temperature difference (C-3) led to a higher overall heat loss, but a lower specific loss per 1 K of the temperature difference between the heated and the adjacent room. This means that little or no insulation needs to be added to prevent losses if the concrete core is made of an insulating material. This point is also illustrated by comparing the wall systems W-4 and W-5 (**Figs. 5 and 8**). The use of an insulating concrete core (W-4) reduced losses by 57% compared to a conductive core with 1 cm of thermal insulation (W-5). Moreover, with the insulating core the output was 8% higher while also providing a certain potential for thermal storage.

A comparison of thermal output for pipe spacing of 5 cm (W-6), 10 cm (W-5) and 15 cm (W-7) in **Fig. 8** showed that a reduction of the spacing from 15 to 10 cm increased the output by 28%. Reducing the spacing to 5 cm increased the output by 48% compared to 15 cm. Additional calculations indicated that the increase in output in W/m^2 per centimeter of pipe spacing was highest close to 5 cm. Further increasing the output can be sensible but may not be so efficient. These results show that it is sensible to reduce the spacing down to at least 5 cm if the construction of the system allows it. This is especially important for cooling systems to maximize output while preventing condensation. A dense pipe spacing allows for higher thermal output of the thermo-active surface per energy input to the generator due to the combined beneficial effect of the increase in the power supplied to the pipe and the homogenization of the surface temperature (**Fig. 6**).

Looking at the differences in the maximum and minimum surface temperatures in **Figs. 9** and **10**, it is seen that the surface temperature is largely non-homogeneous, except for the case W-6 with the very dense pipe spacing. The difference between maximum and minimum surface temperature ($T_{surf,max}$ – $T_{surf,min}$) was about 3 to 4 K for the cases with a pipe spacing of 10 cm. It was even 7 K for a pipe spacing of 15 cm (W-7). This shows that a dense pipe spacing is important, especially for cooling systems. From the cooling point of view, the nonuniformity in the surface temperature

distribution will limit the cooling output of the systems because the minimum surface temperature needs to be above the dew point to prevent local condensation. A higher uniformity of the surface temperature due to a denser pipe spacing allows greater output with a higher water temperature. In other words, the output of the radiant cooling system can be maximized per unit of energy input to the cool source. In addition to a denser pipe spacing, the output could be enhanced and the surface temperature homogenized by using a thermally conductive fin attached to the pipe to improve the temperature distribution. The optimal design of such an element should be the subject of further research.

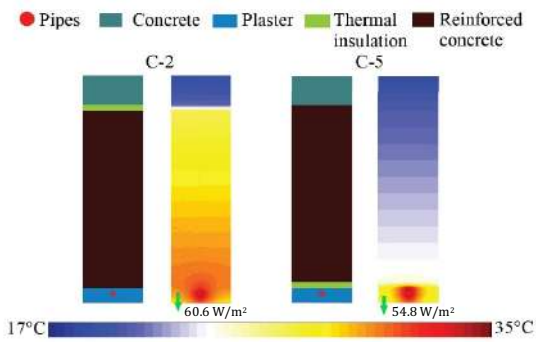

Fig. 4 – Detail of temperature distribution for ceilings

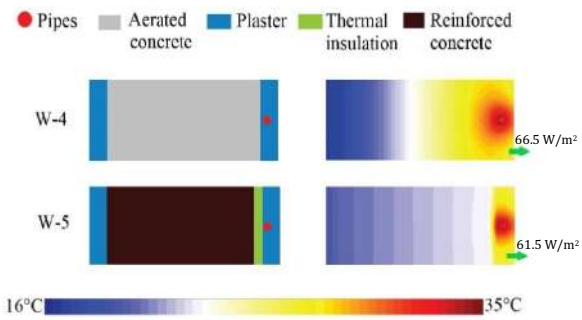

Fig. 5 - Detail of temperature distribution for walls

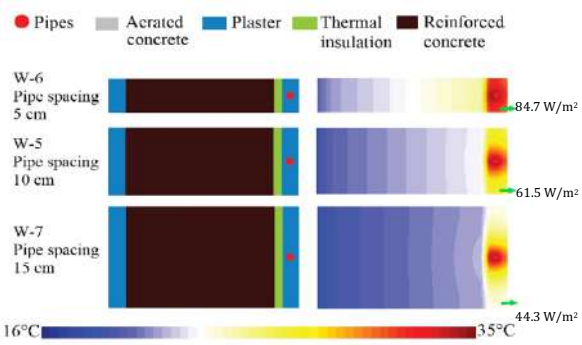

Fig. 6 – Effect of pipe spacing on surface temperature

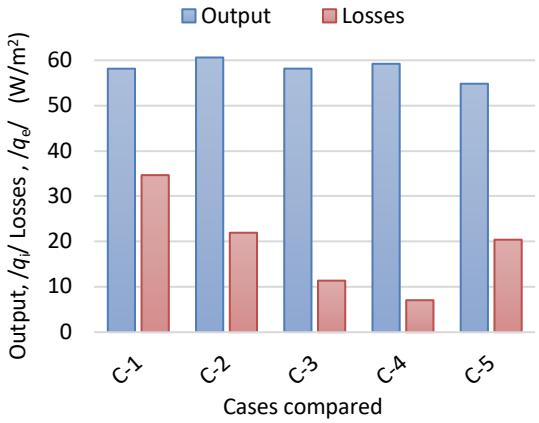

Fig. 7 – Thermal output and losses for radiant ceilings

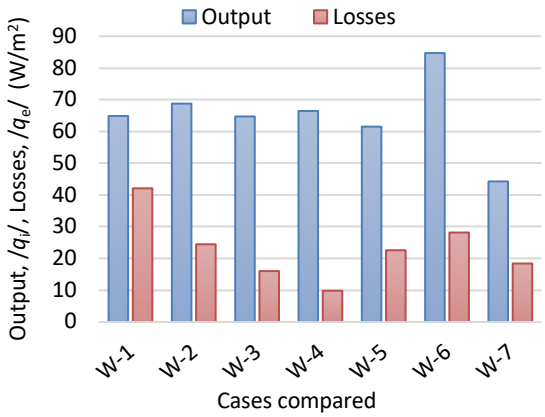

Fig. 8 – Thermal output and losses for radiant walls

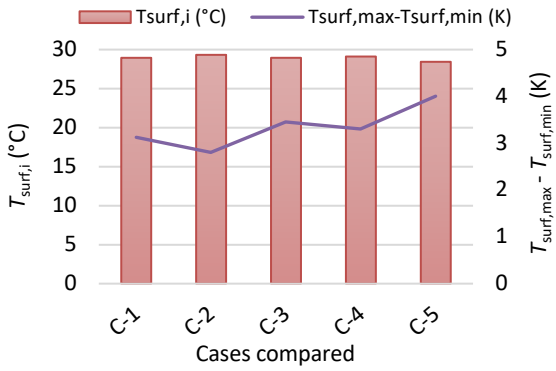

Fig. 9 – Surface temperature for radiant ceilings

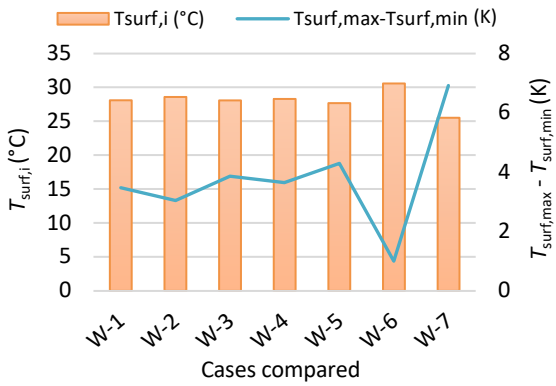

Fig. 10 – Surface temperature for radiant walls

6. Conclusion

This research focused on the effect of the thermal conductivity of the thermal core, the presence and position of the thermal insulation, the spacing of the pipes, and the temperature of the adjoining room on the thermal performance of two radiant heating systems suitable for building retrofit. The main conclusions are summarized as follows:

- With a thermally conductive concrete core, thermal insulation is necessary. For a relatively small temperature difference between rooms, a thin insulation layer (e.g., 1 cm) may suffice. Insulation thicknesses of more than 3 cm may not be efficient.
- If the thermal core is made of an insulating material, thermal insulation may not be needed even at a relatively high temperature difference between rooms.
- A 15 cm pipe spacing was found to be an inefficient design. Reducing the spacing to about 5 cm was efficient in terms in increase in output per 1 cm of spacing.
- For a pipe spacing of 10 cm, the surface temperature was substantially non-uniform due to the pipes located just underneath the surface compared to systems with pipes embedded deeper in the structure. Using a denser pipe spacing made the surface temperature much more uniform. This can be important for radiant cooling systems to achieve greater output while also increasing the required water temperature, thus enhancing the efficiency of the cool source.
- The difference in thermal losses for the placement of insulation on the inner or outer side of the structure was small. However, the output was higher for the insulation placed on the outer side due to a more uniform surface temperature. This configuration also allows considerably higher heat storage capacity.

7. Acknowledgement

This work was supported by the Ministry of Education, Science, Research and Sports of the Slovak Republic grants VEGA 1/0303/21 and 1/0304/21 and KEGA 005STU-4/2021 and Brno University of Technology project FAST-S-22-8060.

The datasets generated during and/or analysed during the current study are not available because of the page limit but the authors will make every reasonable effort to publish them in near future.

8. References

[1] Stetiu C. Energy and peak power savings potential of radiant cooling systems in US commercial buildings. Energy and Buildings 1999;vol. 30:127-138. https://doi.org/10.1016/S0378-7788(98)00080-2.

[2] Kazanci O. Olesen B. IEA EBC Annex 59 - Possibilities. Limitations and Capacities of Indoor Terminal Units. Energy Procedia 2015;vol. 78:2427-2432. https://doi.org/10.1016/j.egypro.2015.11.213.

[3] Bojić M. Cvetković D. Miletić M. Malešević J. Boyer H. Energy. cost. and CO2 emission comparison between radiant wall panel systems and radiator systems. Energy and Buildings 2012;vol. 54:496-502. https://doi.org/10.1016/j.enbuild.2012.04.024.

[4] Guruprakash G. VAV vs. Radiant: Side-by-Side Comparison. ASHRAE Journal 2014;5:16-24.

[5] Babiak J. Olesen B. Petráš D. Rehva Guidebook: Low Temperature Heating and High Temperature Cooling. 2007 ed. Finland.: Rehva; 2007.

[6] Romaní J. Pérez G. de Gracia A. Experimental evaluation of a cooling radiant wall coupled to a ground heat exchanger. Energy and Buildings 2016;vol. 129:484-490. https://doi.org/10.1016/j.enbuild.2016.08.028.

[7] Romaní J. Pérez G. de Gracia A. Experimental evaluation of a heating radiant wall coupled to a ground source heat pump. Renewable Energy 2017;vol. 105:520-529. https://doi.org/10.1016/j.renene.2016.12.087.

[8] Masaryk M. Mlynár P. Solar air-condition by ejector cooling. AIP Conference Proceedings 2000. 2018. pp. 020013-. https://doi.org/10.1063/1.5049920.

[9] Karabay H. Arıcı M. Sandık M. A numerical investigation of fluid flow and heat transfer inside a room for floor heating and wall heating systems. Energy and Buildings 2013;vol. 67:471-478. https://doi.org/10.1016/j.enbuild.2013.08.037.

[10] Myhren J. Holmberg S. Flow patterns and thermal comfort in a room with panel. floor and wall heating. Energy and Buildings 2008;vol. 40:524-536. https://doi.org/10.1016/j.enbuild.2007.04.011.

[11] Kim T. Kato S. Murakami S. Rho J. Study on indoor thermal environment of office space controlled by cooling panel system using field measurement and the numerical simulation. Building and Environment 2005;vol. 40:301-310. https://doi.org/10.1016/j.buildenv.2004.04.010.

[12] Romaní J. Belusko M. Alemu A. Cabeza L. de Gracia A. Bruno F. Control concepts of a radiant wall working as thermal energy storage for peak load shifting of a heat pump coupled to a PV array. Renewable Energy 2018;vol. 118:489-501. https://doi.org/10.1016/j.renene.2017.11.036.

[13] Gwerder M. Lehmann B. Tödtli J. Dorer V. Renggli F. Control of thermally-activated building systems (TABS). Applied Energy 2008;vol. 85:565-581. https://doi.org/10.1016/j.apenergy.2007.08.001.

[14] Arteconi A. Costola D. Hoes P. Hensen J. Analysis of control strategies for thermally activated building systems under demand side management mechanisms. Energy and Buildings 2014;vol. 80:384-393. https://doi.org/10.1016/j.enbuild.2014.05.053.

[15] Oravec J. Šikula O. Krajčík M. Arıcı M. Mohapl M. A

comparative study on the applicability of six radiant floor. wall. and ceiling heating systems based on thermal performance analysis. Journal of Building Engineering 2021;vol. 36. https://doi.org/10.1016/j.jobe.2020.102133.

[16] Krajčík M. Šikula O. Heat storage efficiency and effective thermal output: Indicators of thermal response and output of radiant heating and cooling systems. Energy and Buildings 2020;vol. 229. https://doi.org/10.1016/j.enbuild.2020.110524.

[17] Krajčík M. Šikula O. The possibilities and limitations of using radiant wall cooling in new and retrofitted existing buildings. Applied Thermal Engineering 2020;vol. 164. https://doi.org/10.1016/j.applthermaleng.2019.114490.

[18] Šikula O. Software CalA User Manual. Brno. Czech Republic: Tribun; 2011.

[19] EN ISO 11855:2012 Building Environment Design—Design. Dimensioning. Installation and Control of Embedded Radiant Heating and Cooling Systems. 2012.

Energetic Impact of Temperature Gradients in Heat Recovery in Ventilation in Dwellings

Josué Borrajo Bastero[a], Eline Himpe[a], Jelle Laverge[a]

[a] Research Group Building Physics, Department Architecture and Urban Planning, Faculty of Engineering and Architecture, Ghent University, Belgium

Abstract. The installation of air-to-air heat exchangers in ventilation systems can contribute to reducing the heating demand of the building by recovering the heat from the exhaust air. When there is an active heating demand, the recovered heat becomes useful to reduce that demand. However, as the heat exchanger works independently of the heating needs of the dwelling, the recovered heat may not contribute to the reduction in the heating demand. Furthermore, the indoor temperature gradients in the various rooms/zones of the dwelling can influence the heat recovered by the ventilation system and, consequently, the useful recovered heat. A suitable method to evaluate the effect is based on dynamic multi-zone building energy simulations. In this work, a residential building typology has been modelled with eleven ventilations systems. Some of them work with fixed airflows and others are commercial smart ventilation systems with variable flow rates controlled by CO_2, VOC and humidity sensors. Various systems do not have a heat exchanger due to their ventilation type. Still, the study was extended to those, considering that the unwasted heat as a consequence of using a smart control would be equivalent to the presence of a heat exchanger. The building was heated with two heating strategies: uniform heating in all the zones except for the attic and non-uniform heating with a specific setpoint for three different types of zones. To evaluate the impact of the heat recovery, the annual heating demand and the recovered heat are compared between scenarios with different effectivenesses for the heat exchanger and, to evaluate the effect of the temperature gradients, the results are compared between the two different heating strategies: uniform and non-uniform. The results for the case presented in this study show that centralized heat recovery systems perform better in the scenarios with uniform heating, while distributed ventilation systems perform similarly in both heating scenarios.

Keywords. Temperature gradients, heat recovery, heat exchanger, heating demand, ventilation.
DOI: https://doi.org/10.34641/clima.2022.114

1. Introduction

Ventilation systems are present in dwellings with the sole purpose of having an acceptable indoor air quality by removing stale air from indoors, contributing to improving people's health, comfort and productivity. The ventilation concept, however, is quite inefficient, since it requires extracting the air from inside the building to be replaced with outdoor air, which, hopefully, would have a lower concentration of pollutants. An efficient alternative would be a technology to remove the pollutants from the indoor air by filtering or capturing them. However, these alternatives are not competitive yet, especially to capture CO_2 [1]. The indoor air has been treated by the conditioning system to guarantee a certain level of thermal comfort for the occupants. Then, it is extracted and replaced by air that most of the time does not have the same temperature as the extracted air, which causes an extra heating demand in most heating-dominated climates. Frequently, the extracted air leaves the building without any treatment, meaning that polluted but conditioned air is released into the atmosphere.

Heating, ventilation and air conditioning (HVAC) systems can represent more than 40 % [2] of the energy needs in a new residential building, being 30 % - 50 % heat losses by ventilation and infiltration [3]. Then, one of the aspects to optimize the energy use of the building is to reduce the energy losses caused by the presence of a ventilation system, especially when considering well insulated and airtight buildings, in which transmission and infiltration heat losses are lower.

In centralized ventilation systems, the ventilation process consists of two main airflows for exhaust and supply, which can be connected to a heat exchanger to recover heat that may be useful to reduce the

Copyright ©2022 by the authors. This conference paper is published under a CC-BY-4.0 license.

heating demand of the dwelling. This additional installation requires the investment for the heat exchanger, but it will reduce the extra heating demand needed to compensate for the heat losses in the exhaust with very low or null maintenance costs. The operational costs would be only associated with the increase in fan power to compensate for the extra pressure drop caused by the installation of the heat exchanger.

In decentralized ventilation systems, it is possible to have local heat exchangers in each zone. This solution has more heat exchangers and less piping. It is also more efficient compared to the centralized systems if there were different temperatures in the dwelling since each heat exchanger would recover heat to reach the temperature of the room (happening when using a perfect heat exchanger). On the contrary, in centralised ventilation systems, the maximum reachable temperature (if using a perfect heat exchanger) would be the result of a mixture of temperatures from the airflows of the different zones, which may not be sufficient for some zones and unnecessarily high for other zones.

The different temperature gradients in the dwellings may influence the effect of heat recovery in the reduction of the heating demand, especially in centralized ventilation systems. Furthermore, the configuration of the ventilation system can also have a significant impact on the heating demand. This study tries to estimate the mentioned impact on a specific case-study dwelling through simulations, using constant effectiveness heat exchangers. Some smart ventilation systems without heat exchangers were also included in the study. For those, the heat that is not extracted by the exhaust air (because of the reduced airflows defined by the smart control) is considered equivalent to the recovered heat when a heat exchanger is present. The result in both cases is heat that does not leave the building in the exhaust air.

2. Methodology

In this paper, the impact of the temperature gradients on the heating demand in a dwelling was evaluated using building simulations. The models were developed in Modelica language, using the commercial software Dymola with validated components from the IDEAS library [4] and extended with tailored components to include a better representation of the behaviour of the infiltration through the surfaces from a previous work. Including a detailed model for infiltration causes the simulation speed to decrease by a variable factor (depending on the case, 10 to 100 times slower compared with models with a simplified infiltration network) that makes this study to be limited to a reduced number of ventilation systems and only applied to a single dwelling.

The heat exchanger is an element that works all the time depending only on the temperature difference on both sides of its structure. The exchanged heat can be measured in simulations and in the reality, but the results do not usually give clues on how this recovered heat contributed to a reduction in heating demand. Even on very cold days, when the heating operation is intensive, the total recovered heat is not always useful heat that could reduce the heating demand. When using a heat exchanger, the air temperature in the supply is different all the time with respect to the scenario when no heat exchanger is used, even if the conditioning system is not working, affecting the operation of conditioning the spaces. Then, to know the real impact on the heating demand it is necessary to run two simulations: one with the heat exchanger as it is and another one without the heat exchanger. The difference in heating demand would be associated with the presence of a heat exchanger.

The coefficients η_2 and η_4 were defined [5] to evaluate different aspects of the impact of the ventilation on the heating demand. They are calculated based on the heating demands of three scenarios: 1) Q, representing the heating demand of the actual system with Q_h representing the heat recovered by the heat exchanger; 2) Q_0, representing the heating demand when there is no heat exchanger; and 3) Q_{nv}, representing the heating demand when there is no ventilation system connected to the building.

Equation 1

$$\eta_2 = \frac{Q_0 - Q}{Q_h}$$

Equation 2

$$\eta_4 = \frac{Q_0 - Q}{Q_0 - Q_{nv}}$$

To calculate the coefficients, three simulations are needed. The coefficient η_2 (equation (1)) reflects the useful recovered heat that contributed to the reduction of the heating demand. The coefficient η_4 (equation (2)) represents the reduction in heating demand of the installed system with respect to the increase in heating demand caused by installing a system that does not have a heat recovery strategy. Fig. 1 shows graphically the concepts previously explained. Note that $Q_0>Q>Q_1>Q_{nv}$. Q_h is independent and can be higher or lower than any of the heating demands.

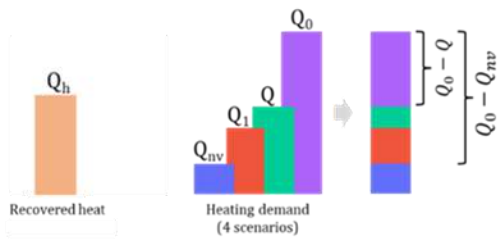

Fig. 1 - Parameters used to calculate the coefficients.

To compare the performance of a system when using non-uniform heating (closer to reality) and uniform heating (closer to regulations) it is possible to get the ratio between η_4 in each heating scenario, which differs only in the heating strategy (uniform and non-

uniform heating). Equation (3) shows the ratio. All parameters associated with the uniform heating scenario are denoted with a "u" subscript.

Equation 3

$$\frac{\eta_4}{\eta_{4u}} = \frac{\frac{Q_0 - Q}{Q_0 - Q_{nv}}}{\frac{Q_{0u} - Q_u}{Q_{0u} - Q_{nvu}}}$$

If the ratio is greater than 1, then the non-uniform heating scenario would be more efficient in recovering energy with respect to its corresponding Q_0 and Q_{nv} scenarios. Also, if the resulting value is below 1, it would indicate that the uniform heating recovers more efficiently the energy than the non-uniform scenario.

The indicators are calculated using specific scenarios applicable to each ventilation system. Consequently, they cannot be used to calculate or estimate annual costs or the thermal performance of the building.

3. Description of the model

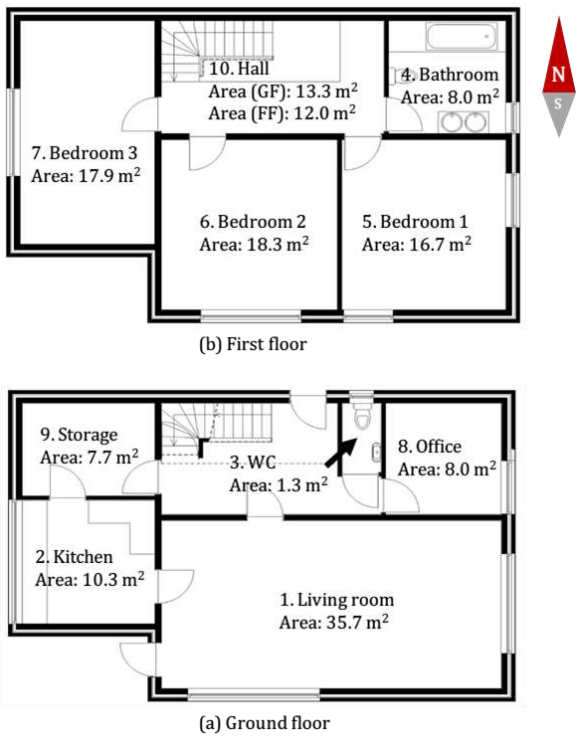

Fig. 2 - Floorplan.

3.1 Building envelope

A representative detached house of the Belgian dwelling stock was selected as the test envelope for this study. The building consists of a living room, a kitchen, an office and a toilet on the ground floor; three bedrooms and a bathroom on the first floor; and an attic on the second floor. The hall, corridor and stairs are combined into a single zone connecting the ground and the first floor. The floorplan of the dwelling is illustrated in Fig. 2, showing the net floor area of all zones. The zone named Hall includes the floor area divided by floor (GF for the ground floor and FF for the first floor). The attic (missing in Fig. 1) is included in the model as a non-conditioned and non-ventilated zone. It occupies almost the entire second floor, except for a part located on top of the Bathroom, Hall and Bedroom 3. The house has a roof with a pitch of 35º. The southern façade is located on the longest dimension of the building, on the side of the kitchen and the living room.

The height of the ground and first floor is 2.55 m, while the second floor has a representative height of 1.8 m. In total, the model has 11 zones shown in Fig. 2. The basement was not included in the model, so the ground floor is in contact with the ground through slabs.

The thermal performance of the building is characterized by the properties of the construction types listed below in Tab. 1. The total heat loss area is 349.9 m^2, which is the summation of all areas listed in the table.

Tab. 1 – Performance of the constructive elements.

Element	Area [m^2]	U-Value [W/m^2/K]	G-Value [-]
Outer Walls	155.6	0.38	-
Roof	88.6	0.48	-
Slabs (ground)	76.6	0.38	-
Win. Glazing	23.9	1.1	0.589
Win. Frames	4.2	0.83	-

3.2 Airflow network

The zones are represented by air volumes and they are connected to other zones and/or boundary conditions representing air or soil. Those connections can exchange energy, air and trace substances carried by the latter. The airflow network is represented by the openings (doors, windows or cavities) between two zones or a boundary condition and a zone; and by the infiltration network, which occurs through the surfaces between zones or between a zone and a boundary condition.

Tab. 2 – Minimum leakage area for doors and windows.

Element	Area [cm^2]
Exterior doors	1
Exterior windows (with frame)	1
Interior doors	70
Interior doors (kitchen)	140

As this study intends to reflect the impact of the temperature gradients in the house, all doors (interior and exterior) and windows remain fully closed all the time, to reduce the mixture of airflows inside the

house that would trend to uniform the temperature in the different zones. It is assumed that the closed doors and windows have a fixed leakage area corresponding to the values shown in Tab. 2:

Doors and windows (including frames) are characterized by their minimum leakage area, while slabs are airtight, considering that on one side there is only soil. Outer walls, roofs, ceilings and floors include submodels that exchange air between both sides. The ruling airflow equation is based on pressure differences and it is proportional to the area of the constructive element. All opaque constructions have the same air permeability, defined by a coefficient that is adjusted during the initialization of the simulation, considering all outer surfaces, to get a global infiltration factor of 2 ACH50. In other words, the model calculates a factor that, when applying a pressure difference of 50 Pa between the interior of the house and the exterior, having all interior openings open (doors) and having all outer openings (windows and doors) closed, the exchanged air through the boundary elements is equal to 2 times the air volume of the house per hour.

For horizontal surfaces (ceilings/floors), the infiltration is represented by one airflow between the upper and the lower connected air volumes, while for non-horizontal surfaces (walls and roofs) there are two airflows at ¼ and ¾ of the height of the surface, used to include the stack effect, characterized by the change in air density in each of the air nodes caused by the weight of the mass of air above, which varies depending on pressure, temperature and moisture.

3.3 Conditioning system

Every zone has its independent conditioning system which is quasi-ideal. It has unlimited power and it reacts almost instantaneously. It can inject or extract heat to or from the conditioned zones, individually, reaching the heating or cooling setpoints immediately. It can work all the time or when someone is present in the zone, depending on the requirements. The share of the heat transfer is 70 % for convective and 30 % for radiative heat, both in heating and cooling modes.

3.4 Setpoint temperatures for conditioning

The setpoint temperatures are defined for the operative temperature (OT) of the zones. The OT is the average between the radiative temperature (the characteristic temperature of the surfaces that enclose the zone node) and the air temperature of the zone.

There are two main scenarios regarding the setpoint temperatures. On one hand, in the uniform-temperature scenario, all conditioned zones in the house are heated up to 18 ºC when heating and cooled down to 26 ºC when cooling operation takes place. For this scenario, all zones in the building are conditioned, except for the attic. In total, 10 zones are conditioned: the living room, the kitchen, the toilet, the office, the storage room, the hall, the bathroom and the three bedrooms. The conditioning system is active all the time in all zones, with or without anybody present.

On the other hand, different setpoints were defined for each type of zone (non-uniform-temperature scenario). A previous study related to thermal comfort dwellings was used to define them [6]. They are based on a reference outdoor temperature ($T_{e,ref}$) which is calculated according to equation (4).

Equation 4

$$T_{e,ref}[ºC] = \frac{(T_{t-0} + 0.8 \cdot T_{t-1} + 0.4 \cdot T_{t-2} + 0.2 \cdot T_{t-3})}{2.4}$$

Where $T_{e,ref}$ is the reference outdoor temperature in [ºC] for the present day, and T_{t-i} ($i \in \{0,1,2,3\}$) the representative temperature of the day i before the present day, which is calculated according to the equation (5):

Equation 5

$$T_{t-i}[ºC] = \frac{T_{\max_{t-i}} + T_{\min_{t-i}}}{2} \; ; i \in \{0,1,2,3\}$$

Where $T_{\max_{t-i}}$ and $T_{\min_{t-i}}$ are the maximum and minimum outdoor temperatures registered on the ith day before the present day, in Celsius degrees. For $i = 0$ the calculations are made for the present day (today).

The same study defines three types of zones for thermal comfort: bathroom, bedroom and the rest of the zones. From $T_{e,ref}$ a neutral temperature (T_n) is calculated for the bathroom (equation (6)), bedroom (equation (7)) and the rest of the zones (equation (8)).

Equation 6

$$T_n[ºC] = \begin{cases} 0.112 \cdot T_{e,ref} + 22.65 & T_{e,ref} < 11 \\ 0.306 \cdot T_{e,ref} + 20.32 & T_{e,ref} \geq 11 \end{cases}$$

Equation 7

$$T_n[ºC] = \begin{cases} 16 & T_{e,ref} < 0 \\ 0.23 \cdot T_{e,ref} + 20.32 & 0 \leq T_{e,ref} < 12.6 \\ 0.77 \cdot T_{e,ref} + 9.18 & 12.6 \leq T_{e,ref} \leq 21.8 \\ 26 & T_{e,ref} > 21.8 \end{cases}$$

Equation 8

$$T_n[ºC] = \begin{cases} 20.4 + 0.06 \cdot T_{e,ref} & T_{e,ref} < 12.5 \\ 16.63 + 0.36 \cdot T_{e,ref} & T_{e,ref} \geq 12.5 \end{cases}$$

All units are in [ºC]. T_n is the temperature at which the least amount of people would not feel comfortable (5 % of dissatisfied people). Fig. 3 shows the neutral temperatures given by the equation (6), equation (7) and equation (8), in function of $T_{e,ref}$.

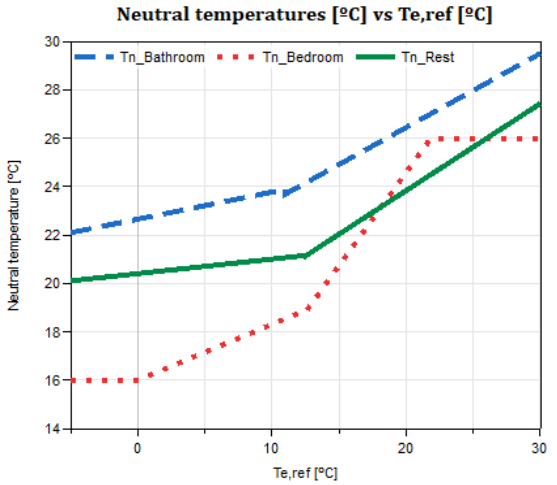

Fig. 3 - Neutral temperatures for bedroom, bathroom and the rest of the zones.

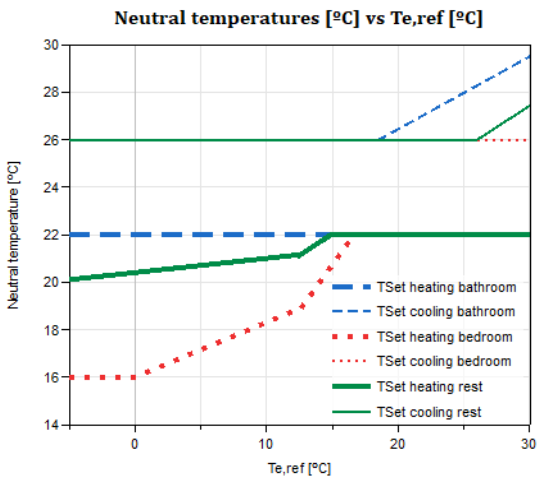

Fig. 4 - Set temperatures for each type of zone for heating and cooling based on T_n.

The conditioning system can provide heating and cooling. Then, using a single setpoint temperature for each type of zone would cause the conditioning system to react to any deviation in the operative temperature around the setpoint in each conditioned zone. This situation would result in higher heating and cooling demands since heating and cooling operations would be required most of the time to compensate for the fluctuations of the operative temperature due to internal and solar gains, as the control is quasi-ideal. Furthermore, looking at the evolution of the setpoints, there are some regions in the setpoints where heating would be discouraged since they correspond to higher values for $T_{e,ref}$, associated with high values for the outdoor temperature (summer). A similar situation can be seen for cooling when looking at the setpoints for lower $T_{e,ref}$ (winter), when cooling should not be activated. To avoid this situation, the heating operation is limited to 22 ºC, while the cooling operation will not take place below 26 ºC. Fig. 3 shows the final setpoint temperatures, for heating and cooling operation, for each type of zone. Between 22 ºC and 26 ºC, the zones will not be heated or cooled.

3.5 Conditioning operation modes

For the uniform-temperature scenario, the conditioning system is activated all the time, so heating or cooling takes place to keep the operative temperature always between 18 ºC and 26 ºC.

For the non-uniform-temperature scenario, the conditioning system is activated exclusively when someone is present in the zone. The conditioning system adjusts the operative temperature immediately according to the defined setpoints when someone enters the zone. Then, the conditioning system is turned off as soon as the room is unoccupied.

3.6 Ventilation flow rates

The building is representative of a dwelling in the Belgian household stock. The requirements for ventilation were calculated according to the national standard NBN D 50-001. The base for the calculated airflow rates is shown in Tab. 3.

Tab. 3 – Airflow requirements.

Zone type	Air flow [l/s]
Habitable spaces	max(1*$Area_{zone}$, 7)
Toilet	7
Bathroom	14
Kitchen	21

Note that the storage room, the hall, and the attic do not have any ventilation requirements, since they are considered non-habitable spaces.

3.7 Ventilation systems

The ventilation systems can be categorized in two ways. Firstly, they can be divided by the ventilation system type (VST) [7], according to the point of air extraction and supply and the way of doing it (mechanical or natural). In this study, VST3, VST4, VST5 and VST7 were investigated. VST3 consist of mechanical exhaust in the exhaust spaces and natural supply using ventilation trickles located in the habitable spaces. VST4 consists of mechanical exhaust in the habitable and exhaust spaces, while the supply consists of trickle vents located in the habitable spaces. Both VST3 and VST4 cannot have a usual heat recovery system, but it is possible to make an equivalence considering that the use of a smart control can avoid releasing heat to the exterior in the exhaust air and count it as a kind of recovered energy. Then, to calculate Q_0, the systems will work at nominal power, without the intervention of the sensors. VST5 consists of direct exhaust in the exhaust spaces (the bathroom, the toilet and the kitchen) and mechanical supply in the habitable spaces (the living room, the office and the three bedrooms). The airflows are centralized and a single heat exchanger can be placed to recover heat from the main exhaust airflow.

Tab. 4 – Design nominal airflows by ventilation system type and ventilation systems. Negative values refer to exhaust.

	Base flows [l/s]	VST3 [l/s]	VST4 [l/s]	VST5 [l/s]	VST5 [l/s]	VST5 [l/s]	VST7 [l/s]
Ventilation systems	**--**	**3a, 3b**	**4**	**5a_c, 5d, 5e, 5f**	**5b_c**	**5c_c**	**7a_c, 7b**
1 Living room	35.7	0	-35.7	35.7	23.8	11.9	-35.7
2 Kitchen	21	-48.4	-21	-48.4	-32.2	-16.1	-21
3 Toilet	7	-16.1	-7	-16.1	-10.7	-5.4	-7
4 Bathroom	14	-32.2	-14	-32.2	-21.5	-10.7	-14
5 Bedroom 1	16.7	0	-16.7	16.7	11.1	5.6	-16.7
6 Bedroom 2	18.3	0	-18.3	18.3	12.2	6.1	-18.3
7 Bedroom 3	17.9	0	-17.9	17.9	11.9	6	-17.9
8 Studio	8.1	0	-8.1	8.1	5.4	2.7	-8.1
9 Storage room	0	0	0	0	0	0	0
10 Hall	0	0	0	0	0	0	0
11 Attic	0	0	0	0	0	0	0
All mechanical supply	96.7	0	0	96.7	64.5	32.2	96.7[2]
All mechanical exhaust	42	-96.7	-138.7[1]	-96.7	-64.5	-32.2	-138.7

[1]The maximum airflow of the real fan is 119 l/s. [2] The trickle vents have two fans: exhaust and supply.

Furthermore, the system is balanced, meaning that the summation of the exhaust airflows is the same as the summation of the supply airflows. Finally, VST7 consist of mechanical exhaust in the exhaust spaces and decentralized exhaust in the habitable spaces using special trickle vents with exhaust fans that can implement heat exchangers to recover heat from the exhaust air. VST1, VST2 and VST6 are not included in the study.

Another division would be between smart and non-smart ventilation systems. The firsts are demand control ventilation systems that use sensors that can measure CO_2 concentration, VOCs concentration and/or humidity located in different zones that are used by the controls to adapt the ventilation flow rates. When the detected signals are below a threshold, the ventilation systems operate at their minimum flow rate. The non-smart ventilation system involves systems that do not have sensors, so they work always at their nominal flow rates.

All smart ventilation systems included in this study are models of commercial systems that can be found in the market. The controls are specific for each system and cannot be published. However, Tab. 4 shows the nominal airflows of each system. The columns for ventilation systems 5b_c and 5c_c represent VST5 systems with reduced airflows (2/3 and 1/3 of the nominal VST5 airflows) for non-smart ventilation systems. It was decided to include these two systems to better understand the impact of the airflows in the heat recovery and to have a non-smart system comparable to smart systems in terms of annual airflows since smart systems optimize the airflows significantly.

3.8 Occupancy profiles

To include human behaviour, a stochastic occupation profile was generated by a modified version of StROBe [8]. The profile is composed of two adults who are full-time workers and sleep in the same bedroom.

Tab. 5 – Presence of people by zone

	presence [%]
1 Living room	3.9
2 Kitchen	11.0
3 Toilet	5.1
4 Bathroom	1.7
5 Bedroom 1	47.0
[6-11] Rest of the zones	0.0
House (anybody at home)	89.4

The profiles appear as direct sources of convective heat, radiative heat, moisture, and CO_2 production for each zone in the model. They vary every 10 minutes and a moving average of a week shows that the profile is quite uniform throughout the year. They include heat and CO_2 production due to metabolic processes, domestic hot water, and appliances such as lights, TV or oven.

The presence in a zone is the ratio between the number of minutes a zone is being occupied by at least one person and the total minutes of the simulation. Tab. 5 shows the presence of the zones, as a percentage. Note that 89.4 % of the time there is at least one

person in the house, so the level of presence is considerable for just two people. This can be explained because their working hours are not the same.

3.8 Weather

The default weather included in IDEAS was used, which is representative of Brussels. The average outdoor temperature throughout the year is 10.8 ºC, which is coincident with the median. The maximum temperature is 19.4 ºC and the minimum is -7.6 ºC, while the first quartile is 5.8 ºC, and the third is 15.6 ºC.

4. Results and discussion

The heating demand is normalized to the net floor area of the building. The ventilation systems are named based on their ventilation system type and those that have the suffix "_c" refer to systems with constant flow rates (non-smart systems). The ventilation system named NV corresponds to the scenario where no ventilation system is installed. Fig. 5 shows the index used to determine the level of IAQ versus the heating demand for all cases, being on the left the uniform heating scenario and on the right the non-uniform heating scenario. The IAQ index is calculated as the summation in all zones of the CO_2 concentration multiplied by the number of people present in each zone and integrated along the year. To have a reference, the horizontal dashed lines represent the indicator for constant CO_2 concentrations. Values below the line of 400 ppm are not possible since this is the ambient CO_2 concentration in the model.

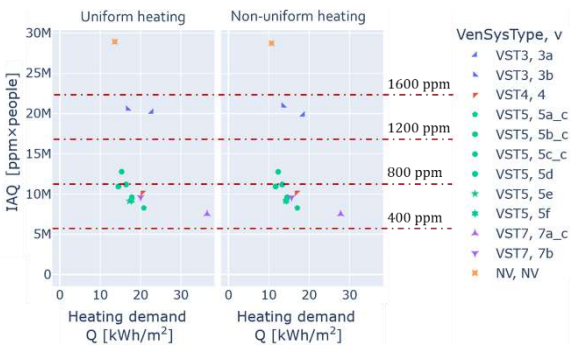

Fig. 5 – IAQ index vs heating demand

The results are very similar for both heating strategies. For IAQ the values are almost the same, while for the heating demand, uniform heating uses around 15 % more heating energy than non-uniform heating. VST4, VST5 and VST7 have quite good behaviour both in IAQ and heating demand, compared to other cases. However, 7a_c has an extraordinary high heating demand (2.5 times the heat used by NV) combined with a comparative very good IAQ, since its exhaust airflows are quite large (see Tab. 4). The system 5d has the lowest energy heating demand (apart from NV). Both VST3 systems have the worst IAQ behaviour (1.5 to 3 times the IAQ values of the rest of the systems). The heating demand of the system 3a is the second most inefficient, while 3b uses similar heating energy as 5b_c, which is a quite low value.

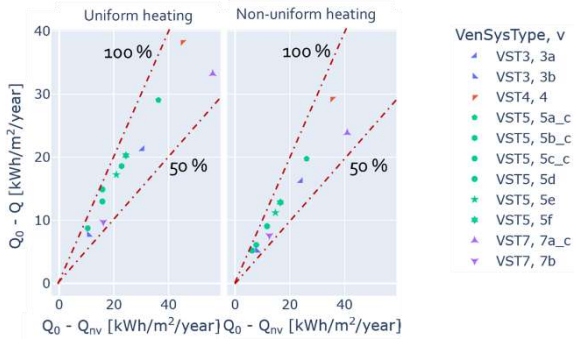

Fig. 6 – η_4: $(Q_0 - Q)$ vs $(Q_0 - Q_{nv})$

The factor η_4, which indicates how much of the heating demand caused by ventilation is successfully reduced by the installation of a heat exchanger (or, in the case of VST3 and VST4 systems, by the installation of a smart control), is shown in Fig. 6. The systems that have lower η_4 belong to VST7, followed by VST3, while VST5 and VST4 tend to have the highest values for η_4. The values for Q_{nv} are smaller for non-uniform heating, which corresponds to the lower heating demand seen before. However, the interest of this work is to look at the ratio η_4/η_{4u}, to see how efficient the systems are depending on the heating strategy. The graphical representation of the factor is shown in Fig. 7. The lowest value for η_4/η_{4u} is for 5d (0.88), which is also the system with the lowest heating demand. The highest value corresponds to 7b (1.01), while 7a_c has a value close to 1.0.

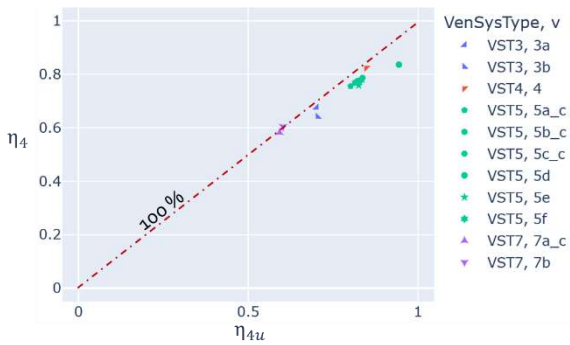

Fig. 7 – η_4 vs η_{4u}

The previous figure shows that only the heat recovery in ventilation systems of VST7 (7a_c and 7b) have an equivalent behaviour when using non-uniform heating than when using uniform heating. The rest of the ventilation systems perform better, in regard to their contribution to their respective heating demand reduction, when using uniform heating. This can be explained because in central ventilation systems the exhaust airflows are merged into a single airflow which temperature is lower than the air in the warmer zones. The recovered heat is distributed among the habitable spaces. Some of them would have a reduction in heating demand, while others will receive the recovered heat although they do not need heating.

As VST7 are distributed systems, they work with the optimal temperatures for each room. Every zone has the potential to recover its exhaust heat, so the heat is not wasted in zones that do not need extra heating. It is important to remark that the ratio η_4/η_{4u} compares two different heating strategies and the result tells how good the recovered heat of each (or unwasted heat, in VST3 and VST4) contributes to reducing the part of the heating demand that is associated with the installation of a ventilation system without any heat exchanger (or with a constant flow for VST3 and VST4). This extra demand is different for each heating strategy and, in all ventilation systems used in this study $(Q_{0u} - Q_{nvu})$ was greater than $(Q_0 - Q_{nv})$ (Fig. 6).
Looking at Fig. 5, the heating demand is 15 % higher in uniform heating scenarios than in non-uniform heating scenarios in all the cases. This situation can be tricky since higher heating demands use more recovered heat (or heat that is not unnecessarily wasted to the exterior in VST3 and VST4) to reduce the demand: more of the recovered heat (unwasted heat for VST3 and VST4) becomes useful heat that contributed to the reduction in the heating demand. This can be seen looking at η_2. Fig. 8 shows this ratio for all ventilation systems that have a heat exchanger. In all cases, η_2 is higher in the uniform heating scenario, meaning that, proportionally, the recovered heat is more useful when using uniform heating.

Fig. 8 – η_2 for all ventilation systems that have one or more heat exchangers.

5. Conclusion

The determination of the impact of temperature gradients on heating demand can be difficult since the recovered heat (or the unwasted heat in systems without heat exchangers) affects the conditions of the zones all the time. Many factors are involved in the analysis, and it becomes difficult to come to a conclusion that could be extrapolated to other cases. For this case study, the factor η_4 is greater for uniform heating than for non-uniform heating, but this could also be affected by a higher heating demand for uniform heating. Centralized heat recovery systems perform better in the scenarios with uniform heating, while distributed ventilation systems perform similarly with both heating strategies.

The shown indicators cannot be used to determine the energy performance of the building in absolute terms. The annual heating demand is different depending on the heating strategy used and additional indicators are needed to make complementary comparisons. Furthermore, the electric power of the fans is not reflected, as the indicators are calculated using the heating demand.

This study needs to be extended with more buildings, as well as typologies, such as schools, offices, etc. to determine the effect of the temperature gradients and check if there is a relation with the results from this study and if it is possible to quantify the effect with the used ratios and get representative results.

6. Acknowledgement

The work presented in this paper has been developed within the frame of the AIVC project *Assessment of the effect of indoor temperature differences and zoning on the performance of energy efficient ventilation strategies for domestic buildings*. This financial support is gratefully acknowledged.

7. References

[1] Kim MK, Baldini L, Leibundgut H, Wurzbacher JA, Piatkowski N. A novel ventilation strategy with CO_2 capture device and energy saving in buildings. Energy and Buildings. 2015 Jan;87:134–41.
[2] O'Connor D, Calautit JKS, Hughes BR. A review of heat recovery technology for passive ventilation applications. Renewable and Sustainable Energy Reviews. 2016 Feb;54:1481–93.
[3] Omer AM. Renewable building energy systems and passive human comfort solutions. Renewable and Sustainable Energy Reviews. 2008 Aug;12[6]:1562–87.
[4] Jorissen F, Reynders G, Baetens R, Picard D, Saelens D, Helsen L. Implementation and verification of the IDEAS building energy simulation library. Journal of Building Performance Simulation. 2018 Nov 2;11[6]:669–88.
[5] Faes W, Monteyne H, De Paepe M, Laverge J. Useful energy transfer in air-to-air heat recovery units in partly heated low energy buildings. In: Proceedings of the 15th IBPSA Conference [Internet]. 2017 [cited 2022 Jan 13]. p. 2701–7. Available from: http://hdl.handle.net/1854/LU-8550254
[6] Peeters L, Dear R de, Hensen J, D'haeseleer W. Thermal comfort in residential buildings: Comfort values and scales for building energy simulation. Applied Energy. 2009 May;86[5]:772–80.
[7] NEN. NEN 1087: 2019 'Ventilatie van gebouwen - Bepalingsmethoden voor nieuwbouw'. 2019;
[8] Baetens R, Saelens D. Modelling uncertainty in district energy simulations by stochastic residential occupant behaviour. Journal of Building Performance Simulation. 2016 Jul 3;9[4]:431–47.

The datasets generated during the current study are not available yet because this work is a part of an ongoing project. They will be released in the following months. Contact the author for further details.

Stratification and draught measurements of ceiling panels, underfloor cooling and fan-assisted radiators

Karl-Villem Võsa[a,b], Egert Eist[b], Jarek Kurnitski [a,b,c]

[a] FinEst Centre for Smart Cities (Finest Centre), Tallinn University of Technology, 19086 Tallinn, Estonia

[b] Nearly Zero Energy Buildings Research Group, Ehitajate tee 5, 19086 Tallinn, Tallinn University of Technology, Estonia

[c] Aalto University, School of Engineering, Rakentajanaukio 4 A, FI-02150 Espoo, Finland

Abstract. This paper reports the results of room conditioning unit measurements carried out in a NZEB test facility in 2021. Ceiling panels, fan-assisted radiators and existing underfloor heating contours were tested in several experimental configurations, operating with relatively high chilled water flow temperatures as these are all non-condensing systems. Time-controlled heating dummies were used to imitate internal heat gains along with the natural solar irradiation to vary the cooling demand. We quantify the vertical temperature gradients due to thermal stratification by measuring air temperatures at various heights. We also present the differences in thermal comfort of the tested systems, as we measure the air velocities and operative temperatures at points of occupancy with a standardised measurement probe. The gradient and operative temperature values affect the cooling emission efficiency which can be compared against an ideal cooling emitter. Measured results can be used to develop a new method for quantification of cooling emission efficiency. The annual emission efficiency can be assessed by applying measured values under different boundary conditions as inputs to simulation models.

Keywords. Cooling, thermal comfort, underfloor cooling, fan-assisted radiator, fan coil, ceiling panel, thermal stratification
DOI: https://doi.org/10.34641/clima.2022.170

1. Introduction

In the face of climate changes, current HVAC system design principles may not be sufficient for sustainable system operation in future climate conditions. Global policies target restricting the median warming to 1.5 °C by year 2100 [1]. Projections indicate more frequent, intense and longer-lasting heat waves [2], which has implications on the cooling loads and energy demands [3], as well as on the well-being of occupants [4], [5]. Therefore, it is of increasing importance to accurately assess emission efficiency of cooling systems.

According to EN 15316-2, space emission system efficiency is evaluated as a sum of different cooling set-point offsets, which reflect system inefficiencies in the distribution, control, and emission of the system [6]. This shifted set-point temperature is then used to calculate the annual cooling energy demand. A discrete set of values default values is given within the latest iteration of the standard, with the possibility of using product-specific values or different tabulated values from national annexes. However, procedures for measuring and calculating these parameter values are not specified in detail.

This study reports results from a set of experimental measurements that are going to be used in annual energy simulations, from which these set-point variations are going to be derived. In particular, thermal stratification, thermal comfort and system cooling capacities are analysed in detail.

2. Research methods

2.1 nZEB test facility

Tests of the cooling devices were conducted in the nZEB test facility at Tallinn University of Technology depicted in **Fig. 1**. Four different cooling devices were installed in the largest room of the facility – a 30 m^2 conference/classroom located on the east side of the building, seen in **Fig. 2**. This room has four windows, two on the east-facing external wall and one on both the north and south facades. The test room has a false ceiling and the whole building has a ventilated crawlspace.

Copyright ©2022 by the authors. This conference paper is published under a CC-BY-4.0 license.

Fig. 1 – Tallinn University of Technology nZEB test facility

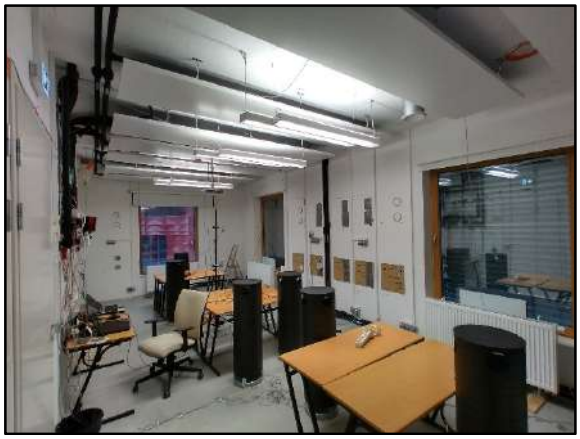

Fig. 2 – General view of the testing premises.

2.2 Ceiling panels

A total of eight ceiling panels (600 x 3000 mm) were installed using suspension cables at an installation height of 2.85 m, or 0.15 m from the ceiling (relative to the room facing side). The ceiling facing side was insulated with manufacturer provided mineral wool insulation plates. These ceiling panels were installed in four pairs, with the panels in series connection within the pair. Detailed geometry, positioning and hydraulic connections of the setup are shown in **Fig. 3.** Nominal conditions and cooling output for a serially connected pair is given in **Tab. 1**.

Tab. 1 - Ceiling panel specifications.

Parameter	Value
Supply temperature, °C	15.0
Return temperature, °C	19.0
Room air temperature, °C	25.0
Volume flow, l/h	76.3
Pressure loss, kPa	13.2
Cooling output per pair, W	354.7

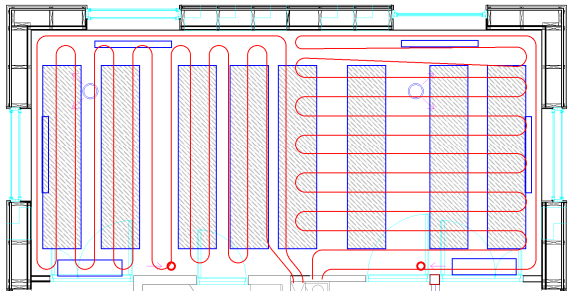

Fig. 3 – Positioning of ceiling panels and underfloor cooling loops.

Fig. 4 – Array of fans with the covering grille removed (left) and view of cooling radiator (right).

2.3 Fan-assisted radiator

Four type 22 steel panel radiators (600 x 1200 mm, two panels two convective fins) were installed in place of previously installed radiators under the windows of the test room. An array of fans is installed on top of the radiator under the cover grille to enhance the cooling output of the radiator. These fans displace air through the channel upwards into the room to prevent a cold down-draught to the floor. This fan speed is controlled according to the temperature difference between the air entering the channel and surface of the cooling panel. The specification and view of these radiators is shown in **Tab. 2** and **Fig. 4**.

Tab. 2 – Cooling radiator specifications.

Parameter	Value
Supply temperature, °C	15.0
Return temperature, °C	17.5
Room air temperature, °C	28.1
Volume flow, l/h	131.8
Cooling output, W	390.0

Tab. 3 – Fan coil unit specifications.

Parameter	Value
Supply temperature, °C	7
Return temperature, °C	12
Room air temperature, °C	27
Air volume flow, m^3/h	390
Fan power input, W	28
Volume flow, l/h	511
Pressure loss, kPa	35.6
Cooling output, W	2120

2.4 Underfloor cooling

Existing underfloor heating loops were used for the testing of underfloor cooling. Supply and return lines before the manifold were retrofitted with 3-way and isolating valves to switch to the cooling circuit. PE-PEX pipes (20 x 2.0 mm) are installed in a 40 mm screed layer with a 300 mm spacing between pipes. The cooling output of this set-up was estimated to be 750 W (25 W/m^2) at operating conditions (14.0/17.0/26.0 °C supply/return/room air temperature). The geometry of the piping is shown in **Fig. 3**.

2.5 Fan coil unit

Two existing wall-mounted FCUs were used. Nominal cooling capacity and operating conditions at the lowest fan speed are listed in **Tab. 3**. The FCUs were operated at the lowest fan speed setting during the measurements.

2.6 Hydraulic installation and cooling generation

Chilled water was produced into a buffer tank with a heat pump. This heat pump operated on a single compressor speed; therefore, the chilled water set-point temperature was set to +10 °C with a hysteresis of ±2 °C to ensure there was sufficiently low temperature delivered to the mixing valve.

A 3-way mixing valve (3 mm travel) was used to control the supply temperature to the cooling devices. The valve was operated with a TA Slider 160 actuator, which got its input signal from a temperature control loop implemented in Python utilizing the simple-PID library. The following controller parameters were used: K_p=1800, K_i=60, K_d=13500, when considering the general PID formulation in equation (1).

$$u(t) = K_\mathrm{p} e(t) + K_\mathrm{i} \int_0^t e(\tau)\,\mathrm{d}\tau + K_\mathrm{d} \frac{\mathrm{d}e(t)}{\mathrm{d}t} \qquad (1)$$

Flow rate to the devices was set using a TA STAD-15 balancing valve. The flow measurement accuracy from the differential pressure over the balancing valve was however insufficient (4 % at best). Instead, a separate ultrasonic water meter was used to measure the volumetric flow rate in the secondary loop.

2.7 Measurement equipment

In the hydraulic part of the system, temperature sensors were installed in thermowells to monitor the chilled water supply and return temperatures both on the primary and secondary sides. Water flow rate was measured with an ultrasonic water meter installed on the return pipe of the secondary side.

A total of 25 sensors were used to measure various air and surface temperatures inside the tested room as well as air temperatures of the bounding rooms (corridor, toilet, two testing rooms) and behind the false ceiling and in the crawlspace. Sensor locations are shown in **Fig. 5** and **Fig. 6**.

A dedicated set of five thermo-anemometers, operative temperature sensor and a relative humidity sensor installed on a tripod were used to measure the gradients and air flow speeds at a pre-determined location for all systems.

FLIR E95 thermal camera was used to capture temperature distribution from the thermal images of the cooling devices. A fog generator was used to visualize the air distribution of the different systems. Ventilation air flow rates were set using both a capture hood and differential pressure manometer with valve position measurement.

Main specifications of the sensors used are listed in **Tab. 4**.

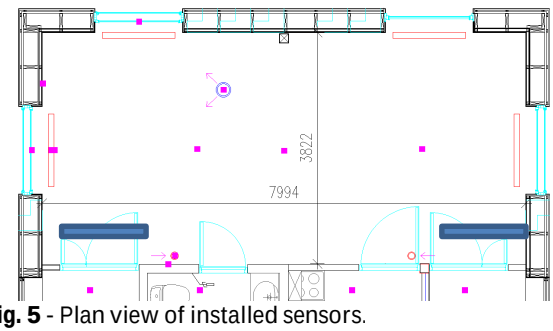

Fig. 5 - Plan view of installed sensors.

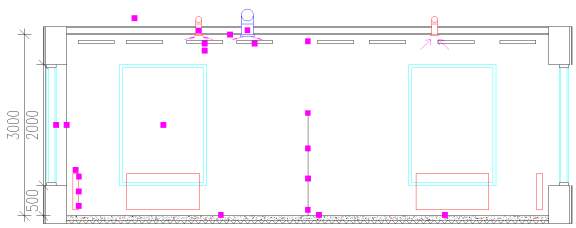

Fig. 6 - Section view of installed sensors.

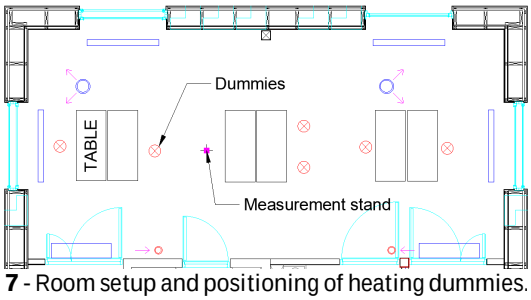

Fig. 7 - Room setup and positioning of heating dummies.

2.8 Internal heat gains

A total of six heating dummies were used in the tests, see the black cylinders in **Fig. 2**. These dummies have 3 incandescent lamps with a rated output of 3x60 W per dummy, in accordance with EN 14240 [7]. Two additional electric radiators with rated heat output of 1000 W were used to further provide a sufficient cooling load. Positioning of the dummies and radiators can be seen in **Fig. 7**.

2.9 Test conditions

The ceiling panels and radiators were tested at two nominal cooling outputs, HIGH output of 800 W (26.7 W/m²) and LOW output of 1200 W (40.0 W/m²), while the FCU was tested only at 1200 W and the underfloor cooling at 800 W. Targeted room air temperature during these tests was 25 °C. Supply and extract air flow rates were set to 1.5 l/(sm²), or 23 l/s per valve. Supplied air temperature was 19±1.5 °C.

Chilled water was supplied at temperatures between 15.0-18.5 °C, depending on the system in use. Volumetric flow rate to devices was kept at 300-350 l/h. External blinds were lowered for all tests to minimize variance from solar loads between the tests. Measurements took place in October-November.

Tab. 4 – Sensor specifications

Sensors	Meas. range	Accuracy
Fluid temperature	-50...+250 °C	±0.15+0.002|t| K
Air temperature	-40...+50 °C	±0.15 K
Surface temperature	-40...+50 °C	±0.15 K
Flow meter	0...3.125 m³/h	±3 %
Thermo-anemometer	0.05...5.00 m/s	±0.02 m/s
	-20...+80 °C	±0.20 K
Operative temp.	0...+45 °C	±0.20 K
Relative humidity	0...100 %	±1.50 %

2.10 Thermal comfort

Air stratification and vertical temperature distribution were assessed in two parts – the vertical air temperature difference γ_1 (head-ankle) according to standard EN16798-1 [8] and the total gradient between the ceiling and floor γ_{TOT}:

$$\gamma_1 = t_{1.1} - t_{0.1} \quad (2)$$

$$\gamma_{TOT} = t_{2.9} - t_{0.1} \quad (3)$$

where t_z is the air temperature at the specified height z in meters. The operative temperature probe was installed at a height of h = 1.10 m reclined to 30° from the vertical position. This value was compared to the air temperature at the same height, to assess whether a higher room air temperature can be allowed while keeping the same sensed temperature level of the occupant. Velocity data from the thermo-anemometers was also logged and analysed from the tripod setup. A typical set-up of this tripod is shown in **Fig. 8**.

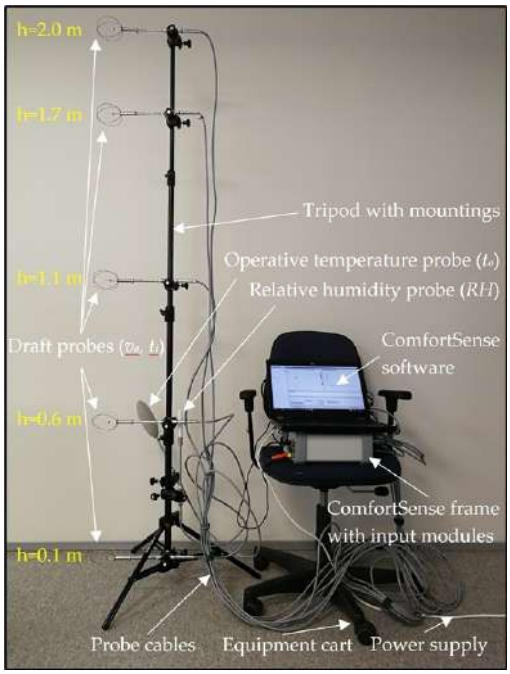

Fig. 8 – Thermal comfort measurement tripod.

3. Results

Hydraulic data and measured cooling outputs for each of the measurements is shown in **Tab. 5**.

3.1 Cooling power output

From **Tab. 5**, it is seen that the measured power is within ±10 % of the intended cooling outputs, except for the FCUs. Such deviations are inevitable, as the test room itself is part of the building susceptible to dynamic processes from both the external as well as internal boundaries (versus tailored test chambers, where all boundary conditions can be carefully measured and controlled).

Measurement accuracy of the cooling output is mostly affected by the low differential temperature in the supply and return temperatures of the chilled water. With temperature differences of 2...4 °C, the worst-case error from the temperature measurements can be 10...20% considering the around ±0.20 °C accuracy of the sensors at the measured temperatures. This could be improved with additional temperature differential sensors.

Tab. 5 – Test conditions, 1 h average.

System	Supply temperature, °C	Return temperature, °C	Room air temperature, °C	Chilled water flow rate, l/h	Cooling power, W	Cooling power, W/m²
Ceiling panels HIGH	15.09	17.96	25.38	335	1128	36.7
Ceiling panels LOW	18.50	20.60	26.66	337	820	26.7
Fan-assisted radiator HIGH	15.00	17.70	24.98	338	1061	34.6
Fan-assisted radiator LOW	15.25	17.41	25.14	345	869	28.3
Underfloor cooling	15.00	17.19	25.84	328	836	27.2
Fan coil units	17.00	21.00	25.88	334	1552	50.6

3.2 Temperature gradients

The underfloor cooling system had the highest temperature gradient by far, with γ_1 = 2.93 K/m and γ_{TOT} = 1.51 K/m (**Fig. 9**). This is the only measured system which at the measured cooling outputs falls into thermal comfort class II according to EN 16798-1 [8]. This falls in line with our expectations, as the cooled air mass near the floor is denser and does not induce a buoyancy effect to mix within the room. Conversely, the fan coil unit has almost no temperature gradient in the occupied zone, with only some temperature rise at h = 2.90 m, γ_1 = 0.14 K/m and γ_2 = 0.57 K/m, respectively ( ). High wall-mount is excellent for buoyancy-driven mixing within the room. The fans also help significantly to diminish the stratification.

Cooling panels and radiators both exhibited similar behaviour at the higher cooling output, with virtually no stratification in the occupied zone (**Fig. 11** and **Fig. 12**). At the lower cooling output, there is some stratification, γ_1 = 1.35 K/m and γ_2 = 0.55 K/m for ceiling panels and radiators, respectively.

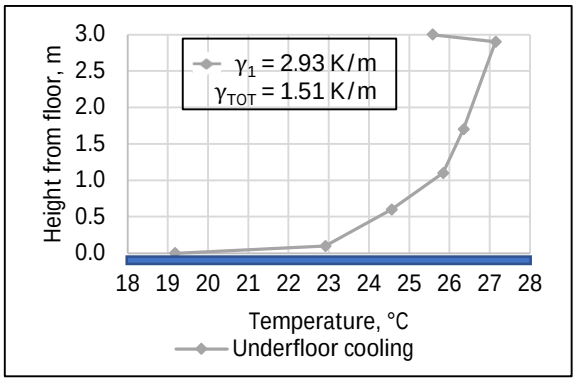

Fig. 9 - Measured gradient of underfloor cooling.

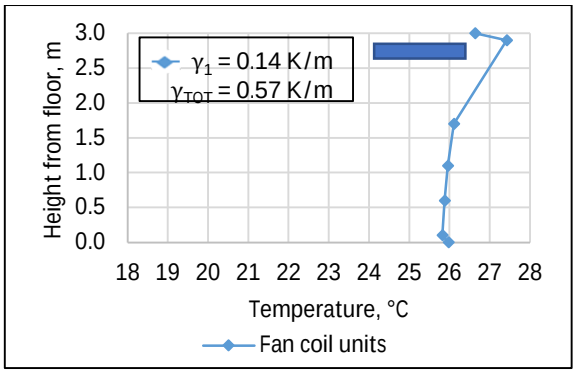

Fig. 10 - Measured gradient of fan coil units.

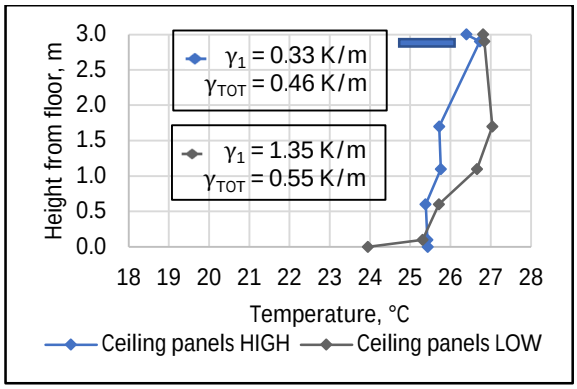

Fig. 11 - Measured gradient of ceiling panels.

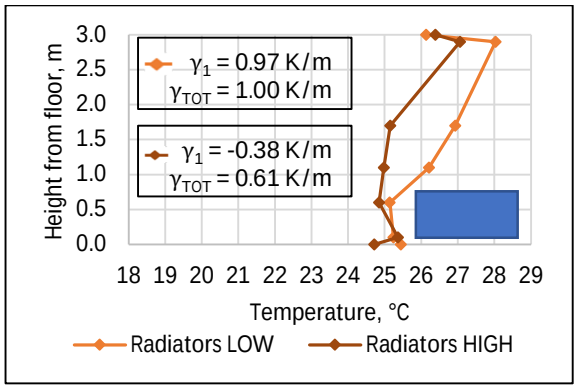

Fig. 12 - Measured gradient of radiators.

3.3 Operative temperature

We measured a sizable difference between the operative and air temperatures as shown in **Fig.** 13. Systems with greater surface areas (ceiling panels and underfloor cooling) have, with a difference as low as -1.28 °C for ceiling panels measured at the lower cooling output. Similarly, the FCUs have the opposite effect, with t_{op}-$t_{1.1}$ = 0.27 °C.

There is a causal effect between the measured gradient and t_{op}-$t_{1.1}$ value, which is why for both the ceiling panels and underfloor cooling, the lower cooling outputs have a higher temperature differential. Higher radiant heat exchange to the colder surface is offset by the lower temperature gradient value.

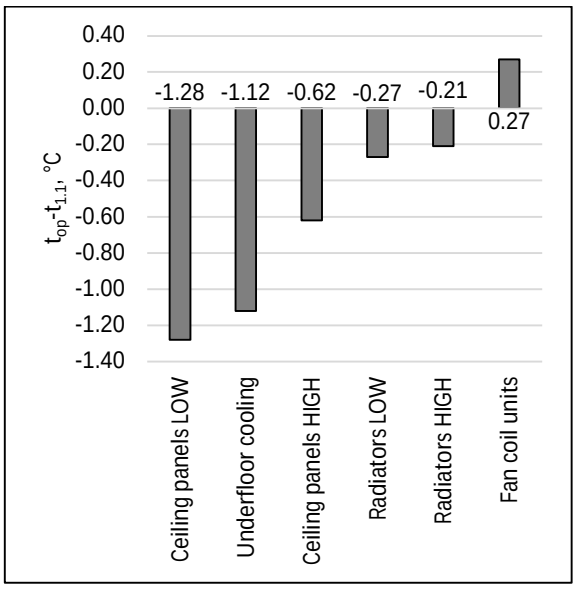

Fig. 13 – Measured operative and air temperature difference.

3.4 Air velocities

Air velocity measurements from the thermal comfort tripod are shown in **Tab 6**. These results are consistent with the thermal stratification seen in the previous section – higher velocities lead to higher mixing of air and vice versa.

For the FCU system, the air velocities in the occupied zone for both a seated and standing occupant are outside category III in accordance with EN 16798-1 [8]. Air velocities for the underfloor cooling are minimal, with average values of 0.02 m/s for both a seated and standing occupant.

We observed higher air velocities in the radiator HIGH tests compared to the radiator LOW tests, which was the excepted result as the fan speed was increased to the maximum output in those tests. Still, the measured air velocities were low enough to stay within the first category of thermal comfort.

Interestingly, this was not the case for ceiling panel HIGH and LOW outputs, with the air velocities being as high as 0.26 m/s at h = 1.70 m for the LOW case. These tests were conducted on different weeks, so it is possible that external factors skewed these measurement results. One would expect that if the higher cooling output achieved Cat. I in thermal comfort, the same would hold true for the lower cooling power.

3.5 Thermal imagery and measured surface temperatures

Thermal imagery of measured systems under selected test conditions are depicted in **Fig. 14**–**Fig. 17**. Visualized temperatures are based on a surface emission of ε=0.95.

The temperature distribution due to the fans drawing air through the radiator's panels can clearly be seen in . The perimeter of the radiator is cooler, as the convective heat transfer is lower due to lower air speeds.

Fig. 14 - Thermal image of radiator HIGH.

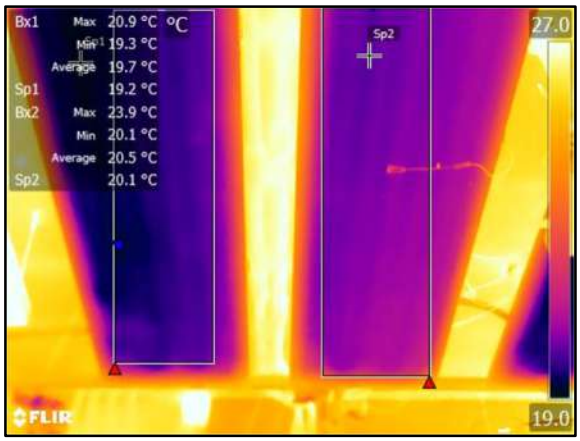

Fig. 15 - Thermal image of ceiling panels LOW.

Tab. 6 – Average air velocities measured on the tripod. Cat. I in green, Cat. II in yellow, Cat. III in orange and exceeding thermal comfort class boundaries in red, white for points outside occupied zone.

Height/ System	Ceiling panels HIGH, m/s	Ceiling panels LOW, m/s	Radiators HIGH, m/s	Radiators LOW, m/s	Underfloor cooling, m/s	Fan coil units, m/s
2.90 m	0.19	0.06	0.11	0.19	0.08	0.19
1.70 m	0.07	0.26	0.08	0.07	0.02	0.88
1.10 m	0.04	0.13	0.12	0.04	0.02	0.45
0.60 m	0.10	0.03	0.09	0.10	0.02	0.25
0.10 m	0.03	0.03	0.06	0.03	0.02	0.61

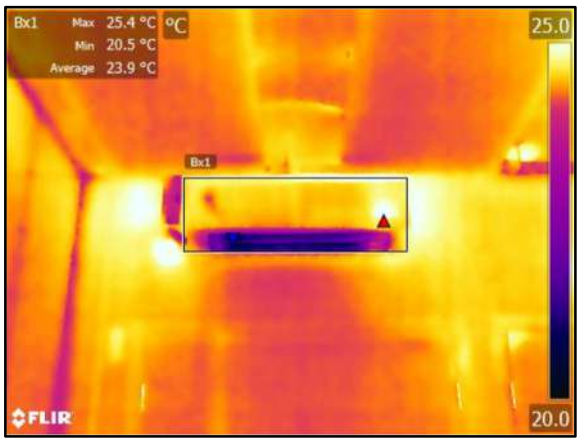

Fig. 16 - Thermal image of FCUs.

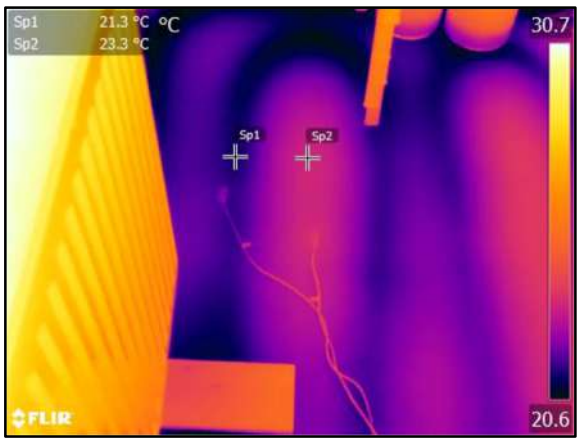

Fig. 17 - Thermal image of underfloor cooling.

Thermal image of a serially connected pair of cooling panels is shown in **Fig. 15**. The panel on the left has lower surface temperatures as it is connected directly to the supply line of the chilled water loop, while the supply of the panel on the right is connected to the return line of the panel on the left. In our measurements, there was an average of 1.0 °C surface temperature difference between the two panels.

The cooling coil of the FCU is seen in **Fig. 16**. This is mainly a convective system, the radiative heat transfer and its effect on operative temperature is minimal as the surface area and solid angle between the occupant and the coil is insignificant.

In **Fig. 17**, a section of the underfloor cooling system can be seen. A temperature difference of 2.0 °C was observed on top of the pipe and between the pipes (Sp1 and Sp2 on the image).

Surface temperatures were also measured at several locations, these results are tabulated in **Tab. 7**.

3.6 Limitations

Some limitations must be pointed out to understand which scope these results and conclusions should be interpreted.

Tab. 7 – Measured surface temperatures.

Device	Sensor	Temp., °C
Ceiling panels HIGH	1st in series	16.30
	2nd in series	17.75
Ceiling panels LOW	1st in series	19.36
	2nd in series	20.38
Radiators HIGH	h = 0.05 m	17.88
	h = 0.30 m	18.61
	h = 0.55 m	-
Radiators LOW	h = 0.05 m	17.37
	h = 0.30 m	19.02
	h = 0.55 m	19.41
Underfloor cooling	On supply pipe	17.85
	b/w supply pipes	19.03
	On return pipe	19.65
	b/w return pipes	20.37

These tests were conducted in autumn months of September-November, which are not in the typical cooling season for Estonia. This was an intentional choice to maintain boundary conditions to make the measurements results less susceptible to uncontrollable solar loads and external temperature swings. Furthermore, the internal heat gains used in the rooms were static loads, while cooling systems typically operate in dynamic conditions both from solar gains and from occupants, equipment, and lights. Thus, the inertia of the systems and control strategies are not assessed in this study.

There is also some effect on the internal surface temperatures and thus the operative temperatures from the chosen season of the tests. This is a function of the insulation of the external walls, which for our case is highly insulated with a thermal transmittance of 0.12 W/(m^{2}K). In poorly insulated boundaries, the mean radiant temperature of these boundaries can be significantly different depending on the outdoor temperature.

Risk of condensation was not assessed in detail. Latent load of the rooms was minimal, primarily from the supply air of the ventilation, which is typically more humid than during the tests. In real application, proper control measures must be taken to avoid condensation on the surfaces of the radiators, ceiling panels and the floor.

The tested systems have a relatively low cooling capacity by design (except the FCUs) and are suitable to be used in spaces where the cooling loads are <50 W/m^2. Furthermore, the measured gradients could vary throughout the room and may not describe the average gradient in the whole room. Therefore, the positioning of sensing equipment is crucial during the measurement and in the interpretation of the results. When considering the temperature gradients for the purposes of energy efficiency assessment, it must be noted that here only one or two cooling

output levels were measured. More measurements at different partial loads would give a more complete overview of the resulting temperature gradients, still subject to the effect of other boundary conditions as well, mainly the ventilation supply temperature and flow rate, but also the internal and external surface temperatures in the room.

4. Conclusions

Four room cooling devices were measured at a nominal cooling output 1200 W (40 W/m^2). This output was not reached for the underfloor cooling, where a capacity of 27 W/m^2 was reached instead at an average floor temperature of 19 °C. In rooms where the cooling loads are higher than 50 W/m^2, only the FCU has sufficient cooling capacity out of the tested devices. Other devices rest rely primarily on radiant heat transfer, which is limited in its cooling capacity.

Significant stratification was observed for the underfloor cooling. For a seated occupant, the head-ankle temperature difference of 2.93 K was measured, which barely achieves category II thermal comfort class for vertical temperature variation, while a standing occupant classifies to category III. Other systems exhibited milder stratification: overall temperature gradients were 1.00 K/m or less, with–all systems achieved thermal comfort category I.

In conjunction with the stratification, the difference between the operative and air temperature was assessed for all systems. In general, systems with larger radiant surfaces showed lower operative temperatures. This is an advantage for the energy efficiency of such radiant systems, as the same comfort level can be achieved at a higher air temperature. It is important to note that this temperature difference is influenced by the vertical temperature distribution as well, and from viewpoint of energy efficiency must be assessed simultaneously.

Finally, air velocities were also analysed. As expected, the fan coil units had the highest average velocities. Even at the lowest fan speed setting, a significant area around the FCU is far beyond the category III limit for air velocity, being unsuitable for typical office work. Other systems had lower velocities classifying to category I, except for the LOW ceiling panel, where likely the upward plume from the heating dummies prevailed instead.

5. Acknowledgement

This work has been supported by the Estonian Ministry of Education and Research, European Regional Fund (grant 2014-2020.4.01.20-0289), the Estonian Centre of Excellence in Zero Energy and Resource Efficient Smart Buildings and Districts, ZEBE (grant 2014- 2020.4.01.15-0016) funded by the European Regional Development Fund, by the European Commission through the H2020 project Finest Twins (grant No. 856602), the Estonian Research Council grant (PSG409) and the Association of the European Heating Industry EHI member companies Orkli, Purmo Group, Zehnder Group and Vasco.

6. References

[1] J. Rogelj *et al.*, 'Scenarios towards limiting global mean temperature increase below 1.5 °C', *Nature Climate Change*, vol. 8, no. 4, pp. 325–332, Apr. 2018, doi: 10.1038/s41558-018-0091-3.

[2] G. A. Meehl and C. Tebaldi, 'More Intense, More Frequent, and Longer Lasting Heat Waves in the 21st Century', *Science*, vol. 305, no. 5686, pp. 994–997, 2004, doi: 10.1126/science.1098704.

[3] D. D'Agostino, D. Parker, I. Epifani, D. Crawley, and L. Lawrie, 'How will future climate impact the design and performance of nearly zero energy buildings (NZEBs)?', *Energy*, p. 122479, 2021, doi: https://doi.org/10.1016/j.energy.2021.122479.

[4] D. M. Hondula, R. C. Balling, J. K. Vanos, and M. Georgescu, 'Rising Temperatures, Human Health, and the Role of Adaptation', *Current Climate Change Reports*, vol. 1, no. 3, pp. 144–154, Sep. 2015, doi: 10.1007/s40641-015-0016-4.

[5] D. Bienvenido-Huertas, C. Rubio-Bellido, D. Marín-García, and J. Canivell, 'Influence of the Representative Concentration Pathways (RCP) scenarios on the bioclimatic design strategies of the built environment', *Sustainable Cities and Society*, vol. 72, p. 103042, 2021, doi: https://doi.org/10.1016/j.scs.2021.103042.

[6] C. E. de Normalisation, 'European Standard EN 15316-2: 2017. Energy performance of buildings. Method for calculation of system energy requirements and system efficiencies. Space emission systems (heating and cooling), Module M3-5', M4-5., Tech. rep., CEN, Bruxelles, BE, 2017.

[7] B. CEN, '14240: 2004 Ventilation for buildings–Chilled ceilings–Testing and rating offers a testing method for chilled ceilings'. CEN, 2004.

[8] EN 16798-1: 2019, 'Energy Performance of Buildings—Ventilation for Buildings—Part 1: Indoor Environmental Input Parameters for Design and Assessment of Energy Performance of Buildings Addressing Indoor Air Quality, Thermal Environment, Lighting and Acoustics—Module M1-6'. European Committee for Standardization Brussels, Belgium, 2019.

Benchmarking the measured energy use of Nordic residential buildings and their Zero Energy-readiness

Andrea Ferrantelli[1,2], Martin Thalfeldt[1,2], Jarek Kurnitski[1,2,3]

[1] FinEst Centre for Smart Cities (Finest Centre), Tallinn University of Technology, 19086 Tallinn, Estonia
[2] nZEB Research Group, Tallinn University of Technology, 19086 Tallinn, Estonia
[3] Department of Civil Engineering, Aalto University, 00076 Aalto, Finland

Abstract. It is well known that buildings are responsible for a nearly 40% share of the total energy consumption; in order to reduce it by improving the energy efficiency of the building stock, it is necessary to first evaluate their performance. Building energy benchmarking provides information to stakeholders and motivates energy retrofits, by evaluating and comparing a building to similar units and/or to a reference building in terms of energy consumption with the minimum amount of data possible.

Towards this end, in this paper we analysed nearly 19000 Estonian Energy Performance Certificates (EPCs) of detached houses. By means of a systematic statistical investigation, we determined the time evolution of EPC labels and evaluated the impact of incentives pre/post renovations, drawing a comprehensive and updated picture of the Estonian detached houses. This allowed evaluating their readiness based on recent trends: unfortunately, new or renovated dwellings are not estimated to achieve the zero-energy status by 2050. Although marginally due also to the use of homeworking during the COVID-19 pandemic, we show that this is mostly determined by changes in the regulations. A benchmarking ranking for each construction type was also created by calculating rating tables based on a 0-100 coefficients scale; this allows comparing with the existing stock any building with known EPC, for energy Audit and other investigations aiming at energy efficiency.

Keywords. Benchmarking, energy consumption, energy management, energy efficiency, statistical analysis
DOI: https://doi.org/10.34641/clima.2022.171

1. Introduction

Building energy audits [1] are an important step in reducing carbon dioxide emissions and the energy consumption of the building stock. These can consist of inspections and surveys aimed at understanding the energy use of the building, starting from e.g. a review of utility bills, to identify opportunities for improving energy efficiency through operational adjustments or system upgrades. Reviewing bills and conducting surveys is called "Simple level Audit" or "Audit Level 1" by ASHRAE, that defines a scale of three stages [2].

As Level 1 can only uncover major problems in the system and does not provide enough data granularity for effective diagnostics and sophisticated statistical analysis, Level 2 and 3 audits are required for a more comprehensive understanding of the building's energy use. These are usually based on data that covers the HVAC system, building envelope etc. and is collected directly through (wireless) sensors. This allows real-time monitoring of the energy usage for efficient interventions on the mechanical and electrical system, as well as testing advanced energy efficiency measures together with their cost-effectiveness [3]. For realising detailed energy audits, it is therefore necessary to acquire a deep and wide knowledge of the energy consumption status of the building stock, to identify eventually problematic sectors or clusters, and to single out representative buildings, or building typologies, for operation monitoring.

Energy Performance Certificate (EPC) databases have a variety of applications [4], as they are directly related to energy consumption. The EPCs in fact are usually defined as the measured or calculated energy consumption of a building during a year. In the European Union (EU), it is common to rate EPCs from A to F (from best to worst) for market classifications, or for building benchmarking. In general, a benchmark is a concept that originated from manufacturing, and it is used to measure the performance of a process. In energy investigations concerning buildings, a building consumption can be used as the indicator to which

Copyright ©2022 by the authors. This conference paper is published under a CC-BY-4.0 license.

the benchmark is compared [5].

A variety of methods have accordingly been formulated in the literature, in order to define accurately a benchmarking procedure that could be extended to diverse construction typologies, for evaluating the present status of the building stock and finding the occurrence of problems and anomalies. Roth [6] propose a benchmarking method based on normalised consumption, by using a non-linear statistical analysis of open-data from 10 cities. Park [7] analysed 1072 office buildings focusing on the US counterpart of the EPC certificate, the Source Energy Use Intensity (Source EUI).

This paper follows those earlier studies and analyses into detail the Detached houses cluster of a larger ~35000 buildings EPC database that was investigated in [8] but did not account for this specific cluster into detail. Here we fill that gap and provide the missing information with a complementary paper that completes the study of the full dataset. Aided by the software R [9], we performed a thorough statistical study of the EPC certificates of over 18000 Estonian dwellings, which were divided into three subcategories according to heated area, following the national legislation's regulations.

2. Research methods

2.1 EPC database and energy labels

Here we address a database of 18689 EPCs of Estonian detached houses, with data categories: building id, construction year, renovation year, heated area, ETA, KEK (an EPC certificate in Estonia can either be ETA if calculated, typically with simulation software, or KEK if measured). The buildings are detached and terraced houses that were further subclassified as portions with dedicated entrance, two or three apartment houses and so on. The EPCs were released between the late 1990's and February 2022 and comprised a few negative values (houses with energy generation e.g. solar panels), as well as a number of outliers with exceedingly large consumption.

As the highest EPC value allowed by the Estonian energy labels classification is 1350 kWh/(m^{2}a), we set 1500 kWh/(m^{2}a) as an upper cut-off for the database, resulting in N=18122 EPCs, with Median equal to 138.0 kWh/(m^{2}a), mean M=143.2 kWh/(m^{2}a) and standard deviation SD=51.04 kWh/(m^{2}a). An important characteristic of the Estonian legislation is that the Detached houses EPC data are subdivided into three groups according to the heated area A, corresponding to A<120 m^2, A=120 m^2-220m^2 and A>220 m^2. We thus labelled the three subclusters with D1, D2 and D3; the boxplot in **Figure 1** and **Tab. 1** shows the breakdown of means and data spread.

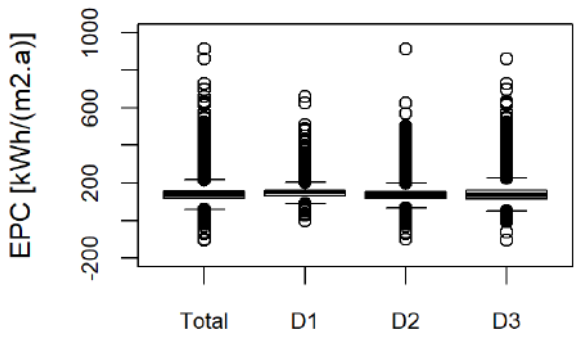

Figure 1 - Boxplot of the EPCs for the database

Tab. 1 – Detatched houses energy classification: number (N), mean (M) and Standard Deviation (SD).

ID	A [m^2]	N	% tot	M	SD
D1	<120	2265	12%	154.8	49.15
D2	120–220	10089	56%	138.9	42.96
D3	>220	5768	32%	146.2	62.68

Such a clustering is reflected in the energy labelling of the national regulation, which runs from A to H as per European Union (EU) standards with the thresholds displayed in **Tab. 2** below.

Tab. 2 – Estonian energy labels for the three categories of detached houses D1, D2 and D3; EPC [kWh/(m^{2}a)].

En. label	D1 (EPC)	D2 (EPC)	D3 (EPC)
A	≤ 145	≤ 120	≤ 100
B	146-165	121-140	101-120
C	166-185	141-160	121-140
D	186-235	161-210	141-200
E	236-285	211-260	201-250
F	286-350	261-330	251-320
G	351-420	331-400	321-390
H	≥ 421	≥ 401	≥ 391

The nZEB level corresponding to class A was first defined in 2013 and then revised in 2018, due to updated cost-optimality calculations and non-renewable primary energy factors for the class A EPC values. The dwellings initially had an EPC value of 50 kWh/(m^{2}a) regardless of the heated floor area A, but the revision increased the corresponding values substantially, also introducing a floor area dependence as well. Furthermore, after 2018 class A must be reached only by the D3 cluster, i.e. dwellings with heated floor area > 220 m^2. D1 and D2 must only meet class B requirements. As we shall explain in Section 3, this turned out to be

crucial for the latest years' trends and for the energy readiness of all three building groups.

Such energy "readiness" is the capability of a specific building cluster to reach the ZEB status and zero emissions by 2050 [9]. By fitting the EPC certificates for recent buildings, namely those that were built or renovated after 2000, we looked at the intersect of the fitting curve with the EPC=0 axis. This allowed for a rough estimation of the ZEB year for the three building subclusters D1, D2 and D3, as well as for the full dataset. The linear fit was computed with a simple linear model lm() in R.

As the fit including the years 2000 through 2022 included also the COVID-19 pandemic period, we wondered whether it could be reflected in the ZEB year estimates. A fit of the data from 2000 until the end of 2019 was accordingly performed and results were compared.

In the following, since the national regulation does not distinguish between ETA and KEK, accepting either certificate as an EPC with units kWh/(m^{2}a), we will mostly mention EPC values, referring to ETA or KEK only when this distinction is significant.

2.2 Fitting distributions and benchmarking

Examining the full dataset histogram in **Figure 3** unveils a clear structure, namely three peaks at 110, 130 and 150 kWh/(m^{2}a), and a very long yet unsubstantial right tail. It can be shown that the D1, D2 and D3 EPC datasets reflect this structure, with the exact same three peaks for D2 and only those at 110 and 150 kWh/(m^{2}a) for D1 and D3.

As our main purpose is benchmarking, namely creating a reference profile for each dataset against which one compares the energy efficiency of a corresponding given building, we need a reliable method to determine where the EPC value of this building sits within this general distribution. In this paper and in [8] we followed Ref. [9] by fitting each of the D1, D2 and D3 datasets of ETA/KEK certificates with a probability distribution, which was then integrated to return the empirical cumulative distribution function (CDF).

This allowed mapping a unique EPC at any given ratio of the dataset; the ranges of EPC values correspond to different quantiles of each original EPC distribution. We also added a 10–100 points scale to embed a rating system that quantified the energy efficiency. This resulted in so-called "benchmarking tables" that are reported in **Tab. 5**, **Tab. 6** and **Tab. 7**. Fitting was non-trivial due to the sharply multimodal nature of the data, to which the ordinary normal or gamma distributions did not apply. The tri- or multimodal distributions were thus handled by means of a Gaussian finite mixture with the R package "mclust" [10], that overlapped either two (D1 and D3) or three (D2) normal distributions and integrated accordingly.

3. Results

3.1 Time trend of EPC labels

The yearly breakdown of EPCs that have been issued since 2010 is illustrated in **Figure 2**. It is clearly seen that after the 2013 remodulation there has been a quick increase in certificates, reaching a steady trend after 2015. A histogram of the full database of 18122 Dwellings is also given in **Figure 3**; **Figure 4** features a plot showing EPC values in function of construction year.

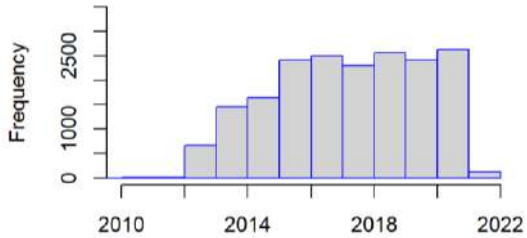

Figure 2 - Yearly breakdown of EPC certificates that were issued since 2010

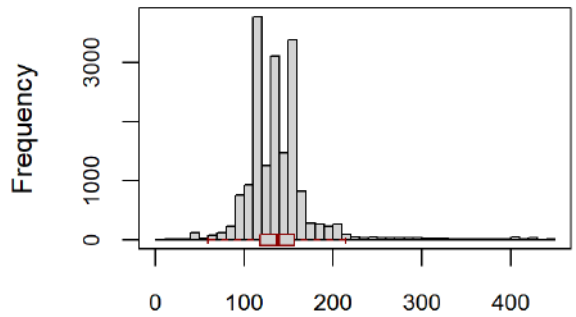

Figure 3 - Histogram of EPC values for the full dataset

A slight accumulation of values below ~300 kWh/(m^{2}a) can be observed in the most recent years, probably determined by the more stringent legislation requirements. Otherwise no clear pattern can be seen, with lower EPCs remaining consistently above 100 kWh/(m^{2}a), i.e. class A. As discussed in Section 2, the EPC certificates for Estonian buildings are comparable until a critical 2013 remodulation, then in 2018 the energy label requirements became more strict; after 01.01.2019 it was required to every newly constructed or renovated building to comply with even stricter bounds.

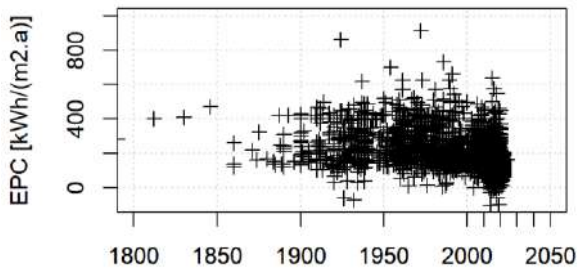

Figure 4 - EPC values for the full dataset in function of construction or renovation year

In this section we accordingly split the data into three clusters according to the EPC certificate

release date: 2013-2017, 2018, 2019-2022. The bar plots in **Figure 5** follow this reasoning and illustrate how for the houses of any size, the most prominent class shifted from C in the period 2013-2018 to B since 2019. A dramatic (yet very welcome) increase in Class A certificates, previously critically scarce, can be observed as well after January 2019.

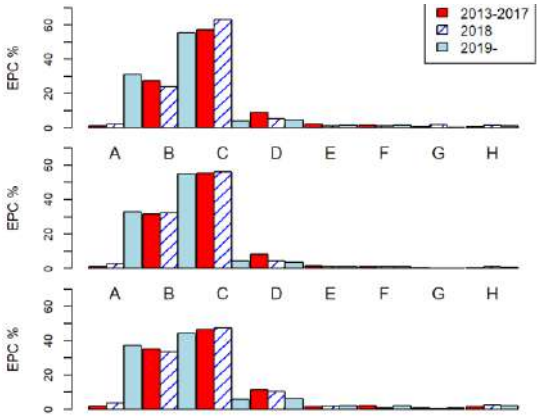

Figure 5 - ETA/KEK certificate classes (percentage over the total) for D1 (top), D2 (middle) and D3 (bottom), grouped by year of certificate release

Another important feature of **Figure 5** is a strong clustering of EPCs towards A, B and C classes. Especially for the D2 dataset, the less energy efficient buildings beyond D Class are negligible.

3.2 Impact of incentives pre/post renovations

How do stricter energy label requirements influence the EPC values? According to **Figure 6**, D1 mostly lies below 160 kWh/(m²a), i.e. within Classes A and B; for D2 the EPCs tend to cluster below 150 kWh/(m²a) after 2019, namely they stay within Class B. D3 exhibits a plateau at about 160 kWh/(m²a), i.e. Class D, consistently with **Tab. 1**.

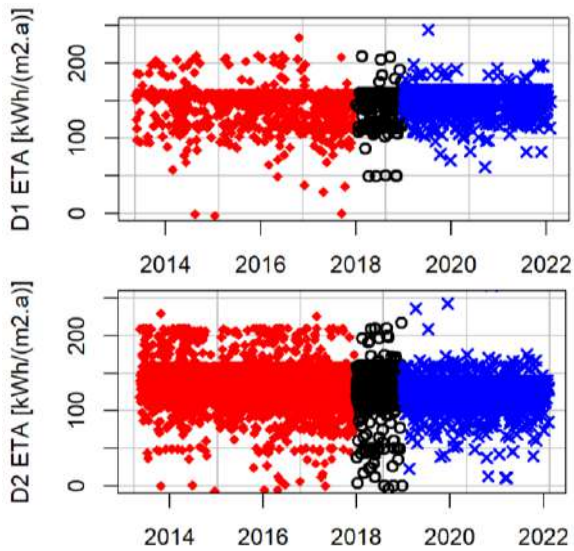

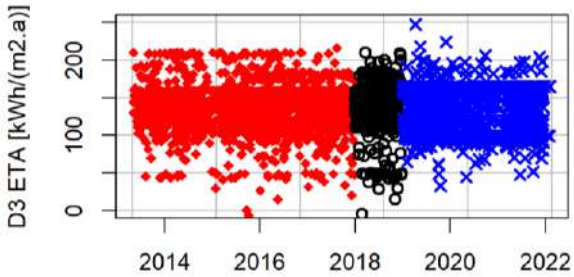

Figure 6 - ETA certificates for D1 (top), D2 (middle), D3 (bottom) versus date of issue: 2013–2017 (red diamonds), 2018 (black circles), 2019–2022 (blue crosses).

Figure 7 features three graphs, one for each Di cluster, where ETA (computed) and KEK (measured) are plotted against construction or renovation year. In all of the cases the ETAs are more frequent after 2013, i.e. when the major remodulation of energy consumption calculations occurred, in agreement with the previous Sections' findings. It is confirmed that a substantial clustering of EPCs below 200 kWh/(m2a) does exist for all building groups.

We observe a substantial increase of certificates since 2013 that is related to a slight reduction in their values. The linear fits (dashed lines), which are computed for EPCs issued after the year 2000, manifest a tendency to a very slow decrease for D1 (the smaller dwellings), while for D2 and D3 the decrease is more pronounced.

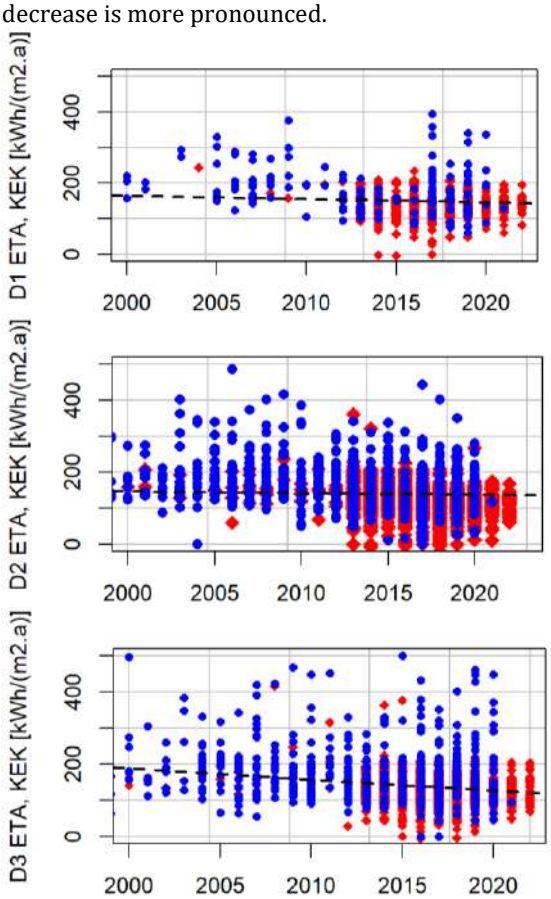

Figure 7 - Top to bottom: EPC values (red diamonds for ETA, blue dots for KEK) versus construction or renovation year for D1, D2 and D3 respectively

3.5 Readiness of the Estonian detached houses

By prolonging the linear fit in **Figure 7**, a rough estimation of the year (ZEB year) when the three building clusters should reach the Zero Energy Building (ZEB) status can be performed. This is illustrated in **Figure 8** below for the full dataset of 18122 EPCs (red solid line for 2000-2022 data.

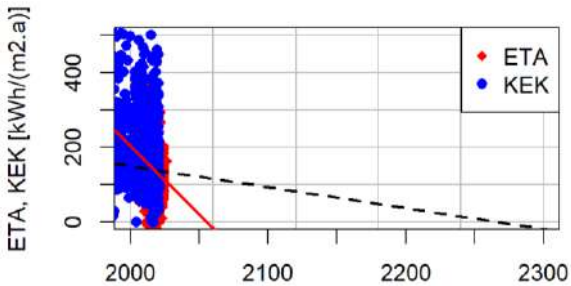

Figure 8 - Estimations of ZEB year for the full 18122 EPCs database, red diamonds for ETA and blue dots for KEK, against construction or renovation year. Dashed line: post-COVID 19, red solid line: pre-COVID-19

Identifying the intersection of the fit with the x-axis, namely the ZEB year, gives 2269 for the full dataset. Distinguishing among the three building categories gives 2178 for D1, 2351 for D2 and 2062 for D3. These are listed in **Tab. 3**.

3.4 Correlations with age and heated area

Pearson correlations between EPC value, heated area A and construction or renovation year have been performed for the three datasets; these are reported in **Tab. 3**. For completeness, also the ZEB year and linear fit slope are added.

Tab. 3 - Correlations for EPC values against Area and construction/renovation Year, ZEB year and fit slope

Dataset	EPC vs A	EPC vs Year	ZEB Year	Slope
D1	-0.082	-0.556	2178	-0.93
D2	-0.181	-0.020	2351	-0.42
D3	-0.217	-0.311	2062	-3.05

The correlations are very weak for all datasets.

3.2 Effect of the COVID-19 pandemic

In order to estimate whether the pandemic has impacted the energy consumption in detached houses, we have compared two ZEB year estimations. The pre-COVID fit was computed with 2000-2019 data, while the post-COVID fit regarded 2000-2022 data, as in **Tab. 3**. The result for the full database and for D1, D2, D3 is reported in **Tab. 4**.

Tab. 4 - Estimates of the COVID-19 impact on the ZEB year for all the building clusters

Data	pre-COVID	Post-COVID	Diff.
TOTAL	2056	2269	+213
D1	2071	2178	+107
D2	2052	2351	+299
D3	2057	2062	+5

At first sight, one might conclude that it was the forced homeworking since 2020 to unquestionably increase the energy consumption of private dwellings to abruptly. However, by breaking down the EPCs into ETA (calculated) and KEK (measured), it can be shown that the main driver of the increase were the regulations, which directly affect the simulations parameters returning the ETAs. We recall indeed from Section 2 that after 2018, class A must be reached only by the D3 cluster, while D1 and D2 must only meet class B requirements. This is perfectly in line with our results, as for D1 and D2 a fit using only ETAs marks a very sharp ZEB year delay. D3 instead exhibited even a slight 7-year ZEB improvement, according to an only-ETA fit.

The KEK (measured) values, conversely, are directly related to occupancy and to COVID-19. These showed only a small delay for the ZEB year for D1 and D3, of order ~5 years, whilst for D2 the year estimation did not even change. In other words, the pandemic effect proved to be very limited, if not even absent.

3.3 Benchmarking tables

The distribution fitting, as explained in Section 2, was performed by means of gaussian mixture [10]. In **Figure 9** we report the result for D1, with a trimodal distribution (overlap of three Gaussian distributions) giving the best fit. D2 also required a trimodal fitting (**Figure 10**) with more distinct modes: the peaks are located at EPC=110, 130 and 150 kWh/(m^{2}a); these correspond to the midpoints of class A, B and C respectively (see **Tab. 2** and **Figure 5**). This is consistent with the full dataset as well, as illustrated in **Figure 3**, because D2 is the largest subcluster, corresponding to 56% of the entire detached houses database. The same holds for D3, which exhibits the same three peaks plus a fourth one at 90 kWh/(m^{2}a), shown in **Figure 11**.

Only D1, namely those buildings with heated area smaller than 120 m^2, carries only two sharp peaks, one at 110 and the other at 150 kWh/(m^{2}a), corresponding to classes A and C.

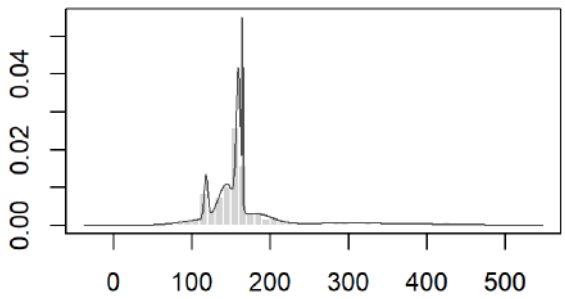

Figure 9 – Trimodal density distribution fit for D1

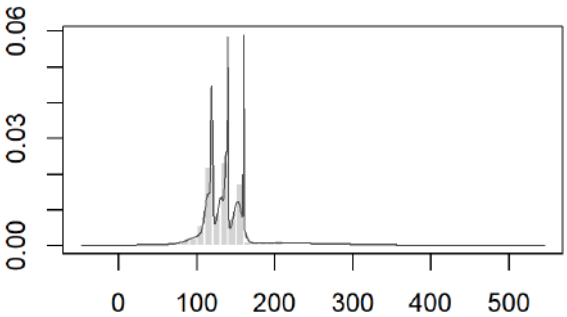

Figure 10 – Trimodal density distribution fit for D2

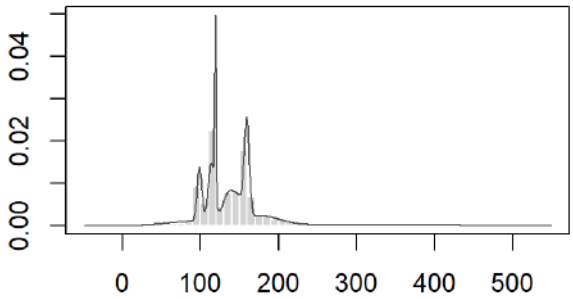

Figure 11 – Multimodal density distribution fit for D3

Through distribution fitting, we were able to construct benchmarking tables for the three clusters D1, D2 and D3 by integrating each distribution and retriving the according cumulative percentage.

Tab. 5 - Benchmarking table for Estonian detached houses D1 with A<120m², EPC [kWh/(m²a)]

Score	Cumul. (%)	EPC ≥	EPC <
100	0	0	64.78
99	1	64.78	87.51
98	2	87.51	105.38
95	5	105.38	116.23
90	10	116.23	119.08
85	15	119.08	124.85
80	20	124.85	132.67
75	25	132.67	137.85
70	30	137.85	145.67
60	40	145.67	153.66
50	50	153.66	157.73
40	60	157.73	160.1
30	70	160.1	163.6
20	80	163.6	182.19
10	90	182.19	∞

Tab. 6 - Benchmarking table for Estonian detached houses D2 with A=120-220 m², EPC [kWh/(m²a)]

Score	Cumul. (%)	EPC ≥	EPC <
100	0	0	48.73
99	1	48.73	75.15
98	2	75.15	96.39
95	5	96.39	109.13
90	10	109.13	113.41
85	15	113.41	116.82
80	20	116.82	118.51
75	25	118.51	119.67
70	30	119.67	128.78
60	40	128.78	135.84
50	50	135.84	139.32
40	60	139.32	146.23
30	70	146.23	155.29
20	80	155.29	160.61
10	90	160.61	∞

Tab. 7 - Benchmarking table for Estonian detached houses D3 with A>220 m², EPC [kWh/(m²a)]

Score	Cumul. (%)	EPC ≥	EPC <
100	0	0	53.98
99	1	53.98	68.61
98	2	68.61	93.97
95	5	93.97	98.88
90	10	98.88	104.39
85	15	104.39	111.84
80	20	111.84	115.32
75	25	115.32	118.07
70	30	118.07	120.46
60	40	120.46	136.84
50	50	136.84	149.32
40	60	149.32	157.68

30	70	157.68	161.85
20	80	161.85	187.84
10	90	187.84	∞

The benchmarking tables for the D1, D2 and D3 datasets are given in **Tab. 5**, **Tab. 6** and **Tab. 7**. The table for the full dataset of detached houses was reported in [8].

4. Discussion

The improvement in energy efficiency of Estonian detached houses is quite evident by looking at **Figure 4**, which displays the time trend of EPCs for the full database. The EPC values have been decreasing steadily during the past six-seven years. This is mirrored by the EPC labels classification that is broken down by heated area, **Figure 5**: a clear shift from C to B class since 2019 exists for all the clusters D1, D2 and D3, together with a substantial increase of A class certificates. One ought to conclude that this should be the effect of renovation incentives. Nevertheless, **Figure 6** and **Figure 7** provide a closer look into the matter. **Figure 6** shows an evident decrease of EPC values for D2 (the largest subcluster by far, 56% of the full database), while for D3 the trend is mostly unchanged and D1 experiences even larger values for 2019-2022. Considering again **Figure 5** is quite enlightening if one looks at the Class A share compared to Class B. This is substantially larger for D3, while D2 and D1 have a much smaller amount of A Class EPCs compared to B Class EPCs. This clearly suggests that renovation campaigns and stricter energy class requirements were successful for larger houses of heated area larger than 220 m^2, while they probably have not been influential for smaller buildings. Notice also how in **Figure 6**, D1 and D2 show a plateau at resp. ~150 and ~160 kWh/(m2a), i.e. at Class B and Class C. D3 exhibits the same behaviour at 160 kWh/(m^2a), the middle of Class D.

Figure 7 is mostly interesting in regard to the structural difference between ETA (computed) and KEK (measured) values. Basically all the outliers for any Di subcluster are KEK, while the calculated EPCs tend to converge rather nicely with the passing of time. However, a steady increment in the lowest ETA values does exist (**Figure 7**) and looking at **Tab. 3**, the absence of correlation between construction (or renovation) year and EPC signify that the whole picture is not so simple. One cannot even suspect the ETA values to have been deliberately underestimated for complying with the regulations, or even the existence of some systematic error in the simulation software.

Keeping in mind the above speculation, a very simple and objective summary of the energy consumption status of the Estonian detached houses is given in **Tab. 3** and **Tab. 4**. The ZEB year provides indeed a simple yet powerful means of judgement: out of the three building subclasses, only D3 (i.e. largest detached houses) are forecast to reach the ZEB status within the next 40 years, in any case well beyond 2050. **Tab. 4** in particular illustrates how the sudden occupancy increment during the COVID-19 emergency was *not* causing the worsening of ZEB year forecasts, if compared to 2000-2019 estimates. On the other hand, the national regulations post-2018 favoured a clustering of EPCs towards class B from class A for D1 and D2, which can be somehow noticed also in **Figure 7**. The effect of regulations and incentives could not be more manifest.

The distribution fitting in **Figure 9** and the benchmarking tables clearly show that the EPCs concentrate within classes A and C, with very long tails beyond class D carrying only a few values. Overall, the three distinct building groups do not exhibit any clustering towards class A. Nevertheless, this seems likely to happen at some point during the next decades anyway at least for D3. Smaller houses, namely the D1 and D2 subgroups, give a very pessimistic forecast as they will tend to cluster around class B for a long time, as in **Figure 5**, unless further restrictions on energy consumption are imposed in the near future.

5. Conclusion

This study examined a large dataset of EPC certificates of nearly 19000 Estonian detached houses (single detached or terraced dwellings, portions with dedicated entrance, two or three apartment houses etc.). This allowed portraying the status of the energy performance of old as well as new or recently renovated buildings.

A thorough statistical investigation unveiled general characteristics as well as specific features of the subgroups D1, D2 and D3, which were created by the national regulation bodies according to heated area. We found that the cluster of largest houses D3, with an area >220 m^2, benefitted from renovation campaigns and is expected to reach the ZEB status in 2062. Smaller dwellings instead showed an EPC clustering towards B Class values, which implied no ZEB status in sight unless stricter regulations, or a coordinated effort, will come into force.

The above considerations are confirmed by a dedicated assessment of the COVID-19 pandemic, which compared ZEB year estimations by fits based on two distinct periods: 2000-2019 (pre-COVID) and 2000-2022 (post-COVID). Contrary to expectations, the forced remote working from home in 2020-2022 was only marginally responsible for the massive delay in the ZEB year forecast of as much as 300 years. We have shown that the culprit was instead the 2018 governmental regulations, inducing a shift in the ETAs from Class A to Class B for some categories. The role of legislation will be thus critical in the future, to ensure that most detached homes will reach the ZEB status by the year 2050 or soon afterwards.

Another novel result is constituted by benchmarking

tables that are obtained via distribution fitting. These can be used to compare a given building with the entire building stock, for evaluating its energy efficiency with a dedicated rating system. Such tables also allow identifying representative buildings for e.g. real-time consumption monitoring; therefore they can be an important tool for detailed energy auditing.

Naturally, the analysis here provided should be updated with newer datasets, extended to other building typologies and refined with more sophisticated statistical methods, especially on the side of readiness forecasting and distribution fitting.

6. Acknowledgement

Support is acknowledged from the European Regional Development Fund via the Estonian Centre of Excellence in Zero Energy and Resource Efficient Smart Buildings and Districts ZEBE, grant 2014-2020.4.01.15-0016, from the Estonian Research Council through the grants PSG409, PRG658, and DigiAudit, from the Estonian Ministry of Education and Research and European Regional Fund (grant 2014-2020.4.01.20-0289), and by the European Commission through the H2020 project Finest Twins (grant No. 856602).

References

[1] A. Magrini, L. Gobbi and F. d'Ambrosio, "Energy audit of public buildings: The energy consumption of a university with modern and historical buildings. Some results," *Energy Procedia,* vol. 101, pp. 169-175, 2016.

[2] ASHRAE, "Procedures for Commercial Building Energy Audits, 2nd Edition," ASHRAE, Atlanta, 2011.

[3] M. C. Baechler, "A Guide to Energy Audits," Pacific Northwest National Lab. (PNNL), Richland, WA (United States), 2011.

[4] A. Hamburg and T. Kalamees, "How well are energy performance objectives being achieved in renovated apartment buildings in Estonia?," *Energy And Buildings,* vol. 199, pp. 332-341, 2019.

[5] W. Chung, Y. V. Hui and M. Lam, "Benchmarking the energy efficiency of commercial buildings," *Applied Energy,* vol. 83, no. 1, pp. 1-14, 2006.

[6] J. Roth, B. Lim, K. J. Rishee and D. Grueneich, "Examining the feasibility of using open data to benchmark building energy usage in cities: A data science and policy perspective," *Energy Policy,* vol. 139, no. 111327, 2020.

[7] H. S. Park, M. H. Lee, L. H. Kang, T. H. Hong and J. W. Jeong, "Development of a new energy benchmark for improving the operational rating system of office buildings using various data-mining techniques," *Applied Energy,* pp. 225-237, 2016.

[8] A. Ferrantelli, J. Belikov, E. Petlenkov, M. Thalfeldt and J. Kurnitski, "Evaluating the energy readiness of national building stocks through benchmarking," *IEEE Access*, vol. 10, pp. 45430-45443, 2022.

[9] H. G. Kim and S. S. Kim, "Development of Energy Benchmarks for Office Buildings Using the National Energy Consumption Database," *Energies,* no. 13, p. 950, 2020.

[10] L. Scrucca, M. Fop, T. B. Murphy and A. E. Raftery, "mclust 5: clustering, classification and density estimation using Gaussian finite mixture models.," *The R Journal,* vol. 8, no. 1, p. 289–317, 2016.

[11] R Core Team;, "R: A language and environment for statistical computing," R Foundation for Statistical Computing, Vienna, Austria, 2020.

NUMERICAL INVESTIGATION OF AN EVACUATED TUBE SOLAR COLLECTOR IN A SOLAR ASSISTED ROOFTOP UNIT

Tunahan Akış [a], Orhan Ekren [a], Kerim Gümrükçüler [b]

[a] Ege University, Solar Energy Institute, İzmir Turkey, tunahannakis@hotmail.com, orhanekren@gmail.com

[b] İmbat Air Conditioning and Cooling Systems Inc., İzmir Turkey, kerim.gumrukculer@imbat.com

Abstract. In this study, numerical analysis of an evacuated tube solar collector integrated into the discharge line in a rooftop air conditioner is carried out. The goal in this system is to increase the efficiency of the unit by reducing the compressor energy consumption with the solar collector. The solar collector consists of vacuum tube collectors. Inside the vacuum tube, there is a copper pipe installation through which the R410a refrigerant in the superheated vapor phase, which is compressed by the compressor, passes. The remaining volume from the copper pipes in the tube is filled with a heat transfer fluid to increase the collector efficiency. In this study, the type of heat transfer fluid filled to the collector for the operating condition of the unit in summer and winter conditions are investigated parametrically and numerically. With the findings obtained, the surface temperature of the copper pipe installation in the collector in the compressor discharge line, depending on the type of heat transfer fluid, is presented comparatively.

Keywords. HVAC & R, solar energy, energy efficiency, computational fluid dynamics
DOI: https://doi.org/10.34641/clima.2022.366

1. Introduction

Today, energy efficiency in HVAC&R systems has become an important issue on a global scale. Among these systems, one of the most widely used devices globally is rooftop air conditioning units. Rooftop air conditioners are a familiar technology but integrating renewable energy sources such as solar energy into the refrigeration cycle is an innovative approach. In the literature studies, two types of such an integration stand out; (i) to meet the fan and compressor power consumption of photovoltaic systems and rooftop air conditioning unit, (ii) to use solar thermal energy as an evaporator in the refrigeration cycle of the refrigerant, as well as to use the solar thermal energy to obtain hot water/air. For the second use method, the placement of the collector before the compressor has been widely studied in the studies conducted in the literature. The purpose of this increasing the evaporation temperature to provide energy efficiency. Torres-Reyes et al. (1998) [1] and (2001) [2], Cervantes et al. (2002) [3] reported that they worked both theoretically and experimentally on a solar assisted heat pump with the direct expansion of the refrigerant in the solar collector and performed a thermodynamic optimization. Chaturvedi et al. (1991) [4] and (1998) [5], Aziz et al. (1999) [6] are carried out on the thermodynamic analysis of two-component, two-phase flow in solar collectors with the application of a direct expansion solar assisted heat pump. Their results show that changes in mass flow rate and absorbed solar heat flux have significant effects on collector tube length and refrigerant heat transfer coefficient. It is observed that changes in tube inlet diameter and collector pressure has a negligible effect on the collector size but had a significant effect on the heat transfer coefficient. The increase in the quality of the refrigerant mixture is observed to be gradual along the main length of the pipe with a rapid rise near the end of the pipe. Apart from these studies, the use of evacuated tube solar collector with direct expansion after the compressor is quite new.

In this study, numerical parametric analyses are carried out on an evacuated tube solar collector integrated into the compressor discharge line, unlike the literature. By filling the different heat transfer fluids in the market into the vacuum tubes, the efficiency of the collector is examined, and the most suitable heat transfer fluid is determined.

2. MATERIAL AND METHOD

2.1 Model and Mesh

The model of the evacuated tube of the solar collector

Copyright ©2022 by the authors. This conference paper is published under a CC-BY-4.0 license.

examined in this study and model is shown in Figure-1. Here, Fig. 1(a) is the top view of the evacuated tube, and Fig. 1(b) is the isometric view. The evacuated tube structure, which is numerically analysed, is in the standard dimensions and has an outer diameter of 53 mm and an inner diameter of 43.8 mm. The inner volume of the tubes is 2.6 liters. Its total length is 1800 mm. The tube consists of two concentric cylindrical glass structures. There is a vacuum gap between these two-cylinder structures. This space provides insulation to store the heat absorbed from the sun in the interior.

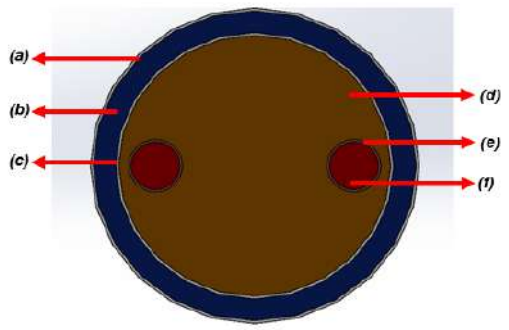

Fig. 1 (a) – Numerical Model, (a) evacuated tube outer glass zone, (b) vacuum zone (c) evacuated tube inner glass zone, (d) heat transfer fluid zone (e) copper tube zone (f) refrigerant zone.

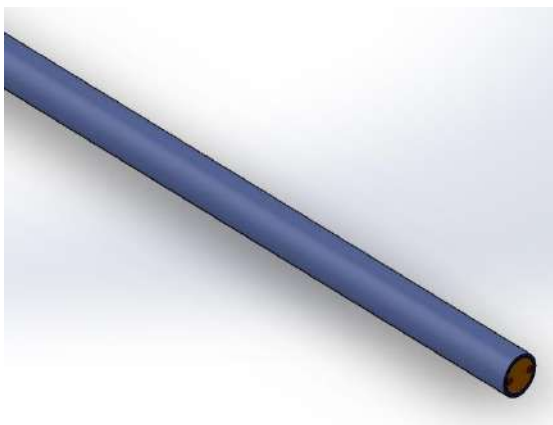

Fig. 1 (b) – Isometric View

In the numerical model, there is a u-shaped copper piping installation inside the vacuum tubes. The diameter of the copper tube is 3/8" (9.595 mm). The refrigerant compressed by the compressor enters the collector from the left side and leaves the collector from the right side in Fig. 1 (a). The goal here is to improve the heat transfer mechanism of the energy taken from the solar radiation to the refrigerant circulating in the copper pipe installation by using the heat transfer fluid and to increase the collector efficiency. The mesh structure of the numerical model is shown in Fig. 2.

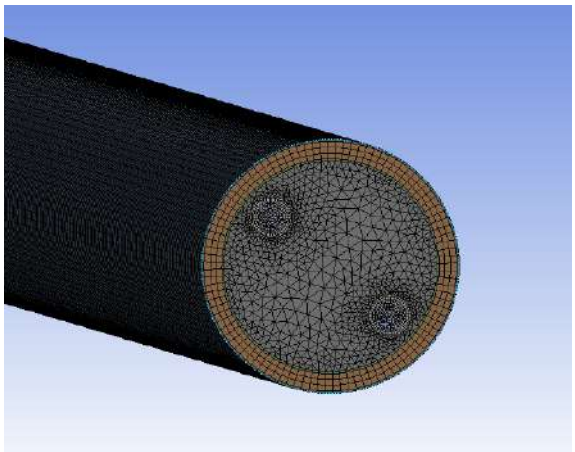

Fig. 2 (a) – Model's Mesh Structure

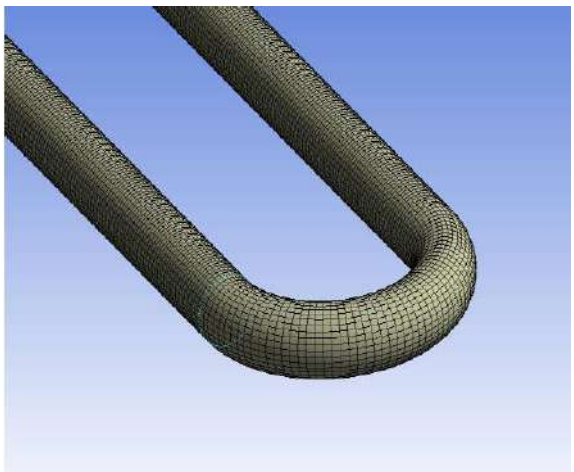

Fig. 2 (b) – Copper Pipe Mesh Structure

Meshing process is done with ANSYS software that is a commercial finite element solver. Fig. 2 (a) shows the isometric view of the mesh structure of the numerical model, and Fig. 2 (b) shows the mesh structure of the copper piping installation inside the evacuated tube structure. Here, hexa structured mesh is knitted for solid volumes. Due to the complexity of the model and the inability to reduce the solution time, the fluid volumes are knitted with a triangular mesh. The triangular mesh structure, which is created with the aim of increasing the mesh structure quality and reducing the solution time, is transformed into a polyhedral mesh structure by improving it in ANSYS-FLUENT, a commercial computational fluid dynamics software. This structure can be seen with Fig. 3.

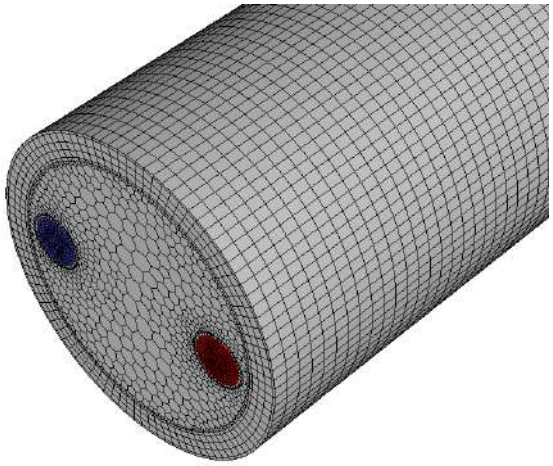

Fig. 3– Polyhedral Mesh Structure

The variation of the refrigerant outlet temperature according to the total number of cells in the mesh structure is given in Table-1. Based on these data, independence from the network structure was achieved with a total number of 7850000 elements for analysis.

Tab. 1 - Refrigerant outlet temperature values according to mesh size

Cell Number	Refrigerant Outlet Temperature [°C]
3750000	81.412
4300000	81.395
5600000	81.252
6000000	81.205
7500000	81.198
7850000	81.197

2.3 Boundary Conditions and Solution Method

While solving the three-dimensional numerical model of the evacuated tube collector examined within the scope of the study, the following assumptions are made

- The thermal losses by radiation and convection to the environment are neglected.
- Modelling of the vacuum field is possible by defining a very small value of conductivity and specific heat value to the relevant volume. For this reason, the thermal conductivity coefficient of the vacuum area is accepted as 10-18 W/mK [8].
- System is accepted in steady state regime
- Heat transfer by radiation between the concentric glass surfaces is neglected.
- The inner glass surface temperature is assumed constant throughout the calculation due to neglect of the variability of seasonal solar radiation.

The solution boundary conditions are given in Fig. 4 and explained in Table-2. The inlet temperature of the refrigerant to the collector varies for summer and winter conditions. The main reason for this can be shown as the change in compressor frequency according to the capacity requirement that the device must meet in different operating conditions. In addition, the inner glass surface temperature varies according to the efficiency of benefiting from solar radiation.

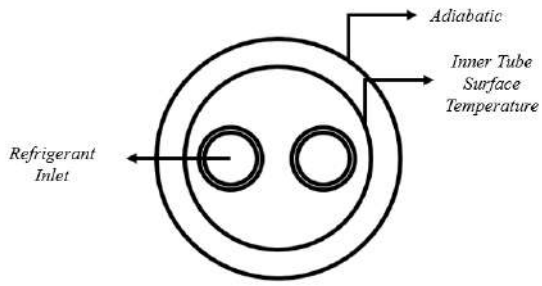

Fig. 4 – Boundary Conditions

Tab. 2 - Boundary conditions according to summer and winter conditions. [7]

Summer		Winter	
Parameter	Value	Parameter	Value
Refrigerant Inlet Temperature [°C]	80.2	Refrigerant Inlet Temperature [°C]	71.5
Inner Tube Surface Temperature [°C]	170	Inner Tube Surface Temperature [°C]	200

The thermophysical properties of the materials used in the analysis are shown in Table-3. These materials are evacuated tube's structure. The thermophysical properties (density, specific heat, conductivity, and viscosity) of the heat transfer fluid used in the analysis change depending on the temperature, and these properties are defined as a function of cell temperatures as a piecewise polynomial to the solver.

Tab. 3 - Thermophysical properties of the used material [8]

Material	Density [kg/m³]	Heat Capacity [J/kg-K]	Conductivity [W/m-K]	Viscosity [kg/m-s]
Glass	2230	980	1.14	-
Vacuum	1.225	0.00001	1e-18	-
R410a	115.4	1327	0.02255	0.00001765

Conservation equations in cylindrical coordinates are discretized with the Power-Law scheme and solved with the SIMPLE algorithm. Conservation equations for cylindrical coordinates are generalized by Equation-1 [9].

$$\frac{\partial(\rho\varphi)}{\partial t} + \nabla\left(\rho\varphi\vec{V}\right) = \nabla\left(\Gamma_\varphi \nabla_\varphi\right) + S_\varphi \quad (1)$$

Here, ρ, φ, $\vec{V}$, S_φ and Γ_φ are the fluid density, the independent parameter, the fluid velocity vector, the source term, and the effective diffusion coefficient, respectively. The refrigerant flow is modeled with the standard k-ε turbulence model. The energy equation is given with Equation-2 [9].

$$\frac{\partial T_f}{\partial t} + \vec{v}\nabla T_f = a_f(\nabla^2 T_f) \quad (2)$$

Here T_f is the fluid temperature. The study is made for the steady-state condition, so the time dependent terms given by Equation-1 and Equation-2 are not included in the solution.

3. Results

The results obtained from the study is analyzed for four different heat transfer fluids (HTFs). In addition, these scenarios are evaluated separately for summer and winter working conditions.

Tab. 4 - Results

HTF	Working Condition	Surface Temperature with Air [ºC]	Surface Temperature with HTF [ºC]
Therminol - 54	Winter	83.10	111.53
	Summer	90.96	117.53
Texol Texotherm HT - 32	Winter	83.10	112.16
	Summer	90.96	122.49
Diphyl DT	Winter	83.10	110.8
	Summer	90.96	116.8
Latema LT4	Winter	83.10	110.54
	Summer	90.96	116.57

The findings indicated in Tab. 4 is obtained as a result of five different analyses. First, in the absence of heat transfer fluid, the surface temperature of the copper pipe while there is air in the evacuated tube collector is examined, and then the surface temperature of the copper pipe by filling this space with four different heat transfer fluids is examined. In the findings, the heat transfer fluid Texol Texotherm HT -32 increased the surface temperature of the copper pipe by 35% compared to the empty state. The temperature distribution in the top view of the collector is given in Fig. 5 together with the empty collector and in the case of using this fluid together with Fig. 6.

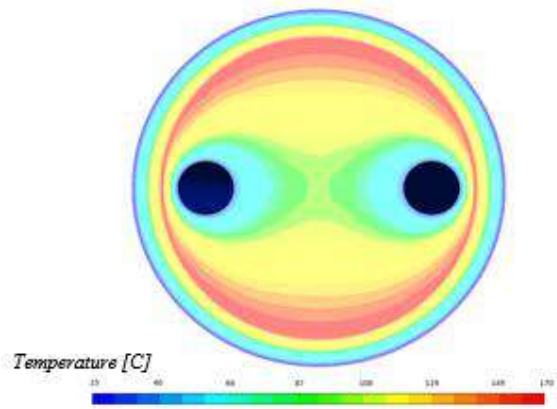

Fig. 5 (a) – Temperature distribution in empty evacuated tube, summer conditions

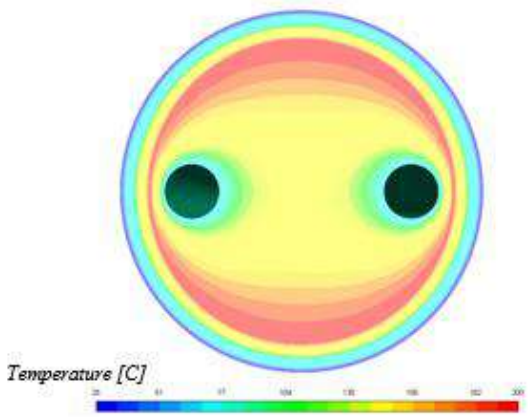

Fig. 5 (b) – Temperature distribution in empty evacuated tube, winter conditions

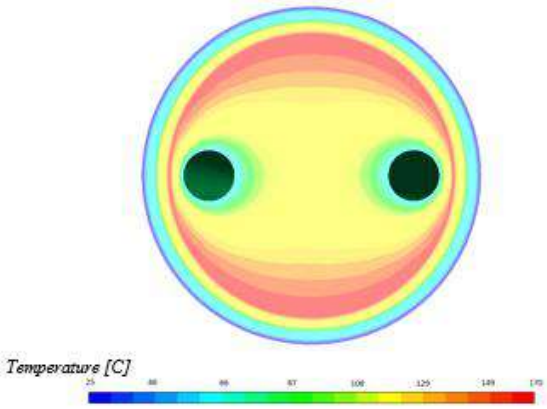

Fig. 6 (a) – Temperature distribution in evacuated tube with the use of heat transfer fluid, summer conditions

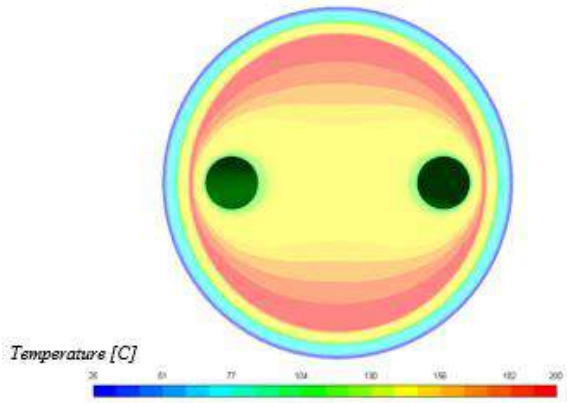

Fig. 6 (b) – Temperature distribution in evacuated tube with the use of heat transfer fluid, winter conditions

When Figure-6 is examined, it is seen that the thermal stratification formed in the space inside the tube decreases compared to an empty collector. However, it can be said that the amount of heat transfer to the copper pipe installation in the evacuated tube has increased. This situation shows that there is an increase in the amount of heat transfer to the refrigerant in the superheated vapor phase in the compressor discharge line. As shown in Tab. 4, the 35% increase in the surface temperature of the copper pipe supports this finding. With the use of Texol Texotherm HT -32 heat transfer fluid, it is observed that the fluid leaves the collector with a temperature increase of 1.02 ^{o}C. Increasing the temperature of the fluid with the thermal energy gained from the collector can be used to decrease the compressor operating frequency. Thus, a part of the condensation pressure (also the high pressure of the cooling cycle) that the compressor should create will be provided by the thermal input from the solar thermal energy.

Cost analysis studies show that the unit liter prices of Therminol - 54 Texol Texotherm HT 32, Diphyl DT and Latema LT4 heat transfer fluids are different from each other. The costs per liter for these fluids are given in Figure - 7. While Therminol - 54 and Texol Texotherm HT 32 fluids have the same unit cost, the unit cost of other fluids is higher.

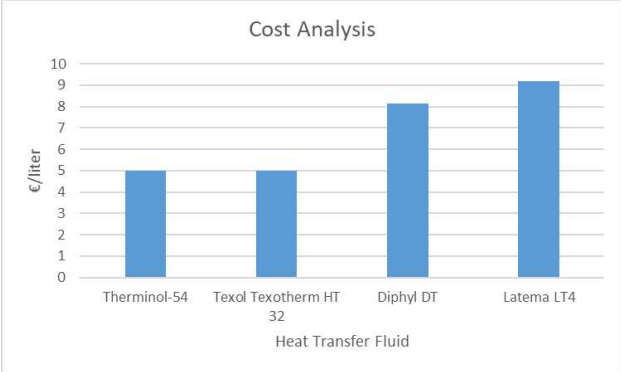

Fig. 7 – Cost analysis of heat transfer fluids

4. Conclusions

In this study, numerical analysis of evacuated tube solar collector integrated into the discharge line of a rooftop unit is carried out using different heat transfer fluids. If the results obtained with the data obtained from the important findings are summarized,

- With the use of heat transfer fluid, temperature up to 35% is observed on the surface of the copper pipe. Due to the location of the collector within the framework of this analysis, the refrigerant in the superheated vapor phase circulates. Currently, providing heat transfer to the refrigerant in this state is a difficult process. For this reason, the space in the evacuated tube structure should be filled with a heat transfer fluid.

- With the use of heat transfer fluid, the thermal stratification between the supply and collection lines of the copper piping in the collector is reduced.

- Improving effect of the other heat transfer fluids used on the collector surface temperature is not far from the effect of the Texol Texotherm HT -32 heat transfer fluid, which is determined as the maximum.

- Results show that performance will be close to each other with all heat transfer fluids, but when cost analysis is made, it is seen that Texol Texotherm HT 32 or Therminol - 54 fluid has a financial advantage. This finding demonstrates that financial research is essential in such an analysis and in such a system design.

5. Acknowledgements

This study is supported by İmbat Air Conditioning and Cooling Systems Inc. and TÜBİTAK university-industry cooperation within the scope of the 1501 TEYDEP projects (project no 3191540). We would like to thank TÜBİTAK for their financial support.

6. References

[1] Torres Reyes E, Picon Nunez M, Cervantes De G. Exergy analysis and optimization of a solar-assisted heat pump. Energy. 1998;23(4):337–44.

[2] Torres-Reyes E, Cervantes de Gortari J. Optimal performance of an irreversible solar-assisted heat pump. Energy Int J. 2001;1(2):107–11.

[3] Cervantes GJ, Torres-Reyes E. Experiments on a solar-assisted heat pump and an exergy analysis of the system. Appl Thermal Eng. 2002;22:1289–97.

[4] Chaturvedi SK, Mohieldin TO, Chen DT. Second-law analysis of solar-assisted heat pumps. Energy .1991;16(6):941–9.

[5] Chaturvedi SK, Chen DT, Kheireddine A. Thermal performance of a variable capacity direct expansion solar assisted heat pump. Energy Convers Manage. 1998;3(4):181–91.

[6] Aziz W, Chaturvedi SK, Kheireddine A. Thermodynamic analysis of two-component, two-phase flow in solar collectors with application to a direct-expansion solar-assisted heat pump. Energy. 1999;24:247–59.

[7] Naik, B. K., Varshney, A., Muthukumar, P., & Somayaji, C. Modelling and performance analysis of U type evacuated tube solar collector using different working fluids. Energy Procedia. 2016; 90, 227-237.

[8] Pawar, V. R., & Sobhansarbandi, S. CFD modeling of a thermal energy storage based heat pipe evacuated tube solar collector. Journal of Energy. 2020; Storage, 30, 101528.

[9] Fluent, 2009, " Documentation," ANSYS, 12.0/12.1, ANSYS Inc., Canonsburg, PA.

Investigation of additively manufactured triply periodic minimal surfaces as an air-to-air heat exchanger

Alper Mete Genç [a,b], Ceren Vatansever [a], Meltem Koçak [b], Ziya Haktan Karadeniz [c]

[a] Graduate School of Natural and Applied Sciences, Izmir Kâtip Celebi University, Izmir, Turkey, alpergenc@eneko.com.tr.

[b] ENEKO, Cigli, Izmir, Turkey, meltemkocak@eneko.com.tr.

[c] Department of Energy Systems Engineering, Izmir Institute of Technology, Izmir, Turkey, haktankaradeniz@iyte.edu.tr.

Abstract. Additive manufacturing provides freedom of production and design of geometries that cannot be produced with traditional methods. Therefore high-efficiency and innovative heat exchanger designs can be produced with 3D printer technology efficaciously. Heat recovery ventilation devices, which meet the indoor air quality requirements with high thermal efficiency, allow heat recovery between the exhaust air and fresh air with the help of the recuperator, which is an air-to-air heat exchanger. In this study, the production processes of triply periodic minimal surfaces (TPMS) with the additive manufacturing method and their performance as an air-to-air heat exchanger are examined. Triply periodic minimal surfaces are three-dimensional and infinite surface geometries that can be expressed with continuous trigonometric functions, forming two separate non-intersecting spaces for fluids. The surface geometry derived from the trigonometric function can be arranged to provide heat transfer between two unmixed fluids at different temperatures. In this study, Schwarz-D, Schwarz-P and Shoen's gyroid geometries are investigated as triply periodic minimal surfaces. During the production of these geometries processes, parameters such as wall and layer thicknesses and printing temperature were changed to achieve the lowest possible wall thickness (0.16mm) with the 3D printer used. The performance of triply periodic minimal surface geometries as air-to-air heat exchangers are determined experimentally in a crossflow experimental setup.

Keywords. Heat exchanger, triply-periodic minimal surface, indoor air quality, additive manufacturing
DOI: https://doi.org/10.34641/clima.2022.172

1. Introduction

According to the International Energy Agency (IEA), world energy demand is incresing by 1.3% each year until 2040 (1). To reduce the increasing energy demand, studies are carried out to improve the energy efficiency of all systems used throughout the world. One of these systems is ventilation systems. Mechanical ventilation systems are now necessary for airtight buildings and are widely used in new residences and building restorations (2). These systems create a stable environment regarding thermal comfort and indoor air quality and create volumes where users can live healthily. The efficiency of ventilation systems depends on the accurate determination of the physiological needs of the users and the climatic variables, making the ventilation load calculations realistically and the correct operation of the systems. In addition, all ventilation system components should be designed to increase system efficiency and be in harmony with each other.

Heat exchangers, one of the most essential elements that significantly affect ventilation systems' energy efficiency and energy savings, are generally made of metal or ceramic materials. Heat exchangers are produced using traditional techniques such as machining or metal forming, which are today's engineering approaches. The efficiency that can be achieved with heat exchangers produced with traditional production technology is limited. This technology is far from flexible enough to meet an architect's aesthetic needs. The transformation created by the digital world we live in in the industry is discussed intensively with the concepts of "Digitalization" or "Industry 4.0". With Industry 4.0, the fourth industrial revolution, additive manufacturing is the latest move in smart automation technology. In this new era, the use of

Copyright ©2022 by the authors. This conference paper is published under a CC-BY-4.0 license.

modern production skills in the context of integrating new information technologies plays a vital role in economic competitiveness (3).

Because of its ability to create complex objects with advanced properties (new materials, shapes), additive manufacturing has become a key technology for producing customised products (4). Thanks to increased product quality, additive manufacturing is now used in various industries such as aerospace, biomedical, manufacturing and ventilation systems (5,6).

One of the basic geometries that can be used for an innovative start in heat exchanger design is the cellular structure family, triply periodic minimal surface (TPMS) porous structures, which consist of unit cells that can be repeated three-dimensionally to form lightweight, high-strength structures (7). The TPMS structures are investigated in a mechanical properties manner by Al-Ketan et al. (8). A comparison study is carried out by examining the topology-property relationship between 3D printed strut-based structures and several classes of TPMS structures. In an overall result, the diamond TPMS structure showed the best mechanical performance among all the tested structures. Abueidda et al. (9) studied three types of 3D printed TPMS structures experimentally and computationally to investigate the mechanical properties. It is found that the Neovius-CM and IPM-CM structures have a similar mechanical response and have higher stiffness and strength than Primitive-CM. TPMS structures are investigated variously along with mechanical properties. An analytical model is generated to investigate the permeability of TPMS structures, i.e., Fisher-Koch S, Gyroid and Schwarz P designs via Computational Fluid Dynamics (CFD) by Asbai-Ghoudan et al. (10). Results showed that the permeabilities of the three structures are increased with porosity at different rates. It is highlighted the importance of pore distribution and architecture. Besides these features that are investigated successfully, the thermal properties of TPMS structures are also studied in various studies. Catchpole-Smith et al. (11) show that the thermal conductivity of TPMS structures (Gyroid, Diamond Schwarz P) is primarily a function of the material properties and volume fraction sample. It is found that the Schwarz P geometry gave the highest conductivity among all the other structures which are manufactured by laser powder bed fusion. Cheng et al. (12) studied the morphology of TPMS structures which has a significant impact on fluid flow, heat/mass transport, and strength performance. Schwarz P, Schwarz D and Gyroid surfaces are investigated, resulting in the P structure having the lowest flow resistance and highest comprehensive heat transfer coefficient. Mechanical and thermal properties of TPMS structures are also investigated numerically to show the influence of geometric factors on the thermal and mechanical behaviour by Gawronska et al. (13). Cubic P, Diamond and Gyroid surfaces are simulated under load and heat transfer, resulting in that with an increasing number of cells, the effective stress values decrease. Considering the constant structure's volume, while the number of cells is increasing, it is shown that the usefulness of TPMS structures is successful.

Additionally, the high surface area to volume ratio is one of the biggest reasons these porous structures are among the potential heat exchanger feature geometry designs. Although the performance of these structures needs to be investigated in future studies, it is possible that they can provide a low-pressure drop with an increase in the surface area required for efficient heat transfer. Also, their large area/volume ratio, continuously bonded surface, inherent structural integrity, and good mixing potential make them suitable solutions for heat exchanger applications produced by additive manufacturing (14). The most studied variations of TPMS are diamond, primitive and gyroid structures, as mentioned. These structures have two separate areas that are continuous but not intersecting. With this feature, two independent channels can be provided. The fluid at two different temperatures can pass without mixing. It creates a structure that allows efficient use as a heat exchanger geometry in the air conditioning sector. Figure 1 shows the most well-known Schwarz P (Primitive), Schwarz D (Diamond) and Shoen's Gyroid TPMS surface models in the literature. Various studies have investigated TPMS structures as heat exchangers experimentally and numerically. Chandrasekaran (15) studied 3D printed Schwarz D geometry designed as heat exchangers experimentally. It is found that among heat exchangers with similar performance, the Schwarz D geometry is 32% smaller than a shell and tube heat exchangers in a manner of pressure drop. Schwarz D, P and Gyroid surfaces are investigated numerically via CFD analysis by Peng et al. (16). A numerical model is developed to optimise TPMS heat exchanger design parameters besides introducing a design workflow to present a streamline of fluid flows. Attarzadeh et al. (17) also studied the Schwarz D architecture by modelling to elucidate the design parameters and establish relationships between velocity, heat transfer and thermal performance at different wall thicknesses.

In this study, 3D printed Schwarz P, Schwarz D and Shoen's Gyroid surfaces are investigated experimentally to demonstrate a comparison between the geometries regarding performance parameters. Thermal efficiencies and pressure drops are obtained for the geometries at different flow rates and porosity ratios.

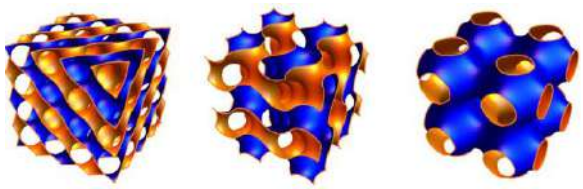

Fig. 1- Surface models of Schwarz D, Shoen's Gyroid and Schwarz P, respectively.

2. Material and method

In the current work, three different TPMS heat exchangers (Gyroid, Diamond and Primitive) with various wall thicknesses are created via Mathematica Programme according to equations 1, 2 and 3, respectively. Then, all geometries are exported. STL format and transferred to a 3-D printer. For each geometry (G, D and P), three different wall thicknesses were selected, and a total of nine heat exchangers were produced.

$$\cos(x)\sin(y) + \cos(y)\sin(z) + \cos(z)\sin(x) = 0 \quad (1)$$

$$\cos(x)\cos(y)\cos(z) - \sin(x)\sin(y)\sin(z) = 0 \quad (2)$$

$$\cos(x) + \cos(y) + \cos(z) = 0 \quad (3)$$

To obtain the thermal efficiency, each heat exchanger was put into the experimental setup, respectively. The experimental setup is shown in Figure 3 and the following assumptions have been considered:

- The inlet temperatures of the air to the system are 40 and 20°C for the hot and cold sides, respectively.
- The flow rate of the fluid is varied in a wide range, between 18 and 53 m^3/h.

In the subsections of material and method, additive manufacturing, pressure drop calculation, experimental setup and heat transfer efficiency have been mentioned.

2.1 additive manufacturing

Along with the fourth industrial revolution, namely Industry 4.0, is the recent movement on intelligent automation technology. In this new era, the utilisation of modern manufacturing skills such as additive manufacturing (AM) within the context of integrating novel information technologies plays a vital role in economic competitiveness [18]. Therefore, it is considered that additive manufacturing (AM) could become a key technology for producing customised products due to its ability to create complex objects with advanced attributes. (new materials, shapes) [18]. Thanks to increased product quality, AM is currently being used in various industries such as aerospace, biomedical, manufacturing and ventilation systems [19, 20]. AM has the potential to drastically change the way components for heat transfer are designed and manufactured [21]. AM provides flexibility to experiment with different complex designs that are otherwise difficult to manufacture with other traditional methods. In addition to advantages, it can reduce lead time such as fast prototyping, acceleration of R&D, on-time delivery of spare parts [22]. In general, AM is the process of building a 3-D object layer by layer. It helps us efficiently use the resources with reduced material waste compared to traditional methods [23]. Fused Deposition Modelling (FDM), Selective Laser Sintering (SLS) and Stereolithography (SLA) are the three 3-D printing techniques that are explored for their feasibility in manufacturing heat exchangers. For this study, FDM will be used to manufacture the heat exchangers because it is the cheaper and most used method to compare other 3-D printing options. FDM is a technology where the melt extrusion method is used to deposit filaments of thermal plastics according to a specific pattern. The layout for FDM consists of a printhead able to move along X and Y directions above a build platform. Nine different geometries, which are shown in Figure 2, were produced by the FDM 3-D printer. Each geometry is produced with a side of 114 mm to be placed in the experimental system. The porosity value of each geometry was obtained differently due to the different equations of TPMSs.

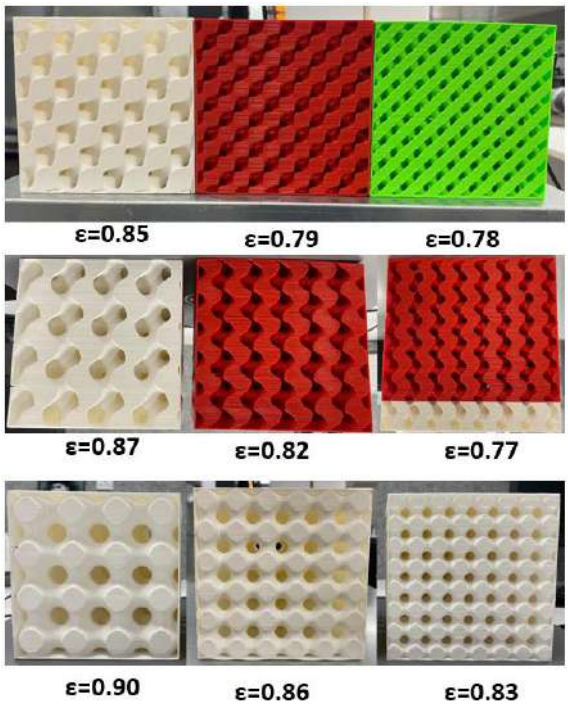

Fig. 2- TPMS heat exchangers produced via FDM

2.2 pressure drop

In the literature, there are several methods to calculate the pressure drop of porous media. One of these methods is presented by Fu et al. (2019) [24], who investigated hydrodynamic and mass transfer performances for three different TPMSs (G, D, P). The following equation is used to calculate the particle or pore diameter (d_p):

$$d_p = \frac{6(1-\varepsilon)}{a_p} \quad (4)$$

Here, ε represents the porosity or void ratio value. a_p is the specific area (m^2/m^3). The rearranged Re

number is as follows:

$$Re = \frac{\rho_G V_G d_P}{(1-\varepsilon)\mu_G} = \frac{3}{2}\frac{\rho_G V_G d_h}{\varepsilon \mu_G} \quad (5)$$

In equation 5, G represents the fluid properties. Also, d_h means the hydraulic diameter. It was stated that the Re number would be in the range of 0-2500, and the fluid velocity would be in the range of 0-3.5 m/s [24]. The pressure drop is calculated by equation 6:

$$\frac{\Delta P}{\Delta L} = \psi \frac{(1-\varepsilon)}{\varepsilon^3}\frac{F_v^2}{d_P} \quad (6)$$

The expression ψ is a resistance coefficient that comes from the Ergun equation (equation 7). F_v^2 represents the amount of pressure exerted by the fluid (equation 8):

$$\psi = \frac{150}{Re} + 1.75 \quad (7)$$

$$F_v = V_G\sqrt{\rho_G} \quad (8)$$

$$f = \frac{\Delta P}{\frac{1}{2}\rho V_g^2 \frac{L}{d_h}} \quad (9)$$

The friction factor (f) is shown in equation 9. Here, L is the length of the heat exchanger.

2.3 experimental setup

The experimental setup is designed to extract data to analyse the actual performance of the heat exchanger. The output of the experiments included four temperature measurements, T_{HI}, T_{CI}, T_{HO}, T_{CO}, flow rates on the hot and cold sides, and the differential pressure across the hot side of the heat exchanger.

A schematic diagram of the experimental setup for better understanding is in Figure 3. The volume flow rates in the experiment were regulated between 0.4 and 1.2 m/s. The temperatures are measured using calibrated Omega K-type thermocouple. These thermocouples can read temperatures up to 200°C. Thermocouples were placed into a small hole drilled in diameter of 6 mm deep into the pipe wall and fixed with thermally non-conductive goop paste. Through, thermocouples placed in the hot and cold airlines were not biased by the ambient temperature. The thermocouples are connected to an IMC STUDIO to record the required temperatures. The thermocouple wires are attached to the connector using hot glue to prevent any leakages. The thermal efficiency for the hot and cold fluid was calculated using the temperatures recorded during the experiments mentioned in chapter 5. We did not expect rapid temperature changes in the system, so the sampling rate was set at 1 S/s (samples/second). The software was developed with the help of Arduino to adjust the fluid velocities. This software has been transferred to an interface. The desired flow rates can be determined by changing the fan operating power. Flow rates can be measured via hotwire probes FTS07 immersed perpendicular to the flow.

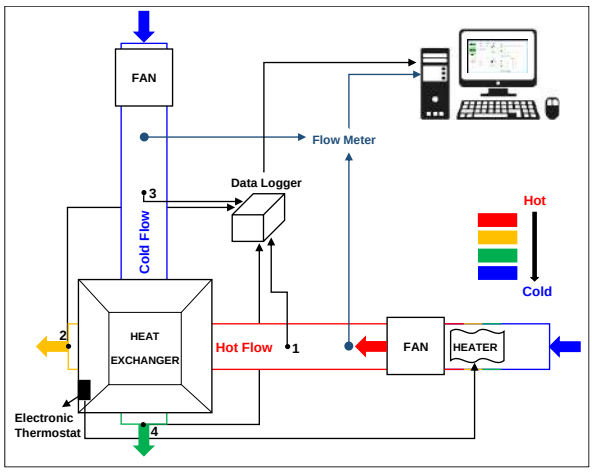

Fig. 3- A schematic diagram of the experimental setup

2.4 heat transfer efficiency

To analyse the experimental values, efficiency is calculated using the TS EN 308 standard [25]. The output of the experiments included 4 temperature measurements, T_{HI}, T_{CI}, T_{HO}, T_{CO}, flow rates on the hot and cold side, and the differential pressure across the hot side of the heat exchanger. The thermal efficiency can be calculated by using (equation 10):

$$\eta_t = \frac{T_{CO}-T_{CI}}{T_{HI}-T_{CI}} \quad (10)$$

In here;

T_{HI}: Hot air inlet temperature
T_{HO}: Hot air outlet temperature
T_{CI}: Cold air inlet temperature
T_{CO}: Cold air outlet temperature

3. Results and discussion

Firstly, internal and external leakage tests were carried out to control the leakage ratio in the system. External leakage tests were performed under 50, 75 and 100 Pa (Table 1). For all pressure values, external leakage ratios were obtained under %3. This means that there is no external leakage in our system.

Tab. 1 - External leakage ratios.

P_{stat} [Pa]	Leakage airflow [m³/h]	Leakage ratio [%]
0	0	0.00
50	0.79	1.58
75	1.02	2.04
100	1.25	2.50

Internal leakage tests were carried out under 25, 50 Pa for all heat exchangers, and the obtained values are shown in Table 2 and 3, respectively.

Tab. 2 - Internal leakage ratios for 25 Pa.

Geometry	Leak. air flow [m³/h]	Leak. ratio [%]
Primitive(ε=0.90)	3.2	6.40
Primitive(ε=0.86)	3.7	7.40
Primitive(ε=0.83)	5.8	11.60
Diamond(ε=0.85)	2.8	5.60
Diamond(ε=0.79)	7.0	14.00
Diamond(ε=0.78)	15.9	31.80
Gyroid(ε=0.87)	1.6	3.20
Gyroid(ε=0.82)	2.5	5.00
Gyroid(ε=0.77)	4.3	8.60
No heat exch.	1.2	2.40

The internal leakage value is below 3% when a heat exchanger is not used under 25 Pa pressure. This shows no leakage in the system under 25 Pa pressure. The rate of internal leakage increases with the addition of heat exchangers to the system. For 25 Pa pressure, the highest internal leakage rate was obtained as 31.8% for Diamond(ε=0.78) geometry. When the tests performed under 50 Pa pressure are examined, the leakage rate for the without heat exchanger has increased and obtained as 6.4%. Also, among the heat exchangers, the leakage rate for the Diamond(ε=0.78) geometry increased to 66%.

Tab. 3 - Internal leakage ratios for 50 Pa.

Geometry	Leak. air flow [m³/h]	Leak. ratio [%]
Primitive(ε=0.90)	5	10.00
Primitive(ε=0.86)	5.6	11.20
Primitive(ε=0.83)	8.4	16.80
Diamond(ε=0.85)	5	10.00
Diamond(ε=0.79)	13.5	27.00
Diamond(ε=0.78)	33	66.00
Gyroid(ε=0.87)	3.2	6.40
Gyroid(ε=0.82)	11	22.00
Gyroid(ε=0.77)	33	66.00
No heat exch.	3.2	6.40

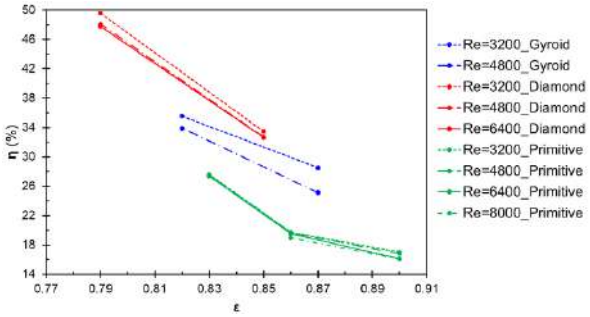

Fig. 4- Efficiency values against porosity

The heat transfer efficiency data are shown in Figure 4. The output of the experiments included four temperature measurements, T_{HI}, T_{CI}, T_{HO}, T_{CO}, flow rates on the hot and cold sides. Temperature values for Gyroid(ε=0.77), Diamond(ε=0.78) and Primitive(ε=0.83) geometries could not be obtained from hotwire probes because the system could not overcome the higher pressure drop. In addition, due to the stated reason, experiments at a Reynolds number of 8000 and 9600 for Diamond(ε=0.79) geometry, 6400, 8000 and 9600 for Gyroid(ε=0.82) geometry, and 9600 for Primitive(ε=0.83) geometry could not be performed. So, the efficiency could not be calculated due to this situation for these geometries. The highest efficiency is derived as approximately %50 for Diamond(ε=0.79) geometry.

Also, according to Figure 4, efficiency decreases with increasing porosity. The same is true for an increase in flow rate. As the flow rate increases, the efficiency decreases. The higher the leakage rate causes, the higher the efficiency due to the mixing of the cold and hot flows.

Pressure drops are calculated by the equations which are given in the pressure drop section. Then friction factor was calculated via pressure drop. Friction factor decreases with increasing Re number for all geometries, which are shown in Figures 5, 6 and 7 for Gyroid, Diamond and Primitive, respectively. Diamond geometries have a higher friction factor due to the more complex geometry compared to Gyroid and Primitive. So, Diamond geometries reach a higher pressure drop penalty with a lower Reynolds number regardless of porosity. Although Gyroid and Diamond have almost the same porosity (0.77 and 0.78, respectively), Diamond has a higher friction factor due to its complex geometry. The curve corresponding to Gyroid surfaces obtains the highest values of f for a given Re due to the dependency on dh factor. Diamond geometries have the lowest dh of the TPMS analysed and this results in a fluctuation of the friction factor values. Also, the friction factor increases with decreasing porosity and, the porosity decreases, the compactness also increases. This ensures the formation of a more rigid structure. On the other hand, increasing the compactness causes a higher friction factor. As a result, it is concluded that the structural integrity in the heat exchangers could not be fully achieved after additive manufacturing, and there are gaps in the exchangers. Heat exchangers need to be remanufactured and tested

using a different AM method such as SLS.

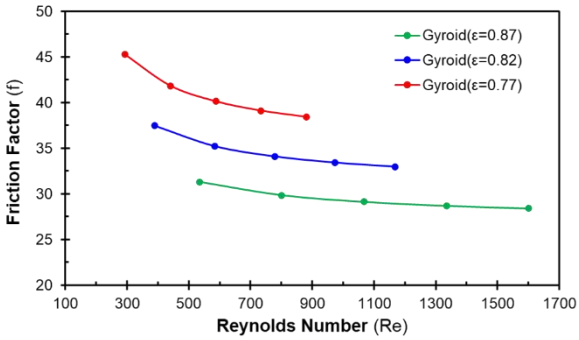

Fig. 5- Friction factor values for Gyroid geometries.

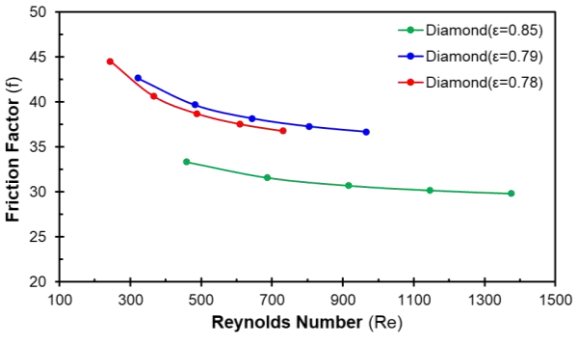

Fig. 6- Friction factor values for Diamond geometries.

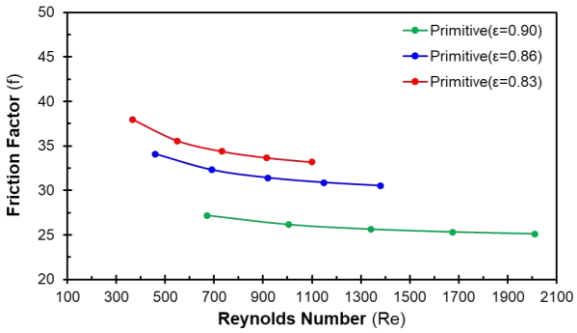

Fig. 7- Friction factor values for Primitive geometries.

4. Conclusion

In this study, 3D printed Schwarz P, Schwarz D and Shoen's Gyroid surfaces are investigated experimentally to demonstrate a comparison between the geometries regarding performance parameters. Thermal efficiencies, pressure drops and friction factors are obtained for the geometries at different flow rates and porosities.

The main conclusions are presented as follows:

- The highest efficiency is derived as approximately %50 for Diamon(ε=0.79) geometry.
- Temperature values for Gyroid(ε=0.77), Diamond(ε=0.78) and Primitive(ε=0.83) geometries could not be obtained from hotwire probes because the system could not overcome the higher pressure drop.
- Diamond geometries reach a higher pressure drop penalty with a lower Reynolds number regardless of porosity due to more complex geometry.
- Friction factor decreases with increasing Reynolds number regardless of TPMS geometries. Also, friction factor is inversely proportional to porosity.
- For all pressure values, external leakage ratios are obtained under %3. This means that there is no external leakage in the experimental system.
- Internal leakage ratios are obtained above %3. Since the structural integrity in the heat exchangers could not be fully achieved after additive manufacturing, and there are gaps in the exchangers. Heat exchangers need to be remanufactured and tested using a different AM method such as SLS.

As a future work, the experiments will be carried out by establishing a system that can overcome the pressure drop. Thus, thermal efficiency and pressure drop values will be obtained for a broader range of flow rates. Due to the gaps in the heat exchangers after additive manufacturing, geometries will be produced with a different additive manufacturing method. In this way, the actual efficiency of the heat exchangers will be obtained.

5. Acknowledgement

The authors would like to thank the anonymous reviewers for their careful reading of the manuscript and valuable suggestions for its improvement. Also, special thanks to Eneko Havalandırma ve Isı Ekonomisi Sistem Teknolojileri A.Ş. for their unwavering support in the use of the laboratory.

6. References

[1] IEA – International Energy Agency - IEA [Internet]. [cited 2022 Jan 10]. Available from: https://www.iea.org/reports/world-energy-outlook

[2] Natural Resources Canada [Internet]. [cited 2022 Jan 10]. Available from: https://www.nrcan.gc.ca/home

[3] Dilberoglu UM, Gharehpapagh B, Yaman U, Dolen M. The Role of Additive Manufacturing in the Era of Industry 4.0. Procedia Manufacturing. 2017 Jan 1;11:545–54.

[4] ASHRAE. Ventilation for Acceptable Indoor Air Quality, Standard 62.1. 2016.

[5] Ayar O, Yalçınkaya M, Karadeniz ZH, Gezgin E. Isı Geri Kazanımlı Havalandırma Cihazları İçin 3

Boyutlu Yazıcı ile Üretilebilecek Isı Değiştirici Tasarımı ve İmalatı. In: 13 Ulusal Tesisat Mühendisliği Kongresi. İzmir; 2017.

[6] Thompson MK, Moroni G, Vaneker T, Fadel G, Campbell RI, Gibson I, et al. Design for Additive Manufacturing: Trends, opportunities, considerations, and constraints. CIRP Annals. 2016;65(2):737–60.

[7] Panesar A, Abdi M, Hickman D, Ashcroft I. Strategies for functionally graded lattice structures derived using topology optimisation for Additive Manufacturing. Additive Manufacturing. 2018 Jan 1;19:81–94.

[8] Al-Ketan O, Rowshan R, Abu Al-Rub RK. Topology-mechanical property relationship of 3D printed strut, skeletal, and sheet based periodic metallic cellular materials. Additive Manufacturing. 2018 Jan;19:167–83.

[9] Abueidda DW, Bakir M, Abu Al-Rub RK, Bergström JS, Sobh NA, Jasiuk I. Mechanical properties of 3D printed polymeric cellular materials with triply periodic minimal surface architectures. Materials & Design. 2017 May;122:255–67.

[10] Asbai-Ghoudan R, Ruiz de Galarreta S, Rodriguez-Florez N. Analytical model for the prediction of permeability of triply periodic minimal surfaces. Journal of the Mechanical Behavior of Biomedical Materials. 2021 Dec;124:104804.

[11] Catchpole-Smith S, Sélo RRJ, Davis AW, Ashcroft IA, Tuck CJ, Clare A. Thermal conductivity of TPMS lattice structures manufactured via laser powder bed fusion. Additive Manufacturing. 2019 Dec;30:100846.

[12] Cheng Z, Xu R, Jiang P-X. Morphology, flow and heat transfer in triply periodic minimal surface based porous structures. International Journal of Heat and Mass Transfer. 2021 May;170:120902.

[13] Gawronska E, Dyja R. A Numerical Study of Geometry's Impact on the Thermal and Mechanical Properties of Periodic Surface Structures. Materials. 2021 Jan 16;14(2):427.

[14] Wadsö I, Holmqvist S. Additively Manufactured Heat Exchangers. [Lund, Sweden]; 2020.

[15] Chandrasekaran G. 3D Printed Heat Exchangers: An Experimental Study. 2018.

[16] Peng H, Gao F, Hu W. Design, Modelling and Characterization of Triply Periodic Minimal Surface Heat Exchangers with Additive Manufacturing. In: 30th Annual International Solid Freeform Fabrication Symposium. Texas-USA; 2019.

[17] Attarzadeh R, Rovira M, Duwig C. Design analysis of the "Schwartz D" based heat exchanger: A numerical study. International Journal of Heat and Mass Transfer. 2021 Oct;177:121415.

[13] Korsavi, S. S., Montazami, A., & Mumovic, D. (2020). Indoor air quality (IAQ) in naturally-ventilated primary schools in the UK: Occupant-related factors. Building and Environment, 106992.

[14] Pegas, P. N., Alves, C. A., Evtyugina, M. G., Nunes, T., Cerqueira, M., Franchi, M., ... & Freitas, M. C. (2011). Indoor air quality in elementary schools of Lisbon in spring. Environmental Geochemistry and Health, 33(5), 455-468.

[15] de Gennaro, G., Dambruoso, P. R., Loiotile, A. D., Di Gilio, A., Giungato, P., Tutino, M., ... & Porcelli, F. (2014). Indoor air quality in schools. Environmental chemistry letters, 12(4), 467-482.

[16] Bluyssen, P. M. (2017). Health, comfort and performance of children in classrooms–new directions for research. Indoor and Built Environment, 26(8), 1040-1050.

[17] Annesi-Maesano, I., Baiz, N., Banerjee, S., Rudnai, P., Rive, S., & SINPHONIE Group. (2013). Indoor air quality and sources in schools and related health effects. Journal of Toxicology and Environmental Health, Part B, 16(8), 491-550.

[18] Dilberoglu, U. M., Gharehpapagh, B., Yaman, U., & Dolen, M. (2017). The role of additive manufacturing in the era of industry 4.0. Procedia Manufacturing, 11, 545-554.

[19] Ayar, O., Yalçınkaya, M. A., Karadeniz, Z. H., Gezgin, E. 2017. "Isı Geri Kazanımlı Havalandırma Cihazları İçin 3 Boyutlu Yazıcı ile Üretilebilecek Isı Değiştirici Tasarımı ve İmalatı" 13. Ulusal Tesisat Mühendisliği Kongresi, 19-22 Nisan, İzmir.

[20] Thompson, M. K., Moroni, G., Vaneker, T., Fadel, G., Campbell, R. I., Gibson, I., ... & Martina, F., 2016. "Design for Additive Manufacturing: Trends, opportunities, considerations, and constraints", CIRP annals: manufacturing technology, 65(2), 737-760.

[21] Catchpole-Smith, S., Sélo, R. R. J., Davis, A. W., Ashcroft, I. A., Tuck, C. J., & Clare, A. (2019). Thermal conductivity of TPMS lattice structures manufactured via laser powder bed fusion. Additive Manufacturing, 30, 100846.

[22] Tirelli, V. (2020, May). Additive Manufacturing in Heat Exchangers and Valves. In Offshore Technology Conference. Offshore Technology Conference.

[23] Danayat, S. S. (2019). Investigating 3-D Printed Polymer Heat Exchanger (Doctoral dissertation, Arizona State University).

[24] Fu, Y., Bao, J., Wang, C., Singh, R. K., Xu, Z., & Panagakos, G. (2019). CFD Study of Countercurrent Flow in Triply Periodic Minimal Surfaces with CO2BOL Solvent (No. PNNL-29590). Pacific Northwest National Lab. (PNNL), Richland, WA (United States).

[25] TS EN 308: Isı eşanjörleri-Havadan havaya ve atık gazlardan ısı kazanımı cihazlarının performansının tayini için deney metotları, 1997.

Data Statement

The datasets generated during and/or analysed during the current study are not publicly available because they could be the subject of future works, but will be available the reason for the need can be requested from the corresponding author by specifying it.

Heat recovery ventilation solutions for school building renovation – case study

Helena Kuivjõgi [a], Henri Sarevet [a], Martin Thalfeldt [a], Jarek Kurnitski [a, b]

a: FinEst Centre for Smart Cities (Finest Centre), Department of Civil Engineering and Architecture, Tallinn University of Technology;

b: Aalto University, School of Engineering, Department of Civil and Structural Engineering, Finland

Abstract.
School building ventilation solutions have been mainly natural ventilation. Only in a few decades has the renovation of ventilation systems in school buildings started. However, there are still many buildings in Estonia that have natural ventilation or mechanical extract ventilation without heat recovery. Last solution can ensure indoor climate requirements in favourable climate conditions if well designed. However, this can lead to excessive heating energy use resulting in not adequate energy performance. Therefore, there is a need of ventilation system renovation to improve both IAQ and energy performance. Two solutions with different cost are studied in this paper: classroom air handling unit (AHU), and central AHU. The aim of this study is to determine which solution is better in energy efficiency if there is demand to renovate ventilation system in school building. The calculations have been done in standard and real use and climate. Study will show the cost-optimality of these solutions in school buildings. Two school building models were composed and building performance simulations (BPS) with the test reference year climate file were conducted to calculate the building energy use based on EN 16798-1:2019 and real use (where the building model was calibrated with monthly measured real energy consumption from year 2014). Previous studies show, that natural ventilation is an electricity saving solution, but not good for indoor climate. This study found that classroom-based solution is easier to build and the initial cost is lower. However, the energy saving for central ventilation solution will exceed the classroom solution of 29 kWh/m^2. Considering energy and cost calculations, the centralized mechanical ventilation with heat exchange will be slightly more cost-optimal solution in this case study as it gained 4 €/m^2 lower global cost than classroom-based solution.

Keywords. School building, mechanical ventilation, heat recovery, cost-optimality, energy efficiency.
DOI: https://doi.org/10.34641/clima.2022.208

1. Introduction

Average school building is more than 30 years old and in acceptable condition, but not with a good indoor environment. The ventilation system has not been the priority of renovation. Quite a few school buildings have natural ventilation or mechanical extract ventilation without heat recovery.

Achieving a good indoor environment for study or work activity requires ventilation rates of the order of 8 l/s per person. That will prevent any impairment of pupils' performance due to inadequate ventilation. [1] The mechanical extract ventilation with window opening will achieve 2.3-3.8 l/s per person [2] and therefore do not fill this recommendation as well the supply temperature will be as low as outdoor air temperature. Furthermore, as mentioned in [2] that the air quality was judged by the students to be the worst in the mechanically ventilated classroom. Therefore, the final solution and maintenance plan should be advised.

The idea of this study is to determine which solution is better in energy efficiency if there is demand to renovate ventilation system in school building. Using a simulation method, the study will consider cost and show the change of heat and electricity energy use if the mechanical extract ventilation system (without heat recovery) will be replaced by mechanical ventilation system with heat exchanger in two possible solutions.

There was considered, that the air change rate is equal to renovated building models ventilation system and correspond to recommendations in [1].

Copyright ©2022 by the authors. This conference paper is published under a CC-BY-4.0 license.

2. Research Method

2.1. Description of the reference building

Fig. 1 - Reference building photo and IDA-ICE model

The reference building (Fig. 1) is one school building in Estonia, Kuressaare. The actual heated area is 5300 m². It includes the main body (classrooms, teacher offices, and library) and functional sections (canteen, hall, gym, and educational centre). The main body ventilation of the building has been renovated in 2005-2006 from natural ventilation solution to mechanical extract ventilation system (without heat exchanger) (Fig. 2). The construction of a ventilation system in the canteen, hall, and gym was in 2003. The educational centre was built as new in 2012 with mechanical ventilation with heat recovery.

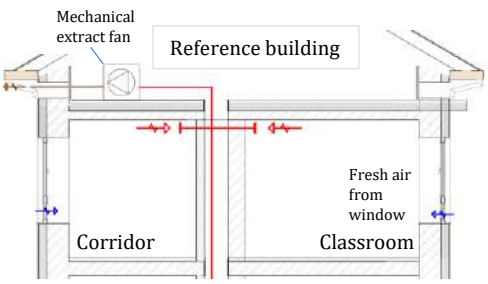

Fig. 2 - Principle of the reference ventilation system in a building

2.2. Simulation Model and Method

The simulation model (Fig. 1) has been built in the well-established and validated simulation software IDA ICE [3]. Model zones are described in Tab. 1.

The simulation model construction U-values was taken as similar as possible to reference building (Tab. 2) and thermal bridge values (Tab. 4) was taken as the average practice and some specific thermal bridges were calculated in the study [4]. Specific air leakage rate was taken 4 m³/(h m²) and infiltration 0.0556 l/(s m² external surface) was calculated according to regulation [5]. The average domestic hot water use is 172 l/m² floor area and year, and the distribution is 50% during 16. June to 14. August. The loss of the distribution system was taken by 3% of the heat delivered by the plant.

Tab. 1 - Building model zones quantity, area and share over total area

Zones	No. of zones	Area, m²	Share
Classrooms	14	1789	33%
Offices	2	191	3.5%
Library	1	86	1.6%
Staircase and corridor	7	2240	41%
Main body	**24**	**4306**	**78%**
Canteen	1	280	5.1%
Hall	3	368	6.7%
Gym	1	315	5.7%
Environmental education center	3	223	4.0%
Other	2	12	0.2%
Total	**34**	**5504**	100%

Tab. 2 - Building envelope area and U-values

Building envelope	Area [m²]	U-value [W/(m² K)]	% of total
Walls above ground	3487	1.06	48.17
Basement wall	319	1.34	5.55
External wall / Educational centre	158	0.19	0.39
Canteen wall	81	1.08	1.14
Staircase wall	342	1.49	6.64
External wall / Hall new part	62	0.19	0.15
External wall / Main	1772	1.11	25.63
External wall / Hall and Gym	707	0.92	8.47
External wall / Gym new part	47	0.35	0.21
Walls below ground	12	1	0.16
Basement wall below ground	12	1	0.16
Roof	1865	0.24	5.88
Roof / Educational center	67	0.14	0.12
Roof / Main	1798	0.25	5.76
Floor towards ground	1925	0.42	10.49
Floor / Educational centre	90	0.21	0.24
Floor / Hall new part	45	0.29	0.17
Floor / Main	1791	0.43	10.07
Windows	1056	1.05	14.41
3 pane glazing, clear, 4-12-4-12-4	1056	1.05	14.41
Doors	19	1.35	0.34
EST External door(2019), heated space	6	1.01	0.07
External door / Gym new part	13	1.49	0.26
Thermal bridges			20.56
Total	8364	0.92	100

Tab. 3 - Model description

	Model 1: Reference building	Model 2: Classroom-based ventilation system	Model 3: Central ventilation system	Required air flow for main body, l/(s*m^2)	Actual air flow in RB, l/(s*m^2)
Classrooms	Mechanical extract ventilation without heat recovery	Classroom-based	Central AHU	2.5-4	0.6
Offices				1.5	0.55
Library				1.5	0.55
Staircase and corridor		Mechanical extract ventilation without heat recovery		1	0.38
Canteen and kitchen	Kitchen AHU	Kitchen AHU	Kitchen AHU	1	1
Hall	Hall AHU	Hall AHU	Hall AHU	1.5	1.5
Gym	Gym AHU	Gym AHU	Gym AHU	1.5	1.5
Environmental education center	Edu Center AHU	Edu Center AHU	Edu Center AHU	2.5	2.5
*Average air flow, l/(s*m^2)*	0.72	1.89	1.89	1.89	0.72

Tab. 4 - Thermal bridges of the reference building

Envelope	Thermal bridge, W/K/(m joint)
External wall / internal slab	0.3
External wall / internal wall	0.0686
External wall / external wall	0.2
External windows perimeter	0.4
External doors perimeter	0.3
Roof / external walls	0.53
Roof / internal walls	0.024
External walls, inner corner	-0.2

After the constructions were set similar to the reference building, the lighting, equipment, and ventilation usage was adjusted until the simulation output will fit with the reference building actual metered energy consumption from utility bills, to calibrate the model. According to ASHRAE guideline 14 [6], the model will be considered calibrated if the building performance simulation (BPS) achieves an approximate mean bias error (MBE) of ±5% and a CV(RMSE) of 15% compared to monthly energy use. This building model energy simulation gets CV(RMSE) 10% and MBE 1.1% for electricity and respectively 17% and -4.9 % for heating energy use. Regarding to that, we have only the main heat and electricity meter and cannot determine the specific energy use, the model considered to be calibrated enough to go further on comparison.

Four simulation models were composed. Models with two different ventilation solutions with required air flows were composed (model dissimilarities are described in Tab. 3). Furthermore, there has been composed two reference building model: one with actual air flows (RB_actual) and another with required air flows (RB_req_air). The principles of the ventilation system are described in Fig. 2, Fig. 3. There are two types of AHU heat exchangers used in the model: cross-flow plate and non-hygroscopic rotor heat exchanger. In detail, see AHU parameters in the Tab. 5.

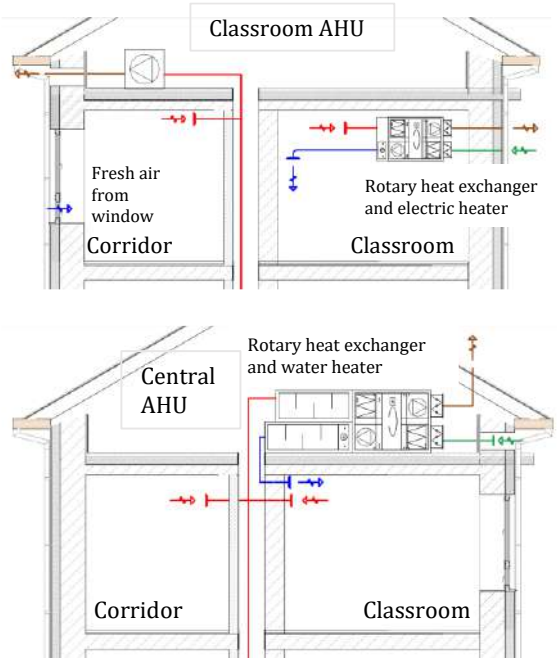

Fig. 3 - Principle of the classroom-based and central ventilation system

Energy simulations for each model for the purpose of comparison, was conducted with real use that is corresponding to calibrated model. The climate file was test reference year (TRY) that is described in T. Kalamees and J. Kurnitski study [7]. Finally, the simulation with standard use from national regulation [5] was done to normalize the usage and climate and find the impact of usage on energy efficiency.

The focus of this study is on the main body of building that include classrooms, offices, library, staircases, and corridors (Tab. 1).

Tab. 5 - Air handling units parameters

AHU (heat exchanger type)	SFP, kW/(m³/s)	Heat exch. Effective-ness, %	Min. allowed leaving temp., °C
Kitchen AHU (plate)	2	70%	0
Hall AHU (plate)	2	60%	1
Gym AHU (plate)	2	70%	0
Edu Center AHU (plate)	1.67	70%	1
Mechanical extract fans (-)	0.9	-	-
Classroom AHU (rotor)	1.5	80%	0
Central AHU (rotor)	1.67	80%	-5

2.3. Indoor Climate Control

The main purpose of these solutions is to ensure good indoor climate conditions in main body of building. Therefore, the concentration of CO_2 and the indoor temperature were considered during simulations. The limits for a good indoor climate are under 800 ppm of CO_2 concentration and room air temperature between 21-25° C. As the building do not have cooling, overheating was considered during 1. May-15. June and 15. Aug-30. Sept

2.4. Economic calculation method

The cost has been asked from representatives who work or have been working in a ventilation contracting or designing company. The authors get one approximate evaluation for each solution and one exact example for the cost of a real school building central ventilation renovation completed in 2020. Both ventilation system solutions have been evaluated in detail, and the cost determined for each part in the system, design and building process. In a classroom-based ventilation solution, the cost has been evaluated for one classroom and then multiplied with 28 classrooms. However, the cost is evaluated by the prices in 2020. The economic prospect has been evaluated by the extra cost per saved delivered energy and global cost calculations according to [8] and EN 15459-1:2017 [9], where the equations 1-3 were used:

$$C_g = \frac{C_I + C_a \cdot f_{pv}(n)}{A_{floor}} \quad (1)$$

where, C_g is the cost related to global incremental energy performance, NPV, €/m²; C_I is the construction cost related to energy performance included in the calculations, €; C_a annual energy cost during starting year, €. For heating energy (district heating) price in 2020 was 0.058 €/kWh and price of electricity 0.076 €/kWh (VAT incl.); $f_{pv}(n)$ is present value factor for the calculation period of n years; A_{floor} is heated net floor area, m².

$$f_{pv}(n) = \frac{1 - \left(1 + \frac{R_R - e}{100}\right)^{-n}}{\frac{R_R - e}{100}} \quad (2)$$

where, R_R is the real interest rate, %; e is escalation of the energy prices of 2%; n is the number of years considered, i.e. the length of the calculation period is 20 years. For the real interest rate the following equation was used:

$$R_R = \frac{R - R_i}{1 + R_i/100} \quad (3)$$

where, R is the market interest rate 5% and R_i is the inflation rate for 2020 -0.5% and for 2019 2.3% according to Bank of Estonia.

3. Results and Discussion

Following section will introduce the results on the energy efficiency and cost-optimality of two school ventilation solutions. The indoor climate condition has been controlled for Model 2 and Model 3. Average air flow for both models is 8 l/s per person (ca 2.9 l/(s*m²)) and the room temperature setpoint during heating period is 21° C. These conditions are providing a good indoor climate: CO_2 concentration is under 800 ppm during all usage time and the room temperature is 21° C during heating period. However, during the cooling period and the school usage time, the room temperature will rise by more than 25° C in total around 400 ° Ch. That is not within the boundaries of national regulation [10]. Therefore, this building needs shading or cooling in the cooling period.

In general, these two solutions are different in the renovation process. The classroom-based ventilation system is easy to build and therefore a faster solution for renovation if there is an urgent need of good air change rate. However, central ventilation solution demands to close the school for several months (Tab. 6).

Tab. 6 - Renovation work for two solutions

	Classroom-based ventilation solution	Central ventilation solution
AHU and ducts installation	classroom	main body
Electrical installation	classroom	at the place of central unit
General construction and finishing work	classroom	main body
Renovation work duration	week	several months

3.1. Two ventilation solution energy consumption

The main body electricity consumption (Fig. 4) did not differ in between the two models with two ventilation solutions that much as for heating consumption (Fig. 5). However, the electric heater increases the electricity use about 3.8 kWh/m²a to the classroom-based system. Therefore, the electricity consumption is higher than for the central ventilation system (Fig. 6). Obviously, the influence is also on AHU fans, but the difference is minor.

Zone heating is the highest energy-consuming component for both models (Fig. 6). However, classroom-based model will consume 32 kWh/m² more heat in zones than model with central ventilation, because of mechanical ventilation without heat exchange in corridors and staircaises (that will occupy 41% of main area (Tab. 1)).

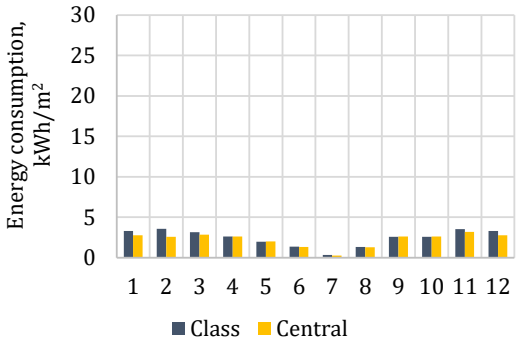

Fig. 4 - Total monthly electricity consumption of the main body for the two ventilation solution models

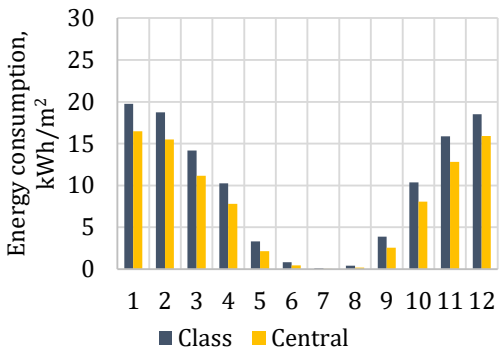

Fig. 5 - Main body total monthly heating energy consumption for two ventilation solution model, kWh/m²

3.2. Total building energy consumption

Energy simulation with whole model of real use shows that the best solution is a ventilation system with central AHU that will service the main body of the building. The primary energy was calculated with PE factors: 0.65 for efficient district heating and 2 for electricity. The lowest primary energy (PE) consumption (Fig. 7) is for model with central ventilation system (159.4 kWh/m²) and almost equal PE consumption is for models RB_actual and Class. Compared to the actual reference building, the delivered energy saving in total is 43 kWh/m² (153 kWh/m² compared to the RB with required air flow) for the model with central ventilation system. Saving is 14 kWh/m² (124 kWh/m² compared with RB with required air flow) for model with classroom-based ventilation system. (Fig. 8)

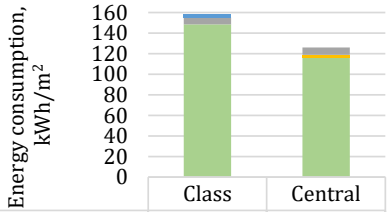

	Class	Central
Electric heating	3.8	0
Fans and pumps	6.6	7.0
AHU heating	0	2.64
Zone heating	148	116
Total el.	10	7
Total heat	148	119

Fig. 6 - Annual energy consumption of the main body for two ventilation solutions

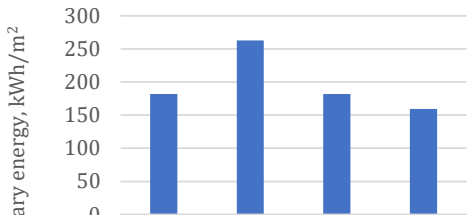

	RB_actual	RB_req_air	Class	Central
EPC, kWh/m2	182.2	263.0	182.3	159.4

Fig. 7-Primary energy consumption for each model

3.3. Comparison of the real and standard use of building

Comparing the BPS based on standard (EN 16798-1:2019) use with real performance (Fig. 8), the energy consumption relative change will vary 6-30%, depending on model. Electricity consumption between the two solutions will differ 2.7 kWh/m² in real use and 0.5 kWh/m² in standard use. However, the heating consumption difference between two solution is 27 kWh/m² in real use, but 58 kWh/m² in standard use. The 31 kWh/m² difference comes as a result of air flow in the building. As for real use, only the main body have 3 l/(s*m²) air flow and other parts have 1-1.5 l/(s*m²). However, in standard use the regulation sets to have a total building of 3 l/(s*m²).

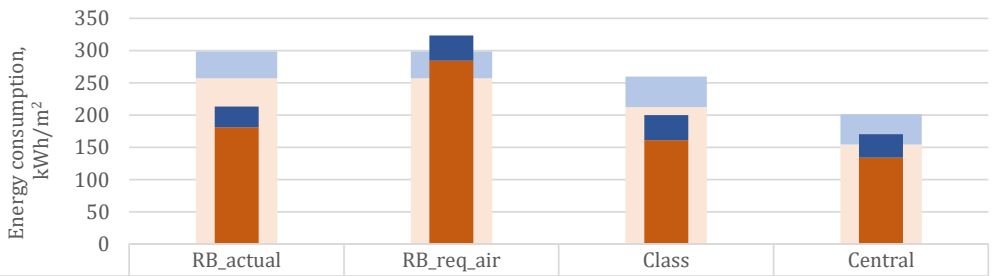

	RB_actual	RB_req_air	Class	Central
Electricity_STD	41.5	41.5	47.4	46.9
Heating_STD	257	257	213	155
Electricity	32.2	39.1	38.7	36.0
Heating	181.3	284.5	161.2	134.4

Fig. 8 - Delivered energy consumption for each model with real and standard (STD) use, kWh/m²

3.4. Practice and Profitability of Two Ventilation Solutions

The renovation of ventilation in school buildings is not straightforward. It needs good preparation and planning. The solutions in this study are almost contrary as explained previously.

Tab. 7 – Renovation cost for two solutions (20% VAT incl.)

	Classroom-based ventilation solution	**Central ventilation solution**
Ventilation system materials and installation, €	312,000	330,000
Additional construction work and finishing, €	56,000	126,000
Electrical installation, €	57,600	50,000
Design and project managing cost, €	17,000	30,000
Margin, %	20%	20%
Total cost, €	531,120	643,200
Total cost, €/m² per renovated section area	123	150
Total cost, €/m² per total heated area	97	117

In this case, the renovation of the central ventilation system will cost about 117 €/m² total heated area and the classroom ventilation solution about 97 €/m² total heated area. However, central ventilation solution is still that much energy efficient, that due to good energy savings, the extra cost per saved delivered energy is almost 2.6 times lower for central ventilation solution. (Fig. 9) Compared to the reference model with the same air flow, the extra cost per saved delivered energy is minimal. (Fig. 10)

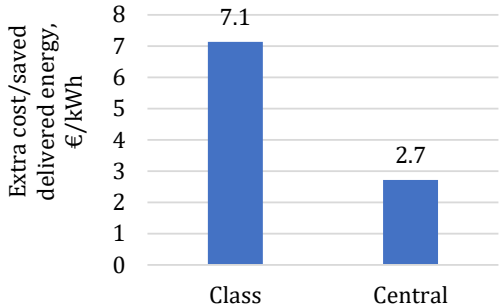

Fig. 9 - Extra cost per saved delivered energy (compared with RB_actual)

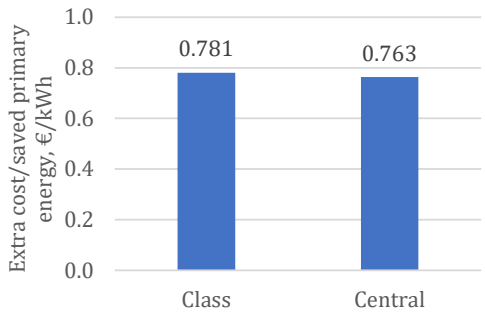

Fig. 10 - Extra cost per saved delivered energy (compared with RB_req_air)

In Fig. 11 and Fig. 12 can see that the central ventilation system will be the best option considering the energy efficiency and cost-optimality with about 4 €/m² lower global cost. The reference building that will achieve indoor climate conditions has almost 10 €/m² higher global cost and 80-100 kWh/m² higher primary energy consumption than renovation solutions. However, the actual case has the lowest global cost, but will not achieve the indoor climate requirements.

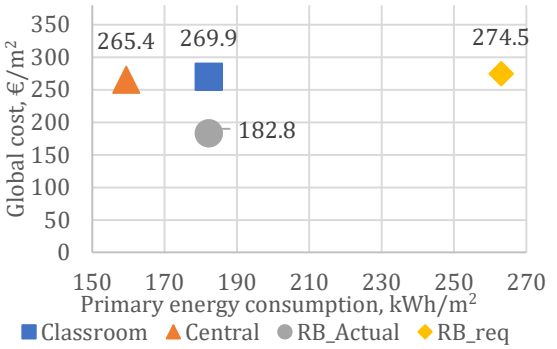

Fig. 11 - Global cost with calculations of 2020 interest rate and inflation

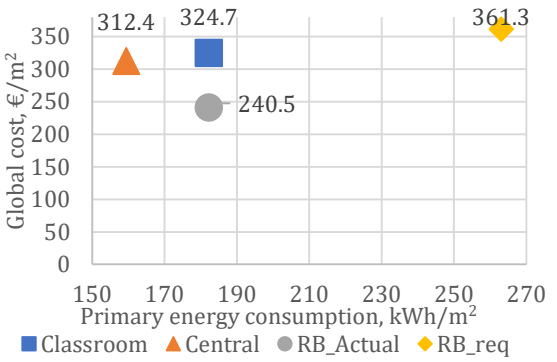

Fig. 12 - Global cost with calculations of 2019 interest rate and inflation

4. Conclusions

Two school building models were composed and building performance simulations (BPS) with the test reference year climate file were conducted to calculate the building energy use according to the EN 16798-1:2019 and the real use. The result of calculations will show the change of heat and electricity energy use if the mechanical extract ventilation system (without heat recovery) will be replaced by mechanical ventilation system with heat exchanger.

There have been compared two possible solutions:

- classroom-based mechanical ventilation with heat recovery that will serve only classrooms (mechanical extract fan for corridors)
- central mechanical ventilation with heat recovery that will serve the main body

Classroom-based solution is easier to built and the initial cost is lower. However, the energy saved is only 14 kWh/m² (124 kWh/m² compared to the RB with required air flow) compared to a central ventilation solution that will save 43 kWh/m² (153 kWh/m² compared to the RB with required air flow). Considering energy and cost calculations, the centralized mechanical ventilation with heat exchange will be the cost-optimal solution in this case study as it gained about 4 €/m² lower global cost. However, the global cost differs only 70-80 €/m² between the cost-optimal solution and the reference building, where the requirements are not up to the standards.

The limitation of this study is the calibration rate, as the model meets only partially the recommendations of calibration due to incomplete energy meter data. Therefore, next studies should be done with buildings that have more specific data on energy consumption. This study considered the savings in test reference year climate. Further studies should calculate saving also in real climate conditions as recommeded in ASHRAE Guideline. Furthermore, the results show that the energy consumption will differ up to 30% between standard and real use. Therefore, next studies should consider normaization aspects in energy calculations. The profitability of solutions is reasonable as it will not consider the indoor climate - in school we can not save energy at the expense of study environment. Further studies should include the indoor environment, so it can be used for government support system.

5. Acknowledgement

The authors are grateful to the TalTech Nearly Zero Energy Buildings Research Group to give me good feedback to promote my paper. This work has been supported by the Estonian Ministry of Education and Research, European Regional Fund (grant 2014-2020.4.01.20-0289), the Estonian Centre of Excellence in Zero Energy and Resource Efficient Smart Buildings and Districts, ZEBE (grant 2014-2020.4.01.15-0016) and Dora Pluss funded by the European Regional Development Fund, by the European Commission through the H2020 project Finest Twins (grant No. 856602), the Estonian Research Council grant (PSG409).

Data sharing not applicable to this article as no datasets were generated or analysed during the current study

6. References

[[1] Z. Bakó-Biró, D. J. Clements-Croome, N. Kochhar, H. B. Awbi, and M. J. Williams, "Ventilation rates in schools and pupils' performance," *Build. Environ.*, vol. 48, no. 1, pp. 215–223, Feb. 2012, doi: 10.1016/J.BUILDENV.2011.08.018.

[2] J. Gao, P. Wargocki, and Y. Wang, "Ventilation system type, classroom environmental quality and pupils' perceptions and symptoms," *Build. Environ.*, vol. 75, pp. 46–57, May 2014, doi: 10.1016/j.buildenv.2014.01.015.

[3] "IDA ICE: validations & certifications." https://www.equa.se/en/ida-ice/validation-certifications.

[4] G. Kuldsaar, "Efficiency analysis of Saaremaa co-educational building," Tallinn University of Technology, 2018.

[5] Estonian Government's Ordinance, "Methodology for calculating the energy performance of buildings," *Riigi Teataja*, 2019. https://www.riigiteataja.ee/en/eli/520102014002/consolide (accessed Aug. 20, 2020).

[6] ANSI/ASHRAE, "ASHRAE Guideline 14-2002 Measurement of Energy and Demand Savings," *Ashrae*, vol. 8400, p. 170, 2002.

[7] T. Kalamees and J. Kurnitski, "Estonian test reference year for energy calculations," no. January, pp. 40–58, 2006.

[8] THE EUROPEAN COMMISSION, *Commission Delegated Regulation (EU) No 244/2012 of 16 January 2012 byestablishing a comparative methodology framework for calculating cost-optimal levels of minimum energy performance requirements for buildings and building elements*. 2012, p. 28.

[9] *EN 15459-1:2017. Energy performance of buildings – economic evaluation procedure for energy systems in buildings - Part 1: Calculation procedures, Module M1-14.* .

[10]. Estonian Government's Ordinance, "Minimum requirements for energy performance of buildings," 2019. https://www.riigiteataja.ee/akt/119012018007?leiaKehtiv.

Numerical analysis of ventilated windows' thermal behaviour under summer condition

Shiva Najaf Khosravi [a], Ardeshir Mahdavi [a]

[a] Department of Building Physics and Building Ecology, Vienna University of Technology, Vienna, Austria, shiva.khosravi@tuwien.ac.at, amahdavi@tuwien.ac.at.

Abstract. Efforts to develop advanced building envelope components have pursued, among other things, ventilated window constructions. To properly configure ventilated windows, both the operation mode and the climatic context must be taken into consideration. In the framework of a previous research project, an instance of a ventilated window (outdoor air curtain mode) was implemented in a testbed and was subjected to experimental studies under summer conditions. In the present contribution, we numerically evaluate the thermal behavior of this system via computational fluid dynamic (CFD) simulation. Specifically, we compared simulation results with measurement data to evaluate the accuracy of the simulation model. Thereby, the main objective was to explore the fidelity of the CFD model and its potential for supporting the design of ventilated windows. To this end, the utility of the CFD was demonstrated in terms the optimization of the design of a ventilation window (exhaust and outdoor curtain mode). In the course of this study, we numerically analyzed the thermal behavior of the two modes of ventilation window operation (exhaust and outdoor curtain mode) under summer conditions. The results of the CFD-based investigation suggest that the application of low-emissivity glazing as the exterior glass pane can improve the cooling effect in both cases. In addition, the exhaust mode of the ventilated window shows a better performance under summer boundary conditions.

Keywords. Heat transfer, ventilated window, CFD simulation, energy performance.
DOI: https://doi.org/10.34641/clima.2022.370

1. Introduction

Ventilated windows have received increased attention due to their potential to contribute to indoor air quality and higher energy efficiency [1]. A ventilated window can regulate, in theory, the interaction between the outdoor and the indoor climate due to its adaptability [2]. This window is composed of a multi-layered structure. In certain instances, it includes transparent panels as an external and internal layer and a ventilated buffer space in between. Operable vents located at the top and bottom of the frames enable, depending on the operation mode, the flow of air in the cavity [3-5]. Ventilated windows can be employed in many regions with various climate conditions [3, 6, 7]. Generally speaking, five main operation modes of a ventilated window can be distinguished, namely i) supply, ii) exhaust, iii) indoor air curtain, iv) outdoor air curtain and v) insulation mode. To properly configure ventilated windows, both the operation mode and the climatic context must be taken into consideration [3].

As the name implies, the main distinction between conventional windows and ventilated windows is the presence of free or forced convection in the interstitial cavity between the window's layers [8]. A ventilated window functions as a solar collector under incident solar radiation. The solar energy passing through the outer glazing warms up the interstitial space and eventually internal glazing surfaces. Re-emitting the trapped heat from these surfaces increases the indoor air temperature. Hence, the thermal behavior of ventilated windows strongly affects the indoor temperature and consequently energy consumption of a building [3].

Predicting the thermal behavior of a ventilated window is not a trivial task. Temperature and airflow patterns evolve due to various dynamic and interdependent thermal and aerodynamic processes. These processes depend on weather conditions, geometry, thermophysical properties of the several constituent components of the ventilated window structure, and the building itself [9-11]. Detailed numerical modeling of ventilated windows to address the full complexity of these systems necessitates the combined representation of heat, mass, and momentum transfer [12]. Modeling and simulation of fluid dynamics in such a system require a high degree of accuracy in details to obtain a high

Copyright ©2022 by the authors. This conference paper is published under a CC-BY-4.0 license.

degree of fidelity toward representation of the reality [4]. As many studies have confirmed, The numerical model (for example, CFD simulations) has the potential to yield a full-scale domain with a complicated boundary layer such as an inner layer, including the thin viscous sublayer or the buffer layer [13]. The numeric analysis of the thermal behavior of ventilated windows has received significant attention in the literature in the last few decades [3, 8, 10, 14-17]. Nevertheless, various approaches to the modeling of heat transfer phenomena in the ventilated windows are seen with a different level of accuracy, depending on the overall goal of the modeling project [4]. For instance, deployment of purely two-dimensional CFD models may be considered as less than ideal [10, 18-20].

In some studies, the dependency of material-related properties on temperature is not considered [10, 20-22]. Likewise, the influence of solar radiation is not included in a number of studies [18, 21, 22]. Most CFD studies model the thermal performance of the window under the assumption of a constant outdoor temperature and do not consider the wind impact. In some cases [16, 23-25], heat transfer coefficients for indoor and outdoor surfaces are considered. These observations imply that, despite significant progress in the CFD-supported study of ventilated windows, the intricate nature of heat transfer and airflow within a ventilated window is far from being fully understood. Therefore, further research in this field is necessary.

The present contribution concerns the thermal performance of an outdoor curtain mode and exhaust ventilated window. This was done by numerically modeling the fluid dynamic and heat transfer in the window and solving the model in a commercially available CFD code. Moreover, available measured data obtained from an exprimental method was applied to evaluate the accuracy of the CFD model. The CFD model was subsequently utilized to compute air temperature, and air velocity distributions. The aim thereby was to cmpare the thermal performance of the two aforementioned ventilated windows in the summer boundary condition.

2. Method

In order to simulate the thermal behavior of the ventilated window, a CFD model was implemented in the finite volume code ANSYS FLUENT 19.0 [26]. The model involves the ventilated window mounted in the façade of a test space. Ansys design modeler and Ansys meshing were applied as a pre-processor to create the geometry, mesh, and the computational domain. In this model, a mesh with hexahedral element was generated. To achieve higher resolution concerning the air movement in the cavity, a finer mesh was applied between the glass sheets. The grid cell size within the cavity was kept to a maximum of 2 mm, as larger dimensions would significantly alter the results. A grid independence study has been performed to ensure the adequacy of the mesh density. Due to the transient outdoor boundary condition, the thermal behavior of the glazing units is rather dynamic. However, due to their relatively small thermal mass, the glazing units react realtively swiftly to the dynamics of prevailing thermal conditions. Based on this observation and considering the computational cost, the thermal processes in the ventilated window were modeled as steady-state mode [27].

In the present study a three-dimensional domain in a steady-state mode was applied. The conservation equation for mass, momentum, and thermal energy, which is known as Reynolds-averaged Navier–Stokes equation was solved to predict the field variables temperature and velocity. The corresponding partial differential equations for continuity (1), momentum (2), and energy (3) are as follows [28]:

$$\frac{\partial}{\partial t}\left(\int_V \rho dV\right) + \oint_A \rho V_r \,.\, da = 0 \tag{1}$$

$$\frac{\partial}{\partial t}\left(\int_V \rho dV\right) + \oint_A \rho v_r \otimes v.\, da = -\oint_A pI.\, da + \oint_V f_b\, dV \tag{2}$$

$$\frac{\partial}{\partial t}\int_V \rho E dV \oint_A [\rho H V_r + v_g p].\,\mathrm{da} = -\oint_A q''.\, da + \oint_A T.\, v dA + \oint_V f_b\,.\, v dV + \oint_V S_E\, dV \tag{3}$$

Thereby, v presents continuum velocity, v_r is the relative velocity; V is volume; a is the area; p is the pressure; I is the unit vector; T presents the viscous stress tensor; E is the total energy; H is the enthalpy; q'' is the heat flux vector; $\otimes$ is kronecker product; S_E radiation energy source.

Buoyancy due to density change was applied in the energy equation. The discrete ordinates (DO) model was applied as the radiation model [29, 30]. This model is capable of modelling glass, a semi-transparent medium [10]. The widely deployed K-ε realizable turbulence model was applied [3, 8, 31, 32]. The pressure based solver was used [17].

For pressure–velocity coupling, the SIMPLE segregated solver was applied[17]. The discretization scheme used for the momentum, energy, turbulent kinetic energy, and specific dissipation rate was the second order upwind scheme. Pressure Staggering Option (PRESTO) was used for the pressure discretization scheme. Gradient reconstruction was done using The Least Squares Cell-based method [17]. The acceptable residual limits were set at $<10^{-3}$ for continuity, x, y and z momentum, turbulent kinetic energy and turbulent specific dissipation, whereas this limit for energy was $<10^{-6}$ [3, 17]. Monitors for area weighted static temperature on the supply vent, maximum velocity in the cavity area and supply vent mass flow rate were setup. Three types of materials were applied in each simulation, namely transparent fluid (air), semi-transparent solids (glazing), and opaque solids (frames and walls). Table 1 summarizes the assumed physical properties of the layers.

As mentioned earlier, in the course of this study, we

numerically analyzed the thermal performance of the two modes of ventilation window operation (exhaust and outdoor curtain mode) under summer conditions. Figure 1 schematically illustrates the vertical section of the ventilated window for the summer case.

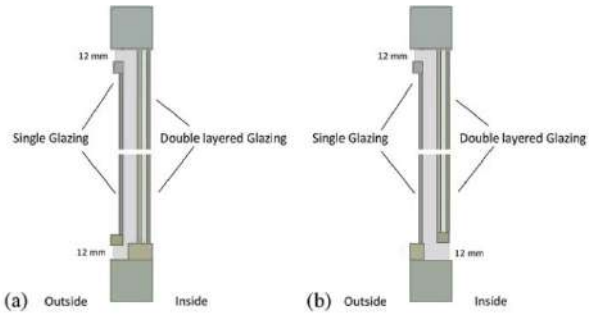

Fig. 1 - Schematic illustration of ventilated window for the summer case; a: outdoor curtain mode, b: exhaust.

Tab. 1 - Assumed properties of simulated glazing units.

	Single glazing (6 mm)	Low-Emissivity double glazing (4+12+4 mm)
Transmittance	0.752	0.305
Reflectance	0.143	0.402
Absorbance	0.105	0.250
Emissivity	0.84	0.148
Thermal conductivity [$W.m^{-1}.K^{-1}$]	1	0.043

2.1 Comparison with measurements

To evaluate the CFD model's reliability, a reference case (outdoor curtain mode) corresponds to the actually implemented experimental setup [33]. During the field trial, the thermal performance of the ventilated window and the effect of solar radiation were evaluated under real outdoor climate conditions [33]. The location of the field trial was Stetten, Austria (Latitude: 48°14'N; Longitude: 16°21'E). A 1.2 m wide and 2.1 m high ventilated window was installed in the Holzforschung test facility [33]. One side of the window was exposed to real weather condition and the other side faced a thermally conditioned room. The measurement accuracy of the air temperature sensors and thermocouples were ± 0.1 K and ± 1.5 K respectively [33]. According to the experimental results, the wind effect was not noteworthy. On the other hand, the solar radiation showed a visible difference in the temperature conditions in the buffer area. During the night, the temperature at the lower measuring position was derived by the outside air temperature. The air temperature at the upper opening was about 5 K higher than at the lower measuring point. On the other hand, during the daytime, the effect of solar radiations was more obvious since the maximum temperature difference between top and bottom opening was about 20-30 K [33]. In this study, a one-hour long segment of measured data from the third day of measurements could be identified as involving relatively small fluctuations of the boundary conditions. We thus could treat this period as quasi steady-state. The registered mean values of the boundary condition during this one-hour period (10:00 AM, July 16th, 2016) were treated as the applicable boundary conditions for the CFD simulation model. Table 2 shows the boundary condition for the summer case.

Tab. 2 - Boundary condition for the CFD simulation.

Variable	Value	Unit
Irradiation	650	$W{\cdot}m^{-2}$
Wind Speed	2	$m.s^{-1}$
Outdoor Temperature	22	°C
Indoor Temperature	25	°C

Figure 2 illustrates the temperature distribution profile (along the depicted path) obtained from the CFD simulation together with the measured temperature at two sensor locations in the window specimen.

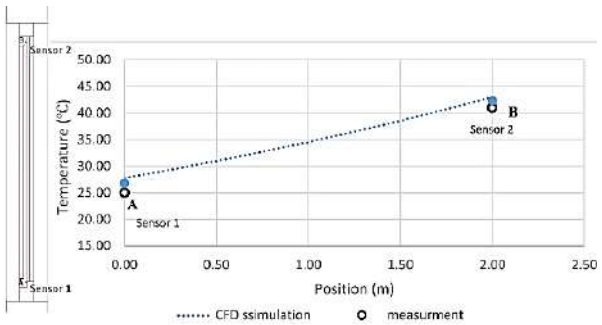

Fig. 2 - Left: schematic section through the examined ventilated window with the position of the two temperature probes; Right: Measured (sensors A and B) and simulated temperature profile. The x-axis denotes the relative distance.

The measurement results reported the effect of solar radiation on warming the air temperature in the interstitial space during the warm season. The CFD simulation slightly overestimates the temperature values. However, simulation results may be suggested to agree in tendency with the measurements.

3. Thermal behavior of exhaust and outdoor curtain ventilated window

As mentioned earlier, one of the goals of this study was to computationally investigate the thermal behavior of ventilated window (exhaust and outdoor curtain mode) during the warm season. To this end, the thermal behavior of two modes of ventilated windows under the identical boundary conditions

and identical dimensions (1 m wide and 1 m high) were estimated. According to the results, in both cases, the temperature difference among openings at the top and bottom opening was between 12-20 K. For the sake of comparison, Figure 3 demonstrates temperature and velocity counters for exhaust (a, b) and outdoor curtain air (c, d) ventilated windows.

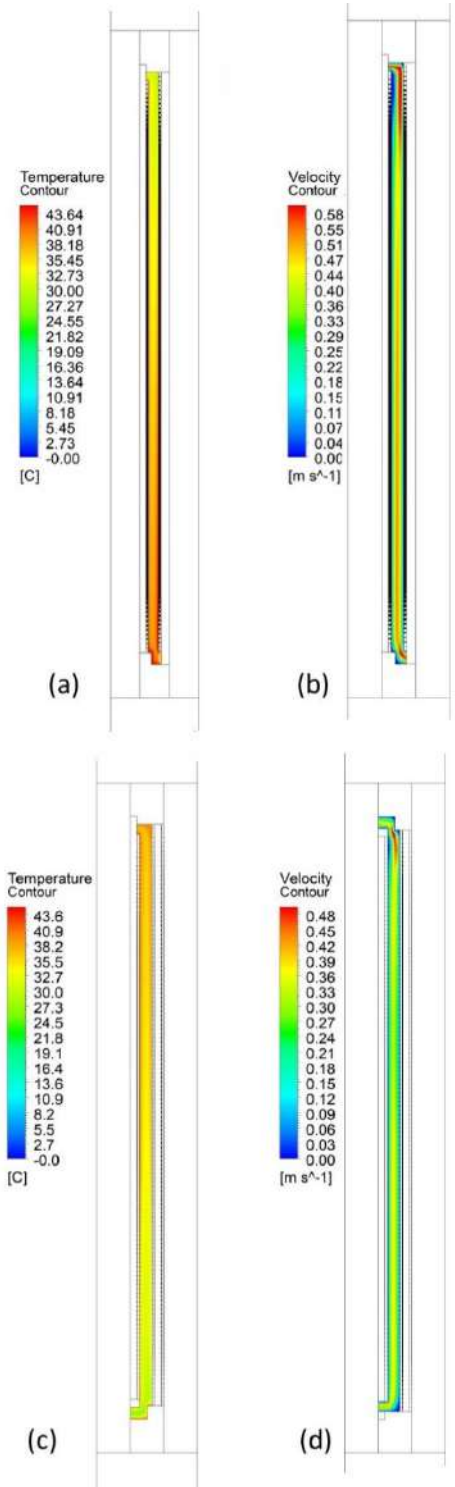

Fig. 3 - Temperature and velocity distribution in the window cavity, a,b: exhaust and b,c curtain air ventilated window.

In the exhaust air ventilated window the mean air temperature and consequently the air velocity is higher. In this type of the ventilated window the buffer space is connected to the indoor air temperature. The solar radiation heats the outside surface of the glass to induce airflow out of the indoor space. The generated negative pressure makes the outdoor fresh air enter from other openings of the room. The system is appropriate when the outdoor temperature is not so high. On the other hand, the Curtain air window expels the accumulated warm air from the buffer space. The solar radiation induces airflow in the interstitial space and consequently reduces heat flux into the room through the glass. This type of the window could represent a proper option for the warm season.

To assess the effect of double-layered glazing location, four cases were considered as per Table 3. The assumed window dimensions are identical in all four cases (1 m wide and high).

Tab. 3 - Summary of the simulated configurations (width of the inlet and outlet opening was assumed to be 12 mm in all cases).

Case	Ventilated window type	Position of the double-layered element
A	outdoor curtain	inside
B	outdoor curtain	outside
C	exhaust	inside
D	exhaust	outside

In order to reduce energy consumption and improve the indoor thermal environment of the buildings, the mean temperature, mean velocity, and inner layer glazing temperature should be considered. Table 4 summarizes the simulation results for the four cases in terms of the mean temperature of the inner layer glazing and buffer space.

Tab. 4 - Temperature difference, mean air velocity and man surface temperature for the simulated scenarios.

Case	Mean temperature (°C)	Mean velocity ($m.s^{-1}$)	Inner layer glazing temperature (°C)
A	34.0	0.31	38.3
B	32.9	0.30	32.5
C	36.2	0.43	41.4
D	34.4	0.41	36.8

The results of the CFD-based investigation suggest that the application of low-emissivity glazing as the exterior glass pane can improve the cooling effect in both cases. According to the results, with help of low-emissivity glazing as the exterior pane, the surface temperature of the interior glass drops, and

consequently, the radiation exchange between this surface and the occupants can be decreased. In addition, the outdoor curtain air mode of the ventilated window reveals a slightly better performance under summer boundary conditions by reducing the temperature difference between the room air and the surface of the interior glass.

4. Conclusion

The present study entailed the thermal analysis of several ventilated window configurations. The thermal performance of the corresponding models was evaluated for summer boundary conditions numerically by a commercially available CFD tool. As remarked at the outset of the paper, the deployment of numerical methods in heat transfer simulation of building details requires careful attention to issues such as the details of the model, mesh generation, and boundary conditions.

To gain confidence concerning the model's reliability, its performance was first compared with field measurement results. The thermal performance of the ventilated windows was assessed in view of four criteria, namely: i) mean air temperature of the interstitial space, ii) mean flow velocity in the cavity, iii) inner layer glazing temperature, iv) The temperature difference between the buffer area and outdoor zone.

Analysing the summer performance of two types of ventilated windows (exhaust and outdoor curtain mode) revealed that the application of low-emissivity glazing as the exterior glass pane can improve the cooling effect in both cases. In addition, the outdoor curtain air mode of the ventilated window displayed a more efficient performance under summer boundary conditions. On the other hand, the operation of the exhaust mode window during periods of milder outdoor conditions lowers the room air pressure. Hence, air may flow into the room from adjacent spaces air via openings and cracks.

Future studies are required to both empirically and computationally determine the annual energy saving potential related to the use of ventilated windows. These investigations would have also to address the monetary and environmental implications regarding the production, installation, and maintenance of ventilated windows.

5. Acknowledgment

The authors gratefully acknowledge Dr. Julia Bachinger of the Holzforschung Austria for the provision of the empirical testing data used in this paper.

6. References

[1] He G, Shu L, Zhang S. Double skin facades in the hot summer and cold winter zone in China: Cavity open or closed? Building Simulation. 2011;4(4):283-91.

[2] Ahmed M, Abdel-Rahman A, Ali PDEAHH, Suzuki M. Double Skin Façade: The State of Art on Building Energy Efficiency. Journal of Clean Energy Technologies. 2016;4:84-9.

[3] Najaf Khosravi S, Mahdavi A. A CFD-Based Parametric Thermal Performance Analysis of Supply Air Ventilated Windows. Energies. 2021;14(9).

[4] Jankovic A, Goia F. Impact of double skin facade constructional features on heat transfer and fluid dynamic behaviour. Building and Environment. 2021;196:107796.

[5] Oesterle E, Lieb R.-D, Lutz M, Heusler W. Double-skin Facades : Integrated Planning. München: Prestel; 2001.

[6] Xu L, Ojima T. Field experiments on natural energy utilization in a residential house with a double skin façade system. Building and Environment. 2007;42:2014-23.

[7] Hien WN, Liping W, Chandra AN, Pandey AR, Xiaolin W. Effects of double glazed facade on energy consumption, thermal comfort and condensation for a typical office building in Singapore. Energy and Buildings. 2005;37:563-72.

[8] Najaf Khosravi S, Mahdavi A. Simulation support for the design of ventilated windows: a case study. Building Simulation 2021; Bruges, Belgium. 2021.

[9] Hensen J, Barták, M, Frantisek D. Modeling and simulation of a double-skin façade system. ASHRAE Transactions. 2002;108(2):1251-9.

[10] Gosselin JR, Chen Q. A computational method for calculating heat transfer and airflow through a dual-airflow window. Energy and Buildings. 2008;40(4):452-8.

[11] Jiru TE, Haghighat F. Modeling ventilated double skin façade—A zonal approach. Energy and Buildings. 2008;40(8):1567-76.

[12] Gavan V, Woloszyn M, Kuznik F, Roux J-J. Experimental study of a mechanically ventilated double-skin façade with Venetian sun-shading device: a full-scale investigation in controlled environment,. Sol Energy. 2010; 84 (2):183–95.

[13] Wilcox D.C. Turbulence modelling for CFD. . DCW Industries1998.

[14] Tanimoto J, Kimura K-i. Simulation study on an air flow window system with an integrated roll screen. Energy and Buildings. 1997;26(3):317-25.

[15] Saelens D, Roels S, Hens H. The inlet temperature as a boundary condition for multiple-skin facade modelling. Energy and Buildings. 2004;36(8):825-35.

[16] Bhamjee M, Nurick A, Madyira DM. An experimentally validated mathematical and CFD model of a supply air window: Forced and natural flow. Energy and Buildings. 2013;57:289-301.

[17] Bhamjee M. A computational fluid dynamics and experimental investigation of an airflow window. Johannesburg, South Africa: University of Johannesburg; 2011.

[18] McEvoy ME, Southall RG, Baker PH. Test cell evaluation of supply air windows to characterise their optimum performance and its verification by the use of modelling techniques. Energy and Buildings. 2003;35(10):1009-20.

[19] Southall R, McEvoy M. Investigations into the functioning of a supply air window in relation to solar energy as determined by experiment and simulation. Solar Energy - SOLAR ENERG. 2006;80:512-23.

[20] Xu X-l, Yang Z. Natural ventilation in the double skin facade with venetian blind. Energy and Buildings. 2008;40(8):1498-504.

[21] Southall R, McEvoy M. Results From a Validated CFD Simulation of a Supply Air 'Ventilated Window'. Air Distribution in Rooms (ROOMVENT). 2000;2:1049-54.

[22] Safer N, Woloszyn M, Roux JJ. Three-dimensional simulation with a CFD tool of the airflow phenomena in single floor double-skin facade equipped with a venetian blind. Solar Energy. 2005;79(2):193-203.

[23]Gloriant F, Tittelein P, Joulin A, Lassue S. Modeling a triple-glazed supply-air window. Building and Environment. 2015;84:1-9.

[24]Parra J, Guardo A, Egusquiza E, Alavedra P. Thermal Performance of Ventilated Double Skin Façades with Venetian Blinds. Energies 2015;8(6):4882-98.

[25] Wang E, Wang H, Deng M, Wang K, Wang Y. Simulation of the ventilation and energy performance of a PV-integrated breathing window. Procedia Engineering. 2017;205:2779-84.

[26] Fluent 19.0, 2018, User's Guide. fluent Inc., Lebanon.

[27] Skaff MC, Gosselin L. Summer performance of ventilated windows with absorbing or smart glazings. Solar Energy. 2014;105:2-13.

[28] Cho, K.-j., Cho, D.-w. Solar Heat Gain Coefficient Analysis of a Slim-Type Double Skin Window System: Using an Experimental and a Simulation Method. Energies. 2018, *11*,1-15.

[29] Torre ATdl, Abel E, Saelens D, Carmeliet J, M. Baelmans. Investigation on airflow and heat transfer of a glazing facade with external louvers 4th International Building Physics Conference; Istanbul2009.

[30] Choudhary R, Malkawi A. A methodology for micro-level building thermal analysis: combining CFD and experimental set-ups. Seventh International IBPSA Conference. 2001:1275-82.

[31] Pasut W, De Carli M. Evaluation of various CFD modelling strategies in predicting airflow and temperature in a naturally ventilated double skin façade. Applied Thermal Engineering. 2012;37:267-74

[32] Launder B, Spalding DB. The Numerical Computation of Turbulent Flow Computer Methods. Computer Methods in Applied Mechanics and Engineering. 1974;3:269-89

[33] Nusser, B.; Bachinger, J.; Schober, K.P. Untersuchungen zur hygrothermischen Funktionsweise des low-tech Window Air Verbundfensters. Holz Forschung Austria, Vienna, 2016.

Data Statement

Data sharing not applicable to this article as no datasets were generates or analysed during the current study.

Passive cooling techniques to improve resilience of nZEBs in Belgium

Alanis S. Zeoli [a], *Vincent Lemort* [b]

[a] Laboratory of thermodynamics, University of Liege, Belgium, alanis.zeoli@uliege.be.

[b] Laboratory of thermodynamics, University of Liege, Belgium, vincent.lemort@uliege.be.

Abstract. Nowadays, buildings are responsible for 40% of energy consumption in the European Union, according to the International Energy Agency (IEA). The urge to build more energy-efficient buildings resulted in the emergence of nearly zero-energy buildings (nZEB). However, the specifications the nZEB design should comply with might not be sufficient to prevent the risk of overheating in summer. To limit the energy consumption rise linked to the upcoming cooling demand increase, passive cooling techniques can be used instead of active ones, that are characterised by a high energy consumption. Passive cooling techniques are investigated through a dynamic simulation of a nearly zero-energy dwelling in Belgium. Their efficiency is assessed based on their ability to improve thermal comfort. The passive cooling techniques can be combined to ensure the resilience of the building to global warming. It was found that the most efficient techniques are the ones relying on ventilative cooling. Solar protections and smart glazing also offer an efficient protection against overheating. The effectiveness of the combined passive cooling techniques is studied over an extreme meteorological event, which is likely to occur by 2100 in Belgium if nothing is done to prevent global warming. Twenty days of intense heat are studied to evaluate the resilience of an nZEB. It was found that the most efficient combination includes night cooling, thermochromic glazing and indirect evaporative cooling. Those techniques allow to decrease the indoor temperature by almost 10 K.

Keywords. Passive cooling, climate change, overheating, resilience, thermal comfort.
DOI: https://doi.org/10.34641/clima.2022.372

1 Introduction

The residential building sector is one of the largest energy consumers in most countries worldwide. Climate change impacts the energy performance of buildings by lessening thermal comfort and increasing the energy demand for space cooling. The energy consumption of buildings affects global warming, which in turn leads to the increment of such consumption, resulting in a vicious circle that needs to be broken to tackle the crucial issues of our generation. From the urge to reduce the environmental footprint of buildings emerged nearly zero-energy buildings (nZEBs). Those buildings are better insulated, hence more energy-efficient [1].

Currently, most Belgian residential buildings are not conditioned. However, together with the emergence of nZEBs and the global warming, the cooling needs of such buildings are expected to rise. Due to their better insulation, extracting heat from nZEBs is more difficult, resulting in a higher overheating risk. Many recent scientific studies focused on this strong link between global warming and building energy performance. All scientists concluded their work by warning the competent authorities about the imminence of the global warming threat and the urge to take actions against the related energy consumption rise. Some of them also investigated the available technologies to reduce or limit the overheating risk in buildings using passive cooling. However, few studies address the combination of passive approaches in residential buildings to improve their energy efficiency. Most studies focus on non-residential buildings. Cooling techniques are gaining attention, especially passive ones, which do not rely on the use of an electricity-driven vapor compression refrigerator. Passive cooling would allow to limit the electricity consumption for residential cooling compared to active cooling. However, the potential of passive cooling capacity is strongly linked to the outdoor climate as colder and drier climates allow for larger capacities. With global warming, the Belgian climate is expected to become hotter and drier [2] and the interest of such techniques in this future climate should be evaluated, as well as their capacity to reduce the imminent risk of thermal discomfort.

The present study aims at assessing the energy consumption and thermal comfort of a residential

Copyright ©2022 by the authors. This conference paper is published under a CC-BY-4.0 license.

building in Belgium and their evolution under global warming. The investigation of the existing passive cooling techniques allows to propose guidelines to ensure resilience of nZEBs to global warming.

2 Research Methods

2.1 Description of the case study

This section gives information about the studied dwelling regarding its geometry, envelope and ventilation system operation (see Tab. 1). The building characteristics are based on the plan of the building, the EPBD, and standard ISO 17772 (See previous work of the author [3] for more details). A 3D model of the studied duplex is shown in Fig. 1. The building is South-oriented with a large window-to-wall ratio (0.6). Fig. 2 is the 2D view of the inside of the duplex. This figure also shows the division of the duplex in thermal zones. Eight thermal zones have been defined. The Walloon Region imposes energy performance standards for buildings through the EPBD, which is reviewed each year. All the walls are compliant with the EPBD 2020. The glazing is triple-glazing. The duplex is equipped with a balanced ventilation system with a heat recovery module of 85% efficiency and a by-pass system. The duplex has currently no cooling system.

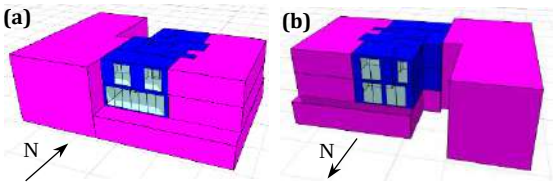

Fig. 1 – 3D model of the building. **(a)** front view **(b)** rear view

2.2 Location and climate

The studied building is in Liege. According to the ASHRAE climate zones, Belgium is part of zone 4A, corresponding to a mixed humid climate. The meteorological files used in this work have been generated at the Laboratory of Climatology of the University of Liege with a regional climatic model called *Modèle Atmosphérique Régional* (MAR) [2]. The MAR being a regional model, it needs to be forced by a general circulation model (GCM) at its boundaries. In this study, two GCMs have been used to better represent the uncertainty spread by 2100 in Western Europe. They are referred to as MPI and BCC. MPI is considered as a colder GCM than BCC. MAR model has been run at 5 km spatial resolution over Belgium. To produce simulations from 2012 to 2100, the GCMs should be coupled with a shared socio-economic pathway that is strongly related to a representative concentration pathway of greenhouse gas. In this paper, the scenario used to account for global warming is SSP5, which describes a society that continues to rely on fossil fuels [4].

Those climate simulation results are used in the BPS program to consider the impact of global warming on the studied building. Fig. 3 shows the evolution of the difference between the simulated average annual temperature and the standard average temperature of Belgium which is 10.9°C. If no measure is taken to lessen global warming, the temperature rise by 2100 is expected to be around 4 K, with a visible global warming effect starting from 2050. It should also be noted that since the circulation models are *global* circulation models, the results obtained with the simulations describe an *average* climate and cannot contain extreme meteorological events.

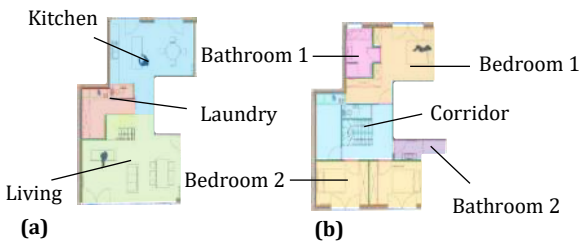

Fig. 2 – Upper view of the duplex **(a)** first floor **(b)** second floor and division in thermal zones.

2.3 Model validation by comparative testing

The building model used in this paper was developed with the IES VE software. The model could not be validated using empirical data. A comparative testing has been performed instead. The building model has

Tab. 1 – General description of the case study.

General information		Envelope		Ventilation system		
Building location	Liege, BE	**Walls**			Supply	Exhaust
Building type	Residential	U-value [W/m²·K]			[m³/h]	[m³/h]
Construction	2020	*External wall*	0.152	Living room	150	-
Nb storeys	9	*Internal wall*	0.452	Kitchen	-	75
Case study	4-person duplex	*Adjacent wall*	0.198	Laundry	-	75
Floor	8-9	*Roofing*	0.081	Bedroom 1	75	-
Orientation	South	*Floor/ceiling*	0.132	Bedroom 2	90	-
Surface	173 m²	**Windows**		Bathroom 1	-	50
WWR	0.6	U-value [W/m²·K]	0.6	Bathroom 2	-	50
Infiltration rate	0.6 ach at 50 Pa	Solar factor [-]	0.5	Corridor	-	65

been developed using two software: IES VE and EES. The outputs of the models (temperature, energy consumption, heating and cooling loads balance) were compared. It appeared that the mean bias error (MBE) and the root mean square error (RMSE) of all the considered variables remain respectively below 5 and 15%. The dynamic behaviour of the building is thus similar in the two simulations and the comparative testing of the model is conclusive [5].

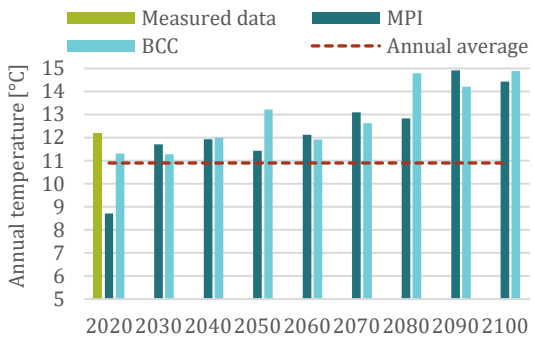

Fig. 3 – Evolution of the annual average temperature with global warming.

3 Thermal comfort analysis

This section focuses on the analysis of thermal comfort in the dwelling and its evolution with global warming. Thermal comfort is evaluated based on the adaptive comfort theory. Studies have shown that in naturally ventilated buildings without any conditioning system, the occupants of the building feel more connected to the outdoor environment and can bear higher temperatures in summer. The maximum adaptive comfort temperature can be expressed by a relationship depending on the mean outdoor temperature:

$$T_{comf,max} = 0.33\, T_{rm} + 21.8 \quad [°C] \qquad (1)$$

where T_{rm} is the running mean outdoor temperature and is calculated as specified by standard NBN EN 15251. This theory can be used if there is no mechanical cooling system and that the occupants can modify their behaviour depending on the climatic conditions, i.e. by adapting their clothing or opening the windows.

Thermal comfort is evaluated in the living room, which is the room with the highest risk of thermal discomfort. It has been decided to study the living room only because it is a South-oriented room, *i.e.* with higher solar gains. Moreover, the living room has a high window-to-wall ratio to account for the fact that new buildings generally tend to have some south-oriented bay windows to increase the illuminance inside the building. It is also a room with more constant and standard internal gains than a kitchen, in which occupants' behaviour can be more difficult to model.

Fig. 4 shows the evolution of the risk of overheating with global warming. This risk is defined according to the percentage of occupation time during which the maximum adaptive comfort temperature is exceeded. If this temperature is exceeded for less than 5% of the occupation time, it is assumed that the overheating risk is negligible and above 10%, an active cooling system becomes mandatory to ensure thermal comfort. Even in 2020, the overheating risk is not negligible and, as expected, it only worsens with global warming, irrespectively of the climate simulation. It is strongly recommended to take some precautions during the conception phase of a building to limit the risk of overheating in the future but also nowadays, as heat waves are becoming more frequent. Passive cooling techniques should be chosen carefully depending on some inherent features of the building, such as orientation or occupancy schedule. Different passive cooling techniques are introduced in the next section.

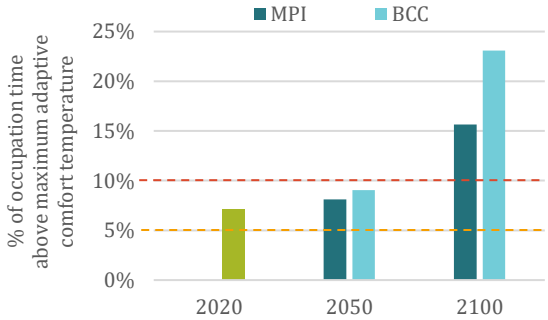

Fig. 4 – Evolution of thermal comfort with global warming.

4 Passive cooling techniques

Maintaining a comfortable environment within a building in a hot climate using passive cooling relies on reducing heat gains into the building and/or fostering the removal of excess heat [6]. The goal of this paper is to show that it is possible to reduce the overheating risk but not completely limit it. The passive cooling techniques principles and models are overviewed all along this section.

4.1 Reducing solar gains

The solar radiation can be blocked either before it enters the building by solar protections or by the glazing itself. The solar protections can be movable or fixed. Generally, movable solar protections cover the entire surface of the window and the orientation of the slats can be adjusted depending on exterior conditions. The impact of shutters is not discussed within this article as it can hamper the passage of wind, reducing the benefits of natural ventilation. Only the fixed solar protection is considered. The principle is illustrated in Fig. 5. There exists an optimum overhang depth which blocks solar beam irradiation from the high summer sun but still allows the low winter sun to shine in to avoid increasing the heating load [7].

Advanced solar glazing is a glazing with a low-emissivity coating that reduces heat gains. Panes absorb solar radiation selectively, more in the near infrared and less in the visible spectrum. With the absorbing pane facing the environment, a large portion of the absorbed radiation is rejected back to

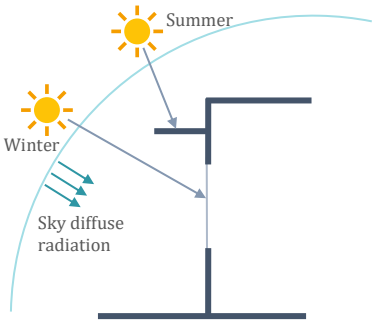

Fig. 5 – Fixed solar protection.

the outdoor environment resulting in a low solar factor [8]. Compared to fixed shading, advanced solar glazing has the advantage to control both direct and diffuse radiation.

Thermochromic glazing is a switchable glazing which can dynamically vary its optical properties. This adaptiveness is allowed by the integration of smart functional materials/layers within glass panes, enabling modulation of the amount of solar radiation transmitted through them. Across a transition temperature, the thermochromic glazing undergoes a structural transformation from "light" to "dark" state. Both states having a different transparency to infrared radiation [9]. Thermochromism being a passive system, it offers no possibility of being manually controlled by the user.

4.2 Removing excess heat

Ventilative cooling uses the cooling capacity of the outdoor air flow by ventilation to reduce or even eliminate the cooling loads, while guaranteeing a comfortable thermal environment. The outdoor air driving force can be either natural, mechanical or a combination of both. Ventilative cooling performances vary between countries due to climate variations, energy prices and other factors [10]. The two ventilation strategies considered are day and night cooling through natural ventilation.

The aim of natural ventilation is to take advantage of the cooler outside air to evacuate the excess heat lingering inside the building. To perform an efficient ventilation, the room should be ventilated if the indoor temperature gets close to 25°C and the outdoor temperature is lower than the indoor temperature. The window opening in the simulation is commanded by a control signal s. A value of 1 means that the window is open.

$$s = \begin{cases} 1, & if\ T_a > 24°C\ and\ T_o > 18°C \\ 0, & otherwise \end{cases} \quad (2)$$

This method is deterministic and not a really good representation of the reality. The building occupants' behaviour can have a negative impact on indoor thermal comfort, as shown by Naspi et al. [11] and Haldi & Robinson [12]. Guaranteeing a good indoor thermal comfort while remaining in the adaptive comfort theory might require occupants' training. Some limitations or constraints on the use of the natural ventilation may be necessary to avoid overheating or overcooling.

The night cooling strategy is typically implemented in temperate climates where night-time temperature is significantly lower than during the day. The basic concept involves cooling the building structure overnight to provide a heat sink that is available during the occupancy period. Night cooling is highly dependent on climatic conditions, as a sufficiently high temperature difference between ambient air and building structure is required to achieve efficient convective cooling of the building mass. The night cooling efficiency has essentially been demonstrated in Europe. However, due to the inherent stochastic properties of weather patterns, a series of warmer nights can occur and passive cooling by night-time ventilation alone might not be sufficient to guarantee thermal comfort at all times [13].

The value of the control signal s that handles window opening is set with a control formula. The formula used in the present work is based on the model developed by Iddon & ParasuRaman [14].

$$s = \begin{cases} 1, & if\ T_a > T_o\ and\ T_a > 20°C \\ 0, & otherwise \end{cases} \quad (3)$$

This formula is only valid between 10 p.m. and 6 a.m. during the cooling season when there is a high risk of overheating. Night cooling is generally used during heat waves when day cooling cannot be relied on as the outdoor temperature is higher than the indoor temperature.

Handling night cooling with natural ventilation has several drawbacks. The opening of a window being a manual action, it is unlikely that the occupants will wake up to close it if the temperature drop is too abrupt or if it rains. In some situations, it could result in overcooling. Night cooling might be associated with automatically controlled windows or used only in extreme cases during heat waves. To cope with those disadvantages, it is also possible to perform night cooling through mechanical ventilation. The advantage of using mechanical ventilation is that it ensures a constant air flow all night long and avoids draughts. One major drawback of overventilation is that the fan power consumption increases as the cubed air flow rate, resulting in a significant increase in electricity consumption.

The last technique that has been studied is indirect evaporative cooling (IEC). It consists in cooling the extracted air by humidification and then, via a heat exchanger, it cools down the incoming outdoor air. The process is illustrated in Fig. 6. The advantage of indirect evaporative cooling over direct humidification of the incoming air is the avoidance of a possible contamination. In summer, this technology provides gentle air conditioning and consumes a minimum energy as it can be coupled with the mechanical ventilation system. The water consumption of this type of systems is also very modest [15]. IEC has been modelled by changing the

Fig. 6 – Schematic of an Indirect Evaporative Cooler.

supply ventilation air temperature. IEC is used when the outdoor air temperature either exceeds 25°C or is higher than the indoor temperature. It is assumed that the extracted air is cooled down to the wet bulb temperature and that the efficiency of the heat exchanger remains unchanged. The temperature of the incoming air can be calculated as:

$$T_{vent,su} = T_o + 0.85 \cdot (T_{wb} - T_o) \quad (4)$$

The advantage of IEC is that it remains efficient even during heat waves, contrary to natural ventilative cooling. A more complete IEC model is currently under investigation to cope with the hypotheses done in this work and evaluate the performance of IEC systems in different climates.

4.3 Comparison of passive cooling techniques

In the previous section, various passive techniques were introduced, and their strengths and limitations were overviewed. Fig. 7 shows how the indoor thermal comfort is impacted by the addition of those passive cooling techniques to the case study. Some passive cooling techniques are efficient but none of them is sufficient to guarantee thermal comfort in 30 or 80 years from now. They can be combined to considerably reduce the overheating risk. To be efficient, a combination of passive cooling techniques should involve at least a solution to decrease the solar gains and one to increase the ventilation losses.

The impact of the combined passive cooling techniques is shown during a period of intense heat when an active cooling system might be the most useful method to prevent the overheating risk. If thermal comfort can be guaranteed during a heat

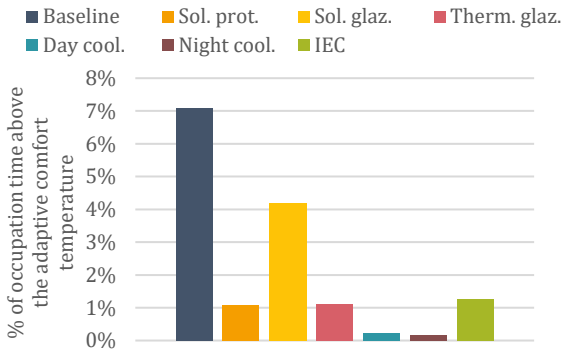

Fig. 7 – Impact of passive cooling techniques on overheating risk.

wave, it can be assumed that the overheating risk has been sufficiently reduced. It also allows to study the resilience of the building. Resilience is defined as the ability of a system to anticipate, absorb, accommodate, or recover from the effects of a hazardous event in a timely and efficient manner, including through ensuring the preservation, restoration, or improvement of its essential basic structures and functions [16]. The hazardous event that has been studied is the heat wave as it is the extreme weather event that is the most likely to occur with climate change in Western Europe.

Fig. 8 shows the evolution of the temperature in the living room during a period of intense heat. The improvements have been added one by one to visualise the improvement generated by each passive cooling technique and determine when the building is sufficiently cooled down to withstand the period of intense heat. The studied passive cooling techniques are presented below in the order they have been added. The legend of the graph shows only the last added technique. The only techniques that have been studied separately are the solar protections as three of them have been investigated.

The first improvement is day cooling as it is the easiest technique to implement in reality. The

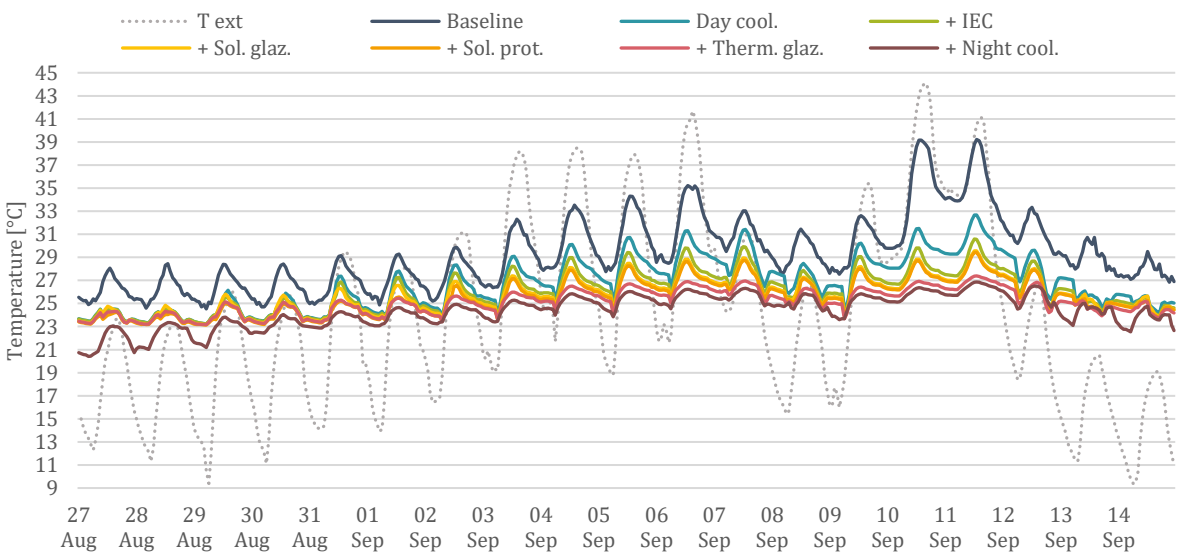

Fig. 8 – Evolution of the indoor temperature during a heat wave considering passive cooling techniques.

efficiency of day cooling appears even before the heat wave. Contrary to the case without improvement, the building has not stored heat within its walls all summer. The thermal inertia of the building is thus available to slow down the temperature increase. But during the heat wave per se, day cooling is helpful only a few hours a day in the morning when the temperature has not yet reached 25°C. Day cooling alone already allows to decrease the temperature by 2.6 K on average.

The second improvement is IEC because it is a promising and easy to implement technique as all new constructions should be equipped with a mechanical ventilation system on which the IEC module can be added. When combined with day cooling, it leads to a further temperature decrease of 0.95 K on average. IEC is expected to become more efficient in the future as the outdoor air will become drier. If the outdoor air and, a fortiori, the indoor air become drier, the temperature decrease due to humidification would be more significant, resulting in a more efficient cooling.

Day cooling and IEC have then been combined with the three solar protections that were considered as the most relevant. Solar glazing and fixed solar protection have almost the same impact on the indoor air temperature. On average, they further decrease the indoor temperature by 0.43 and 0.6 K respectively. Thermochromic glazing allows a temperature reduction of 1.1 K and is the most efficient to decrease solar gains. The characteristics of the glazing are changed continuously depending on the indoor environment conditions and the glazing gets darker as the irradiation becomes more important, smoothing out the temperature peak observed with the other configurations. None of those combinations allows to remain below the threshold of 25°C during the whole heat wave. However, with the use of thermochromic glazing, the maximum indoor temperature is 27°C even when the outdoor temperature reaches 43°C.

A further reduction of the temperature is possible by adding night cooling to the previous passive techniques. Night cooling has been added last although it is a very efficient technique because it can sometimes result in overcooling of the building. Night cooling is particularly efficient because of the outdoor temperature drop during the night. It can also be noted that night cooling impacts the building thermal inertia for several days. During the last days of the heat wave, the outdoor temperature does not fall below 25°C during the night, making night cooling useless. Since the building has been correctly cooled down during the previous days, it allows getting through those days of intense heat. The outdoor temperature is too high to prevent the indoor temperature from exceeding 25°C. However, 25°C is the comfort temperature nowadays and it is not unlikely that in the future, if the temperature rises, people will adapt and be able to withstand higher temperatures.

After the heat wave, it takes less than one day to the building to get back to the same behaviour it had before the heat wave. The resilience of the building is ensured, especially due to natural ventilative cooling.

4.4 Limitations of passive cooling techniques

Theoretically, the building can be defined as resilient and the techniques that are the most efficient to reduce overheating are proper use of ventilative cooling (during the day and especially during the night), thermochromic glazing and, to a lesser extent, IEC. With those techniques, the temperature peaks are smoothed out and remain close to 25°C even though the outdoor temperature significantly increases.

However, in this analysis, one of the most important factors, closely linked to residential building usage, could not be accounted for: the occupants' behaviour. In the simulations, the windows are open and closed exactly when necessary, to avoid overheating during the day and overcooling during the night. Brown & Cole [17] studied the influence of occupants' knowledge on comfort expectations and behaviour. They identified some potential factors that can impact the "performance gap" between simulations and reality. The systems usability or accessibility for the users can strongly impact the building control. The users can lack immediate responsiveness or the sufficient knowledge to manage the building correctly. They also tend to be responsive to an imminent discomfort crisis while it would be more appropriate to continuously optimise the building operation. Building operation should however not entirely lean on the occupants. The human-building interaction should be ongoing and bidirectional by offering immediate and relevant feedback to the occupants for them to know the risks of thermal discomfort. Tam et al. [18] also studied the energy-related occupant behaviour and its implication in energy use. They concluded that the best way to account for and minimise occupant energy-related behaviour is to act instantaneously and make them aware of the implications of their actions in a real-time performance of a building. Moreover, occupants should be well informed of the best practices when dealing with building systems, such as lighting, HVAC, equipment, DHW, etc. Each building should be provided with a user guide towards a better building performance.

The present work tries to remain as general as possible as it aims to the transposition of its conclusions to similar buildings. However, Elnagar & Kohler [19] showed that the building orientation can significantly impact its energy demand. South orientation leads to the smallest heating energy demand while the cooling demand can be decreased with a North orientation. In both cases, a West or East orientation increases the energy demand. They are also the orientations for which external fixed shading devices are the most difficult to design as the Sun has almost the same position in the sky all year round. The passive cooling techniques should also be

adapted depending on the orientation.

5 Conclusion

The thermal model of a nearly zero-energy dwelling has been built with a BPS software called VE. The thermal comfort was studied in the dwelling for 2020, 2050 and 2100 using global warming simulation weather file. The years 2050 and 2100 were simulated assuming a "business as usual" scenario. As expected, it was found that thermal comfort deteriorates with global warming. By 2100, the need for an active cooling system will be bound to happen. Another conclusion of this analysis is that, in South-oriented rooms with high window-to-wall ratio, thermal comfort is not even reached nowadays, meaning that the design of nZEBs has not been conceived to be resilient. The resilience of the buildings should be engineered at design stage by including some passive cooling techniques.

Passive cooling techniques present the advantage to considerably limit the energy consumption increase of the building while significantly improving thermal comfort. The studied passive techniques mainly aim at decreasing the solar heat gains and enhance ventilation losses to remove excess heat from the building. Ventilative cooling was found to be the most relevant cooling technique. It is followed by solar protections and solar glazing. Finally, indirect evaporative cooling has been proven to be useful especially during heat waves. It should be combined with ventilative cooling to guarantee a good thermal comfort.

The resilience of the building has been assessed by analysing its behaviour during a period of intense heat while applying various passive cooling combinations. It was shown that combining night ventilation, indirect adiabatic cooling and thermochromic glazing can reduce the indoor temperature by 10 K.

The purpose of the present work was to study some passive cooling techniques combinations and to apply them to a nearly zero-energy building to reduce the risk of overheating in summer due to the airtightness of new constructions. Some guidelines have been proposed to build more resilient buildings. In any case, it is really important to keep in mind that even though the building has been perfectly designed, the operation strongly relies on the occupants' behaviour. To get rid of that unpredictable variable, buildings should be automated as much as possible. However, a too high level of automation would fail the requirements of the theory of adaptive comfort, narrowing the temperature range considered as pleasant. A balance has to be found between automation and thermal comfort widening by favouring an ongoing and bidirectional human-building interaction. The building should offer immediate and relevant feedback to the occupants so that they know about risks of thermal discomfort.

6 References

[1] Birol DF. The Future of Cooling 2018:92.

[2] Wyard C, Doutreloup S, Belleflamme A, Wild M, Fettweis X. Global Radiative Flux and Cloudiness Variability for the Period 1959–2010 in Belgium: A Comparison between Reanalyses and the Regional Climate Model MAR. Atmosphere 2018;9:262. https://doi.org/10.3390/atmos9070262.

[3] Zeoli A. Using passive cooling techniques to improve resilience to global warming of nearly zero-energy buildings. Université de Liège, 2021.

[4] Hersbach H, Bell B, Berrisford P, Hirahara S, Horányi A, Nicolas J, et al. The ERA5 global reanalysis n.d.:51.

[5] Fabrizio E, Monetti V. Methodologies and Advancements in the Calibration of Building Energy Models 2015:28.

[6] Santamouris M. Passive cooling dissipation techniques for buildings and other structures: The state of the art. Energy and Buildings 2013:21.

[7] Dutta A, Samanta A, Neogi S. Influence of orientation and the impact of external window shading on building thermal performance in tropical climate. Energy and Buildings 2017;139:680–9. https://doi.org/10.1016/j.enbuild.2017.01.018.

[8] Feuermann D, Novoplansky A. Reversible Low Solar Heat Gain Windows for Energy Savings n.d.:7.

[9] Aburas M. Thermochromic smart window technologies for building application_ A review. Applied Energy 2019:21.

[10] Heiselberg P. Ventilative Cooling Design Guide. Aalborg: IEA; 2018.

[11] Naspi F, Arnesano M, Stazi F, D'Orazio M, Revel GM. Measuring Occupants' Behaviour for Buildings' Dynamic Cosimulation. Journal of Sensors 2018;2018:1–17. https://doi.org/10.1155/2018/2756542.

[12] Haldi F, Robinson D. Interactions with window openings by office occupants. Building and Environment 2009;44:2378–95. https://doi.org/10.1016/j.buildenv.2009.03.025.

[13] Artmann N, Manz H, Heiselberg P. Climatic potential for passive cooling of buildings by night-time ventilation in Europe. Applied Energy 2007;84:187–201. https://doi.org/10.1016/j.apenergy.2006.05.004.

[14] Iddon CR, ParasuRaman N. NIGHT PURGE AS A MEANS TO REDUCE COOLING LOAD OF AN OFFICE IN PUNE, INDIA n.d.:7.

[15] Khandelwal A, Talukdar P, Jain S. Energy savings in a building using regenerative evaporative cooling. Energy and Buildings 2011;43:581–91. https://doi.org/10.1016/j.enbuild.2010.10.026.

[16] Zhang C, Kazanci OB, Levinson R, Heiselberg

P, Olesen BW, Chiesa G, et al. Resilient cooling strategies – A critical review and qualitative assessment. Energy and Buildings 2021;251:111312. https://doi.org/10.1016/j.enbuild.2021.111312.

[17] Brown Z, Cole RJ. Influence of occupants' knowledge on comfort expectations and behaviour. Building Research & Information 2009;37:227–45. https://doi.org/10.1080/09613210902794135.

[18] Tam V, Almeida L, Le K. Energy-Related Occupant Behaviour and Its Implications in Energy Use: A Chronological Review. Sustainability 2018;10:2635. https://doi.org/10.3390/su10082635.

[19] Elnagar E, Köhler B. Reduction of the Energy Demand With Passive Approaches in Multifamily Nearly Zero-Energy Buildings Under Different Climate Conditions. Front Energy Res 2020;8:545272. https://doi.org/10.3389/fenrg.2020.545272.

The datasets generated and analysed during the current study are not available because they have been generated during an internship in a private company and are therefore confidential, but the authors will make every reasonable effort to publish them in near future.

'Power gap' in Heat Load calculations – EN12831-1 versus monitoring and simulation results

Paul Van den Bossche[1], Jeroen Van der Veken[1], Sébastien Pecceu[1], Sara Verheyleweghen[1], Stijn Verbeke[2]

[1]Belgian Building Research Institute, HVAC laboratory, Limelette, Belgium; pvdb@bbri.be jvdv@bbri.be

[2]EMIB, UAntwerpen, Belgium

Abstract. For a long time, research and policy has focussed on reducing energy demand and increasing energy efficiency. However, with increasing renewable energy production, also the profile of this energy demand and the potential for demand side management needs to be assessed. Moreover, due to energy distribution restrictions, simultaneous power peaks on the grid need to be reduced or shifted. Regarding dwellings, for which heating still determines the bulk of the energy use in most of the EU, this means that reducing, or at least better characterizing and managing the heat load becomes more important. The current method for the calculation of the design heat load, according to the EN12831-1, is a static method and tends to overestimate the heat load.
This research based on 50 in-situ measurement cases suggest indeed an oversizing between 25% and 100%! Further linear regression analysis and a parametric study based on dynamic building simulation was used to pinpoint possible physical causes for this 'power gap'. Following possible causes could be identified: The standard assumes a 100% simultaneous occurrence of all worst case boundary conditions (low design outdoor temperature – relatively high wind speeds and pressures leading to high infiltration losses – no solar gains – no internal heat gains) which does not occur in reality. Furthermore, the heat load for the heat generator (at building level) is defined as a simple sum of the heat load of each individual space. This might also lead to oversizing, as infiltration or ventilation are not at their maximum in all spaces at the same time. Finally, the difference between monitoring and simulation results suggests that users adapt their behaviour below 0 °C, by reducing their comfort expectations (e.g. less window opening) or other heat loss reducing actions (e.g. keep inner doors closed so that less heat is transferred to unheated zones). Formal conclusions could be used for eventual future standard improvements.

Keywords. Heat load, power gap, sizing of heating systems, thermal inertia, thermal comfort, user behaviour
DOI: https://doi.org/10.34641/clima.2022.134

1. Importance of heat load

With the focus shifting from increasing renewable energy production towards energy distribution issues and finding a continuous grid-match between supply and demand, the need for correct heat load estimations of buildings also increases. Whereas calculations in the past mainly focused on comfort and 'enough power at any moment', a better understanding of the profiles of the required heating power is necessary to bring it in line with renewable energy availability. In addition, the investment costs of highly efficient systems such as heat pumps are more dependent on the installed heat capacity compared with classic fuel burning boiler systems. A clear view on power needs is also required for the sizing of thermal grids, heat distribution and emission systems, geothermal sources and heat storage systems.

It is common practice to adapt distribution and emitter system temperatures in accordance with the real load in order to improve thermal comfort and to optimise the performance of the heating system. For that purpose, a heating curve, often expressed as a linear relation between the outdoor temperature and the distribution medium temperature is used. This assumption fails on various grounds; the heat load does not only depend on the outdoor temperature but also, among others, on wind, solar and internal

Copyright ©2022 by the authors. This conference paper is published under a CC-BY-4.0 license.

gains, resulting in a wide spread of actual heat loads at a certain outdoor temperature.

On top of all that, in order to obtain a grid-match between supply and demand of power, a clear view is required over the load profiles for the following hours or days, and the possibility to shift this load by adapting temperature comfort profiles or adding storage capacity.

2. Calculation standard

Generally, the design heat load is calculated in accordance with the standard EN 12831-1:2017 [1] and its country specific annexe NBN EN 12831-1 ANB:2020 for Belgium [2]. Although this calculation method is elaborate, requiring a lot of input data, the confidence in the market of the resulting heat load is not very high. An oversizing of 20 to 30 % is suspected.

Major possible issues are:

- The heat load is only calculated at the lowest possible outdoor temperature, assuming a simultaneous occurrence of all worst case conditions (no sun, strong wind, no internal heat gains…)
- The lowest possible outdoor temperature is determined on a 24h basis and the resulting heat load is a 24h average, assuming sufficient damping by the building thermal mass. Questions arise whether at 1h time scale higher heating installation power is required, especially in buildings with low thermal inertia.
- The standard calculates a heat load for every room, adding all the individual loads to obtain the required heat load on building level.
- The leak infiltration ratio (LIR) to convert a measured infiltration rate at 50Pa to an infiltration rate at more realistic 24h averaged pressure conditions, is set at 0.1 but has little scientific basis. On building level, the sum of all maximum room infiltrations is assumed.
- Several reheat factors are proposed for temperature setback schemes, taking into account the building mass, the setback temperature, the setback time as well as the reheat time. These factors assume a heat distribution and emission system with step function response (without any inertia) which is very unlikely.
- Room temperatures are defined as operational temperatures, in accordance with the required thermal comfort. However, the calculation uses room air temperatures, that are assumed to be equal with the operational temperatures. In reality, the difference between both depends strongly on the insulation level of the building envelope.
- The standard EN 12831-1 looks to heating, the EN 12831-3 to domestic hot water. The required combined power of both is only assessed in EN 12828 in a very general way.
- The standard uses several assumptions and default values, supposed to lead to a heat load 'on the save side'. A more statistical sound method should be used to treat the distribution of actual values and distinguish dependent and non-dependent parameters and statistical distribution. This should give the designer a better insight in the average safety margins.

3. Methodology

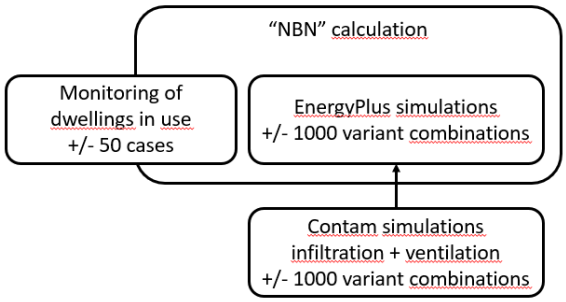

Figure 1: Overview of the set of monitoring, calculation and simulation cases

The research primarily focussed on the comparison of actual used power in dwellings, and the calculated power according to the standard. A monitoring campaign on dwellings provided the necessary data in various weather conditions and in real-life use. However, for a number of monitoring cases some necessary building and user data was missing and the corresponding standard calculation could not be performed. Moreover, the set of the remaining 13 cases is limited in quantity and variation (statistically not evenly distributed), so that is difficult to deduce detailed conclusions from only this data set.

Therefore dynamic simulations are added, with a parametric analysis parallel to the monitoring campaign, aiming to understand the origin of differences between the static standard approach and dynamic building behaviour as well as the influence of individual parameters. Contam simulations of infiltration (and interaction with ventilation) were performed and the resulting air flows are used in the heating demand simulations in EnergyPlus,

4. Monitoring of dwellings

The power delivered to the heating system of some 50 dwellings has been monitored during 2 heating seasons, with a measurement frequency between 5 minutes and 1 day. The resulting heating power is related to the outdoor temperature in next figures, and compared with the calculated load, according to the Belgian annex (referenced in figures as 'NBN'). The resampling time is set at 24h to correspond with

the daily averaged approach in the standard. Resampling on monitoring data with 1h base generally leads to data that is more difficult to evaluate, since 1h power profiles depend more on the control strategy and domestic hot water (DHW). Although the standard calculation only focusses on the heat load at the (lowest) design temperature (depending on the region, i.e. -7°C in the centre of Belgium), the required power is assumed to be proportional to the temperature difference (between indoor and outdoor), and therefore expressed as a straight line in Figure 2.

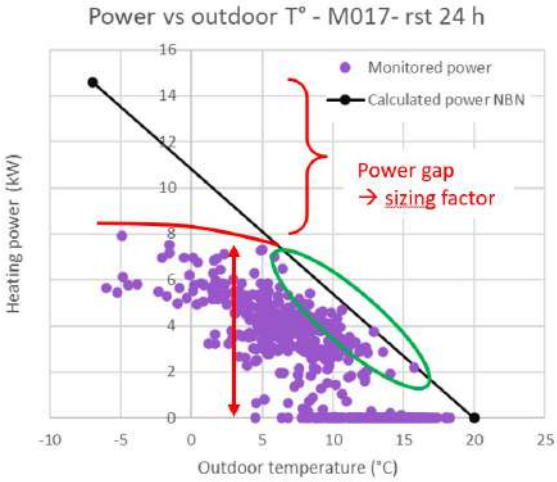

Figure 2: Measured compared to calculated heat load - case M017 - resampling time 24 h

The case in Figure 2 reveals:

- The monitored heating power shows a high variability, even at the same outdoor temperature.
- Within the temperature range between 5 and 15 °C, the maximum used power corresponds closely with the assumed calculated heat load, suggesting that the EN/NBN-standard assumptions in this temperature range are quite correct.
- At lower temperatures (below 0-5°C) the curve with measurement maxima tends to deflect downwards, resulting in a substantial power gap with the standard at the design outdoor temperature (-7°C).

Similar observations could be made for other measured cases. For a sizing factor defined as the ratio between the maximum monitored power and the calculated heat load according to the NBN standard calculation, the values vary between 0.4 and 0.8, as shown in Figure 3 for the 13 most relevant cases. This means that in some dwellings, the actual used heating power is only 40 % of the calculated heat load.

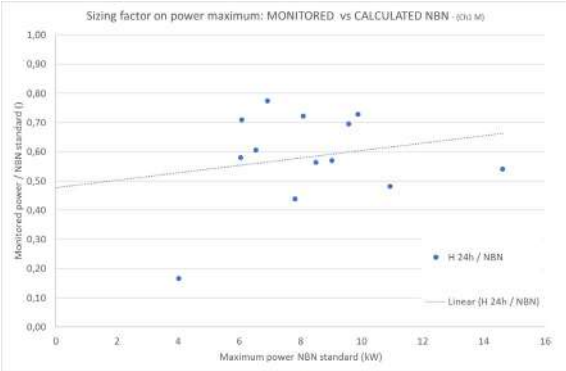

Figure 3: Sizing factor for 13 monitored cases - resampling time 24 h

To understand the lack of correspondence between monitored power data and the pure temperature difference based relationship, following research steps were undertaken:

- A polynomial regression on the monitoring data gives a better understanding of the individual influence of outdoor temperature, wind speed and solar radiation.
- Next paragraphs discuss the use of infiltration simulation (using CONTAM®) and a whole building simulation model (using EnergyPlus®) to analyse some 1000 different variants in a parametric study.

Various polynomial regression equations were evaluated on 10 monitoring cases to find the best fit. A number of the evaluated equations were based on the assumed physics, other evaluated formats were not based on the physics. Used parameters are temperature difference (indoor-outdoor), wind speed and solar irradiation on a horizontal plane Both linear equations and power functions were used. The evaluation of the resulting polynominals was based upon following statistical criteria; a minimal Akaike Information Criterion (AIC) [3,4], a minimal Bayesian Information Criterion (BIC) and average error, but a maximal Pearson correlation coefficient (Rpearson) [5].

Finally the best correlation showed to be:

$$\boldsymbol{\Phi = f1(\theta_{int,i} - \theta_e) + f2w(\theta_{int,i} - \theta_e) + f3Isol,h + c1} \quad (1)$$

with Φ the heat load, θ_{int} the indoor temperature, θ_e the outdoor temperature, w the wind speed, $I_{sol,h}$ the solar irradiation on a horizontal plane (all variables daily averaged) and *f1, f2, f3, c1* different constants. Applying this equation to the measured weather data set, results in **Figure 4** for case M017.

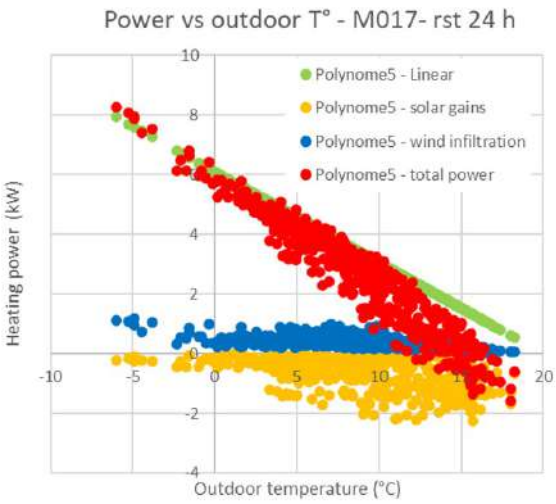

Figure 4: Monitored power breakdown to weather parameters - case M017 – rst 24 h

A distinction can be made between:

- Effects linear to temperature difference such as transmission losses and buoyancy infiltration (stack effect) – green dots.

- Effects related to solar radiation, expressed as a negative heat load – yellow dots. Quite a number of days present hardly any solar gains, but very cold days seem to offer always some gains, although lower values and on daily base, unlikely to be a major source of the curve flattening. At higher outdoor temperatures, solar gains can be very substantial, compared to the total load and even compensate heat losses completely (as from 12 °C for this case).

- Effects of wind, with the wind speed multiplied by the temperature difference – blue dots. Important to notice is that the wind induced heat load at design outdoor temperature (-7 °C in this case) is of the same order of magnitude as the heat load at outdoor temperatures between 5 and 10 °C and could explain the power curve flattening to some extent. This effect finds its origin in the wind distribution in most Belgium weather stations; at very low temperatures, the wind speed is much lower than at higher outdoor temperatures, as shown in **Figure *5***. Be aware that this profile can be different in other climate zones; in Belgium mild South-West winds are prevailing, certainly at higher wind speeds.

Cases with high building envelope permeability present higher wind heat load, reenforcing this flattening effect.

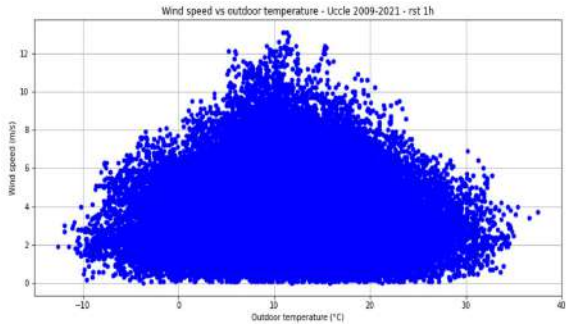

Figure 5: Wind speed versus outdoor temperature – rst 1 h based on RMI data of Uccle (2009-2019) (6)

As a conclusion on this regression analysis, the heat power curve flattening effect can be only partly explained by the absence of days that combine a 100% simultaneous occurrence of power demanding parameters (temperature – wind for infiltration – no solar gains). Other sources of this effect can only be assumed based on the monitoring campaign, not proven. At low outdoor temperatures the occupiers might change their habits: reducing ventilation and IAQ expectations, keeping outdoor (and indoor) doors closed more carefully, reduce the thermal comfort demands, ….

Some other interesting observations can be based upon the monitoring results:

- The monitored maximum power on 1h basis cannot be used for analyses of the real required heating power because this maximum heating power is influenced by the heat generator and its control; especially during reheat intervals the generator will operate at its maximum heat power, but also at other instances the developed heat output can be higher than strictly needed. For this reason most of the analysis is done on a 24h basis.

- Apart from reheat requirements resulting from set-back schemes (considered by the heat load standard in a rather rough way), reheat after priority given to DHW (out of scope of the standard EN 12831-1), we could observe another (third) reheat occurrence, generally not taken into account. In case of underfloor heating, with substantial thermal inertia, this emitter will cool down completely to room temperature when heating is not required for quite some hours, e.g. on a sunny afternoon during a colder day. At sunset, with the heat demand ramping up, the high inertia emitter isn't able to supply this load at once, because it's capacity should be reloaded first. This "high inertia emitter reheat" load is generally not taken into account, and might require some additional power or alternatively an adapted control strategy.

- The standard calculates the design heat load as a 24h average, assuming sufficient damping in the building. Monitoring shows however some important day variations, for instance on cold days with sunny afternoons but very cold mornings. Regardless the 3 above mentioned reheat effects, one could assume that the heat load on shorter time basis (1- 4 h) will be higher, but this is not actually taken into account in the standard. These issues were investigated by dynamic simulation.

5. Infiltration simulation

In the Belgian standard, the leak infiltration ratio (LIR) to convert a measured infiltration rate at 50 Pa to an infiltration rate in real pressure conditions, on a 24 h basis, is set at 0.1. The European standard suggests more differentiated values, taking into account the number of external facades, the height above ground level and the zone height as well as the shielding, but without strong scientific basis.

Based on 4 dwelling models and the multizone airflow simulation software CONTAM® [7,8], the leak infiltration (and ratio) were defined using the combination of a set of variables such as building orientation and wind shielding, various airtightness levels (between 1 and 12 $(m^3/h)/m^2$) and leak distribution, the infiltration was simulated for 10 year weather data (2009-2019) from 3 Belgian locations. A total of 1000 simulations were run and evaluated. A first observation is that the infiltration maximum is higher at moderate outdoor temperatures (as wind reaches higher values between 5 and 10 °C) than at the design outdoor temperature (between -6 and -11 °C in Belgium). This could partly explain the curve deflection observed in the monitoring results (§ 4). Further evaluation is limited to the low design outdoor temperature. Another important element is that infiltration is only accounted as real infiltration when the cold air entering the building exceeds the ventilation requirements. This means that infiltration (and the LIR to be used) is strongly influenced by the ventilation system itself and both cannot be accessed independently; if another ventilation system or control strategy is used, the LIR will alter accordingly.

Figure 6 shows an example of the influence of the Meteorological conditions in 3 locations, with Middelkerke located at the sea coast, Uccle in the country centre and Humain in the Eastern and higher part of Belgium (295 m above sea level). We observe median values far below the Belgian LIR value of 0.1, a value that is closely approached in less than 1 % of the cases. We also obtain some higher values for Humain, where the wind absolute maximum values are lower than at the coast (Middelkerke), but higher wind speeds are observed at the lowest outdoor temperatures.

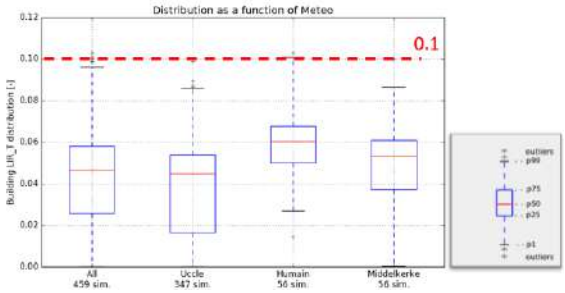

Figure 6: Infiltration ratios as a function of Meteo

Other observations are:

- The LIR values for individual rooms can be much higher than for the building as a whole. A more correct heat load calculation should make a distinction between building level (to size the heat generator) and individual rooms (to size the emission system), with infiltration ratios 2-3 times higher in the latter.
- The resampling time to evaluate the LIR can strongly influence the results, as shown in **Figure 7**. For energy calculations, an resampling time of 1 year results in an LIR of 0.037 (= 1/27). For heat load calculation, the p99 values are 2.5 times bigger on 24 h, and even 3 times on 1 h resampling time.

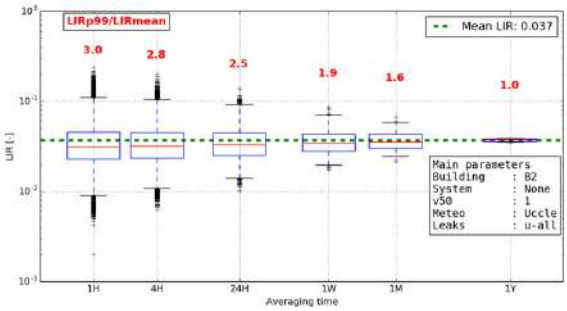

Figure 7: LIR as a function of resampling time (1 specific variant)

6. Heating power simulation

The dynamic building simulation software EnergyPlus® [9] was used to calculate the required heat load for 3 dwelling typologies (row house, semi-detached and lowrise dwelling) and this for each room in the dwelling, as well as the total simultaneous power for the building as a whole. The general set-up of the simulations can be found in the Ph.D of Stijn Verbeke [10]. The particular set of approximately 1000 variants consists of 3 different locations (weather files), 4 building envelope insulation level and 4 infiltration rates (input from the Contam simulations of § 5), 3 solar transmission values of glazing, 3 ventilation systems with different control options, 3 occupancy schedules and internal heat gains, 3 thermal inertias, combined with different temperature and setback schedules.

Regarding the weather files, a selection of cold waves amongst measured climate data of three Belgian locations between 2010 and 2020 was made, so that the dynamic simulations could be run throughout a representative but harsh winter period. Attention is paid to select the real accompanying solar and wind data with these temperature data so that realistic conditions are simulated. It should be noted that this is often not the case when using commercially available datasets for Extreme Cold Weather. This can lead to surprising results; for most of the 1000 variants, the simulated daily maximum heat load isn't reached at the lowest temperatures (daily averaged -10°C for Uccle in February 2012), but at a rather dark December day with an average temperature of -3°C.

The results can be expressed in a similar way as for the monitoring cases in § 4 (heat load in relation to outdoor temperature, resampling time 24 h, compared to the linear assumed calculated heat load according to the Belgian annex ('NBN'). Figure 8 shows this for one specific variant and reveals that the simulated power shows substantial variability at the same outdoor temperature, but less than in monitoring cases, suggesting an underestimation of the variability, probably related to the boundary conditions and user behaviour (e.g. window opening is not considered in the simulation model). The simulated power exceeds the NBN assumptions between 0 and 15 °C. We also observe some downward curve deflection at below 0°C, resulting in a power gap, but smaller than observed in most monitoring cases.

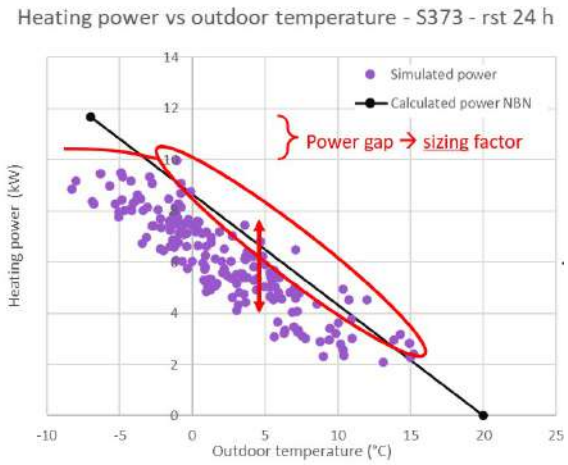

Figure 8: Simulated heating power (building) versus outdoor temperature - variant S373-rst 24h

When applying the same polynomial regression as for monitoring (see § 4), Figure 9 is obtained. We observe some power variation at the same outdoor temperature, as a result from wind and solar influence and some modelled variation in the user behaviour regarding temperature set point and internal heat gain profiles. Lower "wind power" below -5°C, and to a smaller extend the presence of some solar gains, lead to a downward power curve deflection, and, for this variant, to a small power gap.

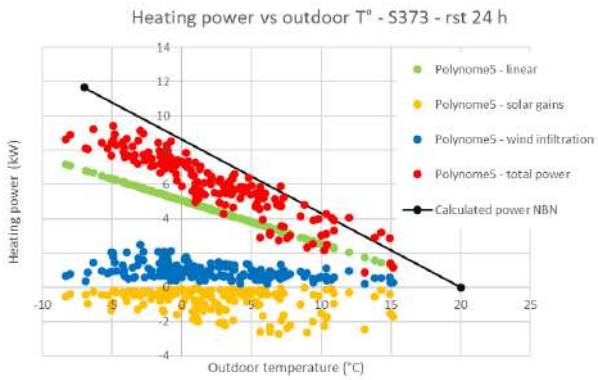

Figure 9: Simulated power breakdown to weather factors - variant S373 – rst 24h

In average a sizing factor of about 0.8 is obtained from the simulations, which is considerably higher compared to the average measured value. The simulated daily average loads are thus higher than the daily measured heat loads and closer to the calculated values following the Belgian annex. Moreover, for quite some variants, the simulated power even exceeds the calculated heat load, suggesting that the standard could underestimate the required power, as can be observed in Figure 10 for the variants with sizing factors above 1.

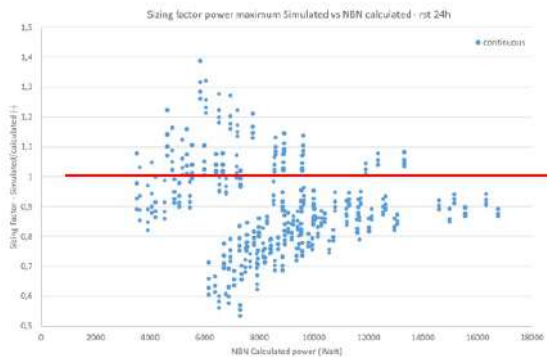

Figure 10: Sizing factor of simulated variants (continuous heating only, well insulated dwellings)

The highest differences in sizing factor are obtained for the different ventilation systems, suggesting that some of the ventilation parameters are not well taken into account in the standard. However, since the interactions between infiltration and ventilation flows was not easy to model, it could be due to modelling issues as well. Further research and analysis should help to scrutinize these results. We can also notice that when the infiltration rates increase, leading to higher NBN calculated heat loads, the sizing factors approaches 1.

While in Figure 10 all dwellings had a good insulation quality, in Figure 11 this insulation quality is varied from a passive standard (Uva – light blue, the lowest heating powers at the left) until non insulated dwellings (Uvi – dark blue – highest heat loads at the right). For the three building types (row house, semi-detached and lowrise dwelling) the same trend is clearly showing; the sizing factor evolves from circa 1 for the best insulated dwellings to circa 0.55 for the

worst insulated dwellings.

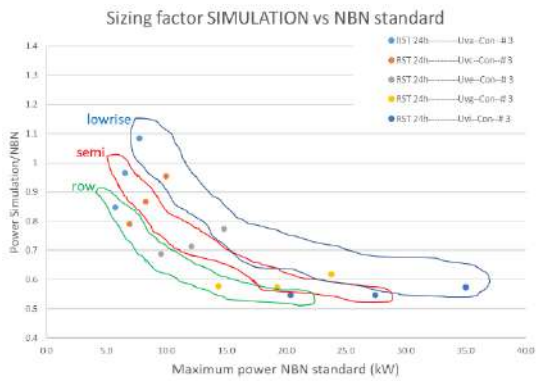

Figure 11: Sizing factor of simulated variants (continuous heating only, varying insulation quality with an average U-value of 0.2 W/m^{2}K for Uva, until 2 W/m^{2}K for Uvi)

This trend is in line with the "physical rebound", which describes that non-heated rooms (or in the philosophy of the heat load standard the rooms that are kept at 10 or 16°C) are only that cold in the worst insulated dwellings, but reach a (much) higher equilibrium temperature for the variants that are better insulated. The better the insulation of the outdoor envelope, the higher average temperatures will be reached in the protected volume. These higher (average) indoor temperatures will cause extra heat losses and therefore also a (relative) higher heat load which is not taken into account for in the standard calculation. Thus, it seems that this 'power rebound' effect is counterbalancing for the best insulated variants other effects that cause the much lower sizing factor becoming apparent for the worst insulated dwellings:

- In reality there are always some internal heat gains so they are included in the measurements and estimated in the dynamic simulations but are not included in the standard calculation
- solar heat gains (idem)
- non-simultaneity of all worst weather conditions and user behaviour

With respect to the resampling time, where the standard assumes that the building mass absorbs hourly variations in heat load, Figure 12 shows that the heat load on 1h basis surpasses the heat load on 24 h average. This is limited from 10 to 40 % for the continuously heated variants, caused by hourly variability during the day (mostly outdoor temperature fluctuation related, but also heat gains vary throughout the day).

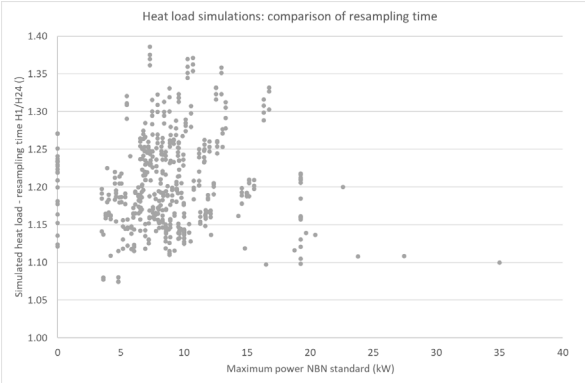

Figure 12: Heat load simulations- comparison of resampling times 1h vs 24h - continuously heated variants only

For the variants with setback schedules and reheat power, however, the simulated sizing factors are much higher, reaching values up to 4 (no figure shown). Since these simulations are run with instantaneous ideal heaters with unlimited heating capacity, this is not a realistic value, though. More simulations have been set up and run with limited emitter capacities, so that the reheat power can be found in relation to realistic reheat times (and building related parameters). Further work is needed to complete this analysis, but the first results show a high non-linearity, so the authors wonder if a small table with reheat values as used in the EN12831-1 is probably an oversimplification of the reality and whether simplified RC models could provide better results.

7. Conclusions

The research was oriented towards possible improvements of the Belgian standard annexe and eventually the European standard EN 12831-1.

Monitoring of real dwellings in use reveal a certain oversizing of the standard on building level, with a 24h horizon. This oversizing can partly be explained by some weather effects, but an important part of this oversizing is probably due to other factors, such as occupant behaviour, without having a method to address it in the standard. Leak infiltration is characterized by a high variability, but new factors couldn't be proposed.

Based on the dynamic simulations we believe that the time horizon of 24h should be reduced, at least for dwellings with lower thermal inertia. This could increase the heat load with 10 to 40 % again, counterbalancing the observed oversizing of the standard on daily base. In addition, the desired flexibility towards smart grids, e.g. as active demand response, can demand extra heating power.

Contrary the actual Belgian standard that assumes the generator capacity as the sum of all room emitter capacities, a distinction should be made between calculations at room and at building level. That will

enable to take into account the increased infiltration and reheat factors on room level (emitter sizing) and the non-simultaneous use of ventilation in all rooms, without increasing the heat load on building level (generator sizing).

Other elements of the standard need clarifications: the definition of temperature comfort and the effect on the air temperature, the definition of ventilation design flow rates and indoor air quality assumptions.

Finally control schedules for heating system operation (e.g. outdoor temperature based heating curves) should take into account the high variability of the required power and the absence of a pure linear relationship between required power (or distribution temperature regime) and the outdoor temperature.

8. Future work

Future research will focus on a simplified RC modelling method to introduce the dynamic behaviour of building and system in the standard calculation. In addition, a more statistical sound method will be investigated in order to avoid oversizing due to the actual simultaneity of all worst case conditions, but enable a more sound choice of parameters that are still on the severe side, but deliver, also when combined, more realistic heat loads.

9. Acknowledgement

This research was partly funded by the Belgian Federal Public Service Economy.

10. References

1. *CEN - European Committee for standardization - EN 12831-1 : Energy performance of buildings - Method for calculation of the design heat load - Part 1: Space heating load (EN 12831-1:2017).*
2. *NBN - Bureau voor normalisatie - NBN EN 12831-1 ANB:2020. Belgian annexe to EN 12831-1:2017, in Dutch and French.*
3. *Payam Refaeilzadeh, Lei Tang, Huan Liu 2008 - Cross-Validation - Arizona State University – USA*
4. *Arshanapalli.F. J. Fabozzi, S. M. Focardi, S. T. Rachev B. G – 2014 - The Basics of Financial Econometrics: Tools, Concepts, and Asset Management Applications - Model Selection Criterion: AIC and BIC - John Wiley & Sons*
5. *Pearson's Correlation Coefficient – 2008 - In: Kirch W. (eds) Encyclopedia of Public Health. Springer, Dordrecht. https://doi.org/10.1007/978-1-4020-5614-7_2569*
6. *RMI - Royal Meteorological Institute - Belgium*
7. *Dols, W. S., & Polidoro, B. J. 2015. Contam user guide and program documentation version 3.2 (No. Technical Note (NIST TN)-1887).*
8. *Peccue S., Van den Bossche P. 2022. Impact Of Building Airtightness On Heat Generator And Heat Emission Equipment Sizing- IAQ 2020 - Athens 2022 – Greece.*
9. *EnergyPlus version 9.4.0; Lawrence Berkeley National Laboratory, U.S. Department of Energy and others.*
10. *Verbeke S. 2017 THERMAL INERTIA IN DWELLINGS - Quantifying the relative effects of building thermal mass on energy use and overheating risk in a temperate climate. Ph.D thesis University of Antwerp*

The full dataset generated and/or analysed during the current study is not publicly available because of GDPR and property issues (most of the cases are measured by HVAC or building companies). However, the authors can be contacted and in function of the research need, a selection of the data can be made available

SunHorizon advanced control system and proactive maintenance tool: Case study in Latvia

Alejandro Martín-Crespo [a], Alejandro Hernández-Serrano [a], Roberto Arnanz [a], Alberto Belda-González [a], Andrea Gabaldón Moreno [a]

[a] Energy Division, CARTIF Technology Centre, Boecillo, Spain, alemar@cartif.es, aleher@cartif.es, robarn@cartif.es, albbel@cartif.es, andgab@cartif.es.

Abstract. Currently, buildings represent a large percentage of the energy consumption in the European Union. Increasing the introduction of renewable energy sources is becoming necessary to achieve an effective reduction of greenhouse gas emissions. SunHorizon project demonstrates the potential of combining solar appliances and heat pumps in buildings for meeting heating and cooling (H&C) demands in Europe. The energy systems are managed by an advanced Python-based control system. Using the forecast of the demand and occupancy of the building, a predictive controller calculates the optimal exploitation of resources and storage use in order to maximize the renewable energy use and cost performance. Furthermore, the control system operates in combination with a proactive maintenance tool that includes fault detection and maintenance surveillance capabilities. This tool is based on the Reliability-Centred Maintenance (RCM) strategy, which focuses on understanding the equipment failure modes, applying all the different possible maintenance strategies and considering consequences and cost of failures. To achieve this goal, several key performance indicators (KPIs) are defined, calculated in real-time operation and compared with simulation data to detect faults. When any failure is obtained, the system triggers specific alarms via web and email, hence notifying house operators or final users. KPIs are also evaluated to calculate their remaining useful life (RUL) and therefore predict future faults. The solution is applied in a building in Riga (Latvia) and the methodology beneath these tools is explained in this paper. The use of prediction for control and maintenance will allow the system to avoid wasting energy, increase self-consumption as well as to save costs on the energy bills.

Keywords. SunHorizon, Heat pumps, Advanced control, Proactive maintenance tool, Latvia.
DOI: https://doi.org/10.34641/clima.2022.106

1. Introduction

In the following years, both residential and tertiary buildings are expected to increase their use of renewable energy, leaving aside conventional technologies and avoiding CO_2 emissions to the environment. Furthermore, in the European Union, the energy associated to heating and domestic hot water (DHW) represents the 79% of total final energy use in households (192.5 Mtoe), and the cooling demand, although smaller, increases significantly in summer months [1]. In addition, climate change threats to increase the cooling energy demand, which may further aggravate electricity peaks in summer [2].

SunHorizon project aims to demonstrate that the proper combination of up-to-date technologies, such as solar panels, heat pumps and storage systems, managed by a controller along with proactive maintenance, can avoid wasting energy, identifying malfunctioning of equipment, maximizing energy coming from renewable energy sources (RES), increasing self-consumption, reducing local energy bills and cutting off greenhouse gases emissions.

In this paper, an advanced control methodology is presented for a case study in Riga. Based on a model of the energy system and using building demand prediction profiles, day-ahead control strategies are calculated optimizing the operation for different criteria, such as maximum self-consumption or minimum operation cost. This predictive optimization uses a combination of the Extended Ant Colony Optimization and Improved Harmony Search algorithms. In addition, a proactive maintenance tool based on the Reliability-Centred Maintenance (RCM) technique is exposed. This tool processes measured and forecast data in order to calculate KPIs and performance indicators (PIs),

Copyright ©2022 by the authors. This conference paper is published under a CC-BY-4.0 license.

which describe the actual health of the system, and trigger alarms in case any problem is detected. Besides, the maintenance tool is able to calculate the RUL of the technologies and their auxiliary elements. All measured and calculated data are stored in a cloud database.

To verify their correct operation, both the advanced control system and the proactive maintenance tool will be tested in the eight demo sites included in SunHorizon project, where several of the H&C devices and management tools designed in the project will be also installed and tested. In this article, the Riga Sunisi house demo intervention and operation are explained.

At the time this article was written, the installation of all devices was in progress, so testing the control system and the proactive maintenance tool with real data was not possible. Instead, simulation tests using historical data were performed.

The remainder of this paper is organized as follows. In Section 2, the Riga Sunisi demo site is described. The advanced control system technique and its implementation are exposed in Section 3. Section 4 shows the proactive maintenance tool developed and adapted to Riga Sunisi. In Section 5, the validation of both tools is included. The conclusion is given in Section 6. Section 7 gathers the acknowledgements. The list of all KPIs and PIs used by the proactive maintenance tool in Sunisi is presented in Section 8 (Appendix A). Finally, Section 9 includes the references.

2. Riga Sunisi demo site description

Riga Sunisi demo site (Fig. 1) consists of a residential house situated in Riga. It was built in 2015 and is composed by a two-floor house and a garage building. The intervention that is been performed in SunHorizon is mainly focused on the heating system, which includes space heating (SH) and DHW systems of the house.

Fig. 1 - Riga Sunisi demo site.

In Fig. 2, a diagram with the technologies which are being installed in Sunisi and their connections is shown.

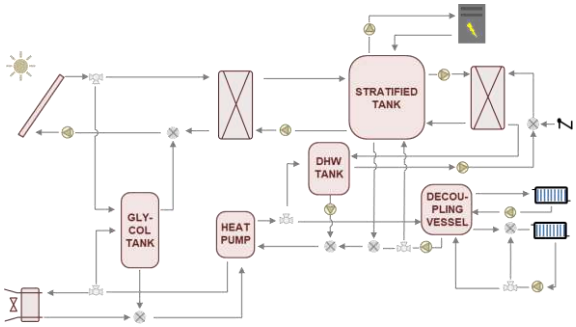

Fig. 2 - Sunisi technologies diagram.

Specifically, the technologies that will be implemented in Sunisi are: hybrid photovoltaic-thermal solar panels (PVT, a natural gas-driven heat pump (HP, a stratified water tank (ST and a glycol tank (GT. The heat output of the PVT is prioritized to store energy in the ST, and, when the outlet temperature of the PVT is not high enough, the heat output of the PVT is stored in the GT. The GT is used to drive the HP when the outdoor temperature is colder than the water stored in the GT, which improves the operation of the DHW and SH loops. The ST pre-heats the DHW and (SH) loops, and the HP supplies the rest of the energy needed. When there is an excess of electrical output from the PVT, a smart electric heater is used to heat up the water inside the ST. The thermal needs of the house include DHW and SH, which is covered using radiators and a radiating floor. The electricity consumption of the house and the technical room are also considered. In order to monitor the SunHorizon system operation, a high number of sensors are being installed at building and room levels.

The energy system is controlled at local level using a rule-based strategy that defines the energy flows to cover the demand, based on temperatures and operation conditions. An advanced controller is used to also consider the prices of gas and electricity to optimize the system's operation (see Section 3). The controller has predictive capabilities to calculate operation strategies that the local controller applies as part of the programmed rules.

The proactive maintenance tool aims to study all the available information in order to provide insights about the current and future status of the previously described system, raising alarms if needed. In the case of Sunisi, both the advanced control and the proactive maintenance tools are executed in a Microsoft Azure server (Fig. 3. This cloud-based virtual machine has been selected because of its advantages, which includes scalability, security and computing power.

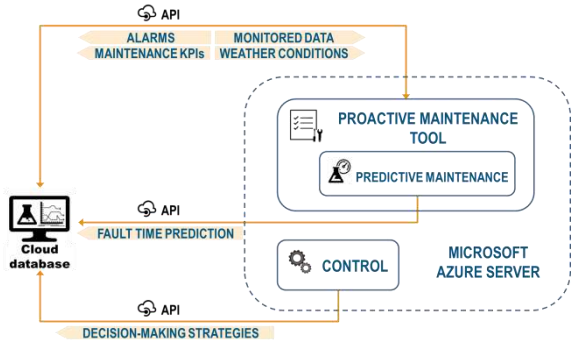

Fig. 3 - Communication flowchart, including Microsoft Azure server.

3. Advanced control system

The heating system of Riga Sunisi incorporates an advanced control system with predictive capabilities, which allows to achieve the optimization of the system in a 24-hours time horizon, to avoid wasting energy, maximize the use of RES and reduce the energy bills.

The advanced controller has been developed in a generic way to be easily adaptable to other cases. Thus, the hybrid controller is implemented on Azure server to avoid the need of any additional architecture at the demo sites (e.g. computer on site). In the particular case of Riga Sunisi, weather forecast data and the predicted demand is provided by IESVE by means of the cloud database [3], and read by the advanced controller through a Python API. Those data are processed and used as an input in a TRNSYS-based model [4]. The model is then co-simulated in TRNSYS and Python and optimized to obtain the predicted optimal status of the system in the next 24 hours to reduce the energy consumption and bills. The general workflow of the advanced controller is shown in Fig. 4.

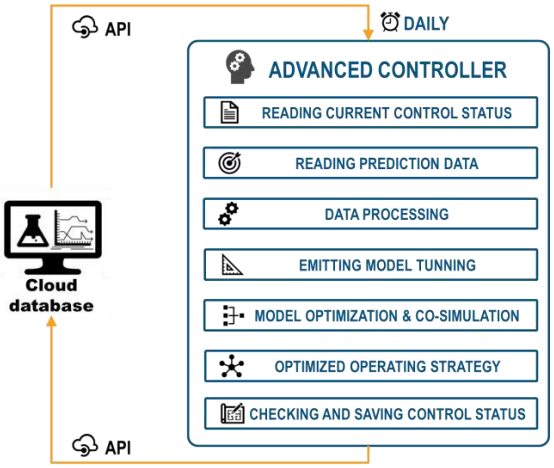

Fig. 4 - Advanced controller flowchart.

In Riga Sunisi, two control decision variables are considered for optimization: the status of the three-way valve that decides whether the PVT stores the thermal output in the ST or the GT, and the amount of power inyected into the smart heater connected to the ST. Costs of gas and electricity are considered to drive the optimization.

For this optimization, the heuristic algorithms Extended Ant Colony Optimization (GACO), Improved Harmony Search (IHS) and Simple Genetic Algorithm (SGA) were used due to their time-efficient computation of integer decision variables, although they do not reach an exact solution, but approximate. The three algorithms were obtained from the pygmo library [5], based on Python, and are compared in Section 5. After testing all of them, IHS was the chosen algorithm to operate the optimization, given that the best results were achieved. In Section 5, the validation results of the advanced controller using IHS are also shown.

4. Proactive maintenance tool

The proactive maintenance methodology in SunHorizon project is based in the Reliability-Centred Maintenance (RCM) strategy, which is a reliability technique used to ensure the inherent designed reliability of a process or piece of equipment through the understanding and discovery of equipment functions, functional failures, failure modes and failure effects. RCM evaluates and applies the different possible maintenance strategies based on consequences and cost of failures, with a strong focus on the proactive maintenance. In this way, RCM integrates traditional preventive, corrective, predictive and condition-based maintenance practices, trying to minimize maintenance and improve reliability throughout the life-cycle. Nowadays, there exist several standards that define the RCM approach, such as [6] and [7].

Following the RCM methodology, the proactive maintenance tool developed in SunHorizon project is focused on the automatic detection and prediction of faults that triggers the maintenance actions defined in the Failure Modes, Effects and Criticality Analysis (FMECA). The tool, which has been developed in Python, includes several steps that are executed once a day (see Fig. 5).

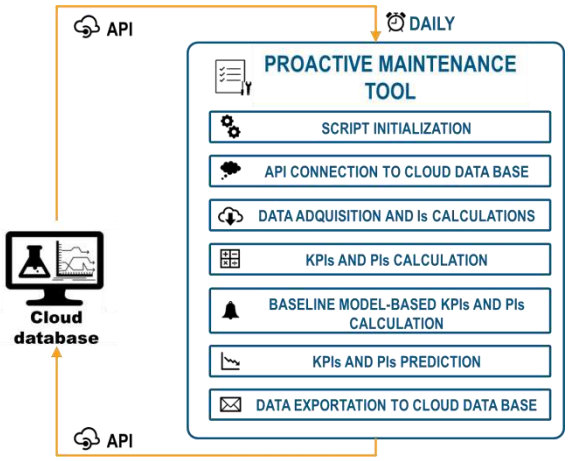

Fig. 5 - Proactive maintenance tool flowchart.

Firstly, the tool gets the monitoring data from a cloud database using an API. Then, KPIs, PIs and other useful indicators (Is) are calculated using their respective formulas (obtained from [8]) and with a different time resolution depending on their characteristics (e.g. 15 minutes, hourly, daily). The complete list of KPIs and PIs calculated in Riga Sunisi can be found in Section 8 (Appendix A). The difference between KPIs and PIs is that the first ones refer to the SunHorizon system as a whole, while the second ones focus on the performance of each of the installed technology. In a third step, the expected KPIs and PIs are estimated using a set of baseline TRNSYS models of the technologies and the real measured data as inputs. The objective of this estimation is performing a comparison between the real and the expected KPIs and PIs, which will help to detect possible faults in the installed devices. Next step is the RUL calculation of the different systems. The KPIs and PIs time series are fit to the predefined fault evolution models, and their prediction is used for the RUL calculation. The RUL value will be very useful for the scheduling of the maintenance tasks. The last step consists of sending to the cloud database all the Is, PIs and KPIs calculated by the proactive maintenance tool and check if any alarm has to be raised comparing real and the expected KPIs and PIs, as previously explained. If any alarm is triggered using the approach in Tab. 1, a notification is sent by web and email. Thresholds from Tab. 1 will be fine-tuned throughout the progress of the project, as well as the evolution of each KPI and PI.

Tab. 1 - Alarms definition.

Alarm level	Formula
Warning	$50\% \leq \frac{Indicator_{actual} - Indicator_{estimated}}{Indicator_{estimated}} \leq 80\%$
Danger	$\frac{Indicator_{actual} - Indicator_{estimated}}{Indicator_{estimated}} \geq 80\%$

5. Validation

In order to validate the operation of the advanced controller and the proactive maintenance tool, simulated data of the building demand have been generated using the models from [4] and uploaded to the cloud database.

Firstly, the three heuristic optimization algorithms selected were studied. The daily costs obtained during one week of February are compared in Fig. 6. Tab 2. shows the average daily cost calculated for that week. IHS is the algorithm that achieves the best performance.

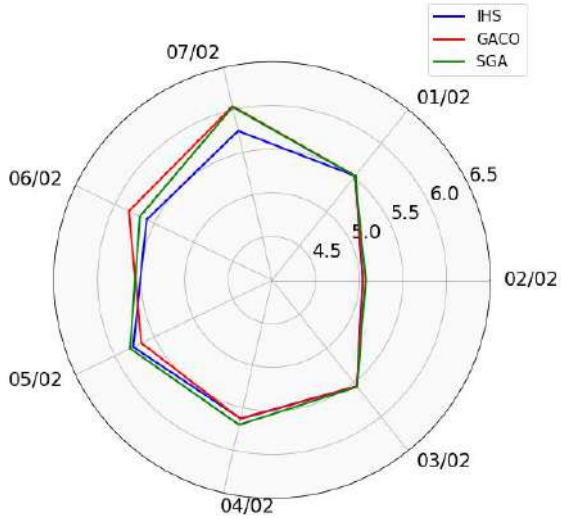

Fig. 6 - Cost comparison between IHS, GACO and SGA algorithms for one week.

Tab. 2 - Average daily cost reached by IHS, GACO and SGA algorithms.

Algorithm	Average daily cost (€)
Improved Harmony Search (IHS)	5.55
Generalize Ant Colony Optimizer (GACO)	5.61
Simple Genetic Algorithm (SGA)	5.63

After choosing the IHS optimization algorithm, the operation of the controller has been validated. One year of simulated data has been used. The results are compared with the "baseline" conditions, i.e. how the system would operate if only rule-based control strategies were applied. As can be seen in Tab. 3, the optimization allows primary energy savings of 4.72%, and a reduction of 9.34% of green-house emissions and 2.88% of operational costs per year.

Tab. 3 - Comparison between baseline and optimized results

Variable	Baseline	Optimized results
Gas consumption (MWh/year)	17.90	14.94
Electricity self-consumption from PVT (MWh/year)	2.92	3.94
Electricity exported (MWh/year)	5.04	4.03
Non-renewable primary energy consumption (MWh/year)	24.52	23.22
Renewable energy ratio (%)	19.11	24.23
Operation costs (€)	1478.66	1436.10

In the case of the proactive maintenance tool, the validation was performed at the functional level. Malfunctioning situations were simulated to ensure the correct alarms calculation and notification.

6. Conclusion

In this paper, a novel advanced control methodology has been presented, along with a proactive maintenance tool. Both developments have been applied to the Riga Sunisi demo site, within SunHorizon project, and have been validated with simulated data. Their combined operation ensures a smart management of innovative H&C devices, resulting in energy, economic and environmental benefits.

Our future work will be focused on the fine-tuning of the advanced controller and the proactive maintenance tool. Once all the devices are installed in the house, real data will be collected, and the operation of all equipment will be analysed and improved.

7. Acknowledgement

This research has been developed as part of SunHorizon project, which has received funding from the European Union's Horizon 2020 Research and Innovation Programme under GA N818329.

8. Appendix A

Tab. 3 and Tab. 4 include all the KPIs and PIs used in Sunisi by the proactive maintenance tool.

Tab. 3 - KPIs of Riga Sunisi demo site.

Name	Unit
Capital expenditure	€
Costumer's bills reduction	€
Customer's satisfaction rate	%
Greenhouse gases emissions reduction	gCO_2
Heating comfort index	°C·h
Levelized cost of heat	€/kWh
Operational expenditure	€
Non-renewable primary energy savings	kWh
Renewable energy ratio	%
Electricity self-consumption fraction	%
Simple pay back	years

Tab. 4 - PIs of Riga Sunisi demo site.

Name	Unit
Dual panels solar electric efficiency	%
Dual panels solar thermal efficiency	%
Dual panels solar thermal fraction	%
Dual panels thermal-electricity ratio	%
Heat pump seasonal gas utilization efficiency	%
Heat pump seasonal performance factor	%
Water tank stratification efficiency	°C
Glycol tank stratification efficiency	°C

9. References

[1] Fleiter T., et al. Mapping and analyses of the current and future (2020-2030) heating/cooling fuel deployment (fossil/renewables). European Commission, Directorate-General for Energy. 2016.

[2] Climate action. https://ec.europa.eu/clima/eu-action/adaptation-climate-change/how-will-we-be-affected/sectors-affected_en

[3] Cabrera A. G., Ntimos D. Comparative study of measurement and verification (M&V) baseline models for quantifying energy savings in building renovations. IOP Conference Series: Earth and Environmental Science. 2020;410(1):012057.

[4] Chèze D., Cuneo A., Macciò C., Porta M., Dino G., Andrea Frazzica A., Gabaldón A. Four innovative solar coupled heat pump solutions for building heating and cooling. EuroSun 2020-13th International Conference on Solar Energy for Buildings and Industry. 2020.

[5] pygmo. https://esa.github.io/pygmo2/

[6] Society of Automotive Engineers. Evaluation Criteria for Reliability-Centered Maintenance (RCM) Processes. SAE JA1011: Society of Automotive Engineers. Rev. 2009.

[7] Society of Automotive Engineers. A Guide to the Reliability-Centered Maintenance (RCM) Standard. SAE JA1012: Society of Automotive Engineers. 2002.

[8] SunHorizon. D2.4 – KPIs assessment based methodology. 2019.

Data Statement

Data sharing not applicable to this article as no datasets were generated or analysed during the current study.

Simplified CFD for pressure drop predictions in ducts

Thijs van Druenen [a], Zakarya Kabbara [b], Ivan Verhaert [b], Twan van Hooff [a]

[a] Building Physics and Services, Department of the Built Environment, Eindhoven University of Technology, PO Box 513, 5600, MB Eindhoven, the Netherlands, t.v.druenen@tue.nl

[b] Energy and Materials in Infrastructure and Buildings (EMIB - HVAC), University of Antwerp, Campus Groenenborger (Building Z), Groenenborgerlaan 171, Antwerp 2020, Belgium

Abstract. In the design of a ventilation system, the ductwork is generally composed based on analytical equations in combination with loss coefficients. This widely used approach can lead to large deviations in the prediction of the total pressure drop. Poor performance optimization could on its turn lead to a higher energy demand. While the use of computational fluid dynamics (CFD) could improve this prediction, it is often not feasible in practice as the use of CFD requires a high computational demand and a high-level of expertise. An alternative could be the use of simplified CFD. In this study the application of several conventional and simplified CFD methods and analytical prediction methods in the ventilation system design process was assessed. The simplified CFD methods include the use of coarse-grid CFD and voxel-based CFD simulations. Measurements on a single and double elbow configuration were performed and were used for validation purposes. For the investigated configurations the analytical prediction started to deviate from the measurements with increasing complexity of the system. For the conventional and coarse-grid CFD methods the prediction of the pressure drop was highly sensitive to the applied near-wall treatment and roughness parameters. For the voxel-based CFD method an average percentage difference of only 3% with respect to the measurements was found for the single elbow configuration. However, it overestimated the measured pressure drop by 64% on average for the double elbow configuration. A general sufficiently accurate method for predicting the pressure drop, which would also be feasible for use in practice ventilation system design, was not yet found. As this paper is part of a larger study, the assessment of additional simplified CFD methods on more complex duct configurations is the subject of future work.

Keywords. Computational Fluid dynamics, Simplified CFD, Ventilation system design, Ducts.
DOI: https://doi.org/10.34641/clima.2022.304

1. Introduction

The design of the ductwork of a ventilation system is primarily based on analytical equations in combination with loss coefficients (e.g. [1,2]). While this is a widely used approach, it is well-known that this can lead to large deviations in the prediction of the total pressure drop [3-5]. Former research indicated that the application of computational fluid dynamics (CFD) simulations could reasonably predict the pressure drop in ventilation systems [6-10]. Shattered agreements were found in early numerical studies. Mumma et al. [6] conducted a numerical study on a configuration of coupled fittings, but found a large underprediction while comparing the calculated loss coefficient for the isolated fittings to the ASHRAE duct fitting database (DFDB). By application of steady RANS and the standard k-ε turbulence model the loss coefficient was underestimated by 28% for a 90° rectangular elbow fitting with a large radius and by 62% for a 90° elbow fitting with a small radius. In a later study, Mumma et al. [7] numerically calculated the loss coefficients for nine fittings. By application of the standard k-ε turbulence model the computed results were within ±15% of those found in the ASHRAE DFDB for seven of the nine fittings. Moujaes and Deshmukh [8] found pressure drop differences of 8% for an elbow fitting, and 8% and 18% for respectively the straight and branch flow in a tee fitting, while comparing their numerical results tot the ASHRAE DFDB. Liu et al. [9] performed CFD simulations and compared the results of three CFD approaches with experimental data from literature. The study found that the calculated pressure drop was very sensitive to the modeled surface roughness in the straight parts of the configuration. After determination of suitable roughness parameters the pressure drop could accurately be predicted by steady RANS methods using the standard k-ε turbulence model or Reynolds stress model. The LES method failed in accurately predicting the pressure drop. However, a relatively coarse grid in terms of LES requirements was used. Manning et al. [10] calculated the loss

Copyright ©2022 by the authors. This conference paper is published under a CC-BY-4.0 license.

coefficient for a flat-oval straight-body lateral and a flat-oval straight-body tee. Their CFD simulations compared well quantitatively against experimental results for the majority of the configurations and considered CFD a viable tool to accurately predict the correct loss coefficient curve-shaped structure as a function of flow rate.

This brief literature review indicated that the performance of CFD was diffuse, but it showed potential of being a valuable tool for predicting the pressure drop. However, application of CFD is not feasible in ventilation design practice as the application of conventional CFD requires large computational resources, long computation time and a high-level of expertise. An alternative could be the use of simplified CFD to lower computation time and limit the required knowledge for performing such simulations ([11-14]). The application of simplified CFD could improve the prediction of pressure drop during the early phases of the design process compared to the use of analytical methods, while limiting the computational demand compared to conventional CFD. Several options are present in literature, for example fast fluid dynamics (e.g. [11]), lattice Boltzmann (e.g. [12]), coarse grid CFD (e.g. [13]), CFD with zero-equation turbulence model (e.g. [14]). Each method has its potential strengths and weaknesses and therefore further analysis is needed.

In this study the application of several prediction methods in the ventilation system design process was assessed. Numerical (CFD) and analytical (ASHRAE) methods were applied to two duct configurations. The CFD methods included the use of high-quality CFD on high-resolution grids and simplified CFD by the use of CFD on low-resolution grids and the use of voxel-based CFD using ANSYS Discovery Live 2020r1 [15]. Measurements on both duct configurations were performed and were used for validation purposes. The purpose of the current project is to find a fast and user-friendly tool, with an improved accuracy over conventional analytical methods, which can be used by engineers without the need for extensive expert knowledge on CFD.

2. Measurements

The full-scale experimental models are shown in Fig. 1. The system was composed of a centrifugal fan, circular air ducts and, depending on the tested configuration, one or two 90° elbows. The system was supported by angle brackets at approximately 1 m height. The circular ducts and elbows had a radius of 100 mm. The elbow characteristics are shown in Fig, 2 with r/D = 1 and D = 200 mm. The components were manufactured of galvanized sheet steel, sealed and connected using steel duct clamps.

Two measurement configurations were tested:

A. Single 90° elbow configuration

B. Double 90° elbow configuration

The measurements were performed according to ASHRAE Standard 120-2017 [16]. This standard prescribes a minimum of eight test velocities, evenly distributed over the total range. The recorded mean flow velocities per configuration are given in Table 1. As the primary goal of this study is the validation of CFD methods, also less-common higher flow rates were investigated. The velocity was unevenly distributed in the duct section. Therefore, velocity measurements were performed at 18 points in the duct's cross sections according to the ASHRAE Handbook [18]. Measurements were performed by the Testo 0635 9542 digital vane probe together with the Testo 480 meter and 10 s average values were noted. The area-average streamwise velocity of this section was taken as the average of these 18 velocity measurements [18].

Tab. 1 - Mean inlet velocities in m/s

A. Single bend	B. Double bend
2.52	2.49
3.22	3.14
4.23	4.13
5.29	5.09
6.68	6.33
7.68	7.52
8.79	8.52
10.09	9.67

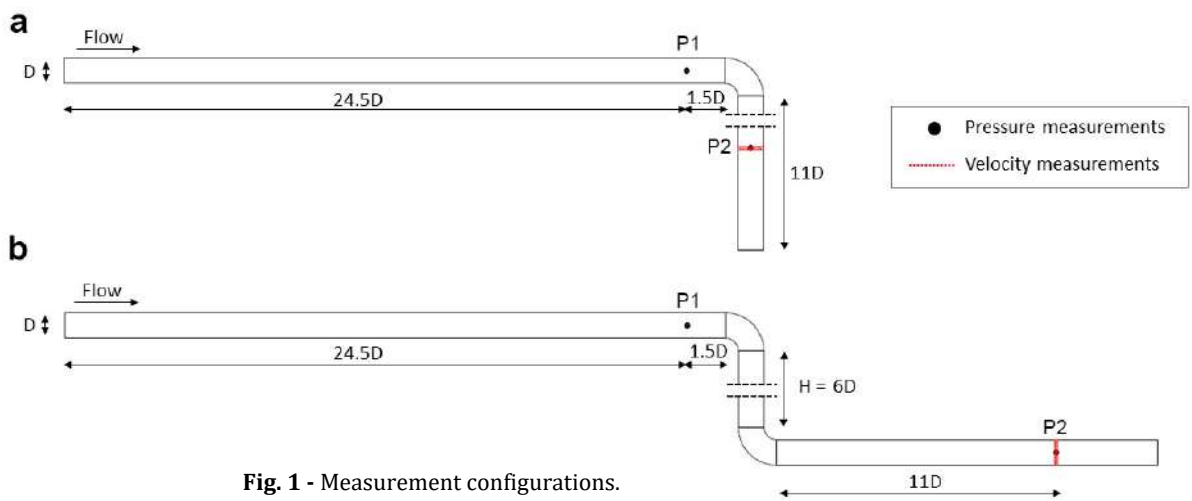

Fig. 1 - Measurement configurations.

A duct length of 4.9 m between the fan and first measurement point P1 was applied to ensure that the air flow was fully developed. A distance of 1.5D (300 mm) was used between P1 and the fitting and the length between the fitting and P2 was 11D (2200 mm). The pressure loss between these points was evaluated for eight flow rates per configuration.

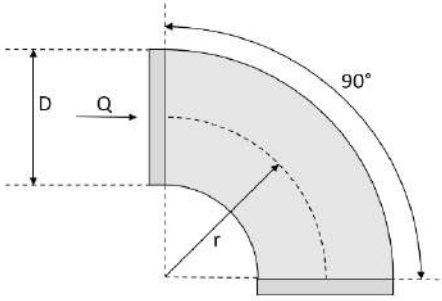

Fig. 2 - Elbow fitting with r/D = 1 and D = 200 mm.

In accordance with the ASHRAE Standard 120-2017 [16] the static pressure differential measurements were performed by simultaneously lowering two pitot-static tubes parallel to the flow in the duct at both P1 and P2. The pitot-static tubes were connected to a Testo 480 pressure transducer [17] and 10 s average values were noted. Measurements of temperature, atmospheric pressure and humidity were performed before each pressure measurement using the Testo 0632 1543 digital IAQ probe together with the Testo 480 meter. The measuring range and accuracy of the instruments is presented in Table 2.

Tab. 2 - Instrumentation details

Instrument	Range	Accuracy
Testo 480 meter	-100 – 100 hPa	±0.3 Pa + 1%
Testo 0635 9542 digital Vane probe	0.6 – 50 m/s	± 1%
Testo 0632 1543 digital IAQ probe	0 – 50 °C	± 0.5°C
Testo 0632 1543 digital IAQ probe	0 – 100% RH	±1.4%
Testo 0632 1543 digital IAQ probe	700 – 1100 hPa	± 3 Pa

The measured friction factor of the circular duct and the loss coefficient of the fitting, both required for the analytical prediction method (see Section 3) were calculated based on straight duct measurements performed in accordance with ASHRAE Standard 120-2017 [16]. Here, configuration A was used (Fig. 1) with exclusion of the elbow fitting. The measured friction factor f_{meas} was determined by:

$$f_{meas} = \frac{\Delta p_{f,1-2}}{p_v/D_h} \quad (1)$$

in which D_h is the hydraulic diameter (0.2 m), p_v the dynamic pressure and $\Delta p_{f,1-2}$ the total pressure loss per meter of straight duct and calculated using:

$$\Delta p_{f,1-2} = \frac{\Delta p_{s,1-2}}{L_{1-2}} \quad (2)$$

Here, $\Delta p_{s,1-2}$ is the measured pressure difference between P1 and P2 and L_{1-2} the length between P1 and P2. The local loss coefficient C_{meas} of the fitting is determined using:

$$C_{meas} = \frac{\Delta p_{t,1-2}}{p_v} \quad (3)$$

In which $\Delta p_{t,1-2}$ is the measured pressure difference $\Delta p_{s,1-2}$ minus the share of the straight duct between P1 and P2 with length L_{SD}:

$$\Delta p_{t,1-2} = \Delta p_{s,1-2} - L_{SD} * \Delta p_{f,1-2} \quad (4)$$

3. Analytical prediction

In this study the analytical prediction of the pressure drop is based on the ASHRAE Handbook [19]. This prediction method distinguishes between friction losses, in straight parts, and dynamic losses due to fittings. For fluid flow in straight ducts the friction loss in terms of total pressure can be calculated by the Darcy equation:

$$\Delta p_{f,calc} = \frac{f L_{SD} p_v}{D_h} \quad (5)$$

Here f is the friction factor, which can be measured (see Equation 1) or calculated by the Colebrook equation:

$$\frac{1}{\sqrt{f_{calc}}} = -2log\left[\frac{\epsilon/D_h}{3.7} + \frac{2.51}{Re\sqrt{f_{calc}}}\right] \quad (6)$$

where ϵ the absolute pipe roughness and Re the Reynolds number of the flow. ASHRAE prescribes a pipe roughness ϵ = 0.09 mm for galvanized steel. Dynamic losses result from flow disturbances caused by duct mounted equipment and fittings that change the airflow's direction or cross-sectional area. For an elbow the total pressure loss over this fitting Δp_e can be calculated by:

$$\Delta p_e = C * P_v \quad (7)$$

Here, C is the loss coefficient for this particular fitting, which can be obtained by measurements (see Equation 3) or be found in manufacturer's datasheets or fitting databases (e.g. [20]). In this study the analytical prediction outlined above was performed for two sets of input conditions. In the first analytical prediction method (AP-I) the friction losses were determined based on f_{calc} (see equation 6) and the loss coefficient C_{ASHRAE} = 0.25 was obtained from a fitting database [20]. In AP-II the measured friction factor f_{meas} was used, which was calculated based on measurements on a straight duct part. The elbow loss coefficient was based on equation 3 in which C_{meas} was calculated from measurements for configuration A.

4. CFD simulations

In this study the performance of several simulation methods on the prediction of the pressure drop was assessed. The methods were classified with respect to theoretical accuracy and simulation time (this included time for pre/post processing). The three categories were named CFD-I, CFD-II and CFD-III, with CFD-I being the most, and CFD-III being the least theoretically accurate and time-consuming method. With respect to simulation time, one can think of CFD-I in the order of days to a week, CFD-II in the order of hours to days and CFD-III in the order of minutes to hours. The CFD-I simulations were characterised by solving the flow down to the viscous sublayer near the wall and is, in essence, required for an accurate prediction of separation and reattachment of the flow. This required a high-resolution grid in these areas. Two turbulence models were assessed, e.g. the realizable k-ε model (RLZ-I) [21] and the k-ω SST model (SST-I) [22]. In the CFD-II approach a simplified form of regular CFD is applied in which the flow was modeled in the near-wall region. This allowed the use of larger cells in these areas. The realizable k-ε model (CFD-II) [21] was used. The CFD-III method included a voxel-based simplified CFD approach using the ANSYS Discovery Live package (CFD-III) [15]. Based on GPU computing, this software allows almost instantaneous simulation results.

4.1 Computational domain

Figure 3a shows the computational domains for the CFD-I and CFD-II methods, for both configuration A and B. The computational domains were constructed with equal dimensions as the ductwork used in the measurements. The surface at the upstream side of the domain was modeled as velocity inlet and the surface at the downstream side of the domain was modeled as pressure outlet. The duct inner surfaces were modeled as no-slip walls and sampling planes P1 and P2 were created at locations similar to the measurements. Due to limitations of the software, only the section between P1 and P2 was modeled for the CFD-III method.

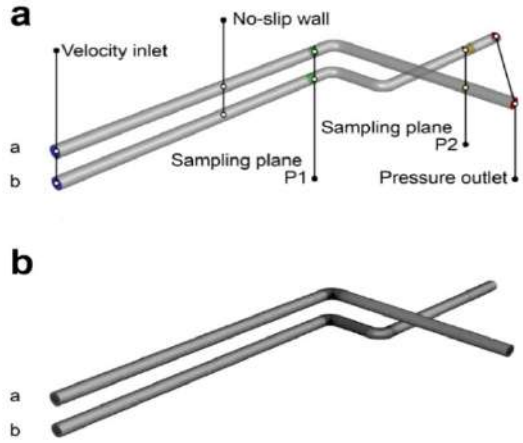

Fig. 3 - Computational (a) domains and (b) indicative grids for CFD-I and CFD-II.

4.2 Computational grid

Grid-sensitivity analyses were conducted for CFD-I and CFD-II methods using configuration A. It was assumed that the resulting grid topology for configuration A (single elbow) was sufficiently fine for configuration B (double elbow) as well. The grids were constructed using a sweep method [23]. Grid topologies are found in Table 3. The surface plane at the inlet of the computational domain was meshed according to the characteristics first cell height, growth rate, cell layers and cells over circumference, after which this meshed surface was swept with given cell lengths to create the 3D volume grid. To resolve the boundary layer at the surface in the CFD-I simulations, the normal distance of the cell center point from the wall surface y_P was determined so that y^* is lower than 2.5 (coarse), 1.3 (medium), 0.6 (fine) and 0.3 (finest) for the highest inlet velocity (≈ 10 m/s). The dimensionless wall unit y^* is defined by $y^*=u^*y_P/\nu$ where u^* is the friction velocity and ν is the local kinematic viscosity. For the CFD-II simulations, y_P was determined so that y^* is higher than 50 for the lowest inlet velocity (≈ 2.5 m/s).

CFD-I required the analysis of four systematically refined grids (see Fig. 4a-d), while for CFD-II the performance on three grids was assessed (see Fig. 4e-g). The results are presented in Section 5.1. The CFD-III simulations did not allow much control on the grid. It automatically constructs a uniform voxel-based grid for its user. By putting the fidelity function at its maximum value the grid was constructed with the highest resolution.

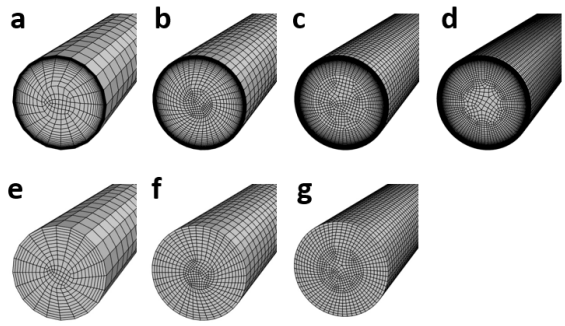

Fig. 4 – (a-d) CFD-I and (e-g) CFD-II grid topologies.

4.3 Computational settings

3D steady RANS simulations were performed in full scale. The CFD-I and CFD-II simulations were performed using the commercial CFD code ANSYS Fluent 21r1 [24], for which pressure-velocity coupling was performed by the SIMPLEC algorithm, gradients were computed with the least square cell based scheme, pressure interpolation was second order and second-order upwind discretization schemes were used for the convection and viscous terms of the governing equations. The simulations were considered converged as an increasing number of iterations did not lead to changes in the monitored pressure drop $\Delta p_{t,1\text{-}2}$.

Tab. 3 – Grid characteristics

Grid resolution		First cell height (mm)	Growth rate	Cell layers	Cells over circumference	Cell length (m)	Cell length in bend (m)
CFD-I a	Coarse	0.08	1.2	28	20	0.06	0.015
CFD-I b	Medium	0.04	1.15	40	40	0.04	0.010
CFD-I c	Fine	0.02	1.1	56	60	0.02	0.005
CFD-I d	Finest	0.01	1.1	60	80	0.01	0.003
CFD-II e	Coarse	5	1.07	10	20	0.06	0.015
CFD-II f	Medium	5	1.07	10	40	0.04	0.010
CFD-II g	Fine	5	1.07	8	60	0.02	0.005

For the CFD-III simulations ANSYS Discovery Live 2020r1 [15] was used. Internal fluid simulations were performed with the steady state fluids solver. This solver is based on a cell-centered Cartesian finite volume discretization according to Ye et al. [25]. Uniform discretization is applied, together with a voxelized level-set approach starting from the geometry. An iterative algorithm similar to the SIMPLE scheme is applied and turbulence is modeled using a standard k-ε model.

4.4 Boundary conditions

At the inlet of the domain a uniform mean velocity was imposed, equal to the magnitude of the mean flow velocity as recorded in the measurements (see Tab. 1). Turbulence was specified by a turbulent intensity of 5% and a turbulent viscosity ratio of 10. Their impact was evaluated to be negligible due to the large distance between the inlet of the domain and P1. Zero static gauge pressure was specified at the outlet. In case the method allowed, roughness was applied at the duct wall surfaces by definition of the equivalent sand-grain roughness height k_S. Fitting with straight duct measurement yielded k_S = 0.0005 m for SST-I and k_S = 0.0006 m for CFD-II.

5. Results

5.1 Grid-sensitivity analyses

The results of the grid-sensitivity analyses were evaluated in terms of percentage deviation in pressure drop $\Delta p_{t,1\text{-}2}$ with respect to that on the finest grid tested and are presented in Figure 5. The results for CFD-II were compared to the results found on the fine grid, while for the CFD-I methods the result were evaluated with respect to $\Delta p_{t,1\text{-}2}$ obtained on the finest grids. The results for CFD-II on both the coarse and medium grids showed differences of 0.2% with respect to the fine grid and therefore the medium grid was retained for the CFD-II method in the remainder of this study. Much larger differences were found for the CFD-I methods and therefore an additional fourth (finest) grid was required. For SST-I differences of 8.2% (coarse), 3.9% (medium) and 1% (fine) were found with respect to the finest grid. Percentage differences of 1.2%, 0.4% and 0.2% were obtained on respectively the coarse, medium and fine grid for RLZ-I. These agreements were considered as nearly grid-independent results and therefore the medium grid was retained for the CFD-I methods.

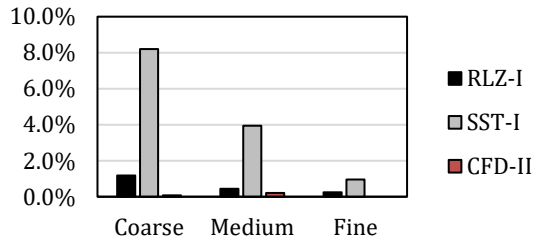

Fig. 5 - Grid-sensitivity analyses results in terms of percentage pressure drop $\Delta pt,_{1\text{-}2}$ with respect to that on the finest grid tested.

5.2 Configuration A: Single elbow

Figure 6 gives the results for all investigated methods for configuration A. The results are presented in terms of $\Delta p_{t,1\text{-}2}$ as function of Q. In agreement with literature, a quadratic relation was observed for all methods. Based on the measurement results, an average loss coefficient C_{meas} of 0.29 was calculated for the 90° elbow fitting using Equations 3 and 4. This loss coefficient C_{meas} was used for the calculation of AP-meas. As a result of this tuning process, the average agreement over all values for Q between AP-meas and the measurements was fair with an average absolute percentage difference *AAPD* of 7%. An AAPD of 13% was calculated for AP-calc. However, the best agreement with the measurements was observed for CFD-III with an AAPD of 3%. SST-I and CFD-II both showed an overestimation of $\Delta p_{t,1\text{-}2}$ with an AAPD of 32% and 16%, respectively. The results for RLZ-I under-estimated the measurements with an AAPD of 14%.

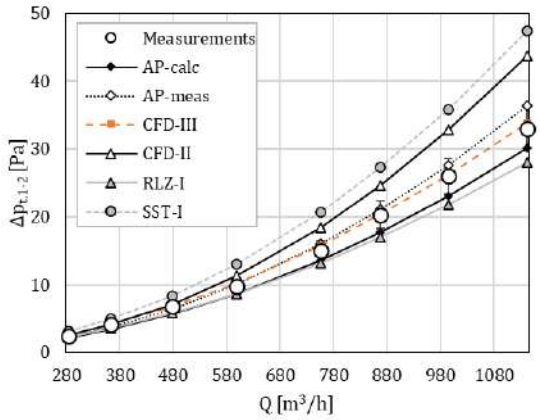

Fig. 6 - Pressure drop $\Delta pt,_{1\text{-}2}$ for configuration A.

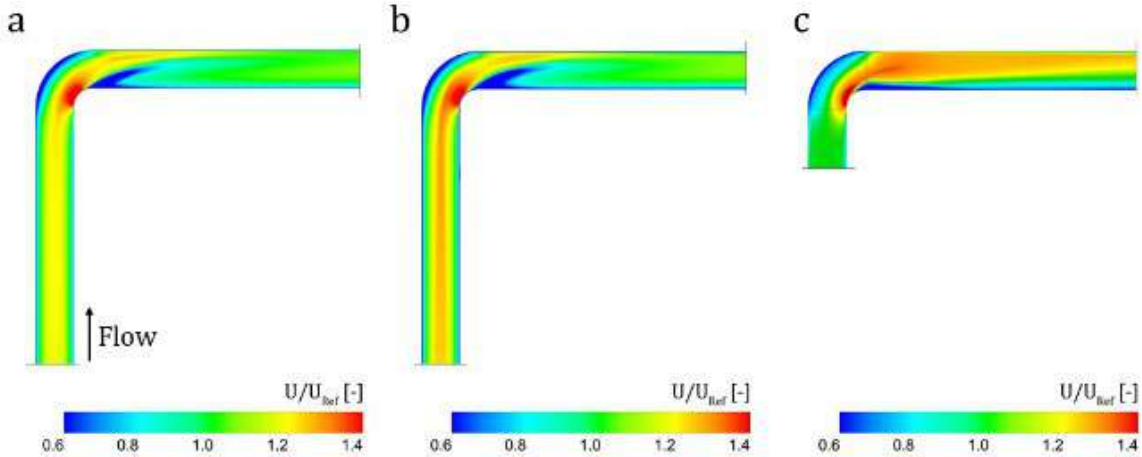

Fig. 7 - Contours of mean velocity ratio U/U_{Ref} for (a) RLZ-I, (b) CFD-II and (c) CFD-III, for configuration A.

Contours of mean velocity ratio are presented in Figure 7 for configuration A. The mean velocity ratio U/U_{Ref} is defined as the mean velocity magnitude U with respect to the inlet mean velocity U_{Ref} = 9 m/s. Differences between CFD methods RLZ-I (Fig. 7a) and CFD-II (Fig. 7b) were as follows. In general, larger regions of low velocity (blue color) were found in the close vicinity of the walls in the straight parts in the configuration for CFD-II (thicker boundary layer). For RLZ-I a larger gradient (thinner boundary layer) was observed near the wall in Fig 7a, while a higher mean velocity ratio was present in the center of the duct for CFD-II (see Fig. 7b) upstream of the elbow. A larger wake region in the region downstream of the elbow was observed for CFD-II. Compared to the CFD-I and CFD-II, a very dissimilar flow field was found for the CFD-III method (Fig. 7c). The size of the wake region downstream of the elbow was very small. Further downstream a large velocity gradient was observed over the complete cross-section of the duct.

5.3 Configuration B: Double elbow

The pressure drop results concerning configuration B are presented in Figure 8. While CFD-III showed a very good agreement with the measurement results for configuration A, for configuration B $\Delta p_{t,1\text{-}2}$ was overestimated with an AAPD of 64%. The pressure drop $\Delta p_{t,1\text{-}2}$ was also mostly overestimated by SST-I (AAPD = 46%), CFD-II (AAPD = 35%), AP-meas (AAPD = 31%) and AP-calc (AAPD = 19%). The best agreement was obtained by RLZ-I with an AAPD of 12%.

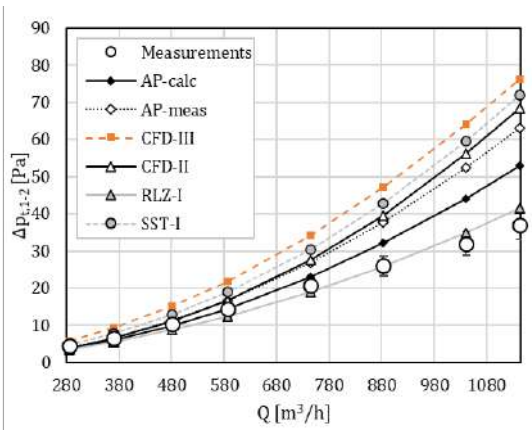

Fig. 8 - Pressure drop $\Delta pt_{,1\text{-}2}$ for configuration B.

For configuration B the contours of mean velocity ratio are given in Figure 9. Comparable flow characteristics were identified as those found for configuration A. Again a higher mean velocity ratio was observed in the center of the duct upstream of the elbows for CFD-II. In addition, the wake regions downstream of both corners were larger compared to those found for RLZ-I. This was most pronounced for the wake region near the downstream elbow. Also similar flow characteristics were observed for the CFD-III method. No recirculation areas in the wake regions downstream of the elbows could be identified and large regions of high mean velocity ratio were present. Downstream of the elbows, it took longer for the flow to stabilize while using the CFD-III method compared to the RLZ-I and CFD-II methods.

6. Discussion

For the single elbow configuration there was a fair agreement between the measured and analytically predicted pressure drops. With AAPDs of 7% and 13% for respectively AP-meas and AP-calc the agreement could be acceptable. However, as the system got more complex and another elbow was added, these AAPDs increased to 31% (AP-meas) and 19% (AP-calc). This large increase in error, especially for AP-meas as it directly used input values based on the onsite measurements, implicates that the flow field in a complex system might be too complex to accurately predict the pressure drop using analytical equations. However, the agreement with the investigated CFD methods was not much better in general. The CFD-III method showed a very good agreement in terms of pressure drop for the single elbow configuration. However, the deviating flow field raised concerns about whether this agreement was largely based on coincidence. These concerns were justified, as the prediction of the pressure drop for the double elbow configuration yielded an AAPD of 64%. Important flow features, like recirculation zones, wake regions and diffusion were not accurately modeled in the presented simulations. As the software only allowed pressure drop calculations over the complete domain, just the part between P1 and P2 was modeled. Therefore, the flow was not completely developed at P1. This could have impacted the results.

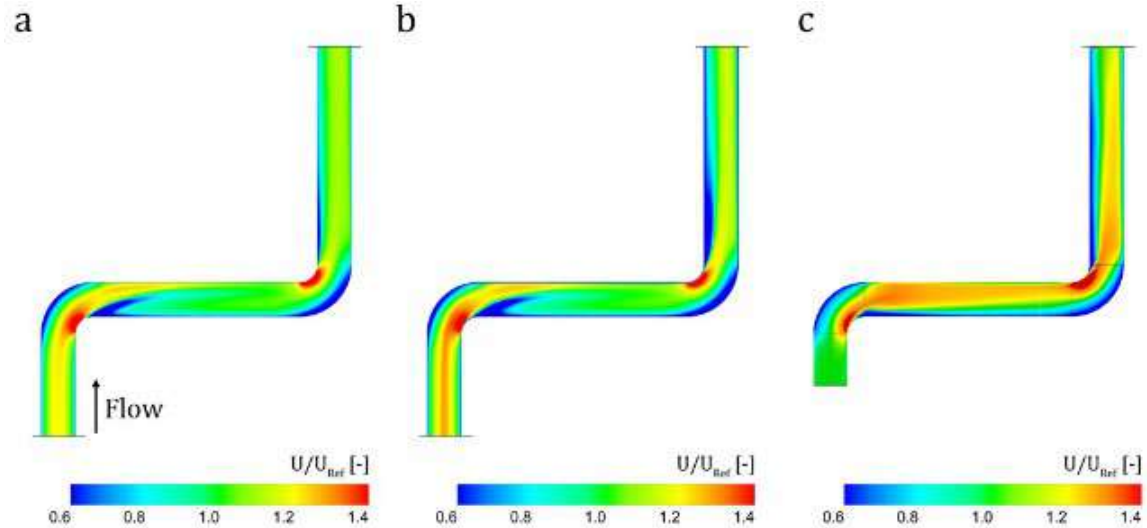

Fig. 9 - Contours of mean velocity ratio U/U_{Ref} for (a) RLZ-I, (b) CFD-II and (c) CFD-III, for configuration B.

For both configurations the CFD-II method overpredicted the pressure drop. A reason for this could be the fact that the k-ε turbulence model, together with wall functions, could overestimate the speed and size of the recirculation areas after flow separation [26, 27]. Wall functions are not capable of accurately predicting the separation point [28]. Overestimation of the wake and recirculation areas contributes to an increase in pressure drop. The CFD-II method used the k-ε turbulence model together with wall functions, while the RLZ-I used the same turbulence model but resolved the flow down to the viscous sublayer at the wall. This would theoretically lead to a better prediction of flow separation and wake regions. However, this method was not capable of modeling the roughness at the wall. This led to a larger velocity gradient near the wall. The decrease in velocity was smaller with no roughness, which partly explains the under-estimation of the pressure drop for using RLZ-I. The other CFD-I method, SST-I, is capable of taking wall roughness into account. However, for both configurations this method overpredicted the pressure drop. In accordance with existing literature on this topic [9] the modeling of roughness had a large impact on the pressure drop prediction. In the remainder of the larger ongoing research project, the use of lower k_S values will be studied as well.

In the current paper only several analytical and CFD methods were included. A general method to predict the pressure drop with satisfying accuracy was not yet found. This paper is part of a larger study in which the performance of additional methods will be assessed as well. At this moment only the use of coarse grids and the use of voxel-based CFD was investigated. As a wide range of simple/fast numerical methods is currently available, the use and performance of more methods will be considered. The aim is to find a fast and user-friendly tool with sufficient accuracy which can be used by engineers without the need for much knowledge on CFD. For benchmark purposes, also the performance of more sophisticated methods, like large eddy simulation or hybrid methods, will be assessed. In addition, measurements on additional complex duct configurations, to be used for validation purposes, is the subject of future work.

7. Conclusion

In this study the application of several CFD and analytical methods on the prediction of the pressure drop in the ventilation system design process was assessed. These included the performance of high-quality CFD on high-resolution grids, the use of simplified CFD by means of coarse-grid CFD and voxel-based CFD, and the use of analytical equations with loss coefficients from either existing literature or self-conducted measurements. Measurements on two duct configurations were performed and were used for validation purposes.

The hypothesis that the analytical prediction starts to deviate from the onsite situation as the system gets more complex holds for the investigated configuration and methods. However, also a satisfying CFD method was not yet found. For the CFD methods that allowed the modeling of roughness at the duct inner surface, the prediction of the pressure drop was highly sensitive to the applied roughness parameters. Though the applied roughness parameters were chosen based on a fitting process with experimental data for a straight duct, these parameters led to overprediction of the pressure drop for the investigated elbow configurations. For the high-resolution CFD method which could not include surface roughness at the walls, the calculated pressure drop was much lower. While the investigated voxel-based CFD method showed an absolute average percentage difference of only 3% with the measurements for the single elbow configuration, it greatly overestimated the measured pressure drop by 64% on average. Based on the investigated methods and configurations in this study, no general sufficiently accurate method for predicting the pressure drop could yet be chosen.

Acknowledgements

This work has been supported by the Flemish Agency for Innovation and Entrepreneurship (VLAIO) in the Flux50 project Smart Ventilation (HBC.2020.2520).

References

[1] Tsal R.J., Behls H.F., Mangel R. T-method duct design – Part 1: optimisation theory and Part 2: calculation procedure and economic analysis. ASHRAE Trans. 1988;94(2): 90–151.

[2] Jorens S., Sörensen K., Verhaert I., de Corte A. Air distribution system design optimisation in non-residential buildings: Problem formulation and generation of test networks. J. Build. Eng. 2017;12: 60-67.

[3] Fischer D. Ventilation duct design by CFD-technology. Proc of Automotive Sim 1991: 169-180.

[4] Smith S.J. Determination of k-factors of HVAC system components using measurement and CFD modelling. PhD thesis, University of Nottingham. 1998.

[5] Beach R., Prahl D. Computational fluid dynamics analysis of flexible duct junction box design. US Department of Energy. 2013.

[6] Mumma S., Mahank T., Ke Y. Close coupled ductwork fitting pressure drop. HVAC&R Res. 1997;3(2): 158-177.

[7] Mumma S., Mahank T., Ke Y. Analytical determination of duct fitting loss-coefficients. Appl. Energy 1998;61: 229-247.

[8] Moujaes S.F., Deshmukh S. Three-Dimensional CFD Predications and Experimental Comparison of Pressure Drop of some Common Pipe Fittings in Turbulent Flow, J. Energy Eng. 2006;132(2): 61-66.

[9] Liu W., Long Z., Chen Q. A procedure for predicting pressure loss coefficients of duct fittings using CFD (RP-1493) HVAC&R Res. 2012;18(6): 1168–1181.

[10] Manning A., Wilson J., Hanlon N., Mikjaniec T. Prediction of duct fitting losses using computational fluid dynamics. HVAC&R Res. 2013;19(4): 400-411.

[11] Liu W., Jin M., Chen C., You R., Chen Q.. Implementation of a fast fluid dynamics model in OpenFOAM for simulating indoor airflow. Numer. Heat. Tr. A-App. 2016;69(7): 748-762.

[12] Khan M.A.I., Delbosc N., Noakes C., Summers J. Real-time flow simulation of indoor environments using lattice Boltzmann method. Build. Simul. 2015;8: 405-414.

[13] Wang H., Zhai J. Application of coarse-grid computational fluid dynamics on indoor environment modeling: optimising the trade-off between grid resolution and simulation accuracy, HVAC&R Res. 2012;18(5): 915-933.

[14] Chen Q., Xu W. A zero-equation turbulence model for indoor airflow simulation, Energy Build. 1998;28(2): 137-144.

[15] ANSYS Inc. ANSYS Discovery Live 2020 R1 User's Guide. 2020.

[16] ANSI/ASHRAE Standard 120-2017. Method of Testing to Determine Flow Resistance of HVAC Ducts and Fittings. 2017. Atlanta, GA: ASHRAE

[17] Testo data sheet, Testo 480 Multi-function VAC measuring instrument. https://static-int.testo.com/media/ff/0a/bbcc0227c912/testo-480-Data-sheet.pdf

[18] ASHRAE Handbook – Fundamentals (SI). 2001. Atlanta. GA: ASHRAE. Chapter 14 – Measurements and instruments.

[19] ASHRAE Handbook – Fundamentals (SI). 2005. Atlanta. GA: ASHRAE. Chapter 35 – Duct Design.

[20] Idelchik I.E., Steinberg M.O., Malyavskaya G.R., Martynenko O.G. 1994. Handbook of hydraulic resistance. 3rd ed. CRC Press/Begell House. Boca Raton. Ann Arbor. London. Tokyo.

[21] Shih T.H., Liou W.W., Shabbir A., Zhu J. A new k-ε eddy-viscosity model for high Reynolds number turbulent flows - model development and validation. Comput. Fluids. 1995;24(3): pp. 227-238.

[22] Menter F. Eddy viscosity transport equations and their relation to the k-ε model. J. Fluids Eng. 1997;119: 876-884

[23] van Hooff T., Blocken B. Coupled urban wind flow and indoor natural ventilation modeling on a high-resolution grid: a case study for the Amsterdam ArenA stadium. Environ. Model. Softw. 2010;25: 51-65

[24] ANSYS Inc, ANSYS FLUENT 2021 R1 User's Guide. 2021.

[25] Ye, T., Mittal, R., Udaykumar, H.S. and Shyy, W., An accurate Cartesian grid method for viscous incompressible flows with complex immersed boundaries. J. Comput. Phys.. 1999;156(2): 209-240.

[26] Murakami S. Comparison of various turbulence models applied to a bluff body. J. Wind Eng. Ind. Aerodyn. 1993;46: 21-36

[27] Tominaga Y., Mochida A., Murakami S., Sawaki S. Comparison of various revised k–ε models and LES applied to flow around a high-rise building model with 1:1:2 shape placed within the surface boundary layer. J. Wind Eng. Ind. Aerodyn. 2008;96(4): 389-411

[28] Menter F.R. Improved two-equation k-turbulence models for aerodynamic flows. NASA technical memorandum. 1992(1) 103975.

Self-adaptive dynamic indoor climate control for museums, archives and libraries. Vast energy savings at Hermitage Amsterdam museum

Rick Kramer [a, b], Marco Martens [c], Edgar Neuhaus [d]

[a] Eindhoven University of Technology, Eindhoven, the Netherlands, r.p.kramer@tue.nl.

[b] DYSECO B.V., Rotterdam, the Netherlands, r.p.kramer@dyseco.nl.

[c] DYSECO B.V., Rotterdam, the Netherlands, m.h.j.martens@dyseco.nl.

[d] DYSECO B.V., Rotterdam, the Netherlands, e.neuhaus@dyseco.nl.

Abstract. The indoor climate in museums usually is conditioned strictly to the "golden standard" of 21°C and 50%RH. It is evident that strict climate control hinders sustainability targets, but also hinders a robust long-term preservation practice. Research at Eindhoven University of Technology (2012-2017) has yielded the concept of dynamic indoor climate control for heritage institutions and its energy saving potential has been validated rigorously. In 2019, the spin-off DYSECO further developed this concept to a control-module that can communicate with any type of Building Management System. The algorithm of the controller calculates optimal adjustments to setpoints for temperature and RH adhering to the boundary conditions set by the user, considering limits and permissible rates of change of temperature and RH. The Hermitage Amsterdam museum has played a vital role in the research and development since 2014 and employs the DYSECO control solution in all exhibition spaces since 2020. Energy data is presented based on 5 years of high-quality data acquisition. The positive effects on collection preservation due to mitigated risk under HVAC failures are demonstrated using state-of-the-art dynamic building simulations with dynamic collection damage models.

Keywords. Climate control, museum, energy efficiency, sustainability, dynamic setpoints.
DOI: https://doi.org/10.34641/clima.2022.305

1. Introduction

For the safe-keeping of collections, one of the main parameters is to create a proper temperature and relative humidity. The indoor climate can pose risks to the collections for multiple reasons: i) an incorrect climate may lead to biological degradation, eg. mould growth; ii) an elevated temperature or relative humidity can lead to a faster rate of chemical degradation and iii) fluctuations in both temperature and relative humidity may cause materials to shrink and expand, eventually creating mechanical damage. Because of the advancements in technology, the general notion has been for a long time: if 50±5% RH is good, 50±3% RH must be better.

One of the major triggers of reducing the range in indoor climate conditions was the evacuation of artifacts during WW2. The London museums moved their collections into caves which have a very constant climate. Restorers, who also moved from London to the caves, noticed that the work they had to do diminished over time: no new damage occurred to the artifacts. So, a constant climate was considered beneficial for preservation purposes [1].

In the 19th century, heating for thermal comfort was adopted in many institutions and governmental buildings, including museums. A comfortable environment became available; e.g. many museums started to exploit cloakrooms and increased temperature even further [2]. Figure 1 illustrates the evolution of the indoor climate in cultural heritage institutions in the 20th century.

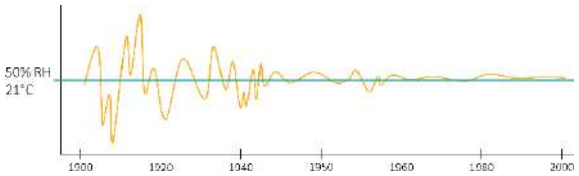

Fig. 1 – Illustration of how the indoor climate became stricter in the 20th century with less fluctuations around the 'golden standard' of 21°C and 50% RH.

Copyright ©2022 by the authors. This conference paper is published under a CC-BY-4.0 license.

A few problems arose from this increasingly stricter paradigm on indoor climate control. Most museums are housed in historic buildings, with a quality of building envelope not suitable for having a constant indoor climate all year round. In climate regions with substantial seasonal variations in outdoor climate, like in western Europe, the indoor air needs a lot of humidification during the heating season to maintain the often desired 50% RH. In historic buildings this often leads to surface condensation, causing mould growth in corners and on window sills, and in case of extensive condensation even wood rot is observed.

Also, climate systems consume a lot of space within the building. Attics and basements are filled with HVAC systems, while ducts and piping run through the entire building. This often negatively affects the integrity of historic buildings.

In the 21st century, sustainability and energy reduction has become increasingly important in the built environment. This conflicts with the existing situation in many museums. Strict climate control leads to excessively high energy demands, while options for historic buildings to reduce energy losses are limited, e.g., insulating the exterior façade is not possible and insulating the interior side often leads to moisture related problems.

One effective way to address the above described issues related to strict indoor climate control is to move from the 'ideal climate' to an appropriate climate' in which limited short-term fluctuations and seasonal variations are allowed [3]. In the last 15 years, many research projects have led to new insights which have resulted in more sophisticated indoor climate requirements, e.g. published by ASHRAE [4]. Kramer et al. [5] have studied and developed energy efficient climate strategies based on the ASHRAE climate classes and integrated thermal comfort requirements. This concept of dynamic climate control determines the optimal course of temperature and relative humidity over time, respecting collection preservation and comfort, at the lowest energy demand possible. However, most building management systems are not suitable to employ dynamic setpoint adjustments. Hence, the spin-off DYSECO has been founded to develop the concept further to an add-on controller that can connect to any Building Management System. Consequently, the advantages of dynamic climate control have become available to the field of cultural heritage. In 2020, the Hermitage Amsterdam museum installed DYSECO controllers at six air handling units for their exhibition spaces. This paper compares the performance of the dynamic climate control mode versus the reference climate control mode, i.e. fixed setpoints of 21˚C and 50% RH. The effects of dynamic climate control, i.e. gradual adjustments of setpoints for ambient air temperature and RH, are evaluated on thermal comfort, collection preservation and energy efficiency.

2. Research method

2.1 Case study Hermitage Amsterdam

The Hermitage Amsterdam Museum played a crucial role in the PhD research of Kramer [6]. The main reasons this museum was chosen were symmetry (left and right wings are identical, in terms of construction and climate systems) and it was state-of-the-art in terms of building physics and HVAC systems, being completely renovated in 2007 – 2009. The historic façade had been insulated, double glazing had been introduced and air tightness had been improved. The all air climate control system was very modern too, with ground cold and heat storage (Aquifer Thermal Energy Storage). The setpoints were 21˚C and 50% RH all year round.

2.2 Measurement setup

The indoor climate and energy demand have been monitored since June 2014 until September 2021. For a comprehensive overview and explanation of the case study museum and the measurement campaign, we refer to a prior publication by Kramer et al. [7]. In summary, for the analysis in this paper, data of the following measurements at the air handling unit have been used: Electricity consumption of the steam humidifier and electricity consumption of the fan, water mass flow rate through the cooling coils and heating coils, water inlet temperature and water outlet temperature of cooling coils and heating coils. All measurements have been logged at a sampling rate of 30 s. From these measurements, the thermal power was calculated for heating, cooling, and dehumidification (sub-cooling).

The reference or 'strict mode' data set, i.e. in which the indoor climate was maintained at 21˚C and 50% RH, has been compiled from the following periods: December 2014 – February 2015 (Winter), March – May 2015 (Spring), June – August 2015 (Summer), September – November 2015 (Autumn). The 'dynamic mode' data set, i.e. in which the indoor climate was controlled via dynamic setpoints, has been compiled from the following periods: December 2020 – February 2021 (Winter), March – May 2021 (Spring), June – August 2021 (Summer), September – November 2021 (Autumn). Although the outdoor climate was not exactly the same, both periods show similar conditions and can therefore be compared. In the dynamic mode, a custom climate class was employed which could be best described as ASHRAE class A1+: Absolute minimum RH = 40%, absolute maximum RH = 60%, permissible short-term RH-fluctuations = ±5% (implemented as a maximum range between upper and lower limit), and the range was allowed to move between the absolute maximum and minimum RH at a rate of 5% per month. Moreover, absolute minimum T = 18˚C, absolute maximum T = 24˚C, permissible short-term T-fluctuations = ±2˚C (implemented as a maximum range between upper

and lower limit), and the range was allowed to move between the absolute maximum and minimum temperature at a rate of 2°C per week.

The thermal energy demands as calculated from the measurements have been divided by generation and distribution process efficiencies to estimate the consumed electricity: the heat pump's COP of 4 for heating, EER of 3 for deep cooling, and an equivalent COP of 25 for high temperature cooling, directly from the Aquifer Thermal Energy Storage. Furthermore, the energy demand is presented as average electricity consumption per week in Winter, Spring, Summer and Autumn.

2.3 Comfort and collection preservation

In a previous study [8], questionnaires were used to ask visitors how they perceived the indoor climate to develop thermal comfort limits for the museum environment. During the course of the project, over 1,250 questionnaires were filled in. The indoor conditions in both strict mode and dynamic mode were evaluated using these adaptive temperature limits.

To assess the effect of the indoor climate conditions on the preservation of objects, the specific climate risk method was used as developed by Martens [9]. The measured indoor climate was assessed with damage functions to find out whether the preservational qualities of the indoor climate were appropriate.

3. Results

3.1 Energy demands

The energy put into the building by the HVAC systems is shown in figure 2; the total values are displayed in table 1. The reference case (REF) uses on average in between 5.270 and 6.200 kWh each week, while the dynamically controlled case (DYSECO) uses in between 1.880 and 4.950 kWh each week. The savings are smallest in Summer (650 kWh weekly, a reduction of 12%) and highest in spring (4.250 weekly, a reduction of 69%). On average, over the whole year the energy demand is reduced with 51%.

When looking at the seasons individually, in Winter a lot of heating energy is saved by lowering temperature, but also humidification was reduced.

Tab. 1 – Total energy demand (kWh/week) per season

	Winter	Spring	Summer	Autumn
REF	6.200	6.180	5.600	5.270
DYSECO	2.550	1.930	4.950	1.880
Reduction	3.650	4.250	650	3.390
Reduction	59%	69%	12%	64%

Because of the lower temperature, the museum is less likely to overheat when many people enter the museum simultaneously, so also on cooling energy a bit is saved. In Spring, heating is hardly needed and also cooling is not needed very often, letting temperature free float for a reasonable amount of time. A bit more humidification is needed, but dehumidification is hardly needed. Both can be explained by an indoor temperature that matches better to the outdoor conditions.

In Summer, because of the higher indoor temperatures in the DYSECO case, more cooling is needed to prevent overheating when visitors are present. Nonetheless, much less dehumidification compensates for this. In Autumn, also a lot is saved on dehumidification and also on heating and cooling.

Tab. 2 – Total electricity use (kWh/week) per season

	Winter	Spring	Summer	Autumn
REF	3.350	1.880	2.220	2.500
DYSECO	1.980	1.480	1.700	1.210
Saving	1.370	400	520	1.290
Saving	41%	21%	23%	52%

Whereas Figure 2 shows the air sided energy demand, Figure 3 shows the related electricity consumption from the air handling processes. Also, table 2 shows the summation of electricity needed. Now, the systems efficiency for each separate step is incorporated, thus leading to purely electrical energy needed.

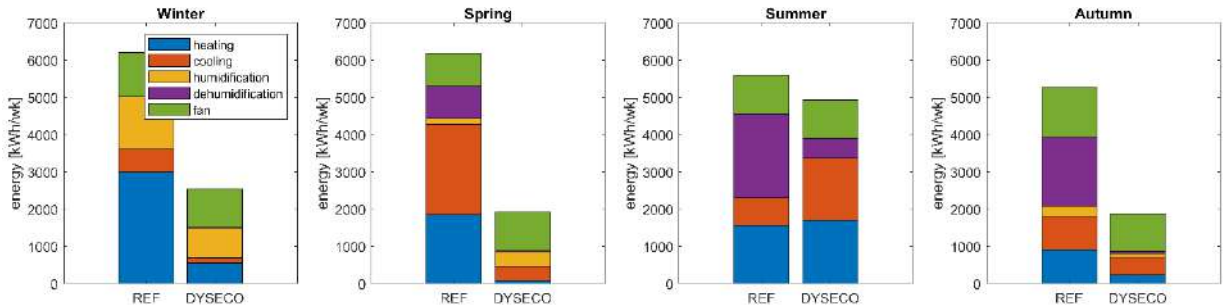

Fig. 2 – Energy demand for each season, for the reference (REF) and dynamically controlled case (DYSECO). Heating is displayed in blue, cooling in red, humidification in orange, dehumidification in purple and fan energy in green. It is expressed in kWh per week; the energy demand is the energy distributed to the air by the HVAC system

When comparing figure 2 and 3, it can be noticed that heating and cooling seem to consume less energy in figure 3 than in figure 2. This is because of the highly efficient ground cold and heat storage. In order to cool or heat, only a small electric pump needs to run to extract the desired amount of cold or warm water from this storage. So, this saves energy compared to an air-to-water heat pump. Humidification and dehumidification are less efficient, because either low water temperatures are needed (lower than the cold storage can supply) or water needs to be evaporated electrically. Also, the fan's electric energy, makes up a greater part than before.

In total an energy reduction of 36% was realised over an entire year. In autumn and winter, savings are highest (52% and 41%), in spring and summer lowest (21 and 23% respectively). Because of the efficiency of the systems, even a seasonal change in the savings can be noticed. Mind that the savings presented in figure 3 are the savings that also reflect the costs savings for the museum.

To further optimize efficiencies, it is advisable to look at methods to more efficiently run the fans and humidification systems in order to improve the sustainability even further.

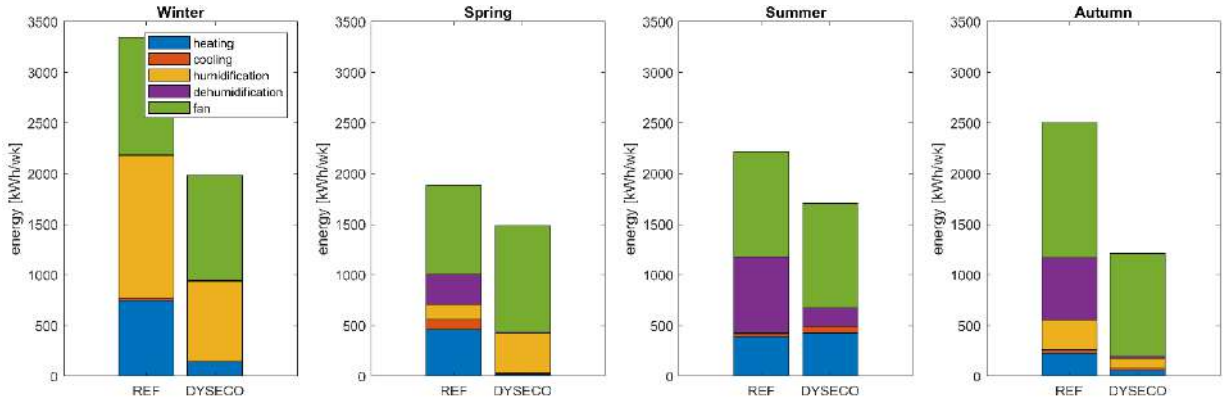

Fig. 3 – Energy consumed by the HVAC systems for each season, in which efficiencies are included. The graph shows electrical energy used. Important to note: because of the ground cold and heat exchanger heating and cooling only require electrical pumps to run during much of the period, leading to a high efficiency. This makes the fan stand out negatively, while in most museums this is only a minor energy user

3.2 Indoor climate comfort

Figure 4 and 5 illustrate the thermal comfort evaluation. Horizontally the outdoor running average temperature over three days is presented; this is the period needed for people to adapt to the weather and e.g. match their clothing. Vertically the indoor temperature is indicated. The areas in blue represent a slightly cool (light blue), a cool (middle blue) and cold (dark blue) sensation. Similarly, an orange colour indicates a slightly warm (light orange), warm (middle orange) and hot (dark orange) experience. The white area is perceived as comfortable by 95 % of all people [8].

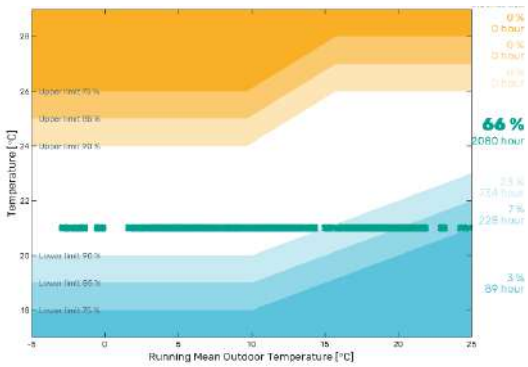

Fig. 4 – Comfort assessment for strict mode data

The questionnaires show that especially during summer the indoor climate was perceived as cool or even cold in the strict control case; 21 °C is experienced as being too low [8]. Figure 4 also indicates this: the green measurement data goes into the blue zone at higher outdoor temperatures.

It makes sense to adjust the setpoint for temperature to follow the outdoor conditions, as was automatically done during the dynamically controlled case. Now temperatures are much more into the neutral (white) zone, as can be seen in figure 5, 73 % of the period temperature was perceived as being neutral or slightly cool, as compared to 66 % during strict control.

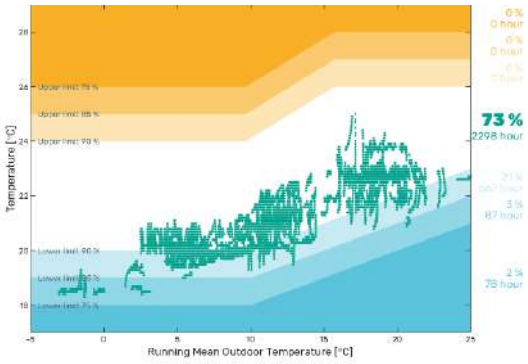

Fig. 5 – Comfort assessment for dynamic mode

More importantly, slightly cold and too cold periods were halved (from 10 % to 5 %).

3.3 Risks for heritage collections

In many museums the ASHRAE climate guidelines are being used [4]. These guidelines, developed by the American Society of Heating, Refrigeration and Air conditioning Engineers provide several climate classes, from strict to basic, each class is associated with some risks for collections. The top classes, AA and A, pose very little risk to almost all museum objects, except for very sensitive ones. AA is considered to be optimal and is meant for long term storage, while in reality many museums strive for AA in their exhibitions while class A would also suffice.

Degradation risks for common museum collections can be calculated from temperature and relative humidity data using specific degradation risk tools [9]. Figure 6 and 7 show the risks calculated for the reference case and dynamic case, respectively. At the top, mould, LM (Lifetime Multiplier), base material and pictorial layer are mentioned as indicators for biological, chemical and mechanical degradation. For three types of objects the risk is presented. The object can be safe (green), have a small risk for degradation (orange) or a high risk (red). In figure 6 only a small risk is noted for the Lifetime Multiplier, which indicates a somewhat higher speed of chemical deterioration.

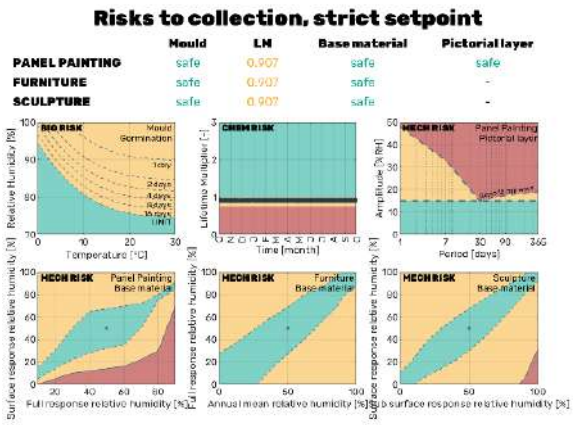

Fig. 6 – Biological, chemical and mechanical risks calculated from measured data for the strict indoor climate in Hermitage Amsterdam.

The difference between figures 6 and 7 is small: the general notion of risks is similar. The dynamic case has a slightly smaller chemical deterioration rate (0.907 versus 0.986, an 8 % longer chemical lifetime for the dynamic case).

The smaller graphs in figures 6 and 7 each represent the behaviour of one of the objects. Figure 8 provides an enlargement for mechanical damage assessment of panel paintings [10].

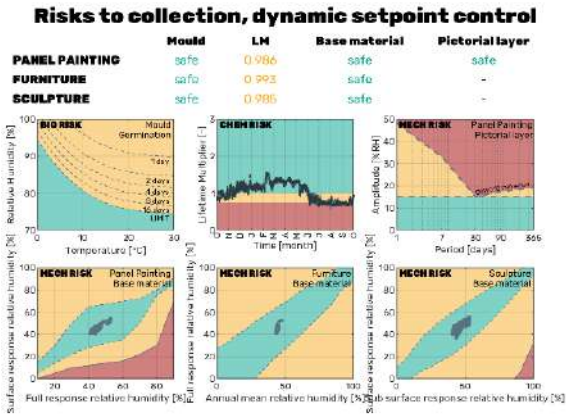

Fig. 7 – Biological, chemical and mechanical risks calculated from measured data for the dynamically controlled indoor climate in Hermitage Amsterdam.

Vertically the RH experienced by the object's surface is indicated, while horizontally the object's core RH is displayed. The surface has a response time of 4 days, while the core has a response time of 26 days to changes in relative humidity. Because of the difference in response time, a gradient within the material occurs over time; this gradient causes tension in and possibly damage to the object. The green area is the safe area, while the red area presents a sudden rupture of the object. The orange area already presents a dangerous situation, causing micro cracks and permanent deformation.

Figure 8 displays the hypothetical situation in which the humidifier malfunctions during a winter week: the relative humidity in the museum drops to a value of about 25% RH, instead of 50% RH in the strict control case (left). It can be seen in the left figure that the surface RH drops, while the full response of the entire object hardly notices this drop at first. This causes the data to go into the orange area of the graph. There is a moderate risk on mechanical damage present during that time. When the humidifier is repaired, a similar jump occurs when the indoor climate goes back to 50% RH: the surface rises fast in RH, while the bulk of the material responds much slower.

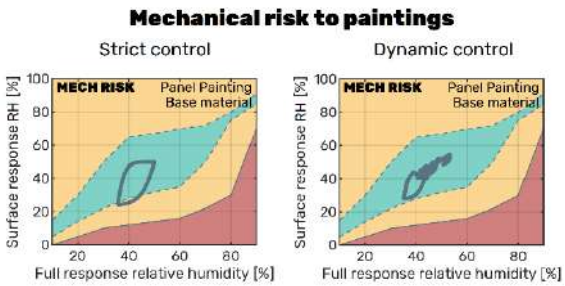

Fig. 8 – Mechanical risk for panel paintings; measured data (grey) fully in green area (right), but also in the orange area during strict control (left)

The right graph of figure 8 shows the exact same situation, but now for the case in which dynamic control is introduced. The data in this graph is not merely a dot at 50% RH, but a 'cloud' of data in

between 40% and 55% RH. Because the starting point was not 50% RH, but around 42% RH when the humidifier failed, the drop is much less severe. Moreover, because of a lower indoor temperature, the RH does not drop to 25% RH, but to a mere 30% RH. This results into a significant risk reduction for the panel painting.

4. Discussion & conclusions

Dynamic setpoints are beneficial in multiple ways. A lot of energy can be saved, both in terms of demand delivered by the system and energy consumed by the system. The latter is mainly the focus point of museums, as institutions are interested in cutting operational costs as well as being more sustainable. Moreover, less risk for collections is encountered in case of a system failure, because of the smaller difference between indoor and outdoor conditions. Moreover, visitors perceive much more comfort because their adaptation to the outdoor climate is accounted for.

Existing systems can benefit from adding the DYSECO controller to the building management system. The demand is reduced and less strain is put on the existing systems. Newly designed systems can benefit even further, because they can be designed with a smaller capacity for most of the components, leading to an increase in efficiency during operation.

It is important to note that no changes were made to the systems at all during the measurements, not in terms of software nor in hardware. Only the existing setpoints were taken over and replaced by dynamic setpoints. It is by no means the goal to take over the control or design of HVAC systems, but simply to make the HVAC systems function more according to the needs for collections and thermal comfort, at the lowest energy demand possible.

5. Acknowledgements

The Hermitage Amsterdam museum played a very important role in this project by handing over the controls of their climate systems to researchers. The authors are grateful for their trust and cooperation.

6. References

[1] Brown JP, Rose WB. Humidity and moisture in historic buildings: the origins of building and object conservation. APT Bull. 1996;27:12–24.

[2] Legnér M. On the Early History of Museum Environment Control. Stud. Conserv. [Internet]. 2011;56:125–137.

[3] Michalski S. The Ideal Climate , Risk Management, the ASHRAE Chapter, Proofed Fluctuations, and Toward a Full Risk Analysis Model. Contrib. to Expert. Roundtable Sustain. Clim. Manag. Strateg. Tenerife, Spain: Getty Conservation Institute; 2007. p. 1–19.

[4] ASHRAE. Museums, Galleries, Archives, and Libraries. In: Owen M, editor. Handb. HVAC Appl. SI edition. Atlanta: ASHRAE; 2019. p. 23.1-23.22.

[5] Kramer R, van Schijndel J, Schellen H. Dynamic setpoint control for museum indoor climate conditioning integrating collection and comfort requirements: Development and energy impact for Europe. Build. Environ. [Internet]. 2017;118:14–31. http://dx.doi.org/10.1016/j.buildenv.2017.03.028.

[6] Kramer RP. Clever Climate Control for Culture: Energy efficient indoor climate strategies for museums respecting collection preservation and thermal comfort of visitors. Eindhoven University of Technology; 2017.

[7] Kramer RP, Schellen HL, Schijndel AWM Van. Impact of ASHRAE ' s museum climate classes on energy consumption and indoor climate fluctuations : Full-scale measurements in museum Hermitage Amsterdam. Energy Build. [Internet]. 2016;130:286–294. http://dx.doi.org/10.1016/j.enbuild.2016.08.016.

[8] Kramer R, Schellen L, Schellen H. Adaptive temperature limits for air-conditioned museums in temperate climates. Build. Res. Inf. 2018;46:686–697.

[9] Martens MHJ. Climate Risk Assessment In Museums: degradation risks determined from temperature and relative humidity data. Eindhoven University of Technology; 2012.

[10] Erhardt D, Mecklenburg M. Relative humidity re-examined. Prev. Conserv. Pract. London: The international institute for conservation of historic and artistic works; 1994.

The datasets generated during and/or analysed during the current study are not publicly available because of privacy reasons for the museum involved but are/will be available after contacting the author and with written permission of the museum.

Grid-impact factors of field-tested residential Proton Exchange Membrane Fuel Cell systems

Nicolas Paulus [a], *Vincent Lemort* [b]

[a] Thermodynamics Laboratory, University of Liège, Liège, Belgium, nicolas.paulus@uliege.be.

[b] Thermodynamics Laboratory, University of Liège, Liège, Belgium, vincent.lemort@uliege.be.

Abstract. Much needed energy transition currently brings focus on micro-combined heat and power (mCHP) systems for residential uses, especially on low-capacity fuel cells (about 1 kW_{el}) because it has been reported that they allow for increased CO_2 savings per kW_{el} compared to engine-based mCHP's [1]. One of those (already commercialized), is a Proton Exchange Membrane Fuel Cell (PEMFC) system hybridized with a conventional gas condensing boiler. It is fed by natural gas; it is designed to cover all the heat demands of residential houses as well as to participate locally in the electrical production. Thanks to high integration levels, it combines a PEMFC of nominal constant power of 0.75kW_{el} and 1.1kW_{th}, a 220L DHW (Domestic Hot Water) tank and a condensing gas boiler, mainly used for peak heat demands, that designed to provide up to 30.8kW_{th}.

The financial incentive representing a major factor in the investor's decision towards such a technological change, focus will indeed be brought on supply and demand cover factors since they are directly linked to how much the citizens are individually billed and since they constitute actual and future unavoidable keys in the energy transition, as more and more intermittent renewable energies will be integrated to the energetic mix.

This study is monitoring two of those installations in residential houses in Belgium, arbitrary chosen, for the whole year 2020. Sampling time of the monitoring hardware is between 2 and 5 minutes but it has been chosen to analyse the grid impacts factors according to average daily values (along with their seasonal trend and yearly figures).

This paper has established yearly supply cover factors between 34 and 36%, which are believed to be higher (based upon literature) that what typical photovoltaics (PV) power plants would have allowed. It unfortunately remains lower than the 37.46% "prosumer" limit considered in the tariffication of Wallonia PV installations [2]. On the other hand, this paper has established yearly demand cover factors of 25 and 33%.

Keywords. Grid-impact factors, PEMFC, CHP, cogeneration, Fuel Cell, supply cover factor, demand cover factor.
DOI: https://doi.org/10.34641/clima.2022.176

1. Introduction

Nowadays, the higher share of intermittent renewables in the electricity mix, especially with PV installations, the more the electrical network is stressed. Around noon, the electrical demand on the centralized power plants drops and the electrical peak consumption of the evening (when most people are coming home from work, are cooking, heating, and globally consuming electrical energy) is not significantly diminished by the PV energy [3]. This means a very steep electrical demand slope is imposed to the electrical network and this effect is commonly represented by a "Duck curve", as shown in **Fig. 1** [4].

It is worsened by the electrification planned for the energy transition (space heat systems, mobility, etc.) that is currently increasing the daily peak demands on the grid. For information, in the future, it would be preferable for the electrical space heating with heat pump to be modulated down while maximum load is requested on the grid, i.e. in the evening, but it is mostly not currently the case.

This "Duck curve" raises tremendous challenges on the infrastructure. The first one is quite trivial as this highly transient electrical demand requires flexibility (of the centralized production) and this is both expensive and difficult to manage. The second one comes from the fact that the electrical network

Copyright ©2022 by the authors. This conference paper is published under a CC-BY-4.0 license.

infrastructures (cables, converters, transformers, centralized power plants) are sized based upon peak power demand. Therefore, if electrification of the society is increasing peak demands and if it is not mitigated by renewables (or by energy consumption mitigation measures such as degrowth, building insulation, teleworking, which are not in this paper's scope), it is likely that the electrical network will have to be refurbished (and that cost must not be forgotten in the energy transition).

Currently, total transmission distribution, and administration costs represent already a significant part of the household electrical bill. For example, those costs have typically been between 0.025 – 0.035 $/kWh since 1980 in the US [5], which represented in 2009 about 20 to 30% of the final customer electrical price [5]). In Wallonia (in South of Belgium), it is even more as they can be established to be equal to about 0.15 €/kWh [2] and that represented in 2020 about 60 % of the end price to the customer (based on the Belgian regulator prices [6]). The main difference is that, in Belgium, the 0.15 €/kWh stated here for transport and distribution include (significant) federal taxes that are imputed by the network company and not directly by the state. In 2020, without considering the taxes, the share of the distribution and transport cost in Belgium in the average household electrical bill drops to 33% (close to the US figure) whereas the electricity generation represented only 23 % of the final customer electrical bill [7].

Thus, in the energy transition that is coming, the shares of the distribution and transport prices (electrical network infrastructure) are likely to account for an even bigger share of the end customer price (at least in a stable geopolitical context).

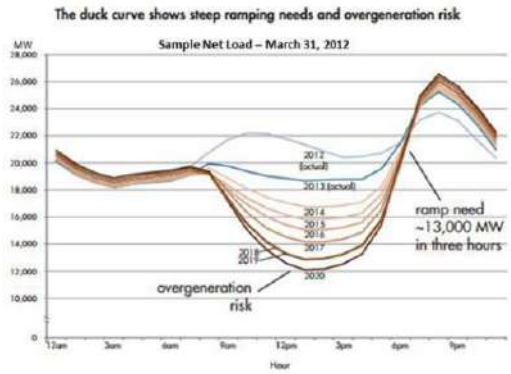

Fig. 1 - "Duck curve" is worsen with higher renewable share (in California) [4]. Figure reproduced from reference with permission.

Therefore, to limit the "stresses" on the electrical network that both the electrification and the renewables are causing, focus is brought on grid impact factors. This is also the case for residential electrical production systems, especially again with high PV penetration, even in developed countries such as Japan where capital investments for distribution lines reinforcement have already been requested [8]. This is why the concept of "prosumer" has been recently established (as agents that both consume and produce energy [9]), which requires some specific regulation framework in electrical markets [10]. In Belgium, these current prosumer regulations are called "the prosumer tariffication" and are designed to bill the energy rejected on the grid [2]. It is therefore critical to mention that economical performance of residential PEMFC systems depend directly on the supply cover factor (and not only on the demand cover factor). This is mainly because the grid energy consumption avoided is far more expensive than the one rejected ("sold") and bought back later on.

2. Research method

Maximizing building load matching factors (demand and supply cover factors, as defined in equation (1) and equation (2) [11]) is thus crucial in order to reduce the impact on the electrical grid. In the energy transition context, this will prevent some additional investments to ensure grid peak power demand or to prevent overvoltage (too much decentralized electrical production at the same time not consumed locally and rejected on the distribution lines).

Supply cover factor γ_s is most critical in a grid configuration as it is the one which maximization would prevent overvoltage (by limiting the power rejected on the grid). Demand cover factor γ_d is also important for obvious economic reasons (while investing in a local electrical production, you would want it to match your power demand as much as possible) and its maximization is critical for off-grid applications. But it is also important for grid configuration as it will mitigate the increasing power demand due to the increasing electrification (less demand from the building on the grid). Actually, both shall be maximized but it is likely that a compromise has to be found between the two factors. It is worth mentioning that whereas those factors should always be considered, there are not the only key design drivers while sizing a local electrical production system. ROI, capital costs, dimensions, load factor, life expectancy, LCA environmental impacts, *etc…* shall be considered as well.

Of course, maximizing cover factors will also have an environmental beneficial aspect as refurbishing the distribution lines might be avoided but also because electrical consumption of the electricity produced locally prevents technical network losses (which can reach about 6-7% in EU [12]).

1.1 Grid-impact factors definition

Both factors are defined as follows [11]:

$$\gamma_s = \frac{\int \min\{P_D, P_S\} dt}{\int P_S dt} = \frac{\text{Onsite consumption (of production)}}{\text{Total onsite production}} \quad (1)$$

$$\gamma_d = \frac{\int \min\{P_D, P_S\} dt}{\int P_D dt} = \frac{\text{Onsite consumption (of production)}}{\text{Total demand of the building}} \quad (2)$$

Where P_S is the local power supply and P_D the local power demand. Both numerators are identical for the two factors, the term $\min\{P_D, P_S\}$ represents the part of the power demand instantaneously covered by the local electrical power supply or the part of the power supply matched by the power demand.

Both cover factors, by definition of equation (1) and equation (2), are defined over a certain period of time. One can consider instantaneous factors (which would be difficult to obtain in this study as it will be stated in ***Section 1.4 Measurement devices*** that sample time of the monitoring hardware is between 2 and 5 minutes) but one can also consider them daily, weekly, monthly, yearly, *etc*. In this case, they have been established daily, and yearly. Also, for both houses, the daily figures have been regressed in order to evaluate seasonal trends.

1.2 The system

The machine is the same in both studied houses and its internal schematics is presented in **Fig. 3**. Its main performance targets, declared by the OEM (Original Equipment Manufacturer) and expressed in Low Heating Value (LHV) are shown in **Tab. 1** and **Fig. 2**.

Tab. 1 - PEMFC gas boiler hybrid expected targets.

Datasheet figures	Values
Maximum electrical production a day	17 kWh_{el}
Fuel cell rated electrical & thermal power	0.75 kW_{el} & 1.1 kW_{th}
Electrical LHV efficiency of the PEMFC	37 %
Max global Fuel cell LHV efficiency	92 %
Max boiler efficiency (at rated power)[a]	108.6 %

[a] Considering HHV to LHV ratio of 1.1085 [13]

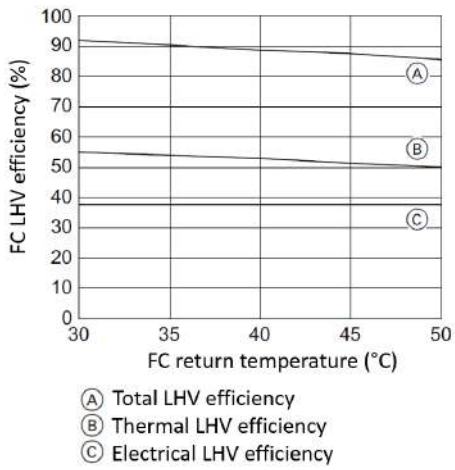

Fig. 2 - OEM's declared LHV efficiency for the PEMFC system only.

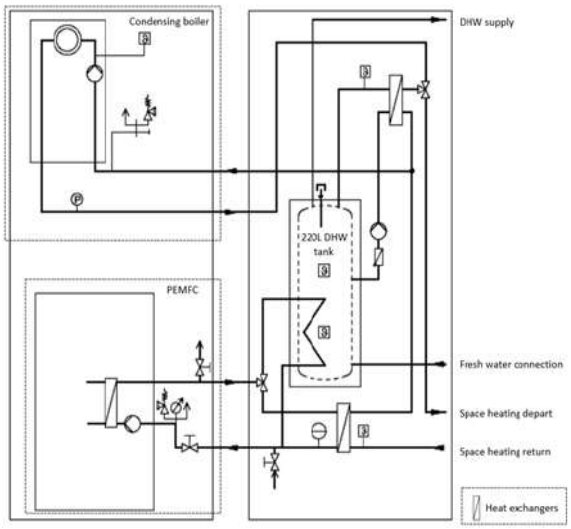

Fig. 3 - System's architecture: high level of integration (through two heat exchangers, several 3-way valves and several pumps) of the PEMFC with the gas condensing boiler and the DHW tank.

As mentioned, the system is fed by natural gas (high methane proportion). It involves an upstream "external" reformer before the PEMFC as temperature within the stack is not sufficiently high for direct "internal" reforming at the electrode [14], only possible with other kinds of technologies, such as solid oxide fuel cells [15]. The hydrogen production is instantaneous so the system is not subjected to the highly constraining safety issues regarding hydrogen storage such as the ICPE (Installation Classée pour la Protection de l'Environnement) authorization in France or similar other legal barriers on EU markets [16].

1.3 The houses

The first house is located in Huy (South-East Belgium) whereas the other one is located in Oostmalle (North of Belgium). From a climatic point of view, one can state that the two houses are located in the same climatic region. The location of the monitoring sites has been presented in **Fig. 4**.

Fig. 4 - Location of the monitoring sites.

The first monitored building (Huy) is a semi-detached house of the early 20th century but significant insulation work of walls and roofs has been conducted. Single-glazing windows have been replaced by double-glazing windows and a balanced ventilation has been installed. However, terminal units still consist of high temperature cast-iron radiators. The family that lives there consists of 2 active adults and 3 children under the age of 10.

The second monitored building (Oostmalle) is a fully detached house from the 70s but tremendous renovation just took place before the study. Insulation has been increased of course, but the whole space heating architecture has also been revisited with the implementation of floor heating for the ground floor. On the first floor, terminal units consist of high temperature radiators such as in the former house. The family consists of a young active couple with one child of a small age.

1.4 Measurement devices

Both houses are equally monitored. Sensors are identical and are placed at the same spots, according to the scheme of **Fig. 5**. Sensor reference, precision and resolution of the acquired data are presented in **Tab. 2**.

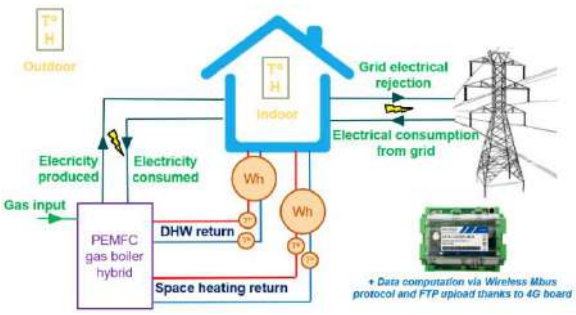

Fig. 5 - Monitored sensors configuration

Last very important parameter not shown in **Tab. 2** is the sampling rate, the frequency of the acquisition, of the measurements. It has been set to a 2-minute time step for the house in Huy and a 5-minute one in Oostmalle. With this data logger, it is impossible to set a time step smaller than 2 minutes due to the fact that it must establish a successful Wireless M-bus (Meter-bus) connection with every sensor, one after the other, and that takes time (a few seconds for each connection). The reason not to have the same sampling rate for all houses is that the faster the rate is, the quicker the battery inside the sensors will be empty. Therefore, reducing the time step to 2 minutes required extra power supply, which was not possible to provide for the second house. Furthermore, for such thermal monitoring applications, a time step of 5 minutes is sufficient for the analyses that have been conducted.

Except for temperatures and humidity, all of those meters are computing energy index values (always increasing).

Tab. 2 - Reference of the monitoring sensors

Sensors	Reference	Resolution	Accuracy
Indoor & Outdoor temperature and humidity	Weptech Munia	0,1 K 0,1 %	± 0,3 K ± 2 %
DHW and space heating heat counters	Qalcosonic E1 Qn2,5 qi=0.025 m^3/h L=130mm	1 kWh 1 L | 0,1 K	Accuracy Class 2 [17]
Machine 2-ways electrical energy counter	Iskraemeco MT174-D2A42-V12G22-M3K0	10 Wh	Accuracy Class 1 [18]
House 2-ways electrical energy counter	Iskraemeco MT174-D2A42-V12G22-M3K0	10 Wh	Accuracy Class 1 [18]
Gas volume counter	BK-G4T DN25 Qmax 6 m^3/h	10 L	<0.5%
Data logger (cloud connection)	Viltrus MX-9	NA	NA

The heat meters are basing their energy index on the integration of their flow rate measurement, combined to (in-pipes) temperature probes on both depart and return lines of the machine (separate measures thanks to PT-500 probes). They are simply following the first thermodynamics principle based on pre-programmed enthalpy laws (internal correlation with temperature is implemented). Sensor pre-programming thus depends on the heat transfer fluid (which is water in both houses). It also depends on the flow meter position (supply or return circuit) as this will impact the flow meter operating temperature, along with the properties of the fluid being measured. Heat meters are preferably placed on the pipe returning to the machine, as the temperature is lower and more stable. The life of the components is thus extended [19] and both sites considered in this study indeed follow this best practice.

Both electrical energy meters are measuring flows both ways: they are able to provide 2 indexes of energy, one for each flow. However, at one particular moment, the net flow is seen and only one of the two indexes can be increasing, following the current direction at that moment. Actually, the machine cannot at the same time consume and produce electrical energy. Since the current always uses the shortest path, in electrical production mode, the machine provides the electricity for its own auxiliaries so no consumption on the meter can be measured. Thus, only the lowered net electrical production is measured, because the power requested by the auxiliaries is taken directly from the gross production of the PEMFC. Same goes for the "grid electrical meter" that measures the net flows

exchanged between the house and the grid. To compute the total electrical demand of the house $\int P_D dt$, one must use equation (3):

$$\int P_D dt = \int P_S dt - W_{el,house,out} + W_{el,house,in} \quad (3)$$

Where $\int P_S dt$ is the monitored electrical energy produced by the machine, $W_{el,house,out}$ is the monitored electrical energy rejected by the house on the grid and $W_{el,house,in}$ is the monitored electrical energy consumed by the house from the grid. Those electrical flows correspond to what is indicated in **Fig. 5**. As explained, there will always be one or several of these flows that will be constant.

3. Results

As shown in **Fig. 6** and **Fig. 8**, the system of Huy has a yearly supply cover factor of 33.84 % whereas it increases to 36.27% in Oostmalle (for the focus year of 2020). For the yearly demand cover factor, it drops to 24.52 % in Huy and 33.48 % in Oostmalle (for the focus year of 2020).

Demand cover factor is lower for Huy mainly because of smaller PEMFC production. It has indeed been observed (and confirmed by the owner) that the heat demand is not smooth enough for the PEMFC to be able to keep dissipating its heat over a long period of time, so the internal regulation of the fuel cell shuts it down. Indeed, the occupants in Huy are manually opening and closing their radiator valves fort a short period of time in the morning and in the evening. On the other hand, smoother heat demand is obtained in Oostmalle simply thanks to floor heating.

Monthly heat and power production are presented for both machines on **Fig. 7**. It can be seen that the heat demand in Oostmalle is higher even though it is believed to have better insulation, and non negligible summer heat demand tends to indicate higher temperature setpoint (for comfort reasons).

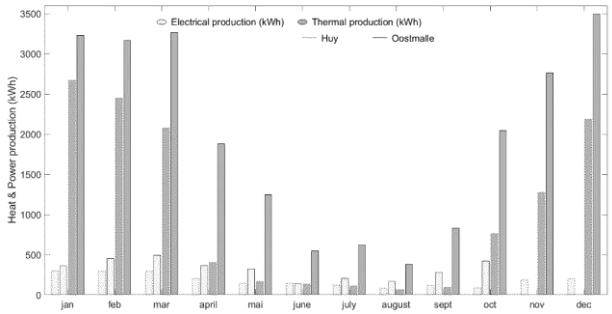

Fig. 7 - Monthly heat and power production for both machines on the year 2020.

The supply cover factor trend increases in the summer mainly because less electrical production occurs (see **Fig. 7**) and this intrinsically leads to less rejection on the grid. On the other hand, lower electrical production in the summer also comes with a lower demand cover factor. The trend curves in Oostmalle are greatly affected by the fact that the PEMFC was shut down (for unknown reasons) at the end of the focus year (also seen in **Fig. 7**). However, one can see that the seasonal trends (summer against winter) are similar for both houses.

In early 2020, Oostmalle demand cover factor reaches almost 70%, which is quite a good performance (compared to yearly performance of PV installations which will be discussed in the following section). Unfortunately, this supply cover factor value could not be maintained the whole year.

Both cover factor trends are nevertheless quite constant over the whole year, which is absolutely not the case with PV installations.

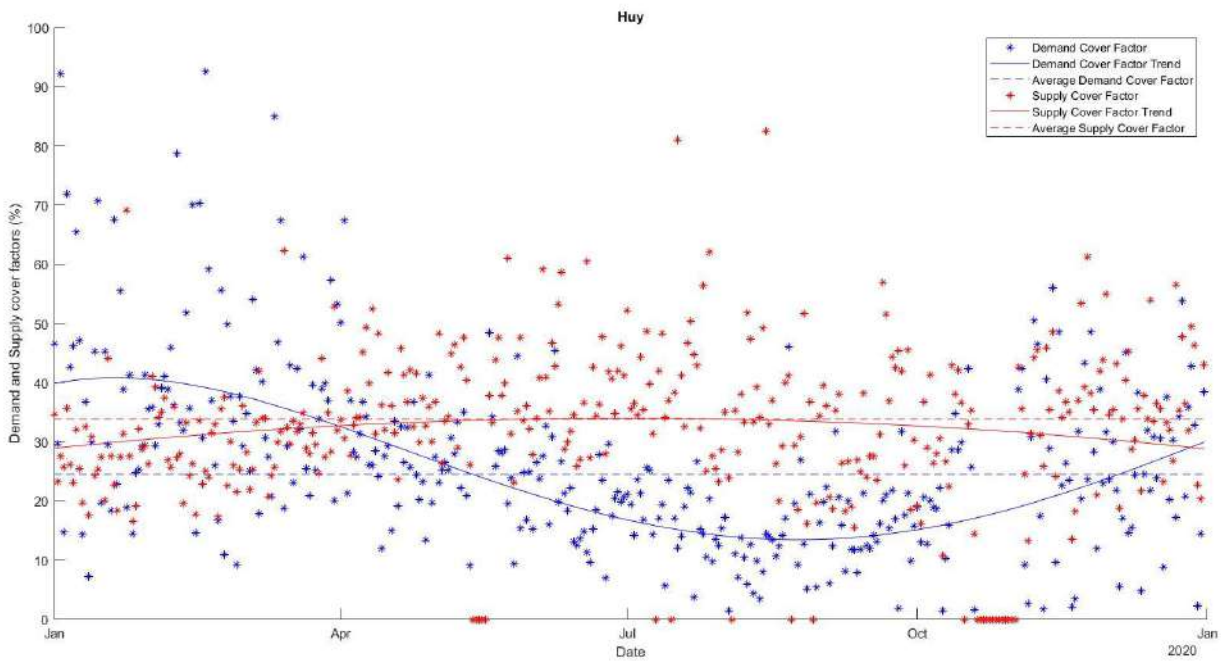

Fig. 6 - Supply and demand cover factors for the year 2020 in Huy.

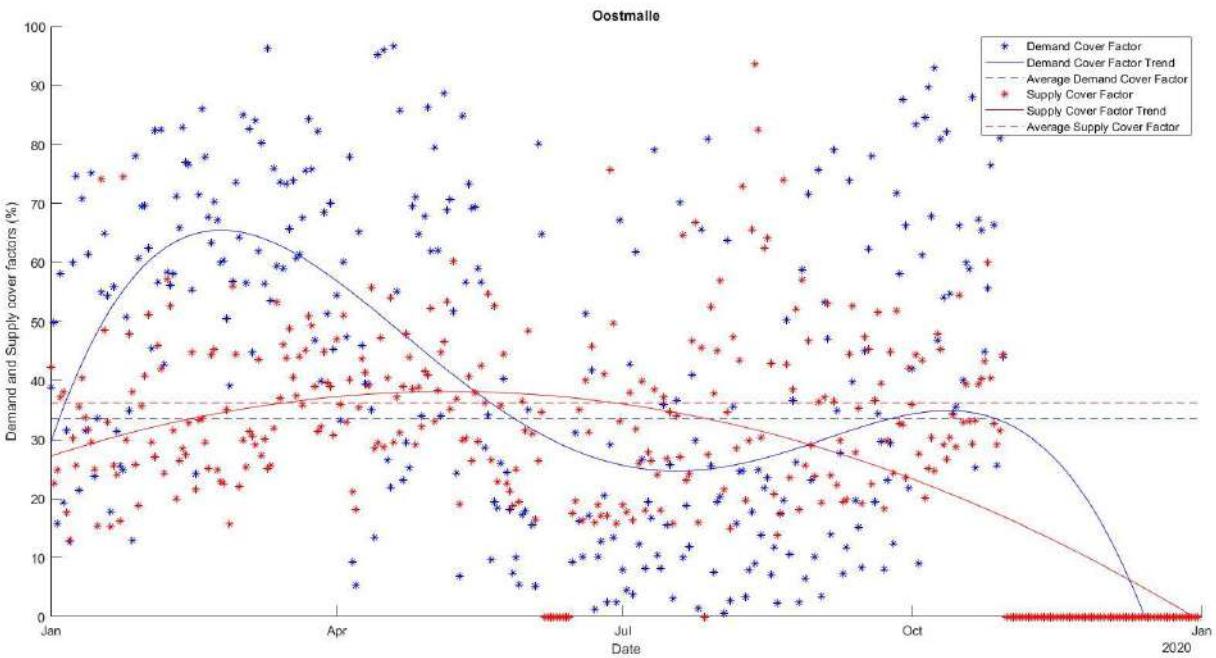

Fig. 8 - Supply and demand cover factors for the year 2020 in Oostmalle.

4. Discussion

It is interesting to point out that this system does not allow the seasonal supply cover factor trend to go higher than 40% (even in the summer) whereas, in its "prosumer tariffication" for PV panels, the Wallonia regulator has assumed a referenced yearly supply cover factor of 37.76% [2]. As established, the yearly values are even below this limit (but close to it). Even if the "prosumer tariffication" assumption for the supply cover factor is not realistic (in order to keep encouraging people to invest in PV installations), it means that this PEMFC system will not be that favorized in Wallonia in terms of electrical rejection compared to PV installations. However, it is worth mentioning that prosumer households with "smart" energy meters (which are mandatory for new electrical installations) are not subjected to this "prosumer tariffication" with the 37.46% assumption of supply cover factor, but they are billed based upon the exact electrical energy rejected on the grid. A "smart" energy meter is an electrical meter that measures both the building consumption and rejection on the grid and that is communicating its energy indexes in real-time to the electrical distribution administrator thanks to wireless communications.

Therefore, the 34 to 36% of supply cover factor obtained with the two houses can still be compared with realistic supply cover factor of PV installations. Of course, PV installations (and household electrical demands) always differ and the resulting supply cover factor can also greatly vary. However, literature can be helpful to obtain examples for those figures. Usually, one must consider the latitude (less PV production at the poles) and also the main electrical appliances of the house (typically, if the house is heated with a heat pump). In Belgium, for residential net zero-energy buildings (ZEBs, which represent a current standard as recommended by EU regulations [20]), supply cover factors have been simulated to reach 26±4% for different building types [11]. All systems have been assumed to be oriented South with an inclination of 34° resulting in the highest annual electricity production [21] and the building's PV plant has been sized to match the yearly electrical demand. The paper mentions heating with heat pumps, which does not account for much energy demand as insulation levels in those kinds of buildings are tremendous. It does not mention any electric vehicle. A similar study conducted on Northern Latitude (Denmark and Sweden ZEBs, also with heat pumps), provides similar supply cover factors of 22 to 24% with simulation and monitoring data [22].

Another study conducted statistical simulations of several building profiles (not only ZEBs) with PV installations (sized based upon total yearly demand) and it stated that, for average European households, the supply cover in the absence of battery varies between 30% and 37% (the value tends to be slightly higher in southern countries) [23]. This study however states that the standard deviation of supply cover factors in the same country with different household profiles is much greater than the difference of the average between countries. For example, for France, it varies from about 18% to about 47% [23].

Therefore, it can be stated that the supply cover factor really depends on the building, on its location, on its occupants. Establishing precisely the supply cover factors that the two monitored houses of this work would have obtained with a PV installation

sized on their yearly demand (or sized on the same yearly electrical production that their PEMFC system has allowed, or sized on a PV installation of similar investment costs) could therefore be performed in further work by simulation with the field-test data. However, based on the existing studies stated here above, it can be assumed that the supply cover factors for those buildings with PV installations would be lower than the ones obtained here with the PEMFC system and probably would be between 20% to 30%. It is worth mentioning that the occupants of the house in Huy have stated that they have been taking some measures in order to increase their supply cover factor (they "are waiting to hear the PEMFC running to launch some appliances such as dishwashers and washing machines"). Therefore, it is likely that they would have done the same with a PV installation so their monitored electrical demand profile shall not be considered directly as is in a PV system supply cover factor simulation.

Unfortunately, the cover factors obtained this paper for these PEMFC are trivially quite case-dependent. Further generalization work might be performed by modelling the PEMFC onsite performance and simulate it according to fictive standardized building demands (established statistically). It is worth mentioning that this system has been modelled in a parallel study [24].

5. Other limitations of this mCHP

As stated, one cannot only look at grid impact factors while considering such a mCHP system. Unfortunately, this particular system has some other limitations.

Firstly, it has been observed that yearly total LHV efficiencies can be at least 10 percentage points behind the reference gas condensing boiler efficiency of 90% (as it is the common assumption of nationally and internationally recognized organizations [25]). For sufficient daily local electrical production (consumed onsite), this relatively low efficiency can be economically compensated but, as it has indeed been stated in a parallel conference, it not exactly the case considering yearly economic performance [26] as expected return on investment is likely to exceed 10 years (based upon the monitoring results and the 2020 Belgian energy prices).

This also results in very questionable CO_2 savings, especially with Belgian electricity mix assumed emissions factors. Calculations are even showing worsen CO_2 emissions compared to reference machines (gas condensing boiler and Belgian electrical mix) no matter the relevant emissions factors that are taken in this study [26].

At last, since the system is not electrically driven (no modulation possible) and since it is designed to provide electricity constantly (as long as possible), the system cannot thus be considered versatile enough to provide flexibility services to the grid.

It is worth mentioning that another limitation of this system is that its PEMFC production has to be periodically stopped for a 2.5-hours regeneration procedure to take place [27].

6. Conclusions

Daily supply and demand cover factors have been established for the two residentials field-test PEMFC-gas condensing boiler mCHP systems for the whole monitored year 2020. Both machines are considered identical and the building they are placed in are similar to the exception that one has floor heating, which demonstrated smoother heat demand and therefore allowed the PEMFC (to keep dissipating its heat and) to run for a longer period of time.

Seasonal trends have also been showed, demonstrating a summer decrease of the demand cover factor while the supply cover factor increases. This is coming from the smaller electrical production that results from lower summer heat demands. Indeed, with few or no heat demand, the PEMFC can no longer release its heat and it shuts down.

On the one hand, yearly demand cover factors of 25 and 33% have been obtained. On the other hand, yearly supply cover factor is about 35% for both houses which is believed to be, based upon literature, 0 to 15 percentage points higher than what would have been obtained for a typical residential PV installation. Unfortunately for this PEMFC technology in Wallonia (South of Belgium), the local electrical regulator is assuming for billing purposes that unmetered residential PV installations are theoretically demonstrating 37,46 % of supply cover factors (even if it is most likely to be lower in reality). Therefore, the current billing framework is rather promoting usual PV installations that such mCHP systems.

However, an advantage of this mCHP system that is currently not considered in the billing framework is that supply and demand cover factors are quite constant over the whole year, which is absolutely not the case with PV installations.

7. Acknowledgement

Authors would like to acknowledge and thank the *Gas.be* (www.gas.be) company for providing much needed fundings to this study (for example, for instrumentation hardware and installation).

8. References

[1] M. M. Maghanki, B. Ghobadian, G. Najafi and R. J. Galogah, "Micro combined heat and power (MCHP) technologies and applications," *Renewable and Sustainable Energy Reviews,* vol. 28, 2013.

[2] CWaPE, "Tarification prosumer - AVIS CD-19k29-CWaPE-1853," CWaPE, 2019.

[3] J. Widén, E. Wäckelgård and P. D. Lund, "Options for improving the load matching capability of distributed photovoltaics: Methodology and application to high-latitude data," *Solar Energy,* vol. 83, no. 11, 2009.

[4] F. Sioshansi, "Chapter 1 - The evolution of California's variable renewable generation," in *Variable Generation, Flexible Demand*, Academic Press, 2020, pp. 3-24.

[5] The University of Texas at Austin - Energy Institute, "The Full Cost of Electricity (FCe-)," 2018.

[6] CREG, "Analyse semestrielle de l'évolution des prix de l'énergie – 2e semestre 2020," CREG, 2020.

[7] CREG, "Comment est composé le prix de l'énergie ?," [Online]. Available: https://www.creg.be/fr/consommateurs/prix-et-tarifs/comment-est-compose-le-prix-de-lenergie. [Accessed 15 01 2021].

[8] O. Gagrica, W. L. Kling and T. Uhl, "Control of micro-inverters as an overvoltage prevention method under high PV- penetration," *Mechanics and control,* vol. 32, no. 2, 2013.

[9] Y. Parag and S. B. K., "Electricity market design for the prosumer era," *Nature Energy,* vol. 1, no. 4, 2016.

[10] S. Lavrijssen and A. Carrillo Parra, "Radical Prosumer Innovations in the Electricity Sector and the Impact on Prosumer Regulation," *Sustainability,* vol. 9, no. 7, 2017.

[11] R. Baetens, R. De Coninck, J. Van Roy, B. Verbruggen, J. Driesen, L. Helsen and D. Saelens, "Assessing electrical bottlenecks at feeder level for residential net zero-energy buildings by integrated system simulation," *Applied Energy,* vol. 96, 2012.

[12] C. Psomopoulos, I. Skoula, C. Karras, A. Chatzimpiros and M. Chionidis, "Electricity savings and CO2 emissions reduction in buildings sector: How important the network losses are in the calculation?," *Energy,* vol. 35, no. 1, 2010.

[13] I. Daoud, "Installer une Cogénération dans votre Etablissement," Ministère de la Région wallonne. Direction Générale des Technologies, de la Recherche et de l'Energie (GGTRE), 2003.

[14] A. Ghenciu, "Review of fuel processing catalysts for hydrogen production in PEM fuel cell systems," *Current Opinion in Solid State and Materials Science,* vol. 6, no. 5, 2002.

[15] N. Paulus and V. Lemort, "Field-test performance of Solid Oxyde Fuel Cells (SOFC) for residential cogeneration applications," in *Herrick 2022 Proceedings*, Purdue, 2022.

[16] F. Dolci, D. Thomas, S. Hilliard, C. Guerra, R. Hancke, H. Ito, M. Jegoux, G. Kreeft, J. Leaver, M. Newborough, J. Proost, M. Robinius, E. Weidner, C. Mansilla and P. Lucchese, "Incentives and legal barriers for power-to-hydrogen pathways: An international snapshot," *International Journal of Hydrogen Energy,* vol. 44, no. 23, 2019.

[17] OIML R 75-, *Heat meters. Part 1: General requirements,* International Organization of Legal Metrology, 2002.

[18] IEC 62053-21, *Electricity metering equipment (a.c.) – Particular requirements. Part 21 : Static meters for active energy (classes 1 and 2),* International Electrotechnical Commission, 2003.

[19] UK Government - Department for Business, Energy & Industrial Strategy, "Heat meter accuracy testing," 2016.

[20] European Parliament, "DIRECTIVE 2010/31/EU on the energy performance of buildings," 2010.

[21] T. Huld and M. Suri, "Photovoltaic Geographical Information System (PVGIS), PV Estimation Utility (EU Science Hub)," [Online]. Available: http://re.jrc.ec.europa.eu/pvgis/. [Accessed 15 11 2021].

[22] J. Salom, A. Marszal, J. Widén, J. Candanedo and K. Lindberg, "Analysis of load match and grid interaction indicators in net zero energy buildings with simulated and monitored data," *Applied Energy,* vol. 136, 2014.

[23] S. Quoilin, K. Kavvadias, A. Mercier, I. Pappone and A. Zucker, "Quantifying self-consumption linked to solar home battery systems: Statistical analysis and economic assessment," *Applied Energy,* vol. 182, 2016.

[24] N. Paulus and V. Lemort, "Field-test performance models of a residential mi-cro-cogeneration system based on a proton exchange membrane fuel cell and a gas condensing boiler," To be submitted.

[25] CWaPE, "Décision CD-5j18-CWaPE relative à "la définition des rendements annuels d'exploitation des installations modernes de référence, ..."," CWaPE, 2005.

[26] N. Paulus, C. Davila and V. Lemort, "Field-test economic and ecological performance of Proton Exchange Membrane Fuel Cells (PEMFC) used in residential micro-combined heat and power applications (micro-CHP)," in *ECOS Proceedings*, Copenhagen, 2022.

[27] N. Paulus and V. Lemort, "Review of probable degradation mechanisms and recovery procedures for reversible performance losses in a residential cogeneration polymer electrolyte membrane fuel cell," To be submitted.

Data Statement

The datasets generated during and/or analysed during the current study are not publicly available because of GDPR (General Data Protection Regulation) but could be available under NDA (Non-Disclosure Agreement) with the data owners, i.e. the *Gas.be* (www.gas.be) company.

Smart thermostatic valves based heat generator control to cut heating bills

Max Boegli[a], Yves Stauffer[a], Nelson Koch[a], Tomasz Gorecki[a] , Renaud Langou[a] Andreas Hutter[a]

[a] Sustainable Energy Center, CSEM, Rue Jaquet-Droz 1, Neuchâtel, 2002, Switzerland ,

Abstract.
The following work aims at demonstrating how a smart thermostatic (radiator) valve network can be used to reduce heating costs by controlling the heat generator (heat-pump, gas boiler, ...) in a more efficient way. Currently, a large proportion of heat generators is controlled by the means of a heating curve, or a similar rule-based logic that mostly rely on outdoor temperature or single point indoor temperature measurements. These simple control laws are in general commissioned to minimize the number of complaints of "cold users". This results in high forward temperatures, that are energetically non-optimal as they create increased losses in the piping network and also have a negative impact on the heat generator efficiency. In the proposed data driven approach, a controller was developed to ensure that the radiators receive fluid with the lowest temperature possible, while satisfying the heating needs. To achieve this goal, smart thermostatic valves are used to monitor the radiator activity. The monitored information is used by a real-time algorithm to adapt the hot water temperature to continuously ensure user comfort. The solution was deployed in a multi-apartment building located in Neuchâtel (Switzerland). The solution has been running with success during the 2020-2021 heating season. The results point out that an average saving of 15% is obtained with respect to the baseline (i.e. heating curve) controller under similar conditions, without any degradation of comfort (under heating in particular). The system will now be deployed on 6 houses in Denmark and remain active at least until 2023.

Keywords. heat generator, control, smart thermostatic valves, radiator, mixing valve, data-driven heat controller
DOI: https://doi.org/10.34641/clima.2022.413

1. Introduction

Space heating (SH) represents a significant part of the energy usage and thus CO_2 emissions. Nowadays, thermostatic valves, conventional or electronic [1] [2], are well established to allow for a well-controlled zone temperature. Nevertheless, to operate properly, the heat emitters, need to be supplied with a heating fluid of a high enough temperature.

Unfortunately, for residential buildings, as for most larger facilities, the heat generator (and mixing valves, if relevant) are still controlled by so called heating curves, which generally provide a linear relationship between the outdoor temperature and desired forward heating temperature. The commissioning of these controllers is in general performed to ensure some overheating, to guarantee user comfort and thus prevent complaints. This results in the generation of heating fluid at too high temperature, which is negatively impacting the coefficient of performance (COP) of the heat generator. In addition, the resulting losses in the distribution piping are also increased.

To overcome these issues, predictive algorithms coupled to optimization have drawn attention [3] [4] [5]. However, in general the commissioning both in terms of hardware to be deployed and software tailoring to be performed, prevent acceptance and thus replication.

In that context, we propose a novel approach that relies on the smart thermostatic valve (STV) information to control the heat generation. The underlying algorithm relies on the STV measured data to continuously adjust the forward

Copyright ©2022 by the authors. This conference paper is published under a CC-BY-4.0 license.

temperature set-point. The method does not require complex commissioning (i.e. tuning of building models or control loops) and achieves energy savings in the order of 15% when compared to the baseline case, without compromising comfort.

The article is organised as follows:

- Section 2.1: highlights the concept
- Section 2.2: introduces the considered key performance indicators (KPI)
- Section 2.3: shows the test site located in the city of Neuchatel (Switzerland)
- Section 2.4: provides details about the test plan
- Section 3: provides the obtained results, per KPI

2. Method

2.1 The concept

A large proportion of heat generators are controlled by the means of a heating curve (i.e. the system is configured to produce water at a temperature that is inversely proportional to the outside temperature), or a similar rule-based logic, for instance night set-back. These simple control laws are in general commissioned to minimize the number of complaints of "users feeling cold". In other words, over-heating is performed to be on the safe side and avoid a technician to be dispatched. In consequence, it is energetically non-optimal. In addition, the method provides no adaptation to modifications in user habits or specific needs. This results in increased losses in the piping network as well as heat generators running at lower efficiencies, as shown in **Fig. 1** (left). Indeed, gas boilers and heat-pumps have higher coefficient of performance (COP) at lower temperatures.

In the chosen approach, **Fig. 1** (right), the radiators receive the minimal temperature required to satisfy the heating needs. To achieve this goal, smart thermostatic valves (STV), shown in **Fig. 2**, are used to monitor the radiator activity, such as the valve opening, which reflects the actual heating needs.

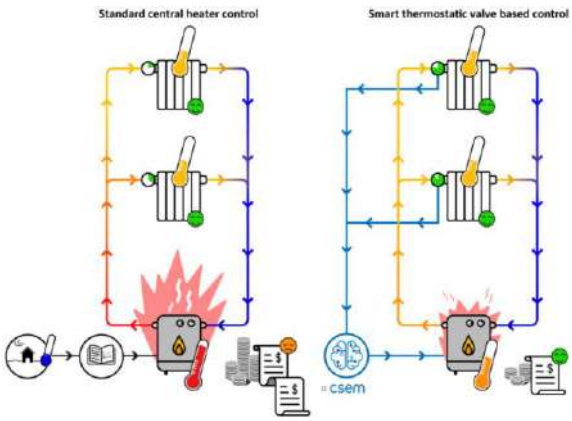

Fig. 1 – Standard central heater control (left), STV based data-driven heat control (right)

The monitored information is used by a real-time algorithm to adapt the hot water temperature to continuously ensure user comfort.

Fig. 2 – Smart Thermostatic Valve (STV)

In previous work [6], validation in simulation showed average savings of 8% on gas condensing and around 18% for heat pumps.

Deployment is simplified as the only needed hardware are STVs and the necessary communication gateways.

A building in Neuchâtel was equipped with all needed material to validate the concept (valves, energy meters & communication gateway). The solution has been running with success during the 2020-2021 heating season.

In the novel approach, the goal of the data-driven heat controller is to reduce the supply heat temperature of each heating circuit based on the real time data provided by the radiator valves. Doing so allows to provide the rooms with the right amount of heat and accordingly lower the needs at the generation level.

2.2 KPI

Key performance indicators (KPI) are defined to evaluate the thermal energy savings of the proposed

method compared to the baseline implementation, while keeping desired comfort for the inhabitants. Following KPIs are defined to assess the thermal energy and comfort:

- **Energy KPI – Daily thermal energy versus average outdoor temperature**. Daily thermal energy per heating circuit is computed as the integration over one day of the thermal power at heating circuit mixing valve level. The total energy consumed at building level is the sum of energy at mixing valves level.

- **Comfort KPI – Underheating and overheating versus average outdoor temperature**. Under / overheating is computed as the difference between the measured room temperature T_{room} and the valve temperature set-point T_{sp}. Daily underheating is the integration over one day of the $\min(T_{room} - T_{sp}^{clip}, 0)$ averaged over all valves, while daily overheating is the integration over one day of the $\max(T_{room} - T_{sp}^{clip}, 0)$ averaged over all valves. To avoid artifacts from out-of-range values from the valve temperature set-point the feasible values were limited in between 16°C and 24°C, i.e. $T_{sp}^{clip} = \text{clip}(T_{sp}, 16, 24)$.

These two KPIs evaluate the energy and comfort of the proposed solution. Results are shown in Section 3.

KPIs are computed for both, the baseline, and the proposed solution with the data-driven heat controller.

For the baseline, a standard heating curve is used to drive the three heating circuits, and in consequence the heat generator.

2.3 Test site

The test site is a mixed (residential and tertiary) building located in the city of Neuchatel (Switzerland). The ground floor is composed of an office and two shops, the four floors host six flats.

The building heat is generated by a gas condensing boiler (Logamax from Buderus that can provide up to 82kW) that serves for space heating and domestic hot water production. Given the building layout, three independent heating circuits (HC1, 2 and 3) each equipped with an independent mixing valve and circulation pump are used (see **Fig. 3**). Each heating circuit is equipped with an individual heat meter, in addition, domestic hot water is also monitored (and removed from space heating).

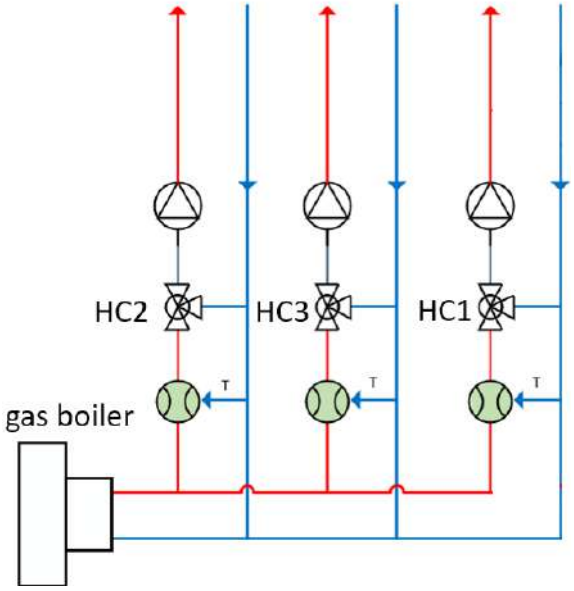

Fig. 3 – Building heat generation and distribution layout showing three heating circuits (HC2, HC3 and HC1 from left to right).

The gas boiler default heating curve set-point can be bypassed thanks to the KM200 gateway from Buderus. This device allows setting the target forward temperature of each heating circuit independently. The boiler oversees generating the heat and driving the mixing valves. For information, the default heating curve is defined by an inversely proportional relationship between the desired forward heating temperature and the outdoor temperature.

The heat emission is ensured by standard steel radiators. The latter were equipped with smart thermostatic valves (SmartDrive MX from HORA and Vicki from MClimate). STV are installed on all radiators, with 14, 5 and 50 units respectively for each heating circuit (i.e. HC2, HC3, and HC1). Among the measured values, the room temperature, room temperature set-point and valve percentage opening are the most critical for the algorithm and results analysis.

A high-level view of the data exchanges is provided in **Fig. 4**. Radiator status is measured by the valves (STV), this information is transmitted to a database located at CSEM. The algorithm is executed on a dedicated server and the computed heating circuit set-points are sent to the KM200 gateway.

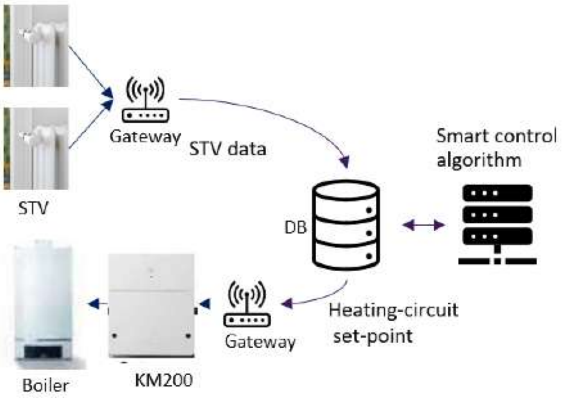

Fig. 4 – Cloud controller

2.4 Test protocol

To evaluate the proposed STV data-driven heat controller and compare it with the baseline, measurements were taken during the winter-spring 2021 seasons from January 15th to June 31st, 2021.

During the preliminary development stage, initial measurements from 15.01.2021 to 12.02.2021 are composed only of baseline data. Then, once the data-driven control algorithm was getting ready, the data-driven heat controller was gradually activated on each heating circuit:

- HC2 starting from 12.02.2021
- HC3 starting from 03.03.2021
- HC1 starting from 23.04.2021

In addition, reverting time to time to baseline operation to have a representative mix of baseline and experiment data spread over a range of outdoor temperature from winter to spring was done[1].

Analysis can be further discriminated between day and night schedule for each heating circuit. The day/night schedule refers to the settings entered by the users at valve level. These settings remain the same during the baseline and optimized control. The configuration of each heating circuit with the number of radiators, day schedule, number of baseline days and experiment days are summarized in **Tab. 1**.

[1] In the follow up heating season, a monthly switching between baseline and data-driven heat control will be done to better analyse and compare both approaches.

Tab. 1 – Heating circuits configuration

Settings	HC2	HC3	HC1
# Radiators	14	5	50
# Baseline days	30	19	48
# Experim. days	69	56	38
Day schedule	9-22h	7-19h	9-22h

Heating circuits HC2 and HC1 supply living spaces with one and six apartments respectively. Heating circuit HC3 supplies a workshop for daily activities.

3. Results

Results are computed for the winter-spring 2021 heating season with energy and comfort KPIs defined in Section 2.2 and test protocol with measurement periods presented in Section 2.4.

3.1 Energy KPI

Energy KPI are computed for each heating circuit with day/night discrimination. Results for daily energy KPI are represented versus the outdoor temperature. Unit of energy KPI is in kWh per day [kWh/d].

The result for the whole building, is provided in **Fig. *5***, where the energy is normalized at 0°C outdoor temperature, in reference to the baseline, and each heating circuits aggregated, so that the whole building energy can be compared between the proposed optimized solution and the baseline. Qualitatively, the thermal power consumption is reduced by 15% for the proposed solution based on the regression at 5°C outdoor temperature.

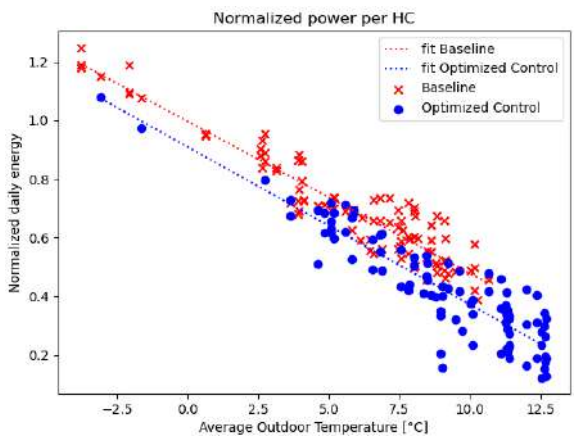

Fig. 5 – Normalized energy results for the whole building (i.e. Energy of HC1, 2 and 3 are normalized at 0°C outdoor temperature, in reference to the baseline, and aggregated)

Energy KPI for HC2, HC3 and HC1 are shown in the appendix in **Fig. 6**, **Fig. 7** and **Fig. 8**, respectively. One can observe a clear reduction of the thermal energy consumption, for the three heating circuits.

Experimental results from heating circuits HC2 and HC3 are promising. Experimental data for heating circuit HC1 are limited, as it was put in service later in the heating season.

3.2 Comfort KPI

Comfort KPI are computed for each heating circuit. Results for underheating and overheating errors KPIs are represented versus the outdoor temperature. Unit of under/overheating error is in Kelvin hour per day [Kh/d].

Global underheating and overheating averaged over all baseline days and experiments days are computed and summarized in **Tab. 2** for underheating and in **Tab. 3** for overheating.

Underheating KPI for HC2, HC3 and HC1 are shown in the appendix in **Fig. 9**, **Fig. 10** and **Fig. 11**, respectively, while overheating KPI for HC2, HC3 and HC1 are shown in **Fig. 12**, **Fig. 13** and **Fig. 14**, respectively.

Tab. 2 – Comfort KPI for underheating

Underheating	HC2	HC3	HC1
for baseline	-0.72	-0.88	-0.31
for experiment	-0.78	-0.93	-0.19

Tab. 3 – Comfort KPI for overheating

Overheating	HC2	HC3	HC1
for baseline	0.26	0.48	0.64
for experiment	0.34	0.46	1.22

Overall observation shows that the underheating and overheating are similar between baseline and experiments for heating circuits HC2 and HC3. For underheating, a value of -0.5 is to be interpreted as: "the average of the valves of the considered heating circuit are 0.5K below the desired set-point over one day".

It is worth pointing out that the savings mentioned in the previous section are not linked to the underheating. Indeed, for HC2 and HC3 the underheating difference between baseline and experiments is only 0.06Kh/day and 0.05Kh/day. Such small differences do not induce 15% energy reduction. Indeed, on average one expects a 1°C indoor temperature difference to impact the energy expenditure by ~7%.

For heating circuit HC1, there is less underheating and more overheating, showing there is a potential for even more thermal energy savings. This result was to be expected, as it was agreed with the building owner that the experiments should be rather conservative in terms of energy savings to prevent any potential discomfort to the tenants.

4. Conclusion

The STV data driven central heating controller was successfully deployed in a real test site. The comparison to the baseline (heating curve) controller shows energy reduction in the order of 15% with no significative impact on comfort.

Future work is aimed to improve the data-driven heat controller with the help of an adaptive scheme to outperform the baseline controller for comfort, while maintaining the energy savings. This new controller will be deployed in six new test sites.

5. Acknowledgement

This research has been financially supported by the research and innovation programme Horizon 2020 of the European Union under the grant agreement nr. 894840 (domOS).

6. Appendix

6.1 Energy KPI details

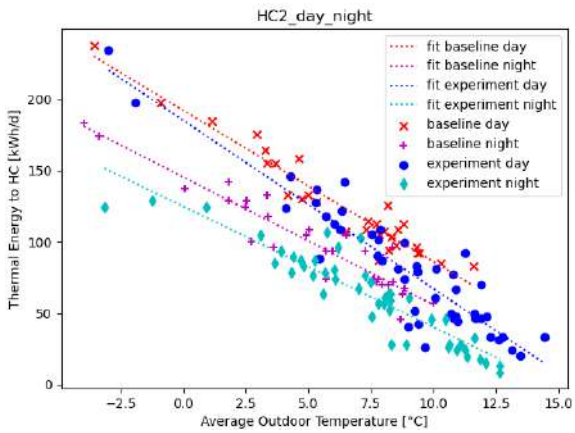

Fig. 6 – Energy KPI with day/night split for the HC2 riser with 14 radiators over 30 days of baseline and 69 days of experiment

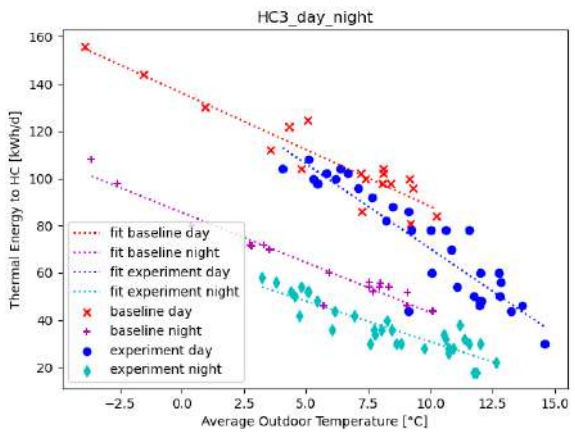

Fig. 7 – Energy KPI with day/night split for the HC3 riser with 5 radiators over 19 days of baseline and 56 days of experiment

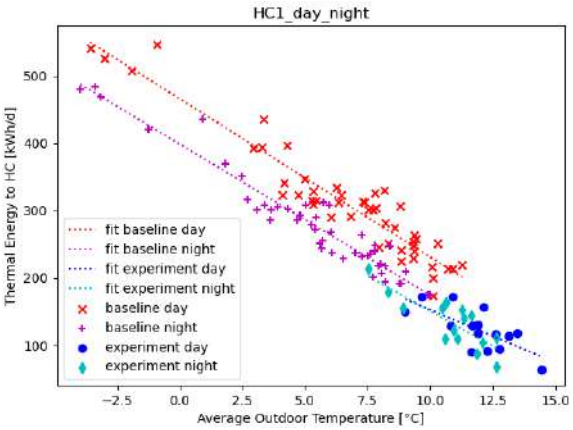

Fig. 8 – Energy KPI with day/night split for the HC1 riser with 50 radiators over 48 days of baseline and 38 days of experiment

6.2 Comfort KPI details

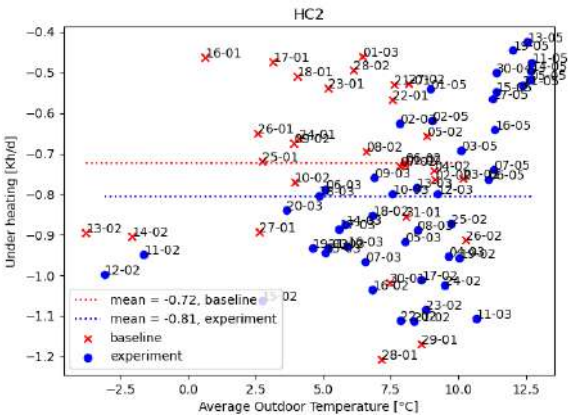

Fig. 9 – Underheating KPI for the HC2 riser with 14 radiators over 30 days of baseline and 69 days of experiment

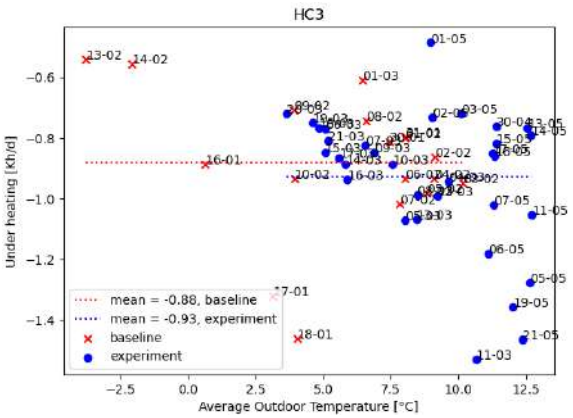

Fig. 10 – Underheating KPI for HC3 riser with 5 radiators over 19 days of baseline and 56 days of experiment

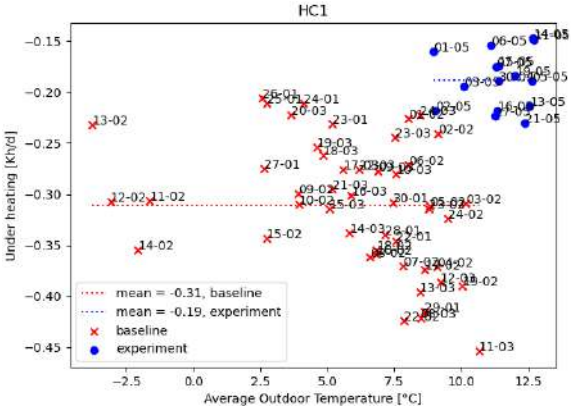

Fig. 11 – Underheating KPI for the HC1 riser with 50 radiators over 48 days of baseline and 38 days of experiment

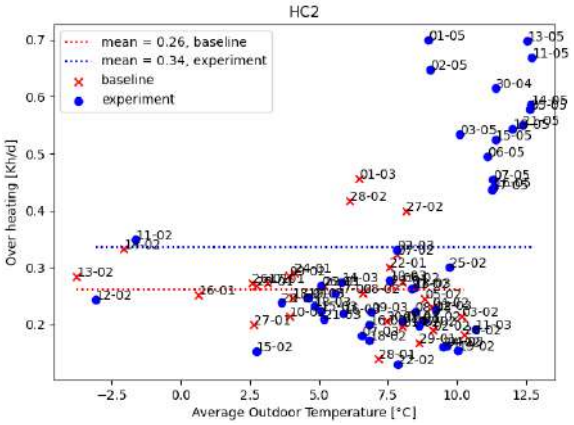

Fig. 12 – Overheating KPI for the HC2 riser with 14 radiators over 30 days of baseline and 69 days of experiment

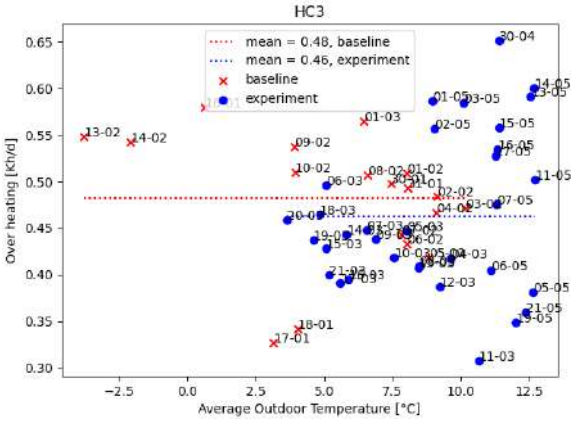

Fig. 13 – Overheating KPI for HC3 riser with 5 radiators over 19 days of baseline and 56 days of experiment

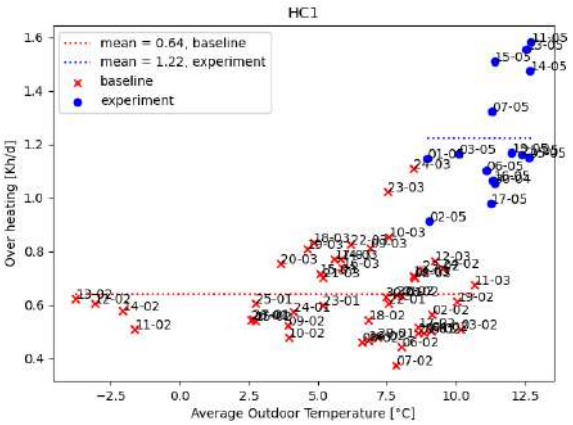

Fig. 14 – Overheating KPI for the HC1 riser with 50 radiators over 48 days of baseline and 38 days of experiment

7. References

[1] "Netatmo," [Online]. Available: https://www.netatmo.com/en-ca/energy/valves. [Accessed 2021].

[2] "Tado," [Online]. Available: https://www.tado.com. [Accessed 2021].

[3] T. Yang and L. Wang, "Control Strategy Optimization for Energy Efficiency and Comfort Management in HVAC Systems," in *IEEE Proceedings of Power & Energy Society Innovative Smart Grid Technologies Conference (ISGT)*, 2015.

[4] A. Mirakhorli and B. Dong, "Occupancy behavior based model predictive control for building indoor climate - A critical review," *Energy and Buildings*, vol. 129, pp. 499-513, 2016.

[5] "Yuon Control," [Online]. Available: https://yuon.ch/Produkt.html. [Accessed 2021].

[6] D. Grivon, P. Riederer, Y. Stauffer and A. Hutter, "Smart Control Strategy for the Reduction of Energy Consumption of Central Heating Systems in Large Buildings," in *IBPSA Building Simulation*, Rome, 2019.

Heat Pumps and Renewables in District Heating – Evaluation of Central and Decentral Approaches

Fabian Ochs [a], Mara Magni [a], Georgios Dermentzis [a]

[a] Unit Energy Effiicent Buildings, University of Innsbruck, Innsbrck, Austria, fabian.ochs@uibk.ac.at.

Abstract. The decarbonization of the building stock and thus of district heating (DH) systems is one of the main future challenges in the building sector. It is controversial which role district heating will play in the future, i.e. to what extent an expansion of DH is beneficial and necessary, but it is undisputed that DH will take or hold a relevant share. With the increasing decarbonisation of the electricity mix, the use of heat pumps (HP) in buildings will be significantly more competitive than (existing fossil-based) DH systems, at least in terms of CO_2 emissions. On the other hand, especially in urban areas and in existing buildings, the use of heat pumps is limited and also technically and economically challenging (source exploitation, space restrictions, architecture, sound emissions, etc.). Decarbonisation of DH might include waste heat, geothermal or solar thermal and heat pumps (in combination with electricity from renewables). Both, decarbonization of DH and electricity mix is challenging and full decarbonization requires electrical and thermal energy storage. Based on the energetic and ecological evaluation of exemplarily DH systems, different variants considering heat pumps integration, i.e. large central HPs central DH or block-wise or decentral i.e. building-wise, or apartment-wise are compared and evaluated. The assessment includes the own-consumption of the Photovoltaic (PV) yield and is then expanded to include various scenarios for the development of the electricity mix and the decarbonisation of DH.

Keywords. Decarbonisation, District Heating, Heat Pumps, Renewables, PV-own consumption, CO_2-Emissions, energetic and environmental evaluation.
DOI: https://doi.org/10.34641/clima.2022.306

1. Introduction

The decarbonization of district heating (DH) is one of the core tasks of the future in the building sector. It is controversial to what extent an expansion of district heating is beneficial and necessary in a future climate compatible energy system, but it is undisputed that DH will take or hold a relevant share. On the one hand, with the increasing decarbonisation of the electricity mix, the use of heat pumps (HP) in buildings will be significantly more competitive than existing DH, at least in terms of CO_2 emissions [1]. On the other hand, especially in urban areas and in existing buildings, the use of heat pumps is limited or at least challenging (source exploitation, space, architecture, sound, etc.).

HPs are effective to reduce energy consumption in buildings and facilitate the integration of renewable sources. While the use of solar thermal and small PV systems combined with HPs is common in single and increasingly also in multi-apartment buildings, HPs in DH is still a slowly growing kind of experimental application. However, DH offers the opportunity to effectively exploit also geothermal energy, industrial waste heat, biomass-based Combined Heat and Power (CHP) and other heat sources, see [2], [3] and [4]. Thus, the integration of HPs in DH systems allows to reduce the share of fossil sources and enables recovering low-temperature heat sources [5]. Possible heat sources are ambient air, ground, sewage and seawater. Among the commercially available heating, ventilation, and air-conditioning (HVAC) systems, ground source HPs outperform the others in terms of energy performance, as shown by [6]. However, depending on the location, exploitation of sources other than air can be challenging and in the case of air as a source, temperature fluctuations have an important influence on the HP performance [7]. A parallel decrease of the heating capacity and the coefficient of performance (COP) as to be accounted for [8].

Partly renewable block heating systems exist as prototypes or demonstrators since many years, but most renewable district heatings rely on biomass, which is a limited resource. A mentionable example of a solar neighborhood is the "Solarsiedlung

Copyright ©2022 by the authors. This conference paper is published under a CC-BY-4.0 license.

Freiburg" that consists of 20 terraced houses [9]. Other concepts are so-called cold DH [10], low-ex [11] or solar assisted DH [12], which can be summarized as so-called 4th generation district heating systems [13].

One main driver to integrate HP into buildings and DH is the possibility to increase the PV own consumption in particular in combination with thermal storage [14], which is mainly motivated because of commonly low PV buyback prices in most European countries [15]. Another motivation increasingly seen is the possibility to use the HPs also for space cooling [16].

1.1 Role of DH in Future Energy System

The shares of renewables, waste incineration, industrial waste heat, CHP and fossile for the DH of Innsbruck (IBK), Vienna, Graz and Lienz are reported in [17]. The largest DH system in Austria is Vienna with a high share of waste incineration. The DH in Graz is dominated by CHP, while in Innsbruck (IBK) there is a high share of biomass and industrial waste heat. There exist several scenarios for the development of DH in Europe. Exemplarily, two different studies, one for Austria and one for Germany are presented to show the wide range of expected contributions of DH in a future energy system. According to [18] in Austria, the assumption is that the buildings will be deeply renovated and in contrast to a further extension of the DH system the share and size in terms of energy remain rather constant. While for Germany, the prediction according to [19] is that the role of DH will significantly increase with a share of 40 %. The share of large-scale HP in the DH in 2050 is assumed to be almost 50 %. It is noteworthy that according to [20] the current German district heating is predominantly fossil-based and the 2030 scenario seems very ambitious in that respect.

1.2 Research Gap and Paper Organisation

The literature review reveals that HPs will play a major role in the heating of buildings as well as in a decarbonized DH system, but a comprehensive investigation is missing on how to optimally integrate HPs. In particular, the evaluation of the efficiency and the environmental impact of the energy supply of multi-apartment residential buildings connected to DH with so-called booster HPs and PV has not yet been investigated.

Based on the energetic and ecological evaluation of two exemplary district heating systems (Innsbruck and Vienna), various variants of integrating heat pumps in district heating are evaluated. By means of a simulation study, the efficiency and the environmental impact of the energy supply of multi-storey residential buildings with DH and HPs are evaluated. Of particular interest in this study is the integration of decentralized so-called booster HPs in combination with photovoltaics (PV) to increase the PV own consumption.

2. Methods

2.1 Reference Building and DH System

Fig. 1 shows a sketch of the reference building used to model the energy demand of a generic DH system and **Tab. 1** summarizes the characteristics of the building.

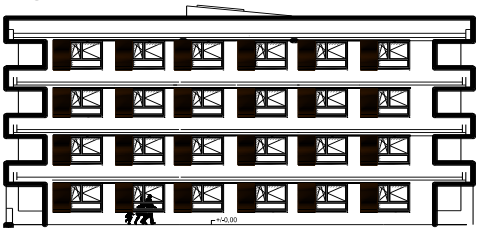

Fig. 1 - Sketch of the reference building, Multi-apartment building with 4 storeys and 16 flats (Neue Heimat Tirol).

Tab. 1 - Overview of characteristic data of the building, variant with Passive House quality [21]

Number of apartments	16
Number of stories	4
Treated area A_T	1295.6 m^2
Design Space Heating (SH) demand	11.0 kWh/(m^2·a)
Number of occupants	48 (design value)
MVHR	2 centralized units
PV (max.)	270m^2 (south 40 °) $A_{PV,max} = 0.6 \cdot A_{Footprint}$
U-value – wall / roof / floor	0.10 / 0.09 / 0.11 W/(m^2·K)
Triple glazed windows with U- and g-value	0.58 W/(m^2·K) and 0.56 [-]
Internal heat gains (design value)	2.7 W/m^2

Standard profiles are used for hot water consumption. [22] resulting in Domestic Hot Water (DHW) demand of 20 kWh/(m^2 a) including storage losses and 25 kWh/(m^2 a) and distribution losses (within the building). Furthermore, standard profiles are used for household electricity [23] resulting in 25 kWh/(m^2 a) of electricity (appliances, lighting, etc.).

2.2 PV and PV own consumption

The building's footprint is 449.4 m^2 with a treated area of 1295.6 m^2. With the realistic assumption of a max. coverage of 60 % of the flat roof with PV (south oriented with 40° slope and an overall system efficiency of $\eta = 12$ %) the annual yield of a PV system is 90.3 kWh/(m$^2_{footprint}$ a), corresponding to 31.3 kWh/(m$^2_{treated\ area}$ a). Because of low PV buyback prices, the share of PV that is directly used in the building shall be optimized (from the economic point of view of the building user/owner).
Typically, the PV own consumption is evaluated in terms of load and supply cover factor as defined by Eq. (1) and (2).

$$LCF = PV_{own}/W_{el,tot} \quad (1)$$

$$SCF = PVown/PVtot \quad (2)$$

In the evaluation of LCF and SCF, the total electricity demand (el) including aux. and appliances should be considered

2.3 District Heating System

A generic DH system is assumed (see **Fig. 2**) that consists of 100 buildings with a normal distribution of SH demands (i.e. 5% with 15 and 80 kWh/(m² a), 24% with 25 and 60 kWh/(m² a) and 40% with 45 kWh/(m² a)).

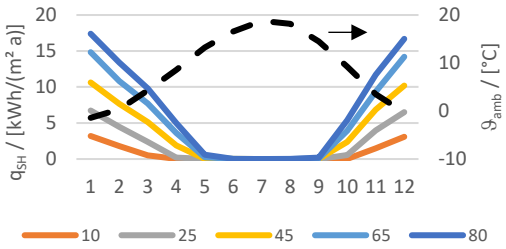

Fig. 2 - Monthly space heating demand of the building with different qualities of the envelope in kWh/(m² a), considering the climate of Innsbruck (site climate acc. to OIB-6_2019)

2.4 District Heating in Vienna and Innsbruck

Because of the high space heating demand in winter, there are strong seasonal variations of the DH load. The DH system in Innsbruck is comparatively small and complex with several small distributed heat sources (Details can be found in [17]). The largest DH system in Austria is Vienna with a high share of waste incineration [24]. The monthly energy balance of the DHs of Innsbruck and Vienna were evaluated.

2.5 Generic District Heating

For the purpose of further investigation, a simplified generic DH system is developed which consists of different shares (in %) of biomass and gas heating: 30-70, 40-60, 50-50, 60-40, 70-30. The overall efficiency of the biomass and gas heater is included in the CO_2 conversion factors, see section 2.9. Fossil gas post-heating is then partly replaced by integrating HPs with different capacities.

2.6 Integration Heat Pumps in District Heating

Generally, the following types of HP integration options are possible (see also **Fig. 3**) :

- DH + central HP (air, ground, water, waste-heat);
- DH + building/block-wise HP for SH;
- DH + building/block-wise HP for DHW;
- DH + decentral/flat-wise air - HP for DHW (PV-own consumption)
- DH + decentral/flat-wise booster or return flow (RF) - HP for DHW (PV-own consumption)
- DH + decentral/flat-wise booster HP for SH and DHW (low-ex)
- Building/Block-wise HP for SH and DHW (no DH)
- Decentral/flat-wise air - HP for SH and DHW (no DH)

Any combination is possible, here the different options are evaluated and compared against each other on a building level and on DH system level.

Typical DH systems are operated with a flow temperature of up to 130 °C in winter and 90 °C in summer with a return temperature of 60 °C. HPs can be integrated as large-scale absorption or compression heat pumps centrally in the DH system. The source is low-grade environmental energy (air or ground) or low-temperature waste heat. The supply temperature of at least 90 °C has to be delivered if (fossil-based) post-heater are not available.

Decentral HPs can be integrated block-wise with a low-temperature distribution system (e.g. 80/30) or building-wise. In low-energy buildings typically 60 °C flow temperature is required for DHW, while space heating can be provided even at lower temperatures (e.g. 35 °C with underfloor heating). Decentral flat-wise heat pumps can deliver DHW at 50 °C to 55 °C.

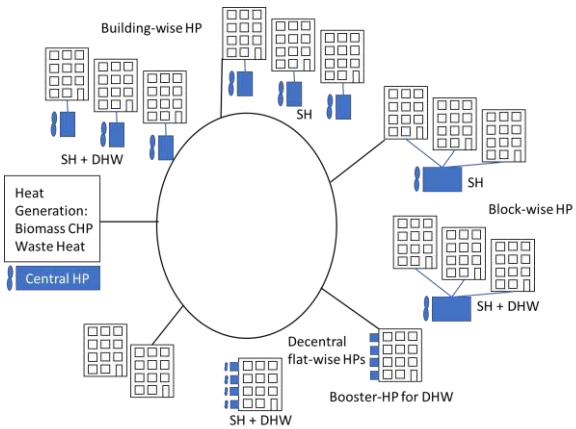

Fig. 3 – Sketch of possible solutions for HP integration (in blue) in a DH system.

2.7 Decentral Booster Heat Pump

There exist different variants of these so-called decentral booster HPs. A common concept is shown schematically in **Fig. 4**. The apartments are heated centrally, i.e. here by means of DH. The heat emission system in the apartments is a low-temperature heating system (i.e. underfloor heating). The central heat supply from a buffer store is controlled via the return temperature. There is a decentral booster HP in each of the apartments for preparing domestic hot water. It consists of a small (1.5 $kW_{thermal}$) water-to-water HP and a small domestic hot water tank of typically 120 l or 150 l. The HP source (evaporator) is connected in parallel to the branches of the underfloor heating. Typically, there is an additional (1.2 kW) heating rod in case backup heating is required. In summer the underfloor heating loops are used to extract heat from the conditioned space (i.e. to provide space cooling) and the central source is only activated if the underfloor heating temperature falls below a threshold or if comfort conditions in the conditioned space cannot be met

anymore. Thus, in summer only a negligible amount of heat is extracted from the district heating, instead.

Another concept is represented by the so-called return flow (RF) HP, where the evaporator of the HP is in series to the floor heating loops see [16], which is not further considered, here.

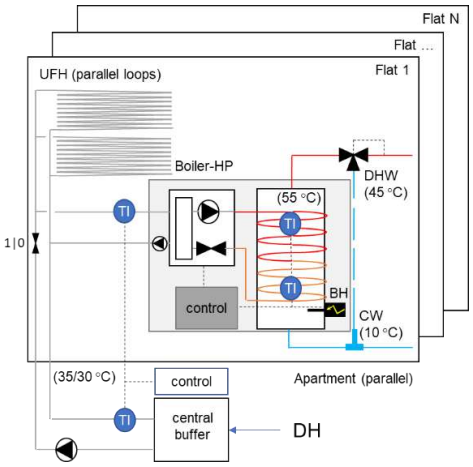

Fig. 4 – Simplified hydraulic scheme of a booster heat pump.

Based on the efficiency (COP) of the HP for DHW preparation of 4.1 at 28 °C and 2.7 at 20 °C source temperature at 55 °C sink temperature, a Carnot performance factor η_C between 0.28 and 0.34 can be determined.

2.8 Modelling Approach

All heat pumps are modelled for sake of simplicity with a Carnot based approach:

$$COP_C = T_{max}/(T_{max} - T_{min}) \quad (3)$$

$$COP = \eta_C \cdot COP_C \quad (4)$$

Different Carnot performance factors η_C and flow temperatures (ϑ_{flow}) are used depending on the type of HP:

Central HP: For the COP of large-capacity high-temperature HPs a cascade system is assumed. The overall COP is approximated with a relative optimistic Carnot performance factor of 0.55 leading with a flow temperature of ϑ_{flow} = 90 °C to a COP in winter conditions of about 2.2 and in summer of 2.8 and a SPF of 2.5.

The Building-/Blockwise HP for DHW and SH is modelled as air sourced HP with a rather conservative Carnot performance factor of 0.35 leading to a SPF of 3.

The Building-/Blockwise HP for SH is modelled as air sourced HP with a conservative Carnot performance factor of 0.35 leading with (ϑ_{flow} = 35 °C for SH and ϑ_{flow} = 55 °C for DHW to a SPF of 3.4.

The Decentral DHW HP is modelled as air-sourced HP that delivers hot water at 55 °C with a Carnot performance factor of 0.35. The SPF results to 2.49.

Decentral Booster HP: As described in section 2.7 above, winter and summer operation has to be distinguished in the case of the Booster HP. In winter, the HP uses the flow temperature of 35 °C (max., with a heating curve) as a source to provide DHW at 55 °C. The relatively high COP of about 5 in winter reduces the energy provided by the DH system to 4/5th.

In summer, the source of the HP is the room temperature (20 °C in the transition seasons and 25 °C in summer) and the COP of the HP is correspondingly lower (i.e. 2.8). In the transition months (May and September) a mixed operation (i.e. average of winter and summer conditions) is assumed.

The seasonal performance factor (SPF) is evaluated on monthly basis.

2.9 CO_2 emissions from DH and HP

The CO_2 emissions resulting from DH strongly depend on the energy mix (see section above). In case HPs are involved, the (European) electricity mix has to be considered, which is also subject to decarbonization. According to [25], and depending on the assumed scenario the share of fossils (coal, oil, gas) will decrease from approximately 50 % to 20 % in 2030 and further to 30 % in 2050 with main contributions from wind, biomass and PV but also nuclear power and imported hydrogen and biofuels.

Both, the DH load curve and the electric load curve depend significantly on the time of the year and to account for that, monthly energy conversion factors are recommended [26]. In this work, the CO_2 conversion factors suggested by OIB-6:2019 [27] are used. Because of the high share of hydropower, the electricity conversion factors are comparatively low in Austria compared to Germany.

In the case of combined heat and power (CHP) the distribution of CO_2 emissions to the electric and the heating part should be calculated using the Carnot Method. CHP has an important contribution in many DH systems, but is disregarded here for sake of simplicity.The CO_2 emissions are evaluated on monthly level using the Eq. (5) where the q_{DH} is calculated according to Eq. (6) and w_{el} according to Eq. (7) and (8). Relative losses of f_{loss} = 10 % related to the space heating (SH) and domestic hot water (DHW) demand and 1 % for auxiliary energy (i.e. pumps), respectively is taken based on measurements of the DH in Innsbruck presented in [17].

$$CO_2 = q_{DH} \cdot f_{CO2,DH} + w_{el} \cdot f_{CO2,el} \quad (5)$$

$$q_{DH} = f_{loss} \cdot (q_{SH} + q_{DHW}) \quad (6)$$

$$w_{el} = w_{el,AUX} + w_{el,HP} \quad (7)$$

$$w_{el,AUX} = f_{AUX} \cdot q_{DH} \quad (8)$$

In the reference DH system the resulting CO_2 conversion factor can be calculated according Eq. (9):

$$q_{DH} \cdot f_{CO2,DH} = Q_{Gas} \cdot f_{CO2,Gas} + Q_{Bio} \cdot f_{CO2,Bio} \quad (9)$$

For the following evaluations conversion factors based on OIB-6:2019 were used:

- Electricity 227 t_{CO2}/MWh;
- Gas 244 t_{CO2}/MWh (incl. 82 % thermal efficiency);
- Biomass/Waste Heat 50 t_{CO2}/MWh.

The CO_2 conversion factors of four generic DH systems with a different share of biomass/waste heat and natural gas are shown in **Fig. 5** and compared with the factors determined for the DH in Vienna and Innsbruck (IBK).

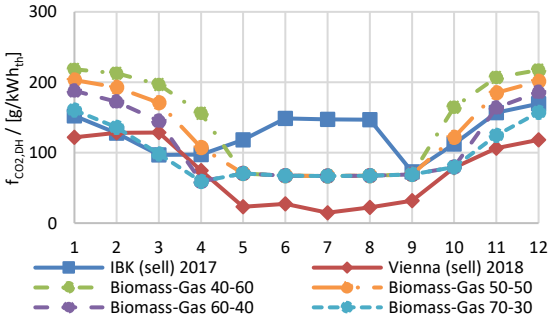

Fig. 5 - CO_2 conversion factors for DH Vienna and Innsbruck (IBK) as well as 4 generic DH systems with different shares of biomass/waste heat and natural gas (own calculations based on [17] and [24]).

CO_2 conversion factors for electricity in Germany (D 2019) and Austria (At, 2019) are taken as a reference [28] and are compared to two scenarios of a generic electricity mix with 10 % hydro, 10 % wind and 10 % PV and 10 % hydro, 30 % wind and 30 % PV, respectively (residual fossil) according to [26] (see **Fig. 6**). For further investigation, the scenario 10-10-10 is used as it might well represent a near-future energy mix for Germany.

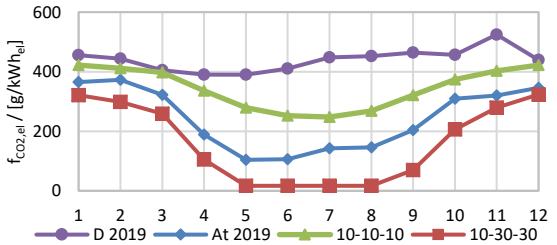

Fig. 6 – CO_2 conversion factors for electricity in Germany (D 2019) Austria (At, 2019) acc. to [28], and acc. to two scenarios of a generic electricity mix with 10 % hydro, 10 % wind and 10 % PV and 10 % hydro, 30 % wind and 30 % PV, respectively (residual fossil) according to [26].

3. Results

The following results apply under the assumption of a limited availability of biomass of (here exemplarily) 32 kWh/(m² a), i.e. in the reference system gas contributes to approx. 60 %. Here, only the case of the reference DH, the central HP and the decentral booster HP are presented examplarily.

3.1 Reference District Heating

Fig. 7 shows the monthly balance of the reference DH system with 40 % biomass and 60 % gas.

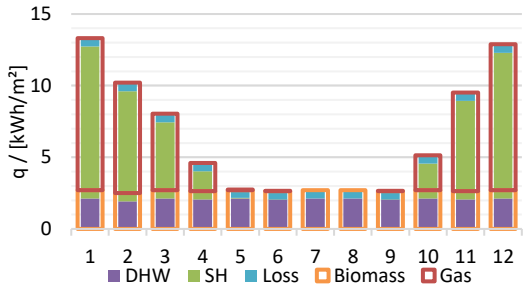

Fig. 7 - Reference DH system with 40 % biomass and 60 % gas.

3.2 District Heating with Central HP

A central HP can be used to reduce the share of fossil gas. Two examples are presented with different heat pump capacities contributing to 16 % and 31 % of delivered heat, respectively (see **Fig. 8**).

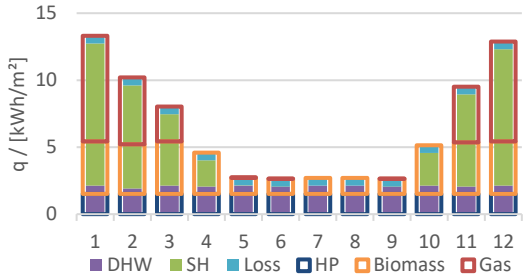

Fig. 8 - DH with central HP 23 %, biomass and gas.

3.3 District Heating with Decentral Booster HP

The monthly balance of a DH heating system with decentral booster HPs is shown in **Fig. 9**.

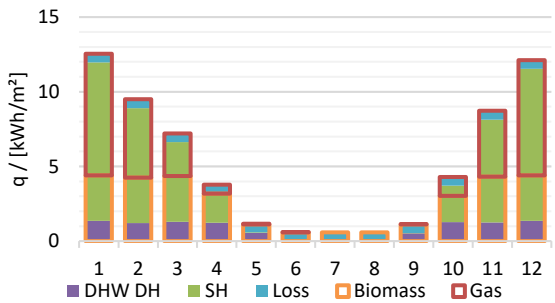

Fig. 9 - Decentral Booster-HP; 40 % Biomass, 60 % natural gas.

3.4 Evaluation of reference DH and DH with HP

Based on the monthly balance, the total annual CO_2 emissions are compared in **Fig. 10**. In all combinations integration of a HP (or replacing DH with HP) leads to a reduction of the CO_2 emissions. The best performance is obtained with either building-wise HP for SH and DHW or DH for DHW and building-wise heat pump for SH. The higher the share of HP and in particular of HP in SH, the larger is the difference between constant CO_2-emission conversion factors and monthly ones according to the scenario "10-10-10". It has to be noted that the assumption of low-temperature heating in (renovated) buildings with an HD of 45 kWh/(m² a) is optimistic. In this sense, the solution with Booster-

HP is not applicable or at least not recommended in buildings with HD higher than 45 kWh/(m² a). The overall performance depends on the number of buildings equipped with a heat pump.

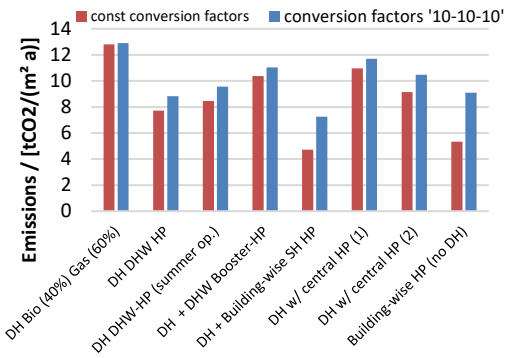

Fig. 10 - CO_2 emissions of the different systems without and with central, building-/block-wise or decentral HP.

3.5 DH level considerations

Given a (rather arbitrary) threshold of 75 % with respect to the energy delivered by the DH without integration of HPs, it can be determined how many buildings in the DH system can be equipped with HP until the operation of the DH system loses economic feasibility. In case of HPs on building (or block level) for SH and DHW, max. 25 % of the buildings can be equipped leading to a building averaged emission of 12 $tCO_2/(m^2\ a)$. In case of building or block-wise SH HPs, 45 % of the buildings can be equipped with HP before the threshold of 25 % is reached. This would result in an average of 10.5 $tCO_2/(m^2\ a)$. However, as the load curve, in this case, is flat and operation of the DH system is constant throughout the year (i.e. relative low power, no peaks) an economic operation of the DH would also be possible with only 65 % of the original energy delivery. In this case (indicated by the dotted line) 60 % of the buildings could be equipped with such as SH HP and emissions would reduce to 9.5 $tCO_2/(m^2\ a)$. Decentral DHW HPs can reduce significantly the CO_2 emissions. However, as such a DH system (with decentral DHW HPs) would have no summer load (except for the losses if the system was operated throughout the year) and would thus feature relatively low operation time and relatively high peaks. Hence, in spite of the remaining high share of energy for SH, for an economic operation of a DH system only a few decentral DHW HPs might be acceptable (indicated by the dotted line) leading to CO_2 emissions of 11.2 $tCO_2/(m^2\ a)$.
Booster HPs do not significantly reduce the DH load except for a few months in summer, when ambient energy is used as a source. Because of the remaining high share of DH demand, all buildings could be equipped with such an HP without threatening economic operation. However, this would also lead to a rather low reduction of the CO_2 emissions from 12.9 $tCO_2/(m^2\ a)$ to 11.0 $tCO_2/(m^2\ a)$. The CO_2 emissions given in the previous figures apply for a constant relative share of biomass in the DH system. Considering that the HP replaces partly biomass, an additional replacement of gas with biomass would be possible.

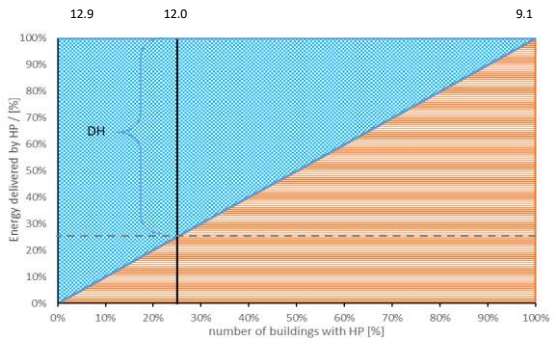

Fig. 11 - DH (for SH and DHW) and HP (for SH and DHW), and specific CO2 emissions in $tCO_2/(m^2\ a)$.

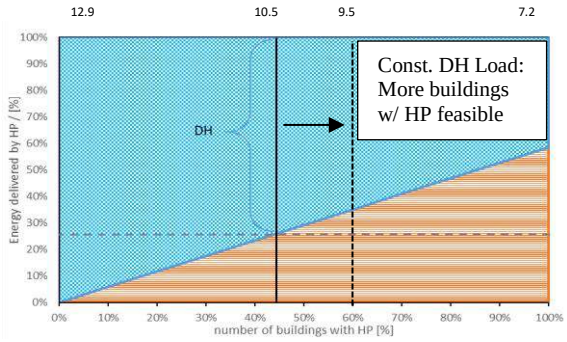

Fig. 12 - DH (DHW) and building-wise HP (for SH), and specific CO2 emissions in $tCO_2/(m^2\ a)$.

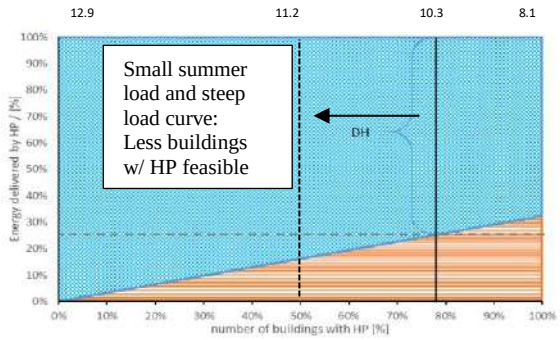

Fig. 13 - Decentral A-W DHW-HP, and specific CO_2 emissions in $tCO2/(m^2\ a)$.

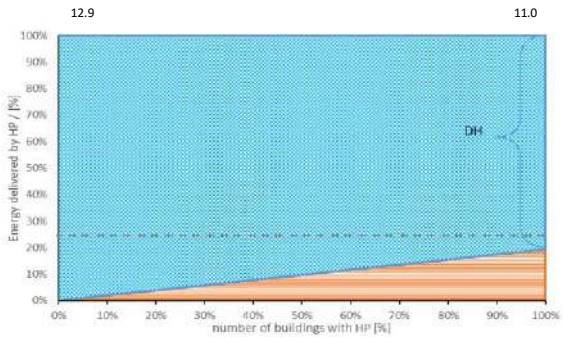

Fig. 14 - Decentral DHW Booster HP, and specific CO_2 emissions in $tCO2/(m^2\ a)$.

3.5 PV own-consumption

To increase the PV own consumption is one of the main motivations for integrating booster HPs in DH systems. The specific PV yield of the 270 m² PV system (2.35 kW_p/flat) is shown in **Fig. 15** together with the own consumption with respect to the Booster HP. With a HP electricity demand of 443.2

kWh/a per flat, the SCF is 10 % and the LCF is 50 % with respect to the electricity demand of the booster HP with a standard control scheme. The CO_2 emissions can be reduced from 11.5 $tCO_2/(m^2\ a)$ to 10.1 $tCO_2/(m^2\ a)$. If the entire DHW production was provided by PV, the emissions could be further reduced to 9.2 $tCO_2/(m^2\ a)$. Various control strategies to increase the PV own-consumption should be taken into account.

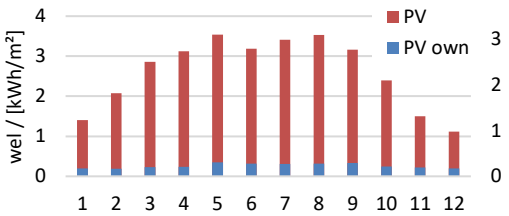

Fig. 15 - specific PV yield in $kWh/m^2_{treated\ area}$ and own consumption with respect to Booster HP.

It is noteworthy that PV own consumption would be higher in the case of DHW-HP and even higher in case of an electric boiler, but this would not lead to a reduction of CO_2 emissions. Furthermore, all PV yield could be used instead to cover the appliances.

4. Discussion

The possible CO_2 emission savings that can be obtained from integrating HPs in DH systems depend on the energy mix of the DH system, the electricity mix and the type of integration. If instead of biomass waste heat is used in the DH, the use of decentral HPs can even lead to an increase of the CO_2 emissions. Generally, the integration of decentral HPs for DHW preparation reduces the summer load thus leading to a more pronounced (relative) winter peak. Typically, DH system operators prefer the reduction of winter load and rather flat load curves.

From the energetic point of view, the application of decentral Booster-HPs in combination with DH is not recommended. In the heating season (typically 7 out of 12 months) the DHW is provided by approximately 1/5th of electricity and 4/5th of DH (COP of 5, the source of the HP is the DH). Only in 5 out of 12 months (or less) the source of the HP is ambient heat. Thus, in spite of reduced distribution (and storage) losses in the building, decentral integration for DHW preparation with Booster-HPs does not show significant savings. The advantage is instead (if the hydraulic configuration allows for it) the possibility to (partly) provide space cooling. Furthermore, the PV-own consumption can be slightly increased, which can be an advantage from the micro-economic point of view (view of the operator and or the tenants of the building), but cannot be recommended from the macro-economic view (see also [14]).

Decentral air-to-water HPs for DHW preparation outperform Booster-HPs. However, their integration into the building/flat is more challenging (air-source, visual/design aspects, sound emissions. However, the application of decentral DHW-HPs leads to a reduction of the base load of the DHW system. In a theoretic DH system with 100 % DHW-HPs, there would be no summer operation. Application of decentral DHW-HPs can be a good solution in the renovation of buildings if DHW distribution in the building is not available and cumbersome to install.

From the exergetic point of view, Booster-HPs in combination with DH seems kind of absurd. The high temperature of the flow of the DH (e.g. 90 °C provided by burning high exergy energy carriers such as biomass and gas) is transferred in a heat exchanger to the building and is then mixed with the return of the heating system (e.g. 30 °C) to provide a low-temperature flow for the underfloor heating (e.g. 35 °C). The flow is "boosted" with the Booster HP by means of exergy (electricity) to 55 °C to provide DHW. Integrating building or flat-wise HP for SH is beneficial in several aspects. For the DH system, the remaining DHW load represents a constant and flat load. HPs can be operated with low sink temperatures and thus with high performance. HPs can be used to provide space cooling when combined with underfloor heating or in combination with air-cooling coils. PV own consumption can also be increased if these decentral HPs are used for cooling. A drawback of building or block-wise SH HPs is the short operation time (only during the winter season) and thus their application might be economically challenging.

5. Conclusions

Heat pumps can significantly contribute to improve the efficiency in buildings for space heating and domestic hot water preparation. The advantage of building- or flat- wise integration of HPs is the lower temperature level (55 °C for DHW and 35 °C or lower for SH with underfloor heating). Contrariwise, central HPs in district DH have typically to provide up to 90 °C in Winter and 60 °C in Summer and even though large HPs typically perform better than small HPs the loss of efficiency due to high sink temperatures cannot be compensated. Assuming an existing DH system additional losses do not occur when a heat pump is integrated.

Thus in the sense of better performance, decentral application of HPs seems to be more favourable. However, the load of the DH system reduces by means of integrating decentral HPs and in particular in case of DHW HPs (both building-wise or flat-wise air-to-water) or decentral boiler HPs the load curve becomes unfavourable: the summer load reduces to close to zero or to zero leading to shorter runtimes of the DH system (only during the heating season from Sept. to May). Furthermore, the possibilities reduce to integrate waste heat or renewables in summer and at least to a lower energy delivery with only insignificantly reduced peak loads in winter and thus to a less economic operation. On a wider perspective, DH systems with a significant amount of buildings with decentral DHW HPs will not be operable in an economic way.

6. Abbreviations

A_T	Treated area
At	Austria
AUX	auxiliaries
Bio	biomass
C	Carnot
CHP	Combined Heat and power
COP	Coefficient of Performance
D	Germany
DH	District Heating
DHW	Domestic Hot Water
el	electricity
g-value	Solar Factor
HP	Heat Pump
HVAC	Heating Ventilation and Air Conditioning
IBK	Innsbruck
LCF	Load Cover Factor
MVHR	Mechanical Ventilation with Heat Recovery
PV	Photovoltaic
RF	Return flow
SCF	Supply Cover Factor
SH	Space Heating
SPF	Seasonal Performance Factor
UFH	Under Floor Heating
U-value	Heat transfer coefficient

7. Acknowledgement

The work presented in this paper is the result of a collaboration within IEA SHC Task 66. Financial support was provided by the Austrian Ministry for Transport, Innovation and Technology and the Austrian Research Promotion Agency (FFG) through the IEA Research Cooperation.The authors thank furthermore Neue Heimat Tirol (NHT) for the funding within the research cooperation in the Project ru27.

8. References

[1] G. Dermentzis, F. Ochs, A. Thuer, and W. Streicher, "Supporting decision-making for heating and distribution systems in a new residential district - An Austrian case study," Energy, vol. 224, 2021.
[2] H. Lund, B. Möller, B. V. Mathiesen, and A. Dyrelund, "The role of district heating in future renewable energy systems," Energy, vol. 35, no. 3, pp. 1381–1390, Mar. 2010.
[3] P. Sorknæs et al., "The benefits of 4th generation district heating in a 100% renewable energy system," Energy, vol. 213, p. 119030, Dec. 2020.
[4] A. Menapace, W. Boscheri, M. Baratieri, and M. Righetti, "An efficient numerical scheme for the thermo-hydraulic simulations of thermal grids," Int. J. Heat Mass Transf., vol. 161,2020.
[5] K. Kontu, S. Rinne, and S. Junnila, "Introducing modern heat pumps to existing district heating systems – Global lessons from viable decarbonizing of district heating in Finland," Energy, vol. 166, 2019.
[6] W. Wu, H. M. Skye, and P. A. Domanski, "Selecting HVAC systems to achieve comfortable and cost-effective residential net-zero energy buildings," Appl. Energy, vol. 212, 2018.
[7] H. Pieper, T. Ommen, J. Kjær Jensen, B. Elmegaard, and W. Brix Markussen, "Comparison of COP estimation methods for large-scale heat pumps used in energy planning," Energy, 2020.
[8] O. Kwon, D. Cha, and C. Park, "Performance evaluation of a two-stage compression heat pump system for district heating using waste energy," Energy, vol. 57, 2013.
[9] M. Heinze and K. Voss, "Goal: Zero Energy Building Exemplary Experience Based on the Solar Estate Solarsiedlung Freiburg am Schlierberg, Germany," J. Green Build., vol. 4, 2009.
[10] M. Pellegrini and A. Bianchini, "The Innovative Concept of Cold District Heating Networks: A Literature Review," Energies 2018, Vol. 11, Page 236, vol. 11, 2018.
[11] S. Dietrich, "Low Temperature District Heating for Future Energy Systems," DHC2018, 2018.
[12] D. Bauer, R. Marx, and H. Drück, "Solar District Heating for the Built Environment-Technology and Future Trends within the European Project EINSTEIN," Energy Procedia,2014.
[13] H. Lund et al., "4th Generation District Heating (4GDH): Integrating smart thermal grids into future sustainable energy systems," Energy, vol. 68, 2014.
[14] F. Ochs, M. Magni, E. Venturi, A. Tosatto, and W. Streicher, "Cost-optimal nZEB HVAC configurations with onsite storage," E3S Web Conf., vol. 246, 2021.
[15] H. Ren, Q. Wu, W. Gao, and W. Zhou, "Optimal operation of a grid-connected hybrid PV/fuel cell/battery energy system for residential applications," Energy, vol. 113, 2016.
[16] F. Ochs, P. Krimbacher, D. Siegele, and W. Feist, "Niedertemperaturheizung in Kombination mit einer dezentralen Boiler-Wärmepumpe," BauSIM, 2014.
[17] W. Streicher, "Fernwärmeverbundsystem der TIGAS für 2017 - Ermittlung des Primärenergiemix für das FW Verbundnetz der TIGAS für 2017 und weiteren Ausbau Innsbruck," 2018.
[18] K. W. Steininger et al., "The Economic Effects of Achieving the 2030 EU Climate Targets in the Context of the Corona Crisis - An Austrian Perspective," no. March, 2021.
[19] P. Sterchele et al., "Wege zu einem klimaneutralen Energiesystem," 2020.
[20] BMWi, "Energiedaten: Gesamtausgabe Oktober 2019," 2019.
[21] Passivhaus Institut, "Passive House Planning Package (PHPP)," 2022. https://passiv.de.
[22] DIN EN 16147, Heat pumps with electrically driven compressors 2017.
[23] APCS, 2022. https://www.apcs.at/de.
[24] Wiener Stadtwerke Gruppe, "Die Welt im Gleichgewicht halten," 2020.
[25] ENTOS-E, "TYNDP 2022 Draft Scenario Report".
[26] F. Ochs and G. Dermentzis, "Evaluation of Efficiency and Renewable Energy Measures Considering the Future Energy Mix," in IBPC2018, 2018, pp. 1271–1276.
[27] OIB-RICHTLINIE 6, "Energieeinsparung und Wärmeschutz," 2019.
[28] M. Ploss et al., Low Cost nZEB. 2022.

The datasets generated during and/or analysed during the current study are not publicly available because the project is ongoing and the database will be further extended but will be available on request by sending an email to fabian.ochs@uibk.ac.at.

Mine water geothermal energy - abandoned mines as a green energy source

Lukas Oppelt[a], Thomas Grab, Timm Wunderlich, Thomas Storch, Tobias Fieback

[a]Chair of technical thermodynamics, Institute of Thermal Engineering, TU Bergakademie Freiberg, Freiberg, Germany, Lukas.Oppelt@ttd.tu-freiberg.de

Abstract. Abandoned mines offer an opportunity to provide renewable energy. Due to almost constant temperatures all year round and the large rock surfacing as heat-transferring surfaces, mine water is ideal for heating and cooling. At sites where water still has to be pumped upwards after mining has ended this water can still be used for heating or cooling supply of industry or districts e.g. in the German Ruhr area. This offers a positive additional effect of the eternal task for old mining areas. In North America and Europe in particular, a number of pilot plants have already been commissioned. These existing and planned mine water geothermal plants worldwide were studied as part of a literature search. The five largest ones have a maximum heating load of about 0.9 to 11 MW. The construction of further plants often stumbles due to the fact that mine water competes with fossil fuels e.g. natural gas or fuel oil. This is compared under economic and ecological criteria within this paper. As a result, mine water geothermal energy is cheaper to operate than fossil fuels such as oil or gas and labour costs below 6ct/kWh are possible. From an ecological point of view, CO2 emissions are reduced by at least 56 % compared to fossil fuels. One important technical risk for mine water plants is the fouling which must be taken into account: impurities in the mine water can reduce the heat transfer in the heat exchanger, which reduces the efficiency of the plant.

Keywords. mine water, geothermal energy, heat pump, district heating cooling.
DOI: https://doi.org/10.34641/clima.2022.55

1. Introduction

Mining has shaped humanity for thousands of years. The first metal ores were mined on the surface in Germany as early as 1000 BC[1]. Over the centuries, mining changed, and from the 10th to the 12th century in particular, more and more silver and copper deposits were deve loped in Europe. The countries with the largest mine production are currently China, Australia and Indonesia [1 - 4]. Nevertheless the individual deposits are also finite; when the resources are exhausted, the abandoned mines are usually flooded and this offers considerable potential: use as a regenerative energy source. Depending on the location, mine water with temperatures between 15 and 40 °C is available and can be used for heating and cooling applications.

2. Technology

Fig. 1 shows a simplified version of the most frequently used functional principle of mine water geothermal energy. First, the mine water is extracted (a). There are various possibilities depending on the available extraction points. At some locations, e.g. in the Ruhr area, the mine water has to be pumped out permanently so as not to endanger the groundwater. These pumped-out waters can be used directly. At other sites, the former mines are drained via galleries, so that the extraction of mine water is possible there. Further extraction possibilities are listed in Fig. 1. After the mine water has been extracted, the heat is transferred in a heat exchanger (b) to a closed intermediate circuit (c) and from there to the consumer or, if the temperature level needs to be

Copyright ©2022 by the authors. This conference paper is published under a CC-BY-4.0 license.

increased, to a heat pump. The cooled / heated mine water is discharged after the heat exchanger, e.g. into surface waters or back into the drainage gallery. Other systems for geothermal use of mine water are described in [5, 6]. The possible consumers also listed in Fig. 1 require different temperature levels, so that different users result based on the general conditions of a former mine site. This is also one of the limitations of mine water geothermal energy: only consumers near abandoned mines can be used. Transporting the heat over longer distances is often not economised.

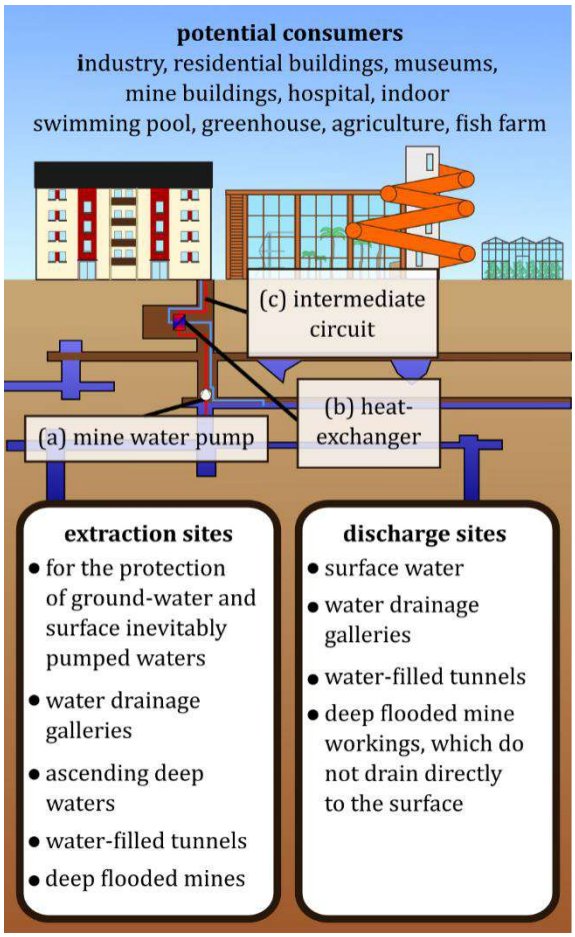

Fig. 1 Basic principle of mine water geothermal energy plant and extraction and discharge sites as well as possible potential users, according to [7]

3. Status quo

Within the framework of literature research, a total of 44 active mine water geothermal plants could currently be researched worldwide. Most of them are located in Germany, Great Britain and the USA [7]. In addition, there are eight decommissioned plants and a large number of planned plants, plants under construction and studies. These are mainly concentrated in Europe and North America. For South America, Africa and Oceania, for example, there is no information on existing or planned plants. Table 1 lists the characteristic values of the five largest plants worldwide.

Tab. 1 –Characteristic values of the currently five largest active mine water geothermal plants worldwide

Novoshakhtinsk	
Location	Novoshakhtinsk, Rostov Region (RU)
Raw Material	coal
Heating power in kW	10.900
Literaturesource	[8]
Zhang-shuanglouCoal Mine	
Location	Xuzhou City (CN)
Raw Material	coal
Heating power in kW	4.750
Literaturesource	[9]
HUNOSA's minesin Cuenca Central	
Location	Mieres, Asturien (ES)
Raw Material	coal
Heating power in kW	3.856
Literature source	[10 bis 13]
Wismut-Schacht 302	
Location	Marienberg (DE)
Raw Material	uranium
Heating power in kW	1.700
Literaturesource	[14, 15]
RothschönbergerStolln	
Location	Freiberg (DE)
Raw Material	silver
Heating power in kW	860
Literaturesource	[16, 17]

One of the first plants in Europe was a plant in Essen, which was opened in 1984. It was used to heat a retirement home [15, 18]. Fig. 2 gives an overview of the number of plants commissioned and shut down per year. The oil price is also shown. It can be seen that there is certain dependence between the rising oil price and the increased commissioning of mine water geothermal plants. A rising oil price also means that the price level for fossil resources rises in general, making the use of alternative energy sources with predictable prices more attractive. Moreover, it must also be taken into account that the reduction of CO_2 emissions is now more important in politics, society and therefore. The expansion of renewable energy sources is to be pushed forward.

Of the currently 18 active plants in Germany, 10 are located in the Ore Mountains in the east of the country. At the moment, for example, energy

utilisation concepts are being developed in the MareEn project for the former coal mining area of Lugau/Oelsnitz (Saxony), in which mine water geothermal energy can be used as the main energy source. For historical reasons, structural change is already more advanced in the Ore Mountains. Currently, however, many plants are also being planned and built in the Ruhr area [7]. For example, in the area of the former mine "Haus Aden", an urban district is to be built on an area of 54 ha, which will be supplied to a large extent with mine water geothermal energy. [19]

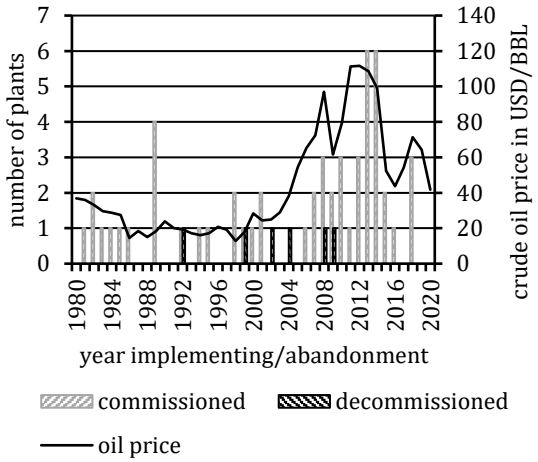

Fig. 2 Comparison of commissioned and decommissioned mine water geothermal plants per year compared to the oil price (according to [7], oilprice: [20])

4. Economic advantages

As a renewable energy source, mine water geothermal energy competes with other renewable and fossil energy sources. The labour costs of the plants depend on various factors. The economic efficiency of the system is subject to various influencing factors:

- Purchase price for electrical power to supply the heat pump, circulation pump, etc.
- Coefficient of performance (COP) of the overall system, depending on e.g.: Temperature range, volumetric flow of mine water, effectiveness of heat exchanger, transport path of the heat, etc.

Figure 3 shows the COP of the overall mine water system and the electricity price in euro cents. From the intersection of these two influencing factors, the labour price for one kWh of heat or cold of the mine water geothermal system can be read. In comparison, the labour costs for a kWh of heat from bioenergy (wood pellets), district heating, natural gas and fuel oil are shown. This is based on the framework conditions and costs of the German market.

As an example, the labour costs are entered for three different plants and scenarios. These are based on monitoring results and electricity prices customary in the respective countries. It becomes clear that at very high work rates (e.g. summer mode at the Reiche Zeche), labour costs for mine water geothermal energy of less than 6 ct/kWh are achieved even at electricity prices > 30 ct/kWh. This makes the energy source competitive with fossil fuels such as gas. The great advantage of this plant is the combined use of mine water for heating and cooling.

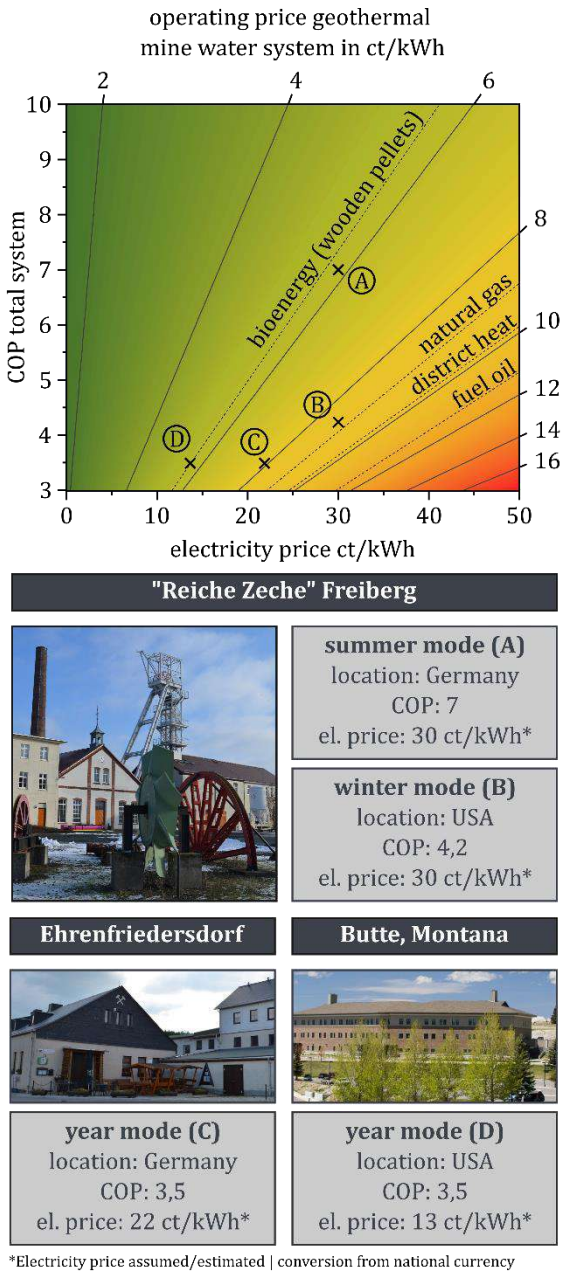

Fig 3. Labour costs of a mine water geothermal plant as a function of COP and electricity price, comparison of different scenarios and to costs of other energy sources (dotted lines) (data, figure Butte: [21])

For cooling, the temperature level of the mine water can be used directly at this location (around 14 °C in summer); no additional effort is required for a secondary system as e.g. a heat pump. Cooling thus represents a large additional benefit, with only little additional effort due to the circulation pumps. For a detailed consideration of the monitoring results of

the "ReicheZeche" plant, please refer to Oppelt et al. 2021 [7]. However, even older systems like the one in Ehrenfriedersdorf/Saxony (year of installation: 1994), which achieve coefficients of performance between 3 and 4, can operate economically if they run effectively and, for example, a more favourable heat pump tariff for electricity supply is possible. The operational costs such as maintenance and servicing along with the consumption-related costs are referred by the energy prices shown in the diagram.

It becomes clear that all the scenarios considered are cheaper than the supply costs for fossil energy sources such as fuel oil, natural gas or the German district heating mix. Only a supply via wood pellets (and thus also renewable) can be cheaper in the scenarios considered. However, heating with pellets does not allow for parallel cooling and large heating capacities are usually not possible or require a great deal of effort to have enough pellets available.

It is also clear that the price of electricity has a decisive influence; with lower coefficients of performance, the system can still be economical. This can be seen in the plant from Butte (D) listed in Figure 3. Due to the lower electricity price in the USA, the plant would even be cheaper under the German framework conditions than a supply with bioenergy.

The CO_2 tax could be an important factor in the future. If additional costs are incurred for the resulting emissions, e.g. for a kWh of gas, this fossil energy source becomes more expensive. We will take a closer look at this in the following section in order to be able to classify the energy source of mine water geothermal energy ecologically.

5. Ecological advantages

For the mine water geothermal plant in Ehrenfriedersdorf (see Figure 3), a life cycle assessment according to DIN EN ISO 14040/44 was carried out as an example. The entire life cycle was considered. Figure 4 shows the result for the following five impact categories:

- Global Warming Potential (GWP)
- Acidification potential (AP)
- Eutrophication potential (EP)
- Ozone Depletion Potential (ODP)
- Photochemical Ozone Creation Potential (POCP)

It is clear that 88 to 96 % of the environmental impacts of the impact categories arise from the operational phase. The reason for this is the electricity mix used as a basis in Germany. Increased use of renewable energy sources in the German electricity mix would enable further reductions here. Only in the case of ozone depletion potential are most of the effects in the construction phase, the cause being the refrigerant. However, it should be noted that this only has a negative impact in the event of leakage or improper disposal. In summary, it is also clear that the disposal of the system usually accounts for less than 1 % of the total impact and thus causes only minor environmental effects.

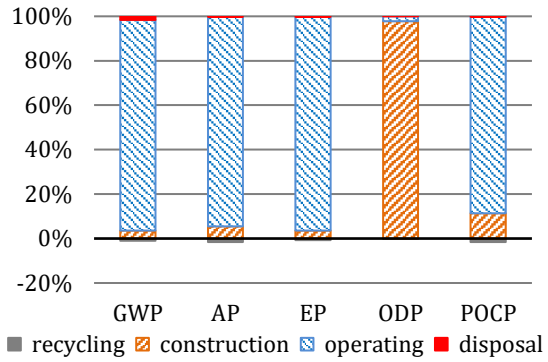

Fig 4 Percentage shares of the life cycle phases in the total impact per impact category

Figure 5 shows a comparison of the energy source mine water geothermal energy to other energy sources based on the CO_2 equivalent. The basis for the calculation for mine water geothermal energy is the analysis of the plant in Ehrenfriedersdorf.

It can be seen that mine water geothermal energy can significantly reduce CO_2 emissions compared to all fossil energy sources. For example, compared to the use of lignite, CO_2 emissions are reduced by around 75%, and by at least 56% compared to natural gas. Here, too, a further reduction is possible if the electricity required for the mine water geothermal system is provided from renewable energy sources.

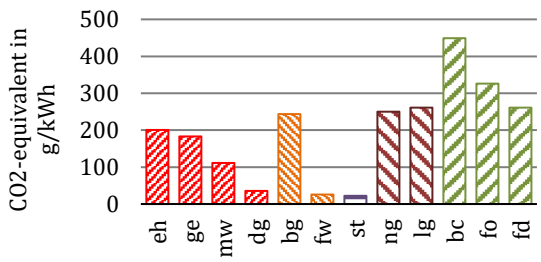

eh	environmentalheat
ge	geothermalenergy (nearsurface)
mw	mine water geothermalenergy
dg	deep geothermalenergy
bg	biogas
fw	firewood
st	solar thermalenergy
ng	natural gas
lg	liquid gas
bc	brown coal
fo	fuel oil
fd	fossil district heat

Fig. 5 Ecological comparison of mine water geothermal energy with other energy sources via CO_2 equivalent for the plant in Ehrenfriedersdorf

6. Technical risk - fouling

Fouling can have a significant impact on the mine water system. Depending on the location, the mine water carries various dissolved/undissolved substances, particles, bacteria, etc. with it. If heat is extracted (heating) or supplied (cooling) in the heat exchanger, this can lead to precipitation in the tubes, filters and in the heat exchanger. An example is shown in figure 6. These deposits cause a reduction in the amount of heat transferred and an increase in pressure loss. As a result, the system works inefficiently: less heat can be extracted from the mine water and other, e.g. fossil, alternative systems have to be used additionally. In addition, the necessary cleaning of the heat exchanger results in downtimes and additional costs. Even with a biofilm of 250 µm, the amount of heat transferred is reduced up to 50 %. [22] In real terms, there are deposits of more than one millimeter.

Currently, the TU Bergakademie Freiberg is investigating possible materials and coatings for the heat exchanger with the goal to reduce the deposits or at least enable complete cleaning. Initial results show that a reduction in heat transfer losses of up to 80 % is possible. It should be noted that the mine water has different characteristics depending on the mine site and therefore site-dependent solutions must be checked and possibly developed.

Fig. 6 Fouling layer on a heatexchangerplate

7. Summary and outlook

Worldwide, the closure of mines offers opportunities to use them as a renewable energy source for heating and cooling. Depending on the site conditions, there are various possibilities to use the mine water, e.g. at sites where the mine water is pumped out to protect the groundwater or can be used directly without additional pumping. Since the 1980s geothermal mine water plants have been built all over the world, and in recent years the number of new plants has increased steadily. Reasons for this include rising energy prices and the political objectives of many countries against climate change. A mine water geothermal plant can compete with fossil energy sources if it is operated effectively (COP high) and at best can provide heating and cooling at constant, calculable energy prices. From an ecological point of view, a reduction in CO2 emissions of at least 56% is also possible compared to fossil energy sources, depending on the boundary conditions. The limits of the technology are that consumers must always be available in the immediate vicinity of the source. Transporting low-temperature heat from mine water is usually not economical. Furthermore, the problem of fouling must be taken into account. The impurities carried in the mine water cause deposits in the heat exchanger and reduce the efficiency of the system. The TU Bergakademie Freiberg is investigating an innovative heat exchanger design to reduce fouling.

8. Acknowledgement

We would like to thank the European Union and the Free State of Saxony for the financial support of the VODAMIN II, GeoMAP and MareEn projects. In addition, we would like to thank all the technicians involved as well as J. Balski and R. Klink, who supported the project work as part of their practical student work.

The datasets generated during and/or analysed during the current study are not publicly available because they are part of the VODAMIN II project and the final version of the final report isn't published now but will be available when the finale report is published.

9. References

[1] Ramos, E. P. u. Falcone, G.: Recovery of the geothermal energy stored in abandoned mines. In: Hou, M. Z., Xie, H. u. Were, P. (Hrsg.): Clean Energy Systems in the Subsurface: Production, Storage and Conversion. Proceedings of the 3rd Sino-German Conference. "Underground Storage of CO2 and Energy", Goslar, Germany, 21-23 May 2013. Springer Series in Geomechanics and Geoengineering. Berlin: Springer; Imprint: Springer 2013

[2] MINERAL COMMODITY SUMMARIES 2021, U.S. Geological Survey, 2021

[3] Bernhard, M.: Die Silberstrasse und ihre Geschichte. [deutsch, English, français]. Leipzig: Sachsenbuch 1992

[4] Symmangk, R.: Bergbau- und Industriegeschichte. Jahrestagung der Deutschen Bodenkundlichen Gesellschaft. Böden ohne Grenzen - Allgemeiner Exkursionsführer. DBG, Bd. 111. 2008, S. 87–99

[5] Grab, T., Storch, T. u. Groß, U.: Energetische Nutzung von Grubenwasser aus gefluteten Bergwerken. In: Bauer, M., Freeden, W., Jacobi, H. u. Neu, T. (Hrsg.): Handbuch Oberflächennahe Geothermie. Berlin, Heidelberg: Springer Berlin Heidelberg 2018, S. 523–586

[6] Walls, D. B., Banks, D., Boyce, A. J. u. Burnside, N. M.: A Review of the Performance of Minewater Heating and Cooling Systems. Energies 14 (2021) 19, S. 6215

[7] Oppelt, L., Grab, T., Pose, S., Storch, T. u. Fieback, T.: Mine water geothermal energy as a regenerative energy source - status quo and results from five years of monitoring. Oil Gas EUROPEAN MAGAZINE 47 (2021) 01/2021, S. 15–19
[8] Energy switch to renewables in Novoshakhtinsk, Rostov region, Russia, UNFCCC, 2007
[9] Guo, P., He, M., Zheng, L. u. Zhang, N.: A geothermal recycling system for cooling and heating in deep mines. Applied Thermal Engineering 116 (2017), S. 833–839
[10] "BARREDO COLLIERY" DISTRICT HEATING, HULLERAS DEL NORTE S.A., S.M.E., 2019
[11] Menéndez, J., Ordóñez, A., Álvarez, R. u. Loredo, J.: Energy from closed mines: Underground energy storage and geothermal applications. Renewable and Sustainable Energy Reviews 108 (2019), S. 498–512
[12] Ordonez, A., Andres, C., Alvarez, R. u. Jardon, S.: Harnessing groundwater as a water supply and energy resource. Sequridad y medioambiente 30 (2010) 118, S. 43–60
[13] Loredo, J., Ordóñez, A., Jardón, S. u. Álvarez, R.: Mine water as geothermal resource in Asturian coal mining basins (NW Spain). 11th International Mine Water Association Congress. Mine Water - Managing the Challenges. 2011, S. 177–181
[14] Lagerpusch, K. H.: Stellenwert Bergbau - Geothermie in Sachsen. Workshop "Bergbau-Geothermie" im Rahmen der ReSource-Arbeitsgruppe "Natürliche Potentiale". Bad Schlema 2010
[15] Wieber, G. u. Ofner, C.: Geothermische Potenziale gefluteter Bergwerke. bbr Jahresmagazin (2008)
[16] Johnson Controls: Hohe Heizkosten sind heilbar: Grubenwasser dient als Energiequelle für zweistufige Ammoniak-Wärmepumpe im Kreiskrankenhaus Freiberg. Fallstudie
[17] Ulbricht, S.: Wieder Pionierrolle für Freiberg. Projekt "Energetische Optimierung im Kreiskrankenhaus Freiberg" nutzt Warmwasser des Supertunnels. Wochenspiegel - regional (2013), S. 3
[18] Wieber, G. u. Pohl, S.: Mine Water: A Source of Geothermal Energy - Examples from the Rhenish Massif. Proc. 10th Int. Mine WaterAssociationCongress. 2008, S. 113–116
[19] Altieri, L., Wagner, H.-J., Gross, M. u. Reiners, T.: Kalte Nahwärmenetze mit Geothermischer Energie aus Grubenwasser. Der Geothermiekongress. Essen 2018
[20] OPEC u. IEA: Average annual Brent crude oil price from 1976 to 2020, 2020. https://www.mwv.de/statistiken/rohoelpreise/
[21] Case Study of the ARRA-Funded GSHP Demonstration at the Natural Sources Building, Montana Tech, Malhotra, M., Liu, X. u. Walburger, A., 2014
[22] Goodman, P. D.: Effect of chlorination on materials for sea water cooling systems: a review of chemical reactions. British Corrosion Journal 22 (1987) 1, S. 56–62

Humidification in healthcare facilities - knowledge base and practice

Marcel Loomans [a], Karin Kompatscher [b], Emelieke Huisman [c], Helianthe Kort [a,c], Wim Maassen [d], Roberto Traversari [b]

[a] Department of the Built Environment, Eindhoven University of Technology, Eindhoven, the Netherlands, ~~M.G.L.C.Loomans@tue.nl~~ ; ~~H.S.M.Kort@tue.nl~~ .

[b] TNO, Delft, the Netherlands, email address, karin.kompatscher@tno.nl ; roberto.traversari@tno.nl .

[c] University of Applied Science, Utrecht, the Netherlands, emelieke.huisman@hu.nl

[d] Royal HaskoningDHV, Rotterdam, the Netherlands, wim.maassen@rhdhv.com .

Abstract. Humidification is not a common procedure in many buildings in the Netherlands. An exception are buildings used for healthcare, especially hospitals. There, e.g. in operating theatres, relative humidity (RH) generally is controlled stringently at levels around 50%. From an energy point-of-view humidification is an energy-intensive activity. Currently, more than 10% of the total energy used in healthcare buildings is spent on humidification. The basis for an RH of around 50%, however, is not clear. Therefore, we pursued a scoping review to find evidence for specific RH thresholds in such facilities. In addition, an inventory was made of the current practice in the Netherlands. After analyzing the title and abstracts, the remaining references were read by two persons and scored on several topics. Guidelines and current practice were analyzed by referring to existing (inter)national guidelines and standards, and by contacting experts from Dutch hospitals through a survey and semi-structured interviews. Outcomes from the literature review were grouped into four different topics: 1) micro-organisms and viruses, 2) medical devices, 3) human physiology and 4) perception. No scientific evidence was found for the currently generally applied RH set-point of ~50%. Some studies suggest a minimum RH of 30% but the evidence is weak, with exception of medical devices if specifications require it. A lack of research that addresses more long-term exposure (a couple of days) and includes frail subjects, is noted. It was found that RH requirements are strictly followed in all hospitals consulted, some only focusing on the hot zones, but in many cases extended to the whole hospital. Steam humidification is mostly applied for hygienic reasons. but is quite energy-intensive. The conclusion t is that there is no solid evidence to support the RH-setpoints as currently applied in the Netherlands. It merely appears a code of practice. Therefore, there appears room for quick and significant energy savings, and CO2 emission reductions, when considering control at lower RH values or refraining from humidification at all, while still fulfilling the indoor environment requirements and not negatively influencing the health risk. This outcome can be applied directly in current practice with the available techniques.

Keywords. Relative humidity, Health, Energy, Hospitals, Literature review, Guidelines, Survey.
DOI: https://doi.org/10.34641/clima.2022.307

1. Introduction

Also in healthcare sustainability is an issue of concern. In order to align with the need to reduce CO_2-emission, a so-called Green Deal Duurzame Zorg [1] (Sustainable Care) has been initiated by the Dutch government. Healthcare facilities are an important energy consumer and effort is put in reducing the energy demand of such type of facilities. The energy demand, amongst others, relates to the conditioning of the indoor environment. Temperature, relative humidity and air quality are examples of indoor environment parameters which are controlled to support the healthcare process. From literature, we

Copyright ©2022 by the authors. This conference paper is published under a CC-BY-4.0 license.

know that the indoor environment affects health, well-being, comfort and productivity [2–4]. The conditions that are set for the parameters that constitute the indoor environment, determine the energy demand in the end. Efficient solutions for realizing these conditions support the reduction of the energy demand. Alternatively, relaxing the requirements (conditions) concerning the indoor environment may also help in reducing the demand, or support the energy flexibility [5]. However, energy savings in healthcare cannot be realized at the expense of the primary process, i.e., availability of functions, patient safety, quality of care and the preconditions within which this care must be provided. In other words, the quality of the healthcare and the performance of the building to support that process cannot be compromised.

Nevertheless, we see that assumptions for indoor environment requirements are not that rigorous. Guidelines for health-based criteria exist when dealing with indoor air quality [6,7]. However, for many contaminants information is still lacking.

Focusing on relative humidity (RH), if values are provided, they generally refer to (thermal) comfort. For healthcare, when related to RH, in the Netherlands current practice heavily relies on past assumptions and codes of practice, e.g. from the former Dutch College Bouw Zorginstellingen [8]. As a result, in the Netherlands, RH in healthcare environments is generally controlled at around 50%. Due to the climatic conditions, then air humidification is required, which therefore is a standard component of the air treatment in HVAC systems for healthcare facilities, particularly in hospitals, but also in long-term care. Nevertheless, the scientific evidence for this code of practice is meager. Notably, air humidification, applying central steam humification, is an energy-intensive process. As a result, humidification is a relatively large energy consumption item (>10%) [9].

Following the above, we see two directions for addressing the sustainability requirement in healthcare settings, related to the RH. First, there is a need to derive more (scientific) evidence for the code of practice as applied currently, that assumes RH values in a relatively small range around 50%. Secondly, current practice with respect to RH-settings and air humidification can provide further insights into how humidification in the Netherlands, in healthcare facilities, is dealt with and what options are available as an alternative.

In view of the situation outlined above and the two clearly different subjects which relate RH to sustainability, this research has been divided into two parts. On the one hand, a literature study was conducted into what limits for relative humidity conditions are in place for the indoor environment, specifically in healthcare settings, in order to achieve a safe environment for patients and staff from the point of view of health and comfort. On the other hand, using current practice as a starting point, an inventory was made to summarize RH set-points and humidification solutions, as currently applied within Dutch hospitals, and assess possibilities (techniques) that could be considered for realising humidification safely and sustainably. This has been translated into two research questions:

1. What is the necessity of humidification, i.e., which RH condition is required in care facilities from the point of view of safety and comfort of the patient and the nursing staff and is there a distinction in functions?

2. In which alternative, more energy-friendly way, can humidification be realised? This taking into account patient safety and comfort requirements of the building users.

2. Methods

2.1 Scoping review (knowledge base)

In order to answer the first research question, a literature study (so-called scoping review) was conducted. The scoping review included studies till November 2020, with a specific supplement on electrostatic discharge till February 2021. It consisted of five different steps: 1. identify the research question, 2. identify relevant studies, 3. select studies, 4. identify themes, 5. report. The steps are based on the framework of Arksey and O'Malley [10] and assume an iterative process. The iterative process makes it possible to go back to earlier steps if new insights are gained that can give more direction to the next step in the review process.

The literature study focused on the necessity of humidification in healthcare buildings from the point of view of patient and staff safety and comfort, and process support. For that, the literature study focused on the following four topics:

1. The effect of RH concerning the survival of micro-organisms and viruses;
2. The effect of RH on the functioning of medical equipment;
3. The effect of RH on human physiology;
4. The effect of RH on perceived human well-being and comfort.

The included databases for the scoping review were: Scopus, Pubmed, Web of Science and Science Direct. The choice was made to search databases from a health perspective and a building perspective so that the theme of air humidification in healthcare buildings was mapped as broadly as possible. The search terms applied were based on the categories indoor air quality, environment, perception, experience and comfort and micro-organisms and viruses.

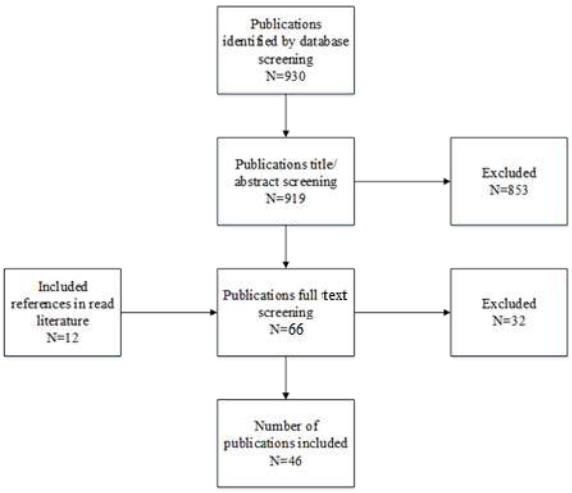

Fig. 1. Flow diagram screening process publications.

The screening process and its outcome are summarized in **Fig. 1**. After processing the results from the search on duplications and the first screening on title and abstract, in total 78 publications were read completely and assessed by two team members. The assessment was performed based on an assessment matrix (rubric) covering topics such as reliability, context, method, usefulness of the results and conclusion. The assessment resulted in a score. The maximum score that could be arrived at was 27. Inclusion or exclusion of an article was discussed if opinions for a publication differed by 5 points or more between the reviewers, or if the score was around 10-20. In general, only articles with a score higher than 15 were included. In the end, a total of 46 publications were included after the screening process.

In the analysis of the information from the articles, the effect of RH on the four topics indicated above was treated separately.

2.2 Practice (inventory)

In the second part of the study, an inventory was made of the current practice, with regard to humidification in Dutch hospitals. This information was obtained through semi-structured interviews with relevant experts in The Netherlands, selected from the research network (e.g., facility management staff and clinical physicists), employed by hospitals and manufacturers of medical equipment. The interview was designed to discuss issues related to (i) requirements set for the relative humidity, (ii) whether requirements differ between functions in the hospital, and (iii) what humidification principles are used for humidification. In total experts from 20 different hospitals were consulted in this way.

In addition, desk research was applied to gather information on standards and guidelines and with respect to techniques applied for humidification, apart from steam humidification.

The concept reports from both studies were presented to a group of experts and persons from practice for peer-review and content validity. These were experts in different fields such as medical specialists (pulmonologist, medical microbiologist), doctors, infection prevention specialist, and technical related experts such as a building services engineer and facility manager. In combination with a rebuttal document to answer the remarks made, their comments were implemented in the final version of the report.

3. Results and discussion

3.1 Knowledge base

The outcomes of the literature study have been gathered in tables that provide information on the type of study performed (e.g., Experiment, Intervention, Case study, Literature study), the environment in which the research was performed (e.g., Hospital, Office, School), and a summary of the specifics of the outcome. A full overview of the tables as developed can be found in [11]. An example of a part of one of the tables developed is shown in **Fig. 2**. Below we summarize the main findings from the literature review and the subsequent analysis.

The information obtained has been grouped according to the four topics indicated: 1) Micro-organisms and viruses, 2) Medical equipment, 3) Physiological aspects and 4) Perception of comfort and well-being. The included studies indicate that RH is often not investigated as a separate parameter but in combination with various other aspects. It, therefore, is not always straightforward to quantify the individual effect of the RH on the outcome.

From the point of view of microbiological organisms, there is a dependency on the type of organism. Temperature and RH conditions outside the host determine the chance/time that for example, a virus, can remain infectious. However, the conditions under which the chance of survival is greatest differ per organism and it is not possible to state a specific value for this. In general, low and high RH values should be avoided. Studies regarding the relationship between RH and transmission of micro-organisms and viruses have not been found.

The lower RH limit used for medical equipment is associated with electrostatic discharge (ESD). To limit ESD, a lower limit of 30% RH is found for medical equipment. The specifications of such equipment are leading for the minimum RH value to be applied, because this can influence the functioning of the equipment. From a comfort point of view, it is also desirable to prevent ESD (shocks when touching surfaces and other people) by using the right material, e.g., footwear (conductive) and bedding (cotton). The RH can reduce this form of ESD, but it cannot completely prevent it.

Subthema / Thema	Score MAX. 27	Omgeving	Type Studie	Micro organismen: Schimmels	Bacteriën	Virussen	Mijten	Allergenen
(Dabisch et al., 2021)	24	AC	EXP			RV 20%-70% [T=10-30°C] inactivitatie SARS-CoV-2 nauwelijks beïnvloed.		
(Wolkoff, 2018)	23	KO	LS			RV > 40% Virus ↓		
(Shajahan et al., 2019b)	22	ZO	LS	RV > 45%-50% bevordert schimmelgroei	RV > 45%-50% beïnvloedt concentratie bacterieen	T=30°C bij een RV 50% om griepvirussen te beheersen		RV > 45%-50% beïnvloedt concentraties allergenen
(Božić, Ilić, & Ilić, 2019)	21	ZO	CS	→ RV 30% - 40% *	→ RV 30% - 40% *			
(Heutte et al., 2017)	21	ZO	EXP	RV kan worden beschouwd als omge-vingsdeterminant van schimmels in de lucht.				
(Pyankov, Bodnev, Pyankova, & Agranovski, 2018)	21	LO	EXP			Overleving neemt af bij hete en droge lucht *		
(Mousavi et al., 2019)Iran	21	ZO	CS	RV 23% - 33% *	coagulase-negative staphylococci (68%), Micrococcus, bacillus RV 23% - 33% *			
(Yang, Elankumaran, & Marr, 2012)	20		LO			Influenza virus en de levensvatbaarheid; RV <50% ↑*		
(Lowen & Steel, 2014)	19,5	ONB	EXP			Transmissie tussen gastheren ~100% bij T=5°C en RV 20% -35%		
(Peccia, Werth, Miller, & Hernandez, 2001)	19,5	AC	EXP		Afname inactivatie bij gebruik UV-C bij RV>50%; Natuurlijke inactivatie wordt niet beïnvloed door RV in range 20%-90% *			

Fig. 2. Example of a part of the table as prepared from the literature review. The example shown is for micro organisms and viruses. Note that the information in the example is in Dutch.

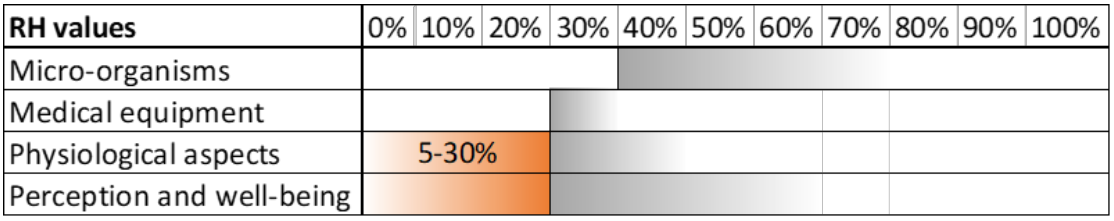

Fig. 3. Summary outcome literature study for the four identified topics investigated. The gradient in colour indicates that there is no fixed value. The orange colour indicates that there is room for lower RH-levels to be applied. An upper RH-limit could not be identified.

Physiological symptoms such as dry eyes, nose complaints, respiratory complaints and headaches can be caused by low RH levels. Many complaints related to physiological symptoms seem to increase at RH lower than 30%. The studies considered, however, often have the limitation that the duration of exposure to these conditions is not explicitly given or is limited (up to a few hours). More long-term exposure (a few days, e.g., related to patient hospitalization) has not been investigated, while this will be the case for the most critical persons (patients) within the care facility. The results available generally are more representative of an outpatient situation. For that matter, there are almost no studies available that address optimal RH-conditions for personnel in such facilities.

In general, significant effects of RH on the perception of dry air seem to be limited. Individual sensitivity may have an effect on this perception. With respect to thermal comfort, the sensitivity to RH, when in normal ranges, is low [12].

Fig. 3 summarises the outcomes of the literature review. It again distinguishes the four topics that were investigated in the context of healthcare buildings. We conclude from the literature available that strict guidelines on RH for healthcare facilities are not to be derived from the current (scientific) information as available in literature. From the overall results, a minimum level of 30% RH may be suggested, but the evidence is weak. In **Fig. 3** the orange colour indicates that there is room for lower RH-levels. We do not propose a higher limit for RH as no information is available to support such a limit for a healthcare environment. Specifications for medical equipment, however, may require such a limit. With respect to air humidification, the lower limit is of most interest, though in practice of course higher RH levels remain possible due to climatic conditions.

The outcome deviates somewhat from reviews such as that from [13]. Sterling et al. propose a RH range between 40% and 60%, at normal room temperatures. The focus of that review is mainly on micro-organisms and a few physiological outcomes and did not focus on healthcare environments. The current review is wider and focuses on healthcare environments.

The concept of dry air in relation to perception and physiological outcomes is complex, as Wolkoff [14] concludes. The closely related link between low RH and indoor air pollution is an underlying explanation for that. In line with the conclusion from Wolkoff, we also find that current research with respect to the

effect of RH on physiological and perceived outcomes is missing. Especially research that resembles realistic situations, in space and time. In this respect there also is an urgent need to distinguish between the 'average' person and the average type of person that is expected to frequent healthcare more often, i.e., frail and aging people.

Following the information gathered from the literature review, there currently is no actual scientific support to keep the RH-level in Dutch hospitals at the generally applied 50% RH. Put otherwise, there is no information available in the current scientific literature that indicates that a RH-level of 50% is best for the people working and staying in healthcare environments. A lower value would still provide for a similar performance on the separately identified topics.

3.2 Practice

Inventory Dutch hospitals

From the inventory, it is concluded that 100% of the surveyed Dutch hospitals (n = 20) apply air humidification as part of their HVAC system for conditioning the supplied air. 72% of the respondents indicated that they use steam humidification as a source for that. The remainder (28%) uses a combination of steam and water humidification. Water humidification alone or combined with steam humidification generally is restricted to low-risk rooms, such as offices. For high-risk rooms, such as operating theatres, steam humidification is applied in all cases because of hygienic assumptions. This is generally done centrally. Decentralized solutions are only applied due to in-use changes of function or rooms. The majority of the hospitals (83%) apply humidification for the entire building. The set-points that are applied vary per hospital surveyed and depend, amongst other things, on the chosen grouping of functions. In 89% of the cases the users of the building are not able to change the RH set-point. That is done centrally by the facility management.

Almost all respondents indicated a subdivision for the operating theatre (hot-zone) and the category 'miscellaneous' which can be considered the remaining functions. Some respondents distinguished these other function groupings with different climatological requirements (e.g., office function, patient room, ICU/CCU, laboratories, pharmacy, lung department, scope department and MRI room). The majority of the set-points used in practice for the operating theatre were ≥50% RH. For the other rooms this was 42.5% RH, with a wider spread in outliers due to the many different function groupings in this category (see **Fig. 4**). According to the respondents, the reason for using strict RH requirements is based on the requirements for medical equipment, comfort, hygiene and perception of wound dehydration, and from guidelines, history and experience.

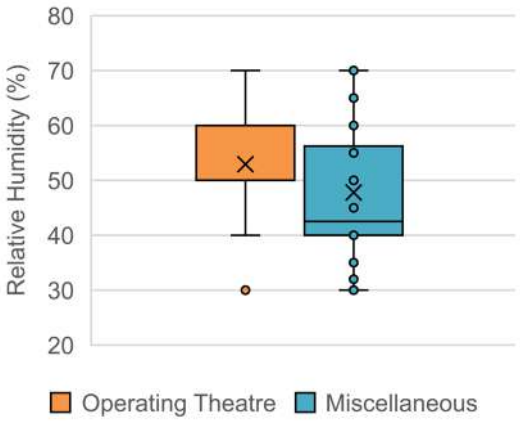

Fig. 4. Distribution of RH set-points as applied currently in practice in the Netherlands.

The inventory of (inter)national standards and guidelines results in an overview of the current recommendations for air humidification. This overview is summarized in tables and can be found in [15]. Standards and guidelines do not show unanimity with respect to the required RH conditions in healthcare settings, and do not provide a scientific knowledge base for suggested RH requirements. An RH of 20% is the lowest lower limit found [16], while a lower limit of 50% RH is used in publications of the former Dutch College Bouw en Ziekenhuisvoorzieningen [8].

Alternatives to (steam) humidification

As could be concluded from the survey, steam humidification is currently the most common technique in Dutch hospitals, when humidification is applied. By heating water (>100°C), steam is produced and supplied to an air stream. The advantage of this technique is the very likely elimination of pathogens.

An alternative to steam humidification is water humidification (i.e., adiabatic humidification). With water humidification, water in its liquid state is supplied into the air flow (i.e., spraying, vaporizing or atomizing) so that no heating of the water is required before addition. However, evaporation of moisture in the air removes heat from the air stream, causing it to cool and requiring additional energy to bring the air flow up to the required temperature before being supplied into a room.

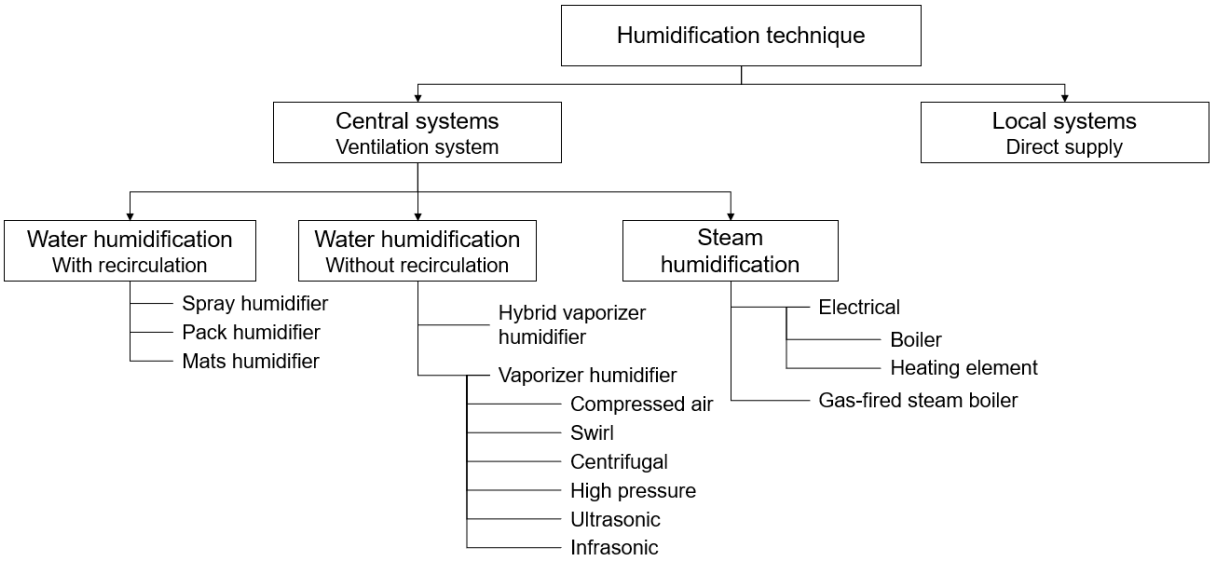

Fig. 5. Overview of available air humidification techniques.

Different types of humidification techniques can be applied when using water humidification. **Fig. 5** provides an overview of the techniques currently available. Techniques with and without recirculation are available. Water humidification with recirculation uses collected water to minimize water consumption. In any case, the microbiological safety, e.g., because of legionella, of this form of humidification still needs to be monitored, in order to gain sufficient certainty about the functioning and safety of such systems in healthcare applications.

Standards and guidelines reflect this precaution by preferring steam humidification over water humidification. Some standards, e.g. DIN194604 [17] only allow the use of steam humification in operating theatres. In the case of water humification, additional requirements are prescribed to assure hygienic performance.

The advantage of water humidification is found in the possibility to apply renewable forms of energy, in combination with a heat pump, to condition the supply air. This is nearly not possible for steam humidification, due to the high temperatures required for that process. On the other hand, hydrogen gas and electricity can be applied to produce steam. Steam production generally is done centrally and therefore prone to heat losses in the distribution process.

4. Conclusion

This study has shown that, in practice, strict requirements are often set for the relative humidity, while the justification for these strict requirements cannot be found in the scientific literature, or is only very limited available or very weak. In general, research on this specific subject, related to healthcare environments, is scarce. This also limits the possibility of providing a good quantitative foundation for the values to be set for the RH in such environments. Based on the available information, an indicative lower limit of 30% RH may be desirable, considering issues such as medical equipment, physiological aspects and well-being and comfort. For micro-organisms and viruses, no general relationship has been found between the occurrence and inactivation of these and the RH. For that matter, more aspects than humidity alone play a role in the transmission and development of infections. An upper limit for RH cannot be advised, as there is no unambiguous optimum for all four topics described in the knowledge base. The emphasis of the studies found and analyzed is on low values for RH. In the context of humidification, the lower limit is of most interest.

In addition to the fact that information on the effect of RH on the identified topics is limited, the connection with the healthcare environment is even more limited. It is concluded that the available research is not well aligned with the situation as found in a healthcare setting. That mainly relates to the duration of the studies performed, generally in the order of hours, and to the subjects involved, healthy (young) people. That is not representative for an in-house patient that is required to stay for a few days in a patient room. There is an urgent need to have research outcomes available that reflect this actual situation better.

Per room or function, primarily a balance will have to be found between presence of (medical) equipment, presence of patients and perception of comfort, with regard to humidity on the one hand and the resulting energy consumption for humidification on the other hand. If there are rooms where medical equipment is used that is sensitive to humidity (high/low RH-values), such as MRI and CT scanners, or other critical equipment, specific requirements can be leading. While in other situations, where no critical equipment or critical processes take place, the need for humidification can be questioned, based on the knowledge base gathered in this research.

5. Acknowledgement

The research was funded by the Dutch association of Hospitals (NVZ), the Dutch Federation of University medical centres (NFU) and the Ministry of Health, Welfare and Sport.

6. Data access statement

The datasets generated and analyzed during the current study are not publically available because of privacy reasons, but they will be available on request and in consultation. The information from the literature review is available through the refered report.

7. References

[1] Anonymous, C-226 Green Deal: duurzame zorg voor een gezonde toekomst, The Netherlands, 2019. https://www.greendeals.nl/sites/default/files/2019-05/Deal tekst GreenDeal 226 Duurzame zorg voor gezonde toekomst_0.pdf (accessed August 28, 2019).

[2] L. Fang, D.P. Wyon, G. Clausen, P.O. Fanger, Impact of indoor air temperature and humidity in an office on perceived air quality, SBS symptoms and performance, Indoor Air, Suppl. 14 (2004) 74–81. https://doi.org/10.1111/j.1600-0668.2004.00276.x.

[3] E.F. Hall, A. Dusseldorp, Gezondheidseffecten van een lage relatieve luchtvochtigheid in woningen, 2008.

[4] J. Razjouyan, H. Lee, B. Gilligan, C. Lindberg, H. Nguyen, K. Canada, A. Burton, A. Sharafkhaneh, K. Srinivasan, F. Currim, S. Ram, M.R. Mehl, N. Goebel, M. Lunden, S. Bhangar, J. Heerwagen, K. Kampschroer, E.M. Sternberg, B. Najafi, Wellbuilt for wellbeing: Controlling relative humidity in the workplace matters for our health, Indoor Air. 30 (2020) 167–179. https://doi.org/10.1111/ina.12618.

[5] C. Papachristou, P.J. Hoes, M.G.L.C. Loomans, T.A.J. van Goch, J.L.M. Hensen, Investigating the energy flexibility of Dutch office buildings on single building level and building cluster level, J. Build. Eng. 40 (2021) 102687. https://doi.org/10.1016/J.JOBE.2021.102687.

[6] A. Dusseldorp, M. van Bruggen, Gezondheidkundige advieswaarden binnenmilieu , een update, (2007) 52. http://www.rivm.nl/bibliotheek/rapporten/609021043.pdf%0Ahttp://www.rivm.nl/rvs/Normen/Milieu/Luchtkwaliteitsnormen.

[7] World Health Organization, WHO global air quality guidelines: particulate matter (PM2.5 and PM10), ozone, nitrogen dioxide, sulfur dioxide and carbon monoxide, Bonn, Germany, 2021. https://apps.who.int/iris/handle/10665/345329 (accessed November 26, 2021).

[8] College bouw zorginstellingen, Gebouwdifferentiatie van een ziekenhuis, 2007.

[9] C.T. Ferreira Porto, Towards zero energy hospital buildings - Energy savings through central steam systems analysis and alternative humidification scenarios Department of the Built Environment Faculty of Architecture Building and Planning Unit Building Physics and Services, Eindhoven, 2020.

[10] H. Arksey, L. O'Malley, Scoping studies: towards a methodological framework, Int. J. Soc. Res. Methodol. 8 (2005) 19–32. https://doi.org/10.1080/1364557032000119616.

[11] M.G.L.C. Loomans, E. Huisman, K. Kompatscher, A.A.L. Traversari, H.S.M. Kort, W. Maassen, Bevochtigingseisen in de zorghuisvesting - kennisbasis, Delft, The Netherlands, 2021. https://www.expertisecentrumverduurzamingzorg.nl/wp-content/uploads/2021/06/Bevochtigingseisen-kennisbasis.pdf.

[12] M.G.L.C. Loomans, The Measurement and Simulation of Indoor Air Flow, Eindhoven University of Technology, 1998. https://pure.tue.nl/ws/portalfiles/portal/1362860/9803293.pdf.

[13] E.M. Sterling, A. Arundel, T.D. Sterling, Criteria for Human Exposure to Humidity in Occupied Buildings, ASHRAE Trans. 91 (1985) 12.

[14] P. Wolkoff, The mystery of dry indoor air – An overview, Environ. Int. 121 (2018) 1058–1065. https://doi.org/10.1016/J.ENVINT.2018.10.053.

[15] K. Kompatscher, A.A.L. Traversari, E.

Huisman, M.G.L.C. Loomans, H.S.M. Kort, W. Maassen, Bevochtigingseisen in de zorghuisvesting - praktijk, Delft, The Netherlands, 2021. https://www.expertisecentrumverduurzamingzorg.nl/wp-content/uploads/2021/06/Bevochtigingseisen-praktijk.pdf.

[16] ANSI, ASHRAE, ASHE, Standard 170-2017 Ventilation of Health Care Facilities, (2017).

[17] DIN, DIN 1946-4:2008 - Ventilation and air conditioning - Part 4: Ventilation in buildings and rooms of health care, 2008. https://webstore.ansi.org/standards/din/din19462008 (accessed December 17, 2021).

Simulation-based seasonal underground sensible heat storage integrated in a district heating network

Bram ter Meulen [a], Rene Geerts [b], Carlos Infante Ferreira [c]

[a] Department Process & Energy, Faculty of Mechanical, Maritime & Materials Engineering, Delft University of Technology, Delft, the Netherlands, bramtermeulen@gmail.com.

[b] Hocosto BV, Zundert, the Netherlands, r.geerts@hocosto.com.

[c] Department Process & Energy, Faculty of Mechanical, Maritime & Materials Engineering, Delft University of Technology, Delft, the Netherlands, c.a.infanteferreira@tudelft.nl.

Abstract. This study assesses the role of (seasonal) thermal energy storage in the next generation renewables based central heating systems for the built environment in the Netherlands. Specifically, the neighbourhood "Karwijhof" in the city Nagele which is transitioning to a collective renewable district heating network incorporating 24 users. The study focus on the technology for storing thermal energy and two different heat collection technologies. The storage of heat is done using an underground seasonal thermal energy storage (USTES), in this case an underground sensible heat storage tank using water as storage medium. The system relies on a small scale district heating network (DHN) for the distribution of heat. For this research two heat collection technologies are considered both incorporating the USTES as main system component. The first system relies on heat collection by solar thermal collectors, the second on an air-water heat pump. Both systems are modelled in Matlab-Simulink making use of KNMI weather data. Different system sizes are evaluated. The investigated components include: volume of the USTES, surface area of the solar thermal collectors, and air-water heat pump capacity. Key performance indicators include the levelised cost of heat (LCOH) and the seasonal COP of the system which gives an indication on the autonomy of the system. To increase the autonomy of the systems a photo-voltaic (PV) array is considered for both systems to offset the electricity use. However, the systems are allowed to exchange electricity with the grid translating into the goal of "zero on the meter" autonomy. The results show that both systems can ensure heat throughout the year for the users considered during this study. However, systems cannot compete with traditional natural gas heating systems based on the LCOH. This is partly due to the high cost of the district heating network. The systems including a PV array show a LCOH that can compete with the traditional natural gas HR-boiler but are constraint by the rooftop area available during this study leading to a non-competitive LCOH. When considering the environmental benefits, the systems are already competitive to the traditional natural gas heating systems.

Keywords. Energy, Renewable and smart energy solutions for buildings and sites, Design of Innovative HVAC systems for optimized operational performances.
DOI: https://doi.org/10.34641/clima.2022.309

1. Introduction

In recent years climate change has gained more awareness among the public and has become an everyday important topic in regional and world politics. Due to the Paris and Glasgow climate agreements of, respectively, 2016 and 2021 the pressure to transition to a sustainable and renewable energy future has been increasing.

Since the Paris agreement countries have been moving towards even more ambitious goals on reducing their greenhouse gas emissions and increase energy efficiencies. In Europe this resulted in the proposition of the 'European Green Deal' setting ambitious goals for various energy consuming sectors including the energy efficiency of the built environment. On this topic the European Commission stated: "The Commission will rigorously enforce the legislation related to the energy performance of buildings [1]." The Netherlands as part of the European Union will take part in the efforts to increase energy efficiency of buildings. Historically buildings in the Netherlands are heated

Copyright ©2022 by the authors. This conference paper is published under a CC-BY-4.0 license.

by fossil resources extracted from the Dutch subsurface. Most building have central heating systems relying on natural gas.

These factors result in the fact that the Netherlands is accelerating its efforts to transition the heating demand of buildings towards renewable energy. The main challenge lies in the transition of the roughly 6-7 million existing buildings with low energy efficiency that are still relying on natural gas for space heating. For existing buildings the transition is more difficult compared to new built homes since systems that are already in place need to be altered to sustain the same level of comfort at a cost competitive price. Another challenge in the transition are the periods in which little energy can be generated with renewable resources due to lack of wind and/or sunlight.

In cooperation with the Dutch government a feasibility project is started to evaluate the opportunity for heating of existing buildings with renewable energy. This project carries the name 'Energiek Nagele'. The houses were built in the 1950's and currently rely on natural gas for their space heating. The main goal of renewable central heating systems is the reduction of greenhouse gas (GHG) emissions. The advancements in renewable energy technologies and cost reductions enable the start of the transition to renewables based central heating for the built environment in the Netherlands. Though, due to the intermittent nature of renewable energy sources, an energy storage solution is needed to ensure energy availability at all times.

The company Hocosto has proposed a method to overcome such periods by introducing a seasonal sensible heat storage tank installed underground. This storage is able to store heat during periods where energy can be generated for instance during summer and use this heat later to serve the heating demand through a small scale district heating network. This paper aims to investigate whether a neighbourhood can rely on a small scale district heating network with local seasonal heat storage and to compare two different thermal energy harnessing methods to charge the storage tank and find the most cost effective solution. The first system, system 1, relies on solar collectors for its heat generation. The second, system 2, uses an air-water heat pump to move energy/heat from ambient air to the storage tank. Both systems have an USTES to overcome periods where due to lack of wind or sunshine no renewable energy can be collected. The solar collectors experience this effect during cold periods with little sunshine, the heat pump is effected during times with low ambient temperatures.

This paper summarizes the work developed by ter Meulen [2] in the frame of the 'Energiek Nagele' project.

1.1 Thermal energy storage in combination with solar thermal collectors

System 1, presented in Fig. 1, starts by collecting heat in solar thermal collectors during summer. The collector arrays are installed on the rooftop of buildings and connected with the USTES by an insulated district heating network (DHN). Here the energy will be stored as sensible heat in water for later use during winter. A water-water heat pump will be installed using the USTES as its source medium to increase the exergy of the water.

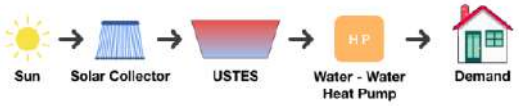

Fig. 1 - System 1, with a solar collector array as main heat source. An USTES is used as heat storage and a water-water heat pump is installed in order to increase the exergy of the water.

1.2 Thermal energy storage using a central heat pump

The alternative system presented in Fig. 2 relies on a central air-water heat pump extracting heat from ambient air and delivering this heat to a heat sink, in this case the USTES. The heat pump will only operate during periods where its coefficient of performance is above a certain threshold. This means the heat pump is turned off during periods of low ambient temperature. During these periods the USTES will cover the heating demand of the households. In this system also a water-water heat pump will be installed to increase the exergy of the water. Photo-voltaic (PV) panels will deliver electricity for the heat pump when possible. However it will not be a fully autonomous system since exchange with the grid will be allowed resulting in a "zero on the meter" system.

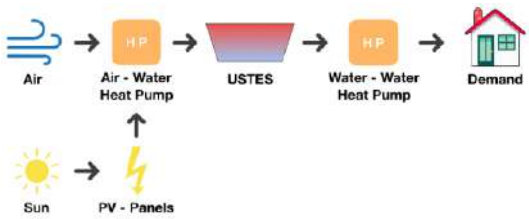

Fig. 2 – System 2, with an air-water heat pump as main heat source. An USTES is used as heat storage and a water-water heat pump is installed in order to increase the exergy of the water.

2. Heating demand of participating households

2.1 Demand profile

The natural gas demand for the 24 participating households in the project 'Karwijhof, Nagele' for the year 2018 is known and displayed in Fig. 3. The graph visualises the natural gas demand of the neighbourhood for one year. However, the natural gas demand profile is not consistent year over year. For instance, demand depends on the demography of the neighbourhood which changes slowly over the years. More significantly does the energy demand

depend on the ambient temperatures in winter which may vary greatly over the years. This effect will be discussed in section 2.2.

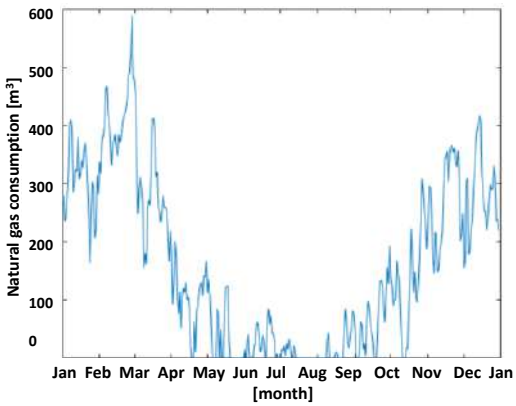

Fig. 3 – Daily gas consumption of the participating 24 users at 'Energiek Nagele' coupled to the outdoor daily mean air temperature measured by the KNMI at Marknesse weather station along the year 2018. The measured total annual gas consumption is 58448 m^3.

The energy demand of the users considered during this study is without any additional measures to improve the energy efficiency of the household. It is not yet known what additional measures can be taken due to the monumental status of the buildings. The monthly energy demand of households in the Netherlands also varies within one year due to seasonal changes. In winter more energy is required for space heating. This results in a higher energy consumption during the cold winter months compared to the warmer summer months. From Fig. 3 a demand profile can be obtained. The figure shows that natural gas consumption peaks in the months November - March and follows a sinusoidal profile. Notice that one of the buildings is a former school which consumes almost 20% of the total.

2.2 Climate effect on energy demand

Climate has a large effect on energy demand for space heating. Therefore, the Dutch meteorological institute (KNMI) uses a definition called "degree days" to account for this climate effect on energy demand. This method is also widely used in literature, for instance by Niessink [3] and Sorknæs [4] among others. Niessink [2] describes a degree day as a day in the year where the outside air temperature is below 18 °C, since only below this temperature a building is assumed to require space heating, otherwise known as the heating limit. Every degree Celsius below this 18 degrees is counted as one degree day. To give an example: if for a given day the outside temperature averaged over 24 hours is 8 degrees, then this accounts for 18-8=10 degree days [3]. The number of degree days gives an indication of the severity of the winter and therefore the need for space heating and its related energy demand. The number of degree days varies greatly over the years. For instance, the (unweighted) difference between 2013 (3078) and 2014 (2385) is 693 degree days where the KNMI climate expectation was 2779 - 2769 degree days respectively. This is a deviation of +11% and -14% respectively from the KNMI expected number of degree days for those years [5]. The degree days are weighted to account for the seasonal changes in solar insolation which contributes to the space heating of a house. Degree-days from November-February are weighted with a factor of 1.1, degree days in March and October have a weight factor of 1 and April-September get a weight factor of 0.8 [6].

2.3 District heating network

The households will be connected to the district heating network (DHN). This DHN will be used to transport the hot water from the heat storage to the houses for space heating and tap water. For this study a traditional two-line network is considered with a supply and return line. The water in the supply line needs to be at a minimum temperature in order to transport enough energy to meet the heating demand, to ensure a certain comfort level, and to ensure the Legionella legislation is met. This translates in the need for a minimum supply or service level temperature of the DHN. The supply temperature is dependent on the energy demand of the households. In general a minimum supply temperature of 70 °C is pre-defined. However, during Autumn and Spring a lower supply temperature is sufficient. Usually the heating temperature is variable from the heating threshold of 18 °C. Though, due to Dutch legionella bacteria legislation it is required for the households to be supplied with water of at least 55 °C for hot tap water production. This results in a relatively flat variable service level with a base temperature of 63 °C. The return flow temperature is constant since with increasing demand the DHN flow rate will increase such that the return temperature remains constant at 40 °C.

The same DHN applies for the two compared systems. The DHN needs to be determined with reasonable accuracy since it impacts on the LCOH. The thermal losses in the pipe network and the electricity consumption of pumps are important parameters since they have impact on the LCOH and the SCOP of the system. The layout of the network is given in Fig. 4.

3. Key performance indicators (KPIs)

The performance of the systems is evaluated based on the levelised cost of heat and on the seasonal coefficient of performance of the system.

3.1 Levelised cost of heat

The levelised cost of heat (LCOH) is defined as the initial investment or capital costs (CAPEX) of the system plus the operational costs (OPEX) divided by the total amount of heat delivered to the households.

Fig. 4 – Layout of the 2-line district heating network (DHN). Participating buildings are indicated in blue, the USTES is indicated in red, and the DHN is indicated by the black lines. Total length of the DHN is 700 m.

$$LCOH = \frac{CAPEX + \sum_{t=1}^{T} \frac{OPEX_t}{(1+r)^t}}{\sum_{t=1}^{T} \frac{E_t}{(1+r)^t}} \quad (1)$$

where T is the total life expectancy of the system (30 year), t is the time in years, r is the discount rate, $OPEX_t$ are the total operating costs in year t , and E_t is the total heat delivered in year t. The discount rate is assumed at 2% since sustainable energy projects generally are subject to low interest rates.

3.2 Seasonal system of performance

The system performance is also based on the seasonal coefficient of performance (SCOP). This represents the ratio between the heat that is delivered to the households and the total electric energy consumed by the system.

$$SCOP = \frac{\sum E_{delivered}}{\sum E_{electricity\ consumed}} \quad (2)$$

4. System design

4.1 System layout and control

For system 1 district heating network heat is generated by solar collectors, stored by a single USTES and has the possibility to use a water - water heat pump when the USTES temperature is below supply temperature level. A schematic overview of the system is given in Fig. 5 (LHS). System 2 consists of a central air - water heat pump for thermal energy generation, the USTES for thermal storage, a water - water heat pump to maximise exergy of the water, and the DHN to supply demand. A schematic overview of the system is given in Fig. 5 (RHS).

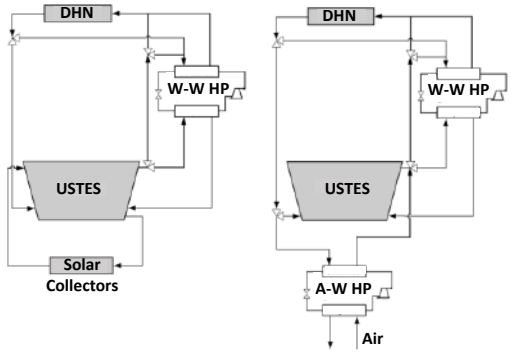

Fig. 5 – LHS: Technical overview of the components making up system 1. Arrows represent piping. The blank triangles represent control valves. RHS: Technical overview of the components in the air-water heat pump based system (system 2).

The system using an air-water heat pump has a control strategy based on the ambient air temperature. If the air temperature ≥ 18 °C then the heat pump will be operational while there is only some tap water demand by the households. The demand will be supplied by the USTES while simultaneously the heat pump is charging the USTES with hot water. If the air temperature is between 10 and 18 °C then there is a space heating demand and the heat pump is operational. The heat pump is charging the USTES. Simultaneously the USTES is discharging into the DHN to meet demand. If the air temperature is lower than the minimal operating temperature of the heat pump then the heat pump is not operational. Heat is supplied directly from the USTES. When the USTES is below supply service level (63 °C) the water - water heat pump will "upgrade" the return heat with energy sourced from the USTES.

The system can discharge into the DHN in three different modes depending on the temperature of the USTES. Due to space limitations these modes will not be discussed here.

4.2 Component modelling

Heat demand The demand is modelled from two input parameters. These are the hourly ambient air temperature provided by the KNMI, and the natural gas consumption of the households provided by the Energiek Nagele project. The two data sets are correlated to obtain the energy demand of the households per degree day, and subsequently degree hour.

USTES Research has shown that in liquid-based, sensible heat storage systems high degrees of stratification can be achieved. This stratification is mostly described using simplified one dimensional models. Cruickshank and Baldwin [7] propose a model of a stratified thermal storage by dividing the tank into N constant volume sections or "nodes". Fig. 6 visualises the node approach applied to the USTES which is a pit storage as proposed by Hocosto. The nodes are assumed to be fully mixed and at uniform

temperature. The resolution of the temperature stratification depends on the number of nodes used. The more nodes the higher the resolution will be, but also the longer the computation time. Cruickshank and Baldwin found that 10 nodes result in an accurate resolution with acceptable computation times, this is therefore the number of nodes used during this study. For each node an energy balance is introduced accounting for the thermal losses to its surroundings and for instance, conduction between the nodes. Each node will represent a sensor installed inside the USTES spaced uniformly in the vertical direction at a distance $\Delta z = z/N_{nodes}$ with z de height of the USTES.

To model the USTES the energy balance for each node needs to be considered. Mass flows leave and enter the nodes at different temperatures changing this energy balance. Also, the USTES is heated up by the solar collector array. The result is an energy balance with various components, these are: heat losses, heat conduction, mixing between nodes (convection), solar energy charging, and heat exchange with the DHN. The previous components are visualised in Fig. 6.

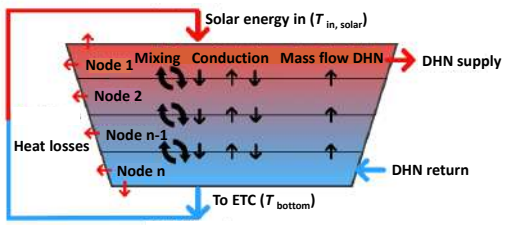

Fig. 6 – Energy flows in the USTES consisting of the heat losses to its surroundings, mixing between nodes, conduction between nodes, mass and heat transport due to solar charging, and mass and heat transport due to heat supply to the users through the DHN.

Solar thermal collectors The quasi dynamic approach proposed by Fischer et al. [8] has been adopted to determine the solar collector thermal output as a function of the local instantaneous radiation data. These data was obtained from the Dutch Meteorological Institute (KNMI). The solar thermal collectors are installed in arrays on the rooftops of the buildings. The rooftops consist of 2 flat surfaces on buildings near the USTES. In this study a separate DHN pipe is assumed to collect heat from the solar collectors and to transport it to the USTES. The solar collectors are installed at a fixed angle of 15 ° oriented 180 ° towards the south. The low inclination angle is imposed since the buildings have a monumental status and the collectors cannot be visible from the street.

Heat pumps The heat pumps have been modelled as proposed in Kiss & Infante Ferreira [9] while the thermodynamic properties of the working fluid (R600a) have been imported into the model from REFPROP (Lemmon et al. [10]). The heat pump has been designed to take full advantage of the large temperature glide of the water flow and includes an internal heat exchanger.

PV panels The performance of the PV panels was obtained as proposed by Smets et al. [11]. The specifications of the Trina Solar Duomax 144 PV panel have been adopted [12].

4.2 Component costs

Table 1 provides a summary of the costs.

Tab. 1 - Cost overview of the system components. In the last column it is indicated whether the costs contribute to the initial capital expenses (CAPEX) or operating costs (OPEX)..

Component	Cost [€]	Capacity	CAPEX/ OPEX
USTES	150	m^3	CAPEX
w-wHeat Pump	500	kW	CAPEX
a-w Heat Pump	450	kW	CAPEX
Evacuated tube collectors	450	m^2	CAPEX
Photovoltaic panels	180	m^2	CAPEX
DHN	150	m	CAPEX
Electricity 0-10000 kWh	0.178	kWh	OPEX
Electricity 10000-2500000 kWh	0.150	kWh	OPEX
Maintenance	1.2%	CAPEX	OPEX

5. Results

The solar collector based system (system 1) has two variable components. These are the USTES volume and the amount of solar collector surface area. The sizing of the air-water heat pump (system 2) is performed by iteration of two variables, the air-water heat pump heating capacity and the USTES volume.

5.1 Optimum LCOH

The optimum LCOH is obtained at its lowest. Fig. 7 (TOP) shows the LCOH of system 1 as function of the USTES volume for different surface areas of the solar collector array. The lowest LCOH is 0.128 €/kWh for an USTES volume of 1600 m^3 and a solar collector area of 800 m^2. The LCOH of the air-water heat pump system (system 2) has a minimum of 0.118 €/kWh at an USTES volume of 1300 m^3 and a heat pump heating capacity of 175 kW. The graph in Fig. 7 (BOTTOM) shows the optimum for the air water heat pump based system.

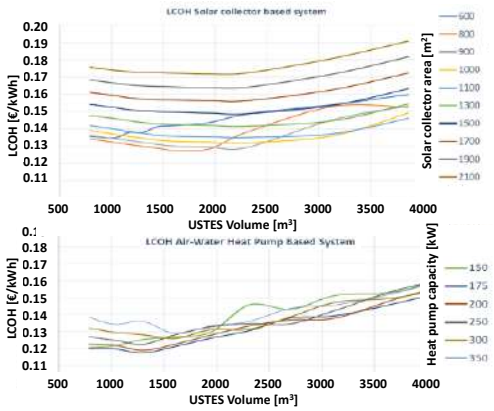

Fig. 7 - LCOH of the system configurations defining an optimum at the lowest point in the graph. Each line of system 1 (TOP) represents a certain solar collector array surface area. The x-axis shows the USTES volume while the y-axis presents the LCOH of the system. For system 2 (BOTTOM) each line represents a certain heat pump heating capacity in kW.

5.2 Optimum Systems COP (SCOP)

The systems seasonal coefficient of performance is optimal when at a maximum value is obtained. This maximum SCOP is theoretically infinite since when no electricity is consumed by the system, no external energy is imported and the system operates fully autonomous. The lower the SCOP the worse the efficiency of the system is. The SCOP of the different system sizes are presented in Fig. 8 with system 1 on top and system 2 at bottom.

For system 1 (Fig. 8, TOP) the SCOP increases with USTES volume and solar collector surface area since auxiliary heating and water-water heat pump operating hours decrease with increasing USTES volume and solar collector surface area.

For system 2 (Fig. 8 BOTTOM) the SCOP optimum approaches a maximum with increasing USTES volume and increasing heat pump capacity. However, the SCOP has a limit related to the COP of the air-water heat pump. The maximum COP of the air-water heat pump based system is 3.1, this is the highest efficiency the system is able to achieve and subsequently the limit to the SCOP of the system.

5.3 CAPEX of systems 1 & 2

The CAPEX of the systems are based on the optimal system configuration as defined in section 5.1. The CAPEX of the solar collector based system (system 1) is 993. k€. The pie chart in Fig. 9 breaks down the cost of components with left system 1 and right system 2. The costs for the DHN are fixed for every configuration and makes up 10% of the total CAPEX of system 1. capacity. Total costs are 493.5 k€.

The CAPEX of the air-water heat pump based system (system 2) is 493.5 k€. From Fig. 9 (RHS) becomes clear that the USTES contributes the largest part of the total CAPEX. The costs for the DHN make up 21% of the total CAPEX of system 2.

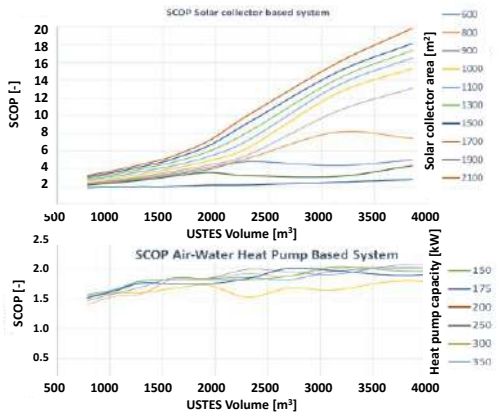

Fig. 8 – TOP: SCOP of the solar collector system configurations increasing with increasing size. Each line represents a certain solar collector array surface area. BOTTOM: Each line represents an installed heat pump heating capacity in kW.

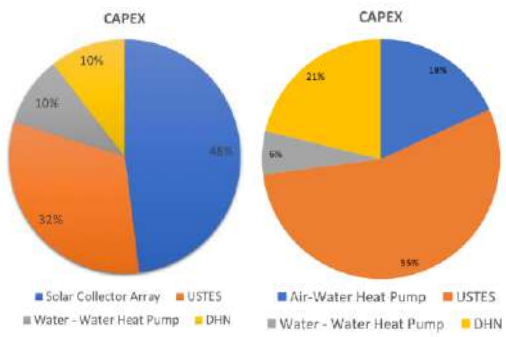

Fig. 9 – LHS: CAPEX cost share of the components for solar collector based system (system 1) with 2100 m³ USTES and 1060 m² solar collectors. Total costs are 993. K€. RHS: CAPEX cost share of the components for the heat pump based system (system 2) with 1800 m³ USTES and 200 kW air-water heat pump heating

5.4 Optimum LCOH of autonomous systems

Both systems 1 & 2 depend on electricity sourced from the grid. To increase the autonomy and renewable share of the system, PV panels can be installed. The solar collector based system does not have the entire rooftop area left since the solar collectors are already taking up a large part of the available space. The heat pump based system does have the entire rooftop area available for additional PV panels. One concern is the mismatch in time between consumption and generation. These systems are therefore not aimed to be fully autonomous but "zero on the meter", meaning the electricity generation is offset to the consumption using the general electricity grid as a "storage".

By installing a PV array the entire electricity use of the systems is compensated. Part of the effective

rooftop area, totalling 1344 m², will be used for the placement of the PV array. This results in an increase of the SCOP to infinity since all energy consumed by the system is also generated within the system. The cost of the PV panels increases the CAPEX of the systems and subsequently the LCOH reaches a new optimum.

For the solar collector based system (system 1) including PV the optimal LCOH is 0.126 €/kWh with a solar collector surface area of 1000 m², a PV surface area of 333 m² and a USTES volume of 3141 m³. Fig. 10 (top) presents the LCOH for different component configurations. The LCOH of this system is limited by the rooftop area available.

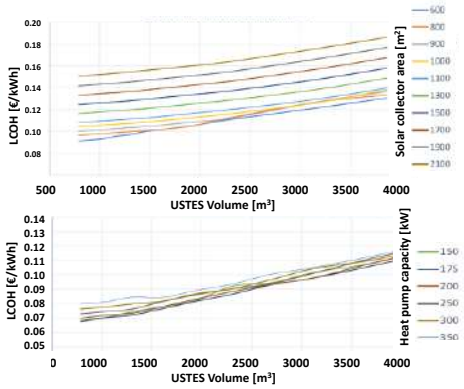

Fig. 10 – Autonomous systems with PV array installed on roofs. TOP: LCOH of the solar collector based system (system 1) including a PV array. BOTTOM: LCOH of the air-water heat pump system (system 2) including a PV array.

The air-water heat pump system consumes more energy compared to the solar collector based system and therefore needs more surface area of PV panels to reach "zero on the meter" autonomy. Fig. 10 (BOTTOM) presents the LCOH for the air-water heat pump system while all electricity use is offset by PV panels. The optimal LCOH for this system is 0.094 €/kWh at a USTES volume of 2709 m³ and a heat pump heating capacity of 250 kW. To ensure all electricity is produced on site a PV array of 1343 m² is needed. This is considered the optimal configuration since the only relevant KPI is the LCOH. The autonomy of the system is equal for all configurations since all electricity is produced by the system. The system is constraint by the rooftop area available. With additional PV panels the LCOH can be reduced further.

5.5 CAPEX of autonomous systems 1 & 2

The CAPEX share for each component of the system is presented in Fig. 11 with system 1 on the LHS and system 2 on the RHS. The PV array entails 5% of the total CAPEX of system 1. The CAPEX of system 1 totals 1182. k€. The CAPEX of the system 2 is 882. k€ and is presented in the RHS of Fig. 11. The PV array entails 27% of the total CAPEX of system 2.

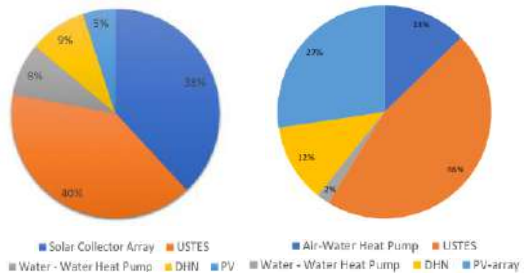

Fig. 11 – LHS: Pie chart of the CAPEX of the solar collector based system including PV. The system consists of 1000 m² of solar collectors, 333 m² of PV panels and 3141 m³ of USTES. RHS: Pie chart of the CAPEX of the air-water heat pump system including PV. The system consists of an USTES of 2709 m³, a 250 kW air-water heat pump, and a 1343 m² PV array.

5.6 Optimal system configuration

The optimal system configuration and sizing for the solar collector based system with PV array is based on "Zero on the meter" at the lowest possible cost while taking into account the rooftop area constraint. This results in a system with 1000 m² of solar collector area, 3141 m³ of USTES volume, and 333 m² of PV panels. The LCOH of the system is 0.126 €/kWh. The LCOH can come down further by installing additional PV panels. However, the rooftop surface area constraints the PV array size. The optimal system configuration and sizing for the heat pump based system with PV array is also determined to achieve "zero on the meter" at lowest cost. This results in a system with 250 kW of air-water heat pump heating capacity, 2709 m³ of USTES volume, and 1343 m² of PV panels. This results in a LCOH of 0.094 €/kWh. Again the LCOH can come down further if not for the rooftop area constraint.

The temperature of the nodes in the USTES over the years is presented in Fig. 12 (TOP) for system 1. From the graph can be seen that the temperature fluctuations are not the same every year but do follow a similar trend. From the figure follows that not all energy comes from the solar collectors but some auxiliary heating is needed with this system sizing. These are the periods for which the USTES reaches a temperature of 5 °C. This implies that using additional solar collectors and USTES volume to ensure demand are more expensive compared to the use of auxiliary heating. This is due to the relatively low cost of electricity and it results in a larger investment, operating and maintenance costs. By installing an PV array the auxiliary heating can also be considered renewable.

The temperature profile of the USTES over the same period is presented in Fig. 12 (BOTTOM) for system 2. To be certain the heat pump is only operating when energy can be added to the USTES, it only operates when the temperature of the bottom node of the USTES is below 80 °C and when there is a return mass flow from the DHN at 40 °C. This translates in the fact that the bottom node appears to be fluctuating between 80-90 °C. From Fig. 12 (BOTTOM) also follows that in the years 2017 and 2018 some auxiliary heating is needed. This

auxiliary heating can be prevented by installing more m³ of USTES. However, based on the KPI's apparently it is favourable to have some auxiliary heating since it leads to a lower LCOH compared to installing additional USTES volume.

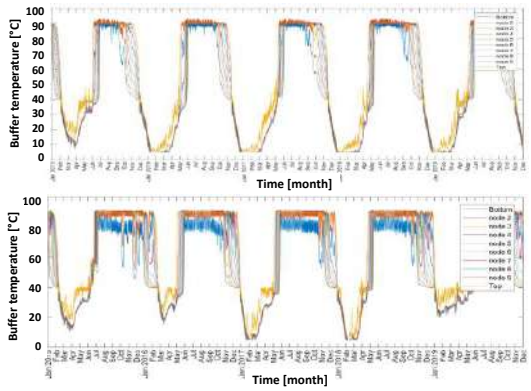

Fig. 12 – TOP: Temperature of the nodes in the USTES during a five year time period with 2100 m³ USTES and 1060 m² solar collectors. BOTTOM: Temperature profile of the nodes in the USTES during the same period with 1800 m³ USTES and 200 kW air-water heat pump heating capacity.

6. Discussion

6.1 Economic feasibility of proposed systems

The results show that it is feasible, both technically and economically, to have a small scale district heating network operating year round based on renewable energy combined with a local seasonal heat storage. To ensure the system is fully renewable a PV array is needed.

6.2 Cost competitiveness

Traditional heat generated by burning natural gas using a HR-boiler operating at a seasonal efficiency of 90% costs 0.088 €/kWh excluding capital costs (the initial costs of the HR-boiler) since the system is already in place. This is the business as usual in the Netherlands for the majority of households. Therefore, this price of heat is the benchmark for renewable heating systems.

The systems including a PV array produce an LCOH of 0.126 €/kWh for the solar collector based system including PV and 0.094 €/kWh for the air-water heat pump based system including PV. The latter is the most competitive with the business as usual case of all system configurations but still cannot compete. With more rooftop area available the systems with PV are able to be cost competitive with the base case.

7. Conclusions

A model to predict the performance of DHN based on renewable resources which make use of high temperature sensible pit heat storage tanks has been developed and implemented in MATLAB/Simulink. The model has been used to optimize the size of the renewable resources and pit storage to reach as low as possible LCOH for a group of 24 buildings in Nagele.

Under the assumptions made, the following has been concluded: The best performance is obtained for the system with an air source based heat pump which delivers heat to the hot pit storage when the environmental temperature is sufficiently high. The air-water heat pump has a heating capacity of 250 kW, the USTES a volume of 2709 m³ and the PV panels an area of 1343 m². The LCOH of the system is 0.094 €/kWh which is only slightly higher than the LCOH with conventional HR-boilers in 2020 (0.088 €/kWh).

Data access statement

The datasets generated during and/or analysed during the current study are not publicly available because MSc thesis [2] is under embargo but will be available at the end of embargo period.

8. References

[1] European Commission. (2019) The European Green Deal. page 9. retrieved from https://ec.europa.eu/info/sites/info/files/european-green-deal-communication_en.pdf

[2] ter Meulen B.P. Underground heat storage. M. Sc. Thesis. Delft University of Technology. 2020; 127 p.

[3] Niessink, R.J.M. (2017) Temperature correction – A Sensitivity Analysis. ECN Amsterdam 2017. https://publicaties.ecn.nl/PdfFetch.aspx?nr=ECN-N--17-039 .

[4] Sorknæs, P. Simulation method for a pit seasonal thermal energy storage system with a heat pump in a district heating system. Energy. 2018;152:533-538.

[5] Centraal Bureau van de Statistiek. Energieverbruik van particuliere huishoudens. 2018. retrieved from https://www.cbs.nl/nl-nl/achtergrond/2018/14/energieverbruik-van-particuliierehuishoudens

[6] Centraal Bureau van de Statistiek. Energie - Cijfers. 2018. retrieved from https://longreads.cbs.nl/trends18/economie/cijfers/energie/#huishoudelijk-energieverbruik

[7] Cruickshank, A.C., Baldwin, C. Sensible Thermal Energy Storage: Diurnal and Seasonal. Storing Energy. 2016;1:91-311.

[8] Fischer, S., Muller-Steinhagen, H., Perers, B., Bergquist, P. (2017) Collector test method under quasi-dynamic conditions according to European Standard EN 12975-2. retrieved from http://www.estif.org/solarkeymark/Links/Internal_links/wp1a/m3wp1ad3.pdf .

[9] Kiss, A.A., Infante Ferreira, C.A. (2017) Heat Pumps in Chemical Process Industry. CRC Press 2017. isbn 978-1-4987-1895-0.

[10] Lemmon, E.W., Bell, I.H., Huber, M.L., McLinden, M.O. (2018) NIST Standard Reference Database 23: Reference Fluid Thermodynamic and Transport Properties-REFPROP, Version 10.0, National Institute of Standards and Technology. 2018. doi: http://dx.doi.org/10.18434/T4JS3C. https://www.nist.gov/srd/refprop

[11] Smets, A., Jager, K., Isabella, O., Swaaij van, R., Zeman, M. (2016) Solar Energy 2016. UIT Cambridge Ltd. isbn: 9781906860325

[12] Trina Solar. Datasheet: Trina Solar DUOMAX dual glass 144 half-cell module. 2019. Retrieved from https://static.trinasolar.com/sites/default/files/PS-M%20A%20Datasheet_Duomax_DEG15H.20%28II%29_NA_2019_A_0.pdf

Optimized district heating system for combined operation with seasonal heat storage

Gijs Wolbert [a], Rene Geerts [b], Carlos Infante Ferreira [c]

[a] Department Process & Energy, Faculty of Mechanical, Maritime & Materials Engineering, Delft University of Technology, Delft, the Netherlands, gijs.wolbert@gmail.com.

[b] Hocosto BV, Zundert, the Netherlands, r.geerts@hocosto.com.

[c] Department Process & Energy, Faculty of Mechanical, Maritime & Materials Engineering, Delft University of Technology, Delft, the Netherlands, c.a.infanteferreira@tudelft.nl.

Abstract. This study optimizes the district heating network side of a high temperature community heating system powered by decentralized solar collectors and seasonal thermal energy storage (STES). Six network configurations are considered which have the potential to improve system performance compared to a base scenario. The base scenario consists of a 2-line network with a fixed supply temperature where the decentralised solar collectors feed in over the heating network. All alternative configurations aim to improve system performance by lowering the temperature of consumed and/or produced heat. Lowering the temperature in the heating network reduces heat losses and decreases heat pump utilization. Lowering the operational temperature of the solar collectors increases their efficiency. The strategies explored by the different configurations include variable supply temperatures, a 4-line network (where the solar collectors do not feed into the heating network), and ways to mitigate temperature constraints imposed by domestic hot water production regulations. In the neighbourhood “”Karwijhof” of Nagele, 24 consumers will make the switch to a solar+storage district heating system. In order to assess their performance, all configurations and the base scenario are modelled in Matlab/Simulink. The system performance is measured in terms of levelised cost of heat (LCOH) and seasonal coefficient of performance (SCOP). They are compared to a scenario where the dwellings are fitted with individual high temperature air to water heat pumps. Making the supply temperature variable (dependent on the ambient temperature) reduces pipeline thermal losses and reduces heat pump utilization. The transition from a 2-line network to a 4-line network where the solar collectors are separately connected to the buffer was found to significantly increase solar collector efficiency. The combination of these two measures reduces the LCOH by 4.5 %. Slightly oversizing the buffer volume and solar area significantly increases the SCOP with small impact on LCOH. When comparing the improved community solar heating system with a scenario where every house is heated with an individual heat pump instead, it is found that the community solar system achieve a 15.7 % lower LCOH while having a SCOP of 4.4 compared to just 2.75 for the heat pump scenario.

Keywords. Energy, Renewable and smart energy solutions for buildings and sites, Design of Innovative HVAC systems for optimized operational performances.
DOI: https://doi.org/10.34641/clima.2022.310

1. Introduction

In the fight against climate change, the Dutch government has vowed to replace current natural gas-based heating systems in buildings for more environmentally friendly alternatives. The need to convert hundreds of thousands of buildings annually, and its accompanying incentives, have sparked a pursuit for low carbon heating systems. A system relatively novel to the Netherlands, is one where solar thermal energy is used to provide the built environment with its heating needs. When such a system is to provide a large portion of the total heating load, energy storage is needed in order to cope with the seasonal mismatch between supply and demand. Until recently, few of these projects were developed due to prohibitively high costs of the high temperature seasonal thermal energy storage (STES). However, the introduction of a new STES design by the company Hocosto has diminished costs

Copyright ©2022 by the authors. This conference paper is published under a CC-BY-4.0 license.

to a point where economic feasibility is achieved for a variety of projects. While Hocosto's solar-plus-storage concept has been tried and tested for several use cases such as individual houses, sport accommodations and schools, arguably the most promising application is the combination with small district heating systems (DHS). In such a system, several consumers would be connected to a central STES by a DHS. This study focuses on decentralised generation, where the consumers generate thermal energy with solar collectors on their own roofs. The concept of having a solar heating network with high temperature STES, offers the appealing benefit that the DHS could operate at a relatively high temperature, mitigating the need to convert participating buildings to be suited for low temperature heating (as is the case for many other low carbon heating concepts). However, having high temperatures in the network has three major downsides:

• Heat losses in the DHS increase

• Higher supply temperatures means more exergy needs to be generated by a heat pump (when the buffer temperature is below the supply temperature, a heat pump needs to supply exergy)

• The solar collectors have to operate at higher temperatures, decreasing their efficiency

This study aims to improve the performance of decentralised solar+storage district heating systems while maintaining the possibility to work with the existing high temperature heating systems. The performance of the system is measured in LCOH, or levelised cost of heat. LCOH takes into account all costs, discounted for the weighted average cost of capital (WACC), divided over the delivered heat. The result is an energy cost expressed in €/kWh. After careful examination of current literature, the improvements potentially leading to a lower LCOH will be sought in (partially) mitigating one or more of the three issues enumerated above. In total, seven different network configurations are considered. The general design and layout of these systems are elaborated. In order to compare the different configurations based on LCOH, they are simulated for several years in a Matlab/Simulink environment. Additionally, to compare how the systems financially hold up to alternative heating systems, they are compared to a scenario where the houses are heated by individual air-water heat pumps. A simple model of a single house and heat pump is introduced. Finally, the comparison between the systems is made. The systems are scaled based on buffer size and solar collector area for the lowest LCOH. Additionally, all systems are also sized for the lowest LCOH with the additional constraint that the seasonal coefficient of performance (SCOP) must be at least 5. This is done because it is reasonable to assume that ecological constraints will be applied in the adoption of such systems. The SCOP is defined as the ratio between the annual consumed thermal energy by the consumers and the total electricity consumption by the entire system (including heat pump, circulation pumps, auxiliary heater and, if applied, DHW boilers). Since the network is small, the energy consumption of the circulation pumps is small (ca. 6000 kWh per year). High comfort levels are to be guaranteed to consumers, while physical space occupation and work required inside dwelling is to be minimized. This paper summarizes the work developed by Wolbert [1] in the frame of the 'Energiek Nagele' project.

2. System configurations

2.1 Alternative solutions

Typical district heating systems (DHS) consist of three main components: An energy source, a distribution network, and more than one end-user. This paper examines solar-based DHS with an additional component: an Underground Seasonal Thermal Energy Storage (USTES). In Nagele, 24 buildings will be connected to a small district heating network powered by decentralised solar thermal energy. The aim of this study is to optimize the district heating part of the system for operation in conjunction with solar collectors and storage. The performance of the system is measured in LCOH. Several network configurations are dynamically modelled and compared. Three main approaches are considered to improve overall system performance; Firstly, the implementation of a four-line network so that the solar collectors do not feed into the heating network, but have their own dedicated network instead; Secondly, an approach where the DHW systems of consumers are altered in order to allow lower supply temperatures; Finally, the introduction of a variable supply temperature based on the ambient temperature. In total, seven different combinations are compared:

• 0-A: Base case, fixed supply temperature, 2-line network, DHW system A

• I-A: Variable supply temperature, 2-line network, DHW system A

• I-B: Variable supply temperature, 2-line network, DHW system B

• I-C: Variable supply temperature, 2-line network, DHW system C

• II-A: Variable supply temperature, 4-line network, DHW system A

• II-B: Variable supply temperature, 4-line network, DHW system B

• II-C: Variable supply temperature, 4-line network, DHW system C

2.2 Two-line and four-line networks

In this study, two main pipeline configurations are considered, both of which are shown in Fig. 1. In both configurations, three heat exchangers per consumer are used to achieve hydraulic separation between the network on one side, and the solar collectors, heating system, and DHW system on the other side.

In system I, there are just two pipelines to which every consumer is connected. Through these pipelines, heat is delivered from the buffer to the consumers, but also the solar energy generated by the solar collectors is transported from the dwellings to the buffer. The biggest benefit of this system is its simplicity and the resulting reduced installation costs since only two pipelines have to be used. System II is unique in the way that it uses a separate network for the solar collectors, much like the Drake Landing solar community in Canada as described by Sibbitt et al. [2].

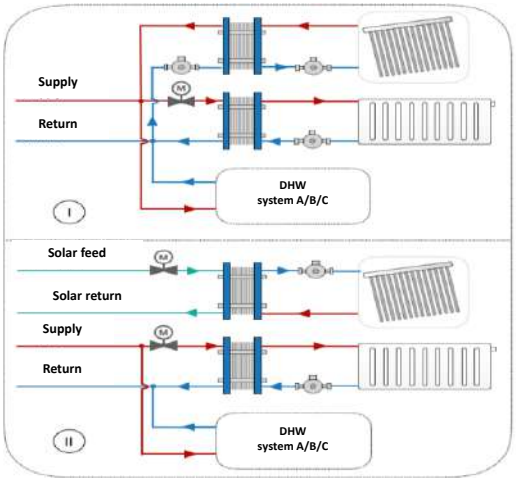

Fig. 1 - Two main network configurations. In configuration II, the solar collectors feed in to their own dedicated network. In configuration I, the solar collectors feed in to the heating network, mitigating the need for this dedicated network for the solar collectors.

The main presumed benefit of this system is an increase in efficiency of the solar collectors since they can operate at lower temperatures. Also, it eliminates the need of one circulation pump per consumer.

2.3 Supply temperatures

Low supply temperatures allow for the use of a wider range of materials and it results in lower return temperatures, which lead to higher solar collector efficiencies. The supply temperature is constrained by several factors: It needs to be sufficiently high to provide enough capacity for space heating, it needs to be high enough to produce DHW according to Dutch legislation, and it is influenced by outlet temperature of the solar collectors. The houses in Nagele are suited so that a supply temperature of 70 °C is sufficiently high to provide enough space heating power year round. However, required space heating power obviously is greatly dependent on weather conditions and is therefore not equal throughout time. Because of that, the supply temperature could be made weather dependent: For higher ambient temperatures, the supply temperature could be lower than the 70 °C needed at low outdoor temperatures. As a result, average network temperatures can be reduced, yielding the advantages listed above. The main constraint in lowering supply temperatures, is the preparation of DHW, since minimum temperatures need to be achieved in order to provide enough comfort and mitigate Legionella growth. The most common method of DHW preparation in district heating networks, is direct preparation through a plate heat exchanger. This method is described by DHW concept A below. Two other concepts (B and C) are conceived which aim to reduce the minimum network supply temperature.

<u>DHW concept A:</u> A single heat exchanger provides all hot water using the heating network as the sole energy source. The minimum DHW supply temperature at tapping locations is 55 °C for non-sanitary purposes, while DHW for sanitary purposes can have temperatures below that. A mean temperature difference over the heat exchanger of 5 K is assumed (based on research by Yang & Svendsen [3]). Also, there will be (small) thermal losses in the pipelines between the heat exchanger and tapping location. The minimum network temperature at the heat exchanger is 61 °C.

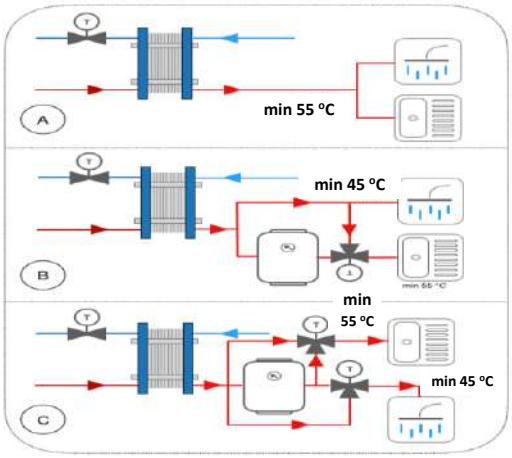

Fig. 2 - Three DHW preparation concepts. Concept A uses only a heat exchanger, requiring the outlet temperature of the heat exchanger to be at least 55 °C. Concept B uses an electric heater to reheat the DHW for kitchen use, reducing the required temperature at the outlet of the heat exchanger to 45 °C. Concept C uses an electric heater to reheat the DHW for all purposes, further reducing the required temperature at the outlet of the heat exchanger. Thermostatic valves are added to limit the outlet DHW temperature to the required level.

<u>DHW concept B</u>. Most of the time, ambient temperatures would allow the minimum supply temperature to be lower than 62 °C. Since this constraint is set by the minimum DHW temperatures, methods are explored to break this constraint. The temperature of DHW for sanitary purposes (which makes up 87.4% of total DHW

demand) is allowed to be below 55 °C in residential environments. Concept B, shown in Fig. 2, makes use of this exception by using an in-line heater to heat non-sanitary water to the 55 °C level. The minimum temperature for sanitary DHW is chosen to be 45 °C, as this seems to be the highest temperature at which consumers shower/bathe. One important component of this concept, is the thermostatic mixing valve after the electric boiler. This allows the hot water tapping temperature to remain constant also for higher boiler temperatures. This is important in Nagele, since space comes at a premium. By using the mixing valve, the boiler temperature can be higher, which increases the stored energy. The advantage is that network temperatures can decrease for relatively high ambient temperatures. The network supply temperature (at consumer level) can vary between 52 and 73 °C. The additional costs compared to DHW concept A are low, since only a small boiler (in the order of 10-15 L) is needed.

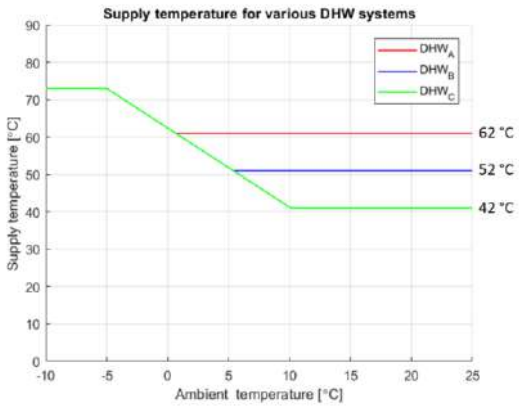

Fig. 3 - Supply temperatures for all DHW concepts as a function of ambient temperatures.

DHW concept C. Concept B is constrained by the 45 °C temperature needed for sanitary purposes. This is resolved in concept C (shown in Fig. 2), where the sanitary water is also heated by the boiler to reach the minimum service level. While theoretically there is no minimum network temperature for this concept since all DHW energy can be supplied by the boiler, this would incur high electricity consumption. Also, there is not enough physical space available at the consumers in Nagele to place sufficiently large boilers. Therefore, the minimum DHW exit temperature of the heat exchanger is chosen to be 35 °C. The reason being that, in combination with a relatively small 40 L boiler at 85 °C, 200 L of 45 °C DHW can be produced, which is assumed to be a very comfortable amount for the consumers. This concept goes further than concept B in achieving lower network temperatures at the cost of higher electrical energy consumption at the consumer level and slightly higher costs of installation. Electrical consumption will be higher when network temperatures are low, but lower average network temperatures have their benefits. In such a configuration, the network supply temperature (at consumer level) can vary between 42 and 73 °C.

Supply temperatures of all systems. DHW systems B and C are conceived in order to reach lower network temperatures than system A allows. In Fig. 3, the supply temperatures of all three concepts are shown. It is clear that for concepts B and C, the system can operate at lower supply temperatures.

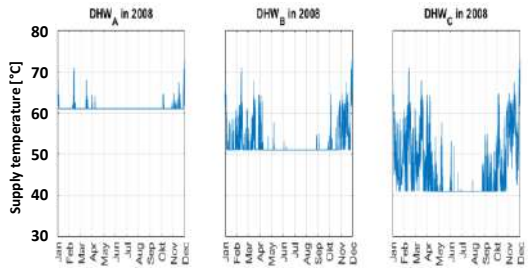

Fig. 4 - Simulated supply temperatures for all DHW concepts for the year 2008.

In Fig. 4, the simulated supply temperatures for the year 2008 is shown for all three concepts. Ambient temperature data from the KNMI [4] for the location Marknesse is used. Marknesse is roughly 13 km from Nagele. When looking at the graph, it can clearly be seen that the peak supply temperature of 73 °C is rarely reached. While it appears that network B and C operate at much lower temperatures most of the time, note that the temperatures displayed are the supply temperatures assumed necessary to properly heat the buildings and provide their DHW. It is the minimum temperature needed in the supply lines of the network at the consumers. Therefore, in the two-line network where the solar collectors feed in over the same pipelines, the actual supply temperatures will be higher at times. Especially at the end of summer when buffer temperatures (and thus solar inlet temperatures) are high, the outlet temperatures of the solar collectors will be significantly higher than the service level temperatures.

3. DHN

The pipelines are sized by imposing a limit on the fluid velocity. In picking an appropriate maximum fluid velocity, it is important to understand that peak power (and thus peak fluid velocity) only rarely occurs in the network. The average power is much lower. Therefore, the economic optimum peak fluid velocity will be relatively high. The pipelines are sized so that this peak fluid velocity does not exceed 2.5 m/s. Two different network configurations are considered in this study: A steel 2-line heating network where the solar collectors feed in to the heating network, and a 4-line network consisting of 2 PE heating pipes and 2 steel solar pipes.

3.1 Two-line network (configuration I)

The two-line network consists of two steel pipelines. The total required pipe length is 691 m. The peak power at every section is determined by either the maximum heating load (space heating + DHW) during cold days, or by the maximum solar yield during hot sunny days, since the solar collectors feed in over the network. The ΔT between supply and return for space heating is assumed to be 20 K, while the ΔT for DHW preparation is assumed to be 50 K. The pump of every solar array is chosen so that it can

provide enough flow to keep the ΔT at a maximum of 30 K during peak power. The DHW peak demand is assumed to be 25% of the absolute peak, since not all consumers will consume DHW simultaneously. In Fig. 5, the resulting pipeline topology and dimensions of network I are shown. In total, 185 m of DN32, 165 m of DN25 and 341 m of DN20 are needed. The peak solar power is leading in diameter selection on every section.

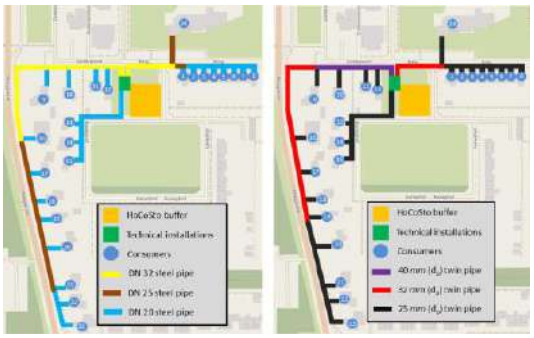

Fig. 5 – LHS: Layout of the steel pipe network which shows pipe diameters for every section. RHS: Layout of the flexible twin pipe network which shows pipe diameters for every section.

3.2 Four-line network (configuration II)

The 4-line network consists of a PE heating network to satisfy space heating and DHW loads, and a steel pipeline network to transport the thermal energy generated by the solar collectors to the buffer. Since the solar yield was leading for diameter selection of the steel pipelines in the 2-line network, the steel network in the 4-line configuration will be equally sized. The PE pipelines are scaled using the peak power in the network: 75 m of DN40, 200 m of DN32, and 416 m of DN25.

4. Seasonal thermal energy storage (STES)

The seasonal thermal energy storage (STES) to be used in the project in Nagele, is one supplied by the company Hocosto. It is an underground seasonal thermal energy storage (USTES) pit type, with water as a heat carrier medium. A patented aluminium frame allows Hocosto to install buffers quickly, and cheaper than any other thermal storage solution. Since the frame can carry large loads, the space above the buffer can be used effectively, for example as a parking lot. Further details of the USTES can be found in a companion paper by ter Meulen et al. [5]. Discharging the buffer is done by extracting fluid from the top of the buffer and returning it to the bottom of the buffer. Charging is done the other way around. The buffer system will be insulated on all sides using XPS (extruded Polystyrene).

5. System model

The model uses KNMI weather data for the 5-year period from 01-01-2008 till 31-12-2012. Because it is important to have realistic buffer temperatures at the start of the simulation, the first year is not used in the results.

5.1 Consumers

In order to simplify the model and reduce simulation times, the 24 consumers in the network have been aggregated in 6 clusters, taking type and size of the dwellings, as well as their locations into account. For every cluster, all heat flows (space heating, hot water demand and solar generation) are simulated (see [5] to see how the model has been calibrated). As a result, the mass flow and inlet/outlet temperatures at every consumer level are calculated. Since the network is branched and bidirectional, fluid flows will occur directly between the solar collectors and the space heating and DHW heat exchangers. Therefore, it cannot simply be assumed that the inlet temperatures of the DHW and space heating heat exchangers are equal to the network supply temperature, and neither can it be assumed that the inlet temperature of the solar collectors is equal to the network return temperature. For that reason, the fluid temperatures at the consumer level are calculated for each time step depending on the fluid flows (and their inlet/outlet temperatures) through each of the three heat exchangers at the consumers, and the flow to or from the network. For example, when the supply temperature of the network is 60 °C, the solar collectors operate at an outlet temperature of 80 °C and 5 L/min , the DHW heat exchanger would have an inlet temperature of 70 °C at 10 L/min. This is especially relevant for the solar collector efficiency, since it is very dependent on its inlet temperature.

DHW: The heating load consists not only of space heating, but also of the production of domestic hot water (DHW). Based on Fuentes et al. [6], demand profiles are generated for all consumer clusters. The demand is separated into three different categories: Showers, baths and tapping (kitchen etc.). The flow rates expressed in L/min of 45 °C for showers and baths, and 55 °C for tapping. Variations are given between households in time of occurrence, longevity, and flow rate. The means are based on DIN 1988-300 [6]. The average drawn volume per household per day is 80, 20 and 28 L/day for showers, baths and sinks, respectively. The heat exchangers for DHW production are scaled so that at maximum power, the temperature difference over the exchanger is 5 K. The mean temperature difference over the heat exchanger for every time step is obtained by assuming a constant UA-value of 500 W/K for the heat exchanger.

One of the most important differences between DHW concepts, will be the boiler electricity consumption. The energy consumption of the electric boilers consists of both energy delivered and heat losses. Since the boilers are kept at a constant temperature, the heat losses of the boiler are introduced as a fixed loss. The loss equals 20 W for the small boilers, and

35 W for the larger boilers.

5.2 Space heating

For the space heating requirement, it is not only important to know the power required by the consumers, but also the mass flows and temperatures of these mass flows. Therefore, a heating system is modelled for every cluster. Fig. 6 shows the energy balance which is made for the clusters.

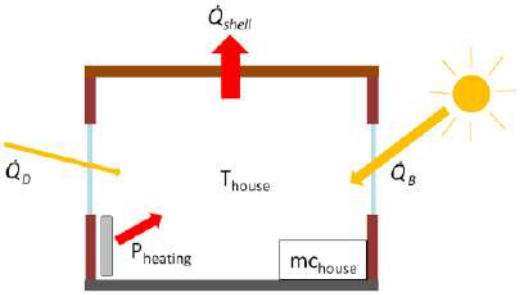

Fig. 6 - Energy balance of a consumer, with the beam (B) and diffuse (D) solar gains, heat losses through the shell (shell) and heating gains (heating + heat capacity).

For each time step, the room temperature is updated using the heat flows in and out of the building. Ventilation and infiltration have been aggregated with the shell losses. The UA-value of each cluster has been calibrated with the measured energy consumption of the cluster.

5.3 Solar collectors

The solar collector output is modelled per time step, depending on the solar irradiance and the solar collector efficiency. The position of the sun and the angles and power of beam radiation on the inclined surfaces have been modelled using methods described by Duffie & Beckman [7].

5.4 Pipelines

The two-line system will use two steel-PUR-PE pipelines, while the 4-line system will use two steel-PUR-PE lines for the solar loop, and PE-twin pipelines for the heating network. The heat losses have been calculated as proposed by Miltenburg [8]. Additionally, considering the discussion by Wallenten [9], when pipes are laid in the ground close to each other their heat losses cannot be calculated independently. The problem of two pipes close to each other in the ground can be divided into two problems: A symmetrical and asymmetrical problem, where the symmetrical problem represents heat loss from the pipes to the surroundings and the asymmetrical problem heat transfer from one to another pipe. While the resulting equations can easily be used to calculate steady state heat losses, implementation in the model is slightly more difficult since both soil surface and fluid temperature are not constant. To overcome the varying soil temperatures, the soil temperature at a larger depth of 0.2 m is taken instead of the surface temperature. The result is that the new environmental temperature is much more stable with just a gradual seasonal variation. Since the resistance over the insulation dominates over the heat resistance of the soil, the assumption that the soil temperature at a depth of 0.2 m is undisturbed seems reasonable. The effects of the variable fluid temperature are ignored, since the thermal resistance of the insulation is much higher than that of the soil. This results in minimal temperature differences of the soil.

5.5 Heat pump

This heat pump has been assumed to achieve a system efficiency equal to 40% of Carnot efficiency. The 40% system efficiency includes the temperature differences over the heat exchangers at both sides of the heat pump.

5.6 Component costs

Table 1 provides a summary of the costs.

Tab. 1 - Cost overview of the system components.

Component	Cost [€]	Capacity
USTES	150	m^3
w-w Heat Pump	500	kW
Delivery kit	1000	consumer
Evacuated tube collectors	450	m^2
Central installations	35000	-
2-line DHN	180	m
4-line DHN	255	m
Electricity 0-10000 kWh	0.178	kWh
Electricity 10000-2500000 kWh	0.150	kWh
Maintenance	1.2%	CAPEX

6. Results

6.1 Comparison of optimum designs

Fig. 7 shows the LCOH for the optimum design of all configurations for both the absolute economic optimum as well as for the situation where an SCOP of 5 has to be met. The economically most attractive system is configuration 2-A with 1100 m^3 of buffer and 900 m^2 of solar collectors. The cost benefit however, is just 0.5 cents per kWh, or 4.5% compared to the base scenario 0-A with 1275 m^3 of buffer and 1100 m^2 of solar collectors. Sizing the buffer volume and solar area slightly larger does not increase LCOH considerably, but does increase SCOP profoundly. This is also seen in Fig. 7, where the systems with a minimum SCOP of 5 are only slightly more expensive than systems without this

constraint.

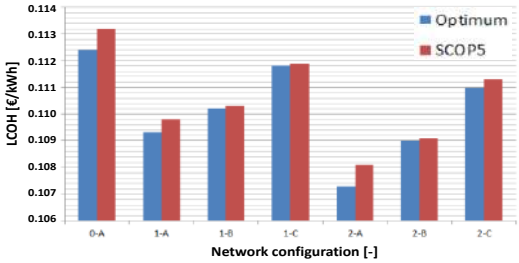

Fig. 7 - Lowest LCOH and LCOH for a minimum SCOP of 5 for every system configuration.

6.2 LCOH of best 2 and 4 line systems

Fig. 8 shows how the LCOH varies with buffer size and solar collector area for the best 2 (TOP) and 4 (BOTTOM) line systems.

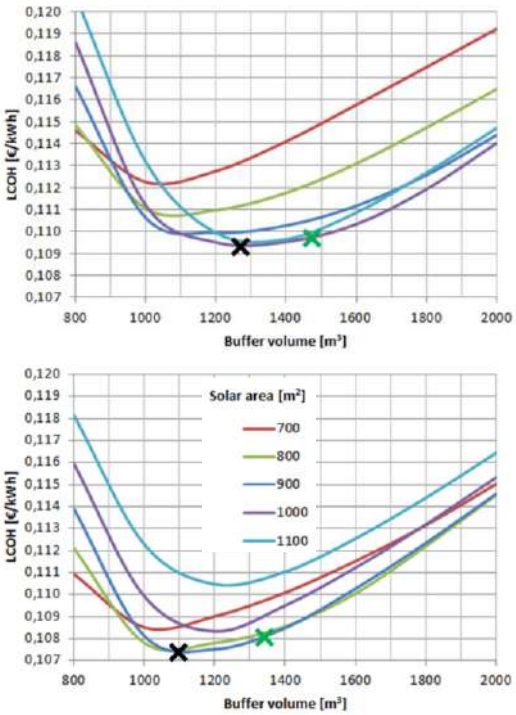

Fig. 8 – TOP: LCOH for configuration 1-A at various buffer volumes and solar areas. BOTTOM: same for configuration 2-A.

Configuration 1-A (Fig. 8 - TOP) is a 2-line network which aims to improve system performance by implementing a variable supply temperature. The minimum supply temperature is restricted to 62 °C due to constraints in the DHW system. This lower supply temperature results in slightly lower pipeline losses, lower heat pump electricity consumption and higher solar collector efficiency. At the absolute economic optimum (1000 m² solar collector area and 1275 m³ buffer), the LCOH is 0.109 €/kWh. Fig. 8 also displays the required design values to reach an SCOP of 5 (1000 m² solar collector area and 1475 m³ buffer). The LCOH is then 0.110 €/kWh.

Configuration 2-A (Fig. 8 – BOTTOM) is a 4-line network where the solar collectors supply heat to the buffer through a separate network. It aims to increase solar collector efficiency by allowing them to operate at lower mean temperatures. The supply temperature of the heating network is variable, but limited to a minimum of 62 °C due to DHW production constraints. Fig. 8 shows the LCOH for various buffer volumes and solar collector areas. The LCOH of 0.107 €/kWh is the lowest attained. When the constraint of having to achieve a SCOP of 5 is to be met, the LCOH increases to 0.108 €/kWh.

6.3 Power consumption and COP of heat pump

Fig. 9 shows the electric power consumption of the heat pump and its corresponding COP for the year 2009. The heat pump is mainly active in late winter and spring. This was expected since these are the periods where the buffer temperatures are low. Correspondingly, it is at these times when buffer temperatures are low that the COP is also lower. Note that the COP is capped at 10, since it is not realistic that higher COP's can be achieved. The impact of this on the results is extremely limited since the heat pump is barely operational when higher COP's could be achieved, as can be seen in Fig. 9.

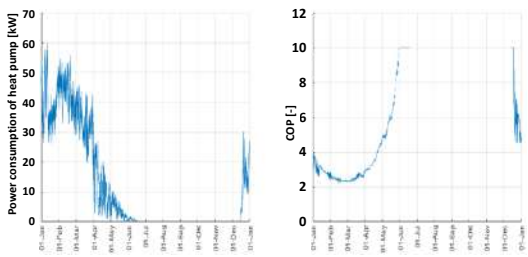

Fig. 9 - Electric power consumption and COP of heat pump in 2009. Configuration 2-A, scaled to have a SCOP of at least 5. 900 m² of solar collectors, 1325 m³ of buffer.

6.4 Performance of configuration 2-A

Configuration 2-A achieves the lowest LCOH for both the absolute cost optimum, as well as for the scenario where a SCOP of at least 5 has to be met.

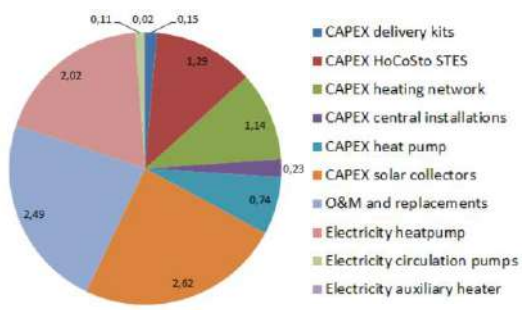

Fig. 10 - Cost breakdown for configuration 2-A in $€_{cent}$/kWh with scaling for SCOP of 5.

Fig. 10 shows a cost breakdown for configuration 2-A sized to reach a SCOP of 5. Slightly oversizing the buffer reduces the electricity consumption from the

auxiliary heater, but increases buffer CAPEX and O&M. The lower auxiliary heater electricity consumption follows from the lowest buffer temperatures which are higher when the buffer is scaled slightly larger, see Fig. 11..

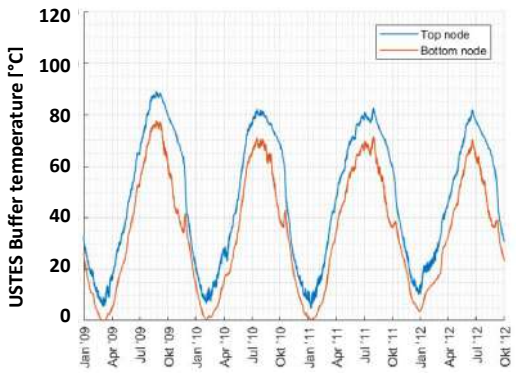

Fig. 11 - Buffer temperatures for configurations 2-A, sized to have a SCOP of at least 5.

6.5 Comparison with individual air-water heat pumps and conventional gas heating

If every participating building is outfitted with an individual high temperature air-water heat pump, the model predicts an average LCOH of 0.127 €/kWh, consisting of 0.87 cents in O&M, 6.87 cents in electricity costs, and 4.99 cents resulting from CAPEX. The SCOP over the 5 simulated years is 2.75, which roughly aligns with claims from air-water heat pump manufacturers. Comparing this scenario with configuration 2-A of the DHS, configuration 2-A achieves an SCOP of 4.4 for a cost of 0.107 €/kWh , the individual heat pump scenario is 18.6 % more expensive, and consumes 63.6 % more electricity. Based on a price of 0.67 €/m^3 of natural gas, a boiler efficiency of 90 %, annual maintenance costs of 100 €, initial CAPEX of 1500 € and 20 year boiler life, the LCOH of heating with natural gas is estimated as 0.082 €/kWh. This is significantly lower than the lowest achieved LCOH of 0.107 €/kWh by the proposed DHS. However, the extra costs related to the damage of the environment are not incorporated into the natural gas heating LCOH.

7. Conclusions

The LCOH decreases when a variable supply temperature is adopted instead of a fixed supply temperature of 73 °C. Best option is when a single heat exchanger provides all hot water using the heating network as the sole energy source and the supply temperature is environmental temperature dependent. Decoupling the solar collectors from the heating network by implementing a 4-line network reduces the LCOH. The decrease of the LCOH results from the significant increase in solar collector efficiency which results from the lower operating temperatures. The advantage is larger for a 4-line network where the operating temperature of the solar collectors can be optimized.

Slightly oversizing the solar collector area and buffer volume greatly reduces the electricity consumption of a system (and so increases the SCOP), without significantly adding to the costs keeping a similar LCOH. A 30 % lower electricity consumption can be achieved when a 1 % higher heating cost is accepted compared to the cheapest sizing. Solutions with supply temperatures requiring additional electrical heating of the DHW in buffers are not cost efficient. The cost increases due to higher CAPEX, increase in thermal losses, and a shift in electricity consumption from the centralised location to decentralised locations (where the electricity tariff is higher). While the proposed DHS can reach LCOH values of 0.107 €/kWh, individual air-water heat pumps in each building results in an LCOH of 0.127 €/kWh.

Data access statement

The datasets generated during and/or analysed during the current study are not publicly available because MSc thesis [1] is under embargo but will be available at the end of embargo period.

8. References

[1] Wolbert G.L.A. Seasonal Energy Storage - An optimized district heating system for solar thermal operation in combination with seasonal heat storage. M.Sc. Thesis, Delft University of Technology. 2020; 77 p.

[2] Sibbitt B., McClenahan D., Djebbar R., Thornton J., Wong B., Carriere J., Kokko J. The performance of a high solar fraction seasonal storage district heating system – Five years of operation. Energy Procedia. 2012;30(1):856–865.

[3] Yang X., Li H., Svendsen S. Evaluations of different domestic hot water preparing methods with ultra-low-temperature district heating. Energy. 2016;109(8):248–259.

[4] Koninklijk Nederlands Metereologisch Instituut. KNMI –Historic Dutch weather data. URL: https://www.knmi.nl/nederland-nu/klimatologie

[5] ter Meulen B., Geerts R., Infante Ferreira C.A. Seasonal underground sensible heat storage. Proceedings of Clima 2022. May 2022, Rotterdam, The Netherlands.

[6] Fuentes E., Arce L., Salom J. A review of domestic hot water consumption profiles for application in systems and buildings energy performance analysis. Renewable and Sustainable Energy Reviews. 2018;81(1):1530–1547.

[7] Duffie J., Beckman W. Solar Engineering of Thermal Processes. 4th Edition. 2013. John Wiley & Sons, Inc.

[8] van Miltenburg R.M. Integration of decentralized solar collectors in Dutch district heating grids. M.Sc. Thesis, Delft University of Technology. 2018.

[9] Wallentén P. Steady-state heat loss from insulated pipes. Lunds Tekniska. Högskola. M.Sc. Thesis. 1991.

Air/water heat pumps: energy and environmental assessment in Mediterranean residential building sector

Carola Lingua [a], Sara Viazzo [a], Stefano Paolo Corgnati [a], Simonetta Lena [b], Leonardo Prendin [b]

[a] TEBE-IEEM Research Group, Department of Energy (DENERG), Politecnico di Torino, Corso Duca degli Abruzzi 24, 10129 Torino (TO), Italy, e-mail: (carola.lingua, stefano.corgnati, sara.viazzo)@polito.it

[b] Rhoss S.p.A., Via Oltre Ferrovia, 33033 Codroipo (UD), Italy, e-mail: (simonetta.lena, leonardo.prendin) @rhoss.com

Abstract. The improvement of buildings energy efficiency represents one of the key objectives of current European policy actions, in order to guide the transition towards a low-carbon society. Indeed, nowadays, it is known that the building sector is responsible for 40% of total energy consumption and that heating is recognised as the main cause of this impact. In this context, heat pumps are recognized as promising solutions both for new constructions and for the renovation of existing buildings. For supporting the transition of the building sector, in Italy, within the "Recovery Decree" (D.L. 34/2020), which has introduced diverse social policies and financial support schemes to face the economic crisis following the COVID-19 pandemic, it is worth mentioning the current Superbonus incentive mechanism, accessible also for the installation of heat pumps. In this context, the paper aims to investigate the effectiveness of the use of air-to-water heat pumps as an alternative to traditional condensing gas boilers in residential buildings, either new or existing. Focusing on single-family houses, different models, differing in building size, envelope characteristics and heating systems were simulated, considering three different climatic zones of Italy. In detail, the energy simulations concerned two main application fields, the former considering the installation of heat pumps in new constructions, characterized by envelopes with high performances, while the latter analysing the use of heat pumps in existing buildings, without intervening on their envelopes with poor performances. The work aims to demonstrate the potential energy and environmental benefits associated with the use of heat pump solutions for space heating and domestic hot water production in both cases. The results allow stressing on the goodness of heat pump technologies in terms of energy savings (expressed in total non-renewable primary energy index) and CO_2 emissions reduction, as well as their capability in improving the energy efficiency classes of the analysed buildings, only with system upgrading intervention.

Keywords. Heat pump, condensing boiler, residential, single-family house
DOI: https://doi.org/10.34641/clima.2022.35

1. Introduction

Improving the energy performance of buildings is fundamental to achieve the desired energy transition. In fact, the increment of buildings energy efficiency represents one of the key objectives of current European policy actions, as outlined by the European Green Deal [1], which aims to achieve climate neutrality and lead Europe towards the transition to a post-carbon society by 2050. Nowadays, the building sector is responsible for 40% of total energy consumption, and building heating is recognized as the main cause of this impact [2]. To decarbonize the building sector, heat pumps are considered the most promising heating solution to be applied in both new constructions and renovated existing buildings [3;4]. In order to support the transition of the building sector, diverse financial mechanisms were introduced, to encourage energy investments in buildings. Recently, focusing on the Italian context, the Decree Law n.34 (D.L. 34/2020) [5], also known as Recovery Decree, was introduced on the 19th May 2020, aiming to provide financial support to face the economic crisis following the Covid-19 pandemic. It is worth mentioning that the Italian Decree introduced an incentive mechanism, the so-call Superbonus, which increased the tax rebate for building interventions from existing 50-65% to 110% [5]. This mechanism involves a considerable amount of actions and technologies, among which the installation of heat pump technologies, aiming to encourage their installation

Copyright ©2022 by the authors. This conference paper is published under a CC-BY-4.0 license.

in new construction or as replacement of existing fossil-fuelled heating systems.
In line with the above, the paper aims to investigate the effectiveness of air-to-water heat pumps as an alternative to the traditional condensing boilers in residential buildings. In detail, the study concerned two main application fields, depending on the type of building intervention: new construction and existing buildings renovation. The former analysis focuses on illustrating the energy and environmental benefits associated to the use of heat pump solutions for space heating and domestic hot water (DHW) services in new residential buildings, excluding the economic evaluation which could be an interesting topic to further explore. Conversely, the second application aims to determine whether an intervention of system upgrading, excluding any actions on building envelope, can guarantee the improvement of two energy efficiency classes for the building under investigation (i.e., a condition required by the D.L. 34/2020 to access the Superbonus 110%) [5]. For both applications, quasi steady-state simulations of a single-family house with different sizes and located in diverse Italian climatic zones were developed, to estimate the energy and environmental benefits that the installation of air-to-water heat pumps can guarantee.
The paper is structured as follows: section 2 describes the methodology used for the analysis, as well as the main parameters considered for the creation of simulation models. Section 3 summarises the main results of the study, divided between new buildings (paragraph 3.1) and existing buildings renovation (paragraph 3.2). Finally, section 4 presents the main conclusive remarks and future perspectives of the work.

2. Research Methods

To estimate the impacts in energy and environmental terms associated to the use of heat pumps in both new and existing buildings, the paper defined specific building models, then simulated through the thermo-technical software EdilClima EC700 v10 compliant with UNI/TS 11300 [6] and validated by the Italian Thermo-technical Committee (CTI, Comitato Termotecnico Italiano).
This paragraph summarises the main assumptions done for the models' construction and simulation, in terms of geometrical characteristics, climate zones, building envelope (paragraph 2.1), reference building systems (paragraph 2.3). After the definition of the reference conditions for the building models, paragraph 2.3 introduces diverse HVAC solutions, focusing on heat pumps, to be installed in both new and existing buildings.
The work focuses on single-family houses (SFHs), belonging to the Italian category E1(1) - dwellings used for residential purposes on a continuous basis, such as civil and rural dwellings. Specifically, two SFH models were defined, presenting different building sizes: a model S (small), characterized by an internal area of 150 m^2, and a model L (large), with an internal area of 220 m^2. Both models S and L present one floor above ground and have a net floor height of 2.7 m. In addition, the south façade of both SFHs has a larger glazed area than the north one, to maximise solar gains and reduce heat loss.

2.1 Building envelope performances

The defined SFHs are considered representative of both new and existing buildings. However, to account for the diverse building envelope performances between these two categories, four levels of envelope performance were considered, in turn characterized by specific thermal transmittance of opaque and transparent envelopes (as reported in Table 2).
Going into detail, all envelopes used in the simulations are in line with the traditional characteristics of Italian single-family house. Generally, bricks and external thermal insulation are used in external walls, and concrete and masonry for floor and ceiling; all windows are equipped with PVC frames with triple low-emissivity glass. Despite a similar structure of the envelope elements, the levels of energy performance are characterized by increased insulation thicknesses, moving from low to very high performance. In order to differentiate the modelled SFHs between new and existing, it was assumed to use envelopes with very high (envelope A) and high (envelope B) performances only for new constructions, while using envelopes with low (envelope C) and very low (envelope D) performances only for existing buildings.
Table 2 summarises the main cited assumptions, reporting the thermal transmittance values of walls, floors, and windows of each model. The 8 models (model S and L, with four level of envelope performance A, B, C and D) were simulated considering three different climatic zones of Italy. In northern Italy, Turin climate was used to represent the climate zone E; in the centre of Italy, the locality of Rome was used for representing the climatic zone D; finally, for the warmer climate of Southern Italy, Palermo was used to represent the climate zone B. Table 1 reported the monthly average temperature for all the three climatic zones of Italy. A total of 24 simulations was carried out; the results obtained in terms of thermal energy requirements for heating ($Q_{h,nd}$) and design thermal load (P_u) are shown in Table 2, calculated according to UNI/TS 11300-1 [6] and UNI EN ISO 12831 [7].

Tab. 1 – Monthly average outdoor temperatures for Turin, Rome and Palermo respectively (unit °C).

	Turin [°C]	Rome [°C]	Palermo [°C]
January	1.20	8.10	11.9
February	3.10	9.10	11.5
March	8.30	11.5	13.6
April	11.9	15.9	16.8
May	18.0	19.2	20.3
June	22.1	22.6	24.1
July	23.6	26.4	27.1
August	22.6	26.6	27.2
September	19.1	21.7	24.1

October	12.3	17.8	20.8
November	6.80	12.7	16.8
December	2.60	8.70	13.1

2.2 Reference system

Once defined the main geometrical and envelope the same reference system, composed of an autonomous heating system, used for the production of domestic hot water combined with the space heating provision. A class A condensing boiler generator, with a 22 kW nominal power and a modulating regulation was considered. For each simulated model, two types of emission terminals were analysed; (1) fan coil with hot water temperature of 45°C and (2) radiant floor with hot water temperature of 35°C. The presence of radiators in the bathrooms characterises all models. Finally, new and existing buildings were diversified only in terms of ventilation system type. Specifically, new buildings (characterized by levels A and B) are equipped with a mechanical ventilation system with heat recovery. On the contrary, existing buildings (characterized by levels C and D) present only natural ventilation through windows opening. It is important to specify that, in this paper, attention is devoted only to heating purposes, without considering the space cooling demands of the SFHs under analysis.

2.3 Proposed heat pump solutions

To estimate the performances of heat pump characteristics of the analysed SFHs, a reference system was identified, with the scope of comparing its energy and environmental performances in the different developed building models with those of heat pumps to be potentially installed in these buildings. All 8 models (i.e., 4 new buildings and 4 existing buildings) are assumed to be equipped with solutions when installed in the modelled buildings, diverse system solutions were proposed, considering the replacement of the reference heat generator and the thermoregulation system. Focusing on electric solutions, the following three air-to-water heat pumps were considered:

(1) one-section air-to-water heat pump space heater, ideal for new buildings with medium-low energy requirements and for renovations;
(2) two-section air-to-water heat pump space heater, ideal for new buildings with medium-low energy requirements, for renovation or for the replacement of existing generators;
(3) two-section air-to-water heat pump combination heater with domestic hot water storage, ideal for new buildings with medium-low energy requirements or for renovations.

Considering that the solutions (2) and (3) are characterized by the same thermal power and Coefficient of Performance (COP), these solutions were simulated only once. In all simulations, heat pumps are evaluated only in heating mode (cooling analyses are out of the scope of this paper). The data of heat pumps performances were gathered from technical documentation of real commercial units.

Tab. 2 – Characterisation of the building envelope energy performance of the simulated models. $Q_{h,nd}$: thermal energy requirements for heating; P_u: design thermal load.

		TURIN	ROME	PALERMO
VERY HIGH PERFORMANCE (Envelope level A) U_{wall}= 0.15 W/m²K, U_{floor} = 0.12 W/m²K, U_{window} = 1.2 W/m²K	Model **SA**	Pu: 7.15 kW, Qh,nd: 31.26 kWh/m²	Pu: 5.07 kW, Qh,nd: 6.55 kWh/m²	Pu: 3.80 kW, Qh,nd: 2.44 kWh/m²
	Model **LA**	Pu: 9.38 kW, Qh,nd: 33.39 kWh/m²	Pu: 6.65 kW, Qh,nd: 8.81 kWh/m²	Pu: 4.98 kW, Qh,nd: 4.03 kWh/m²
HIGH PERFORMANCE (Envelope level B) U_{wall}= 0.28 W/m²K, U_{floor} = 0.21 W/m²K, U_{window} = 1.4 W/m²K	Model **SB**	Pu: 8.42 kW, Qh,nd: 47.75 kWh/m²	Pu: 5.98 kW, Qh,nd: 14.34 kWh/m²	Pu: 4.48 kW, Qh,nd: 6.81 kWh/m²
	Model **LB**	Pu: 10.92 kW, Qh,nd: 47.95 kWh/m²	Pu: 7.74 kW, Qh,nd: 16.41 kWh/m²	Pu: 5.81 kW, Qh,nd: 8.22 kWh/m²
LOW PERFORMANCE (Envelope level C) U_{wall}= 0.86 W/m²K, U_{floor} = 0.5 W/m²K, U_{window} = 2.2 W/m²K	Model **SC**	Pu: 16.61 kW, Qh,nd: 163.8 kWh/m²	Pu: 11.82 kW, Qh,nd: 82.35 kWh/m²	Pu: 8.87 kW, Qh,nd: 46.59 kWh/m²
	Model **LC**	Pu: 22.43 kW, Qh,nd: 160.9 kWh/m²	Pu: 16.02 kW, Qh,nd: 83.66 kWh/m²	Pu: 11.96 kW, Qh,nd: 47.65 kWh/m²
VERY LOW PERFORMANCE (Envelope level D) U_{wall}= 0.86 W/m²K, U_{floor} = 0.5 W/m²K, U_{window} = 4.5 W/m²K	Model **SD**	Pu: 19.01 kW, Qh,nd: 183.2 kWh/m²	Pu: 13.54 kW, Qh,nd: 87.84 kWh/m²	Pu: 10.16 kW, Qh,nd: 50.42 kWh/m²
	Model **LD**	Pu: 25.3 kW, Qh,nd: 176.9 kWh/m²	Pu: 18.06 kW, Qh,nd: 87.46 kWh/m²	Pu: 13.51 kW, Qh,nd: 50.52 kWh/m²

3. Results

The analysis aims to illustrate the energy and environmental benefits associated to the use of heat pump solutions for space heating and domestic hot water purposes for both new and existing buildings. Based on the simulation of the SFHs considering both the reference system and the proposed heat pump solutions, total non-renewable primary energy ($EP_{g,nren}$ for heating, domestic hot water and ventilation) and CO_2 emissions are computed for all models. Specifically, the use of heat pumps in new constructions is explored in paragraph 3.1, while their deployment for the renovation existing buildings heating systems is reported in paragraph 3.2 (considering not to intervene on the building envelope). In all cases, attention is devoted to understanding the possibility for the modelled SFHs to improve of two energy efficiency classes compared to the reference condition, in order to access the Italian tax benefit known as "Superbonus 110%" [4]. The developed graphs provide the results for the three different climatic zones - Turin, Rome and Palermo - and for the diverse emission systems (i.e., radiant floors and fan coils, respectively in blue and red colours). All graphs present on the x-axis the three building system solutions compared (including the reference system) for the three climates; the y-axes report the total non-renewable primary energy on the left and the CO_2 emissions on the right.

3.1 New buildings

Four models of new constructions were developed (models SA, SB, LA and LB), all characterised by the presence of controlled mechanical ventilation and of very high- and high-performance envelopes.

It is clear from the graphs shown in the following figures (from Figure 1 to Figure 4) that the use of one-section and two-section air-to-water heat pump space heater, and two-section air-to-water heat pump combination heater with domestic hot water storage is advantageous both in terms of energy savings and reduced environmental impact, showing a significant reduction in non-renewable primary energy consumptions and CO_2 emissions compared to the use of a condensing boiler (i.e., reference system). All buildings are characterised by an energy efficiency class A+ also with the condensing gas boiler, due to the high building envelope performance considered for new construction buildings. In general, different heat pump solutions provide similar total non-renewable primary energy values in the same country, while the variability of the values in relation to each climate is evident. In addition, from the figures presented below, it can be seen that the performances of the aforementioned heat pumps (whether one-section and two-section air-to-water heat pump space heater, and two-section air-to-water heat pump combination heater with domestic hot water storage) are in line with the minimum performance required by law. A detail discussion of the results for each climate zone is here presented.

In Turin, the one-section heat pump, associated with the use of radiant floor, leads to a consistent amount of energy savings, ranging from 27% (Figure 1) to 38% (Figure 4). Also considering the application with fan coils, the energy savings range between 25% and 32% for SA and LB models, respectively. Analysing the results for the two-section heat pump, the situation is very similar; the presence of a radiant floor leads to energy savings ranging from 22% (Figure 1) to 30% (Figure 2), while with fan coils there is no substantial difference (from 21% to 27% respectively for the SA and SB models). For the location of Turin, the analysis was carried out only for the small size model because the useful thermal power required by the large size model cannot be satisfied by the considered heat pumps.

In Rome, the percentages of energy savings and reduction of CO_2 emissions are slightly lower than the results shown for Turin. The one-section heat pump, associated with the use of radiant floor, leads to energy savings ranging from 22% (Figure 1) to 32% (Figure 4). Considering the two-section heat pump the amount of energy savings ranging from 19% (Figure 1) to 30% (Figure 4). Again, no substantial difference is visible for the combination of heat pumps with fan coils.

Finally, focusing on Palermo climate, the one-section heat pump, combined with the use of radiant floor, results in energy savings ranging from 20% (Figure 1) to 29% (Figure 4); in the scenario with the replacement with two-section heat pump the values come from 19% to 27%, respectively.

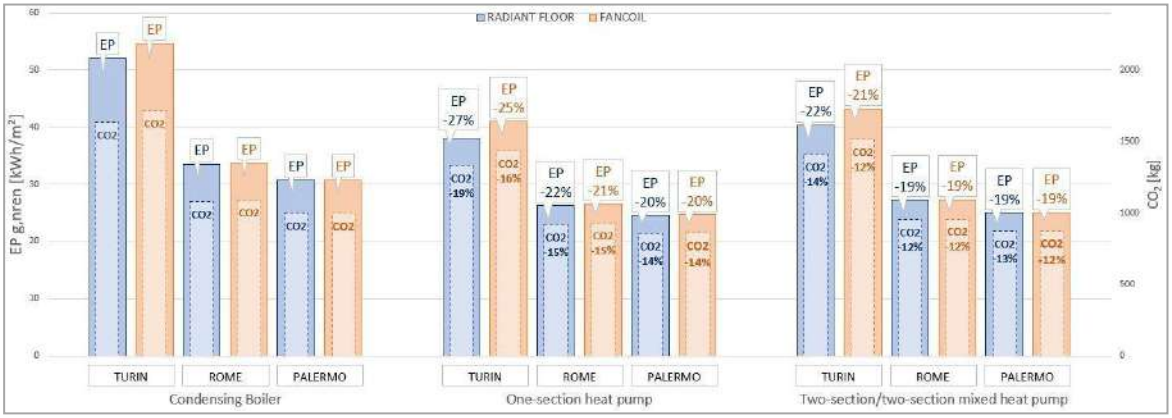

Fig. 1 – Energy- and environmental-related outcomes for model SA.

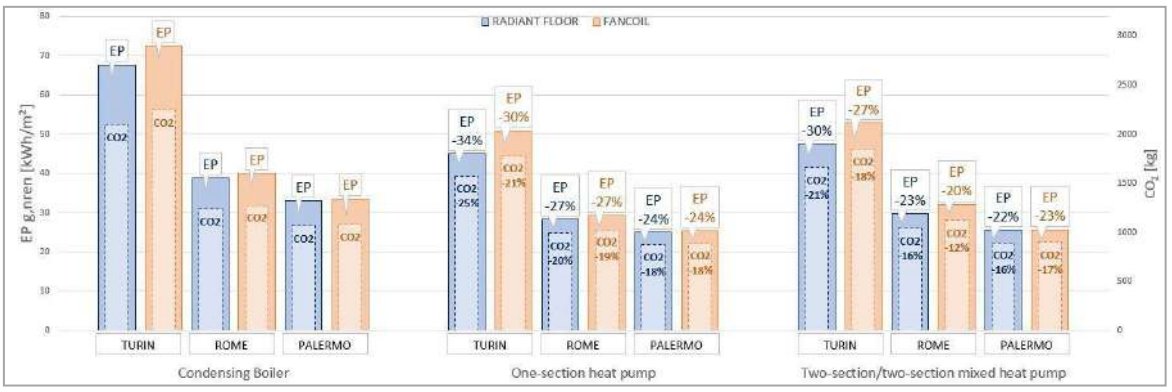

Fig. 2 – Energy- and environmental-related outcomes for model SB.

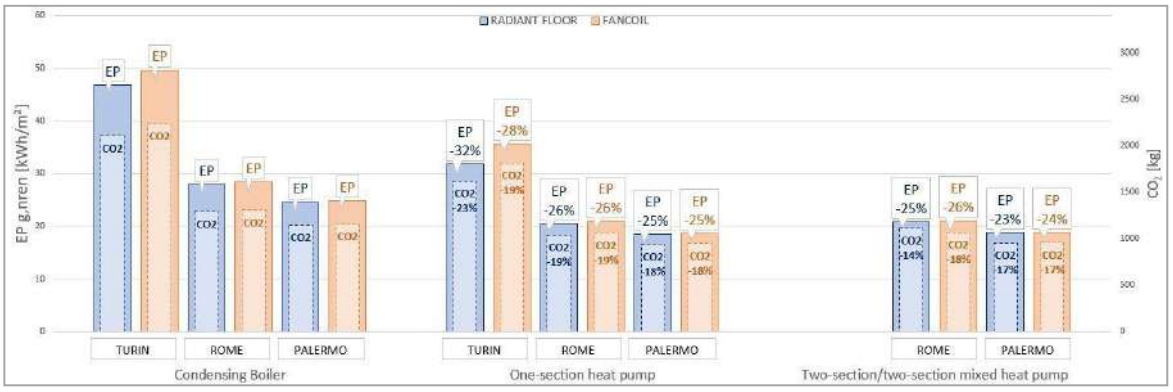

Fig. 3 - Energy- and environmental-related outcomes for model LA.

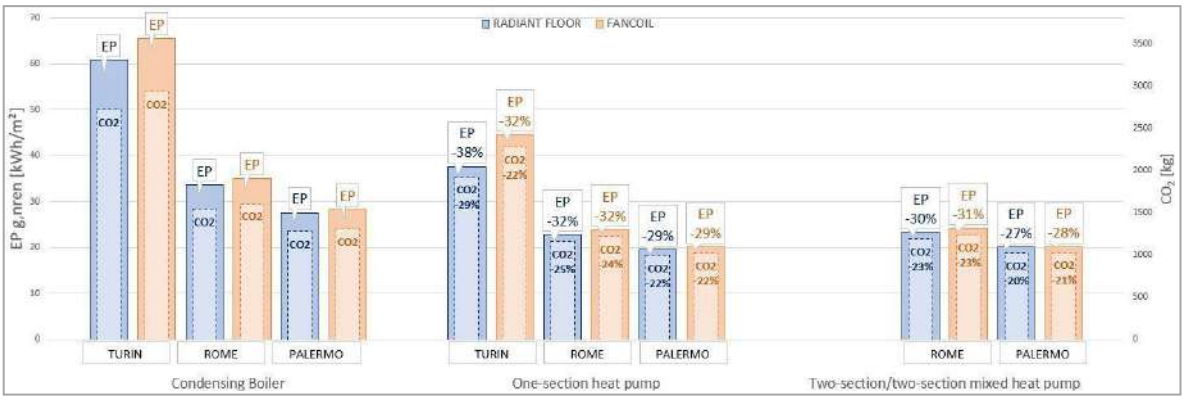

Fig. 4 - Energy- and environmental-related outcomes for model LB.

3.2 Existing buildings renovation

Four models of existing buildings were developed (models SC, SD, LC and LD), all characterised by the presence of natural ventilation and of low- and very low-performance envelopes. As previously mentioned, this section aims to determine whether an intervention of sole system upgrading - the replacement of a condensing boiler with an air-to-water heat pump solution - excluding actions on building envelope, can guarantee the improvement of two energy efficiency classes [5].

As it possible to see from the graphs (from Figure 5 to Figure 8), the results clearly show how the replacement of the condensing boiler with an air-to-water heat pump, both one-section and two-section solutions, makes it possible to achieve an improvement of at least two energy efficiency classes, also without intervening on the envelope. Indeed, this double energy class shift is always verified, both in the presence of radiant floors and fan coils (represented in blue and red, respectively). As far as the environmental analysis is concerned, the graphs show a significant decrease in CO_2 emissions achieved thanks to the use of heat pump technologies. It is important to specify that the analysis is not available for Turin, because the useful thermal power required by both small and large

models cannot be satisfied by the considered heat pumps. Furthermore, the large-size SFHs (models LC and LD, shown in Figure 7 and 8, respectively) were only simulated for Palermo, since the heat pump sizes did not meet the criteria required also for Rome.

In Rome, the one-section heat pump, associated with the use of both radiant floor and fan coils, leads to a consistent amount of energy savings, ranging from 50% to 60% in model SC, as well as in model SD. It can be seen from the graphs that the energy saving achieved leads to 3 to 4 energy class jumps - from class D to A1/A2 in Figure 5 and from class E to B/A1 in Figure 6.

In Palermo, the percentages of energy savings and reduction of CO_2 emissions are quite the same. The one-section heat pump, associated with the use of radiant floor, leads to energy savings ranging from 61% (Figure 5) to 63% (Figure 8). Considering the two-section heat pump the amount of energy savings is equal to 54% in all models. No substantial difference is visible for the combination of heat pumps with fan coils.

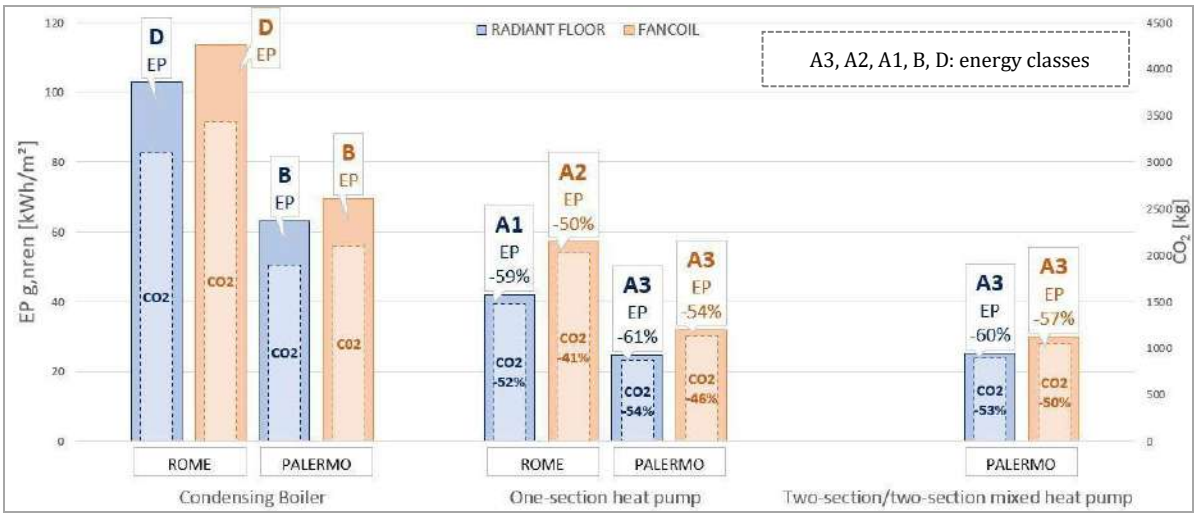

Fig. 5 - Energy- and environmental-related outcomes for model SC.

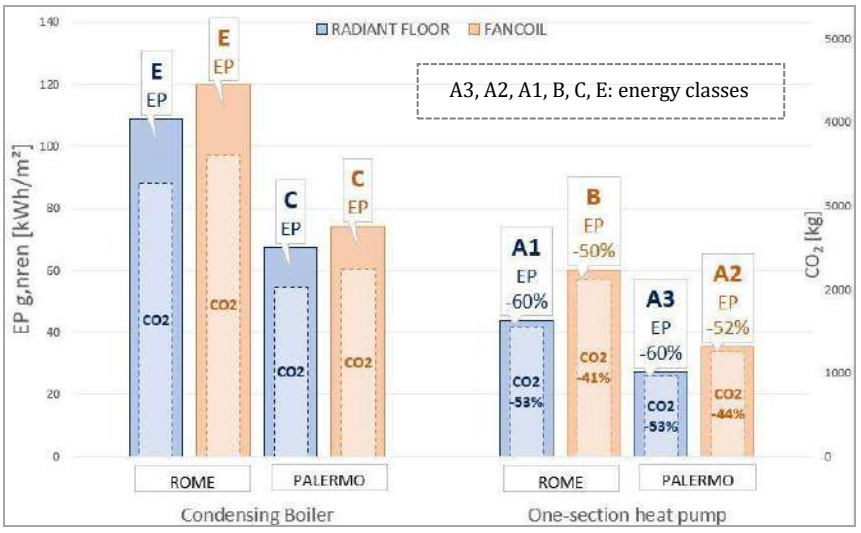

Fig. 6 - Energy- and environmental-related outcomes for model SD.

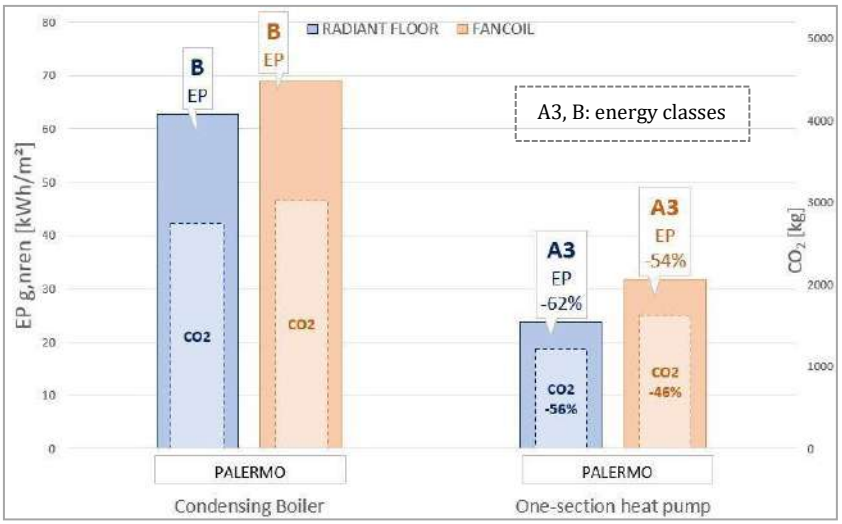

Fig. 7 - Energy- and environmental-related outcomes for model LC.

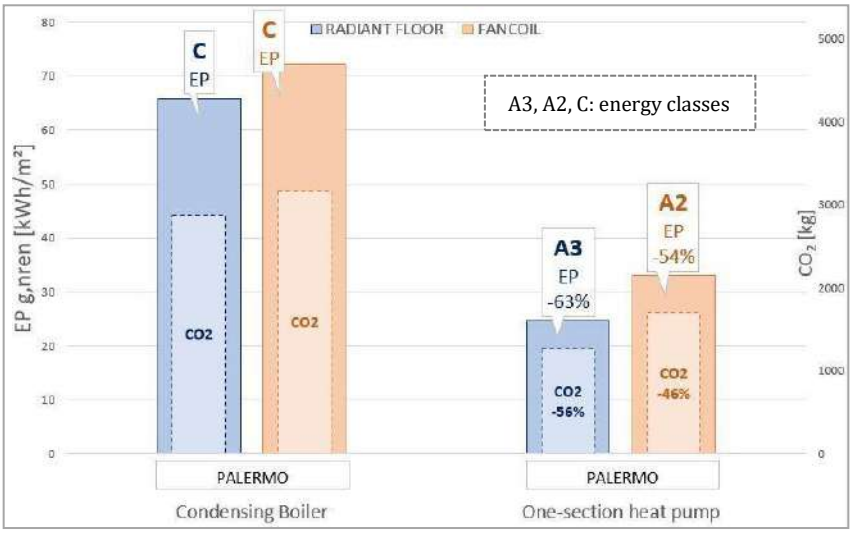

Fig. 8 - Energy- and environmental-related outcomes for model LD.

4. Conclusions

Energy efficiency of buildings represents the key factor of the current European policy actions in order to achieve the energy transition and the energy efficiency of the building sector. Nowadays, the building sector is responsible for 40% of total energy consumption, in which building heating is recognized as the main sources [2]. In this context, a solution is the widespread adoption of heat pump technologies. In fact, in the Italian residential context, the Decree Law 34/2020 [5] increased the tax incentives to 110%, encouraging the replacement of heating systems with heat pump technologies, among various actions. In this context, the paper aims to investigate the effectiveness of air-to-water heat pumps as an alternative to the traditional condensing boilers in residential buildings. In detail, the study concerned two main application fields, depending on the type of building intervention; new construction and existing buildings renovation. In the first analysis the main goal is to illustrate the energy and environmental benefits of using heat pump solutions for the heating and domestic hot water production. The second application aims to determine whether an intervention of system upgrading can guarantee the improvement of two energy efficiency classes.

The results of the analysis shown that the use of one-section and two-section air-to-water heat pump space heater, and two-section air-to-water heat pump combination heater with domestic hot water storage is advantageous both in terms of energy savings and reduced environmental impact, showing a significant reduction in CO_2 emissions compared to the use of a condensing boiler. Furthermore, it has been demonstrated that an intervention of sole system upgrading - the replacement of a condensing boiler with an air-to-water heat pump solution - excluding actions on building envelope, can guarantee the improvement of more than two energy efficiency classes.

The present analysis was carried out on single-family buildings and, in all the simulations, the heat pumps are evaluated only in heating mode. In this view, it might be interesting, as a future development, to consider apartment buildings and to develop the

analysis for the summer season, also considering the cooling mode. In addition, beyond the energy and environmental saving aspect, the impact on the economic value of the building after the energy requalification could be an interesting topic to further explore.

5. References

[1] European Commission, Communication from the Commission to the European Parliament, the European Council, the Council, the European Economic and Social Committee and the Committee of the Regions. The European Green Deal. COM(2019) 640 final. Brussels, 11st December 2019.

[2] European Commission, New rules for greener and smarter buildings will increase quality of life for all Europeans. Brussels, 19th April 2019.

[3] Roccatello E., Prada A., Baggio P., Baratieri M. Analysis of the Influence of Control Strategy and Heating Loads on the Performance of Hybrid Heat Pump Systems for Residential Buildings. Energies 15 (2022), 732.

[4] Ala G., Orioli A., Di Gangi A. Energy and Economic Analysis of Air-to-Air Heat Pumps as an Alternative to Domestic Gas Boiler Heating Systems in the South of Italy. Energy 173 (2019), 59-74.

[5] Decreto-legge del 19 maggio 2020, n.34. Misure urgenti in materia di salute, sostegno al lavoro e all'economia, nonché di politiche sociali connesse all'emergenza epidemiologica da COVID-19. Gazzetta Ufficiale n.128 del 19 maggio 2020.

[6] UNI/TS 11300-1:2014. Energy Performance of Buildings - Part 1: Evaluation of Energy Need for Space Heating and Cooling. Edition, 2nd October 2014.

[7] UNI EN ISO 12831-1:2017. Energy performance of buildings - Method for calculation of the design heat load - Part 1: Space heating load. Edition, 12nd July 2017.

Data statement

Data sharing not applicable to this article as no datasets were generated or analysed during the current study.

Variation in Indoor Thermal Environmental Parameters in an Open Space Office

Arnab Chatterjee [a], Verena M. Barthelmes [a], Dolaana Khovalyg [a]

[a] Integrated Comfort Engineering (ICE), École polytechnique fédérale de Lausanne (EPFL), Fribourg, Switzerland

Abstract. Building energy modelling is an indispensable component of today's design method. However, as per research findings, real-life buildings could utilize almost twice the amount of their ideal energy performance. Thus, it is important to understand the variation in the thermal environmental and thermal sensation parameters in the office buildings during real-life operation. Currently, the design of the indoor environment in buildings is performed based on the appropriate national and international standards. Based on thermal comfort requirements for mechanically conditioned buildings, the temperatures are held within narrow limits, and it is expected that the new and existing buildings adhere to them very strictly. Naturally, the question arises, instead of keeping indoor thermal conditions constant, could it be healthier to make it dynamic. A more dynamic thermal environment that goes beyond the boundaries of comfort zones may be able to provide occupants with thermal comfort, along with instances of thermal delight and positive stimulation.

To this objective, physical measurements were carried out in open office space in Lausanne, Switzerland. Data showing the overall variation of the thermal comfort parameters in space and in time have been presented. The ranges of thermal environment parameters, i.e., operative temperature, relative humidity, air speed, and local discomfort factors consisting of horizontal and vertical radiant temperature asymmetries, vertical temperature differences are discussed. Also, thermal sensation indicators, i.e., PMV and PPD are calculated from the measured values. These values are then compared with the limits specified in the standard ISO 17772. The thermal environmental parameters, particularly operative temperature, mostly lay in the Category II and III. Local discomfort factors did not exceed the limits of Category I. Thermal sensation calculation showed that the conditions were more on the cooler side since PMV was in the range of -0.2 to -1 and, the PPD was between 10-20%.

Keywords. building energy modelling, thermal comfort, energy savings, dynamic thermal environment
DOI: https://doi.org/10.34641/clima.2022.62

1. Introduction

The indoor thermal environment is largely influenced by the activities of the occupants, their metabolic rate and their thermal adaptability. Outdoor temperature also has a significant influence on the indoor thermal environment, even in the mechanically conditioned buildings. In winter, people resort to adaptive behaviours such as consuming hot food and beverages, putting clothing layers, etc. This can widen the range of the comfortable temperatures. The low outdoor temperature helps people to adapt to a cold environment. In studies, it has been found that lower the outdoor temperature and longer the cold climate was, the higher the usage rate of the district heating system in winter, and the longer the heating season was. The outdoor temperature affects the adaptive behaviour, even in heated buildings [1][2][3]. Maintaining a high indoor temperature during the winter is not only a waste of energy; but also nullifies people's adaptation to the environment [4].

The change in the thermal sensation of occupants with space is found to be an important factor determining thermal comfort. Under dynamic

Copyright ©2022 by the authors. This conference paper is published under a CC-BY-4.0 license.

conditions, the change of thermal sensation of people with time has significant effect on the perception of thermal comfort [5]. Dynamic thermal environments, complete with certain natural features, may be more suitable for the human body [6]. Indeed, thermal environments that are beneficial to the human ability of thermal adaptation should be regarded as the healthier. Dynamic thermal environment can be established by allowing more variability of air temperature and/or air velocity. Studies of human responses showed that airflow similar to natural air movement has highest preference. Variation of indoor environmental parameters can result in substantial energy saving while an acceptable indoor climate could be maintained [7].

In rural areas in Northwest China the acceptable temperature ranges for the classrooms in Shaanxi, Gansu and Qinghai Provinces were 12.7-16.9 °C, 11.9-17.1 °C and 15.8-18.7 °C, respectively. Occupants have the ability to adapt to a wide range of temperature [8]. Studies suggest that people originally from cold climates even prefer a little bit lower temperature rather than a neutral temperature [9]. The indoor design temperature should consider the local climate and the clothing thermal resistance, the physiological characteristics, and the psychological adaptability of occupants. Maintaining a high indoor temperature consumes more energy, which is wasteful [10][11]. Results show that often buildings have discomfort due to high temperatures in the wintertime, which is indicative of over-heating [12][2][3].

Feeling of thermal comfort come from dynamic contrast [13]. If the poor thermal environment improves a little, people will feel significantly better [13]. The changes of temperature provide cold or hot stimulation on the human body, which can increase the pleasure of thermal sensation. Average operative temperature value of Europe is much higher than Asia (China). North America holds a narrower operative temperature range [14] thus in North America the indoor conditions have the highest meeting rate (93.5% of data points) of ASHRAE comfort zone. Most of outside-comfort-zone points of Europe are due to overheating, while the outside-comfort-zone points of China are mainly caused by overcooling [14]. The neutral indoor operative temperature during the summer in Beijing was 26.8 °C, while in the winter, it was 20.7 °C [4].

The above studies reveal that cooling and heating setpoints, as specified by the standards, are held within narrow limits. In Table 1, the categorization of the various environmental parameters as per ISO 17772 is tabulated [15][16]. The standard categorizes environmental parameters to "high" or "category I", "medium" or "Category II", "moderate" or "category III" and "low" or "category IV". The definition of each category are as follows:

I. High (Category I) should be selected for occupants with special needs (children, elderly, handicapped)

II. Medium (Category II) are the normal level used for the design and operation (typically used)

III. Moderate (Category III) can still provide an acceptable environment with some risk of reduced performance of the occupants.

IV. Low (Category IV) should only be used for a short time of the year or in the spaces with a very short time of occupancy.

The narrow limits of temperature could lead to the problem of high energy expenditure through overheating and overcooling. Also, it leads to the elimination of the innate thermal ability of the human body to adapt to the mild cold and mild hot conditions and unnecessary waste of energy. There are studies highlighting that exposure to mild cold conditions lead to the activation of Brown fat adipose tissues (BAT) which has been seen to increase the energy expenditure of the human body. Thus, speaking in the long term this can mean a healthier environment to have a mild cold dynamic indoor working condition [17][18].

To this objective, physical measurements are carried out in an open office space in Switzerland. Data showing the overall variation of the thermal comfort parameters in space and in time have been presented. The ranges of thermal environment parameters, i.e., operative temperature, relative humidity, air speed, and local discomfort factors consisting of horizontal and vertical radiant temperature asymmetries, vertical air temperature differences are discussed. Also, thermal sensation indicators, i.e. PMV and PPD, are calculated from the measured values and has been presented in this study. These values are then compared with the limits specified in the standard ISO 17772. The main purpose of the study is to illustrate the thermal environmental parameters during the real operation in an office building in Switzerland and assess their variability.

2. Methodology

The following section is devoted to describing the case study building and the measurement protocols.

2.1 Case Study

The case study building is an office building. The office space is located on the second floor and presents a dominant exposure to north. One smaller part of the open space offices faces east and single offices are exposed to the west. The floor plan (Figure 1) of the studied space consists of open space office (259.1 m2), 2 single offices (21.6 m^2/each), kitchen area (37.9 m2) and separated

Tab. 1 - Categorization of environmental parameters as per ISO 17772

Parameter	Category I	Category II	Category III	Category IV

Operative Temp (T_{op})	21-23 °C	20-24 °C	19-25 °C	17-26 °C
Relative Humidity (RH)	30-50 %	25-60 %	20-70 %	<20, >70 %
Air Speed (V_{air})	<0.1 m/s	<0.16 m/s	<0.21 m/s	>0.21 m/s
Hor. Radiant Asymmetry Temperature (ΔH^*)	<23 °C	-	<35 °C	>35 °C
Ver. Radiant Asymmetry Temperature ($\Delta V^\#$)	<5 °C	-	<7 °C	>7 °C
Vertical Temperature Difference (ΔT_v)	<2 °C	<3 °C	<4 °C	>4 °C
PMV	-0.2–0.2	-0.5–0.5	-0.7–0.7	-1.0–1.0
PPD	<6 %	<10 %	<25 %	>25 %

*For cold wall, #For warm ceiling

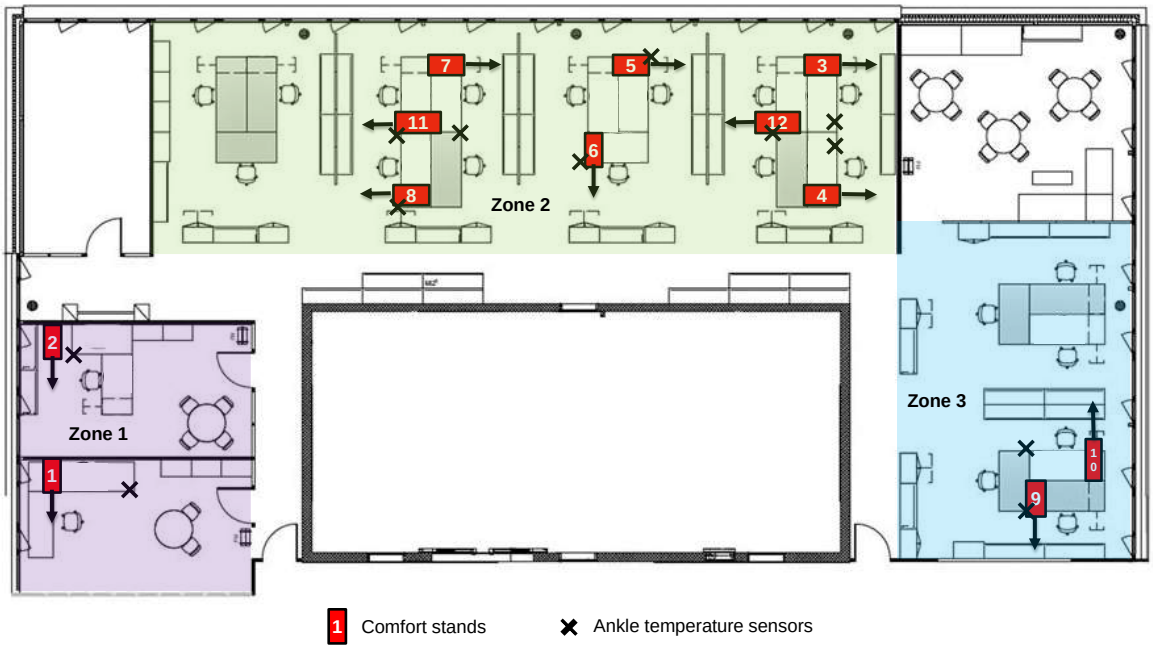

Fig. 1 - Case study plan with the location of the sensors

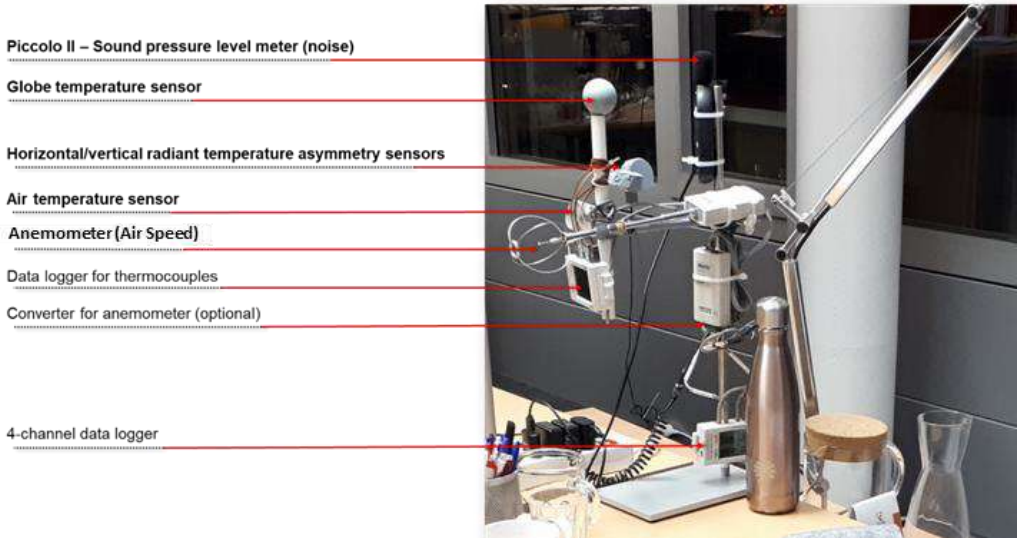

Fig. 2 - Sensor configuration in the stands

printing room that is excluded from the analysis. The floor plan has been divided into three zones out of which Zone 1 consists of two single offices and Zone 2 & 3 are open plan offices. Space heating and cooling is provided by a hydraulic radiant ceiling panel system. The heating/cooling circuit set-point in heating mode is 31°C while set-point in cooling mode is 19 °C. The system is connected to the general heat pump serving multiple buildings in the neighbourhood and an auxiliary heater. The indoor air temperature set-point for all zones is 23 °C and it is not possible to modify the set-point in any individual zones. The changeover between heating and cooling mode is calculated based on the sum of differences between room temperatures in different areas of the building.

The building is equipped with an air handling unit, the set-point of supply temperature depends on the outdoor temperature: if the outside temperature is equal or below 20 °C, the set-point of the supply temperature is 22 °C. The supply set-point than gradually decreases with the increase of outdoor temperature down to 18°C with an outdoor temperature equal or higher than 32 °C. The pressure for air supply and extraction is 180Pa and 140 Pa, respectively. The designed air flow rate for each inlet is 50 m^3/h. The occupants have the possibility to interact with windows and window blinds. Windows are casements windows (tilt-turn) and are all operable. The window blinds are regulated automatically but can be overridden manually. The desk lights are equipped with a motion sensor and turn ON automatically – even though a manual control is possible, it is not used. Ceiling lights installed along the central staircase block are always on during working hours and cannot be individually controlled by the employees.

2.2 Field Study Campaign

The field protocol consists of measurement of thermal environment and local discomfort parameters. The thermal environment variables that are measured and would be discussed in this paper are air temperature, globe temperature, air speed and relative humidity. For the local discomfort factors, ankle level temperature, horizontal and vertical radiant asymmetries are recorded. Air temperature, globe temperature, air speed, horizontal and vertical radiant temperature asymmetries recordings are done every 10 seconds. The ankle temperature measurements have been taken every 5 minutes. Figure 2 shows the typical configuration of the sensors quipped for the current filed study. Figure 1 shows the positioning of the different sensors in the office floor plan. The study was conducted in the winter for a duration of two weeks from 27th January, 2020 to 7th February 2020.

The air temperature, globe temperature and the air speed are measured at a height of 0.6 m above the desk level. It is approximately at the same level as the head of the occupants in a seated position. The ankle temperature sensor is placed near the ankle levels (0.1 m above the floor level). The measurements are used to calculate the vertical temperature differences. Mean radiant temperature and operative temperature are calculated from the measured parameters. Radiant temperature asymmetry sensors are also deployed to measure the horizontal and vertical radiant temperature asymmetry at height of 0.6 m above the desk level to test the presence of local discomfort sources. The globe temperature, air temperature and air speed measurements are accurate to ±0.2 % of the reading. The horizontal and vertical radiant temperature asymmetry are accurate to ±0.6 °C. The relative humidity readings have an accuracy of 2.5 %. And lastly the ankle temperature measurements are accurate to ±0.2 % of the reading. The thermal sensation indicators PMV and PPD was calculated by using the CBE Comfort Tool [19]. Few approximations are made, for example, clothing insulation is considered to be constantly at 0.6 clo and the metabolic rate of 1.1 met is considered which corresponds to seated and light working activity. These values correspond to actual clothing insulation and the activity level encountered in the studied office space.

3. Results and Discussion

In this section the results of the field study are presented along with discussion of the results. All the data represented is for the weekday working hours (7 am to 7 pm). The operative temperature distribution as seen in Figure 3a, shows that during almost all the working hours the temperature is in between 21-25 °C with vast majority of the hours lying in the Category I. The categorization of the parameters has been highlighted in the plots based on the values specified in Table 1. With the exception of a couple of stray spikes, there are almost no hours exposing the occupants to Category IV operative temperature. Similarly, in case of relative humidity (Figure 3b) during majority of the hours, the conditions were in Category I and Category II or between 25-45 %. The air speed lies mostly in the Categories I, II and III i.e. in the range of 0-0.21 m/s. There are also quite a few hours where the air speed lies in the Category IV as can be seen in Figure 3c.

As has already been discussed in the introduction, human beings have the intrinsic ability to adapt to mild cold and mild hot conditions. And this adaptation can be weakened as a result of exposure to constant temperatures for extended period of time. The question that naturally arises is that, would it be better to have a dynamic indoor environment where the temperature, relative humidity and air speed fluctuates within wide ranges rather than always maintaining the indoor conditions within the Category I and II. From the point of view of energy savings, it would definitely be beneficial as operating at lower temperature would save energy which would otherwise have been used for space conditioning.

For the local discomfort parameters, horizontal radiant temperature asymmetry (Figure 3d), vertical radiant temperature asymmetry (Figure 3e) and vertical air temperature differences (Figure 3f) have been presented below. The case study building is equipped with ceiling radiant panels for the cooling and heating purposes. Since the case study has been performed in the winter months, the ceiling panels were working primarily in the heating mode. The presence of these ceiling radiant panels results in vertical radiant temperature asymmetries but since these were working at low temperatures, the vertical radiant temperature asymmetry values are well within the Category I as prescribed by ISO 17772. The range of the values extend between 0-1 °C with a few outliers.

Similarly, the horizontal radiant temperature

asymmetry values are quite low, also within the Category I lying between 0-1 °C. It is mainly due to the fact that there was absence of strong heat sources on the vertical surfaces in the building, except for windows. Based on the measurements, the

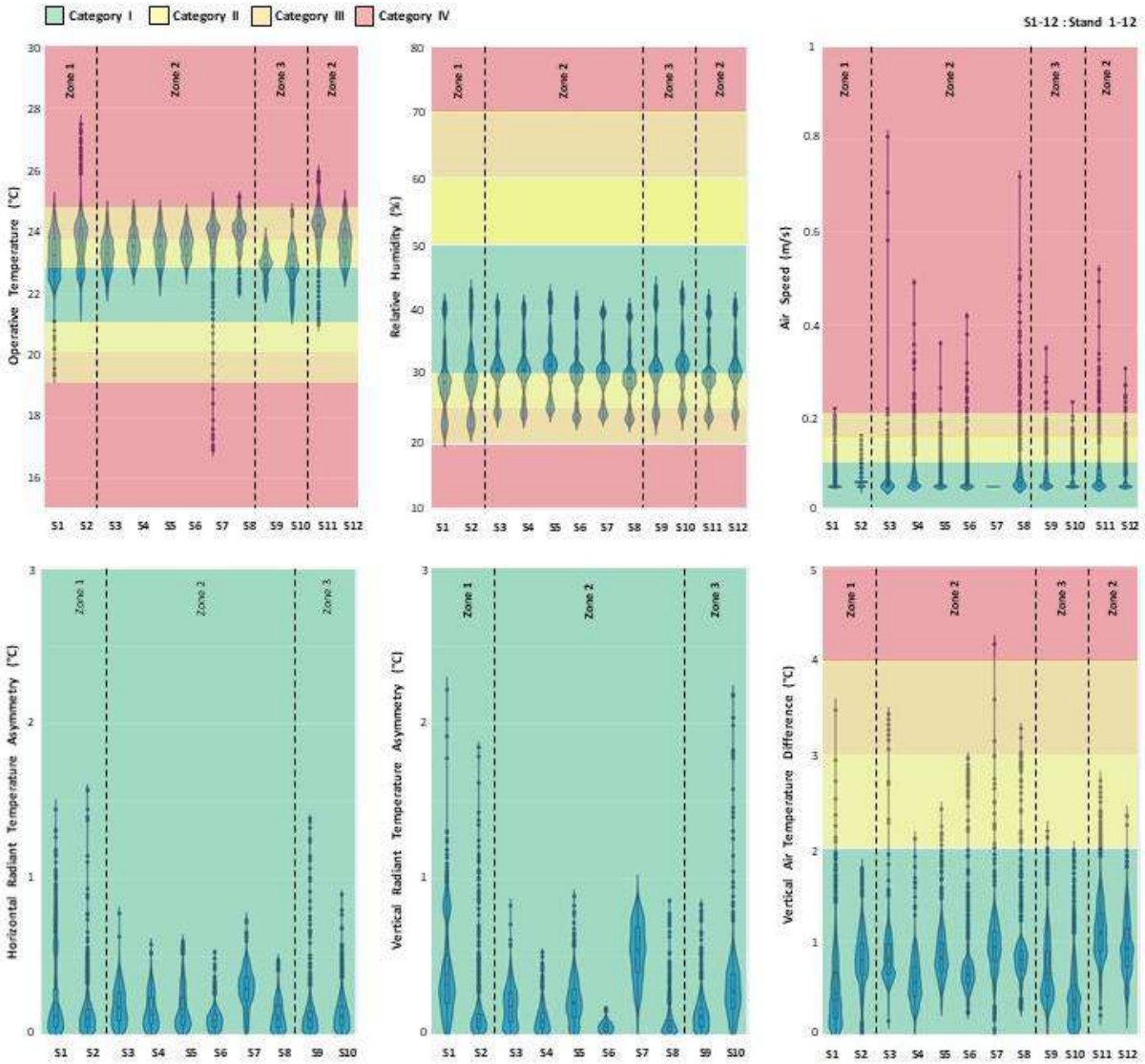

Fig. 3 - Spatial variations in thermal environmental parameters (a) Top, (b) RH, (c) Vair, (d) ΔH, (e) ΔV, (f) ΔT_V

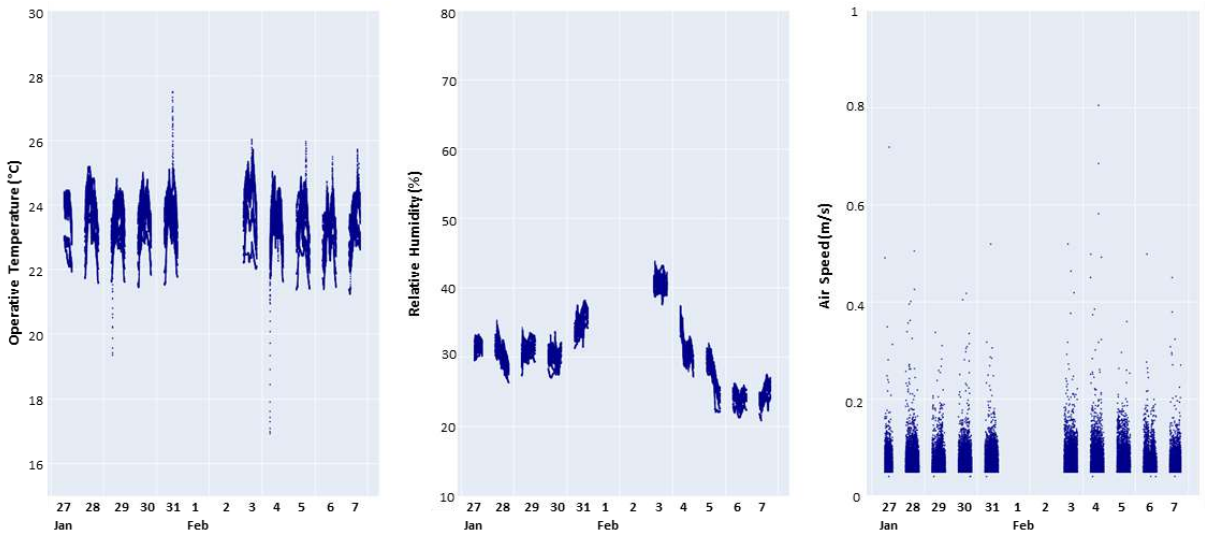

Fig. 4 - Temporal variations in thermal environmental parameters (a) Top, (b) RH, (c) V_{air}

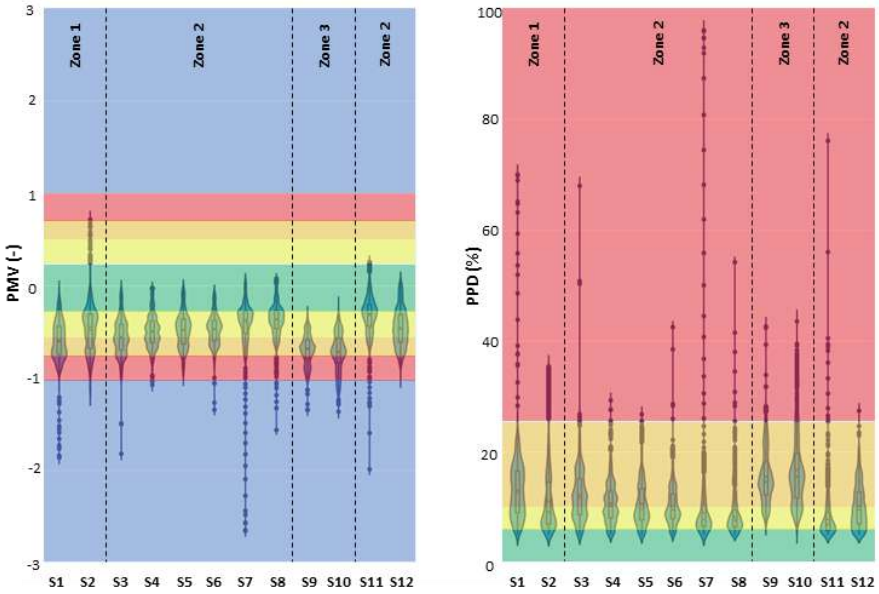

Fig. 5 - Spatial variations in calculated thermal sensation indicators (a) PMV, (b) PPD

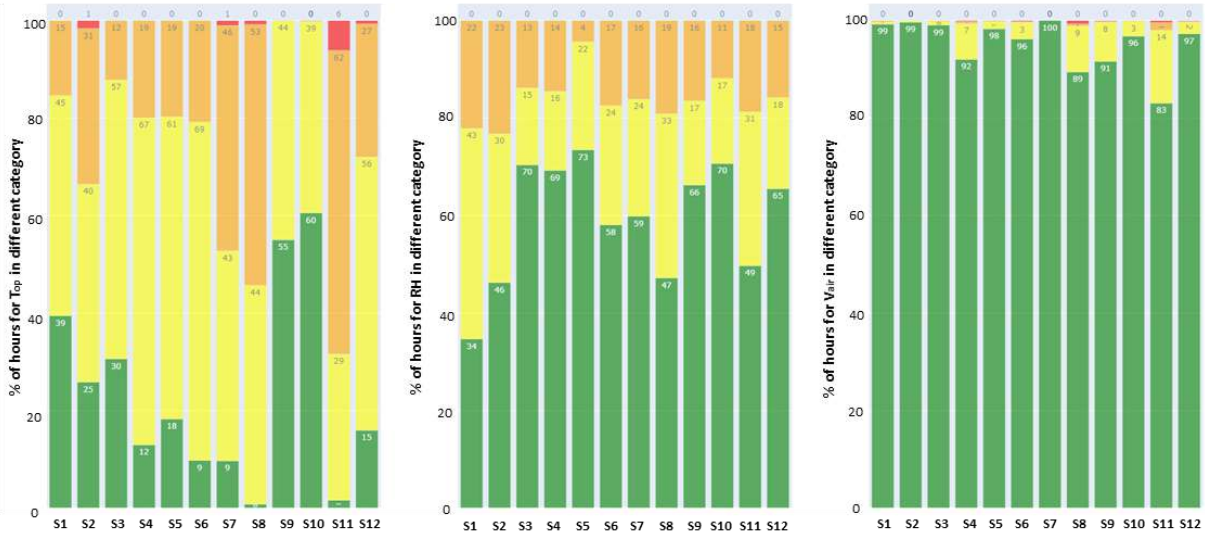

Fig. 6 - Percentage of hours within certain categories of thermal environment for (a) Top, (b) RH, (c) V_{air}

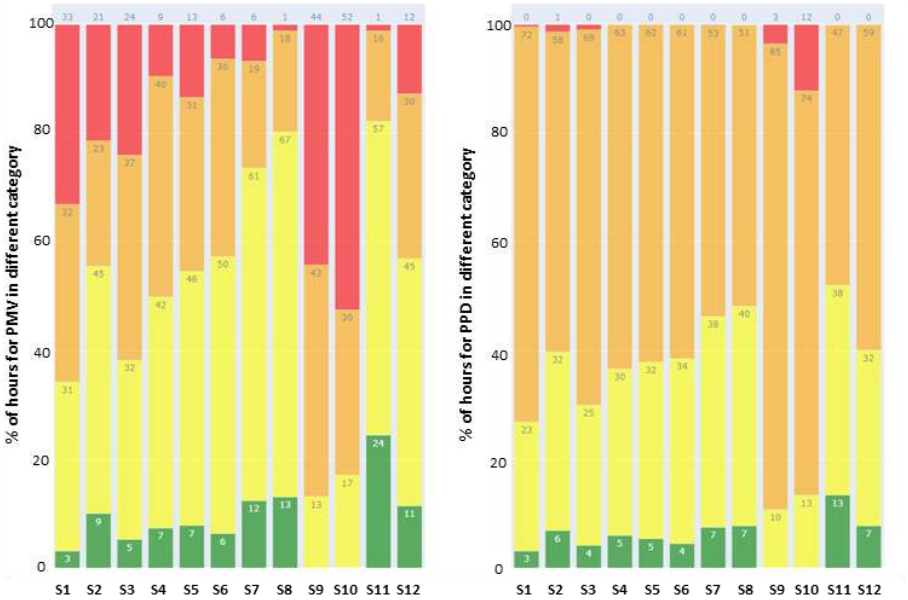

Fig. 7 - Percentage of hours within certain categories of thermal environment for (a) PMV, (b) PPD

shortwave radiation coming through the windows did not have significant effect on radiant temperature asymmetry. The vertical air temperature difference measures the air temperature difference at the head and the ankle level of the occupants. The values range between 0-2 °C with few discrete values above that range. Checking the above values with respect to the limits specified in the standard ISO 17772 for local discomfort parameters, they are within the acceptable range and should not result in uncomfortable condition for the occupants. In Figure 4 we see the temporal variation of the measured and calculated parameters only during the working hours (7 am to 7 pm). In case of the operative temperature a clear pattern can be seen where low temperatures of approximately 21 °C are seen at the beginning and the end of the working hours. While during the peak occupancy hours this temperature goes up to 25 °C. The fluctuations in relative humidity and air speed is apparently not so high to affect thermal comfort. Thus, PMV follows a trend very similar to that of the operative temperature. PMV calculations with respect to ASHRAE Standard 55-2017 leads to PMV values in the range of -0.5 to -1.2.

In the Figure 5a and 5b, the calculated values for Predicted Mean Vote (PMV) and Percentage of People Dissatisfied (PPD) are presented for the whole duration of the field study. They are calculated from the values measured in the study. PMV depends on air temperature, mean radiant temperature, relative humidity, air speed, clothing insulation and metabolic activity level. Mean radiant temperature has been calculated from measured parameters.

All the other values are measured directly and used for the calculation of PMV. As seen in Figure 5, the PMV is mostly on the colder side, lying between -0.2 and -1. This can be attributed to the low clo value of the occupants in this study. PPD is a function of PMV and can be directly calculated from it. Also, the PPD value can be seen to exceed the comfortable limits. In winter normally the occupants tend to wear light sweaters in their office space which can reduce this cool sensation.

Resuming the discussion about dynamic environment, we know that occupants may prefer certain degree of variability in their indoor environment. The changes of temperature provide cold or hot stimulation on the human body, which can increase the pleasure of feelings. In that scenario the above PMV and PPD calculation may not be so significant. Reminding the fact that exposing occupants to narrow range of comfortable temperatures we may be impairing the innate ability of the human body to adapt to mild cold and hot conditions. Our goal should be to make use of this thermal adaptability and promote dynamic indoor environment.

Figure 6 and 7 represents the percentage of hours in different comfort categories for the thermal environmental parameters in the field study. The categorization is with respect to ISO 17772, as seen in Table 1. For the operative temperature in the field study, 10-40% of the working hours lie in Category I, 30-60% in Category II, 10-40% in Category III and almost negligible in Category IV. This translates to the temperature range of 21-26 °C for the majority of hours. In case of relative humidity 35-70% of the occupancy hours lie in the Category I, 15-30% in Category II and about 10% in Category III. While for air speed most of the working hours (about 95%) in all positions lie in Category I according to ISO 17772.

PMV and PPD calculation have been performed by using the web-based tool for thermal comfort calculations developed at the University of California at Berkeley (CBE Comfort Tool). For the PMV values we find that only about 10% of the occupancy hours belong to Category I, 20-50% in the Category II, 20-40% in Category III and 10-20% also in Category IV. Also, for PPD calculations about 85-95% of hours lie in Category II and III. According to the standard ISO 17772, the hours in Category III and IV are supposed to be uncomfortable for the occupants and should be minimized. This is mainly because of the operative temperature which is found to be the in range of 21-26 °C.

Although there are no wild fluctuations in the indoor thermal environment but it is still categorized as uncomfortable according to the limits specified in ISO 17772 which, as we already discussed above, prescribes very narrow limits especially for operative temperature. In the introduction we discussed how temperatures much colder and warmer than 21-26 °C have been regarded as acceptable by the occupants. Thus, the standards need to take into consideration the local climate and thermal adaptability of the occupants when defining comfort category limits. Our objective should be to promote a dynamic indoor environment. The changes of temperature provide cold or hot stimulation on the human body, which can increase the pleasure of thermal sensation. And at the same time, it can reduce the overuse of energy by eliminating overheating and overcooling.

4. Conclusion

A field study was conducted in an open office space in the winter for a duration of two weeks from 27th January, 2020 to 7th February 2020. The field protocol consists of measurement of thermal environment and local thermal discomfort parameters. The thermal environment variables that are measured are air temperature, globe temperature, air speed and relative humidity. For the local discomfort factors, ankle level temperature, horizontal and vertical radiant temperature asymmetries are recorded. The following conclusions can be made:

I) The thermal environmental parameters mostly lie in the Category I, II and III ranges: operative

temperature in between 21-26 °C, relative humidity in between 25-45 % and, the air speed in the range of 0-0.2 m/s. There is a certain degree of dynamicity in the indoor environment particularly as seen in the temperature fluctuations. But the temperature values can be reduced by 4-5 °C to be in the range of 16-21 °C which can increase energy savings and may potentially even provide long term health benefits through increased energy metabolism in the occupants.

II) Local thermal discomfort factors did not exceed the limits of Category I: horizontal and vertical radiant temperature asymmetries lie in between 0-1 °C and, the vertical temperature difference is mostly in the range of 0-2 °C. Thus, the indoor conditions remained comfortable with respect to the presence of local discomfort.

III) Thermal sensation indicators showed that the conditions are more on the cooler side. The PMV is in the range of -0.2 to -1 and, the PPD is in between 10-20 %. ISO 17772 specifies very narrow limits for comfort requirements especially with respect to operative temperature values.

IV) In the case study the indoor conditions are dynamic to some extent but they can be categorized as uncomfortable for most of the hours according to ISO 17772. We remind the fact that by exposing occupants to narrow range of temperatures we may be weakening the innate ability of the human body to adapt to mild cold and hot conditions. Our goal should be to make use of this thermal adaptability and create a dynamic indoor environment.

5. References

[1] Yan H., Yang L., Zheng W., & Li D. Influence of outdoor temperature on the indoor environment and thermal adaptation in Chinese residential buildings during the heating season. Energy and Buildings. 2016;116:133–140.

[2] Yang B., Olofsson T., Wang F., & Lu W. Thermal comfort in primary school classrooms: A case study under subarctic climate area of Sweden. Building and Environment. 2018;135:237–245.

[3] Wang Z., Li A., Ren J., & He Y. Thermal adaptation and thermal environment in university classrooms and offices in Harbin. Energy and Buildings. 2014;77:192–196.

[4] Cao B., Zhu Y., Ouyang Q., Zhou X., & Huang L. Field study of human thermal comfort and thermal adaptability during the summer and winter in Beijing. Energy and Buildings. 2011;43(5):1051–1056.

[5] Zhang Y., & Zhao R. Relationship between thermal sensation and comfort in non-uniform and dynamic environments. Building and Environment. 2009;44(7):1386–1391.

[6] Zhu Y., Ouyang Q., Cao B., Zhou X., & Yu J. Dynamic thermal environment and thermal comfort. Indoor Air.2015;26(1):125–137.

[7] Zaki S., Damiati S., Rijal H., Hagishima A., & Abd Razak A. Adaptive thermal comfort in university classrooms in Malaysia and Japan. Building and Environment. 2017;122:294–306.

[8] Xu C., Li S., Zhang X., & Shao S. Thermal comfort and thermal adaptive behaviours in traditional dwellings: A case study in Nanjing, China. Building and Environment. 2018;142:153–170.

[9] Ji W., Cao B., Geng Y., Zhu Y., & Lin B. Study on human skin temperature and thermal evaluation in step change conditions: From non-neutrality to neutrality. Energy and Buildings. 2017;156:29–39.

[10] Wang D., Jiang J., Liu Y., Wang Y., Xu Y., & Liu J. Student responses to classroom thermal environments in rural primary and secondary schools in winter. Building and Environment. 2017;115:104–117.

[11] Derks M., Mishra A., Loomans M., & Kort H. Understanding thermal comfort perception of nurses in a hospital ward work environment. Building and Environment. 2018;140:119–127.

[12] Diaz Lozano Patiño E., Vakalis D., Touchie M., Tzekova E., & Siegel J. Thermal comfort in multi-unit social housing buildings. Building and Environment. 2018;144:230–237.

[13] Ji W., Cao B., Luo M., & Zhu Y. Influence of short-term thermal experience on thermal comfort evaluations: A climate chamber experiment. Building and Environment. 2017;114:246–256.

[14] Zhang N., Cao B., Wang Z., Zhu Y., & Lin B. A comparison of winter indoor thermal environment and thermal comfort between regions in Europe, North America, and Asia. Building and Environment. 2017;117:208–217.

[15] Khovalyg D., Kazanci O.B., Halvorsen H., Gundlach I., Bahnfleth W., Toftum J., Olesen, B. Critical review of standards for indoor thermal environment and air quality. Energy & Buildings. 2020;213:109-119.

[16] ISO 17772-1:2017. Energy performance of buildings — Indoor environmental quality — Part 1: Indoor environmental input parameters for the design and assessment of energy performance of buildings

[17] Van Marken Lichtenbelt W., Vanhommerig J., Smulders N., Drossaerts J., Kemerink G., Bouvy N., Schrauwen P., Teule G. Cold-Activated Brown Adipose Tissue in Healthy Men. N Engl J Med. 2009;360:1500-8.

[18] Van Marken Lichtenbelt, W. Human brown fat and obesity: methodological aspects. Frontiers in Endocrinology. 2011;2:52.

[19]https://github.com/CenterForTheBuiltEnvironment/comfort_tool. CBE Comfort Tool

Evaluation of tariff structural changes in Spanish households affected by energy poverty

Mariana Jiménez Martínez [a], *Lluc Canals Casals* [a,c], *Joana Ortiz* [c]

[a] Energy Systems Analytics Group, Catalonia Institute for Energy Research (IREC), Barcelona, Spain, mcjimenez@irec.cat

[b] Project and Construction Engineering Department, Polytechnic University of Catalonia, Barcelona, Spain. lluc.canals@upc.edu

[c] Thermal Energy and Building Performance Group, Catalonia Institute for Energy Research (IREC), Barcelona, Spain, jortiz@irec.cat

Abstract. A new structure for regulated tariffs affecting consumers with contracted power up to 15 kW was introduced by the Spanish government in June 2021. According to the National Commission for Markets and Competition the new tariff would impact residential consumers differently, depending on previous contracting conditions. In particular, households under old Time-of-Use tariffs are expected to face a significant increase in their electricity bill, which might be exacerbated by the rising generation costs observed in the Spanish market throughout 2021. This situation becomes more relevant for consumers affected by energy poverty, especially when considering that this group needs to be in a regulated tariff to access social benefits. A set of energy poverty affected households are evaluated during a monitoring campaign carried out in Barcelona's pilot as part of EmpowerMed H2020 project, whose objective is to tackle energy poverty and help improving people's health in the coastal areas of Mediterranean countries, with a particular focus on women. Hourly consumption data is downloaded from the customers' smart-meters, which are accessed through their personal account in the distributor's website. Using this data, the article presents an evaluation of the potential impact that the new tariff structure might have on energy poverty affected households, considering different price scenarios that reflect the observed rising generation costs and the price mitigation measures enacted by the government in an attempt to reduce its impact on domestic consumers.

Keywords. Energy Poverty, Domestic Consumers, Electricity Tariffs, Energy Regulation.
DOI: https://doi.org/10.34641/clima.2022.185

1. Introduction

Although not included as such in the declaration of human rights by the United Nations, the energy use is inherent in almost any human activity and, thus, essential for life [1]. In fact, access to energy, as a human right, has historically been justified as such for being implicit in other effective human rights (i.e. sustainable development right or the right for non-discrimination) [2]. Moreover, since 2015, the 7th sustainable development goal targets to "ensure access to affordable, reliable, sustainable and modern energy" [3], which goes even further than just access to energy.

Nonetheless, this target seems hard to accomplish since, even in Europe more than 15% of the population could be characterized as affected by "fuel poverty" [4]. This situation gets even worse when considering the concept of "energy poverty", which has a wider overview rather than just affordability [5]. This study adopts the concept of "energy poverty" defined by Bouzarovski as "the situation in which a household lacks a socially and materially necessitated level of energy services in the home" [6], which is also used in the EmpowerMed H2020 project that englobes this analysis.

EmpowerMed project aims to mitigate the effect of Energy Poverty (EP) by empowering women (principally) to fight against it [7]. The project has six pilot sites in different regions of the Mediterranean coast where household face difficulties to reach good thermal comfort conditions both in summer and winter. Several approaches are used to this purpose, such as household visit, collective assemblies, do-it-yourself (DIY) capacity activities or workshops. This analysis focusses on the results obtained from the DIY activities carried out in the Barcelona pilot from September 2020 to June 2021, which involved the study of the electricity consumption of a group of EP-affected households through smart meter

Copyright ©2022 by the authors. This conference paper is published under a CC-BY-4.0 license.

monitoring as well as bill optimization analysis [8].

This monitoring campaign showed average potential savings per EP-affected household of 42,0 €/year by optimizing their contract conditions. The choice minimizing participants' costs was a regulated contract – known as PVPC for its Spanish acronym – plus the 2.0DHA tariff, a Time of Use (TOU) option with two pricing periods (peak and valley). Two other tariff structures from the PVPC scheme were also available during the campaign, 2.0A – a flat rate tariff - and 2.0DHS, which was optimized for night EV charging. Customers were also advised to lower their contracted power when their maximum demanded power was significantly below the current contracted value [8].

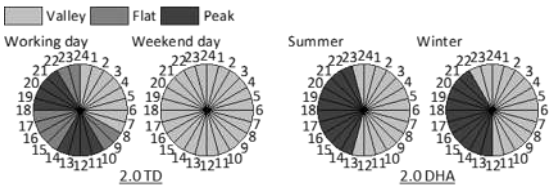

Fig. 1 – Pricing periods considered in tariffs 2.0DHA (abrogated) and 2.0TD (current).

However, a regulatory change introduced in 1st June 2021 put the achieved savings in question as all customers under PVPC contracts were assigned to the 2.0TD tariff, now the only available option under the regulated scheme. This tariff is defined by three pricing periods (valley, flat and peak) as seen in Fig. 1. Weekends and holidays are considered valley, but during workdays, valley hours (late night) are substantially reduced in comparison to the 2.0DHA scheme. Now, hours previously classified as valley are considered flat, which is more expensive. 2.0TD also has differentiated contracted powers for valley and flat-peak times [9]. According to the National Commission for Markets and Competition (CNMC), the new tariff would likely imply larger costs for households previously using the 2.0DHA tariff [10].

In addition, the persistent increase in electricity generation costs has added more concerns, particularly to vulnerable customers. In response, the Spanish government enacted a series of Price Mitigation Measures (PMM) to soften its impact on households' electricity bills. The first set was released in 24th June 2021, being the most relevant for vulnerable customers the transitory reduction of the Value Added Tax (VAT) from 21% to 10% [11]. Other actions were implemented to lower generation costs themselves, but the upward trend was not reversed, which translated into higher active energy prices for PVPC users (Fig. 2).

A second set of PMM was released in 14th September 2021[12]. Among others, it included the reduction of the special tax on electricity from 5,11% to 0,5% and lower access charges imposed to the power-based and active energy components of the 2.0TD tariff. These are responsible for the pattern shift observed in Fig. 2 after this date. In 26th October 2021 [13], the Spanish government released a third set that included larger discounts to beneficiaries of the Social Bonus (SB), a social aid scheme that reduces vulnerable customers' electricity bills up to a certain extent [14]. As happened in June, active energy costs continue rising despite other control actions taken.

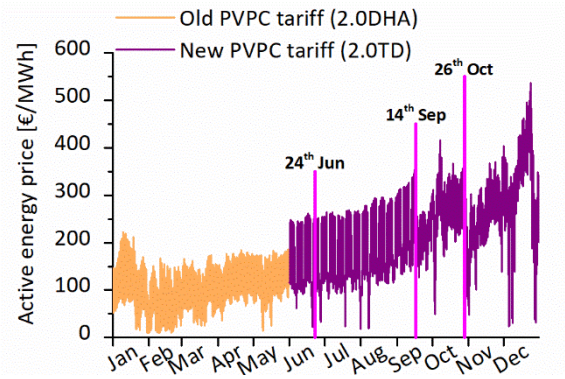

Fig. 2 – Active energy prices registered for the old and new PVPC tariffs during 2021. Pink vertical lines mark the dates on which PMM were applied.

Considering the observed market and regulatory conditions, this article analyses the effect of changing tariff structures under a drastic rise in generation costs to differentiate the impact that each factor has on vulnerable customers. As well, it evaluates the increase or decrease risk to worsening their current EP levels, and the potential role of implemented PMM in softening the negative impact of rising prices on vulnerable Spanish households.

2. Research methods

2.1 Data collection

The EP-affected households included in this study correspond to twelve participants from the EmpowerMed's monitoring campaign carried out in Barcelona from September 2020 to June 2021. Hourly electricity consumption is recovered from the smart-meters installed by the distributor company through a web service. Socioeconomic and energy usage data is gathered using a Google Forms survey. All sampled households attended the collective assemblies organized by the Alliance Against Energy Poverty and had or are in the process of obtaining the Report on Social Exclusion Risk (IRER for its Catalan acronym) issued by social services to officially recognize their vulnerability status [8].

Active energy prices are obtained from the ESIOS platform, operated by the Spanish Transmission System Operator, *Red Eléctrica Española* [15]. The data for the selected pricing periods is downloaded through the platform's Advanced Programming Interface (API) service and cleaned and transformed using a Python script.

2.2 Energy costs calculation

Tariff impact analysis is conducted over two representative weeks for summer (July 6th to 12th 2020) and winter (January 4th to 10th 2021). Data availability from volunteers as well as cooling and heating needs – main drivers for residential electricity demand – are considered in the weeks' selection. During the past 20 years in Barcelona, July has been one of the months with higher reported Cooling Degree Days (CDD), and January with higher Heating Degree Days (HDD) [16]. In particular, the selected summer and winter weeks presented 10 CDD and 71 HDD [17], respectively, which are close to historical average values for both months.

To analyse the impact of price and regulatory changes, nine scenarios are defined as summarized in Tab. 1. Scenarios OT2, NT4 and NT4_NM are evaluated over the winter consumption week, and the rest over the summer week. In all scenarios except NT2_NM, NT3_NM and NT4_NM, all price components and PMM are included based on the actual market and regulatory conditions observed.

Tab. 1 – Characteristics of defined price scenarios.

Scenario	Tariff	Season	PMM
OT1	2.0 DHA	Summer	
OT2	2.0 DHA	Winter	
NT1	2.0 TD	Summer	
NT2	2.0 TD	Summer	✓
NT2_NM	2.0 TD	Summer	
NT3	2.0 TD	Summer	✓
NT3_NM	2.0 TD	Summer	
NT4	2.0 TD	Winter	✓
NT4_NM	2.0TD	Winter	

a. PMM: lower charges on active energy or power-based components, reduced taxes, and larger SB discounts.

The total electricity expenses are calculated considering all the components in the electricity bill, using the methodology set by the government for PVPC tariffs under the old [8] and new schemes [9]. The generation costs used to calculate the active energy component in each scenario correspond to the periods shown in Tab. 2. These are selected considering a Monday to Sunday sequence matching the consumption weeks. The charges imposed over the active energy component are those in force during each considered period, except for NT3_NM and NT4_NM where the regular charges used before the PMM of 14th September 2021 are applied.

The contracted power considered for 2.0DHA scenarios is the Optimal Contracted Power (OCP) established during the DIY campaign and based on the peak power registered by the household during the monitored period. For the new tariff structure that has two different contracted powers, the same value is applied. This was the default option given to customers after the implementation of the tariff 2.0TD; those wanting differentiated values were required to specifically request them [9].

Tab. 2 – Dates considered for the generation costs inputted in each scenario.

Scenarios	Timespan
OT1	24-30 May 2021
OT2	14-20 December 2020
NT1	07-13 June 2021
NT2, NT2_NM	02-08 August 2021
NT3, NT3_NM	20-26 September 2021
NT4, NT4_NM	13-19 December 2021

In scenarios OT1 and OT2, contracted power is charged at 38,04 €/kW-year. For scenarios NT1, NT2, NT2_NM, NT3_NM and NT4_NM a charge of 30,67 €/kW-year is considered for peak-flat periods and 1,42 €/kW-year for valley. In scenarios NT3 and NT4 the reduced charges are applied (23,75 €/kW-year for peak-flat, and 0,98 €/kW-year for valley). The applicable taxes are those in force during the considered timelines, except for scenarios NT2_NM, NT3_NM and NT4_NM where the regular electricity tax (5,11%) and VAT (21%) are applied.

To evaluate the role of the SB as a shielding tool for vulnerable customers, the electricity cost for all scenarios is calculated with and without considering the use of the SB. For this, evaluated households are classified as Vulnerable Customer (VC) or Extremely Vulnerable Customer (EVC) based on their socioeconomic data and the rules defined in [14]. For all scenarios except NT4 a discount of 25% is applicable upon VC's electricity bills and 40% in EVC case. In NT4, 40% and 60% discounts are applicable for VC and EVC as stated in the PMM of 26th October.

2.3 Evaluation metrics

In addition to the cost increase per kilowatt-hour consumed and power contracted in each EP-affected household, the obtained Energy Poverty Ratio (EPR) is selected as a comparison metric. This indicator has been used by the European Energy Poverty Observatory and the Spanish National Strategy against Energy Poverty (2019-2024) as reported by [18] and [19]. The EPR assumes that families with a relationship between energy expenditure and income greater than the national average (2M) – set as 10% by [18] and [19] – are affected by EP. As data about other energy expenses was not available, a modification of the EPR is used in this analysis considering only the electricity expenses incurred by the household (EPR_{elect}). As shown in equation [1], this is calculated on a weekly basis.

$$EPR_{elect} = \frac{Weekly\ electricity\ expense}{Weekly\ household\ income} * 100 \quad [1]$$

The EPR threshold, 2M, is maintained for comparison purposes, but only as an indication of the household increase or decrease risk to suffer EP under the pricing scenarios defined. No final conclusions regarding the households' EP status is intended as there is not enough information to assess it in this study from the broader definition considered in the EmpowerMed project.

3. Results

The main characteristics of the twelve EP-affected households are shown in Tab. 3. The average number of habitants are 2.25 persons per household and the mean monthly household income is 957.60 €/month. Five households are classified as EVC, four as VC, and H2, H3 and H5 are unclassified. Due to lack of income information, H2 and H3 will not be included in the calculations of the electricity bill after the SB discount and the corresponding EPR_{elect}. H5 will be included but no SB discount will be applied over its electricity expenses as its monthly income is above the threshold established in the SB rules.

Tab. 3 – Main characteristics of analysed households.

Key	Hab.	Income [€/month]	OCP [kW]	SB Category
H1	1	1.150	2,40	VC
H2	8	N.D.	3,00	-
H3	1	N.D.	3,45	-
H4	1	430	2,45	EVC
H5	4	2.500	4,60	-
H6	3	1.500	3,50	VC
H7	1	664	2,30	VC
H8	2	1.000	3,30	EVC
H9	2	500	3,45	EVC
H10	1	576	2,42	EVC
H11	2	652	3,45	EVC
H12	1	604	2,20	VC

Households' daily consumption is analysed for the summer and winter weeks in Fig. 3. The consumption of the EP-affected group tends to be stable throughout the summer, with the group's mean consumption per day fluctuating between 6,34 kWh (Sunday) and 7,98 kWh (Monday). The top outliers' values observed during this season, correspond to H7, which presents a mean daily consumption of 19,66 kWh during this week. Notably, households H2, H5 and H10 report mean daily consumptions below 4,0 kWh and H12 below 2 kWh, which might be explained by the restrictive measures used by some EP-affected users to keep their costs down [8].

During the winter week, the group's mean daily consumption is higher than in summer, fluctuating between 7,42 kWh (Friday) and 11,99 kWh (Monday). There is also higher variability among the group members' daily consumptions, especially Monday and Sunday. During the winter week, H6 and H3 report the highest average daily consumption – 26,97 kWh and 20,94 kWh, respectively – and account for the top outlier values reported in this season. Both of these households, in addition to H8, reported to have electrical heating at home. On the other side, households H4 and H7 registered the lowest mean daily consumptions (< 2,0 kWh).

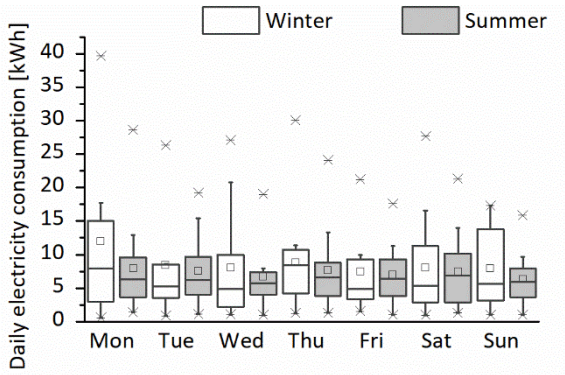

Fig. 3 – Households' mean electricity consumption per weekday (n = 12). Box plot parameters: mean by square; median by horizontal line; 25–75% per-centile by box; 10% and 90% by whiskers; 1% and 99% percentile by cross; minimum and maxi-mum by dash.

In Fig. 4, household's consumption per pricing period is also plotted for the Old Tariff (OT) and New Tariff (NT) scenarios. As observed, most households tend to have lower valley consumptions when considering the new tariff structure, which is expected as valley hours under 2.0TD cover late night and early morning periods when most people are asleep. During flat and peak hours, few households – such as H6 that has high consumption during the flat afternoon period – show differentiated consumptions. For most households, consumption remains stable across flat and peak hours, having a similar distribution between both pricing periods.

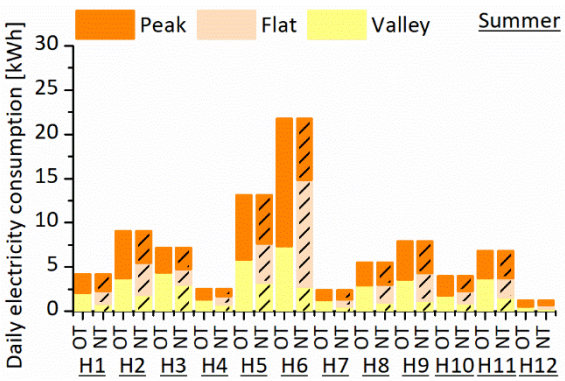

Fig. 4 – Households' mean electricity consumption per hour during the summer week (n = 12). The highlighted pricing periods correspond to tariff 2.0TD.

As explained before, summer peak hours under tariff 2.0DHA were those between 13:00 and 23:00 hours, and the rest were considered valley (Fig. 1). This distribution benefitted most of the households during the target week, as most would take advantage of having longer valley hours, particularly as their consumption tends to rise after 8:00, now considered flat period. H6 is the most benefitted by the new tariff usage as its consumption during flat hours would have been charged with peak prices under 2.0DHA. Having all weekend hours marked as valley instead of two differentiate periods has a soft impact on the sampled households as just three pf them consume considerably more electricity (>10%) in weekends than in workdays during the summer.

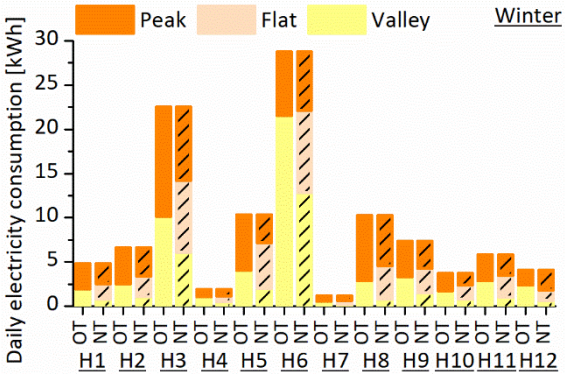

Fig. 5 – Households' mean electricity consumption per hour during the winter week (n = 12). The highlighted pricing periods correspond to tariff 2.0TD.

In winter (Fig. 5), households tend to present larger consumptions and more fluctuating curves, although the lowest consumptions in tariff 2.0TD are also concentrated on the valley hours, except for H6 and H3 that have consumption peaks during the night. It is noticeable that H6's consumption curve changes its peak from a flat period in summer to valley hours in winter, while H5's peak moves from peak to flat hours. H3 and H8 present more pronounced peaks than in summer, which is explained by the use of electrical heating. The rest of households tend to maintain a stable consumption behaviour throughout the day as observed in summer.

Under the old tariff, peak winter hours were those between 12:00 and 22:00 hours. As in summer, such distribution benefitted most of the households, particularly those with no particular peak consumptions during the day.

3.1 Active energy trends during set scenarios

As shown in Fig. 2, active energy prices have been rising consistently in the past following months. This is why the scenarios based on most recent dates tend to have more expensive energy prices than the older ones (Fig. 6 and Fig. 7). The main exception is the scenario OT2 whose prices are higher than those of OT1 even though the latter is more recent. This is due to seasonality effects as, in general terms, winter prices tend to be more expensive than in summer.

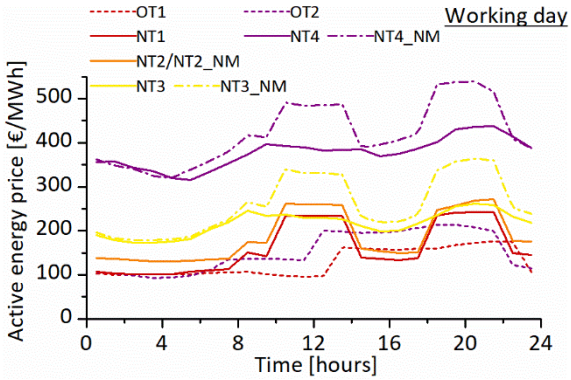

Fig. 6 – Mean active energy price per hour registered in each scenario during workdays.

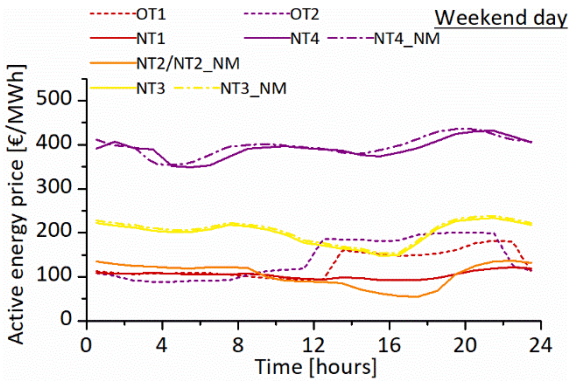

Fig. 7– Mean active energy price per hour registered in each scenario during weekend days.

The effects of the new tariff structure can be clearly identified when comparing the curves of scenarios NT1 and NT2 against those of OT1 and OT2. During working days, the new peak price periods are easily identifiable in NT1 and NT2, having two pricing plateaus instead of one as in the old tariff scenarios (Fig. 6). On the other hand, the curves of NT1 and NT2 are much flatter in the weekends, whereas OT1 and OT2 maintained the observed pricing plateau from Monday to Friday (Fig. 7).

These, however, are dissipated when the reduced charges introduced by the Spanish government in the PMM set of 14th September are considered as observed in the resulting curves for NT3 and NT4 scenarios. These have a stronger impact over workday prices (Fig. 6), as the plateaus observed in NT1 and NT2 flattened, resulting in a similar behaviour to that of the weekends, when only the valley pricing period is considered.

Although the charges applied under the reduced scheme are still differentiated per period, the applied 96% reduction [13] make them less significant in the final active energy price (Fig. 8). In the scenarios in which no reduced charges are considered (NT3_NM, NT4_NM), the peak pricing periods are again distinguishable for workdays. This is not the case of the weekends when considering reduced charges has a minimum impact as they are already quite low for valley hours under normal circumstances.

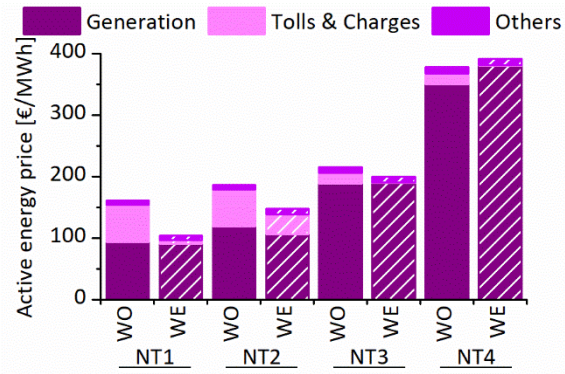

Fig. 8– Mean active energy price per hour registered in each scenario during weekend days.

3.2 Impact on households' electricity expenses

The percentage variation in households' weekly electricity expenses in regards to the old tariff scheme is shown in Fig. 9 (summer scenarios are compared against OT1 and winter scenarios against OT2). For all, except NT4, observed percentage variations remain the same regardless of the SB consideration as the same discounts are applied to all, maintaining an equal relation. The only difference regarding the SB lies on scenario NT4 as larger discounts are used in comparison to the old tariff alternative (OT2) due to the PMM undertaken in 26th October 2021. For that reason, the only distinction between the effect of the SB has been analysed in NT4 (NT4_nSB and NT4_SB, without and with SB).

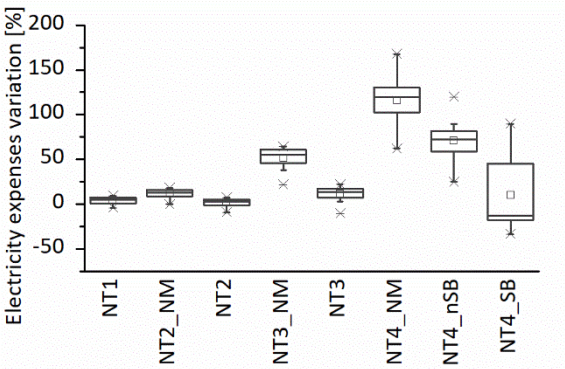

Fig. 9 – Weekly electricity expenses variation from the NT scenarios in comparison to the OT scenarios. Box plot parameters: mean by square; median by horizontal line; 25–75% per-centile by box; 10% and 90% by whiskers; 1% and 99% percentile by cross; minimum and maxi-mum by dash.

As can be observed in the results shown for scenario NT1, the shift to the new tariff scheme does not immediately translate into higher electricity expenses for all households, which together experienced an average increase of 4% under NT1 price conditions. For instance, H4 and H12 show 1% and 4% reductions in their electricity costs. For H12, this is due to its overall low consumption (1.15 kWh/day), which makes more relevant the decrease in contracted power costs introduced in 2.0TD. For H4 – with daily consumption of 7,38 kWh – the results might be explained by the low share of energy it consumes during 2.0TD peak hours: 29%, the lowest in the group.

In scenarios considering more recent dates and no PMM (NT2_NM, NT3_NM and NT4_NM), all households' expenses increase when compared to the old tariff alternatives, particularly in winter scenario NT4_NM in which the mean variation in regard to OT2 is 101%. H4 and H7 present the lowest increases in this scenario; 74% and 52%, respectively. This is explained by the extremely low consumptions (< 2 kWh/day) that both households presented during the representative winter week.

When considering the PMM in scenarios NT2, NT3 and NT4_nSB, households experience still increases in their electricity bills but in a lower degree. In scenario NT2, the lower VAT considered even reduces the final electricity bills of H4, H7 and H12 below OT1 levels; and for all of the users, it reduces the cost in comparison to NT1 levels even though active energy prices were lower in that scenario.

Finally, when considering the larger SB discount in scenario NT4_SB, together with the fiscal reductions imposed, the impact of higher generation costs on sampled households' economy is mitigated. For all households, except H5 and H6, the calculated electricity expenses are lower than for OT2. In the case of H5 because it is not eligible for the SB discount, whereas H6 costs increase are due to their consumption patterns. Specifically, the latter has significant consumptions during the morning that were charged at valley prices during 2.0DHA and now are priced as flat or peak under 2.0TD.

3.3 Observed variations on EPR_{elect}

The households' income and the electricity expenses corresponding to each scenario are used to calculate the EPR_{elect} as explained in the Methodology. During summer, the results obtained indicate that three (H6, H9, H11) out of the ten households surpass the 2M threshold for one or more of the new tariff pricing scenarios without considering the SB (Fig. 10). When applying the SB, H11 manages to move below the threshold, but H6 and H9 still have EPR_{elect} values above 10% for the NT3_NM scenario. Nonetheless, applying the SB plus the PMM manages to keep all households below the 10% threshold during the summer week even during the highest price period considered in this season (NT3).

In winter, the season's higher prices place seven households above the 2M line for at least one scenario when the SB is not considered. If the SB is applied (Fig. 10), three households – H6, H9 and H11 – sill maintain EPR_{elect} values superior to 10%. When considering the government-led PMM (NT4) in addition to the SB discount, EPR_{elect} values lower considerably below the 2M line, and in seven households are even lower than those calculated for OT2. These results highlight the importance of the PMM stablished by the Spanish government in shielding vulnerable customers from price increases.

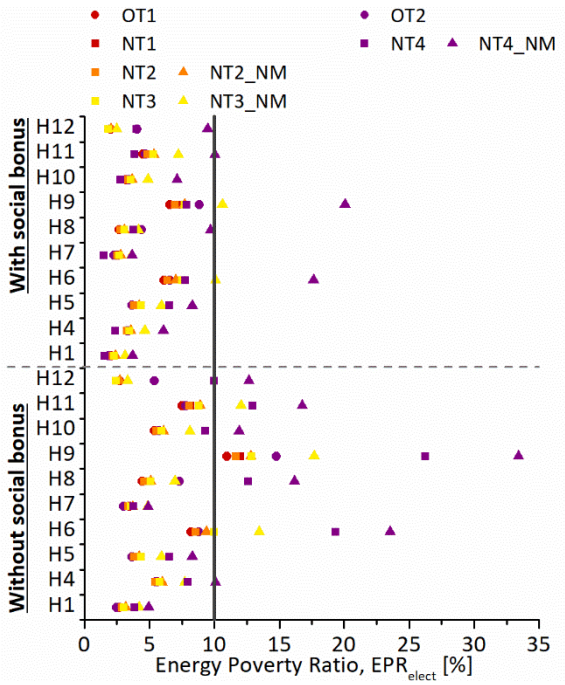

Fig. 10 – EPR_{elect} for analysed households with and without considering the SB (n=10).

4. Conclusions

The implementation of a new tariff structure with three differentiated pricing periods (2.0TD) in June 2021 was expected to impact the electricity expenses of Spanish customers under the regulated scheme, also known as PVPC. This was particularly worrisome in the case of vulnerable customers affected by EP at some level; not only because their economic wellbeing is more sensitive to price increases, but because having a contract under the PVPC tariff is a requirement to obtain the SB, a social scheme that applies a discount over the electricity bill based on the households' vulnerability levels, limiting these users' contracting options.

In addition, the rising generation costs experienced during the past few months that cause the active energy price to spike above historical levels, increased the risk of vulnerable customers with PVPC contracts to worsening its already difficult situation. To protect customers, the Spanish government set in place a number of PMM released in 24th June, 14th September and 26th October of 2021 and still in place by 2022.

The analysis conducted over twelve vulnerable households that participated in the EmpowerMed's monitoring campaign show that the solely consideration of the new tariff scheme might have impacted customers' bill differently depending on their consumption levels and habits, not necessarily resulting in larger expenses. For instance, in the evaluated group, some users actually experienced a reduction in their electricity costs considering the scenario with active energy prices from a few days after the implementation of tariff 2.0 TD (NT1).

Nonetheless, as generation prices increase, all evaluated households end up facing higher electricity expenses when no PMM are taken into account, skyrocketing during the scenario with prices from December 2021 (NT4_NM). This put vulnerable households on risk of worsening their EP status, especially during the winter as active energy prices are the highest of all periods considered.

Without applying any measures or SB, three of the evaluated households have an EPR_{elect} in summer above 10% – the 2M value used as threshold for EP when considering all energy-related expenses – for at least one scenario. In winter, seven households are found in this situation.

During summer, the solely consideration of the SB – without any control measure (NT2_NM, NT3_NM) – seems enough to protect vulnerable customers from a greater risk of worsening their EP situation, as only one household had an EPR_{elect} slightly over the 2M line. But in winter, without considering the PMM, two households report EPR_{elect} above 17% and three more got values close to 10%, which puts them in a higher risk of worsening their EP levels even by applying the SB discount on eligible customers' bills.

Nonetheless, when using the SB in combination with the PMM, all households have an EPR_{elect} below 10% in both seasons This indicates that the introduction of the PMM proposed by the Spanish government seems to serve their purpose, particularly when vulnerable households can access the SB discount.

Up to now, the PMM are considered transitory as a response to unprecedented generation costs. Nonetheless, if the upward trend observed during 2021 continues in 2022, its elimination could put vulnerable customers such as those evaluated in this paper in risk of incrementing its EP levels, with all the associated health and social issues that come with it and that have been discussed in other studies such as [8] and [20].

Finally, it must be remembered that EP is not only a problem for those households that presented EPR_{elect} close or above 10%. As discussed in [8], many EP-affected users have abnormally low consumption as a response to restriction strategies to cope with their fear of facing unpayable electricity bills, which lowers their EPR_{elect} values. Other households use other fuels whose cost must be contemplated for comparison against the 2M threshold.

5. Acknowledgement

This research is part of the EmpowerMed project that has received funding from the European Union's Horizon 2020 research and innovation programme under grant agreement No 847052. Researchers from IREC have been partially supported by the Generalitat de Catalunya (2017 SGR 1219).

6. References

[1] Niu S, Jia Y, Wang W, He R, Hu L LY. Electricity consumption and human development level: A comparative analysis based on panel data for 50 countries. Int J Electr Power Energy Syst Power [Internet]. 2013; Available from: http://dx.doi.org/10.1016/j.ijepes.2013.05.024

[2] Tully S. The Human Right to Access Electricity. Electr J. [Internet] 2006; Available from: https://doi.org/10.1016/j.tej.2006.02.003

[3] Jensen L. The Sustainable Development Goals 2020 [Internet]. 2021. Available from: https://unstats.un.org/sdgs/report/2020/The-Sustainable-Development-Goals-Report-2020.pdf

[4] Halkos GE GE. Evaluating the effect of economic crisis on energy poverty in Europe. Renew Sustain Energy Rev. [Internet] 2021; Available from: https://doi.org/10.1016/j.rser.2021.110981

[5] Li K, Lloyd B, Liang XJ WY. Energy poor or fuel poor: What are the differences? Energy Policy [Internet]. 2014; Available from: http://dx.doi.org/10.1016/j.enpol.2013.11.012

[6] Bouzarovski S. Energy poverty in the European Union: Landscapes of vulnerability. 2014.

[7] European Commission. Empowering women to take action against energy poverty in the Mediterranean [Internet]. Available from: https://cordis.europa.eu/project/id/847052/e

[8] Ortiz J, Jiménez Martínez M, Alegría-Sala A, Tirado-Herrero S, González Pijuan I, Guiteras Blaya M, et al. Tackling energy poverty through collective advisory assemblies and electricity and comfort monitoring campaigns. Sustain. [Internet] 2021;13(17). Available from: ttps://doi.org/10.3390/su13179671

[9] Comisión Nacional de los Mercados y la Competencia – Spain. Circular 3/2020, de 15 de enero, de la Comisión Nacional de los Mercados y la Competencia, por la que Se Establece la Metodología para el Cálculo de los Peajes de Transporte y Distribución de Electricidad. 2020.

[10] Comisión Nacional de los Mercados y la Competencia – Spain. La nueva factura de la luz - 3. Los consumidores domésticos ¿Cómo me afectan los cambios? [Internet] 2021. Available from: https://www.cnmc.es/file/304518/download

[11] Jefatura del Estado – Spain. Real Decreto-ley 12/2021, de 24 de junio, por el que se adoptan medidas urgentes en el ámbito de la fiscalidad energética y en materia de generación de energía, y sobre gestión del canon de regulación y de la tarifa de utilización del agua. 2021.

[12] Jefatura del Estado – Spain. Real Decreto-ley 17/2021, de 14 de septiembre, de medidas urgentes para mitigar el impacto de la escalada de precios del gas natural en los mercados minoristas de gas y electricidad. 2021.

[13] Jefatura del Estado – Spain. Real Decreto-ley 23/2021, de 26 de octubre, de medidas urgentes en materia de energía para la protección de los consumidores y la introducción de transparencia en los mercados mayorista y minorista de electricidad y gas natural. 2021.

[14] Ministerio de Energía Turismo y Agenda Digital – Spain. Real Decreto-ley 897/2017, de 6 de octubre, por el que se regula la figura del consumidor vulnerable, el bono social y otras medidas de protección para los consumidores domésticos de energía eléctrica. 2017;

[15] e.sios Sistema de Información del Operador del Sistema [Internet]. Available from: https://www.esios.ree.es/es?locale=es

[16] eurostat. Cooling and heating degree dats by NUTS 3 regions - monthly data (2000-2020) [Internet]. Available from: https://ec.europa.eu/eurostat/web/energy/data/database

[17] BizEE. Cooling and heating degree days for Barcelona - daily (2019 - 2022) [Internet]. Available from: https://www.degreedays.net/

[18] Bienvenido-Huertas D. Do unemployment benefits and economic aids to pay electricity bills remove the energy poverty risk of Spanish family units during lockdown? A study of COVID-19 induced lockdown. Energy Policy. [Internet] 2021; Available from: https://doi.org/10.1016/j.enpol.2020.112117

[19] Sánchez-Guevara Sánchez C, Sanz Fernández A, Núñez Peiró M, Gómez Muñoz G. Energy poverty in Madrid: Data exploitation at the city and district level. Energy Policy [Internet] 2020;144. Available from: https://doi.org/10.1016/j.enpol.2020.111653

[20] Liddell C, Morris C. Fuel poverty and human health: A review of recent evidence. Energy Policy [Internet] 2010; Available from: https://doi.org/10.1016/j.enpol.2010.01.037

Data Statement

The datasets analysed during the current study are not available due to data protection regulations but the authors will make every reasonable effort to publish them in near future in anonymized way.

Design and energy consumption assessment for a modular hospital in Romania

Ioan Silviu Doboşi [a], Cristina Marincu [b], Silviana Brata [c], Stefan Dună [d], Nicoleta Kaba [e], Ioan Bistran [f]

[a] Romanian Association for Building Services Engineers – Banat Branch, Timisoara, Romania and S.C. DOSETIMPEX S.R.L., Timisoara, Romania, ioansilviu@dosetimpex.ro.

[b] Department of Civil Engineering and Building Services, Politehnica University Timisoara, Timisoara, Romania, cristina.marincu@upt.ro.

[c] Department of Civil Engineering and Building Services, Politehnica University Timisoara, Timisoara, Romania, silviana.brata@upt.ro.

[d] Romanian Association for Building Services Engineers – Banat Branch, Timisoara, Romania and S.C. DOSETIMPEX S.R.L., Timisoara, Romania, stefan@dosetimpex.ro.

[e] Department of Civil Engineering and Building Services, Politehnica University Timisoara, Timisoara, Romania.

[f] S.C. DOSETIMPEX S.R.L., Timisoara, Romania, ioan.bistran@gmail.com.

Abstract. The European Commission has set the goal of making Europe CO_2-neutral by 2050, which requires decarbonising the building sector. Clear steps in this direction were made with the 2010 Energy Performance of Buildings Directive (EPBD), when the concept of nearly zero-energy building (NZEB) was introduced. Currently, NZEB is a mandatory requirement for all new building in the European Union. In Romania, the authorities have established maximum values of total primary energy consumption for NZEB's, out of which at least 30% must be covered form renewable energy sources. Achieving these requirements can be a great challenge, especially in certain building categories such as hospitals. This paper presents a study regarding the NZEB design and the energy performance assessment of a hospital building in Romania. The building in discussion is an infectious diseases hospital, whose aim is supporting potential sanitary system crisis generated by situations such as COVID-19 pandemic. The energy conservation design aimed the minimization of energy need through high thermal insulation, energy efficient windows, ventilation with heat recovery and LED lighting. Also, a renewable energy system consisting in PV panels was proposed. The energy consumption and on-site energy production was assessed by means of monthly method. The aim is to verify if the proposed design solutions assure the achievement of the NZEB standard as it is defined in Romania.

Keywords. Healthcare building, energy assessment, nearly zero-energy building, renewable energy.
DOI: https://doi.org/10.34641/clima.2022.36

1. Introduction

In the last decade, the European Union is strongly focusing on the nearly zero energy building target, as a response to the climate problems generated by the high energy consumption in the building sector. In accordance with the Energy Performance of Buildings Directive, as of 2021, all new buildings in the European Union must be nearly zero-energy buildings (NZEB) [1]. Moreover, Member States must establish strong measures in the building sector to support the transition to a climate-neutral society by 2050. Although the NZEB concept was introduced more than a decade ago, the design, execution and operation of these buildings are still under debate, particularly in case of certain categories of buildings that require special operation conditions, such as hospitals. Following the EPBD requirements, in Romania, 'NZEB' is defined as a building with a very high energy performance, where the energy consumption to provide energy performance is almost zero or very low and is covered at least 30 % with energy from renewable sources, including energy from renewable sources produced on site or nearby [2]. NZEB specific requirements are determined by building category and climate zone in terms of maximum values for specific primary energy consumption and for specific emissions of CO_2. However, at this moment, the document that establishes the values of primary energy and CO_2 emissions is still not in force, although values and limitations were proposed. The COVID-19 pandemic

Copyright ©2022 by the authors. This conference paper is published under a CC-BY-4.0 license.

and associated global crisis has brought into deeper attention the hospital buildings and their fundamental importance in the society. Hospital buildings are unique in terms of energy use as they require energy continuously throughout the year, with energy demand varying greatly depending on the functionality of each area. Medical procedures, laundry rooms, kitchen equipment, sterilization room equipment, laboratory tests, air conditioning, ventilation, and heating are all sources of energy consumption and implicit greenhouse gas emissions in hospitals. The ones connected to air conditioning, ventilation, and heating have the most potential to be improved in terms of energy efficiency among these consumption categories. In the EU, hospital buildings represent 7% of the non-residential building stock and are responsible for 10% of the total energy use in the non-residential building sector [3]. In Romania, the energy consumption in the healthcare sector represents approximately 4% of the total final energy consumption in buildings, while hospitals occupy 1% of the total national building stock [4]. In a study by Merlevede [5] on the energy in the European healthcare the following conclusions on the total energy consumption are presented: 41% to 87.5 % from the total energy consumption is related to heating, 2% to 17% corresponds to cooling and 15% to 40% is occupied by electricity for lighting and equipment. The variation between the minimum and maximum percentages are attributable to the geographical and economic variables, as well as the building's age, composition, and type of systems. Meeting the energy performance requirements in hospitals is a higher challenge than in other categories of buildings. The design and construction of hospital buildings is a complex activity for all specialists involved, especially when energy performance is one of the objectives. The interest in increasing the energy efficiency of hospital buildings has gradually increased throughout time and in the last years and several studies and documents on this topic were developed by researchers or public organizations [6-17]. This paper discusses the energy design and energy performance assessment of a new hospital building for infectious diseases, in the context of mandatory NZEB requirements and sanitary crisis generated by the COVID-19 pandemic. The energy design of the building aims at achieving a low energy consumption and use of renewable energy, while assuring the functionality and indoor environment specific to an infectious disease hospital. The energy assessment aims at verifying if the design of the building leads to a reduced total primary energy consumption and at least 30% share of renewable energy.

2. Methodology

2.1 The case study building

The object of this study is an infectious diseases healthcare facility. More specifically, it consists in the design of a modular hospital to increase the management capacity of the COVID-19 health crisis.

Since the sanitary crisis overlaps with the enter in force of the NZEB mandatory requirements for all new buildings, designing this building became a greater challenge for all the involved specialists. The proposed construction is made of two buildings (from a constructive and dimensional point of view), located at 4.00 m from each other and connected by a secondary building, as seen in the situation plan in Fig.1.

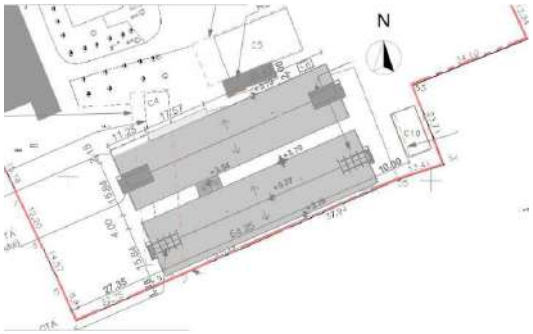

Fig. 1 – Situation plan

From a functional point of view, one part of the building will accommodate the reception area - hospitalizations with the area of investigations and adjacent sterilization and the intensive care unit for severely ill patients and the other part of the building will accommodate the infectious diseases ward for patients with mild or moderate forms, including spaces for medical staff. The whole building has a heated floor area of approximately 1950 m^2 and capacity of approximately 60 beds. Because the investor wants the hospital to be in use quickly, it was decided to have a modular construction system, with a fast execution that would allow the immediate operation of both sections of infectious diseases, in the context of the current pandemic. If necessary, the proposed superstructure can be dismantled and reassembled if the building is to be relocated in the future. Thus, the construction will be made on the structure of modular, repetitive steel frames, with exterior closures and interior partitions from sandwich panels, in compliance with the fire protection conditions of load-bearing and non-load-bearing elements, according to the regulations in force. The floor slab and foundation will be made of reinforced concrete. The enclosure of the modular hospital will remain on exposed sandwich panels. The roof is a smooth-sloping roof-type made of sandwich panels with mineral wool insulation. The design of the HVAC system was performed to comply with the admissible air purity limits required for the hospital spaces according to the Romanian norms, as well as for providing comfort conditions for accommodating patients and conducting hospital activities [17].

2.2 Energy design and assessment

The strategy of energy efficiency design in the case of the case study building consisted in minimization of energy requirements and the implementation of an alternative system for the energy supply from

renewable sources. The energy consumption assessment of the building was performed using the software Doset-PEC, which is a calculation tool available on the Romanian market for the energy certification of buildings. The software performs monthly calculations and is based on the Romanian methodology for calculating the energy performance of buildings [20], [21]. Doset-PEC software tool calculates single-zone energy consumption for heating, cooling, mechanical ventilation, domestic hot water and lighting. When calculating the energy performance of the building, the following aspects were considered: the climatic zone and the orientation of the building, geometry and volume of the building, the composition of the construction elements of the building envelope, number of outdoor air exchanges (infiltration and mechanical ventilation), indoor climate conditions, characteristics of installation systems for heating, air conditioning, mechanical ventilation, and lighting.

To have as minimum as possible heating and cooling energy needs, the envelope elements of the building have low corrected U'-values, below the maximum corrected U-values for non-residential NZEB in Romania (Table 1). The values for U'_{max} are used just as reference values as this moment since the normative that proposes these values is still not in force. In terms of volumetry, the two constructions that compose the hospital have a rectangular shape, with vertical and horizontal geometrical regularity and has just a single level.

Tab. 1 – Thermal transfer resistances.

Envelope element	U' [m²K/W]	U'_{max} [m²K/W]	Area [m²]
Exterior walls	0.20	0.34	1181.9
Windows	0.90	1.11	268.3
Roof	0.16	0.17	2080.2
Ground floor	0.19	0.20	2050

To reduce the losses through mechanical ventilation, the AHUs are equipped with heat recovery units with an efficiency of approximately 70%. Thus, the ventilation of the entire hospital is achieved with the help of 4 air handling units (AHU). The AHUs were dimensioned to ensure that the necessary number of air exchanges were achieved in the rooms connected to each AHU (Table 2).

Tab. 2 – Air handling units serving the whole building

Air handling unit	Served space	Supply/exhaust air flow [m³/h]]
AHU1	Intensive care	7971/8483
AHU2	Patient's access	5184/5729
AHU3	Patient rooms	7265/8007
AHU4	Medical staff access	4315/4729

The number of air changes vary between 3 h^{-1} and 10 h^{-1}. The AHU's have the following characteristics: intermediate fluid heat recovery units, heating/cooling coils, inlet and outlet fans, filters upstream of the air handling unit and after the air intake fan, control for maintaining constant inlet air flow rates regardless of operating conditions, adjusting device to maintain levels of depression in rooms with a lower degree of asepsis than spaces with a higher degree of asepsis. The supply of thermal energy is made from an existing gas central heating.

Cooling is provided with a 250kW air-cooled chiller with built-in hydraulic module, axial fans with frequency converter and low-noise function at night. The transmission of heating and cooling in all rooms is proposed to be made up of the following systems: radiators 95 kW (panel type radiators in hygienic construction), fan coils for heating - 74 kW, AHU heating coils - 291 kW, cooling beams - 52 kW, fan coils for cooling - 52 kW, AHU cooling coils - 177 kW.

The interior air temperature was defined as an average for the whole building, considering the interior air temperature required in each type of space and the corresponding surface area. This simplification is necessary because the used calculation tool does not allow the definition of multiple thermal zones for the building simulation. The interior temperature differs depending on the room destination and were defined in accordance with the Romanian standards. Thus, the interior air temperatures for heating varies between 18°C and 24°C and the average value used in calculation is 21.2°C. The cooling temperature was set to 26°C.

The input data for domestic hot water calculations consisted in the number of use units (60 beds) and the daily specific needs per unit (56 l/unit/day). Lighting energy consumption was assessed considering an installed power of 7 W/m². The energy assessment was conducted using the standard weather for the location of the building.

As a renewable energy source, it is proposed to implement of an ON-GRID photovoltaic panel system on the roof of the building. The available surface on the roof allows the installation of 400 photovoltaic panels with 310 W power each. The system has 4 invertors of 25 kW each. The assessment of the PV energy production was performed using the freely available online platform [18]. This platform provides information about solar radiation and photovoltaic (PV) system performance for any location in Europe.

3. Results and discussion

3.1. Final energy consumption and on-site renewable energy production

Table 3 shows the final energy consumption broken down on energy type and category of consumption, The highest natural gas consumption is associated to

heating while the highest electricity consumption is related to the mechanical ventilation system. The results were compared with other studies conducted at European level [20]. Similar values were obtained for heating and cooling, while significant differences were identified for lighting and ventilation energy consumption.

Tab. 3 – Final energy consumption

Category		Final energy [kWh/(m²year)]
Natural gas		
Space heating		51,12
Domestic hot water		38,36
	Total	89,48
Electricity		
Cooling		8,40
Mechanical ventilation		44,12
Lighting		15,75
	Total	68,27

Fig. 2 shows the monthly energy consumption against monthly electricity produced on-site from PV panels. It is noticeable that from April until August, the PV production is higher than the electrical energy consumption.

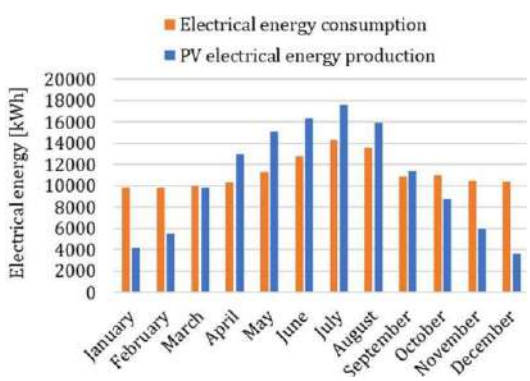

Fig. 2 – Total monthly electricity consumption and on-site PV production

The proposed photovoltaic system is connected to the national electricity grid, without any storage system. This means that in the absence of solar radiation (during the night) and during winter, when the PV production is lower, a major part of the needed energy will be imported from the national grid. Also, in the instances of time when the energy production is higher than what is consumed, the excess energy that is produced is exported to the grid. This means that only a part of the energy produced will be consumed directly on site. To assess the energy balance between imported and exported energy as accurately as possible, hourly energy simulations are the best solutions. However, since this design stage is just a preliminary one, the energy balance was performed considering that the monthly PV electricity production is primarily consumed directly on-site. From the total monthly PV energy production, the remaining difference after covering the building needs is delivered to the grid. The monthly electricity balance is presented in Fig. 3. In this hypothesis, we can see that from April until August, the electrical energy need of the building is covered entirely from PV production, while a lower remaining quantity of PV electricity is exported to the grid. From October until March, the PV panels cover only partially the electricity needs of the building, the rest being taken from the grid.

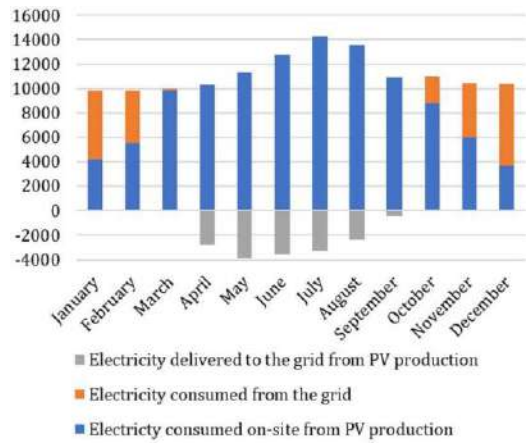

Fig. 3 – Monthly electrical energy balance

3.2 Total primary energy consumption and renewable energy share

The conversion to primary energy was made considering the Romanian conversion factors for each type of energy presented in Tab.3. The values of the primary energy for each energy source are obtained by multiplying the final energy with the corresponding conversion factor. The determination of equivalent CO_2 emissions is made based on primary energy consumption and the factors of conversion of primary energy into CO_2 emissions, depending on the type of energy source (Tab.3). The results of the conversion of final energy into primary energy as well as CO_2 emissions are presented in Table 4.

Tab. 3 – Primary energy conversion factors.

Energy source	Primary energy factor		CO_2 factor
	Non-renewable	Renewable	
Natural gas	1,17	0,00	0,205
Electricity from grid	2,00	0,50	0,299
PV electricity used on-site	0,00	1,00	0,00
PV electricity exported	2,00	0,50	0,00

When calculating the total primary energy, it is considered that the exported energy compensates the imported energy. Also, the on-site renewable

energy production and use is weighted with renewable energy conversion factor 1 and non-renewable factor 0. The primary energy from non-renewable sources is calculated as the difference between the primary energy corresponding to the energy imported from the grid (natural gas and electricity) and the primary energy corresponding to the energy exported to the grid, both accounted with conversion factor 2.5. Thus, the energy exported to the grid is accounted in the energy performance of the building.

Tab. 4 – Primary energy values and CO_2 equivalent.

Category	Primary energy [kWh/(m²year)]	
	Renewable	Non-renewable
Natural gas	-	104.69
Electricity consumed on-site from PV panels	57.03	-
Electrical energy consumed from the grid	5.63	22.50
PV electricity exported to the grid	4.20	16.79
Non-renewable primary energy [kWh/m²year]	106.20	
Renewable primary energy [kWh/m²year]	62.65	
Total primary energy (renewable and non-renewable) [kWh/m²year]	168.84	
Renewable energy share from total primary energy	≈37%	
Total CO_2 equivalent	23.17 kg CO_2/(m²year)	

4. Conclusions and future developments

The advantage of the presented solutions for this investment object, compared to other alternative systems, is that it fits very well with the concept of modular hospital, the photovoltaic panels can be easily relocated and reused when necessary. The total primary energy requirement of the analysed building is approximately 168.84 kWh/ m²/year, out of which 37% represent renewable energy resulting from the proposed system of photovoltaic panels. The estimated annual CO_2 emissions are about 23.17 kg CO_2/(m²year). This is in accordance with the legal provisions in force which stipulate that the total primary energy must be covered by at least 30% renewable energy for NZEB's in Romania. To be considered a NZEB hospital, the total primary energy consumption and CO_2 emissions should be below the values provided by the Romanian authorities for buildings in the healthcare sector. However, when this study was performed (February 2021), these values were not yet officially launched by the Romanian authorities. Nevertheless, to draw some conclusions, the temporarily available values, from documents that were in work at that moment, were used as reference. Thus, for NZEB building in the healthcare sector, located in Romania in climate zone I (where the investigated building is located), the proposed reference value for maximum total primary energy that was used for comparison is 179 kWh/m²/year, while the reference value for CO_2 emissions was 37 kgCO_2/m² /year. Both values are higher than the ones obtained for the case study building. Thus, for the existing conditions when the study was performed, the proposed solutions for the case study building were enough to consider the case study building a NZEB hospital. However, throughout the year of 2021, the new Methodology for Calculating the Energy Performance of Buildings, referred to as MC001 is still work in progress, and some of the reviews might result in changes of the reference primary energy values and CO_2 emissions for building in the healthcare systems. Thus, in order to achieve the NZEB standard for the case study building, compared with the final reference values, supplementary energy conservation measures might be necessary. A primary measure could be reducing even more the heat losses through the building envelope by increasing thermal insulation. Moreover, the implementation of a heating system with renewable energy source such as ground-air heat pump might be a solution to be considered in order to limit the total primary energy consumption of the building.

Healthcare buildings are the most complex buildings in the non-residential sector, in terms of HVAC and operation conditions. Moreover, a variety and types of buildings exist within the healthcare category, starting with general hospitals, infectious diseases hospitals, clinics etc. Each type of healthcare building has specific operation requirements, which can result in very different energy needs from one type of healthcare building to another. Thus, for hospitals that require continuous functioning throughout the day, week and year, hospitals with intensive care units, emergency units, surgery room, the required energy will always be significantly higher than for a dental clinic for example. Therefore, when defining the NZEB limitations for buildings in the healthcare sector, different conditions should be provided depending on the category and type of healthcare buildings. This recommendation is in line with other existing studies [19], which recommend the increase of building types for which separate NZEB definitions are provided, as well as create a new subdivision in healthcare facilities.

References

[1] Directive 2010/31/EU of the European Parliament and of the Council of 19 May 2010 on the energy performance of the buildings, Official Journal of the European Union L153/13, 2010.

[2] Law No. 372/2005 on the energy performance of buildings, republished in 2021.

[3] Building Performance Institute Europe - Europe's buildings under the microscope, (2011)

[4] National Strategy for long-term renovation in Romania. 2020.

[5] Merlevede P. Energy in European Healthcare Institutions: IFHE-EU." International Federation of Hospital Engineering (IFHE) Web site. 5 30. http://www.ifhe.eu/download.php?filid=158c66d67636a2-.

[6] European Commission. 2011. COM (2011) 112 - A Roadmap for moving to a competitive low carbon economy in 2050. Brussels: European Commission.

[7] Bakaimis B., Papanikolau I. "Electrical Energy Saving Policies, Initiatives, Results, Challenges." Procedia Environmental Sciences. 2017:882-889.

[8] Rajagopalan P., Elkadi H. Energy Performance of Medium-sized Healthcare Buildings in Victoria, Australia- A Case Study. Journal of Healthcare Engineering. 2014:247-260.

[9] Somboonwit N., Sahachaisaeree N. Healthcare Building: Modelling the Impacts of Local Factors for Building Energy Performance. ASEAN Conference on Environment-Behaviour Studies. Bangkok: Procedia Social and Behavioural Sciences. 2012:50:549-562.

[10] Gao Z., Li Y., and Ning Y. The survey and analysis on the energy consumption of hospital buildings in Shandong province. Procedia Engineering. 2017:2485-2492.

[11] Franco A., Shaker M., Kalubi D., and Hostettler S. A review of sustainable energy access and technologies for healthcare facilities in the Global South. Sustainable Energy Technologies and Assessments. 2017:92-105.

[12] Singer B.C., Tschudi W.F. High Performance Healthcare Buildings. Environmental Energy Technologies Division Lawrence Berkeley National Laboratory. 2009.

[13] Coccagna M., Cesari S., Valdiserri P., Romio P., Mazzacane S. Journal of Environmental Science 2, 2017:443-452.

[14] Shen C., Zhao K., Ge J., Zhou Q. Analysis of Building Energy Consumption in a Hospital in the Hot Summer and Cold Winter Area. International Conference on Applied Energy (ICAE2018), 22-25 August 2018, Hong Kong, China.

[15] Christiansen N., Kaltschmit M., Dzukowski F. Electrical energy consumption and utilization time analysis of hospital departments and large-scale medical equipment. Energy and Buildings. 2016:131:172-183.

[16] Gonzalez Gonzalez A., Garcia-Sanz-Calcedo J., Rodriguez Salgado D. A quantitative analysis of final energy consumption in hospitals in Spain. Sustainable Cities and Society. 2018:36:169-175.

[17] NP 015 -1997.

[18] https://re.jrc.ec.europa.eu/pvg_tools/en/#PVP

[19] Maassen W., Evaluation Dutch preliminary nZEB requirements for hospital and university buildings. E3S Web of Converences. CLIMA 2019.

[20] Dainese E., Walker S., Maassen W. and W. Zeiler. Towards zero energy hospital buildings: a polyclinic building as case study. E3S Web of Converences. CLIMA 2019.

Analyze the energy-saving benefits of Taiwan's existing advanced energy-saving strategies through energy simulation

Lin Feng-Yi[a], Su Tzu-Ching[b], Yu Pei-Yu[c]

[a] Green Energy and Environment Research Laboratories, Industrial Technology Research Institute, Taiwan, itriA90070@itri.org.tw.

[b] Green Energy and Environment Research Laboratories, Industrial Technology Research Institute, Taiwan, neverending1984@itri.org.tw.

[c] Green Energy and Environment Research Laboratories, Industrial Technology Research Institute, Taiwan, StevenYu@itri.org.tw

Abstract. Building energy consumption accounts for more than 30% of global energy consumption. Nearly zero energy building (nZEB) is an important strategy for energy saving and carbon reduction in the building sector. nZEB design could be separated into two key strategies: "Advanced energy-saving design", which requires highly efficient envelop components and mechanical systems, and "Renewable energy", which requires renewable generations to offset building energy uses.

Taiwan's green building evaluation system provides various advanced energy-saving design strategies to achieve energy-saving beyond the codes. The purpose of this study is to explore the energy saving benefits of Taiwan's existing advanced energy-saving design strategies, especially strategies that were typically used in green buildings. This study first established two reference building energy models, a school building and an apartment, by EnergyPlus. Additionally, we formulated a series of step-by-step advanced energy-saving strategies and determined the maximal energy-saving strategy packages, which could help the two types of buildings achieve the highest rating score in the energy-saving category in Taiwan's green building evaluation system. Following, inputting the strategies into the two models, and simulating their energy efficiencies. The results show that: a school building, which implemented the maximal energy-saving strategy package that achieves the highest energy-saving score in green building evaluation system, could save about 56.2% energy when comparing with a typical school building that complies with the building codes. Regarding apartment building, applying the maximal energy-saving strategy package could reduce 51.3-54.2% apartment energy use when comparing with a typical apartment that complies with the building codes. Moreover, we found out that shading design affects the energy-saving benefits of using efficient building materials. School buildings are generally constructed with side corridors, and the shading effect of the side corridor would reduce the energy saving benefits of using efficient building materials.

Keywords. Building energy efficiency,building energy simulation, advanced energy-saving strategies.
DOI: https://doi.org/10.34641/clima.2022.61

1. Introduction

Building energy consumption accounts for more than 30% of global energy consumption. In Taiwan, residential and commercial sectors account for 35.6% of the total electricity consumption[1]. It is the second largest power consumption category and has great potential for energy saving. Nearly zero energy building (nZEB) is an important strategy for energy saving and carbon reduction in the building sector. In order to promote energy-saving design of buildings, Taiwan has mandatory regulations and voluntary green building evaluation systems for reference. The update of "Building Technical Regulations (Building Codes)" and the green building evaluation system, as well as the formulation of the building energy efficiency evaluation system, have pushed the building towards near zero energy consumption.

There are many design strategies for energy

Copyright ©2022 by the authors. This conference paper is published under a CC-BY-4.0 license.

saving and carbon reduction. Through the preliminary simulation evaluation, the project goals and implementation priorities can be determined[2]. However, there are various building styles and different usage patterns, resulting in different building energy-saving potentials. The energy-saving benefits of the same technology or material in different building cases are often different. In particular, the energy-saving effect of building materials is indirectly dependent on the air-conditioning conditions, which makes it difficult to distinguish and quantify the energy-saving effect. It is not easy for the general public to directly understand the specific energy saving or other benefits of building shading, heat insulation and equipment. In addition, Taiwan lacks typical building energy models and scenario settings with near zero energy consumption. Each study uses different building styles and usage scenarios to evaluate. When evaluating energy-saving effects, different baseline scnarios were used in different studies aswell. As a result, it often leads to a huge gap in the energy-saving benefits of the same technology or policy under different evaluation scenarios. The evaluation results can easily cause misunderstandings by non-professionals.

To effectively evaluate the energy efficiency of residential and commercial buildings and present more widely available evaluation results, the international common practice is to collect local building information and establish a typical scenario as a baseline for evaluating the energy efficiency of various technologies and assessing the potential for achieving near-zero energy consumption. Use energy simulation tools to build building models, assume building usage scenarios, and predict energy consumption of various technologies[3]. The U.S. Department of Energy combined several national laboratories to establish 16 kinds of commercial reference building models of the national building stock. Using these models and setting the situation, it can properly express the local general building style. When performing building energy analysis and evaluation, especially policy-related evaluations, the results will be consistent and representative[4]. ASHARE establishes a model for small and medium-sized offices, and sequentially adds different energy efficiency strategies to the model to quantify the impact of each strategy[2]. Attia et al. established two school baseline models to evaluate the energy performance of nZEB in practice[5]. D'Agostino and Parker used EnergyPlus to simulate and evaluate the design of new houses in 14 different climate zones in Europe. In colder climates, heat insulation and building airtightness are critical, while in warmer places, efficient electrical appliances and Lighting is the key measure[6].

2. Research Methods

This study focuses on school classrooms and multi-dwelling as the simulation object. Draw up the existing advanced energy-saving scenarios in Taiwan, and use EnergyPlus to quantify the benefits of various energy-saving scenarios.

2.1 Model establishment

The scale and form of school classrooms refer to the Taiwan's building regulations[7] and the Ministry of Education's "National Elementary and Secondary School Facilities and Equipment Standards"[8]. For multi-dwelling, refer to building regulations and government sample survey reports[9]. The model details are shown in **Tab. 1**, and the floor plan is shown in **Fig. 1**.

Tab. 1. Model scale.

Object	school classrooms	multi-dwelling
Floor area	72m²/class room	99 m²/ household
Height	3m	3m
Floor	3F	6F
Number of classrooms/houses per floor	3	4
Number of people	30	3
Weather data	Taipei TMY3	Taipei TMY3

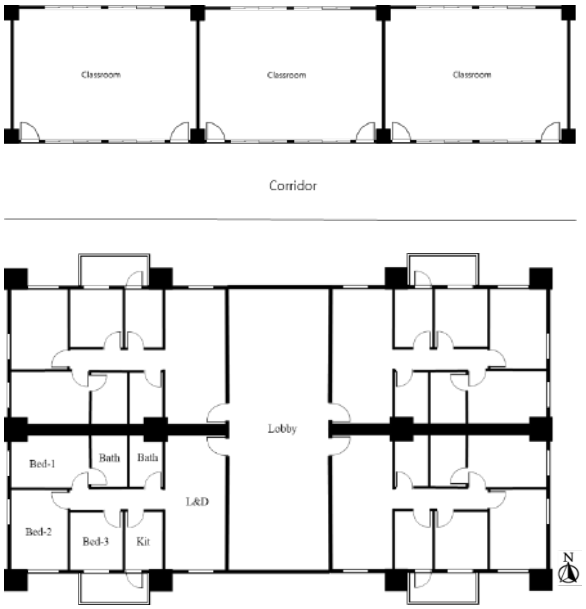

Fig. 1 - Floor plan of school and multi-dwelling.

2.2 Energy-saving scenarios

In the setting of energy-saving scenarios, refer to Taiwan's building envelope and eguipment energy performance standards and the green building evaluation system (EEWH). These two references represent Taiwan's current advanced construction practices in the energy-saving market. The baseline scenario is based on the minimum standards of building regulations, minimum energy performance standard (Meps) for air-conditioning, and

fluorescent lamp design. Prioritize implementation of passive energy-saving measures, and then implement active energy-saving. The five energy-saving scenarios are shown as follows:

1. (Scenario I)Mixed ventilation: mixed use of natural ventilation and air conditioning;
2. (Scenario II)Green building envelope: improviing external shading to reach the highest grade in building envelope criterias in EEWH green building evaluation system;
3. (Scenario III)High-performance building materials: implementing advanced building materials that are beyond green building criterias, such as insulation layers and low-E glases;
4. (Scenario IV)Green building equipment- basic: air conditioning and lighting performances comply with the basic criterias in EEWH green building evaluation system;
5. (Scenario V)Green building equipment-advanced: air conditioning and lighting performances reach the highest grades in equipment criterias in EEWH green building evaluation system.

In particular, in the context of high-performance building materials, the difference between Low-e glass and heat-insulating film glass will be additionally compared for multi-dwelling. In addition to lighting power density (LPD) that meets the EEWH level, the lighting also meets the requirements of classroom illuminance 500-750lux and residential illuminance 150-300lux. The setting details of each scenario are shown in **Tab. 2** and **Tab. 3**.

Tab. 2. Classroom simulation scenario setting.

	Baseline	Scenario I	Scenario II	Scenario III	Scenario IV	Scenario V
Window rate	52%	52%	52%	52%	52%	52%
Shade depth (m)	corridor 4 balcony 0.8	corridor 4 balcony 0.8	corridor 4 balcony 2	corridor 4 balcony 2	corridor 4 balcony 2	corridor 4 balcony 2
Glass (W/m²K)	U=6.07 SHGC=0.8	U=6.07 SHGC=0.8	U=6.07 SHGC=0.8	U=1.38 SHGC=0.48	U=1.38 SHGC=0.48	U=1.38 SHGC=0.48
Roof (W/m²K)	0.8	0.8	0.8	0.467	0.467	0.467
Exterior wall (W/m²K)	3.5	3.5	3.5	1.21	1.21	1.21
LPD (W/m²)	13.5	13.5	13.5	13.5	7.8	3.6
COP	3.31~3.43	3.31~3.43	3.31~3.43	3.31~3.43	3.72	3.74~3.81
AC activation	Open all day	Turn on when the indoor temperature exceeds the upper comfort limit.				

Tab. 3. Multi-dwelling simulation scenario setting

	Baseline	Scenario I	Scenario II	Scenario III	Scenario IV	Scenario V
Window rate	38%	38%	23%	23%	23%	23%
Shade depth (m)	1.2	1.2	2	2	2	2
Glass (W/m²K)	U=6.07 SHGC=0.8	U=6.07 SHGC=0.8	U=6.07 SHGC=0.8	Low-e U=2.56 SHGC=0.26 film U=5.62 SHGC=0.48	Low-e U=2.56 SHGC=0.26 film U=5.62 SHGC=0.48	Low-e U=2.56 SHGC=0.26 film U=5.62 SHGC=0.48
Roof (W/m²K)	0.8	0.8	0.8	0.467	0.467	0.467
Exterior wall (W/m²K)	3.5	3.5	3.5	1.565	1.565	1.565
LPD (W/m²)	6	6	6	6	4.1	1.3
COP	3.63~3.93	3.63~3.93	3.63~3.93	3.63~3.93	3.87~4.21	3.9~4.58
AC activation	Open all day	Turn on when the indoor temperature exceeds the upper comfort limit.				

2.3 Principles of air conditioning activation

Regarding the setting of air-conditioning activation, air-conditioner would not be used in December-March due to the low temperature. In other monthes, air-conditioner would be turned on according to a schedule that determined by the adaptive model of ASHRAE standard 55. When the room is naturally ventilated and the temperature exceeds 90% of the comfortable upper limit, the air conditioner will be turned on. The evaluation according to equation (1).

$$T_{comf} = 0.31 \times T_{om} + 20.3 \quad (1)$$

T_{comf} is the comfortable temperature (°C); T_{om} is the monthly average outdoor temperature (°C), and the monthly average outdoor temperature in Taipei from April to November is 21.2-30.25°C.

3. Result and discussion

3.1 School classroom simulation results

The simulation results of the school classroom are shown in **Fig. 2**. The annual EUI of the classroom in the baseline scenario is 69.12kWh/m². When adopting mixed ventilation(Scenario I), the annual EUI was reduced to 47.52 kWh/m², which is 31.2% energy-saving compared to the baseline. The main reason is that air conditioning is not needed when the thermal comfort upper limit is not exceeded, and only uses natural ventilation, thus reducing the energy consumption of air conditioning by 21.6kWh/m². In scenario II, strengthen the shading performance on the original basis. It was found that the annual EUI was 47.50 kWh/m², which only reduced energy consumption by 0.03% compared with the mixed ventilation scenario. It shows that the original shading design of this classroom model comply with the building codes, and is deep enough to prevent most solar heat gains, as a result, reinforcing the shading design leads to a limited energy reduction. When the exterior walls, roofs and windows were replaced with high thermal insulation materials (Scenario III), the energy consumption of the air conditioner increased by 0.1 kWh. The annual EUI is 47.6 kWh/m². We found that the well-insulated building envlopes prevent the heat gains conducting both outside-in and inside-out. In the case that the indoor heat gains are more than outdoor heat gains, it would lead to a more energy-comsumed result. Since Taiwan is located in in subtropical, cooling dominated climate, when the building has deep shading, continuous improvement of the insulation performance of building materials is not much help to energy-saving. Continuously expanding the shade or using high-performance building materials not only has no obvious energy-saving effect, but also consumes unnecessary costs.

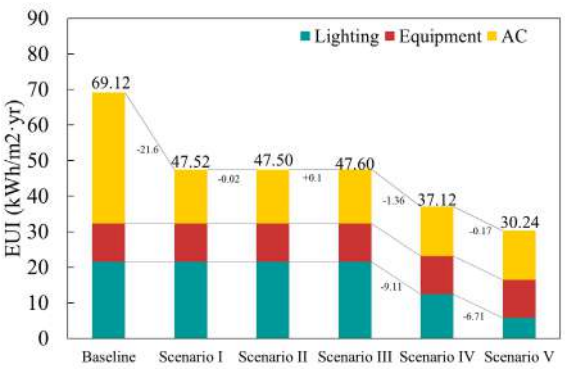

Fig. 2 - The simulation results of the school classroom.

In scenario IV, changing an air conditioner with a COP of 3.31~3.43(energy efficiency level 5) to one with a COP of 3.72 (energy efficiency level 4) reduced 1.36kWh/m². Replace the original lamp with a T5-fluorescent tube, the LPD is reduced from 13.5 W/m² to 7.8 W/m², led to a 9.11 kWh/m² energy saving. In other words, the annual EUI can be reduced to 37.12 kWh/m², which can save 22% energy compared with the high-performance building materials scenario. In scenario V, the air conditioner's COP is increased to 3.74~3.81(energy efficiency level 1), it can save another 0.17 kWh/m². Replace the tube with LED tube, the LPD can be reduced to 3.6 W/m², which can save energy 6.71 kWh/m². The annual EUI is 30.24 kWh/m², which is about 18.5% energy saving compared with the previous scenario. Compared with the baseline, when the envelope, air-conditioning, and lighting all reach the current best levels, energy savings can be 56.2%.

3.2 Multi-dwelling simulation results

The simulation results of the multi-dwelling are shown in **Fig. 3**. The annual EUI of the multi-dwelling in the baseline scenario is 52.59kWh/m². When opening windows with natural ventilation to reduce use air conditioning hours (Scenario I), the annual EUI can be reduced to 33.77kWh/m². It means reducing energy consumption by 35.8%. In scenario II, the original balcony depth is increased to 2m and the fenestration rate is reduced to 23%, the smaller windows would both reduce the heat gains and the opportunity of ventilation, andin this case, less ventilation led to an increase in energy consumption by 0.09 kWh/m², and the annual EUI became 33.86kWh/m², but the impact was infinitesimal. In the high-performance materials scenario (Scenario III), it has a significant energy-saving because the envlope barely has any shading devices. Compared with the previous scenario, energy saving can be 8.5-13.4%, and the annual EUI is 29.31-30.98 kWh/m².

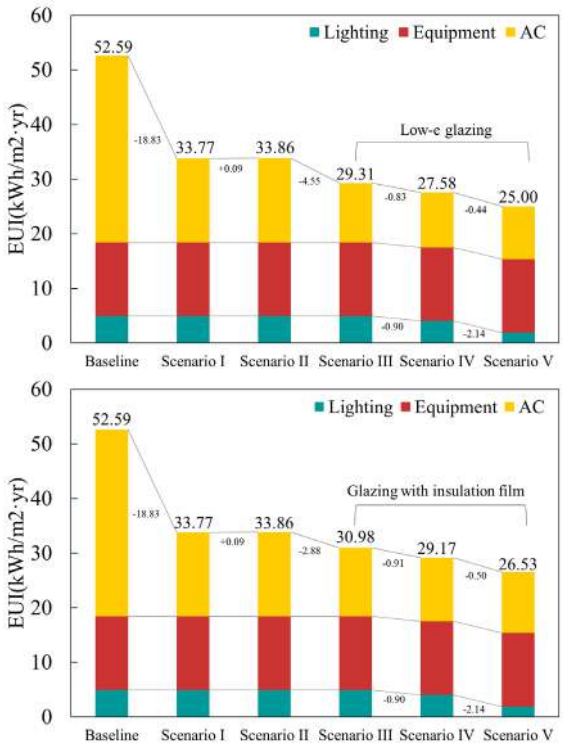

Fig. 3 - The simulation results of the multi-dwelling.

Affected by the performance of building materials, the amount of energy saving varies in different scenarios of high-performance building materials. Using air conditioners with a COP of 3.87~4.21 can reduce 0.9~0.99 kWh/m². When the

air conditioner's COP is increased to 3.9~4.58, another 0.46~0.52kWh/m² would be reduced. Lighting is not affected by the performance of building materials. When the LPD drops to 4.1W/m², it can save 1.57kWh/m², and use LED bulbs to save more energy by 2.30kWh/m². In summary, when air conditioning and lighting meet the EEWH basic criterias (Scenario IV), energy saving is 5.0-5.3% compared to the previous scenario, and the annual EUI droped to 26.85-28.44 kWh/m². When the air-conditioning and lighting reach the best grades in EEWH equipment energy efficiency criterias (Scenario V), it can save 8.1-8.6% more energy. Compared with the baseline, when the envelope, air-conditioning, and lighting all reach the current best levels, energy savings can be 51.3-54.2%.

Further analyze the impact of roofs, exterior walls and glass on the energy saving of air-conditioning. The results show in **Fig. 4**. **Fig. 4 (A)** When the exterior walls and roof are well-insulated and the glass is replaced by a low-e glass, the energy saving per household is 3.71-5.54 kWh/m². Among windows external walls and roofs, windows have the most energy saving effect, accounting for 51.7-63.4%. External walls place the second, accounting for 30.1-38.9%. Roofs have a significant impact on the top floor dwelling units, accounting for 15.1-17.2%. On the other hand, **Fig. 4 (B)** shows a case with the same well-insulated walls and roofs, but changing the low-e window stretegy into insulation film. The energy-saving per household is 2.38-3.39 kWh/m². The energy-saving ratios of glass, exterior walls and roofs are respectively 43.2-53.3%, 37.4-47.8% and 16.2-18.1%. It is ovious that window glass has the greatest impact on the energy consumption of air-conditioning. Therefore, window would be the priority while considering building envelope energy-saving strategies in Taiwan.

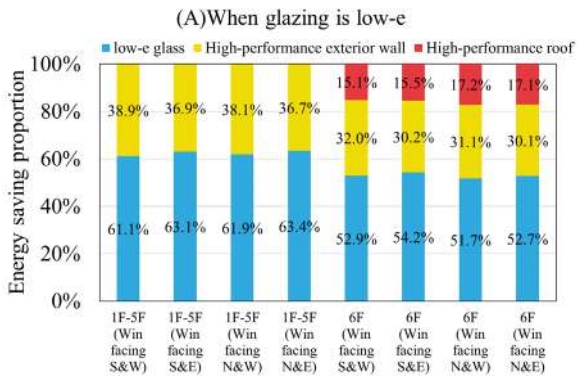

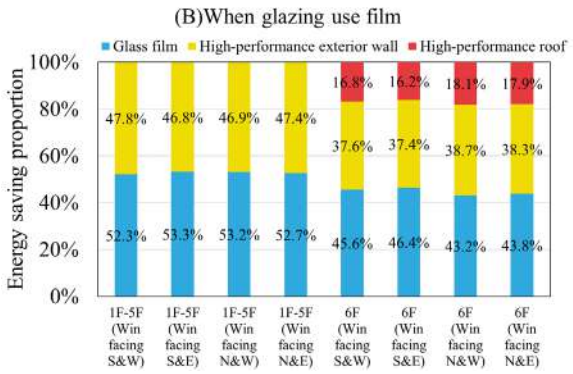

Fig. 4 - Percentage of energy-saving effects of high-performance building materials.

4. Conclusions and recommendation

There are many energy-saving design strategies for buildings. Based on the design and using type of the building, the energy-saving benefits are different. A standard and tipical building model and a series of step-by-step energy efficiency strategies will be a efficient way to evaluate the energy saving benifits. This study focused on school classroom and multi-dwelling, and evaluated the energy performance according to 5 energy-saving scenarios that based on mature but not fully widespread energy-saving technologies in Taiwan. The following are conclusions and suggestions:

1. Natural ventilation, which could reduces indoor temperature and air conditioner uses, is the most economically efficient strategy that should be considered first in any building energy saving design.
2. Well external shading design will reduce the energy-saving benifits of high performance building materials. Among windows, external walls and roofs, windows have the most energy saving benifits. It is recommended to give priority to shading and window design when considering building energy-saving strategy in Taiwan.
3. Since the mixed ventilation strategy greatly reduces the operationg hour of air conditioner, the energy saving that caused by the air conditioner efficiency improving would be reduced; however, equipment energy efficiency still has a significant energy-saving potential. Installing the most efficient level air-conditioners will save 3-5% energy when comparing with installing the basic level ones.
4. Due to the improvement of lighting performance, the LPD can be greatly reduced while maintaining the same illuminance level. Therefore, the use of LEDs can save energy by 13-33% compared with T8-fluorescent tube.
5. When comparing with baseline cases, a beyond-green-building school classroom can save 56.2% energy use, and a beyond-green-building multi-dwelling can save 51.3-54.2% energy use.
6. Compared to countries in temperate zone, Taiwan's air conditioners and lighting performance is similar to international level.

But, the envelope performance is relatively low (compared with passive house, the U value of the outer wall is ≤0.15W/m²k, and the U value of the window is ≤0.8W/m²k). It is worth noting that considering Taiwan's climate and usage, when the envelope, air conditioning and lighting are all upgraded to the highest level of green building in Taiwan, the energy saving effect meets the energy saving level of 20-50% required by ZEB. The rest is to use renewable energy to reach net zero.

5. Acknowledgement

The authors offer their sincere appreciation for assistance in grant to the Bureau of Energy, Ministry of Economic Affairs, R.O.C., under Project no. 111-E0209.

6. References

[1] Bureau of Energy, Ministry of Economic Affairs, "Monthly Energy Statistics Report," Taiwan. 2021.

[2] ASHRAE, Advanced Energy Design Guide for Small to Medium Office Buildings Achieving Zero Energy. 2014.

[3] K.F. Woldekidan et al., "Moving Zero Energy Office Buildings to the Mainstream : Establishing Design Guidelines and Energy Targets Preprint Moving Zero Energy Office Buildings to the Mainstream : Establishing Design Guidelines and Energy Targets Preprint," no. September, 2020.

[4] M.Deru et al., "U.S. Department of Energy commercial reference building models of the national building stock," 2011.

[5] S.Attia, N.Shadmanfar, and F.Ricci, "Developing two benchmark models for nearly zero energy schools," Appl. Energy, vol. 263, no. November 2019, p. 114614, 2020, doi: 10.1016/j.apenergy.2020.114614.

[6] D.D'Agostino andD.Parker, "A framework for the cost-optimal design of nearly zero energy buildings (NZEBs) in representative climates across Europe," Energy, vol. 149, no. 2018, pp. 814–829, 2018, doi: 10.1016/j.energy.2018.02.020.

[7] Construction and Planning Agency, Ministry of the Interior, Building Technical Regulations. 2021.

[8] Ministry of Education, National elementary and junior high school facilities and equipment standards. Taiwan, 2019.

[9] Construction and Planning Agency, "Report on the Sample Survey of Housing Conditions in 2004," 2017.

Data Statement

The datasets generated during and/or analysed during the current study are not publicly available because project requirements but are/will be available confirm by email.

Experimental study on a liquid desiccant dehumidifier with a solution atomization

Soo-Jin Lee [a], Hye-Jin Cho [a], Jae-Hee Lee [a], Yong-Kwon Kang [a], Gyu-Bae Lee [a], Jae-Weon Jeong [a,]*

[a,*] Department of Architectural Engineering, Hanyang University, Republic of Korea, jjwarc@hanyang.ac.kr.

Abstract. The purpose of this study is to improve a dehumidification performance of the liquid desiccant system. The centrifugal atomization technology for spraying the solution was applied to enhance the dehumidification performance by increasing the heat and mass transfer area between the air and solution at low solution flow rate. The experimental study was performed to investigate the effect of the solution atomization for dehumidification performance of the proposed system. The measurement parameters for the test were the inlet air temperature and relative humidity, outlet air temperature and relative humidity, air volume flow rate, inlet solution temperature and density, outlet solution temperature and density, and solution mass flow rate. The dehumidification effectiveness was selected to assess the mass transfer performance of the dehumidifier with the solution atomization using the centrifugal atomizer. To compare the dehumidification performance of the proposed system and conventional packed-bed liquid desiccant system, the simulation was also conducted to estimate the dehumidification effectiveness of the reference system. The thermal load was also estimated of each system to evaluate the energy saving potential of the proposed liquid desiccant system under the conditions that show the same dehumidification performance. The experimental and simulation results indicated that the proposed system required approximately 0.012 liquid-to-gas (L/G) ratio while the reference system needed 0.5 L/G ratio for the same dehumidification effectiveness of 0.58. The most important finding of this result was that the proposed dehumidifier with the solution atomization has improved dehumidification performance at 97.6% lower L/G ratio than the conventional packed-bed type dehumidifier and the proposed system could save 72% cooling load than the reference system.

Keywords. Liquid desiccant, dehumidifier, centrifugal atomization, dehumidification effectiveness, liquid-to-gas ratio.
DOI: https://doi.org/10.34641/clima.2022.40

1. Introduction

As an importance of the humidity control is increasing, previous studies suggested a liquid desiccant based air conditioning systems [1,2]. A liquid desiccant system has been considered as an effective and economic system because of a high dehumidification performance based on non-vapour compression [3,4]. The desiccant solution is also required the renewable or waste heat for solution regeneration, thus, the liquid desiccant based air conditioning systems have energy saving potential in buildings [5].

The liquid desiccant system was based on a heat and mass transfer between the air and desiccant solution. Therefore, the various contact types of the air and solution were studied and the counter-flow and cross-flow packed-bed type dehumidifier was proposed [6,7]. Fumo and Goswami [6] investigated the packed-bed type liquid desiccant dehumidifier and regenerator performance which has counter-flow under various inlet air and solution conditions. The heat and mass transfer between the air and desiccant solution on the cross-flow packed-bed type dehumidifier was also analysed by Dai and Zhang [7]. However, the packed-bed type liquid desiccant dehumidifier consumed massive desiccant solution to ensure sufficient wetting area of the packing materials and it caused a large thermal load for solution cooling and heating.

In view of this, a new design of liquid desiccant system based on a solution atomization was proposed [8,9]. Yang et al. [8] was suggested the ultrasonic atomization dehumidification system (UADS). The solution is atomized with tiny droplets in UADS with approximately 50μm diameter and the liquid-to-air contact area is dramatically increased.

Copyright ©2022 by the authors. This conference paper is published under a CC-BY-4.0 license.

Yang et al. [9] also analysed sensitivity on the performance of UADS. The experiment and simulation were conducted under various operation conditions and the analysis of variance (ANOVA) was applied to investigate the significant operating conditions in the proposed system. However, UADS consisted of complex and expensive components because of an ultrasonic generator, transducer, and voltage stabilizer and it also has a practical problem because of a corrosion issue by the desiccant solution.

Hence, a state-of-the-art technology for solution atomization should be considered to enhance the dehumidification performance of the liquid desiccant dehumidifier. The objective of this study is to propose the liquid desiccant dehumidifier with centrifugal atomization technology and to evaluate the dehumidification performance experimentally. The energy saving potential was also estimated compared with a conventional packed-bed type liquid desiccant dehumidifier via detailed simulation based on experimental results.

2. Experimental setups

2.1 system overview

The liquid desiccant system consisted of a dehumidification and regeneration part, air controller and solution controller. In this system, the hot and humid outdoor air is blown up into a dehumidification chamber in the dehumidification part by an air fan in the air controller. The air and solution contact into the dehumidification chamber and the air is dehumidified by the mass transfer between the air and solution. The main driving force of the mass transfer is a vapour pressure difference and the solution is cooled by the cooler in the solution controller to increase the vapour pressure difference between the air and solution. After the dehumidification process, the dry air is cooled by a cooling coil in the air controller to meet a target supplying condition (i.e., 26°C and 0.010 kg/kg). The weak solution after the dehumidification process is sent to a regenerator for maintenance of a solution concentration. Because the main purpose of this study is to improve the dehumidification performance using solution atomization with fine droplets, experiments and simulation were focused on dehumidification performance of the dehumidifier.

Fig. 1 indicated a conventional liquid desiccant dehumidifier with a packing material. The packing material consists of many layers of cellulose rigid media pads placed in different orientations such as zigzag path to provide the sufficient specific area. Thus, the solution is sprayed onto this packing material in the conventional liquid desiccant dehumidifier and the heat and mass transfer area to achieve a target dehumidification rate can be obtained.

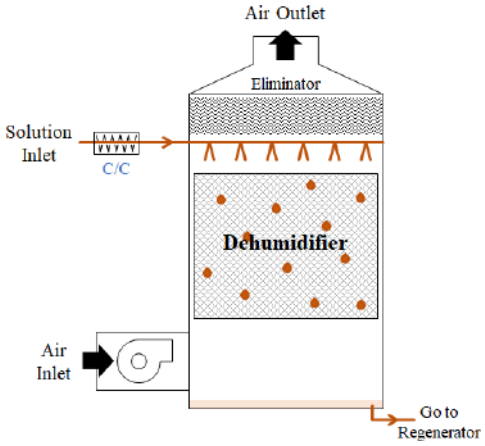

Fig. 1 – Schematic of a conventional liquid desiccant dehumidifier.

As shown in **Fig. 2(a)**, the mainly different part of the proposed system with the conventional system is a contact method of the air and solution in the dehumidification chamber. In the conventional system, the air and solution contact through the packing media, however, the air and solution contact directly in the proposed system. To get an enough contact area for dehumidification rate similar to a packing media, the solution is sprayed as a very tiny droplet by a centrifugal atomization into a dehumidification chamber. **Fig. 2(b)** depicts the test setup.

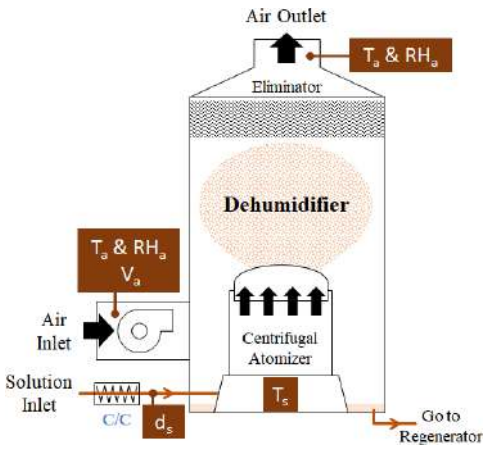

(a) detailed schematic and sensor location

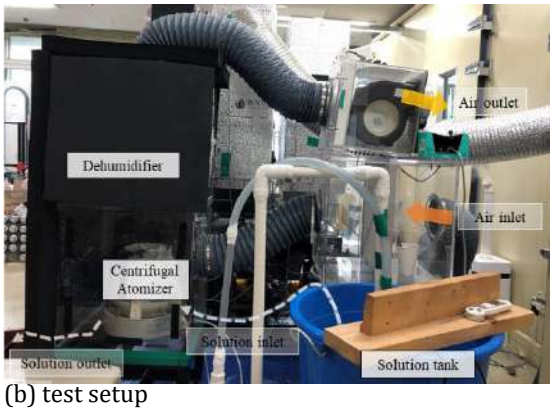

(b) test setup

Fig. 2 – The liquid desiccant dehumidifier with a solution atomization.

Tab. 1 – Specification of the sensors.

parameters	sensor types	accuracy	operating range
air temperature and relative humidity	Negative Temperature Coefficient of Resistance (NTC)	0.3°C	-40 – 120°C
		2.0%	0 – 100%
air velocity	Vane probe ϕ150mm	0.1 m/s (+1.5% of mv)	0.1 – 15 m/s
solution temperature	Pt100	0.2°C (at 50 – 300°C)	-50 – 400°C
solution density	glass hydrometer	1kg/m^3	1000 – 1400 kg/m^3

2.2 measuring instruments

Parameters of the liquid desiccant dehumidifier were measured and recorded with the sensors listed in **Tab. 1** during the dehumidification experiment. The air temperature and relative humidity were measured to evaluate the dehumidification performance. The air velocity was also measured to check the air flow rate. The solution temperature and density were collected to verify the heat and mass balance of the experimental setup during the entire dehumidification process.

Two temperature and humidity sensors were located at the inlet and outlet side of the dehumidifier, and one velocity sensor was located at the inlet air-side. The solution temperature sensor was installed in a sump of a centrifugal atomization to measure the temperature of an atomized solution. The temperature and density sensors were also installed at an inlet solution tank and drain tank. The detailed location of the sensors was illustrated in **Fig. 2(a)**.

The air temperature and relative humidity were logged within 1-s intervals using a Testo 400 data logger and the solution temperature and density were measured intermittently.

2.3 experimental conditions

Experiments were conducted with LiCl as a desiccant solution under the hot and humid air conditions as shown in **Tab. 2**. The air temperature and humidity ratio were the outdoor design conditions of air conditioning in Korea. The air flow rate was set to be a minimum ventilation rate in an office building by ASHRAE Standard 62.1.

The solution flow rate was a specification of a centrifugal atomization used in this study. Thus, the liquid-to-gas (L/G) ratio was set to be about 0.012. The temperature and concentration of the solution were assumed to be a 20°C and 37%, respectively, for satisfying the target humidity ratio of a supply air sufficiently [3,10]. The lithium chloride (LiCl) aqueous solution was used for a liquid desiccant solution. The droplet size of solution was affected with provided spec according to the characteristic of the centrifugal atomization.

Tab. 2 – Test conditions.

component	parameter	value
Air	flowrate	85 m^3/h
	temperature	32°C
	humidity ratio	0.020 kg/kg (relative humidity: 65%)
solution	flowrate	1L/h (L/G ratio: 0.012)
	temperature	20°C
	concentration	37%

3. Analysis of operating data

The energy saving potential of the proposed system was evaluated by analysing the experimental data. The simulation of the reference system was also conducted to compare for a thermal load for the same dehumidification performance.

3.1 measurement data

Fig. 3(a) and (b) show the temperature and humidity ratio behaviours of the process air. The red line means the condition profile measured at the absorber inlets and the blue line means the condition profile collected at the absorber outlets. The process air was supplied at a temperature and humidity ratio of approximately 34°C and 0.020kg/kg. The results indicated that the introduced air was cooled by heat transfer with the cold desiccant solution and significantly dehumidified by the atomized desiccant solution. In detail, the introduced air was pre-cooled to a temperature of approximately 28°C by heat transfer with the cold desiccant solution supplied at a temperature of 20°C as described in **Fig. 3(a)**. As shown in **Fig. 3(b)**, the air was dehumidified from a humidity ratio of 0.020 kg/kg to 0.012 kg/kg during contact with a desiccant solution. In summary, the introduced air was cooled to 28°C and dehumidified to 0.012 kg/kg on average.

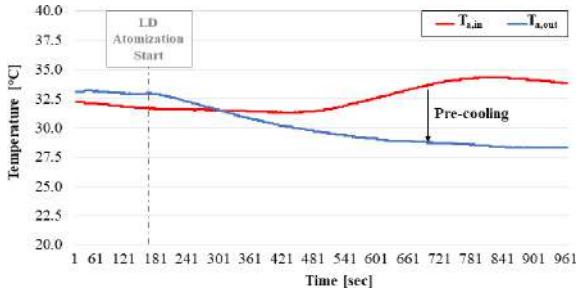

(a) dry-bulb temperature

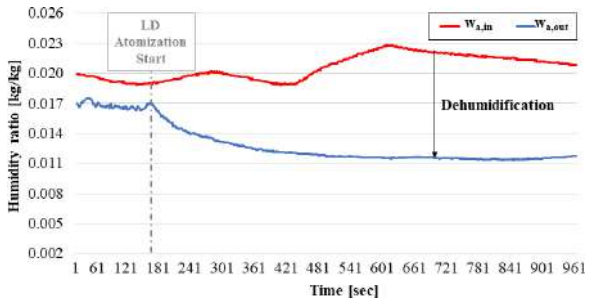

(b) humidity ratio

Fig. 3 – The thermal behaviours of the process air.

3.2 dehumidification performance comparison

To analyse the dehumidification performance using measured data by the experiments, the effectiveness of dehumidification was considered as a performance index. The dehumidification effectiveness (ε_{deh}) can be obtained by inlet ($\omega_{a,in}$) and outlet ($\omega_{a,out}$) air humidity ratio and equilibrium humidity ratio (ω_{eq}) as shown in equation (1). The inlet and outlet air humidity ratio were measured data and equilibrium humidity ratio could be estimated by the previous studies [10].

$$\varepsilon_{deh} = \frac{\omega_{a,in} - \omega_{a,out}}{\omega_{a,in} - \omega_{eq}} \quad (1)$$

The effectiveness of dehumidification was predicted in the reference system for the dehumidification performance comparison with the proposed system. To estimate the dehumidification effectiveness of the reference system, the detailed simulation was performed. It can be estimated by Chung and Luo model for dehumidification effectiveness of a conventional packed-bed type liquid desiccant system [3]. The inlet condition was set a same condition as the experimental setup except L/G ratio.

Fig. 4 illustrates the psychrometric process of the proposed system collected by an experiment and reference system by simulation under the same inlet air and solution condition. In conventional packed-bed type liquid desiccant system, the system has been operated at L/G ratio of 0.8 to meet a target humidity ratio of 0.010 kg/kg. On the other hand, the experimental results indicated that the outlet humidity ratio and effectiveness of dehumidification are 0.012 kg/kg and 0.58, respectively, unsatisfied to a target dehumidification performance. However, the reference system was operated 0.5 L/G ratio while the proposed system required approximately 0.012 L/G ratio to achieve the same performance (i.e., outlet humidity ratio 0.012 kg/kg and 0.58 dehumidification effectiveness). Thus, the proposed system could save about 97.6% desiccant solution consumption.

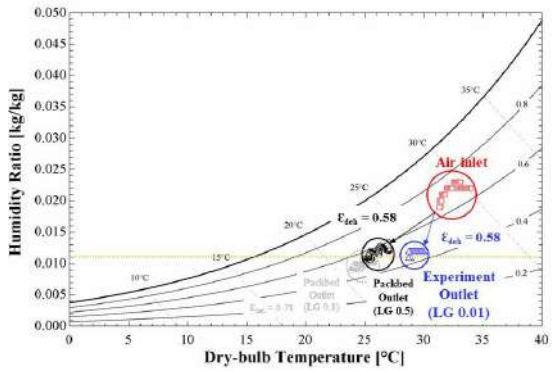

Fig. 4 – Psychrometric process of each system.

3.3 thermal load comparison

To compare the thermal load of each system, the air and solution cooling were considered, simultaneously. The air cooling load ($Q_{a,cooling}$) means the cooling load required to cool the air passed the absorber ($T_{a,abs,out}$) to the target supply air temperature ($T_{sa,target}$). The air cooling load can be calculated by equation (2). The solution cooling was required to satisfy the target solution temperature of 20°C. The solution cooling load ($Q_{s,cooling}$) can be calculated by mass flow rate of the solution ($\dot{m}_s$), heat capacity ($C_{p,s}$), absorber outlet solution temperature ($T_{s,abs,out}$), and target solution temperature ($T_{s,abs,target}$) according to equation (3). In this study, the target supply air temperature and target solution temperature were set to be 26°C and 20°C, respectively.

$$Q_{a,c} = \dot{m}_a \times C_{p,a} \times (T_{a,abs,out} - T_{sa,target}) \quad (2)$$

$$Q_{s,c} = \dot{m}_s \times C_{p,s} \times (T_{s,abs,out} - T_{s,abs,target}) \quad (3)$$

The thermal load of each system was described in **Fig. 5**. The proposed system required the lower solution cooling load than the reference system because of very low flow rate of the solution. However, the heat transfer between the air and solution was also less generated because of the low flow solution in the proposed system. Thus, the proposed system needed an auxiliary cooling for the air to meet a target supply air temperature. On the other hand, the reference system only required a solution cooling because of sufficient cooling of the air by heat transfer with a solution. Finally, the proposed and reference system consumed about 100 Wh and 356 Wh, respectively, during 1 hour and the proposed system could save approximately 72% of cooling load for air and solution.

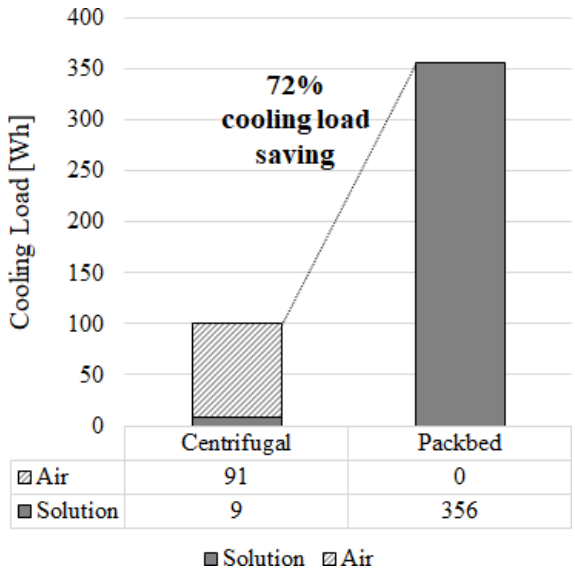

Fig. 5 – Thermal load comparison of each system.

4. Conclusions

The liquid desiccant based air conditioning system is beneficial for hot and humid climate; however, additional cooling and heating load for solution occurred to operate the dehumidifier and regenerator. In this study, the liquid desiccant dehumidifier with a centrifugal atomization technology was proposed to reduce the solution load while maintain the dehumidification performance. The experimental results indicated that the process air was significantly dehumidified from a humidity ratio of 0.020 kg/kg to 0.012 kg/kg under L/G ratio of 0.012. For the same effectiveness of dehumidification, the reference system was operated as 0.5 L/G ratio and the proposed system consumed 97.6% less solution. Finally, the proposed system could save 72% thermal load for air and solution cooling than the reference system.

This study indicated that the feasibility and energy benefits of the liquid desiccant dehumidifier with a centrifugal atomization as a preliminary study. Thus, more comprehensive research is needed for understanding the characteristics of the liquid desiccant dehumidifier with centrifugal atomization technology under various conditions. The consideration about the regeneration process is also required because this study was focused on the dehumidification performance. The whole liquid desiccant system contained regenerator will be manufactured with new atomization technology to control the droplet size in the further study.

5. Acknowledgement

This work was supported by Korea Institute of Energy Technology Evaluation and Planning (KETEP) grant funded by the Korea government (MOTIE) (No. 20202020800360), and this work was supported by Korea Environment Industry & Technology Institute (KEITI) through Prospective green technology innovation project, funded by Korea Ministry of Environment (MOE) (RE202103243).

6. References

[1] Martin V., Goswami D.Y. Effectiveness of heat and mass transfer processes in a packed bed liquid desiccant dehumidifier/regenerator. ASHRAE Trans. 2000;106:20–39.

[2] Al-Farayedhi A.A., Gandhidasan P., Al-Mutairi M.A. Evaluation of heat and mass transfer coefficients in a gauze-type structured packing air dehumidifier operating with liquid desiccant. Int. J. Refrig. 2002;25:330–339.

[3] Chung T.W., Luo C.M. Vapor pressures of the aqueous desiccants. J. Chem. Eng. Data. 1999;44: 1024–1027.

[4] Conde M.R. Properties of aqueous solutions of lithium and calcium chlorides: Formulations for use in air conditioning equipment design. Int. J. Therm. Sci. 2004;43: 367–382.

[5] Kim M.H., Park J.Y., Sung M.K., Choi A.S., Jeong J.W. Annual operating energy savings of liquid desiccant and evaporative-cooling-assisted 100% outdoor air system. Energy Build. 2014;76:538–550.

[6] Goswami D.Y., Fumo N. Study of an aqueous lithium chloride desiccant system: air dehumidification and desiccant regeneration. Sol. Energy. 2002;72:351–361.

[7] Dai Y.J., Zhang H.F. Numerical simulation and theoretical analysis of heat and mass transfer in a cross flow liquid desiccant air dehumidifier packed with honeycomb paper. Energy Convers. Manag. 2004; 45:1343–1356.

[8] Yang Z., Lin B., Zhang K., Lian Z. Experimental study on mass transfer performances of the ultrasonic atomization liquid desiccant dehumidification system. Energy Build. 2015;93:126–136.

[9] Yang Z., Zhang K., Lian Z., Zhang H. Sensitivity and stability analysis on the performance of ultrasonic atomization liquid desiccant dehumidification system. Energy. 2016;112:1169–1183.

[10] Chung T.W. Predictions of moisture removal efficiencies for packed-bed dehumidification systems. Gas Sep. Purif. 1994;8:265–268.

Experimental and numerical performance evaluation of building integrated photovoltaic with thermoelectric generator and phase change material

Yong-Kwon Kang [a], Beom-Jun Kim [a], Soo-Jin Lee [a], Minseong Kim [a], Jae-Won Joung [a], Jae-Weon Jeong [a]

[a] Department of Architectural Engineering, Hanyang University, Republic of Korea, kyk908525@hanyang.ac.kr

[a] Department of Architectural Engineering, Hanyang University, Republic of Korea, bumji21@hanyang.ac.kr

[a] Department of Architectural Engineering, Hanyang University, Republic of Korea, zkdie97@gmail.com

[a] Department of Architectural Engineering, Hanyang University, Republic of Korea, minseongk91@hanyang.ac.kr

[a] Department of Architectural Engineering, Hanyang University, Republic of Korea, jea4527@hanyang.ac.kr

[a] Department of Architectural Engineering, Hanyang University, Republic of Korea, jjwarc@hanyang.ac.kr

Abstract. Building-integrated photovoltaics (BIPVs) are the most promising systems for achieving zero-energy building in cities. However, BIPV has some shortcomings, such as a lack of solar tracking and a rapid increase in the PV surface temperature. Therefore, resolving these shortcomings requires system solutions to eliminate heat from panels or utilize heat sources to improve system efficiency. Heat dissipation methods using phase change materials (PCMs), heat fins, thermoelectric generators, air cooling, and water cooling have been proposed and studied. Among them, the passive technology PCM and thermoelectric generator are attracting attention. Using PCM can reduce the panel temperature without additional energy consumption. In addition, some studies have been conducted on BIPVs with a thermoelectric generator (TEG) or using a working fluid such as water or air to increase the system efficiency. Methods of heat recovery using fluids for conventional PV panels, owing to the characteristics of BIPVs installed on the exterior of building walls, have also been proposed. Some studies have also explored designs that combine TEGs, generating electric power depending on the temperature difference without additional equipment. However, TEGs also have the disadvantage of an extremely low power generation efficiency if they do not achieve a sufficient temperature difference. In this study, to address the shortcomings of each application, a BIPV combined with a PCM and TEG (BIPV-TEG-PCM) is proposed. Herein, the appropriate phase change temperature of the PCM and heat sink design in the PCM container were analyzed through computational fluid dynamics-based simulations and experiments.

Keywords. BIPV, Thermoelectric generator, PCM, Building-integrated photovoltaics, Phase-change material
DOI: https://doi.org/10.34641/clima.2022.216

1. Introduction

The increasing number of people living in cities [1] has led to the enormous energy consumption of buildings. The global Green New Deal requires high energy efficiency equipment and renewable energy. Nevertheless, the reality is that it is challenging to supply a large amount of renewable energy owing to the limited space in cities. Therefore, many studies have been conducted on building-integrated photovoltaics (BIPVs), solar panels integrated with building facades. However, BIPVs are fixed on the exterior building walls, unlike conventional PVs. Therefore, they have a limited time and angle for receiving sunlight. This disadvantage causing reduce the generation efficiency of PV panels. Various solutions have been proposed to improve the efficiency of the BIPVs (Fig 1) [2].

Copyright ©2022 by the authors. This conference paper is published under a CC-BY-4.0 license.

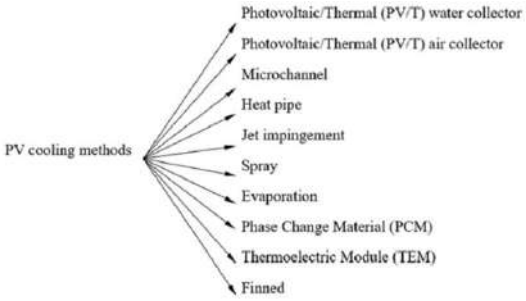

Fig. 1 - Cooling methods of PV panels.

Among the results of previous studies, the convection method had the best heat dissipation efficiency. Koyunbaba et al. (2013) proposed an air-cool-based BIPV thermal (BIPVT) system with a Trombe wall system [3]. An analysis based on the experiments and computational fluid dynamics (CFD) calculations showed that the average electrical and thermal efficiencies of this system could reach 4.52% and 27.2%, respectively. Kaiser et al. (2014) studied a BIPV module system under forced convection conditions [4]. Another study experimentally analyzed the influence of the air gap size and forced convection ventilation system. Under a duct velocity of 6 m/s, the power generation increased by 19% relative to the natural ventilation case. In addition, some studies have focused on water-cooling BIPVT systems. Kim et al. (2014) experimentally analyzed the energy performance of a water-cooled BIPVT integrated on a roof [5]. According to the experimental results, the average thermal and electrical efficiencies of the BIPVT were increased by 30% and 17%, respectively.

However, the fluid convection method is challenging to maintain and requires additional equipment and energy consumption to move the fluids. Therefore, research has been conducted on the BIPV system using a phase change material (PCM) and thermoelectric generator (TEG) to increase the efficiency passively. According to previous studies, the individual energy efficiency of the PV increased by 5.9% relative to that of an existing panel combined with PCMs [6]. Using a TEG, further development of approximately 5% was possible [7]. However, the PCM and TEG have low thermal conductivity and low generation efficiency. In addition, most preceding studies were insufficient considering the substantive problems of building-integrated PVs applied to buildings. Therefore, this study proposes a BIPV-TEG-PCM design considering practical installation, which combines the PV, PCM, and TEG. Furthermore, this study numerically and experimentally analyzed the optimal phase change temperature of the PCM, heat fin spacing, and TEG spacing for BIPV-TEG-PCM.

2. System and simulation overview

2.1 building integrated photovoltaic with thermoelectric generator and phase change material

Applying to the exterior surface of a building wall, BIPV-TEG-PCM is attached directly to the building wall. The integration with the wall using PCMs makes heat rejection possible without an additional power source or fluid for heat dissipation in the PV panel. Moreover, the BIPV-TEG-PCM does not cause infiltration or water-leakage problems from the exterior wall and prevents heat transfer to the interior side, reducing the heat load. The TEGs were located between the PV and PCM containers. The heat in the PV passes through the TEG during the day and is stored in the PCM container. Based on the Seeback effect, the TEG was generated electric power using the temperature difference generated at this time. The electricity generated from the PV and TEG is supplied to the necessary equipment through a battery or external circuit. In addition, the BIPV-TEG-PCM proposed in this study can generate energy at night. In the case of a PCM used to heat a PV during the day, recharging is required. Convection and longwave radiation from the PV surface decreased the surface temperature of the PV panel. The PCM was regenerated based on cooled PV. In this case, the reverse temperature difference between the PV and PCM containers allows the TEG to develop again. The temperature distributions in these processes are illustrated in Figures 1 and 2.

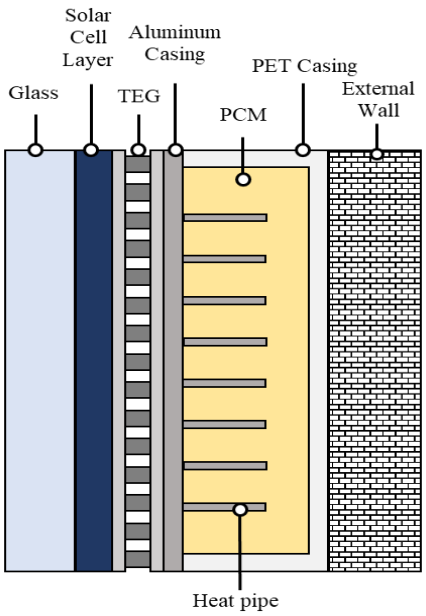

Fig. 2 - BIPV-TEG-PCM design.

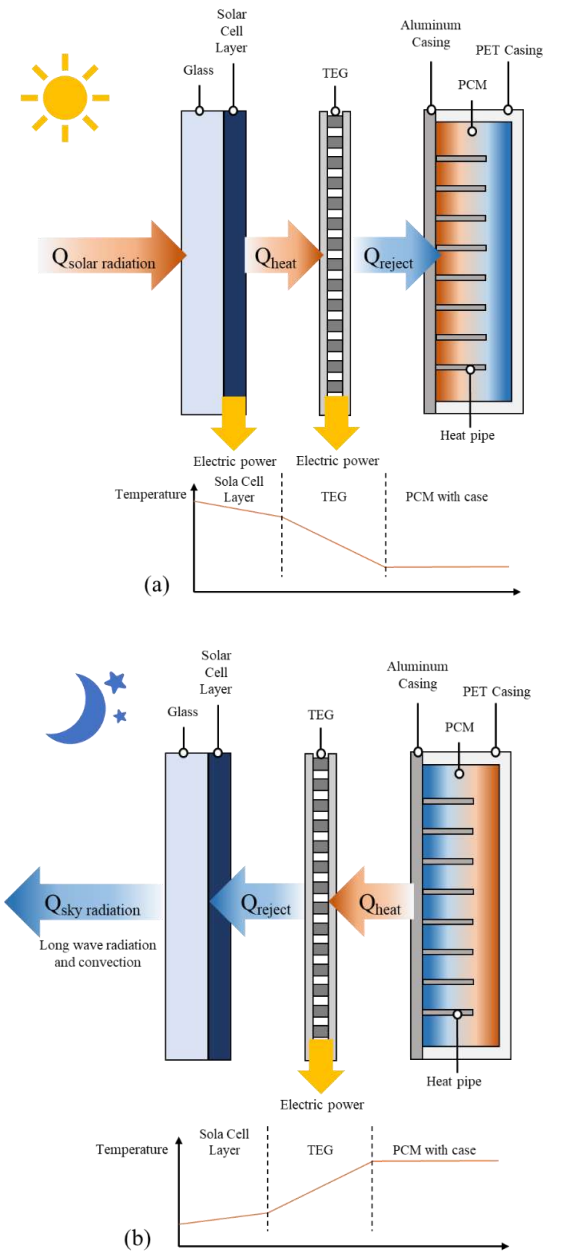

Fig. 3 - (a) BIPV-TEG-PCM operation during the daytime and (b) BIPV-TEG-PCM operation during the night.

2.2 Micro-encapsulated phase change material(mPCM)

In this study, the microencapsulated phase change material (mPCM) applied to easily manufacture and passively reject the heat from the PV panel. Moreover, a BIPV was installed on the outer skin of the building. Therefore, the use of the mPCM can prevent PCM leakage from the PCM container. Typical PCMs require precise containers because the particles are microscopic and easily leak from containers. In the case of mPCM, the particles are larger than the liquid-type PCM. The physical properties of the mPCM used in this simulation are listed in Table 1. Based on the results of the experiments in a preceding study [8], the selected ratio of PCM to tetrabutyl titanate (TBT) for the mPCM was as 6:4. Owing to the characteristics of the PCM, the material values vary slightly depending on the phase-change temperature. In addition, the material properties of the mPCM applied were fixed, and only the phase-change temperature was varied in the simulations.

Tab. 1 - Properties of n-eicosane micro-encapsulated PCM.

Property	Value
Density [kg/m3]	946.4
Specific heat [J/kgK]	1973.1
Latent heat [J/kg]	192660
Thermal conductivity [W/mK]	0.749
Melting point [℃]	25, 35 45
Particle size [μm]	10

3. Experimentation and simulation overview

3.1 Experiment overview

This experimentation conducted on the roof of a building located in Seoul in summer. In this experiment, the surface temperature of the PV panel was compared which the PCM was integrated and the panel without PCM. To monitor the temperature variation of each layer, T-type thermocouples were attached at the PV panel surface, TEG cold side and interior of PCM.

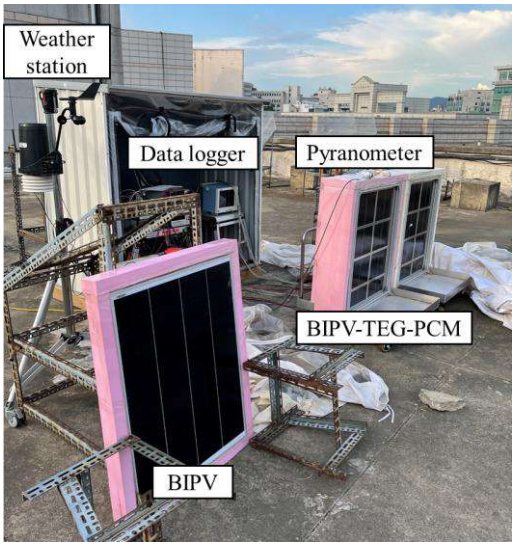

Fig. 4 - Figure caption.

3.2 CFD simulation overview

Transient simulations were conducted using ANSYS FLUENT, a commercially available software package. The purpose of this simulation was to identify the PCM at an appropriate phase-change temperature.

In addition, the PCM used in this study was mPCM in powder form; therefore, the calculation was conducted by assuming a laminar flow because there was no fluid. In addition, most of the heat is transferred within the BIPV-TEG-PCM through conduction. A CFD mesh was constructed using a two-dimensional model. The physical properties of the PCMs used in the CFD settings are listed in Table 1, and other material physical properties are described in previous studies [9–11]. In this simulation, several assumptions were made to reduce the computational time and compare the results in the same environment, and the properties of all objects are unaffected by time and temperature changes. The effects of natural convection were ignored in the PV panel surface. The project was simulated with a size smaller than the actual size.

The total number of nodes was 14,864 (Fig. 5). Based on the PV standard test (STC) conditions of 25 °C and 1000 W/m^2, the heat flux to the PV panel surface was fixed at 1000 W/m^2, and the other surfaces were set under insulation conditions. The total simulation time was four h (i.e., 14400 s), and the results were plotted every second. The properties of the other materials are listed in Table 2.

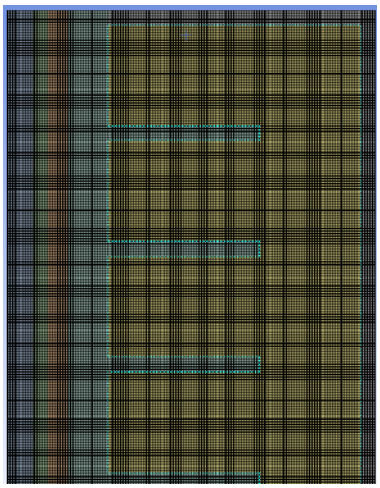

Fig. 5 - Figure caption.

Tab. 2- Properties of BIPV-TEG-PCM.

Material	Density [kg/m3]	Specific heat [J/kgK]	Thermal conductivity [W/mK]
PV	2230	700	148
Aluminium	2719	871	202.4
PET	1500	1200	0.2
TEG	7670	198	1.61

4. Results

4.1 Simulation results

In this study, simulation analysis was performed on heat fin spacing for PCM container, melting temperature of PCM, and TEG spacing to derive an appropriate BIPV-TEG-PCM design. In addition, an outdoor experiment was conducted using a prototype.

The result of optimal heat fin spacing is shown in figure 6 below. In this study, a total of 5 spacings of no fin, 5, 10, 20, and 30 mm were analyzed, and the surface temperature of the PV panel with 5 mm heat fin spacing cases were compared in each PCM melting temperature (i.e., 25, 35 and 45°C). As a result of the simulation, it was found that the 20 mm heat fin spacing could maintain the lowest panel surface temperature regardless of the PCM melting temperature. If the fin spacing is tight, heat transfer is improved, and rapid heat transfer to the PCM is possible. However, due to the decreased amount of the PCM, the melting area of PCM was crated faster than wide fin spacing. Therefore, results showed a faster temperature rise compared to the other fin interval. This phenomenon appeared more clearly as the melting temperature of the PCM was lower, and when the melting temperature of the PCM was increased, a better effect was shown based on rapid heat transfer.

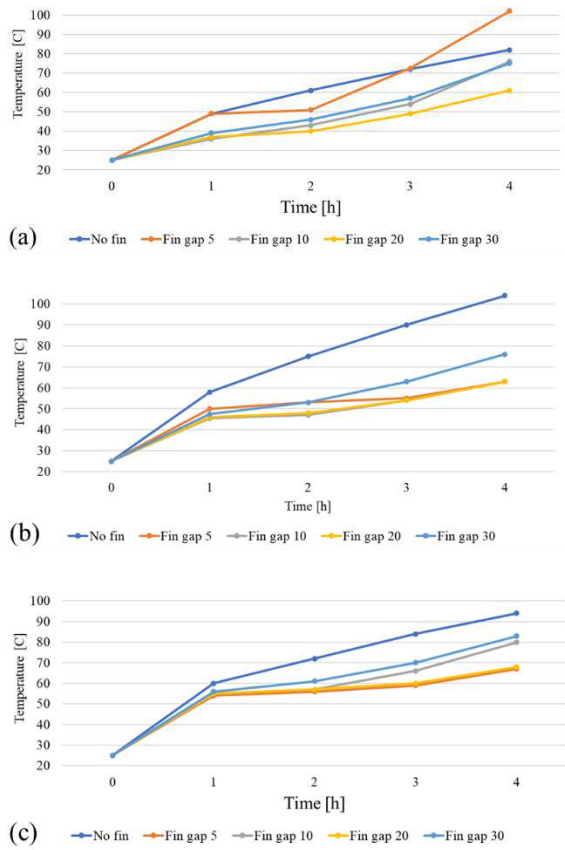

Fig. 6 – PV surface temperature comparison: (a) heat fin spacing with PCM 25 (b) heat fin spacing with PCM 35 and (c) heat fin spacing with PCM 45.

The appropriate PCM melting temperature was compared in each heat fin interval (Fig. 7). As a result of the simulation, the PCM melting

temperature of 25°C shows the best performance for the low PV surface temperature in each case. However, in the case of the close interval heat fin spacing of 5 and 10 mm with PCM 25°C, it was kept low for the first two hours, after two hours showed a steeper temperature rise as the phase change progressed. On the other hand, the high melting temperature PCM with a high temperature showed a similar pattern of increasing gradually at both 35 and 45°C. When the heat fin spacing was narrow, the PCM 35°C showed better performance than PCM 25°C.

Therefore, there may be different combinations depending on the conditions of use. However, using a PCM melting temperature 25°C can maintain the lowest panel surface temperature in STC conditions.

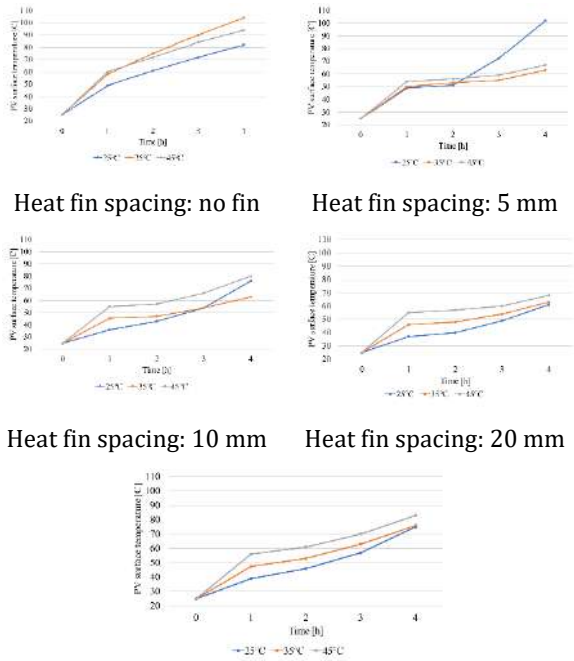

Fig. 7 - PV surface temperature distribution with different melting temperature of PCM.

As shown in figure 8, four TEG intervals were selected for simulation (i.e., 70, 93, 140, and 280 mm). As a result of the TEG spacing simulation, it was found that the temperature difference between the cold and hot sides of the TEG increased as the TEG interval widened. In addition, the panel surface temperature distribution of the remaining cases except for 280 mm was a similar pattern, and it was found that the largest temperature difference occurred when the thermoelectric element was spaced at 140 mm. Therefore, the most appropriate TEG spacing is determined to be 140 mm. The heat transfer rate of the TEG is larger than PCM. Therefore, the closer the distance of the TEG cause, the more heat transfer to the PCM and heat fin. Therefore, it causes the unbalance heat transfer rate between PV to TEG and TEG to PCM. Therefore, the temperature of the cold side and hot side of TEG show similar temperatures.

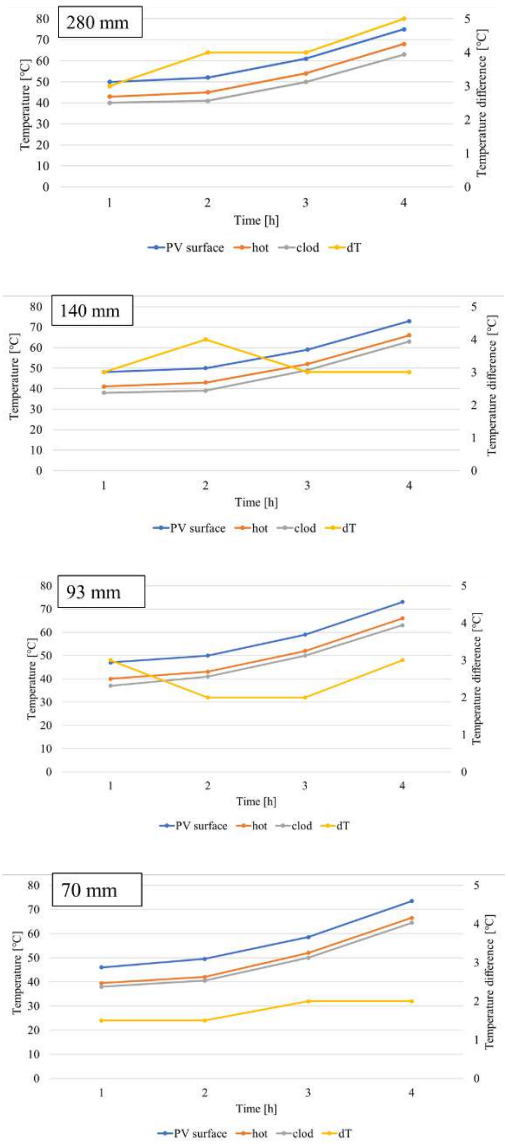

Fig. 8 - PV surface temperature distribution with different TEG interval.

4.2 Experimentation results

As a result of the experiment (Fig. 9), PV surface temperature at the peak was about 20°C lower with the PCM than the panel without the PCM. However, there was no significant difference in surface temperature of the PV panels between the PCM melting temperature at 35°C and 45°C. Therefore, using the PCM and TEG with the PV panel can improve the 13% of PV panel efficiency. As a result of the measurement, it was confirmed that eight TEGs could produce a total of 0.04 Wh of electricity per day. In addition, the amount of power generation changes according to the insolation was confirmed following the characteristic of TEG (Fig. 10).

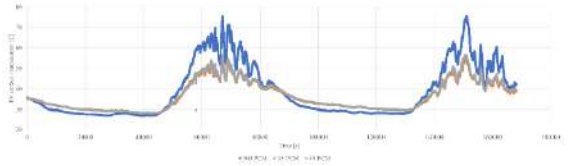

Fig. 9 - PV surface temperature measurement by prototype experiment.

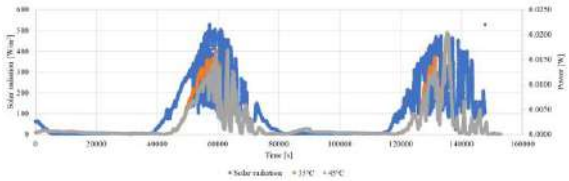

Fig. 10 - TEG power generation during the summer.

5. Conclusion

This study analyzed the impact of the phase change temperature, the heat fin, and TEG arrangement on thermal behavior through CFD transient simulations. In addition, prototype experimentation of the BIPV-TEG-PCM system was conducted to confirm the effect of reducing PV surface temperature by the PCM. As a result of simulation, low phase change temperature helps inhibit an early temperature rise. However, it has been shown that high melting temperature PCM maintain similar or low temperatures for a more extended period if there is a proper design heat fin spacing. Therefore, using a suitable melting temperature PCM with the proper heat fin spacing can increase the efficiency of the panel, which can further contribute to a zero-energy building. In addition, as shown in the experiment results, the PCM can reduce the PV surface temperature by about 20°C lower than the PV panel without the PCM.

Thus, the further study intents to manufacture the second experimental unit of BIPV-TEG-PCM and verify the simulation results through outdoor experiments.

Acknowledgement

This work was supported by Korea Institute of Energy Technology Evaluation and Planning (KETEP) grant funded by the Korea government (MOTIE) (No. 20202020800360), and this work was supported by the Korean Agency for Infrastructure Technology Advancement (KAIA) grants (21CTAP-C163749-01).

6. References

[1] Programme UNE, Construction GA for B and. 2020 Global Status Report 2020.

[2] Bayrak F., Oztop HF., Selimefendigil F. Experimental study for the application of different cooling techniques in photovoltaic (PV) panels. Energy Convers Manag 2020;212:112789.

[3] Koyunbaba BK., Yilmaz Z., Ulgen K. An approach for energy modeling of a building integrated photovoltaic (BIPV) Trombe wall system. Energy Build 2013;67:680–8.

[4] Kaiser AS., Zamora B., Mazón R., García JR., Vera F. Experimental study of cooling BIPV modules by forced convection in the air channel. Appl Energy 2014;135:88–97.

[5] Kim JH., Park SH., Kang JG., Kim JT. Experimental performance of heating system with buildingintegrated PVT (BIPVT) collector. Energy Procedia 2014;48:1374–84.

[6] Hasan A., Sarwar J, Alnoman H, Abdelbaqi S. Yearly energy performance of a photovoltaic-phase change material (PV-PCM) system in hot climate. Sol Energy 2017;146:417–29.

[7] Makki A. Innovative heat pipe-based photovoltaic/thermoelectric (PV/TEG) generation system. PhD Thesis Univ Nottingham 2017:329.

[8] Chai L., Wang X., Wu D. Development of bifunctional microencapsulated phase change materials with crystalline titanium dioxide shell for latent-heat storage and photocatalytic effectiveness. Appl Energy 2015;138:661–74.

[9] Liu XD., Park YH. Structure and transport properties of (Bi1-xSbx)2Te3 thermoelectric materials prepared by mechanical alloying and pulse discharge sintering. Mater Trans 2002;43:681–7.

[10] Niu X., Yu J., Wang S. Experimental study on low-temperature waste heat thermoelectric generator. J Power Sources 2009;188:621–6.

[11] Kazemian A., Salari A., Ma T. A year-round study of a photovoltaic thermal system integrated with phase change material in Shanghai using transient model. Energy Convers Manag 2020;210:112657.

Theoretical analysis on active radiant heat reflector integrated phase change material wall

Gyu-Bae Lee [a], Seong-young Cheon [a], Yong-Kwon Kang [a], Beom-Jun Kim [a], Jae-Won Joung [a] Jae Weon Jeong [a]

[a] Department of Architectural Engineering, Hanyang University, Seoul, Republic of Korea, jjwarc@hanyang.ac.kr

Abstract. Recently, as interest in increasing energy efficiency of buildings increases, a method of reducing indoor heat gain and loss by integrating phase change materials (PCM) into building walls is being studied. The PCM is a type of heat storage material that can reduce energy consumption of the cooling and heating devices of the building by absorbing or releasing heat from outside. However, the PCM which is integrated into the wall of the building cannot fully achieve thermal performance because it absorbs or releases heat according to the temperature change of the surrounding members in the wall. To solve the problem, this study proposed a new system that improves the thermal performance of the PCM integrated wall by controlling radiant heat transfer inside of the wall. The proposed system adjusts the radiant heat transfer in the wall through an active radiant heat reflector, which controls surface emissivity of the PCM in the design conditions. To evaluate the proposed system, a numerical analysis for 1D transient heat transfer was used based on the energy balance equation for the indoor heat gain and loss with the reference systems. The simulation was conducted with Matlab 2021a software, and weather conditions were data from the summer (Jun-August) and winter (December-February) of IWEC2 Seoul. As a result of the simulation, the proposed system confirmed that indoor heat gains and losses were improved in all periods compared to the reference system. The proposed system reduced the total indoor heat gain by 33.3%-44.1% in summer and the total indoor heat loss by 14.2-29.3 in winter compared to the reference systems.

Keywords. PCM integrated wall, Thermal performance, Radiant heat transfer
DOI: https://doi.org/10.34641/clima.2022.107

1. Introduction

According to the international energy agency (IEA), energy consumption in buildings accounts for nearly 36% of the world's total energy consumption [1]. Since using a large amount of energy is closely related to increasing energy costs and environmental issues, the energy consumption of the buildings should be reduced and highly efficient. To increase the energy efficiency of the buildings, some studies have been published about improvement of the building envelope. The building envelope is components of a wall system which separate the interior and exterior environments. Several researchers in the world have demonstrated that the improvement of the building envelope is effective in building energy efficiency [2]. Therefore, improving the building envelope is one of the main key factors which determines the energy efficiency of the buildings and indoor environments.

In recent years, research which integrates phase change materials (PCM) with the building envelope is increasing [3]. The PCM is one of the thermal storage materials which can store large amounts of heat energy as the form of latent heat with small temperature change. This property allows the applications of PCM to integrate in the building envelope as they are effective in reducing space heating and cooling loads of the buildings. However, the heat storage and discharge of the PCM in the building envelope cannot be controlled ideally, which is highly dependent on the surrounding temperature. Because of this, traditional thermal insulation envelopes which have fixed thermal resistance, restrains the energy saving potential of the PCM-integrated building envelope [4]. Therefore, to accomplish complete performance of the PCM, a new building envelope system is needed. Extant researchers [4, 5] have studied the new systems to solve the disadvantages of the PCM integrated envelope. Kishore et al. [4] proposed a novel wall design, comprising a layer of PCM between two layers of dynamic insulation material and system(DIMS). Simulations have confirmed that the proposed system can reduce the annual heat gain by

Copyright ©2022 by the authors. This conference paper is published under a CC-BY-4.0 license.

17-72% and the annual heat loss by 7-38% depending on the buildings. Gracia. [5] proposed a novel concept based on the dynamic use of the PCM in building envelopes. Simulations showed that the proposed system achieves a cooling load reduction of 379% in comparison to a system without PCM with optimum design. The analysis which presented studies support the need to develop additional insulation mechanisms to use the PCM integrated envelope or wall.

This study proposes a new novel insulation mechanism to improve the energy potential of the PCM-integrated building. In the proposed system, the thermal performance of the pcm is improved by controls the radiation heat reisistance inside of the wall with an active radiant heat reflector. To estimate the thermal performance of the proposed system, total indoor heat gains and losses of each summer and winter were evaluated via comparison against reference cases.

2. System overview

2.1 Proposed PCM integrated wall system

Fig. 1 depicts the schematic of the proposed PCM integrated wall system in a vertical building envelope. The system has the PCM layer and an auxiliary insulation layer between the building wall's exterior and interior layer. The cavity is located on the front and rear side of the PCM layer. The PCM layer is composed of microencapsulated PCM (M-PCM), aluminum case, and an active radiant heat reflector.

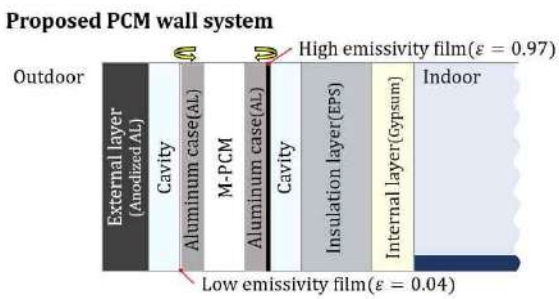

Fig. 1 - Schematic of the proposed PCM wall system in vertical building envelope.

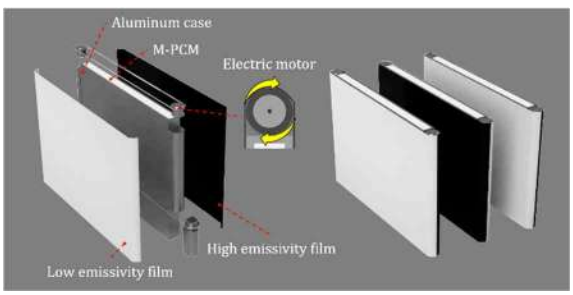

Fig. 2 - Sketch of possible configuration of the PCM with the active radiant heat reflector.

Fig. 2 depicts a sketch of the configuration in the PCM layer with the active radiant heat reflector in the proposed system. The active radiant heat reflector consists of a high-emissivity film part and low-emissivity film part. In the cavity, the high emissivity part increases the radiant heat transfer and the low emissivity part decreases the radiant heat transfer. Each part of the active radiant heat reflector moves through an electric motor to the front and rear side of the aluminum case which contains the M-PCM in the proposed system.

The mechanism, which the active radiant heat reflector controls the radiant heat transfer in the cavity is as follows. **Fig. 3** depicts a schematic of the heat transfer between two different surfaces in the cavity. In **Fig. 3**, the total thermal resistance of the cavity is determined by radiant heat transfer and natural convection heat transfer. From the previous study[6], heat transfer equations on the two different surfaces (i.e., 1&2, $T_1 > T_2$) are as shown in equations (1) and (2) In the equation (1) the amount of the radiant heat transfer is determined by the emissivity of each surface. The higher emissivity transfers more radiant heat, and the lower emissivity transfers less radiant heat between two surfaces. Therefore, if the emissivity of the surface in the cavity may be actively managed, radiant heat transfer in the cavity also may be actively managed. The proposed system attempted to improve the thermal performance of the PCM integrated wall by using the active radiant heat reflector to control the radiant heat transfer of the cavity in the wall.

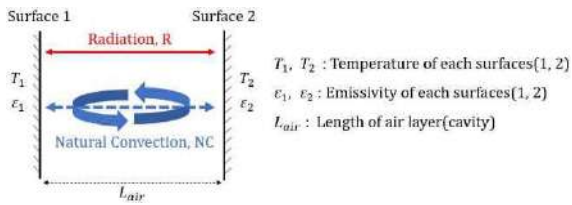

Fig. 3 - Schematic of the heat transfer between two different surfaces in the cross-sectional view (i.e., 1&2).

$$R = A\sigma(T_1^4 - T_2^4)/(\frac{1}{\varepsilon_1} + \frac{1}{\varepsilon_2} - 1) \quad (1)$$

$$NC = k_{air}\, NuA(T_1 - T_2)/L_{air}\ ) \quad (2)$$

2.2 Seasonal operation modes

In this study, the operation of the proposed system was considered and analyzed in summer and winter conditions of the Seoul. In the proposed system, operating modes are classified into four different types according to the season and outdoor temperature to improve the thermal performance of the PCM. The description of the each modes is as follows.

Fig. 4 depicts a schematic of the proposed PCM wall system during the summer season. As shown in **Fig. 4-A**, the outdoor heat flux is transferred to the indoor environment during the day of the summer. While outdoor heat flux is transferred to the indoor, the low emissivity film is located on the external wall side of the PCM. The low emissivity film reduces radiant heat transfer from the exterior wall, delaying heat storage time of the PCM. As a result, the amount of

heat gain from the wall is decreased. As shown in **Fig. 4-B**, heat stored in the M-PCM is released to the outside on the summer nights. While the stored heat of the PCM is released, the high emissivity film is located on the exterior side of the PCM and the low emissivity film is located on the interior side of the PCM. The high emissivity film increases the amount of the radiant heat transfer to the external wall and the low emissivity film decreases the amount of the radiant heat transfer to the indoor environment. As a result, the proposed system can reduce the amount of the indoor heat gain by improving the thermal performance of the PCM during the summer season.

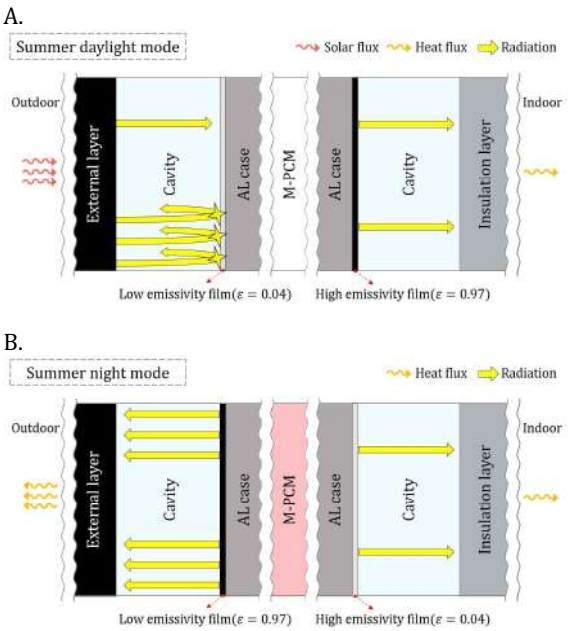

Fig. 4 - Schematic of the proposed system during summer season (A: summer daylight, B: summer night).

Fig. 5 depicts a schematic of the proposed PCM wall system during the winter season. As shown in **Fig. 5-A**, while the sun rises, the heat is transferred from the external wall to the PCM through the solar flux. To maximize the heat storage of the PCM, the high emissivity film moves to the external side of the PCM to increase the amount of the radiant heat transfer. In addition, the low emissivity film is located on the interior side to reduce heat loss from the indoor. **Fig. 5-B** depicts the schematics of the proposed system after the sunset. While the stored heat of the PCM is released, the low emissivity film is located on the exterior side of the PCM and the high emissivity film is located on the internal side of the PCM. The high emissivity film makes The high emissivity film release more heat which is stored at the PCM to the indoor environment. It helps keep the indoor temperature warmer in winter. The low emissivity film restrains the release of heat which is stored in the PCM to the outdoors. As a result, the proposed system can reduce the amount of the indoor heat loss by improving the thermal performance of the PCM during the winter season.

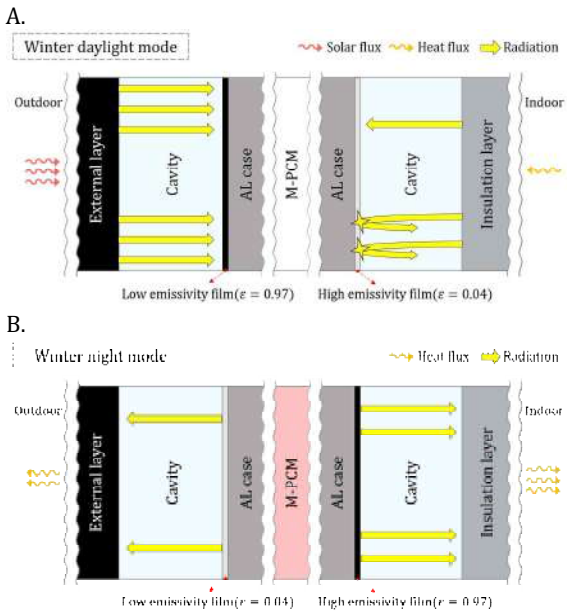

Fig. 5 - Schematic of the proposed system during winter season (A: winter daylight, B: winter night).

3. Simulation setup and overview

3.1 Simulation configuration

Fig. 6 depicts the energy balance equation used in the simulation, briefly. The simulation for each wall system case was conducted using Matlab 2021a by 1-D transient heat transfer method, using the formulas used in previous studies [4,5,6]. The weather data used in the simulation were data from June to August and December to February in IWEC2 Seoul. To simplify the simulation, the time which position of the emissivity films was replaced was fixed, considering the sunrise and the sunset time for each season. **Tab. 1** depicts the basic conditions used in the simulation

Tab. 1 - Basic conditions of the simulation.

Classification	Settings
Weather data	IWEC2 Seoul
Convection heat transfer coefficient	$h_{conv,out} = 25\text{W/m}^2\text{K}$
	$h_{conv,in} = 7.692\text{W/m}^2\text{K}$
Indoor air temperature	$T_{RA} = 24°\text{C}$ (summer)
	$T_{RA} = 18°\text{C}$ (winter)
Emissivity change time(The proposed system)	Summer season:
	08:00 / 24:00
	Winter season:
	09:00 / 17:00
Model scale(A)	0.8m(Height)
	x 0.8m(Width)

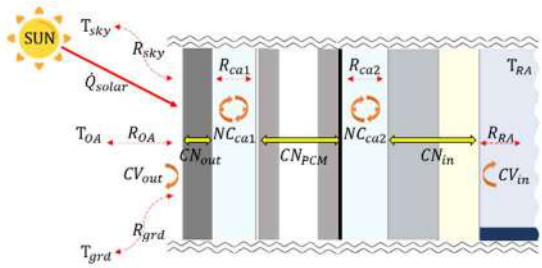

Fig. 6 – Heat transfer model between exterior and interior walls in the simulation.

3.2 Reference wall system cases

To evaluate the thermal performance of the proposed system, those reference wall system cases are selected. Each case is compared and analyzed with the proposed system for indoor heat gain of the summer season and indoor heat loss of the winter season.

Fig. 7 depicts the schematic of the reference case 1 in the vertical building envelope. The case 1 is the conventional PCM integrated wall system which excludes the active radiant heat reflector. The PCM of the case 1 stores and discharges heat through passive heat exchange due to temperature differences.

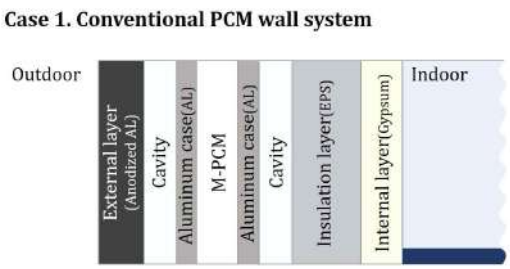

Fig. 7 - Schematic of reference case 1.

Fig. 8 depicts the schematic of the reference case 2 in the vertical building envelope. The case 2 is a wall system using only EPS(Expanded Poly Styrene) insulation without the PCM. The thickness of the EPS which replaced the PCM is same as the proposed system for comparison.

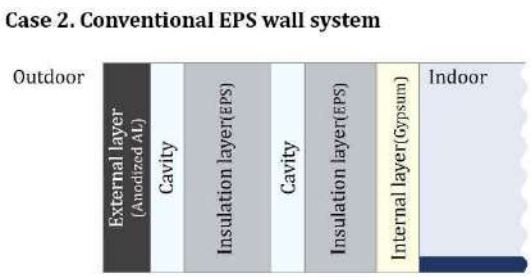

Fig. 8 - Schematic of reference case 2.

Fig. 9 and **Fig. 10** depict schematic of the reference case 9 and 10 in the vertical building envelope. To analysis the effect of radiation transfer which effects the thermal performance of the PCM, reference cases which the emissivity fixed are also simulated. The case 9 and 10 use the same emissivity films as the proposed case, but do not separately control the radiant heat transfer by fixing the position of film.

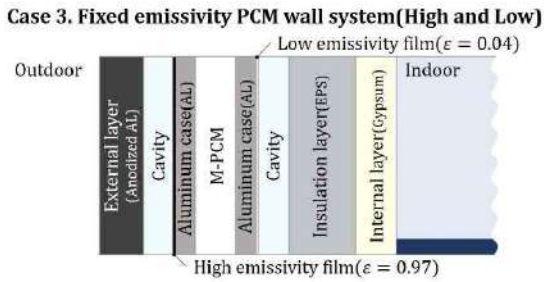

Fig. 9 - Schematic of reference case 3.

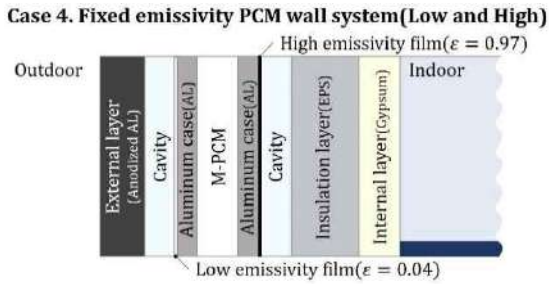

Fig. 10 - Schematic of reference case 4.

3.3 Properties of material of the cases

Each property of the materials of the cases were reflected based on previous studies [6,7,8,9,10]. To compare the thermal performance of the cases, the thermal load to the exterior wall from the outside was set large. In the case of the films, the emissivity value was set for a clear difference in radiant heat resistance value. Also, it was assumed that there was no conduction heat thorough the films because the thickness of the films was very thin. **Tab. 2** depicts the properties of the M-PCM used in this study and **Tab. 3** depicts the properties of the other materials used in this study

Tab. 2 – Properties of the M-PCM.

Classification	Values
Core materials	Paraffin
Melting temperature($T_{m\ et}$)	26℃
Temperature range of phase change(ΔT_{PCM})	±1℃
Latent heat capacity(Q_{PCM})	145 kJ/kg
Specific heat capacity($C_{p,PCM}$)	Solid: 1610 J/kg Liquid: 1995 J/kg
Density(ρ_{PCM})	920 kg/m^3
Thermal conductivity	Solid: 0.24 W/mK Liquid: 0.15 W/mK
Thickness	0.02m

Tab. 3 – Properties of materials of the cases.

Classification	Materials	Thickness (m)	Thermal conductivity ($W/m\,K$)	Density (kg/m^3)	Specific heat (J/kgK)	Emissivity (ε)	Solar absorptance (α)
Exterior wall	Anodized AL	0.02	160	2800	880	0.82	0.95
Insulation	EPS	0.11	0.034	32	1210	0.9	-
Cavity	Air	0.02	0.0255	1.184	1007	-	-
Interior wall	Gypsum board	0.03	0.18	940	1130	0.9	-
Emissivity films	High emissivity	0.0001	-	-	-	0.97	-
	Low emissivity	0.0001	-	-	-	0.04	-
PCM case	AL	0.005	205	2700	910	0.09	-

3.4 Simulation models

The surface temperature of the external wall (T_{ext}) could be determined using equations (3), (4) and (5). The symbols, k_{ext}, ρ_{ext}, C_{ext}, L_{ext} each represent the thermal conductivity (W/mK), density (J/kgK), specific heat (kg/m^3) and length of the external wall. The symbol Δt represents the time interval (s).

$$\dot{q}_{ext} + \frac{k_{ext} A(T^{i+1}_{ext,in} - T^{i}_{ext,out})}{L_{ext}} = \rho_{ext} A \left(\frac{L_{ext}}{2}\right) C_{ext} \frac{\left(T^{i+1}_{ext,out} - T^{i}_{ext,out}\right)}{\Delta t} \quad (3)$$

$$\dot{q}_{ext} = \alpha_{ext} A \dot{q}_{solar} + h_{conv,out} A(T_{OA} - T_{ext}) + \dot{q}_{ext,rad} \quad (4)$$

The radiation heat transfer equation between the outside air and the external wall ($\dot{q}_{ext,rad}$) could be determined by equation (5). The symbol, ε_{ext} represents emissivity of external wall, and the symbol, σ represents the stefan-boltzmann constant

$$\dot{q}_{ext,rad} = \varepsilon_{ext} A\sigma[(1 - F_{sky})\left((T_{OA})^4 - \left(T^{i}_{ext,out}\right)^4\right) + F_{sky}\left((T_{sky})^4 - \left(T^{i}_{ext}\right)^4\right] \quad (5)$$

The temperature of surface B (T_B) among the two surfaces (i.e., $A \cdot B$, $T_A > T_B$) in the cavity could be determined using equations (6), (7), (8).

$$\dot{q}_{cavity,conv} + \dot{q}_{cavity,rad} + \frac{k_B A\left(T^{i}_{B,out} - T^{i}_{B,in}\right)}{L_B} = (\rho_{air} A \left(\frac{L_{air}}{2}\right) C_{air} + (\rho_B A \left(\frac{L_B}{2}\right) C_B \left(\frac{T^{i+1}_B - T^{i}_B}{\Delta t}\right) \quad (6)$$

$$\dot{q}_{cavity,conv} = k_{air}\, Nu(T^{i}_A - T^{i}_B)/L_{air} \quad (7)$$

$$\dot{q}_{cavity,rad} = [\sigma A \left(\frac{\left(T^{i}_A\right)^4 - \left(T^{i}_B\right)^4}{\left(\frac{1}{\varepsilon_A} + \frac{1}{\varepsilon_B} - 1\right)}\right)] \quad (8)$$

The surface temperature of the interior wall (T_{in}) could be determined using equation (9).

$$\varepsilon_{in}\, \sigma A \left(T^4_{RA} - \left(T^{i}_{in,out}\right)^4\right) + \frac{k_{in} A\left(T^{i+1}_{in,out} - T^{i}_{in,in}\right)}{L_{in}} + h_{conv,in} A \left(T_{RA} - \left(T^{in}_{in,in}\right)\right) = \rho_{in} A \left(\frac{L_{in}}{2}\right) C_{in} \left(\frac{T^{i+1}_{in,in} - T^{i}_{in,in}}{\Delta t}\right) \quad (9)$$

The indoor heat gains and losses ($\dot{Q}_{insite}$) by cases through simulation could be determined using equation (10)

$$\dot{Q}_{insite} = \sum_{i=1}^{I}[(T^{i}_{in} + T^{i-1}_{in} - T_{RA})/2]\Delta t \quad (10)$$

4. Results

4.1 Heat gain through building walls in summer

Fig. 11 depicts the comparison of the monthly indoor heat gain of each case when operating during summer. It can be seen that the proposed system obtains less indoor heat gain than each reference case in all periods. Especially in august, when the load of outside air increases, all cases using the PCM excluding the proposed system obtain more indoor heat than case 2 which uses only EPS insulation. The amount of indoor heat gains of case 1, 3, 4 in august increased by 2.51%, 15.35% and 0.05% compared to case2, while the proposed case decreased by 23.68%

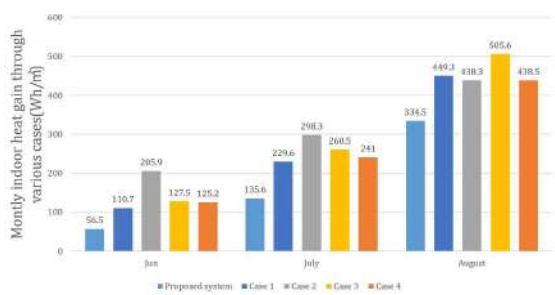

Fig. 11 - Monthly indoor heat gain during summer.

Fig. 12 depicts the comparison of the total indoor heat gain of each case in summer season. Under the summer weather conditions, the proposed system reduced indoor heat inflow by 33.3% compared to case 1, 44.1% compared to case 2, 41.1% compared to case 3 and 34.6% compared to case 4. Therefore, It can be seen that the proposed system obtains less indoor heat gain than each reference case during the summer season. In addition, since the indoor heat inflow amount of cases 3 and 4 using the same emissivity films is significantly different from the proposed system, it can be clearly seen that controlling the radiant heat transfer in the wall improves the thermal performance of the PCM integrated wall.

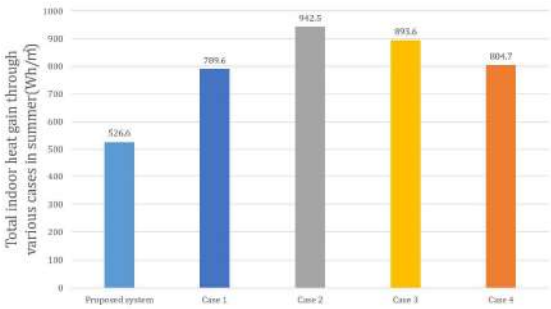

Fig. 12 - Total indoor heat gain during summer.

4.2 Heat loss through building walls in winter

Fig. 13 depicts the comparison of the monthly indoor heat loss of each cases when operating during winter. Since heat can be stored during the daylight through the high solar absorptance of the exterior wall, the cases with PCM had less indoor heat loss than the case 2 that did not. In addition, it can be seen that the proposed system obtains less at least 14% to 24.5% less indoor heat loss than each reference cases during the simulation period.

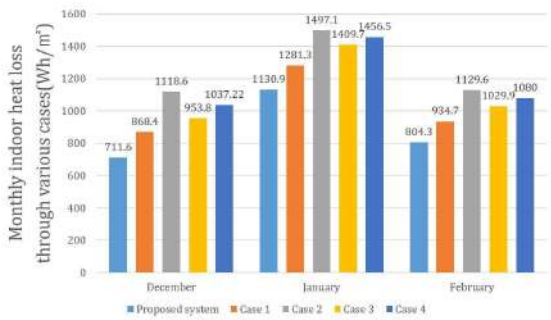

Fig. 13 - Monthly indoor heat loss during winter.

Fig. 14 depicts the comparison of the total indoor heat loss of each case in the winter season. Under winter conditions, the proposed system reduced indoor heat loss by 14.2% compared to case 1, 29.3% compared to case 2, 22% compared to case 3 and 25.9% compared to case 4. It can be seen that the proposed system reduces more indoor heat loss than each reference case during the winter season.

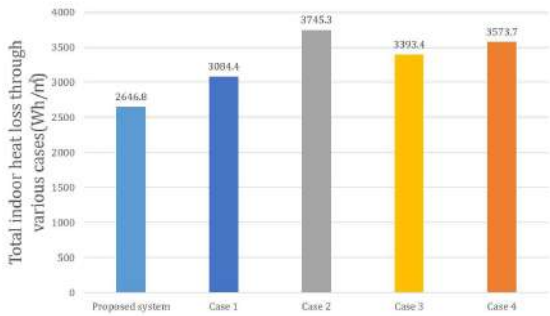

Fig. 14 - Total indoor heat loss during winter.

5. Conclusion

This study proposes a wall system that adjusts the thermal resistance of the cavity in the wall through the active radiant heat reflector to improve the thermal performance of the PCM-integrated wall. In order to compare the thermal performance of the proposed system, the indoor heat gain in summer and the heat the indoor heat loss in winter were compared with the reference cases. The cases were simulated by numerical analysis of 1D transient heat transfer with Matlab 2021a. As a result of the simulation, the proposed system reduced the total indoor heat gain in summer by at least 33.3% up to 44.1% than reference cases. It also reduced the total heat loss in winter by at least 14.2% up to 29.3% compared to the reference cases. Considering that indoor heat gain and loss are directly involved in the cooling and heating load of the building, the simulation results of this study are expected to be effective in terms of energy saving of the building. Also, the annual simulations are being conducted to closely evaluate the thermal performance of the proposed system. In the future, the proposed systems can be considered as one way to reduce energy and increase efficiency of the buildings that integrate PCM and walls.

6. Acknowledgement

This work was supported by Korea Institute of Energy Technology Evaluation and Planning(KETEP) grant funded by the Korea government(MOTIE)(No. 20202020800360), and this work was supported by the Korean Agency for Infrastructure Technology Advancement (KAIA) grants (21CTAP-C163749-01).

7. References

[1] Nundy S., Mesloub A., Alsolami B., Gosh A. Electrically actuated visible and near-infrared regulating switchable smart window for energy positive building: A review. Journal of Cleaner Production. 2021;301:126854.

[2] Sadineni S., Madala S., Boehm R. Passive building energy savings: A review of building envelope components. Renewable and Sustainable Energy Reviews. 2011;15(8):3617-3631.

[3] Liu Z., Yu Z., Yang T., Qin D., Li S., Zhang G.,

Haghighat F., Joybari M. A review on macro-encapsulated phase change material for building envelope applications. Building and Environment. 2018;144:281-294

[4] Kishore R., Bianchi M., Booten C., Vidal J., Jackson R., Enhancing building energy performance by effectively using phase change material and dynamic insulation in walls. Applied Energy. 2021;283:116306.

[5] Gracia A. Dynamic building envelope with PCM for cooling purposes – Proof of concept. Applied Energy. 2019;235:1245-1253.

[6] Cengel Y., Ghajar A., Heat and mass transfer (fundamentals and applications, 4th edition SI units). 2020;McGraw-Hill Education.

[7] Sonnier R., Ferry L., Gallard B., Boudenne A., Lavaud F. Controlled emissivity coatings to delay ignition of polyethylene. Materials. 2015;8(10):6935-6949..

[8] Oh JM., Song JH., Lim JH., Song SY. Analysis of Building Energy Savings Potential for Metal Panel Curtain Wall Building by Reducing Thermal Bridges at Joints between Panels. Energy Procedia. 2016;96:696-709.

[9] Soares N., Gaspar A., Santos P., Costa J. Experimental study of the heat transfer through a vertical stack of rectangular cavities filled with phase change materials. Applied Energy. 2015;142:192-205.

[10] Blanco J., Buruaga A., Rojí E., Cuadrado J., Pelaz B. Energy assessment and optimization of perforated metal sheet double skin façades through Design Builder; A case study in Spain. Energy and Buildings. 2016;111(8):326-336.

Implementation of a shallow geothermal energy system in a multi-source green building

Gavriliuc Robert[a], Catalina Tiberiu[a], Bejan Andrei Stelian[a]

[a] Technical University of Civil Engineering, Faculty of Building Services Bucharest, tiberiu.catalina@utcb.ro

[b] Geoexchange Society robertgavriliuc@yahoo.com

Abstract.
The building stock is responsible for a large share of greenhouse gas emissions (GHG in the European Union. Major emission reductions can be achieved through changes in this sector and the building sector is crucial to achieving the EU's reduction targets. From 2021 all buildings must respect the nZEB standard and must use a certain amount of renewable energy sources. While condensing gas boilers have lower costs these cannot provide cooling and do not use renewable energy. The best alternative is the use of geothermal heat pumps that have high efficiencies and can avoid large amounts of GHG. Currently, geothermal energy sources provide more than 15 GWth for heating and cooling in the European Union, equivalent to more than 4 Mtoe per year, whereby geothermal heat pump systems contribute to the largest part. Shallow geothermal systems are more complex to realize than conventional solutions. Critical aspects include correct design, adequate performance in operation and costs for the installation. The combination with other Renewable Energy Sources (RES like solar energy could improve the return on investment. The main goal of this paper will be to tackle all the above-mentioned areas by developing and demonstrating the potential of shallow geothermal system to be connected in a precise and efficient way to other renewable sources systems, in particular solar thermal energy. This approach is realized by adapting hybrid solutions to reach nZEB standards through a holistic engineering, construction and controls approach. The demo-site was carried out on an energy-efficient house EFdeN House, an active single-family dwelling that was planned and built in Bucharest for academic and research purposes and it is the first Excellence Research Centre in Romania.

Keywords. Renewable Energy Sources, Geothermal Heat Pumps, nZEB energy-efficient house, EFdeN, green building, Geothermal Energy
DOI: https://doi.org/10.34641/clima.2022.108

1. Introduction

The scientific community needs multiple experimental demonstration stands that could be used as a reference in the validation of numerical models for the implementation of ground-to-water heat pumps. Adapting ground-to-water heat pumps to provide the necessary indoor temperature for existing heating and cooling systems that cannot be easily replaced represents a huge challenge. It is also necessary to optimize the energy management of the installations in order to reduce the number of operating hours of the system and to provide support tools to overcome technical challenges in the operation of geothermal systems.

According to the GEO4CIVHIC and CHEAP-GSHP projects [1,2], many research centres in Europe benefit from such experimental stands for testing and coupling geothermal systems with energy-efficient buildings (figure 1).

Our study addresses the main barriers identified in the implementation of geothermal heat pumps by developing and demonstrating the potential of geothermal systems to be connected in a precise and efficient way to other systems using renewable energy sources and especially to solar thermal and photovoltaic systems. This approach is achieved by adapting hybrid solutions in order to achieve nZEB construction standards in a holistic manner.

Copyright ©2022 by the authors. This conference paper is published under a CC-BY-4.0 license.

Fig. 1 - Similar experimental stands in Padua (Italy), Bilbao (Spain), Valencia (Spain), Pikermi (Greece), Mechelen (Belgium) or Dublin (Ireland). This study aims to put Romania on the map of European research centres where the coupling of geothermal systems with heat pumps together with energy efficient buildings are analysed and studied intensively in order to promote and raise awareness of the benefits of implementing this system, to reduce energy consumption and reduce CO_2 emissions, part of the European Union's strategy until 2050 [3].

2. House and system description

The building on which the studies are conducted is carried out on two levels - ground floor and first floor (figure 2 and 3), level hight 2.5m, intended for residential building and exhibition pavilion, with the following geometric characteristics: footprint 96m^2, net area (heated) 133m^2, gross area 170m^2 and total air volume 400m^3.

Fig. 2 – Ground floor plan.

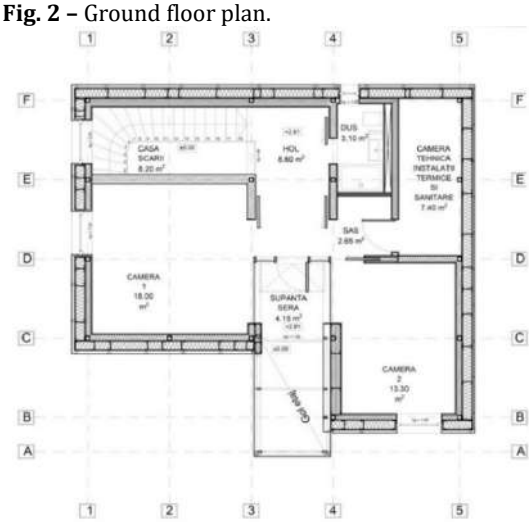

Fig. 3 – Floor plan.

The construction is modular, made of metal structure and is particularly well thermal insulated by approaching the design requirements of passive houses. Table 1 shows the values of the heat transfer coefficients of the construction elements that define the building envelope. The value obtained for the terrace is due to an additional layer of rockwool with variable thickness (thus determining the terrace slope), and the value obtained for the exterior walls is due to an additional layer of rockwool (5cm) present behind the radiant system. heating/cooling, as well as an intermediate layer of air. Plasterboard boards with micro-encapsulated phase change materials are placed in the walls of the house, which have the role of giving thermal mass to the building and of decreasing the energy consumption for cooling during the summer.

Tab. 1 - Heat transfer coefficients of tire elements.

Construction element	U [W/m^{2}K]
Exterior wall	0.129
Flooring	0.124
Terrace	0.121
Interior walls	0.39
Triple glazing windows	0.8

The heating and cooling systems within the studied building were designed to ensure an indoor temperature during the summer of 26ºC, respectively an indoor temperature during the winter of 20ºC, taking into account that the outdoor design temperature for winter (related to climate zone II -Bucharest) is -15ºC, respectively 35.3ºC for summer [4-6].

The existing installation of the EFdeN solar house has as a source an air-to-water heat pump that supplies a buffer used for cooling, a buffer used for heating and a DHW tank used for domestic hot water preparation. The DHW tank and the heating buffer are also connected to a system with two solar panels with vacuum tubes. The indoor installation of the building has a heating / cooling system with radiant panels, positioned within the ceiling and walls of the house. Also, the water flow circulates through the heating/cooling coil after the heat recovery unit used for the fresh air supply. To complete the existing installation, two 3-way valves with servomotor will be provided, and the proposed geothermal installation will represent an independent heating system for the indoor installation. The equipment's that have been implemented to complete the geothermal installation are: Ecoforest ground-to-water heat pump, Ecoforest air-to-water heat pump, plate heat exchanger for passive cooling, pipes for horizontal route geothermal probes, elastomer insulation for installation pipes, buffer 200 litters, 300 litters

trivalent boiler for domestic hot water preparation, expansion vessels, temperature sensors, 3-way valves with modulating servomotor and other accessories (figure 4).

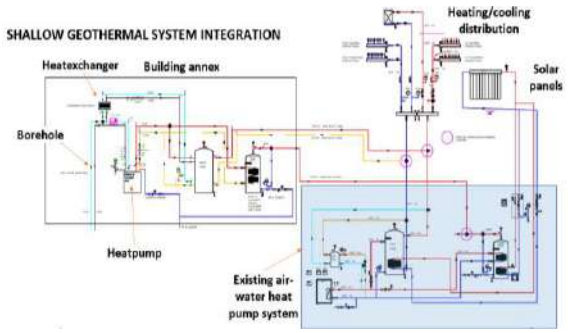

Fig. 4 – System hydraulic schematics

The proposed ground-to-water heat pump will operate in a hybrid system, being complemented by an air-to-water heat pump. The heat pump conducts the water flow to a buffer useful for heating storage and efficient operation of the heat pump and a trivalent DHW tank for domestic hot water preparation connected to the heat pump, thermal solar panels or even an electric heater as back-up. Furthermore, the role of the plate heat exchanger is to ensure the operation of the heat pump in passive cooling mode.

The system proposed within the GEOPILOT project is completely independent of the original building system analysed and it connects to the existing indoor installation through two 3-way valves located before the general distributor-collector that transmits the water flow to the radiant heating / cooling system located in the ceiling and walls of the building (figure 5).

Fig. 5 – Heat pump used within the proposed system

An experimental Ecoforest ecoGEO + 1-6PRO & AU hybrid heat pump will be used in the experimental stand, which can operate in both ground-to-water and air-water mode, in bivalent mode, thus ensuring maximum efficiency of the entire system. The heat pump can provide the functions of heating, cooling and domestic hot water preparation and uses R290 as refrigerant, with a very low GWP value (GWP = 0), with a low impact on the environment. The heat pump has a heating capacity ranging from 1kW to 6kW, COP (B0 / W35) up to 4.9, EER (B35 / W7) up to 5.2 and can supply a water flow with a temperature of up to 70ºC on the installation flow.

3. Preliminary numerical results

The energy modelling of the analysed building was performed with the numerical simulation software Design Builder in order to determine the energy consumption related to the building and the values of thermal loads, for the optimization of the proposed geothermal system (figure 6).

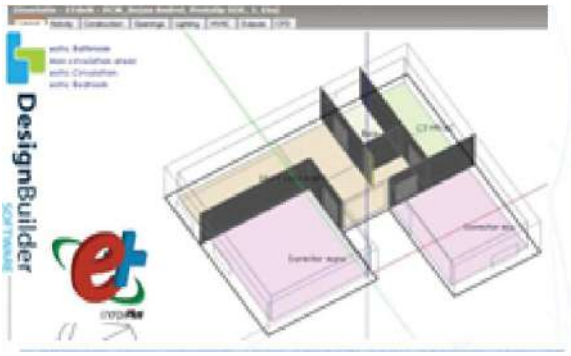

Fig. 6 – Energy modelling of the building in the numerical simulation software Design Builder

In the graphs within figure 7 it can be observed the evolution of winter outdoor temperatures for the climatic zone in which the analysed building is located (-20°C- + 35°C), the evolution of wind speed (0-17m/s), wind direction, position of the sun, atmospheric pressure and intensity of solar radiation (direct and diffuse) for Bucharest.

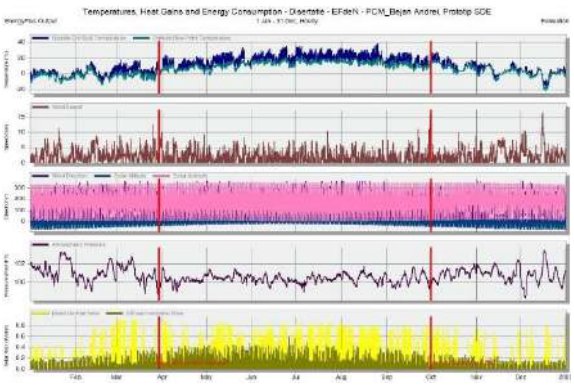

Fig. 7 – Exterior conditions for energy modelling of the building

In table 2 we can observe the values of summer thermal loads for the rooms within the prototype house analysed.

Tab. 2 – Summer thermal loads

Zone	Design capacity [kW]	Sensible [kW]	Latent [kW]
Living	1.66	0.92	0.41

Large bedroom	0.65	0.49	0.04
Small bedroom	0.58	0.44	0.02
Hall	0	0	0
Total	2.89	1.85	0.47

Table 3 shows the values of winter thermal loads for the rooms within the analysed house prototype.

Tab. 3 – Summer thermal loads

Zone	Steady-State Heat Loss [kW]	Design Capacity [kW]
Living	1.49	1.86
Large bedroom	0.55	0.69
Small bedroom	0.49	0.61
Hall	0.52	0.62
Bathroom 1	0.13	0.16
Bathroom 2	0.16	0.19
Total	3.34	4.16

The heating load of the house is 4.16 kW, while the cooling load is 2.89 kW, with the possibility to cover the entire cooling load using passive cooling with radiant panels.

The variation of the thermal loads during a year is highlighted in figure 8:

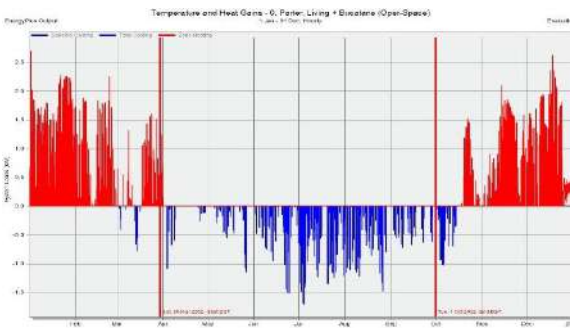

Fig. 8 – The evolution of thermal loads over a period of one year

As can be seen in Figure 9, the total energy consumption for cooling the analysed house is 590 kWh / year, according to the numerical simulations performed. By implementing a cooling system with a ground-to-water heat pump equipped with a passive cooling function, this energy consumption can be reduced by up to 85%; while covering the energy consumption for heating using the energy from the heat pump equipped with the active cooling function, the energy consumption for cooling can be reduced by up to 40%.

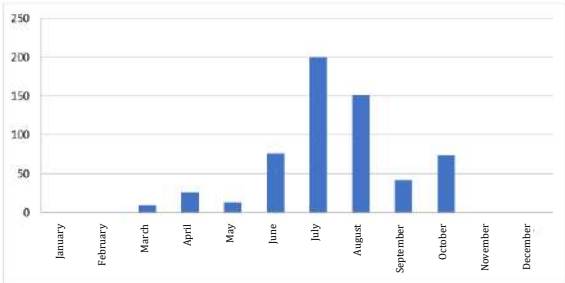

Fig. 9 – Monthly building energy consumption for cooling

As can be seen in Figure 10, the total energy consumption for heating the analysed house is 1878 kWh/year according to the numerical simulations performed. By implementing a ground-to-water heat pump heating system, this energy consumption can be reduced by up to 33%. The evolution of energy consumption during the year is also highlighted in figure 11.

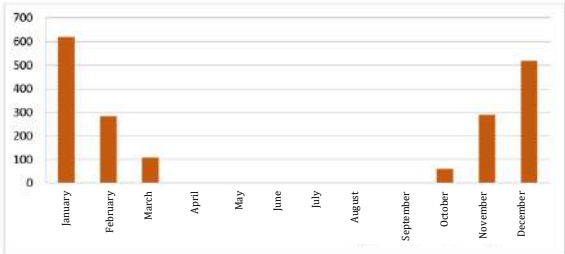

Fig. 10 – Monthly energy consumption of the building, for heating

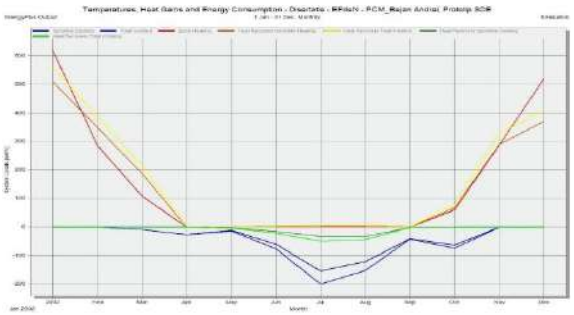

Fig. 11 – Energy consumption during a year

4. Preliminary experimental results

In parallel with the preliminary numerical studies conducted, experimental studies have been performed in order to analyse the energy consumptions for heating and ventilation, where the existing heat pump has a considerable input. These were corroborated with the values of the essential interior comfort parameters according to national and international standards (SR EN 15251: 2007, SR EN 16798-1: 2019) - indoor temperature and CO_2 concentration level [4-6].

The data presented in Figures 12 and 13 were collected during the experimental campaign conducted during the winter and shows the evolution of the values recorded during a reference week, for the main rooms of the building. During the analysed week, the system consumed 38kWh for heating, even if the outdoor temperatures dropped below 5ºC. The indoor air temperature recorded values above those proposed by the standard SR EN 15251 (21ºC for the IDA1 room category and 20ºC for the IDA2 room category) for residential buildings. Moreover, the CO_2 concentration values were within the limits proposed by SR EN 15251 in over 85% of the time for the IDA1 comfort category (below the 800-ppm concentration) and 100% of the time for the IDA3 category (below the 1200 ppm concentration). In order to maintain a low level of indoor CO_2, 10kWh were consumed throughout the week.

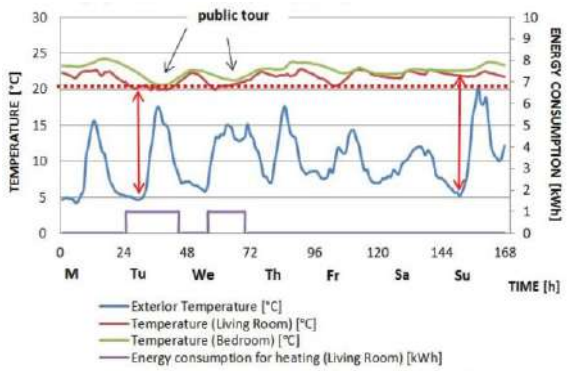

Fig. 12 – Variation of measured temperatures and energy consumption for heating (for a reference week)

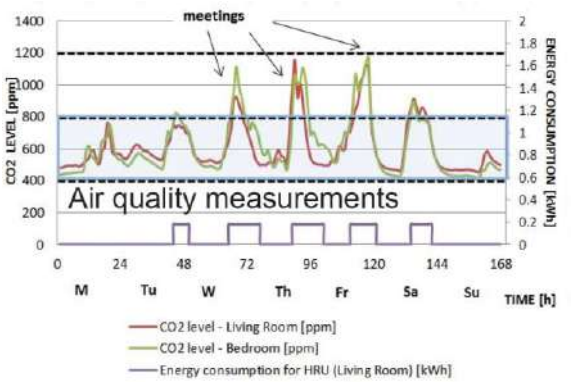

Fig. 13 – Variation of measured CO_2 concentration and energy consumption for ventilation (for one reference week)

Due to the implemented photovoltaic system, the building is not only a passive house, but an active house that produces more energy than it consumes, analysing the annual energy balance. The annual energy production is approximately 6844 kWh / year, while the annual energy consumption is 4330 kWh / year, the surplus energy being injected into the network. (figure 14).

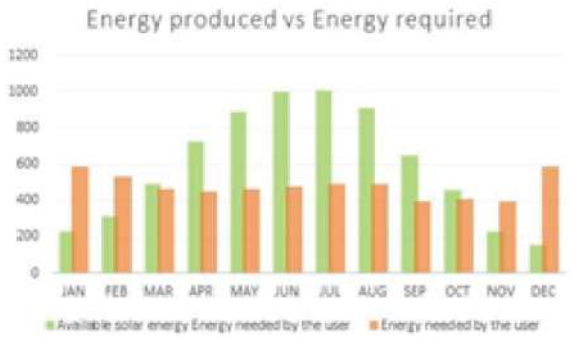

Fig. 14 – Photovoltaic system production and energy consumption of the building

5. Conclusions

The implementation of energy efficient solutions and ground-to-water heat pumps on an nZEB building has a great impact on achieving indoor environmental quality with minimum energy consumptions. By implementing high quality materials, the heating load of the nZEB building studied is only 4.16kW, while the cooling load is only 2.89kW thus being covered only with passive cooling system. Total energy consumption for heating is 1878kWh/year while the total energy consumption for cooling is only 590kWh/year.

6. Acknowledgement

This study was supported by Romanian National Authority for Scientific Research, project GEOPILOT – "Demo geothermal pilot for application in residential buildings nZEB" PN-III-P2-2.1-PED-2019-2881.

7. References

[1] Most easy, efficient and low-cost geothermal systems for retrofitting civil and historical buildings – GEO4CIVHIC Research Project Brochure – www.geo4civhic.eu

[2] Cheap and efficient application of reliable ground source heat exchangers and pumps – CHEAP-GSHPs Research Project Brochure – www.cheap-cshp.eu

[3] Implementing nearly zero-energy buildings (nZEB) in Poland - towards a definition and road map, Buildings Performance Institute Europe (BPIE), 2012

[4] SR EN 15251:2007 - Parametri de calcul ai ambianţei interioare pentru proiectarea şi evaluarea performanţei energetice a clădirilor, care se referă la calitatea aerului interior, confort termic, iluminat şi acustică.

[5] SR EN 16798-1:2019 - Performanţa energetică a clădirilor. Ventilarea clădirilor. Partea 1: Parametrii ambientali pentru proiectare şi

evaluarea performanței energetice a clădirilor, privind calitatea aerului interior, confortul termic, iluminatul și acustica. Modul M1-6

[6] SR EN 16798-1:2019/NA:2019 - Performanța energetică a clădirilor. Ventilarea clădirilor. Partea1: Parametrii ambientali pentru proiectare și evaluarea performanței energetice a clădirilor, privind calitatea aerului interior, confortul termic, iluminatul și acustica. Modul M1-6. Anexă națională

The impact of occupants' energy awareness and thermal preferences on buildings' performance

Florian Regnath [a], Christiane Berger [b], Ardeshir Mahdavi [c]

[a] Department of Building Physics and Building Ecology, TU Wien, Vienna, Austria, florian.regnath@gmx.de.

[b] Department of Architecture, Design and Media Technology, Aalborg University, Aalborg, Denmark, chbe@create.aau.dk.

[c] Department of Building Physics and Building Ecology, TU Wien, Vienna, Austria, amahdavi@tuwien.ac.at.

Abstract. Recent research efforts in building performance simulation increasingly focus on the representation of people's behaviour (specifically, their interactions with buildings' control systems). In this context, the use of agent-based modelling (ABM) is suggested to be a promising approach, as it can capture, in principle, the complexity and dynamics of the patterns of individual occupants' presence and behaviour in buildings. The present contribution describes a related effort, whereby an agent-based model (generated using the NetLogo application) was coupled with a dynamic building simulation model to examine the impact of occupants' energy-related behaviour on buildings' energy performance. To this end, four user types were defined in the agent-based modelling environment. These occupant types were assumed to correspond to different energy awareness levels as well as different tolerance levels with regard to indoor-environmental conditions that are deemed to be desirable. The behavioural model is linked to the dynamic energy simulation tool EnergyPlus via co-simulation using the Building Control Virtual Test Bed tool and Python programming language. A case study object (specifically, six single-occupancy office spaces in an office building) was selected to simulate the impact of different occupant types on the building energy performance. The simulation results suggest that the awareness level of occupants regarding energy conservation issues can have significant influence on the computed energy performance of the case study building. Moreover, occupants' level of tolerance regarding deviations of indoor-environmental conditions from "optimal" settings, was likewise shown to influence energy use. Finally, the case study highlights existing usability challenges concerning co-simulation processes involving both ABM and performance simulation.

Keywords. Occupant behaviour, agent-based modelling, indoor environment.
DOI: https://doi.org/10.34641/clima.2022.406

1. Introduction

A number of past and ongoing research contributions address occupants' behaviour representation in building simulation tools [1-5]. Specifically, much focus has been recently laid on understanding occupants' interaction with buildings' control systems and other building occupants. In this context, different occupant modelling approaches and techniques have been considered [6,7]. Thereby, the agent-based modelling (ABM) approach is proposed to be a promising approach, as it can capture, in principle, the complexity and dynamics of the patterns of individual occupants' presence and behaviour in buildings [8,9]. Within a recent review effort, several ABM research efforts were systematically analysed and discussed [10]. This effort highlighted the potential of ABM to provide a flexible way of representing the dynamic and complex behaviour of occupants' presence and behaviour in buildings. However, a number of limitations and challenges were identified in the reviewed ABM studies.

One main limitation pertains to co-simulation challenges, when coupling a behavioural (agent-based) model with a dynamic energy simulation model. The issue is of relevance to the present contribution, as it involves the coupling of an agent-based model (generated using the NetLogo application) with a building simulation model. Thereby, the main objective is to explore the implications of occupants' energy awareness and thermal preferences for occupants' behaviour in buildings and how this influences buildings' energy performance. Toward this end, a case study building

Copyright ©2022 by the authors. This conference paper is published under a CC-BY-4.0 license.

(including six single-occupancy office spaces in an office building) was selected to simulate the impact of different occupant-related configurations on the building energy performance. The paper presents and discusses the simulation results.

2. Research method

2.1 Case study building

In order to simulate the influence of building users' behaviour on the energy performance, a case study building that is assumed to be located in Vienna (Austria) is selected. The building includes six single-occupied office spaces and comprises a total floor area of 72 m^2 (see Figure 1). Each office space has an operable window with a window to wall ratio of 0.4. The building components are defined in a way to meet the minimum requirements of the Austrian building guideline (OIB Guideline 6 [11]). Table 1 gives an overview of the case study building assumptions, including geometry-related variables (A_w: zone window area; A_{zone}: zone floor area; V_g: gross volume) and construction-related variables (U-values of roof (U_{roof}), floor (U_{floor}), window (U_{window}), and external wall ($U_{ext.wall}$)). Each window is equipped with an internal shading system.

2.2 Occupant behaviour

As alluded to before, the main focus of this research effort is to explore the impact of occupants' energy awareness and thermal preferences on buildings' energy performance. In this context, four different occupant types were defined (see Table 2). The defined occupant types differ in terms of two different levels of energy awareness (low/high) and two different tolerance levels with regard to indoor-environmental conditions (low/high). The assumption is that occupants, who have a higher level of awareness concerning their energy consumption (i.e., Type I and II), tend to carry out a number of adaptive actions (as for example changing their clothing) to enhance their thermal comfort. In contrast, occupants who are less energy-conscious (i.e., Type III and IV), are assumed to be more likely to adapt the heating or cooling setpoint to maintain their preferred thermal condition.

Moreover, the occupant types are assumed to differ in view of their thermally relevant levels of tolerance. As such, occupants with a low tolerance level (i.e., Type II and IV) are more likely to change their indoor-environmental conditions to reach an optimal thermal comfort condition as compared to occupants with a high tolerance level (i.e., Type I and III). The tolerance levels assumed in the model are defined in terms of a function that is based on the PMV (Predicted Mean Vote) concept by Fanger [13]. Figure 2 shows the assumed PMV functions for high and low tolerance levels (in percentage). The respective formulae are given in equation (1) (high tolerance level) and equation (2) (low tolerance level).

Furthermore, it was assumed that the occupant operates the shading elements depending on the level of their energy awareness as well as the contextual circumstances (for additional details see [12]).

$$PMV = 100 - 95 \cdot exp^{(-0.03353 \cdot PMV^4 - 0.2179 \cdot PMV^2) \cdot 0.5} \quad (1)$$

$$PMV = 100 - 95 \cdot exp^{(-0.03353 \cdot PMV^4 - 0.2179 \cdot PMV^2) \cdot 2} \quad (2)$$

In order to explore the influence of different occupant types, four scenarios including a composition of varying occupant types were defined. Figure 3 shows the composition of these four scenarios. Whereas Scenario I exclusively consists of high energy awareness occupants with a high tolerance level, Scenario IV includes only low energy awareness occupants with a low tolerance level. Scenarios II and III include a mix of different occupant types.

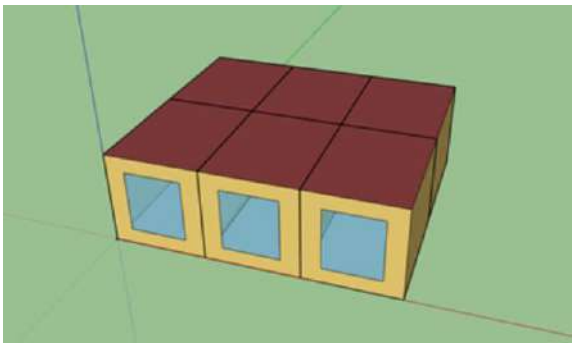

Fig. 1 – Building model in SketchUp [12].

Tab. 1 – Case study building assumptions.

	Variable	Unit	Value
Geometry	A_w	m^2	3.6
	A_{zone}	m^2	12
	V_g	m^3	216
Construction	U_{roof}	$W.m^{-2}.K^{-1}$	0.15
	U_{floor}		0.11
	U_{window}		0.11
	$U_{ext.\ wall}$		0.20

Tab. 2 – Occupant type assumptions.

	Energy awareness	Tolerance level
Type I	high	high
Type II	high	low
Type III	low	high
Type IV	low	low

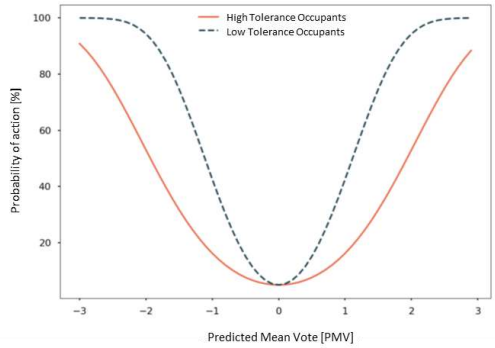

Fig. 2 – Assumed PMV functions corresponding to occupants' high and low thermal tolerance levels regarding thermal conditions [12].

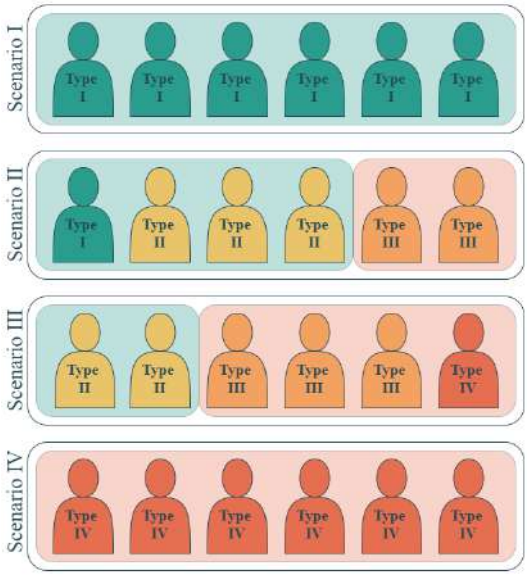

Fig. 3 – Four scenarios with different compositions of occupant types [12].

2.3 Computational configuration

The occupant behaviour model is generated in NetLogo [14], whereas the thermal model is generated in the energy simulation application EnergyPlus [15]. In order to couple the dynamic energy simulation model with the occupant behaviour model, the BCVTB (Building Control Virtual Test Bed) and the Python language were used [16,17]. To obtain the simulation results in a reasonable degree of resolution, the time step duration was set to 30 minutes. Simulations were conducted for a period of four weeks (one representative week per season).

The diagram of the computational configuration and data information exchange is shown in Figure 4. The data exchange process is as follows. At each time step, EnergyPlus simulates the buildings' state (including energy consumption, temperature, illuminance, PMV). The simulated data is communicated via BCVTB and Python to NetLogo. As such, BCVTB is used as a link between NetLogo and EnergyPlus. NetLogo further simulates the building users' actions and communicates this information back to EnergyPlus via Python and BCVTB. EnergyPlus simulates, for the subsequent time step, the updated environmental condition.

Note that a decision-making routine is included in the agent-based model. Thereby, the agent decides, depending on the indoor-environmental condition and the related agents' preferences and tolerance levels, which action will be performed at each time step in order to achieve thermal comfort. In this model, the following possible set of actions is included: *i)* reverse previous action that could have caused thermal discomfort (i.e., close opened window), *ii)* opening or closing the window, *iii)* changing the clothing, and *iv)* changing the heating or cooling setpoint. The likeliness to perform a certain action depends on the user type. Furthermore, limitations for each action are defined (i.e., clothing value limits between 0.6 and 1.4).

An illustrative example of a decision graph is given in Figure 5. This graph depicts a decision routine that pertains to an occupant with a low energy awareness level (i.e., Type III and IV) who perceives the thermal conditions as too warm. As such, the graph shows the relative likelihood of opting for one of these options (alternative control actions) in case of the specific occupant. As alluded to before, the decision routines vary among the different occupant types. Specifically, the likelihood to perform an action is dependent on the energy awareness level of the individual occupants. For instance, a low energy aware occupant (see Figure 5) has a higher likelihood to first change the heating/cooling setpoint (70%) before opening the window (20%) or changing the clothing (10%). Whereas a high energy aware occupant has a higher likeliness to first adapt the clothing (70%) before opening the window (20%) or changing the heating/cooling setpoint (10%).

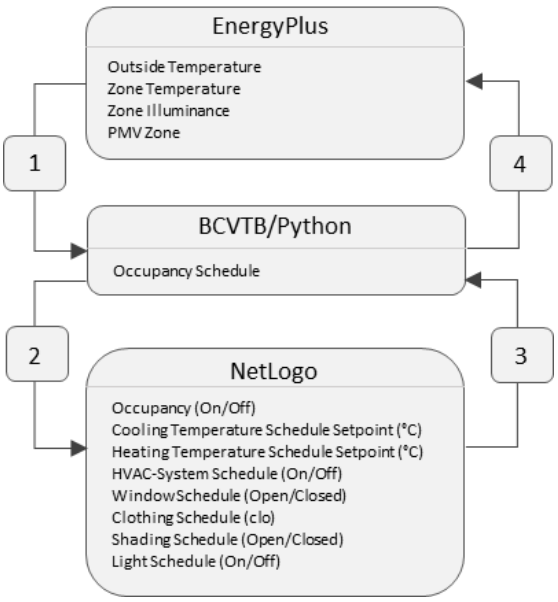

Fig. 4 – Diagram of the computational configuration and data exchange [12].

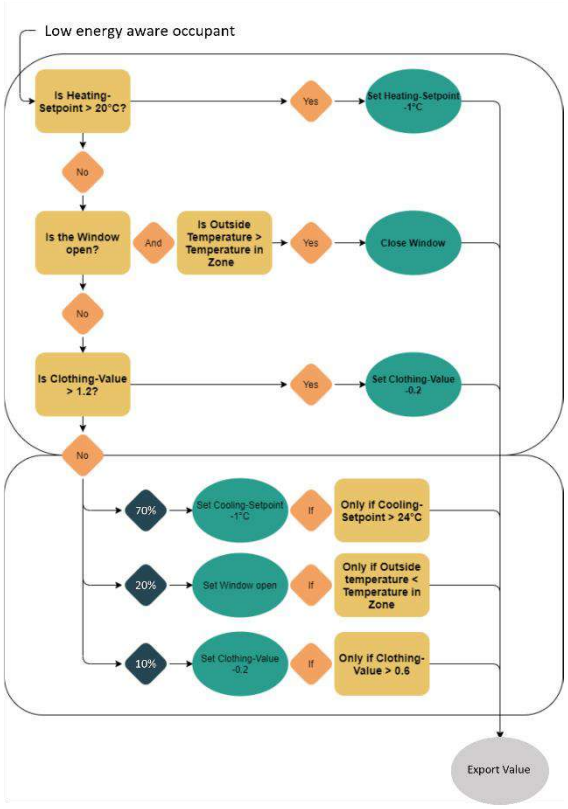

Fig. 5 – Illustrative decision graph for low energy aware users (Type III and IV) [12].

Given the probabilistic aspect of the study, multiple simulation runs were conducted for each scenario. As such, the results illustrated in the following section represent average values over each scenario. The data analysis was performed using Python [17].

3. Results and discussion

The results display, in principle, the significant impact of assumptions regarding occupants' attitudes and behaviour on the buildings' energy loads. Specifically, actions of occupants with low energy awareness result, as it could be expected, in higher heating and cooling loads (see Figure 6). A similar tendency is visible also in Figure 7 and 8, which depicts mean energy loads per scenario (for spring season) in comparison to the Base Case (BC).

The results also suggest that occupants' energy awareness level can contribute to reducing the buildings' overall energy consumption. The results displayed in Figure 9 show the mean energy loads per each occupant type (for the spring season). Note that both the median and the distribution of the results are influenced by the occupants' behaviour. The medians of Type I and II occupants are relatively low. The highest mean energy load corresponds to Type III, which denotes low energy awareness and high tolerance level. This result may appear paradoxical at first but can be explained due to the reduced number of corrective actions resulting from this occupant type's high tolerance level. For instance, an occupant of this type may be oblivious to the fact that very low indoor temperatures in the summer (or very high indoor temperatures in winter) time are detrimental from the energy saving view. A similar trend can be seen in Figures 10 to 12 illustrating the mean energy loads per each occupant type in summer, autumn, and winter.

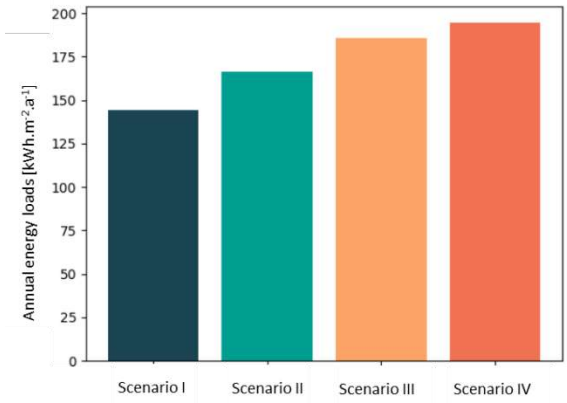

Fig. 6 – Annual energy load per scenario [12].

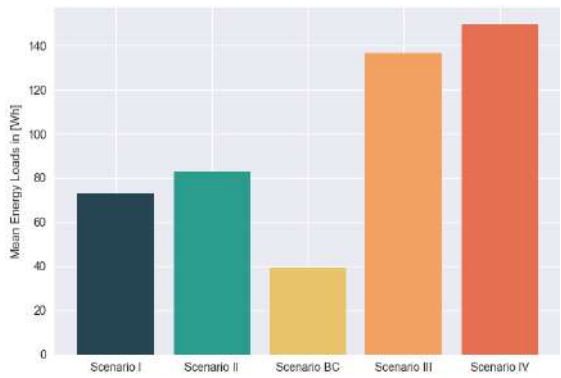

Fig. 7 – Mean energy loads per scenario in spring [12].

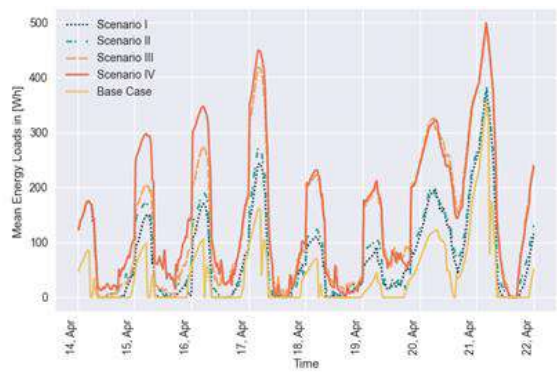

Fig. 8 – Mean energy loads for the Base Case and the four scenarios in spring [12].

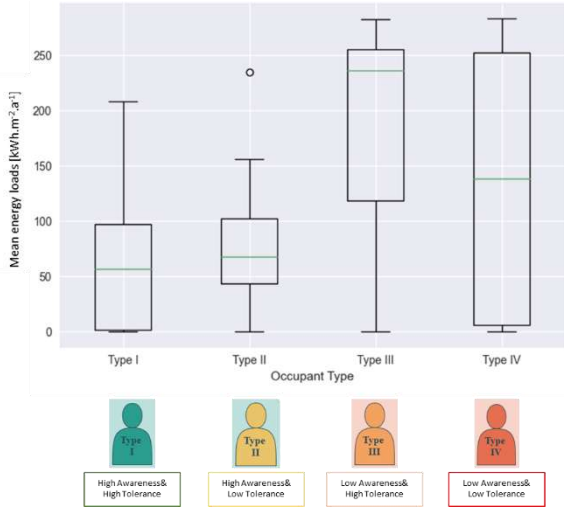

Fig. 9 – Mean energy loads per each occupant type in spring [12].

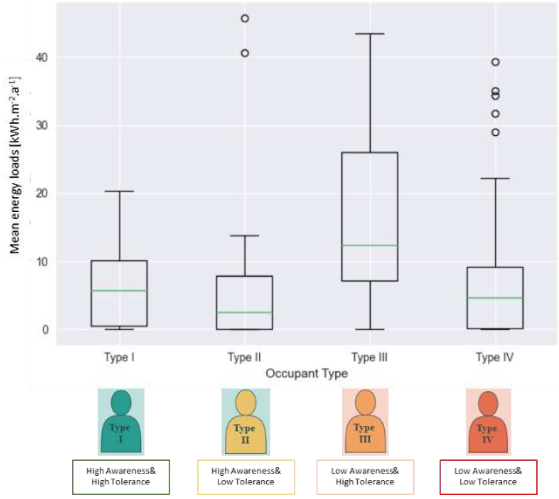

Fig. 10 – Mean energy loads per each occupant type in summer [12].

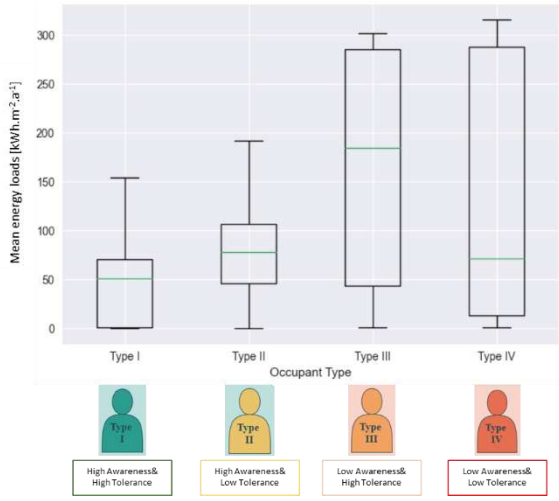

Fig. 11 – Mean energy loads per each occupant type in autumn [12].

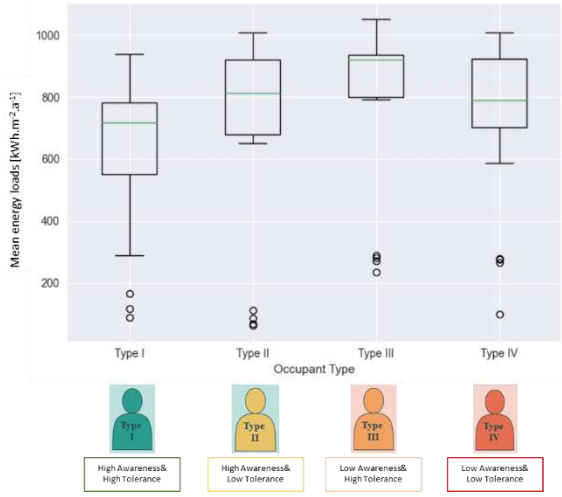

Fig. 12 – Mean energy loads per each occupant type in winter [12].

4. Concluding remarks and future outlook

The study presented in this paper represents an effort to illustrate the potential of ABM integration in energy simulation in order to better capture occupants' attitudes and behaviour. Thereby, several limitations must be acknowledged. For instance, the case study included only single-occupied office spaces. Hence, interactions among multiple occupants, whose modelling could benefit from ABM capabilities, were not taken into consideration. Likewise, the study considered only a limited number of actions that occupants could perform. Future studies could not only address multiple building types and locations, but also include a richer repertoire of occupant types (and associated preferences and behavioural tendencies). It is also important to mention that the ABM implementation presented in this paper, could not be tested against empirical information. As such, the authors would not suggest that the deployed model was validated.

Despite the above limitations, the study presented in this contribution clearly highlights the considerable relevance and importance of occupant-related model assumptions in building performance simulation. The results suggest that computational estimates of buildings' energy consumption are considerably influenced by assumptions pertaining the attitudes (e.g., energy awareness level) or habitual preferences (e.g., thermal conditions in indoor spaces). Specifically, occupants' level of tolerance regarding deviations of indoor-environmental settings from "optimal" thermal conditions could be shown to significantly influence buildings' energy performance.

Aside from the study's main topical concern, a concluding remark regarding the existing usability challenges in ABM applications must be mentioned. These challenges pertain specifically to the necessary co-simulation processes involving both agent-based modeling and building performance simulation. The currently existing complexity of establishing a co-simulation between ABM tools (in this case, NetLogo) and the performance simulation tool (in this case EnergyPlus) requires a considerable level of programming knowledge, which arguably inhibits a broad-scale usage. Advances in this area (including applications for efficient generation and operation of co-simulation environments) could facilitate a richer representational stance regarding the nature and diversity of building occupants' needs, expectations, and actions. As such, a broader understanding of occupants' impact on buildings cannot only facilitate more reliable predictions of building energy use and environmental emissions, but can also contribute to improving occupants' comfort, health, and well-being in the built environment.

5. Acknowledgement

In the writing of this paper, the authors benefited from participation and related discussions in the IEA EBC Annex 79 activities.

6. References

[1] IEA EBC Annex 66, 2021. [updated 2022, cited 2022 Jan 3]. Available from: http://www.annex66.org/

[2] IEA EBC Annex 79, 2021. [updated 2022, cited 2022 Jan 3]. Available from: https://annex79.iea-ebc.org/

[3] O'Brien W, Wagner A, Schweiker M, Mahdavi A, Day J, Kjærgaard MB, et al. Introducing IEA EBC annex 79: Key challenges and opportunities in the field of occupant-centric building design and operation. Building and Environment. 2020 Jul;178:106738. doi: 10.1016/j.buildenv.2020.106738

[4] Yan D, O'Brien W, Hong T, Feng X, Burak Gunay H, Tahmasebi F, et al. Occupant behavior modeling for building performance simulation: Current state and future challenges. Energy and Buildings. 2015 Nov;107:264–278. doi: 10.1016/j.enbuild.2015.08.032

[5] Mahdavi A, Tahmasebi F. People in building performance simulation. In: Building Performance Simulation for Design and Operation, 2019,117-145, doi: 10.1201/9780429402296

[6] Gaetani I, Hoes P-J, Hensen JLM. Occupant behavior in building energy simulation: Towards a fit-for-purpose modeling strategy. Energy and Buildings. 2016 Jun;121:188–204. doi: 10.1016/j.enbuild.2016.03.038

[7] Hong T, Chen Y, Belafi Z, D'Oca S. Occupant behavior models: A critical review of implementation and representation approaches in building performance simulation programs. Building Simulation. 2018 Feb;11:1–14. doi: 10.1007/s12273-017-0396-6

[8] Bonabeau E. Agent-based modeling: Methods and techniques for simulating human systems. Proceedings of the National Academy of Sciences. 2002 May 14;99:7280–7287. doi: 10.1073/pnas.082080899

[9] Putra HC, Andrews CJ, Senick JA. An agent-based model of building occupant behavior during load shedding. Build Simul. 2017 Dec;10(6):845–859. doi: 10.1007/s12273-017-0384-x

[10] Berger C, Mahdavi A. Review of current trends in agent-based modeling of building occupants for energy and indoor-environmental performance analysis. Building and Environment. 2020 Apr;173:106726. doi: 10.1016/j.buildenv.2020.106726

[11] Österreichisches Institut für Bautechnik. OIB-Richtlinie 6. Energieeinsparung und Wärmeschutz. 2019 April.

[12] Regnath F. Application of agent-based modelling to assess the impact of occupant behaviour on buildings' energy use. Master Thesis TU Wien, 2021 Sept. doi: 10.34726/hss.2021.79546

[13] Fanger PO. Thermal comfort: analysis and applications in environmental engineering. Copenhagen: Danish Technical Press. 1970.

[14] Wilensky U. NetLogo. Center for Connected Learning and Computer-Based Modeling, Northwestern University, Evanston, IL. [updated 1999, cited 2022 Jan 3]. Available from: http://ccl.northwestern.edu/netlogo/

[15] U.S. Department of Energy's, EnergyPlus. [updated 2022, cited 2022 Jan 3]. Available from: https://energyplus.net/

[16] Wetter M, Nouidui TS, Haves P, Building Controls Virtual Test Bed. [updated 2016, cited 2022 Jan 3]. Available from: https://simulationresearch.lbl.gov/bcvtb

[17] Python Software Foundation, Python. [updated 2022, cited 2022 Jan 3]. Available from: https://www.python.org/downloads/

Design and experiment study of membrane based isothermal dehumidifier in HVAC system

Seong-Yong Cheon [a], Hye-Jin Cho [a], Su-Young Jo [a], Jae-hee Lee [a], Minseong Kim [a], Jae-Woen Jeong [a,]*

[a,*] Department of Architectural Engineering, Hanyang University, Republic of Korea, jjwarc@hanyang.ac.kr.

Abstract. As passive building systems improve, sensible loads decrease and the air conditioning system takes on a greater role in dehumidification. Isothermal dehumidifier with membrane, which utilizes a vacuum pump to create a partial vapor gradient between membranes, has the potential to save significant energy by operating just for latent cooling as a thermally decoupled system. Although research has concentrated on analyzing the dehumidification and energy performance of isothermal dehumidifiers via simulation studies, their design and experimental analysis for dehumidification systems in HVAC systems remain rare. In this study, we constructed a prototype of an isothermal dehumidifier using hollow fiber membrane modules and vacuum pumps for an air conditioning system. Under different air conditions, the constructed prototype was evaluated for dehumidification characteristics (i.e., isothermal process, moisture removal rate, and dehumidification efficacy). Three factors were used to choose the air conditions for testing the dehumidification performance: air temperature, air humidity, and air velocity. The experiment results indicated that the isothermal dehumidifier dried the air without changing the temperature, and the overall dehumidification performance of the prototype system indicated that the humidity ratio difference was between 3.8 and 14 g/kg, the moisture removal rate was between 0.12 and 1.0 kg/h, and the dehumidification effectiveness was between 36% and 81%.

Keywords. Isothermal dehumidifier, dehumidification performance, Experiment study
DOI: https://doi.org/10.34641/clima.2022.179

1. Introduction

A cooling coil is used in an air conditioning system to dehumidify the air through a condensation process [1]. The method can result in significant energy usage due to excessive dehumidification cooling and air pollution issues due to the wet coil [2]. Desiccant systems, such as desiccant wheels and liquid desiccant systems, are an alternative dehumidification system; however, without a free heat source (e.g., solar thermal or waste heat source), the regeneration process to maintain the dehumidification performance of the systems consumes a significant amount of energy [3].

A vacuum-based membrane dehumidifier has been suggested as a more thermally efficient dehumidification approach than traditional dehumidification systems [4, 5]. The system utilizes gas separation technology that is entirely dependent on the difference in partial vapor pressure between the membranes. A vacuum pump depressurizing the humid air permeates the water vapor in the air via the membrane layer, and then dry air is provided.

The vacuum-based membrane dehumidifier's dehumidification and energy performance are calculated using many impacted parameters: feed air velocity, feed air humidity ratio, water vapor permeability, selectivity, and vacuum pressure. The primary factors that have an influence on the system's dehumidification performance are the membrane selectivity and permeance of the material qualities, as well as the vacuum pressure of the operating energy used to depressurize the vacuum side. Thuan et al. [6] shown that the vacuum-based membrane dehumidifier's theoretical coefficient of performance (COP) is between 2 and 3 under isentropic vacuum pump conditions and infinite selectivity. El-Dessouky et al. [7] suggested a system that combines air conditioning with a vacuum-based membrane dehumidifier. The proposed system is a decoupled air conditioning system that utilizes a vacuum-based membrane dehumidifier for latent cooling and an indirect/direct evaporative cooler for sensible cooling. The simulation findings indicate that the suggested system, which incorporates a vacuum-based membrane dehumidifier, may save up to 86 percent of the energy used by a standard air conditioning system.

Although previous research has primarily used numerical methods or simulations to estimate the dehumidification and energy performance of

Copyright ©2022 by the authors. This conference paper is published under a CC-BY-4.0 license.

vacuum-based membrane systems, experimental analysis of vacuum-based membrane dehumidifiers operating in a variety of air conditions for HVAC systems is extremely rare. We developed a prototype of a vacuum-based membrane dehumidifier for use in an air conditioning system and assessed its dehumidification performance under a variety of settings in this work. A series of experimental data was used to determine the sensitivity of the operating condition on the dehumidification performance of the vacuum-based membrane dehumidifier.

2. Membrane based isothermal dehumidifier

2.1 System overview

As seen in Figure 1, a vacuum-based membrane dehumidifier (VMD) is composed of membrane modules and a vacuum pump. The membrane modules are composed of thick hollow fiber membranes constructed of polymeric materials with a high selectivity and permeability for water vapor. The water vapor in the humid air (i.e., feed side) penetrates to the vacuum side (i.e., permeate side) of the VMD system through the membrane layer due to the partial vapor pressure difference between the membranes. To provide the partial vapor pressure gradient that serves as the dehumidification's driving power, the vacuum pump depressurizes the permeate side to practically vacuum pressure.

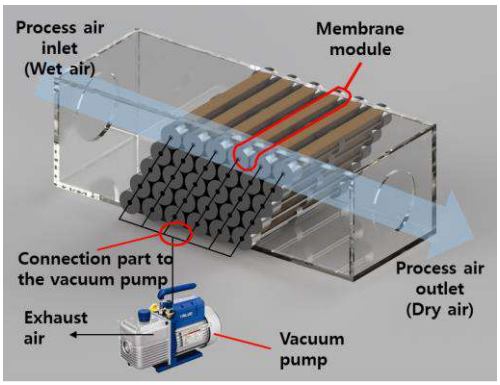

Fig. 1 – Configuration of the vacuum-based membrane dehumidification system

Figure 2 illustrates the VMD's dehumidification procedure in detail. When the system makes advantage of the highly selective and permeance of water vapor to generate a partial vapor pressure difference between the feed and permeate sides, the water vapor with a high chemical potential on the feed side adsorbs to the membrane surface layer. The adsorbed water vapor then diffuses through the membrane and desorption occurs on the permeate side.

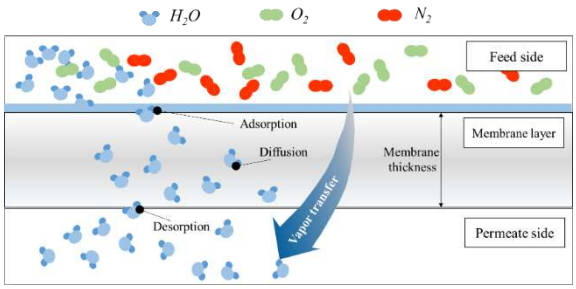

Fig. 2 – Dehumidification process of the vacuum-based membrane dehumidifier

3. Experiment overview

3.1 Experiment setup

The experimental setup for the vacuum-based membrane dehumidifier is shown in Figure 3. The process air is supplied to the shell side of the hollow fiber in the membrane module, while the vacuum pressure depressurizes the permeate side, which is also the shell side of the hollow fiber. Mass transfer happens through the isothermal process in the dehumidification process. The environmental chamber conditions the air entering the VMD system in order to maintain the desired air temperature and humidity ratio.

A variable fan installed on the exhaust side was used to manage the flow rate of the process air. The permeate side vacuum pressure was maintained near vacuum (e.g., 3.3 kPa) using a 1.4 kW commercial vacuum pump. To test the VMD system's dehumidification performance, we examined the inlet/outlet air temperature and humidity, as well as the permeate side vacuum pressure.

Figure 3 depicts the actual experimental setup for the dehumidification test using the vacuum-based membrane dehumidifier. The membrane modules are cylindrical in shape and measure 360 mm in length and 55 mm in diameter. The modules are made of a dense form of hollow fiber membranes 400 μm in diameter. We constructed a complete system of the VMD using 24 membrane modules. To determine the inlet and outflow air conditions, air temperature and humidity sensors with insulation were put at the system's intake and outlet. The variable fan is used to distribute process air in the feed side of the membrane modules, and the airflow rate of the process air is recorded at the system's input by a flowmeter. The permeate side vacuum pressure was determined using a digital pressure sensor connected to the vacuum pump. Each experiment lasted 10 minutes after the system reached steady-state, and data from the sensors were gathered at 1-second intervals to the data recorders. The measuring equipment's ranges and accuracies are reported in Table 1.

Tab. 1 – Sensor characteristics

Variable	Sensor type	Range	Accuracy
Air temperature and relative humidity	Temperature /humidity probe	Temperature: -20 to 60 °C	±0.5 °C
		Humidity: 0 to 100%	±1.8 %
Air velocity	Vane probe	0.1 to 15 m/s	± 0.1 m/s

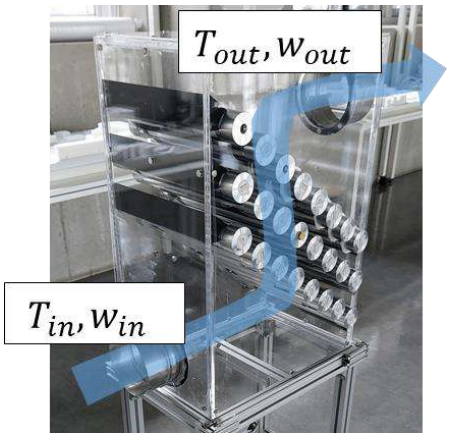

Fig. 3 – Experimental setup of vacuum-based membrane dehumidifier

To conduct the parametric analysis experiments, we evaluated three operational factors that impact the VMD system's dehumidification performance: the air temperature, the humidity ratio, and the air flow rate. In the local standard for a desiccant dehumidifier test condition, the experimental design for the parametric analysis was examined. The VMD was used to perform parametric analysis on five air conditions, with the input temperature set to 25°C to 33°C and the humidity ratio set to 15.96 g/kg to 25.74 g/kg, respectively. The input airflow rate was varied between 18 and 112.5 m^3/h on a four-level basis, while the permeate side vacuum pressure was maintained at 3.3 kPa. Table 2 summarizes the detailed test conditions for the parametric study.

Tab. 2 – Test condition for parametric study

Point	Temperature (°C)	Humidity ratio (g/kg)	Air flow rate (m^3/h)
P1-1	33	25.74	18
P1-2	33	25.74	37.5
P1-3	33	25.74	75
P1-4	33	25.74	120
P2-1	33	20.85	18
P2-2	33	20.85	37.5
P2-3	33	20.85	75
P2-4	33	20.85	120
P3-1	33	15.96	18
P3-2	33	15.96	37.5
P3-3	33	15.96	75
P3-4	33	15.96	120
P4-1	29	20.85	18
P4-2	29	20.85	37.5
P4-3	29	20.85	75
P4-4	29	20.85	120
P5-1	25	20.85	18
P5-2	25	20.85	37.5
P5-3	25	20.85	75
P5-4	25	20.85	120

2.2 Performance index

The humidity ratio difference, moisture removal rate, and dehumidification effectiveness of the VMD system were used as performance indicators for dehumidification. The difference in humidity ratios is defined as the difference between the intake and outlet air humidity ratios (Eq. (1)), which indicates the change in the outlet air state. The moisture removal rate is defined as the process air's dehumidification mass flow rate (Eq. (2)), and the dehumidification effectiveness is defined as the ratio of the water vapor's actual mass flow rate to its maximum mass flow rate (Eq. (3)).

$$\Delta w = w_{f,in} - w_{f,out} \tag{1}$$

$$\dot{m}_d = \dot{m}_a \Delta w \tag{2}$$

$$\varepsilon_d = \frac{\dot{m}_{v,real}}{\dot{m}_{v,max}} = \frac{w_{f,in} - w_{f,out}}{w_{f,in} - w_{eq}} \tag{3}$$

To measure the dehumidification effectiveness, the maximum mass flow rate of water vapor is estimated using Eq (4). The equilibrium humidity ratio is established by the permeate side partial vapor pressure, which is determined by the feed side air conditions (i.e., mass transfer NTU, feed side vacuum pressure, and permeate side partial vapor pressure), as well as the feed side membrane parameters (selectivity, and permeance) as determined by Eq (5).

$$w_{eq} = 0.62198 \frac{P_{p,v,o}}{P_{total} - P_{p,v,o}} \tag{4}$$

$$P_{p,v,o} = f(P_{f,v,i}, NTU_m, P_{p,t}, \text{Sel}, \text{Per}) \quad (5)$$

4. Experiment results

4.1 Temperature

Figure 4 illustrates the effect of air temperature on the dehumidification performance of a vacuum-based membrane dehumidifier. P2, P4, and P5 were the 14 test point sets, which all had the same humidity ratio (i.e., 20.85 g/kg) but with varying airflow speeds. The results indicate that the humidity ratio difference was between 3.8 and 7 g/kg, the moisture removal rate was between 0.12 and 0.55 kg/h, and the dehumidification effectiveness was between 36% and 81%. The parametric study demonstrates that air temperature has no noticeable impact on the difference in humidity ratios and the rate of moisture removal. Increases in the air temperature of the VMD system improve the water vapour permanence of the membrane. However, it had a lesser effect on dehumidification effectiveness owing to fluctuations in the under-air conditioning system's air temperature.

Figure 4.c illustrates the impact of air temperature on the VMD system's dehumidification effectiveness. Additionally, no substantial effect of air temperature is shown, because the driving force of mass transfer, which is the partial vapor pressure between the membrane feed and permeates sides, is unaffected by air temperature.

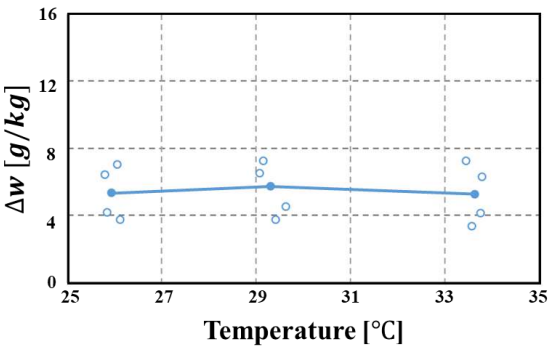

(a) Humidity ratio difference

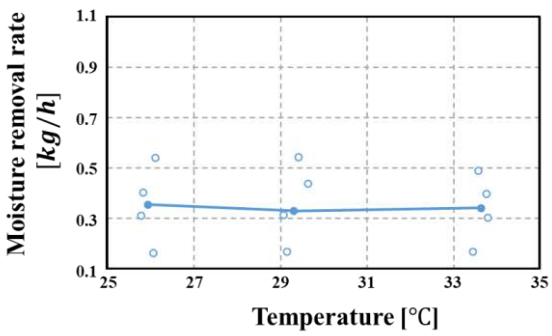

(b) Moisture removal rate

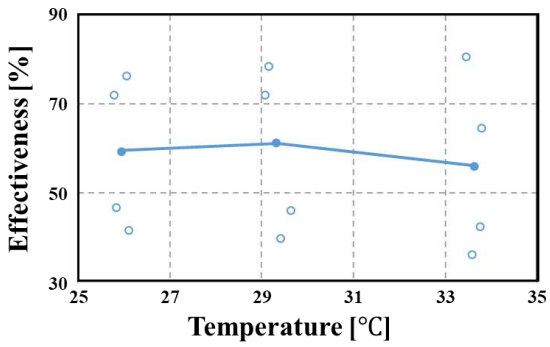

(c) Effectiveness

Fig. 4 - Influence of process air temperature

4.2 Humidity ratio

Figure 5 illustrates the effect of the air humidity ratio on the dehumidification performance of a vacuum-based membrane dehumidifier. P1, P2, and P3 were the 14 test point sets, which all had the same temperature (33°C) but with varying airflow speeds. The findings indicate that the humidity ratio difference was between 3.8 and 14 g/kg, the moisture removal rate was between 0.12 and 1.0 kg/h, and the dehumidification effectiveness was between 36% and 81%. The parametric study shows that the humidity ratio has a significant effect on the humidity ratio difference and moisture removal rate, as the partial vapor pressure difference between the membrane feed and permeate side increases, increasing the VMD system's process air humidity ratio.

Figure 5.c illustrates the impact of airflow rate on the dehumidification effectiveness. The results indicate that there is a less significant effect on the air humidity ratio (positive correlation). Even though the driving force of mass transfer was increased with an increase in the humidity rate, the mass NTU, which is a factor of the permeate flow rate across the membrane, remained unchanged.

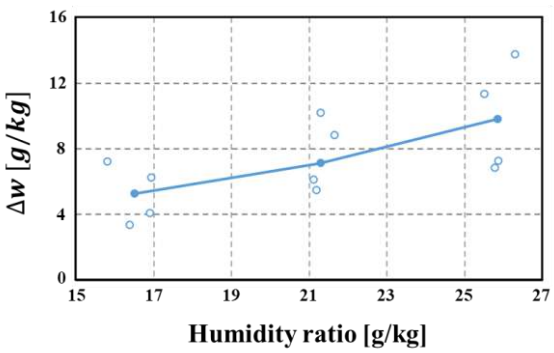

(a) – Humidity ratio difference

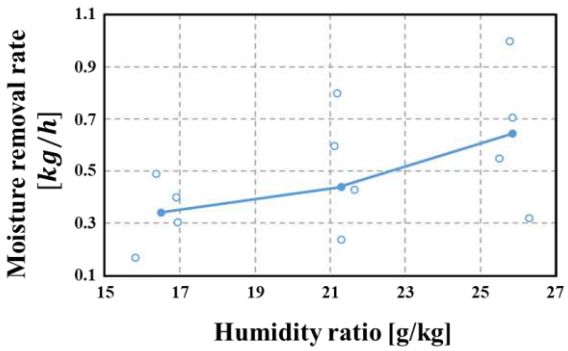

(b) Moisture removal rate

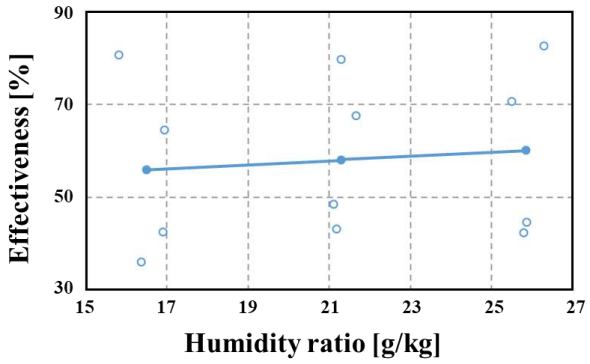

(c) Effectiveness

Fig. 5 - Influence of process air humidity ratio

4.3 Flow rate

Figure 6 illustrates the effect of airflow rate on the dehumidification performance of a vacuum-based membrane dehumidifier. The 24 test point sets were classified as P1–P6, and the data set was organized according to airflow rate. The findings indicate that the humidity ratio difference was between 3.8 and 14 g/kg, the moisture removal rate was between 0.12 and 1.0 kg/h, and the dehumidification effectiveness was between 36% and 81%. The parametric study demonstrates that the humidity ratio has a large negative influence on the difference in humidity ratios owing to the reduction in mass NTU, which increases the airflow rate. The effect of the moisture removal rate, on the other hand, is positive since the impact of decreasing the mass NTU is less than the impact of increasing the airflow rate, as indicated in Eq (2).

Figure 6.c illustrates the impact of airflow rate on the VMD system's dehumidification effectiveness. The data indicate that the greatest negative impact is on the air humidity ratio. Because the mass NTU is inversely proportional to the airflow rate, increasing the airflow rate results in a reduction in the VMD system's dehumidification effectiveness.

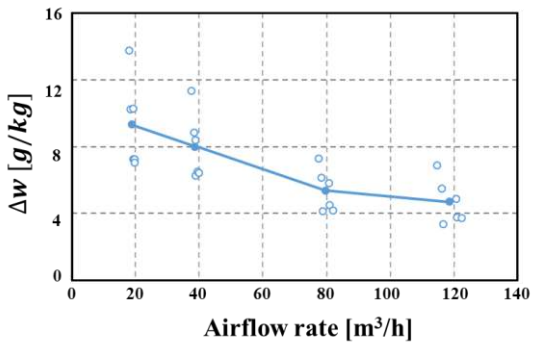

(a) Humidity ratio difference

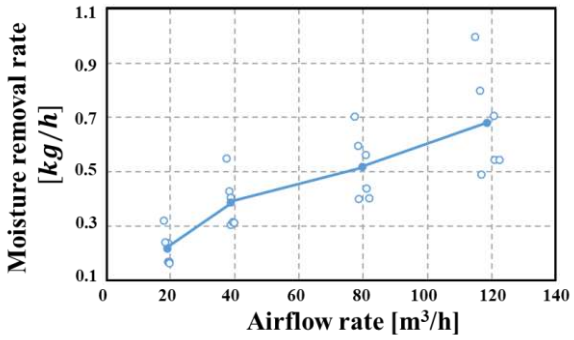

(b) Moisture removal rate

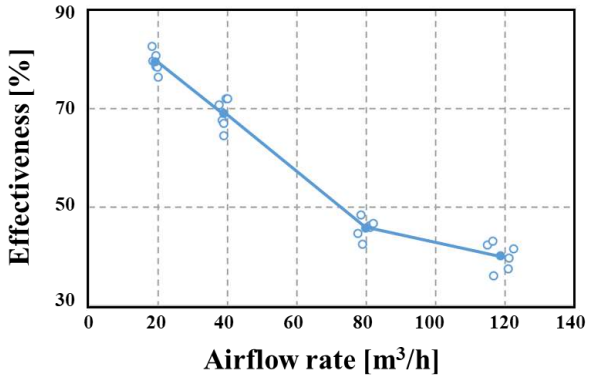

(c) Effectiveness

Fig. 6 - Influence of process airflow rate

In short, air temperature has no influence on dehumidification performance (humidity ratio difference, moisture removal rate, and dehumidification effectiveness). The humidity ratio and airflow rate are the two variables that have the greatest influence on the amount of moisture removal rate. Because variations in the humidity rate correspond to variations in the driving force of mass transfer, while variations in airflow correspond to variations in mass NTU. Additionally, the mass NTU as a function of the change in airflow rate was shown to be the most significant factor affecting the effectiveness.

5. Conclusion

The purpose of this work was to conduct an experimental evaluation of the vacuum-based membrane dehumidifier's dehumidification performance using parametric analysis and to construct an empirical model of dehumidification effectiveness. A series of studies were done in a controlled setting with varying operating conditions. The humidity ratio difference, moisture removal rate, and dehumidification effectiveness were used to evaluate the vacuum-based membrane dehumidifier's performance. On the basis of an experimental design, a parametric study of the vacuum-based membrane dehumidifier was conducted.

According to the testing findings, the overall dehumidification performance of the prototype system was between 3.8 and 14 g/kg, the moisture removal rate was between 0.12 and 1.0 kg/h, and the dehumidification effectiveness was between 36% and 81%, respectively. The parametric study revealed that the inlet humidity ratio and airflow rate had a significant effect on the dehumidification performance of the humidity ratio difference and moisture removal rate. The airflow rate was the primary affect parameter for dehumidification effectiveness. This experimental results demonstrate application to a dehumidifying device (dedicated outdoor air system or air conditioning system) for indoor latent heat removal as a thermally decoupled air conditioning system by demonstrating that isothermal dehumidification is feasible.

6. Acknowledgement

This work was supported by Korea Institute of Energy Technology Evaluation and Planning(KETEP) grant funded by the Korea government(MOTIE)(No. 20202020800360), and this work was supported by the Korean Agency for Infrastructure Technology Advancement (KAIA) grants (21CTAP-C163749-01).

7. References

[1] Murphy J. 2002. Dehumidification performance of HVAC systems. ASHRAE Journal 44:23–31.

[2] Ascione F, Bellia L, Capozzoli A, Minichiello F. 2009. Energy saving strategies in air-conditioning for museums. Applied Thermal Engineering 29:676–686.

[3] Niu JL, Zhang LZ, Zuo HG. 2002. Energy savings potential of chilled-ceiling combined with desiccant cooling in hot and humid climates. Energy and buildings 35:487–495.

[4] Caliskan H, Hong H, Jang JK. 2019. Thermodynamic assessments of the novel cascade air cooling system including solar heating and desiccant cooling units. Energy Conversion and Management 199:112013.

[5] Angrisani G, Roselli C, Sasso M, Tariello F. 2016. Dynamic performance assessment of a solar-assisted desiccant-based air handling unit in two Italian cities. Energy Conversion and Management 113:538–550.

[6] Bui TD, Wong Y, Islam MR, Chua KJ. 2017. On the theoretical and experimental energy efficiency analyses of a vacuum-based dehumidification membrane. Journal of Membrane Science 539:76–87.

[7] El-Dessouky HT, Ettouney HM, Bouhamra W. 2002. A Novel Air Conditioning System. Chemical Engineering Research and Design 78:999–1009.

Experimental investigation on a packaged unit of membrane dehumidification-based ventilation system

Hye-Jin Cho [a], Seong-Yong Cheon [a], Su-Young Jo [a], Soo-Jin Lee [a], Gyu-Bae Lee [a], Jae-Weon Jeong [a]*

[a] Department of Architectural Engineering, Hanyang University, Seoul, Republic of Korea, *jjwarc@hanyang,ac.kr*

Abstract. This study purposed to experimentally investigate the seasonal operating performance of the packaged unit of a hollow membrane-based ventilation system. The packaged unit of the proposed ventilation system was fabricated, and the experiments was conducted based on the test standards for the energy recovery ventilator addressed from air-conditioning, heating and refrigeration institute (AHRI). In addition, for achieving the optimal heat and moisture recovery from the ventilation system under various operating conditions, the seasonal operation modes were suggested for the packaged unit of the proposed ventilation system. The measured data showed that the proposed ventilation unit can provide the ventilation air ait nearly neutral air temperature and humidity ratio in each operation mode. In addition, the average sensible effectiveness, the average latent effectiveness, and the average enthalpy effectiveness of the proposed ventilation system are 70.7%, 75.9%, and 75.6% in mode 1; 44.4%, 74.7%, 80.2% in mode 2; 77.6%, 70.4%, 85.6% in mode 3, which exhibited the higher heat and moisture recovery performance compared to the commercial energy recovery ventilator. In conclusions, the measured data demonstrates that the proposed ventilation system has a great application potential for building ventilation unit in terms of energy recovery performance.

Keywords. Packed-ventilation system, hollow fiber membrane, dehumidification, experiment.
DOI: https://doi.org/10.34641/clima.2022.212

1. Introduction

Recently, net zero energy buildings, which refer to a building with zero-net energy consumption over a typical year, have emerged as buzzwords in heating, ventilation, and air-conditioning (HVAC) research field. To realize net zero energy buildings, there has been many approaches in building design such as the increase in building insulation and airtightness levels. The well-insulated buildings have reduced the total building thermal load, particularly, the sensible cooling load. On the other hand, the buildings with high airtightness level requires higher mechanical ventilation loads for maintaining satisfactory indoor air quality and occupant comfort, which could lead to higher energy consumption in space-air conditioning. Therefore, the demands for energy efficient ventilation systems are growing in building application fields.

Energy recovery ventilators (ERVs), which are widely used in HVAC system, utilize the waste heat and moisture within the exhausted room air instead of releasing it directly to the outsides. Commercial ERVs, which are typically composed of flat sheet hydrophilic polymer, exhibit 50–80% of sensible heat exchange effectiveness and 20–60% of latent heat exchange effectiveness [1]; that is, the latent effectiveness of the commercial ERV is lower than the sensible effectiveness. Therefore, applying an energy recovery ventilation system with high latent cooling efficiency is indispensable to reduce the energy consumption of buildings in hot and humid regions.

Therefore, previous studies have proposed hollow fiber membrane dehumidification-based dual core ventilation system, and evaluated the applicability of the proposed system in HVAC applications via theoretical and experimental approaches. Cho et al. [2] has explored the application potential of a hollow fiber membrane-based latent heat exchanger via experimental approach, and their results showed that the proposed latent heat exchanger exhibits superior latent cooling performance rather than sensible cooling owing to its hollow fiber structure, and exhibits 35.3–82.7% of latent cooling effectiveness. Cho et al. [3] also fabricated a mock-up model of hollow fiber membrane based latent heat exchange module for developing regression models for predicting its latent heat exchange performance under various outdoor air conditions. Then, a series of energy simulations was performed to assess annual energy saving potentials of the proposed ventilation unit compared with the conventional ERV unit [4]. Their results showed that the proposed ventilation unit reduced of 59.7% of ventilation load

Copyright ©2022 by the authors. This conference paper is published under a CC-BY-4.0 license.

and conserved 24% of primary energy consumption in space cooling owing to its higher latent cooling effectiveness and selective heat and moisture reclaims from sensible/latent heat exchange dual core systems.

Subsequently, in this study, a pilot unit of the proposed ventilation unit was constructed, and transient operating behaviours and characteristics were experimentally evaluated.

2. System overview

As shown in Figure 1, the proposed ventilation unit consists of a hollow fiber membrane-based latent heat exchanger (M-LHX) and the sensible heat exchanger (SHX). When the fresh outdoor air (OA) enters the primary inlet air channel and the exhausted room air (RA) enters the secondary inlet air channel, the M-LHX initially reclaims the latent heat from the RA leaving the SHX, and the SHX recovers the sensible heat from RA upstream of SHX.

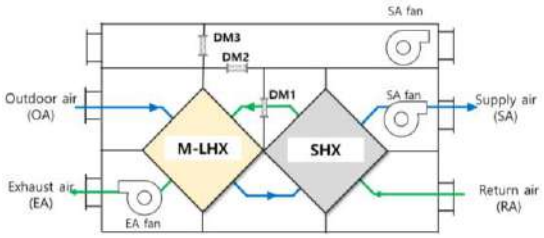

Fig. 1 – Schematic of a proposed packaged ventilation unit

As can be seen in Figure 2, the operating modes of the proposed system are classified into four modes based on OA conditions: the total heat exchange modes (Region 1, 3), the latent heat exchange in cooling seasons (Region 2), and the by-pass mode (Region 4). When the temperature and humidity ratio of OA are higher than those of the room air (RA) or lower than those of the design supply air (i.e., 15 ºC), the M-LHX initially recovers the latent heat from the RA downstream of the SHX. Then, the SHX reclaims the sensible heat from RA. If the temperature of the OA is lower and the humidity ratio of the OA is higher than those of RA, the proposed system operates in latent exchange mode for preventing unnecessary heat exchange from RA. The introduced OA is dehumidified by exchanging moisture with the RA, while the SHX is bypassed. In a sensible exchange mode, when the humidity ratio of the OA is lower and the temperature of the OA is higher than that of the RA, the introduced OA only passes the SHX, and the M-LHX is bypassed. When the temperature and humidity ratio of the OA are lower than that of the RA both the temperature of OA is higher than the design supply air temperature, the bypass mode is activated.

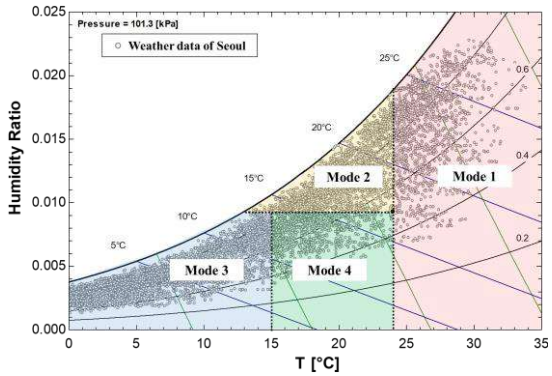

Fig. 2 – Operation modes according to outdoor air conditions on psychrometric chart

3. Experimental overview

3.1 Experiment set up

Figure 3 shows the experimental setup for the pilot unit of the proposed ventilation system. The primary produced by the environmental chamber is blown to the M-LHX facing the tube side, whereas the secondary air is supplied to the SHX. The heat and mass transfer occurs in the primary air and secondary air directions. Polyethersulfone (PES) coated with a hydrophilic polymer was selected as the material for the M-LHX, and the stainless and aluminium are selected as plate and frame material in SHX. The dimensions of the M-LHX and SHX are determined based on the design flow rate of the supply air as 150 m^3/h. Detailed physical information of the proposed ventilation unit fabricated in this study is summarized in Table 1.

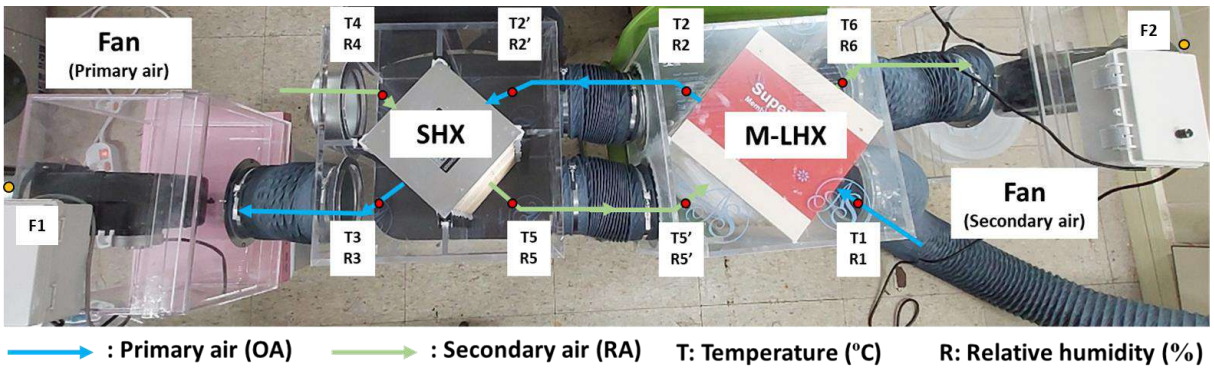

Fig. 3 – Photograph of experimental setup of the proposed ventilation unit

Tab. 1 – Physical information of M-LHX and SHX in the proposed system

Description		Contents
M-LHX	material	polyethersulfone with 9 wt.% of polyvinyl-pyrrolidone
	dimensions	280 mm (W) × 280 mm (D) × 350 mm (H)
SHX	material	Aluminium / stainless
	dimensions	250 mm (W) × 250 mm (D) × 350 mm (H)

3.2 Test conditions

In this study, to investigate the operating performance and feasibility of the proposed system, the transient operating behaviours and characteristics of the critical operating parameters were monitored and for each operating mode 1,2, and 3. The inlet primary air temperature ($T_{a,pri,in}$), the inlet primary air relative humidity ($Rh_{a,pri,in}$), the inlet secondary air temperature ($T_{a,sec,in}$), and the inlet secondary air relative humidity ($Rh_{a,sec,in}$) were selected as four operating parameters. The conditions of the primary air for each mode were determined according to local standard of KS B 6879 heat recovery ventilators [1]. The secondary air conditions for each mode were determined according to the recommend indoor air conditions for cooling and heating seasons. Considering the minimum ventilation rate for a residential or office building with 100 m^2 of floor area, the air flow rate of the primary air and secondary air was set to 150 m^3/h. Table 2 summarized the test conditions for each operation mode. All experiments were conducted in laboratory scale at least 30 minutes.

Tab. 2 – Test conditions for each mode

Mode	Primary air conditions		Secondary air conditions	
	Temp. [ºC]	Relative humidity [%]	Temp. [ºC]	Relative humidity [%]
1	28	72.5	24	50
2	22	72	24	50
3	9	30	20	50

3.3 Performance indices

As performance indices representing the operating performance of the proposed ventilation unit, the sensible heat exchange effectiveness (ε_s), which is defined as the ratio of the temperature variation of the primary air to the theoretical maximum temperature variation (equation 1), the latent heat exchange effectiveness (ε_l), which is defined as the ratio of the humidity ratio variation of the primary air to the theoretical maximum humidity ratio variation (equation 2), and the enthalpy exchange effectiveness(ε_h), which is defined as the ratio of the enthalpy variation of the primary air to the theoretical maximum enthalpy variation (equation 3), were selected.

$$\varepsilon_s = \frac{T_1 - T_3}{T_1 - T_4} \quad (1)$$

$$\varepsilon_l = \frac{\omega_1 - \omega_3}{\omega_1 - \omega_4} \quad (2)$$

$$\varepsilon_h = \frac{h_1 - h_3}{h_1 - h_4} \quad (3)$$

To obtain those three performance indices in each experiment, the inlet primary air temperature (T_1), the inlet primary air relative humidity (R_1), the outlet primary air temperature (T_3), the outlet primary air relative humidity (R_3), the inlet secondary air temperature (T_4), the inlet secondary air relative humidity (R_4) were measured. To respectively assess the operating performance of M-LHX and SHX, the temperature and relative humidity of the primary air downstream of the M-LHX (T_2 and R_2), those of the secondary air downstream of the SHX (T_5 and R_5) were also measured. listed in Table 3, commercial hygrometers were installed at each measuring point for obtaining the temperature and relative humidity of inlet and outlet air conditions. The air flow rate of the primary air (F_1) and the secondary air (F_2) were measured by installing the vane probes downstream of the primary air and secondary air, respectively.

Tab. 3 – Sensor characteristics.

Variable	Sensor type	Range	Accuracy
Temp. /humid.	Thermal hygrometer	-20–60 ºC (Temp.)	±0.5 °C (Temp.)
		0–100% (Humid.)	±1.8% (Humid.)
Air velocity	Vane probe	0.1–15 m/s	± 0.1 m/s

4. Results and discussions

4.1 Uncertainty analysis

Uncertainty analysis was performed for each measured parameter based on ASHRAE guidelines [5]. The overall uncertainty for each variable (U_y) was estimated using equation 4, with the propagated error (B_y), and the random error (P_y). The propagated error was obtained using the fixed error for each variable (b_{x_i}), which can be calculated by multiplying the sensor error and the standard deviation of the measured data (equation 5). The random error was estimated by equation 6 using the standard deviation of the measured data. The overall

uncertainty values of the measured inlet and outlet parameters for each mode are listed in Table 4.

$$U_y = ({B_y}^2 + {P_y}^2)^{1/2} \quad (4)$$

$$B_y = [\sum_{i=1}^{n}(\frac{dy}{dx_i} b_{x_i})^2]^{1/2} \quad (5)$$

$$P_y = \frac{2S_r}{\sqrt{M}} \quad (6)$$

Tab. 4 – Overall uncertainty

Overall uncertainty of measured parameter [%]			
Measuring parameters	Operating mode		
	1	2	3
T_1	1.29	2.26	1.67
R_1	5.13	7.69	4.56
T_2	0.45	2.42	1.56
R_2	4.21	6.45	4.78
T_3	1.84	2.74	2.08
R_3	5.54	7.16	4.65
T_4	0.45	5.35	1.09
R_4	1.74	6.87	4.23
T_5	1.62	5.74	2.24
R_5	3.12	6.38	6.51
F_1	0.77	0.85	0.74
F_2	0.64	0.66	0.71

4.2 Operating characteristics

4.2.1 Operating mode 1

Figure 4 presents the experimental results for the temperature and humidity behaviours of the air flows for operation mode 1. Owing to heat and moisture exchange between the introduced secondary air from the M-LHX, the inlet primary air (28.3 ºC, 19.3 g/kg) was cooled to an average of 27.9ºC, and dehumidified to an average of 11 g/kg when the 23.8 ºC, 8.26 g/kg of the secondary air was introduced. In addition, the primary air entering the SHX was cooled to an average of 25 ºC and maintained 10.8 g/kg of humidity ratio. This results indicate that the proposed ventilation unit could supply the ventilation air at nearly neutral air temperature and humidity ratio by recovering sufficient amount of sensible and latent heat from the secondary air. In addition, one can see that the proposed ventilation unit could provide decoupled heat and moisture recovery performance from M-LHX and SHX.

In terms of the heat and moisture recovery performance, the sensible effectiveness, latent effectiveness, and the enthalpy effectiveness respectively ranged 65–74.4%, 70.3–81.5%, and 72.8–78.3%. Particularly, one can see that the proposed ventilation unit exhibits higher latent effectiveness compared with the commercial ERV (30–60%) from the M-LHX.

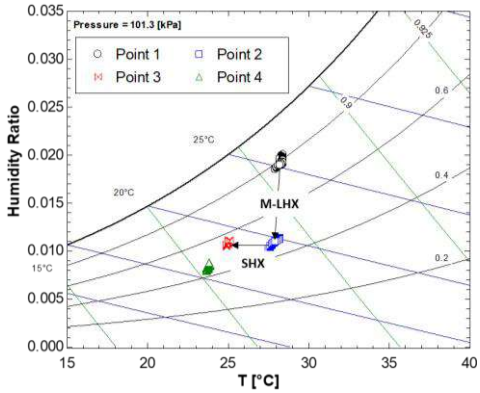

Fig. 4 – Temperature and humidity behaviours of air flows for mode 1

4.2.2 Operating mode 2

Figure 5 presents the experimental results for the temperature and humidity behaviours of the air flows for operation mode 2. The inlet primary air (20.9 ºC, 12.6 g/kg) was dehumidified by M-LHX to an average of 10.2 g/kg, but occurs slight temperature increase to an average of 22.3 ºC when the 24 ºC, 8.96 g/kg of the secondary air was introduced.

The sensible effectiveness, the latent effectiveness, and the enthalpy effectiveness ranged 40.6–48.2%, 70.7–78.6%, and 77.6–82.8%. This results indicate that the proposed ventilation unit could provide satisfactory latent cooling performance, and minimize unnecessary heat exchange with RA only by entering M-LHX.

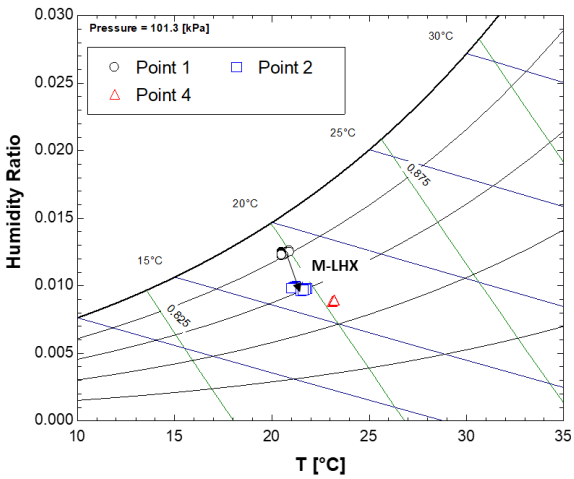

Fig. 5 – Temperature and humidity behaviours of air flows for mode 2

4.2.2 Operating mode 3

Figure 6 presents the temperature and humidity behaviours of the air flows for operation mode 3. The

inlet primary air (9.1 ºC, 2.8 g/kg) was initially heated and humidified by M-LHX to an average of 14.3 ºC and an average of 4.75 g/kg when the inlet secondary air is 20 ºCm 6.67 g/kg. Then, the SHX heated the primary air to an average of 18.6 ºC.

The sensible effectiveness, the latent effectiveness, and the enthalpy effectiveness ranged 71.2–80%, 65.3–73.5%, and 84.4–86.8%. This results indicate that the proposed ventilation unit showed relatively lower latent effectiveness compared with the operation mode in cooling seasons, but the proposed unit showed enhanced sensible and latent heating effectiveness compared with the conventional ERV.

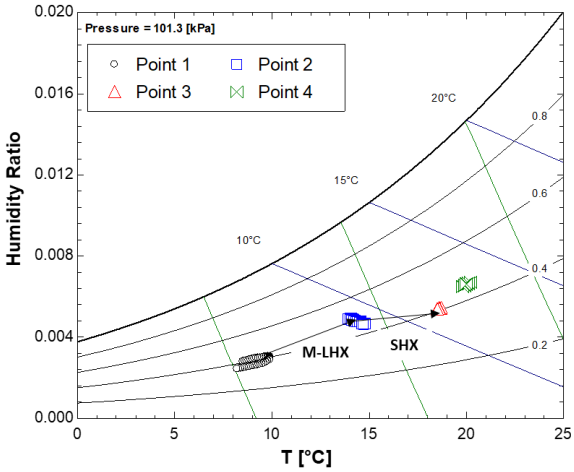

Fig. 6 – Temperature and humidity behaviours of air flows for mode 2

5. Conclusions

This paper experimentally investigated the seasonal operating performance of the packaged unit of a membrane-based ventilation system. The packaged unit of the proposed ventilation system was fabricated, and the experiments was conducted based on the test standards for the energy recovery ventilator addressed from air-conditioning, heating and refrigeration institute (AHRI). In addition, for achieving the optimal heat and moisture recovery from the ventilation system under various operating conditions, the seasonal operation modes were suggested.

The experimental results showed reliable air temperature and humidity behaviors that correspond to the inlet primary and secondary air conditions. In addition, the average sensible effectiveness, the average latent effectiveness, and the average enthalpy effectiveness of the proposed ventilation system are 70.7%, 75.9%, and 75.6% in mode 1; 44.4%, 74.7%, 80.2% in mode 2; 77.6%, 70.4%, 85.6% in mode 3. This indicates that the proposed ventilation system showed higher heat and moisture recovery performance compared with the commercial ERV during annual operation owing to its higher latent heat recovery performance from M-LHX and its selective operation strategies based on OA conditions.

Consequently, this study showed that the proposed ventilation unit has energy saving potential in HVAC application in terms of its energy recovery performance. However, further study should evaluate its fan energy for considering the energy efficiency of the proposed ventilation unit.

6. Acknowledgement

This work was supported by Korea Institute of Energy Technology Evaluation and Planning(KETEP) grant funded by the Korea government(MOTIE) (No. 20202020800360), and this work was supported by Korea Environment Industry & Technology Institute (KEITI) through Prospective green technology innovation project, funded by Korea Ministry of Environment (MOE) (RE202103243).

7. References

[1] AHRI. ANSI/AHRI 1060 2011 standard for performance rating of air- to-air heat exchangers for energy recovery ventilation equipment. Arlington: VA. Air-Conditioning, Heating, and Refrigeration Institute; 2011.

[2] Cho H.J., Cheon S.Y, Jeong J.W. Preliminary study on air-to-air latent heat exchanger fabricated using hollow fiber composite membrane for air-conditioning applications, Energy conversion and management, 251 (2022).

[3] Cho H.J., Kim B.J., Lee J.H. Jeong J.W. Experimental Analysis of Energy Recovery Performance of a Hollow Fiber Membrane-based Ventilation System, Proceeding of ASHRAE Virtual Annual Conference, (2021).

[4] Cho H.J., Cheon S.Y., Jo S.Y., Kim M.S., Jeong J.W. Energy Benefit of a Hollow Fiber Membrane Dehumidification-based Ventilation System in an Office Building, Proceeding of ISHVAC2021, 251 (2021).

[5] ASHRAE Guideline 2-2010. 2010. Engineering analysis of experimental data.

Multi-zone Dynamic Simulations for Investigation of Occupant Behaviour and Building Performance

Elisa Venturi[a], Fabian Ochs[a], Mara Magni[a]

[a] Unit for Energy Efficient Buildings, University of Innsbruck, Technikerstraβe 20, 6020, Innsbruck, Austria, elisa.venturi@uibk.ac.at

Abstract. The study aims to investigate the correlation between occupant preferences, occupant thermal comfort and building energy performances by means of dynamic building simulations. Moreover, the design power of a central heating system is studied in correlation with an increasing number of occupants with non-standard behaviour. A building consisting of 24 office rooms and a common traffic zone, distributed on 3 floors is simulated in MATLAB Simulink environment. The heating demand evaluated considering the climate of Stuttgart accounts for 49 kWh/(m²a), which decreases to 17 kWh/(m²a) when the mechanical ventilation heat recovery is implemented, i.e. thermal building quality according to the Passive House standard. Furthermore, the climates of Rome and Stockholm are considered to take into account the effects of different boundary conditions. A floor heating system is implemented in every office room and the hot water is supplied by a central heat pump. Non-standard behaviour (i.e. setpoint temperature, window shading, window opening and a combination of them) in an increasing number of offices is implemented to study the impact on the heating demand, on the thermal comfort (room temperature and floor temperature) and on the design power of a central heating system. Peculiar behaviours of some of the occupants can have a relative influence on the building performance. For example, extensive ventilation in only one office can have the same impact on the building space heating demand as higher setpoint or shading in several offices at the same time. Results of the dynamic simulations address the robustness of a central heat pump compared to an electric system. Moreover, a general correlation between the number of office rooms with non-standard behaviour and increase of space heating demand cannot be found as the correlation depends on climate and quality of the building envelope. Finally, the position of the office with non-standard ventilation has an impact on the required heating power.

Keywords. Multi-zone simulation, occupant behaviour, building performance, floor heating system, heat pump, space heating demand, design power, robust system
DOI: https://doi.org/10.34641/clima.2022.409

1. Introduction

Occupant behaviour can heavily influence the building performances and it is one of the most common reasons for differences between design energy demand and monitored energy demand (1). Moreover, considering a different input of occupant behaviours has an impact on the building and system performances (2), (3). However, it is not clear if it is possible to foresee the increase of space heating demand due to the increase of occupants with non-standard behaviour (i.e. more energy-consuming behaviours). In addition, an open question is how the design power of the heating system would change if an increasing number of occupants with non-standard behaviour is considered, along with the robustness of the heating system (4). This study investigates these topics, performing multizone simulations in MATLAB Simulink environment. The building model used in the current study is CarnotUIBK (5), which implements elements of the CARNOT toolbox (6). One advantage of the CarnotUIBK building model is the easily rezoning, thanks to the first import of the rooms and the following grouping into thermal zones. The accuracy of CarnotUIBK has been tested in several projects. Among them, a recent study (7) proves the agreements in the results between the CarnotUIBK and the ALMABuild building model, both working in MATLAB environment. Moreover, the study demonstrates the accordance of the evaluated space heating demand when a building is simulated with a single-zone and a multi-zone approach (under

Copyright ©2022 by the authors. This conference paper is published under a CC-BY-4.0 license.

the same inputs), proving the robustness of the model and the possibility to investigate more in detail on zone-level.

2. Methods

In the current study, multizone simulations are performed considering different envelope levels and climates (as described in 2.1), different offices with non-standard behaviour (described 2.2) and different space heating systems (described in 2.3).

2.1 Building description

A simplified building consisting of 24 office rooms (from A1 to H3) and a common traffic zone, distributed on 3 floors (see **Fig. 1**) is dynamically simulated in MATLAB Simulink environment, using the building model CarnotUIBK and the CARNOT toolbox. Simulations are performed in the climates of Stuttgart, Rome and Stockholm.

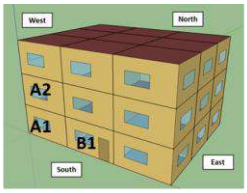

Ground floor			First floor			Second floor		
F1	G1	H1	F2	G2	H2	F3	G3	H3
D1	COMM	E1	D2	COMM	E2	D3	COMM	E3
A1	B1	C1	A2	B2	C2	A3	B3	C3

***Fig. 1** - Sketch of the building and location of the offices.*

Two envelope levels are considered: Low Energy Building (LEB) and Passive House (PH). The properties of the envelopes are presented in **Tab. 1**.

***Tab. 1** - Properties of the LEB envelope and of the PH envelope.*

	LEB	PH
U-value External wall [W/(m² K)]	0.182	0.125
U-value Floor [W/(m² K)]	0.135	0.135
U-value Roof [W/(m² K)]	0.162	0.085
n_{50}	0.6	0.6
MVHR efficiency	0	75%

2.2 Thermal zoning and offices with non-standard behaviour

Multi-thermal zones simulations are performed, considering the offices in the corners (A1, C1, F1, H1, A3, C3, F3, and H3) as different thermal zones, while the remaining offices and common room are considered as a unique thermal zone (called "central thermal zone"). The influence of people on the building performance is investigated, considering standard and non-standard behaviours in the offices, as they are defined in **Tab. 2**.

***Tab. 2** - Properties of offices with standard and non-standard behaviour.*

	Standard behaviour	Non-standard behaviour
Setpoint room temperature	20°C	22.5°C
Shadings	None	Windows shaded (70%) from 08:00 to 18:00 on weekdays
Window ventilation	None	Windows always tilted of 10°

Firstly, the building with all the offices with standard behaviour is simulated. Secondly, a combination of the offices with non-standard behaviour is considered. This approach allows studying the correlation between the number of non-standard offices with the performances of the building and of the system. The building is simulated with 1, 2, 6, or 8 (or none) offices with non-standard behaviour (as shown in **Tab. 3**), which correspond to 4%, 8%, 25%, or 36% (or 0%) of the offices in the building. The 8 offices are those located in the corners of the building. This choice has been made to investigate the non-standard behaviours in the most exposed offices to the external ambient. Afterwards, the non-standard behaviour is implemented at one office at a time, in order to study the influence of orientation and position of the "non-standard office" on the building performances.

***Tab. 3** - Offices with non-standard behaviour.*

Number of offices with non-standard behaviour (and % respect to the total number of offices)	Offices with non-standard behaviour
0 (0%)	None
1 (4%)	A1
2 (8%)	A1, H3
6 (25%)	A1, C1, F1, C3, F3, H3
8 (36%)	A1, C1, F1, H1, A3, C3, F3, H3

2.3 Space heating system

In the central thermal zone, ideal heating and ideal cooling are implemented, to maintain a temperature

of 20°C in winter and 25°C in summer. The offices in the corners are heated with a floor heating (FH) system, while in summer the temperature is not controlled (no cooling system). Eight FH systems are implemented, one for each thermal zone (excepted the central thermal zone).

Each FH system has been implemented in MATLAB Simulink as an ideal floor heating (active power in the floor) and later post-processed to evaluate the required flow temperature of the hydraulic floor heating system and the required power from a central heat pump (HP). The FH power is set to 875 W in each office and the system is controlled in order to meet the setpoint room temperature and to keep the active layer at a maximum temperature of 29°C. For every floor heating system, the mass flow and the flow temperature are calculated as follow (equations (1) and (2)).

The mass flow of the floor heating is evaluated according to equation (1)

$$\dot{m} = \frac{P_{FH}}{c_p \cdot (\vartheta_{flow} - \vartheta_{return})} \qquad (1)$$

The design difference between flow and return temperature of the floor heating is set to 5 K.

The flow temperature is evaluated from equation (2)

$$P_{FH} = U \cdot A \cdot \Delta\vartheta_{log} \qquad (2)$$

where U is evaluated considering both convection and conduction (using the temperature of the active layer, the room temperature and the superficial temperature of the floor).

The performances of a central heat pump, which provides hot water for all the FH systems, are evaluated considering the Carnot COP, knowing the ambient temperature, the flow temperature of the floor heating and a reference COP value of 4 for an air-water HP A7/W35. The flow temperature is evaluated as the maximum of the flow temperature of all the FH systems. The mass flow is evaluated as the sum of the mass flows of all the FH systems.

Moreover, simulations are performed with two different approaches for the heating system:

- Sys1: ideal system (unlimited power). This system is not representative of the reality (especially for floor heating, where the floor temperature cannot exceed 29-30°C for health reasons). However, this approach allows to directly compare the space heating demand among simulations with different number of offices with non-standard behaviour.
- Sys2: real system (limited power), system as described before. This approach represents a real system. The heating power guarantees the comfort in all the thermal zones in standard conditions, but the comfort is not guaranteed when offices have non-standard behaviour. The space heating demand is not directly comparable among simulations with different number of non-standard behaviours.

3. Results

In this section, the space heating demand on building level is compared for different climates, building envelope and number of offices with non-standard behaviour. Moreover, the thermal comfort is discussed considering zones with different behaviour and simulation with the two approaches to the heating system (Sys1 and Sys2). Finally, the power required from a HP system is investigated, considering different numbers, orientations and positions of the offices with non-standard behaviour.

3.1 Space heating demand

The space heating demand in case of all offices with standard behaviour is shown in **Tab. 4**. For sake of simplicity, they will be referred to as "references cases".

Tab. 4 *- Space system demand evaluated with different climates and building envelopes. All offices with standard behaviour (reference cases).*

	Space heating demand [kWh/(m² a)]	
	LEB	PH
Rome	14.6	1.8
Stuttgart	49.5	17.2
Stockholm	67.5	27.6

The increase of space heating demand due to either the change of setpoint temperature or the implementation of shadings or window openings with respect to the reference case of Stuttgart with LEB envelope is presented in **Fig. 2**. Results are shown for an increasing number of offices with non-standard behaviour and for the two approaches of heating system. Due to the ventilation conditions chosen for the current study, the increase of space heating demand is dominated by the ventilation losses, while shadings and setpoint have a similar influence on the space heating demand. The increase of offices with non-standard behaviour leads to a linear increase in space heating demand. **Fig. 2** shows that the extensive window ventilation in only one office has a higher effect on the heating demand than the change of setpoint and window shading applied in 8 offices. A great difference is highlighted

between the two approaches of heating system. In case of 8 offices with non-standard behaviour and windows ventilation, the increase of space heating of 50 kWh/(m²a) in case of Sys2 rises to 113 kWh/(m²a) in case of Sys1. With the combination of the calculated space heating demand, it is possible to evaluate the required energy for a combination of behaviours in the offices, i.e. some standard offices, some offices with only ventilation, others with only shadings, etc.

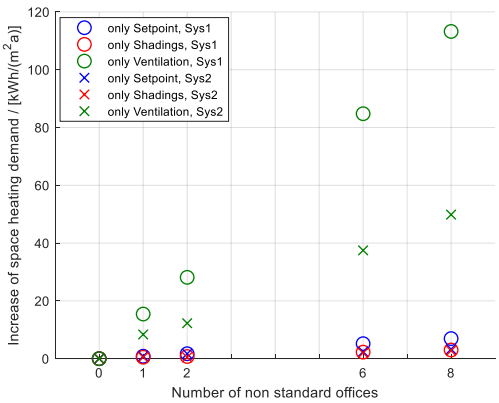

***Fig. 2** - Increase of space heating demand due to increasing number of offices with non-standard behaviour. Comparison of approaches Sys1 and Sys2. Case of Stuttgart LEB.*

In order to consider the maximum possible increase of space heating demand under the conditions of the current study, the investigation proceeds considering the combination of the three user behaviours simultaneously. **Fig. 3** shows the increase of space heating demand for an increasing number of offices with non-standard behaviour considering different climates and different envelope qualities. In case of ideal power (Sys1) – see **Fig. 3(a)** – the climate plays the main role in the space heating demand increase. Nevertheless, when the real system is implemented (Sys2) – see **Fig. 3(b)** – the increase is influenced both by climate and envelope quality. Moreover, in case of Sys2 the required energy is underestimated, as the thermal comfort is not reached in several offices (see next section 3.2).

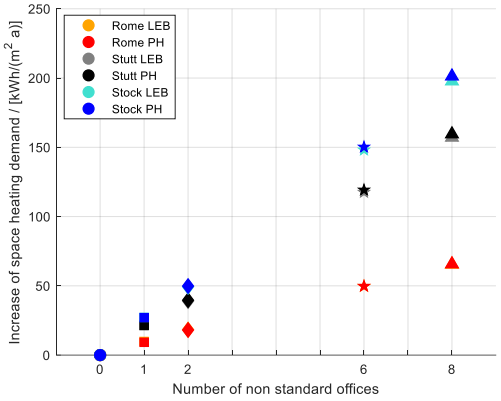

(a)

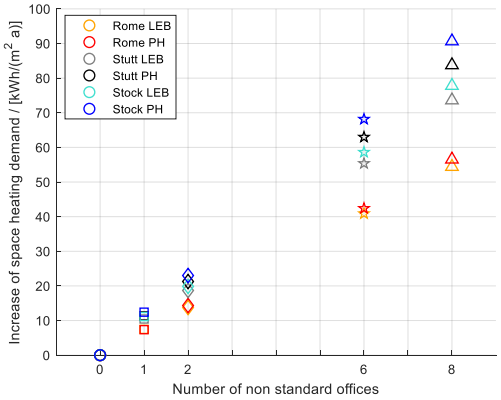

(b)

***Fig. 3** - Increase of the space heating demand with the increasing number of offices with non-standard behaviour. Results with Sys1 (a) and Sys2 (b).*

Monthly values of the space heating demand with different climates and different numbers of non-standard offices are presented in **Fig. 4.** Moreover, the wider and brighter columns represent the approach Sys1, while thinner and darker columns represent results from approach Sys2. In all the climates, the biggest difference in space heating demand between standard behaviour and some offices with non-standard behaviour (Sys1) is highlighted in winter. When the Sys2 is implemented, there is a quite constant increase in space heating demand throughout the months because the comfort is not fulfilled. No difference between Sys1 and Sys2 is presented for reference cases (i.e. all standard behaviour) because the comfort is always guaranteed. The non-standard behaviour of some offices leads to space heating demand also in summer for the climates of Stuttgart and Stockholm.

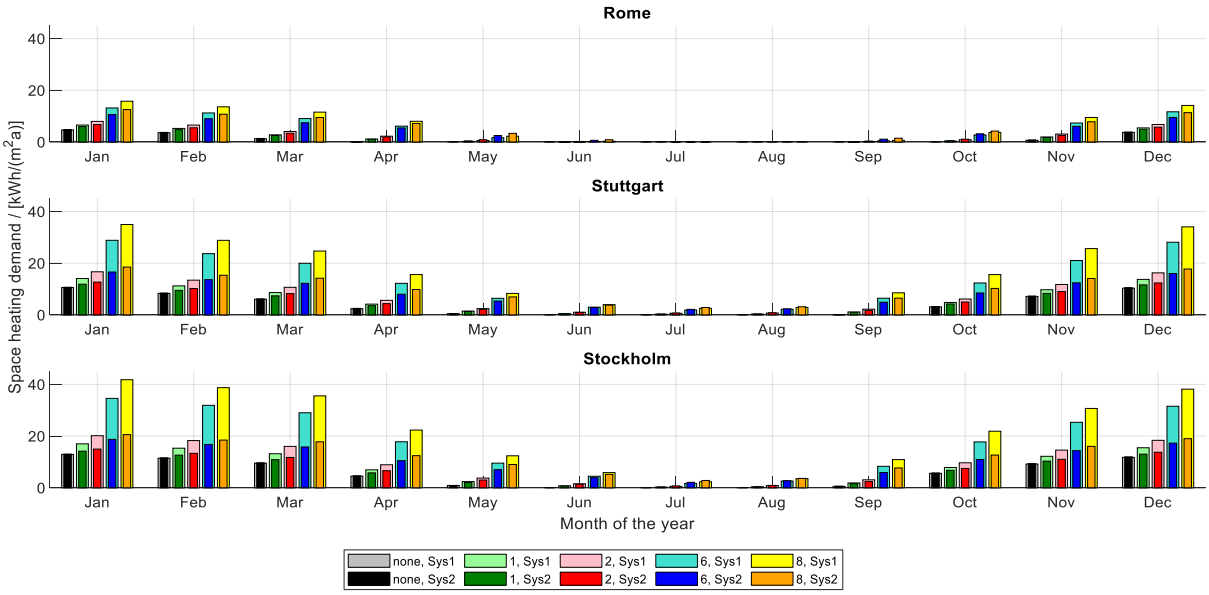

Fig. 4 *- Monthly values of the space heating demand evaluated in three cities with the LEB envelope. Different colours represent different cases for the number of offices with non-standard behaviour and approach to the heating system.*

3.2 Thermal comfort

When the "real system" (Sys2) is implemented, the comfort is not guaranteed for offices with non-standard behaviour. The system working at the maximum power is not able to keep the room temperature at the setpoint. An example is given with **Fig. 5**, results referred to Stuttgart, LEB envelope, non-standard behaviour of the office A1. The room temperature of all the offices meets the thermal comfort, except for office A1 (green line). The temperature of the floor of all the offices is always below 29°C, as required for the comfort of the occupants.

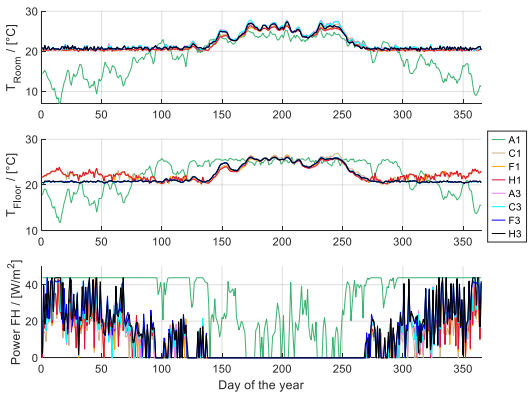

Fig. 5 *- Case of non-standard behaviour of A1, climate of Stuttgart, LEB envelope, "real system" (Sys2). Dynamic temperatures and heating power to study the comfort in the offices.*

When the Sys1 approach for the heating system (infinite power) is applied, the room temperature of the office room A1 always meets the setpoint temperature (22.5°C). The floor temperature is higher than the limit, proving the non-feasibility of this system in the reality (**Fig. 6**).

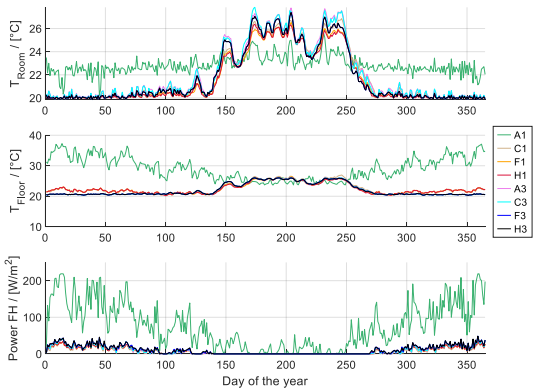

Fig. 6 *- Case of non-standard behaviour of A1, climate of Stuttgart, LEB envelope, "infinite power system" (Sys1). Dynamic temperatures and heating power to study the comfort in the offices.*

3.3 Power of the space heating system

The sorted heating load and the sorted electric power required by a heat pump system in one year are presented in **Fig. 7**. Results are presented for the LEB building in the climate of Stuttgart. The difference between the heating load and the power to be supplied to the HP represents the beneficial effect of the heat pump (COP>1). If a completely electric system is installed, the required power would correspond to the heating load. In case of ideal system (Sys1, **Fig. 7a**), the maximum power (both of heating load and HP power) increases with the increasing number of offices with non-standard behaviour. While with a real system (Sys2, **Fig. 7b**), the maximum heating load of 7kW is common for

every case. Moreover, the maximum heating load in case of 8 offices with non-standard behaviour is constant for 180 days. With both approaches (Sys1 and Sys2) the implementation of a fully electric system would lead to a bigger increase of heating power with the increasing number of offices with non-standard behaviour. Therefore, the HP system is preferable to mitigate the effects of the occupant behaviour.

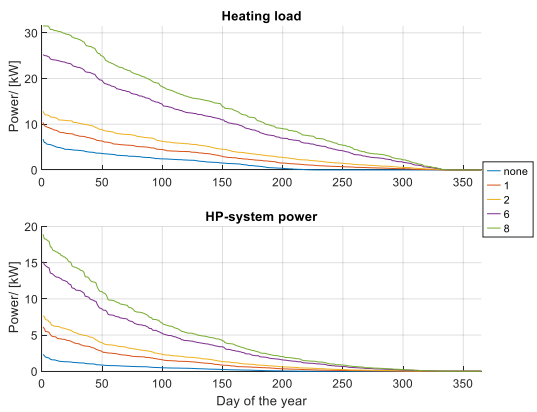

(a)

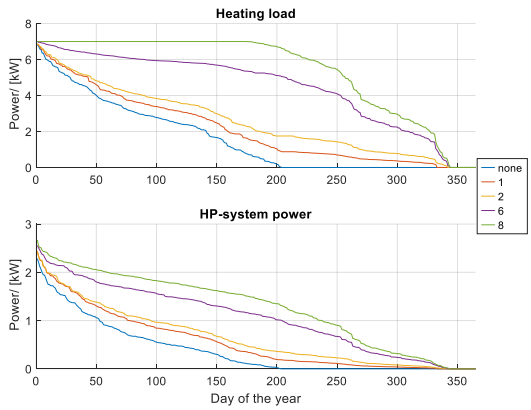

(b)

Fig. 7 *- Sorted heating load and electric power for a HP with approach Sys1 (a) and with Sys 2 (b) considering LEB building in Stuttgart. Comparison among different number of offices with non-standard behaviour.*

In order to investigate the effect of orientation and position of the office with non-standard behaviour, the three behaviours are considered separately. 8 cases are simulated: for each case a different office is considered with non-standard behaviour. Changes in setpoint and shading do not show appreciable differences among the heating power of the 8 cases. On the contrary, the sorted electric power required by the HP in case of only non-standard ventilation in one office presents a clear difference among the considered offices (see **Fig. 8**). The plot presents results for the case of LEB envelope in Stuttgart. A difference is presented between offices with non-standard behaviour on the ground floor and on the second floor. The ones on the ground floor require higher heating power. The orientation of the office doesn't influence the heating power appreciably.

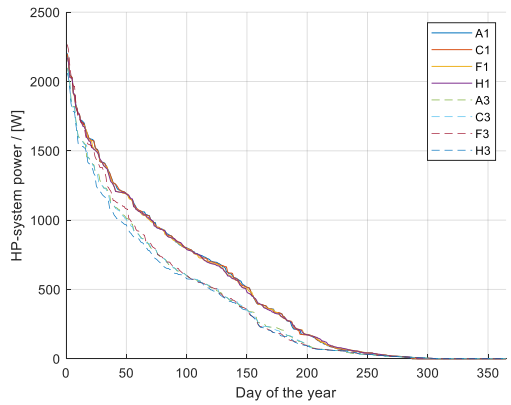

Fig. 8 *- Sorted heating power for a HP system (Sys 2) for cases with one office with only ventilation as non-standard behaviour. Comparison among cases with only one office with non-standard behaviour and different position (solid line for offices on the ground floor, dashed line for offices on the second floor) and orientation in the building. Case of Stuttgart, LEB envelope.*

4. Conclusions

Multizone dynamic simulations have been carried out for an office building considering different envelope qualities, climates, number and position of offices with non-standard behaviour and space heating systems. The increasing number of offices with non-standard behaviour leads to a higher electric power to be provided to the HP (case of infinite power). When a real system is implemented, the maximum power is independent of the number of non-standard offices because comfort cannot be guaranteed. With both approaches (ideal and real system) the increase of power is lower than what would be required from an electric system, proving the robustness of a HP system with the increasing number of offices with non-standard behaviour. A non-standard ventilation in only one office can have the same (or higher) effect on the building space heating demand as the non-standard setpoint or shading in 8 offices at the same time. When the office with non-standard ventilation is located on the ground floor, the heating power is higher than the power required in case the office with non-standard ventilation is located on the second floor. Due to the limited power of the FH system, the thermal comfort of the room temperature cannot be fulfilled when an office has non-standard behaviour. Finally, there is a linear increase of space heating demand with the increasing number of offices with non-standard behaviour (for either non-standard setpoint, non-standard shading, non-standard ventilation and the combination of them). It is not possible to foresee the space heating demand based on the number of offices with non-standard behaviour because climate and envelope lead to different trends.

5. References

1. Liu P, Lin B, Wu X, Zhou H. Bridging energy performance gaps of green office buildings via more targeted operations management: A system dynamics approach. J Environ Manage [Internet]. 2019;238(September 2018):64–71. Available from: https://doi.org/10.1016/j.jenvman.2019.02.111

2. Barthelmes VM, Becchio C, Fabi V, Corgnati SP. Occupant behaviour lifestyles and effects on building energy use: Investigation on high and low performing building features. Energy Procedia [Internet]. 2017;140:93–101. Available from: https://doi.org/10.1016/j.egypro.2017.11.126

3. Calì D, Andersen RK, Müller D, Olesen BW. Analysis of occupants' behavior related to the use of windows in German households. Build Environ. 2016;103:54–69.

4. Calì D, Osterhage T, Streblow R, Müller D. Energy performance gap in refurbished German dwellings: Lesson learned from a field test. Energy Build [Internet]. 2016;127:1146–58. Available from: http://dx.doi.org/10.1016/j.enbuild.2016.05.020

5. Siegele D, Leonardi E, Ochs F. A new MATLAB Simulink Toolbox for Dynamic Building Simulation with B.I.M. and Hardware in the Loop compatibility. Proc Build Simul 2019 16th Conf IBPSA. 2020;16:2651–8.

6. Solar-Institut Juelich. CARNOT Toolbox Ver. 6.3, 10/2018 for Matlab/Simulink R2018b. 2018.

7. Pacillo V, Naldi C, Venturi E, Ochs F, Morini GL, Magni M, et al. Effect of the building zoning on the energy consumption with different dynamic energy simulation tools:ALMABEST versus carnotUIBK. 2021;

Data Statement

The datasets generated during and/or analysed during the current study are not publicly available because of ongoing works, but will be available by contacting and agreeing with the authors.

Energy consumption patterns in a hotel building – A case study

Marek Borowski [a], Klaudia Zwolińska [a], Marcin Czerwiński [b]

[a] Faculty of Civil Engineering and Resource Management, AGH University of Science and Technology, Kraków, Poland, borowski@agh.edu.pl (M.B.), kzwolinska@agh.edu.pl (K.Z.).

[b] Frapol Sp. z o.o., 30-832 Kraków, Poland, marcin.czerwinski@frapol.com.pl.

Abstract. The hospitality industry is one of the most energy-intensive subsectors of the tourism sector. Most of the total energy consumption is due to maintaining an optimal temperature inside the occupied rooms. Conditions inside hotel rooms, hotel infrastructure, including tourist attractions such as swimming pools, restaurants, conference rooms, have a significant impact on the overall energy consumption of this sector. Hotels, unlike other commercial buildings, are characterized by the separation of functional areas. Additionally, the heat loads that change over time are difficult to estimate. The research was carried out in the historic hotel Turówka, which is a reconstruction of the historic salt sales point from 1812. Due to the historical nature of the building (entered in the register of monuments), the thermal modernization of the hotel, adjusting it to the prevailing energy standards, is a big challenge for designers. The work aims to determine the structure of the building's heating and cooling energy demand. Additionally, the factors influencing the building's energy demand in the building during the summer period are determined. The analysis focused on identifying typical patterns of weekly and daily demand and examining the correlation between meteorological parameters and the observed energy consumption. Based on the obtained results, factors that significantly affect the consumption of thermal energy in the building were identified. The article covers the analysis of the energy performance of the building, including the energy demand of three systems in the building: the cooling system, domestic hot water preparation, and the demand of the swimming pool area. Measurements of energy consumption were carried out continuously, using installed heat and cooling energy meters in key places of the installation. An in-depth energy analysis of a building is a necessary element to improve its energy performance and adapt it to the requirements of low-energy buildings. Monitoring the energy consumption of your building system can help you optimize energy use.

Keywords. Energy demand, energy consumption pattern, hotel building.
DOI: https://doi.org/10.34641/clima.2022.187

1. Introduction

Nowadays, reducing energy consumption is one of the fundamental challenges of civilization. This is the result of both economic reasons and environmental aspects. Reducing energy demand allows lower operating costs of the building or installation and minimizes the negative impact of human activity. Together, the building and construction sector accounts for more than one-third of global final energy consumption. There are many methods to reduce energy consumption. Firstly, the crucial sources of energy consumption should be identified. At this stage, an analysis of energy consumption throughout the year is necessary. In this way, the focus may be on the most energy-consuming system or parts of the facilities. The energy consumption in buildings depends to a large extent, on the losses caused by heat exchange between the building and its surroundings. Therefore, the most popular method of reducing energy consumption is to increase the thermal insulation of partitions and to replace the windows. The appropriate management of energy and the environment in buildings can also bring significant benefits. In this way, it is possible to identify areas where savings can be made and implement improvements that increase the energy efficiency of the building.

The hotel is a specific type of facility due to the separation of various zones of use and functionality. Creating the ideal indoor environment in this type of building is crucial, as it affects the economic benefit and profitability of the facility. Requirements for hotels, including those relating to providing customers with adequate thermal comfort - both in

Copyright ©2022 by the authors. This conference paper is published under a CC-BY-4.0 license.

the winter and summer months, make the issues of economic energy management a priority due to the profitability of this type of activity. Hotel facilities rank among the top five in terms of energy consumption in the service sector [1]. The predominant part of the energy consumed in hotels is the energy required to provide a comfortable indoor environment for users. The main energy-consuming activities in hotel buildings include space heating, cooling, lighting, preparing hot water, preparing meals, and systems of swimming pools [1].

The energy consumption of a hotel is influenced by both the physical parameters and operating conditions of the building. Physical parameters include, but are not limited to, the size, structure, facility, its geographic and climatic location, the age of the facility, and the type of energy and water systems installed. Operational parameters that affect energy consumption in hotels include the operating schedules of functional parts, services offered, fluctuations in occupancy levels, differences in customer preferences for indoor comfort. Moreover, crucial factors are local energy-savings practices, the culture, and awareness of resource consumption among users [1] [2].

The literature includes many papers [2-6] on monitoring energy consumption and analysis of energy demand in hotel buildings. Bohdanowicz and Martinac [3] studied water and energy consumption in hotels of two different brands. Besides the difference between the two brands, many important factors that influenced the energy demand in hotels were identified. These parameters include the standard of the hotel, location/climate, size of the facility, occurrence of energy- and water-intensive services, the number of hired rooms, and amount of laundry washed on site. Santiago [4] presented and compared energy models of six hotels in Gran Canaria. According to this study, the highest energy consumption of the facilities is due to the food services, followed by the hot water preparation system. The regression analysis showed that among 31 different characteristics, revenue per available room, swimming pool size, number of guests, and average number of guests per occupied room could explain the total energy demand of the studied hotels. Wang et al. [5] present an analysis of hotel building energy performance using BEMS and energy modelling data. The authors noticed the decisive influence of two parameters on energy consumption: the ambient temperature and the occupancy of hotel rooms.

The paper presents the consumption of heat and cooling energy divided into three systems inside the facility: a cooling system, a system for preparing hot water, and a heating system for the swimming pool. The analysis considered the energy characteristics of the facility from May to September 2019. The variability of parameters on a weekly and monthly basis over the study period was examined.

2. Research Methods

2.1 Characteristics of the building

The subject of the study is the historic hotel Turówka, entered in the register of monuments. The analysed building is a 5-story hotel, four of which are above ground and one underground. The usable area of the hotel facility is 4,620.00 m^2, with a built-up area of 1,370.00 m^2. The facility has 49 double rooms, one single room, and an apartment. The hotel features a recreational facility, including a swimming pool, salt cave, sauna. There is also a restaurant, drink bar, and conference room. The ventilation air is supplied to separate zones using independent installations. Separate installations are equipped in individual air handling units with heat recovery without recirculation. In summer, air cooling is provided by a chilled water system with a chiller located outside the building. The temperature of ventilation air is regulated centrally in the heat exchanger located in the air-handing unit. Additionally, the inside temperature could be controlled locally by using fan coils in rooms. The hot water installation is supplied from the gas boiler room located on the top floor. A detailed description of the systems inside the building can be found in the paper by Borowski et al. [6].

2.2 Measurements and analysis method

The paper includes an analysis of the energy performance of a building. The cooling demand of the facility is examined. The study also considers the heating energy consumption of two systems, i.e., the domestic hot water (DHW) system and the heating system of the swimming pool area. The study covers five months period from May to September 2019. In this period, both heating and cooling energy consumption are observed. The systems were analysed both on a monthly and weekly basis. The systems have been equipped with Kamstrup Multical 403 heat meters. Data were transmitted via a serial communications protocol - MODBUS RTU and stored in a database system. The measurements also included the outdoor temperature directly at the hotel area. Readings were taken at one-minute intervals. Then, to simplify the further analysis, the values were presented with hourly averaging. The prepared data was used to develop variation charts and to examine the impact of identified factors on the energy demand of analysed systems. The factors included outdoor temperature, hotel occupancy, and hour of operation or the day of the week. The occupancy level was assumed as the percentage of occupied rooms in the hotel. To determine the variability of energy demand, one week from each month was selected. Based on this data, a detailed analysis was carried out. The average daily energy demand for each of the systems was also determined separately for the months included in the analysis. The monthly demand for cooling and heating energy was also calculated. The heating energy consumption included both heating systems: a domestic hot water preparation system and a pool area heating system.

3. Results and discussion

The following chapter contains the results of the analysis and the most important observations. Sections below include the preliminary analysis of the collected data, weekly analysis, and the impact of the identified factors on the energy consumption in the hotel.

3.1 Preliminary analysis

In the beginning, the range of measured parameters considered in further analysis was determined. Table 1 contains ranges of the analysed values for five months. As is shown, the observed temperatures dropped even below the value of 5 °C during the analysed period. The occupancy rate varied between 11 and 100%. Energy consumption did not exceed 141.3 kWh/h for the cooling, and 87 kWh/h for the DHW system. The maximum demand for heating energy in the swimming pool area was 63.7 kWh/h.

Tab. 1 - The range of measured parameters.

Parameter/ Energy consumption	Min	Max
Outdoor temperature, °C	3.2	36.2
Occupancy level, %	11.3	100.0
Cooling energy, kWh/h	0.0	141.3
Heating energy (DHW), kWh/h	0.0	87.0
Heating energy (Pool), kWh/h	0.0	63.7

In the next stage, the distribution of external temperature during the research period was analysed.

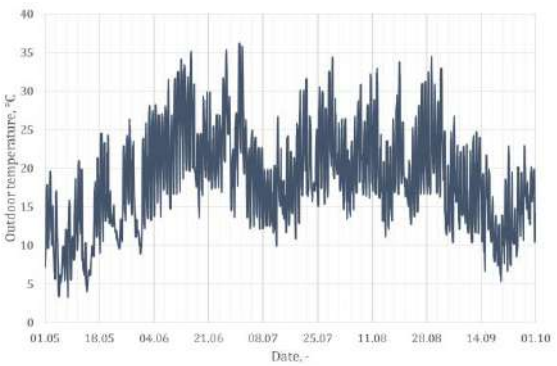

Fig. 1 - Distribution of outdoor temperature on the hotel area from May to September 2019.

In the climate characteristic of this area, the highest temperatures usually occur in July. As can be seen, in the hotel area in 2019, the highest indications were recorded in June. In July, a clear decrease in temperature is visible.

In the next step, the average daily energy consumption for each month was determined. Figure 2 presents the results with the average outdoor temperature marked.

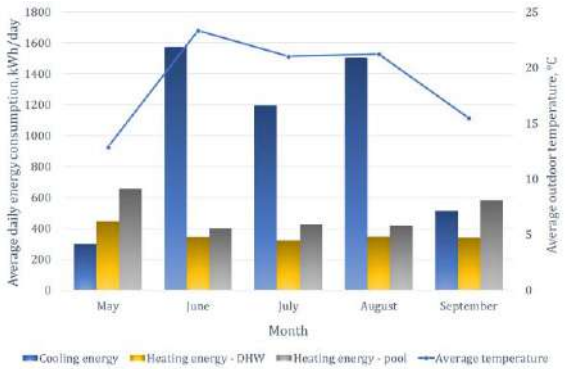

Fig. 2 - Average daily energy demands for each of the systems with the average outdoor air temperature marked.

Then, the monthly energy consumption was estimated with division into individual months of the analysis. Figure 3 shows results with average outside air temperature.

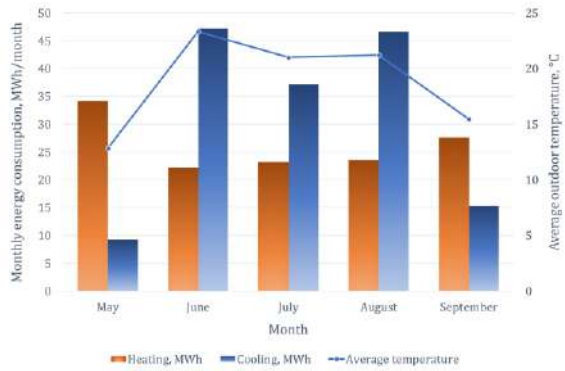

Fig. 3 - Monthly energy demands for the heating and cooling system.

Figure 3 shows that the greatest energy demand is observed in the three hottest months. As shown, during this period, the energy consumption of cooling systems is much higher than heating demand, accounting for even twice the value of heating energy demand.

3.2 Weekly energy consumption variability

The analysis of the energy demand of hotels is a very complex task due to many factors that can affect consumption. At the same time, these factors may change in a very dynamic and often unpredictable way. Due to the wide period of the analysis, it was decided to check the weekly variability of particular parameters. One week was selected from each of the months included in the analysis. The results are presented on the charts below. Figure 4 shows the weekly distribution of demand in May, using the example of days from May 19 to 25, 2019.

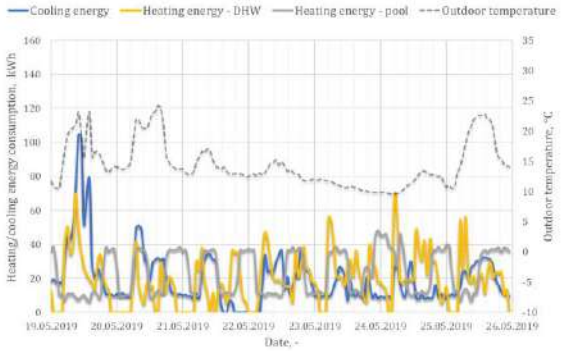

Fig. 4 - Variability of the energy demand of the cooling system, DHW system, and swimming pool heating system - on the example of the period from 19 to 25 May 2019.

During this period, the air temperature is quite low compared to the other months and does not exceed the value of 25 °C. At night, the temperature drops to 9 - 14 °C. Consequently, the cooling demand is kept low. The exception is May 19, when a temporary increase is more than twice the size of the other days. As can be seen, there is also a high demand for the DHW system. It should be noted that on that particular day, the occupancy level amounted to almost the value of 95%. Therefore, the increase may be the effect of a large number of users. Similarly, Figure 5 shows the variation graph for the selected week from June 16 to 22, 2019.

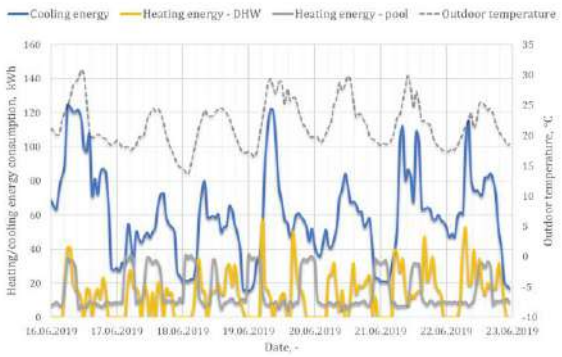

Fig. 5 - Variability of the energy demand of the cooling system, DHW system, and swimming pool heating system - on the example of the period from 16 to 22 June 2019.

The highest temperatures during the entire measurement period were recorded in June Obviously, this also causes an increase in cooling energy consumption this month. The chart shows an increase in consumption during the day (most often in the morning) and a significant decrease in the night hours. The next analysed period is from 21 to 27 July. The graph for this period is shown in Figure 6.

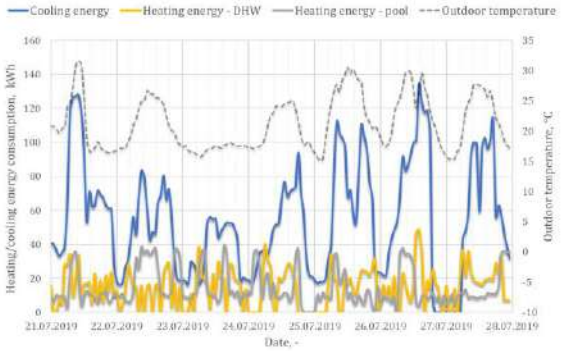

Fig. 6 - Variability of the energy demand of the cooling system, DHW system, and swimming pool heating system - on the example of the period from 21 to 27 July 2019.

Due to the similarity in outside air temperatures and the variability of this parameter during the days, the course of the variability of the demand for cooling energy is analogous to the previous period. As shown in the figure, the temperature decreased below the value of 20 °C on 23 July. It results directly in the reduction of cooling energy consumption this day. In this example, it is noticeable that the outside temperature is a crucial parameter for cooling energy demand estimation. The next chart shows the changes of the analysed values in the period from 18 to 24 August.

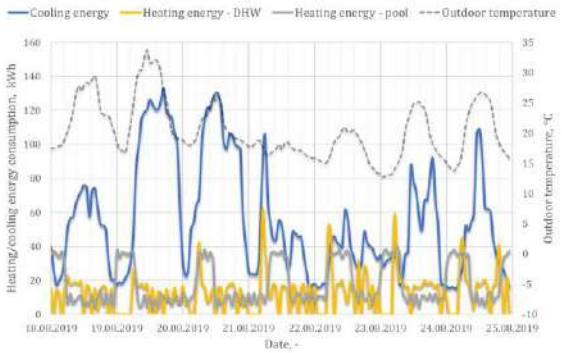

Fig. 7 - Variability of the energy demand of the cooling system, DHW system, and swimming pool heating system - on the example of the period from 18 to 24 August 2019.

Similar to figures for June and July, this chart also allows noticing the importance of outdoor air temperature in the context of changes in cooling demand. In this month, significant fluctuations in the heating energy consumption needed for the DHW system were observed. These values change very dynamically over a wide range and in a short time. The week selected from the last of the analysed months covers the days from 22 to 29 September. The results are shown in Figure 8.

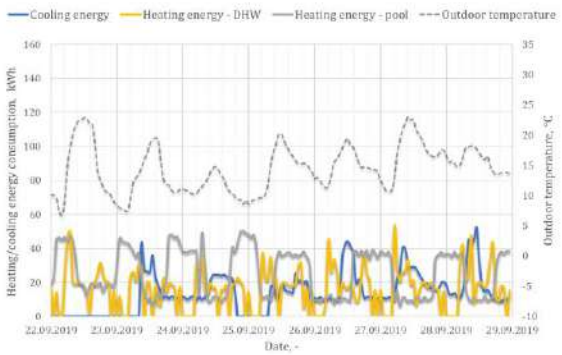

Fig. 8 - Variability of the energy demand of the cooling system, DHW system, and swimming pool heating system - on the example of the period from 22 to 28 September 2019.

In the last of the analysed month, a significant decrease in temperature leads to reducing the cooling demand. It can be seen that despite the temperatures kept below 25 °C during the day and falling below 12 °C at night, some users still use the room cooling system.

Daily energy demand is characterized by clear and repeatable patterns, mainly shaped by changes in the outside temperature and the habits of the average room user. The increase in demand for cooling energy is usually visible around the morning hours, and the amount of consumption depends, among other things, on the temperature of the outside air. The energy demand in the hotel is characterized by typical monthly and daily patterns mainly due to the amplitudes of the outside temperature. The lack of schedules for users' presence and uniform behaviour standards may cause the energy patterns to be less noticeable than, for example, in residential buildings or offices.

3.3 Factors influencing energy consumption

In the next step, the authors decided to check the relationship between the energy demand of individual systems and the parameters defined in the previous chapter. For this purpose, correlation indicators were used, which were calculated for each pair of variables. The results are summarized in Table 2.

Tab. 2 – Correlation coefficients between the hourly energy demand of the systems and defined factors.

Variables	Cooling energy	Heating energy DHW	Heating energy Pool
Outdoor temp	0.831	0.069	-0.410
Occupancy level	0.085	0.137	-0.111
Hour	0.127	0.144	-0.054

Except for the relationship between the cooling load and outdoor temperature, the remaining indicators do not show significant correlations between the variables. Nevertheless, the authors decided also to focus on the relationship between the heating demand of the swimming pool area and the outside temperature. The value of the correlation coefficient for this relation amounts to -0.410. It indicates a slight correlation. As can be seen in the table, the heating demand of the DHW system shows no clear dependence on any of the adopted parameters. Although the time of measurement was expected to affect the results obtained, the coefficient of 0.144 indicates the correlation as low. Figure 9 shows the relationship between the cooling demand and the outside temperature.

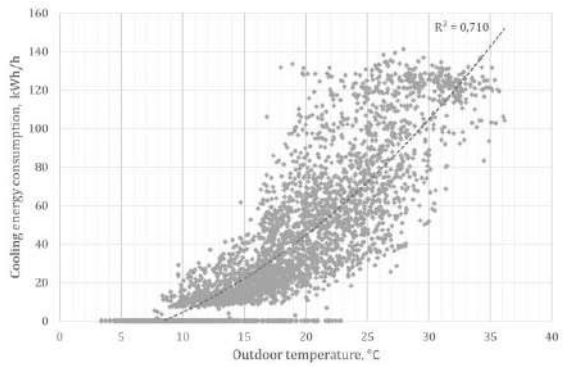

Fig. 9 - The relationship between the hourly cooling demand and the outside air temperature.

Figure 10 shows the relationship between the heating energy consumption for the needs of the swimming pool area and the temperature of the outside air. On the chart, a second-order polynomial trendline was added.

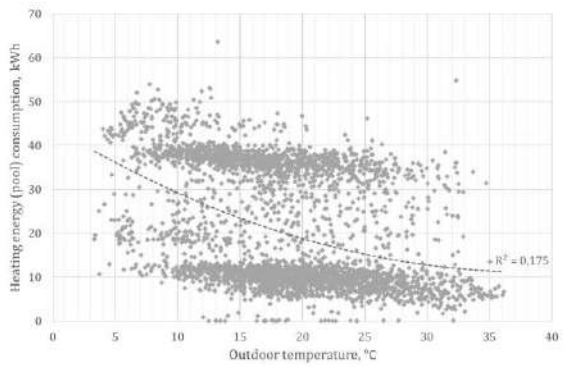

Fig. 10 - The relationship between the hourly heating demand of the swimming pool area and the outside air temperature.

Interestingly, the diagram clearly shows the division of energy consumption results into two groups arranged in parallel sections. However, no parameter has been identified that could lead to such a split.

Due to a large number of measurements and relatively low correlation coefficients in the hourly analysis, it was decided to carry out a correlation analysis for the daily average values. Therefore, the

next step was to determine the correlation coefficients between the daily energy demand of individual systems and the three variables. In this case, the average daily outside temperature, the occupancy level, and day of the week (Monday, Tuesday, Wednesday, Thursday, Friday, Saturday, Sunday) were used. The results are summarized in Table 3.

Tab. 3 – Correlation coefficients between the daily energy demand of the systems and defined factors.

Variables	Cooling energy	Heating energy DHW	Heating energy Pool
Outdoor temp	0.903	-0.355	-0.803
Occupancy level	0.107	0.480	-0.239
Day of the week	-0.040	0.343	-0.106

Of course, the change of the analysis from the hourly to the day values led to an increase in the values of individual factors. In this case, the dependence of the cooling demand and the pool heating energy demand on the outside temperature is determined by the correlation coefficients 0.903 and -0.803, respectively. For the energy consumption of the DHW system, a slight correlation was noticed for each of the three independent variables.

As in the case of the hourly analysis, it was decided to present the relations with the highest correlation coefficient on the chart. Figure 11 shows the relationship between the daily cooling demand and the outdoor air temperature.

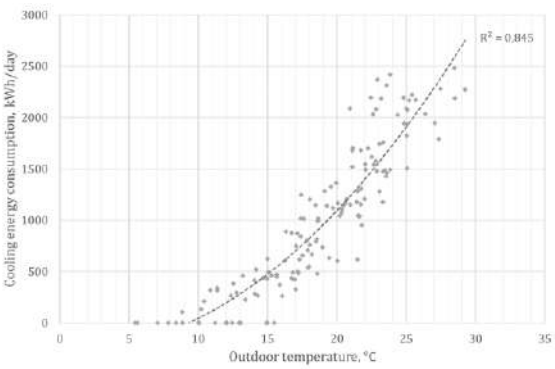

Fig. 11 - The relationship between the daily cooling demand and the outside air temperature.

Similarly, Figure 12 shows the relationship between the daily heating demand for the swimming pool area and the outside air temperature.

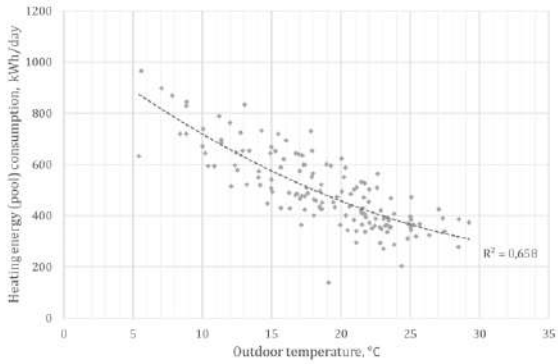

Fig. 12 - The relationship between the daily heating demand of the swimming pool area and the outside air temperature.

The highest correlation coefficient in the case of heating energy consumption for the DHW system was obtained for the relationship with the occupancy level. However, many values deviating from the determined trend were noticed. Therefore, it was decided to present this relationship in a categorized form. The data were divided into nine groups according to the occupancy level. The first category covers days with an occupancy in the range of 10 to 20%. The subsequent groups include ranges of every 10% up to the ninth category, which contains values between 90 and 100%. The results in the form of a box plot are shown in Figure 13.

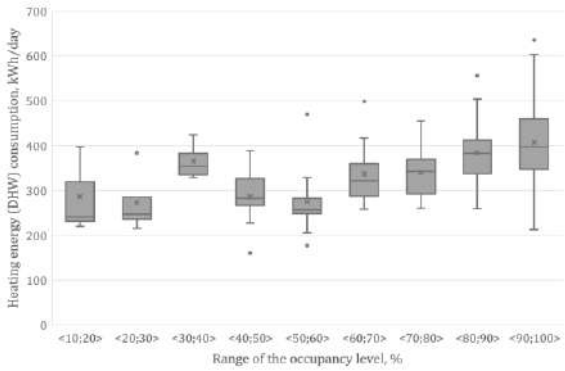

Fig. 13 - Relationship between daily heating demand for DHW and hotel occupancy.

As it is noticeable, there is an upward trend in energy consumption as hotel occupancy increases. The most deviating values were obtained for the range from 30 to 40%. It can be concluded that the presence factor is significant, but it does not completely define the energy demand. In this case, the preferences and habits of users, including the environmental awareness of hotel guests in terms of saving water, may be of key importance.

4. Conclusion

The analysis of the energy performance of the hotel facility was carried out for the summer period and considered both weekly and monthly variability. The research covered the energy demand of three systems of the hotel building, including the cooling system, DHW system, and pool heating system.

An in-depth energy analysis of the building is essential for reducing energy consumption in the facility. It also helps in adapting the building to current trends and energy requirements. As research has shown, in the summer period from June to August, the energy necessary to cool the building was significantly dominant. A relationship between the cooling load and the outside temperature was observed. High-level correlation is noticeable both for the analysis of hourly and daily values. In a daily analysis, for the outside temperature in the range of 10-15 °C, the energy needed for the proper operation of the cooling system is in the range of 0-625 kWh/day. On the other hand, for a temperature of 25-30°C, the energy consumption of the cooling system is in the range of 1500-2500 kWh/day. Such a wide range of changes may result from the preferences of users, who can individually regulate the temperature in their rooms. The average daily cooling demand in the analysed period varies from 299.4 kWh/day for May to 1,573.6 kWh/day for June. For a pool area heating system, the average daily energy consumption varies from 399.6 kWh/day for June to 657.4 kWh/day for May. The average daily heat demand for the DHW system for the research period was 358.6 kWh/day, changing from 322.2 to 445.1 kWh/day for months.

As the analysis showed, the energy performance of a hotel depends on many factors, sometimes very difficult to define and predict. The essential parameter influencing the energy demand in such facilities is the presence of users, including their behaviour, environmental preferences, or environmental awareness. The results showed a significant influence of the outside temperature on the cooling and heating demand of the swimming pool area. The hotel occupancy level is also a significant factor, especially for the DHW system demand. In the future, the research will be extended with other parameters of the outside air. This approach will allow providing a multi-parameter analysis. It may be crucial for their proper management and, as a result, reduction of energy consumption, especially in the case of energy consumption for the swimming pool part and the DHW system.

5. Acknowledgement

The research was carried out in the project entitled „Opracowanie zintegrowanego systemu umożliwiającego precyzyjną kontrolę mikroklimatu w dużych obiektach użytkowych w celu spełnienia wymagań dotyczących budynków o niemal zerowym zapotrzebowaniu na energię (nZEB)" no. POIR.01.01.01-00-0720 / 16 co-financed by the EU European Union from the Regional Development Fund under the Intelligent Development Operational Program for 2014-2020.

6. References

[1] Hotel Energy Solutions, Analysis on Energy Use by European Hotels: Online Survey and Desk Research, Hotel Energy Solutions project publications, 2011.

[2] Borowski M., Zwolińska K. Prediction of Cooling Energy Consumption in Hotel Building Using Machine Learning Techniques. Energies. 2020; 13(23):6226.

[3] Bohdanowic P., Martinac I. Determinants and benchmarking of resource consumption in hotels—Case study of Hilton International and Scandic in Europe. Energy and Buildings. 2007;39(1):82-95.

[4] Santiago D-E. Energy use in hotels: a case study in Gran Canaria. International Journal of Low-Carbon Technologies, 16(4), 2021, 1264–1276.

[5] Wang F., Lin H., Luo J. Energy Consumption Analysis with a Weighted Energy Index for a Hotel Building. Procedia Engineering. 2017; 205: 1952-1958.

[6] Borowski M., Mazur P., Kleszcz S., Zwolińska K. Energy Monitoring in a Heating and Cooling System in a Building Based on the Example of the Turówka Hotel. Energies. 2020; 13(8):1968.

Data Statement

The datasets generated during and analysed during the current study are not publicly available due to privacy restrictions but are available on request from the corresponding author.

Optimal dimensioning power of GSHP with district heating in an educational building

Tianchen Xue [a], Victoria Nadas [b], Juha Jokisalo [a, c], Risto Kosonen [a, c, d], Mika Vuolle [b], Markku Virtanen [a]

[a] Department of Mechanical Engineering, Aalto University, Espoo, Finland.

[b] Equa Simulation Finland Oy, Espoo, Finland.

[c] Smart City Center of Excellence, TalTech, Tallinn, Estonia.

[d] College of Urban Construction, Nanjing Tech University, Nanjing, P.R. China.

Abstract. European Union (EU) have set great goals to reduce carbon dioxide (CO_2) emissions and mitigate global warming trend. In this context, energy performance of buildings should be improved by enhancing the use of renewable energy sources in heating and cooling. For that reason, a hybrid energy system where a ground source heat pump (GSHP) integrated with borehole thermal energy storage (BTES) system is used together with district heating (DH) has become increasingly popular in Finland during the last years. In those hybrid GSHP systems, GSHP is used as a primary energy source and DH is used for supplementing energy during peak heating load period in wintertime. While in summertime, the borehole field is used for free cooling and DH is providing heating energy for domestic hot water. In this study, a large educational building complex in Finland applying a hybrid energy system consisting of a GSHP and DH was modelled in IDA ICE 4.8. Three simulation cases were studied to analyze the effects of the GSHP power ratio on the whole system energy consumption and CO_2 emissions. The results show the total CO_2 emission obtained the minimum when the GSHP heating power ratio was 50%. However, compared to 100% district heating solution, 25% power ratio of GSHP in the hybrid system can already realize 50% reduction of CO_2 emissions as the total cooling demand was fully satisfied by borehole free cooling and 98% DH consumption was reduced.

Keywords. Ground source heat pump, district heating, dimensioning power.
DOI: https://doi.org/10.34641/clima.2022.115

1 Introduction

Currently, European Union (EU) has set two stage targets to diminish carbon dioxide (CO_2) emissions and mitigate the global warming trend: to reduce emissions by 40% by 2030, compared to the 1990 level [1], and to achieve climate neutrality by 2050 [2]. In the EU countries, the building sector accounts for around 40% of the energy consumption and consequent 36% of the CO_2 emissions [3]. Energy performance of new and old buildings should be improved by increasing utilization of renewable energy techniques in the building energy system.

One of the prevalent renewable energy techniques is a ground source heat pump (GSHP) coupled with a borehole thermal energy storage (BTES) system. The hybrid GSHP system where the GSHP integrated with district heating (DH) as a backup heating source has become increasingly popular in Finland during the last years. Hybrid GSHP systems are helpful in several applications including design strategy of demand side management [4] and mitigation of underground thermal imbalance [5]. In the design of the hybrid GSHP system, the GSHP power ratio is an important parameter which needs to be determined properly. However, based on the author's best knowledge, the optimization of the dimensioning power of GSHP based on energy consumption and CO_2 emissions in a hybrid GSHP system with auxiliary DH was not well investigated.

This study aims to investigate the effects of the GSHP power ratio of a hybrid GSHP system connected with DH on building energy consumption and CO_2 emissions of an educational building complex in Finland. The energy simulations of three studied cases with different GSHP power ratio were performed in IDA ICE 4.8. The electricity and DH energy consumptions and the corresponding CO_2 emissions were analyzed for the studied cases. The GSHP power ratio for the optimal CO_2 reduction was suggested.

Copyright ©2022 by the authors. This conference paper is published under a CC-BY-4.0 license.

2 Method

2.1 Building description

The studied building is a large educational building located in Aalto University Campus in Espoo, Finland (shown in Fig. 1). The building was completed by September 2018 and was open to the public since January 2019. The building is a 4/5 storey building with multiple types of spaces including educational area, office, restaurants, gym, workshop, computer rooms, shopping area and a metro station. The heated net floor area of the building is 39670 m^2. Currently, the building is equipped with a ground source heat pump system and connected to a district heating network. The ground source heat pump is coupled with a borehole field containing 74 boreholes with average depth of 310 m.

Fig. 1 - Studied building in Aalto University Campus, Espoo, Finland.

In this study, the building geometry was simplified as a rectangular single storey building model (shown in Fig. 2(a)), which had been calibrated to describe the energy consumption of the building in the previous study [6]. The building space was divided into five zones with room height of 4.6m (shown in Fig. 2(b)). The eventual geometry of each zone was magnified by the zone multiplier of 15.3 to obtain the real net floor area of 39670 m^2.

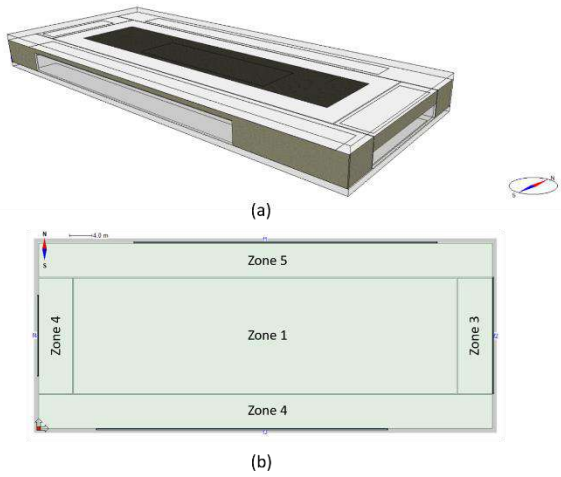

Fig. 2 - The geometry of the building model.

The U-values of the external wall, the roof and the base floor are 0.17 W/m^{2}K, 0.09 W/m^{2}K and 0.18 W/m^{2}K respectively. Each external wall has one window with the U-value of 0.6 W/m^{2}K, solar heat transmittance (g-value) of 0.49 and direct solar transmittance (ST) of 0.41. The windows are equipped with solar shading by blinds between outer panes, which are drawn down when solar radiation level is above 100W/m^2. Moreover, the windows are set to be always closed. The average infiltration air flow rate of the building is 0.045 m^3/hm^2.

The main internal heat gains of the building are from occupants, lighting, and equipment [7]. The internal heat gains used in this study are listed in Table 1. The average occupancy profile is shown in Fig. 3. The average lighting and equipment usage profiles are both set the same as the average occupancy profile.

Tab. 1- Internal heat gains.

Internal heat gains from occupants, lighting and equipment	
Occupants	7378 occupants in the building, which is equal to average occupancy density 0.186 1/m^2 with activity level of 1 met, clothing level of 0.85 ± 0.25 clo
Lighting	Average gain 8.7 W/m^2, internal gain from lighting equals to 16.7 kWh/(m^2, a)
Equipment	Average gain 5.1 W/m^2, internal gain from equipment equals to 11.2 kWh/(m^2, a)

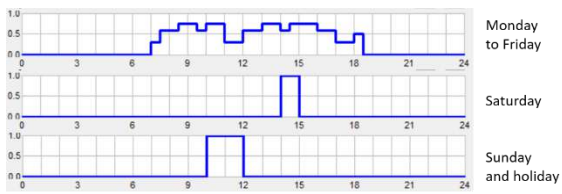

Fig. 3 - The average occupancy profiles. The hours of the day are shown on the horizontal axis and the occupancy is shown on the vertical axis (0 = 0% occupancy, 1 = 100% occupancy).

2.2 Description of heating, cooling and ventilation systems

In order to investigate the effects of different share of GSHP in the total heat power demand of the building, Case 1 using DH for heating and electric air-cooled chiller for cooling is defined as the reference case in this study. The DH substation annual efficiency is 97%. The coefficient of performance (COP) of the air-cooled chiller is 3.0 at the rating conditions (35/7°C). A simplified schematic of the plant model and connections to heating and cooling networks is shown in Fig. 4.

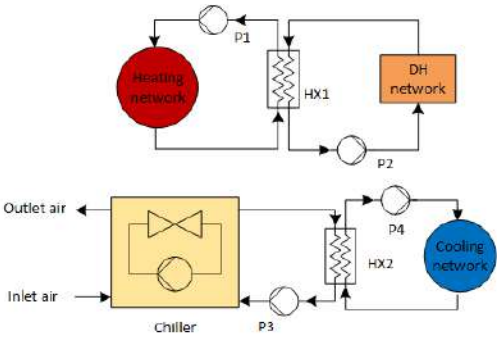

Fig. 4 - Simplified schematic of the plant model and connection in the reference case (Case 1).

In the reference case, the heating set-point temperature is set as 21°C. The heating is delivered through three different circuits: space heating, air handling unit (AHU) heating and domestic hot water (DHW). The space heating is carried out by a hydronic radiator heating system with dimensioning temperatures of 50/35°C. For the space heating, the supply water temperature is controlled according to the control curve shown in Fig. 5. For the inlet water of a reheat coil of the air handling unit, the constant temperature set point of 60 °C is implemented.

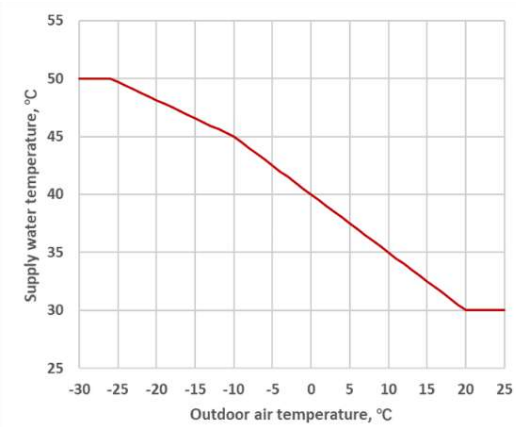

Fig. 5 - Control curve of supply water temperature of radiant panels.

The domestic hot water (DHW) consumption is defined by two main features, the level of consumption and the consumption profile. The annual heat energy consumption level of DHW is 11 kWh/(m², a). The daily DHW consumption profile is shown in Fig. 6. The supply water temperature of the DHW is 55 °C.

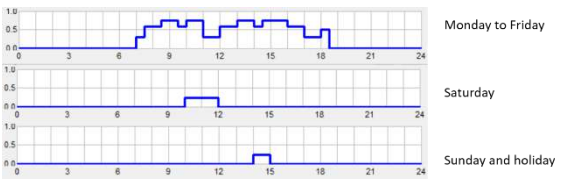

Fig. 6 - The DHW consumption profile. The hours of the day are shown on the horizontal axis and the usage rate is shown on the vertical axis (0 = 0% usage rate, 1 = 100% usage rate).

The cooling is distributed through space cooling and AHU cooling in the building. The space cooling is carried out by a hydronic cooling panel system with the supply water temperature of 15°C. The set-point temperature of space cooling is 25°C. The AHU cooling supply water temperature is set as 5°C constantly.

The building has a mechanical balanced ventilation system with heat recovery. The heat recovery is applied in the AHU with heat exchanger efficiency of 73% on supply air side. In addition, the AHU is equipped with defrost protection on the heat exchanger. The defrost protection is controlled according to the exhaust air temperature after the heat exchanger. When the exhaust air temperature falls below -5°C, the supply air bypasses the heat exchanger.

The ventilation system is a constant air volume system with schedule control, while night ventilation is not applied in this study. The constant supply and exhaust air flow rates are both defined as 2.3 L/(s, m²) during occupied time and 0.76 L/(s, m²) during unoccupied time. The fan operation rates are controlled according to fan operation schedule (shown in Fig. 7). The supply air temperature is controlled by the return air temperature according to the curve shown in Fig. 8.

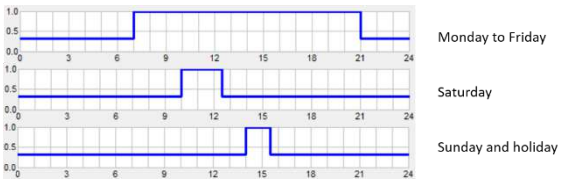

Fig. 7 - The fan operation schedules. The hours of the day are shown on the x-axis and the operation rate of ventilation system is shown on the y-axis (0 = 0% fan operation rate, 1 = 100% fan operation rate).

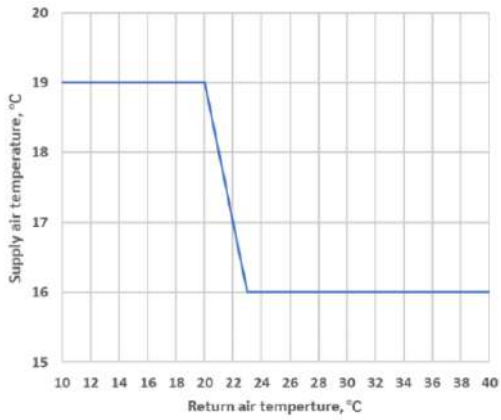

Fig. 8 - Control curve of supply air temperature of AHU.

2.3 Definition of simulated cases

Apart from the reference case (Case 1), two studied cases applying different GSHP power ratios are simulated to investigate the effects of the GSHP power ratio on the whole energy system performance. In Case 1, the total heating power is covered by the DH, and the total cooling power is

provided by the electric air-cooled chiller. In Cases 2-3, a certain part of the total heating power demand of the building is covered by the GSHP, and the rest of the heating power is provided by the DH. Besides, the total cooling power in Cases 2-3 is provided by free cooling from the BTES instead of electric air-cooled chiller. The detailed definitions of these three cases are listed in Table 2. The simulation period of all three cases is year 2019.

Tab. 2 - Definitions of the three simulated cases.

Case	GSHP power ratio	DH power ratio
Case 1	0	100%
Case 2	25%	75%
Case 3	50%	50%

In Cases 2-3, the COP of the simulated GSHP is assumed to be 4.3 at the rating conditions (0/35°C). The borehole numbers are calculated by applying the same ratio of the total maximum heating power of GSHPs and the total length of boreholes (32.2 W/m) in all studied cases as in real the building. The borehole depths are all the same as that in real boreholes (320m).

The GSHP system is used in both heating and cooling seasons. In heating season, the GSHP satisfies the basic heating demand. When the GSHP is unable to produce enough heat for the building, the DH is used as an auxiliary heat source. The condenser side of the GHSP and the DH are both connected to a heating network via a 5m^3 hot water storage tank. In cooling season, the cooling is produced by free cooling from the borehole field. The borehole field is connected to the cooling network via a 3m^3 cold water storage tank.

Fig. 9. shows the simplified schematic of the plant model and connection of heating and cooling networks in Cases 2-3. In heating mode, the GSHP serves as the primary heating source for the heating and DHW generation. The pump P5 is off work during heating season. The GSHP and the pumps P1 and P2 receive permission to start up or shut down according to a temperature set point of the hot water storage tank (HT). The hot water storage tank is used as a buffer tank for storing the hot water generated by GSHP and mitigating temperature variation. If the GSHP cannot produce enough heating energy, the pump P3 will start up and the DH will be used to heat up the water in the hot water storage tank. In cooling mode, the DH is not used as there are not much heating demands in the building. The pump P3 is off work during heating season. The DHW is produced only by the GSHP. Besides, the pump P5 starts up and the BTES produces all cooling energy. The cold water storage tank (CT) serves as a buffer tank to mitigate the temperature variation of the cooling water from the BTES.

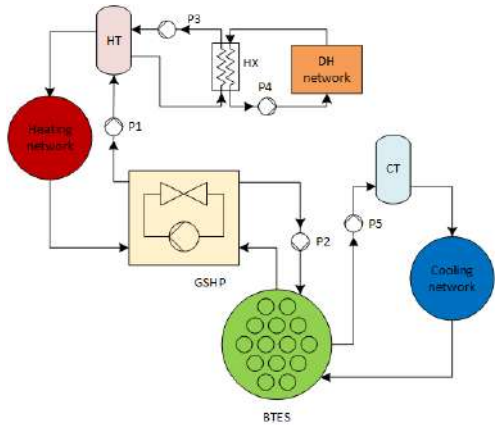

Fig. 9 - Simplified schematic of the plant model and connection in Cases 2-3.

In Cases 2-3, the heat distribution system consists of space heating, AHU heating and DHW in which the parameters are set as the same to those in Case 1. The cool distribution system consists of AHU and space cooling which both adopt the inlet cooling water temperature of 15°C. In the AHU, the liquid side temperature rise of the cooling coil is changed from 5°C to 1°C to simulate a cooling coil with a larger heat transfer area than the default cooling coil used in Case 1. The other parameters of the AHU cooling and space cooling circuits are set as the same to those in Case 1.

2.4 Weather data and simulation tool

According to the classification of Finnish climate zones, the studied building in Espoo is located in climate zone 1, which is the southernmost climate zone in Finland [8].

In this study, the dimensioning heating demand of the building is simulated without internal heat gains under the dimensioning outdoor temperature (-26°C) of southern Finland. The dimensioning cooling demand of the building is simulated with 100% internal heat gains using synthetic weather data of ASHRAE. The design day is chosen according to cumulative frequency of 1 % and the maximum dry-bulb and wet-bulb temperatures are 25.8°C and 17.6°C respectively.

The annual energy simulation uses hourly weather data from Helsinki-Vantaa test reference year (TRY2012). The TRY is developed according to the weather data observations of 30 years (1980-2009) measured by the weather station of the Finnish Meteorological Institute at the Helsinki-Vantaa airport [9]. The annual average temperature in Helsinki-Vantaa region is +5.4 °C. The average number of degree days is 3952Kd under the indoor temperature of 17 °C.

The annual CO_2 emissions due to energy use are calculated by using average Finnish emission factors for electricity and district heating presented in Hirvonen et al. [10]. The CO_2 emissions factor for electricity and district heating are 96 kgCO_2/MWh

and 137 kgCO_2/MWh respectively.

The simulation work of this study is performed by IDA Indoor Climate and Energy (IDA ICE) 4.8 software [11]. The software has been chosen as it is long-developed and reliably applicable in simulating building energy consumption, plant performance, indoor air quality and indoor thermal comfort. It has a detailed and dynamic multi-zone simulation application with variable time step. The IDA ICE has been validated in several studies [12,13], which provides sufficient reasons for using this tool in this study.

3 Results

The results of the power simulations show the maximum heating and cooling demands of the simulated building are 2978 kW and 1685 kW respectively in the design outdoor conditions. Based on these, the dimensioning heating and cooling power are rounded up to the next nearest 100 kW. Therefore, the total heating power is 3000 kW, and the total cooling power is 1700 kW. According to the definition of Cases 1-3, the dimensioning GSHP heating power, DH power and the number of boreholes are listed in Table 3.

Tab. 3 - Dimensioning GSHP heating power, DH power and the number of boreholes in studied cases.

Case	GSHP heating power (kW)	DH power (kW)	Number of boreholes
Case 1	0	3000	0
Case 2	750	2250	70
Case 3	1500	1500	140

Fig. 10 shows the district heating power duration curve for Cases 1-3. Compared to Case 1, the peak load DH power was reduced half in Case 2. However, the total DH duration time also decreased significantly from 6400 h to 580 h. In Case 3 where the GSHP power ratio increasing to 50%, the peak load DH power was decreased to 160 kW, and the total DH duration time was reduced to only 10 h.

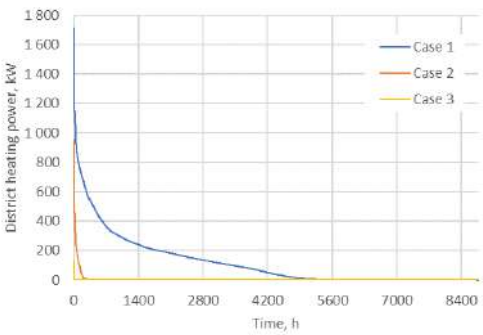

Fig. 10 – District heating power duration curves.

Fig. 11 shows the GSHP heating power duration curve for Cases 2 and 3. In Cases 2 and 3, the peak load GSHP power both reach their dimensioning GSHP heating power. However, from Case 2 to Case 3, the peak load duration time was reduced from 360 h to 8 h while the total GSHP power duration time was the same in these two cases.

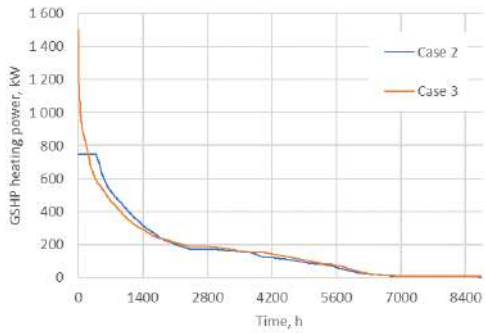

Fig. 11 – GSHP heating power duration curves.

Fig. 12 shows the cooling power duration curve for Cases 1-3. Compared to Case 1, the peak load cooling power and the total cooling duration time were slightly reduced in Cases 2. In Cases 3, the cooling power duration curve almost overlaps that of Case 2, which indicates the borehole free cooling totally satisfied the cooling demand in these two cases.

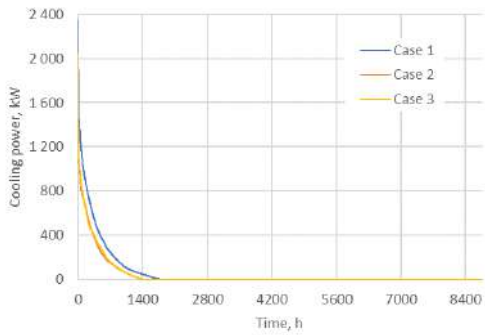

Fig. 12 – Borehole free cooling power duration curves.

Table 4 shows the annual heating and cooling energies of three simulated cases. The result shows the changes of GSHP power ratio slightly affected the produced heating and cooling energy. The difference of heating and cooling energy between the GSHP cases (Cases 2-3) and the reference case (Case 1) can be attributed to the differences of temperature levels.

Table 5 shows the purchased energies of three simulated cases. Although there was no cooling electricity consumption in Cases 2-3, meaning the borehole free cooling satisfied the total cooling demand of the building, the annual total electricity consumptions in Cases 2-3 were still more than that in Case 1. Compared to Case 1, the annual total electricity consumption in Case 2 was 9% higher, as the electricity used for the GSHP and pumps in heating season was more than that used for chiller and pumps in cooling season. Besides, from Case 2 to

Tab. 4 - Breakdown of annual heating and cooling energy for Case 1 (ref), Case 2 (25% of heat covered by GSHP), Case 3 (50% of heat covered by GSHP).

Case	Heating and cooling (kWh/m²,a)							Comparison	
	Space heating	Space cooling	AHU heating	AHU cooling	DHW	Total Cooling	Total Heating	Relative difference of total cooling	Relative difference of total heating
Case 1(ref)	10.8	4.3	14.6	9.3	13.1	13.6	38.6	-	-
Case 2	10.7	4.7	14.6	6.3	13.0	11.0	38.3	-19 %	-0.6 %
Case 3	10.7	4.4	14.6	6.9	13.1	11.3	38.4	-17 %	-0.3 %

Tab. 5 - Breakdown of purchased energies for Case 1 (ref), Case 2 (25% of heat covered by GSHP), Case 3 (50% of heat covered by GSHP).

Case	Electricity (kWh/m²,a)							DH (kWh /m²,a)	Comparison	
	Light-ing	Equip-ment	Electric cooling	GSHP heatin g	Fans	Pumps	Total electr-icity	Total DH	Relative difference of total electricity	Relative differenc e of total DH
Case 1 (ref)	16.7	11.2	4.5	0	15.2	0.05	47.7	39.8	-	-
Case 2	16.7	11.2	0	8.9	15.2	0.15	52.2	0.9	9 %	-98 %
Case 3	16.7	11.2	0	9.4	15.2	0.14	52.7	0	11 %	-100 %

Tab. 6 - Annual CO_2 emissions of Case 1 (ref), Case 2 (25% of heat covered by GSHP), Case 3 (50% of heat covered by GSHP).

Case	CO_2 emissions (ton/a)			Comparison
	Electricity CO_2	DH CO_2	Total CO_2	Relative difference of total CO_2 emissions (%)
Case 1 (ref)	182	216	398	-
Case 2	199	5.0	204	-50 %
Case 3	201	0.1	201	-50 %

Case 3, as the GSHP heating power ratio increases, the electricity used for GSHP heating increased, which mainly contributed to the increase in the total electricity consumption. On the other side, the DH consumption in Case 2 decreased by 98% compared to Case 1. The DH consumption in Case 2 was only 0.9 kWh/(m², a). In Case 3 where the GSHP power ratio increased to 50%, there was even no DH consumption, which indicates the backup heating could be not needed anymore.

Table 6 shows the annual CO_2 emissions of the three simulated cases. With the increase of GSHP heating power ratio, the CO_2 emissions of electricity consumption increased, and the CO_2 emissions of DH consumption decreased. Compared to Case 1, the CO_2 emissions of electricity consumption increased significantly in Case 2. However, as the GSHP ratio increased evenly from Case 2 to Case 3, the CO_2 emissions of electricity consumption changed marginally. On the other side, the CO_2 emissions of DH consumption had a dramatical decrease in Case 2 compared to Case 1. From Case 2 to Case 3, the CO_2 emissions of DH consumption were almost eliminated. The total CO_2 emissions in Cases 2 and 3 both realized 50% reduction. However, from the economical point of view, the 25% GSHP power ratio would be more appropriate for the system design, as the investment could be less on the borehole field.

4 Conclusions

This study investigated the effects of the GSHP power ratio on the total energy consumption and CO_2 emissions of a hybrid GSHP system of an educational building in Finland. The simulation of three studied cases were performed in IDA ICE 4.8. The summary of the results of simulation is listed as following.

- Compared to 100% DH heating, the 25%

GSHP power ratio increase the heating electricity consumption insignificantly, but it can reduce the DH energy consumption by 98%. Besides, the 25% GSHP power ratio can totally satisfy the cooling demand of the building by borehole free cooling. Based on these, the 25% GSHP power ratio can reduce 50% CO_2 emissions.

- As the GSHP power ratio increased more than 25%, the CO_2 emissions remained almost unchanged as the GSHP could meet the total heating demand without using the DH as a backup heat source. Based on economic considerations, the 25% GSHP power ratio was sufficient for the hybrid GSHP system. This result provides a useful reference for designs of hybrid GSHP system.

Acknowledgement

This project has received funding from China Scholarship Counsil (No. 202006370019). The study received further funding from the FINEST Twins project, that is co-funded by the European Union (Horizon 2020 program, grant number 856602) and the Estonian government.

References

[1] European Commission. 2030 Climate & Energy Framework 2018. https://ec.europa.eu/clima/policies/strategies/2030_en.

[2] European Commission. 2050 Long-Term Strategy 2020. https://ec.europa.eu/clima/policies/strategies/2050_en.

[3] Sankelo P, Jokisalo J, Nyman J, Vinha J, Sirén K. Cost-optimal energy performance measures in a new daycare building in cold climate. Int J Sustain Energy 2019;38:104–22. https://doi.org/10.1080/14786451.2018.1448398.

[4] Arteconi A, Hewitt NJ, Polonara F. Domestic demand-side management (DSM): Role of heat pumps and thermal energy storage (TES) systems. Appl Therm Eng 2013;51:155–65. https://doi.org/10.1016/j.applthermaleng.2012.09.023.

[5] You T, Wu W, Yang H, Liu J, Li X. Hybrid photovoltaic/thermal and ground source heat pump: Review and perspective. Renew Sustain Energy Rev 2021;151:111569. https://doi.org/10.1016/j.rser.2021.111569.

[6] Nadas V. Advanced Design and Control Strategies to Optimize a Deep Borehole Field as Long-Term Thermal Storage (Master's thesis). Aalto University, 2020.

[7] Arabzadeh V, Jokisalo J, Kosonen R. A cost-optimal solar thermal system for apartment buildings with district heating in a cold climate. Int J Sustain Energy 2019;38:141–62. https://doi.org/10.1080/14786451.2018.1505725.

[8] Ministry of the Environment (Finland). D3 Finnish Code ofBuilding Regulation: Energy Efficiency of Buildings: Regulations and Guidelines. n.d.

[9] Kalamees T, Jylhä K, Tietäväinen H, Jokisalo J, Ilomets S, Hyvönen R, et al. Development of weighting factors for climate variables for selecting the energy reference year according to the en ISO 15927-4 standard. Energy Build 2012;47:53–60. https://doi.org/10.1016/j.enbuild.2011.11.031.

[10] Hirvonen J, Heljo J, Jokisalo J, Kurvinen A, Saari A, Niemelä T, et al. Emissions and power demand in optimal energy retrofit scenarios of the Finnish building stock by 2050. Sustain Cities Soc 2021;70. https://doi.org/10.1016/j.scs.2021.102896.

[11] Sahlin P. Modeling and simulation methods for modular continuous systems in buildings. Dep Build Sci Div Build Serv 1996.

[12] Alimohammadisagvand B, Jokisalo J, Kilpeläinen S, Ali M, Sirén K. Cost-optimal thermal energy storage system for a residential building with heat pump heating and demand response control. Appl Energy 2016;174:275–87. https://doi.org/10.1016/j.apenergy.2016.04.013.

[13] Niemelä T, Kosonen R, Jokisalo J. Energy performance and environmental impact analysis of cost-optimal renovation solutions of large panel apartment buildings in Finland. Sustain Cities Soc 2017;32:9–30. https://doi.org/10.1016/j.scs.2017.02.017.

Natural indoor climate in St. Charles Borromeo chapel in Telc

*Ondřej Hnilica [a], Stefan Bichlmair [b], Tomáš Fečer [c], Josef Plášek [c]**

[a] Institute of History, Czech Academy of Sciences, Czech Republic

[b] Fraunhofer Institute for Building Physics IBP, Holzkirchen Branch, Germany

[c] Faculty of Civil Engineering, Brno University of Technology, Czech Republic (email: plasek.j@vut.cz)

Abstract: The memorial chapel of St. Charles Borromeo from 1664 in town Telc includes the fresco-secco mural painting in the dome. The natural indoor climate with a height of 12.1 m is analysed for the preventive conservation of the original mural painting. This hygrothermal analysis in the period 2018 - 2021 shows the average indoor air temperature of 10.2 °C and indoor air relative humidity of 75.1 % r.h. This natural indoor climate shows the frequency of Frost risk in 10.72 % days per year, Microbiology risk in 4.85 % days per year, and Dryness effect in 0.01 % days per year. The vertical stratification of indoor climate is obtained for air temperature up to 5.2 K and -24.1 % r.h. for relative humidity. This natural indoor climate in the St. Charles Borromeo chapel is significantly dependent on outdoor weather with time-lag 2 hours.

Keywords: natural indoor climate; mural painting; preventive conservation; measurement
DOI: https://doi.org/10.34641/clima.2022.109

1. Introduction

The chapel of St. Charles Borromeo near town Telc in the Czech Republic is built in 1664 as the memorial chapel on 13th October 1653. On this date, the son Charles of Countess Frantiska Slavatova von Meggau fell to the wolf-pit with a depth of 5 m. The thirteen years old Charles survived October night in the wolf-pit. He was rescued in the next morning by forest workers. This historical legend is the motive of mural painting in the dome, see Fig. 1.

Fig. 1 - *The original photo of mural painting in the dome of the St. Charles Borromeo chapel with the motive of Charles's rescue on day 13th October 1653 is painted about the year 1730 by Heinrich Herwig Hoff.*

1.1 Research Aim

This research study is focused on the preventive conservation of original fresco-secco mural painting in the dome of St. Charles Borromeo chapel in Telc. The hygrothermal analysis of natural indoor climate with a height of 12.1 m is based on experimental measurement over 3 years.

2. Chapel of St. Charles Borromeo

This memorial chapel of St. Charles Borromeo on the hill above Telc is connected with the town by eight stations on the Way of the Cross since 1670, more [1]. This Borromeo chapel is built by the builder Stefano Perti in 1664, see Fig. 2. The polygonal floor plan is composed of a regular octagon with an outer diameter of 9.47 m and the entrance leeward, see Fig. 3. The internal height of the St. Charles Borromeo chapel is 12.1 m (exterior height 16.1 m), and the chapel basement (original wolf-pit) is God's grave with a relics of statue. The peripheral wall with thickness of 1.0 m is built by ceramic bricks up to 9.10 m. This peripheral wall includes four wooden windows (1.25 × 2.50 m) with shutters and double wooden doors (1.34 × 2.60 m). The internal wooden dome with a radius of 3.60 m is created in the octagonal pyramid roof and extended by the lighting lantern. The inner surface of the wooden dome is lime plaster layer with the fresco-secco mural painting. The natural indoor climate is formed only by outdoor weather and natural infiltration. The

Copyright ©2022 by the authors. This conference paper is published under a CC-BY-4.0 license.

liturgical ceremony in the St. Charles Borromeo chapel is organized in summer one time per year.

Fig. 2 - *Photo of St. Borromeo chapel in town Telc* [2].

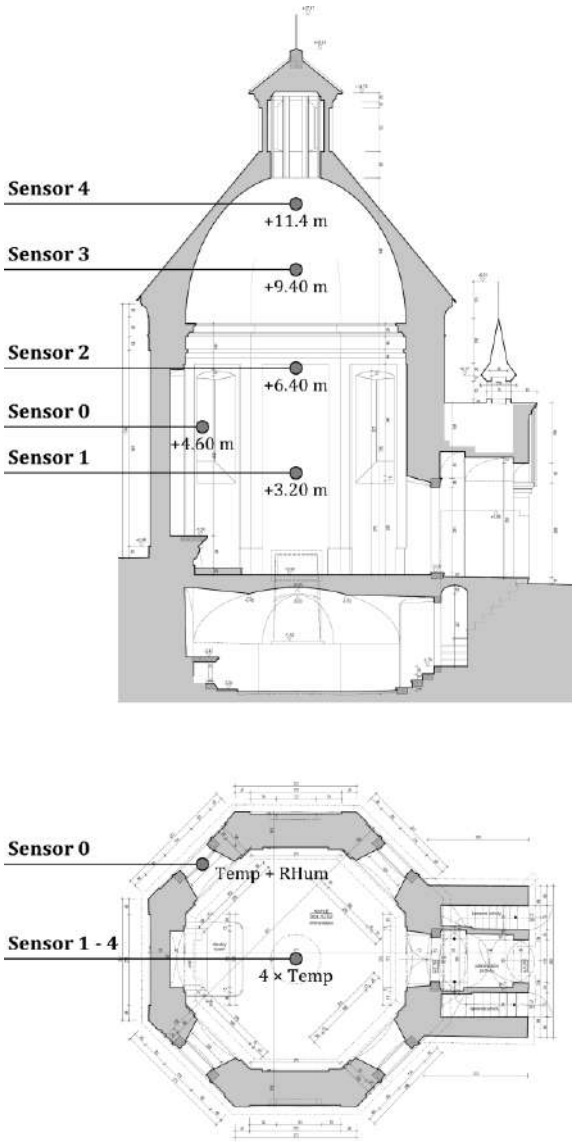

Fig. 3 - *Floor plan and vertical cut of St. Borromeo chapel with the location of hygrothermal probes* [3].

3. Experimental measurement

The natural indoor climate in the St. Charles Borromeo chapel is monitored by a hygrothermal sensor and four temperature probes from 18th June 2018 to 16th October 2021. The hygrothermal data-logger is COMET S3120 with a sensitivity ±0.10 K for air temperature in interval <-30; 70 °C> and the sensitivity ±0.1 % r.h for relative humidity in interval <0; 100 % r.h.>. This hygrothermal data-logger is located on the window (Northwest) with a closed shutter on level 4.60 m (Sensor 0) above the floor. The vertical temperature distribution of natural indoor climate is monitored by four temperature probes COMET Pt1000/3850 ppm with a sensitivity ±0.15 K for air temperature in interval <-30; 180 °C>, more [4]. These temperature probes are suspended in level 3.2 m (Sensor 1), 6.4 m (Sensor 2), 9.4 m (Sensor 3), and 11.4 m (Sensor 4) above the floor, see Fig. 3. The outdoor climate is monitored by professional weather station ITAM (Institute of Theoretical and Applied Mechanics of the Czech Academy of Sciences) in town Telc. The straight distance between the St. Charles Borromeo chapel and this professional weather station ITAM is 2080 m.

4. Results

The natural indoor climate in St. Charles Borromeo chapel is analysed from 4 temperature probes and one hygrothermal sensor (over 28 939 hours) from 18th June 2018 to 16th October 2021 with the respect to mural painting.

4.1 Method of Target range

The appropriate indoor climate for preventive conservation of original fresco-secco mural painting recommends technical standard and scientific studies, see [5-7]. This appropriate natural indoor climate defines a hygrothermal range of indoor air temperature and indoor air relative humidity. The other way is American standard ASHRAE [8] with defined unacceptable indoor climate for the preventive conservation of artefacts.

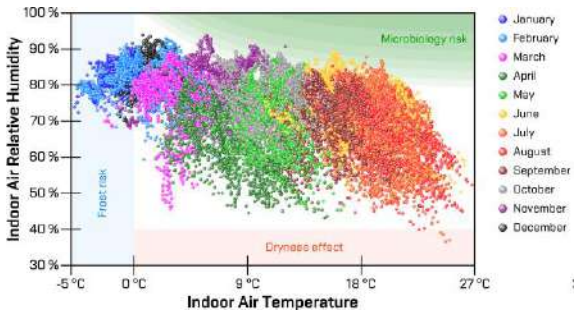

Fig. 4 - *Hygrothermal analysis of natural indoor climate by preventive conservation method of Target range in period from 18th June 2018 to 16th October 2021. The unacceptable indoor climate is defined as Dryness effect (RH < 40 % r.h.), Frost risk (T < 0 °C), and Microbiology risk, according to* [9].

Table 1 - *Frequency of indoor climate in Target range.*

Target range	Frequency	
M.BB.CC. 2001 [5]	2097 hours	7.28 % days
UNI 10829:1999 [6]	2726 hours	9.42 % days
Kadijsky in [7]	617 hours	2.31 % days
Frost risk [8]	4 hours	0.01 % days
Dryness risk [8]	3255 hours	10.7 % days
Microbiology risk [9]	1404 hours	4.85 % days

The year frequency of appropriate indoor climate is 7.28 % days in M.BB.CC. 2001 [5] (range 6-25 °C and 45-60 % r.h.), 9.42 % days in UNI 10829:1999 [6] (range 10-24 °C and 45-65 % r.h.), and 2.31 % days in Kadijsky [7] (range 6-25 °C and 50-55 % r.h.). The year frequency of unacceptable indoor climate is 0.01 % days in the Dryness effect (RH < 40 % r.h.), 10.72 % days in the Frost risk (T < 0 °C), and 4.85 % days in the Microbiology risk [9]. This total year frequency of Microbiology risk is aggregated from risk 3.04 % days in 32 days, risk 1.39 % days in 16 days, risk 0.38 % days in 8 days, and risk 0.04 % days in 4 days. In summary, the natural indoor climate in the St. Charles Borromeo chapel is over 84.4 % days per year without Frost risk, Dryness effect, and Microbiology risk.

4.2 Method of Historical climate

The preventive conservation method of Historical climate respects the natural hygrothermal response of the building. The appropriate indoor climate for preventive conservation is calculated as a 30-days centred moving average (CMA) over a year, and the hygrothermal fluctuation of indoor climate is limited by a lower (7th)/upper(93rd) percentile, more [10].

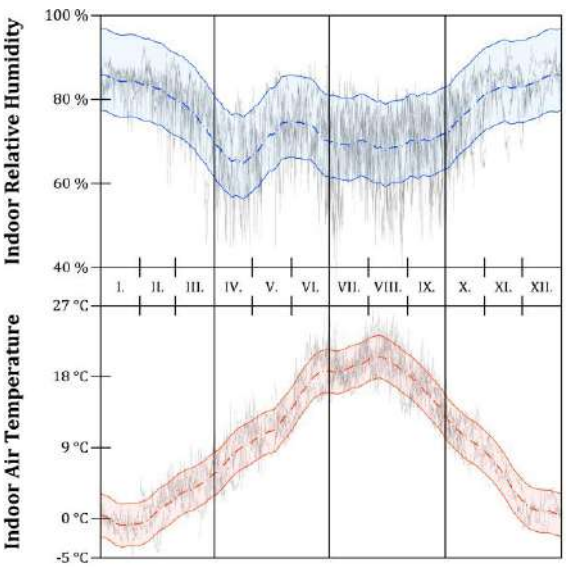

Fig. 5 - *Hygrothermal analysis of natural indoor climate by Historical climate method in period from 18th June 2018 to 16th October 2021.*

The average indoor air temperature is 10.2 °C, and the average indoor air relative humidity is 75.1 % r.h. The CMA of indoor air temperature is calculated in the range from -0.85 °C (18th January at 8 am) to 20.6 °C (8th August at 9 pm) with fluctuation from -2.7 K to 2.7 K. The CMA of indoor air relative humidity is obtained in a range from 64.9 % r.h. (24th April at 6 am) to 85.9 % r.h. (31st December at 23 pm) with fluctuation from -11.0 % r.h. to 8.5 % r.h. This hygrothermal fluctuation of natural indoor climate is caused by natural ventilation through the lighting lantern in the dome.

4.3 Vertical stratification of Indoor climate

The vertical stratification of natural indoor climate show hygrothermal difference between sensors, see Fig. 6. The temperature difference between levels 6.4 m and 3.2 m (red dots) is 0.05 ± 0.26 K in a range from -0.9 to 1.3 K, and the relative humidity shows a median difference -3.7 ± 1.9 % r.h. in a range from -1.2 to -9.4 % r.h. The temperature difference between levels 9.4 m and 3.2 m (grey dots) is 0.10 ± 0.42 K in a range from -1.1 to 2.0 K, and the relative humidity shows a median difference -7.1 ± 3.7 % r.h. in a range from -2.4 to -18.2 % r.h. The temperature difference between levels 11.4 m and 3.2 m (yellow dots) is 0.43 ± 0.74 K in a range from -0.7 to 5.2 K, and the relative humidity shows a median difference -9.4 ± 4.9 % r.h. in a range from -3.2 to -24.1 % r.h. This hygrothermal fluctuation of natural indoor climate increases with the level above the floor, see Fig. 6.

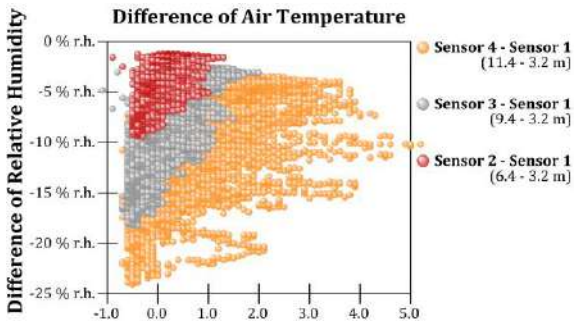

Fig. 6 - *Hygrothermal difference in natural indoor climate between sensors in the period from 18th June 2018 to 16th October 2021.*

The hygrothermal vertical stratification of natural indoor climate shows the temperature gradient 0.136 ± 0.033 K/m in a range from 0.01 to 0.63 K/m, and the relative humidity shows the gradient of 1.49 ± 0.97 % r.h./m in a range from 0.39 to 2.94 % r.h.

4.4 Dependence of Indoor on Outdoor climate

The hygrothermal time-lag between outdoor and indoor climate is calculated for 2 hours by the Fourier transform method with a correlation of 90.2 % for air temperature, 63.3 % for relative humidity, and 95.1 % for specific humidity. The hygrothermal attenuation in the brick envelope of St. Charles Borromeo chapel is obtained by the Root mean square method on a value of 3.87 K for temperature, 13.1 % r.h. for relative humidity, and 0.913 g/kg for specific humidity. This hygrothermal interaction of natural indoor climate with outdoor

climate is plotted for air temperature and specific humidity, see Fig. 7.

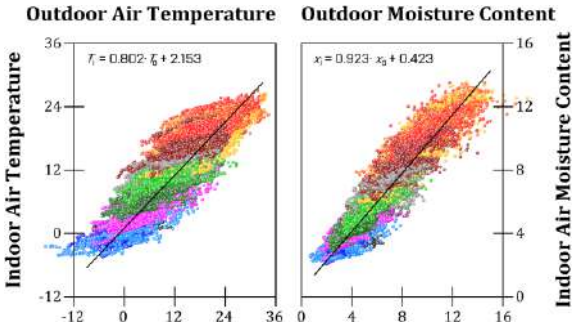

Fig. 7 - *Hygrothermal dependence of indoor climate on outdoor weather in period from 18th June 2018 to 16th October 2021.*

The linear regress between indoor climate (T_i [°C] and x_i [g/kg]) and outdoor weather (T_o [°C] and x_o [g/kg]) is obtained $T_i = 0.802 \cdot T_o + 2.153$ [°C] for air temperature (R^2 value 84 %) and $x_i = 0.923 \cdot x_o + 0.423$ [g/kg] for air specific humidity (R^2 value 92 %). The slope parameter of linear regression close to 1.0 (100 %) shows the hygrothermal dependence of indoor climate on outdoor weather. The intercept parameter of linear regression close to 0 (without gains) shows the hygrothermal source in indoor climate in the St. Charles Borromeo chapel. This hygrothermal source is the impact of heat/moisture loads and heat/moisture storage, sun radiation, etc.

5. Visualisation of Measurement

The colour visualization of hygrothermal behaviour of natural indoor climate in the St. Borromeo chapel uses linear interpolation (colour-map in the figure) between real measured values (numerical value in the figure).

5.1 Spring season

The outdoor weather on 21st April 2019 shows a daily temperature fluctuation from 4.4 °C at 7 am to 20.6 °C at 6 pm. This daily temperature fluctuation (16.2 K per 11 hours) is coupled with the outdoor air relative humidity in a range from 77 % r.h. at 7 am to 25 % r.h. at 3 pm. This hygrothermal fluctuation of outdoor climate is detected in the dome up to 2.1 K and 9 % r.h (Sensor 4) and up to 0.8 K and 4.6 % r.h. in level 3.20 m (Sensor 1). The hygrothermal response of the St. Charles Borromeo chapel shows a stable natural indoor climate during the day, see Fig. 8.

5.2 Summer season

The outdoor weather from 21st June 2018 to 23rd June 2018 shows a sunny warm day with afternoon rain and a following cloudy day. The outdoor air temperature on 21st June 2018 is increased from 16.2 °C at 7 am to 28.8 °C at 3 pm. The indoor air temperature in the dome (Sensor 4) is detected from 20.4 to 20.8 °C. The indoor air specific humidity is obtained from 9.6 to 10.1 g/kg, see Fig. 9.

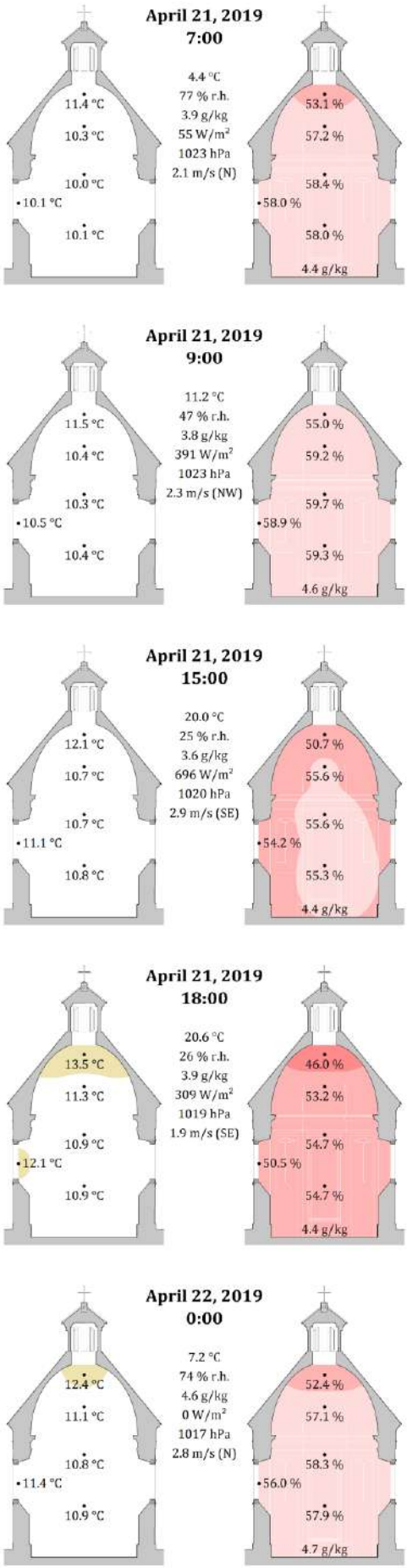

Fig. 8 - *Hygrothermal behaviour of indoor climate in the St. Charles Borromeo chapel in the spring season.*

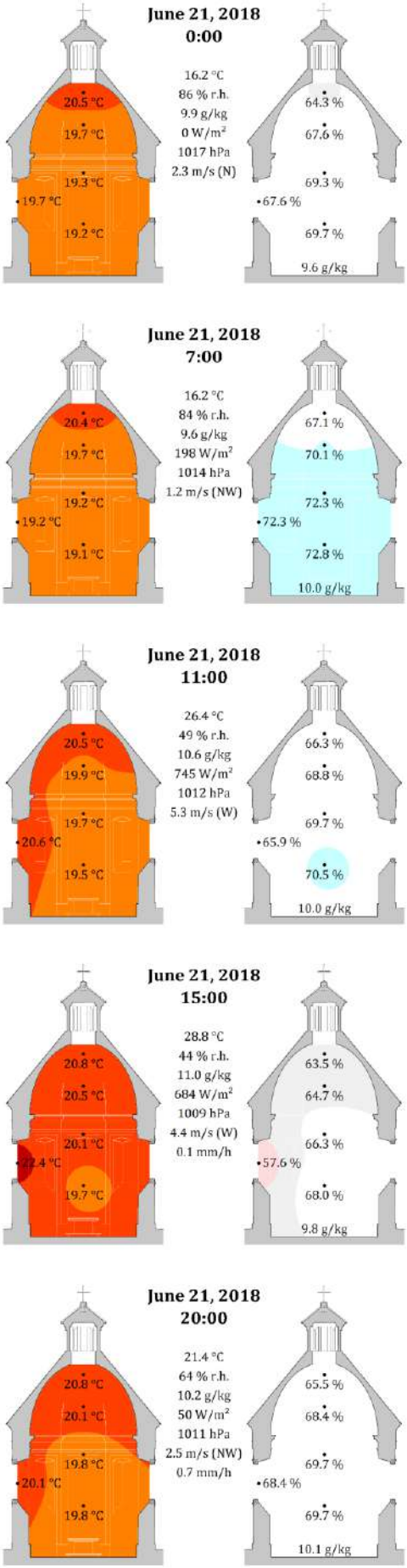

Fig. 9 - *Hygrothermal behaviour of indoor climate in the St. Charles Borromeo chapel in the summer season.*

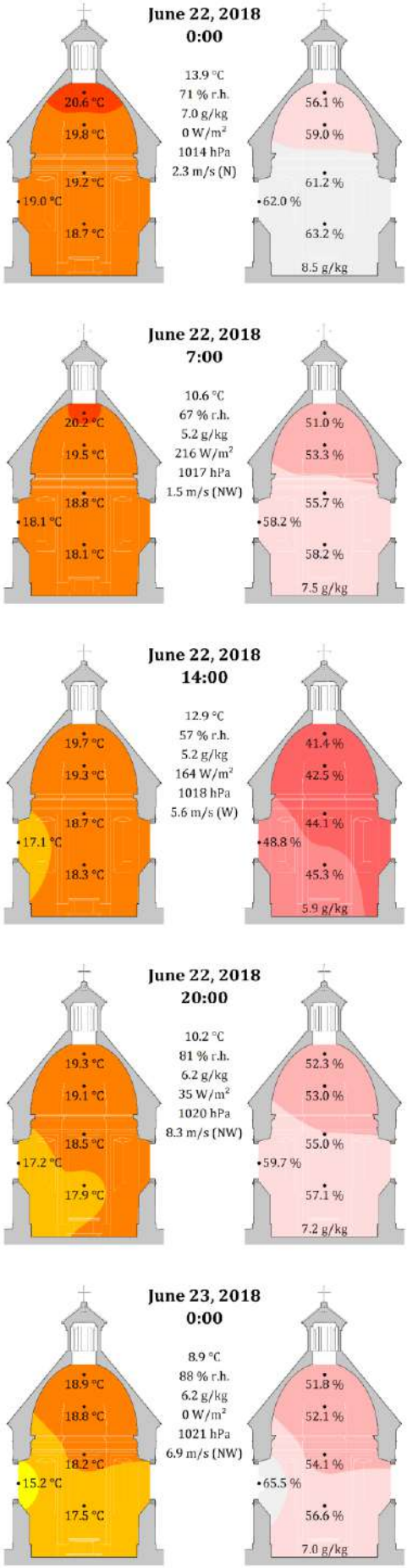

Fig. 10 - *Hygrothermal behaviour of indoor climate in the St. Charles Borromeo chapel in the summer season.*

The outdoor weather on 22nd June 2018 is a windy and cloudy day, see Fig. 10. The outdoor air temperature decreases from 13.9 to 8.9 °C, but the indoor air temperature is over 18 °C. This combination of a warm indoor climate and increased wind speed up to 8.3 m/s at 8 pm causes a drying effect in the St. Charles Borromeo chapel. The indoor air relative humidity decreases up to 41.4 % r.h. in the dome at 2 pm, and the indoor air specific humidity is decreased also from 10.1 g/kg at 8 pm on 21st June 2018 to 5.9 g/kg at 2 pm on 22nd June 2018. This dryness effect of indoor climate is the impact of the natural hygrothermal response of St. Charles Borromeo chapel on the outdoor weather.

5.3 Autumn season

The outdoor weather on 2nd October 2019 shows a windy and cloudy day. The wind speed is measured from 3.6 to 6.5 m/s. The outdoor air relative humidity is obtained from 85 to 90 % r.h. This high outdoor air relative humidity caused by light rain of 0.10 mm/hour is detected in the dome (Sensor 4) by 76.9 % r.h. at 11 am, 80.4 % at 1 pm, 79.2 % r.h. at 3 pm, 79.3 % r.h. at 5 pm, and 69.3 % r.h. at 8 pm after the end of the rain. The indoor air temperature in the dome shows a stable value from 14.1 to 14.2 °C. This hygrothermal response of the St. Charles Borromeo chapel shows the impact of wind on the natural indoor climate.

5.4 Winter season

The natural indoor climate in St. Charles Borromeo shows a low indoor air temperature of -4.7 °C on the northwest window on 26th January 2019 at 4 am. The indoor air temperature is obtained for the outdoor air temperature at -4.8 °C in combination with the northwest wind with a wind speed of 5.2 m/s. This natural indoor climate with the Frost risk on 26th January at 4 am shows indoor air relative humidity in a range from 65.6 % r.h. (Sensor 1) to 73.8 % r.h. (Sensor 0). After the sunrise on 26th January 2019 at 7:33 am, the outdoor air temperature is increased up to 2.1 °C and the wind speed is growing up to 7.4 m/s. The snow layer is melting and the combination with a light rain of about 0.10 mm/hour at 11 am, and 3 - 5 pm increases the indoor air relative humidity up to 88.4 % r.h. (Sensor 3), see Fig. 13 at midnight on 27th January 2019. This obtained result shows the impact of a windy day and high outdoor air relative humidity on the natural indoor climate in St. Charles Borromeo chapel.

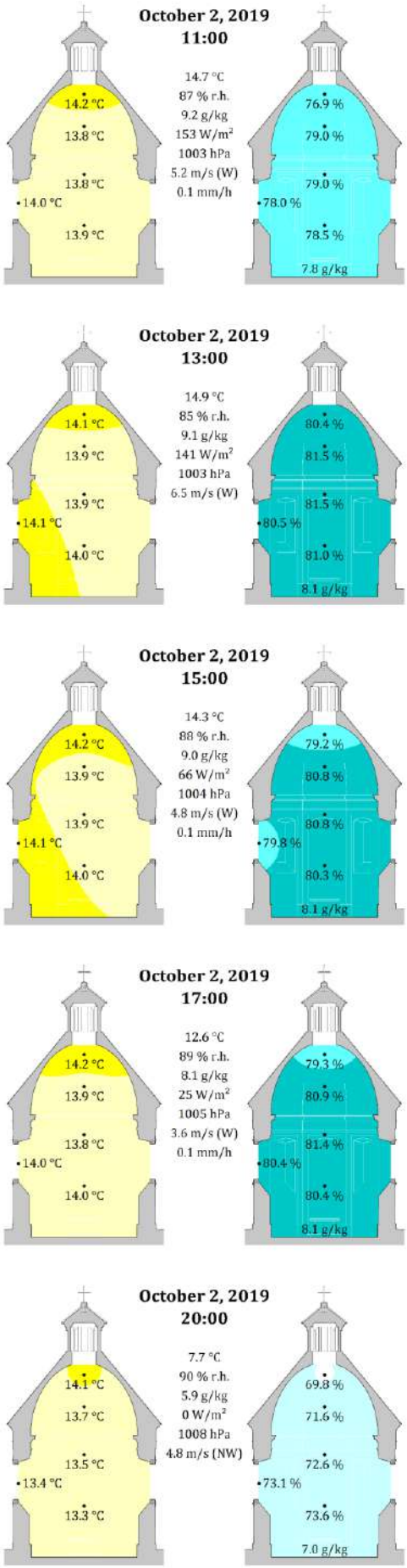

Fig. 11 - *Hygrothermal behaviour of indoor climate in the St. Charles Borromeo chapel in the autumn season.*

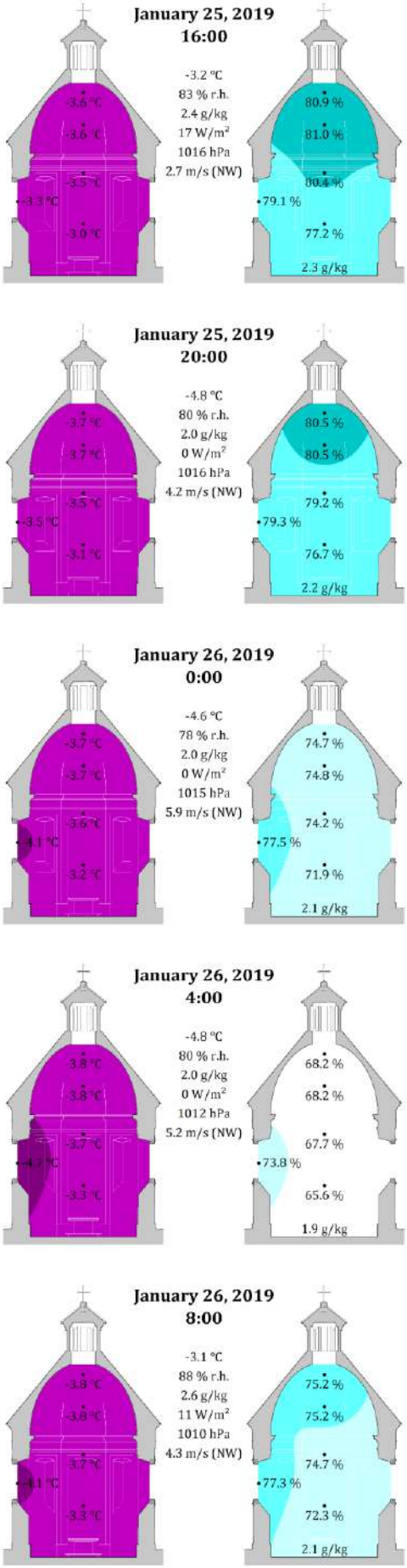

Fig. 12 - *Hygrothermal behaviour of indoor climate in the St. Charles Borromeo chapel in the winter season.*

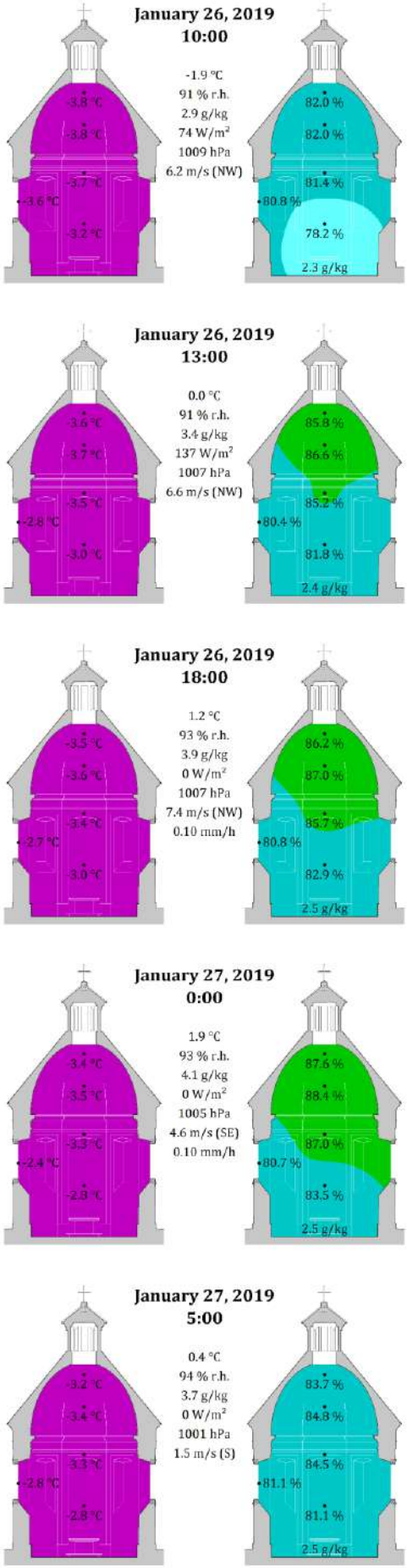

Fig. 13 - *Hygrothermal behaviour of indoor climate in the St. Charles Borromeo chapel in the winter season.*

6. Conclusion

The natural indoor climate in the St. Charles Borromeo chapel is analysed over 28 939 hours in the year 2018 - 2021. This natural indoor climate shows an average air temperature of 10.2 °C and average relative humidity of 75.1 % r.h. The hygrothermal vertical stratification of indoor climate is obtained for air temperature up to 5.2 K and 24.1 % r.h. for relative humidity. These hygrothermal parameters of indoor climate show the Microbiology risk in 4.85 % days per year, the Dryness effect in 0.01 % days per year, and the Frost risk in 10.72 % days per year. Finally, this natural indoor climate isn't a risk for the preventive conservation of original mural painting over 84.4 % days per year.

Acknowledgement

This research project has been created thanks to scientific cooperation between Brno University of Technology, Faculty of Civil Engineering with National Heritage Institute, Regional Branch in Telc and Fraunhofer Institute for Building Physics, Holzkirchen Branch. This contribution has been supported by the research project FAST-J-22-7880.

References

[1] Bobková-Valentová K, Hnilicová P. (editor); *Telč a jezuité, řád a jeho mecenáši. Katalog výstavy*; Historický ústav AV ČR, Národní památkový ústav ÚOP Telč, Ústav teoretické a aplikované mechaniky AV ČR, ISBN 978-80-907357-3-6, Praha 2020.

[2] NPÚ Telč; Photo of St. Charles Borromeo; [https://www.pamatkovykatalog.cz/kaple-sv-karla-boromejskeho-13509673]

[3] Švarc R.; Project documentation of St. Charles Borromeo in Telc; Telc 2016

[4] COMET System s.r.o.; Datasheet of dataloggers; [https://www.cometsystem.cz/userfiles/dokumenty_menu/46/i-log-s3120.pdf]

[5] M.BB.CC. 2001; *Atto di indirizzo sui criteri tecnico-scientifici e sugli standard di funzionamento e sviluppo dei musei D.M. 10.5.2001*; Supplemento ordinario alla G.U. n.244 dal Ministero per i Beni e le Attività Culturali, Ascoli Piceno 2011

[6] Italian Standard UNI 10829:1999; *Works of art of historical importance - Ambient conditions or the conservation - Measurement and analysis*; UNI - Ente Nazionale Italiano di Unificazione, Milan 1999

[7] D'Agostino V.; *Condizioni microclimatiche e di qualità dell'aria negli ambienti museali*; Napoli 2006; [http://www.fedoa.unina.it/1071/]

[8] ASHRAE Handbook; *Museums, galleries, archives and libraries*; USA Society of Heating, Refrigerating and Air-Conditioning Engineers, Atlanta 2011

[9] Sedlbauer; *Vorhersage von Schimmelpilzbildung auf und in Bauteilen*; Fakultät Bauingenieur und Vermessungswesen; University Stuttgart 2001; [http://publica.fraunhofer.de/dokumente/B-78495.html]

[10] European Standard CEN/TC 346, Conservation of Cultural Heritage EN 15757 in year 2010; *Conservation of Cultural Property, Specifications for temperature and relative humidity to limit climate - induced mechanical damage in organic hygroscopic materials*; European Committee for Standardisation, Brussels 2010

Ecological Refrigerant Cascade Systems Replacement in Accordance with the EU Regulations

Tarlea Gratiela [a], Vinceriuc Mioara [b], Temistocle Florin [a,b]

[a] Technical University of Civil Engineering 66 Pache Protopopescu Boulevard, 2nd District, 021414 Bucharest Romania.
[b] Romanian General Association of Refrigeration 66 Pache Protopopescu Boulevard, 2nd District, 021414 Bucharest Romania, e-mail: gratiela.tarlea@gmail.com.

Abstract. The paper analyses ecological refrigeration cascade systems in accordance with Regulation (EU) no. 517/2014 of the European Parliament and Council of 16 April 2014. In present the cascade refrigeration plants work with refrigerants R23/ R404A. In accordance with the Regulation F-gas we will replace R23(GWP=14800) refrigerant with the new refrigerant gas R472A with the lowest GWP value (GWP=353) and R404A refrigerant with R448A. The refrigerant R472A is perfectly compatible with the commercial elements used in cascade refrigeration plants charged with R23. R472A [CO2/R32/134A] refrigerant can be used for ULT (Ultra Low Temperature) applications must reach a temperature lower than or equal to -70°C. The determination of the thermodynamic properties was performed with the help of the Refprop program. The TEWI factor analysis was performed for a cascade refrigeration installation which is located in the Laboratory of the Technical University of Civil Engineering Bucharest, Thermodynamics, Heat and Mass Transfer Department.

Keywords. Refrigerant, alternative mixture, GWP, TEWI factor
DOI: https://doi.org/10.34641/clima.2022.30

1. Introduction

In terms of global warming potential (GWP), at international level regarding the refrigerants, according with the new legislative Regulations [1] ecological alternatives must be founded for refrigeration systems and in this article was studied the case of a testing room, which is located in the Laboratory of the Technical University of Civil Engineering Bucharest, Thermodynamics, Heat and Mass Transfer Department.

Global warming and ozone depletion are two separate environmental problems, but in the end, they are in connection.

The testing room presented in this paper works with a cascade refrigeration system and R23/ R404A refrigerants.

The technology used in the design of this testing room includes thermal insulation materials, super-efficient cooling systems and PC-based control using the powerful WINKRATOS® software package.

2. Ecological Analysis

In accordance with the F-Gas Regulation were replaced R23 and R404A [HFC-125/HFC-143a/HFC-134a] refrigerants with new refrigerant R472A[CO2/R32/134A] and the refrigerant R448A [R32/R125/R134a/R1234ze/R1234yf] with lower GWP values (see table1).

The mixture refrigerant R472A is perfectly compatible with the commercial elements used in cascade refrigeration plants charged with R23 refrigerant.

This refrigerant (R-472A) with low global warming potential (GWP) replace R404A in positive displacement, direct expansion low and medium temperature commercial and industrial applications.

R472A [CO2/R32/134A] refrigerant can be used for ULT (Ultra Low Temperature) applications which must reach a temperature lower than or equal to -75°C.

R448A is an azeotropic blend, which is classified as a non-flammable replacement refrigerant with a low GWP value. It was designed to serve as a replacement for R404A (and R22) in low and medium temperature systems.

The thermodynamic properties (Fig.1, Fig.2 and Fig.3) were determined with the Refprop [2] software.

Table 1 presents some properties of the refrigerant used in this cascade refrigeration system.

Copyright ©2022 by the authors. This conference paper is published under a CC-BY-4.0 license.

Tab. 1 - Comparison between ecological alternatives for the testing room [1,2,3,4,5].

Refrigerant	R404A	R448A	R23	R472A
Safety group	A1	A1	A1	A1
Critical temperature [°C]	72.04	83.65	26.14	44.46
Critical pressure [bar]	37.28	44.95	48.32	68.43
Critical density [kg/m3]	486.54	480.17	526.5	466.17
Molar mass [kg/kmol]	97.60	86.28	70	50.38
ODP	0	0	0	0
GWP	3922	1387	14800	353

Figure 1 presents a thermodynamic comparison between the properties of refrigerants. The pressure evolution vs temperature after simulations of the refrigerants R404A, R23, R472A and R448A can be observed.

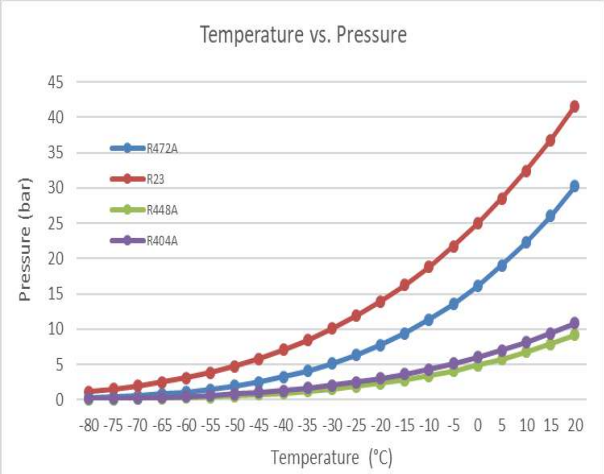

Fig. 1 – Temperature vs. pressure

In the Figure 2 and figure 3 are shown the comparisons between the density and enthalpy in vapour phase for the proposed refrigerants R404A, R472A, R448A and R23.

Some advantages of the new refrigerant R472A are presented. Thanks to miscibility refrigerant R472A is the only gas that makes it possible to use the gas bottle even partially, always ensuring the homogeneity of the mixture both inside the refrigerating plant and in the gas. Quantity remained in the bottle, being reusable in the future.

This is a great advantage for the technicians and students who work with R472A in the laboratory, since they can manage the gas bottles in an extremely easy and safe way, as it is normally the case for other gases commonly used in refrigeration, such as R449A or R452A [9].

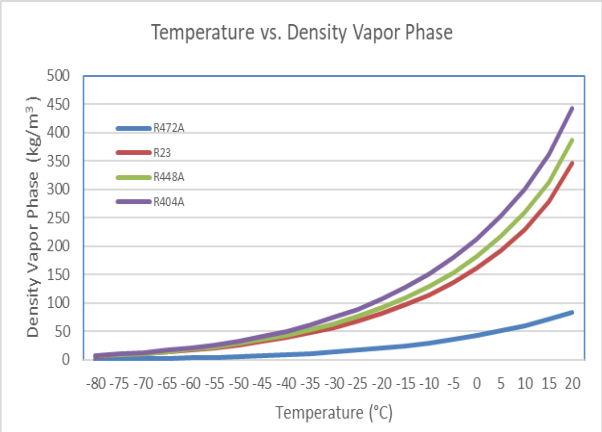

Fig. 2 - Temperature vs. density vapour phase

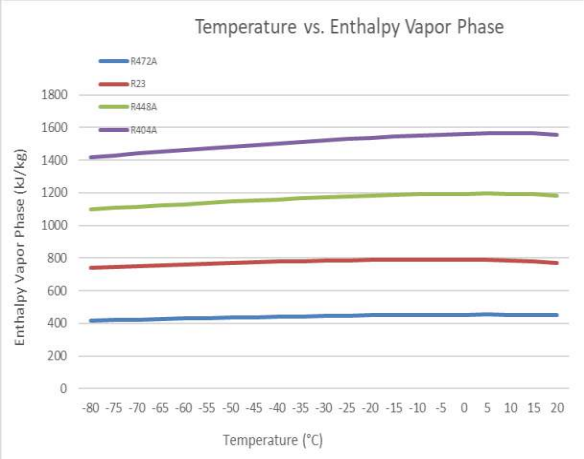

Fig. 3 - Temperature vs. enthalpy vapour phase

R472A is non-flammable and non-toxic: it has obtained the A1 Safety Class by ASHRAE (the American Society of Heating, Refrigerating and Air Conditioning Engineers). Another advantage of this fluid is that R472A has the lowest density vapor phase in comparison with the other refrigerants (Fig.2).

3. Theoretical Study Case

The theoretical comparative study was done for the testing room in a cascade refrigeration system.

The system is loaded with ozone harmless fluids: R404A and R23 but which are in conflict with F-Gas Regulation refrigerants and are not allowed to be used in new refrigeration systems and are strongly restricted.

The testing room has 1200l useful capacity. The environmental humidity and temperature test chamber has an operating temperature range between -70° C and +180°C.

The testing room environmental chambers, continuously improved and up-to date with the latest technologies. Designed to meet the increasingly sophisticated quality and reliability requirements of the humidity and temperature testing chambers [5,6].

The challenge family of chambers always offers superior performances and a striking "high tech" look. The cooling system has been optimized to give maximum thermodynamically efficiency and an accurate temperature control.

Cooling is obtained by the evaporation of the liquid injected into the evaporator.

The compressor compresses the gas refrigerant and after that into the condenser under the effect of the high pressure the cooling gas changes state and becomes liquid. The liquid expands thanks to a thermostatic valve and as it evaporates, it absorbs heat and induces cooling at the same time.

The cycle is completed when the gas is sucked in once again by the compressor.

This cascade refrigeration plants use semi hermetic compressors which are compatible with the characteristics of new refrigerants and the demands of the market related to efficiency, reliability and low noise level [7,8,9].

The characteristics of the compressors are: high C.O.P. values, thanks to fluid dynamic optimisation of the internal flow paths, high efficiency motors and high-tech components, low vibrations and low gas pulsation.

The TEWI factor was calculated in according with UE legislation.

The total global warming potential method calculation (GWP) of Ecological Alternative was done in according with REGULATION (EC) No 842/2006 (from 1 January 2015 REGULATION (EC) No 517/2014).

To calculate TEWI factor were following assumptions: mass of refrigerants made seen in Figure 4.

The leakage of refrigerant was 8% from refrigerant charge with a recovery factor of 0.75. Operating time of the system was 15 years, and CO2 emission was 0,28985 kg / kWh for country where the system is located (Romania).

The TEWI factor was determinate [10,11] taking account of the Standard EN 378-1:

$$TEWI = [GWPx\ Lxn] + [GWPx\ mx(1 - \alpha_{rec})] + [nx\ E_{annual}\ x\beta] \quad (1)$$

Where:

GWP – the global warming potential, CO_2related

L – leakage in kilogrammes per year

n – system operating time in years,

m – refrigerant charge in kilogrammes

α_{rec} - recovery/recycling factor from 0 to 1

E_{annual} – energy consumption in kilowatt-hour per year

β - CO_2 emission in kilogrammes per kilowatt-hour kg/kWh

$[GWP\ x\ m\ x\ (1 - \alpha_{rec})]$ - impact of recovery losses

$[GWP\ x\ L\ x\ n]$ - impact of leakage losses

$[n\ x\ E_{annual}\ x\ \beta]$ - impact of energy consumption.

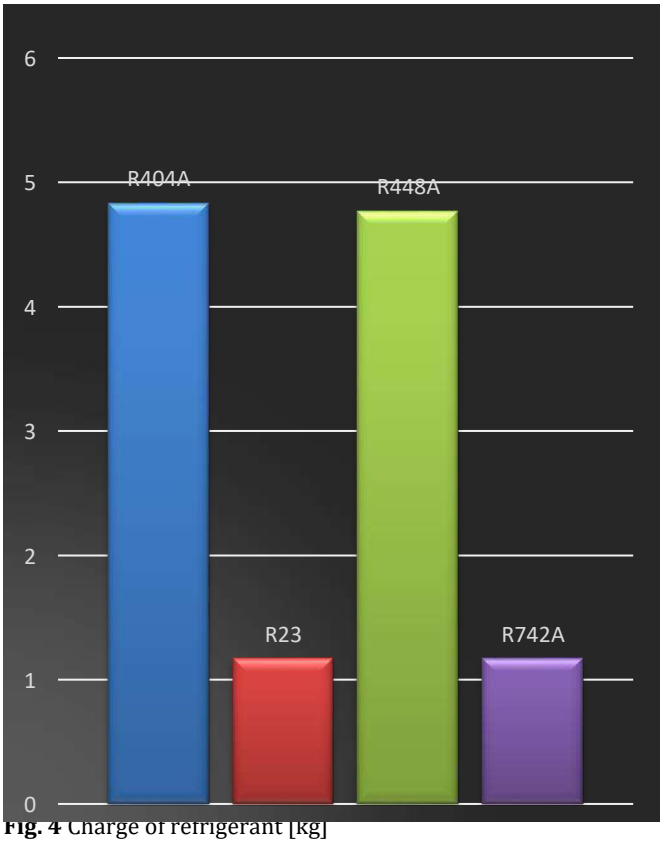

Fig. 4 Charge of refrigerant [kg]

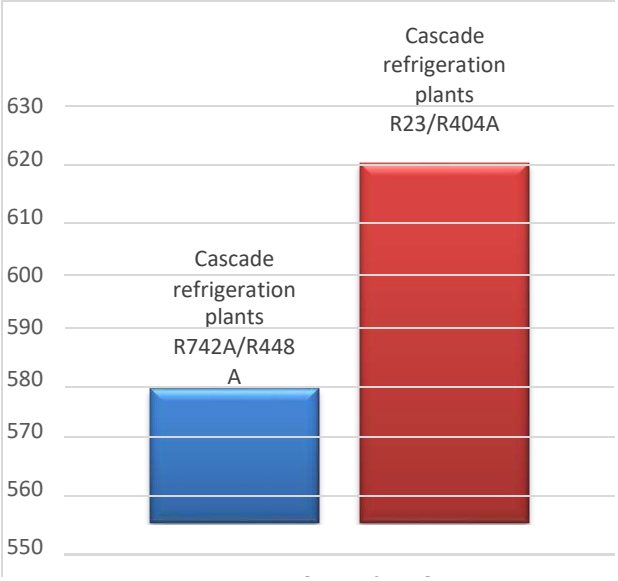

Fig. 5 Comparison of TEWI factor between cascade refrigeration R404A/R23 and R742A/R448A

Higher performance is highlighted when R742A/R448A is used - the reduced amount of refrigerant, a feature with environmental benefits reflected by the TEWI equivalent (Total Equivalent Warming Impact) as it is shown in figure 5.

In the cascade systems, the contribution to warming the atmosphere is both direct (due to the refrigerant) and indirect (through the energy used), the second being the most important [12].

4. Conclusions

Regarding F-Gas Regulation [1], the optimum alternative for this application (testing room with cascade refrigeration plant) from the point of GWP is refrigerant mixture R472A/R448A.

After determinations of the thermodynamic properties, it could be observed (Fig. 1) that the alternative R448A is the best option in comparison with refrigerant R404A because pressure is much lower for temperatures between -70°C ÷ +40 °C.

Also, alternative R472A has the lowest density vapor phase in comparison with the other refrigerants (Fig.2).

From an environmental perspective of lower global warming potential (GWP) alternative R472A has the advantage of 77% lower global warming potential (GWP) than R23.

The molar mass of the alternative 472A has an advantage because it is lower than R23 (Tab. 1)

From an environmental point of view, the theoretical results of the R472A/R448A cascade system have the best TEWI = 575,78 tons of CO2, 7% lower than R404A/R23 (Fig.5).

5. References

[1] Regulation (EU) no 517/2014 of the European Parliament and of the council of 16 April 2014 on fluorinated greenhouse gases and repealing Regulation (EC) No 842/2006

[2] The National Institute of Standards and Technology (NIST) - Refprop version 8.0, USA (2007)

[3] Tarlea G., Vinceriuc M., Temistocle F., Ecological refrigerated cabinets for vaccine storage, presented the Technical Conference - Scientific with international participation, Installations for construction and energy saving", July 1-2, Iasi 2021.

[4] European Standard SR EN 378-1:2016

[5] Ţârlea G. M., 2008, 2009 Codes of Practice (1,2). Domain refrigerating and air conditioning Bucharest, Publisher AGIR.

[6] Ultra-Low Temperature Refrigerator Prospect

[7] ASHRAE – Thermophysical Properties of Refrigerants, -Chapter 20, 2009

[8] Bitzer - Refrigerant Report 2018

[9]https://www.acstestchambers.com/en/services/recovery-of-refrigerant-gases/

[10] Tarlea G., Vinceriuc M., Zabet I., Tarlea A. Theoretically study of ecological alternative for R404A, R507A and R22, published at the 42nd international Congress and Exibition Heating, Refrigeration and Air-Conditioning Belgrade, 30th November – 2nd December 2011: 122-130.

[11] Tarlea G., Vinceriuc M., Zabet, I., Tarlea,A. R404A Refrigerant Retrofit Study Prague, Czech Republic, Clima 2013; 188-194.

[12] Vinceriuc M. Low GWP Alternative for R404A Refrigerant, - presented at the 28th edition of the International Conference of Installations for Constructions and Environmental Comfort, Constantin Avram Amphitheatre of the Faculty of Constructions on April 12, Timisoara 2019; https://www.aiiro.ro/aiiro/aiir-filiala-banat-timisoara/-341.html

Study of Using R290 Refrigerant Replacement in a Heat Pump Application

Tarlea Gratiela [a], Mardare George [a b], Tarlea Ana[b]

[a] Technical University of Civil Engineering 66 Pache Protopopescu Boulevard, 2nd District, 021414 Bucharest Romania.
[b] Romanian General Association of Refrigeration 66 Pache Protopopescu Boulevard, 2nd District, 021414 Bucharest Romania, e-mail: gratiela.tarlea@gmail.com.

Abstract. The study represents a new approach in the research of the advantages obtained by the water-to-water heat pumps. This original system can use a renewable energy resource, respectively groundwater, rivers or sea water and can achieve both the heating and cooling requirements of a location. The study represents also a research in the field of energy efficiency and environmental optimization of heat pumps by changing the refrigerant R407C to R290.
For testing, an open circuit water-to-water heat pump was used, with capillary evaporators in an original spiral shape able to avoid clogging, by continuous self-washing effect.
The simulations showed that the heat pump ensures a reduction of the electricity consumption and Total Equivalent warming Impact by up to 50% compared to an ordinary air conditioning system.

Keywords. Heat pump, EER, COP, TEWI, Capillary Evaporators, Energy efficiency.
DOI: https://doi.org/10.34641/clima.2022.31

1. Introduction

Heat transfer performance is one of the most important areas of research in the field of thermal engineering. There are a large number of refrigerants used in compression refrigeration systems. Their use implies for each case some reservations in terms of environmental impact (R11, R12), toxicity (NH3), flammability (HC) or high pressure (CO2), which gives them degrees of danger accordingly. Ashok G. Matani et al. [1] conducted an experimental study to observe the performance of different ecological refrigeration mixtures (HC and R401a mixture).
The aim of the research is to be part of the preparatory action for the replacement of high GWP freons with environmentally friendly freons and comparatively analyzes the performance of the heat pump when operating with freon R290 and R407C.

2. Method

The research method comprises two stages, respectively:

1. Documentation stage
2. Research stage by testing

Thus, in the first stage, the results of some researchers on this topic were analyzed and quantified, and in the second stage, tests were performed in order to find some conclusions.

E. Halimic et al. [1] tested the operation of a compression refrigeration system using R12, R401A,

R134A and R290 refrigerants. The results (Fig.1) indicated that the performance obtained with refrigerant R134a are close to those obtained with refrigerant R401a but lower than those obtained with refrigerant R290.

E. Navarro et al. [2] conducted a comparative study between R1234yf, R134a and R290, using a piston compressor, with two operating speeds and vaporization temperatures from -20^{0}C to 20^{0}C, with the condensation temperature variation between 40^{0}C and 65^{0}C.

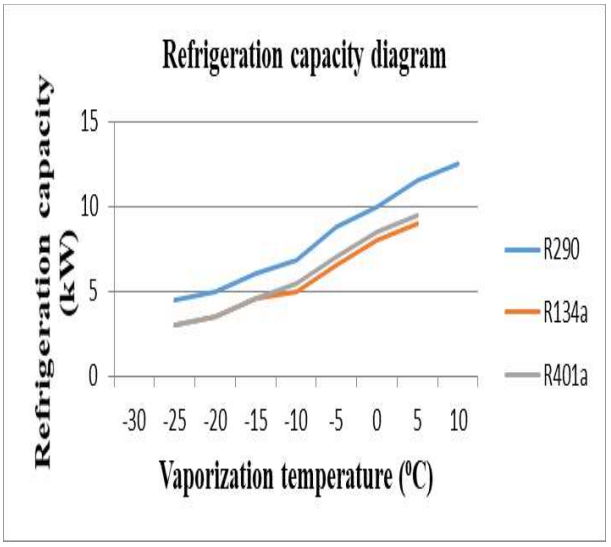

Fig. 1 - Refrigeration capacity analysis

The measurements performed and the subsequent analysis led to the following conclusions:
R-290 has shown a significant improvement in volumetric efficiency, and heat losses are considerably lower than for the other two coolants. It should be noted that R-290 has a significantly higher volumetric capacity than the other two

Copyright ©2022 by the authors. This conference paper is published under a CC-BY-4.0 license.

refrigerants, which may reduce the size of this type of system [3]

The new refrigerant, R-1234yf, has better efficiency compared to R-134a for pressure ratios greater than 8. It has less heat loss than R-134a, but 20% more than R290 [4].

From this study, it can be concluded that R-1234yf and R-290 can be good substitutes for R-134a.

In terms of efficiency, R-290 (Fig.2), demonstrated a better performance for the whole range of conditions tested (improvement on average by 30% of volumetric efficiency and by 15% of compressor efficiency). R-1234yf showed higher heat losses than R290, even with a significantly lower compressor discharge temperature.

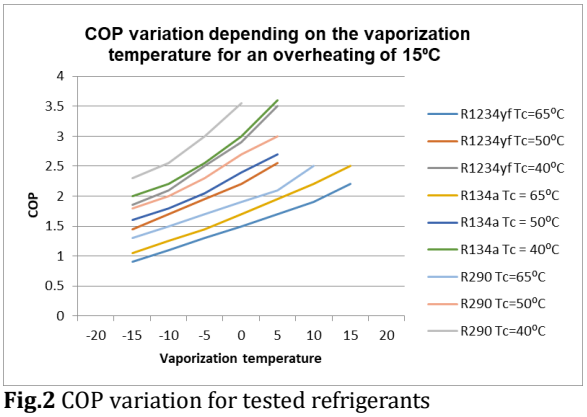

Fig.2 COP variation for tested refrigerants

Ki-Jung Park and others [5] analyzed the performance of two pure hydrocarbons and seven mixtures composed of propylene, propane, R152a and dimethyl ether in order to replace R22 refrigerant in residential air conditioners and heat pumps at evaporation temperatures and condensation of 7 ° C and 45 ° C, respectively. The test results confirmed a value of the performance coefficient of these mixtures up to 5.7% higher than in the case of operation with R22.

The conclusions were that the mixtures used led to superior performance with reasonable energy savings, without any environmental problems and, consequently, can be used in the long term as alternatives for residential air conditioning and heating applications with heat pumps.

Ki-Jung Park and others [6] analyzed the thermodynamic performance obtained with two pure hydrocarbons and seven mixtures composed of propylene (R1270), propane (R290), R152a and dimethyl ether (R170) in order to analyze the possibilities of substituting R22 refrigerant in residential air conditioning installations.

The test results led to COP values up to 5.7% higher than when using R22 refrigerant.

K. Mani and others [7] analysed the operating parameters of a refrigeration system with steam compression using the R290 / R600 mixture (68% / 32%) in order to replace the R12 and R134a refrigerants.

The results showed that the refrigerant R134a showed a slightly lower COP than R12. The R290 / R600a mixture was very close to R12. In conclusion, the mixture R290 / R600a (68/32% by weight) can be considered as a substitute refrigerant for R12 and R134a due to the real ecological advantages.

AS Dalkilic et al. [8] studied the performance of a compression refrigeration plant using mixtures of R134a, R152a, R32, R290, R1270, R600 and R600a refrigerants combined in various ratios and the results were compared with the functional parameters of the same plant using refrigerants R12, R22 and R134a.

The results showed that all alternative refrigerants investigated in the analysis have a COP slightly lower than R12, R22 and R134a for the condensation temperature of 50 ° C and the evaporation temperatures ranging from –30 ° C to 10 °C.

Mixtures of R290 / R600a refrigerants (40% / 60% by weight) can replace refrigerant R12 with close energy results and the mixture of R290 / R1270 refrigerants (20% / 80% by weight) can replace refrigerant R22 with close energy results, having in view the ecological properties of these mixtures.

Vincenzo La Rocca and others [9], analysed the performance of a refrigeration system with vapor compression using refrigerant R22 compared to those obtained by replacing this refrigerant with new refrigerants, HFC, respectively:

R417a, R422a and R422d. The conclusion was that the performances obtained with the new tested refrigerants were inferior to those achieved by operating with the R22 refrigerant.

Yunho Hwang et al. [10] compared the operating performance of a refrigeration system using R404 and R410A refrigerants compared to R290. The conclusion was that the energy performance obtained with R290 refrigerant is lower than that obtained with R404 and R410A refrigerants but the ecological performance of R290 are are absolute.

Venkataramana Murthy et al. [11] considered the possibility of replacing refrigerant R22 with environmentally friendly refrigerants (R134a,R407C and R290) in order to comply with the provisions of the Montreal Protocol using for testinga refrigeration system equipped with a rotary encapsulated compressor using SUNISO4 oil and an air-cooled condenser. The vaporizer used was a 2m long capillary.

The conclusion was that the R290 refrigerant ensures a higher COP, compared to the R134a, R407C

and R22 refrigerants.

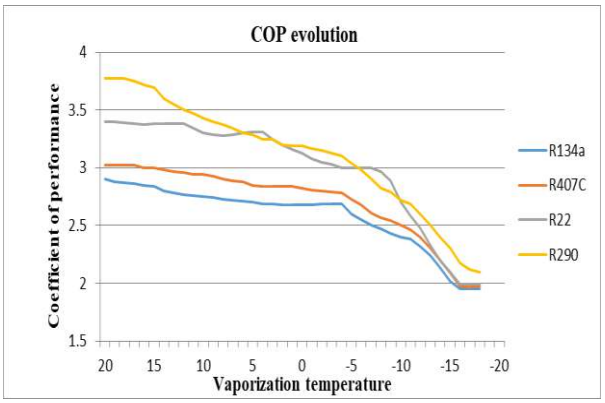

Fig.3 COP evolution for the refrigerants tested in the refrigeration installation

3. Results and discussion

In order to determine the energy performance of the use of the R290 refrigerant compared to the R407C refrigerant at a heat pump, operation simulations were performed using specialized programs provided by the manufacturers, respectively Danfoss and Scroll Copeland. The tests were performed on a capillary heat pump with an Archimedean spiral evaporator.

The COP value was analyzed for the entire usual range of condensation temperatures. Fig. 4-9 represents the COP variation depending on the condensation temperatures.

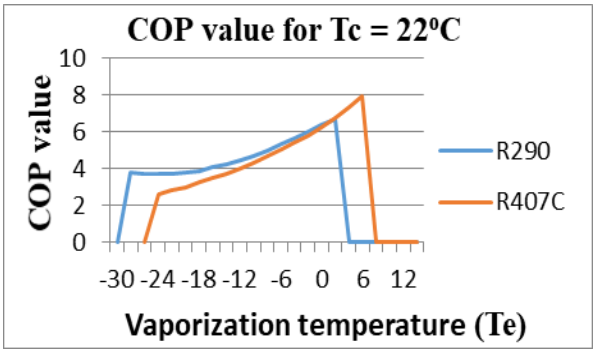

Fig 4. COP value for Tc = 22ºC

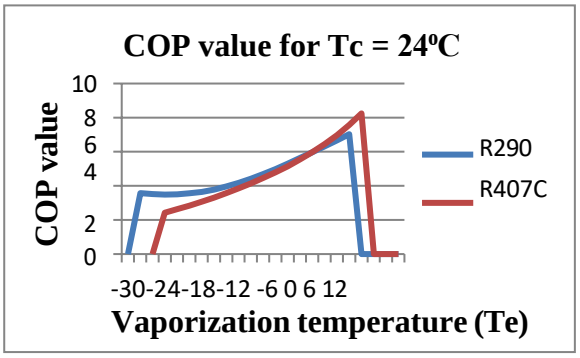

Fig 5. COP value for Tc = 24^{0}C

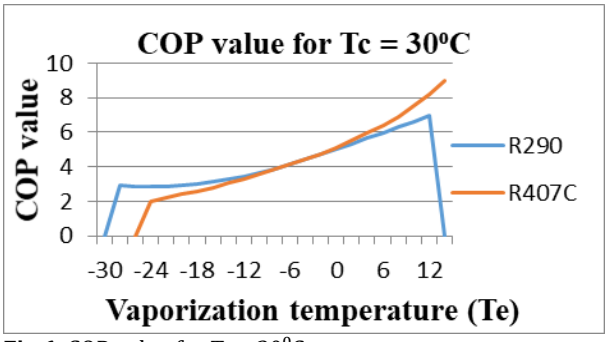

Fig 6. COP value for Tc = 30^{0}C

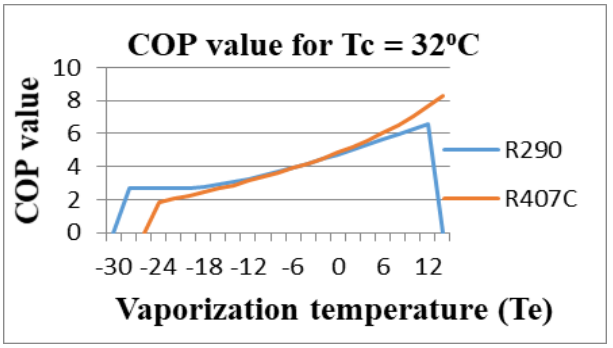

Fig 7. COP value for Tc = 32^{0}C

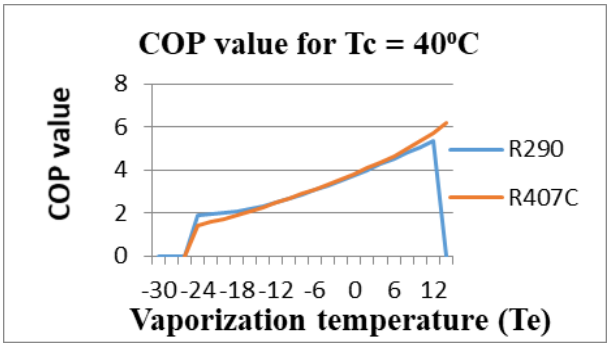

Fig 8. COP value for Tc = 40^{0}C

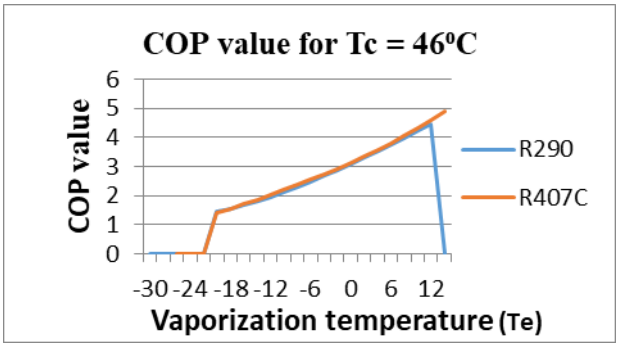

Fig 9. COP value for Tc = 46^{0}C

Tab. 1 - TEWI (Total Equivalent Warming Impact) calculation for R407C and R290

		R407C	R290
GWP		1624	3
L	kg/an	0,09	0,09
n	ani	30	30

m	kg	4,5	4,5
αrecover		0,8	0,8
Eannual	kwh/an	2.462	2.462
β	kg/Kwh	0,28985	0,28985
GWP x L x n		4.384,80	8,10
GWP x m(1-$\alpha_{recover}$)		1.461,60	2,70
n x E_{annual} x β		21.404,8	21.404,8
TEWI in kg CO2		27.251,2	21.415,6
TEWI in tones CO2		27,25	21,42

5. Conclusion

For conclusions, the energetic, ecological and financial parameters were analyzed comparing two systems that use respectively the R407C and R290 refrigerant, using the Pack Calculation pro program.

The results offered by the program were the following:

1) For a year-long operation in climatic conditions in Bucharest, the average COP achieved by the heat pump system using the R407C refrigerant calculated by the program was 2.34 while the system using the R290 refrigerant provides an average COP of3.03;

2) In front of the heat pump that uses the R407C refrigerant, the heat pump that uses the R290 refrigerant achieves an energy saving of 971kWh, which represents at the annual consumption level of the heat pump that uses the R407C refrigerant, a saving of 22%.

3) From the point of view of ecological analysis, during operation, the heat pump that uses the R407C refrigerant generates an indirect CO2 emission of 22,632kg compared to the heat pump that uses the R290 refrigerant at which the amount of CO2 emitted indirectly is only 17,486 kg., As it results fromfig.28

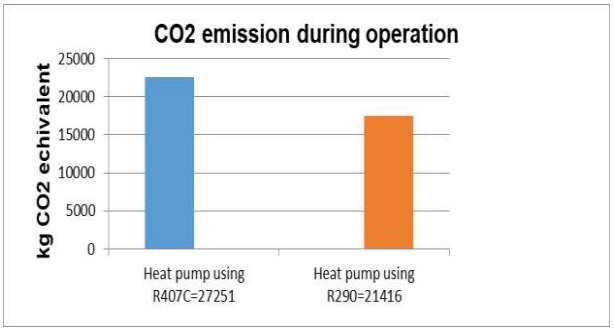

Fig. 10. CO2 emission during operation

The operating tire for the R290 refrigerant is much larger than for the R407C.

4) From the point of view of condensation temperature, the R290 refrigerant operating tire starts at 16^{0}C and ends at 68^{0}C, while the R407C refrigerant operating tire starts at 22^{0}C condensing and ends at condensation temperature of 64^{0}C

5) For condensation temperatures up to 36^{0}C and low vaporization temperatures, between -26^{0}C and -6^{0}C the heat pump with Refrigerant R290 ensures a higher COP than when using refrigerant R407C.

6) For condensation temperatures between 46^{0}C-48^{0}C, the COP is identical for operation with both refrigerants over the entire range of usual values of the vaporization temperature.

7) Operation with the R290 refrigerant ensures the possibility of obtaining condensation temperatures in the range 66-68^{0}C, which exceed the R407C refrigerant operating tire.

8) An important conclusion is that at low values of condensation temperature up to 35° C, corresponding to underfloor heating systems, the use of R290 freon in heat pumps, allows operation at much lower vaporization temperatures than in the case of R407C which allows the use of much colder sources and the obtaining of much better performances than in the case of using the R407C.

9) From the point of view of the TEWI factor, operation with the R290 refrigerant is the ideal option.

6. References

[1] E. Halimic, D. Ross, B. Agnew *, A. Anderson, I. Potts -A comparison of the operating performance of alternative refrigerants Department of Mechanical, Material and Manufacturing Engineering, School of Mechanical and Systems Engineering, University of Newcastle upon Tyne, Newcastle upon Tyne NE1 7RU, UK

[2] E. Navarro, I.O. Martinez-Galvan, J. Nohales, J. Gonzalvez-Macia-Comparative experimental study of an open piston compressor working with R-1234yf, R-134a and R-290-Universitat Polite `cnica de Vale `ncia, Instituto de Ingenierı´a Energe ´tica, Camino de Vera s/n 46022, 46022 Valencia, Spain- 24 November 2012

[3] Brown, J.S., Zilio, C., Cavallini, A., 2010b. Critical review of the latest thermodynamic and transport property data and models, and equations of state for R-1234yf. In: Groll, E.A., Braun, E.A. (Eds.), Proc 13th Int Refrig Air Cond Conf. USA, W Lafayette, IN.

[4] Mathur, G.D., 2010b. Experimental Investigation of AC System Performance with HFO-1234yf as the Working Fluid. SAE Technical Paper 2010-01-1207.

[5] Ki-Jung Park, Taebeom Seo, and Dongsoo Jung, "Performance of alternative refrigerants for residential air-conditioning applications,

Applied Energy, 84, pp. 985–991, 2007.

[6] Ki-Jung Park, and Dongsoo Jung, "Thermodynamic performance of HCFC22 alternative refrigerants for residential air-conditioning applications," Energy and Buildings ,39, pp. 675–680, 2007.

[6] K. Mani, and V. Selladurai, "Experimental analysis of a new refrigerant mixture as dropin replacement for CFC12 and HFC134a," International Journal of Thermal Sciences 47, pp. 1490–1495, 2008.

[7] A.S. Dalkilic, and S. Wongwises, "A performance comparison of vapor-compression refrigeration system using various alternative refrigerants," International Communications in Heat and Mass Transfer, 37, pp. 1340–1349, 2010.

[8] Vincenzo La Rocca, and Giuseppe Panno, "Experimental performance evaluation of a vapor compression refrigerating plant when replacing R22 with alternative refrigerants," Applied Energy, 88, pp. 2809–2815, 2011.

[9] Yunho Hwang, Dae-Hyun Jin, Reinhard Radermacher, Comparison of R-290 and two HFC blends for walk-in refrigeration systems, International Journal of Refrigeration ,30 (2007) 633-641.

[10] Venkataramana Murthy V. Padmanabhan1,* and Senthil Kumar Palanisamy2 1Department of Mechanical Engineering, K. S. Rangasamy College of Technology, Tiruchengode, Namakkal District, Tamilnadu 637-215, India 2Department of Mechanical Engineering, K. S. R. College of Engineering, Tiruchengode, Namakkal District, Tamilnadu 637-215, India- Exergy efficiency and irreversibility comparison of R22, R134a, R290 and R407C to replace R22 in an air conditioning system.

Transparent dynamic insulation: a novel system combining ventilation and insulation for sustainable greenhouse applications

A.J.H. Frijns, L.A. van Schaijk

Eindhoven University of Technology, PO Box 513, 5600MB Eindhoven, the Netherlands,
email addresses: a.j.h.frijns@tue.nl; l.a.v.schaijk@tue.nl

Abstract. Greenhouse horticulture cultivates vegetables, fruits, and flowers in protected glass houses. Approximately 65%-85% of the total energy in greenhouses is used for heating. To reach the climate goals energy reduction is needed. Energy savings cannot only be achieved by improving the insulation value of the greenhouse covers since also the relative humidity of indoor air needs to stay below a critical humidity level to avoid fungus growth. Therefore ventilation is required with an average air change rate (ACH) of 2.5/h. This is often realized by (partly) opening and closing the glass greenhouse cover thereby losing part of the heat. In this paper, we focus on a novel method that improves the thermal insulation of transparent top covers and/or walls while ensuring sufficient ventilation: transparent dynamic insulation (TDI). TDI is based on a concept called Dynamic Insulation, also known as a "breathing wall": infiltrating air flows through the multi-layer insulation panel. While doing this, the incoming air takes up part of the heat and uses this for pre-heating. Thereby it reduces the overall heat transfer value (U-value) and provides pre-warmed, fresh air flow into the greenhouse. The main difference compared to "traditional" dynamic insulation is that its design is transparent for solar irradiation and therefore can be used for greenhouses. In this paper, we show experimental results on a TDI prototype panel using a hot box apparatus with an ACH=2.5/h and prescribed temperature differences between indoor and outdoor of $\Delta T=10^{o}C$ and $\Delta T=20^{o}C$. It is shown that the measured overall U-value for the TDI panel is about 19% lower than for double glass and more than a factor 2 lower than single-layered Hortiplus glass. Therefore it is concluded that TDI is a promising approach to reducing energy consumption in greenhouse horticulture while ensuring sufficient air refreshment for moisture control.

Keywords. Dynamic thermal insulation, ventilation, greenhouses, energy savings
DOI: https://doi.org/10.34641/clima.2022.416

1. Introduction

In greenhouse horticulture, vegetables, fruit, and flowers are grown in protected glass houses. In the Netherlands, in 2018, the annual energy consumption attributed to greenhouses was 100.5 PJ [1]. Hereof, about 77% comprises energy for heating and 23% for electricity. Worldwide these numbers are similar: about 65%-85% of the total energy in greenhouses is used for heating [2]. To reduce the energy consumption, the electricity and heating demand should be reduced. Insulation can be improved by using for example double glazing or, poly-ethylene, polycarbonate, or PMMA covers: energy savings up to 60% compared to single-layer glass covers are reported [2]. Also, additional electricity can be generated in a sustainable way, e.g. by integrated PV panels [3]. In this paper, we focus on the heating demand.

Energy savings can be achieved by improving the insulation value of the greenhouse covers, however also the relative humidity of indoor air needs to stay below a critical RH level of 80% to avoid fungus growth. Therefore also a minimum ventilation rate is required: an average air change rate (ACH) of 2.5/h is needed, which is often realized by (partly) opening and closing the glass greenhouse covers thereby losing also part of the heat. Here we introduce a novel system that improves the thermal insulation of transparent top covers and/or walls of greenhouses while ensuring sufficient ventilation: transparent dynamic insulation (TDI).

2. Transparent Dynamic Insulation

2.1 Dynamic Insulation

Transparent Dynamic Insulation (TDI) is based on a

Copyright ©2022 by the authors. This conference paper is published under a CC-BY-4.0 license.

concept called Dynamic Insulation, also known as a "breathing wall" [4]. In such a system infiltrating air flows through a porous insulation panel that is enclosed between two impermeable walls (Figure 1). While doing this, the incoming air takes up part of the heat (indicated by energy flow C) and uses this for pre-heating the supply air from the outdoor temperature $T_{outdoor}$ to a higher inlet temperature T_{inlet}. Thereby it reduces the overall transmission heat loss (indicated by energy flow D) and improves the overall heat transfer value U [4]. This effective U-value is defined as

$$U = \frac{D}{A\,\Delta T} \qquad (1)$$

where D is the overall heat loss, A the effective surface area, and $\Delta T = T_{indoor} - T_{outdoor}$ is the temperature difference between the indoor and outdoor air. Without the additional airflow through the insulation layer, the heat loss would be larger and thereby the U-values as well. Another advantage is that it provides pre-warmed, fresh airflow into the building.

The required heat input to keep the indoor air at a constant is described by:

$$Q_{req} = D + \dot{m}\,(T_{indoor} - T_{inlet}) \qquad (2)$$

where $\dot{m}$ is the mass flow rate of the incoming air. The second term on the right hand side of equation (2) indicates the amount of heat that is required to heat the incoming air (with temperature T_{inlet}) to the required indoor air temperature T_{indoor}.

Since heat loss D is lowered (lower overall U-value) and T_{inlet} is increased (preheating of the incoming air) less energy is required to keep the indoor space at the same temperature.

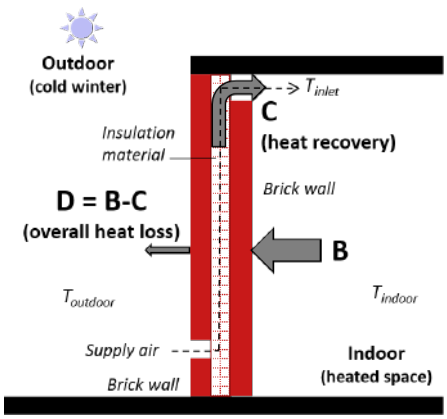

Fig. 1 - Principle of "traditional" dynamic insulation. The heat fluxes are indicated by the arrows. Arrow B indicates the heat loss from the indoor environment. Part of this heat will be taken up by the airflow through the porous insulation material between the inner and outer brick walls (indicated by arrow C), resulting in a lower overall heat loss D. *Picture based on* [4].

2.2 Transparent Dynamic Insulation

For greenhouses solar irradiation is essential. Therefore the material needs to be transparent. That limits the application of wall materials but also prohibits the use of traditional porous insulation materials like glass wool. To achieve a similar insulation effect, an additional transparent plate is added (figure 2). In this way also the path over which the incoming fresh air can take up the heat is prolonged and the temperature rise of the pre-heated incoming air will be larger. The main difference compared to "traditional" dynamic insulation is that its design is transparent for solar irradiation and therefore can be used for greenhouses. In figure 2 a horizontal cover plate is shown, but the panel can also be placed in a vertical orientation, i.e. it can also be used as a wall element.

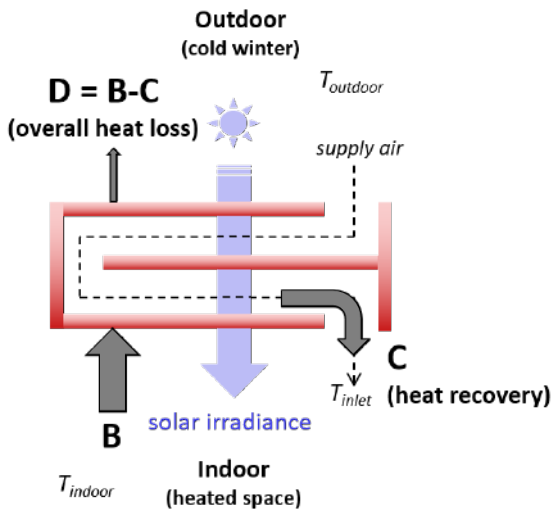

Fig. 2 - Principle of transparent dynamic insulation (TDI) roof cover. The panel walls are made of a transparent material (red lines). Incoming fresh air flows through a double curved channel (dotted line) in between the 3 layered structure while taking up the heat (C) that counterflows from the indoor to the outdoor environment. The overall heat loss (D) is thereby lowered.

2.3 Greenhouse application

In the Netherlands, the most common type of greenhouses is the Venlo-type (Figure 3).

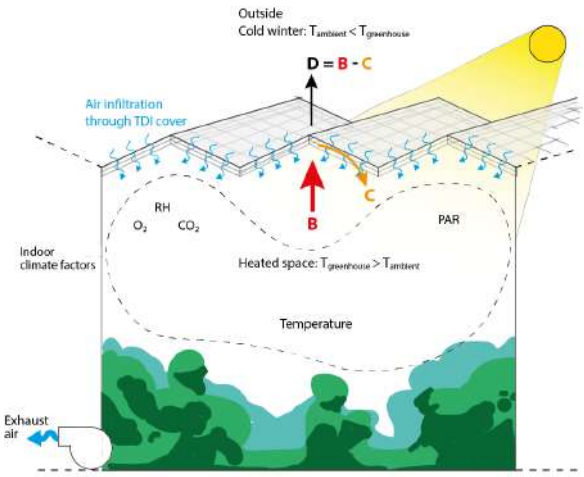

Fig. 3 - Schematic representation of the TDI greenhouse application (Venlo-type). Fresh air is drawn into the TDI cover, offering ventilation needs. The ventilated air regulates RH levels, CO_2 and O_2 concentration levels, and the disposal of moist-laden air. Material transparency allows solar radiation (PAR) to enter the greenhouse. Heat loss to the atmosphere **B** is partly recovered by heat exchange as a result of counterflow with infiltrating air **C**, such that the final heat loss **D** is reduced.

Glass is the most used cover material due to its favourable material properties. Clear, single-layered float glass is most commonly used due to its excellent chemical stability, stable light transmission, and its resistance to weather circumstances. Besides, float glass is easy to clean and relatively cheap. Disadvantages are the relatively high reflective losses, poor thermal performance (high U-values), fragility, and poor tensile strength. Alternative glass and plastic cover materials have entered the greenhouse horticulture market to cover up for the inferior properties of single float glass [5].

In greenhouses, transparency is crucial for the growth of crops. This is quantified by PAR (Photosynthetically Active Radiation). PAR defines a spectral range from 400-700 nm that is used by plants for photosynthesis. The greenhouse cover should be transparent for this spectral range. In table 1 the direct and hemispherical light transmittance within the PAR range (τ_{dir} and τ_{hem}) for the most common cover materials is shown.

Table 1 - glass and polymeric cover material properties, *adapted from* [5].

	Material	τ_{dir} [%]	τ_{hem} [%]	U-value [W/m^2K]
Glass	Float glass	89-91	82	5.8
	Hortiplus	84	69	5.8
	Double glass	81-82	-	2.7
Plastics	Polycarbonate	80/89*	61	3.5/5.8*
	PMMA	89/92*	76	2.8/5.8*

*Single layered panel material
Note that indicated values may differ per manufacturer

The ultimate goal is to design a TDI panel that has better effective insulation properties than horticulture glass at the required ventilation rates, while its transparency is similar.

3. TDI panel

A TDI-prototype panel is designed to study the potential energy savings that can be reached when applying it to a greenhouse. The TDI prototype is made out of PMMA material because of its good transmittance properties and ease of manufacturing. Its thermal properties will be determined at relevant ventilation rates and temperature differences that are representative of typical winter conditions in the Netherlands. An air change rate of ACH=2.5/h is prescribed. Furthermore, temperature differences between indoor and outdoor temperatures of $\Delta T=10^{o}C$ and $\Delta T=20^{o}C$ are used. Finally, a maximum pressure difference over the TDI-element of Δp = 10 Pa is allowed. This pressure difference was chosen such that the maximum force to open a door does not exceed 67 N for exterior hinged doors, and 22 N for interior hinged doors. These values are found in architectural regulations and were set so the elderly and children can also still open doors [6].

Next a TDI-prototype panel was constructed (Figure 4). It was built out of several TDI-unit elements and has a total panel size of LxWxH = 84.5 x 88.2 x 4.2cm.

The direct and TDI prototype PAR transparencies of the TDI-prototype are measured and are found to be $\tau_{dir} = 0.72$ and $\tau_{hem} = 0.59$. This is a bit lower than for Hortiplus glass (table 1) but is not yet optimized. It is expected that it can be improved and can come close to the values of the Hortiplus glass since the basis material is PMMA which has transmittance values that are higher than Hortiplus glass. For example, by decreasing the thickness of the PMMA plates, it is therefore expected that these transparency factors can come closer to those of the Hortiplus glass.

Fig. 4 – PMMA-based TDI-panel prototype of 42mm thickness.

4. Hot Box Experiments

4.1 Set-up

To determine the dynamic U-value of the TDI panel, a hot box apparatus has been used (Figure 5). It is a thermally insulated box that contains 25 temperature sensors, a humidity sensor, a differential pressure sensor, and two heating plates. The averaged indoor air temperature T_{indoor}, the outdoor air temperature $T_{outdoor}$ and the (pre-heated) air entering the climate box T_{inlet} are measured. The walls and bottom of the box are insulated and the TDI panel is placed on top of the setup. Via a pump at the bottom the air change rate (ACH) can be prescribed. The fresh air can enter the climate box via the TDI panel on top (indicated by the blue arrows) or via an inlet tube at the top right side in case it is covered with an airtight test panel (e.g. a double glazed panel).

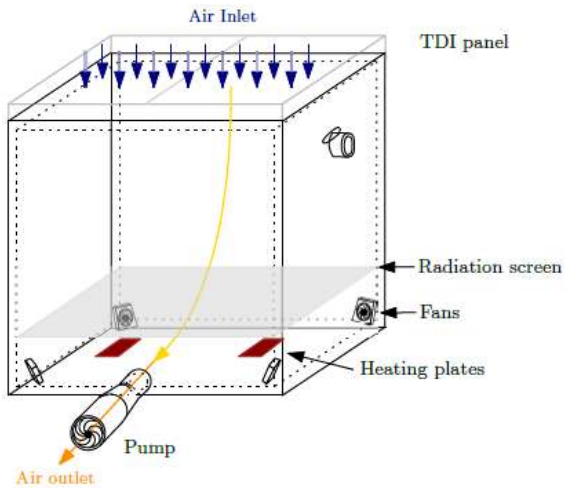

Fig. 5 – Hot box apparatus. The TDI panel is placed at the top of the box. Via heating plates (at the bottom) a temperature difference between the indoor and outdoor air is created. The air change rate (ACH) can be adjusted via the pump at the bottom.

The overall energy balance under steady state conditions is described by:

$$Q_{heaters} = Q_{loss} + Q_{TDI} + Q_{ACH} \qquad (3)$$

Where $Q_{heaters}$ is the power that is delivered by the two heating plates, Q_{loss} is the heat that is lost via the sidewalls and bottom of the hot box, Q_{TDI} *is* the heat flow through the TDI panel (or double glass panel), and Q_{ACH} is the power that is required to heat the incoming pre-heated fresh air with temperature T_{inlet} to the required indoor temperature T_{indoor}:

$$Q_{ACH} = \dot{m}c_p(T_{indoor} - T_{inlet}) \qquad (4)$$

The mass flow $\dot{m}$ is measured via a Testo 410i Vane Anemometer located at the air outlet.

The dynamic U-value of the TDI panel is defined as:

$$U_{TDI} = Q_{TDI}/A(T_{indoor} - T_{outdoor}) \qquad (5)$$

where $Q_{TDI} = Q_{heaters} - Q_{loss} - Q_{ACH}$.

4.2 Results and Discussion

The experiments are performed with a double glass panel (as a reference case) and with a TDI panel. In both cases, an air change rate of ACH=2.5/h is prescribed. For comparison with the literature, in the double glass panel, the insulation value under static conditions (ACH=0) is measured as well. Temperature differences of 10°C and 20°C are prescribed. The results of the experiments are shown in Table 2.

It is seen that the U-values for the measurements with double glass are in the range of 2.5-3.1[W/m^{2}K]. The static U-value is lower than the dynamic value. This is to be expected since the air velocity at the bottom of the panel is increased for the dynamic case and therefore also the convective heat transfer coefficient. Also, additional heat is required to heat the incoming fresh air to room temperature.

Table 2 - Experimental measured dynamic U-values for double glass (reference case) and TDI-panels

	ΔT=10°C	ΔT=20°C
Static U-value double glass (ACH=0) [W/m^{2}K]	2.5	2.8
Dynamic U-value double glass (ACH=2.5/h) [W/m^{2}K]	2.7	3.1
Dynamic U-value TDI (ACH=2.5/h) [W/m^{2}K]	2.2	2.5

The U-value for double glass from the manufacturer is 2.7 [W/m^{2}K] [7]. The measured static U-value is close to the value given by the manufacturer, showing the accuracy of our set-up.

The same setup is used for our TDI prototype. We only considered the dynamic case (ACH=2.5/h) since that is the condition which it is designed for. As can be seen the dynamic U-value for the TDI-panel is about 19% lower than for double glass and more than a factor 2 lower compared to horticulture glass (table 1). This indicates that the thermal insulation of the TDI panel is better than double-glazed windows and single-layer Hortiplus glass. However, it is expected that the thermal performance of the TDI prototype can be further improved: the present prototype is designed such that the sidewalls can be clicked onto the bottom and top plates. No glue is used. The advantage is the ease of manufacturing, while the drawback is that some small gaps are present between the sidewalls and the bottom and top plates. Therefore some shortcuts for the airflow can be present, resulting in a small increase in the U-value. In addition, the walls of the TDI cells can also act as so-called thermal bridges. By making the PMMA walls thinner, as was already proposed to increase transparency, the thermal resistance will increase and thus further decrease the effect of the thermal bridges.

Finally, the TDI panel can also be used with a reversed airflow. Hereby the overall heat transfer value (U-value) will increase. This has a positive effect to prevent overheating of the greenhouses during summertime.

5. Conclusions

In this paper, we introduced the concept of transparent dynamic insulation (TDI) that can be applied to reduce the energy consumption of Dutch greenhouses. We showed that the measured heat transfer value (U-value) for the TDI panel is about 19% lower than for double glass and more than a factor 2 lower compared to the commonly used single-layered horticulture glass. This indicates the saving potential of the transparent dynamic insulation (TDI) concept. Further research is needed to further optimize the TDI design.

6. Acknowledgements

The results are obtained within an ongoing student project. Many bachelor and master students have contributed. We would like to thank the students who contributed to the to the results as shown in this paper: Rhea Buijs, Thijs van Dungen, Max de Lange, Vincent Nieuwenhuis, Casper Poot and Jordie Verstappen. We would also like to thank the lab technicians at the Building Physics laboratory and the Thermal Fluid Engineering laboratory for their support.

7. References

[1] N. Van Der Velden and P. Smit, *Energiemonitor van de Nederlandse glastuinbouw 2018*. 2019. [in Dutch]

[2] M. S. Ahamed, H. Guo, and K. Tanino, "Energy saving techniques for reducing the heating cost of conventional greenhouses," *Biosyst. Eng.*, vol. 178, pp. 9–33, 2019, doi: 10.1016/j.biosystemseng.2018.10.017.

[3] A. Yano and M. Cossu, "Energy sustainable greenhouse crop cultivation using photovoltaic technologies," *Renew. Sustain. Energy Rev.*, vol. 109, no. November 2018, pp. 116–137, 2019, doi: 10.1016/j.rser.2019.04.026.

[4] M. S. E. Imbabi, "A passive–active dynamic insulation system for all climates," *Int. J. Sustain. Built Environ.*, vol. 1, no. 2, pp. 247–258, 2012, doi: 10.1016/j.ijsbe.2013.03.002.

[5] S. Hemming *et al.*, "Optimaal gebruik van natuurlijk licht in de glastuinbouw," *Rapp. / Agrotechnology Food Innov. 100*, no. 100, p., 2004, [Online]. Available: http://edepot.wur.nl/40067%5Cnhttp://scholar.google.com/scholar?hl=en&btnG=Search&q=intitle:Optimaal+gebruik+van+natuurlijk+licht+in+de+glastuinbouw#0. [in Dutch]

[6] *Code of Massachusetts Regulations Title 521: CMR 26: Doors and doorways*. Trial Court Law Libraries Massachusetts Court System, 2018.

[7] "Agc glass configurator," 2021. https://www.agc-yourglass.com/configurator/en.

THERMISTOR NTC SENSOR INACCURACIES IMPACT ON THE HVAC/R COMPRESSOR PERFORMANCE

Adrian Anastase [a], Gratiela Maria Tarlea [a]

[a] Faculty of Building Services, Technical University of Civil Engineering Bucharest, Bucharest, Romania, adrian.anastase@phd.utcb.ro, gratiela.tarlea@utcb.ro

Abstract. Electricity consumption for thermal comfort in urban buildings is estimated to an average of 35%. The aim of this article is to evaluate, theoretically, the impact of sensors inaccuracies on the performance and efficiency of HVAC equipment. Different types of temperature and pressure sensors are considered. The measurement tolerance, from manufacturer's technical data sheet, will be used for the theoretical evaluation of the range in which the operating point of the equipment can vary. Compressor selection software are used for evaluating theoretical COP and electrical energy consumption change in the range of sensor inaccuracies. The study evaluates theoretically the impact on performance of scroll, piston and screw compressors, considering refrigerants used in chillers (R717, R134a, R410A, R32). The operating point of the compressor is considered as normal chiller scenario, with evaporation temperature of +4°C and condensing pressure corresponding to +35°C. The conclusion of the theoretical evaluation is that resistance tolerance bigger than 1% brings a 1% or more variation of compressor's performance.

Keywords. HVAC, sensor impact, COP
DOI: https://doi.org/10.34641/clima.2022.110

1. Introduction

Electricity consumption for thermal comfort in urban buildings is estimated to an average of 35% from global consumption [1] . Recent study [2] shows that there is an increasing trend for residential buildings. That's why research work for better efficiency in HVAC sector is still needed.

This study evaluates, theoretically, the impact of NTC thermistor sensor inaccuracies over the HVAC equipment. In this case is evaluated the theoretical COP and electrical consumption variations due resistance tolerance for a chiller with a cooling capacity of 100 kW.

2. Sensors in HVAC equipment

HVAC equipment like chillers use temperature and pressure sensors for control loop [3] like shown in figure 1.

There are different methods for control loop [4] . In this theoretical evaluation is considered that the compressor is controlled based on the outlet water temperature sensor. The logic diagram is presented in figure 2.

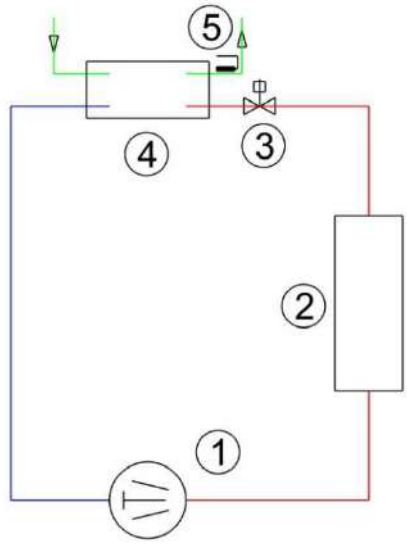

Fig. 1 – System drawing (1-compressor, 2-condenser, 3-expansion device, 4-water heat exchanger, 5-temperature sensor

Copyright ©2022 by the authors. This conference paper is published under a CC-BY-4.0 license.

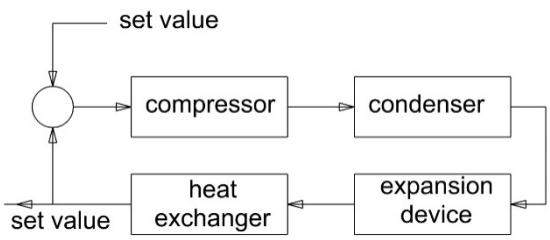

Fig. 2 – Control loop diagram

Thermistor type sensors are one of the most common types [5] used in this kind of application.

One of the main characteristics for thermistor sensor is resistance tolerance and for NTC type this tolerance is in the range of 0.5-10% [6] . For this study was selected, as a reference, a 10kΩ NTC sensor (MEAS PRO4) [7] with main characteristics presented in table 1.

Tab. 1 – NTC sensor characteristics [7].

Nominal resistance at +25°C	Tolerance at +25°C	Temperature range
10kΩ	±1%	-35°C to 105°C

The theoretical values of resistance, based on temperature, were extracted from technical data sheet[7] from the manufacturer. Figure 3 represent the theoretical resistance-temperature curve.

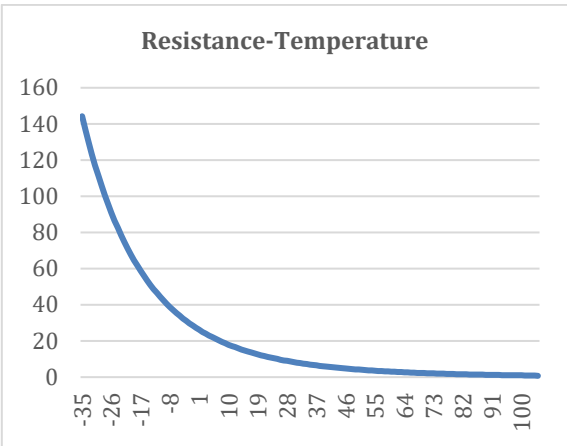

Fig. 3 – Resistance-Temperature curve for NTC sensor.

3. Evaluation method

First step of this theoretical evaluation is to define the temperatures values variation due to the resistance tolerance. Equation (1) is used to calculate the interpolated values.

$$t_3 = (R_3 - R_2)\frac{t_1 - t_2}{R_1 - R_2} + t_2 \quad (1)$$

Calculations were made for resistance tolerance values in the range of 0.5%-10% with steps of 1%.

The values resulted from equation (1) are used to define the range of possible operating points when the reading of evaporating temperature is +4°C.

Using different selection software [8] [9] the theoretical COP range for each situation was extracted. The theoretical electrical power consumption can be calculated using theoretical COP values in equation (3).

$$COP = \frac{Q}{P} \quad (2)$$

$$P = \frac{Q}{COP} \quad (3)$$

The extraction of theoretical COP values was made for different refrigerants: R32 (scroll compressor), R134a (pistons), R717 (pistons), R410a (scroll). The reference operating point is considered t_o=+4°C, t_c=+35°C, Δt_{sh}=10K, Δt_{sc}=2K.

The theoretical COP values and electrical power calculation were made based on 100kW cooling power compressor.

4. Results and discussions

Table 2 present the results for evaporating temperature variation. For each 1% step of resistance tolerance it can be seen the possible theoretical minimum and maximum value of evaporating temperature for a sensor reading of +4°C.

Tab. 2 – Temperature range for operating point.

Resistance tolerance	Temperature resulting values [°C]		
	Max value	Reading	Min value
0.5%	+4.122	+4	+3.878
1%	+4.244	+4	+3.755
2%	+4.489	+4	+3.510
3%	+4.734	+4	+3.266
4%	+4.978	+4	+3.021
5%	+5.223	+4	+2.777
6%	+5.468	+4	+2.532
7%	+5.712	+4	+2.287
8%	+5.957	+4	+2.042
9%	+6.202	+4	+1,798
10%	+6.446	+4	+1.553

Tables 3, 4, 5 and 6 presents the extracted theoretical values for COP using compressor selection software [8] and calculated values for electrical power consumption variation for different refrigerants (R134a, R32, R410A, R717). The 4th column of these tables shows the variation, in percentage, of

electrical power consumption considering the theoretical value, calculated for evaporating temperature of +4°C, as a reference.

The maximum theoretical electrical power consumption variation is about 10% in case of systems with NH3.

Tab. 3 – R32 results.

Resistance tolerance	COP	Electrical power for 100kW cooling power	
	[-]	[kW]	[%]
Reference	5.37	18.62	0
0.5%	±0.02	±0.07	±0.37
1%	±0.04	±0.14	±0.75
2%	±0.08	±0.28	±1.5
3%	±0.12	±0.41	±2.2
4%	±0.16	±0.56	±3.0
5%	±0.21	±0.70	±3.76
6%	±0.25	±0.83	±4.45
7%	±0.29	±0.95	±5.1
8%	±0.33	±1.08	±5.8
9%	±0.38	±1.23	±6.6
10%	±0.42	±1.35	±7.25

Tab. 4 – R134a results.

	[-]	[kW]	[%]
Reference	4.78	20.92	0
0.5%	±0.02	±0.09	±0.43
1%	±0.04	±0.18	±0.86
2%	±0.08	±0.36	±1.72
3%	±0.11	±0.47	±2.25
4%	±0.15	±0.64	±3.0
5%	±0.19	±0.80	±3.82
6%	±0.23	±0.96	±4.58
7%	±0.27	±1,12	±5.35
8%	±0.3	±1,23	±5.88
9%	±0.34	±1.39	±6.64
10%	±0.38	±1.54	±7.36

Tab. 5 – R717 results.

Resistance tolerance	COP	Electrical power for 100kW cooling power	
	[-]	[kW]	[%]
Reference	5.93	16.86	0
0.5%	±0.03	±0.08	±0.5
1%	±0.06	±0.17	±1.00
2%	±0.12	±0.33	±1.98
3%	±0.18	±0.50	±2.95
4%	±0.25	±0.68	±4.05
5%	±0.31	±0.84	±4.97
6%	±0.37	±0.99	±5.87
7%	±0.44	±1,16	±6.91
8%	±0.51	±1,34	±7.92
9%	±0.57	±1.48	±8.77
10%	±0.64	±1.64	±9.74

Tab. 6 – R410A results.

Resistance tolerance	COP	Electrical power for 100kW cooling power	
	[-]	[kW]	[%]
Reference	5.36	18.66	0
0.5%	±0.02	±0.07	±0.37
1%	±0.04	±0.14	±0.74
2%	±0.08	±0.27	±1.47
3%	±0.12	±0.41	±2.19
4%	±0.16	±0.54	±2.90
5%	±0.21	±0.70	±3.77
6%	±0.25	±0.83	±4.46
7%	±0.29	±0.96	±5.13
8%	±0.33	±1,08	±5.80
9%	±0.38	±1.24	±6.62
10%	±0.43	±1.39	±7.43

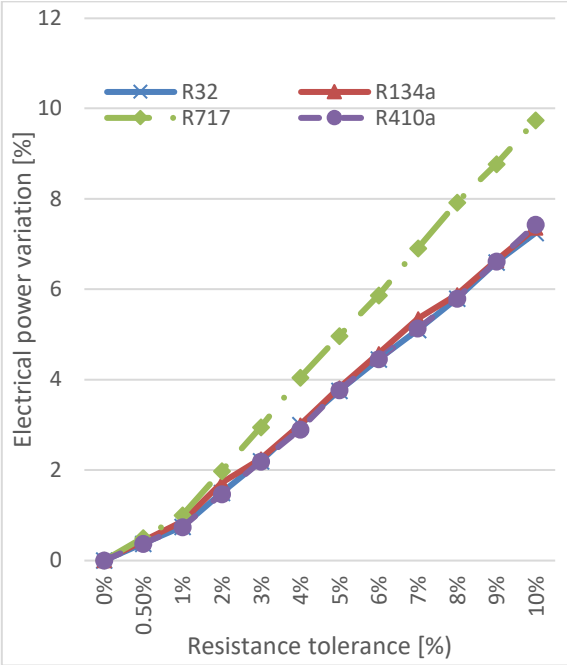

Fig. 4 – Variation of electrical power due to resistance tolerance value.

Figure 4 represents the electrical power consumption variation depending on tolerance. This shows the influence of sensor resistance tolerance on electrical power consumption It seems that systems using R134a, R32 and R410a have similar variations and are very different than NH3 systems.

Also it can be observed that the electrical power consumption has a linear variation, proportional to the resistance tolerance values.

5. Conclusions

When resistance tolerance is bigger than 1%, the electrical consumption variation is bigger than 1%.

The bigger the COP of the system the more influence from resistance tolerance on electrical power consumption.

Depending on application and cooling power, proper temperature sensors must be selected to have an efficient system, preferably with resistance tolerance around 1%.

In case of big resistance tolerance sensors the efficiency can vary until 10%.

Further research regarding the influence from pressure sensor inaccuracies must be done to have a larger view of what inefficiencies can bring sensor tolerances in a HVAC system.

Considering that electricity consumption for thermal comfort in urban buildings is estimated to an average of 35% from global consumption, means that the selection of proper sensors can have a significant impact on global consumption.

Further research that counts together other influences, like time depreciation, should show bigger values, so sensor quality should be neglected for efficiency HVAC systems.

6. Nomenclature

COP – coefficient of performance	(-)
P – electrical power	(W)
Q – cooling power	(W)
R – electrical resistance	(Ω)
t – temperature	(°C)

7. References

[1] Waite M, Cohen E, Torbey H, Piccirilli M, Tian Y, Modi V. Global trends in urban electricity demands for cooling and heating. Energy 2017;127:786–802. https://doi.org/10.1016/J.ENERGY.2017.03.095.

[2] Krarti M, Aldubyan M. Review analysis of COVID-19 impact on electricity demand for residential buildings. Renewable and Sustainable Energy Reviews 2021;143:110888. https://doi.org/10.1016/J.RSER.2021.110888.

[3] Fan Y, Cui X, Han H, Lu H. Feasibility and improvement of fault detection and diagnosis based on factory-installed sensors for chillers. Applied Thermal Engineering 2020;164. https://doi.org/10.1016/j.applthermaleng.2019.114506.

[4] Al-Badri AR, Al-Hassani AH. A control method using adaptive setting of electronic expansion valve for water chiller systems equipped with variable speed compressors. International Journal of Refrigeration 2020;119:102–9. https://doi.org/10.1016/J.IJREFRIG.2020.06.008.

[5] Arman Kuzubasoglu B, Kursun Bahadir S. Flexible temperature sensors: A review. Sensors and Actuators A: Physical 2020;315:112282. https://doi.org/10.1016/J.SNA.2020.112282.

[6] Padilla B (Texas I. Temperature sensing with thermistors 2020. https://www.ti.com/lit/wp/slay054/slay054.pdf?ts=1641758854348&ref_url=https%253A%252F%252Fwww.ti.com%252Fsensors%252Ftemperature-sensors%252Fthermistors%252Foverview.html (accessed January 9, 2022).

[7] GA10K3435STM010 : MEAS PRO4-OVERMOLDED PROBE | TE Connectivity n.d. https://www.te.com/global-en/product-GA10K3435STM010.html (accessed January 7, 2022).

[8] BITZER Software n.d. https://www.bitzer.de/websoftware/Default.aspx?lng=en&lang=en&country=gb (accessed January 8, 2022).

[9] Select Online n.d. https://selectonline.emersonclimate.eu/SelectOnline/main (accessed January 8, 2022).

Energy performance contracting as an innovative tool for financing the building renovation in Slovakia, Central Europe

Veronika Gombošová [a], *Michal Krajčík* [b]

[a] Faculty of Civil Engineering, Slovak University of Technology in Bratislava, Slovakia, veronika.gombosova@stuba.sk

[b] Faculty of Civil Engineering, Slovak University of Technology in Bratislava, Slovakia, michal.krajcik@stuba.sk

Abstract. The possibilities of using Energy Performance Contracting (EPC) are presented for Slovakia, Central Europe, including a case study performed for a building in Bratislava. The case study contained an inspection of the building, an energy audit with a proposal of energy efficiency measures, and profitability calculations for the measures. A package of suitable measures was created, and its suitability for financing by EPC was evaluated. The net present value quotient (NPVQ) was used to indicate the profitability of energy-saving measures. However, for EPC projects, the number of years in which the investment is returned is the most important. Therefore, payback was considered to be a more relevant indicator of profitability for EPC projects. With an adequate combination of energy efficiency measures, a payback period of 15 years was reached. This was acceptable considering that the building belonged to a municipality. The potential drawback of EPC is that it may not be feasible for complex renovations.

Keywords. Energy performance contracting (EPC), energy audit, energy efficiency, net present value (NPV), payback.
DOI: https://doi.org/10.34641/clima.2022.72

1. Introduction

One of the worldwide problems that need to be addressed is high energy consumption. Of all sectors, the most energy is consumed by buildings [1]. As a result, solutions have been researched to reduce energy use by improving the design and operation of building envelope and HVAC systems. The European Directives set minimum requirements and a common methodology to improve the energy performance of newly built and renovated buildings in the EU [2][3]. A significant part of the energy-saving potential in buildings is attributed to building retrofit. Countries within the European Union have made commitments to build energy-efficient buildings between 2019 and 2021 [4]. Especially new buildings are targeted, promoting nearly zero-energy buildings [5], but existing buildings should also be improved with energy retrofits [6][7].

In Slovakia, a substantial part of the building stock was built decades ago. Complex or in-depth renovation of such a building is typically carried out 30 to 40 years after its construction. Based on these facts, special attention must be paid to the quality of current construction or renovation of buildings now, so that they can provide their users with a safe and healthy environment under economically affordable conditions even in 2050.

The biggest obstacle to investing in quality renovation or building construction is, among other things, funding. The most common source of financing is a bank loan. In fewer cases, the financing comes from own capital. However, alternative financing methods exist such as Energy Performance Contracting (EPC). In several countries, a strong commitment of the government to the use of EPC has been observed [8]. In Europe, the European Commission launched an EU-Energy Performance Contracting Campaign (EPCC) to help member states develop a legal and financial framework for the EPC market [9]. The main advantage of EPC is that financing and related risk are taken over by an Energy Service Company (ESCO), which is a company that implements the EPC project. ESCO not only provides clients with upfront capital for project implementation but also monitors the actual performance of newly installed equipment and provides staff training for better system operation and control [10]. In a popular EPC model, the ESCO guarantees the host a certain level of energy savings and compensates for the losses in the event of a shortfall in savings [10].

This study presents the principle of EPC, including related profitability indicators and a case study focused on the possibilities of using EPC for building retrofit in Slovakia. It illustrates the principles to

Copyright ©2022 by the authors. This conference paper is published under a CC-BY-4.0 license.

evaluate the suitability of energy-saving renovation measures for EPC, including the maximum payback durations tolerated for an EPC project.

2. Energy service

An energy service is a service provided under a contract concluded between an energy service provider and a recipient of the energy service. The energy service can be provided as an energy support service and as an energy service with guaranteed energy savings, also called Energy Performance Contracting. The result is a verifiable, measurable, or estimable energy saving which improves energy efficiency and allows for a financial or material advantage for all parties involved due to the more energy-efficient technology or activity. This activity includes the operation, maintenance, or control necessary to provide an energy service [11]. This study focuses mainly on EPC and its principles.

2.1 Legal framework

The energy services provided in Slovakia are based on Act no. 321/2014 Coll. on Energy Efficiency [11], where Energy Performance Contracting is defined. Following the Slovak law, EPC entails an energy service provided under an energy efficiency contract, which must be in written form, with guaranteed energy savings. The specific guidance on how to perform the actions as required by Act no. 321/2014 Coll. are defined in Decree no. 99/2015 Coll. [12]. For example, the Decree provides a sample application for a proficiency test needed to obtain permission to provide EPC. An important part of each EPC project is an energy audit, as it describes the actual state of the objects, the proposal of energy savings measures, and the profitability calculations. The procedure to elaborate the energy audit is provided in Decree no. 179/2015 Coll. on energy audit [13].

2.2 Process of the EPC project

Figure 1 illustrates the principle of an EPC project. In the beginning, the building has a certain energy consumption, also called the baseline, which may be considered too high by the owner. The building owner can see EPC as an option to reduce energy consumption and achieve financial savings. In such a case, the owner bids through public procurement, and the ESCO responds. If the owner is satisfied with the offer from ESCO, they subscribe to the contract. A model contract for Slovakia is published on the website of the Ministry of Economy of the Slovak Republic [14]. The next step is an energy audit of the building, where efficiency measures are proposed, evaluated, and recommended. The contract is usually signed for 6 to 10 years [15]. However, if there is a reliable investor, such as the government or a municipality, the duration of the EPC project can be longer, even up to 15 years. The main principle is that during this period, ESCO guarantees savings and takes all risks that may arise. These savings reduce the energy consumption of the building and pay the initial investment costs paid by ESCO. At the end of the contract period, the building has substantially lower energy consumption compared to the baseline, and the owner now acquires savings, better technologies, services, and a retrofitted building.

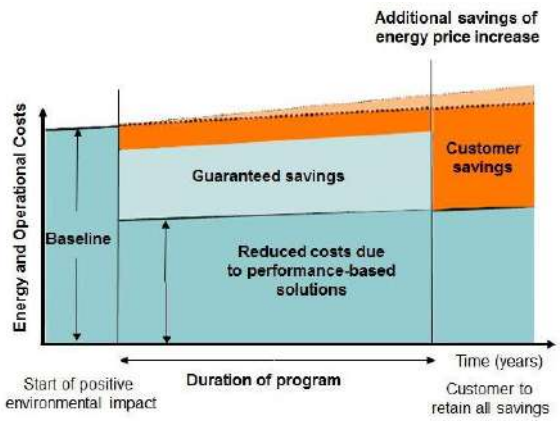

Fig. 1 – EPC project process [11].

2.3 Energy Service Company (ESCO)

Usually, the EPC is provided by an ESCO, which could be a person or a legal entity that provides energy services. At the same time, ESCO assumes the technical and financial risk that arises from the design of energy efficiency measures, their implementation, and operation throughout the project. The project funding can vary; but usually, the ESCO or investors choose a bank loan.

3. Profitability indicators

Economic evaluation is an important part of building retrofit projects. The aim of this evaluation is to find the profitability of individual energy-saving measures and to determine the cash flow of the proposed financing option. The economic parameters that enter into the evaluation are investments, annual savings, economic lifetime, and nominal interest rate. Among the most commonly used profitability indicators are the simple payback, discounted payback, internal rate of return, net present value, and net present value quotient. This study focused on the net present value coefficient and the payback period.

Equation (1) is used to calculate the net present value (NPV) based on the ratio of financial savings per year to the end of the economic life of the equipment ($B_{1\text{-}n}$) and the real interest rate (r), minus initial investments (I). A positive NPV indicates a profitable investment [16].

$$\mathrm{NPV} = \left(\frac{B_1}{(1+r)^1} + \frac{B_2}{(1+r)^2} + \cdots + \frac{B_n}{(1+r)^n}\right) - I \qquad (€)\ (1)$$

A practical way to express the profitability of the measure is the Net Present Value Quotient (NPVQ). It is the ratio of the net present value (NPV) to the value of the total investment (I) [16]. The NPVQ method is suitable for ranking energy-saving measures in terms of profitability.

$$NPVQ = \left(\frac{NPV}{I}\right) \quad (€) \ (2)$$

The discounted return expresses the return of the measure, also considering the discount of the savings over time. According to EN 15459-1, discounted payback (PB_{disc}) is the time when the difference between the initial investment cost for the optional and reference case is balanced with the cumulative discounted annual costs difference in each individual year. It is calculated using eq. (3). The calculation considers the initial investment (CO_{INT}) and the initial investment of the reference solution ($CO_{INT,ref}$). If nothing is done, the value of the reference solution is 0 [17]. In this calculation, the difference in annual costs between the actual solution and the reference solution (CF_t) must also be considered. For better understanding, it can also be explained as the difference in cash flows. The resulting value of the payback period is also affected by the discount rate (RAT_{disc}). The payback period must be lower than the economic lifetime of the energy efficiency measures. In this study, a discount rate of 3% was chosen, as recommended in the Guide to Cost-Benefit Analysis of Investment Projects [18], and 5% for comparison.

$$PB_{disc} = \sum_{t=1}^{TPB} CF_t \cdot \left(\frac{1}{1+RAT_{disc}}\right)^t - CO_{INT} + CO_{INTref} = 0 \quad (a) \ (3)$$

where TPB is the number of years when the sum becomes equal to 0. When calculating the investment in an EPC energy efficiency measure, it is necessary to take into account the additional costs of financing by EPC by increasing the investment in the measure. During the duration of the EPC project, ESCO guarantees energy savings for the entire renovation package. For this reason, additional costs related to risk, management, insurance, or repairs must be reflected in investment costs. These additional costs are expressed as a percentage of the initial investment per measure. These percentages are chosen according to the experience of the entity providing the EPC. A simple payback taking into account the additional investment-related to EPC is calculated as follows:

$$EPC_{SimplePB} = \frac{EPC_{Investment}}{(EPC_{savings} - EPC_{costs})} \quad (a) \ (4)$$

4. EPC projects funding

An essential part of an EPC project is the Energy Performance Contracting Business Model (EPCBM). EPCBM determines the type of contract for EPC projects that has a significant impact on project performance [19]. However, each of the types of EPCBM impacts the EPC project at a different level because various types of EPCBM have their characteristics related to financing and risk-sharing [20][21][22]. EPCBM identifies the roles of the energy customer and the ESCOs and defines the responsibility and risk-sharing of the participants in an EPC project [23][24]. It also clarifies the allocation of cost savings [25]. EPCBM determines the type of contract of the EPC project and has an essential impact on energy savings performance [26].

4.1 Credit and leasing financing

One of the most commonly used financing methods is credit financing. Credit financing means that a lender (financing institution) provides a borrower (customer) with capital for a defined purpose over a fixed period of time. Borrowers in this case can be either ESCO or client. A credit is settled over a fixed period of time with a number of fixed instalments (debt service). These instalments must cover the amount borrowed, plus interest rates, as well as other transaction costs such as administrative fees. Loans are disbursed against proof of purchase in order to secure the earmarked use of the funds. The other often used financing method is leasing. Leasing is a way to obtain the right to use an asset, not the possession of this asset. Assets in our case mean investments in energy conservation measures. When leasing an energy conservation investment, you do not buy it. You only pay for the exclusive right to use it [26].

4.2 Authority/government participation in financing

It is common for the Authority (or other government entities) to participate in the financing of an EPC arrangement. The reasons for an Authority to participate in the financing vary from EPC to EPC, as do the ways in which it may choose to do so. The most common examples are milestone payments (non-refundable) and/or direct provision of EPC assets to the Partner during or at the end of the Construction Phase, loans to the Partner, equity participation in the Partner, financing guarantees and financial incentives (e.g., reduced energy tariffs) and/or exemptions from liabilities (e.g., corporate tax, value-added tax) that the Partner would otherwise incur. But it is necessary to know that European Union financing (e.g. grant, loan) is not counted as government financing [26].

4.3 Funding for EPC projects in Europe and Slovakia

In general, EPC is a financing solution with guaranteed savings, regardless of the funding form. Customers can opt for EPC, regardless of funding [15] to achieve guaranteed savings, thus ensuring the predictability of the economic results of the project, or to use the competitiveness of EPC procurement in the case of complex solutions, so that the best solution for finding a provider can be found to find the most cost-effective solution in terms of cost-benefit.

Based on research carried out by the European market, the most used method was a loan taken by the ESCO. The least-used method in selected European countries as financial leasing. In the case of the Slovak Republic, the most used method was also

a loan taken by the ESCO. The least used method, in this case, was the operating lease [27].

5. Case study – an apartment building in Bratislava

5.1 Building description

The apartment building studied is located in Bratislava, the capital of Slovakia. The built-up area is 1 636 m^2 and the heated volume is 29 135 m^3. The building consists of 2 parts, the entrance building with 3 storeys and the accommodation part with 9 above-ground storeys and one underground storey. The average storey construction height is 2.9 m. Both parts have a simple rectangular shape. Between 2003 and 2005, the building underwent a partial retrofit, consisting of the construction of a single-story vertical extension of the accommodation part and the construction of a two-story superstructure of the entrance building.

The entrance building and most of the accommodation part of the building is built as an aerated concrete wall panel system with a thickness of 300 millimetres. The single-storey superstructure of the accommodation part consists of reinforced concrete with a thickness of 150 millimetres. The perimeter walls of the separate extension consist of full bricks. The roof of the main building is built as an aerated concrete roof panel system. The roof of the separated extension is built as a reinforced concrete roof panel system. All peripheral structures are non-insulated. The opening structures are designed mainly as windows and doors with insulating double glazing and a plastic frame. A small part of the opening structures is still in their original state and does not meet today's normative requirements.

The heating source for the building is a gas boiler room, located on the ground floor in a separate extension with three low-pressure gas boilers. Two boilers operate in alternate operations. The third boiler is outdated and non-functional. The total heat output of the boiler room is 2 190 kW. The efficiency of one boiler is approximately 80%. The heating system is controlled by an equithermal regulation, i.e. based on the external temperature. There are 334 cast iron heaters in the heating system; only a small part of them have a thermostatic head. Horizontal distribution pipes are insulated, but the free risers are uninsulated.

The lighting system has undergone a partial reconstruction. It consists of luminaires with linear fluorescent lamps and classic and electronic ballasts, LED bulbs, or old luminaires with ordinary bulbs, and one halogen lighting. The preparation of domestic hot water is centralized using one storage heater with a volume of 2 000 litres.

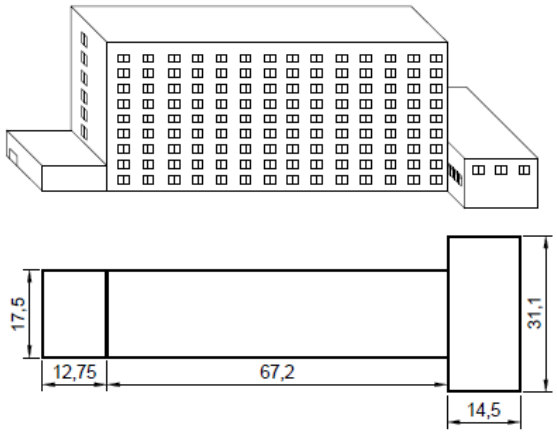

Fig. 2 - The case study apartment building

5.2 Energy inputs

Figure 3 shows the average annual energy costs for the building over three years (2016-2018). The share of energy carriers in annual energy consumption is shown in Figure 4. The average annual electricity consumption was 308.3 MWh, in monetary terms 41 179 € per year. The average annual consumption of natural gas was 129 562 m^3 per year, in monetary terms 54 105 € per year.

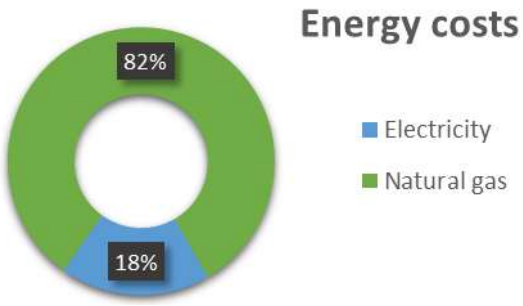

Fig. 3 - Share of energy carriers in average annual energy costs

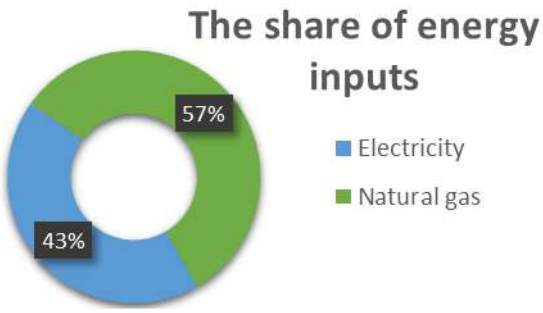

Fig. 4 - Share of energy carriers in annual energy consumption

5.3 Energy calculations

An important part of the EPC project is energy calculations to determine the energy-saving potential of energy-saving measures. The European Committee for Standardization (CEN) provides a set of standards containing procedures for energy balance calculations. The important part is the link

between the energy needs of the building and the energy delivered for space heating and cooling, and the energy requirements for ventilation, domestic hot water, and lighting. For space heating, there is a set of standards EN 15316 with the input of energy need for heating according to EN 52016-1. In addition, national standards and legislation documents provide the specific requirements and input data for the national context and give recommendations and guidelines to specify the methods and inputs for energy balance calculations [28].

The first step is the calculation of the energy needs that represent the only theoretical amount of heat, needed e.g., to keep the room temperature or the water in the tank at a certain level, without considering the losses of the technical systems. The energy need for heating is calculated as defined in EN 52016-1. It is necessary to define the space heating boundaries and calculation method. In this case, a monthly calculation step was used. It is necessary to calculate the specific heat loss by heat transmission and ventilation. Part of the calculation refers to heat gains, which include internal gains and solar gains. According to the national standard STN 73 0540-2, internal heat gains are characterized by the average heat outputs of the internal heat sources. Solar gains depend on the location of the building [29].

To determine the detailed current condition of the building, it was necessary to calculate heat losses by heat transmission through the structures and heat losses through ventilation. The monthly method was used for the calculation, where a different internal temperature was considered for each month. The heat loss of the building is also to some extent influenced by the infiltration rate, which was also considered different for each month. Heat transmission losses were calculated as follows:

$$H_T = \sum b_{x,i}.U_i.A_i + \Delta U.\sum A_i \qquad \text{(W/K) (4)}$$

Heat loss through ventilation was calculated based on air density, specific heat capacity, building volume, and air change rate. The following formula was used for the calculation:

$$H_V = \frac{V}{V_b}.\rho_a.c_a.n_{inf}.V_b/3600 \qquad \text{(W/K) (5)}$$

The next step was the calculation of solar heat gains, which mainly depend on the type of opening structure and internal gains. After calculating the heat losses by heat transmission and ventilation and calculating the heat gains of the building, it was possible to calculate the energy need for heating:

$$Q_H = Q_{ht} - n_{gn}.Q_{gn} \qquad \text{(kWh) (6)}$$

The next step is to calculate the additional energy losses of the technical systems. These consist of heat emission (EN 15316-2 [30]), distribution losses (EN 15316-3 [31]), storage losses (EN 15316-5 [32]), and generation losses (EN 15316-4-1 for boilers [33]). When calculating the energy demand, the calculation process follows a reverse order, from the energy need for heating towards the generation and storage subsystem. For the calculation of the energy demand for heating, the following formula was used (7).

$$Q = Q_H + Q_{em,ls} + Q_{H,dis,ls,an} + W_{H,dis,aux,an} + Q_{s,ls+}Q_{g,ls} \qquad \text{(kWh|(7)}$$

Annual energy saving is the difference between the energy demand before implementation and after implementation of the saving measures. Annual energy savings should also be expressed in monetary terms.

The energy audit also included the calculation of the energy demand for domestic hot water preparation, as well as the energy demand for lighting. Calculating the energy demand for domestic hot water was based on the standards 15316-3 [31] and EN 15316-5 [32] and consisted of the calculation of the energy need for domestic hot water, heat loss from distribution, heat loss from accumulation, and the heat loss from heat generation.

The electricity consumption for lighting was not measured separately. To be able to assess the impact of the lighting system on energy consumption in the building, it was necessary to determine the approximate electricity consumption for lighting based on the individual number of lighting elements and their power consumption and based on the number of lighting hours.

5.4 Energy saving measures considered

After determining the energy demand of the building, energy-saving measures were proposed. These measures focused on the insulation of the perimeter structures of the building, the modernization of the lighting system, the reconstruction of the boiler room and the heating system, and the use of a solar system for domestic hot water. Profitability indicators such as net present value, EPC simple payback, and discounted return were calculated for each of the proposed measures. The proposed measures are shown in Table 1.

To calculate the net present value, formula (1) was used. After calculating the NPV, the net NPVQ was calculated using formula (2). Following EN 15459-1, equation (3) was used to calculate the discounted payback for each of the energy-saving measures [17]. Discount rates of 3% and 5% were selected. Table 2 shows the values of NPV, NPVQ and PB calculated on the basis of a discount rate of 3%. Table 3 shows the values of NPV, NPVQ and PB_{disc} calculated on the basis of a 5% discounted rate. In the calculation of NPV, an economic lifetime of 20 years was considered.

Tab. 1 – Energy-saving measures and investments

Energy-saving measure	Investment (€)
1) Perimeter walls insulation	397 211
2) Heat source reconstruction	82 822
3) Lightning system modernization	61 416
4) Solar system implementation	45 100
5) Reconstruction of DHW distribution	20 630

Tab. 2 – Profitability indicators assuming a discount rate of 3%

Measure	$NPV_{3\%}$	$NPVQ_{3\%}$	$PB_{disc3\%}$
1)	-3 059 626	-6.7	15.0
2)	-1 480 893	-13.3	82.0
3)	+166 705	+14.5	7.0
4)	-551 688	-10.7	27.0
5)	+691 077	+34.5	2.0

* For explanation of the measures 1 to 5 see Tab. 1

Tab. 3 – Profitability indicators assuming a discount rate of 5%

Measure	$NPV_{5\%}$	$NPVQ_{5\%}$	$PB_{disc5\%}$
1)	-3 704 214	-8.3	24.0
2)	-1 512 424	-17.3	<100
3)	+573 753	+10.3	8.0
4)	-646 911	-11.9	40.0
5)	591 337	+29.6	2.0

* For explanation of the measures 1 to 5 see Tab. 1

Tables 4 and 5 describe the EPC simple payback calculation for each of the energy efficiency measures considered. EPC simple payback was calculated using formula (4).

Tab. 4 – EPC Simple payback

EPC investment with funding (€)	EPC saving (€/year)	EPC project costs (€/year)	EPC simple payback (year)
1) 476 654	17 903	15 888	236.5
2) 99 386	7 863	4 141	26.7
3) 73 699	8 294	3 070	14.1
4) 54 120	1 664	2 255	-91.6
5) 24 756	5 214	1 031	5.9

* For explanation of the measures 1 to 5 see Tab. 1

Tab. 5 –EPC project duration

EPC Investment with funding (€)	EPC savings (€/year)	EPC costs (€/year)	EPC simple payback (year)
728 616	40 940	26 387	50.1

Table 5 reports the duration of the EPC project when all energy efficiency measures are considered. By combining these measures, we obtained an EPC simple payback of more than 50 years. As mentioned in Chapter 2.2, the duration of the project is usually 6 to 10 years, sometimes up to 15 years. In this case, a maximum project duration of 15 years was considered. Therefore, it was necessary to find a combination of measures that would fulfil this criterion.

5.5 Suitability of the saving measures for EPC

The basis of an EPC project is the selection of appropriate energy-saving measures. Therefore, in the next step, the measures that had the most significant impact on energy consumption and operating costs were selected while having reasonable profitability. In some cases, the annual cost of the EPC energy efficiency measure may be higher than the related annual savings, resulting in a simple negative return on the specific measure. However, this problem could be solved by using a suitable combination of individual energy efficiency measures to obtain a favourable overall payback for the EPC project. Tables 6 and 7 summarize the energy efficiency measures that were considered appropriate for the case study EPC project.

Tab. 6 – Energy efficiency measures for EPC project

Energy-saving measure	Investment (€)
2) Heat source reconstruction	82 822
3) Lighting system modernization	61 416
5) Reconstruction of DHW distribution	20 630

Tab. 7 – EPC Simple payback

EPC investment with funding (€)	EPC saving (€/year)	EPC project costs (€/year)	EPC simple payback (year)
2) 99 386	7 863	4 141	26.7
3) 73 699	8 295	3 070	14.1
5) 24 756	5 124	1 031	5.9

* For explanation of the measures 1 to 5 see Tab. 1

5.6 EPC project duration

The financial summary of the project without the costs associated with EPC is shown in Table 8. It indicates that based on this initial investment, it is possible to propose financing for the EPC project. Table 9 shows the key parameters of the project, including the associated EPC costs. The EPC simple payback doubled compared to the simple payback in Table 8. None of the selected measures had a negative EPC simple payback. Their combination met the 15-year payback limit. The owner of this building is the city and therefore has several buildings under management. Therefore, it can presumably commit itself to continue to pay the same costs and to ensure that there is no downtime. This reduces the risk to the ESCO and allows for a longer duration of the

project. Therefore, in this case, the duration of the EPC project of 15 years was allowed.

Tab. 8 – Simple payback of project without EPC costs

Investment (€)	Savings (€/year)	Simple payback (year)
164 868	21 373	7.7

Tab. 9 – Simple payback of project including EPC costs

EPC Investment (€)	EPC savings (€/year)	EPC costs (€/year)	EPC Simple payback (year)
197 842	21 373	8 243	15.0

6. Conclusion

The case study on an EPC project for an apartment building confirmed that the renovation of technical systems is often more feasible than the renovation of building structures. Therefore, EPC can be a suitable funding method mainly for the reconstruction of technological systems of buildings. However, in some cases, it is possible to combine it with the reconstruction of building structures. With a suitable combination, it is possible to achieve a return that will be acceptable for the ESCO company as well as for the customer. It also depends on the duration of the contract signed at the begging of the EPC project. In this way, the EPC can be a suitable financing tool even for complex building renovations.

The case study has also shown the important impact of variability in the selected input data, such as, for example, the discount rate. Tables 8 and 9 showed that the additional costs associated with EPC can considerably increase the payback period. The profitability of individual energy efficiency measures can be expressed through various profitability indicators. NPVQ can be used to distinguish the main differences between measures for building structures and measures for technology systems. However, for EPC projects, the number of years in which the investment is returned is the most important. This indicates that PB can be a more relevant indicator for EPC projects than NPVQ.

Nomenclature

Symbol	Definition (Unit)
NPV	Net present value (€)
NPVQ	Net present value quotient
B	Yearly financial savings (€)
r	Real interest rate
n	Economic lifetime (year)
I	Investment (€)
PB_{disc}	Discounted payback (year)
CF_t	Cashflow (€)
RAT_{disc}	Discount rate
t	Time (year)
CO_{INT}	Initial investment (€)
$CO_{INT,ref}$	Initial investment to reference solution (€)
$EPC_{SimplePB}$	Simple payback incl. EPC costs (year)
EPC_{Invest}	Investment to EPC project (€)
$EPC_{savings}$	Financial savings by EPC (€)
EPC_{costs}	Costs associated with EPC (€)
H_T	Heat loss by transmission (W/K)
H_V	Heat loss by ventilation (W/K)
$b_{x,i}$	Factor considering loss to unheated space
U_i	Heat transfer coefficient (W/(m².K))
A_i	Area of the building structure (m²)
ΔU	Loss by thermal bridges (W/(m².K))
$\sum A_i$	Total area of building envelope (m²)
V	Internal volume of building (m³)
V_b	Outer volume of building (m³)
ρ_a	Density of air (kg/m³)
c_a	Specific heat capacity of air (kJ/(kg.K))
n_{inf}	Air change rate in building (1/h)
Q_H	Energy need for heating (kWh)
Q_{ht}	Thermal losses of building (kWh)
n_{gn}	Heat gain utilization factor
Q_{gn}	Heat gains of building (kWh)
Q	Energy demand for heating (kWh)
$Q_{em,ls}$	Heat loss of emission system (kWh)
$Q_{H,dis,ls}$	Heat loss of distribution system (kWh)
$W_{H,dis,aux}$	Auxiliary energy for distribution system (kWh)
$Q_{g,ls}$	Heat loss of generation system (kWh)

7. Acknowledgement

This work was supported by the Ministry of Education, Science, Research and Sport of the Slovak Republic through grants VEGA 1/0303/21 and 1/0304/21 and KEGA 005STU-4/2021.

The datasets generated during and/or analysed during the current study are not available because of the page limit but the authors will make every reasonable effort to publish them in near future.

8. References

[1] Dipasquale, Ch., Fedrizzi, R., Bellini, A., Gustafsson, M., Ochs, F., Bales, Ch. Database of energy, environmental and economic indicators of renovation packages for European residential buildings. Energy & Buildings. 2019;203:1-2.

[2] Directive 2012/27/EU of the European Parliament and of the Council of 25 October 2012 on energy efficiency, amending Directives 2009/125/EC and 2010/30/EU and repealing Directives 2004/8/EC and 2006/32/EC.

[3] Energy Performance of buildings Directive, Directive 2010/31/EU of the European Parliament and of the council of 19 May 2010 on the energy performance of buildings.

[4] EC, EPBD Recast (Directive 2010/31/EU). http://www.eceee.org/policyareas/buildings/EPBD_Recast. 2010.

[5] Marszal A.J., Heiselberg P., Bourrelle J., Musall E., Voss K., Sartori I., Napolitano A. Zero energy building - a review of definitions and calculation methodologies. Energy and Buildings. 2011; 43:971-979.

[6] Brown N.W.O., Bai W., Bjork F., Malmqvist T., Molinari M. Sustainability assessment of renovation for increased end-use energy efficiency for multi-family buildings in Sweden. In: Proceedings of SB11 Helsinki World Sustainable Building Conference, Helsinki. 2011;132-133.

[7] Kurnitski J., Saari A., Kalamees T., Vuolle M., Niemelä J., Tark T. Cost optimal and nearly zero energy performance requirements for buildings in Estonia. Estonian Journal of Engineering. 2013; 19:183-202.

[8] Marino A., Bertoldi P., Rezessy S., Boza-Kiss B. A snapshot of the European energy service market in 2010 and policy recommendations to foster a further market development. Energy Policy. 2011;39(10):6190–6198.

[9] European Commission, Energy Performance Contracting Campaign (EPCC), 2014. Accessed from: http://ec.europa.eu/energy/efficiency/financing/campaign_en.htm

[10] Sorrell S. The economics of energy service contracts. Energy Policy. 2007;35(1):507–521.

[11] Act no. 321/2014 Coll. on Energy Efficiency and on Amendments to Certain Acts, 2014.

[12] Decree of the Ministry of Economy of the Slovak Republic no. 99/2015 Coll.

[13] Decree of the Ministry of Economy of the Slovak Republic no. 179/2015 Coll.

[14] Ministry of Finance of Slovak Republic, EPC contract template [online]. 2020. [cit. 2020-10-05].

[15] The definition of EPC [online]. [cit. 2020-10-05].

[16] Dahlsveen T., Petráš D. Energetický audit budov [Energy audit of buildings], ISBN 80-88905-85-0, 2005; 167-168.

[17] STN EN 15459-1, Energy performance of building – Economic evaluation procedure for energy systems in building – Part 1: Calculation procedures, Brussels, 2017.

[18] Guide to Cost-Benefit Analysis of Investment Projects, ISBN 978-92-79-34796-2, 2015.

[19] Shang T., Zhang K., Liu P., Chen Z. A review of energy performance contracting business models: Status and recommendation. Sustainable Cities and Society. 2017; 203-210.

[20] Lu Z. J., Shuai S. Impacts of government subsidies on pricing and performance level choice in Energy Performance Contracting: A two-step optimal decision model. Applied Energy. 2016;106.

[21] Lee P., Lam P. T. I., Lee W. L. Risks in energy performance contracting (EPC) projects. Energy and Buildings. 2015,92;116–127.

[22] Lee P., Lam P. T. I., Yik F. W. H., Chan E. H. W. (2013). Probabilistic risk assessment of the energy saving shortfall in energy performance contracting projects-A case study. Energy and Buildings. 2013;66:353–363.

[23] Bertoldi P., Rezessy S. Energy service companies in Europe. Status report. 2005;1–72.

[24] Rezessy S., Dimitrov K., Urge-Vorsatz D., Baruch S. Municipalities and energy efficiency in countries in transition – Review of factors that determine municipal involvement in the markets for energy services and energy efficient equipment, or how to augment the role of municipalities as market players. Energy Policy. 2006,34;223–237.

[25] Xu P. P., Chan E. H. W., Qian Q. K. Success factors of energy performance contracting (EPC) for sustainable building energy efficiency retrofit (BEER) of hotel buildings in China. Energy Policy. 2011,39;7389–7398.

[26] Comparison and Evaluation of Financing Options for Energy Performance Contracting Projects, Graz Energy Agency Ltd. 2008.

[27] Project QualitEE, market research. 2019. [cit. 2020-10-05]

[28] STN EN 15316-1:2017, Energy performance of buildings - Method for calculation of system energy requirements and system efficiencies - Part 1: General and Energy performance expression, Brussels, 2017.

[29] STN 73 0540-2, Tepelnotechnické vlastnosti stavebných konštrukcií a budov. Tepelná ochrana budov. Časť 2: Funkčné požiadavky, SÚTN, Bratislava, 2002.

[30] STN EN 15316-2:2017, Energy performance of buildings - Method for calculation of system energy requirements and system efficiencies - Part 2: Space emission systems (heating and cooling), Brussels, 2017.

[31] STN EN 15316-3:2017, Energy performance of buildings - Method for calculation of system energy requirements and system efficiencies - Part 3: Space distribution systems (DHW, heating and cooling), Brussels, 2017.

[31] STN EN 15316-5:2017, Energy performance of buildings - Method for calculation of system energy requirements and system efficiencies - Part 5: Space heating and DHW storage systems (not cooling), Brussels, 2017.

[32] STN EN 15316-4-1:2017, Energy performance of buildings - Method for calculation of system energy requirements and system efficiencies - Part 4-1: Space distribution systems: Space heating and DHW generation systems, combustion systems (boilers, biomass), Brussels, 2017.

Surefit - Sustainable solutions for affordable retrofitting of domestic buildings

Janne Hirvonen [a, b], Yangmin Wang [a], Juha Jokisalo [a, c], Risto Kosonen [a, d]

[a] Department of Mechanical Engineering, Aalto University, Espoo, Finland, janne.p.hirvonen@aalto.fi [b] Faculty of Built Environment, Tampere University, Tampere, Finland

[c] Smart City Center of Excellence, TalTech, Tallinn, Estonia

[d] College of Urban Construction, Nanjing Tech University

Abstract

To reduce greenhouse gas emissions caused by buildings, the EU has declared the Renovation Wave strategy with the goal of retrofitting existing buildings to be more energy efficient. Long-term emission reductions require both speedy and cost-efficient renovation methods. The Surefit project aims to develop practical means for effective building retrofitting. The aim is to reduce emissions and CO_2 emissions by 60%, to reduce installation time by 40% and to demonstrate a payback period of less than 10 years. New modular technologies for improving energy efficiency and indoor conditions will be tested. This study examines three demonstration buildings chosen from three European countries (United Kingdom, Spain and Greece). Each demonstration building was modelled using IDA-ICE and their energy demands simulated to provide the baseline for energy efficiency. Then, various retrofit options were tested using dynamic computer simulations, with the aim of finding out the impact of the different technologies in different climates and under different energy mixes. This study focuses on measures integrated to the building envelope and structure, namely bio-based thermal insulation, solar electric low-energy windows and phase-change materials. Thermal insulation of the building envelope using bio-aerogel reduced CO_2 emissions by 41-43% in continuously heated buildings, but only by 15% in an intermittently heated building. The emission impact of PV glazing was only 3-8%. PV glazing resulted in a slight reduction of overheating in Spain and UK, but increased the temperatures in Greece, because it could not replace the external shading device that was removed when PV glazing was installed. The benefits of PCM were low. A smart ventilation control scheme or a different type of PCM material could help in attaining additional benefits.

Keywords. Surefit, Energy retrofit, Energy efficiency, Emission reduction, Indoor comfort
DOI: https://doi.org/10.34641/clima.2022.210

Copyright ©2022 by the authors. This conference paper is published under a CC-BY-4.0 license.

1. Introduction

Energy use in buildings is the cause about 36% of the CO_2 emissions in the EU [1]. By 2050, most of the current building stock will still be in use, with energy efficiencies much worse than those of new buildings being built now and in the future. The Renovation Wave initiative aims to increase the rate of retrofitting of old buildings to also reduce emissions in the already existing buildings [2].

In this spirit, the Surefit project examines the retrofitting potential of old buildings in various European countries [3]. The goal is to test new energy efficiency technologies and find cost-effective and fast methods for reducing energy use and emissions by 60%. This calls for modular technologies and easy to install packages, which fit typical buildings in each region. In the first stage, the buildings will be modelled and technology impacts will be estimated through dynamic simulation. In the second stage, the retrofits will actually be completed and the new technologies installed in the demo buildings. This is followed by real-time monitoring of energy use and indoor conditions, which will be used to refine the initial simulation models of the buildings.

In this study, we examine some of the technologies and focus on envelope upgrades in three countries: Spain, Greece and the United Kingdom. We also examine the impact of heating schedule on the benefits of thermal insulation.

2. Research methods

2.1 Simulation tool

To obtain the hourly energy demand profiles of the demo buildings, they were modelled and simulated in IDA-ICE 4.8 [4]. IDA-ICE is has been validated for producing accurate results of building energy use and indoor conditions [5] [6].

2.2 Demo building descriptions

The UK demo building is one half of a semi-detached house. Space heating is provided by a gas boiler and hot water heating by a direct electric heater. An additional electric radiator is also utilized in the living room. The building is located in Nottingham, United Kingdom. The region has a temperate oceanic climate with mild summers, cool winters and abundant rain (Köppen climate classification Cfb).

The Spanish building is a terraced house of four apartments. Each apartment has two storeys of living area plus an unheated basement. Space and hot water heating is provided by a gas boiler. The building is located in Valladolid, Spain. It is a region with hot summers and relatively cold winters, with large temperature shifts between night and day (Csb).

The Greek demo building is a small apartment building with two apartments, connected on two sides to neighbouring buildings. Space heating is provided by an oil boiler and hot water by a solar boiler. Cooling is provided by electric air-conditioners. The Greek demo building is located in Athens, Greece. This area has a warm climate with hot summers and mild winters (Csa).

Figure 1. Photographs of the demo buildings. From left to right: UK, Spain, Greece.

Table 1 shows the properties of the building envelope in each demo building before retrofit measures. Some of the data was provided by building owners. Some values were not known, so these data points were obtained from building archetypes shown in the literature. Literature values were used for estimating the envelope U-values for the Spanish demo building and the infiltration value for the Spanish and Greek demo buildings.

Table 1. Properties of the building envelope in the demo buildings before retrofit measures.

	Wall	Roof	Windows	Infiltration
	(W/(m^{2}K))			n_{50} (ACH)
UK	2.1	0.22	2.4 / 2.5	16.1
Spain	1.7 [a]	1.6 [a]	2.8 / 5.7	6.7 [b]
Greece	1.0	3.9	3.5 / 5.9	6.7 [b]

[a] TABULA WebTool [7]
[b] Feijó-Muñoz et al. (2019)[8]

In Mediterranean countries, it is typical to only heat the building intermittently, at certain hours of the day. In regions like the UK, continuous heating is used instead.

The UK demo building was heated continuously to provide 20 °C indoor temperature. The Spanish demo building was heated using a varying setpoint, 18 or 20 °C during the day (hours 14-23) and 17 °C during the night and morning. The Greek building was heated only intermittently, 2 hours in the morning (7-9) and 3 hours in the evening (19-22). This intermittent heating has a big impact on indoor temperatures and energy use. To improve comparability, the building was also simulated using a continuous heating schedule, which always keeps the building at 20 °C during the heating season.

2.3 Model validation

Measured data of building energy use was available, but of varying quality. Monthly consumption was available for the UK demo building. The reference building model was validated by normalizing the measured consumption using monthly heating

degree days and comparing the results to the simulations. Simulated energy demand was within 5% of the measured value.

For the Spanish demo building, bi-monthly energy use data split between 2019-2020 was available for only one of the four apartments. Hot water use according to statistics was removed to obtain the space heating demand. Monthly heating degree days for Valladolid were used to split the bi-monthly energy use data to monthly values and to normalize it to make it comparable to the simulated energy use. The simulated demand was within 12% of the measurements, which was deemed acceptable, considering the uncertainties in both the building envelope properties and energy use data. The monthly comparison is shown in **Figure 2**.

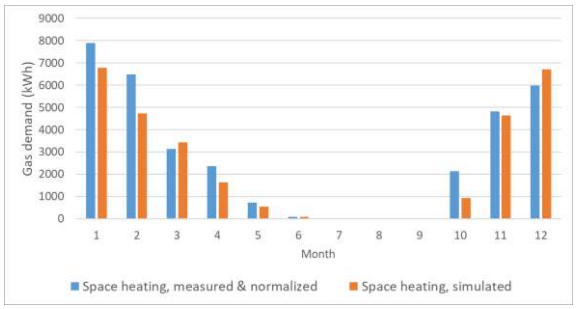

Figure 2. *Measured and simulated space heating fuel use in the Spanish demo building.*

For the Greek demo building only average annual energy use data was available and only for one apartment. Detailed validation was not done due to lack of data. **Table 2** shows the measured and simulated total heating energy use (space heating and domestic hot water) of all demo buildings on an annual level.

Table 2*. Measured and simulated energy demand.*

Heat demand, SH + DHW	UK	Spain	Greece
(kWh/m2)	Monthly	Bi-monthly	Annual
Measured, original	181.5	113.4	36.4
Measured, HDD-corrected	191.3	125	-
Simulated	182.3	115	42.6

2.4 Emissions and primary energy

Each country has a different energy generation mix, which impacts the primary energy and CO_2 emission factors of energy generation. These are shown in **Table 3**.

Table 3. *Emission and primary energy factors.*

	Emission factors (kg-CO_2/MWh)		Primary energy factors (kWh/kWh)	
	Heat	Electricity	Heat	Electricity
UK	203	231	1.13	1.5
Spain	199	190	1.07	1.51
Greece	264	572	1.1	2.9

2.5 Retrofit plan

The envelope retrofit package includes three technologies: bio-aerogel thermal insulation, PV-glazed low U-value windows and phase-change material (PCM). These were applied in sequence to see their impact on building energy efficiency and indoor conditions.

Table 4*. Retrofit measures applied to the buildings.*

-	Installed amount (m^2)		
Technology	UK	Spain	Greece
Bio-aerogel, 5cm on all external walls	81	282	412
Bio-aerogel, 5cm on roof	73	112	108
PV-glazing, on south-facing windows	13	20	11
PCM, 3.2cm on living area ceilings	67	198	154

The bio aerogel was installed on the external walls and roof in a 5 cm layer in each building.

The PV glazing was only installed on the south face of the building exposed significantly to the sun. These windows provide thermal insulation, solar shading and solar electricity generation (though at a low efficiency). There is no such integrated component in IDA-ICE, so the integrated solar electric capacity was modelled as a separate PV system, installed in a vertical position.

The PCM was installed on the ceiling of each room in 3.2 cm layers. The purpose of PCM is to serve as passive energy storage and cooling measure, which absorbs excess heat during the day and releases it during the night. While the salt hydrate product has a nominal melting point of 22 °C, experimental results by the PCM manufacturer show that the phase change happens over a wide range of temperatures. The PCM was modelled in IDA-ICE

using the enthalpy method, such that the temperature range of phase change was divided to sections of varying partial enthalpy values (**Figure *3***). Higher enthalpy values indicate a better capacity for absorbing heat at that temperature value. For solidification, the melting curve was shifted by 2 °C.

Properties of the technologies
Bio-aerogel:
k = 0.024 W/(mK), ρ = 430 kg/m³, c_p = 2260 J/(kgK)

PV glazing:
Window U-value = 0.6 W/(m²K), g-value = 0.53,
electricity generation efficiency η_{PV} = 3.5%

PCM:
rho = 1530 kg/m³, c = 2200 J/(kgK),
k = 0.54 W/(mK),
$h_{f,ave}$ = 200 kJ/kg.

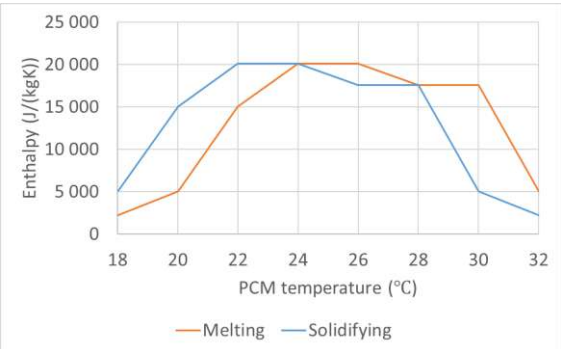

Figure 3. PCM enthalpies used in the simulation.

3. Results and discussion

3.1 Energy use

Figure 4 shows an overview of the emission impacts of the retrofit actions. A more detailed account can be seen in **Table 5**, which shows the fuel, electricity and primary energy use as well as the CO_2 emissions in the examined buildings. Primary energy demand was reduced significantly in the Spanish (-40…-47%) and UK cases (-40…-44%). In the Greek cases utilizing the default intermittent heating, the reduction in primary energy use was much smaller (-15…-25%).

This difference is explained by the intermittent heating pattern used in the Greek building. Since space heating was turned on for only 25% of the heating season, the share of space heating vs. domestic hot water was smaller than in continuously heated buildings. Therefore, measures that reduce space heating demand (thermal insulation and window upgrades) had a smaller impact.

When the Greek demo building was operated under a continuous heating schedule, the reference energy demand was tripled from 37 kWh/m² to 109 kWh/m². As space heating use was more extensive, the energy efficiency measures became more impactful and primary energy demand was reduced by 43 to 51%. This is similar to both the Spanish and British buildings, despite the differences in climate and starting insulation levels.

Table 5. *Specific energy demand and emissions in the buildings before and after retrofitting.*

	Fuel (kWh /m²)	Elec (kWh /m²)	Primary energy (kWh /m²)	Emissions (kg-CO_2 /m²)
UK				
Original	182.3	24.5	242.7	42.7
Bio-aerogel	98.5	22.3	144.8	25.1
Bio-aerogel + PV glazing	93.9	20.0	136.1	23.7
Bio-aerogel + PV glazing PCM	93.1	20.0	135.2	23.5
Spain				
Original	115.0	19,4	152.4	26.6
Bio-aerogel	58.0	19.3	91.1	15.2
Bio-aerogel + PV glazing	51.1	18.2	82.1	13.6
Bio-aerogel + PV glazing + PCM	50.2	18.2	81.2	13.4
Greece, intermittent				
Original	36.8	14.8	67.0	18.2
Bio-aerogel	30.6	13	56.9	15.5
Bio-aerogel + PV glazing	27.9	11.7	51.6	14.1
Bio-aerogel + PV glazing + PCM	27.2	11.5	50.5	13.8
Greece, continuous				
Original	109.3	18.5	152.8	39.3
Bio-aerogel	56.5	14.3	87.7	23.1
Bio-aerogel + PV glazing	46.6	13.4	75.2	20.0
Bio-aerogel + PV glazing + PCM	45.9	13.4	74.5	19.8

The biggest impact on heating energy use came from the thermal insulation of walls. The window upgrades also had a noticeable impact, but the area covered by them was much smaller and limited the potential. The utilizable solar electricity produced by the PV glazing was small in all cases: 2.3 kWh/m² in the UK case, 1.1 kWh/m² in the Spanish case and 1.7 kWh/m² in the Greek case. This reduced purchased electricity consumption by 10%, 6% and 13% in UK, Spain and Greece, respectively.

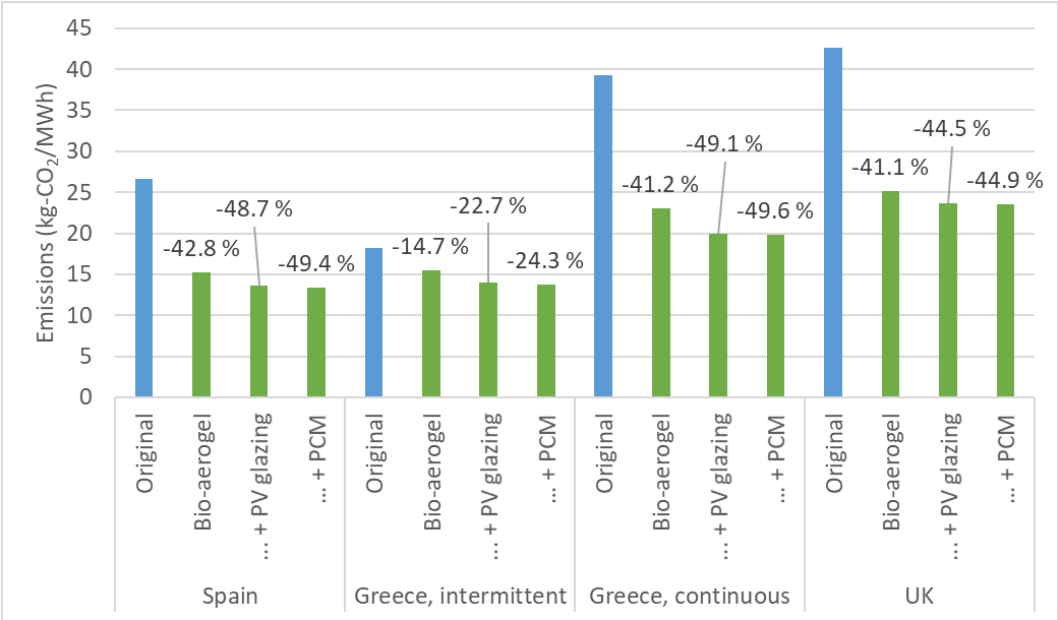

Figure 4. *CO_2 emissions and relative reduction in each demo building before and after retrofitting.*

3.2. Indoor conditions

In each demo building, the envelope upgrades influenced the indoor temperature conditions. The conditions are shown in **Figure 5**. The results show the fraction of time during the whole year that the temperature is above or below the presented limit. It also shows the annual maximum temperature obtained in the simulation.

Less time was spent below the heating setpoint due to the thermal insulation and low U-value windows. Similarly, the low g-value in the windows slightly reduced overheated hours in the UK and Spanish cases. However, in the intermittently heated Greek building, the new windows actually increased overheating by raising the maximum temperature and increasing the time spent above 25 °C. This happened, because an external shading device that covered the balcony in the reference case was removed to see the impact of the PV glazing on preventing overheating. The solar protection effect of the PV glazing was not enough to compensate for the lack of external shading.

Due to intermittent heating, the Greek building was significantly cooled down between the heating periods. This increased the heating power demand when heating was turned on again. Often, the short heating period was not enough to reach the heating setpoint, pointing to a capacity problem. However, improved thermal insulation reduced the time spent below the heating setpoint by 4%-points in the intermittently heated case. The Spanish case was also slightly below setpoint for 5% of the time, but this was reduced to zero by thermal insulation.

The PCM caused a very small reduction (0.4 – 1.9%) of heating demand in the demo buildings. It's main purpose was to reduce overheating, but it only resulted in a 0.4 – 0.6% reduction in the UK and Spanish cases and actually increased overheating in the Greek case with intermittent heating.

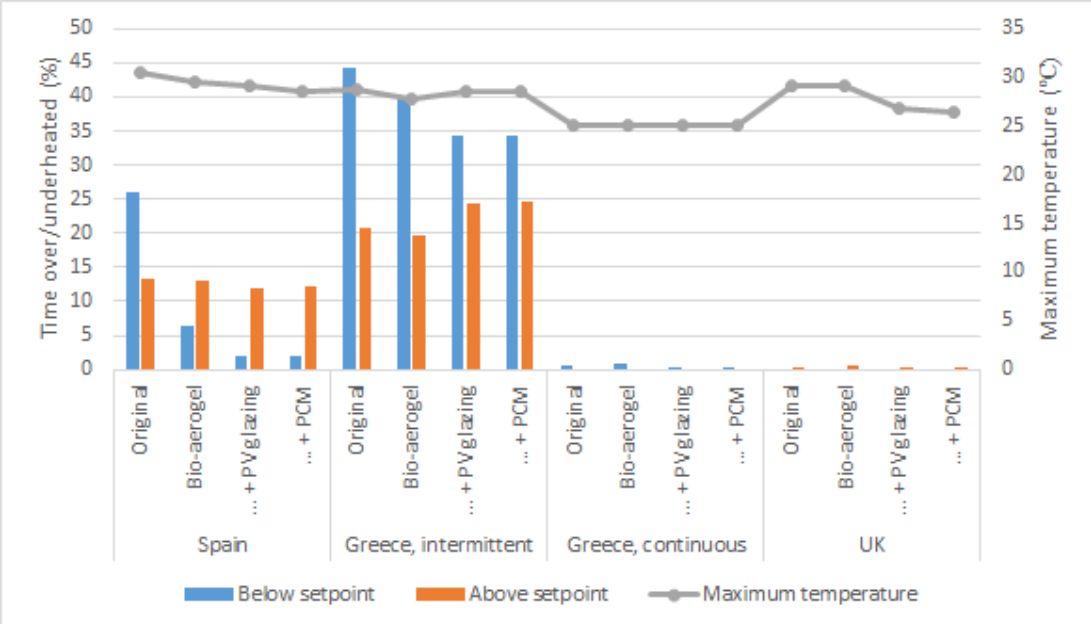

Figure 5. *Indoor conditions in all demo building before and after retrofitting.*

3.3 Discussion

Validation of the specific simulation models was challenging, due to many uncertainties in the data. For example, energy use levels for a whole building had to estimated from measurement data of a single apartment. Some consumption data was given on an annual or bimonthly level, which prevented accurate monthly matching. In addition, infiltration and thermal conduction values of some structural components were uncertain, requiring the use of typical values from statistics.

PCM proved to be of little benefit. In some cases it reduced peak temperatures while in others it raised them, but the impact was only 1 °C or less. The Spanish case had theoretical potential to benefit from the PCM, as even in summer, the outdoor temperatures are reduced significantly during the nights. However, while windows were opened during nights, this was not enough to cool the building and solidify the PCM for significant additional heat absorption. For example, an active blower system might be necessary to benefit from the ambient cooling capacity for both direct space cooling and for PCM regeneration. The wide temperature range for phase change also means that the whole heat capacity cannot be utilized when the temperature remains high for a long time.

In the second stage of the project, the retrofit measures determined to be the most effective by simulations will be installed into the demonstration buildings. Real-time monitoring will be used to assess the accuracy of the simulations and to improve the operational performance through advanced control algorithms. The measurements will be used for validation and further model development.

4. Conclusions

Additional thermal insulation of external walls and roof was very effective for reducing heating energy use. The bio-aerogel insulation reduced CO_2 emissions by 41 to 43% in all demo buildings. Despite the large differences in the initial thermal insulation levels, all buildings received very similar benefits from additional insulation. However, using an intermittent heating profile reduced the impact of insulation on energy use to 15% in the Greek case. Using a continuous heating profile increased the benefit of thermal insulation, because the share of space heating out of the total energy use was higher. This will be important in the cost evaluation phase, as the capital costs of retrofitting will be the same, regardless of the heating strategy. Intermittent heating reduces energy use at the cost of thermal comfort. Continuous heating improves thermal comfort and the potential benefits of energy saving measures, but raises the absolute energy use.

PV glazing provided small additional emission cuts, reducing CO_2 emissions by 3% in the UK, by 6% in Spain and by 8% in Greece. This was mainly due to lower thermal conductivity, with the solar electric generation playing a smaller role. The PV glazing could not replace external solar shading as overheating protection.

The benefit of PCM for passive cooling was questionable. Active night-time ventilation might be necessary to regenerate the PCM for the next day. A material with a more discrete melting temperature range would also help.

Acknowledgement

This project has received funding from the European Union's Horizon 2020 research and innovation programme under grant agreement No 894511. The study received further funding from the FINEST Twins project, that is co-funded by the European Union (Horizon 2020 programme, grant number 856602) and the Estonian government. The authors would also like to thank the partners of the Surefit project, AMSolutions, Faculdade Santa Maria, ISQ Group, PCM Products and the University of Notthingham.

References

[1] European Parliament, "Directive 2010/31/EU of the European Parliament and of the Council of 19 May 2010 on the energy performance of buildings." 2010.

[2] European Commission, "A Renovation Wave for Europe - greening our buildings, creating jobs, improving lives." European Commission, 14-Oct-2020.

[3] Surefit, "Surefit Project," 01-Jan-2021. [Online]. Available: https://surefitproject.eu/.

[4] EQUA Simulation AB, "IDA ICE - Simulation Software," 2019. [Online]. Available: https://www.equa.se/en/ida-ice. [Accessed: 08-Aug-2019].

[5] EQUA Simulation AB, "Validation of IDA indoor climate and energy 4.0 with respect to CEN standards EN 15255-2007 and EN 15265-2007," May 2010.

[6] P. Loutzenhiser, H. Manz, and G. Maxwell, "Empirical validations of shading/daylighting/load interactions in building energy simulation tools," IEA - International Energy Agency, 2007.

[7] T. Loga, J. Calisti, B. Stein, L. Ortega, and B. Serrano, "TABULA WebTool," *TABULA WebTool, building energy efficiency database*, 11-Jun-2017. [Online]. Available: https://webtool.building-typology.eu/#bm. [Accessed: 05-Jan-2022].

[8] J. Feijó-Muñoz, R. A. González-Lezcano, I. Poza-Casado, M. Á. Padilla-Marcos, and A. Meiss, "Airtightness of residential buildings in the Continental area of Spain," *Building and Environment*, vol. 148, pp. 299–308, Jan. 2019.

A comparative study of solar cooling technologies

Beethoven Narváez-Romo [a,b], Eliane Hayashi Suzuki [a], José R. Simões-Moreira [a]

[a] SISEA - Renewable and Alternative Energy Systems Laboratory, Escola Politécnica at University of São Paulo, Brazil.

[b] Grupo de Energía y Termodinámica, Facultad de Ingeniería Mecánica, Universidad Pontificia Bolivariana, Circular 1 No. 70-01, Medellín, Colombia.

Abstract. The environmental impacts of refrigeration and air conditioning applications include synthetic refrigerant fluids use and the high demand for electrical energy for activation, being critical in places whose energy mix depends on fossil fuels. Brazil has advantages due to hydroelectricity and the high incidence of solar irradiation, enabling solar energy technologies in refrigeration cycles. This work aims to study the technical-economic feasibility of photovoltaic energy to drive the vapor compression refrigeration system, and solar thermal energy for the ammonia-water and water-lithium bromide absorption cycles. It developed thermodynamic models of both vapor compression and absorption cycles using the mass and energy conservation equations under steady-state regime. The systems of linear equations were solved by using the *Engineering Equation Solver - EES*. One obtained the air conditioning thermal load profile and the characteristics of the thermal collectors and photovoltaic panels from *EnergyPlus*, from São Paulo-Brazil solar irradiation. Results showed that the monthly energy consumption is reduced from 626 kWh to 196 kWh, achieving a 44% reduction in the value of the electric energy bill for the photovoltaic solar cooling proposed when compared to the conventional one. A 7-years payback time is achieved. For the absorption cycle, the use of a flat thermal collector is unfeasible due to the need for natural gas as a complementary source of energy. It is concluded that solar cooling with photovoltaic has advantages compared to thermal activation, as the overall efficiency has a performance 30% higher than solar cooling by the thermal collector. Results showed that $PREU_{PV}$ is always higher than $PREU_{ST.}$

Keywords. Solar refrigeration, Solar Energy, Absorption refrigeration cycle, Ammonia-water, Water-lithium bromide.
DOI: https://doi.org/10.34641/clima.2022.421

1. Introduction

Air-conditioning refrigeration systems are widely used in commercial buildings to ensure thermal comfort. Compression refrigeration systems are the most commercially used type and convert electrical energy into cooling. However, it presents a high energy consumption and causes energy peaks on the power grid. In addition, air-conditioning system might be responsible for 60% to 80% of the energy consumed in commercial and public buildings [1].

Alternatively, the integration of solar-powered refrigeration systems, known as solar refrigeration, can reduce or eliminate the demand for electrical energy from conventional energy sources. In this way, renewable energy presents a good alternative because of the lower emission of greenhouse gases (GHG) throughout its life cycle, guaranteeing a safe energy supply. The potential depends on exploiting locally available resources and overcoming environmental challenges [2].

The high solar radiation in Brazil favors solar energy capturing and converting into electrical energy or thermal energy. Compression refrigeration cycles require electrical energy, while absorption refrigeration cycles use thermal energy. The most common absorption cooling systems working fluids are ammonia-water and water-lithium bromide. The ammonia-water is employed in applications including refrigeration systems with temperatures below 0°C [3,4]. The water-lithium bromide is used for air-conditioning applications due to the limitations of the water thermodynamic properties.

Three main groups that characterize the technologies available for solar refrigeration are solar photovoltaic, solar thermal, and hybrid. [5] found a return of investment of 22% to 28%, considering an air-conditioning system with photovoltaic energy for two Brazilian cities, São Paulo and Recife. It is worth mentioning that these technologies should be evaluated as a whole by modeling the refrigeration cycles by compression

Copyright ©2022 by the authors. This conference paper is published under a CC-BY-4.0 license.

and absorption to coupling with thermal solar energy. Furthermore, there is no study in the literature comparing different solar refrigeration technologies and providing performance characteristics under the same operating conditions.

This work aims to study the technical-economic feasibility of the vapor compression refrigeration system using photovoltaic energy for partial or total activation, and solar thermal energy for the ammonia-water and water-lithium bromide absorption cycles. To evaluate each of the solar refrigeration settings, it was defined the simple return time and the energy conversion rate dimensionless factor between the input or primary power and the cooling capacity ($kW_{Ref.}/kW_{Prym.}$).

2. Solar refrigeration modeling

Next, the main refrigeration systems are detailed: the vapor compression refrigeration cycles (VCRC) and the absorption refrigeration cycles (ARC). These technologies are coupled with photovoltaic (PV) solar energy, and solar thermal (ST) energy, respectively.

2.1 VCRC driven by PV solar energy.

Figure (1a) shows the simple solar cooling configuration of a VCRC coupled with the PV solar energy under an on-grid electrical connection. VCRC mainly consists of a compressor, condenser, evaporator, and expansion valve. The compressor raises the pressure of the refrigerant gas, which carries out the working fluid from the low-pressure (7) to high pressure (4) sides, increasing the gas temperature at the compressor discharge. Then, the condenser rejects the heat in the high-pressure stage to condense the refrigerant (5). Next, an expansion valve reduces the pressure in an isenthalpic process, and the temperature also decreases due to the Joule-Thomson effect. As a result, a two-phase mixture is achieved in the evaporator inlet with a predominance of the liquid phase (6). After the cooling effect is provided, the refrigerant vapor is directed to the compressor, starting the refrigeration cycle again.

The electrical power demanded by the compressor is supplied by using the group of photovoltaic cells at times of high solar irradiation, and complemented by the electrical network during intermittency, a typical characteristic of renewable energy sources.

To cycle modeling, the mass and energy conservation equations are used. Equation (1) refers to the mass conservation equation for an open control volume in a steady-state regime. Equation (2) defines the conservation of refrigerant species or absorbent fluid, and equation 3 represents the energy conservation, neglecting changes in kinetic energy and potential energy.

$$\sum_{in}^{i} \dot{m}_i = \sum_{out}^{j} \dot{m}_j \quad (1)$$

$$\sum_{in}^{i} x_i \dot{m}_i = \sum_{out}^{j} x_j \dot{m}_j \quad (2)$$

$$\dot{Q} - \dot{W} = \sum_{out}^{j} \dot{m}_j h_j - \sum_{in}^{i} \dot{m}_i h_i \quad (3)$$

2.2 ARC driven by ST energy

Figure (1b) shows the single-stage ARC driven by using ST energy. In contrast with conventional VCRC, ARC demands thermal energy in the generator to separate the refrigerant fluid of the absorbent. So, electrical power is substituted by a thermal compressor system. The ammonia-water not only might be employed in air-conditioning systems but also in freezing applications.

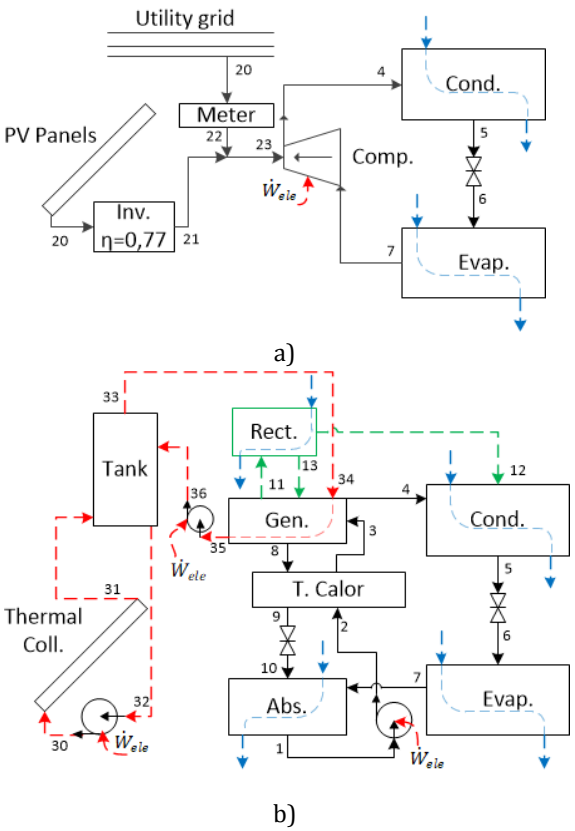

Fig. 1 - Schematic representation of solar refrigeration: a) VCRC coupled with PV solar energy, and b) ARC driven by ST energy.

In ARC, the vapor refrigerant produced in the generator (4) is led to the condenser, expansion valve, and evaporator as a conventional VCRC. The vapor refrigerant leaving the evaporator (7) is absorbed by the absorbent solution becoming the generator (8) after passing the heat recovery (9) and the expansion valve (10). Thus, the solution is pumped to the generator (3) to restart the cycle. For ammonia-water working fluid, a rectification system is coupled to increase the ammonia vapor purity as shown in Figure (1b), points 11, 12, and 13.

Figure (1b) depicts the ARC coupled with the ST energy. A hot water storage tank stores the water of the ST circuit, which is employed to drive the ARC. A natural gas burner is applied to supplement heat for the operating ARC during the low irradiation periods. Similarly, equations 1-3 are employed for ARC modeling.

The coefficient of performance (COP) is defined to evaluate these cooling technologies. The COP sets the ratio between the cooling capacity and the energy rate provided to the cycle. The VCRC uses the compressor's electrical power, and the ARC utilizes the generator. The electrical power of the solution pump is neglected.

Thermodynamic modeling for VCRC and ARC systems is performed with the *Engineering Equation Solver - EES* program. One solved the mass and energy conservation equations as a control volume under steady-state conditions. The results from the thermodynamic model have integrated with the results from the TS collectors and PV panels modeling. A case study of an office environment is defined with a typical thermal load profile and air-conditioning system. The *EnergyPlus* tool is used to evaluate the performance of solar refrigeration technologies.

2.3 Office building case study

An office building with 10.0 m x 10.0 m x 2.8 m in São Paulo is defined as the thermal zone, which is characterized by Cfa humid subtropical climate at Koppën-Geiger classification. The North and West walls are set as external walls with a 45% glazed area, while the East and South are adiabatic. The vertical closures are set with masonry, with a U-factor of 2.3 W/m^2°C, and 5.7 W/m^2°C U-factor laminated glass windows.

The simulation is carried out in *EnergyPlus* 9.4, on the 26th of January, which has a high global solar irradiation incidence according to the São Paulo climate file. The internal thermal loads are set by 5 m^2/person high occupancy density for office environments, 5.4 W/m^2 equipment power [6], and 14.1 W/m^2 lighting power density. The metabolic rate was approximately 110 W/person, a typical office activity [7]. The occupancy schedule was set 100% during most business hours, with 50% at lunchtime. Also, it was considered air renewal of 0.0025 m^3/s per person, plus 0.0003 m^3/s per meter square (m^2), adding up 0.08 m^3/s [8].

The panels were modeled with a 23° inclination from the horizontal in the North orientation. The photovoltaic panels achieved a cell efficiency of 20% with a photovoltaic generator of 150 W. The air-conditioning design settings were 12.4 kW refrigeration capacity demand, with 14 hours of daily operation (from 6 AM to 8 PM) totaling 420 hours per month. The condensation temperature was 45°C, and the evaporation temperature, 7°C. The inverter efficiency was 0.77, and the photovoltaic energy was an on-grid type, generating 20.9 kWh/day or 626 kWh/month. São Paulo's power distribution company defines tariff groups in which the energy cost depends on the contracted demand and peak hour consumption. After modeling it, we used the predictive method proposed by [9] to compare the thermal load profile of the *EnergyPlus* model.

Results of the VCRC and ARC modeling are shown in Table (1). The COP is computed by using an isentropic compression and pumping process. The heat rates are determined for each component of the cycle, for instance, $\dot{Q}_{abs}$ is the rejected absorber heat duty, $\dot{Q}_{gen}$ is the demanded generator heat duty, $\dot{Q}_{con}$ is the removed condenser heat duty, $\dot{Q}_{rec}$ is the removed rectifier heat duty, and $\dot{W}_{ele}$ is the consumed compressor electrical power. It is worthwhile to mention that VCRC only requires electrical power to be driven.

Tab. 1 - Heat duty and power for each component in the cooling technologies.

	Results for $\dot{Q}_{eva}$=12.4 kW, T_{con}=45°C, T_{eva}=7°C,
CRA-H_2O-LiBr COP=0.88	$\dot{Q}_{abs}$=14.0 kW; $\dot{Q}_{gen}$=14.3 kW; $\dot{Q}_{con}$=12.9 kW
CRA-NH_3-H_2O COP=0.68	$\dot{Q}_{abs}$=18.6 kW; $\dot{Q}_{gen}$=19.3 kW; $\dot{Q}_{con}$=12.8 kW; $\dot{Q}_{rec}$=0.85 kW
VCRC-NH_3 COP=6.3	$\dot{Q}_{con}$=14.7 kW; $\dot{W}_{ele}$=2.13 kW

3. Results and discussion

3.1 VCRC driven by PV solar energy.

Figure (2) compares the electrical power required for the VCRC and the power converted by the PV cells throughout the day. The electrical VCRC consumption, obtained by using the *EnergyPlus* along with the COP_{VCRC}, is consistent with the predictive method proposed by [9]. It can be noted that electrical power required by the air-conditioning system follows the same fashion of the photovoltaic energy conversion curve, enabling the solar refrigeration. However, the complementarity with the on-grid electrical grid is mandatory for the activation where energy demand is greater than the solar energy supply. It is determined that the simple payback time is 7 years.

For the case study of São Paulo-SP (Brazil), the results established a photovoltaic area equivalent to

approximately 75% of the climatized area, with a power generator equivalent to 2.23 kWp. The monthly energy consumption is reduced from 626 kWh to 196 kWh, achieving a 44% reduction in the value of the electric energy bill for the photovoltaic solar cooling proposed when compared to the conventional one. Reductions in the electricity bill are limited, as the refrigeration system demand coincides with the low conversion time of photovoltaic energy, i.e. in the first and last hours of the day, and due to the difference in the invoice value at peak hours. On the other hand, the option of photovoltaic generation at off-peak hours to generate credits and consume at peak hours is economically unfeasible, since five times more energy must be generated at off-peak hours to consume at peak hours, demanding greater investment in the photovoltaic collectors acquisition.

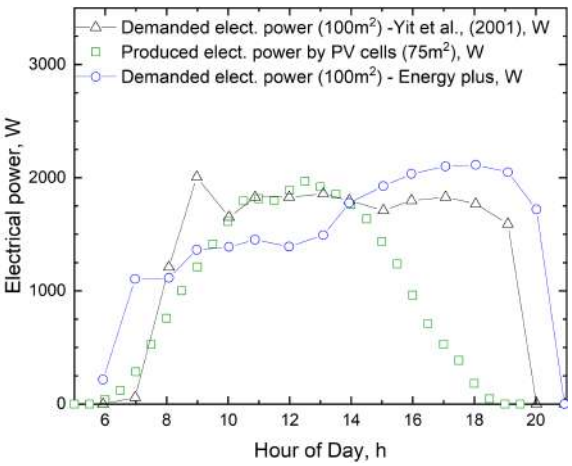

Fig. 2 - Electrical power comparison between the demanded air-conditioning system (VCRC) and the PV generation as a function of the time.

The same analysis was run in five cities with different latitudes to check PV energy generation: Abu Dhabi (24.43°N) in the United Arab Emirates, Acapulco (16.77°N) in Mexico, Bucharest (44.5°N) in Romania, Munich (48.13°N) in Germany, and Seville (37.42°N) in Spain. PV collectors were oriented South and inclined according to their maximum theoretical efficiency.

Simulations were run according to the weather file day's maximum value of incident solar radiation. In this way, the days selected for the cities and the panels' inclinations were Abu Dhabi (May 14/25°), Acapulco (Apr 20/20°), Bucharest (Jun 20/34°), Munich (Jun 9/37°), and Seville (Jun 11/33°).

The daily irradiation was obtained through the design day and converted to solar energy. The energy generated per day was 39.21 kWh for SãoPaulo, 37.31 kWh for Abu Dhabi, 37.19 kWh for Acapulco, 41.36 kWh for Bucharest, 38.63 kWh for Munich, and 39.8 kWh for Sevilla. When comparing these values to São Paulo solar energy generation, given the PV relative performance, results demonstrated that Seville and Bucharest presented positive relative performance of 1.5% and 5.2%, respectively. Abu Dhabi, Acapulco, and Munich showed negative PV relative performance of -5.1%, -5.4%, and -1.5%. Even though Abu Dhabi has a subtropical desert climate, with high solar irradiances peaks, the accumulated energy generated by the PV cells was lower than in São Paulo because of the incidence of radiation distribution along the day on May 14th.

The solar energy generation was similar among the cities, given the highest solar radiation incidence day criteria. Even in different latitudes, it is possible to assign PV solar energy, but it is necessary to consider solar geometry and solar radiation power local characteristics.

3.2 ARC driven by ST energy

Results of solar cooling modeling using the H_2O-LiBr ARC are presented in Figure (3). The thermal load profile is similar to that modeled with the VCRC, as can be seen in Figure (3a). However, the thermal power demanded by the generator, obtained by using the *EnergyPlus* along with the COP_{ARC}, should be constant throughout the day, since ARC does not have the ability to operate at partial loads like VCRC. For the activation of the cycle, thermal solar collectors with a total area equivalent to 35 m^2 are defined.

The study determined that natural gas to complement the water-lithium bromide ARC is economically unfeasible, since the monthly natural gas consumption bill reaches up to three times the value of the local electricity bill when compared to the refrigeration driven with the conventional energy source.

While the water-lithium bromide mixture demands temperatures above 76 °C in the generation process, as shown in Figure (3b), the ammonia-water separation process can require temperatures close to 100 °C. Thus, the economic return is even more critical in the operation of the ARC by using the ammonia-water mixture, due to the higher energy demand and higher operating temperatures of the generator. It is evident that cogeneration can be a better application for the use of ARC, since the residual use of thermal energy can be replaced by the direct burning of natural gas.

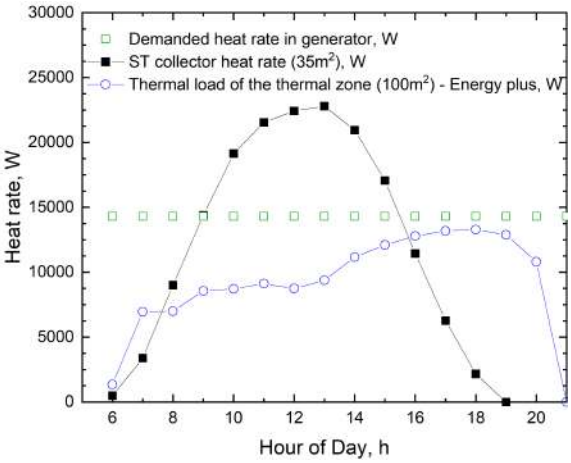

a)

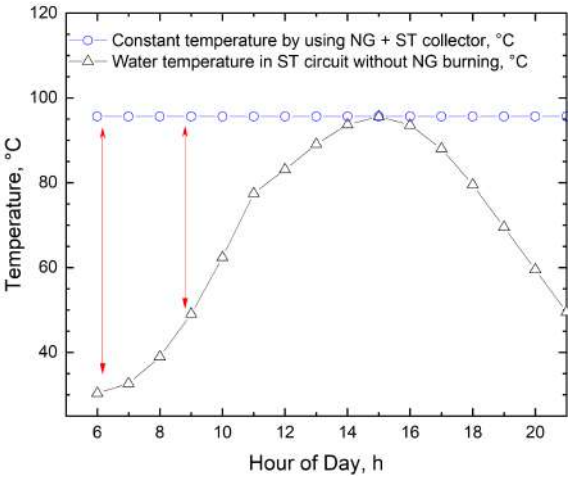

b)

Fig. 3 - Thermal power comparison between the demanded air-conditioning system (ARC) and the ST collector as a function of the time.

3.3 Primary Energy Usage - PEU and Primary Renewable Energy Usage - PREU

Considering the characteristics of the Brazilian electricity mix, which is composed mainly of hydroelectric and thermoelectric plants, as shown in Table (2), an energy conversion rate efficiency of 55.3% is determined [10]. Thus, the Primary Energy Usage – PEU is defined to take into account the energy conversion rate efficiency. This means that for a refrigeration capacity of 12.4 $kW_{Ref.}$, a 3.4 kW_{Prim} of input power is required from the utility grid when operated with a VCRC with a COP of 6.3. In other words, 3.61 $kW_{Ref.}$ cooling capacity are supplied for every 1 kW_{Prim}. of primary energy from the Brazilian electricity mix.

To evaluate solar refrigeration, the Primary Renewable Energy Usage – PREU is defined, considering the energy conversion rate efficiency. For photovoltaic solar cooling, it is found that 1 kW_{Sol} is converted into 0.72 $kW_{Ref.}$ cooling capacity. Finally, ARC are characterized by performances of 0.55 $kW_{Ref.}$ and 0.42 $kW_{Ref.}$ for the water-lithium bromide and ammonia-water solution, respectively.

Tab. 2. A comparison between the PEU (Brazil) and PREU for solar refrigeration.

	Value - $kW_{Ref.}/kW_{Prim\text{-}Sol}$
PEU - VCRC + Utility grid	3.61
$PREU_{PV}$ - VCRC + PV	0.72
$PREU_{ST}$ - NH_3-H_2O ARC+ST	0.42
$PREU_{ST}$ - H_2O-LiBr ARC+ST	0.55

These cooling technologies are a function of the operating parameters such as condensation temperature, evaporation temperature, absorption temperature, and generation temperature, just to mention a few.

Based on the refrigeration cycles simulations, a sensitivity analysis of the COP for different evaporation temperatures was run, fixing the condensation temperature and the other operating parameters of the absorption cycle. Results show a decrease in the COP for lower evaporation temperatures; which affected mainly the compression refrigeration cycles.

Figure (4) comparatively presents the energy conversion rate - PEU ($kW_{Ref.}/kW_{Prim.}$) and PREU ($kW_{Ref.}/kW_{Sol.}$) as a function of the refrigeration cycles evaporation temperature. The use of refrigeration systems with energy from the electricity grid is convenient as compared to the other ones due to the high conversion rates. A 62.5 % hydroelectricity contribution in the Brazilian electrical mix is achieved, explaining the PEU behavior. For solar cooling, the PV solar energy with VCRC should be used for HVAC applications, as this configuration has an advantage when compared to absorption cycles, including water-lithium bromide. On the other hand, ARCs with ammonia-water solar thermal collectors could be used in frozen food refrigeration applications, or in cogeneration.

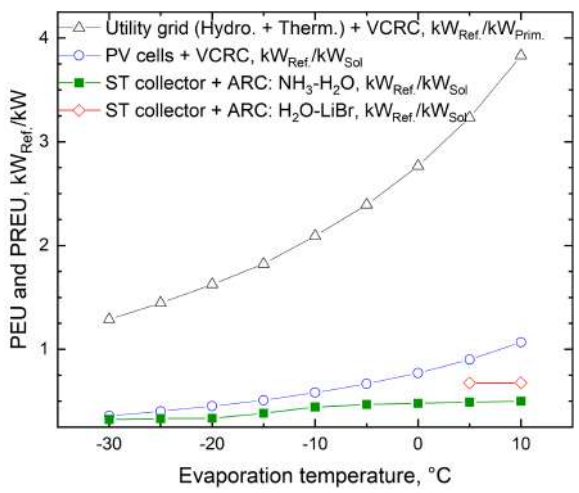

Fig. 4 - PEU and PREU as a function of the evaporation temperature of the cooling technologies.

Spite of the use of conventional hydroelectric energy has better performance than solar renewable sources, more energy demand is growing, thus, solar refrigeration might become a solution for several applications, even though, its usage can be extended for isolated places or as a part of the distributed generation.

4. Limiting efficiency of solar refrigeration

The limiting efficiency of solar refrigeration is defined as a function of the theoretical efficiency of each component. For the PV cells, a tandem solar cell system is calculated by [11]. Semiconductor properties might be neglected over the conversion efficiencies, achieving 68% at 300K when unconcentrated sunlight is employed for one sun. A 33.3 % theoretical maximum efficiency is obtained for a single-junction solar cell [12]. On the other hand, ST collectors might achieve about 80% of the conversion efficiency for extremely low water flow rates. However, the efficiency is a function of the water inlet temperature, surface temperature, glass transmittance, etc. Thus, a 100% of thermal efficiency for the ST collector was assumed, in which no losses are defined.

The theoretical efficiency for refrigeration systems is defined by using Carnot's theory. Efficiencies are only limited by defining the operating temperature; vaporization temperature (eva), generation temperature (gen), absorption temperature (abs), condensation temperature (con). Equation 1 and 2 represent the coefficient of performance for the ARC and the VCRC, respectively. Temperature must be defined as the absolute temperature.

$$COP_{ARC} = \frac{T_{eva}}{T_{gen}}\left(\frac{T_{gen}-T_{abs}}{T_{abs}-T_{eva}}\right) \quad (1)$$

$$COP_{VCRC} = \frac{T_{eva}}{T_{con}-T_{eva}} \quad (2)$$

Figure (5) shows the results of the limiting efficiency of solar refrigeration as a function of evaporation temperature for three different intensities of solar irradiance; 1.2, 1.0 and 0.8 kW/m^2. It can be seen that $PREU_{PV}$ is always higher than $PREU_{ST}$ due to the COP_{VCRC} are greater than COP_{ARC}, about five times for all evaporation temperature range. Moreover, the PREU of the solar refrigeration improves as the intensity of solar irradiance increases.

It can be noted that the operating conditions of the cycle strongly affects the PREU. Higher evaporation temperature and lower condensation temperature enhance the PREU for both cooling technologies. The PREU behavior is more sensible to the operating temperatures than the intensity of the solar irradiance.

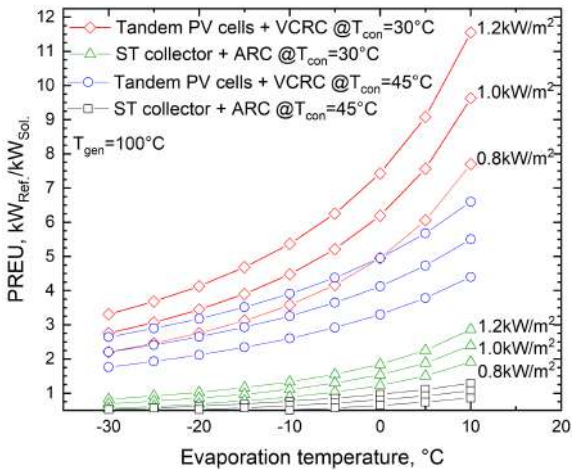

Fig. 5 - PREU of the solar refrigeration as a function of the evaporation temperature for 1.2, 1.0 and 0.8 kW/m^2 intensity of solar irradiance.

5. Conclusions

A study of solar refrigeration with PV cells with VCRC and ST collectors coupled to ARC was carried out. An office building case study was defined to compare both cooling technologies, showing that solar cooling with grid-connected photovoltaic systems might provide a 44% reduction of the electrical energy bill for the 100 m^2 air-conditioned space. The payback time was calculated in 7 years, as the acquisition cost of photovoltaic panels is relatively high.

The ARC solar cooling cycle driven by ST energy presented economic disadvantages compared to the VCRC, as it required energy integration with direct burning of natural gas. The average monthly billing of natural gas was three times higher than the local electric energy bill from the distribution company, making the system unfeasible. The payback time was even more critical for the ammonia-water absorption refrigeration cycle since it requires an even higher operating temperature.

Moreover, it was concluded that solar cooling through the use of PV energy has advantages as compared to ST collectors, as the overall efficiency allows achieving performance values 30% higher than solar cooling by the thermal collector. Even in different locations, those performance ratings are obtained, as the simulated cities presented similar results in energy efficiency. Despite its lower efficiencies, absorption refrigeration with a thermal collector cycle could be used in frozen food applications. Cogeneration can be applied for absorption refrigeration technology since the residual use of thermal energy may be replaced by the direct burning of natural gas.

Additionally, the direct activation of the VCRC with the primary energy use presents advantages over all the solar refrigeration configurations proposed in this work due to the Brazilian electrical mix having high efficiencies in the conversion by

hydroelectricity. Finally, results showed that $PREU_{PV}$ is always higher than $PREU_{ST.}$

The constraints of this paper comprise a set of computational tests with simplified refrigeration modeling, and a hypothetical building and thermal load. Primary Renewable Energy Usage (PREU) present theoretical values. Future works may consider experimental investigation and model validation to compare different solar power supply arrangements.

6. Acknowledgement

Authors would like to thank to the Sao Paulo Research Foundation (FAPESP) for the project funding - Grant No. 2016/09509-1. Moreover, the first author thanks FAPESP for the personal financial support - Grant No. 2020/08211-4, as well as the Colombian Administrative Department of Science, Technology and Innovation - Minciencias - (COLCIENCIAS grant 1.087.046.934-728/2015). The second author thanks to the Coordenação de Aperfeiçoamento de Pessoal de Nível Superior – Brasil (CAPES) – Finance Code 001.

7. References

[1] Opoku R., Edwin I. A., Agyarko K. A. Energy efficiency and cost saving opportunities in public and commercial buildings in developing countries – The case of air-conditioners in Ghana. J Clean Prod;2019;230:937-944.

[2] Hasan M. A., Sumathy K. Photovoltaic thermal module concepts and their performance analysis: a review. Renew Sust Energ Rev;2010;14:1845-1859.

[3] Narváez-Romo B., Chhay M., Zavaleta-Aguilar E. W., Simões Moreira J. R. A critical review of heat and mass transfer correlations for LiBr-H2O and NH3-H2O absorption refrigeration machines using falling liquid film technology, Appl Therm Eng;2017;123:1079-1095.

[4] Narváez-Romo B.; An experimental study of an ammonia-water absorption refrigeration cycle using a novel modified horizontal liquid film absorption system, Ph.D. thesis, University of São Paulo, Brazil;2020.

[5] Leite G. N. P et al. An economic analysis of the integration between air-conditioning and solar photovoltaic systems. Energ Convers Manage;2019;185:836-849.

[6] Associação Brasileira de Normas Técnicas. NBR 16401-1 - Central and unitary air conditioning systems. Part 1: Design of installations. Rio de Janeiro: ABNT, 2008.

[7] International Organization for Standardization. ISO 7730 - Ergonomics of the thermal environment – Analytical determination and interpretation of thermal comfort using calculation of the PMV and PPD indices and local thermal comfort criteria. Geneva: ISO, 2005.

[8] American Society of Heating Refrigerating and Air-conditioning Engineers. ANSI/ASHRAE Addendum to ANSI/ASHRAE Standard 62.1-2016 - Ventilation for Acceptable Indoor Air Quality. Atlanta: ASHRAE, 2019

[9] Yik F. W. H., Burnett J., Prescott I. Predicting air-conditioning energy consumption of a group of buildings using different heat rejection methods. Energ Build;2001;33(2):151-166.

[10] Flórez-Orrego, D.; Silva, J. A. M.; Oliveira, S. Renewable and non-renewable exergy cost and specific CO2 emission of electricity generation: The Brazilian case. Energy conversion and management, 2014, vol. 85, p. 619-629.

[11] De Vos, A.. Detailed balance limit of the efficiency of tandem solar cells. J Phys D Appl Phys;1980;13(5):839.

[12] Alharbi F. H., Kais S. Theoretical limits of photovoltaics efficiency and possible improvements by intuitive approaches learned from photosynthesis and quantum coherence. Renew Sust Energ Rev;2015;43:1073-1089.

Data Access Statement

The datasets generated during and/or analyzed during the current study are not available because the study is under development and has not been finished yet, but the authors will make every reasonable effort to publish them in near future.

Predicting the waterside temperature difference of a cooling coil in part load

Alet van den Brink [a], *Shalika Walker* [b], *Wim Zeiler* [b]

[a] Department O&T, Kropman Installatietechniek B.V., Nijmegen, the Netherlands alet.van.den.brink@kropman.nl

[b] Department of the built environment, Eindhoven University of Technology, Eindhoven, the Netherlands, s.w.walker@tue.nl, w.zeiler@tue.nl

Abstract. Chilled water plants must operate in the most energy efficient way possible. One of the threats to a good energy performance in part load is the 'Low ΔT syndrome', several causes of which are related to the cooling coils. In order to detect deviation behaviour of the waterside temperature difference (ΔT), one needs to know the normal return water temperature during part load operation of the cooling coils. However, until now it has not been possible to predict and quantify the waterside temperature in part load. This paper provides a mathematical derivation to predict the waterside temperature difference in part load. For a constant air and water flow, the performance is only determined by the nominal water leaving temperature and leaving air temperature. Both temperatures determine if the chilled water temperature decreases or increases in part load and the shape of the heat exchanger characteristic of the cooling coil. The result is tested for two known causes of the Low ΔT syndrome, namely 100% outdoor air handling units and economizers. The results show that placing the cooling coil behind (blow through), instead of in front of (draw through), the fan will result in an increased chilled water temperature difference in part load.

Keywords. Cooling coil, part load, low-ΔT syndrome, heat exchanger characteristic
DOI: https://doi.org/10.34641/clima.2022.423

1. Introduction

Cooling is required for indoor climate control in many buildings, and buildings are equipped with Chilled Water (CHW) plants for the purpose of cooling. The cold water can be supplied by chillers or a sustainable source, such as a seasonal thermal energy storage or, a typical Dutch variant, the Aquifer Thermal Energy Storage (ATES). In order to minimize the energy consumption, chillers should operate in the most efficient way. The CHW-plant is designed for full load though generally operates in part load (PL) condition; a good PL efficiency is therefore crucial for a good performance. In PL the Chilled Water Temperature Difference (CHWdT) often differs from the full load condition. One of the causes that threatens a good performance of the CHW-plant is a reduced Chilled Water Return Temperature (CHWR) in PL. This can result in increased energy consumption of circulation pumps and chillers [1–3]. A reduced CHWR with a decreased CHWdT will, for the same capacity, result in increased water flow and pump energy usage. This is especially true for (A)TES systems, because here the pump energy usage is the main source of energy consumption. Many large CHW-plants suffer from a reduced CHWR [2,4] and a series of causes are known as the Low ΔT syndrome: *"A condition whereby a low chilled water return temperature (CHWR) causes an excessive amount of chilled water to circulate to meet system cooling loads and chillers receiving the low temperature CHWR cannot be loaded to their design capacity*"[3,5].

A selection of causes are as follows:

- poorly selected cooling coils [2];
- a reduced set point of the leaving air temperature (LAT) [6];
- economisers and 100% outside air unit [2];
- laminar flow in the cooling coil [7];
- increased chilled water supply temperature (CHWS) in PL [2].

In order to detect the Low ΔT syndrome, the normal CHWdT for the PL of a cooling coil must be known and compared with the actual CHWdT. The definition of the Low ΔT syndrome uses the words "*excessive amount*" and "*low chilled water return temperature*", but in reality, the reduced CHWR can occur without the "excessive amount" of chilled water circulation. This detection is difficult because, to the best of our knowledge, it is for example not possible to

Copyright ©2022 by the authors. This conference paper is published under a CC-BY-4.0 license.

accurately predict or quantify a decreasing (Unfavourable) or increasing (Favourable) CHWdT of the cooling coil in PL, see **Fig. 1**. Therefore, it is not known how the selection of a cooling coil can be improved in order to achieve an increased CHWdT in PL to meet the desired dT condition.

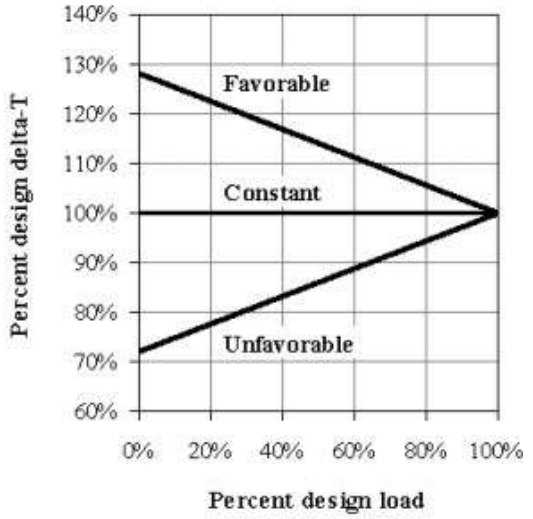

Fig. 1 - Favourable, Constant and Unfavourable CHWdT based on actual data [8]

The main question addressed in this paper is: How will the CHWdT develop – decreasing, constant or increasing – during PL operation?

There has been research done on improving the CHWdT of cooling coils in PL. A summary of this literature is given in **Tab. *1***.

Considering the above-mentioned aspects, the objective of this work is to contribute to the knowledge of the waterside performance of the cooling coil in PL. This enables the evaluation of the PL behaviour of cooling coils during the design and analysis of CHW systems and allows proper measures to be taken, if necessary. As a result, the performance of the whole CHW-plant can be improved. The result is a mathematical formulation to predict an increasing, decreasing or constant CHWdT development in PL. The results are presented in a normalised form based on the nominal conditions.

Tab. 1 - Investigations of part load behaviour of a cooling coil

Author	Investigation	Comment
Yamaguchi et al. [9]	Investigated the PL performance of a cooling coil of six types of engineering models.	The use of the model depends on fields of investigation because waterside results can vary. PL behaviour is not mentioned.
Lu et al. [10]	Presented a performance graph of a cooling coil based on the selection data of the supplier.	Waterside temperatures are not mentioned.
Morisot et al. [11]	A simplified engineering model is discussed to determine the results of a cooling coil in non-design conditions.	Waterside PL behaviour is not studied.
Fiorino [12]	Gave 25 "best practices" to increase the CHWdT in PL.	It recommends selecting an oversized cooling coil. However, it provides no additional knowledge on the CHWdT in PL.
Sekhar & Tan [13]	Studied the dehumidification performance of an oversized (200%) cooling coil in a humid climate.	The waterside results are given but not evaluated.
Zhang et al. [14]	Studied the CHWdT characteristics of chilled water-cooling coils for different geometric configurations and various waterside and airside conditions by means of computer simulation.	It shows that the CHWdT could be higher, equal or lower in PL. A prediction of the CHWdT in PL was not given.

2. Research method

This paper provides a mathematical, normalized model, calculating the CHWdT of a cooling coil as a function of the PL ratio of a cooling coil. This model was obtained by derivation, using three equations describing the heat transfers in a cooling coil. These equations are the waterside capacity, the airside capacity, and the heat transfer capacity using the ε-NTU method [15]. In the derivation, the LAT and the entering chilled water temperature were kept constant. The condition of the cooling coil is

considered dry with constant heat transfer at the airside and the waterside. The normalized form was obtained by using characteristics of the design or nominal condition as used by the authors of [8]. To verify the mathematical model, it is used to create the heat exchanger characteristic, and this is compared with the results from reference [16].

3. Results

The results are presented in two sections. The first section presents the result of the derivation of the CHWdT in PL of a cooling coil. The second section provides the heat exchanger characteristic with verification.

3.1. Derivation of a waterside temperature difference in part load for a constant water flow and a constant air flow

The matching hydraulics for the cooling coil is shown in **Fig. 2**. The heat transfer is kept constant on the waterside by means of a circulation pump (CP) and the capacity is controlled by the two-way control valve (CV). The temperatures entering and leaving the cooling coil are the secondary temperatures, denoted *sec*; the temperatures connected to the main distribution net are called the primary temperatures, denoted *prim*. The nominal waterside temperature difference on the primary side and the secondary side are the same.

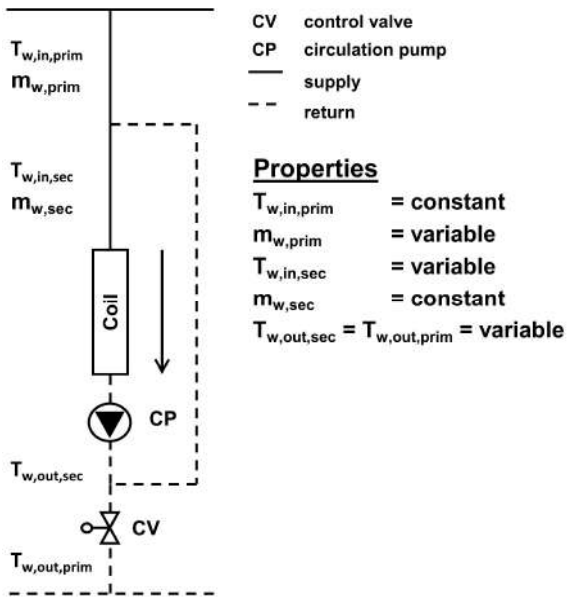

Fig. 2 - Hydraulic configuration of a cooling coil, mixing circuit (module 5) [17]

For any cooling coil, the capacity $\dot{Q}$ [W] can be written for the airside, for the waterside and in terms of heat transfer. The latter is defined by the ε-NTU method [18]. The lumped element model of the cooling coil and the energy balance are given in **Fig. 3**.

First, the airside heat transfer (capacity) equation is written as:

$$\dot{Q} = \dot{m}_a . c_a . \left(T_{a,in} - T_{a,out}\right) \tag{1}$$

Here, $\dot{m}_a$ [kg/s] is the mass flow of the air, c_a [J/kg.K] is the heat capacity of the air, $T_{a,in}$ [°C] the air entering temperature and $T_{a,out}$ [°C] the LAT.

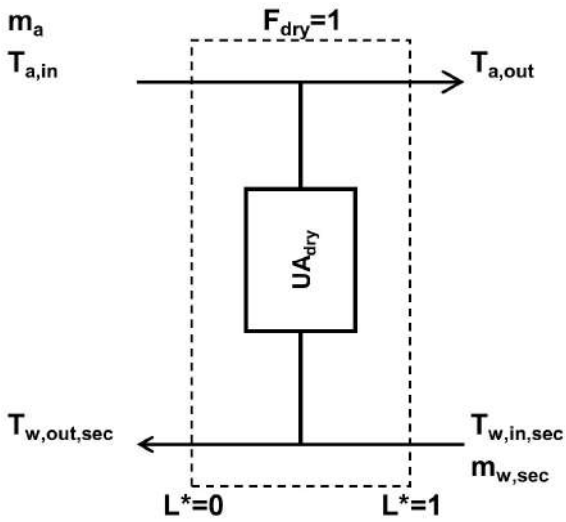

Fig. 3 - Model and energy balance of a dry cooling coil in counter flow

Second, for the waterside:

$$\Delta T_{w,sec} = T_{w,out,sec} - T_{w,in,sec} = \frac{\dot{Q}}{\dot{m}_{w,sec} . c_w} \tag{2}$$

Here, $\Delta T_{w,sec}$ [K] is the secondary CHWdT, $T_{w,out,sec}$ [°C] the secondary CHWR, $T_{w,in,sec}$ [°C] the secondary CHWS, $\dot{m}_{w,sec}$ [kg/s] the secondary water flow and c_w [J/kg.K] the heat capacity of water. Third, from the ε-NTU method we obtain:

$$T_{w,in,sec} = T_{a,in} - \frac{\dot{Q}}{\varepsilon . C_{min}} \tag{3}$$

Here, ε [-] is the effectiveness of the heat exchanger and C_{min} [J/kg] is the minimum capacity flow. $T_{w,out,sec}$ is $T_{w,in,sec}$ (3) increased with $\Delta T_{w,sec}$ (2), where the denominator of the latter is rewritten as the secondary waterside capacity flow $C_{w,sec}$ [J/kg]. Since $T_{w,out,sec}$ [°C] is equal to $T_{w,out,prim}$ [°C], it is written as $T_{w,out}$:

$$T_{w,out} = T_{a,in} - \frac{\dot{Q}}{\varepsilon . C_{min}} + \frac{\dot{Q}}{C_{w,sec}} \tag{4}$$

In order to calculate $\Delta T_{w,prim}$, $T_{w,in,prim,nom}$ [°C] is subtracted on the left and right-hand side of the equation and both sides are divided by the primary ΔT_w of the nominal condition [8]:

$$\frac{T_{w,out} - T_{w,in,prim,nom}}{T_{w,out,nom} - T_{w,in,prim,nom}} = \tag{5}$$

$$\frac{T_{a,in} - T_{w,in,prim,nom} + \dot{Q}\left(\frac{1}{C_{w,sec}} - \frac{1}{\varepsilon.C_{min}}\right)}{T_{w,out,nom} - T_{w,in,prim,nom}}$$

Here, $T_{w,out,nom}$ [°C] is the CHWR in nominal condition. The dimensionless waterside temperature difference T^*_w [-] is defined as equation (6):

$$T_w^* \equiv \frac{T_{w,out} - T_{w,in,prim,nom}}{T_{w,out,nom} - T_{w,in,prim,nom}} \quad (6)$$

$$T_w^* = \frac{T_{a,in} - T_{w,in,prim,nom} + \dot{Q}^*\left(\frac{\dot{Q}_{nom}}{C_{w,sec}} - \frac{\dot{Q}_{nom}}{\varepsilon.C_{min}}\right)}{T_{w,out,nom} - T_{w,in,prim,nom}} \quad (8)$$

The dimensionless capacity $\dot{Q}^*$ [-] is defined as:

$$\dot{Q}^* \equiv \frac{\dot{Q}}{\dot{Q}_{nom}} \quad (7)$$

Here, $\dot{Q}_{nom}$ [W] is the capacity in nominal condition. Now, the left-hand side of (5) is replaced by (6) and $\dot{Q}$ is replaced with (7), and (5) is written as (8):

Both expressions between brackets in the numerator can be rewritten in a CHWdT for the nominal conditions. The left expression between brackets is based on ΔT_w (2) and the right expression between brackets is based on the definition of the ε-NTU method (3):

$$T_w^* = \frac{T_{a,in} - T_{w,in,prim,nom} + \dot{Q}^*\left(\left[T_{w,out,nom} - T_{w,in,nom}\right] - \left[T_{a,in,nom} - T_{w,in,nom}\right]\right)}{T_{w,out,nom} - T_{w,in,prim,nom}} \quad (9)$$

After eliminating $T_{w,in,nom}$, this results in:

$$T_w^* = \frac{T_{a,in} - T_{w,in,prim,nom} - \dot{Q}^*\left(T_{a,in,nom} - T_{w,out,nom}\right)}{T_{w,out,nom} - T_{w,in,prim,nom}} \quad (10)$$

The Entering Air Temperature (EAT) $T_{a,in}$ can be calculated, similar to the nominal condition $T_{a,out,nom}$ [°C] from equation (1), from a known capacity $\dot{Q}$ and with a constant LAT:

$$T_{a,in} = \frac{\dot{Q}}{\dot{m}_a.c_a.} + T_{a,out,nom} \quad (11)$$

The capacity $\dot{Q}$ is rewritten with (7) in the dimensionless form:

$$T_{a,in} = \dot{Q}^*\left(\frac{\dot{Q}_{nom}}{\dot{m}_a.c_a.}\right) + T_{a,out,nom} \quad (12)$$

The term between brackets is the airside temperature difference for the nominal condition, resulting in:

$$T_{a,in} = Q^*\left(T_{a,in,nom} - T_{a,out,nom}\right) + T_{a,out,nom} \quad (13)$$

This expression for $T_{a,in}$ (13) is substituted in (10):

$$T_w^* = \frac{\dot{Q}^*\left(T_{a,in,nom} - T_{a,out,nom}\right) + T_{a,out,nom} - T_{w,in,prim,nom} - \dot{Q}^*\left(T_{a,in,nom} - T_{w,out,nom}\right)}{T_{w,out,nom} - T_{w,in,prim,nom}} \quad (14)$$

Rearranging this equation results in a waterside temperature difference T^*_w, depending only on the capacity $\dot{Q}^*$ and constants of the nominal or design condition:

$$T_w^*(\dot{Q}^*) = \left[\frac{T_{w,out,nom} - T_{a,out,nom}}{T_{w,out,nom} - T_{w,in,prim,nom}}\right] Q^* + \frac{T_{a,out,nom} - T_{w,in,prim,nom}}{T_{w,out,nom} - T_{w,in,prim,nom}} \quad (15)$$

This equation (15) shows that T^*_w of a cooling coil in PL can be written as a linear function of $\dot{Q}^*$ and the temperatures of the nominal condition. The slope represents the favourable, unfavourable and constant T^*_w in PL of **Fig. 1**, which only depends on $T_{w,out,nom}$ and $T_{a,out,nom}$. An unfavourable T^*_w in PL cannot always be avoided. As a result, for two known causes of the low ΔT syndrome (100% outdoor air

handling unit & economizer), it is found that a commonly used definition from the literature is not suitable. Typical, with an economiser in the air handling unit, at a decreasing EAT the recirculation damper closes while the outdoor damper opens to maximise the free cooling capability. Eventually, only outdoor air is processed and the air handling unit is operating as a 100% outdoor air unit. If the EAT drops below the CHWR of the nominal condition, the CHWdT will decrease. The numbers of

Tab. 2 are used to illustrate this for the increasing, constant and decreasing CHWdT, and the accompanying EAT profiles in **Fig 4**. The EAT is normalized using equation (6).

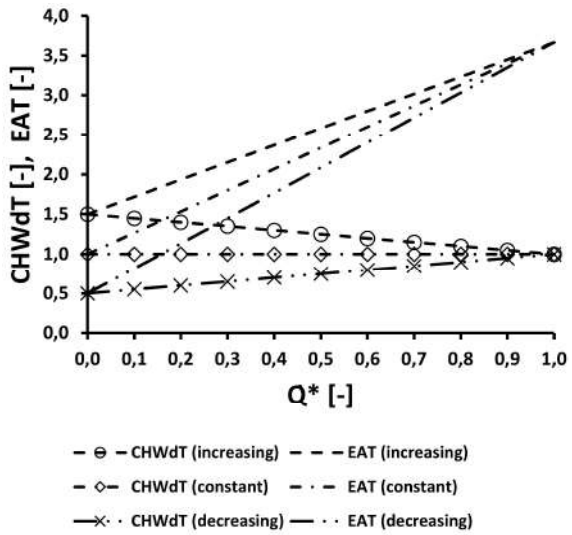

Fig 4 - Increasing, constant and decreasing CHWdT for accompanying EAT profiles

For these cases, the name low ΔT syndrome is misleading since a reduced CHWR can occur during normal conditions without the increased waterflow and therefore during fault-free operation.

3.2. Heat exchanger characteristic of a cooling coil with a constant water flow and a constant air flow

The previous result can be used to create heat exchanger characteristics (HXC), also known as the non-linearity of the cooling coil. The HXC is defined as the capacity as a function of the primary mass flow. It should be noted that the primary mass flow is not constant but variable, and is controlled by the CV (see **Fig. 2**). This HXC can be compared with the characteristics found in the literature for verification. In order to calculate the dimensionless heat characteristic, the primary mass flow $\dot{m}^*_w$ [-] is defined as:

$$\dot{m}^*_w \equiv \frac{\dot{m}_w}{\dot{m}_{w,nom}} \tag{16}$$

Here, $\dot{m}_{w,nom}$ [kg/s] is the primary mass flow at the nominal condition. As a result, $\dot{Q}^*$ can be calculated in the following way:

$$\dot{Q}^* = \dot{m}^*_w . T^*_w \tag{17}$$

With (15) substituted in (17), the full expression for the HXC yields:

$$\dot{Q}^*(\dot{m}^*_w) = \frac{\dot{m}^*_w . \left(\frac{T_{a,out,nom} - T_{w,in,prim,nom}}{T_{w,uit,nom} - T_{w,in,prim,nom}}\right)}{1 - \dot{m}^*_w . \left(\frac{T_{w,out,nom} - T_{a,out,nom}}{T_{w,uit,nom} - T_{w,in,prim,nom}}\right)} \tag{18}$$

Like the CHWdT in PL, the form of the HXC is determined by the same variables. The three different forms are shown in **Fig. 5**, **Fig. 6**, and **Fig. 7** and are based on the numbers of

Tab. 2. These numbers are used to indicate the three different presentations for an increasing, constant, and decreasing waterside temperature difference in PL.

The convex form of the figure of **Fig. 5** is often encountered in literature and is often drawn as a "rule of thumb" and is applicable for a favourable (increasing) CHWdT in PL.

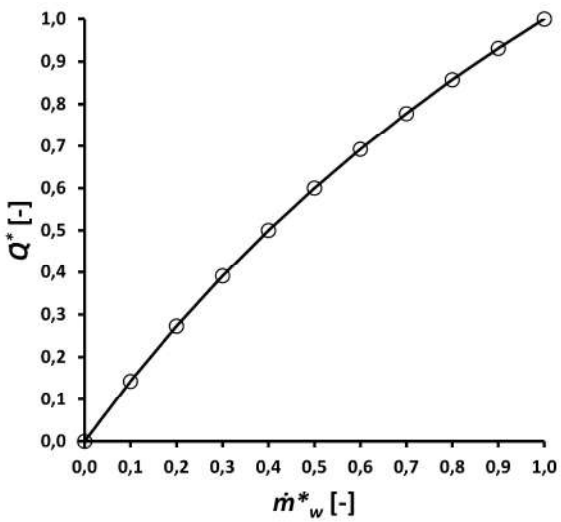

Fig. 5 - Heat exchanger characteristic for a cooling coil with an increasing CHWdT in part load

Fig. 6 shows the linear HXC for a cooling coil with a constant CHWdT in PL. **Fig. 7** shows the HXC of a cooling coil with a decreasing CHWdT in PL, resulting in a concave form. Moreover, the relationship between the T^*_w in PL and the form of the HXCs is, to the best of our knowledge, not available in the literature.

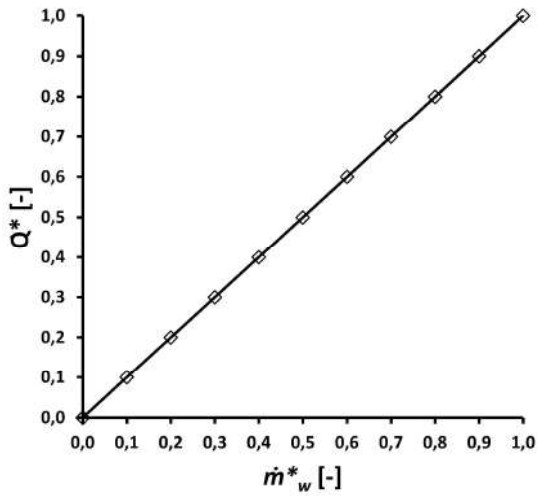

Fig. 6 - Heat exchanger characteristic for a cooling coil with a constant CHWdT in part load

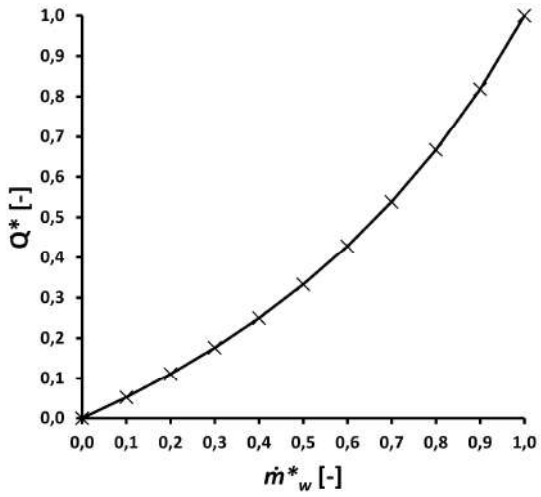

Fig. 7 - Heat exchanger characteristic for a cooling coil with a decreasing CHWdT in part load

For verification, based on the data from **Tab. 2**, all HXCs are created with the same numbers and the equation found in a handbook for a mixing circuit (**Fig. 2**) and a constant LAT [16]. As a result, the current work is successfully verified as there was no difference, with both HXCs being identical.

Tab. 2 - Nominal conditions for three different cooling coils

	Increasing CHWdT	Constant CHWdT	Decreasing CHWdT
EAT	28°C	28°C	28°C
LAT	15°C	12°C	9°C
CHWS	6°C	6°C	6°C
CHWR	12°C	12°C	12°C

The results are summarized in **Tab. 3**.

4. Discussion

By means of a better understanding of the waterside PL behaviour of a cooling coil, the design of a CHW plant can be improved and known causes of the Low ΔT syndrome can be challenged. It is shown that the CHWdT of a dry cooling coil with constant air flow and constant water flow in PL can be written as a linear function based only on the capacity and temperatures of the nominal condition. As a result, during the design phase a decreasing (Unfavourable), constant and increasing (Favourable) CHWdT can be distinguished, and appropriate measures can be considered and possibly implied.

Tab. 3 - Summary of results for CHWdT and HXC in part load

Slope [-]	Key	T^*_w [-]	HXC $Q^*(m_w^*)$
negative slope	$T_{w,out,nom} < T_{a,out,nom}$	Favourable	Convex
Slope = 0	$T_{w,out,nom} = T_{a,out,nom}$	Constant	Linear
positive slope	$T_{w,out,nom} > T_{a,out,nom}$	Unfavourable	Concave

By placing the cooling coil behind the fan (blow-through), the supply fan will add heat before the cooling coil and this must be accounted for during the selection of the cooling coil. The LAT remains the same in contrast with the draw-through configuration, where the fan is placed behind the cooling coil. As a result, to compensate for the fan heat and loss of net cooling capacity, the LAT of the design must be reduced in order to maintain the required cooling capacity of the zone. The effect of 1K fan heat on the favourable and unfavourable configuration of

Tab. 2 is quantified with equation (15) for the draw-through and blow-through configurations and shown in **Tab. 4**.

For both cases, the blow-through configuration leads to an increased CHWdT compared to the draw-through configuration; the slope is smaller. Also, in both cases the highest CHWdT is found for the blow-through configuration at the minimum load condition if $\dot{Q}^*$ approaches zero; the constant value is the highest. The results show that placing the cooling coil behind (blow through) instead of in front of (draw through) the fan will result in an increased CHWdT in PL. Although a comparison between the draw-through and blow-through configuration has been made for cooling and dehumidification performances, the effect on the CHWdT was not considered [19].

Tab. 4 - Change of the slope due to 1K fan heat for the favourable and unfavourable chilled water temperature difference for a draw through and a blow through configuration

	Favourable		Unfavourable	
	Draw-through	Blow-through	Draw-through	Blow-through
slope	-0.33	-0.5	+0.67	+0.5
constant	+1.33	+1.5	+0.33	+0.5

According to the ASHRAE handbook, a conventional building with a traditional all-air system is typically designed at a supply air temperature of 12.8°C [20]. The ASHRAE standard 90.1-2019 [21] states that the design CHWR should not be lower than 13.9°C with a minimum CHWdT of 8.3K (exceptions excluded). With $T_{w,out,nom} > T_{a,out,nom}$, the key of **Tab. 3** shows an unfavourable CHWdT resulting in a slope of +0.13 with equation (15). Circumstances where this can happen include, for example, 100% outdoor air handling units or air handling units equipped with economisers. Here, the EAT can drop below the design CHWR. As a result, the CHWR can never be higher than the EAT. In addition, the increase of the CHWdT during design can increase the risk of the emergence of the low ΔT syndrome. However, this can happen without the "excessive flow" mentioned in the definition of the Low ΔT syndrome. Also, for ATES systems with a high CHWS (~10°C) and large CHWdT up to 10K, this should be considered during PL.

The results can be used to give additional information on existing studies. For example, actual data are simplified to create the favourable or unfavourable CHWdT of **Fig. 1** [8] and these could be reproduced with equation (15). For the same cooling capacity, an unfavourable CHWdT will have a higher chilled water flow compared to the favourable CHWdT, however, in [8] it seems to lack the "excessive flow" from the definition of the Low ΔT syndrome.

5. Conclusions

The knowledge of waterside performance needs to be further extended to mitigate the negative effects of a reduced CHWdT at PL, and to challenge other causes of the Low ΔT syndrome. This work provides a verified mathematical model to qualify and quantify the waterside PL of a cooling coil. With the result of this work, a decreasing waterside temperature difference could be estimated, giving engineers the possibility to take proper measures. Based on this work, the connection between the PL behaviour and the heat exchanger characteristic has been made. The current results are limited to a constant waterside and airside heat transfer, a dry cooling coil with a constant leaving air temperature.

Data Statement

Data sharing not applicable to this article as no datasets were generated or analysed during the current study.

6. Acknowledgement

The research work is funded by the TKI Urban Energy project "Continuous commissioning of low-dT"; and the Eindhoven Engine project "CM-HVAC-FDD".

7. References

[1] Hartman TB. Design issues of variable chilled-water flow through chillers. ASHRAE Trans., vol. 102, San Antonio: 1996, p. 679–83.

[2] Taylor ST. Degrading chilled water plant delta-T: Causes and mitigation. ASHRAE Trans., vol. 108, Atlantic City: 2002, p. 641–53.

[3] Kirsner W. A check valve in the chiller bypass line: Rectifying the primary-secondary paradigm for chilled water plant design To deal with Low ΔT central plant syndrome. HPAC Heating, Pip Air Cond Eng 1998;70:128–31.

[4] Kirsner W. Troubleshooting chilled water distribution problems at the NASA Johnson space center. HPAC Heating, Pip Air Cond Eng 1995;67:7.

[5] Bullet J de. Variable flow chiller plant design. Tech. Sess. #6, 2007.

[6] Kirsner W. The demise of the primary-secondary pumping paradigm for chilled water plant design. HPAC Heating, Pip Air Cond Eng 1996;68:73–8.

[7] Mannion GF. High temperature rise piping design for variable volume systems Key to chiller energy management. ASHRAE Trans., vol. 94, Ottowa: 1988, p. 1427–43.

[8] Bahnfleth WP, Peyer EB. Variable primary flow chilled water systems: potential benefits and application issues. Pen: 2004.

[9] Yamaguchi H, Yoshida H, Niwa H, Watanabe T, Miyata M, Oda H, et al. Experimental Study of a Cooling Coil and the Validation of its Simulation Model for the Purpose of Commissioning. Trans Soc Heating,Air-Conditioning Sanit Eng Japan 2009;34:61–70. https://doi.org/10.18948/shase.34.143_61.

[10] Lu L, Cai W, Xie L, Li S, Soh YC. HVAC system optimization - In-building section. Energy Build 2005;37:11–22. https://doi.org/10.1016/j.enbuild.2003.12.007.

[11] Morisot O, Marchio D, Stabat P. Simplified model for the operation of chilled water cooling coils under nonnominal conditions. HVAC R Res 2002;8:135–58. https://doi.org/10.1080/10789669.2002.10391433.

[12] Fiorino DP. Achieving high chilled-water Delta Ts. ASHRAE J 1999;41:24–30.

[13] Sekhar SC, Tan LT. Optimization of cooling coil performance during operation stages for improved humidity control. Energy Build 2009;41:229–33. https://doi.org/10.1016/j.enbuild.2008.09.005.

[14] Zhang Z, Li H, Liu J. Simulations of chilled water cooling coil delta-T characteristics. ASHRAE Trans 2012;118:349–56.

[15] Shah RK, Sekulic DP. Fundamentals of heat exchanger design. 2003. https://doi.org/10.1002/9780470172605.ch10.

[16] Recknagel H, Sprenger E, E. S. Taschenbuch für Heizung + Klimatechnik. 74th ed. Munchen: Oldenburg Industrieverlag; 2009.

[17] ISSO. ISSO-publicatie 47: Ontwerp van hydraulische schakelingen voor koelen. Rotterdam: 2005.

[18] Kays WM, London AL. Compact heat exchangers. 2nd ed. McGraw-Hill Book company; 1964.

[19] Sarkar M. Theoretical comparison of cooling loads of an air handling unit in blow-through and draw-through configurations. Energy Build 2013;64:239–48. https://doi.org/10.1016/j.enbuild.2013.04.025.

[20] ASHRAE. 2020 ASHRAE Handbook - Heating, Ventilating, and Air-Conditioning: systems and equipment. 2020.

[21] ASHRAE. ASHRAE standard 90.1 Energy Standard for Buildings Except low-rise residential buildings. 2019.

Energy demand with natural ventilation in unheated bedrooms, combined with balanced ventilation

Vegard Heide [a], Laurent Georges [a]

[a] Department of Energy and Process Engineering, Norwegian University of Science and Technology, Trondheim, Norway, vegard.heide@ntnu.no.

Abstract. In Norway, many detached houses are renovated without mechanical ventilation being installed. Many occupants prefer or accept low temperatures in bedrooms and ventilate with regular window openings all year round. In this context, a hybrid ventilation strategy combining ordinary balanced ventilation in warm zones, and natural ventilation in cooler bedrooms, could be appropriate Such a hybrid ventilation strategy might be most relevant for renovation projects where introducing ventilation ducts can be complicated and costly. The aim of this work is to investigate the energy performance using this hybrid strategy when implemented in a detached Norwegian wooden house. Detailed dynamic simulations of a case house are performed using the simulation software IDA-ICE for 2 insulation levels, and 6 different occupant behaviours. In order to reduce the uncertainty of airflow rates through open windows, simulations are done in 3 different simulation modes. Three natural ventilation strategies for bedrooms are compared to the reference with standard balanced mechanical ventilation with heat recovery. Results show that the energy performance of the investigated hybrid ventilation strategies is strongly influenced by occupant behaviour. Given an energy-conscious occupant behaviour (e.g., regarding thermal zoning), it seems possible to achieve a low energy use with natural ventilation in bedrooms. Low temperatures are frequently applied in Norwegian bedrooms so the proposed hybrid ventilation strategies could be applied to a significant share of the renovation market. However, temperature in bedrooms is strongly related to habits and culture. Therefore, the potential of hybrid ventilation can be different for other countries. With the proposed hybrid ventilation strategy, it is possible to create a night setback in the unoccupied zones with mechanical ventilation. This is a technically cheap and simple way to decrease energy use and could be investigated in further research.

Keywords. Hybrid ventilation, natural ventilation, renovation, heating demand.
DOI: https://doi.org/10.34641/clima.2022.32

1. Introduction

More than 30% of Norwegian residential buildings are detached houses built before 1990. This building stock is reaching a stage where major renovations are needed. A recent study (1) found that 60% of the Norwegian detached households made no changes to the ventilation system when performing a renovation, while only 9% installed balanced mechanical ventilation. Renovation usually includes a substantial improvement in air tightness of the building envelope. This reduces the air change due to infiltrations, demanding systematic ventilation measures to provide sufficient indoor air quality (IAQ). The challenge is to develop ventilation concepts that provide good indoor environment and energy performance, while remaining simple and affordable enough to actually be implemented.

Standard one-zone ventilation strategies with balanced cascade ventilation tend to homogenize temperatures in highly insulated buildings. In other words, balanced ventilation reduces the possibility for temperature zoning. In Norway, many users would like colder bedrooms, and a significant part of the occupants open bedroom windows during several hours every night during winter (2-5). Dynamic simulations have shown that this window opening behaviour combined with ordinary balanced cascade ventilation strongly increases the space-heating needs. Simulations also show that control only is unable to create temperature zoning in an energy-efficient way (6, 7). This is an important research gap as it shows that existing systems still do not fully meet the occupants' satisfaction.

A large share of existing detached houses in Norway

have moderate thermal insulation and use natural ventilation. Many occupants ventilate the bedrooms by opening the window when going to bed, and closing it in the morning (8-10). Many people use the bedroom only for sleeping, and keep the bedroom doors closed both day and night. Many do not use local heating in the bedrooms, or rarely. This user pattern is most common for the main bedroom (9). Partition walls in wooden buildings are usually insulated using 75 to 100 mm for acoustic reasons. This limits the heat transfer and makes bedrooms distinct thermal zones. The motivation for accepting low temperatures in bedrooms seem to be habit, reducing energy use as well as good IAQ (10). Keeping thermal comfort with low indoor temperatures is made possible by using thick duvets in beds.

In this context, a ventilation strategy combining ordinary balanced ventilation in warm zones, and natural ventilation in bedrooms, could be appropriate. A key aspect of this strategy is to utilise extensive thermal zoning, meaning lower time-averaged temperatures during the heating season in the natural ventilated rooms. Such a hybrid ventilation strategy might especially be relevant for renovation projects where introducing ventilation ducts can be complex and costly.

The aim of this work is to investigate the energy performance using this new hybrid ventilation strategy, when implemented in a typical detached Norwegian wooden house. A prerequisite for the hybrid solution to be acceptable is that the outdoor air quality (e.g., pollution) and sound levels are low at the building location. Research questions are:

- What is the energy demand for the proposed hybrid strategy compared to ordinary balanced mechanical ventilation with heat recovery?
- How do different occupant behaviour strategies affect the heating demand?
- How does the insulation level of the building envelope affect the energy performance of the hybrid strategy, relative to balanced ventilation?

As far as the authors know, the only work addressing the same questions was performed by Heide in 2013 (11). Similar simulations were done using a more generic building model and a less detailed building simulation tool SIMIEN. Results and general conclusions are similar to this study.

Temperature zoning with different rooms at several intermediate temperatures compared to the ambient are also called temperature cascade. This principle is analysed for a building with natural ventilation, by Suerich-Gulick et al (12) (ref). Results show that the use of temperature cascade can reduce energy demand by more than 50% in moderately hot or cold exterior conditions.

Some studies have analysed heating demand with natural ventilations, but then applied in all rooms. Simonson investigated energy use and heating demand in a detached low-energy house with natural ventilation and no thermal zoning in Finland (13). Calculations based on measurements showed energy demand 10 kWh/m^{2}a (10%) higher than with balanced mechanical ventilation.

An important prerequisite for the proposed hybrid ventilation strategy is sufficient air exchange rate (ACH) to ensure acceptable indoor air quality, and window opening behaviour is crucial for this. Studies from several countries find window opening more common in bedrooms than other rooms, and that habit is an important factor (14-16). Bekø et al. measured ACH in Danish detached houses with natural ventilation. They found higher ACH in summer than winter, and higher ACH when rooms were occupied, showing strong influence from the window opening behaviour (17).

One of the bedrooms monitored in (9) (room H2B2, Fig. 8) had natural ventilation, while the rest of the house had balanced ventilation with heat recovery. The measurements showed acceptable CO2 concentration and regular window opening at night, proving that the hybrid ventilation concept is worth to be investigated.

2. Method

2.1 Building model

Fig. 1 - Case house "Nanne" from Mesterhus (18).

A building test case has been defined based on the work of Selvnes and Georges et al. (7, 19). It is a typical two-storey detached house with three bedrooms located on the second floor, and a total floor area of 173.5 m^2, see Fig. 1. The building is located in Oslo. This building is representative for a great number of well-insulated wooden detached houses, not only in Norway. Thermal dynamic simulation of the case house is performed using the building performance simulation (BPS) software IDA ICE. The building as a lightweight construction in wood with a thermal inertia of 14 MJ/K. Internal gains are defined according to SN/TS 3031 (20) and space-heating is simulated using ideal heaters, as the main focus of our study is on the space-heating needs (not the energy use). The main performance indicator is the net energy demand, including appliances. This indicator enables to include the energy use for ventilation fans in the assessment.

Tab. 1 – Building thermal properties for the two building performance levels.

Insulation level	Uext.wall [W/m²K]	Uext.floor [W/m²K]	Uroof [W/m²K]	Uwindows/door [W/m²K]	n50 [h⁻¹]	Thermal bridge [W/m²K]
PASSIV (NS3700)	0.14	0.13	0.12	0.72	0.6	0.03
TEK07	0.18	0.15	0.13	1.6	4.0	0.05

Two performance levels of the building envelope is investigated: one in accordance with the Norwegian Passive House Standard (21), and one in accordance with the Norwegian building regulations of 2007 (TEK07) (22). Details are shown in Table 1. The building design is based on two occupants in the main bedroom and one occupant in the other bedrooms during the night.

The rated heat recovery efficiency used in the simulations is 70 %, as several field studies show a lower heat recovery efficiency than nominal rated values (23-26). This difference can be caused by several factors: leakages in the ducting system or the heat exchanger, imbalance of airflows, sensible heat not recovered, clogged filters, etc.

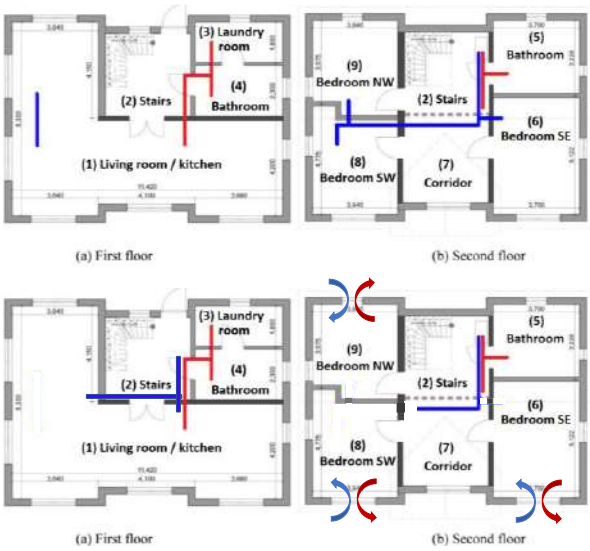

Fig. 2 – Standard balanced cascade ventilation (top), hybrid ventilation with natural ventilation in bedrooms only (lower figure). Supply air duct in blue, extract ducts in red.

2.2 Ventilation strategies

Four ventilation strategies are defined:

1. Balanced cascade ventilation covering all rooms (BAL) see Fig. 2 and 3,
2. Natural ventilation in main bedroom and balanced ventilation covering all the other rooms (MA), see Fig. 3.
3. Natural ventilation in all bedrooms, and balanced ventilation covering the rest (ALL), see Fig. 2 and 3.
4. Natural ventilation in all bedrooms, and balanced ventilation with night set-back for the other rooms (VAV), Fig. 3.

Strategy 1 (BAL) is the common in new detached houses, and serves as a reference. Measurements and surveys (10) show that main bedrooms are much less used (and heated) in daytime than the rooms of children and teenagers. Natural ventilation is less appropriate in bedrooms with occupancy during daytime. IAQ tends to be lower, as people tends to open the window when going to bed, but not before. Cold draft from the window ventilation is more perceptible when occupants are not under a warm duvet. Therefore, natural ventilation only applied in the main bedroom (MA), is explored in addition to strategy 2 with natural ventilation in all bedrooms (ALL).

The other rooms that are not bedrooms, are assumed to have low occupancy during night-time. Consequently, when natural ventilation is used in all bedrooms, the other rooms served by the balanced ventilation system have low occupancy at night. This should allow the introduction of a night set-back with lower airflow rates in these rooms, for example, by reducing the speed of the fans. This is investigated as strategy 4 (VAV). This opportunity to implement night setback is not present in the reference strategy (BAL), as the one-zone cascade ventilation couples all rooms, both the occupied bedrooms and the unoccupied rooms. The system does not allow for a change of the ventilation airflow rate by room, in a technically simple way.

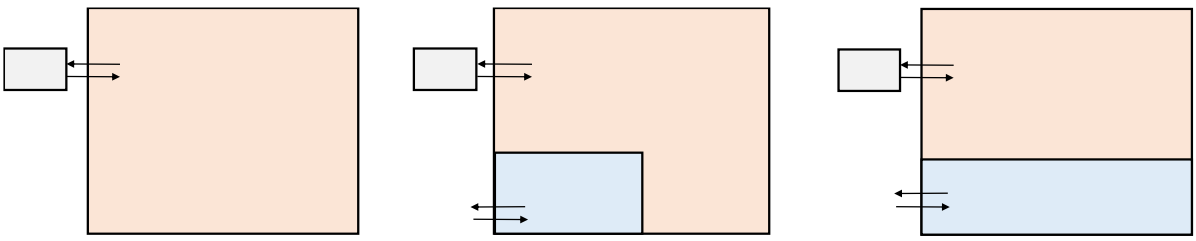

Fig. 3 - The BAL, MAL and ALL ventilation strategies: scenario VAV is equivalent to ALL but with night setback.

2.3 Modelling of natural ventilation

The simplifications for the modelling of airflow rates in BPS should be taken into account. This strongly affects airflow rates through windows and other openings, like infiltrations. Zhai et al. reviewed computational simulation models for natural ventilation (ref). They found that the current airflow network models typically used in BPS tools (like IDA-ICE) can be used to model natural ventilation but it shows low accuracy for single-sided wind-driven ventilation (27). Uncertainty on the computed airflow rates through open windows is to be expected. One way to reduce this uncertainty is to compare different simulation scenarios based on different modelling strategies. Three simulation modes were defined for this purpose:

A. Fixed ventilation airflow rates. ("AHU").
B. Automatic CO_2-controlled window opening (AutW).
C. Fixed window opening size during night-time (FixW).

In simulation mode A, air change rates are fixed and modelled using a decentralized mechanical ventilation (i.e., an additional air handling unit in IDA ICE) with the heat recovery efficiency set to zero. In reality, the airflow will be affected by the wind, the time-varying stack effect as well as the user behaviour. Therefore, real airflows will not be equal to the idealized case A with controlled airflow rates. To evaluate this impact on results, a 50% increase of the overall airflow rate is also briefly analysed (see section 2.6).

In simulation mode B, automatic window opening with a PI-control tracking the CO_2 concentration in the bedrooms was simulated. The setpoint maximum CO_2 concentration in bedrooms is 920 ppm. This is also an idealized model as windows are almost always controlled manually.

In simulation mode C, a constant window opening area was set during night-time. The opening area has been calibrated to reach acceptable maximum CO_2 concentration in the bedrooms. It resulted in a window openings of 90 cm x 9.5 cm for the main bedroom with a maximum CO_2 concentration of 1100 ppm, and an opening of 90 cm x 5 cm in single bedrooms with a maximum CO_2 concentration of 900 ppm. To ensure a minimum ventilation outside occupancy periods (i.e., windows and doors closed), there are also ventilation valves with a constant opening size of 0.005 m^2 in each bedroom, in mode C. The gaps in lower part of the doors of bedrooms with natural ventilation are reduced from 0.01 m^2 to 0.0001 m^2. Windows are generally open during night-time and closed during the day. A time schedule is thus defined for window openings where the night was defined from 23:00 to 07:00.

2.4 Mechanical ventilation airflow rates

Ventilation airflow rates using mechanical ventilation are in compliance with the Norwegian Standard SN/TS 3031 (20), adjusted to follow the requirements in the Norwegian building regulations. These airflows are also used in the natural ventilation using simulation mode A. In bedrooms, it corresponds to ventilation airflow rates of 26 m^3/h per bed. During daytime, these bedrooms with natural ventilation were simulated with the general 1.2 m^3/h pr. m^2 floor area, as they were not assumed to be continuously occupied. In ventilation scenario 4 (VAV), the mechanical ventilation is simulated with a reduction of the ventilation airflow rate during the night of 58% compared to the nominal daytime rate (i.e., 1.2 m^3/m^2*h in daytime, 0.7 m^3/m^2*h during night-time).

Tab. 2 – Definition of the occupant behaviour scenarios and resulting control strategies.

	Warm	Basic	Econ+	Economic	Frugal	Frugal Corr
Other rooms heater setpoint temp.	24	21	21	21	21	21
Bedroom heater setpoint temperature	21	21	10	10	5	No heater
Supply air setpoint temperature	18	16	16	16	16	16
Heat recovery setpoint temperature	20	18	18	18	18	18
Heater in corridor	Yes	Yes	Yes	Yes	Yes	No
Doors open every morning and evening	Yes	Yes	Yes	No	No	No

2.5 Occupant behaviour and control

It is known that the occupant behaviour has a strong influence on the indoor environment and energy use. Occupants define the set-point temperatures (e.g., for the local heaters) and the window and door openings in bedrooms. Consequently, six occupant behaviours are defined in Table 2. Bedroom doors are generally closed, but in the Warm, Basic and Econ+ scenarios they are open half an hour every morning and night. A constant set-point temperature during day and night is applied to the bedroom heater. The set-point supply air temperature defined in Table 2 is only for the mechanical ventilation.

2.6 Sensitivity analysis

In addition, a sensitivity analysis is done to evaluate the influence of the parameter uncertainty. Firstly, the rated efficiency of the ventilation heat recovery is increased from 70% to 80%. Secondly, the influence of bedrooms doors that are always open during daytime is evaluated. Finally, a 50% increase of the airflow rates for the natural ventilation in simulation mode A is analysed.

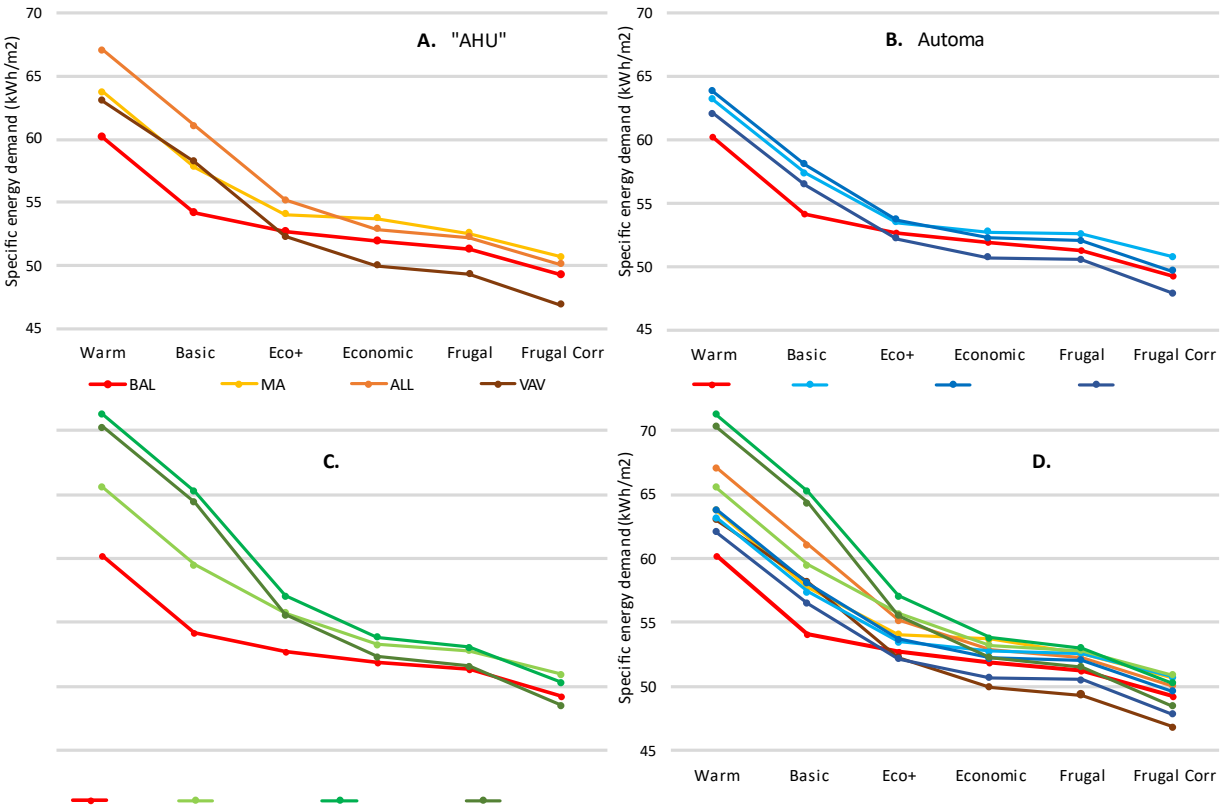

Fig. 4 - Specific energy demand for the Passive building: the figures are grouped by different simulation modes, but all modes are merged in the figure in the bottom right.

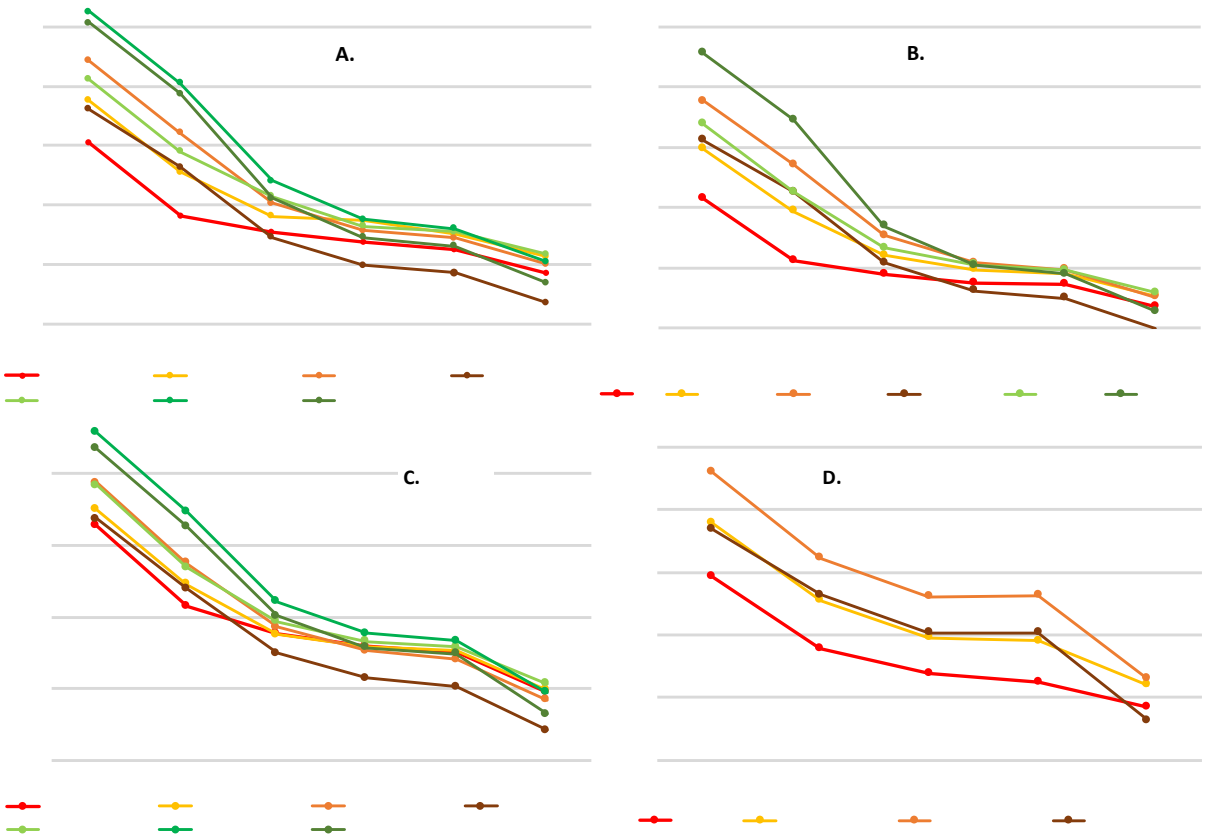

Fig. 5 – Specific energy demand for the total building for several occupant behaviours and simulation modes: different building envelope levels on the left figures, 70% and 80% heat recovery efficiency compared on the top figures while the effect of keeping the bedroom doors open all day is shown by comparing (d) and (a).

3. Results and discussion

Results are presented in Fig. 4 and 5.

The general trend shows a progressive decline in space-heating needs when moving towards occupant behaviours with lower indoor temperatures (meaning more economic behaviour). As expected, strategies using natural ventilation show large space-heating needs when high temperatures are preferred in bedrooms. For the occupant behaviour strategies Warm and Basic, ordinary balanced ventilation clearly shows lower space-heating needs, while the differences with the occupant behaviour Economic and Frugal are much smaller. In other words, the energy performance of the mechanical ventilation (BAL) is more robust regarding the user behaviour.

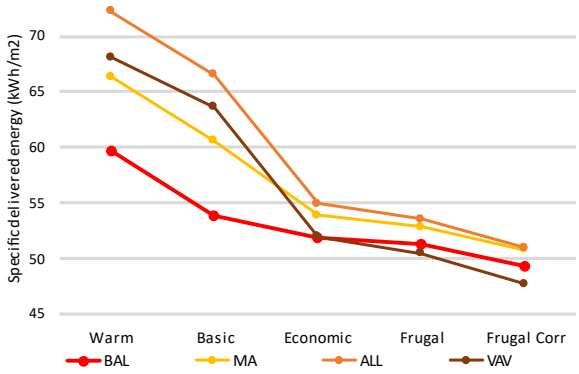

Fig. 6 – Specific energy demand with 50% increased natural ventilation air flow. "AHU" simulating mode, in Passive building.

3.1 Influence of simulation modes

The computed energy needs for the different natural ventilation simulation modes shows similar values. The exception is mode C, with fixed window opening. This mode shows approximately 5% higher energy demand than the other two modes, for occupant behaviour Warm and Basic., When simulating with a fixed night-time opening area all year, it is indeed expected that the airflow rates through the window to be higher than needed (for acceptable IAQ). This is confirmed by a detailed analysis of the output data from the simulations. Fig. 6 shows the influence of an increase of 50% of the airflow rates in simulation mode A and can be compared to Fig. 4(a). Even though this increase of airflow rates is large, the space-heating needs using the natural ventilation in simulation mode A with the occupant behaviour Frugal, is comparable to the balanced ventilation with the user behaviour Basic.

3.2 Bedroom doors

The opening of the bedroom doors influences the energy performance. This is reflected in some of the occupant behaviour modes. In the Warm, Basic and Econ+ scenarios, bedroom doors are opened half an hour every morning and night while the other doors remain closed. The only difference between Econ+ and Economic is the door opening status. The difference in energy demand between these two modes shows that these two short opening events have a significant impact. The effect of having the bedroom doors open all day is shown by comparing Fig 5(a) and 5(d) and in Fig. 7. We can see the impact is substantial: for the mode Frugal the annual specific energy demand increases with 6-7 kWh/m^2.

In Norway, many bedrooms are only used for sleeping (and storing clothes), especially rooms for grown-ups, as reported by Heide et al (9). If the hybrid ventilation strategy was implemented in real houses, one could imagine adapting the building layout to match the ventilation system. Using small bedrooms purely used for sleeping, and other rooms designated for playing and office activities would seem advantageous.

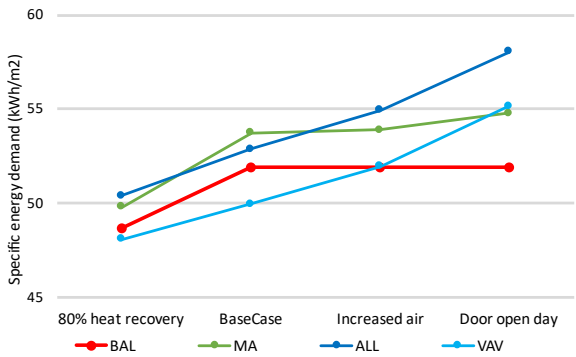

Fig. 7 – Sensitivity analysis on the specific energy demand with the Economic behaviour strategy, in the Passive building.

3.3 Thermal comfort in bedrooms

What are the lowest temperatures in bedrooms with natural ventilation during cold nights? In most of the occupant behaviour scenarios, the minimum temperature in the bedrooms is defined by the set-point temperature applied to the local bedroom heater. Only in the Frugal Corr scenario (with no local heater), the bedroom temperature is free-floating. The resulting minimum temperature here is -0.8°C in the main bedroom, and 3°C in the single bedrooms. This only happens during the coldest nights. When measuring bedrooms with natural ventilation in the field, Heide et al. found temperatures from -2°C to 23°C (9). In the behaviour mode Economic, bedrooms are heated to 10°C, and in Frugal, to 5°C. The annual energy consumption for one of these local heaters is only 80 kWh, and 5 kWh, respectively. This indicates that the number of cold nights is low. According to the authors, a common habit for the coldest or windiest nights, is to close the windows but keep the bedroom door open. In this way the bedrooms are connected to the ventilation of the rest of the house. This can result in less privacy, but this may be acceptable for a few days.

3.4 Sensitivity to the user behaviour

According to the simulation results, the energy performance seems strongly influenced by the

occupant behaviour. A technology that is dependent on certain skills, habits or cultural patterns is user sensitive, and may not fit all occupants. As long as the occupants prefer a cool or cold bedroom, performance of the investigated hybrid strategy may be acceptable. However, if occupants prefer warm bedrooms, the hybrid strategies do not perform as well as a standard balance mechanical ventilation. If they open windows to have acceptable IAQ, with the local heaters on, high space-heating needs is a likely result. Alternatively, if these occupants keep the windows closed at night, in order to keep higher bedroom temperatures, this will result in low air change rates and low IAQ.

3.5 Insulation level of the building envelope

When comparing the two performance levels of the building envelope, the trend shows that the reference (balanced ventilation), shows slightly better performance compared to the hybrid ventilation, with the highest insulation level, see Fig. 5(a) and 5(c). One of the advantages of the hybrid system is the extensive thermal zoning. The lower bedroom temperatures reduce the transmission losses through the external walls of bedrooms. This advantage decreases when the building envelope has better insulation.

3.6 Energy savings using the VAV strategy

The ventilation strategy VAV (with reduced mechanical ventilation airflow rates during night-time) generally shows the lowest energy demand among the natural strategies. For the most energy efficient occupant behaviours, the space-heating needs with this strategy can even be lower than the standard one-zone balanced mechanical ventilation with efficient heat recovery (BAL). This possibility for creating a night set-back is technically cheap and simple. It might be seen as an opportunity provided by the proposed hybrid ventilation strategy. This deserves to be investigated in more details in further work.

3.7 Generalization to other countries

In this study, the simulations are done for a single building. The building test case is however representative for a large number of well-insulated wooden detached houses, also outside Norway. The author has also performed similar but less detailed simulation on a more generic building model, using the BPS software SIMIEN (11). The results and conclusions were in general similar.

An important prerequisite for the proposed hybrid ventilation strategy with extensive thermal zoning, is the use of warm, high-quality duvets and bed clothing. This seems to be important for the acceptance and preference of low bedroom temperatures. Cold bedrooms are not acceptable in all countries, for instance due to the habits related to bedclothes. However, some studies indicate acceptance or tolerance of cold bedrooms is other countries than Norway, like Denmark and China (28-30). The bedroom habits are not frequently reported in the literature so cold bedrooms could in fact be in use in several places in the world. Another important prerequisite for the hybrid solution to be acceptable is that the outdoor air quality (e.g., pollution) and sound levels are low at the building location. This is more challenging in urban areas.

4. Conclusions

The modelling of natural ventilation is based on simplifications in building performance simulation (BPS). Significant uncertainty is expected for window airflow computed using BPS. However, using sensitivity analysis based on different modelling assumptions and different model input parameters, the influence of these uncertainties can be quantified, and the results enable to formulate some general trends.

The energy performance of the investigated hybrid ventilation strategies is strongly influenced by the occupant behaviour. When occupants prefer bedroom temperatures at about 20°C, the investigated hybrid ventilation strategies lead to significantly higher space-heating needs compared to a standard balanced mechanical ventilation with efficient heat recovery unit. When bedrooms are used by occupants accepting (or preferring), low temperatures in bedrooms, and if these rooms are not heated during daytime, the computed space-heating needs are almost as low as standard balanced mechanical ventilation. Given an energy-conscious occupant behaviour (e.g., regarding thermal zoning), it seems possible to achieve a low energy use with natural ventilation in bedrooms. Low temperature in bedroom is frequently applied in Norwegian bedrooms so that the proposed hybrid ventilation strategies could be implemented into a significant share of the renovation market. However, temperature in bedrooms is strongly related to habits and culture. Therefore, the potential of this hybrid ventilation can be different for other countries.

Finally, for the hybrid ventilation strategy where all bedrooms are naturally ventilated, it is possible to create a night setback in the unoccupied zones served by the mechanical ventilation. It is a technically cheap and simple way to decrease energy use. This could be investigated in more details in further research.

5. Acknowledgement

This research work is part of the OPPTRE project on Energy upgrading of wooden dwellings to the nearly-zero energy level (http://opptre.no/). OPPTRE is funded by the Norwegian Research Council.

The datasets generated and analysed during the current study are not publicly available because significant pre-processing and structuring of data is required to make it open-access, but will be available upon request.

6. References

1. Bjørnstad E. Rehabilitering og energioppgradering av boliger. ENOVA SF; 2015.
2. Berge M, Mathisen HM. Perceived and measured indoor climate conditions in high-performance residential buildings. Energy and Buildings. 2016;127:1057-73.
3. Georges L, Wen K, Alonso MJ, Berge M, Thomsen J, Wang R. Simplified space-heating distribution using radiators in super-insulated apartment buildings. Energy Procedia. 2016;96:455-66.
4. Thomsen J, Gullbrekken L, Grynning S, Holme J. Evaluering av boliger med lavt energibehov (EBLE)–samlerapport. 2017.
5. Berge M, Georges L, Mathisen HM. On the oversupply of heat to bedrooms during winter in highly insulated dwellings with heat recovery ventilation. J Building Environment. 2016;106:389-401.
6. Georges L, Selvnes E, Heide V, Mathisen HM, editors. Energy efficiency of strategies to enable temperature zoning during winter in highly-insulated residential buildings equipped with balanced mechanical ventilation. IOP Conference Series: Earth and Environmental Science; 2019: IOP Publishing.
7. Selvnes E. Thermal zoning during winter in super-insulated residential buildings. Trondheim: Norwegian University of Science and Technology (NTNU); 2017.
8. Bjorvatn B, Mrdalj J, Saxvig IW, Aasnæs T, Pallesen S, Waage S. Age and sex differences in bedroom habits and bedroom preferences. Sleep medicine. 2017;32:157-61.
9. Heide V, Skyttern S, Georges L, editors. Indoor air quality in natural-ventilated bedrooms in renovated Norwegian houses. E3S Web of Conferences; 2021: EDP Sciences.
10. Heide V, Georges L, Skytteren S,. Assessing the indoor air quality of natural-ventilated bedrooms in renovated Norwegian houses using detailed field measurements. Healthy Buildings 2021–Europe Proceedings of the 17th International Healthy Buildings Conference 21–23 June 2021; 2021.
11. Heide V. Energieffektivitet med åpent soveromsvindu i passivhus. Passivhus Norden 2013; Gøteborg: Laganhus; 2013.
12. Suerich-Gulick F, Halepaska A, Craig S. Cascading temperature demand: The limits of thermal nesting in naturally ventilated buildings. Building and Environment. 2022;208:108607.
13. Simonson C. Energy consumption and ventilation performance of a naturally ventilated ecological house in a cold climate. Energy and buildings. 2005;37(1):23-35.
14. Andersen R, Fabi V, Toftum J, Corgnati SP, Olesen BW. Window opening behaviour modelled from measurements in Danish dwellings. Building and Environment. 2013;69:101-13.
15. Verbruggen S, Delghust M, Laverge J, Janssens A. Window use habits in Belgian households. The 16th Conference of the International Society of Indoor Air Quality & Climate2020.
16. Levie D, Hoes-van Oeffelen E, Hofstetter H, Janssen S, Spiekman M, Koene F. Determinants of ventilation behavior in naturally ventilated dwellings: Identification and quantification of relationships. Building and environment. 2014;82:388-99.
17. Bekö G, Gustavsen S, Frederiksen M, Bergsøe NC, Kolarik B, Gunnarsen L, et al. Diurnal and seasonal variation in air exchange rates and interzonal airflows measured by active and passive tracer gas in homes. Building and Environment. 2016;104:178-87.
18. Mestergruppen Bolig AS. Mesterhus Nanne 2022 [Available from: https://mesterhus.no/bygge-hus/tradisjonelle-hus/nanne/
19. Georges L, Berner M, Mathisen HM. Air heating of passive houses in cold climates: Investigation using detailed dynamic simulations. Building and Environment. 2014;74:1-12.
20. Standard Norge. SN/TS 3031:2016 Energy performance of buildings. 2016.
21. Standard Norge. NS 3700:2013 Criteria for passive houses and low energy houses (residential buildings). 2013.
22. Direktoratet for byggkvalitet. Norwegian building regulations, TEK07. Oslo2007.
23. Merzkirch A, Maas S, Scholzen F, Waldmann D. Field tests of centralized and decentralized ventilation units in residential buildings – Specific fan power, heat recovery efficiency, shortcuts and volume flow unbalances. Energy and Buildings. 2016;116:376-83.
24. Östin R. Evaluation of a Single Family Low Energy Building in Cold Climate. Energy Procedia. 2017;132:9-14.
25. La Fleur L, Moshfegh B, Rohdin P. Measured and predicted energy use and indoor climate before and after a major renovation of an apartment building in Sweden. Energy and Buildings. 2017;146:98-110.
26. Hurnik M, Specjal A, Popiolek Z. On-site diagnosis of hybrid ventilation system in a renovated single-family house. Energy and Buildings. 2017;149:123-32.
27. Zhai ZJ, El Mankibi M, Zoubir A. Review of natural ventilation models. Energy Procedia. 2015;78:2700-5.
28. Bjørneboe MG, Svendsen S, Heller A. Evaluation of the renovation of a Danish single-family house based on measurements. Energy and Buildings. 2017;150:189-99.
29. Thomsen KE, Rose J, Mørck O, Jensen SØ, Østergaard I, Knudsen HN, et al. Energy consumption and indoor climate in a residential building before and after comprehensive energy retrofitting. Energy and Buildings. 2016;123:8-16.
30. Liu D, Ren Z, Wei S, Song Z, Li P, Chen X. Investigations on the Winter Thermal Environment of Bedrooms in Zhongxiang: A Case Study in Rural Areas in Hot Summer and Cold Winter Region of China. Sustainability. 2019;11(17):4720.

Energy-saving and IAQ control in hospital patient room by bed-integrated ventilation

Zhiqi Wang [a], Mariya Bivolarova [a], Arsen Melikov [a]

[a] International Centre for Indoor Environment and Energy, Department of Environmental and Resource Engineering, Technical University of Denmark, Building 402, Kgs. Lyngby, Denmark.

Abstract. The annual energy-saving potential and IAQ improvement by use of a hospital bed-integrated pollution source control, a ventilated mattress (VM) and local bed ventilation (LBV), was studied. The VM is designed to capture in the bed and exhaust human body bio-effluents. The LBV is supplies clean air close to the breathing zone of the patient in bed and exhausts the polluted (might be infected) exhaled air from the patient before it is mixed with the room air. Exhaled air removal efficiency of the LBV were assumed at 40%, 60% and 80%. Thus, the risk of cross-infection was reduced. Energy use simulations were performed by IDA-ICE software. Intake fraction was used to indirectly assess the risk of cross-infection. Three scenarios were simulated to evaluate the energy-saving potential of the source control methods: 1) a double-patient room (none of patients is infected) using the VM and constant air volume ventilation (CAV), 2) a double-patient room (either one or two patients is infected) using the VM and CAV and 3) a double-patient room (either one or two patients is infected) using the VM, the LBV and CAV. The results reveal that using the VM and the LBV at decreased background ventilation rate can be an effective method for reducing the energy costs needed for hospital wards. Depending on the operation of the VM and the LBV, the energy-saving was between 1880 kWh and 67964 kWh. The annual energy-saving was up to 83.6% when the ward with two infected patients using LBV at 80% exhaled air removal efficiency and CAV at a reduced ventilation rate, compared with the reference cases of only CAV operating at 12 air changes per hour (ACH).

Keywords. Hospital bed ventilation, pollution source control, reduction of airborne cross-infection, indoor air quality, energy-saving
DOI: https://doi.org/10.34641/clima.2022.358

1. Introduction

Indoor air quality (IAQ) has a direct impact on the health, comfort, and productivity of occupants. It is related to indoor pollutant concentration. As the largest indoor pollution source, occupants emit bio-effluents with the exhaled air and body bio-effluent from the skin [1]. In health care facilities like hospitals, exhaled air of infected patients contains pathogenic particles (many of which are airborne), therefore the medical staff and visitors are at the risk of cross-infection [2].

Total volume ventilation is used as a pollution control solution in hospital patient rooms. During the COVID-19 pandemic, several guidelines recommend increasing ventilation rate in rooms to mitigate the risk of airborne cross-infection [3,4]. A HVAC system operating with high ventilation rate consumes a large amount of energy. Generally, the supplied clean air dilutes room air and reduces the contaminants not only in the occupied zone but also in the non-occupied zone. This process is energy inefficient [5].

Instead of total volume ventilation, source control method can be applied to improve indoor air quality at low energy consumption. With this approach pollutants are removed close to the source, i.e., occupant. Ventilation rate can be reduced because the contaminates are removed locally before they spread in the room. As a result, energy-saving can be achieved. In this study, two localized ventilation systems using the source control method were examined. A ventilated mattress (VM) with local heating and a local bed ventilation (LBV). These bed integrated ventilation systems work independently from the background total volume ventilation system.

The studied ventilated mattress is an advanced air distribution system, which evacuates the bio-effluents generated from the occupant's body and thus reduces the contaminate concentration in the room [6]. The ventilated mattress is placed on the top of the bed mattress. Inside the VM there is a three-dimensional spring. As a result, 96% of its inner volume is an air layer. Local exhaust including a small fan is installed at the end of the mattress (on the head

Copyright ©2022 by the authors. This conference paper is published under a CC-BY-4.0 license.

side). There are two exhaust openings on the surface of the mattress under the patient feet (Fig. 1). 1.5-5 L/s of air is extracted from the micro-environment around the lying person through the openings. It has been shown that a filter made of chemically treated carbon fibre installed in the mattress removes efficiently the body-emitted pollution [6]. Thereby, the cleansed air can be released back into the room. The VM enables to capture and remove 98% of the bio-effluents emitted from the patient body [6].

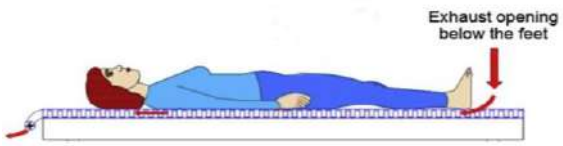

Fig. 1 - Bed-integrated ventilation method: ventilated mattress (Adapted from Bivolarova et al., 2016 [6]).

The airflow through the mattress increases the conductive heat loss from the body of the person in the bed, especially the body part in contact with the mattress. It provides local cooling for the person [7]. With the application of the local heating in the heating season, the ventilated mattress creates a comfortable bed micro-environment.

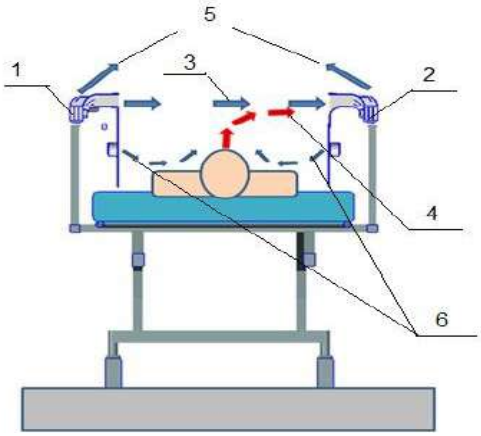

Fig. 2 - HBIVCU working principle: 1 supply ATD; 2 exhaust ATD; 3 horizontal air jet; 4 exhaled air by the patient; 5 vertical upward/inclined air curtains; 6 vertical downward air curtains (Kehayova and Melikov, 2017 [9]).

Hospital Bed Integrated Ventilation Cleansing Unit (HBIVCU), referred in this paper as LBV, is another studied advanced air distribution system that captures and removes human exhaled pollutants [8]. The mobile HBIVCU is installed on the support frame of the hospital bed, and it enables to follow the bed adjustment. Two air terminal devices (ATDs) are mounted on both side of the bed close to the patient head [8]. These devices are connected with air conditioning and distribution box installed at the back of the bed (not shown in Fig.2). HBIVCU working principle is illustrated in Fig. 2.

Room air is extracted in the box (unit 1) by the integrated fan, disinfected from viruses via HEPA filter and UVG light in the unit. The filtered air is then supplied horizontally (3), and gently guides part of the exhaled air toward the box on the opposite side (unit 2). Virus particles are removed in this box (2) and the clean air discharges back to the room. In addition, the clean air is supplied inclined/vertical upward to the ceiling (5) and downward alongside of the patient's head (6). The two upward air curtains are designed to protect a healthy person (medical staff and other occupants) inside the room from exposure to the polluted air coming from the pulmonary activities of the sick person, while it constrains and guides the polluted air upward to an exhaust. The two downward air curtains (6) provide clean air to the breathing zone of the person in bed and also local cooling of his/her head.

The objective of this study was to identify the energy-saving potential of the advanced ventilation system used in hospital room. The energy-saving potential is defined as annual energy-saving property of the hospital room with constant ventilation system (CAV) together with the advanced ventilation system, compared with the hospital room with only CAV.

2. Research Method

2.1 intake fraction

Intake fraction was used to indirectly determine the probability of infection, which was defined as "the proportion of air mass exhaled from the infected person that is then inhaled by the exposed person." [11]. During a certain period, the average intake fraction driven by time was determined with the equation (1):

$$IF = \frac{\int_0^{t_{in}} N_{in(t)} \rho_{in(t)} \dot{V}_{p,in(t)} dt}{\int_0^{t_{ex}} N_{ex(t)}\, \rho_{ex(t)} \dot{V}_{p,ex(t)} dt} \qquad (1)$$

Where:

- $N_{in(t)}\rho_{in(t)}$= concentration of particles in the inhaled air by exposed person, particles/m^3;
- $N_{ex(t)}\rho_{ex(t)}$=concentration of particles in the exhaled air by infected person, particles/m^3;
- $\dot{V}_{p,in(t)}$=the pulmonary ventilation of the exposed person, considered as 1.00×10^{-3}m^3/s;
- $\dot{V}_{p,ex(t)}$=the pulmonary ventilation of the infected person, considered as 1.04×10^{-3}m^3/s;

The concentration of the virus particles was determined based on mass balance. It was related to virus generation rate and air change rate, which is shown in the Appendix of this paper.

2.2 parameters

The energy-saving potential of using the advanced ventilation systems was measured in three types of hospital rooms, namely a general ward, a patient room and an infection isolation room. These three rooms had same layouts (Fig. 3) with dimensions 8.4 m×4.7 m×2.8 m (W×L×H), i.e., 39.48 m^2 [12]. The window with area of 2.27 m^2 (1.2 m×2.27 m, W×L)

was located 1 m above the floor. It was assumed that there were two patients reclined on the beds during the whole day. Their metabolic rate was 0.8 met (corresponding to approximately 73.6 W heat generated by each person with average body surface area at 1.6 m^2 in this position) [13]. Because medical staff spent little time in the room, their influence on the indoor environment was ignored.

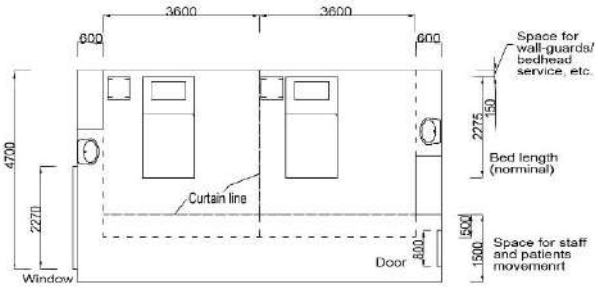

Fig. 3 - Hospital room layout.

It was assumed that the hospital building was located in Copenhagen, Denmark. Its building materials and U-value complied with the Danish Building Regulation [14]. The thermal resistance of the external wall with the window was 0.5372 W/m^2·K. The U-value of the internal walls and the floor were 0.37 W/m^2·K and 2.385 W/m^2·K, respectively. The glazing U-value of the chosen glass was 0.6 W/m^2·K, its solar and visible transmission coefficients were respectively 0.32 and 0.63. The window was oriented to south, its external blind would automatically draw when sunlight exceeded 100 W.

There were nine light-emitted diode lamps installed on the ceiling, each with a power of 5 W. Average heat gain of the medical equipment for each patient was assumed to be 114 W. Thus, the internal heat gain was 402.2 W. The medical equipment operated during the whole day while the lights only turned on from 7:00 to 21:00.

The local bed ventilation consumed 28.5 W during operation. The power of the VM consisted of driving the exhaust air through the mattress at 20W and the local heating. Energy consumption of the local heating depended on the room air temperature, its power was 36 W within the room temperature range of 18-20 ℃ and 18 W in the range of 20-23 ℃. The local heating was only provided when the indoor temperature was lower than 23℃.

2.3 simulated cases

The two hospital beds equipped with VM were used in the ward to enhance indoor air quality (Scenario 1). Neither of the two accommodated patients was infected in this scenario.

The two-bed ward without using the VM was considered as the reference case in Scenario 1. The ward was designed as a common public building room. Due to patients' high requirement of indoor environment quality, the ward was defined as Category Ⅰ, a very-low polluting building. Thus, the required ventilation rate for occupants was 10 L/(s·person) and 0.5 L/(s·m^2) for diluting the generated pollution, i.e., 39.74 L/s (corresponding to 1.30 ACH) for the whole room [13]. It was assumed that half (5 L/s) of the required ventilation rate for occupants is used to dilute body emitted bio-effluents and the other half (5 L/s) to dilute exhaled bio-effluents. The indoor temperature was kept in the range of 21-23 ℃ in the heating season, 23.5-25.5 ℃ in the cooling season. When VM is in operation, 98% of the body-emitted bio-effluents is removed [6]. Therefore, half of the required ventilation rate for occupants, i.e., 5 L/(s·person), was reduced to 2% (corresponding to 0.1 L/(s·person)). As a result, the ventilation rate in the ward with hospital bed equipped with the VM was reduced from 39.74 L/s to 29.94 L/s. Preliminary simulations in IDA ICE showed that this supply air flow rate was sufficient to keep the CO_2 concentration in the ward less than 950 ppm. This CO_2 level complies with the standard requirement for Category I [13]. The ventilation rate and supply temperature set-points of both cases are shown in Tab. 1. The return air temperature was set to 23 ℃.

Tab. 1 -Ventilation system parameters of the simulated cases in Scenario 1 (reference case with only CAV at 1.30 ACH and case with the VM and CAV at reduced ventilation rate in the ward).

Case	Ventilation rate	Min/Max supply temperature
RF-1.30 ACH	1.30 ACH (39.74 L/s)	19/19℃
VM-0.98 ACH	0.98 ACH (29.94 L/s)	19/19℃

In addition, the VM provided local heating and cooling, which created a comfortable bed micro-environment. Therefore, the indoor environment temperature range was set to be from 18 to 28℃. This range still fulfilled the requirement of occupants' thermal satisfaction and medical equipment operation [16]. The design relative humidity was kept between 30%-60% [15].

The local bed ventilation system was used to reduce the risk of airborne cross-infection in the hospital room (Scenario 2). The design temperature range was 21-24℃, return temperature was set to be 23℃ in IDA ICE model. The relative humidity was kept less than 60% and the CO_2 concentration was under 950 ppm as recommended [17].

A patient room without using the LBV was designed as a reference case. One of the two patients present in the room was assumed to be infected and exhaling infectious particles (Scenario 2.1). The design ventilation rate was 6 ACH, i.e., the recommended minimum total ventilation rate in patient rooms to

reduce the risk of airborne transmission and protect uninfected person [4]. This is considered as sub scenario 2.1.1. By using the local bed ventilation, the recommended ventilation rate for airborne transmission control was reduced to achieve energy-saving. Three different exhaled air removal efficiencies (EARE) of the LBV were studied: 80%, 60% and 40%. When using the LBV, the background ventilation rate was reduced to a level which will not result in a higher than 0.0016% intake fraction. IF of 0.016% was obtained at the reference case with only background ventilation (referred in the following as IF=0.0016%). On the other hand, there is a minimum standard requirement of supplying 2 ACH outdoor air to a patient room for maintaining indoor air quality [17]. Therefore, background ventilation rate of 2 ACH was kept in the cases when it could be lower than this. The EARE of the LBV was implemented in equation (1) in order to calculate the intake fraction when the LBV was in operation (see equation 2, 3 and 4 in the Appendix). The corresponding calculated intake fraction for each case is shown in Tab. 2.

Tab. 2 – Intake fraction and ventilation system parameters of the simulated cases in Scenario 2.1.1 (reference case with only CAV at 6 ACH and cases with LBV at 80%, 60% and 40% in conjunction with reduced ventilation rate in the patient room).

Case	Ventilation rate	Intake fraction	Max/Min supply temperature
RF-6 ACH	6 ACH (184.24L/s)	0.016%	20/20°C
LBV - EARE80%	2ACH (61.41L/s)	0.006%	18/19°C
LBV - EARE60%	2ACH (61.41 L/s)	0.012%	18/19°C
LBV - EARE40%	2.8ACH (85.98 L/s)	0.016%	19/19°C

In another sub scenario 2.1.2, the ventilation rate of the reference patient room was designed as 60 L/(s·person), i.e., 3.91 ACH, according to the recommendations in the WHO roadmap [4]. The calculated intake fraction of the uninfected exposed patient was 0.022% under this condition (designated as IF=0.022%). Thus, the background ventilation rate was reduced to levels, which would keep the same or lower IF when the LBV was in operation. The intake fraction and the ventilation system parameters of the cases are shown in Tab. 3.

Tab. 3 - Intake fraction and ventilation system parameters of the simulated cases in Scenario 2.1.2 (reference case with only CAV at 3.91 ACH and cases with LBV at 80%, 60% and 40% in conjunction with reduced ventilation rate in the patient room).

Case	Ventilation rate	Intake fraction	Max/Min supply temperature
RF-120 L/s	3.91 ACH (120 L/s)	0.022%	20/20°C
LBV - EARE80%	2 ACH (61.41L/s)	0.006%	19/19°C
LBV - EARE60%	2 ACH (61.41L/s)	0.012%	19/19°C
LBV - EARE40%	2 ACH (61.41L/s)	0.019%	19/19°C

Scenario 2.2 was a situation of two infected patients present in an airborne infection isolation room. The infection isolation room only with CAV system at 12 ACH (368.48 L/s) was considered as the reference case [17]. In this scenario, only visitors like doctors were under the risk of cross-infection, their intake fraction was 0.009% in the reference case, which was designated as IF=0.009%. Intake fraction and ventilation system parameters of the cases are shown in Tab. 4.

Tab. 4 - Ventilation system parameters of the simulated cases in Scenario 2.2 (reference case with only CAV at 12 ACH and cases with LBV at 80%, 60% and 40% in conjunction with reduced ventilation rate in the infection isolation room).

Case	Ventilation rate	Intake fraction	Max/Min supply temperature
RF-12 ACH	12 ACH (368.48L/s)	0.009%	20/20℃
LBV - EARE80%	2 ACH (61.41L/s)	0.006%	20/20℃
LBV - EARE60%	3.8 ACH (116.69L/s)	0.009%	20/20℃
LBV - EARE40%	6.6 ACH (202.66L/s)	0.009%	20/20℃

In order to improve indoor environment meanwhile reduce the risk of airborne cross-infection, both LBV and VM were used in the patient room (Sub scenario 3.1) and the infection isolation room (Sub scenario 3.2). The air quality level was not evaluated in these scenarios, because the airflow requirement of bio-effluent dilution was undefined. Therefore, the ventilation methods of cases in Scenarios 3.1 and 3.2 were equipped VM on the basis of cases in Scenarios 2.1 and 2.2. All cases in Scenario 3 were shown in Tab.5, 6, and 7. Energy-saving was achieved by extending design temperature range to 18-28 ℃ in simulation cases with the use of VM.

Tab. 5 - Ventilation system parameters of simulation cases in Scenario 3.1.1 (cases with VM and LBV at 80%, 60% and 40% in conjunction with reduced ventilation rate in the patient room).

Case	Ventilation rate	Intake fraction	Max/Min supply temperature
LBVVM - EARE80%	2ACH (61.41L/s)	0.006%	19/21℃
LBVVM - EARE60%	2ACH (61.41L/s)	0.012%	19/21℃

LBVVM - EARE40%	2.8ACH (85.98L/s)	0.016%	20/20℃

Tab. 6 - Ventilation system parameters of simulation cases in Scenario 3.1.2 (cases with VM and LBV at 80%, 60% and 40% in conjunction with reduced ventilation rate in the patient room).

Case	Ventilation rate	Intake fraction	Max/Min supply temperature
LBVVM - EARE80%	2 ACH (61.41L/s)	0.006%	19/21℃
LBVVM - EARE60%	2 ACH (61.41L/s)	0.012%	19/21℃
LBVVM - EARE40%	2 ACH (61.41L/s)	0.019%	19/21℃

Tab. 7 - Ventilation system parameters of simulation cases in Scenario 3.2 (cases with LBV at 80%, 60% and 40% in conjunction with reduced ventilation rate in the infection isolation room).

Case	Ventilation rate	Intake fraction	Max/Min supply temperature
LBVVM-EARE80%	2 ACH (61.41L/s)	0.006%	20/20℃
LBVVM - EARE60%	3.8 ACH (116.69L/s)	0.009%	20/20℃
LBVVM - EARE40%	6.6 ACH (202.66L/s)	0.009%	20/20℃

2.4 HVAC system

Thermal comfort environment in the simulated hospital patient rooms was provided by constant air volume (CAV) system with steam humidifier. A specially controlled steam humidifier and a relative humidity sensor installed to fulfil the standard requirement of 30%- 60% RH [15]. A second heating coil in the AHU installed after the cooling coil was used to dehumidify the supply air in the cooling season. It turned off when there was no need to dehumidify (the case with combination of VM and CAV at reduced ventilation rate in this study). The max and minimum supply air humidity were set at 30% and 90% separately, and the return air humidity set-point was 50%.

The studied room was designed as a typical hospital room. Typical thermal bridge was created in the model as a source of heat loss. Typical infiltration of 0.5 ACH at 50 Pa was chosen based on the wind driven outdoor air. Temperature set-point of the chiller in the default plant was 5℃, its coefficient of performance was 3.8; water set-point of the boiler was 35℃ while its coefficient was set to 90%.

3. Result

3.1 potential energy-saving with the ventilated mattress

Fig. 4 presents results of the annual energy need of the cases with only CAV system (reference case) and the ventilated mattresses with local heating combined with CAV system at reduced background ventilation rate. Compared with the reference case, the annual energy consumption was reduced by 22.5% when using hospital beds equipped with the VM in the ward.

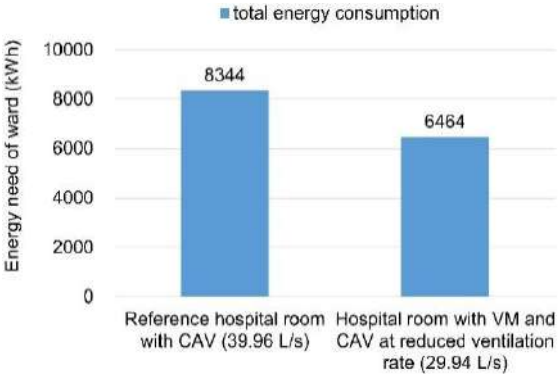

Fig. 4 – Annual energy need of the ward with background ventilation only (reference case) and with the ventilated mattress in conjunction with reduced background ventilation.

3.2 potential energy-saving with the local bed ventilation

Fig.5 presents the results of the annual energy need of the cases focusing on cross-infection reduction. In Scenario 2, the reference cases for the patient room included CAV at recommended 3.91 ACH (60 L/(s·person)) and 6 ACH (184.24 L/s). For the infection isolation room, the reference case included CAV at 12 ACH (368.48 L/s).

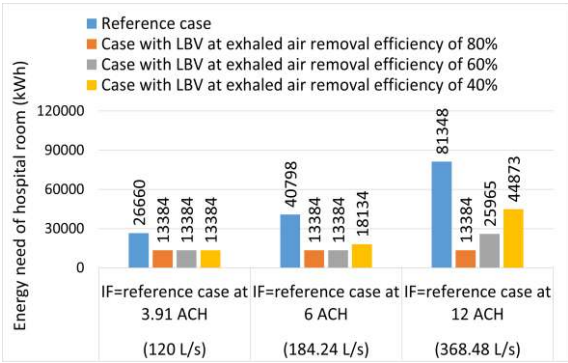

Fig. 5 – Annual energy need of the ward with background ventilation only (reference case) and with the local bed ventilation in conjunction with reduced background ventilation.

Compared with the reference case at 3.91 ACH (120 L/s), 49.8% energy-saving was achieved by the use of the local bed ventilation operated at 40%, 60% or 80% exhaled air removal efficiency (in Fig. 5). Under this condition, the CAV system with reduced background ventilation was maintained at 2 ACH.

The reduction of background ventilation by the use of the LBV at 80%, 60% and 40% exhaled air removal

efficiency led to respectively 67.2 % (2 ACH), 67.2% (2 ACH) and 55.6% (2.8 ACH) energy-saving, compared to the reference case at 6 ACH (184.24 L/s).

With the comparison of the reference case with CAV at 12 ACH (368.48 L/s), the energy-saving of 83.6%, 68.1% and 44.8% was achieved when the LBV operated at respectively 40%, 60% and 80% with reduced background ventilation (2 ACH, 3.8 ACH and 6.6 ACH, respectively) in the infection insolation room.

3.3 potential energy-saving with combination of ventilated mattress and local bed ventilation

Fig. 6 presents the result of the annual energy need of the cases focusing on both cross-infection reduction and indoor air quality improvement.

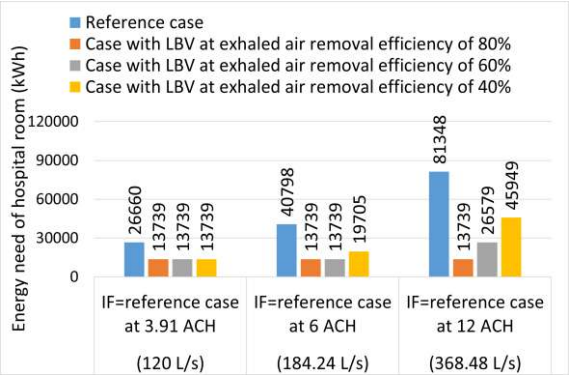

Fig. 6 – Annual energy need of the ward with background ventilation only (reference case) and with the ventilated mattress and the local bed ventilation in conjunction with reduced background ventilation.

48.5% energy-saving was achieved by the use of the VM and LBV operated at 40%, 60% or 80% exhaled air removal efficiency with reduced background ventilation at 2 ACH, compared with the reference case at 3.91 ACH (120 L/s).

The reduction of background ventilation by the use of combination of the VM and the LBV at 80%, 60% and 40% exhaled air removal efficiency led to 66.3 % (2 ACH), 66.3% (2 ACH) and 51.7% (2.8 ACH) energy-saving, compared to the reference case at 6 ACH (184.24 L/s).

Compared with the reference case at 12 ACH (368.48 L/s), the energy-saving of 83.1%, 67.3% and 43.5% was achieved when the LBV operated at respectively 40%, 60% and 80% with reduced background ventilation (2 ACH, 3.8 ACH and 6.6 ACH respectively) in the infection insolation room.

4. Discussion

An important challenge of creating an acceptable indoor air environment while saving energy could be achieved by ventilation based on the source control method. The simulation results of the present study showed that both the ventilated mattress and the local bed ventilation efficiently reduced the annual energy need in the studied hospital room scenarios. The energy-saving potential of the local bed ventilation increased when its exhaled air removal efficiency increased. However, the application of the VM lessened the energy-saving of the room with the combination of the LBV and CAV. More researches are needed to assess the ability of the VM to improve air quality under the risk of cross-infection, which was not considered in the current study.

Because the ventilated mattress removes 98% of the bio-effluents generated from the body, the same indoor air quality level as in the reference case only with mixing ventilation can be obtained but at a reduced ventilation rate. Therefore, less energy is needed for the AHU operation to air-condition the outdoor supply air.

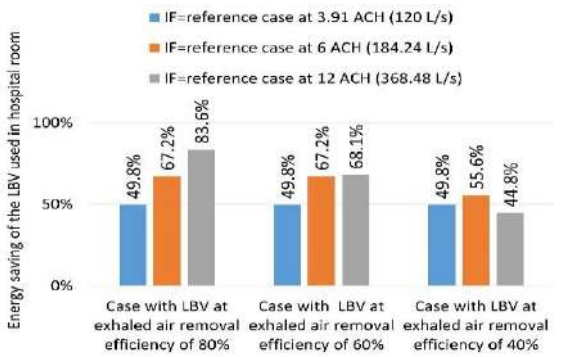

Fig. 7 – Energy-saving of the hospital rooms with the local bed ventilation (LBV) at 80%, 60% and 40% removal efficiency in conjunction with reduced background ventilation.

The energy-saving efficiency of the LBV system (as shown in Fig. 7) was related to the reduction rate of the background ventilation. The local bed ventilation at 60% and 80% EARE had the largest energy-saving capacity and led to highest background ventilation reduction rate in the infection isolation room. In contrast, the energy-saving potential of the LBV at 40% EARE in the isolation room was lower than that of the LBV at same EARE operating the patient room (reference case at 6 ACH, i.e., 184.24 L/s). This is because the background ventilation rate was reduced by 45% (from 12 ACH (reference) to 6.6 ACH) and 52.3% (from 6 ACH to 2.8 ACH) in the case of isolation room and patient room with the LBV with 40% EARE, respectively.

The energy-saving potential of the combination of VM and LBV was slightly lower than in the case when only the LBV was used. This was due to the energy need for local heating in the case with both VM and LBV.

The use of the local bed ventilation might also save initial cost and space for the construction of the HVAC system. Due to noise generation and pressure control, the acceptable air velocity in ventilation ducts connecting the air terminal devices is recommended to be in a range of 1.2 m/s and 2.3 m/s.

The duct diameter of the cases in Scenario 2.1.2 were calculated as an example how building space can be saved when using advanced ventilation systems (as shown in Table 8).

Tab. 8 – Air velocity in a duct and duct diameter (connecting with ATD) of the cases in Scenario 2.1.2.

Case	Ventilation rate	Duct [mm]	Velocity [m/s]
RF-120L/s	3.91 ACH (120 L/s)	315	1.54
Case with LBV	2 ACH (61.41 L/s)	200	1.95

As of November 2021, over 2 billion cases of confirmed Sars-COV-2 have been reported worldwide. Ohsfeldt et al. reported that the median hospitalization day of an infected person was 6 days, and the median cost per day for one patient was $1772 in the USA (intensive care unit required patients were not included) [18]. A healthy and clean indoor environment provided by ventilation systems promotes rehabilitation, reduces the infection risk of exposed person and cross-infection risk. Shorter hospital stays and fewer inpatients mitigate the significant burden on the healthcare system and finances.

This study has several limitations. To simplify the simulation, the models were assumed as a steady indoor environment with constant airflow, air pressure, indoor temperature, internal heat gain, etc. In reality, these factors vary with time and accommodated person movement. Meanwhile, the present energy-saving potential of the advanced ventilation systems were determined in hospitals built in a cold and dry environment (Copenhagen, Denmark). Outdoor climate might somewhat impact the energy-saving capability of these devices. Further studies which consider these variables are required.

The results of the present study were limited by the simulation software. The ventilated mattress and the local bed ventilation were not simulated as advanced ventilation systems. They were built as normal equipment which only generated heat and consumed energy, cooling effect due to air movement was not took into account. In addition, local heating of the ventilated mattress was unable to be incorporated as a heating unit. Instead, it was also simulated as an equipment with certain power.

5. Conclusion

In this study, annual energy consumption of a two-patient hospital room was simulated to determine the energy-saving potential of the ventilated mattress and the local bed ventilation.

The results showed that the use of the ventilated mattresses with local heating achieves 22.5% energy-saving in the hospital room with two uninfected patients. The local bed ventilation performed the greatest energy-saving potential of 83.6% in the infection isolation room with two infected patients, the exhale air removal efficiency of the LBV was 80%. The hospital room with beds equipped with a combination of the local bed ventilation and the ventilated mattress consumed slightly higher energy than equipped with only LBV under the same condition.

The implementation of local bed ventilation will lead to use of smaller HVAC and duct systems and thus space in hospital buildings will be saved.

Further studies might explore the influence of the occupancy schedule, activities of people and outdoor climate. The simulation method should be improved to model the LBV and VM as ventilation units and take local heating into account.

6. Acknowledgement

This research was supported by the Bjarne Saxhof's Foundation for Support of Danish Research, project No 26946.

7. References

[1] Bekö G, Wargocki P, Wang N, Li M, Weschler CJ, Morrison G et al. The Indoor Chemical Human Emissions and Reactivity project (ICHEAR): Overview of experimental methodology and preliminary results. Indoor Air. 2020;30(6):1213-1228.

[2] Douwes J, Thorne P, Pearce N, et al. Bioaerosol health effects and exposure assessment: progress and prospects. The Annals of occupational hygiene. 2003;47(3): 187-200.

[3] Heating, ventilation and air-conditioning systems in the context of covid-19: first update. European centre for disease prevention and control; 2020.

[4] Roadmap to improve and ensure good indoor ventilation in the context of COVID-19. Geneva: World Health Organization; 2021.

[5] Melikov AK. COVID-19: Reduction of airborne transmission needs paradigm shift in ventilation. Building and Environment. 2020;186. 107336.

[6] Bivolarova MP, Melikov AK, Mizutani C, Kajiwara K, Bolashikov ZD. Bed-integrated local exhaust ventilation system combined with local air cleaning for improved IAQ in hospital patient rooms. Building and Environment. 2016;100:10-18.

[7] Nagasawa, S., Sakoi, T., Melikov, A.K. Add-on local sweating simulation system for a dry thermal manikin. Science and Technology for the

Built Environment. 2021;27:7,971-985.

[8] Melikov AK, Bolashikov ZD, Georgiev E. Novel ventilation strategy for reducing the risk of airborne cross infection in hospital rooms. In Proceedings of Indoor Air 2011. 2011;1037.

[9] Kehayova N, Bolashikov ZD, Melikov AK. Exhaled air removal effectiveness of a novel ventilation method for reduction of airborne cross contamination in hospitals. In Healthy Buildings Europe 2017, 2-5 July 2017, Lublin, Poland. 2017.

[10] Bolashikov ZD, Melikov AK, Barova M. Hospital bed ventilation: impact of operation mode on exposure. In Proceedings of ROOMVENT 2014, 13th SCANVAC International Conference on Air Distribution in Rooms. 2014. Paper ID 108.

[11] Bennett DH, Margni MD, McKone TE, Jolliet O. Intake fraction for multimedia pollutants: a tool for life cycle analysis and comparative risk assessment. Risk Anal. 2002;22(5):905-918.

[12] NHS Estates. Ward layouts with single rooms and space for flexibility. The Stationery Office.2005.

[13] ISO 7730. Ergonomics of the thermal environment-Analytical determination and interpretation of thermal comfort using calculation of the PMV and PPD indices and local thermal comfort criteria. 3rd edition. Geneva, Switzerland. International Organisation for Standardization.2005.

[14] BR18. Executive order on building regulations 2018 (BR18). Ministry of Transport, Building and Housing; 2018.

[15] DS/EN 16798-1, Energy performance of buildings –Ventilation for buildings –Part 1: Indoor environmental input parameters for design and assessment of energy performance of buildings addressing indoor air quality, thermal, lighting and acoustics –Module M1-6. Danish Standards Association; 2019.

[16] Heating and ventilation systems, health technical memorandum 03-01: Specialized ventilation for healthcare premises Part a: Design and validation. Department of Health/Estates and Facilities Division; 2007.

[17] ANSI/ASHRAE/ASHE 170-2021, Ventilation of Health Care Facilities. ASHRAE Standing Standard Project Committee 170; 2021.

[18] Ohsfeldt RL., Choong CKC, Mc Collam, PL. et al. Inpatient Hospital Costs for COVID-19 Patients in the United States. Advances in Therapy. 2021;38:5557–5595.

8. Appendix

According to the mass balance, the average virus particle concentration was determined by equation (2).

$$\frac{X_r - X_0}{X_\infty - X_0} = 1 - \mathrm{e}^{-b(t-t_0)} \qquad (2)$$

Where:

- X_0=concentration of pollutant at the beginning, considered as 0, particles/m^3;
- $X_\infty=\frac{\dot{G}}{V_r}$, equilibrium particle concentration of the investigated space, particles/m^3;
- $b=\frac{\dot{V_r}}{V_r}$, air change rate, L/s;
- t=time, s;
- t_0= beginning time, considered as 0, s.

Sars-Cov-2 was considered as the main studied airborne virus, its generation rate was 426 particles/s, corresponding to 2554 particles/exhalation when the patient's exhalation rate is assumed as 10 exhalation/min.

When $(t - t_0) = 5\cdot\frac{1}{b}$, $\frac{X_r - X_0}{X_\infty - X_0} = 0.997$ and the virus concentration in the investigation space keeps approximately constant. Then the average particle concentration for an interval of $[t_0, 5\cdot\frac{1}{\mathrm{b}}]$ could be determined by equation (3):

$$\overline{X_b} = X_\infty + \frac{(X_0 - X_\infty)(\mathrm{e}^{-bt_1} - \mathrm{e}^{-bt_2})}{b(t_2 - t_1)} \qquad (3)$$

$\overline{X_b}$ is the determined average Sar-COV-2 virus concentration. t_1, t_2 is the stating time and ending time of the determined interval.

The studied LBV removes exhaled virus particles at 40%, 60% and 80% close to patient's breathing zone, thus calculated exhaled particles in the investigate space reduce to 60%, 40% and 20%.

Then the virus particle concentration in the hospital room with LBV was determined by equation (4).

$$\overline{X_b{}'} = X_\infty{}' + \frac{(X_0 - X_\infty{}')(e^{-bt_1} - e^{-bt_2})}{b(t_2 - t_1)} \qquad (4)$$

Where:

- $\overline{X_b{}'}$=concentration of pollutant of the investigated space using LBV, particles/m^3;
- $X_\infty{}'=X_\infty(1-\eta_{LC})$, equilibrium particle concentration of the investigated space using LBV, particles/m^3.

Data Statement

Data sharing not applicable to this article as no datasets were generated or analysed during the current study.

Technical-economic and environmental analysis of DHW systems in Spanish climate zones

Emilio-José Sarabia-Escriva [a], Víctor-Manuel Soto-Francés [a], José-Manuel Pinazo-Ojer [a]

[a] Universitat Politècnica de València.

Abstract. There are many systems on the market for domestic hot water (DHW) production. Spanish legislation requires that 60% of the energy needed to produce DHW be of renewable origin. This work analyses the economic, energy and environmental viability of seven DHW production systems installed in six climatic zones of Spain. The systems combine the equipment: gas boiler, solar collectors, heat pump, photovoltaic and electric heater. The calculation tool used for the simulations has been EnergyPlus. Results show that the system that combines solar collectors with gas boiler is the one with the lowest energy consumption and the lowest amount of emissions in all climatic zones, although in areas with intermediate and cold climates, heat pump with photovoltaic system has a similar consumption and emission level. The system with the highest consumption and emissions is the electric boiler. The total life cost analysis includes the capital cost, the annual maintenance and the energy consumption for a 15-year period. In contrast to energy results, the most economical system for the life cycle is the gas boiler for all climatic zones, due to its low capital and maintenance cost. The heat pump system is the best economic alternative to reduce energy consumption and CO_2 equivalent emissions.

Keywords. DHW, heat pump, building efficiency, NetZero Buildings.
DOI: https://doi.org/10.34641/clima.2022.79

1. Introduction

There are different systems for the production of DHW in single-family residential buildings. The choice of one system or another depends on different factors: cost of the system, accessibility to energy sources or even the space required for equipment. This study analyses the energy consumption, the environmental impact and the economic costs associated with the most common DHW systems in single-family homes. The study is carried out in six climatic zones of Spain.

The models of the different DHW systems have been defined and simulated in Energy Plus [1]. Seven systems have been studied: gas boiler, electric boiler with and without PV, solar thermal with gas and with electric boiler and heat pump with and without PV. Systems include different sources: electricity, natural gas and solar energy.

The second section of the paper shows the characteristics of the different climatic zones used in the analysis. Although these are Spanish cities, the most significant climate parameters are described and cities in other countries with similar climates are indicated. This section also details the characteristics of the seven DHW systems used.

The third section shows the results obtained divided into three topics: energy, CO2 equivalent emissions and economic analysis. Each topic includes an assessment and discussion about the results.

Finally, the fourth section presents the conclusion of the study.

2. Methodology

2.1 Climatic zones

Spanish building regulations [2] divide Spain into 13 climate zones. A zone called alpha for the Canary Islands and twelve zones for the peninsula. Peninsular zones are named by a letter and a number. The letter represents the severity of winter weather and ranges from A (mild winters) to E (more severe winters). The numbers range from 1 to 4, from least to most severe in summer.

For this study six peninsular climates have been selected, from warmer to colder: A4 (Almería), B3 (Valencia), C2 (Barcelona), C1 (Bilbao) and E1 (León). According to the Spanish meteorological agency (AEMET) [3], the Köppen-Geiger classification of this climates and similar cities are: Almería-BWk: it is the only desert climate in Europe; Valencia-Csa: Naples (Italy); Barcelona-Csb: Toulouse (France); Bilbao-Cfb: Paris (France) and León-Csb: Porto (Portugal).

Copyright ©2022 by the authors. This conference paper is published under a CC-BY-4.0 license.

Fig. 1 shows the values of the most representative climatic variables in each area: monthly average outdoor temperature, monthly average wet bulb temperature, monthly average temperature of the tap water, direct radiation and diffuse radiation on horizontal surface.

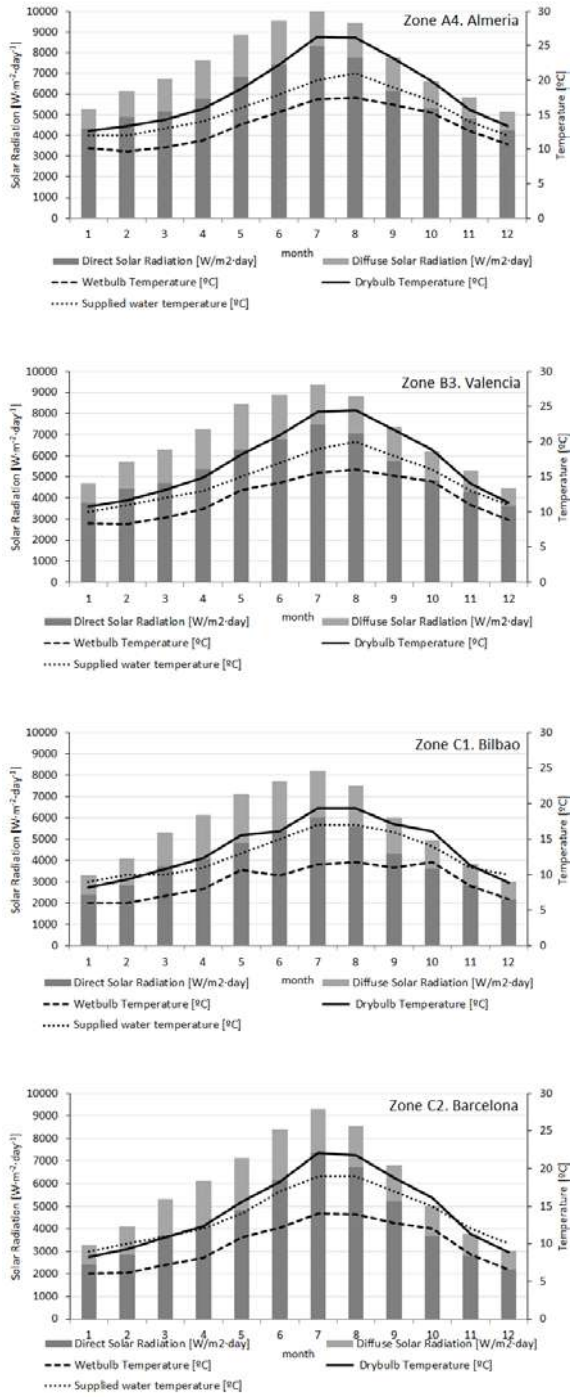

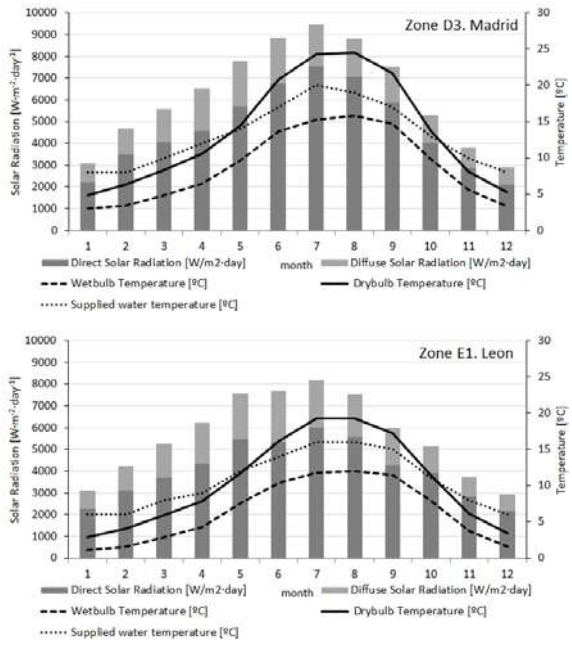

Fig. 1 – Weather data for each climatic zone

2.2 DHW demand

The DHW use profile and daily consumption used in the simulations have been calculated based on Spanish regulations [2] for a house with 4 people. The daily consumption is 165.5 litres of water at 45ºC, distributed as shown in Fig. 2. The highest consumptions are at 8 a.m. and 8 p.m. Simulations made with different profiles have showed similar results [4]. This usage profile is similar to those obtained by Widen for apartments and detached housed [5] on weekdays. There are studies that specify slightly higher daily values for DHW consumption, but do not indicate the water service temperature [6].

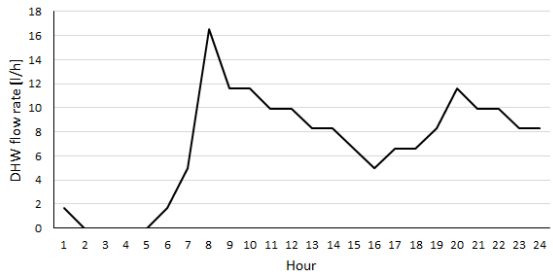

Fig. 2 – DHW demand daily profile.

2.3 DHW systems

The main features of the systems studied are indicated below.

System 1: Gas boiler. Instant production system without accumulation. The boiler has a constant efficiency of 90%. The maximum heating capacity is 20kW with modulating control. The water outlet temperature is 45ºC. The boiler fuel is natural gas.

System 2: Electric boiler. System made of electric heater inside a tank. The loss coefficient per unit area (UA) is 1 W·K^{-1}. The electric efficiency is 100% and its capacity 2.4 kW. The tank volume is 0.2 m^3 and it is located outside. The maximum set point temperature of the tank is 50 ºC.

System 3: Thermal solar with gas boiler. The solar collector area in all zones is 4 m^2. The tilt angle of panels is equal to the site latitude: Zone A4 (Almeria) 36.8ºN, Zone B3 (Valencia) 39.5ºN, Zone C1 (Bilbao) 43.3ºN, Zone C2 (Barcelona) 41.4ºN, Zone D3 (Madrid) 40.3ºN and Zone E1 (Leon) 42.6ºN. The solar collectors are oriented to the south.

The solar tank volume is 0.2 m^3 and its maximum temperature is 80 ºC. The solar collector efficiency is shown in equation (1).

$$\eta = 0.757 - 3.994\frac{\Delta T}{I} - 0.009\frac{\Delta T^2}{I} \qquad (1)$$

In equation (1), $I\left[\frac{W}{m^2}\right]$ is the inclined surface solar radiation and ΔT [ºC] the temperature difference between water and outdoors, equation(2).

$$\Delta T = \frac{T_{w,in}+T_{w,out}}{2} - T_{outdoors} \qquad (2)$$

The boiler is connected in series with the solar system and it turns on when the output temperature of the solar tank does not reach the DHW temperature of 45 ºC. The boiler maximum capacity is 20kW with modulating control.

System 4: Thermal solar with electric boiler. The solar system has the same characteristics as the previous case, but now the system is connected to the tank of system 2, Fig. 3. The specifications of this tank are the same as case 2.

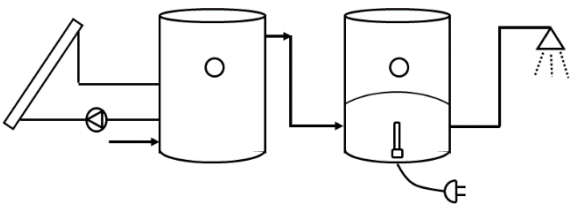

Fig. 3 – Diagram of the thermal solar system with electric boiler.

System 5: Heat pump. This system uses a heat pump as heat generator. For this, the condenser is inside the storage tank. The heating capacity of the condenser and the COP of the heating pump depends on the air and water temperatures. These relations are depicted in Fig. 4 and Fig. 5. The tank volume is 0.2 m^3 and it is located outside. The maximum set point temperature of the tank is 60 ºC.

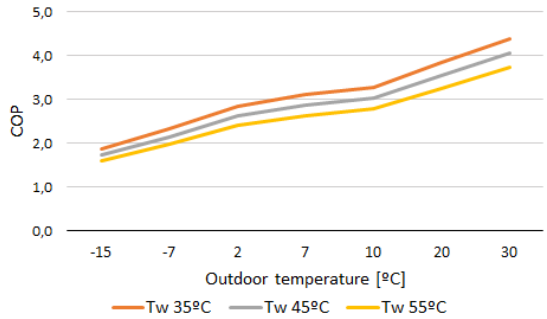

Fig. 4 – Heat pump COP.

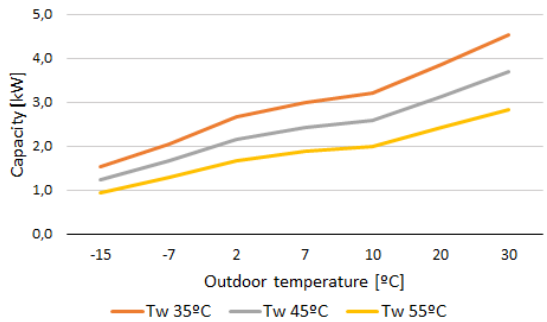

Fig. 5 – Heat pump capacity.

Heat pump reduces its capacity and performance noticeably when outdoor temperature drops below 5 ºC. The minimum outdoor operating temperature is -15 ºC and the maximum 45 ºC.

System 6: Photovoltaic with electric boiler. This system is the same as case 2 with the incorporation of a photovoltaic generator. The electric boiler uses electricity from the photovoltaic system if available. Otherwise, it is connected to the electrical network. The solar panels are oriented to the south and the tilt angle equal to the site latitude. The peak power of the photovoltaic array is 1.82 kW and the inverter efficiency is 0.96.

System 7: Photovoltaic with heat pump. This system is the same as case 5 with photovoltaic generator, Fig. 6. The solar system has the same specifications as the previous case.

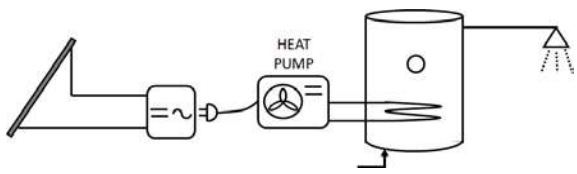

Fig. 6 – Diagram of the photovoltaic system with heat pump.

3. Results and Discussion

3.1 Energy analysis

Tab. 1 shows the energy consumption of each system in each climatic zone. It must be taken into account

that systems 1 and 3 uses natural gas, while the rest electricity. Systems 1 and 2 are the most common in Spain and results show these have the highest consumption.

The most demanding systems are gas boiler and electric boiler. Scoccia [7] obtains a similar trend when comparing systems for DHW production and heating. The system with the lowest energy consumption in all climatic zones is the solar thermal system with gas boiler. The incorporation of solar energy reduces considerably the energy consumption. Comparing system 1 and 3, this reduction con reach 95% in the warmest zone and 69% in the coldest.

Comparing electrical systems 2 and 5 without any kind of solar support, the use of heat pumps reduces the electricity consumption between 65-52%. It is a significant reduction considering that systems require a similar installation. The incorporation of a PV system (systems 6 and 7) represents a reduction of 25-30% in system 2 and 40-50% in system 5. Although this energy reduction is important, it must be taken into account that the cost of the installation increases considerably and with current energy values it is not economically viable, Tab. 4.

Tab. 1 – Final energy in kWh per year.

DHW System	A4	B3	C1	C2	D3	E1
1	2050	2126	2255	2184	2236	2406
2	2306	2394	2552	2475	2534	2732
3	**90**	**176**	**554**	**513**	**539**	**748**
4	330	434	829	781	822	1051
5	791	850	993	955	1096	1306
6	1563	1630	1888	1818	1838	2034
7	397	440	**553**	**531**	641	796

3.2 Renewal percentage

Tab. 2 shows the renewable part of the total energy used for heating the water. This value is calculated with equation (3).

$$Ren(\%) = 100\left(1 - \frac{E_{final}}{E_{total}}\right) \quad (3)$$

The solar thermal systems have in general the greater use of energy from renewable sources. For climates C (template-cold), heat pump system with PV support has a renewable utilization value similar than the solar thermal system.

The use of heat pump (system 5) allows to reduce the consumption of electricity thanks to its high performance. In this system, the renewable energy is between 53-66%. Spanish regulations [2] require a value greater than 60% for newly built homes. This means that this system would comply with the regulations in zones A, B and C. The use of an integrated PV system increases this ratio and allows conforming with the minimum required by the regulations in all climatic zones.

Tab. 2 – Renewable percentage.

DHW System	A4	B3	C1	C2	D3	E1
1	0%	0%	0%	0%	0%	0%
2	0%	0%	0%	0%	0%	0%
3	**96%**	**93%**	**77%**	**79%**	**78%**	**71%**
4	87%	83%	70%	71%	70%	64%
5	66%	65%	62%	62%	57%	53%
6	32%	32%	26%	27%	27%	26%
7	83%	82%	**79%**	**79%**	75%	71%

3.3 CO_2 emissions

CO_2 emissions are related with the final energy consumption of each system and the kind of fuel used. The coefficients used for calculating the equivalent CO_2 emissions are the same used for the energy building certification [8]. The coefficient for electricity is 0.331 $kgCO_2/kWh$ and for natural gas is 0.252 $kgCO_2/kWh$.

This difference in the coefficients slightly favours the systems that uses natural gas (1 and 3). Thus, thermal solar with gas boiler (system 3) has the lowest environmental impact in all climates. Only in zones C, the heat pump and PV has a similar value of equivalent emissions.

These results will be different depending on the conversion coefficients used in each country [9]. In this case, the difference between natural gas and electricity coefficients is not so significant as to alter the existing relationship with the final energy consumption.

Tab. 3 – CO2 equivalent emissions in $kgCO_2$/year.

DHW System	A4	B3	C1	C2	D3	E1
1	517	536	568	550	564	606
2	763	793	845	819	839	904
3	**23**	**44**	**140**	**129**	**136**	**189**
4	109	144	274	259	272	348
5	199	214	250	241	276	329
6	517	540	625	602	608	673
7	100	111	**139**	**134**	162	201

3.4 Economic analysis

The economic analysis has been done taking into account current energy and system prices. Product inflation has not been considered. The subsidies and strategic incentive policies that exist have not been taken into account either (for example for PV installations in Spain). The average price of electricity is 0.17 €/kWh [10] and the price of natural gas 0.0553 €/kWh [11].

The capital price of the installation and the maintenance cost have been obtained by consulting different companies, Tab. 4. Be aware that these prices may fluctuate depending on the demand, the brand of the product and the company. The total cost of the installation has been analysed over a 15-year horizon. The cost includes the capital cost, annual maintenance and the operational cost, assuming a fixed cost of fuel throughout the indicated period.

Tab. 4 –Capital and maintenance cost of systems in €.

DHW System	Capital cost [€]	Annual maintenence [€]
1	380	95
2	330	30
3	**2920**	**285**
4	2870	220
5	1530	75
6	3180	350
7	4380	395

The results obtained for each system in each climatic zone are shown in Tab. 5. These results show the discrepancy between economic and environmental profitability. The simplest systems (with fewer components) are the cheapest in a 15-year life horizon (Systems 1 and 5). This is due to the fact that the low cost of installation and maintenance compensate for the energy inefficiency. Remember that inflation on the price of energy has not been considered, but the difference with respect to the results of the other systems gives a wide margin for this trend to continue. The low price of gas compared to electricity and the simplicity of the gas boiler system make it the most economical, despite having one of the greatest environmental impacts.

Solar systems increase the cost of installation between 750-850% (systems 1,2 vs systems 3,4) and have higher maintenance costs due to the greater number of elements and their exposure to the outside conditions. These drawbacks mean that their current cost does not compensate for the savings caused by reducing energy consumption (in economic terms).

For systems with PV contribution, two scenarios have been considered: the worst (system 6 pess. and 7 pess.), in which the solar system is only used for the DHW system; and the optimal case, (system 6 opt. and 7opt.) in which it is considered that all the energy that is not used in the DHW system is consumed by the building in other uses. Clearly, a PV system dedicated solely to the production of DHW is not economically viable without any type of government incentive. PV support for the heat pump be profitable only in climates with great amount of radiation, taking into account that all the energy produced is consumed in the home (self-consumption).

The cost of annual operation and maintenance of the gas boiler and the heat pump with the current prices of their fuels is very similar. The parameter that makes the cost of the heat pump more expensive is currently its capital cost, which is 4 times higher than the boiler. A decrease in the price of this type of equipment, a government incentive or a decrease in the price difference between gas and electricity would favour the use of the heat pump over the gas boiler and would allow the reduction of equivalent CO2 emissions.

Tab. 5 – Total life cost in k€.

DHW System	A4	B3	C1	C2	D3	E1
1	**3,44**	**3,50**	**3,61**	**3,55**	**3,59**	**3,73**
2	6,56	6,76	7,14	6,96	7,09	7,65
3	7,27	7,34	7,64	7,61	7,63	7,79
4	6,96	7,23	8,22	8,11	8,21	8,78
5	**4,61**	**4,77**	**5,11**	**5,02**	**5,34**	**5,85**
6 pess.	12,20	12,36	13,00	12,85	12,86	13,44
6 opt.	6,51	7,13	8,69	8,36	8,23	9,19
7 pess.	11,20	11,31	11,56	11,51	11,74	12,11
7 opt.	**3,55**	**4,10**	**5,57**	**5,36**	**5,34**	**6,15**

4. Conclusions

The article analyses seven DHW systems for single-family homes: gas boiler, electric boiler with and without PV, solar thermal with gas boiler or electric boiler and heat pump with and without PV. The study includes energy, environmental and economic analysis in six climatic zones: A4, B3, C1, C2, D3 and E1 from the warmest to the coldest.

In energy terms, the incorporation of solar thermal energy implies a reduction in consumption of 69-95% in the gas boiler system, while the incorporation of PV implies a reduction of 40-50% in the heat pump system and 25-30% in the electric boiler. This represents a use of energy from renewable sources of approximately 70-95% in solar thermal systems and 70-83% in PV system with heat pump.

Despite this reduction in energy consumption and with current market conditions, these values are not sufficient to make solar systems economically profitable due to its high capital cost.

The heat pump system seems to be the best economic alternative to the gas boiler to achieve a reduction in the environmental impact of the DHW installations in the residential sector, although economic incentives are still necessary to improve their profitability. In addition, in an optimal scenario, the incorporation of PV would allow a saving of around 50% of energy in the warmest climates and it slightly reduce the total life cost of the system.

5. References

[1] D. B. Crawley, C. O. Pedersen, L. K. Lawrie, and F. C. Winkelmann, "EnergyPlus: Energy Simulation Program," *ASHRAE J.*, vol. 42, pp. 49–56, 2000.

[2] Spanish-Government, "Codigo Tecnico de la Edificacion. Documento Basico HE." http://www.codigotecnico.org/web/recursos/documentos/dbhe/, 2007.

[3] Spanish government, "MAPAS CLIMÁTICOS DE ESPAÑA (1981-2010) Y ETo (1996-2016)," 2016.

[4] U. Jordan and K. Vajen, "Influence of the DHW load profile on the fractional energy savings: A case study of solar combi-system with TRNSYS simulations," *Sol. Energy*, vol. 69, no. prEN 12977, pp. 197–208, 2001.

[5] J. Widén, M. Lundh, I. Vassileva, E. Dahlquist, K. Ellegård, and E. Wäckelgård, "Constructing load profiles for household electricity and hot water from time-use data-Modelling approach and validation," *Energy Build.*, vol. 41, no. 7, pp. 753–768, 2009.

[6] J. C. Evarts and L. G. Swan, "Domestic hot water consumption estimates for solar thermal system sizing," *Energy Build.*, vol. 58, pp. 58–65, 2013.

[7] R. Scoccia, T. Toppi, M. Aprile, and M. Motta, "Absorption and compression heat pump systems for space heating and DHW in European buildings: Energy, environmental and economic analysis," *J. Build. Eng.*, vol. 16, no. July 2017, pp. 94–105, 2018.

[8] IDAE, "FACTORES DE EMISIÓN DE CO2 y COEFICIENTES DE PASO A ENERGÍA PRIMARIA DE DIFERENTES FUENTES DE ENERGÍA FINAL CONSUMIDAS EN EL SECTOR DE EDIFICIOS EN ESPAÑA," 2016.

[9] UK Government, "2018 GOVERNMENT GHG CONVERSION FACTORS FOR COMPANY," no. July, 2018.

[10] Eurostat, "Electricity prices for household consumers." [Online]. Available: http://appsso.eurostat.ec.europa.eu/nui/submitViewTableAction.do. [Accessed: 30-Dec-2021].

[11] Eurostat, "Natural gas prices for household consumers." [Online]. Available: https://ec.europa.eu/eurostat/statistics-explained/index.php?title=Natural_gas_price_statistics#Natural_gas_prices_for_household_consumers.

Modelling of District Heating Systems: Comparative Evaluation of White-box Modelling Approaches

Guokai Chen [a], Ivan Korolija [a], Dimitrios Rovas [a]

[a] Institute of Environmental Design & Engineering, University College London, London, United Kingdom, guokai.chen.17@ucl.ac.uk.

Abstract. District heating systems are prevalent in most European countries, and such energy delivery methods can be crucial to decarbonisation objectives. To appropriately size and design the control of such networks, the modelling of district heating networks should have a good representation of the demand-side, which is the set of buildings connected to the network. Instead of simplified modelling of the demand, whole-building simulation tools can be invoked in this case, like EnergyPlus. More recently, equation-based libraries have been developed in Modelica for component-based simulation of HVAC systems. Modelica-based libraries offer easier model composability and are particularly interesting for control fine-tuning; on the downside, the model setup can be more complex, with more validation needed.
This paper conducts a comparative study of the Modelica LBNL Buildings library against EnergyPlus, based on an archetype-based hypothetical case in the UK with a small-scale district heating system. The methodology resides on models developed in the two tools with the same level of modelling detail. The comparison helps understand software differences in the modelling procedure, computational time, relative accuracy of energy predictions and heating system variables. The results indicate Modelica Buildings library yields similar accuracy in terms of heat transfer calculation through thermal zones as EnergyPlus, whilst capturing additional energy consumption caused by the dynamic changes at system startup and the realistic controllers used in the Modelica district heating models. Meanwhile, the Modelica Buildings library's outputs show the fluctuations of system variables, indicating different operation patterns and control effects against EnergyPlus. This study also proves that the Modelica Buildings library is the better tool for district heating simulation in the context of dynamic performance evaluation and control testing, based on overall capabilities, limitations, and prediction differences.

Keywords. Modelica, Buildings library, EnergyPlus, District heating system, Comparative evaluation.
DOI: https://doi.org/10.34641/clima.2022.359

1. Introduction

District heating systems (DHS) are critical enablers to reduce carbon emissions, as they can improve operational efficiency and integration with distributed renewable energy sources. It is estimated that by 2050, around 18% of heating demand in the UK will be satisfied by district heating networks [1]. With the new generation district heating networks relying on distributed energy sources and digital technologies, advanced control strategies are bound to become more dominant and widely used. Meanwhile, the development of Building Energy Simulation (BES) tools and their integration in design workflows has highlighted the value of building and HVAC system design and operation. As an application of BES software, a proper simulation-based model of district heating system would significantly support the decision-making process, optimise the control strategies, facilitate diagnosis of potential performance gaps and ultimately reduce the energy consumption of district heating system [2, 3].

In recent years, state-of-the-art simulation programs such as EnergyPlus have enabled highly accurate building- and district-level simulations [4]. These tools proved highly successful but also with limitations: the unclear separation of the integration methods with the models imposes restrictions on such tools' modelling capabilities and extensibility. One such example is the modelling of hybrid thermal and electrical energy networks. The more precise separation of concerns led to general-purpose modelling specifications like the Modelica language, which advocates an acausal, component-oriented, equation-based modelling approach. Although de-

Copyright ©2022 by the authors. This conference paper is published under a CC-BY-4.0 license.

veloped initially for other industry verticals, the benefits in energy modelling are now appreciated. Several building-related libraries in Modelica have been developed, such as the LBNL Buildings library [5]. The library provides detailed room models like EnergyPlus and HVAC and controls components for dynamic simulations. Recent research has already found several remarkable merits and weaknesses of the Modelica libraries. Modelica uses acausal couplings between components, brings fewer constraints and general coupling directions during the model development, and adopts variable time steps during simulations [6, 7]. However, as Modelica building-related libraries are brand-new for developers and users, their capabilities and potentials have not been yet evaluated, especially in district heating studies. Therefore, this paper conducts a comparative software assessment to understand the relative differences between the two tools. A comparative evaluation can be practical since models with different levels of detail can be tested without any empirical data from actual buildings [8].

2. Analytical comparison of EnergyPlus and Modelica libraries

In the study of district heating systems, EnergyPlus is a detailed energy simulation tool in demand-side calculations and is suitable for HVAC system simulations [2, 4]. It was initially designed for building-level simulation, but the continued development of EnergyPlus has resulted in the addition of new features, including the capabilities to support district energy simulations. In the demand side calculation, EnergyPlus provides a convenient process to develop 3D geometry of building envelope model assisted by SketchUp plugin, which gives users capabilities to construct detailed building models. Meanwhile, in the HVAC calculation, EnergyPlus allows to build up component-based system layouts by linking "nodes" together and provides idealised system controllers such as the setpoint manager and the system availability manager to adjust temperature setpoints and the on/off states of HVAC systems. As a HVAC component, boiler models are available in EnergyPlus [4], and small-scale district heating systems can be simulated under the plant loop simulation. For example, Andrić et al. [9] used EnergyPlus to simulate the district heating demands, with a plant-loop simulation to compute a small-scale district heating system. Furthermore, as EnergyPlus has been developed for many years, it has been well validated by Building Energy Simulation TEST (BESTEST) and HVAC BESTEST [10], so many industry standards recognise it as the most acceptable tool to be compared with other simulation tools. Hence, EnergyPlus provides a detailed envelope model development procedure and is regarded as a reference tool in the demand-side calculation.

Meanwhile, Modelica is a component-oriented and object-oriented language, initially for large-scale physical models [5]. Recent studies have identified advantages in Modelica compared to state-of-the-art BES tools such as EnergyPlus [11] and TRNSYS [12]. First, Modelica adopts acausal language instead of the causal modelling used in EnergyPlus, which is advantageous for showing system structures and connecting different components. Li et al. [13] and Schweiger et al. [14] concluded that the acausal characteristic of the language could lead to developing more coherent HVAC component models. Conversely, EnergyPlus integrated those numerical solvers with equations, followed by declaring execution sequences and changing program states, so it is tricky to integrate with existing equations when creating new models [6, 15]. Second, Modelica provides capabilities to simulate dynamic components with more advanced controls. At the same time, EnergyPlus usually assumes steady-state and idealised controllers if not enabling the features from Energy Management System in EnergyPlus [7, 16]. In Modelica, the simulation timestep also varies to ensure proper integration and avoid inaccurate results caused by the averaging performance over a fixed time step [6]. Third, unlike single-domain EnergyPlus, a few Modelica libraries have already adapted to multi-scale models and developed the increasing number of systems in district heating domains. Since 2007, the Buildings library has been developing into an open-source tool with over 500 validated components such as detailed envelope models, multi-zone airflow, occupants, fluid dynamics, HVAC components and advanced controllers [5, 17]. With these advantages, it is feasible for us to integrate building-level and district-level components for the district heating simulation. District energy system cases were also tested under the IEA EBC Annex 60 project [7] and are further validated in IBPSA Project 1 [18].

Recently, a developing tool, Spawn of EnergyPlus (SOEP), enables the coupling between the Modelica Buildings library and EnergyPlus [19]. SOEP reuses the calculations of building models in EnergyPlus with the support of HVAC and control models from the Buildings library. It automatically sets up a co-simulation framework and can combine the "best" performance from both EnergyPlus and Buildings library. However, since SOEP is still in development and public users preferred to use a single tool during the modelling rather than co-simulating between tools, this paper mainly focuses on making a standalone-software comparison, highlighting the differences in building-level and system-level simulations, respectively.

3. Methodology

3.1 Case description

A conceptual case of a district heating system was developed and executed in the Buildings library and EnergyPlus, simultaneously following the same modelling procedures to compare software performance in district heating simulations. Different building typologies were considered to form up buildings in the district heating cases. Building ge-

ometry and parameters were selected from English archetypes meta-models generated by Symonds et al. [20], which is based on the 2010-2011 English Housing Survey [21]. According to the top three dominant dwelling types from English Housing Survey, five detached houses (D), two semi-detached houses (S) and three terrace houses (T) were selected to form a street layout in the district model, demonstrated in Figure 1. Each dwelling was regarded as a single thermal zone, and internal surfaces were not detailed since we focused on energy consumption per house. The network shown in Figure 1 was designed as a branch of the radial heating network, with pre-insulated water pipes connected with the heating source.

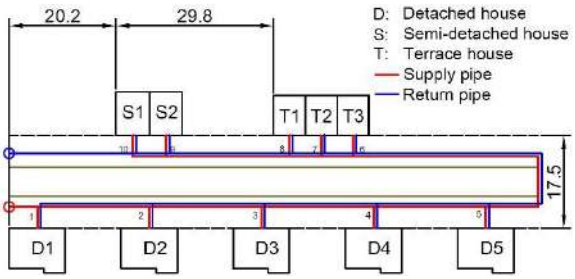

Fig. 1 – Typology of proposed district heating network.

A proper district heating system layout was designed for the two models in the comparative evaluation of white-box modelling approaches. Major components in DHS include boilers as heat sources, distribution network, radiators in each of the ten dwellings as the heating emitters [22]. A bypass connection between the supply pipe and return pipe controls the proper amount of hot water into radiators. The heating network's nominal supply and return water setpoints were 75 °C and 65°C, and the room air setpoint was 20°C, per the British standard [22, 23]. Pipelines, radiators, and boilers were sized correctly and based on the manufacturer database. Other relevant building and HVAC parameters are given in the appendix.

Before forming a complete heating system, a P controller and a PI controller were adopted to adjust the room air temperature and water outlet temperature from the heating source, respectively. In addition, control parameters in the heating system were fine-tuned to reduce system oscillations and avoid unstable operations in the simulation.

As comparative testing, this study obtained all identical building and HVAC parameters and then input those parameters into both tools to control external discrepancy [8]. Hence, we generated the two comparative models in Modelica and EnergyPlus, respectively, demonstrated in Figures 2 and 3. Modelica models were built by simply linking the models of heating system components and their controllers with each other, while in EnergyPlus, all components were connected with a list of nodes, and the control was modelled as a system variable or as a high-level controller attached in the node. Therefore, some control parameters cannot be executed in EnergyPlus, which leads to alternative modelling approaches with similar settings. For the inter-software comparison, we consider the relative deviations in predictions, computational costs, modelling capabilities and limitations as the comparison indices.

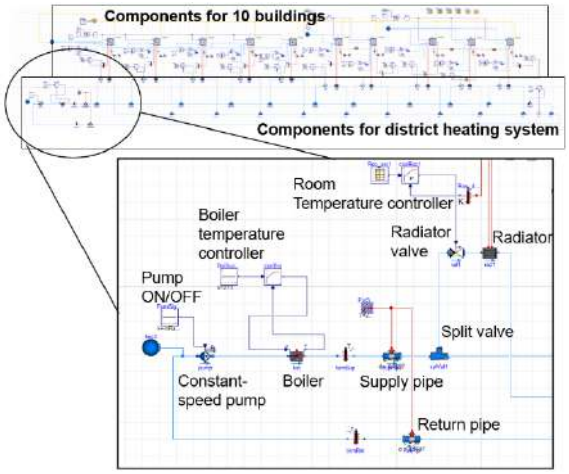

Fig. 2 – Modelica district heating model in Dymola.

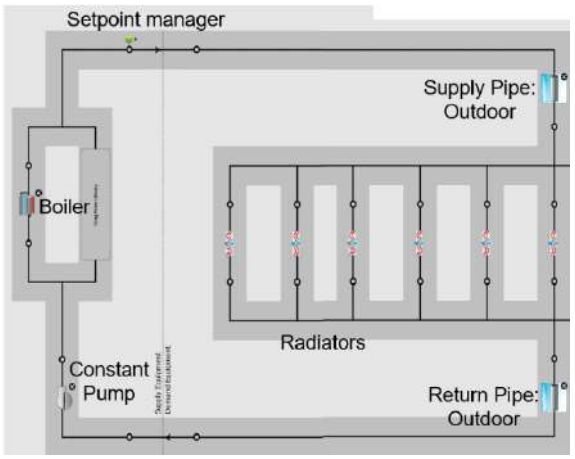

Fig. 3 – District heating model in EnergyPlus, visualized in Openstudio.

3.2 Modelling environment

The Modelica model was developed in Dymola, a commercial implementation of the Modelica specification; this is one option, with others open-source but less mature, such as OpenModelica. The model also used components from the Modelica Standard Library 3.2.3 and the LBNL Buildings library 5.0.1. Comparatively, EnergyPlus version 8.9 was used in the simulation. All simulations in the Modelica Buildings library and EnergyPlus were executed in the same computer with Intel Core i7-7700HQ 8-core 2.80GHz processor. Recommended by the Buildings library, we used the DASSL solver (A Differential/Algebraic System Solver) [24] with a tolerance of 0.001 in the Modelica-related simulation.

3.3 Comparison criteria

We introduced a series of validation steps in the district heating system, in a matter akin to BESTEST [10], to perform a better software comparison. The

iterative validations included building-level comparisons evaluated by the free-floating temperature in Case 1FF, the heating demands in Case 1 and the cross-comparison on heating demands and energy consumption between Cases 2 to 4. Detailed descriptions of the iterative validated steps are shown in Table 1. These iterative validations demonstrated the potential impacts of models with different levels of detail on their simulation results, which facilitated locating the cause-and-effect in the comparative evaluation. The deviations of software accuracy, therefore, would be quantified as the bias error, relative deviation σ and Root Mean Square Error (RMSE), given in equations (1), (2) and (3), respectively, where $\hat{y}(t)$ and $y(t)$ represent the model results from the Buildings library and EnergyPlus respectively at the time n.

$$\Delta(t)=\hat{y}(t)-y(t) \tag{1}$$

$$\sigma = \frac{\hat{y}(t)-y(t)}{y(t)} \tag{2}$$

$$RMSE = \sqrt{\frac{\sum_1^n[\hat{y}(t)-y(t)]^2}{n}} \tag{3}$$

Tab. 1 – Descriptions of iterative validation cases.

Name	Descriptions
Case 1FF	Free-floating buildings
Case 1	Add the ideal air heating system from Case 1FF
Case 2	Add heating components in buildings from Case 1
Case 3	Add the heating network and boiler from Case 2
Case 4	Add heating schedules from Case 3

4. Result analysis

4.1 Heating demands (Case 1 and Case 1FF)

As a part of comparative evaluation of white-box modelling approaches, the accuracy of demand-side modelling could heavily affect the following district heating system predictions. The free-floating temperature was a crucial index to justify the accuracy of heat transfer through the envelope. Figures 4 and 5 illustrate the daily and yearly difference of free-floating temperature of detached house 1 in Case 1FF. Predictions from both tools were quite similar, with mean bias error and RMSE being close to 0. The similarity of the results showed that Modelica simulation could deliver accurate heat transfer calculations as EnergyPlus. However, minor deviations were found, including continuous half-hour delays in the daily results from the Buildings library possibly caused by different translations of weather profiles and a significant variation in the first week of yearly profiles due to the lack of warm-up procedures in the Modelica Buildings library.

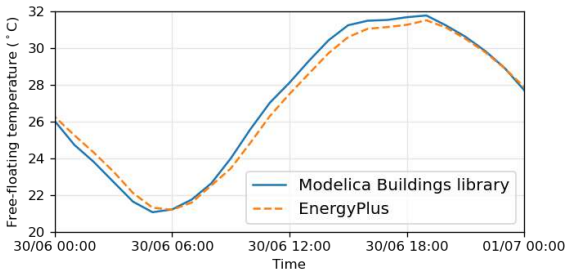

Fig. 4 – Comparison of daily free-floating temperature on Jun 30th.

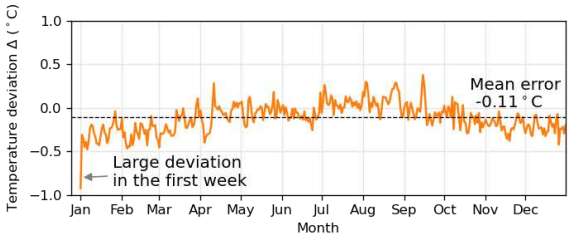

Fig. 5 – Deviations on yearly free-floating temperature.

Table 2 describes the annual heating load in the demand side of each archetype in Case 1. However, it was estimated that the annual heating demands of each archetype in the Buildings library were about 3.3% lower than the EnergyPlus results. This means that Modelica models required less energy to heat the space, attributed to the heat transfer process between the radiators and room air. It could be caused by the room models in the Buildings library were not accounting for detailed geometries, leading to the difference of surface areas. Since the 3% deviation was not significant, it proved that the model developed in the Buildings library had accurate building-level calculation as EnergyPlus even though the models in the Buildings library were built from simplified geometry inputs.

Tab. 2 – Calculation and comparison of each archetype's annual heating demands (kWh/m²) in Case 1.

Archetype	Buildings library	Energy-Plus	Relative deviation
Detached	208.19	215.01	-3.17%
Semi-detached	199.79	206.64	-3.31%
Terrace	181.15	187.16	-3.21%

4.2 Evaluation of iterative cases

A series of iterative cases were tested to identify the effects of model complexity on the model prediction from the Buildings library and EnergyPlus. These four cases were related to different heating system configurations, from simplified to detailed levels. Table 3 and Figure 6 show the daily heating demands in winter. Significant deviations were observed after implementing the district heating system in Case 4 since the mean bias error grew from -5.05 kWh to 10.28 kWh. A higher value of RMSE in Case 4 also indicated that results from the Buildings library had more considerable oscillations. Meanwhile, a lower prediction from EnergyPlus in Case 4

was observed as it adopted idealised controllers instead of realistic and less-ideal PI controllers. Figure 7 demonstrates the case comparison on the annual total energy consumption between these iterative cases from both software, indicating increased deviations observed in more complicated models. From Cases 2 to 4, the Buildings library had higher energy consumption than EnergyPlus by 2.75%, 3.94% and 10.18%, respectively. It could be explained by the extra energy consumption from extra components in Modelica models, such as the valves in the heating network. Thus, these differences in Modelica highlight the energy consumption from realistic HVAC and control components, with more capabilities in the district heating models.

Tab. 3 – Deviations of daily heating demands in Case 1 against Case 4.

Deviations	Case 1	Case 4
Mean bias error (kWh)	-5.05	10.28
Relative deviation (%)	3.39	8.96
RMSE (kWh)	6.14	10.64

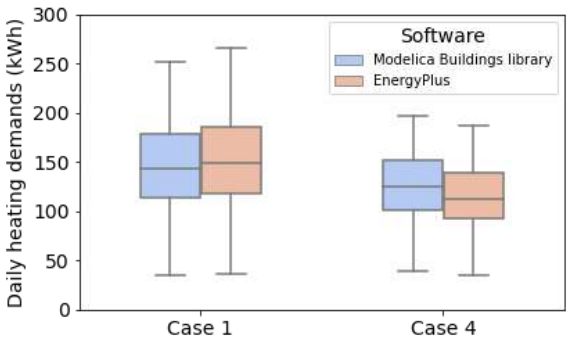

Fig. 6 – Predictions of average daily heating demands of detached house 1 in Case 1 against Case 4 in winter.

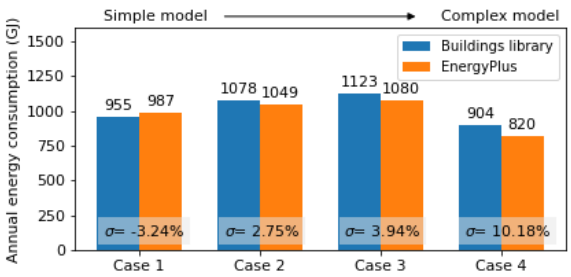

Fig. 7 – Comparison on annual energy consumption of iterative cases: Case 1 to Case 4.

4.3 Heating system variables

Figure 8 depicts a different prediction of hot water return temperature in Case 4, with operation hours displayed in grey. It showed that both tools computed close results, but a lower return temperature was captured in the Buildings library. Moreover, significant discrepancies were found when the heating system switched on. The Buildings library captured a lower return water temperature at around 55 °C before reaching a stable temperature. An analysis of the district heating system done by Kicsiny [25] proved that control errors in a heating system caused this type of fluctuation. By contrast, the temperature in EnergyPlus was kept above 65 °C, as the controllers were idealised without considering the transient process, and the simulation was executed in a fixed time step. Hence, EnergyPlus could only examine limited errors in the system variables, particularly in the transient condition.

Furthermore, a different characteristic was found in the part-load condition when contrasting the boiler's power and water flow rate variables through radiators, given in Figures 9 and 10. It was found that the model in the Buildings library simulated a one-half flow rate at around 0.5 kg/s and a slightly lower heating power at the part-load condition, compared to the results from EnergyPlus. Meanwhile, in Figure 11, the outlet temperature of radiators in the Buildings library was consistently lower than that of EnergyPlus, typically sending water at 50°C at the part-load operation against around 62 °C in EnergyPlus. A possible explanation was that two tools used different ways to compute the hot water distribution in heating networks. EnergyPlus could maximise the flow rate through the radiators to ensure the design temperature difference between the inlet and outlet, and then distribute the extra amount of water into the bypass branch. However, the Buildings library with pressure-based calculations varied the water flow rate according to the resistances in each branch, which caused a dramatic difference in the comparison.

4.4 Computational cost

Simulation time was a crucial index to estimate the computational cost of each modelling tool. Figure 12 shows the simulation time with the average simulation timestep of the free-floating case (Case 1FF) against the district heating case (Case 4) in two modelling environments. In the free-floating case, although Modelica adapted to a longer time step, its computational time was still higher than most simulations in EnergyPlus, due to higher computational cost caused by the transit conduction algorithms in the heat transfer calculation. Moreover, after adding heating system components, the DASSL solver in Modelica simulation reduced its timestep automatically, while its computational time was even higher than the EnergyPlus' one. Therefore, it proves that Modelica spent higher computational costs in a model with more controllers.

5. Discussion

As developed to be the basis of the next-generation tool, the Modelica Buildings library has been validated under BESTEST [5]. In terms of relative accuracy, our findings revealed that the Modelica Buildings library performed proper heat transfer calculations, although the Building library's model did not use the 3D building geometry. The results conclude that lower detail levels in geometry does not affect the overall heating demand calculation significantly.

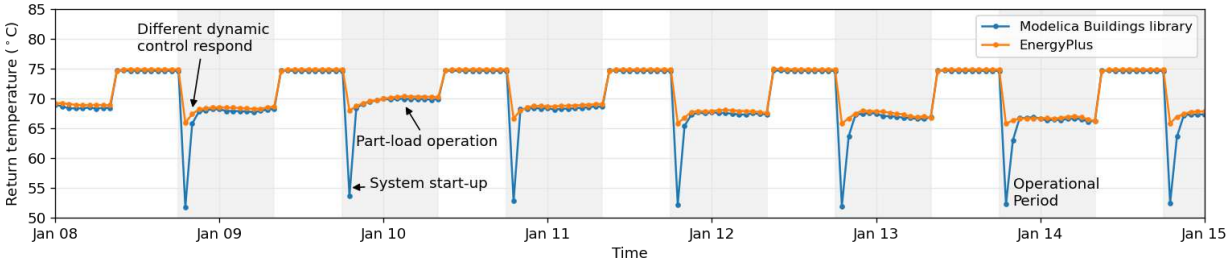

Fig. 8 – Comparison on hot water return temperature in Case 4.

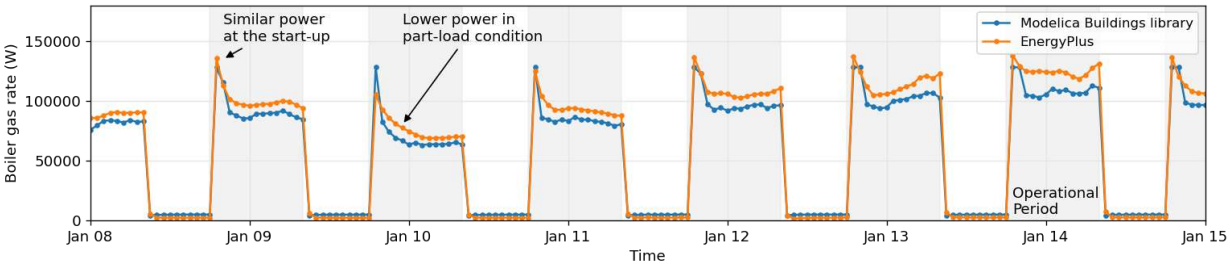

Fig. 9 – Comparison on boiler power rate in Case 4.

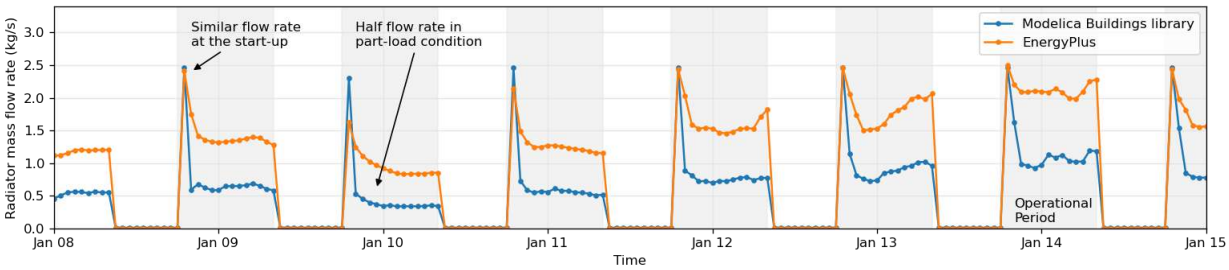

Fig. 10 – Comparison on total mass flow rate of all radiators in Case 4.

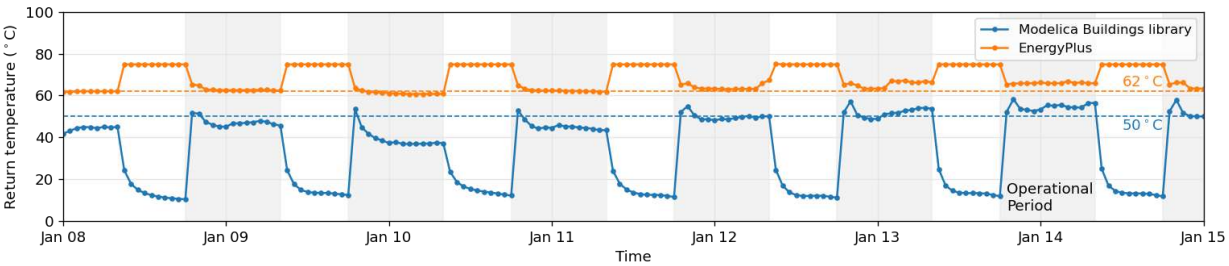

Fig. 11 – Comparison of radiator outlet temperature in detached house 1 in Case 4.

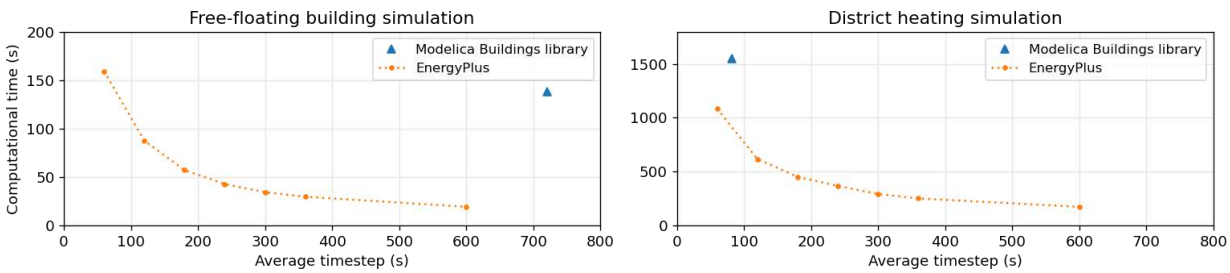

Fig. 12 – Comparison of simulation time in two cases (Case 1FF and Case 4) with different timesteps.

However, a substantial deviation was found when the heating system was involved. On the one hand, discrepancies between Modelica and EnergyPlus grew gradually with a more complicated system introduced, which proves that Modelica Buildings library uses less idealised models than EnergyPlus. On the other hand, the Buildings library captures the dynamic response from the control system, such as the startup period. Wetter et al. [26] stated that modelling an actual control sequence can reduce up to 30% HVAC energy consumption. Therefore, the Buildings library computes dynamic behaviour correctly, provides accurate control modelling, and ultimately reduces the performance gap caused by model simplification.

Surprisingly, the Buildings library did not reduce computation cost in the district heating system model, especially for the free-floating building model. It is probably due to (1) thousands of DAEs lead-

ing to inefficient coding in the detailed zone model; (2) too many closed-loop controllers involved in the model, which leads to higher computational cost when the states or the values of the controllers are changed [27]. These consequence indicates that adopting co-simulation by coupling EnergyPlus with Modelica would be a worthwhile endeavour to reduce computational complexity.

Based on the current findings, we summarise in Table 4 the capabilities and limitations of these two white-box modelling approaches. For example, the Buildings library has more detailed options to model the district heating system but it is more restricted in capturing building geometry. On the other hand, the district heating system implemented in EnergyPlus is entirely controlled by the idealised controllers and has unrealistic assumptions on the bypass water flow rate. Such comparisons and summaries have been acknowledged by the development of SOEP [19], which aims to avoid software limitations and use all capabilities by setting up the co-simulation framework.

Tab. 4 – Capabilities and limitations of the Modelica Buildings library against EnergyPlus.

Level	Simulation aspect	Buildings library	Energy-Plus
Building	Geometry	N	C
	Shadow calculation	N	C
District	Radiator	C	I
	Valve	C	N
	Bi-directional flow	C	N or I
Control		C	I

Note: C: Capable; N: Not capable; I: Idealised.

6. Conclusion

Overall, this study is a comparative evaluation of different white-box modelling approaches, between the Modelica LBNL Buildings library against EnergyPlus, based on a conceptual case of a district heating system. The Buildings library yielded similar outputs as EnergyPlus at the demand side in the case-by-case comparisons. However, significant deviations were found at the district system level after adding realistic controllers into the heating network. It indicates that only the Modelica Buildings library could capture dynamic changes and compute active energy consumption previously omitted by EnergyPlus. The analysis also suggests that the Modelica Buildings library is less computationally efficient than EnergyPlus in a model with higher level of details. This comparative evaluation summarizes different capabilities of two modelling approaches, which is beneficial for the selection of district heating modelling tools. As co-simulation would become more accessible, future work could focus on improving co-simulation frameworks to avoid software limitations and make a trade-off between prediction accuracy and computational cost.

7. Acknowledgements

The datasets generated during and analysed during the current study are available in the repository, https://doi.org/10.5522/04/19393973. The research leading to these results has been partly supported by the European Commission Horizon 2020 project BIMERR under grant agreement No 820621.

8. Appendices

Tab. 5 – Other information for model development.

Parameters	Description
Location	London
Boiler capacity	108800W
Boiler efficiency	0.849
Radiator capacity	14100W (Detached); 8500W (Semi-detached); 7100W (Terraced)
Pipe length	50m (Supply); 50m (Return)

9. References

[1] UK Government. Heat networks - GOV.UK [Internet]; 2021 [cited 2021 Dec 16]. Available from: https://www.gov.uk/guidance/heat-networks-overview.

[2] Allegrini J, Orehounig K, Mavromatidis G, Ruesch F, Dorer V, Evins R. A review of modelling approaches and tools for the simulation of district-scale energy systems. Renewable and Sustainable Energy Reviews. 2015;52:1391–1404.

[3] Harish VSKV, Kumar A. A review on modeling and simulation of building energy systems. Renewable and Sustainable Energy Reviews. 2016;56:1272–1292.

[4] Crawley DB, Lawrie LK, Winkelmann FC, Buhl WF, Huang YJ, Pedersen CO, et al. EnergyPlus: Creating a New-Generation Building Energy Simulation Program. Energy and Buildings. 2001;33:319–331.

[5] Wetter M, Zuo W, Nouidui TS, Pang X. Modelica Buildings library. Journal of Building Performance Simulation. 2014;7(4):253–270.

[6] Wetter M. Modelica-based modelling and simulation to support research and development in building energy and control systems. Journal of Building Performance Simulation. 2009;2(2): 143–161.

[7] Wetter M, Van Treeck C. New Generation Com-

putational Tools for Building & Community Energy Systems: Annex 60 Final Report. [Internet]. Paris, France: International Energy Agency; 2017. September [cited 2021 Dec 16]. Available from: http://www.iea-annex60.org/downloads/iea-ebc-annex60-final-report.pdf.

[8] Judkoff R, Neymark J. International Energy Agency building energy simulation test (BESTEST) and diagnostic method. Golden, CO (United States): National Renewable Energy Laboratory (NREL); 1995 February. Report No. NREL/TP-472-6231.

[9] Andrić I, Gomes N, Pina A, Ferrão P, Fournier J, Lacarrière B, et al. Modeling the long-term effect of climate change on building heat demand: Case study on a district level. Energy and Buildings. 2016;126:77–93.

[10] Neymark J, Judkoff R, Knabe G, Le HT, Dürig M, Glass A, et al. Applying the building energy simulation test (BESTEST) diagnostic method to verification of space conditioning equipment models used in whole-building energy simulation programs. Energy and Buildings. 2002;34(9):917–931.

[11] Crawley DB, Pedersen CO, Lawrie LK, Winkelmann FC. EnergyPlus : Energy Simulation Program. ASHRAE Journal. 2000;42(4):49–56.

[12] Klein SA, Cooper PI, Freeman TL, Beekman DM, Beckman WA, Duffie JA. A method of simulation of solar processes and its application. Solar Energy. 1975;17(1):29–37.

[13] Li P, Li Y, Seem JE, Qiao H, Li X, Winkler J. Recent advances in dynamic modeling of HVAC equipment. Part 2: Modelica-based modeling. HVAC and R Research. 2014;20(1):150–161.

[14] Schweiger G, Larsson PO, Magnusson F, Lauenburg P, Velut S. District heating and cooling systems – Framework for Modelica-based simulation and dynamic optimization. Energy. 2017;137:566–578.

[15] Wetter M, Fuchs M, Grozman P, Helsen L, Jorissen F, Lauster M, et al. IEA EBC ANNEX 60 Modelica Library – An International Collaboration to Develop a Free Open-Source Model Library for Buildings and Community Energy Systems. Building Simulation Conference. 2015:395–402.

[16] Jorissen F, Reynders G, Baetens R, Picard D, Saelens D, Helsen L. Implementation and verification of the IDEAS building energy simulation library. Journal of Building Performance Simulation. 2018;1493:1–20.

[17] Zuo W, Wetter M, Tian W, Li D, Jin M, Chen Q. Coupling indoor airflow, HVAC, control and building envelope heat transfer in the Modelica Buildings library. Journal of Building Performance Simulation. 2016;9(4):366–381.

[18] Wetter M, Van Treeck C, Helsen L, Maccarini A, Saelens D, Robinson D, et al. IBPSA Project 1: BIM/GIS and Modelica framework for building and community energy system design and operation - Ongoing developments, lessons learned and challenges. IOP Conference Series: Earth and Environmental Science. 2019;323(1).

[19] Wetter M, Benne K, Gautier A, Nouidui TS, Ramle A, Roth A, et al. Lifting the Garage Door on Spawn, an Open-Source BEM-Controls Engine. In: 2020 Building Performance Modeling Conference; 2020. p. 518–525.

[20] Symonds P, Taylor J, Chalabi Z, Mavrogianni A, Davies M, Hamilton I, et al. Development of an England-wide indoor overheating and air pollution model using artificial neural networks. Journal of Building Performance Simulation. 2016;9(6):606–619.

[21] Communities and Local Government. English Housing Survey Households 2010-11 [Internet]; 2011 [Cited 2021 Dec 16]. Available from: https://www.gov.uk/government/statistics/english-housing-survey-household-report-2010-to-2011.

[22] CIBSE. CIBSE AM14: Non-domestic hot water heating systems. London, UK: The Chartered Institute of Building Services Engineers; 2010.

[23] British Standard. EN 442-2:2014: Radiators and convectors Part 2 : Test methods and rating. Brussels, Belgium: The British Standards Institution; 2014.

[24] Petzold LR. Description of DASSL: a differential/algebraic system solver. Sandia National Labs., Livermore, CA (USA); 1982.

[25] Kicsiny R. Transfer functions of solar heating systems for dynamic analysis and control design. Renewable Energy. 2015;77:64–78.

[26] Wetter M, Hu J, Grahovac M, Eubanks B, Haves P. OpenBuildingControl: Modelling Feedback Control as a Step Towards Formal Design, Specification, Deployment and Verification of Building Control Sequences. In: 2018 Building Performance Modeling Conference and SimBuild. Chicago, IL; 2018. p. 775–782.

[27] Wang K, Greiner C, Batteh J, Li L. Integration of complex Modelica-based physics models and discrete-time control systems: Approaches and observations of numerical performance. In: Proceedings of the 12th International Modelica Conference. Prague, Czech Republic: Linköping University Electronic Press, Linköping University; 2017. p. 527–532.

Dynamic modeling and simulation of a centrifugal chiller based on MBSE

Yoonjei Hwang, Hanyoung Park, Kangwook Lee, Wansoo Kim, Jongsoo Kim, Yangsoo Lee and Saikee Oh

H&A R&D Center, LG Electronics Inc., 08592 Seoul, Korea, yj.hwang@lge.com

Abstract. Product design by a virtual concept has always been a major subject of many of engineers and manufacturers. Issues should be how close to simulate to the real world by virtual ways. Model Based Systems Engineering (MBSE) in a digital modeling environment provides a methodology to make a virtual mock up easily. In the study, 1D/3D co-simulation was performed on a centrifugal cooling system to check how much accuracy was improved. A specific part of the fields which require to be solved in detail was modeled in 3D for co-simulation while the rest of system remained 1D model. The 1D and 3D solvers run at their respective field domains in parallel and share information. The study considered the multi physics for the components of compressor to refrect the effects of interaction between different physics. An electro magnetics, refrigerant flow & fluid dynamics, heat transfers, power electrics be calculated together to simulate them simultaneously. All 3D models converted to meta model to match time scale with 1D model. This paper shows a case study where a virtual design is successfully applied to the centrifugal chiller system, and dynamic behavior of start up at different cooling loads was simulated and investigated. It can be concluded that the approach by co-simulation as a process of MBSE be able to use to the imposed dynamic behavior on the system. The simulation results under a various load conditions showed that it maintained less than 5% compared with experimental data during from start up to the steady state, moreover, co-simulation showed effective to get a better accuracy.

Keywords. 1D/3D co-simulation, MBSE, virtual product design, multi physics, refrigeration system, centrifugal chiller.
DOI: https://doi.org/10.34641/clima.2022.43

1. Introduction

A centrifugal chiller is an air conditioning equipment that utilizes a centrifugal compressor in a vapor-compression refrigeration cycle. It is popular because they have relatively few moving parts, easy to maintain and long-lived. However, test facilities at a system level are not to be prepared well because of too high heat capacity to be rejected by facility for measuring capacity of a chiller. Moreover, there has a broad spectrum of industrial needs, it is not easy to check for all of quality issues before factory out. The motivation to make a virtual model would be enough to consider at the point of cost and quality. Althrough the product design by virtual concept has been introduced decades ago, it faced a new era by the help of AI technologies under the big umbrella of Digital Transformation(DX). There has been had not much engineering platforms and tools to make a strong simulation model, which was not an environment to use sufficient interfacing technology to communicate well under the condition of multiple physics, different dimensions and different language codes. Before DX, many of simulation model has handicaps to simulate a real world due to not refined data set or there was less ways to melt it into the simulation model even there has. The research focused on dynamic modeling and simulation of the transient characteristics, in which stop–start operating and capacity modulation through various compressor speed, for control purposes. There can find a lot of studies for dynamic modeling, Bendapudi et al.[1] has shown a comparative literature study of refrigeration system for dynamic behaviors. From the reviews, Dhar and Soedel [2] takes a moving boundary approach in the heat exchangers as a coupled pair of lump representing the liquid and vapor phases. He tried to predict the start-up characteristics of compressor by identifying conditions that could lead to liquid slugging, and also as an aid to the system designer to find an optimized condition. Wang [3] presented that a detailed model of the centrifugal compressor is developed from the first principles. He considered the inlet guide vane or pre-rotation vanes form of capacity control, however, the heat exchangers are treated as single entity

Copyright ©2022 by the authors. This conference paper is published under a CC-BY-4.0 license.

lumped effective-NTU. Even there could see a plenty of dynamic models for refrigeration system, most of approach are for a single dimensional model, not included the 3D co-simulation. Moreover, there has not been treated it including the interactions by multi-physics. The study considers 1D/3D co-simulation by the link of different physics at every time interval as time goes on. However, there is no need to make 3D model for all components, in the study, we focused on the modeling for main component of compressor. Heat exchangers are treated as 1D model, it was modeled by a moving boundary method, which is one of single dimensional approach to simulate through the values of inlet/outlet temperatures of chilled and cooling water together with refrigerant properties. The object being modeled for simulation is a commercially available centrifugal chillers, which has two stage compression, magnetic bearings, BLDC motor with variable frequency driver(VFD) and electronic expansion valves(EEVs). Because the 3D models are always heavier than 1D models, co-simulation has to runs at a single dimension basis after taking a reduced order model from 3D full model. The simulation results were compared with the experimental data or the test-based compressor map for validation. The final goal of the study is to make a digital mock up, it can be contributed to development of a scenario based control strategy, performance prediction and quality check by a virtual way.

2. Dynamic modeling approach

2.1 1D modeling for the system

Simulation study was conducted for the centrifugal chiller, with Modelica by Dassualt company. The model calculates thermodynamic properties according to the variation of input parameters at each phases and states. Fig.1 shows a schematic diagram of the system, included instruments and piping. When we plan a model, measuring data from test and experiment set the same parameters from the output of simulation to be matched them in advance for the purpose of adding a control software in the loop simulation(SILS).

The system model should be a virtual model whose dynamic behavior is very similar to the real centrifugal chiller in order to deploy for a failure mode analysis. In the model development, the system is formulated in equations to represent physical system. The basic concept of modeling comes from Thermosys, Alleyne Research Group[4, 5], they suggest a simplified one-dimensional approach to the process of heat transfer and a flow path of heat exchangers, it is capable to simulate a change of an occupied volume according to a phase change of refrigerant. The Thermosys is worth understanding the concept of dynamic approaches of refrigeration system to common users, however, it has to be modified adequately as to apply it for individual's purpose. Shin[6] improved the stability of Thermosys by solving the possibility of diverging caused by initial values. The governing equations be derived from the conservation of mass and energy with assuming one-dimensional refrigerant flow. Terms containing partial derivatives of normalized length can be changed to normal derivatives through the rule of Leibnitz. Since temperature, pressure and the occupied length of phases have the terms of time derivatives, the governing equation represents as a state vector "x" as follows.

$$Z(x,u)\dot{x} = f(\dot{x},u) \qquad (1)$$

The function "f" at the right hand side of equation (1) represents a force vector, it denotes an energy term entering and leaving through a control volume at the equation of energy conservation, at the same time, it can be considered as a variation of mass at the equation of mass conservation. The equation represents dynamic states because derivative term of the state vector x is not be zero. The heat exchangers including economizer, where contained the most of refrigerant during operation, effect a lot on dynamic behaviors than any other components of chiller system. The dynamic behaviors of compressor and expansion valve mainly come from variation of pressure by dynamics of refrigerant besides heat exchangers came from heat transfer related by heat

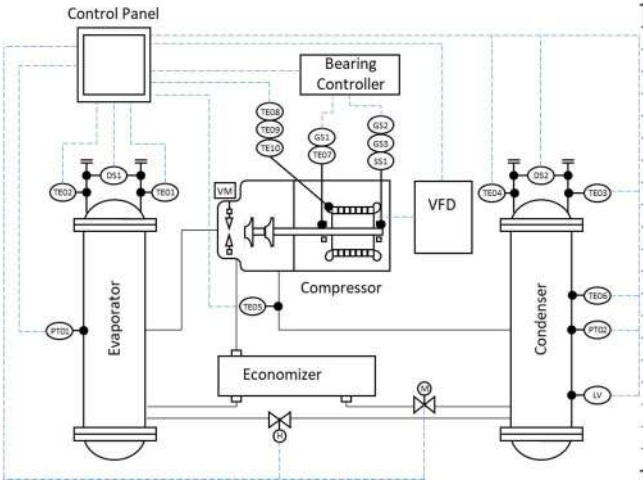

Symbol	Description
TE01	Chilled Water Inlet Temp. Sensor
TE02	Chilled Water Outlet Temp. Sensor
TE03	Cooling Water Inlet Temp. Sensor
TE04	Cooling Water Outlet Temp. Sensor
TE05	Comp. Discharge Temp. Sensor
TE06	Sub-Cooler Temp. Sensor
TE07	Comp. Motor Bearing Temp. Sensor
TE08	Motor Wiring Temp. Sensor (R)
TE09	Motor Wiring Temp. Sensor (S)
TE10	Motor Wiring Temp. Sensor (T)
PT01	Eva. Pressure Transmitter
PT02	Cond. Pressure Transmitter
SS1	Comp. Motor Speed Sensor
SG1	Bearing Gap Sensor (I)
SG2	Bearing Gap Sensor (M)
SG3	Bearing Gap Sensor (Thrust)
VM	Vane Motor
DS1	Diff. Pressure Switch (Chilled Water)
DS2	Diff. Pressure Switch (Cooling Water)
LV	Ref. Level Sensor

Fig. 1 - Schematics of water cooled centrifugal chiller

capacity. The meaning is that there has huge gaps of response time between components. Moreover, it is not easy to make a dynamic model for compressor because of its complexity [7]. Since the compressor model is treated as an abnormal state from the viewpoint of time lapse, 3D modeling of the main components such as motor, inverter driver and impeller was performed for dynamic analysis, followed by co-simulation with the 1D system model.

2.2 1D modeling for heat exchangers

There are two different approaches to make a model for a heat exchanger in refrigeration cycle, which are finite volume method(FVM) and moving boundary method(MBM). In the view of time required at the based on the same calculation results, MBM takes shorter than FVM [8].

Tab. 1 – Nomenclature.

Symbols		Subscript	
P	pressure [Pa]	c	condenser
T	temperature [K]	t	total
x	quality	r	refrigerant
h	enthalpy [J/kg^{-1}]	w	water
u	internal energy [Jkg^{-1}]	in	inlet
Cp	specific heat [Jkg^{-1}K^{-1}]	out	outlet
Z	height [m]	f	saturated liquid
ρ	density [kgm^{-3}]	g	saturated vapor
m	mass [kg]	sat	saturated
ṁ	mass flow rate [kgs^{-1}]	sub	subcooled
A	area [m^2]	u	upside
S	surface [m^2]	d, dn	downside
V	volume [m^3]		
U	overall heat transfer coefficient [Wm^{-2}K^{-1}]		

The main cause comes from how many segments to be considered for calculation. MBM switches set of equations according to the change of phase boundary, and it is relatively simple to calculate heat exchager at transient conditions, besides FVM should be divided it many of small nodes along the flow direction. In case of need to taking the same or similar calculation speed of a model as to match a real product, MBM is better. However, when we takes MBM, there are big issues to find an exact boundary of phase change by comparing the exit enthalpy with the enthalpy at saturation line for good result [9]. At the beginning of caculation, there should have information of length of phase to initiate calculation. In the study, the volume of refrigerant is calculated by the sensing data from a refrigerant level sensor equipped at the heat exchangers. There need five models to represent different phases in heat exchangers, where three models for condenser and two for evaporator. In case of condenser, superheat region can be neglected because the length of superheat region is not appeared significantly,and the capacity of heat at the region is very small. For the evaporator of flooded type, a satuarted refrigerant, where be treated as a superheatd gas with 1.0 of quality, flows into the inlet of compressor because evaporator be designed as the role of accumulator at the same time. Finally, the condenser model can be described as governing equations for two zones, which are two-phase and subcooled region, it represented as equation (2) and (3). Moreover, only one governing equation be needed to describe two-phase zone for evaporator. It is shown as equation (4).

$$\begin{bmatrix} (\bar{\rho}_{r,sub}-\bar{\rho}_{r,sat})\frac{dV_{sub}}{dz} & \frac{\partial\bar{\rho}_{r,sat}}{\partial P_c}V_{sat} & 0 & 0 & 0 & 0 \\ (\bar{\rho}_{r,sub}h_{r,f}-\bar{\rho}_{r,sat}\bar{u}_{r,sat})\frac{dV_{sub}}{dz} & \frac{\partial\bar{\rho}_{r,sat}}{\partial P_c}V_{sat}\bar{u}_{r,sat}+m_{r,sat}\left(\bar{x}\frac{du_{r,g}}{dP_c}+(1-\bar{x})\frac{du_{r,f}}{dP_c}\right) & 0 & 0 & 0 & 0 \\ \bar{\rho}_{r,sub}\frac{dV_{sub}}{dz}(\bar{u}_{r,sub}-h_{r,f}) & 0 & m_{r,sub} & 0 & 0 & 0 \\ 0 & 0 & 0 & m_{w,sub}C_{p,w} & 0 & 0 \\ 0 & 0 & 0 & 0 & m_{w,sat,u}C_{p,w} & 0 \\ 0 & 0 & 0 & 0 & 0 & m_{w,sat,d}C_{p,w} \end{bmatrix} \begin{bmatrix} \dot{z} \\ \dot{P}_c \\ \dot{\bar{u}}_{r,sub} \\ \dot{\bar{T}}_{w,sub} \\ \dot{\bar{T}}_{w,sat,u} \\ \dot{\bar{T}}_{w,sat,d} \end{bmatrix} = X_1 \quad (2)$$

Where,

$$X_1 = \begin{bmatrix} \dot{m}_{r,in} - \dot{m}_{r,out} \\ \dot{m}_{r,in}h_{r,in} - \dot{m}_{r,out}h_{r,f} - U_{sat}\left(A_{t,up} - A_{sub}(z)\right)\left(\bar{T}_{r,sat} - \bar{T}_{w,sat,u}\right) - U_{sat}A_{t,dn}\left(\bar{T}_{r,sat} - \bar{T}_{w,sat,d}\right) \\ 2\dot{m}_{r,out}\left(h_{r,f} - h_{r,sub}\right) - U_{sub}A_{sub}(z)\left(\bar{T}_{r,sub} - \bar{T}_{w,sub}\right) \\ 2\frac{S_{t,sub}}{S_{t,dn}}\dot{m}_{w,sat,d}C_{p,w}\left(T_{w,in} - \bar{T}_{w,sub}\right) + U_{sub}A_{sub}(z)\left(\bar{T}_{r,sub} - \bar{T}_{w,sub}\right) \\ 2(1-\frac{S_{t,sub}}{S_{t,dn}})\dot{m}_{w,sat,d}C_{p,w}\left(T_{w,in} - \bar{T}_{w,sat,u}\right) + U_{sat}(A_{t,up}\ A_{sub}(z)\left(\bar{T}_{r,sat} - \bar{T}_{w,sat,u}\right) \\ 2\dot{m}_{w,sat,d}C_{p,w}\left\{2\frac{S_{t,sub}}{S_{t,dn}}\bar{T}_{w,sub} + 2\left(1-\frac{S_{t,sub}}{S_{t,dn}}\right)\bar{T}_{w,sat,u} - (\bar{T}_{w,sat,d} + T_{w,in})\right\} + U_{sat}A_{t,dn}\left(\bar{T}_{r,sat} - \bar{T}_{w,sat,d}\right) \end{bmatrix}$$

$$\begin{bmatrix} \frac{\partial\bar{\rho}_{r,sat}}{\partial\bar{x}}V_{sat} & \frac{\partial\bar{\rho}_{r,sat}}{\partial P_c}V_{sat} & 0 & 0 \\ V_{sat}\left\{\bar{u}_{r,sat}\frac{\partial\bar{\rho}_{r,sat}}{\partial\bar{x}} + \bar{\rho}_{r,sat}(u_{r,g} - u_{r,f})\right\} & V_{sat}\left\{\bar{u}_{r,sat}\frac{\partial\bar{\rho}_{r,sat}}{\partial P_c} + \bar{\rho}_{r,sat}\left(\bar{x}\frac{du_{r,g}}{dP_c} + (1-\bar{x})\frac{du_{r,f}}{dP_c}\right)\right\} & 0 & 0 \\ 0 & 0 & m_{w,sat,u}C_{p,w} & 0 \\ 0 & 0 & 0 & m_{w,sat,d}C_{p,w} \end{bmatrix} \begin{bmatrix} \dot{\bar{x}} \\ \dot{P}_c \\ \dot{\bar{T}}_{w,sat,u} \\ \dot{\bar{T}}_{w,sat,d} \end{bmatrix} = X_2 \quad (3)$$

Where,

$$X_2 = \begin{bmatrix} \dot{m}_{r,in} - \dot{m}_{r,out} \\ \dot{m}_{r,in}h_{r,in} - \dot{m}_{r,out}h_{r,f} - U_{sat}A_{t,up}(\bar{T}_{r,sat} - \bar{T}_{w,sat,u}) - U_{sat}A_{t,dn}(\bar{T}_{r,sat} - \bar{T}_{w,sat,d}) \\ 2\dot{m}_{w,sat,d}C_{p,w}(T_{w,in} - \bar{T}_{w,sat,u}) + U_{sat}A_{t,up}(\bar{T}_{r,sat} - \bar{T}_{w,sat,u}) \\ 2\dot{m}_{w,sat,d}C_{p,w}\{2\bar{T}_{w,sat,u} - (\bar{T}_{w,sat,d} - T_{w,in})\} + U_{sat}A_{t,dn}(\bar{T}_{r,sat} - \bar{T}_{w,sat,d}) \end{bmatrix}$$

$$\begin{bmatrix} (\rho_{r,f} - \rho_{r,g})\frac{dV_{sub}(z)}{dz} & (V_{tot} - V_{sub}(z))\frac{d\rho_{r,g}}{dP} + V_{sub}(z)\frac{d\rho_{r,f}}{dP} & 0 \\ (\rho_{r,f}u_{r,f} - \rho_{r,g}u_{r,g})\frac{dV_{sub}(z)}{dz} & \frac{d}{dP}(\rho_{r,f}u_{r,f})V_{r,f} + \frac{d}{dP}(\rho_{r,g}u_{r,g})(V_{tot} - V_{r,f}) & 0 \\ 0 & 0 & m_wC_{p,w} \end{bmatrix} \begin{bmatrix} \dot{\bar{x}} \\ \dot{P}_e \\ \dot{\bar{T}}_{w,sat,u} \end{bmatrix} = X_3 \quad (4)$$

Where,

$$X_3 = \begin{bmatrix} \dot{m}_{r,in} - \dot{m}_{r,out} \\ \dot{m}_{r,in}h_{r,in} - \dot{m}_{r,out}h_{r,out} - U_{evap}A_{tot}(\bar{T}_{r,sat} - \bar{T}_w) \\ \dot{m}_wC_{p,w}(T_{w,in} - T_{w,out}) + U_{evap}A_{tot}(\bar{T}_{r,sat} - \bar{T}_w) \end{bmatrix}$$

2.3 3D modeling for compressor

Three dimensional models have been built for the centrifugal compressor, which include an electric motor, inverter driver, two impellers and flow paths of refrigerant such as diffusers, return channel and volute, to reflect interaction of components. Compression system of refrigerant is shown in Fig. 2. The model consists of inlet tube, the 1st impeller, the 1st diffuser, return channel, multiple inlets from economizer, the 2nd impeller, the 2nd diffuser and volute. ANSYS CFX has been used to simulate the compressible turbulence flow and the mesh size is about 33 million of cells. The method of moving reference frame (MRF) is used for rotating impellers, also share stress transport (SST) model is used. The boundary conditions have been set to be able to simulate almost the same range of a real product, where 0.3~228Hz for rotating speed, 300~643kPa for compressor inlet pressure and 2.7~12.7kg/s for mass flow rate of compressor outlet. There has additional mass flow inlet from the economizer before the entrance of the 2nd impeller. The variable frequency driver (VFD) drives a motor by the method of pulse width modulation (PWM). There is a ripple in motor current wave during the PWM process to make the current be sinusoidal and this ripple is transformed as a component of torque ripple whose causes a additional performance degradation due to raise a vibration and noise on motor and add heat up to motor in rotor magnet or copper winding. The study considers motor and VFD together to find out how much influenced it to the system. The normal reduced order model(ROM) for motor is made by Maxwell from ANSYS after considering temperatures at the magnet of motor and stator winding firstly, then the model is connected for calculating total loss of motor to 1D VFD model where after adding a calculation result of PWM current. Twinbuilder provides a role of platform to integrate information of all 1D models. Finally, motor ROM can be obtained after combining normal ROM of motor and 1D VFD model. The calculation range of model for motor set to the same as the other models, whose are component models of compressor for co-simulation. Fig.3 shows a model for VFD and motor.

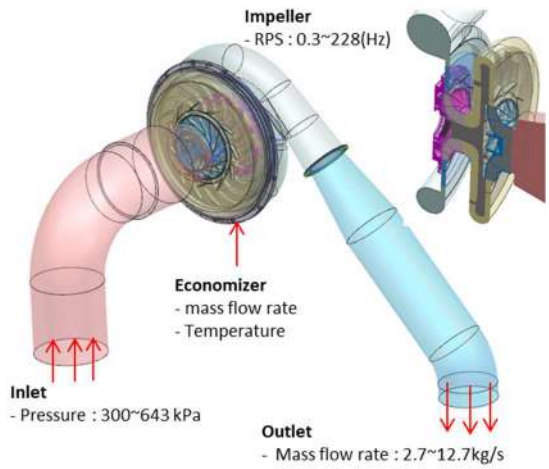

Fig. 2 – The model for a compression system.

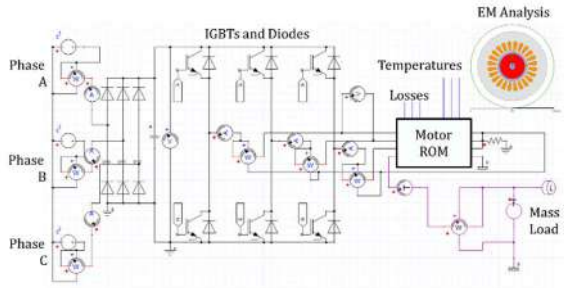

Fig. 3 – The model for VFD and motor.

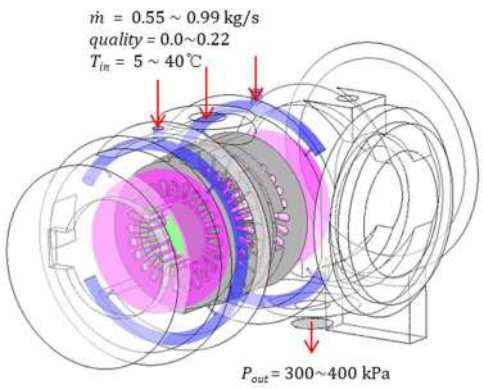

Fig. 4 – The cooling model for motor.

It is essential to cool down at all time for many parts of compressor inside, in the case, motor and inverter circuit are main component for cooling at the model. There is no need to consider for the model to bearings because the system has oil free magnetic bearings. Therefore, the CFD analysis for cooling by refrigerant has done only to the motor and inverter circuit as shown in Fig.4 and Fig5.

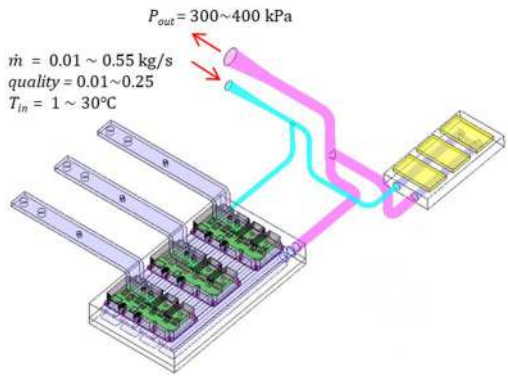

Fig. 5 – The cooling model for IGBT inside of VFD.

The multiple reference frame(MRF) method was introduced for calculation of heat transfer at cooling parts of motor to consider rotational motion of refrigerant flow. To calculate heat transfer between refrigerant and motor surface, a permanent magnet, insulation sheet for bonding, vanish and stator has considered into the CAE model through the 47million grids. After the 3D CAE model of motor converted to a 1D ROM equipped with input and output parameters, 1D ROM exchanges their data with 1D condenser model because refrigerant for cooling comes from condenser. Moreover, for the calculation of heat transfer at inverter driver by refrigerant, IGBTs and Diodes were considered as a main heat source of circuit board.

There have to keep in mind to get a reasonable result by calculation, a model considers a heat transfer coefficient for IGBT dummy and contact surface of circuit parts together with thermal resistance of most of chips. As the same way as motor, 3D inverter model also converted to 1D model for co-simulation. The 12million grids was used for model.

2.4 The cycle modeling for co-simulation

The modeling approach of the study is a 1D dynamic model that can calculate the system, which is to convert 3D models of the compressor's main parts into 1D, respectively, and combine it with the heat exchangers and expansion model already made in 1D. The reason to make a model for the main components of the compressor in 3D firstly, is to observe those components in more detail because the compressor is an important component. Also, the reason to make ROMs for all 3D models is for running co-simulation with different physics at one time for every time intervals. The study had checked soundness of all 1D models after reducing their order because ROM could has a loss of accuracy as compared to the full 3D model in case of inadequate conversion. The normal approach to making a 1D refrigeration cycle model with considering multi-physics is a one-way coupled model, not much for two way coupled model. It comes from a difference of reaction-time between physics, for example a thermal characteristics reacts relatively much slower than an electrical characteristics when operation condition changes according to time, so simulation could be stop. Fortunately, a couple of the software solutions opens an opportunity to simulate a system by two-way coupled situation under the circumstance of multi-physics. Fig.6 shows the parameters to use as input-output between 1D models, it is schematic diagram of co-simulation of refrigeration system.

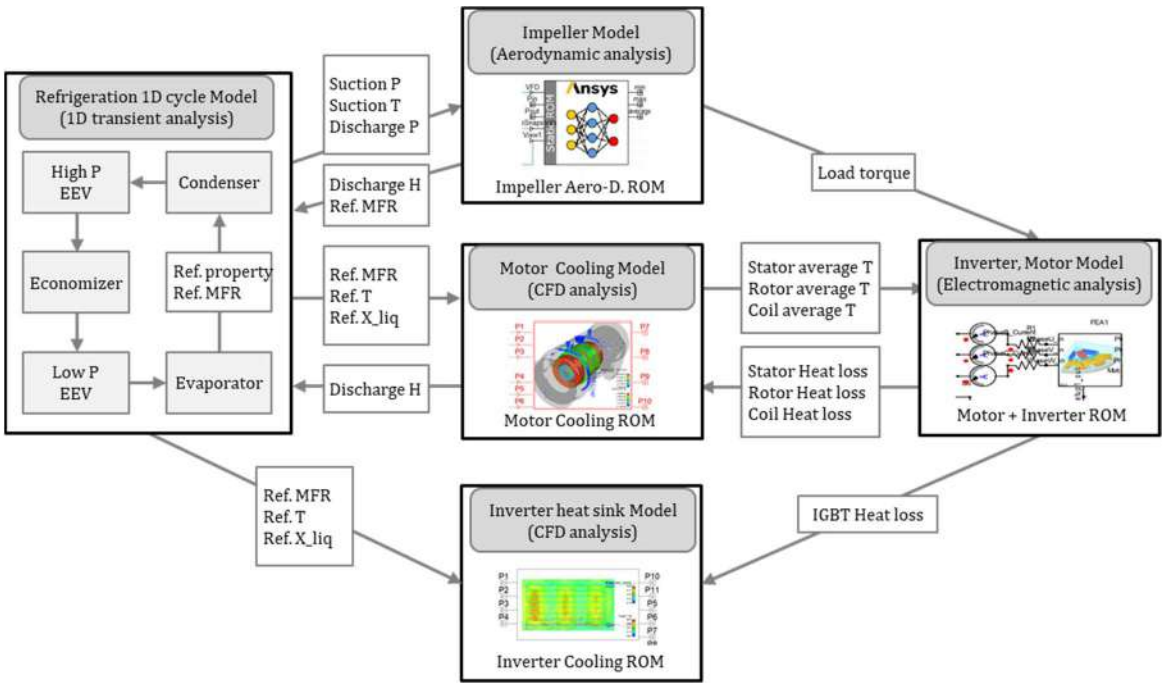

Fig. 6 – The relationship of the single dimensional models for refrigeration cycle.

As you can see at Fig.6, the simulation model for refrigeration cycle is consist of five 1D models, they calculate not only their own properties but also exchange data each other during calculation.

3. Simulation results and discussion

3.1 Model validation under various load conditions

The measured data for validation is an experimental data from the centrifugal chiller whose are manufactured by LG Electronics, it was obtained from the test facility of LGE under start-up and load-change conditions according to AHRI550/590. Simulation has been done from start-up until it reaches a steady state as the same way as doing experiment. The Fig.7~Fig.10 represents that the comparison of the results of the simulation and experiment at various load conditions, figures show a variation of pressure and heat capacity with time.

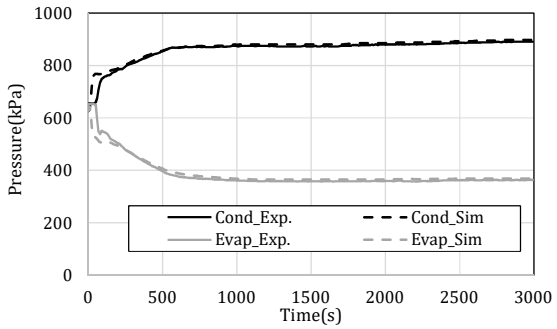

Fig. 7 – The result of simulation to the pressure under 100% load.

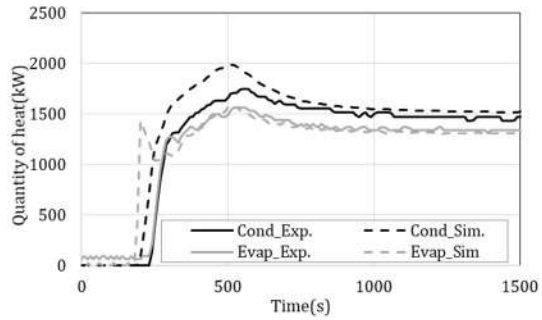

Fig. 8 – The result of simulation to the capacity under 100% load.

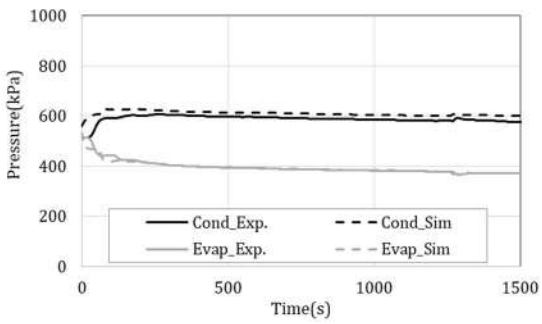

Fig. 9 – The result of simulation to the pressure under 25% load.

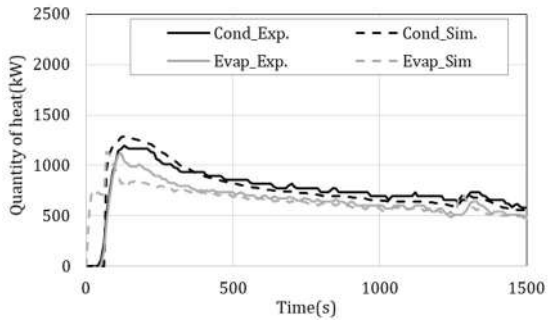

Fig. 10 – The result of simulation to the capacity under 25% load.

There find a reasonable accuracy between simulation and experiment data at all load conditions, however, there has a gap between two values especially for a few minutes after start up. There are two main reasons, first one is that the initial point of calculation could not be set the same as experiment because of their own control strategy of chiller. When an operator pushes the start-up button to turn on a chiller, the controller immediately commands the chiller to run 136Hz, which is the minimum frequency at nothing to do with loads, however, control strategy checks stability of system at every Hz. The result of that, there can be happened a time delay of about 30~45 seconds depending on the communication status. It will be improved by adding the "software in the Loop simulations"(SiLs) as a further study. One other reason is that the simulation model can covers only the same range of operation as experiment, which is from 136Hz to 228Hz. There was not enough data from 0 to 135Hz, so extrapolation method be used to cover the calculation range. It also need to be improved by further study. It would be a common issue when a ROM be introduced for co-simulation in case of less consideration of the model coverage. The accuracy of ROM depends on whether calculation domain is inside of a pre-defined territory. Therefore, diverging could be happen when there be found a case of over-territory during calculation of refrigeration cycle for energy balance under transient condition. It is highly recommended that the separate pre-processing always be required in the 1D/3D interface connection process to ensure that the calculation territory of ROM and the input/output value range of 1D cycle set to be not deviate from each other.

3.2 The effect of co-simulation

The study introduced a concept of the co-simulation not only for improving the prediction accuracy of performance at design stage but also that can be used for manufacturing and quality control. An interaction between physics are normally influenced to a cycle system, co-simulation deserves to be considered. Moreover, 3D CAE model, which will be converted to 1D model, is better to describe a physical phenomenon because it included exact information for the structure and physical dimension. The comparison between two different approaches has shown in Fig.11.

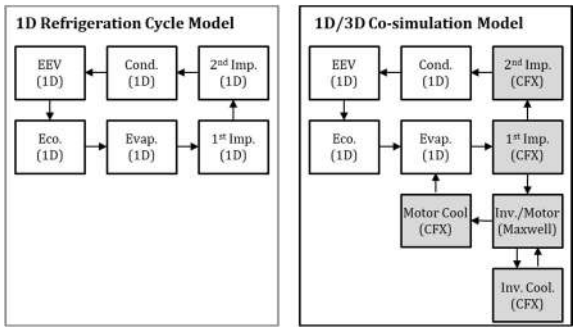

Fig. 11 – The concept of two different modelling approach.

In the co-simulation approach, the impeller aerodynamic characteristics, electromagnetic characteristics of motor, and heat loss, which were difficult to make model at the 1D analysis, were implemented by adding a 3D analysis model. There be shown how much improved accuracy in terms of performance by co-simulation in Fig. 12. The results from "1 D only" simulation both for the capacity of condensing and for evaporating predicted a higher value than experiment while the co-simulation has shown much close value compare to experiment under all load conditions. In the co-simulation, the performance of analysis improved by considering the loss models that could not be reflected in the 1D only model. Moreover, with the help of a detailed 3D analysis for aerodynamics of impellers, the accuracy under low load condition at 25% has also improved.

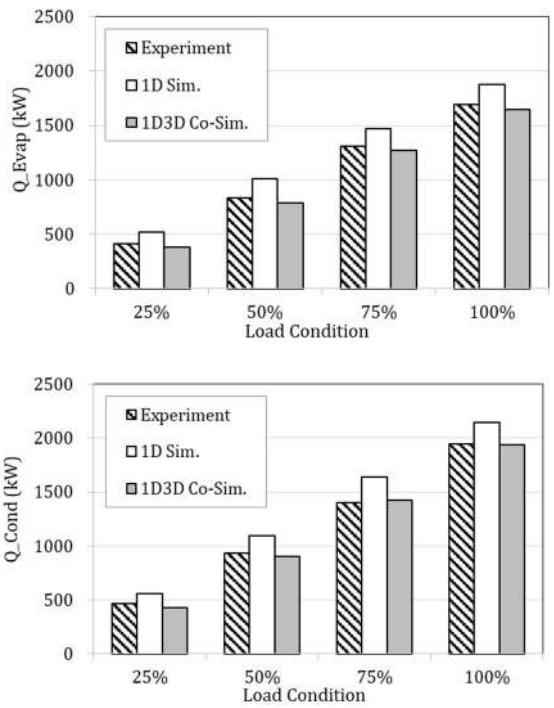

Fig. 12 – The effect of co-simulation on the accuracy of heat capacity.

3.3 Model validation under random change of load

It was observed whether the simulation of the dynamic behavior tracked well under the condition of load scenario. The load scenario was created by selecting 3 pieces of random operation data stored in the real product first, and then attaching them each other to get a series data as long as 50,000 seconds. It becomes a virtual load for model validation. The points with discontinuous data caused by connecting are around 16,000 seconds and 45,000 seconds. Fig. 13 is a dynamic behavior comparing simulation results and scenario data, (a) is a pressure and (b) is an electric current. A capacity of heat can be calculated from the change of electric current because capacity of heat could not directly stored as a data in the control device of chiller. This conversion is one of benefits from doing co-simulation of 1D/3D. Fig.13 shows a pressure and an electric current, the difference between the simulation result and experiment is well tracked within 10%. In case of scenario based analysis, it proceeded from an operating state instead of setting the initial condition as a stop state as shown in Fig. 7~Fig.10. From the results of that, the dynamic behavior of the model is well simulated independent of initial value setting.

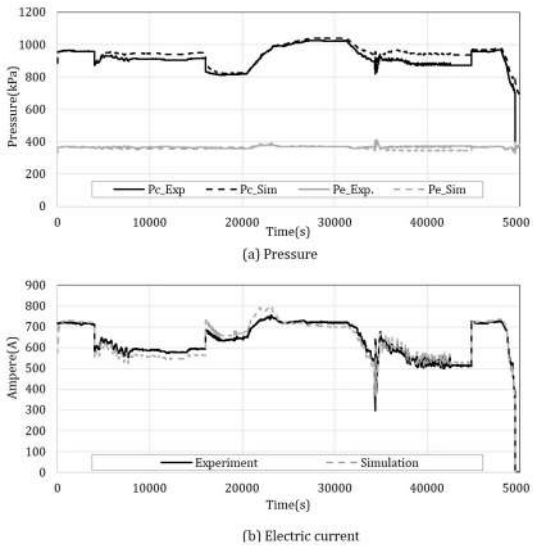

Fig. 13 – The result of simulation on pressure and electric current under the condition of a virtual load.

4. Conclusion

This study presents a detailed modeling approach to a centrifugal chiller as a vapor compression refrigeration system by introduced MBSE methodology of object-oriented structure. The model shows an inaccuracy of less than 2% under the rated condition and 10% under the partial load condition when the simulation result be compared with the experiment. The main contributions brought by the modeling methodology is that 1) the 1D-3D co-simulation significantly improved the accuracy of prediction compared to the 1D analysis only, 2) considering a number of interrelated physics at one time delivered more accurate results if their interaction placed in a state of strong coupled, 3) the

3D models can be converted to 1D model by use of ROM without time lag. At the same time, the accuracy of 1D model maintained as decrease of less than 2% compare to 3D model. The followings are a suggestion as a future study to make a digital mock up by dynamic modeling. 1) At the stage of 1D architecting during MBSE approach, the main component of refrigeration system like a compressor and heat exchangers needs to be refined up to a smaller level, and then make it as an independent library. It is an essential stage for the model to keep expendability even it takes time. 2) In case of adding a 3D modeling for heat exchangers gives a better result than the current model, which did not include 3D model other than compressor. Finally, data domain need to be wide enough so that calculation works well when you making a ROM. Although this study was conducted on a centrifugal chiller system with a centrifugal compressor and a shell & tube heat exchangers, the basic principle of the refrigeration system is the same. Therefore, the result of the study can be applied very similarly to the residential air conditioning system whose have a positive displacement compressor and the fin & tube heat exchangers.

5. References

[1]Bendapudi S., Braun JE. A review of literature on dynamic models of vapor compression equipment. ASHRAE Report. 2002, May;4036-5.

[2]Dhar M., Soedel W. Transient analysis of a vapor compression refrigeration system. Proc. 15th International Congress of Refrigeration, Venice(IT). 1979.

[3]Wang S., Wang J., Burnett J. A mechanistic model of a centrifugal chiller to study HVAC dynamics. Building Services Engineering Research and Technology. 2000;21(2):73-83.

[4]Li B., Alleyne AG. A dynamic model of a vapor compression cycle with shut-down and start-up operations. International Journal of Refrigeration. 2010;33:538-552.

[5]McKinley T. L., Alleyne AG. An advanced nonlinear switched heat exchanger model for vapor compression cycles using the moving-boundary method. International Journal of Refrigeration. 2008;31:1253-1264.

[6]Shin Y., Kim JH., Yoo BJ. Dynamic modeling and simulation of a hybrid heat pump. Korean Journal of Air-Conditioning and Refrigeration Engineering. 2013, July;25(7):406-412.

[7]Shin, Y. A study on diagnosing fouling of heat exchangers of a hybrid heat pump. Korean Journal of Air-Conditioning and Refrigeration Engineering. 2014;26(5):240-246.

[8]Bendapudi S., Braun JE., Groll EA. Dynamic modeling of shell-and-tube heat-exchangers: moving boundary vs. finite volume. International Refrigeration and Air Conditioning Conference. 2004, July;649.

[9]Li P., Li Y., Seem JE. Dynamic modeling and consistent initialization of water-cooled centrifugal chillers. 4th National Conference of IBPSA-USA. 2010, August:386-393.

The datasets generated during and/or analysed during the current study are not publicly available because it is property of LGE but are/will be available depending on purpose. Please contact to yj.hwang@lge.com·

Study on the efficiency of large shallow GSHP Systems. ELI-NP after one year operation

Razvan Silviu Stefan[a], Delia Tinca[a], Radu Mircea Damian[b]

[a] ELI-NP, Romania, razvanstefan80@gmail.com, delia.tinca@eli-np.ro

[b] Technical University of CIvil Engineering, Faculty of Bulding Services, Bucharest, 942rmd@gmail.com

Abstract. This paper is an overview of the performances of the Shallow Ground Source Heat Pump HVAC system from ELI-NP after one year of operation. It approaches the system performances in terms of energy consumption, stability of the indoor comfort parameters and prospective of optimal control. The use of a research facility is different from a classic non-residential building. The large equipment and the large built area of the clean rooms, the high stability of the required comfort parameters imply a high consumption of energy for heating, ventilation and air conditioning. The final goal is to achieve a viable model with replication potential for general use applications (air conditioning of non-residential objectives or district centralized air conditioning). Databases resulting from the continuous real-time monitoring of the system, during 2020, have been analyzed. Deviations of data from the reference values have been interpreted to find solutions for the long-term keeping of indoor microclimate parameters at the required values. The data analysis shows that the system covers the building load / the building energy needs at a high parameters stability. The Energy Intensity Use of the ELI-NP facility (436.13 kWh/ m^2/yr) is less than half of the median EUI for Technology/Science laboratories in the US (1004 kWh/ m^2/yr), as published on the platform Energy Star. The use of the shallow Ground Source Heat Pump HVAC system instead of a traditional fossil fuel one, comes with estimated savings of 60% in the cost of energy consumption of buildings. The next step to follow is a higher accuracy separation of the Ground Source Heat Pump HVAC system electricity consumption. Then an optimization strategy to supply the indoor comfort parameters at the lowest possible energy consumption follows.

Keywords. Heat pumps, buildings, energy efficiency, shallow GSHP
DOI: https://doi.org/10.34641/clima.2022.59

1. Introduction

The Extreme Light Infrastructure – Nuclear Physics Research Infrastructure (ELI-NP) is a European and international center for high-level research on ultra-high intensity laser, laser-matter interaction and secondary sources with unparalleled possibilities. ELI-NP is a very complex facility, which hosts the most powerful LASER in the world.

The main objective the ELI-NP buildings concept design was to create an optimal environment capable of hosting state-of-the-art research equipment and technologically advanced experimental configurations.

Features, such as a clean room of 2400 m^2, large working spaces (i.e. laboratories) without natural lighting, research equipment that require a large cooling capacity, and demands of the environmental parameters, come with significant energy consumption.

The interest of the US authorities to benchmark buildings in terms of energy efficiency generated studies and surveys regarding the energy efficiency of the research laboratories in the US. Based on the available data, the ELI-NP facility was assessed by comparison, in terms of the core activity, to similar facilities as defined on the Energy Star platform, run by the US Environmental Protection Energy.

ELI-NP has been operating for 5 years, of which two years at 70% capacity. After having continuously monitored the buildings in real time, it turns out that the energy consumption rates are lower than expected, the systems providing high parameters stability.

One of the key factors leading to low energy consumption is the HVAC geothermal system the research infrastructure was provided with. The system doesn't use fossil fuels as energy source, the main energy source for both heating and cooling (including technological cooling) is geothermal energy, equipment being powered by electricity.

After observing the performance of buildings and systems, as well as the consumption behavior during the last two years, it came out that there is room for optimization both in terms of control and in terms of energy efficiency. The aim is to optimize both the geothermal HVAC system and the other systems so to get the optimal ratio between consumption and technological requirements.

Copyright ©2022 by the authors. This conference paper is published under a CC-BY-4.0 license.

Currently, optimization strategies applied for smaller geothermal HVAC systems are being studied to determine the one that is best suited to be adapted to the ELI-NP case. Also, additional ways to reduce electricity consumption for lighting and related activities are being investigated.

2. Shallow geothermal HVAC system at ELI-NP

The running of the scientific equipment requires accurate specific conditions, therefore the shallow geothermal system with heat pump units is one of the core systems of the buildings. Its efficiency and proper working are vital for the good functioning of scientific equipment.

The configuration of the site and the breakdown of the total gross area of 33.000 sqm served by the system is shown in Table 1.

Tab.1 - Breakdown of the facility area.

Building / Space	Destination	Gross Built Area (m^2)
Laser Building	research	11.543
Gamma Building	research	13.452
Office Building	support	5.237
Guests House	support	2.568
Other buildings	support	212

The shallow geothermal system, installed on a plot of 27.000 sqm, provides the buildings with all the energy necessary for heating, ventilation, air conditioning, hot water, and technological cooling water.

It has a length of 135 km, and 1080 drills deep of 120 m each. The total installed thermal capacity is approximately 6.2 MW.

Due to the large thermal capacity provided by the shallow geothermal system, the operation of the buildings does not require fossil fuel systems. Thus, the impact of the ELI-NP buildings on the CO_2 emissions is low.

The energy source of the Shallow Geothermal System designed for the ELI-NP facility is the geothermal energy, provided by a closed geoexchange circuit, transferred to the buildings by heat pump units.

The system is a closed-loop made of 1080 boreholes with a depth of 120 m each. Each group of 60 holes is connected to 2 of the 18 existing manifolds. From the existing distributor and collector in each of the 18 manifolds, a pair of geothermal pipe-lines go to the pumping station that performs the management of the extracted energy from the earth throughout the cold season, respectively the injected energy to the earth throughout the warm season.

The required primary thermal agent (water) is pumped from the manifolds to 9 thermal plants equipped with water to water heat pumps that carry out the heating and cooling of the buildings. The secondary thermal agent (water) for cooling and heating prepared with the water-water heat pumps is delivered to the HVAC equipment (air handling units, fan coils units).

The required thermal load of 6,0 MW for heating and 4.2 MW for cooling is provided by 129 water-water heat pumps. On top, 46 water-air heat pumps directly carry out the cooling or heating of the indoor air of some rooms. The heating, ventilation, and conditioning of the buildings is performed by air handling units. Energy recovery is used wherever possible. For the LASER building, a total of 8 handling units are used, out of which 3 are fresh air units that supply a mixed flow rate 85.000 mc/h.

Their major endpoint is to carry out the heating and ventilation of the LASER clean room and of the other existing clean rooms ISO 6 and ISO 7, providing for this purpose 20 air changes per hour with a vertical air flow of 435,000 m^3/h. The required humidity load for the LASER building is provided by steam humidifiers attached to the air handling units.

For the GAMMA building, 2 fresh air handling units are used to supply a flow rate of 80,000 m^3/h each in the experiments rooms.

The shallow geothermal system is digitally controlled by the DDC system. Thus, the temperature and humidity are continuously monitored, recorded and, adjusted, the information being transmitted to the BMS system.

The major endpoint of the SHALLOW GEOTHERMAL SYSTEM is to deliver high stability of the operating parameters.

Some parameters required in the reserch laboratories are presented in Table 2.

Tab.2 – Operating parameters of the Laboratory Buildings

Parameter	Unit	Value	Building
Temperature	^oC	22±0.5	Laser
Temperature	^oC	20±0.5	Gamma
Relative humidity	%	35-50	Laser
Relative humidity	%	30±0.5	Laser
Overpressure	Pa	40	Laser
Negative pressure	Pa	14	Gamma
Cleanliness class	ISO	6, 7	Laser

3. Breakdown of the energy consumption at ELI-NP. Energy Use Intensity

At the same time with the parameters, the total electricity consumption of the research facility was monitored, as the only energy consumption with a precise cost, known based on the supplier's metering and bills.

Figure 1. shows the total consumption during June 2016, when the testing and commissioning of the facility took place, up to December 2021. This period of time covers different stages of occupancy, but years 2020 and 2021 can be considered years of fully operation, meaning full occupancy of the office building, the research equipment and experimental building installed. Only the installation of one equipment is in progress at the moment.

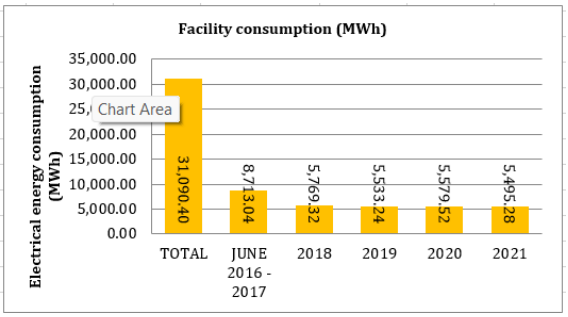

Fig.1 - Total facility consumption begining of the commisioning.

The total electricity consumption from commissioning to the end of 2021 was around 31,100 MWh. The diagram shows that in the last four years of the monitoring period the consumption was relatively constant, with small variations due to environmental factors or the volume of works and tests carried out in the buildings.

The consumption mentioned above means a cost of around 1,3 euro/gross built area m^2, computed considering to the supplier's bills, based on the cost of the electricity on the Romanian free market. This amount includes all the consumptions, meaning: heating, cooling and ventilation of the laboratories and of all the support buildings, hot water, electricity for lighting and office equipment, electricity for the data rooms, electricity consumed to running and cooling the research equipment, exterior lighting of the entire side and the adjacent road.

We found that two-thirds of the electricity consumed comes from the HVAC system together with the technological cooling, both needs being covered by the shallow ground source heat pump system (Figure 2).

For the operating years 2020 and 2021, which we considered as the basis for a future optimization of the energy consumption, the pattern shows, as expected, that the maximum consumption is recorded in the summer months and in the winter months, when the need of cooling or heating is high (Figure 3).

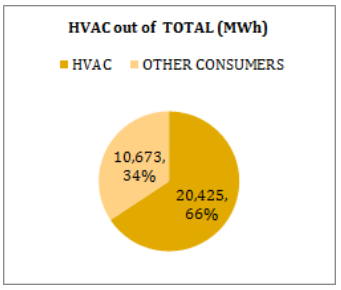

Fig.2 - HVAC consumption out of total begining of the comissioning

Figures 3 and 4 represent the breakdown on months of the total facility consumption for years 2020 and 2021.

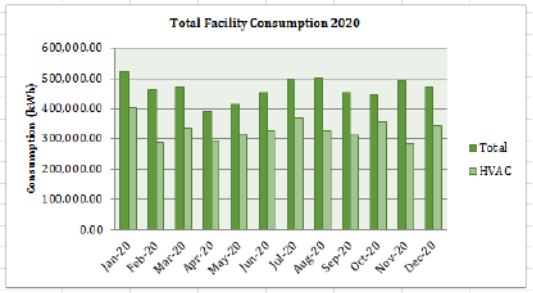

Fig.3 - Breakdown on months 2020

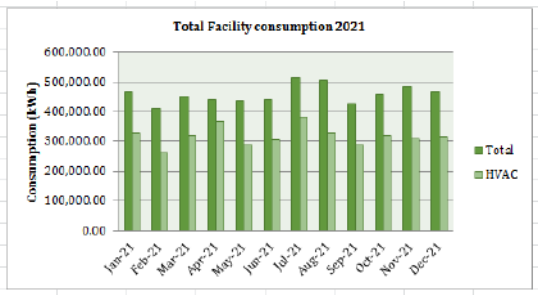

Fig.4 - Breakdown on months 2021

Figures 5 and 6 represent the breakdown on months of the total facility consumtion for years 2020 and 2021.

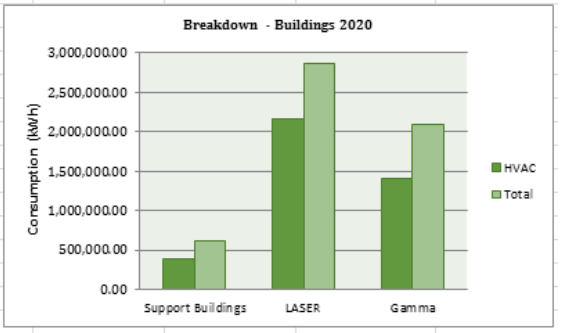

Fig.5 - Breakdown – Buildings 2020

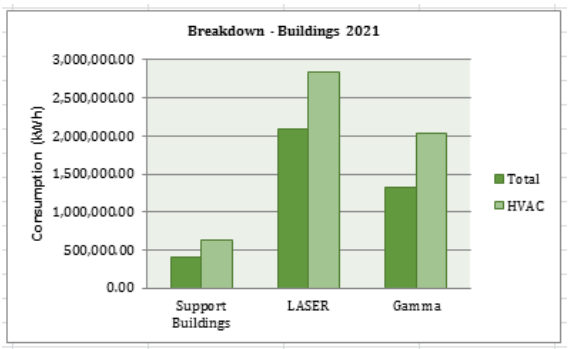

Fig.6 - Breakdown – Buildings 2021

To improve the use of energy, one of the directions followed by authorities was to develop regulations for assessing the energy performance of buildings. Both the existing stock of buildings and the design of new buildings were taken into account.

Rules to rank and evaluate different categories of buildings have been drafted both in the EU and in the US.

The most used key metrics to benchmark buldings in terms of energy performance are:
a. According to EPA (US Environmental Protection Energy) Energy Use Intensity (EUI) is expressed as energy per square foot per year and calculated by dividing the total energy consumed by the building in one year (measured in kBtu or GJ) by the total gross floor area of the building (measured in square feet or square meters) [1].
b. Specific Energy Consumption (SEC) expressed as energy per square meter per year and calculated by dividing the total energy consumed by the building in one year (measured in kWh) by the useful area of the building (measured in square meters).

The calculation of SEC may differ from a country to another or from an author to another [2].

The calculation of SEC explained above is the one used in the Romanian Calculation Methodology of Buildings Energy Performance [3].

Studies indicate that science is more energy intensive than other disciplines.

Therefore the interest in benchmarking the research laboratories in terms of energy performance has grown in recent years to improve the metrics or key performance indicators that score the research facilities [4].

The lack of data on similar infrastructures makes difficult the assessment of the ELI-NP energy performance.

Healthcare facilities, more intensely benchmarked are to some extent similar to ELI-NP in terms of the share of the HVAC system consumption from the total consumption.

The rooms that host the main research equipment are single volume halls, having large areas and considerable heights (maximum height around 16 m), being similar in this respect to event halls and sports facilities.

Therefore, comparison with similar size infrastructures is not relevant due to the fact that research activity comes with high-energy consumption. Comparison with other geothermal systems is also of small relevance due to the fact that there are few geothermal systems of this size.

To achieve our purpose of an assessment in terms of energy consumption, we considered a comparison of the energy performance of the ELI-NP facility with research facilities in the United States.

The EUI of ELI-NP is compared:
a) to the results of a three-year benchmarking study conducted by kW Engineering for the Boston Green Ribbon Commission's Higher Education Working Group [5], [6], [7]and
b) to the median EUI in the United States US for Technology/Science laboratories, published by EPA on the platform Energy Star (programme run by EPA) [1].

Values of source EUI have been compared.

According to EPA the site energy is the annual amount of all the energy the building consumes on-site, regardless of the source and source energy is the total amount of all the raw fuel required to operate your building, including losses that take place during generation, transmission, and distribution of the energy [8].

The conversion factor for electricity (grid purchase) of the site energy to source energy according to the Romanian regulations is 2,62 [3].

According to the glossary of Portofolio Manager application, LABORATORY refers to buildings that provide controlled conditions in which scientific research, measurement, and experiments are performed or practical science is taught [8].

Gross Floor Area should include all space within the building(s) including workstations/hoods, offices, conference rooms, restrooms, storage areas, decontamination rooms, mechanical rooms, elevator shafts, and stairwells [8].

At the time of kW Engineering study the EPA had not provided an ENERGY STAR® rating for lab buildings, and widely used national energy usage datasets contained very limited lab building data. The goal of the study was to construct a new lab building benchmarking dataset comprised of Boston-area higher-education labs, with data quality exceeding that of any other sample.

The data requested from the respondents for each building:

a. Whole-building annual energy usage, meaning energy consumed (from all sources) in one year calendar
b. Building functional requirements: these are the metrics on which buildings are compared, and include total building area, total lab area, number of fume hoods, and predominant lab type (biology/biochem, chemistry, physics/engineering, and other).
c. Building design and operational parameters: these include properties of the buildings that are expected to influence energy consumption but which are not necessarily needed to meet functional requirements. Examples include HVAC system type (e.g. variable air volume with reheat), HVAC control type (e.g. pneumatic), and the use of night airflow setback in labs.
d. Perceived energy efficiency: respondents were asked to rank the buildings in terms of efficiency of original design and efficiency of current operation [5].

The data about the Energy Intensity Use for the studied laboratories have been published in the final report on June 2018 and are presented in Table 3 [7].

Tab.3 - Energy intensity use summary. kW Engineering Study.

LAB TYPE Total area 17k ft²	No. B.	Average SOURCE EUI (kWh/ m²/yr)	Average SITE EUI (kWh/ m²/yr)	Median SOURCE EUI (kWh/ m²/yr)
Bio/ Biochem	46	1.725	921	1.728
Chemistry	13	1.996	1.120	1.908
Physich/ Eng	43	1.363	770	1.217
Other	7	1.709	902	1.741
TOTAL	109	1.615	883	1.599

Later on, EPA updated the Portfolio Manager application on its Energy Star platform with more buildings categories and published the median value of the source EUI for Technology/Science laboratories, based on Commercial Buildings Energy Consumption Survey (CBECS) conducted by the U.S. Department of Energy's Energy Information Administration. The survey considered 11k laboratories totalising an area of 705m ft² [9].

The published median value of EUI for Technology/Science laboratories is 318,2 kBTU/f²/y, meaning 1004 kWh/ m²/y [6].

Regardless of the study considered, it comes out that the ELI-NP research facility has a EUI below the median value of the EUI for research laboratories assessed and scored in the United States. To be noted that the consumption of the technological cooling is not separated from the HVAC, both needs being covered by the shallow ground source heat pump system. Values of the EUI for the entire facility are presented in Table 4 and Figure 7. In Table 5 the value of the EUI for the research purpose building are presented.

Tab.4 - Energy intensity use ELI-NP for the entire Facility

ELI-NP	Cons (MWh)	SOURCE EUI (kWh/m²/yr)	SITE EUI (kWh/m²/yr)
2020	5.579	442.81	169.01
2021	5.503	436.13	166.46

Fig.7 - Source EUI ELI-NP compared to EUI for research laboratories in USA

Tab.5 - Energy intensity use ELI-NP for the Research Purpose Buildings

ELI-NP	Cons (MWh)	SOURCE EUI (kWh/m²/yr)	SITE EUI (kWh/m²/yr)
2020	4.965	518.60	197.94
2021	4.875	509.16	194.34

We consider that an assessment of the ELI-NP facility based on SEC has a high degree of uncertainty due to a) high rate area/volume of the main laboratories (approx. 8.000 m²), b) very large area of the main clean room (approx 2.400 m²).

4. Strategies considered for the HVAC System Optimisation

Two of the optimisation strategies that we investigated have drawn our attention as matching for the shallow Ground Source Heat Pump System ELI-NP.

The first one is a model based strategy proposed by Zenjun Ma and Lei Xia, tested on the geothermal system that serves the Sustainable Buildings Research Centre at the University of Wollongong,

Australia and summarized by the authors in Figure 8.

The developed strategy is suitable for systems equipped with variable speed pump(s) in the ground loop system to modulate the water flow rate and we considered it due to the fact that all hydraulic circuits in the ground loop of the ELI-NP system contain at least one variable speed circulation pump [10].

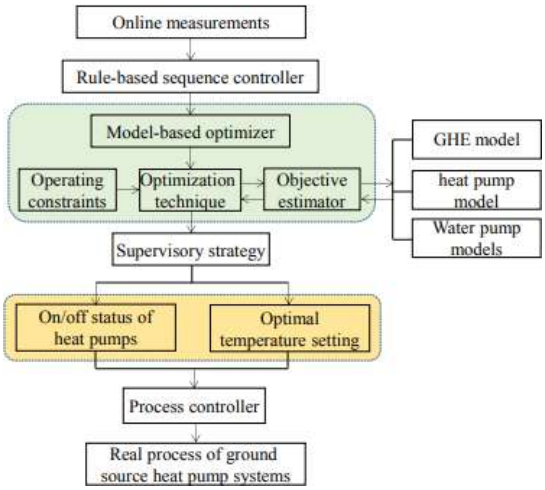

Fig. 8 - Outline of the proposed optimization strategy.

The variable optimized is the outlet water temperature from the ground heat exchanger, which can be used as a set-point to control the operation of the variable speed pumps in the ground loop system. The objective of the optimization is to minimize the system power consumption while providing required building heating and cooling demand.

To estimate the system performance under various trial setting three component models were used: the variable speed circulation pumps in the ground loop, the ground heat exchange and the water to water heat pumps.

The process consists of two steps:
The first step is to use a rule-based sequence controller to determine the operating number of the heat pumps based on the building heating/cooling demand and the capacity of each heat pump as well as the operating constraints of practical applications. The second step is to determine the optimal combination of the outlet water temperature from the GHEs and the water flow rate circulating through the GHEs to minimize the total power consumption of the water pumps in the ground loop and the water-to-water heat pumps.

The exhaustive search method used in this study is not a good search method for real-time control applications due to the nature of its exhaustive search, thereby relatively high computational cost requirement. However, the results obtained using this method can be potentially useful to generate a performance map, which can then be used for real-time control applications.

Although this method comes with only 4.2% energy savings compared to a rule-based control strategy, we considered it due to the fact that we can easily implement it. Also, an extra control is expected over the baseline control strategy we use

The second strategy that we considered is an "in situ" optimisation methodology for ground source het pump system propose by Javier Cervera-Vázquez Carla Montagud José Miguel Corberán Antonio Cazorla-Marín.

The authors previously developed an experimental in situ optimization methodology for the water circulation pumps frequency and then they upgraded it to ensure user comfort. The methodology has been implemented and tested in heating and cooling mode in a real GSHP installation located at the Universitat Politècnica de València in Valencia, Spain [11], [12].

5. Conclusions

The total energy consumption of ELI-NP during operation has been monitored and registered.
Also the consumption for buildings and systems has been registered given that the systems are 85% metered and the HVAC system is fully metered but the consumption of the technological cooling is not separated by the HVAC. To be noted that both needs are covered by the shallow Ground Source Heat Pump System.
A comparison with similar buildings is not an easy task due to the fact that the assessment of the energy performance of research laboratories is recent and the key performance indicators used do not take into account all the characteristics of the research facility with an impact on energy performance.
Beginning of 2021, the EPA included the Technology /Science laboratories in the portfolio of the benchmarked buildings in the United States, publishing their median EUI. The ELI-NP EUI value is 436.13 kWh/ m^2/yr and the median value of EUI for Technology/Science laboratories published on the Energy Star platform is 1004 kWh/ m^2/yr.

After having studied the behavior of ELI-NP in terms of energy consumption, we came to the conclusion that there is room for improving the energy performance of the facility. To be noted that stability of the operating parameters of the systems is of major importance.

We have studied several optimal control strategies proposed by specialists for similar but smaller systems. Our goal is to extend one of these strategies for the ELI-NP geothermal system and eventually to estimate the long-term variation the coefficient of performance of the system.

The total energy consumption of ELI-NP during operation has been monitored and registered.
Also the consumption for buildings and systems has

been registered given that the systems are 85% metered and the HVAC system is fully metered but the consumption of the technological cooling is not separated by the HVAC. To be noted that both needs are covered by the shallow Ground Source Heat Pump System.

A comparison with similar buildings is not an easy task due to the fact that the assessment of the energy performance of research laboratories is recent and the key performance indicators used do not take into account all the characteristics of the research facility with an impact on energy performance.

Beginning of 2021, the EPA included the Technology /Science laboratories in the portfolio of the benchmarked buildings in the United States, publishing their median EUI. The ELI-NP EUI value is below this value.

After having studied the behavior of ELI-NP in terms of energy consumption, we came to the conclusion that there is room for improving the energy performance of the facility. To be noted that stability of the operating parameters of the systems is of major importance.

We have studied several optimal control strategies proposed by specialists for similar but smaller systems. Our goal is to extend one of these strategies for the ELI-NP geothermal system and eventually to estimate the long-term variation the coefficient of performance of the system.

6. References

[1] ENERGY STAR a voluntary U.S. Environmental Protection Agency (EPA) program - What is Energy Use Intensity (EUI)? https://www.energystar.gov/buildings/benchmark/understand_metrics/what_eui

[2] Lawrence A., Thollander P., Andrei M., Magnus K., Specific Energy Consumption/Use (SEC) in Energy Management for Improving Energy Efficiency in Industry: Meaning. Usage and Differences.

[3] Technical University of Civil Engineering of Bucharest, Project produced for Ministry of Regional Development and Public Administration, Methodology of calculation the energy perormance of buildings.

[4] Khoshbakht M., Gou Z., Dupre K., Energy use characteristics and benchmarking for higher education buildings, Januarie 2018, 12

[5] Farmer A., Boston Area Laboratory Energy Benchmarking Study, Year 3 Data Analysis Report University Labs, A Report from the Higher Education Working Group, Boston Green Ribbon Commission, August 2018

[6] Farmer A., Boston Area Laboratory Energy Benchmarking Study, Year 1 Data Analysis Report University Labs, A Report from the Higher Education Working Group, Boston Green Ribbon Commission, May 2017

[7] Farmer A., Boston Area Laboratory Energy Benchmarking Study, Year 1 Data Analysis Report University Labs, A Report from the Higher Education Working Group, Boston Green Ribbon Commission, May 2017.

[8] ENERGY STAR a voluntary U.S. Environmental Protection Agency (EPA) program – Portfolio Manager Glossary https://portfoliomanager.energystar.gov/pm/glossary#SiteEnergy

[9] Energy Information Administration - EIA - Official Energy Statistics from the U.S. Government - COMMERCIAL BUILDINGS ENERGY CONSUMPTION SURVEY (CBECS) https://www.eia.gov/consumption/commercial/data/2018/bc/html/b1.php

[10] Ma Z., Xia L. „Model-based optimisation of ground source heat pump systems," Elsevier, Energy Procedia 111, 2017.

[11] Cervera-Vázquez J, Montagud C., Corberán J. M., Cazorla-Marín A. „Optimal control and operation of a GSHP system for heating and cooling in an office building„" IGSHPA Technical/Research Conference and Expo Denver, Denver, March 14-16, 2017.

[12] Cervera-Vázquez J., Montagud C., Corberán J. M., „In situ optimization methodology for the water circulation pumps frequency of ground source heat pump systems: Analysis for multistage heat pump units," Energy and Buildings, Volume 88, Pages 238-247, 1 February 2015.

Overview and assessment of radiant systems in three administrative buildings

Emília Madarasova [a], Eva Švarcová [b], Dušan Petráš [c]

[a] Faculty of Civil Engineering, Slovak University of Technology in Bratislava, qmadarasovae@stuba.sk

[b] Faculty of Civil Engineering, Slovak University of Technology in Bratislava, eva.svarcov4@gmail.com

[c] Faculty of Civil Engineering, Slovak University of Technology in Bratislava, dusan.petras@stuba.sk

Abstract. Administrative buildings should provide an acceptable environment for people's work where is no excess heat, draught, noise, or low internal air temperatures. It is necessary to provide thermal well-being in each administrative building, but especially in those where the facade is of the prevailing glazed window structures.
The aim is to eliminate thermal gains and to ensure the required conditions for residence and work in administrative buildings. It is necessary to propose appropriate systems of building environment techniques. Radiant systems, low-temperature heating and high-temperature cooling, can suitably ensure an optimal environment throughout the year.
In this contribution, three applications of radiant systems in three different administrative buildings are described. In the first administrative building is the dry application system - suspension radiant covers; in the second administrative building the capillary mats are applied. The concrete core activation system has been applied in the last administrative object. The parameters of the inner environment were examined: air temperature, operating temperature, relative humidity, and airflow rate. The CO2 concentration was measured for further measurement to assess the quality of the internal air. These objective measurements and subsequently subjective evaluations of people located in the measured space were compared with the requirements of international standards for the evaluation of the internal environment. From the measurement overview, we can say that in most measured offices, the parameters of the internal environment meet the normal values of the comfortable environment, suitable for work and residence in the workplace. During the summer season, objective evaluations corresponded to the requirements of the standard, in terms of subjective evaluation, the results were evaluated at the upper range of acceptability. For the winter period, the internal air temperature was slightly increased compared to the standards requirements, but in terms of subjective perception, the space was perceived as favorable.

Keywords. Radiant systems, low- temperature heating, high- temperature cooling, indoor environment, administrative builiding
DOI: https://doi.org/10.34641/clima.2022.33

1. Introduction

A radiant system consists of low-temperature heating during winter and high-temperature cooling to ensure an acceptable environment throughout the year. By combining radiant systems and their placements, we can customize the required demands for any building. The combined system can also be used as one system placed in the same structures. Complying with the recommended values of the Ministry of Health, which describe the internal temperature, air flow rate, and moisture, we will provide the conditions required for the hygro- thermal microclimate. The surface temperatures of the structures are also important in order to avoid thermal discomfort.
The following chapters will describe three radiant systems in three different administrative buildings. The applied heating and cooling systems were subsequently assessed and evaluated in the following chapters. Based on previous measured from 2009 and 2011, a new assessment has been made for the indoor air quality.

Copyright ©2022 by the authors. This conference paper is published under a CC-BY-4.0 license.

2. Types of radiant heating/ cooling systems

Radiant systems that have water as a heat transfer substance transmit heat/cold into the room through the radiation prevailing over convection.

The group of radiant low-temperature heating includes: (2, 3)
- underfloor heating,
- wall heating,
- ceiling heating.

System types radiant heating/ cooling systems:
Insulated pipes from the main building structure: (2, 3)
- TYPE A,
- TYPE B,
- TYPE C,
- TYPE D,
- TYPE G,

Thermo - active building systems (TABS): (2, 3)
- TYPE E,
- TYPE F.

2.1 TYPE A System with pipes built into the plaster - wet system

This system, which has pipes built into in plaster, mortar, or concrete, is called a wet system. It is the most commonly used system in Europe and is applied to underfloor heating. (2, 3)

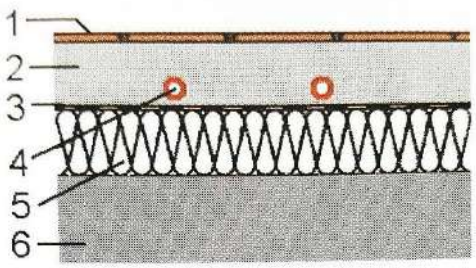

Fig. 1- TYPE A system with pipes built into the plaster: 1= floor covering, 2= carrier and heat distribution layer, 3= protective layer, 4= heating cooling pipes, 5= insulating layer, 6= floor construction (2, 3)

2.2 TYPE B system with pipes built into the thermal insulation layer, dry system

The pipes are stored in a system board, the function of which is as a thermal insulation layer. Temperature transfer from pipe to pipe is limited through the system boards. Well-conductive boards are used to streamline transmission. (2, 3)

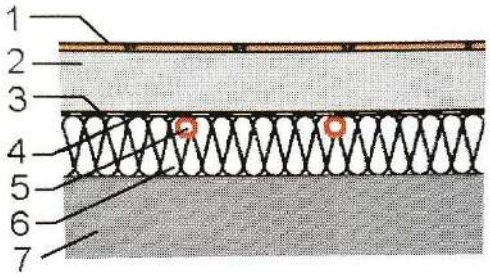

Fig. 2 TYPE B system with pipes built into the thermal insulation layer: 1= floor covering, 2= carrier and heat distribution layer, 3= protective layer, 4= Waterproof layer, 5 =heating/ cooling pipes, 6= insulating layer, 7 =floor construction (2, 3)

2.3 TYPE C system with pipes built into the bulkhead

The tubes in this system are placed in a leveling layer above which there is a second layer of screed, these layers being separated by layers of foil. (2, 3)

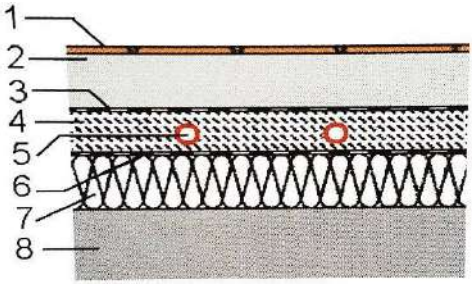

Fig. 3- TYPE C system with pipes built into the bulkhead: 1= floor covering, 2= supporting and heat distribution layer (screed), 3= double separating layer, 4= leveling screed, 5= heating / cooling pipes, 6= protective layer, 7= insulating layer, 8= building construction documents (2, 3)

2.4 TYPE D area system by sections

Instead of a number of single-pipe systems, this system uses extruded plastic panels with small capillary networks of channels in a planar section. This system is rarely used because it is more expensive and its installation is more complicated and depends on the quality of the installation. (2, 3)

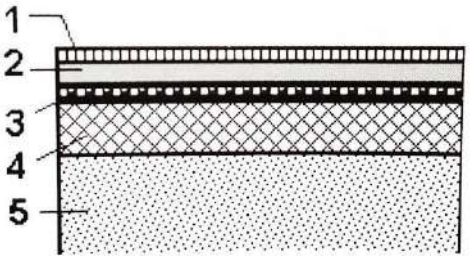

Fig. 4- TYPE D area system in sections: 1= floor covering, 2= load-bearing and heat-distributing layer (screed), 3= surface element, 4= insulating layer, 5= building construction of floors (2, 3)

2.5 TYPE G system with pipes built into a wooden structure

The pipes can also be applied to or under wooden structures, depending on the use of selected methods in construction. They can be fixed to the floor surface or they can be embedded in concrete. The pipes are in the range of 50 to 100 mm intervals. (2, 3)

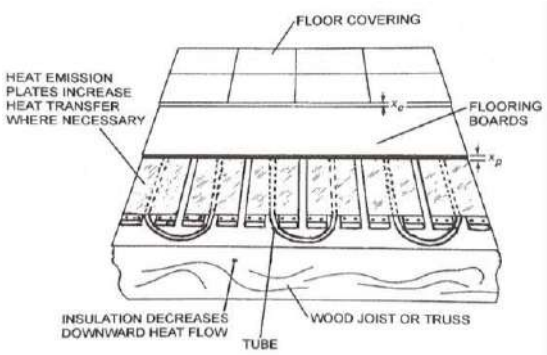

Fig. 5- TYPE G system with pipes built in wooden construction (2, 3)

2.6 TYPE E System with pipes built into the supporting structure

Active ingredients are walls, floors, and ceilings used in which pipes are applied to the neutral center of the concrete slab between the reinforcement, but the position may differ from the composition of the structure. The diameter of the pipes ranges from 17 to 20 mm with a pipe spacing of 150 to 200 mm. (2, 3)

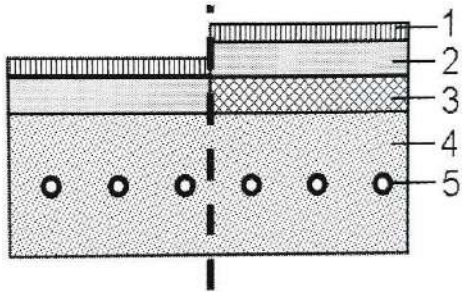

Fig. 6- TABS with and without acoustic insulation: 1 = floor surface covering, 2 = screed material, 3 = acoustic insulation, 4 = building structure, 5 = plastic pipes (2, 3)

This type E of application for radiant heating/ cooling was used in the measured Building C. In the next chapter 3 this system si more described.

2.7 TYPE F capillary mats built into the inner surface layer

Cooling grilles made of small plastic tubes with a diameter of 5 mm, which are placed close together, can be placed in plaster or plasterboard fixed to the ceiling, floor, or wall. (2, 3)

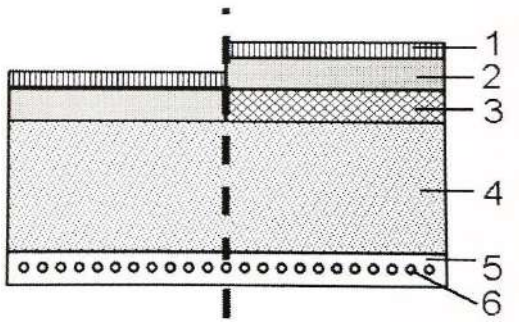

Fig. 7- TABS F with and without acoustic insulation: 1 = floor covering, 2 = screed material, 3 = acoustic insulation, 4 = building structure, 5 = plastic micro pipes, 6 = plaster or gypsum (2)

This type F was applied in Building B, where the measures were made. In the next chapter 3 is described this application.

3. Description of administrative buildings with radiant systems

3.1 Suspended ceiling system - Building A

The administrative building on Tomášikova in Bratislava was built in 2008. The building has two underground floors and eight floors. The facade contains double transparent glazing. The open-space offices and also the classical one local offices are located from the 2nd to the 8th floor. In the administrative part, fresh air is supplied to the office space by air distribution under the floor.

Fig. 8- View of office building A

Heating and cooling of an administrative building A use suspended radiant panels located on ceiling structures. Heating/cooling copper pipes have 8 and 12 mm diameters and are located in panels that are subsequently attached to ceiling structures. Cool panels cover most of the ceiling surface. The ceiling heating/cooling panels are suspended under a concrete plate. The radiant ceiling is composed of: insulation, hangers, pipes, wire net, plaster.

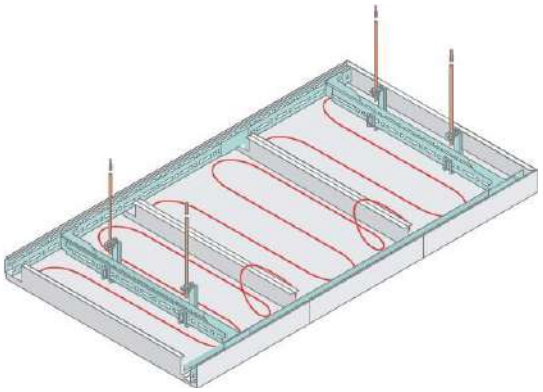

Fig. 9- Radiant heating/cooling system embedded in the ceiling panel (6)

3.2 Capillary pipe system - Building B

Administrative building B is located in Petržalka city district in Bratislava. It consists of two separate blocks: Block A, which has 5 floors, and block B, which has 8 floors. This administrative building B was built in 2009, has a full-glass facade. Fresh air is supplied to the office space by the mechanical ventilation system under the ceiling by slotted air diffusers.

Fig. 10- View of office building B

The capillary mats built into the inner surface layer of the ceiling structure heating or cooling this administrative building B throughout the year. The tubes in the mats have a diameter of 5 mm and are placed 30 mm below the surface plate of the support under the plaster of the ceiling structure. The cross section of construction can be seen in Fig. 7.

3.3 TABS system - Building C

Building C also has a radiant system. The administrative object is located in Bratislava, and has a full facade made of glass. The air supply is provided only by natural ventilation. Building C was built in 2008 and consists of two blocks: block A, which has 7 floors, and block B has 4 floors.

Fig. 11- View of office building C

In this administrative building, the thermal active building system (TABS) is used. Tubes are placed in carrier concrete structures. The diameter of the pipe is 20 mm. This is also called concrete core activation, where the tubes heat/cool the support structure. The cross section of construction can be seen in Fig. 6.

4. Methodology of thermal state assessment

4.1 Objective of the assessment

The surface temperatures of heating/cooling surfaces are due to their physical substance with a dominant parameter in creating thermal well-being in the internal environment.

- Subjective assessment is important for comprehensive assessment of the internal environment. According to this study, the temperature and users were subjectively evaluated by the temperature in the offices.

- One of the most favorable parameters in LTH/ HTC buildings is air flow rate. Mechanical ventilation is used to provide fresh air in the room and not to cool, so the speed and quantity of the supply air is relatively small compared to the conventional cooling methods of similar air buildings.

4.2 Assessed parameters

Experimental measurements were performed in three administrative buildings with glazed facades with various heating/cooling radiation systems. The parameters of the internal environment were measured and also performed in both summer and winter. (7, 8)

Subsequently, the measured values were assessed with the requirements of national and European standards (EN, ISO, CR), subjective assessment of space users.

Local (short-term) measurements were carried out

in each building, during the first week in the summer and during the first week in the winter:
- Inner air temperature (° C), operative temperature (° C), relative humidity φ (%), air flow rate (m/ s).

For local (short-term) heat condition measurements, Brüel & Kjaer 1213 (Indoor Climate Analyzer) was used with appropriate sensors. Measurements were made at individual locations in the office:

• on communication sites in the office - in the head area of a standing person 1.7 m, the center of the body area 1.1 m, and 0.1 m above the floor. Operating temperature was measured only at the height of the center of the body area 1.1 m above the floor.

• in a person's working area - in the head area of the seating man that was 1.1 m, the center of the body area 0.6 m and the ankle area of the seating man 0.1 m above the floor. Operational temperature was measured only in the center of the body area 0.6 m above the floor.

To ensure relevant data from the measurement of quantities, the values were readings: relative humidity and air flow rate up to 3 minutes from the start of measurement and the values for the operational temperature up to 20 minutes.

In Builing A was measured 2 floors 5.th and 8.th, in which there were 10 data loggers on each floor.

In building B, for measurements were done in single offices and also open-plan offices. In the summer 25 data loggers were used. In the winter there were 6 data loggers.

In Building C for measurements were done in single offices on the 3rd and the 5th floor, with 6 data loggers on each floor.

4.3 The results

Inner air temperature θ_a

In winter, the inner air temperatures in building A ranged from 22 to 25.0 ° C (Fig. 12). Building A meets the requirements of III. category from the STN EN 15 251 standards for acceptable heat ranges for heating. (4) The average exterior temperature was typically winter weather during exterior measurements of approximately -4 ° C.

Building B was included in the category III**.** In winter the temperature in the winter ranged from 22.5 to 26 ° C (Fig. 12). It is possible to say that the administrative building is overheated.

In a building C with the built-in TABS system, the temperature during work hours in the winter ranged between 23 to 24 °C (Fig. 12). A great influence on air temperature has natural ventilation windows. Since the building has only a simple facade, the impact of exterior air was very significant. This can be seen in the indoor air temperature values during lunch, when employees were allowed to vent and the temperature decreased significantly. This was also reflected in the high percentage of working time during which the building has fallen into the IV. categories according to STN 15 251. (4)

Most of the internal air temperature, 85% measured in the summer in building A was in the range of 24 to 26.0 ° C and in building B it was 81,9% between 22 to 24.5 ° C (Fig. 12). Building A meets the requirements of II. category according to STN EN 15,251, for acceptable temperature ranges for cooling, while building B with the capillary mats is at the bottom boundary of the II. category up to III. category. (3)

The measurements were made under typical conditions in summer (average daily outdoor temperature 31 to 33 ° C).

Building C: The inner air temperature was about 25 to 26 ° C in the summer.

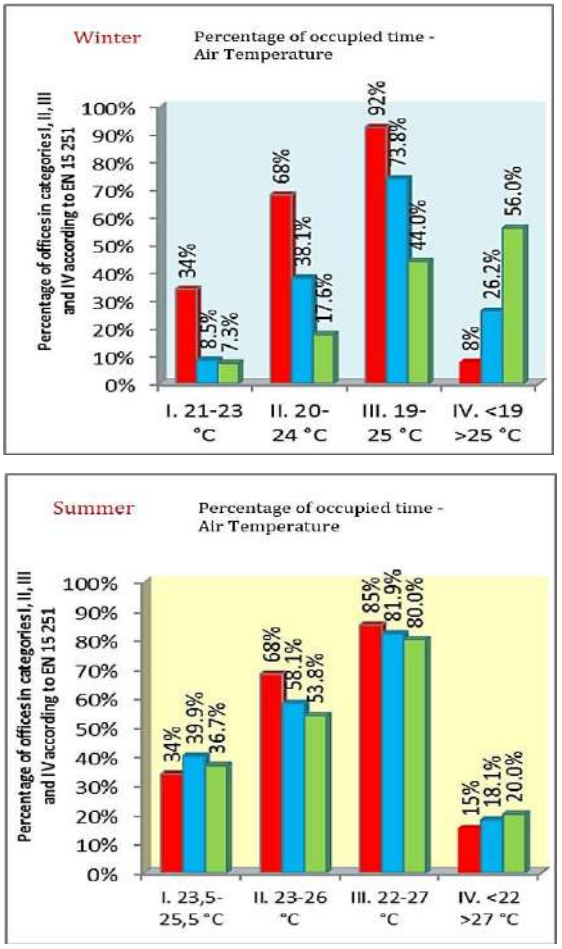

Fig. 12- indicates the percentage of working time during which the air temperature corresponded to individual categories according to STN EN 15 251. (1, 4) (red- building A, blue- building B, green- building C)

Operative temperature θo

In building A: The operating temperature in open-space offices ranged from 24 to 26.0 ° C in winter (Fig. 13). Due to the winter period, this temperature is slightly higher, but still at the acceptable level corresponding to the standard. Compared to subjective assessment (questionnaires), the employees were satisfied with a slightly warm indoor environment. In summer: the operating temperature was 25.8 to 27.0 ° C. In cell offices, the temperature ranged between 24.5 and 26.0 °C. In general, the operating temperature on the highest floors was 0.9 ° C higher than on a typical floor.

Building B: In winter, the operating temperature in building B with capillary mats was equal to the internal air temperature, therefore slightly lower than in building A with a suspended subheading of about 24 ° C.

In summer: the operational temperature was around 23.0 - 24.0 in the capillary mats.

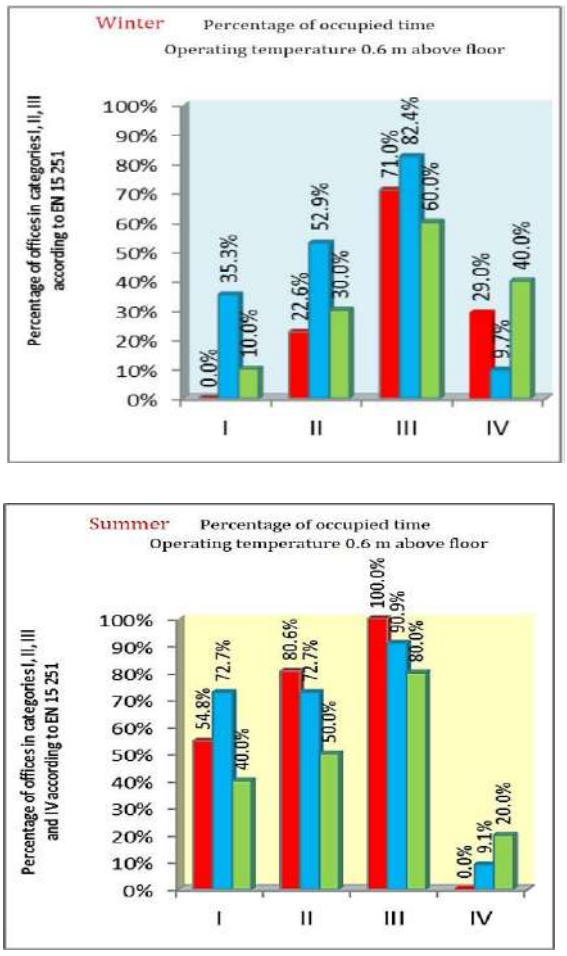

Fig. 13- indicates the percentage of working time during which the operative temperature corresponded to individual categories according to STN EN 15 251. (1, 4) (red- building A, blue- building B, green- building C)

Relative air humidity φ

Relative air humidity ranged from 30% to 40% in both buildings- A and C corresponding to the requirements of the standard STN EN 15 251 (Fig. 14). The values are in view of the winter heating period closer to the lower limit of the permissible standard, but there is still an effect too low humidity for employees.

In building C, there was relative humidity at the lower limit of the standards. However, this condition is caused by air drying due to heating, and the building has no mechanical ventilation, it would only be changed by local air humidifiers.

Relative air humidity in building B in the winter moves below the requirements of the standard (below 30%); therefore, it would be good to increase the moisture to avoid adverse impact.

Relative air humidity was around 50% in the summer, what it is the favorable value of relative humidity for the summer period.

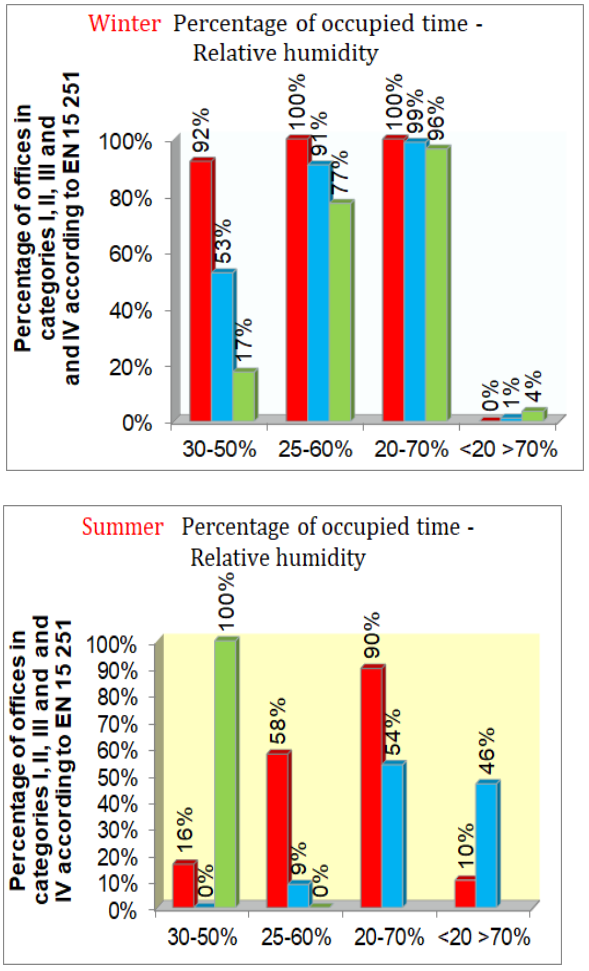

Fig. 14- indicates a percentage of working time during which the relative humidity corresponded to individual categories STN EN 15 251. (1, 4) (red- building A, blue- building B, green- building C)

Air velocity v_a

Building A in the summer and also in winter was similar to air velocity. The average value was 0.09 m/s (Fig. 15). In large offices, the air flow rate was slightly increased in several places, but it still corresponds to the requirements CR 1752. (5)

Building B - the average air velocity was in both heights slightly lower than in building A - moved around 0.05 m/s to 0.1m/s. The difference between head height and ankle height was 0.02 m/s.

The airflow rate in building C was 0.1m/s, which was very low. The exception in the measurements was the office in which the window was opened. However, this condition is temporary and was removed after the window was closed.

All buildings are classified in A category which is defined in this category (<0,15 m/s) according to CR 1752. (5)

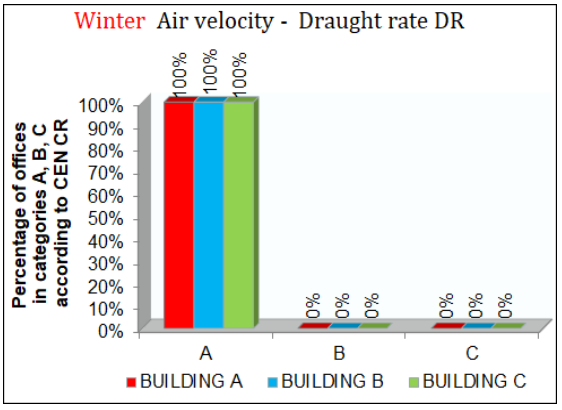

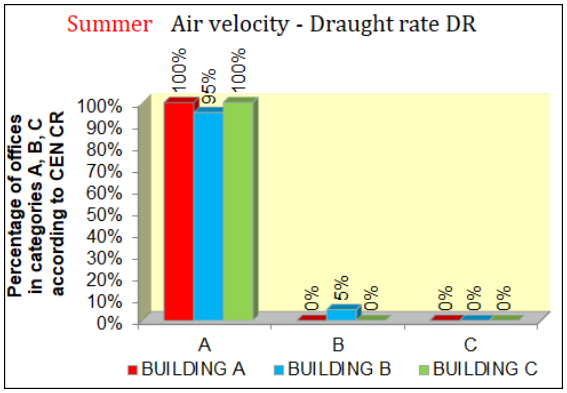

Fig. 15- indicates the percentage of working time in which the final value corresponded to the individual categories of the technical regulation CEN CR 1752. (1, 5) (red- building A, blue- building B, green- building C)

CO2 concentration measurements

Building A: Percentage of occupied time (occupied time), during which the indoor CO2 concentration above the outdoor concentration in the offices fell into the I. category according the standard EN 15 251 in winter (October - April) and in summer (May – September).

Building B and C were not measured for long-term and short-term measurements did not show the full value.

Subjective assessment

Subjective assessment is an important part of the comprehensive assessment of the internal environment. According to the results of the subjective assessment, the internal environment for most users is acceptable in all parameters covered by the questionnaire survey: the acceptability of the environment, the acceptability of the thermal environment, the acceptability of moisture, the flow rate and the quality of the internal air. The thermal sensation in all buildings evaluated users in the winter as slight heat, but the acceptability of the thermal state of the environment was rated as acceptable. It follows that they were happy with this slightly warm environment. However, the findings through objective measurements appeared to be a moderate precursor. In summer, the thermal feeling of users was rated as neutral. Likewise, users considered this condition acceptable.

In two of three building (buildings A and B) subjective evaluation was carried out due to the questionnaires in both summer and winter.

Building A: Percentage of the time the predicted mean vote in offices in categories according the standard ASHREA 55 [9] for winter season are in A category (35,3%), in B category (70,3%) and in last allowed category C (82,4%). For summer season it was 40,0% in A category, 76,5% in B category and in last allowed category C it was 83,6%.

Buiding B: Percentage of the time for winter season are in following categories: in A category (4,6%), in B category (62,7%) in last allowed category C (100%). According to the standard ASHREA 55 [9] for summer season are in following categories: A category (76,8%), in B category (100%) and there was no data outside the allowed categories.

Building C: Percentage of the time the predicted mean vote in offices in categories according the standard ASHREA 55 [9] in the winter season are in A category (8%), in B category (46%) and in last allowed category C (88%). For summer season it was 33% in A category, 80% in B category and in last allowed category C it was 99%.

According to Ashrae [9] the categories were category A (-0,2 < PMV < +0,2), category B (-0,5 < PMV < +0,5) and category C (-0,7 < PMV < +0,7).

5. Acknowledgement

This work was supported by the Ministry of Education, Science, Research and Sport of the Slovak Republic through VEGA Grants 1/0303/21 and KEGA 005STU-4/2021.

6. Conclusion

The internal air temperature in all three buildings moved to the upper limit of standards in winter. Given the user's preference (employees) to a higher temperature led to moderate precursor. But in view of the nature of sitting administrative work, it does not disturb significantly. In the summer, there was very favorable thermal conduct in all buildings. It is clear from year-round measurements that the thermal condition is very stable throughout the year, with little differences thet are not audible or different oriented offices.

The relative air humidity in the building A moved at an acceptable level. In building B and C there was less moisture in winter, it moved closer to the lower limit of standards requirements, but still not at the level at which it could come to the difficulties caused by dry air. The reduction in moisture is due to a higher degree of heating, which naturally occurs in air drying in winter. In summer, relative humidity ranged between 50 to 60%, which is a favorable value in terms of residence.

The air flow rate in all three buildings corresponds to the highest categories of international standards requirements. In the internal space, there is no increased air flow or draft.

In the end, it can be stated that all three types of heating/cooling - with a suspended ceiling system, with capillary mats, and with a concrete core activation system - have a favorable impact on the internal environment and thermal well-being of users without unnecessary risk of creation and beneficial effects on the employees that move in the space.

It is very important to choose the correct type of low-temperature heating system (type E/ type F/ ceiling radiant panels) for different types of buildings (massive construction, light construction, etc.)

7. References

[1] Ďurišová E., Evaluation of indoor environment with low temperature heating / high temperature cooling systems, Ph.D. thesis, Faculty of Civil Engineering, Slovak University of Technology in Bratislava, Bratislava, 2012. (1)

[2] STN EN 1264: 2021, Water based surface embedded heating and cooling systems. (2)

[3] Babiak J., Olesen B., Petráš D. Low temperature heating and hight temperature cooling: Rehva guidebook No.7 Forssan: Rehva, ISBN 2-9600468-6-2, 2007 (3): 43.

[4] EN 15251 Indoor environmental input parameters for design and assessment of energy performance of buildings-addressing indoor air quality, thermal environment, lighting and acoustics 2006. (4)

[5] CEN CR 1752 Ventilation for buildings – Design criteria for the indoor environment (5)

[6] https://www.swegon.com/siteassets/ product-documents/zent-frenger/ en/radiant-ceiling-overview-spread.pdf (6)

[7] Ďurišová E., Petráš D., Evaluation of indoor air in office building in Bratislava - in summer and also in winter period, INDOOR AIR 2011 : Proceedings of the 12th International Conference on Indoor Air Quality and Climate. Austin,Texas, ISBN 9781627482721.

[8] Petráš D., Ďurišová E., Krajčík M., Thermal comfort in the office building with low temperature heating / high temperature cooling and ist influence on the quality of the working environment. Healthy buildings 2009 : 9th International conference. Syracuse, ISBN 9781622769971

[9] ASHRAE 55 – 1992, Thermal Environmental Conditions for Human Occupancy

The datasets generated during and/or analysed during the current study are not publicly available because building operators did not allow us to provide gathered data from measurement but will be available after individual communication and disclosure of data available after authorization.

A study of the sensible and latent heat flux of a ceiling radiant cooling panel with superhydrophobic treatment

Ziwen Zhong [a], Wei Ma [b], Jianlei Niu [a], Shuhuai Yao [b]

[a] Department of Building Environment and Energy Engineering, The Hong Kong Polytechnic University, Hong Kong, China

[b] Department of Mechanical Engineering, The Hong Kong University of Science and Technology, Hong Kong, China

Abstract. Condensation is one of the major factors that limit the application of radiant cooling systems in hot and humid areas. The need for condensation control restricts the temperature difference between a panel surface and indoor spaces, limiting the cooling capacity of the panel. Previous studies indicated that condensation risks of a ceiling radiant cooling panel can be greatly mitigated by applying superhydrophobic surface materials, making a panel usable with a lower temperature even below air dew point. We performed a case study to show how the total heat flux of a ceiling radiant cooling panel with latent heat transfer can be enhanced compared with a panel with only sensible cooling. Based on empirical methods and heat and mass analogy, as indicated by a series of natural convection condensation heat transfer experiments for a ceiling positioning superhydrophobic aluminum surface showing the condensation heat transfer of a superhydrophobic surface can be well predicted by the method, we investigated both the sensible and latent heat flux of a panel placed in the air with a temperature of 25°C and relative humidity between 40% and 70%. The case study shows an increment between 4% and 300% for the total heat flux of the panel compared with only sensible cooling under different humidity conditions.

Keywords. Radiant cooling system, heat flux, condensation, superhydrophobic surface materials.
DOI: https://doi.org/10.34641/clima.2022.202

1. Introduction

Radiant cooling technology has many benefits like energy saving [1], better or equal thermal comfort compared with all-air conditioning [2], and quiet operation [3], but its application is limited in hot and humid areas majorly due to condensation concerns. The principle of condensation control is to maintain the radiant surface temperature above the indoor air dew point, but the raised surface temperature also narrows the temperature difference between the radiant surface and indoor spaces, resulting in a limited cooling capacity of a radiant cooling system.

A vertically positioning metal radiant cooling panel can be operated with condensation on its surface if equipped with a drain unit [4-7]. For ceiling radiant cooling panels (CRCP), however, the cooling capacity is stilled limited as the temperature of the radiant surface facing the occupied space must be controlled [8] to prevent dripping of large condensate droplets. Since panels are usually made of hydrophilic metal alloy materials, droplets with sizes up to 7.3 mm [9] can be formed on a panel surface. Such a large dropping droplet will cause discomfort feelings to space occupants.

Different from hydrophilic surfaces, condensate droplets formed on superhydrophobic surfaces can be much smaller. Condensate droplets can leave a superhydrophobic surface with a tiny size even smaller than people's sensory threshold, hence condensation risk can be greatly mitigated if superhydrophobic surfaces are applied for CRCP [10]. Recent research [11] indicated that the size of condensate droplets formed on certain areas of a superhydrophobic aluminum surface placed on a practical CRCP can be constrained below 150 microns during an 8-hour period of condensation with surface temperature 8°C lower than air dew point under typical indoor air conditions, showing the potential application of CRCP with much lower surface temperature by superhydrophobic surface treatment.

The cooling capacity of a CRCP can be substantially

Copyright ©2022 by the authors. This conference paper is published under a CC-BY-4.0 license.

increased with the expanded temperature difference between the radiant surface and indoor spaces. If the surface temperature is further lowered below air dew point without dangerous condensation, as in the case of the condensation regime on a super-hydrophobic surface, additional latent heat flux can be achieved by the panel. However, there is no discussion revealing the potential cooling capacity of CRCP with latent heat transfer to the best of our knowledge.

On the other hand, the condensation heat transfer coefficient between a ceiling positioning super-hydrophobic surface and humid air under natural convection remains little known, hindering the prediction of the condensation heat flux of a panel with latent heat transfer.

In this paper, we performed a case study of a CRCP placed in indoor space with an air temperature of 25°C and relative humidity between 40% and 70%, attempting to indicate the potential enhancement of the total heat flux of CRCP with superhydrophobic treatment which can be operated with lower surface temperature below air dew point, namely, with latent heat transfer, based on our experimental investigation for the condensation heat and mass transfer of a ceiling placed super-hydrophobic aluminum surface.

2. Methods

2.1 experimental methods for condensation heat transfer of hydrophilic and super-hydrophobic surfaces

Square aluminum plates with a length of 80 mm and a thickness of 5 mm were prepared to fabricate superhydrophobic surfaces by methods mentioned in [11-13]. Same plates were also prepared without any treatment and remained hydrophilic.

The schematic experimental setup is shown in Fig. 1. Condensation experiments were performed in a climate chamber with a size of 4m x 2.7m x 2.9m. To control indoor thermal conditions while avoiding forced airflow, a hydronic radiant panel, a thermal radiator, and a humidifier were placed inside the chamber.

The hydrophilic aluminum plate and super-hydrophobic aluminum plate were mounted onto a cooling stage by bolts and rubber gasket, with a ceiling positioning. The cooling stage was connected to a water chiller. Hence, the plates can be cooled directly by circulated chilled water.

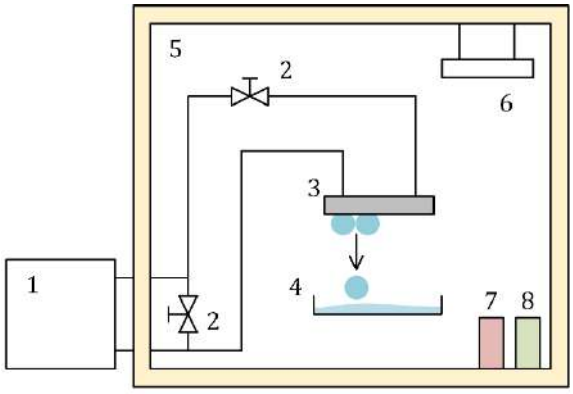

1 - chiller
2 - valve
3 – testing plates
4 – water collection pan
5 - chamber
6 – hydronic panel
7 – thermal radiator
8 - humidifier

Fig. 1 – The schematic experimental setup.

The plate surface temperature was measured by calibrated ultrafine thermocouples attached to the surface via a small foil tape. The condensate rate was measured through the dew collection method. A plastic drain pan was used to collect condensate dripping from the plates. The mass of the condensate was measured using a calibrated weighing scale. The ambient air temperature and humidity were measured by a temperature and humidity transmitter placed near the plates. The accuracy of sensors and calibration devices is shown in Table 1.

Tab. 1 - Accuracy of sensors and calibration devices.

Sensors/Calibration devices	Accuracy
Thermocouples	±0.5°C
Reference thermometer	±0.03°C
Air temperature/humidity transmitter	Temp: ±0.35°C RH: ±2.5%
Weighing scale	0.01 g
Standard weight	0.0005 g

The ambient air temperature (T_a) and relative humidity (RH) in the chamber were maintained at 24.3°C ± 0.5°C and 65% ± 2.5%, and the air dew point was maintained at around 17.3°C. The plate surface temperature was controlled by adjusting the chilled water temperature setpoint (T_{set}) between 5°C and 13°C for different experimental sets to achieve various subcooling degrees. The conditions of each experimental set are shown in Table 2.

Tab. 2 - Experimental sets.

Set	T_{set} (°C)	T_a (°C)	RH (%)
S1	5	24.3 ± 0.5	65 ± 2.5
S2	8		
S3	10		
S4	13		

When performing experiments, the indoor air condition was firstly controlled to the expected level and the chilled water temperature was controlled to the setpoint, then the chilled water valve of the cooling stage was switched on, and the plate was cooled quickly and the plate surface temperature can reach stable in five minutes. After three-hour condensation, the total mass of dew collected in the water collection pan and that remained on the plate surface was measured.

The tiny droplets from the superhydrophobic aluminum plate surface can easily evaporate after falling into the pan, leading to underestimation of the condensate mass. To avoid the error due to the evaporation of tiny droplets, water was added to the water collection pan as a buffer during experiments. The evaporation loss can be firstly measured by implementing a condensation test on the hydrophilic aluminum plate since condensate water film kept remaining on the hydrophilic aluminum surface and won't drip down into the water collection pan during three-hour condensation.

The condensation mass rate $\dot{m}_{cond}$ was calculated by equation (1), considering the dew mass m_{dew} , condensation duration $\Delta\tau$, and the plate surface area A.

$$\dot{m}_{cond} = \frac{m_{dew}}{\Delta\tau A} \tag{1}$$

2.2 methods for the case study of the total heat flux of CRCP with latent heat transfer

The condensate mass rate is considered to be equal to the convection mass transfer rate between humid air and the plate surface, which can be calculated by equation (2).

$$\dot{m}_{cond} = \dot{m}_{conv} = h_m\left(\rho_{vapor,\infty} - \rho_{vapor,sat}\right) \tag{2}$$

Where h_m represents mass transfer coefficient, $\rho_{vapor,\infty}$ is the density of water vapor in ambient air, $\rho_{vapor,sat}$ is the saturated vapor density at the surface temperature.

Heat and mass transfer analogy [14] is applied to estimate mass transfer coefficient.

$$\frac{h}{h_m} = \rho c_p Le^{2/3} \tag{3}$$

Where h is the free convection heat transfer coefficient of a cold horizontal bottom surface, ρ and c_p the density and specific heat capacity of ambient air. Le is the Lewis number, for air, $Le \approx 1$.

Nusselt number (Nu) is defined as equation (4). As recommended in [14], the empirical correlation proposed by Lloyd and Moran [15] is applied to calculate Nu of a cold horizontal bottom surface over a wide range of Raleigh number (Ra).

$$Nu_L = \frac{hL}{k} \tag{4}$$

$$Nu_L = \begin{cases} 0.54Ra_L^{1/4}\ (10^4 \lesssim Ra_L \lesssim 10^7, Pr \gtrsim 0.7) \\ 0.15Ra_L^{\frac{1}{3}}\ (10^7 \lesssim Ra_L \lesssim 10^{11}, \text{All } Pr) \end{cases} \tag{5}$$

Where Ra is calculated based on equation (6).

$$Ra = GrPr \tag{6}$$

Grashof number (Gr) is calculated by equation (7).

$$Gr = \frac{g\beta(T_a - T_s)L^3}{\upsilon^2} \tag{7}$$

Where g is the gravity acceleration, β the coefficient of thermal expansion, T_a the ambient air temperature, T_s the surface temperature, L the length of the plates, υ the kinematic viscosity.

By comparing our experimental data of condensation mass rate and the empirical convection mass transfer rate, it can be determined whether the heat and mass analogy-based empirical methods can be applied to predict the condensation heat transfer of super-hydrophobic surfaces under natural convection in humid air.

To predict the total cooling capacity of CRCP with latent heat transfer, heat flux by thermal radiation, natural convection, and condensation should all be considered.

$$q_s = q_{rad} + q_{conv} + q_{cond} \tag{8}$$

The MRT method [16] was applied to estimate the heat flux by thermal radiation based on the equation (9).

$$q_{rad} = 5 \times 10^{-8}|(t_s + 273.15)^4 - (\text{AUST} + 273.15)^4| \tag{9}$$

Where t_s is the effective panel surface temperature, AUST is the area-weighted temperature of all indoor surfaces excluding active panel surfaces. For simplification, AUST is considered equal to indoor air temperature as in the case of little outdoor exposure of walls.

The natural convection heat transfer coefficient between a cooled ceiling surface and indoor air is

determined by equation (10) [16].

$$h_{conv} = 2.13|t_s - t_a|^{0.31} \quad (10)$$

Then the convection heat flux can be calculated.

$$q_{conv} = h_{conv}|t_s - t_a| \quad (11)$$

The heat flux induced from condensation equals the latent heat released through the condensation process, which can be calculated from the condensation mass rate $\dot{m}_{cond}$ and the vaporization latent heat of water vapor h_{fg}.

$$q_{cond} = \dot{m}_{cond} h_{fg} \quad (12)$$

3. Results and discussions

3.1 condensation heat transfer of a ceiling positioning superhydrophobic surface

The experimental condensation mass rate of the hydrophilic aluminum plate and the super-hydrophobic aluminum plate are compared with the data predicted by the heat and mass analogy and the empirical convection heat transfer coefficient based on equation (4) – (10). The data are displayed in Fig. 2 with relation to the subcooling degrees (SCD) which is defined as the temperature difference between the plate surface temperature and the air dew point. The error between the experimental condensation mass rate of the two plates and the empirical data are both within 15%, proving the applicability of using heat and mass analogy to predict the condensation rate of a superhydrophobic surface. For the hydrophilic plate, all the condensate mass rates are very close to the empirical one, while the condensation mass rate of the superhydrophobic surface is a bit higher than the empirical data when SCD is lower than 8 K. With higher SCD, the condensate mass rate of the superhydrophobic surface becomes closer to empirical data.

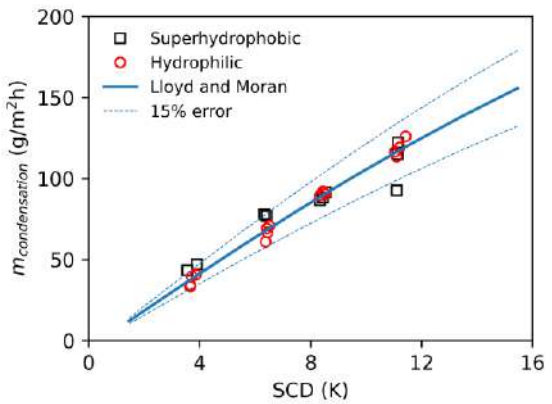

Fig. 2 - The condensation mass rate of the superhydrophobic and hydrophilic aluminum plate, with a comparison with empirical correlation.

Our experimental data showed that the condensation mass rate of the ceiling positioning super-hydrophobic aluminum surface is in the similar range of the hydrophilic aluminum surface under natural convection in humid air, and the comparison with the empirical data shows both the condensate rates can be predicted based on the heat and mass analogy after knowing the convection heat transfer coefficient. Based on the finding, the condensation heat flux of a CRCP with superhydrophobic treatment can be determined using equations (2), (3), and (10).

3.2 the case study of the sensible and latent heat flux of CRCP with latent heat transfer

Studies [10, 11] confirmed that the jumping condensation regime of superhydrophobic surfaces can be applied to mitigate condensation risks of CRCP by constraining the size of dripping droplets, making CRCP usable with a lower surface temperature below air dew point. Under the circumstance, CRCP transfers heat from an indoor space and its enclosure surface by thermal radiation, natural convection, and condensation.

The heat flux through the CRCP is investigated by the method mentioned in section 2.2. In this case study, indoor air temperature is set as 25°C, relative humidity is set between 40% and 70%, the lowest panel surface temperature is set as 10°C to simulate the effective surface temperature of a CRCP with chilled water supplied at 7°C and returned at 12°C.

The heat flux of the CRCP with latent heat transfer in relation to the temperature difference between panel surface and indoor air, ΔT, is shown in Fig. 3. The sensible heat flux is the net heat flux by radiation and convection. The critical temperature difference ΔT_c is the temperature difference between the panel surface and air dew point, which represents the maximum temperature difference a sensible cooling panel can achieve.

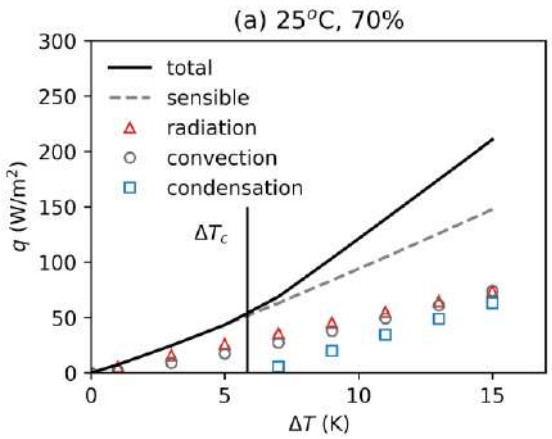

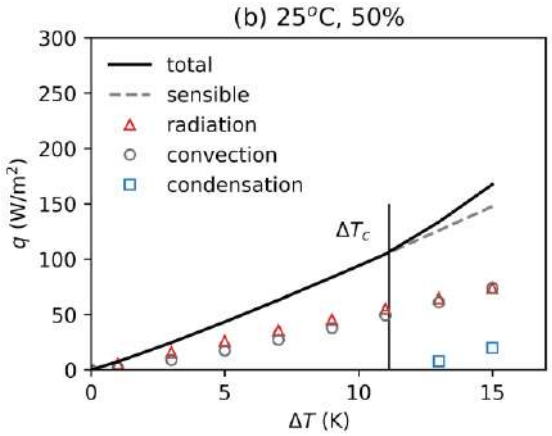

Fig. 3 - The heat flux of CRCP by radiation, convection, and condensation, $\Delta T = |T_a - T_s|$, $\Delta T_c = |T_a - T_{dew}|$. The sensible heat flux is the net heat flux by thermal radiation and convection.

For the highly humid condition (RH = 70%) shown in Fig. 3(a), the heat flux of a sensible cooling panel is limited to 52 W/m² at $\Delta T_c = 5.8$°C. With ΔT further increased, heat flux by condensation is included due to condensation on the panel surface and is increased with increasing ΔT, making the total heat flux higher than the sensible heat flux. With the highest temperature difference $\Delta T = 15$°C in this case, the total heat flux can reach 210 W/m², consisting of 147 W/m² of sensible heat flux and 63 W/m² of condensation heat flux. The ratio of the radiation heat flux is higher than 50% when there is no condensation on the panel surface, but it becomes close to the convection and condensation heat flux when ΔT is near 15°C.

The heat flux of a sensible cooling panel can reach a higher value of 105 W/m² in a relatively dry condition (RH = 50%), as indicated in Fig. 3(b), since ΔT_c can be as high as 11.1°C. If the panel surface is further cooled to the lowest temperature of 10°C, the total heat flux is 168 W/m² with a condensation heat flux of only 20 W/m². The heat flux by radiation contributes to near 50% for sensible heat flux, while the ratio of condensation heat flux can be much smaller when compared with the highly humid condition.

The total heat flux of CRCP with latent heat transfer in relation to the panel surface temperature is shown in Fig. 4. The sensible heat flux is the net heat flux by thermal radiation and convection heat transfer, which represents the heat flux of a CRCP without condensation. The maximum sensible heat flux can reach 150 W/m² at $T_s = 10$°C. When condensation control is considered, however, the sensible heat flux will be hugely limited. In the case of RH = 60%, the maximum sensible heat flux decreased from 148 W/m² to 76 W/m² since the panel surface temperature must be controlled higher than air dew point to prevent dew formation.

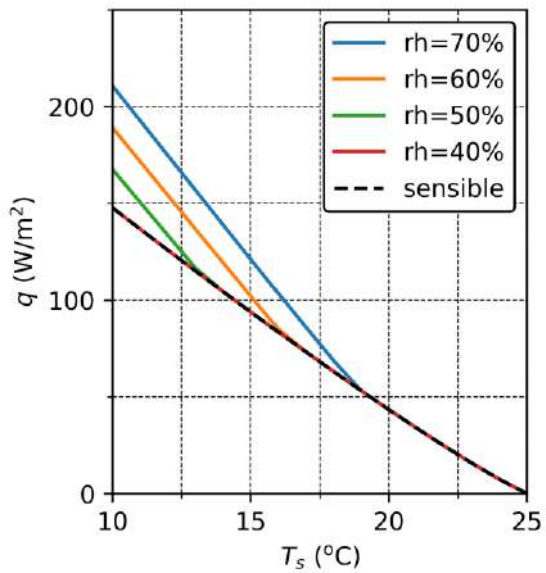

Fig. 4 - The total heat flux of CRCP with latent heat transfer in humid air, $T_a = 25$°C, RH = 40% − 70%, the panel surface temperature is set between 10°C and T_a. The sensible heat flux is the net heat flux by thermal radiation and convection.

An index E_{pl} is proposed to demonstrate the potential enhancement of the heat flux of a CRCP with latent heat transfer. E_{pl} is defined as the ratio of the total heat flux of a CRCP with latent heat transfer under a certain temperature difference between panel surface and indoor air, $q_{tot,\Delta T}$, to the maximum sensible heat flux of a CRCP with only sensible cooling, $q_{\Delta T_c}$.

$$E_{pl} = \frac{q_{tot,\Delta T}}{q_{\Delta T_c}} - 100\% \qquad (13)$$

By equation (13), E_{pl} can show to which extent the total heat flux is increased when latent heat transfer is available compared with only sensible heat transfer.

Fig. 5(a) illustrates the evaluation of $q_{tot,\Delta T}$ and $q_{\Delta T_c}$. The E_{pl} of CRCP with a surface temperature of 10°C in the case is shown in Fig. 5(b). E_{pl} is generally increased with increased air temperature and relative humidity, showing that a more significant enhancement of heat flux of CRCP can be achieved especially in hot and humid weather. In relatively dry conditions (RH = 40%), E_{pl} is relatively small because a large temperature difference can be also achieved for a sensible cooling panel. But in highly humid conditions (RH =70%), E_{pl} shows three times of enhancement of total heat flux compared with only sensible cooling due to the extremely limited cooling capacity for sensible cooling CRCP, indicating the great potential of applying a panel with latent cooling to meet a high thermal load in indoor spaces.

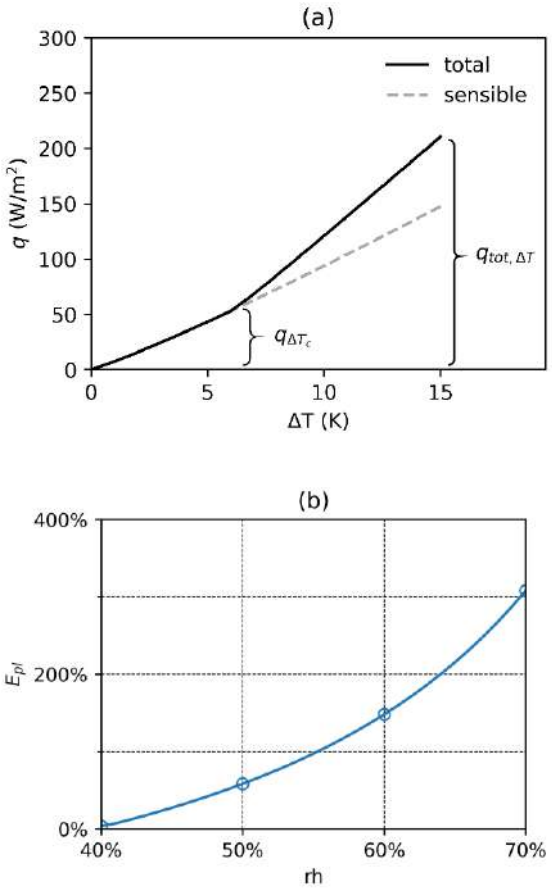

Fig. 5 – (a) The heat flux enhancement index $E_{pl} = \frac{q_{tot,\Delta T}}{q_{\Delta T_c}} - 100\%$, $q_{tot,\Delta T}$ is the total heat flux of CRCP with latent heat transfer at ΔT, $q_{\Delta T_c}$ is the maximum heat flux of a sensible cooling CRCP. (b) E_{pl} of CRCP with latent heat transfer, in this case, $T_s = 10°C$, $T_a = 25°C$, $RH = 40\% - 70\%$.

3.3 cooling effects on air

The cooling effects of CRCP with latent heat transfer are dependent on the falling-escaping-evaporation behavior of tiny droplets jumping from the super-hydrophobic-treated panel surface. If jumping droplets are totally removed from the indoor space, the indoor air can be simultaneously cooled and dehumidified. If jumping droplets totally re-evaporate into the indoor air, the indoor air would be further cooled by an evaporative cooling-like process.

By creating a near-wall flow close to the panel surface through a ventilation system, some droplets can be exhausted and some latent cooling can be achieved. A primary estimation indicates that the ratio of exhausted droplets shall be diminutive. The complex falling-moving-evaporation behavior of tiny jumping droplets in airflow makes it difficult to predict the actual indoor humidity. The computational fluid dynamics technique can be applied to solve the issue in future research.

3.4 limitations of the research

There are also some limitations for this study. The prediction of heat flux by thermal radiation assumes that the panel surface emissivity is 0.9. However, the emissivity of a superhydrophobic surface with condensation has not been thoroughly investigated, though some studies [13] reported that high emissivity and super-hydrophobicity can be integrated on a surface by specific design.

On the other hand, the experimental study is performed with *Ra* between 5 x 10^5 and 10^6, lower than the *Ra* of a practically used CRCP, because the size of our superhydrophobic plate is relatively small compared with practical panels while Ra is highly dependent on the length scale of a surface. The fabrication of a large-scale superhydrophobic surface with mechanical and chemical robustness and good condensation mitigation performance is still a challenge, which is also the major limitation for constructing a practical superhydrophobic CRCP.

4. Conclusions

Condensation issue is the major limitation hindering the application of radiant cooling systems in hot and humid areas. Nonetheless, our case study revealed that the total heat flux of a CRCP can be remarkably enhanced by taking advantage of condensation heat transfer. The results of this study can be summarized as follows.

- The total heat flux of a panel with latent heat transfer can be enhanced by both the increased sensible heat flux due to expanded temperature difference between panel surfaces and indoor spaces, and latent heat flux by condensation of tiny droplets.

- Compared with a panel with only sensible cooling, a significant enhancement of up to 300% can be achieved for the total heat flux of a CRCP with latent heat transfer under a highly humid condition due to 1) the limited maximum sensible heat flux of the sensible cooling panel and 2) the extended total heat flux of the latent cooling panel.

This study draws a clear picture of how the cooling capacity of CRCP can be enhanced via a latent heat transfer process, showing a hidden potential of radiant cooling panels. Since the fabrication of large-scale superhydrophobic materials with mechanical and chemical robustness and good condensation mitigation performance is still a challenge, more efforts are needed to make the panels with latent heat transfer more practicable.

5. Acknowledgment

This study was fully supported by the General Research Funding of the Research Grant Council of the Hong Kong SAR, China (Project No. 15206620).

6. References

[1] J. Niu, L. Zhang, H. Zuo, Energy savings potential of chilled-ceiling combined with desiccant cooling in hot and humid climates, Energy and buildings, 34 (5) (2002) 487-495.
[2] C. Karmann, S. Schiavon, F. Bauman, Thermal comfort in buildings using radiant vs. all-air systems: A critical literature review, Building and Environment, 111 (2017) 123-131.
[3] K.-N. Rhee, B.W. Olesen, K.W. Kim, Ten questions about radiant heating and cooling systems, Building and Environment, 112 (2017) 367-381.
[4] Y. Wu, H. Sun, M. Duan, B. Lin, H. Zhao, Dehumidification-adjustable cooling of radiant cooling terminals based on a flat heat pipe, Building and Environment, 194 (2021) 107716.
[5] H. Teufl, M. Schuss, A. Mahdavi, Potential and challenges of a user-centric radiant cooling approach, Energy and Buildings, 246 (2021) 111104.
[6] H. Shu, X. Bie, H. Zhang, X. Xu, Y. Du, Y. Ma, L. Duanmu, G. Cao, Natural heat transfer air-conditioning terminal device and its system configuration for ultra-low energy buildings, Renewable Energy, 154 (2020) 1113-1121.
[7] D. Song, S. Kato, Radiational panel cooling system with continuous natural cross ventilation for hot and humid regions, Energy and Buildings, 36 (12) (2004) 1273-1280.
[8] W. Zhao, Y. Hu, Y. Wang, W. Qin, Thermal performance of a suspended ceiling fin heat transfer panel with drain pan, Building and Environment, 144 (2018) 622-630.
[9] H. Tang, X.-H. Liu, Experimental study of dew formation on metal radiant panels, Energy and Buildings, 85 (2014) 515-523.
[10] H. Tang, X.-H. Liu, H. Li, Y. Zhou, Y. Jiang, Study on the reduction of condensation risks on the radiant cooling ceiling with superhydrophobic treatment, Building and Environment, 100 (2016) 135-144.
[11] Z. Zhong, J. Niu, W. Ma, S. Yao, M. Yang, Z. Wang, An experimental study of condensation on an aluminum radiant ceiling panel surface with superhydrophobic treatment, Energy and Buildings, 252 (2021) 111393.
[12] Y. Hou, Y. Shang, M. Yu, C. Feng, H. Yu, S. Yao, Tunable Water Harvesting Surfaces Consisting of Biphilic Nanoscale Topography, ACS Nano, 12 (1112(12) (2018) 11022-11030.
[13] W. Ma, Y. Li, C.Y.H. Chao, C.Y. Tso, B. Huang, W. Li, S. Yao, Solar-assisted icephobicity down to −60°C with superhydrophobic selective surfaces, Cell Reports Physical Science, 2 (3) (2021) 100384.
[14] T.L. Bergman, F.P. Incropera, D.P. DeWitt, A.S. Lavine, Fundamentals of heat and mass transfer, John Wiley & Sons, 2011.
[15] J.R. Lloyd, W.R. Moran, Natural Convection Adjacent to Horizontal Surface of Various Planforms, Journal of Heat Transfer, 96 (4) (1974) 443-447.
[16] ASHRAE, ASHRAE Handbook 2016: HVAC Systems and Equipment, ASHRAE, 2016.

Data Statement

Data sharing not applicable to this article as no datasets were generated or analysed during the current study.

Advanced solutions to improve heat recovery from wastewater in a double heat exchanger

Mihnea Sandu [a], Aamjed Albaiyati [b], Ilinca Nastase [a], Paul Danca[c], Florin Bode [a,d],Cristiana Croitoru [a]

[a] CAMBI Research Center, Building Services Faculty, Technical University of Civil Engineering of Bucharest, Bucharest, Romania, Mihnea.sandu@utcb.ro

[b] Kut Technical Institute, Middle Technical University Iraq, aamjed1@yahoo.com.

[c] Department of Renewable Energy Sources, National Institute for R&D in Electric, Engineering ICPE-CA, Bucharest, Romania, paul.danca@icpe-ca.ro.

[d.] Department of Mechanical Engineering, Technical University of Cluj Napoca Cluj, Napoca, Romania florin.bode@termo.utcluj.r

Abstract. One of the main challenges in the world today is reducing energy consumption and CO_2 footprint in existing buildings without major construction work. The main component of energy consumption in buildings is heating, but the demand for the domestic hot water is also very high, especially when daily consumption is high and especially for specific applications. The implementation of technologies using recovery sources for water heating has become very important and one of these technologies involves the recovery of the thermal energy from wastewater. Usually, heat recovery from wastewater is designed to recover residual energy from the hot drainage water and this recovered energy is used to preheat incoming cold water or to heat pumps. The paper presents numerical simulations using a SST k-ω turbulence model in order to compare a regular geometry with a helicoidal one. The second one provides a more turbulent flow that allows an intensification of the outer flow, thus allowing the enhancement of the heat transfer from the inner heated flow to the outer flow.

Keywords. Wastewater, heat recover, energy efficiency, CFD.
DOI: https://doi.org/10.34641/clima.2022.429

1. Introduction

One of the main challenges in the world today is reducing energy consumption and CO2 footprint in existing buildings without major construction work. Many of these buildings represent heritage buildings and the intervention constraints on the original building are much more restrictive for these particular cases. The building sector is one of the world's largest energy consumers, so it is important to seek out and use recovery energies for individual consumers. One of the main component of energy consumption in buildings is the demand for the domestic hot water is also very high, especially when daily consumption is high and especially for specific applications (hotels or laundries for example) This is why the implementation of technologies using renewable energy and recovery sources for water heating has become very important and one of these technologies involves the recovery of the thermal energy from wastewater [1]. Usually, heat recovery from wastewater is designed to recover residual energy from the hot drainage water and this recovered energy is used to preheat incoming cold water or to heat pumps.

Wastewater heat recovery applications are becoming widespread in energy saving applications. This interesting technology is an efficient and inexpensive way to recover thermal energy for reuse also in facilities systems in buildings, such as the production of sanitary hot water or heating. Why do we need such a device? The answer to this question is very simple: even if we are trying now to build energy efficient buildings, we also have to reduce the energy consumption and the CO2 footprint in existing buildings without major construction work. These goals can be met only by using high performance materials, cost-effective energy efficient systems and systems based on renewable energy sources. One of the cost-effective energy efficient system could be the heat recovery system from wastewater.

2. State of the art

We present here a short state of the art of the heat recovery from wastewater as it known at the moment. The literature [2]–[6] stated that the concept of heat recovery from wastewater could be considered highly diversified and the ways of making

Copyright ©2022 by the authors. This conference paper is published under a CC-BY-4.0 license.

use of the available heat are very different. The global system of heat recovery systems from wastewater could be divided into three levels. Level 1 represents the wastewater system, all the way upstream from the water consumption to the final effluent from the wastewater treatment plant, where the potential heat resource exists. Level 2 is the transferring system that connects Level 1 and Level 3, i.e. the technical system that provides heat from resource to the final demand. Finally, Level 3 is the receiving system, i.e. where the heat is finally to be reclaimed. Such a system could be used inside a building, outside on the sewer system upstream or downstream the wastewater treatment plant.

The energy recovered from a wastewater system can be used directly to a specific facility (this is the case for the heat exchangers installed just before the showers) or indirectly via a heat pump. Culha et al. [7] have conducted a review where the wastewater heat exchangers are classified in detail based on multiple features, including utilization and construction methodology. These heat exchangers can be used in different locations to recover the heat from the wastewater: the first location is inside the building, and it is called domestic utilization, the second location is outside and provides larger excess heat from the wastewater to ensure heating/cooling for multiple buildings. Apart from these two locations, waste water heat exchangers can be installed downstream of a wastewater treatment plant to efficiently utilize the energy in the treated waste water at a larger scale. The heat recovery at the sewage treatment plant is technically easier since the energy from the treated wastewater can be extracted more efficiently.

L.Ni et al. [8] proposed a grey water energy recovery system with a multiple function heat pump system. The authors have developed a numerical model for the investigation of the annual energy and water consumptions of the proposed system and the conventional building energy system with gas furnace space heating, package air conditioning and electricity water heater for hot water heating. Based on a case study of a typical residential house with four family members the results show that the proposed system can provide about 33,9% energy savings for space heating, cooling and hot water heating. The study is extended among 15 cities in various climatic zones in the US and the results show energy savings having ranges of 17% - 57.9 %.

Jorgen Wallin & Joachim Claesson [9] have studied the performance of a vertical inline drain water heat recovery heat exchanger. In this case the system recovers the heat with the aid of a heat pump. Investigation of the heat recovery ratio shows that the heat exchanger has the capability to recover more than 25% of the available heat in the drain water at the flow rates investigated.

S. Torras et al [10] investigated also the performance of a vertical drain water heat recovery system as an interesting household technology to reduce energy costs and environmental impact. A specific drain water heat recovery storage-type based on a cylindrical tank with an internal coiled pipe has been built and both numerical and experimental tools have been used to design and study the performance of the device. The DWHR storage had the capacity to recover from 34% to 60% of the energy available in the drain water for the investigated flow rates. However, this type of vertical heat exchangers is not easy to use because of the lack of space and the integration of the horizontal heat exchangers could be interesting from this point of view.

L.T. Wong et al. [11] investigated the potential for shower water heat recovery from bathrooms equipped with instantaneous water heaters in high rise residential buildings of Hong Kong. They proposed a single – passed counter flow heat exchanger horizontally used for preheating the cold water before a water heater. The thermal energy exchange is evaluated in terms of effectiveness-number of transfer units approach and the results indicate that 4 to 15% shower water heat could be recovered through a 1.5 m long single pass counter flow heat exchanger for a drainage pipe of 50 mm diameter. Aonghus McNabola and Killian Shields [12]have also pointed out that the recovery of the waste heat from the domestic wastewater flows is a viable method of improving the energy efficiency of buildings. Their study is of great importance for the proposal here, because they have analysed the efficiency of such a heat exchanger. They have proved that even if many of the existing systems only operate satisfactorily when the heat exchanger is in a vertical orientation due to the nature of wastewater flow within the drainpipes, this orientation requirement presents a barrier to the full-scale implementation because of limited space especially in dwellings. The paper outlines the experimental analysis of a horizontal drain water recovery system for domestic showers and the possibility of increasing the efficiency of such systems. The results also demonstrate that such a system may be economically viable depending on several external factors such as the price of energy, the local climate, the capital cost of the device and the national incentives for energy saving technology. In this case improving the efficiency of such a heat exchanger could be the solution to make them more usable.

There are lot of classical methods to improve the heat transfer through an interface inside a heat exchanger. For example, S. Liu and M. Sakr [13] provide a very detailed state of the art. The passive method generally uses surface or geometrical modifications to the flow channel by incorporating inserts or additional devices, for example, inserts extra component, swirl flow devices, treated surface, extended surface, displaced enhancement devices, coiled tubes, surface tension devices and additives for fluids. There are also active methods to improve the heat transfer such as the use of magnetic fields, surface vibration, fluid vibration, electrostatic fields

or impinging jets which require an external activator/power supply to bring about the enhancement. The two cited categories could be used in combinations such us rough surface with a twisted tape swirl flow device, or rough surface with fluid vibration, or rough surface with twisted tapes. For the convective heat transfer, one of the ways to enhance heat transfer rate is to increase the effective surface area and residence time of the heat transfer fluids. The passive methods are based on these principles by employing several techniques to generate the swirl in the bulk of the fluids and disturb the actual boundary layer to increase effective surface area, residence time and consequently heat transfer coefficient in existing system. The characterization of the heat exchange properties for this kind of interfaces could be done using non-intrusive methods as PIV measurements techniques. There are studies already performed [14], [15] using PIV experimental studies or numerical approaches [16] regarding the flow pattern over rough surfaces in open channel with applicability to the turbulence increasing methods that can be used to enhance the heat flux over an interface.

3. Methodology

The specific goal of this paper is to find a way to improve the efficiency of an horizontal heat exchanger dedicated to recover heat from waste water. We have realized this heat exchanger in the laboratory. The photo of the experimental setup is presented in figure 1a and the schematic of it in figure 1b:

Fig. 1a – Horizontal heat exchanger

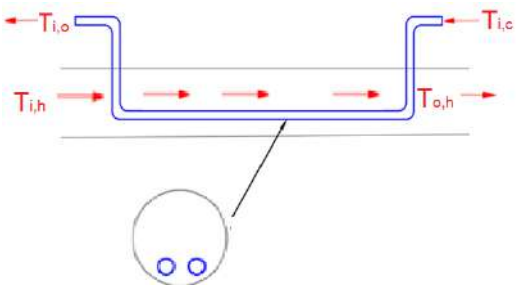

Fig. 1b - Schematic of the heat exchanger

The device is conceived to recover the heat from wastewater from domestic fixtures. There is a circular pipe where the water flows gravitationally which represents the grey water at high temperature coming from sanitary fixtures and two cold water pipes immersed in the greywater flow. This work presents a numerical model of the heat exchanger mentioned above. Several scenarios have been calculated considering flow rates between 3.5 m^3/h and 5 m^3/h for the grey water (free surface flow) and between 0.2 m^3/h and 0.4 m^3/h for the cold water inside the pipes. We will not show all the results in this paper but we have chosen to outline only one scenario in order to explain the results. The main parameters used for our example in this work and their values are the following: $T_{i,h}$ = 40,5°C and $T_{o,h}$ are the inlet and outlet temperatures for grey water and $T_{i,c}$, =10°C $T_{i,o}$ are the inlet outlet temperatures for the cold water. The inlet temperatures have been considered as boundary conditions and the outlet temperatures resulted from calculus. For the flowrates we have considered 4,94 m^3/h for the greywater which correspond to a velocity of 0,17m/s and 0,37 m^3/h for the water inside the copper pipe which correspond to a velocity of 0,7m/s We have envisaged two cases: for the first one we have considered two simple copper pipes for the cold water and for the second one we have added a helicoidal fin on the copper pipes. We have performed numerical simulations to see the difference between the two cases and how much heat recovery is improved by adding the helicoidal layer.

4. Numerical Model

The geometries were created in SolidWorks and after that were imported in DesignModeler under Ansys Workbench 19.2 software. In figure 2a a regular geometry can be seen and in figure 2b is presented the novel helicoidal geometry. At this stage, the geometry was prepared for the numerical simulation.

Fig. 2a – A regular geometry for heat exchanger

Fig 2b. – The novel helicoidal geometry for the heat exchanger

The numerical grid was created for both studied cases in Ansys meshing. Given the fact that the helicoidal geometry is very complex mainly due to the very low thickness of the helicoidal fin (0.4mm) the number of the elements necessary for the numerical simulation was 102 million elements (see figure 3a). A mesh independence test was carried out for this geometry (60, 102, 122 million tetrahedral cells). The main difficulty in creating the mesh was related, as it was stated earlier due to the very low

thickness of the helicoidal fin. Because the helicoidal fin is causing the disturbance in the flow, it was needed to create a very good mesh around the sharp edge of the fin. Also, a boundary layer of eight cells was created on all the walls in the studied geometry. Due to the long geometry this caused the increased number of cells. We created more meshes with a low number of cells but there were not suitable for the numerical simulation.

The numerical grid for the regular geometry was much simpler to be generated because it does not have any complication. Due to the simplicity of the geometry, was even possible to create a polyhedral mesh in this case (see figure 3b). In this case, was also performed a grid independence test which revealed that the numerical grid of 2.66 million polyhedral cells was appropriate for this case (among 1.2, 1.8, 2.66, 3.8 million polyhedral cells). Also, a boundary layer of eight cells was created on all the walls in the studied geometry.

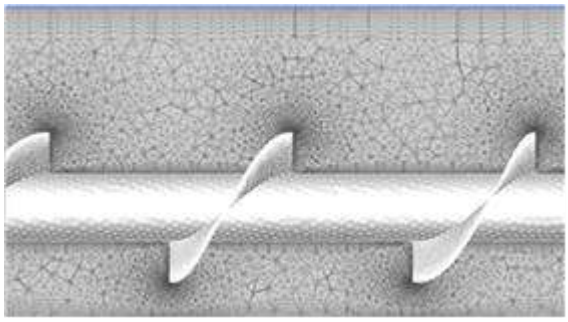

Fig 3a – Numerical grid details for the helicoidal case

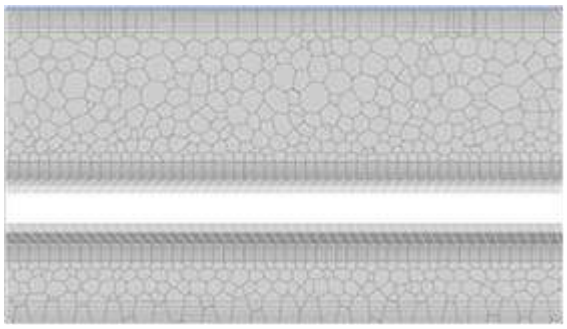

Fig 3b – Numerical grid details for the ordinary case

The numerical simulations were performed in Ansys Fluent 19.2. The turbulence model used for the numerical simulation was SST k-ω due to the high capacity of this model to accurately simulate the flow both in the boundary layer and in the far field [1]. The y+ number had values under 5 on all the wall surfaces from the studied domain which is considered acceptable when using the SST k-ω turbulence model [2].

5. Results

The results are shown in terms of contours of temperature in the exit plane of one of the heated pipes in both analyzed cases. They can be seen in figure 5a,b. Considering the fact, that for both analyzed cases the inlet temperature and flow rate was identic and the single difference between these two cases being the helicoidal fin, it is very clear the great impact in the heat transfer, this fin is adding. The mean temperature at the exit for the helicoidal case was 18.1°C and for the standard case was 13.87°C.

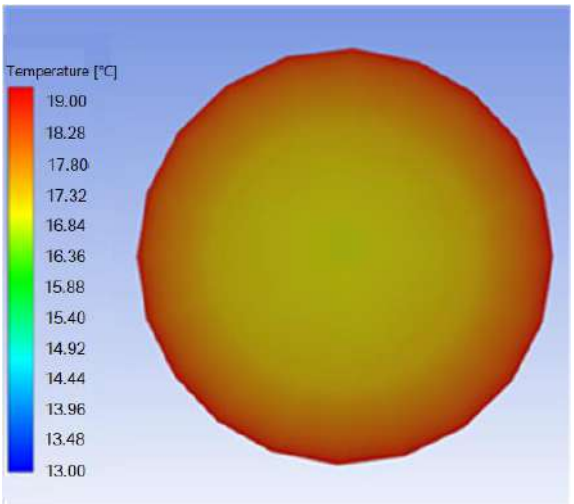

Fig 5a - Contours of temperature in the exit plane of one of the pipes with heated water for helicoidal case

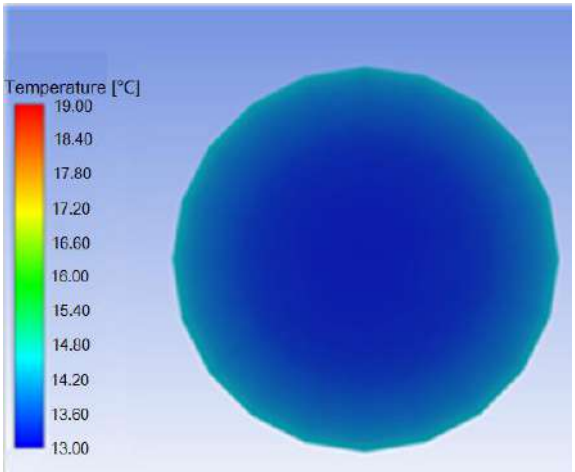

Fig 5b - Contours of temperature in the exit plane of one of the pipes with heated water for the ordinary case

We can show a comparison between the results obtained through numerical simulation for the two studied configurations (the regular geometry and the novel helicoidal geometry) considering the temperatures values and the velocity distributions at several section inside the channel. The previous figures outlined temperatures values inside the cold water pipes while next figures show temperatures values and velocity distribution outside the cold water pipes in the core of the free surface flow.

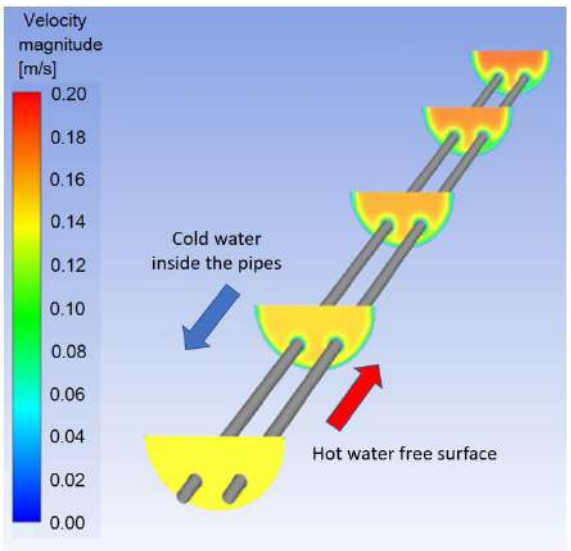

Fig. 6a - Contours of velocity magnitude in subsequent sections of the channel with heated water for the regular geometry

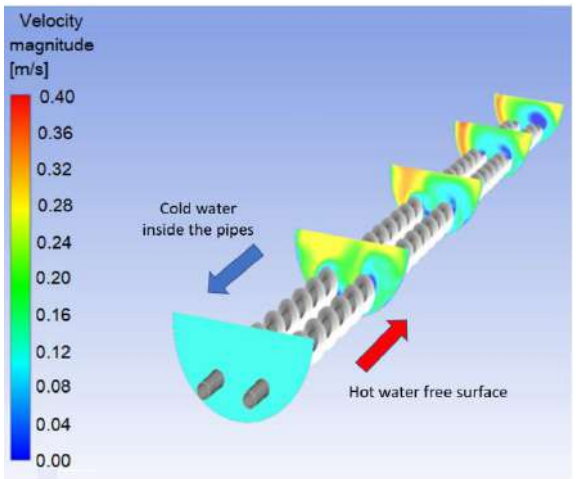

Fig. 6b - Contours of velocity magnitude in subsequent sections of the channel with heated water for the novel helicoidal geometry

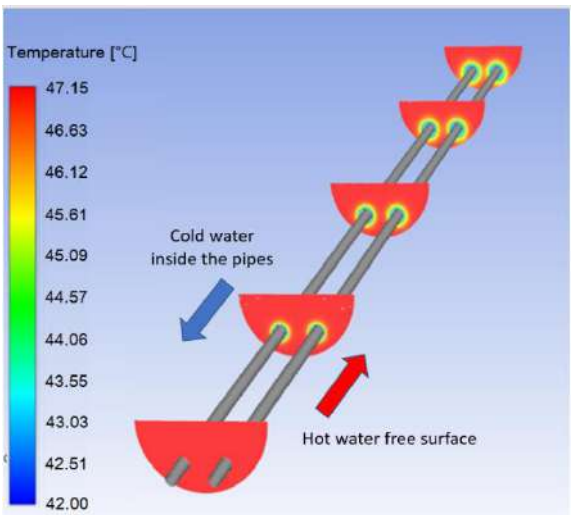

Fig. 7a - Contours of temperature in subsequent sections of the channel with heated water for the regular geometry

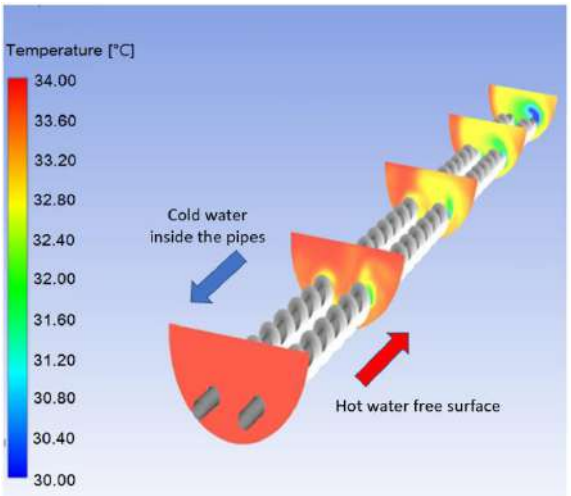

Fig. 7b - Contours of temperature in subsequent sections of the channel with heated water for the novel helicoidal geometry

The same observations as previous might be done, the case with the helical tape provides a more turbulent flow that allows an intensification of the outer flow, thus allowing the enhancement of the heat transfer from the inner heated flow to the outer flow. This is observable on the global distributions of the temperature for the case studied. The evolution of the temperature along the heat exchanger for the cold water inside the pipe considering the helicoidal geometry is shown in figure 8.

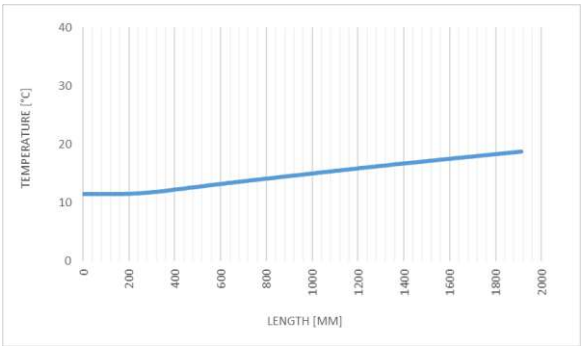

Fig. 8 - Evolution of the temperature along the heat exchanger for the cold water inside the pipe considering the helicoidal geometry

6. Conclusions

The purpose of this study is to develop a water-water heat exchange interface allowing a higher-rate heat flux from the wastewater flow to the cold-water flow to recover maximum of the waste energy.

A regular geometry was compared with a helicoidal one by numerical simulation. The second one provides a more turbulent flow that allows an intensification of the outer flow, thus allowing the enhancement of the heat transfer from the inner heated flow to the outer flow. The heat flux

exchanged between the grey water and clean cool water was 6161.5kW for the helicoidal case and 3206.8kW for the standard case so by adding the helicoidal fin, the performance of the standard heat exchanger was improved by 92.14%.

7. Acknowledgements

This work was supported by a grant of UEFISCDI – 54PTE/2020 – Intelligent System for Water Quality Monitoring – SmartMonWater

8. References

[1] A. Burlacu *et al.*, "Energy efficient heat pipe heat exchanger for waste heat recovery in buildings," *Procedia Manuf.*, vol. 22, pp. 714–721, 2018, doi: https://doi.org/10.1016/j.promfg.2018.03.103.

[2] A. Bertrand, R. Aggoune, and F. Maréchal, "In-building waste water heat recovery: An urban-scale method for the characterisation of water streams and the assessment of energy savings and costs," *Appl. Energy*, vol. 192, pp. 110–125, 2017, doi: https://doi.org/10.1016/j.apenergy.2017.01.096.

[3] S. S. Cipolla and M. Maglionico, "Heat Recovery from Urban Wastewater: Analysis of the Variability of Flow Rate and Temperature in the Sewer of Bologna, Italy," *Energy Procedia*, vol. 45, pp. 288–297, 2014, doi: https://doi.org/10.1016/j.egypro.2014.01.031.

[4] V. Somogyi, V. Sebestyén, and E. Domokos, "Assessment of wastewater heat potential for district heating in Hungary," *Energy*, vol. 163, pp. 712–721, 2018, doi: https://doi.org/10.1016/j.energy.2018.07.157.

[5] M. S. Todorovic and J. T. Kim, "In search for sustainable globally cost-effective energy efficient building solar system – Heat recovery assisted building integrated PV powered heat pump for air-conditioning, water heating and water saving," *Energy Build.*, vol. 85, pp. 346–355, 2014, doi: https://doi.org/10.1016/j.enbuild.2014.08.046.

[6] Y. Wang, Y. Ren, Y. Gu, and Q. Meng, "Comparison and Analysis of Heat Transfer Enhancement for Wastewater Heat Exchanger in Wastewater Source Heat Pump System," *Procedia Eng.*, vol. 205, pp. 2736–2743, 2017, doi: https://doi.org/10.1016/j.proeng.2017.10.190.

[7] O. Culha, H. Gunerhan, E. Biyik, O. Ekren, and A. Hepbasli, "Heat exchanger applications in wastewater source heat pumps for buildings: A key review," *Energy Build.*, vol. 104, pp. 215–232, 2015, doi: https://doi.org/10.1016/j.enbuild.2015.07.013.

[8] L. Ni *et al.*, "Feasibility study of a localized residential grey water energy-recovery system," *Appl. Therm. Eng.*, vol. 39, pp. 53–62, 2012, doi: https://doi.org/10.1016/j.applthermaleng.2012.01.031.

[9] J. Wallin and J. Claesson, "Investigating the efficiency of a vertical inline drain water heat recovery heat exchanger in a system boosted with a heat pump," *Energy Build.*, vol. 80, pp. 7–16, 2014, doi: https://doi.org/10.1016/j.enbuild.2014.05.003.

[10] S. Torras, C. Oliet, J. Rigola, and A. Oliva, "Drain water heat recovery storage-type unit for residential housing," *Appl. Therm. Eng.*, vol. 103, pp. 670–683, 2016, doi: https://doi.org/10.1016/j.applthermaleng.2016.04.086.

[11] L. T. Wong, K. W. Mui, and Y. Guan, "Shower water heat recovery in high-rise residential buildings of Hong Kong," *Appl. Energy*, vol. 87, no. 2, pp. 703–709, 2010, doi: https://doi.org/10.1016/j.apenergy.2009.08.008.

[12] A. McNabola and K. Shields, "Efficient drain water heat recovery in horizontal domestic shower drains," *Energy Build.*, vol. 59, pp. 44–49, 2013, doi: https://doi.org/10.1016/j.enbuild.2012.12.026.

[13] S. Liu and M. Sakr, "A comprehensive review on passive heat transfer enhancements in pipe exchangers," *Renew. Sustain. Energy Rev.*, vol. 19, pp. 64–81, 2013, doi: https://doi.org/10.1016/j.rser.2012.11.021.

[14] M. Iliescu, M. Sandu, I. Nastase, F. Bode, and E. Iatan, "Study of free surface flow in sewage pipes," 2016, doi: 10.5593/SGEM2016/B52/S20.098.

[15] M. Iliescu, M. Sandu, I. Nastase, E. Iatan, and F. Bode, "An Experimental Approach Regarding the Sewage Self-Cleansing Conditions," 2016, doi: 10.1016/j.egypro.2015.12.244.

[16] E. Iatan, M. Iliescu, F. Bode, I. Nastase, R. M. Damian, and M. Sandu, "Numerical Study for Open-channel Flow over Rows of Hemispheres," 2016, doi: 10.1016/j.egypro.2015.12.242.

[17] F. Bode, K. Sodjavi, A. Meslem, and I. Nastase, "Numerical prediction of wall shear rate in impinging cross-shaped jet at moderate reynolds number," *UPB Sci. Bull. Ser. D Mech. Eng.*, vol. 76, no. 2, 2014.

[18] F. Bode, A. Meslem, C. Patrascu, and I. Nastase, "Flow and wall shear rate analysis for a cruciform jet impacting on a plate at short distance," *Prog. Comput. Fluid Dyn.*, vol. 20, no. 3, pp. 169–185, 2020.

Performance analysis of water-to-water CO_2 heat pump in different compressor rotational speed

Yantong Li, Natasa Nord

Department of Energy and Process Engineering, Norwegian University of Science and Technology, Trondheim, Norway, yantong.li@ntnu.no

Abstract. Ozone layer depletion can be weakened when carbon dioxide (CO_2) replaces hydrochlorofluorocarbons and chlorofluorocarbons as the refrigerant in heat pumps. Performance investigations on water-to-water CO_2 heat pumps are still insufficient, especially in real life and experimental conditions. Seldom studies have reported that the compressor frequency may affect the performance of CO_2 heat pumps in some degree. However, the influence of compressor frequency on the performance of the water-to-water CO_2 heat pumps is still unknown. Hence, this study presented the experimental investigations on the water-to-water CO_2 heat pumps in different compressor frequency. The investigated CO_2 heat pump is located in the Energy and Indoor Environment Laboratory in the Department of Energy and Process Engineering at Norwegian University of Science and Technology. It is mainly composed of evaporator, compressor, gas cooler, liquid separator, internal heat exchanger, and expansion valve. The compressor was produced by the Officine Mario Dorin Spa. The plate heat exchangers were applied as evaporator, gas cooler, and internal heat exchanger. The PI controller controlled the discharge pressure by adjusting the expansion valve opening. Experimental cases in which the compressor rotational speed of 1,100 rev/min and 1,300 rev/min were conducted. The coefficient of performance (COP) was calculated by measuring the compressor power and heating capacity in the gas cooler. The analysis on the water-to-water CO_2 heat pump COP in different measured cases was depicted. This study therefore fills the research gap on the performance of the water-to-water CO_2 heat pump in different compressor rotational speed.

Keywords. Water-to-water, CO_2 heat pump, compressor rotational speed, experimental investigation.
DOI: https://doi.org/10.34641/clima.2022.53

1. Introduction

Huge energy needs that are caused by rapidly society development and population increasement, result in increasing the use of non-renewable energy including fossil fuels. This highly intensifies the environmental pollution [1]. Improvement of renewable energy use has become one of the primary tasks for humans. European Union has stated that by 2030 the portion of renewable energy in total energy use would be larger than 32% [2].

Heat pump obtaining thermal energy from ambient media, is one popular technique which enhances the renewable energy utilization. Scholars paid their attention on this aspect. Kosan and Aktas [3] concluded that the utilization of solar collector could enhance the performance of the system. Nikitin et al. [4] analyzed the performance of air-source and ground-source heat pumps in Saint Petersburg. It was found that the coefficient of performance (COP) of the air-source and ground-source heat pumps could reach up to 2.36 and 2.44, respectively. Boahen et al. [5] investigated the performance of the heat pump with different purposes including space heating and domestic hot water use. They found that the increase of returning hot water temperature led to the decrease of the system performance. Ural et al. [6] investigated a textile-based solar-assisted heat pump, and they found that the daily COP of this heat pump was higher than that of the conventional heat pump. Ahrens et al. [7] conducted the analysis of the energy system with the heat pump for both heating and cooling purposes. They concluded that the system COP could reach up to 4.1.

Copyright ©2022 by the authors. This conference paper is published under a CC-BY-4.0 license.

Compared with conventional heat pumps applying chlorofluorocarbons and hydrochlorofluorocarbons as refrigerants, heat pumps applying carbon dioxide (CO_2) as the refrigerant can cause less damage on the ozone layer. CO_2 heat pumps have become the research hotspot. Basso et al. [8] analyzed the performance of the CO_2 heat pump for solar cooling purpose, and they concluded that the COP of the CO_2 heat pump could reach up to 2.4. Humia et al. [9] conducted the study on a solar-assisted CO_2 heat pump, and they found that the maximum COP of the heat pump was approximately 3.67. Rony and Gladen [10] performed the investigation about a photovoltaic-assisted CO_2 heat pump. It was concluded that the COP of the system could reach up to 5.16. Rocha et al. [11] investigated a solar-assisted CO_2 heat pump. Their results indicated that the system COP was improved from 2.19 to 3.12 when solar irradiance increased from 6 W/m^2 to 969 W/m^2. Illán-Gómez et al. [12] studied the effect of different key variables on the performance of the CO_2 heat pump, and they concluded that outlet CO_2 temperature in gas cooler played a significant role on the system performance.

Seldom scholars began to focus on the studies on the effect of compressor rotational speed or frequency on the performance of the CO_2 heat pump, including the studies of Yang et al. [13] and Qin et al. [14]. Although in their studies the effect of compressor rotational speed or frequency on the CO_2 heat pump performance had been analyzed, the investigated CO_2 heat pump was air-source. More studies were urgently needed to verify the conclusions they have summarized. For example, the effect of different compressor rotational speed on the water-to-water CO_2 heat pump was still unknown.

This study therefore performed the experimental studies of the CO_2 heat pump in different compressor rotational speed, i.e., 1,000 rev/min and 1,300 rev/min. The experiments were conducted in the Energy and Indoor Environment Laboratory at the Department of Energy and Process Engineering, Norwegian University of Science and Technology. The PI controller was developed to fix the unchanged discharge pressure. For each compressor rotational speed, five cases with the discharge pressure varying from 7,300 kPa to 8,500 kPa with the interval of 300 kPa were conducted. The analysis on the heating capacity, power, COP, and expansion valve opening in these cases were presented.

The organization for remaining parts of this paper was depicted below. Section 2 presented the CO_2 heat pump experimental setup. The calculation of the uncertainties for measured COP was conducted in Section 3. Section 4 gave the results and detailed analysis for the measured cases. Important conclusions were summarized in Section 5.

2. CO_2 heat pump experimental setup

The CO_2 heat pump was in a laboratory of the Norwegian University of Science and Technology, and its schematic was depicted in Fig. 1. Table 1 depicts the information of important components in the investigated CO_2 heat pump. Note that the rated rotational speed, frequency, and displacement of the compressor were 1,450 rev/min, 50 Hz, and 4.06×10^{-4} m^3/s, respectively. The number of plates in the gas cooler, internal heat exchanger, and evaporator were 30, 12, and 40, respectively. The control of the fixed discharge pressure was conducted by the PI controller. Sensors from Carel having accuracy of ±(0.005×(measured temperature)+0.3) °C were applied for measuring temperature. A variable-area flow meter having accuracy of ±1% [15], was applied for measuring temperature. A sensor from Carel having accuracy of ±1% was applied for measuring pressure. A meter from CARLO GAVAZZI having accuracy of ±1% was applied for recording power.

Tab. 1 - Information of important components in CO_2 heat pump.

Components	Types	Manufactures
Compressor	CD 300H	Officine Mario Dorin Spa
Gas cooler	B18H-30	Swep International A.B.
Internal heat exchanger	CO42-12W-S3	KAORI Brazed Plate Heat Exchanger
Evaporator	CO95-40W-S37	KAORI Brazed Plate Heat Exchanger
Liquid separator	VU8L	Skala AS
Expansion valve	E2V18CS000	Carel

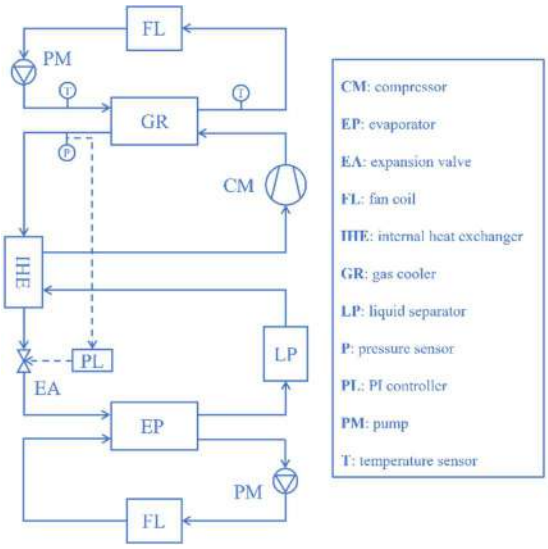

Fig. 1 – CO_2 heat pump experimental setup

3. Uncertainties for measured COP

This section was applied for presenting the calculation for uncertainties of measured variables. The CO_2 heat pump COP was calculated by Eqn. (1):

$$\mathrm{COP} = \frac{\dot{Q}_g}{P_c} \tag{1}$$

where $\dot{Q}_g$ and P_c denote the heating capacity and compressor power, respectively.

$\dot{Q}_g$ was calculated by Eqn. (2):

$$\dot{Q}_g = \dot{m}_g c_g (T_{gi} - T_{go}) \tag{2}$$

where $\dot{m}_g$ and c_g denote the mass flowrate and specific heat of the water in the gas cooler, respectively. T_{gi} and T_{go} denote the inlet and outlet water temperature of the gas cooler, respectively.

The root-sum-square method was applied for calculating uncertainties of measured variables, shown as Eqn. (3) [16]:

$$\varepsilon_v = \sqrt{\sum_{i=1}^{k} \left(\frac{\partial v}{\partial \beta_i} \varepsilon_{\beta_i}\right)^2} \tag{3}$$

where v denotes the analyzed variable. β_i denotes the variable affecting v. ε_v and ε_{β_i} denote the uncertainties of v and β_i, respectively. This method was utilized for calculating uncertainties of measured variables in Eqns. (1) and (2). Uncertainty of COP ($\varepsilon_{\mathrm{COP}}$) was calculated by Eqn. (4):

$$\varepsilon_{\mathrm{COP}} = \sqrt{\left(\frac{\partial \mathrm{COP}}{\partial \dot{Q}_g} \varepsilon_{\dot{Q}_g}\right)^2 + \left(\frac{\partial \mathrm{COP}}{\partial P_c} \varepsilon_{P_c}\right)^2} \tag{4}$$

where $\varepsilon_{\dot{Q}_g}$ and ε_{P_c} denote the uncertainties of $\dot{Q}_g$ and P_c, respectively. $\varepsilon_{\dot{Q}_g}$ was calculated by Eqn. (5):

$$\varepsilon_{\dot{Q}_g} = \sqrt{\left(\frac{\partial \dot{Q}_g}{\partial \dot{m}_g} \varepsilon_{\dot{m}_g}\right)^2 + \left(\frac{\partial \dot{Q}_g}{\partial T_{gi}} \varepsilon_{T_{gi}}\right)^2 + \left(\frac{\partial \dot{Q}_g}{\partial T_{go}} \varepsilon_{T_{go}}\right)^2} \tag{5}$$

where $\varepsilon_{\dot{m}_g}$, $\varepsilon_{T_{gi}}$, and $\varepsilon_{T_{go}}$ denote the uncertainties of $\dot{m}_g$, T_{gi}, and T_{go}, respectively. Using measured data, $\varepsilon_{\mathrm{COP}}$ could be determined by Eqns. (1) to (5). The average and maximum $\varepsilon_{\mathrm{COP}}$ were 3.7% and 4.27%, respectively.

4. Results and analysis

This section gave the results and analysis in different cases with the compressor rotation speed of 1,100 rev/min and 1,300 rev/min, respectively. The discharge pressure (P_d) was maintained at 7,300 kPa, 7,600 kPa, 7,900 kPa, 8,200 kPa, and 8,500 kPa, respectively. The heating capacity ($\dot{Q}_g$), compressor power (P_c), COP, and expansion valve opening (o_e) were selected as performance indicators.

4.1 Measured cases

Tables 1 and 2 presented the information of the measured cases with the compressor rotation speed of 1,100 rev/min and 1,300 rev/min, respectively. The water mass flowrate in gas cooler ($\dot{m}_g$) in these cases was 0.067 kg/s. In Table 1, the varying degree of the inlet water temperature in gas cooler (T_{gi}) in different P_d was small. The smallest T_{gi} was 25.4 °C, occurring when P_d was 7,301 kPa. The largest T_{gi} was 25.7 °C, occurring when P_d were 7,599 kPa and 8,200 kPa. The difference between smallest and largest T_{gi} was only 0.3 °C. The smallest T_{go} was 42 °C, occurring when P_d was 7,301 kPa. The largest T_{go} was 45.6 °C, occurring when P_d was 7,899 kPa. The difference between smallest and largest T_{go} was 3.6 °C. Thus, the difference of T_{go} was larger than that of T_{gi}.

In Table 2, the inlet water temperature in gas cooler (T_{gi}) increased from 25.2 °C to 27.1 °C, when P_d increased from 7,298 kPa to 8,503 kPa. The difference of T_{gi} between the cases with P_d of 7,298 kPa and 8,503 kPa was 1.9 °C. The outlet water temperature in gas cooler (T_{go}) increased from 44.5 °C to 51.5 °C, when P_d increased from 7,298 kPa to 8,503 kPa. The difference of T_{go} between the cases with P_d of 7,298 kPa and 8,503 kPa was 7 °C. The increasing degree of T_{go} was larger than that of T_{gi}, when P_d increased from 7,298 kPa to 8,503 kPa.

Tab. 1 – Measured cases with the compressor rotation speed of 1,100 rev/min.

Cases	P_d (kPa)	$\dot{m}_g$ (kg/s)	T_{gi} (°C)	T_{go} (°C)
1	7,301	0.067	25.4	42
2	7,599	0.067	25.7	43.6
3	7,899	0.067	25.6	45.6
4	8,200	0.067	25.7	45.1

5	8,356	0.067	25.5	45.4

Tab. 2 - Measured cases with the compressor rotation speed of 1,300 rev/min.

Cases	P_d (kPa)	$\dot{m}_g$ (kg/s)	T_{gi} (℃)	T_{go} (℃)
6	7,298	0.067	25.2	44.5
7	7,599	0.067	26.0	46.2
8	7,901	0.067	26.6	47.5
9	8,201	0.067	26.7	50.1
10	8,503	0.067	27.1	51.5

4.2 Effect on heating capacity

Fig. 2 presented the heating capacity ($\dot{Q}_g$) in different cases for different rotational speed: (a) r = 1,100 rev/min and (b) r = 1,300 rev/min. In Fig. 2 (a), when the compressor rotational speed was 1,100 rev/min, meaning that the compressor frequency was 37.9 Hz, $\dot{Q}_g$ was 4,626.3 W, 4,998.3 W, 5,603.7 W, 5,437.2 W, and 5,560.9 W in the Cases 1, 2, 3, 4, and 5, respectively. In Fig. 2 (b), when the compressor rotational speed was 1,300 rev/min, meaning that the compressor frequency was 55.8 Hz, $\dot{Q}_g$ was 5,396.2 W, 5,657.1 W, 5,857.4 W, 6,566.3 W, and 6,831.2 W in Cases 6, 7, 8, 9, and 10, respectively. Thus, when P_d was fixed at the almost same values, the increase of compressor frequency might lead to increase of $\dot{Q}_g$. This finding could be supported by the studies of Yang et al. [13] and Qin et al. [14]. In Fig. 2 (a), $\dot{Q}_g$ increased with the increase of P_d from Case 1 to Case 3. However, $\dot{Q}_g$ in both Cases 4 and 5 were lower than that in Case 3. The reason why $\dot{Q}_g$ in Case 4 and 5 were close might be that the unstable P_d control in Case 5 using PI controller. The setting P_d of 8,500 kPa cannot be maintained, even though the expansion valve opening has been adjusted to the minimum value, i.e., 10%. This is also the reason why P_d was 8,356 kPa in Table 1. In Fig. 2 (b), $\dot{Q}_g$ increased with the increase of P_d. The reason why the variations of $\dot{Q}_g$ was different in Figs. 2 (a) and (b) might be explained according to the study of Yang et al. [13]. In their study, P_d when the peak $\dot{Q}_g$ occurred increased with the increase of the compressor frequency.

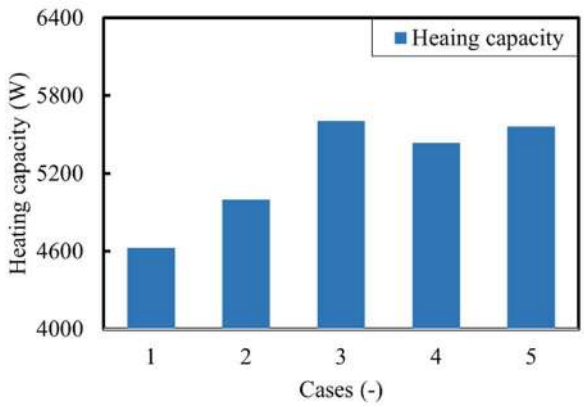

(a) r = 1,100 rev/min

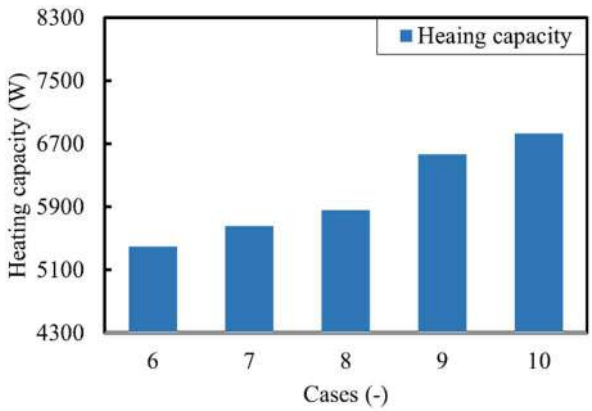

(b) r = 1,300 rev/min

Fig. 2 – Heating capacity in different cases for different rotational speed: (a) r = 1,100 rev/min and (b) r = 1,300 rev/min.

4.3 Effect on compressor power

Fig. 3 presented the compressor power (P_c) in different cases for different rotational speed: (a) r = 1,100 rev/min and (b) r = 1,300 rev/min. In Fig. 3 (a), when the compressor rotational speed was 1,100 rev/min, meaning that the compressor frequency was 37.9 Hz, P_c was 1,066.1 W, 1,158.9 W, 1,235.8 W, 1,308 W, and 1,340.7 W in the Cases 1, 2, 3, 4, and 5, respectively. In Fig. 3 (b), when the compressor rotational speed was 1,300 rev/min, meaning that the compressor frequency was 55.8 Hz, P_c was 1,295.2 W, 1,381.7 W, 1,467.2 W, 1,540.4 W, and 1,610.4 W in the Cases 6, 7, 8, 9, and 10, respectively. Thus, when P_d was fixed at the almost same values, the increase of compressor frequency might lead to the increase of P_c. In addition, the increase of P_d might lead to the increase of P_c. These findings could be supported by the studies of Qin et al. [14].

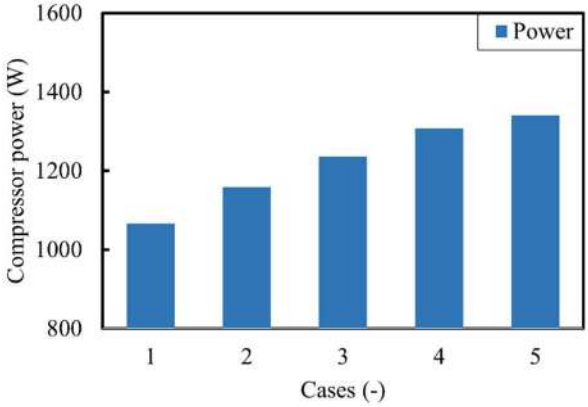

(a) $r = 1{,}100$ rev/min

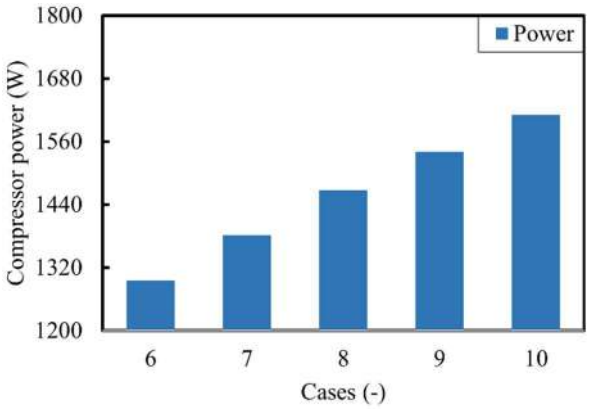

(b) $r = 1{,}300$ rev/min

Fig. 3 – Compressor power in different cases for different rotational speed: (a) $r = 1{,}100$ rev/min and (b) $r = 1{,}300$ rev/min.

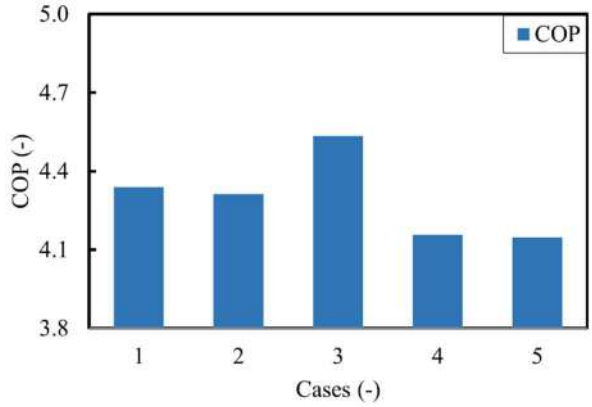

(a) $r = 1{,}100$ rev/min

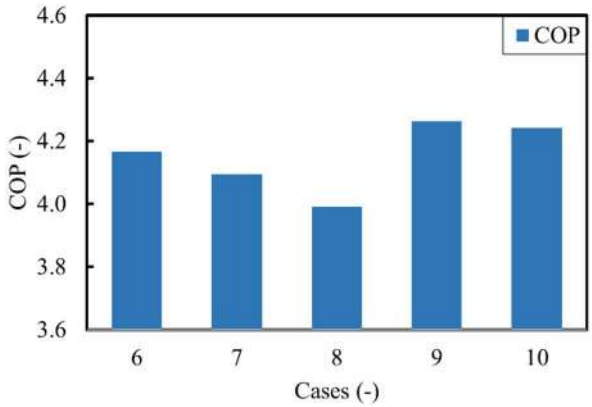

(b) $r = 1{,}300$ rev/min

Fig. 4 – COP in different cases for different rotational speed: (a) $r = 1{,}100$ rev/min and (b) $r = 1{,}300$ rev/min.

4.4 Effect on COP

Fig. 4 presented the COP in different cases for different rotational speed: (a) $r = 1{,}100$ rev/min and (b) $r = 1{,}300$ rev/min. In Fig. 4 (a), when the compressor rotational speed was 1,100 rev/min, meaning that the compressor frequency was 37.9 Hz, COP was 4.34, 4.31, 4.53, 4.16, and 4.15 in the Cases 1, 2, 3, 4, and 5, respectively. In Fig. 4 (b), when the compressor rotational speed was 1,300 rev/min, meaning that the compressor frequency was 55.8 Hz, COP was 4.17, 4.09, 3.99, 4.26, and 4.26 in the Cases 6, 7, 8, 9, and 10, respectively. According to the study of Qin et al. [14], generally the decrease of the compressor frequency might lead to the increase of COP. In their study, there were still the phenomenon that in few cases the increase of compressor frequency might lead to the increase of COP. These could explain the phenomenon why COP in Cases 1, 2, and 3 were higher than that in Cases 6, 7, and 8, respectively, and why COP in Cases 4 and 5 were higher than that in Cases 9 and 10.

4.5 Effect on expansion valve opening

Fig. 5 presented the expansion valve opening (o_e) in different cases for different rotational speed: (a) $r = 1{,}100$ rev/min and (b) $r = 1{,}300$ rev/min. In Fig. 5 (a), when the compressor rotational speed was 1,100 rev/min, meaning that the compressor frequency was 37.9 Hz, o_e was 23.8%, 18.2%, 16.7%, 11.6%, and 10% in the Cases 1, 2, 3, 4, and 5, respectively. In Fig. 5 (b), when the compressor rotational speed was 1,300 rev/min, meaning that the compressor frequency was 55.8 Hz, o_e was 39.5%, 29.6%, 22.4%, 19.5%, and 18.1% in the Cases 6, 7, 8, 9, and 10, respectively. Thus, the increase of expansion valve opening might lead to the decrease of P_d. In addition, for maintaining at the almost same P_d, using higher compressor frequency might lead to larger expansion valve opening.

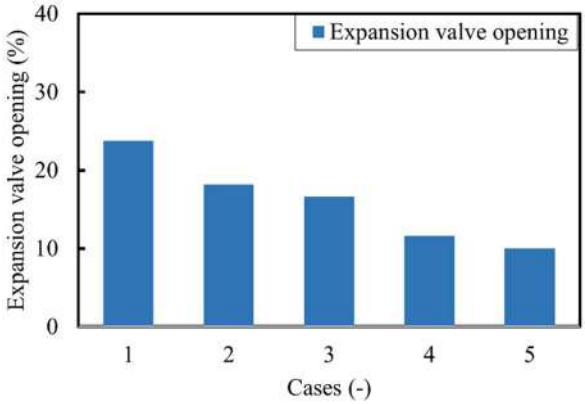

(a) $r = 1{,}100$ rev/min

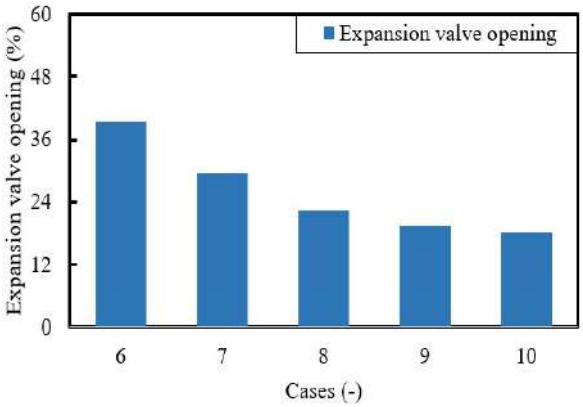

(b) $r = 1{,}300$ rev/min

Fig. 5 – Expansion valve opening in different cases for different rotational speed: (a) $r = 1{,}100$ rev/min and (b) $r = 1{,}300$ rev/min.

5. Conclusions

In this study, the performance of the CO_2 heat pump in different compressor rotational speed, i.e., 1,000 rev/min and 1,300 rev/min, were experimentally analyzed. The cases with the discharge pressure varying from 7,300 kPa to 8,500 kPa with the interval of 300 kPa were presented in experimental conditions. The heating capacity, power, COP, and expansion valve opening in these cases were analyzed. The uncertainties of the COP in these cases were calculated. The maximum and average uncertainties of the COP were 4.27% and 3.7%, respectively. Most findings of this study were compared with the results in the studies of Yang et al. [13] and Qin et al. [14]. Most findings on the effect of the compressor rotational speed on the performance of the CO_2 heat pump were verified. The results indicated that increasing the compressor rotational speed might result in increasing the heating capacity. Increasing the compressor rotational speed might result in increasing the compressor power. In most situations, reducing the compressor rotational speed might contribute to increasing the COP. However, there were still few cases where increasing the compressor rotational speed might contribute to increasing the COP. For maintaining at the almost same discharge pressure, the larger expansion valve opening might be caused by the higher compressor rotational speed. Note that these findings in this study were obtained by the unfixed operating conditions. As shown in Tables 1 and 2, the inlet water temperature of gas cooler in different cases were different. In addition, the measurement uncertainties might affect the results of these findings.

6. Acknowledgement

This project has received funding from the European Union's Horizon 2020 research and innovation programme under the Marie Skłodowska-Curie grant agreement No [895732].

7. References

[1] Ding Z., Wu W. A hybrid compression-assisted absorption thermal battery with high energy storage density/efficiency and low charging temperature. Applied Energy. 2021;282:116068.

[2] Commission E. 2030 climate & energy framework. 2021.

[3] Koşan M., Aktaş M. Experimental investigation of a novel thermal energy storage unit in the heat pump system. Journal of Cleaner Production. 2021;311:127607.

[4] Nikitin A., Deymi-Dashtebayaz M., Muraveinikov S, Nikitina V., Nazeri R., Farahnak M. Comparative study of air source and ground source heat pumps in 10 coldest Russian cities based on energy-exergy-economic-environmental analysis. Journal of Cleaner Production. 2021;321:128979.

[5] Boahen S., Anka SK., Lee KH., Choi JM. Performance characteristics of a cascade multi-functional heat pump in the winter season. Energy and Buildings. 2021;253:111511.

[6] Ural T., Karaca Dolgun G., Güler OV., Keçebaş A. Performance analysis of a textile based solar assisted air source heat pump with the energy and exergy methodology. Sustainable Energy Technologies and Assessments. 2021;47 :101534.

[7] Ahrens MU., Foslie SS., Moen OM., Bantle M., Eikevik TM. Integrated high temperature heat pumps and thermal storage tanks for combined heating and cooling in the industry. Applied Thermal Engineering. 2021;189:116731.

[8] Lo Basso G., de Santoli L., Paiolo R., Losi C. The potential role of trans-critical CO_2 heat pumps within a solar cooling system for building services: The hybridised system energy analysis

by a dynamic simulation model. Renew Energy. 2021;164:472-90.

[9] Marques Humia G., Moreira Duarte W., Jose Garcia Pabon J., de Freitas Paulino T., Machado L. Experimental study and simulation model of a direct expansion solar assisted heat pump to CO_2 for water heating: Inventory, coefficient of performance and total equivalent warming impact. Solar Energy. 2021;230:278-97.

[10] Rony RU., Gladen A.. Parametric study and sensitivity analysis of a PV/microchannel direct-expansion CO_2 heat pump. Solar Energy. 2021;218:282-95.

[11] Rocha TTM., de Paula CH., Maia AAT., Paulino TdF., de Oliveira RN. Experimental assessment of a CO_2 direct-expansion solar-assisted heat pump operating with capillary tubes and air-solar heat source. Solar Energy. 2021;218:413-24.

[12] Illán-Gómez F., Sena-Cuevas VF., García-Cascales JR, Velasco FJS. Analysis of the optimal gas cooler pressure of a CO_2 heat pump with gas bypass for hot water generation. Applied Thermal Engineering. 2021;182:116110.

[13] Yang L-X., Wei X-L., Zhao L-H., Qin X., Zhang D-W. Experimental study on the effect of compressor frequency on the performance of transcritical CO_2 heat pump system with regenerator. Applied Thermal Engineering. 2019;150:1216-23.

[14] Qin X., Liu H., Meng X., Wei X., Zhao L., Yang L. A study on the compressor frequency and optimal discharge pressure of the transcritical CO_2 heat pump system. International Journal of Refrigeration. 2019;99:101-13.

[15] ToolBox TE. Accuracy of variable-area flowmeter. 2021.

[16] Moffat RJ. Describing the uncertainties in experimental results. Experimental thermal and fluid science. 1988;1:3-17.

Decentralized storage in combined heat distribution circuits: how to control?

Stef Jacobs [a], Margot De Pauw [b], Peter Hellinckx [c], Ivan Verhaert [d]

[a] EMIB, Faculty of Applied Engineering - Electromechanics, University of Antwerp, Antwerp, Belgium, Stef.Jacobs@uantwerpen.be.

[b] Kenniscentrum Energie, Thomas More Kempen, Geel, Belgium, margot.depauw@thomasmore.be.

[c] IDLab, Faculty of Applied Engineering – Electronics ICT, University of Antwerp - imec, Antwerp, Belgium, Peter.Hellinckx@uantwerpen.be.

[d] EMIB, Faculty of Applied Engineering - Electromechanics, University of Antwerp, Antwerp, Belgium, Ivan.Verhaert@uantwerpen.be.

Abstract. In apartment buildings, collective heating networks have great energetic advantages. One form gaining more attention for the last decades is a combined heat distribution circuit (CHDC), in Belgium called "combilus". It is a two-pipe system for the distribution of both space heating (SH) and domestic hot water (DHW). The supply temperature is set to the highest needed temperature, which is around 65°C for DHW (considering a temperature difference for enabling heat transfer). However, if decentralised DHW storage tanks in combination with low-temperature emitters for SH are used, the supply temperature could be optimised. In this research, two innovative control strategies were studied for such a CHDC to lower the distribution temperature (to the required temperature for SH) as much as possible by grouping the charging periods of those storage tanks. One control strategy is time-based, with pre-defined charging schemes, while the other is based on two sensors in the storage tanks. In order to test the control strategies, a simulation environment was set up in Matlab that represents the thermal dynamic behaviour of CHDC. However, to fully focus on the evaluation of the control strategies, an idealised central boiler room was assumed, which immediately delivers the desired temperatures. Besides the evaluation of the control strategies, the design of the storage tanks is also optimised by performing sensitivity analyses on the volume, hysteresis and charging flow rates. The results show that larger storage tanks provide better DHW comfort combined with less PE use (for the proposed controls) and that the charging flow rate can significantly reduce the central peak power, while DHW comfort and PE use remain the same. With the time-based control, the charging cycles and volume have a high impact on the performance and comfort. The two-sensor control is always able to reduce PE use and deliver the same or even better comfort than the reference control.

Keywords. Domestic hot water, decentralized storage tanks, combined heat distribution, control strategy, collective heating.
DOI: https://doi.org/10.34641/clima.2022.431

1. Introduction

1.1 Combined heat distribution circuits

Combined heat distribution circuits (CHDC) are collective heating systems in apartment buildings with only one supply pipe and one return pipe (2-pipe system). These pipes distribute heat for both space heating (SH) and domestic hot water (DHW) to the dwellings. By using only one supply pipe, the distribution losses are reduced compared to a 4-pipe system. In Dutch, this system is called "combilus".

Currently, the supply temperature in a CHDC is set at 65°C, the hottest demand, to guarantee the supply of DHW to the end-users at all times without major waiting times. However, this leads to two main disadvantages. Firstly, distribution losses are mostly higher than strictly needed. Secondly, the overall energy efficiency decreases because of high return temperatures [1] when the overflow valve is opened.

Another incentive to regulate the supply temperature in a more adequate way is that the share of SH demand decreases in importance due to

Copyright ©2022 by the authors. This conference paper is published under a CC-BY-4.0 license.

increased insulation [2-3]. Low-temperature emitters, such as underfloor heating and convectors, are becoming more common in the new-built environment. This means that low temperatures can be distributed in the CHDC, if an energy and comfort-friendly solution is provided for the DHW supply. The most promising solutions are decentralised storage tanks [1, 6] and booster heat pumps [6-7] for DHW storage and production at local level, respectively. This research focuses on using decentralised storage tanks for DHW in CHDC.

1.2 Decentralised storage tanks

Decentralised storage tanks are small thermal storage tanks in every dwelling to store DHW. With an internal coil heat exchanger (CHE), the heat from the CHDC is transferred to the water in the tank. This heated water is the consumable DHW for end-users.

Today, decentralised storage tanks are already used in CHDC or district heating networks. However, they are not yet used in combination with an optimised supply temperature control strategy (still set at 65°C), but rather to reduce waiting times for DHW use and make overflow valves unnecessary [8].

Combining low-temperature emitters with decentralised DHW storage tanks provides opportunities for demand-based control strategies in CHDC. During most of the day, the supply temperature could be lowered for SH and when the DHW tanks need to be charged, a temperature of 65°C can be distributed. This has two main advantages: I) reduced distribution losses and II) increased total production efficiencies as low temperatures can be generated by renewable energy sources, such as heat pumps (HP) [7].

1.3 State-of-the-art

Currently, many studies on temperature control optimisations and on decentral storage tanks exists in the scientific literature. Gustafsson et al. [9] investigated the possibilities of supply temperature control in district heating networks to increase the temperature difference between supply and return. They confirm that supply temperature control is usable in collective systems, while guaranteeing comfort. However, the temperature difference was hardly improved. Here, the DHW demand was neglected and it was based on in-situ measurements. In study [1], the performance of six configurations of heat interface units (HIU) in CHDCs and different control strategies were compared, based on return temperature, heat losses and DHW use temperature. However, the control strategies were applied to the overflow valve for recirculation of the CHDC and radiators were considered for SH. Another study [10] presented a general overview of possible concept for DHW production in low-temperature heating systems. A novel control strategy was also introduced, but the focus was again the recirculation loop, and no decentralised storage tanks were considered. In addition, [12] developed an active control strategy with data-based techniques for a district heating network with a CHP. They compared different set-ups, amongst others central storage tanks or decentral storage tanks. The decentral storage tanks yielded the highest possible savings.

Besides proposing new control strategies, the effect of different design choices in the storage tank should be taken into account. As stated in [11, 13], the design has a major impact on the energy performances. Van Minnebruggen et al. [14] validated a dimensioning tool for thermal storage and required heating power in collective heating networks, but the focus lies on the central boiler room, rather than the decentralised storage tanks. In [7], the use of booster heat pumps in combination with decentral storage was assessed for CHDCs. In this study, the focus was on the efficiency of the system by using only heat pumps and on the influence of sizing. The decentral DHW production and storage lead to great energy savings in comparison to CHDCs without decentral storage.

The state-of-the-art lacks optimised control strategies for CHDCs with decentral storage and an evaluation of design choices on the performance of control strategies in CHDCs.

1.4 Outline

The following section explains the used methods and the main principles/assumptions of the simulation environment. Section III is devoted to the description of the proposed control strategies for the supply temperature and the different sensitivity analyses for the storage tanks' design. Afterwards, in section IV, the results for the proposed control strategies are given, with a discussion. Finally, this paper concludes with the main findings of this study.

2. Research Method

2.1 Simulation-based

A dynamic simulation environment is built in Matlab to test control strategies and study the influence of different design choices. By doing so, the boundary conditions and heat demand for DHW and SH could be kept the same for an objective evaluation. The models are based on the doctoral dissertation of Van Riet [15] and are also used in [7,16-18].

This environment represents the dynamic thermal behaviour of the CHDC and its components. The transient behaviour is taken into account by differential equations according to the general equation described in [16]. Only the storage tank model is a partial differential equation both in temperature and along the height (temperature layers). The simulation time step is 10 seconds to have detailed simulations of the DHW use. It is assumed that the CHDC is perfectly balanced, thus the desired mass flow rates are always available. The time-delay in the pipes is taken into account by applying the plug-flow principle [18].

Due to the simulation time step of 10 seconds and the detailed simulation models, the simulation period has been fixed to only one month (January) to reduce the computational time and power.

2.2 Case study

The apartment building of this research consists of 20 identical dwellings, located in Uccle, Belgium. All dwellings have a storage tank for DHW and SH is based on underfloor heating with design temperatures 35°C/30°C. No hydraulic separations (e.g. heat exchangers) are needed as the apartment building is small (no high pressures in CHDC) and the storage tanks separate the DHW from the technical water in the CHDC. All storage tanks have a priority switch for DHW, thus if a tank is being charged, the SH in that dwelling is shut off. The indoor temperature set point is 21°C during the day and 19°C at night. The heat load by design conditions (21°C indoor and -8°C outdoor) is 1340 W. Each dwelling has one shower and two or three other tapping points. They are all occupied by different families of one to three residents. The internal heat gains, occupancy profiles and DHW demand profiles are based on a stochastic "profile generator" developed in the Instal2020 project [4-5]. An example of the DHW profile for all dwellings for two days is given in the appendix to this paper (Fig. A).

The central boiler room consists of a geothermal heat pump (GHP), connected to a storage tank, and a boiler in series. The boiler room is considered as ideal, thus it can instantaneously deliver the demanded supply temperature and mass flow rate by the control strategy. This approach is chosen, as it allows us to focus on evaluating the control strategy, without the effects of transient behaviour in production units or incorrectly set PID controllers. An overview of the case study is shown in Fig. 1.

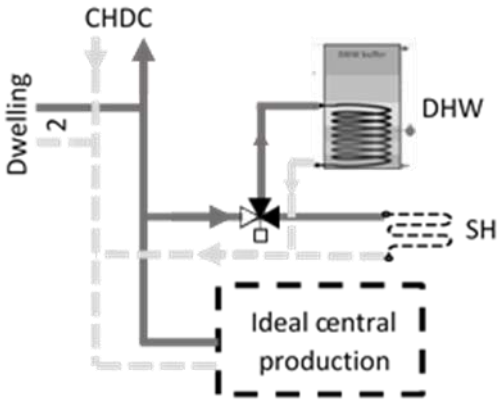

Fig. 1 – Overview of the case study. The ideal central production consists of a geothermal heat pump and a boiler. Every dwelling in the CHDC has a storage tank for DHW and underfloor heating.

2.3 Model of DHW storage tanks

The stratified thermal storage tank has an internal coil heat exchanger (CHE) in the lower half of the tank and two ports at 0% and 100% of the height. The model is based on Type 60 of TRNSYS [19] and described in [15]. The tank is divided in different homogeneous water layers. Heat transfer to the adjacent layers due to conduction and advection is considered, as well as losses to the surroundings and heat gains from the internal heater. A temperature inverse algorithm is added to take account of the buoyancy effect. At the in- and outlet, no account is taken of buoyancy, but rather of mixing. It is possible to add an electrical resistance in one of the layers. The dimensioning (UA-value [W/K]) of the internal CHE is based on lab measurements of a 90 l storage tank and technical information from *Collindi* [20]. When larger volumes are simulated, a larger coil with increased nominal power is foreseen and UA is modified as such. For different charging flow rates, a constant UA value is assumed, which means that the internal CHE is smaller and longer.

2.4 Key Performance Indicators

To compare the control strategies and analyses, four key performance indicators (KPI's) are used:

First is the total primary energy (PE) use of the system (PE_{use}[kWh]). The PE use of the ideal central boiler room is calculated and, if any, summed up with the PE use of the electric resistances in the storage tanks. The GHP's set point is 45°C. Its Coefficient of Performance (COP) at 45°C/37°C is assumed to be 4.8 and adjusted to the return temperature (T_{ret} [°C]) according to the EPB calculation method [21], shown in equation (1)). If the supply temperature is above 45°C, the boiler will provide the extra heat with an efficiency of 100%. The conversion factor for electricity to PE is 2.5 in Belgium. This KPI is important since this research aims at reducing the energy use.

$$COP = 4.8 \cdot (1 + 0.01 \cdot ((45 - T_{ret}) - 8)) \qquad (1)$$

Next is the Primary Energy Ratio (PER). This is the total efficiency in terms of PE, i.e. the ratio of PE_{useful} to PE_{use}. PE_{useful} [kWh] is the useful energy for SH and DHW. A higher PER indicates a higher heat pump's share in energy delivery and lower heat losses.

The relative duration of DHW temperature lack [%] is introduced as a KPI. This is the proportion of the total tapping times of all storage tanks that the DHW temperature is lower than 40°C. This KPI refers to the situation where the storage tanks are getting empty at the end of a tapping period. In contrast to a temperature lack that occurs at the beginning of a tapping, which is related to pipe lengths, this discomfort is due to sizing or late recharging of tanks (control strategies). The smaller this percentage, the less time the end-users experience discomfort on average. The distribution pipes from the storage tanks to the tapping points are not considered.

Finally, the central peak power (CPP) [kW] is used as KPI. This is the highest power delivered by the

central boiler room over a time period of 10 minutes. This larger timeframe is chosen to have more realistic values, since an ideal production without inertia – and thus providing unrealistic temperature increases - is assumed. The lower this peak power, the smaller the boiler and GHP can be designed, which reduces investment costs and increases the overall energy performance.

3. Experiments

3.1 Control strategies and sensitivity analyses

The control strategies are considered for a CHDC that can operate at both low (38°C) and higher (65°C) temperatures. A straight forward control strategy is to raise the distribution temperature each time one of the storage tanks demands heat. Although the temperature can be lowered outside these charging cycles, simulations show that low distribution temperatures rarely occur for such a basic control strategy. Hence, the proposed control strategies are meant to increase the simultaneity of the charging storage tanks and thus minimise the time period with high distribution temperatures. As a result, primary energy use is expect to decrease as described in 1.2.

The impact of two optimized control strategies on energy use and DHW comfort is assessed and compared to the reference control strategy, where the distribution temperature is high (65°C) both for SH and DHW demand. The design parameters are set according to a case study measured in Malle [22]: the reference volume is 90 l (for one shower per dwelling). The tanks have one sensor at 2/3th of the height and a set point of 58°C with an ON/OFF control hysteresis of +- 3°C. The charging flow rate of the storage tanks is initially set at 600 kg/h.

The first optimized strategy is a time-based control. The distribution temperature is raised at some pre-defined time slots and all tanks, with demand according to one sensor at the bottom of the tank, are thermally loaded. It is important to define the size of the storage tank and the charging time slots to ensure DHW comfort in between. Therefore sensitivity analyses are performed for these parameters.

For the second strategy, two sensors are used in each tank. If there is a demand according to the upper sensor of one tank, distribution temperature is raised and all tanks with demand according to their lower sensor are loaded simultaneously. This control strategy can be optimized by improving the hysteresis and the size of the storage tanks, which is also subject of this research.

Due to the increased simultaneity, the CPP is expected to increase with the proposed control strategies. Therefore the impact of lowering the charging mass flow is assessed for both strategies.

4. Results and discussion

4.1 Time based control (TB-control)

Fig. 2 shows PE and DHW discomfort for January when a time based control (TB-control) is used, compared to the reference as described in 3. In the following figures, the shape refers to the volume of the storage tank (150, 200 or 300 litre), the colour to the charging flow rate (from 100 kg/h to 600 kg/h). For each combination of volume and flow rate, 5 different time slots are considered, with a total charging time of 1, 2, 3, 4 or 6 hours. This total charging time is divided equally between a morning and evening charging cycle, because this proved to give better comfort results almost without affecting the energy consumption. So, the rightmost datapoints, with the largest PE, are for a charging time of 2*3h. As the charging time shortens, energy use decreases and the points move to the left on the graph. They are indicated with smaller data points. Finally, it should be mentioned that the data points for the 3 volumes, with 100 kg/h and a 2*0.5h charging cycle, have discomfort percentages up to 65% and fall outside the limits of the graph.

Fig. 2 makes clear that, compared to the reference case, TB-control leads to lower energy use, while DHW discomfort highly depends on the storage volume and the duration of charging cycles. For 300l storage, a charging time of 2*1 h (>=300 kg/h) or 2*1.5 h (100 kg/h) results in nearly no DHW discomfort. Extending the charging time is not recommended, as this only leads to higher energy use. For smaller storage volumes, and the considered time slots, there is always some discomfort. However, it is possible to maintain at least the comfort level of the reference with a charging time between 2*1 h and 2*2 h (depending on volume and flow rate). For smaller volumes, extending charging times or increasing flow rates improves DHW comfort, but despite higher energy use.

Given the limited place in apartments, increasing the storage temperature (+10°C) might be preferable instead of larger volumes. Another way to provide a better DHW comfort for smaller storage volumes, is adding an electrical resistance (ER) in the storage tank. These datasets are added in Fig. 3, outlined in red and in green, resp. Only the cases with a flow rate of 100 kg/h are included here (for readability). Fig. 3 shows that taking these measures do indeed improve DHW comfort, but at the expense of increased PE use. The increase in PE is limited when increasing the storage temperature, but when local ERs are added, the total PE exceeds even the reference control. It should be mentioned that this conclusion highly depends on the assumed PE conversion factor for electricity (for Belgium; 2.5). If PV panels are present, the cases with local ERs will be more advantageous.

The TB- strategy is intended to combine the charging cycles of the different storage tanks and therefore result in higher CPP (see Fig. 4) compared to the

reference. However, also a significant reduction of CPP is possible when the charging flow rate of the storage tanks is reduced. This also results in PE saving (Fig. 2 and Fig. 4). It is concluded that, based on PE, DHW comfort and CPP, the best option is to work with reduced flow rates (100 kg/h) and a volume of 300 l with a charging time of 2*1.5 h. However, good results can be obtained with smaller volumes, but charging time should be adjusted to the other parameter settings and comfort requirements.

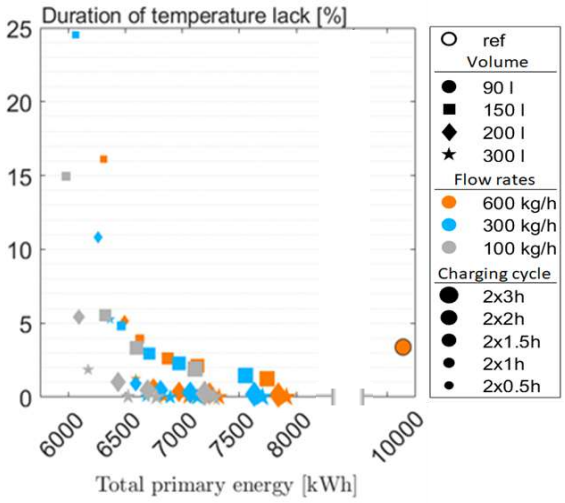

Fig. 2 – TB-control: PE and DHW discomfort for different storage volumes, flow rates and charging cycle.

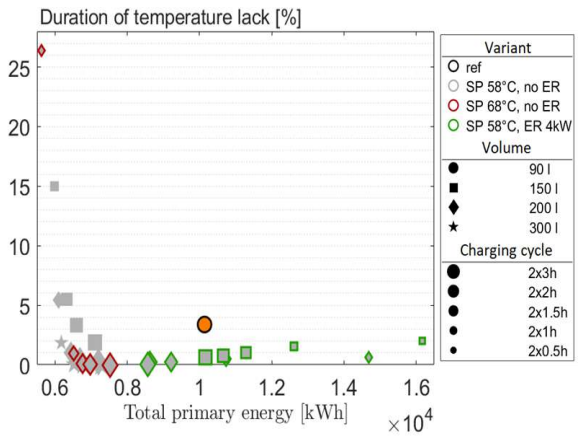

Fig. 3 – TB-control: PE and DHW discomfort, variants on storage temperature and electrical resistance.

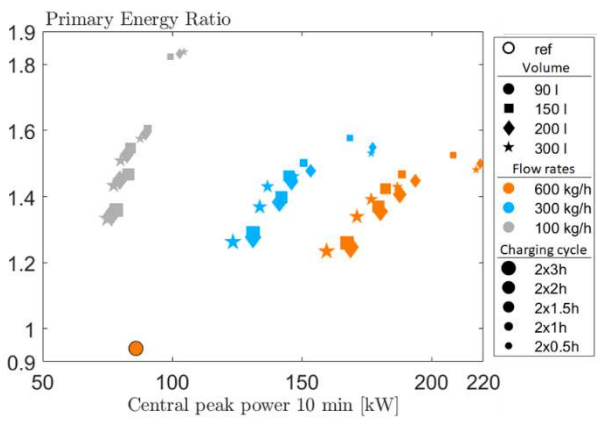

Fig. 4 – TB-control: central peak power and PER for different storage volumes, flow rates and charging cycle.

4.2 Two-sensor control (2SC)

The second proposed control strategy, based on two sensors, is called "two-sensor control" (2SC). The set point of the sensors in the storage tanks is always 58°C. In following figures, the shape refers to the volume (90, 150 or 200 litre), the colour to the charging flow rate (from 100 kg/h up to 600 kg/h) and the darkness of the (same) colour refers to the hysteresis (light colour variant is +-3°C, the darkest variant of a colour is +-5°C). These variations on the reference control strategy (always supply temperature of 65°C and with a hysteresis of +-3°C) are also given, slightly outlined in black.

Fig. 5 shows for all variants the PE use vs. the discomfort of DHW in % of tapping time (see section 2.4 for exact definitions). A few conclusions are drawn from this chart. Firstly, the influence of the volume on the discomfort for DHW is clearly visible. For both the reference and the 2SC, a larger storage tank consequently improves the comfort level for DHW. While the reference control requires approximately the same PE (same charging flow rate considered, i.e. colour), and the 2SC reduces PE use by up to 25% (when the charging rate is 600 kg/h for 200 litre tanks) compared to its reference. In fact, with the 2SC, PE savings are achieved for each variant, while DHW comfort is roughly the same or even better than with the reference control. The PE use is similar for different tank sizes in reference control, because of similar storage losses (all between 3 and 4% of the total energy demand). The PE savings with the 2SC is due to the simultaneous charging, as the supply temperature is low during longer periods for larger tanks.

Secondly, for the 2SC, the charging rate has nearly no influence on the comfort and PE use for the larger storage tanks. For the 90 l tanks, the discomfort increases when using a smaller charging rate and the PE use is slightly smaller. In contrast, the charging rate has a high influence on the PE use of the reference control. The effect on DHW comfort is also larger for smaller tanks in reference control. These different results are due to simultaneous charging of tanks. With the 2SC, many tanks are simultaneously

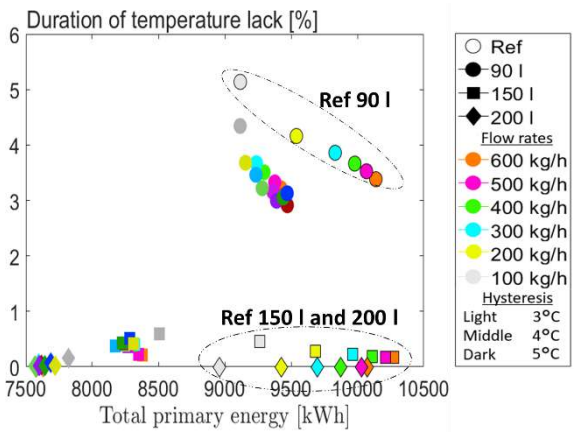

Fig. 5 – Two-sensor control: Pareto analysis on the DHW discomfort [%] and total PE use [kWh] for different charging rates, volumes and hysteresis.

charged. When the charging rate decreases, the return temperature during charging is lower, which increases the production efficiency. However, the smaller charging rate leads to a high distribution temperature for longer periods. The increased distribution losses and efficiency gains cancel each other out for 2SC, resulting in similar PE uses. In reference control, the discomfort increases, since small charging rates are not sufficient, certainly not for small tanks. The PE use decreases due to higher production efficiencies (lower return temperatures).

Finally, the hysteresis (only shown for two-sensor control) does not seem to have a pronounced effect on the larger volumes, but on the 90 litre tanks it can be used to optimise the DHW comfort.

Now the different influences on comfort and PE use are clear, the influences on the required central peak power (CPP) over a period of 10 minutes in relation to the PER is examined in Fig. 6.

For the 2SC, the required CPP increases with higher charging flow rates and larger storage tank volumes. The larger the tank, the larger the relative reduction for smaller charging rates is. The standard deviation of the PER for each volume separately is low from 600 to 300 kg/h. For larger tanks with a charging rate of 200 and 100 kg/h, the PER decreases. The effects on the PER are related to the PE use from previous discussion (Fig. 5). In reference control, the CPP also decreases with a decreased charging rate, but to a lesser extent than in 2SC. Due to the non-simultaneity charging moments, the effect of the flow rate is smaller. On the other hand, the PER increases in a greater extent, which is also consistent with the findings on PE use (Fig. 5).

For the 2SC it is possible to indicate an optimal variant for every volume of the storage tank. For 90l, a charging flow rate of 400 kg/h with hysteresis of +-4°C, is preferred. The comfort is better than the reference control, with the least PE use. For 150 l and 200 l, smaller flow rates will slightly decrease DHW comfort (but always less than 0.6% of tapping time), while the CPP decreases significantly (up to 54%). Thus, a charging rate of 100 kg/h is preferred. For the reference control and the best variant of the 2SC,

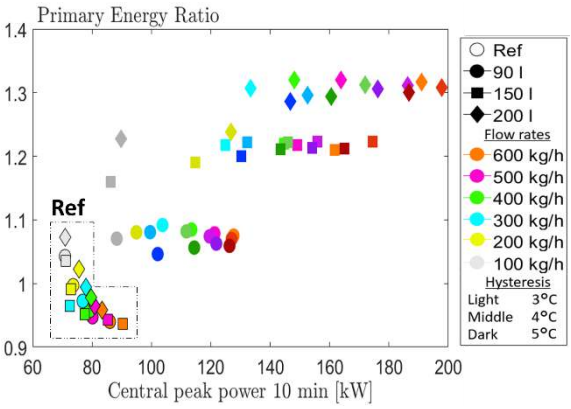

Fig. 6 – Two-sensor control: Pareto analysis on PER and central peak power.

Fig.7 presents the influence of the number of dwellings on both PE use and DHW discomfort.

As the number of dwellings decreases, the 2SC makes it more difficult to maintain a good DHW comfort. The reason is a decreased probability of a top sensor in a particular tank that gives a signal. Thus, the CHDC will supply more often low temperatures and tanks will be recharged less frequently, resulting in smaller effective storage volumes. On the other hand, the relative PE savings for an apartment building with fewer dwellings is larger, because of these lower supply temperatures. As expected, the central peak power decreased with the number of dwellings, while the PER increases slightly.

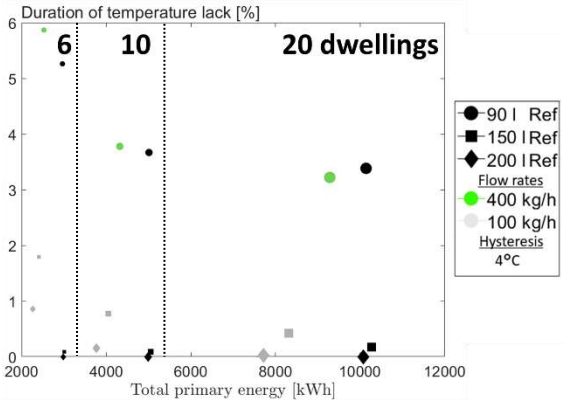

Fig. 7 – Influence of number of apartments for best variants of 2SC and on the reference control.

4.3 Comparison of control strategies

In 4.1 and 4.2 is shown that optimized control strategies allow to decrease PE use and at the same time, achieve a better DHW comfort. Those refined control strategies require sufficient attention to the settings of the significant parameters. Fig. 8 summarises the results. While the TB-control saves more energy with smaller charging cycles, it impacts the DHW comfort, and larger volumes are required (a compromise must be found between these KPI's). For the 2SC it is possible to specify an optimal variant for each volume, and saving more energy with increasing volume.

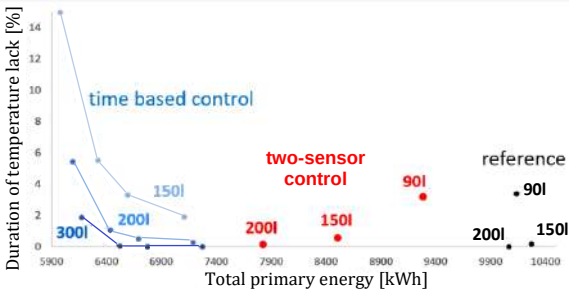

Fig. 8 – DHW discomfort and PE use for reference control (600 kg/h) and proposed control strategies (100 kg/h).

As mentioned before, all analyses were performed considering an ideal central boiler room. It is expected that PE savings would be less for a realistic boiler room, because the losses in the boiler room, and the delay of valves etc. are not considered. In addition, the efficiency of the boiler is set at 98%,

while the COP of the GHP is calculated as done in EPB [21]. Besides these technical simplifications, the distribution temperature would not immediately be increased from 38°C to 65°C in reality, and thus this would also affect the DHW comfort. However, the goal was to compare different control strategies and these assumptions were made for both the reference control as the proposed control strategies.

4. Conclusions

Currently, the supply temperature control of CHDCs is set at 65°C to supply DHW at all times. However, with DHW storage tanks and low-temperature emitters in the dwellings, there are possibilities to optimise this supply temperature control. The goal is to reduce the supply temperature to the SH design temperatures for most of time by grouping charging times of all storage tanks as much as possible.

In this respect, this research proposes two control strategies. The first is a time-based control strategy, where one or two charging moments are pre-defined. The second one is based on two sensors. If the upper sensor in one of the tanks measures a too low temperature, the central supply temperature is set to 65°C. All storage tanks that are too cold at the bottom sensor will be charged. Afterwards, the central supply temperature is set back to 38°C for SH (design temperature of underfloor heating is 35°C/30°C). Both controls have a priority rule for DHW, so no SH is enabled in a given dwelling when its storage tank is being charged. Besides new control strategies, sensitivity analyses were performed on storage volumes, sensor's hysteresis and charging flow rates.

In order to test the two control strategies and to compare it to the reference control, a simulation environment is built in Matlab. The models are based on previous research [7, 15-18] with differential equations to simulate the dynamic thermal behaviour of the system. The central boiler room is considered as ideal, so it delivers directly the desired temperature to the CHDC. The DHW profiles, internal heat gains, occupancy patterns are based on a profile generator from Instal2020 [4-5]. The simulation time step is 10 seconds to simulate DHW demand in detail.

The proposed control strategies offer opportunities to lower PE use in CHDCs. At the same time, choosing the right settings to preserve DHW comfort and to limit peak demand, could pose some challenges. In summary, the main conclusions of performed analyses are: I) increase the volume of storage tanks, as this will increase the DHW comfort level, while the total PE use is similar for the reference control and decreases even further for the proposed controls. II) The time-based control strategy is quite simple to introduce and has the potential to perform better than the reference control. However, an under- or overestimation of charging time and/or flow rate will have significant (negative) effect on resp. DHW comfort or PE. Besides, larger volumes (than 90 l) are required to provide the DHW comfort. III) The two-sensor control reduces the PE use (up to 25%), while delivering similar or improved DHW comfort (less than 0.6% discomfort). However, the control is way more complex to implement. IV) If one of the proposed control strategies is applied, the charging flow rate should be reduced to lower the central peak power, and thus reducing the investment cost of the central boiler room and the sizing of the piping. By reducing the flow rate from 600 kg/h to 100 kg/h, half the peak power is required, while maintaining the level of comfort with a similar PE use.

In future work, the position of sensors for the 2SC could be analysed. It is expected that these sensors will influence the level of comfort, but also the optimisation potential. Concerning the TB-control, different DHW profiles should be investigated. It is expected that a more flattened profile would complicate this strategy. The proposed control strategies should also be tested in a simulation environment with a realistic central boiler room to research the influence of thermal inertias and the influence of PID controllers. Finally, using artificial intelligence to optimise control strategies is an interesting follow-up research.

5. Acknowledgements

This research is funded by two instances. First, by a TETRA-project concerning qualitative heating networks (www.warmtenet.info) sponsored by VLAIO. Secondly, by FWO with grant number 1S08622N from the panel SBWT7B.

6. Appendix

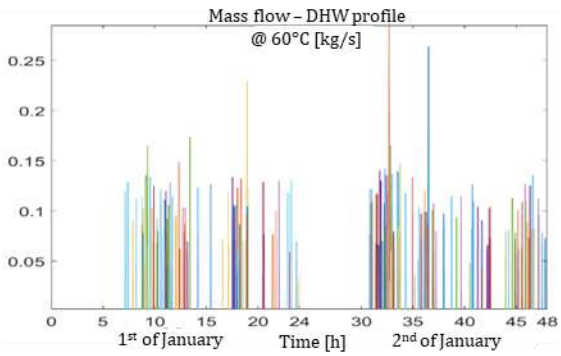

Fig. A – Example of DHW profile for the 1st and 2nd of January. The colors represent the different dwellings.

7. References

[1] Vaillant Rebollar J, Himpe E, Laverge J, Janssens A. Influence of recirculation strategies in collective distribution syste on the performance of dwelling heating substations. CIER 2015. Proceedings of VIII International Conference for Renewable Energy, Energy Saving and Energy Education; 2015 May; La Habana, Cuba; 2015.

[2] Bøhm, B. Production and distribution of domestic hot water in selected Danish apartment buildings and institutions. Analysis of consumption, energy efficiency and the significance for energy design

requirements of buildings, Energy Conversion & Management 67,(2013)152-159.

[3] Buffa, S, Cozzini, M, D'Antoni, M, et al. 5th generation district heating and cooling systems: A review of existing cases in Europe. Renewable and Sustainable Energy Reviews. 2019;104:504-522.

[4] WTCB. Instal2020 [internet]. Brussel (Belgium): WTCB; 2018 [cited 2021 Dec 8]. Available from: https://www.instal2020.be/projectresultaten/

[5] De Schutter J, Verhaert I, De Pauw M. A methodology to generate realistic random behavior profiles for space heating and domestic hot water simulations. Proceedings of REHVA annual Meeting Conference; Low carbon technologies in HVAC; 2018 April 23, Brussels, Belgium; 2018.

[6] Ibrahim Tol H, Svendsen S. A comparative study on substation types and network layouts in connection with low-energy district heating systems. Energy Conversion and Management 2012;64:551–561.

[7] Jacobs S, Van Riet F, Verhaert I. A collective heat and cold distribution system with decentralised booster heat pumps: a sizing study. BS2021. Proceedings of Building Simulations 2021 Conference; 2021 Sept 1-3, Bruges, Belgium; in press.

[8] EMIB UA. Warmtenet [internet]. Antwerp (Belgium): EMIB UA; 2021 [cited 2021 Dec 9]. Available from: http://www.warmtenet.info/

[9] Gustafsson J, Delsing J, van Deventer J. Experimental evaluation of radiator control based on primary supply temperature for district heating substations. Applied Energy. 2011;88(12):4945-51.

[10] Benakopoulos T, Vergo W, Tunzi M, et al. Overview of Solutions for the Low-Temperature Operation of Domestic Hot-Water Systems with a Circulation Loop. Energies. 2021;14(11):3350.

[11] Stalinski D, Duquette J. Development of a simplified method for optimally sizing hot water storage tanks subject to short-term intermittent charge/discharge cycles. Journal of Energy Storage. 2021;37:102463.

[12] Vanhoudt D, Claessens B.J, Salenbien R, et al. An active control strategy for district heating networks and the effect of different thermal energy storage configurations. Energy and buildings. 2018;158:1317-27.

[13] Verhaert I, Bleys B, Binnemans S, Janssen E. A Methodology to Design Domestic Hot Water Production Systems Based on Tap Patterns. CLIMA 2016. Proceedings of 12th REHVA World Congress; 2016 May 22-25; Aalborg, Denmark; 2016.

[14] Van Minnebruggen S, Verhaert I. In-situ valiation of a new sizing methodology for combined production and distribution for domestic hot water and space heating. BS2021. Proceedings of Building Simulations 2021 Conference; 2021 Sept 1-3, Bruges, Belgium; in press.

[15] Van Riet F. Hydronic design of hybrid thermal production systems in buildings [dissertation]. Antwerp (Belgium): University of Antwerp; 2019.

[16] De Pauw M, Van Riet F, De Schutter J, et al. A methodology to compare collective heating systems with individual heating systems in buildings. Paper presented at: The REHVA Annual Meeting Conference; 2018 Apr 23; Brussels, Belgium.

[17] Ghane S, Jacobs S, Casteels W, et al. Supply temperature control of a heating network with reinforcement learning. IEEE. Proceedings of 2021 IEEE International Smart Cities Conference (ISC2); 2021 Sept 7-10; Manchester, United Kingdom; 2021. p. 1-7.

[18] Van Riet F, Steenacker G, Verhaert I. A novel approach to model transport delay in branched pipes. Proceedings of the 10th International Conference on System Simulation in Buildings. 2018 Dec 10-12; Liège, Belgium; 2018.

[19] TRNSYS. Mathematical Reference Type 60 (Stratified fluid storage tank with internal heat exchangers).

[20] ClimaWays. Collindi: geïndividualiseerde collectieve verwarmingssystemen: collective heating management [brochure]. Available from: https://climaways.be/professioneel/producten/verwarmingssatellieten/collindi/#downloads

[21] Vlaams Energie – en Klimaatagentschap. BijlageV – Bepalingsmethode EPW [internet]. [cited 2021 Dec 9]. Available from : https://www.energiesparen.be/bouwen-en-verbouwen/epb-pedia/epb-regelgeving/energiebesluit/bijlage-v

[22] S van Minnebruggen, J Schelkens. Personal communication in conversation on 27 Aug 2021.

Data Statement

The datasets generated and/or analysed during the current study are not publicly available because it is part of ongoing research, but are/will be available on request by mail to the corresponding author.

Phase change materials in facades of buildings for solar heating and cooling

Martin Tenpierik [a], Michela Turrin [a], Willem van der Spoel [a]

[a] Faculty of Architecture and the Built Environment, Delft University of Technology, Delft, the Netherlands, {m.j.tenpierik, m.turrin, w.h.vanderspoel}@tudelft.nl.

Abstract. Phase change materials (PCMs) have already been used in buildings and building services for several decades, mostly integrated into walls or ceilings to passively increase the building's thermal inertia, or integrated into the HVAC system for (pre-)heating or (pre-)cooling fresh air. More recently, the use of PCMs in facades is being explored for solar heating. This paper presents the results of a several years of research into the use of PCMs in rotatable Trombe walls and sun-shading for passive heating and cooling purposes. Simulations used a custom-made model of a room in Matlab/Simulink, in which all relevant heat transfer paths and mass components are accounted for. Once the behaviour of PCM was modelled, the model was connected with the optimisation platform modeFRONTIER to study the (best) performances under different scenarios. The results show that a significant reduction in the energy demand for heating and cooling can be achieved in different climates. The results also show that the shading and insulating effect of the solar wall have the highest impact on the reduction of the cooling respectively heating demand, followed by the thermal mass effect. The paper ends with the development of a prototype of a Trombe wall which was installed in an office at the Green Village (a living lab in Delft).

Keywords. Phase change materials, heating and cooling demand, Trombe wall, solar wall
DOI: https://doi.org/10.34641/clima.2022.91

1. Introduction

In 2019, buildings and activities inside buildings (households plus commercial and public services) accounted for 41% of the final energy use in the European Union [1]. The built environment will face a daunting challenge to reduce its (fossil) energy use and related carbon emissions to meet the targets set by the Paris Agreement. Besides producing renewable energy, buildings need to become more energy-efficient by among others reducing the demand for space heating and cooling, at the same time maintaining comfort for its occupants. Several strategies can be used like climate responsive design.

One novel group of materials that could work well in conjunction with the principles of climate responsive design are phase change materials (PCMs). PCMs are materials that can store or release significant amounts of heat latently by a change of phase (e.g., solid-liquid) without significant change in temperature. Examples of PCMs are salt hydrates, paraffin, eutectics, and bio-based materials using palm oil or rape seed oil.

PCMs have been applied in buildings and building services for several decades. One of the first documented applications in buildings dates back to 1948 when Glauber's salt was stored in drums inside the Dover house [2]. In recent decades, PCMs have been used to increase the thermal inertia of buildings (walls, floors, ceilings, roofs, sun-shading), or as mass inside ventilation systems to pre-heat or pre-cool fresh air supply, in floor heating systems to stabilise the system, and in heat recovery units [3, 4, 5].

Over the past years, the authors have investigated the application of PCMs in facades of buildings, with one application addressing their use in Trombe walls for passive solar heating and cooling. A Trombe wall is a structure made of a 10-20 cm thick solid wall placed behind a layer of glass with a thin layer of air in-between [6, 7]. Generally, in winter the wall heats up due to insolation and temporarily buffers this heat in its mass. Due to conduction the heat will slowly conduct towards the other side of the wall where it with a time delay will transfer the heat towards the space behind the wall. Many Trombe walls also have grills at their bottom and top which can be opened in the afternoon and at night to allow for a flow of warm air from the cavity to the room further enhancing the heat transfer. As a result of the time delay, the heat is available when occupants are at home at night reducing the energy demand for heating.

Copyright ©2022 by the authors. This conference paper is published under a CC-BY-4.0 license.

These traditional walls, however, have several drawbacks: they are very heavy and thick; they are not suitable for refurbishment projects; they block the admittance of daylight into the building; and they cannot be adjusted to the varying outdoor and indoor conditions. Among the first studies that investigated lightweight thermal storage systems in façades are the studies conducted by Kienzl [8], Manz et al. [9], Weinläder et al. [10] and Fiorito [7]. Although these studies investigated the possibilities for lightweight systems, none of these were adjustable to varying circumstances as they were developed as static building components. Our research into Trombe walls explored a system that can be tuned concerning heat absorption and radiation for both winter and summer using PCM as a lightweight thermal buffering material, and thereby save on energy demand for heating and cooling.

2. Research method

2.1 Trombe wall principle and materials

The Trombe wall is made of phase change material of 10 to 60 mm (as a variable) on one side and of 10 mm translucent aerogel grains on the other side, encased in a thin plastic container, and rotates twice a day at sunrise and sunset. In winter between sunrise and sunset the PCM faces the window and between sunset and sunrise it faces the room; in summer between sunrise and sunset the PCM faces the room and between sunset and sunrise it faces the window. Furthermore, in summer at night vents are opened in the façade which enables a natural flow of outdoor air along the PCM in order to release the stored heat into the outdoor environment (Fig. 1).

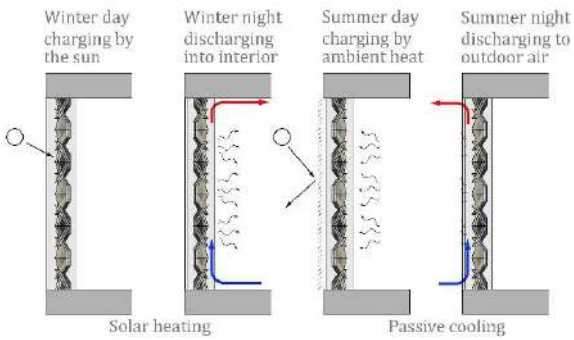

Fig. 1 - Principle of the latent heat storage unit [11].

The thickness of the air cavity between the glass and the wall is considered a variable and varies between 10 and 160 mm. For the façade with window, the window-to-wall ratio is fixed to 80%, whereas the size of the Trombe wall in relation to the window is variable ranging between 40 and 90% (If not mentioned for the specific simulation, it is 90%). The orientation of this façade can vary.

For aerogel the following properties were used: a thermal conductivity of 0.012 $W \cdot m^{-1} \cdot K^{-1}$, a bulk density of 75 $kg \cdot m^{-3}$ and a specific heat of 1440 $J \cdot kg^{-1} \cdot K^{-1}$. A layer of 10 mm aerogel transmits and absorbs 91% respectively 9% of the incoming solar radiation.

The PCM used in this study is a salt hydrate with a melting temperature (mid-point of melting range) as a variable ranging between 20 and 26 °C (if not mentioned for the simulations it will be 25 °C). Also the latent heat of fusion is considered a variable ranging between 160 and 240 $kJ \cdot kg^{-1}$ (if not mentioned for the simulations it will be 180 $kJ \cdot kg^{-1}$); it is modelled as a temperature dependent specific heat capacity, c_p, as shown in Figure 2. The thermal conductivity is set to 0.6 $W \cdot m^{-1} \cdot K^{-1}$, the bulk density to 1450 $kg \cdot m^{-3}$ and the sensible specific heat capacity to 2000 $J \cdot kg^{-1} \cdot K^{-1}$. Most PCMs exhibit hysteresis which means that the melting cycle differs from the solidification cycle. A hysteresis dead band of 2 °C was included in the simulations.

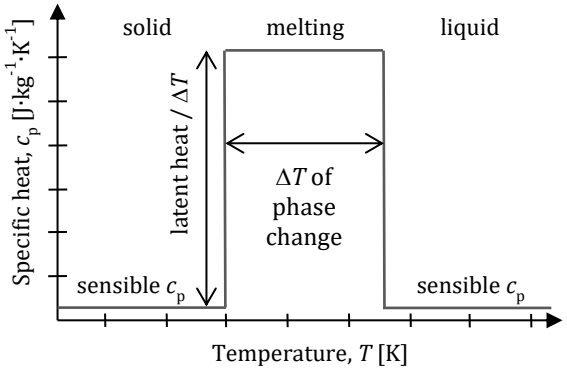

Fig. 2 – Modelling of the latent heat as part of the specific heat capacity.

2.2 Simulation model

For this research an energy performance simulation model in Matlab/Simulink was developed that includes a rotating Trombe wall with latent heat storage properties. Three of our MSc students, Carlos Chang Lara [12], Jeroen van Unen [11] and Kees-Jan Hendriks [13] added features specific for their research. The model is set-up as a multi-nodal model with nodes for the room air, the cavity air, the outdoor environment, the walls, ceiling and floor (two surface nodes and two inner nodes each) and multiple nodes for the Trombe wall. Between these nodes conductive, radiative and/or convective heat transfer and in some case air flow is taking place. Figures 3a and 3b show examples of heat transfer modes between several of the nodes. Air exchange between the nodes of the cavity and the indoor space and between the cavity and the outdoor air (night flushing) is modelled using the stack effect formula for which the relevant coefficients were obtained from an air flow network model.

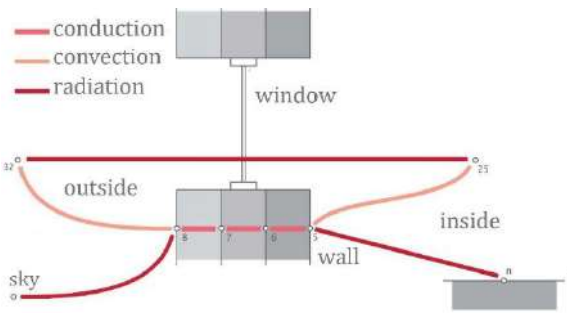

Fig. 3a – Heat transfer between nodes near window without Trombe wall [12].

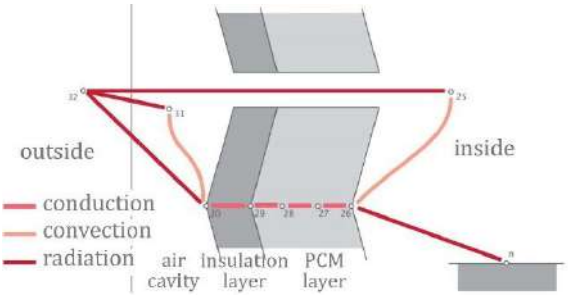

Fig. 3b – Heat transfer between nodes near window with Trombe wall [12].

The basic room (Fig. 4) has three adiabatic walls, an adiabatic floor and ceiling, and one façade which exchanges heat with the outdoor environment via infiltration, transmission and solar radiation gains. Balanced mechanical ventilation with heat recovery is implemented providing fresh air to the occupants of the space. Besides, a simplified heating and cooling system (COP=1) is implemented in the model that provides a stable temperature inside the room based on a set-point temperature and PID controller for the times the space is occupied. The set-point for heating is 20 °C and for cooling 26 °C. The output of the model thus is the energy demand. A complete description of the model is provided in [11], [12] and [13].

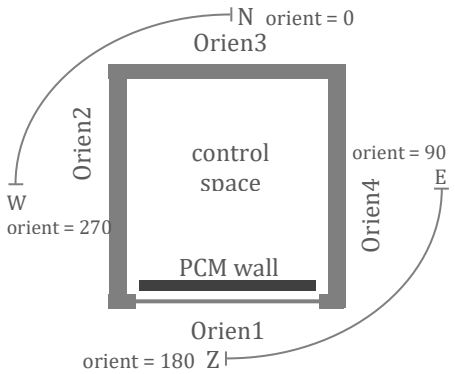

Fig. 4 – Floor plan model of the simulated room. The orientation may vary in the model.

Table 1 provides an overview of the most important properties and settings of the simulation model for both the offices and housing simulated.

2.3 Optimisation model and settings

For running the optimisations, the Matlab/Simulink model was connected to the optimisation platform modeFRONTIER. ModeFRONTIER creates a direct connection between the two platforms. Once the optimisation is set with optimisation objectives, design variables, eventual constraints and other relevant features, modeFRONTIER drives the optimisation process through simulations in Matlab/Simulink. Several optimisation objectives were defined of which only here are shown:

1.) Minimisation of the energy demand for cooling;
2.) Minimisation of the energy demand for heating;
3.) Minimisation of the year round energy demand.

The self-adaptive multi-strategy optimisation algorithm pilOPT [14] in modeFRONTIER was used to drive the optimisation process. This algorithm combines Response Surface Methodology (RSM) with a Genetic Algorithm (in our case NSGA-II), which increases the robustness of the process and the quality of the optimisation. Around 4000 generations were sufficient to have good convergence of the results towards a Pareto front.

2.4 Climates

Several climates were included in these studies: Cold (Stockholm), temperate (Milan), dry (Cairo) and tropical (Singapore) [13]. Weather data for these cities were extracted from the website of EnergyPlus. Also the town De Bilt was included in another optimisation run for which weather data based on the Dutch standard NEN5060: 2018 was used [11]. This standard includes a reference meteorological year for the Netherlands for energy simulations.

Tab. 1 – Settings and properties of simulation model.

variable	value	
building function	offices	housing
room size	small: 3.6 x 5.4 x 2.7 m^3 big: 7.2 x 10.8 x 3.0 m^3	
façade orientation	North, East, South or West	
radiat./convect. (ins./outs.) surface heat transfer coef.	5.0 / 2.7 /25 W·m^{-2}·K^{-1}	
%openings in Trombe wall	10%	
U-value / SHGC of glass	double: 1.6 W·m^{-2}·K^{-1} / 0.7 triple: 0.7 W·m^{-2}·K^{-1} / 0.5	
R_c-value opaque facade	old buildings: 2.0 m^2·K·W^{-1} new buildings: 4.5 m^2·K·W^{-1}	
Infiltration rate	old buildings: 0.8 ach new buildings: 0.2 ach	
total internal heat load	office: 25 W·m^{-2}	housing: 6 W·m^{-2}
Occupancy, intern. heat load and vent. schedule	8.00-18.00 h (Mon-Fri)	18.00-8.00 h (Mon-Fri) 0.00-24.00 h (Sat-Sun)
heating set-point temperature	20 °C	
cooling set-point temperature	26 °C	
mech. vent. rate	2.0 ach	0.7 ach
efficiency of heat recovery	90% bypassed: $T_{int,op}$>T_{ext} & $T_{int,op}$>24 °C	
nat. vent. (rate) at night to flush PCM	$A_{in} = A_{out} = 0.025 \cdot A_{facade}$ C_d = 0.8 (stack eff. formula) on: $T_{int,op}$>T_{ext} & $T_{int,op}$>24 °C	
sun-shading operation	closed: T_{ext}>24 °C & q_{sol}>100 W·m^{-2} [13] or 22 °C & q_{sol}>100 W·m^{-2} [11]	
SHGC sun-shading	0.25	

3. Results

3.1 Different climates

Figures 6a/b show the effect of the PCM based rotatable Trombe wall on the heating respectively cooling demand of all simulated offices and homes for cold, temperature, warm dry and tropical climates. In cold climate the Trombe wall mostly impacts the heating demand, in warm dry and tropical climates the cooling demand and in temperate climates both the heating and cooling demand. Since the different spaces simulated were of different sizes, the absolute differences also depend on room size. Percentile differences show that energy demand reduction of 5 to 100% can be achieved using this type of Trombe wall, the exact amount depending on the available thermal mass in the room, the thermal quality of the façade, the window-to-wall ratio, the internal heat loads, the amount of ventilation, etc.

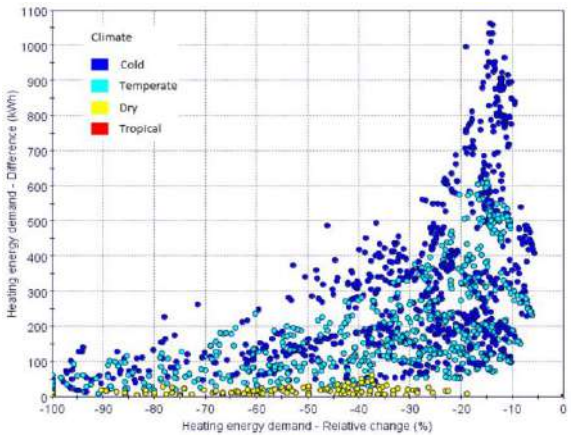

Fig. 6a – Difference in heating demand (absolute and relative) between room without and with Trombe wall for different climates [13]. Positive absolute values / negative percentages denote that the Trombe wall leads to an energy saving.

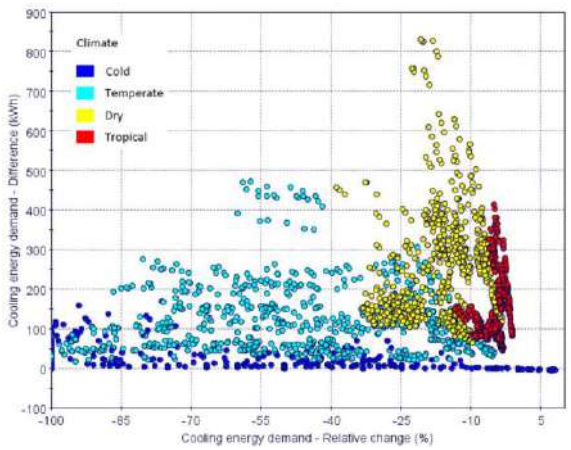

Fig. 6b – Difference in cooling demand (absolute and relative) between room without and with Trombe wall for different climates [13]. Positive absolute values / negative percentages denote that the Trombe wall leads to an energy saving.

3.2 Offices versus housing

Figures 7a/b show the difference between housing and offices for all simulated cases. For both offices and housing the heating demand reduction of the PCM based Trombe wall is of the same order of magnitude looking at all cases as a whole. However, in summer the cooling demand reduction in general is higher for residences than for offices.

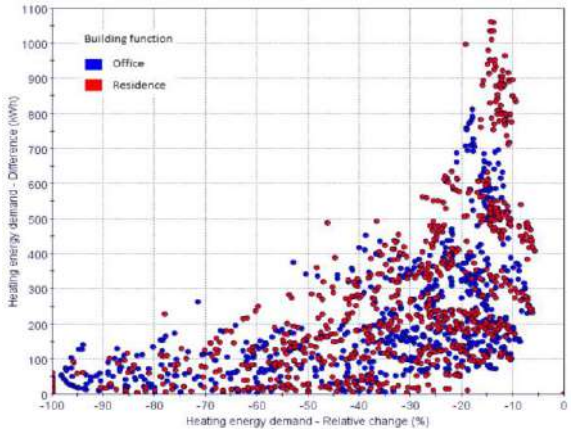

Fig. 7a – Difference in heating demand (absolute and relative) between room without and with Trombe wall for offices versus houses [13]. Positive absolute values / negative percentages denote that the Trombe wall leads to an energy saving.

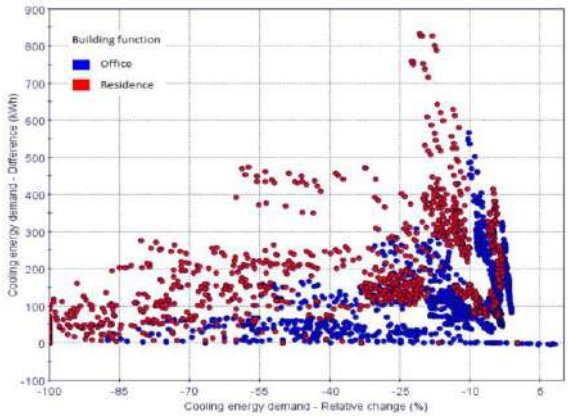

Fig. 7b – Difference in cooling demand (absolute and relative) between room without and with Trombe wall for offices versus houses [13]. Positive absolute values / negative percentages denote that the Trombe wall leads to an energy saving.

3.3 Orientation of Trombe wall

Also the impact of the orientation of the Trombe wall was investigated: North, West, South or East. Looking at Figures 8a/b a first conclusion is that the PCM based Trombe wall leads to heating and cooling demand reductions for all façade orientations. A closer look at Figure 8a shows that in general the South orientation appears more often towards the left upper corner (yellow data points) meaning that a South oriented Trombe wall in general leads to higher energy savings for heating. To get a better understanding of the impact of orientation three rooms were investigated more closely and the green

arrows in Figure 8a show how these cases move in the chart when their orientation changes from North/East/West to South. The performance of the Trombe wall is similar for North, East and West orientations but is better for South orientations (in relative terms).

Also for the cooling demand reduction three data clusters were further investigated (green circles in Figure 8b). Concerning cooling demand reduction, the performance of the Trombe wall is similar for all orientations. This can also be explained by the fact that in that case the wall is cooled at night using outdoor air and is taking up heat from internal heat sources throughout the day. Such performance is hardly impacted by orientation.

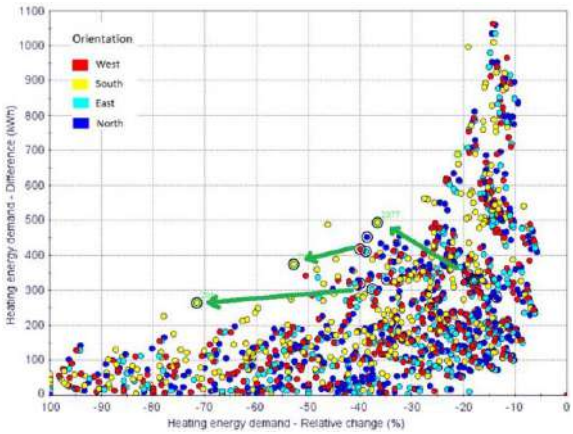

Fig. 8a – Difference in heating demand (absolute and relative) between room without and with Trombe wall for different orientations [13]. Positive absolute values / negative percentages denote that the Trombe wall leads to an energy saving. The green arrows denote how certain cases change if their orientation changes.

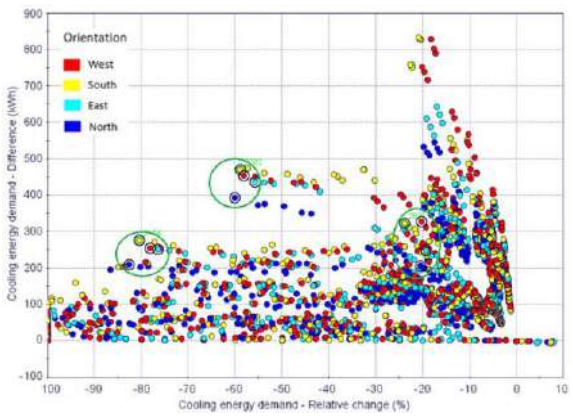

Fig. 8b – Difference in cooling demand (absolute and relative) between room without and with Trombe wall for different orientations [13]. Positive absolute values / negative percentages denote that the Trombe wall leads to an energy saving. The green circles denote how certain cases change if their orientation changes.

3.4 PCM thickness: offices in the Netherlands

The results of the simulations show that on a mild summer day the indoor air temperature is hardly affected by the thickness of the PCM layer in the Trombe wall [11]. On warm and sunny summer days, however, thicker layers of the PCM are better able to stabilise the room air temperature. If no proper sun-shading is used, the temperature of the PCM can easily overheat to temperatures above its maximum operating temperature as stated by the manufacturer. Thicker layers are better able to reduce this overheating. The same applies to sunny winter days on which the sun-shading is not used. In that case a minimum thickness of around 30 mm is needed.

Table 2 provides the reduction of the heating and cooling demand for an office in the climate of the Netherlands with a PCM with melting temperature of 25 °C and latent enthalpy of 180 kJ·kg^{-1}. These results show that generally thicker layers of PCM in the Trombe wall lead to higher performance. However, increasing the thickness from 10 to 20 mm has more effect than from 50 to 60 mm; a thickness beyond 30 mm hardly adds to additional energy savings in the Netherlands. Also from a cost perspective, considering a bulk (>10,000 kg) price range of between 2-4 €·kg^{-1} for inorganic and 4-10 €·kg^{-1} for organic PCMs [11], it would be advisable to limit the thickness.

Tab. 2 – Difference in heating and cooling demand (absolute and relative) between an office space without and with Trombe wall for different thickness of the PCM layer using NEN5060 weather data [11]. PCM melting range between 23-26 °C (latent heat peak at 25 °C). Positive absolute and percentile values denote that the Trombe wall leads to an energy saving.

PCM thick-ness (mm)	Cooling demand reducti on (%)	Heating demand reducti on (%)	Cooling demand reduction (kWh/m^2)	Heating demand reduction (kWh/m^2)
10	49	51	9.2	2.8
15	53	60	10.0	3.3
20	58	64	10.9	3.5
25	59	72	11.1	3.9
30	60	72	11.3	3.9
40	62	77	11.6	4.2
50	62	**80**	11.6	**4.4**
60	**63**	**80**	**11.8**	**4.4**

An important consideration, however, is that for thicker layers of PCM the melting process becomes uneven. Some of the authors have performed CFD simulations to investigate this phenomenon [15]. A 30 mm thick, 200 mm high block of PCM with a melting temperature of 25 °C exposed to solar radiation for 8 hours was simulated. The results showed that after several hours a free-convective fluid flow develops inside the melted PCM which transports heat from the bottom to the top, speeding up the melting at the top. By segmenting the block of PCM in height the melting process can be made more even. Figure 9 shows some of these results. Also segmenting the block with one or two vertical barriers would be beneficial.

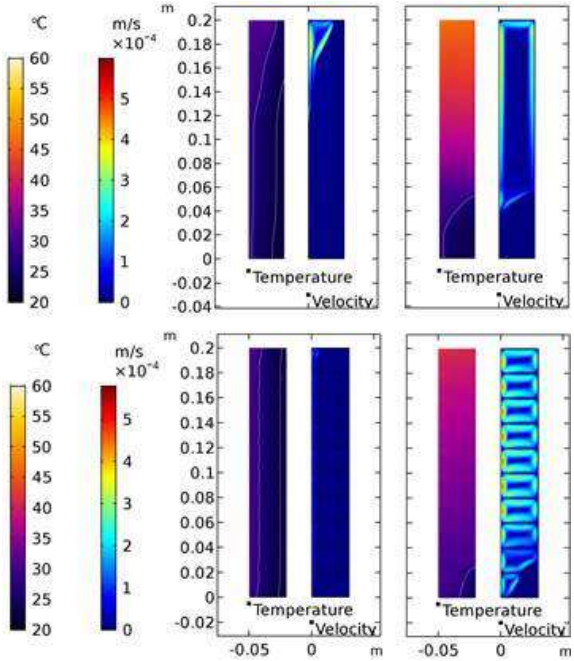

Fig. 9 – Temperature and fluid flow inside a block of PCM with a melting temperature of 25 °C and a thickness of 30 mm exposed to a radiation source of 300 W·m^{-2}, after exposure of 4 (left) and 8 hours (right). The top image shows an unsegmented block of PCM; the bottom image shows a segmented block of PCM (2 cm). [15]

3.5 Melting temp.: offices in the Netherlands

Figure 10a and 10b show the temperature development of the PCM and the room air when the PCM based Trombe wall is used, for different melting temperatures of the PCM (20 °C up to 26 °C; mid-point of melting range). The figures show that in general PCM with a high melting temperature has the best performance under both summer and winter conditions. In summer the room air temperature remain coolest for the PCMs with higher melting temperatures; in winter the daily average room air temperature is higher and more stable for higher PCM melting temperatures. The higher PCM temperatures in winter as compared to summer are a result of the activation of the sun-shades in summer.

Table 3 shows the effect of the PCM melting temperature on heating and cooling demand reduction. These results confirm that for summer a relatively high melting temperature is beneficial but also that the improvement per unit change of the melting temperature becomes smaller. In winter, a melting temperature of around 23 °C performs best for offices. The annual best performance is found for a melting temperature of about 25 °C. A remarkable finding is that the optimal melting temperature for PCM applied in a Trombe wall is higher than what would generally be advisable for indoor PCM use as a passive stabiliser of room air temperature.

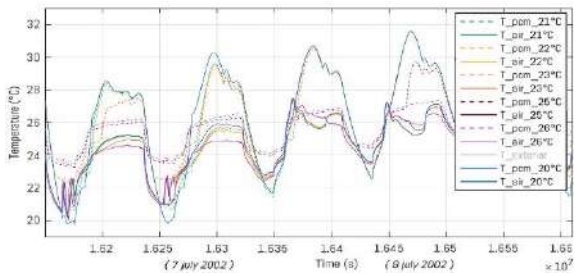

Fig. 10a – Temperature of the PCM and room air of an office space of 60 m² for different PCM melting temperature (mid-point of range at 20 to 26 °C with ΔT of 3 °C) under warm summer conditions using NEN5060 weather data [11].

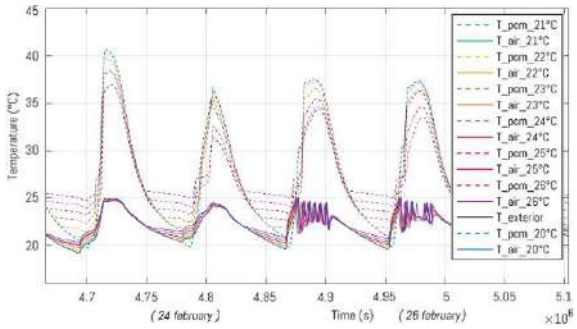

Fig. 10b – Temperature of the PCM and room air of an office space of 60 m² for different PCM melting temperature (mid-point of range at 20 to 26 °C with ΔT of 3 °C) under sunny winter conditions using NEN5060 weather data [11].

Tab. 3 – Difference in heating and cooling demand (absolute and relative) between an office space without and with Trombe wall for different PCM melting temperature using NEN5060 weather data [11]. PCM layer thickness is 25 mm and has a ΔT of 3 °C. Positive absolute and percentile values denote that the Trombe wall leads to an energy saving.

PCM T_{melt} (°C)	Cooling demand reduction (%)	Heating demand reduction (%)	Cooling demand reduction (kWh/m²)	Heating demand reduction (kWh/m²)
20	42	59	7.9	3.2
21	44	67	8.2	3.7
22	47	72	8.8	3.9
23	50	**73**	9.4	**4.0**
24	54	72	10.2	3.9
25	59	72	11.1	3.9
26	**61**	64	**11.5**	3.5

4. Prototype development

4.1 Impact of shape, position and holes

The results presented in the previous section dealt with a flat wall PCM-based rotatable Trombe wall. Additional research was performed by the research team working on the Double Face 2.0 project [16] and MSc student Eve Farrugia [17] using the heat transfer and fluid flow modules of the software

Comsol, to investigate the melting and solidification process of the PCM and the impact of the overall shape of the Trombe wall. More specifically, these simulations investigated how surface geometry, variation in thickness, holes inside the wall and position in relation to the glass impacted the capture of solar heat on a winter day, the release of heat via convection and infrared radiation towards the room on a winter evening, the capture of internal heat via convection and infrared radiation on a summer day and the release of heat via convection on a summer night. Figure 11 shows an example of CFD simulations along several surface geometries.

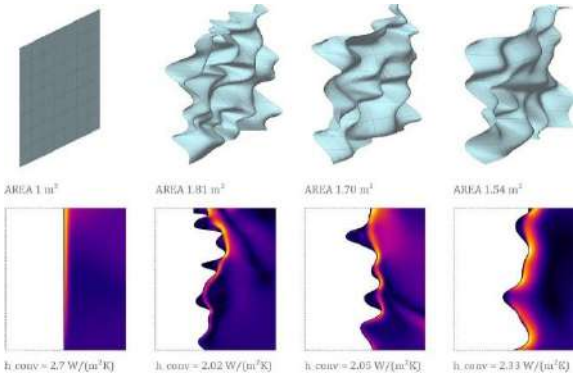

Fig. 11 – Effect of surface geometry on convective heat transfer coefficient [17].

Main conclusion from these simulations was that the melting of the PCM due to exposure to solar radiation, even in winter, is fast but that the cooling down by convection and infrared radiation exchange is slow. This means that, to reduce the risk of overheating the PCM to beyond its service limits, sun-shades are needed in front of the wall for conditions with high solar radiation. The PCM volume also needs to be subdivided into smaller pockets to have good control over the melting and solidification process. A small percentage of holes in the Trombe wall of less than 10% of the surface area does not largely impact the thermal performance of the wall. And a PCM of higher melting temperature could be used in the upper one-third of the wall.

4.2 Developed prototype

Some previous plus aesthetical considerations resulted in geometrical complexity in the design. For this and to facilitate options for product customisation, it was decided to use Additive Manufacturing (Fused Deposition Modelling) with an extruder connected to a robotic arm for producing the prototype. This decision, in addition to the thermal considerations, involved that the design process from the onset integrated considerations deriving from the possibilities and limitations of the 3D printing technique. The research and design process developed by the researchers Tudor Cosmatu, Yvonne Wattez and Stravroula Tsafou led to the design of a prototype as shown in Figures 12, 13 and 14. The thermal response of this wall was monitored for several months after installing it in a meeting room; the data will soon become available.

Fig. 12 – Robotically 3D printing of the prototype of the developed PCM based Trombe wall.

Fig. 13 – Installed full panel of the prototype of the developed PCM based Trombe wall in a meeting room.

5. Conclusion

The research into the use of PCMs in facades of buildings for solar heating and passive cooling has shown that a PCM-based rotatable Trombe wall with a thickness of around 35-40 mm (25-30 mm PCM and 10 mm aerogel) can lead to an important reduction of the heating and/or the cooling demand of both offices and houses, in different climates. The exact reduction depends on the use and characteristics of the room and the façade, and the type and amount of PCM. This reduction is not only because of the presence of the PCM but also because the Trombe wall creates an additional insulating layer behind the glass in winter and a solar shading layer in summer.

It is important to mention that a solution like this would only be cost-effective for thin layers of PCM. In the case of a 25 mm thick Trombe wall, in a 100 m^2 modern apartment with approx. 25 m^2 of facade with a WWR of 0.75, the heating and cooling demand can be reduced by 326-369 and 369-458 kWh/yr respectively in a temperate climate. Assuming a SCOP/SEER of 3 and a cost of 4 €·kg^{-1} for the PCM and 0.3 €·kWh^{-1} for electricity, the payback time would be 30-35 yrs. A similar analysis for a 10 mm thick Trombe wall leads to a payback time of 15-18 yrs. Interesting next steps, therefore, would be to explore thinner curtain-like layers having higher user-friendliness and shorter payback time.

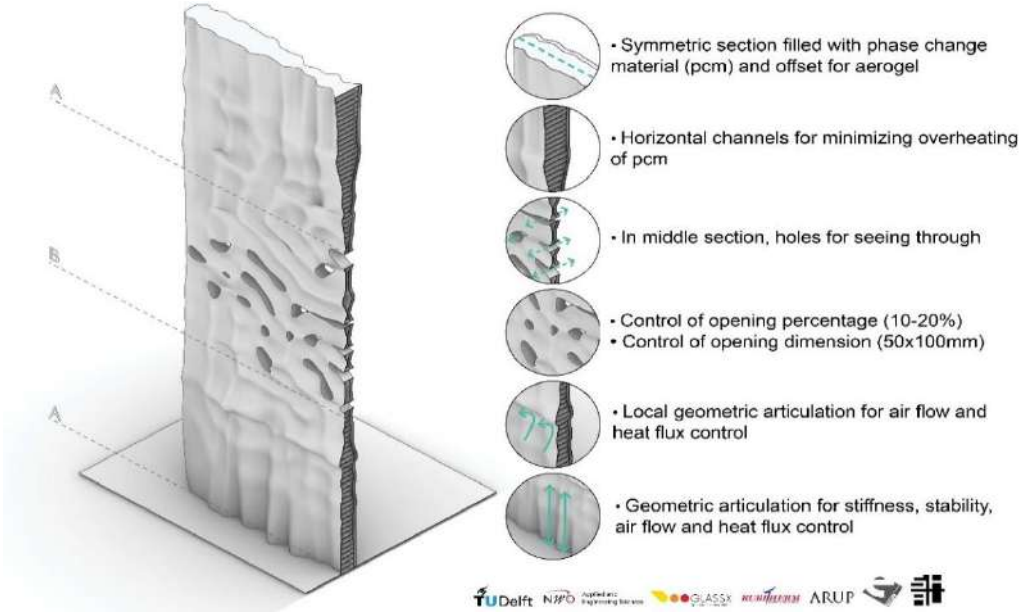

Fig. 14 – Final design of the prototype of the Double Face 2.0 PCM-based rotatable Trombe wall.

6. Acknowledgement

The Double Face research project was part of the lighthouse program, which was financed by the 4TU Centre of Excellence for the Built Environment (4TU.Bouw). The Double Face 2.0 project was part of the research program Research through Design with project number 14574, which was financed by the Netherlands Organization for Scientific Research (NWO) and Taskforce for Applied Research SIA.

The authors are also grateful for the support by the project partners from industry: Shau Architecture and Urbanism, GlassX AG, Esteco SpA, Rubitherm GmbH and Arup. We would also like to thank MgM Robotics for the technical support and advice when using a Comau robot, which was used for the construction of the prototype.

We also thank all staff (Yvonne Wattez, Tudor Cosmatu, Stavroula Tsafou, Paul de Ruiter, Arend-Jan Krooneman, Arno Freeke, Hans Hoogenboom, Aytaç Balci) and students (Carlos Chang Lara, Jeroen van Unen, Kees-Jan Hendriks, Eve Farrugia, Despoina Pouniou) involved.

7. Data statement

The datasets generated during and/or analysed during the current study are available in the MSc theses and project report, which can be obtained from the TU Delft repository, https://repository.tudelft.nl/.

8. References

[1] Eurostat. Final Energy Consumption by Sector. [online]. accessed 9 September 2021. <https://ec.europa.eu/eurostat/databrowser/view/ten00124/default/table?lang=en>.

[2] Harland, A., Mackay, C., Vale, B. Phase Change Materials in Architecture. In: Proceedings of the SB10 Sustainable Building conference. May 26-18, 2010. Wellington, New Zealand. pp. 1-11.

[3] Baetens, R., Jell, B.P., Gustavsen, A. PCMs for building applications: A state-of-the-art review. Energy and Buildings. 2010; 42: 1361-1368.

[4] Kalnaes, S.E., Jelle, B.P. Phase change materials and products for building applications: A state-of-the-art review and future research opportunities. Energy and Buildings. 2015; 94: 150-176.

[5] Bland, A., Khzouz, M., Statheros, T., Gkanas, E.L. PCMs for residential building applications: A short review focused on disadvantages and proposals for future development. Buildings. 2017; 7, 78: 1-18.

[6] Saadatian, O., Sopian, K., Lim, C.H., Asim, N., Sulaiman, M.Y. Trombe walls: a review of opportunities and challenges in research and development. Renewable and Sustainable Energy Reviews. 2012; 16: 6340-6351.

[7] Fiorito, F. Trombe walls for lightweight buildings in temperate and hot climates. Exploring the use of phase-change materials for performance improvement. Energy Proceedia. 2012; 30: 1110-1119.

[8] Kienzl, N. Advanced Building Skins. Translucent Thermal Storage Elements. MSc thesis. 1995. Technical University of Munich, Munich.

[9] Manz, H., Egolf, P., Suter, P., Goetzberger, A. TIM-PCM external wall system for solar space heating and daylighting. Solar Energy. 1997; 61(6): 369-379.

[10] Weinläder, H., Beck, A., Fricke, J. PCM-façade-panel for daylighting and room heating. Solar Energy. 2005; 78: 177-186.

[11] Hendriks, K.J. A change of state. A thermodynamic and cost-effective optimized Trombe wall based on latent heat storage (LHS) for year round application. MSc thesis. 2019. TU Delft, Delft.

[12] Chang Lara, C., Tenpierik, M., Spoel, W. van der Turrin, M. Double Face. Thermal Simulations. Report. 2015. Delft University of Technology, Delft.

[13] Unen, J.A. van. The Energy and Comfort Performance of a Lightweight Translucent Adaptable Trombe Wall in Different Buildings. MSc thesis. 2019. TU Delft, Delft.

[14] https://www.esteco.com/modefrontier

[15] Tenpierik, M., Wattez, Y., Turrin, M., Cosmatu, T., Tsafou, S. Temperature Control in (Translucent) Phase Change Materials Applied in Facades: A Numerical Study. *Energies*. 2019; 12(17): 1-16.

[16] Tenpierik, M.J., Wattez, Y.C.M., Turrin, M., Cosmatu, T.E, Tsafou, E.S. Double Face 2.0. A lightweight adjustable translucent Trombe wall. Report. 2018. TU Delft, Delft.

[17] Farrugia, E. Thermal Morphology. A Geometrically Optimised Trombe Wall. MSc thesis. 2018. TU Delft.

FASTLANE – Dynamic approach to low carbon and energy producing real estate portfolios – case Amsterdam Universities

Thomas Verhoeven [a], Rowan Boeters [b,c], Wim Maassen [a]

[a] Royal HaskoningDHV, Rotterdam, the Netherlands, thomas.verhoeven@rhdhv.com, wim.maassen@rhdhv.com.

[b] University of Amsterdam, Amsterdam, The Netherlands, r.boeters@hva.nl.

[c] Amsterdam University of Applied Sciences, Amsterdam, The Netherlands, r.boeters@hva.nl.

Abstract. In The Netherlands Municipalities, Universities and Healthcare organizations all have targeted to meet the Paris agreement targets, 'Nett Zero Carbon' namely 95% CO_2-emission reductions compared to 1990, long before 2050. To support these organizations on their journey to meet their targets effective and efficient, regarding Carbon emissions as well as costs, a dynamic approach called FastLane is developed. FastLane has already been used for more than 1,000 buildings in more than 75 portfolio roadmap plans to reduce in total 1-3 Mton CO2 emissions by 2050. Implementing all these plans, we can reduce up to 1-3 Mton CO_2 by 2050. This approach deals with three important challenges of the energy transition: only limited time and budget available, close the energy gap between calculated and measured Carbon emissions and provide a dynamic insightful tool to monitor and control the energy transition. These challenges require a different approach than traditional energy studies to identify and select measures. In this paper the requirements, demands and benefits of the developed approach, consisting of a methodology, smart tools using databases and strong insightful presentations in dashboards, are explained.

The approach is illustrated with the case of University of Amsterdam & Amsterdam University of Applied Sciences with a combined portfolio of 50 buildings. Insights are given how Amsterdam University aims to reach their targets and how they are in control doing so during their journey. A roadmap with the most important renovation measures is presented including the possibilities of dynamic interventions adapting to possible changes in the future. Enabling an optimized timing of applying the measures. This already saved Amsterdam University up to 20% of the costs for the energy transition and optimizing the implementation along the way will guarantee the most effective and efficient energy transition of the real estate portfolio.

Keywords. FastLane approach, Energy, Carbon emissions, Roadmap, University Buildings, Real Estate Portfolio.
DOI: https://doi.org/10.34641/clima.2022.221

1. Introduction

In The Netherlands Municipalities, Universities and Healthcare organizations have targeted to meet the Paris climate agreement targets (Conference of Parties November 2015), 'Nett Zero Carbon' namely 95% CO_2-emission reductions compared to 1990, long before 2050. To meet these energy transition targets millions of buildings need to be made more sustainable over the next thirty years. This requires thoughtful planning to accelerate the right decisions and effective implementation.

To enable organizations to realize the energy transition with their building portfolio in time there are three important challenges on strategical, tactical as well as operational level.

The first one is about making roadmaps, long term plans for a period of 30 years, for not one but a portfolio of buildings. Since there is no time to waste this must be done in a short period of time to set the target and reserve the required investment budget. Traditional approaches use energy studies for every single building and use different software tools to calculate the energy performance and cost, taking the maintenance plans into account. To develop the roadmap a new approach is required because the

Copyright ©2022 by the authors. This conference paper is published under a CC-BY-4.0 license.

traditional approach is to slow, time consuming, with too much detail and unnecessary expensive.

The second one is the energy gap between calculated and measured energy use and consequently the gap between calculated and measured CO_2-emissions. Evidence on the magnitude of the gap is adding up fast, suggesting buildings tend to use 1.5 to 2.5 times more energy than predicted in their design [4] [5]. Traditional approaches use mainly calculations to make predictions without fitting the predictions to the actual energy use and CO_2-emissions. However, in the end we need to reduce the actual measured energy use and CO_2-emission. Therefore, the required approach should explicitly focus on these actual reductions instead of calculated theoretical energy and CO_2-emission reductions [6].

The third challenge is the dynamic character of the energy transition with an increasing number of technological innovations and legislation changing rapidly. To manage the energy transition, monitoring compliance and the realised increasing energy performance, of each building and the portfolio of buildings as a whole, is required.

2. FastLane approach

The FastLane approach is a development of Royal HaskoningDHV and is designed to deal with the challenges mentioned above. It focusses on the energy saving measures to be taken at building and portfolio level with starting point the usage of the building and the possibilities and energy infrastructure in the vicinity of each building. The approach consists out of 5 steps, see Figure 1.

Fig. 1 – Visualisation of the 5 steps in the FastLane approach [1].

Deskresearch - The first step is to collect and validate the existing data very thoroughly. In most cases a lot of data is already available. The data is checked on validity and added when required with some assumptions based on benchmark data in a database.

Inspection - Next in step two on-site inspections are performed to validate data and assumptions and, in the meantime, already check practical feasibility of intended measures. The data aggregated with on-site visits including photo's is archived and is already valuable for building owners.

Expert session - In step three, the collected data, information and proposals are discussed with your organization during an expert session, integrally per building, and assessed by a team of experts (energy transition scout, energy expert, structural engineer, cost expert). The aim of this session is to identify the possibilities and impossibilities together with the property managers and building managers to select the most promising measures.

Calculation - Based on these results, in step four, the energy expert and cost expert calculate CO_2-emission reduction, the investments and savings of each measure. With the software module the calculated measures from the library are fitted to the actual energy use of the building. Then the measures of a selected scenario with a package of measures is plotted. The measures can be planned in line with the Multi-Year Maintenance Plan.

Scenario's - In step five the scenarios with packages of measures are selected for each building and the portfolio of buildings. Afterwards it will still be possible to make changes in the digital platform to optimize the scenario's and/or update the baseline to the actual situation. The digital platform offers a set of dashboards to optimize the planned measures and to monitor the calculated and realised performance, see Figure 2.

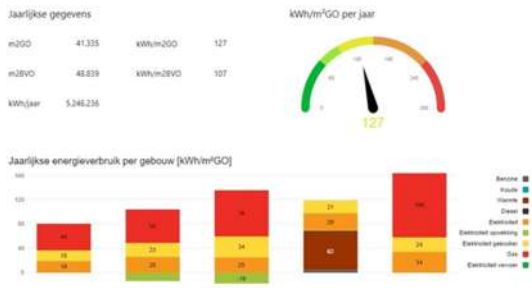

Fig. 2 – Visualisation of dashboard and a dynamic monitoring and control on tablet [1].

3. Case study – Amsterdam Universities

The Dutch universities have committed themselves to the Climate Agreement by means of the sectoral roadmap. This roadmap indicates that the sector will contribute to achieving the climate objectives. By means of an institutional roadmap, the universities are expected to demonstrate their annual contribution. To draw up the institutional roadmap, an inventory and calculation is required of the possible and intended sustainability measures per building. Based on the components described below, we provide our vision and principles for creating a successful roadmap. The University of Amsterdam and the University of Applied Sciences in the city are taking the lead in the energy transition. They are preparing their entire building portfolio to meet the targets of the Paris Climate Agreement targets by 2040.

The two universities house around 100,000 students, teachers, and support staff in a real estate portfolio of 650,000 m² which includes centuries-old inner-city buildings and historic monuments, see Figure 3.

Fig. 3 – Impression of the different types of University Buildings within the four campuses [3]

The different building styles and functions vary too - from laboratories and lecture halls to offices and student accommodation. It makes the transition to low-carbon buildings complex and challenging.

4. Results

The FastLane approach provided an overview across the entire portfolio of more than 50 buildings. In Figure 4 the energy consumption for a selection of buildings is presented including the target energy consumption for 2050.

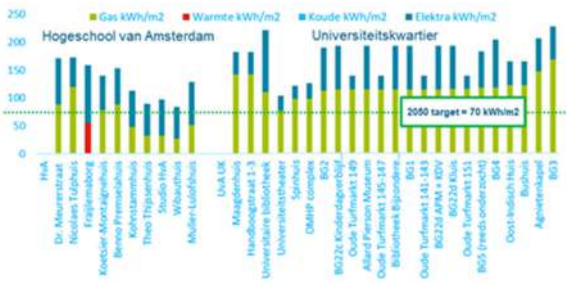

Fig. 4 – Baseline (2018) energy use of some buildings [1], [3].

After executing the first two steps of the FastLane process, a series of expert sessions with representatives from the university and partner organisations to discuss and identify appropriate measures and timings for implementation were held. Decisions were made at the level of individual buildings and the impact across the whole portfolio tracked. Through structured data collection, it was possible to adjust and optimize the plan when there were new insights.

The measures for a typically old and new building are presented in Figure 5 and Figure 6. Here we did calculate the CO_2 that should be reduced by the Paris Climate Agreement. To reach the remaining CO_2-emission reduction of 95%, the net supplier will need to make the electricity net more sustainable upcoming years.

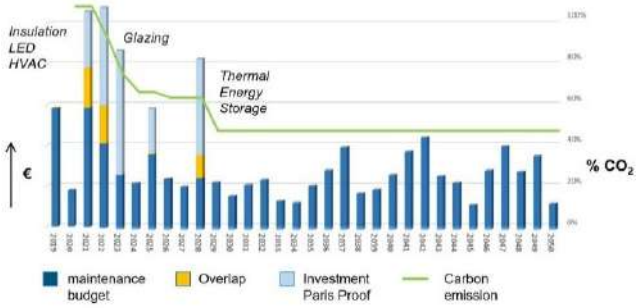

Fig. 5 – Yearly CO_2-emission reduction and required investments for a typical old building < 1800 [1], [3]. If we include indirect effects of net supplier, it will come close to 95% CO_2-emission reduction.

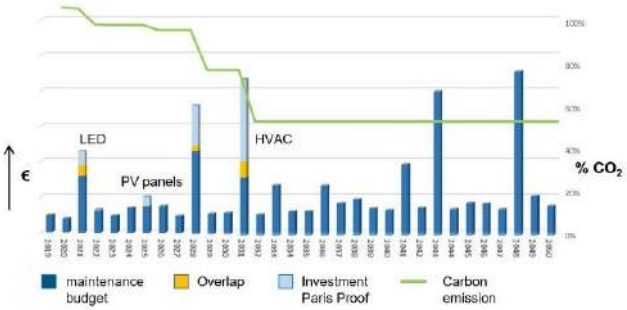

Fig. 6 – Yearly CO_2-emission reduction and required investments for a typical modern building > 2004 [1], [3]. If we include indirect effects of net supplier, it will come close to 95% CO_2-emission reduction.

An overview of the most effective energy saving measures is given in the Table 1. Here we see that especially the changing of energy source will bring a higher efficiency. This in combination with improving the insulation and windows in the façade, replacing the air handling Units and integrating LED lighting in the buildings.

Tab. 1 – Calculated results for different scenario's [3].

Measures	Reduction CO_2-emissions [ton/a]
Aquifer Thermal Energy Storage in combination with Heat Pump	950
New Air Handling Unit with Heat Recovery	350
New wooden frames with HR++ windows	300
Inside facade insulation	250
Replacement single glass windows with HR++ windows	125
Twincoil Heat Recovery in existing Air Handling Units	100
Replacement of TL by LED lighting	50

Typical and effective energy saving measures for older buildings are:

- Insulation of roof and facade
- Applying LED lighting including smart daylight and motion control
- Replacing and upgrading the Air Handling Units

For newer buildings applying LED lighting including daylight and motion controls and photovoltaic solar cells are effective measures.

All buildings will benefit from a newly developed Aquifer Thermal Energy System combined with heat pumps. Of course, the heating and cooling systems in the connected buildings need to be upgraded to low temperature heating and high temperature cooling.

The automatically generated result of all buildings together for the so-called scenario ''all electric'' is presented in Figure 7. The CO2 emission reduces every year until 2040. Here we did calculate the CO_2 that should be reduced by the Paris Proof agreement. The remaining CO_2 will be reduced by the net supplier of the electricity upcoming years.

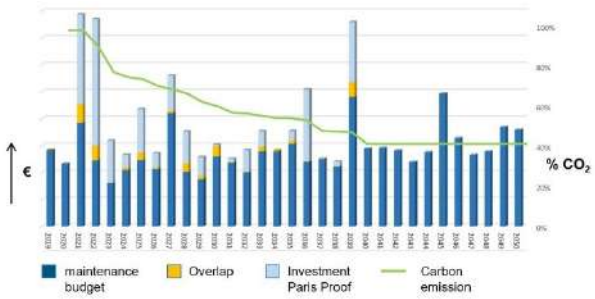

Fig. 7 – Yearly CO_2-emission reduction and required investments for building portfolio of campus 'Universiteitskwartier' [1], [3]. If we include indirect effects of net supplier, it will come close to 95% CO_2-emission reduction.

The results of the selected All electric scenario is presented next to 3 other scenario's that were evaluated in Table 2.

Tab. 2 – Calculated results for different scenarios.

Scenario	Reduction CO_2 emissions* [%]	Payback time [a]
Quick wins	5%	3
Business case	17%	25
All electric	37%	82
Max CO_2-reduction	44%	93

*The indirect effects of net supplier are excluded. If we include effects of net supplier, the All electric scenario will come close to 95% CO_2-emission reduction.

The University of Amsterdam and Amsterdam University of Applied Sciences developed their roadmap using the FastLane approach and now know the measures they need to take, the costs involved, have included them in their maintenance and investment plans and used this information in their energy roadmap report [2]. They are herewith one of the frontrunners in the Netherlands with a practical plan to realize energy transition targets for their building portfolio.

Additionally, by applying the FastLane approach they also completed 80% of the work to comply with Dutch energy legislation for the Energy Efficiency Audit (EED) and Information Requirement (EML) was completed.

5. Conclusions

- A new approach called FastLane, including a digital platform and database, is developed that enables building owners to plan, steer and monitor the energy transition of each building and the whole building portfolio.
- The resulting digital portfolio roadmap is fully secured in the building owner organization as an easily accessible, current, and living document with calculations fitted on the real energy usage and the flexibility to make changes and monitor the performance. Because all information is stored in a database it is easy to later make changes. In this way it is possible to make changes if this is needed for current and upcoming legislation.
- There is a big advantage of using real time energy in combination with energy performance. The effects of the measures can be checked with real-time energy meters. In this way it is possible to monitor the progress daily, monthly, and yearly. This is a great time saver compared to more theoretical approaches where for an update a new calculation is needed. In this way the first steps are made in the direction of energy management conform ISO 50001.
- Key in the approach is to gather and combine up-to-date information and knowledge: data in archives, data from on-site inspections, information of facility and maintenance managers and multidisciplinary expertise of consultants.
- Integration of measures in existing processes yields quality gains and savings. University buildings are being adapted continuously. Through DMJOP integration in these processes, higher savings can be realized in the realization costs.

- The Fastlane approach is successfully applied at the University of Amsterdam and Amsterdam University of Applied Sciences. It enabled this organization to:

    - update and archive data of the buildings, the use of the buildings and building services in a dynamic database that also allows automated analyses to select, plan and present the most effective CO_2-emission reduction measures. It provided a good overview and insight in the complex portfolio of buildings which was already very valuable;

    - develop and implement their dynamic energy transition roadmap, instantly calculating costs and the impact on energy use and CO_2-emissions;

    - Identify and select the measures that will realize the most CO_2-emission reduction each and in total together 1,850 ton: Aquifer Thermal Energy Storage in combination with Heat Pump; New Air Handling Unit with Heat Recovery; New wooden frames with HR++ windows; Inside façade insulation;

    - plan the implementation of different measures in line with natural moments of replacement and maintenance, which saved 20% in costs;

    - Organize and realize decision making by the board of the organization on ambition and budgets;

    - comply with legislation EU Energy Efficiency Audit (EED) and NL Information Requirement (EML).

6. Recommendations

The FastLane approach can be further improved and developed by expanding and keeping up to date of the database with benchmark energy data of different building functions and advised/applied measures.

Furthermore it is recommended to take notice of some lessons learned in the presented case and be prepared when applying the FastLane approach:

- Start with insulation and quickwins, the earlier you start the more CO_2 you can save;

- Trias energetica could be neglected if the aforementioned insulation measures are postponed and rising energy costs lead to faster sustainable energy generation;

- Plan the implementation of different measures in line with natural moments of replacement and maintenance. The number natural replacements until 2050 are scarce and may happen only once. The earlier you start, the more money, energy and CO_2-emissions you can save;

- Sustainable process knowledge and engineering is needed to turn a FastLane idea into an actual plan. This requires more from the operator than standard maintenance and additional expertise must be attracted for it. A balanced budget must also be abandoned within 1 year or the process must be arranged in such a way that in complex engineering assignments 20% of the preparation costs are released 1 or two years before the actual implementation;

- Collaborate with the building users to integrate their functional demands and achieve the highest perfomance of the energy saving measures;

- The approach consists of a tour of many complex buildings, but no detailed study of the BMS system. Some identified control measures were already implemented and others couldn't be implemented as stand-alone measures, but are part of a management contract with the major technical parties;

- Certain groups of measures have been found to be unprofitable after research or involve technical risks. Increasing room temperatures in MER/SER rooms resulted in the failure of UPSs and the application of an air scrubber requires much more than the indicators indicate;

- Implementation of insulation measures requires better real estate planning and are less suitable for inclusion in DMJOP because of the nuisance it entails. Many measures only have a natural moment during renovation and are postponed until then. Less is also possible according to monument care and well-being;

- Reserve enough time for preparation and execution and take some extra time into account for internal discussions on topics with more than one stakeholder and/or different opinions;

- Market developments must be translated

into budgets;

- Monitor the effect of measures and keep the digital dynamic roadmap up-to-date for maximum control on the energy transition of the building portofolio. Integrate this in your energy and building management system.

7. Acknowledgement

The execution of FastLane project for the presented case study was funded by University of Amsterdam and Amsterdam University of Applied Sciences.

8. References

[1] Verhoeven T., Case study: Digital Platform FastLane dashboard with projectnr. BG9341, December 20th 2019, [online] https://global.royalhaskoningdhv.com/projects/dynamic-roadmap-to-low-carbon-real-estate-for-amsterdam-universities

[2] Roadmap University of Amsterdam and Amsterdam University of Applied Sciences: https://student.uva.nl/binaries/content/assets/studentensites/uva-studentensite/nl/nieuws/routekaart-energietransitie-uva.pdf

[3] Verhoeven T., Boeters, R. Royal HaskoningDHV-Webinar: Strategical energy transition scenarios for a portfolio of buildings combined with regular maintenance and replacements - Case: University of Amsterdam and Amsterdam University of Applied Sciences. July 17th 2020.

[4] C. Menezes, A. Cripps, D. Bouchlaghem and R. Buswell. Predicted vs. actual energy performance of non-domestic buildings: using post occupancy evaluation data to reduce the performance gap. Applied Energy 97 (2012) 355-364.

[5] CarbonBuzz, website at www.carbonbuzz.org (last accessed January 13th 2022).

[5] TVVL, Dutch Green Building Council, WEii protocol - An energy efficiency indicator based on the actual energy use of a building, Version 1.1, March 2021, [Omline] https://www.weii.nl/english-5

Data Statement

The datasets generated during and/or analysed during the current study are not publicly available because of privacy of the client but could be made available in further consultation to the client.

Total Cost of Ownership of Sensor Faucets in Commercial and Healthcare Construction

Marie Patterson [a], Blake Wentz [b], Tim Wentz [c]

[a] Faculty of Construction Management, California State University, Chico, Chico, CA, United States, mepatterson@csuchico.edu

[b] Dean of the College of Engineering, Computer Science and Construction Management, California State University, Chico, Chico, CA, United States, bwentz@csuchico.edu

[c] Professor Emeritus of Construction Management, University of Nebraska-Lincoln, Lincoln, NE, United States, twentz1@unl.edu

Abstract. Owners who are pursing the construction of new commercial and healthcare buildings are very interested in the sustainability, energy efficiency, life cycle costs and cleanliness of their proposed projects. Owners are requiring designers and construction companies to develop innovative strategies to lower their utility use and total cost in their projects. One area of opportunity to meet this owner need is the decision to use either battery-powered or hardwired restroom faucets. Several construction projects of various types and locations were analyzed to determine the total cost of ownership of both types of faucets over a 12-year and 25-year timeframe. The results of the unit cost calculation showed that the battery-powered faucets had a lower cost of ownership at 12 years, while hardwired fixtures installed in intervals of six had the lower cost of ownership over 25 years. Although, when researching actual construction projects, where installation of multiple faucets in a row isn't realistic, battery-powered faucets had the lower cost of ownership over the hardwired options in both the 12-year and 25-year timeframes in all building types.

Key Words: Sustainability, Life Cycle Cost, Energy Efficiency, Water Efficiency, Plumbing.
DOI: https://doi.org/10.34641/clima.2022.117

1. Introduction

Owners who are engaged in building new commercial and healthcare projects have many different requirements and expectations for their projects. These requirements and expectations must be met if the project is to be successful for both the owner and the designers. As owners are the key stakeholder for construction projects in this market, it is critical to identify their ultimate needs within the building (Alshubbak, Pellicer, Catala, & Teixeira, 2015). Many owners are concerned about energy efficiency and interested in strategies to reduce their operational costs. A study by Gliedt and Hoicka in 2015 showed that many owners/property managers were motivated by economic return and made technology and funding decisions based at least in part on the expectation of direct or indirect economic returns.

The commercial building sector in the United States consists of 93 billion square feet of real estate and accounts for 18% of U.S. primary energy use (U.S. Energy Information Administration, 2020). Based on the building size, the decisions owner's make during the design stage can have substantial impacts on energy use, and their maintenance costs after construction. Depending on the building type and expected occupants, different buildings have different needs to be met. In recent years owners have become more knowledgeable in the sustainability, energy efficiency, life cycle costs, and ease of maintenance of their buildings. The increased prevalence of rating systems such as Leadership in Energy and Environmental Design (LEED), Energy Star, and American Society of Heating, Refrigeration and Air Conditioning Engineers (ASHRAE) Building Energy Quotient (bEQ) have shown that owners are making energy and water efficiency a requirement of their projects more common.

One option that is often investigated in commercial and healthcare projects is the decision to use faucets with sensing technology with either battery-powered or hardwired power supplies. Faucets with sensing technology allow for water savings as the faucets automatically shut-off the flow of water while the faucet is not in demand. In addition to water saving technology, faucets with sensors also provide a hands-free operation, which helps reduce the spread of disease and viruses (Sloan, 2011), especially important in healthcare.

William Sloan patented his flushometer style toilet flush valve in 1906, which revolutionized the plumbing industry by reducing water and energy

Copyright ©2022 by the authors. This conference paper is published under a CC-BY-4.0 license.

without the need of a tank. Plumbing manufacturing companies have continued to improve and introduce new technical innovations in their products. Companies such as Sloan Valve Company (Sloan), Delta Faucet Company, and Kohler Company offer a variety of products such as faucets with hands-free sensing technology with battery-powered operation and power-harvesting technologies, such as solar and inline water turbine products. The variety of products give designers of new construction projects many options in function, aesthetics, upfront cost, energy efficiency, and water efficiency.

Sensing faucets require some form of power supply, typically battery or hardwired, to operate an internal solenoid valve to turn on and off the flow of water. Each option has its advantages and disadvantages, and each is prevalent in projects worldwide. Battery-powered faucets reduce the up-front cost of coordination and installation by eliminating the electrical wiring to the device. Battery technology is constantly evolving which has led to improved battery life, extending the time between battery replacement, therefore lowering the maintenance cost of these systems. Many owners continue to prefer the hardwired faucets because of the reliability, reduced maintenance, and perception that this will lead to lower maintenance expenses. This study investigated which of these two options had the lower total cost of ownership over the estimated lifespan of the faucet to help owners make more informed decisions.

One of the key benefits of sensing faucets according to manufacturers is the water efficiency achieved (Sloan, 2011). Non-sensing faucets are turned on manually by the occupant while starting to wash one's hands, while continue to run while lathering, when the water is not in demand. Sensing faucets automatically sense an individual's hand placement and turn the water on and off based on the integrated sensor. While each use may save only a small amount of water, when this is multiplied by multiple faucets uses each day per occupant, over many days, the amount of water saved can be substantial.

However, studies have been done to determine if sensor faucets are actually more efficient than manually operated faucets. One such study by the ASHRAE that investigated the energy efficiency of photovoltaic water heaters showed that when the researchers switched their faucet configuration from a manual faucet to a sensor faucet, average daily hot water volume increased 58% (Fanney, Dougherty, & Richardson, 2002). Another study at the Millennium Dome in London over a one-year period showed that the manual faucets used significantly less water, roughly half, than an infrared sensor faucet (Koeller, 2012). Both studies indicate a water and energy savings by using a manual faucet, contradicting manufacturer's claims.

Another key benefit of sensing faucets is the hands-free benefit that decreases the transmission of disease and viruses (Sloan, 2011), especially of importance during recent pandemics. Although users often believe flush handles are the dirtiest touch point in a restroom, sink areas are usually more germ-laden, as this is where bacteria are shed from hands during washing (Lozier, 2016). This was further studied by Kurgat et al. (2019) that showed in an office building the most contaminated areas of the building were the refrigerator, drawer handles, sink faucets, the push bar on the main exit of the building, and the soap dispensers in the women's restroom.

When analyzing the faucet's life cycle, the estimated life of the products installed must be taken into consideration. Product life cycle cost includes three primary phases: production, use and final disposal (Kalbusch & Ghisi, 2016; Gnoatto, Kalbusch, & Henning, 2019). For production, the analysis should involve the manufacturing of the faucets in both scenarios, and the amount of conduit and wiring compared to battery production. For the use phase, the analysis should include maintenance and operation (evaluated as part of this study), in addition to the energy use and battery cost. For the disposal phase, the analysis should include disassembly and recycling of the electrical wire and conduit compared to battery disposal. Batteries, depending on the type, can be easily recycled, or taken to a manufacturer for recycling. All phases would ultimately include the evaluation of water consumption, energy consumption and global warming potential for all manufactured components (Gnoatto et al., 2019).

The total cost of ownership of different construction materials relates to the interest of owners in energy efficiency. There have been studies on individual components, such as a 2014 study by Mader and Madani, that showed the total cost of ownership of various control systems for an air-water heat pump. Manufacturers of plumbing fixtures list varying advantages of their products, such as ease of use, reduced maintenance, as well as energy efficiency. But after reviewing the literature there are no peer reviewed studies on the total cost of ownership of battery-powered vs. hardwired faucets.

2. Research Methods

The researchers partnered with Sloan Valve Company to evaluate their faucets for the purpose of comparing different faucet power applications in order to identify any significant differences in installation costs and applications. The goal of this research is to help clients make informed decisions on the best products for their building projects in terms of the total cost of ownership.

Sloan Valve Company identified which models of faucets were most popular in terms of use and provided the product data sheets on these items. Sloan Valve Company also provided the preventative maintenance frequency for individual components,

replacement part costs, typical life span, and recommended battery replacement. The researchers and Sloan determined that the following products would be used for this study based the popularity of use based on historic sales for the corresponding building types of the study:

- Sloan Optima Sensor Faucet EBF-425 AA battery-powered (optional turbine) with underdeck mounted manifold
- Sloan Optima Sensor Faucet EAF-350 6V battery-powered with integral temperature mixer
- Sloan Optima Sensor Faucet ETF-420 wired
    - Hardwired with transformer
    - Hardwired for plug-in
- Sloan Basys Sensor Faucet EFX-275 solar-powered

The researchers evaluated the total cost of ownership in common types of buildings that Sloan faucets were often installed, commercial office and healthcare buildings. In order to gather the project information, the researchers enlisted a variety of construction firms, including General and Mechanical Contracting companies in the United States to participate in the data collection for this research. Companies were recruited from different geographic areas of the United States in order to get a cross-section of projects. The firms that participated in the study were Turner Construction Company, Mortenson Construction Company, DPR Construction Company, JF Ahern Company, and Southland Industries.

Each company was asked via email to participate in the study, and a conference call was followed up to confirm the request and to discuss timeline expectations and project deliverables. The firms were asked to provide the researchers at least two projects in both a commercial and healthcare category for evaluation. They were asked to provide the design drawings and documents and upload through a cloud-based folder structure. The researchers requested a variety of projects in terms of size, scope and geographic location, but no other parameters were given. The construction documents were received, and the researchers then evaluated each project submitted for inclusion in the study.

For the installation costs, the installation instructions provided by Sloan were reviewed, and the researchers consulted with the mechanical and electrical contracting firms to develop the steps and materials necessary for installation. The labor hours were then calculated from the installation steps to ensure the total cost of installation was captured. Since the plumbing of hot and cold-water supply was the same for all faucets, the labor and material cost was not included in the researchers study. Table 1 shows the installation steps necessary between the different types of faucets evaluated.

The installation of all battery-powered faucets included the labor for plumbing skilled trades' people for the installation of the faucet and activation of the sensor. No electrical hours are included, as an electrician is not required for the installation of battery-powered faucets.

The installation of all hardwired faucets required electrical tradespeople for the rough-in electrical work, including running conduit and wire from the closest electrical panel to near the location of the faucet. The electrician also had finish work to complete once the drywall was completed to complete the hardwiring for the transformer model or install the electrical outlet for the plug-in model. For the transformer wired faucets there is the opportunity to power up to six faucets from one transformer, reducing the per faucet installation costs when intervals of six faucets were installed. For the plug-in faucets there is also the opportunity to daisy-chain up to six faucets together to plug into one outlet, also reducing the cost per fixture. The plumbing trade also was required to set the faucet and sensor activation unit.

For the maintenance costs, the data provided by Sloan identified the timeframes, parts, and costs for the recommended maintenance of the faucets. The recommended battery replacement was every three years for normal-use restrooms for battery-powered faucets; every six years for the solar-powered faucets; and every ten years for hardwired fixtures that had a battery backup. Each faucet was evaluated over a 12-year and 25-year maintenance period to determine if length of operation affected the total cost of ownership.

The labor hour durations for installation and maintenance requirements were estimated by the mechanical and electrical contracting firms. The U.S. national average labor rates were used as provided by the Mechanical Contractors Association of America (MCAA) and the National Electrical Contractors Association (NECA). Union plumbers were assumed for installation of the faucets, activation of the sensors, plug-in of wired faucets, and all preventative maintenance and repair items.

Tab. 1 - Installation steps of primary faucet types

Installation Steps	Battery Deck Mount and Solis	Battery Underdeck Mount	Hardwired Transformer	Hardwired Plug-In
Install conduit and wiring from panel to transformer	-	-	X	X
Install transformer and wiring to faucets	-	-	X	X
Surface mount control box and connect faucet wires	-	X	X	X
Connect control box cable to faucet	-	X	X	X
Install battery pack	X	X	-	-
Activate sensor	X	X	X	X

Union electricians were assumed for the installation of all conduits, wiring, and transformers required for the hardwired option. The battery replacement was assumed to be by custodians. There was no shared time savings to perform maintenance and battery replacement simultaneously as it was determined that these are typically different maintenance tasks performed by different trades.

Material costs were provided by the electrical contractors based on large project pricing and battery costs were provided by Amazon. Maintenance and labor costs did not take into account inflation, escalation or wage rate increases. Sloan provided the faucet and replacement part costs.

The researchers then calculated the total cost of ownership of the various faucets in both an individual analysis to determine unit cost, as well as cost per each building project. This allowed for total and average costs per building type for comparison purposes. For the quantity take off the researchers used a PDF reader and excel spreadsheet to keep track of each restroom and faucet. Electronic dots were used to mark each item as taken off. Different colors of dots were used to identify gender counts; red for women, blue for men, and lavender for individual or unisex restrooms. Each project had quantities taken off calculating the total number of restrooms for both women, men and unisex, and also the number of faucets in each women's restrooms, men's restrooms, and individual unisex restrooms. For the wired fixtures, if there were two restrooms that shared a wall with one another, and the faucets were both on either side of the wall, similar to shown in Figure 1, those faucets were identified as sharing a transformer or outlet to identify installation costs savings; instead of individually wired faucets. Figure 1 also shows one of the ideal layouts for a restroom to maximize the installation efficiency of the hardwired faucets. The preferred restroom would either be three faucets back-to-back as shown, or six faucets in a row.

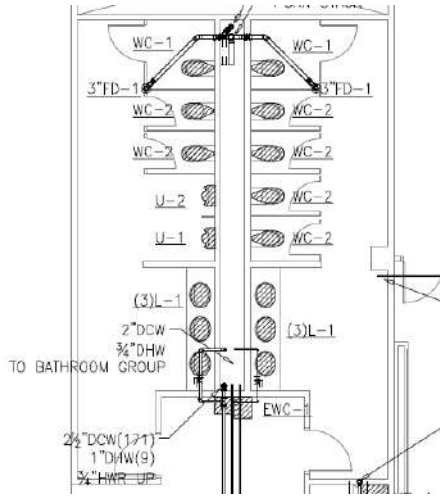

Fig. 1 - Ideal restroom of three faucets back-to-back to maximize hardwire configuration.

3. Results

A total of thirteen projects were submitted by the partnering contracting firms for use in this study. There were seven healthcare buildings and six office buildings submitted and all were included in this study. Of the healthcare buildings, four are located in Wisconsin, two in California, and one in Illinois. For the office buildings, four are located in Wisconsin and two in California.

While evaluating the installation steps, it was discovered that for both battery-powered and hardwired faucets, there were multiple installation options that could affect the cost. For the battery-powered faucets the battery pack could be either deck mounted (above the countertop) or underdeck mounted (under the countertop). Both options were evaluated. For the battery-powered faucets there is an option for an internal turbine that can be used to generate power and that option was also evaluated.

For the hardwired faucets, each faucet could be wired using a plug-in power connector that could be daisy chained together, or a bank of up to six faucets could be hardwired together in series with a

transformer. Both of the options varied the electrical installation and were therefore evaluated. There was also the option to have hardwired faucets include a battery back-up, or not. Owners may want this option to have an additional power source in the event of a power outage. After consulting with Sloan, they stated that most owners want the battery back-up as a safety measure. The only way to offset this issue would be to make sure that the circuit the faucets were connected to were tied to an emergency generator, or other form of back-up power. Based on this discussion, the unit rate cost for hardwired with no battery-backup was calculated and found to be most advantageous over 25 years, but the estimated installed costs still did not outperform the battery-powered faucets.

The quantity take-offs for each building were completed and all maintenance costs were tabulated for each option on each project. Table 2 shows the results of the total cost of ownership for each faucet option in a 12-year timeframe as well as a 25-year timeframe for office building projects. Table 3 shows the total cost of ownership for healthcare buildings.

The data shown in Table 2 shows that the total cost of ownership is lowest for deck mounted, battery-powered faucets compared to all other styles. Generally speaking; the traditional battery-powered faucets are the most cost effective in all applications except for the SOLIS solar-powered faucet and the SOLIS turbine option. It is interesting to note that the two SOLIS faucets become the most expensive option at the end of the 25-year period. This is due to the high cost of replacement parts for the solar components and turbine at the end of the maintenance period.

Tab. 2 - Total cost of ownership for faucets in office building projects.

Faucet	Average Count per Project	12-Year Total	25-Year Total	Percent Increase 12-Year	Percent Increase 25-Year
Battery – AA Deck Mount	38	$39,420.82	$62,089.34	-	-
Battery – AA Underdeck	38	$39,873.78	$62,542.30	1.011	1.007
Battery – SOLIS	38	$43,903.68	$68,073.96	1.114	1.096
Battery – Turbine (SOLIS)	38	$43,980.06	$68,150.34	1.116	1.098
Hardwired – Transformer	38	$45,601.16	$65,032.08	1.157	1.047
Hardwired – Plug-in	38	$45,743.38	$65,174.30	1.160	1.050

Tab. 3 - Total cost of ownership for faucets in healthcare building projects.

Faucet	Average Count per Project	12-Year Total	25-Year Total	Percent Increase 12-Year	Percent Increase 25-Year
Battery – AA Deck Mount	70	$72,172.70	$113,674.84	-	-
Battery – AA Underdeck	70	$73,002.00	$114,504.14	1.011	1.007
Battery – SOLIS	70	$80,380.05	$124,631.65	1.114	1.096
Battery – Turbine (SOLIS)	70	$80,519.88	$124,771.49	1.116	1.098
Hardwired – Transformer	70	$90,856.05	$126,430.70	1.259	1.112
Hardwired – Plug-in	70	$92,861.00	$128,435.65	1.287	1.130

For healthcare projects as shown in Table 3, the total cost of ownership for deck mounted battery-powered faucets is lower than that of other battery and hardwired applications when compared during both the 12-year and 25-year timeframe, which is the same as what was found for the office building projects. Also, the same phenomenon of having the SOLIS faucets become the most expensive at the end of the 25-year period also presents itself in this building type. But when comparing the two building types, the total ownership cost per faucet is almost identical within each faucet type.

Results show that over a 25-year timeframe that hardwired sensors showed a total cost of ownership of less than 1.047-1.287% from the lowest battery-powered faucet.

4. Conclusions

The results show that the deck mounted and underdeck battery-powered faucets have a slightly lower cost of ownership over the life of the product compared to hardwired faucets and the SOLIS faucets. There are significant up-front costs for

installation for the hardwired faucets because of the electrical conduit and wiring, which is not present in the battery-powered fixtures. The overall maintenance cost for the battery faucets is not significantly more than that of the hardwired faucets, with the exception of the SOLIS units, and over the life of the faucet this is not enough to overcome the additional upfront installation costs of the wiring.

Ultimately, it is up to the owner to determine their project needs and communicate them to the designers and contractors. They should understand the potential use requirements as to whether battery-powered or hardwired is more beneficial based on the use of their building and intended occupants. The estimated life of the building is critical component of the analysis and, additionally, whether the initial additional costs are worth the reduced maintenance and inconvenience after construction is complete.

Owners of healthcare and commercial construction projects can be well informed by the results of this study to allow them to make informed decisions about which types of faucets will produce the lowest total cost of ownership. There are many owners, architects, and construction firms that may intuitively believe the total cost would be lower by selecting the hardwired options, and they may be giving inaccurate advice believing that the maintenance costs of the battery-powered and specifically the battery replacement would eventually have a higher total price. The results of this study indicate that owners of these types of projects should select a deck mounted, battery-powered faucet for all of their bathrooms to achieve the lowest cost of ownership. Based on the unit cost, owners wishing for hardwired fixtures should coordinate and request designers to maximize the installation of six, or multiple, faucets to minimize the installation costs as much as possible.

One item that was raised during the research was the variability in how owner's facilities staff monitor the battery-powered faucets for maintenance during the life of the product. After further research, it was found that sensors on the faucets have an indicator light to notify facilities staff that a battery is weakening and needs to be replaced. This is up to the staff proactively monitor the fixtures so that batteries are replaced before failure. This will require additional training for the custodial staff to not only monitor the faucets, but also how to properly replace the batteries. This study assumed all custodial staff were trained, followed the recommended replacement procedures and did so in a timely manner. Failure to do so could result in non-operational faucets, increase total costs, and may change the results of the study. Future research can be conducted to study the level of understanding of custodial staff in these procedures as well as their effectiveness and associated costs in how they are currently maintaining their faucets.

Another area of possible future research would be to investigate the actual use of the faucets to determine if the recommended maintenance schedules and battery replacement provided by the manufacturer are indeed accurate. The methodology used in this study did not account for actual use, and some buildings may be high-use, or low-use and that could cause the maintenance and battery life to increase or decrease accordingly. Future research could also be conducted on various other building types such as educational facilities, and athletic facilities to see if the conclusions of this study are valid for those building types. Remodel projects also were not investigated as part of this research, and future research on these types of projects may indicate different results because of the unique constraints of those projects.

A final item that could be investigated is the life cycle analysis and costs of the faucets. This project only investigated the total cost of ownership to the owner of the building project, but life cycle costs include additional costs of the product that could have impact to the client as well as to the community. A study could be done to determine these additional costs as well as the environmental impacts to determine the true overall impact of these devices.

5. Acknowledgement

Sloan Valve Company provided manufacturing data and costs. The general, mechanical and electrical contracting companies listed in the report provided installation and maintenance costs and methodologies.

6. Data Access Statement

The datasets generated during and/or analysed during the current study are not available because of privacy restrictions from building project owners but the authors will make every reasonable effort to publish them in near future.

References

Alshubbak, A., Pellicer E., Catala, J., & Teixeira, J. (2015). A model for identifying owner's needs in the building life cycle. *Journal of Civil Engineering and Management* (pp. 1046-1060).

Fanney, A., Dougherty, B., Richardson, J. (2002). Field Test of a Photovoltaic Water Heater. *ASHRAE Transactions*, [online], https://tsapps.nist.gov/publication/get_pdf.cfm?pub_id=860840 (Accessed January 5, 2022).

Kalbusch, A., & Ghisi, E. (2019). Energy consumption in the life cycle of plumbing fixtures. *Water Supply,* 19, (pp. 70–78). doi: https://doi.org/10.2166/ws.2018.053

Kalbusch, A., & Ghisi, E. (2016). Comparative life-cycle assessment of ordinary and water-saving taps. *Journal of Cleaner Production*, 112, (pp. 4585–4593). https://doi.org/10.1016/j.jclepro.2015.06.075

Koeller, J. (2012). More or Less? Studies Find that Actual Results Contradict Efficiency Claims About Sensor-Activated Valves. *Official*, Volume 34, Number 4, (pp26-27).

Kurgat, E., Sexton, J., Garavito, F., Reynolds, A., Contreras, R., Gerba, C., Leslie, R., Edmonds-Wilson, S., Reynolds, K. (2019). Impact of a hygiene intervention on virus spread in an office building. I*nternational Journal of Hygiene and Environmental Health*, Vol. 222, Issue 3, pp. 479-485

Lozier, Paige. (2016). Electronic Sensor Faucets Improve Hygiene and Conserve Water in Commercial Restrooms. *Architect*, Vol. 105, Issue 1, pp. 74-77.

Mader, G. and Madani, H. (2014). Capacity control in air-water heat pumps: Total cost of ownership analysis. *Energy and Buildings*, Volume 81, pp. 296-304.

Gliedt, T. and Hoicka, C. (2015). Energy updates as financial or strategic investment? Energy Star property owners and managers improving building energy performance. *Applied Energy*, Volume 147, pages 430-443.

Gnoatto, E. L., Kalbusch, A., & Henning, E. (2019). Evaluation of the environmental and economic impacts on the life cycle of different solutions for toilet flush systems. *Sustainability (Basel, Switzerland)*, *11*(17), 4742–. https://doi.org/10.3390/su11174742

Gonçalves, F., Kalbusch, A., & Henning, E. (2018). Correlation between water consumption and the operating conditions of plumbing fixtures in public buildings. Water Science & Technology. *Water Supply*, 18(6), (pp. 1915–1925). https://doi.org/10.2166/ws.2018.013

Sloan Valve Company. (2011). The battery balancing act - technology vs. application needs. White Paper [online], https://sloan.com/resources/education/white-papers/battery-balancing-act-technology-vs-application-needs (Accessed November 15, 2021).

U.S. Energy Information Administration (2020). Annual Energy Outlook 2020. [online] https://www.eia.gov/outlooks/aeo/ (Accessed January 2, 2022).

Concise cycle test methods to evaluate heating/cooling systems with multiple renewable sources

Robert Haberl [a], Maike Schubert [a], Thibault Péan [b], Iván Bellanco [b], Francisco Belio [b], Jaume Salom [b], Daniel Carbonell [a]

[a] SPF Institute for Solar Technology, OST Eastern Switzerland University of Applied Sciences, Switzerland, Robert.Haberl@ost.ch.

[b] Catalonia Institute for Energy Research (IREC), Spain, jsalom@irec.cat.

The goal of the project TRI-HP is to develop systems based on electrically-driven natural refrigerant heat pumps coupled with photovoltaics to provide heating, cooling and electricity to multi-family buildings with an on-site renewable share of 80 %. The implementation of different energy sources for such a system often leads to a complex architecture of the overall system. The performance evaluation of such systems is not trivial and cannot be done via steady-state measurements of individual components. Instead, dynamic measurements using the hardware-in-the-loop approach are performed to test the performance of the newly developed systems. A method called concise cycle test (CCT) has been developed for this purpose. This method was adapted to the systems to be tested and applied in different versions. The CCT method is based on the selection of several representative periods of the year, and shows the behaviour of a complete system for heating and cooling under relevant conditions in these periods, enabling then to extrapolate the results for a whole year operation. Two different approaches were used to select the test sequence. For the measurement of a dual source/sink system, the annual weather data were divided into four clusters, from each of which representative days were selected. For the solar-ice-slurry system, a single, contiguous test cycle of typical days from throughout the year was selected. This allows both, to test the functionality of the ice-slurry storage and the advanced energy management strategies by performing experiments only on selected days. For the tests, the complete system including a heat pump and thermal and electrical storages are installed on a test rig. The test rig emulates a building, including the space heating and cooling distribution system, the domestic hot water draw offs, the solar collector field or ground heat exchanger depending on the system tested and the photovoltaic installation. The system tested must act completely autonomously to cover the demand for heating and cooling of the building and the draw-offs during a test cycle. In this work, the methodology has been applied to two different cases of complete systems adapted to different climates (Switzerland and Spain).

Keywords. hardware-in-the-loop, emulation, whole system test, test cycle, heat pump.
DOI: https://doi.org/10.34641/clima.2022.390

1. Introduction

1.1 H2020-TRI-HP

The overall goal of the TRI-HP project is the development and demonstration of flexible energy-efficient and affordable trigeneration systems. The systems are based on electrically driven natural refrigerant heat pumps coupled with renewable electricity generators (PV), using low temperature thermal and/or electrical storages to provide heating, cooling and electricity to multi-family residential buildings with a self-consumed renewable share of 80 %. The innovations proposed should reduce the CAPEX system cost by at least 10-15 % compared to current heat pump technologies with equivalent energetic performances. Two natural refrigerants with very low global warming potential, propane and carbon dioxide, are used as working fluids. Two system concepts were developed for two different combinations of heat sources for the heat pumps, i) dual ground/air source/sink and ii) solar with ice-slurry as intermediate storage. These two concepts combined with the two heat pump types developed (CO_2 and propane) lead to three complete systems (CO_2-ice, propane-ice and propane-dual) that are being tested in the laboratory.

1.2 Purpose and general procedure of the Concise Cycle Test

Copyright ©2022 by the authors. This conference paper is published under a CC-BY-4.0 license.

The implementation of different energy sources for systems for space heating (SH), space cooling and domestic hot water (DHW) preparation often leads to a complex architecture of the overall system. The efficiency of the resulting system is highly dependent on dynamic operating conditions due to transient on/off cycles, component interactions, thermal storage, hydraulic designs, overall system control, and other factors. Performance evaluation of such systems is not trivial and cannot be done via steady-state measurements of individual components. For this reason, the Concise Cycle Test (CCT) [1,2,3] as a hardware-in-the-loop approach was developed at the institutes SPF and IREC.

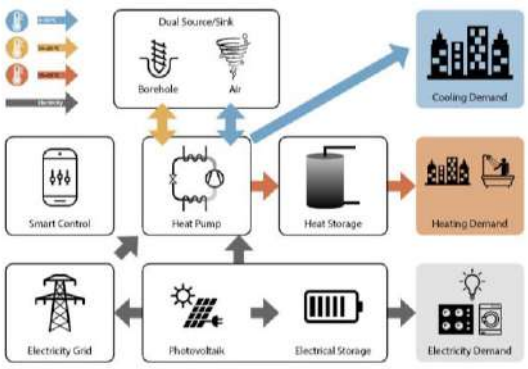

Fig. 1 - *Dual source/sink system*: ground/air system concept for cooling-dominated climates

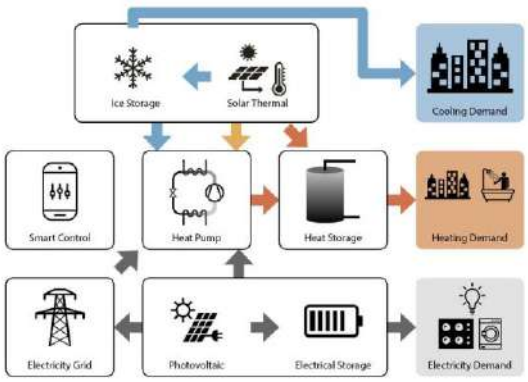

Fig. 2 – Solar-ice slurry system (CO_2 and propane HP): solar-ice-slurry system concept for heating-dominated climates.

The CCT shall show the behaviour of a complete system for heating and cooling under real-life conditions at different days of the year. In TRI-HP, the functionality of an ice-slurry storage will be tested in the system test as well as an advanced energy management (AEM) control developed within the project. Therefore, the complete system will be installed on a test rig. The test rig emulates a building, including the SH and cooling distribution system, the DHW draw offs, the solar collector field and the photovoltaic (PV) installation. The system under test must act completely autonomously to cover the demand for heating and cooling during a test cycle. This test cycle is composed of a number of representative days of a real year, which vary from four to seven depending on the goal of the test, e.g. benefits of the advance energy management system or quantification of the yearly energetic efficiency. The selected days are put together to a consecutive test-cycle.

1.3 Procedure for online simulation and emulation

Emulation can be based on load files or on real-time online simulations. In order to emulate a realistic response that is dependent on the behaviour of the tested system, real-time online simulations are used to calculate the behaviour of the components interacting with its environment. The emulated components are: solar thermal collectors, PV field, the building with the heating and cooling distribution systems and the ground source heat exchangers.

The procedure for simulation and emulation can be described as follows: at the end of each simulation/emulation time step, measured values are passed from the test bench control software to the system simulation software. Based on these values, the simulation software is simulating the response of the emulated device for the next time step and returns the result to the test bench control software, which controls the emulation of the emulated time step at the beginning of the next time step. Meanwhile, the simulation software pauses and waits for the next input of measured values from the test bench control software. The input data for the simulation is then based on measurements that were acquired before the emulated time step. The actual values may deviate from those values during the current time step. In order to minimize the error resulting from this deviation, the time steps of the simulation shall not be larger than 2 min. Components whose behaviour is independent of the rest of the system are implemented using predefined load profiles: a draw-off profile for the DHW consumption and a household electricity profile.

2. Tested systems and boundary conditions of climate and load

2.1 Overview

As described above, the newly developed systems are aimed for different climatic conditions. Concept schemes of the systems are shown in Fig. 1 and Fig. 2. In the TRI-HP project, prototypes of the most important new developments of individual components of the system were built and measured individually. The prototypes were sized for laboratory-scale measurements. The main developments are related to the heat pumps including the innovative natural refrigerant based circuits with the new heat exchangers as well as the advance energy management of the complete system.

This chapter describes the assumed annual climate data and electrical and thermal demands of the final applications as well as the load adjustments done in

order to to measure a functional overall system at laboratory scale.

2.2 Dual source/sink system

The dual source heat pump is able to use both a ground source heat exchanger and the ambient air as heat source (or sink), and can provide both, heating and cooling depending on the season. The system is completed by thermal storages, photovoltaic panels and a battery for the electrical part (Fig. 3).

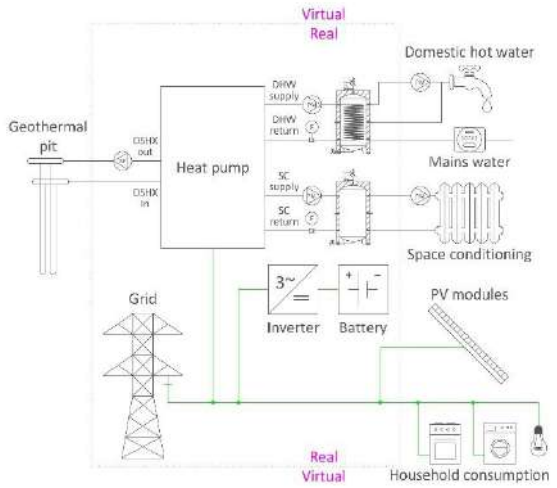

Fig. 3 – Sketch of the hydraulic and electrical components of the system test of the dual source/sink system.

A renovated building in the city of Tarragona, Spain was defined for this system. This climate zone represents a significant cooling load. Furthermore, the renovated version of the building corresponds to the current standards of the Spanish Building Code, which is in force for all new constructions. The weather for Tarragona was retrieved from the software Meteonorm, which produces a typical year file based on historical records from official weather stations covering the years 1991 to 2007. The yearly average temperature is 17.4 °C, while the yearly total horizontal irradiation sums up to 1665 kWh/m².

Apart from the weather, different profiles of occupancy have been implemented in the modelling environment. The internal gains from occupants, lighting and equipment are defined from the CTE (Spanish Building Code) [4]. Considering these assumptions, the peak heating load of the building amounts to 43.9 kW, while the peak cooling load amounts to 28.3 kW. The DHW tapping profile is generated with the tool DHWcalc [5] that enables to distribute the DHW load stochastically, keeping a certain pattern and a global energy demand corresponding to the number of families in the building. The electricity consumption from appliances (not considering HVAC) is also generated as a 10 minutes stochastic profile, with a peak load of 44.7 kW (99 % percentile at 29.5 kW).

2.3 Solar-ice-slurry system

The solar-ice-slurry system uses solar thermal energy as a source for the heat pump as well as to partly cover the heating and DHW demands directly. When possible, the solar energy is stored in an ice slurry storage, which serves as a source for the heat pump when solar radiation is not available. Additionally, a PV plant delivers electricity for the heat pump and the household electricity and a battery is included to reach the goal of 80 % renewable onsite share.

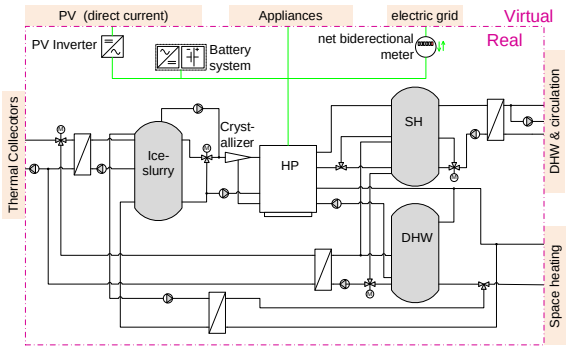

Fig. 4 – Sketch of the hydraulic and electrical components of the system test of the solar-ice-slurry system.

For selection of days, weather conditions of the city of Bern are chosen. Bern represents the dense populated Swiss midlands with rather cold winter and foggy periods. The SIA weather data is used, which is based on the standard SN EN ISO 15927-4 to generate a collection of so-called Design Reference Years. This collection is based on measurement data from the years 1984 to 2003. It contains weather data of 40 different locations in Switzerland, each with an extreme warm, an extreme cold and a normal design reference year as described in [6]. In order to be able to analyze the cooling potential in the system tests, SIA-warm weather data is used. The average ambient yearly temperature for warm weather data in Bern is 12.3 °C and the yearly total horizontal irradiation is 1230 kWh/m².

Other boundary conditions are the user profiles for household electricity, DHW consumption and internal gains in the building due to the presence of the people themselves and the equipment and lighting used. Individual profiles of each household were obtained from the load profile-generator [7] tool for a total of 6 apartments.

2.4 Scaling of laboratory systems

The dual source heat pump prototype has a nominal thermal capacity of 10 kW, compared to 44 kW needed for the multi-family building of Tarragona, therefore the scaling factor is around 4.5. All boundary conditions have been scaled down with this factor, notably the building floor area and capacity, the DHW and household electrical demand profiles. The capacities of the thermal storages have also been reduced accordingly. In the case of the electrical systems, the electrical cabinets present in the lab are also limited to 7.5 kW, therefore the scaling factor is slightly higher in that case, and these systems are a bit undersized relatively to the rest of the systems.

The final sizes of the systems to be tested in the lab are summarized in Tab. 1.

The retrofitted multifamily building in Bern (MFB90) serving as the load case for the solar-ice-slurry system has about 50 kW heating capacity. The size of the building (building capacity, floor and roof area and as a result the heating demand), all additional demands (DHW, household electricity) as well as internal gains and sizes of the energy system (ice storage, thermal collector field area, PV area, battery) have been sized to one fifth of the initial size of the reference system. As roof space is limited, and solar-thermal collectors and PV are both used in the ice-slurry system, the PV field is distributed to the roof and the southward directed façade. In this case 60 % of the PV modules are on the roof and 40 % on the façade. The sizes of the system tested within the system test are summarized in Tab. 1.

Tab. 1 - Summary of the component sizes for both systems tested in the system test.

		dual source	ice-slurry
Heat Pump	[kW]	10	10
DHW storage tank	[l]	500	1000
SH storage tank	[l]	300	600
Battery capacity	[kWh]	10	7
PV plant	[kWp]	7.5	8.2
Solar thermal	[m²]	-	33.3
Ice-storage tank	[m³]	-	2

The yearly simulations of both the scaled system and the original system were compared and resulted in the same yearly energetic efficiency. From the scaled simulation, the days for the system tests were selected. In order to test the system in the test rig the ice storage was scaled down to a size of 2 m^3 in order to represent its behaviour as seasonal storage in a seven day test. The ice storage will be emulated first and installed as a prototype within the test rig in the system test in a later stage.

3. Selection of periods

3.1 Overview

This chapter presents two different methods for determining test sequences for system testing. The different methods are necessary because of the characteristics of the systems or the components used: The measurement of a system with intelligent controller, which makes a prediction for the next 24 hours based on the current boundary conditions, requires a continuous sequence with weather data with a fluctuation that corresponds to the annual course. The measurement of a system with seasonal storage, on the other hand, should optimally reproduce the course of a year in order to be able to map the interaction of heat sources and heat sinks.

3.2 Dual source/sink system

The selection of the most representative days for the system's operation over the whole year are based on the developed method K-meansGA. This method uses the classification method K-means and optimization based on a genetic algorithm (GA). Meteorological and demand data are used for obtaining the results for Tarragona. First, the weather data is classified in a number k of clusters. For this, the k-means algorithm from the python library sklearn is used. The clusters are generated by the data distribution. Each data point is classified using the lowest quadratic distance to the nearest centroid. The centroids are the mathematical centres of the cluster and are not actual data points. In each iteration, the centroids position change until the distance between each data point and their centroid is minimum. The closest point to the centroid is the final result. Secondly, a genetic algorithm is used, based on natural selection applied to optimization problems. In each iteration, random "parent" solutions are selected, crossed and mutated, generating "descendent" solutions for the next iteration. In the end, the most fitted solution is found.

For the test of the advanced energy management (AEM) algorithm, the days selected must be consecutive rather than different days of the year put together, so as to observe the behaviour of the AEM systems over several consecutive days (e.g. storing PV energy on a sunny day for the next day with less production). Because of this, the algorithm selects all the possible combination of consecutive days of the year (e.g. series 1: day 1, 2, 3 and 4, series 2: day 2, 3, 4 and 5). Therefore, each data point is a series of 4 consecutive days. For the current application, the daily average temperature and the daily solar irradiation are used for the k-means. The algorithm does not take into account the chronological order of the days. Therefore, each cluster has points from various dates of the year. The intermediate results of the k-means are one series of four days for each cluster, each one representing different conditions of the year. This result is used for the genetic algorithm as seeds for the solutions. Also, cluster classification is used. The function to optimize by the GA is the minimum difference between the extrapolated load of the selected series of days (load of the selected days multiplied by the number of days in the cluster) and the total load of the cluster. The algorithm searches for series of days that minimize that difference and are near the centroids.

The genetic algorithm can optimize for different loads at the same time. For this project, three different load types were considered: space conditioning, DHW and electrical power consumption from the appliances. Space conditioning is the main load associated with the heat pump, divided into space heating during the cold season and space cooling during the warm season. In the following we analyse if adding the DHW and appliances consumption to the

optimization to select the days could improve the results.

For DHW, stochastic data was used to obtain the extraction profiles along the year. Space heating and DHW can be added together as a total heating demand. However, the result may lead to a selection of days where one type of demand is dominating and the other is not correctly represented. To avoid this, SH and DHW are considered as two different variables to optimize.

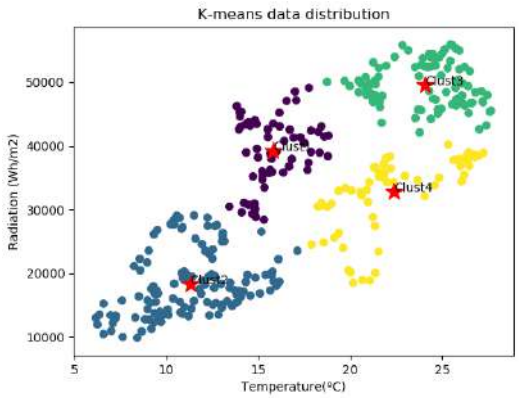

Fig. 5 – K-means clusterization of Tarragona. The solar radiation is the sum of the 4 days series and temperature the average. Each cluster is shown with a different colour. The red stars are the centroids of the clusters.

The stochastic distribution and the lack of seasonality of the DHW made it hard to select representative days throughout the year. Only one of the eight solutions changed when adding the DHW to the optimization. In that case, the results do not show enough improvement to justify the consideration of the DHW demand in the selection process. Therefore, the DHW demand will not be considered for optimization.

For the appliances, the electric consumption is based on a typical yearly profile. This annual profile does not present seasonality. When optimizing based on the appliances consumption, half of the results changed while the other half stayed the same as when considering only space conditioning. For the ones that changed, the results for space conditioning worsened. The improvement of the results for the appliances consumption is not enough to justify the worsening of the space conditioning load prediction.

Taking into account the test objectives, the use of only space conditioning as the input load data was considered the most appropriate option. The k-means algorithm considers the climatic data which affects the photovoltaic generation, while the GA algorithm selects the days which best extrapolate the load for the whole year.

Fig. 5 shows the clusterization of the climate data from Tarragona. Cluster 3 corresponds to the warmest days of the year, while cluster 4 are the coldest ones. Cluster 1 and 2 are in the middle, being the latter the one with less radiation. Cluster 1 and 4 have heating demand, while clusters 2 and 3 have cooling demand. The climate of Tarragona is cooling dominated.

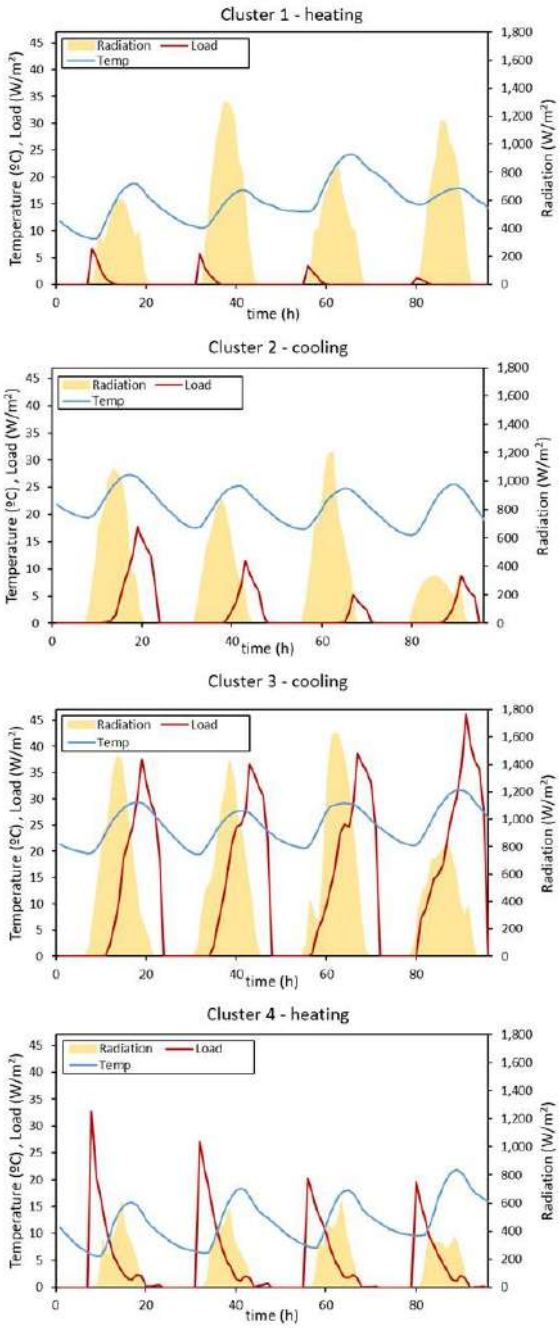

Fig. 6 – Hourly profiles of temperature, solar radiation and load for the selected series of days for Tarragona.

3.2 Solar-ice-slurry system

The first goal of testing the solar-ice system in a system test is to proof the functionality of the complex system. Additionally, a real installation of an ice-slurry storage with supercooling water in the evaporator of the heat pump and generating ice-slurry by means of a crystallizer will be tested as well. To achieve this goals, a period of 7 days was selected representing a year in a way that the ice-

slurry storage reaches its maximum ice fraction only in a small period of time. The CCT test will be performed with the propane heat pump during spring 2022 and with the CO2 heat pump during autumn 2022. Additionally, the simulation model should be validated with the results of this system test in order to evaluate the system performance with a reliable, validated model in a yearly simulation.

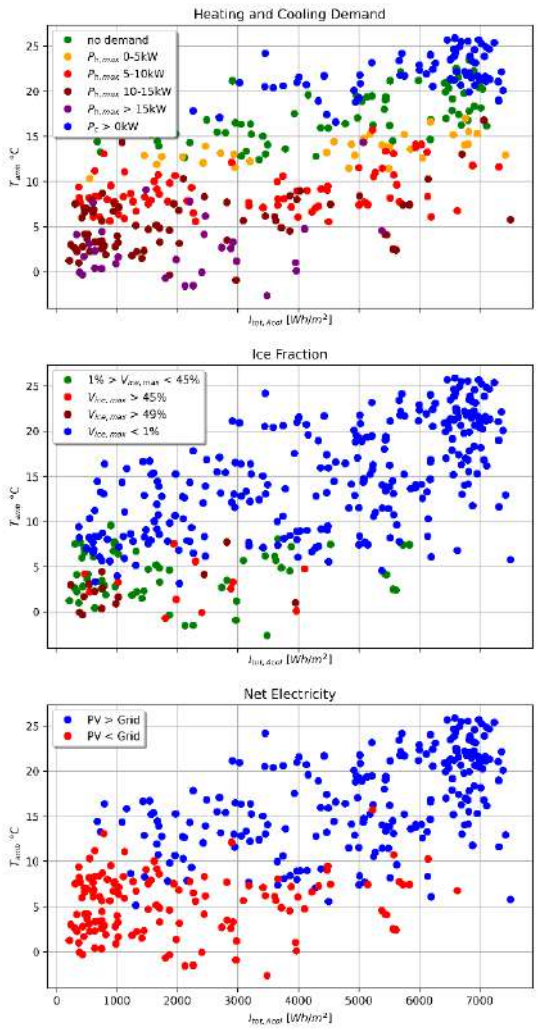

Fig. 7 – Ambient temperature vs total solar irradiation in the collector plane in Wh/m² for all days in a year. The colours represent the values of several variables (up) heating and cooling, demand, (mid) ice fraction and (bot) net electricity.

The first step for selecting the days for the system test is to get an overview about the distribution of different weather conditions and their influence in the heating system over the year. However, as a difference of the method presented in the above section 3.1, here we also need to consider the charge/discharge status of the ice storage, which cannot be pre-processed like the energy demands and weather data, but it needs to be simulated. Fig. 7 shows the distribution of the daily averaged ambient temperatures with the daily sum of solar irradiation into the collector field. The colour code indicates different situations in terms of the heating and cooling demands and the ice fraction of the ice storage. The days with low irradiation and low temperatures tend to have a high heating demand but very different status of the ice fraction. The ice fraction on days with high heating demand is deciding on system efficiency. A system with an SPF of 4 reaches the maximum ice fraction only on 3.5 % of the days.

In the yearly simulations, 60 % of the days have heating demand, 20 % have cooling demand and 20 % have neither. The seven days were chosen in a way that they represent this distribution as far as possible, reaching the fully iced ice storage only for a part of a day in order to be comparable with the yearly simulation. The ambient temperature and the total horizontal irradiation are shown in Fig. 8. The ambient temperature was smoothed at the transitions between the days to get a temperature profiles without unrealistic steps. For the system simulation of the seven days, the ice storage was scaled down further to a lab-size of 2 m³. These profiles of the seven days as well as a seven day profile for household electricity and DHW was then fed into the system simulation and results for the seven day period were calculated.

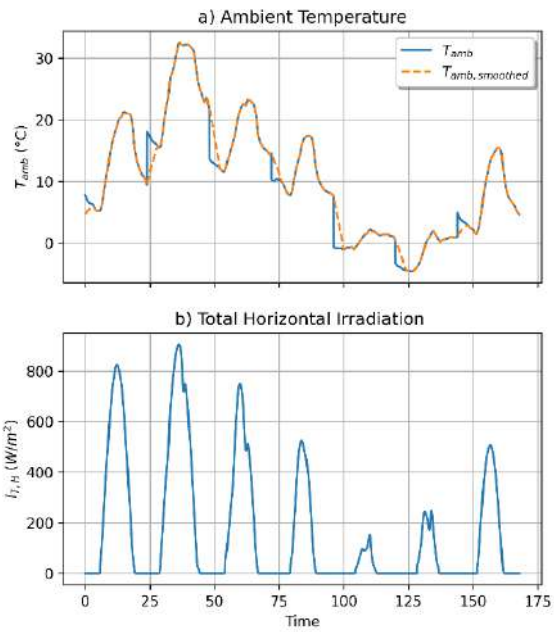

Fig. 8 – Ambient temperature and total solar irradiation in Wh/m2 for different conditions as a function of the time for the seven test days.

The system test with the propane heat pump using the seven days selected should serve for validation of the simulation model. The results of the system test will be compared with the simulation results of the seven selected days and the simulation model will be calibrated. Afterwards, a yearly simulation will be carried out with the calibrated model to calculate the energetic yearly system efficiency.

The building respects medium insulation standard of a retrofitted, old building and has a high thermal

capacity. Such heating up in warm weather periods or cooling down in cold periods takes some days. To get realistic building temperatures corresponding to the actual ambient temperature for the system test, the temperature of the building is reinitialized every day at midnight with the temperature of the following day from the yearly simulation. In this way, the cooling and heating demand in the system test is not influenced by the short-term change of seasons.

Tab. 2 – Comparison of the KPI for yearly simulation and the simulation of the selected 7 days.

	annual simulation	7-day simulation
$R_{RE,loacal}$	81 %	82 %
SPF	4.1	4.3

The TRI-HP goal of reaching at least 80 % of onsite renewable share is fulfilled for the ice-slurry system in yearly simulations as well as in the simulation of the seven representative days selected (see Tab. 2). Additionally, the electricity produced by the onsite PV plant is about the amount of electricity used by the heating system (including pumps and inverter/battery losses) and the households in the yearly simulation.

4. Test procedure and evaluation of results

4.1 Dual source/sink system

The storage units installed on the consumer side, both thermal and electrical, lead to inertia in the overall system. To start the test in a more realistic state, an additional day of pre-conditioning will be carried out in the experiments: the day before the chosen series of 4 days will also be tested in real time in the experiments, in order to bring the tanks into a usual stratification state that corresponds to a normal operation. We will, however, discard this first day of pre-conditioning, and only consider the 4 actual days of the test for the analysis. Since the capacity of the installed storage units does not exceed the respective daily demand, no further conditioning measures are necessary.

It could happen that because of the control strategy or the test conditions, the states of the storage are different at the start and at the end of the 4 days test period. Therefore, the differences in charged/discharged energy will be calculated for all the storage elements (thermal mass of the building, storage water tanks, electrical battery) and taken into account in the energy balances.

As described, four different 4-day sequences including one additional conditioning day each are used. From the sequences, quantities such as the useful heat or cold as well as the electricity demand can be extrapolated. The sum of the four extrapolated data then results in the annual value, from which the defined KPI can be calculated.

4.2 Ice-slurry-system

After the installation and commissioning of the whole system, the controller must be parameterized. For this purpose, some preliminary tests are required to check the speed of the pumps, the heating curve of the controller and the domestic hot water mixing valves. Before the actual start of the test, all tanks included must be conditioned. This means that the DHW tank should be in the upper range between 50 °C and 60 °C and the heating buffer at about 40 °C. The ice slurry storage should have an ice content of about 50 %, and the battery should be discharged to just above the maximum depth of discharge. Once the test has started, no changes or interventions in the system or its controllers are allowed until it is completed. The tested system must operate autonomously to meet the building's heating, cooling and household electricity needs. After 7 days or 168 hours, the end of the test cycle is reached. However, the test is not stopped then, but continues seamlessly, starting again at day 1. The end of the test is not reached until the so-called Concise Cycle criterion is reached. This ensures that no energy is stored within the system, or that the state of the system is identical at the beginning and end of the test. The Concise Cycle criterion for the termination, or the successful completion of the test, consists of three key aspects: energy consumption and storages state of charge as explained in the following:

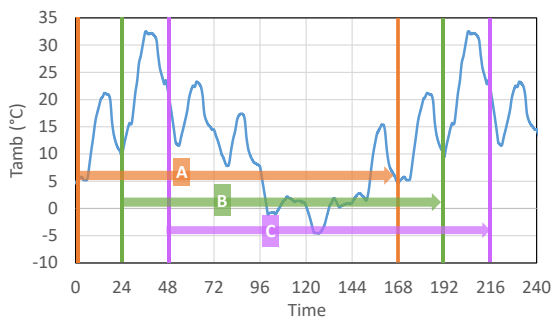

Fig. 9 – 7-day test sequence as a cycle, which is seamlessly aligned, respectively repeated. The test can be completed successfully if the evaluation of two consecutive phases is identical (A = B or B = C etc.).

El. energy consumption: At the end of the eighth test day, the consumption of electrical energy in the period 0 h to 168 h (cf. phase "A" in Fig. 9) can be compared with the consumption of electrical energy in the period 24 h to 192 h (phase "B"). These values have to be identical (±1 %), if not the test is continued to compare phase "B" with phase "C".

Storage tank temperature: The storage tank temperature is measured by means of contact sensors on the storage tank wall. This temperature measurement can be used to determine an average storage tank temperature and thus its state of charge.

This temperature must be identical at the beginning and end of the test cycle (±0.5 K). If the temperature does not match, this means that the conditioning of the storage tank was not correct and the energy content of the storage tank has changed during the test period. In this case, the test must continue for at least 24 h and at the end of the next day the initial and final temperature has to be compared again.

Battery state of charge: The state of charge of the battery must be identical at the beginning and at the end of the test cycle. This can be done either by the display of the battery itself, or by balancing the supplied and discharged electrical power.

The test cycle used for ice-slurry systems was created with the aim of combining all relevant operating conditions in one test cycle while providing a directly extrapolated result. The comparison of the 7-day simulations and the annual simulations from the selection of test sequences shows that this has been achieved. However, this is only true if, on the one hand, the test confirms the expected efficiency from the simulations carried out in advance and, on the other hand, the dimensioning of all components is suitable for the load of the test. In case of a deviation, the source temperature of the heat pump changes and thus also its efficiency. For this reason, the measured data will be used to calibrate the already existing simulation model of the tested system. If the simulation results from the 7-day simulation match the measured data we can assume a well set simulation and the parameter study can be extended with annual simulations for different locations.

5. Conclusions

The CCT method will allow a proof of concept of the two heating and cooling heat pump systems developed within the project TRI-HP at laboratory size: for warm regions in southern Europe, the dual source/sink system was developed with a propane-dual heat pump. This system makes use of ground source heat exchangers and air as heat sources for the heat pump. For colder regions in central Europe, the ice-slurry system was developed with a propane heat pump for retrofitted buildings with a rather low share of DHW demand on the total heat demand and with a CO_2 heat pump for with a share of DHW demand about 50 % of the total heat demand.

The methods for selecting the representative days are different for both systems. The proposed methodologies demonstrate an efficient selection of the test periods representative for the operation of the system over a whole typical year, and they allow an accurate assessment of the dynamic behaviour of the system and its energetic efficiency.

For testing the AEM, the weather data is divided into four different seasonal clusters. Representative days for each clusters are selected and used for the system tests in order to evaluate the behaviour of the advanced management control method and their cost-economic advantages compared to a rule-based control.

For selecting the representative days for the ice-slurry system, the weather data and heat demands alone are not sufficient as the system efficiency depends on whether the ice storage freezes completely or not and by how long. Therefore, system simulations were used to select the representative days comparing the KPIs obtained for one year simulations with the ones corresponding to the seven consecutive days selected. It will serve as a proof of concept for an ice-slurry storage prototype integrated into a heating system. With the results from the concise cycle test the simulation model will be checked and adjusted for getting reliable results for a simulation study for testing the viability of both systems for different climates in Europe.

6. Acknowledgement

The research conducted in this paper is partially funded by the European Union's Horizon 2020 research and innovation program under grant agreement No.814888 (TRI-HP).

7. References

[1] Peter Vogelsanger. The Concise Cycle Test Method - a 12 Day System Test. A Report of IEA SHC. IEA-SHC Task 26 Solar Combisystems, Paris, France: 2002.

[2] Haller MY, Haberl R, Persson T, Bales C, Kovacs P, Chèze D, et al. Dynamic whole system testing of combined renewable heating systems – The current state of the art. Energy and Buildings 2013;66:667–77. https://doi.org/10.1016/j.enbuild.2013.07.052.

[3] T. Péan, J. Romani, E. Fuentes, J. Salom (2020). Treballs tècnics relatius al potencial de les bombes de calor aerotèrmiques d'alta eficiència energètica per a climatització i generació d'aigua calenta sanitària a Catalunya. Technical report for ICAEN.

[4] Ministerio de Fomento de España. Código Técnico de la Edificación CTE - Documento Básico HE - Ahorro de Energía. (2019)

[5] Jordan, U. and Vajen, K. DHWcalc: Program to generate domestic hot water profiles with statistical means for user defined conditions, ISES World Congress, Orlando, 2005.

[6] SIA. SIA Merkblatt 2028: Klimadaten für Bauphysik, Energie- und Gebäudetechnik 2010.

[7] Pflugradt N. Load Profile Generator Version 1.3.5. Chemnitz: Prof. Technische Thermodynamik, Germany; 2010.

Development of an energy analysis tool for data center free cooling technologies modelizzation and comparison in different climate conditions

Mauro Mantovan [a], Carlo Bissaro [a], Fabio Poletto [a], Michele De Carli [b], Angelo Zarrella [b]

[a] Hiref S.p.A., Viale Spagna, 31/33, 35020 Tribano PD, Italy. E-mail: mauro.mantovan@hiref.it

[b] Department of Industrial Engineering, University of Padova, Italy. E-mail: angelo.zarrella@unipd.it

Abstract. Data Centers are currently undergoing a great period of change. Developments in business and personal data transfer together with new technologies such as virtualisation and cloud computing are transforming Data centers into dynamic environments with greater power demands unexpectedly. The cooling requirements of the Data Center infrastructure form a large part of the overall power requirements and it is therefore critical to ensure correct optimisation to achieve the desired energy efficiency levels. In Planning data centers for the future, it is imperative that the design matches the infrastructure with greater scalability and integration enabling Data Centrers to evolve to cope with less power demands and lower running costs. This work brings together the main layouts of high efficiency IT cooling systems, highlighting their operation and efficiency in the case of an IT room with a thermal load of 1 MW and three different climatic scenarios. The efficiency of the systems is evaluated through a calculation routine in which all the components of each cooling system are modelled and the regulation logics of the software of these units are implemented. The climatic scenarios for 3 different locations (Palermo, Milan, and Frankfurt) are represented according to the hourly distribution of temperatures and humidity in order to evaluate the seasonal performance of each cooling system. The results give an overview of the consumption referred to each IT cooling technology in relation to the application climate. The calculation routine developed allows to choose the most suitable technology for the climate and the installation considered, also leaving the possibility of a subsequent optimization of the unit design based on the most appropriate technology.

Keywords. Data center, cooling technologies comparison, cooling efficiency, energy analysis tool, energy simulation.
DOI: https://doi.org/10.34641/clima.2022.393

1. Introduction

Worldwide web, online services, cloud computing are increasing and there is the need for arranging reliable facilities to process, store and transmit these data. This increases the energy consumption of Data Centers: half of the energy is normally consumed by servers while the other half is for electrical power supply and for the cooling system. IT devices also need a close controlled temperature and humidity environment in Data Centers in order to work properly and to provide a reliable and efficient service. Suppliers of servers advise Data Center owners to keep computing rooms within recommended hygrothermal limits throughout their whole working life. As can be seen in Fig. 1, these limits have been constantly widened in recent years, allowing to maximize the annual hours of free cooling, and reducing the consumption of electricity dedicated to the cooling, while ensuring the proper functioning and duration of the servers. The objective of this study is to develop a data center cooling system energy performance evaluation tool that can provide a comparison between different cooling layouts and technologies, driving to an early design choice that should be the best for a particular climate zone considering also installation available footprint and costs of energy and eventually of water when adiabatic cooling is considered.

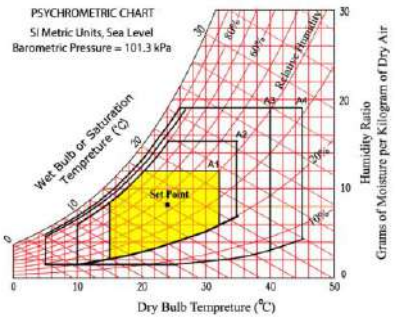

Fig. 1 – Computing rooms hygrothermal limits from class A1 to A4 according to ASHRAE specifications

2. Energy performance in data centers

2.1 Power Usage Effectiveness

Data Center efficiency is measured by DCiE (Data Center infrastructure Efficiency) and PUE (Power

Copyright ©2022 by the authors. This conference paper is published under a CC-BY-4.0 license.

Usage Effectiveness), as defined by The Green Grid, a global consortium of IT professionals aiming to increasing the energy efficiency of Data Centers. The biggest challenge for IT organizations to manage Data Centers is the reduction of energy for cooling and for power supply: this is the only way to let Data Centers grow. Efficient Data Centers let IT providers better manage the increasing demands on the network, computing, and storage requirements with lower energy costs, thus with lower running costs (operating expense). A higher efficiency in the end leads to more competitiveness and readiness in answering to the market demands. As can be seen in Eq. (1) Power Usage Effectiveness (PUE) is a measure of how efficiently a Data Center uses the input energy:

$$PUE = \frac{Total\ Facility\ Energy}{IT\ Equipment\ Energy} \quad (1)$$

In particular, it shows how much energy is used for the IT System compared to that used for Cooling and Power Supply. The DCiE is the reciprocal of PUE:

$$DCiE = \frac{1}{PUE} \quad (2)$$

The ideal PUE of a data center should be 1.0, which means that all the energy consumed by the facility is used to power ICT (Information and Comunication Techonology) equipment. In real applications, as shown in Fig. 2, the total power consumption, the electricity used (by ICT equipment, cooling, lighting, etc.) need to be measured to calculate the effectiveness.

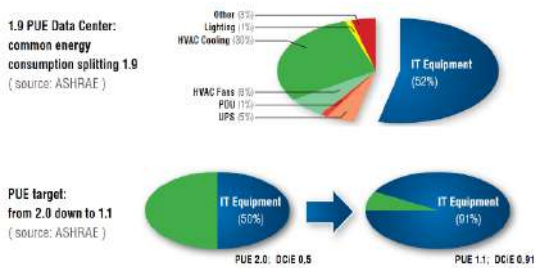

Fig. 2 – Data center energy consumption splitting example.

2.2 Water usage effectiveness

Another index to consider in the case of adiabatic cooling systems is the WUE (Water Usage Effectiveness), that has received increasing interest with increasing usage of adiabatic cooling systems, where a large amount of water evaporates to get the desired cooling effect. WUE is a measure of the amount of water used in the Data Center per unit of IT equipment energy:

$$WUE = \frac{Annual\ site\ water\ usage}{IT\ Equipment\ Energy} \quad (3)$$

The ideal WUE of a data center should be 0.0, but if the goal is to minimize water use at a global level, then a low WUE can have an adverse impact that needs to be considered. In fact electricity generation needs a significant amount of water that depends on the generation method used, but the majority of electricity generation today is still very water intensive. So reducing water use at the site may increase electricity use, which will likely result in increased water use at the power-generation source. Depending on many factors like location, business strategy, and financial considerations, increasing water use and decreasing energy use may be the desired outcome, or increasing energy use and decreasing water use (as in a desert location) may be the desired outcome. Regardless of the outcome, PUE and WUE are helpful tools to guide business decisions.

3. Free Cooling

As temperature limits inside computer rooms have increased in the last years, many more places around the world can achieve the needed cooling capacity for the servers as Free-Cooling capacity, using (directly or indirectly) fresh air from outside. The cooling system can work in Free-Cooling operation when the outdoor temperature is below that o fthe computer room. The required cooling can be achieved by letting the outdoor air directly into the racks (direct Free-Cooling) or exchanging heat between outside and indoor air (indirect Free-Cooling) or between the outside air and the chilled water circuit (indirect water Free-Cooling). A larger operation field in terms of indoor hygrothermal conditions lead to a larger number of hours for Free-Cooling, a larger number of countries where Free-Cooling is achievable and higher chilled water temperatures for CRAC units, thus more indirect Free-Cooling hours.

3.1 Air quality and direct free cooling

When in direct Free-Cooling operation a Data Center uses outside fresh air which is directly blown into the server room, so outside air quality strongly affects the IT devices performances and behaviour.
ASHRAE recommends, besides hygrothermal values, particulate contamination limits and gaseous contamination limits. The reference norm for particulate contamination is ISO 14644-1: the quality of the air is defined by nine different classes (1 to 9 ISO class) as the number of particles in each cubic meter of air. Each particle is considered with its size. ASHRAE claims that air filters used must achieve ISO 8 class cleanliness. According to ANSI/ASHRAE Standard 127-2007 the indoor air must have filtration class MERV8, while the air entering the Data Center must have filtration class MERV11/MERV13 depending on the outdoor air quality and specific computer room conditions. When dedicated measurements show that outdoor air can not be directly used for cooling purposes (ISO class greater than class 8) then specific filters with a high efficiency must be used.
The reference standard for gaseous contamination is ANSI/ISA S71.04-1985: different corrosivity levels (from G1 to Gx) define each gas reactivity

level according to concentration. ASHRAE's book "Particulate and Gaseous Contamination in Datacom Environments" of 2009 recommends level G1 for Data Centers. In the end direct Free-Cooling is the best solution thermodynamically, but the following aspects must be considered:

- high efficiency filtration causes high air pressure drops, therefore the fans' energy consumption may reduce the global efficiency of the system.
- the replacement of old filters may be expensive
- a strict control of gaseous contamination with chemical filters is necessary
- the upper humidity limit must be controlled (dehumidification may be needed)
- the lower humidity limit must be controlled (humidification may be needed)

4. Evaluated Cooling technologies

In the current work all the considered cooling units are equipped with free cooling modules comparing performances of direct free cooling CRAC, Indirect Free Cooling CRAC, Indirect Evaporative Cooler, Free Coolig Chiller and Adiabatic Free Coolig Chiller, with typical return air condition for a compartmentalized room of 36°C and RH 27%. While CRAC units and Indirect Evaporative Cooler are working directly on data centre indoor air, chillers are producing chilled water that is supplied to dedicated free fans CRAC units. For each cooling technology a data hall with a thermal load of 1 MW and (n+1) redundancy have been considered.

4.1 Direct free cooling CRAC – Case 1

This layout consists in a typical close control unit used for perimetral cooling in data center rooms where the free cooling is obtained by means of the regulation of a damper which allows to select if recirculate return air from hot aisle, let external ambient air enter the data center or have a mix of these two airflows to match the target supply air temperature. When the free cooling is not available or insufficient, mechanical cooling guarantee the maintenance of the set point. Units are equipped with a remote condenser, and condensation control is achieved by partialization of the condenser ventilation. Standard refrigerant R410A is considered, 2 scroll compressors are installed in 2 separated circuits (one On-Off compressor and one inverter driven compressor), (9+1) redundancy has been adopted for seasonal energy analysis.

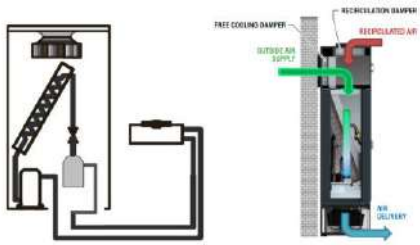

Fig. 3 – Direct free cooling CRAC principle scheme and direct free cooling damper.

4.2 Indirect Evaporative Cooler – Case 2

These units are based on the use of a cross flow heat exchanger that keeps internal and external airflows separated. The evaporative system, by cooling down external air all along his path through the recovery system, increases the heat exchange capacity of the recovery system, thus allowing indirect free cooling to be extended to a wider range of external thermo-hygrometric conditions reducing the field of action of mechanical cooling. Extra costs due to the increase in water consumption and water treatment and pumping requirements are compensated by limited compressor operation. These units can be installed on the external perimeter of the data center or on the roof, taking zero indoor space. Standard refrigerant R410A is considered, 2 scroll compressors are installed in a single circuit (one On-Off compressor and one inverter driven compressor), (5+1) redundancy has been adopted for seasonal energy analysis.

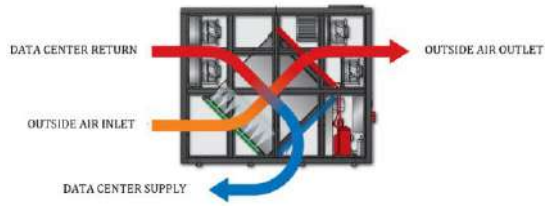

Fig. 4 – Indirect evaporative cooler principle scheme

4.3 Adiabatic Free Coolig Chiller + CW CRAC – Case 3

This case scenario is based on a traditional air cooled liquid chiller with V shaped condenser coils. In these units are also installed free cooling coils with the same V shape and a 3 way valve regulating the amount of water flow in the free cooling module. Upstream of the free cooling coils, evaporative pads are installed which allow the outside air temperature to be lowered by adiabatic saturation, increasing the number of free cooling hours per year and reducing consumption. Standard refrigerant R134a is considered, 2 screw compressors are installed in 2 separated circuits (one On-Off compressor and one inverter driven compressor), (3+1) redundancy has been adopted for seasonal energy analysis. Chilled water on supply is sent to an indoor CRAC free fan unit working with (9+1) redundancy.

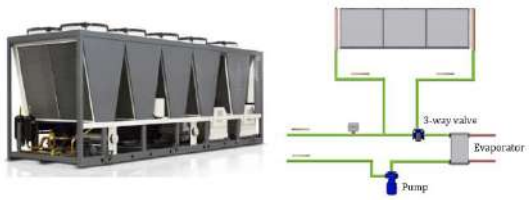

Fig. 5 – Evaporative free cooling chiller and free cooling module principle scheme

4.4 Free Coolig Chiller + CW CRAC - Case 4

Same scenario of Case 3 without adopting evaporative pads.

4.5 Indirect Free Cooling CRAC - Case 5

Indirect Free Cooling CRAC provide free cooling by cooling glycol water through an external dry cooler if the external air temperature allows it. The cooled water is sent to the indoor unit in a finned coil dedicated to cooling the return air from the datacentre. If free cooling is not available or sufficient, mechanical cooling guarantees the maintenance of the set point, using the water leaving the free cooling coil for condensation on a dedicated plate condenser. In the case of negligible contribution from free cooling, a 3-way valve diverts the water arriving from the dry cooler directly to the plate condenser, reducing the pressure drops of the hydraulic circuit. Condensation control is guaranteed by means of a flooding valve which allows a reduction of the exchange surface of the condenser by flooding a portion on the refrigerant side. Standard refrigerant R410A is considered, 2 scroll compressors are installed in 2 separated circuits (one On-Off compressor and one inverter driven compressor), (9+1) redundancy has been adopted for seasonal energy analysis.

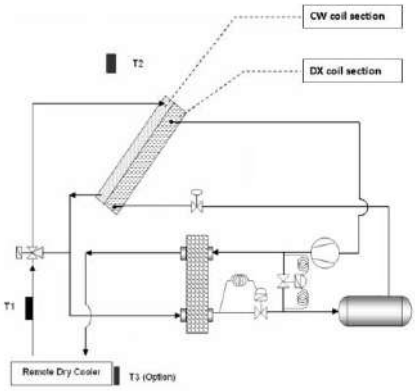

Fig. 6 – Indirect Free Cooling CRAC principle scheme

5. Cooling unit's components and numerical modelling

All the units considered are equipped with a free cooling module and a backup/integration mechanical cooling system. The components are sized in order to guarantee the necessary cooling capacity in the worst climatic conditions with a unit in failure/maintenance, while the energy analyzes are conducted on the assumption that all the units are active with load partialization. Below are the main components common to all the layouts that make up the free cooling and mechanical cooling modules, describing their numerical implementation in the seasonal energy analysis routine.

5.1 Compressors

Regardless of the type, compressors behaviour is always modelled according to the polynomials provided by the manufacturer in order to predict the cooling capacity, the electrical absorption, and the thermal power to be disposed off to the condenser according to a given number of rpm and given temperatures of evaporation and condensation. The adopted polynomials have a standardized form exposed in Eq. (4).

$$y = c1 + c2 * to + c3 * tc + c4 * to^2 + c5 * to * tc + c6 * tc^2 + c7 * to^3 + c8 * tc * to^2 + c9 * to * tc^2 + c10 * tc^3 \quad (4)$$

5.2 Finned Coils

Finned coils are used as evaporators, condensers, chilled water-cooling coil, and dry cooler's/free cooling heating coil on modelled units. Refrigerant fluid properties are evaluated by literature available equations, while air properties are evaluated through standard psychrometric relations for humid air. Fins and tubes geometries and spacing are the inputs of the model with airflow rate, air temperature and humidity, and evaporation/condensation temperatures. The finned coil model provides an iterative method that converge matching refrigerant side and air side exchanged power, solving heat transfer on each side with empirical correlations developed by units constructor. The synthetic flow chart shown in Fig. 7 groups the main steps of the calculation model. The various functioning modes of the finned coil share the same calculation method with evaluation of refrigerant's properties, and formulation of the heat transfer coefficients dedicated to the specific case.

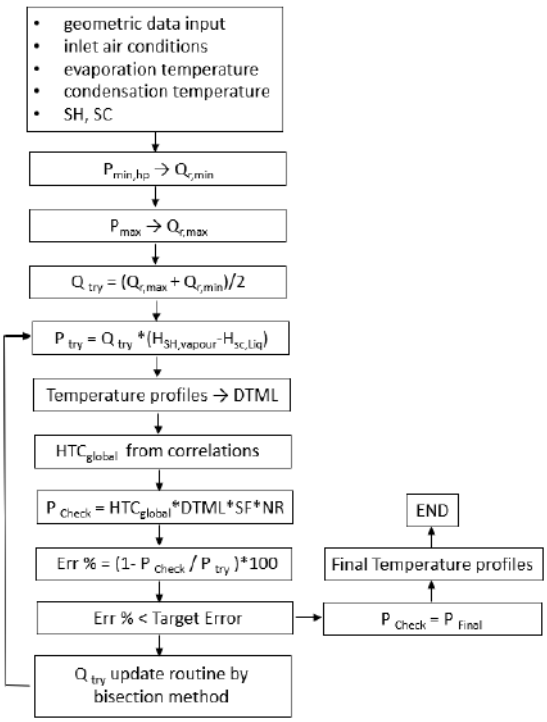

Fig. 7 – Finned coils general flow chart

5.3 Plate heat exchangers

Plate heat exchangers are used as water cooled condensers on modelled CRAC units. Compressor discharge temperature, refrigerant properties, and water/glycol mixtures properties are evaluated through the use of Refprop. Plates geometry and spacing, exchanged power, condensation temperature, water inlet temperature and water volumetric flow are the inputs of the model. Water channel is modelled with standard correlation for parallel plates flow, while refrigerant side is solved with empirical correlations. The output of the model is the margin of the exchanger over required working conditions.

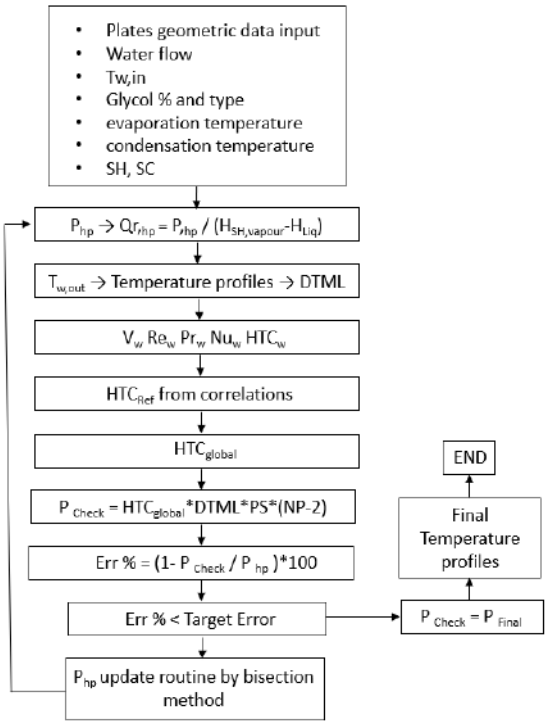

Fig. 8 – Finned coils general flow chart

5.4 Radial and axial fans

Fans are modelled using constructor 's data for head and absorbed power at full speed, scaling performances at variable rpm with affinity laws indicated in Eq. (5, 6, 7).

$$Q2 = Q1 * \left(\frac{N2}{N1}\right) \tag{5}$$

$$H2 = H1 * \left(\frac{N2}{N1}\right)^2 \tag{6}$$

$$HP2 = HP1 * \left(\frac{N2}{N1}\right)^3 \tag{7}$$

5.5 Wetted Cross flow heat exchanger

Calculations are based on a Finite Element Method, that starts from boundary conditions to solve mass and energy balance of each element of the recuperator. Calculation are based on NTU (number of transfer units) that are calibrated with the constructor polynomials for a given working condition and water evaporation on external air side is accounted through heat and mass transfer analogy with dedicated Lewis number evaluation and surface wettability factor. For heat transfer mechanism between internal and external air is schematized in Figures 9 and 10.

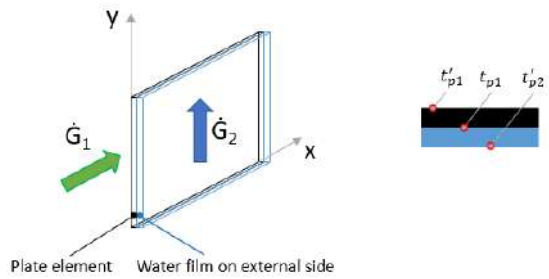

Fig. 9 – Heat exchanger plate – water film interface in crossflow heat exchanger model

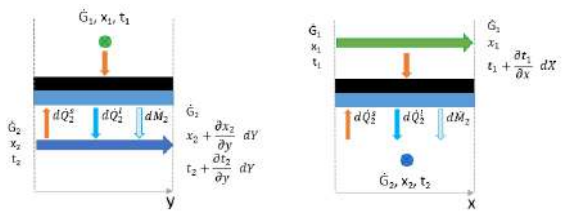

Fig. 10 – Differential control element of the crossflow heat exchanger model

Governing equations for external airflow are listed in Eq. (8, 9) while internal airflow is described by Eq. (12). Energy balance between internal and external flows is guarantee by Eq. (10, 11).

$$\frac{dt_2^{(k,l)}}{d\overline{Y}} = NTU_2'\left[\left((t_2^{(k,l-1)})' - t_2^{(k,l-1)}\right) + \left(\frac{\sigma_p}{Le}\right)_2 \left(\frac{c_g}{c_p}\right)_2 \left((t_2^{(k,l-1)})' - t_2^{(k,l-1)}\right)\left((x_{p2}^{(k,l-1)})' - x_2^{(k,l-1)}\right)\right. \tag{8}$$

$$\frac{dx_2^{(k,l)}}{d\overline{Y}} = NTU_2'\left(\frac{1}{Le_2}\right)\sigma_{p2}\left((x_{p2}^{(k,l-1)})' - x_2^{(k,l-1)}\right) \tag{9}$$

$$\left(\frac{W_1}{W_2}\right)NTU_1\left(t_{p1}^{(k,l-1)} - t_1^{(k,l-1)}\right) + NTU_2\left((t_2^{(k,l-1)})' - t_2^{(k,l-1)}\right) + NTU_2\left(\frac{\sigma_p r_0}{c_p Le}\right)_2\left((x_{p2}^{(k,l-1)})' - x_2^{(k,l-1)}\right) = 0 \tag{10}$$

$$\left(\frac{\lambda_{plt}}{\delta_{plt}}\right)\left(t_{p1}^{(k,l-1)} - \left(t_{p2}^{(k,l-1)}\right)'\right) = \alpha_1\left(t_1^{(k,l-1)} - t_{p1}^{(k,l-1)}\right) \tag{11}$$

$$\frac{dt_1^{(k,l)}}{d\overline{X}} = NTU_1\left(\frac{t_{p1}^{(k-1,l)} + t_{p1}^{(k,l)}}{2} - t_1^{(k-1,l)}\right) \tag{12}$$

5.6 Adiabatic pads

Adiabatic pads efficiency is modelled by interpolation of constructor data taking into consideration external air temperature and relative humidity, and air flow speed through the pads. Also additional pressure drops has been considered as a function of air speed.

6. Main energy analysis calculation routine

The code related to the modelling of each component has been inserted into a higher level calculation routine that allows to evaluate the seasonal behaviour of the various IT cooling technologies considered. A data upload section by the user allows to enter data relating to the load and the thermo-hygrometric conditions of the room. The user also enters the model and the number of cooling units to simulate, thus recalling the components relating to the selected unit from a specific database. By selecting the desired location, the data relating to temperature, relative humidity and hourly distribution for seasonal simulation are obtained from the database. As the ventilation in the room is a closed loop, the first step of the calculation is always regarding the solution of the aeraulics, to account for additional load related to user fans dissipations. After this stage, in accordance with external climatic conditions, an evaluation of the available amount of free cooling is made, givin as a result the call for a full free cooling regulation, a mechanical top up cooling request, or a full mechanical cooling request if free cooling is not available or not advantageous. While the convergence cycle for the mechanical cooling and it's regulation requires lot of iterations and involve subroutines dedicated to condensation control, compressor's envelope limits control and so on, only a simplified flow chart valid for all the cooling units is reported in Fig. (11).

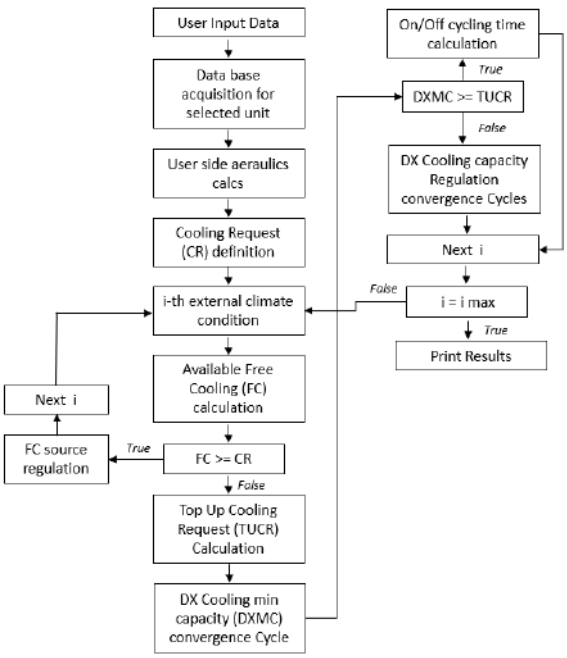

Fig. 11 – Seasonal energy analysis calculation flow chart

7. Climatic conditions for the considered data center locations

The Cities of Palermo, Milan and Frankfurt has been considered for the camparison of seasonal performances of the different cooling technologies. The distribution of seasonal hourly temperature and the annual average relative humidity for each temperature are shown in the graphs in Fig. 12 for each of the three cities considered.

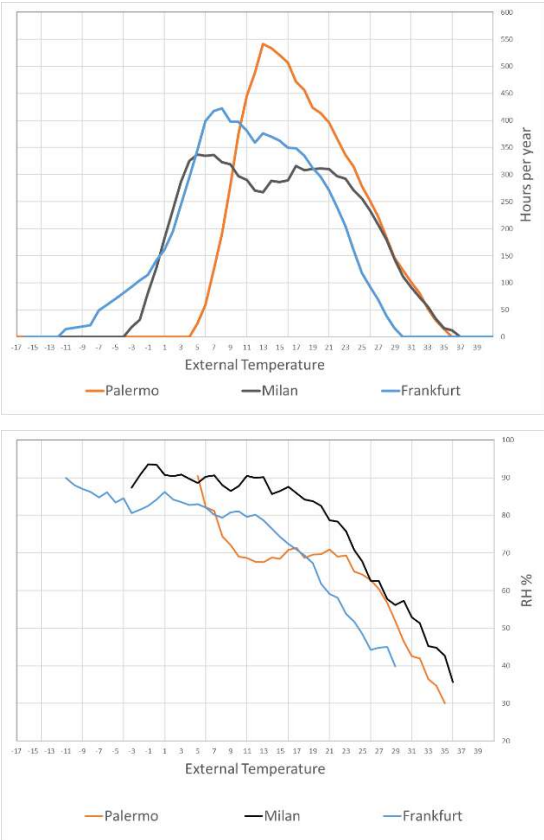

Fig. 12 – Seasonal temperatures and humidity distributions for three considered locations

8. Results comparison

In Tab. 1 all the results in terms of PUE and also in terms of WUE for units that are equipped with evaporative cooling modules are listed. An indication of the footprint split in indoor and outdoor is also reported.

8.1 Energy analysis

Depending on temperature distribution, on annual basis, the absorbed energy and the cooling energy delivered by the systems are calculated and synthesized in Figure 13 (Frankfurt), 14 (Milan) and 15 (Palermo). This helps highlight the extent of each cooling method and each component consumption contribution (fans, compressors, pumps).

Tab. 1 – Results comparison of seasonal energy analysis of each cooling technology for all the considered locations

	PUE			WUE			Footprint Indoor	Footprint Outdoor
	Palermo	Milan	Frankfurt	Palermo	Milan	Frankfurt	m² per 1MW data hall	m² per 1MW data hall
Case 1 (Direc Free Cooling CRAC)	1,073	1,068	1,056	0	0	0	22,3	29,7
Case 2 (Indirect Evaporative Cooler)	1,089	1,083	1,062	0,93	0,64	0,59	0,0	83,5
Case 3 (Adiabatic Free Coolig Chiller + CW CRAC)	1,142	1,122	1,093	0,49	0,26	0,25	15,7	44,2
Case 4 (Free Coolig Chiller + CW CRAC)	1,159	1,126	1,102	0	0	0	15,7	44,2
Case 5 (Indirec Free Cooling CRAC)	1,156	1,130	1,112	0	0	0	22,3	47,0

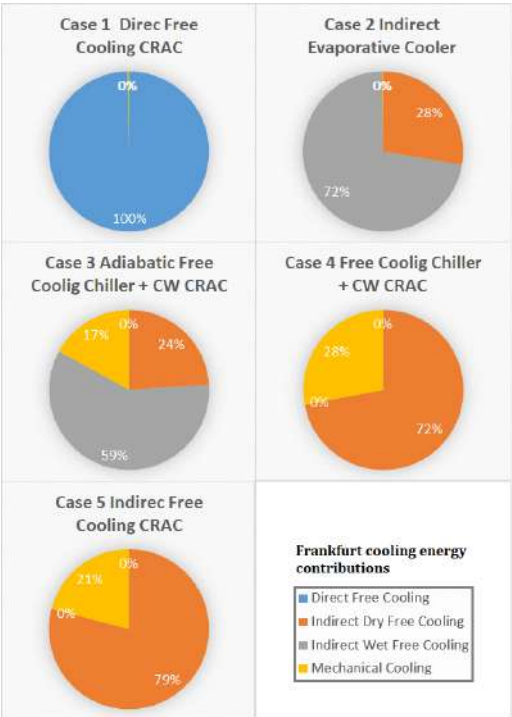

Fig. 13 – Cooling energy contributions from each cooling technology with Frankfurt climate data

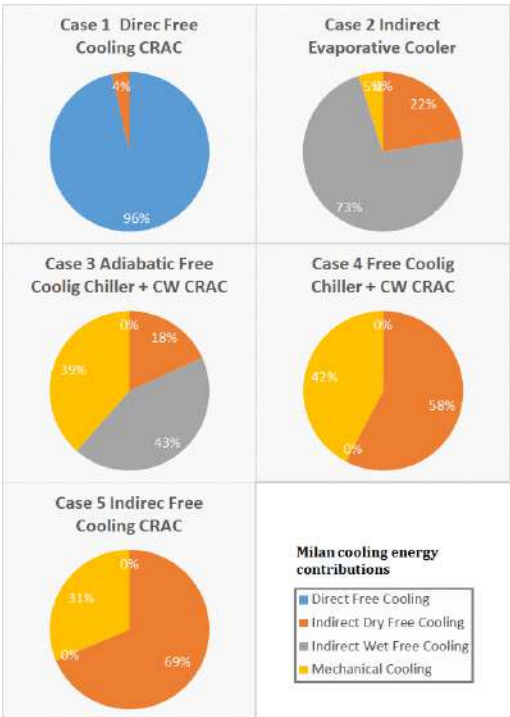

Fig. 14 – Cooling energy contributions from each cooling technology with Milan climate data

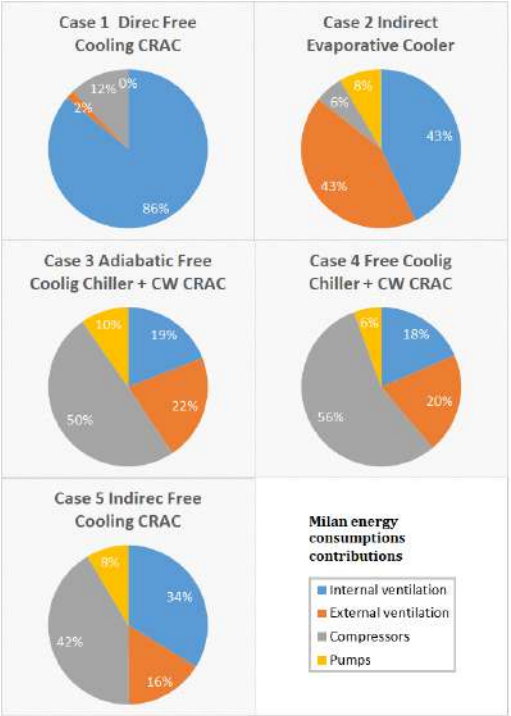

Fig. 15 – Energy consumptions contributions from each cooling technology with Palermo climate data

9. Conclusions

By comparing different values obtained by simulations, it is clear that from a strictly thermodynamic point of view the direct free cooling technology is extremely convenient, even more due to the adopted conditions of return air from the data center with high temperatures that allow full free cooling to be pushed beyond 90% of the annual hours even in a Mediterranean climate like the one of Palermo. The negative aspect of this technology concerns the limitations in terms of quality and pollution of the outdoor air in large cities where data centers are currently built up.

The only units with indirect free cooling capable to obtain results close to direct free cooling in terms of seasonal PUE are the IECs (Indirect evaporative coolers), which take advantage of large heat exchange surfaces and the use of large quantities of water to feed the evaporative cooling system of the outdoor air.

Following the efficiency classification in terms of seasonal PUE visible in Tab. (1) it is evident that from case 3 onwards the technologies are penalized by the fact that free cooling is based on the use of a carrier fluid that acts as a medium between external air and indoor air, introducing an extra step in the heat exchange process and reducing its efficiency. In chillers with adiabatic free cooling this problem is mitigated by the effect of lowering the external temperature through adiabatic pads, which have lower water consumption than indirect evaporative systems with cross flow heat exchanger (see WUE values in Tab. (1)).

Hence the most efficient solution is not the one usually adopted, since other factors should be considered such as the impact on costs of ordinary and extraordinary maintenance (filter replacement, water treatment, nozzle replacement, etc.) as well as the variability of cooling loads on a daily and/or seasonal basis (data traffic fluctuations) and environmental, space and noise requirements for each specific application. A financial analysis should also be carried out to estimate the initial investment rate of return, which may also differ significantly from one solution to another. In this context, the developed calculation tool fits perfectly to produce the data necessary for a technical-economic analysis, allowing to evaluate the best choice for the cooling system starting from the early design stages of the data center in the climatic context of interest.

10. References

[1] Belady, Christian L; Beaty, Don. Roadmap for Datacom Cooling ASHRAE Journal; New York Vol. 47, Fasc. 12, (Dec 2005). Pages 52-55.

[2] V. Avelar, D. Azevedo, A. French. PUE : A comprehensive examination of the metric. The Green Grid, White Paper #49, 2012

[3] M. Patterson. Water Usage Effectiveness (WUE): A Green Grid data center sustainability metric. The Green Grid, White Paper #35, 2011.

[4] Thermal Guidelines for Data Processing Environments. Fourth Edition. ASHRAE Datacom Series; book 1. ASHRAE, 2015.

[5] IT Equipment Power Trends. Third Edition. ASHRAE Datacom Series; book 2. ASHRAE, 2018

[6] Data Center Power Equipment Thermal Guidelines and Best Practices. Whitepaper by ASHRAE TC 9.9. ASHRAE, 2016.

[7] EN ISO 14644-1:2015. Cleanrooms and associated controlled environments - Part 1: Classification of air cleanliness by particle concentration (ISO 14644-1:2015)

Data statement

Data sharing not applicable to this article as no datasets were generated or analysed during the current study.

Performance analysis of heat pump assisted desiccant cooling system through experiment

Tae-Ha Leigh [a], Se-Jin Lee [b], Chang-Ho Jeong [c], Myoung-Souk Yeo [d]

[a] Department of Architecture and Architectural Engineering, Graduate School, Seoul National University, Seoul, Korea, redsky2969@snu.ac.kr

[b] Department of Architecture and Architectural Engineering, Graduate School, Seoul National University, Seoul, Korea, qkqhtpwls@snu.ac.kr

[c] Division of Architecture for Urban Planning & Real Estate Development, The University of Suwon, Hwaseong, Korea, chjeong@suwon.ac.kr

[d] Institute of Construction and Environmental Engineering, Department of Architecture and Architectural Engineering, Seoul National University, Seoul, Korea, msyeo@snu.ac.kr

Abstract. The building heat resistance performance and air tightness are more and more developed. According to this, especially in hot and humid climate, the latent load easily increases and occupant comfort decrease. Because of this the importance of dehumidification grow higher and higher. Heat pump assisted desiccant cooling (HPDC) system is one of the systems to control the indoor humidity while using less energy than conventional condensation dehumidification and general desiccant cooling system by using condensation heat as regeneration heat for desiccant. And the disadvantage of HPDC system, which is hard to control the temperature, is supported by using radiant ceiling panel (RCP) to control the room temperature. The object of the paper is analyzing the energy performance and thermal comfort satisfaction of HPDC system and analyze the adaptability of HPDC system combined with RCP (HPDC w/RCP) through experiments. In experiment 1, HPDC system used 55% lower energy consumption compared to packaged air conditioning system (PAC) and can satisfy comfort zone rather than PAC system, especially in humidity comfort range. In experiments 2, HPDC w/RCP system satisfied ASHRAE comfort zone 12% more than HPDC system and used 5% lower energy. The experiment performed in this study can prove that the HPDC system is a possible alternative system of conventional cooling and dehumidification systems and HPDC w/RCP also has possibility to enhance the thermal comfort and energy saving.

Keywords. Heat pump assisted desiccant cooling system. Radiant ceiling panel. Dehumidification. Energy consumption. Thermal comfort.
DOI: https://doi.org/10.34641/clima.2022.397

1. Introduction

As Passive house researches aim to get Zero Energy Building (ZEB) goes deeper and deeper, the insulation and air tightness performance grow better and better. For this growth, especially in hot and humid climate, latent load increase and satisfaction decrease are easily occurred. Also, the requirement of fresh outdoor air and changing lifestyle of occupants leads the increase of latent load ratio to total indoor load [1]. Besides, it was demonstrated that the growth of bacteria and melds affecting human health problem can be inhibited easily under 40~60% relative humidity conditions [2].

For above reasons, thermal discomfort due to increased humidity become main issue of indoor environment control because the conventional air-conditioning systems do not contain the effective dehumidification capacity. Condensation dehumidification is mostly selected method in conventional air-conditioning system due to the compactness and convenient maintenance. Subcooling and re-heating process to perform condensation dehumidification causes unnecessary energy consumption [3, 4]. Because of this, prior researches focused to desiccant systems, especially solid desiccant systems for their compactness compared to liquid desiccant systems. Heat pump assisted desiccant cooling system (HPDC) is the dehumidification and cooling systems using solid desiccant. Because this system uses condensation heat as regeneration heat for solid desiccant, it can reduce the need for regeneration heat source and also can

Copyright ©2022 by the authors. This conference paper is published under a CC-BY-4.0 license.

control the zone humidity [3]. It was verified that the installation of cooling coil for pre-cooling in front of solid desiccant wheel increases the performance of dehumidification system [5]. However, when use this method, there is difficult at controlling the outlet temperature of the system because of the temperature increase while dehumidification. To solve this problem, there are two methods; one way is using cooling coil at front of desiccant wheel while stopping dehumidification, the other way is using other sensible heat control system like radiant cooling panel.

When using conventional air systems like packaged air conditioning (PAC) system, it consumes more energy than radiant ceiling panel (RCP). According to this research results, there has been researches applying RCP to the desiccant dehumidification system [6, 7]. It was announced that when using HPDC combined with RCP can satisfy users' comfort rather than when using PAC as cooling and dehumidification system [7].

In this paper, the performance of HPDC is analysed through experiment with comparative analysis between HPDC system and PAC system. Additionally, adaptability of HPDC w/RCP is also analysed through additional experiment compared with HPDC system.

2. Performance evaluation experiments

2.1 Experiment 1 (HPDC v.s. PAC)

HPDC is main target of the study and to confirm the possibility of HPDC, in experiment 1, comparative analysis was carried out between the HPDC system and conventional system (PAC). HPDC system used DX HP as heat source which is inside the HPDC system, and used air in laboratory (LA), maintained 26°C, and PAC system used electric heat pump (EHP) as heat source and used outdoor air (OA), which is 15°C at the experiment period. Fig. 1 and Fig. 2 shows the schematic diagram of HPDC system and PAC system.

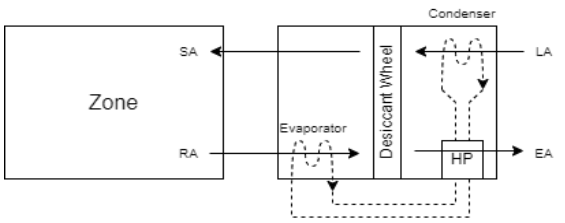

Fig. 1 – Schematic diagram of HPDC.

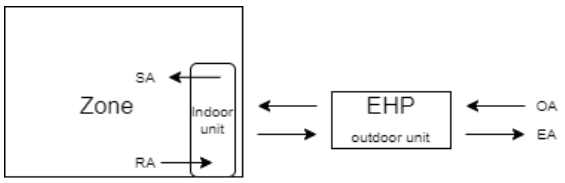

Fig. 2 – Schematic diagram of PAC.

2.2 Experiment 2 (HPDC v.s. HPDC w/RCP)

In experiment 2, adaptability of HPDC combined with RCP to resident building was analysed compared with HPDC system. When operate HPDC w/ RCP, LA also used as inlet air-source for the desiccant dehumidification and OA is used to produce chilled water used at RCP. Fig. 3 shows the schematic diagram of HPDC w/RCP. HPDC can control room air temperature and relative humidity by itself. But by using RCP, the energy use for cooling and dehumidification will be reduced and comfort also be increased.

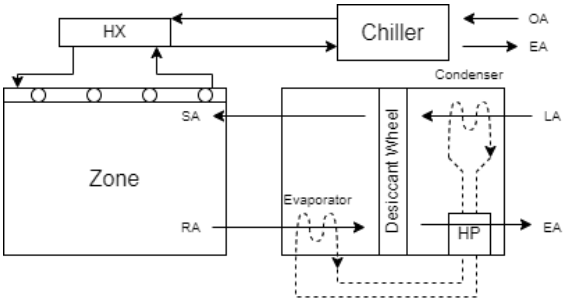

Fig. 3 – Schematic diagram of HPDC combined with RCP.

2.3 Experiment Criteria

Main target of the study is resident building in hot and humid climate (e.g. Seoul, South Korea). Considering this, the living room located at the inside part of the building was traced to the experiment chamber. Because the inside part of the building is traced, only internal heat gain was considered (especially the load due to people. Other loads like solar radiation and loads due to lighting and device were ignored).

Cooling and dehumidification are main subject of the study, cooling season is selected as experimental environment, Outdoor temperature is traced as 32°C at the outdoor air chamber. The initial condition of chamber at experiment 1 is assumed as 28°C, 40%. At experiment 2, to discriminate the performance of HPDC system and HPDC w/ RCP system, which have very similar consistence, initial condition goes higher by 30, 80%, Set point temperature and set point relative humidity were selected as 26°C, 50% for each and temperature is prior control variable.

The number of occupants and internal load due to occupants were calculated according to floor area. To implement the internal load due to occupants, four 60W dummies consisted with light bulb to describe sensible load and one 157W humidifier to describe latent load were installed inside the chamber.

Both experiment 1 and experiment 2 were performed at the same environment conditions mentioned above (Tab. 1) for equality.

Tab. 1 – Experiment environment summary.

Criteria	Value
Chamber size	4.2 m x 5.5m x 3.0m
No. of Users	3.4 people
Sensible load	238 W
Latent Load	153 W
Sensible load Imitate	60 W dummy 4ea.
Latent load Imitate	157 W humidifier 1ea.
Chamber initial Temp.	30 ℃
Chamber initial Hum.	80 %
Set Temp.	26 ℃
Set Hum.	50 %

Experiment 1 was excuted during the autumn season (at average OA temperature 15). To get exact results, experiment 1 lasted 12 hours for each case to meet the stable room conditions. Experiment 2 was excuted during wintre season (at OA temperature -2). To simply confirm the adaptability of HPDC w/RCP, experiment 2 lasted 1 hours for each case to reach the set point temperature and set point relative humidity.

At each case, cooling and dehumidification systems were controlled only by on/off control to compare basic energy consumption and comfort which is not affected by specific control method. However, especially HPDC, to control the temperature and humidity only with the HPDC, HPDC was operated in cooling mode and dehumidification mode alternately. And inlet chilled water temperature (T_{CWS}) of RCP system was controlled with PI control.

Tab. 2 – Experiment cases.

Case	System	Heat Source	Control
Exp 1, Case 1	HPDC	Attached HP	Set point On/Off Dehumidification mode / cooling mode
Exp 1, Case 2	PAC	Air source EHP	Set Temp. On/Off
Exp 2, Case 1	HPDC	Attached HP	Set point On/Off Dehumidification mode / cooling mode
Exp 2, Case 2	HPDC	Attached HP	Set. Hum. On/Off
	RCP	Chiller	Set. Temp. On/Off T_{CWS} PI control

2.4 Evaluate methods

To evaluate the energy usage of PAC and HPDC, power meter was use to log the electric energy use. And to estimate the energy use at chiller for RCP, heat removed by radiant panel and chiller COP was used as equation.

$$Q_{chiller} = (T_{CWR} - T_{CWS})\dot{m}_{CW}/COP_{chiller} \quad (1)$$

Fig. 4 – Experiment facilities. (a) indoor chamber. (b) HPDC system. (c) PAC system. (d) RCP. (e) chiller for RCP. (f) 60W light bulb dummy for sensible load trace. (g) 157W humidifier for latent load trace.

And to evaluate the thermal comfort, comfort zone announced at ASHRAE 55 was used. The operative temperature and humidity ratio data of each case were scattered in psychrometric chart and discriminated whether the data was inside the comfort zone or not. The satisfaction of occupants' thermal comfort was expressed with comfort zone satisfaction ratio as can confirm at equation (2).

$$\frac{(The\ number\ of\ data\ at\ the\ comfor\ zone)}{(Total\ number\ of\ data)} \quad (2)$$

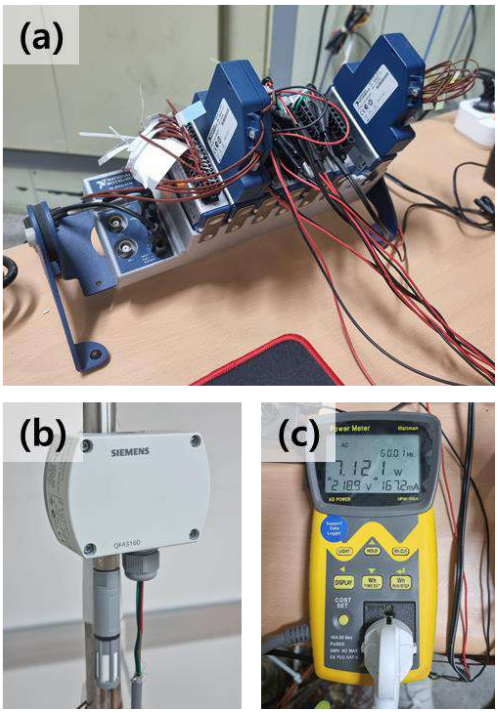

Fig. 6 – Sensors. (a) NI device for data collector and data transmission. (b) Relative humidity data logger. (c) Power meter.

3. Experiment Results

3.1 Thermal Comfort

Fig. 7 and **Fig. 8** shows the comfort distribution of the experiment 1.

The results show that Exp 1 Case 1, which used HPDC system controlled the temperature and humidity almost perfectly. There were no data which not satisfy the humidity range and just about 5.8% of data were dissatisfied the temperature comfort range.

Exp 1 Case 2, which used PAC system controlled not perfectly as HPDC. Lots of data were not inside the comfort zone. About 72.9% of data did not satisfy the humidity comfort range, only 0.8% of data did not satisfy the temperature comfort range in contrast.

With both results, the fact that HPDC system can control the indoor environment more perfectly in aspect of totally (temperature and humidity). However, as focus on temperature only, PAC system can control even more perfectly than HPDC system. On the other hand, PAC system also could not control the humidity well.

Through **Fig. 9** and **Fig. 10** shows the comfort distribution of the experiment 2.

The results show that Exp 2 Case 1, which used HPDC system mostly dissatisfied comfort zone because of the high initial condition and short experiment time. This is because, as designed, the experiments were carried out to just reach the set point and aim to confirm the reach speed. About 62.5% of data dissatisfied the temperature comfort range and 19.6% of data were dissatisfied the both temperature and humidity comfort range. Total 17.9% of data were satisfied comfort zone.

Exp 2 Case 2, which used HPDC w/RCP system also mostly dissatisfied due to the same reason of Exp2 Case 1. About 60.6% of data did not satisfy the temperature comfort range, and 11.5% of data were dissatisfied the both temperature and humidity comfort range. Total 27.9% of data were satisfied comfort zone.

With both results, HPDC w/RCP system can reach the comfort zone faster than HPDC system. And HPDC w/RCP can control the temperature better than HPDC system, according to the number of data satisfied the temperature comfort range. Thus, there is a possibility to adapt HPDC w/RCP system to resident building to get faster and better thermal comfort.

3.2 Energy Consumption

Energy consumption of each case can be found in **Fig. 11** and **Fig. 12.** Mentioned above, the energy consumption of PAC system and HPDC system were measured by power meter (**Fig. 6 (c)**). And the energy consumption of chiller used to make chilled water for RCP system were calculated by equation (1), which need the inlet and outlet temperature of chilled water used as RCP system. When calculate the energy consumption of chiller, the heat loss at distribution systems were ignored.

The energy consumption of Exp 1 Case 1 was much lower than Exp 1 Case 2 by 55%. Due to the energy wasted to perform subcooling and re-heating, PAC system consume much more energy than HPDC system.

The energy consumption of Exp 2 Case 1 was little bit higher than Exp 2Case 2 by 5%. HPDC system perform the cooling and dehumidification by itself using cooling mode and dehumidification mode alternatively. HPDC w/RCP system additionally used RCP for cooling compared to HPDC. HPDC system cools indoor air by convection using cooling coil.

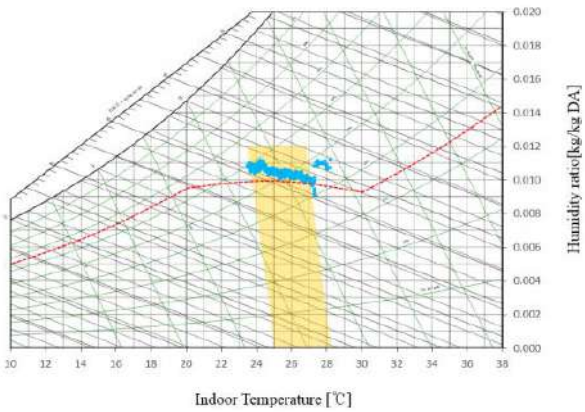

Fig. 7 – Comfort distribution of Exp 1, Case 1 data

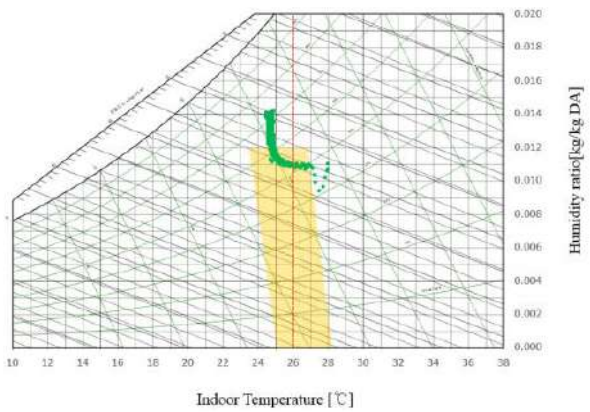

Fig. 8 – Comfort distribution of Exp 1, Case 2 data

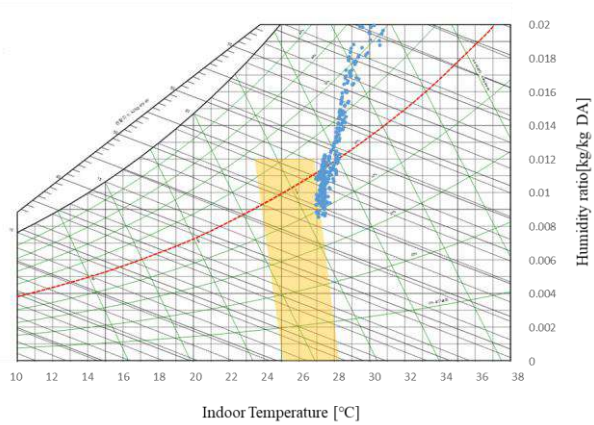

Fig. 9 – Comfort distribution of Exp 2, Case 1 data

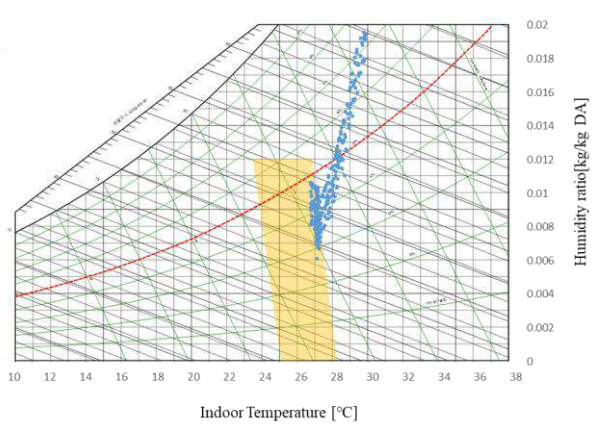

Fig. 10 – Comfort distribution of Exp 2, Case 2 data

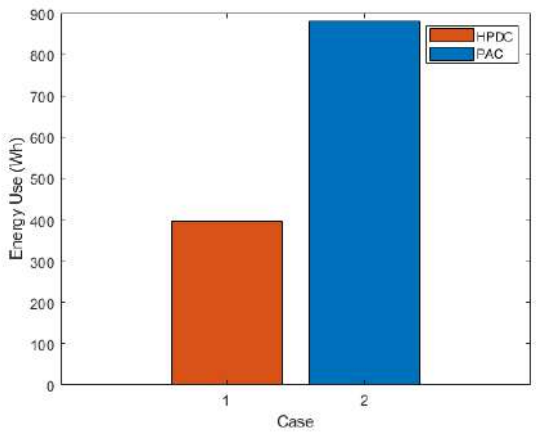

Fig. 11 – Energy consumption in Exp 1

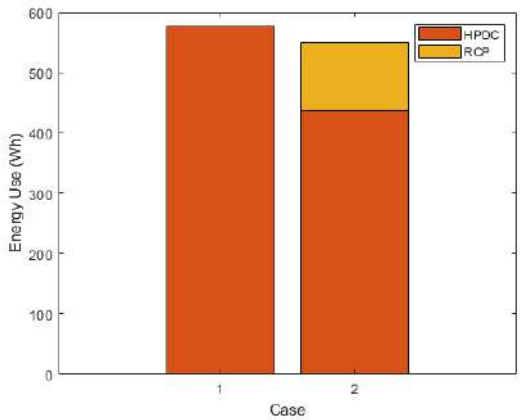

Fig. 12 – Energy consumption in Exp 2

And to be used at cooling coil for cooling mode, refrigerant inside the attached HP need to be cooled to temperature ranged at 7℃. However, when use RCP for cooling, sensible heat removed by radiation and, for that, the chilled water send to the RCP system does not need to be low temperature; it needs to be just 18℃. To make the 18℃ chilled water by heat exchanger between chiller and RCP, chiller only needs to make chilled water temperature at 12℃, which is much higher temperature than HPDC system. The difference between the temperature of evaporator

side needed to be produced leads to the difference of energy consumption between Exp 2 Case 1 and Exp 2 Case 2.

4. Conclusions

In this study, performance of HPDC w/ RCP was evaluated by experiment and analysed with comparative analysis with PAC system and HPDC system. Results are follows.

(1) Shown in experiment 1 results (**Fig. 7, 8, 11**), using HPDC system has lower frequency which are at the outside of ASHRAE comfort zone rather than PAC system. When using HPDC system, the non-comfort data (about 5.8% of data) were at out of comfort temperature range and there were no data out of comfort humidity range. And at the view of energy consumption, HPDC system used much less energy compared to PAC system by 55%.

(2) Shown in experiment 2 results (**Fig. 9, 10, 12**), using HPDC system combined with radiant ceiling panel can reduce the energy consumption by 5% compared to HPDC system used case. Furthermore, data of HPDC combined with RCP, which located at outside of ASHRAE comfort zone, is less than data of HPDC system by 12%. This means that using HPDC combined with RCP has possibility to be used for energy saving and thermal comfort.

(3) The experiment performed in this research is carried out during the autumn and winter season in Seoul, South Korea. However, the verification targets were cooling systems, Therefore the outdoor air temperature used at experiments were not suitable to exact comparative analysis because some heat sources (PAC system and chiller for RCP) uses outdoor air. For more exact and reasonable evaluation, experiment during the cooling season (summer) should be performed in further study.

Acknowledgement

This work was supported by the National Research Foundation of Korea grant (2021R1A2C1014415) funded by the Ministry of Science and ICT (South Korea) (MIST). We thank Humaster Co. for technical data support in desiccant wheel modelling.

References

[1] Katili AR, Boukhanouf R, Wilson R. Space Cooling in Buildings in Hot and Humid Climates—A Review of the Effect of Humidity on the Applicability of Existing Cooling Techniques. Proc 14th Int Conf Sustain Energy Technol. 2015;(August):25–7.

[2] Arundel A V., Sterling EM, Biggin JH, Sterling TD. Indirect health effects of relative humidity in indoor environments. Environ Health Perspect. 1986; 65(3):351–61.

[3] Liu S, Jeong CH, Yeo MS, Characteristic analysis of PTAC w/reheat system and heat-pump assisted hybrid solid desiccant cooling system, 2021 SAREK Winter Annual Conference, pp. 809-812.

[4] Fong KF, Lee CK, Chow TT, Fong AML. Investigation on solar hybrid desiccant cooling system for commercial premises with high latent cooling load in subtropical Hong Kong. Appl Therm Eng. 2011. 31(16):3393–401.

[5] Liu S, Jeong CH, Yeo MS. Effect of Evaporator Position on Heat Pump Assisted Solid Desiccant Cooling Systems. Energies, 2020, 13(22): 5918.

[6] Niu JL, Zhang LZ, Zuo HG, Energy savings potential of chilled-ceiling combined with desiccant cooling in hot and humid climates, Energy and Buildings, 2002, 34. pp. 487-495.

[7] Jang HS, Jeong CH, Yeo MS, Kwon YS. Applying Sensible·Latent Decoupling Cooling System through the Comfort Zone in Apartment Buildings in Summer, autumn annual conference of AIK, 2021, pp. 397-398.

Biomass in District Energy Systems: Overview and Perspectives for an Italian Case-Study

Lorenzo Teso [a], Tiziano Dalla Mora [a], Piercarlo Romagnoni [a]

[a] Department of Architectures and Arts, IUAV University of Venice, Venezia, Italy.
LT: lorenzo.teso@iuav.it, TDM: tiziano.dallamora@iuav.it, PR: piercarlo.romagnoni@iuav.it

Abstract. Buildings are one of the major users of energy in the European Union, accounting for almost half of the total consumption. In this scenario, renewable energy sources play a fundamental role in the transition towards a low-carbon society, and promoting their use is vital for the future of Europe. This work focuses on the use of district heating networks supplied with energy from biomass as a form of sustainable development for cities and communities, with attention to the Italian situation. After a first introductory part dealing with the European context of district energy networks, the focus shifts to Italy. It is introduced the diffusion on the national territory of district systems with a description of the most used energy sources that power these systems. To demonstrate how the use of biomasses in district energy networks represents a valid alternative to fossil fuels an analysis of the utilization of forests for wood harvesting in the Italian energy sector is carried out, showing how greenwoods and forests can withstand even greater exploitation for the collection of wood material for energy production. In order to prove the feasibility of the switch, a case study district, representative of the Italian residential building stock, is analysed. The district is firstly studied to evaluate the energy demand for space heating, and subsequently investigated by comparing different strategies for its energy efficiency improvement, all dealing with materials coming from wood processing, and switching from a decentralized energy system based on fossil fuels to a centralized network supplied by biomass. The results of the analysis show interesting results in primary energy consumption savings at least 38%, highlighting the potential of the demonstrated approach. Final remarks explain that, with the correct support of policies and awareness on the status of national forestry ecosystems, benefits are achievable through more intensive use of forests, leading to a higher share of natural feedstock in materials for the energy enhancement and energy production, that will help in reaching European sustainability goals.

Keywords. Solid biomass; Building energy demand; Energy efficiency; Renewable energy sources; Italy.
DOI: https://doi.org/10.34641/clima.2022.398

1. Introduction

To comply with climate agreements, the European Union (EU) has important goals to achieve by 2030 and 2050, focusing mainly on the penetration of renewable energy sources (RES) in the energy landscape, and increasing the efficiency of buildings to decrease consumption and harmful emissions.

Heating and cooling in industries and buildings represent half of the energy consumption of the EU [1]. European households use 79.2% (222.7 Mtoe) of the total energy they consume for heating and DHW. The largest share of energy used to cover buildings' needs comes from fossil fuels (66%), while just the remaining percentage (34%) is generated using RES [2].

In Europe, natural gas is the most widely used primary fuel for heating, accounting for around 44%. The use of coal, although halved since 1990, is still present in the European residential stock with a share of about 10%. Oil is also still used as a primary energy source, accounting for about 15%. Biomass has seen an increase of about 20% from 1990, but as with oil, about 95% of its supply is used in individual heating systems. The remaining renewables (e.g. solar, wind) only count for 3%. The switching from fossil fuels to less armful sources, coupled with energy efficiency works on buildings, has contributed to a decrease in harmful emissions since 1990, reaching the objectives of the EU of a reduction of at least 20% by 2020 [2,3].

In most European Member States (MS) heating is the largest final energy consumption in residential buildings. To curb energy use and emissions, energy efficiency measures are of paramount importance, but they are often not enough. While policies and directives are strongly implemented by the EU their application is often unsatisfactory. A further way to reach the EU sustainability goals is to improve the

Copyright ©2022 by the authors. This conference paper is published under a CC-BY-4.0 license.

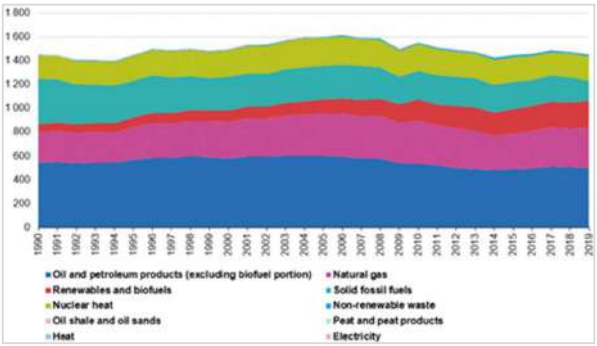

Fig. 1 - Gross inland energy consumption by fuel from 1990 to 2018 for the European MSs (EU-27) in million tonnes of oil equivalent. Data from [4]

efficiency of heat generators. In some cases, by modernizing the existing systems with more performing machines. There are other cases where alternative solutions exist. In areas with high heat density, district heating (DH) networks can be an interesting solution. Their versatility allows exploiting local heat surplus and possible integration with RES, but also more performing and efficient technologies such as combined heat and power (CHP). In favour of this switch towards network solutions, several studies claim that the heat demand in Europe is sufficient for the development and expansion of DH systems, even though currently only 12% of the energy needs are supplied by DH [5,6].

Heat Roadmap Europe studies, indicate how DH is more efficient than decentralized systems, also allowing higher shares of renewables [2]. Network systems are usually chosen also because a single plant means less maintenance and lower running costs, a reduction of the carbon emissions and improved air quality related to the switch from fossil fuels to RES. This latter aspect helps in the uptake of renewable energy, reduce fuel poverty, and create competitiveness in heating costs [7,8]. The goal of this paper is to provide an example of sustainable renovation for an Italian district located in the historical city of Venice through the development of a replicable methodology accompanied by an application to a case study of the renovation works on buildings' envelopes and the switching from a traditional heating solution based on natural-gas-boilers to a DH network powered by biomass.

1.1. DH networks across Europe and Italy

Although EC's plans for the development of DH systems are quite recent, Europe is one of the places where the highest number of DH networks are located. It is a widespread technology across the whole continent with more than 10,000 different networks installed [9]. Several small systems found application in Germany, mainly in cities where outdated heating systems were replaced by DH systems to reduce fire hazards in historical buildings containing art fortunes [10]. Scandinavian, the Baltic countries, and Central Europe present a higher degree of DH systems expansion because of the high consideration for the environmental and energy independence aspects. The climatic characterization is another important aspect: with its long and cold winter reflected in a high number of heating degree-days (HDD) (above 3,000), Central and Nordic Europe have a high heat demand index, resulting in major investments into expanding and improving the existing DH systems. Contrary to that, DH systems are not so common in southern European regions where the dominant energy sources are gas and fuel oil, and the density of buildings is lower. Exceptions of these considerations are cities: in countries where the climate is more temperate, the majority of DH systems can be found in densely built-up areas [11].

In Italy individual systems, mainly powered by electricity and natural gas, are used to meet heating and cooling needs. The last census shows that in 2018, 368 DH networks were operating, satisfying the thermal needs of 350 million m^3 of built-up spaces These systems are mainly located in the northern part of Italy, with higher concentrations in alpine areas, due to the rigid temperatures. However, since half of the Italian territory is characterized by cold winters (more than 2,000 HDD), is not unusual to find examples of these systems used in the central region of Italy, where the large availability of geothermal heat fuels numerous plants. Cities play an important role in the distribution of DH networks along the Peninsula: almost 200 examples are in contexts where the high density of heat demand made DHs the ideal solution for heating. A mix of different energy sources is used. The most widely used fuel is natural gas representing 64% of the total, RESs are still the smallest fraction, but increasing in recent years, in particular woody biomass-fuelled networks accounts for 13% [12]. Regarding the sizes, on average, small power plants are more common in Italy: 54% are smaller than 6 MW, 31% are in the range of 6 MW to 50 MW, and only the remaining 16 % are bigger than 50 MW [13].

1.2. Woody biomass harvesting in Italy

In the whole EU forests and their ecosystems are growing. In recent years the surfaces covered by woods have increased by about 13 million hectares. About 55% of the forested areas are currently used for harvesting wood for biomass [14]. In Italy, the situation is a bit different. Data from Italian Ministry of Agriculture, Food and Forestry Policies show that after actualizing the data considering the life cycle of the trees, out of a total of 241,800 ha (hectares) available for woody biomass harvesting, only 25% is used for extracting woods for energy reasons [15]. Therefore, it is possible to suppose an increase in the utilization of the available areas for wood harvesting and this scenario is foreseen in the Italian energy strategy (Strategia Energetica Nazionale, SEN): the growth in the use of RES for thermal energy production is acknowledged, but measures to promote and support this development are needed [16]. Optimizing the use of biomass can significantly improve the energy sector. To do so, measures to

stimulate the use and gradual expansion of the biofuels are needed.

2. Methods

The EC has in recent years supported the development of methodologies for the renovation of the building sector through projects and funding. In particular, the district scale approach is the one in which the scientific community believes most. The aim of this work is to demonstrate how the use of energy from renewable sources, together with improvements in the building envelope, could be a winning strategy to achieve the 2050 targets set by the EC. To do this, the methodology suggested by the IEA EBC Annex 75 project was used [17]. The work begins with the selection of a neighbourhood in desperate need of renovation. The decision fell on the residential neighbourhood of Santa Marta, located in the western part of the historic city centre on the island of Venice. The district was studied and digitally reconstructed through the use of QGIS software [18]. Once the model is digitally reconstructed, the buildings are assigned the thermophysical characteristics of the elements that compose it, the composition and structure of the heating and hot water production systems, and the usage characteristics. The model is then simulated using the City Energy Analyst (CEA) software developed by ETH Zurich [19]. Within the software environment all other settings necessary for the correct functioning of the model are set. A first simulation is carried out to create a baseline corresponding to the actual state. In the following steps, improvement scenarios are simulated by applying previously defined energy conservation measures on the building envelope elements and from the point of view of the plant systems. By comparing the results, it is possible to derive the energy saving potential of each scenario and to define the best of the scenarios in terms of costs, energy or somewhere in between [20].

The developed methodology is applied in the following paragraphs for the aforementioned case study of Venice.

3. Case study

The Italian political class aimed to end the insecure situation in which the low-income population found itself since the turn of the twentieth century. Luigi Luzzatti, an Italian lawmaker, founded the Istituto Case Popolari in 1903. (Public Housing Institute; ICP). The purpose of this organization was to provide low-cost housing that adhered to the most up-to-date sanitary and hygienic laws. In Venice, a chapter of ICP was founded in 1914 with the same goal: to improve the living conditions of the poor. The ICP's name changed several times over the years until it was renamed "Aziende territoriali per l'edilizia residenziale" (Local Agency for Residential Buildings) in the mid-90s.

The district under investigation, known as "Santa Marta IACP housing," was part of this wave of social housing building. It is located in the western portion of Dorsoduro, one of the six districts that make up Venice's old town, towards the city's southwest end. The district is irregularly shaped, but its dimensions are roughly 400 m × 160 m, with a total surface area of 3.78 hectares (ha) (equal to 0.04 km^2). The municipality began construction of the first set of 14 buildings for a total of 148 housing units in this neighbourhood in 1920, with the intention of accommodating low-income workers from adjacent enterprises and nautical workshops. These structures were finished in 1928. A second intervention in the area in 1930 ensured the construction of 365 more units in more than 21 new buildings.

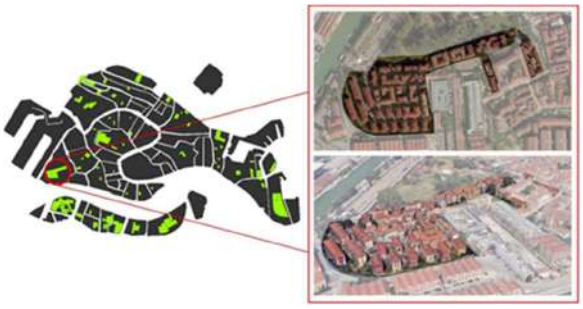

Fig. 2 - Map of Venice's historic centre, showing in green the social housing for low-income families within the Sestrieri. Moreover, satellite view and 3D visualization of the Santa Marta district in Venice

Most of the buildings in the case study are multifamily. The structure may be classified into two groups based on their age, and the geometry of the buildings varies slightly. The first series of buildings, constructed between 1920 and 1928, had a standard rectangular shape with lengths varying from 18 to 50 metres on the long side and a consistent 12.5 metres on the short side. Each building has four stories and two to six flats per floor, depending on the size of the building. The buildings in the second group, finished in 1936, have more complicated and variable geometries: they are typically structured around a central void or in a "C" shape. The sizes of these structures vary greatly, ranging from 170 m^2 footprints to complexes of over 1,500 m^2. The number of floors and flats varies as well, ranging from small two-story cottages with one flat per level to substantial five-story structures with up to 14 flats per floor.

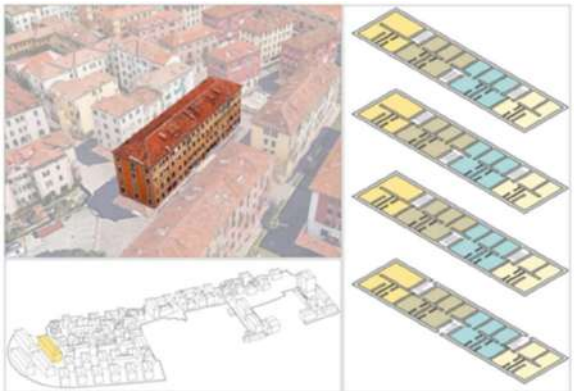

Fig. 3 - Representative building of the first group built between 1920 and 1928, with a regular rectangular shape. Aerial view from Google Earth, 3D map and plans.

The construction technologies used for the building envelope were the same in the two phases: two-headed solid masonry and plastered buildings, wooden roofing, hollow core slabs, wooden frame windows and single glazing. There is no insulation. Some differences can be found in the transparent envelope: double-glazed wooden frame windows have replaced some single glazed systems with a wooden frame, depending on the owners' willingness to retrofit the flat. The building's installations are standard and have undergone several updates while remaining faithful to the original supply network. The heating is provided to the flats by a centralized gas boiler installed in each building, although a single system for flat has been installed in some condominiums and in this case the generator is arranged for both heating and DHW. Cooling systems were not foreseen at the time of construction and are not currently present in most buildings. In some cases, a simple monosplit or multisplit air conditioner for one flat has been privately installed over the years by the users (owners or tenants). Domestic hot water (DHW) is provided by an electric water heater installed in each flat which, in the case of condominium heating, only works in summer. For heating, the overall efficiency used to define the boiler characteristics considers the efficiencies of generation, distribution, emission and regulation, provided that the pipes are not commonly insulated due to the age of the building, and that the heat is mainly emitted by cast iron radiators. The overall efficiency of this type of system is 80%.

The main parameters for setting the district model are described in Table 1.

Tab. 1 - Calculation parameters for the type of buildings in the neighbourhood

Parameter	Unit	Building typology
Building information		
number of buildings per typology		54
Construction period		1920-1936
Geometry		
Gross heated floor area (GHFA)	m^2	58,605.96
Net heated floor area (NHFA)	m^2	51,392.86
Heated volume	m^3	138,249.51
Façade area incl. window area	m^2	50,753.28
Roof area if pitched roof	m^2	15,241.27
In case of pitched roof: Is room below roof heated or not?	Yes/No	Yes
Area of windows to North	m^2	1,569.25
Area of windows to East	m^2	2,239.31
Area of windows to South	m^2	1,571.48
Area of windows to West	m^2	2,232.96
Number of floors above ground	-	1-5
Usage		
Type of use		Residential
area per occupant	m^2 / person	30.45
Typical indoor temperature (for calculations)	°C	20
Average electricity consumption per year and m^2 (excluding heating, cooling, ventilation)	$kWh/(m^2.a)$	28
HVAC systems		
Type of existing heating system (boiler, heat pump, etc.)		Boiler
Existing energy carrier (Gas, Electricity, etc.)		Natural gas
Is ventilation system without heat recovery installed?	Yes/No	No
Is ventilation system with heat recovery installed?	Yes/No	No
Efficiency of heat recovery	%	/
Ventilation rate	ach	0.3
Is cooling system installed?	Yes/No	No
Hot water consumption	l/person/day	40

3.1. Calculation parameters and scenarios

A thermal renovation of the selected case study has been proposed, considering five different scenarios of renovation measures on the building envelope.

Tab. 2 – List of the proposed scenarios with their interventions on the envelope of the buildings. Codes M3 to M6 refers to EPS application, M7 to M10 to WF.

Code	Description
M 1	no interventions
M 2	windows replacement
M 3, M 7	façade insulation
M 4, M 8	roof insulation
M 5, M 9	windows replacement and façade insulation
M 6, M 10	windows replacement, insulation of façade and roof

Two different insulating materials have been considered, expanded polystyrene (EPS) panels and wood fibre panels (WF), by application in the inner side of external walls due to the restrictions by Superintendency of Cultural Heritage to preserve the external envelope of buildings in the historical centre of Venice. This action has major repercussions on the price for the initial investments, since no needs for scaffoldings reduce the cost of intervention.

The following table resumes the data for energy performances and a global cost calculation adopted for each scenario.

Tab. 3 - Summary of the measures of intervention on the envelope with performance of the building component and investment and maintenance costs according to the type of insulation material selected. For the intervention in the transparent envelope, only one type with a wooden frame and triple glazing with low emission is intended. The service life is 30 years.

WALL	Unit	Reference	EPS	WF
U-values	W/m^2K	1.71	0.25	0.25
Investment costs	EUR/m^2		38.93	67.02
Maintenance costs	EUR/m^2y	1.27	1.52	1.71
ROOF	**Unit**	**Reference**	**EPS**	**WF**
U-values	W/m^2K	2.70	0.20	0.20
Investment costs	EUR/m^2		119.94	139.70
Maintenance costs	EUR/m^2y	2.09	2.87	3.00
WINDOW	**Unit**	**Reference**	**New**	
U-values	W/m^2K	5.8	1.00	
Investment costs	EUR/m^2		333.8	
Maintenance costs	EUR/m^2y	1.60	3.78	

In the present scenario, each flat is equipped with a condensing boiler fuelled by natural gas, with a water-based distribution system. For the purpose of the study, a centralized heat distribution system is planned considering two combined heat and power (CHP) generators, a natural gas fired, and a biomass powered (Table 4) [21]. The selected systems present a difference in costs: the investment costs assumed for gas CHP is 830 €/kW, coupled with 29 €/kW of yearly maintenance, while for a biomass generator the costs are respectively 500 €/kW and 17 €/kW year.

Tab. 4 - Summary of the measures of intervention on the system with sizing referred to the needs calculated for each scenario of intervention on the envelope. The service life is 15 years.

Parameter	Unit	M 1	M2	M 3	M 4	M 5	M 6
I1 - Central heating system 1 (Natural Gas CHP)							
Capacity	kWe	2,241	1,810	1,717	1,797	1,375	1,012
I2 - Central heating system 2 (Biomass CHP)							
Capacity	kWt	604	524	499	521	407	309

All the different heat supply systems are coupled with all the energy efficiency measure scenarios, totalling 21 cases, including the scenarios in which no envelope interventions are foreseen, only the substitution of the heating generators.

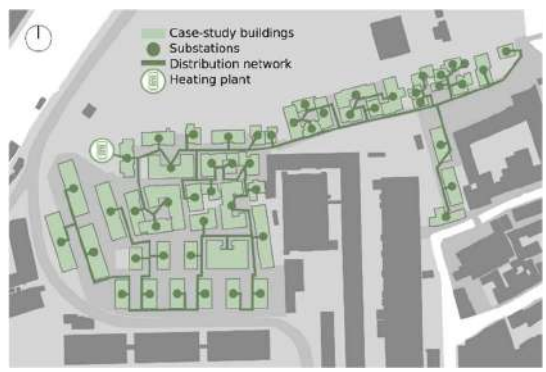

Fig. 4 - Plan of centralized network, CEA elaboration.

The design of the supply network and its substations is considered by using the CEA tool, in which the characteristics of the selected plants are implemented in the model and a district network is calculated.

For the case study of the Santa Marta district, the network is defined as in and extends for 1,782.72 m. The main power plant was located to the east of the area for a number of logistical and feasibility reasons: it is a large port area where the connecting infrastructure network, i.e., road, tram and marine networks with their landing stages, are still in use and would facilitate the storage and transport of materials such as biomass to Venice main island. In addition to dimensioning the length according to the route, each pipe section of the network is dimensioned according to the energy needs for heating and hot water of each building (better each

substation). The parameters of length and diameter of the network influence the installation costs. In the present case, parametric costs from literature and professionals are applied, as shown in Table 5. Also costs for the substation installation are adopted at the parametric level, counting 30% of the total pipeline installation cost, white the maintenance costs are evaluated as 10% of the total cost of pipeline and network over the service life period. Therefore, the cost of a centralized system network is a function of the shorter length and smaller diameter, i.e., it is related to the geometric density of the district and the energy needs of the buildings.

Tab. 5 - Supply and placement of the network pipework parameterized according to the length and diameter of the segment.

Diameter [mm]	Cost [€/m]
20	100
25	114
32	123
40	133
50	145
65	226
80	361
100	415
125	471
150	517
200	620
250	700
300	775
350	930
average	402

The scenarios are combined according to the following scheme, in which interventions on the envelope have code M, and installations have code I.

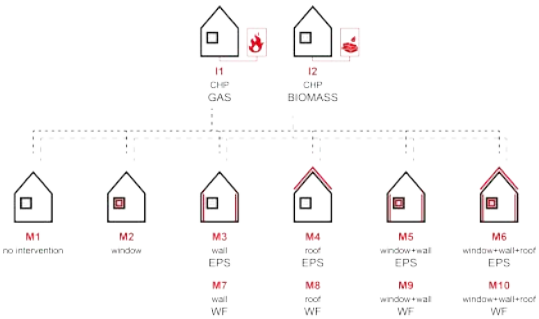

Fig. 5 - Overview of selected scenarios combined by measures of intervention on envelope (M) and new centralized system (I).

4. Results

The proposed scenarios were simulated and analysed in comparison with the Reference case to identify Primary Energy consumption, GHG emissions and Global Costs, as shown in the table below. Some notes can be made on the results obtained. The planned measures lead to energy efficiency that halves primary energy consumption for most scenarios. Among the measures in the envelope, the most efficient are those that consider an insulation intervention of the whole envelope (M6 and M10). Moreover, it should be underlined how the substitution of energy system (M1 code, without envelope intervention) could halve the energy use of Reference case, reducing the Primary Energy from 508 kWh/m^2 yearly to 313 kWh/m^2 yearly by adoption of a Natural Gas CHP and 268 kWh/m^2 yearly for Biomass CHP.

Tab. 6 - Summary of the calculated outputs, highlighting the minimum (in green colour) and maximum (in red colour) values for each parameter. Values are expressed per unit of net conditioned area (NHFA). Global costs is the sum of investment, maintenance and energy costs

Scenario	Primary Energy [kWh/m^2 y]	GHG Emissions [kg CO2eq/m^2 y]	Investment [€/m^2 y]	Maintenance [€/m^2 y]	Energy Cost [€/m^2 y]	Global Cost [€/m^2 y]
Reference	508	118	45	61	709	815
Natural Gas CHP						
I1_M1	313	74	47	97	504	648
I1_M2	281	66	89	99	454	642
I1_M3	271	64	70	94	438	603
I1_M4	291	68	75	96	469	640
I1_M5	232	54	113	98	379	591
I1_M6	192	45	140	99	317	556
I1_M7	271	64	94	99	438	631
I1_M8	291	68	81	98	469	647
I1_M9	232	54	137	103	379	619
I1_M10	192	45	172	126	317	614
Biomass CHP						
I2_M1	268	63	27	81	417	525
I2_M2	236	56	74	88	377	540
I2_M3	225	53	57	84	364	505
I2_M4	245	58	61	85	389	535
I2_M5	187	44	103	90	320	513
I2_M6	146	34	133	93	275	501
I2_M7	225	53	80	89	364	533
I2_M8	245	58	66	87	389	542
I2_M9	187	44	126	95	320	541
I2_M10	146	34	164	99	275	538

The choice of material represents a question of cost as both proposed materials must guarantee the same requirement of equivalent thermal transmittance and therefore the factor that influences is the unit cost, in this case higher for wood fibre. The Global Costs have been calculated with an interest rate of 3% for a service life of 30 years. The best cost-effective solution is given by the scenario in which a centralized grid system is installed with a Biomass CHP generator combined with the insulation of the full envelope (I2_M6). In analytical terms, the table shows that, looking at the energy efficient solutions, the investment and maintenance costs are certainly much higher to be sustained and amortized over time

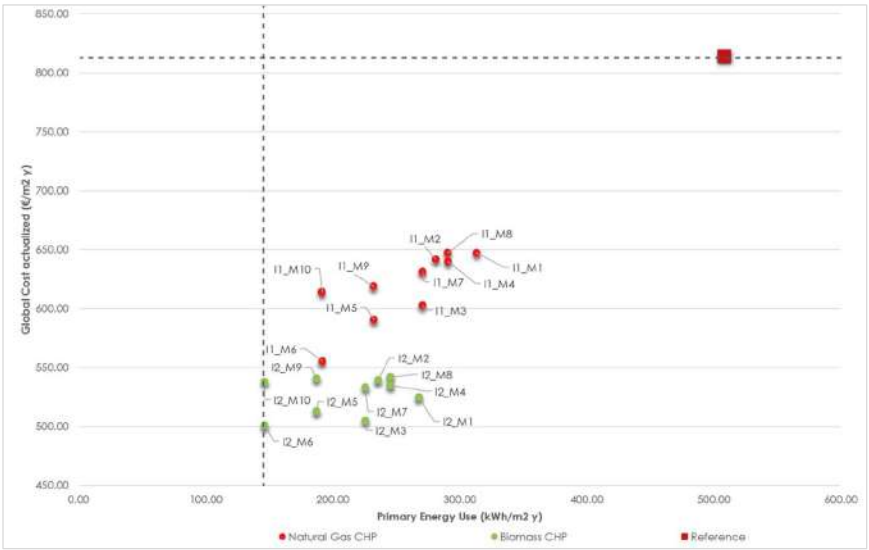

Fig. 6 - Chart Global Cost and Primary Energy to identify the optimal intervention solution: the horizontal and vertical dotted lines indicate respectively the margin downwards of the cost-effective solutions in relation to the Reference and the margin of the most efficient solutions to the left in relation to the optimal solution.

(133 €/m² and 93 €/m² respectively for the I2_M6 scenario), but the total energy costs would be lower due not only to the better performance of the system (and therefore lower consumption of primary energy), but also to the lower unit cost of the energy vector. In fact, for this study the applied conversion values are shown in the Table 7 and energy costs and CO_2 emissions are also included.

Tab. 7 - Primary energy conversion factors, prices and emissions of the energy carriers adopted.

Energy Vectors	*Primary Non-Renewable Energy Fp,nren [-]*	*Primary Energy Renewable Fp,ren [-]*	*Total Primary Energy Fp,tot [-]*	*Unit price [€/kWh]*	*CO2 emissions [kg CO_2eq/kWh]*
Electricity	1.950	0.470	2.420	0.219	0.483
Natural Gas	1.050	-	1.050	0.081	0.250
Wood pellets	0.200	0.910	1.110	0.067	0.030
Wood chips	0.200	0.910	1.110	0.028	0.032
Oil	1.070	-	1.070	0.170	0.267
DHN electric	1.200	0.300	1.500	0.150	
DHN gas	0.640	0.920	1.560	0.068	
DHN biomass	0.300	1.200	1.500	0.060	

Biomass values are divided by type of wood chips and pellets according to the different cost on the market and the CO_2 emission factor, while for district heating the values certified by plant operators present on the Italian territory have been considered, with relative application of tariffs to the consumer. The prices adopted for the final consumer are referred to the year 2018, for the energy carrier electricity and natural gas they are elaborated from the Eurostat database [22], while for biomass reference is made to the 2018 report of the Italian Agroforestry Energy Association AIEL [23].

Looking at the summary graph (Figure 6) of the results in terms of global costs and primary energy, the cost optimal solution is identified in the I2_M6 scenario, that coincides with the most energy efficient one. Compared to the Reference case, the costs are reduced by 38%, but in general the graph shows the influence of the installation of centralized biomass plants. The scale of the graph may influence the evaluation as the overall costs vary by about 50 €/m² y, but in the case of the district they are equivalent to about 86,000 € per year.

5. Discussion and conclusions

The results of calculation on the presented case study demonstrates the validity to install a DHN with biomass energy vector to reduce energy consumption and GHG emission in comparison to fossil fuels. Even if the simulation shows the cost-effectiveness of intervention both on envelope and energy system, the adoption of Biomass system halves the Primary Energy use and could be the first step to district building refurbishment with the aim to reduce also GHG emissions. The increased use of biomass in the national energy mix is foreseen by Italian energy strategies and is justified by the analyses presented above. Currently only a quarter of the potentially available woody biomass is used for energy purposes. In the transition to a more sustainable future, biomass represents a viable alternative to fossil fuels due to its renewable nature and lower harmful emissions into the atmosphere.

Furthermore, the possibility of creating a district network to replace individual boilers per building is a step towards greater sustainability of the energy sector in the Italian residential sector. However, to achieve even better results it is necessary to optimise the biomass cycle by stimulating its use with ad hoc policies and financial and technical support.

Future developments in this research will focus on defining scenarios in which the entire set of interventions is carried out with wood-based materials. In the case study, the most cost-effective and energy-efficient choice was the use of polyurethane insulation, but with a more careful analysis of the life cycle of the insulation materials it will be possible to make the entire set of interventions on both the building envelope and the energy supply wood-based.

6. References

[1] Review of Available Information on an EU Strategy for Heating and Cooling, (2016).

[2] F. Tobias, R. Elsland, M. Rehfeldt, J. Steinbach, U. Reiter, G. Catenazzi, M. Jakob, C. Rutten, R. Harmsen, F. Dittmann, P. Rivière, P. Stabat, Profile of heating and cooling demand in 2015, (2020).

[3] Odyssee-Mure, Odyssee 2017, (n.d.). http://odyssee.enerdata.net/home/ (accessed December 27, 2019).

[4] Eurostat, Gross inland energy consumption by fuel, EU-27, 1990-2018, (2019). https://ec.europa.eu/eurostat/statistics-explained/index.php/Energy_statistics_-_an_overview.

[5] BloombergNEF, Sector Coupling in Europe: Power Decarbonization, 2020.

[6] A. Volkova, V. Mašatin, A. Siirde, Methodology for evaluating the transition process dynamics towards 4th generation district heating networks, Energy. 150 (2018) 253–261. https://doi.org/https://doi.org/10.1016/j.energy.2018.02.123.

[7] L. Liu, P. Rohdin, B. Moshfegh, Investigating cost-optimal refurbishment strategies for the medieval district of Visby in Sweden, Energy Build. 158 (2018) 750–760. https://doi.org/10.1016/j.enbuild.2017.10.002.

[8] X. Zhang, G. Strbac, N. Shah, F. Teng, D. Pudjianto, Whole-System Assessment of the Benefits of Integrated Electricity and Heat System, IEEE Trans. Smart Grid. 10 (2019) 1132–1145. https://doi.org/10.1109/TSG.2018.2871559.

[9] Euroheat & Power, District Heating and Cooling Country by Country - 2015 Survey, 2015.

[10] S. Frederiksen, S. Werner, District Heating and Cooling Development, in: Dist. Heat. Cool., Studentlitteratur AB, 2013: pp. 541–560.

[11] M.A. Sayegh, J. Danielewicz, T. Nannou, M. Miniewicz, P. Jadwiszczak, K. Piekarska, H. Jouhara, Trends of European research and development in district heating technologies, Renew. Sustain. Energy Rev. 68 (2017) 1183–1192. https://doi.org/10.1016/j.rser.2016.02.023.

[12] AIRU, Il Riscaldamento urbano Annuario 2018, AMARC DHS Srl. (2018) 375.

[13] A. Grossi, Stato e prospettive della regolazione del settore del teleriscaldamento e teleraffrescamento Introduzione al seminario, (n.d.).

[14] M. Mikoláš, K. Ujházy, M. Jasík, M. Wiezik, I. Gallay, P. Polák, J. Vysoký, M. Čiliak, G.W. Meigs, M. Svoboda, V. Trotsiuk, W.S. Keeton, Primary forest distribution and representation in a Central European landscape: Results of a large-scale field-based census, For. Ecol. Manage. 449 (2019) 117466. https://doi.org/10.1016/j.foreco.2019.117466.

[15] Ministero delle Politiche Agricole Alimentari e Forestali Ispettorato Generale - Corpo Forestale dello Stato, CRA - Unità di Ricerca per il Monitoraggio e la Pianificazione Forestale, INFC 2005 - Inventario Nazionale delle Foreste e dei Serbatoi Forestali di Carbonio, 2007.

[16] Ministero dello Sviluppo Economico, Ministero dell'Ambiente e della Tutela del Territorio e del Mare, Strategia energetica nazionale (SEN) 2017, 2017. http://www.enea.it/it/seguici/le-parole-dellenergia/glossario/parole/strategia-energetica-nazionale-sen (accessed April 4, 2019).

[17] J.M. Hidalgo-Betanzos, IEA Annex 75 | Cost-Effective Building Renovation at District Level Combining Energy Efficiency & Renewables - Workshop document, 2019. https://annex75.iea-ebc.org/ (accessed February 19, 2021).

[18] QGIS - A Free and Open Source Geographic Information System, (n.d.). https://www.qgis.org/en/site/ (accessed February 27, 2020).

[19] J.A. Fonseca, T.A. Nguyen, A. Schlueter, F. Marechal, City Energy Analyst (CEA): Integrated framework for analysis and optimization of building energy systems in neighborhoods and city districts, Energy Build. 113 (2016) 202–226. https://doi.org/10.1016/j.enbuild.2015.11.055.

[20] T. Dalla Mora, L. Teso, L. Carnieletto, A. Zarrella, P. Romagnoni, Comparative Analysis between Dynamic and Quasi-Steady-State Methods at an Urban Scale on a Social-Housing District in Venice, Energies. 14 (2021) 5164. https://doi.org/10.3390/en14165164.

[21] L. Carnieletto, S. Graci, M. De Carli, Hypothesis for a more efficient and sustainable development of a district heating in Padova, integrating renewable energies and existing generation plant, E3S Web Conf. 111 (2019) 6021. https://doi.org/10.1051/e3sconf/201911106021.

[22] Prices - Energy - Eurostat, (n.d.). https://ec.europa.eu/eurostat/web/energy/methodology/prices (accessed January 10, 2022).

[23] AIEL Associazione Italiana Energie Agroforestali, Mercati & prezzi, 12 (2020) 1–8. https://www.aielenergia.it/public/pubblicazioni/162_M_P_1-2020.pdf.

Examination of life cycle cost in nZEB design

Makiko Ukai [a], Masaya Okumiya [b], Gyuyoung Yoon [c], Hideharu Niwa [d]

[a] Graduate School of Environmental Studies, Nagoya University, Nagoya, Japan. ukai@nuac.nagoya-u.ac.jp.

[b] Nagoya Industrial Science Research Institute, Nagoya, Japan. masayaokumiya@yahoo.co.jp

[c] Graduate School of Design and Architecture, Nagoya City University, Nagoya, Japan. yoon@sda.nagoya-cu.ac.jp. [d] Nikken Sekkei Research Institute, Tokyo, Japan. niwah@nikken.jp

Abstract. In this paper, the feasibility and net present value of life cycle cost (LCC(NPV)) of nZEB under the meteorological conditions of Sapporo, Japan was examined for the model building. The procedure for examining the feasibility of nZEB is as follows. First, a building with envelope and equipment that meets the performance standards of the Japanese Building Energy Conservation Law is set as a reference building. Then the energy performance improvement measures of strengthening the thermal insulation performance, installing energy-saving lighting equipment, improving the efficiency of the heat source, installing the total heat exchanger, a combined heat and power and PV power generation were applied in order of cost effectiveness. And the change in LCC(NPV) was calculated. When all measures except PV power generation and ground source heat pump were adopted, the primary energy consumption was reduced by about 53%, which reached the level of ZEB Ready in Japan's ZEB evaluation. Furthermore, the installation of PV power generation reduced the primary energy consumption to about 25%. This is a nearly ZEB in Japan's ZEB evaluation. The point of becoming the cost optimum (minimum LCC(NPV)) was the level at which the primary energy consumption was about 50%. From this result, it was possible to show the importance of deciding the policy of ZEB while considering energy consumption and LCC(NPV) at the same time.

Keywords. Life cycle cost, nZEB, Net present value.
DOI: https://doi.org/10.34641/clima.2022.111

1. Introduction

International joint research by the Federation of European Heating, Ventilation and Air Conditioning Associations (REHVA) and The Society of Heating, Air-Conditioning and Sanitary Engineers of Japan (SHASE) started in April 2018. In this joint research, we are conducting research on the comparison of energy performance of nearly zero energy buildings (hereinafter, nZEB) in countries with different climates.

So far, we have examined the methods of comparing the energy performance of nZEB and confirmed the difference in the conditions of energy performance evaluation between Europe and Japan. Then, a model building was defined, and a method for comparing the energy requirement performance of nZEB under different conditions was examined [1)].

The move toward a carbon-free society has become a global trend, with the EU Green Deal "Achieving Climate Neutrality in 2050" in 2019, the "Net Zero Emissions of Greenhouse Gases by 2050" in the Byden Plan and China's "carbon neutrality by 2060" in 2020. And in Japan, in October 2020, former Prime Minister Suga declared that "Japan aims to reduce greenhouse gas emissions to zero as a whole by 2050, that is, to realize a carbon-neutral, carbon-free society in 2050."

At COP26 held in Glasgow, England in 2021, in order to pursue efforts to limit the temperature increase to 1.5℃ above pre-industrial levels, contracting parties were urged to take measures against carbon neutrality in the middle of this century and ambitious climate change toward 2030. In parallel with these, the greenhouse gas or CO_2 reduction targets of each country were strengthened, and in October 2021, the Global Warming Prevention Headquarters decided the strengthened Nationally Determined Contribution (NDC) of Japan, as "Japan aims to reduce its greenhouse gas emissions by 46 percent in fiscal year 2030 from its fiscal year 2013 levels, setting an ambitious target which is aligned with the long-term goal of achieving net-zero by 2050. Japan will continue strenuous efforts in its challenge to meet the lofty goal of cutting its emission by 50 percent. "The breakdown of 46% is 51% in the Commercial and others sectors and 66% in the

Copyright ©2022 by the authors. This conference paper is published under a CC-BY-4.0 license.

Residential sector, and these reduction targets are very strict compared to other sectors. Furthermore, in the "Green Growth Strategy for 2050 Carbon Neutral" announced in December 2020, " The houses/building field is a key field for carbon neutrality in the home/business sector, and once built, becomes a long-term stock; and is a field that should be addressed immediately." Then the spread of ZEH and ZEB is mentioned as a priority issue.

ZEB's design flow begins with reducing the load of air conditioning, lighting, etc. as much as possible by making full use of architectural energy saving measures (passive measures) while maintaining indoor thermal comfort. Building service such as highly efficient air conditioning systems and artificial lighting is applied to this reduced load and active renewable energy utilization (energy creation) to aim net zero level. And in the actual design, while these flows are the basis, various energy saving methods should be introduced after careful consideration of cost benefits in order to realize nZEB at an appropriate cost. In addition, the final decision should be made after understanding the optimal cost level while considering changes in energy consumption and life cycle cost.

Based on the above background, this paper examined the feasibility and life cycle cost of nZEB under the meteorological conditions of Sapporo, Japan, for the model building adopted in previous paper [1)] as part of the international joint research.

2. Method

2.1 model building, input data and BEI

Figure 1 shows a reference building model [1)], which has a net floor, envelope and window areas of 4451.8 m^2, 3993.9 m^2 and 1326 m^2, respectively. The reference building is used as an office building in Sapporo , Japan and its input data is shown in Table 1. The heating degree day of Sapporo is 2,267 (2021,IWEC weather data) and the cooling degree day is 687.

Figure 2 shows the definition of Japanese ZEB according to the present regulation. Energy performance requirements in Japan are regulated by BEI indicator, which is the ratio of design and standard value representing so-called reference-building method. BEI = 1.0 is the minimum requirement and BEI = 0.5 is set for ZEB Ready with the aim to reduce primary energy by 50% compared to the present energy requirement. Primary energy includes energy uses for HVAC, domestic hot water and lighting. The standard value of primary energy is determined by multiplying the reference factor by each floor area and summing them. The reference factor for each energy use has been defined depending on the 8 climate regions, 8 building types, and 201 room types. The reference value for HVAC is estimated according to the heat load calculated based on the input data as shown in Table 1. Official tool, WEBPRO is used to simulate the standard value as well as the designed value. WEBPRO has been produced by the Japanese National Building Research Institute [2)3)].

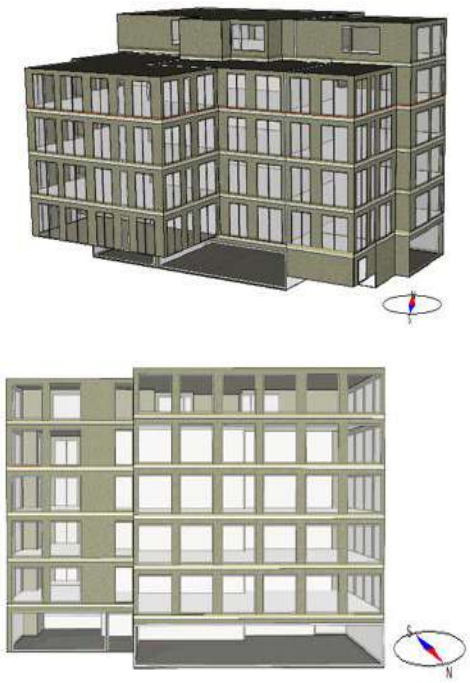

Fig.1 Views of simulated reference building model

Tab. 1 Input data for the reference building

Input data	[a]Japan (Sapporo)
Occupant, m^2/person	10
Appliances, W/m^2	12
Lighting, W/m^2	[b]16.3/7.5
Air volume flow by re-circulation, m^3/h. m^2	[c]17.1
Appliances & lighting operation hour	8:00-21:00
Usage factor	0.89
DHW, l/m^2 a	91.58
Fan operation hour	7:00-21:00
Ventilation rate, l/m^2 s	1.39
Heating set point, °C	22
Cooling set point, °C	26

[a] Relative humidity during heating season should not be less than 40% and not more than 50% during cooling season;
[b] Lighting power for 2016 and ZEB ready are 16.3 and 7.5 W/m^2, respectively;
[c] Re-circulation was used only with 2016 regulation and was not applied to Japanese nZEB

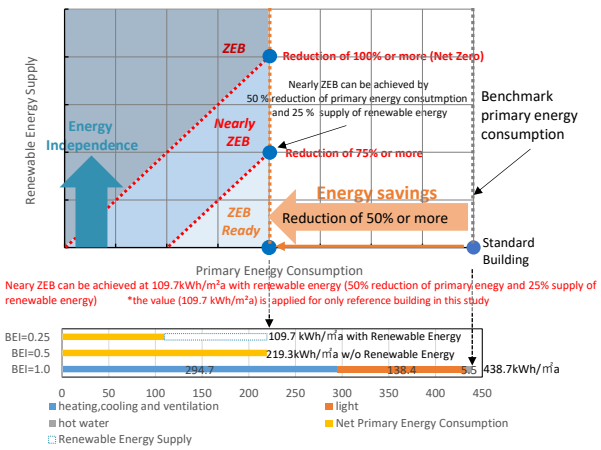

Fig. 2 Energy performance of reference building according to present regulation

2.2 calculation method for energy consumption

In this subsection, the reference building and system specification and the energy conservation measures are described.

Energy performance of the reference building were estimated with using the WEBPRO. Table 2 shows the building and system specifications for baseline calculation with input data listed in table 1. BEI for the baseline for further analysis is 0.98.

Tab. 2 Building properties and system specification for baseline with BEI=0.98

Building properties	
U- value (Outer wall) [W/㎡K]	0.32
U-value (Roof)	0.61
U value (Windows)	2.8
Solar radiation heat acquisition rate [-]	0.79
Systems	
specifications	**Installed number**
Air- source heat pump Cooling/Heating capacity: 252 kW/513kW COP for cooling/Heating : 3.23/2.95 Primary circulation pump: 11.7 kW	2
Secondary pump 31.4㎥/h, 4.8kW (constant water flow)	2
Outdoor air handling unit Cooling/Heating capacity: 106kW/280kW 13268㎥/h (CAV), 11kW for fan Total heat exchanger efficiency:60%	1
Fan coil unit Cooling/heating capacity:2.5kW/4.2kW	225
Gas-fired hot water supplier Capacity: 2.0 kW, primary energy efficiency: 0.66	6

In this study, 10 energy conservation measures are applied to the design building; 1) better performance of insulation and windows, 2) lower hot water supply temperature for heating, 3) LED lighting and its control, 4) installing higher performance of domestic hot water supplier, 5) installing higher performance of heat source equipment, 6) installing higher efficiency of total heat exchanger, 7) variable volume control of secondary pump, 8) installing CHPs, 9) installing PV on the roof, and 10) installing ground source heat pump (hereafter, GSHP).

1) Insulation and windows

The U-value of the outer wall and roof for the baseline is 0.61 w/㎡K and 0.32 W/㎡K respectively. The improved value for the outer wall and roof is 0.27 and 0.18 W/㎡K respectively.

The U-value of windows for the baseline is 2.8 W/㎡K, and the solar radiation heat acquisition rate is 0.79. The improved U- value and solar radiation heat acquisition rate are 0.82 and 0.33 respectively.

2) Lower hot water supply temperature for heating

The setpoint of hot water supply temperature for heating for baseline case and energy conservation case is 45℃ and 40℃ respectively.

3) LED lighting and its control

As shown in Table 1, the internal heat gain from lighting equipment was reduced from 16.3W/m² to 7.5 W/m². In this study, time schedule control, illuminance control, human presence control, and function of illuminance initial correction are installed as energy conservation measures.

4) Higher performance of domestic hot water supplier

The primary-energy- based efficiency of the gas-fired hot water heater is improved from 0.66 to 0.9. In addition, the piping is insulated as energy conservation measures.

5) Higher performance of heat source equipment

Table 3 listed the specification of the heat source for energy conservation case. For the baseline case, two air-source heat pumps are installed shown in table 2. For the energy conservation case, 10 air-source module heat pumps are adopted in order to operate with higher efficiency when the cooling/heating heat load is small.

Tab. 3 Specification for the heat source for the energy conservation case

Specifications	**No.**
Air-source module heat pump Cooling/Heating capacity: 53.6 kW/53.6kW COP for cooling/Heating : 4.12/4.19 Primary circulation pump: 0.375 kW	10

6) Higher efficiency of total heat exchanger

For the baseline case, the efficiency of total heat exchanger is 60%. To achieve high efficiency of total heat exchanger, the bigger size of the total heat exchanger is selected and the face velocity is reduced. The value is improved to 77% for the energy conservation case.

7) Variable volume control of secondary pump

For the baseline case, the variable volume control of secondary pump is not installed, in other word, the water flow volume of secondary pumps is constant. For the energy conservation case, the variable volume control of the secondary pumps is installed and its minimum frequency ratio is set at 30%.

8) CHPs

For the baseline case, CHPs are not installed. For the energy conservation case, a CHP is installed listed in table 4. The exhaust hot water from a CHP is utilized for heating in winter. In summer, exhaust hot water from the CHP is not used.

Tab. 4 specifications of CHP

Installed number	1
Electricity [kW]	34
Power generation efficiency [%]	33.5
Exhaust hot water generation efficiency [%]	54.5

9) PV on the roof

Crystalline photovoltaics on the roof are installed for the case, the capacity of which is 131kW, facing the south. Its angle of inclination is 43°. The efficiency of the power conditioner is 0.93.

10) GSHP

Two out of 10 air source module heat pumps are replaced with GSHP. Table 5 shows the specification of GSHP. The length of the total ground source heat exchanger is 2000m with 25 boreholes (80m/each borehole).

Tab.5 Specification of GSHP

Installed number	2
Capacity (cooling/heating) [kW/each]	41.2/46.4
COP (cooling/heating)	5.42/4.18
Circulation volume of chilled/hot water [l/min/each]	118/133
Circulation volume for ground sour heat exchanger (cooling/heating) [l/min/each]	139/101
Electricity consumption of primary pump [kW/each]	0.4
Electricity consumption for ground source heat exchanger pump [kW/each]	0.75

For the estimation of energy consumption for the case with GSHP, LCEM tool [4)5)6)] is used for considering the actual performance of GSHP based on the cooling and heating load provided by the WEB-Based program.

2.3 Cost-effectiveness calculation

The cost-effectiveness of different energy conservation measures was estimated with net present value of life cycle cost (hereafter, LCC(NPV)) defined with eq.(1) to eq.(3). In the paper [7)], maintenance cost was not included in the economic calculation, however, in this study, maintenance cost is considered for each conservation measure.

$$C_{g(t)} = C_i + \sum_{i=1}^{15} \left(C_{ao,i} \times R_d(i) \right) + C_m \qquad eq.(1)$$

where t means the calculation period (in this study 15 years), $C_{g(t)}$ is total cost over the calculation period t [YEN], C_i is initial investment cost for a measure or a set of measures [YEN], $C_{ao.i}$ is annual operation energy cost during year i [YEN], Rd(i) is a discount factor for year i, C_m is maintenance cost [YEN].

Depending on the refurbishment of the systems, the cost-effectiveness calculation period was chosen to be 15 years.

$$C_m = K0 \times C_i \qquad eq.(2)$$

where K0 is the maintenance cost factor (=0.02).

The cost-effectiveness of the additional costs related to each energy conservation measure that was needed to meet the requirement of the nearly ZEB was assessed in these calculations.

$$\nabla \mathrm{LCC(NPV)} = \frac{\left(C_{g(t)}^{nZEB} - C_{g(t)}^{ref} \right)}{A_{floor}} \qquad \text{eq. (3)}$$

where, $C_{g(t)}{}^{nZEB}$ is global energy performance related cost included in the calculations of nZEB [YEN], $C_{g(t)}{}^{ref}$ is global energy performance related cost included in the calculations of reference building [YEN], and cooled/heated net floor are [㎡].

Initial additional costs compared to the baseline case for each conservation measure are estimated as follows.

1) Insulation and windows

$$dC_{ins} = (C1_{ins} - C0_{ins}) \times S \times (1 + k1) \times (1 + k2) \text{eq. (4)}$$

where, dC_{ins} is an additional cost for insulation [Yen], $C1_{ins}$ is a unit price with insulation 100mm [Yen/㎡], $C0_{ins}$ is a unit price with insulation 50mm [Yen/㎡], S is an area of outer walls and ceiling, K1 is delivery cost ratio (0.1) and K2 is expense ratio (0.2).

$$dC_{wind} = (C1_{wind} - C0_{wind}) \times S \times k3 \qquad \text{eq. (5)}$$

where, dC_{wind} is an additional cost for window glazing and flame [Yen], $C1_{wind}$ is a unit price with both windows and its sash for baseline case [Yen/㎡], $C0_{wind}$ is unit price with both window glazing and its flame for improved case [Yen/㎡], K3 is expense ratio.

Improving the thermal performance of the building envelope is expected to decrease the heat load and thus HVAC equipment capacity. However, this study does not consider the cost reduction due to the reduction in equipment capacity.

2) Lower hot water supply temperature for heating

There is no additional cost for this energy conservation measure.

3) LED lighting and its control

The additional cost for LED lighting and its control is set with the reference to the result of a similar project.

4) Higher performance of domestic hot water supplier

The additional cost for higher performance of domestic hot water supplier is set with the reference to the result of a similar project.

5) Higher performance of heat source equipment

The additional cost for higher performance of heat source equipment is set with the reference to the result of a similar project.

6) Higher efficiency of total heat exchanger

The additional cost for higher efficiency of the total heat exchanger is provided based on the quotation by the general contractor.

7) Variable volume control of secondary pump,

The additional cost for higher efficiency of the total heat exchanger is provided based on the quotation by the general contractor.

8) CHPs

$$dC_{CHP} = C1_{CHP} \times CAP_{CHP} \qquad \text{eq. (6)}$$

where, dC_{CHP} is the additional cost for CHP [Yen], $C1_{CHP}$ is the unit price per capacity of CHP, CAP_{CHP} is the electrical capacity of CHP .

9) PV on the roof

$$dC_{PV} = C1_{PV} \times CAP_{PV} \qquad \text{eq. (7)}$$

where, dCpv is the additional cost for PV [Yen], C1pv is the unit price per capacity of PV, CAPpv is the capacity of PV.

10) Ground source HP

$$dC_{gshp} = C1_{gshp} + C1_{boreholes} \times L_{boreholes} + C1_{hspump} \quad eq. (8)$$

where, dC_{gsgp} is the additional cost for GSHP, $C1_{gshp}$ is the cost for ground source HP itself, [Yen], $C1_{boreholes}$ is the unit price for digging boreholes, pile construction and piping work [Yen/m], $L_{boreholes}$ is the total length of the boreholes [m] and $C1_{hspump}$ is an additional cost for circulation pump of heat source water.

$C1_{gshp}$ is assumed to be zero because, as indicated in section 2.2. 10), two out of ten air source heat pump is replaced with ground heat source, therefore, there is no additional cost for GSHP itself.

2.4 Evaluation Indices

BEI and primary-energy-based energy consumption are the indices to evaluate the building energy performance. In this study, the order of applying energy conservation measures is followed by the philosophy of nZEB that passive design measures must be prioritized. In the evaluation, the energy conservation measure for building property including better insulation and windows is the first measure to apply. Then, the energy conservation measure will be adopted in the order of the lowest pay-back year.

The cost-effectiveness of different solutions was estimated using LCC(NPV) described in 2.3.

3. Results and discussion

Figure 3 shows the results of BEI for baseline case and energy conservation cases. The value in parentheses shows the annual unit energy consumption [kWh/m^{2}year]. The number in the square brackets from one to ten means applied set of energy conservation measures as listed in table 6. The effect of the energy consumption is accumulated from baseline (BL), that is, in the example, the value 0.92 is the results of installing better insulation and windows and lower hot water supply temperature for heating.

The figure indicates that a set of the energy conservation measures including better performance of insulation and windows, lower hot water supply temperature for heating, LED lighting and its control, high performance of domestic hot water supplier, high performance of heat source equipment, and high efficiency of total heat exchanger does not achieve BEI=0.5 (ZEB ready). In addition to the above measures, when the energy conservation measures including variable volume control of secondary pump, installation of CHP, PV and GSHP can achieve BEI=0.26 which is certified by almost Nearly ZEB. These results show that it is necessary to apply the further energy conservation measure to achieve nZEB requirement [BEI=0.25] in

Japan. In other words, it shows that Japanese nZEB requirement is ambitious requirement.

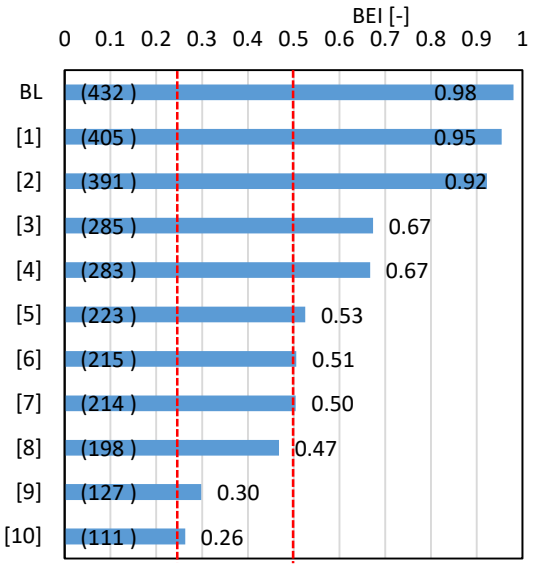

Fig. 3 Results of the BEI

Tab. 6 List of the set of energy conservation measures

Num.	set of energy conservation measures
[1]	Higher insulation and better windows
[2]	[1] and lower hot water supply for heating
[3]	[2] and LED lighting and its control
[4]	[3] and higher performance of domestic hot water supplier
[5]	[4] and higher performance of hear source
[6]	[5] and higher efficiency of total heat exchanger
[7]	[6]and variable volume control of secondary pump
[8]	[7] and CHPs
[9]	[8] and PV on the roof
[10]	[9] and GSHP

Table 7 shows the summary of the BEI, simple pay-back years, energy reduction cost of operation, construction cost, operation cost for 15 years and maintenance cost.

As shown in 2.4, although the simple pay-back years for better insulation and windows (27 years) is longer than some of the other energy conservation measures, it is first adopted to the baseline case as priority. The longest simple pay-back years is marked at installing GSHP because the digging cost is calculated based on a conservative unit price which might be significantly lower due to technological innovation, in addition because of the underestimating of energy-saving amount by replacing conventional heat source equipment to GSHP, because the ASHP module of the LCEM-tool used in this study does not consider the performance characteristic while the ASHP is under the defrost operation. As indicated in section 2.3, the calculation period in this study is 15 years. Insulation, windows and boreholes for GSHP have longer lifespan than 15 years, therefore these simple pay-back years are underestimated. Figure 4 shows the relation between accumulated reduction of operation cost and accumulated initial cost. From the case introducing lower hot water supply temperature for heating to the case installing CHP, their effects on accumulated reduction of operation cost is relatively high. PV on the roof has large impact both initial cost and operation cost.

Figure 5 shows the relation between LCC(NPV) and primary energy consumption. The lowest value of LCC(NPV) is marked at almost BEI=0.5, which means it would be certified by ZEB ready. In this study, the non-energy benefits of the improved thermal performance of the building envelope regarding thermal comfort are not considered. If these benefits are considered, the increase in LCC(NPV) due to that in the figure may be different. And the BEI with minimum LCC(NPV) was 0.5 as a result of prioritizing the installing enhanced thermal performance of building envelope, but different results would be derived depending on this priority.

From the viewpoint of the balance between BEI and LCC(NPV), construction of buildings with the level of ZEB ready is estimated by the lowest LCC(NPV). And it is expected that Nearly ZEB would be achieved at the similar level of LCC(NPV) of BL case.

As for the level of Nearly ZEB with BEI=0.25, the value of LCC(NPV) gets high because of the increase of initial cost. So, it should be needed that LCC(NPV) considers not only energy-benefits but also none energy-benefits to encourage the motivation to achieve ZEB further

4. Conclusion

In this paper, as part of the international joint research, the feasibility and LCC(NPV) of nZEB under the meteorological conditions of Sapporo, Japan was examined for the model buildings.

The procedure for examining the feasibility of nZEB is as follows. First, a building with envelope and equipment that meets the performance standards of the Japanese Building Energy Conservation Law is set as a reference building. Then the energy performance improvement measures of strengthening the thermal insulation performance, installing energy-saving lighting equipment, improving the efficiency of the heat source, installing the total heat exchanger, a combined heat and power, and PV power generation were applied in order of cost effectiveness. And the increase of LCC(NPV) was calculated.

When all measures except PV power generation and GSHP were adopted, the primary energy consumption was reduced about 53%, which reached the level of ZEB Ready in Japan's ZEB

Tab. 7 summary of the BEI, simple pay-back years, energy reduction cost of operation, operation cost for 15 years, and maintenance cost. The vaues of cost for BL are the reference, therefore each cost is to be zero.

	primary energy consu-mption	BEI	Invest-ent: P	Effect: M	P/M	Accumul-ated initial cost	Accum-ulated reducti-on cost of operati-on	Operati-on cost for 15 years	Mai-ntenan-ce cost	SUM
			Additio-nal initial cost	Reducti-on cost of operati-on	Simple pay-back years					
	kWh/㎡a	-	Yen/㎡	Yen/㎡	year	Yen/㎡	Yen/㎡	Yen/㎡	Yen/㎡	Yen/㎡
BL	432	0.98	0	0	0	0	0	0	0	0
[a][1]	405	0.95	6014	220	27	6014	220	-3,051	120	3,083
[a][2]	391	0.92	0	108	0	6014	328	-4,548	120	1,586
[a][3]	285	0.67	570	836	1	6584	1164	-16,145	132	-9,429
[a][4]	283	0.67	27	21	1	6611	1185	-16,435	132	-9,692
[a][5]	223	0.53	884	476	2	7495	1662	-23,040	150	-15,395
[a][6]	215	0.51	840	64	13	8335	1726	-23,925	167	-15,424
[a][7]	214	0.50	100	5	19	8435	1731	-23,997	169	-15,394
[a][8]	198	0.47	1910	124	15	10345	1855	-25,713	207	-15,161
[a][9]	127	0.30	17656	568	31	28001	2423	-33,593	560	-5,032
[a][10]	112	0.26	6811	114	60	34812	2537	-35,177	696	331

[a] the number in brackets are listed in table 6

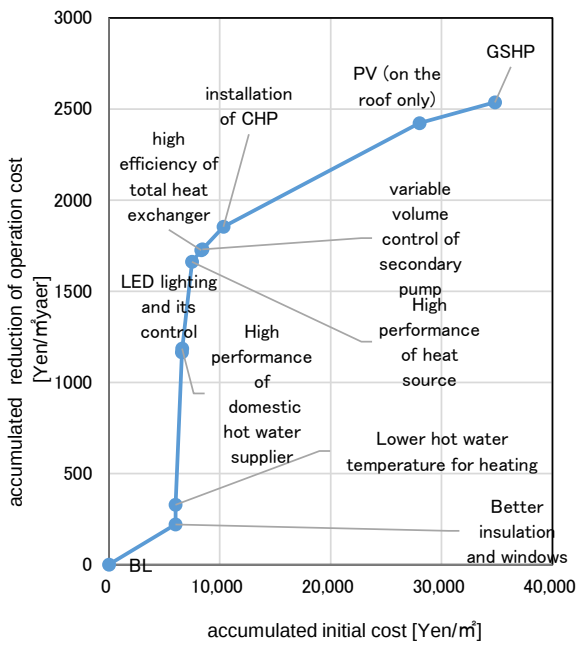

Fig. 4 the relation between accumulated initial cost and accumulated reduction of operation cost

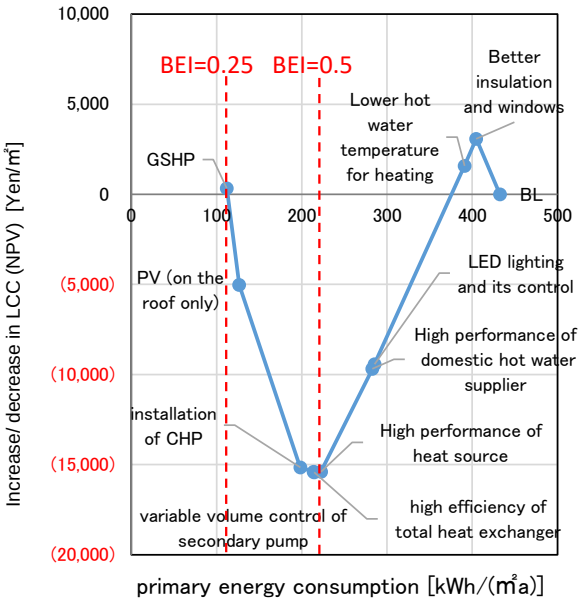

Fig. 5 relation between increase/decrease in LCC(NPV) and primary energy consumption.

evaluation. Furthermore, the installation of PV power generation reduced the primary energy consumption to about 25%. This is a nearly ZEB in Japan's ZEB evaluation.

The point of achieving the cost optimum (minimum LCC(NPV)) was the level at which the primary energy consumption was about 50%, marked at almost BEI=0.5, which means it would be certified by ZEB ready. And it is expected that Nearly ZEB would be achieved at the similar level of LCC(NPV) of BL case. From this result, it could be said that policy initiatives such as financial support are needed to raise motivation to achieve ZEB. Several research is also being conducted on the multiple benefits of energy efficiency improvement and the co-benefit of ZEB[8)9)10)]. Therefore, as the next step of the study, in addition to the LCC(NPV) composed of initial cost

and energy cost, the co-benefits such as thermal comfort, air quality, increased productivity, lower staff turnover, and reduced sick leaves will be considered for the evaluation of ZEB.

The specific values of energy performance and cost shown in this study depend on the conditions of the country or region such as weather conditions, material costs, labor costs, and manufacturing costs. On the other hand, these results show that the feasibility study and the LCC(NPV) analysis are very helpful measure to qualitatively and quantitatively understand how ambitious ZEB requirement are under the different climate and other conditions. In addition, these analyzes can be performed by utilizing simulation tools that are usually used in each country.

5. Acknowledgements

This research was supported by the Special Committee for Joint Study on NZEB between SHASE and REHVA, The Society of Heating, Air-Conditioning and Sanitary Engineering of Japan (SHASE). We would also like to thank Prof. Kurnitski Jarek for his advice in advancing this research.

6. References

[1] K. Ahmed, G. Yoon, M. Ukai, J. Kurnitski, How to compare energy performance requirements of Japanese and European office buildings. CLIMA2019. 2019;E3Ss Web of Conference 111; 03038.

[2] Building Research institute, National Research and Development Agency, Japan. WEBPRO. https://building.app.lowenergy.jp/ last accessed on 5th January 2022

[3] M. Miyata, T. Sawachi, Y. Kuwasawa, Y. Miki and Y. Akamine, Web-based simulation Tool for the 2013 Energy Efficiency Standard for Commercial Buildings in Japa, Asim 2014, IBPSA Asia Conference, Nagoya, Japan, November. 2014.

[4] Ministry of Land, Infrastructure Transport and Tourism. LCEM tool. https://www.mlit.go.jp/gobuild/sesaku_lcem_lcem.html last accessed on 5th January 2022

[5] R. Kobo, T. Kondo, et. Al., Development of Simulation Tool for HVAC system Combining with Ground-source Heat Pump, Part.3 Evaluation of system performance and accuracy verification of developed module, Technical paper of annual meeting, SHASE.J 2017.

[6] M. Ito, S. Murakami, et. Al., Development of HVAC System Simulation Tool for LCEM (Life Cycle Energy Management), Proceedings of Clima 2007 WellBeing Indoors

[7] J. Kurnitski, Cost Optimal and nearly Zero-Energy Buildings (nZEB). 2013. Springer, London

[8] International Energy Agecy, Multiple Benefits of Energy Efficiency

[9] M. Ferreira, M. Almeida, A. Rodrigues, Impact of co-benefits on the assessment of energy related building renovation with a nearly-zero energy target, Energy and Buildings, Energy and Buildings, Volume 152, 1 October 2017, Pages 587-601

[10] CRAVEzero, D6.4: Co – Benefits of nZEBs (https://www.cravezero.eu/wp-content/uploads/2020/05/CRAVEzero_D64_CoBenefits.pdf)

Development of a building thermal solution using solar renewable energy production

Eusébio Conceição [a], João Gomes [b], M. Inês Conceição [c], M. Manuela Lúcio [a], Hazim Awbi [d]

[a] Faculdade de Ciências e Tecnologia, Universidade do Algarve, Faro, Portugal, econcei@ualg.pt; maria.manuela.lucio@gmail.com.

[b] CINTAL, Universidade do Algarve, Faro, Portugal, jgomes@ualg.pt.

[c] Instituto Superior Técnico, Universidade de Lisboa, Lisboa, Portugal; ines.conceicao@tecnico.ulisboa.pt.

[d] School of Built Environment, University of Reading, Reading, United Kingdom; h.b.awbi@reading.ac.uk.

Abstract. This paper presents a numerical study of the development of a thermal solution in buildings using solar renewable energy production in winter cold conditions. The Building Thermal Modelling numerical model, using solar sources through a DSF (Double Skin Facade) system, in a virtual small building, calculates the energy distribution, the internal variables and the thermal comfort level. The study considers a virtual small building equipped with two DSF systems, installed in south-facing windows, equipped with a duct system connected to an internal ventilation system, based on a mixing ventilation system. Each DSF is used to heat two or more spaces. The DSF systems are built with two transparent surfaces, forming an internal canal used to transport the warm air and to produce thermal energy, and are equipped with a set of internal lamella. The Building Thermal Modelling numerical model uses energy and mass balance integral equations for the opaque bodies, transparent bodies, internal bodies and internal air and contaminants. The study, made in winter cold conditions, in Mediterranean environment, evaluates the internal temperature and thermal comfort level evolution that the occupants are subjected. Without DSF system, the spaces equipped with windows turned south are thermally uncomfortable by positive PMV values, while the spaces equipped with windows turned North and East are thermally uncomfortable by negative PMV values. With DSF system, in general, all spaces are thermally comfortable. When the spaces with east and south facing windows are occupied the acceptable thermal comfort is verified by negative PMV values. When the north facing space is occupied the acceptable thermal comfort is verified in the noon by positive PMV values and in the final of the afternoon by negative PMV values.

Keywords. Energy production, Building Thermal Modelling, Double Skin Façade, Energy and mass integral equations, Thermal Comfort levels.
DOI: https://doi.org/10.34641/clima.2022.70

1. Introduction

In the development of a building thermal solution is frequent used solar renewable energy production in a Double Skin Facade (DSF) system. The DSF system is developed and implemented, mainly, in south-facing windows, is built with two transparent glasses, formed an internal channel, and works by natural, forced or hybrid ventilation.

Inside the air channel various types of devices, such as venetian blinds or photovoltaic cells, are frequently installed. Some studies about this topic can be seen in Pasut and De Carli [1], Ghadamian et al. [2], Hazem et al. [3], Parra et al. [4], Luo et al. [5], Ghaffarianhoseini et al. [6], Poirazis [7], Catto et al. [8], Xue et al. [9], Lee et al. [10], Lee et al. [11] and Li et al. [12]. Pasut and De Carli [1] analysed the CFD model in the evaluation of airflow in natural ventilated DSF system. Ghadamian et al. [2] studied the energy simulation of DSF system applied in buildings. Hazem et al. [3] analysed the numerical study of the airflow ventilation to evaluate the behaviour of the DSF system. Parra et al. [4] studied the thermal response of a ventilated DSF with Venetian-type blinds. Luo et al. [5] made a study of a DSF system in winter conditions. Ghaffarianhoseini et al. [6] analysed some advantages of DSF systems. Poirazis [7] made a literature review of DSF systems in office buildings. Catto et al. [8] presented a study about the simulation of DSF system. Xue et al. [9] analysed a method for thermal study of natural ventilation in a DSF system. Lee et al. [10] studied the natural ventilation system and energy of a DSF

Copyright ©2022 by the authors. This conference paper is published under a CC-BY-4.0 license.

system. Lee et al. [11] analysed the natural ventilation and the acoustical systems in a DSF system. Finally, Li et al. [12] studied the thermal performance of an DSF system in buildings.

The numerical study presented in this study considers a Building Thermal Modelling numerical model. This model was developed by the authors over the last years, and it was applied, as example, on the studies of Conceição et al. [13] and Conceição and Lúcio [14].

The solar radiation, the glass radiative proprieties and the convection heat transfer coefficients were introduced in the study of Conceição et al. [15]. The results obtained in each space of the Building Thermal Modelling are used in software that simulates the coupling of Computer Fluid Dynamics and Human Thermal Modelling in order to evaluate the comfort (see Conceição et al. [16]).

The ventilation system, considered in occupied buildings, is used to improve the thermal comfort and indoor air quality. The thermal comfort is usually evaluated by the Predicted Mean Vote (PMV) and the Predicted Percentage of Dissatisfied (PPD) people indexes, presented in the work of Fanger [17], and making part of ISO 7730 [18] and ASHRAE Standard 55 [19]. In the Building Thermal Modelling numerical model, the thermal comfort is evaluated based on the human thermal physiology (see Conceição et al. [20]). The indoor air quality is frequently evaluated using the carbon dioxide concentration, used as indicator (see ASHRAE 62 [21]). In the Building Thermal Modelling numerical model, the evolution of carbon dioxide concentration is calculated in occupied spaces. Examples of this issue can be seen in Conceição and Lúcio [22], for buildings, and in Conceição et al. [23], for vehicles.

The main objective of this numerical work is to evaluate the influence of two DSF, located in facing-south windows, on the building thermal response and thermal comfort inside an occupied virtual building. Each DSF system is connected by ducts with two or more spaces: one space facing south and others facing north. The comparative study, for winter conditions, is made with and without DSF system.

2. Numerical Model

The Building Thermal Modelling numerical model, presented in this work, was developed by the authors in the last years. This numerical model considers a building design and an energy and mass balance integral equations system.

The building design is developed by the Computer Aided Design, CAD, numerical methodology. All geometry of the building is considered. The building geometry, developed previously and used as input in the numerical model, is used to developed the energy and mass balance integral equations for the opaque, transparent and indoor bodies and for the indoor spaces:

- Each opaque body considers a group of energy equations for the different layers (doors, floor, brick, double brick, roof and others);
- Each transparent body, namely the glass, considers one energy equation;
- Each indoor body considers one energy equation;
- Each space considers one energy equation and a group of mass equations for all contaminants (carbon dioxide concentration and others) and water vapour.

In the geometry is also necessary to introduce the boundary conditions. These boundary conditions define the heat transfer fluxes inside the building. The numerical model is nodal, except when calculating radiation and radiative exchange, in which the numerical model is discretized using, at least, meshes with 10×10 elements.

Building Thermal Modelling numerical model considers energy and mass balance integral equations. These equations are used to calculate, in transient conditions, the temperature fields of the opaque, transparent and internal bodies and internal air, and the water and contaminants mass fields inside the spaces. The energy and mass balance integral equations are solved by the Runge-Kutta-Felberg method with error control

The energy balance linear integral equations consider the convection, conduction and radiation phenomena as follows:

- Heat transfers by natural, forced and mixed convection are evaluated using dimensionless coefficients, which are used in the opaque and transparent bodies;
- Heat transfer by conduction is verified within the opaque bodies, between the different layers;
- In the incident solar radiation, the numerical model considers a sun trajectory during all day, for all days in the year. In this calculus all contaminants in the atmosphere are considered;
- In the absorbed, transmitted, absorbed and reflected solar radiation in transparent (glasses) bodies the numerical model considers all radiative proprieties of the grass;
- In the absorbed solar radiation by opaque bodies the numerical software considers the surface proprieties.

The radiation phenomenon considers all shading devices. In this calculus all surfaces of the building geometry are considered. The study calculated the shading devices considered in the external surfaces and the shading devices considered in the internal surfaces. In the second situation, for each indoor space, the external surfaces are also considered.

The energy balance integral equations are used to evaluate the temperature opaque bodies (door, walls, floor and ceiling), transparent (glazed) bodies, indoor bodies and internal air of the virtual buildings. In the DSF system, the Building Thermal Modelling numerical model calculates the temperature in Venetian-type blind, inner and outer glasses, DSF surrounding structure and air inside the ventilated DSF.

The mass balance integral equations consider the convection and diffusion phenomenon. This equation system is used to evaluate the mass concentration of the water vapour and contaminants concentration inside the building indoor space. In the DSF system this equation system is also used to evaluate the mass concentration of the water vapour and contaminants concentration

As input data, the numerical model considers the geographical data, the environmental data, and other details. In the environmental conditions the external air temperature, air relative humidity, air velocity and wind direction, for all day, are considered.

All numerical models were validated in winter conditions and in summer conditions, with different conditions, for school buildings and experimental chamber:

- In school buildings the indoor air temperature calculated by the numerical model and measured experimentally was considered in transient conditions (see Conceição and Lúcio [24] for winter conditions and Conceição et al. [25] for summer conditions);

- In the experimental chamber the surrounding surfaces (floor, ceiling, wall and indoor bodies temperatures), in steady state conditions, are considered (see Conceição and Lúcio [26]).

3. Methodology

The building geometry, considered in this work is presented in Fig. 1. Fig. 1a) represents the building scheme, while Fig. 1b) and Fig. 1c) represents the building grid generation. The grid generation considered in the numerical simulation, namely in the calculus of the solar radiation field in external and internal surfaces, can be analysed in Fig. 1. The main facade of the building (including the door and two windows, one larger and the other smaller) faces south. The building also has two more windows: a small one facing north and another facing east.

The numerical simulation considers one external space, five internal spaces, a loft and two DSF systems, namely:

- Space 1 – external space. The air temperature and relative humidity, wind velocity and wind direction are used as input data.

- Space 2 – non-permanent occupation. Is equipped with a door facing south.

- Space 3 – two occupants between 19 to 24 hours. Is equipped with a window facing south.

- Space 4 – two occupants between 12 to 14 hours and one occupant between 18 to 19 hours. This space is equipped with a window facing north.

- Space 5 – two occupants between 0 to 8 hours. This space is equipped with a window facing east.

- Space 6 – one occupant between 18 to 19 hours. This space is equipped with a window facing south.

- Space 7 – loft. This space is used to regulate the temperature in the building.

- Space 8 – Small DSF system. This space is used to heat two spaces: the space 6 (with window equipped with this DSF system) and the space 5.

- Space 9 – Large DSF system. This space is used to heat two spaces: the space 3 (with window equipped with this DSF system) and the space 4.

A comparative study, with and without DSF system, is made. This work is divided into two parts:

- Without DSF system: the heating process is made using only direct solar radiation;

- With DSF system: the heating process is made using direct solar radiation and heat transported by ducts from the DSF located in the south window to the uncomfortable cold spaces located in the north-facing area of the building, in order to improve the thermal comfort conditions of these spaces.

The two DSF systems, in the present study, consider an airflow from the:

- DSF number 8 to the space number 6 during all day with an airflow rate of 0.005 m^3/s;

- DSF number 8 to the space number 5 during all day with an airflow rate of 0.02 m^3/s;

- DSF number 9 to the space number 3 between the 14 to 24 hours with an airflow rate of 0.01 m^3/s;

- DSF number 9 to the space number 4 between the 0 to 14 hours, with an airflow rate of 0.02 m^3/s and between the 14 to 24 hours, with an

airflow rate of 0.01 m^3/s;

- DSF number 9 to the space number 5 between the 0 to 14 hours with an airflow rate of 0.02 m^3/s.

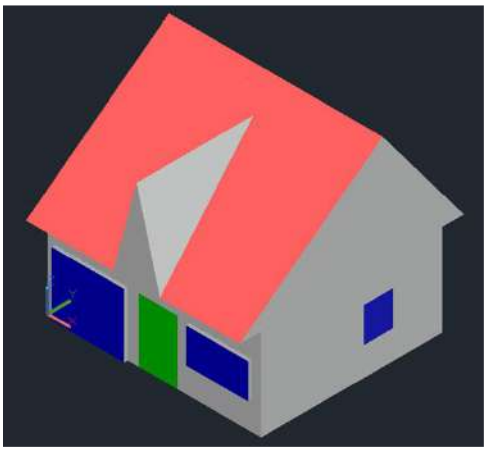

a)

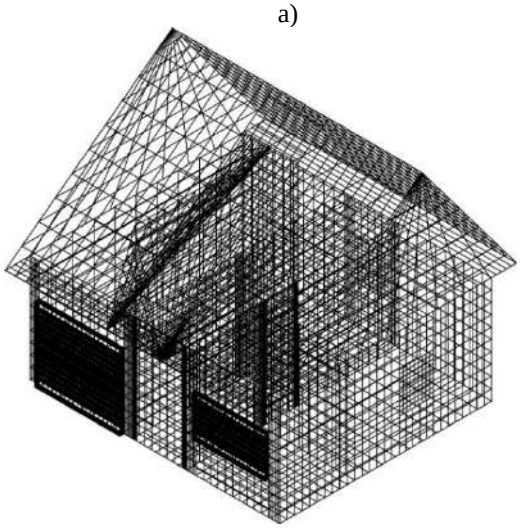

b)

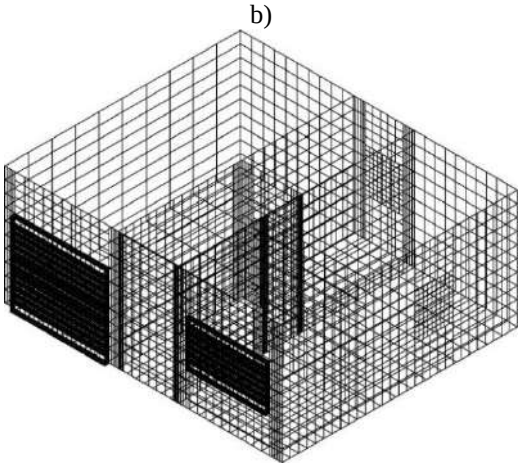

c)

Fig. 1 – Building occupied space. External surface a), grid generation in all building b), and grid generation in occupied building spaces c).

The values of the previous airflows were selected in order to guarantee conditions of thermal comfort when the spaces are occupied.

The study considers a virtual small building equipped with two DSF systems, installed in windows facing south, equipped with a duct system connected to an internal ventilation system, based on a mixing ventilation system.

Without DSF system, an airflow rate of 35 m^3/h by person, only when the space is occupied, suggested by the standards for an occupation of two persons, was used in the numerical simulation.

Each DSF is built with two glazed surfaces and a surrounding structure. The Venetian-type blind is constituted by an adjustable set of six aluminium lamellae and it is installed in the air cavity of the DSF system (see Fig. 2). The small DSF system is equipped with six lamellas, while the larger DSF system is equipped with twelve lamellas.

The input data of the numerical simulation are the outdoor air temperature, air relative humidity, wind velocity and wind direction, obtained in a winter typical day by a weather station located in the South region of Portugal. The simulation was done for 24 hours supposing clean sky. A typical winter day, as the 21st December, was used to determine the evolution of solar radiation on that day. In the numerical simulation the five previous days were considered in order to obtained the real build thermal behaviour.

In the assessment of the PMV index, a metabolic rate of 1.2 met and a clothing insulation level of 1 clo were used [18].

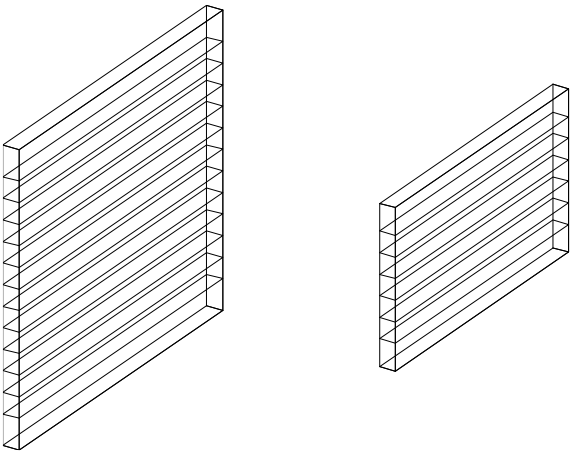

a) b)

Fig. 2 – DSF used in the numerical simulation. Small a) and large b) DSF.

In Fig. 3 the existing air flows can be seen when the DSF are not used (Fig. 3a) and when the DSF are used (Fig. 3b and Fig. 3c), the latter in the situation existing after 14 hours).

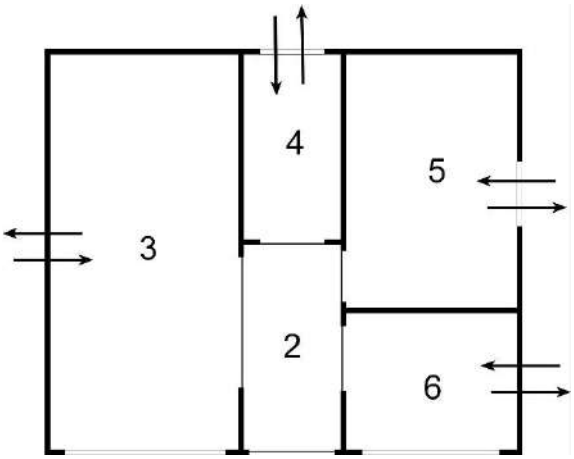

a)

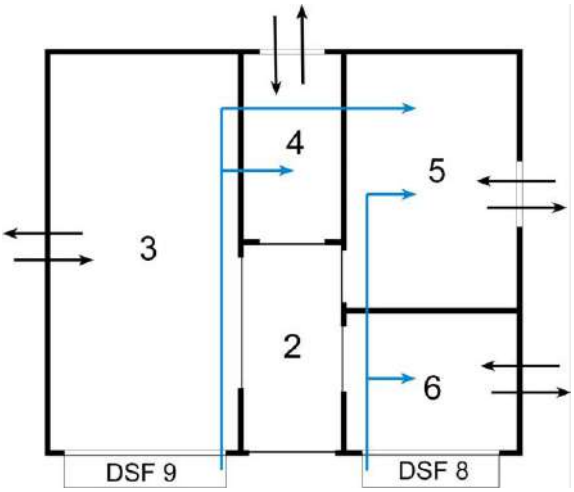

b)

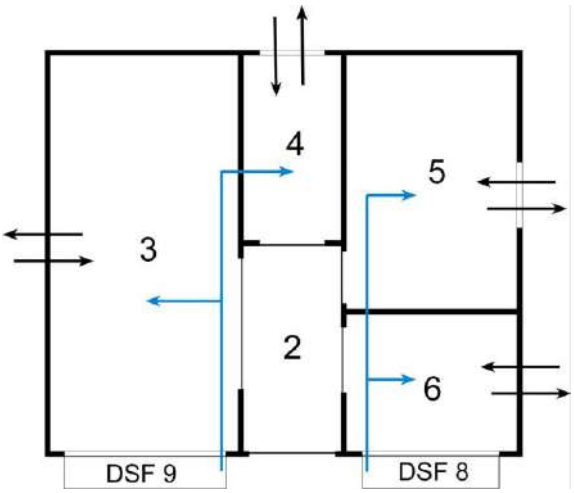

c)

Fig. 3 – Airflow without DSF a) and airflow with DSF until b) and after c) 14 hours.

4. Results and discussion

In Fig. 4 is presented the evolution of the air temperature in the internal space without (point a) and with (point b) DSF system. In the Fig. 4, the spaces numbers 2, 3, 4, 5, 6 and 7 are presented.

Without DSF, the evolution of temperature is higher in spaces facing-south (number 3 and 6). Spaces numbers 2 (without window), 4 (with window facing-north), 5 (with window facing east) and 7 (loft without window) present internal air temperature evolution with low values.

Thus, in accordance with obtained results, two DSF systems were developed in order to improve the temperature distribution. In order to increase the internal air temperature in occupied spaces numbers 4 and 5 a DSF system was installed in each window of the space 3 and 6. The internal air temperature spaces 4 and 5 increase, mainly when the spaces are occupied, to values near the space number 3. The internal air temperature of the space number 3 and 6 decreases.

Fig. 5 shows the evolution of the air temperature in the external environment (space 1) and DSF spaces (8 and 9) system.

In accordance with the obtained results, the larger DSF space present higher internal air temperature than the small DSF system.

Fig. 6 shows the evolution of the PMV index in the internal spaces, namely the spaces number 3, 4, 5 and 6. The point a) is associated without a DSF system, while point b) is associated with a DSF system.

The thermal comfort level, evaluated by the PMV index, when is not used a DSF system, is uncomfortable by positive values in spaces with windows facing south (3 and 6) and is uncomfortable by negative values in the space with window facing north (space number 4) and in the space with window facing east (space number 5).

However, in accordance with the obtained results, with DSF system, the following conclusions are verified:

- The thermal comfort level is acceptable, by negative PMV values, in the space number 3 during the afternoon and the night, mainly, when the space is occupied during the night. In this space the DSF system improves the thermal conditions to acceptable values;

- The space number 4 presents comfortable thermal comfort levels, by negative PMV values, in the morning, in the evening and at night. On the other hand, it presents comfortable thermal comfort levels, by positive PMV values, in the early afternoon. Thus, when the space is occupied at noon the thermal comfort level is acceptable, by positive PMV values, and in the early night the thermal comfort level is acceptable, by negative PMV values;

- The space number 5 presents acceptable thermal comfort conditions, by negative PMV values, during the night, in the early morning and in the late afternoon and presents acceptable thermal comfort conditions, by positive PMV values, during the late morning and during the early afternoon. Thus, when the space is occupied (during the night) the thermal comfort conditions, by negative PMV values, is verified;

- Finally, the space number 6 presents acceptable thermal comfort conditions, by negative PMV values, during the afternoon and morning and unacceptable thermal comfort conditions, by negative PMV values, during the night. When the space is occupied (in the late afternoon) the acceptable thermal comfort conditions are verified.

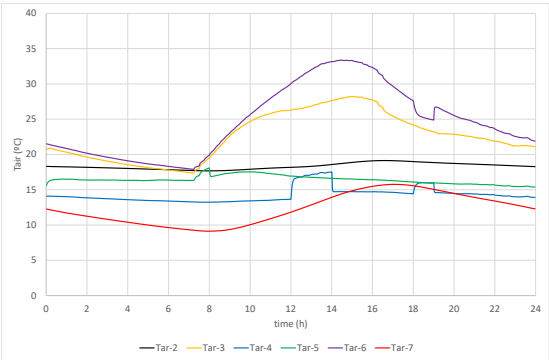

a)

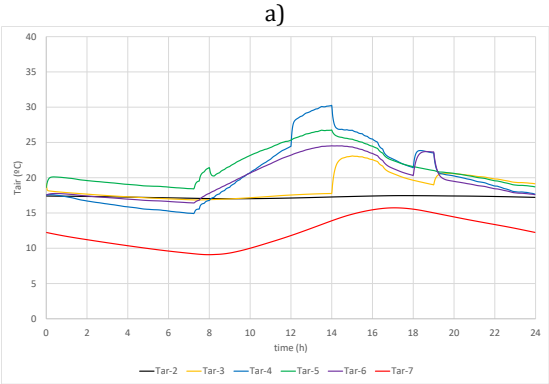

b)

Fig. 4. Evolution of the air temperature in the internal spaces (2, 3, 4, 5, 6 and 7), without a) and with b) DSF system.

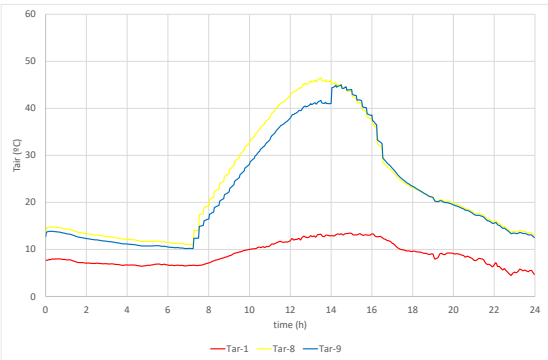

Fig. 5. Evolution of the air temperature in the external and DSF spaces (1, 8 and 9) system.

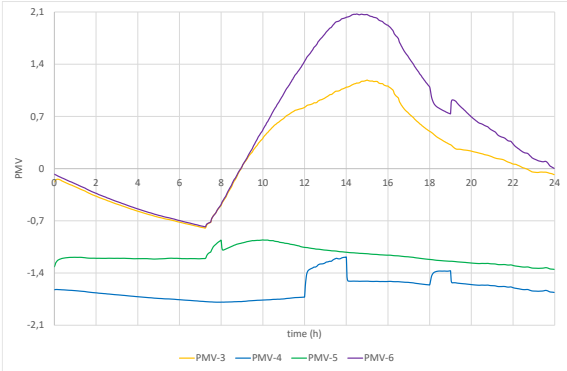

a)

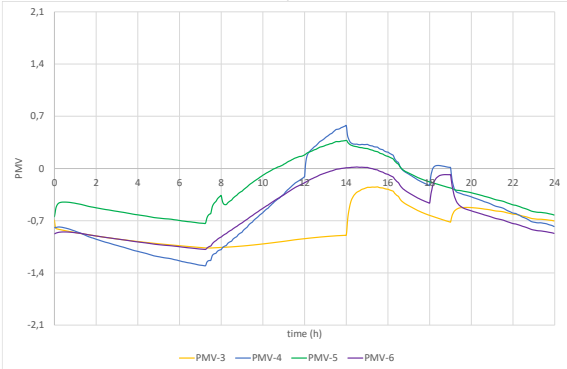

b)

Fig. 6. Evolution of the PMV index in the internal spaces (3, 4, 5 and 6), without a) and with b) DSF system.

5. Conclusions

In this paper is presented a numerical study of the development of a sustainability thermal solution in buildings using solar renewable energy production in winter cold conditions. The comparative study is done considering the building without DSF system and equipped with two DSF systems, each one connected by ducts to two spaces.

In general, without DSF system the spaces equipped with windows facing south are thermal uncomfortable by positive PMV values, while the other spaces are thermal uncomfortable by negative PMV values.

When is used the DSF systems, in general, all spaces are thermal comfortable when the space is occupied. When the spaces number 3, 5 and 6 are occupied the acceptable thermal comfort is verified by negative PMV values. When the space number 4 is occupied the acceptable thermal comfort is verified in the noon by positive PMV values and in the late afternoon by negative PMV values.

In accordance with the obtained results, the larger DSF transports higher energy level than the necessary, while the small DSF transports lower energy level than the necessary. Thus, in future work is important to implement and developed new energy management in order to optimize the energy distribution promote by the DSF system.

6. Acknowledgement

The authors acknowledge to the project (SAICT-ALG/39586/2018) from Algarve Regional Operational Program (CRESC Algarve 2020), under the PORTUGAL 2020 Partnership Agreement, through the European Regional Development Fund (ERDF) and the National Science and Technology Foundation (FCT). The authors grateful the collaboration of the Margarida Conceição in the project design development.

7. References

[1] W. Pasut and M. De Carli, "Evaluation of various CFD modelling strategies in predicting airflow and temperature in a naturally ventilated double skin faade," *Appl. Therm. Eng.*, 2012, doi: 10.1016/j.applthermaleng.2011.11.028.

[2] H. Ghadamian, M. Ghadimi, M. Shakouri, M. Moghadasi, and M. Moghadasi, "Analytical solution for energy modeling of double skin façades building," *Energy Build.*, 2012, doi: 10.1016/j.enbuild.2012.03.034.

[3] A. Hazem, M. Ameghchouche, and C. Bougriou, "A numerical analysis of the air ventilation management and assessment of the behavior of double skin facades," *Energy Build.*, 2015, doi: 10.1016/j.enbuild.2015.05.057.

[4] J. Parra, A. Guardo, E. Egusquiza, and P. Alavedra, "Thermal performance of ventilated double skin façades with venetian blinds," *Energies*, 2015, doi: 10.3390/en8064882.

[5] Y. Luo, L. Zhang, Z. Liu, L. Xie, X. Wang, and J. Wu, "Experimental study and performance evaluation of a PV-blind embedded double skin façade in winter season," *Energy*, 2018, doi: 10.1016/j.energy.2018.09.175.

[6] A. GhaffarianHoseini, A. GhaffarianHoseini, U. Berardi, J. Tookey, D. H. W. Li, and S. Kariminia, "Exploring the advantages and challenges of double-skin facąds (DSFs)," *Renewable and Sustainable Energy Reviews*. 2016, doi: 10.1016/j.rser.2016.01.130.

[7] H. Poirazis, "Double Skin Façades for Office Buildings Literature Review," *Div. Energy Build. Des. Dep. Constr. Archit. Lund Inst. Technol. Lund*, 2004.

[8] E. Catto Lucchino, F. Goia, G. Lobaccaro, and G. Chaudhary, "Modelling of double skin facades in whole-building energy simulation tools: A review of current practices and possibilities for future developments," *Building Simulation*. 2019, doi: 10.1007/s12273-019-0511-y.

[9] F. Xue and X. Li, "A fast assessment method for thermal performance of naturally ventilated double-skin façades during cooling season," *Sol. Energy*, 2015, doi: 10.1016/j.solener.2015.01.040.

[10] J. Lee, M. Alshayeb, and J. D. Chang, "A Study of Shading Device Configuration on the Natural Ventilation Efficiency and Energy Performance of a Double Skin Façade," 2015, doi: 10.1016/j.proeng.2015.08.432.

[11] J. Lee and J. D. Chang, "Influence on Vertical Shading Device Orientation and Thickness on the Natural Ventilation and Acoustical Performance of a Double Skin Facade," 2015, doi: 10.1016/j.proeng.2015.08.431.

[12] Y. Li, J. Darkwa, and W. Su, "Investigation on thermal performance of an integrated phase change material blind system for double skin façade buildings," 2019, doi: 10.1016/j.egypro.2019.01.688.

[13] E. Z. E. Conceição, J. M. M. Gomes, N. H. Antão, and M. M. J. R. Lúcio, "Application of a developed adaptive model in the evaluation of thermal comfort in ventilated kindergarten occupied spaces," *Build. Environ.*, vol. 50, 2012, doi: 10.1016/j.buildenv.2011.10.013.

[14] E. Z. E. Conceição and M. M. J. R. Lúcio, "Numerical study of the influence of opaque external trees with pyramidal shape on the thermal behaviour of a school building in summer conditions," *Indoor Built Environ.*, vol. 19, no. 6, 2010, doi: 10.1177/1420326X10377546.

[15] E. Z. E. Conceição, M. C. G. Silva, J. C. S. André, and D. X. Viegas, "A computational model to simulate the thermal behaviour of the passengers compartment of vehicles," *SAE Tech. Pap.*, 1999, doi: 10.4271/1999-01-0778.

[16] E. Z. E. Conceição, C. I. M. Santiago, M. M. J. R. Lúcio, and H. B. Awbi, "Predicting the air quality, thermal comfort and draught risk for a virtual classroom with desk-

type personalized ventilation systems," *Buildings*, vol. 8, no. 2, 2018, doi: 10.3390/buildings8020035.

[17] P. Ole Fanger, "Thermal comfort. Analysis and applications in environmental engineering.," *Copenhagen Danish Tech. Press*, 1970.

[18] ISO, "ISO 7730: Ergonomics of the thermal environment Analytical determination and interpretation of thermal comfort using calculation of the PMV and PPD indices and local thermal comfort criteria," *Management*, 2005, doi: 10.1016/j.soildyn.2004.11.005.

[19] ASHRAE-55, "Thermal environmental conditions for human occupancy," *ANSI/ASHRAE Stand. - 55*, 2017.

[20] E. Conceição, J. Gomes, and H. Awbi, "Influence of the airflow in a solar passive building on the indoor air quality and thermal comfort levels," *Atmosphere (Basel).*, vol. 10, no. 12, 2019, doi: 10.3390/ATMOS10120766.

[21] ASHRAE, "Ventilation for Acceptable Indoor Air Quality," *J. Phys. A Math. Theor.*, 2016, doi: 10.1088/1751-8113/44/8/085201.

[22] E. Z. E. Conceição and M. M. J. R. Lúcio, "Air quality inside a school building: Air exchange monitoring, evolution of carbon dioxide and assessment of ventilation strategies," *Int. J. Vent.*, vol. 5, no. 2, 2006, doi: 10.1080/14733315.2006.11683743.

[23] E. Z. E. Conceiçäo, M. C. G. Silva, and D. X. Viegas, "Air quality inside the passenger compartment of a bus," *J. Expo. Anal. Environ. Epidemiol.*, vol. 7, no. 4, 1997.

[24] E. Conceição, A. Silva, and M. Lúcio, "Numerical study of thermal response of school buildings in winter conditions," in *Proceedings of the 9th Conference on Air Distribution in Rooms (Roomvent 2004), Coimbra, Portugal*, 2004, pp. 5–8.

[25] E. Z. E. Conceição and M. M. J. R. Lúcio, "Numerical study of thermal response of school buildings in summer conditions," in *HB 2006 - Healthy Buildings: Creating a Healthy Indoor Environment for People, Proceedings*, 2006, vol. 3.

[26] E. Z. E. Conceição and M. M. J. R. Lúcio, "Numerical simulation of the application of solar radiant systems, internal airflow and occupants' presence in the improvement of comfort in winter conditions," *Buildings*, vol. 6, no. 3, 2016, doi: 10.3390/buildings6030038.

Performance evaluation of a R-290 dual-source heat pump for heating and cooling

Laura Alonso [a], Xabier Peña [a], Felipe Trebilcock [a], Julen Hernandez [a], Aitor Agirre [a]

[a] Efficient Thermal Energy Systems / Energy, Climate and Urban Transition / TECNALIA, Basque Research and Technology Alliance (BRTA). Azpeitia, Spain. laura.alonso@tecnalia.com

Abstract. In this paper, the performance of a 10 kW reversible heat pump using R290 as refrigerant and using a dual source/sink is presented. The heat pump design is oriented for its integration with solar photovoltaic energy in multifamily near Zero Energy Buildings, with the objective to reach a high onsite renewable share. The development is part of TRI-HP project: Trigeneration systems based on heat pumps with natural refrigerants and multiple renewable sources. The heat pump has a specifically designed dual source heat exchanger (DSHX) working as the outdoor unit of the heat pump. This element is able to work as a condenser (cooling mode) or evaporator (heating mode), exchanging heat between the refrigerant and air or water/brine as heat source (in heating mode) or sink (in cooling mode). Both sources can also be simultaneously used as heat source or sink. The design procedure and used correlations for the DSHX are described. The heat pump has been experimentally tested in a climatic chamber in all the possible different working modes (Heating with air, heating with brine, cooling with air, cooling with brine), showing in general a good agreement with the design values. Results for coefficient of performance, heating/cooling capacities and compressor consumption are presented for different air/brine temperatures and different compressor velocities. The experimental campaign has served to validate the developed models for designing the DSHX. Future work includes an improved redesign of the heat pump with a more compact DSHX and a simplified refrigerant circuit, which will be experimentally tested in an analogous experimental campaign.

Keywords. Dual-source, heat exchanger, heat pump, R290.
DOI: https://doi.org/10.34641/clima.2022.381

1. Introduction

According to the Roadmap to a Resource Efficient Europe, Europe must reduce its greenhouse gas emissions by 80-95% by 2050 [1]. Cities and the construction sector play a decisive role in the process of energy transition and reduction of the carbon footprint in the EU. Within this context, the generation of heat and cold in buildings can and should play an important role towards the change of model.

Heat pumps have characteristics that make them very interesting for use in near-zero energy buildings (EECN). These buildings are designed to have a very low energy demand, which is largely covered by energy from renewable sources, including self-production of renewable energy. In this context and considering residential energy consumption, the heat pump is imposed as a technology for the future. Due to its consideration of renewable, versatility and high energy efficiency, the development of heat pump technology will be crucial in this transition towards almost zero energy buildings.

The use of low-impact refrigerants is a need that is already covered by regulations, and is expected to increase in the future. This is due to the fact that traditional refrigerants have a high global warming potential (GWP), and their use has begun to be restricted for certain applications. The F-Gas regulation [2] has determined a series of restrictions on the use of refrigerants until the year 2030. As of January 1, 2022, fluorinated gases with a GWP ≥ 150 will be prohibited in sealed commercial equipment except equipment for evaporation <-50 °C or with a fluid load less than 40 tCO2eq. In this context, the use of natural refrigerants is spreading in cases where it is technologically safe and economically feasible.

The use of dual systems combining geothermal and aerothermal is considered an innovative alternative to the use of aerothermal or geothermal heat pumps [3]. Jin et al. [4] analysed the potential of a hybrid system combining ambient air and geothermal energy, obtaining COP improvements of 28.1% and 4.7% for the system in heating and cooling operating modes, respectively. Man et al. [5] presented simulations of a hybrid

Copyright ©2022 by the authors. This conference paper is published under a CC-BY-4.0 license.

aerothermal/geothermal system, with supplemental air sinks for a residential building in Hong Kong. The economic analysis showed a savings in investment costs of 34.3% compared to a conventional geothermal system; with a saving in operating costs of 53.6% in a period of 10 years.

However, all current hybrid aerothermal/geothermal systems use two exchangers in parallel, a cooling-air exchanger (coil) and a cooling-water/brine exchanger (geothermal exchanger). In this project, the designed heat pump performs the exchange with both energy sources in the same device, the dual heat exchanger.

2. Dual-source heat pump design

2.1 Dual-source heat pump concept and system integration

The designed dual-source heat pump (DSHP) uses R290, a natural refrigerant, and is envisaged to be integrated in multi-family residential buildings, and be powered by largely renewable electricity (from photovoltaic panels with battery electrical storage). Fig. 1 shows a diagram of the proposed heat pump integrated into the building's thermal system.

The heat pump is equipped with a space conditioning heat exchanger (SCHX) and a desuperheater (DSH) in the demand side, and can provide heating or domestic hot water (DHW) using both exchangers or use them simultaneously to provide both services at different temperatures. It also allows the provision of cooling and DHW simultaneously, thanks to the use of the compressor discharge heat in the DSH. The external heat exchanger, which is dual-source, allows the use of geothermal and/or aerothermal energy, depending on the most favourable conditions. In addition, the system allows free cooling directly from the ground. It is, therefore, a versatile system which makes possible multiple modes of operation.

The main innovation of the heat pump is the use of a dual-source heat exchanger (DSHX) in the source/sink side. This feature of the heat pump allows the length of the geothermal boreholes to be reduced by around 50% compared to a conventional geothermal heat pump system, which leads to considerable savings in investment costs.

2.1 Dual-source heat exchanger design

A DSHX has been designed such that it can exchange heat with the water/brine (ground), air or with both simultaneously depending on environmental conditions. Moreover, the design allows to use this heat exchanger as evaporator or condenser in order to reverse the heat pump cycle. The working modes of the DSHX include:

- **Heating air-water.** DSHX working as an evaporator, exchanging heat between air and R290.
- **Cooling air-water.** DSHX working as a condenser, exchanging heat between air and R290.
- **Heating water-water.** DSHX working as an evaporator, exchanging heat between water and R290.
- **Cooling water-water.** DSHX working as a condenser, exchanging heat between water and R290.

The geometry of the DSHX consists on an external air finned coil with an internal coaxial bare tube. The air exchanges heat with the refrigerant, which flows through the annular space between the two coaxial tubes. The water flows through the inside of the internal tube, therefore being able to exchange heat with the refrigerant. A scheme of the DSHX is shown in Fig. 2.

In order to perform the design, four different design tools, each one corresponding to the working modes of the DSHX, have been defined for determining the capacity of each working mode and it's required heat exchange surface. The dimensioning tools have been implemented as deterministic models in EES (Engineering Equation Solver) [6] based on the geometry of each heat exchanging part:

- Geometry of air source heat exchanger or coil, for air source/sink evaporator/condenser and,
- Geometry of coaxial tube heat exchangers, for geothermal source/sink evaporator/condenser.

Wang et al. [7] correlation has been used to calculate the air side heat transfer coefficient of the DSHX.

Different correlations have been used for the sensible heat transfer coefficient on the refrigerant side and on the water side of the DSHX, depending on the regime:

- Correlation proposed by Shah and London [8] for laminar regime (Re < 2300).
- An interpolation between results for laminar flow and turbulent flow is applied for transitional flow (2300<Re<3000), as proposed by Nellis and Klein [9].
- Correlation proposed in VDI Heat Atlas [10] for Re numbers between 3000 and 10000.
- Correlation of Dittus-Böelter [11] for turbulent regimes (Re > 10000).

For the calculation of the HTC in the condensing zone the correlation recently proposed by Shah [12,13] has been implemented.

On the other hand, the correlations proposed by Mishima et al. [14] and Shah [15] have been implemented for the evaporation zone.

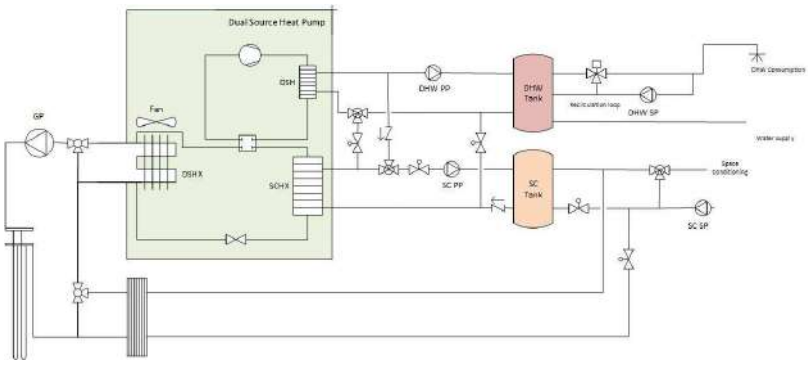

Fig.1 - DSHP integrated into the building's thermal system.

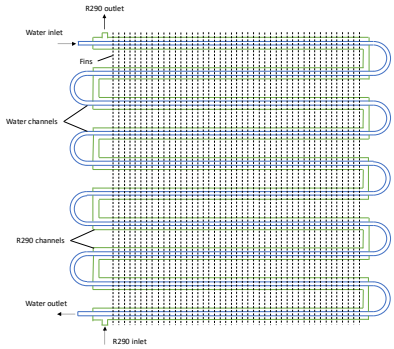

Fig.2 – DSHX scheme.

3. Dual-source heat pump testing

The R290 DSHP prototype has been experimentally tested inside a climatic chamber in the laboratory (Fig. 3). The main achievements of the first testing campaign have been:

- Measuring heat pump capacity and efficiency for different operation modes.
- Generating data for testing a simple heat pump model for further simulations.
- Detecting problems and potential for optimization.

The climatic chamber of the laboratory can be partitioned into two chambers, having two symmetric dissipation and energy producing systems, which can work at the same conditions when the chamber is unique, or separately at independent conditions when it is separated in two chambers. The DSHP prototype is located in Chamber number one (hereinafter Chamber1), which contains the following dissipation and energy generation equipment:

- 5 impeller pumps. Impulsion pump number 2 (hereinafter Pump2), is the one which is linked to the demand side of the HP, and will provide the water flow rate to the SCHX (at heating, cooling and DWH modes) and the DSH (at heating, heating+DHW, cooling+DHW modes).
- 3 heat exchangers.
- A 885 l buffer tank.

Fig.3 - DSHX test bench installed inside the climatic chamber.

Fig. 4 shows the scheme of Chamber1, where the DSHX test bench has been installed. In order to reach to the desired testing conditions in Chamber1, an Air Handling Unit (AHU) is used. The AHU comprises different heat exchanging coils. In the AHU, two fans blow the air coming from the chamber through the heat exchanging coils until it is expelled uniformly through hoppers. The air is treated in the different heat exchanging coils inside the AHU, achieving the desired conditions.

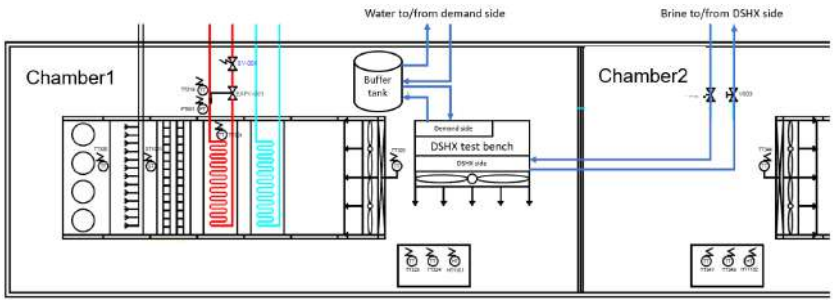

Fig.4 – Scheme of the DSHX test bench installed in the climatic chamber.

As the DSHX can work with air or water/brine, it needs to be connected to another heat source/sink, so a connection with Chamber number two (hereinafter Chamber2) was implemented, providing a water flow rate to the DSHX. Air conditions and demand side conditions are controlled from Chamber1; DSHX source/sink conditions when it is working with water/brine, are controlled from Chamber2. A buffer tank of 250 l was installed between the test bench and the demand side circuit to gain stability. Inside Chamber1 there are two sensors, an NTC sensor for measuring ambient dry bulb temperature, and a relative humidity sensor. Besides these two sensors, the additional metering instrumentation shown in Table 1 has been included for the testing of the unit. During the initial tests, the PIDs of the climatic chamber have been adjusted in order to get the maximum possible stability in the measurements.

Testing has been conducted following EN 14511 procedures [16], in the different possible working modes. Fist, the room is preconditioned and when the required tolerances are met, it is maintained in steady-state operation for sufficient time, then calculating the heating and cooling capacities based on the measurements on the demand-side fluid (water).

• **Heating air-water.** The DSHP was tested for 7 °C ambient air temperature, producing warm water from 30 °C to 35 °C, from 40 °C to 45 °C, from 47 °C to 55 °C and from 52 °C to 60 °C. The testing campaign was developed with the compressor at its nominal operating point, 70 rps, and at different partial loads: 50 rps, 60 rps and 90 rps (full load).

• **Cooling air-water.** The DSHP was tested for different ambient temperatures: 27 °C, 35 °C and 45 °C; chilling water from 12 °C to 7 °C and from 23 °C to 18 °C, at its nominal operating point with compressor working at 70 rps and at different partial loads: 40 rps, 50 rps, and full load 90 rps.

• **Heating water-water.** The DSHP was tested for different water source temperatures: 7 °C, 12 °C and 16 °C; producing warm water at 35 °C and 45 °C. Several compressor speeds have been tested, from 50 rps to 90 rps.

• **Cooling water-water.** The DSHP was tested for different water sink (rejection) temperatures: 25 °C and 30 °C. A cold-water supply from 12 °C to 7 °C was tested. The compressor speed varied from its nominal operating point at 70 rps, to different partial loads at 50 rps, 60 rps, and full load 90 rps.

4. Results and discussion

In the following subsections the achieved experimental results are presented for each working mode in all the testing points defined. The experimental values have not been compared for the different sources, as the idea behind the dual-source heat pump is to switch between one mode (air as source/sink) or the other (brine as source/sink) depending on the external conditions, mainly air temperature as the ground temperature is going to be more constant. Also, for the same experimental points (same temperatures with air and with brine), quite similar performance is encountered for air/brine modes.

4.1 DSHP in heating mode using air as heat source

Heating capacity, measured at SCHX, and Coefficient of Performance (COP) are increasing with decreasing SCHX water supply temperature, therefore reducing the pressure ratio / required temperature boost, as can be seen in Fig. 5 and Fig. 6. Fig. 7 shows the compressor electrical power in the different testing conditions. On the one hand, the highest heating capacity values at SCHX and electrical consumption values are achieved with the highest compressor speed. On the other hand, the highest cycle efficiencies are achieved with the lowest compressor speed. The calculated COP for high supply temperatures is around 2.5, which is rather low.

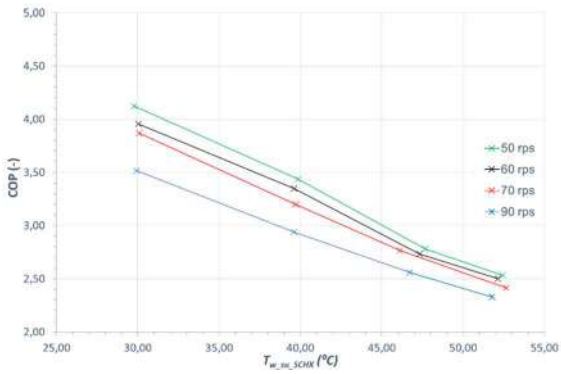

Fig.5 – COP for different water supply temperatures to the SCHX and compressor speeds (rps). Heating air-water mode.

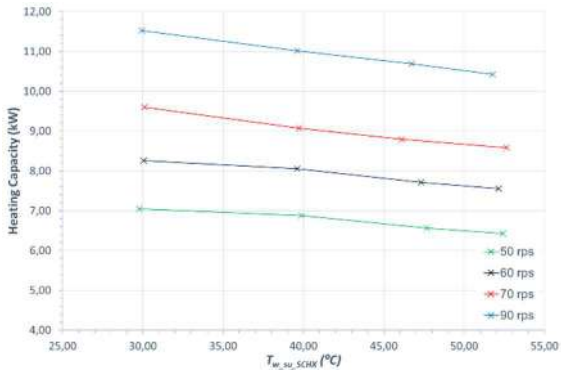

Fig.6 – Heating capacity for different water supply temperatures to the SCHX and compressor speeds (rps). Heating air-water mode.

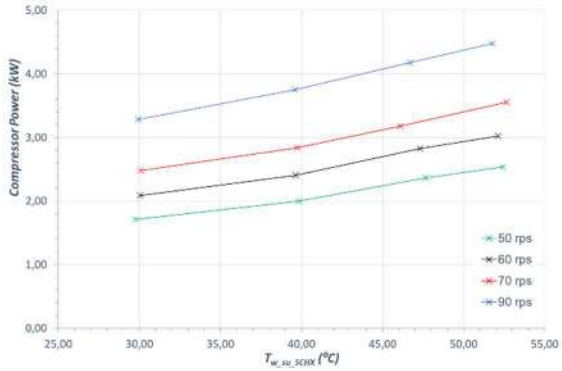

Fig. 7 – Compressor power for different water supply temperatures to the SCHX and compressor speeds (rps). Heating air-water mode.

This is due to abnormal refrigerant pressure drop on the DSHX, observed when the device is working in heating mode. This leads to lower values than predicted with the developed models.

Fig. 8 shows the deviation between the DSHX capacity estimated by the dimensioning tool and the experimental results. The deviation is below 10 % for all of the testing points. Therefore, the numerical model can be used for predicting the capacity of the DSHX as air source evaporator. The capacity calculated with the thermodynamic model is obtained by introducing correction factors which account for the refrigerant pressure drop values obtained experimentally.

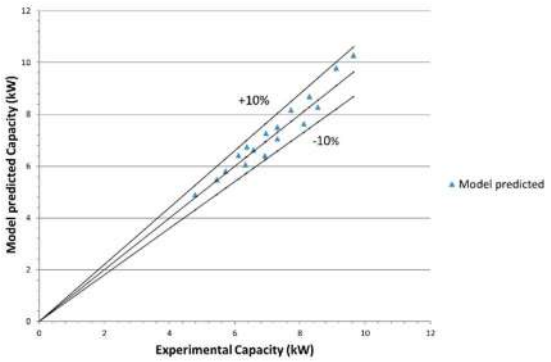

Fig.8 – Capacity deviation between thermodynamic model and tested values for DSHX working as evaporator with air.

4.2 DSHP in cooling mode using air as heat sink

Cooling capacity at SCHX and Energy Efficiency Ratio (EER) are increasing with decreasing ambient temperature, therefore reducing the pressure ratio / required temperature boost, as can be seen in Fig. 9 and Fig. 10.

Fig. 11 shows the compressor electrical power in the different testing conditions. On the one hand, the higher the compressor speed, the larger the cooling power and electrical consumption values. On the other hand, the lower the compressor speed, the higher the cycle efficiency. Nevertheless, the EER values achieved with low compressor velocities 40 and 50 rps are really close. The calculated COP for high ambient temperatures is between 2.5 to 3.2, aligned with the expected values. As expected, the highest the ambient temperature, the lower the cooling capacity in the SCHX, due to the higher pressure-ratio.

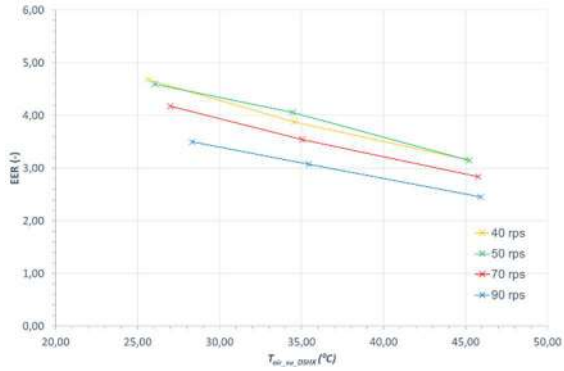

Fig.9 – EER for different water supply temperatures to the DSHX and compressor speeds (rps). Cooling air-water mode, producing cooling from 12 °C to 7 °C.

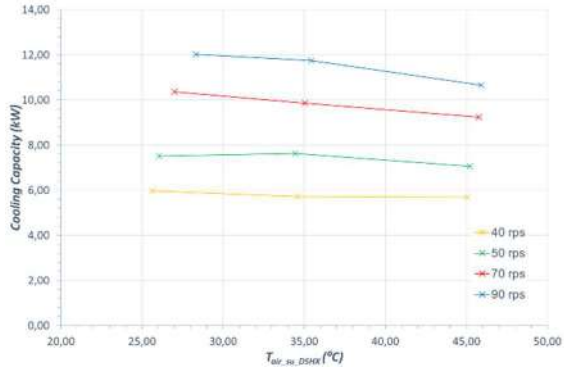

Fig.10 – Cooling capacity for different water supply temperatures to the SCHX and compressor speeds (rps). Cooling air-water mode, producing cooling from 12 °C to 7 °C.

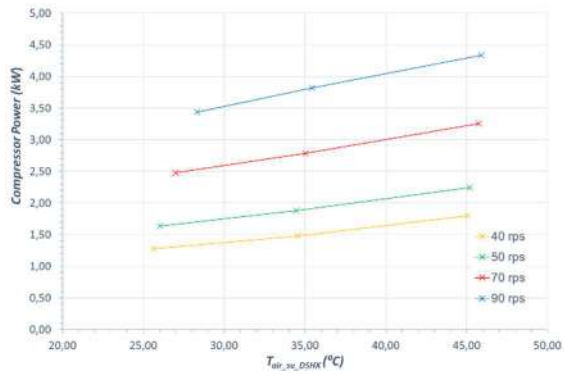

Fig.11 – Compressor power for different water supply temperatures to the SCHX and compressor speeds (rps). Cooling air-water mode, producing cooling from 12 °C to 7 °C.

Fig. 12 shows the deviation between the condenser capacity estimated by the dimensioning tool and the experimental results. The model tends to slightly over-predict the behavior of the DSHX in air

condenser mode, but deviations below 10 % are found for all the testing points, and are considered acceptable.

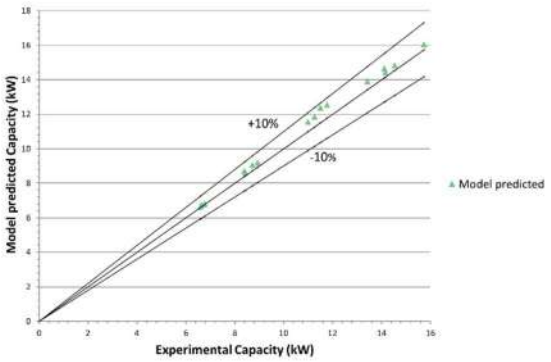

Fig.12 – Capacity deviation between thermodynamic model and tested values for DSHX working as condenser with air.

4.3 DSHP in heating mode using water as heat source

Tendencies showing the influence of compressor speed on the COP can be observed in Fig. 13, and on the heating capacity in Fig. 14, for different DSHX water/brine supply temperatures and maintaining the SCHX supply temperature at 40 °C for all cases represented. Fig. 15 shows the compressor electrical power in the different testing conditions. DSHP heating capacity and electricity consumption increase as compressor speed increases, achieving higher capacities when the pressure ratio is reduced. Respect to the DSHP efficiency, the lower the pressure ratio, the higher the achieved COP values. In addition, the lower the compressor speed, the higher the COP.

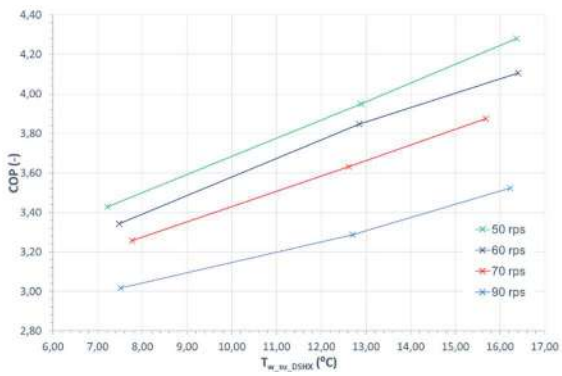

Fig.13 – COP for different water supply temperatures to the DSHX and compressor speeds (rps). Heating water-water mode, producing heating from 40 °C to 45 °C.

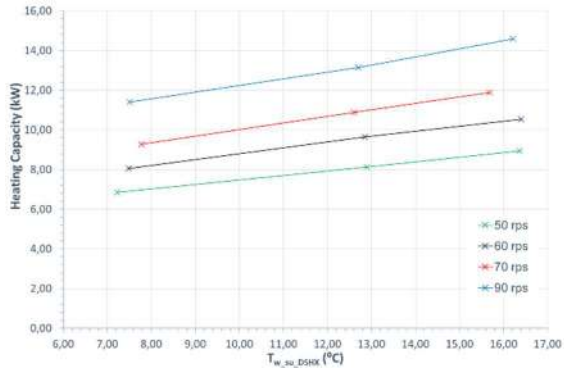

Fig.14 - Heating capacity for different water supply temperatures to the DSHX and compressor speeds (rps). Heating water-water mode, producing heating from 40 °C to 45 °C.

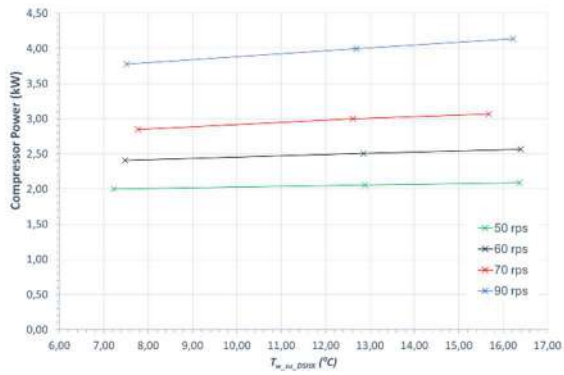

Fig.15 - Compressor power for different water supply temperatures to the DSHX and compressor speeds (rps). Heating water-water mode, producing heating from 40 °C to 45 °C.

Fig. 16 shows the deviation between the evaporation heat obtained by the numerical model and the experiments. As can be seen the deviation is below 10% for all of the testing points. Therefore, the numerical model predicts the evaporation heat with a good accuracy and could be used as dimensioning tool.

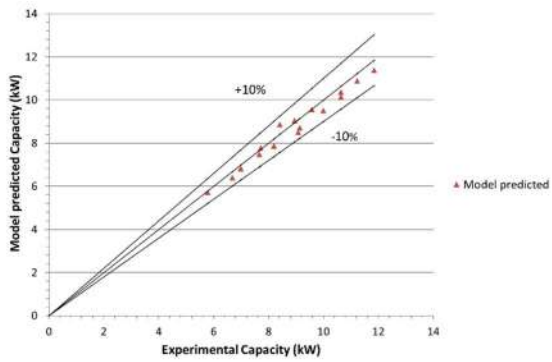

Fig.16 – Capacity deviation between thermodynamic model and tested values for DSHX working as evaporator with water.

4.4 DSHP in cooling mode using water as heat source

EER values increase when DSHX supply stream temperatures decrease, therefore reducing the pressure ratio / required temperature boost, as can be seen in Fig. 17. But this enhancement is only due to the higher compressor electricity consumption, because the cooling capacity seems to remain constant for both DSHX supply temperatures, as can be observed in Fig. 18. On the one hand, the higher the compressor speed, the larger electrical consumption, as can be seen in Fig. 19. On the other hand, the lower the compressor speed, the higher the cycle efficiency (EER), but not for 50 rps at 25 °C DSHX supply temperature. Nevertheless, the EER values achieved with low compressor velocities, 50 and 60 rps are really close at 30 °C DSHX water supply temperature. The calculated EER values for high water supply temperature (30 °C) are between 3.2 to 3.8, aligned with the expected values.

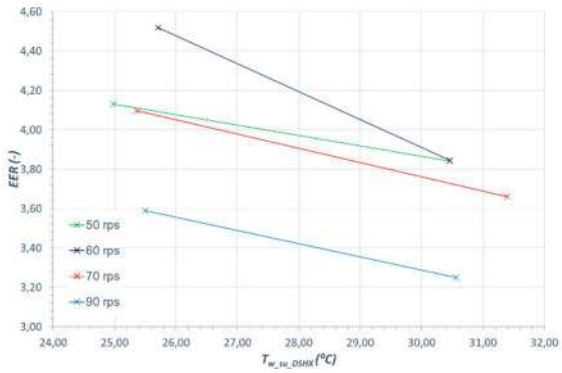

Fig.17 – EER for different water supply temperatures to the DSHX and compressor speeds (rps). Cooling water-water mode, producing cooling from 12 °C to 7 °C.

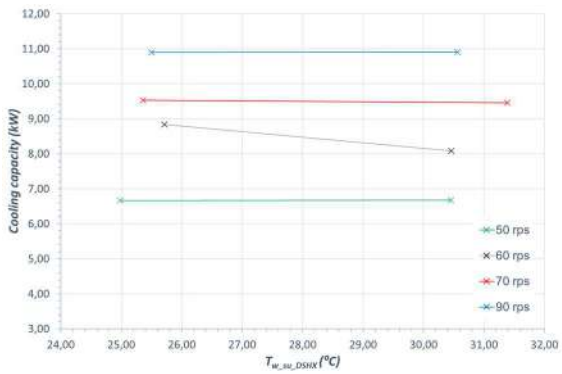

Fig.18 - Cooling capacity for different water supply temperatures to the DSHX and compressor speeds (rps). Cooling water-water mode, producing cooling from 12 °C to 7 °C.

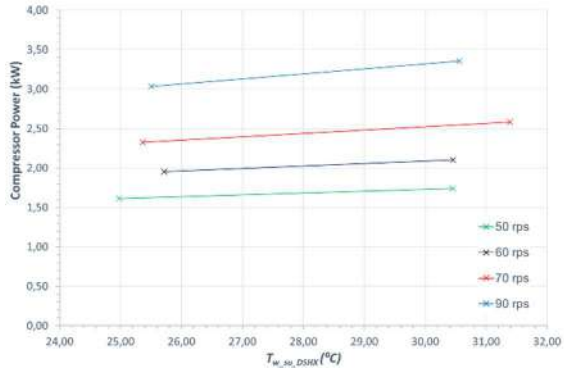

Fig.19 - Compressor power for different water supply temperatures to the DSHX and compressor speeds (rps). Cooling water-water mode, producing cooling from 12 °C to 7 °C.

Fig. 20 shows the comparison between the model predicted capacity and the experimental values, showing deviations for the same testing conditions below 15% for all the points tested. The model overpredicts slightly the behaviour of the DSHX at ground source condenser mode, but the difference could be considered acceptable.

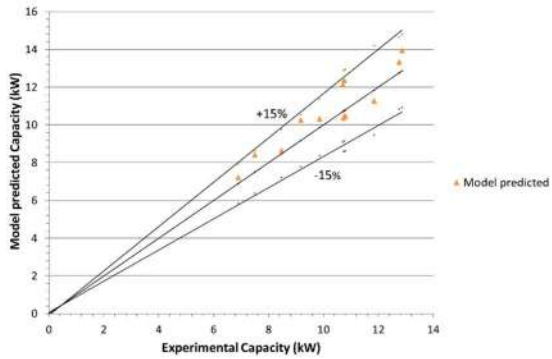

Fig.20 – Capacity deviation between thermodynamic model and tested values for DSHX working as condenser with water.

5. Dual-source heat pump redesign and future work

Based on the results and the problems encountered during the testing of the DSHP, a new design has been carried out and a new prototype has been built. The unit includes a more compact DSHX, based reduced diameters for the tubes and internally enhanced external tubes. This change has allowed an important reduction of the DSHX volume, and thus, the refrigerant charge has been reduced by 70%.

The refrigerant circuit has been optimized, also focusing on the compactness of the unit. It has been simplified, especially regarding the DSHX inlet and outlet parts, as during the experimental campaign of the first prototype an excessive pressure drop was measured in evaporator mode.

Fig. 21 shows the second manufactured prototype, which will be tested in an experimental campaign analogous to the one carried out with the first prototype. Additionally, combined air-water modes in the DSHP (air and water as a source or sink simultaneously in the DSHX) are planned for testing, in order to explore the whole set of possibilities which the DSHX can offer.

Fig. 21 – Second prototype of the DSHP.

The experimental results of the DSHP and the new designed unit will be used to evaluate the energy performance of the whole system, which is focused in multi-family buildings and designed in order to achieve a high renewable share.

6. Acknowledgement

The authors are grateful for the funding received from the EU Horizon 2020 program, within contract no. 814888, corresponding to the TRI-HP project "Trigeneration systems based on heat pumps with natural refrigerants and multiple renewable sources." in which this analysis is framed.

https://www.tri-hp-.eu

7. References

[1] Roadmap to a Resource Efficient Europe. Available at: https://eur-lex.europa.eu/legal-content/EN/TXT/PDF/?uri=CELEX:52011DC0571&from=EN

[2] EU F-Gas Regulation Handbook, EIA, 2015.

[3] Rees, Advances in ground-source heat pump systems. Woodhead Publishing, 2016.

[4] Jin, T. M. Eikevik, P. Nekså, and A. Hafner, "A steady and quasi-steady state analysis on the CO2 hybrid ground-coupled heat pumping system," International Journal of Refrigeration, vol. 76, pp. 29 – 41, 2017.

[5] Man, H. Yang, and J. Wang, "Study on hybrid ground-coupled heat pump system for air-conditioning in hot-weather areas like hong kong," Applied Energy, vol. 87, no. 9, pp. 2826 – 2833, 2010.

[6] Engineering Equation Solver. F-Chart Software. http://www.fchart.com

[7] W. Chi-chuan, H. Yi-chung, and L. Yur-tsai, "Convective heat transfer for plain ns. performance of plate finned tube heat exchangers under dehumidifying conditions," Journal of Heat Transfer, vol. 119/1, pp. 109 – 117, 1997.

[8] Shah, R., London, A., Heat transfer in pipe flow. laminar flow forced convection in ducts, Academic Press, vol. 192, p. 98, 1978.

[9] Nellis, G., Klein, S., Heat Transfer. Cambridge University Press, 2008.

[10] V. D. Ingenieure, VDI-Heat Atlas. Springer, 1993.

[11] Incropera, F., DeWitt, P., David, P., Fundamentals of Heat and Mass Transfer, 6th ed. New York Wiley, 2007.

[12] Shah, M., Comprehensive correlations for heat transfer during condensation in conventional and mini/micro channels in all orientations, International Journal of Refrigeration, vol. 67, pp. 22–41, 2016.

[13] Shah, M., Prediction of heat transfer during condensation in inclined plain tubes, Applied Thermal Engineering, vol. 94, pp. 82–89, 2016.

[14] L. Sun and K. Mishima, An evaluation of prediction methods for saturated _ow boiling heat transfer in minichannels, International Journal of Heat and Mass Transfer, vol. 52, pp. 5323 – 5329, 2009.

[15] Shah, M. M. Chart correlation for saturated boiling heat transfer: equations and further study, ASHRAE Transactions, vol. 88, pp. 185 – 196, 1982

[16] EN 14511-3:2018 Air conditioners, liquid chilling packages and heat pumps for space heating and cooling and process chillers, with electrically driven compressors - Part 3: Test methods.

Data Statement

The datasets generated during and/or analysed during the current study are not publicly available at the moment of the publication of the paper, but will be available under the TRI-HP Data Research Community in Zenodo in the near future. TRI-HP Research Data Community | Zenodo

Energy performance retrofits targeting national strategy development for typical Turkish school building

Hazal Kızıldağ [1], Gökçe Tomrukçu [2], Gizem Avgan [3], Ayşe Özlem Dal [4], Neşe Ganiç Sağlam [5], Ece Kalaycıoğlu Özdemir [6], Touraj Ashrafian [7]

[1] Graduate School of Engineering and Science, Department of Architecture, Ozyegin University, Istanbul, Turkey, hazal.kizildag@ozu.edu.tr

[2] Graduate School of Engineering and Science, Department of Architecture, Ozyegin University, Istanbul, Turkey, gokce.tomrukcu@ozu.edu.tr

[3] Graduate School of Engineering and Science, Department of Architecture, Ozyegin University, Istanbul, Turkey, gizem.avgan@ozu.edu.tr

[4] Graduate School of Engineering and Science, Department of Architecture, Ozyegin University, Istanbul, Turkey, ozlem.dal@ozu.edu.tr

[5] Faculty of Architecture and Design, Department of Architecture, Ozyegin University, Istanbul, Turkey, nese.saglam@ozyegin.edu.tr

[6] Faculty of Architecture and Design, Department of Architecture, Ozyegin University, Istanbul, Turkey, ece.kalaycioglu@ozyegin.edu.tr

[7] Faculty of Architecture and Design, Department of Architecture, Ozyegin University, Istanbul, Turkey, touraj.ashrafian@ozyegin.edu.tr

Abstract. Today, most existing buildings should be retrofitted to reduce the negative impact on the environment. According to the EPBD, Member States should prepare national action plans to increase nZEB. Therefore existing buildings must go under deep refurbishment. Educational facilities are a critical segment of the public sector, and a frequently used building type with high energy needs. In Turkey, more than 17 million students spend the majority of their time in school buildings, hence increasing energy efficiency in existing educational buildings not only contributes to the environment and can create healthy and comfortable indoor conditions for the students, but also creates an awareness of the youth and increases their learning performance. This study focuses on analyzing the effects of various retrofitting applications of the building envelope and HVAC systems on the energy performance of a school building to improve existing energy consumptions. Analysis of the building envelope is an important primary step towards achieving a low energy level, as other energy efficiency measures such as buildings' HVAC systems' efficiencies. The aim is to reduce the heating and cooling demand of the selected building and to increase its energy performance. The analysis of the case study showed that there is no insulation layer on the outer wall as a result of the measurements. Therefore, the first step is to observe how the appropriate insulation layer affects the energy performance of the building. The methodology consists of energy modeling of the case study building in DesignBuilder and obtaining energy performance results by EnergyPlus software. Various retrofit scenarios were prepared into packages which include alternatives of thermal characteristics of the opaque elements such as external walls and roof, application of different glazing units, and implementation of solar control elements. These variables were combined and compared in terms of their effects on total primary energy consumption, heating and cooling demand. Based on the results, technical suggestions were given according to the best performing scenarios. It is expected that the research outcomes will contribute to the studies to improve the energy performance in educational buildings.

Keywords. energy consumption, educational buildings, energy performance, energy retrofit
DOI: https://doi.org/10.34641/clima.2022.382

Copyright ©2022 by the authors. This conference paper is published under a CC-BY-4.0 license.

1. Introduction

Global energy use is rapidly increasing day by day. This demand for energy causes a lack of resources, pollution to our environment, and worldwide catastrophes such as global warming and climate change that we can sense the consequences even today. The construction sector consumes an unignorable high amount of energy. Therefore the energy efficiency analysis of the present buildings and retrofitting strategies is vital to take precautions against energy overconsumption. This issue has affected the national protocols and legislations. In order to meet their aims, the European Union (EU) has established several laws under the Kyoto Protocol to improve energy efficiency, reduce energy consumption, and eliminate waste. In 2002, the Energy Performance of Buildings Directive (2002/91/EC, EPBD) was introduced [1]. One of the requirements is the implementation of minimum standards in new and some renovated structures.

The monitoring of the existing buildings' energy efficiency is an important strategy for preventing energy overconsumption in the construction sector. It is one of the fundamental challenges in moving towards sustainable buildings. Demolition of existing structures to construct new ones is not a reasonable method in terms of high budget, effort, or pollution to the environment, and it also consumes more energy [2]. To ensure adequate performance, the initial option is to lower the energy demand of buildings through passive solutions, followed by the retrofitting of building envelope layers. Preventing heat transmittance between outside and interior spaces is crucial for achieving the energy efficiency goal of sustainable buildings. The envelope of a building is like the skin of a human body, is the boundary between the inside and outside spaces that determine heat gain and heat loss. To provide optimum indoor comfort for the occupants as well as preventing over consumption of energy, heat loss prevention must be ensured with possible envelope alternative solutions with the assistance of efficient HVAC systems. Identifying the most significant material and insulation thickness requirements in the early design stages is vital. Presently, the majority of building thermal parameters' efficiency is computed using simple energy models of building envelope dynamics [3]. The thermal permeability is the most important parameter in these computations in case of comparing characteristics of thermal performance given by Turkish national standards and to evaluate thermal performance of educational buildings' envelopes suited for thermal insulating purposes. In the literature, various building parameters are analyzed on the retrofitting of educational buildings towards NZEB with cost efficiency in the process of refurbishment design [2,4,5,6]. The building envelope features, insulation thickness, HVAC system's effectiveness and role of solar shadings are analyzed in studies to evaluate building energy performance [7,8,9]. The occupancy schedules, parameters related to occupant behaviors input in computational programs affect the energy efficiency analysis results [4].

This study is a part of an ongoing project funded by Scientific and Technological Research Council of Turkey (TUBITAK) that focuses on analyzing the energy performance of a school building located in İstanbul, Turkey to determine the effects of envelope design elements and highlight key HVAC features' impacts.

2. Methodology

At the first step of the research, the building geometry is modeled in DesignBuilder [10] with all structural features including the materials, envelope details and HVAC systems to perform a dynamic energy simulation. The energy performance of the case study building is validated for the whole year of 2019 through the obtained electricity and natural gas bills. After calibrating the energy model by conducting simulations using DesignBuilder and Energyplus [11], the next step presented in this paper focuses on retrofit measurements on the building envelope and HVAC system to reduce the energy consumption of the building. Initially, the current energy use is observed in terms of annual heating and cooling consumption (kWh/m2a) and primary energy use (kWh/m2a). The energy usage is analyzed from both the bills and validated simulation results obtained from EnergyPlus. Then the variables that affect the energy demand are identified, such as material properties of walls, roof and glazing. Secondly, several alterations on building envelope components such as changing the thickness of insulation materials and also enhancing the mechanical system made within the simulation packages. Then the best performing individual packages are combined to analyze an overall effect.

2.1 Case Study Building

The case study building (Fig 1,2) is an elementary school located in Bakırkoy, Istanbul. The climate of Istanbul is classified as Csa according to Köppen [12], which has a mild Mediterranean climate. The selected building consists of four typical floors and a basement with a gross area of approximately 4435.78 m^2 . Since the case study building is a typical school building commonly constructed in Turkey, the retrofitting strategy can be generalized and suitable for other school buildings. Hence, it may be a guideline for future constructions in Turkey. The construction of the building was completed in 2008 and opened for use. The school building is used between 09:00-14:40 on Friday and 09:00-16:20 for the rest of the weekdays. The geometry, thermophysical features, mechanical systems, internal gains, and user schedules were modelled and calibrated using electricity and natural gas bills obtained from the school administration.

Fig. 1 - Exterior view of the case study building.

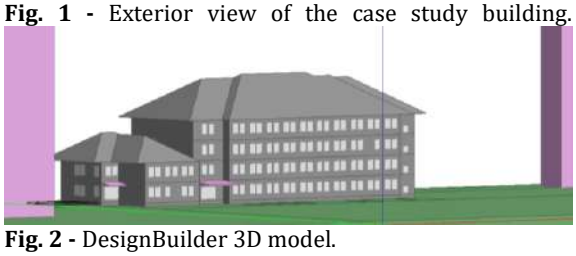

Fig. 2 - DesignBuilder 3D model.

2.2 Existing Building Properties

The external walls of the building are entirely cast concrete as it is located in one of the earthquake zones. The U-value of the external wall was measured on the field, and the rest of the material information was obtained from the school municipality and technical drawings. However, it has been observed that the thermal transmittance of the wall does not meet the permitted value by the national standard for Istanbul [13] which is 0.6 W/m2-K, while the existing U-value of the wall is 1.663 W/m2-K. Other construction details with material specifications are given in Table 1.

Tab. 1 Construction materials of the case building.

	Material	Conductivity (W/mK)	Specific Heat Capacity (J/kgK)	Density (kg/m3)	Thickness (m)	U value (W/m2-K)
External Wall	gypsum plaster	0,42	840	1200	0,03	1,663
	cast concrete	1,13	1000	2000	0,35	
	gypsum plaster	0,42	840	1200	0,03	
Floor	ceramic floor tile	0,8	850	1700	0,03	1,815
	floor screed	0,41	840	1200	0,07	
	cast concrete	1,13	1000	2000	0,35	
Roof	roofing tile	0,84	800	1900	0,01	0,507
	polyester resin	0,19	1200	1400	0,02	
	oriented strand board	0,13	1700	650	0,02	
	air gap	n.a	n.a	n.a	0,5	
	MW stone wool	0,038	840	40	0,05	
	reinforced concrete	2,3	1000	2300	0,12	
	cement plaster	0,72	840	1760	0,03	
Internal Wall	plaster	0,16	1000	600	0,03	1,184
	brick	0,62	800	1700	0,13	
	plaster	0,16	1000	600	0,03	

The glazing consists of air-filled double glazed windows (4+12+4) with a light-grey colour covering on the interior glass (Table 2). Additionally, there is no external shading; only the internal blinds are used for shading purposes.

Tab. 2 -Glazing materials of the case building.

Material	Thickness (mm)	Visible Transmittance (Tvis)	Solar Heat Gain Coefficient (SHGC)	U value (W/m2-K)
clear glass	4	70%	50%	2,7
air	12			
light grey-coloured glass	4			

The mechanical system information was gathered during the field observations, and it was determined that the heating system consists of a non-condensing hot water boiler with radiators.The single boiler has a 300 kW capacity. However, according to the latest regulation released in 2018 [14] it is forbidden to use non-condensing boilers that have a capacity under 400 kW. In terms of cooling, there are split air conditioners in several rooms such as the principal's room, teachers' room, kindergarten classrooms and elementary classrooms facing the south façade. Using air conditioners in classrooms is not common among public elementary schools. Since there is no use of an active cooling system in the building, there is an overheating problem affecting occupancy thermal comfort in the southern part of the building.

2.3 Existing Building Energy Performance

According to the U value measurement on the wall, the U value of the case study building is very high as stated above. It is clear that this situation directly affects the energy performance of the building. Annual heating demand is calculated as 42,931.54 kWh/m^{2}a, cooling demand is 0.4183 kWh/m^{2}a, and the primary energy consumption is calculated as 83,134.71 kWh/m^{2}a. The lack of insulation material in the building envelope and the lack of maintenance of the boiler caused an increase in the energy consumption of the building.

3. Results

3.1 Retrofit Strategies of External Wall

To ensure the energy performance improvements of the building, the current U value was measured during a site visit on 24th of May 2021. The measured U-value was recorded as 1.663 W/m^2-K. It has been observed that the building has a high U value according to the climate type and strategies have been developed for energy improvements. The selection of the materials for enhancing the building envelope was conducted according to the best performing materials available in TS 825 [13]. According to the measurements and information obtained from the technical personnel of the school, it is determined that there was no insulation layer on the outer walls. At the first step, expanded polystyrene (EPS) material is added to the outer walls (W1), and the resulting U-value is 0.685 W/m^2-

K which is appropriate for the Istanbul region. Secondly, the U-value is decreased to 0.432 W/m^2-K by increasing the thickness of this insulation material (W2). The improvement scenarios are shown in Table 3.

Tab. 3 Retrofit scenarios of the exterior wall.

Wall	Material	Thickness	Conductivity	Specific Heat	Density	U Value
		M	W/mK	J/ Kg-K	Kg/m3	W/m2-K
WO (Existing)	Cement Plaster	0.03	0, 42	840	1200	1,663
	Cast Concrete	0.35	1,13	1000	2000	
	Cement Plaster	0.02	0, 42	840	1200	
W1	Cement Plaster	0.03	0, 42	840	1200	0,685
	Cast Concrete	0.35	1,13	1000	2000	
	EPS Expanded Polystrene (Heavyweight)	0.03	0, 035	1400	25	
	Cement Plaster	0.02	0, 42	840	1200	
W3	Cement Plaster	0.03	0, 42	840	1200	0,432
	Cast Concrete	0.35	1,13	1000	2000	
	EPS Expanded Polystrene (Heavyweight)	0.06	0, 035	1400	25	
	Cement Plaster	0.02	0, 42	840	1200	

Results showed that (Fig. 3) the building's need for heating energy is decreased. Currently, the building has a heating demand of 42.93 kWh/m^{2}a, but with the addition of the insulation layer, this demand is lowered to 33.97 kWh/m^{2}a. Finally, if the thickness of the insulation material is increased, the heating requirement becomes 31.72 kWh/m^{2}a. A reduction of 11.21 kWh/m^{2}a is achieved according to the heating needs of the existing building. On the other hand, while the cooling load is 0.41 kWh/m^{2}a at the beginning, it has decreased to 0.35 kWh/m^{2}a in the W2 scenario. This situation also affected the primary energy consumption of the building. In the current situation, the primary energy consumption of the building is 83.13 kWh/m^{2}a per year. In comparison, the primary energy consumption obtained in the W1 scenario is 74.12 kWh/m^{2}a and in the W2 scenario is 71.85 kWh/m^{2}a. Therefore, in general, both the primary energy consumption and the need for heating and cooling have decreased, especially when the insulation layer is added to the building.

Fig. 3 - Comparison of wall scenarios

3.2 Retrofit Strategies of Roofing System

In order to reduce the energy consumption of the building, an improvement proposal is also developed on the roofing system (Table 4). Currently, the U-value of the roof is 0.503 W/m^{2}K. The insulation layer of the roof, which was 0.05 m, is changed to 0.07 m by increasing the thickness of the MW stone wool layer. The revised U-value of the roof is calculated as 0.398 W/m^{2}K.

Tab. 4 Retrofit scenarios of the roof.

Roof	Material	Thickness	Conductivity	Specific Heat	Density	U Value
		M	W/mK	J/ Kg-K	Kg/m3	W/m2-K
RO (Existing)	Roof Tile	0.025	0,84	800	1900	0, 503
	Polyester Resin	0,02	0, 19	1200	1400	
	Oriented Strand Board	0.02	0, 13	1700	650	
	Air Gap	0.5	N.A	N.A	N.A	
	Mw Stone Wool	0.05	0, 038	840	40	
	Concrete Reinforced with %1 steel	0.12	2, 3	1000	2300	
	Cement Plaster	0.03	0, 72	840	1760	
R1	Roof Tile	0.025	0,84	800	1900	0, 398
	Polyester Resin	0,02	0, 19	1200	1400	
	Oriented Strand Board	0.02	0, 13	1700	650	
	Air Gap	0.5	N.A	N.A	N.A	
	Mw Stone Wool	0.07	0, 038	840	40	
	Concrete Reinforced with %1 steel	0.12	2, 3	1000	2300	
	Cement Plaster	0.03	0, 72	840	1760	

The results obtained in the comparison of the roof scenario showed that the difference between primary energy consumption and yearly heating and cooling demand is not so apparent as in the wall scenarios (Fig. 4).The primary energy consumption, which is currently 83.13 kWh/m^{2}a, has been analyzed as 83.09 kWh/m^{2}a after the roof improvement. On the other hand, the heating demand was initially 42.92 kWh/m^{2}a, and it is 42.89 kWh/m^{2}a in the R1 scenario. As the results did not meet the expected outcomes, it is evident that retrofit measurements on the roof system require different strategies.

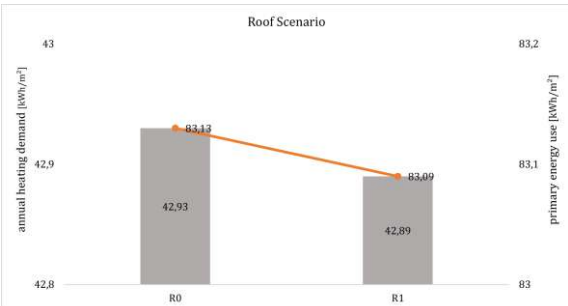

Fig. 4 - Comparison of roof scenarios

3.3 Retrofit Strategies of Glazing System

Another analysis to improve the energy performance of the selected building is conducted on glazing systems. Currently, it is double glazing, and the interior glass is grey coated. The existing U-value is

2.665 W/m^{2}K. The first recommended glazing system (G1) is double Low-E glazing filled with air. The U-value of this glass is 1.5 W/m^{2}K. The second scenario (G2) contains double solar Low-E glazing on outer glass and the system's cavity filled with argon gas with a U-value of 1.1 W/m^{2}K (Tab. 5).

Tab. 5 -Retrofit scenarios of the glazing system.

Glazing	Material	U Value	Total Solar Transmittance	Visible Transmittance
		W/m2-K	SHGC	Tvis
G0 (Existing)	Dbl Clr 6mm/13mm Air (Grey)	2,665	0, 47	0, 38
G1	Dbl LoE 6mm/13mm Air	1,5	0, 54	0, 78
G2	Dbl Solar LoE 6mm/18mm Argon	1,1	0, 42	0, 71

According to the results (Fig. 5), low-E glass has reduced primary energy use and annual heating and cooling demand. The primary energy consumption, which was 83.13 kWh/m^{2}a at the beginning, decreased to 78.27 kWh/m^{2}a with Low-E and 78.22 kWh/m^{2}a as a result of filling the space inside with argon instead of air in the G2 scenario. While the heating demand is 42.92 kWh/m^{2}a at the existing state, the value reached in the second scenario (G2) is 40.26 kWh/m^{2}a. While the cooling demand is 0.41 kWh/m^{2}a in its existing situation, it decreased to 0.39 kWh/m^{2}a.

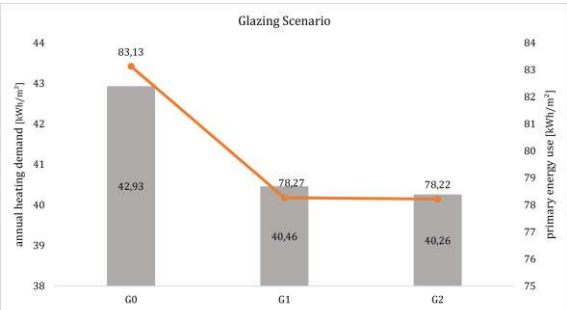

Fig. 5 - Comparison of glazing scenarios

3.4 Retrofit Strategies of HVAC System

Apart from the building envelope, enhancement of the mechanical heating system is proposed. Accordingly, there is a non-condensing single hot water boiler with a 300 kW capacity that has 75% efficiency at the current state (H0) . Replacing the existing boiler with a 300 kW capacity condensing boiler that has 95% efficiency (H1) has drastically reduced annual heating demand by 25.3%. Also, primary energy use is decreased from 83,13 kWh/m^{2}a to 72,25 kWh/m^{2}a (Fig. 6). It is evident that boiler efficiency has a considerable impact on energy consumption mainly in heating demand.

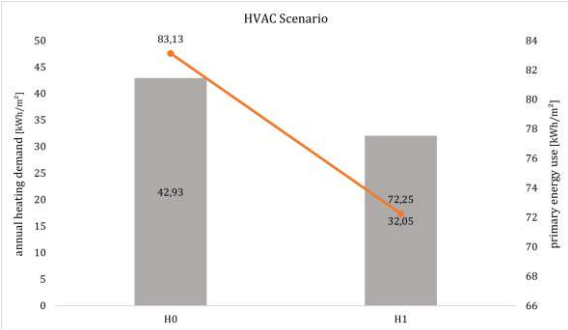

Fig. 6 - Comparison of HVAC scenarios

3.5 Combination of Retrofit Scenarios

At this stage of the research, the best performing retrofit scenarios (W2, R1, G2, H1) are selected to measure their combination's outcome. Among the analyzed scenarios, W2-R2-G2 scenarios with high insulation and low U values are selected for the wall, roof, and glass system. The HVAC system aims to increase the efficiency with the condensing option of the existing boiler. As a result of combining these scenarios, the heating demand, which was initially 42.93 kWh/m^{2}a, is reduced to 19.93 kWh/m^{2}a; hence the building will need less energy for heating. Considering the primary energy consumption, it is decreased by 25.31 kWh/m^{2}a from 83.13 kWh/m^{2}a. While the cooling requirement was 0.41 kWh/m^{2}a at the initial state, it is dropped to 0.32 kWh/m^{2}a.

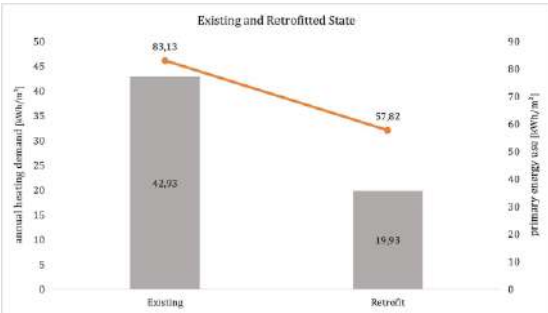

Fig. 7 - Comparison of existing and retrofitted state

3.6 Combination of Retrofit Scenarios with Exterior Shading

Another strategy to reduce the energy performance of the building requires that the shade elements are designed and applied in accordance with the climate and the structure. It is essential for students' performance, especially in educational buildings. As a result of the observations made in the case study building, there is an overheating problem, especially in south-facing spaces in summer. For this reason, indoor air temperature is controlled by air conditioning in these places. However, this situation increases the energy consumption of the building. Therefore, wooden overhang elements are included in the simulation scenarios. Adding shading elements to the south-facing spaces of the best-combined package has increased the need for overall heating and lighting. However, since it reduces the need for cooling, especially in summer, the overall reduction in energy consumption has been analyzed. While the

primary energy consumption was 57.82 kWh/m^{2}a in the combined scenario, it is decreased to 55.31 kWh/m^{2}a with the addition of shadow elements.

4. Discussion & Conclusion

In this paper, energy performance analysis and retrofit strategies were analyzed in order to decrease energy consumption. For this purpose, a school building selected as a case study is modeled in DesignBuilder, and energy performance analysis is conducted in EnergyPlus. Firstly the effect of external walls and roof on energy performance is observed by adding and increasing insulation layers. The lack of insulation layer in exterior walls in the building caused the building's energy consumption to be high. Secondly, different glazing systems are implemented with lower U-values as the glass systems must not leak the ambient air. In addition, the HVAC system's increased efficiency by high capacity hot water boilers has a significant impact on fuel consumption for heating energy. After that, the combinations of individual retrofit packages are simulated. Results showed that adding 0.6 m EPS insulation in external walls, 0.07 m stone wool insulation in the roof, installing argon filled double solar Low-E glazing system, and enhancing the boiler with an efficiency of 95% have a dramatic effect on both annual heating, cooling demand, and primary energy consumption. The outcomes showed that the primary consumption was significantly reduced from 83.13 kWh/m^{2}a to 57.82 kWh/m^{2}a. Lastly, the effect of exterior shading on energy performance is analyzed by adding overhangs on the south façade. Overall, the combination of retrofit scenarios and shading elements decrease the primary energy use by 33.4%.

5. Acknowledgements

This research is a part of project 'Developing National Approach of Long-term Renovation Strategies for Existing Educational Campuses in Turkey towards Nearly Zero Energy Target' (219M552) funded by TUBITAK. We would like to pay our special regards to the administration and students of the case study buildings for their help.

6. References

[1] EPBD Directive 2002/91/ECDirective of the European parliament and of the council on the energy performance of buildingsThe European Community Official Journal, L001 (2003), pp. 0065-0071

[2] Moazzen N, Ashrafian T, Yilmaz Z, Karagüler ME. A multi-criteria approach to affordable energy-efficient retrofit of primary school buildings [Internet]. Vol. 268, Applied Energy. Elsevier BV; 2020. p. 115046. Available from: http://dx.doi.org/10.1016/j.apenergy.2020.115046

[3] Trgala K, Pavelek M, Wimmer R. Energy performance of five different building envelope structures using a modified Guarded Hot Box apparatus—Comparative analysis [Internet]. Vol. 195, Energy and Buildings. Elsevier BV; 2019. p. 116–25. Available from: http://dx.doi.org/10.1016/j.enbuild.2019.04.036

[4] O' Donovan A, O' Sullivan PD, Murphy MD. Predicting air temperatures in a naturally ventilated nearly zero energy building: Calibration, validation, analysis and approaches [Internet]. Vol. 250, Applied Energy. Elsevier BV; 2019. p. 991–1010. Available from: http://dx.doi.org/10.1016/j.apenergy.2019.04.082.082

[5] Ascione F, De Masi RF, de Rossi F, Ruggiero S, Vanoli GP. NZEB target for existing buildings: case study of historical educational building in Mediterranean climate [Internet]. Vol. 140, Energy Procedia. Elsevier BV; 2017. p. 194–206. Available from: http://dx.doi.org/10.1016/j.egypro.2017.11.135

[6] Kwiatkowski J, Mijakowski M, Trząski A. The measures for achieving nZEB standard of retrofitted educational building for specific polish location – case study [Internet]. Kaźmierczak B, Kutyłowska M, Piekarska K, Jouhara H, Danielewicz J, editors. Vol. 22, E3S Web of Conferences. EDP Sciences; 2017. p. 00098. Available from: http://dx.doi.org/10.1051/e3sconf/20172200098

[7]Fathalian A, Kargarsharifabad H. Actual validation of energy simulation and investigation of energy management strategies (Case Study: An office building in Semnan, Iran) [Internet]. Vol. 12, Case Studies in Thermal Engineering. Elsevier BV; 2018. p. 510–6. Available from: http://dx.doi.org/10.1016/j.csite.2018.06.007

[8] Korjenic A, Bednar T. Validation and evaluation of total energy use in office buildings: A case study [Internet]. Vol. 23, Automation in Construction. Elsevier BV; 2012. p. 64–70. Available from: http://dx.doi.org/10.1016/j.autcon.2012.01.001

[9] Cetin KS, Fathollahzadeh MH, Kunwar N, Do H, Tabares-Velasco PC. Development and validation of an HVAC on/off controller in EnergyPlus for energy simulation of residential and small commercial buildings [Internet]. Vol. 183, Energy and Buildings. Elsevier BV; 2019. p. 467–83. Available from:

http://dx.doi.org/10.1016/j.enbuild.2018.11.005

[10]DesignBuilder. Gloucestershire: DesignBuilder Software Ltd; 2002. https://designbuilder.co.uk/

[11] EnergyPlus. U.S.: National Renewable Energy Laboratory (NREL); 2018. https://energyplus.net/

[12] Yılmaz E, Çiçek İ. Detailed Köppen-Geiger climate regions of Turkey<p>Türkiye'nin detaylandırılmış Köppen-Geiger iklim bölgeleri [Internet]. Vol. 15, Journal of Human Sciences. Uluslararasi Insan Bilimleri Dergisi; 2018. p. 225. Available from: http://dx.doi.org/10.14687/JHS.V15I1.5040

[13]Turkish Standards Institute. TS 825 - Thermal insulation requirements for buildings [Internet]. 1998 [revision 22 May 2008; cited 2022 Jan 9].

[14]Turkey. Ministry of Science, Industry and Technology. Regulation on amending the regulation (92/42/EC) on the efficiency requirements of new liquid and gas fueled hot water boilers 2018 (Act No. 1 of 12). Official Gazette of the Republic of Turkey. No: 30374.

Validation process of energy performance simulation: A Turkish school building case

Gökçe Tomrukçu [1], Hazal Kızıldağ [2], Gizem Avgan [3], Ayşe Özlem Dal [4], Neşe Ganiç Sağlam [5], Ece Kalaycıoğlu Özdemir [6], Touraj Ashrafian [7]

[1] Graduate School of Engineering and Science, Department of Architecture, Ozyegin University, Istanbul, Turkey, gokce.tomrukcu@ozu.edu.tr

[2] Graduate School of Engineering and Science, Department of Architecture, Ozyegin University, Istanbul, Turkey, hazal.kizildag@ozu.edu.tr

[3] Graduate School of Engineering and Science, Department of Architecture, Ozyegin University, Istanbul, Turkey, gizem.avgan@ozu.edu.tr

[4] Graduate School of Engineering and Science, Department of Architecture, Ozyegin University, Istanbul, Turkey, ozlem.dal@ozu.edu.tr

[5] Faculty of Architecture and Design, Department of Architecture, Ozyegin University, Istanbul, Turkey, nese.saglam@ozyegin.edu.tr

[6] Faculty of Architecture and Design, Department of Architecture, Ozyegin University, Istanbul, Turkey, ece.kalaycioglu@ozyegin.edu.tr

[7] Faculty of Architecture and Design, Department of Architecture, Ozyegin University, Istanbul, Turkey, touraj.ashrafian@ozyegin.edu.tr

Abstract. Buildings produce one-third of the world's carbon emissions. It is estimated that the energy needs of buildings will increase by 40% until 2040 unless measures are taken. A significant portion of the energy in Turkey is consumed by non-residential construction sectors such as educational buildings. Therefore, efforts to improve the energy performance of educational buildings are essential to minimize the environmental impacts of the building stock. Building's energy simulation provides the possibility of testing various scenarios to define their pros and cons. However, the difference between the simulation results and the actual energy consumption should be minimized in practice. The study aims to monitor energy consumption and validate the simulation results of typical school buildings in Istanbul, Turkey. The approach consists of creating dynamic energy performance simulation models and validating with onsite measurements, energy bills and climatic data of the measurement period. At the first step, the detailed schedule of the occupants and mechanical systems, the building envelope materials, the lighting system, devices information, capacity, and efficiency values of mechanical systems and electrical equipment were obtained and defined in the DesignBuilder software. The U-values of the exterior walls were obtained through in-site measurements. In the next step, interior temperature, relative humidity, and CO2 in the building was measured based on related standards and regulations (ISO 7726 and ASHRAE Guideline 14). As a result, the validated energy model based on a comparison of simulation and measured data can be applied and tested to achieve a high energy performance level in the school building.

Keywords. validation, energy consumption, educational buildings, energy performance, simulation
DOI: https://doi.org/10.34641/clima.2022.383

1. Introduction

According to IEA's 2021 energy report, Turkey's current energy demand mostly relies on imported gas and oil. For improving energy security and decreasing the high imported energy demand, there are important steps taken by the Turkish government such as National Energy Efficiency Action Plan (NEEAP), which targets to reduce Turkey's energy consumption by %14 in different sectors, including buildings, power and heat, in 2017-2023 [1]. The non-residential buildings account for 41% of the construction sector's energy usage, and the educational facilities have a significant

Copyright ©2022 by the authors. This conference paper is published under a CC-BY-4.0 license.

share. It has become crucial to study on school buildings since they are one of the most used public buildings on a daily basis [2]. Therefore, this study focuses on how to improve existing school buildings' energy performances in Turkey. One of the steps to be taken is to determine the correct reference building data by examining the national building stock. Validation is done with the model's intended purpose in mind. For instance, various purposes may need varying degrees of forecast accuracy. Comparing simulated and observed values in model validation necessitates evaluating uncertainty in these data [3]. The current situation of energy performance in educational buildings is examined [4], as well as existing simulation tools for building energy retrofit, gaps, and difficulties in measuring instruments [5].

To achieve national energy efficiency action plans, retrofitting has gained importance. Therefore the simulations' accuracy has become more significant. A study in Ireland aims to close the gap between measured data and energy performance simulation results for the home prototypes, providing new approaches on future building performance measurements, as well as monitoring and updating energy simulation softwares [6]. The study on analyzing the gap between simulation and measurements provides new information about predicting the performance gap using a probabilistic approach by evaluating the correctness and precision of the simulated results compared to the reference values [7].

This study is a preliminary part of a project funded by the Scientific and Technological Research Council of Turkey (TUBITAK) that aims to verify the current buildings' energy performances by conducting an energy simulation of two educational buildings in Istanbul. The study aims to validate the chosen two educational case study buildings' energy simulation with onsite measurements. By validating the energy efficiency simulations, this research may be an important step as a reference study for future studies on the energy efficiency of educational facilities.

2. Methodology

The methodology consists of four steps. Firstly, two case studies were selected. Secondly, by making onsite observations and field measurements, data for energy performance simulations was collected, such as consumption habits and user-related variables. After that, the buildings were modeled, and the collected data were transferred to the simulation program. Then, the existing bills and measured interior temperatures were compared with simulation results and analyzed. The error rate between the indoor air temperatures obtained from the simulation and the measurement results were calculated by the Root Mean Square Error (RMSE) method [8].

2.1 Case Study Buildings

Existing educational buildings in Istanbul were selected (Table 1). Among the factors that played a role in selecting the buildings, they were chosen because they have typical plan types and materials, can be generalized in terms of user calendars, and allow for detailed analysis of the data collection process. Both buildings have no insulation layers on the exterior walls. The main difference is that Type A building's exterior walls consist of cast concrete, whereas Type B building has brick material in external walls.

Tab.1-Case Study Buildings Properties

		Building Properties	
		TYPE A	TYPE B
Picture of building geometry		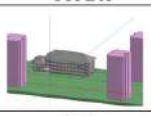	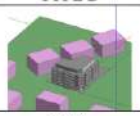
U value of the building envelope (W/m2-K)	External	1.55	1.74
	Roof	0.507	0.537
	Window	2.7	2.8
Heating system		Gas Boiler (Non-condensing) and radiators	Gas Boiler (Condensing)and radiators
Nominal thermal eff (%)		81	85
Cooling system		PTAC air conditioner	PTAC air conditioner
Hot water system		Electric water heater	Electric water heater
Set Point °C	Heating	22	21
	Cooling	24	24
Air change rate (1/h)		0.6	0.7

The obtained data were transferred to the DesignBuilder and EnergyPlus program for performance analysis. The simulations were made using the real climate data of the measurement period. Internal heat gains data, the physical properties, and the materials used were defined. To calculate the energy performance correctly, data such as the number of people and electrical equipment that can generate heat gain inside, the activity schedule, indoor temperatures, and the power of the devices were transferred to the program by making onsite observations and measurements.

3. Data Collection and Field Measurements

The thermal characteristics of external walls greatly impact total building energy performance. Therefore it is crucial to measure the actual U-value of the external walls onsite as the performance of the buildings may change over time. The U-value measurement was held on Feb 15 in both school buildings (Figure 1). The outdoor temperature was relatively cold, and the heating system was active. In order to achieve high accuracy the recommended difference between interior and exterior air temperature is 10 °C [9]. The interior temperature in the selected room in Type A was 20.9°C. It was 21°C in Type B while the outside temperature was 10.8°C. The observed U value for Type A is 1.55 W/m^2K and for Type B is 1.74 W/m^2K, and both of them are

inappropriate for the Istanbul (Region 2) region [10].

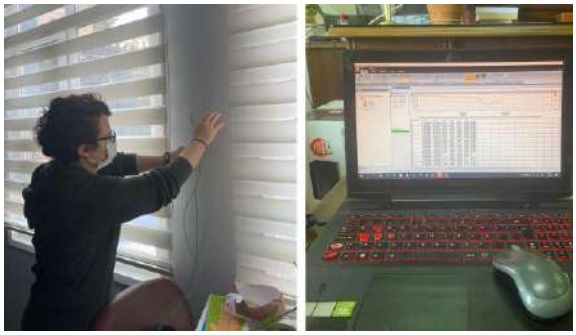

Fig. 1 - Onsite U-Value Measurements of the external wall

Fig. 2 - Placement of Testo 160 Indoor Air Quality (IAQ) Data Logger

To measure indoor temperature, relative humidity, and CO2, DataLogger devices were used (Figure 2). The selection of the device's location is based on several parameters, such as the room should be in the middle floors and the device should be placed on an internal wall. The inner walls of the selected rooms were examined with a thermal camera, and the inner wall that did not receive direct sunlight was selected. Façade photographs were taken with a thermal camera to detect the leaks and thermal bridges that may occur in the systems carrying steam, hot water, and hot air (Figure 3).

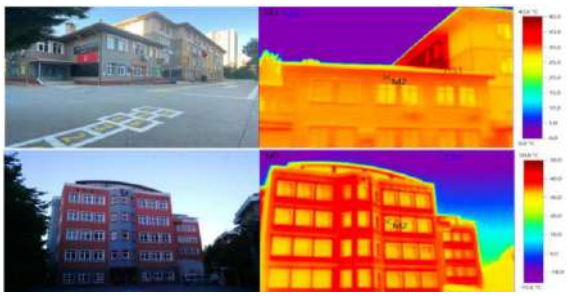

Fig. 3 - Thermal Exterior Photos of the Buildings (Building Type A on up and Building Type B presented below)

4. Modeling and Simulation

The energy efficiency of two school buildings is investigated by using DesignBuilder and EnergyPlus for the simulations (Figure 4). EnergyPlus is used to run several annual and monthly simulations, and the monthly gas and electricity consumption rates from the ESO file are noted as results for calibration.

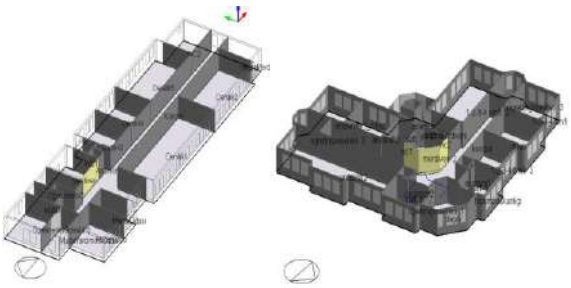

Fig. 4 - Building Modelings in DesignBuilder (Building Type A on the left and Building Type B presented on the right)

4.1 Climate data

The buildings are located in Istanbul, in which summers are hot and dry, and winters are rainy and warm. Weather information was requested from the General Directorate of Meteorology (MGM) and the files were arranged using the Elements software program to generate EPW files for EnergyPlus.

4.2. Building zoning and construction input

Building geometry was modeled with architectural plans obtained from the school administration. The real-life application can be different; hence field observations and measurements were conducted in both schools, and several alterations were observed. After revising the plans and elevations, zoning was made according to several parameters such as function, user schedule, and mechanical system. Rooms with the same parameters and adjacent to each other were combined into one zone. Construction details are obtained from field measurements and detailed sections. A measured U-value was used to determine the materials of the external wall. Material properties for other construction elements such as slab, roof and internal walls are obtained from TS 825 [10]. The label information was used for the glazing system, and the performance details were calculated for the Tvis, SHGC and U-value of the windows.

4.3 Internal heat gains and losses

The main parameters that are critical for the validation process are variables that cause heat gains, and losses are explained below in detail.

Occupancy input: The maximum number of people using a zone is determined from occupancy activity information obtained from observations and defined in DesignBuilder. The occupancy schedule is determined by the education period and holidays in 2019 and lecture-break hours. The school year of 2019 started on 09.09.2018 and ended on 14.06.2019. The semester holiday was between Jan 27 and Feb 4. The mid-holiday was between 18 November-22 November [11]. The lecture-break hours in Type A are 09:00-16:20 from Monday to Thursday and 09:00-14:40 for Friday.

For Type B, it is 09:40-16:00 for weekdays. The fraction for student occupancy in a classroom zone during the lecture hours is assumed as 1, whereas it is 0.1 for break-time as the majority of the students leave the classroom on break. For occupancy in circulation areas such as corridors, the fraction during lesson hours is entered 0 and 0.25 in the break times.

Lighting input: Each armature in a zone was counted and the power (Watts) was determined by observations. The values were defined by Watt/h in DesignBuilder. It is assumed that the lighting is on during school hours if the illuminance is under 400 lux in rooms [12]. For circulation areas such as corridors and stairs, lighting is always on during school hours, while for toilets and kitchen, it is on only during the usage hours.

Electrical equipment input: Electrical equipment such as split air conditioners, interactive whiteboards, computers, kitchen utensils etc., affect internal gains. These were counted and label information was observed on the site to obtain power values (Watts). The usage schedule was made according to the fraction method. For instance computers are being used for 2 hours a day on average in an office during school hours in Type B, hence the fraction is 0.3.

Natural ventilation: Natural ventilation depends on the window opening/closing habits of the occupants. According to ASHRAE Standard 62-1 [13], there is no fixed value for air changes per hour (ACH); however, it is recommended that ACH can be accepted in a range between 5-6 for school buildings. Based on this standard, several simulations were conducted with different ACH values within this range for both school buildings to observe the difference between consumption rates and interior temperature values.

Air infiltration: Air infiltration depends on the quality of construction and maintenance of the buildings and it is one of the main reasons for heat losses and affects energy performance. Values in an appropriate range that is recommended in the CIBSE standard [14] were defined in several simulations in order to reduce the differences between simulation results and energy bills. For Type A the infiltration rate of 0.6 1/hr is found to be suitable and for Type B it is 0.7 1/hr.

4.4 Mechanical System

The mechanical system information was obtained during the field observations. Type A school has a heating system working with a single natural gas-fired non-condensing boiler with radiators. There are split air conditioners for cooling in several zones, such as the principal's room and some of the classrooms that are located in the southern part of the building. There is a natural ventilation system in the building; the below-grade storey has windows that are opened by areaway. In Type B school, the heating system consists of a condensing boiler with radiators. There is a natural ventilation system, and in below-grade storeys with no windows, the fresh air is supplied by outlets located on the ceiling. The cooling system is dependent on the split air conditioners in several rooms. There is a theater hall that has a duct-type split air conditioner and a dining hall on the top floor which has a fan coil unit.

Boiler efficiency: Boiler efficiency can vary according to type, usage, maintenance, flue gas performance, fuel type and boiler insulation. In both cases boilers have been used for over 20 years and annual maintenance is not done regularly. Therefore, different boiler efficiency rates corresponding to these data were defined in simulations within the recommended value range which are 80-85% for non-condensing boilers and 85-90% for condensing boilers [15], and the value that reduces the difference between energy bills and simulation results was determined as 0.81 for Type A and 0.85 for Type B.

Heating and cooling setpoint temperature: There is no thermostat system that measures the indoor temperature in both buildings. The thermostat system located only outdoors measures the external air temperature. When the outdoor temperature is below 15 C°, the boiler starts to operate. Based on the literature and standards, the range for heating setpoint temperature is 20-23 C° and for cooling setpoint temperature is 24-28 C° for students' thermal comfort [16]. For defining accurate setpoint temperatures, values within this range were defined in various simulations and the results were compared with energy bills and measured internal temperatures. The heating setpoint is defined as 22 C° for Type A and 21 C° for Type B. The cooling setpoint is 24 C° in both school buildings.

5. Validation of the simulation

5.1 Validation with electricity and gas bills

In order to validate the actual energy consumption, the electricity and natural gas bills are compared with the simulation results. Because of the Covid-19, occupant behavior and schedule have changed due to the distance education and lockdowns. These variations inevitably lead to limitations in the comparison of actual energy consumption and simulation results. Therefore, this consumption data represents 2019 in which there was no pandemic. Simulations are conducted for both a whole year and monthly basis using weather data from 2019. The annual total and monthly electrical and gas consumptions and simulation results are presented in Table 2.

Firstly, annual simulations are performed and the total amount of consumption for a year is compared with the bills. As the case study buildings are schools, there are no students but a few administrators and teachers are present during the summer holiday months (Jun, Jul, Aug). Also, the heating system is not active between March and November. The gas

Tab. 2 - Actual electricity and gas consumptions and simulation values for Type A(left) and Type B(right)

Month	Type A-2019		Simulation			Err. (%)
			Annual		Monthly	
	Ele. (kWh)	Gas (kWh)	Ele. (kWh)	Gas (kWh)	Gas (kWh)	Monthly Gas
Jan	9,946.76	36,599.42	7,586.32	32,480.62	36,124.85	1.2
Feb	9,370.40	39,463.79	9,938.09	43,924.05	40,419.01	2.4
Mar	8,750.80	34,069.61	11,420.28	40,281.03	34,692.23	1.8
Apr	7,412.52	11,867.08	7,505.43	16,986.53	11,367.29	4.2
May	3,130.88	329.04	3,405.95	329.04		
Jun	2,287.20	6,775.00	2,485	6,775.00		
Jul	2,473.52	6,775.00	302	6,775.00		
Aug	7,383.84	242.16	225.02	242.16		
Sept	8,179.64	614.48	2,402	614.48		
Oct	6,591.12	704.88	3,457	704.88		
Nov	10,011	25,304.13	14,881.52	50,057.67	24,193.74	4.3
Dec	8,963.68	37,176.21	12,102.61	34,059.27	38,442.67	3.4
Total	84,501.36	186,384	75,711.17	186,339.21		
Annual Err (%)			10.40	0.02		

Month	Type B-2019		Simulation			Err. (%)
			Annual		Monthly	
	Ele. (kWh)	Gas (kWh)	Ele. (kWh)	Gas (kWh)	Gas (kWh)	Monthly Gas
Jan	15,754.92	57,755.07	11,955.98	53,436.46	57.599.90	0.27
Feb	16,006.86	52,550.42	11,816.91	56,753.94	54.983.50	4.62
Mar	16,613.82	47,081.76	13,217.46	47,459.00	47.938.78	1.82
Apr	15,651.36	37,394.40	13,121.02	32,921.87	39.049.96	4.42
May	14,676.60	11,625.95	13,611.71	11,625.95		
Jun	9,457.68	2,595.81	10,854.94	2,595.81		
Jul	6,878.28	2,320.06	9,019.58	2,320.06		
Aug	7,972.62	2,320.06	8,977.82	2,320.06		
Sept	7,383.84	269.28	11,687.39	269.28		
Oct	13,502.58	4,154.96	13,631.15	4,154.96		
Nov	12,561.36	5,193.02	12,591.11	10,126.98		
Dec	17,922.42	40,075.06	13,570.13	47,233.37	38.842.16	3.07
Total	154,382.34	263,335.85	144,055.20	271,217.74		
Annual Err (%)			6.68	2.99		

consumption available in the bills for May, June, July, August, September, and October represents mainly the consumption of kitchen appliances. To find the gas usage of the kitchen, the gas bill of October is used in which the heating system is closed, but the kitchen is active. Accordingly, it is ~700 kWh in Type A, and ~4000 kWh in Type B. These consumption rates are added to the corresponding months of simulation results. For Type A, the annual error rate for electricity is %10.04 and for natural gas is %0.02. For Type B, the annual error rate for electricity is %6.68 and for natural gas is %2.99. According to the ASHRAE Guideline 14 [18], these error values are in an acceptable range. Secondly, the monthly simulations are conducted and results are obtained and validated only for natural gas consumption. Monthly inspection of electricity consumption is an ongoing study. For monthly validation of natural gas consumption, simulation results are available only for the time and months that the heating system is active; therefore, the error rates are presented for January, February, March, November, and December. However, in Type B, the date of the gas bill of November does not contain the time interval in which the heating system is active and it has not been included in monthly gas validation. All monthly gas error rates are in an acceptable range that is %5 for both schools [18].

5.2 Validation with indoor temperature

The indoor air temperature was measured in hourly intervals from Apr 29 2021 until Jan 9 2021. Due to the lockdowns and distance education there were no occupants, and mechanical systems were not active. It inevitably caused several limitations such as the effect of user behavior and internal gains cannot be obtained correctly. However, measuring indoor air temperature while lockdown has several benefits such as it is possible to validate the thermophysical and geometrical properties of the model more accurately without human-based parameters, which highly affects the error rates in simulation. Hence internal air temperature measurement results from lockdown dates (Apr 29- May 17 2021) [17] are selected to compare with the simulation (Figure 6). Firstly, simulation input data was revised by changing schedules for people, lighting, electrical equipment, mechanical systems, and natural ventilation to be off 24/7. The simulation run period was arranged for April 29th to May 17th. The weather data obtained from MGM is applied. Fig. 5 presents the differences between measurement and simulation. The simulation's max, min and average temperatures are 26.7, 18.44, 21.39 C° and in observed data are 22.5, 18.9, 20.6 C° for Type A. For Type B the max, min, and average temperatures in the simulation are 25.11, 18.34, 21.72 C° and in observed data are 24.2, 20, 21.73 C°. Considering the measurement tools have ±0.5°C error rate, the differences between the measured and the simulated temperature show that there is no significant error.

$$\text{RMSE}(\hat{O}) = \sqrt{MSE(\hat{O})} = \sqrt{E((\hat{O} - O)^2)}$$

(1) Root mean square error (RMSE) equation Obtained from Sedki et al. [18]

The Root Means Square Error (RMSE) (1) was used for an hourly basis to calculate the error between the simulation and measured values [8]. The error rate for Type A is 1.53 and for Type B is 0.6. According to Maamari et al. [19] the difference between the actual and predicted values should be between 10-20%. As results show, the error rates obtained in Type A and B schools are satisfactory. In addition to the measurement during the pandemic period and without internal gains, another measurement was held on November 25th 2021. During this time, the school was open and the training was face to face. Internal gains, human factors, and climate data inputs were revised in the simulation. The measured internal air temperature is 24.1 C°, and it is 24.5 C° in the simulation for Type A (Figure 5). For Type B measured internal air temperature is 21.9 C° and 21 C° in simulation, which shows no significant error.

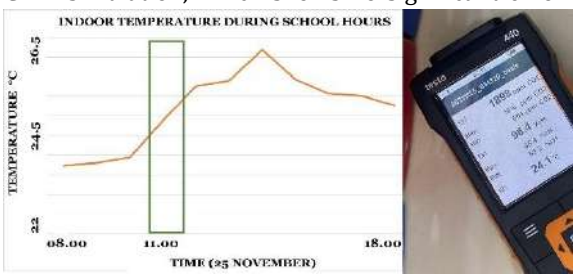

Fig. 5 -Example of indoor temperature measurement on November 25th 2021, Type A Building.

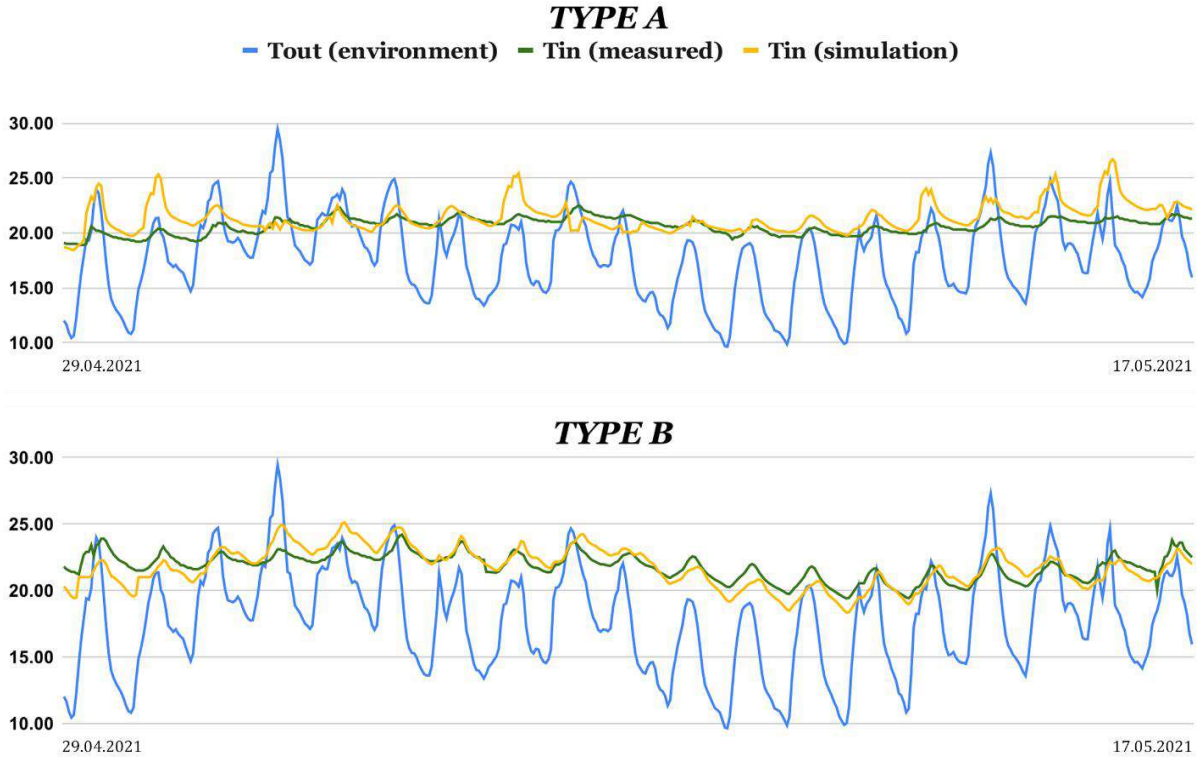

Fig. 6 - Measured and simulated indoor air temperature comparison

6. Discussion

Minimizing the challenges encountered while validating the model and calculating the energy performance of buildings as close to reality is critical for the transition to the next phase of the project that proposes retrofit strategies to reduce the energy consumption of the school buildings. The most significant parameters that risk the validation of energy simulation models are discussed below.

-*Climatic and environmental data:* Weather data directly affects the energy needed to provide the appropriate indoor temperatures for the users' comfort in the simulations. Although the climatic data were obtained through meteorology, missing data emerged in several days and hours. This challenge was resolved by taking the average values of the former and latter that day and hour. Still, some parameters such as radiation gain could not be obtained. Problems with these parameters can cause errors in simulations.

-*Building thermophysical properties:* Envelope properties such as air infiltration is one of the critical parameters that affect natural gas consumption. Different infiltration rates within a recommended range were defined in simulation to analyze their effects on the gap between actual gas consumption and simulation outcome. It is possible to state that 0.1 change in air infiltration rate affects the gas consumption by 4-6%.

User behavior: The human factor affects the heat gain or loss in buildings such as opening windows for fresh air and occasionally turning on lights during the day. This should be observed and precisely defined into the software. In this study, onsite observations and surveys were made and parameters suitable for user behaviors were transferred to the software. For instance, more Air Changes per Hour (ACH) are expected to provide thermal comfort in the summer months. In the EnergyPlus simulation, higher values are defined compared to the winter months. However, it is not possible to determine an exact value for ACH rate for each month. Therefore, different ACH values from the range of 5-6 [20] were defined in software and the results were compared with the natural gas bills. Findings showed that 0.1 difference of ACH values affects natural gas consumption by 09% to 1.3%.

-*Mechanical System:* Boiler efficiency and heating setpoint temperature variables are the most critical parameters that affect the simulation results of natural gas consumption and internal air temperature. According to the simulation results, ±0.10 change in boiler efficiency can cause a 12-14% difference in gas consumption. Additionally, the lack of a thermostat system in both buildings has caused limitations in terms of defining proper heating setpoint temperature, which can significantly impact simulation results. Also this situation inevitably increases gas consumption. For instance, according to the different simulation results with different heating setpoint temperatures, ±1 change in heating setpoint temperature affects the natural gas consumption by 12-15%.

-*Internal air temperature:* Measuring internal air temperature and comparing the data with simulation outcome is one of the methods that was used in the study. Internal temperature is dependent on air infiltration, window opening, internal gains,

mechanical systems and window to wall ratio. Based on these there are differences between Type A and Type B schools. When the internal temperatures measured during the quarantine period during April and May are compared, the internal temperatures in Type A are lower than Type B because of the fact that the window to wall ratio is higher in Type B school. Therefore, it has caused the interior spaces to become warmer. In addition, when the measurement results from November, in which the education was face-to-face, were compared, the internal temperature of Type A was greater than Type B because internal heat gain due to the occupants and equipment is high. Additionally, measured internal air temperature during the heating period is greater than the heating setpoint temperature of the system because of the high internal gains in school buildings.

-*Pandemic Situation:* During the pandemic, internal temperature measurements were made while switching to online education in schools. Although this has negative effects on the operation of the project, problems arising from user behavior have been eliminated by measuring when there is no user during the quarantine. It also allowed for building envelope analysis without internal gains or losses. On the other hand, more ventilation was needed to ensure fresh air flow during the training period and the user capacities of some places were different from the normal situation. It may cause some limitations between the simulation and the observed values.

7. Conclusion

In this study, simulation is the first step taken to improve buildings' energy performance, including the validation of the observed results. Necessary details for simulation were obtained by making onsite observations at two school buildings in Istanbul and analyzed using Designbuilder and EnergyPlus programs. The most important step in data collection is to gather information from schools' users. Therefore, authors had meetings with the school administration to learn user habits. Another significant matter is mechanical system information obtained from on-site visits, standards, and consultants. The simulation results were compared with the devices placed in schools that measure the indoor air quality in terms of temperature, humidity, and CO_2. Because of the Covid-19, there is a lockdown during the measurement time interval. Therefore these measurements were used to validate only the geometrical and thermophysical properties of case buildings by comparing simulation and measured internal air temperature. These outcomes present necessary information of the material properties as well as infiltration rates. The internal air temperature error rate between simulated and measured data was calculated by the REMS method and verified. To validate energy consumption, electricity and natural gas bills obtained from schools and simulation outcomes were compared in terms of natural gas consumption and confirmed monthly with ASHRAE standards [13]. Additionally, internal temperatures were observed on November 25th in schools to observe indoor temperature while the heating system is active and education was face-to-face.

Energy efficiency in buildings is becoming a more significant and critical concept day by day. The initial step of energy optimization involves validating the simulations with the actual building. Additionally, there are pandemic-related limitations in the study that cause alterations in methodology. However, studies on this subject are very limited. It is expected that this study will fill the existing gap and serve as a guide for similar studies. In addition, this work is an ongoing project and the future study is the development of energy-efficient strategies for these buildings whose next phase is validated.

8. Acknowledgement

This research is a part of the project entitled 'Developing National Approach of Long-term Renovation Strategies for Existing Educational Campuses in Turkey towards Nearly Zero Energy Target' funded by TUBITAK with 219M552 ID. We would like to pay our special regards to the administration and students of the case study buildings for their help.

9. References

[1]Turkey 2021. IEA. [cited 2022 Feb 17].Doi:https://www.iea.org/reports/turkey-2021

[2]Aksin FN, Arslan Selçuk S. Energy performance optimization of school buildings in different climates of Turkey. Future Cities and Environment. 2021;7(1). Doi: 10.5334/fce.107

[3]Ohlsson KEA, Olofsson T. Benchmarking the practice of validation and uncertainty analysis of building energy models. Vol. 142, Renewable and Sustainable Energy Reviews. Elsevier BV; 2021. p. 110842. Doi:10.1016/j.rser.2021.110842

[4]Loreti L, Valdiserri P, Garai M. Dynamic Simulation on Energy Performance of a School. Vol. 101, Energy Procedia. Elsevier BV; 2016. p. 1026–33. Doi: 10.1016/j.egypro.2016.11.130

[5]Hu M. Existing Energy Performance and The Potential of Role of Simulation in School Building Design – A Review. Building Simulation Conference proceedings. IBPSA; Doi:10.26868/25222708.2019.210336

[6]Beagon P, Boland F, Saffari M. Closing the gap between simulation and measured energy use in home archetypes . Vol. 224, Energy and Buildings. Elsevier BV; 2020. p. 110244.Doi:http://dx.doi.org/10.1016/j.enbuild .2020.110244

[7] Ekström T, Burke S, Wiktorsson M, Hassanie S, Harderup L-E, Arfvidsson J. Evaluating the impact of data quality on the accuracy of the predicted energy performance for a fixed building design using probabilistic energy performance simulations and uncertainty analysis. Vol. 249, Energy and Buildings. Elsevier BV; 2021. p. 111205. Doi: http://dx.doi.org/10.1016/j.enbuild.2021.111205

[8] Hyndman RJ, Koehler AB. Another look at measures of forecast accuracy. Vol. 22, International Journal of Forecasting. Elsevier BV; 2006. p. 679–88. Doi:http://dx.doi.org/10.1016/j.ijforecast.2006.03.001

[9] Giebeler, M. Testo Ltd. U-value measurement on a wall of unknown materials with the testo 635.. BAU-EXPERT Engineering Consultants; 2014.Doi:https://www.testo.com/en-US/products/products

[10] Turkish Standardization Institute (2013) TS825, Thermal insulation requirements for buildings, Ankara.

[11] Turkish Republic the Ministry of Education. 2018-2019 Academic Year Calender; 2018 Jun.

[12] Chel A. Performance of skylight illuminance inside a dome shaped adobe house under composite climate at New Delhi (India): A typical zero energy passive house. Alexandria Engineering Journal. 2014 June 1st;53(2):385-97.

[13] ASHRAE Guideline 14 Measurement of Energy, Demand, and Water Savings, ASHRAE inc, 2014

[14] Chartered Institution of Building Services Engineers. Guide A - Environmental Design. 2015, London.

[15] Turkey. Ministry of Science, Industry and Technology. Regulation on amending the regulation (92/42/EC) on the efficiency requirements of new liquid and gas fueled hot water boilers 2018 (Act No. 1 of 12). Official Gazette of the Republic of Turkey. No: 30374

[16] European Standards. BS EN 16798-1:2019 Energy performance of buildings. Ventilation for buildings Indoor environmental input parameters for design and assessment of energy performance of buildings addressing indoor air quality, thermal environment, lighting and acoustics.

[17] Ministry of Interior. Partial Closing Circular to 81 Provincial Governorships. Turkey: Ministry of Interior; 2021. Available from:https://www.icisleri.gov.tr/81-il-valiligine-kismi-kapanma-genelgesi-gonderildi

[18] Sedki A, Hamza N, Zaffagnini T. Field Measurements to Validate Simulated Indoor Air Temperature Predictions: A case study of a residential building in a hot arid climate. Building Simulation Cairo Conference: Towards Sustainable & Green Built Environment. Cairo: EEER - IBPSAEgypt; 2013 [cited 9 January 2022]. p. 338-347.

[19] Maamari F, Andersen M, de Boer J, Carroll WL, Dumortier D, Greenup P. Experimental validation of simulation methods for bi-directional transmission properties at the daylighting performance level. Vol. 38, Energy and Buildings. Elsevier BV; 2006. p. 878–89.Doi:http://dx.doi.org/10.1016/J.ENBUILD.2006.03.00

[20] ASHRAE Standard 62-1 Ventilation for Acceptable Indoor Air Quality, ASHRAE inc, 2019

Bioclimatic Design and Advanced Strategies' Impacts on Energy Performance of Residential Buildings

Gizem Avgan [1], Touraj Ashrafian [2]

[1] Graduate School of Engineering and Science, Department of Architecture, Ozyegin University, Istanbul, Turkey, gizem.avgan@ozu.edu.tr

[2] Faculty of Architecture and Design, Department of Architecture, Ozyegin University, Istanbul, Turkey, touraj.ashrafian@ozyegin.edu.tr

Abstract. The construction sector covers a significant percentage of the energy consumption in the world. Human actions on energy use are gradually being identified as the primary cause of climate change, global warming, and significant environmental changes. In response to these problems, the concept of sustainability has become one of the most crucial solutions for reducing the construction sector's high energy demand. Bioclimatic architecture is a sustainability approach that brings forward the strategies of vernacular architecture into the present by adapting the building systems to their climatic and topographic conditions. It is also an option for affecting the building sector in Turkey to prevent energy overconsumption by initiating efficiency improvements. This study examines the design requirements and physical characteristics of a building in the Marmara region (Turkey) and how these features impact its overall energy consumption. The case study building is a 9 storey apartment building in Erenköy, İstanbul, located in the humid-temperate climatic region of Turkey. Since that, the design scenarios consisting of different bioclimatic strategy combinations are chosen about this climatic region's features. The software DesignBuilder, empowered with an EnergyPlus simulation engine, is used to test the design scenarios' impacts on final energy consumption. The present condition of the case study building is monitored to calculate its energy consumption to evaluate the difference between the design scenarios. The impact on the primary energy use of different passive strategies, HVAC systems, electricity generation, and a bioclimatic set of standards implemented to the building was then assessed using parametric analysis of various scenarios. The results showed that the combination of passive strategies with earth pipe installation and thermal assisted radiant floors reduced the energy use by approximately 30%. Passive strategies significantly impact the residential building systems' energy efficiency showing how bioclimatic architecture criteria can meet the requirements of high-efficiency standards in the humid-temperate climatic region of Turkey.

Keywords. Bioclimatic Architecture, Residential Buildings, Building Energy Performance, Advanced Energy Efficiency Strategies
DOI: https://doi.org/10.34641/clima.2022.354

1. Introduction

In Turkey, rapid population growth in the last two decades has resulted in a significant increase in energy demand. Nonetheless, Turkey's economy is still driven by fossil fuels, with considerable reliance on imports, particularly oil and gas (93% and 99%, respectively). As a result, Turkey's reforms and policies have focused on liberalization and domestic production. Turkey has made expanding local exploration and production a priority to lessen its reliance on imported oil and gas. Given the constraints on upstream supplies and the need to reduce emissions, Turkey should focus on cost-effective demand-side initiatives like efficiency improvements [1].

There are numerous ways to reduce the high energy consumption of the construction sector by following efficient passive system strategies on the buildings. Bioclimatic architecture is vital to increase the overall energy efficiency, achieve thermal occupancy comfort, use renewable energy sources and local materials while considering cost-efficiency.

Throughout history, people have been trying to

Copyright ©2022 by the authors. This conference paper is published under a CC-BY-4.0 license.

adapt their buildings to the environment to form better living conditions [2]. Since each climatic region has its unique conditions, the bioclimatic design strategies vary in every location. Local environmental factors greatly influence the implementation of thermal design solutions for buildings.

A psychrometric chart is analyzed in ClimateConsultant with Istanbul's obtained weather data. The outside temperatures rise in the summer, whereas in winter, the temperatures may be low, with high precipitation creating discomfort. In temperate-humid climate regions, natural ventilation is possible throughout the year. However, heat recovery is recommended as a means of energy conservation. The earth can be utilized as a heat source for a heat pump or renewable cooling. Surface cooling systems may be proper to operate. Direct radiation accounts for a higher share of total radiation than diffuse radiation. Solar thermal systems can heat water and provide supplemental heating during transitional months. Integrated photovoltaic systems are also helpful [3].

In the literature, bioclimatic design strategies have been studied in different climate regions and locations. Buildings' energy performances and the impacts of passive cooling, heating, and ventilation strategies on occupants' comfort are analyzed for different locations. Bioclimatic research was done on traditional Turkish houses and outdoor spaces [4]. Other studies focus on feasible climate control approaches and techniques that have been used in vernacular architecture with bioclimatic methods and combining them with the innovative and parametric design processes, addressing current sustainability needs in case studies [5 and 6]. The use of passive system strategies' impacts on building energy performances is also studied [7].

This paper aims to assess the energy performance of a residential building located in the temperate-humid climate region, Istanbul, Turkey, by comparing the energy efficiencies between the existing situation of the building and the same building with bioclimatic strategies implemented. It is expected to see the impacts of bioclimatic strategies and innovative systems' assistance on building energy performance.

2. Research Methodology

This study uses DesignBuilder (v7.0.0.116) to analyze the effects of bioclimatic strategies and various building HVAC systems on the energy efficiency of a residential apartment in the Marmara region. The building model with envelope characteristics and HVAC systems is created to conduct energy simulations.

The obtained weather data for İstanbul, Turkey, is used. The thermal zones are based on the occupancy use, activity, and schedule (Figure 1.b); living room (lounge), kitchen, bedroom, and circulation area. The key characteristics assigned to each zone are (Figure 1.c.) HVAC zones are assumed: the living rooms and bedrooms are conditioned with radiator heating and PTAC; kitchens are conditioned only with radiator heating.

Occupancy activity is entered for using lighting and miscellaneous equipment as domestic family schedules, including 08:00-12:00 and 16:00-23:00 for weekdays and 08:00-23:00 for the weekends. According to Turkish regulations, the room temperatures in the independent sections heated by central systems should be adjusted to be at least 15 °C [8]. For heating, the night setback temperature is set at 15 °C, and during the day, the setpoint temperature is at 21 °C [9], [10]. The minimum supply air temperature for the cooling system operation (PTAC) is set at 15 °C, and the setback temperature is 28 °C to 25 °C. The internal doors of the floors are assumed to be open through the simulation hours.

An analysis is conducted for various HVAC system designs and bioclimatic strategies' impacts on overall energy consumption. The measures for simulations are selected according to the climatic data input from the literature review. Firstly, the envelope characteristics and the HVAC systems are simulated. Subsequently, the passive design integrations (building volume/area, window/wall, and orientation variations) are combined with HVAC systems. Annual primary energy usage (kWh/m^2) and carbon dioxide emissions are calculated for scenarios' comparison. The site-to-source conversion factor is accepted as 2,36 for electricity end-use and 1,00 for natural gas end-use. The annual primary energy usage (EP) (kWh/m^2) in this study is calculated considering electricity end-use (EE), natural gas end-use (EG) as in the equation below;

EP=[(EEx2,36)+(EGx1,00)]/net conditioned area

The carbon dioxide emissions are calculated as the following equation;

CO_2=[(EEx0,626)+(EGx0,234)]/net conditioned area

2.1 Case Study Building Presentation

Güney Apartmanı (Fig. 2a) is a residential apartment building with 9 storeys and 16 flats located in Erenköy, Istanbul, Turkey. The layout is rectangular, with a fire staircase mass joined.

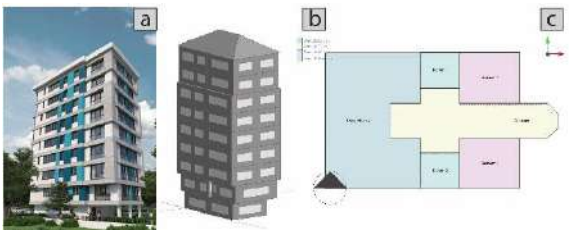

Fig. 1 - Case Study Building Render (a), Building Energy Model (b), Floor Zones in DesignBuilder (c).

The case study building was constructed in 2018 within the urban transformation process of Istanbul led by the municipality. The ground-level floor is being used as an entrance lobby. Each floor above the ground floor has two symmetrical flats consisting of one bedroom, one living room, one bathroom, and one kitchen. The total building area is 1496 m². The net conditioned building area is 1385 m² which was included in the calculations of primary energy usage of the building in energy simulations.

The window to wall ratio of the building is 30%. The building entrance (narrower façade) is oriented towards the west direction.

The rooms on the plan layout are concatenated towards the East and the West (Fig. 1.c). The humid weather can specify a temperate-humid climate in almost all seasons, rainy days in summers, and temperate winter months. The maximum temperature is around 28 °C in summer and 10 ° C in winter, whereas the minimum temperature is approximately 20 °C in summer and 5 °C in winter times [11].

Tab. 1 – Base Case Envelope and HVAC System Features

Building Features	Construction Details	Conductivity (W/m-k)	Specific Heat Capacity (J/kg-K)	Density (kg/m³)
External Walls Uvalue: 0,400 (W/M2-K)	0,013 m Gypsum Plastering	0,4	1000	1000
	0,25 m Aearated Concrete Blocks	0,24	1000	750
	0,04 m Rockwool	0,047	840	92
	0,03 m External Rendering	0,5	1000	1300
Internal Walls Uvalue: 2,929 (W/M2-K)	0,025 m Gypsum Plasterboard	0,25	1000	900
	0,01 m Air Gap	-	-	-
	0,025 m Gypsum Plasterboard	0,25	1000	900
Pitched Roof Uvalue: 0,591 (W/M2-K)	0,005 m Roofing Felt	0,19	837	960
	0,06 m Stonewool	0,04	840	30
	0,025 m Clay Tile (Roofing)	1	800	2000
Floors Uvalue: 0,426 (W/M2-K)	0,2 m Aerated Concrete Slab	0,16	840	500
	0,03 m Floor Screed	0,41	840	1200
	0,004 m Plywood (Lightweight)	0,15	2500	560
Ground Floor Uvalue: 0,426 (W/M2-K)	0,03 m Epoxy Resin	0,2	1400	1200
	0,05 m Floor Screed	0,41	840	1200
	0,1 m Cast Concrete	1,13	1000	2000
	0,13 m Urea Formaldehyde Foam	0,04	1400	10
Glazing Units	Double Glazing 2,5mm/6mm Air, clear	Uvalue (W/m2k)	Solar Heat Gain Coefficient	Visible Transmittance
		2,724	0,72	0,81
Radiator Heating		Living Room & Kitchen & Bedrooms		
Boiler HW		Central System		
PTAC		Living Room & Bedrooms		
Lighting		Ceiling Mounted & Recessed		

The building design is a synthesis of many decisions analyzed from the characteristics of the weather conditions that can be aimed at lowering energy use of the building by additional passive strategies and innovative tactics.

2.2 Model Calibration

For the calibration of the simulations and the present energy consumption of the case study building, the accessible electricity bill of February-March 2021 and the gas bill of August-September 2020 are obtained.

In the yearly analysis of the base energy simulation in DesignBuilder, electricity end-use per conditioned building area accounts for 33,18 kWh. The conditioned area of each flat of the case study building is 70 m^2. The electricity end-use of a flat is 2310 kWh in a year. For a month, it equals 192,5 kWh. The actual electricity use on the bill is 202,29 kWh. The accuracy difference between simulation and bill of electricity is 4,79%.

The natural gas end per condition conditioned building area accounts for 35,98 kWh. For each flat, the natural gas end-use for a year equals 2518 kWh and 209,9 kWh for a month. The obtained natural gas use on the bill is 221,89 kWh. The accuracy difference between simulation and bill of natural gas is 5,03%.

2.3 Case Study Building's Energy Consumption

The base case is simulated in current conditions (base simulation), including all energy performance indicators to compare each scenario's efficiency. The envelope features are entered (Table 1). The heating system of the building is a radiator heating system. The cooling system is packaged terminal air conditioner (PTAC). The glazing system is double glazing (3 mm panels- 6 mm air gap). The electricity end-use (EE) for the current situation is 38331,83 kWh. The natural gas end-use (EG) is 41575,94 kWh. The total energy for heating with natural gas is more than the total energy for cooling and lighting demand. The net conditioned area for the building is 1155,36 m^2.

For the current situation's calculation, the annual primary energy usage (EP) is equal to 114,283 kWh/m^2. The simulations after are compared with this primary energy consumption (EP) value.

3. Results and Discussion

3.1 Envelope and HVAC System Scenarios

Different envelope characteristics and HVAC systems were tested after determining the case study building's energy performance (Table 2). Initially, building envelope characteristics, the exterior wall, roof insulations' thickness variations, and glazing unit type were indicated and simulated separately.
Among advanced energy systems, the shading panel integration, cooling ceiling with cooling tower, solar thermal system assisted surface heating, heating and

cooling with earth pipe installation are selected to be analyzed in the study [3]. Additionally, power generator systems, electricity generation with photovoltaics, and micro-cogeneration system (CHP), which produces electricity and provides heat recovery, are modeled and tested [12].

Parameters		Features
Wall Insulation	W1	8cm exterior insulation thickness (rockwool) Uvalue: 0,333 (W/M²-K)
	W2	12cm exterior insulation thickness (rockwool) Uvalue:0,259 (W/M²-K)
Roof Insulation	R1	11 cm roof insulation thickness (stonewool) Uvalue: 0,340 (W/M²-K)
	R2	16 cm roof insulation thickness (stonewool) Uvalue: 0,239 (W/M²-K)
Glazing	G1	triple glazing Uvalue:0,9 (W/M²-K)
Shading	S1	double glazing 1 m overhang
Cooling Ceiling	C1	cooling ceiling integration/cooling tower
Surface Heating	H1	solar thermal system/surface heating
Earth Pipe	E1	earth pipe/incoming air prewarming
Photovoltaics	PV1	photovoltaic panel integration
Micro-Cogeneration (CHP)	MC1	generator - internal combustion engine integration to DHW loop

Tab. 2 - Envelope and HVAC System Scenarios

For the shading panel integration (S1), the glazing units are kept as double glazing, U-Value: 2,724, 3 mm panels, and 6 mm air gap with 1 m overhangs integrated. With this method, the simulated total electricity end-use is 32855,53 kWh, whereas the total natural gas end-use is 49221,5 kWh. The calculated primary energy use is 109,7 kWh/m^2. This method performs more efficiently than the base simulation (114,28 kWh/m^2) (Figure 2).

For the cooling system, instead of the packaged terminal air conditioner (PTAC), the cooling ceiling integration (C1) with the cooling tower had been used with a regular radiator heating system. The cooling ceiling usage simulation resulted in the total electricity end-use of 38257,02 kWh total natural gas end-use of 43845,98 kWh. The calculated primary energy use is 116,09 kWh/m^2. This system performs less efficiently than the base simulation.

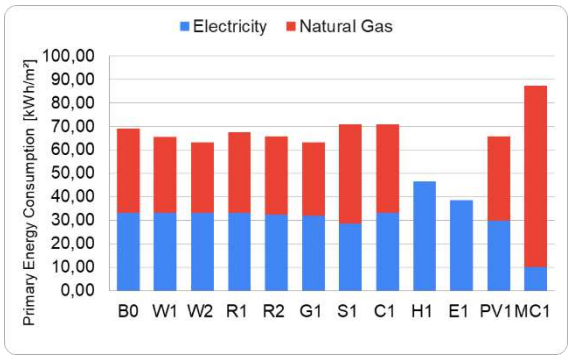

Fig. 2 – Natural Gas and Electricity Primary Energy Consumptions under different Envelope and HVAC Scenarios

Another strategy for bioclimatic architecture is to use renewable energy sources. In this context, solar energy is selected for the simulation H1. This simulation tests surface heating instead of radiator heating with a central hot water system with a boiler. The hot water source for surface heating corresponds with solar thermal energy. Compared to the base simulation, there is no need for natural gas for heating besides electricity. A solar thermal panel on the South facing roof surface and storage are used. The system resulted in 53.639 kWh total electricity end-use and zero natural gas use. In this case, the primary energy calculation resulted in 109,99 kWh/m^2.

The simulation with earth pipe integration (E1) is selected to compare the radiator heating system's energy efficiency and earth pipe usage's energy efficiency. The pond heat exchanger template is selected in the earth pipe scenario (E1) for the ground heat exchanger. The pipes are connected to a chilled water plant loop with a chiller system and a hot water loop with a heat pump system. The supply pipes are connected to the radiant surfaces conditioned zones. In this way, the heating and cooling demand corresponded with a passive system strategy of using the temperature difference of earth and outside temperature. The earth pipe integration simulation (E1) resulted in 44481,69 kWh total electricity end-use and zero natural gas consumption. It is the common conditioning system for heating and cooling demand. The calculated primary energy use is 90,86 kWh/m^2. This method performs much more efficiently than the base simulation.

The photovoltaic panel integration (PV1) and five photovoltaic panels (5m x 0,548m) were placed on the South facing roof surface. These panels generate 3889,389 kWh of electricity. It is reduced from the total electricity end-use (38.467 kWh). The remaining electricity used is 34578 kWh for the building. The calculated primary energy use is 106,62 kWh/m^2 for this case. Compared to the base simulation, this method performs efficiently but not significantly by itself (Figure 3).

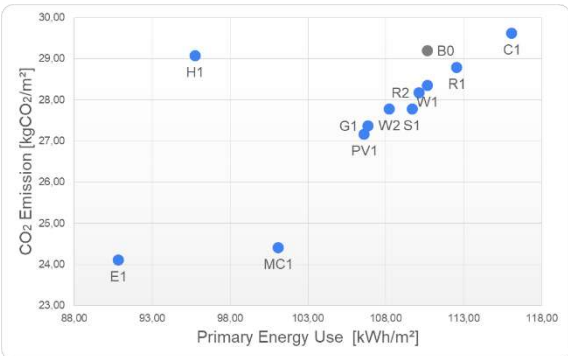

Fig. 3 – Primary Energy Consumptions vs. CO_2 Emissions under different Envelope and HVAC Scenarios

The micro-cogeneration system (MC1) is a DHW loop hot water tank heated by a hot water loop with a natural gas sourced generator incorporated and functioning as a heating source. Suppose the heat produced by the generator is insufficient to fulfill the heating load. In that case, the hot water tank contains

an internal built-in gas boiler that provides backup heating for the building heat requirement. The generator type in this study is an internal combustion engine. The generator is operated to supply the building's thermal demand and generates electric energy as a product [13]. This method consumes more natural gas than a boiler system (Figure 4). However, the satisfied electricity load is %76,22 from fuel-fired power generation, and water-side heat recovery is %24,34. Consequently, the primary energy use is 101,12 kWh/m^2, and CO_2 emission is 28198,47, which is an efficient system (Figure 3).

In these initial scenarios, the earth pipe installation and micro-cogeneration system result efficiently compared to buildings' existing situation (approximately %10 decreases in final energy end-use).

3.2 Bioclimatic Design Parameters Scenarios

A quantitative study is performed to determine the influence of alternative HVAC system configurations and bioclimatic parameters used in the building on overall energy consumption. After the envelope combinations (W1R1G1, W2R2G1), these two packages (P1, P2), and other passive strategies; the building volume/area ratio (P3, P4), building orientation (P5, P6), window to wall ratio (P7, P8) are combined with advanced system scenarios (Figure 4). Seventy final scenarios are combined and analyzed for the comparison of different configurations.

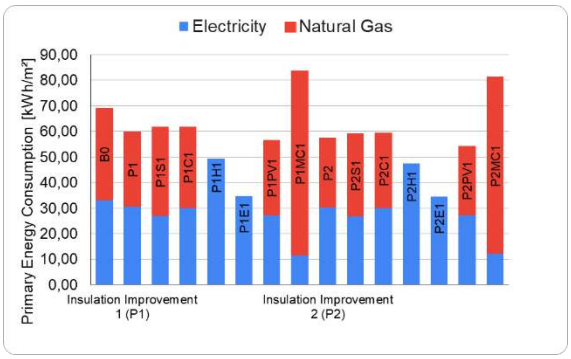

Fig. 4 - Natural Gas and Electricity Primary Energy Consumptions under different Building Envelope Improvements

The shading devices integration with first envelope parameters (P1S1), which uses shading panels (1m overhang), resulted in 18,81% less total electricity end-use and 2,83% less total natural gas end-use. The thicker insulation (P2S1) resulted in 19,53% less total electricity end-use and 9,39% less total natural gas end-use. In comparison, the difference is minor between the scenarios. The differentiation between these packages is the insulation thicknesses. Natural gas demand is more reduced with a thicker insulated envelope than the base simulation. The shading devices provide a reduction in building cooling energy demand causes a decrease in electricity usage. Thus, the thicker insulation may be efficient for heating and cooling energy demand with shading devices used in buildings.

The chilled ceiling with a cooling tower is tested instead of air conditioning units for cooling the building (P1C1, P2C1). The system combined with the first insulation scenario resulted in 9,15% less electricity end-use and 11,89% less natural gas end-use. In contrast, the second scenario resulted in 9,69% and 18,17% fewer end uses. The electricity reductions are not high compared to the present condition for the cooling need. If this system is chosen for cooling interiors, thicker insulations may be required in terms of energy saving.

For analyzing the envelope measures with heating system variations, the heating floor with the solar thermal system usage (P1H1, P2H1) is tested instead of natural gas sourced radiators. This system resulted in more (42,94% and 42,94% respectively) electricity use, but no natural gas consumption. This scenario's primary energy uses are 116,72 and 111,92 kWh/m^2. Compared to base case conditions, the primary energy calculation of P1H1 is slightly more. In early design phases, heating floor systems with solar thermal assistance with a well-insulated envelope can be considered instead of radiator heating for this climatic region.

Earth pipe integration (P1E1, P2E1) resulted in similar electricity end-use as the base conditions. The advantage of the system is that it does not consume natural gas. The primary energy use calculations for these simulations' results are 82,22 and 81,45 kWh/m^2. Compared to the building's present condition, the energy consumption is dramatically reduced. Providing the heating and cooling need of the building, the system can be considered in the early phases of building design for energy efficiency.

Power generative systems' analysis with envelope parameters (P1PV1, P2PV1, P1MC1, and P2MC1) results in less electricity end-use. Photovoltaics' integration reduces the electricity demand by 18,14%, whereas the micro-cogeneration system corresponds to 65,77% of the electricity load. The envelope improvements can be considered since these systems do not reduce heating demand. Overall, the building envelope's insulation improvements positively impact primary energy use and carbon dioxide emissions (Figure 5).

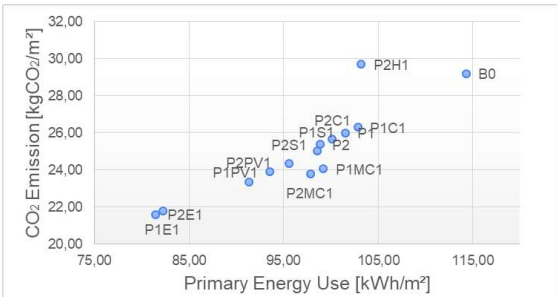

Fig. 5- Primary Energy Consumptions vs. CO_2 Emissions under different Building Envelope Improvements

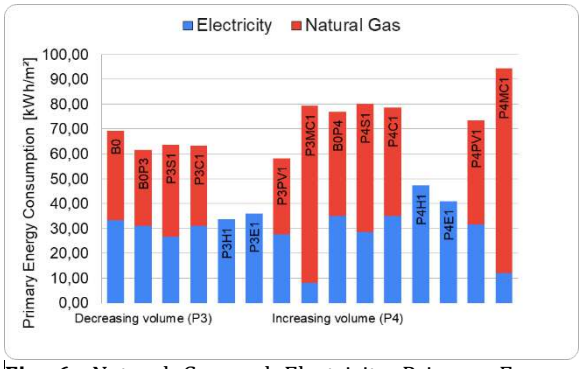

Fig. 6- Natural Gas and Electricity Primary Energy Consumptions under different Building Volume to Area Ratios (V/A)

Building volume to area ratio (V/A) is combined with initial scenarios to evaluate the impact of building volume changes on advanced building systems' energy performance. Firstly, the V/A ratio is decreased by %15. This method is applied to the base scenario (B0P3). The total electricity end-use and the natural gas end-use slightly decreased (6,25% and 15,37%, respectively). Conversely, the increase in V/A with no advanced system used increases energy uses (5,57% EE and 16,11% EG). Next, the method is applied to the HVAC scenarios (Figure 6).

The decrease in the V/A ratio results in 19,62% end-use electricity reduction with shading panels (P3S1) but a 2,91% increase in natural gas end-use. The decline in electricity demand is mainly from the cooling demand. Compared with B0S1, a reduction in the V/A ratio reduces the need for cooling by 9,37%.

The heating and cooling systems, chilled ceiling, radiant heated floors, earth pipe integration performs more efficiently in decreased volumes since the temperature conditioning of interiors need less energy in fewer volumes. The chilled ceiling integration to the base scenario (B0C1) has not affected the primary energy use. On the contrary, the system performs 7,47% less energy consumption in decreased volumes. The P3H1 scenario resulted most efficiently with a 30% decrease in primary energy use. Similarly, the P3E1 scenario outcome presents a reduction of 25,58% primary energy use compared to the base simulation (Figure 7).

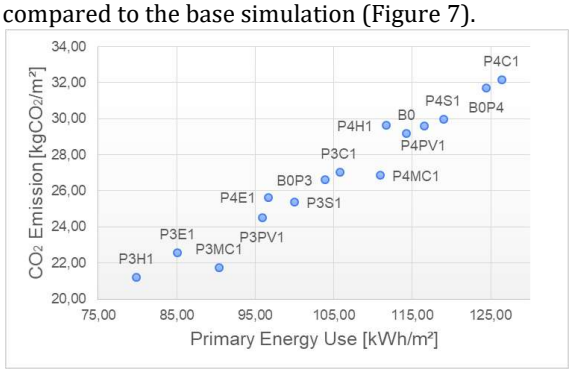

Fig. 7 - Primary Energy Consumptions vs. CO_2 Emissions under different Building Volume to Area ratios (V/A)

The photovoltaic panel integration into the V/A ratio reduced model results in 16,40% electricity end-use reduction and 15,37% natural gas reduction. The micro-cogeneration system provides 70,36% of the electricity load. Compared with B0MC1, the system performs 18,89% more efficiently in decreased volume.

Ultimately, the volume decreases resulted in fewer primary energy end-uses and carbon dioxide emissions. On the contrary, the 15% increase in volume has increased the building's primary energy end-use. Higher volume residential buildings may be more efficient with HVAC system improvements (Figure 7).

Another passive strategy tested on advanced systems in this study is the orientation of the building. At the current stage, the building's larger façade is facing the South direction. To examine the HVAC strategies performances, the building is rotated between 30°-90° angles in four steps. The significant differences that occurred (45° and 90°) are presented in Figure 8. Initially, the 45° change in orientation is applied to the base simulation. The electricity end-use is almost resulting no change. In contrast, the heating demand of the building is slightly increased and caused a minor (4,14%) increase in natural gas end-use.

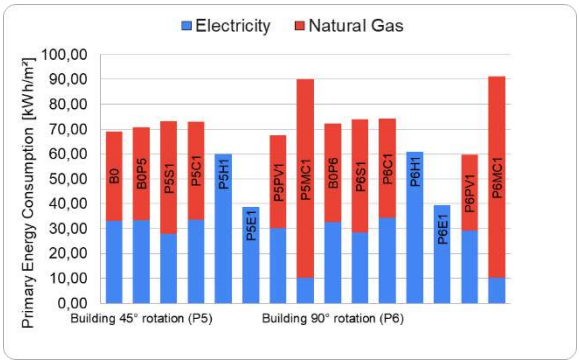

Fig. 8 - Natural Gas and Electricity Primary Energy Consumptions under different Building Orientations (45°, 90°)

The shading device applied South-West facing façade (P5S1) results in a 15,67% decrease in EE and a 25,60% increase in EG. On the other hand, the 90° rotation (P6S1) resulted in similar outcomes (-14,25%, +26,42%). Hence, the heating demand is in correlation with the building orientation. The Southern orientation performs more efficiently with

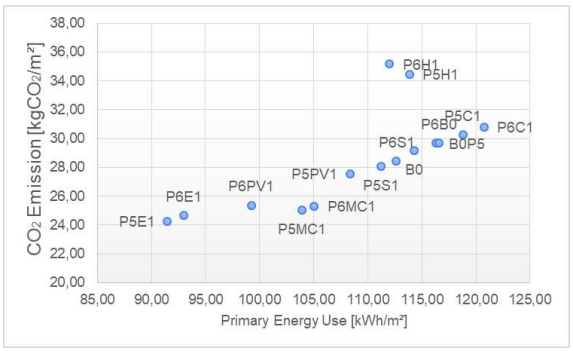

Fig. 9 - Primary Energy Consumptions vs. CO_2 Emissions under different Building Orientations (45°, 90°)

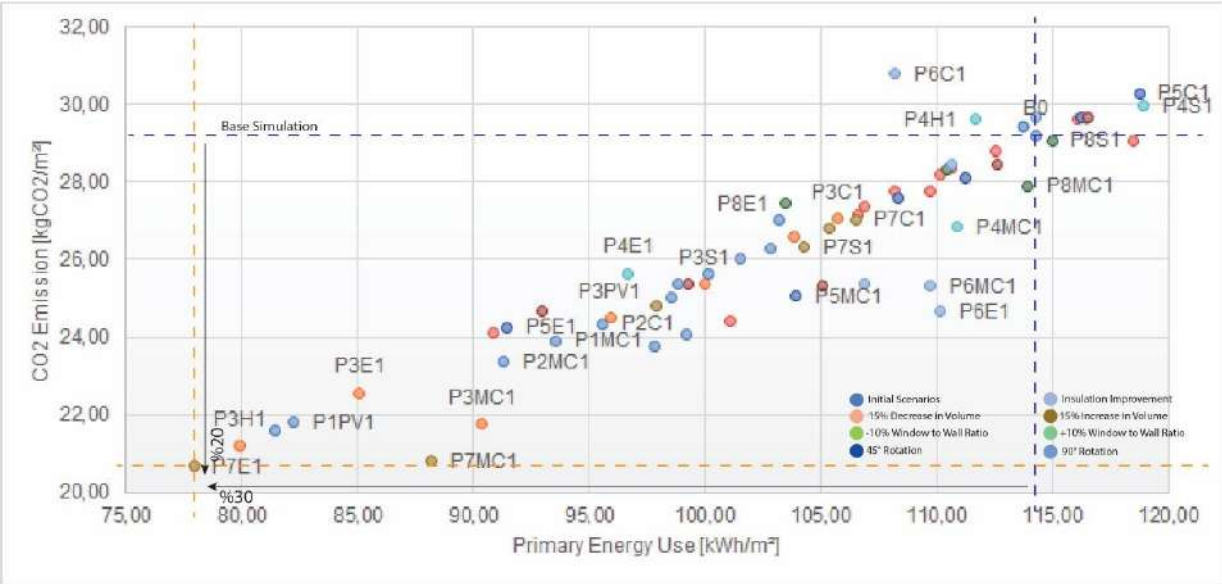

Fig. 12 – Bioclimatic Strategies Impacts on Primary Energy Use and CO_2 Emissions

shading elements. That being the case, this method presents more significant outcomes with HVAC system variations.

The chilled ceiling systems result in minor differences in electricity end-use. However, the natural gas end-use outcomes 15,18% less demand for heating energy than shading device scenarios. Compared to B0P5 and B0P6, the chilled ceiling implementation scenarios result in 3,97% and 5,68% more primary energy end-use. This cooling system method should be considered with optimum building orientation. The earth pipe integrated scenarios (P5E1, P6E1) result in 16,80% and 18,74% more electricity end-use. Indeed, the primary energy uses in both scenarios are approximately 20% less than the base scenario since the thermal loss is more with increased window dimensions. Given these points, the 45° and 90° rotation from the South direction lead to more primary energy end-use and CO_2 emissions. Despite this result, some systems in this study, like shading elements, earth pipe usage, and generative power systems, still present less primary energy use than the base simulation (Figure 9).

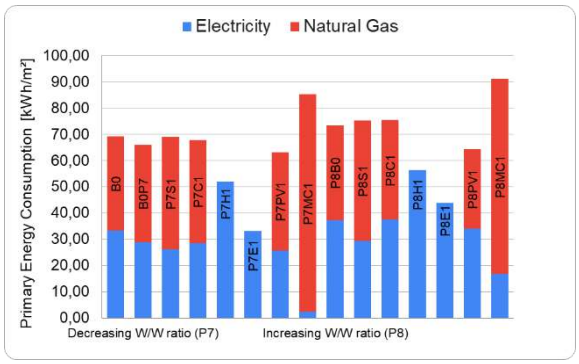

Fig. 10 – Natural Gas and Electricity Primary Energy Consumptions under different Window to Wall Ratios (±10%)

The window to wall ratio differentiations' impacts on energy performance is analyzed as a final step. The case study building has a 30% window to wall ratio. First, this ratio is decreased by 10% (P7). This method decreased 7,82% in electricity end-use and 8,23% in natural gas end-use. Second, the ratio is increased by 10% (P8). The obtained outcomes present an 8% increase in energy end-uses. These variations are applied to initial system simulations (Figure 10). The shading devices' combinations with the first window to wall ratio (P7S1) have a 21,72% decrease in electricity end-use, whereas this scenario results in a 19,54% more natural gas end-use. When the ratio is increased to 40% (P8S1), the decrease in electricity end-use is smaller (11,65%). In this scenario, the natural gas end-use is 27,33% more.

The chilled ceiling integration scenario's (P7C1) outcome presents a 14,11% decrease in electricity end-use compared to the base scenario, and the natural gas end-use differs 9% more. If the window-wall ratio is increased (P8C1), these differentiations are not majorly changed. The earth pipe integrated scenarios (P7E1, P8E1) result in 16,80% and 18,74% more electricity end-use. Indeed, the primary energy uses in both scenarios are approximately 20% less than the base case (Figure 11). The CHP system performs best when the thermal loss by windows is minimized.

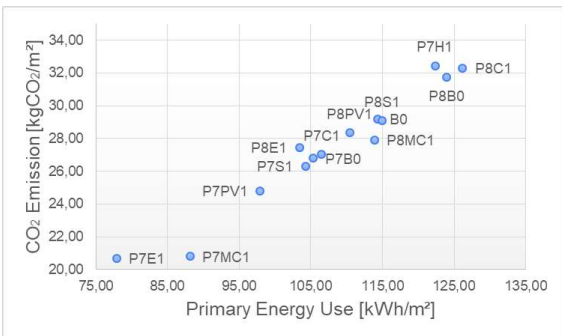

Fig. 11 – Primary Energy Consumptions vs. CO_2 Emissions under different Window to Wall Ratios

(±10%)

The most efficient scenario in envelope improvements is earth pipe installation (P2E1) with 28,72% reduction in primary energy use and 25% reduction in C02 emission. In -10% V/A scenarios, solar-assisted radiant floor usage (P3H1) performs the best with reducing primary energy usage by 30% and C02 emission by 27,82%. The building orientation efficiency is the best when the larger façade is oriented towards the South. The variations in degrees may increase the primary energy by 4% (P5C1). In -10% W/W scenarios, the earth pipe usage decreases the primary energy by 31,81% and C02 emission by 29,19%. Overall, amongst the bioclimatic strategies, the decrease in the W/W ratio performs the best (Figure 12).

4. Conclusion

One of the most critical challenges in contemporary architecture is to design high-performance buildings. Bioclimatic strategies can harmonize buildings with the climate, thus conveniently improving building performance. The analyzed parameters by bioclimatic principles influence the control of all factors related to energy conservation. As a result, there is a need for optimizing and estimating the performance of the bioclimatic design criteria, particularly during the early design phase. The dynamic simulation calculations performed for the case study reveal that a suitable design for a bioclimatic building may easily lead to achieving the requirements for an energy-efficient building. The findings also highlight the need to analyze passive methods with building systems to optimize energy savings. Variations in window dimensions and building volume among bioclimatic strategies create the most significant changes. It was also shown that, notably in a humid-temperate climate, renewable solar energy could be a critical source in lowering the energy demand for heating. The solar-assisted radiant floor integration and surface heat exchanger (earth pipe installation) reduced the primary energy use, around 30%. The contributions of photovoltaic panels and savings in micro-cogeneration systems are also significant in reducing energy consumption by power generation. This framework, however, solely pertains to building energy performance analysis. The bioclimatic strategies' impacts on thermal comfort and cost efficiency should be considered in future studies.

5. Acknowledgement

Special thanks to Yelkovan Grup for the permission to study their projects and provide the documents.

6. References

[1]Turkey 2021. IEA. Available from: https://www.iea.org/reports/turkey-2021

[2]El-Masry D, Farag E, Salem L, Katafygiotou M. Bioclimatic principles towards sustainable, comfortable and energy-efficient societies. Qatar Green Building Conference 2015 - The Vision. Hamad bin Khalifa University Press. Doi: 10.5339/qproc.2015.qgbc.7

[3] Hausladen G, Saldanha Mde, Liedl P. Building to suit the climate: A Handbook. Basel: Birkhauser; 2012.

[4]Özdeniz MB. Bioclimatic analysis of traditional Turkish houses. Vol. 17, Environment International. Elsevier BV; 1991. p. 325–36. Doi: 10.1016/0160-4120(91)90019-M

[5]Chronis A, Liapi KA, Sibetheros I. A parametric approach to the bioclimatic design of large scale projects: The case of a student housing complex. Vol. 22, Automation in Construction. Elsevier BV; 2012. p. 24–35. Doi: 10.1016/j.autcon.2011.09.007

[6] Convertino F, Di Turi S, Stefanizzi P. The color in the vernacular bioclimatic architecture in Mediterranean region. Vol. 126, Energy Procedia. Elsevier BV; 2017. p. 211–8. Doi: 10.1016/j.egypro.2017.08.142

[7] Ashrafian, T. & Moazzen, N. & Karagüler, M. Wind-catchers' Impact on the Energy Performance of Buildings in Hot & Arid Climate of Iran; 2017.

[8] Heating And Sanitary Hot Water Expenses In Central Heating And Sanitary Hot Water Systems Regulation On Sharing. Official Gazette of the Republic of Turkey. No: 26847.

[9]European Standards. BS EN 16798-1:2019 Energy performance of buildings. Ventilation for buildings Indoor environmental input parameters for design and assessment of energy performance of buildings addressing indoor air quality, thermal environment, lighting, and acoustics.

[10]Turkish Standards Institute. TS 825 - Thermal insulation requirements for buildings. 2008, TSE, Ankara.

[11]Weather Observation Station Data Set - İBB: https://data.ibb.gov.tr/tr/dataset/meteorology-observation-station-data-set

[12]Filoğlu E. Türkiye'de Mikro Kojenerasyon. [retrieved at 2022 Mar 1]. Available from: https://www.emo.org.tr/ekler/1d7156ffb1bc9a4_ek.pdf

[13]Generators - modeling guide. Available from: https://designbuilder.co.uk/helpv6.0/Content/GeneratorsModellingGuide.htm [retrieved 2022 Mar 1]

Economic and Energy Performance of Heating and Ventilation Systems in Energy Retrofitted Norwegian Detached Houses

Vegard Heide [a], Bianca Kjellberg [a], Sondre Valstad Johansen [a], Håkon Selstad Thingbø [a], Anne Gunnarshaug Lien [b] and Laurent Georges [a]

[a] Department of Energy and Process Engineering, Faculty of Engineering, Norwegian University of Science and Technology, Trondheim, Norway, vegard.heide@ntnu.no

[b] SINTEF community, Trondheim, Norway.

Abstract. The aim of this study is to compare the life cycle costs (LCC) and energy performance of different heating and ventilation systems (HVAC) in deep-energy renovation of Norwegian detached houses. More specifically, the relative performance of nine different HVAC combinations based on heat pumps is compared using two case buildings with four different insulation levels for the building envelope. The case buildings are small wooden dwellings without hydronic heating system, which is representative for existing Norwegian detached houses. The energy performance was simulated using the dynamic software IDA-ICE, in compliance with Norwegian Standards. The standard NS-EN 15459 (2017) was mainly used for the cost performance assessment. HVAC combinations with low investment costs (e.g., EAHP, balanced ventilation and air-to-air heat pump) showed lowest global costs, but the highest delivered energy. Low energy consumption can be achieved with different balances between investments on energy measures for the building envelope versus HVAC systems. Heat pumps can contribute significantly to the reduction of the energy use. In many cases, the cost uncertainty within one HVAC combination is larger than the difference between the combinations. The global cost and delivered energy diagram show a Pareto front relatively flat over a long range of energy use, so that some HVAC combinations can significantly decrease the energy use for a small increase in global costs. The compact heat pump and ground source heat pump fall into this category. For the investigated cases, the current governmental subsidies in Norway do not seem large enough to make investments in deep energy renovation profitable. Finally, results show that the prebound effect should be taken into account to make a realistic analysis of the cost performance of energy retrofit.

Keywords. Deep-energy retrofit, life cycle costs, energy performance, heat pumps.
DOI: https://doi.org/10.34641/clima.2022.350

1. Introduction

The Norwegian residential sector is characterised by a large share of detached wooden houses, privately owned. They are responsible for more than half of the total energy use in the Norwegian building stock. A great number of these houses were built between 1950 and 1990, and are now ready for major renovation. If these houses undergo deep energy renovation, it would contribute significantly to the national target of 10 TWh/year energy saving for existing buildings by 2030. A large share of these houses have direct electric heating, some supplemented with wood stoves. Heat pumps have been installed in recent years, the majority being air-to-air. Unlike many other countries, few detached houses from this period have a hydronic heat distribution system installed (1). A history of low electricity prices, and high investments costs in buildings, heating and ventilation systems (HVAC), have contributed to this situation. The additional cost to install a hydronic system can strongly affect the cost-effectiveness of heat pumps with hydronic space-heating distribution.

The aim of this study is to evaluate the performance of different HVAC solutions used in energy renovation of Norwegian wooden detached houses. Both life cycle costs (LCC) and energy performance are considered. The goal is to understand pros, cons and trade-offs between different HVAC combinations, according to different insulation levels and building sizes. The research questions are:

Copyright ©2022 by the authors. This conference paper is published under a CC-BY-4.0 license.

- What is the balance between LCC and energy performance and for different HVAC solutions?
- How is this affected by insulation level?
- How do prebound effects affect this?

This work is based on an architecture competition in the OPPTRE project (2). Energy renovations were proposed for six existing dwellings built between 1950 and 1990. More information about OPPTRE can be found in Moschetti et al (3). Two of the OPPTRE houses are used as case buildings in our study.

The number of existing studies on HVAC systems in energy renovation of detached houses in a cold climate are limited. The Norwegian context is different from most other countries due to renewable electricity at low prices and little use of hydronic distribution. Several studies investigated different technologies, but few have assessed both the costs and energy performance. Dermentzis et al. (4) investigated the use of a compact (exhaust air) heat pump in a renovated multi-family house in Germany, and found the system to be cost efficient due to prefabrication. Gustafsson et al. (5) compared energy performance of three HVAC systems for a renovated semi-detached house, and found that balanced ventilation combined with a micro heat pump, and exhaust air heat pump (EAHP) had the lowest energy consumption in Stockholm climate. Ekstrøm et al (6). evaluated the renovation of detached houses to Passive House level in Sweden, and found EAHP, and also ground source heat pumps (GSHP) the most cost-effective. Langdal investigated cost-effectiveness of energy renovation of Norwegian detached houses and found air-to-air heat pumps to be cost-efficient. He also found governmental grants crucial for profitability of the general upgrading (7). Felius et al. studied the potential of different energy renovation measures on detached and multi-family case houses in Norway, and estimated that an air-to-air heat pump had greater energy-saving potential than reducing heat loss through the building envelope (8).

2. Method

2.1 Evaluation of economic performance

The cost performance calculations were done on basis of the Norwegian and European standard NS-EN 15459-1:201 (9). The investment costs, the payback time and the total discounted costs were used as indicators. The following assumptions and parameters have been considered:

- The calculation period is 20 years. If energy measures have a longer lifetime, the residual value of the system at the end of the calculation period is discounted to present value.
- The electricity price is assumed constant in this study at 1.5 NOK/kWh. Prices in Norway have historically been low. However, the increase seen the last years is expected to continue, due to several new international connection cables. An alternative analysis is also done, based on the average Norwegian price from 2012 to 2020, rounded up to 1.0 NOK/kWh (10).
- The reference scenario for the calculation of the payback time of different HVAC combinations is the building after the upgrade of the building envelope with all-electric heating and natural ventilation. Thus, costs for building envelope upgrade is not considered in the payback time.

Tab. 1 - Parameters for calculating the economic performance.

Parameter	Value
Calculation period (TC) [years]	20
Inflation rate [%]	2
Real discount rate [%]	3
Electricity price [NOK/kWh]	1.5

2.2 Two case houses

The two case houses were selected because they represent a certain diversity:

- Malvik house: built in 1957, 2 storeys, 184 m^2 heated area.
- Kristiansand house: built in 1972, 2 storeys, cold attic, 214 m^2 heated area, basement floor with a studio apartment.

The two houses had no hydronic distribution system.

2.3 Three building envelope upgrade levels

In addition to the pre-retrofitted state, three performance levels of the building envelope were analysed: TEK10, OPPTRE and PASSIV. TEK10 is mostly in accordance with Norwegian building regulations of 2010. OPPTRE is based on proposals from OPPTRE's architect competition (2). PASSIV is mainly in accordance with the Norwegian passive house standard NS3700 (11). Thermal properties of each performance level are summarized in Table 2.

Tab. 2 – Thermal properties for the two case houses for the different building envelope performance.

Parameter	Unit	Existing Kristians.	Existing Malvik	TEK10	OPPTRE	PASSIV
U-value external wall	$W/(m^2.K)$	0.45	0.44	0.22	0.18	0.11
U-value roof	$W/(m^2.K)$	0.5	0.3	0.18	0.14	0.08
U-value basement wall to ground	$W/(m^2.K)$	0.87	3.5	0.33	0.2	0.11
U-value external floor	$W/(m^2.K)$	0.54	4.3	0.3 (4.3*)	0.18 (4.3*)	0.11
U-value internal walls	$W/(m^2.K)$	0.47	0.6	0.47	0.47	0.47
U-value windows and doors	$W/(m^2.K)$	2.6	2.6	1.6	1.0	0.8
Normalized thermal bridge value	$W/(m^2.K)$	0.07	0.07	0.7	0.5	0.3
Infiltration	h^{-1}	6.0	6.0	3.0	1.5	0.6

*U-value 4.3 in the Malvik house

2.4 Cost of envelope upgrade

Investment costs to upgrade the building envelope are included in the LCC analysis. Only measures to improve energy efficiency are included (i.e., other measures due to necessary maintenance or renovation was not included). A lifetime of 60 years was assumed for the envelope.

2.5 Nine HVAC combinations

Nine different HVAC combinations were analysed, see Table 3. These combinations are mainly named after the heat pump technology even though the combinations also include a ventilation measure. Eight have heat pumps and four of them have hydronic space-heating distribution. Six have balanced ventilation with heat recovery and two have exhaust ventilation with EAHP. No systems are based on fossil fuel or biomass.

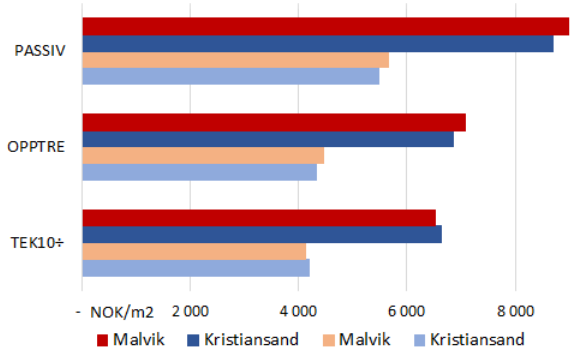

Fig. 1 - Specific cost of envelope upgrading: pale colours show the cost with the discounted residual value.

Tab. 3 - Description of the different HVAC combinations: heat pump and ventilation system.

Combination	Description
BalVent	Electric panel heaters, electric floor heating in bathroom (as for the reference scenario) Balanced mechanical ventilation with heat recovery
A2A	Air-to-air heat pump, electric panel heaters, electric floor heating in bathroom. Balanced mechanical ventilation with heat recovery
A2Asolar	Air-to-air heat pump, electric panel heaters, electric floor heating in bathroom. Solar collectors for heating of domestic hot water. Balanced mechanical ventilation with heat recovery
A2W	Air-to-water heat pump for space heating and domestic hot water. Hydronic distribution system. Balanced mechanical ventilation with heat recovery
GSHP	Ground source heat pump for space heating and domestic hot water where the borehole heat exchanger does not exist and should be created. Hydronic distribution system. Balanced mechanical ventilation with heat recovery
CHP	Compact heat pump unit for heating of domestic hot water. Electric panel heaters, electric floor heating in bathroom. Balanced mechanical ventilation with heat recovery integrated in HP unit.
CHPcomb	Compact heat pump for space heating and heating of domestic hot water, and some ventilation air heating Hydronic distribution system. Balanced mechanical ventilation with heat recovery integrated in HP unit.
EAHPDHW	Exhaust air heat pump for heating of domestic hot water. Electric panel heaters, electric floor heating in bathroom.
EAHPcomb	Exhaust air heat pump for space heating and heating of domestic hot water. Hydronic distribution system.

2.6 Cost of HVAC combinations

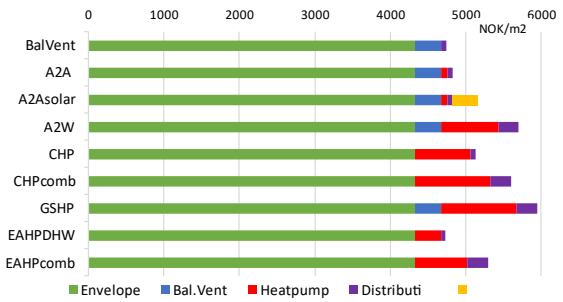

Fig. 2 - Total specific investment costs for both envelope and HVAC systems for the OPPTRE scenario: residual values are discounted

Maintenance costs, replacement costs and residual value were included in the analysis. As this paper is limited to Norwegian dwellings and climate, the costs are based on the current Norwegian market. Most of the costs were collected directly from suppliers and building companies or their webpages. Where this was not possible, generic costs from reports and statistics were used (12, 13). Uncertainty on costs was considered by collecting several prices and using a cost range (i.e., uncertainty). Systems were dimensioned according to simulated net heating demand for the different scenarios,. An example of total investment costs for both the envelope and HVAC systems are shown in Fig. 2.

2.7 Energy analysis

The energy performance was evaluated using the dynamic software IDA-ICE, in compliance with the Norwegian Standard NS-NSPEK 3031 (14). Ventilation airflow rates are adjusted to follow the requirements in the Norwegian building regulations. Only Oslo-climate was used in the simulations.

2.8 Heat pump efficiency

The seasonal performance factors (SPF) of the heat pump system in our simulations are shown in Fig. 3 while the energy coverage factor is shown in Fig. 4. Among key factors influencing the energy coverage factor and the SPF, it can be mentioned: the power coverage factor of the heat pump, the type of space-heating distribution subsystem, the layout of the floor plan and the share of DHW covered by heat pumps. As it can be seen, the energy coverage factor has a strong influence on the system SPF. To make sure that the simulation results are realistic, the SPF value can be compared to the literature, here shown in Table 4. The literature generally reports slightly more favorable SPF than our simulations.

Tab. 4 - SPF values in cold climate reported in literature.

Heat pump	Reported SPF	Study
Air-to-air	2.1	Fältmätning
	2.1	Nordman et al (15)
Air-to-water	3.1 - 3.3	Nordman et al (16)
	2.1 - 4.2	Miara et al (17)
GSHP	3.3 - 4.7	Nordman et al (16)
	2.2 - 5.4	Miara et al (17)
Compact	1.7 - 2.4	O'Sullivan et al (18)
EAHP	1.43	Saini et al (19)
	1.91 - 2.09	Thalfeldt, et al (20)

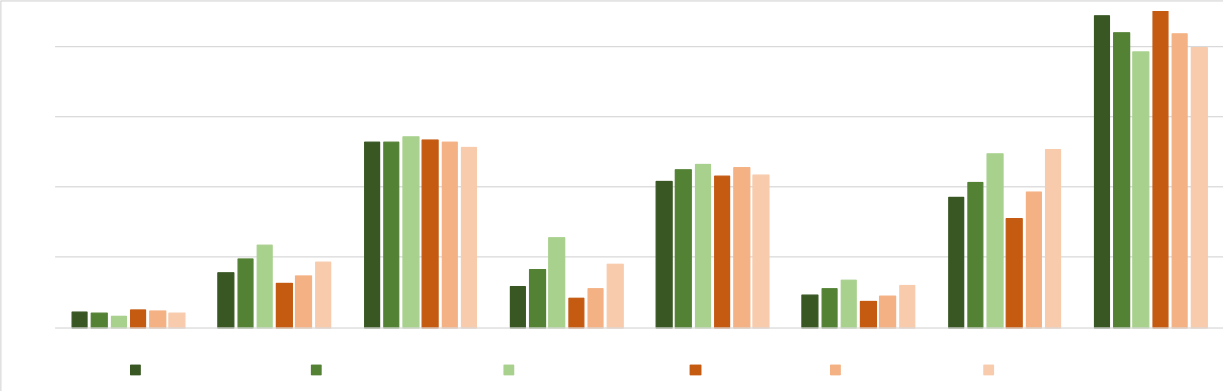

Fig. 3 – Seasonal performance factor for heat pump system in both houses.

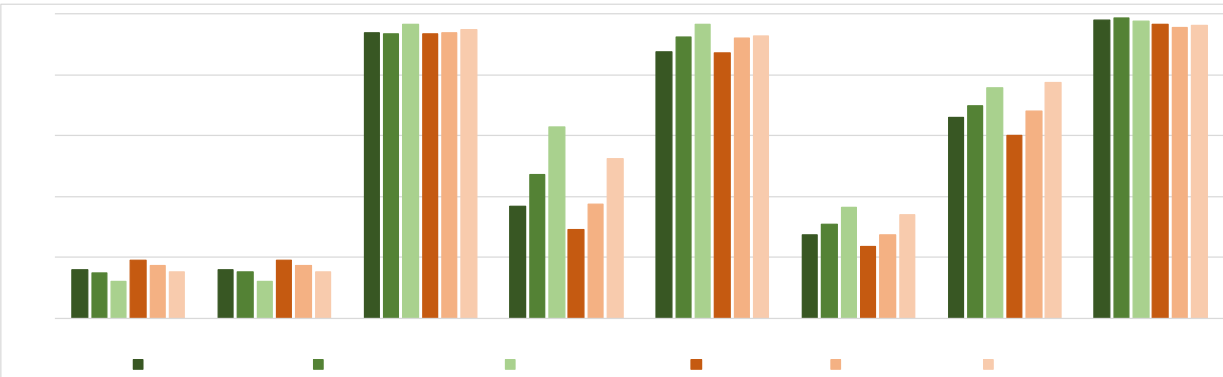

Fig. 4 – Energy coverage factor of the heat pump in both houses (i.e., fraction of heat demand covered by heat pump).

2.9 Prebound effect

The most common way to evaluate energy measures is to use standardised energy calculations before and after renovation. However, the real energy use can be different, typically due to the occupants' behaviour (i.e. the performance gap). The measured delivered electricity was available in five of the six case houses in the OPPTRE architecture competition and the average deviation was 60% of the standardised calculation. This indicates a large prebound effect. The reasons for this performance gap are unknown. It can be caused by lower temperatures and thermal zoning, or low ventilation airflow rates. Sandberg et al. analysed a larger set of buildings and found a prebound effect of 25% for houses of this segment, which is used for the assessment in this paper (21).

3. Results and discussion

3.1 Delivered energy

The delivered energy is shown in Figs. 6 and 7. There is a large spread in the energy performance: 51 to 135 kWh/m² annual delivered electricity. Several different combinations can be used to achieve a low energy demand. Most of the analysed combinations are below the target on delivered energy in the OPPTRE architecture competition, of 108 kWh/m², see Figs. 6 and 7. This target can be reached by different means, and different balance between energy measures on the building envelope versus the HVAC systems. Combinations with efficient heat pumps and hydronic distribution show the lowest energy use (GSHP, A2W, CHPcomb). The hydronic distribution allows a high energy coverage factor for the heat pump. This indicates that the contribution

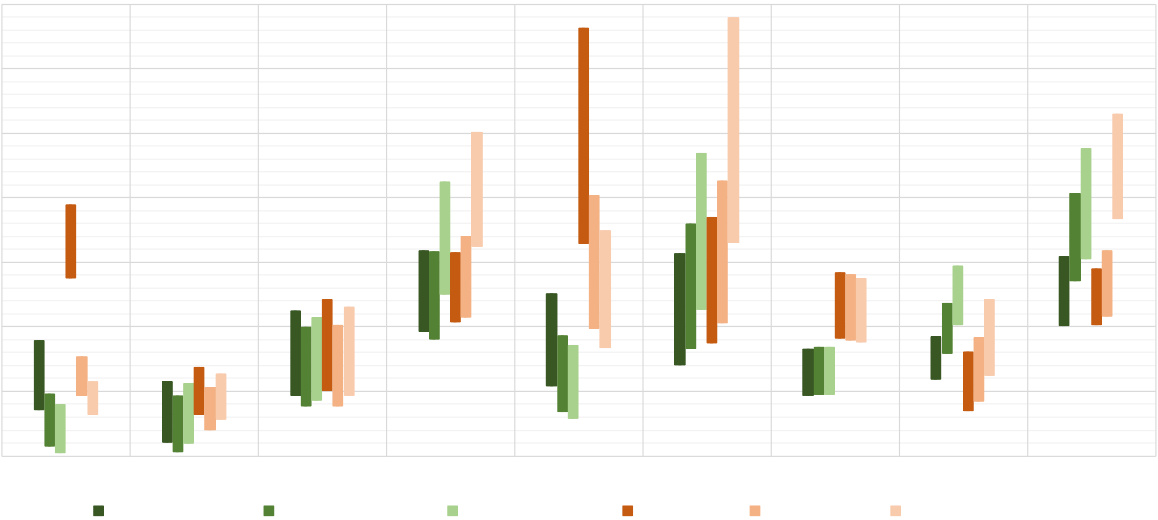

Fig. 5 – Payback time for the analysed HVAC combinations.

from these heat pumps is important. The figure also illustrates that, by using heat pump systems with high SPF, like GSHP, the OPPTRE target can be reached with lower insulation levels than in our study.

3.2 Payback time

Payback times for the HVAC combinations are presented in Fig. 5. Most combinations have a payback time close to the calculation time period, i.e. 20 years, which is critical. The combinations with the lowest payback times for both case houses are A2A. For the BalVent combination, the payback time decreases with a better performing building envelope. This can be explained by the reduced infiltration, causing a larger part of the air change to pass through the heat exchanger. For most of the combinations with a heat pump used for space heating, the payback time increases along with the increasing insulation level of the building envelope. The reason for this is the reduced space-heating needs for higher insulation levels, resulting in less energy saved by installing more efficient energy supply solutions. This is clearly seen for combinations with high investment and a high energy coverage factor: A2W, CHPcomb, EAHPcomb and GSHP. This indicates that efficient energy supply solutions with higher investment costs are less profitable for buildings with low heating demand. The payback time of the combinations mainly covering domestic hot water are less affected by the insulation level of the building envelope, as illustrated by the EAHPDHW. This is because the DHW heating needs are unaffected by the different levels of the envelope retrofit.

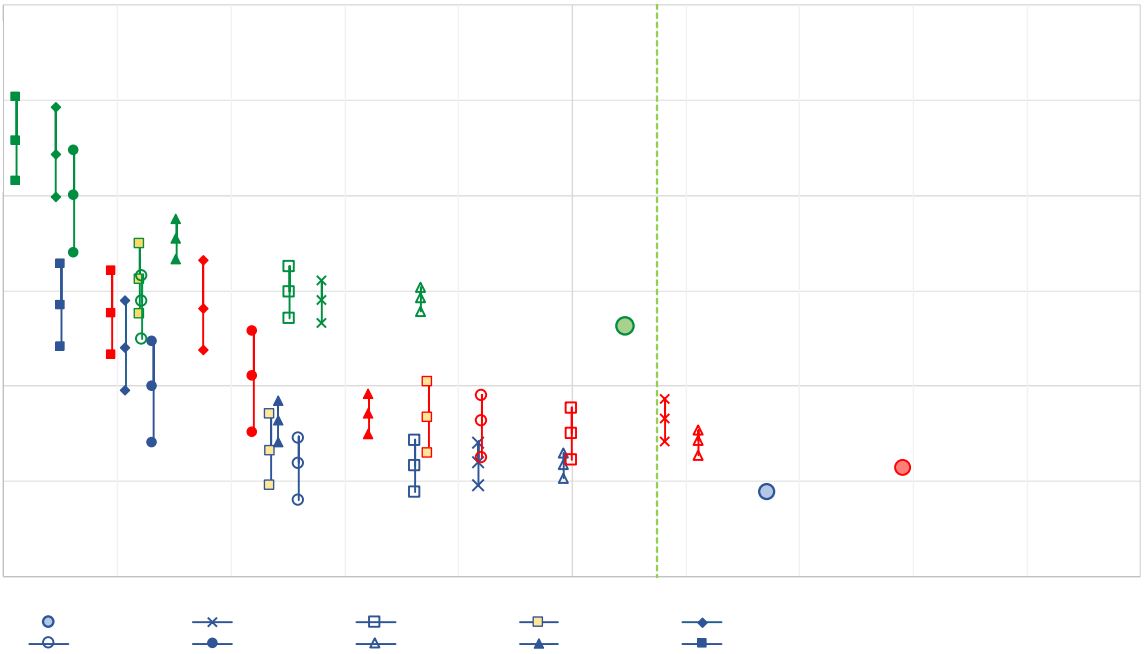

Fig. 6 – Specific global costs and delivered energy of the Kristiansand house: TEK10 in red, OPPTRE in blue, PASSIV in green, and the vertical line shows the minimum energy requirement from the OPPTRE architecture competition.

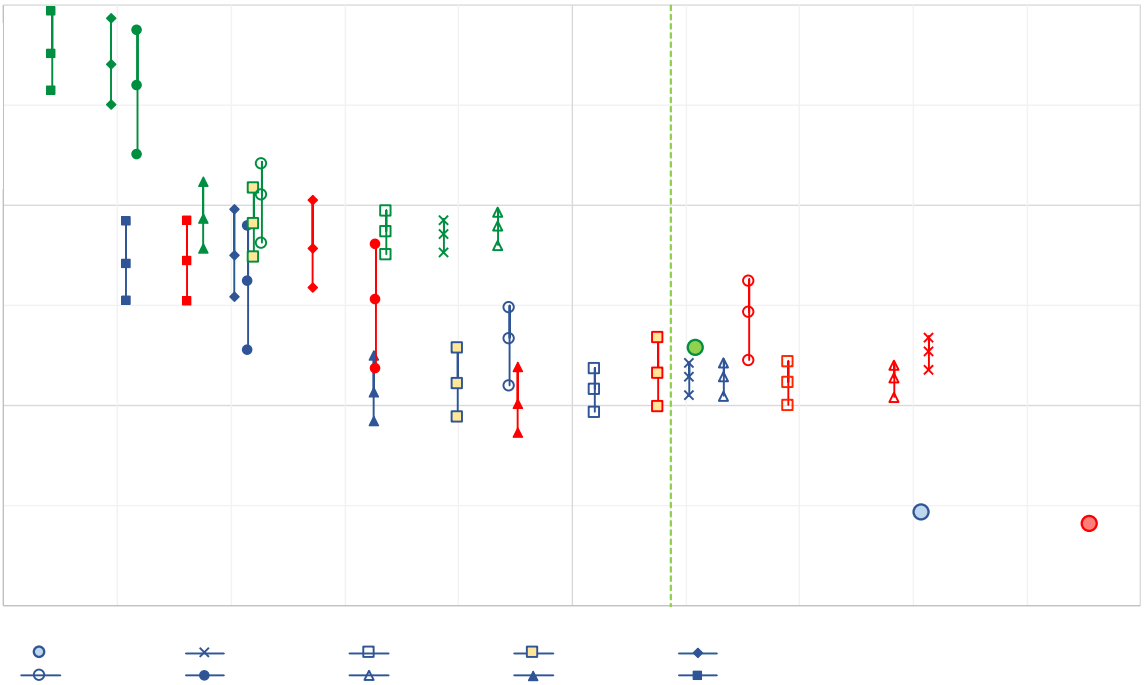

Fig. 7 – Specific global costs and delivered energy of the Malvik house: TEK10 in red, OPPTRE in blue, PASSIV in green, and the vertical line shows the minimum energy requirement from the OPPTRE architecture competition.

3.3 Global costs

Global costs including the investments and energy costs during the calculation period are shown in Figs. 6 and 7. The case only considering the envelope upgrade and the cases also including the HVAC combinations are shown. The Pareto front between 60 and 100 kWh/m^{2}year is flat, showing many HVAC combinations in the same range of global cost. This leads to the following conclusions:

- In many cases, the cost span inside a combination (resulting from the data range in collected investment costs) is larger than the difference between the neighbouring combinations. This indicates uncertainty regarding which combinations are optimal. The best solution can eventually depend on the choice of HVAC manufacturer and company installing the equipment.
- For both houses, a number of combinations show approximately the same low global cost, but with a wide range in delivered energy. These combinations generally have low or medium investment costs. Among these, the CHP and EAHPcomb, show the best energy performance, for the Kristiansand and Malvik house, respectively.
- No solution is optimal for both energy use and costs. Neither a scenario with low energy use but high global costs, nor a scenario with low global costs but only small improvements in the energy performance are desirable. Therefore, a compromise between achieving low global costs and low energy consumption is preferable, satisfying both the household budget and energy use. For the largest house in Kristiansand, the compact heat pump seems to be the optimal trade-off. For the house in Malvik, the larger investment in the GSHP can be mitigated by the energy savings so that the total costs remain moderate but with an excellent energy performance.

Comparing the BalVent and the A2A combinations, the balanced ventilation system contributes more to reduced energy use than the air-to-air heat pump, especially for the high preforming envelopes. This is more pronounced with the PASSIV scenario, as the low space-heating demand implies a small contribution from the heat pump, while the ventilation heat demand is the same regardless of insulation level. In addition, due to lower air infiltration, more heat is recovered by the AHU. As for payback time, combinations with lower investment (such as BAL, A2A or EAHP) perform relatively better with increasing envelope insulation.

Finally, it is worth mentioning that some of the combinations with low investment costs may provide a lower thermal comfort. With the EAHP for example, supply ventilation air is not preheated. Due to possible cold draft, some occupants may experience this as a less comfortable.

3.4 Electricity price

A calculation with electricity price of 1.0 NOK/kWh is also done. The global costs are then lower, but the measures are clearly less cost efficient. Therefore, the combinations with lower investment costs (EAHP, BalVent, A2A) are relatively more favourable.

3.5 Governmental grants

Governmental subsidies and grants for improving energy efficiency in buildings are not included in the baseline analysis in this study. When including the

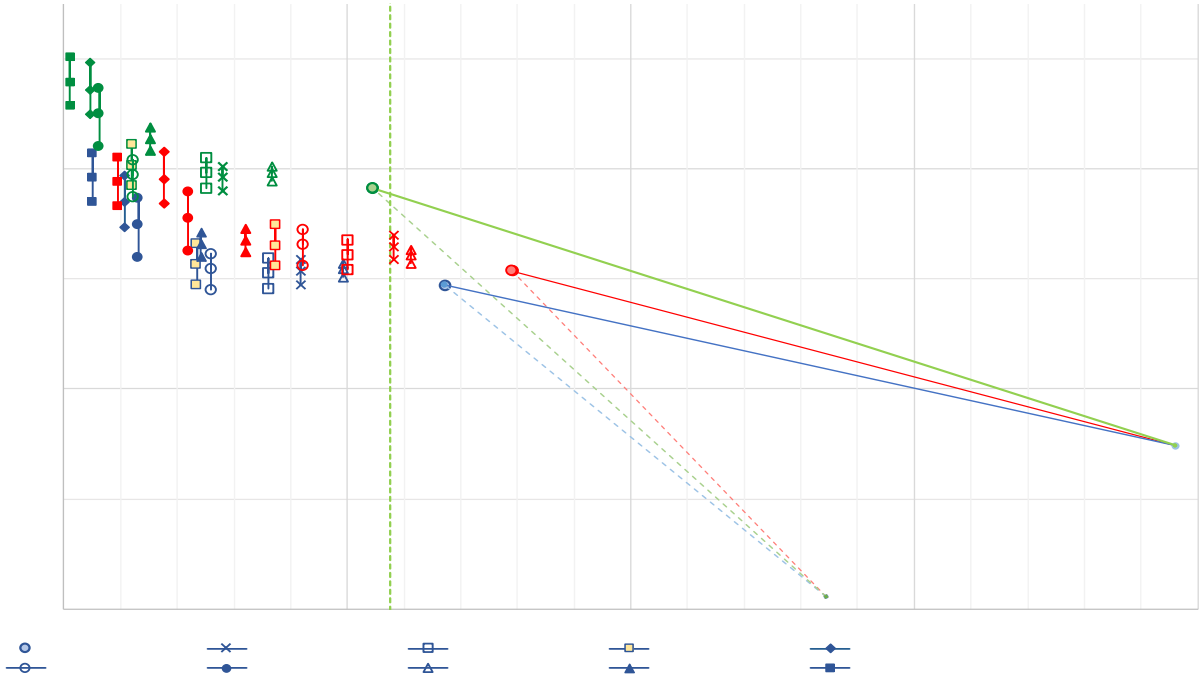

Fig. 8 – Specific global costs and delivered energy of the Kristiansand house with the situation before upgrading to the far right: the lines show the effect of envelope upgrade, dotted lines and the lowest point considers the prebound effect.

Norwegian grants, the global costs of some of the measures with high investment cost are relatively more favoured. However, with the electricity price used in this study, these grants do not seem large enough to support high investment costs in deep energy renovation of detached houses.

3.6 Envelope upgrade level

For both houses, upgrading to the PASSIV envelope shows higher global costs, which means the investment costs are higher than the savings in energy costs it provides. The OPPTRE envelope shows slightly lower global costs than TEK10 for Kristiansand house. This conclusion is stronger if government grants are included.

3.7 Envelope versus technical systems

The results show that low delivered energy demand can be reached with different balance between energy measures on the building envelope versus the HVAC systems. Determining this optimal balance between measures on the building envelope and the technical systems is challenging. Fig. 8 visualises some of these aspects. The starting point before retrofit is to the far right, and the lines represent the upgrade of the envelope only. The other symbols show the situation after also adding the different HVAC combinations. The steeper the line, the larger the increase in global costs per kWh reduction of the annual delivered energy. If the retrofit of the envelope and the HVAC are done in two separate steps, the order of the implementation of these measures influences the analysis. If HVAC measures were implemented first and the economic performance of envelope upgrade was analysed afterwards, the relative contributions would probably be different.

3.8 Prebound effects

The point in the bottom part of Fig. 8 displays the building before upgrading with a prebound effect of 25% lower energy use. When using this as the starting point before renovation, the upgrading measures seem even less profitable. In addition, the literature tends to show a rebound effect for highly-insulated buildings. This rebound effect has not been introduced for the renovated cases in our study and should be investigated in further studies.

4. Conclusions

Results can be summarized as follows:

- Many combinations have longer payback time than the economic lifetime of the project.
- Low energy consumption can be achieved with different balances between investments on energy measures for the building envelope versus HVAC systems. Heat pumps can contribute significantly to the reduction of the energy use (especially with hydronic distribution).
- In many cases, the cost uncertainty within one HVAC combination is larger than the difference between the combinations.
- HVAC combinations with low investment costs (e.g., EAHP, balanced ventilation and air-to-air heat pump) showed lowest global costs, but the highest delivered energy.
- The global cost and delivered energy diagram show a Pareto front so that no HVAC combination is the absolute optimum; a solution is optimal for a given energy use. However, the Pareto front is relatively flat over a long range of energy use (between 60 and 100 kWh/m^{2}year) so that some combinations can significantly

decrease the energy use for a small increase in global costs. These combinations have a great potential for energy savings. The compact heat pump and the GSHP fall into this category for the Kristiansand and Malvik houses, respectively.

- Increasing envelope insulation favours HVAC combinations with lower investment and higher energy use. Combinations with higher investments are less profitable with the highest envelope performance.
- The most ambitious envelope upgrade, i.e., the Passiv level, shows higher global costs, and only slightly lower energy use compared to the other envelope performance investigated.
- For the investigated cases, the current governmental subsidies in Norway do not seem large enough to make investment in deep energy renovation profitable.
- The prebound effect should be taken into account to make a realistic analysis of the cost performance of energy retrofit.

5. Acknowledgement

This work is part of the OPPTRE project, on Energy upgrading of wooden dwellings to nearly zero energy level (http://opptre.no/). This project is funded by the Norwegian Research Council.

The datasets generated and analysed during the current study are not publicly available because significant pre-processing and structuring of data is required to make it open-access, but will be available upon request.

6. References

1. Bøeng AC, Halvorsen B, Larsen B. Oppvarming i boliger: Kartlegging av oppvarmingsutstyr og effektiviseringstiltak i husholdningene. NVE, SSB; 2014.
2. Sørlie KH, Lien AG, Brekke T, Hauge PK, Heide V, Jelstad E, et al. Architecture competition "OPPTRE". Energy upgrading of wooden dwellings to nearly zero energy level. NAK; 2021.
3. Moschetti R, Time B, Gullbrekken L, Heide V, Georges L, Lien AG, editors. Analysing energy upgrading projects of single-family houses towards a Norwegian nZEB level. Journal of Physics: Conference Series; 2021: IOP Publishing.
4. Dermentzis G, Ochs F, Siegele D, Feist W. Renovation with an innovative compact heating and ventilation system integrated into the façade – An in-situ monitoring case study. Energy and Buildings. 2018;165:451-63.
5. Gustafsson M, Dermentzis G, Myhren JA, Bales C, Ochs F, Holmberg S, et al. Energy performance comparison of three innovative HVAC systems for renovation through dynamic simulation. Energy and Buildings. 2014;82:512-9.
6. Ekström T, Bernardo R, Blomsterberg Å. Cost-effective passive house renovation packages for Swedish single-family houses from the 1960s and 1970s. Energy and Buildings. 2018;161:89-102.
7. Langdal J. Energisparepotensiale og lønnsomhet ved energioppgradering av 50- og 80-talls enebolig. Trondheim: Norwegian Univerity of Science and Technology (NTNU); 2019.
8. Felius LC, Hamdy M, Dessen F, Hrynyszyn BD. Upgrading the Smartness of Retrofitting Packages towards Energy-Efficient Residential Buildings in Cold Climate Countries: Two Case Studies. Buildings. 2020;10(11):200.
9. Standard Norge. NS-EN 15459: Energy performance of buildings - Economic evaluation procedure for energy systems in buildings - Part 1: Calculation procedures, Module M1-14. 2017.
10. Statistisk Sentralbyrå. Elektrisitetspriser 2021 [Available from: https://www.ssb.no/elkraftpris
11. Standard Norge. NS 3700:2013 Criteria for passive houses and low energy houses (residential buildings). 2013.
12. Ericson T. Varmepumper i energisystemet. Status og muligheter. NVE; 2016.
13. Weir DE. Kostnader i energisektoren. Kraft, varme og effektivisering. NVE; 2015.
14. Standard Norge. SN-NSPEK 3031 Energy performance of buildings — Calculation of energy needs and energy supply. 2021.
15. Nordman R, Andersson K, Axell M, Lindahl M. Calculation methods for SPF for heat pump systems for comparison, system choice and dimensioning. SP Rapport, ISSN 0284-5172. 2010;2010:49.
16. Nordman R, et al. Demonstration of Field Measurements of Heat Pump Systems in Buildings – Good Examples with Modern Technology. 2016.
17. Miara M, Günther D, Langner R, Helmling S, Wapler J, editors. 10 years of heat pumps monitoring in Germany. Outcomes of several monitoring campaigns. From low-energy houses to un-retrofitted single-family dwellings. 12th IEA Heat Pump Conference; 2017.
18. O'Sullivan P, Colclough S, Morehead J, O'Donovan A, editors. Evaluation of the theoretical and in-use performance of Exhaust Air Heat Pumps. E3S Web of Conferences; 2021: EDP Sciences.
19. Saini P, Paolo B, Fiedler F, Widén J, Zhang X. Techno-economic analysis of an exhaust air heat pump system assisted by unglazed transpired solar collectors in a Swedish residential cluster. Solar Energy. 2021;224:966-83.
20. Thalfeldt M, Kurnitski J, Latõšov E. Exhaust air heat pump connection schemes and balanced heat recovery ventilation effect on district heat energy use and return temperature. Applied Thermal Engineering. 2018;128:402-14.
21. Sandberg NH, Sartori I, Inderberg Vestrum M, Brattebø H. Using a segmented dynamic dwelling stock model for scenario analysis of future energy demand: The dwelling stock of Norway 2016–2050. Energy and buildings. 2017;146:220-32.

Next-Generation Energy Performance Certificates, What novel implementation do we need?

Lina Seduikyte [a], Phoebe-Zoe Morsink-Georgali [b], Christiana Panteli [c], Panagiota Chatzipanagiotidou [d], Koltsios Stavros [d], Dimosthenis Ioannidis [d], Laura Stasiulienė [a], Paulius Spūdys [a], Darius Pupeikis [a], Andrius Jurelionis [a], Paris Fokaides [b]*

[a] Faculty of Civil Engineering and Architecture, Kaunas University of Technology, Kaunas, Lithuania, lina.seduikyte@ktu.lt*, laura.stasiuliene@ktu.lt, paulius.spudys@ktu.lt, darius.pupeikis@ktu.lt, andrius.jurelionis@ktu.lt

[b] Frederick Research Center, Frederick University, Nicosia, Cyprus, res.gp@frederick.ac.cy, eng.fp@frederick.ac.cy

[c] Cleopa Gmbh, Hennigsdorf, Germany, c.panteli@cleopa.de

[d] Centre for Research and Technology Hellas, Information Technologies Institute, Thessaloniki, Greece, phatzip@iti.gr, skoltsios@iti.gr, djoannid@iti.gr

Abstract. Energy performance certificates are being utilized through the European Union Member States to document and asses the energy performance of the building stock, while they are used as measures to investigate and adopt policies that would lower the final energy consumption and environmental footprint. After several years of implementation, the current EPC schemes have enlighten the domain energy efficiency in the building sector, but at the same time they have been identified with several challenges and deficiencies that deteriorate the quality of the results. This study performed under the H2020 project "Next-generation Dynamic Digital EPCs for Enhanced Quality and User Awareness (D^2EPC)", aims to analyze the quality and weaknesses of the current EPC schemes and aspires to identify the technical challenges that currently exist, setting the grounds for the next generation dynamic EPCs. The present work reveals that current EPCs schemes are based on a cradle-to-gate rationale, completing their mission after the certificate to the building user, overlooking the user's behavior and the actual energy performance of the building that might change dynamically within time. In this study, the idea of the dynamic EPCs is introduced, a certificate that will allow the monitoring of the actual performance of buildings and the users' behavior profiles on a regular basis. The introduction of novel indicators and the integration of BIM and GIS are also discussed.

Keywords. EPC, SRI, LCA, BIM, DT, GIS, human comfort, D^2EPC.
DOI: https://doi.org/10.34641/clima.2022.348

1. Introduction

Energy Performance Certificates (EPCs) are a mandatory requirement for the European Union (EU) Member States (MS) when constructing, selling, or renting a building. EPCs serve as a transparent information instrument for building owners and real estate stakeholders. They are among the most important information sources regarding energy performance in the EU's building stock. EPCs could act as a criterion for decision-making on energy efficiency property improvements by providing recommendations for cost-effective or cost-optimal upgrading of buildings. Existing procedures and tools used in assessing buildings' energy performance across Europe present several drawbacks and discrepancies.

As a promising technology in the construction industry, the building information model (BIM) concept became widespread on the market early in the 2000s. BIM is more than a three–dimensional (3D) building tool, which can become a multidimensional information model [1-2]. Well-defined semantic and geometric data for each element and the ability to enable collaboration between stakeholders during the life cycle of the facility can be referred to as a key feature of BIM [3]. According to the purpose of BIM, its application is observed throughout all stages of the asset life cycle. Architects, engineers, and constructors use BIM throughout the design and construction stage, while gaining benefits from errors reducing, improving construction efficiency, communication and data exchange, and costs and time monitoring [4-5].
The aim of the study, performed under the H2020 project "Next-generation Dynamic Digital EPCs for

Copyright ©2022 by the authors. This conference paper is published under a CC-BY-4.0 license.

Enhanced Quality and User Awareness (D^2EPC)", is to create the concept of the next generation dynamic EPCs. The aim is reached through the following steps: (i) identification of the quality and weaknesses of the current EPC schemes, (ii) identification of the novel indicators for EPC (iii) evaluation of posibilities of integration of BIM, DT and GIS in EPC, (iiii) presentation of the developed D^2EPC system architecture.

2. Methodology

Desk research was performed to identify the current status of EPCs, limitations, and information for the gaps in the existing schemes, the calculation procedures, and standards.

An overview of reports was performed to identify the current EPC schemes' challenges, needs, and opportunities, as well as the emerging future market requirements. The documented statements within the collected reports provide evidence on current practices in the EU MSs.

3. Quality and weaknesses of current EPC schemes

The main findings of the conducted study are presented below:

- At this moment, there is no obligation for MSs to use Building Information Model (BIM) software. Most EU countries do not use BIM documentation and literacy or digital logbooks for the issuance of EPCs. Furthermore, the current EPC practises in most EU MSs don't include GIS information, which could be exploited for issuing, validating, monitoring, and verifying the processes of the EPC calculation.
- Environmental/LCA-related indicators are not considered for the EPC issuance.
- The human comfort factor is combined in assessment systems, but it is not calculated in the analysis. Indoor environmental quality indicators are not covered in current EPC regimes and are not included in the calculation procedure.
- In certain countries, only parts of the building stock are examined visually or estimated according to the calculations.
- 1/3 of the EU countries do not have systematic and regular evaluation/ assessment of energy assessor's competence and skills.
- Smart metering and real-time data are not utilized in the calculation procedures of the EPC in many MSs.
- Energy-related financial indicators are not found to be included in current EPCs schemes and procedures in any EU MSs.
- There is a need for an openly accessible EPC registry of all EPCs in Europe MSs, addressed by the European Energy Performance of Properties Analysis.

4. The novelty of the dynamic EPC

The aforementioned shortcomings of national EPC schemes urge the development of a holistic framework that will strengthen and improve the quality and application of EPCs. The former can be achieved with the introduction of novel and cost-effective approaches for assessing the energy performance of building envelopes and systems. According to the collected information, the introduction of novel aspects in the certification process and the simplification thereof, the strengthening of its user-friendliness, as well as the conformity with national and European legislations, can be accomplished using a standard collection of indicators based on a specific methodology. All upgrade needs of EPCs can be met by choosing acceptable output indicators supported their automated estimation.

4.1 New indicators

The introduction of novel aspects into the energy performance certification process includes three indicators – the smart-readiness level of the buildings (SRI), human comfort-related indicators, and environmental aspects (LCA).

Smart readiness indicator. The scheme for rating the smartness of buildings was presented in 2018 in a revision of the Energy Performance of Buildings Directive (EPBD). It was established that the smart readiness of buildings should be optionally evaluated by the smart readiness indicator (SRI) [6]. According to the EPBD, this indicator reflects the building's ability to adapt to the needs of its occupants and outdoor energy infrastructure, improving its overall energy performance.

To define the smartness of buildings' services, three main functionalities of smart readiness are introduced in the methodology:

- The ability of the building to adapt its energy consumption based on the needs in an energy-efficient way;
- The ability of the building to adapt its operation to occupant's needs;
- The building's flexibility to its overall electricity demand, as well as its ability to participate in demand-response, in relation to the grid.

The SRI scheme includes the following nine services' domains: heating, cooling, domestic hot water, controlled ventilation, lighting, dynamic building envelope, electricity, electric vehicle charging, and monitoring and control. Each domain can be evaluated with a different degree of smartness (functionality levels) and includes various impact criteria (i. e. energy savings, maintenance and fault prediction, comfort, convenience, health and wellbeing, information to occupants, grid flexibility, and storage) that can be delivered by several

building services.

The functionality levels could be evaluated in ordinal numbers on a scale from 2 to 5. The higher the functionality level, the more impact the building, its occupants, or the outdoor energy infrastructure will have on the final rating. A multi-criteria assessment method, that includes the diverse domains and criteria, is used to calculate the SRI. The smart readiness score is described as a percentage of how close (or far) the building is to the maximum smart readiness that it could reach.

In a study performed by Fokaides et al. [7], SRI was calculated for a D energy efficiency class building. The total SRI score of the examined case study was relatively high and equal to 52%. Such a result demonstrates that SRI, as a methodology, does not follow the EPC class and additional attention is needed to align these two schemes.

Within the H2020 D^2EPC project, both SRI and EPC methodologies will be included in the same calculation engine allowing, where possible, to merge these two methodologies to progress the SRI to a higher level.

Human comfort. People in developed countries spend more than 90% of their time in closed environments - buildings and transport [8]. Air quality indoors is 2-5 times lower than outdoors [9]. These values can be even lower if we consider the future effects of climate change (extreme temperatures, heat waves, heavy rainfalls, air pollution). Therefore, significant attention should be paid from researchers, businesses, and standardization organizations to the field of indoor environment quality (IEQ) [10-12].

The main indicators that assess the IEQ of a building and human comfort/wellbeing can be described by an integrated multi-comfort concept that includes indoor air comfort/quality, thermal, visual, and acoustic comfort. The indoor air quality (IAQ) examines how fresh the air is in a building and the concentration in the air of certain pollutants (e.g. CO_2, VOC). Thermal comfort provides a state of satisfaction with the existing thermal environment. Visual comfort ensures that the luminance levels are within acceptable levels. Acoustic comfort creates a comfortable acoustic environment without uncomfortable noise or vibrations.

Many worldwide-accepted certification schemes of building energy efficiency and environmental impact are developed and applied widely. The schemes assess the impact of buildings throughout their life cycle. They include a number of factors, e.g. heating and cooling energy consumption, water consumption, operational processes, indoor environmental conditions, land use, transportation, sustainability, etc. The following parameters for human comfort/wellbeing indicators estimation or calculation are addressed in LEED [13], BREEAM [14], and WELL [15] certification systems: temperature, relative humidity, ventilation rate (rate of fresh air supply), air speed, concentrations of TVOC, formaldehyde, CO_2, CO, PM10, PM2.5, ozone, ambient noise and reverberation time, illuminance level, daylight factor, spatial daylight autonomy, PMV/PPD (WELL v2). Furthermore, these parameters are also found in other green buildings certification systems over Europe and the world, e.g., Level(s) (EU), OsmoZ (France), klimaaktiv (Austria), DGNB (Germany), NABERS (Australia). The WELL certification scheme also examines radon, benzene (same as LEVEL(s)), NO_2, CS_2, and trichloroethylene levels. The SRI scheme evaluates human comfort/wellbeing parameters indirectly via the functionality score of the technical building services (TBS) (IAQ and thermal comfort) or the climate adjustments on the domain weights used in the calculation (thermal and visual comfort). The schemes assign credits to four IEQ components: thermal environment, IAQ, acoustic environment, and visual environment. The LEED system gives 35% for visual comfort, 12% for acoustics, 47% for IAQ and 6% for thermal comfort, while BREEAM gives 33%, 22%, 28% and 17% and WELL gives 13%, 25%, 50% and 13%, respectively. According to the existing framework, the SRI methodology gives 26% for visual comfort, 0% for acoustics, 47% for IAQ, and 26% for thermal comfort. Currently, in the case of LEVEL(s), only two components are considered and allocated half the credits of the total IEQ credits: IAQ and thermal comfort.

Within the H2020 D^2EPC project, human comfort/wellbeing parameters will be measured and used in the calculation engine allowing dynamic input for dynamic EPCs.

Life cycle assessment. LCA indicators such as "energy savings", expressed in "embodied energy/m^2" and "carbon reductions", expressed in "carbon dioxide equivalent/m^2", will be included in the dynamic EPCs calculation engine. This will provide to the building design team the option to improve and optimize the environmental performance of the building, based on changes to be integrated at the initial design stages of the building.

In the D^2EPC project, the LCA Indicators for EPCs will allow maximizing energy saving and carbon reduction of the buildings, introducing this way the aspect of building's sustainability as part of the EPC issuance process. This could speed up the transaction into NZEBs as well as control the building's energy demand, reduce carbon emissions, and enhance public awareness.

The D^2EPC project will propose additional indicators, which will demonstrate the environmental performance of buildings, for their introduction in the next-generation EPCs.

4.2 The Introduction of BIM and Digital Twin Concepts for the Next-Generation EPCs

The use of BIM technology helps to improve the collaboration of stakeholders from the design to asset maintenance phases. Benefits can be obtained in various design and construction stages such as

clash detection, scheduling, simulations during building design, as well as quality control and validation, safety management, logistic solutions during building construction and maintenance phases. While BIM delivers static data, Digital Twin (DT) focuses on linking physical objects to their respective digital replicas using periodically updated (dynamic) data flow. The key features of DT are sensing and monitoring, data linkage, Internet of Things (IoT) implementation, simulation, predictions, and controls.

As prediction and control features are concerned, the integration of the physical asset monitoring systems with the DT becomes a prerequisite feature. The rest part of the DT consist of geometrical representation of the physical objects and "attached" alphanumerical information related to various types of properties, features and attributes. A sufficient and mature BIM model can be employed as an efficient information repository. The BIM model can deliver semantically rich object-based information related to the asset and the processes involved in the asset or its part.

As far as DT is concerned for the employment in the Operation and Maintenance (O&M) management [16], the main aspects and features of DT can be linked and employed for the improvement of the EPC and its issuing procedures. Since DT enables the connection of sensing and actuating tools with the digital representation of the physical asset during the O&M phase, it can be employed for the asset and operational rating evaluation procedures. In the following are presented three use cases for the employment of DT at the EPC procedures:

1) Use of the DT to predict, visualize, and inform end-user of its behavior impact for energy consumption of the building and predict users' actions impact for EPC.

2) Employment of transformative DT to achieve and sustain the building's highest available energy efficiency class. At this point, DT's ability to take control of building appliances plays a significant role in eliminating user faults regarding energy savings. It can be utilized from the most straightforward actions such as switching off the lights to HVAC and other systems adaptation to users' behavior.

3) DT can be adopted to monitor appliances' performance and inform the user and stakeholders about inefficient or deteriorated devices and their impact on energy uses. This feature can be utilized as well for highlighting and/or disarming inefficient appliances.

Fig. 1 represents the definition of BIM and DT concept regarding the energy efficiency of the building throughout its life cycle stages: plan and design > produce and construct > use and maintain. "Asset", "Analysis/change", and "Digital data" layers in the figure represent different types of approach.

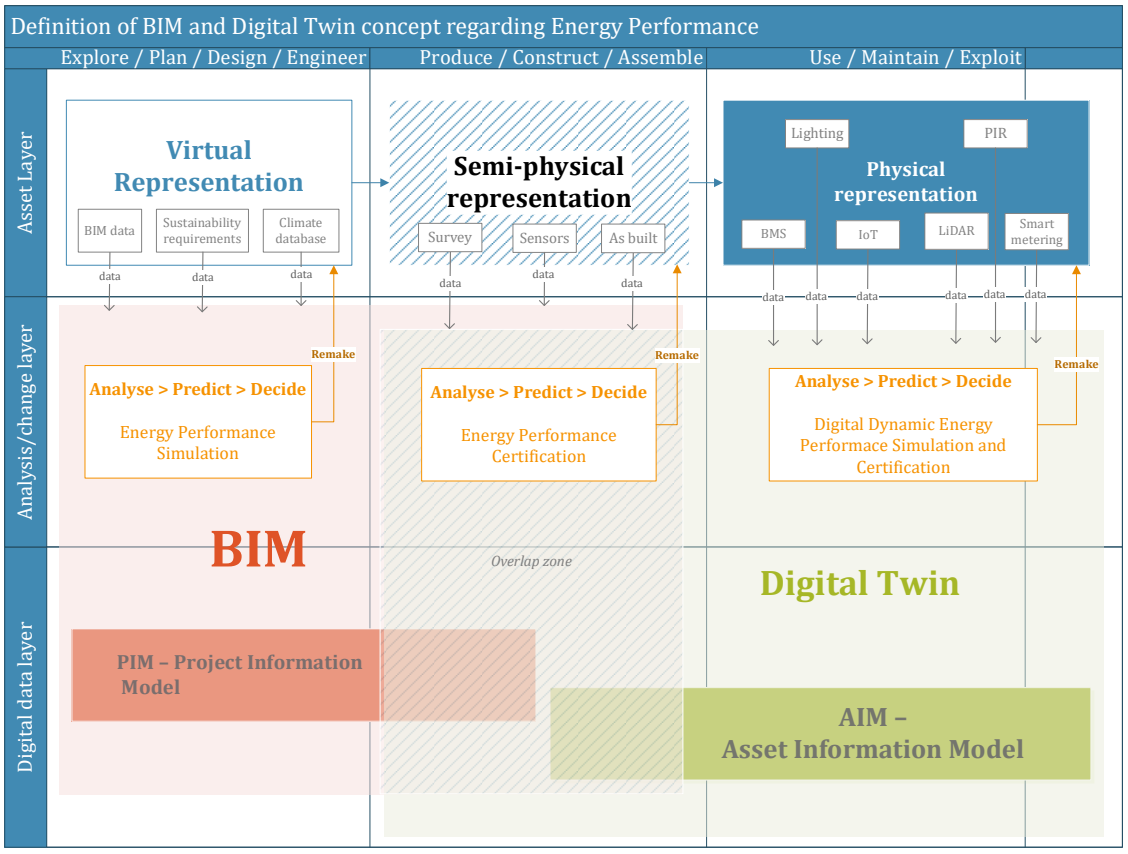

Fig. 1. Definition of BIM and DT concept regarding energy performance

Considering the "Asset layer", it delivers information on the virtual, semi-physical, and physical development of assets, including stored information such as requirements, BIM model, sensors, BMS, and other related data and documentation.

While the "Asset layer" is responsible for data storage and collection representation, the "Analysis/change layer" plays a significant role in optimizing energy efficiency-related actions throughout all asset life cycle stages. The "Analysis/change layer" presents a common logic of utilizing digital data received from the "Asset layer" for the energy efficiency analysis required for asset design. It can also be employed during construction and maintenance phases to achieve the best possible energy efficiency decision considering physical and operational data.

The bottom layer represents the main constituents of the BIM model according to the group of information management standards [17]. The first part is for defining concepts and principles, while the second is focused on the information delivery phase of the asset. Part 3 is based on information management during the operational phase. It is stated in the standards that a project information model (PIM) is an information model relating to the delivery phase of an asset, and an asset information model (AIM) is an information model relating to the operation of an asset. It is evident that BIM and DT overlap in the construction phase since BIM can deliver object-based data utilized for the DT.

4.3 Introduction of GIS in EPC

In the D^2EPC project and GIS context buildings are described and considered in the concept of BuildingsExtended3D, i. e. with correct geometric dimensions, proportions, scale, but not considering geolocation of a particular building. These 3D designs depict the correct building proportions and scale, but the correct geolocation is yet to be defined. To this end, several methods of geolocation can be applied, depending on the existence and availability of data: If the building under study is already correctly geo-referenced (projection information can be obtained from cadastral information and/or other spatial databases), a simple projection procedure should be applied.

In the case of not geo-referenced EPCs for buildings or lack of information, two data acquisition methods can be applied. The first is geolocating the building/parcel using a GPS/GNSS procedure to provide the best and most reliable accuracy results. The other approach is addressing geocoding method used to collect appropriate geolocation data.

In parallel with the geo-referencing procedure, it is also essential to determine the unique geographical location of each building. By adopting a common reference coordinate system for all the under-study regions/cases, a unique code can be created in many possible ways, using the coordinates of each plot of land. A simplified way to create a unique geocode for the case studies is to convert a polygon shape feature into a centroid point and extract 2D coordinates from this centroid point.

The definition of the Z - height value of a unit (building, apartment, etc.) - is as important an EPC element as the aforementioned geolocation features. Same as for geolocation, the different data acquisition scenarios may be applied: a) Floor/height information is available in official registries, spatial governmental agencies. b) If there is no known recorded and registered data, there are few options for data acquisition. The first is to use GPS/GNSS measurements taken on-site, which will give an accurate altitude. Another approach is the application of a widely agreed assumption that the height of one floor equals 3 meters; in this scenario, it is possible to identify the floor number in each building (floor = building's height / 3).

The use of geospatial technologies and accurate data location could improve the processes related to the data needed to assess the energy performance and needs of buildings and urban areas. In addition, the use of geolocation practices can increase decision-making effectiveness by different stakeholders (policymakers, technicians, citizens). Online and web-based tools that can provide near real-time data on the actual energy performance of buildings at the building or regional level could provide public authorities, governments and energy service companies with crucial regional insights. A unified scheme for monitoring and evaluating energy efficiency policies and practices, using a standard set of spatial data (dwellings, buildings, neighborhoods), could improve the synergies between existing energy initiatives and the adoption of new initiatives.

4.4 Introduction of financial schemes

Introducing financial schemes in EPC is suggested in this study. Based on the well-established principle of lifecycle costing, a set of financial indicators could be developed to allow the individual elements of buildings' energy efficiency to be interpreted into standardized numerical values. The delivery of such indicators could allow the use of EPCs for the financial evaluation of energy upgrading measures for buildings. For example, financial awards (e.g. tax reliefs) should be included if the building owner exceeds new EPC requirements and class. In the opposite case – penalties should imposed based on the "polluter pays" principle.

5. D^2EPC System Architecture

A novel methodology for dynamic EPC is being developed within the H2020 D^2EPC project, which introduces the aspects of SRI, occupant comfort, LCA, integration with DT, and GIS systems. Key functionalities of D^2EPC architecture are presented in Fig. 2.

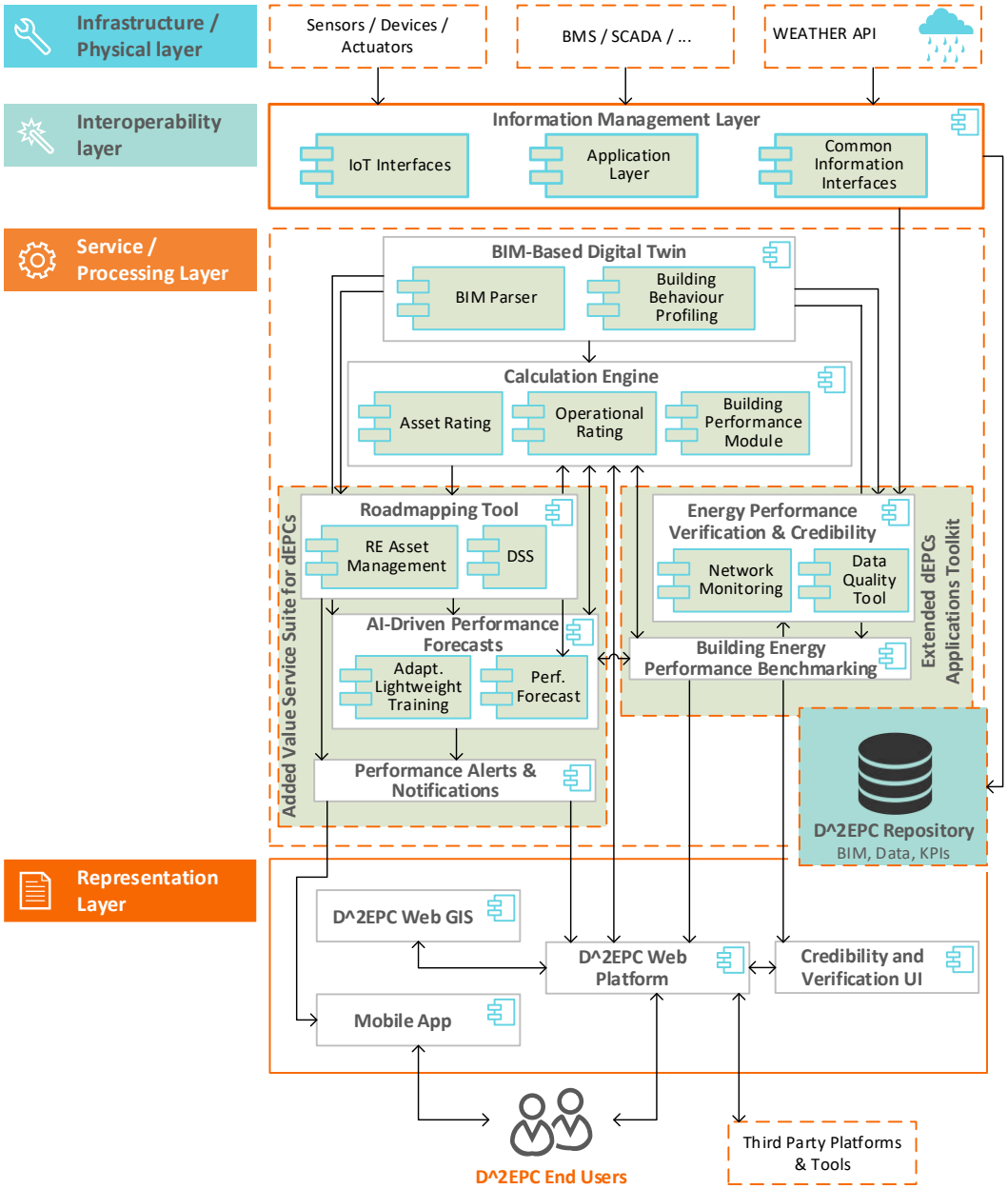

Fig. 2. D^2EPC System Architecture [18]

D^2EPC framework consists of four layers:

- Infrastructure/Physical Layer,
- Interoperability Layer,
- Service/Processing Layer, and
- Representation Layer [18].

Infrastructure/Physical Layer. All devices, sensors, actuators, and systems are included in this layer, including BMS (Building Management Systems) and SCADA (Supervisory Control and Data Acquisition), enabling dynamic EPCs. Weather data can be fed on-site or through external weather APIs from the weather stations.

Interoperability Layer. This layer is responsible both for the managementt of the received information from the Infrastructure/Physical Layer and the interoperability of the various interconnected devices. It retrieves the necessary information and streams it into the D^2EPC repository in the proper data format. As current IoT solutions, either available on-site or installed, are quite diverse in terms of communication protocols, data acquisition, etc., interoperability is considered one of the most cumbersome challenges when deploying and integrating a digital solution for dynamic EPCs [18]. D^2EPC will employ IFC4 standard to ensure data interoperability".

Service/Processing Layer. Processing and decision-making functionalities are included in this layer of D^2EPC architecture. State-of-the-art methodologies allow the evaluation of incoming data's quality and credibility, the mapping of static and dynamic

building (near) real-time information, as well as the calculation of a wide variety of metrics and indicators. Furthermore, recommendations for cost-effective building upgrades and benchmarking are also introduced here. This layer employs the BIM-based Digital Twin concept, which means operational data are collected, represented, and used for analytics, and in turn, the assessment process is automatic.

One of the main components of the D^2EPC architecture is the Calculation Engine. It consists of three modules which deal with the Asset and Operational Rating schemes, while the third sub-module is related with the calculation of certain KPIs related to the overall performance of a building. A variety of indicators are calculated relevant smart readiness, comfort and wellbeing, financial and life cycle assessment aspects, to enrich the EPC procedure.

The Roadmapping Tool for performance upgrade will enable novel decision support algorithms for strategic scenarios generation, enabling user-centered suggestions on building performance and upgrades.

The module AI Driven Performance Forecasts utilizes artificial intelligence algorithms to train dedicated models. These models will be used for forecasting the future energy performance of the building taking into account the both the data streams as received from the building, as well as outside parameters that affect the building's energy performance. A lightweight approach will be employed to reduce the need for the processing power and the actual forecasting should only be used when needed.

The actual performance of the building is monitored through the Performance Alerts & Notifications component, which will also enable the occupants to personalize their indoor environment settings.

An automatic and continuous verification process will be enabled with the Energy Performance and Credibility component, which analyses the IoT data streams and performs a constant check on sensor's health and data quality.

The classification and comparison of the particular building data with reference to certain metrics will be carried out through the Building Energy Performance Benchmarking component, which is linked to the Roadmapping tool for increasing the building performance.

Representation Layer. The representation layer enables the D^2EPC platform interaction with the end-users and third-party platforms. The Web Platform will enable the representation of different KPIs and provide dashboards and analytics results, while the Web-GIS module will provide geospatial information using maps and 3D models.

6. Conclusions

The following new indicators are suggested to be included in the dynamic EPC: SRI, human comfort-related indicators, LCA, and financial schemes.

By integrating BIM into the EPC scheme, it is possible to obtain object-based information related to a particular asset (e. g. class, related properties and processes, aggregation, etc.). A semantically rich BIM model can be considered the basis for a digital twin, which can be used for energy performance modelling from the design to the maintenance phases of the asset. Complemented by sensors/BMS/IoT and other data, the DT can visualize and inform the users about the impact of their behavior on EPC. As DT can take management action to eliminate user culpability, it can be used to achieve the highest possible energy performance class for a building. In addition, the sensing and monitoring functions of DT can be used to prevent inefficient energy impacts of the appliance through smart assets or the IoT.

Correctly locating the geographic location of the dynamic EPC will provide a better understanding of the energy performance status of each dwelling/building over a given monitoring period. In addition, the EPC can be tailored to spatially and visually relate the exact location of the building to other relevant climatic factors (climate change indicators, the greenness of the neighborhood, incoming sunlight, etc.). At the same time, it will help to explore innovative geolocation practices to overcome the lack of existing cadastral data.

New technologies that didn't existed at the time when the current EPCs schemes were developed, enable new approaches towards building energy certification. D^2EPC platform aims to integrate IoT, AI, and other novel technologies to enhance end-user awareness and facilitate a more sustainable life cycle of buildings. Nevertheless, integrating these technologies into a coherent unified tool is still a challenging task. D^2EPC aims to provide a demonstrator platform that will help increase the understanding of European building stock's EPCs.

7. Acknowledgement

This work is part of the D^2EPC project that has received funding from the European Union's Horizon 2020 research and innovation program under grant agreement No. 892984.

8. References

[1] Mattaraia, L.; Fabricio, M.M.; Codinhoto, R. Structure for the Classification of Disassembly Applied to BIM Models. 2021, doi:10.1080/17452007.2021.1956420.

[2] Pupeikis, D.; Daukšys, M.; Navickas, A.A.; Morkūnaitė, L.; Abromas, S. Possibilities of Using Building Information Model Data in

Reinforcement Processing Plant. Journal of Sustainable Architecture and Civil Engineering 2021, 28, 80–93, doi:10.5755/J01.SACE.28.1.27593.

[3] Munir, M.; Kiviniemi, A.; Jones, S.; Finnegan, S. BIM-Based Operational Information Requirements for Asset Owners. Architectural Engineering and Design Management 2020, 16, 100–114, doi:10.1080/17452007.2019.1706439/SUPPL_FILE/TAEM_A_1706439_SM9537.DOCX.

[4] Theißen, S.; Höper, J.; Drzymalla, J.; Wimmer, R.; Markova, S.; Meins-Becker, A.; Lambertz, M. Using Open BIM and IFC to Enable a Comprehensive Consideration of Building Services within a Whole-Building LCA. Sustainability 2020, Vol. 12, Page 5644 2020, 12, 5644, doi:10.3390/SU12145644.

[5] Heaton, J.; Parlikad, A.K.; Schooling, J. Design and Development of BIM Models to Support Operations and Maintenance. Computers in Industry 2019, 111, 172–186, doi:10.1016/J.COMPIND.2019.08.001.

[6] "BPIE of the European Parliament and of the Council of 30 May 2018 on the energy performance of buildings (recast)".

[7] P. Fokaides, C. Panteli and A. Panayidou, "How Are the Smart Readiness Indicators Expected to Affect the Energy Performance of Buildings: First Evidence and Perspectives," Sustainability, p. 9485, 2020.

[8] U.S. Environmental Protection Agency. 1989. Report to Congress on indoor air quality: Volume 2. EPA/400/1-9/001C. Washington, DC.

[9] U.S. Environmental Protection Agency. 1987. The total exposure assessment methodology (TEAM) study: Summary and analysis. EPA/600/6-87/002a. Washington, DC.

[10] ASHRAE, "Indoor Air Quality Guide Best Practices for Design, Construction, and Commissioning, Guide", 2012.

[11] ASRHAE, "Position paper on IEQ", 2015.

[12] American Society on Heating, Refrigeration and Air-Conditioning Engineers, "Standard 55. (2004) Thermal Environmental Conditions for Human Occupancy", 2004.

[13] U.S. Green Building Council, "LEED v4 for interior design and construction," 2014 .

[14] BREEAM UK , "new construction – Non-domestic buildings Technical manual," 2014 .

[15] I. W. B. I. pbc., "THE WELL BUILDING STANDARD," 2020.

[16] Lu, Q., Xie, X., Parlikad, A.K., Schooling, J.M. and Konstantinou, E., (2020). Moving from building information models to digital twins for operation and maintenance. Proceedings of the Institution of Civil Engineers – Smart Infrastructure and Construction.

[17] EN ISO 19650 Organization of information about construction works —Information management using building information modelling.

[18] Koltsios S., Tsolakis A.C., Fokaides P.A., Katsifaraki A., Cebrat G., Jurelionis A., Contopoulos C., Chatzipanagiotidou P., Malavazos C., Ioannidis D., Tzovaras D. D^2EPC: Next Generation Digital and Dynamic Energy Performance Certificates. 6th International Conference on Smart and Sustainable Technologies, Bol and Split, Croatia, 2021.

Data Statement

Data sharing not applicable to this article as no datasets were generated or analysed during the current study.

Optimal design and operation for heat prosumer-based district heating systems

Haoran Li [a], Juan Hou [a], Natasa Nord [a]

[a] Department of Energy and Process Technology, Norwegian University of Science and Technology, Kolbjørn Hejes vei 1 B, Trondheim 7491, Norway.

Abstract. Heat prosumers will become important participants for future district heating (DH) systems. However, the current unidirectional heating price models reduce interest in prosumers and hinder the promotion of prosumers in DH systems, because the prosumers gain no economic benefit from supplying heat to the central DH system. This study aimed to break this economic barrier by introducing water tank thermal energy storage (WTTES) and optimizing the operation of heat prosumers with WTTESs, considering the widely used heating price models in Norway. Firstly, a generalized heating price model was introduced, which could represent the current widely used heating price models in Norway. Secondly, the WTTES was integrated into the heat prosumer to improve the self-utilization rate of the prosumer's heat supply from its distributed heat sources, meanwhile, shave the prosumer's peak load. Afterwards, an optimization framework was formulated to optimize the operation of the prosumer with the WTTES under the generalized heating price model. Finally, a numerical method for solving the proposed nonlinear optimization problem was given. A case study showed that the proposed method could cut the prosumer's annual heating cost by 7%, and the investment of WTTES could be recovered in four years.

Keywords. nonlinear optimization, thermal energy storage, heating price, distributed heat sources.
DOI: https://doi.org/10.34641/clima.2022.347

1. Introduction

The widely used heating price models in Norway charge a heat prosumer's heating bill mainly based on heat prosumer's heat use and peak load [1]. Accordingly, two potential ways to minimize a heat prosumer' heating cost in a district heating (DH) system are: 1) decreasing the heat supply from the central DH system by increasing the heat supply from prosumer's distributed heat sources (DHSs), which are free and may come from renewables and waste heat, and 2) shaving the peak load by shifting the heat supply from peak hours to non-peak hours.

Thermal energy storages (TESs) may be used to achieve the above two goals. Firstly, TESs can increase the self-utilization rate of the heat supply from DHSs, because for the periods when the heat supply from the DHSs is higher than the demand of the prosumer, the surplus heat can be stored into the TESs and used for later heat supply instead of being fed into the central DH system [2, 3]. Secondly, TESs can shave the prosumer's peak load, because the peak demand can be satisfied by the stored heat from the non-peak hours [4, 5]. However, TESs are investment intensive. The high investment costs and the long payback periods are hindering the implementation of TESs in DH systems.

This study proposed a comprehensive method for optimal design and operation of prosumer-based DH systems with short-term TESs. The method was based on the heating price models in Norway but can also give references for DH systems outside Norway.

2. Method

This section explains the proposed method. Firstly, a generalized heating price model is introduced, which may represent the current widely used heating price models in Norway. Secondly, WTTES is integrated into the heat prosumer-based DH system to improve the self-utilization of the heat supply from the DHSs and shave the peak load. Afterwards, an optimization framework is formulated to optimize the operation of the proposed DH system under the generalized heating price model. Finally, a numerical method for solving the proposed nonlinear optimization problem is given.

Copyright ©2022 by the authors. This conference paper is published under a CC-BY-4.0 license.

2.1 The method to obtain a generalized heating price model

Although heating price models may vary in Norway, this study introduced a generalized heating price model, which could approximate and generalize the widely used heating price models. According to the review article [1], a heating price model may include four components: energy demand component (EDC), load demand component (LDC), fixed component (FXC), and flow demand component (FDC). The EDC is charged based on the heat use, and it is used to cover the fuel cost. The LDC is charged according to the peak load, and it aims to maintain a certain capacity of heat production. The FXC is the fee for connecting to the central heating grid. The FDC motivates the low return temperature, and it is charged based on the volume of the circulating water.

Fig. 1 gives the existence and the average share of each component for investigated heating price models in Sweden. Firstly, it can be found from Fig. 1 that, the LDC and the EDC are the most important components, which together share 96% of the total heating cost. Moreover, 87% of the investigated heating price models have the LDC and all the heating price models have the EDC. In contrast, the FXC and FDC play limited roles in the investigated heating price models, which only share less than 2% of the total heating cost. Furthermore, only about half of the investigated heating price models have the FXC and FDC.

Based on the above situations, a generalized heating price model used to approximate a prosumer's heating cost was introduced as Equation (1), in which the total heating cost includes the LDC and the EDC.

$$C_{tot} = C_{ldc} + C_{edc} \tag{1}$$

where C_{tot} refers to the total heating cost, C_{ldc} and C_{edc} are the LDC and the EDC, respectively, which can be obtained by Equation (3) and Equation (4).

$$C_{ldc} = LP \cdot \dot{Q}_{pea} \tag{2}$$

$$C_{edc} = \int_{t_0}^{t_f} EP(t) \cdot \dot{Q}(t) dt \tag{3}$$

where LP and $EP(t)$ are the LDC heating price and EDC heating price, respectively. $\dot{Q}_{pea}$ refers to the yearly peak load [6, 7] and $\dot{Q}(t)$ is the heat supply flow rate.

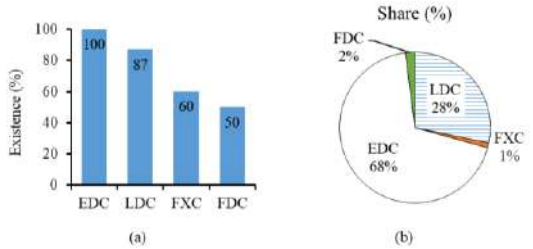

Fig. 1. The existence (a) and average share (b) of each component in investigated heating price models [1]

2.2 System design for heat prosumer-based DH system with TES

As introduced in Section 2.1, to minimize the heating cost of a heat user, it is required to decrease the LDC and the EDC heating cost, which are related to the peak load and the heat use, respectively. Moreover, as explained in Section 1, TESs may be used to achieve the above goals. Fig. 2 illustrates the proposed system for a heat prosumer-based DH system, which integrates a TES. In Fig. 2, DHS was a low-temperature heat source utilizing free heat from renewables or waste heat. DHS was integrated into the prosumer's local DH system using the R2R mode, in which DHS extracted water flow from the return line and fed it back into the return line after the heating process. The R2R mode was used because it is preferable for a low-temperature heat source [8].

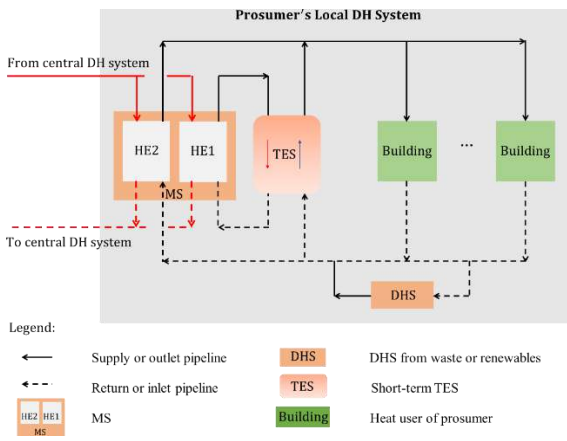

Fig. 2. System design for a heat prosumer's local DH system with TES

Moreover, MS in Fig. 2 referred to the main substation, which connected the central DH system with the prosumer's local DH system. Two types of heat exchanger (HE) were installed in the MS. HE1 was used for charging the TES. For the period with low heat demand, HE1 supplied heat to the local DH system through TES when the heat supply from the DHS was not enough. For the period with high heat demand, HE1 was used for peak load shaving by charging heat at non-peak hours. HE2 in the MS functioned as a high-temperature heat source, it boosted the supply temperature of the local DH system to the required level when the water temperature after the DHS was not high enough.

In addition, the TES was a short-term TES. As introduced in Section 1, the TES functioned in two ways to minimize the prosumer's heating cost. Firstly, it improved the self-utilization rate of heat supply from the DHS. For the period with low heat demand, the DHS from renewables and waste heat may have a higher heat supply than the demand, and the surplus heat supply would be stored in the TES and for later use instead of being supplied to the central DH system. Secondly, the TES may shave the prosumer's peak supply from the central DH system. For the periods around the peak periods, the central DH system may charge the TES at non-peak hours and the stored heat may shave the heat supply at the peak hours.

Fig. 2 gives an example of a community heat prosumer, which has a cluster of buildings as the heat users. However, for the cases of individual heat prosumers, the heat user is a single building.

2.3 Optimization framework for the operation of heat prosumer-based DH system

An optimization framework for the operation of a heat prosumer-based DH system is proposed in this section. The framework was based on the system design presented in Section 2.2, considering the generalized heating price model introduced in Section 2.1. The mathematical formulation of this framework is presented in Equations (4), (5), (6), (7), and (8). Equation (4) is the objective function, in which the first part is the EDC heating cost, and the second part is the LDC heating cost. Equation (5) represents the effort to shave the peak load, Equation (6) describes the system dynamics and Equation (7) defines the initial states of the system. Equation (8) is the system constants.

Minimize:

$$\int_{t_0}^{t_f} EP(t) \cdot \dot{Q}(t)dt + LP \cdot \dot{Q}_{pea} \tag{4}$$

subject to:

$$\dot{Q}(t) \leq \dot{Q}_{pea} \tag{5}$$

$$F(t, \boldsymbol{z}(t)) = 0 \tag{6}$$

$$F_0(t_0, \boldsymbol{z}(t_0)) = 0 \tag{7}$$

$$z_L \leq \boldsymbol{z}(t) \leq z_U \tag{8}$$

where $\dot{Q}(t)$ is heat supply flow rate from the central DH system. $\dot{Q}_{pea}$ is the peak load, which is a parameter to be minimized. LP and $EP(t)$ are the heating price for the LDC and the EDC, respectively. $\boldsymbol{z} \in \mathbb{R}^{n_z}$ are the time-dependent variables, including the manipulated variable $\boldsymbol{u} \in \mathbb{R}^{n_u}$, the differential variable $\boldsymbol{x} \in \mathbb{R}^{n_x}$, and the algebraic variable $\boldsymbol{y} \in \mathbb{R}^{n_y}$. $z_L \in [-\infty, \infty]^{n_z}$ and $z_U \in [-\infty, \infty]^{n_z}$ are the lower bounds and upper bounds, respectively. The system dynamics described in Equation (6) contained the dynamics of the MS, DHS, TES, distribution network, and buildings. The interactions between these subsystems were defined in Equations (9), (10), (11), (12), and (13).

$$\dot{Q}(t) = \dot{Q}_{HE1} + \dot{Q}_{HE2} \tag{9}$$

$$\dot{Q}_{HE1} + \dot{Q}_{HE2} + \dot{Q}_{DHS} = \dot{Q}_{Bui} + \dot{Q}_{TES} + \dot{Q}_{loss,TES} + \dot{Q}_{loss,pip} \tag{10}$$

$$\dot{Q}_{HE1} = c \cdot \dot{m}_{HE1} \cdot (T_{HE1,sup} - T_{HE1,ret}) \tag{11}$$

$$\dot{Q}_{HE2} = c \cdot \dot{m}_{HE2} \cdot (T_{HE2,sup} - T_{HE2,ret}) \tag{12}$$

$$\dot{Q}_{DHS} = c \cdot \dot{m}_{DHS} \cdot (T_{DHS,sup} - T_{DHS,ret}) \tag{13}$$

where $\dot{m}_{DHS}$, $\dot{m}_{HE1}$, and $\dot{m}_{HE2}$ refer to the water mass flow rate of DHS, HE1, and HE2, respectively. $\dot{Q}_{DHS}$, $\dot{Q}_{HE1}$, and $\dot{Q}_{HE2}$ represent the heat supply flow rate of the DHS, HE1, and HE2, respectively. $\dot{Q}_{TES}$ is the heat flow rate of the TES for discharging (negative values) and charging (positive values). $\dot{Q}_{Bui}$ represents the building heat demand. $\dot{Q}_{loss,pip}$ and $\dot{Q}_{loss,TES}$ refer to the heat loss flow rate from the pipeline and the TES, respectively. $T_{DHS,sup}$, $T_{HE1,sup}$, and $T_{HE2,sup}$ represent the supply temperature of DHS, HE1, and HE2, respectively. $T_{DHS,ret}$, $T_{HE1,ret}$, and $T_{HE2,ret}$ refer to the return temperature of DHS, HE1, and HE2, respectively. c is the specific heat capacity of water.

The manipulated variables $\boldsymbol{u}$ in this study were $T_{HE1,sup}$, $T_{HE2,sup}$, $\dot{m}_{HE1}$, $\dot{m}_{HE2}$, and $\dot{m}_{Bui}$.

This article focuses on the introduction of the optimization framework, the detailed information on the sub-system models is given in the journal articles [9] and [10].

2.4 Algorithm to solve the optimization problem

Section 2.3 defines a dynamic optimization problem, which is challenging to solve because of the nonlinearity of the dynamic model. This study used the direct collocation method [11] to transform the original infinite-dimensional nonlinear programming (NLP) problem into a finite-dimensional NLP, which could be solved by NLP solvers.

Fig. 3 illustrates the direct collocation method. A time grid from t_0 to t_N was created over the optimization horizon by dividing the horizon into N internals with a constant interval. Afterwards, the state variables $x(t)$ were discretized on each time

grid, and thus the state points from s_0 to s_N were obtained. The manipulated variables $u(t)$ were parameterized at each time grid, and thus on each interval $[t_k, t_{k+1}]$, a constant control signal q_k was yielded. Moreover, for each collocation interval $[t_k, t_{k+1}]$, a set of collocation points were generated from $t_{k,1}$ to $t_{k,d}$, and then a polynomial $p_k(t,\ v_k)$ was used to approximate the trajectory of the state within the interval. Therefore, Equation (6) was discretized into Equation (14) in the time interval $[t_k, t_{k+1}]$.

$$c_k(v_k, s_k, q_k) = \begin{bmatrix} v_{k,0} - s_k \\ F(\dot{p}_k(t_{k,1}, v_k), v_{k,1}, t_{k,1}, q_k) \\ \vdots \\ F(\dot{p}_k(t_{k,i}, v_k), v_{k,i}, t_{k,i}, q_k) \\ \vdots \\ F(\dot{p}_k(t_{k,d}, v_k), v_{k,d}, t_{k,d}, q_k) \end{bmatrix} = 0 \tag{14}$$

Besides, continuity conditions should be satisfied at the time grid points $k = 0,1,\cdots N-1$, i.e., the lengths of the red lines in Fig. 3 should be zero. Therefore, Equation (15) was added for these points.

$$p_k(t_{k+1}, v_k) - s_{k+1} = 0 \tag{15}$$

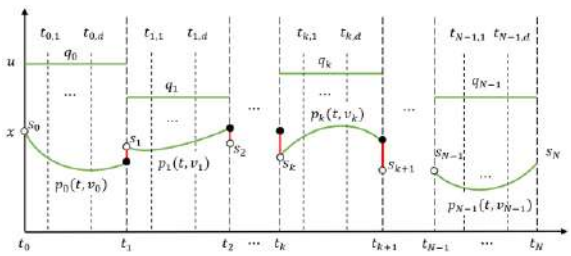

Fig. 3. Illustration of the direct collocation method

Finally, an NLP was yielded and it can be described in the following general form as Equations (16), (17), (18), (19), and (20).

Minimize:

$$\sum_{k=0}^{N-1} L_k(v_k, s_k, q_k) \cdot (t_{k+1} - t_k) + P \tag{16}$$

subject to:

$$x(0) = s_0 \tag{17}$$

$$c_k(v_k, s_k, q_k) = 0 \tag{18}$$

$$p_k(t_{k+1}, v_k) - s_{k+1} = 0 \tag{19}$$

$$h(s_k, v_k) \leq 0 \tag{20}$$

where $k = 0,1,\cdots N-1$. Equation (16) is the discretized form of Equation (4). In Equation (16), the first term approximates the integration term of Equation (4), and the second term represents the parameter to be minimized in Equation (4). Equation (17) represents the initial conditions described in Equation (6), Equations (18) and (19) discretize the system dynamics in Equation (6), and Equation (20) is the discretized constraints in Equation (8).

The NLP was solved by NLP solvers. Firstly, the inequality constraints were got rid of using the interior-point method, and then a local optimum was obtained via solving the first order Karush-Kuhn-Tucker condition using iterative techniques based on Newton's method. The optimization process was conducted using the open-source platform JModelica.org [12].

3. Case study

A DH system at a university campus in Norway was used as the case study, as presented in Fig. 4. The studied DH system was a prosumer, which got heat supply from the central DH system via the MS, meanwhile, recovered the waste heat from the university DC [2, 3].

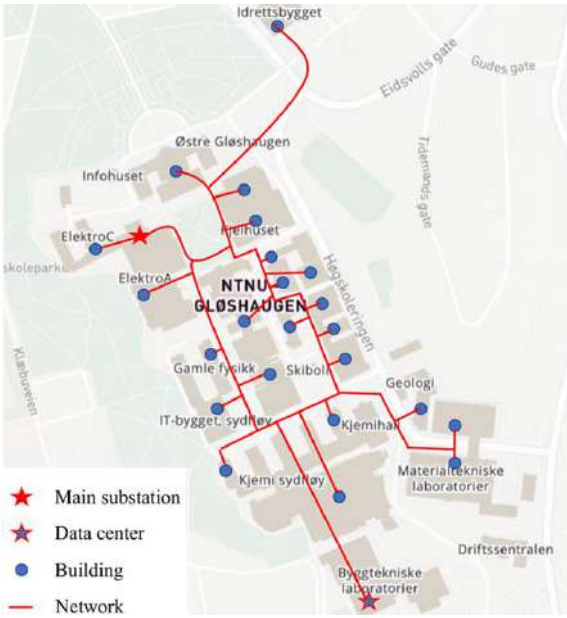

Fig. 4. DH system at the university campus [2, 3]

Fig. 5 presents the measured building heat demand and waste heat supply. The following problems can be observed 1) the mismatch between the waste heat supply from the DC and the building heat demand, which led to the surplus waste heat supply as shown with the red line in Fig. 5 and reduced the self-utilization rate of the heat supply from DHSs. 2) the high peak load during the wintertime as shown with the yellow line in Fig. 5.

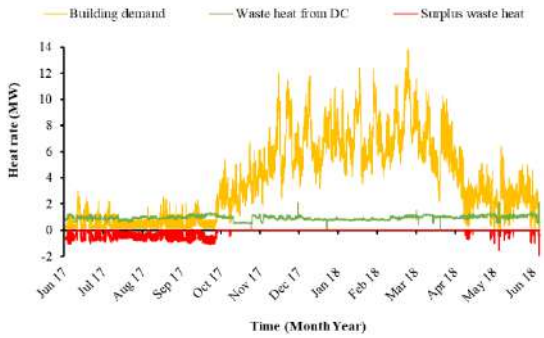

Fig. 5. Measured building heat demand, waste heat supply from the DC, and surplus waste heat

This study introduced a WTTES into the university DH system as proposed in the system design in Section 2.2 and used the optimal operation strategy proposed in Section 2.3 to optimize the economic performance of the studied DH system. The size of the WTTES was 1,700 m^3 and the heating price was obtained from the website of the local DH company [13].

4. Results

This section presents the simulation results, which demonstrate the improved economic performances of the heat prosumer by applying the proposed method. The scenario Ref and WTTES refer to the situation before and after introducing WTTES, respectively.

Fig. 6 and Fig. 7 present the annual heat use and the yearly peak load for the scenario before and after introducing WTTES, respectively. These two indicators quantified the heat supply from the central DH system to the heat prosumer through the MS. It can be observed from Fig. 6 that introducing WTTES reduced the annual heat use from 26.2 GWh to 25.9 GWh, meaning a heat use saving of 1%. Compared to this less significant heat use saving, a more obvious peak load shaving was obtained as shown in Fig. 7, the yearly peak load was shaved from 12.4 MW to 9.5 MW, a shaving of 24%.

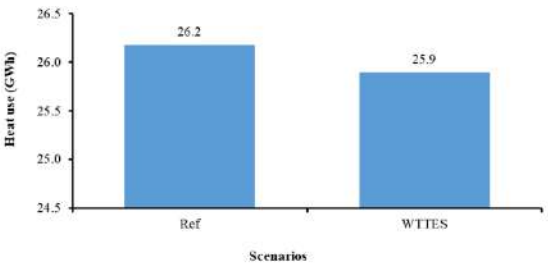

Fig. 6. Annual heat use for the scenario before and after introducing WTTES

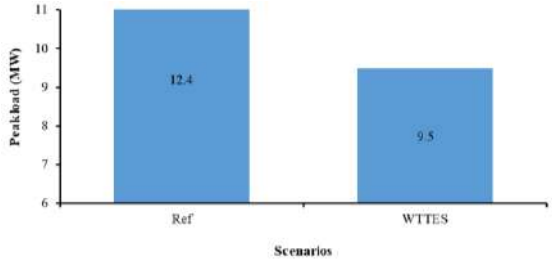

Fig. 7. Yearly peak load for the scenario before and after introducing WTTES

The resulting annual heating cost for the scenario before and after introducing WTTES is presented in Fig. 8. The proposed method cut the annual heating cost from 20.7 million NOK to 19.3 million NOK, which meant a cost saving of 7% was achieved. Moreover, this cost-saving could recover the investment of the WTTES in four years. These economic performances proved that the proposed system design and the operation strategy were economically feasible.

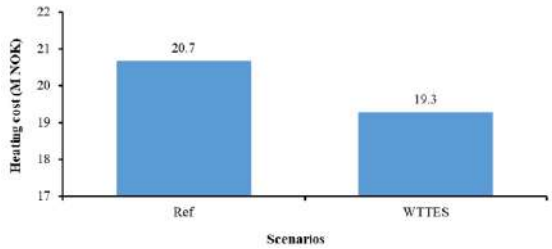

Fig. 8. Annual heating cost for the scenario before and after introducing WTTES

5. Conclusions

This study proposed a method to improve the economic performance of heat prosumers under the heating price models in Norway. The method included a type of system design, which integrated a WTTES into the heat prosumer-based DH system, and an operational strategy to minimize the heating cost considering the widely used heating price models in Norway. A case study showed that the proposed method was economically feasible. The method could cut the prosumer's annual heating cost by 7% and recover the investment of WTTES in four years.

6. References

[1] Song J, Wallin F, Li H. District heating cost fluctuation caused by price model shift. Applied Energy. 2017;194:715-24.
[2] Li H, Hou J, Nord N. Using thermal storages to solve the mismatch between waste heat feed-in and heat demand: a case study of a district heating system of a university campus. 2019.
[3] Li H, Hou J, Hong T, Ding Y, Nord N. Energy, economic, and environmental analysis of integration of thermal energy storage into district heating systems using waste heat from data centres. Energy. 2021;219:119582.

[4] Harris M. Thermal Energy Storage in Sweden and Denmark: Potentials for Technology Transfer. IIIEE Master thesis. 2011.
[5] Li H, Hou J, Ding Y, Nord N. Techno-economic analysis of implementing thermal storage for peak load shaving in a campus district heating system with waste heat from the data centre. vol. 246. EDP Sciences, p. 09003.
[6] Sernhed K, Gåverud H, Sandgren A. Customer perspectives on district heating price models. International Journal of Sustainable Energy Planning and Management. 2017;13:47-60.
[7] Song J, Wallin F, Li H, Karlsson B. Price Models of District Heating in Sweden. Energy Procedia. 2016;88:100-5.
[8] Li H, Nord N. Transition to the 4th generation district heating- possibilities, bottlenecks, and challenges. Energy Procedia. 2018;149:483-98.
[9] Li H, Hou J, Tian Z, Hong T, Nord N, Rohde D. Optimize heat prosumers' economic performance under current heating price models by using water tank thermal energy storage. Energy. 2022;239:122103.
[10] Li H, Hou J, Hong T, Nord N. Distinguish between the economic optimal and lowest distribution temperatures for heat-prosumer-based district heating systems with short-term thermal energy storage. Energy. 2022;248:123601.
[11] Amrit R, Rawlings JB, Biegler LT. Optimizing process economics online using model predictive control. Computers & Chemical Engineering. 2013;58:334-43.
[12] Åkesson J, Gäfvert M, Tummescheit H. Jmodelica- an open source platform for optimization of modelica models. Conference Jmodelica- an open source platform for optimization of modelica models.
[13] Charging method for heating bill in Trondheim, https://www.statkraftvarme.no/globalassets/2-statkraft-varme/statkraft-varme-norge/om-statkraft-varme/prisark/20190901/fjernvarmetariff-trondheim-bt1.pdf, accessed September 2020.

An aquifer thermal energy storage model for efficient simulations of district systems

Elisa Scalco [a,b], Angelo Zarrella [a], Alessandro Maccarini [b], Alireza Afshari [b]

[a] Department of Industrial Engineering, University of Padova, Padova, Italy, elisa.scalco.2@studenti.unipd.it, angelo.zarrella@unipd.it.

[b] Department of the Built Environment, Aalborg University, Copenhagen, Denmark, amac@build.aau.dk, aaf@build.aau.dk.

Abstract. Thermal energy storage systems are valuable assets to enable high penetration of renewable energy sources into district heating and cooling (DHC) systems. One of the main benefits of using thermal storage is that it can contribute to matching energy supply and energy demand when they do not coincide in time.

Aquifer thermal energy storage (ATES) is an attractive technology to provide sustainable heating and cooling to buildings through DHC systems. In ATES systems, storage and recovery of thermal energy is achieved by extraction and injection of groundwater using wells. To calculate the energy performance of ATES, most of the studies use detailed simulation models developed using computational fluid dynamics software. However, such programs have limited capability of simulating the integration of ATES into building and district energy systems.

The aim of this research study is to develop a simplified ATES model, which is suitable for coupling with building and district energy simulation programs. The model has been developed using a finite-difference approach in the MATLAB computing platform to solve the transient heat and mass transfer equations in porous media in two dimensions. The aquifer around the wells is modelled as two independent radially symmetric discs with an inner radius and an outer radius. The model has been validated by comparing predicted warm/cold well temperatures with measurements data from literature. Since the model is developed in MATLAB, it can be coupled with building energy software (such as TRNSYS, Modelica, EnergyPlus) via co-simulation.

Keywords. ATES system, building energy simulation, MATLAB, thermal storage, district heating, district cooling.
DOI: https://doi.org/10.34641/clima.2022.346

1. Introduction

According to literature, the building sector has become the largest source of greenhouse gas (GHG) emissions and it is responsible of 40% of global energy consumption and one-third of global GHG emissions [1]. When considering residential buildings, space heating and space cooling represent the two most energy demanding end-uses [2]. Therefore, research in the field of efficient building energy systems is crucial to reduce the global GHG emissions and mitigate the effects of the climate change.

A large body of the literature has attempted to identify the main factors affecting the building sector's carbon emissions and Gholipour et al. [3] concluded that the main drivers of buildings' CO_2 emissions and energy demand are income, energy price, and outdoor temperature, followed by population and heated floor area. Thermal energy is vital also for industry process that are usually very demanding, with most of the heat demand currently met through fossil-fuel based sources.

A more sustainable energy system requires the adoption of renewable energy, and in order to fill in the time gap between production and demand, thermal energy storage is a key solution. There are essentially four main groups: hot water thermal energy storage (HTES), gravel-water thermal energy storage (GWTES), borehole thermal energy storage (BTES) and aquifer thermal energy storage (ATES).

Copyright ©2022 by the authors. This conference paper is published under a CC-BY-4.0 license.

Thermal storage focuses on saving thermal energy that would otherwise be wasted. Guo et al. [4] studied a large-scale industrial waste heating system integrated with borehole thermal energy storage, running with temperatures above 200°C. Another example of underground large-scale thermal energy storage system was proposed by Zhou et al. [5] in China, whose energy demand has exceeded that of the United States [6] and where coal is still used with respiratory diseases reaching 30%. In this case it reveals that USTES (underground seasonal thermal energy storage) has significant economic, social and environmental benefits. However, large heat loss and low solar fraction are still common challenges for large-scale applications.

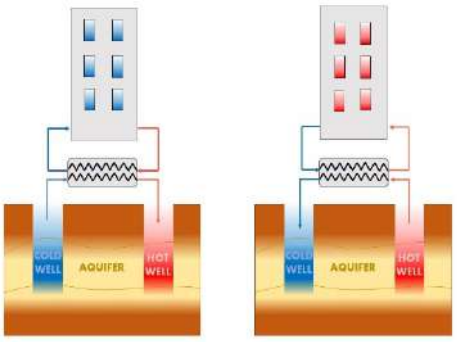

Fig. 1 – Cooling and heating configuration in ATES.

The low-grade waste heat is more suitable for district heating usage, due to its low exergy level. On a district level, ATES systems are a very promising technology when it comes to tackle heating and cooling energy demand. They enable up to 40% of energy savings [7], by providing sustainable space cooling and space heating for buildings through seasonal storage of heat in already existing aquifers, underground layers of water-bearing permeable rock mixed with other materials such as gravel and sand. ATES systems consist of at least two wells, a hot and cold one, used to either inject or withdrawal the groundwater. They usually work on a seasonal cycle. In winter, when heating mode is to be set, hot water is extracted from the hot well and is sent towards the internal heat exchanger of the building, that could be also provided with a heat pump to better adjust the temperatures needed by the users. The return cold water is sent towards the cold well to be stored for use in the following season when cooling mode will be needed. These systems though are not only meant for seasonal storage. As proved by De Schepper et al. [8] in the context of demand-side management and geothermal energy production also shorter frequencies of storage can provide good results.

As pointed out by Rostampour et al. [9] the spatial layout of ATES systems is a key aspect for the technology, as thermal interactions between neighbouring systems can degrade the performances. Considering this issue, current planning policies for ATES aim to avoid thermal interactions. However, under such policies, some urban areas already lack space for the further development of ATES, limiting achievable energy savings.

While these systems conventionally work on a range of 5-25°C and referred to as low temperature ATES, high temperature ones (HT-ATES) also exist and are gaining more and more attention by the research community thanks to their higher storage temperature, which can exceed 90°C. This enables the use of waste heat coming from a wider range of sources, such as CHP plants for example. With such temperatures, they could also provide energy for electricity generation baseload power. Organic Rankine cycle generators can use hot water between 80°C and 350°C, binary cycle geothermal power plants can exploit temperatures ranging from 70°C to 180°C, while flash steam power plants typically use hot water up to 300°C [10].

Unfortunately, when injecting warm/hot water there is a potential risk of minerals precipitation and also microorganisms' growth. The higher the operating temperature, more likely to be affected by this risk. HT-ATES therefore are usually located in deeper aquifers to reduce this environmental impact, meaning the requirement of deeper drilling and so higher overall costs.

The main benefit of a higher fluid temperature is a higher energy density, and therefore higher economic benefits. As stated by Huang et al. [11] operating at higher temperatures could eliminate the need for the heat pump that raises the temperature of the fluid before it enters district heating networks, thereby reducing investment costs. One must also take into account that when increasing the storage temperature, the number of waste heat sources in fact increases but the overall storage efficiency decreases as more heat will be lost to the surroundings [7].

Finally, ATES systems are widely recognized as a valuable solution for saving energy. Compared to traditional cooling/heating systems, about 90-95% of energy savings can be achieved when ATES are used directly. When coupled with heat pumps, they can lead to about 60-85% of energy savings [12]. By using the available subspace in cities, these systems can be optimally linked and integrated on a urban level. As presented in a case study in Finland, the integration of ATES systems with balanced pumping volumes in summer and winter with GWHP for DC and DH had a positive result in terms of system's efficiency, impact on the surrounding groundwater areas and techno-economic feasibility [13].

As in all systems, an evaluation of the thermal behaviour of an ATES system is fundamental to improve the application and quantify the benefits. Common ATES systems simulation models are for example MODFLOW or belong to the MT3D family [14]. They are finite-difference software that work on groundwater transport modelling and require groundwater flow equations solving. They mainly

focus on the aquifer itself, by working on its hydrogeologic characteristics and by the means of hydrologic boundaries. As anticipated in the abstract, the aim of this research study is to develop a simplified lumped-element model for ATES systems that is capable of being connected and could properly work with building energy simulation programs at district level. To reach this result, a series of simplifications and assumptions have been made in order to develop a model that is simple, yet flexible enough for the purposes just mentioned but without affect the quality of the results.

2. Model description

2.1 Overview

Both wells have been considered as two independent cylinders for which the height has been initially set (coinciding with the ATES thickness), together with the radius, beyond which an undisturbed ground temperature was considered. The first interest was studying the time and spatial variation of the temperature only on the radial direction, so an axial symmetry has been assumed, with the temperature kept constant along the depth of the aquifer, z direction in **Fig. 2**.

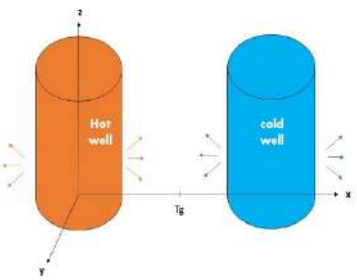

Fig. 2 – Hot and cold wells discretization.

As far as it concerns the methodology, the numerical model was developed in MATLAB and the starting point has been solving the transient heat and mass transfer equations in porous media in one dimension with a finite-difference approach.

2.2 Numerical model

A 1D discretization was considered to study how the temperature within the aquifer changes in the radial direction. To assess the behaviour of the aquifer, it was used a lumped-parameter system where for each node, representing a certain distance from the axis of the well, a thermal resistance and a thermal capacitance were assigned.

For the sake of simplicity, the following sections show the equations used in the model for a 3-node system.

2.3 1D model with heat conduction and heat advection

The following system consists of three active nodes, from *1* to *3*, and two boundary conditions in node *0* (representing the bore wall) and node g at T_g (representing the undisturbed ground).

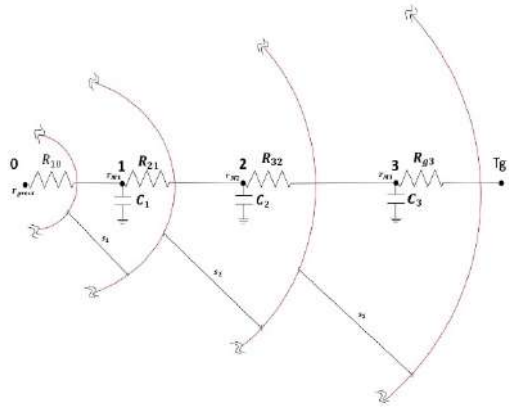

Fig. 3 – Lumped discretization for 3-node system.

For each thermal node (except the boundary conditions, nodes *0* and g) there is a thermal resistance and a thermal capacitance. Each node with a lumped thermal capacitance is placed into the barycentric medium radius, r_M, of the corresponding annulus. Each annulus is spaced from the previous one according to an expansion coefficient c, that is arbitrary, and it is set at the beginning of the simulation. It is usually assumed between 1.1 and 1.2 and it is used to increase the thickness of the annulus starting from the grout radius. For example, for node 1:

$$s_1 = c * r_{grout} \tag{1}$$

$$r_{ext,1} = r_{grout} + s_1 \tag{2}$$

$$r_{M1} = \sqrt{\frac{r_{ext,1}^2 + r_{grout}^2}{2}} \tag{3}$$

For each node the energy balance equation was written, taking into account in this example just the heat conduction:

Node 1:

$$\frac{T_0^p - T_1^p}{R_{10}} + \frac{T_2^p - T_1^p}{R_{21}} = C_1 \frac{T_1^p - T_1^{p-1}}{\Delta\tau} \tag{4}$$

Node 2:

$$\frac{T_1^p - T_2^p}{R_{21}} + \frac{T_3^p - T_2^p}{R_{32}} = C_2 \frac{T_2^p - T_2^{p-1}}{\Delta\tau} \tag{5}$$

Node 3:

$$\frac{T_g^p - T_3^p}{R_{g3}} + \frac{T_2^p - T_3^p}{R_{32}} = C_3 \frac{T_3^p - T_3^{p-1}}{\Delta\tau} \quad (6)$$

For each active node there are three contributions. A heat conduction flow for each surrounding node (on the left side of the equation) and the contribution due to the stored heat (on the right side of the equation), expressed through the thermal capacitance.

In Equations (4-6) the superscripts "p-1" and "p" indicate the time dependence of the equations. The finite difference solution restricts the temperature to discrete points (nodes) in space but also in time. In fact, calculations were made at successive times, each one separated by a certain time step, $\Delta\tau$, set by the user. So that:

$$t = p\Delta\tau \quad (7)$$

Therefore, the calculation starts at time "p-1" for a generic *n* node, the input system will be T_n^{p-1} and the output will be the temperature at the current time, T_n^p.

When working with an ATES, there are three distinct phases. First the system is charged with a certain water flow, this is the injection period. Once the ATES is charged it will have reached a certain temperature, this is the storage period. Finally, when it needs to be activated, the water flow will be extracted and sent to the complex of buildings, this is the withdrawal period.

The next step deals with a water flow to essentially model the injection and withdrawal phases.

During the injection phase a certain water flow is being injected into the aquifer through the grout at a certain known temperature.

With **Fig. 3** as reference, these are the correlated equations:

Node 1:

$$\frac{T_0^p - T_1^p}{R_{10}} + \frac{T_2^p - T_1^p}{R_{21}} + \rho c_p \dot{V}\left(T_0^p - T_1^p\right) = C_1 \frac{T_1^p - T_1^{p-1}}{\Delta\tau} \quad (8)$$

Node 2:

$$\frac{T_1^p - T_2^p}{R_{21}} + \frac{T_3^p - T_2^p}{R_{32}} + \rho c_p \dot{V}(T_1^p - T_2^p) = C_2 \frac{T_2^p - T_2^{p-1}}{\Delta\tau} \quad (9)$$

Node 3:

$$\frac{T_g^p - T_3^p}{R_{g3}} + \frac{T_2^p - T_3^p}{R_{32}} + \rho c_p \dot{V}(T_2^p - T_3^p) = C_3 \frac{T_3^p - T_3^{p-1}}{\Delta\tau} \quad (10)$$

During the storage phase there is no water flow involved, as the system is still. Therefore, it is ascribable to the model here presented.

Finally, when it comes to the withdrawal, the system works in reverse compared to the injection. The water flow then will stream in the other direction. This time though the withdrawal temperature, T_0, is unknown.

Still referencing to **Fig. 3:**

Node 0:

$$\frac{T_1^p - T_0^p}{R_{10}} + \rho c_p \dot{V}(T_1^p - T_0^p) = 0 \quad (11)$$

Node 1:

$$\frac{T_0^p - T_1^p}{R_{10}} + \frac{T_2^p - T_1^p}{R_{21}} + \rho c_p \dot{V}(T_2^p - T_1^p) = C_1 \frac{T_1^p - T_1^{p-1}}{\Delta\tau} \quad (12)$$

Node 2:

$$\frac{T_1^p - T_2^p}{R_{21}} + \frac{T_2^p - T_2^p}{R_{32}} + \rho c_p \dot{V}(T_3^p - T_2^p) = C_2 \frac{T_2^p - T_2^{p-1}}{\Delta\tau} \quad (13)$$

Node 3:

$$\frac{T_g^p - T_3^p}{R_{g3}} + \frac{T_2^p - T_3^p}{R_{32}} + \rho c_p \dot{V}(T_g - T_3^p) = C_3 \frac{T_3^p - T_3^{p-1}}{\Delta\tau} \quad (14)$$

To sum up:

- Storage and injection systems working with *n* nodes will require solving *n* equations.
- Withdrawal system working with *n+1* nodes will require solving *n+1* equations.

2.4 2D model with heat conduction and heat advection

The following step focuses on the modelling of the upper and lower layers of the aquifer. This meant studying not only the radial direction, but also the vertical one.

As it can be seen in **Fig. 4**, two layers (above and below) have been added to the pre-existent aquifer model. This new space discretizes the ground adjacent to the aquifer. To keep the model simple enough, a limited number of nodes have been added, where only heat conduction takes place.

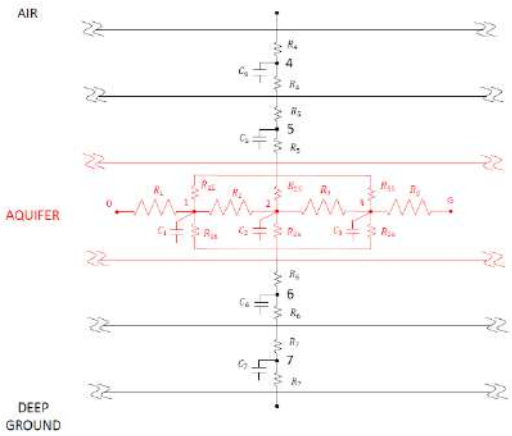

Fig. 4 – Final discretized ground.

Compared to the previous situation, heat conduction through these new layers has been added (in the vertical direction) in each thermal balance equation.

Still referencing to **Fig. 4**, during the injection phase:

Node 4

$$\frac{T_{air}^{p}-T_4^p}{R_4}+\frac{T_5^p-T_4^p}{R_4+R_5}=\frac{C_4(T_4^P-T_4^{P-1})}{\Delta\tau} \tag{15}$$

Node 5:

$$\frac{T_5^p-T_4^p}{R_4+R_5}+\frac{T_1^p-T_5^p}{R_{15}+R_5}+\frac{T_2^p-T_5^p}{R_{25}+R_5}+\frac{T_3^p-T_5^p}{R_{35}+R_5}=\frac{C_5(T_5^P-T_5^{P-1})}{\Delta\tau} \tag{16}$$

Node 1:

$$\frac{T_0^p-T_1^p}{R_1}+\frac{T_2^p-T_1^p}{R_2}+\rho c_p\dot{V}(T_0^p-T_1^p)+\frac{T_5^P-T_1^p}{R_{15}+R_5}+\frac{T_6^p-T_1^p}{R_{16}+R_6}=\frac{C_1(T_1^P-T_1^{P-1})}{\Delta\tau} \tag{17}$$

Node 2:

$$\frac{T_1^p-T_2^p}{R_2}+\frac{T_3^p-T_2^p}{R_3}+\rho c_p\dot{V}(T_1^p-T_2^p)+\frac{T_5^p-T_2^P}{R_{25}+R_5}+\frac{T_6^p-T_2^p}{R_{26}+R_6}=\frac{C_2(T_2^P-T_2^{P-1})}{\Delta\tau} \tag{18}$$

Node 3:

$$\frac{T_2^p-T_3^p}{R_2}+\frac{T_g^p-T_3^p}{R_3}+\rho c_p\dot{V}(T_2^p-T_3^p)+\frac{T_5^p-T_3^P}{R_{35}+R_5}+\frac{T_6^p-T_3^p}{R_{36}+R_6}=\frac{C_3(T_3^P-T_3^{P-1})}{\Delta\tau} \tag{19}$$

Node 6:

$$\frac{T_7^p-T_6^p}{R_6+R_7}+\frac{T_1^p-T_6^p}{R_{16}+R_6}+\frac{T_2^p-T_6^p}{R_{26}+R_6}+\frac{T_3^p-T_6^p}{R_{36}+R_6}=\frac{C_6(T_6^P-T_6^{P-1})}{\Delta\tau} \tag{20}$$

Node 7:

$$\frac{T_{ground}^{p}-T_7^p}{R_7}+\frac{T_6^p-T_7^p}{R_7+R_6}=\frac{C_7(T_7^P-T_7^{P-1})}{\Delta\tau} \tag{21}$$

To each new node a new equation has been added, alongside with two new boundary conditions, the air temperature above and the deep ground temperature below.

For the aquifer nodes (1 to 3) there is the new contribution of heat conduction due to node 5 and node 6.

During the withdrawal phase as shown before there will be an additional equation related to node 0.

3. Model validation

The final step has been validating the model. To do so data from a research paper by Carotenuto et al. [15] has been used as reference. In this paper, an ATES system placed in Capua (Italy) was studied and tested. The experiment consisted of charging the aquifer, storing the heat and then withdrawing the water flow. **Fig. 5** outlines the aquifer located at 42 m underground. It is described as coarse sandy and gravelly.

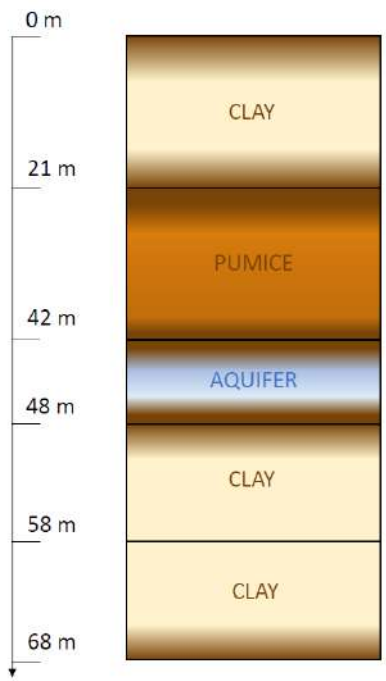

Fig. 5 – Simplified stratigraphy section of the case study.

The experiment was based on two wells (W1, W2). During the injection phase the water flow was

pumped into W1, after been heated, and following the storage period was pumped back into W2. The experiment was carried out during July and August of 1990 in the following way:

- a 34 m^3/h water flowrate at 16°C was pumped from W2, heated via a plate heat exchanger up to 40°C and finally injected into W1. After a period of settlement, this water flow was extracted and pumped back into W2.

- The injection period lasted 15 days, the storage 7 days and 15 hours and the withdrawal another 15 days.

Tab. 1 and **Tab. 2** describe all the input data that has been used to run the simulation.

In order to validate the model, simulation results have been compared to measured temperature data provided by the paper. **Fig. 6** shows the three different trends.

Tab. 1 – Thermophysical properties

layer	cv	λ
	[J/(m³K)]	[W/(m K)]
Pumice	$2.4 \cdot 10^6$	1
Aquifer	$2.6 \cdot 10^6$	1.3
Clay	$2.3 \cdot 10^6$	0.8

Tab. 2 – Boundary Temperatures

Node	T °C
Air	10
(Deep) Ground	16
Aquifer	16
(Aquifer) Ground	16
Grout	40

The yellow curve is the data related to the actual measured temperature on the site during the experiment. This is the average temperature measured by three thermocouples positioned in the aquifer at 46.5, 45.0 and 42.5 m of depth. The green curve is the temperature trend as result of the 1-dimensional model simulation while the brown one is the 2-dimensional one.

Before the first phase, the temperature node (placed at 10 m from the well) is at 16°C. Once the injection starts, a hot water flow (around 40°C) is pumped into the well and the node temperature slowly increases, reaching the set point after 100 hours (about 4 days). During this phase, the two simulations provide results quite alike because the vertical heat conduction is negligible. Compared to the yellow curve, the simulated aquifer is in both cases a bit slow during this charge. The little stall in the yellow curve after 40 hours and again after 100 hours could be related to some measuring error. Injection finishes after 360 hours.

During the storage phase the two models start to differentiate from each other. This is where the vertical heat losses come into play. Given that the aquifer has a temperature of 40°C, the ΔT between the aquifer and the other layers is now large enough that vertical heat conduction becomes relevant.

Finally, in the withdrawal phase, the 2D simulation model shows better results in comparison to the 1D simulation model. The 2D aquifer compared to experimental data is quite slow in this final phase. This effect could be due to the groundwater leaks that are not considered in the model.

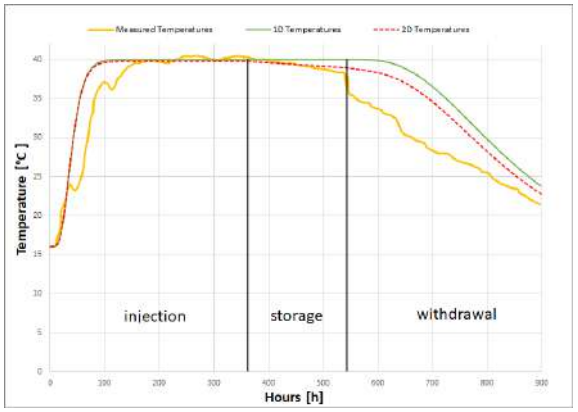

Fig. 6 – Average temperatures plotted vs time at 10 m from W1

4. Conclusions

This work presented a first approach for a simplified model to evaluate the thermal behavior and application of ATES in design planning. The model was based on a lumped parameter approach and was compared with measurements presented in literature. Despite the simplifications, the model for a single well has proved itself to work fine and give good enough results in terms of temperatures. The interaction between adjacent wells will be the future aspect that will be considered. The key feature of the model is its ability to be linked to building and district simulation tools. This feature will be further implemented in the future in order to evaluate the benefits of ATES in different contexts.

5. Data availability

The datasets generated during and/or analyzed during the current study are not publicly available because measurements were not carried out by the Authors but are/will be available upon request

6. Acknowledgements

This work was supported by the Danish Energy Agency, under the Energy Technology Development and Demonstration Program (EUDP), journal no. 64019-0575.

This research emerged from the Task 32 project; an international project conducted under the umbrella of the International Energy Agency (IEA) within Energy Storage Technology Collaboration Programme (ES TCP).

7. Nomenclature

C thermal capacitance [J/K]

c_V volume specific capacity [J/(m^{3}K)]

c_p thermal specific capacitance [J/ (kg K)]

c expansion coefficient [-]

λ thermal conductivity [W/ (m K)]

Δτ time step [s]

r_M barycentric medium radius [m]

ρ density [kg/m^3]

R thermal resistance [K/W]

r_I annulus radius [m]

s annulus thickness [m]

t time [s]

T temperature [°C]

V volumetric water flow [m^3/s]

Subscripts and superscripts

p: time instant

g: aquifer ground

8. References

[1] Yang T., Pan Y., Yang Y., Lin M., Qin B., Xu P., Huang Z. CO2 emissions in China's building sector through 2050: A scenario analysis based on a bottom-up model.2017,06,1;

[2] Bloemendal M., Jaxa-Roxen M., Olsthoorn T. Methods for planning of ATES systems. 2018,2,22;

[3] Gholipour H., Arjomandi A., Yam S. Green property finance and CO2 emissions in the building industry. 2022,2;

[4] Guo F., Zhu X., Li P., Yang X. Low-grade industrial waste heat utilization in urban district heating: Simulation-based performance assessment of a seasonal thermal energy storage system. 2022,1,15;

[5] Zhou X., Xu Y., Zhang X., Xu D., Linghu Y., Guo H., Wang Z., Chen H. Large scale underground seasonal thermal energy storage in China. 2021,1;

[6] Wilberforce T., Olabi A., Sayed E., Elsaid K., Maghrabie H.M., Abdelkareem M. A review on zero energy buildings – Pros and cons.2021,07,24;

[7] Mahon H., O'Connor D., Friedrich D., Hughes B. A review of thermal energy storage technologies for season loops. 2021,9,28;

[8] De Schepper G., Paulus C., Bolly PY., Hermans T., Lesparre N., Robert T. Assessment of short-term aquifer thermal energy storage for demand-side management perspectives: Experimental and numerical developments. 2019,05,15;

[9] Rostampour V., Jaxa-Rozen M., Bloemendal M., Kwakkel J., Keviczky T. Aquifer Thermal Energy Storage (ATES) smart grids: Large-scale seasonal energy storage as a distributed energy management solution. 2019,05,15;

[10] Heather A. Sheldon, Andy Wilkins, Christopher P. Green. Recovery efficiency in high-temperature aquifer thermal energy storage systems.2021,11;

[11] Huang Y., Pang Z., Kong Y., Watanabe N. Assessment of the high-temperature aquifer thermal energy storage (HT-ATES) potential in naturally fractured geothermal reservoirs with a stochastic discrete fracture network model.2021,12;

[12] Bozkaya B., Li R., Labeodan T., Kramer R., Zeiler W. Development and evaluation of a building integrated aquifer thermal storage model. 2017,6,28;

[13] Todorov O., Alanne K., Virtanen M., Kosonen R. A method and analysis of aquifer thermal energy storage (ATES) systems for district heating and cooling: A case study in Finland. 2019,9,20;

[14] MODFLOW https://www.usgs.gov/software/modflow-6-

usgs-modular-hydrologic-model

[15] Carotenuto A., Fucci F., La Fianza G., Reale F. Physical model and demonstration of an aquifer thermal energy store. 1991,11(2-3):169:180;

Numerical analysis of a thermal energy storage tank charged with a flat type solar air collector

Guven Hasret Yilmaz [a], *Mustafa Zeki Yilmazoglu* [b]

[a] Faculty of Engineering, Gazi University, Ankara, Turkiye, ghyilmaz@gazi.edu.tr

[b] Faculty of Engineering, Gazi University, Ankara, Turkiye, zekiyilmazoglu@gazi.edu.tr

Abstract. As energy and sustainability issues related to climate change gain importance day by day, the significance of energy storage systems is increasing. Carnot Batteries, where energy can be stored thermally, constitute one of the most outstanding alternatives for the storage of excess electrical energy produced from renewable energy in the concept of smart cities. The energy is stored in the Carnot Batteries during the hours when the electricity demand is lower than the electricity production, the energy stored in the Carnot Batteries is converted into electricity during the hours when the electricity demand is higher than the electricity production. In this respect, Carnot Batteries can offer a good solution to the imbalance between energy demand and production, which is a crucial problem in energy use, and therefore, it is likely that they will be an indispensable part of the future and smart city systems. In this study, a simulation covering the charging and discharging processes of a Thermal Energy Storage tank, which receives its energy from flat type solar thermal collectors, was carried out in MATLAB. In the simulation, a 6 m height tank was divided into 60 cells and discretized, the solar radiation values were calculated locally and a solar path was created. At the time of charging, the Thermal Energy Storage tank received its energy from the solar collectors, depending on the determined solar path. In the simulation, the effects of variables related to the energy storage media such as sphericity, void fraction, charging time were investigated.

Keywords. Carnot battery, energy storage, charge, discharge, solar thermal collectors, Organic Rankine Cycle.
DOI: https://doi.org/10.34641/clima.2022.339

1. Introduction

In today's world, the tendency towards renewable energy sources is increasing. While developed countries meet most of their electricity production from renewable resources, developing countries are constantly increasing their orientation towards renewable resources. Although renewable energy systems have many advantages, these also have some disadvantages such as intermittent operation characteristics. On the other hand, the increase in renewable energy investments will cause energy supply-demand imbalance at certain times during the day. Thermal energy storage systems can offer an effective and economic solution to the supply-demand imbalance. The motivation of this study will be to examine the effects of thermal energy storage in low temperature systems. The goal is to create a modeling code to include high-temperature systems. The storage of the produced energy is one of the most current research topics. So far, many different types of energy storage systems such as supercapacitor, battery and flow batteries, Compressed Air Energy Storage, Superconducting Magnetic Energy Storage, Pumped Hydroelectric Energy Storage, Thermal Energy Storage or Pumped Thermal Energy Storage, flywheel and Hydrogen Storage are in different technological stages (Benato A. and Stoppato A., 2018a). Among these systems, Pumped Hydroelectric Energy Storage, Compressed Air Energy Storage, Thermal Energy Storage, and Flow Batteries can be considered as mature, while other systems are still under research. Pumped Hydroelectric Energy Storage system offers high efficiency at low cost with longer operating hours. Compressed Air Energy Storage systems can offer high efficiency at low cost. Flow Batteries have higher energy density than Pumped Hydroelectric Energy Storage and Compressed Air Energy Storage systems, but have a shorter lifespan (Benato A. and Stoppato A., 2018b). Pumped Hydroelectric Energy Storage and Compressed Air Energy Storage systems cannot be installed in any region as these require certain geographical conditions. On the other hand,

Copyright ©2022 by the authors. This conference paper is published under a CC-BY-4.0 license.

Pumped Thermal Energy Storage systems can be an important alternative to other energy storage systems with their high energy densities, high efficiencies, low costs and long lifetimes. Besides, there is no need for any geographical conditions in Thermal Energy Storage systems.

In Thermal Energy Storage systems, or Carnot Batteries, electrical energy is stored as heat energy. The basic principle in these systems is to store energy in the form of heat into the materials with thermophysical properties suitable for energy storage, such as water, oil, paraffin, wood, sand, concrete, brick, glass wool, and granite. When the electricity demand exceeds the electricity generation, the energy stored as heat is drawn from the storage media by means of a working fluid to generate electricity by conventional cycles, Rankine, Organic Rankine, Brayton etc.

In Pumped Thermal Energy Storage systems, the charging process takes place in two different ways. In these systems, either a heat pump or an electrical resistor is used during the charging process. In the discharge process, a gas turbine, Rankine cycle or a hybrid system is used. The storage part is realized in three different ways as sensible heat storage, latent heat storage, and thermochemical storage. Latent heat storage is done with substances called phase change materials. These materials also store and/or use an extra phase energy by changing phase during storage and/or discharge of thermal energy. However, the costs and total cycle availability of these materials should be considered. In sensible heat storage, materials with high thermal permeability, non-toxic, non-flammable and inexpensive are used. Rocks, metals, stones, concrete, sand, and salts are suitable materials for use in sensible heat storage.

Singh et al., (2008) numerically investigated a Thermal Energy Storage system powered by solar collectors. As a result of the 8-hour charging process, it was found that the maximum energy stored in the tank to be approximately 175 MJ by assuming the solar radiation as constant. Peterson (2011) examined a Thermal Energy Storage system consisting of a heat pump, a heat engine, and a latent heat storage tank. The effect of isentropic efficiency of compressor and turbine on system efficiency was investigated. Morandin et al. (2012) investigated a Thermoelectric Energy Storage system consisting of transcritical CO_2 cycles (heat pump and Rankine cycle). As a result, the efficiency of the Pumped Thermal Energy Storage system was found to be 60%. Henchoz et al., (2012) performed a thermoeconomic analysis of an energy storage system including solar thermal collectors. The optimum efficiency was found to be 43.8% – 84.4% in the system, the working fluid was ammonia. Kuravi et al., (2013) designed a sensible heat storage system for concentrated solar power plants. Air was used as the working fluid and it was observed that the increase in the air flow rate decreased the energy storage time. Steinmann (2014), examined a latent heat storage system operating on the conventional Rankine cycle. Okazaki et al., (2015) examined three different energy storage systems. It was observed that the wind powered Thermal Energy Storage system using a heat generator is more economical than other systems. Vinnemeier et al., (2016) investigated the Pumped Thermal Energy Storage system integrated into a number of different thermal power plants. As a result, the maximum exergy of the system was found to be 70%. Ayachi et al., (2016) constructed a thermodynamic model of a Pumped Thermal Energy Storage system consisting of transcritical CO_2 cycles, geothermal energy storage and a ground heat exchanger. According to the results, it was stated that the system efficiency is 50%, however, it is possible to reach up to 66% with more complex systems. Guo et al. (2016) examined Pumped Thermal Energy Storage and Pumped Cryogenic Energy Storage systems. It was found that the overall performance of the Pumped Thermal Energy Storage system is better than the overall performance of the Pumped Cryogenic Energy Storage system. Benato (2017) reviewed Pumped Thermal Energy Storage system with an electric heater and heat exchanger and the materials stored. Air was used as the working fluid and the system was modelled as 1D. It was concluded that the configuration with the lowest specific cost and the highest energy density was the packed bed consisting of aluminum oxide spheres. Frate et al., (2017) studied a hybrid Pumped Thermal Energy Storage system utilizing a low-grade heat source. Different working fluids were considered in the model and it was found that the system efficiency can be over 100%. Roskoch and Atakan (2017) investigated the thermodynamic potential of a Pumped Thermal Energy Storage system consisting of a compression heat pump, latent heat energy storage tank, and organic Rankine cycle. The results show that the system efficiency increased with increasing storage temperature and increased superheating effect at the expander inlet. Smallbone et al., (2017) performed an economic analysis of a Pumped Thermal Energy Storage system and compared this system with other energy storage systems. It was reported that the Pumped Thermal Energy Storage system can compete with the Compressed Air Energy Storage system economically, and that it can even compete with the Pumped Hydroelectric Energy Storage system, since the Pumped Thermal Energy Storage system does not need any geographical conditions. Georgiou et al., (2018) analyzed and compared the Liquefied Air Energy Storage and Pumped Thermal Energy Storage system thermodynamically and economically. It was revealed that the efficiency of the Pumped Thermal Energy Storage system is higher, but the Energy Storage system with Liquefied Air is more economical. Farres-Antunez et al., (2018) examined a hybrid system consisting of Liquefied Air Energy Storage and Pumped Thermal Energy Storage systems. In the thermodynamic analysis-based study, the efficiency of the hybrid system was found to be 70%. It was also reported that the energy density of the hybrid system is higher than that of the Liquefied Air Energy Storage system and the Pumped

Thermal Energy Storage system. Pillai et al., (2019) examined a Carnot Battery consisting of a heat pump and Organic Rankine cycle from a thermodynamic perspective. In the simulated Carnot Battery, it was also examined the latent and sensible heat behavior and tried various working fluids in the simulations. In addition, it was reported that the highest exergy amount was in the HFO-1336mzz(E) fluid, and the lowest exergy amount was in the R1234ze(Z) fluid. Attonaty et al., (2019) investigated a Thermal Energy Storage system with a capacity of 200 MWh, consisting of an electric heater and a Brayton-Rankine hybrid cycle. The system efficiency was found to be 50% at a storage temperature of 900°C. Dietrich et al., (2020) analyzed a Thermal Energy Storage system consisting of the Joule/Brayton cycle exergo-economically. As a result of the transient numerical studies, it was found that the efficiency of the Thermal Energy Storage system is 42.9%. It was also concluded that the examined system has the highest power-specific cost compared to other installed systems. Frate et al., (2020) investigated a Thermal Energy Storage system consisting of a heat pump and Organic Rankine Cycle. In the analytical study, it was observed that the efficiency of the system can exceed 50%, provided that the temperature of the waste heat source does not exceed 60°C. As a result of the literature review, it was seen that there are many studies on Thermal Energy Storage systems. Thermal Energy Storage systems are quite suitable for today's energy policies, but it is expected to become a necessity in the near future.

In this study, a Thermal Energy Storage (TES) system, in which solar radiation will be used as a variable according to the region and the day of the year, is numerically simulated. A solar path, giving the hourly solar radiation is created and the charging and discharging characteristics of the system are obtained according to this solar path. Sensible energy storage media with different physical properties is modelled. On the power side, an Organic Rankine cycle with a working fluid R245fa is considered. The efficiency of the power side during dischange process is also obtianed.

2. METHODOLOGY AND NUMERICAL MODEL

Thermal Energy Storage systems can be configurated in many ways. However, the selected media and subsystems can affect the charge and discharge properties of the storage systems. Heat pump or electrical resistance is generally used in the charging process of the TES systems. Rankine cycle, Organic Rankine cycle, gas turbine cycle or hybrid systems can be considered in the discharge process. In this study, flat type solar collectors are considered for the charging process. Organic Rankine Cycle (ORC) is considered for the discharge part of the investigated system. A sensible heat storage tank is considered due to its lower cost and availability. The main components of the simulated system is shown in Fig. 1.

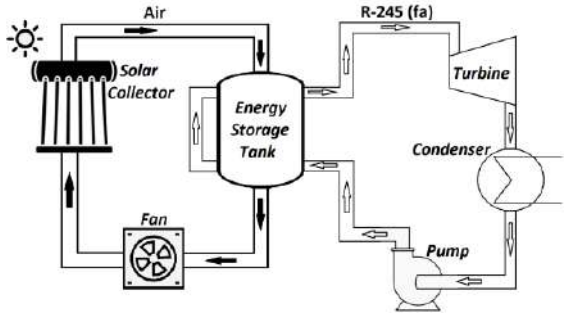

Fig. 1. Schematic of the simulated system

The system consists of a flat type solar air collector, fan, heat storage tank, and Organic Rankine cycle. The working fluid for the charging process is air and for the discharge process the working fluidi s R245fa. Initially, the air in the system is drawn towards the tank by the fan. The drawn air is heated in the solar air collectors. The heated air moves towards the tank filled with rocks after the solar collectors. The hot air raises the tank temperature to a certain temperature level after a charging period of 8 hours. After the charging process, the discharge process starts as the refrigerant enters the hot tank and heats up. At this stage, the refrigerant passed through copper pipes placed in the tank, unlike air. The pipes are designed in multiple bundles, straight and placed along their length. The energy storage tank acts as evaporator for the ORC. The working fluid expands in the turbine to generate electricity.

Numerical analysis of the TES is performed in a MATLAB code. The tank is divided into “n” cells and discretized, and the charging and discharging processes are calculated by repeating for each determined unit time step. Besides, a solar path is created that calculates solar radiation based on the coordinates of the region and the day of the year. The model chosen for use in each discretized control volume is a hybrid model that consists of the Mumma and Marvin model and thermal resistance analogy.

Validation of the model

A validation study is carried out for testing the Mumma and Marvin model (Singh et al., 2008). The charging process of the tank that receives its energy from a solar air collector is investigated. Singh et al., and used air as the working fluid in the simulations. The air at room temperature warmed up from the solar collectors and then entered the energy storage tank filled with storage material. The air warmed the tank to a certain extent after a charging time of 8 hours. Besides, the effects of changing the material values such as the sphericity and void ratio of the storage materials is investigated. The parameters used by Singh et al., are given in Table 1.

Table 1. Validation case material properties

Parameter	Value/Range
Volume of packed bed	15 m^3
Length of packed bed	6 m
Number of bed elements	60
Initial bed temperature	25°C

Sphericity of material element	0.55 – 1.00
Void fraction	0.31 – 0.63
Density of storage material	1920 kg/m³
Density of air	1.1 kg/m³
Specific heat of storage material	0.835 kJ/kgK
Specific heat of air	1.008 kJ/kgK
Thermal conductivity of storage material	0.70 W/mK
Dynamic viscosity of air	0.0000185 kg/ms
Ambient temperature	25°C
Inlet air temperature to bed	40°C
Insolation	500 W/m²

The charging characteristics of the energy storage tank and the Mumma and Marvin model is validated. In the simulations, the energy storage tank subjected to a charging period of 8 hours and examined the results obtained according to different void ratios and sphericity values. Likewise, in this study in which the Mumma and Marvin model will be used, a validation study is carried out by using the parameters and equations. To show the consistency and compatibility of the validation the temperature values at the end of the 4-hour charging period and the 8-hour discharging period according to the different void ratios of the energy storage tank are compared (Fig. 2) and the results are in aggrement.

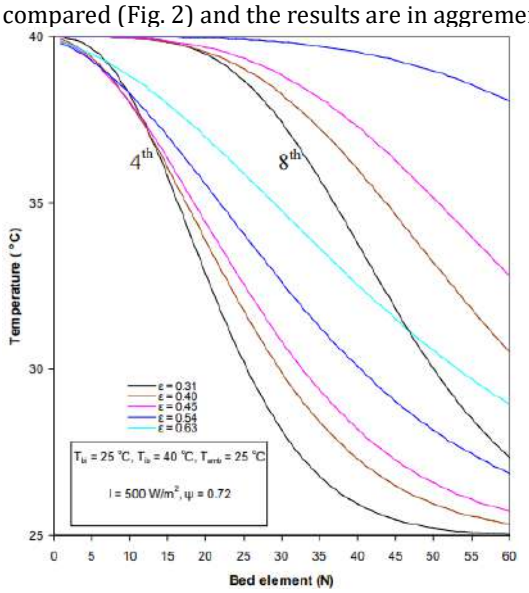

(a)

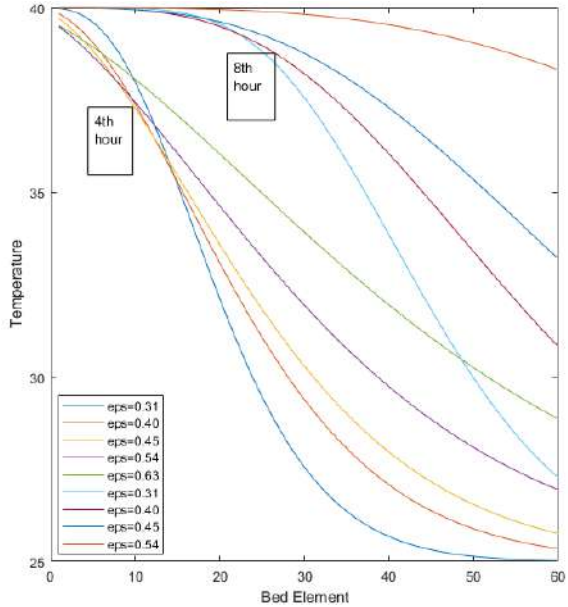

(b)

Fig. 2. Comparison of the results for the validation (a) reference work (b) this study The temperature change according to the different void ratios of the energy storage tank at the end of the 4 and 8 hour charging periods.

The Mumma and Marvin Model

The energy storage tank is divided into 60 control volume (Fig. 3). The generated equations are solved for each cell. At the same time, the equations created for each control volume were also repeated for each time step.

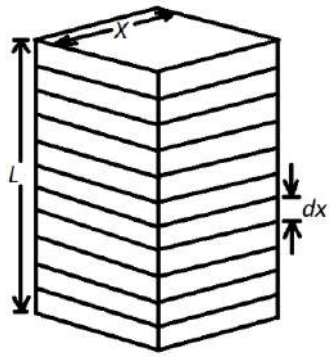

Fig. 3. The discritized view of the tank

The thermal energy storage tank is considered as a rectangular prism. While the cross-sectional area of the tank is 1.5x1.5 m², its height is assumed to be 6 m. The tank is discretized by dividing it into 60 compartments along its height. The useful heat energy is calculated from Eq. 1.

$$Q_u = A_c[S_t F_R(\tau\alpha) - F_R U_l(T_i - T_{amb})] \qquad (1)$$

In Eq. (1), A_c collector surface area (m²), S_t insolation (W/m²), F_R heat removal factor, (τα) effective transmittance-absorption product, U_l overall heat

transfer coefficient (W/m²K), T_i air inlet temperature to the collector (°C) is T_{amb} outside temperature (°C). Q_u is the amount of useful heat transfer (W). The useful heat transfer amount Q_u is also included in Eq. 2.

$$Q_u = \dot{m}C_p(T_o - T_i) \quad (2)$$

which, $\dot{m}$ is the mass flow rate of the air (kg/s), and C_p is the specific heat of the air (kJ/kgK). T_o is the exit temperature of the air from the collector. The equations that are solved by repeating in the discretized tank are as follows.

$$T_{a,m+1} = T_{s,m} + (T_{a,m} - T_{s,m})e^{-\emptyset_1} \quad (3)$$

$$T_{s,m\,(t+\Delta t)} = T_{s,m\,(t)} + \Delta t[\emptyset_2(T_{a,m} - T_{a,m+1}) - \emptyset_3(T_{s,m\,(t)} - T_{amb})] \quad (4)$$

which $T_{a,m+1}$ is air temperature at outlet of control volume element "m" (°C), $T_{a,m}$ is air temperature at inlet of control volume element "m" (°C), $T_{s,m\,(t)}$ is mean temperature of control volume element "m" at time t (°C), $T_{s,m\,(t+\Delta t)}$ is mean temperature of control volume element "m" after time interval Δt (°C). Δt is the time step (s). Also, $\emptyset_1$, $\emptyset_2$ and $\emptyset_3$ are empirical coefficients.

$$\emptyset_1 = \frac{h_v AL}{N(\dot{m}C_p)} \quad (5)$$

$$\emptyset_2 = \frac{N(\dot{m}C_p)}{\rho_s AL(1-\varepsilon)C_s} \quad (6)$$

$$\emptyset_3 = \frac{(UA_s)}{N(\dot{m}C_p)}\emptyset_2 \quad (7)$$

which A is the cross-sectional area of the tank (m²), L is the height of the tank (m), N is the number of compartments in which the tank is discritized, ρ_s is the density of the storage material (kg/m³), C_s is the specific heat of the storage material (kJ/kgK), and ε is the void ratio. hv is the volumetric heat transfer coefficient (W/m³K) and at the same time the volumetric heat transfer coefficient, Nusselt number and Reynolds number can be found from the equations below;

$$h_v = \frac{KNu}{D_e^2} \quad (8)$$

$$Nu = 0.437(Re^{0.75})(\Psi^{3.35})(\varepsilon^{-1.62})\{\exp[29.03((log\Psi)^2)]\} \quad (9)$$

$$Re = \frac{\rho V D_e}{\mu} \quad (10)$$

Here, ρ_a is the density of the air (kg/m³), D_e is the equivalent diameter of the storage materials (m), K is the thermal conductivity of the air (W/mK), and Ψ is the sphericity. The pressure loss is calculated with Eq. 11.

$$\Delta P = \frac{fG^2}{\rho_a D_e} \quad (11)$$

which ΔP is the pressure loss (Pa), G is the mass velocity of the air (kg/m²s), f is the friction coefficient.

$$f = 4.466(Re^{-0.2})(\Psi^{0.696})(\varepsilon^{-2.945})\{\exp[11.85(log\Psi)^2]\} \quad (12)$$

The sphericity and void ratio values are obtained from Eq. 13 and 14.

$$\Psi = \frac{a_s}{a_e} \quad (13)$$

$$\varepsilon = \frac{V_t - V_s}{V_t} \quad (14)$$

In Eq. 13 and 14, a_s is the surface area of a sphere with a volume equal to the volume of the storage material (m²), while a_e is the surface area of the storage material (m²) (Benato, 2017).

RESULTS

The temperature change in the tank during the charging and discharging processes is investigated according to the height of the tank and time. It is repeated according to different void ratios and sphericity values. During the discharge process the efficiency of the ORC is also investigated. To observe the availability of the energy stored thermally in the tank and then converted into electricity via the ORC, the hourly electrical efficiency is calculated. The most important parameter for the charging process of the Carnot Battery system, which is powered by solar collectors, is the solar radiation. In this study, solar radiation is not considered as a constant and varied according to the day of the year and the latitude of the region. In this context, a hot day of the year and the Ankara (Turkey) are chosen.

The solar radiation reached its maximum value around 12:00 and the sun rays reached the earth from the atmosphere for about 14 hours a day. During this 14-hour period, an effective 8-hour period is selected and the charging process is considered. The temperature profiles are obtained along the height of the tank in the charging process and at different time intervals (Fig. 5).

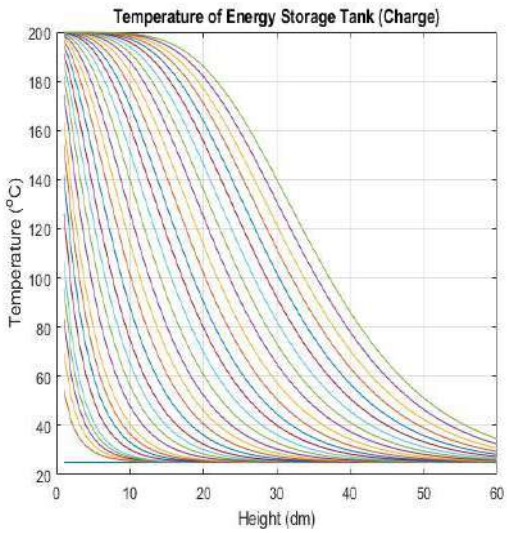

(a)

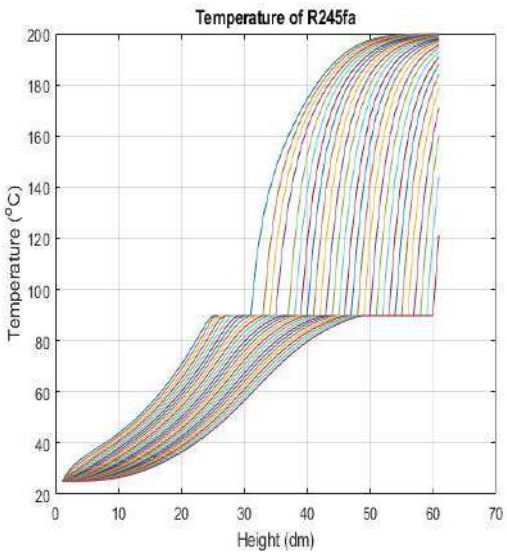

(b)

Fig 5. Temperature distribution of the energy storage tank for the charge process (a) and the temperature of the fluid for the discharging process (b)

In the TES tank, it is seen that the temperature decreases as it progresses along the height axis. This shows that thermal stratification is complied with in the simulation. It was also observed that this stratification continued as time passed and the temperature increased over the entire height of the tank. Each of the lines in Fig. 5 represents the temperature lines of the tank at different time intervals. The temperature of the tank from one end to the other increases as time passes during the charging stage. The temperature change of the fluid during discharge is shown in Fig. 5b. While the temperature of the fluid increased until and after the phase change, its temperature remained constant in the phase change region. After the charging process was completed according to different parameters, the discharge process is started. For the discharge process, the working fluid is passed through the tank for a discharge period of approximately 7 hours. While the tank temperature has its maximum temperature at the beginning of the discharge process, it decreased to its minimum temperature at the end of the discharge process as it transfered thermal energy to the working fluid.

The efficiency of the ORC is calculated as the ratio of net energy, which is the difference of the energy obtained in the turbine and the energy consumed in the pump and heat delivered by the thermal energy storage tank to the fluid. In the model, the thermal storage continues to be used until about 10°C above the saturation temperature, depending on the degree of the quality of the working fluid at the turbine inlet. The small increase in efficiency after the 5th hour in the discharge state can be explained by the decrease in the heat energy transferred to the working fluid. The variation of the efficiency of Organic Rankine cycle according to the discharge process hours is given in Fig. 6. The efficiency progressed steadily at 12% for approximately 7 hours.

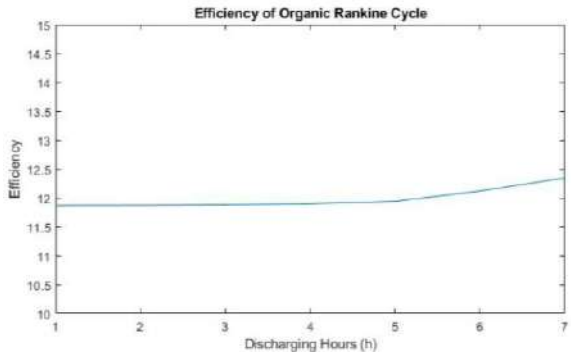

Fig 6. Efficiency of Organic Rankine Cycle according to discharging hours

CONCLUSION

In this study, the thermal storage of solar energy and the generation of electricity from stored energy with ORC are discussed. On the solar side, flat type solar air collectors are used and the working fluid of the solar side is air. On the power side, the working fluid is R245fa. Sensible heat storage on a solar path in Ankara conditions is considered. In the numerical model, the transient solution of the storage tank is considered. In case of discharge, the total efficiency of the system is obtained. According to the results, it was calculated that the electrical efficiency of the system will be approximately 12% in case of discharge. The temperatures of the storage tank with working fluids are obtianed according to the time step.

In the next step of this study, storage with Carnot batteries will be discussed. In this structure, which started to gain importance with the concept of smart cities, the conversion of excess electricity into heat and its storage and then its conversion to electricity in case of demand will be discussed. It is aimed to expand this study with exergy and economic analysis.

REFERENCES

[1] Singh, R., Saini, R.P., Saini, J.S. (2008). *Simulated Performance of Packed Bed Solar Energy Storage System having Storage Material Elements of Large Size - Part I. The Open Fuels & Energy Science Journal, 11(1), 91-96. doi: 10.2174/1876973X00801010091*

[2] Peterson, R. B. (2011). *A concept for storing utility-scale electrical energy in the form of latent heat. Energy, 36(10), 6098–6109.* doi:10.1016/j.energy.2011.08.003

[3] Morandin, M., Maréchal, F., Mercangöz, M., & Buchter, F. (2012). *Conceptual design of a thermo-electrical energy storage system based on heat integration of thermodynamic cycles – Part A: Methodology and base case. Energy, 45(1), 375–385.* doi:10.1016/j.energy.2012.03.031

[4] Morandin, M., Maréchal, F., Mercangöz, M.,

& Buchter, F. (2012). *Conceptual design of a thermo-electrical energy storage system based on heat integration of thermodynamic cycles – Part B: Alternative system configurations. Energy, 45(1), 386–396.* doi:10.1016/j.energy.2012.03.033
[5] Henchoz, S., Buchter, F., Favrat, D., Morandin, M., & Mercangöz, M. (2012). *Thermoeconomic analysis of a solar enhanced energy storage concept based on thermodynamic cycles. Energy, 45(1), 358–365.* doi:10.1016/j.energy.2012.02.010
[6] Kuravi, S., Trahan, J., Goswami, Y., Jotshi, C., Stefanakos, E., & Goel, N. (2013). *Investigation of a High-Temperature Packed-Bed Sensible Heat Thermal Energy Storage System With Large-Sized Elements. Journal of Solar Energy Engineering, 135(4), 041008.* doi:10.1115/1.4023969
[7] Steinmann, W. D. (2014). *The CHEST (Compressed Heat Energy STorage) concept for facility scale thermo mechanical energy storage. Energy, 69, 543–552.* doi:10.1016/j.energy.2014.03.049
[8] Okazaki, T., Shirai, Y., & Nakamura, T. (2015). *Concept study of wind power utilizing direct thermal energy conversion and thermal energy storage. Renewable Energy, 83, 332–338.* doi:10.1016/j.renene.2015.04.027
[9] Vinnemeier, P., Wirsum, M., Malpiece, D., & Bove, R. (2016). *Integration of heat pumps into thermal plants for creation of large-scale electricity storage capacities. Applied Energy, 184, 506–522.* doi:10.1016/j.apenergy.2016.10.045
[10] Ayachi, F., Tauveron, N., Tartière, T., Colasson, S., & Nguyen, D. (2016). *Thermo-Electric Energy Storage involving CO 2 transcritical cycles and ground heat storage. Applied Thermal Engineering, 108, 1418–1428.* doi:10.1016/j.applthermaleng.2016.07.063
[11] Guo, J., Cai, L., Chen, J., & Zhou, Y. (2016). *Performance optimization and comparison of pumped thermal and pumped cryogenic electricity storage systems. Energy, 106, 260–269.* doi:10.1016/j.energy.2016.03.053
[12] Benato A. Performance and cost evaluation of an innovative Pumped Thermal Electricity Storage power system. Energy 2017;138:419–36. doi:10.1016/j.energy.2017.07.066.
[13] Frate, G. F., Antonelli, M., & Desideri, U. (2017). *A novel Pumped Thermal Electricity Storage (PTES) system with thermal integration. Applied Thermal Engineering, 121, 1051–1058.* doi:10.1016/j.applthermaleng.2017.04.127
[14] Roskosch, D., & Atakan, B. (2017). *Pumped heat electricity storage: potential analysis and orc requirements. Energy Procedia, 129, 1026–1033.* doi:10.1016/j.egypro.2017.09.235
[15] Smallbone, A., Jülch, V., Wardle, R., & Roskilly, A. P. (2017). *Levelised Cost of Storage for Pumped Heat Energy Storage in comparison with other energy storage technologies. Energy Conversion and Management, 152, 221–228.* doi:10.1016/j.enconman.2017.09.047
[16] Benato, A., & Stoppato, A. (2018). *Heat transfer fluid and material selection for an innovative Pumped Thermal Electricity Storage system. Energy, 147, 155–168.* doi:10.1016/j.energy.2018.01.045
[17] Benato, A., & Stoppato, A. (2018). *Pumped Thermal Electricity Storage: A technology overview. Thermal Science and Engineering Progress, 6, 301–315.* doi:10.1016/j.tsep.2018.01.017
[18] Georgiou, S., Shah, N., & Markides, C. N. (2018). *A thermo-economic analysis and comparison of pumped-thermal and liquid-air electricity storage systems. Applied Energy, 226, 1119–1133.* doi:10.1016/j.apenergy.2018.04.128
[19] Farres-Antunez, P., Xue, H., & White, A. J. (2018). *Thermodynamic analysis and optimisation of a combined liquid air and pumped thermal energy storage cycle. Journal of Energy Storage, 18, 90–102.* doi:10.1016/j.est.2018.04.016
[20] Pillia A., Kaya A., De Paepe M., Lecompte S. (2019). Performance Analysis of an Organic Rankine Cycle for Integration in a Carnot Battery. 5th International Seminar on ORC Power Systems
[21] Attonaty, K., Stouffs, P., Pouvreau, J., Oriol, J., & Deydier, A. (2019). *Thermodynamic analysis of a 200 MWh electricity storage system based on high temperature thermal energy storage. Energy.* doi:10.1016/j.energy.2019.01.153
[22] Dietrich A., Dammel F., Stephan P. (2020). Exergoeconomic analysis of a pumped heat electricity storage system based on a Joule/Brayton cycle, DOI: 10.1002/ese3.850

c.The datasets generated during and/or analysed during the current study are not available because [due to the ongoing thesis study] but the authors will make every reasonable effort to publish them in near future.

Thermal performance of a supply-air window with triple heating glazing inserted in building envelope

Salem Zeiny[a], Yassine Cherif[a], Stéphane Lassue[a], Thierry Chartier[a]

[a] Univ. Artois, IMT Lille Douai, Junia, Univ. Lille, ULR 4515, Laboratoire de Génie Civil et géo-Environnement (LGCgE), F-62400 Béthune, France, stephane.lassue@univ-artois.fr

Abstract. Nowadays, no one ignores that the building envelope plays a major role in terms of energy consumption and greenhouse gas production. Successive regulations have mainly resulted in a reinforcement of thermal insulation and an improvement of the airtightness of the envelopes. But this often results in poor estimations of consumption, condensation problems on the walls and poor air quality.

Our project consists in analyzing the contributions of a glazed, supply air and heating façade component that provides the ventilation, the heating of the building and the recovery of solar and fatal energy. It is based on a supply-air window of type "Paziaud" in which a heating glass has been inserted. A prototype has been installed on the façade of a building and has been extensively instrumented. Measurements of surface temperatures and air temperatures, pressure difference and velocity are completed in an original way by a fluxmetric instrumentation placed in the ventilated air gaps of the window and on the surfaces in contact with the interior and exterior environments.

This paper will allow us to share and discuss the first results obtained in this in-situ configuration. Our experimentation highlights the difficulties that arise in the interpretation of measurements in real sites, more or less disturbed during the day and at night by the variations of meteorological parameters. It is also a question of coming back to the definition of the performance indicators by comparing theoretical formulas and practical results. In particular, it is necessary to take a closer look at the definition of the outside temperature, which is involved in the expression of a surface transmission coefficient adapted to the component and to discuss an efficiency factor for the window which functions as an exchanger. It is also important to take into account the different heat sources (solar radiation, electricity and recovered waste heat), the heat convective exchanges coefficients that take place in the air gaps and the definition of performance indicators.

Keywords. Heated Supply air window, Experimental prototype, Heat fluxmeter, Building ventilation
DOI: https://doi.org/10.34641/clima.2022.338

1. Introduction

This project (NTE-VARIETO supported by ADEME (French ecological transition agency) is conducted in the framework of a collaboration between two French university laboratories, the LGCgE (University of Artois - Béthune) and the LASIE (University of La Rochelle) and also with a joinery company (Ets RIDORET). The objective is to obtain information allowing the characterization of the performances of a supply air heating window. This window of the Paziaud type [1] is relatively well known. Originally, its operating principle is to allow the transfer of air renewal through the window by circulating between three panes forming a U-shaped channel. In this configuration, the air circulation is ensured by the depression of the building under the effect of a mechanical controlled or natural assisted ventilation device. The air that circulates in the window is the fresh ventilated air and here the interest being that in winter, it is introduced more or less preheated in the building. The preheating is achieved by convection by recovering part of heat losses by transmission and some of the incident solar energy absorbed by the glazing. In recent years, the work of Gloriant [2,3] and Greffet [4] have allowed significant progress in the study of these windows and have also allowed the transition to industrialized component through official technical notice and to the consideration by the building thermal regulations.

In the "VARIETO" project, the interior glazing is replaced by an electrically powered heated glazing.

Copyright ©2022 by the authors. This conference paper is published under a CC-BY-4.0 license.

This disposition must allow to propose an element of the building envelope which is also a heat emitter. The contribution to heating is made both by a warm air supply (fresh air heated in the window) and by radiation and convection on the interior surface. The heated glass can reach a surface temperature of about 45°C, (maximum chosen for the safety of the occupants). In this project, the LGCgE is in charge of several experiments, one of which concerns the implementation of a ventilated heating window in-situ on the south façade of a building of the University of Artois in Béthune. This one is the subject of this paper.

2. Experimental device

- This prototype of window has the advantage of being able to be open as a fan-like model (figure 1 and thus allow us to access to all the six sides of the three panes.

- The exterior glazing is 6mm thick, without any special treatment.

- The central glazing is 4mm thick with one low-emissivity face (the one facing outwards and which will be numbered "3" in this work).

- The interior glazing is 8 mm thick. It is a laminated glass, two panes of 4mm each, with a resistive film of some µm thickness at the interface which will act as a heating resistor. This resistive film, like the low-emissive coating, has an attenuating effect on the transfer of solar (visible) radiation.

Fig 1 The prototype of parietodynamic window

The instrumented window (Fig 2) is located on the south façade of one of the buildings of the Faculty of Applied Sciences in BETHUNE. The objective is to carry out in-situ measurements by recording the external climatic conditions (air temperature, sunlight, IR radiation, wind speed), the heat fluxes passing through the glazing and the surface temperatures and air temperatures in the window. In this paper, we will focus on winter nights. These are the periods for which the interpretation of the measurements is the simplest. Indeed, when the window is exposed to solar radiation, the measurements of heat fluxes and surface temperatures are difficult to exploit.

Fig. 2 Instrumented window on the south façade of a faculty building in Bethune

In addition to the air temperature measurement, a pyranometer, a pyrgeometer and an anemometer are used to characterize the outdoor environment. The figure 3 shows the layout of thermocouples and tangential gradient fluxmeters.

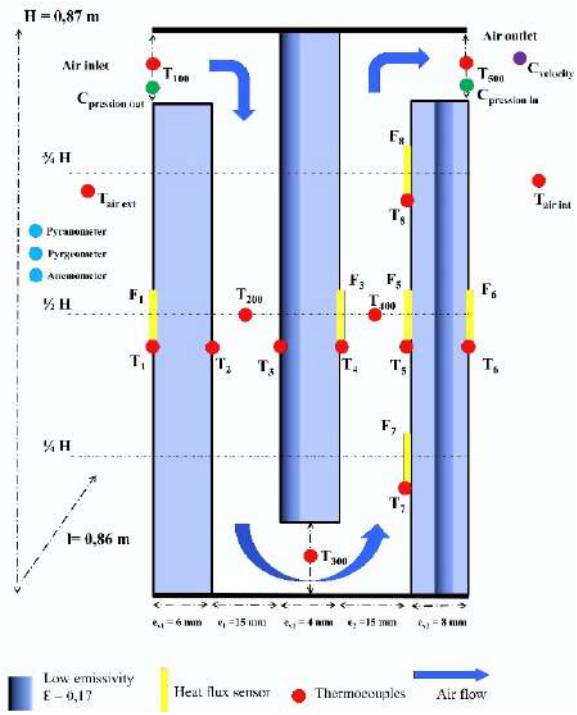

Fig 3 Sensors localization in the prototype

One of the particularities of a supply-air window is the variation that exists in the thermal flux densities for each of the panes (Figure 4). We aimed to highlight this particularity by placing in the window, thermal flux sensors (numbered from 1 to 6 according to a horizontal plane) and two others (7 and 8) arranged on the internal face of the heating glass (face 5) and at different heights (see Figure 2 and 3).

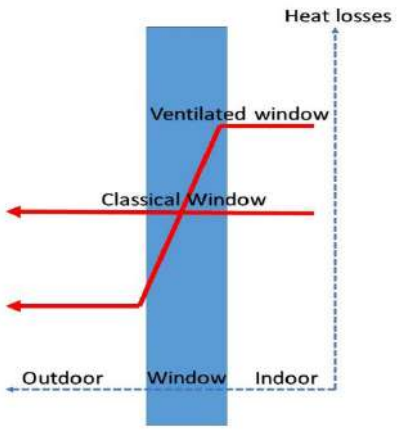

Fig 4 Comparison of the evolutions of the heat flux through a conventional window and in a parietodynamic window

These tangential gradient fluxmeters (Figure 5) were developed by our laboratory several decades ago [5]. They are now manufactured by the Captec® company and calibrated by our team. They have a very low thickness (< 0.2 mm) and thermal resistance and are well adapted to our measurement problem. These sensors have an average sensitivity of about 20 microvolts for an heat flux density of 1 W/m².

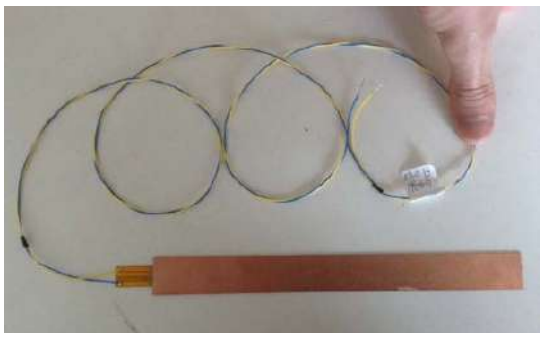

Fig 5: View of one of the fluxmeters used to instrument the supply air window

Originally made of raw copper, the faces of the fluxmeters were painted here to obtain an emissivity close to that of the glazing on both faces (~0.87). After gluing them with a very thin layer of thermal grease, the visible faces, facing the outside, were covered with a white adhesive to limit the absorption of solar radiation during the day.

Type T thermocouples were used for air and surface temperatures measurements. For surface temperatures measurements, the thermocouple junctions have a diameter of about 0.1 mm. They were bonded to the glass with an adhesive heat-conducting aluminum pad, a few mm in diameter. This was then covered with a white adhesive in order to reflect as much as possible the solar incident radiation on the probe. A Kapton adhesive, which has transparency and emissivity properties similar to those of glass, was used to keep the very fine thermocouples wires in position, so as not to disturb the air flow between the panes. On the low emissivity face of pane (number 3), a thermocouple has been glued with a very small (some mm diameter) reflective and low emissivity aluminum pad to reduce as much as possible the effect of the probe on the measurement.

The air temperature measurements in the window are made with T-type thermocouples of 0.05 mm diameter. At the window exit, a plenum was installed and connected to a 100 mm diameter PVC duct, itself connected to an air extractor (Figure 7)

Fig 7 View of the experiment

3. Experimental results - Simple supply-air window

The graphs 8, 9, 10 and 11 show us the first measurements made (16 to 18/11/2019) without activation of the heating resistor. We are then in the case of a classic supply-air window. The average airflow measured at the extraction is 23.45 m³/h. This flow rate is representative of common values, between 15 m³/h and 30 m³/h at the level of the air inlets with classic joineries.

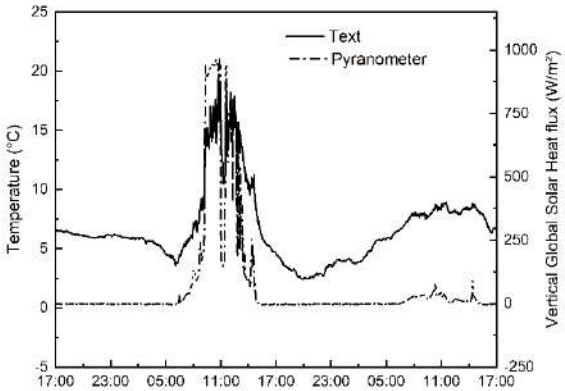

Fig 8 Global solar irradiation and outdoor temperature.

The figure 8 shows two days recordings of outdoor temperature and solar global radiation. On the first day, the incident solar radiation measured by the pyranometer reaches a maximum of almost 1000 W/m². This value is very important. This is due to a white roof under the window reflecting part of the incident radiation that it receives. It can be observed that the outside temperature seems to be also strongly affected by this.

The T100 thermocouple that measures the air temperature at the window entrance gives almost identical results (Figure 10). The outside air temperature measured very locally is not the same as the one that would be measured under shelter by a weather station. It is close to the temperature of the air entering the window (T100) and therefore probably also to the temperature of the air near the exterior glass surface. This point is particularly important to emphasize when determining performance indicators.

3.1 Temperatures

On the figure 9 we can observe the evolution of the surface temperatures of glazings for these two days. We note, here again, that the solar radiation is undoubtedly disturbing the measurements.

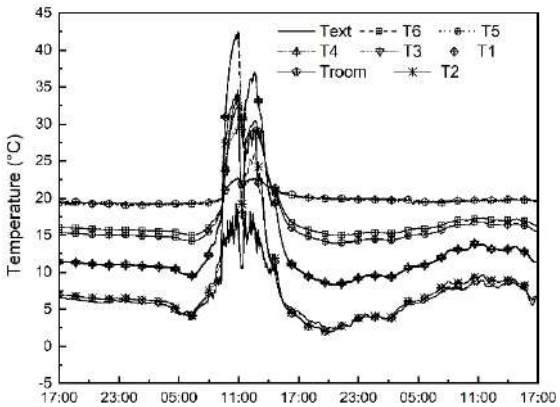

Fig 9: Ambient and surface temperatures

On the other hand, at night and on cloudy days, the measurements seem to be directly exploitable and very interesting. We can clearly see on the figure 9 the decrease in temperature from the inside to the outside of the building. The temperature differences between the two sides of the same pane are very small (at the limit of the measurement accuracy). One could not use this difference to deduce the flux through the glass by conduction heat transfer.

These results are complementary to the air temperatures (Figure10) flowing through the window. (See also Figure 3). The temperature T500 is measured in the plenum at the window outlet.

Here again the solar disturbance is such that the results of fluxmetric measurements cannot be easily exploited during the day.

Nevertheless, the white surfaces of the fluxmeters are very small compared to those of the glazing so the heating of the air by parietodynamic effect is clearly preponderant. It is of the order of 6 to 8°C during the night or when covered sky. It rises to a maximum of 15°C when the sun shine.

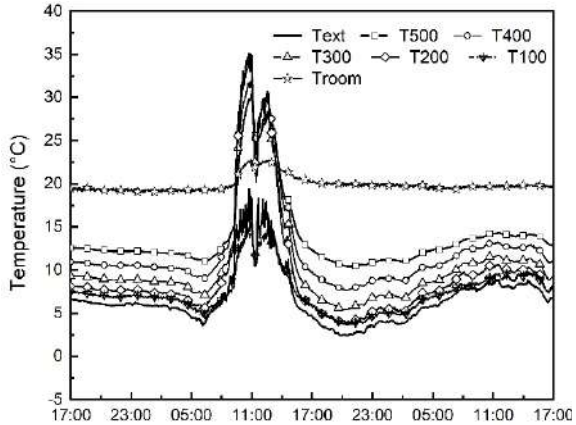

Fig 10 : Air temperatures

3.2 Heat fluxes

Finally, the figure 11 represents the evolution of the flows for the same period.

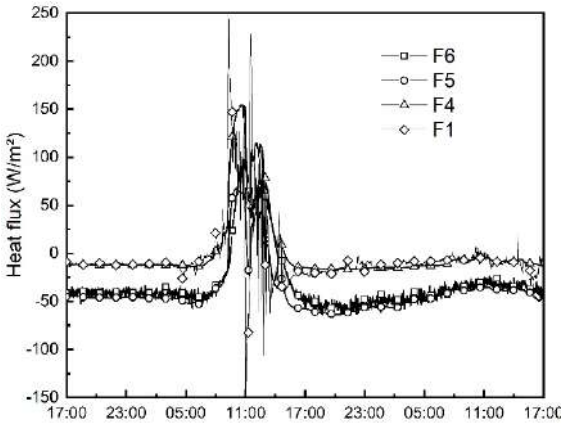

Fig 11 : Heat fluxes through the window

Here again the sunny period is not exploitable. It is interesting to note that the F1 (exterior glazing) and F4 (intermediate glazing) flows are very close and relatively low. This confirms that the outer air gap is not very active in terms of heat recovery, as it was noted in simulations in previous work [6]. In the second air gap, the increase in air temperature from the bottom to the top causes that F7 > F6 > F8. The fluxes F5 and F6 measured at mid-height on either side of the inner pane are very close.

3.3 Performances Indicators

By defining different control areas, Gloriant in his thesis [3] proposed performance indicators for the supply air window. If we consider control zone "1" (Figure 12), the fresh air enters the zone at the outside temperature as for a conventional window and it is the flux at the outside glazing that is used to calculate the U-value. This is the same definition used by Wright [7].

$$U_e = \frac{F_1}{T_{int} - T_{ext}} \quad (1)$$

If we consider the control zone "2", this time, the air

enters the zone after being preheated in the window's air gaps. The U-value is defined from the value of the flux at the interior glazing:

$$U_{dyn} = \frac{F_6}{T_{int} - T_{ext}} \quad (2)$$

In winter, this coefficient will be much greater than the previous one because of the increased transfers through the first glazing (from inside the building). But a large part of this energy is recovered by the ventilation air which is preheated and returns to the control zone. It is therefore necessary to add to the U-value another value which will be an indicator of the efficiency of heat recovery by the air in the supply air window.

$$\eta_{dyn} = \frac{T_{preheated\ air}(T_{500}) - T_{ext}}{T_{int} - T_{ext}} \quad (3)$$

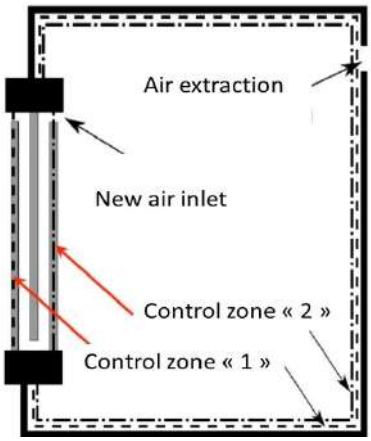

Fig 12 Control zones for defining performance indicators

Using the flux densities and the measured temperatures, we can estimate the Ue of the window with and without activation of the heated glass. To do this, we will take into account the measurements of thermal flux in pane 1. In the middle of the night from 17 to 18/11 the flux F1 is equal to about 10.8 W/m² on average. We note that F6 is a little noisier, due to exchanges by natural convection with the air of the room whereas the fluxmeter F5 is in contact with a laminar air flow in forced convection at low speed. The average temperature in the room for the same period is 19.5°C and the average outside temperature is about 6°C.

This gives us an "experimental" U_e in the order of 0.8 W/m²°C for a simple supply air window, a U_{dyn} of 3.22 W/m²°C and a recovery efficiency η_{dyn} = 0.45. These calculations are based on the average values of the flows and temperatures measured over the period.

The U_e (U_g) should be lower for a conventional supply air window than for an efficient triple glazing. This value is indeed quite high, far from the lower theoretical values obtained in modelling [2]. To improve the results, in reality the outdoor temperature to be taken into account experimentally is different from the air temperature because the IR radiation measured by a pyrgeometer gives here an environmental temperature of -7°C for the same period. Taking this temperature into account will tend to increase the temperature difference between the indoor and outdoor environments and the experimental U-value will be reduced. It should be noted that the measured outdoor temperatures are generally assimilated to air temperatures for heat loss calculations. Our results are indicative of an inaccuracy difficult to remove but generally accepted in the calculations. On the other hand, it is the air temperature that must be used for the energy balance on the ventilation air.

The advantage of the supply air window being here to preheat the fresh ventilated air, the energy balance is always very favourable even if the value obtained for the Ue is relatively high compared to the expected results based on models. It must be taken into account that these models were developed on 2-dimensional window diagrams, without taking into account the effects of the frame of the joinery, the thermal bridges and the sealing defects which can exist between the air gaps. The truth is probably somewhere in between.

4. Heated supply air Window

We now look at the behavior of a supply air window with active heated glazing. We are now in December. Over the period from December 1 to December 5, it appears very sunny days, with a very clear sky which increases the difference between the air temperature and the environmental temperature deduced from the pyrgeometer measurements. (ex Fig 13)

The days from the 6th to the 8th (not very sunny) will be more adapted to the analysis of our measurements (see Fig 14).

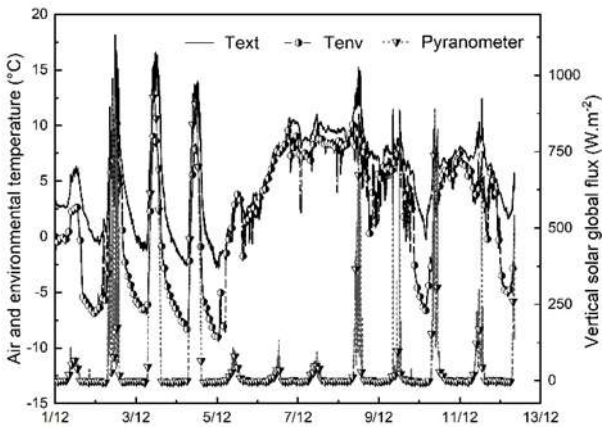

Fig 13 : Global solar irradiation and outside temperatures

It should be noted that from the first of December, the power supply to the window is 208.7 Volts, which is equivalent to a power dissipated by Joule effect in the window of about 354 W/m², with an average air flow rate in the window of 23,45m³/h.

In this paper we will focus on the period from 6 to 8 December. The graph below Fig 14 represents the evolution of the outdoor and indoor ambient temperatures as well as the different temperatures of the glazing. It allows to realize the impact of the solar radiation on these values. The sunny periods do not seem conducive to reliable analysis given the solar radiative disturbances on the measurements.

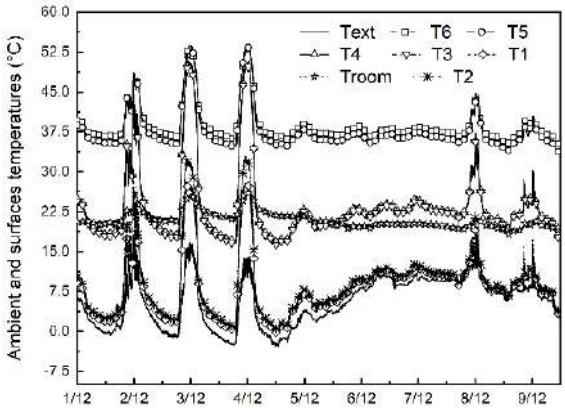

Fig 14: Glazing temperatures and ambient temperatures

Looking in more detail at the temperature curves of the glass panes, we can see that they go well in pairs with small differences between the two sides of each pane. On the other hand, the differences are important between the panes. The heated glass has an average temperature of about 37 °C while the temperature of the intermediate glass is around 22,5 °C. This difference is important and undoubtedly has consequences on the evolution of the exchange coefficients in this air gap. In the same way, in the external air gap, the difference is significant (about 12°C) between the two panes, probably reinforced by the low-emissivity coating on side 3. The external pane remains cold, close to the external air temperature.

4.1 Heat flux

On figure 15, we can note that the heat flux F6 becomes negative (according to the conventional direction we have chosen, positive heat flux is oriented from the inside to the outside). The flux is reversed here because the heated inner pane is active.

At the heart of this glass, a deposit of metal oxides forms a flat, heating electrical resistance. The night conditions are very stable. As in the case "without heating", the temperatures increase between side 1 and side 6. (Figure 16) A significant decrease in the value of the flux can be observed as one moves from the inside to the outside. The difference corresponds largely to the energy recovered by the air coming from outside at about 9°C and blown into the room at about 22°C. This is a very interesting result that the valuew of the F4 and F1 fluxes are very low. This indicates a priori a very good recovery of the power supplied by the electric power supply and of the heat losses crossing the window.

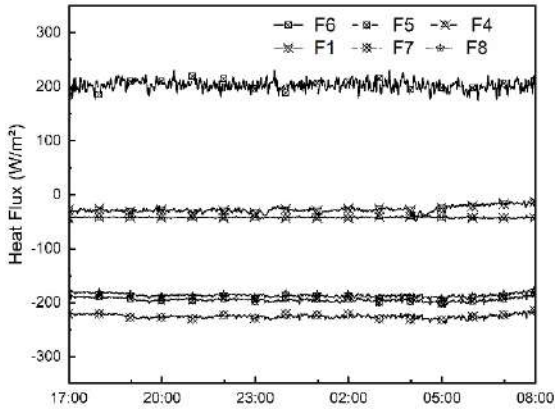

Fig 15 Thermal heat flux in the window between 07/12 at 5 pm and 08/12 at 6 am

A power of about 354 W/m^2 is injected into the heating element. The average thermal flux F5 measured is 195 W/m^2. The F6 flux is on average (and in absolute value), 203 W/m^2. The sum of the two fluxes exceeds the 354 W/m^2 supplied to the heating glass.

4.2 Temperatures

As in the previous test, we can see (figure 16) that the temperature differences between the two sides of the same pane are very small (maximum 1.3°C for the heated pane).

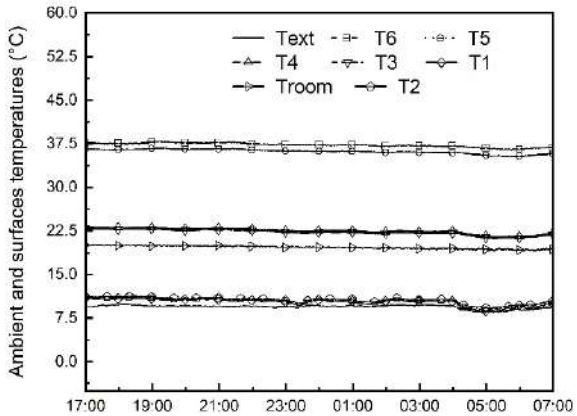

Fig 16: Surface temperatures of glazing in the window between 07/12 at 5 pm and 08/12 at 6 am

The average surface temperature of the heated glass is then around 37°C, transforming the glass into a radiator/convector. A flow of fresh air at an average temperature of 22,5°C (T500 - figure 17) is blown into the room (while the outside air temperature is around 9.5°C on average. The gain in fresh air preheating is therefore about 12.5°C. Here the energy gain by the air is relatively equivalent if we consider the two air gaps. (T300-T100 ~5,2°C) and T500-T300 ~6,7°C, which does not correspond to the expected results. The T300 temperature measured near the frame of the joinery and at the change of direction of the airflow is probably disturbed.

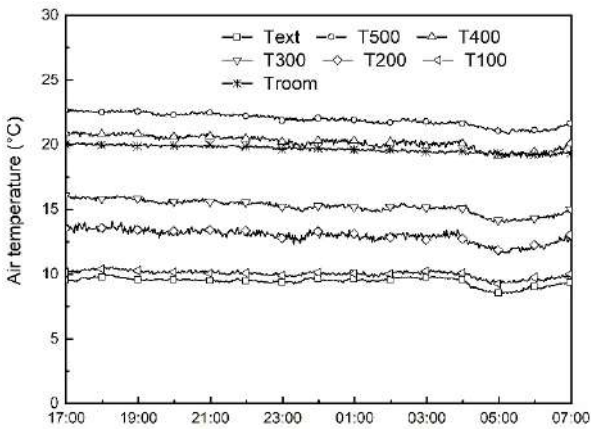

Fig 17: Temperatures of air circulating in the window between 07/12 at 5 pm and 08/12 at 6 am

Since the low-emissivity layer of the central pane is located on side 3 (exterior side), it does not prevent the absorption of energy transfer by radiation from the heated pane. The central pane then transmits heat into the two air gaps. It is conceivable that turning this low-emissivity pane inward would result in greater heating of the heated pane and an imbalance in convective transfers between the two air gaps. The question arises as to the best efficiency between the two options. The first experimental results presented here allow to highlight the role of preheater of fresh air played by the window and the role of heat emitter when the interior pane is heated. Figure 7 gives us an output flux (F1), in absolute value, of 26 W/m². Figure 6 shows an interior temperature of 19.5°C and an exterior temperature of 9.5°C. In the end, we have a Ug of 2.6 W/m²°C.

The average thermal power win by the air on the considered period is about 100W (0,34Wh/m³.K x 23,45m³/h x12,5°C) that we have to add to the power transmitted to the room by the interior glazing (~200 W/m² x (0,87x0,87 m²) = 151,4 W. The electric power furnished to the window *Pelec* is (354W/m²) x (0,87x0,87 m2) = 266W

Then we can think that there is about 15 W which are dissipated in the window through the frame, and we can hope that a majority of this power is transmitted to the room.

We have to consider that the power supplied is distributed over the entire surface of the glazing while the measurements made by the fluxmeters are local (in the center of the window). The fluxmeters are sensitive to the dissipation of the electrical energy supplied, but also to the different exchange conditions with the interior environment of the room and the air flow from the outside through the window. We must not forget that the sweep of the glazing surfaces temperature is not uniform and that there are probably dead zones related to the 3D geometry of the flow. These results must be taken with caution.

Indeed, in the case where the glazing is heated, new performance indicators are to be proposed.

4.3 Performance indicators

To characterize the performance of this window, i.e. to evaluate how well it insulates, the energy it provides and the energy consumed, it is necessary to define indicators of performance by blowing and the heat lost from the interior of the room (exponent "off" or "on" depending on whether the window is heated or not) [8,9,10]

Thermal flux entering the interior space

$$\mathrm{F}_{int}^{on} = \mathrm{F}_{air} + \mathrm{F}_{int} \ (\mathrm{W/m^2}) \qquad (4)$$

where F_{air} is the power gained by the fresh air in relation to the glazed area of the window (W/m²).

F_{int} is the heat flux density for the glazing on the interior side (heated room)

Heat transmission coefficient

$$U_g = \frac{\mathrm{F}_{ext}^{on}}{T_{int} - T_{ext}} \ (\mathrm{W/m^2K}) \qquad (5)$$

F_{ext}^{on} the heat flux density for the outer glazing representing here the heat losses

Window efficiency

$$E_w = \frac{\mathrm{F}_{ext}^{off} + \mathrm{F}_{in}^{on}}{Pelec} \qquad (6)$$

F_{ext}^{off} the flux density that would exist if the heated window was not activated.

Efficiency of the heating film

$$E_{film} = \frac{\mathrm{F}_{int}^{on}}{Pelec} \qquad (7)$$

Equations 4, 5, 6 and 7 define the performance indicators. From the measurements of heat flux, temperature and power, we can evaluate the energy performance of the window. A coefficient classically noted g (ISO 15099 [11]) will be used in the presence of solar radiation.

calculation of the coefficient g

$$g = \frac{F_{transmis} + (F_{éch} - F_{int})^{sol} - F_{ext}}{F_{sol\ incident}} \qquad (5)$$

It is difficult at present to determine precisely the values of the performance factors of the heated window because they are based on the evaluation of heat fluxes transferred to the environments at any time. We show that it is possible to measure these fluxes correctly at night but very difficult to do so when the window is under the influence of sunlight. It is also difficult to know the share of energy recovered from the heat losses, from the solar

absorption of the glazing and from the power supplied to the heated glazing by using Kurnitski's equations.

In these equations there is an "off" and an "on" heatflux depending on whether the heating is activated or not. And it is currently difficult to find the value of one when measuring the other. A numerical simulation model is actually built to solve this problem.

5. Conclusion

In this paper we have presented the first results of an experimentation aiming at better understanding the functioning of a heated supply air window and establishing performance indicators. These results show the interest of the window in terms of preheating or heating of new ventilation air. Here we are in a room of about 350 m^3 with 5 windows of the same dimensions and equipped with hot water radiators. In an application framework, it will be necessary to dimension the window surfaces according to the room to be heated. There are undoubtedly great advantages to using heated windows. In fact, it eliminates the problem of cooling of the interior glazing in winter in the case of ventilated windows, thus eliminating the risk of condensation and improving thermal comfort. Another advantage is the removal of heat emitters that take up space in the room. However, the calculation of the Ug-value gives here apparently too high values, they are equivalent to that of a normal triple glazing. In the case of the addition of a heating glass, the first results are interesting but to be confirmed in detail. We can show here the problem of the definition for the performance indicators when a façade component is also an essential part of the ventilation system and also an heat emitter highly perturbated by meteorological parameters. (global sun radiation and outdoor temperature (air and environment).

[1] Paziaud J., 1983. Fenêtre à isolation dynamique par circulation d'air. Patent 8205279. 30 septembre 1983.

[2] Gloriant F., Joulin A., Tittelein P., Lassue S., 2014. Modeling a triple-glazed supply-air window. Building and Environment. 2014. DOI 10.1016/j.buildenv.2014.10.017. Volume 84, January 2015, Pages 1-9

[3] Gloriant François, 2014. Caractérisation et modélisation d'une fenêtre pariéto-dynamique à trois vitrages. Université d'Artois.

[4] Greffet R. 2016. Etudes expérimentales et numériques des performances energétiques d'une fenêtre pariétodynamique. Thèse de doctorat CIFRE - Université de la Rochelle.

[5] Leclercq D, P. Thery 1983 Apparatus for simultaneous temperature and heat-flow measurements under transient conditions Rev Sci Instrum, 54 , pp. 374-380

[6] Gloriant F., Joulin A., Tittelein P., Lassue S., Using heat flux sensors for a contribution to experimental analysis of heat transfers on a triple-glazed supply-air window, Energy, Vol. 215, Part A, 15 January 2021, 119154

[7] Wright J.L., Effective U-values and shading coefficients of preheat/supply air glazing systems, Proc Sol. Energy Soc. Can., Winnipeg, Canada (1986), pp. 219-224

[9] Kurnitski 2002. Efficiency of electrically heated windows, Helsinki University of Technology, HVAC-Laboratory, Finland: the 9th International Conference on Indoor Air Quality and Climate.

[10] Kurnitski J, Jokisalo J. , Palonen J., Jokiranta K. , Seppänen O. 2004. Efficiency of electrically heated window. Energy and Building, pp. 1003-1010.

[11] Kaboré M., Rapport d'avancement projet NTE-ADEME – Varieto - Analyse de sensibilité et études paramétriques d'une fenêtre pariétodynamique intégrant un film chauffant. (2018). Paris

[12] ISO-15099. 2003, "Thermal Performances of Windows, Doors and Shading Devices - Detailed Calculations". Technical report.

Data sharing not applicable to this article as no datasets were generated or analysed during the current study.

Life cycle analysis of warehouse-type constructions

Ionut Emil Iancu [a], Ligia Mihaela Moga [b]

[a] Faculty of Civil Engineering, Technical University of Cluj-Napoca, Cluj, Romania, iancu_ionut_emil@yahoo.com

[b] Faculty of Civil Engineering, Technical University of Cluj-Napoca, Cluj, Romania, ligia.moga@ccm.utcluj.ro

Abstract. This paper conducts a comparative analysis of the life cycle for industrial warehouse-type buildings, intending to compare the embodied emissions and the embodied energy for the assessed cases and at the same time draw practical conclusions for practitioners. The analysis aims to identify the optimal solutions for the conformation of industrial buildings as well as the sustainability, from components choice and structural solution approach.
Four industrial buildings with different structural solutions, building envelope components, and destination are assessed: 1st case: a steel structure with production and storage as the main activity, having the destination of warehouse construction and energy storage and distribution; 2nd case: a mixed structure made of steel and wood used as a production space, namely glued laminated timber production; 3rd case: a commercial warehouse made of prefabricated concrete elements, intended for storage and sale of construction materials; 4th case: a commercial warehouse made of prefabricated concrete elements with metal roofing, intended for storage and sale of household goods. The analysis was performed using the Athena Impact Estimator software by imputing the description for all the materials describing the components, the locations of the buildings, the destination of each building, and other relevant data. Based on the preliminary results it was concluded that the industrial building made of prefabricated concrete elements (i.e. 3rd case scenario) is the most balanced and sustainable in terms of carbon and embodied energy.

Keywords. Life Cycle Analysis, industrial warehouse, embodied energy, embodied carbon.
DOI: https://doi.org/10.34641/clima.2022.329

1. Life cycle analysis of industrial buildings

The life cycle analysis of a construction (fig.1) calculates the impact it has incorporated from "cradle to grave": namely the effects of extracting the necessary resources, manufacturing and transporting products, proper construction, maintenance / replacement of products and demolition / deconstruction / disposal (1).

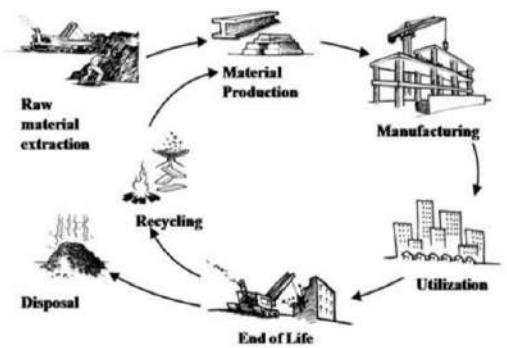

Fig. 1 - Representation of life cycle assessment from raw materials to end of life (cradle to grave) *(2)*

This analysis also includes operating energy and impact beyond life (the possibility of reusing / recycling resources) (1).

2. The evaluation method of the calculation program

In order to perform the needed analysis, the chosen program used in this assessment is Athena Impact Estimator (3). The program performs an analysis by modelling the building's complete structure and envelope over the entire life of the building. It takes into account the maintenance and replacement carried out, by building type and location. By entering the quantities of each material used to execute a construction, broken down into modules and stages of execution (4), the software takes into account the environmental impacts of material manufacturing and related transportation, on site construction, building type and regional variations of energy use and transportation, maintenance and repair over its lifespan, implications of demolition at the end of its life and operating energy emissions.

Copyright ©2022 by the authors. This conference paper is published under a CC-BY-4.0 license.

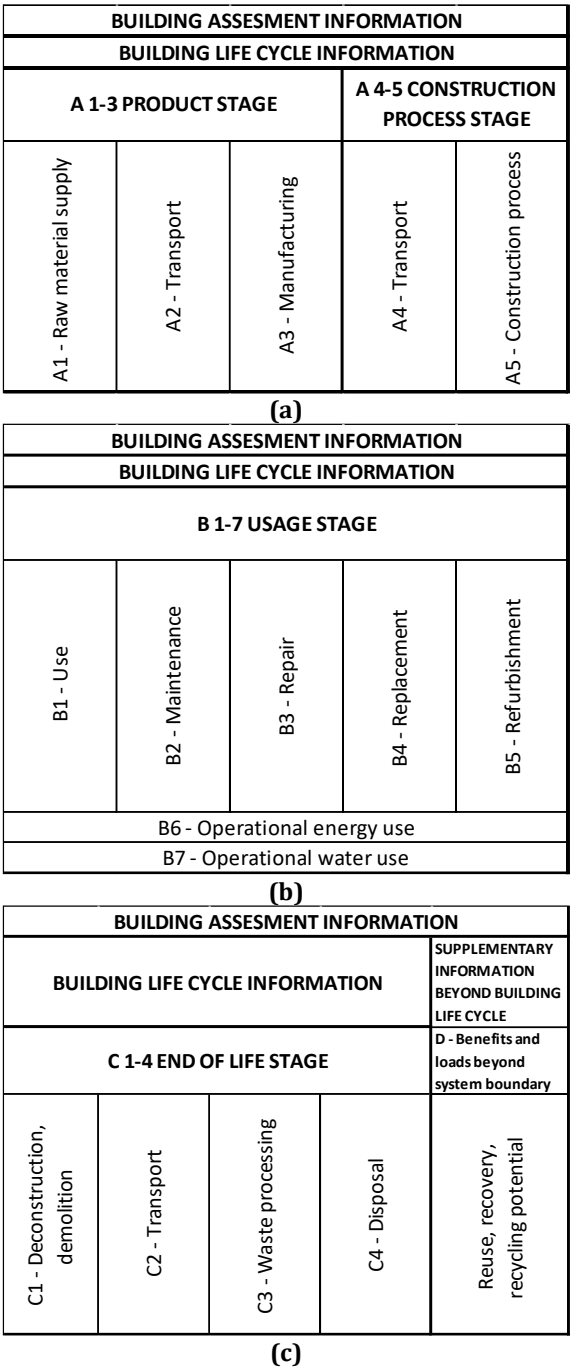

Fig. 2 - LCA analysis modules (adapted from *(5)*)

Thus, we have modules A1-A3 (fig. 2a) that describe the supply of raw materials, transport and manufacturing of the products to be put into operation, modules A4-A5 (fig. 2a) regarding the transport of products, the execution and the commissioning of the construction.

Modules B from 1 to 7 (fig. 2b) are the effects produced by use, maintenance and reconditioning.

Modules C1-C4 (fig. 2c) are related to the end-of-life effects of a construction, namely demolition, waste transportation and processing.

Therefore, all modules starting from A1 up to C4 provide the figures for the Building life cycle for the assessed case, while the last module, D (fig. 2c), provides data regarding the benefits obtained from recycling, recovery and reuse of the used materials.

3. Presentation of the analyzed industrial warehouses

Similar studies were performed using the Athena Impact Estimator tool by Moore et al (6) and Chen et al (7) with the aim of presenting a comparative analysis between buildings made up from different materials. Walter P. Moore concluded that metal buildings performed better in LCA analysis than concrete and masonry (6). The second study (7) conducted a comparative analysis on two high-rise buildings constructed from cross-laminated timber and reinforced concrete. For high-rise buildings, the study concluded that mass timber buildings perform better (7).

For the present analysis, four industrial buildings with different structural solutions, were assessed. Each building is described by its main function, as it follows:

1st case - Arc Park Industrial: a steel structure with production and storage as the main activity, having the destination of warehouse construction and energy storage and distribution;

2nd case- Lunca Ilvei: a mixed structure made of steel and wood used as a production space, namely glued laminated timber production;

3rd case- Hornbach: a commercial warehouse made of prefabricated concrete elements, intended for storage and sale of construction materials;

4th case- Kaufland: a commercial warehouse made of prefabricated concrete elements with metal roofing, intended for storage and sale of household goods.

Considering the varied detailing of each case study, the analysis of a variety of structural systems and envelope elements was performed. A short presentation of each case study is offered.

3.1 Production and storage warehouse Arc Parc Industrial, Dej, Cluj county (fig.3)

Fig. 3 - Rendering of architecture Production and storage warehouse Arc Industrial Park *(8)*

The warehouse has a total area of 5130 m^2, with an attic height of 7.60m and a total ridge height of 11.50m .

The infrastructure consists of a system of isolated reinforced concrete stepped footings, with the foundations for the perimeter base and for the masonry walls inside the building made of reinforced cantilever footings.

The building consists of the resistance structure, frame-type with metal pillars and beams with bars on the transverse and longitudinal direction, and the docking areas made of reinforced concrete diaphragms, with a reinforced concrete slab at the top.

The envelope elements are made of BCA blocks, the confined masonry type and thermally insulated metal panels (sandwich) of 80mm, and the roof is of the framework in two waters, with the structure of lattice beams, metal panels and the cover made of 80mm thickness sandwich panels.

3.2 Wood production warehouse Lunca Ilvei, Bistrita Nasaud county (fig. 4)

Fig. 4 - Rendering of architecture Wood production warehouse Lunca Ilvei (9)

The warehouse has a floor area of 9911 m^2, ground floor height regime and a building height of 14.60 m. Being a production unit, it is also equipped with overhead cranes.

The infrastructure consists of isolated reinforced concrete footings under the metal columns of the warehouse and continuous footings under the annexes of the hall. These foundations stand on a compacted ballast cushion and are connected to each other by reinforced concrete cantilever beams.

The building has a metal resistance structure with centrally braced frames. The main beams of the roof are made of laminated timber and the roof panels are made of laminated wood beams arranged on the main beams.

The building envelope is made of 2 types of sandwich panels as walls, with the following composition from the inside to outside: laminated wood 10-12 cm and thermal insulation 10 cm, vertical uprights / air layer 6 cm, wooden sleepers 4 cm, laminated exterior wood 3 cm. These walls are mounted on the entire perimeter of the warehouse over a 2 m high concrete base with a sandwich type structure from inside to outside: reinforced concrete layer 15 cm - thermal insulation 15 cm - reinforced concrete layer 10 cm. The BCA masonry walls are thermally insulated with 10 cm of mineral wool and covered with laminated wood on the outside in the manner of sandwich walls. The compartments are made of 12 cm layered wood walls, and the roof is made of 10 cm thick sandwich insulation panels.

3.3 Hornbach commercial warehouse, Cluj-Napoca, Cluj county (fig. 5)

Fig. 5 - Rendering of architecture Hornbach commercial warehouse *(10)*

The warehouse has a floor area of 10953 m^2 with ground floor and partial 1st floor, with a building height of 8 m.

The infrastructure consists of isolated footings, specific to the prefabricated reinforced concrete structures. Perimetrically, there is a three-layer prefabricated reinforced concrete base, 14 cm of reinforced concrete + 10 cm of polystyrene (thermal insulation) + 6 cm of reinforced concrete with the role of thermal insulation protection.

The suprastructure is made of prefabricated reinforced concrete columns and beams.

The envelope is made of exterior sandwich type wall panels with PIR core 15 cm (Polyisocyanurate) and glass facade, and the interior partitions made of plasterboard panels mounted on a metal structure. There are also interior walls made of reinforced concrete, and the roof of the warehouse is made of corrugated metal panels and thermal insulation of 20 cm (basalt mineral wool).

3.4 Kaufland commercial warehouse, Sibiu, Sibiu county (fig. 6)

Fig. 6 - Rendering of architecture Kaufland commercial warehouse *(11)*

The warehouse has a floor area of 5232 m^2 with ground floor regime and a building height of 6.78 m.

The infrastructure consists of isolated concrete footings under each pillar. On the upper face of the footings, the prefabricated panels consisting of three-layer base with a resistance layer of 16 cm, thermal insulation of 8 cm and the outer protective layer of 10 cm, are mounted. Continuous footings are made under the masonry walls inside the warehouse.

The suprastructure is made of prefabricated reinforced concrete columns and beams and metal structure for the roofing.

The envelope is made of two types of facade panels: three-layer prefabricated panels with a resistance layer of 16 cm, thermal insulation of 8 cm and the outer protective layer of 10 cm; monolayer prefabricated panels with a resistance layer of 16cm. The partition walls are made of 24cm thick and 12.5cm thick masonry and have a concrete belt at the top. Reinforced concrete columns were placed at the intersection of the walls. At the technical spaces, reinforced concrete floors with a thickness of 15 cm are provided. There are also structural boxes with thermal insulation and sinusoidal metal sheet on the walls and trapezoidal metal sheet with thermal insulation and waterproofing on the roofs.

4. Results and discussions

Tables 1-4 summarize the quantities of materials used in the construction of the warehouses.

The materials used in the execution of the resistance structure and the component materials of the envelope elements were taken into account. The materials and products for finishing were not taken into account in this analysis.

Table 1 - Materials used in the analysis of Arc Parc Industrial production and storage warehouse

Material	Unit	Total quantity
Insulated Metal Panel	m2	9366.67
Concrete C8/10 and C16/20	m3	1745.50
Concrete C20/25	m3	156.45
Autoclaved aerated concrete	m2	1773.45
Glass Fibre	kg	21168.00
Hot Rolled Sheet	Tonnes	155.86
Rebar, Rod, Light Sections	Tonnes	54.40

Table 2 - Materials used in the analysis of Wood production warehouse Lunca Ilvei

Material	Unit	Total Quantity
Coarse Aggregate Crushed Stone	Tonnes	3497
Concrete C20/25	m3	4464.18
Concrete C30/37	m3	221.55
Concrete C40/50	m3	573.51
Cross Laminated Timber	m3	546.41
Expanded Polystyrene	m2 (25mm)	46641
Fine Aggregate Natural	Tonnes	457.2
Glass Fibre	kg	44625
GluLam Sections	m3	816.4537
Hot Rolled Sheet	Tonnes	258.61858
MBS Metal Roof Cladding	m2	20492.9
Mortar	m3	221.95
Mineral wool	m2 (25mm)	1514.94
Rebar, Rod, Light Sections	Tonnes	346.75623

Table 3 - Materials used in the analysis of Hornbach commercial warehouse

Material	Unit	Total Quantity
Gypsum Board	m2	2,015.20
Concrete C20/25	m3	3,064.95
Concrete C30/37	m3	9.41
Concrete C40/50	m3	197.21
Concrete C50/60	m3	708.49
Double Glazed Hard Coated Argon	m2	1,010.00
PVC membrane	m2	36,875.10
Metal Roof Cladding	m2	11,062.53
Metal Wall Cladding	m2	10,048.38
Mortar	m3	110.4
Mineral wool	m2 (25mm)	110,808.60
Polypropylene fibers	Tonnes	6.64
Rebar, Rod, Light Sections	Tonnes	241.49
Wide Flange Sections	Tonnes	64.69

Table 4 - Materials used in the analysis of Kaufland commercial warehouse

Material	Unit	Total Quantity
Cold Rolled Sheet	Tonnes	0.15
Concrete C8/10 and C16/20	m3	82.32
Concrete C20/25	m3	251.49
Concrete 30/37	m3	453.6
Concrete 50/60	m3	182.7
Hot Rolled Sheet	Tonnes	1.11
Metal Roof Cladding	m2	5,353.00
Mineral wool 140mm for roof	m2 (25mm)	27,825.00
Mineral wool 80mm for wall	m2 (25mm)	1,365.00
Rebar, Rod, Light Sections	Tonnes	98.04
PVC Membrane	m2	17,843.33
Softwood Plywood	m2 (9mm)	1,071.00
Welded Wire Mesh	Tonnes	9.38
Wide Flange Sections	Tonnes	1.36

The impact that the construction and operation of these types of warehouses have during their lifetime is outlined based on the materials used. In terms of final results, the following indicators are of interest::

- global warming potential - through greenhouse gas emissions (kgCO_2 equivalent);

- acidification potential - air pollution is converted into acidic substances (kg equivalent Sulfur dioxide);

- emissions of fine particles into the air (kg of fine matter - particulate matter);

- eutrophication potential - increase of nitrates in water and soil (kg nitrate equivalent);

- potential for ozone depletion - ozone decomposition due to emitted gases (kg chlorofluorocarbon equivalent);

- potential for smog formation - involves the formation of a layer of ozone and other gases in a lower layer of the atmosphere, which generates a number of lung diseases and adverse weather effects;

- total primary energy incorporated;

- non-renewable energy and depletion of fossil fuels.

Graphs 1-4 show for each studied warehouse, by comparison, the embodied (blue) and operational (green) CO_2 input over the entire standard life of the warehouses (taken 50 years).

Graph 1 - Embodied carbon for the Arc Parc Industrial production and storage warehouse

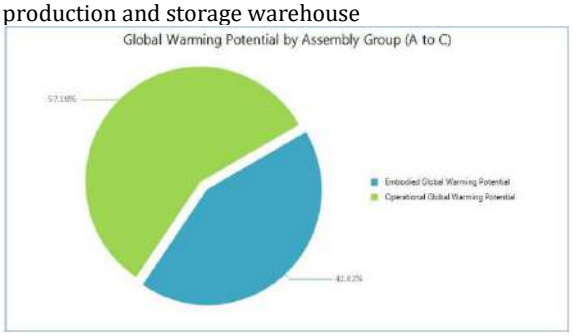

Graph 2 - Embodied carbon for the Lunca Ilvei wood production warehouse

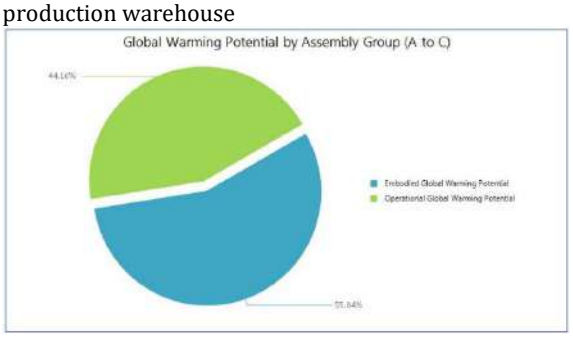

Graph 3 - Embodied carbon for the Hornbach Commercial warehouse

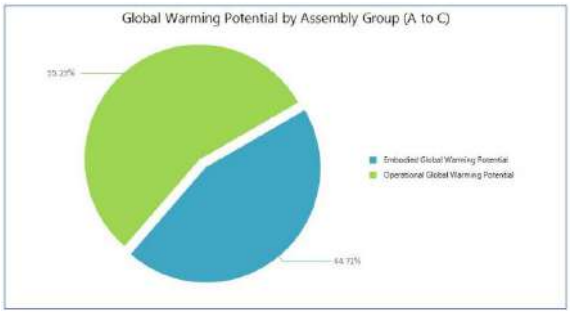

Graph 4 - Embodied carbon for the Kaufland Commercial warehouse

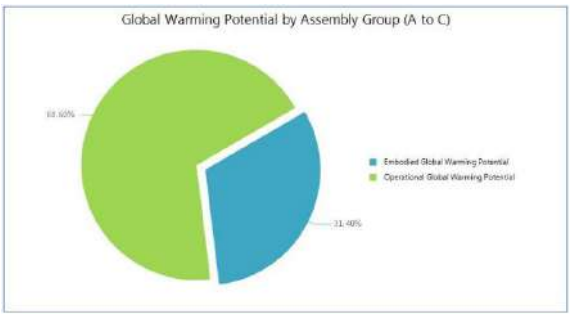

The embodied primary energy input (blue) and the operational primary energy (green) is figured in graphs 5-8 for each of the studied warehouses.

Graph 5 - Embodied energy for the Arc Parc Industrial production and storage warehouse

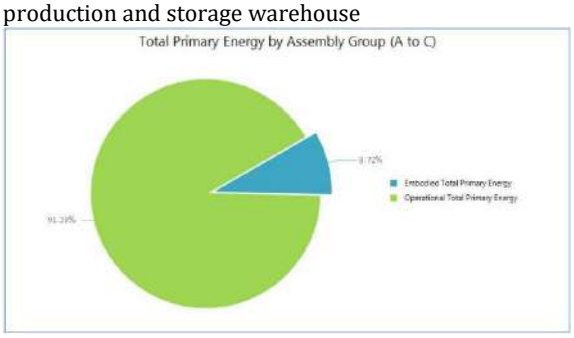

Graph 6 - Embodied energy for the Lunca Ilvei wood production warehouse

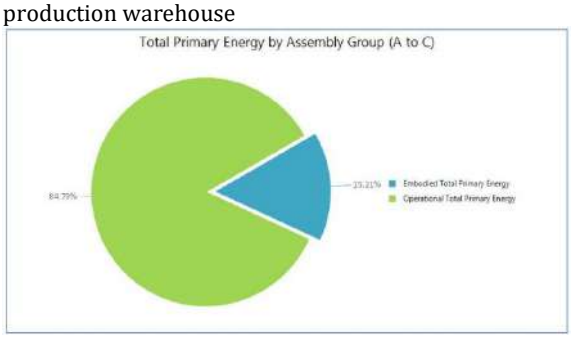

Graph 7 - Embodied energy for the Hornbach Commercial warehouse

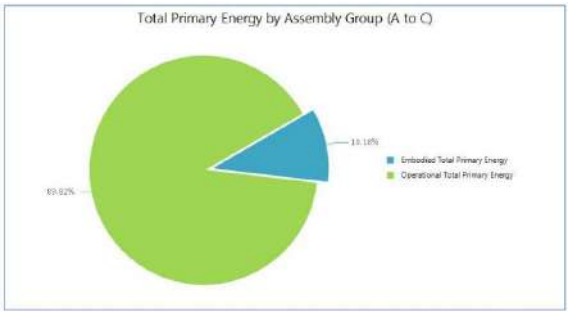

Graph 8 - Embodied energy for the Kaufland Commercial warehouse

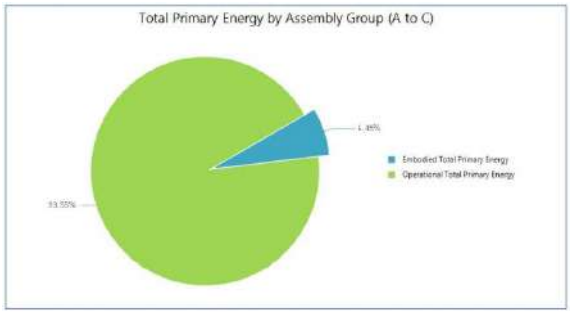

The comparative results show the absolute values (in graphs 9 and 10) of the CO_2 emissions for the 4 warehouses in the situation "cradle to grave A-C" and "cradle to cradle A-D". We notice that the warehouses with the largest surfaces, Hornbach and Lunca Ilvei recorded the highest emissions and the largest amount of energy incorporated. But on the forefront stands the Lunca Ilvei wood production warehouse. Following its material analysis, we found that higher quantities of materials were used, which led to this result.

Graph 9 - Embodied carbon for modules A to C

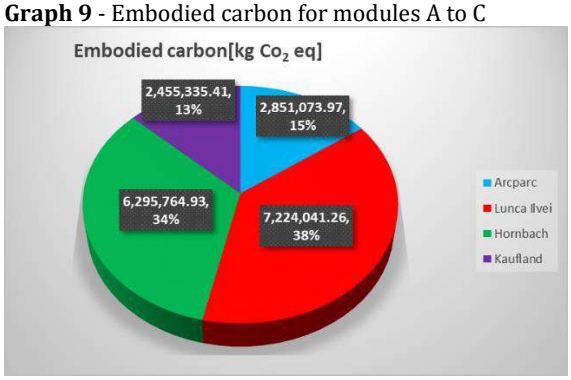

Graph 10 - Embodied carbon for modules A to D

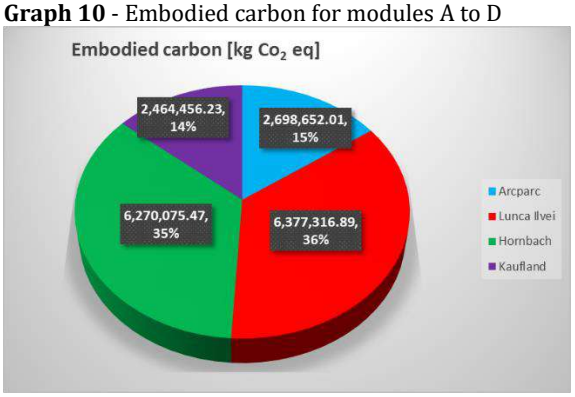

The values of the emissions related to the surface of the units (see graphs 11 and 12) is indicating that although Hornbach and Lunca Ilvei warehouses have the highest incorporated CO_2 amounts, if one takes into account the fact that the former has the largest footprint and useful area, we can deduce that its structural solution along with its building envelope components lead to a more favorable result / m^2.

Graph 11 - Embodied carbon for modules A to C relative to surface

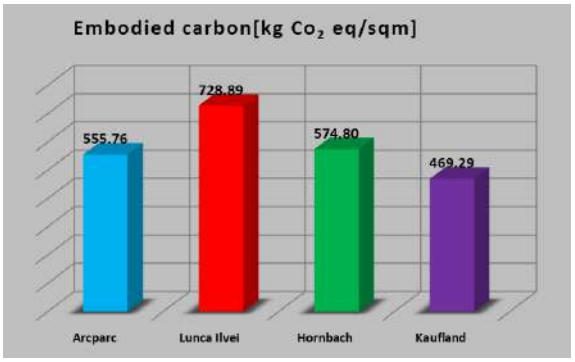

Graph 12 - Embodied carbon for modules A to D relative to surface

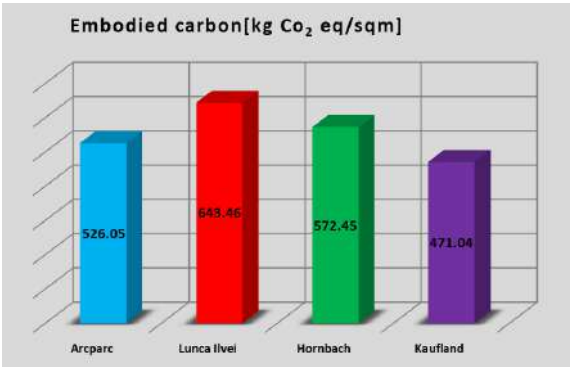

By comparing the materials used (table 5) in the construction of the warehouses,

Table 5 - Centralization of materials used in all warehouses

Material	Unit	Arcparc	Lunca Ilvei	Hornbach	Kaufland
concrete	m^3	1,902.00	5,481.00	4,090.45	970.00
steel	t	210.26	605.00	306.17	110.00
masonry	m^2	1,773.45	0.00	2,015.00	0.00
insulation	m^2	29,973.34	48,155.94	110,808.60	29,190.00
wood	m^3	0.00	1,362.86	0.00	0.00
surface	**m^2**	**5130**	**9911**	**10953**	**5232**

graphs 13 to 15 show the share of the quantity of the three predominant materials in all the four.

Graph 13 – Quantity of the used concrete [%]

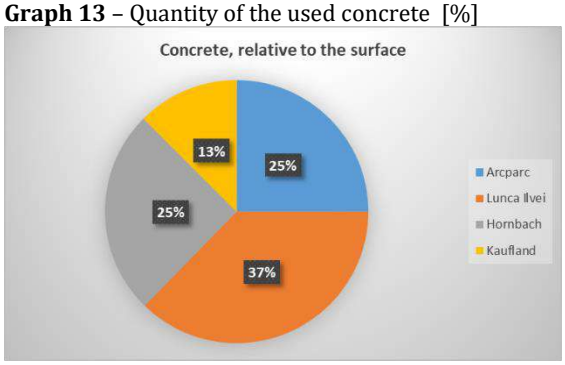

Graph 14 – Quantity of the used steel [%}

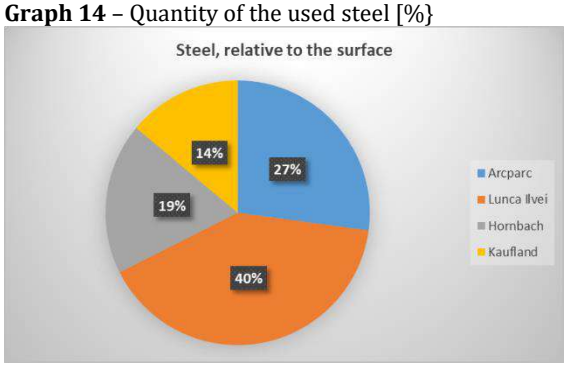

Graph 15 – Quantity of the used thermal insulation [%]

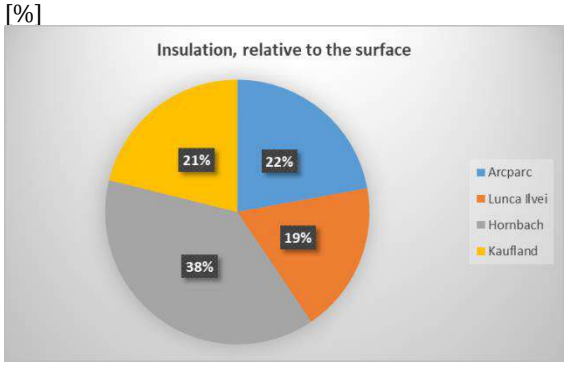

Thus, the amount of concrete and steel component is high in Lunca Ilvei warehouse while the amount of thermal insulation is the lowest in Lunca Ilvei compared to the other buildings. The other 3 industrial buildings have a balanced ratio of materials, as one can see in graphs 13 to 15.

And in order to indicate the contribution of the material in the amount of emissions and incorporated energy, a parallel study to LCA analysis on these four warehouses was conducted on the material. Thus, the impact of 1 m^3 of reinforced concrete (2500 kg), 2.5 tonnes of steel and 2.5 tonnes of glued timber was verified.

The following were obtained: wood has the best behavior in terms of carbon emissions both during life cycle and after. Steel has the greatest negative impact on the environment, both through the embodied carbon and through the embodied energy; but it also has the highest percentage of reuse / recycling. Concrete is the most balanced: the embodied carbon is medium, the embodied energy is the lowest of the 3 materials analyzed.

5. Conclusions

Construction occupies a significant percentage in the process of environmental degradation in all stages of life, from design, production of construction materials, transport and commissioning, operation and maintenance, to demolition and recycling (12).

Construction is a sector that, by its nature, has a major impact on the environment. Globally, the cumulative impact of construction processes has increased exponentially due to the accelerated development of the urban environment. It is reported that the operation of buildings (maintenance, occupation) contributes to a third of global greenhouse gas emissions and more than 40% of the use of energy resources globally. Population growth and migration to large urban centers are the premise for the need to develop new homes, shopping centers, industrial buildings, etc (13).

Responsible use of construction materials, products and technologies can significantly contribute to a better environmental performance of buildings throughout their life cycle and thus to their sustainability. Methods for analyzing the impact on the environment as well as potential reductions, improvements and savings can be brought from the design stage by implementing an LCA analysis in the design stage of the buildings.

As it can be seen from the analysis conducted on the 4 industrial buildings, the ones with the highest concrete content (i.e. Hornbach and Kaufland) and the lowest content of the other materials (steel, wood) have the highest sustainability as well as durability, taking into account the surfaces to which they refer, as well as the energy consumption in operation, during the normal duration of their use.

The present study consisted in assessing existing warehouse buildings. Thus, the authors are not able to provide an assessment at the initial design phase. The aim was to do a comparison study between existing buildings from an LCA perspective.

Future research directions should be directed towards prefabricated concrete industrial buildings, as they present the optimal solution in terms of sustainability and durability.

6. References

1. Guiyuan Han, M.Sc. and Jelena Srebric, Ph.D. Life-Cycle Assessment Tools for Building Analysis.
2. Life cycle assessment of villas , comparison between wood and brick facade. Fiskarhedenvillan. June 2018, Vol. Energy Efficient Built Environment No . 2.
3. Athena EcoCalculator for Commercial and Residential Assemblies: Inner Workings Synopsis. s.l. : Athena Sustainable Materials Institute, 2012.
4. Institute, Athena Sustainable Material. Impact Estimator for Buildings V. 5 User Manual and Transparency Document. 2019.
5. EN 15804:2012. 2021 : s.n.
6. Associates, Walter P. Moore and. Athena Impact Estimator Case Studies. 2015.
7. Comparative Life-Cycle Assessment of a High-Rise Mass Timber Building with an Equivalent Reinforced Concrete Alternative Using the Athena Impact Estimator for Buildings. Zhongjia Chen, Hongmei Gu, Richard D. Bergman and Shaobo Liang. s.l. : MDPI, 2020.
8. project no 216. Dej : designed by SDC Proiect, 2014.
9. project no 199. Lunca Ilvei : designed by SDC Proiect, 2013.
10. project no 379. Cluj Napoca : designed by SDC Proiect, 2017.
11. project no 234. Sibiu : designed by SDC Proiect, 2014.
12. Dan Georgescu, Adelina Apostu. Impactul constructiilor din beton armat asupra mediului.
13. Buildings and Climate Change. United Nations Environmental Programme. 2009, Sustainable Buildings & Climate Initiative.

The datasets generated during and/or analysed during the current study are not publicly available because of the commercial satus of the projects but are/will be available uppon request, under certain confidenciality therms.

Going active: How do people envision the next generation of buildings?

Elli Nikolaidou [a], Ian Walker [b], David Coley [a], Stephen Allen [a], Daniel Fosas [c]*

[a] Department of Architecture and Civil Engineering, University of Bath, Bath, United Kingdom

[b] Department of Psychological Sciences, University of Surrey, Guildford, United Kingdom

[c] School of Engineering, University of Edinburgh, Edinburgh, United Kingdom

Abstract. With several countries having declared a climate emergency and set decarbonisation targets, the built environment is expected to change radically. Several building standards have been developed to reduce carbon dioxide emissions from buildings, but they do not provide a clear pathway to a net zero future. The recently launched Active Building Code (ABCode) offers guidance on minimising the environmental impact of the next generation of buildings termed Active Buildings (ABs). This is achieved through their synergetic relationship with the grid. This paper presents our two-stage investigation into the stakeholder perceptions of ABs. In stage 1, we collected thoughts on the future of the built environment through a series of online focus group discussions with 30 industry experts. In stage 2, we quantified the ideas that arose from stage 1 through an online survey of 30 academics and researchers. Participants answered four questions, namely: (i) what is missing from existing regulations and standards; (ii) what is an AB; (iii) how should the performance of ABs be assessed; and (iv) what are the challenges to the popularisation of ABs. The data that was collected from the focus groups and the survey was analysed visually and statistically using logistic regression to identify the aspects stakeholders find important when envisioning the next generation of buildings. No significant differences were, in general, observed between the two groups, with industry and academia agreeing that whole-life carbon, energy demand, and energy flexibility should be used for the performance assessment of ABs – therefore aligning with the metrics suggested by the ABCode. Both groups interpreted 'activeness' as responsiveness, with industry experts highlighting the need to better define the relationship between buildings and the grid. They also regarded people's mindset as the biggest challenge faced by ABs, due to the general tendency to make decisions based on capital cost. Academics and researchers also worried about the cost of technologies involved, which is however expected to drop over time. Results should be used to inform regulations and standards to make sure these are comprehended by all stakeholders and ultimately drive down carbon on all building projects.

Keywords. Active Buildings, decarbonisation, stakeholder engagement.
DOI: https://doi.org/10.34641/clima.2022.325

1. Introduction

With human-induced global warming having caused multiple changes in the climate system [1], several countries have now declared a climate emergency. To act on it, countries will have to shift onto a path of decarbonisation, setting targets and timelines for net zero carbon. Countries will thus have to achieve a balance between the amount of carbon they add to the atmosphere and the amount they remove from it [2]. Aiming to achieve such a balance and ultimately stop its contribution to global warming by 2050, the UK was the first major economy to pass a net zero emissions law [3]. The building sector is expected to play a critical role in reaching this net zero target, as buildings are associated with approximately 40% of total carbon dioxide (CO_2) emissions in Europe [4]. However, reports produced by experts, such as the LETI Climate Emergency Design Guide [5], state that current building regulations are seriously lagging behind the trajectory required to achieve net zero and stop global warming. In a similar way, voluntary building standards do not push the decarbonisation agenda far enough, as they do not always encourage holistic solutions, nor do they offer incentives for well-performing buildings [6].

In more detail, buildings commonly draw the energy

Copyright ©2022 by the authors. This conference paper is published under a CC-BY-4.0 license.

they require to satisfy the needs of their occupants from the grid. Hence, they are commonly regarded as passive users of energy, not as active parts of the energy infrastructure. Thanks to technologies such as solar panels and batteries, buildings are however able to support a bi-directional relationship with the grid. Such a relationship can provide the grid with a greater energy flexibility, which is vital to meeting net zero – given the time-varying renewable energy generation [7]. Active Buildings (ABs) aim to exploit this missed opportunity [8]. These are buildings that produce, store, and share energy (Fig. 1) based on the needs of their occupants, as well as of the grid [9]. Thanks to their active interaction with the grid, ABs can help both the building and energy sectors reach net zero. At the same time, such a synergetic relationship can reduce peak demands and thus the need to invest in energy infrastructure. It can also transform building occupants into prosumers (that is, producers and consumers of renewable energy) and hence reduce their energy bills.

If we are to adopt such an approach, stakeholders would need some form of guidance on what an AB is and how its performance should be assessed during the design and in-use stages. The easiest way to do this would be via some form of building code. Given that building technologies and energy infrastructure are rapidly evolving and that creativity in design is necessary, any proposed Active Building Code needs itself to be active – i.e., to evolve over time. ABCode1 is our initial proposition for an Active Building Code (ABCode) [10]. Additional iterations (e.g., ABCode2, ABCode3, etc.) may emerge in the future to account for any advances in the building and energy sectors, and ensure that we are on track for decarbonisation.

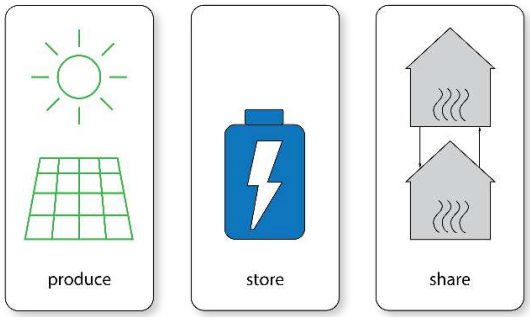

Fig. 1 – Going active: Produce, store, and share energy.

This paper presents our two-stage investigation into the stakeholder perceptions of the next generation of buildings called Active Buildings (ABs), aiming to:

1) Identify the aspects that are missing from existing regulations and standards, which should be accounted for when developing or revising relevant frameworks;

2) Justify our initial proposition for an Active Building Code (ABCode) and provide a clear definition of ABs and a suitable framework for assessing their performance; and

3) Identify the barriers to the popularisation of ABs, which should be dealt with by future iterations of the ABCode.

2. Research Methods

Section 2 describes the data collection and analysis process applied in this study.

2.1 Data collection

The first stage of our investigation aimed to help us get an insight into industry thinking. The focus group method was used, as this is recommended for cases where researchers wish to get a feel for an emerging topic, and an understanding of what is important to a given population [11] – but may not yet know what questions must be asked quantitatively [12]. Twelve focus group discussions were conducted, with each group comprising two or three industry experts and the moderator/facilitator (i.e., one of the authors of this paper). These were decided to be online – and not face-to-face – due to COVID-19. Online focus group discussions are accompanied by great savings in time, cost, and CO_2 emissions [13].

Each discussion lasted for approximately one hour. Initially, participants briefly introduced themselves. They then engaged in a general discussion about the future of the built environment in view of the net zero target – including the extent to which existing building regulations and standards support such a target. Finally, they participated in a more specific discussion about ABs, providing their definition of 'active' without having any knowledge of the term. They also shared their thoughts on the performance assessment of ABs, as well as on the barriers to their acceptance. Each of the sessions was videorecorded upon agreement of all participants, with the help of Microsoft Teams. As focus group discussions do not seek to sample representatively from a population, participants were all selected on the basis of their extensive experience within the building and energy sectors. In particular, they are experienced industry practitioners across the whole value chain, having a variety of backgrounds and work experience (i.e., architecture, engineering, sustainability consulting, energy management, and housing development).

This sampling strategy is called purposive sampling, as participants are selected purposely to yield rich information [14]. 30 industry experts were recruited in this study. The total number of participants – and therefore of focus groups – was dictated by the so-called 'saturation point'; i.e., the point at which no new information was emerging from the discussions [15]. An initial round of five focus groups were here conducted. As no saturation was reached, additional participants were recruited, and a second round of seven focus groups were conducted – until no new information was emerging. Regarding the size of the groups, a low number of participants per group was here selected due to the complexity of the topic. In more detail, triads and dyads were preferred as they

offer a balance between the individual and the group context, and therefore allow participants to become familiar with the topic and reflect on what they hear from others [16].

The second stage of our investigation aimed to help us get an insight into academic thinking. An online survey was used, as this would help us quantify the ideas that emerged from the first stage (i.e., the focus group discussions). The survey included four close-ended questions to reflect the themes that emerged from the discussions with the industry experts. The options that were given to participants reflected the most popular responses among the industry experts. The survey was completed by a total number of 30 academics and researchers, who had the freedom to select up to two options per question.

2.2 Data analysis

Grounded Theory was here used to analyse the data that was collected from the focus group discussions in the first stage of our investigation. This is a well-known approach to theory generation, developed by Barney Glaser and Anselm Strauss in the 1960s [15]. After becoming familiar with the data by listening to all the recordings and keeping notes, we completed the coding step by attaching labels to text segments. Coding was essential for generating core categories (themes), which can provide an easily recognisable description of any valuable data. Four themes arose through constant comparison (i.e., the definition of codes and their comparison to previously identified codes). These were then expressed in the form of questions (as presented in Section 3) – which were subsequently posed to academics and researchers through an online survey in the second stage of our investigation. The data that was collected from the focus group discussions and the survey was analysed visually (in Python), and statistically (in R, using a logistic regression model).

Focusing on the statistical analysis of the responses, a generalised linear model was here used to predict the binary outcome (i.e., whether a specific option is selected by a person, or not). The $lme4$ package for R and, in particular, its $glm()$ function was used to fit such a model and to analyse the fitted model. The fitted model revealed the interaction or not between options and the two groups of stakeholders. That is, it showed whether industry experts, and academics and researchers, tend to respond in a different way, or not. Note that, analysis automatically used the first option (i.e., the first label of the x axis in Fig. 2–5) as the reference category. It then showed whether the rest of options are significantly different from it, or not. In other words, each pair of responses (i.e., of blue and green circles in Fig. 2–5) was compared to the reference category. Finally, the odds ratios from the binary logistic regression were calculated in R using $exp(model\$coefficients)$ to demonstrate the options that are more likely to be voted for by any stakeholder – and that should be hence prioritised when designing the next generation of buildings. It is worth pointing out that conclusions refer to the collected data. In the future, additional observations could be collected to boost statistical power.

3. Results

Section 3 presents results in the form of four major themes. These express the topics that emerged from the online focus group discussions with the industry experts. They also reflect the close-ended questions that were then posed to academics and researchers. These had the freedom to select up to two responses (among the most popular responses provided by the industry experts, as shown on the x axis in Fig. 2–5).

3.1 Theme 1: What is missing from existing regulations and standards?

The great majority of the industry experts regarded *performance verification* as the aspect that is mainly missing from regulations and standards (Fig. 2). In more detail, all focus groups brought to discussion

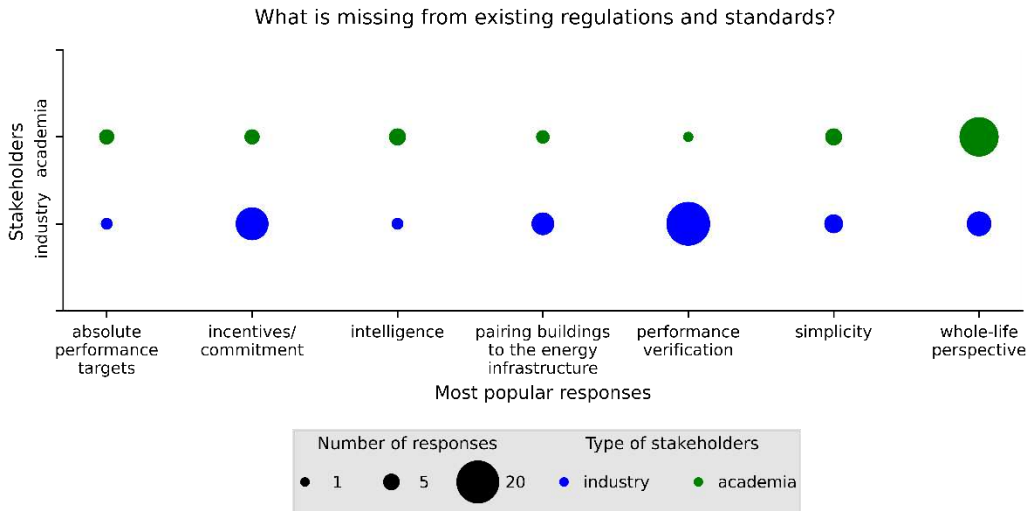

Fig. 2 – The aspects that are missing from existing regulations and standards, according to the 30 industry experts (blue) and the 30 academics and researchers (green).

the lack of a compulsory scheme for post-occupancy evaluation for all building types, expressing worry that this may prevent buildings from achieving net zero carbon in operation. The second most popular response was *incentives/commitment*. Almost half of the industry experts stated that the current lack of carbon incentives does not motivate stakeholders to invest in greener solutions. Another omission is that there is not any agreement that forces stakeholders to commit to a high level of performance in use. In the case of academics and researchers, none of these two aspects were popular responses, as they were voted by one and four persons, respectively. *Whole-life perspective* was the most popular response for these stakeholders, who appear to believe that the whole-life performance of buildings is not dealt with sufficiently by existing regulations and standards.

Focusing on the statistical analysis of responses, the logistic regression model in R indicated that options and groups interacted significantly in the case of the following options: *performance verification* (p-value = 0.002); *incentives/commitment* (p-value = 0.03); and *pairing buildings to the energy infrastructure* (p-value = 0.05). This implies that, in these occasions, academics and researchers responded significantly differently from industry experts – using *absolute performance targets* as the reference category. The analysis also showed that these three options as well as *whole-life perspective* were significantly different from the reference category. The calculation of the odds ratios confirmed the popularity of *performance verification*, *commitment*, *whole-life perspective*, and *pairing buildings to the energy infrastructure*. In more detail, it showed that the odds of someone voting for these options are greater than the odds of someone voting for *absolute performance targets* by a factor of 21, 10.71, 6, and 5.1, respectively.

3.2 Theme 2: What is an AB?

When asked to provide their own definition of active without any prior knowledge of the term, industry experts highlighted the importance of designing and delivering buildings that are *responsive to the needs of the energy infrastructure* (Fig. 3). ABs should thus be active parts of the grid, playing an important role in its decarbonisation and also minimising its need for upgrade – which can be very expensive. Around one third of the industry experts connected the term 'activeness' with the *responsiveness to internal and external conditions*. ABs are thus expected to directly respond to inputs, such as the weather, with the aim of optimizing building energy performance. Another interpretation of activeness was the *responsiveness to the needs of occupants*. ABs are hence expected to interact with their end users to satisfy their needs, such as heating and cooling, and ultimately maximise their health and wellbeing. This was chosen by half of the academics and researchers who participated in the survey, while the *responsiveness to the needs of the energy infrastructure* was selected by only one academic. The *responsiveness to conditions* was the most popular response for this type of stakeholders.

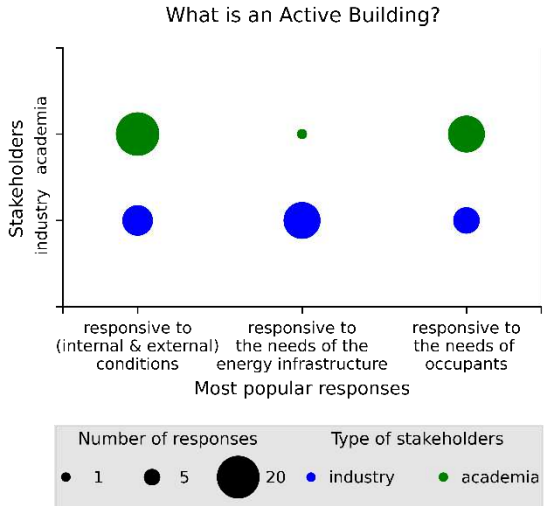

Fig. 3 – The definition of an Active Building, according to the 30 industry experts (blue) and the 30 academics and researchers (green).

The logistic regression model in R showed that the interaction between options and groups was highly significant just in the case of the *responsiveness to the needs of the energy infrastructure* (p-value = 0.0004). This is thus the only occasion where academics and researchers responded significantly differently from industry experts. No other significant difference was found as none of the options is significantly different from the reference category (as a pair of responses). The calculation of the odds ratios suggested that the odds of someone voting for the *responsiveness to the needs of the energy infrastructure* are slightly greater than the odds of someone voting for *responsiveness to internal and external conditions* by a factor of 1.5.

3.3 Theme 3: How should the performance of ABs be assessed?

Evaluating the performance of buildings during the design and in-use stages is critical in ensuring that we are always on track for decarbonisation. It is still an open question though what metrics must be used. This question yielded a consensus of opinion among stakeholders, as the most popular response for both groups (i.e., industry and academia) was *whole-life carbon* (Fig. 4). That is, the majority of stakeholders support the use of a target for the whole-life carbon performance of buildings, with the aim of increasing potential savings in their operational and embodied carbon sides – and ultimately mitigating the climate emergency. The second most popular response was *energy demand*. Several stakeholders stated that this metric will gain popularity over the next few years, as electricity is getting closer to its decarbonisation. They also claimed that this can be easily measured in real life and judged against predicted performance values. Other proposed metrics were *comfort*, *energy flexibility*, and *peak demand*. The latter was found to be important for three industry experts, but was not selected by any academic or researcher.

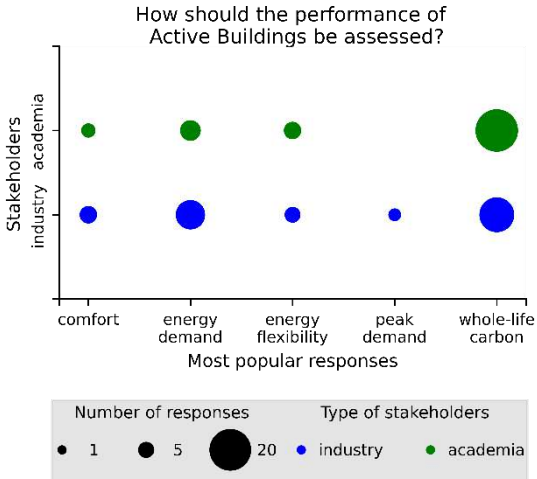

Fig. 4 – The metrics for assessing the performance of Active Buildings, according to the 30 industry experts (blue) and the 30 academics and researchers (green).

The logistic regression model verified that the two groups responded in a similar way, as there was no occasion where the interaction between options and groups was statistically significant. It also indicated that *whole-life carbon* (p-value < 0.0001) and *energy demand* (p-value = 0.02) were significantly different from *comfort*. The calculation of the odds ratios confirmed the popularity of *whole-life carbon*, and *energy demand*, followed by *energy flexibility*. That is, it showed that the odds of someone voting for them are greater than the odds of someone voting for *comfort* by a factor of 7.54, 2.7, and 1.1, respectively.

3.4 Theme 4: What are the challenges to the popularisation of ABs?

The industry experts also referred to the potential challenges to the popularisation of ABs (Fig. 5). *Our culture* was found to be the biggest challenge, as our cultural mindset determines the acceptance – or not – of a new concept and therefore drives the market. Embedding net zero carbon in people's mindset may prove to be challenging, as the carbon fluency of the general population is not there yet. This means that people do not automatically do things that improve the carbon performance of buildings, but have to be nudged into doing the right thing. It is also difficult to convince people to care about the life-cycle carbon performance of buildings at the expense of capital cost. The *lack of evidence* was also considered as a main challenge. In particular, given that this is a new concept, a database of evidence has not been built yet. This is however essential for demonstrating the real-world benefits of the concept and ultimately for convincing the various stakeholders to adopt it. The *lack of combined authorities* was also found to be a challenge to the popularisation of the AB concept. It is thought that there is a lack of local connectivity, as well as a lag between planning policies and best practice – as the former often refer to a performance that barely passes the building regulations, and thus not force stakeholders to opt for greener solutions. *Expensive technologies* was only mentioned by two industry experts, but was the most popular answer for academics and researchers. This was followed by *our culture* and *skills shortage* – as there is still a shortage in terms of labour, but also of professionals with a knowledge and experience of how to deliver well-performing buildings. None of the academics or researchers voted for the *lack of evidence*.

The logistic regression model showed that options and groups interacted significantly only in the case of *expensive technologies* (p-value = 0.005). In other words, this option led to a different response pattern as it was considered as the most significant challenge by academics and researchers, but as the smallest challenge by industry experts. *Our culture* (p-value = 0.002), the *lack of evidence* (p-value = 0.007), and the *lack of combined authorities* (p-value = 0.04) were significantly different from *data control*, as the latter was not a popular response for either group. The calculation of the odds ratios confirmed that *our culture* is the most likely response, with the odds of someone voting for it being greater than the odds of someone voting for *data control* by a factor of 9. The latter is the least likely response, followed by *skills shortage*.

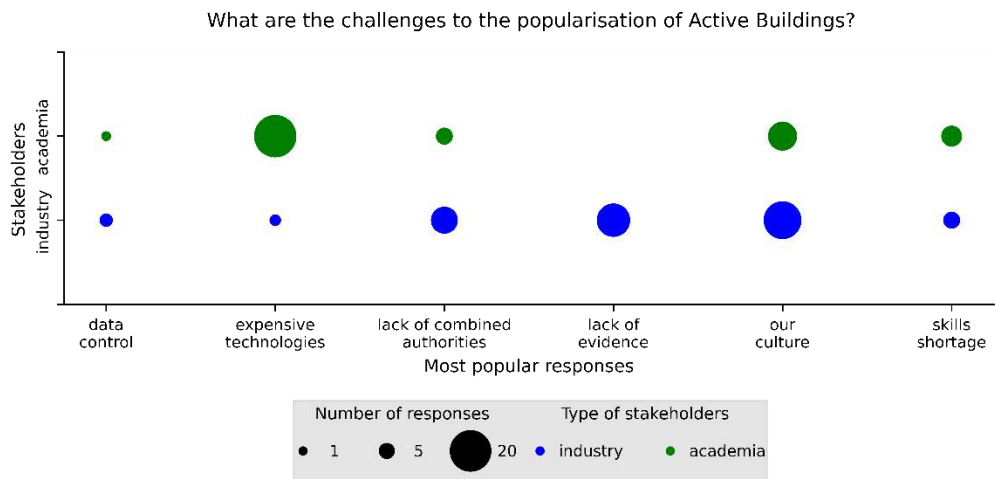

Fig. 5 – The potential challenges to the popularisation of Active Buildings, according to the 30 industry experts (blue) and the 30 academics and researchers (green).

4. Discussion

Section 4 discusses the stakeholder perceptions of the next generation of (active) buildings, as revealed from the focus group discussions with the industry experts, as well as from the survey of the academics and researchers.

4.1 Current situation

The discussions with the industry experts revealed the immediate need to re-evaluate how we design, construct, and operate buildings – if we are to reach net zero and tackle the climate emergency. Existing building regulations and standards will have to be revised accordingly as they were found to be missing aspects that are vital for achieving decarbonisation. The aspects that were mentioned by the majority of industry experts were *performance verification* and *incentives/commitment*. That is, there is a need for a compulsory scheme for post-occupancy evaluation to ensure that buildings are truly net zero carbon in their operation. There is also a need for incentives to motivate different stakeholders to invest in low carbon solutions.

The online survey of the academics and researchers highlighted another aspect that is currently missing from regulations and standards, namely, a *whole-life perspective*. That is, a more holistic way of thinking and acting is needed in terms of minimising the CO_2 emissions of (new and existing) buildings. This calls for a whole-life carbon assessment to be embedded in the decision-making process. As we are gradually moving towards a better operational performance of buildings, the consideration of and reporting on embodied carbon is becoming even more crucial.

The importance of these three aspects was verified by the statistical analysis of the responses of both groups (i.e., industry and academia). These aspects were followed (in order of importance) by *pairing buildings to the energy infrastructure* and *simplicity*. Hence, to achieve decarbonisation, it is important to encourage and legislate the synergetic relationship between buildings and the grid. To ensure the wide adoption of any standard even from the early design stages, it needs to rely on a simple, well-understood formula. Finally, the revision of existing standards or the development of new ones should account for *absolute performance targets* and *intelligence*. That is, assessing the performance of buildings in relation to notional buildings (as currently proposed by the regulations) was reported to often lead to inefficient building shapes. Absolute performance targets are hence needed to prevent designers from developing poor design solutions. Despite their important role in ensuring the optimal performance of buildings, smart building technologies were also found to be commonly neglected by regulations and standards.

4.2 Going active

Aiming to cast light on the characteristics of the next generation of (active) buildings, both groups were asked to interpret 'activeness', without having any prior knowledge of the term. All industry experts perceived activeness as 'responsiveness', with the great majority of them referring to a *responsiveness to the needs of the energy infrastructure*. That is, to minimise the detrimental effect of both the building and energy sectors on the environment, buildings will have to be reactive to the needs of the grid. This agrees with the ABCode which was built around two main principles: whole-life sustainability and energy network support. Most of academics and researchers interpreted activeness as *responsiveness to internal and external conditions*. This emphasises the need to design buildings that react to changes in real time (e.g., a temperature drop), but also in the long term (e.g., a new building use). Another interpretation of the activeness was the *responsiveness to the needs of occupants*. That is, the design of buildings should include a user-centred control system that ensures the health, wellbeing, and comfort of occupants.

Another topic that arose from the discussions with the industry experts was the use of a suitable metric for assessing the performance of (active) buildings. This topic yielded a consensus, as the majority of the participants in both groups advocated the adoption of *whole-life carbon*, followed by *energy demand*, and *energy flexibility*. This also aligns with the metrics suggested by the ABCode, namely: embodied carbon, energy consumption, renewable energy production, and energy flexibility. As with the embodied carbon, energy flexibility is becoming increasingly critical in achieving decarbonisation. In more detail, achieving a stable and decarbonised grid is calling for the use of storage technologies – and hence for a metric that incentivises their use. The inclusion of *comfort* and *peak demand* in the evaluation framework for ABs was also brought to discussion. The former echoes the importance of user experience, and the latter is a reflection of the direct impact of buildings on the energy infrastructure.

4.3 Challenges and opportunities

The discussions also revealed the challenges to the popularisation of ABs, with the majority of industry experts regarding *our culture* as the biggest barrier. That is, according to industry experts, stakeholders tend to be driven by the capital cost of buildings. It may hence be challenging to convince them to opt for a solution that is associated with a higher capital expenditure, even if the payback period is short. The *lack of evidence* was found to be the second biggest challenge. This is also related to the way of thinking and acting of stakeholders who, in the absence of sufficient evidence, may not be convinced that it is worth adopting a new concept. The *lack of combined authorities* was also found to be a barrier, showing the catalytic role of stakeholders – and in particular of local authorities – in the wide adoption of such a new concept. In more detail, industry experts stated that there is an absence of local connectivity which detrimentally affects decision-making, as it does not

encourage stakeholders to commit to building to a better standard. Interestingly, the great majority of academics and researchers considered the *high cost of technologies* as the main challenge to the adoption of the AB concept. This was mentioned by only two industry experts, with both of them stating that this is expected to change over the next years, given the rising demand for such technologies. *Skills shortage* and *data control* are also potential challenges. The former refers to the lack of experience in delivering high-performance buildings and the associated skills gap. The latter indicates the existing reticence with sharing data, which may prevent data management from reaching its full potential.

In addition to drawing attention to the barriers the wide adoption of the AB concept may possibly face, the discussions with the industry experts indicated future opportunities. In other words, they revealed approaches and technologies that are expected to be gaining popularity on our way to decarbonisation – and that should thus be further expanded in future iterations of the ABCode. Focusing on social aspects, there is an increasing demand for healthy buildings, which was accelerated due to COVID-19. The ability of ABs to boost the *health, wellbeing, and comfort* of their occupants, should hence be further promoted. The applicability of the AB concept to a community of buildings should also be underlined as, in addition to any environmental and financial benefits, it offers a sense of *collectiveness* that adds value to the user experience. The growing interest in *circular economy* is another opportunity that should be henceforth harnessed by the ABCode, which already encourages users to consider the life-cycle environmental effect of buildings. Regarding any technical aspects, the ability of ABs to provide energy flexibility should be expanded by harnessing emerging technologies e.g., *smart technologies*, *storage systems*, *electric vehicles*, and *digital twin*.

5. Conclusions

As countries declare a climate emergency one after another, setting targets and timelines for net zero carbon is becoming crucial. The building sector is a major contributor to carbon dioxide emissions, and hence a vital player in addressing the climate crisis. Nevertheless, building regulations and standards are failing to promote holistic solutions, hence seriously lagging behind the trajectory needed to achieve net zero. Despite the direct link between buildings and the grid, regulations and standards lack a synergistic way of thinking and acting. This is certainly a missed opportunity for the decarbonisation of both sectors. In this context, we recently introduced the Active Building Code (ABCode) [10]. This is a new building standard that promotes the synergetic relationship between the electrical grid and the next generation of buildings termed Active Buildings (ABs), in order to help both the energy and building sectors reach net zero.

This paper presented the stakeholder perceptions of ABs, as arose from the focus group discussions with 30 industry experts and the survey of 30 academics and researchers. Existing regulations and standards were found to be missing valuable aspects, namely (in an order of importance, as defined by the two groups of stakeholders): *performance verification*, *incentives and commitment*, *whole-life perspective*, *pairing buildings to energy infrastructure*, *simplicity*, *absolute performance targets*, and *intelligence*. The need to pair buildings to the energy infrastructure was also revealed by the definition of an AB, as provided by the majority of industry experts. That is, an AB is a building that is *responsive to the needs of the energy infrastructure*, being in line with the definition included in the ABCode. Academics and researchers interpreted activeness as *responsiveness to internal and external conditions* or *responsiveness to the needs of occupants*, hence further highlighting the need for adaptive buildings. With respect to the metric(s) for assessing the performance of ABs, both groups of stakeholders stated that *whole-life carbon*, *energy demand*, and *energy flexibility* should be the way forward. This again aligns with the metrics that are proposed in the ABCode. The inclusion of *comfort* and of *peak demand* was also brought to discussion. Finally, the barriers that must be removed to drive the scale-up of ABs were also revealed: *our culture*, *lack of evidence*, *lack of combined authorities*, *high cost of technologies*, *skills shortage*, and *data control*.

To conclude, the (visual and statistical) analysis of responses revealed the aspects that are more likely to be voted for by any stakeholder – and that should be prioritised when designing the next generation of buildings. No significant statistical differences were in general observed between the responses from the two groups of stakeholders. In the future, additional responses should be collected to increase statistical power, and hence draw safer conclusions about the response patterns of different stakeholders. Future research should also build on the opportunities that arose from the focus group discussions. These may cover both social and technical aspects, in order to further improve the carbon performance of ABs and ensure these are delivering the best user experience. The stakeholder perceptions that were expressed in this study could be useful in writing regulations and standards that not only drive down carbon, but are also widely comprehended and accepted.

Acknowledgement

This study was conducted in the context of the Active Building Centre Research Programme (EP/V012053 /1). The programme brings together several leading universities, businesses, as well as service providers to develop innovative ideas and technologies which will enable the construction industry to transform into a net zero emissions sector. It is funded through the UKRI Transforming Construction Challenge.

We would like to warmly thank each industry expert who participated in the focus group discussions, and each academic or researcher who participated in the

survey for their valuable input. We would also like to thank Dr Emma Cliffe for her valuable advice on the statistical analysis of the collected data.

References

1. Hoegh-Guldberg O, Jacob D, Taylor M, Bindi M, Brown S, Camilloni I, et al. Impacts of 1.5°C of global warming on natural and human systems. World Meteorological Organization. 2018.

2. National Grid. What is net zero? [Internet]. 2021 [cited 2022 Jan 13]. Available from: https://www.nationalgrid.com/stories/energy-explained/what-is-net-zero

3. UK Government. The Climate Change Act 2008 (2050 Target Amendment) Order 2019. 2019.

4. European Commission. Clean energy for all Europeans. 2019.

5. LETI. Climate Emergency Design Guide. 2020.

6. Nikolaidou E, Fosas D, Roberts M, Allen S, Walker I, Coley D. Buildings as energy infrastructure, not passive consumers. Active Building Centre Research Programme (University of Bath). 2020.

7. National Grid. Flexibility [Internet]. 2021 [cited 2022 Jan 13]. Available from: https://www.nationalgrideso.com/future-energy/future-energy-scenarios/fes-2021/system-flexibility

8. Active Building Centre Research Programme. The Active Building concept [Internet]. 2022. [cited 2022 Jan 10]. Available from: https://abc-rp.com/about-us/

9. Bankovskis A. One million homes constructed as"buildings as power stations". SPECIFIC Innovation and Knowledge Centre; 2017.

10. Fosas D, Nikolaidou E, Roberts M, Allen S, Walker I, Coley D. Towards active buildings: Rating grid-servicing buildings. Build Serv Eng Res Technol. 2021;42(2):129–55.

11. Kontio J, Bragge J, Lehtola L. The focus group method as an empirical tool in software engineering. In: Guide to advanced empirical software engineering. London: Springer; 2008. p. 93–116.

12. Kamberelis G, Dimitriadis G. Focus groups: Contingent articulations of pedagogy, politics, and inquiry. In: Collecting and interpreting qualitative materials. Los Angeles: SAGE Publications; 2008.

13. Stewart DW, Shamdasani P. Online focus groups. J Advert. 2017;46(1):48–60.

14. Patton MQ. Qualitative research. In: Encyclopedia of Statistics in Behavioral Science. Chippenham: John Wiley and Sons; 2005.

15. Glaser BG, Strauss AL. The discovery of grounded theory: Strategies for qualitative research. New Brunswick: Aldine Transaction; 1967.

16. Finch H, Lewis J, Turley C. Focus groups. In: Ritchie J, Lewis J, McNaughton Nicholls C, Ormston R, editors. Qualitative research practice: A guide for social science students and researchers. London: SAGE Publications; 2013.

17. Nikolaidou E, Walker I, Coley D, Allen S, Fosas D. Dataset for “Going active: How do people envision the next generation of buildings?”. University of Bath Research Data Archive; 2022. Available from: https://doi.org/10.15125/BATH-01125

Data access statement

The data that was collected and analysed during this study is available at the University of Bath Research Data Archive [17].

Hybrid photovoltaic-thermic system with enhanced cell energy efficiency

Marius Brănoaea [a], Andrei Burlacu [a,], Marina Verdeş [a], Vasilică Ciocan [a], Marius Costel Balan [a] and Robert Ştefan Vizitiu [a]*

[a] "Gheorghe Asachi" Technical University of Iasi-Romania, Faculty of Civil Engineering and Building Services, Blvd. Mangeron, No. 1, 700050, Iasi, Romania

* marius.branoaea@student.tuiasi.ro

Abstract. Interest towards green energy has been increasing over the past decades, due to the increasing effect climate change and unsustainable energy sources pose to the planet. Among the renewable energy sources only solar, hydropower and wind provide substantial potential, while geothermal, wave energy, and biomass provide a local solution.
Solar energy has the potential of being one of the world's largest energy providers, due to the fact it is present in every corner of the earth and can be converted with ease in the electric energy and thermal energy using photovoltaic (PV) and solar panels.
Hybrid systems generate significant quantities of electricity and also generate heat. Photovoltaic-Thermal (PVT) systems have the potential to reduce the energy consumption in buildings, reducing both thermal and electrical energy, thus reducing the operation costs.
This study aims to design, model, and test the energy efficiency of a PVT system in order to overcome the main drawbacks of photovoltaic panels.
The main challenge photovoltaic panels face is overheating that leads to a reduction in the cells efficiency and energy production, a method of overcoming this is through cooling, recovering the excess heat with the cooling agent. At the same time using the recovered thermal energy to supply the needs of the building in terms of heating and hot water, either directly or as a preheated primary agent, a further reduction in terms of the building energy requirements is achieved.
This study analyses the performance and efficiency of three original design hybrid photovoltaic systems by cooling a photovoltaic panel using water as a cooling agent.
By cooling a photovoltaic panel with a cooling agent with various flow rates, the efficiency of the photovoltaic cells is maximized, and by keeping their temperature as close to the nominal operating cell temperature (NOCT), the study aims to prevent degradation through overheating and cooling cycles during the day and night.
By cooling a PV panel with water as a coolant, the efficiency of the photovoltaic cells is increasing from 17.85 in the case of the uncooled panel to over 19% in the case of the water-cooled systems at a flow rate of v = 3 l / min and v = 5 l / min.
Keywords. Photovoltaic Cooling, Photovoltaic Cell Efficiency, Energy Efficiency, Cooling Methods, Computational Fluid Dynamics.
DOI: https://doi.org/10.34641/clima.2022.321

1. Introduction

Based on the Global Energy review made by the International Energy Agency global energy consumption has increased over the past decades, the only year when this was not the case was the year 2020 which marked the debut of the SARS-CoV-2 viral pandemic, the energy consumption of 2021 surpassing both the values of 2020 and 2019. Moreover, even though the demand for renewable energy sources has been increasing yearly due to an omnipresent energy crisis, the demand for fossil fuel increased significantly, following the decline in 2020 the demand for coal in the year 2021 rising upwards to 60% in comparison to all renewable sources combined (1).

In terms of energy consumption, the buildings sector is responsible for over 40% of the global energy consumption, and regarding emissions, the buildings

Copyright ©2022 by the authors. This conference paper is published under a CC-BY-4.0 license.

are responsible for 30% of the global CO2 emissions. This is a result of the development of the world and factors such as an increase in indoor residence time, rapid urbanization coupled with significant deforestation (2).

Recently the development of the energy sector was centered on sustainability and green energy. Among all clean and sustainable sources of energy, the sun is one of the most important sources because it is responsible directly or indirectly for the majority of the renewable energy sources, furthermore, it is a direct progenitor of the conventional fuels as well, considering a significant portion of these fuels are a result of the photosynthesis process. Solar energy in comparison to other types of renewable energy sources presents the potential of being not only one of the largest suppliers of energy among renewable sources but one of the largest suppliers of energy among all sources, through its accessibility, being implementable on every continent. Furthermore, solar radiation can be converted directly to thermal energy or electrical energy with the use of thermal or photovoltaic (PV) modules (3,4).

Through the implementation of PV systems, the energetic vulnerability of the European Union is reduced, through the production of energy locally without the use of fossil fuels that originate outside the European community. At the same time taking into consideration that with the current technology, PV systems have an increased service life and their CO_2 emissions are reduced and the potential to stabilize the energy market and prevent future shortages in terms of energy supply or energy crises (5,6,7).

According to the literature, if the cell temperature of a polycrystalline silicon, monocrystalline, and amorphous silicon photovoltaic cell increases by 1 °C, the electrical efficiency of the photovoltaic unit will decrease by 0.45%, 0.45%, and 0.25% (8,9).

2. Photovoltaic panels

Photovoltaic (PV) panels are made of PV cell arrays that directly convert the energy radiated by the sun into electric energy. The conversion of solar energy into electrical energy in comparison to other types of energy production presents several advantages: apart from the initial cost, the energy is free, due to the fact that the electricity production is done without any moving parts the maintenance costs are reduced and it is fully renewable and in terms of emissions, PV panels do not produce greenhouse gasses, waste or noise.

In terms of environmental parameters that influence the lifetime and efficiency of a PV panel, the most notable ones are solar radiation, the wind direction and velocity, ambient temperature, dust, humidity, shading, and cell temperature (10,11). A majority of these parameters are meteorological parameters, which cannot be controlled. Moreover, there are parameters that even though in comparison with the environmental parameters, which seem random, can be controlled, such as orientation, tilt angle, and positioning, in a vast majority of cases these parameters are not managed, especially in the case of typical PV systems. However, a parameter that can be controlled and one that has a significant impact on the efficiency of the PV cells is their operating temperature, and keeping the cell temperature as close to the nominal operating cell temperature (NOCT) is a way to maximize the cell temperature (12,13,14).

Unfortunately, through the energy generation process a portion of the solar radiation is not converted into electrical power, thus increasing the temperature of the PV cells, which translated to a reduction of the efficiency of the energy conversion through a reduction of the current intensity and voltage inversely proportional with the temperature of the cells. This phenomenon was studied by Fesharaki et al and Qiang et al in their respective researches, highlighted in Fig. 1 and Fig. 2. (15,16).

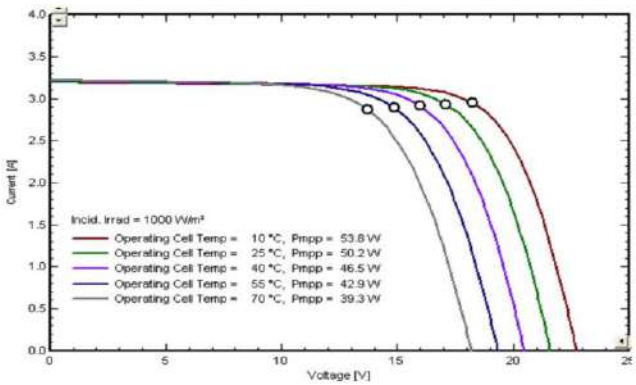

Fig. 1 - Photovoltaic Cell current intensity and voltage variation based on cell temperature

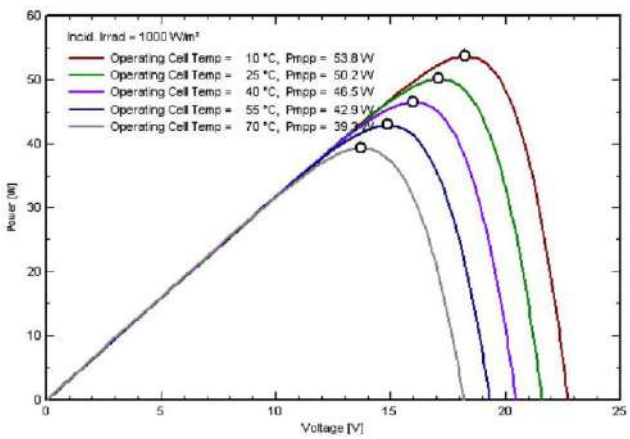

Fig. 2 - Photovoltaic Cell power output and voltage variation based on cell temperature

Taking into consideration the effect temperature has on the performance of the photovoltaic cell, it can be said that cooling is a requirement in some cases in order to maximize the efficiency of the electrical conversion (15).

In terms of energy production and efficiency, the current efficiency of the solar cells in a majority of commercial photovoltaic systems is below 20% (17).

Through scientific research and the evolution of technology, the production cost of advanced solar cells is decreasing, these cells provide higher efficiency in comparison to commercial cells, with an advanced cell, in a single p-n junction, in theory, the achievable efficiency is 29.4% (18).

2.1. Photovoltaic cooling

Taking into consideration the significant impact the environmental parameters pose on the photovoltaic cell efficiency; the research community has studied various cooling methods in order to ensure the optimal cell temperature and the cell operation at optimal parameters.
All types of cooling techniques can be characterized into two categories:
Active photovoltaic cells cooling, which employs a cooling agent in order to reduce the temperature of the cells. The most commonly used coolants are air and water but scientists analyzed the use of specially designed cooling agents such as refrigeration agents or nanofluids, but these have the major drawback of being very expensive to produce (19). The main advantage of active cooling methods is the increased effectiveness caused by the possibility to control the flow rate of the agent with a fan or a pump and the main disadvantage of these types of cooling is the operating cost (20,21,22,23).
The second type of cooling method is passive cooling. This type of cooling focuses on adding extra components on the rear of the photovoltaic panel with the aim of better natural convection. The added components function as heat exchangers, extracting the heat from the PV cells and dispersing it into the surrounding air. During their research scientists analyzed the use of heat sinks, heat pipes, and even phase change materials (PCMs). The use of heat pipes, in particular, is intensely studied, their field of applications ranging from the buildings sector to the IT sector (24,25,26). Passive cooling techniques present the advantage of being cheaper to install and operate, the only cost being the initial cost of the added components but their main drawback is the fact that it is impossible to control the heat transfer and their efficiency is thus reduced in comparison to active cooling techniques (27,28).
In terms of active cooling, cooling the photovoltaic panel using fluid is more efficient in comparison to air cooling methods because fluids present increased heat-carrying capacity in comparison to air (29).
Boumaarafa et al. studied a hybrid photovoltaic/ thermal (PVT) system with a serpentine heat exchanger and revealed that through the combination offers a significant cumulative efficiency, the overall thermal efficiency reaching 79.43% (30).

3. Research Methodology

In order to improve the electrical efficiency of a photovoltaic panel and reduce the energy waste, as is the case for most passive cooling systems, hybrid systems called photovoltaic-thermal systems (PVTs) were conceptualized through adding a heat recovery system to the rear of the PV panel, absorbing the excess heat generated by the sun and using it to produce thermal energy, decreasing the temperature of the PV cells which translates to a better electrical output. PVTs function as cogeneration systems and their use in domestic applications has a significant effect on the environment (31).
Even though the interest towards PVT systems is great and a large number of research papers have been published on the subject, there is little research that treats the enhancement of flow parameters such as inlet flowrate on multiple designs of PVT simultaneously.
The paper addresses multiple numerical simulations on three types of transient PVT models, employing the use of CFD numerical simulations with the Autodesk CFD Software in order to study the thermal distribution of all the systems during operation. This was made to demonstrate the most effective design for the cooling system in increasing the performance and the electrical production efficiency of the photovoltaic cells.
For the study, a common monocrystalline Si-based PV panel (Jinko Eagle PERC JKM315M-60-V) was analyzed because of the advantageous position of the junction box with the main parameters presented in (Table 1) (32).

Tab. 1 - PV module technical characteristics.

	STC	NOCT
Maximum Power (Pmax)	315Wp	235Wp
Maximum Power Voltage (Vmp)	33.2V	31.2V
Maximum Power Current (Imp)	9.49A	7.56A
Open-circuit Voltage (Voc)	40.7V	37.6V
Short-circuit Current (Isc)	10.04A	8.33A
Module Efficiency (%)	19.24%	
Temperature coefficients of Pmax	-0.37%/°C	
Temperature	-0.28%/°C	

coefficients of Voc	
Temperature coefficients of Isc	0.048%/°C
NOCT	45±2°C

The heat recovery systems were designed in three constructive methods, a cooling system comprised of vertical pipes through which water flows from a distributor towards a collector (Fig. 4 – A), a cooling system comprised of a serpentine through which flows water (Fig. 4 – B) and a cooling system made of multiple serpentines connected by a distributor and a colector at the top and bottom (Fig. 4 – C).

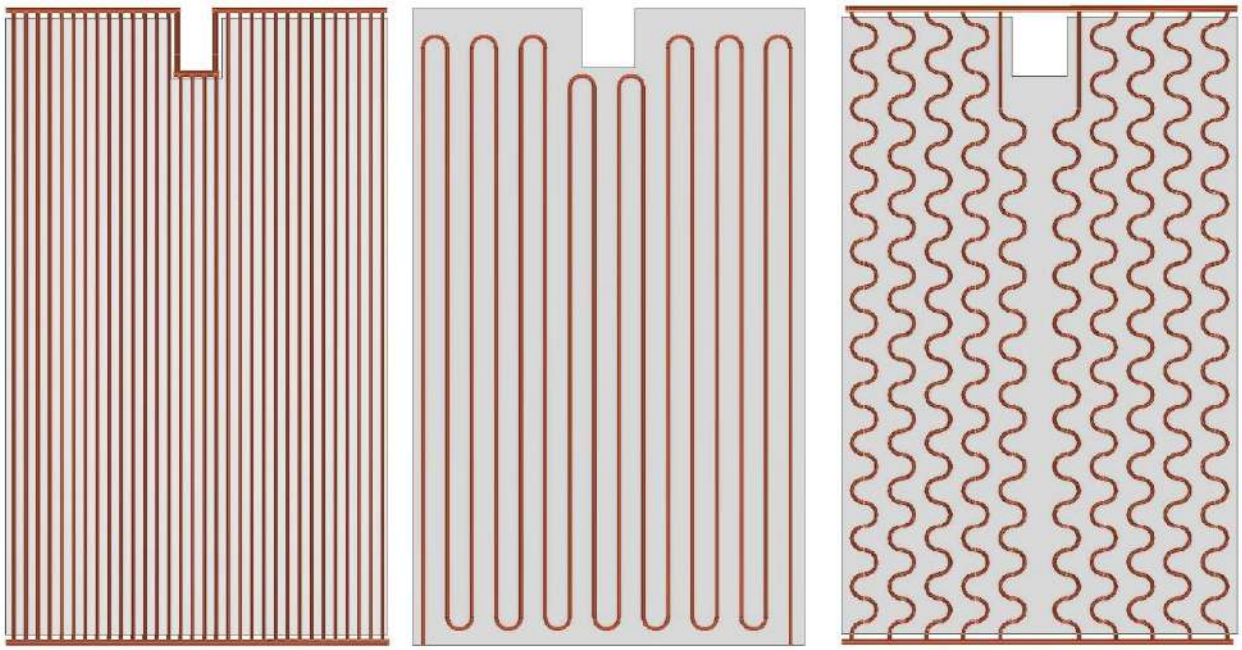

The photovoltaic panel consists of 60 photovoltaic cells of 156x156 mm with a thickness of 5 mm made of monocrystalline silicon. The efficiency of the photovoltaic cells is 19.24% at the nominal operating cell temperature of, T_{NOCT} = 45°C. The decrease in the efficiency of the photovoltaic cells is 0.37% /ºC.
In the first phase, it was necessary to model each part using the Auto-desk Inventor Professional 2021 software.
The panel is comprised of a metallic frame (3) L = 1650 mm, w = 992 mm, d = 35 mm, 60 photovoltaic cells (5), L = 156 mm, w = 156 mm, d = 5 mm, enclosed in a glass protective layer (4), L = 1650 mm, w = 992 mm, d = 5 mm and cooled with a heat recovery system (6), through which water flows from an intel (1) to an outlet (2). The components of the models can be viewed in Fig. 3.

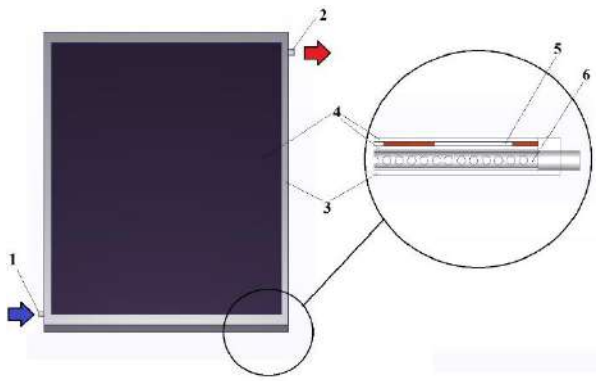

Fig. 3 – PVT model elements.

Fig. 4 – Heat recovery plates designs

For the water in order to have a pertinent comparison between the three cooling designs, four values for the velocity were considered: a lower flow rate of 1 l/min, a higher flow rate of 10 l/min, and two intermediary flow rates of 3 and 5 l/min.

The next step consisted in assigning the simulation parameters by setting each component the material it is made of, followed by the meshing process and afterwards imposing the boundary conditions.
Because photovoltaic panels are under the influence of solar radiation, they can heat up significantly, the temperature of 65 ºC was used for the temperature of solar cells as an initial condition during operation.

4. Results and discussion

After running the simulations, the average temperature of the water outlet was recorded for each case as well as the average temperature for the photovoltaic cells, as exemplified in Fig. 5.

In figure 6 it can be observed the backside of the panel for every type of cooling system analysed as well as the temperature distribution.

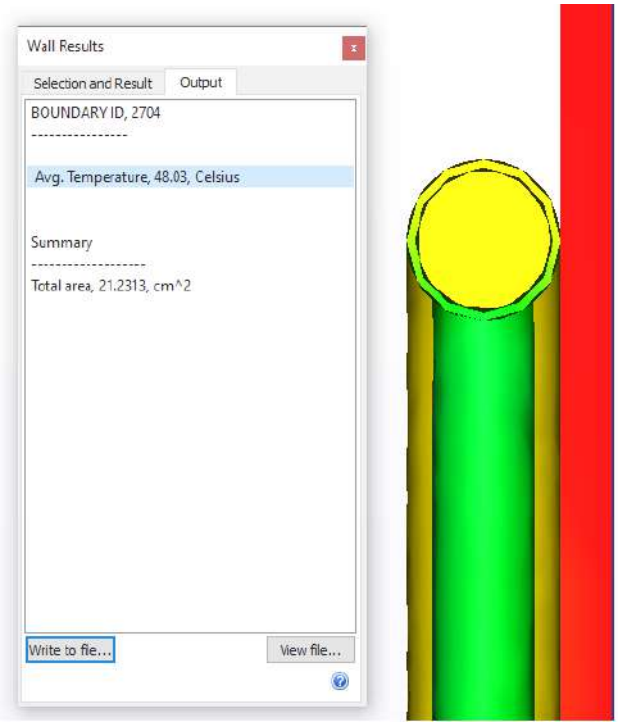

Fig. 5 – Water outlet temperature

Tab. 2 – Simulation Results

	Water flowrate [l/min]	Cell temperature [°C]	Water temperature [°C]
PV	0	64.53	12
Vertical tubes	1	57.19	59.07
	3	50.34	48.03
	5	43.5	36.98
	10	35.36	28.62
Serpentine	1	56.83	64.08
	3	47.32	54.63
	5	37.81	45.19
	10	29.85	32.55
Multiple Serpentines	1	56.55	64.16
	3	46.91	54.74
	5	37.27	45.33
	10	29.48	34.07

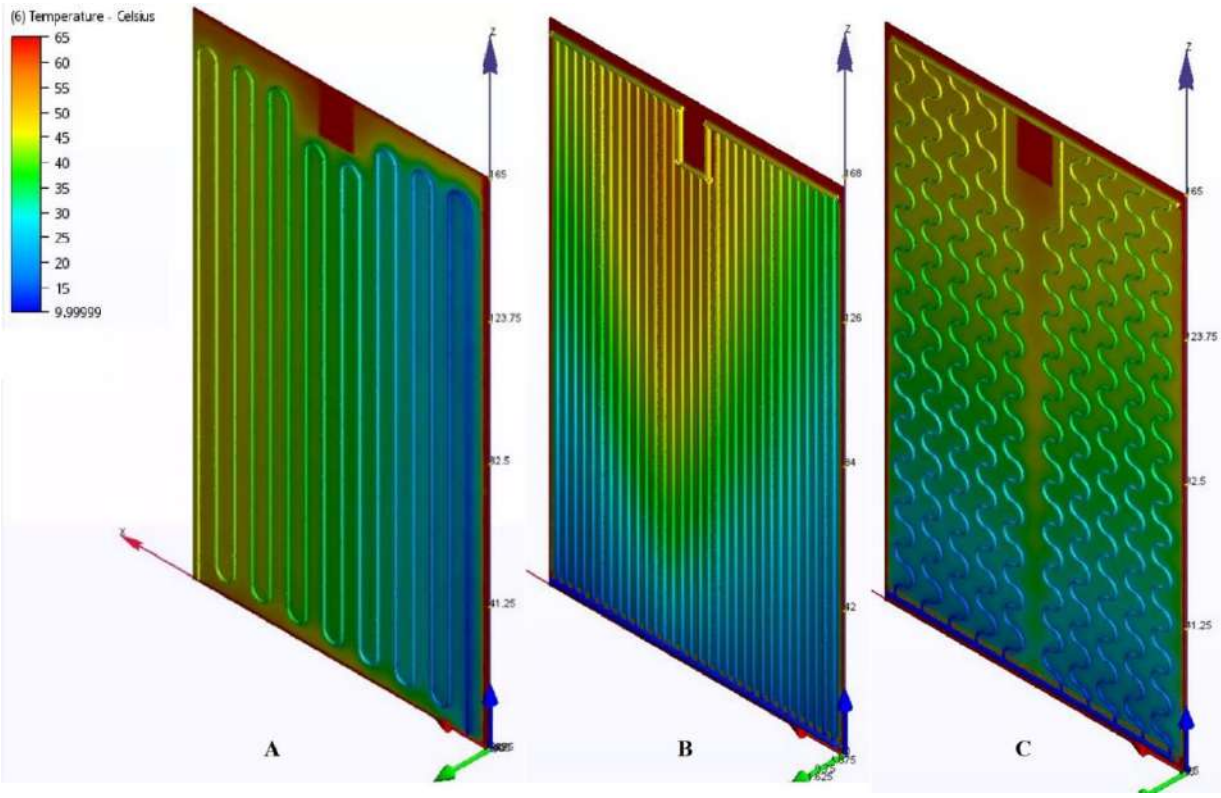

Fig. 6 – The temperature distribution of each cooling system

The pronounced effect that PV operating temperature has upon PV electrical efficiency (η_c) is well documented (10)

$$\eta_c = \eta_{ref} - [\beta_{ref} \times \eta_{ref} \times (T_c - T_{ref})] \qquad (1)$$

β_{ref} = solar radiation coefficient ≈ 0.004 K

T_{ref} = reference temperature (°C)

The values of T_{ref} and η_{ref} are normally provided by the module's manufacturer.

The energy conversion efficiency was determined and displayed in Tab.3.

Tab. 3 – Cell Efficiency

	Water flowrate [l/min]	Cell temperature [˚C]	Cell efficiency [%]
PV	0	64.53	17.85
Vertical tubes	1	57.19	18.37
	3	50.34	18.86
	5	43.5	19.13
	10	35.36	18.55
Serpentine	1	56.83	18.40
	3	47.32	19.07
	5	37.81	18.73
	10	29.85	18.16
Multiple Serpentines	1	56.55	18.42
	3	46.91	19.10
	5	37.27	18.69
	10	29.48	18.14

For an easier visualization of the efficiency of each cooling system at every flowrate, all the data was introduced in the graphs presented in Fig. 7. and Fig.8.

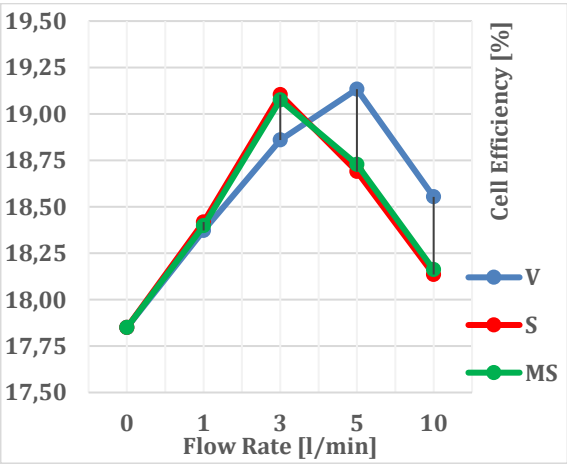

Fig. 7 – Cell efficiency graph

The maximum efficiency was obtained for the vertical tube cooling system (V), with a value of 19.13% with a water flow rate of 5 l/min.

Through cooling, the PV panel the efficiency of the electric production increased by almost 7% in the case of cooling it using the single serpentine (S) and multiple serpentines (MS) at a flow rate of 3 l/min and for the vertical tube cooling system (V) at a flow rate of 3 l/min.

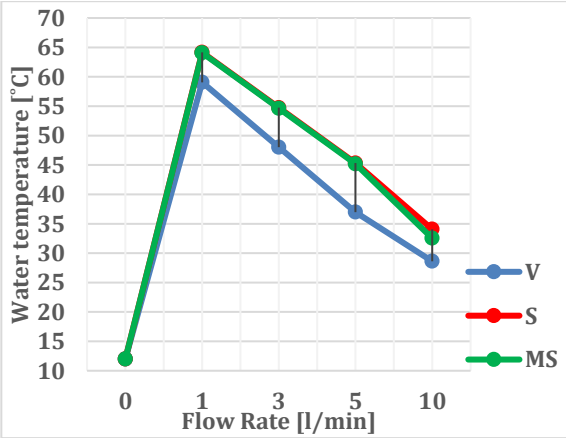

Fig. 8 – Water temperature graph

The cooling system comprised of a single serpentine (S) and the cooling system comprised of multiple serpentine (MS) present comparable results and similar trends but among these two the system comprised of multiple serpentines presents a better temperature distribution.

In terms of thermal performance, the maximum value for the outlet water temperature was 64.16 ˚C at a flowrate of 1 l/min and the water temperature for the flowrate of 3 l/min, which corresponds to a cell temperature close to the NOCT value, the water temperature reached 54.74 ˚C in the case of the multiple serpentines (MS) system.

Among these 3 systems, the most suitable one for cooling a PV panel is the multiple serpentines (MS) system, due to the fact it provides a comparable increase in cell efficiency at a lower flow rate in comparison to the vertical tube cooling system (V) and provides a more uniform temperature distribution than the single serpentine (S) cooling system.

5. Conclusions

Hybrid systems generate significant quantities of electricity and also generate heat. Photovoltaic-Thermal (PVT) systems have the potential to reduce the energy consumption in buildings, reducing both thermal and electrical energy, thus reducing the operation costs.

This study analyses the performance and efficiency of three original design hybrid photovoltaic systems by cooling a photovoltaic panel using water as a cooling agent.

Through cooling a PV panel with water as a coolant, the efficiency of the photovoltaic cells is increasing from 17.85 in the case of the uncooled panel to over 19% in the case of the water-cooled systems at a flow rate of v = 3 l / min and v = 5 l / min.

The water reached a temperature ranging from 28.62 to 64.16 ˚C, and the water temperature for the best-

case scenario, the multiple serpentines (MS) at a flow rate of v = 3 l / min reached a temperature of 54.74 ˚C, an ideal temperature for the water to be used as domestic hot water or even as a heating agent.

Among these 3 systems, the most suitable one for cooling a PV panel is the multiple serpentines (MS) system, due to the fact it provides a comparable increase in cell efficiency at a lower flow rate in comparison to the vertical tube cooling system (V) and provides a more uniform temperature distribution than the single serpentine (S) cooling system.

Acknowledgments: This work was supported by a grant of the Romanian Ministry of Education and Research, CCCDI-UEFISCDI, project number PN-III-P2-2.1-PED-2019-3112, within PNCDI III.

Data access statement: Data sharing not applicable to this article as no datasets were generated or analysed during the current study.

6. References

1. IEA (2021), Global Energy Review 2021. [Online]. Available from: https://www.iea.org/reports/global-energy-review-2021.
2. Cao X, Dai X, Liu J. Building energy-consumption status worldwide and the state-of-the-art technologies for zero-energy buildings during the past decade. Energy and Buildings. 2016; 128: 198–213.
3. AlAmri F, AlZohbi G, AlZahrani M, Aboulebdah M. Analytical Modeling and Optimization of a Heat Sink Design for Passive Cooling of Solar PV Panel. Sustainability. 2021; 13(6): 3490.
4. Kopnina H. Energy Policy in the European Union: Renewable Energy and the Risks of Subversion. In Governance and Security Issues of the European Union.:.M.C. Asser Press, The Hague; 2016. p. 167-184.
5. Kuznetsov P, Yuferev L, Voronin D, Panchenko V, Jasiński M, Najafi A, et al. Methods Improving Energy Efficiency of Photovoltaic Systems Operating under Partial Shading. Applied Sciences. 2021; 11(22): 10696.
6. Colarossi D, Principi P. Indoor and Outdoor Performance of an Enhanced Photovoltaic Panel through Graphene/Fins/Phase Change Materials. Applied Sciences. 2021; 11(19): 8807.
7. Why Europe's energy prices are soaring and could get much worse. [Online].; 2021. Available from: https://www.euronews.com/2021/10/28/why-europe-s-energy-prices-are-soaring-and-could-get-much-worse.
8. AL-Musawi AIA, Taheri A, Farzanehnia A, Sardarabadi M, Passandideh-Fard M. Numerical study of the effects of nanofluids and phase-change materials in photovoltaic thermal (PVT) systems. Journal of Thermal Analysis and Calorimetry. 2019; 137: pages623–636.
9. Kalogirou SA, Tripanagnostopoulos Y. Hybrid PV/T solar systems for domestic hot water and electricity production. Energy Conversion and Management. 2006; 47(18-19): 3368-3382.
10. Skoplaki E, Palyvos JA. On the temperature dependence of photovoltaic module electrical performance: A review of efficiency/power correlations. Solar Energy. 2009; 83(5): 614-624.
11. Skoplaki E, Palyvos JA. Operating temperature of photovoltaic modules: A survey of pertinent correlations. Renewable Energy. 2009; 34(1): 23-29.
12. Dubey S, Sarvaiya N, Seshadri B. Temperature Dependent Photovoltaic (PV) Efficiency and Its Effect on PV Production in the World – A Review. Energy Procedia. 2013; 33: 311-321.
13. Kamuyu WCL, Lim JR, Won S, Ahn HK. Prediction Model of Photovoltaic Module Temperature for Power Performance of Floating PVs. Energies. 2018; 11(2): 447.
14. Idoko L, Anaya-Lara O, McDonald A. Enhancing PV modules efficiency and power output using multi-concept cooling technique. Energy Reports. 2018; 4: 357-369.
15. Fesharaki VJ, Dehghani M, Fesharaki JJ. The Effect of Temperature on Photovoltaic Cell Efficiency. In Proceedings of the 1st International Conference on Emerging Trends in Energy Conservation - ETEC ; 2011; Tehran.
16. Qiang F, Tong N. A Complex-Method-Based PSO Algorithm for the Maximum Power Point Tracking in Photovoltaic System. Second International Conference on Information Technology and Computer Science. 2010;: 134-137.
17. Abdullah MF, Alghoul MA, Naser H, Asim N, Ahmadi S, Yatim B, et al. Research and development efforts on texturization to reduce the optical losses at front surface of silicon solar cell. Renewable and Sustainable Energy Reviews. 2016; 66: 380-398.
18. Richter A, Hermle M, Glunz W. Reassessment of the Limiting Efficiency for Crystalline Silicon Solar Cells. IEEE Journal of Photovoltaics. 2013; 3: 1184-1191.
19. Salari A, Taheri A, Farzanehnia A, Passandideh-fard M, Sardarabadi M. An updated review of the performance of nanofluid-based photovoltaic thermal systems from energy, exergy, economic, and environmental (4E) approaches. Journal of Cleaner Production. 2020;: 124318.
20. Al-Waeli AHA, Chaichan M, Sopian , Kazem HA. Modeling and experimental validation of a PVT system using nanofluid coolant and nano-PCM. Solar Energy. 2019; 177: 178-191.
21. Bambrook SM, Sproul AB. Maximising the energy output of a PVT air system. Solar Energy.

2012; 86(6): 1857-1871.

22. Dubey S, Solanki SC, Tiwari A. Energy and exergy analysis of PV/T air collectors connected in series. Energy and Buildings. 2009; 41(8): 863-870.
23. Brănoaea M, Burlacu A, Verdeş M, Balan MC, Vizitiu RŞ. Enhancing the Energy Efficiency of Photovoltaic Cells Through Water Cooling. Lecture Notes in Networks and Systems. 2022 January; 386.
24. Reay DA, McGlen RJ, Kew PA. Heat Pipes, 6th Edition, Theory, Design and Applications: Elsevier Ltd. ; 2014.
25. Brănoaea M, Burlacu A, Ciocan V, Verdeş M, Vizitiu RŞ. Numerical Investigation of a Novel Heat Pipe Radiant Floor Heating System with Integrated Phase Change Materials. Proceedings of The 14th International Conference on Interdisciplinarity in Engineering—INTER-ENG 2020. 2020;(63): 15.
26. Vizitiu RŞ, Burlacu A, Abid C, Şerban A, Verdes M, Ciocan V, et al. EXPERIMENTAL INVESTIGATION ON THE OPTIMUM FILLING RATIO OF HEAT PIPES USED FOR HEAT RECOVERY SYSTEMS. Proceedings Of International Conference Building Services And Energy Efficiency, Sciendo. 2020;: 154-161.
27. Wu S, Xiong C. Passive cooling technology for photovoltaic panels for domestic houses. International Journal of Low-Carbon Technologies. 2014;(9): 118-126.
28. Hudişteanu SV, Cherecheş NC, Popovici CG, Verdeş M, Ciocan V, Balan M, et al. Effect of cooling on power generated by photovoltaic panels. IOP Conference Series: Materials Science and Engineering. 2021;(1141): 012008.
29. Gomaa MR, Hammad W, Al-Dhaifallah M, Rezk H. Performance enhancement of grid-tied PV system through proposed design cooling techniques: An experimental study and comparative analysis. Solar Energy. 2020 November; 211: 1110-1127.
30. Boumaaraf B, Boumaaraf H, Slimani MEA, Tchoketch_Kebir S, Ait-cheikh MS, Touafek K. Performance evaluation of a locally modified PV module to a PV/T solar collector under climatic conditions of semi-arid region. Mathematics and Computers in Simulation. 2020; 167: 135-154.
31. Sahota L, Tiwari GN. Review on series connected photovoltaic thermal (PVT) systems: Analytical and experimental studies. Solar Energy. 2017; 150: 96-127.
32. Jinko. [Online]. [cited 2021 11 5. Available from: http://jinkosolar.com.au/wp-content/uploads/2021/12/Eagle-JKM315M-60-A2-EN.pdf.

Evaluation Dutch final nZEB requirements for University buildings

Mike van Osta [a], Wim Maassen [a,b]

[a] Royal HaskoningDHV, Rotterdam, the Netherlands, wim.maassen@rhdhv.com .

[b] Department of the Built Environment, Eindhoven University of Technology, Eindhoven, the Netherlands, wim.maassen@rhdhv.com

Abstract. The need for (nearly) Zero Energy Buildings (nZEBs) in the Netherlands becomes increasingly important due to climate change, increasing energy prices, scarcity of fossil fuels and increasing geopolitical conflicts. In line with the EU EPBD, from January 2021 new buildings, including hospital and university buildings, have to fulfill more strict energy requirements. Besides that, also the energy requirements for existing buildings will become stricter to realize an energy neutral built environment by 2050. On request of the Dutch Universities (WO) and the Dutch Academic Medical Centre's (UMC), the Netherlands Enterprise Agency (RVO) assigned Royal HaskoningDHV to study the effect of the nZEB requirements on this real estate of the sector. The feasibility of the final nZEB requirements has been assessed for eight representative, recently designed and realized university buildings. The results show that:

- Compared to the provisional nZEB requirements it has become less difficult to fulfil the final nZEB requirements and sometimes even less difficult than using the former method (NEN 7120) and requirements (EPC);
- Five of eight university buildings comply with all nZEB requirements and three buildings do not comply with the nZEB requirement on primary energy (BENG 2);
- Effective and necessary measures in general are: good thermal isolation, energy efficient lighting with daylight and occupancy control, ventilation with heat recovery and CO2/occupancy control, Aquifer Thermal Energy Storage with Heat Pumps and local PV solar panels.

Although the nZEB requirements are feasible, organizations should keep in mind that fulfilling these requirements for only their new buildings is not enough to meet the 95% CO2 emission reduction target in line with the Paris Climate agreement in 2050. A roadmap with all measures to reach this target, including the existing buildings, should prevail when making design and energy transition decisions for the campus energy infrastructure and each building.

Keywords. nZEB Netherlands, Energy, University Buildings, Feasibility, Case Studies.
DOI: https://doi.org/10.34641/clima.2022.320

1. Introduction

Finally, after some delay, the Dutch nZEB regulation is put into practice on January 1st 2021. Not only new requirements are introduced, but also the calculation method is altered. The provisional nZEB requirements were already proposed in 2015 and led to many questions regarding their feasibility, in particular regarding the demand for more than 50% renewable energy generation on site, see [5]. These provisional requirements from 2015 were updated in 2018. In 2019 the final nZEB requirements were introduced together with the calculation method NTA8800 that replaced the former calculation method NEN 7120.

Among most concerned organisations are universities and hospitals which own and use large multistorey buildings with high energy demand. The consequences of new regulations need to be known before renovations and new constructions can be planned. Therefore several nZEB feasibility studies have been performed [2-7]. In this paper the results of the last study are presented, answering the following questions:

- How do 8 selected recently realised and/or designed sustainable university buildings perform in regard to the set final nZEB requirements?
- How do the results of the new calculation method NTA8800 compare to the former method NEN 7120?
- Does complying with the new nZEB

Copyright ©2022 by the authors. This conference paper is published under a CC-BY-4.0 license.

requirements interfere with CO2 emission reduction target of -/- 95% in 2050 for the university building portfolio?

2. Approach

A straightforward approach is followed. Calculations with the new NTA8800 and old NEN 7120 method were made and analysed.

The following calculation methods are used as given in Table 1.

Tab. 1 – Calculation methods used to compare the case studies

	Quantity	*Calculation method*	*Case*
1	Ecalc/Eref	commercial program Enorm (version: 2009;2015)	all Buildings
2	BENG(2017)	with commercial program Enorm (version 2017)	all Buildings except EUT Flux Building
3	BENG (2019)	NTA8800-excel calculation	only for EUT Flux Building different variants were calculated
4	BENG(2020)	NTA8800 with commercial program VABI-program (version 2020)	all buildings

For the EUT Flux building different scenarios are compared. For seven other buildings, only the design as built is compared. It was checked if the buildings comply with the nZEB requirements and the differences between the calculations with different methods were analysed. Next looking at the results and the CO2 emission reduction target in 2050, it was analysed and explained if fulfilling the nZEB requirements automatically leads to the best solutions to achieve the CO2 emission reduction targets in 2030 and 2050.
We developed and used a Five-step method that was also previously published [1]. The characteristics of each building or variant were analysed by using the so-called 'Five-Step Method'. This is an upgraded version of the 'Trias Energetica' with the explicitly separated steps: demand and behaviour (step 1) and energy exchange and storage systems (step 4) [2], see Figure 1.

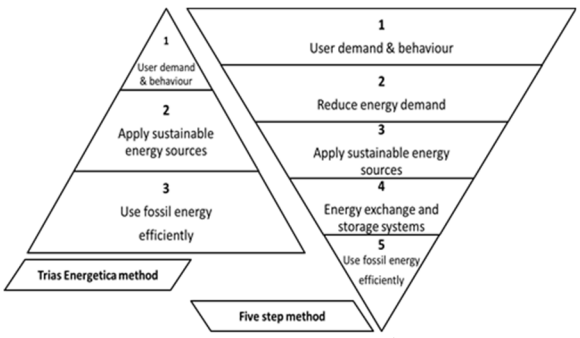

Fig. 1 - Building design approaches: 'Trias Energetica' versus the upgraded 'Five Step Method' [1].

3. Theory

The Dutch energy performance requirements for new buildings, which had to be met until 2021, are expressed in the dimensionless number E_{calc}/E_{ref}, which is the quotient of the calculated and the set admissible amount of primary Energy use and calculated according to the Dutch standard NEN 7120 [8]. Only the energy use of the Heating Ventilating and Air Conditioning (HVAC), lighting and sustainable energy are included and the energy use of appliances/equipment is excluded.

From January 1st 2021 the calculation method NTA 8800 is introduced. This is a new and more detailed calculation method, which is based on the developed EU EPBD CEN standards [11]. Together with the introduction of the new calculation method also the Primary Energy Factor for the electricity form the grid was changed from 2.56 to 1.45. This PEF is in line with the actual situation in the Netherlands and leads already to a significant reduction of the primary energy use related to the consumption of electricity from the grid.

In the Dutch nZEB method 3 energy performance indicators (EP 1, EP 2 and EP 3) are calculated which each need to fulfil for each type of building function a set requirement (BENG 1, BENG 2 and BENG 3):

- EP 1 with requirement BENG 1: Thermal Energy Demand consisting of heating and cooling. Influencing the geometry, insulation, infiltration, orientation, solar irradiance, internal heat production, thermal mass.

- EP 2 with requirement BENG 2: Total Primary Energy taking the different Primary Energy Factor of offsite energy into account. The same energy posts are considered as in the former NEN7120 calculation method: Heating, Cooling, Lighting, Fans, Domestic Hot Water, Humdification, (excl. Equipment) -/- Sustainable energy (PV, Wind, Aquifer Thermal Energy Storage (ATES) etc). The EP2 has the same meaning as E_{calc} in the EPC.

- EP 3 with requirement BENG 3: Fraction of locally generated sustainable energy, e.g. PV, Wind, ATES, Heating Source for Heat Pump.

For a whole building each BENG requirement is a weighted value based on the floor area of each available building function, e.g. an education building consists of an education function, but also an office function.

The nZEB requirements were adjusted several times in the years before they came into effect. The final

nZEB requirements for some individual building functions are presented in Table 2.

Tab. 2 - Final (2019) nZEB requirements to be calculated with NTA8800 for some building functions.

Function	*BENG 1 – Energy demand [kWh/ (m².a)]*	*BENG 2 – Primary fossil energy consumption [kWh/ (m².a)]*	*BENG 3 – Percentage renewable energy [%]*
Office	$A_{ls}/A_g \leq 1,8$: 90 $A_{ls}/A_g > 1,8$: 90 + 30 x (A_{ls}/A_g - 1,8)	40	30%
Assembly function	$A_{ls}/A_g \leq 1,8$: 90 $A_{ls}/A_g > 1,8$: 90 + 30 x (A_{ls}/A_g - 1,8)	60	30%
Education	$A_{ls}/A_g \leq 1,8$: 190 $A_{ls}/A_g > 1,8$: 190 + 30 x (A_{ls}/A_g - 1,8)	70	40%
Healthcare without bed area	$A_{ls}/A_g \leq 1,8$: 90 $A_{ls}/A_g > 1,8$: 90 + 35 x (A_{ls}/A_g - 1,8)	50	40%
Healtcare with bed area	350	130	30%

A_{ls}: Building Shell Area including facade and roof.
A_g: Nett Floor Area

It should be noted that the nZEB requirements are design requirements that calculate a theoretical energy consumption based on a reference building usage and assuming an optimal condition of the building and the building services. Consequently, the measured energy consumption in operation can differ from the calculated value if the building usage and/or building and building services conditions differ. Furthermore, special attention should be paid to the indoor environment and requirements to avoid negative effects, e.g. (i) increasing indoor temperatures during summer that can lead to additional cooling and/or (ii) less ventilation that can lead to a loss of productivity or the application of additional ventilation systems when the building is in use, when applying measures to comply with nZEB requirements.

4. EUT Flux Building

The Eindhoven University of Technology Flux building was selected for a more in-depth analysis. It's a 26,200 m² facility, with around 9,852 m² offices, 5,945 m² education, 190 m² shops, 2,564 m² meeting spaces and shared corridors. Three different cases have been evaluated, trying to comply with the required energy use 53 kWh/(m².a), according to the nZEB requirements based on the combination of the building functions. Table 3 presents selected parameters of the reference scenario and changes that have been implemented in the three following cases. Building characteristics and changes are listed in order of the five step method.

Tab. 3 - Changes introduced in Cases Var 1, Var 2 and Var 3 compared to the reference case: REF.

	REF
1	Lighting control based on precense detection, sweep and daylight control
2	Rc= 3.5; 5.0 and 5.0 m²K/W (floor, facade, roof) HR++ glazing (U=1.6 W/m²K, g-value 0.35) Shades Infil.: 0.42 l/s.m², Heat recovery: 70% Lighting: 7 W/m²
3	Heatpump
4	Heat and cold storage
5	Electroboiler

	Changes REF ↔ Var. 1
1	
2	
3	2,250 m² PV (50% roof area)
4	
5	

	Changes REF ↔ Var. 2
1	
2	Rc= 3.5; 5.0 and 6.0 m²K/W (floor, facade, roof); Ventilation heat recovery 80% with bypass; Ventilation flow rate 140% requirements building code; Lighting : 4 W/m²
3	2,250 m² PV (50% roof area)
4	
5	

	Changes REF ↔ Var. 3
1	Mechanical ventilation with CO2 sensors controlled in different zones;
2	Rc= 3.5; 5.0 and 6.0 m²K/W (floor, facade, roof); Ventilation heat recovery 90% with bypass; Ventilation flow rate 140% requirements building code; Lighting : 4 W/m²
3	2,250 m² PV (50% roof area)
4	
5	

Various changes have been introduced to reduce the energy consumption. These three cases are presented on Figure 2, together with the reference case of the current situation.

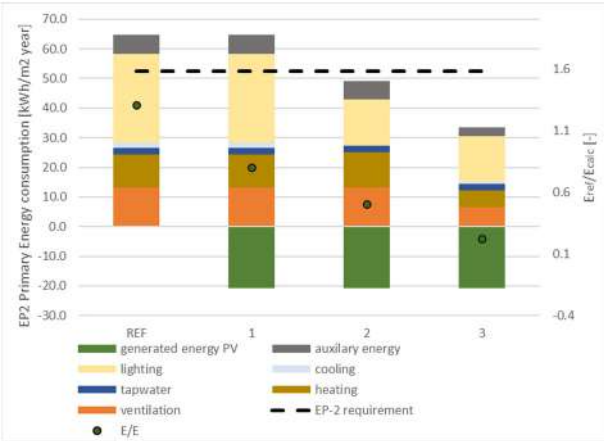

Fig. 2 - Results of the analysis of four cases, aiming to

reduce the energy usage and comply with nZEB regulations.

The results are summarised in Table 4.

Tab. 4 - Summarized results of the case study for the EUT Flux Building.

Variant	Energy demand [kWh/(m^2.a)]	Energy use [kWh/(m^2.a)]	Renewable energy [%]	E_{calc}/ E_{ref} [-]
Requirement	< 122	< 53	> 33%	<1.0
Ref	95	65	43%	1.3
Var. 1	95	44	61%	0.8
Var. 2	95	28	65%	0.6
Var 3	85	13	75%	0.2

The BENG 1 requirement for the energy demand of the building is already fulfilled with the standard characteristics of the reference building. The same goes for the BENG 3 requirement for minimum use of renewable energy. The Flux building is connected to an aquifer thermal storage system (ATES).

Energy from this source is counted as renewable energy, together with air – water heat pumps, biomass, combined heat and power and energy generation by PV, wind and solar thermal collector.

The BENG 2 requirement is fulfilled, even without additional energy generation, if a highly efficient heat recovery system is used, the ventilation flow rate is lowered to a minimum required flow rate and lighting power is reduced. Furthermore, it is possible to fulfil the requirements if PV panels are introduced in the design.

From the case study can be concluded that for this building:

- The nZEB requirements are less strict than the former EPC requirement. After all, EP 2 is only 10% above BENG 2 for the REF variant, while the calculated primary energy with the EPC is 30% above the requirement (E_{calc}/E_{ref}=1.3)

- nZEB requirements are already feasible for the EUT Flux building with less than 50% PV on the roof.

5. Case studies

The energy performance of eight different recently realised and/or designed sustainable university buildings, see Figure 3, is investigated. The buildings are: (1) Eindhoven University of Technology Flux - EUT FLUX, (2) Faculty of Geological Sciences University Utrecht - UU GEO, (3) Education cluster University Utrecht - UU OWC, (4) Energy Academy Europe University of Groningen - RUG EAE, (5) Eindhoven University of Technology Atlas - EUT Atlas), (6) Delft University of Technology Pulse – TUD Pulse, (7) new Building Rotterdam University

Tab. 5 - Building characteristics of the case studies

Nr =>	***1***	***2***	***3***	***4***	***5***	***6***	***7***	***8***
Building =>	***EUT Flux***	***UU GEO***	***UU OWC***	***RUG EAE***	***EUT Atlas***	***TUD Pulse***	***HR KZ***	***TiU N2***
NFA [m^2]	21,561	14,095	10,440	9,363	33,204	4,542	12,404	2,847
Heating	HP	HP, CHP	HP	HP HE	HP	HP	HP	HP
Cooling	ATES	ATES	ATES	ATES	ATES	ATES	ATES	ATES
Ventilation	MB 60% red HR 70%	MB 20% red HR 70%	MB 20% red HR 60%	MB 40% red HR 70%	MB 40% red HR 70%	MB 20% red HR 76%	MB 60% red HR 75%	MB 20% red HR 75%
Windows	U=1.6 W/m^{2}K SHF=0.35	U=1.6 W/m^{2}K SHF=0.35		U=0.97 W/m^{2}K SHF=0.15-0.5	U=0.8 W/m^{2}K SHF=0.25	U=1.65 W/m^{2}K SHF=0.4	U=0.9 W/m^{2}K SHF=0.35	U=1.5 W/m^{2}K SHF=0.6
Shades	S,W,E	S	Overhang	Solar panels	S,W,N,E	no	no	S
Lighting	9 W/m^2 dl and md	8 W/m^2	8 or 13 W/m^2	4.5 - 16 W/m^2	7 W/m^2 dl and md	5 or 8.8 W/m^2 dl and md	5 W/m^2 on/off	8 W/m^2 dl and md
PV [m^2]			500	3,030	4,300	948	2,250	
PV/NFA [-]	*0.00*	*0.00*	*0.05*	*0.32*	*0.13*	*0.21*	*0.18*	*0.00*

NFA	Net Floor Area	HR	Heat Recovery
HP	Heat Pump	U	Isolation [W/(m^2.K)]
HP HE	Heat Pump High Efficiency	SHF	Solar Heating Factor [-]
ATES	Aquifer Thermal Energy Storage	dl	daylight control
CHP	Combined Heat and Power	md	motion detector
MB	Mechanical Balance	PV	Photovoltaic panels
red	% ventilation flow reduction	S,W,N,E	South, West, North, East

of Applied Sciences – HR KZ and (8) Tilburg University Building nr 2 – TiU N2.

Some characteristics of these buildings are described in Table 5 and more information can be found on the websites that are included in the Appendix.

In Table 6, the energy performance calculated with NEN 7120 and expressed in E_{calc}/E_{ref} are given.

Tab. 6 - The university buildings and the calculated E_{calc}/E_{ref} with NEN 7120.

Nr.	Building	Built [a]	A_g [m²]	EPC date	E_{calc}/E_{ref} [%]
1	EUT Flux	2014	21,561	1-jan-15	131%
2	UU GEO	2017	14,095	18-aug-15	84%
3	UU OWC	2015	10,440	6-nov-12	81%
4	RUG EAE	2016	9,363	8-dec-16	1%
5	EUT Atlas	2018	33,204	20-oct-20	47%
6	TUD Pulse	2018	4,542	20-jul-16	9%
7	HR KZ	2022	12,404	nvt	nvt
8	TiU N2	2021	2,847	29-mai-20	-15%

TU/e Flux is above 100% because the original calculation which had to fulfil the requirements of 2009 were recalculated with the more strict requirements from 2015. In Table 6 for every E_{calc}/E_{ref} calculation is indicated which requirements were used. The 2009 requirements for educational buildings became 45% more strict in 2015.

The energy performance expressed in the three EP indicators was first calculated in 2017 based on the old calculation method NEN 7120. Results from this study are given in Table 7. In 2020 the EP indicators were calculated again based on the new calculation method NTA8800. The results are given in Table 8.

Tab. 7 - Results comparison energy performance in BENG based on calculation method NEN 7120 and intended requirments in 2017.

Nr.	Building	BENG 1 [kWh/m².a]	EP 1 [kWh/m².a]	BENG 2 kWh/m².a]	EP2 [kWh/m².a]	BENG 3 [%]	EP 3 [%]
1	EUT Flux	124	93	61	105	34	32
2	UU GEO	50	41	60	91	50	10
3	UU OWC	50	74	60	127	50	27
4	RUG EAE	50	29	60	-11	50	132
5	EUT Atlas	50	61	60	39	50	49
6	TUD Pulse	50		60	-	50	
7	HR KZ	50		60	-	50	
8	TiU N2	50	59	60	-6	50	107

Tab. 8 - Results comparison energy performance in BENG based on final calculation method NTA 8800 and final requirements in 2020.

Nr.	Building	BENG 1 [kWh/m².a]	EP 1 [kWh/m².a]	BENG 2 kWh/m2.a]	EP2 [kWh/m².a]	BENG 3 [%]	EP 3 [%]
1	EUT Flux	122	95	53	65	33	43
2	UU GEO	97	63	47	76	31	32
3	UU OWC	164	141	67	94	37	59
4	RUG EAE	97	57	47	-35	31	170
5	EUT Atlas	164	122	64	28	37	70
6	TUD Pulse	171	137	68	43	38	77
7	HR KZ	134	86	62	0	34	101
8	TiU N2	171	154	68	3	38	98

Explanations by Table 7 and 8:

- *Results' type style means: does not meet the NZEB requirement and **does meet the NZEB requirement**;*
- *BENG are the requirements and EP are the calculated values;*
- *at TU/e Flux, the BENG score of 2019 with excel model NTA8800 has been entered in BENG Score 2017. This was available for TU/e Flux and not for the other buildings.*

Fig. 3 - The university buildings which have been considered in this study.

The results in Table 7 and 8 show:

- The RUG EAE, EUT Atlas, TUD Pulse, HR KZ and TiU N2 buildings comply with the nZEB requirements;
- The buildings EUT Flux, UU GEO and UU OWC UU do not comply with the BENG 2 requirement;

• Compared to the EP scores in 2017, it has become easier to fulfil the BENG 1, 2 and 3 requirements.

6. nZEB requirements versus former E_{calc}/E_{ref} requirement

Table 9 shows for each building the percentage wherein the E_{calc}/E_{ref} and EP2/BENG2 demand is exceeded. Besides, the table indicates whether the EPC requirement for 2009 or 2015 was applicable. The 2009 EPC requirements were less strict than the 2015 EPC requirements.

Tab. 9 - Results comparison energy performance in E_{calc}/E_{ref} and EP2/BENG based on final calculation method and final requirements in 2020.

	EPC	*BENG 2*	*EPC-eis*	
			in 2009	*in 2015*
EUT Flux	31%	23%		yes
UU GEO	-17%	62%	yes	
UU OWC	-19%	39%	yes	
RUG EAE	-99%	-175%	yes	
EUT Atlas	-53%	-56%		yes
TUD Pulse	-91%	-37%		yes
HR KZ				
TiU N2	-115%	-96%		yes

Taking into account that the E_{calc}/E_{ref} requirements have become stricter by approximately 45% in 2015 than in 2009, it can be concluded the BENG 2 requirement has become stricter except for the EUT Flux, RUG EAE and EUT Atlas building.

Tab. 10 – The 7 Energy Performance Indicators

7. nZEB requirements versus 2050 Carbon emission reduction targets

In general, it can be stated that fulfilling the nZEB requirements does not automatically lead to the right steps towards the climate agreement goals of 2050. The nZEB requirements only set performance requirements for 1 new building and do not take other buildings, existing buildings and in future changes in buildings and energy infrastructure into account.

Furthermore, the BENG 2 requirements is currently (2021) focusing on reducing primary energy consumption and the associated direct and indirect CO2 emissions in a cost-effective way. It is a short-term goal/measure, based on current economic feasibility.

For the built environment, the Climate Agreement focuses on the reduction of direct CO2 emissions in the long term (2030, 2050), for which roadmaps are being developed. For a new gas-free/fossil-free building. The BENG 2 requirement will have no direct influence on the reduction of direct CO2 emissions.

Only designing according to the nZEB requirements can lead to sub-optimal solutions because it is not (explicitly) based on the long term and the roadmap for the buildings of the organization. Part of the roadmap can be a future transformation of the energy infrastructure near the building. This could be for example the development of sustainable central energy plant on the campus,

whereby requirements are also set for the buildings to be linked, e.g. a maximum connection capacity or energy demand. It includes a building that must

Name	*Goal*	*Energy performance indicator*	*Unit*	*Explenation*
Energy demand	Reduction building related energy demand	EP 1	[kWh demand/m^2 floor area]	Thermal energy demand without building services, not calculated to primary energy
Primary energy consumption	Reduction total (direct and indirect) CO2 emission	EP 2	[kWh primary/m^2 floor area]	Same as scope EPC with NEN 7120. Building related energy consumption taking into account efficiencies of the local systems and from energy generation on country level
Share renewable energy	Stimulating local renewable energy generation	EP 3	[%]	Excluding purchased energy, because allocated energy is in the Netherlands not allowed in EP 3, see also EP 7.
User energy	limit energy and internal heat load not related to building	EP 4	[kWh electric/m^2 floor area]	Outside scope EP 1 - 3.
Real energy consumption (on the meter)	Limit externally purchased energy that will eventually be fully renewable	EP 5/ Real energy consumption	[kWh/m^2 floor area]	Energy reduction for EP 1 has also effect on EP5
Direct CO2 emission	Reduce direct CO2 emissions (Goal of the climate agreement for buildings)	EP 6	[kWh CO2 direct/ m^2 floor area]	
Share purchased renewable energy	Stimulating energy transition energy sector	EP 7	[% kWh reality]	The share of renewable energy of all purchased energy

comply with the nZEB requirements, which can also be seen as part of the roadmap for the buildings, including the future planning in energy infrastructure and the available capacity

To evaluate a building design against longer-term goals, it is recommended to add 4 energy performance indicators (User energy, Actual energy, direct CO2 emissions and share of renewable energy purchased) to the 3 BENG indicators for the building, see Table 10. In this way it is possible to monitor and manage the energy performance of buildings as part of the energy transition more effectively, in line with the corresponding goals of these additional energy performance indicators, see Table 10.

8. Conclusions

The nZEB requirements (BENG 1,2 and 3) can easily be fulfilled for university buildings with the new NTA8800 method. In some cases, the nZEB requirements are even less strict than the former EPC requirement E_{calc}/E_{ref} requirement with method NEN 7120.

The BENG 1 requirement appears to be most easy to be fulfilled. Although the insulation value of the investigated buildings is lower than the current building decree level. Consequently, it is concluded that BENG 1 is not a strict requirement for university buidings.

In addition to sustainability measures such as an air-water heat pump, PV panels are always required to meet the requirements in order to achieve BENG 2 and 3.

Fan energy and lighting are the largest energy posts for Flux and the Energy Academy Building. At the UU Geo building it is visible that heating has a large share in the primary energy caused by the use of natural gas for the CHP system.

9. Recommendations

The final nZEB requirements are further differentiated per building function, e.g. there are now requirements for a healthcare building function with beds and healthcare building function without beds. However, no distinction has been made for educational buildings, except for an indirect distinction within BENG 1 based on the ratio of the building shell (facade and roof) and nett floor area. However, it is also important to make a distinction in BENG 2 and BENG 3 based on the number of floors and the total nett floor area, e.g. educational buildings with only 1 floor can have much more advantage (in energy per m^2 nett floor surface) of PV-panels on the roof than larger educational buildings with more floors.

The BENG 1 requirement should be stricter and at least in line with the current building decree levels and also stimulate the optimization of the design and facade that will have a long lifetime with consequently long pay back times for adjustments when the building is in use.

Only complying with the nZEB requirements does not automatically lead to the best design choices to meet the energy and climate goals in the longer term. It is therefore important to always take into account the roadmap with which the buildings of an organization will contribute to the targets of the climate agreement.

To assess a building design against longer-term goals, it is recommended to add 4 energy performance indicators (User energy, Actual energy, direct CO2 emissions and share of renewable energy purchased) to the 3 BENG indicators for the building.

The datasets generated during and/or analysed during the current study are not publicly available because the datasets are the property of each building owner but will be made available after the permission of each building owner.

10. Acknowledgement

The evaluation studies were funded by the Netherlands Enterprise Agency (RVO).

11. Appendix

More information about the case studies can be found on the following websites:

1. TU/e Flux gebouw https://www.tue.nl/en/news-and-events/news-overview/28-08-2015-tue-halves-gas-consumption-with-the-official-opening-of-the-flux-building/
2. Faculteit Geowetenschappen Universiteit Utrecht (GEO UU) https://www.uu.nl/en/organisation/real-estate-and-campus/campus-utrecht-science-park/development/construction-projects-in-progress/new-office-building-for-geosciences
3. Onderwijscluster Universiteit Utrecht (OWC UU) https://www.ectorhoogstad.com/projects/owc-%E2%80%93-victor-j-koningsberger
4. Energy Academy Europe RUG (EAE RUG) https://www.rug.nl/groundbreakingwork/projects/eae/?lang=en
5. TU/e Atlas (TU/e Atlas) https://www.tue.nl/en/our-university/about-the-university/sustainability/atlas/the-

most-sustainable-building-of-education/

6. Pulse TUD https://campusdevelopment.tudelft.nl/en/project/pulse/
7. Hogeschool Rotterdam KZ Bouwdeel C (HR KZ) https://paulderuiter.nl/en/projects/hogeschool-rottterdam-bouwdeel-c/
8. Tilburg Universiteit Nieuwbouw 2 (TiU N2) https://www.tilburguniversity.edu/campus/developments/educational-building

12. References

[1] Gvozdenović, K., W.H. Maassen, W. Zeiler, and H. Besselink. 2015. Roadmap to nearly zero energy buildings in 2020. REHVA Journal 2:6–10 [Online]. Available https://www.rehva.eu/rehva-journal/chapter/roadmap-to-nearly-zero-energy-buildings-in-2020

[2] Maassen, W.H., REPORT (nearly) Zero Energy Hospital Buildings, Reference: I&BBE3112R001F0.1, Revision: 0.1/Final, Date: 25 January 2017, [Online]. Available: https://tc0906.ashraetcs.org/I&BBE3112R001D01%20nZEB%20Hospital%20Buildings%201701125.pdf

[3] REHVA Journal 2017/05, HVAC in Health Sector, nZEB Hospitals case studies, October 2017, [Online]. Available: https://www.rehva.eu/fileadmin/REHVA_Journal/REHVA_Journal_2017/RJ5/RJ1705_WEB.pdf

[4] Maassen, W.H., Peeters, B., RAPPORT - BENG eisen en Utiliteitsgebouwen voor Hoger Onderwijs en Universitair Medische Centra/Ziekenhuizen, Studie naar haalbaarheid BENG eisen, Reference: I&BBF1511R001D1.2, Date: October 27th 2017, see https://www.royalhaskoningdhv.com/nl-nl/nederland/nieuws/papers-en-artikelen/voorgenomen-beng-eisen-c-struikelblokken-voor-ziekenhuizen-en-hoger-onderwijs-q/7985

[5] Maassen, W.H., Evaluation Dutch preliminary nZEB requirements for hospital and university buildings, REHVA 13th HVAC World Congress CLIMA2019, 26th-29th May 2019, Bucharest, Romania

[6] Maassen, W.H., Osta van, M., BENG eisen voor Hoger Onderwijs en Ziekenhuizen - Studie naar haalbaarheid BENG eisen volgens methode NTA 8800, Referentie: BF1511IBRP1902181538, 18 februari 2019, Available: https://www.royalhaskoningdhv.com/nl-nl/nederland/nieuws/nieuwsberichten/onderzoek-naar-haalbaarheid-van-de-beng-eisen-voor-ziekenhuizen-en-hoger-onderwijsgebouwen/9050

[7] Maassen, W.H., Osta van, M., Feasibility nZEB requirements for University Buildings (NL: Haalbaarheid BENG gebouwen HO), Report, Royal HaskoningDHV proj.nr. BH5096, RVO ref. EGO2000086, March 9th 2021

[8] NEN 7120 Energy performance of buildings - Determination method

[9] NEN NTA8800: Energy performance of buildings - Determination method, https://www.gebouwenergieprestatie.nl/bepalingsmethode/

[10] Software NTA8800: Vabi EPA NTA 8800, versie 3, https://www.vabi.nl/product/vabi-epa-u/

[11] [Online] REHVA EPB (Energy Performance of Buildings) Standards: https://www.rehva.eu/activities/epb-center-on-standardization/epb-standards-energy-performance-of-buildings-standards

Experimental and CFD comparison of driver's thermal plume with classical air diffusers

Amaury Jamin [a], Paul Alexandru Danca [b], Bart Janssens [a], Florin Bode [b], Ilinca Nastase [b], Walter Bosschaerts [a]

[a] Department of Mechanical Engineering, Royal Military Academy, Brussels, Belgium, amaury.jamin@mil.be

[b] CAMBI Research Center, Building Services Faculty, Technical University of Civil Engineering of Bucharest, Bucharest, Romania, paul.danca@utcb.ro, ilinca.nastase@utcb.ro

[c] Department of Mechanical Engineering, Technical University of Cluj Napoca Cluj, Napoca, Romania florin.bode@termo.utcluj.ro

[d] Department of Renewable Energy Sources, National Institute for R&D in Electric, Engineering ICPE-CA, Bucharest, Romania, paul.danca@icpe-ca.ro

Abstract. In confined spaces, such as vehicle cabins, airflow is one of the most critical factors affecting thermal comfort and pollutant dispersion. To develop innovative and energy-efficient HVAC systems, a deep understanding of the jet flows' interaction from air diffusers on the thermal plume became essential to improve our knowledge of airflow patterns for optimizing ventilation system design, thermal comfort, and indirectly, energy efficiency. We have developed a 1:1 scale mock-up with transparent walls, replicating a Renault Megane's interior in a climatic chamber and associated complex numerical models. PIV and IR measurements were firstly performed for the pure thermal plume with a thermal manikin in a driver's seat in this 1:1 scale mock-up. The experimental and numerical results showed good agreement regarding ranges and distributions. This paper presents experimental and numerical comparisons performed without and with ventilation systems to evaluate this interaction for classical air diffusers as a part of our larger project. The flow structure in the car cabin is complicated with existing large- and small-scale vortices. With an active ventilation system, the thermal plume is stronger in front of the head, the opposite of what has previously observed back the head. The airflow moves forward along the ceiling. The presence of the steering wheel distorts the flow direction at the thigh level. The additional velocity field on convective upward velocity in the shoulders' region is caused by impinging jets from diffusers. The Coanda effect caused by the central diffuser's flow creates a nonuniform and asymmetrical air distribution in the shoulders' region. A qualitative comparison of the jets' velocity distributions shows that the velocities are more uniform with innovative LAG diffusers than with the classical ones. This shows clearly the benefits of passive flow mixing to improve the thermal sensation.

Keywords. Human thermal plume, jet flow, PIV, IR, car cabin ventilation, CFD modeling.
DOI: https://doi.org/10.34641/clima.2022.314

1. Introduction

In recent decades, thermal comfort and air quality for passengers with reduced energy consumption are among the automotive industry's leading research and development goals. Driver stress or fatigue, driver and passenger health, energy consumption, and emissions are parameters that significantly impact a comfortable thermal environment [1-2].

Controlling thermal conditions in the passenger compartment remains a challenge for engineers because the fast dynamic behaviour of these systems makes it difficult to predict the optimal parameters for achieving thermal comfort. The inhomogeneity of the surface temperature distribution due to thermal convection effects directly affects the airflow at the precise locations. Moreover, the airflow patterns and their effects on the thermal sensation should be studied in more detail in the future. Due to thermal gradients and the presence of the passengers, the overall flow path (convection effects) can deviate significantly from the direction predicted by the guided vanes of the air diffusers. Therefore, the airflow distribution is one of the most critical factors for thermal comfort and pollutant dispersion in car cabins [3-4]. Indeed, in car cabins, a deep understanding of airflow patterns is essential for removing excess heat and diluting contaminants [5], which results from the interaction between human airflows, mainly thermal plumes from passengers and conditioned air delivered by the air HVAC systems [6].

Therefore, to develop innovative and energy-efficient HVAC systems, a better understanding of the following phenomena could provide fundamental information for the optimization of the design of

Copyright ©2022 by the authors. This conference paper is published under a CC-BY-4.0 license.

these systems: i) human thermal plume; ii) airflow, especially in the vent outlet and jet stream areas; iii) interaction of the jet flow from classical or innovative air diffusers on the development process of the human thermal plume. In passenger compartments, human thermal plumes generated by body heat loss significantly impact passenger comfort, pollutant dispersion, and air quality. The cabin interior's geometry, the air vents' manufacture and location, the grid vanes' design, and the HVAC's flow parameters set affect strongly influence the airflow in the jet stream area. For designing a mixing ventilation system, thermal comfort, air quality and energy consumption are the crucial parameters. In fact, a high induction level is desirable in these ventilation systems, allowing optimal mixing of the ventilating jet with the ambient air. From previous research, the innovative idea was to introduce lobed geometries passive control for improving air diffusion in buildings and vehicles with 12 studies regarding different configurations in UTCB and the French university of La Rochelle. Optimizing the design of innovative air diffusers, such as lobed ailerons, orientable lobed spherical nozzles, and cross-shaped lobed perforated panels, with passive flow mixing to improve the thermal sensation of the occupants appeared as an efficient, cost-effective solution to reduce the energy consumption for conventional, electric, or hybrid vehicles using an intelligent air diffusion strategy [7-9].

This type of phenomenon can be investigated experimentally using many different measurement techniques. PIV, an optical flow visualization method, is the most suitable method for studying the human thermal plume air distribution [10-11], characterized by low-velocity fields and transient behaviour and the velocity distribution of jet streams (large-scale PIV) [4,12,13]. In PIV measurements, the main difficulty is maintaining thermal equilibrium and achieving the most homogeneous seeding particle concentration. However, the main limitations of the experimental investigation are the parametric study and the reproducibility of specific boundary conditions. Computational Fluid Dynamics (CFD) has become very powerful in the automotive industry because it can provide a large amount of information relatively quickly and at a relatively low cost. From a numerical point of view, the human thermal plume is one of the most difficult to be reproduced correctly due to its unstable nature governed by buoyancy forces. A key factor in numerical simulations is validating and verifying the computational data. When the human thermal plume interacts with other flows in the microenvironment of the human body, the validation or calibration of the models becomes even more complicated. This microenvironment is extremely confined inside a vehicle, with unevenly distributed surface temperatures and high velocities near the human body and its plume. In our effort to study and understand the influence of air distribution in the car cabin on the thermal sensation of the human body, complex numerical models are developed.

To this end, we have developed a full-scale experimental model of a vehicle cabin that replicates the interior of a Renault Megane, with a real dashboard and associated air distribution system and real seats (see Fig. 1). This model -mostly transparent- allows the investigation of the involved flows through optical methods of measurements. In a previous study [14], we performed PIV and IR measurements of the thermal plume of a sophisticated Thermal Manikin (TM) in the driver's seat in a 1:1 scale mock-up of a Renault Megane car cabin in a climatic chamber where all active walls with surface temperatures controlled by a hydraulic and automation system were set up at constant temperature and without a ventilation system to validate the numerical model. Two conditions were checked to capture the pure thermal plume air distribution without ventilation. First, the new thermal equilibrium of the cabin must be achieved without any internal thermal energy being extracted by the A660 A/C laboratory unit. Secondly, the momentum of the seeding airflow introduced in the cabin mock-up must be negligible compared to the thermal plume [15]. Case 1 (without ventilation) was made to improve the understanding of this phenomenon separately in a confined space as a reference.

The results obtained with both methods showed good agreement regarding ranges and distributions of velocity and temperature in the sagittal and coronal planes [16-18]. The paper presents the experimental and numerical comparisons performed with no active and active ventilation system intended to evaluate the interaction of the jet flow from a classical vehicle air diffuser on the development process of the human thermal plume in the sagittal and coronal planes as the first step in our global plane. In the current literature, for the first time, the thermal plume of a seated person inside a vehicle is captured by optical measurement methods and compared with numerical models without (case 1) and with (case 2) ventilation systems from a classical air diffuser.

2. Experimental setup

A full-scale experimental model (see Fig. 1) was set up in an environmental chamber measuring 2.5 x 3.6 x 3.6 m, which is equipped with active walls and whose surface temperature is controlled by a hydraulic and automatic system for PIV and IR measurements. All active walls were set up at 20°C to have a constant temperature with an active ventilation system in the climatic chamber. An A660 A/C laboratory unit was used to control the injected air's mass flow, temperature, and humidity into the car cabin. The total volume flow rate was 191.3 m^3/h. A nude TM with a neuro-fuzzy control system named Suzi [19], characterized by a standard human size of 1.7 m and a total surface of 1.8 m^2 was used to generate the thermal plume's flow. A uniform body surface temperature of 34°C was imposed over the entire TM because it is easier to capture the thermal plume than a nonuniform surface temperature. The

TM is controlled by in-house software in LabVIEW based on a neuro-fuzzy system, allowing the user to specify setpoints for each of the 79 areas of surface temperature.

Fig. 1 – Experimental setup – 1:1 scale cabin mock-up with transparent walls.

The monitoring system can record the temperature evolution of the 395 available temperature sensors, 5 sensors in each of the 79 zones, and record the power consumption of each segment. Non-reflecting painting and material were used to mask all reflecting surfaces inside the cabin.

PIV measurements were carried out in a climatic chamber, using a TM in the driver's place inside the scale 1:1 mock-up. The purpose of PIV measurements was to experimentally verify the CFD velocity distribution around the TM's head (See Fig. 3: green planes) and CFD jet velocity distribution in the middle plane of air diffusers (See Fig. 3: blue planes). A PIV system, composed of a FlowSense EO camera with 2048x2048px as spatial resolution combined with a 50 mm lens and a Dual Power green (532 nm) Litron laser with an energy of 200 mJ, was used to measure the thermal plume and jet velocity profile. The maximum trigger rate of the PIV system between two pairs of images was 7.5 Hz. The time between pulses was 500-2000 μs, with 500 images for the thermal plume and 150-250 μs, with 250 images for the jet flow acquired for each measurement. The vehicle cabin was seeded with a high-volume liquid seeding generator from Dantec Dynamics that produced olive oil particles (0.5 μm). An air compressor was used to supply the seeding generator with compressed air. During the PIV measurements, the seeding generator was turned off. A calibration target with tiny dots formed a grid with dimensions of 100x100mm [24]. The size of each captured image was 250x250mm for the thermal plume and 380x380mm for the air jet. A FLIR E40 IR camera was used to measure the manikin's temperature gradient and evaluate the thermal plume around the head, using a thin metallic sheet with equidistant points 30 mm apart in the horizontal and vertical direction as a reference scale.

Fig. 2 – PIV calibration targets for air jet.

3. Numerical setup

Numerical simulation is widely used to study vehicle cabins' thermal and flow environments [7-9]. Based on this 1:1 scale cabin mock-up, the numerical model was designed and implemented in Ansys Fluent software (see Fig. 3).

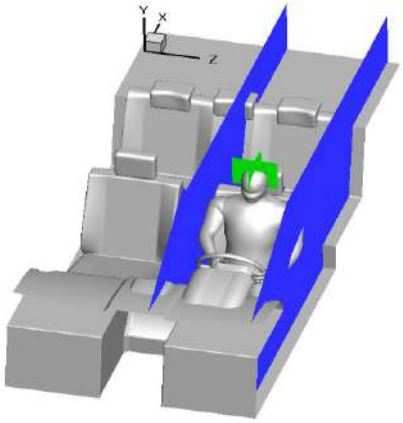

Fig. 3 – Side view of the studied geometrical model.

Steady-state RANS simulations were performed with the SST k-ω turbulence model. Different turbulence models in vehicle cabins were studied [20-21], advising the SST k-ω model for induced jet streams and the thermal plume [8]. For density models, ideal and incompressible-ideal gas and Boussinesq approximation were chosen and compared. The boundary conditions (BCs) for the manikin and the car cabin (windshield, front, ceiling, floor, rear window, left and right side) were set up with no-slip wall with a fixed temperature of 34°C and 20°C. The inlet BC of the air vents was set at 20°C and with an imposed mass flow rate of 0.0285 kg/s for the side air vents and 0.0354 kg/s for the central air vents based on experimental measurements and a constant turbulence intensity of 5% (see Tab. 1) being calculated using an empirical method [22]. We considered an isothermal uniform flow. As described in [22], the initial values of kinetic energy k, specific dissipation rate ω, and eddy viscosity ν_t were approximated. The governing equations were solved on a grid of polyhedral elements.

Tab. 1 – Calculation for Boundary conditions for air inlets.

	Left	Central left	Central right	Right
$\dot{m}$ [kg/s]	0.0136	0.0193	0.0161	0.0149
D_h [m]	0.076	0.074	0.074	0.076
Re	8273	11472	9422	9974
I [%]	5.2	5	5.1	5.1

Gradients were calculated with least-square-cell-based method. Coupled solver was chosen for pressure-velocity coupling scheme. Second-order upwind scheme was chosen to calculate the convective terms. The initialization was set to hybrid. Different meshes were considered and tested for the grid dependence test based on a previous study [14]. The CFD domain comprises 18 million polyhedral elements which, the boundary layer with prisms consists of 8 layers where the first cell height of 0.75mm and a growth factor of 1.2. Three refined mesh zones were created using the body influence technique as a critical area (see Fig 4).

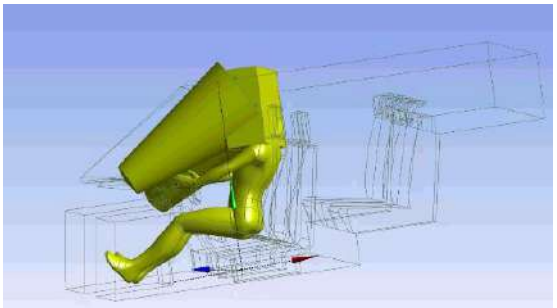

Fig. 4 – Mesh detail for the refining zones.

4. Results and discussion

Measurements and numerical simulations were performed in a full-scale passenger compartment considering only one HVAC volume flow rate (191.3 m^3/h). When comparing both results for the air velocity and temperature distributions in the sagittal and coronal planes (case 2), a good agreement was found regarding the ranges and distributions. An average correlation method to extract the velocity profiles was used for the PIV postprocessing in Dynamic Studio 7.2 software. Due to reflections, an image mask was defined to hide noisy vectors, such as vectors close to the Plexiglas roof or steering wheel.

4.1 Human thermal plume

Figures 5-12 present the thermal plume velocity and temperature distribution in sagittal and coronal planes. The thermal plume air and temperature distribution are asymmetrical in both cases. The flow structure in the car cabin is complicated with existing large- and small-scale vortices (See Fig. 13). For case 2, the thermal plume is stronger in front of the head, which is the opposite of case 1 back the head due to the following contributions. The airflow moves forward along the ceiling (see Fig. 13). The presence of the steering wheel distorts the flow direction at the thigh level (see Fig. 13). The additional velocity field on convective upward velocity in the shoulders' region is caused by impinging jets from diffusers. The Coanda effect caused by the central diffuser's flow creates a nonuniform and asymmetrical air distribution in the shoulders' region (see Fig. 13-14).

Tab. 2 – PIV/CFD comparison for velocity distribution.

V [m/s]	Sagittal		Coronal	
	PIV	CFD	PIV	CFD
Case 1	0.09-0.012		0.07-0.85	0.07-0.09
Case 2	0.15-0.2		0.12	0.12-0.15

The values determined in the sagittal and coronal planes for the temperature distribution of the thermal plume obtained by the numerical and experimental methods are very similar.
In both sagittal and coronal planes, the main upward-moving stream was observed, and the surrounding cold air flowed into the area that the hot plume left.
The thermal plume air and temperature distribution are also asymmetrical on the two measurement planes as previously.

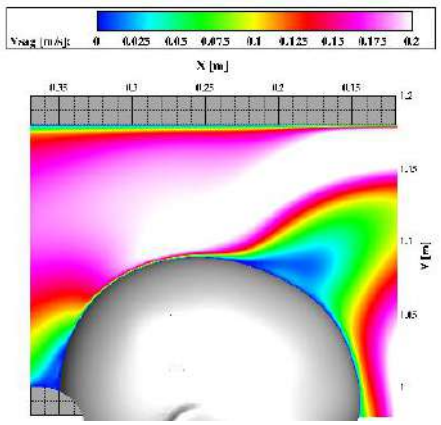

Fig. 5 – Thermal plume velocity distribution in sagittal plane (CFD).

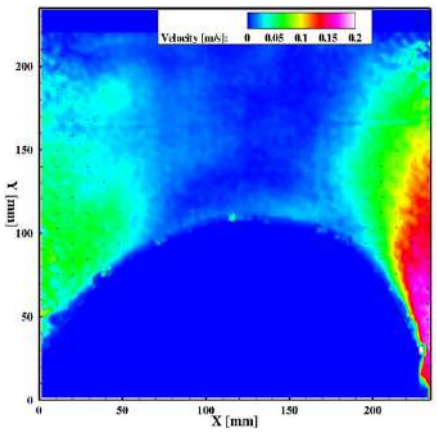

Fig. 6 – Thermal plume velocity distribution in sagittal plane (PIV).

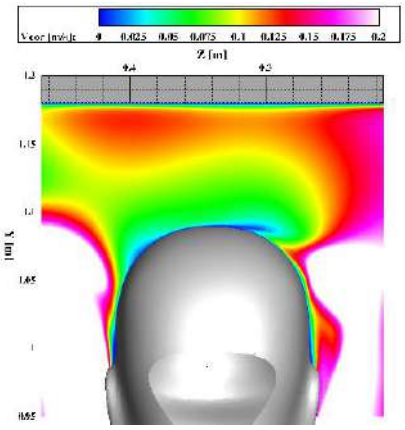

Fig. 7 – Thermal plume velocity distribution in coronal plane (CFD).

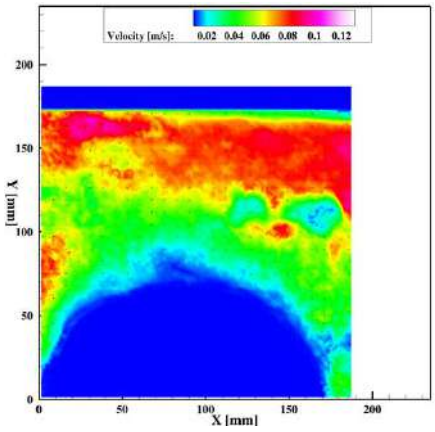

Fig. 8 – Thermal plume velocity distribution in coronal plane (PIV).

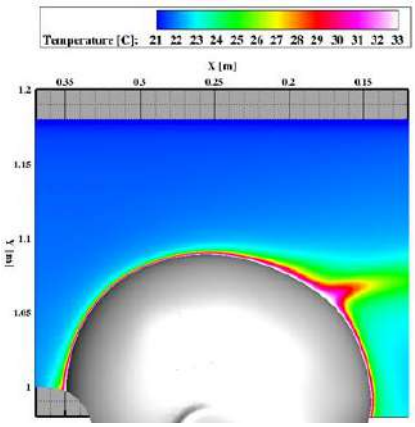

Fig. 9 – Thermal plume temperature distribution in sagittal plane (CFD).

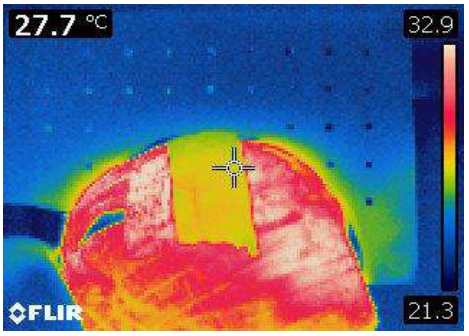

Fig. 10 – Thermal plume temperature distribution in sagittal plane (IR).

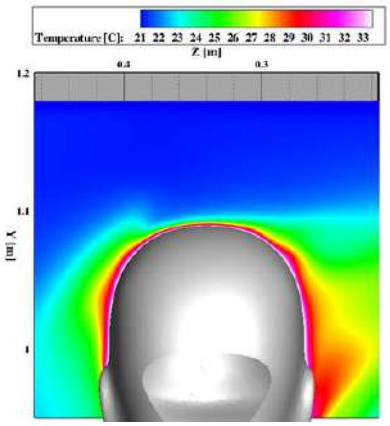

Fig. 11 – Thermal plume temperature distribution in coronal plane (CFD).

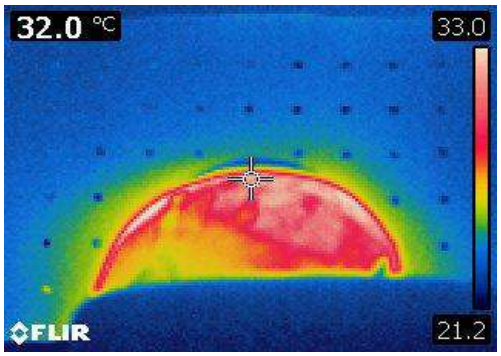

Fig. 12 – Thermal plume temperature distribution in the coronal plane (IR).

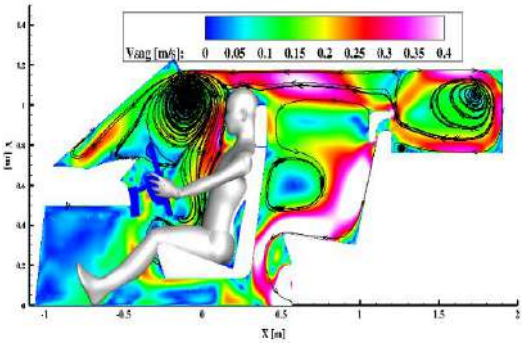

Fig. 13 – Velocity field in the driver's seat centre plane.

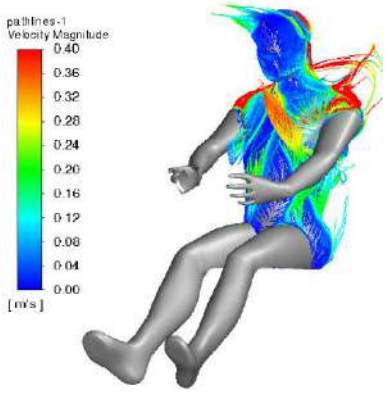

Fig. 14 – Pathlines showing the thermal plume on the manikin's body**.**

The distribution of the convective fluxes allows us to have a more precise idea of the thermal plume dynamics and heat transfer for each body's part. For case 2, a nonuniform and asymmetrical heat transfer can be observed (see Fig. 15).

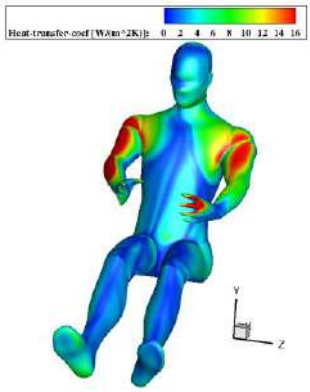

Fig. 15 – Convective heat flux on manikin surface.

4.2 Air jet

Figures 16-21 present the velocity distribution for CFD isothermal uniform flow and PIV measurements in the middle plane of the central left/ left side Classical Grilles (CG) and Lobed Aileron Grilles (LAG) diffusers. The results show that this qualitative comparison with PIV measurements is not too bad despite having a CFD isothermal uniform flow of air jets in terms of velocity range and the general shape of the jet stream. A disadvantage of this working assumption for the uniform flow is that the same velocity across the inlet area is an unrealistic situation. If a uniform air velocity is assumed as a BC, the airflow distribution in the cabin will change, and the passenger's thermal sensation will also change. PIV qualitative comparison of the jets' velocity distributions shows that with an innovative LAG diffuser, the velocities are more uniform than with the classical one since the flow injected through the lobed diffuser train more air and mix better with air from the cabin. This greater uniformity in the flows for LAG diffusers has been demonstrated in previous studies [25-26] with a critical value of 30^0 for the lobe inclination. If this critical value is not respected, there will be a separation of the two flows than the desired effect of mixing the two flows bounded by the sheet. It shows clearly the benefits of passive flow mixing to improve the thermal sensation.

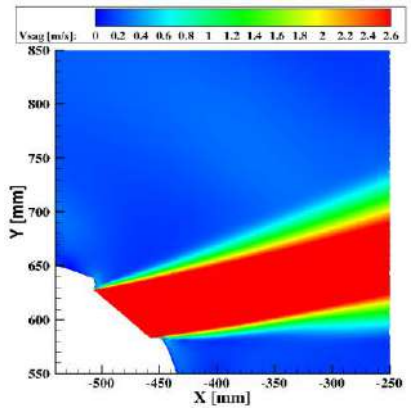

Fig. 16 – CFD velocity Distribution in the middle plane of the central left diffuser.

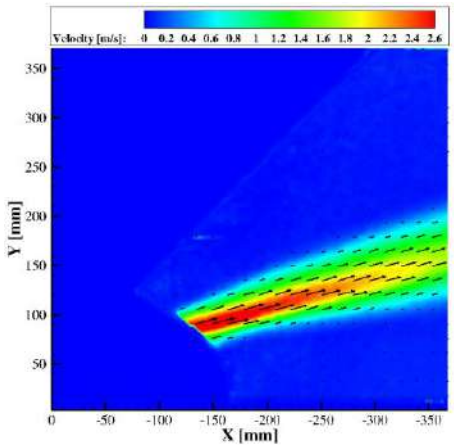

Fig. 17 – PIV velocity distribution in the middle plane of the central left CG diffuser.

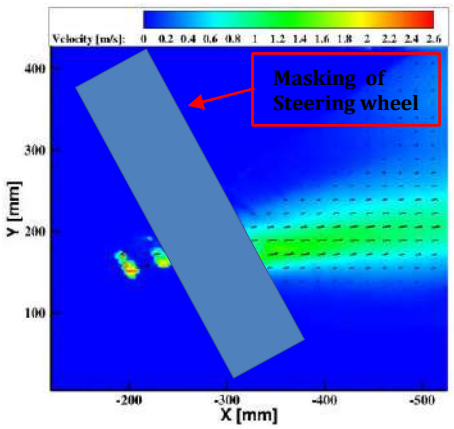

Fig. 18 – PIV velocity distribution in the middle plane of the central left LAG diffuser.

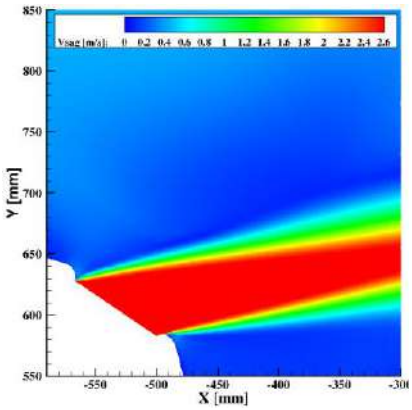

Fig. 19 – CFD velocity Distribution in the middle plane of the left side diffuser.

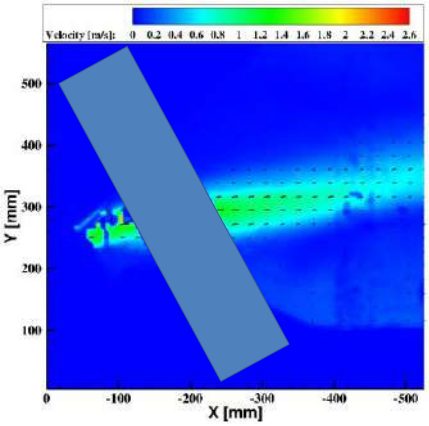

Fig. 20 – PIV velocity Distribution in the middle plane of the left side CG diffuser.

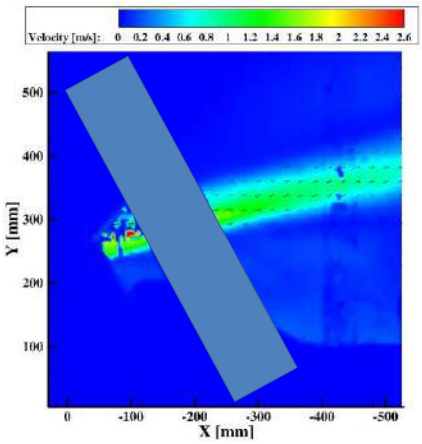

Fig. 21 – PIV velocity Distribution in the middle plane of the left side LAG diffuser.

5. Conclusion and perspectives

The results obtained by numerical and experimental methods showed good agreement regarding ranges and distributions in both planes for the thermal plume in case 2, where an isothermal uniform flow as CFD BC was used. The asymmetrical behaviour was observed in both planes for the thermal plume airflow and temperature distributions. The thermal plume is stronger in front of the head, which is the opposite of what was previously observed in the head [14] due to four different contributions, as explained in section 4.1.

To investigate thermal plume air distribution with PIV measurements, it is crucial to check the cabin's thermal equilibrium and the momentum of the seeding airflow.

A qualitative comparison of the jets' velocity distributions shows that with an innovative LAG diffuser, the velocities are more uniform than with the classical one since the flow injected through the lobed diffuser train more air and mix better with air from the cabin.

For future validations of this interaction, the next step will be to compare the PIV measurements for three different HVAC volume flow rates with two different approaches:

- Real 3D scanned ducts will be simulated separately from the car cabin to reduce computation time (see Fig. 22).
- BC's of air velocity distribution from LDV data.

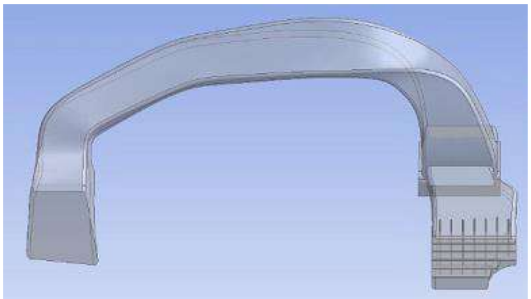

Fig. 22 – Geometry of real 3D scanned air ducts.

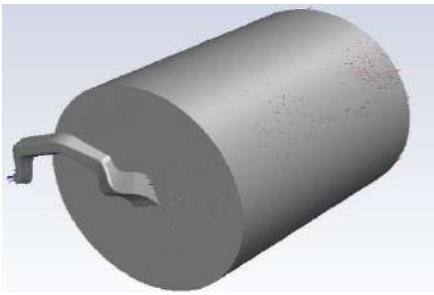

Fig. 23 – CFD domain of real 3D scanned air ducts.

6. Acknowledgement

This work was supported by a grant from the Romanian Ministry of Education and Research, CCCDI-UEFISCDI, project number PN-III-P2-2.1-PED-2019-4249, within PNCDI III, XTREME – Innovative system to extend the range of electric vehicle at improved thermal comfort.

7. Data access statement

Data sharing is not applicable to this article as no datasets were generated or analyzed during the

current study.

8. References

[1] Zhang B, Xue T, Hu N. Analysis and improvement of the comfort performance of a car's indoor environment based on the predicted mean vote–predicted percentage of dissatisfied and air age. Advances in Mechanical Engineering. 2017 Apr;9(4):1687814017695693.

[2] Croitoru C, Nastase I, Bode F, Meslem A, Dogeanu A. Thermal comfort models for indoor spaces and vehicles—Current capabilities and future perspectives. Renewable and Sustainable Energy Reviews. 2015 Apr 1;44:304-18.

[3] Zhang H, Dai L, Xu G, Li Y, Chen W, Tao W. Studies of airflow and temperature fields inside a passenger compartment for improving thermal comfort and saving energy. Part II: Simulation results and discussion. Applied Thermal Engineering. 2009 Jul 1;29(10):2028-36.

[4] Lee JP, Kim HL, Lee SJ. Large-scale PIV measurements of ventilation flow inside the passenger compartment of a real car. Journal of visualization. 2011 Dec;14(4):321-9.

[5] Mangili A, Gendreau MA. Transmission of infectious diseases during commercial air travel. The Lancet. 2005 Mar 12;365(9463):989-96.

[6] Kühn M, Bosbach J, Wagner C. Experimental parametric study of forced and mixed convection in a passenger aircraft cabin mock-up. Building and Environment. 2009 May 1;44(5):961-70.

[7] Bode F, Patrascu C, Nastase I. Heat and mass transfer enhancement strategies by impinging jets: A literature review. Thermal Science. 2021;25(4 Part A):2637-52.

[8] Amina M, Nastase I, Bode F, Beghein C. Optimization of a lobed perforated panel diffuser-a numerical study of orifice arrangement. International Journal of Ventilation. 2012 Dec 1;11(3):255-70.

[9] Nastase I, Meslem A, El Hassan M. Image processing analysis of vortex dynamics of lobed jets from three-dimensional diffusers. Fluid Dynamics Research. 2011 Nov 7;43(6):065502.

[10] Cao X, Liu J, Jiang N, Chen Q. Particle image velocimetry measurement of indoor airflow field: A review of the technologies and applications. Energy and Buildings. 2014 Feb 1:69:367-80.

[11] Cao X, Liu J, Pei J, Zhang Y, Li J, Zhu X. 2D-PIV measurement of aircraft cabin air distribution with a high spatial resolution. Building and Environment. 2014 Dec 1:82:9-19.

[12] Yang JH, Kato S, Nagano H. Measurement of Airflow of Air-Conditioning in a Car with PIV. Journal of visualization. 2009 Jun;12(2):119-30.

[13] Huera-Huarte FJ, Cort X, Aramburu E, Vizcaino X, Casto L. DPIV Measurements of the HVAC Aerodynamics Inside a Passenger Car. In23rd SAE Brasil International Congress and Display 2014 Sep 30 (No. 2014-36-0214).

[14] Jamin A, Janssens B, Bosschaerts W, Bode F, Danca PA, Nastase I. Experimental Validation of the Human Thermal Plume of the Driver Inside a Vehicle Cabin. In2021 10th International Conference on ENERGY and ENVIRONMENT (CIEM) 2021 Oct 14 (pp. 1-5). IEEE.

[15] Li J, Liu J, Wang C, Jiang N, Cao X. PIV methods for quantifying human thermal plumes in a cabin environment without ventilation. Journal of Visualization. 2017 Aug;20(3):535-48.

[16] Danca P, Bode F, Nastase I, Meslem A. CFD simulation of a cabin thermal environment with and without human body–thermal comfort evaluation. InE3S Web of Conferences 2018 (Vol. 32, p. 01018). EDP Sciences.

[17] Li J, Cao X, Liu J, Mohanarangam K, Yang W. PIV measurement of human thermal convection flow in a simplified vehicle cabin. Building and Environment. 2018 Oct 15;144:305-15.

[18] Li J, Liu J, Pei J, Mohanarangam K, Yang W. Experimental study of human thermal plumes in a small space via large-scale TR PIV system. International Journal of Heat and Mass Transfer. 2018 Dec 1;127:970-80.

[19] Ursu I, DG CC, Danca P, Nastase I. Advanced TMPrototype with Neurofuzzy Control System. COBEE 2018. 2018.

[20] Heider A, Konstantinov M, Lauenroth G, Rütten M, Werner F, Wagner C. Experimental and numerical investigations of cabinflow in a mini-van. In: Aero- dynamics of Heavy Vehicles III: Trucks, Buses and Trains (2010). https://elib.dlr. de/67185

[21] You R, Chen J, Shi Z, Liu W, Lin CH, Wei D, Chen Q. Experimental and numerical study of airflow distribution in an aircraft cabin mock-up with a gasper on. Journal of Building Performance Simulation. 2016 Sep 2;9(5):555-66.

[22] Jaramillo JE, Perez-Segarra CD, Rodriguez I, Oliva A. Numerical study of plane and round impinging jets using RANS models. Numerical Heat Transfer, Part B: Fundamentals. 2008 Aug 7;54(3):213-37.

[23] Ullrich S., Buder R., Boughanmi N., Friebe C., Wagner C. Numerical study of the airflow distribution in a passenger car cabin validated with PIV. In Symposium der Deutsche Gesellschaft für Luft-und Raumfahrt (pp. 457-467). Springer, Cham. 2018.

[24] Tacutu L, Bode F, Năstase I, Croitoru C, Dogeanu A. Experimental and numerical study on the thermal plumes of a standing and lying human in an operating room. Science and Technology for the Built Environment. 2022 Jan 2;28(1):2-0.

[25] O'sullivan M. N., Krasnodebski J. K., Waitz I. A., Greitzer E. M., Tan C. S., & Dawes W. N. Computational study of viscous effects on lobed mixer flow features and performance. Journal of Propulsion and Power, 1996, 12(3), 449-456.

[26] NASTASE I. Analyse des jets lobés en vue de leur intégration dans les Unités Terminales de Diffusion d'air. 2007. Thèse de doctorat. La Rochelle.

New forecast control of heat for heating

Tomasz Cholewa[a,], Alicja Siuta-Olcha[a], Piotr Wolszczak[b], Andrzej Smolarz[c], Piotr Muryjas[c], Łukasz Guz[a], Martyna Bocian[a]*

[a]Faculty of Environmental Engineering, Lublin University of Technology, Nadbystrzycka 40B, 20-618 Lublin, Poland, email address: t.cholewa@pollub.pl

[b]Faculty of Mechanical Engineering, Lublin University of Technology, Nadbystrzycka 36, 20-618 Lublin, Poland

[c]Faculty of Electrical Engineering and Computer Science, Lublin University of Technology, Nadbystrzycka 38A, 20-618 Lublin, Poland

Abstract.
In many existing buildings, the reduction in energy consumption has already been made by carrying out the thermal modernization of the building envelope. Therefore, other renovation measures, aimed at further increasing the level of energy efficiency in such a buildings, will focus in particular on improvement of control and automation of the processes of supply, as well as storage and use of energy.
This paper presents the field results of applying forecast control of heating system, which can be easily employed in existing buildings (time of installation in existing buildings: below 2 hours) and may work with existing, widely used weather controller. The new methods (applied in forecast controller) used for the creation of real energy model of the building (energy characteristics of buildings and their heating systems) and for forecast of heat power for heating are presented. The field research was conducted for a multi-family building located in Poland for part of a single heating season. The analyzed multifamily building in the first part of research was regulated only by a traditional weather-based controller, whereas forecast control system was used in the second part of research. The application of the proposed forecast control allowed decreasing the supply temperature of heating medium, lower the heat power supplied and in such a way generate energy savings of above 10%.

Keywords. forecast control of heating system, load forecasting, energy in buildings, energy efficiency
DOI: https://doi.org/10.34641/clima.2022.313

1. Introduction

Existing buildings use around 42% of total final energy in the European Union [1] and about 80% of this energy is used for space heating [2]. Therefore, in order to increase the energy efficiency of existing buildings, several opportunities including the envelope and services such as heating, ventilating and air-conditioning (HVAC) are available. The measures which are easy applicable are preferred. One of such solutions may be optimization of HVAC control. In this light and with the development of technology, the demand for intelligent building control increases. Intelligent control of heating, ventilation and air conditioning (HVAC) generates potentially large energy savings at relatively low installation costs. For efficient building management, the influence of several atmospheric factors should be taken into account. These are in particular the outdoor air temperature, solar radiation, relative humidity and wind speed [3]. One of the methods of controlling HVAC systems is the Model Predictive Control (MPC) [4-6]. For example, it allows reducing the energy consumption for cooling in the office by 58.5% and decreasing the electricity consumption in the conference room by 36.7%, in relation to the previously used control method. Additionally, owing to the use of MPC in both rooms, an improvement in thermal comfort is observed [7]. An important aspect used to determine the heat demand in MPC is the weather forecast. Several methods are used to define it. One of them involves artificial neural networks that mimic biological neural networks. This allows for adapting the principle of the network operation towards changing initial conditions.

However, such a control of heating system is not easy applicable, especially in existing buildings. Therefore, this work shows the results of preliminary field test of forecast control of heating system. However, detailed presentation of the

Copyright ©2022 by the authors. This conference paper is published under a CC-BY-4.0 license.

method for forecast control of space heating in existing buildings will be included in an journal article [8]. This manuscript is organized as follows: section 2 presents the object and methods of analysis. Section 3 presents the main research findings regarding the heat power delivered to analysed building without and with forecast control of space heating system.

2. Materials and methods

The subject of the research was a multi-family building located in Poland before and after the application of the forecast control of space heating systems. The studied building is located in the 3rd climatic zone for the winter period in Poland, where the designed outdoor temperature is -20°C, and the average annual outdoor temperature is 7.6°C. The building is a 5-storey building. The heating system in buildings is a traditional system with vertical risers and radiators connected from one side. The heating installation is made of steel pipes, convection radiators with thermostatic radiator valves. The heating installation is supplied with the heating medium (80/60°C by outdoor air temperature equal to -20°C). Individual thermal station for heating and hot water purposes is located in the lowest part of the building. The control of heat supply is realized by weather base control which uses heat curve dedicated for this building. The building was equipped with a calibrated heat meter, which is installed in the main circuit of the heating system. The heat power supplied to the heating system and the temperature of heating medium on supply and return were monitored on an hourly basis and sent to information system (*IS*), which was to perform future calculations using algorithms.

The research included in this manuscript was conducted for four weeks in heating season 2020/2021 during which for two weeks the heating system was regulated only by traditional weather base control, and by two following weeks by forecast control system which cooperates with the existing weather base control.

The new forecast control system uses existing weather base control and allowed for the appropriate modification (only increase) of the current outdoor temperature, taking into account the building energy model (in form of T_{eq}), the forecast of user profiles and the forecast of weather conditions ($T_{outdoor}$, V, $Insol$).

This forecast control system has the ability to take into account in advance (what may be set individually in the control system) the impact of the forecasted changes in weather parameters (especially the forecasted increase in outdoor temperature and the occurrence of solar radiation) and use the thermal inertia of the building. Therefore, owing to such functions, this system allows increasing the value of the outdoor temperature sent to the existing controller of heating system, which lowers the supply temperature and allows for energy savings, which will be presented in Chapter 3.

3. Results and discussion

The new forecast control module was installed (beginning of 2021) in the investigated building first to create the data-driven real building energy model in the form of equivalent outdoor temperature (T_{eq}). This building energy model of the investigated building was created based on the data from February 2021 till mid-April. In this period the heating system was controlled by existing weather base control. The building energy model includes a correction of T_{eq} due to wind speed (T_v^{rev}) and correction due to solar radiation (T_{insol}^{rev}) – see [9] for more details. The influence of wind speed on the heat power delivered to building (T_v^{rev}) was estimated based on the data from night hours (11 p.m. – 4 p.m.), because then the influence of users and solar radiation is minimized. In turn, the data from Monday to Friday at 10 a.m. – 2 p.m. for wind speeds below 3 m/s were used to determine T_{insol}^{rev}. For these conditions, the influence of wind speed and users (who are usually away from home during these hours) is limited.

The equivalent outdoor temperature (T_{eq}) is presented in Equation 1.

$$T_{eq}=T_{outdoor}-(1.23\cdot V-2.16)+(0.01\cdot Insol+0.47)[°C] \quad (1)$$

Where: $T_{outdoor}$ is outdoor air temperature in °C, V- wind speed in m/s; $Insol$- solar radiation in W/m^2.

When calculating the energy model for the analyzed building, the coefficients of determination were 0.91 and 0.89 for T_v^{rev} and T_{insol}^{rev}, respectively. The details about validation of building energy model in the form of T_{eq} are provided in [9].

The minimum training period of creating a building energy model is 1 month, but 1 heating season is preferable.

Besides the building energy model above presented, also the profile of equivalent indoor temperature as the parameter related to the effect of the building occupant behaviour (see [10] for more details) was taken into account. This profile is updated for the analysed building on the weekly base. The forecast system is integrated with API meteo, owing to which the forecast of outdoor meteorological parameters for specific location is provided. The main output from the calculations made on *IS* are the outdoor temperature settings for 6 hours in advance. Then, the forecast control module emulates in the specific manner the outdoor temperature, which is the input to existing weather base control.

In such a way, the forecast system has the possibilities to react in advance to changing outdoor meteorological parameters. Owing to such a way of control of heating systems, it is possible to lower the supply temperature of heating medium for the investigated building by 7%, which is presented in **Figure 1**.

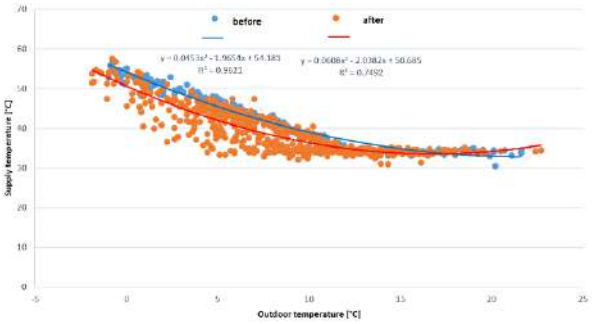

Fig. 1 – Supply temperature before and after the installation of forecast control.

Owing to lower supply temperature (in comparison to the period before the use forecast control of heat supply), the energy savings may be achieved (**Fig. 2**), which account for about 12.7% for the analysed buildings.

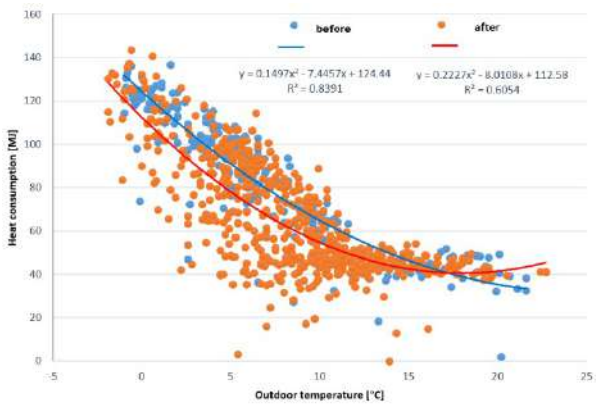

Fig. 2 – Heat consumption before and after the installation of forecast control.

Regarding the possible application of the proposed forecast control of heating system and easy extrapolation for other buildings, it should be emphasized that the proposed system may cooperate with the weather based controller already existing in a given building. Therefore, it takes no more than 2 hours to install the proposed system in an existing building. Additionally, for the purposes of building an energy model, it is not necessary to have a building (or a heating system) documentation, because this is data-driven real building energy model in the form of equivalent outdoor temperature (T_{eq}), which significantly simplifies the installation process. The proposed system also has a user friendly interface that allows adjusting individual settings (for example amount and period for data used) for creation of the building energy model of the building, the control process and allows setting additional indoor temperature reductions at night or during the day – see more details in [8].

4. Conclusions

Nowadays, there is limited numbers solutions others than weather base control of heating system in the existing buildings. In this manuscript, the preliminary results of new forecast control of space heating were shown. It has been observed based on the research conducted in existing building, that the use of forecast control allowed decreasing the supply temperature of heating medium and lower the heat consumption by 12.7% for the analysed building. This methodology may be widely applied in different countries, where central heating of buildings is applied. The detailed presentation of the method for forecast control of heating system will be presented in scientific journal paper.

5. Acknowledgement

This study was supported by research project, financed from European Funds (under the Intelligent Development Programme) by the Polish National Centre for Research and Development. Project number: POIR.04.01.02-00-0012/18.

6. References

[1] EU Energy in Figures. Statistical Pocketbook 2019. Luxembourg: Publications Office of the European Union. Available online: https://ec.europa.eu/energy/en/data-analysis/energy-statistical-pocketbook.

[2] International Energy Agency - IEA, Energy efficiency market report 2015, OECD/IEA; 2015.

[3] Chen S., Zhang G., Xia X., Setunge S., Shi L. A review of internal and external influencing factors on energy efficiency design of buildings. Energy and Buildings. 2020;216: 109944.

[4] Prívara S., Siroky J., Ferkl L., Cigler J. Model predictive control of a building heating system: The first experience. Energy and Buildings. 2011;43:564–572.

[5] Široky J., Oldewurtel F., Cigler J., Prívara S. Experimental analysis of model predictive control for an energy efficient building heating system. Applied Energy. 2011;88:3079–3087.

[6] Ascione F., Bianco N., De Stasio C., Mauro G.M., Vanoli G.P. Simulation-based model predictive control by the multi-objective optimization of building energy performance and thermal comfort. Energy and Buildings. 2016;111:131-144.

[7] Yang S., Wan M.P., Chen W., Ng B.F., Dubey S.

Model predictive control with adaptive machine-learning-based model for building energy efficiency and comfort optimization. Applied Energy. 2020;271:115147.

[8] Cholewa T., Siuta-Olcha A., Smolarz A., Muryjas P., Wolszczak P., Guz Ł., Bocian M., Balaras C.A. An easy and widely applicable forecast control for heating systems in existing and new buildings: First field experiences. Journal of Cleaner Production. 2022; (in press).

[9] Cholewa T., Siuta-Olcha A., Smolarz A., Muryjas P., Wolszczak P., Anasiewicz R., Balaras C.A. A simple building energy model in form of an equivalent outdoor temperature. Energy and Buildings. 2021;236:110766.

[10] Cholewa T., Siuta-Olcha A., Smolarz A., Muryjas P., Wolszczak P., Anasiewicz R., Balaras C.A. On the short term forecasting of heat power for heating of building. Journal of Cleaner Production. 2021;307:127232.

Data Statement

The datasets analysed during the current study are not publicly available because privacy reason but will be available on request.

Flexibility deployment of a heating system with heat pump in residential towers

Beatrix Bos [a], Pieter-Jan Hoes [b], Jan Hensen [b], Ingrid van Prooijen [c], Christina Papachristou [c]

[a] Sustainable Energy Technology, Department of Mechanical Engineering, Eindhoven University of Technology, Eindhoven, the Netherlands, b.r.a.bos@student.tue.nl.

[b] Building Physics and Services, Department of the Built Environment, Eindhoven University of Technology, Eindhoven, the Netherlands, p.hoes@tue.nl.

[c] BAM Energy Systems, Royal BAM, Bunnik, the Netherlands, ingrid.van.prooijen@bam.com.

Abstract. The transition from fossil fuel energy sources to renewable energy sources requires flexible use of our energy consumption to prevent congestion in the electricity grid. The heating systems of buildings are large energy consumers and can play an important role in matching electricity generation and demand. This research evaluates the amount and value of the potentially available flexibility from the heat pump in a case study on the heating system of two residential towers in The Netherlands, named Stoker & Brander. The thermal mass of the buildings is used to store energy to prevent heating during moments when grid congestion is likely to occur or when renewable energy production is low while maintaining comfortable indoor temperatures. To assess the potential energy flexibility, a building performance model and a financial model are developed to compare the influence on the energy flexibility when using different thermostat setpoint schedules. The total heat demand, the shifted load, the comfort, and the saved costs when deploying flexibility are selected as key performance indicators. With the model, 9 different thermostat setpoint schedules are tested with varying preheating duration and with varying timing before peak hours. In general, the schedules with a 2-hour preheating duration show the best results in terms of comfort and potential saved costs, while the timing before the peak hours has less effect on the results. The analysis on the saved costs is done with electricity prices of 2019, representing the current market, and with 4 price scenarios for 2030, representing the future market. The savings significantly increase for 2030, showing a large future potential for flexible deployment. However, it remains difficult to make a correct estimation of the predicted future savings as the scenarios show large differences between each other due to large uncertainty about the future prices. Nevertheless, for all scenarios at least 20% of the electricity purchase costs can be saved in 2030.

Keywords. Energy flexibility, heat pump operation, thermal mass, thermostat setpoints, electricity price scenarios
DOI: https://doi.org/10.34641/clima.2022.295

1 Introduction

1.1 Background information

To mitigate the effects of climate change, The Netherlands has decided to gradually reduce the natural gas consumption of buildings to zero by 2050 [1]. Common alternatives for heating with natural gas are all-electric heat pumps, collective heating systems or green gas. The electricity for the heat pump can be provided by renewable energy sources like solar or wind energy. These sources are characterized by their intermittent nature, which can result in an energy surplus when the weather circumstances are beneficial, yet in zero energy production when the weather is less beneficial. Renewable sources are implemented decentralized in the electricity grid, which often leads to grid congestion at places with a large renewable energy penetration and low grid capacity. The combination of these two characteristics leads to an increased pressure on the electricity grid and eventually to grid congestion, which is increasingly becoming a problem in the Netherlands (see this map). To alleviate these electricity grid problems a certain flexibility is required in demand and supply of electricity. Electricity should be used *where* it is generated and *when* it is generated. One way to offer this energy flexibility is by using Demand Side Management (DSM) in which the demand loads are adapted to the grid requirements [2]. Examples of Demand Side Management are load shifting and peak shaving of the peak electricity demand. In this research the focus lies on shifting the building energy demand to *when* electricity is generated.

The ability of a building to manage its energy demand according to local climate conditions, user needs and

Copyright ©2022 by the authors. This conference paper is published under a CC-BY-4.0 license.

grid requirements is addressed as the Energy Flexibility of a building [3]. In this research we focus on the energy flexibility that can be offered by using the heating system of a building in combination with the building's thermal mass. The working principle is based on the thermal inertia of a building, i.e., the indoor temperature responds relatively slow due to thermal energy buffering in the thermal mass [4]. When (green) electricity is available or cheap, heat can be produced and stored in the thermal mass without changing the indoor temperature too much. When generation from renewable energy sources is low or when congestion is expected, the stored heat in the thermal mass can be used to maintain a comfortable temperature, while reducing to building's heating energy demand [5]. This is referred to as load shifting. However, it is important to keep in mind that the operative temperature should always be kept within the limits of the occupants' thermal comfort.

1.2 Case description: project Euroborg - Stoker & Brander

In this research, the potential of using a heat pump for energy flexibility deployment is investigated by using a case study building. Royal BAM Group, hereafter indicated with BAM, has constructed two residential towers in Groningen, named Stoker & Brander. Each of these towers is home to 90 apartments with different lay-outs divided over 25 levels [6]. BAM acts as an Energy Service Company (ESCo), and is therefore responsible for the design, installation, and maintenance of the heating & cooling system of the towers. The system consists of a large heat pump that uses an underground heat and cold storage as thermal energy source (an Aquifer Thermal Energy Storage (ATES) system). The heat pump provides space heating to all apartments through an underfloor heating systems. For domestic hot water, the installation of gas boilers was required to achieve higher temperatures

1.3 Research objective

The main research objective of this project is to *quantify and value the potential energy flexibility of the heat pump in the heating system of two residential towers, Stoker & Brander, by utilizing the thermal mass of the buildings as heat storage medium*. This research explicitly focuses on making use of the existing heating system to keep additional investment costs in new infrastructure and storage capacity as low as possible. Next to that, this research is restricted to the condition that thermal comfort of the residents should always be guaranteed.

The following three main questions are formulated to support the research objective:

1. What is the current performance of the heating system in Stoker & Brander?
2. What is the energy flexibility of the current space heating system? Additional sub-questions can help to answer this question: What Key Performance Indicators are relevant? How can the energy flexibility be modeled and which building performance simulation models are suitable? What model complexity is appropriate?
3. What are the current and future monetary savings when the energy flexibility is deployed or not deployed?

2 Methodology

2.1 Research steps

In this research the flexibility of Stoker & Brander is quantified and valued by using a computational model that consists of multiple parts. To create this model, several steps are taken.

In the first step an analysis on historical data of the buildings is executed as well as having multiple conversations with BAM's management and operations team working on these buildings leading to detailed information about the current performance of the buildings. Second, the architectural drawings are taken as starting point to find an appropriate spatial resolution for the model. The appropriate spatial resolution is identified for one apartment by experimenting with certain modeling resolutions and their impact on the KPIs, after which the choices are converted to the geometries of the other apartments. In step 3 information about the occupant behavior, lighting settings, heating system and its settings, and the simulation periods are added to the model by using an iterative process. In the 4th step, varying temperature setpoint schedules are tested on one apartment to investigate the flexibility deployment by using the heat pump. In the next step, all different apartment types are simulated. In the last step, the results of all apartment types are combined with the outputs of the first step. Besides the quantification of flexibility, the valuation of this quantity requires a financial analysis. This analysis looks at both the current expected value and the future expected value.

2.2 Simulation workflow

In order to execute the research steps, different software tools are used that complement each other. An overview is presented in Figure 3. On the left side, the used inputs for the software tools are shown, in the middle is shown which part of the model is made with which tool and on the right side the outputs are represented. In red is indicated if and where the output is used as input for another software tool.

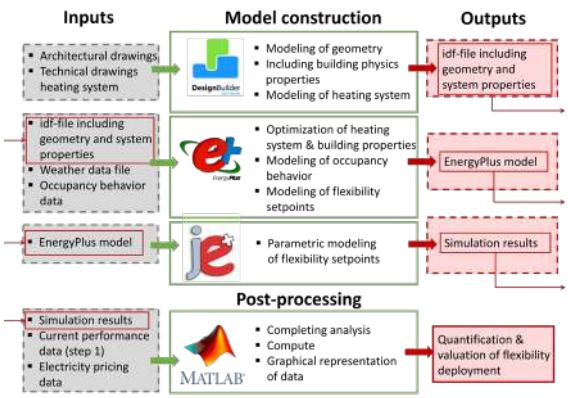

Fig. 1 - Graphical representation of the used software tools and their in- and outputs.

3 Case study description

As explained previously, BAM acts as an Energy Service Company for the buildings Stoker & Brander. The benefits of an ESCo are that the building owners (and tenants) are care-free and not responsible for the heating and cooling provision. A key component of the relation between the owner(s) and the ESCo is the energy performance contract. Generally, in these contracts, long-term guarantee of the performance is secured and, optionally, agreements are made on the energy savings. The ESCo agreement on these buildings, that runs for 30 years, provides an incentive for optimization of the system and its operational costs. Residents pay a fixed amount to BAM for their consumed heat. If BAM can generate the delivered heat more efficiently, they can benefit from higher profit margins while the clients pay a flat, predictable rate. However, the risk of producing heat against higher costs is also for BAM. Making smart use of the heat pump and the expected fluctuating electricity prices could save on the operational costs. Based on their point of view, the Key Performance Indicators are formulated.

3.1 Key Performance Indicators

The quantification and valuation of the flexibility deployment is assessed by using a set of Key Performance Indicators (KPIs). To assess the energetic performance of the system when deploying flexibility, the shifted load and the total energy consumption are evaluated. The amount of increase or decrease of the electricity demand after a (price) signal is the shiftable load for one signal. The summation of the shifted loads of all signals during one heating seasons is used as the *total shifted load*, which can be used to express the amount of flexibility [7]. Besides the shifted load, it is good to keep an eye on the *total energy consumption* to make sure that the energy consumption when deploying flexibility does not increase. The KPI's value can be seen as a boundary condition that should be satisfied. The valuation of the flexibility deployment is expressed in the saved operational costs of the heat pump. The operational costs mostly consist of the electricity costs. These *saved costs* are expressed in absolute saved costs in [€] and relative to the total electricity costs in [%] for the heating system. As is the case with the total energy consumption, the *thermal comfort* also places limits to the amount of flexibility that can be deployed. Therefore, thermal discomfort is defined as the number of hours when the occupants are present of which the operative temperature falls outside the 90% bandwidth of the Dutch adaptive comfort limits.

3.2 Building characteristics

As real-life buildings function as case buildings, a lot of information is known. Three aspects are of interest: the (thermal) building properties, the functioning of the heating system and information about the residents. Based on the architectural drawings, most building properties have been deduced. Second, information about the installed heat system is analyzed and converted into more simple, schematic overviews showing the main components of the installation and their connections. Due to privacy laws, not much information is known about the residents. Therefore, demographic information of the neighborhood gives an indication of the residents' profiles. Five different household types are identified: 1-adult household (39%), 2-adult household (13.9%), 1-senior household (21%), 2-senior household (15.1%), Family household (11%).

4 Current performance analysis

As described in the section Research steps, the first step entails the analysis of the current performance of the case buildings. The results of this analysis are used as inputs to construct the model. Key figures that are of interest are the energy flows, distribution losses and the performance of the heat pump. To get an idea of the total performance of the system, the total energy flow over one heating season is presented in a Sankey diagram, see Figure 4.

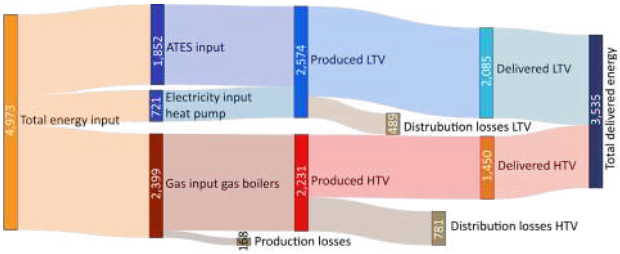

Fig. 2 - Sankey diagram of the energy flow in Stoker and Brander for 2019

The total amount of produced thermal energy for Low Temperature Heating (Lage Temperatuur Verwarming - LTV), which is used for space heating, is the combination of the electricity consumed by the heat pump and the thermal energy extracted from the ATES source. During the delivery of the LTV from the installation room to the apartments, the distribution losses are 18 to 19%. The total amount of produced thermal energy for the High Temperature Heating (Hoge Temperatuur Verwarming - HTV), which is mainly used for Domestic Hot Water (DHW), depends on the gas consumption and the efficiency of the gas boilers, which is assumed to be 93% and is common for gas boilers. Due to the higher temperatures of the HTV, higher distribution losses are found of 35 to 36%. For both streams, the losses are lower than the design values of 20 and 40% respectively. Though, it should be kept in mind that the losses vary over the years. As no significant amount of electricity is used to supply cooling to the apartments, the energy flows for cooling are not regarded in this analysis and thus, the thermal energy from the cold source is not included.

The heat pump is a crucial asset of the heating system. At moments where the heat pump does not function as designed, the gas use increases enormously, having a negative effect on the environmental and financial costs. Over the years that the heat pump was in normal operation, an average COP of 3.6 was found. Histograms of the data show that most of the time, the COP was even higher

than 3.6 but the average performance is decreased by some low outliers (that can occur during malfunctioning of the heat pump).

5 Model construction

The construction of the simulation model is split into three sections. The first section focuses on the modeling of the geometry of the building, the second on the simulation settings and the third section explains the financial model.

5.1 Geometric modeling

Stoker & Brander are similar in terms of most building properties and floor plans**,** moreover they are connected to the same heating system. The largest difference between the towers is the orientation of the buildings. Stoker is oriented 36.6° relative to the north axis, where Brander is oriented -2.5° relative to the north axis. This difference results in a varying solar incidence per wall. To check whether the orientation influences the thermal heat demand, the smallest and the biggest apartment are simulated for both orientations. The difference between the smallest apartments is 5.8% and between the largest apartments 1.9%. As the differences are small, it is assumed that the differences are insignificant, and this research continues with the modeling of one of the two buildings.

Within one building there are 90 apartments for which 11 different apartment types can be identified based on their position, size and floor plan. The types are indicated with the letters A, B, C, D, E, F, G, H, J, K and L. For every apartment type, at least one apartment should be simulated to investigate the impact of the apartment type on the results. To prevent creating 90 different models per building, the model is simplified by using the method of [10] In Fig. **5** the colored apartments indicate how this method is translated to the apartments of Stoker & Brander. Note that level -2 is uninhabited due to leakage problems.
To decrease the complexity of the geometries within the apartments, different thermal zone designs are tested for one type of apartment to find an optimum between the complexity of the model and accuracy the results. Four common zone configurations are modelled [9]: *single-thermal zone*, where the entire apartment is modelled as one thermal zone, *zone per orientation*, where there are always five zones, one

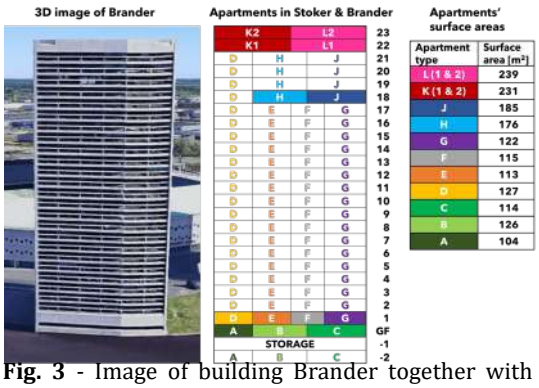

Fig. 3 - Image of building Brander together with a schematic overview of the apartment types, their floor level and surface area.

for each orientation and one in the middle, *zone per function*, where rooms with the same function can be combined, and *zone per room*, which entails the highest complexity. Simulations show that single-thermal zoning has the highest deviation in the relevant KPIs, and is therefore less suited, which is in accordance with the literature on multistorey buildings [9][10]. A choice is made for the *zone per function* as this can result in the simulation of the least thermal zones with comparable results.

5.2 Simulation settings and assumption

With the geometry of the buildings being modelled, a representation of the heating system is chosen. As this study is interested in shifting electricity consumption, only the space heating system is modelled as the DHW-system is mostly consuming natural gas. The space heating system can be modelled in three parts: the underfloor heating system to release the heat, the distribution system of heat and the heat generation in the installation room. As the efficiency of the heat pump and the distribution system of the case buildings are known (see Section 4), this part can also be calculated during the post-processing of the results to decrease the complexity of the simulation model. Therefore, the heat generation and distribution system are represented in the models by a district heating system that directly delivers its heat to the apartment, while the underfloor heating system is modelled per apartment in more detail.

However, the consumption of the heating system depends greatly on the behavior of the occupants, that is characterized by personal preferences and lifestyle. Similarities between these characterizations can be grouped in different household types that are common in the Dutch housing stock, as defined in Section 3.2. Per group, characteristics like occupant presence and desired temperature setpoints can be assigned in the form of profiles. The data for these characteristics is extracted from the WoonOnderzoek Nederland (WoON) [11] and composed to profiles in previous work [10][12]. These profiles show the presence or desired temperature setpoint per hour of the day. When the presence is 0, an occupant is not at home at that hour, when the presence is 1, an occupant is at home, and in between 0 and 1 the occupant is present at that moment for a part of the week. The temperature profiles show when the setpoint temperature is preferred (20°C or for seniors 22°C), or when the setback temperature is preferred (16°C or for seniors 18°C), which is the minimal value for the room temperature that must be maintained. By means of simplicity these profiles are equal for the weekends and the weekdays.
Next, it is determined in what level of detail the simulations should take place. As the time span of heat storage in thermal mass is relatively small, this study requires a large level of simulation detail. Therefore, the 5-minute interval shows the most realistic results and is therefore used for all further simulations.

Due to this large level of detail, simulating the entire heating season would require large calculation load.

To reduce the computational load, three different weeks in the heating season are simulated and translated back to the heating seasons. These three weeks are chosen by their different weather characteristics for several consecutive days to represent the different outdoor circumstances that could occur during the heating season. The characteristics of the weeks are shown in Table 1.

Tab. 1 - Characteristics of the three weeks chosen as simulation periods.

	Average year based on E+ weather file	Colder year	Warmer year
Week A	8	10	4.5
Week B	11	10	13
Week C	15.5	14.5	17

During preliminary simulations of one entire heating season, the energy demand during the chosen three weeks is compared to the other weeks of the heating season, based on the EnergyPlus weather file for Groningen [13]. This gives an indication of how many times each week should be included in the model to represent one heating season. Though, as not every year is identical - one year can be colder or warmer than other years – a warmer and a colder year is created to cover the differences per year. To generate the colder and warmer variations on the average year, the reference years in NEN5060 are used.

Tab. 2 - Translation of simulated weeks to entire heating season showing how many times a week occurs.

	Dates	$T_{out,m}$ [°C]	Total GHI [W/m²]	Average wind speed [m/s]
Week A	9-15 Feb	-3.7	6353	2.76
Week B	16-22 Jan	5.2	4531	6.52
Week C	7-13 Nov	8.3	3714	3.74

Generally, it shows that their 2018 reference climate year is significantly warmer than the weather file of Energy Plus for Groningen. It is more likely that the future years getting warmer than colder. This is also expressed through their 1% & 5% exceedance probability reference years. Though, NEN5060 also shows that extreme cold consecutive days with similar temperatures as week A are not rare and could still occur. Therefore, based on this information a slightly colder year than the average year is constructed but a significantly warmer year than the average year is included, see Table 2.

5.3 Financial model

To calculate the saved costs by deploying flexibility, a financial model is developed. For a realistic cost estimation, historical data from the EPEX day-ahead market, where BAM is also likely to purchase their electricity from, is used to calculate the electricity costs per time step. The prices of the winter of 2019-2020 are used as this is the most recent heating season before the impacts of the COVID-19 crisis. However, there is a discrepancy between the weather profile of EnergyPlus for Groningen influencing the simulations and the actual weather that can have influenced the prices of 2019-2020. Therefore, days from 2019-2020 with similar weather profiles for the outdoor temperature, wind speed and Global Horizontal Irradiance to the EnergyPlus Groningen weather file are selected to create a new time series for electricity costs [14].

Furthermore, it is expected that the weather will increasingly influence the electricity prices besides all other market changes. Predictions for future prices can be used to give a better estimation of the future costs saving potential. CE Delft developed four scenarios for the day-ahead market prices in 2030 that differ in two factors with each two options: high or low renewable energy supply (RES) and high or low coal, gas & CO2 prices (prices). More details about these options can be found in their report [15]. The four scenarios are indicated with *2030A*, having low coal, gas & CO2 prices and low RES, *2030B*, having low prices but high RES, *2030C*, with high prices and but a low RES, and *2030D*, having both high prices and high RES. Based on descriptive data from CE Delft, that has a negative skewness, new price scenarios are created by using a Pearson system. For each scenario 5 data sets are created to anticipate on random generator errors. The data sets are placed in logical order based on the price profile of 2019-2020. This results in five time series for the four 2030-scenarios for the three different weeks of which one is shown in Fig. **6**.

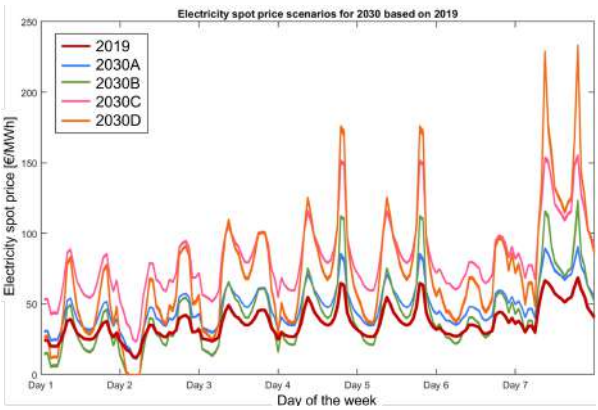

Fig. 4 - Time series of the 2030 electricity spot price scenarios for week A.

6 Flexibility deployment

With the model in place, different operation settings can be simulated to test whether the electricity use of the heat pump can be shifted over time. To do so, flexibility events are defined in two steps: first, it is investigated during which moments it is desirable to decrease the electricity use, the so-called peak hours. The peak hours are here defined as the moments where the electricity price is high, mostly caused by a large electricity demand or low renewable electricity production. The peak hours function as signal or penalty for the electricity demand, as referred to in Section 3.1. To find realistic timings for these peak hours, the moments where simultaneously the Dutch electricity spot prices and the electricity use of the heat pump of Stoker & Brander are high, are considered [16]. It appears that the prices and consumption are high between 07.00 and 10.00 and between 16.00 and 20.00, which are therefore defined as the peak hours. Second, taking

these peak hours into account, the temperature setpoint profiles described in the previous section are adjusted in such a way that the set-back temperature falls within the peak hours. Therefore, the timing of the setpoints is advanced to before peak hours, see the yellow profile in Fig. **7**.

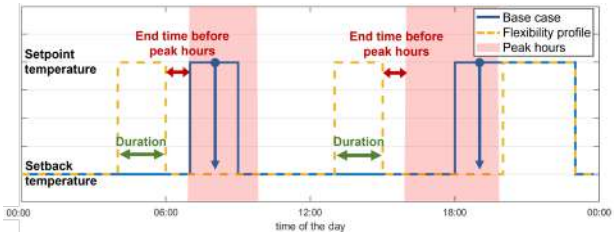

Fig. 6 - Schematic graph of the conversion of the base case to the flexibility schedules

To investigate for how long and at which time the system should preheat to remain comfortable, several schedules are designed to test the differences. The different durations test how much thermal energy should be added to the building to remain comfortable. The different end times before the start of the peak hours are varied to create 'smarter' schedules in comparison to the base case temperature schedules, that ensure to have achieved a comfortable room temperature at the start of the peak hours. Combining the different characteristics leads to 9 different schedules, see Tab. **1**.

Tab. 1 - The new temperature setpoint schedule characteristics that aim to deploy energy flexibility

	Duration	End time before peak hours	Name
Schedule 0	-	-	No flex
Schedule 1	2 hours	0 min	2h-0min
Schedule 2	2 hours	30 min	2h-30min
Schedule 3	2 hours	1 hour	2h-1hour
Schedule 4	1 hour	0 min	1h-0min
Schedule 5	1 hour	30 min	1h-30min
Schedule 6	1 hour	1 hour	1h-1hour
Schedule 7	30 min	0 min	30m-0min
Schedule 8	30 min	30 min	30m-30min
Schedule 9	30 min	1 hour	30m-1hour

7 Results

The apartments are all simulated for the different flexibility schedules and this section will discuss the results. The results on building level are analyzed for one of the two buildings during one heating season, using the extrapolation method explained in Section 5.2. The following observations can be made when analysing the data presented in Fig. ***9***:

- More than 50% of the total load is shifted in time.
- The differences between the flexibility schedules are very small for the shifted load and the heat demand. This is because during the peak hours the temperature setpoints in all flexibility schedules are set to the lower setpoint, preventing the heating system to switch on. Consequently, the only heating demand that can occur during the peak hours comes from the bedrooms, which is for every schedule almost the same. This would imply that based on these two KPIs it would not matter which schedule to be used.
- Though, when analyzing the uncomfortable hours, the schedules show that the shorter the preheating duration, the more uncomfortable hours. The end time before the peak moment does not seem to have an influence on the comfort. The schedules with a preheat duration of 30 minutes show a very high number of uncomfortable hours, which is not desirable. Though, it should be noted that most of these hours are a result of the simulations during the cold weeks. Therefore, it is too early to conclude that all schedules with a preheat duration of 30 minutes should not be used.

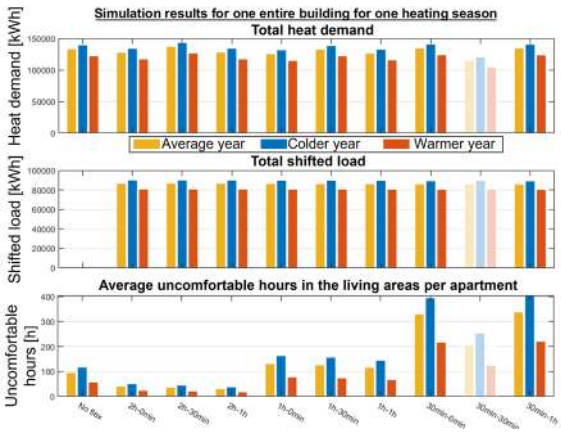

Fig. 5 - Results for 3 of the 4 KPIs for one building, presented for an average, colder and warmer year.

When looking into differences between the apartment types, the most important findings are the amount of shifted load per m² is higher for the larger apartments, however the range of the number of uncomfortable hours is also larger for larger apartments. Between the household types, the largest difference can be seen at the senior household types. As they have a higher heat demand, they also show a larger shiftable load, however without any uncomfortable hours. This can be explained by the fact that the adaptive comfort model is not specifically targeted to seniors, however, on average they do prefer a higher indoor temperature. Therefore, these results do not indicate that the seniors are always feeling comfortable.

The 30min-30min schedule shows a lower heat demand for all household types and all apartment types than the other two 30-minute schedules, and especially a lower number of uncomfortable hours. When comparing the times series of this schedule to the other schedules to track the cause, it shows that the total consumption is consistently lower while the indoor temperatures are higher. The deviating results are hard to explain as the only change to the model per schedule are the setpoint schedules. For these reasons, this schedule is not trusted, and will therefore be excluded from all results to come.

Looking at the remaining KPI, the amount of saved costs, the savings relative to the total costs are considered. Fig. ***10*** shows the savings as a share of the total electricity costs and the electricity purchase costs of Stoker & Brander. The grey bars refer to the current total electricity costs which include taxes, sustainable energy fees, transport costs, connection costs, measurement costs and the rent for the

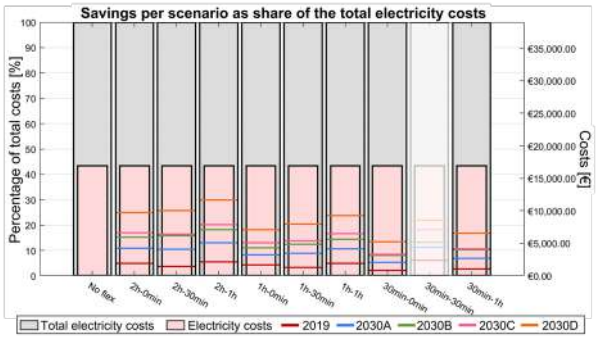

Fig. 7 - Results for the saved costs with 2019 prices and for the 2030 price scenarios for the assumed household combination presented as percentage of the total costs (left axis) and as absolute costs (right axis).

transformer. The pink bar explicitly shows what part of the total electricity costs is spent at the actual purchasing of electricity. The graph only includes the results for the average year as it is found that the different years do not impact the results significantly. The graph shows that currently, around 5% of the total electricity costs can be saved per year, while in 2030 this could be around 25 to 30% of the total electricity costs. Though, it is remarkable that the amount of savings is influenced by the different flexibility schedules while the total demand or the shifted load do not vary significantly between these schedules. The schedules with a 2-hour preheat duration can achieve double the amount of savings, probably as heating only occurs at the set moments with low electricity pricing. In the contrary, for the schedules with a 30-minutes preheat duration the heating system also needs to operate during other, more expensive moments as comfort limits are not reached due to insufficient preheating, leading to higher costs. In addition, the heating peak of the 2-hour schedule occurs further away from the peak hours, profiting from lower prices. Besides the influence of the schedules, the price scenarios have a significant influence on the potential savings. The scenarios for 2030 all show an increase of at least double the amount of cost savings compared to the prices of 2019. Especially scenario 2030D (high prices and high RES), shows larger savings due to the increased fluctuations in electricity prices.

8 Discussion

This section will further discuss the interpretations, implications, accuracy and limitations of the model and its results, together with a translation of this research into practice.

It can be questioned if the three chosen weeks are representative enough for an entire heating season since no other week in the year can be completely equal to the simulated weeks, and no day is the same. Simulating day by day would give more accurate results, although it requires more computational load and adds additional complexity and uncertainty to the analysis. However, more accurate modeling is not assumed to be necessary for this research as the objective is to investigate the flexibility *potential* of the buildings in contrast to a detailed quantification.

Currently, it is not investigated if combining different schedules throughout the year would give better results. It would be interesting to perform an optimization study to find valuable combinations, for example by using model predictive control instead of rule-based control. To determine which temperature schedule to be used, the weather or the electricity price profiles can be leading. This requires accurate weather and price forecasting models to base the heating strategy on.

At the moment, the financial investigation is only based on cost savings due to variable electricity prices. However, potential flexibility incentives from distribution system operators (DSO) are not taken into account. This additional incentive can be valuable for BAM with respect to their Stoker & Brander ESCo and can increase their cost savings.

To bring the theory of this entire research into practice, it is important to place the findings in a practical context and to acknowledge possible limitations from practice. To begin with, it is looked at what should be changed to the installation to apply energy flexibility in the way that is investigated in this study. Generally speaking, this only means that the temperature setpoints of the occupants' thermostats need to be set to the temperature schedules as defined in this study. Preferably, this is done from a distance without any interference from the occupants, both to prevent errors and to unburden the occupants. This will require close communication with the occupants and agreements on the privacy of their data.

Yet, the operation and responsibility of BAM on the system in Stoker & Brander reaches until the delivery sets, but not beyond. However, the heat pump can also be controlled in another way. By lowering the temperature of the outflow of the heat pump, less thermal energy, and thus less electricity, is required by the heat pump. This will also mean that the incoming flow at the delivery set has a lower temperature, meaning that less heat is provided to the occupants. If an occupant experiences discomfort, the occupant can overrule this by increasing their thermostat temperature. Though, this way of flexibility deployment is not investigated in the model and therefore it is unsure if the same flexibility potential can be reached. It could be investigated if, for new ESCo projects, it would be interesting to also operate and deploy the underfloor heating system and the thermostat.

It should not be forgotten that before having the possibility to save costs as a result of load shifting, BAM should become an active participant in the electricity market. This means that they will purchase their electricity directly from the market without any electricity supplier in between (e.g. Eneco). This means that accurate forecasting of the demand of the ESCo is required to prevent large imbalance costs, also for the cooling season, when load shifting will probably not play a role.

Lastly, it is advised to closely collaborate with the local distribution system operator (DSO) to determine when load could be shifted. The DSO could provide information about potential local grid congestion and the local renewable energy rate. This could also be done by using the GOPACS platform.

9 Conclusion

In general, shifting the electricity load from the residential buildings Stoker & Brander with the heat pump is possible without exceeding the comfort limits when sufficiently preheating the apartment. Little differences are shown between an average, a colder and a warmer year, indicating that over the years, similar results can be expected. With this load shifting, a significant part of the electricity costs can be saved, especially when considering future electricity price scenarios. This shows that the potential for flexibility deployment can gain momentum during the coming decade. Moreover, the buildings can play a role in smart consumption of the generated renewable energy and preventing grid congestion as this investigation shows that under certain conditions the buildings can potentially shift more than 50% of the electricity demand of its heat pump. The analysis on the differences between schedules shows that the schedules with a 2-hour preheating duration have better results in terms of cost savings and comfort than the schedules with the 1-hour and 30-minutes preheating durations. Note that longer preheating does not necessarily lead to a higher heat demand as the schedules with a shorter preheating duration have to compensate with additional heat demand during other moments, resulting in a similar heat demand for all schedules. The end time of the preheating before the start of the peak hours shows to have less effect on the comfort, however, it does appear that the 1-hour before end time schedules can save more costs as their timing is further away from the peak hours and, therefore, they profit from lower prices. Regarding the cost savings, when comparing the simulated saved costs to the electricity purchase costs for Stoker & Brander, a maximum of around 10% of the purchase costs can be saved based on electricity prices for 2019. However, when calculating the saved costs with the electricity price scenarios for 2030, the potentially saved costs can go up to two-third of the purchase costs. The uncertainty about the future prices makes it difficult to conclude whether it is worth it or not to proceed with investing in flexibility deployment. Nevertheless, at least 20% of the purchase costs can be saved in 2030 and these reoccurring, annual savings are interesting for BAM as their ESCo contracts run for around 25 to 30 years. During a pilot, field tests should show if the comfort of the occupants is truly not affected and if no additional complaints arise when flexibility is deployed. Note that this paper is a shortened version of a full thesis where more details about the study can be found [17]. The datasets generated during and/or analyzed during the current study are not publicly available because the data is privately owned by BAM but are available on request by email.

10 References

[1] RVO. Energiecijfersdatabank - energiemix, 2019.

[2] Thibault Q. Péan, Jaume Salom, and Ramon Costa-Castelló. Review of control strategies for improving the energy flexibility provided by heat pump systems in buildings. Journal of Process Control, 74:35–49, 2 2019.

[3] IEA-EBC. EBC Annex 67 Energy Flexible Buildings. (December):32–36, 2014.

[4] Xue Li, Wenming Li, Rufeng Zhang, Tao Jiang, Houhe Chen, and Guoqing Li. Collaborative scheduling and flexibility assessment of integrated electricity and district heating systems utilizing thermal inertia of district heating network and aggregated buildings. Applied Energy, 258:114021, 1 2020.

[5] Hicham Johra, Per Heiselberg, and Jérôme Le Dréau. Influence of envelope, structural thermal mass and indoor content on the building heating energy flexibility. Energy and Buildings, 183: 325–339, 1 2019.

[6] Royal BAM Group. Eerste bewoners trekken in appartemententoren Stoker (Euroborg, Groningen), 2009.

[7] Christina Papachristou. Designing a decision support tool for high performance office buildings focusing on energy flexibility: supporting decisions on thermal comfort control strategies and building design parameters. PhD thesis, Eindhoven University of Technology, 2019.

[9] Sara Elhadad, Chro Hama Radha, István Kistelegdi, Bálint Baranyai, and János Gyergyák. Model simplification on energy and comfort simulation analysis for residential building design in hot and arid climate. Energies, 13(8):1876, 4 2020.

[10] Sultan Çetin-Öztürk. Net-Zero Energy Renovations of High-Rise Apartments in The Netherlands. Technical report, Eindhoven University of Technology, 2018.

[11] Dutch Ministry of the Interior and Kingdom Relations (BZK). WoON - WoonOnderzoek Nederland, 2012.

[12] O. Guerra-Santin and S. Silvester. Development of Dutch occupancy and heating profiles for building simulation. Building Research and Information, 45(4):396–413, 5 2017.

[13] EnergyPlus. Weather Data by Region, 2020.

[14] Pieter-Jan Hoes. Computational performance prediction of the potential of hybrid adaptable thermal storage concepts for lightweight low-energy houses. PhD thesis, Eindhoven University of Technology, 2014.

[15] Maarten Afman, Sebastiaan Hers, and Thijs Scholten. Energy and electricity price scenarios 2020-2023-2030: Input to Power to Ammonia value chains and business cases. Technical report, CE Delft, 2017.

[16] Nord Pool. Historical Market Data, 2019.

[17] Beatrix Bos. Flexibility deployment of a heating system with a heat pump in residential towers. MSc thesis, Eindhoven University of Technology, 2021.

Analysis of the application of ventilative cooling in different regions of Turkey

Asli Birturk[a], M. Zeki Yilmazoglu[b]

[a] Solar Energy Institute, Ege University, Izmir, Turkiye, birturkasli@gmail.com

b Dept. of Mechanical Engineering, Faculty of Engineering, Gazi University, Ankara, Turkiye, zekiyilmazoglu@gazi.edu.tr

Abstract. Energy efficiency practices have gained momentum in recent years and continue to invest. The main motivation of this study is whether an effect can be achieved with ventilative cooling in terms of energy efficiency in buildings with mechanical ventilation, especially in transition seasons. In this context, the potential of ventilative cooling in different provinces of Turkey, where hourly average temperature values are taken, has been examined. According to the results obtained, ventilative cooling can be considered as an energy efficienct application.

Keywords. Ventilative Cooling, energy efficiency, mechanical ventilation
DOI: https://doi.org/10.34641/clima.2022.220

1. Introduction

Energy efficiency applications have become one of the current research topics around the world, especially after the Paris Climate Change Agreement. Reducing energy intensity on a country-by-country basis and the amount of greenhouse gas emissions that need to be provided will also bring sanctions. Emissions trading and energy efficiency practices are supported by many different subsidy mechanisms. Although studies on this subject in Turkey have shifted to rooftop photovoltaic system applications in recent years, there is an important potential in buildings that has not been evaluated until now. While insulation applications come to the fore in new buildings, there are many buildings that do not even have insulation.

The use of natural ventilation in buildings has come to the fore again with increasing energy costs and the research for natural ventilation opportunities in new building designs has come to the fore. Considering that the energy consumption of fans in mechanical ventilation is around 5-15 W/m^2, there is a significant energy saving with natural ventilation. In addition, improvements to be made in heating or cooling systems, especially in the transition seasons, reveal a significant potential [1]. Examples of windows consists of phase-change materials in buildings also emphasize ventilation in order to reduce energy consumption [2]. Besides, the combination of phase change materials with night ventilation has shown that an energy saving of around 73% can be achieved [3]. Kigawata et al. [4] investigated the potential of ventilation cooling with radiant floor cooling systems in hot and humid regions. The results showed that horizontal pivot windows improve thermal comfort due to ventilation cooling. Increasing insulation thicknesses and airtight designs due to energy efficiency in buildings cause a continuous cooling load, especially in office buildings. Yu et al. [5], reviewed novel system solutions for cooling and ventilation in office buildings.

Belleri et al. [6], analyzed the ventilative cooling potential tool (VC tool) to assess the potential effectiveness of ventilative cooling strategies by considering also building envelope thermal properties, occupancy patterns, internal gains and ventilation needs. Grosso et al. [7], simulated ventilative cooling effectiveness in an office building. O'Sullivan et al. [8], also analyzed ventilative cooling potential for 14 international cases. Brambilla et al., [9] offered a performance indicator for a life cycle driven approach to evaluate the potential of ventilative cooling and thermal inertia. Chiesa and Grosso [10], analyzed the applicability of the natural ventilative cooling in the Mediterranean area. Simulations were performed for 50 cities in Design Builder and Energy Plus. The results showed that controlled natural ventilation as a heat dissipation technique has a fairly high potential in all Mediterranean region.

Copyright ©2022 by the authors. This conference paper is published under a CC-BY-4.0 license.

Overheating, on the other hand, is an important problem encountered in the cooling season due to the increased internal heat loads in well-insulated buildings. To overcome this problem, ventilative cooling is recommended by Annex 62 in the standards. In this context, although overheating will not be expected due to excess insulation in Turkey, it was investigated whether the thermal comfort conditions are provided by increased air flow rates before the cooling groups are activated, especially in buildings with mechanical ventilation during the transition seasons.

2. Ventilative Cooling Method

Ventilative cooling is a method for taking advantage of the cooling capacity of outdoor air through ventilation, that provides fresh air to the indoor environment [11]. According to the report, published by Annex 62 working group of International Energy Agency, five different cooling modes are recommended for ventilative cooling evaluations [12]:

- *Ventilative Cooling Mode 0:*

When the outdoor air temperature is lower than the heating temperature for the indoor environment, there is no need for cooling.

- *Ventilative Cooling Mode 1:*

The indoor environment is ventilated with the minimum air flow rate determined depending on the comfort conditions. At this point, if the outdoor temperature exceeds the indoor comfort temperature, the required minimum air flow rate is used in the calculations.

- *Ventilative Cooling Mode 2:*

If the outdoor environment has a temperature compatible with the indoor comfort temperatures, In the ventilative cooling system, the required fresh air can be given to the indoor environment by increasing its flow rate. In this case, the required air flow rate is calculated to keep the indoor temperature comfort stable.

- *Ventilative Cooling Mode 3:*

If the outdoor temperature is above the upper temperature limit, indoor comfort is provided by including direct evaporative cooling.

- *Ventilative Cooling Mode 4:*

If the outdoor temperature is above the upper temperature limit and the direct evaporative cooling outlet temperature exceeds the comfort conditions, the indoor environment becomes unfavorable. Therefore, the air change rate for night ventilation needs to be balanced.

2.1 Sample Designs for Ventilative Cooling

In this study, ventilative cooling requirements were determined for a hospital room with an area of 40 m^2 and a height of 3.5 m. It is accepted that there are 3 occupants in the hospital room. Ventilative cooling designs of the sample hospital room in the study were evaluated depending on the climatic characteristics of 5 different cities in Turkey. In terms of climate data diversity, Ankara from Central Anatolia region, Istanbul from Marmara region, Izmir from Aegean region, Erzurum from Eastern Anatolia region and Antalya from Mediterranean region were preferred for this study. Considering the general climatic characteristics of the regions:

- The Central Anatolia region has a cold and semi-arid continental climate.
- Marmara region has a moderate climate. In addition, intense humidity in summers and strong winds in winters are among the effective climate characteristics in the region.
- The Aegean region has a climate with mild and rainy winters and hot and dry summers.
- Eastern Anatolia region has a harsh continental climate.
- The Mediterranean region has a climate that is hot and dry in summers, mild and rainy in winters.

Ventilative cooling requirements are designed for each selected city through the ventilative cooling potential analysis tool developed by Annex 62. In the analysis, many parameters were calculated in detail, especially important parameters such as location, indoor volume, occupancy density per square meter, and minimum required ventilation rate.

The required minimum air flow rate was determined by choosing the 2nd category (normal level of expectation) given in standard EN 15251 or the revised standard EN 16798. The recommended air flow rates in the standard for the 2nd category can be selected in the tool prepared by the Annex62 working group.

3. Results

In this study, according to the data obtained from hourly temperature profile, the monthly average diurnal temperature swings are higher in Ankara and Erzurum, and lower in İzmir, Antalya, and Istanbul.

Additionally, internal heat gains that can be offset for night-time ventilation vary depending on the months for each city.

- In Ankara, an average of 13 W/m^2-ACH internal heat is gained between April and October.
- In Istanbul, an average of 9 W/m^2-ACH internal heat is gained between May and September.
- In İzmir, an average of 6 W/m^2-ACH internal heat is gained in July and August.
- In Erzurum, an average of 15 W/m^2-ACH internal heat is gained between June and September.
- In Antalya, an average of 5 W/m^2-ACH internal heat is gained between May and November.

The modes proposed by Annex 62 are studied in a ventilative cooling design for five different cities. In the graphs below for each city, red represents Mode 0, yellow represents Mode 1, medium dark blue represents Mode 2, light blue represents Mode 3, and very dark blue represents Mode 4.

According to the findings of the study:

- For the hospital room in Ankara climate conditions, Mode 2 was determined as the most suitable ventilative cooling design with a percentage of 59% annually (Figure2). Mode 2 has a high rate in all months of the year except December. In December and January, it is seen that Mode 0 and Mode 2 have very close percentage values (Figure 1). In summers, Mod 2 and Mod 3 usage time percentages are close to each other.

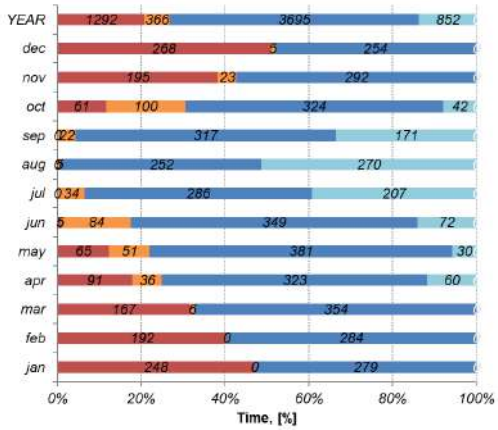

Fig. 1- Usage period of ventilative cooling design depending on months for Ankara climate conditions

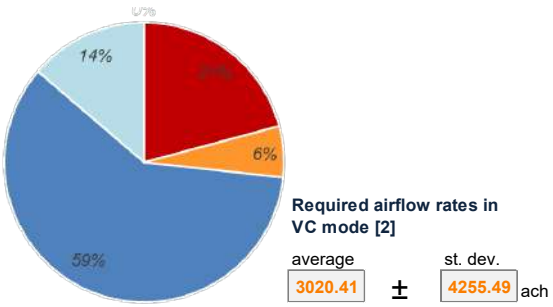

Fig. 2- Annually percentage diagram of the evaluated ventilative cooling modes for Ankara climate conditions

- For the hospital room in İstanbul climate conditions, Ventilative Cooling Mode 2 seems to be suitable with a high rate in all months of the year. As in the design in Ankara, it is seen that the terms of use for Mode 0 and Mode 2 in December and January are close to each other in percentages (Figure 3 and Figure 4).

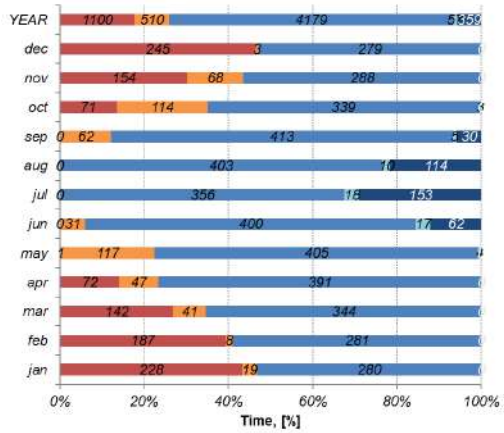

Fig. 3- Usage period of ventilative cooling design depending on months for İstanbul climate conditions

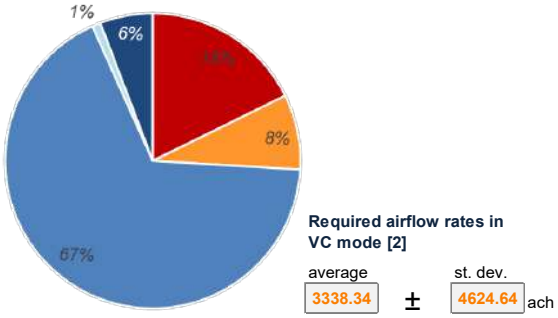

Fig. 4- Annually percentage diagram of the evaluated ventilative cooling modes for İstanbul climate conditions

- For the hospital room in İzmir climate conditions, it is seen that Mode 2 has the highest rates in all months of the year, and Mode 2 is 100% suitable for the design in summer months (Figure5). On an annual basis, the Mode 2 usage time is given in Figure 6 with a percentage of 73%.

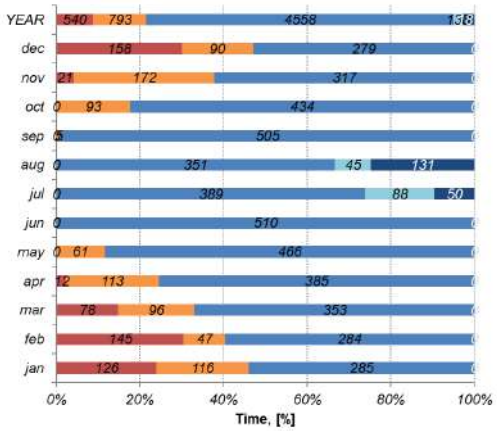

Fig. 5- Usage period of ventilative cooling design depending on months for İzmir climate conditions

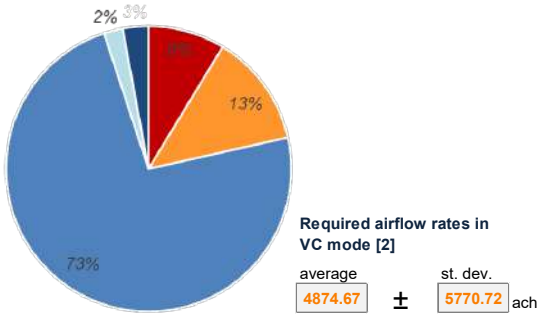

Fig. 6- Annually percentage diagram of the evaluated ventilative cooling modes for İzmir climate conditions

– For the hospital room in Erzurum climate conditions, it is seen that Mod 2 has a high percentage compared to other Mods in all months of the year. In addition, it is understood that Mode 0 has the second highest significant usage percentages in all months except summer (Figure 7).

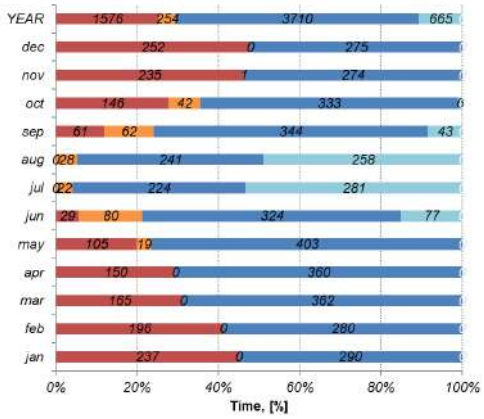

Fig. 7- Usage period of ventilative cooling design depending on months for Erzurum climate conditions

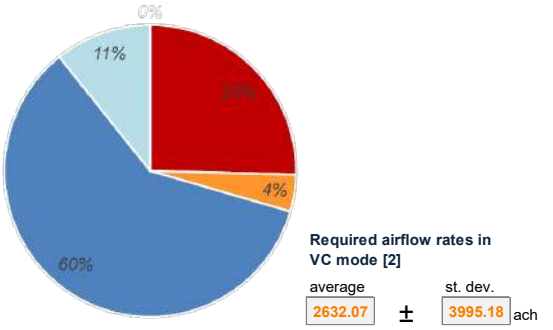

Fig. 8- Annually percentage diagram of the evaluated ventilative cooling modes for Erzurum climate conditions

– For the hospital room design in Antalya climate conditions, it is understood that Mode 2 has by far the highest percentage of usage time and the most suitable ventilative cooling design in all months except summer. In July and August, Mode 3 has much higher percentages than any other mode (Figure 9).

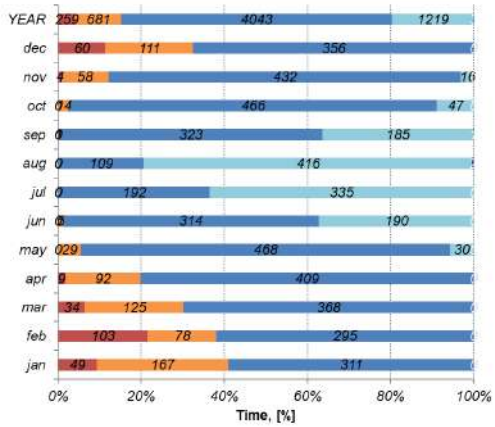

Fig. 9- Usage period of ventilative cooling design depending on months for Antalya climate conditions

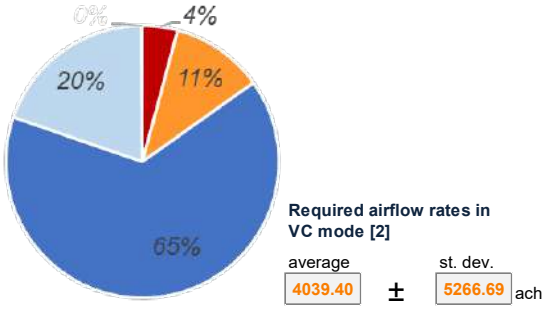

Fig. 10- Annually percentage diagram of the evaluated ventilative cooling modes for Antalya climate conditions

4. Conclusion

Within the scope of the study, hourly climatic data was taken as a basis for each city. Based on climatic data, it was analyzed using the ventilative cooling calculation tool developed by Annex 62. This calculation tool defines the useful time using ventilative cooling as a percentage based on months. At the same time, ventilation rates for day and night can be determined to benefit from the capacity of the heat in the building mass.

5. References

[1] Carillho da Graça G. and Linden P., Ten questions about natural ventilation of non-domestic buildings, Building and Environment, 107, 263-273, 2016.

[2] Hu Y., Heiselberg PK, Guo R, Ventilation cooling/heating performance of a PCM enhanced ventilated window - an experimental study, Energy and Buildings, 214, 109903, 2020.

[3] Barzin R., Chen JJ, Young BR, Farid MM, Application of PCM energy storage in combination with night ventilation for space cooling, Applied Energy, 158, 412-421, 2015.

[4] Kigatawa H, et al., Optimization of window design for ventilative cooling with radiant floor cooling systems in the hot and humid climate of Indonesia, Building and Environment, 188, 107483, 2021.

[5] Yu T, Heiselberg P, Lei B, Pomianowski M, Zhang C, A novel system solution for cooling and ventilation in office buildings: A review of applied technologies and a case study, Energy and Buildings, 90, 142-155, 2015.

[6] Annamaria Belleri, Marta Avantaggiato, Theofanis Psomas & Per Heiselberg (2018) Evaluation tool of climate potential for ventilative cooling, International Journal of Ventilation, 17:3, 196-208, DOI: 10.1080/14733315.2017.1388627

[7] Mario Grosso, Andrea Acquaviva, Giacomo Chiesa, Henrique da Fonseca, Seyyed Sadegh Bibak Sareshkeh, Maria José Padilla, Ventilative cooling effectiveness in office buildings: a parametrical simulation, 39th AIVC Conference "Smart Ventilation for Buildings", Antibes Juan-Les-Pins, France, 18-19 September 2018.

[8] Paul D O'Sullivan, Adam O'Donovan, Guoqiang Zhang, Guilherme Carrilho da Graca, Design and performance of ventilative cooling: a review of principals, strategies and components from International case studies, 38th AIVC Conference "Ventilating healthy low-energy buildings", Nottingham, UK, 13-14 September 2017

[9] Brambilla A, Bonvin J.,Flourentzou F, Jusselme T, Life cycle efficiency ratio: A new performance indicator for a life cycle driven approach to evaluate the potential of ventilative cooling and thermal inertia, Energy and Buildings, 163, 22-33, 2018.

[10] Chiesa G., Grosso M., Geo-climatic applicability of natural ventilative cooling in the Mediterranean area, Energy and Buildings, 107, 376-391, 2015.

[11] International Energy Agency (IEA), 'Ventilative Cooling Case Studies - IEA-EBC Annex 62 Ventilative Cooling', 2018.

[12] International Energy Agency (IEA), 'Ventilative Cooling potential tool User guide', 2017.

Renewables the frontiers towards low carbon resilience – Are they shaping the landscapes of Energy Markets?

Prachi Ugle Pimpalkhute

[a] ESDW2021- ESDW European Wide Initiative Organizer, Lead and Mentor for Mission De Facto Cities and Communities, Founder and Climate Change Crusader Eco Endeavourers Network, IUCN Union Commission Member Environmental Management, Environment, Economic and Social Policy, SPP Sustainable Procurement Ambassador, UN SDG Ambassador, ACT4SDGs Ambassador, Campaigner & Champion, Association of Commonwealth Universities Higher Education and the SDGs Network Member, UN Partnership for SDGs Platform Member, prachiugle@gmail.com

Abstract. As we are transitioning towards low carbon economy, renewables have become a compelling investment for foraying ahead in shaping global energy sector landscapes. Upfront higher costs are an impending challenge for the global renewable market. Ways and means to channelize and inflow of capital into renewables is of utmost priority. Innovation, co-creation and bonds are some approaches towards creating an equally accessible and allocable renewable energy portfolio with reduced credits risks. Credit risks and policy risks are the two major constraints that are undermining the mobilization of finance in renewable energy projects. Hedging solutions per se and reducing barriers better facilitate and manage shall need varied tools, instruments, mechanisms and rating models. This paper aims to put forth the valid policies, practices, frameworks and tools –on improving the access and allocation of green energy projects and credit risk management with better solutions for ease of implementation for future trajectories. Varied policies and tools that reduce barriers and mitigate risks include a) Enabling policies and tools which are divided into Financial policies and regulations, Project Preparation Facilities, Project facilitation tools, on-lending facilities, and Hybrid structures b) Financial Risk Mitigation Instruments which include Guarantees, currency hedging instruments, liquidity facilities, Resource risk mitigation tools and c) Structured Finance Mechanisms and Tools which includes Standardization, Aggregation, Securitization, Green bonds and Yieldcos, The policy push for systems integration of renewables and enabling technologies (such as energy storage) should focused primarily on increasing power system flexibility and control, as well as grid resilience. Flexibility, in particular, is an important requirement for systems integration of renewables as the share of VRE (Variable Renewable Energy) generation rises. The key deliverables from the paper include: policies which should advance the integration of both centralized and distributed VRE and increase the flexibility of the power system pertaining to, for example: market design, demand side management, transmission and distribution system enhancements, and grid interconnections. Since, countries have renewable energy support policies, they should now promote renewable portfolio standards (RPS), other quota obligations, incentives, feed-in policies (tariffs and premiums), renewable power tenders and auctions, incentives and community choice aggregation programmes.

Keywords. Renewable energy, low carbon economy, risk, mitigation, grid, VRE, Storage
DOI: https://doi.org/10.34641/clima.2022.237

1. Introduction

Developing countries are aggressively investing in renewable energy capacity, which reflects the priorities of government policies, as distributed renewable energy projects are crucial for expanding access to electricity in poor regions (OECD, 2020) there is a increase in market competition. In lieu of it is essential to price deals for risk correctly, and this calls for granular and robust assessment of the two main risk factors: first the likelihood that a project will default on its obligations – probability of default (PD). And secondly, what losses will the lender incur if the project does default – loss given default (LGD). Tools and methodologies already exist for lenders to conduct a rigorous internal assessment of a project finance deal. A robust project finance credit risk tool rests on the following pillars:

Copyright ©2022 by the authors. This conference paper is published under a CC-BY-4.0 license.

• Default and recovery data – either internal or provided by external ratings agencies – that can be used to calibrate PD and LGD models empirically

• Comprehensive experience of the industry leaders, for example from relevant professional associations and internal teams in assessing project finance projects to developing and using the appropriate credit risk frameworks

• Predictive analytical models that are tested for predictability against project finance data and/or external ratings of the various asset classes.

2.Objective:

The objective of the paper is to know how evolved renewables are towards low carbon resilience and are they shaping the landscapes of Energy Markets frontiers ?

3.Methodology

Each type of renewable energy technology and each project needs to be evaluated on its own merits, but there is a common set of credit risk drivers that apply across all the renewable energy sub-sectors. These include operational risk, the regulatory environment, the competitiveness of the market in which the project operates, geographical conditions and how these impact production capacity, and the experience and management structure of the project team. Technological considerations are particularly important in assessing risk in the renewables industry because of constant innovation and refinement of existing technologies and the resulting questions surrounding their efficacy and reliability. What is necessary in the current set up is increasing investment in renewable energy which requires identification, evaluation, and monitoring of credit risk in project finance investments. Renewable energy companies and investment projects typically have high volatility in terms of returns on investment, hence the need for standardized credit risk metrics, particularly probability of default (PD) and loss given default (LGD). Also included are notching factors which refers to factors that can notch the PD up or down, including strength of structuring, refinancing risk, construction risk, termination payment, and capital expenditure management. (OECD).

3.1. Renewable Energy Tools

I. Enabling Policies and Tools:

- *Financial policies and regulations*
- *Project Preparation Facilities*
- *Project facilitation tools*
- *On-lending facilities*
- *Hybrid structures*

II. Financial Risk Mitigation Instruments

- *Guarantees*
- *Currency hedging instruments*
- *Liquidity facilities*
- *Resource risk mitigation tools*

III. Structured Finance Mechanisms and Tools

- *Standardization*
- *Aggregation*
- *Securitization*
- *Green bonds*
- *Yieldcos*

3.2. How to manage currency risk :

• Currency risk is one of the major barriers to the financing of clean energy projects in developing countries. The high degree of political and country risk associated with developing countries increases the risk premium, thereby increasing the cost of clean energy. It also has an indirect impact on the financing of clean energy projects, in which it acts as a factor in credit assessment, thereby resulting in low ratings for projects. Foreign investors generally use long-term currency swaps to cover the currency risk.

3.3. How would structured finance mechanism help in enabling capital market financing for clean energy ?

Use of structured finance mechanisms could help in enabling capital market financing for clean energy. Clean energy assets are typically small scale and illiquid in nature, which makes the refinancing of such projects difficult. Measures like warehousing and securitization can help in transforming illiquid assets into liquid and tradable instruments and can assist in the refinancing of the projects. Warehousing is a process in which it is possible to aggregate smaller projects to reach a scale and securitize them into a special-purpose tradable asset. Rating agencies assess these securitized assets for default and then trace them in the secondary market as fixed-income instruments. The bundling of securities could diversify the risk for such instruments and can help in securing high credit ratings.

4. Results and Discussions

4.1. Policy Support for enabling Renewable Energy:

Policy support for renewable energy can be categorised as direct policy and indirect policy. Direct policies such as mandates or financial incentives, explicitly target the increased deployment of renewables and enabling technologies. Indirect policies support effective operating conditions and the integration of renewables and enabling technologies into energy systems and markets. Policies to advance renewable energy production and use can be targeted at any and all end-use sectors, including heating and cooling (in buildings and industry), transport and electricity. Renewable energy policy can exist across all levels of governance, including international and regional; national, state and provincial; and municipal governments. In jurisdictions with regulated power systems, national and sub-national public utility commissions (also called energy commissions or energy regulators) develop policies that apply to regulated utilities (REN, 21).

Trade policy also has an impact on the production, exchange and development of renewable energy products, as well as renewable energy demand levels within specific countries. Renewable Energy and Climate Change Policy include :

• Net zero Emission Targets
• Both NetZero Emission targets and Carbon Pricing Policy
• Carbon Pricing Policy
• Sub-National Carbon Pricing Policy

Carbon pricing policies include emissions trading systems and carbon taxes. Net zero emissions targets mentioned are binding and include those that are in law or policy documents, as well as those that have already been achieved.

• Also in place are Nationally Determined Contributions (NDCs) for emission reduction under Paris agreement.

• Policy mechanisms that promote large-scale, centralised renewable power include renewable portfolio standards (RPS) and other quota obligations, feed-in policies (tariffs and premiums), renewable power tenders and auctions, financial incentives (for example, grants, rebates and tax credits) and more recently we have the community choice aggregation programmes. In 2019, the shift continued away from feed-in policies and towards mechanisms such as auctions and tenders. Feed-in policies have been used to promote both large-scale, centralised renewable energy and decentralised renewables. Many small-scale residential and commercial installations benefited from net metering policies, which compensate system owners for surplus electricity fed into the grid. Virtual net metering (VNM) has emerged as a mechanism to facilitate participation in shared renewable energy projects, in which multiple customers can receive net metering credits tied to their portion of a single distributed system.

4.2. Policies to support mobility infrastructure

Electric vehicle (EV) policies are not renewable energy policies by themselves. While EVs may not always increase the renewable energy share in the transport sector, they do offer the potential for greater penetration of renewable electricity, increased efficiency and lower emissions. Policies to support the increased uptake of EVs include binding targets, financial incentives, public procurement and public support for charging infrastructure. Incentives such as congestion charging, free parking and preferred access also can contribute to greater EV uptake. Targets and financial incentives are two of the most common forms of policy for EVs. The creation of low-emission vehicle zones could increase the uptake of both EVs and biofuels. Through community energy arrangements: residents, businesses and others within a relatively small geographic area initiate, develop, operate, own, investing and/or directly benefit from a renewable energy project. Communities vary in size and shape (for example, schools, neighbourhoods, city governments, etc.), and projects vary in technology, size, structure, governance, funding and motivation. Policy plays a crucial role in permitting or fostering the deployment of community renewable energy projects. FIT schemes, net metering and VNM, and policies dedicated to supporting community energy arrangements all have the potential to incentivise community renewable energy initiatives. At a municipal level, community choice aggregation (CCA) programmes (also called municipal aggregation) allow municipalities and other local governments to procure renewable energy on behalf of their residents and businesses while still receiving transmission and distribution services from existing utilities. By aggregating the demand of multiple residents, communities gain leverage to negotiate better rates and opt for renewable energy sources.

Technology		Risk
Wind	Onshore	Low
	Offshore	High
Solar	Crystalline Silicon PV	High, Medium and Low
	Thin Film PV	High, Medium
	Concentrator PV	High
	Concentrated	High
	Solar Power	
Biofuels	First Generation	Low
	Second	High
	Generation	
Biomass and Waste	Incineration	Low
	Other biomass	Medium
Geothermal		Medium
Ocean/Marine		High
Small Hydro		Low

Fig. 1 - Technology Risk Classification for Various Renewable Energy Technologies,

5. Conclusions

Flexibility, is an important requirement for systems integration of renewables as the share of VRE generation rises. Policies that can advance the integration of both centralised and distributed VRE and increase the flexibility of the power system pertain to, for example: market design, demand side management, transmission and distribution system enhancements, and grid interconnections. Policies also may support the deployment of enabling technologies, such as energy storage, which in addition to supporting power systems in general may help to integrate renewable electricity into the transport and heating and cooling sectors. The key reason for the low penetration of renewables in the final end-uses of thermal and transport energy is the lack of supporting policies in these sectors. As renewable energy policies typically are enacted at a single level of governance and tend to focus on a single end-use sector.

Strategies to align renewable energy policy across multiple levels of governance and across multiple economic sectors are rare. Although most renewable energy policies are not integrated or co-ordinated across sectors or levels of governance, examples of integration and co-ordination are emerging.

Co-ordinated policy efforts often are organised under national or state-/provincial-level energy or climate change strategies. Key workable should include :

- Reduce prices
- Increase subsidies on renewables
- Cap the production
- Cap the consumption
- Do not cap price as it widens gap
- Deploy BAT (Best Available Technologies) invest in renewables and not divest the portfolio as its a short term gain and other future proofing tooler.

Targets are a primary means of expressing commitment to renewable energy and sending a positive signal to market players. Although targets on their own are generally insufficient to stimulate investment in renewables, they may be converted into action through the adoption and implementation of complementary policies. Globally, most renewable energy targets are aimed exclusively at the power (electricity) sector. However, some jurisdictions have enacted independent targets in the heating and cooling and transport sectors, and some (although fewer) have committed to cross-sectoral, economy-wide renewable energy targets.

The way we treat the grid shapes the renewable market, low carbon resilience answer lies in man management ie the approach towards access, allocation distribution and end use technologies are additionality.

6. Acknowledgement

I extend my sincere thanks to my associated partners with whom I work, ESDW-ESDN, IUCN Commission on Environmental Management, Protected Areas, Education and Communication and Environment, Economic and Social Policy, SPP Sustainable Procurement Pledge SDG, Teaching SDGs, Association, of common wealth Universities in Higher Education and UN SDGs Platform with whom I work, collaborate and cocreate best practices policies for being the source of motivation to work on varied verticals and shape strategies and processes that benefit wider stakeholders.

7.References

1. REN 21, https://www.ren21.net/

2. OECD https://data.oecd.org/energy/renewable-energy.htmLee

Evaluation of the intrinsic thermal performance of an envelope in hot period.

Outdoor experiment at a 40m³ test cell

Arnaud Jay [a], *Marie Tanchou* [a], *Hafsa Fares* [a], *Jocelyn Anger* [a]

[a] Univ. Grenoble Alpes, CEA, Liten, INES, ITE INES.2S, 73375 Le Bourget du Lac, France

Abstract. Ensuring the proper thermal performance of a building's envelope upon reception is an important stage in the life cycle of the building. Several methods already exist for this purpose, and continue to be improved, such as co-heating, ISABELE, EPILOG, QUB and SEREINE. All these methods follow the common protocol consisting of heating the measured building with an electrical system. These measurement protocols quantify the dynamic evolution of interior and outdoor temperatures, and the thermal power injected into the building. These data are used in calibration algorithms to determine, by an inverse method, a heat loss value. These methods require a difference of a few degrees between the interior and the exterior which can cause in summer periods a risk of damaging the building, as the outside temperature may already be high. The objective of this work is to explore the possibility of determining the intrinsic thermal performance of a building's envelope in the summer period using a cooling hydraulic system. Some encouraging experiments have been done on a square meter scale cell in an indoor environment. The focus of this paper is to test a similar method in an outdoor Passys test cell of 40m³ and explore the capacities and limitations of the method at this scale by varying several stress parameters of the enclosure. First, some electrical heating modes are run acting as reference values. Then, a hydraulic system is used to estimate the HLC value and gives comparable results to the electrical mode considering an uncertainty of 2 W/K. Third step is to setup cooling scenario with the hydraulic system. Some of the results are also comparable with the heating mode and some limits are highlighted such as the cooling power limitation to avoid water condensation into the cell. This impact of condensation is then studied and seems to have a limited impact on the results for this experiment.

Keywords. Envelope thermal performance; assessment; performance guarantee; Cooling; Experimentation
DOI: https://doi.org/10.34641/clima.2022.436

1. Introduction

Ensuring the proper thermal performance of a building's envelope, whether new or renovated, upon its reception is an important step in the life cycle of the building. It allows to quantify the performance gap and to ensure the good consistency between the design phase and the implementation during the construction work, in order to consider possible corrective actions to reduce its environmental impact. Several methods exist for this purpose and continue to be improved such as co-heating(1), ISABELE (2), EPILOG, QUB (3) or SEREINE methods. The objective is to determine the thermal performance of an envelope which can be quantified by the Heat Loss Coefficient (HLC in [W/K]), which is the sum of the heat loss due to infiltration (H_{inf}) and the heat loss due to conduction through the walls (H_{tr}) (towards the exterior and the ground). These values will partly depend on the test conditions including the indoor and outdoor pressure difference and the operative temperature inside, the outside air temperature for H_{inf} and the convective heat transfer coefficient under real conditions for H_{tr}. All these methods have the common point to stress the building over a certain period using a heating system. These protocols measure the dynamic evolution of the indoor temperatures, the thermal power injected into the building and the outdoor conditions. For most of these methods, these data are then used in a calibration algorithm using a RC model to determine, by an inverse method, the model parameters and thus deduce the HLC (Heat Loss Coefficient). These methods require an indoor temperature a few degrees higher than the outside temperature, a gap that is potentially no longer acceptable in summer periods without the risk of damaging the measured building. The aim of the work is consequently to develop a test methodology with a cooling system in order to be able to measure a HLC coefficient even in summer periods.

Copyright ©2022 by the authors. This conference paper is published under a CC-BY-4.0 license.

2. Research Methods

2.1. Research objective

The overarching objective of this work is to develop a test methodology with a cooling system in order to be able to measure a HLC coefficient even in summer periods. Some previous work (4) have been done to sketch and test such method at a 1m³ indoor cell using a water/air heat exchanger. The test consists of cooling the air inside the cell and measuring the dynamic evolution of the injected cooling power and the temperature inside and outside the cell. The power required to compensate the heat losses with the exterior is then estimated leading to the HLC coefficient of the cell using the SEREINE calibration method. More specifically, the work presented here aims to test this methodology on a larger cell, about 40m³ positioned in an outdoor environment. This will need to solve two technical and scientific barriers, the first related to the change of scale and the second to the added perturbations due to solar radiation and day/night temperature variation.

2.2. Existing methods

As mentioned in the introduction, several methods exist to determine the proper thermal performance of a building's envelope such as HLC. These tests need an unoccupied building from one to 30 days depending on the methods to estimate a HLC coefficient. First, a blower door test is done to estimate the infiltration flow rate's characteristics of the building. Secondly, the thermal behaviour of the envelope is monitored. For that, a specific thermal stress scenario is set into the building thanks to electric fan coils. During this test, the indoor temperature, the electrical consumption and the weather conditions are dynamically monitored. These data are then used in mathematical models to identify the model parameters and deduce H_{tr} and HLC as shown in **Fig. *1*** from (5)

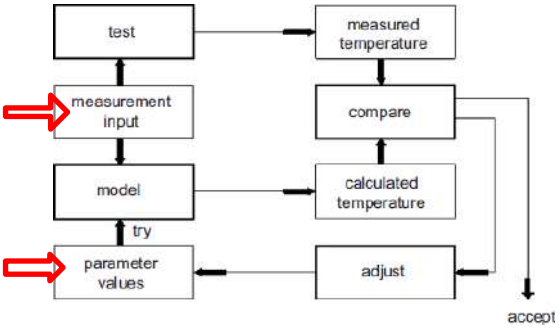

Fig. 1 - Process steps *(5)*

The purpose of the optimization algorithm for the calibration is to find the set of parameters (of the RC model retained) which minimizes the difference between measured interior temperature and the simulated one based on the experimental data (injected power inside and the outside temperature). The algorithm used is taken from the numerical code used in SEREINE method, currently under development. This algorithm is an evolution of the versions used in previous methods (ISABELE (2) and EPILOG), and is partly based on the pySIP uncertainty propagation algorithm (6).

The present analysis consists in calculating by inverse method the HLC of an envelope, from a RC model (7) (8) from the SEREINE tool.

The aim of this work is to validate that the calibration method works with a cooling scenario, allowing to make changes only for the thermal stress of the building and the energy consumption measurement technique.

2.3. From electric to hydraulic energy source

One major change in our methodology is to switch from an electrical to a hydraulic thermal source. In order to produce and dissipate cool into the cell, we are using a hydraulic system instead of the conventional electrical fan coils. This implies to change the way to calculate the energy dissipated into the cell. In the existing methods, power sensors measure the electrical consumption of the equipment put into the cell and suppose that the energy consumption is equal to the energy loss by the envelope with a thermal performance ratio of the electrical fan coils and other equipments of 1. The uncertainty of the electrical power sensor used is 2% on the range used. For the hydraulic system, the power injected by the fluid into the cell is estimated thanks to the fluid flow rate, the temperature difference of the fluid entering and leaving the cell as mentioned in equation (1). The energy loss/gain by the envelope (P_{in} [W]) is the sum of energy captured by the fluid (negative) (P_{hydrau}) and the electrical consumption of the fan (P_{fans}), which aims to optimize the heat exchanger's performance and homogenizes the indoor air temperature in the building.

$$P_{hydrau} = \dot{m}_{water} . Cp_{water} . (T_{water-out} - T_{water-in}) \quad (1)$$

$$P_{in} = P_{Hydrau} + P_{fans} \quad (2)$$

With P_{hydrau}, the power released by the fluid inside the cell in [W], $\dot{m}_{water}$ the volume flow rate of water flowing into the heat exchanger in [kg/s], Cp_{water} the thermal capacity of water (fluid used in the thermal bath) in [J/(kg.K], $T_{water-out}$ and $T_{water-in}$ the water temperatures exiting and entering the cell, in [°C or K].

The uncertainty on the hydraulic power is estimated to be:

$$\frac{\Delta P_{hydrau}}{P_{hydrau}} = \sqrt{\left(\frac{\Delta m_{eau}}{\dot{m}_{eau}}\right)^2 + \left(\frac{\Delta(\Delta T_{eau})}{\Delta T_{eau}}\right)^2 + \left(\frac{\Delta C_p}{C_p}\right)^2} \quad (3)$$

2.4. From heating to cooling methods

Another challenge in this method, which implies to change from a heating method to a cooling method, is the questioning of the condensation. Indeed, bringing cool fluid into a closed cell might generate some condensation phenomena at the cooled pipes surface. If condensation appears in the cell / building,

it generates a phase change energy sink. So part of the energy brought by the hydraulic system will be used for phase change (from vapour to liquid) and not to compensate the heat flux through the walls. So either we need to avoid condensation or at least we need to quantify it dynamically.

In previous work (4), the feasibility of this method on a small indoor 1m^3 scale have been demonstrated. Some barriers to change scale to real one and validate the method in outdoor conditions are the interest of this article using the same methodology.

3. Case study

3.1. Experimental cell description / envelope to measure

The test cell used in this study is a Passys cell (**Fig *2***) of around 40m3 developed in the project PASLINK (9) and which presents 5 faces highly insulated (~40cm of insulation), and an adaptive facade. In our case, the adaptive facade was south oriented partly glazed (standard double glazing) and poorly insulated woodframe wall for the rest (R~0.5 m^{2}K/W). The opposite face which is one of 5 highly insulated faces separates the cell of a technical room.

Fig 2 – Outside view of a Passys cell

3.2. HVAC system for energy source.

The cooling/heating transmitter is an air/water exchanger placed inside the cell as illustrated in **Fig. *3***. The water circulating in this exchanger is cooled or heated by a thermal controlled bath **Fig. *4*** with a variable flow pump to set the water flow running through the hydraulic circuit. The heat exchanger is paired to an electric fan, its purpose is to stir the air that runs through the exchanger and to homogenize the interior atmosphere of the cell. The power consumption of the fan is calculated upstream and is taken into account in the overall thermal power that is injected into the experimental cell, considering that the electrical power consumed by the fan is dissipated into heating power. A second ventilator is set to homogenize the indoor air temperature.

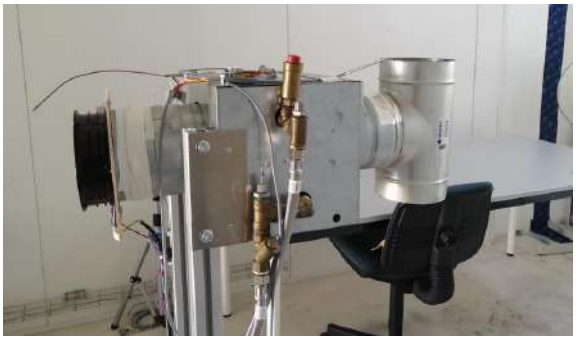

Fig. 3 – Water/Air heat exchanger inside the cell

Fig. 4 - Heating/Cooling systems, left: Generation - Thermal bath, right: View of inside the Passys Cell

3.3. Sensors

The physical quantities measured inside the cell are air, surfaces and water temperatures, the heat fluxes through certain walls, the relative humidity of the air, as well as the water flow rate. A weather station situated on site gives the data for the outdoor temperature and the solar radiation. The setup and position of the sensors is summarized in Table 1. The temperature probes were calibrated upstream of the tests with their complete acquisition chain. The data from the sensors are pre-processed to feed the algorithm presented in the following paragraph. An average indoor air temperature is calculated from the sensors installed.

Tab. 1 - Setup and position of the sensors.

Type of sensors [Unit]	Position	Setup	Nb
Temperature [°C]	Inside Cell – Air	At different points of the cell	11
	Inside cell – Air	Inlet and outlet of heat exchanger	2
	Inside Wall Surface	Center of Each cell face	5
	Outside Cell - Air	Adjacent Room	1
		Outdoor	1
	Outside Wall Surface		

	Hydraulic loop	Cell Inlet	1
		Cell Outlet	1
Flowmeter [kg/h]	Hydraulic loop	Cell Inlet	1
Hygrometer RH [%]	Air	Outlet of heat exchanger	1
		Adjacent Room	1
Heat-flux [W/m²]	Indoor walls	Top/Bottom /Right/Left	4

In the usual methods, electrical resistors are used as heat sources. The dissipated power is then measured directly by monitoring the electrical consumption. One of the challenges in cooling mode is to be able to measure with a sufficient accuracy the thermal power injected into the enclosure. In our case, it is calculated by adding the calorific power supplied by the hydraulic system to the electrical power supplied by the fan. The calorific power is calculated using the water flow rate and the water temperature measurements of the hydraulic circuit taken at the inlet and outlet of the cell [eq (2)].

The power of the fans was calculated before the presented tests by measuring the intensity of the current running through the fan using a multimeter for various voltage values, and gives the following values:

$$P_{fan_HE} = 42{,}6\,W\ ;\ P_{fan_cel} = 24{,}8\,W$$

3.4. Scenarios setup

Tests were ran between May and December 2021 with different families of scenarios that had been ran with both electrical and hydraulic system.

With the electrical system, the scenarios are a co-heating system and 3 pseudo-random scenarios. The co-heating, which will serve as a reference value, lasts 17 days with a fixed set point temperature at 35°C. During the co-heating, the heating power varies automatically to compensate the indoor/outdoor temperature difference and maintain the indoor set point temperature. Pseudo Random scenario (inspired from SEREINE project and named PSA in this article) consist of sequences with heating source ON and OFF with variable duration from a few minutes to a few hours as shown in **Fig. *5*** for 2 types of PSA (short and long). Pseudo Random scenario test the dynamical behaviour of the building as explained in (5). In this scenario, when heat is ON, the heat power is fixed and is stop only if the temperature limit is reached (35°C) in order to not damage the building/cell.

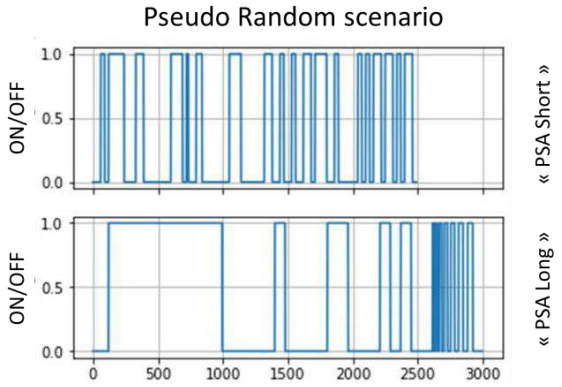

Fig. 5 - Pseudo Random scenario

Tab. 2- Scenario setup

Type	*Mode*	*Set Point*	*Scenario*	*tests nb*	*Exploitable results*
Hydraulic	Heating	35 °C	Steady	Hy.1	YES
			PSA short	Hy.7	YES
			PSA long	Hy.17	NO
		30 °C	Steady	Hy.11	YES
		25 °C	PSA long	Hy.8	NO
	Cooling	18 °C	PSA short	Hy.2, Hy.3	NO
		15 °C	Steady	Hy.4, Hy.6	NO
			PSA short	Hy.5	NO
		10 °C	Steady	Hy.9, 10, Hy.12, 13, Hy.14	YES
			Shifting	Hy.15	YES
	Alter-nation	10 - 35 °C	Shifting	Hy.16	YES
Electric	Heating	35 °C	Co-heating	El.1	YES
			PSA short	El.2, EL.3	YES
			PSA long	El.4, El.5	YES
		200 W	Steady	El.6	YES

Second family of scenario is using the hydraulic system. For them, two parameters were controlled: the set point temperature of the thermal bath fluid which is then entering the PASSYS cell, and the flow rate of the water getting through the heat exchanger in the Passys cell. Contrary to the electrical scenario, neither the indoor temperature nor the heat flux are controlled in the hydraulic scenario. Three kinds of scenario with the hydraulic system have been tested. Some steady state scenario lasting from 2 to 5 days, both in cooling or heating mode depending of the weather forecasts, some Pseudo Random scenario, following the same spirit as the one with the electrical system and finally scenarios with thermal

bath set point temperature shifting from cooling mode during the day to a heating mode during the night.

As illustrated in **Tab. *2***some of the scenarios were implemented several times in order to verify the repeatability of the experiment.

3.5. Mathematical model used

The mathematical model used in our calibrations is the RC TWTI model from the SEREINE tool (or M2_TmTi model in (7)), where TW indicates the presence of a capacitance associated with two transmittances modelling the envelope and Ti indicates the presence of a capacitance modelling the internal mass. In our case, this internal mass is supposed to model the internal air volume to be cooled. It requires as input data the power supplied, the indoor temperature given by the air temperature sensors, and the equivalent exterior temperatures of the enclosure.

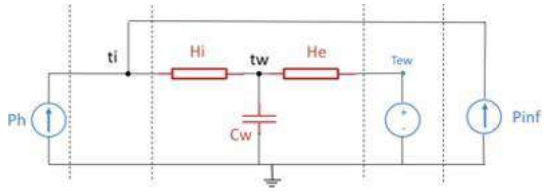

Fig. 6 - RC model used for the calibration.

As far as the exterior temperature is concerned, taking only the outside air temperature around the cell is not enough, because we won't consider the solar radiation on the outside surface of the Passys cell. To take into account the impact of solar radiation into the cell, an equivalent outside temperature $T_{ew-meteo}$ is calculated using meteorological data and surface caracteristics of the test cell.

4. Results

4.1. Passys cell airtightness

As mentioned in paragraph 2.2, in order to be able to separate the impact of infiltration to heat loss, it is important to measure the airtightness of the building. To estimate the infiltration flow rate of the cell, some blower tests have been done and give a Q_{50} value of 138 m³/h at 50 Pa and an equivalent surface ELA of 0,0026m² as mentioned in **Tab. *3***. Thanks to this last value, we estimate the infiltration flow rate thanks to the model defined by the LBNL model defined by Sherman in (10) depending on the indoor/outdoor temperature difference and the wind velocity, according to equation (4)

$$Q_{inf} = ELA * \sqrt{f_w^2 * v^2 + f_s^2 * |\Delta T|} \quad (4)$$

Where Qinf is the infiltration flow rate (m³/s), fw=0,13 et fs=0,12 m/(s.K$^{1/2}$) are constant coefficients linked to wind and thermal effects. We estimate the thermal loss due to infiltration thanks to the following formula:

$$P_{inf} = Q_{inf} * \rho_{air} * Cp_{air} * \Delta T \quad (5)$$

$$H_{inf} = \frac{P_{inf}}{\Delta T} \quad (6)$$

Tab. 3: Blower Door results

Estimated quantity	Value
Q_{50} (m³/h)	138
ELA (m²)	0,0026

With P_{inf} the power loss due to infiltration in [W], Cp_{air} the thermal capacity of air in [J.kg/K], and ΔT the temperature difference of air between inside and outside the cell. For the Passys cell, we aim to estimate: $H_{inf} = 2{,}3\frac{W}{K}$ considering an average velocity of 5m/s

4.2. H_{tr} theoretical estimation

A first estimation of the Heat Transfer loss by the walls is calculated thanks to the cell specifications (dimensions and material properties) and is summarized in the following graph and table. The H_{tr} is estimated to be greater than 13W/K, regarding that the thermal bridges due to singular points were not fully quantified, and so adding the infiltration loss leads to a HLC greater than 15.3 W/K, which means that the infiltration loss represents a maximum of 15% of the envelope thermal loss.

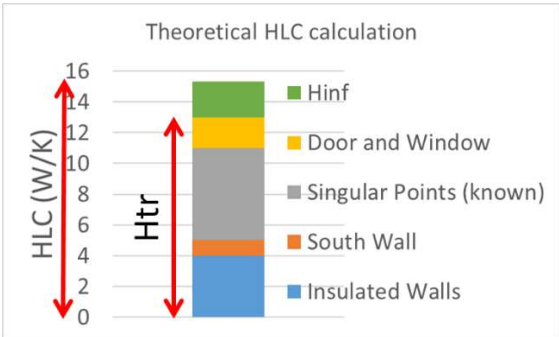

Fig. 7 - HLC theoretical estimation

4.3. Results with an electric scenario

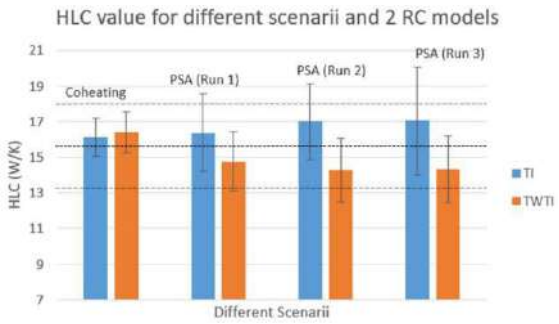

Fig. 8 - Electrical results

Some scenarios have been run with fan coils to get some values with existing methods. A 17 days scenario with a constant temperature at 35°C (named Coheating in the following figure) gives a HLC value estimated to 16.4 W/K with an uncertainty of 1.2 W/K with TWTI RC models from SEREINE

method. 3 PSA scenarios with different durations of heating and relaxation mode succession give HLC values between 14 and 17 W/K, all included in a +/- 15% range around the estimated theoretical value of 15.3 W/K.

4.4. Results with a hydraulic scenario

The **Fig. *9*** shows the data monitored for a 3-day scenario, its upper side shows a graph of the evolution of the injected power P_inj and the effective power Ph, received by the cell, which is, in a cooling mode, lower than P_inj because of the heating power released by the electric devices in the cell. The lower graph shows the evolution of the internal air temperature (Ti) and the equivalent outdoor temperature T_{ew-1BC} as mentioned in paragraph 3.5. The power gets stabilized after less than one day around 200 W and the small daily variations are due to the same variations observed in the evolution of the internal temperature, in the second part of the graph. The internal temperature has the same stabilization time and then follows the external temperature but shifted and highly dampened.

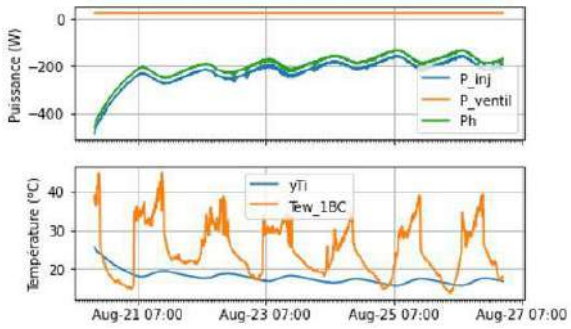

Fig. 9 - Evolution of Power injected and temperatures for a scenario

A series of tests were monitored with the scenario mentioned as "Steady" (section 3.4) , in the cooling mode as well as in the heating mode and the results for a calibration process using the TWTI model (section 3.5) are displayed in **Tab. *4***. The values of HLC obtained under the same control temperature, high temperatures (e.g. 35°C) as well as cold ones (e.g. 10°C), and same scenario are repeatable and gathered within the range [14.5, 17.5] W/K, with a global uncertainty lower than 3 W/K. These HLC values were obtained after a stabilization time included between one and four days, because of the cell's volume and the relatively low power injected, depending on the internal temperature and the control one. A comparison of these values with the theoretical one (section 4.2), contained in this range, can validate the model. However, some discrepancies can be observed in the HLC value when the control temperature changes, and even if it can be explained by the uncertainties, a further investigation could lead to a better understanding of the phenomenon.

Tab. 4 - Results with hydraulic mode for both cooling and heating tests

Test nb	Set Point [°C]	HLC [W/K]	ΔHLC [W/K]	Test Duration (Day)
Hy.1	35	14.9	2.8	2.8
Hy.7	35	15.4	1.8	1.9
Hy.9	10	17.1	1.9	5.0
Hy.10	10	17.5	1.5	5.7
Hy.11	30	17.0	1.9	3.2
Hy.12	10	17.3	1.4	6.8
Hy.13	10	15.5	1.0	4.6
Hy.15	10	15.6	1.7	2.1

Another series of tests were lead with Pseudo Random scenarios as mentioned in section 3.4. It was not possible to estimate a correct value of HLC with these scenarios due to the energy injected in the cell was to small to lower the indoor air temperature and to compensate the external gains. Indeed, it is necessary to create a difference of temperature, either positive (for heating method) or negative (for cooling method), between the indoor and outdoor environments, in order to notice the heat gains or losses through the walls. Thus, the energy injected should both be able to compensate the heat losses or gains through the walls but also to cool down the air temperature in the cell at the beginning of the experiment. With the relatively small value of power injected in the cell, the periods in all the PSA tested were not long enough to cool down the cell. Indeed, the modules used in the SEREINE method provide a constant power between 700 W and 2 kW instead of the maximum of 500 W that we observed in these experiments with an hydraulic system and an intermittent operation due the Pseudo random scenario. It can explain the lack of results observed when this kind of scenario in a cooling mode were lead.

An increase of the power injected, by means of lowering control temperature or increasing the waterflow, needs to be explored to check its feasibility.

4.5. Condensation wonderings

Working with a cooling method implies to choose between a temperature not too low to avoid condensation in the cell but which limits the heat flux of the heat exchanger or a lower temperature to increase the power generation but this leads to condensation in the cell. As mentioned in paragraph 2.4, it is important to control condensation since this generates a new term in the energy flux equation. So if condensation appears in the cell, a part of the power injected is used for phase change, and need to be quantified to estimate the correct HLC value.

Regarding the low heat flux generated thanks to a

water temperature at 15 and 18°C, it has been decided to test the method with a lower temperature (10°C) which generates condensation phenomena. Indeed, with a humidity varying between 8 and 10 g/kg in the cell, a control temperature of 10°C was lower than the dew point temperature, according to the psychrometric chart. During different tests working in the cooling mode, condensation appeared and was observed thanks to pictures captured at a time step of 10 minutes. Two elements rose from this observation:

- some water drops appeared on the pipe all along the test
- during the first hour of each test, a puddle under the inlet pipe closed to its entrance in the cell increased and then started to decrease until it stabilized, which might be due to a probable evaporation, possibly due to the relative higher temperature of the floor.

Following these observations, condensation was neglected, since it was considered to reach a stationary state at the cell's scale, due to the equilibrium between condensation on the entering pipe and evaporation on the floor. Two tests were, then, lead under the same set point temperature and indoor humidity. For one test, the pipes were insulated, preventing from condensation on the pipe. The HLC value was 16,2 ± 2,4 W/K in the insulated case and 17,3 ± 1,4 W/K in the other one. Thus, both results are within the range considered in previous section, validating the previous consideration: in these conditions, condensation can be neglected, since no real discrepancies in the HLC value are noticed.

5. Conclusion

During this work, some experiments have been done to estimate the HLC value of a Passys cell with different thermal stress methods. Two systems were tested: an electrical one thanks to fan coils, and a hydraulic system thanks to a thermal bath coupled to a water to air heat exchanger. Both heating and cooling tests have be tested. The thermal stress scenarios vary from a steady state scenario (a 17 days co-heating test serving as a reference value) to Pseudo Random scenario with sequences of heat sources On/Off varying from a few minutes to a few hours. All these experimental Data were then used in the SEREINE calibration tool to estimate the HLC value.

It has been shown that it is possible to estimate the HLC value of a Passys cell (40m^3 cell in real outdoor condition) in an acceptable range of uncertainty for both electrical and hydraulic system and for both heating and cooling methods. The HLC value of this cell is around 16 W/K, which is too low to be representative of a real size building, but still presents some strong interest in the method development.

Some limitations of the cooling method with this hydraulic system appeared and began to be investigated. The power injected with the hydraulic system used in a cooling mode needed an inlet temperature under the dew point temperature. So, condensation could not be avoided. However, condensation seems not to impact the ability to estimate the HLC of the Passys cell.Another limitation is that Pseudo Random scenario which are really promising to reduce the duration of tests with electrical fan coils was not successful in these experiments mainly due to a low energy injected to the cell with the system coupled to its intermittent operation.

Finally, further works need to be investigate to check the feasibility of such a method at a real scale house

6. Acknowledgement

The algorithm used for the calibration process has been developed in the scope of the project SEREINE part of PROFEEL program. This work was supported by the French National Program "Programme d'Investissements d'Avenir - INES.2S" under Grant ANR-10-IEED-0014-01

7. References

1. Bauwens G, Roels S. Co-heating test: A state-of-the-art. Energy Build. oct 2014;82:163-72.

2. Thébault S, Bouchié R. Refinement of the ISABELE method regarding uncertainty quantification and thermal dynamics modelling. Energy Build. nov 2018;178:182-205.

3. Ahmad N, Ghiaus C, Thiery T. Influence of Initial and Boundary Conditions on the Accuracy of the QUB Method to Determine the Overall Heat Loss Coefficient of a Building. Energies. 6 janv 2020;13(1):284.

4. Jay A, Fares H, Rabouille M, Oberle P, Thebault S, Challansonnex A, et al. Evaluation of the intrinsic thermal performance of an envelope in the summer period. J Phys Conf Ser. 1 nov 2021;2069(1):012093.

5. Baker PH, van Dijk HAL. PASLINK and dynamic outdoor testing of building components. Build Environ. févr 2008;43(2):143-51.

6. Raillon L, Rouchier S, Juricic S. pySIP: an open-source tool for Bayesian inference and prediction of heat transfer in buildings. Congrés français de thermique. 2019;

7. Thebault Simon. Contribution à l'évaluation in situ des perfomances d'isolation thermique de l'enveloppe des bâtiments [Thèse de Doctorat]. INSA Lyon; 2017.

8. Rouchier S, Rabouille M, Oberlé P. Calibration of simplified building energy models for parameter estimation and forecasting_

Stochastic versus deterministic modelling. Building and Environment. 134e éd. 2018;181-90.

9. Baker PH, van Dijk HAL. PASLINK and dynamic outdoor testing of building components. Build Environ. févr 2008;43(2):143-51.

10. Sherman MH. Estimation of infiltration from leakage and climate indicators. Energy Build. 1 févr 1987;10(1):81-6.

Data Statement

The datasets generated during and/or analysed during the current study are not available because of time necessary to clean and extract the specific data but the authors will make every reasonable effort to publish them in near future.

Methodology for the development of temporally high-resolved and spatially accurate tapping profiles

Mark Distelhoff, Peter Pärisch, Carsten Lampe

Institute for Solar Energy Research Hamelin, Emmerthal, Germany, distelhoff@isfh.de.

Abstract. Within the framework of a current research project, different types of drinking water installations in flats are analysed and compared in a simulation study with regard to drinking water hygiene criteria. The planned modelling of the temperature, stagnation and flow behaviour of individual pipe sections requires the development of particularly detailed tapping profiles. The paper at hand shows a methodology to derive tapping profiles in the required level of detail. A spatially accurate resolution requires that each of the selected draw-off points - washbasin, kitchen sink, shower, bathtub, WC, dishwasher and washing machine - receives its own tapping profile, separated into hot and cold water. The high temporal resolution is the prerequisite for an adequate recording of short tappings lasting only seconds. The basis of the tapping profiles is a statistical database of tapping quantities and frequencies for three different types of residents (couple, family, retirees). In the next step, the DHWcalc tapping profile generator is configured and used to create spatially accurate tapping profiles. Subsequently, an Excel VBA tool refines the time step from 1 min to 5 s and shortens the tapping time for small tapping quantities. By means of simulations with the software TRNSYS an exemplary compact T-piece installation is set up to account for transient effects, like temperature adjustment processes at the shower. With the presented methodology, tapping profiles can be created for different installations that clearly exceed the level of detail of DWHcalc and are suitable for detailed simulative analyses.

Keywords. Tapping profile, drinking water hygiene, simulation, DHWcalc, TRNSYS
DOI: https://doi.org/10.34641/clima.2022.229

1. Introduction

The high temperature in central domestic hot water heaters in multi-family houses (MFH) is an obstacle for the use of heat pumps. The aim of the research project "Trans2NT-TWW" is to reduce this temperature in a hygienically safe way. With regard to hygienical requirements in drinking water installations, the cold water temperature and the frequency of water exchange also needs to be addressed beneath the hot water temperature. There are different types of drinking water installations available on the market (e.g. T-piece, loop and ring installation), which will be evaluated in future system simulations. As a basis for the planned work, this paper presents a method that enables to generate tapping profiles for hot and cold water that are accurate in terms of draw-off location and highly resolved in terms of time. A high level of detail is necessary to determine the exact flow and stagnation behaviour, as well as the temperature changes of individual pipe sections. This allows conclusions to be derived regarding the quality of the drinking water. Existing tapping profile generators, such as DHWcalc (v.2.02) [1], do not meet the detailed requirements because there is insufficient temporal resolution or it is not possible to separate hot and cold water demands or individual draw-off points. Chapter 2 introduces statistical basics of typical water demand, which are implemented in the DHWcalc (v.2.02) tool in chapter 3. This tapping profile generator is used to generate precise profiles for three different types of residents with different water demands. In the next step, the obtained time increment of 1 min is refined to 5 s and at the same time small tapping quantities are temporally compressed to a shorter tapping period. The final step in chapter 4 requires the simulation software TRNSYS to account for installation-specific effects. This separates hot and cold water flows, due to mixing processes at the tapping and increases the demand due to stagnation effects.

2. Statistical basics

2.1 Selection of the draw-off points

The selection of the draw-off points is based on the floor plans of a statistically representative apartment building that was investigated in the project "MFH-re-Net" carried out at the ISFH [1]. The floor plan section in Fig. 1 shows the arrangement of the draw-off

Copyright ©2022 by the authors. This conference paper is published under a CC-BY-4.0 license.

points used. In addition to the kitchen sink, a dishwasher and a washing machine are installed in the kitchen. The bathroom has a washbasin, WC and bathtub with shower fittings (shower tray).

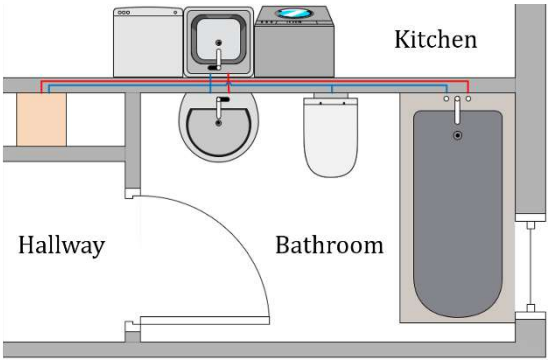

Fig. 1 - Arrangement of the draw-off points.

2.2 Resident types

The definition of three resident types allows the consideration of different tapping behaviour with regard to the daily tapping quantity and the temporal distribution of the tappings. Resident type “couple” is a childless young couple working full-time. Both are absent a lot and use the drinking water installation relatively little. Resident type “family” is a family of three with a school-age child. One parent works full time, the other parent works part time. Resident type “retirees” is a retired couple who have no regular absences. The drinking water installation is used evenly throughout the day.

2.3 Presence profiles

Part of the daily tapping does not take place in one's own household, but for example at work or at school. With the help of presence profiles, it is possible to calculate the share of the daytime the resident types spend outside their own household. The corresponding absence times serve as a factor for reducing the tapping frequencies and quantities at the washbasin, WC and kitchen sink. It is assumed that the shower and bathtub are used exclusively in the household. The presence profiles are drawn up on the basis of the time use survey of the Federal Statistical Office of Germany [2].

Tab. 1 shows the times when tapping is likely and unlikely on working days. The category "likely" means that 95 % of all tappings fall into these periods. The remaining tappings occur evenly at unlikely times of the day and night. No regular or prolonged absences are assumed at weekends in this study. However, there is a shift of 30 min of the night's rest into the evening.

Tab. 1 - Presence profiles of resident types and percentage of absence on weekdays.

	Couple	Family			Retirees
		Parent 1	Parent 2	Schoolchild	
Likely	06:30-08:00	06:00-08:00	06:00-08:00	06:00-07:30	06:30-21:30
Unlikely	08:00-17:30	08:00-17:30	08:00-13:00	07:30-13:30	-
Likely	17:30-22:30	17:30-22:30	13:00-22:30	13:30-21:30	-
Night’s rest	22:30-06:30	22:30-06:00	22:30-06:00	21:30-06:00	21:30-06:30
Absence time	39.6 %		Ø 28.5 %		0.0 %

2.4 Water demand at the draw-off points

In 2018, the average water consumption in private households in Germany was 115.5 l per person and per day (p·day) [3]. Fig. 2 shows the differentiation of water use in households. It is assumend that the categories "cleaning, gardening, etc." and "eating, drinking" occur at the kitchen sink. The categories "washing dishes" and "laundry" are completely assigned to the household appliances dishwasher and washing machine. The category "personal hygiene" can be subdivided into tappings at the shower, the bathtub and the washbasin. The division is based on further literature data ([4], [5], [6]). From this, a consumption of 32.9 l (28.5 %) for the shower, 5.8 l (5.0 %) for the bathtub and 7 l (6.1 %) for the washbasin per person and day can be determined.

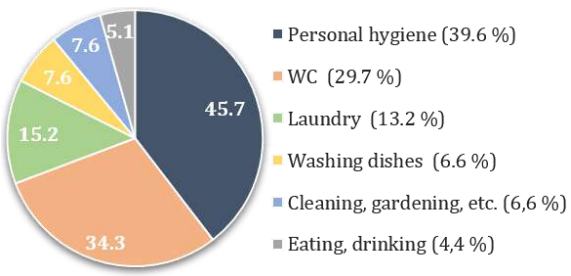

Fig. 2 - Water usage in the household in l/(p·day); own illustration based on [3].

2.5 Tapping frequencies

Tab. 2 lists the tapping quantities and frequencies of the individual draw-off points. The lower part of the table shows the reductions determined according to Tab. 1 due to the absence times, as well as the predefined target mixing temperatures.

Following the default settings of DHWcalc, the tapping frequencies and quantities of the kitchen sink

and washbasin given in Tab. 2 are based on a representative survey by Dichter (1999) [7], [8]. However, adjustments are made to the statistical average values determined in Fig. 2, as well as increases with regard to frequency, since three tappings at the kitchen sink or seven tappings at the washbasin per p·day seems to be unreasonably low. According to DIN 1385:1988-05, a WC cistern holds between six and nine litres of water [9]. Based on this, five flushes of 7.5 litres per p·day are assumed, which correlates with the statistical demand quantities according to Fig. 2.

Tab. 2 - Average tapping quantities, frequencies and duration, as well as reductions due to absences.

	Kitchen sink	WC	Shower	Bathtub	Washbasin
Ø Water demand/tapping	3.0 l	7.5 l	48 l	140 l	0.7 l
Ø Water demand /(p·day)	12.7 l	35 l	32.9 l	5.8 l	7.0 l
Ø Tappings/(p·day)	4.22	5	0.6857	0.0415	10
Tapping duration	≤ 1 min	1 min	6 min	14 min	≤ 1 min
Ø Water demand after reduction due to absences [l/(p·day)]					
Couple (39.6 %)	7.7	21.1	-	-	4.2
Family (28.5 %)	9.1	25.0	-	-	5.0
Retirees (0.0 %)	12.7	35.0	-	-	7.0
Target mixing temperature	42 °C	-	39 °C	42 °C	35 °C

2.6 Dishwasher and washing machine: cleaning sequences

The underlying cleaning programme of a dishwasher consumes an average of 11 l of water [10] within 120 min. During this time, there are three tappings: The pre-rinse cycle requires 4 l of water at the beginning. After 45 minutes, the dirty water is pumped out and fresh water is poured in for the intermediate rinse cycle. After 90 minutes, the water is changed again for the clear rinse cycle with 3 litres of fresh water. The washing machine consumes 48 l of water within the standard programme of 150 min. During this time, there are a total of five rinse cycles with evenly distributed fresh water tappings of 9.6 l each (based on [11], cf. Tab. 3).

Tab. 3 - Statistical database for generating a dishwasher and washing machine sequence.

	Dishwasher	Washing machine
Water consumption per cleaning cycle	11 l	48 l
Cleaning cycles per year (couple; family; retirees)	209; 313; 261	140; 175; 140
Duration of the cleaning programme	120 min	150 min
Number of tappings per cleaning cycle	3	5
Timing of tappings	0; 45; 90 min	0; 30; 60; 90; 120 min
Tapping quantity per tapping	4; 4; 3 l	9.6 l each
Tapping duration per tapping	1 min	1 min

3. Generation of the tapping profiles

3.1 Tapping profile generation with DHWcalc

With the exception of the dishwasher and the washing machine, two tapping profiles are initially created with DHWcalc for each resident type and for each draw-off point (30 in total): one tapping profile for the weekdays and one tapping profile for the weekends. The separation is necessary because the daily tapping quantities differ due to the presence profiles. The tapping profiles for weekdays cover 261 days and consider the tapping volume reductions due to the presence profiles (cf. Tab. 1 and Tab. 2). The daily tapping quantity, the volume flow and the tapping duration are set in DHWcalc to match the values displayed in Tab. 2. The settings for the probability distribution of the tappings correspond to the presence profiles according to Tab. 1. The tapping profiles for the weekends cover 104 days accordingly and do not take absences into account. Generally, the smallest possible time step setting of 1 min is selected in DHWcalc [12]. Holiday periods are not considered in this step, since they can be inserted individually afterwards (e.g. in the resulting text file or in TRNSYS).

3.2 Merging the tapping profiles

A tool implemented in Microsoft Excel - Visual Basic for Applications (VBA) merges the separate tapping

profiles according to working days and weekends. The sorting is done by the VBA tool periodically creating a gap in the weekday tapping profile after 7,200 time steps of 1 min (5 days) and then copying in 2,880 time steps (2 days) from the weekend profile. Fig. 3 visualises the sorting process. A total of 15 tapping profiles remain (5 per resident type), each covering a year.

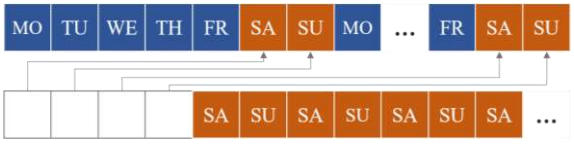

Fig. 3 - Principle of merging weekday and weekend tapping profiles.

3.3 Refinement of the time step and temporal compression of small tapping quantities

In everyday life, very short tappings, lasting only a few seconds, often occur at the kitchen sink and washbasin. Examples include filling a kettle or wetting a toothbrush. With a time step of 1 min, these tappings cannot be represented realistically by DHWcalc, as even the smallest tappings, e.g. 0.1 l, are always assumed to last 60 s. From the point of view of drinking water hygiene, it can be assumed that pipes and their surroundings heat up more the longer a hot water tapping lasts.

A tool, also realised with Excel-VBA, refines the time step width of the tapping profiles from 1 min to 5 s (the desired simulation time step) and compresses tappings at the kitchen sink and the washbasin in terms of time. Tab. 4 shows the categories for compressing small tappings. Based on the default settings in DHWcalc, the assumed maximum flow rate is 7.2 l/min.

Tab. 4 - Categories for compressing small tappings.

Category	Volume [l]	Duration [s]
1; 2	> 0.0 - 0.6; > 0.6 - 1.2	5; 10
3; 4	> 1.2 – 1.8; > 1.8 - 2.4	15; 20
5; 6	> 2.4 - 3.0; > 3.0 - 3.6	25; 30
7; 8	> 3.6 - 4.2; > 4.2 - 4.8	35; 40
9; 10	> 4.8 - 5.4; > 5.4 - 6.0	45; 50
11; 12	> 6.0 - 6.6; > 6.6	55; 60

Fig. 4 shows the principle of time step refinement and the compression in terms of time according to small tapping quantities by the VBA tool. Each time step value of the tapping profiles created with DHWcalc is read in successively, converted to 5 s values in terms of quantity and the resulting array of 12 is written to a new text file. If, for example, a time step in the tapping profile for the shower has the value 8 (l/min), the tool transforms this entry into 12 new time steps of 0.67 (l/5 s) each. If, for example, a time step has the value 2.5 (l/min), this results in the following transformation: The first 5 entries contain the value 0.5 (l/5 s), the remaining 7 entries receive the value 0.0. With this method, the tapping volume of 2.5 l is compressed from 60 s to 25 s, increasing the flow rate from 2.5 l/min to 6 l/min.

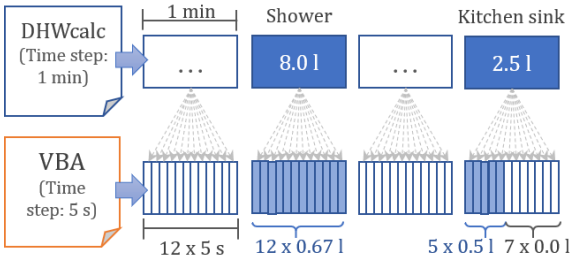

Fig. 4 - Principle of time step refinement and temporal compression of small tapping quantities.

3.4 Tapping profile generation for dishwasher and washing machine

The generation of the tapping profiles for the dishwasher and the washing machine is done in the same way and requires two steps. In the first step, markers are set in an empty tapping profile defining the start of a dishwasher or washing machine sequence. This step is done with the help of the random function in Excel. In the random distribution, absence times and night rest are left out according to Tab. 1. The number of markers depends on the resident types (cf. Tab. 3). Using the example of the dishwasher for resident type couple, 209 randomly selected markers are set in the course of the year (family: 313, retirees: 261).

The second step involves the actual tapping profile generation with a tool implemented in Excel VBA. It reads in the previously formed marker profiles and generates new profiles with a time step resolution of 5 s. A marker triggers a cleaning sequence. As described in chapter 2.6, this consists of 3 or 5 tappings of 1 min each at defined intervals. The volume flow is 0 l/min during the periods before, after and between the tappings. Fig. 5 illustrates how the washing machine and dishwasher sequences are integrated into the tapping profile. With the dishwasher and washing machine cold water tapping profiles created, each resident type receives a total of 7 tapping profiles.

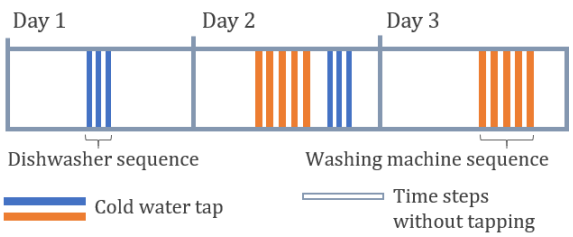

Fig. 5 - Exemplary integration of dishwasher and washing machine sequences.

4. Optimisations in TRNSYS

The water consumption in households determined in chapter 2.4 does not distinguish between hot and cold water demand. However, simulative detailed analyses of drinking water installations require this

distinction in order to be able to model the flow, stagnation and temperature behaviour of individual pipe sections. Therefore, the simulation tool TRNSYS (v17.01.0028) is used to create a model for a drinking water installation in order to separate the hot and cold water flow streams (cf. chapter 4.1). Based on the chosen draw-off points in Fig.1, Fig. 6 shows the structure and pipe lengths of the T-piece installation which is implemented in the TRNSYS model.

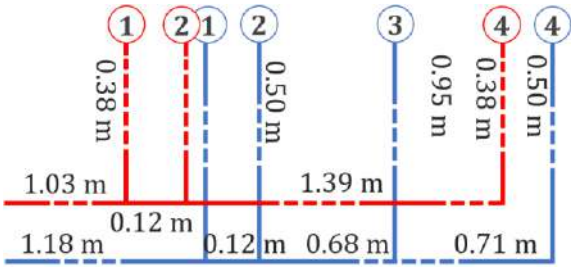

Fig. 6 - Structure of the T-piece installation implemented in TRNSYS; 1: washbasin, 2: kitchen sink, dishwasher, washing machine, 3: WC, 4: shower tray

The selected simulation parameters are listed in Tab. 5. In the framework of the TRNSYS model, flow extensions due to temperature adjustment processes are added (cf. chapter 4.2).

Tab. 5 - Simulation parameters regarding to pipes and temperatures used in the TRNSYS model

Pipe diameter (inner; outer)	16; 18 mm
Pipe material	Copper
Insulation thickness (PWH; PWC)	4; 4 mm*
Pipe total length (PWH; PWC)	3.68; 5.14 m
Total volume	1.773 l
Temperature input (PWH; PWC)	Ø 48; 15 °C
Ambient room temperature	Ø 23.5 °C
*λ = 0.04 W/(m·K); c.f DIN 1988-200 [13]	

DIN 1988-200:2012-5 recommends the insulation of PWH pipes to avoid corrosion and to provide for mechanical protection [13]. The temperatures are implemented as sinus functions, which show a range of 0.8 °C (PWH), 1.8 °C (PWC) and 4.1 °C (ambient room temperature) around the temperatures given in Tab. 5. The time intervals are 6 h, 18 h and 4.380 h. The sinus function of the ambient room temperature is widely stretched and shifted on the time axis. The maximum temperature is reached in the summer, the minimum temperature is reached in the winter.

4.1 Separation of hot and cold water

The required hot and cold water volume flows to achieve the target mixing temperatures specified in Tab. 2 can be determined according to formula (1) and (2). Constant heat capacitances are assumed.

$$\dot{V}_{PWC} = \frac{\vartheta_{PWH} - \vartheta_M}{\vartheta_{PWH} - \vartheta_{PWC}} \cdot \dot{V}_{SUM} \quad (1)$$

$$\dot{V}_{PWH} = \left(1 - \frac{\vartheta_{PWH} - \vartheta_M}{\vartheta_{PWH} - \vartheta_{PWC}}\right) \cdot \dot{V}_{SUM} \quad (2)$$

ϑ_M, ϑ_{PWH}, ϑ_{PWC}: Target mixing temperature [°C], Warm- and cold water temperature[°C]

$\dot{V}_{PWH}$, $\dot{V}_{PWC}$, $\dot{V}_{SUM}$: Volume flow[l/min] of warm- and cold water, Total volume flow [l/min]

Fig. 7 illustrates exemplarily the implementation of the mixing rule in TRNSYS for one of the warm water draw-off points: kitchen sink, washbasin, shower and bathtub. In the central element, the equation, the formulas (1) and (2), as well as the target mixing temperature ϑ_M of the respective draw-off point are stored. The tapping profiles are read in with a data reader and provide the total volume flow $\dot{V}_{GES}$ as input for the mixing rule. The hot and cold water connections of the draw-off points are implemented as pipe types. These calculate the time-varying discharge temperatures $\vartheta_{PWH}(t)$ and $\vartheta_{PWC}(t)$. In each simulation time step (à 5 s), the required mixing ratio of $\dot{V}_{PWH}$ and $\dot{V}_{PWC}$ is determined from these data. Both volume flows are fed back as input to the pipe types in order to map the respective flow of the pipe sections. The Delay (Type 661) is only present at the shower tap and is used to implement the temperature adjustment process described in chapter 4.2.

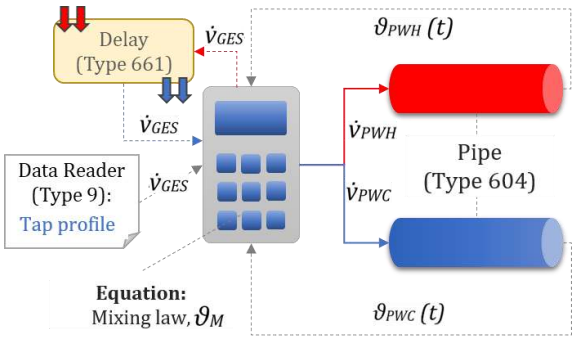

Fig. 7 - Implementation of the mixing rule in TRNSYS.

4.2 Temperature adjustment process

The water temperature in the pipes approaches the ambient room temperature during a stagnation period. In this case, the maximum PWH supply temperature is available with a delay after the start of tapping, as the stagnant water must first drain off. In this context, the temperature adjustment process means the process of adjusting the target mixing temperature using the mixer tap at the beginning of a tapping. The process typically proceeds in such a way that initially only hot water is requested by using the lever position of the mixer tap until an increasing heating of the outflowing water is perceived. The subsequent step-by-step adjustment of the lever position leads to an admixture of cold water until the target mixing temperature is reached. The water flowing out during this process flows unused into the drain. This must be distinguished from the volume flows defined

in the tapping profiles, which refer exclusively to tappings when the target mixing temperature is reached. The temperature adjustment process takes place before the actual tapping and leads to an increase in the tapping duration and volume compared to the data from the tapping profiles. Superimposing the original tapping profiles with the tapping volume that has flowed off unused during the temperature adjustment process results in new, so-called "extended tapping profiles" (cf. Fig. 8).

The consideration of the temperature adjustment process in TRNSYS including the tapping extension is limited to the shower tap. For reasons of comfort, the desired water temperature is typically adjusted before entering the shower. For short tappings at the washbasin and kitchen sink (e.g. for washing hands or filling a kettle), the significance of the water temperature reached at the start of the tapping is negligible. The same applies when filling a bath.

The implementation of the temperature adjustment process in TRNSYS is realised with the help of the equation shown in Fig. 7 in connection with the Type 661 ("Delayed Output Device"; in this version called "delay-type"). A test condition is stored in the equation which passes on the volume flow from the tapping profile to the delay type if the mixing temperature at the outlet of the pipes is below the target mixing temperature during a tapping (ϑ_M, shower = 39 °C). The delay-type stores the volume flow for the duration of the shower tapping (72 time steps of 5 s each) and then returns it to the equation. Fig. 8 shows the volume flows from the tapping profile and the delay-type that enters the equation. The superimposition results in a summed volume flow (extended tapping profile) from which the required mixing ratio ($\dot{V}_{PWH}$ and $\dot{V}_{PWC}$) is calculated and transferred to the pipes. Thus, on the one hand, the original tapping profile is extended by the time required for the temperature adjustment process. On the other hand, the tapping volume is increased by the amount of water that previously flowed off unused.

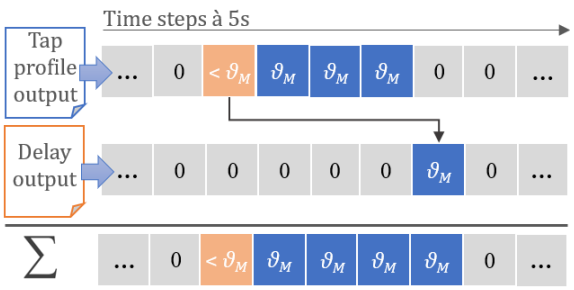

Fig. 8 - Volume flow superimposition: Extended tapping profiles.

5. Results

5.1 Exemplary tapping profile cut-outs

Fig. 9 and Fig. 10 each show an exemplary daily course (working day) of the extended tapping profiles for the resident types couple and retirees. In the time interval of the night's rest (cf. Tab. 1), tapping takes place only in exceptional cases (e.g. 3:00 AM). The direct comparison of the two resident types clearly shows the influence of the presence profiles. In the case of the couple, there is an accumulation of tappings in the morning and a subsequent stagnation until 4 PM. In the case of the retirees, the tappings are distributed quite evenly throughout the day without longer stagnation periods.

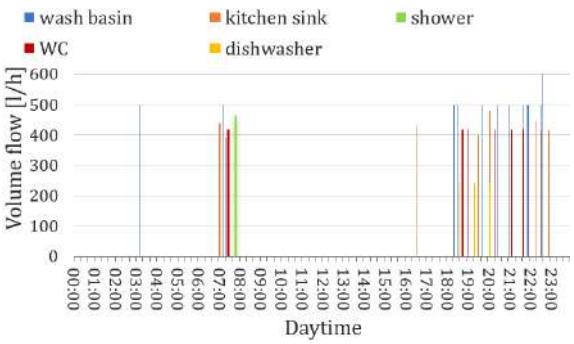

Fig. 9 - Tapping profile cut-out; resident type couple.

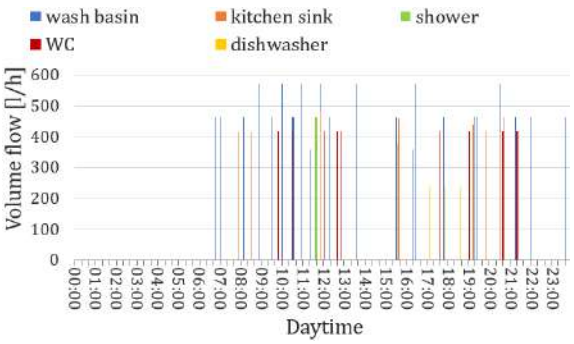

Fig. 10 - Tapping profile cut-out; resident type retirees.

Fig. 11 shows an example of the implementation of the dishwasher and washing machine sequences in the tapping profile for the resident type family. The night and absence times do not contain any tappings.

Fig. 11 - Dishwasher and washing machine sequences; resident type family.

5.2 Mixing rule, temperature adjustment process and tapping extension

Fig. 12 shows the flow rate and temperature curve of two exemplary shower tappings at intervals of around 20 min. At the beginning of the first shower tapping, a clear spike in the volume flow of the hot water pipe ($\dot{V}_{PWH}$) can be seen as long as the target mixing temperature of 39 °C is not reached. At the

same time, the temperature (ϑ_{PWH}) at the outlet of the PWH-pipe rises up to a flow temperature of 48 °C (instantaneous water heater). The cold water volume flow ($\dot{V}_{PWC}$) is added with a slight time delay after the PWH setpoint temperature has been reached. The dashed line of the cold water temperature (ϑ_{PWC}) shows, that stagnant water that is close to the ambient room temperature (approx. 22 °C), initially flows out until fresh cold water with a temperature of 14 °C follows. The water that flows off during this temperature adjustment process does not count as part of the actual shower tapping and leads to an extension of the tapping time. The volume flow from the original tapping profile ends approx. with the vertical, green dotted line. The tapping extension takes place via the delay type and corresponds to the temperature adjustment process in terms of duration and quantity.

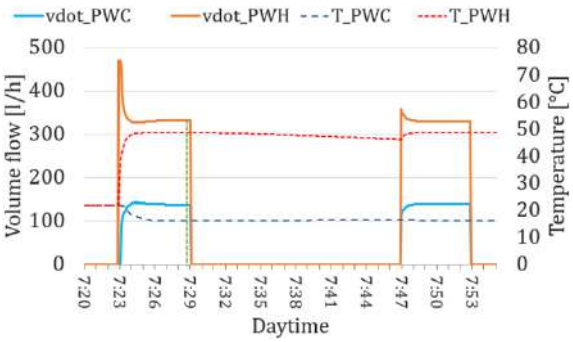

Fig. 12 - Shower tappings with temperature adjustment process.

Between the first and second shower tapping, the water temperatures in the pipes change only slightly. There is no need for an initial temperature adjustment process at the beginning of the second shower tapping, because a sufficiently high PWH temperature is already available to reach the target mixing temperature. That is why there is only a small peak in the $\dot{V}_{PWH}$-line. In contrast to the first shower tapping, the cold water volume flow is added immediately.

Simulations were performed for each resident type to determine the additional consumption at the shower due to the temperature adjustment process. Tab. 6 shows the original and extended annual tapping quantities at the shower (lines 1 and 2), as well as the relative additional consumption (line 3). Line 4 shows the relative additional consumption in relation to the respective total consumption of the resident types.

Tab. 6 - Additional consumption due to the temperature adjustment process at the shower tap

Resident type	Unit	A	B	C
Original shower profile	l/a	24,000	36,000	24,000
Extended shower profile	l/a	24,410	36,632	24,472
Add. consumption (shower tap)	%	1.7	1.8	2.0
Add. consumption (annual total)	%	0.67	0.92	0.61

6. Discussion

The high time resolution compared to DHWcalc enables a realistic consideration of short-term tappings. In the context of drinking water hygiene, this is particularly relevant in a simulation model when depicting pipe heating. With the definition of three different types of residents, individual consumption quantities and times are included. In the following studies, the influence of usage behaviour on drinking water hygiene can be analysed. The overall effort is relatively high due to the research of statistical data, as well as the implementation of the three consecutive steps with different software (DHWcalc, VBA-Tools, TRNSYS). Changes, for example with regard to draw-off points or resident types, require the repetition of at least some steps.

The additional consumption at the shower during temperature adjustment (cf. Tab. 6) increases the statistical demand quantity of the resident types by less than 1 % each. The relatively small additional demand is due to the compact drinking water installation with low pipe volume. In addition, the PWH flow temperature is immediately available at the inlet of the pipe structure in the TRNSYS model. Therefore, the cooled stagnation water drains off quickly and hot water follows without delay. Although the additional consumption is small, it may still have an impact on drinking water hygiene due to prolonged flushing and heating of the PWH pipe.

The used demand quantity refers to average values of the total German population (cf. Fig. 2). Individual tapping behaviour deviates from this. Looking at the developed extended tapping profiles, the reference to reality is still given. A general reduction of the tapping quantity in the original tapping profile should be avoided, as not every shower tapping involves a temperature adjustment process (cf. Fig. 12).

7. Conclusions

The described methodology enables the generation of suitable, spatially accurate and temporally highly resolved tapping profiles for detailed simulation analyses. For each individual hot and cold water pipe to the selected draw-off points, individually suitable

volume flows are available. Due to the lack of available software solutions, the degree of automation is low. However, the tapping profiles created in this work already cover various typical tapping behaviours and can be used e.g. for detailed analyses or as summed tapping profiles for entire apartments or buildings. For the optimisation of the tapping profiles with regard to an adequate separation of hot and cold water proportions, as well as the temperature adjustment process, the use of simulation software such as TRNSYS is indispensable. For these calculations, time-step accurate state variables of the system are necessary (e.g. current temperature of the hot and cold water pipes). Looking at the planned simulative hygiene analyses, the temperature adjustment process plays an important role. The prolonged flushing of the hot water pipe leads to stronger pipe heating, which surely effects on a nearby cold water pipe, for example. This could sometimes make it difficult to maintain important hygienic temperature limits and reveal weak points in the drinking water installation types. Further extensions of the tapping profiles within TRNSYS are conceivable. This includes, for example, the addition of holiday periods or the variation of the supply temperatures in order to analyse the effects on the temperature adjustment processes.

8. Acknowledgement

The work is carried out within a joint project of the Institute for Solar Energy Research GmbH (ISFH), together with the Fraunhofer Institute for Energy Economics and Energy System Technology (IEE), the Rhenish-Westphalian Institute for Water Research (IWW), DME Consult GmbH and Solvis GmbH under grant number 03EN1027C (Trans2NT-TWW). The authors gratefully acknowledge the support of the State of Lower Saxony and the Federal Ministry for Economic Affairs and Climate Action (BMWK). Further thanks are due to Delta Systemtechnik GmbH and Taconova GmbH for their support. The authors are responsible for the content of the publication.

9. References

[1] Mercker O, Arnold O. Abschlussbericht zum Vorhaben: Ansätze zur Reduktion der konventionell erzeugten Wärmeverteilverluste in solar unterstützten Mehrfamilienhäusern; 2017.

[2] Statistisches Bundesamt. Zeitverwendungserhebung: Aktivitäten in Stunden und Minuten für ausgewählte Personengruppen; 2015.

[3] Bundesverband der Energie- und Wasserwirtschaft e.V. (BDEW). Trinkwasserverwendung im Haushalt; 2019.

[4] Bonin J. Wärmepumpen: Fehler vermeiden bei Planung, Installation und Betrieb: Beuth Verlag GmbH, Fraunhofer IRB Verlag; 2018.

[5] Hildebrandt A. Bonin J. Wärmepumpen: Fehler vermeiden bei Planung, Installation und Betrieb: Beuth Verlag GmbH, Fraunhofer IRB Verlag; 2018: Springer-Verlag; 2020.

[6] Schlomann B, Gruber E, Eichhammer W, Kling N, Diekmann J, Ziesing H, et al. Energieverbrauch der privaten Haushalte und des Sektors Gewerbe, Handel, Dienstleistungen (GHD): Abschlussbericht an das Bundesministerium für Wirtschaft und Arbeit; 2004.

[7] Jordan U, Vajen K. Influence of the DHW-load profile on the fractional energy savings: A case study of a solar combi-system with TRNSYS simulations; 2000.

[8] Dichter E. Dusch- und Badeverhalten: Bericht zu einer Repräsentativumfrage. Bern: Eidgenössische Dr.-Sachen- und Materialzentrale; 1999.

[9] Klosettbecken mit angeformtem Geruchsverschluß: Beuth Verlag; 1988.

[10] Bundesministerium für Wirtschaft und Energie (BMWi). Spülmaschine: Bei Wasserverbrauch und Stromkosten sparen [Internet]. c13.8.2021 [updated 2021 Aug 13; cited 2021 Aug 13]. Available from: https://www.deutschland-machts-effizient.de/KAENEF/Redaktion/DE/Standardartikel/Dossier/A-geschirrspueler.html.

[11] Grond A. Das richtige Programm - und wie es wirkt: Was läuft bei den Spezialprogrammen in einer Waschmaschine technisch ab? Elektrohändler 2008.

[12] Jordan U, Vajen K, Brass H. DHWcalc: Werkzeuge zur Generierung von Trinkwasser-Zapfprofilen auf statistischer Basis; 2017.

[13] Technische Regeln für Trinkwasser-Installationen. Beuth Verlag; 2012.

The datasets generated during and/or analysed during the current study are not available because because the study is currently still being carried out and will be extended and possible changes may occur but the authors will make every reasonable effort to publish them in near future.

Monitoring a deep energy renovated building

Matthias Haase [a]

[a] Institute of Facility Management, Zurich University of Applied Sciences, Waedenswil, Switzerland, Matthias.haase@zhaw.ch.

Abstract. A typical residential building from 1937 located near Wurzburg in Germany, was deep retrofitted in 2013. The energy use and costs could be drastically reduced compared to the old building. However, increase in energy costs can thread economic success. Therefore, it is important to monitor also the performance of the different technical systems. A measurement campaign of a real building with energy consumption and production ("prosumer model") proves the concept of prosumer over time. The total energy costs were 387 € in 2018 and have increased to 839 € in 2021. This is an increase of 217%., changes in energy prices and tariff structures might influence the lifetime energy costs as well as the savings. Electricity use of the compact unit was measured, share of ventilation and heat (heating and DHW) was calculated based on standard models. Electricity use is illustrated and contrasted with electricity production from a 7.95 kW solar PV system.

Keywords. performance monitoring, electricity use and production, economic evaluation **DOI**: https://doi.org/10.34641/clima.2022.248

1. Introduction

Residential use of energy is responsible for 28% of EU energy consumption [1]. The barriers to consumer energy saving have been known for more than 30 years but are still present. in particular split incentives (e.g. tenants vs. landlords). lack of information. high initial investment in energy-efficient equipment and habits of energy users [2].

Likewise. while awareness of the existence of renewable energies has improved considerably in the last years. there is still a lack of understanding of how to use and optimize them in practice.

The EPBD requires nearly zero energy buildings (nZEB) from 2021. There are many approaches to this goal and several pilot buildings have been built and extensively measured [3]. The theoretical approach is normally based on three pillars; first, energy saving measures have to be applied that ensure a massive reduction of heating energy. The second pillar is energy efficient equipment and third the production of renewable energy on-site [4]. All measures have been applied in this case.

2. Energy renovation (motivation)

A residential building from 1937 located near Wurzburg in Germany was deep retrofitted in 2013. The project received funding from the German Bank for Rebuilding (KfW) in the class kfW55 which uses 55% of the energy budget defined in the existing German building code (EneV) [5]. More ambitious levels (e.g. KfW40 or any type of zero energy buildings) do not exist for refurbishments (only new constructions). There were, however, additional funding schemes for heating systems and Feed-in tariff (FIT) for photovoltaics (PV) [6]. Today, the funding schemes as well as FIT are under revision [7].

The old building was equipped with an oil boiler connected to central heating system with radiators in each room. In the energy renovation strategy towards nZEB, the following steps were followed:

1. Reduction of heat losses through the building envelope).
2. Supply heat with efficient equipment; supply heat with efficient heat pump, underfloor heating, and ventilation air.
3. Installation of 7.95 kW_p PV to produce electricity.

The new energy concept is based on a heat pump with balanced ventilation which provides heating through the central heating system as well as through an underfloor heating in the kitchen and living room 1. The successful renovation was reported in 2016 [8]. In addition, a greywater system was installed which reduces water consumption.

2.1 Building envelope

Roof. façade and ceiling in the basement were highly insulated and thermal bridges were minimized. Windows were replaced with three-layered glazed windows with wood-aluminium windows [8]. The roof was additionally equipped with a 7.95 kW PV

Copyright ©2022 by the authors. This conference paper is published under a CC-BY-4.0 license.

system which produces electricity. This is used in the building for covering the household electricity, the remaining electricity is fed into the grid (FIT).

2.2 Balanced ventilation system

The compact unit also comprises a balanced ventilation system as illustrated in Fig. 2. The fresh air rates are adjustable in three levels (140, 185 and 220 m3/h, i.e. 0.36, 0.48, 0.57 ACH) and flow rates required for indoor air quality are used. In 2018 and 2019 night-time flow rates of 140 m3/h (0.36 ACH) were used. But in 2020 it was switched to 185 m3/h (0.48 ACH). This was done because the building is fully occupied during night-time and less occupied during daytime. However, it was decided not to reduce daytime airflow rates further (but remain on level 2).

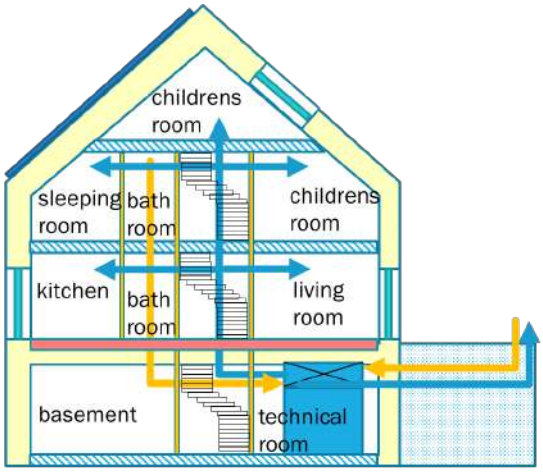

Fig. 2 – Ventilation concept.

This delivers 185m3/h to all the rooms (except storage room in 2. floor; 35m^2) as shown in Figure 2 with a supply and extract fan (with dampers). A cross-plate heat exchanger with 85% thermal efficiency was included in the compact unit. The ventilation ducts were integrated into the existing chimneys. Fan power is kW/(m3/s).

2.3 Compact unit

A compact unit (balanced ventilation system with integrated air-to-water heat pump) was installed. Exhaust air is used as heat source as shown in Figure 1. An underfloor heating system was installed in the kitchen. The electricity used for the compact unit is monitored in a separate meter. This is the know "classical" compact unit: all building services are realized in one appliance: heating, ventilation and domestic hot water. In this case, the hot water is connected to the central heating system and with a mixture valve also to the underfloor heating system. Supply water temperatures for domestic hot water (DHW) are 55°C and then cascade to 30 – 38 °C for the central heating and 25 – 30 °C for the underfloor heating system.

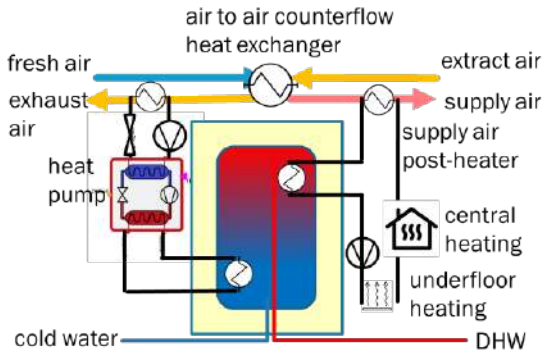

Fig. 1 – Compact unit.

The temperatures are controlled by the outdoor temperature, so that low outdoor temperatures result in higher supply temperatures (heating curve) and pump power is 600 W/(l/s) (with a water flow rate of 0.05 l/s.

2.4 PV system

A 7.95 kW solar PV system was installed on the south-west facing roof. It consists of 30 modules and covers 42m^2. An inverter was placed in the technical room and connected to the household grid and equipped with a two-lane meter.

3. Objectives

This paper reports the long-term measurement results of a comprehensive energy renovation (towards nZEB). The energy use and costs could be drastically reduced compared to the old building. However, increase in energy costs can thread economic success. Therefore, it is important to monitor also the performance of the different technical systems. Therefore, the energy use (and savings) of a residential building located in Wurzburg, Germany was monitored over a period of four years. Consumption pattern can be used to evaluate standard key performance indicators, like energy use, electricity use, production and costs.

4. Method

A measurement campaign of a real building with energy consumption and production ("prosumer model") proves the concept. Electricity use of the compact unit was measured, share of ventilation and heat (heating and DHW) was calculated based on standard models. Electricity use was illustrated and contrasted with electricity production from a 7.95 kW solar PV system.

Electricity use of the compact unit was measured. This is used for heating, fans and pumps.

Specific fan power is given to SFP = 2.5 kW/(m^3/s). Specific pump power is given to SSP = 0.6 kW/(m^3/s) so that total energy use of ventilation can be determined.

Thus, the energy demand for heat could be calculated:

$Q_H = Q_h + Q_{DHW}$ (1)

$SPF = Q_H / E_H$ (2)

$E_{HP} = E_H + E_V$ (3)

$E_V = E_{vent} + E_{pump}$ (4)

Q_h is the heating demand of the building

Q_{DHW} is the heat demand for DHW

SPF is the seasonal performance factor. Here, the boundaries for SPF used includes fan and pump power.

E_{vent} is the electricity demand of the fans and can be calculated by

$E_{vent} = V_{vent} * SFP * t$ (5)

E_{pump} is the electricity demand of the pumps

SPF is the specific fan power of the fans

$E_{pump} = V_w * SPP * t$ (6)

SPP is the specific pump power

with

- SPF (specific fan power) = 2.5 kW/(m^3/s)
- V_{vent} = 185 m3/s (level 2) (140 m^3/s (level 1: night level in 2018 and 2019))
- SPP = 0.6 kW/(l/s)
- t = time of use

The SPF was derived from COP tables of HP provider, with following formula.

$SPF = 2.4 + (0.1*T_{out})$ (7)

With
Tout = outdoor temperature (°C)

There are several energy tariffs for different electricity streams. At least four different tariffs have been considered:

- Electricity purchased for household
- Electricity purchased for heat pump (divided into HT and LT for day and night-time)
- PV electricity self-consumed
- PV electricity sold to grid

The energy price is including working tariff, fixed fees (transfer pricing and fixed performance price) and all taxes which are included in the bill. For the electricity of the self-consumed electricity from PV production only the working tariff plus taxes (electricity tax and value added tax) have been considered. For the electricity supply a special 'heat-pump' tariff was chosen (HT: during daytime; LT: during nighttime).

5. Results

Electricity measurements were monitored:

- Electricity purchased from the grid
- Electricity sold to the grid
- Electricity produced by PV
- Electricity costs

Fig. 3 shows electricity purchased and sold from and to the local provider. It can be seen that the energy purchased is slightly higher than energy sold. Therefore, the building does not reach NZEB

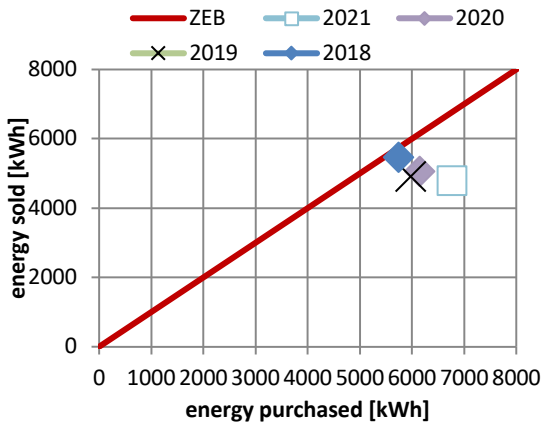

Fig. 3 – Annual electricity purchased and sold (2018-2021).

5.1 Domestic hot water (DHW)

DHW is produced by the compact unit. The amount of water consumption was measured and calculated to hot water and energy need for this was calculated. In 2020 the greywater system was not in operation.

Tab. 1 – Domestic hot water use in 2020.

month	days/month	litres/month	kWh/month
1	31	4617,52	269,4
2	24	3574,86	208,5
3	31	4617,52	269,4
4	25	3723,81	217,2
5	28	4170,67	243,3
6	27	4021,71	234,6
7	31	4617,52	269,4
8	14	2085,33	121,6
9	21	3128	182,5
10	31	4617,52	269,4
11	24	3574,86	208,5
12	28	4170,67	243,3
sum	315	46920	2737

Thus, the freshwater consumption could be measured without recovery which amounted to 138 m³. According to a water consumption survey (IWU) 34% is used for DHW. This amounts to 128 l/d. The DHW use was calculated to liters per month and energy demand for DHW was derived. Table 1 gives the values for 2020. The calculations were done for the other years accordingly, as shown in Table 1.

5.2 Ventilation

The balanced ventilation system consists of two main distribution ducts from the basement up to ground floor and first and second floor. It provides fresh air in living room 1 and 2, the office rom (in ground floor) and the sleeping/children rooms in second and third floor. Extract openings are located in the two bathrooms in ground floor and first floor. The total energy use of ventilation is Event = (1125 + 526) kWh = 1751 kWh.

5.3 Heating (heat pump)

The heat pump is a compact unit (Stiebel Eltron) with 420 l storage tank.

The temperature dependent SPF was then calculated as shown in Fig. 4 and Fig. 5.

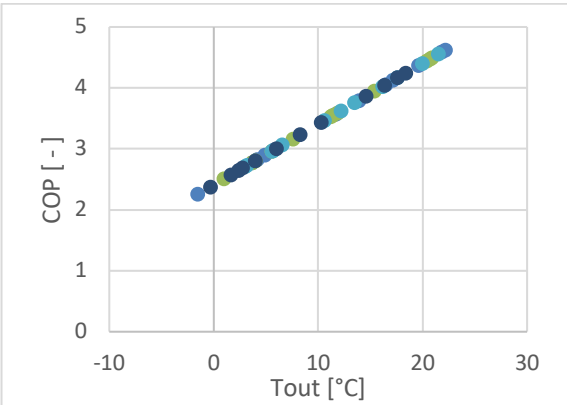

Fig. 4 – COP for air/water HP depending on outdoor air temperature.

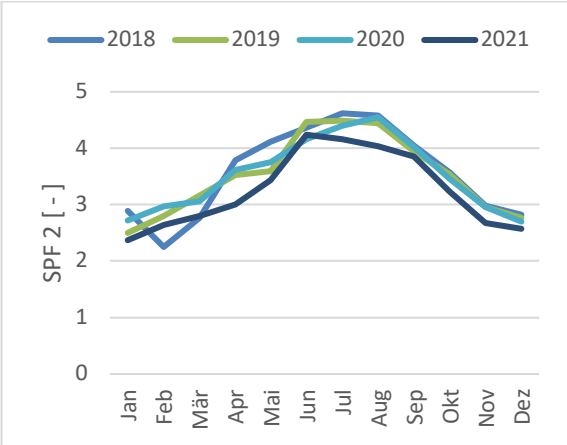

Fig. 5 – SPF for heat pump (2018 – 2021).

5.4 Electricity costs / tariffs

The energy tariffs for different electricity streams as summarized in Table 2. It can be seen that electricity tariff for household electricity ranges between 0.34 and 0.39 ct/kWh.

Tab. 2 – Electricity tariffs (2018 – 2021)

year	house-hold	heat pump HT	heat pump LT	PV (OC)	PV (FIT)
2018	0.3411	0.2281	0,.073	0,3411	0.454
2019	0.3700	0.2390	0.2182	0,3700	0.1454
2020	0.3863	0.2610	0.2401	0,3863	0.1454
2021	0.3863	0.2610	0.2401	0,3863	0.1454

(FIT: Feed-in tariff); HT: high tariff; LT: Low tariff)

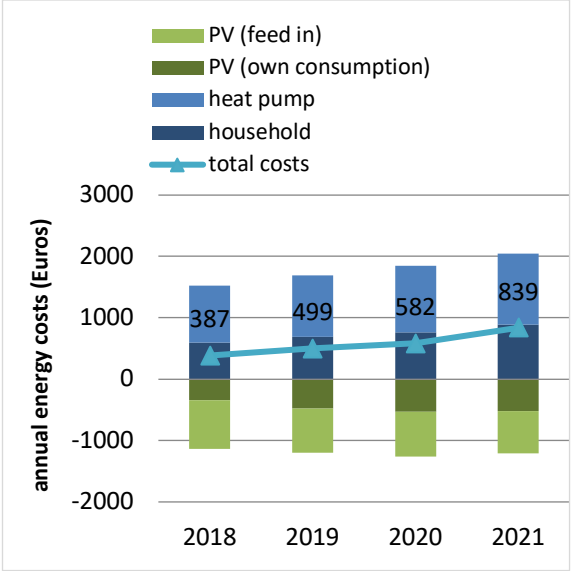

Fig. 6 – Economic figures for 2018 - 2021.

Fig. 6 summarizes annual electricity costs for heat pump, household, self-consumption and electricity use (for household). For comparison reasons, the figure also includes energy costs revenues for PV sold. It can be seen that total energy costs (blue line) as well as household energy costs (dark blue) have increased since 2018.

The revenue from PV electricity production (counted as negative) consists of revenue from selling electricity to the energy provider plus the revenue from saved electricity costs from self-consumption (dark green).

The total energy costs were 387 € in 2018 and have increased to 839 € in 2021. This is an increase of 217%. It should be noted that energy costs amounted to 4897 € (1415 € for electricity; 3482 € for heating (oil)) before renovation. This could have decreased to 4358 € in 2018 and increased to 4679 € in 2021. There are still energy cost savings due to the renovation measures, but the increase of energy costs influences the payback calculations of the renovation measures considerably.

6. Discussion

The deep energy renovation was very successful and energy use and costs could be drastically reduced. However, several technical systems were installed which need to be monitored in more detail. The compact unit was measured separately but still some performance indicators are good to check, e.g. the SPF.

This measurement campaign was done in a building in operation. Not all boundary conditions could be monitored. For example, the building operation was paused in short periods for maintenance. Also, the opening and closing of windows and doors was not monitored. But the household is a rather typical one, with six persons sharing 158.5 m^2 it is rather densely occupied. But water consumption is rather low compared with figures from other surveys.

The performance of the PV system was not in focus of this report.

7. Conclusions

7.1 Energy renovation

The energy use and costs could be drastically reduced compared to the old building. However, increase in energy costs can thread economic success. Therefore, it is important to monitor also the performance of the different technical systems. The PV system is also an important system, but it was not in focus of this report.

7.2 Heat pump

There is an optimization potential for the operation of the compact unit, but it is rather difficult to make improvements and to monitor the improvements in performance. A digital twin could be useful to run in the shadow, not only to quantify improvements in the planning phase but also in order to be able to quantify improvements in operation

7.3 Economic appraisal

Combined energy consumption and production profiles represent a new type needs further recognition. An optimization of the energy costs can be achieved by improving the operation of the building and of the PV system. However, changes in energy prices and tariff structures might influence the lifetime energy costs as well as the savings.

7.4 Proposal for future work

We suggest setting up a Digital twin. This will help to analyse further performance influencing factors.

An analysis tariff structures and their changes over time (decades) will be helpful.

An analysis of PV system (not only parameters orientations, shading, size, costs) by also considering different tariff structures will become even more important when considering additional energy storage options.

It is advised to apply sensitivity analysis of PV system over a longer period (several years) and analysis with weather data to get a better understanding of the influencing parameters.

8 Acknowledgement

This work was written within the project “PEB”. Financial assistance from ZHAW is greatly acknowledged.

9 References

[1] Energy strategy for Europe (2012) Energy market country report 2011 – Belgium. European Commission.

[2] BPIE 2013. Data Hub for the energy performance of buildings. Source: http://www.buildingsdata.eu/

[3] EPBD. 2010. Energy Performance in Buildings Directive 2008/0223. European Commission. Brussels. revised 2010. http://eur-lex.europa.eu/LexUriServ/LexUriServ.do?uri=OJ:L:2010:153:0013:0035:EN:PDF. access date: April 2015

[4] Lysen E.H (1996) 'The Trias Energetica - Solar Energy Strategies for Developing Countries', in: Proceedings of the Euro sun Conference; Freiburg

[5] Energieeinsparverordnung 2014. (EneV). http://enev-2014.info/. access date Jan 2016

[6] Act on the Development of Renewable Energy Sources ((Renewable Energy Sources Act RES Act 2014). (in German: Erneuerbare Energien Gesetz EEG 2014). http://www.erneuerbare-energien.de/EE/Redaktion/DE/Gesetze-Verordnungen/eeg_2014_engl.pdf?__blob=publicationFile&v=4. access date: jan 2016

[7] Bergner, J. And Quaschning, V., Sinnvolle Dimensionierung von Photovoltaikanlagen für Prosumer, in German: Meaningful sizing of PV systems for prosumers, Verbraucherzentrale NRW e.V, https://pvspeicher.htw-berlin.de/, access date: 21.12.2021

[8] Haase, M., Case study of deep retrofitting of a residential building towards plus energy level, proceedings IEECB&SD conference (IEECB&SD2016), 16-18 March 2016, Frankfurt, Germany

Optimization of Novel Air-to-Refrigerant Heat Exchangers for Lower-GWP Refrigerants in Air-Conditioning Systems

James Tancabel[a], Vikrant Aute[b], Jiazhen Ling[c]

[a]PhD Candidate, Center for Environmental Energy Engineering, Department of Mechanical Engineering, University of Maryland, College Park, Maryland, USA. jmtanc@umd.edu.

[b]Research Scientist & Co-Director, Center for Environmental Energy Engineering, Department of Mechanical Engineering, University of Maryland, College Park, Maryland, USA. vikrant@umd.edu.

[c]Associate Research Professor, Center for Environmental Energy Engineering, University of Maryland, College Park, Maryland, USA. jiazhen@umd.edu.

Abstract. Air-to-refrigerant heat exchangers (HXs) are fundamental components in HVAC&R systems, and considerable research has focused on reducing the airside thermal resistance, which can exceed 70-90% of the overall resistance. Traditional HX design ideology utilizes secondary heat transfer surfaces (fins) to reduce the airside thermal resistance by increasing the airside heat transfer area. However, fins also have inherent deficiencies such as increased airside pressure drop, material costs, and HX fouling/frosting potential. Recent advancements in simulation tools such as Computational Fluid Dynamics (CFD) and Finite Element Analysis (FEA) and also in optimization algorithms have enabled researchers to apply shape and topology optimization to the primary heat transfer surfaces (e.g., tubes) to design high performance, highly compact HXs which do not require fins. These novel HXs feature reduced size, weight, cost, and refrigerant charge compared to current state-of-the-art HXs while maintaining or improving system-level performance, thereby reducing the overall environmental impact. Such factors are especially important given the recent governmental and industrial shifts to low-GWP flammable and mildly-flammable refrigerants, which have highly regulated charge amounts. In this paper, an HX optimization framework featuring automated CFD and FEA simulations and approximation-assisted optimization is utilized to optimize a residential A/C condenser for three different refrigerants: (i) R410A (industry-standard for US residential A/C units), (ii) R32 (most popular lower-GWP replacement for R410A in the EU), and (iii) R454B (another lower-GWP alternative to R410A). Preliminary findings show that the optimal HXs achieve at least 20% reductions in airside pressure drop and envelope volume, up to 11% reduction in tube material volume, and more than 40% reduction in tube internal volume while delivering similar capacity to the state-of-the-art baseline HX. The differences between the refrigerant-specific optimal HXs are also discussed in detail to shed light on how the refrigerant choice impacts the final HX designs. By using systematic optimization, it is possible to arrive at highly compact and lighter HX designs for any of the new lower-GWP replacement refrigerants.

Keywords. heat exchanger, optimization, low-GWP, R32, R454B.
DOI: https://doi.org/10.34641/clima.2022.245

1. Introduction

Air-to-refrigerant heat exchangers (HXs) are fundamental components in all HVAC&R systems. Compact HXs, i.e., HXs with tube characteristic diameters smaller than 6.0 mm [1], are of particular interest to researchers since their intrinsically high heat transfer area to envelope volume ratio can yield significant size reductions. However, these small characteristic diameter tubes do not have adequate primary heat transfer area to achieve the required thermal resistance to satisfy the HX capacity requirements. Thus, compact HXs typically utilize fins to increase the airside heat transfer area and satisfy the thermal resistance requirements. However, fins have inherent drawbacks including increased airside pressure drop, material consumption, and fouling/frosting potential. Recent

Copyright ©2022 by the authors. This conference paper is published under a CC-BY-4.0 license.

research [2] has noted that as characteristic diameter decreases, finless surfaces have superior airside thermal-hydraulic performance compared to similarly-sized finned surfaces. Additionally, small diameter, round tube HXs have been well-studied throughout the literature [3-6].

More recently, Bacellar et al. [2,7] argued that classical HX design paradigms should evolve to leverage modern computational and manufacturing capabilities. To this end, the authors developed a comprehensive multi-scale analysis and shape and topology optimization framework capable of designing finless compact HXs which utilize novel, small diameter, non-round tubes. Their methodology was experimentally validated using an additively manufactured proof-of-concept HX design, further strengthening the case for implementing shape optimization and additive manufacturing into HX design ideology.

In a related work, Radermacher et al. [8] suggested that non-round, shape-optimized tube designs may lack the required mechanical strength for pressure-holding, thereby requiring detailed structural analyses to verify pressure-holding capabilities of all candidate geometries. Additionally, Tancabel et al. [9] noted that no air-to-refrigerant HX shape and topology optimization studies explicitly considered tube mechanical strength.

In this paper, we present the application of an HX design optimization methodology which features integrated multi-scale and multi-physics analyses and shape and topology optimization [10-11] to optimize a residential air-conditioning (A/C) unit condenser using novel, shape-optimized non-round tubes which can be conventionally (i.e., non-additively) manufactured. We consider three different refrigerants: (i) R410A (GWP = 2,088), the industry-standard for US residential A/C units, (ii) R32, a lower-GWP (GWP = 677) alternative to R410A which is the most popular replacement for R410A in the EU [12-16], and (iii) R454B, an even lower-GWP (GWP = 466) alternative to R410A (compared to R32) [16-19]. Comparisons between the optimal HX designs for each refrigerant are discussed in detail to shed light on how the refrigerant choice impacts the final HX design.

2. Methodology

2.1 Design Optimization Framework

The HX design optimization framework (Fig. 1) utilizes Approximation-Assisted Optimization (AAO) [20] involving automated Computational Fluid Dynamics (CFD) [21] and Finite Element Analysis (FEA) simulations [10-11], Kriging metamodels [22], and optimization with a multi-objective genetic algorithm (MOGA) [23].

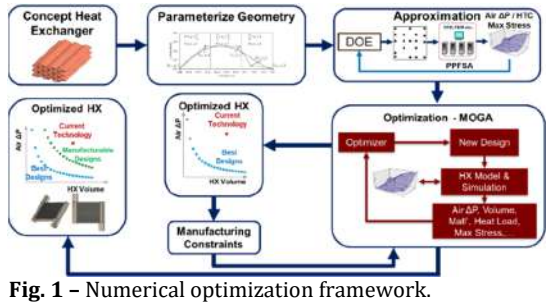

Fig. 1 – Numerical optimization framework.

2.2 Problem Description

High performance HXs featuring novel, non-round tubes have been investigated for many applications [10-11, 24]. In this research, the optimization framework is utilized to design novel, finless, air-to-refrigerant condensers for residential A/C applications using lower-GWP alternative refrigerants. The baseline HX is a commercially-available, state-of-the-art nominal 5.28 kW (1.5-Ton) tube-fin air-to-R410A condenser. Three refrigerants are investigated: (i) R410A, (ii) R32, and (iii) R454B. The inlet conditions for each refrigerant are taken from commercially-available residential A/C units with nominal 5.28 kW (1.5-Ton) capacity [25]. Sample schematics for a representative tube-fin HX and a finless HX with shape-optimized tubes are shown in Figure 2.

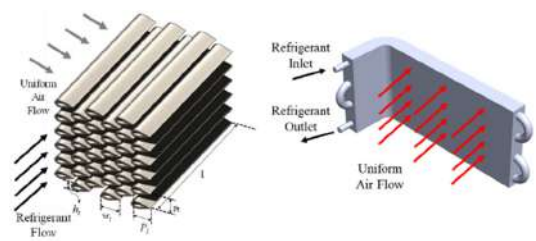

Fig. 2 – (Left) Generic HX with shape-optimized tubes; (Right) Generic multi-pass tube-fin condenser.

The HXs are in cross-flow, and all HX models assume the following: (i) uniform normal inlet air velocity on the HX face, and (ii) fully-developed, uniform refrigerant flow. The airside thermal-hydraulic performance is predicted using CFD, and the tube-level mechanical performance is computed using FEA. Refrigerant-side performance is computed using existing correlations for single and two-phase flow in small diameter channels.

The framework utilizes fourth-order Non-Uniform Rational B-Splines (NURBS) [26] to represent the novel, non-round tube shapes (Fig. 3). The tube shape considered herein [2] has been conventionally manufactured in both copper and aluminum. Burst pressure testing and FEA modelling of the copper tubes showed minimal deformation up to 20.0 MPa, validating the tube structural strength [27]. We therefore consider the copper version herein.

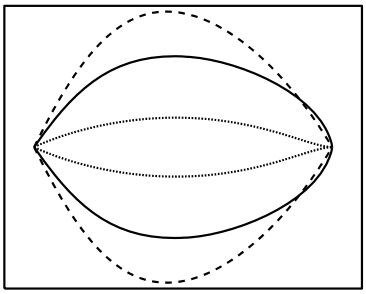

Fig. 3 – Sample non-round tube shapes.

2.3 Parallel Parameterized Fluid & Structural Analysis

It is impractical to simulate an entire multi-variable Design of Experiments (DoE) manually, and thus the entire simulation process must be automated to reduce the computational time burden. To this end, Abdelaziz et al. [21] developed Parallel Parameterized CFD (PPCFD) to automate CFD simulations, resulting in more than 90% engineering time savings. Similarly, Tancabel et al. [10-11] integrated automated FEA simulations into the PPCFD framework for use in multi-physics analyses of HXs utilizing shape and topology optimized tubes. Their framework was termed Parallel Parameterized Fluid & Structural Analysis (PPFSA).

As mentioned above, the modelling and experimental validation of the copper tube structural integrity eliminates the need to consider the structural component of PPFSA. Thus, it is only necessary to consider the CFD component of PPFSA, which is explained in detail in the following sections. All present analyses utilize the ANSYS® 18.0 platform [28-29]. Geometry and meshing are performed using Gambit® 2.4.6 [28], and all CFD simulations are run using Ansys® Fluent 18.0 [29].

2.4 CFD Modelling, Post-Processing, & Uncertainty Analysis

The airside CFD computational domain (Fig. 4) is a two-dimensional cross-section of the HX in the depth-wise direction wherein all end effects are negligible and the working fluid is dry air. In the near-wall region, an inflation layer mesh is employed with a growth ratio of 1.2 to more accurately capture the boundary layer physics. The core mesh is a pave mesh scheme where the average element size is equal to the last row of the inflation layer.

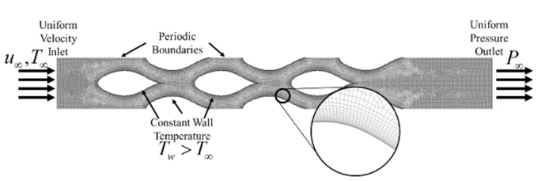

Fig. 4 – Sample CFD domain, mesh, & boundary conditions.

The left boundary is a uniform velocity and temperature inlet, and the right boundary is a uniform atmospheric pressure outlet. The tube walls are fixed to a constant temperature, and periodic boundaries are applied at the upper and lower domain boundaries. The dry air thermophysical properties are computed using polynomial curve fits as a function of temperature, while the density is computed using the ideal gas law. The realizable k-ε (RKE) model [30] is utilized to model turbulence. The convergence criteria utilized is maximum residuals, and the limits are set to 1E-05 for continuity and momentum, 1E-06 for energy, and 1E-03 for turbulence. If these convergence criteria are not met, but the simulation stabilizes to a solution, the simulation is considered converged if the standard deviation of the final 100 iterations is less than 0.5% of the average of those same 100 iterations.

The CFD simulations are utilized to determine the airside thermal-hydraulic performance only, and thus the wall and refrigerant thermal resistances can be neglected. This allows for the airside heat transfer coefficient to be easily computed using UA-Log Mean Temperature Difference (UA-LMTD) method as given in equation (1) [31], while the airside pressure drop is computed as the difference between the inlet and outlet static pressures as given in equation (2).

$$h_{air} = \frac{\dot{m}c_p}{A_w} \cdot \ln\left[\frac{T_w - T_{in}}{T_w - T_{out}}\right] \tag{1}$$

$$\Delta P_{air} = P_{in} - P_{out} \tag{2}$$

The CFD modelling grid resolution uncertainty is quantified using the Grid Convergence Index (GCI) method [32-35] for all boundary designs using three grid resolutions and a constant refinement ratio of 1.3. The GCI for a given design is computed using the absolute relative difference for a metric of interest (in this case, h_{air} and ΔP_{air}) between two consecutive grid sizes [34-35]. All CFD uncertainty quantification results are tabulated in Table 1.

Tab. 1 – CFD uncertainty quantification using GCI.

Metric	h_{air}	ΔP_{air}
Designs with GCI ≤ 10%	96%	91%
Max	16.5%	54.6%
Average	0.9%	1.25
Median	2.0%	3.3%

2.5 Metamodeling

If a new CFD simulation were required for each individual generated by the optimizer during a single optimization run, tens of thousands of CFD simulations would be required. To reduce this computational burden, this research employs approximation-assisted optimization [20], wherein a simplified model, sometimes called a metamodel, which is capable of accurately representing the simulation behaviour is utilized to carry out the optimization. In this case, metamodels are utilized to

quickly and efficiently compute the airside thermal-hydraulic performance.

A 5000-sample Design of Experiments (DoE) generated using Latin Hypercube Sampling (LHS) [36] was simulated using PPFSA, and Kriging metamodels [22] were built using 2673 converged samples. The metamodels were then verified by comparing the predicted (metamodel) responses to simulated (CFD) responses for 544 converged random samples. The Metamodel Acceptance Score (MAS) [37] was utilized to quantify the metamodel accuracy. The MAS gives the percentage of predicted responses whose absolute relative error compared to the simulated response is less than a prescribed threshold. The metamodel verification results are summarized in Table 2 and Figure 5.

Tab. 2 – Metamodel verification statistics.

Metric	h_{air}	ΔP_{air}
Mean Absolute Error	6.30	14.27
Root Mean Square Error	13.51	41.70
MAS (10%)	97.97%	70.95%
MAS (20%)	99.26%	90.99%

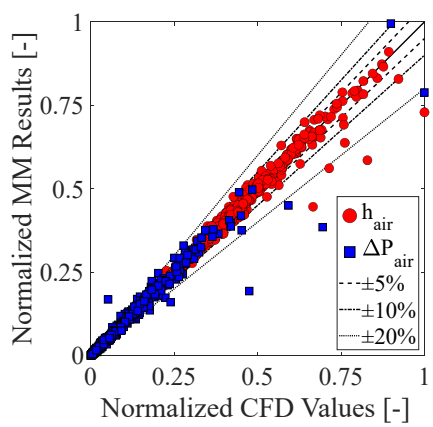

Fig. 5 – Metamodel verification results.

2.6 Multi-Objective Optimization

This research presents the application of a multi-scale and multi-physics analysis with shape and topology optimization methodology [2,7,10-11] which leverages a Multi-Objective Genetic Algorithm (MOGA) [23] to model full HXs with novel tube shapes and topologies. Full HX models are built and simulated using an in-house, experimentally-validated air-to-refrigerant HX modelling tool [39]. CFD-based metamodels are utilized to predict the airside thermal-hydraulic performance (h_{air}, ΔP_{air}). Refrigerant-side thermal-hydraulic performance is evaluated using empirical correlations for single-phase flow and (condensing) two-phase flow in small channels (Tab. 3). Refrigerant thermodynamic property calculations utilize NIST REFPROP v10.0 [39] augmented with polynomial curve fits as proposed by Aute and Radermacher [40].

Tab. 3 – Thermal-hydraulic performance correlations.

Operating Mode	h_{ref} Correlation	ΔP_{ref} Correlation
Air	CFD Metamodels	
Liquid refrigerant	Gnielinski (1976) [41]	Churchill (1977) [42]
Two-phase refrigerant	Shah (2019) [43]	Xu-Fang (2013) [44]
Vapor refrigerant	Gnielinski (1976) [41]	Churchill (1977) [42]

3. Optimization Results & Discussion

3.1 Optimization Problem Formulation

This research considers a bi-objective optimization problem as defined in equation (3) where the objectives are to minimize airside pressure drop and HX core envelope volume. The overall objective is to design air-to-refrigerant condensers featuring the novel non-round tube shape which was conventionally manufactured in copper as discussed above [25, 27] for three different refrigerants: (i) R410A, (ii) R32, and (iii) R454B. For each refrigerant, the inlet air (temperature, volume flow rate) and refrigerant states (temperature, pressure, mass flow rate) are fixed to that of commercially-available residential units with nominal 5.28 kW (1.5-Ton) capacity [25].

$$\begin{gathered} \min \Delta P_{air}, V_{HX} \\ \text{s.t.} \\ \Delta P_{air} \le 2.0 \cdot \Delta P_{air,BL} \qquad V_{HX} \le V_{HX,BL} \\ 0.5 \le H_{HX}/L_{HX} \le 2.0 \qquad A_f \le A_{f,BL} \\ \Delta T_{SC,BL} - 1.0\,\text{K} \le \Delta T_{SC} \le \Delta T_{SC,BL} \end{gathered} \tag{3}$$

All optimal HXs have a 60%/40% two-fluid-pass configuration, i.e., the first fluid pass contains 60% of the tubes, and the second fluid pass contains the remaining tubes. The airside pressure drop cannot exceed two times the baseline value, and the HX frontal area cannot exceed the baseline value. Moreover, the HX frontal aspect ratio (height-to-length ratio) is constrained such that the HX is no more than two times as tall as it is long or vice versa. The HX capacity constraint is considered by constraining the condenser outlet subcooling to be at least the same, but no more than 1.0 K more, compared to the baseline value. Note that the problem statement is sufficiently general, and it is possible to find additional promising designs by examining other pass configurations and removing the HX face area constraint. In total, five (5) design variables are considered: tube horizontal spacing, tube vertical spacing, number of tube banks, number of tubes per bank, and inlet air velocity.

Five separate optimization runs are conducted for each refrigerant (R410A, R32, & R454B). The optimal designs presented in the following sections are the

non-dominated set of designs found by combining the output from all optimization runs (for each refrigerant separately) and conducting non-dominated sorting to find the best designs for each refrigerant respectively. Additional MOGA settings are summarized in Table 4.

Tab. 4 – MOGA settings.

Type	Unit	Value
Optimization runs per refrigerant	-	5
Population size	-	50
Replacement	%	20
Iterations	-	300

3.2 Optimization Results

Figures 6 – 8 present a summary of the optimization results coloured by HX face area (Fig. 6), core material volume (Fig. 7), and core internal volume (Fig. 8). All metrics are normalized with respect to the baseline, and the dashed lines represent the 20%-20% improvement region for each objective. For the baseline airside pressure drop, the optimal designs for each refrigerant can achieve ~46% reduction in HX core envelope volume, ~30% reduction in HX face area, ~7% in tube material volume, and ~50% reduction in tube internal volume. For the baseline HX core envelope volume, the optimal designs for each refrigerant can achieve ~46% reduction in airside pressure drop, ~9% reduction in HX face area, and ~20% reduction in tube internal volume. However, for those designs, the tube material volume is ~27% greater than the baseline, which would result in significantly higher manufacturing costs. From an environmental standpoint, the significant tube internal volume reductions will correspond to significant charge reductions and thus lower the overall environmental impact, while the significant face area reductions are highly advantageous to HX manufacturers since face area is directly related to system footprint [25]. These results clearly emphasize that by using systematic optimization, we can arrive at highly compact and lighter HX designs for any of the new lower-GWP replacement refrigerants.

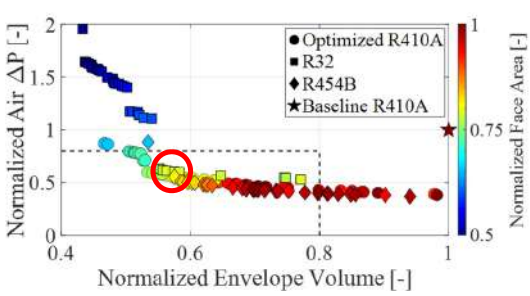

Fig. 6 – Optimization results (Colour: face area).

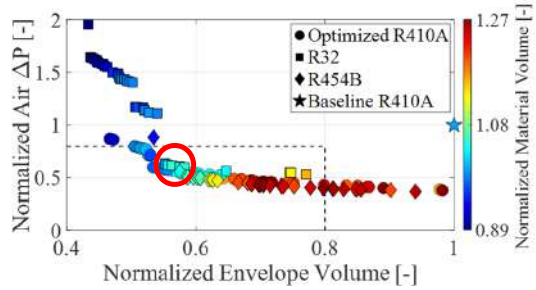

Fig. 7 – Optimization results (Colour: material volume).

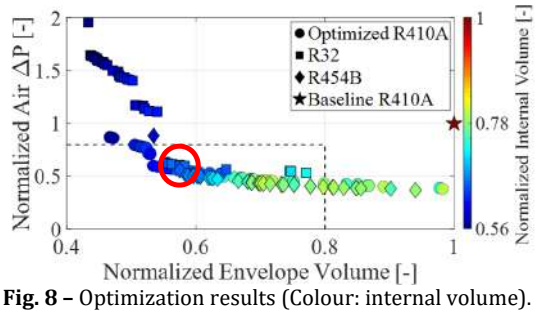

Fig. 8 – Optimization results (Colour: internal volume).

3.3 Comparison of Optimal Designs for each Refrigerant

It is of interest to directly compare the optimal HX designs from each refrigerant case to one another to gain valuable insights into whether, and if so, to what extent, the refrigerant's unique thermophysical properties impact the final HX designs. First, consider the entire set of optimal designs for each refrigerant as a whole. The similarities and differences in across the optimal designs are listed below:

- All HXs have very similar tube pitches and numbers of tube banks, resulting in all HXs having similar airside pressure drops and HX core depths.
  - All R410A and R454B HXs have 4 tubes banks.
  - Most R32 HXs have 5 tube banks, the rest have 4 tube banks.
- On average, R32 HXs have the fewest tubes per bank, while R454B HXs have the most.
  - This could be the result of R32 HXs having more tube banks, which then requires fewer tubes per bank to achieve the desired capacity.
  - Fewer tubes per bank reduces the HX core height, resulting in the R32 HXs having the smallest face areas. Because the air volume flow rate is fixed, the R32 HXs have large inlet air velocities, which could lead to undesirable fan noise / tube aeroacoustics challenges.

Next, we consider three HX designs (one design per refrigerant) as highlighted with red circles in Figures 6 – 8. Note that these HXs were chosen since they are all close together in the objective space (~40% reductions in both HX core envelope volume and

airside pressure drop). The normalized values of different performance metrics for these HXs are highlighted in Table 5, and additional normalized values of HX geometry are listed in Table 6. As mentioned above, all HXs have the same tube shape and similar tube pitches, and thus these values are not listed.

Tab. 5 – Comparison of normalized performance metrics for three optimal HX designs. All values are normalized with respect to the baseline R410A HX.

Fluid	V_{HX}	ΔP_{air}	A_f	V_{Mat}	V_{Int}	Charge
R410A	0.58	0.56	0.81	1.04	0.65	0.63
R32	0.57	0.60	0.79	1.03	0.65	0.52
R454B	0.58	0.56	0.81	1.04	0.65	0.55

Tab. 6 – Comparison of normalized HX geometry values for three optimal HX designs. All values are normalized with respect to the optimal R410A HX.

Fluid	*Number of tube banks*	*Number of tubes per bank*	H_{HX}	L_{HX}
R410A	1.0	1.0	1.0	1.0
R32	1.0	0.73	0.71	1.36
R454B	1.0	0.97	0.97	1.04

It is clear from Tables 5 and 6 that, while the HXs have very similar performance metrics, the HXs themselves are quite different. First and foremost, the R32 and R454B HXs have 15-20% lower refrigerant charge compared to the R410A HX, which is especially advantageous given that R32 and R454B are mildly flammable refrigerants. Additionally, as noted above, the R32 HX has much fewer tubes per bank, but this is compensated by having ~36% longer tubes compared to the R410A HX, while the R454B HX is almost identical to the R410A HX. Looking from a strictly HX standpoint, i.e., assuming that all other system components (e.g., compressor, flammability considerations, etc.) are changed to enable the use of R32 and R454B, the following conclusions can be drawn:

- R32 should not be used as a direct drop-in replacement to R410A HXs. Instead, HX optimization should be done specifically for R32.
- R454B could serve as a near drop-in replacement to R410A in HXs originally designed for R410A.
    - Soft optimization methods (component selection, operating condition tuning, etc.) could be sufficient to efficiently transition R410A HXs to R454B.

4. Conclusions

This paper presents the application of a multi-scale, multi-physics analysis and tube shape and topology optimization methodology, which is utilized to design residential A/C unit condensers for three different refrigerants: (i) R410A and two lower-GWP alternatives (ii) R32, and (iii) R454B. The novel, non-round, shape-optimized tube geometry considered herein has been conventionally manufactured. The optimal HX designs deliver the same capacity as a state-of-the-art baseline tube-fin condenser while achieving at least 20% reductions in airside pressure drop and envelope volume, up to 11% reduction in tube material volume, and more than 40% reduction in tube internal volume, thus showcasing the viability of tube shape and topology optimization for the design of HXs using alternative refrigerants. Detailed comparisons of optimal HXs designs for each refrigerant were also presented, and it was found that the R32 HX geometries showed many differences compared to the R410A HXs, while the R454B and R410A HX geometries were largely similar. This suggests that when considering R32 to replace R410A, separate HX optimization studies may be required to ensure that the HXs are delivering the desired performance. On the other hand, R454B could serve as a near drop-in replacement in HXs originally designed for R410A so long as appropriate soft-optimization techniques such as component selection and operating condition tuning are also considered. In summary, this study highlights how systematic optimization can result in highly compact and lighter HX designs for any of the new lower-GWP replacement refrigerants.

5. Nomenclature

A_f	[m^2]	HX face area
c_p	[Jkg^{-1}K^{-1}]	Specific heat
GCI	[-]	Grid convergence index
GWP	[-]	Global warming potential
h	[Wm^{-2}K^{-1}]	Heat transfer coefficient
H_{HX}	[m]	HX core height
L_{HX}	[m]	HX core length
$\dot{m}$	[kgs^{-1}]	Mass flow rate
P	[Pa]	Pressure
T	[K]	Temperature
u	[ms^{-1}]	Fluid velocity
$\dot{V}$	[m^{3}s^{-1}]	Volumetric flow rate
V	[m^3]	Volume
ΔP	[Pa]	Pressure drop
ΔT_{SC}	[K]	Refrigerant subcooling
Subscripts		
air		Air
BL		Baseline
HX		Heat exchanger
in		Inlet
int		Internal
mat		Material
out		Outlet
ref		Refrigerant
w		Wall

6. Acknowledgement

This material is based upon work supported by the U.S. Department of Energy's Office of Energy Efficiency and Renewable Energy under the Building Technologies Office Award Number DE-EE0008221. The views expressed herein do not necessarily represent the views of the U.S. Department of Energy or the United States Government. This work was also supported in part by the Modeling & Optimization

Consortium at the Center for Environmental Energy Engineering at the University of Maryland.

7. Data Access Statement

The datasets generated during and/or analysed during the current study are not publicly available due to the on-going nature of the research project, but the authors will make every reasonable effort to publish them in near future upon project completion.

8. References

[1] Kays, W. & London, A., Compact Heat Exchangers, 1984; McGraw-Hill, New York.

[2] Bacellar, D., Aute, V., Huang, Z., & Radermacher, R. Design optimization and validation of high-performance heat exchangers using approximation assisted optimization and additive manufacturing. Science & Technology for the Built Environment, 2017; 23(6): 896-911.

[3] Paitoonsurikarn, S., Kasagi, N., & Suzuki Y. Optimal design of micro bare-tube heat exchanger. Symposium on Energy Engineering, 2000; 972–979: Hong Kong, China.

[4] Saji, N., Nagai, S., Tsuchiya, K., Asakura, H., & Obata, M, Development of a compact laminar flow heat exchanger with stainless steel micro-tubes. Physica C, 2001; 354(1-4): 148-151.

[5] Kasagi, N., Suzuki, Y., Shikazono, N., & Oku, T. Optimal design and assessment of high performance micro bare-tube heat exchangers. 4th International Conference Compact Heat Exchangers and Enhancement Technologies for the Process Industries, 2003; 241-246: Crete, Greece.

[6] Chen, H.T., Lin, Y.S., Chen, P. C., & Chang, J.R. Numerical and experimental study of natural convection heat transfer characteristics for vertical plate fin and tube heat exchangers with various tube diameters. International Journal of Heat & Mass Transfer, 2016; 100: 320-331.

[7] Bacellar, D., Huang, Z., Tancabel, J., Aute, V., & Radermacher, R. Multi-scale analysis, shape optimization and experimental validation of novel air-to-refrigerant heat exchangers, 9th World Conference on Experimental Heat Transfer, Fluid Mechanics, and Thermodynamics, 2017; Iguazu Falls, Brazil.

[8] Radermacher, R., Bacellar, D., Aute, V., Huang, Z., Hwang, Y., Ling, J., Muehlbauer, J., Tancabel, J., Abdelaziz, O., & Zhang, M. Miniaturized Air-to-Refrigerant Heat Exchangers, 2017; United States Department of Energy Report for Project Award DE-EE0006114.

[9] Tancabel, J., Aute, V., & Radermacher, R. Review of Shape and Topology Optimization for Design of Air-to- Refrigerant Heat Exchangers. 17th International Refrigeration and Air Conditioning Conference, Purdue University, 2018; Paper 1965: West Lafayette, Indiana, USA.

[10] Tancabel, J., Aute, V., Ling, J., & Radermacher, R. Multi-scale and multi-physics analysis of novel high performance, reduced charge evaporators with novel tube shapes. 9th International Conference on Compressor and Refrigeration, 2019; Xi'an, China.

[11] Tancabel, J., Aute, V., Ling, J., & Radermacher, R. Design optimization of high performance, reduced charge condensers with novel tube shapes. 25th International Congress of Refrigeration, 2019; Montreal, Quebec, Canada.

[12] Li, H. By, R. System Soft-Optimization Tests of Refrigerant R-32 in a 3-ton Split System Air-Conditioner. Air-Conditioning, Heating, and Refrigeration Institute (AHRI) Low-GWP Alternative Refrigerants Evaluation Program (Low-GWP AREP) Test Report #32; 2015.

[13] Alabdulkarem, A., Eldeeb, R., Hwang, Y., Aute, V., & Radermacher, R. Testing, simulation and soft-optimization of R410A low-GWP alternatives in heat pump system. International Journal of Refrigeration, 2015; 60: 106-117.

[14] Mota-Babiloni, A., Navarro-Esbrí, J., Makhnatch, P., & Molés, F. Refrigerant R32 as lower GWP working fluid in residential air conditioning systems in Europe and the USA. Renewable and Sustainable Energy Reviews, 2017; 80: 1031-1042.

[15] Heredia-Aricapa, Y., Belman-Flores, J.M., Mota-Babiloni, A., Serrano-Arellano, J., & García-Pabón, J.J. Overview of low GWP mixtures for the replacement of HFC refrigerants: R134a, R404A and R410A. International Journal of Refrigeration, 2020; 111: 113-123.

[16] Nair, V. HFO refrigerants: A review of present status and future prospects. International Journal of Refrigeration, 2021; 122: 156-170.

[17] Panato, V.H., Pico, D.F.M., & Bandarra Filho, E.P. Experimental evaluation of R32, R452B and R454B as alternative refrigerants for R410A in a refrigeration system. *International Journal of Refrigeration*, 2021.

[18] Shen, B., Li, Z., & Gluesenkamp, K.R. Experimental study of R452B and R454B as drop-in replacement for R410A in split heat pumps having tube-fin and microchannel heat exchangers. *Applied Thermal Engineering*, 2021; 204: 117930.

[19] Sieres, J., Ortega, I., Cerdeira, F., & Álvarez, E. Drop-in performance of the low-GWP alternative refrigerants R452B and R454B in an R410A liquid-to-water heat pump. *Applied Thermal Engineering*, 2021; *182*: 116049.

[20] Simpson, T. W., Poplinski, J. D., Koch, P. N., & Allen, J. K. Metamodels for computer-based engineering design: survey and recommendations. Engineering with computers, 2001;17(2): 129-150.

[21] Abdelaziz, O., Aute, V., Azarm, S., & Radermacher, R., Approximation-assisted optimization for novel compact heat exchanger designs, HVAC&R Research 2010; 16(5): 707-728.

[22] Cressie, N., Statistics for Spatial Data, 1993; John Wiley & Sons, New York.

[23] Deb, K. Multi-objective Optimization using Evolutionary Algorithms, 2001; John Wiley & Sons, New York.

[24] Tancabel, J., Aute, V., & Ling, J. Optimization of R290 Heat Exchangers using High-Performance, Non-round Tubes. 14th IIR-Gustav Lorentzen Conference on Natural Refrigerants; 2020.

[25] Private communications, 2019.

[26] Tiller, P.L., The NURBS Book. 1995; Springer, New York.

[27] Radermacher, R. Design and Manufacturing of High Performance, Reduced Charge Heat Exchangers (HPRC-HX), 2019; United States Department of Energy BTO Peer Review.

[28] ANSYS, Inc. Ansys® GAMBIT, Release 2.4.6, 2018.

[29] ANSYS, Inc. Ansys® Academic Research Fluent, Release 18.0, 2018.

[30] Shih, T.H., Zhu, J., & Lumley, J.L., A new Reynolds stress algebraic equation model, Computer Methods in Applied Mechanics and Engineering, 1995; 125(1-4): 287-302.

[31] Bergman, T.L., Incropera, F.P., DeWitt, D.P., & Lavine, A.S. Fundamentals of Heat and Mass Transfer – 7th Edition. 2011; John Wiley & Sons: Hoboken, NJ.

[32] Roache, P.J., Quantification of Uncertainty in Computational Fluid Dynamics, Annual Review of Fluid Mechanics, 1997; 29(1): 123-160.

[33] ASME, Standard for Verification and Validation in Computational Fluid Dynamics and Heat Transfer, ASME V&V 20-2009, 2009; American Society of Mechanical Engineers: New York, New York, USA.

[34] Oberkampf, W., Roy, C., Verification and Validation in Scientific Computing, 2010; Cambridge University Press, Cambridge, UK.

[35] Roy, C., Oberkampf, W., A Comprehensive Framework for Verification, Validation, and Uncertainty Quantification in Scientific Computing. Computer Methods in Applied Mechanics and Engineering. 2011; 200(25): 2131–2144.

[36] McKay, M.D., Beckman, R.J., & Conover, W.J., Comparison of Three Methods for Selecting Values of Input Variables in the Analysis of Output from a Computer Code, Technometrics, 1979; 21(2): 239-245.

[37] Hamad, H., A New Metric for Measuring Metamodels Quality-of-Fit for Deterministic Simulations. 38th conference on Winter Simulation, 2006; 882-888: Monterey, California, USA.

[38] Jiang, H., Aute, V., & Radermacher, R., CoilDesigner: A General Purpose Simulation and Design Tool for Air-to-Refrigerant Heat Exchangers, International Journal of Heat and Mass Transfer, 2006; 29(4): 601-610.

[39] Lemmon, E.W., Bell, I.H., Huber, M.L., & McLinden, M.O. NIST Standard Reference Database 23: Reference Fluid Thermodynamic and Transport Properties-REFPROP, Version 10.0, 2018; National Institute of Standards and Technology, Standard Reference Data Program, Gaithersburg, MD.

[40] Aute, V. and Radermacher, R. Standardized polynomials for fast evaluation of refrigerant thermophysical properties. 15th International Refrigeration and Air Conditioning Conference, Purdue University, 2014; Paper 1499: West Lafayette, Indiana, USA.

[41] Gnielinski, V. New equations for heat and mass transfer in turbulent pipe and channel flow. International Chemical Engineering, 1976;16(2): 359-368.

[42] Churchill, S.W. Friction-factor equation spans all fluid-flow regimes. Chemical Engineering, 1977: 91–92.

[43] Shah, M.M. Improved correlation for heat transfer during condensation in conventional and mini/micro channels. International Journal of Refrigeration, 2019; 98: 222-237.

[44] Xu, Y. and Fang, X. A new correlation of two-phase frictional pressure drop for condensing flow in pipes. Nuclear Engineering and Design, 2013; 263: 87-96.

Parameter analysis of air-conditioning systems for high-tech cleanrooms considering climate impact

Wenxuan Zhao [a], *Hangxin Li* [a, b], *Shengwei Wang* [a, b]

[a] Department of Building Services Engineering, The Hong Kong Polytechnic University, Kowloon, Hong Kong

[b] Research Institute for Smart Energy, The Hong Kong Polytechnic University, Kowloon, Hong Kong

Abstract. The air-conditioning systems for high-tech cleanrooms are usually energy-intensive, due to strict temperature, humidity and particle concentration requirements. Their system performance strongly depends on the operation parameters and climate/weather conditions. But few studies have investigated such impacts for high-tech cleanrooms. Therefore, this study has quantified the impacts of operating parameters on the performance of high-tech cleanroom air-conditioning systems under different climate conditions via parametric and sensitivity analysis. A typical high-tech cleanroom located in Chinese five climate zones is selected to examine each parameter's impact using Energyplus/Matlab platform. Results indicate that the system annual energy consumption shows nearly linear changing trends when varying the operation parameters. The outdoor air exchange rate and MAU (make-up air handling unit) outlet air temperature are the most sensitive parameters in cold zones. The studied results can help practitioners improve air-conditioning system design and operational performance for high-tech cleanrooms through carefully determining parameters with heavy impacts.

Keywords. High-tech cleanroom, Air-conditioning system, Energy performance, Climate impact, Parameter sensitivity
DOI: https://doi.org/10.34641/clima.2022.281

1. Introduction

High-tech cleanrooms have been growing very fast in terms of the total floor area and production quantity. It has large applications in today's industrial manufacturing, i.e., semiconductor manufacturing, TFT-LCD (thin-film transistor liquid-crystal display) panel manufacturing, microelectronics aerospace and other electronics. Such highly skilled and technology-intensive fabs basically require ultra-clean environment, which are highly energy-intensive [1]. The annual electricity consumption of a typical semiconductor fab is as high as 20,908 kWh/m^2 [2], which is around three times the average consumption of data centers worldwide [3] and even 100 times that of public buildings [4].

As the primary facility system to provide the novel production environment for manufacturing processes, the air-conditioning systems are also energy-intensive, which account for 30–35% of the total energy use in a high-tech industry [1, 2, 5, 6]. The main reasons are as follows. (***i***) High-tech cleanrooms need extensive supply air exchange rate to maintain the clean environment for high-precision manufacturing. (***ii***) High-tech cleanrooms need large outdoor air exchange rate to compensate for the large exhaust air generated from the manufacturing. (***iii***) The machines/equipment in the high-tech cleanrooms generate a great amount of heat. Therefore, the energy performance of such energy-intensive applications strongly depends on the operation parameters (e.g. supply and outdoor air exchange rate). Improper determination of these operation parameters often occurs that much energy has been wasted [7].

There are a few publications that have investigated the impacts of various operation parameters on the performance of high-tech cleanroom air-conditioning systems. Hu et al. [8] investigated the energy consumption of a Taiwanese semiconductor manufacturing fab, and indicated that lowering the dry-bulb temperature of the MAU (make-up air handling unit)-supplied air from 14°C to 11°C could result in 8.63% energy savings. Hu et al. [9] further quantified the corresponding reduced energy of 5.82% by reducing the MAU exit temperature of 1°C interval. Chang et al. [10] discussed the impacts of cleanroom dry bulb temperature and relative humidity setpoints, supply air volume flowrate and MAU exit temperature on the annual power consumption for a TFT-LCD fab by adjusting their values. The above researches focused on identifying the possible reduced energy use when changing the operation parameters (i.e. MAU exit temperature, supply air volume). The impacts of other important

Copyright ©2022 by the authors. This conference paper is published under a CC-BY-4.0 license.

parameters, such as indoor cooling load, outdoor air volume, are still not clear. Meanwhile, very few studies are found concerning the parameter sensitivity analysis in air-conditioning system designs of high-tech cleanrooms considering the climate variety.

Therefore, this study conducts the parametric and sensitivity analysis to systematically investigate the impacts of key operation parameters on the energy performance of air-conditioning systems for high-tech cleanrooms under the full range of climate conditions. The climate-dependent sensitivity of each operation parameter on system performance is also identified and analyzed. This study aims to provide valuable information for parameter determination with expected energy savings, for high-tech cleanroom air-conditioning systems.

2. Methods

2.1 A typical high-tech cleanroom air-conditioning system and key operation parameters

A typical high-tech cleanroom air-conditioning system, i.e., MAU+DCC (dry cooling coil) +FFU (fan filter unit) system, is selected for parameter and sensitivity analysis. The MAU+DCC+FFU system is the most updated and commonly-used air-conditioning system for high-tech cleanrooms today [11, 12]. Its system configuration and year-round operating principle are shown in Fig. 1. The air-conditioning system provides constant supply and outdoor airflow rates to guarantee strict space temperature, relative humidity, cleanliness, static pressure controls. Specifically, the MAU and DCC separately condition outdoor air and return air, respectively, to fully-decoupled control the space relative humidity and dry-bulb temperature. The FFU cycles and delivers the supply air via the orifice plate air supply outlet facilitated with HEPAs (high-efficiency particulate air filter), to the high-tech cleanroom space.

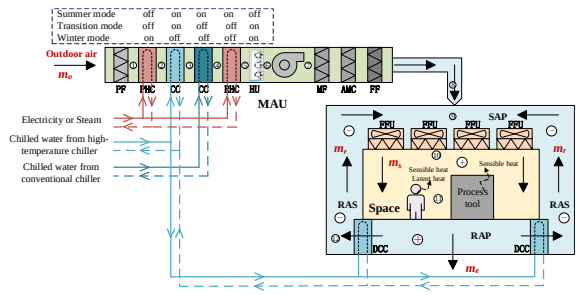

(a) system configuration

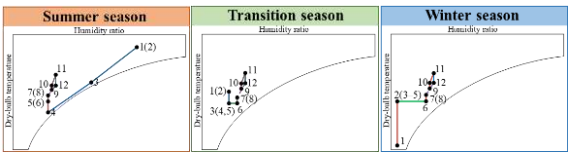

(b) operating principle

Fig. 1 - A typical air-conditioning system for the high-tech cleanroom.

Five key operation parameters are selected to evaluate their impacts, i.e., indoor design condition (t_i, w_i), indoor cooling load index (Q_{tot}), supply and outdoor air exchange rates (A_s, A_o), MAU outlet air temperature (t_{MAU}). Because they significantly influence the energy performance of high-tech cleanrooms, and they are primarily determined during the design stage and easy to adjust during the operation stage without any extra expenditure.

2.2 System energy model

Assuming that the indoor temperature and relative humidity in the high-tech cleanroom are perfectly controlled at the indoor design condition (t_i, w_i), its annual cooling load profile (Q_{tot}, W_{lat}) can be calculated by Energyplus. The required supply air (h_s, t_s, w_s) and outdoor air (w_{ro}) states for offsetting the indoor total and latent cooling loads (Q_{tot}, W_{lat}) are first determined based on the heat and mass balance equations of cleanroom (Eqs. (1–4)). Then the operating mode is identified by comparing the outdoor air condition with the required state (w_{ro}). The loads of cooling coils ($Q_{fc,MAU}$, $Q_{sc,MAU}$, Q_{DCC}), heating coils ($Q_{he,MAU}$) and humidifiers ($Q_{hu,MAU}$) can be thus calculated using Eqs. (5–9). Finally, the total energy consumption, including electricity for chillers (E_c) and fans (E_f), and electricity or steam for heaters (E_{he}) and humidifiers (E_{hu}), can be computed and converted to the primary energy using Eqs. (10–12). The overall coefficients of performance (COPs) of the cooling systems (conventional: COP_{cc}, high-temperature: COP_{hc}) vary with the wet-bulb temperature of outdoor air [13-15]. The above system energy model is developed in the Matlab platform after validation.

$$h_s = h_i - \frac{Q_{tot}}{m_s} \tag{1}$$

$$w_s = w_i - \frac{W_{lat}}{m_s} \tag{2}$$

$$t_s = \frac{h_s - 2501 w_s}{1.006 + 1.86 w_s} \tag{3}$$

$$w_{ro} = w_i - \frac{W_{lat}}{m_o} \tag{4}$$

$$Q_{fc,MAU} = \begin{cases} m_o(h_1 - h_3), & w_o > w_{fc} \\ 0, & w_{ro} < w_o \le w_{fc} \\ 0, & w_o \le w_{ro}, t_o < t_{MAU} \\ m_o(h_1 - h_3), & w_o \le w_{ro}, t_o \ge t_{MAU} \end{cases} \tag{5}$$

$$Q_{sc,MAU} = \begin{cases} m_o(h_3 - h_4), & w_o > w_{fc} \\ m_o(h_1 - h_4), & w_{ro} < w_o \le w_{fc} \\ 0, & w_o \le w_{ro} \end{cases} \tag{6}$$

$$Q_{DCC} = m_r(h_{11} - h_{12}) \tag{7}$$

$$Q_{he,MAU} = \begin{cases} m_o(h_5 - h_4), & w_o > w_{ro} \\ m_o(h_2 - h_1), & w_o \le w_{ro}, t_o < t_{MAU} \\ 0, & w_o \le w_{ro}, t_o \ge t_{MAU} \end{cases} \tag{8}$$

$$Q_{hu,MAU} = \begin{cases} 0, & w_o > w_{ro} \\ m_o h_{fg}(w_6 - w_5), & w_o \le w_{ro} \end{cases} \tag{9}$$

$$\begin{aligned} E_{tot} &= E_c + E_{he} + E_{hu} + E_f \\ &= \frac{Q_{fc,MAU} + Q_{DCC}}{COP_{hc}\eta_p} + \frac{Q_{sc,MAU}}{COP_{cc}\eta_p} + \frac{Q_{he,MAU}}{\eta_s} \\ &\quad + \frac{Q_{hu,MAU}}{\eta_s} + \frac{W_{f,MAU}}{\eta_p} + \frac{W_{f,FFU}}{\eta_p} \end{aligned} \tag{10}$$

$$W_{f,MAU} = \frac{V_o \Delta P_{MAU}}{\eta_1 \eta_2} \tag{11}$$

$$W_{f,FFU} = \frac{V_s \Delta P_{FFU}}{\eta_1 \eta_2} \quad (12)$$

2.3 Climate/weather conditions

As China has a vast territory and climates show large diversities in different geographical regions, its typical climatic locations are selected in this study to assess the parameter impacts for high-tech cleanroom air-conditioning systems. Five typical cities, i.e., Harbin, Beijing, Shanghai, Guangzhou and Kunming in the five climate zones, i.e., severe cold, cold, hot summer cold winter, hot summer warm winter, as well as mild zones, are selected to locate the high-tech cleanroom [16]. The Typical Meteorological Year [17] weather conditions of each city are used to identify the operation mode and calculate the load and energy consumption of the air-conditioning system.

2.4 Sensitivity quantification

The sensitivity of each parameter is quantified and evaluated by the sensitivity factor *S(x)*, as shown in Eqs. (13).

$$S(x) = \frac{\Delta E_{tot}(x_r + \Delta x) - E_{tot}(x_r)}{E_{tot}(x_r)} \Big/ \frac{\Delta x}{x_r} \quad (13)$$

Where, *S(x)* is the sensitivity factor; x_r is the reference value of a certain parameter; Δx is the change of the parameter. A larger absolute value of *S(x)* represents a more sensitive relationship between the change of energy consumption and the change of parameter.

3. Results and discussions

3.1 Parameter impacts on system annual energy consumption

The individual impacts of the five key parameters (i.e., indoor design condition, indoor cooling load, supply and outdoor air exchange rates and MAU outlet air temperature) on the annual energy consumption of high-tech cleanroom air-conditioning systems are illustrated in Fig. 2.

It can be found that the system annual energy consumption varies nearly linearly with the changes of five operation parameters in all five climate zones. Either increasing the indoor cooling load, supply/outdoor air exchange rate and MAU outlet air temperature would increase the system annual energy consumption. However, the energy increasing rates are different when increasing the operation parameters in different climate zones. (***i***) As the indoor cooling load increases by 100W/m^2, the hot zones increase more annual energy consumption of 1.06 and 1.30GJ/m^2, compared with the cold zones and mild zone of 0.74, 0.87, and 0.98GJ/m^2, respectively. This is because the increment of indoor cooling load can be partially removed by the cold outdoor air in cold climates. (***ii***) As the outdoor air exchange rate increases by 1h^{-1}, the cold zones increase more annual energy consumption of 1.32 and 1.03GJ/m^2, compared with the hot zones and mild zone increase by 0.84, 0.88 and 0.63GJ/m^2, respectively. This is because more outdoor airflow rate requires more preheating energy demands in cold climates, which is larger than the increased outdoor air dehumidification demands in hot and mild climates. (***iii***) However, as the supply air exchange rate increases by 10h^{-1}, the five zones increase nearly the same annual energy consumption of 0.63, 0.64, 0.66, 0.67 and 0.65GJ/m^2, respectively. This is because the increased energy consumption is mainly used for fan power on delivering more supply airflow rate. (***iv***) Similarly, as the MAU outlet air temperature increases by 1°C, the five zones increase nearly the same annual energy consumption of 1.01, 1.01, 1.13, 1.16 and 1.05GJ/m^2, respectively. This is because the increased energy consumption is used to preheat and reheat outdoor air. (***v***) For the indoor design condition, higher indoor requirements of temperature and humidity are good to the hot and mild zones, where the hot and humid days occupy the most of year time and less cooling and dehumidification energy consumption is needed.

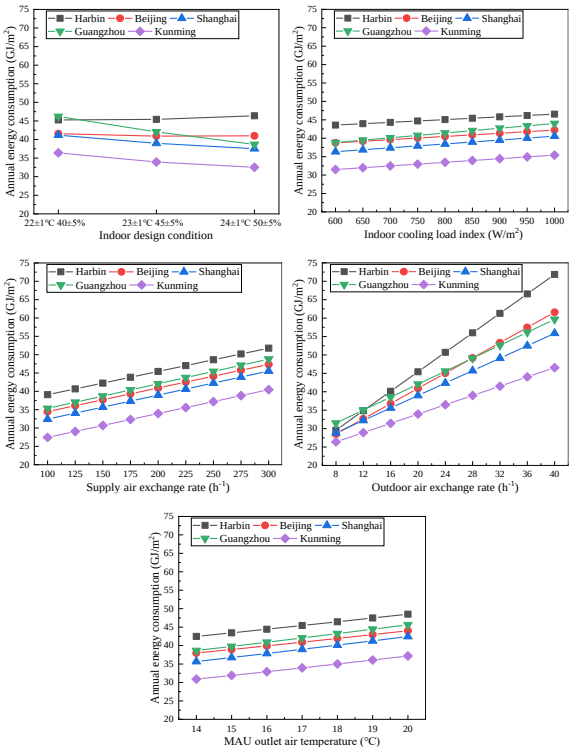

Fig. 2 - The impacts of five key operation parameters on the system annual energy consumption.

3.2 Parameter sensitivity on system annual energy consumption

In light of the impact differences of different operation parameters in the different climates, the sensitivity factors *S(x)* of five parameters in the five climate zones are shown in Fig. 3.

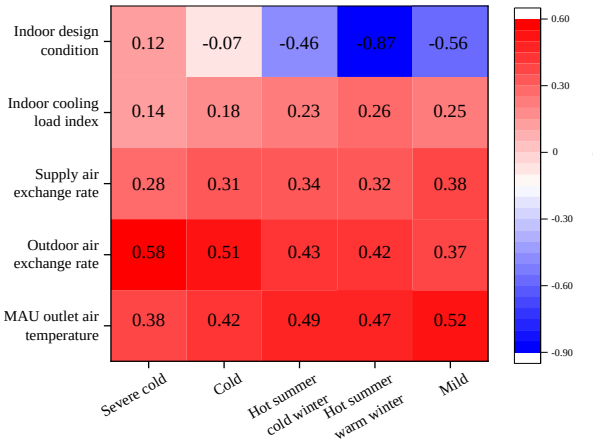

Fig. 3 - Sensitivity factors of five operation parameters under different climate zones.

For the severe cold and cold zones, the most sensitive parameter is the outdoor air exchange rate, followed by the MAU outlet air temperature. For the hot and mild zones, the most sensitive parameters are the MAU outlet air temperature and indoor design condition, followed by the outdoor air exchange rate. However, the indoor cooling load has the lowest contribution in all five climate zones. Therefore, the most energy-sensitive parameters in the specific climate zone should be well determined and adjusted during the design and operation stages, for considerable energy savings.

4. Conclusions

In this study, the quantitative impacts of operating parameters on the energy performance of high-tech cleanroom air-conditioning systems are investigated in different climates. The major conclusions are as follows.

- The annual energy consumption of high-tech cleanroom air-conditioning systems shows nearly linear changing trends when varying the operation parameters.
- As the supply air exchange rate and MAU outlet air temperature change, the energy consumption of high-tech cleanrooms in different climates changes nearly the same, i.e., 0.63–0.67GJ/m^2 per 10h^{-1} and 1.01–1.16GJ/m^2 per 1°C, respectively. However, as the indoor cooling load and outdoor air exchange rate change, the high-tech cleanrooms located in different climates show different performances.
- The outdoor air exchange rate and MAU outlet air temperature are the most sensitive parameters in cold zones, while the indoor cooling load index has the lowest contribution in all five climate zones.

5. Acknowledgment

The research work presented in this paper is financially supported by a General Research Grant (152075/19E) of the Research Grant Council (RGC) of the Hong Kong SAR.

6. Nomenclature

Abbreviations	
AMC	Airborne molecular contaminant filter
CC	Cooling coil
COP	Overall coefficient of performance of cooling system
DCC	Dry cooling coil
E	Energy consumption (kW)
FF	Final efficiency particulate air filter
FFU	Fan filter unit
HEPA	High-efficiency particulate air filter
HU	Humidifier
h	Enthalpy (kJ/kg)
MAU	Make-up air handling unit
MF	Medium efficiency particulate air filter
m	Air mass flow rate (kg/s)
PF	Primary efficiency particulate air filter
PHC	Preheating coil
Q_{tot}	Space total cooling load (kW)
RAP	Return air plenum
RAS	Return air shaft
RHC	Reheating coil
SAP	Supply air plenum
t	Temperature (°C)
W_{lat}	Space latent cooling load (kg/s)
w	Humidity ratio (kg/kg)
Greek letters	
η_p	Power generation efficiency
η_s	Steam generation efficiency
η_1	Pressure efficiency
η_2	Motor efficiency
Subscripts	
c	Cooling system
cc	Conventional cooling system
f	Fan
fc	First cooling coil
hc	High-temperature cooling system
he	Heating system
hu	Humidification system
i	Indoor air
lat	Latent
o	Outdoor air
r	Return air
s	Supply air
sc	Second cooling coil
tot	Total

7. Reference

[1] ASHRAE. ASHRAE Handbook: Heating, Ventilating, and Air-Conditioning Applications. 2019.

[2] Yin J, Liu X, Guan B, Zhang T. Performance and improvement of cleanroom environment control system related to cold-heat offset in clean semiconductor fabs. Energy and Buildings. 2020;224:110294.

[3] 2019 Green data center white paper. China Electronics Standardization Institute.
[4] 2020 Annual research report of China building energy efficiency. China Building Industry Press.
[5] Zhao Y, Li N, Tao C, Chen Q, Jiang M. A comparative study on energy performance assessment for HVAC systems in high-tech fabs. Journal of Building Engineering. 2021;39:102188.
[6] Hu SC, Tsai YW, Fu BR, Chang CK. Assessment of the SEMI energy conversion factor and its application for semiconductor and LCD fabs. Applied Thermal Engineering. 2017;121:39-47.
[7] Kircher K, Shi X, Patil S, Zhang KM. Cleanroom energy efficiency strategies: Modeling and simulation. Energy and Buildings. 2010;42:282-9.
[8] Hu SC, Lin T, Fu BR, Chang CK, Cheng IY. Analysis of energy efficiency improvement of high-tech fabrication plants. International Journal of Low-Carbon Technologies. 2019;14:508-15.
[9] Hu SC, Lin T, Huang SH, Fu BR, Hu MH. Energy savings approaches for high-tech manufacturing factories. Case Studies in Thermal Engineering. 2020;17:100569.
[10] Chang CK, Lin T, Hu SC, Fu BR, Hsu JS. Various energy-saving approaches to a TFT-LCD panel fab. Sustainability (Switzerland). 2016;8:907.
[11] Yin J, Liu X, Guan B, Ma Z, Zhang T. Performance analysis and energy saving potential of air conditioning system in semiconductor cleanrooms. Journal of Building Engineering. 2021;37:102158.
[12] Hu SC, Tsao JM. A comparative study on energy consumption for HVAC systems of high-tech FABs. Applied Thermal Engineering. 2007;27:2758-66.
[13] Lu Q. Energy saving analysis of cooling tower cooling technology in data centers. HV&AC. 2019;49:56-62.
[14] Liu J, Su L, Dong K, Liu X. Critical temperature of free cooling using indirect opening cooling tower in data centres: a review. International Journal of Ambient Energy. 2019:1694069.
[15] Zhang T, Liu XH, Li Z, Jiang J, Tong Z, Jiang Y. On-site measurement and performance optimization of the air-conditioning system for a datacenter in Beijing. Energy and Buildings. 2014;71:104-14.
[16] GB 50176-2016 Code for thermal design of civil building. Ministry of Housing and Urban-Rural Development of the People's Republic of China; 2016.
[17] Marion W, Urban K. User’s manual for TMY2s: Typical meteorological years: Derived from the 1961-1990 national solar radiation data base: National Renewable Energy Laboratory; 1995.

Optimal dispatch strategy for building aggregators to fully utilize the energy flexibilities

Hong Tang [a], Shengwei Wang [a,b]
a Department of Building Environment and Energy Engineering, The Hong Kong Polytechnic University, Hong Kong S.A.R. (China)
b Research Institute of Smart Energy, The Hong Kong Polytechnic University, Hong Kong S.A.R. (China)

Abstract. Well-managed demand-side flexibility can effectively alleviate the pressure on the reliability of the power system and the advanced development of smart grid technologies creates win-win opportunities for the power system operators and demand-side users. The building sector, as one of the largest consumers of electricity, has great flexibility potential through smart load control and natural thermal mass storage. However, few studies have investigated the potential contribution of buildings in providing multiple flexibility services without sacrificing the occupants' comforts. Another major hurdle to utilizing the building energy flexibility is that individual buildings usually cannot reach a sufficient size to bid the flexibility services in the electricity market. Therefore, this paper proposes an optimal dispatch strategy for building clusters using mixed-integer non-linear programming (MINLP) to aggregate and utilize full-scale energy flexibilities of variable controllable loads, the passive thermal mass storage and active electrical storage systems. The building cluster consisting of five commercial buildings is selected in the case study to test the proposed strategy and analyze the practical relevance based on a real-life electricity market. Results show that the proposed dispatch strategy reduces the electricity costs of the building cluster by 11.6% from multiple revenue streams, including energy arbitrage, regulation service and operating reserve service. Active electrical storage systems can increase revenues by 2.3 times and the unlocked flexibility of building thermal and lighting loads can achieve 152 $ daily revenues. This study addresses the issue that the energy flexibility of individual buildings is too small to bid flexibility services, and the findings may stimulate the investment of the distributed storage system at the aggregated level, as the building aggregator is a promising business model in future flexibility markets.

Keywords. Demand-side flexibility, building aggregator, bidding strategy, multiple flexibility services.
DOI: https://doi.org/10.34641/clima.2022.414

Abbreviations and Nomenclature.

P^E	Total purchased energy	A_{bui}	Effective building surface
π^E	Energy price	Cap_{min}	Minimum bid capacity
π^{Rs}	Reserve service price	SOC_{ES}	State of charge of the electrical storage
π^{Rg}	Regulation service price	COP	Coefficient of performance
ΔQ_{ch}	Cooling supply alteration	LO	Lowest operating limit
β_L	Acceptable level of lighting regulation	ES	Electrical storage
γ_L	Acceptable level of lighting reserve	Rev	Revenues from ancillary services
T_i	Indoor temperature	lig	Lighting system
T_o	Outdoor temperature	k	Time slot k
$R_{bui,o}$	Outer thermal mass resistance	i	Building cluster
$R_{bui,i}$	Inner thermal mass resistance		
C_{bui}	Thermal capacitance of per square		

1. Introduction

Renewable generation is increasingly integrated into the modern power system to achieve energy transitions and environmental targets (e.g., carbon neutrality), while it raises pressure on the reliability of the power grid due to the uncertain and intermittent nature of solar and wind power [1]. Well-managed demand-side flexibility can effectively alleviate the pressure and the advanced

Copyright ©2022 by the authors. This conference paper is published under a CC-BY-4.0 license.

development of smart grid technologies creates win-win opportunities for the power system operators and demand-side users. Multiple electricity services are introduced in the electricity markets for economic energy dispatch and short-term power balancing, e.g., energy arbitrage and ancillary services. The balancing services in the wholesale electricity market are gradually open to the direct demand-side participants who have great flexibility potential to provide such services. For example, the integration of electric vehicles into the grid cannot be only considered as the charging loads, but can also be the flexibility aggregator to bid the flexibility services in the electricity markets [2, 3]. Besides microgrids and virtual power plants consisting of multiple loads, storage resources and distributed generation, demand-side aggregator [4] is also an emerging business model in the market trading, which can effectively help demand-side participants avoid the spike price in the wholesale markets [5].

The building sector, as one of the largest consumers of electricity, has great flexibility potential through smart load control and natural thermal mass storage. Numerous studies have investigated the demand response potential of both individual buildings and the building clusters, on load shifting [6, 7], grid frequency regulation [8] and power reserve capacity [9]. However, few studies have investigated the potential contribution of buildings in providing multiple flexibility services and on how to optimally allocate the flexibility capacity to different flexibility services without sacrificing the occupants' comforts [10]. Moreover, in some real-life electricity markets, there usually exists the requirement of the minimum bid capacity for flexibility services. For example, the minimum bid capacity for ancillary services in PJM (Pennsylvania, New Jersey, and Maryland) and CAISO (the California Independent System Operator) markets are 100 kW and 500 kW, respectively. Individual buildings usually cannot reach a sufficient size to bid the flexibility services in the electricity market, which is the major hurdle to be overcome when utilizing the building energy flexibility. The business model "building aggregator" can effectively address this issue by aggregating a cluster of buildings and optimally dispatch their flexibility capacities.

Therefore, this paper proposes an optimal dispatch strategy for building aggregators to fully utilize the building energy flexibilities using mixed-integer non-linear programming (MINLP). The coordinated control of multiple flexibility resources, including variable controllable loads, the passive thermal mass storage and active electrical storage systems, is optimized to maximize the economic benefits of building clusters considering multiple revenue streams in the electricity markets. A case study is conducted to test the proposed strategy and analyse the practical relevance.

2. Methods

2.1 Multiple flexibility services in the electricity markets

As shown in Fig. 1, there are three stages in the planning and scheduling of the power system, including system balancing, energy-economic dispatch and capacity planning. Therefore, multiple electricity products are introduced in the electricity markets, where frequency regulation and operating reserve are two ancillary services for power balancing requiring the service provider to respond within a few seconds or minutes. Dynamic hourly and sub-hourly energy tariffs are scheduled which stimulate the market participants to optimize the energy dispatch. It is reasonable to assume that the building energy flexibilities can be transformed to bid the energy and capacity bands in joint energy and ancillary services markets, as multiple flexibility resources enable the building to respond at different time scales. In this paper, the day-ahead joint market referring to CAISO (the California Independent System Operator) is considered where energy trading and ancillary services are co-optimized at the same time.

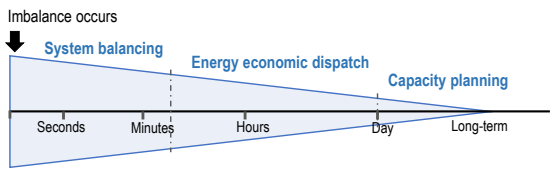

Fig. 1 - Three stages of power system planning and scheduling.

2.2 Bi-level optimal dispatch strategy of the building aggregator

In the building aggregator model as shown in Fig. 2, all individual buildings interface with aggregators through building energy management systems (BEMS) and send the storage information and flexibility quantification results of variable loads. After that, the aggregator can allocate the flexibility capacity to different flexibility services to maximize the profits or minimize the electricity costs according to the service prices. In this paper, the aggregator is assumed as the price-taker.

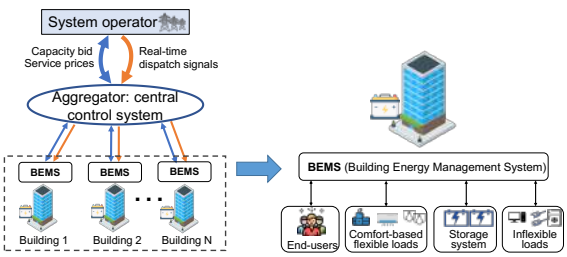

Fig. 2 - Structure of the aggregator control system and the building energy management system.

The dispatch optimization of the aggregator can be formulated as a cost minimization problem as shown in Eq. (1), equal to the energy cost minus the revenues from regulation and reserve services. The constraints are presented by formulation (2)-(12).

$$min\ \ Cost = \sum_{k\in T}(\pi_k^E P_k^E - Rev_{reg,k} - Rev_{res,k}) \quad (1)$$

$$P_k^E = \sum_{i\in N}\left(P_{ES,i,k}^E + P_{lig,i,k}^E + P_{HVAC,i,k}^E + P_{others,i,k}^E\right) \quad (2)$$

$$Cap_k^{Rs} = \sum_{i\in N}(Cap_{ES,i,k}^{Rs} + Cap_{lig,i,k}^{Rs} + Cap_{HVAC,i,k}^{Rs}) \quad (3)$$

$$Cap_k^{Rg} = \sum_{i\in N}(Cap_{ES,i,k}^{Rg} + Cap_{lig,i,k}^{Rg} + Cap_{HVAC,i,k}^{Rg}) \quad (4)$$

$$Rev_{reg,k} = \begin{cases} 0 & Cap_k^{Rg} < Cap_{min}^{Rg} \\ \pi_k^{Rg} Cap_k^{Rg} & Cap_k^{Rg} \geq Cap_{min}^{Rg} \end{cases} \quad (5)$$

$$Rev_{res,k} = \begin{cases} 0 & Cap_k^{Rs} < Cap_{min}^{Rs} \\ \pi_k^{Rs} Cap_k^{Rs} & Cap_k^{Rs} \geq Cap_{min}^{Rs} \end{cases} \quad (6)$$

$$-P_{ES,i,k}^{\vee} - Cap_{ES,i,k}^{Rs} - Cap_{ES,i,k}^{Rg} \geq -P_{ES,i,rated} \quad (7)$$

$$P_{ES,i,k}^{\wedge} + Cap_{ES,i,t}^{Rg} \leq P_{ES,i,rated} \quad (8)$$

$$SOC_{ES,i,k+1} = SOC_{ES,i,k} + \frac{\eta_i P_{ES,i,k}^{\wedge} - P_{ES,i,k}^{\vee}/\eta_i}{E_{ES,i,rated}} \quad (9)$$

$$SOC_{ES,i,k,max} = SOC_{ES,i,k} + Cap_{ES,i,k}^{Rg} * 0.5/E_{ES,i,rated} \quad (10)$$

$$SOC_{ES,i,k,min} = SOC_{ES,i,k} - \frac{Cap_{ES,i,k}^{Rg} * 0.5 + Cap_{ES,i,k}^{Rs}}{E_{ES,i,rated}} \quad (11)$$

$$\underline{SOC}_{ES,i} \leq SOC_{ES,i,k}, SOC_{ES,i,k,max}, SOC_{ES,i,k,min} \leq \overline{SOC}_{ES,i} \quad (12)$$

At the building level, the model-based flexibility quantification method is used to evaluate the flexibility capacity of the comfort-based loads including thermal and lighting loads, as presented by formulation (13)-(21) [10]. Where L is the horizontal illuminance on the working plane. P is the light power input. LE is the luminous efficacy of each lamp (80 am/W). UF is the utilization factor (0.4~0.6). MF is the maintenance factor (Good condition: 0.7). A simplified building thermal storage model (RC model) is used to predict the alternation of building cooling demand when utilizing the building thermal mass as the flexibility resource.

$$L_{w,k} = \frac{LE \times UF \times MF \times (P_{lig,k}^E - Cap_{lig,k}^{Rg} - Cap_{lig,k}^{Rs})}{Area} \quad (13)$$

$$L_{min} \leq L_{w,k} \leq L_{max} \quad (14)$$

$$Cap_{lig,k}^{Rg} \leq \beta_L P_{lig,k}^E \quad (15)$$

$$Cap_{lig,k}^{Rs} \leq \gamma_L P_{lig,k}^E \quad (16)$$

$$\Delta Q_{ch,k} = \frac{T_{opt,k} - T_{base,k}}{R_{bui,o} + R_{bui,i}} \times \left(1 + \frac{R_{bui,o}}{R_{bui,i}} \times e^{-\frac{t}{\tau}}\right) \times A_{bui} \quad (17)$$

$$\tau = \frac{R_{bui,o} \times R_{bui,i}}{R_{bui,o} + R_{bui,i}} \times C_{bui} \quad (18)$$

$$\Delta P_{Ch,k}^E = \Delta Q_{ch,k}/COP \quad (19)$$

$$Cap_{Ch,k}^{Rg} \leq min\ (P_{Ch,rated} - P_{Ch,k}^E, P_{Ch,k}^E - P_{Ch,LO}, \Delta P_{Ch,k}^E) \quad (20)$$

$$Cap_{Ch,k}^{Rs} = min\ (P_{Ch,k}^E - P_{Ch,LO}, \Delta P_{Ch,k}^E) - Cap_{Ch,k}^{Rg} \quad (21)$$

3. Description of the case study

The building cluster consisting of five 40-floor commercial buildings (1*low-weighted, 3*middle-weighted, 1*high-weighted) is selected in the case study to test the proposed strategy and analyse the practical relevance based on the real-life electricity market. All individual buildings are equipped with an active electrical storage system (224 kWh, 80 kW). Fig. 3 (a) shows the time-varying prices of different market services including the energy, reserve, and regulation (sum of up and down) services. The minimum bid capacity for regulation and reserve services is 500 kW. Table. 1 shows the RC parameters of the building clusters. The weather data is adopted from available Hong Kong TMY (typical meteorological year) data, as shown in Fig. 3 (b). The occupied period is 8:00-20:00 with a constant indoor temperature setting of 24°C and humidity of 60% RH in the baseline case. The lighting density is assumed to be 15W/ m2 following the given baseline schedules. In the flexibility quantification, the maximum allowed indoor temperature increase is 2K and the minimum indoor illuminance is 300 lux.

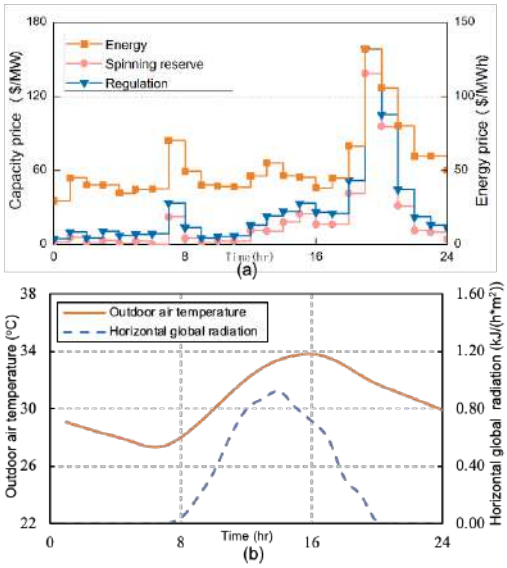

Fig. 3 – (a) Hourly energy prices and ancillary service revenues from CAISO; (b) Outdoor weather on the test day.

Tab. 1 - RC parameters of building thermal model [11].

Building type	Low weighted	Middle weighted	High weighted
Cbui (j/m2.k)	248621	467878	696082
Rbui,o (m2.k/W)	0.9236	0.6551	0.5266
Rbui,i (m2.k/W)	0.2133	0.1477	0.1134
Rbui (m2.k/W)	0.1733	0.1205	0.0933

4. Results

The optimization target of the dispatch strategy is programmed as the mixed-integer non-linear problem via YALMIP [12], and solved with CPLEX solver using a computer with an eight-core Intel Core i7 CPU.

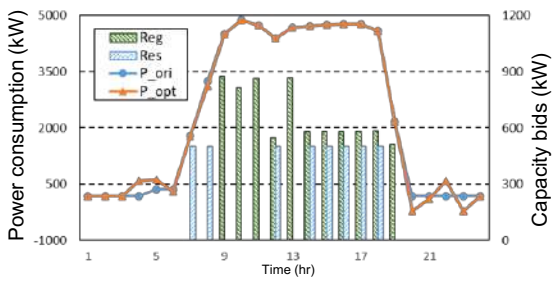

Fig. 4 - The optimal bidding result of the building aggregator.

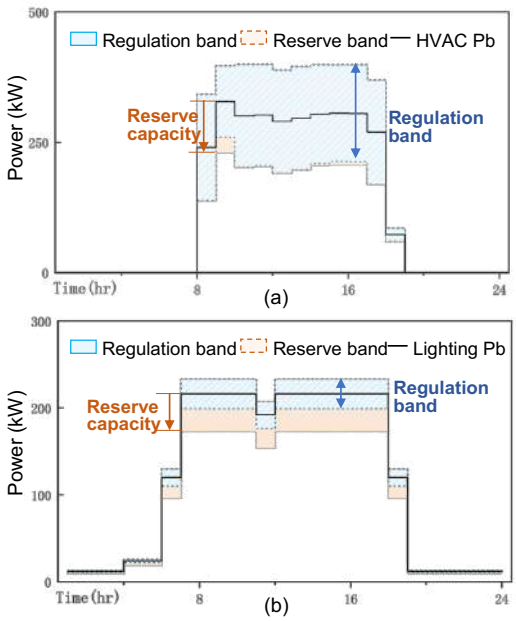

Fig. 5 - The power baseline and flexibility capacity of (a) the HVAC system and (b) the lighting system of the high-weighted building.

Tab.2 - Revenues of the building aggregator from different flexibility services.

Multiple services	Cost saving
Energy arbitrage income($)	33.6
Regulation revenue income($)	220.8
Reserve revenue income($)	78.2
Total cost saving ($)	332.7 (11.6%↓)

Fig. 4 shows the optimal bidding results of the building aggregator during a 24-hour period. Fig. 5 shows an example of the hourly power baseline and flexibility capacities (i.e., regulation band and reserve capacity) of the high-weighted building. If individually optimizing the dispatch of each building, only 80.2 $ daily cost saving can be achieved in total from load shifting by the storage system, since the flexibility capacity of individual buildings is too small to bid ancillary services. Through the coordinated dispatch of the active storage systems from aggregator central control systems, the flexibility of building thermal and lighting loads can be utilized to provide regulation and reserve services. The financial results are presented in Table. 2. Results show that the proposed dispatch strategy reduces the electricity costs of the building cluster by 11.6% from multiple revenue streams, including energy arbitrage, regulation service and operating reserve service. Active electrical storage systems can increase revenues by 2.3 times and the unlocked flexibility of building thermal and lighting loads can achieve 152 $ daily revenues. The total cost saving can reach 332.7 $, in which the flexibility of comfort-based loads contributes to 45.7% of the revenues and the active storage systems contribute to 54.3%.

5. Conclusion

Aggregated control of multiple flexibility resources can maximize the economic benefits of building clusters by ensuring a minimum capacity and optimally allocating the capacity to multiple services in the electricity market. This study addresses the issue that the energy flexibility of individual buildings is too small to bid flexibility services, and the findings may stimulate the investment of the distributed storage system at the aggregated level, as the building aggregator is a promising business model in future flexibility markets. The main conclusions are as follows:

1) The model-based flexibility quantification method is effective to evaluate the flexibility capacity of the comfort-based loads of the building.
2) The building aggregator business model can maximize the economic benefits of building energy flexibilities by providing multiple qualified services in electricity markets. The total electricity costs can be reduced by 11.6%.
3) The centralized control of the storage systems can be an economic and effective measure to unlock the energy flexibilities of the comfort-based loads which contribute to 45.7% of the revenues.

6. Acknowledgement

The research presented in this paper is financially supported by a research grant under strategic focus area (SFA) scheme of the research institute of sustainable urban development (RISUD) in The Hong Kong Polytechnic University and a general research grant (152165/20E) of the Hong Kong Research Grant Council (RGC).

7. References

[1] Yamujala S, Kushwaha P, Jain A, Bhakar R, Wu J, Mathur J. A stochastic multi-interval scheduling framework to quantify operational flexibility in low carbon power systems. Applied Energy. 2021;304:117763.
[2] Zheng Y, Yu H, Shao Z, Jian L. Day-ahead bidding strategy for electric vehicle aggregator enabling multiple agent modes in uncertain electricity markets. Applied Energy. 2020;280:115977.
[3] Peng C, Zou J, Lian L, Li L. An optimal dispatching

strategy for V2G aggregator participating in supplementary frequency regulation considering EV driving demand and aggregator's benefits. Applied Energy. 2017;190:591-9.
[4] Lu X, Li K, Xu H, Wang F, Zhou Z, Zhang Y. Fundamentals and business model for resource aggregator of demand response in electricity markets. Energy. 2020;204:117885.
[5] Marwan M, Ledwich G, Ghosh A. Demand-side response model to avoid spike of electricity price. Journal of Process Control. 2014;24:782-9.
[6] Klein K, Herkel S, Henning H-M, Felsmann C. Load shifting using the heating and cooling system of an office building: Quantitative potential evaluation for different flexibility and storage options. Applied Energy. 2017;203:917-37.
[7] Patteeuw D, Henze GP, Helsen L. Comparison of load shifting incentives for low-energy buildings with heat pumps to attain grid flexibility benefits. Applied Energy. 2016;167:80-92.
[8] Wang H, Wang S. A hierarchical optimal control strategy for continuous demand response of building HVAC systems to provide frequency regulation service to smart power grids. Energy. 2021;230:120741.
[9] Vrettos E, Andersson G. Scheduling and provision of secondary frequency reserves by aggregations of commercial buildings. IEEE Transactions on Sustainable Energy. 2015;7:850-64.
[10] Tang H, Wang S. A model-based predictive dispatch strategy for unlocking and optimizing the building energy flexibilities of multiple resources in electricity markets of multiple services. Applied Energy. 2022;305:117889.
[11] Xue X, Wang S, Sun Y, Xiao F. An interactive building power demand management strategy for facilitating smart grid optimization. Applied Energy. 2014;116:297-310.
[12] Lofberg J. YALMIP: A toolbox for modeling and optimization in MATLAB. 2004 IEEE international conference on robotics and automation (IEEE Cat No 04CH37508): IEEE; 2004. p. 284-9.

A common European EPB Assessment and Certification scheme. U-CERT's proposal

Pablo Carnero [a], Dick van Dijk[b], Niccolò Mignani[c], Gabriela Ana [d]

[a] Instituto Valenciano de la Edificación, València, Spain, pcarnero@five.es

[b] Energy Performance of Buildings (EPB) Center, Rotterdam, the Netherlands, dick.vandijk@epb.center.

[c] Alma Mater Studiorum Università di Bologna, Bologna, Italy, niccolo.mignani@studio.unibo.it.

[d] Energy Performance of Buildings (EPB) Center, Rotterdam, the Netherlands, ga@epb.center.

Abstract. Buildings are responsible for great share of the global GHG emissions. Increasing buildings' energy efficiency is crucial to decarbonise the EU. For energy performance policies and requirements to have actual impact on buildings' direct and indirect emissions is crucial to develop robust, accurate, meaningful and user-friendly assessments and certification schemes. This paper presents a methodology .to calculate building energy performance fully compliant with EPB Standards. Also, it proposes a selection of holistic indicators aiming to overcome shortcomings of national energy performance certificates, while being compliant with the latest version of the Energy Performance in Buildings Directive (EPBD). The results have the ambition of laying the foundation for a common European EPB assessment and certification scheme.

Keywords. EPB standards, EPC, EPBD, user-friendliness, digitalisation, indicators, calculation.
DOI: https://doi.org/10.34641/clima.2022.279

1. Introduction

Anthropogenic climate change stands as the greatest menace humanity must face in the XXI century. Hence, the adhesion to the International Paris Agreement [1] and the climate and environment declaration by the European Parliament [2]. Consequently, the European Green Deal [3] established the mission for Europe to be net zero emissions by 2050. The checkpoint of cutting greenhouse gas (GHG) emissions by 55% in 2030 compared to 1990 levels was defined by the Climate Target Plan [4].

Decarbonising our societies calls for multidimensional action, it is widely acknowledged that buildings shall play a key role. During their use and operation, buildings are responsible of over 40% of the energy consumption and represent approximately one third of direct and indirect GHG emissions [5]. Direct emissions caused by their low energy performance and fossil-fuel use [6]. Indirect due to the high energy demand, which strains the power and heat sector. Almost 75% of EU's building stock is inefficient, and over 85% of the buildings that exist today will still be standing in 2050. However, the weighted annual energy renovation remains sunk at 1% [7]. Thus, the 'Fit for 55' package [8] was published with a view to revising the entire climate and energy framework. As a result, the proposal for the Energy Performance in Buildings Directive (EPBD) was released at the end of 2021 [7]. The document aims at being the definitive push to national building regulation towards delivering the ambitious EU climate targets. A core instrument is the revision of Energy Performance in Building (EPB) Assessments and Certification schemes.

1.1. EPB Assessments and Certification schemes

The first version of the EPBD [9] laid down the general framework for calculating buildings' energy performance. Such energy performance shall be assessed in a transparent manner that allowed to verify compliance with minimum requirements established for buildings. Moreover, it should also feed building's energy performance certificates (EPC), posed as the key informative instrument aiming to provoke a shift in the market in favour of efficient constructions. Despite the cardinal rule EPB assessment represented, the specific methodology to obtain it was left to each member state. The definition of a comprehensive procedure capable of assessing buildings' energy performance was far from trivial. When facing such titanic effort, each country defined its own EPB assessment and certification scheme, which generated great discrepancies across the EU [10][11]. In the interest of clarity, the EPBD was recast in 2010 [5]. It further detailed the minimum requirements for energy performance calculations in buildings and mandated member states to consider the existing European

Copyright ©2022 by the authors. This conference paper is published under a CC-BY-4.0 license.

standards when developing their national assessment methodologies. A revised version of the EPBD was published in 2018. The document mandated member states to *"describe their national calculation methodology following the national annexes of the overarching standards, namely ISO 52000-1, 52003-1, 52010-1, 52016-1, and 52018-1"* [12]. These standards are part of a coherent set of internationally harmonized procedures developed to assess buildings' energy performance in a systemic manner. They are often referred to as EPB standards and were developed supported by mandate M/480 from the European Commission to CEN.

Many researchers and initiatives have considered the question of EPB assessments and certification schemes in buildings. However, to date, research has given considerable more attention to cross-country comparison and identification of shortcomings [13][14][15][16][17]or auxiliary tool development [18][19], rather than proposing a common-EU methodology considering the set of EPB standards [20].

The main scope of this paper is to propose a methodology for a new energy performance in building (EPB) assessment and to define the corresponding EPC. The remainder of this paper is structured as follows: Section 2 presents the methodology used in the research. Section 3 presents results and discusses them. Finally, in Section 0, conclusions are set together and policy recommendations are given.

2. Research Methods

The research is performed in the scope of the U-CERT project. U-CERT is a Coordination and Support Action funded under the Horizon 2020 programme aiming to define the next-generation EPB assessment and certification scheme leveraging the set of EPB standards.

2.1. EPB Assessment methodology

The project deeply mapped the state of the art regarding national EPB assessments and certification schemes in 11 countries (i.e., The Netherlands, Sweden, Estonia, Hungary, Spain, Slovenia, Romania, Italy, Bulgaria, France and Denmark) [21]. The gathering of all available National Annexes, as mandated by [12], was taken as the baseline for the definition of a converged set of EPB standard choices defining the common EU assessment methodology. The procedure was to categorise the EPB Standards to facilitate the identification of the most relevant ones. Next, all Annex A choices were structured and prioritised. Lastly, expert discussions were held in dedicated task forces, using available National Annexes as benchmark, to come to a final decision on U-CERT National Datasheets.

As a result, from the 61 overviewed EPB standards, 10 were finally selected as core of the U-CERT EPB calculation methodology (i.e., EN ISO 52000-1, EN ISO 52010-1, EN 16798-1, EN ISO 52016-1, draft ISO/FDIS 520232-1, EN 15316-4-2, EN 16798-7, EN 16798-5-1, EN ISO 52003-1, and EN ISO 52018-1). Thus, a total of 237 Annex A choices were made. For a detailed description of the selected choices, refer to [22].

Although U-CERT considers measured procedures as valid methods to estimate energy performance in buildings, the lack of EPB standards comprehensively addressing whole building assessments hindered its thorough analysis.

2.2. EPC report

Once having defined the EPB assessment methodologies, U-CERT approached the task of defining the set of indicators and the visual layout of the next-generation EPC. For this purpose, the latest provisions from [7] have been considered.

Apart from the detailed analysis of the two overarching standards dealing with energy performance indicators (i.e., EN ISO 52003-1, and EN ISO 52018-1), an investigation of the latest developments in Energy Voluntary Certification schemes (EVCS) was also performed [23]. Moreover, parallelly to the technical investigation, users' perception regarding EPCs in each of the countries was analysed leveraging ethnographic research techniques [24]. Consequently, to overcome the shortcomings identified in national EPCs (e.g., lack of user-friendliness, reliability, acceptance, etc.), the following briefing for next-generation EPCs was obtained. The objective was to define a flexible EPC, which shall be sensible to the user (i.e., expert and non-expert), to object (i.e., new and existing building), and to assessment type (i.e., calculated and measured). The 'silo-thinking' regarding energy performance should be abandoned, exploiting synergies with other complementary building assessments, such as Indoor Environmental Quality (IEQ), smart readiness, and cost. Furthermore, the next-generation EPC should be designed in a modular fashion, laying the foundation for a digitalised report.

3. Results

Although, EPB assessments are often focused on standardised calculations (i.e., estimating building energy use under normal use and typical climate conditions), U-CERT allows to produce other types of assessment, as depicted in Tab. 1. They can be mainly clustered in calculated and measured.

Tab. 1 - EPB Assessment types. Adapted from [25].

Type	Building situation	Use	Climate
Calculated	Design for new construction	Standard	Standard
		Project	Project
	As built existing building	Standard	Standard
		Actual	Actual
	Design for renovation	Standard	Standard
		Project	Project
		Actual	Actual
Measured	As built existing building	Actual	Actual
		Standard	Standard

The calculated assessment can be applicable to all building situations. In the design for a new construction, the calculations can be arranged to represent standard use and climate, or other project conditions. The first option is usually preferred when dealing with official EPB assessments, whereas the second option is always available for any other tailored analysis. Similarly, when having an existing building, standard or actual conditions can be applied to calculations representing the as built status. In the case of design for renovation, the calculated EPB assessments can reflect standard conditions, usually applicable for checking requirements or fulfilling regulatory obligations; or project conditions, which can be related to actual building use. The latter of special relevance when envisioning tailored-to-actual use renovation roadmaps. In contrast, the measured assessment is only applicable to as built existing buildings since they require having access to metered data. However, such measurements can be normalised to reflect standard conditions or left as measured to represent actual building use and climate influence and as such to be compared with a tailored calculation. Note that measured EPB assessment can't include an estimation of the building renovation potential.

With respect to the selection of indicators, to be included in the EPC report, there are four categories: energy performance (EP), IEQ, smart readiness and cost. These categories of indicators are sensible to whether they are embedded in calculated or measured EPB assessments, as shown in Tab. 2 and Tab. 3.

Tab. 2 – Calculated EPB Assessment indicators.

Category	Indicators	U-CERT Included	U-CERT Left as voluntary
General information		X	-
EP	Overall	X	-
	Partial	X	-
Smart Readiness	SRI	X	-
IEQ	ALDREN Thermal score	X	-
Cost	Cost	-	-

Tab. 3 – Measured EPB Assessment indicators.

Category	Indicators	U-CERT Included	U-CERT Left as voluntary
General information		X	-
EP	Overall	X	-
	Partial	-	X
Smart Readiness	SRI	-	X
IEQ	ALDREN Thermal score	-	X
Cost	Cost	X	-

Note that the indicators included in U-CERT's selection vary depending on the type of assessment. However, all assessments contain general information (e.g., contextual data, identification of the building and the assessor, link to databases, etc.). In the next subsections greater detail is given on the specific indicators within each category.

3.1. Energy Performance

The selection of energy performance indicators can be found in Data access statement

Data sharing not applicable to this article as no datasets were generated or analysed during the current study.

Appendix A. The main EP indicator defines the EP rating, according to a single reference point scale ranging from A to G, with the A+ subclass.

3.2. Smart Readiness

Smart Readiness refers to the capability of buildings or building units to adapt their operation to the needs of the occupant, also optimizing energy efficiency and overall performance, and to adapt their operation in reaction to signals from the grid. Smart Readiness consideration in the scope of U-CERT's EPB assessment is done by means of the Smart Readiness Indicator, as defined in [26]. This assessment produces an SRI rating.

The fully-fledged SRI assessment could be regarded as a parallel analysis to be included as an annex in EPB Assessments and Certification schemes.

ALDREN's EVC goes in this direction [18]. U-CERT is aware that the complete inclusion of SRI as independent from EPB Assessments could represent too much extra work for EPB assessors further hindering the uptake of next generation EPCs. However, if smoothly integrated in the EPB assessment process, added value could be given to EPCs, while not overburdening assessors. For a detailed identification of the overlapping elements between SRI and U-CERT's EPB Assessment, refer to [27].

3.3. IEQ

U-CERT decision with respect to including IEQ indicators in EPB assessments and certification schemes is to use the discomfort indicators defined as overall EP indicators (i.e., summer, winter and DHW thermal discomfort), along with the thermal score defined by the ALDREN project in [20].

3.4. Cost

In EN ISO 52000-1's Annex B a weighting factor is foreseen for the energy cost. However, U-CERT considers that for an asset EPB assessment, introducing a cost indicator may be counterproductive. This is because the asset EPB assessment represents the calculated EPB performance under standard conditions and standard weather data. Thus, any cost indicator that builds on such theoretical energy calculations won't provide meaningful information to both final users and EPB experts, who would tend to compare the cost indicator with the information present in the energy invoices.

A calculated cost indicator could be meaningful if it were performed under tailored conditions, rather than standardized. If the EPB assessment were configurated to reflect the actual use conditions (e.g., thermostatic setpoints, control strategies, occupant behaviour, etc.) and under actual weather influence, - tailored-to-actual conditions- then the cost indicator could be closer to reflect the actual energy expenditure. Moreover, it could be valuable to use it as baseline model for the ideation of tailored renovation roadmaps.

3.5. EPC report

The U-CERT project performed the selection of indicators with a view to easing the integration into building logbooks and EPC databases. Moreover, the EPC report, although produced in a static fashion, it has been structured and designed envisioning evolution to a digital environment. The most relevant feature is the concept of extended and reduced report. The former contains all the indicators and detailed information relevant to an expert user, while the latter just contains the basic insights addressed to a non-expert user. A summary can be found in Tab. 4 and Tab. 5.

Tab. 4 – Calculated EPC report. Content overview.

Calculated EPB Assessment	Reduced	Extended
Existing building or new building		
General information	X	X
Main EP rating in scale	X	X
Thermal comfort rating in scale	X	X
Smart Readiness in scale	X	X
Overall EP indicators	-	X
Partial EP indicators	-	X
SRI report	-	X
ALDREN Thermal score report	-	X
Voluntary indicators as annexes	-	X
Renovation potential *per each renovation action*		
Description of renovation action	X	X
Main EP rating in scale	X	X
Thermal comfort rating in scale	X	X
Smart Readiness in scale	X	X
Cost of renovation action	X	X
Overall EP indicators	-	X
Partial EP indicators	-	X
SRI report	-	X
ALDREN Thermal score report	-	X
Voluntary indicators as annexes	-	X
for the complete renovation scenario		
Description of renovation scenario	X	X
Main EP rating in scale	X	X
Thermal comfort rating in scale	X	X
Smart Readiness in scale	X	X
Cost of renovation scenario	X	X
Overall EP indicators	-	X
Partial EP indicators	-	X
SRI report	-	X
ALDREN Thermal score report	-	X
Voluntary indicators as annexes	-	X

Tab. 5 – Measured EPC report. Content overview.

Measured EPB Assessment	Reduced	Extended
Existing building or new building		
General information	X	X
Main EP rating in scale	X	X
Thermal comfort rating in scale (if performed)	X	X
Smart Readiness in scale (if performed)	X	X
Overall EP indicators	-	X
Partial EP indicators (if	-	X

performed)		
SRI report (if performed)	-	X
ALDREN Thermal score report (if performed)	-	X
Voluntary indicators as annexes	-	X

The EPC report template design has not been reproduced here due to space restrictions. It can be found in [27].

4. Conclusions

U-CERT sets the foundation of next-generation EPB assessments and certification schemes by producing a calculation methodology fully compliant with EPB Standards. Moreover, proposes a selection of holistic indicators, covering energy and complementary-to-energy dimensions, and a design of an EPC report which aims to overcome the shortcomings of national procedures. These results have been produced considering the latest provisions from [7]. Thus, they have the ambition of laying the foundation of a common European EPB assessment and certification scheme. Member states may find in U-CERT's value propositions a valuable stepping stone when aiming to renew their national procedures when having to transpose the EPBD to their national regulation.

Although progressing on existing research, this investigation is not exempt from limitations. In the scope of the project it was possible to retrieve users' perception on existing national EPCs from 11 countries. Nevertheless, replicating the methodology with the new EPC report was not possible during project duration. Furthermore, the calculation methodology has not been transferred to a functional simulation software. The EPC report could not be digitalised. These last two endeavours are left to future research.

5. Acknowledgement

The research was performed under the U-CERT project. Thus, the authors would like to acknowledge the technical support from the project consortium and the financial support of the European Commission under the H2020 programme. U-CERT received funding from the European Union's Horizon 2020 research and innovation programme under grant agreement number 839937.

6. Data access statement

Data sharing not applicable to this article as no datasets were generated or analysed during the current study.

7. Appendix A

The indicators considered for U-CERT's EPB assessments can be classified into overall and partial indicators. The overall indicators include the following:

- Overall non-renewable primary energy use [kWh/m^2] [kWh]. Calculated according to H5 in Annex H in ISO 52000-1 [2]; thus, considering compensation between different energy carriers and the effect of exported energy.

This indicator assesses the final global impact the energy performance of the building has. An excess consumption during certain moments during the year may be balanced by surplus of energy in others. It constitutes the main EP indicator. This is in line with ALDREN project [18].

- Overall total primary energy use [kWh/m^2] [kWh]. Calculated according to H4 in Annex H in ISO 52000-1 [2]; thus, not considering compensation between different energy carriers nor the effect of exported energy.

This indicator assesses the total primary energy the building requires to operate according to the energy needs, technical building system efficiency and renewable contribution to the onsite energy use. It seeks to prevent buildings to balance a poor envelope and inefficient systems with oversized renewable generation.

- Summer thermal comfort [K·h].

This indicator serves to account for overheating during the cooling period. It refers to the amount of (weighted) occupation hours the temperature is above a certain reference temperature.

- Winter thermal comfort. [K·h].

This indicator serves to account for underheating during the heating period. It refers to the amount of (weighted) occupation hours the temperature is below a certain reference temperature.

- Domestic Hot Water thermal comfort [K·h].

This indicator serves to check that sanitary hot water is provided, when there is demand, at a certain minimum reference temperature.

Additionally, the following overall indicators are considered of informative nature.

- Overall non-renewable primary energy use [kWh/m^2] [kWh]. Calculated according to H4 in Annex H in ISO 52000-1 [2]; thus, not considering compensation between different energy carriers nor the effect of exported energy. This indicator is also compliant with Level(s).

- Overall renewable primary energy production [kWh/m^2] [kWh]. Considering the whole renewable primary energy production, regardless of whether consumed onsite or exported to the grid.

- Overall renewable primary energy use [kWh/m²] [kWh]. The portion of the previous indicator compensating the energy demanded by the uses considered in the assessment.

- Overall equivalent CO_2 emissions [kg/m²]. Calculated following H5 in Annex H in ISO 52000-1 [2]; thus, considering compensation between different energy carriers and the effect of exported energy.

- Renewable electricity generation by onsite PV, wind turbines or CHP [kWh/m²] [kWh].

- Renewable electricity from onsite PV, wind turbines or CHP self-used [kWh/m²] [kWh].

- Renewable electricity exported to non-EPB uses by onsite PV, wind turbines or CHP [kWh/m²] [kWh].

- Renewable electricity exported to the grid by onsite PV, wind turbines or CHP [kWh/m²] [kWh].

- Energy needs per service – heating, cooling, domestic hot water, humidification and dehumidification, and mechanical ventilation - [kWh/m²].

For the case of the lighting, the metric proposed would be the Daylight Autonomy (DA). Thus, the indicator of the lighting energy needs would be the percentage of the occupied hours of the year when artificial lighting is needed, because daylight alone can't meet the minimum illuminance threshold [19].

- Energy use per system service – heating, cooling, domestic hot water, humidification and dehumidification, mechanical ventilation, and lighting - and energy vector [kWh/m²] [kWh].

The partial indicators cover physical and technological elements, which could have strong connection with building and system inspections. They can be subdivided into envelope, technical building systems and renewable electricity production performance indicators.

The envelope performance indicators selected to be included in U-CERT are the following:

- Per opaque envelope construction.
  - Thermal transmittance [W/(m²·K)];
  - Colour outside layer;

Additionally, a description of the layered materials should be included. It should cover (from outer to inner element), at least name, thickness, and conductivity of the material. Other features, such as density or specific heat may also be included.

- Per window/skylight:
  - Thermal transmittance [W/(m²·K)];
  - Opening control (e.g., manual or fixed windows, open/closed detection to act on HVAC, based on sensor data, etc.)
  - Solar shading of glazings:
    - Presence;
    - Technology (e.g., awning, blinds, shutters, etc.);
    - Control (e.g., manual, motorized, automation based on sensor data, combined control with HVAC, predictive control, etc.)
    - Solar shading potential [%], according to ISO 18292 [20];
  - Glass thermal transmittance [W/(m²·K)];
  - Glass solar factor [-];
  - Frame thermal transmittance [W/(m²·K)];
  - Frame colour or absorptance.
  - Air permeability class, according to EN 12207.

Additionally, a description of each representative window/skylight should be included.

- Thermal bridges, per type of junction (e.g., corner, slab-façade, pillar, etc.):
  - Linear thermal transmittance Ψ [W/(m·K)].
  - Length [m].

- Air leakage:
  - Air change rate at 50Pa [1/h].

This indicator should be measured by means of a Blower Door test according to EN 13829 [21] whenever possible, and its value should be included in the calculations.

Continuing with the infrastructure present in the building, the technical building systems per service also provide valuable information about the energy performance of the building, as a whole.

- Technical Building Systems per service or combination of services.

Additionally, to the categories presented below, a general description of the installation should be included.

  - Service or services linked to the system.
  - Overall installation efficiency.
  - Generation:
    - Technology (e.g., conventional boiler, condensing boiler, air-to-air heat pump, electric heater, etc.);
    - Energy carrier;
    - Nominal power [kW];
    - Effective rated output [kW];
    - Nominal efficiency [%];
    - Renewable contribution (if applicable);
    - Metering;
    - Control (e.g., on-off control; control according to fixed priority list; control according to dynamic priority list; control according to dynamic priority list and predicted information; control according to dynamic priority list, predicted information and external

signals).
  - Storage:
    - Capacity [m^3].
    - Control (e.g., continuous storage operation, scheduled storage operation, load prediction-based storage operation, flexible control according to external signals, etc.).
  - Distribution:
    - Typology of circuit (e.g., two-pipe, four-pipe, recirculation, etc.);
    - Insulation of pipes;
      Further detail may be included.
    - Circulation device (e.g., pumps, fans, etc.).
      Further detail may be included.
    - Control (e.g., on-off control, multi-stage control, variable speed circulation device control based on internal signals or on external signals).
  - Emission:
    - Technology (e.g., radiators, heated floor, fancoils, etc.);
    - Control (e.g., central automatic control, individual room control, individual room control with communication between controllers and to BACS, individual room control with communication and occupancy detection).
  - Reporting of performance (e.g., central reporting of KPIs, historical data, forecasting and/or benchmarking, predictive management, and fault detection, etc.).

The aim is to characterize the main elements of the Heating, Cooling, DHW, Humidification & Dehumidification, and Mechanical Ventilation technical systems.

With respect to Lighting, the following may apply:
- Technology (e.g., LED, dichroic, fluorescent, etc.).
- Nominal power;
- Control (e.g., manual, sweeping extinction signal, automatic detection, etc.).

If there is a certain service which lacks technical building system, it should be explicitly mentioned.

U-CERT proposes including the following indicators about renewable electricity production.

- Photovoltaics:
  - Technology (e.g., monocrystalline, etc.).
  - Installed peak power [kWp].
  - Nominal efficiency [%].
  - Orientation [°].
  - Inclination [°].
  - Possibility to export electricity to the grid.
  - Inverter type (e.g., central inverter, power optimizer + inverter, or microinverters).
  - Reporting of performance (e.g., current generation data, actual values and historical data, performance evaluation including forecast and/or benchmarking, predictive management, and fault detection, etc.).

- Wind turbine:
  - Technology.
  - Installed peak power [kWp].
  - Nominal efficiency [%].
  - Possibility to export electricity to the grid.
  - Reporting of performance (e.g., current generation data, actual values and historical data, performance evaluation including forecast and/or benchmarking, predictive management, and fault detection, etc.).

- CHP:
  - Installed peak power [kWp].
  - Technology.
  - Nominal efficiency for thermal and power generation.

- Storage:
  - Technology (e.g., dedicated battery storage, dedicated thermal energy storage, etc.).
  - Installed peak capacity [kWh].
  - Control (e.g., direct storage of on-site production, controlled based on grid signals, optimising the use of locally generated electricity, possibility to feed back into the grid, etc.).
  - Reporting of performance (e.g., current state of charge, actual values and historical data, performance evaluation including forecast and/or benchmarking, predictive management, and fault detection, etc.).

In the case the building or building unit is connected to an energy community or district heating/cooling network it should also be made explicit.

8. Data Access Statement

Data sharing not applicable to this article as no datasets were generated or analysed during the current study.

9. References

[1] The Council of the European Union, *Council Decision (EU) 2016/1841 of 5 October 2016 on the conclusion, on behalf of the European Union, of the Paris Agreement adopted under the United Nations Framework Convention on Climate Change*. Brussels: The Council of the European Union, 2016.

[2] T. Haahr, "The European Parliament declares climate emergency." European Parliament, 2019, [Online]. Available: https://www.europarl.europa.eu/news/en/press-room/20191121IPR67110/the-european-parliament-declares-climate-emergency.

[3] European Commission, "The European Green Deal," *European Commission*, vol. 53, no. 9.

European Comission, Brussels, p. 24, 2019, [Online]. Available: https://eur-lex.europa.eu/legal-content/EN/TXT/?qid=1588580774040&uri=CELEX:52019DC0640.

[4] European Commission, "2030 Climate Target Plan," 2020. https://ec.europa.eu/clima/policies/eu-climate-action/2030_ctp_en (accessed May 02, 2021).

[5] European Parliament, *Directive 2010/31/EU*. European Parliament and the Council of the European Union, 2010.

[6] Eurostat, "Disaggregated final energy consumption in households for EU28," 2021. https://ec.europa.eu/eurostat/databrowser/view/NRG_D_HHQ__custom_937958/default/table?lang=en (accessed May 01, 2021).

[7] European Parliament and The Council of the European Union, *Directive of the European Parliament and of the Council on the energy performance of buildings (recast)*, vol. 0426, no. COM(2021) 802 final. 2021, pp. 1–79.

[8] European Commission, "Fit for 55 - Delivering the EU's 2030 climate target on the way to climate neutrality," *Eur. Comm.*, p. 15, 2021, [Online]. Available: https://eur-lex.europa.eu/legal-content/EN/TXT/?uri=CELEX:52021DC0550.

[9] European Parliament, *Directive 2002/91/EC*. European Parliament and the Council of the European Union, 2003.

[10] I. de Graaf, "Capitalising Energy Efficiency in Housing Markets: an Investigation into the Impact of Energy Performance Certificates (EPCs) on Transaction Prices in Selected European Countries," TU Wien, 2016.

[11] R. Hitchin, K. E. Thomsen, and K. B. Wittchen, "Primary Energy Factors and Members States Energy Regulations," 2018. [Online]. Available: https://www.epbd-ca.eu/wp-content/uploads/2018/04/05-CCT1-Factsheet-PEF.pdf.

[12] European Parliament, *Directive (EU) 2018/844*, vol. 276 LNCS, no. May 2010. European Parliament and the Council of the European Union, 2018, pp. 98–107.

[13] G. Hofer, W. Hüttler, K. Leutgöb, M. Emilia-Cerna, and D. Popescu, "Immovalue - D3.1 Overview report on different energy performance certificate approaches and their assessmentin the context of property valuation," 2011. [Online]. Available: https://immovalue.e-sieben.at/project-reports.html.

[14] S. Geissler, S. Vlachos, H. Petran, and N. Urban-incerc, "Enerfund - D2.1 Report on current status of EPC in targeted countries, relevant data from existing initiatives, and on EPC implementation on the real state market," 2016. [Online]. Available: http://enerfund.eu/wp-content/uploads/2018/04/D2.1_Report-on-EPC_Existing-Initiatives_Real-Estate-Market_HP.pdf.

[15] S. Gokarakonda, M. Venjakob, and S. Thomas, "QualDeEPC - D2.1 Report on local EPC situation and cross-country comparison matrix." QualDeEPC project, pp. 1–120, 2020, [Online]. Available: www.qualdeepc.eu.

[16] Y. Li, S. Kubicki, A. Guerriero, and Y. Rezgui, "Review of building energy performance certification schemes towards future improvement," *Renew. Sustain. Energy Rev.*, vol. 113, Oct. 2019, doi: 10.1016/j.rser.2019.109244.

[17] The European Commission, "Concerted Action EPBD," *Outputs*. https://epbd-ca.eu/ca-outcomes (accessed Dec. 30, 2021).

[18] J. Las-Heras-Casas, L. M. López-Ochoa, L. M. López-González, and J. P. Paredes-Sánchez, "A tool for verifying energy performance certificates and improving the knowledge of the residential sector: A case study of the Autonomous Community of Aragón (Spain)," *Sustain. Cities Soc.*, vol. 41, pp. 62–72, Aug. 2018, doi: 10.1016/j.scs.2018.05.016.

[19] Z. Magyar and G. Nemeth, "D3.4 TripleA-reno combined performance label on energy, indoor environment and well-being," 2020. [Online]. Available: https://triplea-reno.eu/wp-content/uploads/2020/09/TripleA-reno-Deliverable-3.4.pdf.

[20] J. Bendžalová, J. Zirngibl, and D. Muskatová, "ALDREN - D2.2 - ALDREN Methodology note on energy rating procedure," 2020. [Online]. Available: https://aldren.eu/wp-content/uploads/2021/11/D2_2.pdf.

[21] REHVA and U-CERT project partners, "U-CERT - D2.1 Report on implementation of EPC schemes in U-CERT partner countries," 2021.

[22] EPB Center, "U-CERT - D3.1 Proposed converged set of national data sheets for the set of EPB standards," 2021.

[23] Tallinn University of Technology and U-CERT project partners, "U-CERT - D2.4 Review of building performance indicators based on measured data relevant for holistic EPCs."

[24] IRI-UL and U-CERT project partners, "U-CERT - D2.3 Report on users' perception about EPC scheme in U-CERT partner countries."

[25] ISO/TC 163 and CEN/TC 371, "EN ISO 52000-1. Energy performance of buildings. Overarching EPB assessment. Part 1: General framework and procedures." 2017.

[26] S. Verbeke, A. D, G. Reynders, Y. Ma, and P. Waide, "Experimental calculation sheet for SRI assessment method A and/or B (version 3.0A and 3.0B)." SRI technical support study, 2021.

[27] P. Carnero Melero, D. Van Dijk, M. Spiekman, and G. Ana, "U-CERT - D3.2 Development of a set of user centred and effective overall and partial indicators, using SRI," 2021.

Improving Roofs to Reduce Energy and Protect Occupants from Climate Change

Delia D'Agostino[a], *Danny Parker*[b]

[a] European Commission, Joint Research Centre (JRC), Ispra (VA), Italy. Email: delia.dagostino@ec.europa.eu

[b] FSEC Energy Research Center, University of Central Florida, USA. Email: dparker@fsec.ucf.edu

Abstract. Refurbishing existing buildings to reduce energy use is a priority worldwide to reduce greenhouse gas emissions. Millions of buildings have poorly insulated old roofs with large roof surface areas. Covered by photovoltaic (PV) arrays, these roofs could potentially provide significant renewable energy generation. Uninsulated, they increase needs for heating and cooling, while also posing health risks for top-floor occupants during summer heat waves. Such heat waves look to become increasingly common with future climate change. Suspended air conditioning from power interruptions are likely due to excessive system electric demand, earthquake or storm. We analyze an uninsulated apartment building in Milan for several scenarios to save energy while improving occupant comfort in top floor apartments. We evaluate three strategies: added roof insulation, increased roof solar reflectance and covering PV arrays above the roof. We estimate heating and cooling energy savings as well daily temperatures of a roof-adjacent top floor flat under peak summer conditions. We evaluate using current weather TMY 2018 files as well as another morphed to anticipated 2060 weather for the 90% IPCC scenario which represents extreme warming.

Keywords. Roof, insulation, energy, climate change, photovoltaics, comfort.
DOI: https://doi.org/10.34641/clima.2022.69

1. Introduction

Interest in reducing energy consumption in buildings is recognized worldwide as a priority [1]. Buildings account for about 40% of global energy consumption, and 36% of associated CO_2 emissions [2]. Therefore, retrofit is a key factor to achieve the European (EU) 2030 Energy and Climate targets [4]. At the same time, the need to electrify energy demand to facilitate greenhouse gas emission reductions, and reduce both climate change warming potentials and energy dependance, makes it important to locate new available areas for renewable energy production [5]. Building rooftop solar photovoltaic (PV) arrays are a demonstrated means for addressing building energy use since roof areas experience full solar radiation and are freely available for such utilization [6]. World building floor area and associated roof expanses are enormous (223 x 10^9 m^2 globally) [7].

Renewable energy generation from PV production and designing new buildings at nearly or net zero energy consumption has proved feasible around the world [8]. However, achieving effective energy reduction is much more difficult for existing buildings. Insulation retrofit for envelope elements is a frequent intervention in buildings **Error! Reference source not found.**. In particular, roof retrofit is one of the first options selected in building design optimization [10]. Roofs in existing residential buildings are often old and poorly insulated, increasing needs for heating and cooling [11]. Also, poor levels of roof insulation can lead to overheating of top floor apartments during summer [12]. This issue may become crucial under foreseen climate change scenarios of temperature increase and anticipated heat waves [13]. A harmonized approach for roof retrofit is still missing and many interventions are implemented without a comprehensive knowledge of the potential savings and costs [14].

Accordingly, this paper aims at investigating different common scenarios to save energy adding roof insulation, increasing roof solar reflectance, and covering roof with PV arrays. The connected occupant comfort in top floor apartments is included in the analysis.

2. Methodology

We perform an example analysis for an older five-story apartment complex in Milan, Italy. The prototype building is drawn from previous research examining the potential of roofing insulation [15]. Several parameters are defined: roof insulation with materials and thicknesses, with/without PV). We also examine shading from raised stand-off PV arrays and how this influences heat gains and insulation performance.

We consider a fully-electric apartment complex with both current weather as well as weather files

Copyright ©2022 by the authors. This conference paper is published under a CC-BY-4.0 license.

morphed to the year 2060 with the risk of the 90% extreme weather case from the IPCC scenarios. Given the risk of "brown outs" and power interruption during future climate change, we evaluate the risk of high temperatures upper floor apartments in the event of power interruption and not cooling. To address the health risk as well as energy implications, we examined roof insulation, roof reflectance and PV installation to evaluate impacts.

We also examine how improving roof insulation or altering roof surface reflectance might reduce heating and cooling energy consumption while improving comfort in roof-adjacent dwellings. At the same time, we evaluate how much electricity can be generated through combined PV installation at the same time that roofs are thermally improved. For the evaluation, we used the well-accepted EnergyPlus and TRNSYS simulation software, implemented within BEopt, driven by hourly recent weather data, both recent and morphed to the future given expectation of climate change.

3. Retrofit Potential and PV Array Shading of Roofs

Thermal retrofit to building roof and walls are among most implemented interventions for building energy refurbishment. Improving the building envelope is key to controlling thermal losses to outdoor weather extremes and can have strong influences on resulting space heating and cooling needs [16]. Other research has shown the highly reflective roofs are very effective at cutting summer cooling loads, but with negative benefits in winter during heating conditions [17].

Taking advantage of PV systems to generate renewable energy is of growing importance to both cover building energy needs (e.g. equipment and appliances), and contribute delivery to the grid. PV panels are becoming commonplace worldwide and more often integrated as a building material (Fig.1).

Fig.1. a) Examples of rooftop PV systems in existing buildings in Northern Italy with a) showing solar array shading of apartment roof complex.
b) Visible and IR image illustrating impact of shading from photovoltaics on thermal heat gain. Colour is proportional to temperature: white/ red hottest, and black and blue coolest.

However, a remaining advantage of stand-off PV arrays, with an air space below the panels, comes from roof shading and modification to roof surface long-wave radiation to the sky, that affect thermal transmittance and, consequently, cooling and heating loads. Fig.1b provides an empirical evidence of the PV shading influence on roof heat gain from thermography. The shading impact of a South-facing stand-off PV array is evident: the roof surface is hotter outside the PV array shadow and much lower underneath. Thermal impacts of PV stand-off array on roof heat transfer performance underneath are complex depending on array shadow, spacing, tilt, wind as well as roof view factor to the sky.

Although impacts are small save for insulated roof assemblies, they can be important, however, for existing residential buildings that cannot be easily insulated. Tsurusaki et al. [18] observed an average 26% reduction in monitored space cooling after rooftop PV panels were installed atop Japanese buildings. Dominguez et al. [19] saw a 38% reduction in roof heat gain during the cooling season in San Diego, California. Kapsalis and Karamanis [20] measured and simulated a 17.6% decrease to space cooling in Western Greece. Decreased solar irradiance in winter, can potentially increase heating through lost roof solar absorption, but altered long-wave re-radiance may provide a partially compensating effect. Estimation of impact is accomplished within the EnergyPlus simulation by assuming that the PV array covered portion of the roof has a 90% interruption of incident solar radiation compared to the exposed sections. However, the long-wave emittance of this covered section is also altered from 0.92 for fully exposed sections vs. 0.10 for the covered segments.

3.1 Baseline building prototype

Using the Tabula classification [21], we created a multi-story apartment complex prototype to represent residential urban level density. Characteristics are detailed (Tab. 1).

Tab. 1. Roof description for analysis of the apartment complex.

Insulation level	Description	heat transfer coefficient (W/m²K)	Scheme
No	Flat roof with reinforced brick-concrete slab.	2.00	
Low		0.80	
Medium		0.60	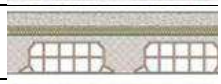
High		0.35	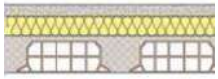
Very high		0.20	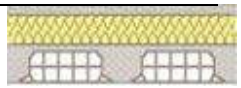
Extra high		0.15	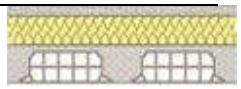

Typical roof type for the apartment complex was identified from the Tabula research, differentiated into six different insulation levels (Tab. 2).

The overall U-factor of heat transfer depends on the insulation of the roof/ceiling. Overall conductance varies was estimated from 2.00 and 0.15 W/m²K depending on insulation level. However, buildings older than 1976 had generally lower or no insulation with typical conductance of ~2 W/m²K. Based on previous evaluation of a cost effective retrofit for apartment complexes that considering PV with electrical storage and likely economic parameters, we showed the very high insulation level (0.15 W/m²K) was justified [14]. We thus confined our evaluation for Milan to the uninsulated case or an insulated one with 0.20 W/m²K.

The structure has five floors and a total of 50 apartments (81 m² each) separated on either side by an access corridor. In future years, all-electric buildings in Europe will likely be advocated. Recent world events emphasize the need to reduce dependency on natural gas and oil. Thus, we assumed a future with all-electric buildings with efficient heat pumps (COP=3.5 heating/ COP 4.1 for cooling).

Tab. 2. Summary and thermal characteristics of the existing apartment prototype.

Building type	Apartment complex
Example	
Model rendering	
Area (m²)	4056
Units	50
Roof area (m²)	811
Available PV area (m²)	650
PV power capacity DC (kW)	138
Windows	120m² with double clear glass (2.2 W/m²K); 24 m² corner apartments
Walls	Low insulation (0.8 W/m²K)
Ceiling	Uninsulated (2 W/m²K)
Doors	Uninsulated (2.86 W/m²K)
Air leakage	4 ACH at 50Pa blower door pressure
Heating system	Air source heat pump; COP= 3.5
Cooling system	COP 4.1 mini-split cooling system
Hot Water	Electric boiler providing 76 l per day at 55°C per unit (50 units)
Mechanical ventilation	13.7 l/s per apartment, continuous with 72% ERV(50 units)

3.2 Installed Rooftop PV Array

The number of high-efficiency PV modules that fit on the building's roof was estimated by calculating the available roof area, assuming that each 21.4% efficient 345 W module has a 1.63 m² footprint with 80% of the gross roof area available for array installation and access. The flat apartment complex roof was modelled as a conventional concrete surface with an 80% solar absorptance and a 92% far-infrared emittance. When a 400 module stand-

off PV array is placed above the roof, they provide solar shading, and also block the surface-view factor and the far-infrared emittance linked to sky radiative heat transfer. Using the approach by Peng and Yang [22], we accounted for PV shading by altering the roof total solar absorptance and the far-infrared emittance. We assumed that the roof under the PV arrays has no effective view factor with limited solar exposure or long-wave heat transfer.

4. Energy simulations and results

Energy simulations were performed using BEopt, developed by the U.S. National Renewable Energy Laboratory [23]. The tool performs hourly energy calculations using the EnergyPlus simulation developed by the Lawrence Berkeley National Laboratory and the U.S. Department of Energy]. It estimates energy loads related to heating, cooling, water heating and appliances. Renewable energy production from photovoltaic systems is predicted using the state-of-the-art TRNSYS simulation [24]. To evaluate interaction with expected climate change we used TMY 2018 files morphed to expected conditions in the year 2060 under the IPCC 90% scenario that would approximate extreme future warming [25][26]. Results are in Tab. 3.

Tab. 3. Predicted energy performance with and without PV shading using 2018 and 2060 Extreme Weather.

Insulation level	Cooling (kWh)	Heating (kWh)	Total (kWh)	Cooling savings (%)	Heating savings (%)	Heat/cool energy savings (%)
2018 TMY						
Without PV shading						
No Insulation	18256	53215	71471	0.0	0.0	0.0
U-0.2W/m²K	14768	36222	50990	19.1%	31.9%	28.7%
Reflective Roof	14710	59332	74042	19.4%	-11.5%	-3.6%
With PV shading						
No Insulation	15240	53429	68669	16.5%	-4.0%	3.9%
U-0.2W/m²K	14393	36418	50811	21.1%	31.2%	28.9%
2060 Extreme Weather (90% IPCC Scenario)						
Without PV shading						
No Insulation	40191	31521	71471	0.0	0.0	0.0
U-0.2W/m²K	33391	19056	50990	16.9%	39.5%	28.7%
Reflective Roof	34308	35308	69616	14.6%	-12.0%	2.6%
With PV shading						
No Insulation	35783	30947	66730	11.0%	1.8%	6.6%
U-0.2W/m²K	32781	19071	51852	18.4%	31.2%	27.5%

As seen in Tab. 3, the savings derived from added insulation level were 28.7% of total energy for heating and cooling. For the 2018 weather data, the 138 kWDC rooftop PV system is predicted to produce 146817 kWh annually. Total annual energy use for all end-uses (appliances, lighting and miscellaneous in addition to heating and cooling) is estimated at 297233 kWh for the apartment complex, such that with added insulation (consumption falls to 276633) the generated renewable electricity is 46.9% of annual consumption. For the 2060 extreme conditions, similar thermal influences are seen although heating is significantly lower in Milan and cooling is more than doubled. Total predicted annual energy end uses for 2060 are 284338 kWh, down to 263857 with insulation against 164,818 kWh produced by the PV system. PV output is grows with climate change as winter skies are expected to exhibit reduced cloud cover [27].

As PV-related shading in 2018 reduced cooling by 16.5% (3016 kWh savings) when added to the uninsulated apartment complex (Tab. 3). Little impact on heating was observed (+214 kWh/year). The impact of shading fell sharply when insulation was added. Shading reduced cooling by 2.5% (375 kWh) when added to a well-insulated roof, it increased heating by 0.5% (196 kWh). A reflective membrane (70% reflectance) added to the uninsulated roof is very effective to reduce space cooling, but significantly increased space heating in winter.
Accordingly, this option does not appear well suited for Milan. It may do very well, however, in other Mediterranean locations with negligible winter heating—particularly within future climate.

4.1 Rooftop PV shading as aid to lack of cooling or summertime power interruption

Roof insulation retrofit with added PV can also have large potential impacts on comfort and safety in existing apartment buildings during summer heat waves. Many flats in older apartment buildings with low levels of insulation in Europe lack cooling systems. With increased summertime heat waves expected from climate-related warming, the top floor apartments adjacent to the roof deck under full sun can experience much higher levels of heat accumulation during summer heat waves that can endanger the health of occupants, particularly the elderly [28][29][30].

Even in flats with cooling systems, there is the possibility of equipment failure. Also with increased heatwaves in the future, there are increased chances that utilities may experience “brownouts” where power for cooling and or heating systems are temporarily unavailable [31][32]. Under full sun, the upper floor apartments can become exceedingy hot and are notoriously difficult to ventilate with limited cross ventilation [33] [34].

With simulation, we examined the air temperatures within the top floor apartment flats with the cooling system disabled on the hottest summer day. We examined predicted performance both with and without insulation and a shading cover from an expansive rooftop PV system (Fig.2).

Shading from the rooftop PV system appeared effective in controlling excess heat accumulation in the top floor dwellings, particularly when matched with insulation. On 18 July, the hottest day on the Milan weather file, the elevated indoor temperatures in simulated inside flat 47 next to the uninsulated roof were much more moderate with the PV system overhead. During evening hours around 10 pm on this very hot day, the peak inside air temperature in the uncooled and uninsulated flat was predicted at 40.7 °C against 35.6 °C with insulation added.

However, providing PV shading over the top of the roof in the apartment complex with insulation as well was predicted to drop the inside flat temperature without cooling to 33.6 °C, only slightly above the outdoor temperature. While not comfortable, is indicates a very significant improvement in interior comfort and one to less dangerous to vulnerable occupants. As seen with the much hotter extreme weather for 2060 (peak outdoor temperature is 40 °C), the differences in heat accumulation could easily impact occupant mortality as the differences in insulation and shading represent a 7 °C difference in peak room temperatures without mechanical cooling.

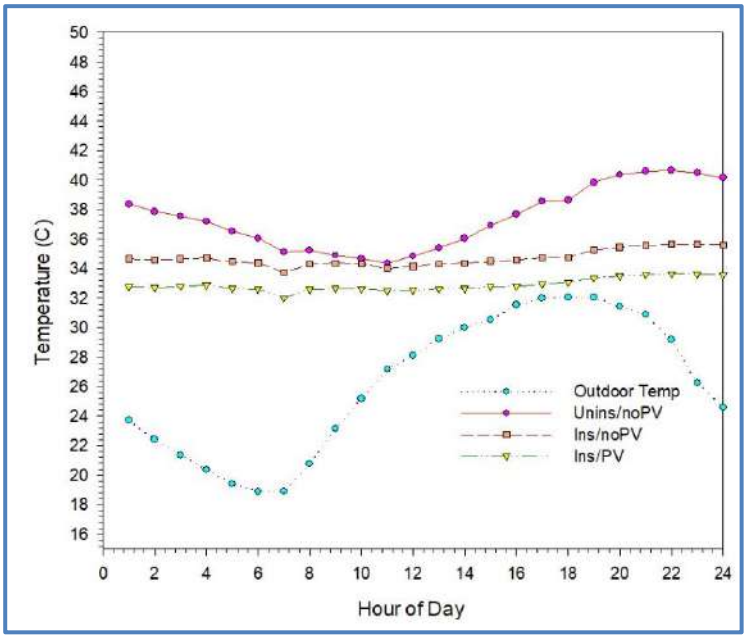

a)

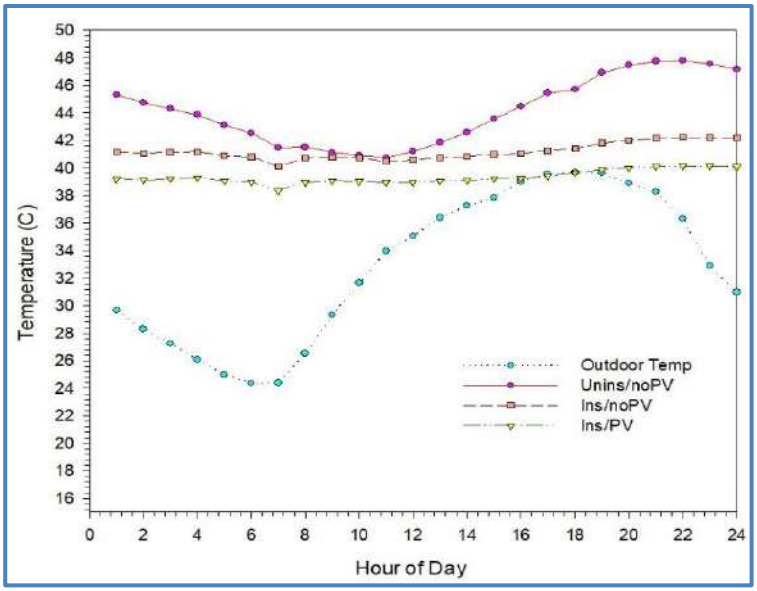

b)

Fig.2. Comparison of simulated top floor apartment air temperatures adjacent to roof on summer peak day with and without roof shading from PV arrays and insulation (*Unins/Ins*). Blue dotted line and symbols are the outdoor temperatures on 18 July on the 2018 TMY Milan weather file. Fig. 2b shows the same date for a weather file morphed to the 90% IPCC condition in 2060.

5. Conclusions

Roof retrofit for existing buildings becomes a priority compared to other measures when considering potentials to reduce energy use, generate PV electricity and improve power interruption resiliency. Around the world, poor roof insulation can lead to considerable overheating of top-floor apartments during summer heat waves with increased mortality for some occupants paricularly the health-challenged. Full electrication is also desireble along with efficiency to prevent interruption of natural gas supplies from threating comfort and well being.

We conducted an evaluation of potential energy savings from combining roof insulation with PV electricity generation. For the first time, the overhead shading of solar and long-wave roof irradiance associated with stand-off PV arrays was approximated as part of the evaluation.

Our example analysis for Milan, Italy evaluated a roof insulation retrofit to the roof of an apartment complex combined with or without the installation of rooftop PV. Simulations show that adding insulation to uninsulated apartment prototype was shown to cut heating by 31.9% and cooling by 19.1%. Meanwhile, PV generation can provide up to 46% or

more of annual energy needs for a fully electrified complex. We summarize key conclusions:

- Shading from stand-off PV arrays can reduce overheating of uninsulated roofs during summer. Predicted energy required for cooling can be reduced by up to 16.5%.
- PV arrays that cover and shade building rooftops can improve interior comfort in top floor dwellings which may not have cooling systems or whose cooling systems may not be functional. In particular, this provides important protection for health and safety of top-floor apartment dwellers. We saw decreases in temperature in roof adjacent flat without mechanical cooling of 5-7 °C —depending on the presence of insulation and shading from an overhead PV system. These differences are potentially significant to occupant safety, particularly for the elderly.
- Weather files morphed to represent extreme future climate suggest insulation and shading of upper floor apartment roofs may be important to public safety during heat waves if power is interrupted.

In summary, ourresults suggest adding insulation and rooftop PV arrays can not only save energy and produce significant electricity (nearly half for a an electrified apartment complex), but can also help protect building occupant health and safety. in the event of energy interruption.

6. Acknowledgments

The views expressed are purely those of the authors and do not represent any official position of the European Commission or the University of Central Florida. The authors wish to thank Christian Thiel and Maurizio Bavetta (JRC) and James Fenton (FSEC/UCF) for supporting this research.

7. References

[1] International Energy Agency, 2017. Tracking clean energy progress 2017 informing energy sector transformations. http://www.iea.org/publications/freepublications/publication/TrackingCleanEnergyProgress2017.pdf

[2] D'Agostino D, Tsemekidi Tzeiranaki S, Zangheri P, Bertoldi P, Assessing Nearly Zero Energy Buildings (NZEBs) development in Europe, Energy Strategy Reviews, https://doi.org/10.1016/j.esr.2021.100680.

[3] Congedo PM, Baglivo C, Zacà I, D'Agostino D, High performance solutions and data for nZEBs offices located in warm climates, Data in Brief, Volume 5, Pages 502–505, December 01 2015, DOI 10.1016/j.dib.2015.09.041

[4] Congedo PM, Lorusso C, De Giorgi MG, Marti R, D'Agostino D, Horizontal air-ground heat exchanger performance and humidity simulation by computational fluid dynamic analysis, Energies, Volume 9, Issue 112016, DOI 10.3390/en9110930

[5] D'Agostino D, Cuniberti B, Bertoldi P, Data on European non-residential buildings, Data in Brief, Volume 14, Pages 759 – 762, October 2017, DOI 10.1016/j.dib.2017.08.043

[6] Poul Alberg Østergaard, Neven Duic, Younes Noorollahi, Hrvoje Mikulci, Soteris Kalogirou, Sustainable development using renewable energy technology, Renewable Energy, Volume 146, February 2020, 2430-2437,https://doi.org/10.1016/j.renene.2019.08.094

[7] Giorgos S. Georgiou, Paul Christodoulides, Soteris A. Kalogirou, Optimizing the energy storage schedule of a battery in a PV grid connected nZEB using linear programming, Energy 208 (2020) 118177.

[8] Wang Ran, Feng Wei, Wang Lan, Lu Shilei, A comprehensive evaluation of zero energy buildings in cold regions: Actual performance and key technologies of cases from China, the US, and the European Union, Energy, https://doi.org/10.1016/j.energy.2020.118992

[9] D'Agostino Delia, Zacà Ilaria, Baglivo Cristina, Congedo PaoloMaria, Economic and thermal evaluation of different uses of an existing structure in a warm climate, Volume 10, Issue 59, May 2017. Article number 658, DOI 10.3390/en10050658

[10] Delia D'Agostino, Danny Parker, Data on cost-optimal Nearly Zero Energy Buildings (NZEBs) across Europe, Volume 17, Pages 1168 – 1174, DOI 10.1016/j.dib.2018.02.038

[11] D'Agostino D, Tsemekidi Tzeiranaki S, Zangheri P, Bertoldi P, Data on nearly zero energy buildings (NZEBs) projects and best practices in Europe, Data in Brief, 2021, 39,107641, 10.1016/j.dib.2021.107641

[12] Aditya L., Mahlia T.M.I., Rismanchi B., Ng H.M., Hasan M.H., Metselaar H., Oki Murazaf, H. Aditiya, A review on insulation materials for energy conservation in buildings, Renewable and Sustainable Energy Reviews 73 (2017) 1352–1365.

[13] Zacà Ilaria, D'Agostino Delia, Congedo PaoloMaria, Baglivo Cristina, Assessment of Cost-Optimality and Technical Solutions In High Performance Multi-Residential Buildings in The Mediterranean Area, Energy and Buildings, http://dx.doi.org/10.1016/j.enbuild.2015.04.038.

[14] Delia D'Agostino, Danny Parker, Paco Melià, Giovanni Dotelli, Optimizing photovoltaic electric generation and roof insulation in existing residential buildings, Energy and Buildings, Volume 255, 2022.

[15] D'Agostino, D., Parker, D., Melià, P., Dotelli, G., Data on roof renovation and photovoltaic energy production including energy storage in existing residential buildings , Data in

Brief 41,107874
[16] Collier, Z. A., Wang, D., Vogel, J. T., Tatham, E. K., Linkov, I., 2013 Sustainable roofing technology under multiple constraints: a decision-analytical approach. Environ Syst Decis (2013) 33:261–271.
[17] Piselli C., Saffari, M., de Gracia, A., Pisello, A., Cotana, F., Cabeza, L., Optimization of roof solar reflectance under different climate conditions, occupancy, building configuration and energy systems, Energy&Buildings 151 (2017) 81–97.
[18] Tsurusaki T., Tanaka A., Nakagami H., Evaluation of Photovoltaic Power Generation Systems in Residential Homes in Japan: A Partnership Program of Utility and Consumers' Cooperative, 2000, Proceeding of the ACEEE 2000 Summer Study on Energy Efficiency in Buildings, Vol.1, 355-366, American council for an Energy Efficient Economy, Pacific Grove, CA.
[19] A. Dominguez, J. Kleissl, J.C. Luvall, Effects of solar photovoltaic panels on roof heat transfer, Sol. Energy. 85 (2011) 2244-2255. https://doi.org/10.1016/j.solener.2011.06.010.
[20] V. Kapsalis, D. Karamanis, On the effect of roof added photovoltaics on building's energy demand, Energy Build. 108 (2015) 195-204. https://doi.org/10.1016/j.enbuild.2015.09.016.
[21] Ballarini, I., Cognati, S.P., Corrado, V. (2014). Use of reference buildings to assess the energy saving potentials of the residential building stock: the experience of TABULA project. Energy Policy: 273–284, DOI: 10.1016/j.enpol.2014.01.027.
[22] Peng, C., Yang, J., The Effect of Photovoltaic Panels on the Rooftop Temperature in the EnergyPlus Simulation Environment, International Journal of Photoenergy, 2016, http://dx.doi.org/10.1155/2016/9020567
[23] Rhodes Joshua D., Gorman William H.,. Upshaw Charles R, Webber Michael E., Using BEopt (EnergyPlus) with energy audits and surveys to predict actual residential energy usage, Energy and Buildings 86 (2015) 808–816, http://dx.doi.org/10.1016/j.enbuild.2014.10.076
[24] Klein SA, et al. TRNSYS 17: a transient system simulation program. Madison, USA: Solar Energy Laboratory, University of Wisconsin; 2010. http://sel.me.wisc.edu/trnsys.
[25] D. D'Agostino, D. Parker, I. Epifani, D. Crawley, L. Lawrie, How will future climate impact the design and performance of nearly zero energy buildings (NZEBs)?, Energy, Volume 240, 2022.
[26] S.E. Belcher, J.N. Hacker, D.S. Powell Constructing design weather data for future climates Build Serv Eng Technol, 26 (1) (2005), pp. 49-61.
[27] Hou, Xinyuan & Wild, Martin & Folini, Doris & Kazadzis, Stelios & Wohland, Jan. (2021). Climate change impacts on solar power generation and its spatial variability in Europe based on CMIP6. Earth System Dynamics. 12. 1099-1113.
[28] Conti S, Meli P, Minelli G, Solimini R, Toccaceli V, Vichi M, Beltrano C, Perini L. Epidemiologic study of mortality during the Summer 2003 heat wave in Italy. Environ Res. 2005 Jul;98(3):390-9.
[29] Kovats, R.S., Kristie, L.E, 2006, "Heat Waves and Public Health in Europe," European Journal of Public Health, Vol. 16 (6), (2006), 592-599.
[30] Quinn, A., Kinney, P and Shaman, J. "Predictors of summertime heat index levels in New York City apartments," Indoor Air, 2017, Jul: 27(4) 840-851.
[31] Añel, J.A., Fernández-González, M., Labandeira, X, López-Otero, X. and de la Torre, L., "Impact of Cold Waves and Heat Waves on the Energy Production Sector," Atmosphere, 2017, 8, 209.
[32] D'Agostino, D., Tzeiranaki, S.T., Zangheri, P., Bertoldi, P., Assessing Nearly Zero Energy Buildings (NZEBs) development in Europe, Energy Strategy Reviews 36,100680, 10.1016/j.esr.2021.100680
[33] D'Agostino, D., Parker, D., Melià, P., Environmental and economic data on energy efficiency measures for residential buildings, Data in Brief 28,104905, 10.1016/j.dib.2019.104905
[34] D'Agostino, D., Mazzarella, L., Data on energy consumption and Nearly zero energy buildings (NZEBs) in Europe, Data in Brief 21, pp. 2470-2474, 10.1016/j.dib.2018.11.094

Data Statement

The datasets generated during and/or analysed during the current study are not available because not yet published, but the authors will make every reasonable effort to publish them in near future.

Predictive and flexible system controller for hybrid power supply systems

Martin Knorr [a], Tim van Beek [a], Maximilian Beyer [a], Lars Schinke [a], Joachim Seifert [a]

[a] Chair of Building Energy Systems and Heat Supply, Institute of Power Engineering, Faculty of Mechanical Science and Engineering, Technische Universität Dresden, Dresden, Germany, martin.knorr@tu-dresden.de.

Abstract. Regarding the overall efficiency of hybrid power supply systems, a system controller as an addition to device controllers was developed to contribute to its increase. An essential premise in the development of such a controller was the modular structure and the implementation as an open source solution. By using the MQTT protocol, the controller can operate within an IoT-network and hence be used universally, e.g. in a Software- (SiL) or in the Hardware-in-the-loop (HiL) environment as well as in field test. In order to make optimal use of the flexibilities provided by thermal or electrical storages, MPC (Modell Predictive Control) functionalities were implemented in the controller, which, however, are supported by rule-based algorithms on a "fallback level". The target values of the control can be adjusted variably and include economical as well as ecological aspects in a weighted way. The open structure of the controller makes it possible to easily include other system components in the control concept and also to operate the controller either locally, in an edge device or in a cloud environment. The performance of the controller was demonstrated by SiL- and HiL-tests. Here, annual characteristic values were determined on the basis of representative days. The representative days were selected using a cluster procedure. Overall, energy and cost savings can be demonstrated by using the controller, which are particularly effective in the optimized use of electricity from photovoltaic systems in combination with heat pumps.

Keywords hybrid energy systems, heat pump systems, sector coupling, renewable energies, carbon footprint, model predictive control.
DOI: https://doi.org/10.34641/clima.2022.278

1. Introduction

Driven by efforts to save energy and decarbonize the building sector, hybrid systems for supplying energy to buildings are becoming increasingly important [1]. Here, generators using fossil fuels or heat pumps are often combined with renewable energies. A central system controller or energy manager is required to ensure that the individual components, which are often highly developed, also achieve high energy efficiency values in the overall system. Particularly noteworthy in this context is the possibility of combining diverse components from different manufacturers into a complex energy system and supporting the sector coupling between electricity and heat. For the improvement of the self-consumption share and economic efficiency of photovoltaic systems, energy management systems with predictive features are beneficial. In a research project, a cross-platform system controller was therefore developed and tested in a Software-in-the-loop (SiL) and further in a Hardware-in-the-loop (HiL) environment. The procedure using HiL and SiL investigations was pre-developed and successfully tested in previous research projects [2], [3], [4], [5], [6]. An essential premise in the development of the controller is the use of an open source software structure, which, due to its modular design and the use of the MQTT protocol, allows a rapid adaptation to a wide range of energy systems. This approach distinguishes the controller from other state-of-the-art solutions, which are partly proprietary or have been strongly adapted to specific energy systems. With regard to the energy management functions, MPC algorithms allow the utilisation of further savings potentials compared to rule-based functions [7]. Thus, MPC functions were implemented for a setup with a thermal and an electrical storage. The following article presents the software architecture of the controller and the description of selected services. In addition, a use case is described in the article and economical and ecological effects of the controller operation are shown and discussed.

2. Architecture of the controller

2.1 Fundamental consideration

Python was chosen as the programming language for the development of the platform controller. To ensure a stable workaround (interpreter, package versions, etc.), poetry [8] is also used, where corresponding requirements are defined and the system controller can be executed in a virtual environment. The MQTT protocol [9] is used for the machine-to-machine (M2M) data transfer, which means that network access is a minimum requirement for using the system controller. MQTT is considered a standard protocol in the IoT sector and is particularly suitable for the data transport of telemetry data, such as sensor values, etc.

Copyright ©2022 by the authors. This conference paper is published under a CC-BY-4.0 license.

In the context of the project, MQTT is used via TCP (transmission control protocol). The quality of service (QoS) is set to zero, i.e. each message is sent at most once. The QoS is adjustable if a higher reliability of the data transport is required. The possible QoS are:

- QoS = 0: The message is sent at most once
- QoS = 1: The message is sent at least once
- QoS = 2: The message is sent exactly once.

The message broker (server) used is Eclipse Mosquitto [10], which is available as open source software. There exist many alternatives and it could also be replaced by cloud solutions, for instance. In the context of the project, the "localhost" as a broker address is used, i.e. the end device on which the platform controller is executed also serves as a broker.

The system controller thus represents a client in the client-server structure of MQTT and communicates with all system components that are also MQTT-capable. If no MQTT interface is available, it is conceivable to upgrade the component (e. g. through MQTT gateways), which can convert the MQTT messages into any signals (e. g. serial communication standards as RS-485). Due to the broad application of MQTT in the IoT area, various gateways are already established on the market.

2.2 Structure of the system controller

The system controller has a modular structure and is supplemented by corresponding scripts as functions are expanded. According to Fig. 1, each component of the real plant system is mapped as a separate client in the platform controller and is both publisher (source) and subscriber (sink).

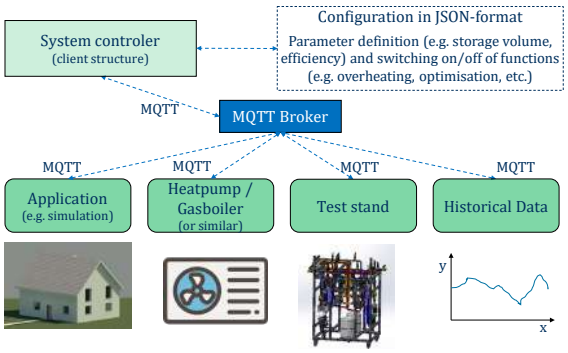

Fig. 1 – Structure of the system under consideration

The individual clients are configured via configuration files in JSON format. Each client is assigned to a specific JSON file (client-JSON pair). Within the configuration files, a unique assignment of parameters and their values ('key-value' assignment) is made, which can be adapted to the desired system. On the one hand, these can be constant parameters, such as a nominal power. On the other hand, the assignment can be to a specific address (topic) through which the clients send or receive their (transient) measured values to or from the broker in real time.

The heart of the system controller is an energy manager to which all measured and calculated values of the clients are transferred. Based on these values, rule-based decisions are made here. Depending on the configuration, the energy manager decides, among others, whether to switch-on the energy converters in a hybrid system, whether to feed-in or charge a battery using photovoltaic yield, and whether to switch between heating and cooling mode using heat pumps with cooling function. An overview of the decisions about switching-on the energy converters in the current project is provided in the Fig. 2.

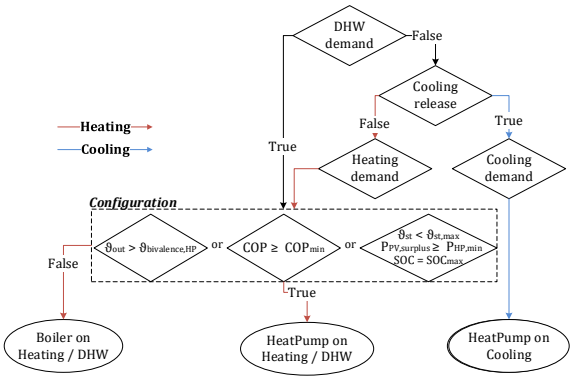

Fig. 2 – Decision tree of the energy manager

If part of the energy system, a photovoltaic system can be taken into account while deciding whether an electrically driven heat pump or an electric heating element is to be preferred. Moreover, the system controller provides an overheating function to heat up thermal storages using photovoltaic yield while there is no heating demand. For this purpose, energy characteristics of the appliances, status information of the thermal storage units as well as a weather forecast must be taken into account for the prediction of the heat pump efficiency. As mentioned, it is necessary that the components are MQTT-capable for this. Each of the components is configured as a controller client in the platform controller and can be added via TRUE/FALSE assignments in the energy manager (see Fig. 3).

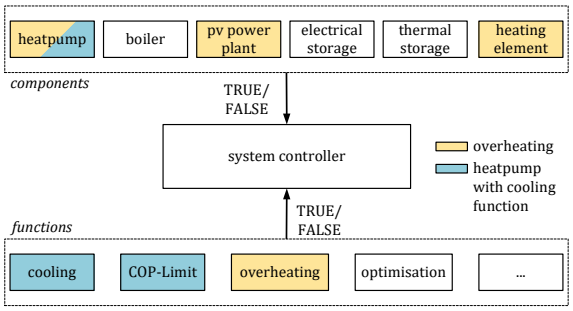

Fig. 3 – Possible assignments of the system controller

2.3 Model Predictive Control (MPC) algorithm

For the MPC control function, forecast data of the weather, energy generator and the PV yield are necessary. Within the project, the forecast values are, among others, determined both from measured data using regression and from known annual load and yield profiles. The last mentioned is thus considered as a perfect forecast and essential for determining the maximum possible benefit. For determining the forecasts from historical data and in addition to the implementation of appropriate measuring equipment, a data storage function must be implemented, which saves historical data on a sliding basis over a certain period of time (e.g. the last 72 hours). A snapshot is provided by the Fig. 4. Fine-tuning or improving forecasting functions is not intended to be part of this project. In the system controller, the possibility of both reading profiles and determining the forecasts based on historical data are implemented and can be selected accordingly.

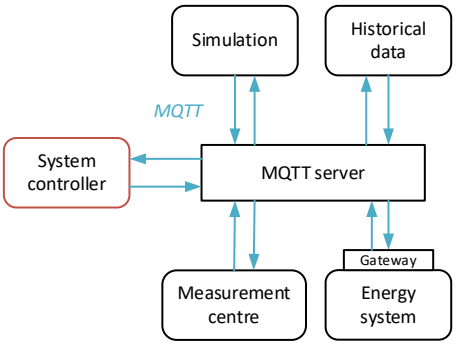

Fig. 4 – Basic communication structure of the system

The forecasts are determined for the following parameters:

- Heating/Cooling energy demand
- Energy demand for domestic hot water
- Electrical energy demand of the single-family house (without energy supply)
- Photovoltaic output
- Outside temperature (for determining COP/EER for heatpump)

The *heating energy demand* forecast is a form of trend forecast using linear regression. The method was used and validated in multiple studies [11], [12], [13]. The basis of the trend procedure is historical data of the heating load and the outdoor temperature ($Q_{i,j}$ and $\vartheta_{a,i,j}$ respectively) based on 72 hours (≙n=3 days). The heating energy demand for the next timestep Q_{i+1} is calculated according to the equations (1) to (3).

$$Q_{i+1} = m_i \cdot \vartheta_{a,i+1} + t_i \tag{1}$$

with

$$m_i = \frac{\sum_{j=0}^{n}(\vartheta_{a,i,j} - \bar{\vartheta}_{a,i}) \cdot (Q_{i,j} - \bar{Q}_i)}{\sum_{j=0}^{n}(\vartheta_{a,i,j} - \bar{\vartheta}_{a,i})^2} \tag{2}$$

$$t_i = \bar{Q}_i - m_i \cdot \bar{\vartheta}_{a,i} \tag{3}$$

Within the scope of the project, an annual load profile of a single-family house is used to enable a perfect forecast for the *electrical energy demand.* If no profile is available, the average value of the last few days at the respective time can be determined and used as an alternative. In the mean value procedure, weekdays are not taken into account, as otherwise a large amount of historical data would be required.

The *photovoltaic output* is determined either via the persistence method using a "clear-sky" factor or via an annual load profile. In the scope of the project, an annual load profile was used. The persistence method is presented as follows: A clear-sky factor $f_{sky,i}$ is determined from the ratio of the instantaneous value $W_{PV,i}$ to the maximum photovoltaic yield $max(W_{PV,j})$ of the historically considered time, see equation (4).

$$f_{sky,i} = \frac{W_{PV,i}}{\max(W_{PV,j})} \tag{4}$$

The clear-sky factor is then used to determine the photovoltaic output forecast for the next timestep, see equation (5).

$$W_{PV,i+1} = W_{PV,i} \cdot f_{sky,i} \tag{5}$$

3. Case study

3.1 Use cases

For the simulation investigations and as software within the coupling in the HiL test, the numerical simulation programme (TRNSYS-TUD) [14] is used. This is a comprehensively revised and expanded program version of the commercial simulation program TRNSYS. The reliability of the source code has been extensively tested in numerous studies [14], [15], [16].

Building under consideration

The project examines a single-family building with an underfloor heating system in TRNSYS-TUD (see Fig. 5).

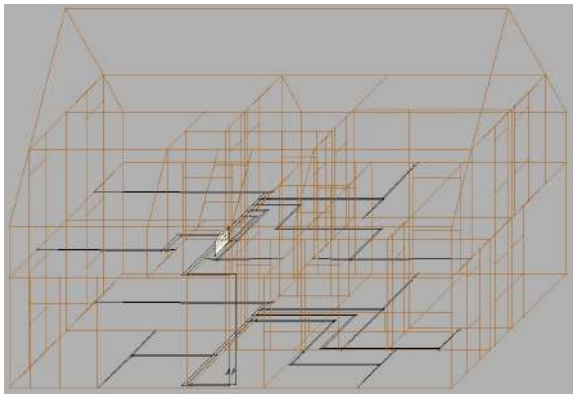

Fig. 5 – Single-family building in TRNSYS-TUD

A detailed description of the model can be found in [17]. The building is set up as follows:

- Heated floor space: 158 m^2
- Heating load according to DIN EN 12831 [18]: 53 W/m^2
- Domestic hot water profile "L" according to EN 13203-4 [19]

Energy system

The energy system contains the following parts (see Fig. 6):

- Underfloor heating system according to DIN EN 1264-3 [20]
- Air-to-water heat pump with cooling function, outdoor installation
- Gas condensing boiler
- Photovoltaic plant
- Thermal storages (heating and cooling)
- Electrical storage

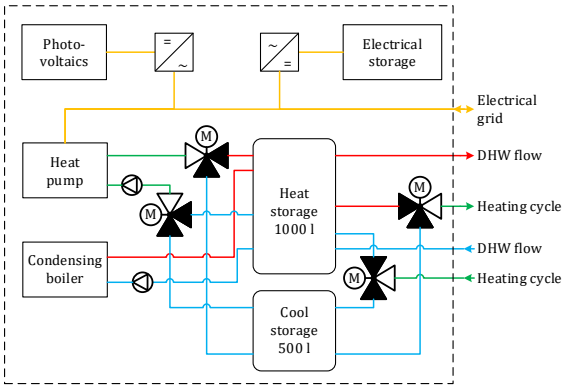

Fig. 6 – Energy system under consideration

Software-in-the-loop (SiL)

The system controller was first tested in a software-only environment. The communication via MQTT thus only took place between simulation and system controller, i.e. both the building and the energy system were simulated. A variant study with year-simulations was carried out in which the system controller, starting from a "basic configuration" with the heat pump and the condensing boiler, was increasingly extended with functions and clients to improve the operation of the energy producers. The variants with the operational premises to switch on/off the heat pump according to Fig. 7 were considered.

Starting from switching-on the heat pump only considering a fixed bivalence temperature (variant 1), the heat pump in variant 2 is switched-on if a predicted COP value exceeds a specified limit value. In variant 3, a PV system is added and PV yield is used for driving the heat pump. To use more of photovoltaic yield, the thermal storage can be overheated additionally in variant 4. With a battery in variant 5, the flexibility on the electrical side can also be used for the system control. Variant 6 includes all options and controls the system with an MPC algorithm.

Nr.	Variant	Components	Operational premises
1	Basic configuration		Bivalence temperature
2	+ COP-Limit		Bivalence COP (e.g. based on energy price)
3	+ PV system		Power to heat
4	+ Overheating		Thermal storage is loaded above the target temperature coming from heat curve
5	+ Electrical storage		Power to heat
6	+ Optimisation		Power to heat, MPC-optimisation provides optimised target temperatures

Heat pump Gas boiler PV panel Battery

Fig. 7 – Variants executed in the variant study

The objective function of MPC is the reduction of total system operational costs, which are eventually composed of the costs for operating the condensing boiler and the heat pump and the income from the feed-in tariff, see equation (6). The MPC result is used to determine optimised target temperatures for the thermal storages. The flexibility resulting from the system energy demand, generator outputs and storage capacities, the so called "energy trend band", is used for this purpose. This basic approach has already been successfully tested in further scientific projects with a focus on sector coupling in regional virtual power plants [12], [21]. The whole algorithm is shown in Fig. 8.

$$C_{tot} = \min\left(\sum_{t=0}^{T} C_{HP,t} + C_{boiler,t} - I_{PV,t}\right) \qquad (6)$$

Hardware-in-the-loop (HiL)

In a parallel step, the energy system was transferred from the simulation to the real environment, named as "Combined Energy Lab 2.0" [22] shown in Fig. 9 and 10. The Combined Energy Lab 2.0 consists of three main test facilities that are coupled together. Test facility 1 is the indoor climate room used for testing heat transfer and indoor air quality / thermal comfort issues. Test facility 2 is the outdoor climate room with the capability to set the humidity and air

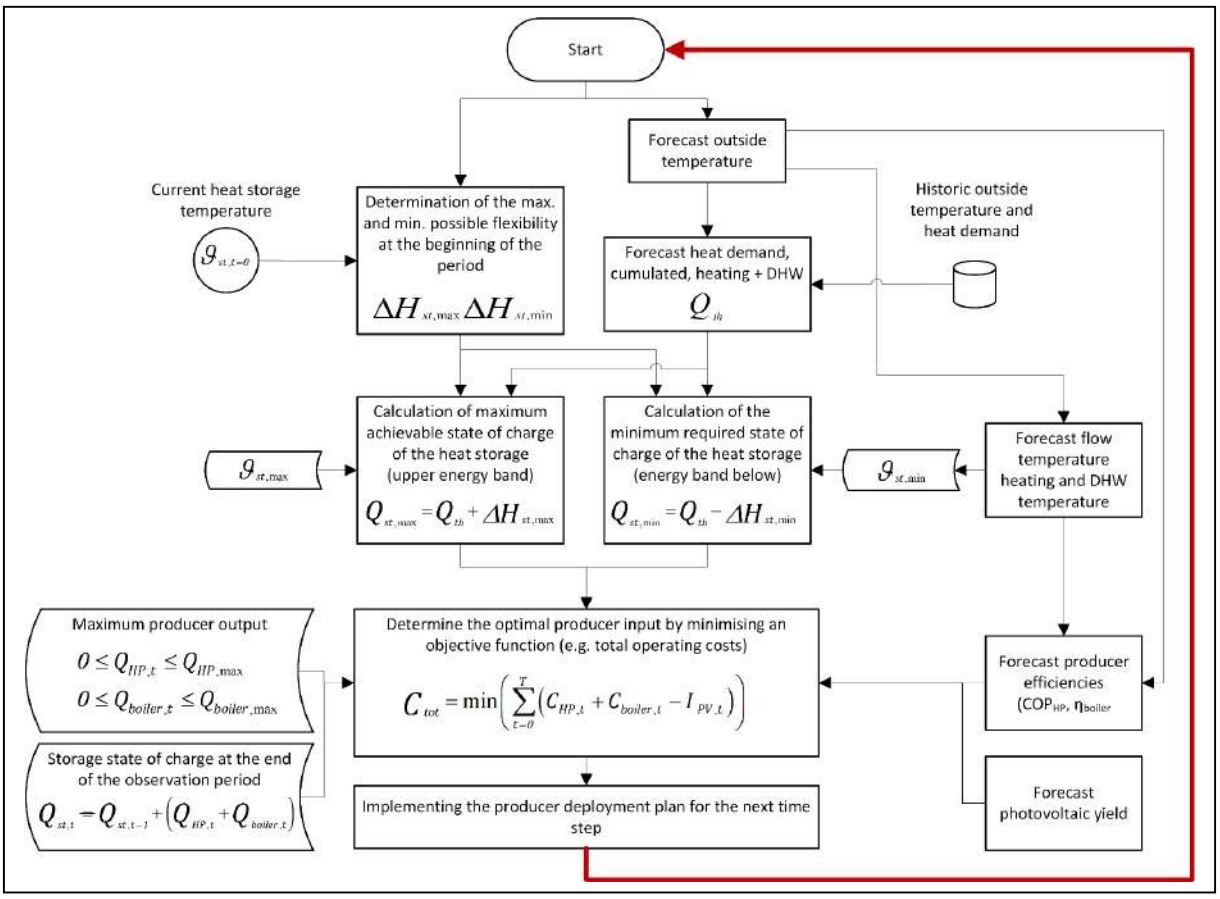

Fig. 8 – Basic MPC algorithm

temperature in a range from ϑ_a = -18 °C … 35 °C, which is used e.g. for testing heat pumps. To ensure the reaction of the building and to be able to perform real-time tests, the so called "energy park" is necessary. The energy park includes heat generators, thermal storage tanks and a hydraulic module for coupling with the building simulation. On the one hand, the required measured values are obtained at the hydraulic module and, on the other hand, the return values from the simulation are set via control valves.

Within the energy park, a low-voltage emulator is also integrated, with which it is possible to vary the characteristics of the electrical distribution network.

The Combined Energy Lab 2.0 offers the possibility to analyse complex energy supply structures. However, since the test time is limited to real time, a type day procedure was developed with which an annual test can reduced to 5 representative type days. Details of the method are documented in [17].

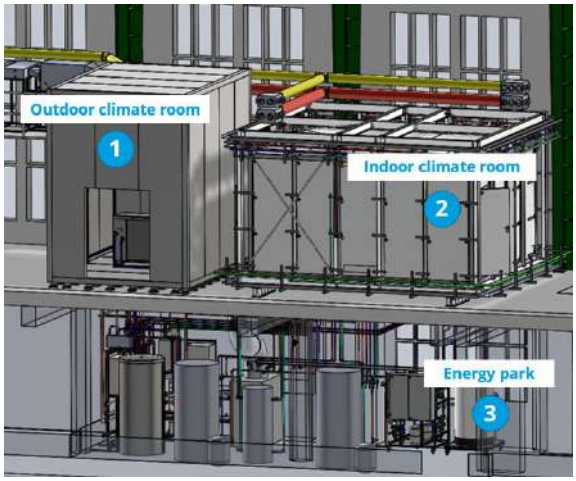

Fig. 9 – Overview about the Combined Energy Lab 2.0

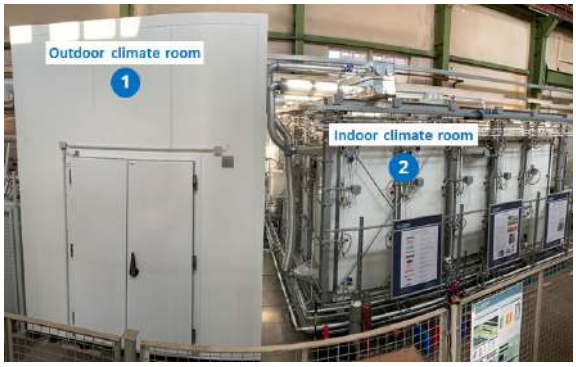

Fig. 10 – Photography of the Combined Energy Lab 2.0

3.2 SiL results

Due to the increasing extensions of the functionalities of the system controller, an increasing needs-based cost reduction can be achieved, as shown in Fig. 11. Regarding e.g. the costs, a reduction of 48 % in the latest expansion stage is possible, depending on the system under consideration. The MPC algorithm can also be used to minimise the CO_2 emissions. However, this was not in the scope of the project.

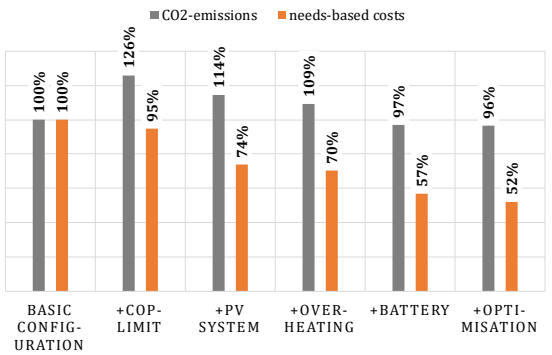

Fig. 11 – SiL results regarding CO2 emissions and needs-based costs

At the same time, it can be seen in Fig. 11 that the MPC control itself provides relatively small cost savings of 5% compared to variant 5 (rule-based algorithms). Here, object-related cost-benefit analysis is required to determine whether the additional expenditure is economical specifically for the forecasts. Furthermore, it can be seen that variants 2-4 lead to higher CO_2 emissions compared to variant 1. This can be explained by the energetically optimised mode of operation, which causes the gas boiler to be switched on more often.

The cost saving of variant 4 compared to variant 5 is caused by the significant increase in the share of self-use of the photovoltaic yields, as the corresponding proportions according to Fig. 12 illustrate. The controlled overheating of the thermal storage tank can also considerably increase the proportion of solar electricity that is used for self-consumption (variant 4 compared to variant 3).

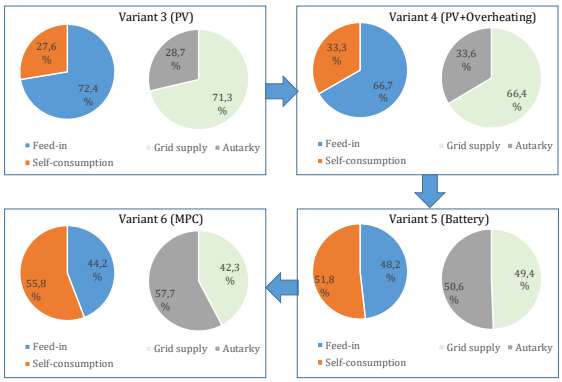

Fig. 12 – SiL results regarding proportions of electrical energy use

3.3 HiL results

The HiL method is particularly useful for repeating tests with identical boundary conditions. Furthermore, there is no longer any dependence on simulation models of the power generation system. Within the project, the reproducibility of representative days can be ensured with a high accuracy. An example is shown in Fig. 13 for a cold representative day, which was conducted three times in total.

Further analyses with regard to the real system behaviour in comparison to the simulation are currently being carried out.

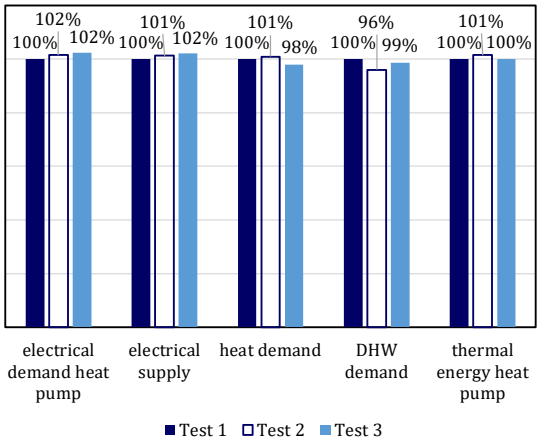

Fig. 13 – HiL reproducibility accuracy of a cold representative day

4. Conclusion

This paper presents the structure, mode of operation and the potential of a system controller in the context of the internet of things. The results are representative but exclusively valid for the system under consideration. Using the highest expansion of the system controller, a needs-based cost reduction of 48 % is possible. However, rule-based algorithms can already reduce costs significantly compared to simple control. Of course, the additional installation costs for the considered additional components must be taken into account. In particular, the MPC-algorithm is able to reduce or expand its influencing factors or change the objective function. Regarding HiL (or field tests), the system controller can be located completely elsewhere than the energy system or the building (simulation), e.g. in cloud-services, and transient Key Performance Indicators (KPI) can be determined.

5. Acknowledgement

This publication is based on a research project which were supported by the German federal ministry of economics and energy under the code 03ET1595B.

6. Symbols and abbreviations

C_{tot}	Total costs	€
$C_{HP,t}$	Total costs for the heat pump	€
$C_{boiler,t}$	Total costs for the boiler	€
$f_{sky,i}$	clear-sky factor	
$I_{PV,t}$	feed-in income	Wh
m_i	Slope	Wh/°C
Q_{i+1}	Heating energy demand forecast	Wh
$Q_{i,j}$	Past heating energy	Wh
$\bar{Q}_i$	Mean past heating energy	Wh
ϑ_a	Outside temperature	°C
$\vartheta_{a,i+1}$	Outside temperature forecast	°C
$\bar{\vartheta}_{a,i}$	Mean past outside temperature	°C
t_i	Ordinate intercept	Wh
$W_{PV,i}$	PV energy output	Wh
$W_{PV,i+1}$	PV energy output forecast	Wh

7. References

[1] V. Quaschnig, Sektorkopplung durch die Energiewende, HTW Hochschule für Technik und Wirtschaft Berlin, 2016.

[2] K. Huchtemann, H. Engels, P. Mehrfeld, M. Nürenberg und D. Müller, „Testing method for evaluation of a realistic seasonal performance of heat pump heating systems: Determination of typical days," in *CLIMA 2016 - proceedings of the 12th REHVA World Congress: volume 3*, Aalborg, Denmark, 2016.

[3] H. Harb, J.-N. Paprott, P. Matthes, T. Schütz, R. S. and D. Müller, "Decentralized scheduling strategy of heating systems for balancing the residual load," *Building and Environment, No. 86,* pp. 132-140, 2015.

[4] M. Knorr, J. Seifert, L. Schinke, P. Mehrfeld and M. Nürenberg, "Using the Hardware-in-the-Loop concept for energetic evaluation of heat generators," in *CLIMA 2019 - proceedings of the REHVA 13th HVAC World Congress*, Bucharest, Romania, 2019.

[5] P. Mehrfeld, M. Nürenberg, M. Knorr, L. Schinke, M. Beyer, M. Grimm, M. Lauster, D. Mülle, J. S. und K. Stergiaropoulus, „Dynamic evaluations of heat pump and micro combined heat and power systems using the hardware-in-the-loop approach," *Journal of Building Engineering 28,* 2020.

[6] A. Adlhoch, A. Hasert, P. Knoll und M. Becker, „Hardware-in-the-Loop Werkzeuge für den Entwurf und den Test von energieeffzienten Raumautomationssystemen in Gebäuden," in *IBPSA BausSim*, RWTH Aachen, 2014.

[7] J. Drgona, J. Arroya, I. C. Figueroa, D. Blum, K. Arendt, D. Kim, E. P. Ollé, J. Oravec, M. Wetter, D. L. Vrabie and L. Helsen, "All you need to know about model predictive control for buildings," *Annual Reviews in Control 50,* pp. 190-232, 2020.

[8] „Poetry packaging and dependency management," 2021. [Online]. Available: https://python-poetry.org/.

[9] „MQTT - Message Queuing Telemetry Transport," 2021. [Online]. Available: https://hivemq.com.

[10] „Eclipse mosquitto, MQTT broker," 2021. [Online]. Available: https://mosquitto.org.

[11] J. Lipp, „Flexible Stromerzeugung mit Mikro-KWK-Anlagen: Experimentelle Untersuchung der Möglichkeiten einer flexiblen Stromerzeugung von Mikro-KWK-Anlagen mit Hilfe einer Wärmebedarfsprognose und einem intelligenten Speichermanagementsystem," Thesis, TU München, 2015.

[12] J. Seifert, J. Werner, P. Seidel and e. al., "RVK II - Praxiserprobung des Regionalen Virtuellen Kraftwerks auf Basis der Mikro-KWK-Technologie," VDE Verlag, 2018.

[13] P. Seidel, „Ein Beitrag zur energetischen Analyse von vernetzten Energiesystemen am Beispiel von Klein-KWK-Anlagen (virtueller Verbund)," Thesis, TU Dresden, 2019.

[14] A. Perschk, „Gebäude und Anlagensimulation - Ein "Dresdner Modell"," *gi Gesundheits-Ingenieur - Haustechnik - Bauphysik - Umwelttechnik,* Bd. 131, Nr. 4, 2010.

[15] C. Frenzel und M. Hiller, „TRNSYS 17: Neuerungen und Anwendung der IEA Besttest Multi-Zone Non-Airflow In-Depth Diagnostic Cases MZ320-MZ360," in *IBPSA Bausim*, Wien, 2010.

[16] C. Felsmann, „Ein Beitrag zur Optimierung der Betriebsweise heizungs- und raumlufttechnischer Anlagen," Thesis, TU Dresden, 2002.

[17] J. Seifert, M. Knorr, L. Schinke and M. Beyer, Instationäre, energetische Bewertung von Wärmepumpen und Mikro-KWK-Systemen, VDE Verlag, 2017.

[18] EN 12831, *Energy performance of buildings - Method for calculation of the design heat load,* 2017.

[19] EN 13203-4, *Gas-fired Domestic Appliances Producing Hot Water - Part 4: Assessment of Energy Consumption of Gas Combined Heat and Power Appliances (mCHP) Producing Hot Water and Electricity,* 2016.

[20] EN 1264-3, *Water based surface embedded heating and cooling systems - Part 3: Dimensioning,* 2021.

[21] J. Seifert, P. Schegner, A. Meinzenbach, P. Seidel, J. Haupt, L. Schinke, J. Werner and T. Hess, Regionales Virtuelles Kraftwerk auf Basis der Mini- Mikro-KWK-Technologie, VDE Verlag, 2015.

[22] J. Seifert and L. Schinke, "Neuer Klimaversuchsraum an der TU Dresden," *Gebäudetechnik in Wissenschaft und Praxis GI,* 2016.

[23] J. Seifert, „Zum Einfluss von Luftströmungen auf die thermischen und aerodynamischen Verhältnisse in und an Gebäuden," Thesis , TU Dresden, 2005.

Data access statement

The datasets generated and analysed during the current study are not available because patent protection law votes are currently being carried out but the authors will make every reasonable effort to publish them in near future.

Decision tree for early-stage design of hybridGEOTABS office buildings

Mohsen Sharifi, Eline Himpe, Rana Mahmoud, Jelle Laverge

Building physics group, Department of Architecture and Urban Planning, Faculty of Engineering and Architecture, Ghent University, Jozef Plateaustraat 22, B-9000, Gent, Belgium

Abstract. Hybrid GEOthermal heat pump system coupled to Thermally Activated Building Systems (hybridGEOTABS) utilises the high thermal capacity of TABS to smooth out the building thermal loads and downsize the production units. Moreover, hybridGEOTABS has achieved remarkable carbon emissions saving. However, the optimal design of hybridGEOTABS is not achieved with current design methodologies. This article provides a decision tree for early-stage design of hybridGEOTABS office typology. To derive the decision tree, a design methodology which has been previously developed and verified was applied on nearly 40,000 office building case studies with variety of parameters such as climate, insulation level, and internal gains. The methodology exploits multi-zone dynamic simulation of building energy performance and optimal control of TABS for peak-shaving to offer an optimal sizing of the HVAC components. To analyse the results of the numerous simulations and to drive the decision tree, supervised machine learning, specifically a classification technique, was deployed. The application of the decision tree is exemplified in this article using three case studies. The decision tree also enables architects to practice the influence of different parameters on the sizing and performance of the HVAC system. Thus, designers may use it to optimise the building physical design to increase the possible share of geothermal system as a sustainable core for providing thermal comfort in buildings.

Keywords. hybridGEOTABS, ground source heat pump, TABS, optimal design, early-stage design, decision tree, energy performance optimization
DOI: https://doi.org/10.34641/clima.2022.234

1. Introduction

GEOTABS is a combination of a geothermal heat pump and thermally activated building systems (TABS). TABS is a radiant heating and cooling emission system in which the heating/cooling pipes are embedded in the mass of the building elements (for example, concrete floors), activating them as thermal storage. This thermal storage enables the decoupling of demand and supply moments on an intraday time window, as well as the shave of demand peaks, both of which are advantageous for providing flexibility. TABS can provide very low-temperature heating (as low as 22-30°C) and high-temperature cooling (as high as 15-23°C) by converting entire floor or ceiling surfaces into heavy-weight emission systems. These temperatures are similar to those found in the ground's shallow layers, allowing geothermal heat pumps to operate at high efficiency. The geothermal source acts as a seasonal storage facility, allowing heat to be extracted during the heating season and injected again during the summer. The hybridGEOTABS concept deploys GEOTABS core as a sustainable heating, cooling, and air conditioning (HVAC) system supplemented with secondary heating and/or cooling emission systems to maintain thermal comfort when TABS is not the most efficient emission system. When the building thermal loads fluctuates significantly, TABS may have difficulty providing efficient thermal comfort. At the production level, complementary energy sources can help to maintain the thermal balance of the geothermal source, increase financial flexibility, and improve the system's environmental performance. The key components of hybridGEOTABS are ground source heat pump (GSHP), passive cooling heat exchanger (PCHX), borefield, TABS, and secondary systems in heating and cooling modes depicted in Fig. 1. A secondary emission system such as fan coil unit (FCU) is also considered to assist TABS. hybridGEOTABS is a flexible and future-proof HVAC concept that provides comfort to buildings by utilising hybrid renewable energy systems and activating the building's thermal storage capacity [1].

Copyright ©2022 by the authors. This conference paper is published under a CC-BY-4.0 license.

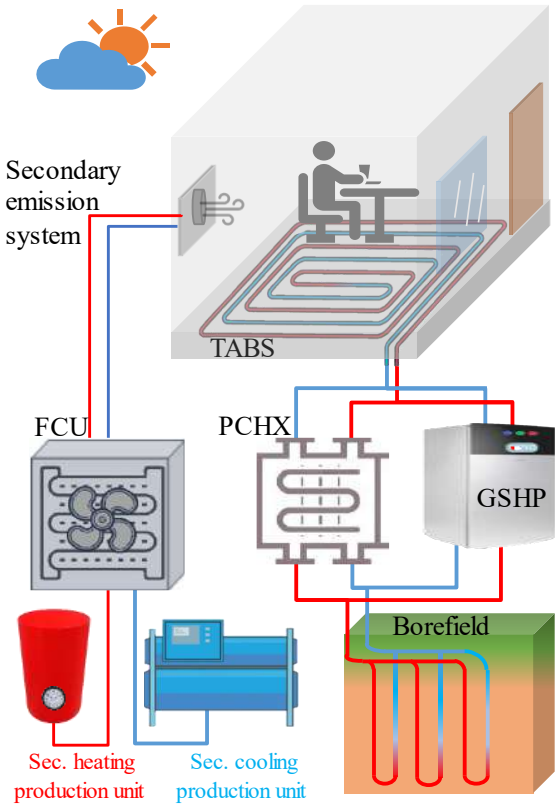

Fig. 1 key components of hybridGEOTABS [2]

The design of a hybrid and storage-integrated system such as hybridGEOTABS, consequences challenges during the HVAC-design. The main questions are what shares of the heating and cooling demands can be optimally covered by GEOTABS and secondary system respectively, and what are the resulting sizes of the key HVAC-components (the heat pump, geothermal borefield and secondary system). As a result of their thermal inertia, and if optimally controlled, the heat inputs to the TABS can be smoothed out over time, resulting in peak shaving and reduced size of the heat pump. On the other hand, as it takes some time to charge and discharge this thermal storage, a sudden change from heating to cooling mode of the system would lead to energy losses. Therefore in such situations, it is often more desirable to engage a secondary fast-reacting emission system (e.g. fan coil units, air handling systems, radiators…). Yet, another element to consider is the effect of the optimal control on the component sizing and load shares. An optimal control strategy optimises the system performance, and has knowledge of the building and system properties and behaviour (by using a model) and of future disturbances (by using predictions such as weather predictions).

The aforementioned dynamic aspects influence the sizing and load share of the hybridGEOTABS system. As a result, the critical conditions for the sizing of the system(s), typically appearing at the warmest and coldest days of the year, are no longer valid for hybridGEOTABS buildings and will lead to an oversizing of the system and increased investment costs. Furthermore, optimal load split between the two systems cannot be answered by only observing the critical moments of the year. Therefore, classical steady-state heat loss calculations are insufficient for sizing hybridGEOTABS.

Instead, the state-of-the-art design of GEOTABS buildings today relies on detailed, case-by-case dynamic building energy simulations (BES), performed by experts. Moreover, detailed design procedures are available when the building design has been finalised and when sufficient detailed information of the building is available. As a result, feedback from the HVAC designer to the architect might require an architectural correction with significant financial impacts on the building's design.

Alternatively, an early-stage design methodology rely on limited number of inputs from the designer and deliver sufficient data to assess the optimal design of the building and the HVAC and, if needed, alter the design accordingly. However, simplified design methodologies for innovative HVACs are not available. Hence, designers inevitably deploy the methodologies developed for conventional HVACs which results in inaccurate estimation of the design indicators, such as energy use, key components nominal power, costs, and environmental impacts.

This paper briefly recapitulates a simulation-based design methodology. The methodology incorporates the dynamic behaviour of the building and the HVAC as an indispensable part of hybridGEOTABS optimal design. The methodology offers optimal energy use and sizing through efficient use of high thermal capacity of TABS. Accordingly, the key components are sized. The methodology was applied on over 40,000 of office building case studies to provide pre-engineering data for designers. The data were analysed using a supervised machine learning technique. The outcomes are presented in this paper as an early-stage design decision tree.

In section 2.1, it is explained how the simulations have been run for thousands of case studies to provide pre-engineering results. The systematic approach for analysing the outcomes of thousands of simulations is elaborated in section 2.2. The results section starts with excerpt of intermediate outcomes of the simulations (section 3.1) to give insight how the final decision tree was developed. Section 3.2 documents the final early-stage design decision tree. Three case studies are introduced in 4.1 to exemplify the application of the decision tree section 4.2.

2. Methodology:

2.1 Simulation-based design methodology

The first step in sizing the components of an HVAC system is estimating the building's heating and cooling (peak) loads. In general, the load can be calculated statically using existing standards or dynamically using BES tools. Varity of studies (such

as [3]) have revealed a significant impact of dynamic behaviour of the building, HVAC-system, and control of hybridGEOTABS buildings on the design. Thus, the simplified early-stage design procedure, which is a decision tree in this article, must be built upon the results that account for the dynamic behaviour of the building and HVAC.

Mahmoud et al. [4, 5] provided a BES database of time series of dynamic building simulation result for one year. They conducted a building stock analysis and organised building physical and geometrical parameters to achieve thousands of different office building designs in three climates. As a result, their database is enriched with a remarkable amount of building design possibilities. They characterised building geometrical design with 176 different archetypes using building geometrical parameters such as total surface area, number of floors, layout, height, width, and length. Moreover, they defined variety of insulation, internal gains, and window to wall ratio. They developed a python code to call the simulation program (Modelica) to automatically model a building using high level building parameters from the database. Then, the Modelica model runs hourly simulations for each case study of their database. Their database was chosen as the starting point to develop pre-engineering design decision trees.

Sharifi et al. [7] developed an algorithm called optimal load split algorithm (OLSA) to optimally split the building thermal load between the TABS and the secondary system on an hourly level. Their algorithm contains an optimisation core inside and a surrogate model of the TABS and building [6] to simulate the dynamic behaviour of them with low mathematical complexity. They achieved to keep the calculation time of their algorithm in the order of a minute so that it can be applied on thousands of case studies from the aforementioned database. OLSA guaranties thermal comfort and minimum energy use. It also utilises the load-shifting ability of TABS to shave the building thermal loads peaks. Consequently, OLSA facilitates optimal design of hybridGEOTABS, while it is not a sizing tool. Thus, the outcomes of OLSA must be post-processed to achieve the final sizing of hybridGEOTABS components.

The post processing methodology was developed and verified as elaborated in [8]. It removes the high thermal peaks of the heat pump and the borefield by smoothing out the time series of the thermal loads. The smoothing is allowed thanks to the high thermal inertia of TABS. Accordingly, central moving average of the heat pump power time series with a 24 hours interval was applied. This avoids oversizing of the borefield and the heat pump. The borefield length was estimated according to standard VDI [9]. Note that if the annual borefield thermal loads in heating and cooling modes are not balanced, the secondary system is used to cover the excessive load that will cause the imbalance. Sharifi et al. [3] showed that the financial viability of hybridGEOTABS is threatened when the imbalance part of the building thermal load is supplied with the borefield. This is due to the fact that the thermal imbalance between heating and cooling can adversely affect the system performance. The imbalance can decrease or increase the borefield temperature, also called depletion of the borefield. The imbalance can be solved in variety of ways; for instance, increasing the borefield length, regeneration of the borefield, and using a secondary system to cover the imbalance part of the demand. However, these options must be evaluated in the detailed design stage. Finally, the CO_2 emissions were also estimated using the system efficiencies and conversion factors reported in the Appendix.

2.2 *Meta-analysis methodology*

The entire simulation-based design methodology was verified as elaborated in [10]. The methodology was later translated to an automated python code. The code reads the data from the BES database and automatically calls the OLSA and thus optimally splits the load between the primary system (GEOTABS) and the secondary system. Then, it calculates the design indicators such as energy use, components maximum load, and CO_2 emissions with the explained post-processing steps. The code was used to design hybridGEOTABS for all the case studies from the BES database. This provided a rich database that relates the predictor variables (design variables such as climate, insulation level, glazing area) to the predicted parameters (design indicators such as energy use, components sizing, and CO_2). The whole dataset can be statistically divided to subgroups according to their similarities. To find the similarities in subgroups of the dataset, recursive partitioning technique was used. Recursive partitioning is a classification technique and a subsection of supervised machine learning technique [11]. Accordingly, a predictor variable is chosen and the data are split to two or more subgroups

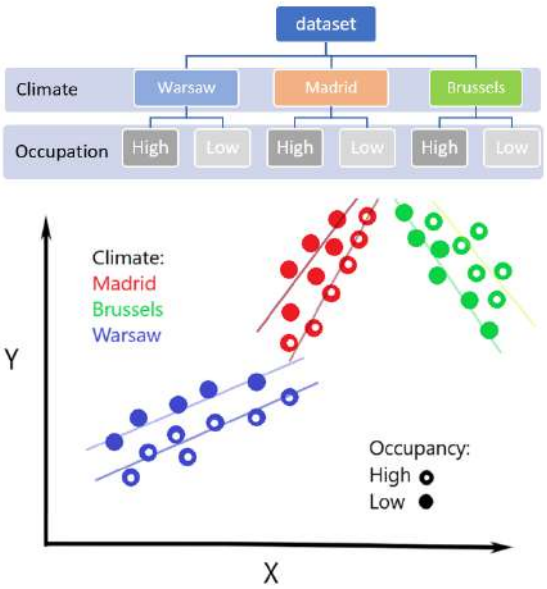

Fig. 2 Partitioning approach leading to a decision tree [8]

(branches) according to the values of the predictor. A line is regressed to the data to relate the predicted variables and predictor parameter. For instance, if the predictor is "climate", the dataset is divided to subgroups of Warsaw, Madrid, and Brussels (Fig. 2, on the top) as the three climates that were used in the simulations. Statistical tests are performed between branches and if the null-hypothesis is rejected, the subgroups are significantly different and the predictors is considered a root for the tree. Next, another predictor variable is chosen and partitioning into subgroups is repeated. The final outcome will be a decision tree whose final subgroups are the fitted regression lines for subgroups (Fig. 2).

To systematically apply the methodology on the dataset, an R code was developed and the function "*ctree*" from the package "*partykit*" was used [12]. The function *ctree* builds the tree by applying statistical tests on the dataset to find the optimum meaningful subsets of the data. It finds the optimum split based on a greedy algorithm looking for the variable that meets the growing criterion better than the other variables in each step. The function has different stop criterion. Naturally, a bigger tree always brings more accuracy. However, the interpretation of a bigger tree is not easy and the amount of branches can become prohibitive. Considering the main target of developing the decision tree, we aimed at a rather small and easily interpretable decision tree. Therefore, we manually controlled the decision tree development whereas the size of tree was chosen as the stop criterion to prevent having a vast decision tree.

3. Results

3.1 Intermediate results

Fig. 3 shows violin plots that conducts a relation between heat pump specific power (vertical axis) and the distribution of the cases studies according to their climate, insulation level, and occupancy rate. The violin graph depicts the difference between heat pump sizing that is caused by differences in building parameters. For instance, the design for high and low dense occupancy is different despite the fact that the box-plot (inside the violins shows) a symmetrical distribution in one group. This means that the right side of the violins might be significantly different with the left side. As another example, with high dense occupancy for medium insulated cases in Brussels, the graph shows two distinct groups. These high-level observations confirm the relationship between the specific heat pump size of the building design characteristics.

3.2 Early-stage design decision tree

Fig. 4 documents the final decision tree for the office typology. Note that in the decision tree, L"," M", and "H" respectively stand for "Low", "Medium" and "High" for different parameters. The parameter's value associated to "Low", "Medium", and "High" for is documented in Annex . The decision tree requires the designer to find its building using the climate, insulation level, occupancy rate, window-to-wall ratio, and shading system and accordingly guides the user towards the design indicators which are listed in Table 4 in Appendix.

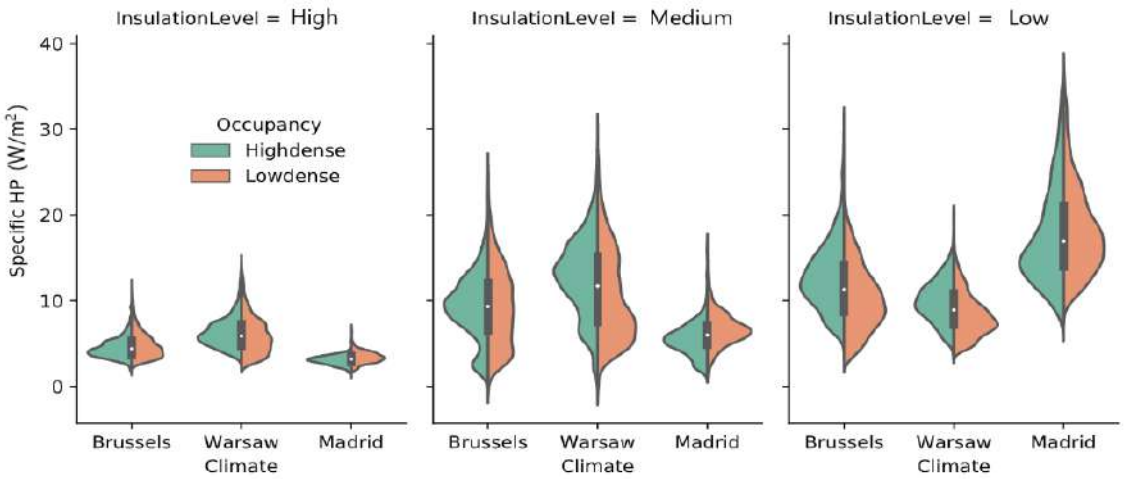

Fig. 3 Distribution of the specific maximum HP power in office cases related to different design parameters

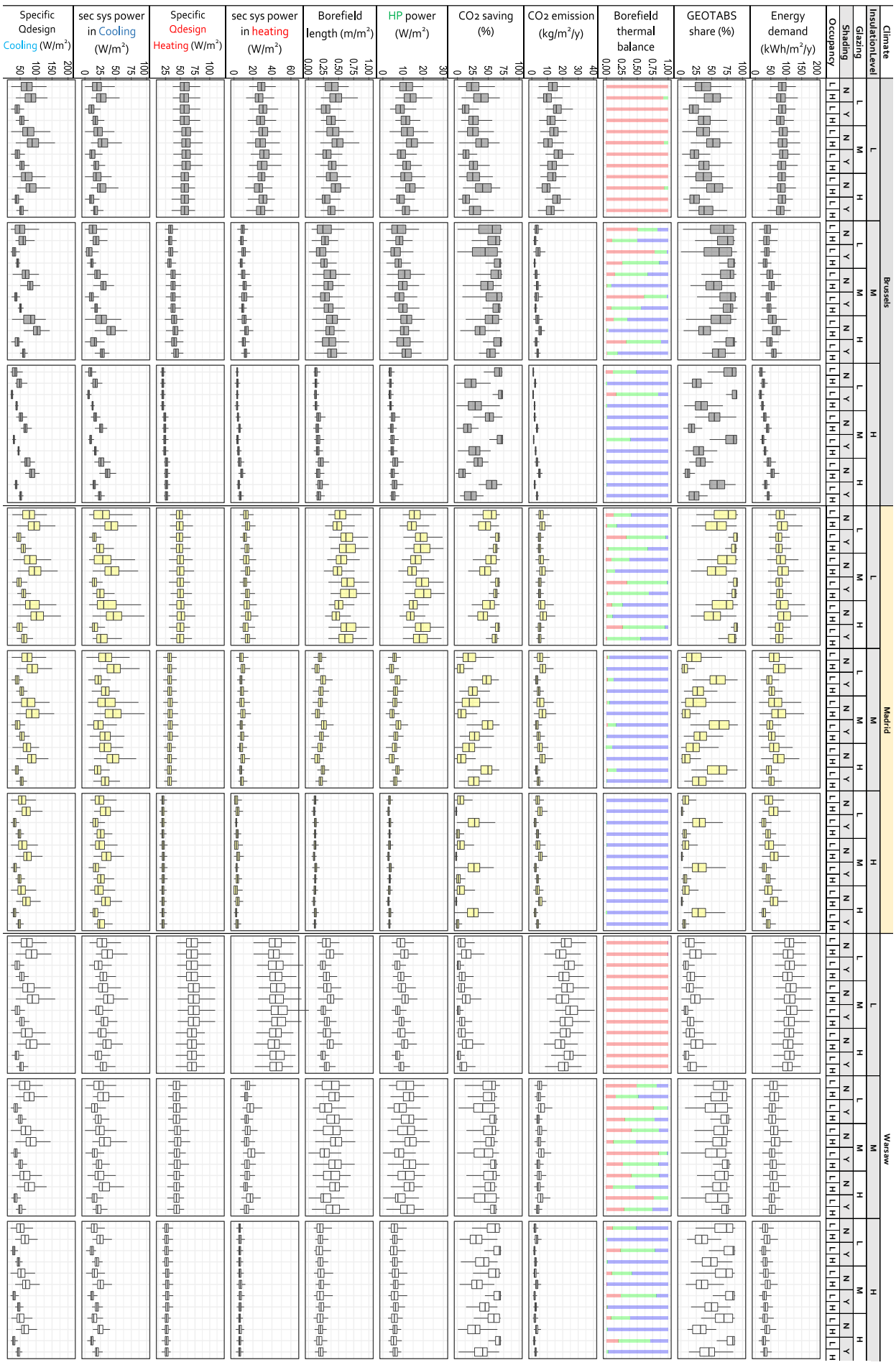

Fig. 4 hybridGEOTABS early-stage design decision tree for office buildings

4. Application of the decision trees

4.1 *Case studies*

Three case studies are introduced to exemplify the use of the decision tree. The three cases are located in **Brussels** with similar geometrical parameters as listed in Table 2. To practice the influence of different physical parameters, a combination of the parameters were chosen to form three random design A, B, and C as listed in Table 3.

Table 2 *Geometrical properties of the three case studies*

Geometrical variables	***Value***
Conditioned area (m^2)	*2390*
Volume (m^3)	*8532*
Heat loss surface area (m^2)	*4325*
Height (m)	*6.4*
Number of floors	*2*
Window to wall ratio (%)	*40*
Compactness	*1.9*

Table 3 three groups of building design A, B, and C used as case studies

Case	Insulation	Occupancy	Shading	Orientation
A	Medium	Low-dense	yes	North
B	High	High-dense	yes	North
C	Low	High-dense	No	West

4.2 *hybridGEOTABS design using decision trees*

Using the proposed decision tree, hybridGEOTABS was designed for the three case studies. As the decision tree mostly provides the design indicator values per unit of conditioned floor area, the estimated values from the tree were multiplied by the conditioned area (2390 m^2) where applied and the absolute values were derived. The estimated design indicators for the three case studies are listed in Table 1. The values are rough approximations used in the early-stage of the design procedure. We used the maximum value of the box in the box-plots (the 75% quartile of the distribution) for each indicator. The designer may decide to use the maximum value of the whiskers for a more conservative estimation. Moreover, it is possible to use more conservative scenarios for one indicator, e.g the secondary system in heating and a less conservative scenario for the (usually more expensive) primary system.

In comparison to the maximum steady-state thermal load of the building, as a traditional way of sizing HVAC components, a remarkable downsizing of the components is observed. The thermal balance of borefield (second indicator) shows that case *C* is definitely heating dominated and case *B* is cooling dominated. Case *A* seems the best design as the GEOTABS share is the highest and the CO_2 emission and saving is high.

Table 1 design indicators derived from the decision tree

Case study	***A***	***B***	***C***
Total heat demand (kWh/m2/y)	55	40	105
Share of heating form the total annual load (%)	60	10	85
GEOTABS share (%)	90	25	65
Heat pump power (kW)	31	12	35
Borefield length (m)	950	430	1195
Secondary system power in heating (kW)	24	18	71
Secondary system power in cooling (kW)	43	60	84

5. Discussion

The decision tree offers an easy-to-use tool for the designers to practice optimal design of hybridGEOTABS. The financial design indicators associated with the technical design indicators can be easily derived from the results. The tool offers all the means to estimate operational and investment costs of each design. This option was not elaborated in this article due to the limitation on the article length.

The borefield length was estimated using a simplified method that did not involve dynamic simulations. As a result, a conservative assumption was used to ensure thermal balance in the borefield and avoid long-term consequences. However, in imbalanced cases, this conservative assumption limited the share of GEOTABS. Hence the results should be interpreted as the hybridGEOTABS concept's minimum possible improvement in terms of sustainability. The designer can utilise the decision tree to possibly change the building design and increase the share of the renewable core of the HVAC concept. Thus, the share of GEOTABS can appear higher in the detailed design.

This work assumed conventional HVAC solutions such as a gas boiler and chiller to simplify and generalise the problem. To improve environmental performance even further, the designer is encouraged to use additional renewable sources such as solar panel and solar boilers in secondary systems and/or envisage an air source heat pump as the secondary system.

6. Conclusion

Combination of geothermal heat pumps with thermally activated building systems (GEOTABS) is applicable to every building if a secondary system is potentially assumed in the design procedure. Then the concept is called hybridGEOTABS. hybridGEOTABS design contains challenges that cannot be overcome with existing methodologies. The current methodologies are either based on steady-state calculation methodologies which are inaccurate, or case specific detailed design procedures which are inaccessible. This paper documented a decision tree for the use of early-stage design of hybridGEOTABS. The tree was derived from the database built upon results from dynamic simulations of 40,000 case studies. The aforementioned dynamic thermal loads were used for developing a fast and automated sizing methodology for hybridGEOTABS components. As a first important step, an optimal load splitting algorithm called OLSA, developed in-house was used to split the building thermal load between the primary and the secondary system. OLSA guarantees the thermal maintaining thermal comfort and takes into account the dynamic thermal behaviour of TABS. The main outcomes of the OLSA are time series of the primary and the secondary system power for one year. The time series are then used were used for sizing the key components of hybridGEOTABS and estimating the environmental performance for the case studies in the database. Meta-analysis of the data was carried out using classification technique.

The final outcome of the whole procedure is a decision tree providing the most crucial inputs for the designer to consider in the early-stage of design. While using the decision tree for design is very fast and easy, the results are close to the results coming from detailed and time consuming algorithms, and are thus an added value for the designer to assess the feasibility of hybridGEOTABS for their design. Moreover, architects can see the influence of different parameters on the sizing and performance of the system. Thus, they may use it to optimise the building physical design to increase the possible share of GEOTABS as a sustainable core for the building heating and cooling energy use. The application of the decision was exemplified with three case studies. It was shown how the decision tree guides the designer to compare the impact of the different building parameters on the design of the hybridGEOTABS.

Acknowledgement

This research, as part of hybridGEOTABS project, has received funding from the European Union's Horizon 2020 research and innovation programme under grant agreement No 723649 (MPC-.GT, 2016-2021).

Appendix

This appendix documents four tables containing assumed efficiencies for the production systems, CO_2 conversion factors, primary energy factor, and building parameters used in the modelling.

Table 4 Description of the design indicators reported decision tree.

Design indicator	Description
Energy demand (kWh/m^2/year)	sum of net heating and cooling demands of the building assuming an ideal heating and cooling system (22-24°C indoor temperature range)
GEOTABS share (%)	share of the heating and cooling demands covered by GEOTABS
Borefield thermal balance	relative frequency of heating dominated (red), balanced (green) or cooling dominated (blue) cases in that subgroup of the database
CO_2-emissions (kgCO2/m^2/year)	estimated CO_2-emissions for heating and cooling the building
CO_2-savings (%)	savings in CO_2-emissions as compared to a non-GEOTABS scenario (100% of heating and cooling provided by a boiler and chiller)
HP-power (W/m^2)	specific power of the heat pump per conditioned floor area
Borefield length (m/m^2)	length of the geothermal borefield (m) per conditioned floor area (m^2)
Sec Sys power in heating (W/m^2)	specific power of the secondary heating system per conditioned floor area
Specific Q_{design} in heating (W/m^2)	steady-stated heating demand of the building reported as a common indictor
Sec Sys power in cooling (W/m^2)	specific power of the secondary cooling system per conditioned floor area
Specific Q_{design} in cooling (W/m^2)	quasi steady-stated cooling demand of the building reported as a common indictor

Table 5 Primary energy and CO_2 emission conversion factors

	Primary energy factor Total (-)	CO_2 emissions factor (g/kWh)
Natural Gas	1.1 [13]	220 [13]
Electricity EU 2020	2.0 [14]	260 [14]

Table 6 Production efficiencies for the different systems

Type of production unit	*efficiencies*
SPF Heat pump heating (primary heat production)	6
SPF Heat pump cooling (Cold production)	5
Gas boiler (secondary heat production)	0.95
Secondary emission system	0.95
Electric chiller (Cold production) EER	3
Passive cooling (Cold production)	20

Table 7 Summary of the parameters used in the modelling and simulation

Parameter	Decision tree label		value
Window to wall ratio	High		20%
	Medium		40%
	Low		60%
Orientation (large facade)	S		South
	W		West
Shading System	YeSh		No-Shading
	NoSh		External screen is on at 150 (W/m^2)
Envelope performance	Low	Envelope U-value	0.5 (w/m^2.k)
		Window U-value	2.5(w/m^2.k)
		Glass g-value	0.6
		air-tightness n50	5.0 (h^{-1})
	Medium	Envelope U-value	0.27 (w/m^2.k)
		Window U-value	1.5 (w/m^2.k)
		Glass g-value	0.56
		air-tightness n50	2.0 (h^{-1})
	High	Envelope U-value	0.15 (w/m^2.k)
		Window U-value	0.8 (w/m^2.k)
		Glass g-value	0.4
		air-tightness n50	0.6 (h^{-1})
Building mass	Low		390 (kg/m^2)
	High		630 (kg/m^2)
Internal heat gains	Low	Density	1 Person/20m^2
		Occupancy	5.0 (W/m^2)
		Lighting	8.0 (W/m^2)
		Appliances	5.5 (W/m^2)
		Total	18.5 (W/m^2)
	High	Density	1Person/10m^2
		Occupancy	10.0 (W/m^2)
		Lighting	8.0 (W/m^2)
		Appliances	15.0 (W/m^2)
		Total	33.0 (W/m^2)
Ventilation flow rate	Constant		36 (m^3/h)

References

1. Boydens W, Helsen L, Olesen BW, Ferkl L, Laverge J, Himpe E (ed.). Renewable and storage-integrated systems to supply comfort in buildings. A&S/books. Ghent, Belgium, 2021.

2. Sharifi M, Figueroa IC, Mahmoud R, Himpe E, Helsen L, Laverge J, et al. Early-stage Optimal Design of hybrid GEOTABS Buildings in Terms of Costs and CO_2 emissions, Energy Convers Manag 2022;257:115392. https://doi.org/10.1016/j.enconman.2022.115392.

3. Sharifi M, Jorissen F , Himpe E, Helsen, L, Laverge, J. (2020). Quantified differences in optimal TABS, HP and GSHX sizing for MPC and RBC. EU-H2020-hybridGEOTABS project Deliverable 2.4. https://doi.org/10.5281/zenodo.4892351

4. Mahmoud, R., Himpe, E., Delghust, M., & Laverge, J. A modelling approach to reduce the simulation time of building stock models. Proceedings of Building Simulation, 16th Conference of IBPSA (Vol. 16, pp. 1491–1497). 2019.

5. Mahmoud R, Borrajo Bastero J, Himpe E, Laverge J. D2.2: A set of parametric geometries for the (sub)typologies studied. https://doi.org/10.5281/zenodo.4769719

6. Sharifi M., Borrajo Bastero J., Mahmoud R., Himpe E., Laverge J. Developing a Simplified Methodology for Simulating Energy Performance of Buildings with Thermally Activated Building Systems. In proceedings of international building simulation conference 2021. Brugge, (Belgium), 1-3 September 2021.

7. Sharifi M, Mahmoud R, Himpe E, Laverge J. A heuristic algorithm for optimal load splitting in hybrid thermally activated building systems. J Build Eng 2022;50:104160. https://doi.org/10.1016/j.jobe.2022.104160.

8. Sharifi M, Mahmoud R, Borrajo Bastero J, Himpe E, Laverge J. D2.5: hybridGEOTABS key component sizing: methodology and guidelines. https://doi.org/10.5281/zenodo.4704647

9. Verein Deutscher Ingenieure (VDI). Thermal use of the underground – ground source heat pump systems; 2001.

10. Himpe E, Sharifi M, Mahmoud R, Jorissen F, Helsen L, Boydens W, Laverge J. Development of the hybridGEOTABS design methodology for feasibility study and pre-design, In Proceedings of International Building Simulation Conference 2021 Brugge, Belgium, 1-3 September 2021.

11. Loh W. "Fifty Years of Classification and Regression Trees." International Statistical Review 82 (3): 329–48, 2014. https://doi.org/10.1111/insr.12016.

12. https://cran.r-project.org/web/packages/partykit/partykit.pdf

13. ISO 52000-1:2017. Energy performance of buildings — Overarching EPB assessment — Part 1: General framework and procedures.

14. Hamels S, Himpe E, Laverge J, Delghust M, Van den Brande K, Janssens A, et al. The use of primary energy factors and CO2 intensities for electricity in the European context - A systematic methodological review and critical evaluation of the contemporary literature. Renewable and Sustainable Energy Reviews [Internet]. 2021;146(April):111182. Available from: https://doi.org/10.1016/j.rser.2021.111182

Assessment of Use Cases Involving Data from the Energy Performance Certification Process for Buildings - From Individual Buildings to Regional Scale

Gerfried Cebrat [a,c], Alessandra Manzini [b], Christiana Panteli [b], Claudia Julius [c]

[a] effiziente.st Energie- und Umweltconsulting e.U., Hermann-Bahr-Gasse 5, 8020 Graz; g.cebrat@effiziente.st

[b] Cleopa Gmbh, Neuendorfstraße 18B, 16761 Hennigsdorf, Germany; amanzini@cleopa.de

[c] SEnerCon Gmbh, ,Hochkirchstraße 11, 10829 Berlin, Germany; c.julius@senercon.de

Abstract. The main objective of this paper is to analyse use-cases which are based on data from the Energy Performance Certification (EPC) process. This data, which is often collected for compliance checks by authorities, can be used exploited for multiple purposes. The most basic service is energy consulting by engineers, based on a living document from the EPC process, depicting the buildings thermal characteristics and specification of the HVAC system. But also, the design of regional decarbonization can be data driven, and the drafting of energy policies supported, investigating effect of renovation and decarbonization incentives. When using data from EPC software export files to set up thermal building models for digital twins, peak load shifting at the individual building and district level can be initiated. A high coverage with EPC as source for digital twins can be achieved by marketing for pre-planning decarbonisation of quarters. This paper is originating from the work in the research project EPC4SES which is funded in the ERANet RegSys program and by HORIZON, and develops six use-cases and analyses strengths, weaknesses, opportunities, and threads of services making use of data from the EPC process.

Keywords. Open data, EPBD, Digitalisation, Digital Twin, Decarbonisation, EPC, Regional Energy Planning.
DOI: https://doi.org/10.34641/clima.2022.112

1 Objective for the research

The hypothesis of this research in the project EPC4SES is that valuable information from the energy performance certification EPC does exists which might be exploited to the good of reducing energy demand and CO2 intensity for heating/colling of buildings. This assumption is also backed by literature that "EPC data to add value for policy making, monitoring and research analysis" (Pasichnyi, Wallin, Levihn, Shahrokni, & Kordas, 2018). Such information from EPC was available publicly in an open data registry for England and Wales until Sept. 2021 (Department for Levelling Up, Housing & Communities, 2022). Depending on the regional schemes in the EU member states extended information – to be uploaded to EPC registries – may also be available to the building owners. Such data is embedded in transfer formats (usually XML) and can contain all information to model the thermal behaviour of buildings. In the Austrian Province of Vorarlberg, we find a many fold more detailed data model (Energieausweis-Zentrale, 2017) compared to the Viennese WUKESA system. The ZEUS system in Austria which was adopted by four regions (Archiphysik, 2020) has a similar data model than Germany, and presents a registry functionality for the erectors, EPC issuers and authorities. Since the data model of the transfer files varies across one country and the EU the project shall make a statement with regards to the EPC data usage scenarios. The project EPC4SES shall investigate exploitation of such data to build digital twins for buildings, allowing microscopic simulation of buildings and Model Predictive Control to data owners being building owners or entities which have been allowed to use that data, like operators of district heating networks or Distribution System Operators, DSO. EPC4SES shall validate whether significant savings of energy and CO_2 might be achieved in this way. With correct data from the EPC-process, thermal modelling of buildings is possible and state of the art (Richter, 2009). It shall be possible to divide buildings into zones when modelling and take into consideration energy conversion and heat loss of piping and ducts in the simulation since respective parameters are entered into the EPC-software and are exported via XML. In nine EU member states building characteristics are stored in EPC register databases (Arcipowska, Anagnostopoulos, Mariottini, & Kunkel, 2014). Authorities demand XML uploads for quality checks of the EPC and for controlling compliance to building codes. Thus, we shall investigate the usage of

Copyright ©2022 by the authors. This conference paper is published under a CC-BY-4.0 license.

building and HVAC characteristics from the exported XML and not primarily the result of the EPC assessment which is also stored in the XML. Unfortunately, in case of consumption based operational EPC, which is allowed in some member states, such direct exploitation of EPC data is very limited. But the application of the so called ''invoice/bill based" operational EPC type was cancelled in France in 2021, thus giving access to the building characteristics from asset-based EPC in future (ISOVER, 2022).

2 Project description EPC4SES

The project EPC4SES is exploiting input data that are collected for the issuing of Energy Performance Certificates (EPCs). This data, respectively building models based on it, may be used for optimal planning and operational control of smart energy systems and for defining innovative applications. The best evaluated model-based prediction applications are implemented in the project as research prototypes with real data from the pilots in four pilot regions, Andalusia, Berlin, Salzburg, and Vienna, to determine impact and evaluate effort when establishing virtual (digital) twins of buildings.

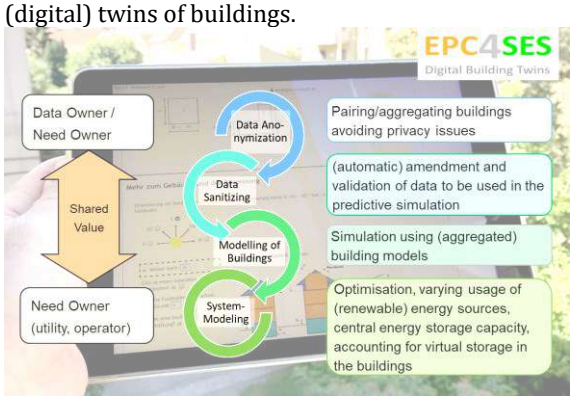

Figure 1 Working hypothesis EPC4SES

All results of the ongoing project including approaches to support decarbonization through virtual storage and interoperable smart energy systems will be fed back to the scientific community of ERANet. The final aim of the project is to exchange information between energy supplier and/or DSO and energy users over standard interfaces like shown in Fig. 2, to allow increase of renewable energy utilization. Using physical and/or virtual storage will allow to increase utilization of feed-ins from heat waste (or anergy) and solar in thermal networks and increase utilization of PV and wind energy in the power grid.

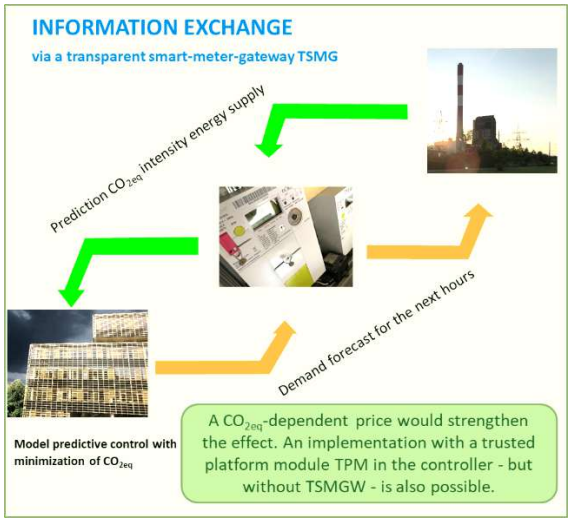

Figure 2 Bidirectional information flow between Smart Energy Systems via Transparent smart meter

The project EPC4SES – EPC based Digital Building Twins for Smart Energy Systems – aims also at decarbonizing heating & cooling energy demand through load shifting by adding model predictive control (MPC) functionality utilising CO_2 prognosis data from networks/grids. Model-based simulation of demand is considering the thermal capacity of buildings and behavioural models for consumer attitudes based on preferences. MPC allows single building owners, energy communities and facility managers to compile a demand forecast which is based on the optimisation and to transmit the prognosis to local DSO and/or energy suppliers. In the case of Energy communities, the load forecasting would consist of a whole community prognosis, taking into consideration optimized internal energy exchange.

3 Policy Context

3.1 Regulatory Background

The Energy Performance Certificates (EPCs) were introduced in 2002 by the Energy Performance of Buildings Directive (EPBD, Directive 2001/91/EC) [1] as a mandatory requirement for the EU Member States. The current certification scheme, regulated by the EPBD directive 2018/844 [5], which amended the Directive 2010/31/EU, had not modified the articles related to issuing and displaying of the energy performance certificate (Articles 11, 12 and 13). Basically, the directive requires the Member States to lay down the necessary measures to establish a system of certification of the energy performance of buildings, including a methodology for the calculation of the energy performance of buildings which shall be transparent and open to innovation.

The recasts of the Energy Performance of Buildings Directive in 2010 (2010/31/EC) [2] and in 2018 (2018/844/EC) [3] reinforced the EPCs obligation for the Member States and delivered detailed provisions for the energy performance certificates (EPCs). Particularly, according to the article 9 of the

2010 directive (2010/31/EC2), Member States should develop a joint methodology of calculating the energy performance of buildings. The member states are eligible to amend their methodology to include not only thermal characteristics but also other significant parameters which may affect the energy consumption such as HVAC equipment, renewable energy applications, passive heating and cooling, shading, indoor air-quality, as well as other elements. Moreover, according to article 10, Member States are required to set national minimum requirements for the energy performance of buildings and building elements as well as to review them on a regular basis, in accordance with the status of the technological progress. These requirements should be set, based on the target of achieving cost-optimal balance between the investments involved and the energy costs saved throughout the lifecycle of the building. The lack of sufficient quality assurance requirements from the initial directive of 2002, was addressed in the succeeding recasts of the directive, establishing the required framework to improve EPCs 'quality. An independent control system was introduced in the 2010 recast, specifying the verification of EPC schemes such as the validation of the input data, the verification of results and recommendations, the on-site visit of the building as well as other equivalent measures. However, the current regulations have led to the status that the energy performance certificates do not generate any further benefit beyond the presentation of energy performance certificates when building, renting, selling and renovating properties. In some countries operational EPC are called display EPC and are applied for larger public buildings. Allowing a low-cost, low-quality approach for EPC deprives authorities of investigating the thermal renovation potential.

3.2 Standardisation process

The issuance of EPCs is framed by the EU regulations, which allow the adoption of national regulatory provisions. The EU member states are also responsible to establish rules to comply to the GDPR while implementing EPC register schemes. An alternative in the project context would be to exchange forecasts instead of disclosing building data, so only interfaces shall be standardised. However, this is not applicable for pre-planning cases lacking the output of a model predictive Building Energy Management System. An IEC 62559 based standardisation of the digital twin and data model would start with the requirements for those applications which are utilising data from the EPC process.

The project includes work on XML schemas or Document Type Descriptions DTD for defining the XML files, harmonising the approaches in the regions and member states. EPC4SES found small deficits in the XML schemas like lacking thermal capacity figures and orientation or inclination of transparent elements in some cases but also ways adding adiabatic energy storing internal elements. EPC4SES proposes to develop a European open-source XML format for storing energy related building data as a specification to facilitate the development of applications in transnational approaches on the standardisation level and for software industry and ESCOs. Modelling building energy performance in MPC is dynamic by nature and thus could be nearer to 13786:2017 than to ISO 52000-1.

3.3 Barriers to implementation

To make data derived from the EPC process useful for citizens, academia, and business, accessibility has to be improved, since it varies among the member states and among their provinces if federated systems are enacted. Inaccessibility to aggregated EPC data causes challenges for national policy makers, and for anyone wanting to access and compare information about EPCs issued in different parts of the country (Altmann-Mavaddat, Tinkhof, Simader, Arcipowska, & Weatherall, 2015). Also the variance interpreting EU regulations is an actual barrier. Making EPC mandatory for all buildings will benefit regional energy planning because of the higher coverage of the building stock. Data privacy is highly relevant for European citizens, but aggregation makes possible even to exploit data from single family homes if it is shown as one pixel on a 1 km x 1 km grid, whereas in city centres 100 m x 100 m are possible without a GDPR problem. Considering the priorities to be tackled within the climate emergency, apart from policy makers all actors in the energy market and researchers should be able accessing that data. Apart from the indirect use of EPC data without house owner involvement it is possible to set up contracts between district heating supplier and building owners to make available detailed data or the results from prognosis of the building energy management system. Application could be the model predictive control of the connected energy system featuring Renewable Energy RE storage.

The accuracy of data collected in the EPC process is vital for modelling. So, quality of EPC input data shall be improved. Most trivially the surfaces of building elements and its characteristics are erroneous. While the first could be overcome by comparing to or using GIS/LIDAR, validity checks using data from similar buildings can improve quality of building element data, namely u-values windows to wall ratio etc.. Data fusion when compiling EPC - taking data from 3D models - can help to minimize errors. Introducing concrete rewards like better EPC rating or funding in the smart readiness initiative will help to introduce building energy management systems having model predictive control in need of EPC derived data.

3.4 Preconditions

EPCs are reflecting the current thermal standard of the respective building at the time they were issued, and in some countries also reflect the optimal renovated status as benchmark. Operational EPCs based on energy consumption data are biased by the behavioural influences of the building occupants, which should be levelled out by the rule that only buildings with more than four flats might have operational EPC. Those operational EPC are lacking

detailed information for the building envelope which would be provided by asset based EPCs. For the planning of a large-scale building renovation, including their future energy supply, preferably based on renewables, data from both types of EPC are required. On the building level, for the evaluation of a modernization plan it is essential to prioritize the recommendations given in the EPC and implement them step by step. The success of each step should be evaluated via frequently recurring operational EPC to adjust for possible mistakes in the implementation. Here the boundaries to energy monitoring are fluent, but it important to ensure that with operational EPC original consumption data is stored additionally to the normalized data.

Smart meters are beginning to diffuse based on EU regulations which targets distribution system operators DSO, (electric meters are leading, gas meters following). They are allowing monitoring the energy used for space heating/cooling/ventilation and lighting (heating for gas and district heating smart meters). Those meters will provide real-time energy consumption of buildings as base value for load prognosis. But smart meters can also act as gateway to establish communication between market participants and customers, which is assumed in the project to transmit prognosis of CO_2 intensity and load forecast to DSO and energy suppliers (Fig. 2).

At EU level, the aim is to constantly improve the quality of energy certificates and their usefulness. Decarbonisation is high on the agenda, but it also needs data to plan it. Designing new carbon free settlements and energy networks is often difficult because the necessary data is not always available. The same applies to existing buildings and energy networks, where the lack of data for a digital twin makes prognosis and model-based control in operation difficult.

The quality assurance activities for EPC are supporting the use cases. Correct and accessible building element and HVAC equipment data is the key to many applications orchestrating the decarbonisation and efficiency improvement process, either for property owners, (public) network operators, public authorities, but also for the renovation industry. Energy consulting for individual buildings, based on data from the energy performance certification (EPC) can extend the XML data model and produce a living document. Persistence and accessibility of that information - also via QR - code is a precondition for some use cases.

Finally, model predictive control and decentral load prognosis needs accurate and affordable weather predictions, also including solar irradiation.

4 Use Cases

In this chapter we describe six use cases for data collected in the EPC process and stored in a standardised format. The use case scenarios imply a multilevel perspective of implementation ranging from individual to regional scale.

4.1 UC1 Energy consulting for individual buildings, based on energy performance certificate (EPC) data (extended XML), XML as living document, also accessible via QR code.

The quality of the individual consulting for property owners shall be made more efficient and be based on quality assessed building data used in EPC. Energy performance certificate (EPC) data contained in extended XML could be provided by commercial or public entities as living document being updated each time an EPC is due and made accessible via QR code for building owners and contracted entities like energy consulters. This would help energy consultants not to start from scratch but from input data to EPC. Enriching with actual data for energy price and renovation cost it is used to define reduction measures for the energy related cost and CO_2 footprint of a building. As the extended EPCs provide a continuous picture of the building, energy consultants issuing EPCs can build up a steady relationship with customers to accompany them on the modernization path of their buildings. The application of digital twins could help to forecast energy savings and CO_2 reductions for each modernization step and at the same time keep EPCs up to date. Thus, by controlling energy efficiency improvement via the extended EPCs, the quality of the individual consulting for property owners is made more efficient and based on quality assessed building data used in EPC. This is an outstanding service, not yet available on the market. Moreover, EPC software providers can innovate their solutions and provide a new service module including new business networks with ESCOs that can connect their services to EPCs to forecast and evaluate the success of their services.

4.2 UC2 Support of market development for thermal refurbishment through Big Data approach using anonymous EPC data

In a big data approach, commercial entities of the energy efficiency market may either address trusted aggregators to retrieve predefined detailed statistics stemming from the EPC process or postulate SQL queries with a minimum geolocation area not to create privacy problems. This can have a positive effect on the energy efficiency market as it helps the refurbishing industry to better estimate the demand of cost-efficient products. Anonymous aggregated EPC XML data from enhanced EPC registers allow the refurbishing industry to adapt their portfolios according to the most demanded refurbishing measures and materials of the respective building stock market. One example might be analysis of data uploaded into the Salzburg province EPC registry

ZEUS, where tendency to switch heat converter type with building reconstruction might be quantified (Prieler, Leeb, & Reiter, 2017).

4.3 UC3 Support of energy policy by using EPC data (forecasts, scenarios, revealing deficits...)

Energy policies shall be based on empirical data, employing data science on enhanced EPC register data. An open harmonised information basis is vital for a good energy oriented urban planning, especially if geolocation is available (Schardinger, et al., 2021). Implementing Directive 2003/4/EC on public access to environmental information the bodies or authorities in charge shall allow researchers access to anonymized EPC XML based data (stored in database fields). In UC3 also statistics are exploited but different to UC2 the focus is on efficiency of policy measures. So, the renovation rate may be correlated with the existence of monetary and non-monetary incentives. Funding is correlated with changes in energy demand and public funding of renovation also triggers issuing of new EPC if they are mandatory for obtaining funding. Researchers, energy agencies or officers from responsible public entities may correlate renovation measures with funding schemes.

Using EPC register data and applying data fusion, the design of funding schemes can be optimized and tailored to the actual situation of the building stock. Also, using data from EPC registries the effect of funding different renovation measures on the total energy demand and funding exchange of oil and gas furnaces CO2 footprint can be evaluated.

Such models to calculate energy demand and CO_2-footfrint shall be calibrated with the help of manual input (Pfeifer, 2017), also coping with the fact that for private buildings not rented out no EPC is mandatory.

4.4 UC4 Pre-planning of energy systems (e.g., rural district heating networks or energy communities) with the help of EPC data acquired from potential customers.

This use case involves different actors. An example of implementation could imply a contract among the energy system designers and building owners of a settlement to get accurate data for planning smart energy systems starting from the conduction of an asset-based EPC. Energy system designer use the geo located digital twins to simulate extension of networks or planned networks. Building owners commit to deliver the data in return to a free EPC. The digital twin might also be offered by third parties processing EPC data to be used in a simulation tool for the energetic performance of the building in the network context.

Another example is the application within an energy community. Pre-planning for a community with different degrees of urbanization is one of the fields of application. The energy community could be seen as a guarantor of the policy implementation. If the energy community has enough power or weight or organization, it could modulate the behaviour of the DSO. To achieve this the energy community can plan a demand responsive system managing a multitude of peak prognosis related to different single units rather than managing just the one of a whole energy community. The market power of an energy community or a federation of them could be important introducing local renewable energy production and model predictive control of storage facilities maximising solar yield or yield from heat pumps.

4.5 UC5 Building energy management with model predictive control (MPC) based on own EPC data (accessed via link or QR-code)

This use case foresees a commitment of energy suppliers or grid/network managing entities to provide prognosis of CO_2 intensity digitally via API like we see with (Prognosis, 2022). While conducting asset-based EPC, the building data is collected and used for a digital twin which is then used for model predictive control minimizing energy demand/CO_2 intensity based on the CO_2 prognosis for the energy supply. In one example the building owner procures an EPC with the possibility to export an enhanced XML, this could be then used in a digital twin in the building energy management system (BEM). The EPC issuer uploads the data to the BEMS. The BEMS producer foresees interfaces to import that building data and read weather forecasts. The BEMS features a simulation model for the building. Literature in this case is very optimistic estimating a 35% cut in energy consumption and 50 to 100 % cut in carbon emissions (Lukesh, 2021). Especially for larger buildings the cost for a Building Energy Management System can be paid back rapidly.

4.6 UC6 MPC for local energy systems (with fluctuating RE feed-in) using forecasts from the customer's building MPC.

This use case is a further development of the above-described UC 5, extending the application by renewable energy utilised on the network level. While active elements for UC5 are the building thermal mass, and if available buffer and DHW tanks, UC5 focuses on DH-network/grid . Modulating energy conversion and storage using model predictive control with load prognosis data from clients and weather forecast data, efficiency, renewable energy yield resp. utilisation rate can be increased. Without forecast provision from single buildings this use can also be linked to UC4 since the digital twins from planning may also be used for MPC at the network level.

4.7 Use Case Application in different markets

To structure the use cases they were arranged in a triangle according to their purpose (*Figure 2*).

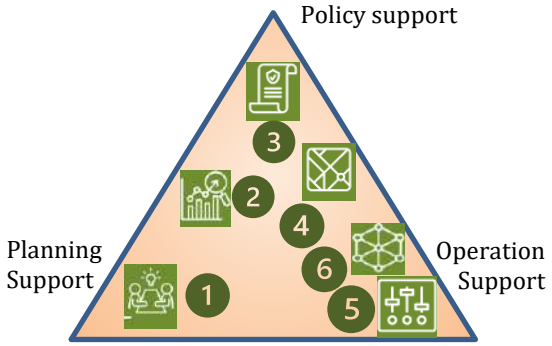

Figure 3 Strategic purpose of the use cases

In the following we undertake a qualitative assessment of the use cases. In Germany, **Use Case 1** is the most promising use case with business potential. The other use cases based on EPC registers don't have many chances now in Germany, as up to date no accessible national, regional, or local EPC registers exist which are featuring the data collected for quality control of EPC by the DIBt (Deutsches Institut für Bautechnik). Thus, as a pre-condition for the other use cases, data already collected via XML should be stored in national or regional accessible building registers.

In Austria, **Use Case 1, 2** and **4** have the most business potential as EPC data registers exist in four of the federal regions (Salzburg, Styria, Vorarlberg, and Burgenland). They have a different pace in terms of adopting new rules and data access to the public but the situation is converging. The roll-out of Use Case 4 depends on the acceptance of future clients to provide enhanced EPC data, which is required for the higher accuracy of the model.

In Norway, **Use Case 3 and 4** are most promising. In Spain theoretically **Use Case 6** should be very attractive, given the high potential of renewable energy. On the other hand, constant weather conditions would require long term forecast and long-term storage.

4.8 Use Case Evaluation

The use cases were analysed in terms of data availability (feasibility), the theoretical CO_2 saving potential, the potential overall market size, the acceptance amongst stakeholders, and the existence of usable technological solutions, in Table *1*:

Table 1 Evaluation of use cases

UC	EPC based data availability	CO_2 saving	Applicable building stock	Accep-tance	Techno-logical maturity	Total
UC1 Energy consulting	+++	+	+++	+++	++	++++++++++++
UC2 Market support	+	+	+++	++	+++	++++++++++
UC3 Policy support	+	+++	+++	++	+	++++++++++
UC4 Pre-planning of energy systems	+	+++	++	++	++	++++++++++
UC5 Building energy Management	+++	++	++	++	++	+++++++++++
UC6 Energy system management	++	++	++	+++	+++	++++++++++++

Some rating of use cases depends on the actual quality of the legislation, so acceptance of use cases may be replaced by compliance to regulations. The most promising start seems to be **UC6 model predictive control of smart energy systems using heating demand prognosis from connected buildings**. This is an upgrade from statistical approaches employing multivariate regression with parameters like outside temperature and sunshine hours. The more demanding the use of fluctuating renewable energy is, the better prognoses should be, being based on user preferences and real status and characteristics of the building. UC5 Building energy management using MPC will then become part of UC6. UC1 to UC4 have quite high marks, so they should be implemented in parallel. UC1, UC2 and UC3 not only depend on the data model for the EPC registry, but also on the coverage. So, in a less perfect world, UC1 is to be preferred, because lacking data might be acquired during energy consulting and stored in the living EPC document, representing the building. This not only would enable simulating savings with renovation by energy consulters but allow to connect a notification service if the prices change, or new funding is introduced.

5 Validation of the approach

5.1 Aim

For the projects pilots the main focus was on use case 5 and partly 6, which have very severe requirements for the building data. To validate the hypotheses, we need to evaluate the results applying MPC and to test the automated production of RC thermal building models.
The results of the retrieval of the XML files should be identical whatever software is used for producing the exported XML transfer file to be uploaded in the EPC control scheme.

5.2 Methodology

The savings in energy and CO_2 were calculated on the basis of an experimental approach as described in (Cebrat, Chan, Kofler, Manzini, & Brunauer, 2021) .The preliminary findings show that taking more active elements into the MPC, like Domestic Hot Water DHW tanks or central district heating storage benefits the CO_2 savings significantly.
In the validation report of the interoperability of the project the following methodology was applied. XML exports from two different EPC software products were used, from one XML files for different Austrian ZEUS based XML collection regimes were exported. The PHP scripts then analysed the results of the production of R and C but also checked parallel data exchange via SOAP and HTTP request.

5.3 Results

From building electrical analogue RC models, which are depicting the thermal behaviour and testing extraction of such models from exported XML to different regional requirements in the Austrian EPC registry scheme ZEUS, we can deduct the following:

- In some XML schemes some characteristics of the hull elements is lacking, like orientation of windows, which is necessary to calculate solar gains and specific heat of building elements, which is necessary to calculate the C (heat capacity);
- EPC software allows to enter adiabatic interior elements like floors/ceilings, but data entry staff (which often is not identical to the authorized issuer of the certificates) must be urged to do so to be able to calculate correct thermal capacity of the building;
- Correctness of those XML exports should be validated before upload so it can be utilised in digital twins.

6 Policy recommendations to enable the market uptake

6.1 General Comments

With the introduction of EPC, the EU hoped that a renovation and behavioural change with buyers or renters of apartments and buildings would have been induced. Since the years until 2021, the energy price was low and apartments scarce , this strategy did not work out. Quality of EPC deteriorated with the absence of quality control, correlating with lowered prices for EPC. Also, public authorities did not make sufficient use of the big EPC data, so data quality was not an issue. However, the situation has improved much for all those points. The EU has updated the EBPD directive, introducing mandatory quality measures and energy prices increased. Public authorities begin to provide EPC data after issuing them in an electronic form.
Currently, funding schemes are triggering new EPCs, if EPCs are mandatory when applying for fundings. However, the big enabler would be to legislate a minimum standard of insulation for all buildings, to be documented in a living document, where data for compiling EPC resides. The more future buildings will be available for planning Smart Energy Systems, the better the accuracy of regional energy plans based on EPC derived data will be. EPC drafts should therefore be available from the first phase of the building development, which is implemented in schemes where building codes are checked from that data by authorities.
Smart readiness characteristics of course may improve actual performance, so indicators should be included in the XML. Science might contribute with an assessment of the impact including prebound and rebound effects.

6.2 SWOT

The paper elaborates the best strategy for usage of EPC data, based on enhanced SWOT. The following SWOT analysis in Table 2 reflects the evaluation of strengths, weaknesses, opportunities, and threads for all use cases.

Strengths	**Opportunities**
Usage of data generated during the EPC process is an enabler of planning and operational efficiency.	Usage of data from the EPC process depends on correctness of this data and frequent data usage will put more emphasis on EPC quality.
Weaknesses	**Threats**
Quality of data, and its availability are key points for success.	Member states do not support usage of data from the EPC process in legislation and do not define a minimum data model for EPC register data. Privacy concerns and lack of resources with public authorities may prevent exploitation

Figure 2 SWOT analysis of the use cases

Combining strengths and threats, member states shall create ecotopes for using EPC related data in regional contexts. A minimum specification for required data for EPC register data allows to test applications in other markets. Combining weaknesses and opportunities, the usage of EPC related data will automatically require higher EPC quality. There is also the possibility to combine asset-based and operational EPC to calibrate EPC, if Smart Metering develops.
We propose the following list of points necessary to bring forward digitalisation of energy systems in the building sector:

- A mandatory description of EPC schemes in English for all EU regions allowing in depth review and harmonisation attempts.
- An EPC register database with minimum data set and both individual owner access and public access to aggregated data.
- Mandatory publication of CO_2 prognosis' in networks/grids
- Provision of regional weather prognosis (including irradiation) by energy agencies for free for private persons.
- Standard for communicating load prognosis for buildings stemming from the digital building twins.
- DIN SPEC on negotiating demand control using digital twins.
- Public GIS support for horizons, supporting shading calculation.
- Special funding on connected big thermal and power storage making use of the digital twins.

7 References

Altmann-Mavaddat, N., Tinkhof, O. M., Simader, G., Arcipowska, A., & Weatherall, D. (2015). Report on Existing Monitoring Initiatives and Databases to Retrofit Action: How European Countries are using Energy Performance Certificate (EPC) Database System. Retrieved from Desliverable to the REQUEST2ACTION project: https://www.energyagency.at/fileadmin/dam/pdf/projekte/gebaeude/Report_on_existing_monitoring_initiatives_and_databases.pdf

Archiphysik. (2020). *Energieausweis Datenbanken und ihr Hunger nach Daten.* Retrieved from https://archiphysik.at/wip-energieausweis-datenbanken-und-ihr-hunger-nach-daten/

Arcipowska, A., Anagnostopoulos, F., Mariottini, F., & Kunkel, S. (2014). *Energy Performance Certificates Across the EU.* Retrieved from https://bpie.eu/wp-content/uploads/2015/10/Energy-Performance-Certificates-EPC-across-the-EU.-A-mapping-of-national-approaches-2014.pdf

Energieausweis-Zentrale, L. V. (2017). *Datenverwendung - Welche Daten werden erfasst?* . Retrieved from https://eawz.at/FileDownload/downloadSecureFile/6fd3b08fadb0fb5de7e7d8ec28fae6bb75312853dbf4b209e433e09d5b9a2146dbf5c86f53f75e9b4c5990a1fa9b33249fc3a3442c1e7b0764dd0374c5de7f13/art/2142721742/41747

ISOVER. (2022). *Tout savoir sur le nouveau Diagnostic de performance énergétique (DPE)* . Retrieved from https://www.toutsurlisolation.com/tout-savoir-sur-le-nouveau-diagnostic-de-performance-energetique-dpe

Lukesh, T. O. (2021). Digital twin: the Age of Aquarius in construction and real estate. *EY Building a Better World, (May)*, Retrieved from https://www.ecmag.com/sites/.

Pasichnyi, O., Wallin, J., Levihn, F., Shahrokni, H., & Kordas, O. (2018, 10 15). *Energy Performance Certificates — New Opportunities for Data-enabled Urban Energy Policy Instruments?* Retrieved from Energy Policy Journal: https://www.researchgate.net/publication/330359991_Energy_performance_certificates_-_New_opportunities_for_data-enabled_urban_energy_policy_instruments

Pfeifer, D. (2017). *Entwicklung, Untersuchung und Bewertung von Berechnungsmodellen zur Erstellung von kommunalen Energiebilanzen im Gebäudebereich.* Retrieved from https://www.uibk.ac.at/bauphysik/lehre/dissertationen/abgeschlossen/documents/pfeifer.pdf

Prieler, M., Leeb, M., & Reiter, T. (2017). *Characteristics of a database for energy performance certificates.* Retrieved from 11th Nordic Symposium on Building Physics, NSB2017, 11-14 June 2017, Trondheim, Norway: https://pdf.sciencedirectassets.com/277910/1-s2.0-S1876610217X00295/1-s2.0-S1876610217348543/main.pdf?X-Amz-Security-Token=IQoJb3JpZ2luX2VjEGUaCXVzLWVhc3QtMSJHMEUCIDLkm9Xepck8o3d%2FKkQ0AyzWUZm%2FzRwviKQgiqFSjBMTAiEA5L3ZRdg1Z38q8VHoJnY9%2BnjIawCWw4IbaYu%2F

Richter, S. M. (2009). *EDV-Programme für Gebäude-Energiekennzahlen.* Retrieved from https://zidapps.boku.ac.at/abstracts/download.php?dataset_id=7265&property_id=107

Schardinger, I., Vockner, B., Atzl, C., Kinzl, H., Gampe, L., Hemis, H., & Rehbogen, A. (2021). *Enerspired Cities - offene harmonisierte Informationsgrundlagen für die energieorientierte Stadtplanung.* Retrieved from https://nachhaltigwirtschaften.at/resources/sdz_pdf/schriftenreihe-2021-9-enerspired-cities.pdf

Determining the infiltration and exfiltration in Supertall and Mega Tall Buildings

Peter Simmonds [a], Ph.D., Fellow Life Member ASHRAE, FIBPSA

Duncan Phillips [b], Ph.D., MASHRAE

[a] Building and Systems Analytics, Los Angeles and Bergen, the Netherlands

[b] RWDI, Guelph, Ontario, Canada N1G 4P6.

Abstract. Most traditional heating and cooling load calculations are based on weather conditions measured at a height of 10 m. But how appropriate is this in Super-Tall buildings 300m+ and Mega-Tall Buildings 600m+? This paper will present some specifics of evaluating building designs and performance in Tall Buildings.
From previous designs and research, we know that outdoor conditions vary with height. and the outside climate can have both a positive and a negative effect on the space conditions within the building. This paper illustrates the fluctuation of pressure differentials on the heating and cooling loads of spaces over the height of the building.
Rarely does the design of the upper level of the building capitalize on this phenomenon. Furthermore, wind, temperature, and pressure conditions at the top of a tall building are considerably different, therefore façade leakage rates and the buildings stack effect must be carefully assessed. If sufficient data is known about this difference, it can be incorporated to optimize the overall building design.
This novel paper explores the nuances of the ambient climate on tall buildings and the effects on the performance of the building.

Keywords. Mega Tall Buildings, Stack Effect, Energy Consumption
DOI: https://doi.org/10.34641/clima.2022.253

1. Introduction

Stack effect is a phenomenon that causes challenges in tall building design and subsequent operation. Temperature and air density differences between the indoors and outdoors cause stack effect driven pressure differences to be created that drive airflows through the building envelope. The pressure differences are created because the density of air inside the building is less than that outside. This results in the weight of the column of air inside being lighter than that outside in winter months. The weight difference results in inward flows at lower levels in winter and flows out at the top. Somewhere up the height of the building the inward flows transition to being outward. This transition is typically where the indoor-outdoor pressure difference is zero. During cooling months (e.g., the summer) the pressure differences are typically less as the temperature difference is not as severe as during winter conditions. This results in a lower pressure differential between the shaft and the outside compared to those under winter temperature differences.

2. Background Information

In most tall buildings there are shafts/risers that run top to bottom in the building. From the floorplate layouts we have been using in this and previous papers we have two emergency exits stairways and two freight elevators. There are also other risers such as plumbing chases and electrical chases, but these are not considered in this exercise.

The dimensions of the stair and elevators shaft openings such as doors and cracks are provided in the NPL calculations provided in previous papers.

3. Calculating Location of Neutral Plane Level (NPL)

To get the sum of the effective crack area openings we use a resistance formula:

$$\text{ECA} = \frac{1}{\frac{1}{\Sigma AF} + \frac{1}{\Sigma S + E}} \qquad (12)$$

Where: ΣAF is the crack opening areas such as:

- Entrance doors
- Exterior wall leakage cracks

And ΣS+E is the crack opening areas such as:

- Stair shaft wall
- Stair shaft doors
- Elevator shaft wall
- Elevator doors

The crack opening areas effectively act as a passage for air flow with a resistance in place. In a manner analogous to electrical circuits, the flow network established by these resistances across doors, through walls, facades, up and down ducts etc. create a resistance network. Hence the objective is to calculate an effective crack area on each floor and then calculate a height weighted average and turn that into an estimate of the NPL (Simmonds and Phillips, 2022).

The design engineer will determine the number of elevators, transfer floors, refuge floors and other such elements as shown on the architectural drawings.

The exterior wall leakage rate in this case is 1.96 cm2/m2. The area of the exterior walls is 756 m2. The crack area is 1.96*756 = 1481.76 cm2 or 0.148 m2. This term is called AF, 1/AF = 6.7

The leakage rate of the stair shaft is 0.4 cm2/m2, the area of the stairwell = 62.1 m2 and the crack area =25.5 cm2 or 0.0025 m2

The leakage of the elevator doors = 187.5 cm2 per elevator, there are 6 elevators giving a total crack area of 1125 cm2 or 0.1125 m2.

The leakage rate of the elevator wall is 1.57 cm2/m2, the elevator wall area = 100.8 m2 giving a total crack area of 158.25 cm2 or 0.0158 m2.

The total stairwell and elevator (S+E) area is 0.0025+0.1125+0.0158 = 0.128 m2. This term is called S+E, 1/S+E = 7.792.

The sum of the crack areas = 1/ (1/AF +1/S+E) =0.0687 (at the highest level)

For details of areas and leakage rates see ASHRAE Fundamentals (2021) Chapter 16 and 24, also ASHRAE Applications Handbook (2019) Chapter 4 and Chapter 54.

Stack Effects

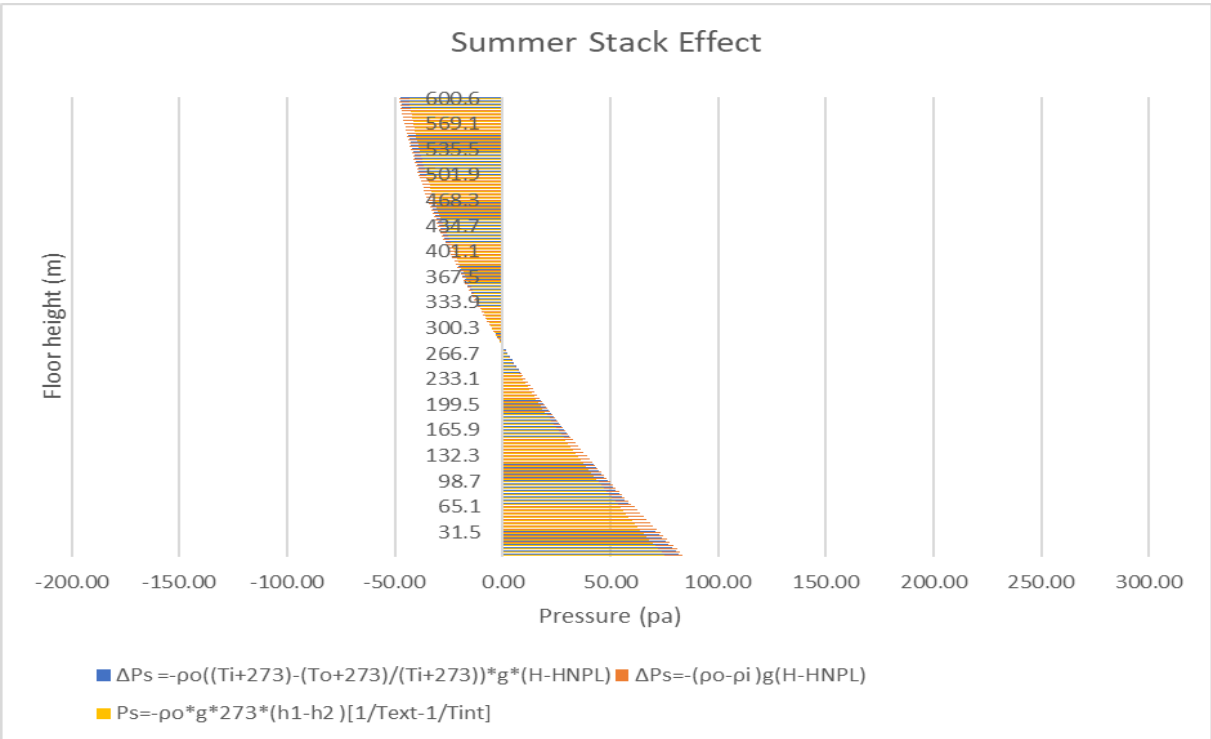

Figure 1 Stack effect driven indoor-outdoor pressure difference as a function of height in summer given the position of the neutral plane assuming the building is a single zone.

Figure 1 presents the indoor / outdoor pressure difference for the reference building for summer conditions with the outside temperature 32°C and the indoor temperature 24°C. This pressure difference is created exclusively

because of the temperature difference between the indoors and outdoors.

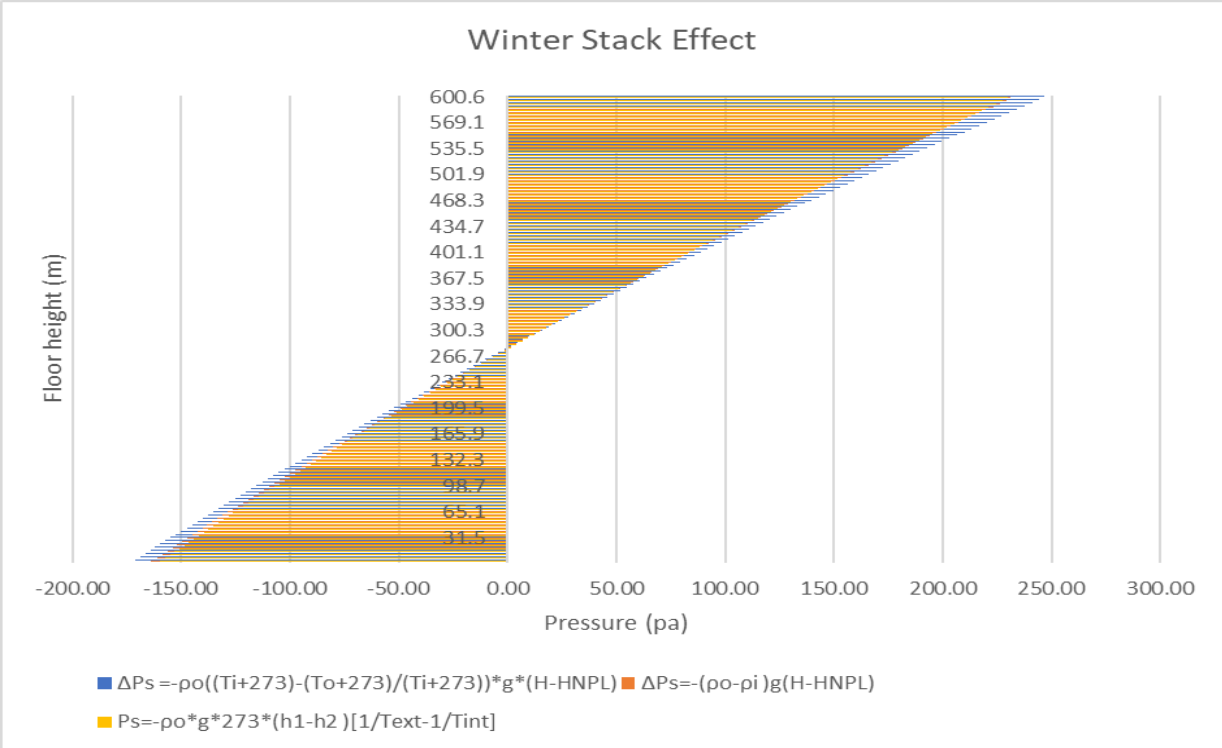

Figure 2 Stack effect driven indoor-outdoor pressure difference as a function of height in winter given the position of the neutral plane assuming the building is a single zone.

Figure 2 presents the indoor / outdoor pressure difference for winter conditions: the outdoor temperature is 6°C and the indoor temperature 20°C. The total delta P for the building is approximately 330 Pa. Clearly the slope here is less steep indicating a higher temperature difference: a vertical plot would mean zero temperature difference and a more horizontal slope would reflect a very high temperature difference.

4. Static air pressure in the shafts.

Static pressure, or hydrostatic pressure as it is sometimes called, is the pressure exerted by a fluid at rest. A fluid is any substance that does not conform to a fixed shape. This can be a liquid or a gas. Since the fluid is not moving, static pressure is the result of the fluid's weight or the force of gravity acting on the particles in the fluid.

Static pressure is the weight of the fluid above the point being examined. The pressure difference between two elevations can be calculated using the following equation:

$P = \rho * g * \Delta h$

Where:

P = the hydrostatic pressure (Pa)

ρ= the density of the air at height h

Δh = the height difference between the two points being examined

For this paper we are assuming the building to be 600m tall, we calculate the hydrostatic pressure at each floor starting at the top of the building. As we go down the building the pressure of the air at the floor above is integrated with the hydrostatic pressure at the floor being considered. At the bottom of the building there is a height of 600m creating the hydrostatic pressure difference.

5. Calculating Static Pressure Differences

Using the data shown in tables 1 through 4 above we can calculate the static pressure of the air in a shaft.

summer temp ©	summer density (kg/m3)
18	1.212

Table 1: Summer conditions in the stair shaft

Winter temp ©	Winter density (kg/m3)
14	1.229

Table 2: Winter conditions in the stair shaft

summer temp ©	summer density (kg/m3)
28	1.172

Table 3: Summer conditions in the elevator shaft

Winter temp ©	Winter density (kg/m3)
18	1.212

Table 4: Winter conditions in the elevator shaft

Using the above temperatures and resultant densities we calculate the pressures in the shafts

6.Calculating Flow Driven by Predicted Pressure Differential on Each Level

To calculate the air movement either from the shaft to the outside or vice versa we use the following formula:

$$Q = C_p A\sqrt{2\,\Delta P_{tot}/\rho} \qquad (1)$$

Where:

Q = airflow, m3/s

Cp =flow coefficient (0.61 was used for these calculations)

A = cross-sectional area of opening (e.g., the cracks in the case of infiltration), m2

ΔP_{tot} = total pressure difference between the vertical shaft and outdoors at the elevation of interest {Pa}

ρ = air density, kg/m3

The following formula is used to express the total pressure differential between a shaft and the outside.

$$\frac{1}{C_p^2}\left(\frac{Q}{A}\right)^2\frac{\rho}{2} = \Delta P_{tot} \qquad (2)$$

If we work with just the elevator shafts and assume the stair shafts are not participating in the stack effect:

$$\Delta P_{tot} = \Delta P_F + \Delta P_E \qquad (3)$$

The total pressure from is the pressure differential across the façade and the pressure differential across the elevator doors.

$$\Delta P = \frac{\rho}{2}\frac{1}{C_p^2}\left(\frac{Q_F}{A_F}\right)^2 + \frac{\rho}{2}\frac{1}{C_p^2}\left(\frac{Q_E}{A_E}\right)^2 \qquad (4)$$

Where:

Q_F = air flow through the façade

Q_E = the air flow through doors and cracks

A_F = the area of the façade

A_E = the area of doors and cracks

Formula 4 is derived from expanding formula 3 with formula 2.

Simplifying formula 4 we get,

$$\Delta P = \frac{\rho}{2C_p^2}\left(\frac{Q_F}{A_F} + \frac{Q_E}{A_E}\right)^2 \qquad (5)$$

As the air flows through the two sets of cracks (e.g. elevator and façade) are equal, we get,

$$Q_F = Q_E \qquad (6)$$

The next step is to assess the infiltration or exfiltration through the elevator shaft and the infiltration or exfiltration through the façade,

$$\Delta P = \frac{\rho}{2C_p^2}\,(Q_F A_E + Q_E A_F / A_F A_E)^2 \qquad (7)$$

Simplifying formula 7 we get

$$\Delta P = \frac{\rho}{2C_p^2}\,(2Q(A_E + A_F)/A_F A_E)^2 \qquad (8)$$

Further simplifying formula 8, we get

$$Q = \sqrt{2\,\Delta P/\rho}\,\frac{C_D}{2}\,(A_E A_F)/(A_E + A_F) \qquad (9)$$

To identify the pressure differential across the façade we get

$$\Delta P_F = \Delta P_{tot} - \frac{\rho}{2C_p^2}\left(\frac{Q}{A_E}\right)^2 \qquad (10)$$

This equation permits one to split the total pressure difference at any elevation into that across the façade and elevator doors based on the relative leakiness of the elements. To use this approach, the designer needs to acquire the following information:

- Equivalent façade leakage areas (at a known pressure difference) over the height of the building.

- Emergency exit stair shafts (these are usually the height of the building).
- Openings in stair shafts that lead to leakage including gaps underneath the doors.
- All elevator shafts, including goods and firefighter's elevators as well as the height of each elevator shaft.
- Openings in elevator shafts that lead to leakage including the gaps around the elevator doors; and,
- Any required building sections such as refuge floors.

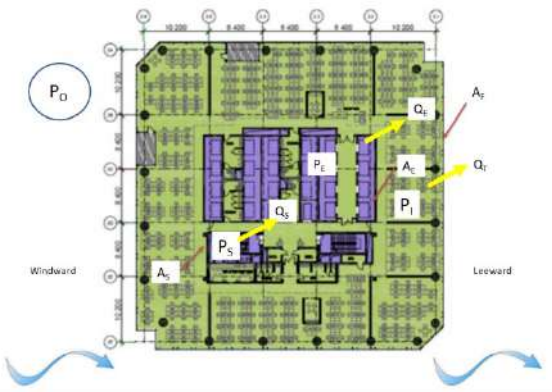

Figure 3:Typical floorplan of the building under consideration. There are two emergency staircases and two freight elevators

Leakage performance data is sometimes specified as a flow at a given pressure difference – this typically for the façade. For other components, for example operable windows, the leakage performance data is specified as a leakage area per linear distance of component. Finally, leakage area could be specified per unit (e.g., per door). To perform the calculation, the equivalent leakage areas should be calculated for all components which removes the pressure-based relationship of flow vs. pressure difference.

7. Pressure Predictions

Due to the dynamics of the interaction between outside conditions and temperatures in unconditioned spaces the study was conducted using three steps. The first step was to assume the outside temperature was constant over the height of the building, the second step was to assume a variable temperature over the height of the building and the third step was to assume a variable temperature and pressure over the height of the building.

The pressure in the stair shaft and elevator shaft were calculated for each floor and then the pressure in the floor above is integrated with the pressure from the floor below to provide a pressure head at that point.

The following figures show the results of comparing the pressure differential between the stair shaft and outside and the pressure differential between the elevator shaft and the outside.

From figures 1 and 2 we can see the building has a different characteristic fir the Summer and for the Winter. During the summer the flow of pressure is from the outside to the inside above the neutral plane. This means outside air will infiltrate the building and will add an extra cooling load to the conditioning system. In the winter the flow of pressure is from the outside to the inside below the neutral plane. This results in outside air infiltrating the building and will increase the heating load.

The goal of this research is to quantify the energy effects of the outside air infiltration due to the pressure differential between shafts and the outside.

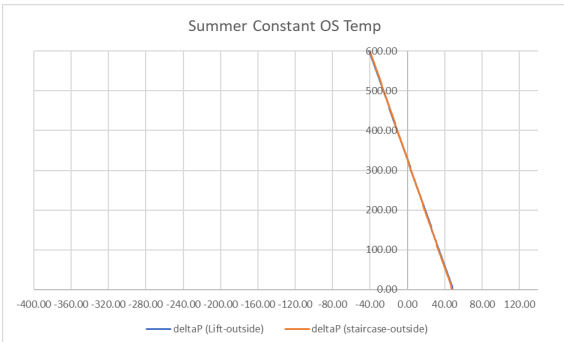

Figure 4 shows the pressure differential between the shafts and the outside when the outside temperature is assumed to be constant over the height of the building.

The pressure differential is from -40 Pa at the top of the building to +40 Pa at the bottom of the building. As the temperature differentials between shafts and outside are relatively small, 80 Pa.

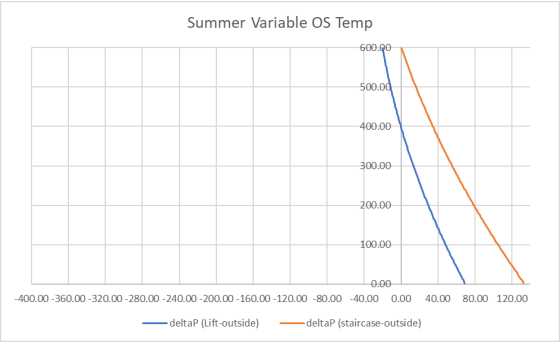

Figure 5 shows the pressure differential between the shafts and the outside when the outside temperature is assumed to be variable over the height of the building

Figure 5 shows a curved relationship this is due to the temperatures in the shafts being constant, but the outside temperature reduces over the height of the building. The pressure differential between the elevator shaft and outside is from -- 40 Pa at the top of the building to +80 Pa at the bottom of the building. The pressure differential between the Stair shaft and outside is from 0 Pa at the top of the building to +130 Pa at the bottom of the building.

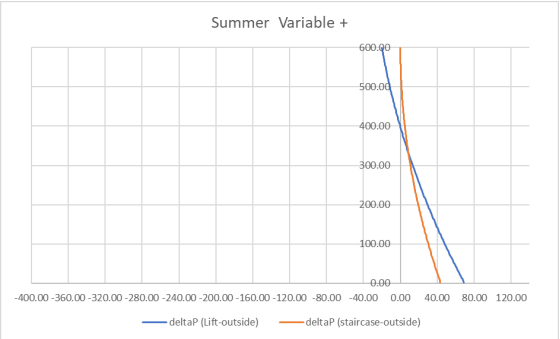

Figure 6 shows the pressure differential between the shafts and the outside when the outside temperature and pressure is assumed to be variable over the height of the building

Figure 6 shows the sensitivity of the pressure relationships. The pressure differential between the elevator shaft and outside is from -- 20 Pa at the top of the building to +70 Pa at the bottom of the building. The pressure differential between the Stair shaft and outside is from 0 Pa at the top of the building to +40 Pa at the bottom of the building.

Both stair and elevator shafts to outside pressure differentials are lower than the pressure differentials shown in figure 5.

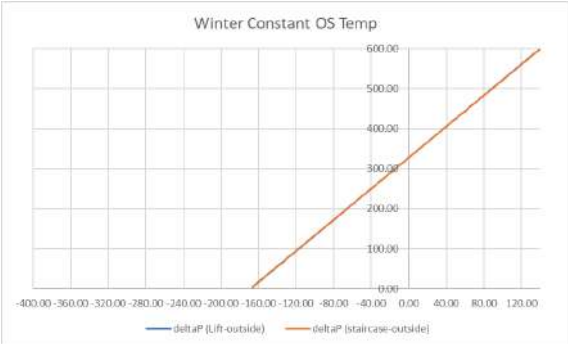

Figure 7 shows the pressure differential between the shafts and the outside when the outside temperature is assumed to be constant over the height of the building.

The pressure differential is from +130 Pa at the top of the building to -160 Pa at the bottom of the building. As the temperature differentials between shafts and outside are large, 290 Pa.

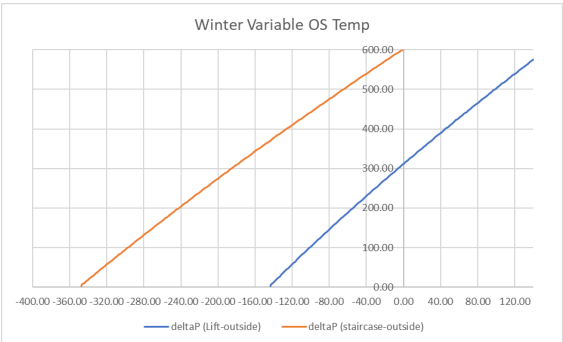

Figure 8 shows the pressure differential between the shafts and the outside when the outside temperature is assumed to be variable over the height of the building

Figure 8 shows a curved relationship this is due to the temperatures in the shafts being constant, but the outside temperature reduces over the height of the building. The pressure differential between the elevator shaft and outside is from +130 Pa at the top of the building to -140 Pa at the bottom of the building. The pressure differential between the Stair shaft and outside is from 0 Pa at the top of the building to -350 Pa at the bottom of the building. Both pressure differentials are much higher than the summer calculation and this is due to the larger temperature differential between the shafts and the outside.

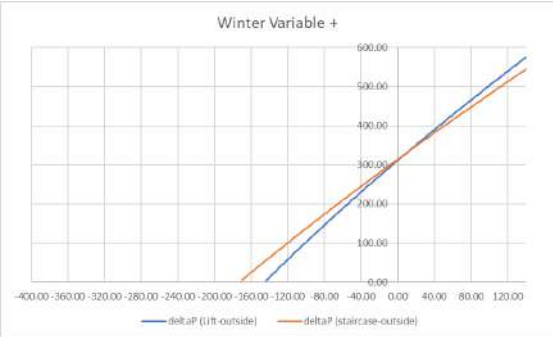

Figure 9 shows the pressure differential between the shafts and the outside when the outside temperature and pressure is assumed to be variable over the height of the building

Figure 9 shows the sensitivity of the pressure relationships. The pressure differential between the elevator shaft and outside is from +130 Pa at the top of the building to -140 Pa at the bottom of the building, which is 270 Pa. The pressure differential between the Stair shaft and outside is from +130 Pa at the top of the building to -170 Pa at the bottom of the building, which is 300 Pa.

8. Flow Predictions

The following results are for a single stair shaft and a single elevator shaft. For combinations of multiple stair and elevator shafts we refer to a future paper that will include these complicated calculations.

Using the following data from the preliminary analysis:

ρ stair

ρ elevator

ΔP stair to outside

ΔP elevator to outside

AS = Area of the stair openings

AE = Area of the elevator openings

AF= area of the facade

And using formula 9 we get the following results

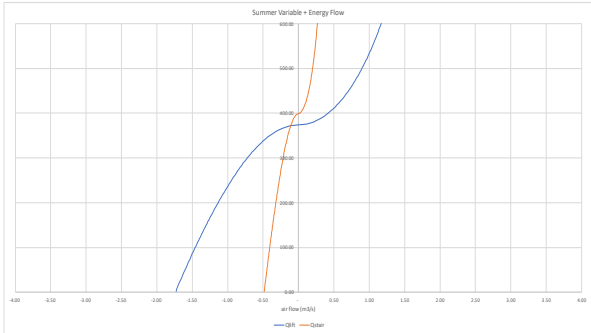

Figure 10 shows the volume of air flow infiltrating and exfiltrating the building in the summer.

When the flow is positive outside air will infiltrate the building. In the summer the infiltration of outside air will increase the space cooling load. The increase in cooling load is estimated at 149*1*1.172*(30-24) = 1,047.7 kW, on the design day.

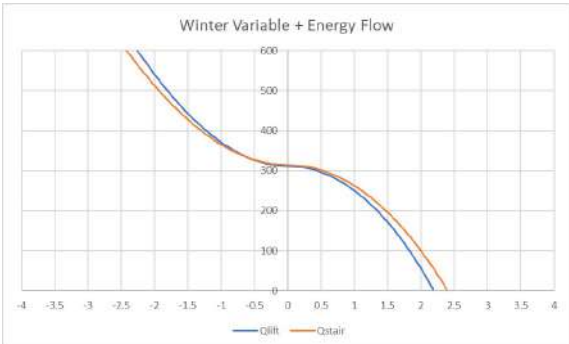

Figure 11 shows the volume of air flow infiltrating and exfiltrating the building in the Winter at 6 C outside temperature.

When the flow is negative outside air will infiltrate the building. In the winter the infiltration of outside air will increase the space cooling load. The increase in cooling load is estimated at 110*1*1.172*(20- 6) = 1,804 kW, on the design day.

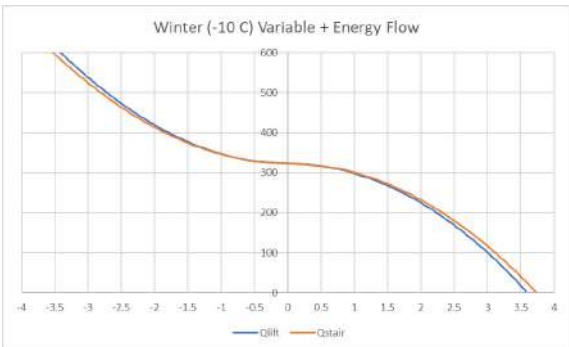

Figure 12 shows the volume of air flow infiltrating and exfiltrating the building in the Winter at -10 C outside temperature.

When the flow is negative outside air will infiltrate the building. In the winter the infiltration of outside air will increase the space cooling load. The increase in cooling load is estimated at 121*1*1.19*(20- -10) = 4,319.7 kW, on the design day.

9. Conclusions

The results clearly show that when calculation heating and cooling loads for Tall, Supertall and Megatall buildings the actual outside temperature differentials at different building heights need to be incorporated into the calculations.
The critical period is the winter as the temperature differential between internal shafts and the outside are largest, also the infiltration of outside air is at a lower temperature.
The actual outside air infiltration will be much higher than specified and who will be responsible for the increase in infiltration.
What pressure should the façade be tested to? What outside air infiltration rate has been included in the heating and cooling load calculations?
At present, there are no commercially available load calculation programs that use a variable outside temperature in the calculations.
This paper shows how the variable outside temperature can be used when calculating a buildings heating and cooling loads in a spreadsheet. These hand calculations should be recommended for Tall, Supertall and Megatall buildings.
It is, of course, essential that the vertical weather data be made available for such calculations.
The façade air infiltration rate specified by the architect should be appropriate for the overall height of the building.

Data Access

The datasets generated during or analysed during the current study are not publicly available because they are owned by RWDI.

References

ASHRAE. (2019). Standard 62·1-2019. Ventilation for Acceptable Indoor Air Quality, ASHRAE: Atlanta, Ga 30329.

ASHRAE. (2021). Chapter 16 and Chapter 24 Fundamentals Handbook 2021. ASHRAE: Atlanta, Ga 30329.

ASHRAE. (2019). Chapter 4 and Chapter 54, Applications Handbook 2019. ASHRAE: Atlanta, Ga 30329.

Lovatt, J. E. and Wilson, A. G. (1994). Stack effect in tall buildings. ASHRAE Transactions 100(2), pp. 420~431.

Nylund, P.O. 1980. Infiltration and ventilation. Report D22:1980. Swedish Council for Building Research, Stockholm.

Raymond, W. H. (2000). Estimating Moisture Profiles Using a Modified Power Law, Journal of Applied Meteorology 39(7), pp. 1059~1070.

Ross, D. (2004). An HVAC design guide for tall commercial buildings, ASHRAE.

Persily, A.K., and R.A. Grot. 1986. Pressurization testing of federal buildings. In Measured air leakage of buildings, STP 904, p. 184. H.R. Trechsel and P.L. Lagus, eds. American Society for Testing and Materials, West Conshohocken, PA.

Phillips, D, (2014) Personal Correspondence.

Phillips, Duncan A. (2021), Managing Infiltration in Tall Buildings to Control Energy Loss, Minimize Pathogen Transport and Enhance Air Quality, Presented at the ASHRAE January 2021 Conference, Seminar 75.

Simmonds, P., and Zhu, R., Stack Effect Guidelines for Tall, Mega Tall and Super Tall Buildings, International Journal of High-Rise Buildings, December 2013, Vol 2, No 4, 1-8

Simmonds, P., The new ASHRAE Design Guide for Tall, Supertall and Megatall Building Systems, ASHRAE 2015 and second edition 2020

Simmonds, P., and Phillips, D., A unique way to determine the Neutral Plane height in Stack Effect calculations. ASHRAE Journal, 2022

Tamblyn, R. T. (1991). Coping with air pressure problems in tall buildings. ASHRAE Transactions 97(1), pp. 824~827.

Tamura, G.T., and C.Y. Shaw. 1976a. Studies on exterior wall air tightness and air infiltration of tall buildings. ASHRAE Transactions 82(1):122. Paper DA-2388.

Tamura, G.T., and C.Y. Shaw. 1976b. Air leakage data for the design of elevator and stair shaft pressurization system. ASHRAE Transactions 82(2):179. Paper SE-2413.

Tamura, G.T., and A.G. Wilson. 1966. Pressure differences for a nine-story building as a result of chimney effect and ventilation system operation. ASHRAE Transactions 72(1):180.

Tamura, G.T., and A.G. Wilson. 1967a. Pressure differences caused by chimney effect in three high buildings. ASHRAE Transactions 73(2): II.1.1.

Tamura, G.T., and A.G. Wilson. 1967b. Building pressures caused by chimney action and mechanical ventilation. ASHRAE Transactions 73(2): II.2.1.

Solar hybrid collectors analysis - Experimental and numerical study

Catalina Tiberiu[a], Listarhov Ana[a], Teodosiu Catalin[a], Popescu Razvan[a], Popescu Lelia[a], Lungu Catalin[a]

[a] Technical University of Civil Engineering, Faculty of Building Services Bucharest, Tiberiu.catalina@utcb.ro .

Abstract. The resource economy is currently a global priority and the preservation of the planet and its resources are becoming the main international objectives. In this regard, EU states must establish clear lines and long-term strategies. Also, the goal of developed countries must involve reducing emissions by 80-95% by 2050. The global economic context leads to an intense concern in the field of unconventional sources, with solar energy occupying an important place. Solar energy can be collected and transformed either into electricity using photovoltaic or thermal technologies, through the use of different types of solar thermal panels or through the use of hybrid panels (PV/T Hybrid solar photovoltaic - thermal collectors, often known as PV/T are systems that simultaneously convert solar radiation into electricity and heat - operating in cogeneration. The paper includes experimental measurements and numerical analysis of a hybrid solar panel. A decrease in the surface of the panel was observed, thus an increase in electricity production by up to 6%. The original part is the experimental protocol used and the comparison of two solutions of energy production under the same conditions. The numerical campaign accompanies the experimental study and provide interesting data.

Keywords. Solar hybrid panels, experimental measurements, numerical simulations.
DOI: https://doi.org/10.34641/clima.2022.119

1. Introduction

The global economic context leads to an intense concern in the field of unconventional sources, solar energy occupying an important place. Renewable energy sources can be a form of energy production with a minimal impact on the environment and a low cost of implementation/operation. Of these, solar-powered systems are easy to implement and can become accessible in areas with solar potential, with a relatively short payback period. Solar energy can be captured and transformed either into electricity using photovoltaic technologies, or into thermal energy by different types of solar thermal panels.

According to Wu J. et al. [1] PV/T collectors could become a potential solution, as the simultaneous production of electricity and heat leads to a higher overall conversion of solar energy (94%) than independent collectors.

Based on the findings from the literature review, four general types [2] of PV/T installations can be identified: PV/T collectors with air, PV/T collectors with liquid - small scale, PV/T with liquid on a large scale where heat pumps and the latest category of PV/T concentrators mounted on the roof of industrial buildings and on non-residential buildings are also included.

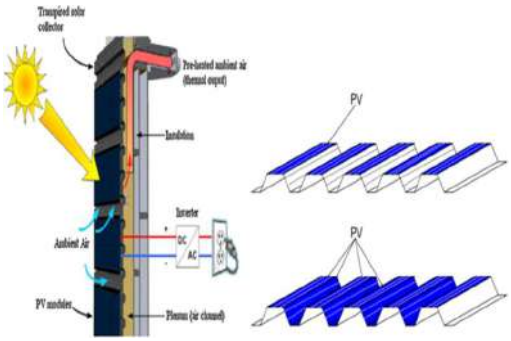

Fig. 1 – Conceptual scheme of hybrid PV / T collectors for facades and roofs [3,4]

The thermal efficiency of PV/T collectors can be improved by adding a layer of glass, while in PV collectors the efficiency decreases in this case. A compromise on photovoltaic and thermal efficiency must be considered in order to achieve the best performance for PV/T collectors in practice. [5].

Other major benefits of PV/T (according to Al-Waelia Ali HA, Sopiana K, Kazemb Hussein A, Chaichan Miqdam T.) [6]:

- more efficient use of the entire solar spectrum with photovoltaic and thermal components in a single unit;
- reduction of installation and space costs;
- decreasing the thermal load of the entire

Copyright ©2022 by the authors. This conference paper is published under a CC-BY-4.0 license.

building;

- a better architectural aesthetic integration compared to two individual collectors (one photovoltaic and one thermal).

China is by far the largest solar thermal market in the world, with 86% of the market and 64% of total installed capacity [7,8]. PV/T systems are not at the heart of research and development in China, but there is a growing interest in PV/T systems for water heating and direct connection to heat pumps. PV/T hot water systems are expected to become one of the main solar systems in buildings in China. [9]. Over the last 26 years, energy consumption in Sweden has been stable in the range of 46 to 53 Mtons (equivalent to millions of tons of petrol) compared to global energy consumption. [10] This is mainly due to the decrease in the use of fossil fuels but also a slight increase in the use of renewable energy sources, an increase from 38% to 64% in the period 1990-2016, but also in the future it is estimated that Renewable energy sources (solar and wind power) will have a continuous average increase of 2.8% per year between 2015 and 2040. [11] In Sweden a target has been set, in 2040, electricity will be 100% of renewable sources, solar energy will contribute 5-10% to electricity generation, compared to 2017 when the contribution was 0.1%. [12]. In Sweden PV/T collectors (used for electricity but especially for hot water) can be integrated into constructions in several variants (installation on the floor, on the roof, walls, balcony but even integration in windows in new buildings but also in old buildings) [13,14,15], PV/T collectors are able to connect with complex heating systems such as: district heating systems [16], desalination [17], industrial processing [18], waste heat recovery [19], electricity generation [20,21].

Grammer Solar & Bau in Germany currently have a commercially available PV/T product, the PV / T panel is air-conditioned and preheats the ventilation air. The product is available in 4 different module sizes ranging from 50 kWp to 250 kWp per module. [22.23,32]

In 1993, the Japanese government invested more than 1,200 million yen to test photovoltaic panels. One area of interest has been the development of PV / T collectors for buildings in Japan. A prototype for residential buildings was developed, which was tested on a house in Japan. PV / T collectors consist of photovoltaic cells supported by a thermal absorber, the collectors produce daily about 3.2 kWp of electricity and 25 kW of thermal energy for domestic water [24]. In Japan, Sekisui Chemical Co., Ltd installs the PV/T collector that converts about 10% of solar energy into electricity and 30% for average hot water annually.

At the Mataro Spain Library, PV/T collectors are mounted on the façade and on the skylights on the roof. The PV / T collectors used are those with air, the air is used to preheat the water in the conventional heating system. [25]

Yellow House in Aalborg, Denmark has 5 different groups of PV / T installations on the facade. [26-30]

Millennium Electric's Multi Solar System with a daily power of 2 to 4 kWh of electricity and 6,000 kcal of hot water has been installed in residential homes in Klil, a small mountain community in northern Galilee, Israel. . The systems have been in operation and have been monitored since 1991 [31,32].

The Canadian company Conserval Engineering has developed a PV / T air collector (SolarWall PV / T). The PV / T concept was developed at Concordia University, Montreal, and the demonstration system was installed at the university in 2007 [33].

In the UK, the number of PV / T installations has grown rapidly over the last decade. Newform Energia claims to have hundreds of installations across the country, from small systems to multiple complex sources of energy installations [34].

One example of a warmer climate is the Cogenra installation on a building at the University of Arizona Tech Park, which supplies the building with 191 kW of heat and 36 kW of electricity [35]. The project was partially funded by a local incentive program.

Solar energy is a significant source of renewable energy for buildings that have the same type of construction. The efficiency of electricity generation of photovoltaic systems is affected by the temperature of the photovoltaic panel. As the temperature of the panel increases, the efficiency of electricity production decreases due to the increase in resistance. To overcome this drawback, photovoltaic (PV / T) systems were introduced in the 1970 [36,37].

The purpose of this paper is to analyze by means of experimental measurements and later on using numerical simulations the performance of a hybrid solar panel compared to a classic photovoltaic one.

2. Experimental set-up

The experimental set-up was placed in the courtyard of the Faculty of Building Services Bucharest.

The activity within this stage are preparation of the experimental protocol (see Figure 2 and 3) , the installation of sensors (temperature, pyranometer, energy meters) and the effective measures with the related analysis. The equipment's are:

- 2 solar panels (one hybrid PV/T and one

photovoltaic)

- 2 microinverters
- 2 storage tanks
- 2 flow meter
- 2 circulation pumps
- 1 acquisition station
- ALMEMO temperatures
- 1 thermal imaging camera
- 1 power acquisition station
- electrical panel

Fig. 2 – Experimental campaign – during October 2021

Fig. 3 – Photos with the Almemo temperature acquisition system, electrical connections, and water storage tanks

Using the infrared thermal camera multiple images were taken and it can be seen that the hybrid solar panel are colder by up to 10°C due to the water circulation inside it.

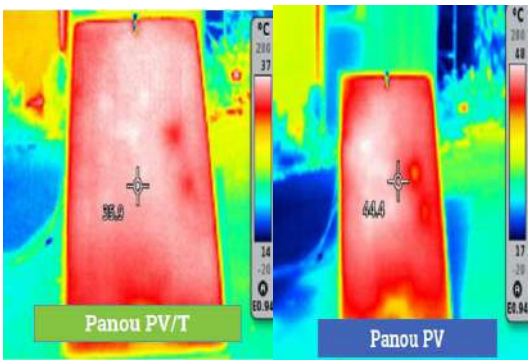

Fig. 4 – Thermal camera images for the two analyzed panels

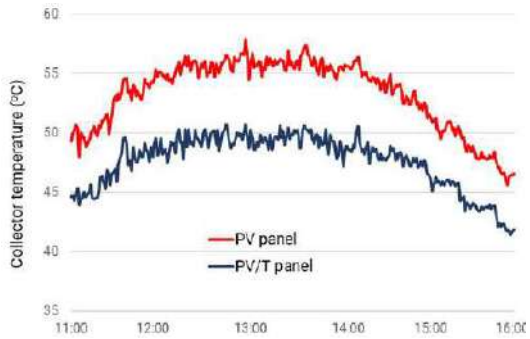

3. Numerical simulations

The built numerical model will allow the investigation of the operation of the PV / T hybrid solar panel and in other working conditions.

It is mentioned that the Ansys R15.0 software (Academic) was used to develop the CFD numerical model. The construction of the model took into account the real geometry resulting from the experimental stand (Fig. 1). The geometry of the computing domain thus includes the following elements: the panel itself, the thermal insulation layer and the copper coil.

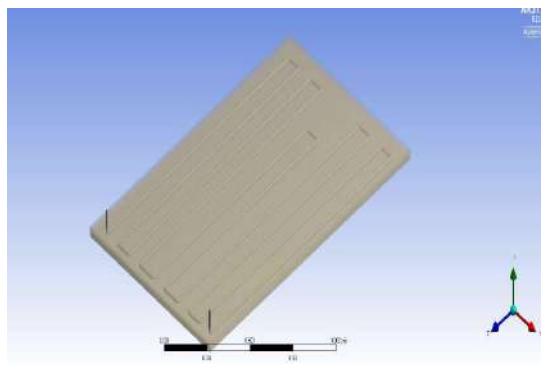

Fig. 1 – 3D geometry of the hybrid panel

The total number of finite volumes resulting from the discretization operation of the computational domain is 281,376 (Fig. 2 a). It is also shown in Fig. 2 b a detail with the discretization network made. It is specified that for the serpentine a finer discretization was made in order to be able to correctly capture its geometric shape, as well as the physical phenomena involved at its level (Fig. 4).

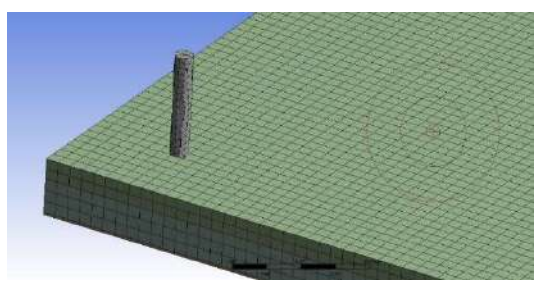

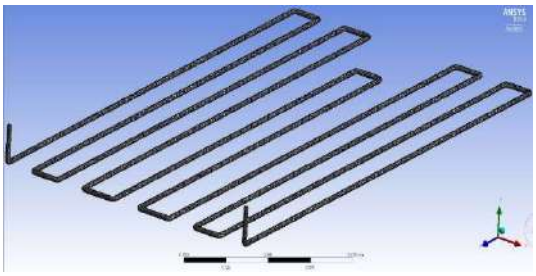

Fig. 2 – Discretisation detail (a) and serpentine (b)

The main hypotheses, physical models and numerical methods used are summarized in Table 1.

Tab. 1 - The main components of the numerical model

Element	Description
Flow	3D, turbulent, non-isothermal, permanent mode
Turbulence model	k-epsilon standard
Flowing near solid borders	Wall functions
Numerical solution	Default solver "segregated"; diffusive terms: schemes centered by ordinal 2; convective terms: ordinal up-wind scheme 2; SIMPLE algorithm (pressure-speed coupling)

The boundary conditions imposed in the numerical model were as follows:

• upper panel face: temperature imposed on the surface, constant value 50°C (according to experimental data)

• lower face of the panel (thermal insulation): temperature imposed on the surface, constant value, 25 ° C (according to experimental data),

• serpentine inlet: «velocity inlet», imposed speed - value that would allow obtaining the water flow from the experimental study, respectively 2.5 l/min; imposed temperature: 10°C

• coil outlet: «outflow»

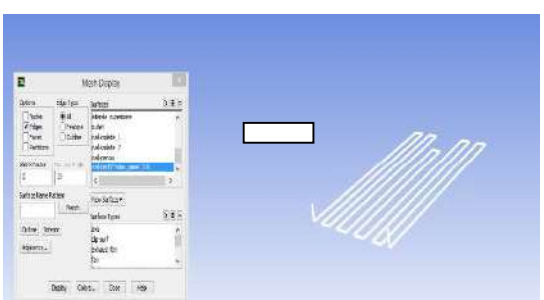

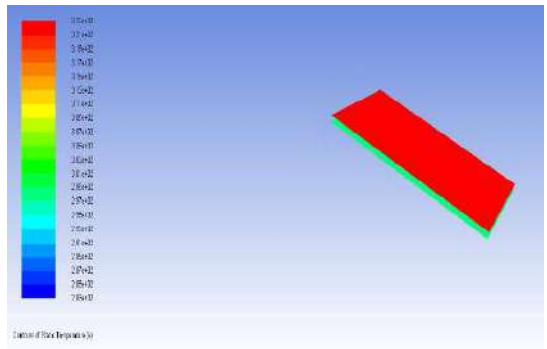

Fig. 3 – Boundary conditions inlet/outlet serpentine (a) and solar panel surfaces (b)

The main result of the numerical simulations consists in the water temperature at the exit of the coil with which the PV/T hybrid solar panel was provided. The temperature obtained was 13.78°C - practically a difference of 3.78 °C from the inlet. The experimental data showed an outlet-in-water temperature difference between 5°C and 6°C. Future calibrations and simulations will seek to improve the numerical prediction of water heat transfer within the analyzed PV/T hybrid solar panel. On the other hand, it is mentioned that the simulation results showed a more than acceptable balance (lower than the value of 10-6) in terms of the water inlet flow /water outlet flow ratio. This first numerical study highlighted the ability of the developed CFD model to accurately represent the heat transfer and fluid flow phenomena within the analyzed PV/T hybrid solar panel. The numerical model can also be used for other working conditions to extrapolate the results. Also, based on the developed CFD model, research will continue for the integration of aspects related to the insertion of phase change materials in the PV / T hybrid solar panel.

4. Conclusions

Using an experimental set-up several parameters were measured for two types of solar panels: one hybrid PV/T and another one PV. It can be concluded that the PV/T surface temperature was on average by 10oC colder than the PV solar panel which is translated in better performance in terms of energy production. From the energy data from both panels we have calculated that the electric energy production for a PV/T panel is higher by 5-6% than a classical PV panel. The second part of the paper was dedicated to the numerical modelling of the hybrid solar panel. Using the input data from the experimental measurements (water flow, temperatures) we were able to simulate the heat flow. The numerical study represents the first step in optimizing further the solar panel by introducing phase change materials for example. A decrease in the surface of the panel was observed, thus an increase in electricity production by up to 6%.

5. Acknowledgement

The project was funded by the Romanian Research Ministry and Technical University of Civil Engineering Bucharest. The project reference is UTCB-CDI-2021-001.

6. References

[3] McInnes D., Bollen J. Learning on the job: metaphors of choreography and the practice of sex in sex-on-premises venues. Venereology. 2000;13(1):27-36.

[1] Wu J, Zhang X, Shen J, et al. A review of thermal absorbers and their integration methods for the combined solar photovoltaic/thermal (PV/T) modules. Renew Sustain Energy Rev 2017;75:839–54.

[2] Clara Gooda, Jinfeng Chenb, Yanjun Daib, Anne Grete Hestnesa, "Hybrid photovoltaic-thermal systems in buildings – a review" Energy Procedia 70 (2015) 683 – 690

[3] Athienitis Andreas K, et al. A prototype photovoltaic/thermal system integrated with transpired collector. Sol Energy 2011;85:139–53

[4] Delisle, Veronique; Collins, Michael R.. Model of a PV/thermal unglazed transpired solar collector. In: Proceedings of 32nd Solar and Sustainable Energy of Canada Inc. conference, Calgary, Alberta, Canada; 2007. p. 10–13

[5] Yaxiu Gua, Xingxing Zhangb, Jonn Are Myhrenb, Mengjie Hanb, Xiangjie Chenc, Yanping Yuand (2018), "Techno-economic analysis of a solar photovoltaic/thermal (PV/T) concentrator for building application in Sweden using Monte Carlo method" Energy Conversion and Management 165, 8–24

[6] "Al-Waelia Ali HA, Sopiana K, Kazemb Hussein A, Chaichan Miqdam T. "Photovoltaic/Thermal (PV/T) systems: status and future prospects. Renew Sustain".Energy Rev 2017;77:109–30."

[7] Chow TT, et al. Performance evaluation of a PV ventilated window applying to office building of Hong Kong. Energy Build 2007;39:643–50.

[8] Dubey Swapnil, Solanki SC, Tiwari Arvind. Energy and exergy analysis of PV/T air collectors connected in series. Energy Build 2009;41:863–70

[9] Dubey Swapnil, Sandhu GS, Tiwari GN. Analytical expression for electrical efficiency of PV/T hybrid air collector. Appl Energy 2009;86:697–705

[10] Enerdata Yearbook.<https://yearbook.enerdata.net/>

[11] "International Energy Outlook.<https://www.eia.gov/outlooks/ieo/pdf/0484(2017) .pdf>"

[12] Swedish energy agency. Proposals for strategy for increased use of solar.<https:// energimyndigheten.a-w2m.se/Home.mvc ResourceId = 5599>

[13] Zondag HA, Helden WGJ, Elswijk MJ, Bakker M. PV-thermal collector development - an overview of the lessons learnt. In: Proceeding the 19th European PV solar energy conference and exhibition, 7–11 June 2004, Paris, France.

[14] X10 PV/T.<http://www.absolicon.se/product/absolicon-x10-pvt>

[15] "Strebkov D, Litvinov P, Kuzhnurov Y, Tveryanovich E, Tyukhov I, Kivalov S. Integrating PV/thermal concentrator systems into buildings. In: Proceedings of thesolar world congress 2005: bringing water to the world, including proceedings of 34th ASES annual conference and proceedings of 30th national passive solar conference.p. 1091."

[16] "Alba Ramos, Ilaria Guarracino, Alexander Mellor, Diego Alonso-Álvarez, Peter Childs, Nicholas J. Ekins-Daukes, Christos N. Markides. Solar-Thermal and Hybrid Photovoltaic-Thermal Systems for Renewable Heating. Grantham Institute, Briefing paper No 22; May 2017 .<https://www.imperial.ac.uk/media/imperial-college/ grantham - institute /public/publications/briefing-papers/2679_Briefing-P-22-Solarheat_web.pdf>"

[17] Arunkumar T, Denkenberger David, Velraj R, Sathyamurthy Ravishankar, Tanaka Hiroshi, Vinothkumar K. Experimental study on a parabolic concentrator assisted solar desalting system. Energy Convers Manage 2015;105:665–74.

[18] Riggs BC, Biedenharnb R, Dougher C, et al. Techno-economic analysis of hybrid PV/T systems for process heat using electricity to subsidize the cost of heat. Appl Energy 2017;208:1370–8.

[19] Xing Ju, Chao Xu, Liao Zhirong, Xiaoze Du, Wei Gaosheng, Wang Zhifeng, et al. A review of concentrated photovoltaic-thermal (CPVT) hybrid solar systems with waste heat recovery (WHR). Sci Bull 2017; 62:1388–426.

[20] Buonomano Annamaria, Calise Francesco, Palombo Adolfo. Solar heating and cooling systems by absorption and adsorption chillers

driven by stationary and concentrating photovoltaic/thermal solar collectors: Modelling and simulation. Renew Sustain Energy Rev 2018;82:1874–908.

[21] Powell Kody M, Rashid Khalid, Ellingwood Kevin, Tuttle Jake, Iverson Brian D. Hybrid concentrated solar thermal power systems: a review. Renew Sustain Energy Rev 2017;80:215–37.

[22] http://www.grammersolar.de/solarthermie/pvkollektor.htm.

[23] https://grammer-solar.com/de/

[24] www.nrel.gov/ncpv/documents/japan.html]

[25] "The Library of Mataro description and first results of monitoring", Article by Dr. Antoni Lloret, Labotatoire des Interfaces et des Couches Minces Ecole Polytechnique, 91128 Palaiseauu cedex, France.

[26] "The Yellow House- An innovative solar renovation of multi storey housing" O. B. Jørgensen, Esbensen Consulting Engineers Ltd. 1997, proceedings from 7th. International Conference on Solar Energy at High Latitudes – North Sun `97, Espoo-Otaniemi, Finland

[27] "Integration of Solar Energy in future renovation of multi storey housing - The Yellow House" O. B. Jørgensen, Esbensen Consulting Engineers Ltd. 1997, proceedings from EuroSun `96, Freiburg, Germany

[28] "Monitored results from the Yellow House" O. B. Jørgensen and L. T. Nielsen, Esbensen Consulting Engineers Ltd. 2000, paper presented at EuroSun 2000 in Copenhagen, Denmark

[29] "The Yellow House-Final Report" Esbensen Consulting Engineers Ltd and SBS Byfornyelse, 2002, Copenhagen, Denmark.

[30] "The Importance of Hybrid PV-Building Integration", Paper by M. Posnansky, Atlantis Energy Ltd. 3012 Bern, Switzerland,

[31] Dr. A. Elazari, "Multi Solar System, Field Experience In Israel", Several articles obtained from Dr. Elazari at Chromagen in Tel Aviv

[32] Miroslav Bosanac, Jamal Badran et al, "Photovoltaic/Thermal Solar Collectors and Their Potenţial in Danmark" Final Report EFP project 1713/00-0014, 2003

[33] A.K. Athienitis, J. Bambara, B. O'Neill, J. Faille, A prototype photovoltaic/thermal system integrated with transpired collector, Solar Energy, 85 (2011) 139-153.

[34] Newform Energy, http://www.newformenergy.com/

[35] New Solar Technology Deployed at the UA Tech Park's Solar Zone Gains Momentum, Tech Parks Arizona, https://techparks.arizona.edu/new-solar-technology-deployed-ua-tech-park's-solar-zone-gains-momentum, 2013.

[36] S. Rasoul Asaeea,∗, Sara Nikoofarda, V. Ismet Ugursala, Ian Beausoleil-Morrison "Techno-economic assessment of photovoltaic (PV) and buildingintegrated photovoltaic/thermal (BIPV/T) system retrofits in the Canadian housing stock" Energy and Buildings 152 (2017) 667–679

[37] R. Kumar, M.A. Rosen, A critical review of photovoltaic–thermal solar collectors for air heating, Appl. Energy 88 (11) (2011) 3603–3614

Intelligent building envelope solutions in Finnish new and old apartment buildings

Azin Velashjerdi Farahani[1], Juha Jokisalo[1,2], Natalia Korhonen[3], Kirsti Jylhä[3], Heikki Ihasalo[1], Jaakko Ketomäki[1], and Risto Kosonen[1,2,4]*

[1] Aalto University, Espoo, Finland
[2] Smart City Center of Excellence, TalTech, Tallinn, Estonia
[3] Finnish Meteorological Institute, Helsinki, Finland
[4] Nanjing Tech University, Nanjing, China

Abstract. This study investigated the effects of intelligent building envelope solutions (automated blinds, openable windows, and awnings as well as electrochromic windows) in Finnish old and new apartment buildings. Moreover, the results are compared to the passive solutions (manual blinds and solar protection windows). The main goal was to compare the performance of each solution in improving the indoor temperature conditions in Finland's current climate. Thus, the solutions were simulated with the usage of a mechanical cooling system in the living room to see the effects on both the energy demand of the buildings and indoor temperature conditions in the warmest bedroom. Furthermore, indoor temperature conditions were analyzed in the warmest bedroom of the new building without an active cooling system, as well. According to the results, electrochromic and solar protection windows are the solutions with the lowest cooling electricity consumption in the old building. However, in the new building, the lowest cooling electricity consumption is for the case with the automated openable windows and the next effective solutions are solar protection and electrochromic windows. Considering the results of indoor temperature conditions, the combination of solar protection windows and manual blinds is the most effective solution in the old building. While automated openable windows have the best performance in the new building with or without the active cooling system. Overall, passive solutions are more effective in both the old and new apartment buildings except for automated openable windows in the new building.

Keywords: Intelligent building, residential building, Energy efficiency, automated solutions
DOI: https://doi.org/10.34641/clima.2022.438

1 Introduction

One of the highest energy consumptions is for the building sector in Europe [1]. It is mentioned by the EU commission provisions that the level of energy consumption should be lower in future buildings [2].

On the other hand, climate change and increasing ambient temperature have been a growing concern and their effects on energy consumption are not questionable [3]. Based on the literature, climate change is likely to increase the cooling energy demand and decrease the heating energy demand in most of Europe [4]. Thus investigating the ways to reduce cooling energy seems to be necessary.

Intelligent control of building facilities has been an approach to making buildings more energy-efficient in recent decades [5]. However, there is still a need for evaluating their effects on energy efficiency as well as occupants' comfort in different buildings.

This study aims to determine the energy efficiency of intelligent building envelope solutions and their effects on indoor temperature conditions in Finnish old and new residential buildings. Furthermore, their performance will be compared to passive solutions.

2 Methods

2.1 Example building

The studied buildings are two 5-story (four living floors and a basement) apartment buildings with the same

* Corresponding author: azin.velashjerdifarahani@aalto.fi

Copyright ©2022 by the authors. This conference paper is published under a CC-BY-4.0 license.

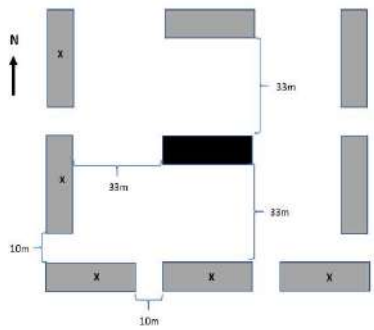

Figure 2. The simulated example building (black box) and the surrounding buildings (grey boxes).

Figure 1. The geometry of the building.

geometry and orientation in Helsinki. Fig. 1 shows the geometry of these buildings. The heated net floor area of each building is 1943.5 m^2. Both buildings are surrounded by similar buildings as shown in Fig. 2.

These two buildings are different in their construction year. Thus, their ventilation systems, envelop properties, window to wall ratio, and window properties are different as well. The new building belongs to the period after 2012 and the old one to the 1960s. The new and old buildings' properties are reported in Table 1.

Table 1. The properties of the studied building.

	New building	Old building
Year of construction	after 2012	The 1960s, 1950s
Heated net floor area (m^2)	1943.5	
U-value of the external wall (W/m^{2}K)	0.17	0.6
U-value of external window (W/m^{2}K)	1	2.5
Airtightness of building envelope (q_{50}) (m^3/h,m^2)	4	6
Heating system	District heating, 70/40°C water radiators, 65 W/m²	District heating, 70/40°C water radiators, 100 W/m²
Ventilation system	Constant air volume (CAV) mechanical supply (17°C) and exhaust ventilation system, Heat recovery efficiency: 0.65	Mechanical exhaust (CAV) ventilation
	total air exchange rate of the building: 0.52 ACH.	
Split cooling unit (not in all the cases)	COP: 3, Living rooms, the Cooling capacity of the units: 45 W/m²	

A mechanical exhaust constant air volume (CAV) ventilation system is used in the old building with specific fan power (SFP) of 0.7 kW/m³/s. The ventilation system of the new apartment building is a CAV mechanical supply and exhaust ventilation system with the SFP of 1.8 kW/m³/s. The setpoint temperature of supply air heating is 17 °C and it is assumed that supply and exhaust air temperature increase by 1 °C due to fans and ducting. There is no mechanical cooling in the air handling unit (AHU). The AHU is equipped with a district-heated reheat coil which is used for heating supply air. The floor plan, room types, and exhaust airflow rates (negative values) in different rooms of the old and new apartment and supply airflow rates (positive values) in each room of the new building are shown in Fig. 3. The air leakage rate of building envelope q_{50} at 50 Pa pressure difference is 4 m^3/hm^2. The total ventilation air exchange rate of both buildings is 0.52 ACH.

The occupancy density is 1 occupant per 28 m^2. The activity level is assumed to be 1.2 MET and an adjustable clothing level of (0.85 ± 0.25 CLO) is used in the simulations. It is assumed that there are no heat gains from occupants in the staircase and base floor. The presence of the occupants corresponds with the lifestyle of working people.

The heating system of both old and new buildings is district heating (DH) and the efficiency of the heat exchanger in the DH substation in the building is 97%. 70/40°C water radiators with a heat distribution efficiency of 80% are used. However, the space heating system capacity is 65 W/m^2 in the new building and 100 W/m^2 in the old building. The temperature setpoint for the space heating is 21 °C in the living spaces and 22 °C in the bathrooms. The setpoint of space heating is 17 °C for the staircase and basement floor. It is assumed that the living room of each apartment is equipped with a split cooling unit with a Seasonal Coefficient of Performance (SCOP) of 3 and a cooling capacity of 45 W/m². The temperature setpoint of space cooling is 25 °C in the apartments. However, there are some simulation cases in the new building without a mechanical cooling system which will be discussed in the next section.

The annual net heating demand of domestic hot water (DHW) in both buildings is 35 kWh/m^2, per total heated net floor area. The DHW is heated via the district heating system and its consumption is constant with time. Heat losses of the DHW circuit are 0.56 W/m² and 50% of the heat losses can be assumed to end up with internal heat gains in the zones. The total annual electricity consumption of household equipment is 21.0 kWh/m^2, per heated net floor area. The electric power of the appliances (W/m^2) is evenly distributed by the floor area of all the spaces of the apartments and the appliances are used every day between 7:00-23:00. There are no appliances on the staircase or base floor.

The total annual electricity consumption of indoor lighting is 7.9 kWh/m^2, per total heated net floor area. The

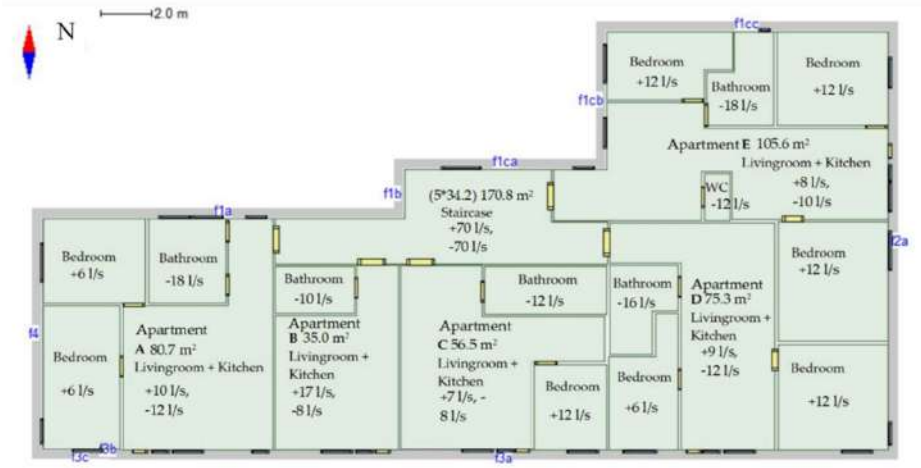

Figure 3. Floor plan and room types in the studied building**.**

electric lighting power (W/m^2) is assumed to be evenly distributed by the floor area of all the spaces in the apartments and by the floor area of the staircase. It is assumed that there are no heat gains from lighting on the base floor. The usage time of the lights are:

May to August: between 21:00-23:00

Sep to Apr: between 6:30 - 9:00 and 15:00 – 23:00

The internal door of the bathrooms or WCs is always closed but the other internal doors inside the apartments are always open. The airtightness of the closed doors is considered in the simulation and the equivalent leakage areas at 4 pa pressure difference are 0.02, 0.1, and 0.08 m^2 for the bathroom door, doors between the apartments and the staircase, and the outdoor door of the staircase, respectively.

Except for some of the simulations cases, there are no blinds for the windows. Additionally, the buildings are not equipped with lighting controls as any typical apartment building in Finland.

2.2 Climatic data and simulation tool

The study is done using the validated dynamic simulation tool IDA-ICE 4.8 [4]. The time resolution of the simulation results is 1 hour.

The test reference year (TRY2020) of the Helsinki-Vantaa weather station describing the current climatic conditions of Southern Finland was used in the study.

2.3 Simulation cases

Three groups of simulation cases are defined for both the old and new buildings. First, the reference cases are as described in the previous section. Second group, passive solutions: manual blinds, solar protection (S.P) windows, and the combination of S.P windows and manual blinds. Third, automated solutions: automated blinds, automatically controlled openable windows, automatically controlled awnings, and electrochromic windows. All these cases are simulated with the mechanical cooling system in the living rooms in both buildings. Table 2 describes these simulation cases. Moreover, the base case, the case with the combination of S.P windows and manual blinds, and all the automated solutions in the new building are simulated without the mechanical cooling system to see the effects of the solutions on indoor air temperature. These cases are shown by * in Table 2. All over, there are 8 cases in the old building and 14 cases in the new building.

2.4 Target values of indoor air temperature

The target value is used in this paper to compare the effects of the solution on indoor temperature conditions. Thus, the requirements suggested by the Ministry of the Environment are used. As in the design phase, the maximum allowed design indoor air temperature is 27°C [6]. The annual hourly indoor air temperature profiles for the warmest bedroom of each building are simulated. In the cases without mechanical cooling, the annual degree hours above 27 °C are calculated and compare

3 Results

The results are presented in two different parts, in the first one, the annual district heating and space cooling electricity consumption of each case are compared. The second one is an assessment of the indoor air temperature in the warmest bedroom of the buildings to find out the effects of each solution on indoor conditions.

3.1 Energy consumption

A summary of the breakdown of space and AHU district heating and space cooling electricity consumption in the old and new buildings are presented in Tables 3 and 4, respectively. The effects of each solution on district heating demand for space heating and the reheat coil of ventilation and cooling electricity will be discussed for each building.

Table 2. Brief description of simulation cases.

	Cases	Description
Base Case	Old-Base	The reference case.
	New-Base*	
Passive solutions	Old-Manual blind	Manual blinds between the outer windowpanes according to the occupancy schedule during the whole year, all the windows except the staircase windows.
	New-Manual blind	
	Old-S.P windows	Solar protection windows, U value: 1 W/m^{2}K, g-value: 0.19, ST: 0.16
	New-S.P windows	
	Old-Manual blind & S.P. windows	Combination of manual blind and solar protection windows.
	New-Manual blind & S.P. windows*	
Automated solutions	Old-Auto blind	Blinds Between the outer windowpanes are in use when the intensity of solar radiation on the façade exceeds 100 W/m^2 for all the windows except the staircase windows.
	New-Auto blind*	
	Old-Openable windows	10% of the largest window of each room (cross ventilation) opens when the outside air temperature is between 12 °C and 22°C and the zone air temperature is between 23 °C and 25°C. Not in the staircase.
	New-Openable windows*	
	Old-Auto awning	Electrically controlled awning. Awnings on the windows without a balcony open when the wind speed is less than 8 m/s and outdoor air temperature exceeds 15 °C meanwhile the intensity of solar radiation on the façade exceeds 100 W/m^2. All the windows except the large atrium windows, small windows of the atrium at the street level have awnings. The depth and height of the awning are equal to 30% of the window height.
	New-Auto awning*	
	Old-Electrochromic windows	Electrochromic windows. U value 0.97 W/m^{2}K, when the outdoor solar radiation on the façade exceeds 450 W/m^2 the darkest state of the glazing is on ST: 0.29-0.01, g-value: 0.31-0.05, Tvis: 0.61. All the windows.
	New-Electrochromic windows*	

As Table 3 shows, the space heating and AHU district heating consumption in the cases with solar protection windows and the combination of solar protection windows and manual blinds in the passive group and the case with electrochromic windows in the automated group, has decreased by 3-4% (around 5 kWh/m^2) in the old building. The lower U value of these windows compared to the existed poorly insulated windows has caused this decrease. While in the new building (Table 4) with the existing well-insulated windows, these cases have caused an increase of 2-3% (around 1 kWh/m^2) in district heating consumption because of the reduction in solar gains. Manual blinds have slightly increased the district heating consumption in both buildings. Compared to electrochromic windows, other automated solutions have had a smaller effect on district heating consumption in both buildings. This difference is because of the lower U value of these windows in the old building and their lower solar gains in the new building.

On the other hand, all the solutions have decreased the space cooling electricity consumption in both buildings. However, the absolute value of the cooling electricity is small (around 2 kWh/m^2), even if the percentage of decrease caused by each solution is high. The highest decrease levels in the old building are for the cases with solar protection windows and the combination of solar protection windows and manual blinds, electrochromic windows, and openable windows, with more than 60%. In the new building, the case with the openable windows has the lowest cooling electricity consumption (0.4 kWh/m^2). The next two cases with the lowest cooling electricity consumption are the ones with solar protection windows and a combination of solar protection windows and manual blinds with a more than 30% decrease. Manual blinds had the lowest effect on cooling electricity consumption in the new building with around 9%.

In the cases with openable windows, the windows are open when the indoor temperature is between 23-25 ℃. The simulation results showed that the indoor temperature of the old building is in this range for a shorter period than the new building. Thus, the effects of this solution in the new building are more significant.

Table 3. Breakdown of annual energy consumption in the old building (kWh/m^2).

Systems	Old-Base	Old-Manual blind	Old-S.P windows	Old-Manual blind & S.P. windows	Old-Auto blind	Old-Openable windows	Old-Auto awning	Old-Electrochromic windows
Space heating + AHU	136.1	136.7	131.7	131.9	138.1	136.5	136.3	130.6
Space cooling electricity	2.1	1.8	0.8	0.7	1.1	0.8	1.5	0.8
Difference (%) of Space heating + AHU in comparison to Base case		0.4	-3.2	-3.1	1.5	0.3	0.1	-4.0
Difference (%) of Space cooling electricity in comparison to Base case		-14.3	-61.9	-66.7	-47.6	-61.9	-28.6	-61.9

Table 4. Breakdown of annual energy consumption in the new building (kWh/m^2).

Systems	New-Base	New-Manual blind	New-S.P windows	New-Manual blind & S.P. windows	New-Auto blind	New-Openable windows	New-Auto awning	New-Electrochromic windows
Space heating + AHU	34.9	35.0	36.1	36.1	35.0	35.1	34.9	35.7
Space cooling electricity	2.3	2.1	1.6	1.5	1.9	0.4	2.0	1.8
Difference (%) of Space heating + AHU in comparison to Base case		0.3	3.4	3.4	0.3	0.6	0.0	2.3
Difference (%) of Space cooling electricity in comparison to Base case		-8.7	-30.4	-34.8	-17.4	-82.6	-13.0	-21.7

3.1 Indoor temperature conditions

The indoor air temperature is analyzed in all the cases in both buildings with the mechanical cooling system. Then the degree hours above 27 °C in the cases with the lowest energy consumption without the usage of the mechanical cooling system are calculated and compared in the new building.

The indoor air temperature in the warmest bedroom of both building types is investigated. The warmest bedroom is in Apartment D, on the middle floor, and faces to the south and is shown in Fig.4.

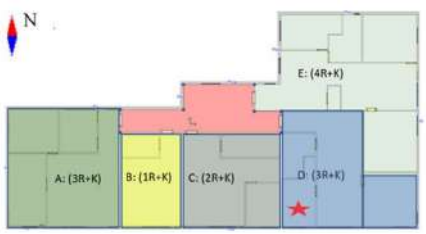

Figure 4. The location of the warmest bedroom (red star) in the buildings.

The indoor temperature duration curves for the old and new are shown in Fig.5 and 6, respectively. As the figures show, the maximum temperature in the old building is higher than in the new building but the new building is warmer most of the time.

Among the passive solutions, the cases with solar protection windows (combined with manual blinds or alone) have the most effects on indoor temperature conditions in both buildings, and manual blinds have not been effective. Regarding the automated solutions, all of them have decreased the indoor air temperature in both buildings. openable windows, electrochromic windows have had the highest effect. Among all the passive and automated solutions, it seems that openable windows, the combination of solar protection windows, and electrochromic windows are the most effective ones in both buildings, respectively.

Since the curves are close together, for a more detailed comparison between the effects of passive and automated solutions on indoor temperature conditions, the degree hours above 27 °C are calculated in the new building. Table 5 reports the degree hours above 27 °C in the cases with the lowest energy consumption without the usage of the mechanical cooling system in the new building. The openable windows have decreased the degree hours above 27 °C by 100%. The combination of solar protection windows and manual blinds, as well as electrochromic windows, are the next solutions with a 58% and 43% decrease. Auto blinds and auto awnings are also effective. However, the percentage of decrease in degree hours above 27 °C is around 30% in the cases with these two solutions.

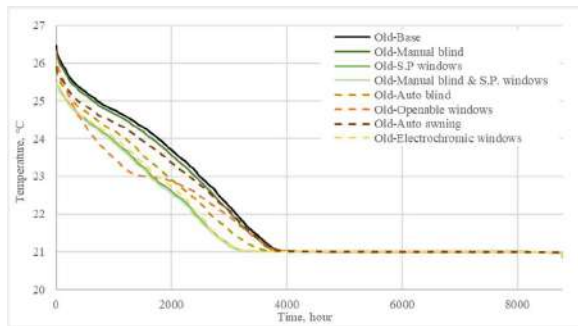

Figure 5. Indoor air temperature duration curve of the old building.

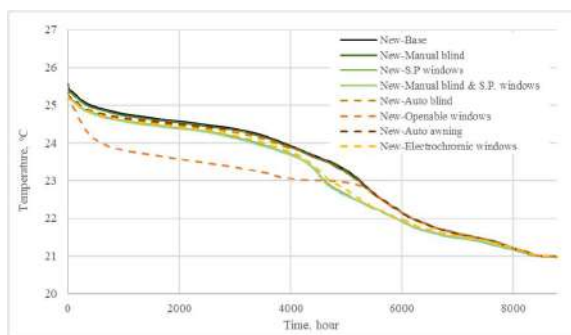

Figure 6. Indoor air temperature duration curve of the new building.

Table 5. Degree hours above 27 °C in the selected cases of the new building without the usage of mechanical cooling.

Cases	Degree hours above 27 °C	The decrease in degree hours (%) in comparison with the Base case
New-Base	3938	-
New-Manual blind & S.P. windows	1636	58
New-Auto blind	2568	35
New-Openable windows	0	100
New-Auto awning	2770	30
New-Electrochromic windows	2232	43

5 Conclusions

This study defined the energy efficiency of intelligent envelope solutions in Finnish old and new apartment buildings along with their effects on indoor temperature compared with passive solutions.

The lowest district heat consumption is for cases with electrochromic windows and solar protection windows in the old building. While these two solutions may increase the district heat consumption in the new building. Other solutions have no noticeable effect on district heat consumption in both buildings.

The three lowest cooling electricity is for cases with electrochromic windows and solar protection windows, and electrically controlled openable windows in the old building, respectively. The electrically controlled openable window is the case with the lowest cooling electricity consumption in the new building. Cases with solar protection windows and electrochromic windows are the next two.

Considering indoor temperature conditions, the maximum temperature in the old building is higher than in the new building. However, the new building is warmer in general.

The three best solutions with the lowest indoor air temperature in the old building are the cases with the combination of solar protection windows and manual blinds, solar protection windows, and openable windows, respectively. While in the new buildings the case with openable windows is the one with the lowest indoor air temperature with zero degree hours above 27 °C and the cases with the combination of solar protection windows and manual blinds and solar protection windows are the next two ones.

All over, among the passive solutions, solar protection windows can reduce the energy consumption (both district heating and cooling electricity) in the old building. However, they may increase the district heating consumption in the new building, despite the decrease in the cooling electricity consumption. In both of the studied buildings, solar protection windows are among the best solutions with the lowest indoor air temperature. Among the automated solutions, in both studied buildings, openable windows, can reduce the cooling electricity consumption without any noticeable change in district heating consumption. Alongside, they are among the best solutions with the lowest indoor temperature in both buildings. However, they may cause some difficulties such as excessive noise and air pollution coming from outside the spaces. The next automated solution may be the electrochromic windows with the lowest energy consumption in the old building.

References

1. European Commission. Energy statistical country datasheets.
2. European Commission. DIRECTIVE (EU) 2018/844 OF THE EUROPEAN PARLIAMENT AND OF THE COUNCIL of. 2018;(May).
3. IPCC 2021: Masson-Delmotte V, Zhai P, Chen Y, Goldfarb L, Gomis MI, Matthews JBR, et al. Climate Change 2021: The Physical Science Basis. Contribution of Working Group I to the Sixth Assessment Report of the Intergovernmental Panel on Climate Change [Internet]. 2021. Available from: www.ipcc.ch
4. Jylhä K, Jokisalo J, Ruosteenoja K, Pilli-Sihvola K, Kalamees T, Seitola T, et al. Energy demand for the heating and cooling of residential houses in Finland in a changing climate. Energy and Buildings. 2015 Jul;99:104–16.
5. Mofidi F, Akbari H. Intelligent buildings: An overview. Energy and Buildings. 2020;223:110192.
6. Ministry of the Environment. Decree (1009/2017) on the indoor climate and ventilation of the new building. (Ympäristöministeriön asetus uuden rakennuksen sisäilmastosta ja ilmanvaihdosta). Helsinki, Finland; 2017. p. 3–4.

Study regarding the impact of the new EPB standards on the energy performance evaluation

Ioan Silviu Doboşi [a], Silviana Brata [b], Ioan Bistran [c], Stefan Dună [d], Cristina Marincu [e]

[a] Romanian Association for Building Services Engineers – Banat Branch, Timisoara, Romania and S.C. DOSETIMPEX S.R.L., Timisoara, Romania, ioansilviu@dosetimpex.ro.

[b] Department of Civil Engineering and Building Services, Politehnica University Timisoara, Timisoara, Romania, silviana.brata@upt.ro.

[c] S.C. DOSETIMPEX S.R.L., Timisoara, Romania, ioan.bistran@gmail.com.

[d] Romanian Association for Building Services Engineers – Banat Branch, Timisoara, Romania and S.C. DOSETIMPEX S.R.L., Timisoara, Romania, stefan@dosetimpex.ro.

[e] Department of Civil Engineering and Building Services, Politehnica University Timisoara, Timisoara, Romania, cristina.marincu@upt.ro.

Abstract. Energy Performance of Buildings (EPB) set of standards offer an accurate methodology for calculating the energy performance of buildings, thus supporting the implementation of the EPBD. In recent years, the Romanian authorities have started the process of updating the national methodology for calculating the energy performance of buildings to align with the set of European EPB standards. At present, the energy certification of buildings in Romania is based on the Methodology for Calculating the Energy Performance of Buildings (Mc001-2006) but the new methodology has been approved and is about to enter into force. This paper proposes a comparison between the calculated energy consumption with the existing and upgraded calculation procedure. For this purpose, a residential building in Romania was investigated in terms of energy need for space heating, domestic hot water and artificial lighting. This study aims at enhancing the main differences between the two calculation procedures in terms of input data and results.

Keywords. Energy performance calculation, EPB standards, energy calculation software.
DOI: https://doi.org/10.34641/clima.2022.37

1. Introduction

According to the Energy Performance of Buildings Directive (EPBD) [1], the energy performance of buildings should be calculated based on a methodology, which may be differentiated at national and regional level. Moreover, the calculation methodology should consider existing European standards. The set of Energy Performance of Buildings standards, developed by CEN under mandate M/480, constitute the basis for an accurate methodology for calculating the energy performance of buildings, thus supporting the implementation of the EPBD. The use of an European set of standards as basis for national calculation methodologies among the Member states aims at obtaining an internationally harmonised procedure for the assessment of the overall energy performance of buildings. According to [2], the use of European standards allows for better comparison of best practices within Member States, as well as improving accessibility, transparency, and objectivity of energy performance assessments. The first Romanian Methodology for Calculation the Energy Performance of Buildings, referenced as Mc001-2006, was launched in 2006 [3]. The technical regulation Mc001-2006, aimed to establish a coherent method of evaluation and certification of energy performance for both new and existing buildings, transposing the provisions of the Directive of the European Parliament and of the European Council 2002/91/EC [4] on the energy performance of buildings through Law no. 372/2005 on the energy performance of buildings [5]. In recent years, the Romanian authorities have started the process of updating the national methodology for calculating the energy performance of buildings to align with the set of European EPB standards. According to the Romanian laws [3], the calculation methodology should be defined based on general standards, namely ISO 52000-1, 52003-1, 52010-1, 52016-1 and 52018-1 [6-10]. The methodology sets out the

Copyright ©2022 by the authors. This conference paper is published under a CC-BY-4.0 license.

minimum energy performance requirements for both new and existing buildings or building units and applies them differently to different types of building categories. The requirements provided in the methodology consider the conditions of a comfortable and healthy indoor climate, including adequate indoor air quality [5]. At present, the energy certification of buildings in Romania is still based on the Methodology for Calculating the Energy Performance of Buildings (Mc001-2006). The new methodology Mc001-2021 has been approved on 13th September 2021 by the Ministry of Development, Public Works, and Administration and on 10th January 2022 by the Technical Regulations Information System at European level. This paper proposes a comparison between the energy needs calculated with the existing and upgraded calculation procedure. For this purpose, a residential building in Romania was investigated in terms of energy need for space heating/cooling, domestic hot water energy need, and artificial lighting energy consumption. The study aims at enhancing differences between the two calculation procedures in terms of input data and energy consumption results. For this purpose, an energy certification software available on the Romanian market was used. The first version of the program Doset-PEC was validated in Romania in 2010 and follows Mc011-2006 and will be referenced as Doset-PEC v1007. Currently, the software is in the process of update in accordance with the new methodology Mc001-2021, referenced as Doset-PEC v1008.

2. Overview of the calculation of energy performance of buildings software

2.1 General description

The Romanian software Doset-PEC, based on Mc001-2006 [3], is a commonly used tool in Romania for determining the building energy performance class and energy performance certificate. The calculation program Doset-PEC for the energy performance of flats was validated in Romania in 2010. In the following years, it was completed with the modules for determining the energy consumption for mechanical ventilation and cooling. The energy needs for heating and cooling are determined using monthly calculation procedures and allows the calculation of a single thermal zone. However, in the program there is an additional calculation module for three unheated spaces in the case of buildings: unheated technical basement, unheated staircase, and unheated attic. Unheated technical basements are characteristic of most existing blocks of flats in cities. The supply of these multi-storey buildings is made partially through a centralized system of preparation and distribution of the thermal agent for heating. The new version of the software, currently under development, is based on the Romanian methodology Mc001-2021 and the set of European standards for determining the energy performance of buildings.

2.2 Energy certification and labelling

According to the Mc001-2006 methodology [3], the energy performance of a building and the classification in energy classes are determined according to the final energies calculated at the level of technical systems. The certificate also highlights the renewable energies used on each technical system. The energy rating scale is the same for all categories of buildings. The classification in the energy performance class is made based on the final energy consumption. One of the major changes in Mc001-2021 is related to the way the energy performance of the building is expressed. In the energy certificate, the classification of buildings in energy classes is made according to the total annual specific consumption of primary energy expressed in kWh/ m^2/year (usable floor area of the building). Furthermore, there are several energy classes defined for eight categories of buildings and the 5 climatic zones of Romani. This is a major change in comparison with the previous methodology, which had the same energy scale, regardless of the building category or climatic zone. In the new energy performance certificate, the specific annual consumptions of primary energy calculated accordingly for each technical system are highlighted, the specific annual consumptions of energy from renewable sources and share of renewable energy from total energy consumption. Depending on the total primary energy consumption, the building falls in a certain energy performance class. Also, depending on the total primary energy and the share of renewable energy, the building can be classified as nearly zero-energy building, Moreover, based on the greenhouse gas emissions expressed in kg CO_2 /m^2 year, the building falls into a certain class that expresses the level of pollution.

2.3 Calculation features – energy needs

In order to align with the EPB standards and Mc001-2021, a major upgrade of the software Doset-PEC consists in the fact that allows the subdivision of a building in several thermal zones and service areas, following ISO 52000-1:2017 [6]. The monthly calculation method is still used because there is no official input data at national level for the hourly calculation. The overall energy performance assessment of the buildings follows the general framework and procedure indicated in EN ISO 52000-1 [6] for determining the heating and cooling energy needs. The procedure implies the assignment of the heating and cooling needs to heating and DHW system service areas, respectively cooling service areas. The energy consumption of technical systems is calculated in accordance with the standardized methods which considers the retention of recoverable thermal system losses retention for the next calculation interval when these losses are accounted as internal heat gains. With respect to the heating energy need, the new software takes into consideration the solar contributions through

opaque and transparent envelope elements and a monthly extra heat flow due to thermal radiation to the sky. In the current version, this flow was considered only for cooling energy need for opaque envelope elements. Also, in the new version of the program, the possibility to consider the different influence of shading devices when calculating energy needs for heating and cooling was created. Thus, a separate simulation is no longer necessary in the case of solar input through windows during the winter and summer, respectively.

The heat transfer through ground is also an important aspect, which suffered important update in the new software version. As the requirements regarding the thermal performance of NZEB type buildings at the level of 2021, 2022 and for the following years are more restrictive from the point of view of energy consumption, it was necessary to update the calculation module of the thermal fluxes transmitted by elements in thermal contact with de ground in accordance with the European standard ISO 13770: 2017 [11]. The calculation is more flexible and covers any situation existing in energy certified buildings. In the current program version, it is possible to simulate the influence of slab-on-ground floors in four cases, considering the outer wall uninsulated or thermally insulated and the floor on the ground uninsulated or insulated. The thickness of the insulation is imposed at a usual value that ensures the minimum requirement regarding the thermal transmission of the slab on the ground imposed by Mc001-2006.

2.4 Calculation features – technical systems

In the upgraded software, the definition of the technical systems and the corresponding service area that deserves the thermal zones of the building is made based on the algorithm indicated in Figure 1. For each technical system the following are defined: space heating/cooling emission sub-system including control, the distribution system, the storage sub-system and the generation system. For all these subsystems additional heat/cooling losses are determined, highlighting recoverable losses and auxiliary energy consumed. The energy consumption of the technical systems of the building will be satisfied based on priorities by the generation subsystem. The electrical uses can be partially or entirely covered by on-site electricity production. The excess production can be exported to the grid. The energy performance of a building can be determined either without accounting the energy that is exported to the grid (calculation step A) or considering the exported energy (calculation step B), in accordance to EN ISO 52000-1 [6].

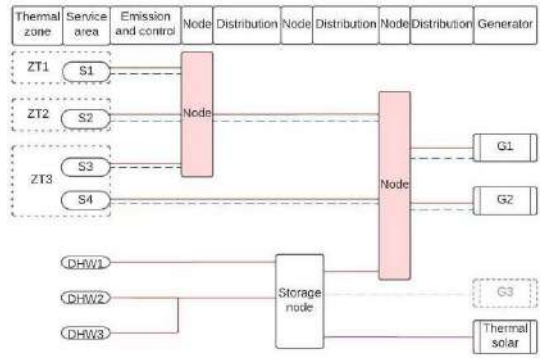

Fig. 1 – Technical systems definition.

Domestic hot water (DHW) demand and lighting energy calculations have been updated in the new software version, following Mc001-2021 and the European standards [12-13, 16]. In case of DHW energy demand, the calculation method is similar to the one in Mc001-2006, with some differences that will be enhanced through the case study. Currently, the determination of the electricity consumption for lighting, in case of residential buildings is made using a tabular method in accordance with Mc001-2006. which provides standard values of the specific energy consumption for lighting that were obtained by direct measurement for collective multi-storey residential buildings.

2.5 Renewable energy systems

In order to respond to the market needs related to the design and energy certification of nearly zero-energy buildings, the new version of the software will also include renewable energy calculation modules, thus allowing the analysis of buildings that have such systems. For this purpose, a calculation module that estimates the monthly energy production from photovoltaic systems has already been implemented and is functional. Other calculation modules for renewable energy that are in process of implementation include: thermal solar panels based on EN 15316-4-3:2017 [14] and heat pumps following standard SR EN 15316-4-2:2017 [15]. This ensures a standardized calculation at European level, but also a compact calculation by running the Doset-PEC program, without the need for separate calculations with the help of other specialized programs and the subsequent introduction of the results obtained in the basic program.

3. Case study

The case study presented in this chapter aims at providing a comparison between Mc001-2006 and Mc001-2021, by applying the calculation procedures to a collective residential building. Doset-PEC v1007 software was used for the assessment based on Mc001-2006 and the new version was used for the energy assessment based on the new methodology Mc001-2021. Because the Doset-PEC v1008 is not fully updated with all the calculation modules, the

study was limited in comparing the heating and cooling energy needs, DHW energy need and electrical energy consumption for lighting.

3.1 Building description

The case study building is a residential building with 5 floors, including the ground floor. It is composed of 10 apartments per storey and has a total usable and heated area of approximately 3538.09 m². The characteristics of the envelope of the building can be seen in Table 1. The U'-values are below the maximum required for new NZEB buildings in Romania through Mc001-2021.

Tab. 1 – Envelope characteristics of the case study buildings.

Envelope element		Area [m²]	U'-value [W/m²K]
Ground floor		770.2	0.19
Flat roof		770.2	0.14
Exterior walls	NE	441.3	0.24
	NW	318.0	
	SE	318.0	
	SW	428.4	
Windows	NE	286.1	0.90
	NW	100.4	
	SE	100.4	
	SW	299.0	

The building is located in west side of Romania, climatic zone II, where the outdoor conventional temperature for calculations during winter is -15°C.

3.2 Heating and cooling energy need

This subchapter will only discuss a comparison between the energy needs for heating and cooling determined using Doset-PEC v10007 and Doset-PEC v1008. Both assessments follow monthly calculation procedures. The results of the assessments are presented as monthly values in Figure 2 and Figure 3. As we can see the two calculation procedures led to very close results in monthly values.

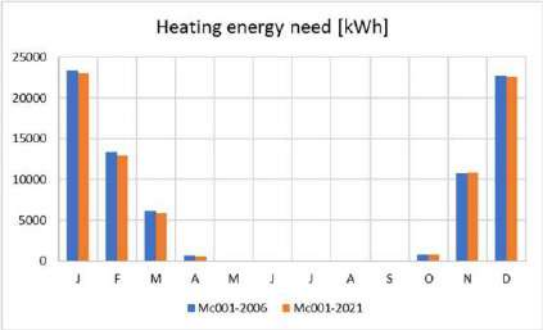

Fig. 2 – Heating energy demand.

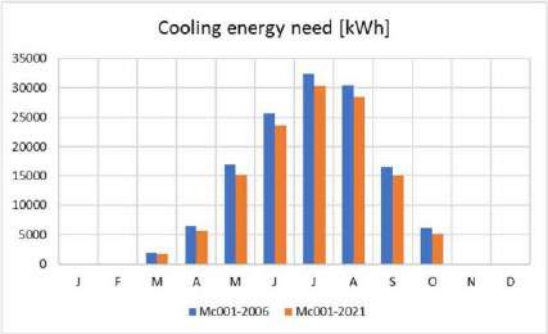

Fig. 3 – Cooling energy demand.

Table 2 presents the specific annual heating and cooling energy demand for the two calculation procedures.

Tab. 2 – Annual heating/cooling energy need.

	Mc001-2006 Doset-PEC v1007	Mc001-2021 Doset-PEC v1008
Annual heating energy demand [kWh/m²]	21.96	21.64
Annual cooling energy demand [kWh/m²]	38.61	35.32

In case of heating, DOSET-PEC v1008 leads to a slightly lower energy demand, approximately 2% lower than the heating energy demand resulted in DOSET-PEC v1007. For cooling energy demand, the difference is a bit higher. In this case, DOSE-PEC v1008 leads to a value that is approximately 9% lower than the value obtained in Doset-PEC v1007. The obtained differences for heating can be attributed in the first place to the different calculation procedures for elements in contact with ground (as explained in chapter 2) and also due to the fact that Doset-PEC v1008 also takes into account solar gains through opaque envelope elements and a monthly extra heat flow due to thermal radiation to the sky. In case of cooling the difference can be mainly attributed to different consideration of the utilisation factors (with different conditions).

3.3 DHW energy need

This subchapter will discuss the calculation procedures for the energy needs for domestic hot water. In both Doset-PEC v1007 and Doset-PEC v1008, the energy needs for domestic hot water depends on the delivered hot water volume and on water temperatures. The main difference consists in the value of daily volume of domestic hot water, which in case of Doset-PEC v1007 is determined considering the number of persons in the building and specific volume of hot water needed daily per person. The value of the specific volume of hot water needed daily per person is determined using a tabular method, depending on the building category and type of domestic hot water system. For this case study, 60 l/person/day was used, corresponding to

residential buildings and for hot water preparation using gas boilers. In Doset-PEC v1008, daily volume needs for domestic hot water is determined depending on the specific daily needs for domestic hot water and the number of equivalent consumers. Thus, following the procedure in Mc001-2021 based on EPB standards, the equivalent number of consumers were calculated, resulting 68 consumers and 40.71 l/person/day. In both cases, the temperature for preparing the hot water was considered 60°C, while the cold-water temperature 13.5°C. The number of persons/consumers was set to 68 for both calculations, thus the only difference consisting in the daily hot water volume. The assessment results are presented in Table 3.

Tab. 3 – DHW energy need.

	Mc001-2006 Doset-PEC v1007	Mc001-2021 Doset-PEC v1008
Specific DHW energy needs [kWh/m^2]	26.65	18.89

By analysing the results and the input data for the two calculations, it cand be said that while in Mc001-2006, the volume of hot water needed for a person daily, had a fixed value, depending on the category of building and DHW system, in Mc001-2021, this daily volume/person is calculated depending on the usable area of the building and can have a maximum value of 40.71 l/person/day. As seen in Tab.2, this leads of course to lower energy needs for DHW in residential buildings.

2.1 Lighting energy consumption

As mentioned in the previous chapter, in Mc001-2006 an implicitly in the current Doset-PEC v1007, the specific energy consumption for lighting in case of residential buildings is determined using a tabular method. Thus, the corresponding values for each type of apartment were selected and further an average specific energy consumption for the entire building was obtained (Tab.1). Doset-PEC v1008 has a lighting energy calculation module which is based on Mc001-20021 and SR EN 15193-1 [13]. The calculation procedure can be used for both residential and non-residential buildings. The calculation can be performed separately for each type of room, and it requires information such as: the time tD in which the lighting of the building/building zone is ensured also using natural light, the time tN in which the lighting of the building/building zone is ensured using only artificial light, the total installed electric power of the luminaires, for recharging batteries and automation devices, the space occupancy factor Fo, the factor for dependency on constant lighting level FC. Using the mentioned input data, Doset-PEC v1008 performs annually calculation and the result of the calculation is the energy consumption expressed in kWh/year, and LENI, expressed in kWh/m^2/year. The results are presented in Table 4.

Tab. 4 – Lighting energy consumption.

	Mc001-2006 Doset-PEC v1007	Mc001-2021 Doset-PEC v1008
Specific lighting energy consumption [kWh/m^2]	11.43	14.08

The specific energy consumption for lighting calculate with Doset-PEC v1008 is higher than the one determined using Doset-PEC v1007, which means that the current method in Doset-PEC v1007 tends to underestimate the energy use for lighting. However, the calculation procedure implemented in Doset-PEC v1008 requires very accurate information related to the lighting systems. This means that the accuracy of the energy consumption results is strongly dependent on the knowledge of the software user but also on the information available for the analysed building.

4. Conclusion and discussion

This study aimed at enhancing some of the differences between the Methodology for Calculating the Energy Performance of Buildings in Romania Mc001-2006 and the new one Mc001-2021 as they were implemented in the Romanian software Doset-PEC. Although most of the calculation principles are similar in the two methodologies as they follow monthly calculation methods, the approach is different starting from the very beginning with the process of thermal zoning and ending with the energy certificate of buildings.

The case study is limited to heating and cooling energy demand, DHW energy demand and lighting energy demand as these are the modules that were implemented and fully tested until now in DOSET-PEC v1008, which follows Mc001-2021 and EPB standards. The heating and cooling energy demand obtained with Doset-PEC v1008 have very close values with the ones obtained with Doset-PEC v1007, even though there are differences in the calculation procedures. Higher differences are noticed in case of energy consumption for lighting and DHW energy demand. Nevertheless, a more comprehensive study will be conducted in the future, which will go beyond energy needs and will include energy losses final energy consumption as well for heating and cooling. Moreover, primary energy, renewable energy and renewable energy ratio are to be calculated. The new methodology Mc001-2021, based entirely on the EPB standards, provides very complex calculation procedures for all the situations that can be encountered when assessing the energy

performance of a building. However, due to its complexity and multitude of possible situations, the implementation in a calculation software can be extremely difficult and time consuming.

5. References

[1] Directive 2010/31/EU of the European Parliament and of the Council of 19 may 2010 on the energy performance of the buildings, Official Journal of the European Union L153/13, 2010.

[2] Van Dijk D., Hogeling J. The set of EPB standards in CEN and ISO: common characteristics. REHVA Journal, December 2016.

[3] Mc001 – 2006. Methodology for Calculating the Energy Performance of Buildings.

[4] Directive 2002/91/EC of the European parliament and of the council of 16 December 2002 on the energy performance of buildings.

[5] Law No. 372/2005 on the energy performance of buildings, republished in 2021.

[6] EN ISO 52000-1:2017. Energy performance of buildings — Overarching EPB assessment — Part 1: General framework and procedures.

[7] EN ISO 52003-1:2017. Energy performance of buildings — Indicators, requirements, ratings and certificates — Part 1: General aspects and application to the overall energy performance.

[8] EN ISO 52010-1:2017. Energy performance of buildings — External climatic conditions — Part 1: Conversion of climatic data for energy calculations.

[9] EN ISO 52016-1:2017 Energy performance of buildings — Energy needs for heating and cooling, internal temperatures and sensible and latent heat loads — Part 1: Calculation procedures.

[10] EN ISO 52018-1:2017. Energy performance of buildings — Indicators for partial EPB requirements related to thermal energy balance and fabric features — Part 1: Overview of options.

[11] EN ISO 13370:2017. Thermal performance of buildings — Heat transfer via the ground — Calculation methods.

[12] EN 12831–3:2017 (DHW systems heat load & needs). Energy performance of buildings – Method for calculation of the design heat load – Part 3: Domestic hot water systems heat load and characterization of needs, Module M8–2, M8–3.

[13] EN 15193–1:2017. Energy performance of buildings – Energy requirements for lighting – Part 1: Specifications, Module M9.

[14] EN 15316-4-3:2017. Energy performance of buildings - Method for calculation of system energy requirements and system efficiencies - Part 4-3: Heat generation systems, thermal solar and photovoltaic systems, Module M3-8-3, M8-8-3, M11-8-3.

[15] EN 15316-4-2:2017. Energy performance of buildings - Method for calculation of system energy requirements and system efficiencies - Part 4-2: Space heating generation systems, heat pump systems, Module M3-8-2, M8-8-2

[16] EN 15316-1:2017. Energy performance of buildings - Method for calculation of system energy requirements and system efficiencies - Part 1: General and Energy performance expression, Module M3-1, M3-4, M3-9, M8-1, M8-4.

Potential of WASTE WATER HEAT RECOVERY in reducing the EU's energy need

MSc. Pavel Sevela[a], MSc. Johannes Frenger [a], Dr. Jürgen Schnieders [b], Assoz. Prof. Dr.-Ing. Rainer Pfluger [a]

[a] Unit of Energy Efficient Building, University of Innsbruck, Innsbruck, Austria, bauphysik@uibk.ac.at.

[b] Passive House Institute, Darmstadt, Germany, mail@passiv.de.

Abstract. After extensive research, **Waste-Water Heat-Recovery (WWHR)** technology was identified as the most promising technology to unlock the under-addressed potential in reducing the energy need for water heating.
Particularly interesting application of WWHR is for showering, which accounts for about 70 to 82 % of the daily residential hot water tapping profile. Shower-wise installed heat-exchangers offer a cost-effective way of utilizing otherwise wasted heat for preheating cold fresh water, thus reducing the temperature span covered by the water heater. The total energy demand **savings for hot water heating can be up to 40 %**. The unique advantage of WWHR, is achieving high thermal energy savings without compromising on user comfort with low material and monitary needs. The cost-effectiveness of WWHR is best in climates with cold ground temperatures and in cases where showers are used extensively.
At European level, the WWHR itself is theoretically capable of surpassing the energy savings targets planned in the "Fit for 55" climate action in the hot water sector, if all buildings are equipped accordingly. If between 2022 and 2030, every second anyways renovated or newly constructed building in Europe were equipped with the WWHR system, **35.7 TWh less energy would have to be generated and 6,6 Megatons of CO2e emissions less emitted.**
Although WWHR has been a well-proven technology for decades in some countries; it is still unknown in most European regions. Further action, in particular the creation of a European legal framework, the training of professionals and the granting of subsidies, is needed to accelerate the adaptation of this promising, sustainable technology into practice.

Keywords. Waste-Water Heat-Recovery, Fit for 55 climate action, EPBD, hot water production, system losses, energy efficiency first, ZEB, state of the art.
DOI: https://doi.org/10.34641/clima.2022.439

1. Problem statement

Buildings are the single largest energy consumer in Europe. Heating, cooling and domestic hot water account for 80% of the energy that we, citizens, consume [1].

The EU has committed to reduce the greenhouse gas (GHG) emissions by at least 55 % by 2030, compared to 1990 levels. This climate act known as the "Fit for 55" package is the EU's contribution under the "2015 Paris Agreement", with a target of limiting the increase of global temperature to just 1.5°C compared to pre-industrial levels. For the EU building sector, it means to reduce its energy consumption of heating and cooling by 18%, compared to energy consumption (delivered energy) levels in 2015 [2].

As illustrated in **Fig. 1**, the energy for space heating has decreased significantly in the past decades especially thanks to applied insulation, however this has not been the case for water heating. According to Eurostat, the hot water preparation in the current residential building stock represents 14.8% of the whole energy consumption in buildings [3].

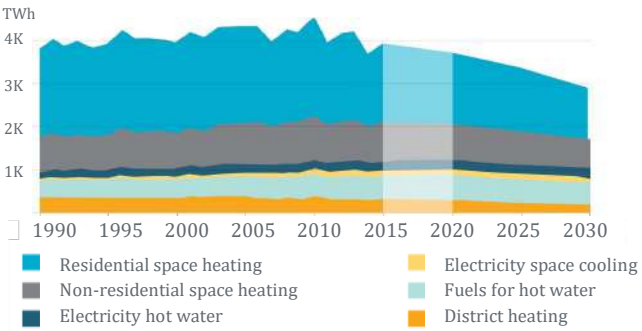

Fig. 1 - Final energy demand in residential and non-residential buildings by energy use [4].

Copyright ©2022 by the authors. This conference paper is published under a CC-BY-4.0 license.

Since the cold water temperature is naturally given by geographic location and the desired hot water draw-off temperature and duration is set by the user, the only way to reduce the energy demand for water heating is to reduce the flow rate or to pre-heat the cold water to reduce the temperature rise by the water heater. The WWHR is the last unaddressed systematical thermal leak in the building thermal envelope, as lightly illustrated on **Fig.2**.

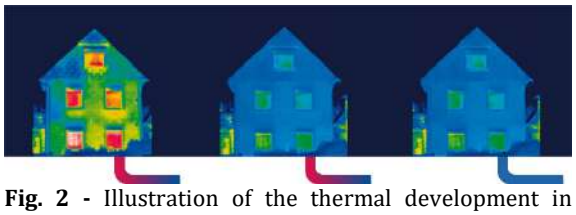

Fig. 2 - Illustration of the thermal development in building technology as an infrared thermography.

Using **wastewater heat recovery (WWHR)** technology, lowering comfort by reducing hot water flow rates is not necessary while reducing the domestic hot water (DHW) energy demand. WWHR can utilize the waste heat that leaves the building and would otherwise end up in the environment. With this technology, the heat is recovered from the warm wastewater and transferred to the cold fresh water and thus the amount of energy required to reheat the cold water is reduced.

For wasting energy from hot water, showering plays the dominant role, accounting for about 70-82% of the daily hot water tapping profile [5] [6]. Furthermore, the duration of most other hot water draw-offs or its temperature is not great enough to overcome the dynamics at the beginning of the WWHR process. Therefore, **showering is the most effective application of WWHR technology**, as the hot water draw-off at a high temperature level and the fresh cold water supply occur simultaneously and takes on average between 4,5 – 8,5 minutes [7].

2. State of the art of WWHR

For decades, heat recovery has been a standard for reducing energy demand in industrial processes by transferring waste heat to another fluid via a heat exchanger that separates the media materially but allows the heat to conduct through. Different techniques to recover energy from warm domestic wastewater are also applied. From municipal applications to centralized (building-wise) installed heat exchangers or de-centralized (shower-wise) devices, the latter shows the most **promising potential and a number of certified products** are already in existence.

Decentralized heat exchangers (**Fig.3**) are placed as close as possible to the source of the warm wastewater (typically 32-36°C). If the heat exchanger is placed further away from greywater source, the warm effluent cools and could be mixed with other colder effluents. Most widespread decentralized devices are screed embedded linear shower drains with horizontal exchanger tubes or vertically installed devices replacing appx. two meters of sewer pipe, which benefit from "no maintenance" at low prices compared to the horizontal ones. However, the space and access required to the floor below can cause difficulties with retrofits. So-called active heat recovery systems pump the shower water into a heat exchanger and are often driven with a vertical heat exchanger but can be installed on the shower level.

Other preinstalled shower units are even equipped with a primary heat source e.g. an electrical water heater. Those benefit from synchronized components without complex plumbing and high circulation losses. As independent hot water modules, they can be evaluated with the existing EU energy label. Beside a smaller hot water storage volume, the WWHR decreases the required power of flow heaters. Almost loss-free DHW production on demand can get a future technology, especially when combined with electric mobility via power-load throw-off.

Fig. 3 - Shower water heat exchanger for vertical (left), horizontal (middle) application; active heat exchanger (right) source: Counter Flow Products B.V., Joulia ltd., Hamwells Nederland B.V.

The energy saving potential of various decentralized WWHR system are mainly influenced as follows:

- Efficiency of heat exchanger device

Counterflow driven exchangers with high thermal length and fluid turbulence result in best efficiencies. The robust design for highly polluted wastewater and the double wall construction according to EN1717 limit the efficiency of those heat exchangers. The steady-state efficiency of typical devices range between 37-60% for horizontal systems, 57-78% for vertical systems and 60-82% for active systems [8].

- Hydraulic connection of heat exchanger

Maximum energy transfer in the exchanger also relies on a balanced flow rate of fresh and wastewater side, see **Fig. 4**. When applying a decentralised heat exchanger for a shower, wastewater only equals the freshwater flow if the preheated water feeds the shower mixer and the water heater. If the preheated water from the heat exchanger feeds only the shower mixer or the DHW heater, the waste water and fresh water flows in the heat exchanger are unequal, and therefore the efficiency of the heat exchanger could decrease due to the lower possible energy transfer.

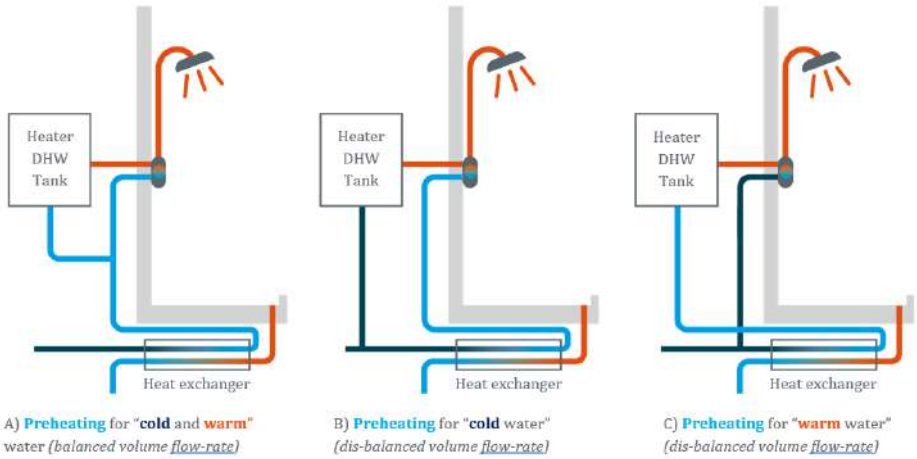

Fig. 4 - Hydraulic connection possibilities of a WWHR device

- Water temperatures and shower duration

Low shower temperatures combined with high freshwater temperatures e.g. in the EU´s southerly member states, have to be considered as less benefitting from WWHR. With increasing shower duration, the dynamic heat exchanger efficiency approaches its steady-state value and obviously supports the absolute energy savings.

3. Methodology of the energy savings calculation

In order to demonstrate the potential energy saving effect of DHW systems including WWHR, a calculation based comparison study was performed. Saving calculation on household level are based on PHPP [9].

(1) A vertical tube-in-tube heat exchanger with a typical efficiency of 67% was chosen [8], which causes costs of approx. 1000€ for the device itself and additional installation effort.

(2) One WWHR system per dwelling unit is assumed, with an European average occupation of 2.3 persons per dwelling unit [10]. Each person uses the equivalent of 32 l of domestic hot water at 60°C per day, of which 24 litres are shower water.

(3) The calculations were carried out under the assumption that the preheated water outlet is hydraulically connected to the water heater and the shower mixing valve.

(4) The data used for the upscale calculation on EU Level was extracted from each member in the EU´s 2019 statistics [3].

4. Results and interpretation of energy saving calculations with WWHR

4.1 Energy saving potential on household level

It is important to note that WWHR saves the same amount of energy needed for water heating in combination with all three used DHW systems. This means the amount of recovered heat is not depending on the DHW technique.

WWHR **savings in delivered energy (electricity, gas, etc.) vary depending on the water heating technique** due to significant differences in hot water distribution and storage thermal losses, as well as the efficiency of the actual heater, see **Fig. 5**.

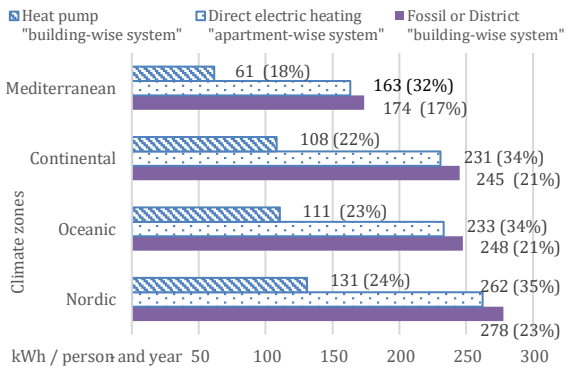

Fig. 5 - Savings in delivered energy for total DHW with WWHR in combination with various hot water systems per person (in brackets: as percentage of total delivered energy)

A clear trend towards higher yields in colder climates can be observed. This can be referred mainly to the colder ground water temperatures in the Nordic climate zone. Possible differences in user behaviour e.g., tendentially warmer and longer showers in northern regions, which makes the WWHR more effective was neglected in this study to provide a conservative view of the results.

An obvious difference is that WWHR accounts for a larger share of the delivered energy by direct electric water heating; that is close to the actual energy need for DHW; as this system is a decentralized system with zero tank and circulation losses and lower distribution heat losses as by the central DHW system. **These losses account in average for about 1/3 of the delivered energy**

for DHW in the EU but in some systems can represent more than 50%. The less efficient energy conversion when burning fossil fuels causes slightly higher possible energy savings.

The savings in energy consumption by WWHR in combination with a heat pump are lower in absolute terms than for the other two systems, since a heat pump requires a lower proportion of delivered energy (electricity) to produce the same amount of heat, thanks to its electricity to heat conversion factor (COP). Nevertheless, cold climate supports the application of WWHR combined with heat pumps because of the colder ambient and hence worse conversion rates of heat pumps. WWHR in heat pump systems can therefore be very cost effective, especially when used with shower-intensive tapping profiles.

4.2 Possible contribution of WWHR to the zero-emission building standard

The possible effect of WWHR on an example household is examined, assuming a 104 m² single family house occupied by 2.3 persons in oceanic climate zone. The intention was to evaluate the impact of the application of WWHR in this particular scenario on the reduction of "delivered electrical energy" .

The building thermal envelope and HVAC were considered to be state of the art to meet the requirements of the **"zero-emission building" (ZEB) standard, coming into force in 2030.**

Assuming a heat pump-based water and space heating system with a yearly average COP of 2.4, the **annual savings correspond to 13% of the "total delivered energy"**, as seen in **Fig. 6.** In the context of the EPBD, which specifies a maximum primary energy of 60 kWh/m2/a for ZEB in this climate zone, the **WWHR reduce primary energy consumption by ca 7 kWh/m²/a when a primary energy factor of 2.1 is assumed.** Therefore, in cases of already advanced thermal envelopes or efficient heating technologies, WWHR can play the key role to reach this ambitious standard.

4.3 Energy and GHG saving potential depending on country

To evaluate a population independent saving potential, **Fig. 7** shows the annual energy and emission savings per installed WWHR device by country. Actual GHG emissions for electrical power consumption were applied. The "steps" in energy savings are due to the use of reference values for

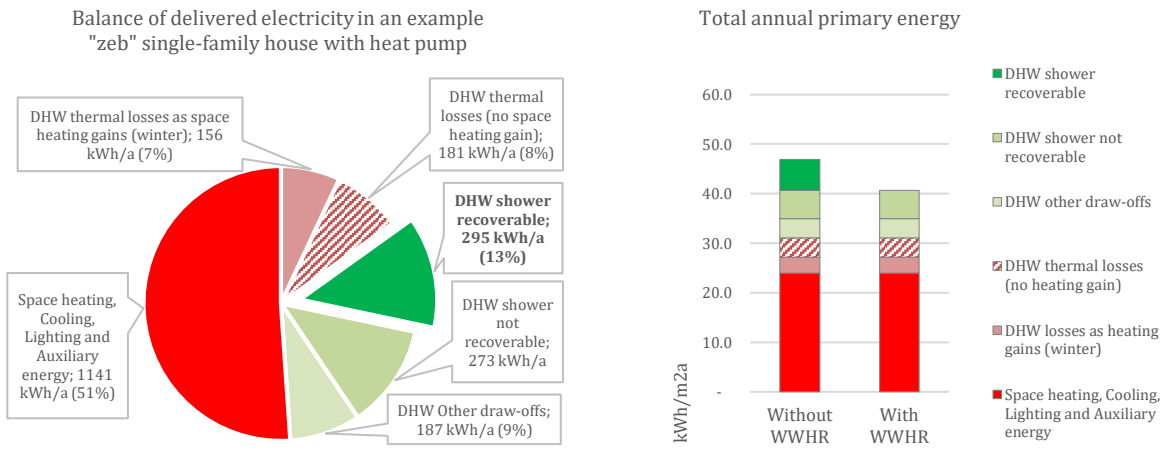

Fig. 6 - Delivered energy with respect to the recoverable share with WWHR in a single family "ZEB" house

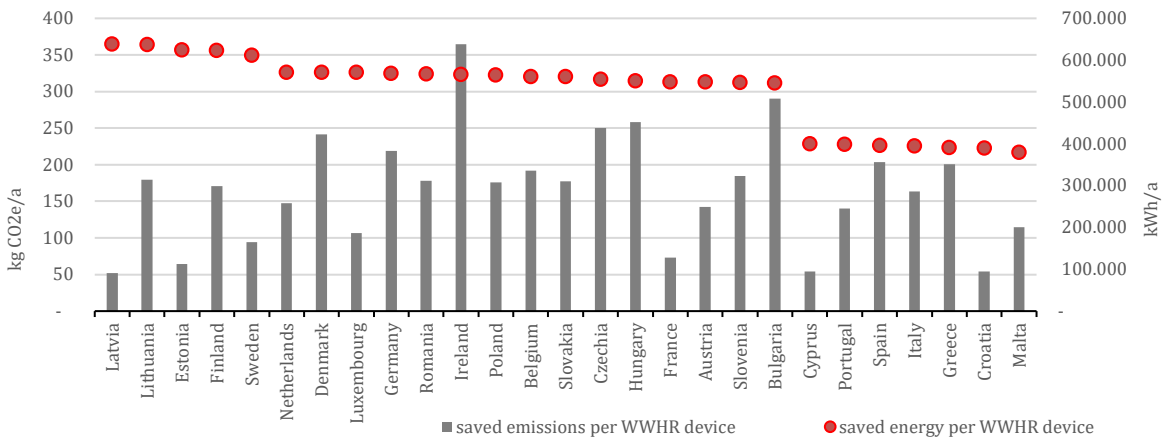

Fig. 7 - Annual energy and emission savings per WWHR device per country

mains water temperature and climate data for each climate zone. **Most promising energy savings are seen in northern countries** due to low mains water temperatures. At the same time, GHG emission savings are considerably lower in northern countries due to generally "low-carbon" energy production and high district heating supply rates. **Warm climatic regions with high-emission-power-production can therein still play an important role, despite its relatively lower energy savings.**

4.4 Energy saving potential on EU-27 level

To achieve the at least 55% European emissions reduction target for 2030, proposed by the Commission in September 2020, the **EU must reduce greenhouse gas emissions in the building sector by 60% and thus the energy consumption of heating and cooling by 18%, compared to delivered energy consumption level in 2015** [11].

The possible energy and emission savings with WWHR were scaled up to EU-27 level to show the role of WWHR in the EU's "renovation wave" in different scenarios. A hypothesis was made by applying the WWHR in four scenarios with a share of 20, 50, 80 and 100% of the **total of 35 million renovated and 15 million newly built buildings between 2022 and 2030.** WWHR technology could be incorporated up to three-times more often as any bathroom or shower renovation is an opportunity for integration of WWHR. The amount of total installed devices and its savings were accumulated linearly during this time.

Fig. 8 shows the impact in the hot water sector referring to the 18% energy savings goal compared to the consumption in 2015, although the energy savings by WWHR actually apply to the already higher energy consumption from 2020 onwards. Depending on the scenarios, approx. 4%; 11%; 16% or 25% of the planned energy reduction can be covered by WWHR only. If every renovated or newly built building in Europe were to be equipped with WWHR starting 2022, 25% of the 2030 "Fit for 55" goals in the warm water sector could be expected. If the total current building stock would be equipped with the described WWHR until 2030, **a significant consumption-drop of 100 TWh/a could be observed and the energy conservation goals for hot water would be surpassed by WWHR only.**

5. Conclusion

The main message of this paper is that there is a **14.8% share of the energy consumption in buildings (DHW)** [12] that has been overlooked and unaddressed by the main EU policies in recent decades.

WWHR saves usable energy for water heating from going down the drain, especially for the shower, which is the largest consumer of hot water in the home. **With WWHR, the delivered energy for today´s water heating in Europe could be reduced by 24 %** (100 TWh/a); see **Fig. 6**; if "business as usual" is continued. Further savings potential lies in reducing heat losses from hot water circulation, distribution and storage, since WWHR cannot actively reduce these losses that represent on average about 1/3 and in some cases even more than 50% [7] of the delivered energy for DHW heating. It should be also noted that WWHR does not affect the energy required for not simultaneously tapped hot water, for example in a bathtub. On this background, **suitable devices integrated into a DHW system with optimized distribution, storage and circulation losses can reduce the amount of delivered energy water heating by about 40%.**

WWHR also contributes to minimize DHW technology, especially by systems with high investment costs per kW such as heat pumps with geothermal probes. With the WWHR the DHW systems can become also easier to operate by renewable energies. As the EC states: "**The energy efficiency and the deployment of renewable energy complement each other**" [13].

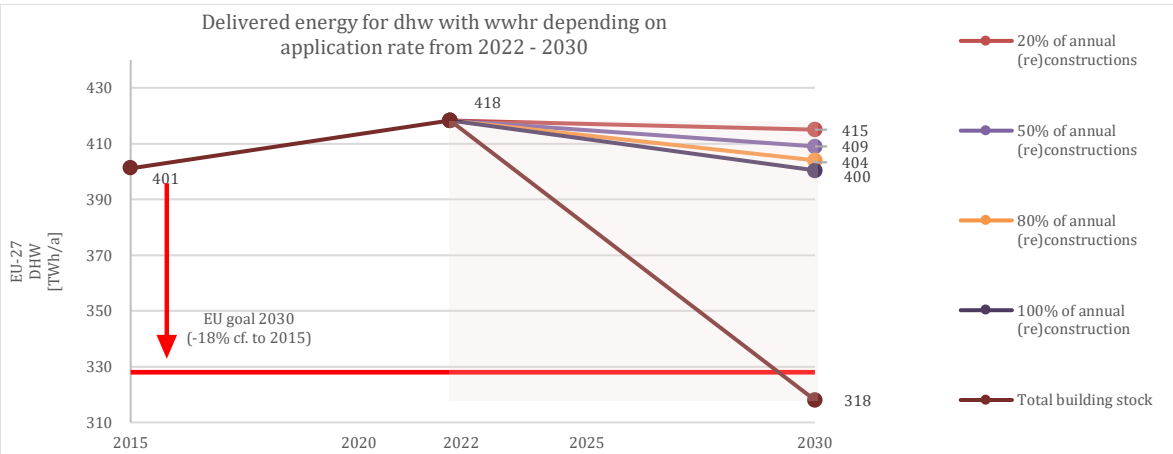

Fig. 8 - EU-27 (Targeted) Energy demand for DHW in 2030 depending on application rate of WWHR

The economy is particularly good by application with multiple users such as sport facilities, businesses and hotels but also in climates with colder ground water. In all three technological scenarios, the **"price of energy saved", hence a fixed energy price for the next decades when using WWHR, is around or below the average energy price in the first quarter of 2021, rising since then.** One WWHR device can save more than a 100 € per family on the hot water operational costs every year.

Due to its high energy efficiency and level or recyclability, the life-cycle of WWHR devices (>20 years) causes a **minimal ecological footprint that is balanced by CO2 savings already during the first year of its operation.**

The quick decarbonization of the building stock is limited by the low renovation rate of buildings; currently below 1% [14]. in the EU. **The building stock can be upgraded about three times faster with WWHR than with regular energy-saving measures** such as insulation of the building envelope. This is due to the fact that the renovation rate of HVAC systems is about three times higher, according to the Zentralverband Sanitär Heizung Klima, Germany. This makes WWHR a very effective tool with a rapid uptake in the resident market.

The WWHR is in some EU member countries an established technology, recognized as one of the top 10 most promising energy saving opportunities, scoring in several countries on a first rank, according to the Member State Annex Report done by EC [15]. WWHR is an emerging technology bringing a number of benefits that are in line with the EU climate action plan. These are the identified barriers and measures that need to be taken for the European legal framework to unlock the WWHR´s potential of in the EU and globally:

- The WWHR is currently **not officially recognized in the EPC, EPBD or other building rules** and thus the application of WWHR does not bring constructors any legal improvements in the energy efficiency, despite the obvious energy savings.

- **New European norms** on planning and hygiene criteria of application of WWHR system in the buildings shall be created as well as a common certification procedure for the WWHR units. The adoption of **WWHR in the Eco-design Directive** could convey the benefits of combining WWHR with water heating systems in an easy and understandable way, through established energy labelling.

- The **WWHR may be included in the EU's toolbox** as an effective measure for energy-efficient renovations and new constructions. As WWHR is in some regions a new technology, it needs to be **promoted** and **professionals need to be trained** on its benefits and planning. Together with further incentives this procedure can be an effective way to overcome the well-known psychological effect of "status quo bias", making the professionals more hesitant about new technologies they are not familiar with yet.

- **Scaling-up** the number of applications shall make the WWHR system more affordable due to higher cost-efficiency in production. Although double-wall heat exchanger construction is currently required by law in Europe, **single-wall designs** could increase cost-effectiveness if sufficient drinking water safety is provided. In the NL and UK an exemption has been granted (status by 04.2022) to the active systems where the heat exchanger is located above tile level with an air brake for drainage (overflow).

Removing the barriers and making the energy efficiency measures more attractive and simpler to apply will decide if every well-done renovation and new construction will bring Europe closer to its goals, or if it will become a missed opportunity that could lock-in untapped energy savings and associated emissions in the coming decades.

6. Acknowledgement

This study was commissioned by the European Copper Institute at the University of Innsbruck and the Passive House Institute.

7. Appendices

Link to the full article:
https://diglib.uibk.ac.at/7640369

Annotation

45,26 m2 living area / person [16]

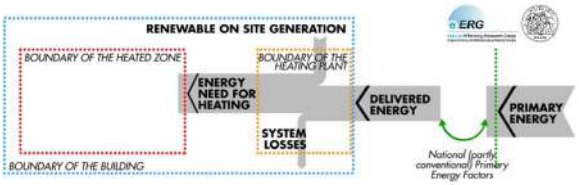

Fig. 9 - Methodological explanatory to the EPBD [17]

Abbreviations

COP	Coefficient of performance
EC	European Commission
EPBD	Energy Performance of Buildings Directive
EPC	Energy Performance Certificates
EU	European Union
FSE	Final sewage effluent
GHG	Green House Gas
HE	Heat Exchanger
HVAC	Heating, ventilation, and air conditioning
nZEB	nearly-Zero-Energy Building
PHPP	Passive House Planning Package Tool

WWHR Waste Water Heat Recovery
DVGW German society for gas and water installations
ZEB Zero-Emission Building

Tab. 1 – Current standard

Country	Efficiency	Hygiene
Germany	PHI (Certified Passive House Components) ; DIN 94678 (in preparation)	DVGW
Netherland	KIWA NEN 7120	
France	CSTB CAPE/RECADO-PQE	Th-BCE/RT2012
UK	CAPE/RECADO-PQE or KIWA NEN 7120	WRAS
Switzerland	KIWA NEN 7120; Minergie	SVGW
EU	EU No 812/2013 (in preparation)	

8. References

[1] European Commission; EPBD-Facts and figures; https://energy.ec.europa.eu/topics/energy-efficiency/energy-efficient-buildings/energy-performance-buildings-directive_en

[2] Comission to the European parliament; A Renovation Wave for Europe; Brussels 2020

[3] Eurostat database; https://ec.europa.eu/eurostat/de/data/database

[4] Roscini et al.; contributions from the building sector to a strengthened 2030 climate target; BPIE 2020

[5] Anna Marszal-Pomianowska et. al; Comfort of Domestic Water in Residential Buildings: Flow, Temperature and Energy in Draw-Off Points: Field Study in Two Danish Detached Houses; Energies 2021

[6,7] Bertrand et. al ; Characterization of domestic hot water end-uses for integrated urban thermal energy assessment and optimization; Applied Energy 2017

[8] Passive House Institute; Component Database as of 2021; https://database.passivehouse.com/de/components/list/heat_recovery

[9] Passive House Planning Package (PHPP) https://passivehouse.com/04_phpp/04_phpp.htm

[10] Eurostat/size of housing https://ec.europa.eu/eurostat/cache/digpub/housing/bloc-1b.html?lang=en

[11] A Renovation Wave for Europe - greening our buildings, creating jobs, improving lives; Brussels, 14.10.2020 COM (2020): 662 final

[12] Eurostat database; https://ec.europa.eu/eurostat/de/data/database

[13] Comission to the European parliament; A Renovation Wave for Europe; Brussels 2020

[14] European Comission; EPBD-Facts and figures; https://energy.ec.europa.eu/topics/energy-efficiency/energy-efficient-buildings/energy-performancebuildings-directive_en

[15] Technical assistance services to assess the energy savings potentials at national and European Level, Member State Annex Report; Yeen Chan et.al; European Commission; 2021

[16] Eurostat/size of housing https://ec.europa.eu/eurostat/cache/digpub/housing/bloc-1b.html?lang=en

[17] Explanatory note from eceee regarding the EPBD draft Annex I; European Council for an Energy Efficient Economy; 1 December 2017

Data Statement

The team at the University of Innsbruck will be happy to answer further inquiries, share their practical experience and hands on knowledge in WWHR research and development. pavel.sevela@uibk.ac.at

CIRCULARITY

Application of circular technical services in a living lab in Ghent

Lode Lefevre [a], Cihan Kayaçetin [b], Hilde Breesch [c], Lieven Smeyers [d], Alexis Versele [e]

[a] Building Physics and Sustainable Design, Faculty of Engineering Technology, KU Leuven, Technology campus Ghent, Belgium, lode.lefevre@kuleuven.be

[b] Building Physics and Sustainable Design, Faculty of Engineering Technology, KU Leuven, Technology campus Ghent, Belgium, cihan.kayacetin@kuleuven.be

[c] Building Physics and Sustainable Design, Faculty of Engineering Technology, KU Leuven, Technology campus Ghent, Belgium, hilde.breesch@kuleuven.be

[d] Litobox, Arendonk, Belgium

[e] Building Physics and Sustainable Design, Faculty of Engineering Technology, KU Leuven, Technology campus Ghent, Belgium, alexis.versele@kuleuven.be

Abstract. The construction industry in the EU possesses great potential for mitigating environmental impacts because of its large share in resource use and waste production. The Circular Economy Action Plan of the EU stimulates the sector to adopt more circular principles and bio-based material use. The European Interreg 2 Seas project "Circular Bio-Based Construction Industry" (CBCI) is in line with these European ambitions researching technical, economical, legal and, social aspects. In the course of the project, a prototype for a terraced single-family house called the living lab (LL) Ghent is developed and constructed in close collaboration with multiple stakeholders of the construction sector. The building implements and tests the research outputs in a real-life setting. During the development of LL, the circularity of building components was taken into account by utilizing the layers of Brand approach. Among those layers are structure, skin, technical services and, space plan. On the one hand, each layer has its specificity (e.g. life duration). For example, for technical services and space plan, components are subject to upgrades and/or replacement more often than those in other layers. The retention and reuse of valuable materials and components need to be anticipated. This calls for circular strategies and solutions corresponding to each layer. On the other hand, the layers are interdependent and integrated in terms of energy performance and spatiality. This interconnectedness compromises the efficacy of the applied circular strategies. Despite the need for such circular strategies, existing assessment tools seldom focus on technical services due to a lack of appropriate design methods and increased investment costs of components suitable for reuse. This paper documents the translation of existing European assessment tools as method and related design strategies for layers of structure, skin and space plan to the layer of technical services. The selected design strategy was an iterative process ensured by a design & build procurement and the solution for the integration of technical services was determined as a plug-in unit which is part of a modular CLT technical core. It is expected that the technical unit will continue its lifetime beyond the lifetime of LL Ghent.

Keywords. Circular and integrated building design, Design for Disassembly, Product Life-Cycle Strategies, Component Reuse and Remanufacturing, decision-support.
DOI: https://doi.org/10.34641/clima.2022.298

1. Introduction

Improving methods of construction and the use of buildings in the EU would decrease the European energy consumption by 42%, greenhouse gas emissions by about 35%, water consumption by 30% and, only 50% of the current extraction of materials would take place [1]. Existing policies for promoting energy and resource efficiency in buildings need to be further strengthened and should consider the

Copyright ©2022 by the authors. This conference paper is published under a CC-BY-4.0 license.

environmental impacts across the life-cycle of buildings and infrastructure. Life-time costs of buildings should be taken into account rather than just the initial costs, including waste production (both during construction and at end-of-life (EoL) and residual value. Enabling this accounting, calls for elaborate approaches for evaluation of circular construction materials and methods.

The development of 'ISO 59020, Measuring circularity framework' is currently in progress [2]. This paper aims to address the gap in applicability for technical services in buildings in mentioned standard by sharing the user experience of circular assessment tools. It is estimated that the share of the embodied impact of technical services in buildings, on average, is around 10 to 12% [3, 4]. In case of industrial buildings, it accounts for an even higher number. Despite the importance of this characteristic, there is a lack of environmental evaluation methods to assess and mitigate the impact of the embodied energy of technical services. In the next sections, relevant indicators from an inventory of circular assessment tools are retrieved for an analogous assessment of the technical services. In Living Lab Ghent, which was developed in the scope of the Interreg CBCI Project, a stand-alone HVAC system in a housing project is described to demonstrate the circular application of technical services. The concept was developed with a special focus on circular principles, which was purchased using a Product-as-a-service business model, will be monitored during the use phase and at end-of-life when the HVAC system is demounted and retrieved from the building.

2. Literature Review

In preparation for deriving a list of indicators for assessing the circularity of the 'service layer' [5], an inventory and categorisation of characteristics of existing assessment tools regarding circularity and flexibility is compiled. A systematic market and literature research is carried out focusing on micro and meso scale (see Figure 1) to give a complete overview of such assessment tools. Subsequently, the review framework of Lindgreen et al. [6] will be applied.

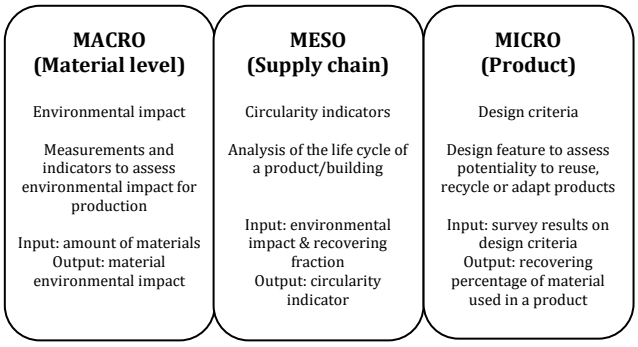

Fig. 1 - Methodology for circular assessment tools [7].

The methodology used can be divided into the following steps:
- Defining concepts for the inventory
- Carrying out literature and market analysis resulting in an inventory
- Application of the review framework

2.1 Defining concepts for the inventory

Compiling suitable assessment tools requires a definition of circular construction. According to 'Vlaanderen Circulair' [8] circular construction strives for an efficient and effective use of resources. The aim is to create or at least maintain economic, social and ecological (added) value. During the construction process, the existing legacy and future opportunities specific to the built environment is taken into account. Flexible or future-oriented construction [9] also aims to reduce the environmental impact of the construction sector by, at the start of projects, anticipating future changes in expectations and use of the building.

Assessment tools are set up to gain insight into the performance of a particular subject (company, product, process, etc.). This research is specifically concerned with circularity and helping to increase the implementation of circularity into the technical services by making the performance transparent, communicable and comparable, making improvement possible in the long term. A multitude of such tools are available in the absence of a legislative framework and standardisation for measuring circularity. The development of ISO 59020 is expected to address this gap.

Furthermore, it is important to note the methodological difference between measuring and assessing circularity. As far as circularity is concerned, it is considered impossible to carry out a purely quantitative valuation, as circularity is a very broad and abstract concept and thus not a measurable quantity. Tools that work on a numerical basis cannot be called purely quantitative in their principle, as qualitative characteristics are often translated numerically. Van Oppen et al. [10] makes a division according to Table 1.

Tab. 1 - Breakdown measuring vs. assessment according to Van Oppen et al [10].

Measuring	Assessing
Quantitative	Qualitative
Objective	Objectified by methodology

The assessment level should be considered. Given the CBCI Living Lab context, both the micro level (component level) and the meso level (supply chain) seem to be important. Cottafava et al. [7] address the need and make a proposal for an interaction between macro, meso and micro level assessment data (see Figure 1).

2.2 Carrying out literature and market analysis resulting in an inventory

Existing literature reviews on academic papers on assessment methodologies for circularity indicate that there is an oversupply of tools and more specifically developed methodologies documented in academic publications [6]. In addition, according to a recent study by Lovrenčić Butković et al. [11], the number of available methodologies increases in an exponential line through time (see Figure 2).

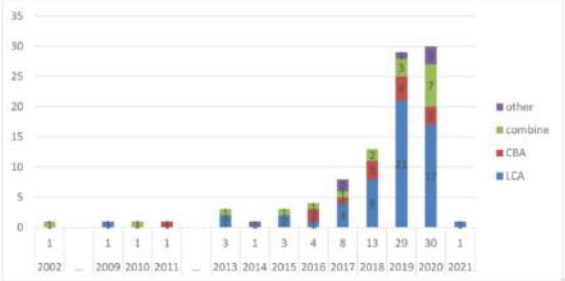

Fig. 2 - Annual distribution of available circular assessment tools [11]

Sources used are databases for academic papers, conference papers, grey literature and web-based assessment tools of the last 5 years (2016-2021). Search terms can be divided into several themes; circularity and assessment. More specifically, they are respectively circularity, circular economy, change-oriented, flexible and assessment tool, assessment tool, methodology, measurement, valuation. A set of inclusion and exclusion criteria was used to oversee the multiplicity of tools as presented below in Table 2.

Tab. 2 – Criteria for inclusion and exclusion

Inclusion criteria
Micro (and meso) scale
Building and component level
New methodologies regarding CE
Assessment methodology transparent
Published and working version
Exclusion Criteria
Macro level
Product or company
Conventional methodologies like LCA
Unpublished underlying methodology
Beta version

This resulted in the following tools; De Material Circularity Indicator (MCI) by the Ellen McArthur Foundation, The BCI & demountability index by Alba Concepts, Cb'23 by Platform CB'23, Calc-C by Cenergie, Circulariteitsindicator by Madaster, CBA by BAMB, Flex 4.0 by Geraedts TUDelft, Circularity tool by One-Click, GRO by OVAM, Circulair gebouw by WTCB/VCB, Circulaire peiler by Circularie bouweconomie NL, CPG GPR gebouw by W/E adviseurs, KIEM.CIE by Saxion, Levels by the EU commision, Circulaire handtekening by Upcyclea and Veranderingsgericht bouwen by OVAM.

2.3 Review framework

The selected tools were characterised and categorised according to the revised review framework developed by Lindegreen et al. [5].

Tab. 3 – Revised review framework

Perspective	Goal	Characteristic	Clarification
General	Description of characteristics	Name	Reflection on the general characteristics of the tool
		Age	
		Source/ Country	
Descriptive	Inventory of underlying methodologies	Scale	Micro or meso scale [6]
		Sector specific	Construction sector specific or otherwise
		Indicators	Assessment tools are often based on more fundamental methodologies such as LCA/MFA/input-output/... An understanding of this basis allows to appreciate the tool more.
		Case study	In case practical examples are available in the methodology, it is easier for the users to apply the tool correctly.
Normative	Pillars of sustainability	Three pillars integrated	In the context of CE assessment, the question is: "What should be the ideal outcome of the application of CE for the concept to be of value?" The concept of CE is interpreted here as only being valuable if it achieves greater sustainability (three pillars).
		CE specific	
Prescriptive	Suggestions and Lessons learned	Insights in results	How can better decisions be made? Are lessons learned or points of improvement provided?
		End score	How is the overall performance communicated?

The framework consists of four perspectives; a) general, b) descriptive, c) normative and d) prescriptive, further described in Table 3. The inventory and analysis of existing tools results in a shortlist of underlying methodologies and subsequent indicators (descriptive perspective). A summary of the indicators, according to their main overarching objective, is given in Figure 3.

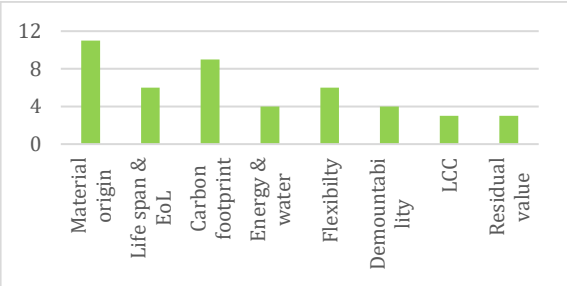

Fig. 3 – Summary of indicators

The first four indicators all relate to Life Cycle Assessment (LCA) calculations. Literature shows that efforts have already been made to develop methodologies for LCA, specifically applied to technical services [12]. However, the underlying indicator types relating to LCA are influenced by other aspects; among which the reusability of components and the end of life (EoL) scenarios, which in turn, are influenced by the manner of integration of the components in the building (Flexibility) and the methods for design-for-disassembly (Demountability). Demountability is defined as the degree to which objects can be dismantled within buildings so that the object can retain its function and high-quality reuse can be realized [13]. These two concepts form the basis of research in this paper, resulting in a component-level demountability and building level integration and flexibility of the technical services.

3. Methodology

3.1 Design for Disassembly

The inventory shows many tools assessing the potential for reuse, yet those seldomly take into account the preconditional aspect of demountability and if so, adhere to a limited and qualitative or quantitative approach. OVAM, One-Click and Flex4.0 only qualify whether demountability is considered. CBA quantifies the share of the total building that is demountable. Only C-calc and BCI (demountability index) apply a more in-depth assessment, with BCI using the most advanced approach with the so-called Demountability Index.

The Demountability index is based on four factors which are defined as follows; (i) type of connections, (ii) accessibility to the connections, (iii) crossings (level of integration), (iv) form enclosure (composition of objects). These factors are assessed for each object between 1,00 being the best score and 0,10 being the worst. A distinction is made between the Demountability Index of the connection (Dlc) and the Index of the composition (Dls) of the element, respectively influenced by the connection between objects and influenced by the composition of objects. As shown in Figure 4, the demountability index is a combination of both indexes.

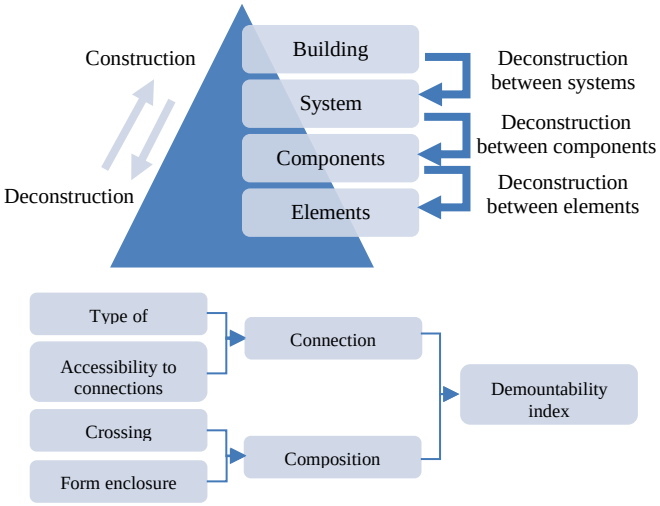

Fig. 4 – Demountability index calculation and levels of material composition [13]

To determine to what level of detail the calculations should be done, Van Vliet [14] refers to the diagram in Figure 4 of the 'Transformable Building Structures' by Durmisevic [15] showing the different levels. The described assessment methodology is applied for all types of components with the same pre-set values, regardless of the layer of Brand the component belongs to. However, it is considered that these values are not specific enough to be applied efficiently to technical services. A converted list of pre-set values and supplementary factors is given in Table 4. In addition, supplementary factors are listed in Table 5 based on the early work of Van Vliet [16] and Durmisevic [15] which formed the basis for the Demountability Index development.

Tab. 5 – Supplementary factors for demountability assessment of technical services.

Supplementary factor	Clarification	Pre-set values
Assembly direction	The assembly sequence sets a mirror image for the disassembly sequence. [14]	Direct disassembly possibility Multiple actions needed before disassembly
Tolerance between components	The provision of space with adjacent components to allow for separation	Tolerance included in connection, outside connection No tolerance foreseen
Required tools	The required tools to disassemble products, range in complexity	Standard tools required Specialize tools required

3.2 Integration

The method of BCI manages to qualitatively asses the demountability of components, while going as far as, yet not exceeding, the boundaries of the layers of Brand. Additionally, the spatial interdependency and integration of the layer of technical services in the Brand model should be assessed, in other words, how the whole layer is integrated in the building and not only its individual components. This aspect is almost entirely missing in available tools apart from FLEX4.0, which considers the location of the facilities, disconnection of facility components, independence of user units and anticipation for future adjustments to the system. In order to assess demountability and circularity, the following concepts can be assessed additionally:

Accessibility of all the components in relation to the other layers Brand. The demountability Index considers accessibility only while demounting, that is the whole building, not accessibility during use for maintenance of replacement. This can be further nuanced by considering the four main segments separately; production, distribution, delivery and storage. Integration, layout and compactness of the overall concept. While the individual components could be easily accessible, the entire system can be integrated into the building to a varying extent, ranging from widely spread to very lean and centralised. Further divisions could be made, again based on the four segments. For instance, considering centralisation of vertical distribution in a technical shaft.

Tab. 4 – Converted list of factors and pre-set score for demountability assessment of technical services.

Factor original	Pre-set value original	Factor converted/ supplementary	Factor converted/supplementary
Type of onnection		**Type of Connection**	
Dry connection	Dry connection	Dry connection	Reversible dry connection
	Click connection		Reversible click connection
	Velcro connection		Magnetic connection
	Magnetic connection		Tapered fitting
Connection with added elements	Bolt-and-nut-connection	Connection with added elements	Bolt-and-nut-connection
	Spring connection		Spring connection
	Angle connection		Angle connection
	Screw connection		Screw connection
	Connection with added elements		Connection with added elements (clamps)
Direct integral connection	Pin connection	Direct integral connection	Pin connection
	Nail connection		Nail connection
			Press fitting connection
Soft chemical connection	Kit connection	Soft chemical connection	Kit connection
	Foam connection		/
Hard chemical connection	Glue connection	Hard chemical connection	Glued connection
	Connecting pour		Soldered connection
	Welded connection		Welded connection
	Cement connection		Hard chemical connection
	Chemical anchor		/
	Hard chemical connection		/
Accessibility of the connections		**Accessibility of the connections**	
	Freely accessible		Freely accessible
	Extra operation resulting in no damage		Extra operation resulting in no damage
	Extra operation resulting in damage		Extra operation resulting in partial damage of components
	Non-accessible		Extra operation resulting damage of all components
			Non-accessible
Crossings		**Crossings**	
	Modular zoning of objects		Modular zoning of objects
	Intersection of objects		Intersection of objects
	Full integration of objects		Full integration of objects
Form enclosure		**Form enclosure**	
	Open		Open
	Overlap single sided		Enclosed single sided
	Closed single sided		Enclosed double sided
	Fully closed		Fully Enclosed

4. The application for LL Ghent

The CBCI LL Ghent is a prototype for a terraced single-family house. Several scenarios for structure and technical services have been generated and evaluated in a multi-criteria assessment. In this section, the definitive design case is explained in parallel with circularity concepts that were provided in the previous sections.

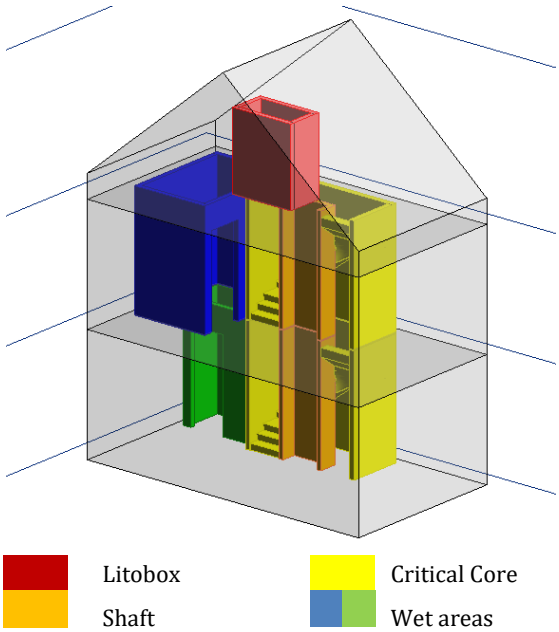

Fig. 5 – Location of technical services in LL Gent

Both structure and technical services in LL Ghent are designed in a modular fashion around a 'critical core'. The critical core is a CLT structured staircase which wraps around the technical shaft in the centre of the building. Technical services are based on the top level above the critical core, in the form of a pre-fabricated technical room, the Litobox (see Fig 5). The previously listed indicators for demountability assessment are converted to the building concept in the sub-sections below;

Demountability assessment

The connections of messing fittings and clamping fixings are highly reversible dry connections that are freely accessible. The simple and organized layout of both the Litobox, the technical shaft, and floor integration make all components individually and freely accessible.

Concerning integration, layout, and compactness, the Litobox centralizes all production in a prefab box, whereas the technical shaft (vertical) and subfloor (horizontal) make up for an orderly integration. Any crossings in vertical or horizontal direction are avoided as such; (i) Litobox with a direct access to production and storage components, (ii) the technical shaft that is open on one side for maintenance and (iii) the integration of the piping in the subfloor combined with a demountable floor finish, make the whole system easily accessible (see Figure 6). In this configuration, the system is considered as having an open enclosure which enables removal of a certain component without intervening with another one.

As a result, the technical system becomes a 'plug-in-system which has a practical sequence for the mounting and demounting of the main components. In the application for LL Gent, the Litobox is the main component that was mounted only before the roof was enclosed. In its location, it would be considered as accessible for regular maintenance at a 'material level'. In case of a major revision, it would also be possible to remove the whole 'component' with minimum amount of intervention on the structure. That would also imply that at higher scales of built environment, one can demount the mechanical system as a whole easily (just after the roof is demounted) and reuse it at another building.

For educational and demonstrative purposes, the system was accessible for stakeholders during the construction phase and will be monitored during the use phase in the KU Leuven Technology Campus in Gent for learning purpose.

Fig. 6 – Integration of the technical services

5. Conclusions

The literature review shows there is a lack of circular assessment methods specifically for technical services, both on micro and meso scale. This study reviews the existing assessment tools that can also be utilized on technical services. A list of converted indicators based mainly on the demountability index and partially on additional tools is presented. Supplementary indicators considering several levels of a building and integration are provided as well.

The CBCI LL Gent demonstrated the real-life implication of the collected indicators. Not only can integration be considered in the end result, but also in the process to come to said result. It was seen that the vertical piping in the critical core can be pre-mounted off site. This would also increase the demountability of the critical core together with installation system.

Realising high accessibility to the technical system may result in a decrease in performance on other criteria, for instance the acoustic barriers will be less effe. This aspect will be monitored during the use phase of the LL Gent. It was also noted that the Litobox had to be placed just before the roof was enclosed. Then, this requires a different mounting order and additional attention to protect the system during the remaining exterior and interior works.

Further analysis of the demounting phase is necessary to validate the first insights gained in this study. Such a future study would contribute to close the gap in case studies and examples on demounting of structural and technical components.

6. Acknowledgement

The Circular Bio-based Construction Industry (CBCI) project is funded by the European Union Regional Development Fund Interreg 2 Seas Mers Zeeen (2S05-036). Data sharing not applicable to this article as no datasets were generated or analysed during the current study.

7. References

[1] Marton Herczeg, David McKinnon, Leonidas Milios, Ioannis Bakas, Erik Klaassens, Katarina Svatikova, Oscar Widerberg. Resource efficiency in the building sector (2014) DG Environment.

[2] Claudio Perissinotti Bisoni, Carlo Brondi, Claudio Rosso, & Laura Cutaia. Towards a Global Framework to Measure and Assess Circular Economy. Symphonya, (1), 2020; 88-100.

[3] Hitchin R. RR9 Embodied carbon and building services. CIBSE Research Report. 2013.

[4] Kiamili, C., Hollberg, A., & Habert, G. Detailed assessment of embodied carbon of HVAC systems for a new office building based on BIM. Sustainability (Basel, Switzerland). 2020; 12(8), 3372.

[5] Brand, S. How buildings learn: What happens after they're built. NY: Penguin Books. 1994.

[6] Lindgreen, Erik Roos, Salomone, Roberta, & Reyes, Tatiana. A critical review of academic approaches, methods and tools to assess circular economy at the micro level. Sustainability (Basel, Switzerland). 2020; 12(12), 4973.

[7] Cottafava, Dario, & Ritzen, Michiel. Circularity indicator for residential buildings: Addressing the gap between embodied impacts and design aspects. Resources, Conservation and Recycling, 2021; 164, 105120.

[8] Vlaanderen Circulair. Circulaire economie in de Vlaamse Bouwsector. 2021.

[9] OVAM. Veranderingsgericht bouwen: ontwikkeling van een beleids- en transitiekader. 2016.

[10]Van Oppen Cécile, Croon G., Bijl de Vroe D. Circular Procurement in 8 Steps. First edition, Copper, 2018.

[11]Lovrenčić Butković, L., Mihić, M., & Sigmund, Z. Assessment methods for evaluating circular economy projects in construction: A review of available tools. International Journal of Construction Management, 2021; 1-10.

[12]Finnegan, S. Embodied carbon of sustainable technologies. In *Embodied Carbon in Buildings: Measurement, Management, and Mitigation* (pp. 287–300). Springer International. 2018.

[13]Bos, M.: Circulair bouwen: Rapport losmaakbaarheid beschikbaar. Retrieved from https://www.w-e.nl/rapport-losmaakbaarheid-bij-circulair-bouwen. 2019.

[14]Van Vliet, M., Van Grinsven, J., Teunizen, J.:. Circular buildings—Meetmethodiek Losmaakbaarheid. V 2.0. Alba Concepts. 2021

[15]Durmisevic, A.: Transformable building structures design for disassembly as a way to introduce sustainable engineering to building design & construction. 2006

[16]Van Vliet, M. Disassembling the steps towards building circularity redeveloping the building disassembly assessment method in the building circularity indicator. 2018.

BIM-based circular building assessment and design for demountability

Tetiana Lukianova [a], Cihan Kayaçetin [b], Lode Lefevre [c], Alexis Versele [d], Ralf Klein [e]

[a] KU Leuven, Department of Civil Engineering, Building Physics and Sustainable design, Technology Campus Ghent, Belgium; tetiana.lukianova@kuleuven.be.

[b] KU Leuven, Department of Civil Engineering, Building Physics and Sustainable design, Technology Campus Ghent, Belgium; cihan.kayacetin@kuleuven.be.

[c] KU Leuven, Department of Civil Engineering, Building Physics and Sustainable design, Technology Campus Ghent, Belgium; lode.lefevre@kuleuven.be.

[d] KU Leuven, Department of Civil Engineering, Building Physics and Sustainable design, Technology Campus Ghent, Belgium; alexis.versele@kuleuven.be.

[e] KU Leuven, Department of Civil Engineering, Building Physics and Sustainable design, Technology Campus Ghent, Belgium; ralf.klein@kuleuven.be.

Abstract. The on-going transformation of the linear economy model (LE) to a sustainable circular economy (CE) creates new challenges for information management, evaluation methods, and information exchange. This impacts also the traditional definitions of roles and processes in the AEC sector. OpenBIM and a proper definition of the design process and the key decision points based on EN ISO 19650 and using the IDM framework (EN ISO 29481) can help to master these challenges. This is complemented by the need for reliable product data that could be satisfied by implementing EN ISO 23386 and 23387 together with the more specific EN ISO 16757 tailored for the needs of the HVAC sector. While the general methodology has recently been defined in these international standards, the concrete application for sustainable design and many implementation details remain still open. This paper presents a BIM-based scoring approach for Circular building assessment (CBA). It defines the information needs at different design stages: from the requirements in an early design stage to the solutions chosen in the detailed design stage. The same methodology can be applied to structural elements of the building envelope as well as to technical equipment and HVAC systems, providing a common framework for the integrated design of sustainable buildings. Besides the methodology, this paper describes a first implementation for the case of the Living Lab (LL) building, a prototype dwelling in Ghent (Belgium) built in the scope of the Circular Bio-Based Construction Industry (CBCI) project funded by the EU Interreg 2 Seas program. The aim of this paper is to demonstrate how BIM can be used to partly automate decision-making and evaluation for the specific needs of CBA and design for demountability. The proposed solution based on Alba Concept is creating an efficient link between an external database and the BIM model. This is performed by extracting the necessary object information and integrating it for further evaluation during the lifecycle of the building including the design, construction, operation, end-of-life and re-use phases.

Keywords. Building Information Modelling (BIM), circular building, demountability assessment, circular building assessment, decision making process, BIM model adaptation, Dynamo.
DOI: https://doi.org/10.34641/clima.2022.291

1. Introduction

Building Information Modelling (BIM) support in the construction industry is an important component due to increased interdisciplinary activities and the amount of construction data.

To unlock the full potential of a collaborative BIM-based design and construction process as well as support for circularity, the data management and exchange needs to be based on open, standardized data-structures and exchange formats. While the framework is already described for a big part in European standards, the application to different

Copyright ©2022 by the authors. This conference paper is published under a CC-BY-4.0 license.

disciplines within the construction sector and the implementation are still work in progress.

However, owing to an impetus and governmental support, the CE has gained momentum and considering the latest EU commission publications [1] it can be envisaged that the circular building approach will become an integral part of the design process. These concepts involve data management across the entire building lifecycle and the need to integrate circular methodology into the BIM environment and define appropriate data structures. Future proof approaches like OpenBIM based on the above-referenced standards can help to master these challenges.

The aims of this conference paper are:

1. to provide an overview of the existing BIM tools that are available to support sustainable circular economy (CE) focused on demountability assessment;

2. to provide more insight in the current evolution of European (CEN) and international (ISO) standardisation in order to provide workflows and data management for construction projects that can be implemented and used today and will allow a smooth transition once the standardisation framework will be fully implemented.

3. to present a framework that was developed in the scope of the Living Lab (LL) prototype in the CBCI project, while considering the future possibility of its applicability to, not only the building envelop but in a latter phase also the HVAC and electrical systems.

This paper focusses on the development of the framework and lessons learned from the workflows and information needs of the design phase of the case study.

Numerical results of the demountability assessment and a comparison of different assessment methods are outside the scope of this paper.

2. Methodology and current state of the art

The use of BIM as a supporting tool for research and application is on a rise in the last decade. Several points of research interest are environmental impact, circular design and optimization of BIM processes. This study focuses on the integration of BIM with LCA and DfD research efforts as seen in Figure 1.

LCA is a comprehensive environmental impact assessment framework as defined in the ISO 14040:2006 standard which takes into account the whole life cycle of a product or building. Design for Deconstruction (DfD) is an emerging concept that focuses on demountability of building components.

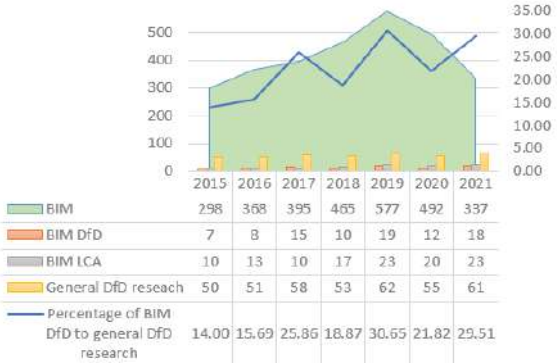

	2015	2016	2017	2018	2019	2020	2021
BIM	298	368	395	455	577	492	337
BIM DfD	7	8	15	10	19	12	18
BIM LCA	10	13	10	17	23	20	23
General DfD reseach	50	51	58	53	62	55	61
Percentage of BIM DfD to general DfD research	14.00	15.69	25.86	18.87	30.65	21.82	29.51

Fig. 1 - Number of publications and its distribution on the topic "BIM", "LCA" and "DfD" in engineering technology, building and architectural construction sector (Scopus, Mendeley, Web of Knowledge).

Research has focused initially on quantitative resource performance indicators for Life Cycle Assessment (LCA) and dynamic LCA [2], but an increased focus towards a DfD direction can also be seen, which emphasizes the attention of LCA for the required adaptability, usability and maintenance for building materials throughout the entire lifecycle.

Prior to 2014, only one-third of LCA tools were BIM integrated, but none considered the aspects of deconstruction. For this reason, this study was conducted on existing information from 2015 onwards. However, a fluctuating line illustrates the recent three trends of BIM-focused studies to the total amount of DfD research and keep its level near 23-30% for the last 3 years.

The first two are oriented to the demountability calculation by considering the detached component (covers the information requirements of "Level of detail" (LOD 350)) as well as an element level (LOD 200) defined by the American Institute of Architects (AIA)) [3]. And, respectively, the third is based on time and cost analysis of assembly works based on 4D and 5D modelling [4].

Several BIM integrated DfD concepts have been developed and published. BCI Gebouw is a standalone platform that gives an overview of the possibility of disconnecting a building based on a measurement method developed by Platform CB'23 based on the list of indicators considering waste and material flow (Circular Construction 2023) [5]. The BAMB project works on the BIM-integrated Reversible Building Design Tools, including aspects of reuse potential reversibility and disassembly, with significant attention to the interrelationships between components [6].

To our best knowledge there are no existing studies that mention the DfD BIM concept for HVAC systems. In the early studies, Shuo Chen [7] focuses on materials in his environmental impact analysis and treats HVAC systems as recyclables with transportation taken into account. Also identified

are early studies [8] incorporating some performance criteria into Fuzzy multi-criteria evaluation. Recent studies include HVAC systems as a full component of LCA analysis methods, but do not take into account demountability factors [9].

2.1 Technical barriers preventing the DfD integration into BIM

A significant barrier in the DfD development linked to the AEC sector is the lack of a well-defined and standardized methodology, thereby also affecting the evolution of other interlinked related studies such as LCA and material passport certification [10].

However, to analyze interrelationships among different factors one can deduce, that a collaborative study of DfD BIM provides a better understanding of the general methodology's needs due to the identification and analysis function of component attributes. There are several key concerns in data extraction automation: differing techniques and rules for 3D model design, use of different classification and nomenclature systems between partners, collaborative work with various linked files, and software compatibility issues. Therefore, particular attention should also be paid to the data-structure and the exchange format, e.g. the IFC (Industry Foundation Classes) format [11] to ensure correct data exchange and model coordination.

Furthermore, the absence of a database of connectors and their associated characteristics increases the amount of required manual entry during the design phase. Consequently, at some point, it becomes inappropriate to modify the 3D model. Such databases with a standardized data structure, provided for example by the manufacturer of components, would allow improving visualization and usability for the demountability process, in addition, to incorporating DfD into parametric designs maintaining the object attributes, behaviours and constraints.

Also contributing to complexity is the fact that the Revit API [12] inheritance hierarchy structure for various objects is different and the method syntax needs to be clarified in the case of custom input, for example: "loadable families", adaptive components, etc.

2.2 European and international standardization and its current implementation

To be able to exchange information digitally and take full advantage of a collaborative project development, standardization is key.

The technical committees ISO/TC 59 SC 13 and CEN/TC 442 have developed standards for data structures that are published as EN ISO 12006-3, EN ISO 23386 and EN ISO 23387. More specifically to the HVAC sector a series of standards is under development. It is based on work that was published as a German guideline, the VDI 3805. The EN ISO 16757 series aims at a complete framework for reliable product data exchange for HVAC. While part 1 and 2 are already published, current work is dedicated to align this standard with the other standards for data templates and to define a scripting language that is integrated into the exchange format IFC and enables the definition of dynamic system properties of HVAC components like the pressure drop of a duct component depending on the volume flow.

Further work is required for implementation, specifically the governance, maintenance and hosting of the required databases. The definition of product properties will be done in close collaboration with other CEN/TC's. CEN/TC 442 is working on the methodology, while other TC's have the necessary competence to apply that methodology to their domain and define the actual content.

So currently it is common practice in construction projects to use proprietary BIM software and data-structures, that are ad-hoc defined for a project, aligned with company standards or in the best case following local guidelines.

To make the transition to a fully implemented, standardized framework for product data according to EN ISO 23386 and 23387 it is essential to gain more insight into the required information at different stages in the lifecycle of a built asset.

The case study presented in the following chapter contributed to this aim, as information requirements have been analysed and translated into the implementation of a tailor-made software tool based on the REVIT API.

While the implementation of standardised product data is still under development, the methodology for project setup and workflows is already fully defined in the EN ISO 19650 series. These standards describe a proper definition of the design process and the key decision points. Following this standard enables the creation of BIM-based collaborative projects.

3. The CBCI case study

The research is based on a case study which was conducted as a part of the CBCI project which investigates the efficient and sustainable use of building materials and technologies in the construction industry, thereby reducing environmental impact, e.g. CO2 emissions. This study aims to achieve project task automation and calculations support (mainly assessment tools for environmental impact and circularity measures) based on model data created in the BIM tool used by

the project partners (REVIT).

Several circular construction tools were used to assist the CBCI objectives and were tested in the real-life case study during the design and construction phase of the LL Ghent. The design is a 2-storey residential building (including an attic) with a 98.8 m2 total gross area, designed according to the 19th-20th century terraced houses typology (Fig.2). The total front facades (west, east) measures 56 m2 and the side facades (north, south) add up to 129 m2. The window area in all facades is 22.7 m2. The roof area is 46m2 with a 19.1 m2 roof-top window area.

Fig. 2 - 3D and exploded view of the CBCI LL Ghent.

Based on preliminary studies of the building envelop [13], it was decided to develop a tool that can reduce the time needed for an expert design and evaluation based on the Alba Concept method [14]. The tools' methodology represents four technical factors for the assessment, which are connection type, accessibility of connections, crossing type, form enclosure, which are detailed in the Tab.1.

Tab. 1 - The rating types of the technical factors [14].

Type	Score
Connection type	
Dry connectors (dry, velcro, spring)	1.00
With additional connectors (bolt/nut, ferry, corners, screw)	0.80
Direct integral connect(pin, nails)	0.60
Soft chemical connect (organomercuric, foam)	0.20
With the hard chemical connections (glue, weld, recycling mat, cement, chem. anchors)	0.10
Accessibility of connections	
Freely accessible	1.00
Accessible with additional actions, don't cause damages	0.80
Accessible with recoverable damage weight	0.40
Inaccessible - irreparable damage to objects	0.10
Crossings type	
Modular zoning of objects	1.00
Intersections between one/more objects	0.40
Full Objects integration	0.10
Form enclosure	
Open, no inclusions	1.00
Overlap on one side	0.80
Closed on one side	0.20
Closed from several sides	0.10

These technical factors are rated between 1.00 and 0.10. A difference is made between the connection demountability Index (Dlc) and the composition demountability Index (Dls) of each item, which is respectively influenced by the connection between the elements (Fig.3). The demountability index is a combination of both indexes, taking into account the volumetric parameter as a normalization factor [13]. To define a level of detail during the modelling and calculation phase, BB/SfB, a Belgian version of the international classification system CI/SfB - was applied [15].

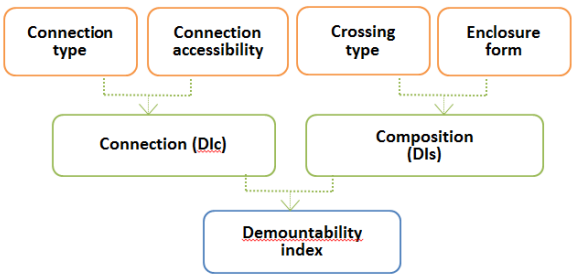

Fig. 3 - Demountability index assessment.

4. Workflows and tool implementation

The developed tool in this research is based on a Dynamo [16] script through which the assessed elements can be selected and have a connection type assigned with subsequent simulations and calculation. Dynamo is a Revit-based visual programming interface that enables users to build code with algorithmically linked nodes (data and operations), thereby setting up and automating the workflow of building information data. The automated script was written within both the standard and custom nodes using Python and Revit API programming languages by supporting the following general workflow (Fig.4).

For the CBCI framework, the script works not only as a data delivery tool, but also as a calculation engine, and can be divided into six sections, each with various functions:

- GUI (graphical user interface) activation;
- object selection;

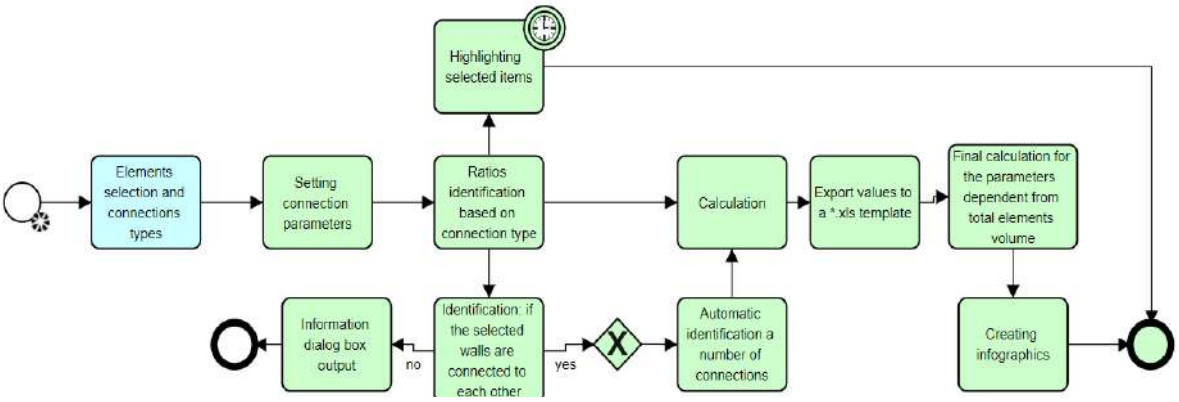

Fig. 4 - CBCI demountability index calculation tool workflow.

- connection type assignment;
- database reading;
- mathematical calculation and data export to Excel.

During the initial phase, the Dynamo script activates the GUI (graphical user interface) by which users select elements for assessment (Fig.5, 1) and their connection types and connection accessibility based on expert evaluation (Fig.5, 2).

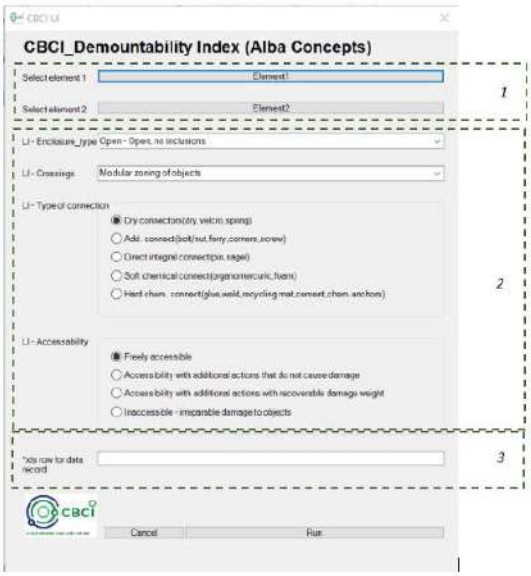

Fig. 5 - GUI (graphical user interface) for the CBCI demountability tool.

After the required experts' input, the script starts the element connection checking process, extracts the necessary geometric attributes from the model, and directly assesses formulas. In a final step, the collected intermediate results are averaged and normalized to rate the considered structure in one single score.

Accordingly, all input and output building data can be classified into various categories. General attributes provide an element identification by their ID, family type and BB/SfB code. Geometric attributes provide the element dimensions and its materials' densities. Coordination attributes provide an automated determination of the number of attached elements. Selective attributes provide the data stored internally within the assessment scenario to identify the type and coefficients of connections.

A Demountability Index normalized (DI_n) parameter was taken out of the main analysis in the Dynamo script as it is based on the total volume of all elements. It is technically possible to implement in the extra-functional nodes group with the additional data import from the same excel template, but as a consequence, it increased the speed of data processing. As a final result, the user obtain a CBCI excel template containing all imported data and assessment results, diagrams subdivided into 'Structure', 'Skin', 'Services', 'Space plan' layers [13]; and element filtering tool (Fig.6).

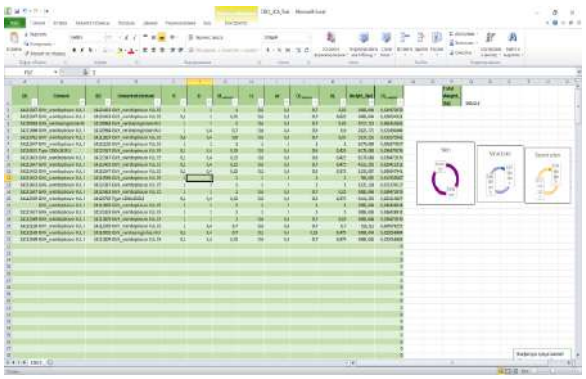

Fig. 6 - A sample of a visual display of the results window.

After conducting tests, several improvements were integrated into the CBCI tool with the aim to improve its usability, such as the dialog box (a message notification that specifies whether the elements are connected) and function for highlighting of selected objects in the 3D model.

5. Discussion

During the intermediate simulation, it occurred that connected elements were defined as not connected because of the minimum distance between elements (e.g., for design reasons). For this problem, the team

developped a strategy in which indicators were created at the corners of the elements to determine an intersected element. They are illustrated by the blue lines in Fig. 7. Along the selected element's edges, at the top and base points, the six lines are automatically generated in various orientations by a user-defined length. As a next step, the developed tool determines whether these lines are intersecting with a surface geometry of the second selected element and generates a message. These indicators have their advantages and complexities and should be studied and improved further in the future. The disadvantage of this strategy is that these indicators are based on geometric nodes, which are quite capacious and complicated for the script workflow. But this concept can be applied for automation and identification of two other factors of the four defined; being accessibility connections and crossings type for the HVAC system for the purpose to identify adjacent elements.

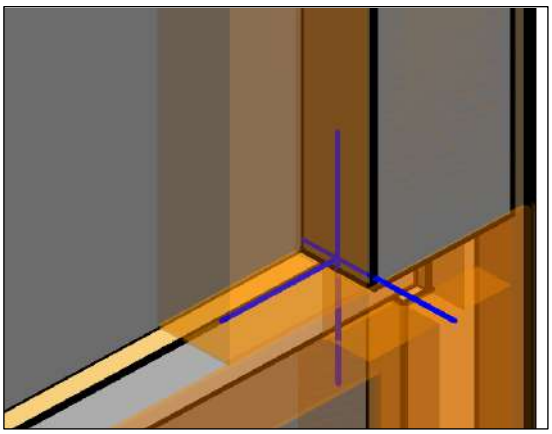

Fig. 7 - The CBCI wall indicators illustration (lines were enlarged for better visual clarity).

Besides this first strategy, two other strategies were tested throughout the work on the main concept. The first one is the adaptive family strategy which uses a set of key parameters for expert assignment. The second strategy is to examine the framework, also peculiar to the BCI Gebouw tool [17], which is supporting an assessment method developed by the CB'23[5], but its concept includes the "one element, one connection" hypothesis. This structure and hypothesis cannot be practical for structural building components and HVAC elements with multiple connections, for example: floors, ceilings, girder slab system, T-ducts, etc. In addition, another critical aspect to consider with this approach is that the absence of IFC format support reduces the model's data interaction within the platform, hence in the case of random/user-based connection identification; the attached elements cannot be transparent to other users.

The indicated gaps in research and tool application lead to the conclusion that a tool for HVAC models is needed. The conceptual analysis and CBCI LL test-case demonstrate the functionality and feasibility of this methodology for HVAC systems. Facilitating future research is the fact that the developed script can be adapted for data structural changes and other modifications such as an additional data requirements or functionality. The final evaluation and comparative studies will be published in the further thematic project reports, whereas the data related to this paper will be presented at the conference.

6. Conclusions and future work

From the review of existing studies it can be concluded that the DfD topic is interconnected with the general LCA research area, material reuse potential and environmental impact. However, only a few papers currently published are focusing on the technical feasibility to integrate DfD or LCA calculations into a BIM environment. A key research contribution is the BIM-integrated development approach based on the Dynamo Revit interface, which supports demountability analysis based on the Alba concept method. This visual programming script represents an algorithm with a graphical interface that automates obtaining geometric element data and expert value data with a subsequent assessment using a connection type database as well as a built-in mathematical computation. In the course of the CBCI LL test-case analysis, it was confirmed that this framework can also be applied to HVAC systems.

On the basis outlined in the previous chapters, several research perspectives and improvement potential in relation to the BIM area were identified, that arise from the practical experience of our team and project partners. In addition to the methodological work, potential in-depth automation is planned to cover the following items:

1. In-depth process analysis and effective data management between DfD experts and BIM/CAD modelers.
2. To continue the work on the existing tool, by further extension with a deconstruction plan, and as a result, create a direct Revit plug-in.
3. It is appropriate to investigate technical features to automate the identification and visual representation of connection type and subsequently reduce the manual work and expert decision, as well as the creation of a connectors' database integration to the BIM environment.
4. It is essential to perform a specific study and to evaluate the possibility of adapting the DfD assessment methodology to Algorithm-Aided Design (AAD) and existing BIM adaptive design tools.
5. A proof of concept implementation as a tool for detailed investigation of the workflows and the information requirements for DfD has been done. Additional step(s) from this proprietary solution towards a more general solution based on the described open, standards based framework, can be taken as soon as the required implementations become available.

7. Acknowledgement

Funding by the European Union's Regional Development Fund Interreg 2 Seas Mers Zeeen for the "Circular Bio-based Construction Industry (CBCI)" project (2S05-036) is gratefully acknowledged.

The datasets generated during and/or analysed during the current study are not available yet because the project is not finalized and IP issues have to be checked with the project partners, but the authors will make every reasonable effort to publish them in near future.

8. References

[1] European Commission - Circular Economy - Principles for Building Design [Internet]. [cited 2021 Dec 2]. Available from: https://ec.europa.eu/docsroom/documents/39984.

[2] Akinade OO, Oyedele LO, Ajayi SO, Bilal M, Alaka HA, Owolabi HA, et al. Design for Deconstruction (DfD): Critical success factors for diverting end-of-life waste from landfills. Waste Manag. 2017 Feb 1;60:3–13.

[3] Vandervaeren C, Galle W, Stephan A, De Temmerman N. More than the sum of its parts: Considering interdependencies in the life cycle material flow and environmental assessment of demountable buildings. Resour Conserv Recycl [Internet]. 2022 [cited 2021 Dec 13];177:106001. Available from: http://creativecommons.org/licenses/by/4.0.

[4] Guerra BC, Leite F, Faust KM. 4D-BIM to enhance construction waste reuse and recycle planning: Case studies on concrete and drywall waste streams. Waste Manag [Internet]. 2020 Oct 1 [cited 2021 Dec 13];116:79–90. Available from: https://pubmed.ncbi.nlm.nih.gov/32791461.

[5] Platform CB'23 (Circular Construction 2023). Core method for Circular economy assessment in the construction sector. [Internet]. [cited 2021 Dec 13]. Available from: https://platformcb23.nl/english.

[6] Durmisevic E, Jorissen A, Nijsen R, Broek K, et al. Circular economy in construction design strategies for reversible buildings. 2019 [cited 2022 Jan 10]. Available from: https://www.bamb2020.eu/wp-content/uploads/2019/05/Reversible-Building-Design-Strateges.pdf.

[7] Chen S, Zhang K, Setunge S. Comparison of three HVAC systems in an office building from a life cycle perspective. 2012 [cited 2022 Jan 1]. Available from: www.semanticscholar.org/paper/dc4e5bbf9c0889545c05ceb5a4e2cd5e457418d.

[8] Wang JJ, Jing YY, Zhang CF. Fuzzy multi-criteria evaluation model of HVAC schemes in optimal combination weighting method. Building Services Engineering Research & Technology. 2009;30(4):287–304.

[9] Ylmén P, Peñaloza D, Mjörnell K. Life Cycle Assessment of an Office Building Based on Site-Specific Data. Energies 2019, Vol 12, Page 2588 [Internet]. 2019 Jul 4 [cited 2021 Oct 27];12(13):2588. Available from: https://www.mdpi.com/1996-1073/12/13/2588/html.

[10] Charef R, Morel JC, Rakhshan K. Barriers to implementing the circular economy in the construction industry: A critical review. Sustain. 2021;13(23):1–18.

[11] Industry Foundation Classes (IFC) [Internet]. buildingSMART International. 2019 [cited 2022 Jan 10]. Available from: www.buildingsmart.org/standards/bsi-standards/industry foundation-classes.

[12] Revit API Docs [Internet]. Revitapidocs.com. [cited 2022 Jan 10]. Available from: https://www.revitapidocs.com/.

[13] Kayaçetin NC, Verdoodt S, Lefevre L, Versele A. Evaluation of Circular Construction Works During Design Phase: An Overview of Valuation Tools. Smart Innov Syst Technol. 2022;263:89–100.

[14] Van Vliet, M., Van Grinsven, J. and Teunizen, J. (2021). Circular Buildings – Meetmethodiek Losmaakbaarheid. V 2.0. Alba Concepts.

[15] De Troyer F, Neuckermans H, Havenne D, Simon F. BB/SfB Tabellen 1990 [Internet]. BB/SfB Tabellen 1990. Regie der Gebouwen; Brussel; 1990.

[16] Dynamo [Internet]. Autodesk.com. 2021 [cited 2022 Jan 9]. Available from: https://www.autodesk.com.

[17] BCI [Internet]. Bcigebouw.nl. [cited 2022 Jan 9]. Available from: https://bcigebouw.nl.

Open BIM-based LCA of HVAC and circularity assessment using the Madaster platform

Theißen Sebastian [a], Pelzer Björn [c], Höper Jannick [a], Drzymalla Jan [c], Frank Claudius [b], Bergmann Patrick [b], Meins-Becker Anica [a]

[a] Institute of Building Information Modeling, Faculty of Architecture and Civil Engineering, Wuppertal, Germany, sebastian.theissen@uni-wuppertal.de.

[b] Madaster Germany GmbH, Berlin, Germany.

[c] Institute of Building Services Engineering, Faculty of Process Engineering, Energy and Mechanical Systems, TH Köln (University of Applied Sciences), Cologne, Germany.

Abstract. In Life Cycle Assessments (LCA) of buildings and circularity assessment, Heating Ventilation and Air-Conditioning (HVAC) systems are almost completely ignored due to the lack of regulation requirements, simplified consideration in green building certification and high complexity. Therefore, there is a lack of relevant information that enables a comprehensive whole building LCA and a circularity assessment of materials in HVAC. Using a digital Material Passport (MP) for buildings enables combining whole building LCA with qualitative and quantitative assessments of circularity. The open Building Information Modeling (BIM) method and the open data exchange format Industry Foundation Classes (IFC) offer a high potential for the efficient creation and management of a MP, as data can be integrated, linked and exchanged in 3D models with a high degree of semantics. This work analyses the life cycle assessment and circularity of two design variants of Ventilation and Air-Conditioning (VAC) systems of an office building within an open BIM-based process. Thereby, the embodied carbon of the VAC design variants was analyzed within an open BIM-based LCA. As a second step, the VAC models were assessed regarding their circularity using the Madaster Circularity Indicator (MCI) and detachability index within the Madaster platform as a case study. The results show that the impact of VAC materials is very important to consider within a whole building LCA, as VAC cause high material-related embodied impacts. In addition, the circularity assessment, using MCI and Detachability index, shows that the reduction of material mass does not influence the assessment. Instead, Design for Disassembly (DfD) turns out as a very important factor, which can also provide information for a more realistic assignment of end-of-life scenarios, effecting LCA results interpretation in the future. However, therefore various competencies in planning, data modelling and sustainability assessment need to be more connected. The open BIM approach already offers the tools to make this more efficient and automated. The research shows advantages and obstacles of open BIM based LCA and circularity assessment of HVAC and provides insights for further research regarding a more holistic assessment of buildings.

Keywords. LCA, Circularity Assessment, MCI, detachability, technical building services, HVAC, open BIM, IFC, material passports.
DOI: https://doi.org/10.34641/clima.2022.184

1. Introduction

The decision of the Paris Climate Agreement of 2015 and the climate goals agreed in December 2019 have intensified the requirements for the reduction of greenhouse gases (GHG) emissions at both European and national levels. The European Green Deal sees a sustainable transformation in the most GHG-intensive sectors in terms of climate protection, resource conservation and digitalization as important solutions. The construction and building sector plays a key role in this context, as it is the world's largest consumer of materials and the largest emitter of GHG emissions, and also generates the largest share of global waste production [1]. The EU Taxonomy Regulation, as a part of the European Green Deal, is a classification system for sustainable financial products. In this context, pressure is also exerted on real estate industry players through the fulfillment of sustainability requirements as well as their transparent

Copyright ©2022 by the authors. This conference paper is published under a CC-BY-4.0 license.

disclosure. For example, Life Cycle Assessment (LCA) of buildings is required. As a standardized method LCA is used. This method has already become established in certification systems for sustainable buildings. Thereby, a whole building LCA is used to evaluate environmental impacts and resource consumption over the entire life cycle of the building. However, technical building services (TBS), meaning Heating Ventilation and Air-Conditioning (HVAC) electrical and plumbing systems, is usually only included in a simplified way and therefore usually insufficiently evaluated. TBS is not only an underestimated part within whole building LCAs. It is also usually not considered in circularity assessments [2], although TBS contains strategically and economically valuable raw materials, such as copper, aluminum, steel and rare earths [3]. Since LCA is only partially suitable for assessing circularity, further evaluation methods are needed. For example, installation situation and the accessibility as well as the connection to other building elements are not covered or considered using whole building LCAs. However, these are crucial for the Design for Disassembly (DfD) and the assignment of a correct possible End-of-Life scenarios within whole building LCAs [4]. Methods, such as the Madaster Circularity Indicator (MCI) or the Urban Mining Index (UMI), represent initial approaches in this regard. However, these circularity assessment methods focus on structural elements and do not consider TBS so far.

At this point, the method of open Building Information Modeling (BIM) offers a high potential for the detailed consideration of TBS in whole building LCAs and the assessment of circularity. It also reduces the manual effort of the necessary data collection and calculation processes compared to day-today planning. Through the lifecycle, open and transparent exchange of data within the open BIM approach, data of architecture, structural engineering, TBS as well as LCA and circularity can be linked. In addition, it can be evaluated as well as communicated and documented. In this way, the open BIM-based calculation of LCA and circularity creates many added values for sustainable design, construction, operation, renovation and deconstruction. However, only two works in the field of open BIM-based LCA including TBS are known [5,6]. Work on open BIM-based assessments of circularity of TBS is not known. In this paper, an open BIM-based LCA and circularity assessment of two design variants of a Ventilation and Air-Conditioning (VAC) system of an office building is presented. The aim is to investigate the importance of VAC for whole building LCAs and circularity assessments. In addition, the challenges and potentials that arise during the modeling and data exchange within an open BIM process were identified.

LCA in the building and construction industry is standardized in EN 15978 and EN 15804. While EN 15978 defines for example the general scope and system boundaries, EN 15804 standardizes which types of environmental impacts must be considered in which phases of a life cycle. A total of 38 different environmental indicators are currently defined, such as the Global Warming Potential (GWP), which need to be indicated in the life cycle phases: Product phase (A1-A3), Construction phase (A4-5), Use phase (B1-7) and End-of-Life (C1-4) phase. The phases are supplemented with a module D, which indicate benefits resulting from reuse, recovery or recycling outside of the life cycle and system boundaries. Currently, whole building LCA finds its main application in the assessment of environmental quality within green building certification systems, such as the one of the German Sustainable Building Council, called DGNB. These systems define currently the only (voluntary) requirements that offer the possibility of taking HVAC into account.

DGNB provides a simplified or complete calculation approach, based on the standards of EN 15978 and 15804. In practice, however, HVAC is currently only represented using the simplified approach [7]. The main reasons for this in early project phases are that the design progress of HVAC for whole building LCA is too poorly developed. In late project phases, incomplete LCA data of HVAC make a detailed LCA more difficult. Also, the additional manual effort required for a detailed assessment of the various HVAC system components based on 2D planning documents is very high. Therefore, the simplified procedure is preferred in certification systems like DGNB. In more detail, it is only necessary to include the generator systems, e.g., the air handling units of a VAC system, in whole building LCA. The remaining system infrastructure and components are therefore only included as an additional share of 20%, meaning a factor of 1.2 is multiplied with LCA results. This means that the environmental impacts and resource consumption of, e.g., piping, air ducts and outlets, are not considered in detail. Instead, their embodied impacts are represented by the factor of 1.2 depending on the LCA results of the building structure.

However, studies show that TBS, including HVAC, can cause significantly higher environmental impacts [8]. For example, GHG emissions of HVAC are higher than 20% or 30%. Depending on the building type and energy standard, GHG emissions can cause up to 80% in special cases [9]. However, a detailed assessment of the environmental impacts and resource consumption of HVAC using only LCA is not sufficient to show the true environmental impacts. Also, it can lead to incorrect statements when optimizations are made. For example, if piping for an underfloor heating system is selected only on the basis of embodied carbon, plastic pipes (PEX) account for about the half of the embodied carbon as copper pipes. This is shown by a functionally equivalent comparison based on ÖKOBAUDAT datasets [10]. However, it is unlikely that plastic pipes are (up-)cycled at the end of their service life. Instead, often only incineration takes place. As an opposite, copper is very likely to be materially recycled. In addition, composite pipes made of PEX will incur high disposal costs at the end of their service life, while copper promises an increasing raw material value in the future. Therefore, a combined assessment of environmental impacts as well as circularity is very important in the

environmental selection of building construction and HVAC materials and products in order to provide a more holistic decision support.

There is currently no standard for the assessment of circularity that unifies the currently different methods that assess circularity for the building and construction sector. However, one of the first and so far best known methods was developed by Madaster [11]. It is a validated scientific method, called the Madaster Circularity Indicator (MCI). This method is based on the Material Circularity Indicator developed by the Ellen MacArthur Foundation [12]. The MCI measures the quality of circularity, score from 0-100%, in three different phases:
(1) Construction phase: What is the ratio between the volume of “virgin” materials and the volume of “recycled, reused or renewable” materials?
(2) Use-phase: What is the expected functional lifecycle of the products used, as opposed to the average functional lifecycle of similar products?
(3) End-of-life: What is the ratio between the volume of "waste", and the volume of "reusable and/or recyclable" materials and products derived from a building when it is refurbished or demolished?
To calculate the MCI-score, the measurement method uses the weighted average. The weighted average is based on the mass of the materials and products used. In addition, in calculating the MCI-score, the result is multiplied with a correction factor. This factor is based on the comprehensiveness of the model in terms of the percentage of the mass for which the materials are known.

At a higher level, such as the building product, component or building level, additional attention must be given to DfD and deconstruction in terms of circular construction methods. This means that information on the installation situation, accessibility or detachability with other materials must also be available. In this respect, the detachability index, also 0-100%, has recently been added to the MCI method to better evaluate the DfD and deconstructability [13]. The index is based on the revised version of the report "Circular Buildings - a measurement method for detachability 2.0". The following criteria are taken into account [14]:
(1) Connection type: dry connections are preferred over connections with added elements and direct, integral connections take precedence over soft and hard chemical ones.
(2) Accessibility of the connection: how easily one can (physically) reach the connecting elements and to what extent this causes damage to nearby objects.
(3) Intersections: indicates the extent to which products overlap or are integrated with each other. The higher the integration, the more actions required to disassemble an element at the end of its life.
(4) Product edges inclusion: assessment of how products are placed in a composition and whether it is open or closed. A 'locked up' product can only be dismantled in the reverse order of construction.

The Madaster platform is also the only known solution to date that enables open BIM-based assessments of the circularity of entire buildings and individual building products [15].

The BIM method integrates different actors and software systems. This requires an exchange of data between the individual software systems. Open BIM describes the exchange of data between different programs using open data formats. This is intended to ensure that no manufacturer-specific application restrictions prevail in the projects. The basic data model in the open BIM method is the non-proprietary data exchange format IFC, which is standardized in ISO 16739. IFC is an object model and represents more than 700 classes. The classes are technically defined and are formally mapped via object-related relations to other classes, in addition to the inheritance relations. These definitions are generally concretized in the IFC data model by so-called entities, functions, rules, attributes as well as relations. In addition, there are the functions of quantity sets and property sets (Psets), which can be used to define dynamically expandable property sets in a modular way.

So far, only a few options are available in the current IFC4 standard via IfcClasses and Psets that represent information of LCA or circularity assessment in a standardized way. For example, in the field of LCA, service life can be covered by the previous structure of Pset_EnvironmentalImpactIndicator and Pset_EnvironmentalImpactValues. In general, however, these are outdated and not EN 15804 compliant [16]. In the field of circularity, the fastener type can be described and exchanged in a standardized way via IfcFastener as a relevant criterion of circularity. Nevertheless, there is a lack of possibilities to describe the accessibility and installation situation. Furthermore, it is not possible to exchange information on the disassembly effort, the reuse potential, or the disposal path of a material in a standardized way via the IFC model. The information must therefore be created and exchanged as user-defined Psets. For example, a "Pset Madaster" can be used to enrich various information and transfer them using IFC. Thereby, third-party software, in this case the Madaster platform, can read and process the information. Currently, the Madaster platform can read the following important properties from the IFC file via the Pset_Madaster and process them for circularity assessments:

- GUID, Volume, Area, Length, Width, Height, Type, Building phase, Classification, MaterialOrProductName, GTIN, Product code, Building Number, Flooring, IFC-type
- DetachabilityConnectionType, DetachabilityConnectionTypeDetail
- DetachabilityAccessibility
- DetachabilityIntersection
- DetachabilityProductEdge

2. Method

In pursuing the objectives of this paper, a BIM-based LCA was performed, followed by the circularity assessment. Due to the limited scope of this paper, only a part of the HVAC was considered. Since VAC accounts for the largest mass and embodied carbon share with over 55% of the total HVAC in office buildings [8], we focused on VAC only. The approach starts in the first step with the design and creation of a VAC BIM model based on a reference office building. Based on this, a second VAC variant was created in which optimizations were made with regard to the volume flow rate due to a reduced occupancy rate. When dimensioning the VAC models, all necessary calculations and designs were carried out according to German standards and legal requirements. Subsequently, the LCA for the two variants was performed using an open BIM-based LCA software program. Both BIM models were then uploaded to the Madaster platform via IFC upload to evaluate the variants from a circularity perspective. Finally, the results of the circularity assessment were compared with the LCA results and discussed.

2.1 Implementation Case Study MH Software/DESITE BIM/Madaster

The planning and dimensioning of the VAC models in terms of air volumes, sound protection, central unit dimensioning was performed with Microsoft Excel and manufacturer-specific dimensioning software. The subsequent modeling of the ventilation and air conditioning system was done with the software solution MH-Software in version 6.0 BIM. DESITE BIM from thinkproject GmbH was used as an information management program to enrich the VAC models with additional information. Unlike MH software, this tool cannot be used for geometric modeling. Instead, semantic information can be enriched, modified and individually evaluated by DESITE BIM allowing holistic access to all data and information in the model. For example, models imported in IFC format can be checked, analyzed and extended in many ways on the basis of self-programmed analysis rules. Based on the results of the research project "Life Cycle Assessment and BIM in sustainable construction" [16], Höper [17] developed a EN 15978 compliant BIM & LCA tool within DESITE BIM, which can also conduct a whole building LCA including TBS. In addition, it is possible to combine different sub models, e.g.. architecture and TBS, into one coordination (linked) model. Furthermore, external databases such as ÖKOBAUDAT can be integrated. In addition to the dynamic calculation of the LCA of the VAC models, DESITE BIM was also used for the data enrichment of the Pset_Madaster. Madaster is a central platform where the identity, quality and location of materials and components in buildings can be registered. It has an Excel as well as IFC import interface. The goal of the platform is to store information about materials and components over the lifecycle of a building, even with changing owners, and make it available during renovation and deconstruction. The platform can combine multiple IFC models. Uploaded BIM models can be subsequently edited and linked to other databases to perform circularity assessments.

2.2 Data for LCA and circularity assessment

The data basis for whole building LCA is ÖKOBAUDAT (version 2021-I) and IBU.data as well as additionally developed TBS LCA data extensions. For example, the service lives of standard VDI 2067 for TBS were added. The Madaster database has been individually adapted to the country-specific situation of the circular economy for each country in which the platform is available. In Germany, the data comes mainly from databases provided by Madaster, producers or public databases (e.g. ÖKOBAUDAT). One Madaster database provides data that consists of primary raw materials and no recycling is assumed. The second Database is a "C2C database" within Madaster that contains ideal scenarios for the same building products. These ideal scenarios are based on the technically best possible reuse and recycling processes today. They are based on the WECOBIS database provided by the federal government.

2.3 Modeling of a reference and optimized VAC model

For the planning and modeling of the VAC model, a reference building based on standard VDI 6009 was used.

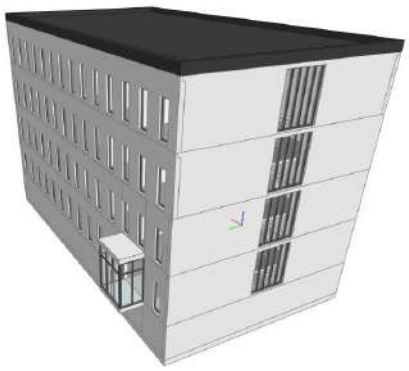

Fig. 1 – BIM model of reference building according to standard VDI 6009.

The office building has five full floors, which are divided into a basement and four above-ground floors. The area according to standard DIN 277 is 2259.36 m^2. The location of the building is assumed to be in Cologne, Germany. This BIM model formed the basis for the design and modeling of the VAC system. Furthermore, an optimized variant for the VAC model was planned and modeled on this basis. Preliminary investigations revealed that a reduction in air volumes can have a positive effect on the total mass and thus the embodied carbon of the VAC. Therefore, for all office and meeting rooms, the approaches of the number of persons related to the floor area were adjusted and the total volume flow for the building was calculated. Based on the adjustment of the person occupancy density, the required outdoor air volume

flow could be reduced from 12,370 m^3/h to 9,130 m^3/h. This corresponds to a reduction of 26%. Taking the recalculated outdoor air volume flow as a basis, the entire distribution network as well as all necessary components were redesigned and constructed as an optimized VAC model.

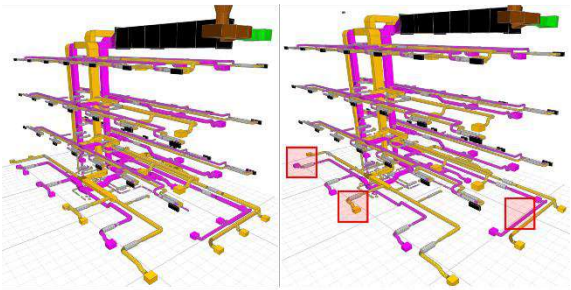

Fig. 2 – Comparison of the reference and optimized VAC model, including exemplary marking of the changes on the first floor.

2.4 Conduct of LCA using specific open BIM-based LCA tool

The basis for the LCA of the two VAC models is described by the following:

Tab. 1 – Summary of LCA framework conditions

Life span	50 Jahre
Data basis	ÖKOBAUDAT 2021-I, IBU.data and VDI 2067
Calculation method	EN 15978 und DGNB ENV1.1 (version 2018, 8. edition), without module B6. complete calculation approach for VAC system
Life cycle impact assessment	CML; Global Warming Potential

The ÖKOBAUDAT provides the parameters for the environmental impacts per unit and specified smallest nominal size. Using the weight information from the LCA data, the conversion to the defined functional unit was performed. This is the reason why the number of units of the components is partly listed as rounded values in the following.

Tab. 2 – Summary of Life Cycle Inventory

Part of VAC system	Material and type	Amount FE	Service life
Duct segment	Angular, steel	428.25 [m^2]	30 a
Duct fitting	Angular, steel	166.10 [m^2]	30 a
Duct segment	Spiral duct round, steel	425.65 [m^2]	30 a
Duct fitting		83.56 [m^2]	30 a
Insulation	Mineral wool, aluminium-covered	42.97 [m^3]	30 a
Fire damper	Angular, stainless steel,	19.96 Pcs.	20 a
Fire damper	Round, steel, plastics	10.37 Pcs.	20 a
Volume flow controller	Constant, round, plastics, steel	17.13 Pcs.	20 a
Volume flow controller	Variable, angular plastics, steel	2.00 Pcs.	20 a
Volume flow controller	Variable round, plastics, steel	102.35 Pcs.	20 a
Silencer	Angular steel plastics,	2.00 Pcs.	20 a
Silencer	Round, steel plastics,	132.50 Pcs.	20 a
Air handling unit	Steel, plastics, aluminium	1.237 Pcs.	20 a
Air outlet	Slot diffuser plastics, steel	42.00 Pcs.	20 a
Air outlet	Poppet valve plastics, steel	38.35 Pcs.	20 a
Air outlet	Swirl outlet, plastics, steel	71.78 Pcs.	20 a
Air outlet	Deflector hood	1.00 Pcs.	20 a
Air outlet	Grid, steel	1.00 Pcs.	20 a

The LCA was conducted using the open BIM&LCA tool by Höper. A full description how this tool works can be found be found in [5].

2.5 Conduct of a circularity assessment using Madaster

Both models, with the identical information of table 2, form the basis for the evaluation of circularity using the Madaster platform. Beforehand, the VAC models were additionally enriched with properties described in 2.4 and assigned to Pset_Madaster.

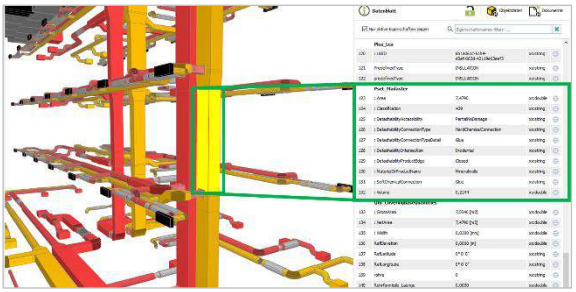

Fig. 3 – Enrichment of Pset_Madaster

Subsequently, an IFC export was performed, which was uploaded to Madaster.

Fig. 4 – Conduct of a circularity assessment using the Madaster platform

Based on the previously fulfilled modeling requirements, Madaster automatically assigns the VAC model to the materials of the Madaster database as far as possible.

3. Results

3.1 LCA results

Figure 4 shows the GWP of the VAC system in kg CO_2-equivalent/m^2/a. The components shown in Table 2 were grouped into five categories: air ducts total without insulation, insulation total, components, air handling unit, air outlets. The sixth column shows the total GWP of the VAC system. Each column is subdivided into the different life cycle modules according to EN 15804 and focused on the relevant life cycle modules according to DGNB: A1-A3, B4, C3, C4 as well as D. Overall, a saving of 19% was achieved for the optimized variant compared to the reference. With regard to the individual components of the VAC system, it is clear that the air ducts have the largest share in the reference and the optimized variant. The reason for this is the generally large total area of the air ducts and the resulting total weight. Therefore, significant GWP savings could be achieved, especially in reducing the mass of the air ducts. Furthermore, there was a shift from the square designed fire dampers to the round design. The reason for this is the reduction of the volume flow at the shaft outlet, which made it possible to dimension the fire dampers smaller resulting in material and thus GWP savings. The same applies to the volume flow controllers. Since the outdoor air volume flow of the meeting rooms and open-plan offices was generally reduced due to the occupant density, the diffusers could be reduced in number or size. With focus on the differentiation of life cycle modules, it was shown that B4, i.e., the GWP due to replacement, had the highest impact in each group. This can be explained by the relatively short replacement cycles of the VAC components compared to a life span of 50 years according to DGNB.

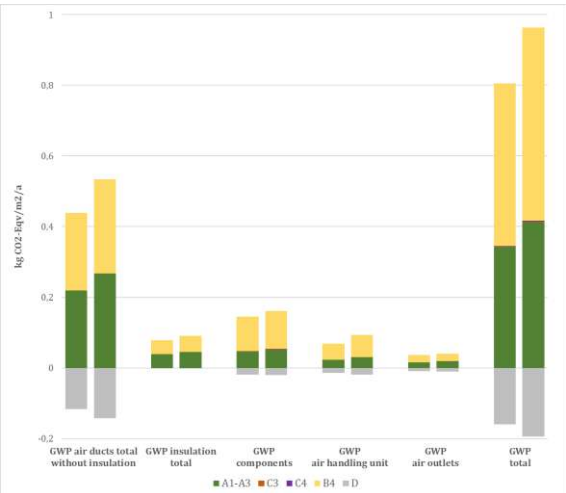

Fig. 5 – Comparison of the GWP of the optimized and the reference VAC model

3.2 Circularity assessment results

As there is currently no possibility to directly compare variants in Madaster, the results of the two VAC variants were compared in a separate overview. For this purpose, the MCI and the circularity in the construction, use and end-of-life phase were compared. Furthermore, the detachability index was presented. All values are between 0 and 100%, with 100% representing the target value. The evaluation of the MCI and its three indicators shows no changes for the reference as well as for the optimized variant. This can be explained by the fact that no other materials with different circularity properties were used. Only the quantities and masses changed. Therefore, the detachability index did not change either.
The reduction of material masses, e.g., galvanized steel, can be observed via a detailed overview of the materials used in Madaster. Thus, there is only an influence on LCA and raw material values.

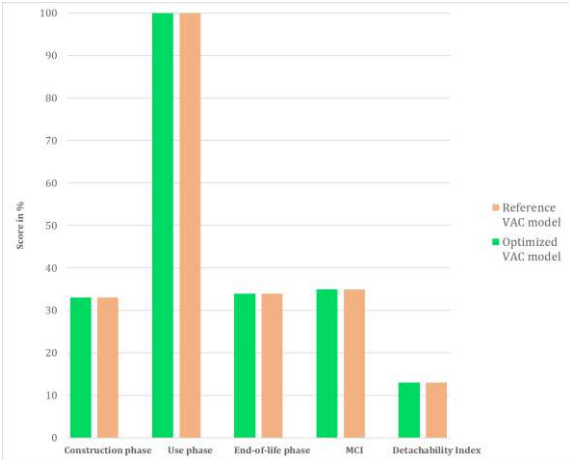

Fig. 6 – Comparison of MCI, consisting of construction, use and end-of-life phase, as well as Detachability Index of the optimized and the reference VAC model

4. Discussion

The discussion focuses on four main points: (1) Importance of VAC for whole building LCA. (2) Suitability of MCI and Detachability Index to assess circularity of VAC (3) Effects of circularity assessment on LCA. (4) Challenges and further potentials.

4.1 Importance of VAC for whole building LCA

As other studies on whole buildings LCAs have already shown, the simplified approach representing TBS with an additional factor of 20% is not sufficient to consider the TBS adequately in a whole building LCA. This paper confirms this finding when the following reference is made to the DGNB LCA benchmark for new construction of office buildings: Multiplying the benchmark of 9.4 CO_2-Eqv/m^2/a, which only includes embodied impacts of TBS generator plants, by the factor of 1.2 leads to a total value of 11.28 CO_2-Eqv/m^2/a. This corresponds to a premium of 1.88 kg CO_2-Eqv/m^2/a as an absolute value for all components of TBS. The LCA of the air ducts as well as the other components of the reference VAC system of this work show an absolute value of 0.87 CO_2-Eqv/m^2/a. In relation to the absolute value of 1.88 kg CO2-Eqv/m^2/a, of the DGNB LCA Benchmark, 46% would already be covered by the materials of the VAC system and the replacement cycles. Against the background of a 50 year DGNB life span of an office

building even higher environmental impacts are to be expected, while the building construction, especially in the support structure, generally does not require any costly material replacements. In addition, further material related embodied carbon from heating, sanitary, electrical and other TBS systems, which also have large distribution networks and short replacement cycles, can be expected to have significantly higher GWP impacts than the remaining 1.01 kg CO_2-Eqv/m^2/a. Thus, it become clear that TBS is underrepresented using just a factor of 1.2. The importance of TBS needs to be considered in whole building LCAs more. This can be achieved if, on the one hand, an increased factor is introduced within the framework of the simplified approach or, on the other hand, the effort for detailed consideration of TBS is further simplified.

4.2 Suitability of MCI and Detachability Index to assess circularity of VAC

The circularity assessment shows that the MCI as a single indicator is not sufficient to meaningfully evaluate circularity for TBS. While the C2C database within Madaster can be used to simulate material optimization through alternative materials and/or different material circularity properties for the VAC system, this is not sufficient without more information on how materials are connected or installed. Evaluations of service life show that if a TBS material has a longer service life than the reference service life of 15 years of TBS, 100% can already be achieved in the use phase. This standardization is to be regarded as critical, since TBS can have very different service life spans, e.g., ranging from one year of fine filters up to 40 years of pipelines in accordance with VDI 2067. In addition, problems arise if the installation situation is not considered. In the example of the air duct, a 100% evaluation within the use phase can be considered with a standard service life of 20 years. However, since the ducts run above an attached plasterboard ceiling, destruction must be planned for maintenance or replacement in order to achieve accessibility to the ducts.

The Detachbaility index therefore provides a starting point to include the DfD, too. However, it is necessary to enrich the data using the Pset_Madaster and a BIM coordination model as well as simultaneous expertise in the planning and execution of the VAC system. However, when assigning these properties, it is not possible to specify the project-specific installation or connection to another element/component. This means that it can be defined for mineral wool insulation that an adhesive connection is present, but it is not possible to further define to which component, e.g. ventilation duct, the mineral wool is glued. So, the (quantitative) assessment of the DfD of HVAC systems provide research potential. In addition, this qualitative assessment of defining properties of detachability and accessibility within the Pset_Madaster results in subjective influence, e.g., in the assessment of accessibility and the extent to which damage can occur in preceding structures. The detachability index is therefore dependent on the subjective evaluation of the planner. Quantitative evaluations will be important in the future and represent also a need for further research, e.g., to what extent installation situations can be (automatically) analyzed from coordination models. This combination of necessary competencies for this also shows how new tasks and new job profiles for sustainable design and construction will arise in the future, in which BIM, HVAC design and sustainability assessment must be considered holistically.

4.3 Effects of circularity assessment on LCA

While Madaster has so far been used primarily as a documentation tool after the completion of a building, the use of the tool in early phases has proven useful in the course of conducting the assessments in this work. In particular, conclusions for a better DfD understanding, e.g., in the suspended ceiling, could be identified during the evaluation of the installation situation and accessibility. Thus, the circularity assessment in the open BIM process can be used as an optimization tool already for earlier planning phases by ideally influencing how VAC is accessible as well as connected and installed already before execution. This can provide important decision-making support, e.g., when choosing a fully revisable metal ceiling instead of plasterboard. Another point of interest is that the assessment of DfD can help to identify the end-of-life scenario for LCA in module D. By having the information whether materials are readily separable from each other, it is possible to assess to what extent direct reuse, recycling, incineration, or landfilling are possible. However, therefore it is useful to know the specific installation situation and connection to other elements/materials. If this is possible in the future, this could mean that findings from the circularity assessment must ideally be available at the same time or prior to LCA in order to select realistic scenarios in Module D for the LCA. This is particularly relevant for the DGNB LCA, since the benefits from Module D are included here. However, there are currently only a few LCA datasets where several scenarios are already available, as required by EN 15804:2020.

4.4 Challenges and further potentials

The enrichment and analysis of information in a BIM coordination model is essential in order to implement LCA and circularity assessment of HVAC in the open BIM process. Only by using the BIM coordination model could the installation situation and accessibility for the VAC system be evaluated in a meaningful way. This in turn requires the use of open BIM and the data exchange of non-proprietary data formats. In doing so, the different software applications, e.g., BIM authoring tool for architecture and TBS, are able to exchange and read BIM models created by different BIM software. Furthermore, the issue of data quality and quantity is an important point. For example, there is no data set for air handling units in Madaster. This had to be created individually. This in turn was problematic because hardly any manufacturer data on material types and their proportions is

publicly available. The quantity of LCA data in ÖKOBAUDAT is also still very low. In the area of quality, image files for conversion of channel sizes and their GWP share complicate machine readability and integration into BIM-based LCA tools. During modeling, not all components of the VAC are usually modeled. Threaded rods and the suspension of air ducts are often not part of the modeling. Accordingly, information on material quantities/masses is also missing here. In addition, there is also a difference between installation and execution planning in the area of modeling. While the suspension structure of air ducts has to be modeled for execution in installation planning, there are usually no more adjustments in the BIM model after execution. This means that the as-built situation is no longer documented. Accordingly, there is no 100% correct digital twin. Reasons for this are often additional and costly efforts. To ensure urban mining in the future, however, it is essential to provide as-built quality with the completion of the building, to make a complete and meaningful basis about material passes for the further life cycle phases of the building available.

5. Conclusion / Outlook

This work has shown that TBS is an important part in the environmental assessment of buildings, which must be considered much more in the future. Open BIM solutions already offer the technical possibilities for this today. Madaster proved to be the only solution that already allows an open BIM-based assessment of circularity of TBS, even if it still needs optimization in many points. From this first investigation, many important insights could be found. For example, how advantages in the combined evaluation of LCA and circularity assessment can be used for a more holistic environmental design support. In this context, also the individual design phases merge into each other, as planning and execution know-how grow together more and more.

Open BIM-based material passports and software make it possible to handle the large amounts of data and to analyze them more easily. However, this also requires connecting different competencies in the planning process, which creates new tasks and processes for planning teams and generates much further need for research.

6. References

[1] Global Alliance for Buildings and Construction, 2020 Global Status Report for Buildings and Construction: Towards a zero-emissions, efficient and resilient buildings and construction sector. 2020.

[2] Cheshire D., Russett S., et al., Resource efficiency of building services: TM56: 2014; Chartered Institution of Building Services Engineers. 2014, Vol. 56.

[3] Köhn A., Urban Mining: Entwicklung einer Methodik zur Ermittlung zukünftiger Rohstoffströme aus Gebäudetechnik. 2018.

[4] Rosen A., Urban Mining Index: Entwicklung einer Systematik zur quantitativen Bewertung der Kreislaufkonsistenz von Baukonstruktionen in der Neubauplanung; Fraunhofer IRB Verlag. 2021.

[5] Theißen S., Höper J., et al., "Using Open BIM and IFC to Enable a Comprehensive Consideration of Building Services within a Whole-Building LCA," Sustainability. 2020, Vol. 12, 5644.

[6] Figl H., Ilg M., Battisti K., "6D BIM–Terminal: Missing Link for the design of CO 2 -neutral buildings," IOP Conf. Ser.: Earth Environ. Sci. 2019, Vol. 323.

[7] Deutsche Gesellschaft für Nachhaltiges Bauen – DGNB, Benchmarks für die Treibhausgasemissionen der Gebäudekonstruktion: Ergebnisse einer Studie mit 50 Gebäuden. 2021.

[8] Lambertz M., Theißen S., et al., "Importance of building services in ecological building assessments,". 2019, Vol. 111, 3061.

[9] Royal Institution of Chartered Surveyors, Whole Life Carbon Assessment for the Built Environment, 1st edition. 2017.

[10] Bundesministerium des Innern, für Bau und Heimat, ÖKOBAUDAT: Informationsportal Nachhaltiges Bauen, http://www.oekobaudat.de/, accessed 22-10-2021.

[11] Rau T., Oberhuber S., Material matters: Wie wir es schaffen, die Ressourcenverschwendung zu beenden, die Wirtschaft zu motivieren, bessere Produkte zu erzeugen und wie Unternehmen, Verbraucher und die Umwelt davon profitieren; Econ. 2019.

[12] Madaster Services B.V., Madaster Circularity Indicator explained: v1.0. 2021.

[13] Madaster, Madaster Release Notes 2021: Version 10.0. 2021.

[14] Dutch Green Building Council, Circular Buildings - a measurement method for detachability 2.0. 2021.

[15] European Commission, Building logbook state of play: report 2 of the study on the development of a European Union framework for buildings' digital logbook; Publications Office.

[16] Lambertz M., Wimmer R., et al., Life Cycle Assessment and BIM in sustainable construction: Final report. 2020.

[17] Höper J., Development of a method for the automation of whole building Life Cycle Assessment using the Building Information Modeling method. 2020.

The datasets generated during and/or analyzed during the current study are not available because they are part of ongoing PhD thesis, but the authors will make every reasonable effort to publish them in near future.

The circularity of renovation solutions for residential buildings

Kalle Kuusk[a], Michiel Ritzen[b], Patrick Daly[c], Dimitra Papadaki[d], Cecilia Mazzoli[e], Guzide Aslankaya[f], Jure Vetršek[g], Targo Kalamees[a]

[a]Tallinn University of Technology, Tallinn, Estonia

[b]VITO NV, Mol, Belgium

[c]Technological University Dublin, Dublin, Ireland

[d]National and Kapodistrian University of Athens, Athens, Greece

[e]Alma Mater Studiorum - Università di Bologna, Bologna, Italy

[f]PichArchitects, Barcelona, Spain

[g]Institute for Innovation and Development of University of Ljubljana, Ljubljana, Slovenia

Abstract. Construction and demolition waste accounts for approximately a third of all waste generated in the EU. Adopting circularity principles to the construction processes aims to reduce waste generation. The focus of the study was on circular renovation solutions as renovation is becoming increasingly important. The renovation wave for Europe sets a target to double annual energy renovation rates in the next ten years. This study analyses circularity of the renovation concepts for the pilot renovation cases in seven countries in different climate zones in Europe. Analyses were carried out within the DRIVE 0 project funded by the European Union's Horizon 2020 research and innovation program. Pilot buildings are detached houses and apartment buildings with different renovation interventions. Design for Disassembly criteria and embodied energy and embodied CO_2 analyses combine design and material use aspects. Results show that in terms of design for disassembly indicators, prefabricated modular solutions have much higher circularity potential than the traditional wall insulation systems due to the low disassembly and reusability potential of external thermal insulation composite systems (ETICS. The environmental impact of the prefabricated insulation solutions is lower than and ETICS solutions. Although the difference between prefabricated and ETICS solutions in terms of environmental impact is smaller than in terms of disassembly and recovery options.

Keywords. Circular renovation, design for disassembly, embodied energy, embodied carbon.
DOI: https://doi.org/10.34641/clima.2022.333

1. Introduction

Adopting circularity principles to the renovation processes helps reduce waste generation in the construction industry. Construction waste generated during renovation works is an important issue because the renovation wave for Europe sets a target to double annual renovation rates in the next ten years.

Previous research has shown that the construction sector is resistant to circularity and the need to develop disassemblable building products is necessary (1). The sustainability of deep renovation solutions is often not assessed during the design phase. Current deep renovation solutions are mainly based on operational energy use and do not consider the carbon footprint aspects.

Practices for circularity in the construction industry aim at reducing the amount of waste generated at the end of the life cycle of a building (2). An essential aspect of increasing the reuse possibilities of building materials and products is modularity. Previous research and development projects have demonstrated prefabricated modules for building renovation (3). The next step would be to link prefabrication and modularity with circularity.

This study analyses circularity of the modular and non-modular external wall insulation solutions for pilot renovation cases in Europe. The pilot renovation cases were selected as part of an EU-funded project DRIVE 0 (4), developing circular deep renovation solutions. The goal for DRIVE 0 is to provide solutions to speed up the deep and circular renovation process.

Copyright ©2022 by the authors. This conference paper is published under a CC-BY-4.0 license.

2. Methods

There is currently no single methodology for circularity assessment and many different indicators exist for evaluating the circularity of construction products and buildings. Some indicators are based on one characteristic (durability, the recycled share of materials, etc), and some indicators include wider impacts (economic, environmental, etc). In the current study, circularity assessment includes design for disassembly criteria and environmental impact. The purpose of the method selection was to have an approach with few input data which would be useful also for practitioners.

2.1 Circularity assessment

Methodology for circularity assessment is based on the design for material recovery principles (5). The indicator used to assess the degree of circularity of the renovation solutions is the simplified version of the DfD criteria proposed by AlbaConcept (6). Circularity is assessed based on four variables with relative weights depending on specific components and joint features.

Circularity assessment criteria:
1. type of connections,
2. accessibility of connections,
3. crossings,
4. form containment.

Tab. 1 - Type of connection.

Dry connection	Dry connection	1.0
	Click connection	
	Velcro connection	
	Magnetic connection	
Connection with added elements	Ferry connection	0.8
	Corner connections	
	Screw connection	
	Bolt and nut connection	
Direct integral connection	Pin connections	0.6
	Nail connection	
Soft chemical compound	Kit connection	0.2
	Foam connection	
Hard chemical connection	Glue connection	0.1
	Pitch connection	
	Weld connection	
	Cement bond	
	Chemical anchors	
	Hard chemical connection	

Tab. 2 - Accessibility of connection.

Freely accessible	1.0
Accessibility with additional actions that do not cause damage	0.8
Accessibility with additional actions with reparable damage	0.4
Not accessible - irreparable damage to objects	0.1

Tab. 3 - Crossings.

Modular zoning of objects	1.0
Crossings between one or more objects	0.4
Full integration of objects	0.1

Tab. 4 - Form containment.

Open, no inclusion	1.0
Overlaps on one side	0.8
Closed on one side	0.2
Closed on several sides	0.1

On a product level, material selection is also added as a criterion to assess the circularity of materials used for renovation:
1. Repaired: restoring to good working order, fix, or improving the damaged condition.
2. Reused: using an item for its original purpose or to fulfill a different function.
3. Recycled: converting waste material into reusable material by breaking down items to make new materials.
4. Refurbished: restore to original order & appearance with new materials.
5. Remanufactured: using a combination of reused, repaired, and new parts.

Tab. 5 - Materials and products.

Locally repaired, reused building components and materials	1.0
Biobased materials	0.8
Recycled and upcycled building components and materials	0.6
Refurbished, remanufactured materials	0.4
Non-biobased virgin materials or products made from non-biobased pure materials	0.1

The circularity index is calculated based on the average of the five subcategories. To achieve a high degree of circularity, the average index of the subcategories must be above 0.80.

Assessing degree of circularity:
1. index < 0.60 Low degree
2. index ≥ 0.60 Medium degree
3. index ≥ 0.80 High degree

2.2 Environmental impact assessment

Methodology for environmental evaluations is based on embodied energy and embodied carbon of the buildings (7).

Embodied energy and CO_2 for each component are assessed by filling the material spreadsheet. For each material, the quantity and the total amount are specified. The existing building envelope is excluded from the analysis, as existing constructions are often not changed during the renovation.

Tab. 6 – A material spreadsheet.

Mass of materials	kg; kg/m^2
Embodied Energy of materials	MJ; MJ/m^2
Embodied CO_2 of materials	kg; kg/m^2

The data results in an overview of material mass, embodied energy, and embodied CO_2. The ICE (8) database for the built environment was used for the materials embodied energy and embodied CO_2.

Tab. 7 – Embodied energy and CO_2 of materials.

Material	Embodied energy, MJ/kg	Embodied CO_2, kgCO_2/kg
Sawn timber	7,4	0,2
Stone wool	16,8	1,12
Glass wool	28	1,35
Cellulose wool	2,12	0
Fibre cement panels	15,3	1,28
Expanded Polystyrene	88,6	3,29
General plaster	1,8	0,13

2.3 Case studies

Seven demonstrators were selected to analyze different residential buildings in different climate zones in Europe. All buildings are residential buildings but have different functionalities: detached houses, semi-detached house, terraced house, and apartment buildings.

Table 8 shows the brief description for each case study building, and Figures 1-7 shows a photo of the building.

Tab. 8 - Case studies description.

Country	Floor area, m^2	Type
Netherlands	144	terraced house
Estonia	2415	apartment building
Greece	109	detached house
Ireland	80	semi-detached house
Italy	470	rural manor villa
Slovenia	232	detached house
Spain		apartment building

Fig. 1 - Dutch pilot.

Fig. 2 - Estonian pilot.

Fig. 3 - Greek pilot.

Fig. 4 - Irish pilot.

Fig. 5 - Italian pilot.

Fig. 6 - Slovenian pilot.

Fig. 7 - Spanish pilot.

2.4 Description of the renovation solutions

Dutch pilot: The assessment of circularity on the product level consist of wooden prefabricated elements of WEBO, indicated in Figure 8.

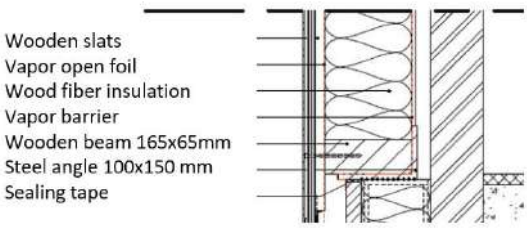

Fig. 8 – Cross-section of façade insulation element.

Estonian pilot: The circularity assessment on product level has been done for the prefabricated façade insulation element. The cross-section of the façade element is shown in Figure 9.

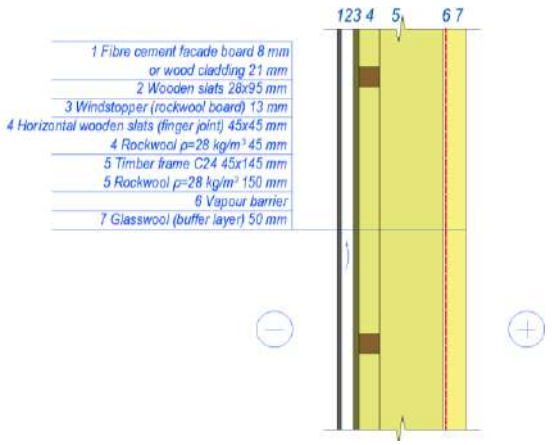

Fig. 9 – Cross-section of façade insulation element.

Greek pilot: The circularity assessment on product level has been done for external thermal insulation composite system (ETICS) based external wall insulation solution.

Irish pilot: The product-level circularity assessment has been done for the prefabricated 2D façade insulation element. The cross-section of the façade element is shown in Figure 10.

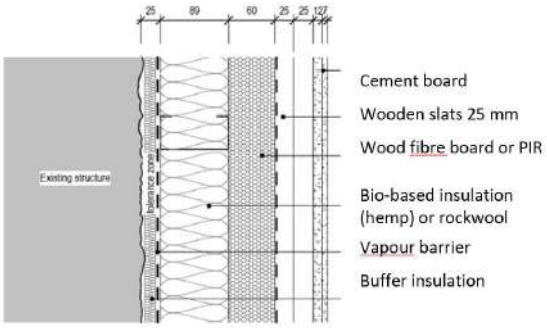

Fig. 10 – Cross-section of façade insulation element – Design Proposal (Coady Architects).

Italian pilot: The assessment of circularity on product level has been done both for the 2D plug&play prefab panels, composed of two layers of high and low-density rock wool (to be applied to the North and West oriented façades), and for the traditional ETICS system in rock wool (to be used to the South and East oriented façades). The final solution that will be implemented may differ from the one presented in the paper, depending on the company's technical requirements during the construction. The cross-section of the façade element is shown in Figure 11.

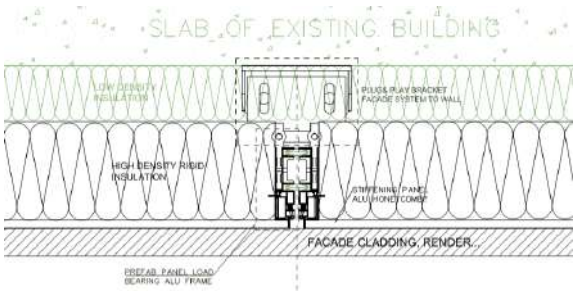

Fig. 11 – Cross-section of façade insulation element – Design Proposal (ALIVA).

Slovenian pilot: The circularity assessment on product level has been done for external thermal insulation composite system (ETICS) based external wall insulation solution.

Spanish pilot: The product-level circularity assessment has been done for the prefabricated green wall façade elements with building-integrated PV panels. The cross-section of the façade element is shown in Figure 12.

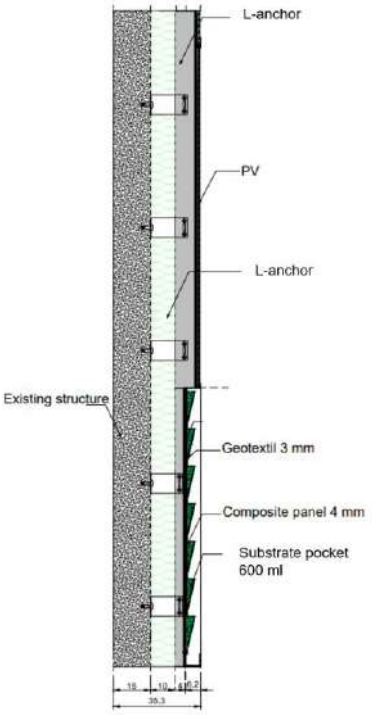

Fig. 12 – Cross-section of façade elements – Design Proposal (Pich Aguilera Arquitectos S.L.).

3. Results and discussion

3.1 Circularity

An example of the Design for Disassembly calculation for Estonian pilot renovation is shown in Table 9. On a product level, a medium degree of circularity has been achieved. Type and accessibility of connections, crossings, and form containment showed a high degree of circularity (>0.8) and material use showed a low degree of circularity (<0.6).

The structure of the insulation element is a timber frame made from finger-jointed structural timber. The circularity of the timber frame is high as timber is biobased material and the use of finger joints reduces production waste. Frame connections are made with screws which allow relatively easy disassembly. Insulation, wind barrier, and façade cladding materials are not biobased or reused. Façade insulation element with cellulose insulation would achieve a higher score but cellulose insulation cannot be used because of fire safety regulations. Estonian pilot building is a TP1 class building that requires at least fire resistance class A2 for insulation material. Cellulose wool has fire resistance class B1.

Results of the Design for Disassembly calculations for all pilot cases are summarized in Table 10. Category averages for external wall insulation solutions are shown for the type of connections, accessibility of connections, crossings, form containment, and materials. Calculations were performed for all layers, and averages of the whole prefabricated insulation elements are presented.

Prefabricated modular solutions have higher circularity potential than the traditional wall insulation systems system due to the low demountability and reusability potential of ETICS.

Although it may be debated whether the circularity benefits of biobased materials are adequately weighted as the material indicators are only 1/5th of the score, and the circularity assessment is mainly based on DfD, bio-based materials show better material circularity potential.

The indicators are also not weighed or proportioned with the material amount (volume or mass), and small elements (vapour barrier) can have a disproportional impact on the results.

Tab. 9 – Circularity of renovation solutions.

	Element	Type of Connection		Accessibility of connection		Crossings		Form containment		Materials	
1	Connection to existing wall	Corner and screw	0.8	No damage	0.8	Modular zoning	1.0	Overlaps on one side	0.8	-	
2	Buffer insulation (glass wool)	Screw and line	0.8	No damage	0.8	Modular zoning	1.0	Open, no inclusions	1.0	Recycled material	0.6
3	Timber framing	Screw	0.8	No damage	0.8	Modular zoning	1.0	Open, no inclusions	1.0	Biobased material	0.8
4	Insulation (stone wool)	Dry	1.0	No damage	0.8	Modular zoning	1.0	Open, no inclusions	1.0	Mainly virgin material	0.1
5	Wind barrier (stone wool)	Screw	0.8	No damage	0.8	Modular zoning	1.0	Open, no inclusions	1.0	Mainly virgin material	0.1
6	Wooden lath	Screw	0.8	No damage	0.8			Open, no inclusions	1.0	Biobased material	0.8
7	Facade cladding (fibre cement)	Screw and seal	0.8	Freely accessible	1.0	Modular zoning	1.0	Open, no inclusions	1.0	Mainly virgin material	0.1
Category average			**0.83**		**0.83**		**1.0**		**0.83**		**0.42**
Circularity indicator		**0.78**				**Medium degree of circularity**					

Tab. 10 – Circularity of renovation solutions.

	Type of Connection	Accessibility of connection	Crossings	Form containment	Materials	Circularity index	Degree of circularity
Dutch (2D prefab)	0.68	0.87	0.83			0.80	high
Estonian (2D prefab)	0.83	0.83	1.00	0.83	0.42	0.78	medium
Greek (ETICS)	0.50	0.10	1.00	0.10	0.10	0.36	low
Irish (2D prefab)	0.84	0.64	1.00	0.83	0.44	0.75	medium
Italian (2D prefab)	0.71	0.88	1.00	0.70	0.54	0.77	medium
Italian (ETICS)	0.27	0.40	0.10	0.10	0.43	0.26	low
Slovenian (ETICS)	0.27	0.40	0.83	0.10	0.10	0.34	low
Spanish (PV facade)	0.82	0.85	1.00	0.82	0.49	0.79	medium

Many building materials would have excellent circularity properties; however, they could not be used for practical reasons. Main obstacles with the use of recycled or biobased materials:

- Absence of necessary certificates (recycled materials)
- Fire safety regulations (a common issue for most of biobased materials)
- Hygrothermal properties (risk for mold growth)
- Higher maintenance need (repainting of the wooden cladding)
- "Factory friendliness" (factories favor rigid wind barrier because of prefabrication effectiveness and to guarantee the angularity of the element)

3.2 Embodied energy and embodied carbon

The Embodied energy and embodied CO_2 calculations are shown in Figures 13 and 14.

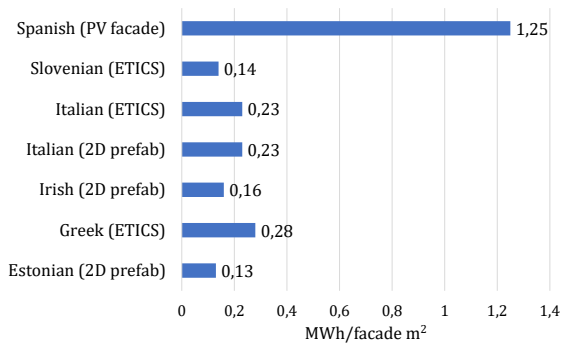

Fig. 13 – Embodied energy of m² of façade area

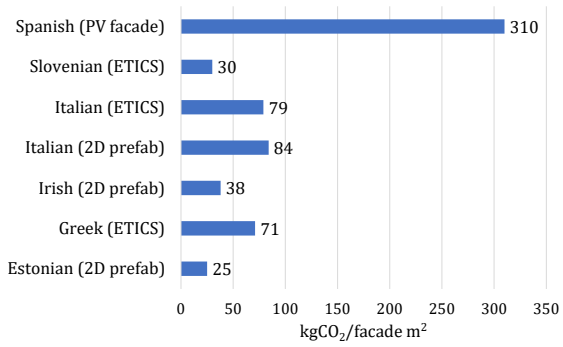

Fig. 14 – Embodied CO_2 of m² of façade area

The high embodied energy and embodied CO_2 content of the Spanish pilot renovation is mainly caused by the steel frames needed to install the PV panels.

Based on embodied energy and embodied CO_2, the environmental impact of the prefabricated insulation solutions and ETICS solutions are in the same range. This is due to differences in the mass of the materials. For example, embodied energy and embodied CO_2 per kg of expanded polystyrene is much higher than materials used in prefabricated solutions but because the expanded polystyrene is light, the embodied energy and embodied CO_2 per square meter of façade can be in the same range as a prefabricated solution with more environmentally friendly materials. Prefabricated insulation panel with timber frame, 200 mm of insulation, and fibre cement board for cladding weigh ~50 kg/m², ETICS solution with expanded polystyrene weighs ~20 kg/m².

4. Conclusions

The research goal was to analyze the circularity of the renovation solutions used for pilot renovations. The indicators used to assess the degree of circularity of the renovation concept are Design for

Disassembly (DfD) criteria and building environmental (with embodied energy and embodied CO_2 as indicators).

The main advantage of modular prefabricated elements is the greater potential for disassembly and reusability. ETICS can only be recycled and cannot be reused without remanufacturing process. Embodied energy and embodied CO_2 of the prefabricated insulation solutions are lower than and ETICS solutions. Prefabricated solutions also allow a wider choice of materials (bio-based insulation materials and cladding) to achieve a low environmental impact. Although the difference between prefabricated and ETICS solutions in terms of environmental impact is smaller than in terms of disassembly and recovery options.

Some building materials have excellent properties in terms of circularity; however, for practical reasons, they could not be used. The main concerns with using recycled or biobased materials were the absence of necessary certificates, fire safety, hygrothermal properties, and higher maintenance need. The final selection of the design solution is a balance between the circular, practical, and financial sides.

Assessment of the circularity of renovation concepts through design aspects (design for disassembly) and material use is a suitable approach. However, the assessment method for design aspects does not consider the proportion of scores relevant to material mass. Materials with low total mass can disproportionately affect the results (for example, air and vapor barrier). At the same time, the additional weighting factor would make the calculation more complex. It's the point of discussion on whether the design for disassembly methodology would benefit from scoring disassembly and material re-use potential based on the mass of the material.

5. Acknowledgement

This research was supported by the European Commission through the H2020 projects DRIVE0 (grant No. 841850) and Finest Twins (grant No. 856602), by Estonian Centre of Excellence in Zero Energy and Resource Efficient Smart Buildings and Districts, ZEBE (grant No. 2014-2020.4.01.15-0016), and by the Estonian Research Council (grant No. PRG483).

6. References

1. Giorgi S, Lavagna M, Wang K, Osmani M, Liu G, Campioli A. Drivers and barriers towards circular economy in the building sector: Stakeholder interviews and analysis of five european countries policies and practices. Journal of Cleaner Production [Internet]. 2022 Feb 15 [cited 2022 Jan 13];336:130395.
2. Machado N, Morioka SN. Contributions of modularity to the circular economy: A systematic review of literature. Journal of Building Engineering. 2021 Dec 1;44:103322.
3. Veld PO t. MORE-CONNECT: Development and Advanced Prefabrication of Innovative, Multifunctional Building Envelope Elements for Modular Retrofitting and Smart Connections. Energy Procedia. 2015 Nov 1;78:1057–62.
4. DRIVE 0 project website (Accessed: 8 March 2022). Available at: https://www.drive0.eu/
5. Akinade OO, Oyedele LO, Ajayi SO, Bilal M, Alaka HA, Owolabi HA, et al. Design for Deconstruction (DfD): Critical success factors for diverting end-of-life waste from landfills. Waste Management. 2017 Feb 1;60:3–13.
6. Alba Concepts (Accessed: 8 March 2022). Available at: https://albaconcepts.nl/circulairbouwen/
7. Ramesh T, Prakash R, Shukla KK. Life cycle energy analysis of buildings: An overview. Energy and Buildings. 2010 Oct 1;42(10):1592–600.
8. Inventory of Carbon & Energy (ICE) Version 2.0 .

The datasets generated during and/or analysed during the current study are not available because the project reports containing the analysed data have not been published but the authors will make every reasonable effort to publish them in near future.

Embodied Energy and Carbon of Residential Buildings: Towards an Actual nZEB Concept

Nazanin Moazzen [a], *Touraj Ashrafian* [b]

[a] Faculty of Architecture and Design, Maltepe University, Istanbul, Turkey, nazaninmoazzen@maltepe.edu.tr

[b] Faculty of Architecture and Design, Özyeğin University, Istanbul, Turkey, touraj.ashrafian@ozyegin.edu.tr

Abstract. Over the past few decades, energy efficiency policies have concentrated more on buildings' energy consumption and performance. EU established strategies by energy performance of buildings directive and its amendments for all new and retrofitted buildings to achieve nearly Zero Energy Buildings (nZEBs). Most of the studies and approaches cover the operation phase of the building life cycle, while, by observing the building's whole life cycle, it is determined that buildings are accounted for energy consumption during not just the operation phase and also the construction and demolishing stages. Consequently, the most prominent buildings should progress towards nearly Zero Energy Buildings by evaluating the energy consumption during the whole life cycle and not just during the operation. The embodied energy that covers the energy consumed in the process and manufacturing of the material, transportation, and installations on-site, is intensive energy consumed in a short period compared to the operation energy.

Residential buildings are accounted for extensive energy consumption among different building typologies due to their size and number. According to various studies on residential buildings, in conventional and low energy buildings, the share of embodied energy has varied between 6 and 20%, and 26 and 57%, respectively. It means that embodied energy of the buildings is not negligible.

Consequently, a logical method for residential buildings to reach the nZEB level using energy-efficient measures and proper materials considering the life cycle of buildings is inevitable. The paper aims to investigate the possibility of obtaining nearly zero energy levels in residential buildings reflecting the whole life cycle. The paper has concentrated not only on the operation energy but also on the embodied energy and carbon commencing from applying various measures to the building. The embodied energy and carbon data for building materials have been obtained from the Intergovernmental Panel on Climate Change (IPCC) database. All primary energy consumption of the building and improvement measures during the operation phase are computed with dynamic simulation tools, EnergyPlus and DesignBuilder. The life cycle energy consumption and CO_2 emissions of various measures have been calculated. Optimum alternatives have been proposed in the temperate-dry climatic zones of Turkey.

Keywords. Life Cycle Energy, Embodied Energy, Embodied Carbon, Residential, Nearly Zero Energy Buildings.
DOI: https://doi.org/10.34641/clima.2022.290

Abbreviations

ACH – Air Change per Hour
CFL - Compact Fluorescent Lamp
EC – Embodied Carbon
EE – Embodied Energy
GHG – Greenhouse Gas
LCA – Life Cycle Analysis
LCE – Life Cycle Energy
LCEA – Life Cycle Energy Assessment
LCEC – Life Cycle Energy Consumption
LCCO2E – Life Cycle CO_2 Emissions
LCI – Life Cycle Inventory
nZEB – nearly Zero Energy Building
RB – Reference Building
PEC – Primary Energy Consumption

Copyright ©2022 by the authors. This conference paper is published under a CC-BY-4.0 license.

1. Introduction

Buildings are responsible for a significant share of energy use. Improving the buildings' energy efficiency, reducing carbon emissions and increasing renewable energy uses are essential to cope with climate change [1]. The buildings sector is in charge of about 35% of worldwide energy consumption. Assessment of building during operational energy use is crucial; nevertheless, the energy used for production, transportation of building materials, construction, and demolition should be considered. The construction sector's Embodied Carbon (EC) is accountable for 11% of global GHG emissions, equal to 28% of the building sector's GHG emissions.

The whole life cycle of building construction has generated environmental impacts. Life Cycle Energy Analysis (LCEA) is a widespread and popular method for assessing energy uses and CO_2 emissions during buildings' lifespans. LCEA is comprised of manufacturing, operational, and demolition energy. The manufacturing energy includes the energy content of all materials and components entitled the embodied energy and the transportation energy. Operational energy consists of the whole energy used for HVAC, domestic hot water, lighting, and home appliances during the building operation. Demolition energy is the energy required to demolish a building at the end of its useful life and transport the material to storage areas or recycling facilities [2].

The proportion of embodied energy and carbon of energy-efficient buildings in whole life cycle energy consumption (LCEC) is high enough not to be neglected. Most researchers have addressed the operational energy, but less attention is on embodied energy and embodied carbons. The growing building renovation towards nearly zero energy building standards is expected to lead to a relative increase in embodied energy and embodied carbon emissions. All the new construction has critical roles in embodied carbon and energy. This paper focuses on the life cycle of nearly zero energy residential buildings. The environmental impact and embodied energy and carbon are evaluated during the life cycle framework.

2. Literature review

There are several works of literature on LCE of different building typologies. Ramesh et al. [2] identified 73 case buildings across 13 countries, including residential and office buildings. They concluded that operating energy has about 80–90%, the embodied energy (10–20%), and the demolition energy is negligible with a little percentage share in LCE. Mangan et al. [3] have investigated residential building performances for different climatic zones of Turkey regarding LCE and life cycle cost efficiency. More recent evidence highlights the importance of embodied energy and embodied carbon. Some studies have concentrated on LCE and cost-efficiency. Ferrari et al. [4] assessed the existing office building by some representative retrofit options for achieving zero buildings. Pikas et al. [5] considered energy efficiency and cost optimality of office building fenestration design. The investigation evaluated different measures to achieve the nZEB level. Sicignano et al. [6] have investigated identifying the construction system with the lowest embodied energy and carbon. Thormark [7] studied that the embodied energy was 40% of the total energy needed for a life expectancy of 50 years. The embodied energy can be decreased by approximately 17% through material adjustment.

However, few studies have focused on LCE terms and embodied energy and carbon of materials simultaneously. Chastas et al. [8] have shown an increasing share of embodied energy in the transaction from conventional to passive, low energy, and nZEB. The share of embodied energy in low energy buildings is 26%-57%, and nearly zero energy buildings are 74%-100%, respectively. In passive buildings, the percentage of embodied energy varies between 11% and 33%. Shirazi et al. [9] evaluated that up to 30% of a building's life cycle energy (LCE) and emissions are associated with the embodied phase. Ohta [10] investigated that the material added for better energy efficiency and CO_2 emissions generated during the manufacturing and construction periods positively affected reducing the Life Cycle CO2 Emission (LCCO2E) of homes. The ratio of LCCO2E for a zero-energy home becomes relatively high compared with a conventional home. Cabeza et al. [11] discussed the Low carbon and low embodied energy materials. Different materials are defined as cement and concrete, wood, bricks, rammed earth, and sandstone as low carbon materials referred. Xiaodong Li et al. [12] evaluated the embodied carbon impacts of three types of residential buildings in China. Morini et al. [13] indicated that it is possible to use reliable software with embodied energy and carbon footprint metrics to assess the environmental problem early in development and materials selection. Khadra et al. [14] considered three different renovation packages used in multi-family buildings from an economic perspective.

3. Methodology

Four stages should be considered in the LCA of energy-related building renovation. These stages define the scope, life cycle inventory, impact assessment, and interpretation. The methodology of this paper was also divided into four parts. The first stage was the definition of the scope of study and the initial analyses. A residential building was selected to be the reference building (RB). The energy modelling was conducted. It includes calculating operational energy use and emissions. The energy model was made in DesignBuilder and then transferred to the EnergyPlus to calculate the operational energy and carbon emissions.

The second step of the LCA outlines the methodology used to analyze embodied energy and embodied CO_2eq emissions arising from the production of building materials. The Life Cycle Inventory (LCI) phase is generally considered the most significant obstacle since the data collection process is very time-consuming. As there are no LCI databases available in Turkey, in the study, the LCI database of the University of Bath's Inventory of Carbon and Energy has been used [15].

The third step outlines the various alternatives to improve the RB. Different envelope, lighting, mechanical components, and renewable energy alternatives are determined in this step. The LCE and LCCO2E have been calculated for individual and combined single measures during the building life cycle. The building lifespan is considered 50 years. The fourth step is related to interpreting the LCEC, LCCO2E and EE of all parameters and evaluating them.

4. Reference Building

The five-story apartment building, which represents a detached apartment located in Ankara, is a case building. This city has a tempered-dry climate. This 6-floor building (5 occupied floors and an unoccupied underground floor) has a gross area of about 2752.1 m^2; from this amount, 440 m^2 belongs to the sloped roof area that is unoccupied. The building has four dwelling units with about 85 m^2 and 90 m^2 areas on each floor. Each unit has two bedrooms and one living room. Each unit's height is 2.8 m from above to below the floor. Most of the living areas are faced to the south. Other physical information about the reference building is presented in table 1.

Tab. 1 - RB's physical properties.

Physical properties of the RB.	
Location	Ankara-39.93° N-32.85° E
Orientation	0°
Floor area (m^2)	440
Total floor area (m^2)	2312.1
Floor height (m)	3.20
Facade surface area (m^2)	1557
Elevation (m)	752
Roof area (m^2)	442.54
Glazing area (m^2)	327.40
Glazing ratio (%)	20
Number of floors	6 (1+5 typical floor)
Number of apartments	20
Number of the apartment on the floor	4

The building energy modelling is done by dynamic simulation tools design-builder and energy plus. Figure 1 shows the floor plans drawings and 3D views of the Reference Building (RB).

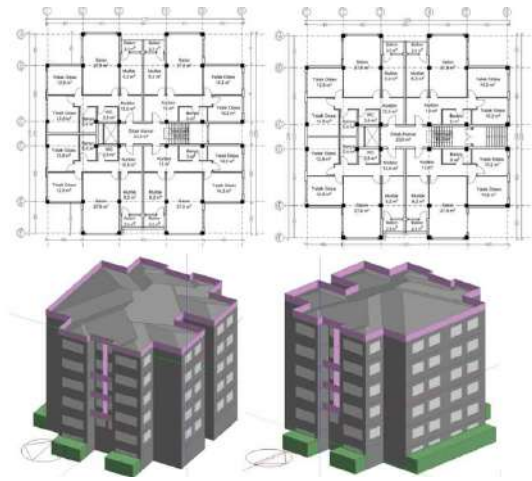

Fig. 1 - Drawings of floor plans and 3D views of 5-story reference building apartment.

The building envelope materials are chosen based on TS825-2013 standards [16]. According to TS825-2013, Ankara is located in third-degree day zones. The U-values of reference building for walls, roofs, and ground floor are 0.48, 0.28, and 0.43 W/m^2°K, respectively. Also, the minimum U-value of the glazing system is 1.8 W/m^2°K. The Visible transmittance of glazing and the solar heat gain coefficient are 0.56 and 0.32, respectively. Table 2 indicates the primary characteristics of the building components and their materials, including embodied energy and embodied carbon.

Tab. 2 - Thermo-physical properties of the RB.

	Material layers (from outside to inside)	E.E. (kWh/kg)	EC (kgCO2/kg)	U value (W/ m^2 °K)
External Wall	Cement rendering	0.37	0.21	0.48
	Extruded polystyrene	24.61	2.55	
	Brick	0.83	0.24	
	Gypsum Plastering	0.50	0.12	
Roof	ceramic	3.33	0.74	0.28
	cement mortar	0.37	0.21	
	Reinforced concrete	0.31	0.16	
	water insulation	14.17	0.38	
	Extruded polystyrene	24.61	2.55	
	water barrier	14.17	0.38	
	concrete	0.24	0.10	
	Reinforced concrete	0.31	0.16	
	Gypsum Plastering	0.50	0.12	
Ground Floor	Hardcore	0.13	0.02	0.43
	Concrete	0.24	0.10	
	Water insulation	14.17	0.38	
	Cement mortar	0.37	0.21	
	Extruded polystyrene	24.61	2.55	
	Water barrier	14.17	0.38	
	Dry pine	0.02	0.00	
	Parquet	4.44	1.05	
Glazing	Clear glazing	4.17	0.85	1.8
	PVC frame	597.23	110.00	

Like the envelope, the interface part of buildings, the renovation measures on envelope measures affect the building's energy use. Thus, construction elements like internal walls or floors do not affect the building's energy performance. Based on Turkey's Building Energy Performance (BEP-TR) [17], the setpoint temperature for cooling and heating is set to 26°C and 20°C, respectively. The reference building's heating system is a natural gas-based combi boiler with an internal radiator (Baseboard Hot Water Convector). In contrast, the cooling system is an individual system with a packaged terminal air-conditioner in each case. A mechanical ventilation system is not used in the building, and natural ventilation works solely. The boiler produces the Domestic Hot Water (DHW) system. Also, all lamps are 40W Compact Fluorescent Lamp (CFL). There are lighting controls in living spaces. It is estimated that during occupancy hours, except for sleeping hours, one of the bedrooms can be used as a study room and living room. When the illumination level provided by natural lighting is below the required amount (200 LUX for the bedroom and 150 LUX for the living room), the lighting system is on; otherwise, the system is off in those rooms. Table 3 includes the features of building HVAC systems.

Tab. 3 - Energy systems' characteristics.

Heat production	Boiler efficiency = 0.8 COP (Coefficient of Performance)
Heat distribution	Hot water radiator-Natural gas
Domestic Hot Water (DHW)	Boiler – Natural Gas
Cooling Generator	Individual System
Cooling System	Air Conditioning (Electricity)
Ventilation System	Natural Ventilation
Heating & Cooling Setpoints	Heating Periods=20 °C, Cooling Periods =26 °C
Lighting System	Compact fluorescent- Lighting Control
Infiltration Rate	0.5 Air Change per Hour (ACH)

4.1 Definition of the Energy Efficiency Improvement Measures.

Different measures on envelope, lighting, and mechanical systems are defined to reach the nZEB level. Three thermal insulation levels on walls, roof, and ground floor are used at the first, second, and third stages. The primary material of third measures on walls is Autoclaved Aerated Concrete (AAC) blocks. In other measures and the ERB, the primary wall material is brick. Two different improvement measures are defined for glazing systems. The first measure is double glazing with a 1.3 W/m^{2}K U-value, and the second measure is a triple glazing system with 1.3 W/m^{2}K U-values. Another measure on the envelope is added Polyethylene wick for reducing air filtration from 0.5 ACH to 0.3 ACH. For improving the lighting systems, all CFL lamps were replaced with LED lamps.

Besides, the mechanical system is modified for improving the heating system. At the first level, boiler modification with central systems by natural gas fuel condensing boilers is projected. The current heating system is replaced with a condensing boiler, underfloor heating, and central floor heating systems at the second, third, and fourth levels. The photovoltaic system is added to the RB and four other improvement measures. The photovoltaic system type is monocrystalline (Mono-CSI) cells. Table 4 indicates individual renovation measures characteristic of the RBs. The RBs U-values are according to the Turkish Insulation standard, TS825-2013. Table 5 displays the possible individual and combination energy-efficient measures.

Tab. 4- Single energy efficiency improvement measures.

ID	Single Improvement Measures
O1	Brick- Wall= XPS 12 cm; Roof=Glass wool 15cm; Ground Floor=XPS 14cm
O2	Brick- Wall= XPS 17 cm; Roof=Glass wool 20cm; Ground Floor=XPS 18cm
O3	Autoclaved Aerated Concrete – Wall= XPS 17 cm; Roof=Glass wool 20cm; Ground Floor=XPS 18cm
GL1	Double Glazing- 4+16+4 (air) - 1.3 W/m^{2}K; 0.44 SHGC; 0.71 Tvis
GL2	Triple Glazing - 4+12+4+12+4 (Air) - 0.9 W/m^{2}K; 0.48 SHGC; 0.69 Tvis
LI1	LED Bulb
A1	Air filtration 0.3 ACH
H1	Central Systems- Gas fuel condensing boilers between 150.000-200.000 kcal / h
H2	Condensing Boiler - 20.000 kcal / h
H3	Individual Floor Heating-
H4	Central Floor Heating
PV	60 number of Monocrystalline silicon 13.9%

4.2 Life Cycle Inventory

LCA's foremost significant part is a life cycle inventory (LCI) or data collection. As there is insufficient inventory data in Turkey, the embodied energy and carbon emission of materials are based on the IPCC and the University of Bath's Inventory of Carbon and Energy (ICE) database. PV system's EE and EC were derived directly from the literature [17]. However, all calculations do not consider EE and EC of lighting and mechanical systems measurements.

RB's the most embodied energy percentages allocated to reinforcement concrete, brick, and concrete which are 52%, 24%, and 9%, respectively. The building lifespan is assumed to be 50 years. The primary energy consumption is considered for calculating the energy consumption of operational energy. Primary energy conversion factors are 1.00 for natural gas and 2.36 for electricity in Turkey [18]. Additionally, for calculating CO_2 emission during the operation stage, the emission factors for natural gas and electricity were taken as 0.234 and 0.626 kg.eq.CO_2/kWh, respectively [19].

Tab. 5- Energy efficiency improvement packages.

ID	Opaque System	Transparent System	Infiltration	Lighting System	Mechanical systems	Photovoltaic System
RB+PV	-	-	-	-	-	PV
P01	O1	-	-	-	-	-
P02	O2	-	-	-	-	-
P03	O3	-	-	-	-	-
P04	-	GL1	-	-	-	-
P05	-	GL2	-	-	-	-
P06	-	-	-	LI	-	-
P07	-	-	A1	-	-	-
P08	-	-	-	-	H1	-
P09	-	-	-	-	H2	-
P10	-	-	-	-	H3	-
P11	-	-	-	-	H4	-
P12	O1	GL2	A1	LI	H3	-
P13	O2	GL1	A1	LI	H3	-
P14	O2	GL2	A1		H3	-
P15	O2	GL2	A1	LI	H3	-
P16	O1	GL2	A1	LI	H2	-
P17	O2	GL1	A1	LI	H2	-
P18	O2	GL2	A1	-	H2	-
P19	O2	GL2	A1	LI	H2	-
P20	O1	GL2	A1	LI	H1	-
P21	O2	GL1	A1	LI	H1	-
P22	O2	GL2	A1	-	H1	-
P23	O2	GL2	A1	LI	H1	-
P24	O1	GL2	A1	LI	H1	PV
P25	O2	GL1	A1	LI	H1	PV
P26	O2	GL2	A1	-	H1	PV
P27	O2	GL2	A1	LI	H1	PV

5. Results

By overview of the primary energy consumption of the reference building, heating is more imperative than cooling. Ankara is located in a tempered-dry climate zone; hence, most of the reference building's primary energy consumption belongs to heating with 72.51 kWh/m^2.a. In contrast, the lowest primary energy consumption belongs to cooling with 5.03 kWh/m^2.a. After heating that is accounted for 57% of the whole primary energy, HVAC components (pumps and fans), lighting, and cooling are located with %4, %22, and %17, respectively. Figure 2 shows the distribution of the primary energy consumption by different systems in the reference building.

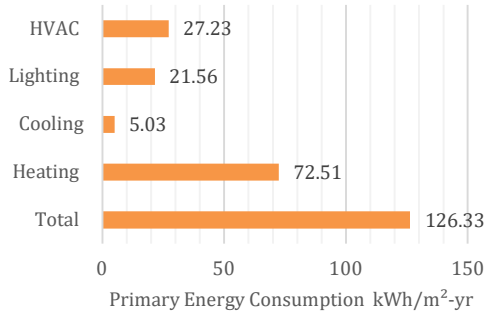

Fig. 2 - Distribution of RB's primary energy consumption.

Considering the PEC of all measures, the most reduction in single and combination steps is related to the P24 and P27 with 46% and 57.4% saving, respectively. The results show that adding thermal insulation to the envelope makes it possible to reduce PEC between 13.2% and 16.8%. P11 reveals that it can minimize operation energy by 19.3% with individual mechanical renovation. By modifying lighting systems to LED bulbs (P6), PEC saving is only 2.2%, the lowest saving among packages. P24, P26, and P27 support by renewable systems have the most PEC savings among all packages. Figure 3 demonstrates the annual PEC of RBs and improvement packages.

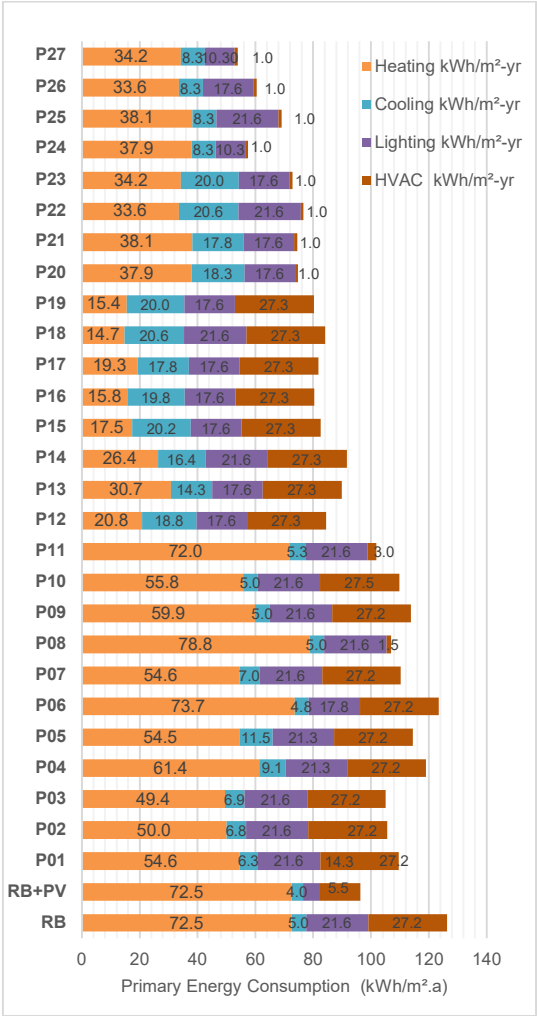

Fig. 3 - Annual Primary Energy Consumption of RBs and improvement packages.

Figure 4 illustrates the LCE and LCCO2E saving values of individual and combined improvement measures. P24, P25, P26, and P27 are the most LCE and LCCO2E savings scenarios among combination measures. Not surprisingly, all these alternatives contain PV system. RB+PV package and P11 have the most savings among single measures. Generally, single packages are not as efficient as combination measures. The lowest amount of LCE and LCCO2E savings are related to P6, P4, and P5.

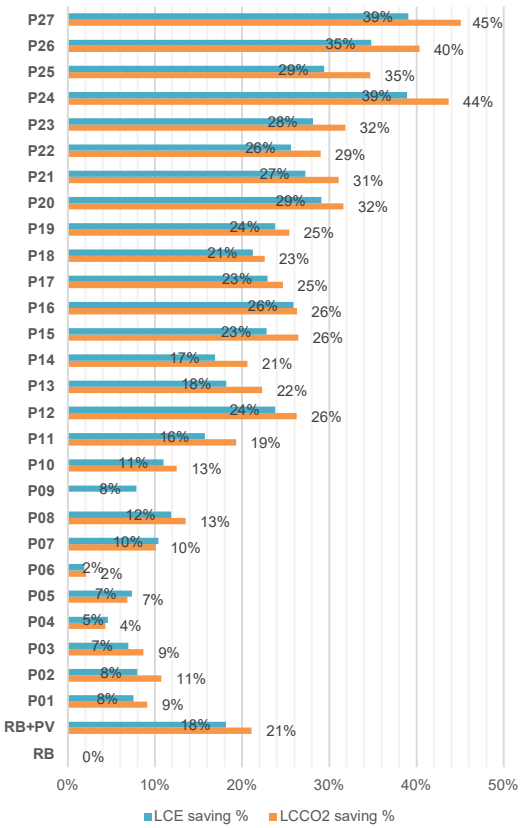

Fig. 4 - LCE and LCCO2E emission saving values.

RB has a low EE while it has the highest amount of LCEC. It is fundamental to note that the LCEC of renovation measures has been reduced by increasing the EE of measures. Not surprisingly, the highest EE options are related to the PV systems. Figure 5 displays the distribution of LCEC versus EE in different improvement scenarios.

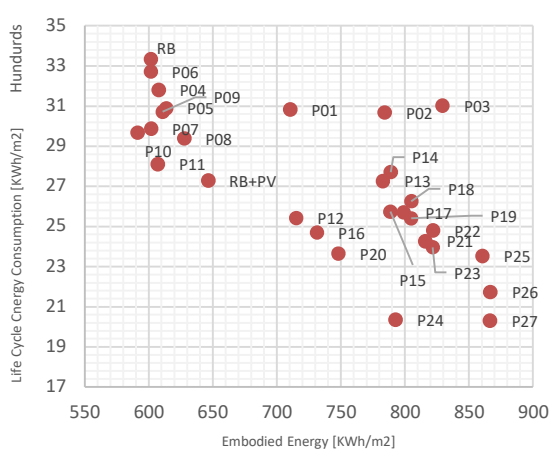

Fig. 5 - LCEC versus Embodied Energy of different improvement scenarios.

RB has the highest amount of LCEC and LCCO2E among all packages. In contrast, the least LCE and LCCO2E are P27, P24, and P26, respectively. Consequently, these packages are the most efficient LCE and LCCO2E measures. However, P6 and P4 have the most LCEC and LCCO2E among measures. Figure 6 demonstrates the LCE versus LCCO2E of renovation measures.

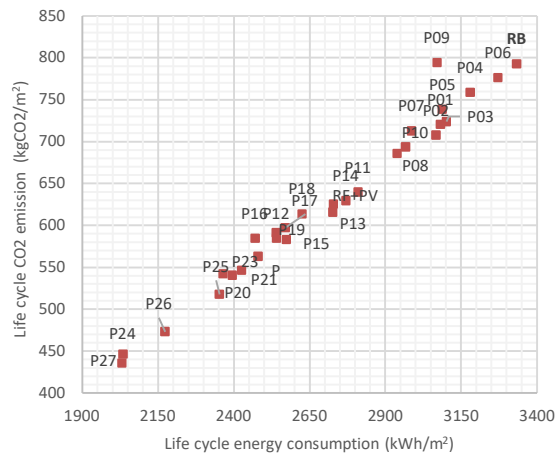

Fig. 6 - LCEC versus LCCO2E of renovation measures.

The results indicate that measures with almost the same LCEC and LCCO2E saving can have different EE. P24 and P27 have almost equal saving potentials. However, P24 has a comparable low EE. RB's embodied energy and operational energy share are approximately 18% and 82%, respectively. While, in nZEB scenarios, P27, P24, P26, and P25, the share is 40% to 60% for EE and operational energy. Consequently, by reaching nZEB, the embodied energy exceeds 18% to 40%. In comparison, the operational energy is decreased from 82% to 60%. Table 6 summarised the energy and CO_2 emissions for the RB and nZEB scenarios during the building life cycle.

Tab. 6 - Summary of the results for RB and measures located in the nearly zero-energy ranges.

Parameters		nZEB Scenarios		
	RB	P.24	P.26	P.27
PEC (kWh/m².a)	126.3	57.47	60.43	53.86
Primary Energy Saving (%)	n.a.	54.5	52.2	57.4
LCEC (kWh/m²)	3333.7	2035.5	2173.4	2031.2
LCCO2E ($kgCO_2/m^2$)	792.6	446.3	472.9	435.4
LCCO2E Saving ($kgCO_2/m^2$)	n.a.	346.3	319.7	357.2
LCCO2E Saving (%)	n.a.	44%	40%	45%
Embodied Energy (MWh)	1391.4	1832.9	2003.7	2003.2
Embodied Carbon ($TonCO_2$)	334.1	383.8	401.2	401.4

6. Conclusion

In conventional buildings, the energy consumed in material production is almost a quarter of the operating energy consumption. A large amount of carbon is released in the material formation and transportation process. The operational energy is consumed during the building operation, which has a comparatively long span than the material formation

and transportation. It means that the embodied energy is very intensive than operational energy. That's why Embodied Energy should play a pivotal role in building energy analysis.

Considering the life cycle of the building, it is obvious that zero energy buildings indeed are not actually zero energy. Due to the excess of components and materials used in these buildings, the materials' formation energy and carbon emissions are higher than in conventional buildings. Although this situation should not be considered an obstacle for buildings being developed with zero energy concepts, ignoring it may cause more significant challenges. Therefore, building materials with lower embedded energy and carbon emissions should be integrated into the zero energy building concept and all related initiatives. In addition, materials with these features should be disseminated with the necessary legal regulations.

The paper has focused on the life cycle impact of a case study building under different improvement measures. The results show that the measures with similar life cycle energy consumptions and CO2 emissions have different embodied energy consumption and CO_2 emissions. The study data is based on an international database. However, a national database is necessary to have more reliable outcomes from the studies on building life cycle. The embodied energy and CO_2 emission data for the HVAC system is not available in the literature. This deficiency also should be fulfilled to have an inclusive approach.

References

[1] Life Cycle Assessment for Cost-Effective Energy and Carbon Emissions Optimization in Building Renovation (Annex 56), Energy in Buildings and Communities Programme, March 2017, International Energy Agency.

[2] T. Ramesh, Prakash R., Shukla K.K. Life-cycle energy analysis of buildings: an overview. Energy and Buildings. 2010; 10:1592–1600.

[3] Mangan S. D., Koçlar Oral G. Assessment of residential building performances for the different climate zones of Turkey in terms of life cycle energy and cost efficiency. Energy and Buildings. 2016 ;110: 362–376.

[4] Ferrari S., Beccali M. Energy-environmental and cost assessment of a set of strategies for retrofitting a public building toward nearly zero-energy building target. Sustainable Cities and Society. 2017; 32: 226–234.

[5] Pikas E., Thalfeldt M., Kurnitski J. Cost optimal and nearly zero energy building solutions for office buildings. Energy and Buildings. 2014; 74:30–42.

[6] Sicignano E., Di Ruocco G., Melella R., Mitigation Strategies for Reduction of Embodied Energy and Carbon, in the Construction Systems of Contemporary Quality Architecture, Sustainability, 2019, vol. 11, issue 14, 1-14

[7] Thormark C. The effect of material choice on the total energy need and recycling potential of a building. Building and Environment. 2006; 41:1019–1026.

[8] Chastas P., Theodosiou T., Bikas D. Embodied energy in residential buildings-towards the nearly zero energy building: A literature review. Building and Environment. 2016;105: 267-282.

[9] Shirazi A., Ashuri B. Embodied Life Cycle Assessment (LCA) comparison of residential building retrofit measures in Atlanta. Building and Environment. 2020;171: 106644.

[10] Ohta I. Embodied CO2 Evaluation of a Zero Life-Cycle CO2 Home: A Case Study of an Actual Industrialized Home. Journal of Asian Architecture and Building Engineering. 2017;16(1): 231-237.

[11] Cabeza L. F., Boquera L., M. Chàfer, D. Vérez. Embodied energy and embodied carbon of structural building materials: Worldwide progress and barriers through literature map analysis. Energy & Buildings. 2021; 231:110612.

[12] Lia X., Yanga F., Zhub Y., Gao Y. An assessment framework for analyzing the embodied carbon impacts of residential buildings in China. Energy and Buildings. 2014; 85:400–409.

[13] Augusto Morini A., Ribeiro M. J., Hotzac D., "Early-stage materials selection based on embodied energy and carbon footprint", Materials and Design. 2019 ;178:107861.

[14] Khadra A., Hugosson M., Akander J., Myhren J. A. Economic performance assessment of three renovated multi-family buildings with different HVAC systems. Energy & Buildings. 2020;224: 110275.

[15] Hammond G. P., Jones C. I. Embodied energy and carbon in construction materials. Proceedings of the Institution of Civil Engineers – Energy. 2008; 161 (2): 87-98.

[16] Turkish Standardization Institute, TS825-Thermal insulation requirements for buildings. 2013.

[17] Diaz Al. C., Energy Life Cycle Assessment (LCA) of silicon-based photovoltaic technologies and the influence of where it is manufactured and installed, Master thesis of renewable energy and energy sustainability, University of Barcelona, 2013- 2014.

[18] Turkish Ministry of Public Works and Settlement, Building's Energy Performance of Turkey (Bep-Tr), Official Gazette. 2008; 27075.

[19] Turkish Green Building Council (CEDBIK), Green Building Certification Guide for New Houses. 2019.

Should we ventilate differently in an adaptable context? An exploratory LCA-study

Oskar Seuntjens [a], Bert Belmans [a], Matthias Buyle [a], Zakarya Kabbara [a], Sandy Jorens [a], Amaryllis Audenaert [a]

[a] Faculty of Applied Engineering, University of Antwerp, Antwerp, Belgium, Oskar.seuntjens@uantwerpen.be.

Abstract. Currently a great number of buildings, that are not able to meet the evolving needs of building owners and users, are being demolished before reaching their technical life span. To avoid such waste, it is crucial that buildings have an adaptable design in order to allow for flexible building usage. Ventilation is crucial in this transition as a flexible building usage can lead to fluctuating ventilation requirements. However, knowledge about how to choose between ventilation systems in an adaptable context is sorely lacking. In this research, an exploratory LCA-study will be carried out on two ventilation systems in an adaptable context over a period of 15 years. The case study concerns a school building where a reconfiguration of the floorplan design is planned every five years. The first ventilation system concerns a centralized balanced mechanical ventilation system which uses a heat recovery system and ductwork to distribute the air to all the classrooms. The second ventilation system is a ductless exhaust ventilation system which uses three exhaust fans to extract air and vents above windows to supply air naturally. Despite the centralized balanced ventilation system having a higher energy efficiency, the environmental impact of this ventilation system is 40% higher than the impact of the ductless exhaust ventilation system. This is caused by the use of a great amount of ductwork and an air handling unit. The largest share of the environmental impact of the ductless exhaust ventilation system is related to the additional energy that is needed to condition the temperature in the classrooms. Further research should include other ventilation systems and flexibility scenarios as well. Moreover, follow-up research should not only quantify the environmental impact but also assess the financial impact of ventilation systems in an adaptable context.

Keywords. Adaptability, Circularity, Ventilation systems, Life cycle assessment
DOI: https://doi.org/10.34641/clima.2022.284

1. Introduction

As buildings are becoming increasingly energy efficient, the share of material-related environmental impact has gained importance, both in absolute and relative terms [1]. To reduce this material-related environmental impact, the circular economy advocates using all materials and components to their maximum value [2]. However, a great part of our current building stock is being demolished long before its technical lifespan has been reached [3]. One of the main reasons that buildings are being dismantled prematurely, is that they cannot meet evolving needs from building owners and users. These evolving needs can vary [4–6]. To avoid this much building waste, buildings must be adaptable in order to allow for a more flexible usage.

The current state-of-the-art regarding adaptable buildings mainly stresses the importance of a smart spatial configuration [7–9] and the oversizing of building components to avoid future lock-in effects [10,11]. To ensure that an adequate indoor environment can be guaranteed over the entire life cycle of a building, ventilation systems should be considered in terms of adaptability as well. As a result, HVAC designers are facing a new challenge in designing ventilation solutions for an adaptable building practice. Instead of only considering the short term requirements, ventilation systems should be designed bearing the buildings entire life cycle in mind in order to ensure comfort, health, and energy efficiency under a wide range of possible future use scenarios.

As a flexible usage can lead to fluctuating ventilation requirements, ventilation systems are found to be a key factor with respect to the possibilities of adaptable buildings [12,13]. Changes in occupancy, floorplan layout and function of a room can result in a different normative air flow rate. Also in the long term a degree of adaptability is required, as the lifespan of ventilation systems is shorter than the lifespan of the entire building [14]. Therefore it is

Copyright ©2022 by the authors. This conference paper is published under a CC-BY-4.0 license.

important that the components of ventilation systems can be easily replaced by new ones once their lifespan has been reached. Moreover, considering the long term, it is also important that ventilation systems do not hinder large refurbishments. Unfortunately, in many cases the ventilation systems have proven unsuitable to coping with an adaptable context [15,16].

This paper is innovative, as it is the first to quantify the environmental impact of two ventilation systems in an adaptable context. It concerns an exploratory case study of a school building where a reconfiguration of the floorplan layout is planned every five years. A life cycle assessment (LCA) will be carried out on two different ventilation strategies. The first one concerns a centralized balanced mechanical ventilation system. The second system is a ductless mechanical exhaust ventilation system with natural air supply through vents. The environmental impact of both ventilation systems will be compared over a period of 15 years.

2. Research Methods

In this research, an exploratory LCA-study will be carried out on two traditional ventilation strategies. A part of a school building will be used as a case study. Every five years the floorplan design will be reconfigured. The CO2 concentration in all classrooms will be simulated and the environmental impact of both ventilation systems will be assessed.

2.1 Case study

A part of a school building that is located in Belgium will be used as a case study. As this research focusses on adaptability, it is presumed that the floorplan design is reconfigured every five years. The original configuration contains six relatively small classrooms that are separated by demountable and reusable interior walls. In the second configuration four small classrooms are turned into two larger classrooms and in the final configuration there are only three large classrooms. The smaller classrooms are occupied by 20 persons and the larger classrooms by 30 persons. The three configurations are illustrated in Fig. 1.

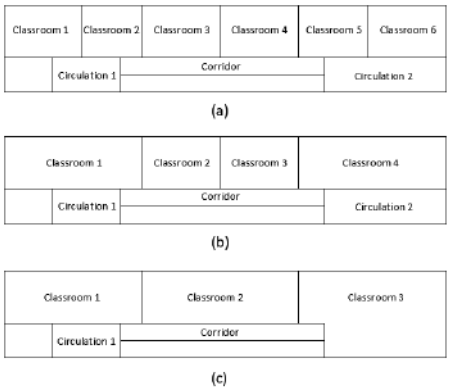

Fig. 1 - (a) Configuration 1; (b) Configuration 2; (c) Configuration 3

Two ventilation strategies will be compared to each other. The first one is a centralized balanced ventilation system with an inlet and outlet in all six classrooms. To ensure an adequate indoor air quality in classroom 3 for the third configuration, an additional inlet is provided in circulation room 2. This inlet will only be used when the last configuration is in use. The ductwork is designed so that the air velocity in the ducts is always between three and five meters per second. The central air handling unit is placed above classroom 3 and 4. This air handling unit does not include a heating or a cooling battery, but it does include a heat exchanger. The second strategy is a ductless mechanical exhaust ventilation system with natural air supply. There are three exhaust fans in use; one in each circulation room and one in the corridor. Fresh air will be naturally supplied through vents that are placed above a window in all six classrooms. The designs of both ventilation systems are illustrated in Fig. 2.

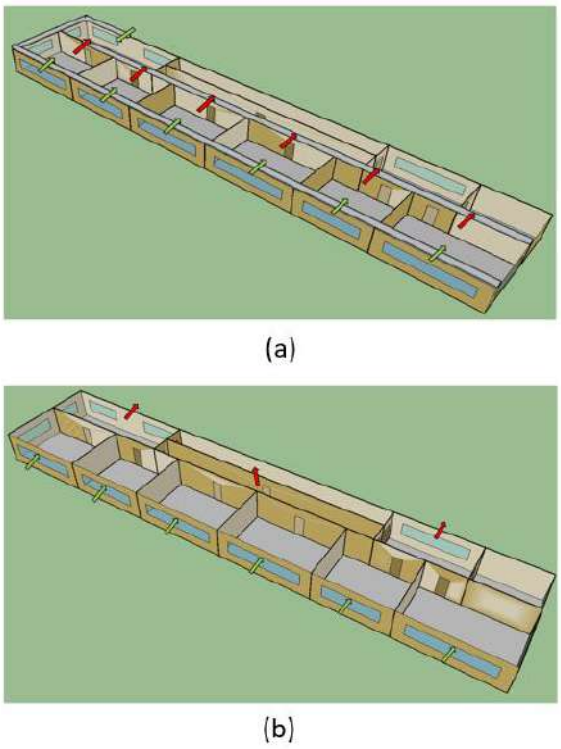

Fig. 2 - (a) Centralized balanced ventilation system ; (b) Ductless exhaust ventilation system

2.2 LCA

To quantify the environmental impact from both ventilation systems, an LCA-study will be carried out. As described in the framework provided by ISO 14040/44 [17], the following steps will be followed: Goal and scope definition, life cycle inventory (LCI) and life cycle impact assessment (LCIA).

Goal and scope. To create a level playing field, both ventilation systems are compared to each other with respect to the following functional unit: *a part of a school building where, during school hours over a period of 15 years, the maximum occurred CO_2 concentration is between 960 and 1000 ppm in all*

classrooms for every configuration and the temperature in the classrooms is at least 21 °C during school hours and 15.6 °C after school hours. The entire life cycle of all the ventilation components are taken into account: the production-, the use- and the end-of-life-phase. In the case of ductless exhaust ventilation with natural air supply, the additional energy use that is needed for space heating, compared to the centralized balanced ventilation with heat recovery, is taken into account as well. Maintenance of the air handling unit and ductwork is not included in this study. Consequential LCA will be used over attributional LCA. Consequential LCA aims at describing how environmentally relevant flows will change in response to possible decisions [18]. Moreover, as this case study is situated in Belgium, the Belgian electricity mix will be used.

LCI. In Tab. 1 and Tab. 2 an overview is given of all the used materials and energy flows for both ventilation systems that are being included in this LCA-study. The air handling unit contains the fans and the heat recovery system. For the transport of materials to the site and the end-of-life-phase of materials, the scenarios provided by TOTEM [19] were used.

Tab. 1 - Life cycle inventory centralized balanced ventilation system.

Material	Unit
Air handling unit	Pieces
Ductwork	Meter
Wiring and control for centralized ventilation	Pieces
Energy consumption fans	kWh
Energy consumption heat exchanger	kWh

Tab. 2 - Life cycle inventory ductless exhaust ventilation.

Material	Unit
Exhaust fans	Pieces
Exhaust air outlet wall	Pieces
Exhaust air outlet roof	Pieces
Wiring and control for decentralized ventilation	Pieces
Energy consumption fans	kWh
Additional energy consumption for space heating	kWh

LCIA. To calculate the environmental impact of both ventilation systems, the Simapro software and the Ecoinvent database were used. The ReCiPe 2016 method is used and the environmental impact is presented as a single score.

2.3 Simulations

The software EnergyPlus (version 9.6) is used to carry out the energetic and indoor air quality simulations. An entire school year was simulated for every configuration for both ventilation strategies. Belgian holidays were included, except the months of July and August because school is closed during these months. The required energy needed for the fans and space heating for every configuration for both ventilation strategies was derived from these simulations and multiplied by five (as every configuration will be used for a period of five years). To calculate the required air flow rate from the fans to keep the CO_2 concentration between the range mentioned in the functional unit, the air flow network from EnergyPlus was used. The energy consumption by the fans was calculated manually. The energy consumed by the fans was calculated manually.

3. Results

In this section the results of the study will be discussed. First, the results derived from the simulations in EnergyPlus will be discussed. Hereafter, the results from the LCA-study will be discussed. All the precise calculations and the simulations can be found in the supplementary materials.

3.1 Space heating

The kind of ventilation system that is used will also have an impact on the amount of energy that is needed to condition the temperature in the classrooms. As stated in the functional unit, the heating system is scheduled to heat the classrooms up to 21 °C during school hours and up to 15,6 °C after school hours. A cooling system is not included in this case study. The results of the needed energy consumption for space heating are shown in Tab. 3. It can be deduced that the total energy that is needed to condition the temperature of the classrooms after 15 years, but also for every configuration, is less than half the amount in the case of the centralized balanced ventilation system compared to the case that uses a ductless exhaust ventilation system. This could be expected, since in the case of the ductless exhaust ventilation system, unconditioned cold air is taken into the classrooms through vents while the centralized balanced ventilation systems uses a heat recovery system. As a consequence, the heating system needs to deliver more energy to reach the required temperatures in the case of the ductless exhaust ventilation.

Tab. 3 - The energy needed to condition the temperature of the classroom for both ventilation systems.

	Centralized balanced VS [kWh]	Ductless exhaust VS [kWh]

Configuration 1	45429	93772
Configuration 2	37825	83781
Configuration 3	33602	69575
Total	116856	247128

3.2 Fans

Both ventilation systems should ensure an acceptable indoor air quality. As defined in the functional unit, the maximum CO_2 concentration that can occur in the classrooms is 1000 ppm. The maximum CO_2 concentration should also be above 950 ppm, in order to create a level playing field for both ventilation systems. In Tab. 4, the maximum CO_2 concentrations are shown for both ventilation systems and for every configuration that will occur in all six classrooms. From these results, it can be concluded that for every classroom the maximum concentrations are always within the predefined range.

Tab. 4 - Maximum CO_2 concentrations in all classrooms for both ventilation systems and all configurations.

	Centralized balanced VS [ppm]			**Ductless exhaust VS [ppm]**		
	Configuration 1	Configuration 2	Configuration 3	Configuration 1	Configuration 2	Configuration 3
Cl.1	985	967	972	991	984	979
Cl.2	986	959	974	991	999	970
Cl.3	985	968	972	972	999	994
Cl.4	986	973	*N/A*	972	980	*N/A*
Cl.5	990	*N/A*	*N/A*	999	*N/A*	*N/A*
Cl.6	990	*N/A*	*N/A*	999	*N/A*	*N/A*

Since the CO_2 concentrations meet the predefined requirements, the next step is to calculate the energy consumptions of the fans for both ventilation systems. As stated in the previous section, the energy consumption of the fans has been calculated manually. The results of the energy consumption from the fans can be found in Tab. 5. The energy consumption of the centralized balanced ventilation system contains the energy consumption from the supply and exhaust fan that are located in the air handling unit. The energy consumption of the ductless exhaust ventilation contains the energy consumption from the three exhaust fans that are located in the two circulation rooms and in the corridor. The results show that a much higher energy consumption is required in the case of centralized balanced ventilation. The reason for this is twofold. Firstly, in the case of the ductless exhaust ventilation system where the air supply happens naturally through the vent, a lower ventilation rate of the exhaust fans is required as natural forces such as wind also contribute to the ventilation of the classrooms. Secondly, the centralized balanced ventilation system has to cope with a lot more pressure losses because of the presence of extensive ductwork and other components such as a heat exchanger, which results in a higher energy consumption of the fans.

Tab. 5 - Energy consumption of the fans.

	Centralized balanced VS [kWh]	**Ductless exhaust VS [kWh]**
Configuration 1	16231	1309
Configuration 2	11584	574
Configuration 3	11486	281
Total	39302	2164

3.3 LCA

With the simulations and calculations of the energy consumption required for space heating and the use of the fans, everything is now in place to carry out the LCA-study. In **Error! Reference source not found.** and **Error! Reference source not found.**, an overview is given of the amount and the environmental impact of all the material- and energy related components in both ventilation systems. The environmental impact of all the used materials covers the impact of the production of these materials, the transport to the site as well as the end-of-life phase. The latter is accompanied with a negative impact since a large part of these materials will be recycled and thus partly avoids the production of new products.

When looking at the results from the centralized balanced ventilation system, it can be concluded that the ductwork has the largest environmental impact, followed by the air handling unit. These two components contribute up to more than 75% of the total environmental impact of the entire ventilation system. The energy consumption that is required for the fans and heat exchanger have the third and fourth largest environmental impact, respectively. The control and wiring have the smallest impact from the entire ventilation system.

Tab. 6 - Environmental impact centralized balanced ventilation system.

Material and energy usage	**Amount**	**Unit**	**Impact [Pt]**
Air handling unit	1	Pieces	460

Ductwork	114	Meter	765
Wiring and control	1	Pieces	14
Energy use fans	39302	kWh	329
Energy use heat exchanger	6278	kWh	53

The largest environmental impact of the ductless exhaust ventilation system is caused by the additional energy that is needed to condition the temperature in the classrooms. The environmental impact related to this energy consumption is responsible for more than 95% of the total environmental impact of this ventilation system. All the other components of this ventilation system and the energy consumption of the exhaust fans have an environmental impact that is relatively low. By contrast, the largest part of the environmental impact of the centralized balanced ventilation system was caused by the used materials and not by the energy consumption.

Tab. 7 - Environmental impact ductless exhaust ventilation system

Material and energy usage	Amount	Unit	Impact [Pt]
Exhaust fans	3	Pieces	3
Exhaust air outlet wall	2	Pieces	3
Exhaust air outlet roof	1	Pieces	4
Wiring and control	3	Pieces	20
Energy use fans	2164	kWh	18
Energy use space heating	130272	kWh	1090

In *Fig. 3*, the total environmental impact of both ventilation systems are compared to each other after a period of 15 years. From this graph it can be deduced that the environmental impact of the ductless exhaust ventilation system is approximately 30% lower than the impact of the centralized balanced ventilation system. Despite a great amount of additional energy being needed to condition the temperature of the classrooms in the case of the ductless exhaust ventilation system, the environmental impact of the great amount of ductwork and the air handling unit turns out to be higher still. However, once the school building is used more extensively, i.e. not only during school hours, the environmental impact related to the additional energy that is required to condition the temperature of the school building will increase. The environmental impact of the energy consumption by the fans in the centralized balanced ventilation system is also much higher than the energy consumption by the exhaust fans in the ductless exhaust ventilation system. The main reasons for this are the higher air flow rate and the pressure drops because of the ductwork and the use of a rotary wheel as a heat exchanger.

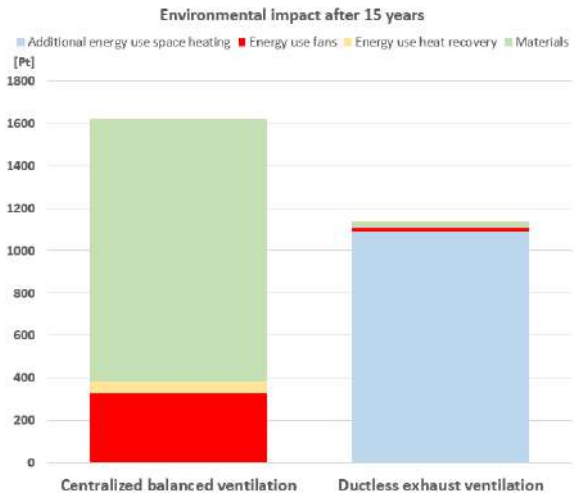

Fig. 3 - Comparison environmental impact.

4. Discussion

To obtain a better understanding on the meaning of this study, the results from this LCA-study will be analysed and discussed more thoroughly in this discussion section. Moreover, some recommendations for further research are formulated.

4.1 Discussion of results

The results from the LCA-study have shown that the environmental impact of the centralized balanced ventilation system is larger than the impact of the ductless exhaust ventilation system. The largest part of the environmental impact of the centralized balanced ventilation system is caused by the used materials, and not by the energy consumption of the fans. It is stated by Blengini and Di Carlo [20], that as buildings have become increasingly energy efficient, the share of material-related environmental impact has gained importance, both in absolute and relative terms. This also holds true for centralized balanced ventilation systems, based on the results from this LCA-study. While this ventilation systems is certainly more energy efficient than the ductless exhaust ventilation system, the environmental impact of the materials used for this ventilation system is much higher. In this specific case, the impact of the used materials is even so high, that the total environmental impact of this ventilation system is higher than the environmental impact of a ventilation system that is significantly less energy efficient. Yet a great number of studies focus mainly on the energy efficiency of ventilation systems, e.g.

Salcido et al. [21] and Jacobs and Knoll [22]. LCA-studies on ventilation systems, such as the study carried out by Fong et al. [23], are rather scarce.

However, it is important to stress that a ductless exhaust ventilation does not have a lower environmental impact than a centralized balanced ventilation system per definition. In this particular case, the building is only occupied during school hours. Once this school building is used in a more extensive way, the additional energy that is needed to condition the temperature of the classrooms will increase, and consequentially the environmental impact will as well. Therefore, it is possible that a ductless exhaust ventilation system has a higher environmental impact in a situation where the school building is being more frequently used. On the other hand, if a very energy efficient heating system is in use, the share of the environmental impact related to the additional energy needed to condition the temperature of the classrooms decreases.

Finally, it should also be stated that although some boundary conditions were imposed in this study, i.e. the maximum CO_2 concentration and the minimum temperature in the classrooms, the level of comfort both ventilation systems can guarantee is not completely equal. Parameters such as the relative humidity, draught and the maximum temperature were not included as this is only an exploratory case study which can form a basis for further research in the topic of ventilation in an adaptable context.

4.2 Further research

This is the first LCA-study carried out on two ventilation systems in an adaptable context. There are, however, many more ventilation systems that can allow for a flexible building usage. The environmental impact of these systems should be assessed as well. Moreover, there are also far more ways of using a building in a flexible manner than merely by altering the floorplan layout. For example, school buildings can be used after school hours as well. The activities that take place in school buildings can also fluctuate over time. It is important to understand how other kinds of flexible building usage influence the environmental impact of several ventilation systems.

Moreover, the records from ventilation components from the Ecoinvent database that were used in this LCA-study are rather outdated. Therefore it is important for follow-up research to use more accurate data about all the components used, i.e. the materials they consist of, where and how these components are made, the maintenance these components require and what happens with these components after their technical life span has been reached.

Finally, the authors also encourage carrying out a life cycle cost assessment (LCCA) on ventilation systems in an adaptable context, besides only an LCA-study. An example of such a study, is the study carried out by Buyle et al. [24] where both the environmental and financial impact of several internal walls were compared to each other over a period of 60 years with a reconfiguration of the floorplan design layout planned every 15 years. Based on both the environmental and financial consequences of a ventilation system, building owners can then make an informed decision on which system they prefer. Flexibility scenario's must be taken into consideration as a building is often used in a flexible way.

5. Conclusion

In this paper an exploratory LCA-study was carried out on two different ventilation systems in an adaptable context over a period of 15 years. A part of a school building where the configuration of the floorplan layout was changed every five years was used as a case study. The first ventilation system concerns a centralized balanced ventilation system which uses a heat recovery system and a great amount of ductwork to distribute the air. The other system was a ductless exhaust ventilation system. Air was supplied naturally through vents placed above windows in all classrooms and air was extracted through three exhaust fans. Despite the centralized balanced ventilation being more energy efficient, it has a higher environmental impact than the ductless exhaust ventilation system. This is caused by the environmental impact related to the great amount of ductwork and the air handling unit. The largest environmental impact of the ductless exhaust ventilation system is related to the additional energy that is required to condition the temperature of the classrooms. In this case study, the school building was only occupied during school hours. If the school building were to be used more extensively, the environmental impact of the ductless exhaust ventilation system would increase and might even be higher than the environmental impact of the centralized balanced ventilation system.

Further research should also include other ventilation systems and take into account other flexibility scenarios, e.g. a more extensive building usage and other types of building usage. Besides quantifying the environmental impact, the financial impact should be quantified as well by means of an LCCA-study. Based on these results, building owners can then make an informed decision on which ventilation system they prefer.

6. Acknowledgement

We thank the Research Foundation Flanders (FWO-Vlaanderen) for supporting Matthias Buyle with a post-doctoral fellowship (Postdoctoral Fellow - junior; 1207520N).

The datasets generated during and/or analysed during the current study are available in the

Supplementary data.zip repository, https://blackboard.uantwerpen.be/bbcswebdav/xid-32842002_1·

7. References

[1] Belussi L, Barozzi B, Bellazzi A, Danza L, Devitofrancesco A, Fanciulli C, et al. A review of performance of zero energy buildings and energy efficiency solutions. J Build Eng 2019;25:100772. https://doi.org/10.1016/j.jobe.2019.100772.

[2] Çimen Ö. Construction and built environment in circular economy: A comprehensive literature review. J Clean Prod 2021;305. https://doi.org/10.1016/j.jclepro.2021.127180.

[3] O'Connor J. Survey on actual service lives for North American buildings. Woodframe Hous. Durab. Disaster Issues Conf., Las Vegas: 2004.

[4] Kelly G, Schmidt R, Dainty A, Story V. Improving the design process for adaptability: Linking feedback and architectural values. Assoc. Res. Constr. Manag. ARCOM 2011 - Proc. 27th Annu. Conf., vol. 1, 2011, p. 43–52.

[5] Bullen PA. Assessing sustainable adaptation of existing buildings to climate change. Int. Constr. Res. Conf. R. Inst. Chart. Surv., 2004.

[6] Mansfield J. Sustainable refurbishment: policy direction and support in the UK. Struct Surv 2009;27:148–61. https://doi.org/10.1108/02630800910956470.

[7] Safarzadeh G. Agility, Adaptability + Appropriateness: Conceiving, Crafting & Constructing an Architecture of the 21st Century. ARCC 2012;9.

[8] Geraedts RP. Design for Change; Flexibility Key Performance Indicators. 1st Int Conf Ind Integr Intell Constr 2008:11.

[9] Julistiono EK, Hosana N, Liemansetyo F, Wijaya IF. Spatial and Structural Aspects of an Adaptable Building. Dimens (Journal Archit Built Environ 2017;44:87–94. https://doi.org/10.9744/dimensi.44.1.87-94.

[10] Conejos S, Langston C, Smith J. Designing for better building adaptability: A comparison of adaptSTAR and ARP models. Habitat Int 2014;41:85–91. https://doi.org/10.1016/j.habitatint.2013.07.002.

[11] Geraedts RP, Prins M. FLEX 3 . 0 : An Instrument to Formulate the Demand for and Assessing the Supply of the Adaptive Capacity of Buildings. CIB World Build Congr 2016 Vol V Adv Prod Serv 2016:679–90.

[12] Geraedts RP. Design for Change; Flexibility Key Performance Indicators. 1st Int. Conf. Ind. Integr. Intell. Constr., 2008, p. 11.

[13] Kronenburg R. Flexible: Architecture that Responds to Change. London: Laurence King Publishing Ltd; 2007.

[14] Durmisevic E. Transformable Building Structures: Design for disassembly as a way to introduce sustainable engineering to building design & construction. Technische Universiteit Delft, 2006.

[15] Gann DM, Barlow J. Flexibility in building use: The technical feasibility of converting redundant offices into flats. Constr Manag Econ 1996;14:55–66. https://doi.org/10.1080/01446199600000007.

[16] Geraedts R. Future Value of Buildings 2014.

[17] ISO 14044:2006 Environmental management — Life cycle assessment — Requirements and guidelines. 2006.

[18] Buyle M, Braet J, Audenaert A. Life cycle assessment in the construction sector: A review. Renew Sustain Energy Rev 2013;26:379–88. https://doi.org/10.1016/j.rser.2013.05.001.

[19] OVAM. Environmental profile of building elements. Mechelen: 2018.

[20] Blengini GA, Di Carlo T. The changing role of life cycle phases, subsystems and materials in the LCA of low energy buildings. Energy Build 2010;42:869–80. https://doi.org/10.1016/j.enbuild.2009.12.009.

[21] Salcido JC, Raheem AA, Issa RRA. From

simulation to monitoring: Evaluating the potential of mixed-mode ventilation (MMV) systems for integrating natural ventilation in office buildings through a comprehensive literature review. Energy Build 2016;127:1008–18. https://doi.org/10.1016/j.enbuild.2016.06.054.

[22] Jacobs P, Knoll B. Diffuse ceiling ventilation for fresh classrooms. 4 th Intern. Symp. Build. Ductwork Air tightness, Berlin: 2009.

[23] Fong ML, Lin Z, Fong KF, Hanby V, Greenough R. Life cycle assessment for three ventilation methods. Build Environ 2017;116:73–88. https://doi.org/10.1016/j.buildenv.2017.02.006.

[24] Buyle M, Galle W, Debacker W, Audenaert A. Sustainability assessment of circular building alternatives: Consequential LCA and LCC for internal wall assemblies as a case study in a Belgian context. J Clean Prod 2019;218:141–56. https://doi.org/10.1016/j.jclepro.2019.01.306.

DIGITIZATION

Verification of Energy Efficiency Measures in Three Apartment Buildings Using Gaussian Process

Sakari Uusitalo [a]

[a] Faculty of Building services, Tampere University of Applied Sciences, Tampere, Finland, sakari.uusitalo@tuni.fi.

Abstract. The aim of this work was to examine whether the Gaussian process as a machine learning method is suitable for modelling time series data collected from buildings and whether it can be used to verify the effects of energy efficiency measures on three apartment buildings. A Gaussian process regression model was created using outdoor temperature and time information as inputs including information about the day of the week and the hour of the current day. Correspondingly, the output of the model was to estimate the hourly heating power demand corresponding to these inputs. The results provided by the created model were used as a reference point to verify the effects of energy efficiency measures taken on these residential buildings. The model was trained with 2016 hourly data. The 2017 data was used as test data to evaluate the functionality of the model. The impact assessment of the energy efficiency measures was performed with the measured data of 2019, which was compared with the results given by the model. Based on the performed modelling, it can be stated that using the Gaussian process, the need for hourly power of buildings was reasonably well modelled with even small amount of input variables. It can be assumed that the biggest uncertainty factor in the modelling is related to the domestic hot water consumption and the resulting power requirement. By measuring hot water consumption, modelling accuracy could probably be significantly improved. Based on the reviews, it could also be verified that the energy efficiency measures taken have had an impact on the peak power needs of residential buildings as well as on total energy consumption. For all three buildings, peak power needs appear to have decreased and overall energy consumption is lower than it would have been without the actions taken.

Keywords. artificial intelligence, machine learning, intelligent building, building services, energy efficiency, energy, power.
DOI: https://doi.org/10.34641/clima.2022.63

1. Introduction

In Finland energy efficiency measures in buildings are often targeted specifically at the heating system, but the challenge is to assess the impact of the actions taken as outdoor conditions and the occupancy rate of a building can vary considerably. To verify the impact of energy efficiency measures on the need for the heating power and energy consumption of a building, we need a model of the building. The model allows us to look at the situation where no measures has been taken and to compare the actual data with the results of the model.

We can use a computer program, based on dynamic model, to calculate the need for heating power at different outdoor temperatures. An example of such a simulation program is IDA ICE [1]. However, to build a model, we need a considerable amount of information about the properties affecting the dynamics of the building. For example, we need to find out the structures and areas of walls and windows, heat transfer coefficients, ventilation airflows, building use profiles and numerous other features affecting the need for heating capacity.

On the other hand, we may use a machine learning algorithm that is able to learn the dynamics of a building from the collected history data. For example, the algorithm can learn how the heating demand of a building depends on the outdoor temperature and time. In other words, we do not have to find out so much information about the building itself. It is enough that we know the outdoor temperature at any given time and the corresponding need for heating power.

This study examines how machine learning is suitable for modelling a building's heating power demand. The used algorithm is called Gaussian process, which is widely used in machine learning applications. The goal is to verify the effects of energy efficiency measures on three apartment buildings with student housing. Actual energy efficiency

Copyright ©2022 by the authors. This conference paper is published under a CC-BY-4.0 license.

measures are not presented because they are secondary to work. However, they have been designed to reduce the peak power needs and overall energy consumption of the buildings. The subject of the comparison has been the hourly power needs of the buildings and the monthly and annual energy consumption. By comparing the hourly capacities, an attempt has been made to examine whether the measures taken have been able to cut the greatest power requirements of the buildings.

2. Gaussian process

In this section the basic idea of Gaussian process is introduced. For more complete definitions and descriptions please check out the book written by Rasmussen and Williams [2]. For visual introduction to Gaussian process, you should visit a web site authored by researchers from University of Konstanz [3].

2.1 Idea of a Gaussian process

Let $\mathbf{X}$ be a m $\times$ n -matrix in which each horizontal row $\mathbf{x}_\mathrm{i}$ represents one observation point. Each horizontal row item x_{ij} indicates the status of a particular property at that observation point. Each element $y_i = \mathrm{f}(\mathbf{x}_i) + \epsilon_i$ of the vertical vector $\mathbf{y}$, where ϵ_i is a measurement error, describes the observation of the phenomenon at the observation point. The purpose of the Gaussian process is to get to know the phenomenon under consideration by means of observations made at points and to find out the unknown events of the phenomenon at points $\boldsymbol{y}_*$ at points $\mathbf{X}_*$. Learning takes place by forming a conditional multidimensional normal distribution of the functions $\mathbf{f}$ (actually the values of the functions) suitable for the observations. The best estimate of the unknown events $\mathbf{y}_*$ of a phenomenon at the points $\mathbf{X}_*$ is the mean value vector $\boldsymbol{\mu}_*$ of that distribution. The aim of the process is not to find a function describing the actual phenomenon, but only the values produced by the function. [2]

In many cases, modelling tasks are more interested in the values produced by the function and their uncertainty than the function itself. [4]

2.2 Definition of a Gaussian process

According to the definition of Rasmussen and Williams [2], the Gaussian process is a collection of random variables, each of which follows a common normal distribution. The Gaussian process can be thought of as a generalization of the multidimensional normal distribution. Where a multidimensional normal distribution is a vector distribution, the Gaussian process is a distribution of functions, and the random variable is now the value of the function $\mathrm{f}(\mathbf{x})$ at the point $\mathbf{x}$. We can illustrate this with the follofing presentation:

$$\begin{pmatrix} f(\mathbf{x}_1) \\ f(\mathbf{x}_2) \\ \vdots \\ f(\mathbf{x}_n) \end{pmatrix} \sim \mathcal{N}\left(\begin{pmatrix} m(\mathbf{x}_1) \\ m(\mathbf{x}_2) \\ \vdots \\ m(\mathbf{x}_n) \end{pmatrix}, \begin{pmatrix} k(\mathbf{x}_1, \mathbf{x}_1) & \cdots & k(\mathbf{x}_1, \mathbf{x}_n) \\ \vdots & \ddots & \vdots \\ k(\mathbf{x}_n, x_1) & \cdots & k(\mathbf{x}_n, \mathbf{x}_n) \end{pmatrix} \right) \quad (1)$$

where $\mathrm{m}(\mathbf{x})$ and $\mathrm{k}(\mathbf{x}, \mathbf{x}')$ are a mean function and a covarince function (kernel). Rasmussen and Williams [2] have defined Gaussian process distribution as follows:

$$\begin{aligned} & f(\mathbf{x}) \sim \mathcal{GP}\big(m(\mathbf{x}), k(\mathbf{x}, \mathbf{x}')\big) \\ & m(\mathbf{x}) = E[f(\mathbf{x})] \\ & k(\mathbf{x}, \mathbf{x}') = cov[\mathbf{x}, \mathbf{x}'] \\ & = E\big[\big(f(\mathbf{x}) - m(\mathbf{x})\big)\big(f(\mathbf{x}') - m(\mathbf{x}')^{\mathrm{T}}\big)\big] \end{aligned} \quad (2)$$

2.3 Formation of a Gaussian process

In forming the Gaussian process, the covariance function plays an important role in determining the form of the function to be estimated. The covariance function looks at the distance (similarity) between two points $(\mathbf{x}, \mathbf{x}')$, connecting the different observations to each other. The selection of the appropriate covariance function plays a key role in the success of the modelling task. The most typical covariance functions and their properties are presented, for example, in [3] and [5]. Covariance functions often contain also free hyperparameters which should be optimized by an appropriate method using training data [2]. To form a Gaussian process, the covariance function must be computed between all possible points, giving three matrices: $\mathbf{K_{XX}}$, $\mathbf{K_{X_*X}}$ and $\mathbf{K_{X_*X_*}}$. Each value of the function to be searched is normally distributed, so that a combined normal distribution [2]

$$\begin{pmatrix} \mathbf{y} \\ \mathbf{y}_* \end{pmatrix} \sim \mathcal{N}\left(\mathbf{0}, \begin{pmatrix} \mathbf{K} & \mathbf{K}_*^{\,T} \\ \mathbf{K}_* & \mathbf{K}_{**} \end{pmatrix} \right) \quad (3)$$

can be formed from the training and estimated observations assuming that the mean function $m(\mathbf{x}) = 0$. The most probable values $(\boldsymbol{\mu}_*)$ of the function $f(\mathbf{x}_*) = y_*$ at the estimated points $(\mathbf{X}_*)$ can now be found by forming a conditional distribution [2]

$$p(\mathbf{y}_* \mid \mathbf{X}_*, \mathbf{X}, \mathbf{y}) \sim \mathcal{N}\begin{pmatrix} \mathbf{m}_* + \mathbf{K}_*\mathbf{K}^{-1}(\mathbf{y} - \mathbf{m}_*), \\ \mathbf{K}_{**} - \mathbf{K}_*\mathbf{K}^{-1}\mathbf{K}_*^T \end{pmatrix} \quad (4)$$

By assumption $\mathbf{m}_* = \mathbf{0}$, the best estimate of values $\mathbf{y}_*$ obtained by the function $\mathbf{f}_*$ is now a mean vector of the distribution

$$E[\mathbf{y}_*] = \boldsymbol{\mu}_* = \mathbf{K}_*\mathbf{K}^{-1}\mathbf{y} \quad (5)$$

and the uncertainty of that estimate is described by the variance of the distribution

$$var[\mathbf{y}_*] = \mathbf{K}_{**} - \mathbf{K}_*\mathbf{K}^{-\mathbf{1}}\mathbf{K}_*^T. \quad (6)$$

Figure 1 shows an example of a situation where $x_* \in [-5,5]$ and the goal is to find out the values $\mathbf{y}_*$ obtained by the function $f(x_*)$ in that range. The left side of the figure shows the situation when no observations have been made of the function values and the right side of the figure shows the situation when six noisy observations have been obtained. The solid bold line describes the best estimate of the values obtained by the function in both cases. The dashed line in right side is the real function to be estimated and the grey area is the 95 % confidence interval obtained from the variance of the distribution.

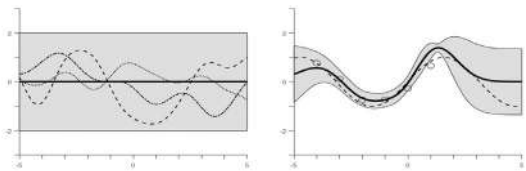

Figure 1 - Three samples of possible functions, when there are no observations about the function values and an estimated function when there is six observation points about the function values.

3. Verifying energy efficiency measures

In this section the used data and main results is presented.

3.1 Used data

The heating power demand in a building depends on the temperature difference between the indoor and outdoor temperatures. The hourly averages of the Finnish Meteorological Institute's Tampere Härmälä measuring station were used as the outdoor temperature. Wind strength can also have a large effect on heating power demand in certain situations, but no detailed information on wind strength was available for these explicit buildings, so it was decided to exclude it. The heating power required to heat domestic water depends, of course, on how much water is used and when. In principle, therefore, this may be entirely incidental. However, it is assumed that there is some correlation between the need for heating power in terms of the day of the week and the time of day. This assumes that the routines of apartment dwellers, such as washing and cooking, will remain reasonably similar. However, it is precisely the assessment of the power required to heat domestic water that involves the greatest uncertainty.

The measures taken on buildings date back to 2018 and possibly 2019. Data from 2016, 2017 and 2019 were used in the study. Data from 2016 have been used as a training data while 2017 has been used as a test year. As the systems and use of the buildings have been very similar in 2016 and 2017, the modelled data should correspond quite well to the data measured for 2017. Measures have been taken in the buildings during 2018. In 2019, the measures have had an impact throughout the year. So, when comparing the modelled and measured data for 2019, it should show the effects of the measures taken in terms of reduced peak power and energy consumption.

The outdoor temperature and time data, which included information about the day of the week and the hour of the current day, were used as inputs for the model built in the study. The output of the model was an estimate of the hourly average heating power demand corresponding to these inputs. Since time is cyclical, time information must be transformed into a form from which the used algorithm also understands its cyclical nature. Thus, the algorithm must in practice understand, for example, that the last hour of the day is close to the first hour of the following day. Therefore, the input used as a time information has been converted to cyclic using sin and cos transformations.

Before the actual construction of the model, the data were cleaned by removing e.g., clearly erroneous readings as well as moments of time that lacked relevant information such as outside temperature or heating power information. Many times, in modelling tasks like this, the data is collected from many different sources, in which case it may be incomplete in some respects and contain erroneous readings. Making data usable is often one of the biggest and most time-consuming jobs before the actual analysis and modelling work.

3.2 Building the Gaussian process model

The GPstuff function library for Matlab, made by Vehtari et al. [6], was used to build the Gaussian process model. In these studies, the addition of the squared-exponential and periodic covariance function was used. Additivity allows strong assumptions to be made about the individual components that make up the sum [5]. Other variations of the covariance function were also tested but were not found to have a significant effect on the modelling results. However, it is good to note that using the right kind of covariance function or a combination of them can have a significant impact on the success of the modelling.

3.3 Error review

Table 1 shows the RMSE values of the models for 2017 monthly. The RMSE values describe the distance between the prediction and the observation vector and cannot in themselves be used to draw conclusions about the goodness of the model. In this study, RMSE values were mainly used to define the Gaussian process model to be used when testing the effect of different covariance functions, and their combinations, on the modelling results. However, the table 1 shows that the RMSE values for building 1 are the smallest. Building 2 values are slightly higher and building 3 values are clearly higher than the other two buildings. This is natural, as the hourly outputs

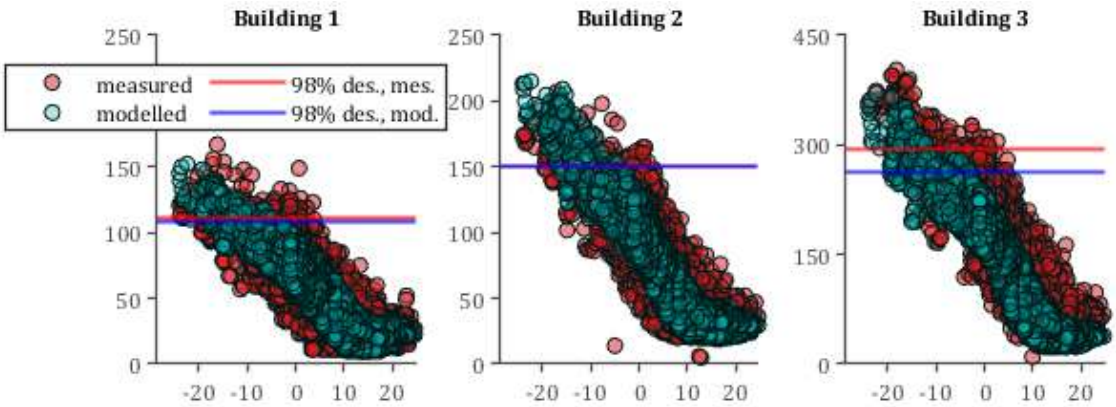

Figure 3 - Modelled and measured hourly powers of buildings from 2017.

themselves are higher for buildings 2 and 3. Building 3 also differs considerably in the actual power demand from buildings 1 and 2. Maximum power demand at building 3 is about $400\frac{kWh}{h}$, while buildings 1 and 2 have maximum power requirement slightly below and above $200\frac{kWh}{h}$. In this case, relatively equal errors in the modelling may appear as a larger absolute error in those buildings where the power range is also larger.

Table 1 - Year 2017 model RMSE-values.

	Building 1	Building 2	Building 3
jan	10.5	13.5	32.8
feb	10.6	16.0	27.9
mar	10.3	12.9	25.1
apr	12.3	16.5	27.7
may	12.4	16.5	34.5
jun	8.7	9.5	25.9
jul	6.4	7.0	19.6
aug	6.7	7.9	29.9
sep	10.6	12.1	49.2
oct	11.0	13.6	46.4
nov	11.0	17.6	40.5
dec	12.4	15.8	34.0
year	10.4	13.7	34.3

The figure 2 shows the distributions of the residual values of the 2017 models. The distribution shows that the expected values of the residual values of buildings 1 and 2 ($\mu_1 = -0.57$ and $\mu_2 = -1.50$) are close to zero, which can be considered as one of the properties of a successful regression model. Instead, the residual values of object 3 are slightly weighted to the right of zero ($\mu_3 = 22.40$), suggesting that the modeled values would appear to be smaller than the measured values.

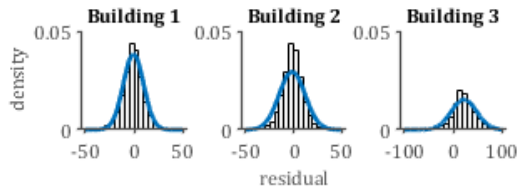

Figure 2 - Distributions of residuals between 2017 measured and modelled values.

3.4 Hourly power comparison

The figure 3 shows the modelled and measured hourly power of buildings in relation to the outdoor temperature in 2017. The figure also shows the lines indicating the level below 98% of all hourly power values. As can be seen from the figure for buildings 1 and 2, for both the modelled and measured values, the lines are very close to each other. This suggests that the modelling has been reasonably successful and in 2017 the technical systems and users of the building have performed similarly as in 2016. Instead for building 3 the line of the modelled values is lower than the measured values, so the modelled values would appear to be lower than the measured ones. This can also be clearly seen by looking at the points. The points produced by the model would appear to compress to the left edge of the point cloud of measured values.

The same comparison for 2019 is shown in figure 4. The figure shows two things. First, the image also shows how some of the actual hourly power points of the harshest frosts have dropped lower, forming their own small point cloud. In addition, the 98% limit for measured values has dropped lower in all three buildings. These findings support the claim that actions taken to the buildings have succeeded in limiting the maximum hourly powers.

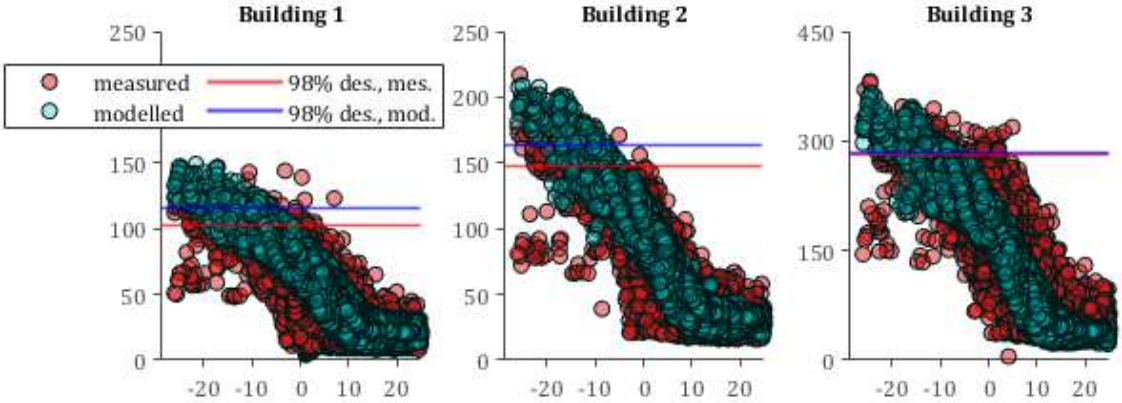

Figure 4 - Modelled and measured hourly powers of buildings from 2019.

In addition to limiting the maximum power requirement, the actions taken in the buildings also aimed at lower energy consumption. Figure 5 shows the monthly energy consumption of buildings for 2017 and Figure 6 for the whole year. It can be seen from the figures that the measured and modelled consumptions correspond quite well to each other, but small deviations occur, especially at the monthly level. For building 3, the differences are larger and follow the same regularity as when comparing hourly power needs.

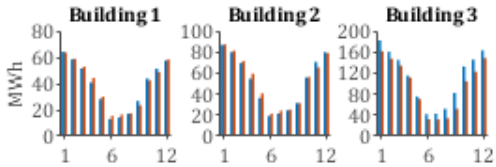

Figure 5 – Measured (blue) and estimated (orange) monthly energy consumption of buildings in 2017.

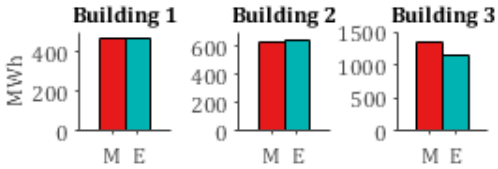

Figure 6 - Measured (M) and Estimated (E) annual consumption of buildings 2017.

Figures 7 and 8 show the same thing for 2019. Figure 7 shows that the measured consumption is lower than the modelled ones every month, except for building 3. However, for building 3 it can also be seen that the difference between the measured and modelled consumption has narrowed compared to 2017. Of course, the effect is also visible on an annual basis, and the figure 8 shows that for buildings 1 and 2, the actual total energy consumption in 2019 is significantly lower than the modelled one. For building 3, the difference between actual and modelled consumption has narrowed since 2017.

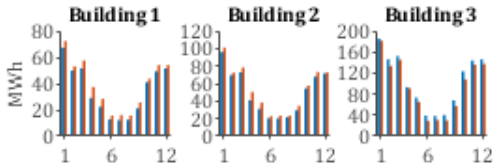

Figure 7 – Measured (blue) and estimated (orange) monthly energy consumption of buildings in 2019.

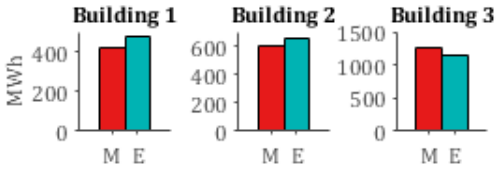

Figure 8 - Measured (M) and Estimated (E) annual consumption of buildings 2019.

4. Discussion

Based on the modelling performed, it can be stated that the method succeeded in modelling the hourly power demand of buildings with even small amount of input variables. It can be assumed that the biggest uncertainty factor in the models is related to the domestic hot water consumption and the resulting power requirement. By measuring hot water consumption, modelling accuracy could probably be significantly improved. On the other hand, information about the position of the hot water heating control valve is already often available in building automation system. Also, taking this information as one additional variable could improve the accuracy of the modelling.

It can also be said that the energy efficiency measures in buildings have had a positive effect both in limiting the maximum hourly power needs and in reducing overall energy consumption. Although the effects are clear, their absolute magnitude, especially on an hourly basis, is difficult to assess. To make hourly absolute impact assessments, the model should be more accurate, which could be achieved, for example, with the hot water consumption data described before. Regarding the annual consumption of the model, a reasonably good estimate can be made of the actual energy savings of buildings 1 and 2. In contrast, for building 3, there was more uncertainty in the modelling. This may be due, for example, to

changes in the building in question that were not known and had an impact on power demand in 2017. On the other hand, modelling for this building also suggests that measures have been taken during 2018 reduced overall energy consumption compared to the situation without measures.

Machine learning can have significant applications in the analysis of building operations and the development of more intelligent control methods. In addition to the impact assessment of energy efficiency measures discussed in this work, potential applications could also include model-based predictive control, maintenance cost forecasting based on utilization rate, fault diagnosis by identifying various deviations, and clustering-based intelligent control. However, these are just a scratch on the surface of potential applications, and the construction industry also offers considerable opportunities for innovation in the use of artificial intelligence and machine learning. However, the implementation of various methods and applications still requires considerable further research and development. There are many questions that still need to be answered. What kind of information is relevant? How is the information collected and who owns it? What are the possibilities of different methods and what limitations do they have? How to get methods into the production? And many others.

5. References

[1] EQUA Simulation AB. IDA Indoor Climate and Energy URL: https://www.equa.se/en/ida-ice (referred 3.1.2022).

[2] Rasmussen, Carl Edward., and Christopher K. I. Williams. Gaussian Processes for Machine Learning. Cambridge, Mass: MIT Press, 2006. Print.

[3] J. Görtler, R. Kehlbeck ja O. Deussen. A Visual Exploration of Gaussin Processes. URL: https://www.jgoertler.com/visual-exploration-gaussian-processes/ (referred 3.1.2022).

[4] Géron, Aurélien. Hands-On Machine Learning with Scikit-Learn and TensorFlow: Concepts, Tools, and Techniques to Build Intelligent Systems. Sebastopol: O'Reilly Media, Incorporated, 2017. Print.

[5] Duvenaud, David. Automatic model construction with Gaussian processes. Dissertation. 2014.

[6] Vanhatalo, J., Riihimäki, J., Hartikainen, J., Jylänki, P., Tolvanen V., and Vehtari, A.. GPstuff: Bayesian Modeling with Gaussian Processes Journal of Machine Learning Research. 2013; 14(Apr):1175-1179.

Data Statement

The datasets generated during and analysed during the current study are not publicly available because the data is owned by the local energy company and the housing associations but will be available anonymously on request.

Next generation energy performance assessment methods for EPCs using measured energy data

Jan Verheyen [a,b], Evi Lambie [c,d], María Fernández Boneta [e], Iná Maia [f], Lukas Kranzl [g], Theresa Urbanz [h], David Frick [i]

[a] Unit Smart Energy and Built Environment, VITO, Mol, Belgium, jan.verheyen@vito.be

[b] EnergyVille, Thor Park, Genk, Belgium, jan.verheyen@energyville.be

[c] Unit Smart Energy and Built Environment, VITO, Mol, Belgium, evi.lambie@vito.be

[d] EnergyVille, Thor Park, Genk, Belgium, evi.lambie@energyville.be

[e] Energy in Buildings Department, National Renewable Energy Centre, Navarra, Spain, mfboneta@cener.com

[f] Technische Universität Wien, Austria, maia@eeg.tuwien.ac.at

[g] Technische Universität Wien, Austria, kranzl@eeg.tuwien.ac.at

[h] Energie Agentur Steiermark gGmbH, Graz, Austria, theresa.urbanz@ea-stmk.at

[i] Energie Agentur Steiermark gGmbH, Graz, Austria, david.frick@ea-stmk.at

Abstract. The European Union (EU) aims at net-zero greenhouse gas emissions by 2050, with intermediate quantified targets in 2030. To achieve these long-term objectives, the renovation rates in the building sector should be increased. Therefore, as part of the European Green Deal, the EU has initiated the renovation wave initiative with the ambition to at least double the annual renovation rate and to foster deep renovation. An important tool to raise awareness regarding the building energy performance and the need for renovation is the energy performance of buildings certification (EPC). The EPC was already introduced in the Energy Performance of Buildings Directive (EPBD) in 2002 (2002/91/EC) and is a specific focus of the upcoming revision of the EPBD. Currently, EPCs are mostly based on calculation of theoretical performance. Despite challenges such as correction for actual occupant behaviour and weather conditions, the inclusion of measured data of building energy use may lead to additional benefits, improve the quality, reliability and usability of next-generation EPCs. On the one hand, energy performance indicated based on actual energy use data relates better with non-experts understanding of energy consumption and bills. On the other hand, the actual energy use data can attribute to a more efficient and accurate reflection of the actual energy performance of a building. Such aspects are important for augmenting user acceptance and increasing trust in the market, which in turn may lever renovation rates.

This paper presents energy performance indicators based on measured building energy use, either to replace or to supplement EPC indicators currently in use. First, state of the art approaches for energy performance evaluation based on data of measured energy use or related parameters are described. Next, implementation cases are presented that are being developed in the frame of EU H2020 research projects ePANACEA and X-Tendo. Finally, the outline of future work within these projects is given.

Keywords. Energy performance certification, Measured energy performance, Operational rating, Smart buildings, Data driven modelling.
DOI: https://doi.org/10.34641/clima.2022.260

1. Introduction

The EU has set forward the ambition to attain net-zero greenhouse gas emissions by 2050, with intermediate quantified targets in 2030, which were recently updated and aim at a reduction of the CO_2 emission with 55% by 2030 compared to 1990 levels. Since buildings are responsible for approximately 40% of energy consumption and 36% of CO_2 emissions in the EU [1], the energy performance in the building sector needs to be improved to achieve the long-term objectives. Policy

Copyright ©2022 by the authors. This conference paper is published under a CC-BY-4.0 license.

measures in relation to new or thoroughly renovated buildings have been deployed, expanded and tightened throughout the recent 1,5 decade, but efforts to reduce the greenhouse gas (GHG) emissions in the existing building stock need to accelerate. Currently only 1% of European building stock undergoes energy-efficient renovation every year [2], while an average annual renovation rate – expressing the (equivalent) share of building stock that undergoes deep renovation - of more than 3% is required [3]. Therefore, as part of the European Green Deal launched in 2020, the EU has initiated the Renovation Wave initiative with the ambition to at least double the annual renovation rate in the next 10 years and to foster deep renovation.

An important tool to raise awareness regarding the building energy performance and the need for renovation is the energy performance of buildings certification (EPC), which was already introduced in the Energy Performance of Buildings Directive (EPBD) in 2002 (2002/91/EC), followed by implementation starting from 2006. EPCs could effectively instigate renovation in the EU if the full potential was explored [4]. There is a need to provide an improved and more reliable service tailored to the end-users [4] [5]. A report by Buildings Performance Institute Europe (BPIE) published in 2014 indicates that EPCs are mostly based on a theoretical calculation [6], a situation that barely changed since [4]. Despite challenges such as correction for actual occupant behaviour and weather conditions, the inclusion of measured data of building energy use or related aspects may lead to additional benefits, improve the quality, reliability and usability of next-generation EPCs. On the one hand, energy performance indicated based on actual energy use data relates better with non-experts understanding of energy consumption and bills. On the other hand, the actual energy use data can attribute to a more efficient and accurate reflection of the actual global or part energy performance of the building and more accurate energy assessments of energy efficiency measures. Such aspects are important for augmenting user acceptance and increasing trust in the market, which in turn may lever renovation rates.

It is shown that significant differences between energy use determined on calculation and actual energy use can occur, a phenomenon known as the 'energy performance gap' [7] [8] [9] [10] [11]. The actual energy use in buildings could be as much as 2,5 times the predicted or simulated energy use [11], but no clear or definitive quantification is available [10]. The most important causes contributing to the energy performance gap can be attributed to occupant behaviour (the use of thermostats, windows, blinds, etc…), micro-environment (outdoor climatic conditions) and design versus as-built issues [11] including the use of conservative default values as an input in case of missing or incompliant information [12]. There is also the aspect of modelling; calculation methods and simulation tools – especially the simplified ones – do not accurately represent the full details of physical reality. Apart from this inaccuracy of such EPC assessment methods, the resulting indicators also cause confusion for the end-users because of the difference with metering or billing information and the expression in primary energy instead of final energy.

In order to explore the potential of advanced performance assessment methods and to evolve towards next-generation EPCs, a call for proposals was launched on "Next-generation of Energy Performance Assessment and Certification" as part of the H2020 program [13]. This paper is based on synergies and discusses the results in relation to introducing energy consumption data in 'next generation EPCs' investigated in two co-funded projects, X-tendo, "eXTENDing the energy performance assessment and certification schemes via a mOdular approach", https://x-tendo.eu/ and ePANACEA, "Smart European Energy Performance AssessmeNt And CErtificAtion", https://epanacea.eu/.

X-tendo aims to support public authorities in the transition to next-generation EPC schemes, including improved compliance, reliability, usability and convergence. X-tendo envisions a toolbox as a key output: a freely available online knowledge hub that will contain 10 innovative EPC features that can be implemented in addition to existing EPC practices. The 10 innovative features are categorized into two main groups. Group one consists of the innovative EPC indicators, including smart readiness, comfort, outdoor air pollution, real energy consumption and district energy. Group two comprises the Innovative EPC data handling functionalities, including EPC databases, building logbook, enhanced recommendations, financing options, and one-stop-shops.

ePANACEA aims to overcome the current EPC challenges with a special focus on the performance gap between calculated and actual consumption patterns, incorporation of the user dimension and the improvement of clarity of the information provided by the EPC. ePANACEA develops a holistic methodology based on three different energy assessment methods and its decision matrix, covering technical building innovations and the use of actual building data for energy modelling. The whole methodology will be integrated on a prototype online platform SEPAP (Smart Energy Performance Assessment Platform). The vision is ePANACEA becoming a relevant instrument in the European energy transition through the building sector.

2. State of the art approaches for energy performance assessment based on measured energy use

Distinction between approaches that include measured data in energy performance assessment can be made according to different categorization aspects. The approaches can be categorized according to for instance the mathematical calculation principles applied, the type of corrections that are implemented, the resulting output(s) or the purpose they serve.

A review of approaches using measured data in (part) energy performance assessment methods is included in the X-tendo deliverable 3.1. Table 1, adopted from the publication, gives an overview of characteristics of energy performance assessment methods, categorized according to the type of method applied. In view of selecting approaches suitable for integration in EPC practices, the approaches are categorized in the report according to three types; Building-level simple approach; Building-level detailed approach and Stock-level model development. Further details on the approaches can be found in the X-tendo deliverable report D3.1 [12].

Tab. 1 – Overview of energy performance assessment methods and characteristics [12].

Method	Inputs	Accuracy	Applications	Restrictions
Engineering calculations	Simplified building information	Variable	Design, end-use evaluations, Highly flexible	Limited accuracy
Simulation	Detailed building information	High	Design, Compliance, Complex buildings, Cases where high accuracy is necessary	Dependent on user skill and significant data collection
Statistical	Dataset of existing buildings	Average	Benchmarking systems, Simple evaluations	Dependent on statistical data, Limited accuracy
Machine learning	Large dataset	Average to high	Buildings with highly detailed data collection, Complex problems with many parameters	Model construction is complicated, Do not consider direct physical characteristics
Limited postprocessing	Data of measured energy use	Variable	Simple evaluation, Historical benchmark	Including non-standard influences

In EN 52000-1 [7] distinction is made within the measured energy performance approaches between actual, climate corrected, use corrected and standard measured energy performance, depending on what corrections are applied to the measured energy use input data.

Energy performance assessment methods based on measured energy use data vary from very simple to relatively complex approaches. In its simplest form, the energy use data of a previous one-year period of the in-use building is directly included in an EPC after some limited processing of the data. Such processing consists of essential corrections required to consider the resulting output as an energy performance indicator [7]. These corrections mainly aim to exclude the non-EPC related energy uses and correct for non-standard influences of user behaviour and climate for the purpose of inter-building comparison and comparison of the energy performance over time.

Statistical techniques are implemented in data-driven modelling [14], using data of energy use complemented by other data such as the outdoor climatic conditions. These can be further subdivided in black-box modelling (including machine learning [15]), in which the structure of the model and the model parameters are determined solely from the measurement data, and grey-box modelling, a hybrid approach that combines a mathematical description of the building's physical model with data-driven statistical modelling techniques [16]. Such approaches are also implemented for the characterization of parameters related to the energy performance of the building or components of it. These parameters can serve directly as a part energy performance indicator or as an accurate input of (simplified) energy performance calculation methods. An example of such approaches to determine a part energy performance parameter is the whole building heat loss coefficient characterization [17]. In addition to these characterization methods, specific data-driven modelling techniques exist that enable the disaggregation of energy use across its constituent parts, such as the separation between gas use for domestic hot water and for space heating, or the quantification of electrical energy use for appliances [18] [19].

The energy performance of a building may also be determined by detailed dynamic energy balance simulation models that are calibrated based on measurements of the building energy use [20]. Such approach is currently considered less suitable for integration in EPC frameworks because of its complexity and related issues [12].

3. Implementation

3.1 X-tendo MEPI method

In the X-tendo project an EPC indicator is developed that expresses the energy performance of a building unit based on measured energy use and related data; Measured Energy Performance Indicator (MEPI). It can be applied to most types of buildings; residential single family houses, individual apartment units, multi-family houses, commercial and public buildings. It is not intended to be applied

to industrial buildings. The MEPI can be used for certification potentially replacing existing energy performance indicators or it may solely serve informative purposes for instance for use in addition to existing EPC indicators currently applied in practice.

The MEPI determination method follows the general principles as described in EN 52000-1 series [7] and is inspired by other methods, such as the Swedish energy performance determination method based on measured energy used data [21].

The main input on the building level consists of measurement data of energy delivered to and exported from the building unit per energy carrier and per application. The meters required in the monitoring infrastructure can consist of electricity, gas, oil, heat meters or several of those. The number, type and location of the (sub)meters depend on the system and building architectural configuration. It is expected that availability, prevalence and quality of low cost sensor devices will increase substantially in the upcoming years. It was nevertheless acknowledged within the X-tendo consortium that the required monitoring infrastructure in most cases is not present in the existing building stock. The calculation tool is therefore complemented by a report with options to process real energy use data to represent part or global energy performance that may be used in cases with limited amount or detail of information or in very complex buildings (e.g., malls, hospitals) where the theoretical approach would be time consuming and costly. This additional report is planned to be published in the upcoming months.

Default corrections are applied to the space heating and cooling energy delivered to the building unit for external climatic conditions by means of heating degree-days and cooling degree-days method. Correction methods for solar irradiation, for domestic hot water energy and for indoor temperature are included optionally, with the default choice to also implement these corrections.

In the calculation procedure, a distinction is made between two types of energy carriers for the reason that energy carriers delivered from on-site are restricted in the amount of energy available for delivery to the building and obtain priority, while others are considered to be able to deliver the remaining energy that is required within normal conditions of climate and use.

The output of the MEPI methodology contains more than one indicator member states can choose from to adopt within their existing EPC practices. The default indicator is the non-renewable primary energy performance EPnren for the case Minus exported on-site produced electrical energy. This represents the annual specific primary standard measured energy performance calculated using the non-renewable primary energy conversion factors and taking into account the electrical energy produced on site and exported. The latter is accounted for as a reduction of the primary energy use by the avoided impact of electricity from the grid. Also as default indicators, the Renewable energy ratio RER and specific CO_2 equivalent emissions CO2eq both for the case Minus exported on-site produced electrical energy are reported.

A calculation spreadsheet [22] with accompanying guidelines [23] of the measured energy performance indicator including a description of the calculation algorithms is available on the X-tendo website (www.X-tendo.eu).

3.2 ePANACEA methodology

Within ePANACEA, several methods are developed to identify the energy performance based on on-board-monitoring data. Hereto, the data of 15 real-life cases (both residential and non-residential) is used to iteratively validate and improve the developed methodologies. One of the methods developed within ePANACEA elaborates the MEPI tool of X-tendo, which is possible because of the availability of more detailed high frequency (sub-)hourly data. Three alterations/additions are applied;

1) The heating and cooling degree days are calculated from measured high frequency outdoor and indoor temperatures, by comparing with the outdoor temperature of no heating/cooling required. In the MEPI tool, heating degree days (HDD) and cooling degree days (CDD) are calculated with a default indoor temperature and national or regional monthly outdoor temperatures. Correction for a deviating average indoor temperature during heating season is optional.

2) The domestic hot water is corrected for the number of default occupants and then extrapolated to the full year by means of the number of days. In the MEPI tool, in case the system efficiency is known, the energy demand for domestic hot water (DHW) is replaced by a calculated average value for the respective building characteristics. If efficiency is not known, the measured energy delivered for domestic hot water is corrected to the actual occupancy rate.

3) Self-consumption is derived based on the actual hourly measurement of the PV generation, which is linearly extrapolated and calibrated to the full year by means of solar radiation hourly profile from a standard year. In the MEPI tool, correction for actual solar irradiation is optional. In case the option is not retained, the measured energy yield from solar systems is recalculated to a full year based on standard national or regional values for solar irradiation.

Often the consumption for final energy usage per application (e.g. heating, DHW, cooling) is not

measured separately. Instead, it is available as an energy carrier quantity (e.g. gas, oil, electricity). Depending on the frequency of the measurement, several methods are specifically developed and investigated in ePANACEA for disaggregation of energy carrier quantity data to the final energy uses of the various applications.

The ePANACEA methods allow to derive input parameters from measured values to replace theoretical inputs in existing energy performance calculation methods or enable the determination of additional energy performance indicators. The methods can thus be implemented to increase accuracy and reliability of the EPC indicator in use in local practice or as an extra energy performance indicator providing valuable additional information.

3.3 example with virtual buildings

The specifications, the technical functionalities, the usability and sensitivity of the calculation procedure were analysed by executing the calculation procedure of the MEPI with all options included for a set of theoretically composed residential reference buildings for 3 locations in Europe (Palermo, Bratislava and Helsinki).

Definitions of the climatic zones for Northern (N), Central (C) and Southern (S) EU are adopted from the Aldren project [24].

A reference single family house (SFH) and a reference apartment unit (APT), adopted from ISO/TR 52016-2 [25] - example 1 and 2 respectively - are used in the verification calculations. For each building case, two variants were considered; one to represent low energy performance level of the current building stock (Old) and one to represent a new or renovated building energy performance level (New). Missing characteristics to complete MEPI calculation inputs are further specified, such as system specifications. These include for the New cases good airtightness, a demand controlled mechanical exhaust ventilation system, PV and a new air/water heat pump for space heating and domestic hot water. Old cases have stock representative thermophysical properties and system efficiencies, natural ventilation and no PV. The actual number of inhabitants is set to 4 for SFH and 2 for APT. The annual energy use data per energy carrier and per application are based on building stock net energy use indicators from JRC IDEES library [26] (data of 2018) for the location of Belgium and translated to the three climatic zone locations using HDD for space heating energy use, CDD for space cooling energy use and solar irradiation for PV delivered electrical energy estimation.

The results of these verification calculations are included in table 2 and evaluated based on expert judgement to be in line with what in general can be expected.

Tab. 2 – MEPI verification calculation results.

Case	EPnren [kWh/(m^2.a)]	RER [-]	C2_eq [kg/(m^2.a)]
SFH_New_N	141	0,36	26
SFH_Old_N	309	0,00	61
APT_New_N	125	0,40	23
APT_Old_N	394	0,00	77
SFH_New_C	53	0,51	10
SFH_Old_C	175	0,01	35
APT_New_C	29	0,67	5
APT_Old_C	179	0,01	35
SFH_New_S	19	0,73	3
SFH_Old_S	113	0,05	22
APT_New_S	-7	1,15	-1
APT_Old_S	119	0,05	24

The energy gap is clearly present in the results from the table. The prebound effect- occupants use on average less energy compared to the calculated energy use and this increases with increasing calculated energy use [27] - is shown: the energy performance of old cases is better (lower EPnren values) than estimated by calculations. Vice versa, the rebound effect – occupants tend to use more energy compared to calculated energy use in low energy buildings [27] - is identified for the new cases, which perform not as good (higher EPnren values) as expected, although part of it is also explained by the fact that energy use data originate from 2015 and energy performance requirements have evolved since.

The insulation levels were not adapted to the climatic zones, which is reflected in poorly performing building cases in Northern EU climate. The new building variants in this climate perform rather poorly compared to those in the other climatic zones, which can be partly explained by a low efficiency of the heat pump: the air source heat pump efficiency depends on the outdoor air temperature .

When exported energy outweighs the delivered energy in the balance – which also is reflected in a RER value exceeding 1 – EPnren (default case is Minus exported on-site produced electrical energy) show negative values. Old cases in Central and Southern EU do not have heat pumps nor PV but also have RER values higher than one due to the space cooling air-conditioner outdoor condenser that contributes to ratio of renewable energy RER. In Northern EU climatic zone, energy delivered for space cooling is assumed equal to zero, so RER for Old cases there is equal to zero.

The verification outcomes do not reveal errors,

anomalies or unexpected outcomes. The analysis described above verifies the outcomes which confirms correct implementation of the MEPI calculation method in the calculation tool. The results of the findings on aspects of functionalities, usability and clarity of the calculation tool from the verification calculations were used to improve the calculation and guideline tools, currently released as a beta version of the MEPI Calculation tool.

3.4 real-life case examples

The Within ePANACEA measurement data of 15 real-life cases located in 5 European countries are used to develop, improve and validate the three assessment methods. In this paper, the results of the EPANACEA method 1 for a Belgian case (BE) and an Austrian case (AT) are shown as an example and compared to results of the X-tendo MEPI tool. In the MEPI-tool, we opted to correct for (1) an indoor temperature that deviates from the default value, (2) DHW with known system efficiency and (3) the default solar radiation. Importantly, the X-tendo MEPI method is applied although the data does not comply to the requirements of duration of monitoring period; only two month period data are available, while MEPI requires uninterrupted period of at least 12 entire months. It is decided to proceed with these short period datasets within the context of this paper to enable comparison.

The Belgian case is a terraced house located in the city of Ghent, which was originally constructed in 1904 and renovated in 2017. For the period from the 1st of December 2017 until the 31st of January 2018 measurements were performed for a set of parameters, amongst others: the energy use, indoor climate, outdoor climate and user behaviour. As a result, an average indoor temperature of 18.8°C and outdoor temperature of 5.7°C was defined for the monitoring period, and additionally the total gas consumption was found to be 3006.8 kWh and the electricity consumption 511 kWh. To be able to split the gas consumption into energy use for space heating and domestic hot water (DHW), a questionnaire was performed to get insight in occupant-related characteristics, which enabled to estimate the energy use for DHW. It should be noted that there is no renewable energy system in this case.

The Austrian case is a newly built terraced house constructed in 2018, which is part of a multi-family building block. Measurement data was available from the 17th of October 2019 till the 31st of December 2019 for a similar set of parameters as the Belgian case. For the monitoring period, the average indoor temperature in the living room was 22.5°C, while the average outdoor temperature was 5.1°C. The total electricity use of the building was found to be 561.1 kWh, while for space heating 1318.8 kWh and for domestic hot water 405.3 kWh was used for a biomass boiler.

Starting from this monitoring data, the corrected energy use for a full year could be estimated, using the X-tendo and the ePANACEA correction methods respectively. Hereby the default outdoor climate and a constant indoor temperature of 18°C were considered as boundary conditions. The results are summarized in Fig. 1.

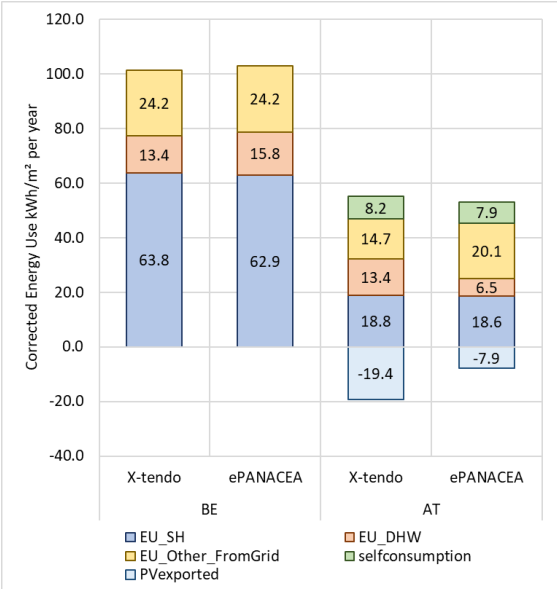

Fig. 1 - Results of the correction of the two real-life cases of ePANACEA and X-tendo (Belgian case BE and Austrian case AT). Note that the X-tendo method is applied using short period data, which does not comply to the requirements of duration of the monitoring period.

Fig. 1 distinguished different types of energy uses: space heating (EU_SH), domestic hot water (EU_DHW), electricity from the grid for other appliances (EU_Other_FromGrid), the generated electricity that is consumed on site (selfconsumption) and the generated electricity that is exported to the mains grid (PVexported). This shows that for the Belgian case the results of the two methods are very similar for space heating and the electricity use from the grid, but not for the domestic hot water. For the electricity from the grid there is no difference (since the same method is used), while for space heating the difference is only 2%. For the energy use of domestic hot water the difference is more significant (18%), since the energy demand for DHW is replaced by a default value within the MEPI methodology, while the ePANACEA method corrects the measured energy demand.

For the Austrian case, on the other hand, only the energy use for space heating is similar for the two methods while for the other energy flows the differences are more significant. The energy use for space heating differs with only 1%, while the energy use for domestic hot water is 50% lower for the ePANACEA method, and the electricity use from the grid is about 30% higher. The generated electricity exported to the main grid also differs significantly

(60% lower for the ePANACEA method).

This indicates that incorporating the heating degree day method at a higher frequency has rather a limited impact on the correction results, while calculating the energy use for domestic hot water based on the number of occupants and a detailed self-consumption calculation have a large impact. However, it is impossible to quantify the accuracy of the two methods. Furthermore, the impact of the use of short term monitoring data instead of a minimum duration of monitoring of an entire year for the X-tendo MEPI method is not quantified. As the X-tendo method should only be applied for data of a monitoring period of at least one year, the magnitude of the comparative results from X-tendo and ePANACEA methods should be interpreted considering a possible and likely bias as a result of this, as well as the very limited number of cases (2). Which method should be preferred strongly depends on the implementation context and correction parameters.

4. Conclusions

State of the art methods and implementation examples of energy performance assessment methods based on actual energy use data as developed in EU H2020 research projects X-tendo and ePANACEA are presented together with theoretical and real-life cases. Results from the example cases contribute to verification of the method's results and hint at extending the real-life case analysis programme in the next steps. As it is known that inclusion of actual energy used data in EPC may improve the quality, reliability and usability of EPCs, such methods support public authorities in the transition to next-generation EPC schemes.

5. Outline of future developments

In a next step of the presented approach, there is a need for validating the methods by applying them on a larger set of case studies. These real life cases should also include long-term monitoring period for correct implementation of the X-tendo MEPI method and also more cases need to be included to compare results from both X-tendo and ePANACEA methods. Currently the MEPI methodology also is tested in actual buildings in 4 countries.

Within ePANACEA, the developed methods are demonstrated and validated with regard to their reliability, accuracy, user-friendliness and cost-effectiveness through 15 case studies in 5 European countries (Austria, Belgium, Finland, Greece and Spain). These methods will be implemented in the Smart Energy Performance Assessment Platform. Additionally, a decision matrix will be developed in order to provide guidance or recommendation on the most suitable method to use with reasonable accuracy and uncertainty levels. Beyond ePANACEA, the SEPAP is a customizable tool that could be adapted to particularities and requirements at member state level. It also allows the joint implementation of energy performance certification with other policy instruments. The digitalization of information through the use of common data bases, including actual building data, easily accessible through web platforms, like the SEPAP, that also allow implementing different assessments is a key aspect to build the link between all of these policy instruments. Then, a common use of data sources can be established for all of them, also ensuring common data formats (interoperability) for information exchange between different platforms.

6. Acknowledgement

The information published in this paper contains results of research partly funded by the European Commission within the Horizon 2020 programme; Grant Agreement number: 845958 — X-tendo — H2020-LC-SC3-2018-2019-2020/H2020-LC-SC3-EE-2018; Grant Agreement number: 892421 — ePANACEA — H2020-LC-SC3-2018-2019-2020 / H2020-LC-SC3-EE-2019.

7. Data access statement

The datasets generated during and/or analysed during the current study are not available because the privacy of the inhabitants must be respected (GDPR regulations) but the authors will make every reasonable effort to publish them in near future.

8. References

[1] European Commission. New rules for greener and smarter buildings will increase quality of life for all Europeans. European Commission; Brussels, Belgium; 2019.

[2] European Commission. Renovation wave. European Commission; Brussels, Belgium; 2021 Aug.

[3] Laski J., Burrows V. From thousands to billions coordinated action towards 100% net zero carbon buildings by 2050. World Green Building Council; Torronto, Canada; 2017.

[4] Volt J. et al. Energy performance certificates - Assessing their status and potential - X-tendo deliverable 2.1. Buildings Performance Institute Europe (BPIE); 2020 Mar;

[5] Li Y., Kubicki S., Guerriero A., Rezgui Y. Review of building energy performance certification schemes towards future improvement. Renew. Sust. Energ. Rev. 2019 Oct;113:109-244.

[6] Arcipowska A. et al. Energy performance certificates across the EU: a mapping of national approaches. Buildings Performance Institute Europe (BPIE); Brussels, Belgium; 2014 Oct. 60p.

[7] European Committee for Standardization. EN ISO 52000-1: Energy performance of buildings – Overarching EPB assessment –Part 1: General framework and procedures. European Committee for Standardization (CEN); Brussels, Belgium; 2017 Jul.

[8] Borgstein E.H., Lamberts R., Hensen J.L.M. Evaluating energy performance in non-domestic buildings: A review. Energy Build. 2016 Sep 15;128:734-55.

[9] Laurent M.-H., Allibe B., Oreszczyn T., Hamilton I., Tigchelaar C., Galving R. Back to reality: How domestic efficiency policies in four European countries can be improved by using empirical data instead of normative calculation. Proceedings of the ECEEE summer study: Rethink, renew, restart; 2013 Jan;2057-70.

[10] Shi X., Si B., Zhao J., Tian Z., Wang C., Jin X., Zhou X. Magnitude, causes, and solutions of the performance gap of buildings: a review. Sustainability 2019 Feb;11(3):937.

[11] Zou X.W., Xu X., Sanjayan J., Wang J. Review of 10 years research on building energy performance gap: Life-cycle and stakeholder perspectives. Energy Build. 2018 Sep 5;178:165-81.

[12] Zheikh Z. et al. Exploring innovative indicators for the next generation energy performance certificate features – X-tendo Deliverable 3.1. Buildings Performance Institute Europe (BPIE); Brussels, Belgium; 2020 Jun. 155p.

[13] European Commission. CORDIS EU research results – Next-generation of Energy Performance Assessment and Certification. European Commission; 2018 Nov.

[14] Madsen H. et al. IEA-EBC Annex 58: Reliable building energy performance characterization based on full scale dynamic measurements; Report of subtask 3, part 2: Thermal performance characterization using time series data – statistical guidelines. KULeuven; Leuven, Belgium; 2016 Nov 28. 85p.

[15] Seyedzadeh S., Rahimian F. P., Glesk I., Roper M. Machine learning for estimation of building energy consumption and performance: a review. Vis. in Eng. 2018 Oct 2;6.

[16] Janssens A. IEA-EBC Annex 58: Reliable building energy performance characterization based on full scale dynamic measurements – Report of Subtask 1b: Overview of methods to analyze dynamic data. Ghent University; Ghent, Belgium; 2016 Jun. 64 p.

[17] Senave M. Characterisation of the Heat Loss Coefficient of Residential Buildings Based on In-use Monitoring Data [Phd-thesis]. [Belgium, Leuven]: KU Leuven; 2019 Dec.317 p.

[18] Bacher P., de Saint-Aubin P., Christiansen L., Madsen H. Non-parametric method for separating domestic hot water heating spikes and space heating. Energy Build. 2016 Oct 15;130:107-12.

[19] Senave M., Reynders G., Sodagar B., Saelens D. Uncertainty in building energy performance characterization: Impact of gas consumption decomposition on estimated heat loss coefficient. Proceedings of the 7th International Building Physics Conference (IBPC); 2018 Sep 23-26; Syracuse, NY, USA:1491-6.

[20] Krstić H., Teni M. Review of methods for buildings energy performance modelling. IOP Conf. Ser.: Mater. Sci. Eng. 2017;245.

[21] Boverket. Boverkets författningssamling (Swedish building code regulation). Boverket (the Swedish National Board of Housing, Building and Planning); Sweden; 2017 Jun 26.

[22] Verheyen J. et al. X-tendo Feature 4: Real energy consumption: Calculation spreadsheet – Beta-version. VITO; Genk, Belgium; 2021 Aug.

[23] Verheyen J. et al. X-tendo Feature 4: Real energy consumption: Guidelines – Beta-version. VITO; Genk, Belgium; 2021 Aug. 44p.

[24] Bendzalova J. et al. D2.2 - ALDREN Methodology note on energy rating procedure. ENBEE; Slovakia; 2019 Apr 30. 140p.

[25] European Committee for Standardization. ISO/TR 52016-2: Energy performance of buildings - Energy needs for heating and cooling, internal temperatures and sensible and latent heat loads - Part 2: Explanation and justification of ISO 2016-1 and ISO 52017-1. European Committee for Standardization (CEN); Brussels, Belgium; 2017 Jul.

[26] Nijs W., Ruiz P. 02_JRC-EU-TIMES Building Stock Module. European Commission, Joint Research Centre (JRC) [Dataset] PID: http://data.europa.eu/89h/c2824007-5e24-4380-ac02-e391fdb1e9de. 2019.

[27] Sunikka-Blank M., Galvin R. Introducing the prebound effect: the gap between performance and actual energy consumption. Build. Res. Inf. 2012 Jun 1;40(3):260-73.

Placement and utilization of CO_2 measurements in the ventilation and occupancy assessments

Antti Mäkinen [a], Sampo Saari [b], Sakari Uusitalo [a], Jussi-Pekka Juvela [a], Leila Kakko [c]

[a] School of Built Environment and Bioeconomy, Tampere University of Applied Sciences, Tampere, Finland, antti.j.makinen@tuni.fi, sakari.uusitalo@tuni.fi, jussi-pekka,juvela@tuni.fi

[b] School of Pedagogical Innovations and Culture, Tampere University of Applied Sciences, Tampere, Finland, sampo.saari@tuni.fi

[c] School of Business and Media, Tampere University of Applied Sciences, Tampere, Finland, leila.kakko@tuni.fi

Abstract. Continuous carbon dioxide measurements have typically been used to adjust the demand-based ventilation. With the global COVID-19 pandemic, the use of measurements to ensure the functionality of ventilation and to assess the utilization rate of the space has increased in importance due to the significant impact of air exchange on the spread of the disease via aerosols. The work aimed to examine the spread of carbon dioxide in the room and how the location of the sensors and space users affects the measurement result. In our study, six carbon dioxide sensors were placed in the room that serves as a teaching restaurant. Five sensors were placed in the space itself and one sensor in the exhaust valve. Two meals were arranged, each attended by 10 people. The location of the persons in the space was also monitored. Based on the measurements, it was assessed how the air distribution of the space and the location of the users affected the measurement result of carbon dioxide. It was found that the carbon dioxide content measured close to diners differed from the result measured in the exhaust duct. Because the air in the exhaust duct is mixed with more fresh supply air than in the vicinity of the dining table, it can be thought that the concentration measured in the exhaust duct can indicate better the air variability of the whole space. On the other hand, sensors located closer to the seating area are potentially better positioned from the demand-based ventilation point of view. In the future, it will be necessary to study the issue in more detail for different types of premises and to examine the application of ventilation and space utilization assessment to real-time monitoring of the risk of airborne infectious diseases, for example.

Keywords. Ventilation, Carbon Dioxide, COVID-19, Occupancy
DOI: https://doi.org/10.34641/clima.2022.68

1. Introduction

Over the recent years, measuring room carbon dioxide levels in buildings and using this information to either control ventilation or collect data on the conditions has increased. A question that arises, however, is how well the installed measurement corresponds to the actual levels of CO_2 in a room and which are the factors that may cause discrepancies between the two.

Since the beginning of 2020 SARS-CoV-2 virus and its different variations have spread throughout the world and there have been numerous research papers attempting to describe the transmission of the virus in different kinds of settings. Some papers, for example, emphasize the role of airborne transmission and consequently, the role of ensuring sufficient indoor ventilation becomes one of importance. [5] Mathematical models have been formulated to estimate the probability of transmission of respiratory pathogens in indoor settings. One of these models is the Wells–Riley infection model which among other factors takes into account the room ventilation rate. [2]

CO_2 can be used as a control parameter for demand-based room ventilation control. Additionally, it can also be used in the evaluation of the sufficient room ventilation rate. Thus, indirectly a connection between CO_2 levels and virus transmission probability may be formulated further underlining the need for reliable CO_2 measurements.

In this paper, we present a pre-study test and demonstration methodology for examining the effect of placement of the CO_2 measuring devices on the measured results. The placement is examined in

Copyright ©2022 by the authors. This conference paper is published under a CC-BY-4.0 license.

relation to supply and extract terminals of ventilation but also in relation to occupant placement and distribution. Additionally, we demonstrate a concept of data collection on CO_2 levels and occupancy rates that may be used to further examine sufficient ventilation rates and airborne infection risk probabilities.

1.1 The effect of carbon dioxide on human health and cognitive abilities

As humans spend time indoors exhaling produces carbon dioxide and this will elevate the concentration of CO_2 in the room. The effects of elevated CO_2 levels on human health and decision-making have been widely discussed. For example, Satish et.al. have found that some moderate decrements in decision making may occur already on CO_2 levels between 600…1000 ppm [7]. On the other hand, some studies critique that some of the research on the issue may be inconclusive. Du et.al. argue that some cases may have failed to achieve uniform distribution of CO_2 inside the room where experiments on cognitive performance have been made and thus the inhaled amount of CO_2 is not accurately known [3]. This begs the question: If the CO_2 concentration is non-uniformly distributed, could this happen in any significant amount, and if so, in what kind of settings could this occur?

1.2 CO_2 measurements and mechanical ventilation control

CO_2 concentration can be used to control mechanical ventilation inside a room via a variable air volume ventilation system. This can be achieved for example by setting a corresponding air exchange volume to the CO_2 concentration value. The air exchange rate will in this case increase linearly as the CO_2 concentration rises. This kind of control is typically used to restrict ventilation to a minimum level needed to maintain indoor conditions thus saving the fan power and energy needed to heat or cool the air.

Additionally, if it's assumed that air is fully mixed inside the room, dependence between the room ventilation rate, the number of occupants, and the CO_2 concentration can be derived using a fully mixed mass balance model. If two of these are known, the third one can be calculated. For example, Franco et.al. [4] have used that model in their article as follows:

$$V\frac{dC_{CO2}(t)}{dt} = \dot{r}\, n_{occ} - \dot{m}\,(C_{CO2}(t) - C_{ext})$$

where C_{CO2} is the concentration of CO_2 inside the room, V the total volume of the room, n_{occ} the number of occupants, $\dot{r}$ the CO_2 generation rate per person, $\dot{m}$ the airflow rate due to ventilation, and C_{ext} is the CO_2 concentration in the supply air. [4] Thus, if the number of occupants is known the CO_2 concentration can be used to determine the ventilation rate. Conversely, if the ventilation rate is known CO_2 concentration can be used to determine occupancy.

1.3 SARS-CoV-2 transmission mitigation

Ventilation has been found to play a major role in mitigating the transmission risk of the SARS-CoV-2 virus.
Many respiratory pathogens may spread through small respiratory aerosols that can stay airborne for extended periods of time [8].

One of the key factors in the probability of transmission of a virus pathogen via indoor air is the airborne concentration of infectious quanta (quanta/m^3). The larger the quanta the higher the probability of the infection is. Naturally, the amount of ventilation in the room will influence the quanta and studies have found that increased ventilation will reduce the risk of infection as it will lead to diluted quanta concentrations. For example, Miller et.al. show the modelling of the Skagit Valley Chorale super spreader event using the Wells–Riley formulation and what role the ventilation rate would play in such an event [6]. Burridge et.al. studied the applicability of CO_2 measurements in airborne infection risk modelling and concluded that there is a clear need for better mitigation of the airborne spread of the SARS-CoV-2 virus. Building on this notion they also recommend more widespread use of CO_2 monitoring in occupied spaces to ensure sufficient ventilation. [1]

2. Research Methods

2.1 Test room and participants

Catering Studio, a learning environment for Hospitality Management students was the test room in this study. It is composed of two different kitchens, a bar, and a restaurant area. All the measurements were done in the restaurant area, and it worked as a living lab situation to study customers' behaviour while having a buffet lunch. Two one-hour settings were served with ten customers in each. All the diners were taking part in the study voluntarily. Participants got information about the study, hand hygiene, and safe distances.

During the experiments, the room was mechanically ventilated. The air distribution system is mixing ventilation with supply air terminals located in the ceiling in the middle of the room and extract air terminals in the ceiling at the end of the room. The placement of the terminals is presented in Fig. 1. The ventilated airflow was 400 L/s supply and 400 l/s extract air. This air exchange rate corresponds to 5,3 L/s, m^2 and 40 L/s per person (10 persons in the room during the study). The ventilation airflows were observed via the building automation system.

2.2 CO_2 measurements

The CO_2 measurement system consisted of 6 sensors that measured temperature and CO_2 value. The sensors were placed in the locations shown in the floor plan (Fig. 1). The sensors 1, 3 and 5 were on the

floor about 1.6 meters high, which is close to the typical installation height of a room sensor and also close to the average height of breathing of a standing person. The table-level sensors (2 and 4) were about 0.5 meters above the table surface. In addition, one sensor was placed in the exhaust air duct (sensor 6). In addition to the CO_2 sensors, the data for the building automation measurement of the space were stored. The sensors used were Miran DLS-system sensors for CO_2 and relative pressure (Fig. 2). As the purpose of this experiment was to test and demonstrate the method it was not seen necessary to further calibrate the sensors at this point and thus, they were in factory calibration. This can be seen as a possible source of some inaccuracies in the results.

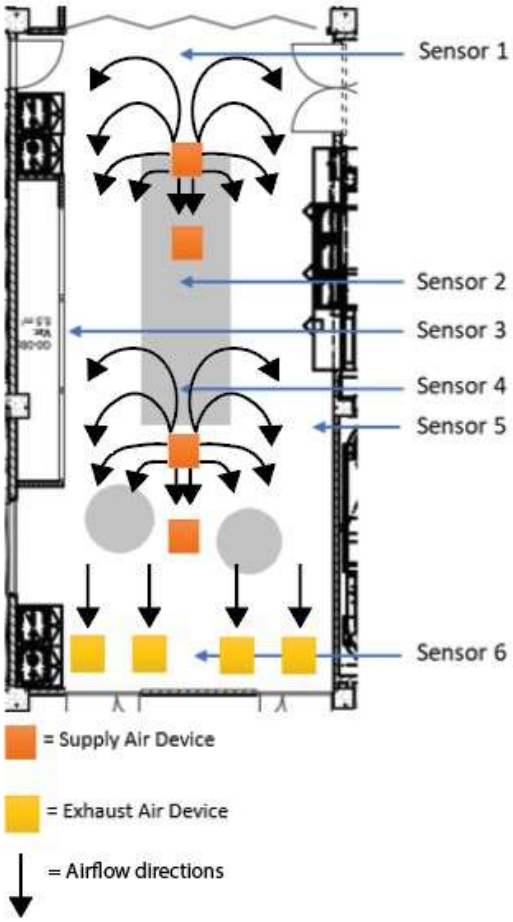

Fig 1: Positioning of the CO_2 sensors, air devices and estimated airflow directions in the room.

Fig 2: Miran DLS IAQ.THB+CO2+DP sensor used in CO_2 measuring

2.3 Personal position tracking

Noccela ID Badge is a UWB based proximity detection device for social distancing and contact tracing, and it sends the contact data to the server via a UWB beacon for Contact Tracing (noccela.com). In this study, it was used to get the position data of the persons in the test room. When the customers entered the restaurant area, they were given these personal badges and they carried them during the lunch.

3. Results

Temporal variations of CO_2 concentrations in the room measured by the sensors are shown in Fig. 3. All the sensors showed a CO_2 level increase when the persons entered the room, but there were some differences between the sensors based on their location in the room. Also, the tracked position of the persons affected the results. Position data of the persons in the room is shown in Fig. 4.

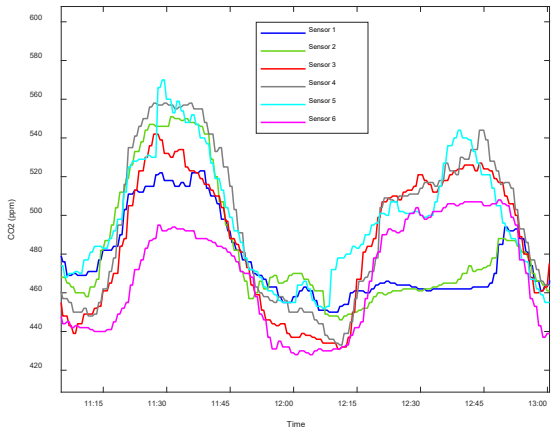

Fig 3: CO_2 concentrations in the room measured by the sensors 1-6.

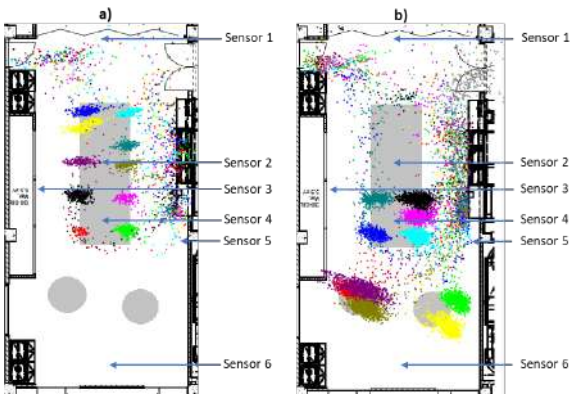

Fig. 4: Positional data of persons in the room **a)** during the first setting (11:00–12:00) and **b)** during the second setting (12:00–13:00). The colours indicate different persons.

During the first setting (11:00-12:00) all the persons had their position mostly at one table far away from the exhaust duct. CO_2 levels of the sensors 2, 4, and 5 showed the highest concentrations as they were located close to the breathing zone of the persons. The sensors 3 and 1 showed a bit lower levels as they were not located so close. The sensor 6 in the exhaust duct showed the lowest CO_2 level. The difference in the breathing zone sensors 2 and 4 was about 70 ppm due to CO_2 dilution before the exhaust duct. The difference in the time of the rising CO_2 between the exhaust duct sensor 6 and the other sensors is about 5 min.

During the second setting (12:00–13:00) the persons chose their seats at three different tables. Now, the sensors 2, 3, and 5 showed the highest values and similar trends as they were located close to the breathing zone. The sensors 1 and 2 showed the lowest CO_2 levels as they were located not so close to the persons and upstream of the airflow in the room. Interestingly, the sensor 6 in the exhaust duct showed higher values compared to the sensors 1 and 2 and similar values compared to the sensors 2, 3, and 5.

4. Discussion and recommendations

Measuring indoor carbon dioxide concentration can have many purposes. On the other hand, it can be used to control mechanical ventilation but also it is usable for monitoring the indoor air quality to ensure healthy indoor conditions. Both aforementioned uses of CO_2 measurements are can already be found in mechanically ventilated spaces. We propose another use for the measurement in the mitigation of transmissible respiratory pathogens. As CO_2 concentration inside a room can be used to derive the ventilation rate in the room it can also be used to derive the approximate probability of the infection. CO_2 measurements provide real-time data, and the infection probability can also be modelled in real-time. Zivelonghi et.al. also discuss this possibility in their research. [9]

Based on the presented results, it can be said that positioning of the sensors in relation to the air stream and persons in the room is important. The CO_2 sensor in the exhaust duct gives an average status and variations of CO_2 levels in the room, but using more sensors, especially close to the breathing zone, provides more accurate information about the exposure to CO_2 and other compounds in exhaled air including also potential pathogens.

While the modelling and calculation of infection probability with different models cannot be considered to provide absolute probabilities but only approximations, the connections between CO_2 concentration, ventilation rates and infection probability in occupied spaces are clearly shown. This lays an interesting foundation for future studies where infection probability could be calculated in dynamically altering situations based on real-time data collection. This could, in effect, lead to the real-time presentation of the infection risk. It's important to note, however, that it should also be studied further how this information on infection probability could or should be effectively used in mitigation.

5. Conclusions

The concept of several CO_2 sensors and personal position tracking data were tested in the restaurant setting to study CO_2 levels in different locations in the room in relation to persons and ventilation. The location of CO_2 sensors is important: human exposure to CO_2 and other respiratory compounds and potential pathogens is best obtained when the sensors are close to the breathing zone.

The CO_2 measurements can traditionally be used for different functions involving the control of ventilation and indoor air quality. Additionally, in this paper, we support another proposal for the mitigation of transmission of respiratory pathogens. Furthermore, as the CO_2 concentration is unlikely to be uniformly distributed inside a room the placement of the sensor will have importance on the reliability and accuracy of the measured data.

In this paper, we demonstrated a data collection method that can be used to evaluate the effect the placement of a CO2 sensor has on the results and also how occupant placement and distribution can simultaneously be monitored. Further research is needed in different kinds of settings to weigh how each factor may affect the measured results and what practical importance it may have. For example, different purposes i.e., ventilation control, pathogen mitigation and occupancy estimation may demand different kinds of considerations for CO2 sensor placement. The method demonstrated in this paper can be used to take these different factors into consideration i.e., placement and height of the sensor, the amount of ventilation and the number and location of occupants.

6. Acknowledgement

This experiment was done in cooperation between two research projects at Tampere University of Applied Sciences. The involved projects were Licence to Breathe a Business Finland funded Co-Creation project which aims to support businesses in SARS-CoV-2 mitigation and the Surface hygiene project concerning surface hygiene in different spaces and tested for the presence of viruses in the Living Lab and practical work environments.

We also thank Saul Wiinamäki for arranging and handling the sensors needed for measurements.

7. References

[1] Burridge, H.C., Fan, S., Jones, R.L., Noakes, C.J. and Linden, P.F., 2020. Predictive and retrospective modeling of airborne infection risk using monitored carbon dioxide. arXiv preprint arXiv:2009.02999.

[2] Dai, H., & Zhao, B. (2020). Association of infected probability of COVID-19 with ventilation rates in confined spaces: a Wells-Riley equation based investigation. MedRxiv.

[3] Du, B., Tandoc, M.C., Mack, M.L. and Siegel, J.A., 2020. Indoor CO2 concentrations and cognitive function: A critical review. Indoor air, 30(6), pp.1067–1082.

[4] Franco, A. and Schito, E., 2020. Definition of optimal ventilation rates for balancing comfort and energy use in indoor spaces using CO2 concentration data. Buildings, 10(8), p.135.

[5] Klompas, M., Milton, D. K., Rhee, C., Baker, M. A., & Leekha, S. (2021). Current Insights into Respiratory Virus Transmission and Potential Implications for Infection Control Programs: A Narrative Review. Annals of Internal Medicine, 174(12), 1710–1718.

[6] Miller, S.L., Nazaroff, W.W., Jimenez, J.L., Boerstra, A., Buonanno, G., Dancer, S.J., Kurnitski, J., Marr, L.C., Morawska, L. and Noakes, C., 2021. Transmission of SARS-CoV-2 by inhalation of respiratory aerosol in the Skagit Valley Chorale superspreading event. Indoor air, 31(2), pp.314–323.

[7] Satish, U., Mendell, M.J., Shekhar, K., Hotchi, T., Sullivan, D., Streufert, S. and Fisk, W.J., 2012. Is CO2 an indoor pollutant? Direct effects of low-to-moderate CO2 concentrations on human decision-making performance. Environmental health perspectives, 120(12), pp.1671–1677.

[8] Wang, C.C., Prather, K.A., Sznitman, J., Jimenez, J.L., Lakdawala, S.S., Tufekci, Z. and Marr, L.C., 2021. Airborne transmission of respiratory viruses. Science, 373(6558), p.eabd9149.

[9] Zivelonghi, A. and Lai, M., 2021. Mitigating aerosol infection risk in school buildings: The role of natural ventilation, volume, occupancy and CO2 monitoring. Building and Environment, 204, p.108139.

Data access statement

The datasets generated and analysed during the current study are not available because unfinished studies and agreements between cooperating projects, but the authors will make every reasonable effort to publish them in near future.

Quality requirements for forecasts in HVAC operation optimization

Thomas Oppelt

Air-conditioning department, Main Department Ventilation and Air Conditioning,
Institut für Luft- und Kältetechnik gemeinnützige GmbH, Dresden, Germany, klima@ilkdresden.de

Abstract. Optimizing HVAC operation by taking into account predictions for presence, occupancy and inner loads, weather (mainly air temperature and solar irradiation) and thermal behaviour of the room or building can lead to significant energy savings while maintaining thermal comfort for the occupants. However, the quality of forecasts plays an important role for the success: High prediction qualities are essential for achieving the objectives in energy saving and thermal comfort. In the present paper, a simulation study is presented for the example of an office room with up to three occupants. Perfect and real (non-perfect) forecasts are applied for simulating predictive HVAC control in the course of one year. For evaluating the impact of forecast quality, the annual reduction of cooling energy demand and the decrease of thermal comfort are considered. Results show that there is a complex interaction between the different forecasts: The combined quality of all forecasts determines the benefit which can be reached from predictive control. If forecasts are not good enough, thermal comfort decreases significantly compared to perfect forecasts or the reference case without predictive control. Here, especially the forecast of room temperature development (thermal behaviour of the room) was found to be very important. If the forecasts are good, the annual cooling energy demand can be decreased by 19 % in the example while maintaining high thermal comfort.

Keywords. building model, machine learning, thermal comfort, energy saving
DOI: https://doi.org/10.34641/clima.2022.96

1. Introduction

The operation of HVAC systems can be optimized by considering forecasts for the control system. Control actions might be tested in advance by means of simulating the system behaviour for the next time range (model-predictive control, MPC). Thus, different advantages are provided: For example, oscillations in the system (e.g. alternating heating and cooling) are avoided, room heating is deactivated or reduced when solar heat gains are expected for the next time, offices are cooled only if they are really used. Improvements in both energy savings and thermal comfort can be achieved by operating HVAC systems based on appropriate forecasts. Machine learning algorithms can be applied for approaching optimal control [1, 2]. Different concepts and methods were proposed which consider forecasts of weather and occupancy [3, 4] and achieve for example 18 % savings in cooling energy demand [5]. Some studies took into account the uncertainty of weather predictions [6, 7] and showed the influence on MPC performance. It was also shown that reliable cooling load predictions are required for MPC [8].

Thus, the performance of predictive HVAC control strongly depends on the quality of the forecasts which are required for the optimization. If the quality of such forecasts is not sufficient, lower thermal comfort and higher energy consumption may occur than without using forecasts. Well performed predictions are an important basis for successful optimization of operation. In the present paper, a simulation study is presented which compares the application of perfect and real (non-perfect) forecasts. It is shown which forecasts are required for HVAC predictive control in offices and how their quality influences energy savings and thermal comfort.

Here, an office room is modelled numerically as a basis for the study. An operation in the course of one year is simulated with predictive HVAC control applying varied prediction models for presence, occupancy, weather and thermal behaviour of the room. For evaluating the performance, cooling energy savings and thermal comfort are analysed.

Copyright ©2022 by the authors. This conference paper is published under a CC-BY-4.0 license.

2. Research Methods

2.1 Example room

The study is based on the numerical model of a theoretical office room with the dimensions 3.92 m x 8.00 m x 3.16 m (volume 99 m^3) situated in Potsdam, Germany. The room can be occupied by up to three people. The outer walls contain windows with a total area of 22.4 m^2. For the sake of simplicity, horizontal orientation of the windows is assumed. For non-horizontal windows, the sun's position determines the irradiation to the room for a given irradiation measured on the horizontal surface. For starting with a basic model for room temperature forecast, this dependency has not been considered yet. Therefore, the influence of solar altitude on the irradiation to the room is neglected in this stage of research.

For modelling the transient thermal behaviour of the room, the room model described in VDI 6007 Part 1 [9-11] is used as a basis. This is a second-order model which divides the building mass into two thermal capacitors. One capacitor subsumes all non-adiabatic components (e.g. outer walls), the other one represents the adiabatic components (e.g. wall to neighbour rooms with the same thermal conditions). The transient solution for the system of capacitors and resistances is found by analogy to electric circuits. The model is based on a time step of 1 h, but can be adopted to smaller time steps. Here, some simplifications for thermal radiation were made to decrease the calculation duration for a small time step of 1 min (no absorption or emission on opaque outer surfaces, no emission from inner surfaces).

Thermal loads within the room are the following:

- base heat source: 200 W (50 % convective, 50 % radiative)
- heat source per occupant: 75 W (person) + 200 W (IT), 50 % radiative
- lighting: 150 W (50 % radiative)

These are practical values for different kinds of offices, e.g. with CAD-workstations. For the HVAC system, the following typical parameters are assumed:

- air supply per person: 40 m^3/h
- supply air temperature: 24 °C for heating, 18 °C for cooling
- setpoint value for room air temperature during active operation time: 21 °C
- minimal and maximal room air temperature during passive operation time (night, weekend): 18 °C/27 °C
- active operation time: 6:30 to 18:30 on weekdays (if not derived from occupancy forecast)
- start-up time before active operation: 1 h
- decay time before end of active operation: 1 h (During decay time, heating/cooling is reduced and the room air temperature is allowed to deviate from the set-point value because a slight increase or decrease is acceptable for the occupants before they leave the office.)

2.2 Forecasts

For predictive HVAC control, different forecasts are required. These are described in the following and details on the machine learning models are given in Table 1.

(1) Presence forecast (PF): For optimal control, information is required on when there are people in the room or building and when not. For an office room, especially the arrival time of the first occupant in the morning and the time when the last occupant left the room in the afternoon (departure time) are relevant, because these times define the period when comfort requirements are to be met. If a forecast predicts the presence of people in a room or building, the room temperature can be kept at the required value and restricted to this time for the sake of energy savings.

The target values in presence forecasting are for example the arrival time of the first person and the departure time of the last person on a specific day. Relevant features (influence parameters) can include the weekday, the month, school holidays yes/no, working day yes/no. Here, a random forest model is used. Alternatively, presence forecast can be derived from occupancy forecast (see below): When the predicted occupancy is at least one, somebody is present in the room.

(2) Occupancy forecast (OF): The occupancy (number of people in a room or building) predicted for a certain time horizon allows for optimal operation of the HVAC system both with regard to user comfort and reaction to inner thermal loads (heat emission of people, devices, machines and lighting). This allows for example to avoid overshooting of the room temperature. The occupancy can be predicted based on the same features as used for presence forecast. Additionally, the time is an important parameter.

For the study described here, synthetic occupancy data were created for an office room with three desks and flexible work time. 5 min values were generated for a total period of two years. They take into account the individual holiday and working time preferences of the people being modelled. The particular times of arrival, lunch break and departure at each day are

Tab. 1 – Models applied for forecasts. Machine learning models are taken from scikit-learn [12]; validation performance given as root mean square error (MSE)

Forecast	ML model	Details	Performance
Presence (PF)	random forest regression	arrival time of first person in seconds at day based on features weekday, working day departure time: same method as for arrival time	arrival time: MSE = 2743 s departure time: MSE = 2806 s
Occupancy (OF)	random forest regression	number of people being present at current time step based on features weekday, working day, time, occupancy in previous time step	MSE = 0.1
Weather (WF)	none	simple model: ambient temperature and global solar irradiation from same time at previous day	temperature: MSE = 3.4 K irradiation: MSE = 115 W/m^2
Room temperature (RF)	linear regression	room air temperature based on features ambient temperature, solar irradiation, convective and radiative inner heat sources (including heating/cooling systems), temperature in previous time step	MSE = 0.2 K

subject to random distribution within the respective typical time windows. A random forest model has been trained and validated with the data for the first year while the second year data are used for the application in the predictive HVAC control study.

(3) Weather forecast (WF): If it is known that high solar irradiation will affect the room within the next hours, heating can be deactivated anticipatorily. Weather companies provide forecast data for air temperature, solar irradiation and other parameters. Solar irradiation data might be split into direct and diffuse irradiation or consolidate these parts into global irradiation. Generally, provided irradiation data are related to one square meter of horizontal surface. As the effect of solar irradiation on the room or the building depends on the current solar position and thus e.g. on calendar day and time, conversion by an analytical or numerical model (could also be a machine learning model) is necessary. For limiting the complexity of the study presented here, this conversion has been avoided by assuming horizontal windows.
For the most cases studied here, a perfect weather forecast was applied because the focus was on the building-specific predictions (presence, occupancy, thermal behaviour). In the case with weather prediction, a simple model using the values from the same time at the previous day was applied.

(4) Thermal behaviour of the building (room temperature forecast RF): For finding the optimal HVAC control, the development of the room air temperature depending on thermal loads, room or building properties and HVAC system operation needs to be predicted. This forecast can be conducted by means of an analytical or numerical room/building model or with a machine learning model. Here, a linear regression model is used which was trained and validated with data from the room model.

2.3 Predictive HVAC control

For optimizing HVAC operation, the active operation time of the system is not fixed but depending on the presence forecast. At the beginning of each day (0:00), this forecast is generated for the present day and the active operation time is derived from the result. At the defined start-up time before the (predicted) active operation (see Figure 1; here: 1 h), the system starts to heat or cool in order to reach the setpoint value when the first occupant arrives.

The predicted departure time of the last occupant defines the end of the active operation time. As a slight decrease or increase of temperature might be acceptable for the user before leaving the room, a decay time (here: 1 h) is assumed before the end of the active operation time. During this time, heating or cooling is reduced or deactivated.

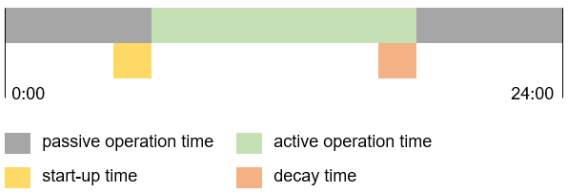

Fig. 1 – Nomenclature of time periods.

Heating the room when cooling would be required shortly afterwards or vice versa should be avoided. To this end, a defined "preview time" is considered here. The preview time is a defined time horizon from the current real time to the future which is considered for predictive control. This means that forecasts are conducted e.g. for the following hour to

check if a change from cooling to heating or from heating to cooling becomes necessary. If this is the case, cooling or heating will already be stopped at the current time. For the preview time, inner and outer thermal loads are estimated based on the occupancy forecast and the weather forecast, respectively. The development of the room temperature is predicted by the forecast model for the thermal behaviour as described in section 2.2.

In the optimized operation, the air change/the air supply to the room is set according to the real occupancy.

The predictive HVAC control modelled here is only a basic example because the main focus was to investigate the influence of forecast quality. Much more advanced strategies and optimization algorithms are possible and desirable.

2.4 Metrics

The aim of predictive HVAC control is to reduce energy demand while ensuring thermal comfort for the occupants. Here, the following metrics are used for evaluating energy demand and thermal comfort, respectively:

- Cooling energy reduction: The relative change of cooling energy in the room during one year compared to the reference case without predictive control shows the energetic advantage. Heating energy was studied as well, but is not shown here because it follows the same trends.

- Temperature deviation hours: A temperature deviation hour of 1 Kh means that during the presence of at least one person the room air temperature deviates from the setpoint value plus tolerance (here 1 K) by 1 K for one hour. The summarized value for one year is used here as an indicator for thermal comfort.

2.5 Cases

Perfect and real predictions are used in the cases. "Perfect" means that the real value, e.g. the number of people being present in the next time step, is known in advance. "Real" predictions are the forecasts made by the machine learning models named in section 2.2.

The following cases are investigated:

- Case 0: Reference case without any predictions. The HVAC system runs with fixed active operation time and start-up time as given in section 2.1. There is no decay time, air supply is constant at 120 m^3/h during active operation time. Thus, the setpoint temperature is met during all times when people are present.

- Case 1: As case 0, but air supply is controlled according to a perfect occupancy prediction. That means that the air supply is adjusted to the real number of persons at each time.

- Case 2: As case 1, but with a decay time of 1 h before the fixed end of active operation time.

- Case 3: As case 2, but with a preview time of 1 h for predictive HVAC control. For simulating the preview time, perfect predictions for occupancy, weather and thermal behaviour of the room are used. The active operation time remains fixed, no presence forecast is used.

- Case 4: As case 3, but with real occupancy forecast.

- Case 5: As case 4, but with real presence forecast used during preview time simulation.

- Case 6: As case 5, but with active operation time based on real presence forecast.

- Case 7: As case 6, but with real forecast of thermal behaviour and perfect forecast for presence, occupancy and weather.

- Case 8: As case 7, but with real occupancy forecast.

- Case 9: As case 7, but with real presence forecast.

- Case 10: As case 9, but with real occupancy forecast.

- Case 11: As case 10, but with real weather forecast- Thus, no perfect forecasts are used in this case.

The case configurations are summarized in Table 2. One year of operation is simulated for each case, the simulation time step is 1 minute.

3. Results and discussion

The resulting metrics for the 11 cases are shown in Figure 2.

For case 1, there is no temperature deviation because the setpoint of the room temperature is maintained during the fixed active operation time. However, cooling energy demand can be reduced by 9 % compared to the reference case (case 0) by adjusting the air supply to the number of people being present.

Cases 2 to 6 show cooling energy reductions between 15 and 20 %. These reductions are accompanied by deviations between the setpoint and the real room air temperature during certain hours. For the whole year, temperature deviation hours are below 50 Kh and might thus be acceptable.

Tab. 2 – Case overview: Forecasts for presence (PF), occupancy (OF), weather (WF) and thermal behaviour of the room (RF); p = perfect, r = real; n.d. = no decay time; n.a. = active operation time not based on forecast.

	Forecast			
Case	PF	OF	WF	RF
1	-	p (n.d.)	-	-
2	-	p	-	-
3	-	p	p	p
4	-	r	p	p
5	r (n.a.)	r	p	p
6	r	r	p	p
7	p	p	p	r
8	p	r	p	r
9	r	p	p	r
10	r	r	p	r
11	r	r	r	r

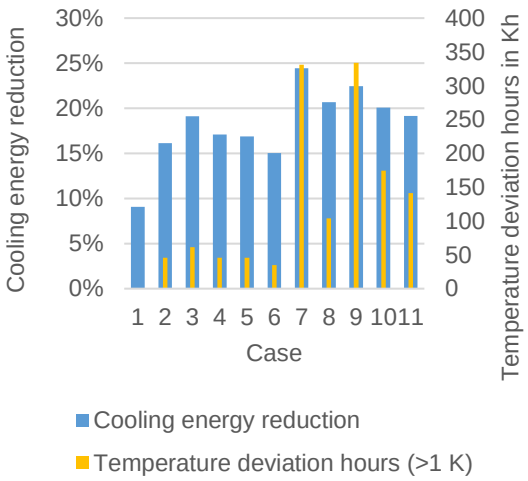

Fig. 2 – Cooling energy reduction and temperature deviation hours for one year depending on the case.

The cases up to 6 have in common that a perfect forecast for the thermal behaviour of the room is used. Switching to a real prediction (cases 7 to 11) leads to significant increase of temperature deviation hours and thus a loss in thermal comfort. The reason is that in certain hours the forecast says that no cooling is required for example, but the real temperature development is different and the room gets too warm.

From case 3 to 6, further perfect forecasts are replaced by real forecasts. Cooling energy reduction decreases, but temperature deviation hours decrease as well. Thus, the real forecasts lead to less success in energy savings, but no comfort problems are produced by the real forecasts compared to the perfect forecasts in the example considered here.

Cases 7 to 11 show that the success of predictive HVAC control depends on the combination of forecast qualities: Case 7 with real forecast of thermal behaviour and perfect forecasts for all other parameters shows poor thermal comfort (temperature deviation hours: 330 Kh). Replacing the perfect occupancy forecast by the real one (case 8) leads to significant comfort improvement (104 Kh). Case 9 with real presence forecast, but perfect occupancy forecast is much worse again. Tis shows the complex interaction of the different forecasts.

Basing the predictive HVAC control only on real forecasts (case 11) provides cooling energy savings of 19 % compared to the reference case while there are 141 Kh temperature deviation hours. This might be acceptable, but could be improved by increasing forecast accuracy (see case 3 with the same cooling energy savings, but less than half of the temperature deviation hours due to perfect forecasts).

In the cases presented here, preview time is set to 1 h. Figure 3 shows for the example of case 3 what happens if this value is varied.

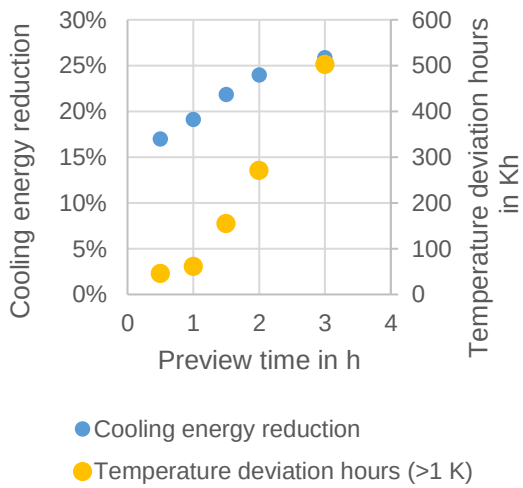

Fig. 3 – Influence of the preview time length on cooling energy reduction and temperature deviation hours (based on case 3)

With more than one hour of preview time, thermal comfort decreases significantly. The relative increase of cooling energy reduction is much smaller and does not justify the loss of thermal comfort. Thus, preview time length needs to be chosen carefully.

4. Conclusions

For the example of an office room with three occupants, the influence of the forecast quality on the performance of predictive HVAC control was investigated. Results show that the complex interactions of the different forecasts (presence, occupancy, weather, thermal behaviour of the building/room) have a strong influence on the energy savings which can be achieved while

maintaining an acceptable level of thermal comfort. If forecasts are not reliable, thermal comfort decreases significantly compared to perfect forecasts or the reference case without predictive control. Here, especially the forecast of room temperature development (thermal behaviour of the room) was found to be very important. A machine learning model applied for this forecast needs to be well-suited to the room or building. Alternatively, an analytical or numerical building/room model could be applied. Modelling and parametrization effort might be higher than for a machine learning model, but the forecast quality is expected to be better as well if the analytical or numerical model is an appropriate representation of reality.

The example studied here cannot be generalized. The thermal behaviour of buildings and rooms is very individual and depends on many parameters as for example thermal capacity of the envelope, ratio of transparent to opaque areas, etc. Thus, the results shown here are supposed to give an impression on the effects that can be expected depending on the forecasts which are available, but further studies are required. The room model will be improved by taking into account the orientation of windows and the sun's position. Furthermore, other room types (e.g. meeting rooms) will be studied and experimental validation of the findings needs to be conducted.

5. Acknowledgements

The project underlying this paper was funded by the German Federal Ministry for Economic Affairs and Energy under the code MF180093.

6. References

[1] Zhang Z., Chong A., Pan Y., Zhang C., Lam K. P. Whole building energy model for HVAC optimal control: A practical framework based on deep reinforcement learning. Energy & Buildings. 2019;199:472-490.

[2] Drgona J., Picard D., Kvasnica M., Helsen L. Approximate model predictive building control via machine learning. Applied Energy. 2018;218:199-216.

[3] Dong B., Lam K. P., Neuman, C. P. Integrated building control based on occupant behaviour pattern detection and local weather forecasting. Proceedings of Building Simulation 2011: 12th Conference of International Building Performance Simulation Association, Sidney, 2018;193:200.

[4] Dobbs J. R., Hencey B. M. Model predictive HVAC control with online occupancy model. Energy and Buildings. 2014;82:675-684.

[5] Dong B., Lam K. P. A real-time model predictive control for building heating and cooling systems based on the occupancy behaviour pattern detection and local weather forecasting. Building Simulation. 2014;7:89-106.

[6] Oldewurtel F., Parisio A., Jones C. N. et al. Use of model predictive control and weather forecasts for energy efficient building control. Energy and Buildings. 2012;45:15-27.

[7] Petersen S., Bundgaard K. W. The effect of weather forecast uncertainty on a predictive control concept for building system operation. Applied Energy. 2014;116:311-321.

[8] Fan C., Liao Y., Zhou G., Zhou X., Ding Y. Improving cooling load prediction reliability for HVAC system using Monte-Carlo simulation to deal with uncertainties in input variables. Energy and Buildings. 2020;226.

[9] VDI 6007 Sheet 1: Calculation of transient thermal response of rooms and buildings – Modelling of rooms. 2012.

[10] Lauster M., Brüntjen M.-A., Leppmann H., et al. Improving a low order building model for urban scale applications. Fifth German-Austrian IBPSA Conference, Aachen, 2014.

[11] Monti A., Pesch D., Ellis K., Mancarella P. Energy Positive Neighborhoods and Smart Energy. Academic Press, 2016.

[12] scikit-learn: Machine learning in Python. https:/www.scikit-learn.org, 2022.

Data Statement

The datasets generated during or analysed during the current study are not publicly available but will be available upon direct request to the author.

Detection of the low ΔT syndrome using machine learning models

Anand Thamban [a], Alet van den Brink [b], Shalika Walker [a], Wim Zeiler [a]

[a] The Department of the Built Environment, Eindhoven University of Technology, Eindhoven, the Netherlands, a.thamban@tue.nl , s.s.walker@tue.nl , w.zeiler@tue.nl

[b] Afdeling O&T, Kropman Installatietechniek B.V., Nijmegen, the Netherlands, alet.van.den.brink@kropman.nl

Abstract. The low ΔT syndrome has been a prevalent issue in many chilled water systems, leading to an increase in the pump energy consumption, increase in the chiller energy consumption, and/or failure to meet the cooling loads. It is therefore important to detect the low ΔT syndrome using suitable fault detection and diagnosis methods. One such fault detection method is the data-based approach using machine learning algorithms. The main signs indicating the low ΔT syndrome include a reduced return water temperature from the cooling coil and an increased mass flow rate through the cooling coil. Since the mass flow rate of water is not measured in all chilled water installations, the cooling coil valve position is measured instead. This research aims to compare the performance of different machine learning regression models which predict the return water temperature and the cooling coil valve position, based on the R^2 score and root mean square error. The different machine learning algorithms compared for the study include Support Vector Regression, Artificial Neural Network and eXtreme Gradient Boosting. The data required for the analysis was obtained from fault-introduced experiments conducted in an office building. The different fault cases include stuck cooling coil valve at 50%, stuck cooling coil valve at 75%, reduced supply air temperature by 2K and reduced supply air temperature by 1K. The regression models are expected to predict the fault-free data ($X_{predicted}$) of the system such that faulty data (X_{actual}) can be identified with residuals ($X_{predicted} - X_{actual}$). The results showed that XGBoost was the best performing algorithm in terms of model accuracy. The XGBoost based prediction models for return water temperature and cooling coil valve position were able to successfully detect anomalies for 3 out of the 4 fault cases.

Keywords. Low ΔT syndrome, XGBoost, ANN, SVR, fault detection and diagnosis.
DOI: https://doi.org/10.34641/clima.2022.121

1. Introduction

The built environment contributes to about 35% of the total energy consumption in the Netherlands [1]. With an increasing trend of warming witnessed every year, the cooling demand is expected to increase in the European continent [2]. To cope with this rising cooling demand, the energy consumption for cooling is also expected to increase. Around 75% of this cooling energy use comes from Heating, Ventilation and Air-Conditioning (HVAC) systems [1]. The HVAC system aims to maintain thermal comfort and the required indoor air quality for human occupation. Research has shown that retro-commissioning of HVAC systems can lead to a 5-15% savings in energy use [3,4]. Therefore, there is a potential to reduce about 1.3 - 3.9% of the total energy consumption in the Netherlands if all systems are continuously monitored for faults, and frequent replacements of components are made to ensure that they run efficiently.

The low ΔT syndrome is an infamous phenomenon related to the chilled water system in a building/plant, and if left unaddressed, can have a negative impact on the energy consumption of the system. The problem has been widely discussed by many researchers, some of whom have identified its presence in almost all big distributed chilled water systems and suggested alternative design changes [5] and some who have identified its main causes, as well as solutions to mitigate the problem [6]. In a chilled water system, the capacity of the cooling coil is mainly attributed to the water-side temperature difference during part-load conditions. A smaller temperature difference between the supply water and return water will lead to an inefficient chilled water system, reducing cooling output and causing energy wastage to operate extra chillers and pumps to keep up with demand [5]. This phenomenon of a

Copyright ©2022 by the authors. This conference paper is published under a CC-BY-4.0 license.

reduced temperature difference across the cooling coil with an increased demand of flow to keep up with system demand is called the low ΔT syndrome [5].

The low ΔT syndrome can be caused by abrupt faults (control failure, physical failure etc.), incipient faults (fouling, equipment degradation) or design faults (three-way valves, improper coil selection) [6]. In this study, only the abrupt faults will be addressed.

One of the ways to identify and solve the low ΔT syndrome is by using fault detection and diagnosis (FDD) tools. FDD tools are used in the maintenance of building installations with the main purpose of detecting faults and diagnosing them, such that corrective measures can be taken to fix the system. The aim of an FDD tool is to detect a fault (in this case, the low ΔT syndrome) by observing certain signs (reduced return water temperature (RWT), increased mass flow rate etc.) and then diagnose the causes (stuck cooling coil valve, reduced supply air temperature (SAT)) leading to the fault. Few studies have been conducted which used grey box models to detect low ΔT syndrome [7,8] but they are limited to fouling related faults and/or just the low ΔT syndrome in large distributed chilled water plants.

FDD processes can be classified into data-driven and knowledge-driven methods [9]. Data-driven methods include classification and regression models which rely on large amounts of data with the capability of learning complex patterns from it. But these methods are largely black-box thus making it difficult to interpret what goes on behind the model. Knowledge-driven models include Bayesian networks, fuzzy logic etc., and are largely supported by expert knowledge in the particular field.

Using the data-driven methods, anomaly detection is a popular way of detecting faults in the data by identifying unexpected or abnormal data from normal fault-free data. This is usually done using supervised learning regression models which predict fault-free data and is then compared with the measured data. When large residuals are identified between the expected value (fault-free) and the measured value (faulty), it can be assumed that a fault exists in the system. Different kinds of machine learning (ML) algorithms have been used for regression purposes including Artificial Neural Networks (ANN), Support Vector Machines (SVM) or Support Vector Regression (SVR), Decision Trees, Random Forest and eXtreme Gradient Boosting (XGBoost). Each of these algorithms is advantageous over the other depending on the characteristics of the dataset.

SVM or SVR is an algorithm used for both classification as well as regression problems. It has the advantage of performing well with a limited amount of data compared to other models. But the computational time required for model development is considerably higher than other ML algorithms like ANN and Random Forest [10]. Decision trees are also regression algorithms that are based on the approach of splitting a dataset while evaluating certain conditions. Ensemble algorithms are based on the ML theory that a group of weak learners create a much stronger ensemble than a single strong learner [11]. XGBoost is one such ensemble algorithm that has proven to be a well-performing ML algorithm in several studies [12–14] and has been previously used for fault detection in HVAC systems [15]. Since previous research clearly showed the benefits of ensemble algorithms compared to individual Decision Trees [11], Decision Trees are not included in this study. ANN has also been used to develop regression models to predict continuous variables like energy consumption [10], temperature [16] and cooling coil valve position [17]. But ANN is more complex in nature compared to SVR and requires precise adjustment of its many hyper-parameters [18]. Neural networks also perform better with larger amounts of data, which could be a drawback if limited data is available [18].

Since each of the algorithms has its advantages and disadvantages, it is necessary to compare their performance to see which algorithm can make predictions with the least amount of error, which is an essential factor for anomaly detection. The purpose of the study is to develop an FDD tool to detect the low ΔT syndrome using a suitable ML algorithm which can be replicated in most kinds of chilled water systems. It is important to note that in this research only the fault detection aspect of the low ΔT syndrome is addressed and not the fault diagnosis part.

2. Methodology

The low ΔT syndrome is detected by two main phenomena: the increase in mass flow rate through the cooling coil and the decrease in the RWT from the cooling coil. Since many installations do not have mass flow rate meters, one way to get an idea of the flow demand from the system is to observe the cooling coil valve position (CCVP). Therefore, the low ΔT syndrome can be detected by monitoring the CCVP and the RWT.

The CCVP and RWT prediction models were developed by following a structured procedure shown in Fig. 1. The different steps are as follows:

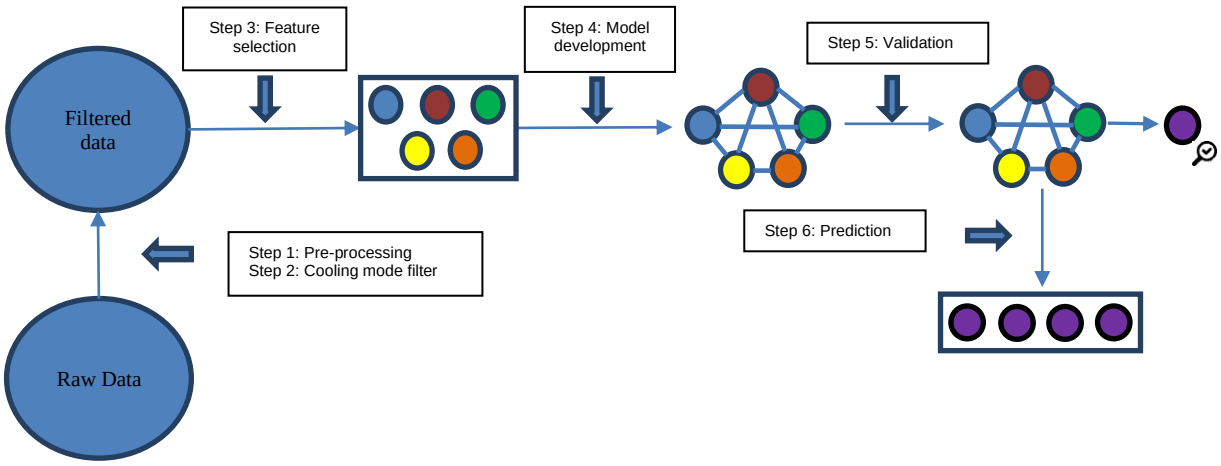

Fig. 1 - ML model development process

Step 1: Pre-processing of raw data to remove noise and missing data
Step 2: Filtering of data for cooling mode
Step 3: Feature selection
Step 4: Model development
Step 5: Validation and error calculation
Step 6: Prediction

If the CCVP prediction model showed a positive residual (residual = actual value – predicted value) and the RWT prediction model showed a negative residual, then it could be said that low ΔT syndrome was detected in the system.

2.1 Description of raw dataset

The analysis in this study was done using raw data collected from an office building located in Breda, the Netherlands. The office building is a living lab with multiple sensors placed both in the indoor environment as well as the HVAC installations. The building offers an ideal environment for conducting studies related to occupant comfort, energy demand predictions and HVAC fault simulations.

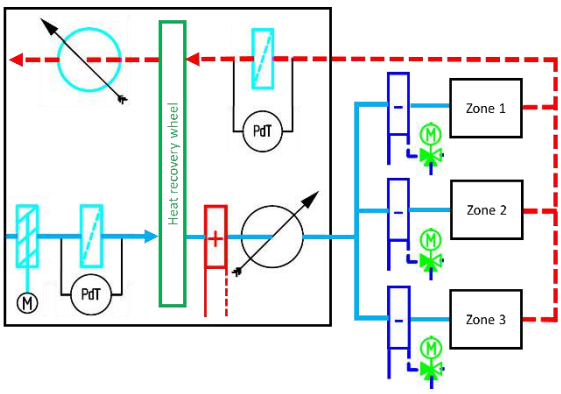

Fig. 2 - Schematic of the AHU in the use case building

The building has an air handling unit (AHU) in a constant air volume system which supplies conditioned air to three zones. The cooling coils are situated outside the AHU and act as after-coolers. Fig. 2 shows the schematic of the AHU and the zones supplied with conditioned air.

The raw data used in the study was collected from January 2017 up to September 2021. In this setup, extra sensors were installed near the cooling coil to measure the mass flow rate of water, inlet and outlet water temperatures and pressure difference of air over the cooling coil. These sensors were installed in March 2021, therefore the raw data used for RWT prediction was available only from April 2021 to September 2021. The mass flow rate sensor is not used in the fault detection process because it is not usually present in all chilled water installations. The temperature sensors used to measure the inlet and outlet water temperatures are Kamstrup Pt500 sensors which have a reaction time of 5s, and a maximum deviation of 0.1K for a temperature difference of 15K (i.e. ± 0.1K) between the inlet and outlet ports.

2.2 Fault simulation

Certain faults were introduced into the HVAC system from June 2021 to September 2021 in order to collect faulty data. These faults include:

1. Stuck cooling coil valve (50% and 75%)
2. Reduced SAT (1K and 2K)

These specific faults were introduced into the system because they were observed from computer simulations to be the abrupt faults that have the highest impact on the energy consumption of the pumps as well as occupant comfort.

2.3 Step 1: Pre-processing of raw data to remove noise and missing data

Before the model was developed, the data collected from the building management system (BMS) was cleaned to remove noisy and missing data points. Data for a particular timestamp where one or more features were absent were completely dropped. Interpolation was not done to fill in the missing data points because it could lead to incorrect values being fed into the dataset, leading to a faulty training dataset.

Moreover, some features in the dataset had incorrect values due to errors in the reporting system from the BMS, e.g., the CCVP signal was multiplied by a factor of 10. This had to be scaled down to be within the limits of 0 to 100%.

2.4 Step 2: Filtering of data for cooling mode

Once the data had been pre-processed, the next step was to ensure that the correct data was used for the ML model development. Since the focus of the study was to detect the low ΔT syndrome which occurs only when the AHU operates in cooling mode, it is more efficient to filter data when the AHU operates in cooling mode and then use the filtered data for the model development. The data was filtered using two conditions applied together:

1. The CCVP signal > 0
2. The chiller water outlet temperature < 8°C

Condition 1 is more generalizable since almost all HVAC installations have sensors to measure the cooling coil valve position. A value greater than 0 indicates that chilled water is demanded by the system and cooling is required.

Condition 2 is another criterion to see if the system is in cooling mode. The outlet water temperature from the chiller is a good indication of whether cooling is required by the system or not.

2.5 Step 3: Feature selection

To have a good quality prediction, it is necessary to choose the features which have the most impact on the predicted variable. In the case of fault detection, it is also necessary to avoid those features which can be influenced by the fault, e.g., a stuck valve fault can impact the SAT coming from the outlet of the cooling coil. If the SAT is used as a feature, then the prediction from the model would be biased to the fault hence giving a smaller residual than usual.

Feature selection can be done either manually by looking at a cross-correlation heat map and selecting the features with the highest cross-correlation score or by automatically selecting them using Recursive Feature Elimination using Cross-Correlation (RFECV). Both methods were used in this research.

The main features available for the study include inlet air temperature, inlet air relative humidity, inlet air absolute humidity, airflow rate, chilled water supply temperature, outdoor air temperature, SAT setpoint for a zone, measured and setpoint return air temperature, pressure across the supply and return filters, and fan speed.

2.6 Step 4: Model development

The purpose of the model is to predict the CCVP and cooling coil RWT in a fault-free mode such that when faults occur in the system, large residuals are generated to indicate faults in the system. The model was trained with fault-free data in the system to ensure the predictions are always fault-free. Three different ML models namely SVR, ANN and XGBoost were developed and compared in Python using the sci-kit learn library and XGBoost library.

2.7 Step 5: Validation

All the ML algorithms were validated using the k-fold cross-validation method [10]. K-fold cross-validation is a commonly used statistical method to determine the performance and accuracy of an ML model. In this method, the dataset is split into k folds (groups), where one group is held as a test set and the rest (k-1) groups are held as the training set. The model is then fit with the training set, evaluated with the test set and discarded while retaining the values. The process is then continued for the other k-1 test groups, eventually giving a summarized score of the model. In this study, 10-fold cross-validation is used.

The accuracy of the model was identified by two metrics [10]: the root mean square error (RMSE) and the coefficient of determination (R^2).

RMSE is used to measure the differences between values predicted by an estimator and the actual values observed. It is a measure of accuracy to compare forecasting errors of different models for a particular dataset and not between datasets, as it is scale-dependent. The RMSE is calculated using equation (1), where $\hat{y}_i$ is the estimated value, y_i is the actual value and N is the number of samples.

$$RMSE = \sqrt{\frac{\sum_{i=1}^{N} (\hat{y}_i - y_i)^2}{N}} \quad (1)$$

The coefficient of determination is a statistical parameter that measures the proportion of variation in the dependent variable that is predictable from the independent variable. It is a measure of how well the model is able to replicate outcomes, based on the proportion of total variation of all the outcomes the model replicates. The R^2 value is determined using equation (2) where $\bar{y}_i$ is the mean value.

$$R^2 = \frac{\sum_{i=1}^{N} (y_i - \hat{y}_i)^2}{\sum_{i=1}^{N} (y_i - \bar{y}_i)^2} \quad (2)$$

2.8 Step 6: Prediction

The models developed using the different algorithms generated predictions for the same data set. They were then evaluated and compared based on the average RMSE and R^2 value from k-fold cross validation.

The model with the best performing algorithm was then used to detect anomalies in the fault simulated experimental data.

3. Results

The results section is divided into two parts: the comparison of different ML algorithms for the prediction of CCVP and RWT, and the detection of low ΔT syndrome using the best performing algorithm. The comparison of the different ML algorithms is done based on the R^2 score and the RMSE.

3.1 Comparison of ML algorithms

The different ML algorithms were compared for two models – CCVP prediction and RWT prediction. Fig. 3 shows the comparison of R^2 values between different algorithms for the prediction of RWT.

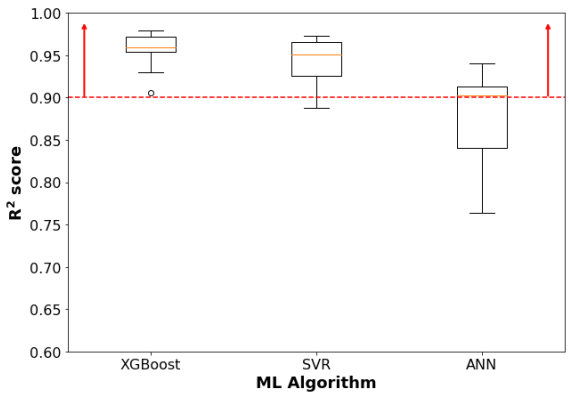

Fig. 3 - Comparison of R^2 values for RWT prediction

The boxplot shows the results obtained with the k-fold cross validation. For a good regression model with lower chances of false positives or true negatives, it is ideal to have R^2 values larger than 0.9 (red dotted line). It is evident that XGBoost and SVR perform well with their median values close to 0.95. ANN on the other hand has its interquartile range between 0.84 and 0.91. XGBoost, therefore, performed the best in terms of R^2 value for RWT prediction.

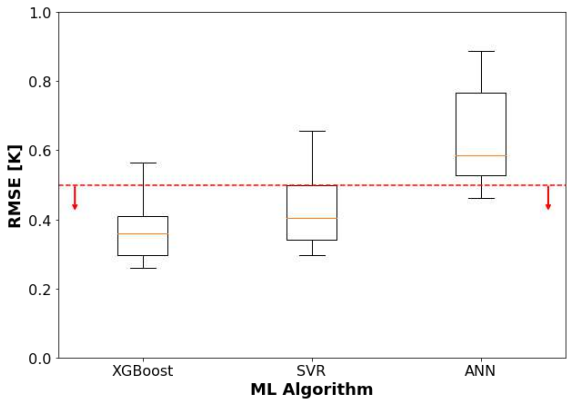

Fig. 4 - Comparison of RMSE values for RWT prediction

Fig. 4 shows the comparison of RMSE values between different algorithms for the prediction of RWT. XGBoost shows to produce the least amount of error, compared to the other algorithms. Since the RWT usually reduces by small values, it is essential to choose a model with relatively low error, so that the model can detect anomalies in the data if faults exist. Therefore, a threshold of 0.5K is chosen for selecting the appropriate algorithm.

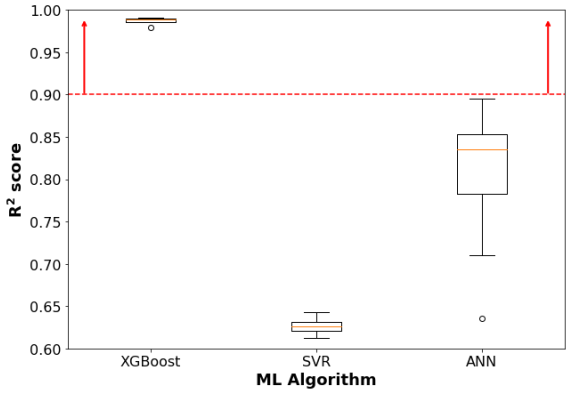

Fig. 5 - Comparison of R^2 values for CCVP prediction

Fig. 5 shows the comparison of R^2 values between different algorithms for the prediction of CCVP. In the figure, it is seen that XGBoost is the only model which performs well, with R^2 values above the threshold of 0.9, whereas the other models perform poorly.

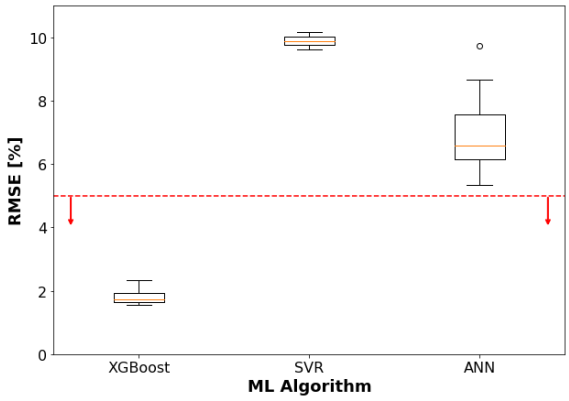

Fig. 6 - Comparison of RMSE values for CCVP prediction

Fig. 6 shows the comparison of RMSE values between different algorithms for the prediction of CCVP. XGBoost shows to have the least amount of error compared to the other models. A threshold of 5% valve position units is chosen to ensure a minimum number of false positives and true negatives among the predictions.

3.2 Fault detection

From the results shown in the previous subsection, it was found that XGBoost was the best performing model in terms of the R^2 value as well as the RMSE. The next step is to use the developed RWT and CCVP prediction model on the chilled water system to detect the low ΔT syndrome.

Fig. 7 shows the comparison between the predicted RWT (red line) and the actual RWT (blue line) for the fault use case where the CCVP is stuck at 75%. The generated negative error residual (green line) is greater in magnitude than the threshold of 0.5K and clearly shows the presence of a fault in the system.

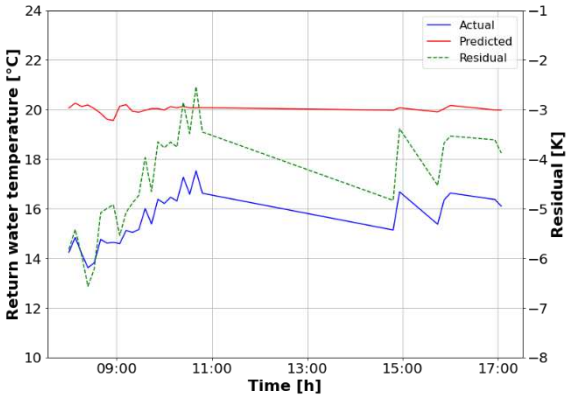

Fig. 7 - RWT prediction for CCVP stuck at 75%

Fig. 8 shows the comparison between the predicted CCVP and the actual CCVP for the same fault use case where the CCVP is stuck at 75%.

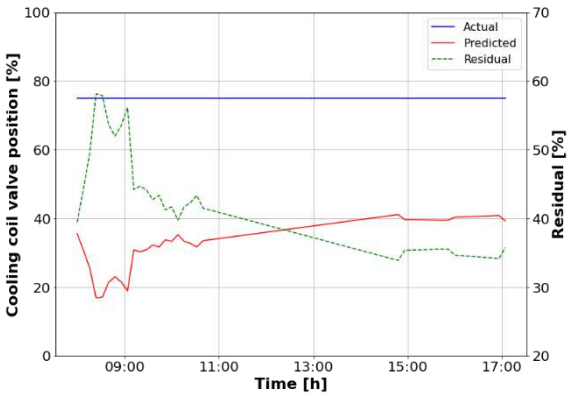

Fig. 8 - CCVP prediction for CCVP stuck at 75%

The generated positive error residual is greater than the threshold of 5% and clearly shows the presence of a fault in the system.

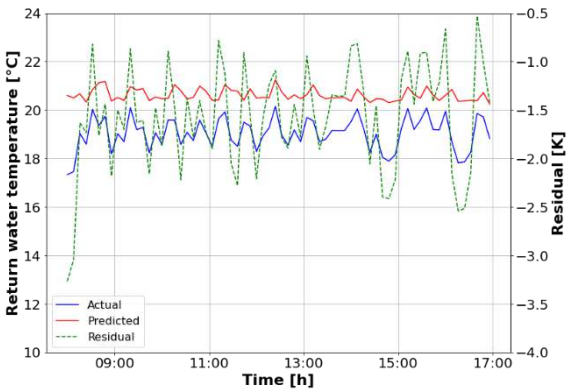

Fig. 9 - RWT prediction for CCVP stuck at 50%

Fig. 9 shows the comparison between the predicted RWT and the actual RWT for the fault use case where the CCVP is stuck at 50%. The generated negative error residual is on an average greater in magnitude than the threshold of 0.5K and therefore shows the presence of a fault in the system.

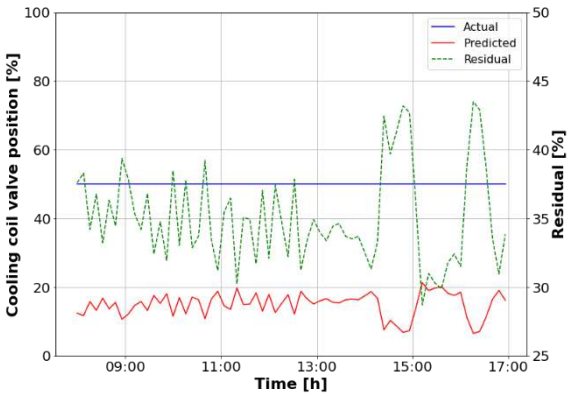

Fig. 10 - CCVP prediction for CCVP stuck at 50%

Fig. 10 shows the comparison between the predicted CCVP and the actual CCVP for the fault use case where the CCVP is stuck at 50%. The generated positive error residual is greater than the threshold of 5% and therefore clearly shows the presence of a fault in the system.

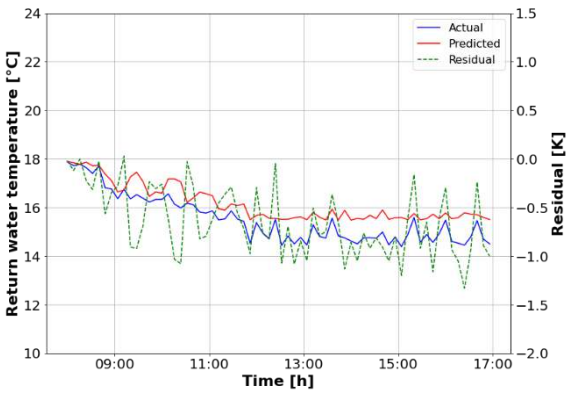

Fig. 11 - RWT prediction for reduced SAT by 2K

Fig. 11 shows the comparison between the predicted RWT and the actual RWT for the fault use case where the SAT setpoint is reduced by 2K. The generated negative error residual on an average is greater in magnitude than the threshold of 0.5K and therefore shows the presence of a fault in the data.

Fig. 12 shows the comparison between the predicted CCVP and the actual CCVP for the fault use case where the SAT setpoint is reduced by 2K. The generated positive error residual is greater than the threshold of 5% for certain periods (8 am to 12 pm and 3 pm to 5 pm) and therefore shows the presence of a fault in the above-mentioned time period, although the fault was present throughout whole period (7 am to 5 pm). The prediction (12 pm to 3 pm) becomes very close to the actual measured value reducing the chances of fault detection.

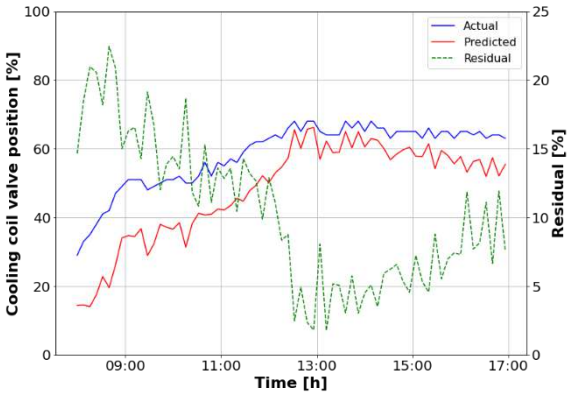

Fig. 12 - CCVP prediction for reduced SAT by 2K

Fig. 13 shows the comparison between the predicted RWT and the actual RWT for the fault use case where the SAT setpoint is reduced by 1K. It is observed that the predictions are quite close to the actual value and therefore sufficiently large residuals are not generated.

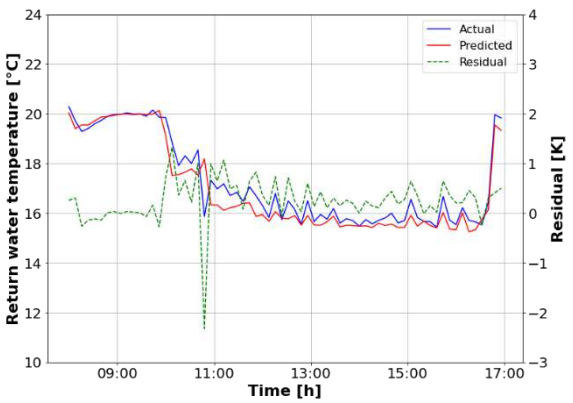

Fig. 13 - RWT prediction for reduced SAT by 1K

Fig. 14 shows the comparison between the predicted CCVP and the actual CCVP for the fault use case where the SAT setpoint is reduced by 1K.

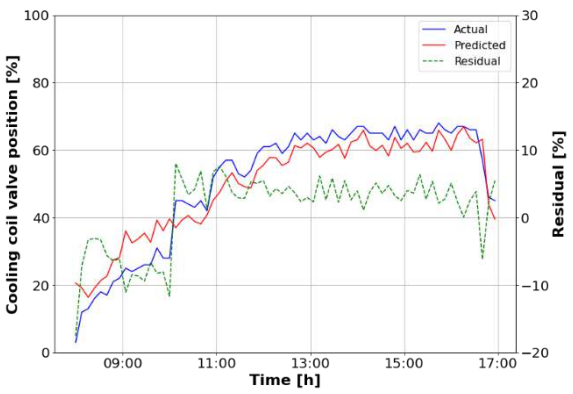

Fig. 14 - CCVP prediction for reduced SAT by 1K

Similar to the RWT prediction model, it is observed that the predictions are close to the actual value and therefore sufficiently large residuals are not generated. The reduction of the SAT by 1K does not seem to have much of an impact on the CCVP either.

4. Discussion

This study compared the capability of different ML algorithms in the detection of low ΔT syndrome using two different fault conditions. From the comparison, it is evident that XGBoost performed the best. SVR also performed well for a limited amount of data, which is seen in the RWT prediction. But its performance drops when large amounts of data are used. ANN did not perform well in all cases and did not cross the required thresholds for model acceptance. Apart from the model performance, the model development process for an ANN was also more complicated than XGBoost or SVR. ANN did not support RFECV thus requiring manual feature selection. This is a time-consuming and inefficient method of identifying the correct features. The automated feature selection capability supported by XGBoost and SVR is highly desirable, especially for commercial implementation of the FDD tool.

The XGBoost prediction model for RWT and CCVP was tested for different fault use cases conducted at the experiment site. The models show the ability to generate predictions (positive for CCVP and negative for RWT) with sufficiently large residuals which indicate the presence of the low ΔT syndrome in the system. The cooling coil stuck valve faults show a significant impact on the RWT (residual > 0.5K) and CCVP prediction (residual > 5% CCVP). The reduction of SAT by 2K fault on the other hand did not show very large residuals but were large enough for certain periods throughout the day indicating the presence of a fault. The reduction of SAT by 1K had little to no impact on the RWT or the CCVP and therefore did not show any anomalies. This is because the reduction of SAT by 1K did not lead to a significant increase in the mass flow rate.

It is important to note that during the experiments for reduced SAT, the outdoor air dry-bulb temperature did not go above 23°C. Therefore, there wasn't a very high cooling demand from the building. The reduction in SAT would have caused a small increase in the mass flow rate which would be difficult to detect. This could be a possible explanation for the smaller impact of the reduced SAT faults on RWT and CCVP.

5. Conclusions

This study shows that XGBoost is a suitable model for predicting RWT and CCVP in HVAC installations and can be confidently used for fault detection of low ΔT syndrome. Even though the low ΔT syndrome was detected in 3 of the 4 fault cases, the impact and intensity of the fault varied for each use case. The stuck cooling coil valve fault had a very high impact on RWT and CCVP and therefore was easily detected by the system. The reduced SAT fault on the other hand had a smaller impact.

6. Recommendations

It would be beneficial to conduct further experiments for reduced SAT when the outdoor air dry-bulb temperature is higher than 25 °C. This is also a more practical fault simulation since usually the SAT would be reduced only if the cooling demand is very high on hot days. The extension of the current study to another building would also be valuable to confirm the trend of the findings.

7. Acknowledgement

The research work is funded by the TKI Urban Energy project "Continuous commissioning of low-dt" and the Eindhoven Engine project "CM-HVAC-FDD". We would like to express our gratitude to all the other partners in the project. A special thanks to Roel Vos and John Verlaan of Kropman Breda for helping in setting up and coordinating with the experiments at the use case building.

8. References

[1] Agentschap NL. Monitor Energiebesparing Gebouwde Omgeving. 2019.

[2] Lhotka O, Kyselý J, Farda A. Climate change scenarios of heat waves in Central Europe and their uncertainties. Theor Appl Climatol 2018;131:1043–54.

[3] Friedman H, Piette MA. Comparative guide to emerging diagnostic tools for large commercial HVAC systems. Lawrence Berkeley Natl Lab 2001.

[4] Mills E. Building commissioning: A golden opportunity for reducing energy costs and greenhouse gas emissions in the United States. Energy Effic 2011;4:145–73.

[5] Kirsner W. The demise of the primary-secondary pumping paradigm for chilled water plant design. HPAC Heating, Piping, Air Cond 1996;68:73–8.

[6] Taylor ST. Degrading chilled water plant delta-T: Causes and mitigation. ASHRAE Trans 2002;108 PART 1:641–53.

[7] Gao D ce, Wang S, Sun Y, Xiao F. Diagnosis of the low temperature difference syndrome in the chilled water system of a super high-rise building: A case study. Appl Energy 2012;98:597–606.

[8] Gao D ce, Wang S, Shan K, Yan C. A system-level fault detection and diagnosis method for low delta-T syndrome in the complex HVAC systems. Appl Energy 2016;164:1028–38.

[9] Zhao Y, Li T, Zhang X, Zhang C. Artificial intelligence-based fault detection and diagnosis methods for building energy systems: Advantages, challenges and the future. Renew Sustain Energy Rev 2019;109:85–101.

[10] Walker S, Khan W, Katic K, Maassen W, Zeiler W. Accuracy of different machine learning algorithms and added-value of predicting aggregated-level energy performance of commercial buildings. Energy Build 2020;209:109705.

[11] Zhou Z-H. Machine Learning. Springer; 2021.

[12] Pan B. Application of XGBoost algorithm in hourly PM2.5 concentration prediction. IOP Conf Ser Earth Environ Sci 2018;113.

[13] Mo H, Sun H, Liu J, Wei S. Developing window behavior models for residential buildings using XGBoost algorithm. Energy Build 2019;205:109564.

[14] Yao L, Cai M, Chen Y, Shen C, Shi L, Guo Y. Prediction of antiepileptic drug treatment outcomes of patients with newly diagnosed epilepsy by machine learning. Epilepsy Behav 2019;96:92–7.

[15] Chakraborty D, Elzarka H. Early detection of faults in HVAC systems using an XGBoost model with a dynamic threshold. Energy Build 2019;185:326–44.

[16] Montazeri A, Kargar SM. Fault detection and diagnosis in air handling using data-driven methods. J Build Eng 2020;31:101388.

[17] Wang S, Jiang Z. Valve fault detection and diagnosis based on CMAC neural networks. Energy Build 2004;36:599–610.

[18] Seyedzadeh S, Rahimian FP, Glesk I, Roper M. Machine learning for estimation of building energy consumption and performance: a review. Vis Eng 2018;6.

Data Statement

The datasets generated during and/or analysed during the current study are not publicly available because they are provided by a company and has to be kept private owing to privacy and security concerns but are/will be available if the concerned parties contact us and explain the reason for the data requirement, but the final decision lies with the company and access cannot always be guaranteed.

Applying MTP-concept for the standardization of building automation and control systems

Michael Krüttgen (M. Eng.)[a] *, Jochen Müller (Prof. Dr. rer. nat)* [a]

[a] TH Köln - University of Applied Sciences, Institute of Building Services Engineering, 50674 Cologne, Germany

Abstract. Energy requirements for buildings and their technical systems are becoming stricter and interfaces of technical systems more complex. Today's processes for monitoring applications are inefficient in planning, commissioning and operation due to the high effort involved. This is caused by lack of semantic specifications in existing standards. A basis for their economic implementation is not given.
This paper proposes a lifecycle spanning standardization of production related technical building equipment systems. The standardization work is based on the information model of the I4.0 Asset Administration Shell including the application of an online repository. Unified properties are defined from aspects of engineering to operation for technical plants. As a result, monitoring applications are possible with little effort. By applying Module Type Package, an information model is available for manufacturer-neutral and service-oriented plant control. A prototype is used to illustrate the advantages and engineering by means of Module Type Package. Quality assurance as an aspect of the commissioning is supported by the development of digital twins. Finally, the effort in the lifecycle phases of engineering, commissioning and operation is reduced. The standards developed will be published in a NAMUR recommendation.

Keywords. *Industry 4.0, NAMUR, Asset Administration Shell, Module Type Package (MTP), Asset-Monitoring, Production-related Building Automation.*
DOI: https://doi.org/10.34641/clima.2022.138

1. Introduction

Due to the current lack of standards, information on assets (components of production related technical building equipment (TBE)/building automation (BA)) are only available with increased engineering effort. Necessary properties for plant control, simulation and plant asset management are not available or are only available to a limited extent. Studies in practice [1] show that due to a lack of standards, non-uniform information models and the variety of subsystems (communication, applications), engineering efforts for data integration in e.g. energy- or asset-monitoring applications are often higher than their benefits. In practice, islands of information and data with an increased administrative effort get created. Thus, monitoring applications for energy- or asset-management are possible with increased effort and not widely available.

From perspective of legislation [2], buildings should have functions by 2025 that allow continuous monitoring, among other things. Selected systems for this purpose must benchmark the energy efficiency of buildings, report malfunctions to responsible persons and provide automated information about savings potential. Networked and interoperable system technology is required [3]. In order to achieve these targets and to be able to show the efficiencies, various monitoring applications are needed. As in administrative buildings, requirements for economic and efficient processes apply equally in production buildings, if not with a greater impact of efficiency on a building's emissions.

The NAMUR working group 1.7 "Production related building automation" and the TH Cologne-University of Applied Sciences developing information standards for industrially widespread asset types of production related TBE. The aim is to reduce efforts in processes of engineering, commissioning and operation of production-related building automation. By applying a uniform information model, hurdles to widespread application will be reduced. Monitoring, optimization and maintenance applications of HVAC systems can thus become an economically applicable standard. Figure 1 gives an overview about standardization work for production related TBE. The shown aspects of plant asset management, quality assurance of automation functions and plant control are getting standardized.

Copyright ©2022 by the authors. This conference paper is published under a CC-BY-4.0 license.

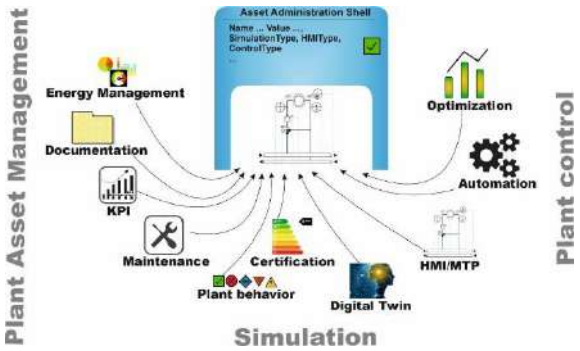

Fig. 1- Overview of standardization work

Standardization of production related TBE through suitable information models is a lever to aim the requirements according to [2] through the simplified availability of properties for energy management and asset monitoring applications. The information model of Industry 4.0 Asset Administration Shell (I4.0-AAS) [4] and Module Type Package (MTP) [5] are applied as a solution approach. An I4.0-AAS represents a lifecycle spanning and manufacturer-independent information model, which extends from planning to operation. For the area of automation and plant control, the MTP-concept is available by process industry.

2. Today's Standards and guidelines

Today's standards for building automation [6-11] do not include information technology descriptions for asset types and macro functions for TBE systems. Only the task of room automation is covered by macros [12]. Related functions or services for TBE systems, e.g. as macros for automation functions according to [7, sheet 3.2], are expected to be available from 02/2023.

Despite the standardization of interfaces and protocols, manufacturer-neutral communication and field bus systems [13-15] can only be integrated into an overall system with a huge effort in engineering. A Leading protocol in building automation is BACnet [6] with a service-oriented structure. BACnet standardizes input and output functions; templates or macros are not available. An analysis of the discussed standards shows that there is a gap for an area of manufacturer-independent automation with templates and HMI for building automation. MTP-concept is currently the only applicable information model for manufacturer-independent and service-oriented automation including HMI visualization. Its application in practice is currently limited to process automation. This standardization work demonstrates that MTP-concept is of importance for building automation. Essential factors for the use in building automation are the manufacturer independence, the service-based automation, the machine-readable data exchange by means of [16] and the integrability into a central information model.

Time-consuming quality assurance of automation functions through simulation is simplified by the creation of digital twins. There are various software tools for creating those [17, 18]. Using existing libraries, e.g. [19-21], linked and complex plant simulations with different targets can be created. A common software environment is Modelica, with the open source version OpenModelica [17]. Various open source libraries are available for simulation processing with Modelica. Another well-known open source library is the CARNOT library [22]. This is an extension of the MATLAB Simulink environment and is tailored to plant and building simulations. Requirements of Good manufacturing practice [23, 24] are spread in the pharmaceutical industry. In relation to the building automation there is only a small impact given and thus, GMP is not part of the standardization work.

Monitoring and observation of processes or procedures in building technology is implemented through technical monitoring according to [25]. For asset condition monitoring, asset monitoring is used according to [26]. With [25, 26], standards are given that can describe the states of the processes and assets. In practice, these standards are applied through complex and manual engineering during operation.

Planning of buildings is increasingly built on BIM (Building Information Modelling). Informational bookkeeping in BIM is based on the Industry Foundation Classes (IFC-standard) [27]. IFC describes a lifecycle-spreading model for planning and operating of buildings. In practice, currently the entire application of the IFC model is missing, thus data for later operation are not available through the meta model of the IFC standard.

In total, there is a lack of a lifecycle-spreading central information model for building automation that can map the in Figure 1 shown aspects of plant control, quality assurance and plant asset management. In fact of standards explained above are each without semantic characteristics, phase-specific information- and data-islands emerge e.g. BIM in the area of planning.

3. I4.0-AAS as central Information-model

The information model based on the Industry 4.0 metamodel is used to map the characteristics of assets across the life cycle [4]. Submodels available through the information model can be used as a generic approach for all assets. As well, the MTP concept can be mapped to the I4.0 AAS information model, as already shown in [28]. The IFC [27] metamodel of BIM, on the other hand, requires separate type developments for each asset type. The lack of practical application of BIM for the operational data of buildings and assets leads to choose that the I4.0-AAS as leading information model for this standardization work.

3.1 Structure and application of the I4.0-AAS

I4.0 Asset Administration Shells represent the connection between the physical asset and the Internet of Things and Services (I4.0 component consisting of an asset and its Administration Shell [4]). The Asset Administration Shell (AAS) of a TBE asset or component represents standardized functional aspects as a virtual image, e.g. properties, configuration parameters, states, capabilities and offered services. A central component of the I4.0-AAS are submodels that describe a wide variety of asset functions (simulation, HMI, operation, maintenance, etc.) using a structured set of standardized characteristics and capabilities [4]. In concrete terms, this means that management applications can access the features of submodels of I4.0 AAS. Figure 2 shows the structure of the submodels based on the planning and construction process according to [29, 30].

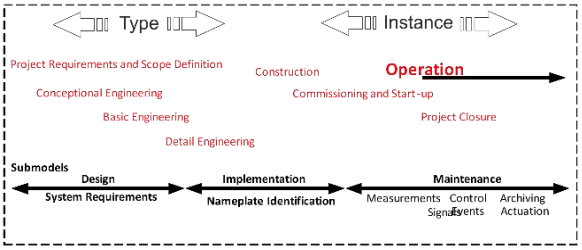

Fig. 2-Lifecycle-sketch in relation to submodels

Several years can pass from the planning process to a regulated and ready-to-operate TBE. With the planning phase, types of the I4.0 AAS are available. By entering product-specific characteristics of the aspects named in Figure 1, the I4.0 AAS is instantiated. Due to the lifecycle spanning approach of the information model of the I4.0 AAS, planning and commissioning information is available for later applications through the type and instance model, as the type information remains available even after instantiation through the submodels. During a performance evaluation of plants and components in operation, a comparison of operational data with planning data of respective assets can be carried out in order to identify potential weak points in actual operation.

3.2 Application in production-related building automation

In addition to the Bill of Material, the mtp-file is available as a separate *Module* Type *Package* sub-model for use in third-party applications. Figure 3 shows an excerpt of the I4.0 AAS information structure. If the information of the I4.0 AAS is viewed by using an XML viewer [31], the features with attributes are recognizable, e.g. the file path of the mtp-file, as marked in Figure 3.


```
</Attribute>
<ExternalInterface
 Name="FileDataReference"
 ID="31c079b4-e1c9-4a1c-9f42-cd25676c97b3"
 RefBaseClassPath="AssetAdministrationShellInterfaceClassLib/FileDataReference">
 <Attribute
  Name="MIMEType"
  AttributeDataType="xs:string">
  <Value>application/mtp</Value>
 </Attribute>
 <Attribute
  Name="refURI"
  AttributeDataType="xs:anyURI">
  <Value>/aasx/files/20211104_HeatingCircuitA.mtp</Value>
 </Attribute>
</ExternalInterface>
<RoleRequirements
 RefBaseRoleClassPath="AssetAdministrationShellRoleClassLib/File" />
</InternalElement>
```


Fig. 3-Extract from the AAS-file

Figure 4 shows the prototypical implementation of a TBE, using the example of a heating circuit and the composition as a composite component. All belonging I4.0 components of heating circuit are linked to the composite component.

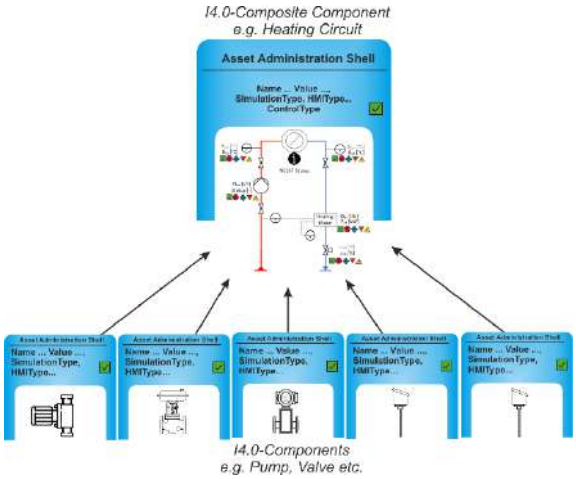

Fig. 4-Sketch of an I4.0 AAS composite component

Heating circuits of a HVAC-system are standardized by means of information model of the I4.0 AAS. By using AAS Package Explorer [32], as one possibility of AAS generation, the I4.0-AAS "Heating Circuit" has been set up as composite components. Composite components themselves do not represent a physical asset. A composite component represents a relationship complex of two or more AAS, which contains a higher and new functionality [33]. This results in a composite component that represents the entire heating circuit in addition to the individual AAS of temperature sensors, valve, pump and heat meter. A composite component maps the comprehensive information such as energy requirements and consumption, the MTP file and overall performance on a system-specific basis.

4. MTP for building automation

MTP-concept describes the modularization of complex production plants in terms of operation, visualization, alarming, communication, etc. [5]. Production related process equipment assemblies (PEA) are defined, which can consist of several modular functional units. Scope of standardization are systems of production related TBE, which includes HVAC and room automation systems.

MTP concept is currently applied in the process industry. Due to the characteristics of service-based automation and the availability of an information model applicable to building automation, the MTP-concept is applied to plant control aspect of this standardization work. With use of I4.0 AAS information model as the leading information model, MTP-concept must be integrated into it. Application of submodels of the I4.0 AAS enables this integration, as Figure 5 shows.

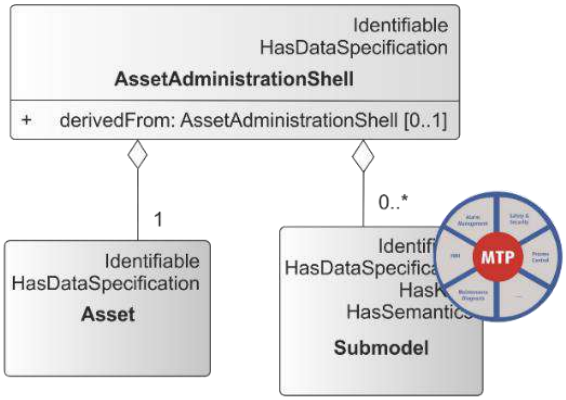

Fig. 5-Integration of the MTP into the I4.0 Asset Administration Shell [28]

The combination of PEA in complete systems requires an orchestration. Thus, a *Process Orchestration Layer* (POL) [1] is used which represents the automation and information technology level for the operation of modular plants. Goal is manufacturer-independent use with the same representation of a PEA by the HMI of MTP. An asset with multiple functions or partial functions, provides a separate service for each individual function. For example, a ventilation system, depending on the equipment, contains the services heating, ventilating, cooling, humidifying and dehumidifying. These defined services are available to the user in an executable form without having to carry out the engineering or create the visualization. A parameter set with setpoints is supplied with the service call for each PEA. HMI are available through templates. Service-oriented modelling and the use of templates for HMI of complete plant components, result in a reduction of engineering effort and simplification of configurations.

4.1 Application in production-related building automation

Figure 6 shows how visualization aspects are standardized in terms of information technology. HMI of a heating circuit with function template of pump for operation is shown.

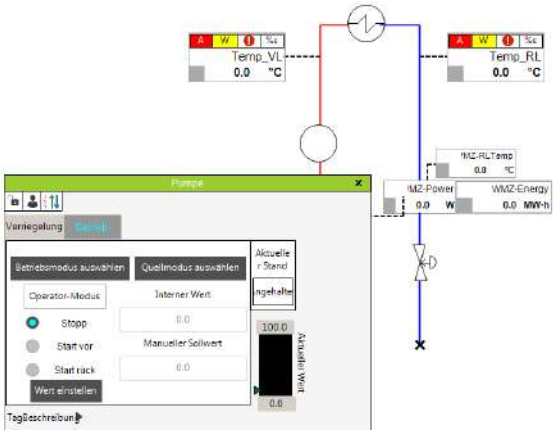

Fig. 6-View visualization with function template

Structure of TBE systems is developed and specified by users in Namur working group. The information technology standardization of assets is independent of the TBE structure. A basis for the information technology standardization of assets is the mapping of ISO/IEC standard ECLASS [34]. By specifying ECLASS version and ECLASS-IRDI, described data point can be represented unambiguously. Target systems, such as a POL, can represent the data point correctly by applying the semantic specification.

Heating circuit is automated by means [5, sheet 4]. State machines define a service-oriented interfaces for calling plant-control functions. A state machine executes fixed defined functions based on certain input status. Without functional requirement, the state machine is in *IDLE mode*. The executable program is started by the status word *Start.* As with the request of a service, a status word is also required for termination. *Complete* terminates the service in a controlled manner and the state machine is set to the initial state *IDLE.* Figure 7 shows entire state machine including intermediate states Pause, Cancel, Hold and Stop. Service-oriented plant control uses the advantage that not every field device control is processed individually in the state machine, but a single service (e.g. heating) can be executed. A service call leads to a predefined sequence of functions and processes in execution, e.g. continuous setpoint control. State machines can change the execution of the service by means of defined status words (start, abort, end, stop, completion, etc.).

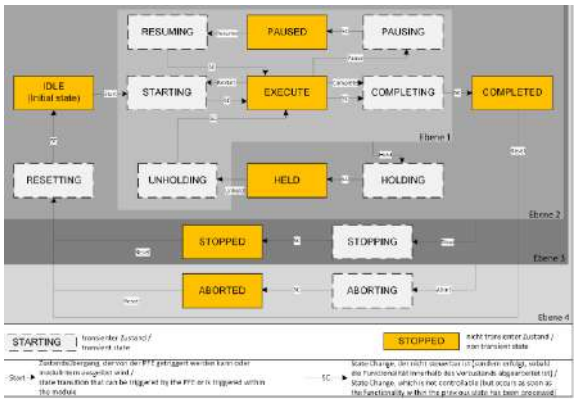

Fig. 7: Service State Machine [5]

PEA to be developed within the framework of the standardization work are always to be understood as integrable modules, which are integrated into a POL in a fully specified functional manner. In addition to the standardized HMI and function templates, the respective services are developed as program code. Each service has at least one procedure that processes the service. Services can only operate and be called in defined procedures, which are executed exclusively as continuous procedures. If several services are required that are to be processed in one procedure, e.g. cooling and humidification in an air conditioning system, recipes are written that structure the sequence of the individual services. As part of standardization work, HVAC-systems etc. are developed as independent PEA.

Applied to a heating circuit, this results in the service Heating, which is executed by the *Start* status word or terminated by the *Complete* status word. With the *Start* command, *the* required parameters (temperature setpoint, volume flow) are transferred to PEA. If service is executed in the *Execute* status, PEA continuously controls temperature setpoint and volume flow. New parameters are only applied when service is terminated and restarted. The decision as to how long which service is to be executed is therefore made in the higher-level POL.

5. Quality assurance of automation functions

TBE are brought together into an overall system by many technical installations at great expense. Technical systems from different manufacturers are to fulfil one or more tasks together. Due to heterogeneous field of technical systems and manufacturers, interfaces are unavoidable. Therefore, it makes sense to test the technical installations and systems of TBE systems virtually for quality assurance purposes before commissioning. One possibility is to simulate automation functions of digital twins for building automation. A digital twin can be defined as a representative of an asset in simulation environments, which simulates its dynamic behavior. Virtual representatives thus enable a check of building automation control functions before commissioning, e.g. by hardware in the loop [35]. Furthermore, certifications of systems or components are made possible based on the simulation models. For user, simulation represents an element for quality assurance of automation functions. Incorrect or missing parameters as well as process errors in control code become visible through virtual commissioning and the dynamic system behavior is tested.

Regardless of software used, the digital twins are linked as a file in I4.0-AAS and made available for higher-level simulation tasks. By means of [36], these simulation models can be exported as a Functional Mock-Up Unit (FMU). The FMI standard represents an exchange format for simulation models based on xml- and C-coded program code. This FMU is available for third-party applications for simulation in complete systems. In an appropriate simulation environment, generated FMU can be integrated for simulation without loss. With the standardization work, digital twins are developed for the individual assets and made available for quality assurance. Users of production-related automation practice demand, that quality assurance measures are required even before commissioning. [42]

6. Asset monitoring

Requirement for continuous monitoring according to [2] is not limited to energy monitoring. It is necessary to monitor and evaluate system conditions in order to enable efficient operational management.

In practice, the means of technical monitoring described in [25] are used to implement energy monitoring. This includes plant monitoring for recording and analysis of operating states for technical plants. Asset monitoring according to [26], which is known in the process industry, describes value-preserving and value-increasing maintenance by processing condition information of plant components. While asset monitoring according to [25] is carried out through limit value monitoring, characteristic value formation and elaborate graphical methods, asset monitoring in process industry uses concrete condition information of assets. This information is used to evaluate health status and plant behavior, e.g. with [37].

Due to a lack of uniform semantics, monitoring applications can only be implemented through costly engineering. Since effort currently exceeds the benefit, the aspect of low-effort asset monitoring is implemented through standardization work. Submodels of information model of I4.0 AAS are used to make asset information available for monitoring applications. For energy management applications according to [11, 38, 39] or asset, plant and maintenance monitoring according to [26, 40], status information of respective assets is provided without configuration.

Semantics missing in previous standards are provided by the online repository ECLASS [34]. For example, energy consumption of a heating circuit is measured by a heat meter. The consumption value is represented in I4.0 AAS by *Measurement* sub-model with the property *Total cumulative thermal energy (meter reading)*. The energy monitoring applications can reference through ECLASS-IRDI *0173-1#02-AAE300#006* that it is a feature on the *energy consumption of conventional heating* [34]. The procedure applies equally to asset monitoring applications. *Condition Based Maintenance / Breakdown Maintenance* submodels provide, for example, the status according to NE107 [37], which can be referenced with the ECLASS-IRDI *0173-1#02-AAV962#00.*

Through standardization work and use of an online repository, features with semantic characteristics are made available. This means that the contents can be accessed in a machine-readable way, which in practice leads to a simplification in engineering and in subsequent operational management.

7. Conclusion

Information standards are created based on the meta model of I4.0 AAS for TBE. This results in benefits for plant planners and operators throughout the entire life cycle. Engineering effort is reduced by predefined asset types. Measures of quality assurance of automation functions are already possible before commissioning through digital twins, and effort of commissioning is reduced through manufacturer-independent integration of MTP-file into an overall plant. During operation, applications for energy and asset monitoring, maintenance and service management, as well as performance evaluation are available with less configuration and reduce effort of asset management. The engineering process of a complete system will be based on standardized asset types and application of Namur recommendation.

The described procedure for implementing a technical building equipment system by means of information modelling of I4.0 AAS and MTP concept, represent the beginning of a series of standardizations. After completion of the prototypical implementation of a heating circuit, results will be transferred to cooling circuits. Subsequently, remaining trades of cost group 400 [41] will be processed, including ventilation and air-conditioning and room automation systems. The standardization work is limited to systems in area of production related building services.

Results of standardization are documented in a Namur Recommendation. All achieved results of the standardization work will be made available and published as an open source library consisting of digital twins, I4.0 AAS and amL files.

8. References

[1] Schuhmann et.al.: Effort for the integration of machines in asset monitoring applications, Internal study BASF, 2019

[2] EPBD 2018-European Directive on the Energy Performance of Buildings: Directive (EU) 2018/844 of 30 May 2018;

[3] Hug P., Wetzel A., VDMA: Energiemanagement in der Gebäudeautomation erfüllen zukünftige gesetzliche Anforderungen schon heute. 2018, 13, 09.;

[4] Plattform Industry 4.0: Details of the Asset Administration Shell, Part 1 - The exchange of information between partners in the value chain of Industry 4.0 (Version 2.0), 2019

[5] VDI 2658: Automation engineering of modular systems in the process industry; Verein Deutscher Ingenieure. 2019/10

[6] DIN EN ISO 16484. Building automation and control systems (BACS);

[7] VDI Building3814, Automation and Control Systems (BACS), Association of German Engineers. 2019

[8] DIN V 18599 part 11: Energy efficiency of buildings, Calculation of the net, final and primary energy demand for heating, cooling, ventilation, domestic hot water and lighting - part 11: Building automation; 2018/09.

[9] DIN EN 15500: Energy Performance of Buildings - Control for heating, ventilating and air conditioning applications. 2017

[10] DIN EN 17609. Building automation systems - Control application. 2020/12.

[11] Arbeitskreis Maschinen- und Elektrotechnik staatlicher und kommunaler Verwaltungen (AMEV). Notes for planning, execution and operation of building automation in public buildings - Building Automation 2019. brochure no. 145.

[12] VDI 3813, Building automation and control systems (BACS), Fundamentals for room control; Verein Deutscher Ingenieure. 2011

[13] Industrial communication networks - Fieldbus specifications - Part 4-3: Datalink layer protocol specification - Type 3 elements. 2020/08

[14] DIN EN 62769-115-2. Field Device Integration (FDI) - Part 1152: Profiles - ModbusRTU. 2018/10

[15] DIN EN 13757, part 2, Communication systems for meters. Wired M-Bus communication. 2018

[16] IEC 62714. Engineering data exchange format for use in industrial automation systems engineering -Automation markup language - Part 1: Architecture and general requirements. 2019/02

[17] Modelica Homepage; https://www.modelica.org/documents; Aufruf am 08.12.2021

[18] IDA Indoor Climate and Energy (IDA ICE); EQUA Solutions AG, Untermüli 3, 6300 Zug (headquarters) Switzerland; https://equa.se/de/ida-ice

[19] Modelica Buildings Library: Lawrence Berkeley National Laboratory,

https://simulationresearch.lbl.gov/modelica/ ; accessed 03.03.2021

[20] AixLib: RWTH Aachen, https://www.ebc.eonerc.rwth-aachen.de/cms/E-ON-ERC-EBC/Forschung/OPEN-SOURCE/~modh/AixLib58/; accessed 03.03.2021

[21] Nytsch-Geusen Chr. Huber J. Ljubijankic M. Rädler J. Modelica Buildingsystems-Eine Modellbibliothek zur Simulation komplexer Energietechnischer Gebäudesysteme. Berlin University of the Arts, Institute for Architecture and Urban Development

[22] SIJ Solar-Institut Jülich der FH Aachen, Solar Campus Jülich, Heinrich-Mußmann-Str. 5, 52428 Jülich, CARNOT Toolbox; https://www.fh-aachen.de/forschung/solar-institut-juelich/carnot/

[23] Bundesministerium für Gesundheit, Bekanntmachung zu § 2 Nummer 3 der Arzneimittel- und Wirkstoffherstellungs-verordnung - AMWHV vom 2. Dezember 2014.

[24] Code of Federal Regulations Title 21. Volume 2. CITE: 21CFR117.145. Sec. 117.145 Monitoring.

[25] VDI 6041, Facility Management, Technical monitoring of buildings and building services; Verein Deutscher Ingenieure. 2017

[26] Namur Recommendation NE91. Requirements for Online Plant Asset Management Systems; NAMUR e.V., User Association for Automation in Process Industries. 2001-11-01

[27] DIN EN ISO 16739: Industry Foundation Classes (IFC) for data exchange in the construction industry and asset management (ISO 16739:2013);

[28] Dr. Matthias Freund et.al.: "Das Module Type Package und die Verwaltungsschale-An Ansatz zur Integration"; Automation 2020 (video presentation), 30.06.2020

[29] Namur Worksheet NA35. PCT Planning and Processing in the Process Industry. NAMUR e.V., User Association for Automation in Process Industries. 2019-01-17

[30] Namur worksheet NA180. Comparison of phase model NA 35 and HOAI. NAMUR e.V., User Association for Automation in Process Industries. 2020-12-02

[31] AutomationML Editor. Josef Prinz, inpro. Berlin. Version 5.3.3.0. AutomationML e. V. 2019

[32] AAS Package Explorer. Festo AG & Co. KG. Hoffmeister, M., Orzelski, A. et al. , Version v2021-08-18

[33] Working Paper: Relationships between I4.0 Components - Composite Components and Smart Production. Continuation of the Development of the Reference Model for the I4.0 SG Models and Standards. Federal Ministry for Economic Affairs and Energy (BMWi). 2017/06

[34] ECLASS: ECLASS - Standard for Master Data and Semantics for Digitisation. (https://www.eclass.eu/index.html) Call on 13.12.2021

[35] VDI/VDE 3693: Virtual commissioning. Association of German Engineers. Association of Electrical, Electronic & Information Engineers. August 2016

[36] Pohlmann U. Wagner R. Use of the FMI/FMU standard for early simulation of software and hardware models of complex mechatronic systems. System Engineering Day 2012

[37] Namur Recommendation NE107. Self-Monitoring and Diagnosis of Field Devices. NAMUR e.V., User Association for Automation in Process Industries. 2017-04-10

[38] DIN EN 50001. Energy management systems - Requirements with guidance for use. 2018/12

[39] Arbeitskreis Maschinen- und Elektrotechnik staatlicher und kommunaler Verwaltungen (AMEV). Technical Monitoring 2020. Technical Monitoring as an Instrument for Quality Assurance. 2020. Recommendation No. 158

[40] DIN EN 17485. Maintenance -Maintenance40 within physical asset management - Framework for improving the value of the physical assets through their whole life cycle. 2021/08

[41] DIN 276 - Costs in construction; December. 2018

[42] NAMUR Annual General Meeting 2021, Virtual Workshop Session: AK1.7 Prozessnahe Gebäudeautomation: Aktuelles / Zwischenergebnisse Forschungsarbeit; 2021-11-04

Data Statement

The datasets generated during and/or analysed during the current study are not available because the study is still in progress. But the authors will make every reasonable effort to publish them in near future.

Building Assessment Framework from Whole Building to Components: A Danish Case Study

Kamilla Heimar Andersen [a,], Simon Pommerencke Melgaard [a], Rasmus Lund Jensen [a], Thomas Fehr [b], Anna Marszal-Pomianowska [a], Per Kvols Heiselberg [a]*

[a] Department of the Built Environment, Aalborg University, Aalborg, Denmark, [*] Kahean@build.aau.dk

[b] EK Energiekonzepte AG, Zürich, Switzerland

Abstract. Well-functioning buildings are crucial for the occupant's health and comfort and for reducing the CO_2 emissions from the building sector. A first step in assessing a well-functioning building is to know the current state of the building by, for example, relevant Key Performance Indicators (KPIs). Choosing suitable KPIs to provide a clear message can be challenging; however, beneficial to convey a message to the building actors. This study proposes a Building Assessment Framework to mitigate the latter, consisting of 1) a flexible and novel KPI tool and 2) a step-by-step KPI assessment methodology applicable to all buildings, systems, subsystems, and components. The KPI tool provides the user with a list of KPIs suited for all building systems, and with a separate backend and frontend, it is an easy tool to use. The KPI assessment methodology will guide the user through 5 steps and propose visualization of the chosen KPIs. The step-by-step KPI assessment methodology consists of 5 steps: 1) identification of the selected building resolution level 2) selection of the KPIs for the resolution level 3 + 4) recognition and cross-referencing of necessary sensors 5) choice of benchmarking for the data. The results from the KPI assessment using historical data from a university building located in Denmark demonstrate that the KPI tool is generic, making it applicable to all levels of a building and its systems. The Building Assessment Framework is flexible; it can be used over short and long periods (instantaneous to several years) and implemented in the building management system. However, it is necessary to be used with historical data, allowing for the real-time performance evaluation of the selected buildings or systems, thereby enabling the users to spot potential abnormal behavior that can lead to faults in the systems.

Keywords. Key Performance Indicators (KPIs), building systems, building assessment, energy use, rotary heat exchanger, air handling unit (AHU), open historical data
DOI: https://doi.org/10.34641/clima.2022.317

1. Introduction

Recent developments in Danish national policies [1] and the European Commission highlight the importance of reducing energy use in buildings [2], thus decreasing CO_2 emissions. Since the newly built share accounts for only 1% annually, to reduce CO_2 emissions from the building sector, controlling and operating the existing building stock efficiently and transparently is essential. Key Performance Indicators (KPIs) have been shown to incentivize building actors such as building owners, managers, and occupants to reduce the energy use in buildings [3]. The development and use of KPIs and assessments have notably increased in the last decade [4] [5] [6]. The latter aims to calculate the performance of buildings, systems, and components and thus provide easily accessible and valuable information to the building actors.

Previous studies regarding the development of KPIs have mainly focused on comparisons with the designed value from a numerical calculation (e.g., simulation) [7]. It is known that this comparison can create a performance gap due to the difference between the assumptions in the numerical calculations and the real-life operational behavior of the building systems [8]. With the increased instrumentation monitoring and access to data from buildings [9] [10], a deeper assessment with real-life data of building systems is feasible. Another research gap identified was adapting KPIs to all building systems, from whole building to component level [7]. Also, there is still a lack of knowledge on selecting the appropriate KPIs, depending on the building monitoring level (data quality & frequency and measured variables) and analytic methods (KPI assessment type and data acquisition).

Copyright ©2022 by the authors. This conference paper is published under a CC-BY-4.0 license.

The Horizon2020 "SATO" (Self-Assessment Towards Optimization of Building Energy) project https://www.sato-project.eu/ aims to develop and implement a cloud-based platform that can perform self-assessment and optimization of energy-consuming devices in a building so-called the SATO platform. The SATO platform will use an artificial intelligence approach combined with 3D BIM-based visualization to provide an accurate vision of the real-life energy performance of buildings and appliances. In this project, definitions of key performance indicators got substantial attention as they play a prominent role in the self-assessment and self-optimization platform [11]. The first part of the SATO platform is the development of the SATO KPI Tool, providing a list of KPIs used to assess the whole building level to the component level.

This study presents a developed Building Assessment procedure using the SATO KPI Tool. Further, the step-by-step KPI assessment procedure is presented using real-life data from a campus building at Aalborg University. The future purpose of the proposed Building Assessment procedure is to be integrated into the SATO platform. Combined with the building management system (BMS), that will facilitate a more efficient real-time operation.

1.1 SATO KPI Tool

The SATO KPI Tool is currently an Excel (.xlsm) based tool to be integrated into the SATO platform, with a frontend and a backend. The full description of the SATO KPI tool, including a detailed list of KPIs, can be found in [12].

The backend of the SATO KPI Tool consists of two main tabs (Tab 1 and Tab 2) shown in Fig. 1 and is not intended to be changed by the general user but to support the selection of KPIs in the frontend. Tab 1 describes the energy system terminology and the SATO KPI Tool user-manual, which describes the content and scope. Tab 2 concerns the Key Performance Indicators, Input for KPIs, Necessary measured variables, Data acquisition methods, and Required time resolution.

The frontend consists of a "Parameter selection" tab (Tab 3) which supports the user in selecting desired KPIs for the chosen building system.

The green color indicates the introduction, the energy system terminology used throughout the KPI Tool, and the user manual. The blue color is the backend content, and the red color is the frontend, which is the only tab the user needs to change.

2. Step by step KPI assessment methodology

This chapter presents the step-by-step procedure of the KPI assessment and can be seen in Fig. 4.
A more detailed and explained step-by-step assessment procedure can be seen in chapter 4 applied to the case study. However, two more aspects must be foreseen before performing a KPI assessment. This consists of mapping the building resolution level and determining the data benchmark. The KPI assessment procedure uses the SATO KPI Tool and identifies specific information about the selected building of choice, the building resolution level, and the data benchmark. The use of the SATO KPI tool is not restricted to this framework, and it can also be used to select individual KPIs for stand-alone monitoring. However, knowledge of building systems is necessary to use this assessment procedure. This is because the KPI tool will assist in selecting KPIs, but the user determines the final choice.

Fig. 1 – Overview of the SATO KPI Tool. It consists of an introduction (green), a frontend (blue), and a backend (red).

2.1 Step 1: Building resolution level

To determine which KPIs are applicable, it is essential to identify which inputs from the building systems are available. A proposed subdivision of a geometry-based and a system-based building resolution is proposed in Fig. 3 and Fig. 4. This type of subdivision can provide proper boundaries and insight into necessary and available inputs for the building and/or systems.

2.2 Step 2: Selection of KPIs

The KPI selection is conducted with the SATO KPI tool. It is expected that the SATO KPI Tool will be available online in April 2022 on this webpage: https://www.sato-project.eu/project-deliverables

2.3 Steps 3 and 4: Identify and cross-reference sensors

Steps 3 and 4 are performed partly with the SATO KPI Tool and manual sorting. Here the SATO KPI Tool will support to identify the physical sensors, resolution, and KPI method necessary for the selected KPI(s) for step number 3. Then, the manual cross-reference of needed sensors and already installed sensors in step number 4.

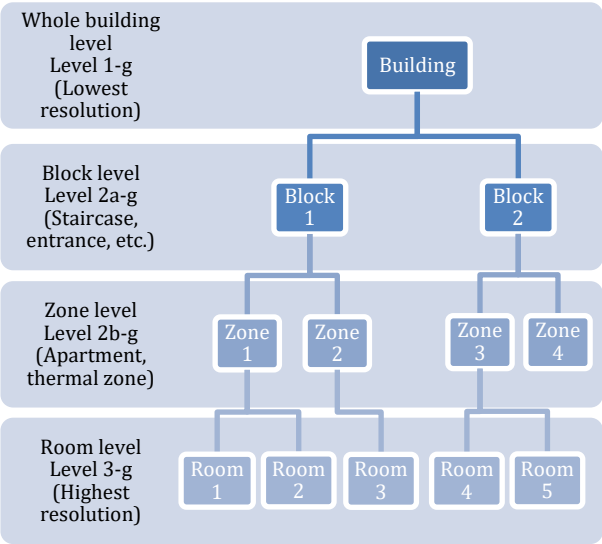

Fig. 2 – Building geometry-based resolution overview.

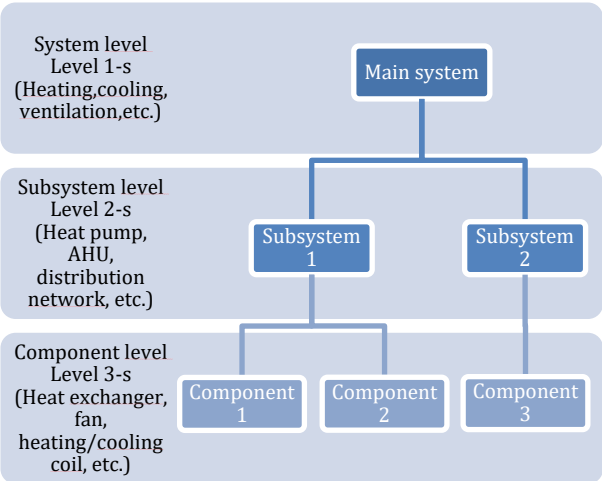

Fig. 3 – Building system-based resolution overview.

2.4 Step 5: Data benchmarking

The SATO project has developed three data benchmarks suggestions (Reference, Actual and Contextual), and one additional benchmark (Historical) is proposed below with examples and applicability.

Reference: Based on numerical simulation/model with standardized input values consisting of manufacturer data or standardized inputs according to standards/guidance compared with historical data from the same building, system, and area.
Example: The dimensioned SFP for an AHU compared to historical data, where the operating conditions are similar to the conditions for the dimensioned SFP.

Actual: Based on a numerical simulation/model with calibrated input values from the actual conditions compared with historical data from the same building, system, and area.

Example: A numerical simulation with calibrated values according to the historical data conditions, e.g., internal loads such as occupancy, lights, or weather for yearly heating use compared with historical data for yearly heating use.

Contextual: Based on historical data from the system and how well a specific service is achieved. Thereby indicating how efficient service is provided and if a higher target of the service causes possible higher/lower energy use.

Example: Heating energy use for a zone or room, compared to the level of thermal comfort provided.

Historical: Based on historical data from the current time period and compared to historical data from previous time periods for the same building, system, or area. If only the current time period is used, it gives an overview of the current performance, while if the previous time period(s) are used, an indicator for the change in performance is obtained. This benchmark is highly dependent on a high share of historical data as it is purely data-driven.

Example: Heating energy use for a year, compared to the heating energy use for the previous years. Coefficient of performance (COP) of a heat pump for a year, compared to the COP for the previous year.

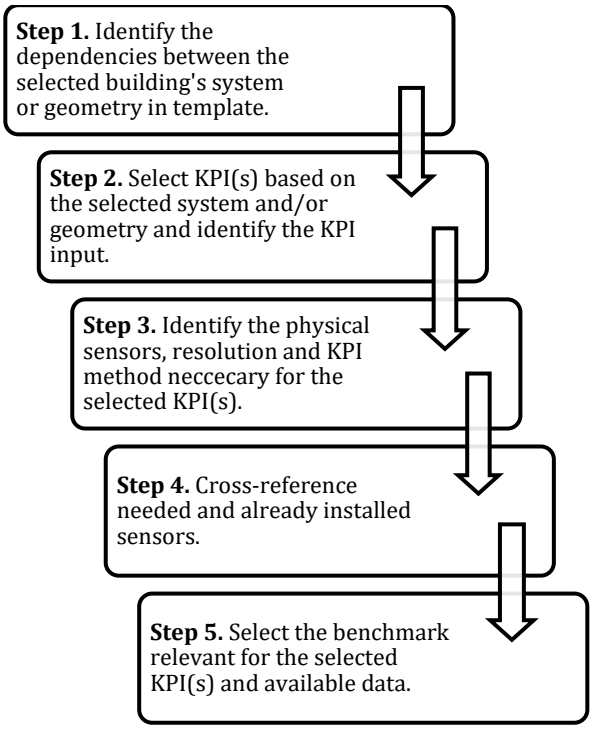

Fig. 4 – SATO KPI Tool step-by-step assessment procedure.

3. Case study

The case study is a university building located in Aalborg, Denmark, which houses the department of the Built Environment (BUILD) at Aalborg University, see Fig 6.

The building is ~9000 m² spread over four stories, with the area split into roughly 1/3 for laboratories and 2/3 for offices. The focus in this case study is only on the Air Handling Unit (AHU) supplying the western part of the offices, for example the 3rd floor can be seen on Fig. 5.

Fig. 5 - Thomas Manns Vej 23, 3rd floor coverage by AHUs, the blue area is covered by the AHU used in this paper.

The data for the case study is retrieved from the BMS system (Schneider Ecostruxure) and the energy management program (EMT Nordic EnergyKey) at Aalborg University. The data used are for the period from August 1st to December 23rd, 2021, with a 1-minute resolution.

Fig. 6 – Department of The Built Environment University building "Build department building" in Aalborg, Denmark.

4. Results and discussion

4.1 KPI Assessment

This subsection presents the result from the KPI assessment of the case study. The results are presented according to the step-by-step assessment procedure in section 2.

Step 1: Building resolution level
In this case study, the focus was on the AHU, so only the system-based building resolution level is shown in Fig. 7.

Step 2: Selection of KPIs
Based on the system from step 1, the SATO KPI tool is used to choose **three** KPIs, **one** for the **AHU** and **two** for the **rotary heat exchanger**. The selected KPIs are shown in Tab. 1.

Tab. 1 – Location, KPI, and the input needed for the KPI identified for the Build department building.

Location	KPI	Input needed for the KPI
Subsystem (AHU)	Specific AHU power (electricity use per m³ air)	Electricity use ; Air flow
Component (rotary heat exchanger)	Temperature efficiency ; Heat recovery	Efficiency ; outdoor air temperature

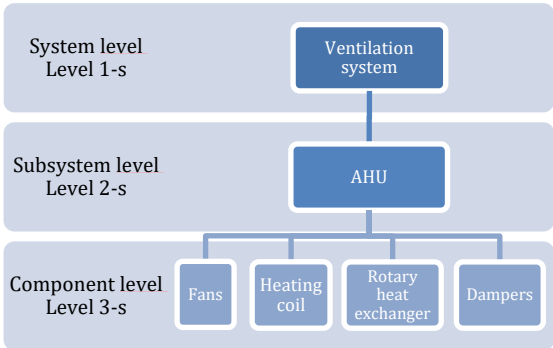

Fig. 7 – The Build department building system-based building resolution level for the ventilation system.

Step 3: Identify sensors and methods for calculating KPIs
From the previous step, the necessary input for each KPI is obtained; based on these, the KPI tool provides the sensor type, resolution, and if necessary, any sub inputs. These are all seen in Tab. 2 below.

Besides the input data, the methods for calculating the KPIs are also obtained. For the specific AHU power (per m³ air), the algorithm is shown in Equation 1.

$$AHU_{el} = \frac{E_{el}}{\sum_{i=1}^{60} Q_{air,i}} \quad (1)$$

AHU_{el} is the electricity use per m³ air $\left[\frac{kW}{\frac{m^3}{s}}\right]$
E_{el} is the electricity use per hour $[kW]$
$Q_{air,i}$ is the sum of the supply and extraction air flow per minute $\left[\frac{m^3}{s}\right]$

For the temperature efficiency and the heat recovery KPIs for the rotary heat exchanger, the algorithm for the temperature efficiency is shown in Equation 2.

$$HE_{eff} = \frac{T_{sup,out} - T_{sup,in}}{T_{ext,in} - T_{sup,in}} \quad (2)$$

$T_{sup,out}$ is the temperature on the supply-side after the heat exchanger $[°C]$
$T_{sup,in}$ is the temperature on the supply side before the heat exchanger (intake temperature) $[°C]$

$T_{ext,in}$ is the temperature on the exhaust side before the heat exchanger (extraction temperature) [$°C$]

Tab. 2 - Sensors and methods for calculating KPIs for the Build department building. S = sensor, CAL = calculation (Lower resolution than sensor), VS = virtual sensor (Same resolution as sensor), ES = external sensor (Sensor not located in the system/geometry), M = metadata (Static value from producer, design, etc.).

Parameter	Sensor type	Reso-lution	Input
Electricity use of AHU	S	1 hour	-
Air flow	CAL	1 hour	Supply air flow Extraction air flow
Supply air flow	S	1 min	-
Extraction air flow	S	1 min	-
Efficiency of HE	VS	1 min	Intake temperature Temperature after HE Extraction temperature
Outdoor air temperature	ES	1 min	-
HE rotation speed	S	1 min	-
Intake temperature	S	1 min	-
Temperature after HE	S	1 min	-
Extraction temperature	S	1 min	-

Step 4: Cross-reference needed and already installed sensors

Once the necessary input for the KPIs has been identified from the KPI tool, they must be checked against the sensors which are already installed; if all are available, there are no adjustments needed. If some are missing, these sensors must either be installed, or the SATO KPI tool can be used to check if another sensor can replace them. This case is shown in Tab. 3, where the air flows are not measured, so they must either be measured or replaced by a virtual sensor using the fan speeds and data sheets to calculate the air flow.

As this case did not have direct measurements for the air flow, it was chosen to make instead a virtual sensor based on the fans datasheet and take the fans control signal (recalculated to fan speed) and the dimensioned pressure increase over the fan as inputs. This adds uncertainty to the air flow, but, realistically, it will frequently occur in buildings, as many older systems do not measure flow directly.

The virtual sensor was created from the datasheet using points where fan speed, pressure increase, and air flow were known. The model was created according to the following Equation 3 in Python/Spyder 5.

$$Q_{fan,air} = \omega^a * b + p^c * d + (\omega * p)^e \qquad (3)$$

$Q_{fan,air}$ is the air flow across a fan $\left[\frac{m^3}{h}\right]$
ω is the rotational speed of the fan $[min^{-1}]$
p is the pressure across the fan $[Pa]$
a, b, c, d, e are coefficients for the model

The trained model had a Root Mean Square Error (RMSE) of 654 m3/h and a Coefficient of the Variation of the Root Mean Square Error (CV-RMSE) of 8,2% as calculated according to ASHRAE Guideline 14-2014 [13], indicating that it performs reasonably well. The most considerable uncertainty when using this kind of virtual sensor is the pressure loss of the distribution system. However, it is not a relatively large problem, as the system maintains a constant pressure in both the supply and extraction distribution network.

Tab. 3 - Already installed sensors and sensors needed to install in the Build department building.

Already installed sensors	Sensors needed to be installed	Can be replaced by
Electricity use of AHU	Supply air flow	Virtual sensor based on supply fan speed and the fan datasheet
Outdoor air temperature	Extraction air flow	Virtual sensor based on extraction fan speed and the fan datasheet
HE rotation speed	-	-
Intake temperature	-	-
Temperature after HE	-	-
Extraction temperature	-	-

Step 5: Data benchmark

Once it is confirmed that all necessary sensors are present, the benchmark is chosen. In this case study, the reference benchmark is selected for the temperature efficiency of the rotary heat exchanger and the historical benchmark for the heat recovery of the rotary heat exchanger, and the specific AHU power for the AHU.

*****The selected KPIs for visualization*****

The three KPIs are visualized with one or two of their most essential dependencies. The specific AHU power is plotted in Fig. 8 with the total air flow, which is the intake and exhaust air flow sum because this is the main parameter influencing the KPI as a reference benchmark. The heat exchanger's heat recovery is plotted in Fig. 9 with the outdoor air temperature and rotation speed because these

parameters will have an essential influence on the efficiency of the heat exchanger. The heat exchanger temperature efficiency is plotted in Fig. 10, with the intake and extraction temperatures, to see which ranges are used to compare with the reference performance.

Fig. 8 illustrates one of the selected KPIs: the specific air handling unit power with respect to the total air flow. As one can observe in Fig. 8, the specific AHU power decreases as the flow increases, thereby becoming more efficient, indicating that for this case, the AHU performs the best when running at the higher air flows.

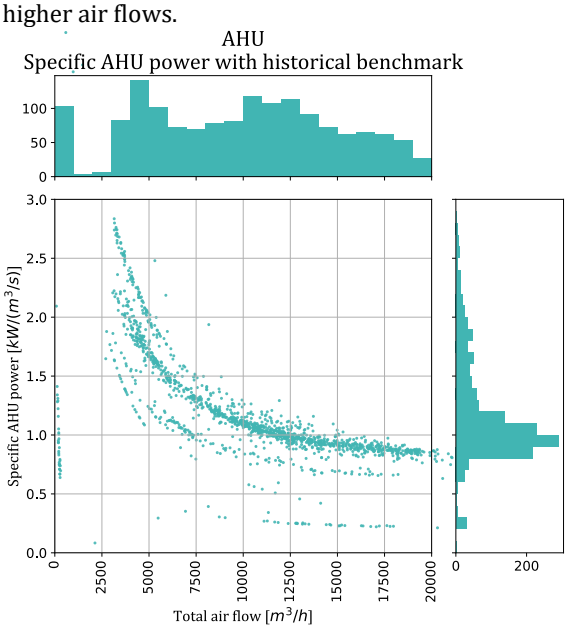

Fig. 8 - The KPI "Specific AHU power" is shown with the total air flow through the AHU (the sum of intake and exhaust air flow). The top and right plots are histograms for the total air flow and specific AHU power representing the number of data points within each range.

Fig. 9 shows that even though there is some variance in the HE efficiency, it follows the same trend. The efficiency increases as the outdoor air temperature decrease until it reaches approximately 5 °C. Naturally, this trend is observed to be due to the rotation speed of the heat exchanger; as it decreases with rising temperatures, so does the efficiency. This might not be a problem, as it could be due to the lowered need for heat recovery, but this cannot be concluded from this KPI alone.

Fig. 10 shows the temperature efficiency of the rotary heat exchanger under conditions as close to the manufacturer's calculation conditions as possible in the measured data. The conditions for performing this calculation are the rotation speed should be at max, and the flow should be balanced at a flow of 10000 m³/h on both the supply and exhaust. The rotation speed is fulfilled, while for the flow, they are balanced, but not all are at the dimensioning flow of 10000 m³/h. The lower flow will influence, but it is still possible to make a comparison near the manufacturer's conditions, to assess the performance of the components. For this component, it is necessary to accept a range for the different conditions, as for example, the intake temperature will very rarely be at the dimensioning conditions in Denmark, with the manufacturers intake temperature being -15 °C, which has only happened in one year within in the last 5 years.

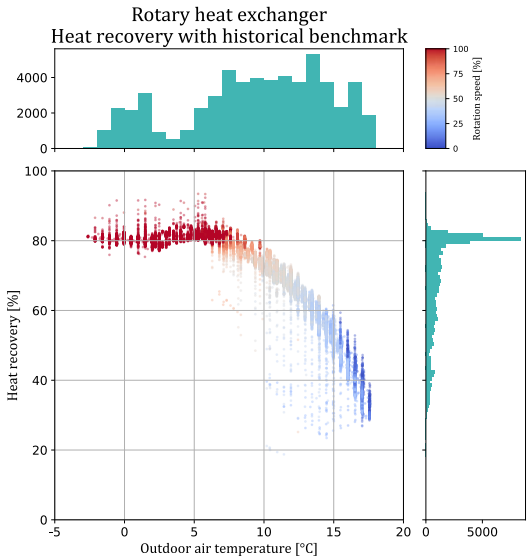

Fig. 9 - The KPI "Rotary heat exchanger (HE)", heat recovery with the historical data benchmark is shown with the outdoor air temperature and the rotation speed. The top and right plots are histograms for the outdoor air temperature and HE efficiency, representing the number of data points within each range.

4.2 Strengths and limitations

There are already existing studies developing and testing KPIs for building systems. However, to the best of our knowledge, no study was found to investigate KPIs for the full range of a building and system levels, with most studies investigating whole building or component level. The developed KPI assessment methodology can be applied to all building categories and suggests several benchmark options. The benchmarks encourage using historical data from the building or systems, providing realistic insights. This by comparing the historical data from the building or system with benchmarks based on real-life operating conditions. The KPI assessment methodology is developed to be an easy and understandable procedure for users.

Nevertheless, as all the benchmarks are partly data-driven, real-life operational data is needed. Also, as the developed KPI Tool is a selection tool, programming- and expert knowledge are still necessary. If the visualization is to be integrated into a BMS, expert knowledge on Information Technology (IT) is needed. However, adapting real-time building assessment and making clear guidelines is a significant task required to establish a valuable framework for building performance assessment and enable its practical use by the building industry.

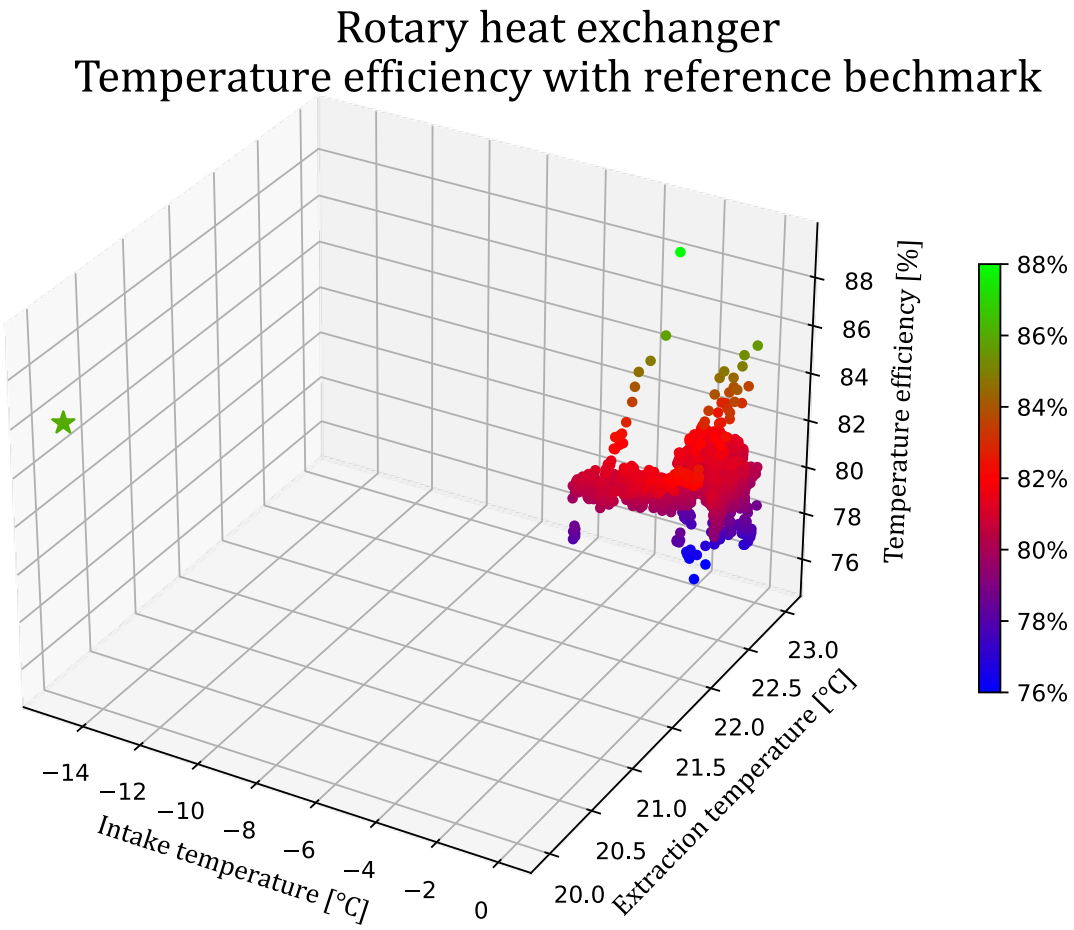

The measured values are based on 2912 points	Manufacturer value	Measured average value	Measured standard deviation
Temperature efficiency	86%	80.4%	0.8%
Intake temperature	-15°C	-1.4°C	1.1°C
Extraction temperature	20°C	22.6°C	0.2°C

Fig. 10 - The KPI "Temperature efficiency" is shown in relation to the intake and extraction temperature. The star is the manufacturers data point with the accompanying efficiency, and the dots are the measured data points. The table underneath the 3D plot shows the summation of the results and inputs.

5. Conclusion and future opportunities

This study sheds light on a flexible and novel Building Assessment Framework consisting of 1) the SATO KPI tool designed explicitly for applicability of KPIs in all building systems and 2) a KPI assessment methodology that will guide the user through a KPI selection and visualization procedure. The KPI assessment can be used for any building category and interconnected systems.

A KPI assessment using the proposed methodology is presented in this study with three selected KPIs for visualization, 1) the specific AHU power for the AHU, 2) the heat recovery for the rotary heat exchanger, and 3) the temperature efficiency of the rotary heat exchanger.
From the three KPIs visualized, it can be seen that to provide useful insight on the building and systems, 1) a KPI should not necessarily be a single number but instead a function of the essential parameters, thereby indicating the performance over the entire working range of the system. 2) It is found that the dimensioning point from the manufacturer does not necessarily correspond to the operating points of the system or component, thereby making comparisons between the expected and achieved performance challenging.

Continuing to visualize desired KPIs will allow the actors to better understand and use their building to the best of its potential, consequently reducing energy and optimizing occupant's comfort and health.

The KPI assessment is designed for utilization over short and long time periods (instantaneous to several years), and in conjunction with the visualized KPI graphs, allows the actors to get a better idea of the building and systems performance in the different parts of the operating range, thereby

allowing for detection and optimization of abnormal behavior. These capabilities are planned to be further explored and expanded in the author's future building systems.

The visualization code created in Python/Spyder 5 and the historical data from the university building is available on the author's GitHub repository: https://github.com/aauphd2024/CLIMA22_data_code

6. Acknowledgments

The authors gratefully acknowledge the support from the European Commission through the research project "Self-Assessment Towards Optimization of Building Energy" (SATO, https://www.sato-project.eu/), Grant agreement number: 957128.

The authors also gratefully acknowledge Campus Service at Aalborg University for access to the data used in this study.

7. References

[1] Government Danish, "Aftale mellem regeringen (socialdemokratiet) og venstre, dansk folkeparti, socialistisk folkeparti, radikale venstre, enhedslisten, det konservative folkeparti og alternativet om: National strategi for bæredygtigt byggeri," 2021. Available: https://im.dk/Media/C/4/Endelig%20aftalekst%20-%20B%C3%A6redygtigt%20byggeri%20-%205.%20marts%202021.pdf

[2] *Progress made in cutting emissions*. Available: https://ec.europa.eu/clima/eu-action/climate-strategies-targets/progress-made-cutting-emissions_en.

[3] Faria, P. *et al*, "A methodology for energy key performance indicators analysis," *Energy Inform,* vol. 4, *(1),* pp. 1-15, 2021. Available: https://link.springer.com/article/10.1186/s42162-021-00140-0.

[4] Wiik, M. K. *et al*, "A Norwegian zero emission neighbourhood (ZEN) definition and a ZEN key performance indicator (KPI) tool," *IOP Conference Series. Earth and Environmental Science,* vol. 352, *(1),* pp. 12030, 2019. Available: https://iopscience.iop.org/article/10.1088/1755-1315/352/1/012030.

[5] Cabeza, L. F. *et al*, "Key performance indicators in thermal energy storage: Survey and assessment," *Renewable Energy,* vol. 83, pp. 820-827, 2015. Available: https://dx.doi.org/10.1016/j.renene.2015.05.019.

[6] S. Lavy, "A Literature Review on Measuring Building Performance by Using Key performance Indicators," 2012. Available: https://doi.org/10.1061/41168(399)48.

[7] Li, H. *et al*, "System-level key performance indicators for building performance evaluation," *Energy and Buildings,* vol. 209, *(C),* pp. 109703, 2020. Available: https://dx.doi.org/10.1016/j.enbuild.2019.109703.

[8] C. Carpino *et al*, "Energy performance gap of a nearly Zero Energy Building (nZEB) in Denmark: the influence of occupancy modelling," *Building Research and Information : The International Journal of Research, Development and Demonstration,* vol. 48, *(8),* pp. 899-921, 2020. Available: http://www.tandfonline.com/doi/abs/10.1080/09613218.2019.1707639.

[9] *Volume of data/information created, captured, copied, and consumed worldwide from 2010 to 2025*. Available: https://www.statista.com/statistics/871513/worldwide-data-created/.

[10] *State of the IoT 2018: Number of IoT devices now at 7B – Market accelerating*. Available: https://iot-analytics.com/state-of-the-iot-update-q1-q2-2018-number-of-iot-devices-now-7b/.

[11] *Self-Assessment Towards Optimization of Building Energy*. Available: https://www.sato-project.eu/.

[12] Andersen, K. H., Melgaard, S. P., Marszal-Pomianowska, A., Jensen, R. L., Fehr, T., & Heiselberg, P. (2022). Development and description of the SATO KPI Tool. Institut for Byggeri, By og Miljø (BUILD), Aalborg Universitet. DCE Technical Reports No. 302 Available: https://vbn.aau.dk/en/publications/development-and-description-of-the-sato-kpi-tool

[13] Society of Heat, Refrigerating and Air Conditioning Engineers, "ASHRAE guideline 14-2014. measurement of energy, demand, and water savings." Available: https://upgreengrade.ir/admin_panel/assets/images/books/ASHRAE%20Guideline%2014-2014.pdf

Digital Twin for Heat Pump Systems - Description of a holistic approach consisting of numerical models and system platform

Joachim Seifert [a], Lars Haupt [a], Lars Schinke [a], Alf Perschk [a], Thomas Hackensellner [e], Stephan Wiemann [a], Martin Knorr [a]

[a] Chair of Building Energy Systems and Heat Supply, Institute of Power Engineering, Faculty of Mechanical Science and Engineering, Technical University of Dresden, Dresden, Germany, joachim.seifert@tu-dresden.de.

[e] Glen Dimplex Deutschland GmbH, Kulmbach, Germany, thomas.hackensellner@glendimplex.de

Abstract. Numerical building simulation is a tool that has been used intensively for years to analyse systems engineering in buildings. In the past, the focus of the development work was increasingly on the creation of detailed partial models and the coupling to other simulation programs, which was called co-simulation in the professional world. The development work regarding the coupling of building and plant simulation programs with programs of the numerical flow simulation is to be mentioned here. Currently, the coupling to measurement technology is pushed more strongly, whereby the focus is seen on the parallel use of the numerical model to a real system. This development is called "digital twin" of components or subsystems in power engineering. The following article addresses this development and would like to describe the system concept of a digital twin using the example of a heat pump technology. Based on the characterization of a special use case, the digital twin will first be divided into the development phase, field test phase, and deployment phase of heat pumps. Different model accuracies of the digital twin are assigned to the individual phases. In a second step, the different models for the component's compressor, heat exchanger, expansion valve, and the necessary piping are described. The coupling to a building simulation program is also part of the article. Furthermore, an essential point is the interaction with a cloud platform, in which the comparison between measured values and values from the digital twin takes place. Here, the focus is on the data exchange formats and the additional analysis tools that were used in the system concept. The paper concludes with a demonstration of an example under laboratory conditions within the Combined Energy Lab (CEL) of the TU Dresden.

Keywords. Digital twin, heat pump systems, sector coupling, renewable energies, carbon footprint
DOI: https://doi.org/10.34641/clima.2022.376

1. Introduction

The need for CO_2 reduction, especially in the building sector, leads to new system solutions. While in the past there was a transition from low-temperature gas technology to gas condensing technology and from low-temperature oil technology to oil condensing technology, development is currently focusing very strongly on heat pump technology and fuel cell technology. Fig. 1 shows the numbers of sold heat pumps in Germany during the last years. Within the heat pump technology, the air-to-water systems are in great demand, whereas the heat pump systems with ground coupling or groundwater coupling are less in focus.

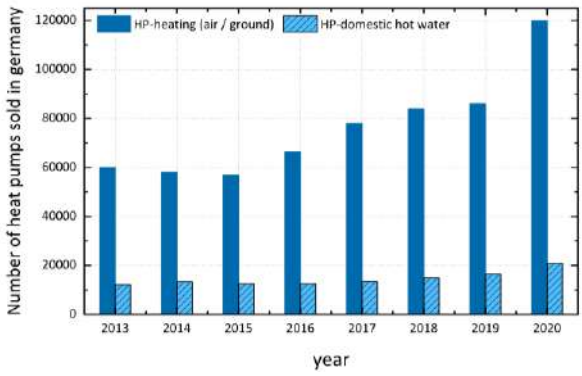

Fig. 1 – Number of sold heat pumps in Germany during the last years (air-to-water heat pumps / ground heat pumps and heat pumps for domestic hot water production) [1]

Copyright ©2022 by the authors. This conference paper is published under a CC-BY-4.0 license.

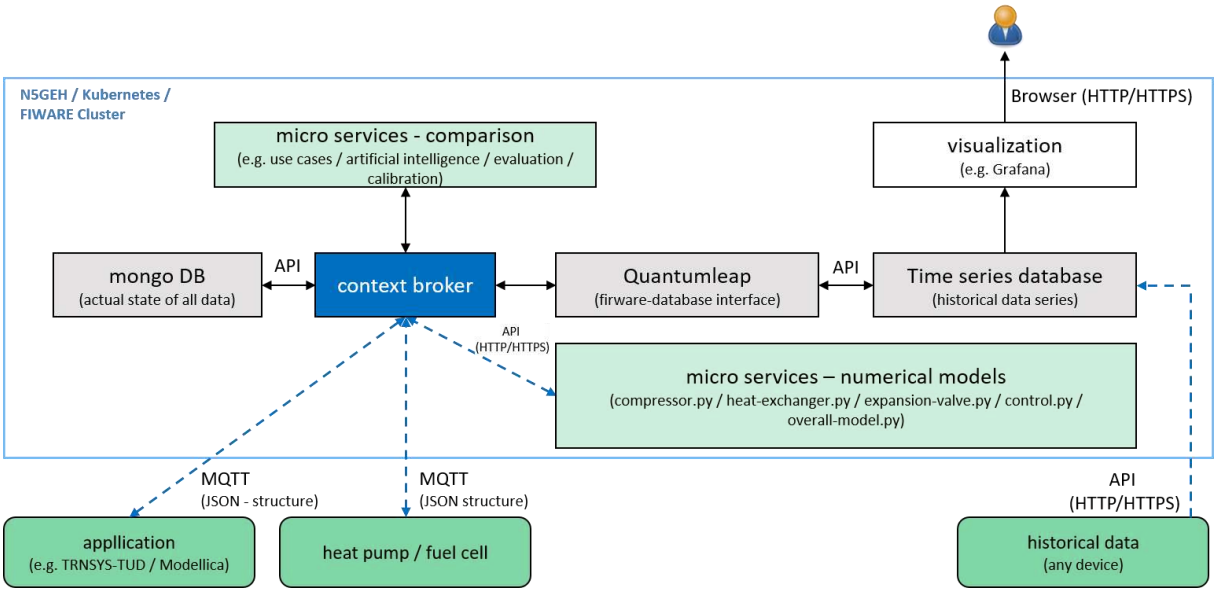

Fig. 2 – Digital twin for heat pump and fuel cell systems [2]

Heat pumps to produce hot water are also showing an increase in sales, but not as strong as air-to-water heat pumps. Heat pump technology is highly efficient, but also more dependent on external conditions than gas condensing technology. Against this background, it is advisable to carry out a comprehensive analysis of the thermal behaviour of the individual components of a heat pump during the development of new heat pump units. The following article will present a methodology for the analysis of heat pumps, which focuses on a digital twin.

2. Methodology of the digital twin

2.1 Fundamental consideration

The literature contains a wide variety of explanations of digital twins. The concept is particularly well established in production engineering [2], [3], [4]. In energy technology, with a focus on heat pump technology, reference can be made to [5]. A digital twin can be defined as follows:

"A digital twin is a digital representation of a tangible or intangible object from the real world in the digital world. Digital twins enable an overlapping exchange of data. They are more than just data and consist of models of the represented object and can also contain simulations, algorithms, and services that describe or influence the properties or behaviour of the re-presented object or process or offer services about it."

Essential features for the digital twin are

- representation of reality utilizing numerical models,
- data analysis and comparison of numerical and real systems as well as
- service functions based on the selected data.

All these functionalities were combined in a digital twin for heat pump systems. Fig. 2 documents the developed structure, which is based on a cloud architecture.

With reference to Fig. 2, various applications within the cloud architecture make up the components of the digital twin. These components also utilize external services, such as Trnsys TUD [7] or Modellica [8]. Furthermore, the corresponding real devices are connected to these services and applications. The IoT framework FIWARE is used to collect and process all the necessary data coherently. FIWARE's approach to linked data and its support for extensive data models allows not only for a comprehensive set of data points regarding the current status of an entity but also for a uniform method to store all relevant metadata like relationships or geolocations. All data passes through the context broker, which manages metadata and subscriptions. Subscriptions define where specific data is processed (e.g., time-series data is passed on to the database) and which components should receive an update of this data. Additional data can also be queried on-demand, or a subscription can be configured to be triggered only when predefined conditions are met. The subscription-based data-forwarding facilitates a modular service architecture in which a service is receiving data as soon as it is available at the context broker and all components can be built upon a uniform API. External applications and entities are preferably

connected to the cluster through the MQTT [9] protocol which offers a similar data exchange mechanism and very good scalability.
Within the cloud structure, various database systems, the micro-services, and the central visualization processes were arranged. The Grafana [10] program was used for visualization. The microservice “comparison” and the microservice “numerical models” are the two main components of the digital twin. In the microservice "numerical models", all components of the heat pump were mapped numerically using the scripting language Phyton. This is described in detail in the following section. In the micro-service "comparison" the comparison between numerical data and real data measured on the device is realized. In addition, functionalities for clustering and data analysis are implemented in this microservice.

2.2 Micro-service “numerical models”

For the development of the "numerical models" service, the initial focus was on the representation of an air-to-water heat pump. The implemented cooling circuit can be seen in Fig. 3. This consists of the air-refrigerant heat exchanger, the compressor, an intermediate heat exchanger, the refrigerant-water heat exchanger on the useful side, and the expansion valve.

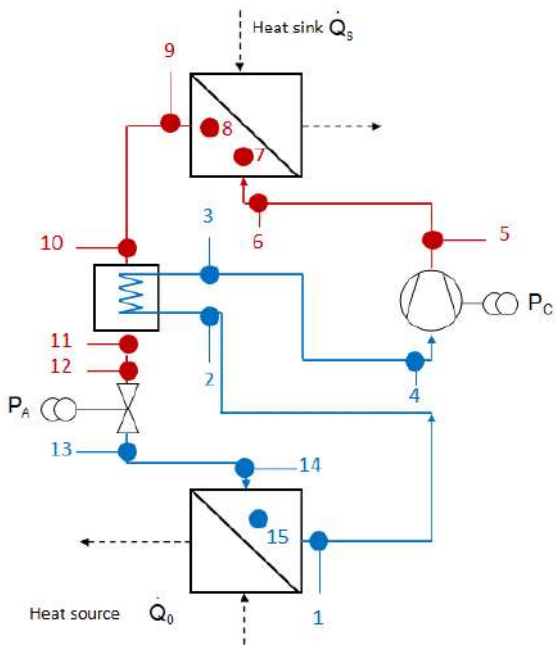

Fig. 3 – Refrigeration circuit of an air-to-water heat pump

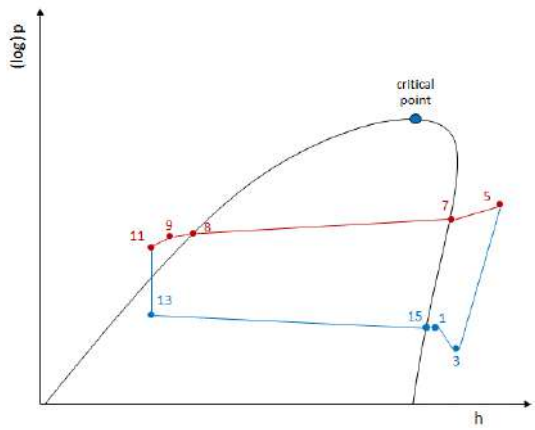

Fig. 4 – Process sequence in (log) p - h diagram

In the first step of modelling the internal heat exchanger was not considered. This means that the state points 2 and 3 as well as the state points 10 and 11 are omitted. The process sequence of the refrigeration cycle under these boundary conditions with temperature glide of the refrigerant and pressure losses can be seen in Fig. 4.
The numerical model of the heat pump should be able to be used in different phases of the product utilizing the digital twin. It is planned to use the digital twin

- in product development,
- in a field test phase
- as well as in the series product (and its use).

For the product development phase, very detailed models must be used to clarify construction details, for example. The time step sizes for the calculation are rather small here. It is advantageous to work with grey-box models [11] which are close to the high detailed white-box model approach (CTW). In the field test phase as well as in the real use phase of the product, simple models are required, since the number of data points is limited here, and the real-time capability of the models is important. It is advisable to use grey-box models which are close to the low detailed black-box model approach (CTB) for this purpose (see Fig. 5).
Figure 5 shows a classification of the digital twin with regard to the application area. The left diagram documents the requirements during the development phase of heat pumps. Very detailed models are needed here. The middle diagram documents the first field test phase of the prototype. Here rather robust models are needed. In the continuous operation of the devices, Black-Box models are required, which allow low computation times and allow a comparison to measurements.

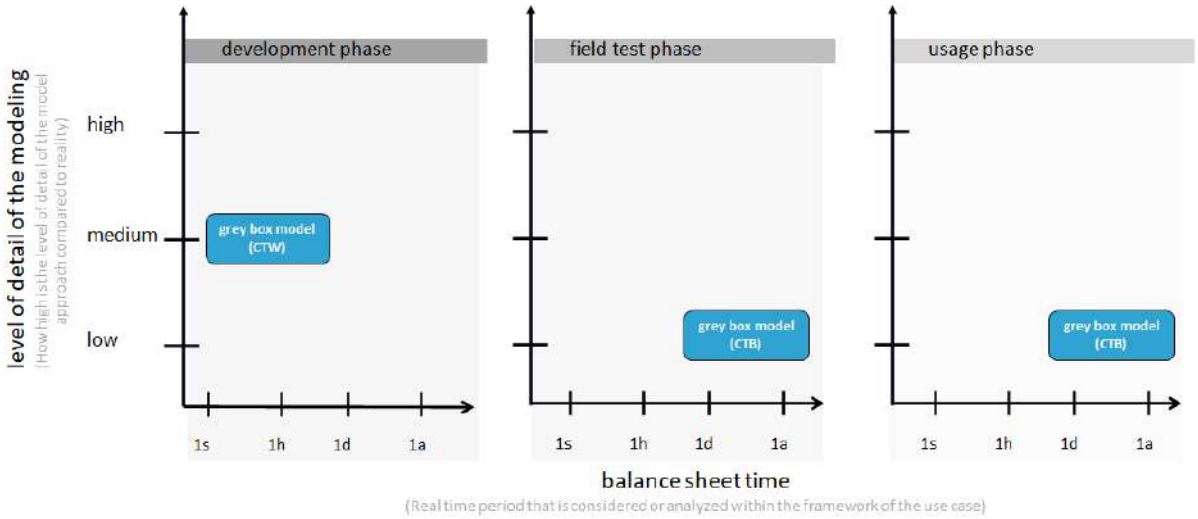

Fig. 5 – Numerical models – level of detail depends on development and usage phase

Figure 5 shows a classification of the digital twin with regard to the application area. The left diagram documents the requirements during the development phase of heat pumps. Very detailed models are needed here. The middle diagram documents the first field test phase of the prototype. Here rather robust models are needed. In the continuous operation of the devices, Black-Box models are required, which allow low computation times and allow a comparison to measurements.

As a result, the digital twin must contain a variety of models that can be flexibly combined depending on the usage requirements. In this case, at least one grey-box model (CTW) and one model (CTB) were created for each component of the heat pump (heat exchanger, compressor, expansion valve). Fig. 6 shows the possible combinations.

component	model 1	model 2	model 3
heat exchanger	X	O	...
compressor	X	O	...
expansion valve	X	O	...

X grey-box model (CTW – close to White-Box Model)

O grey-box model (CTB – close to Black-Box Model)

Fig. 6 – Heat pump subcomponents and their combination

Not all models can be described in detail here. For this reason, only the heat exchanger calculation and the overall model will be presented below as an overview. The interconnection of the subcomponents in the overall cycle process for the simulation is illustrated in Fig. 7. In the iterative algorithm, the condenser model calculates the refrigerant mass flow rate in dependence on the pressure values determined by the other subcomponents.

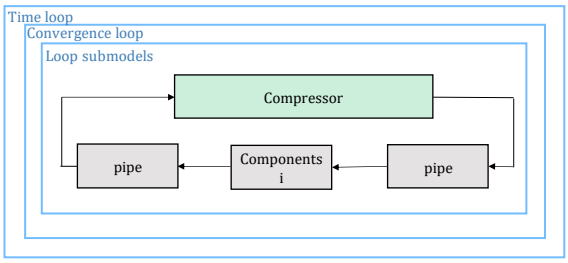

Fig. 7 – Simulation loops of the cycle process

As a simplified alternative to the detailed simulation of the heat exchanger with a cell model, a model based on the operating characteristics was implemented as follows. According to Fig. 8, the heat exchanger is therefore divided into 3 parts. For the condenser, the sub-processes a) cooling-superheating, b) condensing, c) sub-cooling are considered. The three different areas in the heat exchanger are required for the exact mapping of the heat transfer processes on the condenser side. On the evaporator side, only one subdivision into two areas is necessary.

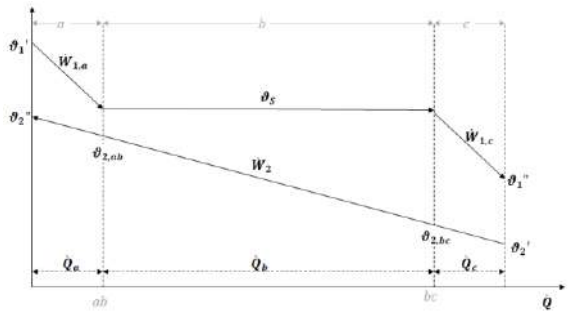

Fig. 8 – Temperature curves with trisection of the heat exchanger with condensation according to [12].

Here, the known design total heat transfer surface $(UA)_{des}$ is divided among the 3 different parts. Initially, the distribution is not known, so with a known boiling temperature, a solution must be determined by iteration. Knowing the outlet temperature of the refrigerant determined in the iteration, the unknown temperatures can be calculated from energy balances (see equations (1) to (3)).

$$\vartheta_{2,bc} = \vartheta_2' + \frac{\dot{W}_{1,c}}{\dot{W}_{2,c}} \cdot \left(\vartheta_S - \vartheta_1''\right) \tag{1}$$

$$\vartheta_{2,ab} = \vartheta_{2,bc} + \frac{\dot{m}_1 \cdot \left(h_{1,ab} - h_{1,bc}\right)}{\dot{W}_{2,b}} \tag{2}$$

$$\vartheta_2'' = \vartheta_{2,ab} + \frac{\dot{W}_{1,a}}{\dot{W}_{2,a}} \cdot \left(\vartheta_1' - \vartheta_S\right) \tag{3}$$

with $\dot{W}_{1,i} = \dot{m}_1 \cdot c_{1,i}$, $\dot{W}_{2,i} = \dot{m}_1 \cdot c_{2,i}$, $R_{2,i} = \frac{\dot{W}_{2,i}}{\dot{W}_{1,i}}$

Index i = a, b, c

With the temperatures according to equations (4) – (6), the dimensionless temperature changes (temperature effectiveness) P and from this the number of transfer units NTU are calculated.

$$P_{2,a} = \frac{\vartheta_2'' - \vartheta_{2,ab}}{\vartheta_1' - \vartheta_{2,ab}} \tag{4}$$

$$P_{2,b} = \frac{\vartheta_{2,ab} - \vartheta_{2,bc}}{\vartheta_S - \vartheta_{2,bc}} \tag{5}$$

$$P_{2,c} = \frac{\vartheta_{2,bc} - \vartheta_2'}{\vartheta_S - \vartheta_2'} \tag{6}$$

$$NTU_{2,i} = \frac{1}{1 - R_{2,i}} \cdot \ln\left(\frac{1 - R_{2,i} \cdot P_{2,i}}{1 - P_{2,i}}\right) \tag{7}$$

From the sum of the NTU values, the total heat transfer area $(UA)_{calc}$ can be calculated (see equation 8). With these results, a new outlet temperature of the refrigerant ϑ_1'' is determined by the iteration algorithm until the deviation between $(UA)_{calc}$ and $(UA)_{des}$ is below a present value.

$$(UA)_{calc} = \sum\left(NTU_{2,i} \cdot \dot{W}_{2,i}\right) \tag{8}$$

3. Validation of the digital twin

Different procedures are available for validating the models within the digital twin. In the first step, measurement data from companies can be used. This data can be transferred into the cloud system via the "historical data" interface. The second possibility is the targeted measurement in the Combined Energy Lab of the TU Dresden [13]. The Combined Energy Lab consists of three main test facilities that are coupled together. Test facility 1 is the outdoor climate room which is used for testing heat pumps. Test facility 2 is the indoor climate room used for heat transfer tests and indoor air quality / thermal comfort issues. To ensure the reaction of the building and to be able to test realistically, an energy park is necessary. Fig. 9 (CAD view) and Fig. 10 (real implementation) show the different experimental setups.

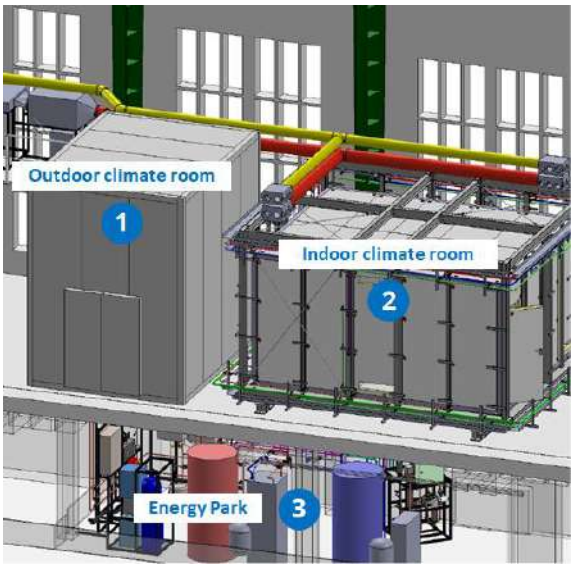

Fig. 9 – Overview about the Combined Energy Lab 2.0

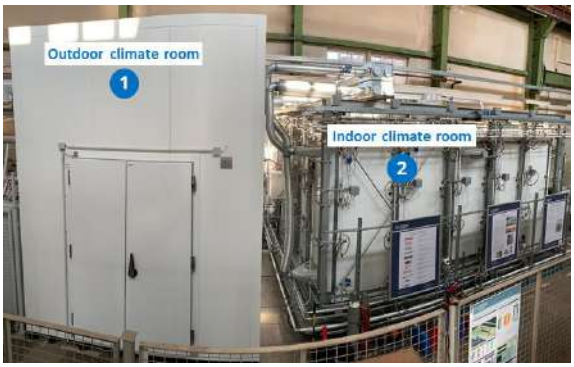

Fig. 10 – Photography of the Combined Energy Lab

Within test environment 3, a low-voltage emulator is also integrated, with which it is possible to vary the characteristics of the electrical distribution network.

With the Combined Energy Lab 2.0, it is possible to analyse complex energy supply structures. However, since the test time is limited to real-time, a type day procedure was developed with which an annual test can be reduced to for example four representative type days. These type days are used to validate the digital

twin. Details are documented in [13][1].

4. Conclusion

This paper presents the methodology of a digital twin for heat pumps. The main component of the digital twin is a cloud structure which, in addition to the numerical representation of the refrigeration cycle including the control system, also includes a comparison of the numerical data with field test data. The exchange can be adapted to the granularity of the task. The main component of the digital twin is the numerical model, which was implemented in Phyton. It consists of some grey-box models (CTW, CTB) for each component, which can be combined in any way. The strong structure of the presented numerical model is to be understood as a positive system property since it is possible to generate digital twins or digital system twins for other heat and cold generation systems very quickly.

However, concerning the development of numerical models, it must be noted that there are some limitations in the Python scripting language. Especially the overall convergence for the calculation of the refrigeration cycle is difficult and should be completely revised for future development.

5. Acknowledgement

This publication is based on a research project which was supported by the German Federal Ministry of Economics and Energy under the code 03EN1022 A-D (A = TU Dresden; B = RWTH Aachen; C = Glen Dimplex; D = Viessmann)

6. Symbols and abbreviations

	specific enthalpy	J/kg
c	specific heat of fluid	J/(kg K)
	mass flow rate	kg/s
NTU	number of transfer units	-
$\dot{Q}_S$	heat transfer rate (building)	W
	pressure	Pa
$\dot{Q}_0$	heat transfer rate (air, water, ground)	W
P	temperature effectiveness	-
P_C	electric power (compressor)	W
P_a	electric power (auxiliary energy)	W
R	heat capacity ratio	-
$(UA)_{calc}$	calculated product of overall heat transfer coefficient and total heat transfer area	W/K
$(UA)_{des}$	product of overall heat transfer coefficient and total heat transfer area (designed)	W/K
$\dot{W}$	flow stream heat capacity rate	W/K
x	dimensionless temperature change	-
ϑ_1'	inlet temperature	°C
ϑ_1''	outlet temperature	°C
ϑ_2'	inlet temperature	°C
ϑ_2''	outlet temperature	°C

1…x	points of calculation
1	refrigerant side
2	heat sink - side
a, b, c	index of the calculation (sections)

7. References

[1] BWP: Statistics on heat pump systems, German Heat Pump Association, https://www.waermepumpe.de/, 2021.

[2] J. Seifert, L. Haupt, L. Schinke, A. perschk, T. van Beeck, M. Knorr: „Digitaler Zwilling (DZWi) – Digitaler Zwilling von Wärmeerzeugersystemen als Wegbereiter für die Entwicklung emissionsarmer Gebäudeenergietechnik", - Interim Report to the research project, Technische Universität Dresden, 2021

[2] Virtual Twin: Manufacturing Excellence through Virtual Factory Replication, Grieves, M. White-Paper. 2018.

[3] Glaessgen, E. u. Stargel, D.: The Digital Twin Paradigm for Future NASA and U.S. Air Force Vehicles. Structures, Structural Dynamics, and Materials Conferences. 53rd AIAA/ASME/ASCE/AHS/ ASC Structures, Structural Dynamics and Materials Conference. 2012

[5] Boss, B., Malakuti, S., Lin, S.-W., Usländer, T., Clauer, E., Hoffmeister, M. u. Stojanovic, L.: Digital Twin and Asset Administration Shell Concepts and Application in the Industrial Internet and Industrie 4.0. An Industrial Internet Consortium and Plattform Industrie 4.0 Joint Whitepaper

[6] R. Jentsch, J. Aizpuru, M. Lauermann, T. Barz: Digitaler Zwilling einer Wärmepumpe für die

[1] The presentation of the paper at the 2022 Climate Change Conference will feature the initial test results, as they were not finalized at the time the paper was submitted.

prognosebasierte Betriebsführung, KI- Kälte / Luft / Klimatechnik, 04/2021

[7] A. Perschk, „Gebäude- und Anlagensimulation - Ein "Dresdner Modell",“ *gi Gesundheits-Ingenieur - Haustechnik - Bauphysik - Umwelttechnik,* Nr. Jg. 131 Nr. 4, 2010.

[8] The Modelica Association, https://www.modelica.org, 2021

[9] MQTT – Massage Queuing Telemetry Transport, https://www.hivemq.com, 2021.

[10] Grafana: The open observability platform, https://grafana.com/ 2022.

[11] E. F. Silvia, I. Merts, B. De Ketelaere, J. Lammertyn: Development and validation of “grey-box” models for refrigeration applications: A review of key concepts, International Journal of Refrigeration-revue Internationale Du Froid - INT J REFRIG, Volume 29, Pages 931-946, 10.1016/j.ijrefrig.2006.03.018., 2006

[12] J. Seifert, M. Knorr, L. Schinke, M. Beyer: Instationäre, energetische Bewertung von Wärmepumpen und Mikro-KWK-Systemen, VDE-Verlag, 2017

[13] J. Seifert, L. Schinke: Neuer Klimaversuchsraum an der TU Dresden, Gebäudetechnik in Wissenschaft und Praxis GI; DIV Deutscher Industrieverlag München, 2016

Data Statement

The datasets generated and analysed during the current study are not available because patent protection law votes are currently being carried out but the authors will make every reasonable effort to publish them in near future

Deep learning for CFD analysis in built environment applications: a review

Giovanni Calzolari [a], *Wei Liu* [b]

[a] Division of Sustainable Buildings, Department of Civil and Architectural, Engineering, KTH Royal Institute of Technology, Stockholm, Sweden, gcal@kth.se.

[b] Division of Sustainable Buildings, Department of Civil and Architectural, Engineering, KTH Royal Institute of Technology, Stockholm, Sweden, weiliu2@kth.se.

Abstract. The study and control of the airflow in indoor environment is of great importance since it directly affects human daily life primarily in terms of health and comfort. Fast and accurate airflow predictions are therefore desirable when it comes to built environment applications of inverse design, system control, evaluation, and management. Computational fluid dynamics (CFD) enables detailed predictions through numerical flow simulations and it has been consistently used to simulate airflow motion, heat transfer, and contaminant transport in indoor environment. However, CFD still faces many challenges mainly in terms of computational expensiveness and accuracy. With digitization, recent interest is posed on new data driven tools to either substitute CFD typically for faster predictions or aid the CFD simulation for improved accuracy. More specifically, the abilities of deep learning and artificial neural networks (ANN) as universal non-linear approximator, handling of high dimensionality fields, and computational inexpensiveness are very appealing. This work reviews current deep learning applications in built environment research, which are only limited to surrogate modeling as replacement for expensive CFD simulation. ANN enables fast and sometimes even real-time prediction, but usually at a cost of a degraded accuracy. For this reason, we also critically review what it is done and presented in fluid mechanics simulations research in general, to propose and inform about different techniques other than surrogate modeling for built environment applications and possibly improve the predictions quality as well. More precisely, ANNs can enhance the turbulence model in various way for coupled CFD simulations of higher accuracy, improve the efficiency of POD decompositions methods, leverage crucial physical properties and information with physics informed deep learning modeling, and even unlock new advanced methods for flow analysis such as super-resolution techniques. All these methods are very promising and largely yet to be explored in the built environment scene. Together with promising advancements, deep learning methods come with challenges to overcome, such as the availability of consistent large flow databases, the extrapolation task problem, and over-fitting, etc.

Keywords. Artificial intelligence, Neural networks, Fluid Mechanics, Turbulence, Built Environment, Digitization, Computational Fluid Dynamics.
DOI: https://doi.org/10.34641/clima.2022.139

1. Introduction

The advent of the era of digitization is enabling the use of machine learning tools to provide advances to many areas of research in scientific and engineering disciplines. Specifically, within machine learning, deep learning can leverage the growing amount of data available to infer predictions over a broad range of different problems, such as airflow simulations. Computational Fluid Dynamics (CFD) is a field where data driven models are showing much potential in the latest years [1]. Standard CFD deals with numerical simulations of fluid flows by solving physical flow equations. It is a useful, and widely used tool that enables detailed predictions. However, it has unfortunately some limitations, mainly in terms of computational expensiveness. The most accurate CFD approach that tries to fully capture turbulence phenomena of the flow, called *Direct Numerical Simulation* (DNS), is in fact still unfeasible in most practical applications due to the extremely high computational power required to solve the equations for the discretized grid. Other common CFD approaches are the so-called *Large Eddy Simulations* (LES) and *Reynolds Averaged Navier*

Copyright ©2022 by the authors. This conference paper is published under a CC-BY-4.0 license.

Stokes equations (RANS) methods. The latter in particular is significantly less computational demanding than DNS but introduces assumptions and turbulence models which eventually increase the number of uncertainties and lower the overall accuracy of the simulation [2]. Besides, the problem with CFD simulations in built environment is that, even with small indoor domain, the airflow is quite complex, making even RANS simulations quite demanding in processes where fast predictions and control are necessary. Even though very fast or real time predictions are unfeasible, RANS represents the industry standard and it is widely used in the indoor environment to simulate turbulent airflow [3], heat transfer [4], and contaminant transport [5]. It is also used in the urban environment to simulate wind flow around buildings [6] or at pedestrian level [7] and tracking pollutants [8]. While new improved CFD techniques, algorithms and models are appearing, recent interest is posed on new data driven tools, deep learning, to either substitute or aid CFD simulations. This work will review the current research on the interaction between built environment fluid dynamics simulations and deep learning algorithm. Deep learning is the supervised learning class based on *Artificial Neural Networks* (ANNs) [9], which task is to map the function between inputs and outputs. ANNs are composed of a number of hidden layers between input and output, Figure 1 shows an ANN in its most standard architecture: the *Multi-Layer Perceptron* (MLP) [9].

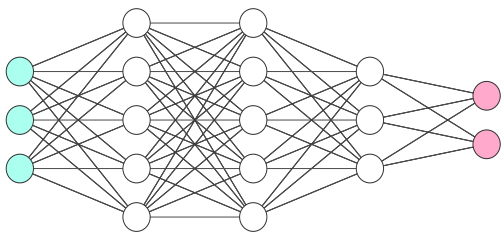

Fig. 1 - A four Layer MLP, with a 3 nodes input layer colored in light blue, 3 hidden layers of 5-5-3 nodes respectively in white, and a 2 nodes output colored in pink.

Applications with deep learning architectures of different types will be reviewed. Besides MLPs the most common to be found are *Convolutional Neural Networks* (CNNs) [10] and *Recurrent Neural Networks* (RNNs) [11]. CNNs are developed and adapted for computer vision tasks and pattern recognition. RNNs, instead, are specialized in working with time sequence data thanks to the presence of a feedback loop. In recent years, deep learning algorithm proved to be extremely flexible, highly scalable and universal approximator of non-linear functions, such as equations of the fluid flows.

2. Research Methods

The primary objective of this review paper is to inform and propose new interactions between built environment CFD simulations and deep learning algorithm. This interaction is not exactly new or never explored before. There are already some works that substitute CFD simulations with deep learning algorithm using the ANN as surrogate model of the numerical simulation, which are going to be reviewed in section 3. Surrogate modeling generally solves one of the main problems of CFD simulations being their general expensiveness. Depending on the specific problem, surrogate modeling can allow for order of magnitudes [12] faster airflow prediction, even **real-time** predictions in some cases [13]. However, the landscape of interaction is mostly limited to surrogate modeling, and what is generally wanted and desired is to obtain fast, but also accurate predictions of flow quantities such as velocity, pressure, temperature and pollutant concentrations to provide and control thermal comfort to indoor environments. Even though the main objective of surrogate modeling is to reduce computational cost while keeping the same order of accuracy [14], the computational inexpensiveness usually comes at the cost of degraded accuracy. Surrogate modeling is often built from and compared with RANS simulations, which still present all the uncertainties stated above. In the best cases ANNs produce very similar results in terms of accuracy, but worse in others. This review aims to show that surrogate modeling is not the only way to make use of deep learning architecture together with CFD simulations. By critically reviewing in section 4 some major applications of deep learning that have been attempted in fluid mechanics research, hints and opportunities for future research on integration of ANNs and CFD for built environment applications are proposed. The number and kind of deep learning interactions in fluid mechanics is in fact much larger allowing for a systematic review of different techniques such as turbulence model tuning and enhancement, surrogate modeling, POD, and super-resolution. Finally, section 5 offers a discussion about possible opportunities, but also challenges for deep learning methods to aid, substitute, or improve CFD simulations for the built environment.

3. Built Environment applications

Numerous indoor environment applications are strictly connected to the study and simulations of fluid flows. Fast and accurate predictions of variables such as velocity, pressure and temperature profiles are desirable in this context. Some examples of CFD simulations that are consistently performed in the indoor environment for inverse design are thermal comfort analysis, pollutant dispersion, HVAC system control, etc. For the outdoor environment, the simulations of wind and tracking pollutants are conducted at various urban levels. Thermal comfort in the indoor environment, such as vehicle cabins of cars but also aircraft is a challenging problem which has been attempted to solve with increased popularity by inverse design. Together with these methods, deep learning models have started to cover an important place in these applications. Deep learning techniques have already been widely

applied since the early 2000s in specific topics such as building energy predictions [15,16,17] or HVAC system control [18,19]. However, data driven interactions with CFD simulations are still limited in quantity and diversity of approach. The vast majority of applications are limited to substituting surrogate modeling for expensive CFD simulations to achieve faster predictions. CFD simulations can in fact be very computationally demanding, especially in the design process, emergency management and control, where fast predictions are necessary, or in the outdoor environment where the simulation domain is usually large. The main objective of surrogate modeling is to reduce computational cost while keeping the same order of accuracy [14]. Section 3.1 reviews the studies on the topic.

3.1 Deep learning surrogate modeling in the built environment

In the work by Hintea et al. [13], from a minimalistic set of cabin environment sensors, several different machine learning algorithm, including a standard MLP network and a random forest algorithm, are used and compared to approximate equivalent temperature inside a car to obtain real-time predictions. The equivalent temperature is measured at eight body locations to provide a direct estimation of thermal comfort. Eventually the fastest prediction is delivered by a simpler linear regression model, while the MLP obtains the highest accuracy overall. As shown instead by other works (Zhang et al. [20,21] and Warey et al. [22] for instance), CFD simulations are not discarded completely, but still used as high fidelity solution necessary for training the deep learning algorithm. Warey et al. [22] (see Figure 2) use deep learning models to quantify the thermal comfort of indoor vehicle cabins for different boundary conditions of air temperature, but also air velocity, humidity, glazing conditions, etc. To better assess the indoor thermal comfort this time not only an equivalent temperature analysis is performed, but also on more advanced evaluation scores, the predicted mean vote and the predicted percentage of dissatisfied people. These scores evaluate thermal comfort from a more rational perspective [23]. CFD simulations previously validated with wind tunnel experimental measurements are generated to be used to train the deep learning algorithm, which was then applied also to different fields with real time predictions. Instead, Zhang et al. [20] first use a shallow standard MLP in general indoor environments with CFD as training data to solve the inverse design problem and identify a possible relationship between thermal comfort and inlet boundary condition. Later on in another work, Zhang et al. [21] apply the based knowledge on a simplified first class aircraft cabin environment. This time the deep learning surrogate model is integrated inside a genetic algorithm and the results are compared against a 57% more computationally expensive classic genetic algorithm without deep learning tools. Three shallow MLPs are singularly trained to obtain the predicted mean vote, the air age and the draft rate, the latter assessing the local discomfort for humans.

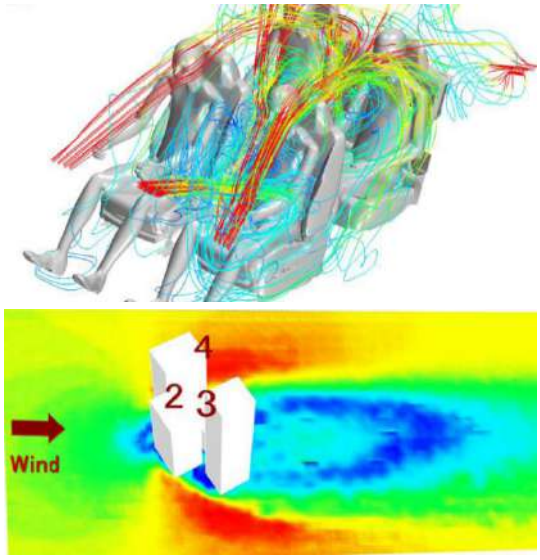

Fig. 2 - Two examples of deep learning surrogate modeling for built environment applications. Above the study of thermal comfort for indoor vehicles cabin by Warey et al. [22]. On the bottom, the optimization study of urban wind flow simulations by Tanaka et al. [12].

Upgrading the scale of simulations from indoor to external environments, like urban cities, accuracy deterioration and struggle to consider other boundary conditions such as traffic or weather are inevitable. Tanaka et al. [12] (see Figure 2), study urban flow simulations where the location, dimension and shape of four tall buildings were optimized in a restricted area with the construction of a CFD optimization tool. The objective is to reduce wind forces on buildings and mitigate local strong winds at pedestrian level. The focus of the paper still resides on CFD RANS simulations, which are eventually used to train a deep CNN encoder-decoder for *ultra-fast* (0.005 seconds) predictions. They estimate the CNN predictions to be about fifty thousand times faster than RANS. However, the ANN predictions show lack of accuracy compared to CFD simulations especially in specific case that the network was not trained for, such as different wind directions. In Tanaka et al. [12] case, the deep learning method has to be viewed more as a parallel tool to the CFD simulation, useful in the early design process for example. A similar example is also given by the work of Ding et al. [24], which develop data driven regression model for coupled indoor-outdoor flow analysis together with CFD simulations. Eventually, surrogate modeling main advantage resides in the possibility to obtain really fast and inexpensive predictions, otherwise unfeasible with CFD simulations. It also comes with limitations such as being strongly case dependent, without good generalizability, and in need of large training data sets. In most indoor environment studies, only the case related data were used for training. Then the trained ANN was very likely unfeasible for another case that the network was not trained for. Its limited accuracy can become an important factor in practice. Many possibilities of utilization of deep learning

models that section 4 will cover are yet to be explored in the built environment, possibly to further increase also the accuracy of the analysis and create more trusty models.

4. Deep learning applied to Fluid Mechanics

The range of applicability of ANNs is in general much richer than what highlighted in section 3. This section aims to inform about possible different techniques and applications of ANNs to drive forward the research in the built environment. Starting from the beginning of the 1900s with the first applications with very shallow ANNs [25,26], the architectures, models and types of interaction are becoming over the year more and more improved and advanced. Fluid mechanics research is not only looking at deep learning methods for computational efficiency but also increased accuracy. Nowadays, fluid mechanics deep learning techniques sees numerous possible applications. Some of them make use of data-driven machine learning models as an aid for augmenting the CFD simulations and their turbulence models. Some others instead present deep learning architectures as surrogate model of fluid dynamics numerical simulation, similarly of what is also done in the built environment. Besides straightforward substitution of CFD with ANN, model order reduction and POD techniques are also reviewed. There are some other applications that use completely different new emerging methods such as super-resolution techniques.

4.1 Turbulence modeling

As remarked already, deep learning techniques can be utilized in conjunction with CFD simulations to increase the accuracy of simulations. Turbulence models introduce a number of constant coefficients varying from model to model, determined experimentally. Therefore, the RANS turbulence models are not universally capable for every flow, but actually depend on the specific flow features. A first obvious way to utilize deep learning algorithm on turbulence models is for *constant tuning*, finding for different flow applications the best values of the coefficients of a particular turbulence model. For example, Yarlanki et al. [27] estimated the temperature in data centers using a tuned standard RANS turbulence model, allowing a reduction of the absolute average error in by 35%. Another example is the work by Luo et al. [28]. The main difference between the two is that Luo et al. [28] provide a **physics informed** neural network by combining the high-fidelity labeled output of DNS simulations with prior knowledge on the mathematical representation of the RANS model. In general, tuning coefficients can increase the accuracy of CFD predictions, but the value of the coefficients of the turbulence models are problem related, with scarce generalizability. Furthermore without proper caution, tuning coefficient techniques could actually introduce more uncertainties to the analysis, compensating for example for experimental errors, inaccurate boundary conditions, etc. Physics informed deep learning modeling can help to contain this problem and increase generalizability so that the same architecture can be applied to different flow fields.

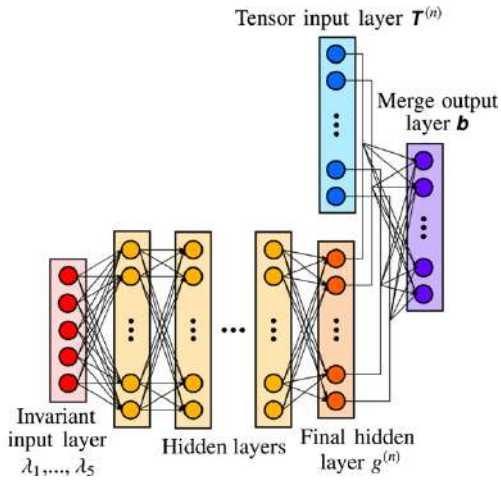

Fig.3 - TBNN architecture used by Ling et al. [37]. It presents a further input layer called Tensor input layer, which makes sure that the ANN embeds the physical property of rotational invariance.

Deep learning algorithm can actually achieve much more when interacting with turbulence modeling. Research is focusing on new ways of enhancing turbulence models by acting directly to the source of uncertainties. An idea is to use deep learning algorithm to build a *representation* of turbulence modeling closure terms. Tracey et al. [29] take a one-equation turbulence model and try to reproduce the same results by replacing its source term of the model with a classic shallow MLP. They established a methodology for future studies where the training data becomes more accurate DNS or well resolved LES simulations. The enhanced model in practice learns the behavior of turbulence leading to better prediction over a wider range of flows. In 2016, Ling et al. [30], for instance, explore the opportunity of using DNS data as labeled output, which accuracy tops RANS's. They act directly on the eddy-viscosity hypothesis, substituting it with an ANN model. The ANN used is a very deep architecture of more than 10 hidden layers, an advanced alternative to MLP, called Tensor Basis Neural Network (TBNN), shown in Figure 3. This custom deep architecture makes use of a tensor basis set to impose within the ANN prior physical knowledge about fluid flows. In particular, it embeds symmetry and physical property of Galilean-rotational invariance, which is ultimately fundamental for accuracy of the CFD solution. Similar applications focusing on augmenting turbulence modeling is for instance the work of Geneva et al. [31] using the same TBNN architecture from Ling et al. [30] coupled with Bayesian statistics. Deep learning can even reveal new hidden correlations where the physical laws are still not known *a priori*. A perfect example of this interaction is given by Font et al. [32] for turbulent flow analysis. They make use of a remarkable custom architecture, being an advanced deep Multiple Input-Multiple Output CNN (MIMO-

CNN). Overall, turbulence model enhancement techniques allow for impressive accuracy improvements, and perhaps most importantly even the discoveries of new equations and correlations about turbulence phenomena that were not known before.

4.2 Surrogate modeling

As shown in section 3 for the built environment, ANNs can also be used to marginally or completely substitute CFD simulations in the analysis of fluid flows. In general, computational efficiency of reduced order based methods can be 1-2 orders higher compared to conventional CFD methods [33], even allowing real-time prediction in some cases. For example, Guo et al. [34] develop a CNN algorithm that performs at least two orders of magnitude faster than equivalent CFD solution with slightly less accurate solution. Fukami et al. [35] instead analyze the feasibility of five different deep learning architecture for aerodynamic design predictions in three different regression problems, including the estimation of force coefficients of wake flows. Sensor measurements were used as labeled output for the network training. The multiple works done primarily by Guastoni et al. [36,37], apply deep learning models to an open channel extremely expensively boundary layer DNS simulation. It is one clear example of the computational efficiency advantage of data driven models surrogate over brutal numerical simulations. In the next sections applications of two methods that are conceptually similar to simple surrogate modeling will be reviewed: POD, and super-resolution.

4.3 POD

Already in 2002, Milano et al. [38] was modeling near wall turbulent flows with POD. POD belongs to the branch of order reduction models and decomposes a physical field into a basis along the principal component analyses, allowing for example to quantify the structure of turbulence through recognized basic patterns [39]. The limitations raised by POD resided in the inherent linearity of the mode decomposition. Milano et al. [38] showed ANNs can actually be viewed as generalization of POD, but with improved architecture consisting of non-linear layers that eliminates the linear limitations of POD. Since the work by Milano et al. [38], the development of model order reduction using POD with ANNs has been uninterrupted. Fresca et al. [40] develop a strategy to make the offline training dramatically faster by performing a prior dimensionality reduction through POD and a pre-training stage where different models are combined to initialize the parameters of the algorithm. Improved ANNs architectures have also been researched over the years. For example, in 2018 Wang et al. [41] applies the LSTM-RNN architecture with POD techniques in the study of ocean currents and flow around cylinder. POD deep learning techniques are eventually an interesting and efficient form of order reduction modeling, which allows much faster predictions while maintaining reasonable accuracy [41].

4.4 Super-resolution

Borrowed from computer vision and image recognition, super-resolution imaging refers to the class of techniques that aims at obtaining a high-resolution image output from a low-resolution image. Deep learning has already been extensively used for super-resolution and lately mainly through CNNs [42], given their predisposition for visual pattern recognition. The same concept could be applied to flow fields by treating them as *images*. Using an offline database of high-resolution snapshot of flow field (for example DNS data) as labeled output, it is possible to give input from low resolution data either from experimental measurements as done by Erichson et al. [43] or from fast and computationally inexpensive simulation. The method consequently reconstructs the turbulent field to high resolution with the ANN. More specifically, Erichson et al. [43] first reconstruct a 2D cylinder with 10 sensors and getting DNS data as high resolution output and subsequently also apply the same architecture to the study of isotropic turbulence. Fukami et al. [14,44] take DNS high-resolution data and purposely down-scale them with a pooling operation to obtain the low-resolution input data. Using two different neural network architecture, one a classic CNN and another improved hybrid ANN algorithm that can handle the multi-scale nature of the flow, Fukami et al. [14,44] successfully reconstruct the same cylinder wake of Erichson et al. [43] and even 2D decaying isotropic turbulence. In all these cases, the model super-resolves the low-resolution field without assuming any *a priori* knowledge of the physics, which demonstrate the strength of data-driven super-resolution techniques. At the same time, the super-resolution opens the possibility to incorporate the knowledge of the physics into the learning process for improved accuracy in future studies. Gao et al. [45] develop a physics-informed deep learning based super resolution solution using a CNN. The aim of a physics-informed algorithm is to guarantee that the super-resolved fields are faithful to the physical laws and principles. As shown, super-resolution techniques eventually offer a new and efficient way to study turbulent flows, with enormous potential especially when coupled with CNNs.

5. Opportunities and challenges in the built environment

Most RANS turbulence models are designed for aeronautics applications with high speed flow, while built environment simulations usually present low velocity fields. The standard coefficients of the models might be inadequate in various scenarios as highlighted by Yarlanki et al. [27]. Tuning coefficients with the use of ANNs is a practical scope that can already decrease error in quantities of interest. By acting on augmenting the turbulence models, further

substantial accuracy improvements can be reached. However, the computational efficiency in built environment design problems still needs to be addressed. Coupled deep learning CFD might be unfeasible for some applications, especially when fast predictions are needed, such as in control, design or optimization tasks. On the other hand, surrogate modeling inevitably allows faster computations, but the predictions quality is usually affected. Surrogate modeling is also able to obtain results without any prior physical knowledge about the problem, thanks to a large amount of training data. This is advantageous in some respects, as it is not required previous deep physical knowledge and experience on the problem, but it can be problematic in others. For example, without prior physical knowledge, the trained ANN could provide adequate level of accuracy on the variables trained, but critically non-physical results overall. Physics informed modeling is another possible step into higher quality predictions, which could also increase the generalizability of the model. About the direction of turbulence modeling research, Duraisamy et al. [46] note that one should not throw away the existing knowledgebase in turbulence modeling but rather build on top of it. Some modeling base concepts, such as dimensional analysis and Galilean invariance in turbulence modeling should be preserved in the deep learning architecture. Numerous physics informed modeling have been reviewed in section 4. With the availability of large amount of data, deep learning models are also capable to find hidden correlations or equations that were unknown [46]. This can be extremely important since human preconception and knowledge can harm new discoveries instead of helping achieve them. For example, forcing to fit deep learning models from RANS models when the closure is renowned to fail in multiple cases will certainly not allow great performance improvements. Instead, data driven models might even bypass the traditional ways of hypothesis-driven model creation and instead generate models free from human intuition [46]. A similar philosophy could also be applied in the built environment. The accuracy of simple surrogate modeling and coefficient tuning is highly dependent on the training procedure. The corresponding ANNs show the highest struggle in adapting to cases where the ANN was not trained for, even for simple variables changes as seen in the work by Tanaka et al. [12]. Super-resolution and POD are in general less sensitive in this regard, but they still require a large training data set to achieve good accuracy. Turbulence model augmentations provide a tool to overcome the limitations of standard turbulence models and they should provide the highest generalizability and robustness in applications to different flow scenarios. Finally, the addition of physical information with physics informed modeling can definitely help in improving overall performance of deep learning.

It is important to notice that the power of ANNs in specific tasks reside almost completely in their capacity to interpolate the data. The performance on the test set will be adequate if the test and training set are under similar distribution. A big challenge for deep learning instead resides in the extrapolation process, where ANN can fail even in simple cases [43]. One obvious example of extrapolation task is when the data has the form of a time sequence and the objective of the deep learning algorithm is to inference about future predictions, given historical data as training data (crucial in climate modeling for instance). The deep learning model fails in extrapolating the fields which belong to a different statistical distribution. Therefore, for transient indoor/outdoor airflow, the application of super-resolution requires further investigation. Directly linked to interpolation ability is the renowned ANN hunger for large dataset. In computer vision tasks, the available training data are usually massive. In fluid mechanics, the availability of data is still limited, despite various efforts in the latest years to create fluid mechanics databases of simulations. The research community is still not used to consistently work with open and large shared databases and often prefer to generate simulation data themselves, especially in the built environment, which eventually harm the development of better data driven models. Besides, the scarce availability of large data makes the classic over-fitting problem during the ANN training procedure even more relevant.

6. Conclusions

Thanks to digitization, new data driven tools are starting to make an impact in engineering applications as CFD simulations in the built environment. The objective of this study is to perform a comprehensive review of the current state of the art of the interaction between deep learning models and fluid mechanics simulations, update on the state of the built environment research in the topic, and propose possible advancements in the field. The vast majority of applications in fluid mechanics analysis in the built environment involves deep learning as surrogate modeling for faster predictions, justified by the expensiveness of CFD simulations. Most often, fast predictions come at a cost of degraded accuracy. Fluid mechanics research and applications in general offer inspiration for possible different interaction which could benefit not only prediction speed but also accuracy performance. Above all, physics informed deep learning modeling, turbulence model enhancement with different techniques, and super-resolution techniques are the most promising methods that are largely yet to be explored in the built environment, for both indoor and outdoor simulations. Unfortunately, together with promising advancements, deep learning methods come with challenges to overcome, such as the availability of consistent large flow databases, the extrapolation task problem, over-fitting and others.

7. Acknowledgement

This work was partially supported by the Digital

Futures, C3.ai Digital Transformation Institute, and the Energimyndigheten (Swedish Energy Agency, grant No. 50057-1).

8. References

[1] Brunton SL, Noack BR, Koumoutsakos P. Machine learning for fluid mechanics. Annual Review of Fluid Mechanics. 2020; 52: 477–508.

[2] Schmitt FG. About Boussinesq's turbulent viscosity hypothesis: historical remarks and a direct evaluation of its validity. Comptes Rendus Mécanique. 2007; 335: 617–627.

[3] Wang M, Chen Q. Assessment of various turbulence models for transitional flows in an enclosed environment (RP-1271). Hvac&r Research. 2009; 15: 1099–1119.

[4] Stamou A, Katsiris I. Verification of a CFD model for indoor airflow and heat transfer. Building and Environment. 2006; 41: 1171–1181.

[5] Srebric J, Vukovic V, He G, Yang X. CFD boundary conditions for contaminant dispersion, heat transfer and airflow simulations around human occupants in indoor environments. Building and Environment. 2008; 43: 294–303.

[6] Liu J, Niu J. CFD simulation of the wind environment around an isolated high-rise building: An evaluation of SRANS, LES and DES models. Building and Environment. 2016; 96: 91–106.

[7] van Druenen T, van Hooff T, Montazeri H, Blocken B. CFD evaluation of building geometry modifications to reduce pedestrian-level wind speed. Building and Environment. 2019; 163: 106293.

[8] Lauriks T, Longo R, Baetens D, Derudi M, Parente A, Bellemans A, et al. Application of improved CFD modeling for prediction and mitigation of traffic-related air pollution hotspots in a realistic urban street. Atmospheric Environment. 2021; 246: 118127.

[9] Goodfellow I, Bengio Y, Courville A. Deep Learning: MIT Press; 2016.

[10] LeCun Y, Bengio Y, others. Convolutional networks for images, speech, and time series. The handbook of brain theory and neural networks. 1995; 3361: 1995.

[11] Medsker LR, Jain LC. Recurrent neural networks. Design and Applications. 2001; 5.

[12] Tanaka H, Matsuoka Y, Kawakami T, Azegami Y, Yamamoto M, Ohtake K, et al. Optimization Calculations and Machine Learning Aimed At Reduction of Wind Forces Acting on Tall Buildings and Mitigation of Wind Environment. International Journal of High-Rise Buildings. 2019; 8: 291-302.

[13] Hintea D, Brusey J, Gaura E. A Study on Several Machine Learning Methods for Estimating Cabin Occupant Equivalent Temperature. In Proceedings of the 12th International Conference on Informatics in Control, Automation and Robotics; 2015. p. nil.

[14] Fukami K, Fukagata K, Taira K. Super-Resolution Reconstruction of Turbulent Flows With Machine Learning. Journal of Fluid Mechanics. 2019; 870: 106-120.

[15] Wong SL, Wan KKW, Lam TNT. Artificial neural networks for energy analysis of office buildings with daylighting. Applied Energy. 2010; 87: 551–557.

[16] Yokoyama R, Wakui T, Satake R. Prediction of energy demands using neural network with model identification by global optimization. Energy Conversion and Management. 2009; 50: 319–327.

[17] Kalogirou SA. Artificial neural networks in energy applications in buildings. International Journal of Low-Carbon Technologies. 2006; 1: 201–216.

[18] Wei T, Wang Y, Zhu Q. Deep reinforcement learning for building HVAC control. In Proceedings of the 54th annual design automation conference 2017; 2017. p. 1–6.

[19] Wang Z, Hong T, Piette MA. Data fusion in predicting internal heat gains for office buildings through a deep learning approach. Applied energy. 2019; 240: 386–398.

[20] Zhang Th, You Xy. Applying Neural Networks To Solve the Inverse Problem of Indoor Environment. Indoor and Built Environment. 2013; 23: 1187-1195.

[21] Zhang Th, You Xy. A Simulation-Based Inverse Design of Preset Aircraft Cabin Environment. Building and Environment. 2014; 82: 20-26.

[22] Warey A, Kaushik S, Khalighi B, Cruse M, Venkatesan G. Data-Driven Prediction of Vehicle Cabin Thermal Comfort: Using Machine Learning and High-Fidelity Simulation Results. International Journal of Heat and Mass Transfer. 2020; 148: 119083.

[23] Carlucci S, Bai L, de Dear R, Yang L. Review of adaptive thermal comfort models in built environmental regulatory documents. Building and Environment. 2018; 137: 73–89.

[24] Ding C, Lam KP. Data-driven model for cross ventilation potential in high-density cities based on coupled CFD simulation and machine learning. Building and Environment. 2019; 165: 106394.

[25] Thibault J, Grandjean BPA. A neural network methodology for heat transfer data analysis. International Journal of Heat and Mass Transfer. 1991; 34: 2063–2070.

[26] Lee C, Kim J, Babcock D, Goodman R. Application of Neural Networks To Turbulence Control for Drag Reduction.

Physics of Fluids. 1997; 9: 1740-1747.

[27] Yarlanki S, Rajendran B, Hamann H. Estimation of turbulence closure coefficients for data centers using machine learning algorithms. 13th InterSociety Conference on Thermal and Thermomechanical Phenomena in Electronic Systems. 2012 May.

[28] Luo S, Vellakal M, Koric S, Kindratenko V, Cui J. Parameter Identification of RANS Turbulence Model Using Physics-Embedded Neural Network. In Lecture Notes in Computer Science.: Springer International Publishing; 2020. p. 137-149.

[29] Tracey BD, Duraisamy K, Alonso JJ. A Machine Learning Strategy to Assist Turbulence Model Development. In 53rd AIAA Aerospace Sciences Meeting; 2015 January. p. nil.

[30] Ling J, Kurzawski A, Templeton J. Reynolds Averaged Turbulence Modelling Using Deep Neural Networks With Embedded Invariance. Journal of Fluid Mechanics. 2016; 807: 155-166.

[31] Geneva N, Zabaras N. Quantifying Model Form Uncertainty in Reynolds-Averaged Turbulence Models With Bayesian Deep Neural Networks. Journal of Computational Physics. 2019; 383: 125-147.

[32] Font B, Weymouth GD, Nguyen VT, Tutty OR. Deep Learning of the Spanwise-Averaged Navier-Stokes Equations. Journal of Computational Physics. 2021; 434: 110199.

[33] Zhang W, Wang B, Ye Z. High efficient numerical method for limit cycle flutter analysis based on nonlinear aerodynamic reduced order model reduced order model. In 51st AIAA/ASME/ASCE/AHS/ASC Structures, Structural Dynamics, and Materials Conference 18th AIAA/ASME/AHS Adaptive Structures Conference 12th; 2010. p. 2723.

[34] Guo X, Li W, Iorio F. Convolutional Neural Networks for Steady Flow Approximation. In Proceedings of the 22nd ACM SIGKDD International Conference on Knowledge Discovery and Data Mining; 2016 August. p. nil.

[35] Fukami K, Fukagata K, Taira K. Assessment of Supervised Machine Learning Methods for Fluid Flows. Theoretical and Computational Fluid Dynamics. 2020; 34: 497-519.

[36] Guastoni L, Güemes A, Ianiro A, Discetti S, Schlatter P, Azizpour H, et al. Convolutional-network models to predict wall-bounded turbulence from wall quantities. arXiv preprint arXiv:2006.12483. 2020.

[37] Srinivasan PA, Guastoni L, Azizpour H, Schlatter P, Vinuesa R. Predictions of Turbulent Shear Flows Using Deep Neural Networks. Physical Review Fluids. 2019; 4: 054603.

[38] Milano M, Koumoutsakos P. Neural Network Modeling for Near Wall Turbulent Flow. Journal of Computational Physics. 2002; 182: 1-26.

[39] Berkooz G, Holmes P, Lumley JL. The Proper Orthogonal Decomposition in the Analysis of Turbulent Flows. Annual Review of Fluid Mechanics. 1993; 25: 539-575.

[40] Fresca S, Manzoni A. POD-DL-ROM: enhancing deep learning-based reduced order models for nonlinear parametrized PDEs by proper orthogonal decomposition. arXiv preprint arXiv:2101.11845. 2021.

[41] Wang Z, Xiao D, Fang F, Govindan R, Pain CC, Guo Y. Model identification of reduced order fluid dynamics systems using deep learning. International Journal for Numerical Methods in Fluids. 2018; 86: 255–268.

[42] Yang W, Zhang X, Tian Y, Wang W, Xue JH, Liao Q. Deep Learning for Single Image Super-Resolution: a Brief Review. IEEE Transactions on Multimedia. 2019; 21: 3106-3121.

[43] Erichson NB, Mathelin L, Yao Z, Brunton SL, Mahoney MW, Kutz JN. Shallow Neural Networks for Fluid Flow Reconstruction With Limited Sensors. Proceedings of the Royal Society A: Mathematical, Physical and Engineering Sciences. 2020; 476: 20200097.

[44] Fukami K, Fukagata K, Taira K. Machine-learning-based spatio-temporal super resolution reconstruction of turbulent flows. Journal of Fluid Mechanics. 2021; 909.

[45] Gao H, Sun L, Wang JX. Super-resolution and denoising of fluid flow using physics-informed convolutional neural networks without high-resolution labels. arXiv preprint arXiv:2011.02364. 2020.

[46] Duraisamy K, Spalart PR, Rumsey CL. Status, emerging ideas and future directions of turbulence modeling research in aeronautics: National Aeronautics and Space Administration, Langley Research Center; 2017.

Data sharing not applicable to this article as no datasets were generated or analysed during the current study.

Real-time diagnostic tool for hygienic and energy parameters of air handling components

Christian Friebe, Thomas Oppelt, Hannes Rosenbaum

Air-conditioning department, Main Department Ventilation and Air Conditioning, Institut für Luft- und Kältetechnik gemeinnützige GmbH, Dresden, 01309, Germany, klima@ilkdresden.de

Abstract. Material and surface properties in air conditioning systems are subject to change, e.g. due to aging, wear or fouling. This is why regular inspections, maintenance or even cleaning measures are mandatory. In the course of quality assurance and the striving for sustainability and energy efficiency, heat- and mass-transferring air conditioning components particularly require permanent metrological monitoring. This goes beyond the conventional data recording in air conditioning components. With the aim of parameter-guided maintenance management, this means a comprehensive monitoring of function and properties based on design and process data. An extensive exchange of information throughout the entire value chain and life cycle (Industry 4.0) also is essential. ILK Dresden has developed a measurement-based diagnostic tool especially for a new type of membrane heat and mass transfer unit for air humidification and sorptive dehumidification. The aim was to process real-time measurement data, considering long-term data, and to apply it for statistical evaluations of changing material parameters, for target-performance comparisons and for risk assessments (e.g. mould growth). The central element of the tool was programmed in Python and is a script for the direct and simultaneous iterative calculation of the ideal reference process and the real characteristic values of the heat and mass transfer process in the membrane heat exchanger. In addition to the thermodynamic calculation, the mould growth risk can be determined with this algorithm. The basis for assessing the mould growth risk is based on a known algorithm comprising different thermodynamic parameters. This method in addition with a detection of special events (load curves, maintenance, faults, etc.), provided by machine learning algorithms is the basis for a process optimisation, quality assurance and sustainable system operation. This presentation will illustrate the technical parameters and the function of the diagnostic tool. Furthermore, the results of the initial test phase under laboratory conditions will be presented as well as an overview of further development steps and potential areas of application.

Keywords. liquid sorption, humidity recovery, enthalpy recovery, HVAC, textile heat exchangers, hygiene, energy efficiency, evaporative cooling, closed-loop-system.
DOI: https://doi.org/10.34641/clima.2022.98

1. Introduction

Increasing energy efficiency requirements lead to higher demands on air conditioning systems, too. One approach to cope with this is the application of a desiccant cooling system with a lithium-chloride (LiCl)-brine [1]. Since open systems have disadvantages with regard to corrosion, enclosed heat exchangers e.g. with semipermeable membranes as diaphragms are the subject of ongoing research projects (e.g. Rosenbaum [2–4]). One of the most interesting possibilities is the combination of more than two different fluids within one heat exchanger. Applying such a heat exchanger provides the opportunity to e.g dehumidify an air stream with a LiCl-brine whilst the intrinsic solution enthalpy is balanced with a cooling water circuit. At the opposite, an air stream might be cooled and humidified at the same time by applying a cooling water circuit and a hot water circuit in combination.

All these different options suffer from the same problem: The heat exchanger performance cannot be solved explicitly by applying the known equations. Therefore the supervision and optimisation of an air conditioning system with such a heat exchanger is challenging.

Secondly, mould-growth is one of the major problems to be solved in air conditioning systems, especially under humid operation conditions. Mould can course severe health problems when spores or mycotoxins are transported as airborne particles to the occupants of rooms equipped with this problematic air conditioning system, leading to Upper Respiratory Tract symptoms, Cough, Wheeze or Asthma [5]. For

Copyright ©2022 by the authors. This conference paper is published under a CC-BY-4.0 license.

this reason, strict regulations for design, installation, operation and maintenance of an air conditioning are state of the art (e.g. [6], [7][6]).

Nevertheless, a deeper insight into the actual conditions of an air conditioning system is of interest with respect to the reduction of maintenance work and correct handling of current issues, e.g. the replacement of filters in case of increased mould-growth risk [8].

The purpose of this article is to provide information on a proposal to manage the requirements of a modern air conditioning system in terms of implementation in IoT and cloud-based systems. The theoretical background and investigations at a heat exchanger with textile-based materials of a closed-loop circuit will be explained in the following sections.

2. Theoretical Background

2.1 Thermodynamic calculation of the heat exchanger

The thermodynamic calculation of the heat exchanger is based upon a numerical discretisation of several fluid layers with up to three different fluids species, as illustrated in Fig. 1. The fluid can be chosen as air, water or a brine of LiCl and water. Each of this layers allows a fluid a movement within the x,y-plane and each layer comprises a n_x,n_y-matrix of unit cells. The flow-direction is described as an initial boundary condition. The boundary of each flow normal to the flow direction at every x,y-plane is defined as adiabatic in terms of heat and mass transfer.

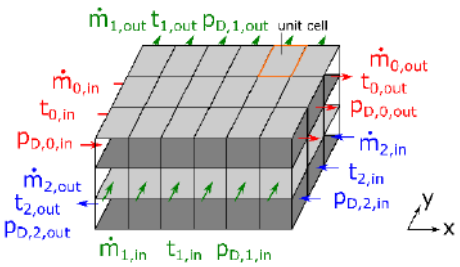

Fig. 1 – Model scheme

The contact conditions between two layers are defined separately. Thus, the outlet parameters of each layer are calculated referring to the very contact conditions and the inlet parameters by solving the heat and mass transfer equation (according to Fig. 2) with respect to the flow-direction, starting at the inlet and ending at the outlet.

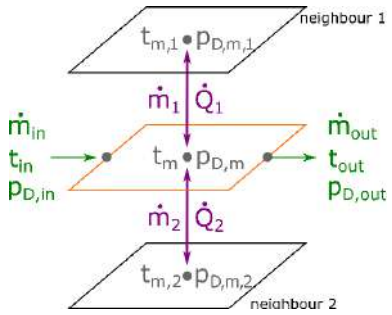

Fig. 2 – heat and mass transfer at single element

Each unit cell is divided into subsections in order to stabilise the numerical interpolation. As depicted in Fig. 3, a linear interpolation is applied to calculate the representative parameters. This avoids non-physical numerical effects like crossing temperature lines in neighbouring cells.

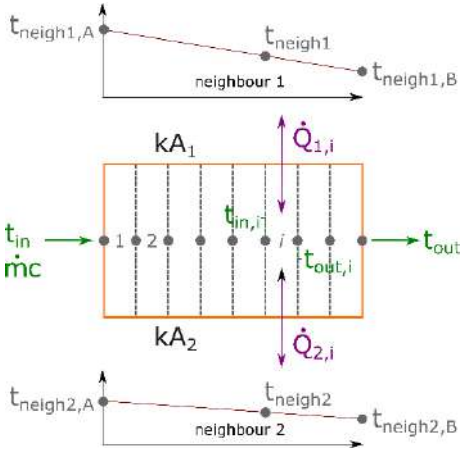

Fig. 3 – Heat transfer between unit cell and heat transfer to neighbour cells, division of the unit cell into single sections

The objective of this numerical model is the calculation of

- transient heat and mass transfer,
- fluids in parallel-, cross- and counter-flow regime
- temperature- and pressure-dependent material data
- dilution enthalpies, condensation- and evaporation enthalpies.

The temperature- and pressure-dependent material properties of humid air and LiCl-brines are calculated by means of Conde [9] and Conde [10], respectively.

2.2 Calculation of mould-growth risk

Currently, several models for mould-growth exist. All these models have different advantages and disadvantages and were compared by several authors, e.g Vereecken et al. [11]. One of the most common models is the updated VTT (uVTT) model as described by Ojanen et al. [12]. Based on the calculation method developed by Hukka and Viitanen [13] the calculation was extended from wood to other materials. The risk of mould-growth is

described by the mould-index M. This index correlates to the description according to Tab. 2. The parameters of influencing are

- the relative humidity,
- the temperature and
- the substrate.

A second well-established model (WuFi) was developed by Sedlbauer [14]. Instead of calculating a risk as in the uVTT-model, this model calculates the mycelium growth and sperm germination depending upon the specimen of the fungi.

Tab. 1 – Description of the mould-index M

M	Description
0	no growth
1	Small amounts of mould on surface (microscope), initial stages of local growth
2	Several local mould growth colonies on surface (microscope)
3	Visual findings of mould on surface, < 10% coverage, or < 50% coverage of mould (microscope)
4	Visual findings of mould on surface, 10%–50% coverage, or > 50% coverage of mould (microscope)
5	Plenty of growth on surface, > 50% coverage (visual)
6	Heavy and tight growth, coverage about 100%

Within this project the uVTT-model is used for mould-growth calculation due to the consideration of ambient conditions, where mould is not growing or even reduces. Contrary to the WuFi-model, a reduction of mould on a surface is considered in the uVVT-model.

Nevertheless, a correlation of the results (M-index and growth rate) of both models (uVTT and WuFi) is suggested by Viitanen et al. [15]. Cabrera et al. [16] applied a combination of both methods in order to calculate the mould-growth risk for future climate conditions.

The calculation is based on the change rate of the M-index according to eqs. (1) - (5) and the parameters as provided in Tab. 2. Herein t represents the time in hours, RH the relative humidity in %, T the temperature in $°C$, W the timber species, SQ the surface quality (if the substrate is not wood, then $W, Sq = 0$) and c_{mat} the decline coefficient.

$$\frac{\partial M}{\partial t} = \begin{cases} (7e^{k_0})^{-1} k_1 k_2 & RH \geq RH_{crit} \\ -0.00133\, c_{mat} & RH < RH_{crit} \quad t - t_1 \leq 6 \\ 0\, c_{mat} & RH < RH_{crit} \quad 6 < t - t_1 \leq 24 \\ -0.000667\, c_{mat} & RH < RH_{crit} \quad t - t_1 > 24 \end{cases} \tag{1}$$

$$k_0 = -0.68 \ln T - 13.9 \ln RH + 0.14\, W - 0.33\, SQ + 66.02 \tag{2}$$

$$k_2 = \max\left[1 - e^{2.3(M - M_{max})}, 0\right] \tag{3}$$

$$M_{max} = 1 + A \frac{RH_{crit} - RH}{RH_{crit} - 100} - B \left(\frac{RH_{crit} - RH}{RH_{crit} - 100}\right)^2 \tag{4}$$

$$RH_{crit} = \begin{cases} -0.00267\, T^3 + 0.16 T^2 - 3.13 T + 100 & T \leq 20 \\ RH_{min} & T > 20 \end{cases} \tag{5}$$

Tab. 2 – Description of the mould-index M

	K1		M_{max}			RH_{min}	c_{mat}
	M<1	M≥1	A	B	C	%	
vs	1.000	2.000	1.0	7	2.0	80	1.00
s	0.578	0.386	0.3	6	1.0	80	0.50
mr	0.072	0.097	0.0	5	1.5	85	0.25
r	0.033	0.014	0.0	3	1.0	85	0.10

3. Setup of the investigated heat exchanger

3.1 Experimental setup

The analysis was performed with a closed-loop heat exchanger as illustrated in Fig. 4. This system comprises two heat exchangers connected with a water circuit for cooling the outdoor/supply air (ODA/SUP) of an air handling unit by means of indirect evaporative cooling at a second heat exchanger at the extraction air (ETA) – exhaust air (EHA) section of this air handling unit. A membrane heat exchanger as described by Rosenbaum and Franzke [17], [18] comprising three different fluids (air, water, water for evaporation) with a semi-permeable membrane between air and evaporating water was used for cooling water from inflow to outflow of the respective water. The semipermeable membrane enables the mass transfer of gaseous water between air flow and water flow.

The closed loop system was equipped with several measurement probes. At each inlet and outlet the average temperature was calculated from five temperature probes. Additionally to the five temperature probes, two probes for the relative humidity were installed. All water temperatures where measured with one probe at each connection of the heat exchangers. Furthermore, the mass flows were saved in a measurement file. The files were updated every 30 seconds. The measurement period lasted from 2020/07/07 to 2020/12/18.

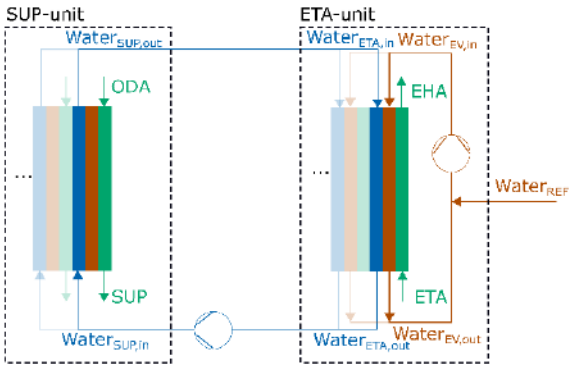

Fig. 4 – Schematical drawing of the closed-loop system used in this investigation

3.2 Numerical setup

For the first calculations, only the ETA-unit of the closed-loop system was considered. The heat exchanger has a numerical resolution of 450 cells. This value was proven to be reasonably feasible by a convergence study, for which the results are printed in Fig. 5.

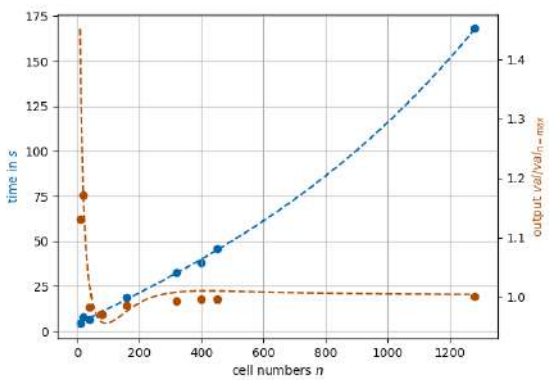

Fig. 5 – Results of the convergence study with different cell numbers at x-axis, time for full iteration of the heat exchanger at the left y-axis and the resulting output at the right y-axis, performed at an I7-7600 @ 2.8 GHz

For the further calculation of the heat exchanger thermodynamics, the values recorded by the measurement were averaged in one-hour time slots and the calculation was performed for the first 1054 hours. The numerical inlet conditions of the heat exchanger were set to these measured values (ETA, Water$_{EV,in}$, Water$_{ETA,in}$) in order to calculate the outlet conditions by predefined thermodynamic parameter settings of the heat exchanger as thermal conductivity, mass transfer coefficient, active surface and permeability.

The mould-calculation was performed using the described code and was applied to the temperature and the humidity at EHA. The sensitivity of the substrate to the mould was set after 62.5 days from 'mr' to 's' and after additional 62.5 days to 'vs'. Such an increase in sensitivity may be caused by a gathering of biological non-inert matter at the surface of the textile heat exchanger.

For mould-calculation, the processing of 664,311 data points took about 78 s at an I7-7600 @ 2.8 GHz. The heat exchanger is operated continuously for about 158 days, followed by a dry-out phase.

4. Results

The results of the calculation of the outlet conditions of air, water and evaporation water in comparison with the measured data are provided in Fig. 6. The measured inlet conditions are represented by a solid line whilst the measured outlet are represented in a dashed line style. The calculated outlet conditions are printed as dots. There is a slight deviation between measurement and calculation.

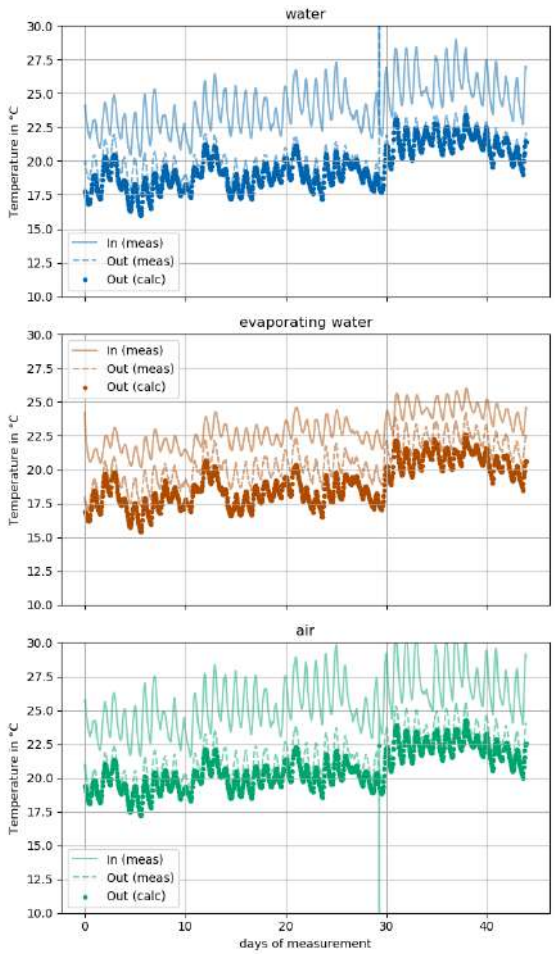

Fig. 6 – Temperature profiles of the measured conditions at the ETA-unit at inlet and outlet (lines) in comparison to the calculated outlet conditions.

The mould-calculation was performed for the whole measurement period and different sensitivities where assumed. The results shown in Fig. 7 provide the course of the M-index for constant sensitivities of the substrate to mould. The profile of the M-index for time-dependent sensitivities from 'mr' to 's' is presented in Fig. 8.

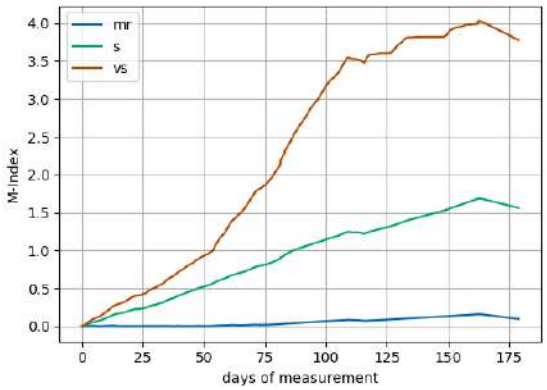

Fig. 7 – Profile of the M-index over the whole measurement period for the sensitivities of 'mr', 's' and 'vs'

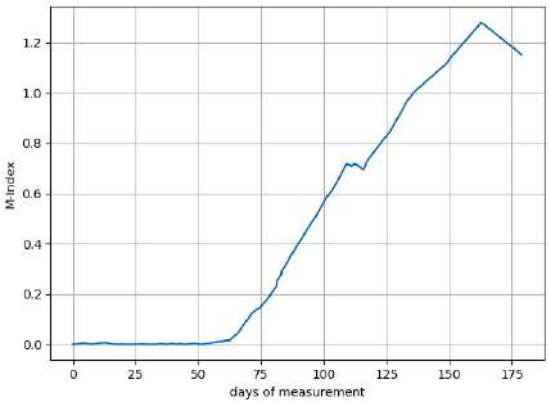

Fig. 8 – Profile of the M-index over the whole measurement period (sensitivity 'mr', 's' and 'vs' at 0, 62.5 and 125 days, respectively)

The formation of mould colonies is strongly dependent on the sensitivity of the heat exchanger material. If the heat exchanger material is tendentiously inert ("mr"), the growth of moulds can only be detected with the help of microscopy, if at all. In cases with higher sensitivity, mould formation is stronger to the point of being visible to the eyes. In the assumed situation of deterioration of the resistance of the surface, mould growth is retarded, but there is a tendency to form a higher risk of mould after the dry-out phase. Here there is still a high sensitivity of the biologically contaminated heat exchanger material to mould growth.

5. Discussion and Conclusions

The measured values of the heat exchanger proof the stable operation of such a textile heat exchangers with three different fluids.

The presented results of the heat exchanger calculations indicate an overall good coincidence with measured values at the outlet. Nevertheless several deviations have been detected. A better adaption of the calculation parameters to the measured data is mandatory. This refers to the inclusion of the currently neglected thermal inertia of the heat exchanger, too.

The calculation established in the numerical heat exchanger analytics is too slow for time resolved investigation (e.g. 30 s for one time step). One of the underlying reasons is based in the air property calculations. We expect an improvement by changing from the scientific calculation to industrial style of the parameters according to the IAPWS formulas.

The coincidence of the calculated mould-growth risk was not verified by separate investigations at the heat exchangers surface. This challenging issue should be topic of further investigations.

For this project, the mould-growth risk was calculated for the outlet conditions (EHA). In future, a risk depending upon the internal calculated conditions might provide better information on the actual state of the hygienic conditions. By applying the analysis only at the outlet (or inlet) conditions, the mould-growth risk might be underestimated.

Caused by the operation of the heat exchanger within a controlled environment, no deviations from the acceptable parameters where recorded, unfortunately. By applying this algorithm at a unit installed within a more practically operated system will provide better data for establishing a machine learning algorithm for fault detection and improper unit operation. This challenge coincidences with the reduction of measurement probes to a very limit.

6. Acknowledgement

This work was funded by the Federal Ministry for Economic Affairs and Energy of the Federal Republic of Germany under Contracts no. MF 180112.

The datasets generated during or analysed during the current study are not publicly available but will be available upon direct request to the authors.

7. References

[1] CONDE-PETIT, MANUEL ; ETHZ, DR SC TECH: Liquid desiccant-based air-conditioning systems—LDACS. In: *Proc. of the 1st European Conference on Polygeneration—Technologies and Applications* : Citeseer, 2007, pp. 217–234

[2] ROSENBAUM, H.: Membran-Kühldecke mit kondensatfreier Luftentfeuchtung. Messtechnische Analyse einer ersten Pilotanwendung dezentraler Flüssigsorptionsprozesse, Membrane-based cooling ceilings with condensate-free Dehumidification. Measurement Analysis of a first pilot application of decentralized liquid sorption. In: *KI - Kälte, Luft, Klimatechnik*, *KI - Kälte, Luft, Klimatechnik*. vol. 50 (2014), Nr. 3, pp. 26–30

[3] ROSENBAUM, H.: Sorptionsgestützte Klimatisierung und Membran-Kühldecken. In: *DKV-Tagung, Deutsche Kälte-Klima-Tagung, 40*, *DKV-Tagung, Deutsche Kälte-*

Klima-Tagung, 40, 2013 — ISBN 978-3-932715-49-5, pp. 1–14

[4] ROSENBAUM, H.: Textiler Wärmeübertrager – Enthalpierückgewinnung zwischen örtlich getrennten Luftströmen. In: *Die Kälte + Klimatechnik* (2020), Nr. 9, pp. 30–35

[5] INFRASTRUCTURE, ALBERTA ; TRANSPORTATION: *Mould in Indoor EnvironmentsRisk Assessment and Management - Program Handbook* : Alberta Research Council - Toxicology Unit, 2006

[6] VDI 6022 Blatt 1 2018-01: Raumlufttechnik, Raumluftqualität - Hygieneanforderungen an raumlufttechnische Anlagen und Geräte (VDI-Lüftungsregeln) : Verein deutscher Ingenieure, 2018

[7] EUROPE, WORLD HEALTH ORGANIZATION. REGIONAL OFFICE FOR: *WHO guidelines for indoor air quality: dampness and mould* : World Health Organization. Regional Office for Europe, 2009 — ISBN 9789289041683

[8] KRAUSE, RALPH ; OPPELT, THOMAS ; FRIEBE, CHRISTIAN ; DÖGE, SABINE ; HERZOG, RALF: Machine learning for filter pollution control. In: . Moscow, Moscow State Technical University n.a. N.E. Bauman (Bauman MSTU) : 3rd International Conference «REFRIGERATION AND CRYOGENIC ENGINEERING, AIR CONDITIONING AND LIFE SUPPORT SYSTEMS»,19-20 November 2019, 2019

[9] CONDE-PETIT, MANUEL: Thermophysikalische Eigenschaften der feuchten Luft: Modelle (2014)

[10] CONDE-PETIT, MANUEL: Aqueous solutions of lithium and calcium chlorides: property formulations (2014)

[11] VEREECKEN, EVY ; SAELENS, DIRK ; ROELS, STAF: A comparison of different mould prediction models. In: *Proceedings building Simulation, 12th Conference of International Building Performance Simulation Association, Sydney*. vol. 14, 2011, p. 16

[12] OJANEN, TUOMO ; VIITANEN, HANNU ; PEUHKURI, RUUT ; LÄHDESMÄKI, KIMMO ; VINHA, JUHA ; SALMINEN, KATI: Mold growth modeling of building structures using sensitivity classes of materials. In: *Proceedings Building XI* (2010)

[13] HUKKA, A. ; VIITANEN, HANNU: A mathematical model of mould growth on wooden material. In: *Wood Science and Technology* vol. 33 (1999), pp. 475–485

[14] SEDLBAUER, KLAUS: *Vorhersage von Schimmelpilzbildung auf und in Bauteilen*, Lehrstuhl fur Bauphysik, 2001

[15] VIITANEN, HANNU ; KRUS, M. ; OJANEN, TUOMO ; EITNER, V. ; ZIRKELBACH, D.: Mold Risk Classification Based on Comparative Evaluation of Two Established Growth Models. In: *Energy Procedia*. vol. 78, 2015

[16] CABRERA, PAMELA ; SAMUELSON, HOLLY ; KURTH, MARGARET: Simulating Mold Risks under Future Climate Conditions. In: *Building Simulation*, 2019

[17] ROSENBAUM, HANNES: Membranbasierte Raumklimatisierung. In: *Die KÄLTE + Klimatechnik* (2011), Nr. 12, pp. 48–51

[18] FRANZKE, UWE ; FRIEBE, CHRISTIAN ; ROSENBAUM, HANNES: Air Conditioning with liquid sorption solution. In: *9th IIR Gustav Lorentzen Conference*. Sydney : IIR, 2010

Transient analysis of individual return temperatures in hydronic floor heating systems

Simon Thorsteinsson [a], *Henrik Lund Stærmose* [b], *Jan Dimon Bendtsen* [a]

[a] Section of Automation and Control, Department of Electronic Systems, Aalborg University, Denmark, sith@es.aau.dk.

[b] Neogrid Technologies ApS, Niels Jernes Vej 10 - 9220 Aalborg east, Denmark, hls@neogrid.dk.

Abstract. In this work, we investigate some potential benefits and opportunities gained from monitoring the return temperature of all the circuits in a *hydronic floor heating* (FH) system. It is for example possible to obtain information on the flow distribution in the FH system. Since flow sensors are relatively expensive, most currently installed FH systems do not provide any information on the flow entering the forward manifold, let alone flows in the individual circuits. This lack of information inhibits analysis of performance and prevents commissioning of more advanced control methods. The approach proposed here, based on temperature sensors mounted on the exterior of the pipes, provides a possible cheap alternative to measuring the flows directly. Further, we argue that this retrofitted solution can be applied to most already installed floor heating systems. The paper contains a description of the retrofit kit and a dynamic model, which is shown to be able to replicate the behaviour of measurements acquired from an actual FH system installed in a single-family house, as well as a method for calculating the relative flows. The results show that flow-related parameters such as circulation time are, under the right circumstances, directly observable in the data. Overall, we conclude that measuring the individual return temperatures provides valuable information when monitoring the health and performance of a floor heating system.

Keywords. Floor Heating, Flow, Retro-fit, Estimation, Simulation
DOI: https://doi.org/10.34641/clima.2022.140

1. Introduction

In this paper we discuss the potential benefits of continuously measuring the return temperatures of the individual circuits in a *hydronic floor heating* (FH) system placed in a single family house, and propose a method to roughly estimate the *flow distribution* (FD) and thereby the distribution of energy consumption in the different FH pipes. The word *distribution* signals that only a relative, and not an absolute, measure of the heat consumption of the individual circuits is obtained.

On the topic of energy efficiency, single family houses are interesting and problematic. Interesting because they cover a significant amount of heated area (about 55 % in Denmark) [1]. Problematic since this large share is distributed over many small units, which means the potential for energy savings in each unit is relatively small. Further, a majority of these units are owned by the residents themselves [2], meaning that any investment into energy efficiency has to be understood from a perspective of a relative low budget. The consequence is that, without any active incentive programs, energy efficiency solutions for single family houses have to be highly cost effective. Solutions for retrofitting existing buildings are, in this text, characterized into two main groups, passive, where changes are made to the physics of the building, and active, which covers changes in the operation under the existing conditions. The active solutions to a large extent cover exchanging existing controllers, together with updating the set of sensors and actuators, in order to operate the overall system more efficiently.

Returning to the theme of this paper, a question arises: why is the FD, in a FH system, interesting and useful information? To answer this, it is helpful to visit a class of controllers called Model Based Controllers. Among controllers classified as model based, *Model Predictive Control* (MPC) is the most widely known. The method combines a model with an objective function, which assign costs to states and inputs over a control window. To obtain the specific model it has to be constructed and identified. In [3] the authors used a grey-model method called *Maximum Likelihood* (ML) to estimate the dynamics of an arctic low-energy house heated by FH. For the

Copyright ©2022 by the authors. This conference paper is published under a CC-BY-4.0 license.

identification of the parameters, the heat flow, based on forward/return temperature and mass flow of the water, is used as input for each circuit. A *Least Squares* (LS) method is used by [4] to fit the parameters in a grey-box model. In [5] the authors use an *Unscented Kalman Filter* (UKF) to online estimate the parameters of a five room building. Common for the mentioned texts is that they assume the heat flows from the HVAC systems to be known. This is rarely the case in single family houses. The text in [5] touches upon this problem and discusses numerical instabilities, related to not providing a scaled input for the different rooms. Although, the scale here refers to the difference of actual heat flows between individual rooms, we argue that on room level a relative scale based on e.g. FD is enough, since it is possible to further scale the relative estimates, if a central measure of the heat consumption is available. This is e.g. the case if the house is provided by district heating, since the overall heat consumption is needed to settle the energy bill. The authors of [3] do something similar when they correct the individual estimated heat flows according to the measured total heat consumption obtained centrally. Further, being able to scale FH circuits is useful in MPC. If all circuits are considered equal the MPC cannot ration the energy appropriately. If the actual heat consumption of the rooms are not obtainable, then it is at least useful to know whether one circuit is twice as expensive as the other. The notion of flow distribution and relative heat distribution is not new, [6] defines it as *relative heating coefficient* (RHC). The authors derive and compare an array of RHCs, which are used to rate the heat efficiency of the rooms of an office building. The work carried out in [6] lays the foundation for the work of this paper. Having established the importance of knowing the flow distribution and relative heating distribution, we pose the hypothesis: *It is possible to obtain a relative flow and heating distribution, based on measuring the forward/return temperature and control-valve state for all circuits. This approach outperforms scaling circuits using only floor area distribution.*

The rest of the paper contains an introduction to the system and retrofit-kit. Sec. 2. describes a simulation, which is used to investigate the method under ideal circumstances, followed the experiment conducted in the test house. Section 3. contains results from the simulation and test house before Sec. 4. concludes.

2. Method

This section presents the retrofit kit, simulation and derivation for the relative heating coefficient.

2.1 System

Figure 1 presents the system which is considered in this paper. The system reflects a common installation seen in many single family houses. The heat source provides a common forward temperature for the FH circuits. Each floor heating circuit is ON/OFF controlled with hysteresis based on temperature difference between measured room temperature and reference. The actuators are wax-motor valves [7]. The mass flow in circuit j, q_j combined with the total flow entering the forward manifold q are considered unknown.

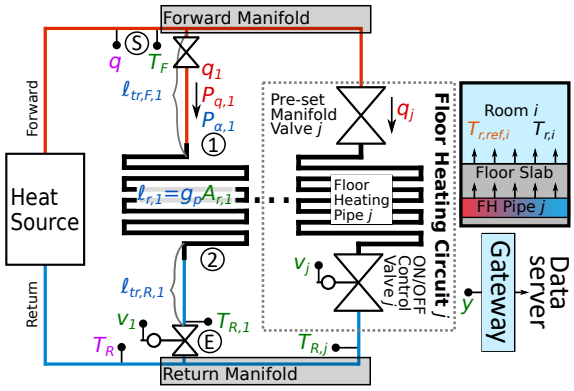

Fig. 1 – The system diagram containing the important signals. The signals are color coded: (green) measured signals or known inputs, (blue) estimated parameters, (magenta) measured for validation and (red) unknown but desired variables.

The FH system is placed in a test house, where data is gathered using the retrofit kit presented in the upcoming section. The house is built according to the BR2020 standard and heated using an air-to-water heat pump. There are 15 FH circuits distributed on two manifolds. The FH circuits are controlled using temperature feedback from the rooms. Each room has one thermostat. Rooms with more than one FH circuit are controlled using the same thermostat. Two rooms have two circuits, one has three, and the remaining have one each.

Assumption 1 (Constant flow)**.** The flow in an open circuit is constant, regardless of the state of the other FH circuits.

Assumption 2 (Common cross-area)**.** The cross area of the pipe A_p is the same for all FH circuits.

Assumption 3 (Measured return temperatures)**.** The return temperature for each FH circuit is measured.

Assumption 4 (Common pipe length per m^2 floor)**.** Pipe length per square meter floor, g_p, is the same for all rooms. This is shown in Fig. 1.

Assumption 5 (Floor area)**.** The area covered by the floor heating pipe is assumed known.

We are aware that Assumptions 1, 2 and 4 are not always satisfied, but they are considered

acceptable in a retrofit situation. In the next section, we shall address a way to satisfy Assumption 3.

2.2 The retrofit kit

The retrofit kit, used to measure the return temperatures, consists of three components. Firstly, surface mounted temperature sensors are placed on each pipe before the collector manifold. The sensors, circled in red in Figure 2, are covered by insulation to lower effects from air temperature and heat radiation. The common forward temperature are measured in the same way. Second, the inputs to the ON/OFF control valves are monitored. The data samples are, in our case, sent via a gateway to an the online data server, provided by Neogrid Technologies ApS, but any sample-based data acquisition method may of course be employed. Third, the gateway supports overwriting control signals. Therefore, if the natural fluctuation of return temperatures is insufficient for estimation, reference manipulation is used to force control valves to open and close on demand.

Fig. 2 – Shows temperature sensors placed under the insulation of each return pipe. Although the retrofit solution is the same, the picture is not from the test house discussed in this text.

2.3 Relative heat consumption

The heat consumption at time t for FH pipe j is in this text, defined as the instantaneous heat transferred from the water in the pipe to the floor. We denote this function as $\dot{Q}_{\mathrm{FH},j}(t)$. This heat transfer is dependent on multiple factors such as flow rate, temperature profile along the pipe and floor temperature, making it difficult to use in practice. To simplify the measure, the heat transferred is assumed well approximated by the difference between energy entering and exiting the pipe as seen in Eq. (1):

$$\dot{Q}_{\mathrm{FH},j}(t) \approx c_{\mathrm{w}} q_j(t) \left(T_{\mathrm{F}}(t) - T_{\mathrm{R},j}(t)\right) \tag{1}$$

With c_{w} being the heat capacity of water, T_{F} the forward temperature and $T_{\mathrm{R},j}$, q_j, the return temperature and mass flow of circuit j, respectively. The total heat consumption of the FH is given as the sum of the consumption of each circuit or as the total flow times temperature difference.

$$\dot{Q}_{\mathrm{FH}} = \sum_{j=1}^{N} \dot{Q}_{\mathrm{FH},j}(t) = c_{\mathrm{w}} q(t) \left(T_{\mathrm{F}}(t) - T_{\mathrm{R}}(t)\right) \tag{2}$$

The return temperature, T_{R}, and total flow, q, are given as sums of contributions as well.

$$T_{\mathrm{R}}(t) = \sum_{j=1}^{N} \frac{q_j(t)}{q(t)} T_{\mathrm{R},j}(t) \quad q(t) = \sum_{j=1}^{N} q_j(t) \tag{3}$$

As mentioned, both the total flow q and the circuit flows q_j are considered unknown, meaning that Eq. (2) cannot be computed in practice. Alternatively, as suggested in [6], one can introduce a *relative heating coefficient* (RHC) denoted β, which describes the relative consumption between the circuits. Instead of using the absolute flow a nominal distribution of flows is used. The term nominal distribution is used to indicate that the flow is a percentage share of the total and that the flows are independent of each other as stated in Assumption 1. The RHC derived in this test is seen in Eq. (4), and it is based on the advective heat flow of the circuit.

$$\beta_{q,j}(t) = v_j(t) \alpha_j \left(T_{\mathrm{F}}(t) - T_{\mathrm{R},j}(t)\right) \tag{4}$$

Here, α_j is the flow distribution scalar and v_j binary valve state. The total relative consumption is given by Eq. (5).

$$\beta(t) = \sum_{j=1}^{N} \beta_j(t) \tag{5}$$

Eq. (4) is equivalent to Eq. (2) if Assumption 1 holds. The factor is $q_{\max} c_{\mathrm{w}}$.

$$\dot{Q}_{\mathrm{FH}} = q_{\max} c_{\mathrm{w}} \beta_q \tag{6}$$

To get the by room percentage share of consumed heat, normalize the total heat transferred:

$$\mathcal{P}_{\beta,j}(\beta_j(t)) = \frac{\int_0^T \beta_j(t) \mathrm{d}t}{\int_0^T \beta(t) \mathrm{d}t} \tag{7}$$

The next section shows the derivation of the scalar α_j presented in Eq. (4)

2.4 Nominal flow distribution

We start by stating the two common flow equations for pipe with constant flow and pipe area.

$$q_j = v_j A_{\mathrm{p}} \rho \tag{8}$$

$$v_j = \frac{\ell_{\mathrm{r},j}}{\Delta t_{\mathrm{r},j}} \tag{9}$$

where v is the velocity of the water, A_{p} is the area of the cross section of the pipe and ρ is the mass density of water, ℓ_{r} is the length of the pipe under the floor and Δt_{r} is the time water spends under the floor in the circuit. Since the pipe is buried in

the floor, the length is unknown, but if Assumption 4 is true, the length is given by

$$\ell_{\mathrm{r},j} = g_{\mathrm{p}} A_{\mathrm{r},j} \tag{10}$$

where g_{p} is the common pipe length per area floor. Inserting Eq. (9) and (10) into (8) gives

$$q_j = A_{\mathrm{p}} g_{\mathrm{p}} \rho \frac{A_{\mathrm{r},j}}{\Delta t_{\mathrm{r},j}}. \tag{11}$$

According to Assumptions 4 and 2 the pipe area A_{p}, mass density of water ρ and pipe length factor g_{p} are common for all circuits, meaning that the flow in circuit q_j is proportional to the ratio $A_{\mathrm{r},j}/\Delta t_{\mathrm{r},j}$.

$$q_j \propto \frac{A_{\mathrm{r},j}}{\Delta t_{\mathrm{r},j}} = \alpha_j \tag{12}$$

2.5 Measuring the round trip time Δt_j

According to assumption 5, the room areas are assumed known, but the circulation time $\Delta t_{\mathrm{r},j}$ for circuit j is not, meaning it has to be measured. To measure the round trip time Δt_j of circuit j, time series measurements from the forward temperature T_{F} and individual return temperatures $T_{\mathrm{R},j}$ are used.

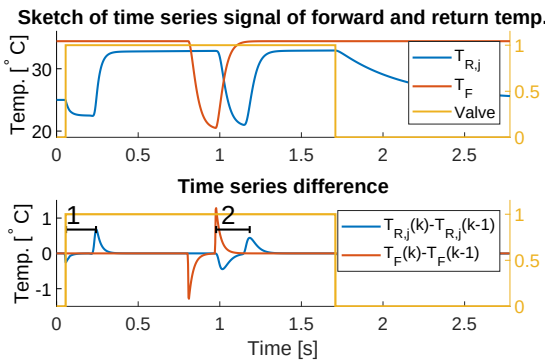

Fig. 3 – Shows a sketch of the measured forward and return temperature of a circuit. The figure presents two events that can be used for measuring the round trip time. The first (marked 1) is the time after a circuit opens. In this period old cooled water is replaced by fresh warm. The second event (marked 2) is caused by a large step on the forward temperature. Note that k indicates sample number.

Events, shown in Figure 3, with rapid changes in the forward temperature can be observed on both the forward and return temperature sensor. First on the forward temperature sensor, then later in a low pass filtered version on the return sensor. The challenge lies in figuring out when to start and stop the timer. It has been observed from measurements that the steepest gradient on the signal marks a sufficient and often clear point in the data; this claim is explained in more detail in Section *3.1*. By taking the time series difference, the slope graph is obtained, and the round trip time is easily measured as the time distance between the two peaks.

2.6 Considerations on circulation time Δt_r

Having shown that the flow is proportional to room area over room circulation time, this section deals with the estimate of the circulation time. The simple expression in Eq. (11) is derived under the assumption that the circulation time under floor, denoted $\Delta t_{\mathrm{r},j}$, is measured. This is equivalent to measure from (1) to (2) in Fig. 1. In practice, however, it is the time from point (S) to (E), denoted Δt_j, which is measured. Eq. (13) shows the relation between the measured, Δt_j, and desired time, $\Delta t_{\mathrm{r},j}$:

$$\Delta t_j = \Delta t_{\mathrm{r},j} + 2\Delta t_{\mathrm{tr},j} \tag{13}$$

where Δt_{tr} is the transport time from the manifold to the floor. The time Δt_{tr} is scaled by two because the water has to be transported to and back from the floor. If the transport time is not considered, a significant bias is introduced. It is a weakness of the method that it is the round trip time, and not the time spent under the floor, that is measured. This said, it is possible to compensate for this bias by using information from the system. To obtain the corrected circulation time one has to obtain an estimate of the percentage share of the full pipe length placed under the floor, $\mathcal{P}_{\mathrm{r}}$. The percentage share $\mathcal{P}_{\mathrm{r}}$, seen in Eq. (14), is calculated using estimates on the length of the transport pipe $\hat{\ell}_{\mathrm{tr}}$ and the length of pipe per square meter floor $\bar{g}_{\mathrm{p}}$.

$$\begin{aligned}\hat{\Delta t}_{\mathrm{r},j} &= \Delta t_j \frac{\ell_{\mathrm{r},j}}{\ell_{\mathrm{r},j} + 2\ell_{\mathrm{tr},j}} \\ &= \Delta t_j \frac{\bar{g}_{\mathrm{p}} A_{\mathrm{r},j}}{\bar{g}_{\mathrm{p}} A_{\mathrm{r},j} + 2\hat{\ell}_{\mathrm{tr}}} = \Delta t_j \mathcal{P}_{\mathrm{r},j}\end{aligned} \tag{14}$$

This means that the estimate of the pipe length under the floor ℓ_{r}, is based on an assumption of a linear relationship between floor area and pipe length. The pipe density g_{p} is often between 3 and 6 m/m^2. The transport length $\ell_{\mathrm{tr},j}$ can be estimated with some uncertainty, based on distance from room to manifold. Inserting Eq. (14) into (12) gives the corrected proportionality constant:

$$q_j \propto \frac{A_{\mathrm{r},j}}{\Delta t_j \frac{\bar{g}_{\mathrm{p}} A_{\mathrm{r},j}}{\bar{g}_{\mathrm{p}} A_{\mathrm{r},j} + 2\hat{\ell}_{\mathrm{tr}}}} = \frac{A_{\mathrm{r},j} + \frac{2\hat{\ell}_{\mathrm{tr}}}{\bar{g}_{\mathrm{p}}}}{\Delta t_j} = \alpha_j \tag{15}$$

The updated expression seen in (15) is used to calculate the RHC coefficient α_j.

2.7 Simulation

To investigate the claim that the maximum slope measures the complete circulation time, a simulation of a simple floor heating system is implemented. As seen in Figure 4, the model consists of six parts. A room modelled as a first order system, a floor, a water pipe (under floor

and two transport sections), a piece of pipe placed in the heating room and a simple sensor model attached to this pipe. Note that indexes such as i and j refer to partitions of one pipe and not circuits, since the model is representative for all circuits.

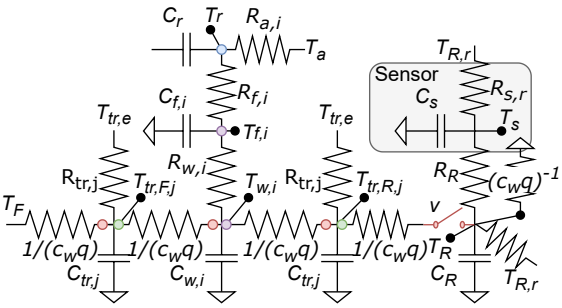

Fig. 4 – Shows the resistor-capacitor equivalent of the simulation model. The green dot indicates that this model section is repeated M_{part} times. The purple dot indicates that the section is repeated N_{part} times. The blue dot describes a summation point, where the heat contribution from all the floor parts are collected. The red dots indicate circuit breakers. If the binary valve indicator is 1 the circuit is closed and the water is flowing, and 0 stops the flow.

The model of the transport pipe (tr), for both directions are shown in Eq. (16a).

$$C_{\text{tr},\{\cdot\},j}\dot{T}_{\text{tr},\{\cdot\},j} = c_{\text{w}}q\left(T_{\text{tr},\{\cdot\},j-1} - T_{\text{tr},\{\cdot\},j}\right)v + \frac{1}{R_{\text{tr},i}}\left(T_{\text{tr},e} - T_{\text{tr},\{\cdot\},j}\right) \quad (16a)$$

with C being the heat capacity, T the temperature, q the nominal mass flow, $v \in \{0,1\}$ the valve indicator variable and R the heat resistance. The placeholder $\{\cdot\}$ indicates that the equation is valid for both the *forward* (F) and *return* (R) pipe. This is the case since they are modelled as being equally long. The pipes have M_{part} partitions each, with $j \in \{1, ..., M_{\text{part}}\}$. The equation consists of a term describing the water being transported within the pipe and one describing transport loss. Eq. (16b) describes the water in the pipe under the floor:

$$C_{\text{w},i}\dot{T}_{\text{w},i} = \frac{1}{R_{\text{w},i}}\left(T_{\text{f},i} - T_{\text{w},i}\right) + c_{\text{w}}q\left(T_{\text{w},i-1} - T_{\text{w},i}\right)v \quad (16b)$$

Again a term describes the water transport and one describes the transfer of energy to the *floor* (f) slab. Note that losses to the ground or other rooms are not considered. There are N_{part} partitions, with $i \in \{1, .., N_{\text{part}}\}$. Eq. (16c) shows the equation for floor partition i. There is an equal number of floor and water pipe partitions, since they are paired together.

$$C_{\text{f},i}\dot{T}_{\text{f},i} = \frac{1}{R_{\text{w},i}}\left(T_{\text{w},i} - T_{\text{f},i}\right) + \frac{1}{R_{\text{f},i}}\left(T_{\text{f},i} - T_{\text{r}}\right) \quad (16c)$$

The floor partition is nothing more than a capacitance and two resistances placed between the the pipe and room. Eq. (16d) describes a *room* (r) with an equal distributed air temperature.

$$C_{\text{r}}\dot{T}_{\text{r}} = \sum_{i=1}^{N}\frac{1}{R_{\text{f},i}}\left(T_{\text{f},i} - T_{\text{r}}\right) + \frac{1}{R_{\text{a},i}}\left(T_{\text{a}} - T_{\text{r},i}\right) \quad (16d)$$

The energy flow from the floor is the sum of the flow from each floor partition. The other term describes the heat loss to the environment. Eq. (16e) describes the part of the return pipe (R) placed in the heating room.

$$C_{\text{R}}\dot{T}_{\text{R}} = c_{\text{w}}q\left(T_{\text{tr,R},N_{\text{part}}} - T_{\text{R}}\right)v + \frac{1}{R_{\text{R,r}}}\left(T_{\text{R,r}} - T_{\text{R}}\right) + \frac{1}{R_{\text{R}}}\left(T_{\text{s}} - T_{\text{R}}\right) \quad (16e)$$

Eg. (16e) has three terms, the water flow, a small heat loss to the sensor and the loss to the heating room. Eq. (16f) describes the temperature sensor as a small first order capacity. The state T_{s} describes the measured value.

$$C_{\text{s}}\dot{T}_{\text{s}} = \frac{1}{R_{\text{s,r}}}\left(T_{\text{R,r}} - T_{\text{s}}\right) + \frac{1}{R_{\text{R}}}\left(T_{\text{R}} - T_{\text{s}}\right) \quad (16f)$$

$$T_{\text{tr,F},1} = T_{\text{F}} \quad T_{\text{r}} \in \mathbb{R} \quad \mathbf{T}_{\text{f}} \in \mathbb{R}^{N_{\text{part}}} \quad \mathbf{T}_{\text{w}} \in \mathbb{R}^{N_{\text{part}}}$$

The water pipe is divided into two *transport* (tr) sections and the part embedded in the floor. The floor and pipes are discretized along the length, which makes the model a high order system. The length of each partition ℓ_{part} in the floor and transport pipe is decided by a exchange percentage α_{p}, meaning a certain percentage of water needs to be exchanged at each sample.

$$\ell_{\text{part}} = \frac{qdt}{\rho_{\text{w}}\pi r_{\text{p}}^2\alpha_{\text{p}}} \implies \ell_{dt} = \alpha_{\text{p}}\ell_{\text{part}} \quad (17)$$

where ℓ_{dt} is the distance the water travel each simulation sample period dt. To create a correlation between coefficients in the simulation, a number of relations can be formulated for heat capacities, $C_{\{\cdot\}}$, and resistances $R_{\{\cdot\}}$.

$$C_{\text{w},i} = C_{\text{tr},\{\cdot\},j} = c_{\text{w}}\rho_{\text{w}}A_{\text{p}}\ell_{\text{part}} \quad (18)$$

$$C_{\text{R}} = c_{\text{w}}\rho_{\text{w}}A_{\text{p}}\ell_{\text{R}} \quad (19)$$

$$C_{\text{f},i} = \frac{A_{\text{r}}g_{\text{f}}}{N_{\text{part}}} \qquad C_{\text{r}} = V_{\text{r}}c_{\text{a}}\rho_{\text{a}} + A_{\text{r}}g_{\text{e}} \quad (20)$$

$$R_{\text{w},i} = \frac{N_{\text{part}}}{2\pi r_{\text{p}}u_{\text{w}}g_{\text{p}}A_{\text{r}}} \quad R_{\text{tr},i} = \frac{1}{2\pi r_{\text{p}}u_{\text{tr}}\ell_{\text{part}}} \quad (21)$$

$$R_{\text{R,r}} = \frac{1}{2\pi r_{\text{p}}u_{\text{R,r}}\ell_{\text{R}}} \quad (22)$$

$$R_{\text{a},i} = \frac{N_{\text{part}}}{u_{\text{a}}A_{\text{r}}} \qquad R_{\text{f},i} = \frac{N_{\text{part}}}{u_{\text{f}}A_{\text{r}}} \quad (23)$$

$$R_{\text{R}} = \frac{1}{U_{\text{R}}} \qquad R_{\text{s,r}} = \frac{1}{U_{\text{s,r}}} \quad (24)$$

$$q = g_q A_{\text{r}} \quad (25)$$

with A_p being the cross area of the pipe and ρ, c the density and specific heat capacity, respectively. Volumes are denoted as V. The heat capacity per square meter floor is given as g_f. The heat conduction per square meter is u and heat conduction is U. The ratio between floor area and wall capacity and flow is given by g_e and g_q, respectively. The model can then be summed up as an switched-input linear model. The state space version is seen in (26):

$$\mathbf{C}\dot{\mathbf{T}} = v\mathbf{A}_\mathrm{on}\mathbf{T} + (v-1)\mathbf{A}_\mathrm{off}\mathbf{T} + v\mathbf{B}T_\mathrm{F} + \mathbf{E}d \tag{26}$$

where $\mathbf{A}$, $\mathbf{B}$, $\mathbf{C}$ and $\mathbf{E}$ are matrices and $\mathbf{T}$ a vector of temperatures. The model is simulated with a time period of dt using first order Euler integration.

$$\mathbf{T}(k+1) = [\mathbf{I} + v(k)\mathbf{A}_\mathrm{on}dt + (v(k)-1)\mathbf{A}_\mathrm{off}dt] \\ \mathbf{T}(k) + v(k)dt\mathbf{B}T_\mathrm{F}(k) + dt\mathbf{E}d(k) \tag{27}$$

2.8 Experiment in test house

The test house used in this project has a flow-meter on the common circuit of the FH system. This flow-meter is used to establish a baseline flow distribution. To obtain the distribution, the flow is measured with only one circuit open. This is done for all circuits. Note, the distribution obtained from this approach does not account for any saturation effects on the circulation pump occurring at high flow rates.

To obtain the round trip times Δt_j used for Eq. (15), all circuits are opened. Then a step in the forward temperature is performed by turning of the heat source while circulating the water. In this particular case the heat pump turned off periodically. This is illustrated as event two in Fig. 3 and seen in Fig 5.b. The data from the return sensors is sampled with a period of 20 seconds and low-pass filtered to reduce noise and quantization effects. Multiple samples are carried out and averaged. In practice the experiment can be carried out without forcing the circuits open.

3. Results

This section presents the results from the simulation based sensitivity analysis and the experiment on the inhabited test house.

3.1 Simulation results

In Sec. *2.5* it is claimed that round-trip time can be measured using the return sensors. In this section, the simulation from Sec. *2.7* is used to investigate whether this is consistent under varying conditions and configurations.

Tab. 1 – The distribution of random parameters

Parameter	Distribution	Unit
A_r	$\mathcal{U}(5,30)$	$[m^2]$
g_q	$\mathcal{U}(0.002,0.005)$	$[kg/(m^2s)]$
g_f	$\mathcal{U}(24000,36000)$	$[J/(m^2K)]$
g_e	$\mathcal{U}(12000,17000)$	$[J/(m^2K)]$
g_a	$\mathcal{U}(0.3,1)$	$[\cdot]$
r_p	$\mathcal{U}(0.01,0.02)$	$[m]$
u_a	$\mathcal{U}(0.45,0.55)$	$[W/(m^2K)]$
u_f	$\mathcal{U}(3.5,4.5)$	$[W/(m^2K)]$
u_w	$\mathcal{U}(6,12)$	$[W/(m^2K)]$
u_tr	$\mathcal{U}(2,4)$	$[W/(m^2K)]$
$u_\mathrm{R,r}$	$\mathcal{U}(0.05,0.15)$	$[W/(m^2K)]$
U_R	$\mathcal{U}(0.5,0.5)$	$[W/K]$
$U_\mathrm{s,r}$	$\mathcal{U}(0.05,0.15)$	$[W/K]$
ℓ_tr	$\mathcal{U}(3,25)$	$[m]$
C_s	$\mathcal{U}(80,120)$	$[J/K]$
$\mathcal{P}_\mathrm{p}$	$\mathcal{U}(0.5,0.5)$	$[\cdot]$

The analysis is performed by repeating a 10 room simulation, supplied with randomly drawn coefficients, 100 times. The coefficients are distributed according to Tab. 1 where $\mathcal{U}$ denotes the uniform distribution. The pipe distribution g_p, follows Assumption 4. Fig. 5 shows the transient response from the simulation compared with the measured one.

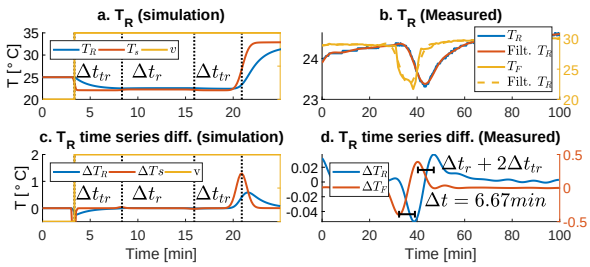

Fig. 5 – Column one: shows an example of the simulated transient response and time series diff. for the simulation. Column two: shows one the measured values. Note that $\Delta T_R = T_R(k) - T_R(k-1)$.

The simulation allows us to investigate otherwise inaccessible states such as transport time Δt_tr and the actual water temperature T_R. As mentioned in Sec. *2.5*, the peak for ΔT_R, seen in Fig. 5.c, exactly measures the total round trip time. We think this is the case, since this is the time where the new front of warm water arrives at the sensor. Further, it can be seen that the measured value T_s has a slower time constant, since the heat needs to propagate through the pipe. To measure the performance the root mean square error seen in (28), is computed for the difference between the actual flow distribution $\mathcal{P}_q \in \mathbb{R}^N$ and the particular flow distribution estimates $\mathcal{P}_{x,j}$ with $x \in \alpha, A_\mathrm{r}$. The subscript α indicates that the distribution is based on Eq. (15), and A_r that it is

based purely on area distribution.

$$RMSE_x = \frac{1}{N}\sum_{j=1}^{N}\left(\mathcal{P}_{q,j} - \hat{\mathcal{P}}_{x,j}\right) \tag{28}$$

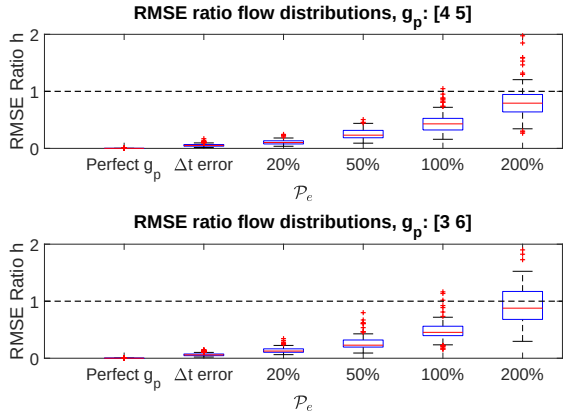

Fig. 6 – Upper and lower show the RMSE ratio of the test performed with the pipe density g_p drawn uniformly between 4 and 5 and 3 to 6 m/m^2, respectively The x-axis shows the results with increased error on the transport pipe estimate. The first entry contains the results using perfect information. The second shows the results where only the error from measuring the round-trip time affects the result. $\mathcal{P}_e$ is the percentage error.

To quantify the results, the root mean square error calculated from the simulations are formulated as a ratio h seen in Eq. (29).

$$h = \frac{RMSE_\alpha}{RMSE_{A_\mathrm{r}}} \tag{29}$$

This ratio allows us to evaluate whether the overall distribution improved. If h is zero, it means that the fit is perfect, and if it is greater than one, it would be better to distribute based on area alone. The estimates for the flow distribution, $\mathcal{P}_{\alpha,j}$, is calculated using the normalized version of (15) with $\bar{g}_\mathrm{p} = 4.5$ and $\hat{\ell}_\mathrm{tr}$ as the real transport length plus estimation error:

$$\hat{\ell}_\mathrm{tr} = \ell_\mathrm{tr} + e_\mathrm{tr} \tag{30}$$

The error is correlated with the actual length of the transport pipe and normally distributed according to the following 3σ rule.

$$e_\mathrm{tr} \sim \mathcal{N}(0, (1/3\mathcal{P}_e\ell_\mathrm{tr})^2) \tag{31}$$

where $1/3\mathcal{P}_e\ell_\mathrm{tr}$ is the standard deviation of the error of the one-way transport distance, meaning that 99% of the errors are within plus/minus this range. Figure 6 and 7 show the results of the simulations. As can be seen in Figure 6, it is important to have a good estimate of the length of the transport pipe, since it has a large effect on the quality of the estimate. The outliers, seen with red crosses, have been related to bad measurements where the wrong peak is obtained.

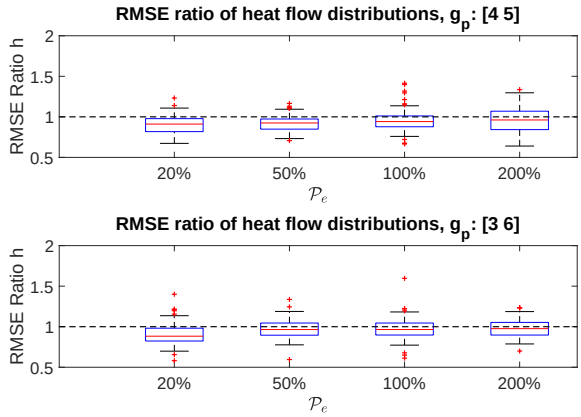

Fig. 7 – Sums up the results for the calculated heat distributions. The figure has the same structure as Fig. 6. The RMSE resulting from using the RHC in Eq. (4) is divided by the RMSE from Eq. (32).

The heat distributions, defined as the percentage share of accumulated heat consumption, are also calculated from the simulations. The heat distribution is based on the RHC in Eq. (4) and compared with Eq. (32) taken from [6].

$$\beta_{A_\mathrm{r},j}(t) = A_{\mathrm{r},j}\frac{T_\mathrm{F}(t) - T_{\mathrm{R},j}(t)}{\ln\left(\frac{T_\mathrm{F}(t)-T_{\mathrm{r},j}(t)}{T_{\mathrm{R},j}(t)-T_{\mathrm{r},j}(t)}\right)} \tag{32}$$

This RHC also uses the return temperature together with the room temperature $T_{\mathrm{r},j}$ and floor area over the circuit. The RHC in Eq. (32) assumes that the specific heat conduction from water to room is the same for all rooms. The final heat distribution is obtained by integrating the RHC using Eq. (7). As in the case with pipe density, the specific heat conductance's in the floor are varied with each simulation, but kept constant between rooms in any given simulation. This is done to avoid punishing the method based on Eq. (32) unnecessarily. Considering the heat distribution the improvement is not that clear. It has to be mentioned that real floors do not have equal resistance, due to varying floor types and the effects caused by the interior of the room.

3.2 Demo house comparison

To collect evidence for or against the ability of the method to estimate the flow distribution in real houses, the method was carried out on a test house having a flow meter on the common pipe of the FH system. The measurement results of round-trip time Δt_r are seen in Tab. 3. Two measurements are made and the average value is used. Note that the times differ quite significantly between the two tests, and the reason for this is unexplained. It is worth noting, though, that if the values are plotted, the pattern is preserved. Besides the measured times, the actual measured flow for each circuit is shown in liters per hour. The areas and assumed transport lengths are presented too. Figure 8 shows the results of the estimated flow distribution. As can be seen, 12

out of 15 circuits improved when compared to the measured distribution.

Tab. 2 – Shows the RMSE and *mean absolute error* (MAE) of the estimates for the nominal flow distribution based on floor area and Eq. 15

Measure	A_r	$\frac{A_\mathrm{r}}{\Delta t}$	Ratio h
RMSE	0.014	0.0093	0.62
MAE	0.012	0.0077	0.63

Tab. 3 – Results for room 1-15

Room	1	2	3	4	5	6	7	8
$q[l/h]$	173	135	87	154	158	184	119	132
$\Delta t^1_{\mathrm{r},j}[s]$	460	500	440	480	420	420	280	480
$\Delta t^2_{\mathrm{r},j}[s]$	420	440	380	480	340	340	240	440
$A_\mathrm{r}j[m^2]$	12.7	9.2	3.6	9.5	9.3	9.6	4.8	9.5
$\hat{\ell}_{\mathrm{tr},j}[m]$	8	5.5	7	1.5	3	3	1.5	5.5
Room	9	10	11	12	13	14	15	
$q[l/h]$	126	184	150	140	165	156	95	
$\Delta t^1_{\mathrm{r},j}[s]$	440	520	520	480	360	460	300	
$\Delta t^2_{\mathrm{r},j}[s]$	340	500	460	400	300	360	280	
$A_{\mathrm{r},j}[m^2]$	9.5	15	14.6	7.7	9.6	13	5.5	
$\hat{\ell}_{\mathrm{tr},j}[m]$	5.5	11.5	2.5	8.5	3	2	2	

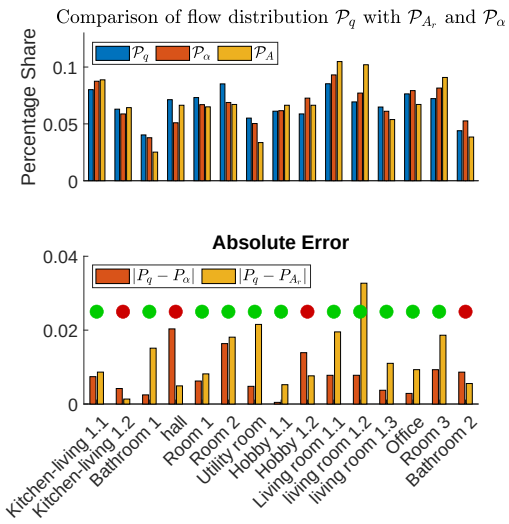

Fig. 8 – Upper: Comparison of real percentage share of flow with estimate based on α and A_r. Lower: difference for each room plus improvement indicator.

4. Conclusion

In this work we investigated the use of retrofitted sensors on the return pipes to estimate the flow distribution in a FH system. Simulation and experimental results suggest that it is possible to observe round-trip time in the data, and the flow distribution resulting therefrom is better than the one merely based on floor area distribution. The method improved the estimate in a test house by 38%. Work to be done, is to carry out a statistic, which either supports or disproves the result presented in this text. The results also suggest that measuring the temperature in the pipe could improve the results substantially.

The datasets generated during and/or analysed during the current study are available in the git repository, `https://gitlab.com/Thorsteinsson/clima-2022.git`.

References

[1] Danish Energy Agency, "Data, tabeller, statistikker og kort Energistatistik 2019," da, Danish Energy Agency, Tech. Rep., ISSN: 0906-4699 year: 2019, p. 60. [Online]. Available: `https://ens.dk/sites/ens.dk/files/Statistik/energistatistik2019_dk-webtilg.pdf` (visited on 05/07/2021).

[2] Statistics Denmark, *Boligbestanden*, da, 2021. [Online]. Available: `https://www.dst.dk/da/Statistik/emner/borgere/boligforhold/boligbestanden` (visited on 11/25/2021).

[3] P. D. Andersen, M. J. Jiménez, H. Madsen, and C. Rode, "Characterization of heat dynamics of an arctic low-energy house with floor heating," en, *Building Simulation*, vol. 7, no. 6, pp. 595–614, Dec. 2014, ISSN: 1996-8744. DOI: `10.1007/s12273-014-0185-4`.

[4] I. Hazyuk, C. Ghiaus, and D. Penhouet, "Optimal temperature control of intermittently heated buildings using Model Predictive Control: Part I – Building modeling," en, *Building and Environment*, vol. 51, pp. 379–387, May 2012, ISSN: 0360-1323. DOI: `10.1016/j.buildenv.2011.11.009`.

[5] P. Radecki and B. Hencey, "Online Model Estimation for Predictive Thermal Control of Buildings," *IEEE Transactions on Control Systems Technology*, vol. 25, no. 4, pp. 1414–1422, Jul. 2017, Conference Name: IEEE Transactions on Control Systems Technology, ISSN: 1558-0865. DOI: `10.1109/TCST.2016.2587737`.

[6] J. Ploennigs, A. Ahmed, B. Hensel, P. Stack, and K. Menzel, "Virtual sensors for estimation of energy consumption and thermal comfort in buildings with underfloor heating," en, *Advanced Engineering Informatics*, Special Section: Advances and Challenges in Computing in Civil and Building Engineering, vol. 25, no. 4, pp. 688–698, Oct. 2011, ISSN: 1474-0346. DOI: `10.1016/j.aei.2011.07.004`.

[7] T. M. Kull, M. Thalfeldt, and J. Kurnitski, "Modelling of Wax Actuators in Underfloor Heating Manifolds," en, *E3S Web of Conferences*, vol. 246, p. 11 009, 2021, Publisher: EDP Sciences, ISSN: 2267-1242. DOI: `10.1051/e3sconf/202124611009`.

Customized Neural Network training to predict the highly imbalanced data of domestic hot water usage

Caroline Risoud, Amirreza Heidari, Dolaana Khovalyg*

Ecole Polytechnique Fédérale de Lausanne (EPFL), Integrated Comfort Engineering (ICE), CH-1700 Fribourg, Switzerland, *caroline.risoud@epfl.ch

Abstract. Despite space heating and cooling, the energy use for hot water production has not changed significantly over time and accounts for a big share in modern, well-insulated buildings. The main challenge of hot water generation lies in the highly stochastic nature of the domestic hot water (DHW) demand. Prediction of DHW demand can significantly help to a more efficient operational strategy in water heating systems. However, the time-series data of hot water demand is very sparse and imbalanced, including many zero demands, which makes it challenging to be predicted properly by Machine Learning methods. This study uses data recorded from a single-family building in South Africa and aims to understand how the customizations of a neural network for learning imbalanced datasets can affect the prediction of hot water demand. Four different customizations (Random over-sampling, Random under-sampling, Weight Relevance-based Combination Strategy, Synthetic Minority Over-sampling Technique for Regression) are compared with the baseline model to predict the hot water demand data. The performance of 9 different simulations is compared and the challenges are outlined. The over-sampling technique shows promising results for practical implementation by over-predicting high peaks by up to 20%, which will guarantee enough hot water production at peak usage.

Keywords. Hot water demand, Occupant behaviour, Machine Learning, Imbalanced data, Neural network, Time series
DOI: https://doi.org/10.34641/clima.2022.141

1. Introduction

Hot water production accounts for a big share of energy use in modern buildings [1]. While the energy use of heating and cooling systems has significantly decreased through the generations of buildings [2], the hot water energy use has not significantly decreased. Actual water heating systems do not account for stochastic behavior of occupants and follow a conservative operational strategy to ensure that hot water is available whenever it is demanded. A control strategy that can learn and predict the hot water use behavior of occupants and adapt the hot water production to the demand can significantly reduce the energy consumption [3].

The aim of this project is to learn and understand how the LSTM (Long Short-Term Memory Network) neural network can predict stochastic hot water use behavior. The work copes with the challenge of predicting a continuous target variable within a highly imbalanced dataset, by implementing modifications that resample the training dataset in order to counterbalance the biases towards zero values. The practical implementation of such models could lead to smart, dynamic water heating systems that would adapt to the predicted demand. This could lead to significant energy savings on the large scale since buildings' energy consumption in 2016 represented almost 40% of total EU energy consumption. Finally, this could contribute towards reaching Europe's 20% energy efficiency target for 2020 and beyond [4].

Only limited research has focused on predicting the highly stochastic DHW demand. Heidari et al. [3] proposed a set of Machine Learning (ML) models including Single models, Sequential Multi-task models, and Parallel Multi-task models, to predict the DHW in residential buildings. Then an adaptive water heating system that follows the predicted demand was proposed and compared to the conventional systems. In another study, Heidari et al. [5] proposed the implementation of attention mechanism and time series decomposition to improve the prediction performance of the LSTM neural networks for predicting hot water demand energy use. Ferrantelli et al. [6] developed prediction formulas based on analytical modelling to predict hourly hot water demand in Finland. Gelazanskas and Gamage [7] proposed stochastic models to forecast hot water demand at the individual building

Copyright ©2022 by the authors. This conference paper is published under a CC-BY-4.0 license.

level. Ritchie et al. [8] also evaluated the energy-saving potential by an optimal control strategy based on demand predictions. Previous studies have not addressed the imbalanced nature of hot water demand data which is the main challenge for achieving higher accuracies in predictions. The main objective of this work is to evaluate and compare few potential customizations that are developed to cope with imbalanced datasets used for ML.

2. Methodology

2.1 Case study description

This study used the data recorded from a single-family building in South Africa [9]. The data was recorded over approximately 8 months from 18.01.2018 to 15.08.2018. It captures the outflow from the water heater in [ml/m] (millilitres per minute) every 20 minutes. 52% of the timesteps have zero hot water consumption and therefore the dataset can be considered as being imbalanced and biased towards zero values of hot water consumption.

2.2 Performance Metrics and Model Evaluation

Three metrics are used in this work: MAE (Mean Absolute Error), which is an average of the sum of absolute differences between actual and predicted values. RMSE (Root Mean Squared Error), which is an average of the sum of the squares of the error. R2 (R-squared score), which measures the quality of prediction by expressing the percentage of variance explained by the model.

2.3 Baseline model

The baseline model is a LSTM, which is a neural network that is trained using backpropagation through time and overcomes the vanishing gradient problem. LSTM is selected in this study due to its better memory for long-term dependencies. The effects of different architectures (number of LSTM layers, units per layer, presence of dropout layer, presence of dense layer) and hyperparameters (number of epochs, batch size) and input data are analysed to define the best performing baseline model.

2.4 Modifications

The goal of the following sampling methods is to re-balance the distribution of the zero values and the non-zero values.

2.4.1 Random under-sampling

This method performs under-sampling (value removal) on the "*uninteresting values*" of the training set. If the training sample is $D = \{\langle \bar{x}, y \rangle\}_{i=1}^{N}$, the 2 following parameters are defined by the user: t, the threshold on the dataset, and r, the ratio of under-sampling. The values above the threshold are considered as "important" data (which are desired to be predicted with good accuracy). In other words, the domain of the target values can be split into two sub-domains: a domain of rare values, which is of greater importance to the user, and the domain of uninteresting values. The ratio r represents the ratio between the potential candidates for under-sampling in the new (customized) dataset and the potential candidates for under-sampling in the actual (initial) dataset. If the dataset of the rare values is $D_{rare} = \{\langle \bar{x}, y \rangle \in D: y > t\}$ and D_n is the dataset with the remaining observations $D_n = \{\langle \bar{x}, y \rangle \in D: y \leq t\}$ then $r = \frac{|D_{n,New}|}{|D_{n,Actual}|}$. So, if r=0.8 and t=0, then 20% of the zeros were removed from the actual dataset. Noting here that, on one hand, too large values of r will result in a new training dataset that is still too imbalanced and, on the other hand, too small values of r will result in a training data set that is too small or too different [10]. The cases to be under-sampled are then randomly selected from the potential candidates in the dataset. The following three simulations are presented: 1) t=0 and r=0.8 (under-sampling of 20% of the common cases); 2) t=0 and r=0.7; 3) t=2 and r=0.8.

2.4.2 Random over-sampling. Similar to the random under-sampling, the definition of threshold t on the dataset and ratio n that represents the ratio of rare cases to be oversampled have to be specified by the user. Here, $\mathbf{n} = \frac{|\mathbf{D_{rare,New}}|}{|\mathbf{D_{rare,Actual}}|}$. The cases to be oversampled are then randomly selected from the potential candidates in the dataset. Then, they are copied and randomly reintroduced in the new dataset. The training sample resulting from this approach will be larger than the original dataset. The following two simulations are presented: 1) t=0 and n=1.2 (over-sampling of 20% of the rare cases); 2) t=4 and n=1.8.

2.4.3 Weight Relevance-based Combination Strategy (WECS). In this approach, over- and under-sampling are combined. In contrary to the previously discussed methods, the cases are no longer over- or under-sampled randomly. This strategy uses the relevance values as weights to select data points for over- and under-sampling [11]. Previous work [12] proposed the use of a relevance function to map the domain of continuous variables into a [0,1] scale of relevance, i.e., $\phi(Y):Y \rightarrow [0,1]$. This function attributes levels of importance to ranges of the target variable. In this work, the choice of a shifted sigmoid function has been made in order to capture the effect of increased importance for larger DHW values and a relevance score of almost zero for zero DHW demands. This function is expressed by the following equation 1.

$$\mathbf{relevance}(\mathbf{x}) = \boldsymbol{\phi}(\mathbf{x}) = \frac{1}{1+e^{(x-5)}} \quad (1)$$

With x being the target variable (value of hot water consumption) in [ml/m] (millilitres per minute).

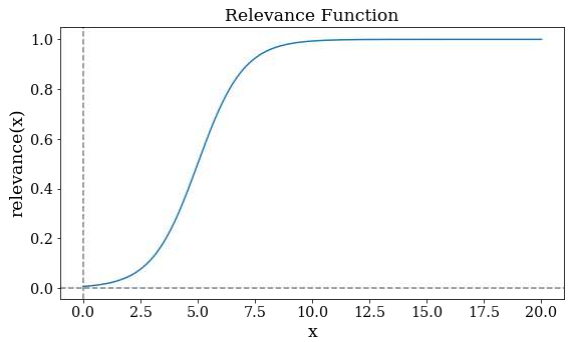

Fig. 1: Chosen relevance function

The key idea of this strategy is to use the relevance function scores as probabilities for resampling. A threshold of t=0 is fixed, so that the relevance scores are only used for over-sampling while the under-sampling is strictly performed on zero DHW values. Before performing over- and under-sampling, the relevance scores are translated into probabilities for each DHW value being an over-sampling candidate in the training set as shown in equation (2).

$$\mathbf{p_i^{over}} = \frac{\phi(y_i>t)}{\sum_{i=1}^{N}\phi(y_i>t)} \quad (2)$$

With $(\mathbf{y_i} > \mathbf{t})$ representing the candidates for over-sampling (target values in the dataset that are bigger than the user-defined threshold t), **N** is the total number of over-sampling candidates. In that way, the higher the relevance for a DHW value, the more likely it is to be selected for over-sampling. Two simulations are performed using this strategy, namely: 1) 300 data points are oversampled and 300 data points are undersampled; 2) 300 data points are oversampled and 200 data points are undersampled.

2.4.4 SMOTE for Regression (SMOTER). This method combines under- and over-sampling [13] and is a modification of the classical SMOTE algorithm so that it is suitable for regression tasks [14]. This time, the over-sampling candidates are not just copied and inserted in the training set; "synthetic" cases with rare target values are generated as an interpolation of the values of its k-nearest neighbours [15]. Again, the relevance function from equation (1) is used and the threshold is held at t=0 in this method. The two following simulations are performed: 1) Over-sampling rate [%] = 100, Under-sampling rate [%] = 100, k (number of nearest neighbours to use for the generation) = 2; 2) Over-sampling rate [%] = 300, Under-sampling rate [%] = 200, k=2.

3. Presentation and Analysis of the results

The goal is to compare the 9 (2 over-sampling, 3 under-sampling, 2 WECS, 2 SMOTER) sampling approaches against the baseline model and to identify which methods could lead to a better prediction of the true DHW demand. Table 1 summarizes the numerical results . Figure 2 shows the results as a plot for the specific period between 10-12 July 2018.

Tab. 1: Comparison of accuracy metrics achieved by the different methods

	Base-model	Over-sampling1	Over-sampling2	Under-sampling1	Under-sampling2	Under-sampling3	WECS 1	WECS 2	SmotR 1	SmotR 2
MAE	1.692	3.044	3.130	3.017	3.035	3.033	3.086	3.061	1.739	1.774
RMSE	3.306	5.959	6.165	5.859	6.002	5.911	6.064	6.071	3.360	3.459
R2 score	0.352	0.322	0.256	0.340	0.345	0.340	0.294	0.313	0.311	0.350

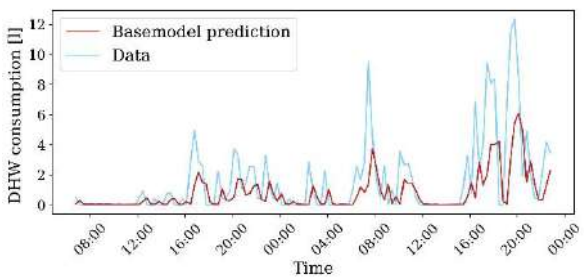

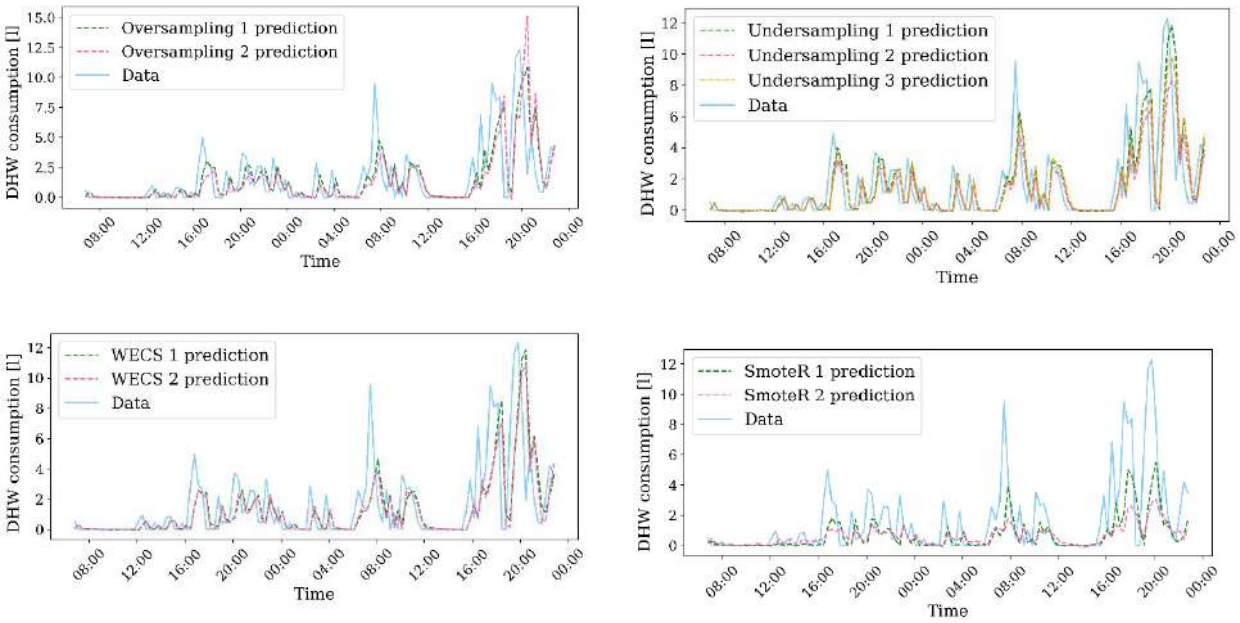

Fig. 2: Predicted versus actual demand (Data) by the proposed methods for the period between 10-12 July 2018

It is clear that all applied modifications work, zero values are very well predicted and the general trends are respected for each simulation. The basemodel predictions clearly show the problem of predicting an unbalanced dataset. Almost all non-zero values are underpredicted while zero-values are well predicted. However, the non-zero values are the most important values to predict accurately.

Neither of the implemented modifications overperformed the baseline model, which performed the best. WECS 1 shows the worst results. The over-sampling 2 simulations predicted higher DHW demand than the actual demand during peak hour around 8 PM. This is a real benefit given that the peak demand is the most crucial demand that has to be guaranteed. In order to guarantee the DHW demand at peak usage, predictions have to be slightly higher than the actual demand to account for the potential uncertainty while guaranteeing the peak demand.

The fact that the modifications did not perform better is due to the shift in the forecast, which means that the forecasted and the actual data are shifted by one time-step. Shifts in time-series predictions are a well-known issue [16], to which we propose the following modifications and improvements:

1. Using an alternative performance metric to evaluate the model which would be more adapted to imbalanced regression tasks. An evaluation framework for forecasting rare extreme values of a continuous target variable (precision and recall for regression) is proposed by [10]. Their key idea is weighting the error also by its relevance and not only by its magnitude.

2. Improving the input data by adding categorical features (month of the year, day of the month, hour of the day) and additional features such as the total number of hot water demands until the current moment.

3. Reformulating the problem as a multi-class classification problem. A classification task will make the forecasting much easier for the model and could overcome the shift issue. This implementation could easily be practically applied by creating a storage tank with different 'levels' where each level corresponds to a new class.

4. Conclusion

Based on the obtained results, the following conclusions can be drawn:

a. Predicting the exact value and time of hot water demand is a very challenging task for ML due to the stochastic nature of occupants' behavior. Thus, the proposed models usually underestimate the demand and show a shift in predicted time versus actual time of demand.

b. The SMOTER method is capable of reaching almost the same performance as the baseline model.

c. The Random Over-sampling method is very promising by being able to predict higher values at peak hours.

In sum, if the proposed strategies to cope with the

time-series shift can be introduced, the over-sampling technique shows promising results for practical application by over-predicting high peaks, which will guarantee enough hot water production at peak usage. Still, further research is required to better predict the highly stochastic occupant behavior by ML models.

5. References

[1] Diana Ürge Vorsatz et al. "Heating and cooling energy trends and drivers in buildings". In: *Renewable and Sustainable Energy Reviews* 41 (Jan. 1, 2015), pp. 85–98. ISSN: 1364-0321. DOI: 10.1016/j.rser.2014.08.039.

[2] Zhihua Zhou et al. "Heating energy saving potential from building envelope design and operation optimization in residential buildings: A case study in northern China". In: *Journal of Cleaner Production* 174 (Feb. 10, 2018), pp. 413–423. ISSN: 0959-6526. DOI: 10.1016/ j.jclepro.2017.10.237.

[3] Amirreza Heidari et al. "Adaptive hot water production based on Supervised Learning". In: *Sustainable Cities and Society* (Dec. 1, 2020), p. 102625. ISSN: 2210-6707. DOI: 10.1016/ j.scs.2020.102625.

[4] European Commission. *Towards reaching the 20% energy efficiency target for 2020, and beyond.* European Commission. 2017. URL: https : / / ec . europa . eu / commission/presscorner/detail/en/MEMO_17_ 162 (visited on 01/04/2021).

[5] Amirreza Heidari and Dolaana Khovalyg. "Short-term energy use prediction of solarassisted water heating system: Application case of combined attention-based LSTM and time-series decomposition". In: *Solar Energy* 207 (Sept. 1, 2020), pp. 626–639. ISSN: 0038- 092X. DOI: 10.1016/j.solener.2020.07.008.

[6] Andrea Ferrantelli et al. "Analytical modelling and prediction formulas for domestic hot water consumption in residential Finnish apartments". In: *Energy and Buildings* 143 (2017), pp. 53–60. ISSN: 0378-7788. DOI: https://doi.org/10.1016/j.enbuild.2017.03.021.

[7] L. Gelažanskas and K. A. A. Gamage. "Forecasting hot water consumption in dwellings using artificial neural networks". In: *2015 IEEE 5th International Conference on Power Engineering, Energy and Electrical Drives (POWERENG).* 2015 IEEE 5th International Conference on Power Engineering, Energy and Electrical Drives (POWERENG). ISSN: 2155- 5532. May 2015, pp. 410–415. DOI: 10.1109/PowerEng.2015.7266352.

[8] Michael Ritchie, Jacobus Engelbrecht, and M.J. (Thinus) Booysen. "Practically-Achievable Energy Savings with the Optimal Control of Stratified Water Heaters with Predicted Usage". In: *Energies* (Apr. 1, 2021). DOI: 10.3390/en14071963.

[9] Joshua Siegel. "*Single Family Hot Water Flow Data*". fr. In: (Sept. 2019). type: dataset. DOI: 10.7910/DVN/BQEHMU. URL: https://dataverse.harvard.edu/dataset.xhtml? persistentId=doi:10.7910/DVN/BQEHMU (visited on 11/02/2020).

[10] Luís Torgo and Rita Ribeiro. "Precision and Recall for Regression". In: *Lecture Notes in Computer Science*. Vol. 5808. Oct. 3, 2009, pp. 332–346. ISBN: 9783642047466. DOI: 10 . 1007/978-3-642-04747-3_26.

[11] Paula Branco, Luís Torgo, and Rita Ribeiro. "Pre-processing Approaches for Imbalanced Distributions in Regression". In: *Neurocomputing* 343 (Feb. 1, 2019). DOI: 10 . 1016 / j . neucom.2018.11.100.

[12] Luís Torgo et al. "Resampling strategies for regression". In: *Expert Systems* 32 (Aug. 2014). DOI: 10.1111/exsy.12081.

[13] Luís Torgo et al. "*SMOTE for Regression*". In: vol. 8154. Sept. 2013, pp. 378–389. DOI: 10.1007/978-3-642-40669-0_33.

[14] Luís Torgo and Rita Ribeiro. "*Utility-Based Regression*". In: Sept. 2007, pp. 597–604. ISBN: 9783540749752. DOI: 10.1007/978-3-540-74976-9_63.

[15] Aleksandra Deis. *Regression Addressing Extreme Rare Cases*. en. 2019. URL: https://kaggle. com/aleksandradeis/regression-addressing-extreme-rare-cases (visited on 11/02/2020).

[16] Flovik, V. (2018, June 7).In towardsdatascience: https://towardsdatascience.com/how-not-touse-machine-learning-for-time-series-forecasting-avoiding-the-pitfalls-19f9d7adf424

Data Statement

The dataset analyzed during the current study is available in the Harvard Dataverse, https://dataverse.harvard.edu/dataset.xhtml? persistentId=doi:10.7910/DVN/BQEHMU (visited on 11/02/2020).

CONVERGE: low energy with active passiveness in a transparent highly occupied building

Peter van den Engel [a], Regina Bokel [a], Eleonora Brembilla [a], Luigi de Araujo Passos [b], Peter Luscuere [a]

[a] Faculty of Architecture and the Built Environment, Delft University of Technology, Delft, the Netherlands, P.J.W.van denEngel@tudelft.nl

[a] Faculty of Architecture and the Built Environment, Delft University of Technology, Delft, the Netherlands, R.M.J.Bokel@tudelft.nl

[a] Faculty of Architecture and the Built Environment, Delft University of Technology, Delft, the Netherlands, E.Brembilla@tudelft.nl

[b] Faculty of Mechanical, Maritime and Materials Engineering, Delft University of Technology, Delft, the Netherlands, L.A.deAraujoPassos@tudelft.nl

[a] Faculty of Architecture and the Built Environment, Delft University of Technology, Delft, the Netherlands, P.G.Luscuere@tudelft.nl

Abstract

This research gives an overview of the current comfort and energy performance, and optional future design of highly transparent and lightweight buildings. The transparent Co-Creation Centre in the Green Village at the TU Delft, has a combination of active and passive climate control measures. The aim of the research is to show how transparent buildings with a high glass/floor percentage (here 122 %) perform and how these could be optimized. An overview of the research project and system integration is presented, with the focus on energy, comfort and working of the BMS-system. Energy and comfort performances are measured and simulated. Validation has been executed of daylight, solar heat access, and thermal performances. A large Phase Change Material (PCM) buffer in the air handling unit reduces the heating and cooling demand. Making use of passive qualities of the outdoor and indoor air temperature and solar energy requires a more complex control strategy than usual. A Model Predictive Control (MPC) strategy has been investigated and can optimize the energy consumption.

Keywords. transparency, passive, PCM, ventilation

1. Introduction

Transparency is since long mainstream in architecture. However, this may lead to a higher heating and cooling load due to a lower insulation of the transparent material and its higher solar transmission. The variability of solar load also leads to an unstable indoor climate. These factors make it more difficult to use passive or active climate control strategies. The climate control system will become more complex and less robust. A high degree of transparency will also effect indoor visual comfort, due to high luminance levels and sharp contrasts between sunlit and shaded areas.

The new fully transparent building, the Co-Creation Centre, see figure 1, was erected at TU Delft, Green Village [1] in 2020. The Co-Creation Centre is both a meeting centre and a research facility. The building consists of large meeting space, with a service cabin connected to it. The meeting space is used for different functions like conferences, educational and office functions. The occupancy is extremely variable from low to very high. The large glass hall can be seen in figure 1 at the left side. The service centre with a kitchen, toilets and ICT-functions at the right side.

The fully transparent triple glazed façades are state of the art in glass engineering, the columns are even of glass. The building has large overhangs and automatic outdoor sunshades to prevent overheating. The building was initially designed for 30 people but was redesigned to hold 240 people in a meeting setting (prior to the introduction of Covid restrictions). A so-called climate tower, visible on the left in figure 1, makes sure that the building is comfortable. The building, with PV panels on the tower, aims to become energy neutral or positive,

Copyright ©2022 by the authors. This conference paper is published under a CC-BY-4.0 license.

which is even better than the Dutch BENG-standard. The building is also a research facility to investigate if a transparent building could be passively heated, cooled and ventilated without loss of comfort. The building has an extensive sensor network for continuous monitoring. This paper describes the building and all its climate controls and shows the first results of the investigation.

Fig. 1 – Co-Creation Centre with blinds down and climate tower at the South-side.

2. The building and its control options

2.1 The building

The building has a limited size (315 m^2). The fully transparent façades consist of triple glazing with a U-value of 0.53 W/m^2K. The building has 34 PV-panels of 300 Wp on the climate tower, leading to 6,000 – 7,000 kWh/y electricity production per year. However, on the circa 400 m^2 roof much more panels could be installed.

In winter the building is heated by the sun through the transparent façade and by preheated displacement ventilation via the floor. Heating is provided by an air-based heat pump in the climate tower. The climate tower was originally designed as a solar chimney, but later reconfigured as a large air handling unit. The ventilation is controlled by the indoor CO_2 concentration, to minimize the amount of air changes in the heating season. A counter-flow heat exchanger further reduces the heating energy necessary for ventilation.

In summer blinds are used to reduce the solar load from the sun, see figure 1. Overhangs and trees reduce the amount of sun in summer too. A PCM battery with 1,170 panels (2,106 kg, 181 kWh) of calcium chloride hexahydrate with a phase change temperature between 20 and 23 °C adds additional cooling or heating power to building. The PCM battery can be cooled by ventilation at night and heated up by warm return air. In the cooling season skylights and doors can also be used for natural ventilation during the day and cooling at night. Extra cooling is also possible via the heat pump with return air or the ground as its source.

2.1 Passiveness

The degree of passiveness is here defined as the time of the year that the building does not need additional electricity for heating, cooling and ventilation while maintaining a comfortable indoor climate. The energy necessary for controlling the blinds and the airflow and for opening the skylights is not considered in this definition of passiveness. Several key performance indicators, such as energy consumption, indoor temperature, illuminance, and CO_2-levels are measured. Furthermore, occupants' comfort is evaluated. However, due to Covid-19 restrictions, this is only indicative at this stage of the research.

2.2 Control options

The following main control options are available:

Blind control: the blinds can be individually controlled for all four facades, to all tilt angles and to all vertical heights. Four different shading control strategies are being developed and evaluated: (a) fixed passive strategies; (b) sun-tracking dynamic control; (c) energy-based dynamic control; and (d) visual comfort-based dynamic control. The first strategy (a) is based on passive lighting control provided by fixed shading elements, such as the overhangs and the deciduous trees behind the building. Strategy (b) is based on a traditional sun-tracking algorithm, which controls the tilt of the lamellas so that they always block direct sunlight. Strategy (c) controls the blinds based on the amount of available solar energy and on the amount of heat that is required within the building at any specific moment. On a hot summer day this behaves similarly to the sun-tracking control mode, but on a colder day, the blinds are more open to let more sunlight inside and heat the building. The last control strategy (d), still in development, is controlling the blinds based on the combined requirements of preventing discomfort glare and guaranteeing a view out whenever possible. The control of the blinds is based on illuminance data read by sensors installed on the Co-Creation Centre roof and on simulation data from synchronous daylight modelling algorithms.

Indoor thermal comfort: the indoor thermal comfort is controlled by the air temperature set-point. A different set-point is chosen for summer and winter. The air temperature set-point takes also the radiant temperature of the glass into account maintaining the operative midwinter-temperature above 21 °C.

Fresh air supply: the airflow is firstly controlled based on the CO_2 concentration when the building is occupied. When the CO_2 concentration is below 800 ppm (Covid values) the airflow can follow different paths through the climate tower.

Airflow control for passive heating and cooling: the heat exchanger can be enabled between 0 and 100 %.

Exhaust air can either pass or not pass through the PCM.

Airflow control for PCM heating and cooling: the air can pass through the PCM to heat up or cool down the inlet air. The air can pass through the PCM with an airflow percentage between 0 and 100 %. This is the control strategy when the building is occupied. When the building is unoccupied or when the indoor air is within the temperature boundaries for thermal comfort, (part of) the air can pass through the PCM to heat up or cool down the PCM to store heat or cold.

Airflow control as a source of the heat-pump: a limitation is that the exhaust air is the source of the heat-pump, requiring an increased indoor and outdoor airflow to obtain enough heating power of the heat pump.

Heating and cooling via water flowing via piles in the ground: soon the heat pump will be connected to energy stored in the ground via energy piles under the building. The energy piles are able to replace the outdoor condenser and are expected to increase the COP of the heat pump significant. The cold in the ground can also cool the building indirectly without using the heat-pump.

Controlled natural ventilation: rooflights can be automatically controlled for cooling in summer. The doors can be opened manually to further increase air exchange rate. It is estimated that the building does not need HVAC for 20-30% of the year, while keeping CO_2-levels and temperatures within comfort-range.

2.3 PID and MPC

The control system includes an automatic operation mechanism to deal with the dynamics of people occupancy and heat exchanges across the building. The controller relies on the temperature measurements collected in situ and algorithms implemented to optimally follow the set of strategies presented in Section 2.2. The purpose is keeping the tracking error e (the difference between the temperatures read by the sensors and the desired value) close to zero. While several methods can be considered, a PID (Proportional-Integral-Derivative) controller has currently been implemented since it is known to be an accurate and reliable control method [2]. The PID continuously balances selected inputs (e.g. shades aperture, ventilation flow rates, and heat pump power) by a correction factor u that depends on the tracking error feedback as follows:

$$u = K_\mathrm{p} e + K_\mathrm{i} \int_0^t e\, dt + K_\mathrm{p} \frac{de}{dt} \qquad (1)$$

where K_p and K_i are control parameters tuned for the current controller.

Moreover, a MPC (Model Predictive Control) has been theoretically investigated through MATLAB simulations [3], as it shows promising results when evaluating the control performance in comparison to PID controller. With MPC, the controller draws on system models and on the SQP (Sequential Quadratic Programming) method [4] to determine the set of optimal inputs that minimize an objective function over a selected time horizon, such that:

$$\min_{\mathrm{x}} \sum_0^t \dot{q}_\mathrm{hp} + e^2 \qquad (2)$$

where x is the controllable input, and $\dot{q}_\mathrm{hp}$ the heat pump power consumption. Therefore, the MPC builds on the capability of knowing the system dynamic in advance instead of acting over sensor feedback, which is certainly helpful when dealing with different disturbances and heat capacities.

3. Methods of research and design

3.1 Set-points

The measurements are performed with dummy persons in the room to simulate the internal heat production of 30 persons. The dummy persons are spread over the room, creating a more or less realistic situation. The occupancy times are 9:00 - 17:00 h in the measurement periods. The air temperature set-points have the following values:

Tab. 1 – Set-points during the measurements °C

season	min/max occupied	min/max unoccupied
spring	20/23	15/25
summer	20/23	15/30
autumn	20/23	15/25
winter	21/23	18/25

The set-points for occupied hours are based on Category A or B of the EN 15251. Ultimately an adaptive control strategy will be implemented to reduce energy even more. Outside occupancy time temperatures may be lower or higher to save energy or load the PCM-battery.

3.2 Measurements

More than 100 sensors are used in the building and integrated in the online Priva Display website. Figure 2 gives an indication of all the sensors and controls. The sensors log measurements every 5 minutes, except for the energy sensors which log measurements every 15 minutes. Additional measurements were also manually collected to validate the simulations, besides the long-term data series recorded by the sensor network.

Weather data are measured at a weather station established on the roof of the Co-Creation Centre and by a pyranometer managed by the faculty of EWI of the Delft University of Technology. Four illuminance sensors are place on the Co-Creation Centre roof:

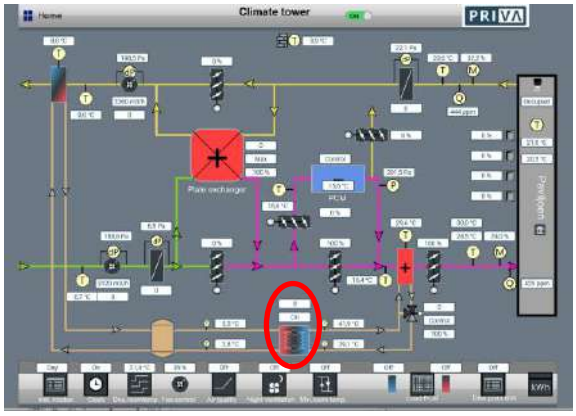

Fig. 2 – Schematic overview of the climate tower and the sensors on the accompanying Priva website. The red box in the middle is the heat exchanger, the blue box the PCM-battery and at the bottom, circled, the air to air heat-pump can be seen.

one is positioned horizontally and looks upward, while the other three are positioned vertically and respectively look towards the East, South, and West directions (approximately, as the longitudinal axis of the building is tilted of -22° from due North). The focus of this evaluation is only on the thermal and comfort achievements in relation to the energy consumption. Occupant feedback was also collected but due to Covid 19 and in this stage of the project the results only consist of random samples.

3.2 Simulations

Simulations with DesignBuilder, Phoenics (CFD), Radiance, and Matlab/Python were used for calibration and yearly predictions of energy and comfort. Also, the effect of the cooling set-point was investigated. The thermal behaviour of the PCM-battery is predicted via a CFD- (Phoenics) and MATLAB-model. These models are discussed in more details elsewhere [5].

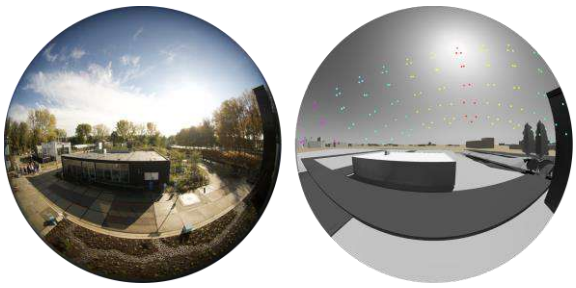

Fig. 3 – Fisheye photograph taken from the viewpoint of the South facing illuminance sensor (left) and virtual reconstruction of the same scene used for Radiance simulations (right).

Radiance was used to simulate the illuminance reaching of each of the four outdoor illuminance sensors, as a first step towards the validation of the blind control algorithms. This step allowed the quantification of errors due to the luminance distribution model used within the simulation (Perez All-Weather) and to the modelling of the environment surrounding the Co-Creation Centre.

4. Results

4.1 Measurements

Measurements with the same internal heat over two weeks in spring, summer, autumn and winter are executed. The exact period of measuring was depending on the availability of the building.

Summer temperatures

Measurements in the summer period are presented in figure 4. The set-point for the maximum temperature was 23 °C during working hours. The minimum temperature set-point was 15 °C. The highest indoor temperatures are in the weekend, without occupancy.

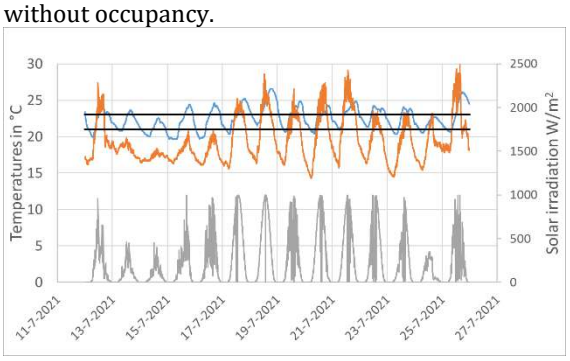

Fig. 4 – Measurements 12 – 25 July 2021. The line at the top is the indoor temperature (blue) and in the middle, the outdoor temperature (orange). The lower line is the solar irradiation (W/m²). The two black lines are the boundary conditions for occupied weekdays.

Occupants last summer often experienced the space as "too cold" suggesting that the cooling set-point of 23 °C could be higher.

Autumn temperatures

In autumn, the temperature drop between day and night is only around 3 °C, see figure 5. The blinds are mostly closed, but the blind settings were not optimized at that time.

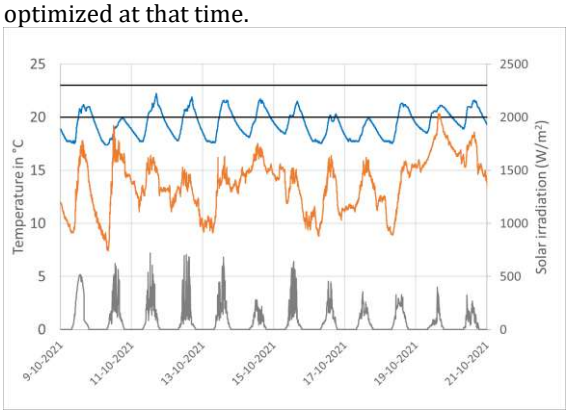

Fig. 5 - Measurements 9 – 21 October 2021. The line at the top is the indoor temperature (blue) and, in the middle, the outdoor temperature (orange). The lower line is the solar irradiation (W/m²). The two black lines are the boundary conditions for occupied weekdays.

The building is heated by the heat-pump, as shown in figure 6. Here the air temperature of the air coming from the heat-pump is shown to reach 35 °C.

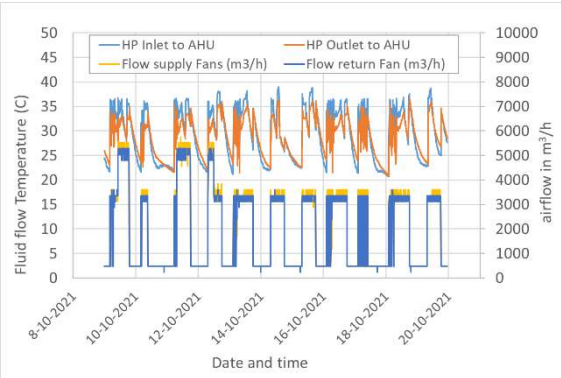

Fig. 6 - Autumn measurement period (9 – 21 October). The fluid flow temperatures (around 35 °C) to and from the heat-pump to the heat exchanger (HP inlet and outlet to AHU) which heats up the air to the room and the air flows via the fans (m^3/h) are presented.

The air flows (3,000 to 5,500 m^3/h) are very large for the limited simulated amount of people (30) inside, see figure 6. With 30 m^3/h per person, 900 m^3/h would have been sufficient.

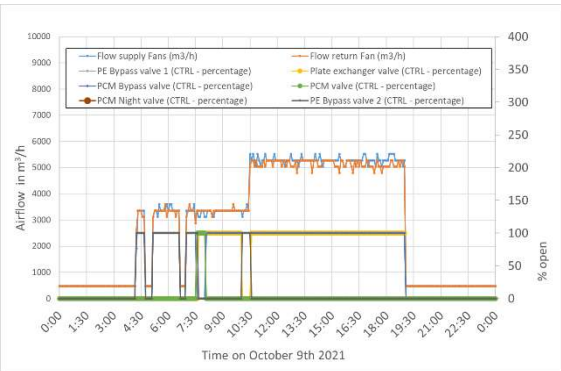

Fig. 7 – Control actions on October 9th.

In the following section some initial problems with fine-tuning of a complex climate system are presented. The measurements in figure 6 show an airflow of more than 3,500 m^3/h in the early morning. In more detail, see figures 7 and 8, on Saturday October 9th the building valve opens at around 4:00 a.m. when the inside temperature is below 18°C. This is caused by the heat-pump only working when there is an air flow. At 4:00 am the temperature of the airflow from the heat-pump (supply temperature) rises when the heat-pump starts to work. The heat-pump tries to keep the indoor temperature above 20 °C within the occupied time, i.e. from 7:30 h (figure 8, yellow line in the middle). Under the night setting, when the building is unoccupied, the heat exchanger was not used. As a result, the heat-pump needs to heat the cold outside air instead of air preheated by the heat exchanger. Figure 7 shows that during occupancy, i.e. from 7:30 onwards, the heat exchanger is active except for the short period when the airflow rate increases, around 10:00. Figure 8 shows the measured temperatures as a result of all the control actions shown in figure 7. The stored heat in the PCM is only checked at the start of the day for the 9th of October but is not actively used. The PCM temperature is slightly higher than the average outside air temperature.

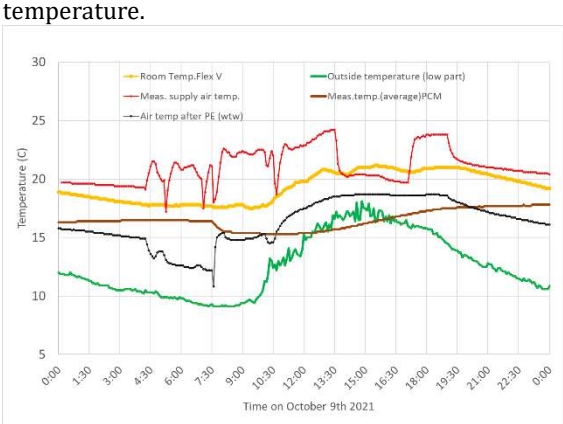

Fig. 8 - Temperature measurements at 9th October.

Another not yet logical control setting is a combination of using the heat exchanger first to load the PCM with internal heat, making this less efficient (not visible in these figures).

Winter measurements

Measurements of the heat-pump for a whole year show a total electrical energy consumption for heating and cooling of 12,700 kWh (40 kWh/m^2), excluding the energy for the fans in the condenser. The energy consumption is expected to become much lower once the ventilation is optimized and the ground storage is connected to the heat-pump.

Noise

A disadvantage of the current design is the choice of a high efficiency fan with a too small diameter. The diameter of the fan is 0.31 m, whereas a 0.62 m diameter and a maximum velocity of 10 m/s would be more appropriate for a low pressure and low noise system. The maximum velocity in the fan is 37 m/s at 10,800 m^3/h with a measured pressure difference of 2,000 Pa. The noise level, based on manufacturer data, is 87.6 dB(A) at 8,000 m^3/h. On top of that there is an Aeolian sound effect caused by one of the ventilation grilles. An air flow of circa 6,000 m^3/h produces circa 52 dB(A) at 49 m distance outside, whereas the Dutch Building Code requires 40 dB(A), and 37 dB(A) within the building. 6,000 m^3/h should already be sufficient for the high maximum number of 240 occupants.

Solar access results

Global horizontal irradiance is recorded by a commercial pyranometer installed on the Co-Creation Centre roof. Measurements collected by this device were compared to irradiances measured by a research-grade pyranometer installed on the roof of one of the nearby campus buildings. Figure 9 shows the correlation between the two datasets, for measurements collected during the July test weeks. The bias error is zero, indicating a good agreement between the two instruments overall. However, there is a noticeable scatter (R^2=0.72) and a relative Mean Absolute Error (rMAE) of 22%. Measurements

recorded during high sun altitude instances seem to be particularly affected by errors and under-prediction.

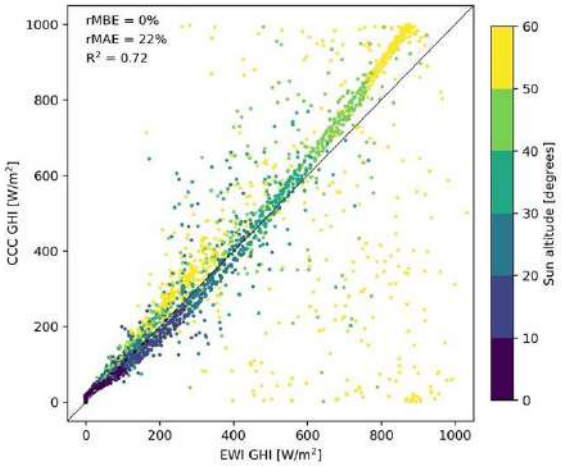

Fig. 9 – Scatterplot showing the correlation between Global Horizontal Irradiance (GHI) values (in W/m²) recorded by a research grade pyranometer on a building on campus (EWI) and by the commercial pyranometer installed on the CCC roof.

4.2 Simulations

DesignBuilder-simulations

For the DesignBuilder calibration simulations and the yearly energy demand the 2021 data of the weather station of Rotterdam Airport has been used, as provided by the KNMI [6].

Heating Season (winter)

DesignBuilder simulations of the winter show that the temperature is allowed to drop to as low as 10 - 12 °C at night. Even with a low heating capacity of 15 kW and heating starting 3 hours before occupancy time, the required comfort-temperature can be realized. The large diurnal temperature drop shows a potential weakness of the concept of a lightweight building with fully glazed facades. In buildings with sufficient thermal mass and a limited glass percentage the diurnal swing in winter would only be several degrees, whereas the Co Creation Centre can reach a 10 °C temperature drop. The air-to-air heat-pump should - after optimization - lead to an yearly energy consumption for heating of minimal 6,500 kWh/y (20 kWh/m²y) with a COP of circa 2. However, this COP-value will become much higher with a COP of circa 5 with a connection to the storage in the ground in combination with an efficient running PCM-battery (COP > 27 [5]). Simulation results shows that most of the heating is provided by the sun. In order to reduce the heating energy more, a façade with 30 % glass, combined with an opaque part with a U-value of 0.2 W/m² would lead to a thermal heating energy consumption of only 5,000 kWh instead of 13,000 kWh, with almost the same usage of electrical lighting energy (70 kWh above 1030 kWh). A transparent design with adaptive façade isolation could be a future option.

Cooling Season (summer)

At a cooling set-point of 26 °C and a low average occupancy of 30 people (9:00 - 17:00 h) the simulated thermal cooling energy consumption is only 300 kWh/y. Due to the low g-value of the glass with outside louvres (design value g=0.03), a large overhang and trees on the West-side, the solar transmission in summer is very low when the louvres are down. This prevents overheating.

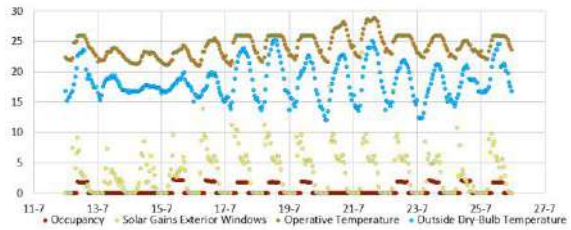

Fig. 10 – DesignBuilder simulations for 12 – 25 July. The cooling set-point is 26/27 °C (adaptive range Category C). The operative temperature is shown at the top with the outdoor temperature below that line. The solar gains are low in summer: maximal circa 10 kW, due to usage of the blinds (circles at the underside). The dark line below those circles is the internal heat load. The left axis shows temperatures or kW's.

Cooling set-points

The energy-consumption for heating remains almost the same, so choosing a higher set-point is energy-efficient. The cooling load due to the sun in the cooling season is around 50 % lower due to a full row of high trees at the West-side, see figure 1. Most of the heat loss is caused by transmission through the 5 m high triple glazing with a U-value of 0.53 W/m²K. The CO_2-level based ventilation (a maximum of 1200 ppm only at very low outdoor temperatures) is, apart from the isolation of the glass, the most relevant parameter to reduce the heating energy. The limited heat loss through ventilation explains the fact that, without a heat exchanger, the thermal energy consumption increases only from 45 to 54 kWh/m². In table 2 the results of DesignBuilder simulations are presented. The set-points for cooling have almost no effect on the discomfort hours that comply with the EN 15251 Category C.

Tab. 2 – Set-points, thermal energy and comfort*

Set-point cooling	Cooling Energy kWh	Heating Energy kWh	Hours Cat. C EN 15251
26 °C	300	13,116	7,5
25 °C	1,078	13,078	8,0
24 °C	3,165	12,916	5,5
23 °C	3,565	12,809	5.5

*The blinds go down at an inside temperature above 21 °C, combined with a solar tracking-mode of the blinds. There are 30 persons inside, Mo – Fri from 9:00 - 17:00 h. The CO_2-level is maximal 1200 ppm.

The simulated amount of energy that can be stored in the PCM-battery is 181 kWh for one load. When 1200 kWh = 600 sunny hours of 20 kW could be delivered in the heating season in the simulated year of 2021 (see table 2) the heat-pump would not be necessary. However, in the months November till the end of February there is not enough sun at all times. The heat pump still has to run to compensate for the sunless days as can be seen in figure 11:

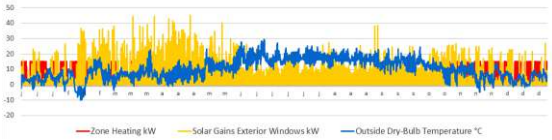

Fig. 11 – DesignBuilder-simulations of the whole year. The set-point for cooling is 26/27 °C (adaptive range Category C). Red = heating load (kW), yellow solar load and blue outside temperature. The left axis shows temperatures or kW's.

The operative temperature is not presented here but is at least 20 °C during occupancy. The solar gains are high in the heating season, maximum circa 40 kW, the number of leaves on the trees is then decisive.

Radiance simulations

As shown in figure 12, the simulations performed for the outdoor illuminance sensors resulted in relatively small errors (relative Mean Bias Errors, rMBEs, lower than 7% and rMAEs lower than 27%). except for the West looking sensor.

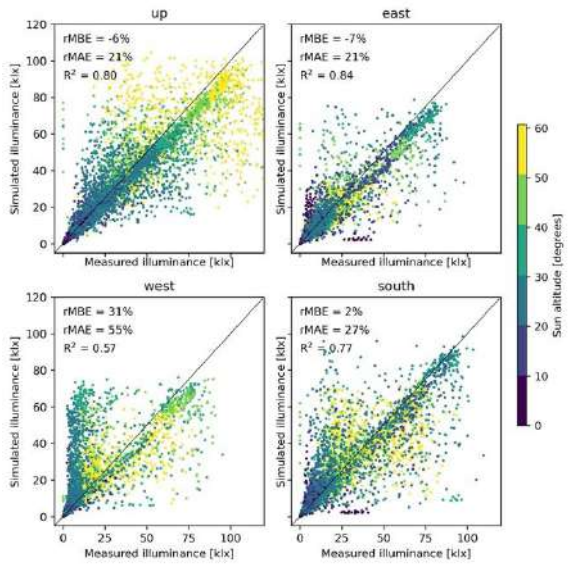

Fig. 12 – Scatterplots showing the correlation between measured and simulated illuminances for the four roof sensors. The points colour indicates the sun altitude at the time of measurement.

Such sensor is significantly obstructed by trees, a challenging element for the correct modelling of the environment. During the middle of the day errors are less pronounced but simulation results are characterised by more frequent fluctuations than measured values. To exemplify the role of obstructions on results, figure 13 shows measured and simulated illuminance data for a clear sky day within one of the test periods (July 18th 2021). It can be noticed that for low sun altitudes (morning and evening) the obstructions on the horizon lead to more discrepancies between measurements and simulations, especially noticeable for the East and West looking sensors. These might be due to the luminance distribution model implemented in the simulation.

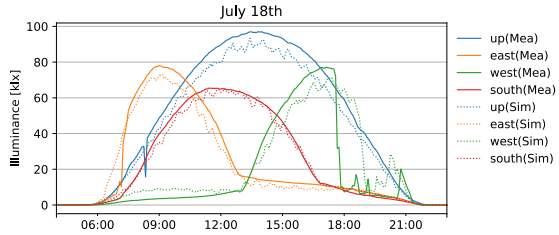

Fig. 13 – Example of illuminance data recorded by the four roof sensors (solid lines) and corresponding results from the simulation (dotted lines), during a clear day (July 18th). The results for the west looking sensor are affected by nearby obstructing trees.

5. Evaluation

5.1 Overheating?

At the start of the project, it was expected that overheating would be a major problem, but due to a very effective sunshade, the opposite is true and reduction of heat loss via the façade and ventilation needs more attention to reach the goal of delivering an almost passive building.

5.2 All air system for a fully glazed system?

The indoor climate is based on an all-air system-principle. Even though this is often seen as too energy-intensive, for buildings with a low heating and cooling load this is a realistic option again. The building has displacement ventilation via perforated tiles under the carpet, making the contaminant removal efficiency favourable as well. A comfortable climate for 240 occupants was a main design starting point, which could be realized. For the default usage with a number of 30 persons a much lower air flow (≥ 750 m³/h) will be already sufficient.

5.3. Heating using an air-based heat pump

In the current design the air flow is connected to the heat-pump which uses the return air as a heat source. The heat-pump requires a minimal air flow of circa 3,400 m³/h, which is circa 1/3 of the ventilation capacity. It is also more difficult than expected to heat up the building because of the low capacity (surface) of the heat exchanger in the supply air. The building makes use of a low-pressure cross flow heat exchanger with a high efficiency of 93 %. According to DesignBuilder a reduction of heat recovery efficiency from the current 93 % to, for instance, 70 % for a twin-coil would have limited effect on energy consumption. A twin-coil could be an option

for a design substantially based on buoyancy forces.

5.4. Climate Tower

The usage of the natural pressure difference (buoyancy) is very limited within this design because fresh, but cold, outdoor air enters via the top of the chimney and leaves the building at ceiling height. The original design was based on a low position of the air inlet at floor level and exhaust at the top.

5.5 Energy and visual comfort

With high outside temperatures a high solar load is unwanted. When the outside temperatures are low a higher solar load inside will reduce the heating load of the heat-pump. A high glass percentage produces contrast differences giving the occupants the feeling that there is insufficient light in the centre of the building which leads to occupants turning on the artificial lighting [7]. This effect is increased by the black and grey colours of the ceiling and floor. The dark colours also reduce the reflections of the floor, blinds and ceiling, making the lighting less efficient. On top of that, with closed louvres a spectacular "mausoleum"-effect is created. An entirely different atmosphere can be created with lighter colours and natural materials as can be seen in the house of Philip Johnson and the Barcelona gallery of Mies van der Rohe. At high wind-velocities the outdoor sunshade cannot be used so indoor sunshade will shortly be added to prevent glare and this could make the interior less dark. The mausoleum effect can also partly be compensated by opening louvres in a strategic way, i.e. opening the blinds at the sides where the sun is not shining or only blocking only the direct solar beams. The combination of lighter colours and a smart control in DesignBuilder reduces the electrical energy for lighting (> 300 lux, 3 W/m^2 LED) from the measured 3,500 kWh to 1,000 kWh.

6. Conclusion and recommendations

It should be possible to design a lightweight fully glazed building with an acceptable to good visual comfort, which can be energy positive against a limited amount of solar panels. At the moment the heating energy is too high, but this is probably due to unnecessary ventilation at the start and an unconnected energy storage in the ground for the heat pump. On top of that electricity consumption for lighting is much higher than expected.
A building with a lower glass percentage would lead to less heating and cooling energy, lower investment and maintenance costs and an easier to realize good visual comfort. This also depends on the glass-floor ratio, window-height and thermal mass, so there is no final answer.
Architects need to have very good reasons to design fully transparent buildings and in some circumstances these are realistic. Partly transparent buildings, where transparency is an added value on strategic locations, is often a better choice [8, 9]. A comparable building-design with a more limited heat loss could have, for instance, even better isolating glass or screens at the in- or outside. In order to realize an even better energy positive building with a good thermal and visual comfort, optimization of all components need more attention. Additional options are: reduction of resistance of the ventilation system, using buoyancy, a modulating heat-pump, a larger heat exchanger for air supply and a light-coloured interior. Complexity reduction of the installations and a more user-friendly control system (BMS) are other connected relevant issues for sustainable transparent designs of the future.

7. Acknowledgement

The research is made possible via the Dutch TKI program Urban Energy, grant Converge**.** The evaluation of project will be continued.

8. References

[1] "The Green Village," www.thegreenvillage.org. [Accessed 10 January 2022]

[2] Borase R. P., Maghade D. K., Sondkar S.Y., Pawar S.N. A review of PID control, tuning methods and applications, International Journal of Dynamics and Control (9), p. 818-827, 2020.

[3] Ceha T.J., Araujo Passos L.A. de, Baldi S., Schutter B. de. Model predictive control for optimal integration of a thermal chimney and solar shaded building. Mediterranean Conference on Control and Automation. 2021.

[4] Fletcher R., "The Sequential Quadratic Programming Method," Lecture Notes in Mathematics, 2010.

[5] Engel P.J.W. van den, Malin M., Venkatesh M.K, Araujo Passos L.A. de. Performance of a Phase Change-battery in a transparent building. Journal of Fluid Dynamics & Materials Processing. 2022 (under review).

[6] "KNMI," https://www.knmi.nl/home [Accessed 10 January 2022]

[7] Naves C., Amorim D., Svabo L. Brasilia: daylighting analysis of public buildings designed by Oscar Niemeyer. PLEA2006.

[8] Napier J. Climate Based Façade Design for Business Buildings with Examples from Central London. Buildings (5), p. 16-38, 2015

[9] Short C.A. The Recovery of Natural Environments in Architecture. Air, Comfort and Climate. Routledge 2017.

The datasets generated during and/or analysed during the current study are not available, because it requires specific data-acquisition rights and skills, but the authors will make every reasonable effort to make them available in the near future.

An early prototype for fault detection and diagnosis of Air-Handling Units

Shobhit Chitkara [a], Alet van den Brink [b], Shalika Walker [a], Wim Zeiler [a]

[a] Department of the Built Environment, Eindhoven University of Technology, Eindhoven, the Netherlands, s.chitkara@tue.nl, s.s.walker@tue.nl, w.zeiler@tue.nl.

[b] Afdeling O&T, Kropman Installatietechniek B.V, Nijmegen, the Netherlands, alet.van.den.brink@kropman.nl.

Abstract. The built environment is responsible for nearly 35% of energy consumption and is undergoing a digital transformation. Up to 30% of energy is consumed inefficiently due to inadequate setup and/or incomplete utilization of available data. An efficient fault detection and diagnosis (FDD) strategy for air handling units is key to addressing this gap. Even though numerous FDD approaches have been published, real-world applications are far more complex and rarely discussed. This paper deals with FDD tool prototyping and integration aspects and discusses its development for air handling units deployed at 2 case-study buildings located in the Netherlands. The design and development of the FDD tool follows a structured 4 step process. Firstly, literature research is utilized to narrow the design space and establish a complete use case for developing the FDD tool. Secondly, the developed use case is handled utilizing a data-driven strategy to generate fault symptoms using a state-of-the-art extreme gradient boosting algorithm (XGBoost). Thirdly, the detected faults are isolated with a diagnostic Bayesian network. This way the fault detection and diagnosis aspects are separately handled. Lastly, integration of the prototyped tool with a commercially operated continuous monitoring system, currently being utilized to monitor 400 buildings, is discussed. Upon experimental validation, diagnosis specificity exceeding 90% is realized. It is further observed that the prototyped FDD tool could prevent up to 33% of chiller consumed energy. Moreover, the results presented will contribute to the adoption and deployment of AI-based FDD strategies in commercial applications.

Keywords. Air Handling Unit, Fault Detection and Diagnosis, Symptoms, Diagnostic Bayesian network, Artificial Intelligence
DOI: https://doi.org/10.34641/clima.2022.318

1. Introduction

The direct and indirect CO_2 emissions from energy use in buildings surpassed 10GtCO2 in 2019, the highest recorded level [1]. Space cooling and heating applications are key drivers of this demand [1]. Despite the efficiency gains due to digitization realized in other sectors such as banking, media etc. this potential is underleveraged in buildings. Up to 30% energy could be saved through the effective use of data collected through deployed continuous monitoring systems (CMS) [2].

Air-Handling Units (AHU) are the most widely studied sub-systems in the Heating, Ventilation, and Air-Conditioning (HVAC) system [2]. In their recent review of Automated Fault Detection and Diagnosis studies (AFDD), Shi et al. in [3] highlighted that there remain limited real-life applications despite much research. Further, the users that have currently adopted state-of-the-art FDD practices typify early adopters or innovators on the technology adoption curve [4].

Considering these aspects, the direct contribution of this paper is to add to the limited real-life demonstrations of FDD and inspire its widespread adoption. More specifically, the design, development, and validation of an FDD tool prototype that utilizes artificial intelligence (AI) methods is discussed. Further, the tool is integrated with a commercially operated CMS that has been utilized to monitor over 400 buildings in the Netherlands.

2. Related Work

Granderson et al. in [5] surveyed commercially deployed and under development FDD tools. It can be observed from their survey that FDD tools being utilized by the industry typically rely on a combination of expert rules or first principles. For example, in [6] proposed a cloud-based AFDD tool for AHUs. Their tool utilizes AHU performance assessment rules (APAR) [7]. Some of the common issues identified with using this approach are listed below:

Copyright ©2022 by the authors. This conference paper is published under a CC-BY-4.0 license.

a) Rules-based systems heavily rely on the sensed information. Due to the sensitivity of building owners to initial project costs, most building installations only have sensors limited to their control functionality [8]. Due to the lack of this additional information and the uncertainty associated with deployed sensors, it is difficult to develop reliable quantitative or qualitative models for FDD.

b) The limits utilized for generating alarms using the rule-based approaches are typically set at a higher threshold than desired to minimize the number of false positives [2]. This reduces the ability of an FDD system to detect faults with lower severity.

c) There is a lack of a unified framework for developing generic key-performance indicators (KPIs) and associated detection rules [9].

Bayesian inference-based approaches have been successfully demonstrated by authors of [10] and [11] for HVAC applications. In general, these models can handle circumstances when incomplete, uncertain, or conflicting information is presented as their outputs are fault probabilities instead of Boolean fault outcomes [11].

Besides, for the deployment of advanced algorithms from the machine learning (ML) domain lack of labelled faulty data is a key impediment [12]. Regression model-based or residual generation approaches offer an alternative to working with labelled data [2].

Often, the published research methods utilizing novel FDD techniques start with utilizing a prepared dataset. However, the practical application of these methods with operational CMS is rarely discussed. Granderson et al. [13], in their survey of 14 commercially deployed tools noted that whilst their software stack was proprietary several vendors offer application programming interface (API) to support integration.

Some desirable characteristics proposed by authors of [3] and [14] for an FDD system are categorized as functional and realization design requirements [15], (see **Tab. 1**). They serve as guiding indicators for the prototyped FDD tool.

3. Design Methodology

The design methodology for the tool is based on the systems thinking approach. For its software level deployment, Python is utilized as it is now the most popular programming language and has a large collection of continuously maintained packages supporting AI-based development. Further, the proposed software architecture is modular and can be expanded in-depth and at scale. This addresses the scalability and interoperability aspects stated in **Tab. 1**.

Tab. 1 - Desirable characteristics for an FDD system

Functional Aspects	Realization Aspects
High accuracy	Adaptability
Quick detection and diagnosis	No need for handcrafted AFDD algorithms
Robustness	Low Cost
Explanation facility	Interoperability
Isolability - ability to distinguish between multiple failures	Low storage and computational requirements
Novelty identifiability	Limited modelling requirements
Heuristic observations as evidence	Automation level in configuration
Multiple fault identifiability	Evaluation and decision support capabilities

In section 3.1, the overall software architecture for the proposed tool is introduced. In section 3.2, the business layer of the proposed tool is revealed, and in section 3.3, the integration aspects are discussed.

3.1 FDD Tool Overview

The overall architecture of the FDD tool is presented in **Fig. 1**. Herein, the implemented workflow is represented with solid arrows. The architecture comprises several layers namely data acquisition, pre-processing, business, post-processing, and visualization. The data acquisition layer is where all aspects concerning data transactions, protocol, and security are maintained.

The design of the FDD tool hereafter can be envisioned as *user agnostic* and *user specific* as shown in **Fig. 1**. The *user agnostic* development concerns design of data preparation and data mining operations on acquired data. The data preparation is carried out using Python libraries such as *Pandas*, and *NumPy*. For data mining, the business layer that wraps the fault detection and diagnosis approach is dwelled upon in section 3.2.

The *user specific* development is to help users efficiently realize outputs from the FDD business layer and enable human-in-the-loop diagnostics. The outputs are post-processed in an intermediary layer before being parsed through to the data visualization layer. The objective of this layer is to provide limited yet valuable evaluation and decision support capabilities for the user as identified in **Tab. 1**. The data visualization layer is designed using an open-sourced web development framework called *Dash by Plotly*. It wraps underlying layers of HTML, JavaScript, and CSS code blocks in a Pythonic syntax. Using this approach, an end-to-end Python-based

tool that's reliable, scalable, customizable, and quickly deployable is realized.

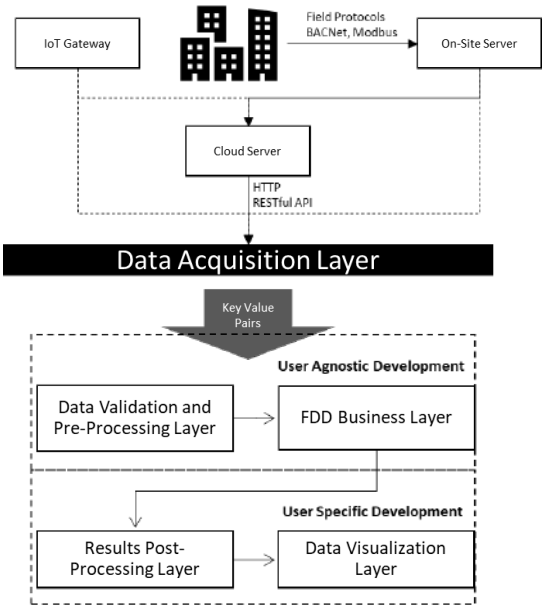

Fig. 1 - FDD tool prototype architecture

3.2 FDD business layer

For the design of the FDD business layer, 4S3F (four symptoms and three faults) framework is utilized (see **Fig. 2**) [16]. The 4S3F framework combines systems thinking approach with Bayesian probabilistic models. It addresses key aspects such as robustness, isolability, and early fault detection and diagnosis as identified in **Tab. 1.** At its core, the framework is aligned with the design and implementation of the HVAC system, thus making the designed FDD business layer interpretable.

The proposed approach isolates fault diagnosis or root-cause elimination process from fault detection or anomaly detection process. This separation between layers is highly recommended as it allows for multiple techniques from various domains and sub-domains to be combined in a common framework. For example, in this paper, an advanced AI algorithm called XGBoost (extreme gradient boosting) is utilized in the fault detection process [17]. The detected anomalies using XGBoost are then isolated in the diagnosis process.

In the 4S3F framework, the relationship between the faults and the symptoms are characterized using a belief network or also alternatively referred to as the Diagnostic Bayesian network (DBN) [18]. Here the operational state (OS) symptom nodes represent a deviation in the operational state from its expected state. The OS symptoms can be derived from building management system (BMS) data and are further classified as control-based OS indicators and design-based OS indicators [9]. For the demonstrated prototype both control-based and design-based OS indicators have been utilized. The other three kinds of symptom nodes namely Energy Performance (EP), Energy Balance (EB), and Additional (Add.) symptom nodes have been left out of the scope of this paper.

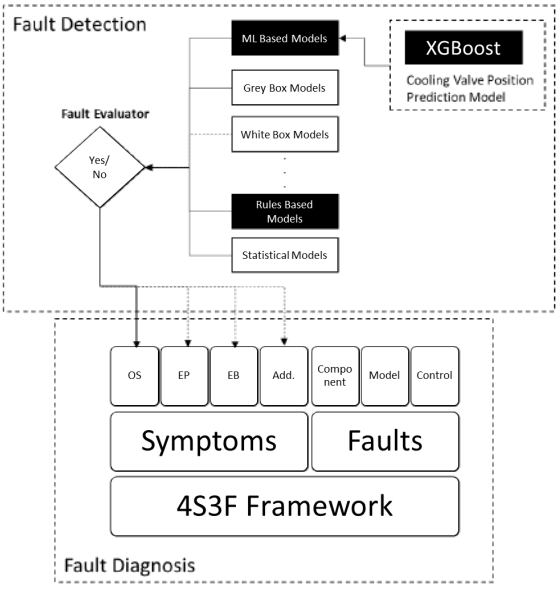

Fig. 2 - FDD Business Layer

DBN is a directed acyclic graph that encapsulates causal relationships between faults and symptoms in its structure. The DBN structure is further explained by initial beliefs mapped as prior and conditional probability tables [17]. For the faults studied, the prior probabilities are derived using literature research [10]. The conditional probabilities are derived using HVAC expert knowledge. Once, a DBN is finalized the posterior fault probabilities are inferred using the Bayes theorem. Using a sensitivity analysis authors of [18] revealed that if the probability values are reasonably set, the likely diagnosis is not affected by their magnitude.

Faults to be included for developing the initial DBN structure can be prioritized considering the impact of the fault. For AHUs, Gunay et al. in [19] surveyed over 20 years of literature for most studied faults and categorized them by their impact on energy and comfort. From this list, faults namely stuck or leak control valve, fouled or leaking duct, fouled or broken filter, stuck or complete fan failure, and inappropriate supply air setpoints are shortlisted as faults for prototyping the FDD tool. These faults have been prioritized for development considering their high energy impact.

The fault detection layer comprises a modelling layer and a fault evaluation layer. A fault is an unpermitted deviation of at least one characteristic property or feature of the system from an acceptable, usual, standard condition [20]. To realize these acceptable, usual, or standard conditions fault detection models are prepared. These fault detection models can be classified into data-driven and knowledge-driven based methods [9]. The knowledge driven-based methods in this classification are non-AI based

methods. Amongst, the data-driven based approaches regression-based approach has been utilized due to the unavailability of fault labels apriori.

For regression modelling, XGBoost is utilized given its superior performance [21]. To select relevant features for the XGBoost algorithm an iterative process is utilized beginning with a coarse feature selection process. This is followed by a wrapper-based feature selection method known as recursive feature elimination and cross-validation (RFECV). Lastly, Shapley additive explanations (SHAP) framework is invoked at the end to further drop features [22]. Minimal possible features are selected to prevent the uncertainty in sensor measurements from spilling over to the inference process.

The FDD business layer is validated by artificially introducing faults in the case study buildings discussed in section 4. For validation of the prototyped FDD tool refer to section 5.2.

3.3 FDD Tool Integration

Besides the veracity of the business logic, a robust coupling between the FDD tool and the deployed CMS is key to its usefulness. The data is acquired over an API, enabled at the server end by the project partner (see **Fig. 1**). For interfacing with remote servers, Python's *requests* package is utilized and is implemented in the data acquisition layer. Here, data is acquired over secure HTTPS. The data acquisition layer has been customized to the case-study buildings, however, it can be expanded to interface directly with on-premises servers or Internet of Things (IoT) gateways. This is the first step toward ensuring the interoperability of the designed system (see **Tab. 1**).

As the proposed tool utilizes an AI-based approach, the software architecture needs to attune to this atypical programming environment. Emmanuel Ameisen in [23] discussed how the development of ML applications at their core comprises two pipelines namely training and inference. For instance, for deploying the XGBoost fault model two data pipelines are stitched. The training pipeline starts with data acquisition over the API. Downstream, includes a key step of filtering out data for AHU's cooling mode operation. Besides, the model is trained until a satisfactory performance is achieved. Cross-validation root mean squared error (CV-RMSE) is utilized as KPI to determine the model's accuracy [24].

In the inference pipeline, data is requested over the same API and results are inferred using a saved model from the training pipeline. Given the use case, the data pipeline unfolds into two data streams. One is utilized for plotting results from the trained model for visual diagnosis and the other passes straight through to the fault evaluator (ref. **Fig. 2**) and further into the diagnosis pipeline. The training and inference pipelines for other ML models as well as the Bayesian network are designed using a similar approach. To encode the proposed DBN in Python, *pomegranate* package is utilized [25].

4. Case Study Description

For validating the prototyped FDD tool two case study buildings located in the Netherlands are utilized. In section 4.1, the first case study, a medium-sized office type building located in the city of Breda is discussed. In section 4.2, the second case study, an educational building located in Nijmegen is discussed.

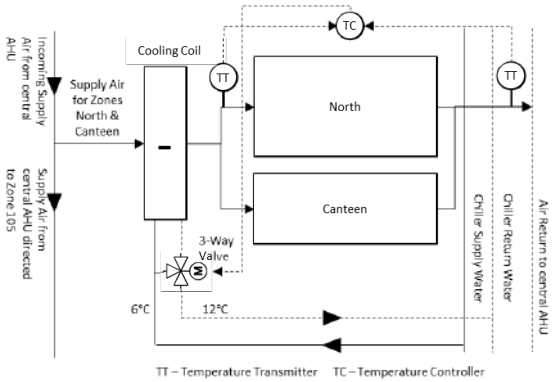

Fig. 3 - P&ID Breda office building - North and Canteen Zone

4.1 Case study 1: Breda office building

The office building was commissioned in 1993 and renovated in 2009. The heating and cooling demand for the building is fulfilled by an onsite gas boiler and electric chiller unit respectively. The central AHU supplies three centrally conditioned zones. This constant air volume (CAV) AHU contains a supply and return fan, heating coil, supply, and return filter, and heat recovery wheel (HRW).

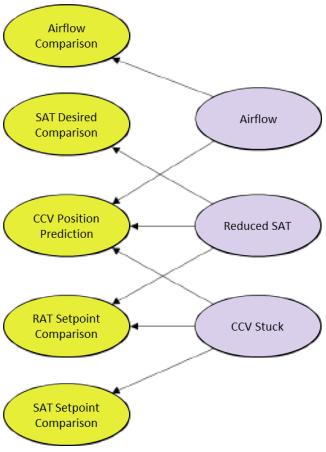

Fig. 4 - DBN Breda office building

In the air path of the AHU post supply fan, three individual cooling coils have been placed for each of the supply zones. A portion of the P&I diagram for zones North & Canteen is shown in **Fig. 3**. For this

paper, this zone and cooling operation of the AHU is considered. The design of the DBN contained in the FDD business layer emanates from this P&ID subsection. The component fault nodes are depicted in purple in the DBN shown in **Fig. 4** and are in line with the prioritized faults discussed in section 3.2. The airflow fault node is an abstraction for any upstream air side faults in components such as ducts, fans, or filters that can alter the supplied airflow to the zone. Reduced supply air temperature (SAT) and cooling coil valve (CCV) stuck nodes depict reduced setpoint and cooling coil control valve stuck faults respectively.

Tab. 2 – DBN symptom nodes and states description

#	Symptom node	Symptom state	Rules for setting the state
1	Airflow Comparison	High	F_{act}-F_{pred} >Θ
		Low	F_{act}-F_{pred}<-Θ
		Fault-free	F_{act}-F_{pred}<=Θ
2	SAT Desired Comparison	Negative	T_{set}-$T_{set,des}$<-Θ
		Fault-free	T_{set}-$T_{set,des}$<=Θ
3	CCV Prediction	Positive	X_{ccv}-$X_{ccv,pred}$>Θ
		Negative	X_{ccv}-$X_{ccv,pred}$<-Θ
		Fault-free	X_{ccv}-$X_{ccv,pred}$<=Θ
4	RAT Setpoint Comparison	Positive	T_{ra}-$T_{ra,set}$>Θ
		Negative	T_{ra}-$T_{ra,set}$<-Θ
		Fault-free	T_{ra}-$T_{ra,set}$<=Θ
5	SAT Setpoint Comparison	Positive	T_{sa}-$T_{sa,set}$>Θ
		Negative	T_{sa}-$T_{sa,set}$<-Θ
		Fault-free	T_{sa}-$T_{sa,set}$<=Θ

Key:

F - Flow Rate in m3/s, **T** - Temperature in °C, **X** - Control Position in %, **Θ** – Threshold, **act** – Actual, **pred** – Predicted, **ccv** – Cooling coil valve, **des** – Desired, **sa** – Supply air, **ra** – Return Air, **set** – Setpoint

The symptom nodes depicted in yellow in **Fig. 4** are generated using a combination of multiple modelling approaches. The rules for passing evidence to the symptom nodes are enlisted in **Tab. 2**. Airflow comparison node and CCV position prediction nodes are activated using predictions from a statistical and ML model respectively. Features selected for training the ML model are provided in **Tab. 3**.

4.2 Case study 2: Nijmegen school

The second building is a school located in Nijmegen. It was commissioned in the year 2010. The HVAC installation at the building comprises an Aquifer Thermal Energy Storage (ATES) system supported by a heat pump on the generation side. On the distribution side, two AHUs are installed. The AHUs operate with a CAV control strategy. Their supply air temperature is maintained using two-way control valves that throttle supply water through a common cooling and heating coil. In comparison with the discussed office building, here a single casing houses all of the AHU components.

Tab. 3 - XGBoost model features

Breda office building	Nijmegen school
Supply air temperature (central AHU), Chiller entering water temperature, Supply air temperature setpoint (Zone north), Supply air temperature setpoint (central AHU), Chiller leaving water temperature, Supply air pressure, Week of year	Supply water temperature (coil), Suction air temperature, Return water temperature (coil), Supply air temperature (SAT) post-HRW, SAT setpoint, Supply & Return pressure drop, Supply airflow speed, Week of year, SAT post supply fan, Return air temperature, SAT post coil, Control HRW, HRW (on/off)

As with case study 1, the operation of the AHU in its cooling mode operation is considered. The DBN for the cooling operation emanates from the P&ID of the installed HVAC system. Despite the differences in HVAC configuration between the two case studies, the DBN structure does not differ beyond the Reduced SAT fault node shown in **Fig. 4**. This alteration is required since the supply air temperature setpoint is feed-forward controlled based on the outdoor air temperature alone. In contrast at the Breda office, the zone supply air temperature setpoint is controlled using two variables return air and outdoor air temperatures. From the symptom nodes listed in **Tab. 2**, the RAT setpoint comparison node is excluded, and the rest are retained in the developed DBN for this case.

5. Designed FDD tool and its experimental validation

In this section, an early prototype of the FDD tool is presented. In section 5.1, the dashboard layout is shown. Thereafter in section 5.2, results from experimental validation of the underlying FDD business layer are discussed. Lastly in section 5.3, a savings analysis to estimate the benefit of deploying the FDD tool is presented.

5.1 FDD Tool

The developed FDD application utilizes the React.js framework in its underlying layers and is accessed using a standard web browser interface.

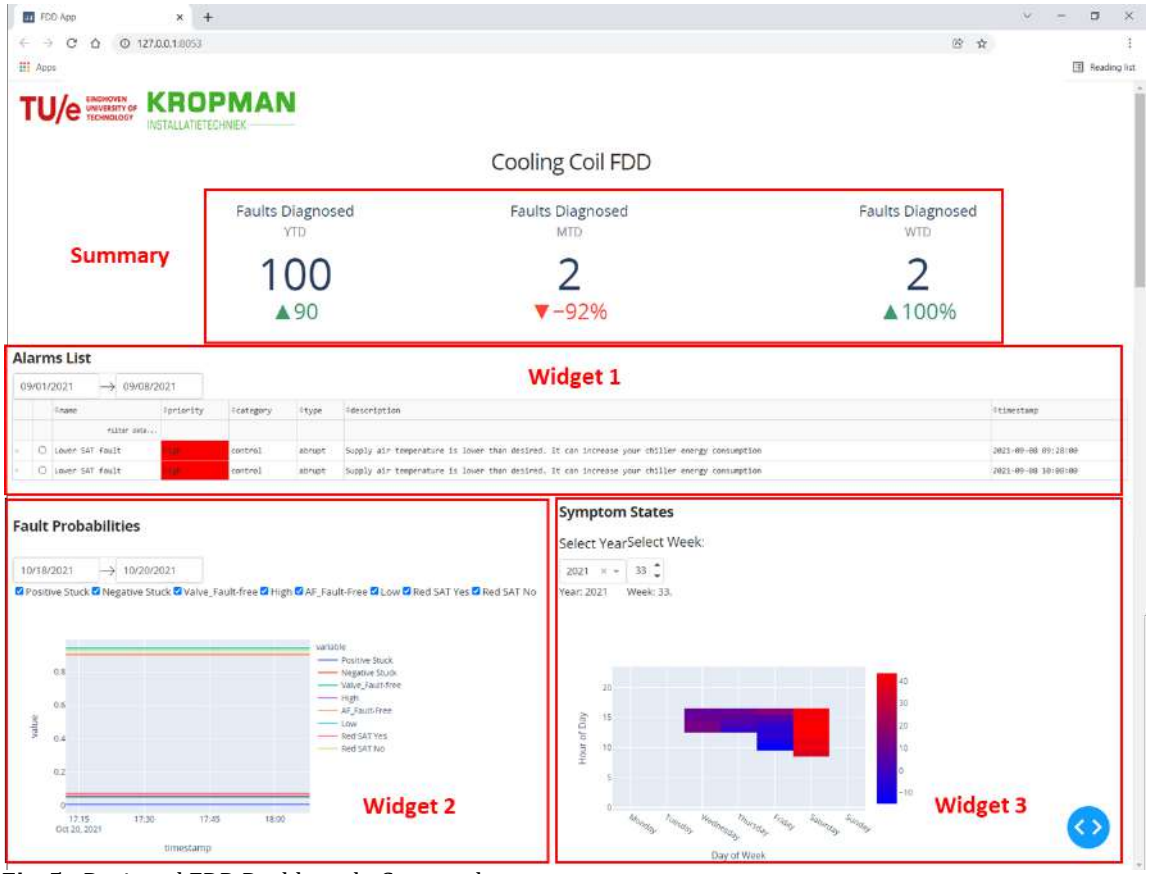

Fig. 5 - Designed FDD Dashboard - Case study one

The application is currently deployed locally, however, is extensible to a cloud environment. A dashboard for the cooling coil diagnosis at Breda with its key performance indicators are presented across multiple widgets in **Fig. 5**. The data presented in the figure is for representation purposes alone. In the *summary widget*, summary statistics describing the faults diagnosed by the FDD tool across various time horizons such as year to date (YTD) are shown. In *widget 1*, faults diagnosed by the FDD tool are presented as alarms for users. Alongside each alarm, qualitative information such as fault priority, category, type, description about the raised alarm is provided. Further, the user is equipped with filtering, searching, and sorting functionalities for an enhanced user experience. In *widget 2*, the probabilities of various fault states are plotted as time series. In *widget 3* using a heat map representation, the intensity of the residual generated using the XGBoost model can be found. *Widgets 2 & 3* have been developed to augment the capabilities of a building manager to quickly identify anomalies and aid human-in-the-loop diagnostics.

5.2 FDD Validation Results

For validating the discussed FDD business layer (see section 3.2), experiments were carried out at both buildings. During these experiments, faults were artificially introduced into the system to simulate faulty behaviour. In this paper results from introducing two faults (one in each case study) are discussed.

On 16th July 2021, an experiment was carried out and a stuck valve fault was introduced in the north zone cooling coil at Breda. The position of the three-way control valve that regulates the flow was fixed at 75% at 15:30 using a BMS override. It can be observed from **Fig. 6** that the predicted valve position deviates significantly from the measured actual valve position post introduction of this fault and generates a large residual. Also, the computed probability of the fault state (Positive Stuck) changes from a low (less than 5%) to a high likelihood (~70%) of fault presence. The user can observe this probability shift and change in residual using *widget 2* and *widget 3* respectively presented in **Fig. 5**. An alarm generated automatedly under such an event can be found in *widget 1* in **Fig. 5**.

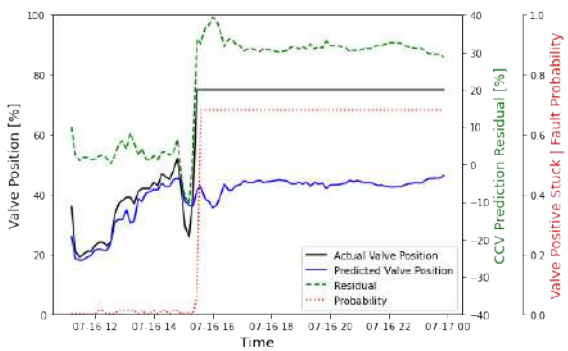

Fig. 6 - Stuck valve experiment at Breda

On 3rd August 2020, the supply air setpoint was reduced to 17°C to simulate a reduced setpoint fault

scenario at AHU one at the Nijmegen school. As can be observed from **Fig. 7** the desired setpoint given the prevailing outdoor air temperature should have neared 21°C under a normal scenario. However, the automated setpoint determining logic was manually overwritten in the BMS to introduce this fault. The designed DBN was able to confirm (with more than 85% likelihood) this fault when a large positive residual is observed on the valve position prediction state.

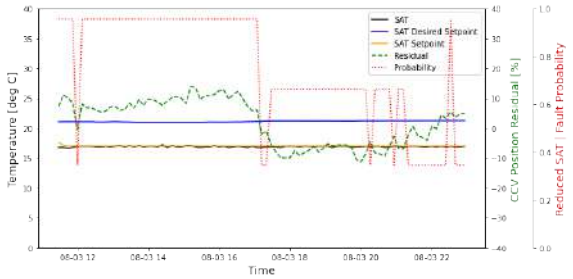

Fig. 7 - SAT setpoint experiment at Nijmegen

Besides the reported experiments additional experiments spread over nearly two months were carried out to validate the prototyped tool across multiple faults scenarios at both locations. During this period, diagnosis sensitivity of 67% and specificity of 92% were recorded at the Breda office. At Nijmegen school diagnosis sensitivity of 84% and specificity of 94% were observed. The realized results validate the veracity of the developed FDD business layer for both locations.

5.3 Potential Savings: Breda office building

Through the validation process faults introduced in the system were successfully diagnosed with the tool. Using the case presented in **Fig. 6**, preventable energy waste is estimated. The fault was introduced late Friday afternoon and corrected the following Monday. The chiller's energy consumption between the periods 16:00-17:00 was compared on both days to estimate the energy savings. Using an energy meter, a 63% increase in the chiller's energy consumption was measured during the faulty operation. As faults were simultaneously introduced in all cooling coil control valves, the measured increase is apportioned in the ratio of airflow through each zone. Using this approach, nearly a 33% increase in the chiller's energy consumption is estimated as attributable to the stuck valve fault in the north zone's cooling coil control valve.

6. Conclusion

An early prototype of the proposed FDD tool along with its design architecture is presented. Further, integration with an operational CMS is demonstrated for two case study buildings. The business layer of the tool combines state-of-the-art techniques from the AI domain and automates the FDD process. The designed tool is scalable, reliable, rapidly deployable, and interoperable. DBN structure and modelling processes are scaled for both the studied cases possessing different HVAC characteristics. Hence, alluding to generalizability.

Upon experimentally validating the designed tool, encouraging results (diagnosis specificity exceeding 90%) across two use-case environments are obtained. The continuous monitoring setup at these installations can be augmented with the prototyped tool and energy penalties due to faults can be avoided. At the cooling coil installation at Breda, nearly 33% of energy savings are estimated, and consequent additional emissions are thus preventable.

For further development of the tool following areas have been identified:

- The presented tool does not feature any framework for uniformly identifying building metadata such as Project Haystack or Brick Schema, which is highly desirable for addressing large scale deployments.
- Currently, the DBN model doesn't exhibit any learning character which can be improved by updating conditional probabilities dynamically.

7. Acknowledgement

The research work is funded by the TKI Urban Energy project 'Continuous commissioning of lowdT'; and the Eindhoven Engine project 'CM-HVACFDD'. The work is also supported by Kropman Installatietechniek. Special thanks to Joris de Ruiter, Jan-Willem Dubbeldam, John Verlaan, and Roel Vos at Kropman for facilitating the experiments, data collection and software integration process.

8. References

[1] IEA. Tracking Buildings 2020. Paris; 2020.

[2] Kim W, Katipamula S. A review of fault detection and diagnostics methods for building systems. Science and Technology for the Built Environment. 2018 Jan 2;24(1):3–21.

[3] Shi Z, O'Brien W. Development and implementation of automated fault detection and diagnostics for building systems: A review. Vol. 104, Automation in Construction. Elsevier B.V.; 2019. p. 215–29.

[4] Lin G, Kramer H, Granderson J. Building fault detection and diagnostics: Achieved savings, and methods to evaluate algorithm performance. Building and Environment. 2020 Jan 15;168:106505.

[5] Granderson J, Singla R, Mayhorn E, Ehrlich P, Vrabie D, Frank S. Characterization and Survey of Automated Fault Detection and Diagnostics Tools | Energy Technologies Area [Internet]. 2017 [cited 2021 Mar 16]. Available from: https://eta.lbl.gov/publications/characterization-survey-automated

[6] Bruton K, Raftery P, O'Donovan P, Aughney N, Keane MM, O'Sullivan DTJ. Development and

alpha testing of a cloud-based automated fault detection and diagnosis tool for Air Handling Units. Automation in Construction. 2014 Apr 1;39:70–83.

[7] Schein J, Bushby ST, Castro NS, House JM. A rule-based fault detection method for air handling units. Energy and Buildings. 2006 Dec 1;38(12):1485–92.

[8] Zhao Y, Li T, Zhang X, Zhang C. Artificial intelligence-based fault detection and diagnosis methods for building energy systems: Advantages, challenges and the future. Vol. 109, Renewable and Sustainable Energy Reviews. Elsevier Ltd; 2019. p. 85–101.

[9] Taal A, Itard L. P&ID-based symptom detection for automated energy performance diagnosis in HVAC systems. Automation in Construction. 2020 Nov 1;119:103344.

[10] Zhao Y, Wen J, Wang S. Diagnostic Bayesian networks for diagnosing air handling units faults – Part II: Faults in coils and sensors. Applied Thermal Engineering. 2015 Nov 5;90:145–57.

[11] Xiao F, Zhao Y, Wen J, Wang S. Bayesian network based FDD strategy for variable air volume terminals. Automation in Construction. 2014 May 1;41:106–18.

[12] Fan C, Liu X, Xue P, Wang J. Statistical characterization of semi-supervised neural networks for fault detection and diagnosis of air handling units. Energy and Buildings. 2021 Mar 1;234:110733.

[13] Granderson J, Lin G, Singla R, Mayhorn E, Ehrlich P, Vrabie D, et al. Commercial Fault Detection and Diagnostics Tools: What They Offer, How They Differ, and What's Still Needed. 2021 Jun 28 [cited 2021 Oct 19]; Available from: https://escholarship.org/uc/item/4j72k57p

[14] Yu Y, Woradechjumroen D, Yu D. A review of fault detection and diagnosis methodologies on air-handling units. Vol. 82, Energy and Buildings. Elsevier Ltd; 2014. p. 550–62.

[15] Zeiler W. Basisboek Ontwerpen. Noordhoff Publishers; 2014.

[16] Taal A, Itard L, Zeiler W. A reference architecture for the integration of automated energy performance fault diagnosis into HVAC systems. Energy and Buildings. 2018 Nov 15;179:144–55.

[17] Chen T, Guestrin C. XGBoost: A Scalable Tree Boosting System. Proceedings of the ACM SIGKDD International Conference on Knowledge Discovery and Data Mining [Internet]. 2016 Mar 9 [cited 2021 Aug 19];13-17-August-2016:785–94. Available from: https://arxiv.org/abs/1603.02754v3

[18] Hu M, Chen H, Shen L, Li G, Guo Y, Li H, et al. A machine learning bayesian network for refrigerant charge faults of variable refrigerant flow air conditioning system. Energy and Buildings. 2018 Jan 1;158:668–76.

[19] Taal A, Itard L. Fault detection and diagnosis for indoor air quality in DCV systems: Application of 4S3F method and effects of DBN probabilities. Building and Environment. 2020 May 1;174:106632.

[20] Gunay B, Shen W, Yang C. Characterization of a Building's operation using automation data: A review and case study. Vol. 118, Building and Environment. Elsevier Ltd; 2017. p. 196–210.

[21] Isermann R. Fault-diagnosis systems: An introduction from fault detection to fault tolerance. Fault-Diagnosis Systems: An Introduction from Fault Detection to Fault Tolerance. Springer Berlin Heidelberg; 2006. 1–475.

[22] Miller C, Arjunan P, Kathirgamanathan A, Fu C, Roth J, Park JY, et al. The ASHRAE Great Energy Predictor III competition: Overview and results. Science and Technology for the Built Environment [Internet]. 2020;26(10):1427–47. Available from: https://doi.org/10.1080/23744731.2020.1795514

[23] Lundberg SM, Lee S-I. A Unified Approach to Interpreting Model Predictions. In: I. Guyon, U. V. Luxburg, S. Bengio, H. Wallach, R. Fergus, S. Vishwanathan, et al., editors. Advances in Neural Information Processing Systems 30 [Internet]. Curran Associates, Inc.; 2017 [cited 2021 Nov 26]. p. 4765–74. Available from: http://papers.nips.cc/paper/7062-a-unified-approach-to-interpreting-model-predictions.pdf

[24] Ameisen E. Building Machine Learning Powered Applications. O'Reilly UK Ltd.; 2020. 250.

[25] Walker S, Khan W, Katic K, Maassen W, Zeiler W. Accuracy of different machine learning algorithms and added-value of predicting aggregated-level energy performance of commercial buildings. Energy and Buildings. 2020 Feb 15;209:109705.

[26] Schreiber J. Pomegranate: fast and flexible probabilistic modeling in python. 2017 Oct 31;

Data Statement

The datasets generated during and/or analysed during the current study are not publicly available because they are provided by a company and has to be kept private owing to privacy and security concerns but are/will be available if the concerned parties contact us and explain the reason for the data requirement. However, the final decision lies with the company and access cannot always be guaranteed.

Interoperability of semantically heterogeneous digital twins through Natural Language Processing methods

Alina Cartus [a], Maximilian Both [a*], Nicolai Maisch [a], Jochen Müller [a], Christian Diedrich [b]*

*First Authors

[a] Institute of Building Services Engineering, TH Köln, University of Applied Sciences, Cologne, Germany, {acartus; maximilian_alexander.both; nicolai.maisch; jochen.mueller}@th-koeln.de.

[b] Institute of Automation Technology, Otto von Guericke University Magdeburg, Magdeburg, Germany, christian.diedrich@ovgu.de.

Abstract. Self-organizing systems represent the next stage in the development of automation technology. For being able to interact with each other in an interoperable manner, it requires a uniform digital representation of the system's components, in the form of digital twins. In addition, the digital twins must be semantically interoperable in order to realize interoperability without the need for costly engineering in advance. For this purpose, the current research approach focuses on a semantically homogeneous language space. Due to the multitude of actors within an automation network, the agreement on a single semantic standard seems unlikely. Different standards and vendor-specific descriptions of asset information will continue to exist. This paper presents a method extending the homogeneous semantics approach to heterogeneous semantics. For this purpose, a translation mechanism is designed. The mapping of unknown vocabularies to a target vocabulary enables the interactions of semantically heterogeneous digital twins. The mapping is based on methods from the artifcial intelligence domain, specifically machine learning and natural language processing. Semantic attributes (name, definition) as well as further classifying attributes (unit, data type, qualifier, category, submodel element subtype) of the digital twins' attributes are used therefore. For the mapping of the semantic attributes pre-trained language models on domain specific texts and sentence embeddings are combined. A decision tree classifies the other attributes. Different semantics for submodels of pumps and HVAC systems are used as the evaluation dataset. The combination of the classification of the attributes (decision tree) and the subsequent semantic matching (language model), leads to a significant increase in accuracy compared to previous studies.

Keywords. Semantic interoperability, Natural Language Processing, Decision Tree, Asset Administration Shell
DOI: https://doi.org/10.34641/clima.2022.143

1. Introduction

The change to self-organizing systems is shaping the next development stage of automation technology. In automation technology, the digital, global networking of systems with self-x capabilities is being pushed. Self-x capabilities are understood as functionalities of a system that enable intrinsic automatisms for network exploration, self-configuration, -diagnosis and -optimization. Self-x capabilities of systems enable interoperability and automation based on it. Interoperability means that systems actively collaborate across specific product, system, and process boundaries to meet common functional fulfillments [1, 2]. If this cooperation is automated, manual configuration and control efforts are reduced and result in an optimization of the value chain.

If interoperability is guaranteed for systems of technical building equipment (TBE), a self-configuration of interactions (e.g. the integration of energy values into a monitoring application) can be realized by means of automatically executable rules and engineering efforts can be avoided or essentially reduced. A prerequisite for the interoperability of systems is their digital, uniform representation, as well as the guarantee of semantic interoperability (SI) of the systems. SI refers to the ability to correctly exchange data among themselves and to understand what they mean [3].

Copyright ©2022 by the authors. This conference paper is published under a CC-BY-4.0 license.

To achieve SI, the current research approach focuses on semantically homogeneous descriptions of systems [2, 4]. This homogeneity comes from standardization and harmonization activities of information for different components of industry and TBE (e.g. [5–8]). If, for example, properties for the power consumption of different components are based on a uniform vocabulary, they can be automatically integrated into a monitoring application (Figure 1) [9].

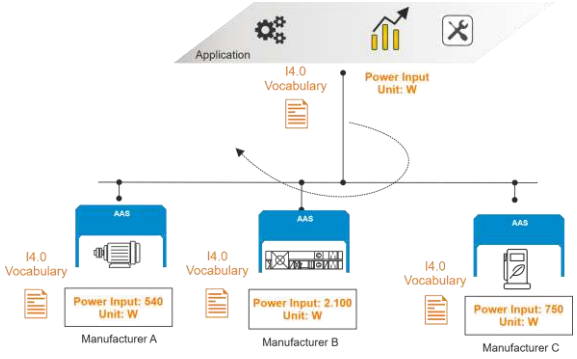

Fig. 1 – Semantically homogeneous AAS

However, if systems are based on heterogeneous vocabularies, interactions must be configured through manual effort and expert knowledge. This is the current state of the art for the majority of industrial and building applications. Because of the effort involved, operators carefully weigh the implementation of multi-vendor applications, such as plant asset management applications, against their benefits. The high configuration effort stands in the way of the wide availability of these applications. [10]

This paper contributes to extending the research approach from interactions of semantically homogeneous to heterogeneous systems. The interoperability of semantically heterogeneous systems can be achieved by mapping heterogeneous descriptions, to the, underlying semantic standard of the respective components. This paper presents the method of automated matching, which allows systems to map semantically heterogeneous descriptions to their own standard independently and without configuration (Figure 2).

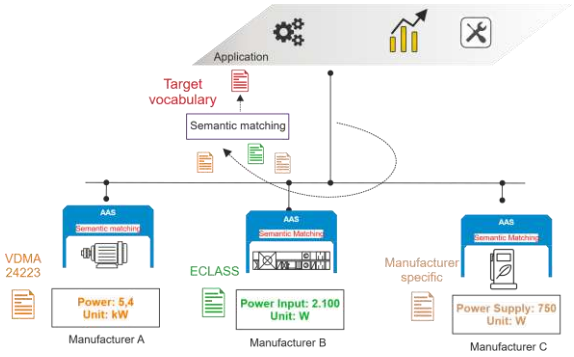

Fig. 2 – Semantically heterogeneous AAS

The starting point for matching is the information from the digital representations of the components. These are available in a uniform structure, but do not follow a semantically uniform standard. Methods from Natural Language Processing (NLP) [11] serve as the basis for matching semantic attributes.

In a first draft [12] the semantic attributes "name" and "definition" of heterogeneously labeled pump properties from the project [8] were used for automated matching. The mapping of heterogeneous semantics to a defined target vocabulary was achieved using a pretrained language model (PLM). For technical language understanding, extended pretraining of the PLM was performed with technical literature (Step 1, Figure 3). Combined with sentence embeddings (SeEm), the PLM was then refined on general paraphrase identification (PI) datasets to learn the matching task (Step 2, Figure 3). [12]

In this paper, the extended pretraining (Step 1, Figure 3) is considered on additional domain-specific literature. In addition, the evaluation dataset is extended to include properties from air handling units (Step 3, Figure 3). However, the focus of the extension of the first model design from [12] is the integration of meta-information of the properties as complementary parameters for a previous classification of the properties (Steps I-II, Figure 3).

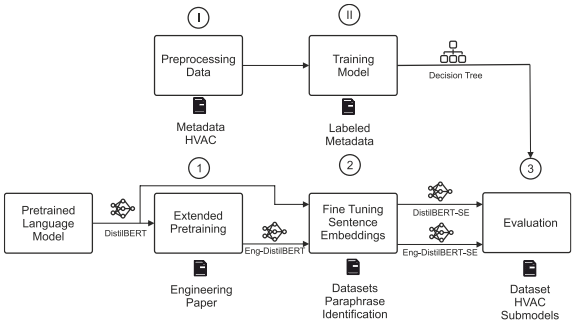

Fig. 3 – Training process

2. Background

Interoperability is a central pillar in the efforts to transform systems of automation technology into self-organizing systems [2]. It requires a digital representation of systems and the structured provision of their information. SI is required for mutual understanding of the information.

2.1 The Asset Administration Shell

For the digital representation of technical components, different concepts like [13] or [14] have been established in the technical domain. In this paper, we build on the concept of the asset administration shell [14] (AAS) as the digital representative of an asset. In this respect an asset can be understood as any entity (physical or logical) being of value to an enterprise [15]. The AAS originates from the field of Industrie 4.0 (I4.0), but can also be used for the digitalization of TBE. The

composition of asset and AAS is referred to as an I4.0-component [14].

A prerequisite for the automated exchange of information is the representation of all component information in standardized digital form within an AAS. This is realized by structuring the content into standardized submodels, which represent topics such as identification, design and configuration[14]. In the submodels, associated properties and functionalities of the asset are represented as submodel elements (SEs). SEs inherit mandatory and optional meta-level attributes from higher-level classes (Figure 4) [14].

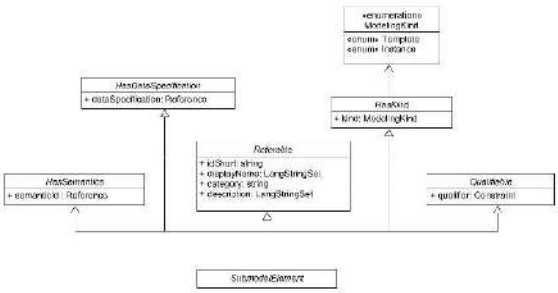

Fig. 4 - Class of the SE with its superordinate classes (own representation based on [14])

The class HasSemantics prescribes, for example, the mandatory definition of a SemanticID, which references a semantic definition of the SE. Further is the data type and the definition of the SE derivable as mandatory information from the class HasDataSpecification. [14]

2.2 Semantic Interoperability with homogenous semantics

To ensure interoperability according to the I4.0 research approach, the contents of the submodels must be standardized. Various initiatives standardize submodels for industrial components, e.g. pumps or drives[5, 8].

In addition to the uniform structure of the submodel contents by the information model, a uniform semantic language understanding of the information is required for the interoperable interaction of I4.0 components [4]. The integration of the submodels into dictionaries such as the ECLASS standard [16] enables the unambiguous identification of the submodels, as well as their SE, thus paving the way for homogeneous semantics.

Accordingly, the I4.0 approach requires a uniform structure (information model management shell) and semantics (homogeneous language space) to achieve interoperability. [14] Heterogeneous language spaces, i.e. language spaces that are not captured in standardized dictionaries, such as those available in manufacturer-specific descriptions, are not captured in the current I4.0 approach.

2.3 Semantic Interoperability with heterogeneous semantics

To achieve SI, it is possible to map heterogeneous semantics to each other in addition to using a uniform language space. This can be done either by semantically unique links to each other (Linked Data) or by automated matching.

Linked Data describes the use of ontologies to semantically describe entities. Ontologies represent knowledge structurally in machine-readable format. By using standardized ontological markup languages, entities of different ontologies can be linked together, creating a semantic network, e.g. [17]. In the context of I4.0, linking allows the recognition of SEs' semantics of one AAS by other AASs. The use of Linked Data in the technical domain requires knowledge of different ontologies and the creation of links between entities. In a comprehensive I4.0 value network, a large number of domain-specific ontologies of different components can be expected. Linking these requires a high level of analysis and engineering effort [18]. This complicates the use of Linked Data models.

Automated matching is another mapping possibility. This is pursued in this paper. The method used here is based on concepts of NLP and enables configuration-free translation of vocabularies. It requires neither a common semantic standard nor a manual linking of heterogeneous language spaces.

NLP is a subfield of artificial intelligence that enables computers to understand natural language (textual and phonetic) in order to perform tasks/actions based on it [11]. State of the art NLP models are based on the transformer architecture [19]. It is characterized by an encoder-decoder structure. The encoder is used for speech analysis and classification and the decoder for speech generation tasks. To cover more specific requirements in the areas of classification or generation, current models are usually characterized by either an encoder (e.g. [20]) or decoder structure (e.g. [21]). The model architecture for the semantic matching developed within this paper is based on an encoder architecture.

The training of current LMs is divided into pretraining and finetuning [22]. First, LM are pre-trained on large amounts of text and thus already learn a general understanding of the language. Based on this understanding, LM are adapted to specific tasks in a second training (finetuning) [23]. LM's language understanding is based on the representation of words in vectorized form, the word embeddings (WE). These WE are adapted during pretraining with different texts to represent the semantic meaning and relationships of the words. Thus, they are already capable of recognizing similarities or relationships, e.g., whether a word pair like Berlin and Germany has the same relationship as Madrid and Spain. In finetuning, the

WE are refined with specific data sets of a concrete use case. For automated matching of heterogeneous descriptions, this paper builds on the PLM DistilBERT [24].

2.4 The ISO-DistilBERT-SE Model

The general DistilBERT model was pretrained on English literature in the form of the BooksCorpus [25] and English Wikipedia [24]. Research shows that PLMs for domain-specific use cases achieve better results with a second phase of pretraining on specific literature [26]. Therefore, DistilBERT was extended with training on ISO standards [27–33] to form the ISO-DistilBERT model (Step 1, Figure 3) [12].

Subsequently, the model was used to be refined into ISO-DistilBERT-SE using data sets from the PI domain (Step 2, Figure 3). PI refers to the ability of a model to detect whether two sentences have the same meaning [34]. Here, the methodology of the Sentence BERT [35] model is adapted. The WE are combined into a Sentence Embedding (SeEm) with fixed dimension. Using cosine similarity, it is possible to check whether the SeEm of two sentences are similar and thus determine whether they are paraphrases [35]. The datasets used are the general datasets MultiNLI [36], STS-Benchmark [37] and QQP [38].

The model was then evaluated on a dataset created for this purpose (Step 3, Figure 3). For the ISO-DistilBERT-SE model, this dataset contains different definitions and names for SEs from the pump identification and design domain.

The ISO-DistilBERT-SE model achieves an accuracy of 94.33%. This shows that the use of the SeEm is an effective method to determine the similarity of SE based on the name and definition. Furthermore, an increase in accuracy of 2.46 percentage points was achieved by the extended pretraining [12].

3. Extension of the Semantic Matching Model

In order to be able to use the model in concrete application scenarios, such as extensive plant asset management, the evaluation dataset will be extended to include additional SEs and associated paraphrases from the field of air handling system (AHs) technology. In addition, the following model developments will be made: More domain-specific literature will be added to the extended pretraining. Metadata will be integrated as a classification feature to increase the accuracy of the model.

3.1 Extension of the evaluation data

The data set for the evaluation of the model is extended from SE of pumps to SE of an entire air handling system. Each component of the AHS, as well as the AHS as a whole, have up to twelve submodels, which are divided into the topics identification, design, maintenance, control, etc. [8] In total, the target vocabulary is thus extended from a pump's 39 SE to 427 SE of an AHS. For each SE, up to eleven paraphrases consisting of name and definition are created. Thus, a total of 1052 paraphrases for the 427 SEs of the target vocabulary are available for the evaluation of the model. The model is tested to match any name and definition of a SE from the paraphrase dataset to the matching SE of the 427 possible SEs in the target vocabulary. The larger the target vocabulary, the more difficult it is for the model to predict the matching SE of the target vocabulary from the possible SEs.

3.2 Extended pretraining on domain-specific literature

The extended pretraining from DistilBERT to ISO-DistilBERT is based on ISO standards [12]. This is complemented with another dataset on Eng-DistilBERT. The dataset includes 81.1M academic English papers from several disciplines [39]. These were filtered by engineering discipline, leaving 228,000 papers for the extended pretraining. Thus, the model learns complementary, subject-specific vocabulary of the engineering domain. The pre-trained model Eng-DistilBERT is then refined to the PI task following the presented procedure in [12] with the creation of SeEm. The refined model is referred to as Eng-DistilBERT-SE.

3.3 Extension of the model through metadata classification

The fault evaluation of the automated matching from [12] shows that errors occur mainly because different SE are often designated and defined very similarly. For example, there are several similarly defined pressure limits for a pump. For a more precise delimitation of the SEs among each other, a classification performed in advance is introduced in this paper. This is based on additional attributes, the metadata of the SE. Pressure limit values, which differ e.g., only by the time of their definition (definition during manufacturing vs. planning), can be distinguished from each other by an appropriate meta information and thus do no longer qualify as mutual paraphrase.

The first step is to select the metadata categories according to which a classifying algorithm delimits the SEs from each other. Since the whole model is based on the AAS information model, the metadata defined there are used for SE. The first metadata category *AAS_Spec* distinguishes the SE into the different subclasses property, file or SE collection. The properties, representing the majority of the SE, are further differentiated by the meta information of the *category* from the class Referable (Figure 4) according to the attribute Variable, Parameter or Constant. From the HasDataSpecification class (Figure 4), the *data type* and *unit* of an SE are taken as metadata categories. The *qualifier* according to

[41] is included as the last metadata to differentiate SEs according to their lifecycle status. The metadata selection is tailored to the present AHU plant evaluation dataset in order to characterize the existing SEs according to the most meaningful metadata possible. For this purpose, the metadata categories with their expressions in every possible combination are elaborated and labeled for a classification algorithm (Table 1). Since not all meta information is mandatory according to [14] and [41] e.g. the case that no qualifier is defined for an SE is also considered as a possible combination.

Tab. 1 – Label of possible metadata combinations

AAS_ Spec	Qualifier	Category	Unit_ Categ	Meta-label
File	OP	-	-	1
File	-	-	-	1|2
File	SUP	-	-	2

Thus, an SE can be labeled based on its metadata. The task of automated labeling places a multi-class requirement on a classification algorithm. For this purpose, a decision tree (DT) is trained according to [42] , which forms a structure of as few goal-directed decision paths as possible from the data set of possible metadata specifications in order to classify the data effectively. The points on a path where the next data decomposition is decided are called nodes. The tree structure of the "Decision Tree Classifier" according to [42] prescribes the maximum formation of two classes per node. Thus, questions are asked in a node, which can be answered binary with yes or no. The structure of the DT and the formation of the next node is determined automatically according to the best Gini-Impurity [42] calculation of the algorithm. The data basis of the DT are the possible metadata combinations and associated labels to be predicted (excerpt in Table 1). Figure 5 shows a section of the decision tree created.

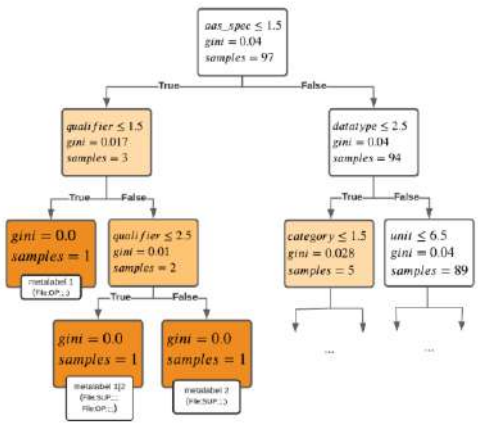

Fig. 5 - Detail of the decision tree

The metric used to evaluate the model is accuracy.

$$accuracy = \frac{correct\ predictions}{all\ predictions}$$

Training the DT on possible metadata combinations achieves 100% accuracy.

3.4 Combination of the Classifier and the LM Eng-DistilBERT-SE

The processing of the metadata of an SE is used for pre-filtering, indicating which SE of the target vocabulary should be reasonably used for comparison, in order to find the correct paraphrase. Thus, the SEs of the target vocabulary that cannot represent a paraphrase due to different metadata are dropped. By reducing the number of possible paraphrases, the probability of a wrong assignment is minimized.

Both the LM Eng-DistilBERT-SE and the DT are trained separately on their task to be solved. Eng-DistilBERT-SE processes the semantic information of an SE. The DT assigns one or more possible metadata classes to the SE. In Semantic Matching (SM), first, the SeEms and the metadata class(es) of the SE in the target vocabulary are formed and the information is linked. For unique identification, the SEs of the target vocabulary are indexed. In the use case, an unknown SE is labeled with metadata class(es) and then receives the indices of the SEs of the target vocabulary that qualify as paraphrases based on their metadata class. The LM Eng-DistilBERT-SE then compares the SeEm of the SE only with the SeEm of the SE that is in the indexed selection(Figure 6).

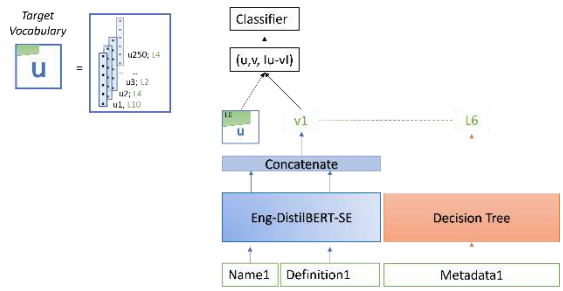

Fig. 6 - Advanced model MetaEng-DistilBERT-SE

Thus, the additional information of the metadata class(es) acts as a filter for the PI of the LM. The fused model is called MetaEng-DistilBERT-SE.

4. Evaluation

Table 2 presents the results of the different models on the newly created evaluation dataset. Increasing the target vocabulary from 39 to 427 decreases the accuracy of the original DistilBERT-SE model from 94% to 64.7%. The improvement of the accuracy by 2.3 percentage points of the model ISO-DistilBERT-SE to DistilBERT-SE in [12] already showed that pretraining with technical literature is promising. This is confirmed by the renewed increase in accuracy by another 2.5 percentage points by adding

engineering papers to the pretraining (Eng-DistilBERT-SE).

Using the integrated metadata model, the MetaEng-DistilBERT-SE model achieves an increase in accuracy of another 16.3 percentage points in the PI of SE task. This confirms the positive effect of classification by metadata in parallel with the processing of semantic information from SE to PI.

Tab. 2 - Semantic Matching results

Model version	Accuracy
DistilBERT-SE	64.7%
ISO-DistilBERT-SE	67.0%
Eng-DistilBERT-SE	69.5%
MetaEng-DistilBERT-SE	85.8%

Table 3 shows the influence of each metadata category on the model's output.

Tab. 3 - Analysis of different variants of the metadata model MetaEng-DistilBERT-SE

MetaEng-DistilBERT-SE	Acc
w/all Metadata	85.8%
w/o AAS_Spec	85.7%
w/o Datatype	85.6%
w/o Qualifier	85.4%
w/o Unit	79.9%
w/o Category	68.8%

The greatest influence on the model is the classification of the data according to the meta information of *category*. It differentiates SEs from each other by distinguishing variable from parameterized and constant values. This not only helps to distinguish measured values from nominal values, but also covers life cycle status. Values defined by the manufacturer in the design phase are defined as constant. In contrast, the designer's specifications are classified as parameters, and operational values are classified as variable. One of the main sources of error in the Eng-DistilBERT-SE model was the distinction between similarly defined features that differ only in their life cycle status. Therefore, solving this problem by defining the *category* is particularly influential on overall performance. Since the *qualifier* is only optionally present in the data, it has less significance as a category than the compulsorily defined *category* of the SEs. The *unit* category helps to differentiate measurement values among themselves whose metadata are not distinguished from each other by the other categories. The omission of one of the metadata categories *data type* and *AAS_Spec* exerts little influence on the model since the remaining categories of the SE already unambiguously determine the metadata class in the respective version. A constant SE of the dataset is e.g., in 98.5 % of the cases a SE of the datatype String or Real. Without specification of the data type these two classes are nevertheless distinguished by the specification of the *unit* with physical SE. Overall, the influence of individual categories for the classification of SE depends on the available data distribution. However, the clear improvement of the PLM can be statued by the inclusion of a metadata classification.

5. Conclusions

The results extend the current I4.0 research approach to the interaction of semantically homogeneous to semantically heterogeneous AAS. For this purpose, a combination of LMs, for mapping heterogeneous semantics, and a DT, for prior classification of the SE, was used. The results show that classification by the DT produces a significant increase in accuracy (70 to 86%). However, this needs to be further increased for acceptance in practice. For this purpose, other methods from the NLP field are applied to investigate how the accuracy can be increased. In addition, the information model of the AAS will be analyzed with respect to further metadata that can be used for classification.

Besides improving the model, it will be prototypically implemented as an I4.0 service in an I4.0 environment [43]. For this purpose, an I4.0 interface is specified that can be used within AAS to implement an SM service. The results are fed into relevant specification work to extend the interaction manager of AAS with an SM service.

The datasets generated during the current study are available in the Labor GART repository, https://github.com/thcologne-gart

6. Acknowledgement

The authors gratefully acknowledge financial support from the KSB Foundation in the project Automatic interaction of semantically heterogeneous Industrie 4.0 Asset Administration Shells by means of generic translation mechanisms based on methods of Natural Language Processing (1.1359.2020.1).

References

[1] Federal Ministry for Economic Affairs and Energy (BMWi). 2030 Vision for Industrie 4.0: Shaping Digital Ecosystems Globally; October 2019.

[2] Federal Ministry for Economic Affairs and Energy (BMWi). Position Paper: Interoperability – Our vision for Industrie 4.0: Interoperable communication between machines within networked digital ecosystems;

November 2019.
[3] International Electrotechnical Commission. Semantic Interoperability: Challenges in the digital Transformation Age: IEC Whitepaper 2019.
[4] VDI. Language for I4.0 components: Structure of messages. VDI/VDE-Gesellschaft Mess- und Automatisierungstechnik (GMA); 2020 04.2020.
[5] ZVEI - Zentralverband Elektrotechnik und Elektronikindustrie e. V. Antrieb 4.0 – Vision wird Realität: Merkmale, Daten und Funktionen elektrischer Antriebssysteme in Industrie 4.0 für Hersteller, Maschinenbauer und Betreiber; November 2018.
[6] DIN, DKE, STANDARDIZATION COUNCIL INDUSTRIE 4.0. Deutsche Normungsroadmap Industrie 4.0: Version 4; März 2020.
[7] Federal Ministry for Economic Affairs and Energy (BMWi). Submodel Templates of the Asset Administration Shell: ZVEI Digital Nameplate for industrial equipment (Version 1.0); November 2020.
[8] Both M, Müller J. Digitization of pumps – Industry 4.0 submodels for liquid and vacuum pumps. 4th International Rotating Equipment Conference 2019.
[9] Ostermeier M, Maisch N, Both M, Ulmer R, Müller J. BIM im Betrieb durch lebenszyklusübergreifende Verfügbarkeit von Anlagendaten auf Basis von I4.0-Verwaltungsschalen. In: Automation 2021. VDI Verlag 2021; 131–40.
[10] Clemens Rohde, Patrick Plötz, Lisa Nabitz, *et al.* Branchen- und unternehmensgrößenbezogene Ermittlung von Klimaschutzpotenzialen (Schwerpunkt KMU) durch verstärkte Umsetzung von Energiemanagementmaßnahmen in der Wirtschaft: Abschlussbericht; 2018.
[11] Jurafsky D, Martin JH. Speech and language processing: An introduction to natural language processing, computational linguistics, and speech recognition. 2. ed., Pearson internat. ed. Upper Saddle River, NJ: Prentice Hall Pearson Education Internat 2009.
[12] Both M, Müller J, Diedrich C. Automatisierte Abbildung semantisch heterogener I4.0-Verwaltungsschalen durch Methoden des Natural Language Processing. at - Automatisierungstechnik 2021; 69(11): 940–51 [https://doi.org/10.1515/auto-2021-0050]
[13] Kaebisch et al. Web of Things (WoT) Thing Description; 2020 [cited 2021 November 13] Available from: URL: https://www.w3.org/TR/wot-thing-description/.
[14] Federal Ministry for Economic Affairs and Energy (BMWi). Details of the Asset Administration Shell: Part 1 - The exchange of information between partners in the value chain of Industrie 4.0 (Version 2.0.1). Berlin; May 2020.
[15] VDI/VDE-Gesellschaft. Industrie 4.0 Begriffe/Terms: VDI Statusreport; April 2019.
[16] ECLASS. ECLASS - Standard für Stammdaten und Semantik für die Digitalisierung [cited 2020 November 17] Available from: URL: https://www.eclass.eu/index.html.
[17] Linked Open Data Cloud. The Linked Open Data Cloud [cited 2020 November 16] Available from: URL: https://lod-cloud.net/.
[18] Automated Ontology Matching in the Architecture, Engineering and Construction Domain - A Case Study. Schneider, Georg. The 7th Linked Data in Architecture and Construction Workshop 2019.
[19] Vaswani A, Shazeer N, Parmar N, *et al.* Attention Is All You Need; 2017 Jun 12.
[20] Devlin J, Chang M-W, Lee K, Toutanova K. BERT: Pre-training of Deep Bidirectional Transformers for Language Understanding; 2018 Oct 11.
[21] Radford A, Wu J, Child R, Luan D, Amodei D, Sutskever I. Language Models are Unsupervised Multitask Learners Alec; 2019.
[22] Ruder S, Peters ME, Swayamdipta S, Wolf T. Transfer Learning in Natural Language Processing. In: Sarkar A, Strube M, editors. Transfer Learning in Natural Language Processing. Stroudsburg, PA, USA: Association for Computational Linguistics; 15–8.
[23] Peters ME, Ruder S, Smith NA. To Tune or Not to Tune? Adapting Pretrained Representations to Diverse Tasks; 2019 Mar 14.
[24] Sanh V, Debut L, Chaumond J, Wolf T. DistilBERT, a distilled version of BERT: smaller, faster, cheaper and lighter; 2019 Oct 2.
[25] Zhu Y, Kiros R, Zemel R, *et al.* Aligning Books and Movies: Towards Story-like Visual Explanations by Watching Movies and Reading Books; 2015 Jun 22.
[26] Gururangan S, Marasović A, Swayamdipta S, *et al.* Don't Stop Pretraining: Adapt Language Models to Domains and Tasks; 2020 Apr 23.
[27] ISO. ISO TC 115: Pumps [cited 2020 December 11] Available from: URL: https://www.iso.org/committee/51766.html.
[28] ISO. ISO/IEC JTC 1/SC 17: Cards and security devices for personal identification [cited 2020 December 11] Available from: URL: https://www.iso.org/committee/45144.html.
[29] ISO. ISO/IEC JTC 1/SC 31: Automatic identification and data capture techniques [cited 2020 December 11] Available from: URL: https://www.iso.org/committee/45332.html.
[30] ISO. ISO/TC 184/SC 4: Industrial data [cited 2020 December 11] Available from: URL: https://www.iso.org/committee/54158.html.
[31] ISO. ISO/TC 46/SC 4: Technical interoperability [cited 2020 December 11] Available from: URL: https://www.iso.org/committee/48798.html.
[32] ISO. ISO/TC 46/SC 9: Identification and description [cited 11.12.20] Available from:

URL:
https://www.iso.org/committee/48836.html.
[33] ISO. ISO/TC 59/SC 2: Terminology and harmonization of languages [cited 11.12.20] Available from: URL:
https://www.iso.org/committee/49076.html.
[34] Socher R, Huang EH, Pennington J, Ng AY, Manning CD. Dynamic Pooling and Unfolding Recursive Autoencoders for Paraphrase Detection. In: Dynamic Pooling and Unfolding Recursive Autoencoders for Paraphrase Detection; 2011. Red Hook, NY, USA: Curran Associates Inc; 801–9.
[35] Reimers N, Gurevych I. Sentence-BERT: Sentence Embeddings using Siamese BERT-Networks; 2019 Aug 27.
[36] Williams A, Nangia N, Bowman S. A Broad-Coverage Challenge Corpus for Sentence Understanding through Inference. In: A Broad-Coverage Challenge Corpus for Sentence Understanding through Inference; 2018. Association for Computational Linguistics; 1112–22.
[37] Cer D, Diab M, Agirre E, Lopez-Gazpio I, Specia L. SemEval-2017 Task 1: Semantic Textual Similarity Multilingual and Crosslingual Focused Evaluation. In: SemEval-2017 Task 1: Semantic Textual Similarity Multilingual and Crosslingual Focused Evaluation; 2017. Vancouver, Canada: Association for Computational Linguistics; 1–14.
[38] Iyer S, Dandekar N, Csernai K. First Quora Dataset Release: Question Pairs: Quora [cited 2020 November 23] Available from: URL:
https://www.quora.com/q/quoradata/First-Quora-Dataset-Release-Question-Pairs.
[39] Lo K, Wang LL, Neumann M, Kinney R, Weld D. S2ORC: The Semantic Scholar Open Research Corpus. In: Jurafsky D, Chai J, Schluter N, Tetreault J, editors. S2ORC: The Semantic Scholar Open Research Corpus. Stroudsburg, PA, USA: Association for Computational Linguistics; 4969–83.
[40] DIN Deutsches Institut für Normung e.V. DIN EN 62569-1 Allgemeine Regeln zur Erstellung von Produktspezifikationen: Teil 1: Grundsätze und Methoden; 2018.
[41] Pedregosa et al. Scikit-learn: Machine Learning Library for Python; 2011.

Automated performance monitoring of HVAC components by artificial intelligence

Maximilian Both [a], Nicolai Maisch [a], Björn Kämper [a], Alina Cartus [a], Jochen Müller [a], Christian Diedrich [b]

[a] Institute of Building Services Engineering, TH Köln, University of Applied Sciences, Cologne, Germany, {maximilian_alexander.both; nicolai.maisch; bjoern_klaus.kaemper; acartus; jochen.mueller}@th-koeln.de.

[b] Institute of Automation Technology, Otto von Guericke University Magdeburg, Magdeburg, Germany, christian.diedrich@ovgu.de.

Abstract. Energy management systems are an important tool for increasing the energy efficiency of buildings. However, the widespread availability of such systems is offset by the high complexity and high costs of implementation, as well as a lack of data. By using standardized digital twins of technical components, these obstacles can be addressed. In combination with homogeneous semantics of the digital twins and standardized interfaces as uniform access points to the information, the implementation of an energy management system can be simplified. If all technical components of a building have the same information technology structure in the form of digital twins and make their standardized information uniformly available for query, simple query rules can be implemented. These enable the automated integration of the information into an energy management system. However, given the large number of different manufacturers of the technical components, agreement on a common semantic standard in particular seems unlikely. Studies show that methods from the field of Natural Language Processing can be used to process heterogeneous semantics. Agreement on a common vocabulary is no longer necessary. Instead, different semantics can be used and matched to a target vocabulary. In order to use semantic matching in Industrie 4.0 environments, it must be provided as an Industrie 4.0 service. The service provides a translation mechanism from a foreign vocabulary to one's own. For this purpose, a standardized Industrie 4.0 interface consisting of two operations is specified. This interface is implemented prototypically as an API to show how it can be used. The specified interface can be used within the digital twins to process heterogeneous semantics and map them to its own. Extending the Industrie 4.0 approach from homogeneous to heterogeneous semantics can help simplifying the implementation of energy management systems. Simpler implementation lowers the barriers to the use of such systems, which in turn can lead to their higher availability.

Keywords. Industrie 4.0 Interfaces, Natural Language Processing, Energy management systems, Digital twins
DOI: https://doi.org/10.34641/clima.2022.144

1. Introduction

Increasing energy efficiency in every sector of industry is an important aspect of meeting the agreed climate targets of Germany and other countries [1]. In order to identify and leverage energy efficiency potentials, energy management measures, in particular energy management systems (EMS), energy audits, Eco-Management and Audit Schemes (EMAS) and environmental management systems can be used. Although these systems are generally considered useful to increase the energy efficiency of buildings, they are not yet widely used. Studies show that the percentage of companies with EMSs is between 18 and 23% [2]. Barriers to the use of such systems include the high complexity of these, high costs, and a lack of data to identify potential savings [2]. In order to increase the spread of EMS, these obstacles must be overcome: the complexity of the systems must be reduced, the costs lowered and the data basis expanded. Concepts from the areas of Industry 4.0 (I4.0) and Internet of Things (IoT) are ideal for this purpose. The basis of these two concepts is the digital representation of assets. If the digital representation, in the form of a digital twin (DT), is based on a uniform standard (e.g. [3, 4]), the information can be accessed automatically. For this purpose, the DT can also provide standardized interfaces via which its information can be accessed by other DTs. [5]. In addition, a standardized semantics of the DTs' information content is necessary in order to be able to process the information in an automated way [4]. The standardized characteristics can be stored in digital

Copyright ©2022 by the authors. This conference paper is published under a CC-BY-4.0 license.

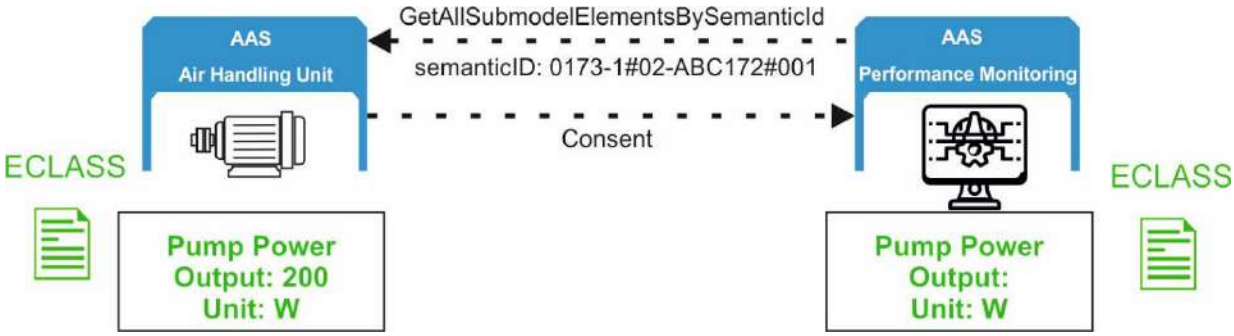

Fig. 1 - Interaction between two Digital Twins

repositories, e.g. [6–8], making them retrievable and available at any time.

An example of an interaction between an EMS and the DT of a pump is shown in Figure 1. Here, the energy management application also has a DT. Specifically, both DTs follow the concept of the asset administration shell (AAS) [4] and are thus based on the same standard. Both AAS have the standardized interface "GetAllSubmodelElementsBySemanticId". Via this interface the EMS application can query the AAS of the pump whether it has the property with the standardized semanticID. This is from the ECLASS standard [6] and is the ID of the "Pump Power Output" property. Since the semantics of the pump's AAS is also based on the ECLASS standard, it can return the requested property and can be integrated into the EMS.

If the three prerequisites (standardized DT, interfaces, semantics) are present, an EMS can be easily set up. Within the EMS, automated rules can be implemented that check new components of a building for their standardized information. One such rule is the query for the "Pump Power Output" and the "Manufacturer Name" of a pump. If these two pieces of information are available in standardized form for all pumps in a building and can be queried via the same interface, they can be automatically integrated into the building's EMS. A manual examination of the information household of components is no longer necessary. This in turn leads to a reduction in complexity (automated creation of the EMS), reduces costs (less manual engineering) and results in a better data basis (standardized information of the DTs).

However, if one of the three conditions is not met, the automated creation of an EMS becomes more difficult (Figure 2).

The EMS and the heat pump both have an AAS and the standardized interface "GetAllSubmodelElementsBySemanticId". However, while the AAS of the EMS is based on the ECLASS standard, the AAS of the heat pump uses a manufacturer-specific vocabulary: the two AASs are based on heterogeneous semantics. Therefore, the ECLASS semanticID is not recognized and the value of the requested property cannot be returned. Thus, an automated query and integration of energy-relevant values into an EMS is not possible. Instead, the semantics of the properties would have to be analyzed and manually linked to an EMS. This in turn leads to increased complexity and rising costs.

One way to solve the problem of heterogeneous semantics is to use Semantic Matching (SM) [9, 10]. Here, methods from the field of artificial intelligence, specifically natural language processing (NLP), are used to map heterogeneous semantics to each other.

This paper designs interfaces that AAS can use to implement an SM service. The interfaces are first specified in a technology-neutral way and then as an API. Additionally, the specified interfaces are implemented prototypically to show how they can be integrated into an AAS. By means of the interfaces it is also possible to process heterogeneous semantics. This further simplifies the implementation of EMS.

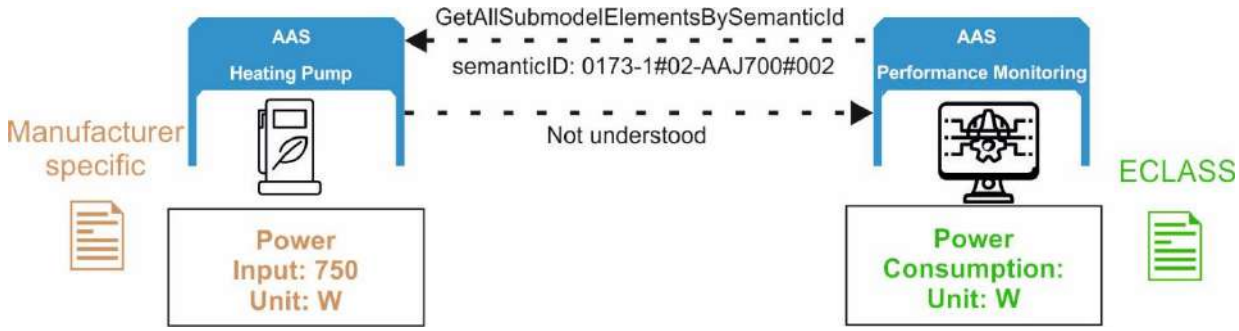

Fig. 2 - Failed Interaction of two Digital Twins

2. Background

I4.0 interfaces and NLP methods are used to implement an SM service.

2.1 The Asset Administration Shell

The transformation from rigid value chains to flexible, highly dynamic and globally networked value networks characterizes the current efforts of organizations towards I4.0. Various fields of action are being addressed for this purpose, one of the central ones being the topic of interoperability [11]. In the field of I4.0, the concept of the AAS has established itself as the basis for interoperability. The AAS is the digital representative of an asset in the digital world [12]. Here, an asset can be any entity that has value for an organization [13]. The information model of the AAS defines the structure of how information of different assets must be arranged[4]. The composition of AAS and asset is called I4.0-component. The central building blocks of the AAS are submodels, which represent the properties and functionalities of the assets and their contents in the form of submodel elements (SE) [4]. Submodels represent, for example, identification, design, or configuration. In addition to the specified structure through the information model, a unique semantics is required for the interaction of I4.0-components [12, 14]. This is achieved if the submodels are available in standardized form and their semantics are also uniformly standardized. The semantics of submodels or SEs can be uniquely described by semantic IDs to locally stored or online available repositories or ontologies.

Various initiatives standardize submodels for technical components, e.g. pumps or drives [15, 16]. The integration of the submodels in vocabularies available online [6–8] enables the unambiguous identification of the submodels and their SEs and thus paves the way for unambiguous semantics. In the current I4.0-approach, interoperability is achieved through a uniform structure (information model AAS), semantics (homogeneous language space) and the provision of services based on standardized interfaces.

2.2 Industrie 4.0 Interfaces

The access to the information of an AAS is realized by interfaces, provided by the AAS. To enable automated access to the interfaces of different AAS, these interfaces are standardized. According to [5] the I4.0-service model describes four levels that are passed through during the standardization of interfaces. First, at a technology-neutral level, the interfaces and associated operations are described in a general textual form. The second level describes how these general descriptions can be applied in different technologies (e.g., HTTP/REST, OPC UA, MQTT). The third level is called the implementation level and includes the implementation of the interfaces using a concrete language such as Python or Java. The last level describes the runtime level, i.e., the concrete implementation of the interfaces in an I4.0-environment. [5]

In [5] the levels 1 and 2 of different interfaces are described, e.g. "GetSubmodel". This interface can be called to retrieve a specific submodel of an AAS. The general interfaces can be provided in different services. A service consists of different interfaces [13]. A basic distinction is made between "Infrastructure Services" and "Application relevant Software Services". Infrastructure services refer to general services that can be reused in concrete application services. Asset-related services, which are provided by AAS, represent a subcategory of application services. [17]

2.3 Semantic Matching for Industrie 4.0 Administration Shells with heterogenous semantics

Currently, the I4.0 research approach focuses on homogeneous semantics to achieve semantic interoperability and interoperability based on it. If AAS with heterogeneous semantics are used, interoperability cannot be guaranteed [4]. To extend this approach to heterogeneous semantics, a method is developed that can automatically map heterogeneous semantics to each other. This method is called semantic matching (SM) [10]. The basis of SM are methods from the NLP domain. The goal of NLP is to make computers understand human language and realize interactions based on it [18]. For this purpose, Language Models (LM) (e.g. [19–24] are used. The training of these takes place in a two-stage process. In the first step, the models are trained on large amounts of general text (pretraining). In the second step (fine tuning) the models are trained for specific NLP tasks (e.g. text classification or question answering). Based on these LMs and the specific NLP task of paraphrase identification [25] heterogeneous semantics can be processed.

The developed approach is based on the idea that two SEs can have different names and definitions, though having the same semantic content, like the example in Figure 2. In the applied model (DistilBERT-SE), name and definition of two SEs are passed through forming sentence embeddings [26] first. In the form of vectors, these embeddings contain the semantic information of the SEs' names and definitions. Using cosine similarity, the similarity of the sentence embeddings is checked and output whether the two SEs are paraphrases, i.e. whether they have the same semantic meaning. In initial studies, this approach was investigated using heterogeneous pump SEs as an example. The results with an accuracy of 94% show that this approach provides first promising results [10].

To improve the results, the DistilBERT [22] model was additionally trained on domain-specific literature [27]. Furthermore, additional attributes (e.g. unit) of SEs in AAS of pumps and HVAC systems

were used to classify the semantics of SEs. A decision tree was implemented for this purpose. The combination of the decision tree and the LM "Eng_DistilBERT-SE" results in the overall model "MetaEng-DistilBERT-SE" (Figure 3), which is described in more detail in [9].

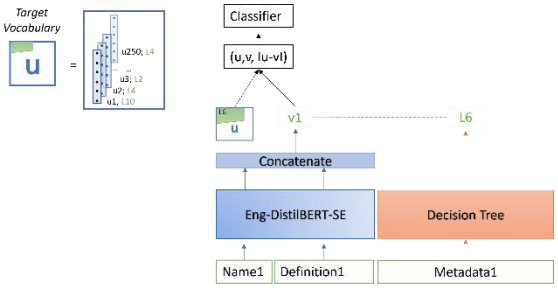

Fig. 3 – The MetaEng-DistilBERT-SE model

This model will be used in the further course of the implementation of the interface.

3. Industrie 4.0 Interface for Semantic Matching

This paper specifies the "Semantic Matching" interface. For this purpose, the first three levels of the I4.0-service model are developed. In addition, it is shown how this can be used within an EMS to enable the automated integration of semantically heterogeneous information into such an EMS.

3.1 Technology-neutral specification

The SM interface is composed of two interface operations. The first operation is called "PostAssetAdministrationShellEmbeddings" (PAASE) (Appendix A). The input to the operation is a component's own AAS. The operation is called from its own AAS and therefore has no output parameter that is returned to another AAS. With the help of this operation, the content of an AAS, specifically the individual SEs of it, passes through the model "MetaEng-DistilBERT-SE" (Figure 4).

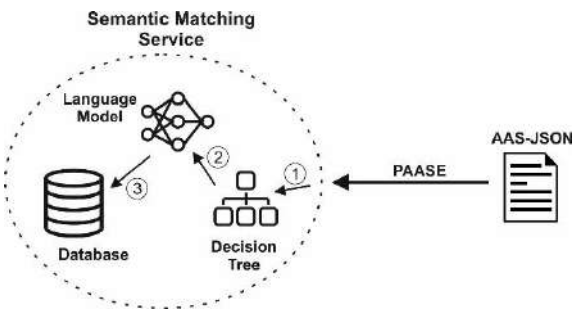

Fig. 4 - Operation PostAssetAdministration-ShellEmbeddings

First, the metadata is processed in the decision tree and assigned to one of the pre-trained classes. The attributes of the SE from Table 1 are first mapped to the parent classes (Watt to Power, Real Measure to Real) and then assigned to class 28 by the decision tree. This class acts as the index of the database to be created. In parallel, the name and definition of the SE run through the "Eng-DistilBERT-SE" model and the sentence embeddings are formed. These embeddings are then concatenated and written to the matching index of the database together with the semantic ID of the SE. This database is initialized and created when the operation is called.

Tab. 1 -Example for an SE from an AAS

AAS Metamodel	**AAS Pump**
Submodel Element	Property
Category	VARIABLE
Qualifier	Operation
Unit	Watt
Data type	REAL_MEASURE
Preferred name	Pump power output
Definition	measured useful mechanical power transferred to the fluid during its passage through the pump
Semantic ID	0173-1#02-ABC172#001

The second interface operation is called "GetAllSubmodelElementsBySemanticIdAndSemanticInformation" (GASEIBSIASI) (Appendix B). The goal of this operation is to return the matching SE of its own AAS (Figure 5).

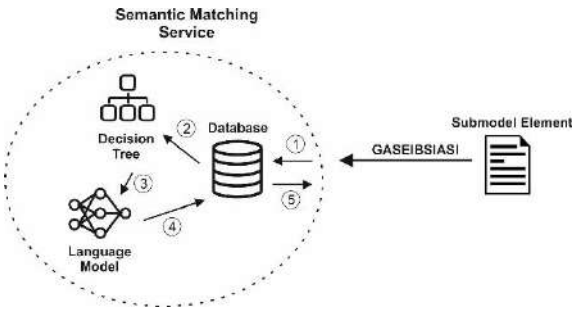

Fig. 5- Operation GASEIBSIASI

The input parameters of this operation are the attributes of the SE to be matched. First, the semantic ID is used to check whether the two AASs use a homogeneous language space. The semantic ID of the SE to be matched is first compared with all semantic IDs in the database of the SEs of the own AAS. If a semantic ID returns a match with the semantic ID to be matched, this SE is returned as matching. Matching based on the other attributes does not need to be performed since the same vocabulary is used. If no match is found, the attributes are passed to the "MetaEng-DistilBERT-SE" model (step 2), classified and the sentence embeddings are formed. According to the class formed on the basis of the meta

information, all embeddings of the own AAS belonging to this class are returned from the database.

Each of these sentence embeddings is then compared to the requested SE using cosine similarity. The SE with the highest similarity is classified as a paraphrase and returned as an output parameter along with the corresponding cosine similarity.

3.2 Technology-specific and implementation level

In the technology-specific level, the generally specified interface SM and the two operations are mapped to a specific API. In this paper, HTTP/REST is used as the technology. The implementation of the interface and the associated operations is carried out using Python. The Python framework FastAPI [28] is used to implement the API. The API provided via FastAPI for calling the two operations is shown in Figure 6.

Fig. 6 – Interface Semantic Matching

When an AAS is passed to the PAASE operation, the model is first run and the results are stored in a database [29].

When the operation "GASEIBSIASI" is called, it is first checked with the database whether a common language space is used. If not, the SM is subsequently performed and the result is returned to the requesting AAS. An example of such a call is given in Figure 7.

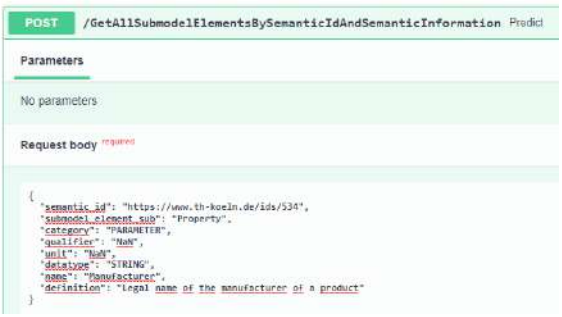

Fig. 7 – Calling the operation GASEIBSIASI

An own SE can be defined via the mask. The necessary attributes for calling the operation must be filled in here. If, as in the example, no unit is available, the value can be left empty, this is intercepted via the function. This request is made to the API and processed. The response is shown in Figure 8.

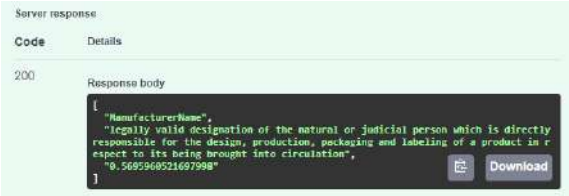

Fig. 8 – Response of the server

The semantics of the requested AAS is based on the ECLASS standard. The SE defined in the mask, however, is not based on any standard. Therefore, a homogeneous language space does not exist. After the implemented model has been run through, the appropriate SE is returned as the response.

The example shows that as a request the name of the manufacturer was asked. Although the requested AAS is based on a different vocabulary and the name and definition do not match the requested name and definition, the matching SE was still returned. Accordingly, the model processed the request correctly and interpreted the semantics of the requested SE correctly.

The example shows the basic flow of the SM. The following chapter describes how this can be integrated into an I4.0-environment in further developments and made available for an automated EMS.

3.3 Integration of the Semantic Matching Service into an I4.0-environment

The interface is deployed as a Docker Image. Docker Images can be downloaded from Docker Hub and used as a Docker Container as one application on one system. All installations required for this application are included on the image. [30]

The SM interface has been implemented as a Docker image so that it can be easily used in an I4.0 environment (Figure 9).

The AAS of the heat pump provides the endpoint for API access to the SM interface to other AASs. The EMS's AAS then sends a request, as in Section 3.2 to the heat pump's AAS, requesting the SE. This AAS has implemented the Docker image as a Docker container within its runtime environment and can thus access the operations of the container. The simple implementation of the container makes it possible to implement this interface within AAS.

If several AAS are implemented by different components in a building, an EMS can now simply be set up. If, for example, energy-relevant variables such as power consumption, power demand, etc. are to be integrated from each component, the individual AAS of the components can be queried for these variables. If positive feedback is received about the existence of these variables, they can be integrated into the EMS. Time-consuming examinations of all SEs of each AAS for the appropriate energy-relevant variables are no longer necessary. The setup of an EMS in a building

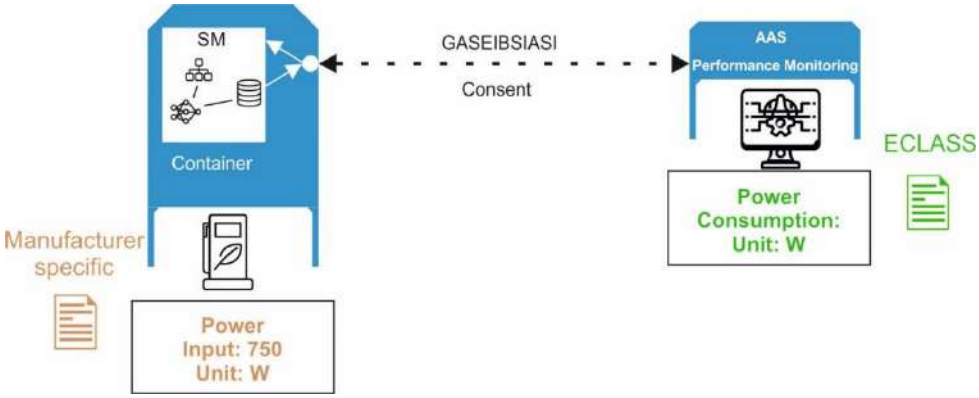

Fig. 9 - Interaction EMS with heat pump based on heterogeneous sematics

is significantly simplified by the SM service.

4. Conclusions

The results extend the current I4.0-research approach to the interaction of semantically homogeneous to semantically heterogeneous AAS. For this purpose, NLP methods were used to implement an automated SM on a target vocabulary. The SM service was specified as an I4.0-interface and is composed of two operations that are called when the interface is used. The interface was expressed and prototyped as an HTTP/REST API. This demonstrated that the interface can be used to process heterogeneous semantics. However, for the interface to be used by AAS, standardization is necessary. For this purpose, the interface will be brought into the corresponding I4.0 working groups to perform a standardization.

EMS are an important factor to increase the energy efficiency of buildings. In order to simplify the

implementation of these and reduce costs, the use of DTs of technical components must be pushed further. In this context, the presented SM service represents a possibility to process heterogeneous semantics of components and thus reduces a potential conflict in the widespread use of EMS. In this paper, the AAS was used as the digital representation. In order to cover further specifications of DTs the SM service must be adapted to their structure.

The datasets generated during the current study are available in the Labor GART repository, https://github.com/thcologne-gart

5. Acknowledgement

The authors gratefully acknowledge financial support from the KSB Foundation in the project Automatic interaction of semantically heterogeneous Industrie 4.0 Asset Administration Shells by means of generic translation mechanisms based on methods of Natural Language Processing (1.1359.2020.1).

6. Appendices

Appendix A

Operation Name	PostAssetAdministrationShellEmbeddings	
Explanation	Takes all submodel elements of the submodels of an Administration Shell, forms embeddings and writes them to a database	
Name	**Type**	**Description**
Input Parameter		
aas	AssetAdministraionShell	AssetAdministration Shell object

Appendix B

Operation Name	GetAllSubmodelElementsBySemanticIdAndSemanticInformation	
Explanation	Returns all submodel elements of the Submodel with a specific Semantic-Id or based on Semantic Matching	
Name	**Type**	**Description**
Input Parameter		
Semantic ID	String	Identifier of the semantic definition
Preferred name	String	Preferred Name of the Submodel Element
Definition	String	Definition of the Submodel Element
Data Type	DataTypeIEC61360	Data type of the Submodel Element (i.e. String, Real etc.)
Submodel Element	String	Subtype of the Submodel Element (i.e. Property, Capability, File etc.)
Category	String	Category of the Submodel Element (Constant, Parameter, Variable)
Qualifier	String	Qualifier of the Submodel Element
Unit	String	Unit of the Submodel Element (i.e. Pascal, Kelvin etc.)
Output Parameter		
Payload	Submodel Element	Matched Submodel Element
Cosine Similarity	Float	The calculated cosine similarity as a measure of the accuracy of matching

References

[1] Walter Kahlenborn, Sibylle Kabisch, Johanna Klein, Ina Richter, Silas Schürmann. Energy Management Systems in Practice: ISO 50001: A Guide for Companies and Organisations; 2012.

[2] Clemens Rohde, Patrick Plötz, Lisa Nabitz, *et al.* Branchen- und unternehmensgrößenbezogene Ermittlung von Klimaschutzpotenzialen (Schwerpunkt KMU) durch verstärkte Umsetzung von Energiemanagementmaßnahmen in der Wirtschaft: Abschlussbericht; 2018.

[3] Web of Things (WoT) Thing Description: W3C Recommendation 9 April 2020; 2020 [cited 2021 November 30] Available from: URL: https://www.w3.org/TR/wot-thing-description/.

[4] Federal Ministry for Economic Affairs and Energy (BMWi). Details Of the Administration Shell: Part 1 - The exchange of information between partners in the value chain of Industrie 4.0 2020.

[5] Federal Ministry for Economic Affairs and Energy (BMWi). Details Of the Administration Shell: Part 2 - Interoperability at Runtime – Exchanging Information via Application Programming Interfaces 2021.

[6] ECLASS e.V. ECLASS: ECLASS - Standard für Stammdaten und Semantik für die Digitalisierung [cited 2021 November 30] Available from: URL: https://www.eclass.eu/index.html.

[7] IEC. IEC Common Data Dictionary [cited 2021 November 30] Available from: URL: https://cdd.iec.ch/cdd/iec61360/iec61360.nsf/TreeFrameset?OpenFrameSet.

[8] buildingSMART. buildingSMART Data Dictionary [cited 2021 November 30] Available from: URL: https://www.buildingsmart.org/users/services/buildingsmart-data-dictionary/.

[9] Both M, Cartus A, Maisch N, Müller J, Diedrich C. Interoperability of semantically heterogeneous digital twins through Natural Language Processing methods. CLIMA 2022.

[10] Both M, Müller J, Diedrich C. Automatisierte Abbildung semantisch heterogener I4.0-Verwaltungsschalen durch Methoden des Natural Language Processing. at - Automatisierungstechnik 2021; 69(11): 940–51 [https://doi.org/10.1515/auto-2021-0050]

[11] Federal Ministry for Economic Affairs and Energy (BMWi). 2030 Vision for Industrie 4.0: Shaping Digital Ecosystems Globally; October 2019.

[12] VDI. Language for I4.0 components: Structure of messages. VDI/VDE-Gesellschaft Mess- und Automatisierungstechnik (GMA); 2020 04.2020.

[13] VDI/VDE-Gesellschaft. Industrie 4.0

Begriffe/Terms: VDI Statusreport; April 2019.
[14] Federal Ministry for Economic Affairs and Energy (BMWi). Position Paper: Interoperability – Our vision for Industrie 4.0: Interoperable communication between machines within networked digital ecosystems; November 2019.
[15] Both M, Müller J. Digitization of pumps – Industry 4.0 submodels for liquid and vacuum pumps. 4th International Rotating Equipment Conference 2019.
[16] ZVEI - Zentralverband Elektrotechnik und Elektronikindustrie e. V. Antrieb 4.0 – Vision wird Realität: Merkmale, Daten und Funktionen elektrischer Antriebssysteme in Industrie 4.0 für Hersteller, Maschinenbauer und Betreiber; November 2018.
[17] Functional View of the Asset Administration Shell in an Industrie 4.0 System Environment: Discussion Paper; April 2021.
[18] Jurafsky D, Martin JH. Speech and language processing: An introduction to natural language processing, computational linguistics, and speech recognition. 2. ed., Pearson internat. ed. Upper Saddle River, NJ: Prentice Hall Pearson Education Internat 2009.
[19] Devlin J, Chang M-W, Lee K, Toutanova K. BERT: Pre-training of Deep Bidirectional Transformers for Language Understanding; 2018 Oct 11.
[20] Clark K, Luong M-T, Le V Q, Manning CD. ELECTRA: Pre-training Text Encoders as Discriminators Rather Than Generators; 2020 Mar 23.
[21] Liu Y, Ott M, Goyal N, *et al.* RoBERTa: A Robustly Optimized BERT Pretraining Approach; 2019 Jul 26.
[22] Sanh V, Debut L, Chaumond J, Wolf T. DistilBERT, a distilled version of BERT: smaller, faster, cheaper and lighter; 2019 Oct 2.
[23] Lewis M, Liu Y, Goyal N, *et al.* BART: Denoising Sequence-to-Sequence Pre-training for Natural Language Generation, Translation, and Comprehension; 2019 Oct 29.
[24] Radford A, Wu J, Child R, Luan D, Amodei D, Sutskever I. Language Models are Unsupervised Multitask Learners Alec; 2019.
[25] Socher R, Huang EH, Pennington J, Ng AY, Manning CD. Dynamic Pooling and Unfolding Recursive Autoencoders for Paraphrase Detection. In: Dynamic Pooling and Unfolding Recursive Autoencoders for Paraphrase Detection; 2011. Red Hook, NY, USA: Curran Associates Inc; 801–9.
[26] Reimers N, Gurevych I. Sentence-BERT: Sentence Embeddings using Siamese BERT-Networks; 2019 Aug 27.
[27] Lo K, Wang LL, Neumann M, Kinney R, Weld D. S2ORC: The Semantic Scholar Open Research Corpus. In: Jurafsky D, Chai J, Schluter N, Tetreault J, editors. S2ORC: The Semantic Scholar Open Research Corpus. Stroudsburg, PA, USA: Association for Computational Linguistics; 4969–83.
[28] FastAPI: FastAPI framework, high performance, easy to learn, fast to code, ready for production [cited 2021 December 3] Available from: URL: https://fastapi.tiangolo.com/.
[29] Elasticsearch: Das Kernstück des kostenlosen und offenen Elastic Stack [cited 2021 December 3] Available from: URL: https://www.elastic.co/de/elasticsearch/.
[30] Docker Docs [cited 2021 December 3] Available from: URL: https://docs.docker.com/.

Effect of measurement resolution on data-based models of thermodynamic behaviour of buildings

Thea Hauge Broholt[a], Louise Rævdal Lund Christensen[a], Steffen Petersen[a]

[a] Department of Civil and Architectural Engineering, Aarhus University, Denmark, thb@cae.au.dk.

Abstract. Multiple studies have investigated and shown a theoretical potential in utilising Model Predictive Control (MPC) of residential heating systems to lower CO_2-emissions. However, there are several practical issues in realising this potential. This paper reports on a simulation-based study focused on two of these issues both related to the data-based identification of a black-box state-space model for MPC. First, it is investigated how the measurement resolution of the heating energy consumption affects the precision of the model used for MPC. Second, the resolution analysis is combined with an investigation on whether it is possible to obtain appropriate models using data generated from excitation signals that in theory do not lead to occupant discomfort. The performance of the models was evaluated by combining different resolutions of data with different types of excitation signals. The results show that a Pseudo-Random Binary Sequence signal within a temperature span from 20 to 24 °C, and a time and data resolution of one hour and 0.1 kWh, respectively, of the heat consumption is expedient to ensure black-box models sufficient for MPC purposes.

Keywords. Black-box model, Data resolution, Model Predictive Control, Space heating.
DOI: https://doi.org/10.34641/clima.2022.196

1. Introduction

The CO_2-emissions from energy use for heating in buildings has a large impact on reaching EU climate goals of being climate neutral by 2050 [1]; in 2019, 63.6 % of energy consumption in European households went to space heating [2]. In Denmark, and many other European countries, the heat supply is district heating. Therefore, district heating plays a large role in lowering the total energy consumption.

Multiple simulation studies show that the CO_2-emission from heating of buildings can be lowered through Model Predictive Control (MPC) of space heating systems. Knudsen and Petersen [3], compare a regular PID controller to an MPC, and find that MPC using forecast of CO_2-emissions as control signal lead to relatively large CO_2-reductions. A similar outcome is reported by Pedersen, Hedegaard and Petersen [4] who demonstrate that the CO_2-reducing effect of a similar MPC scheme on an apartment building is enhanced by energy retrofits. Avci et al. [5] compare MPC to a regular thermostat using both simulations and field tests and find that MPC lead to 5 % and 8 % energy reduction compared to the thermostat using fixed or variable temperature set points, respectively. Prívara et al. [6] implement an MPC in a real university building and obtain energy savings of 17-24 % compared to the original control system. Cigler et al. [7] use both simulation and a field test where they reach energy savings of 15 % and 28 % compared to the original well-tuned control strategy. All these studies show a significant potential in MPC for lowering CO_2-emissions from space heating.

An important aspect of MPC for space heating is to obtain a thermodynamic model of the thermal zone to be heated. This model can be obtained in different ways but is typically involving a calibration process using heating data from the thermal zone. The resolution of this data varies across studies. Knudsen and Petersen [3] and Pedersen, Hedegaard and Petersen [4] all use hourly time resolution of the heat load for their MPC, Avci et al. [5] use a sampling time of 15 minutes, and Cigler et al. [7] use a sampling interval as low as five minutes. Yu et al. [8] evaluates sampling times between 2.5 minutes and one hour. In most Danish households, the available heat consumption data is truncated kWh on an hourly basis as described in Kristensen and Petersen [9]. An example of truncation is as follows. If the heat consumption of hour 1 is 1.4 kWh, 1 kWh will be registered for hour 1, and 0.4 kWh will be added to the next hour (hour 2). Consumption in hour 2 is 5.8 kWh but as 0.4 was transferred from hour 1, a consumption of 6 kWh will be registered for hour 2, and 0.2 kWh will be added the next hour (hour 3), and so on. The question is whether this form of readily available data is useful for generating a model for MPC – let alone operate the heating system with MPC.

Copyright ©2022 by the authors. This conference paper is published under a CC-BY-4.0 license.

The purpose of this study is therefore to investigate whether this truncated data is sufficient to create high performing models. Literature typically indicate that a high model accuracy is a model fit between 80 % and 100 % [4,5,10], to name a few. However, for MPC purposes a model fit of approximately 70 % has been shown to be enough [11,12]. The investigation is performed by comparing the model performance from input with truncated data to input of finer resolution data. The study will then determine which resolution is needed to create models with sufficient accuracy for MPC purposes.

2. Method

The following sections briefly describe the EnergyPlus [13] model of the case building (section 2.1), the black-box model structure (section 2.2), the different excitation signals used for generating data for system identification (section 2.3), and heat consumption datasets with different precision and resolution (section 2.4).

2.1 Case building

The case building was a single-family residential building of 81 m^2. Fig. 1 shows a floorplan and an illustration of the building. A detailed description on the building construction is found in [14] (table 1). Three walls were exposed to the outdoors while the east wall was adiabatic. For the sake of simplicity, the building was modelled as one thermal zone, where internal walls were modelled as a heat capacity with the EnergyPlus class *InternalMass*. Windows and the living room door were modelled with a U-value of 0.74 W/(m^{2}K) and a solar heat gain coefficient of 0.5 corresponding to a 3-layer low-E coated glazing, while the entrance door was modelled as non-transparent with a U-value of 0.67 W/(m^{2}K).

Fig. 1 – Case building. Top: floorplan. Bottom: building illustration.

The building was natural ventilated with a design ventilation rate of 0.21 l/s per m^2, and a design infiltration rate of 0.09 l/s per m^2, i.e. a total rate of 0.3 l/s per m^2 in accordance with the Danish building regulation [15]. The actual ventilation rates were calculated by the EnergyPlus *BLAST* algorithm [16] leading to a ventilation rate that varies with windspeed and indoor/outdoor temperature difference. The heating system was managed with a PI-controller, with a proportional band of 2 °C and an integral time of 600 seconds. The anti-windup technique *conditional integration (clamping)* was modelled for the integration part. This was modelled with EnergyPlus *EnergyManagerSystem:Program*. The ground temperature was modelled using default settings of the EnergyPlus class *Foundation:Kiva*, with exposed foundation perimeter set to the outer circumference of the case building.

Weather data for the simulation was obtained from [17], a service providing EnergyPlus weather files for user-defined locations in Denmark. Data from 2018 for a city near Aarhus (longitude: 10.0, latitude 56.06) was used.

2.2 Building model

The model used for MPC purposes was assumed to be a black-box model formulated as the linear state space model given in equation (1) and (2). This formulation is similar to the one in Knudsen and Petersen [10].

$$x[k+1] = \boldsymbol{A}x[k] + \boldsymbol{B}u[k] + \boldsymbol{K}e[k] \quad (1)$$
$$y[k] = \boldsymbol{C}x[k] + e[k] \quad (2)$$

where k is time step, $x[k] \in \mathbb{R}^n$ is system state, $y[k] \in \mathbb{R}^p$ is output (indoor air temperature [°C]), $u[k] \in \mathbb{R}^m$ is input (outdoor temperature [°C], global horizontal solar irradiation [W/m^2] and heat from building heating system [W]) and $e[k] \in \mathbb{R}^p$ is output prediction error. $\boldsymbol{A} \in \mathbb{R}^{n\times n}$ is state matrix, $\boldsymbol{B} \in \mathbb{R}^{n\times m}$ is input matrix, $\boldsymbol{K} \in \mathbb{R}^{n\times p}$ is Kalman gain matrix, $\boldsymbol{C} \in \mathbb{R}^{p\times n}$ is output matrix.

The matrices $\boldsymbol{A}$, $\boldsymbol{B}$, $\boldsymbol{C}$ and $\boldsymbol{K}$ were initially estimated with the MATLAB method *N4SID* and afterwards refined with prediction error minimization (*PEM*). If *PEM* failed to create a model, the $\boldsymbol{K}$-matrix from *N4SID* was replaced by a zero-matrix. The settings for *N4SID* and *PEM* are given in Tab. 1 and Tab. 2, respectively. The settings were chosen because they provide the best accuracy of the model. Default settings were used when nothing else was given.

Tab. 1 – Chosen settings for *N4SID.*

Setting	Choice
Form	Companion
Model order	2
Time step (k)	One hour
Weight	CVA
Focus	Simulation
Horizon	Auto

Tab. 2 – Chosen settings for *PEM.*

Setting	Choice
Initial state	Estimate
Search method	Lm
Max iterations	500

The model was calibrated and validated through winter and transitional seasons (September to May). The calibration and validation period depend on the excitation signals described in the following section.

2.3 Excitation signals

When training the models for MPC, most studies have used the excitation signal Pseudo Random Binary Sequence (PRBS) signal, which one would expect to lead to discomfort for the occupants due to the highly varying heat load from the heating system. Examples of studies using such a signal are [3,4,18]. A few studies such as [8,14,19] compare PRBS signals to other types of signals. Broholt et al. [14] compare the model performance of models calibrated with a PRBS signal to models calibrated with a night-boosting signal. They find the performance of models calibrated with a PRBS signal is only marginally better than models calibrated with a night-boosting signal. Yu et al. [8] evaluate model performance of models trained with a night set-back signal and validated with a PRBS signal. They conclude that the night set-back signal is a good excitation signal. Knudsen et al. [19] compare the performance of an MPC based on a PRBS signal with an MPC based on an MPC signal. They find no significant difference in the performances.

The effect of excitation on the model accuracy was tested in this study by evaluating two types of excitation signals: The typically used PRBS signal, and a Night Boost (NB) signal like a signal usually observed in previously mentioned MPC studies. Two types of PRBS signals were tested:

1) lower and upper bound of 20 °C and 24 °C, respectively (see example in Fig. 2).
2) bounds between 21 °C and 23 °C.

There are different ways to design a PRBS signal to excite the heating system in buildings; Yu et al. [8] follow the guidelines of IEA EBC Annex 58 [21] that proposes to combine two different PRBS signals to identify both short and long time constants in a building using a short (e.g. 20 min.) and a long (e.g. 20 hour) period (T). Hedegaard et al. [20] also ensures a signal that identify the short and long time constants in the building. In this study, T is set to one hour. The goal is to train models for MPC that adjust heating setpoint on hourly basis, why a control signal with a T below one hour is not relevant. Models were both calibrated and validated with data where the heating system was excited with a PRBS signal. The calibration period with PRBS signal was the first 382 hours (15.9 days) each month (September-May), equal to a combination of two full-length PRBS signals of seventh and eighth order. The validation period was the last 255 hours (10.6 days) of each month, equal to a full length PRBS signal of eighth order.

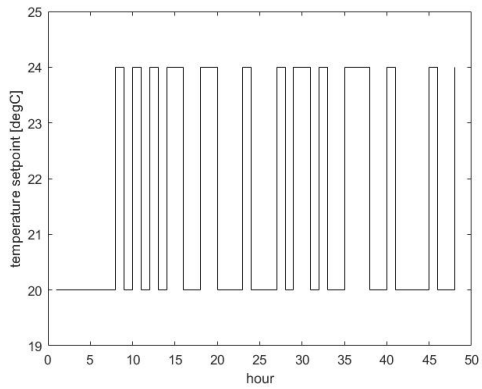

Fig. 2 – Example of the PRBS signal (first 48 hours of the seventh order signal).

Four different types of NB signals were constructed:

1) Boosting to 24 °C from 3 a.m. to 5 a.m. (see example in Fig. 3)
2) Boosting to 23 °C from 3 a.m. to 5 a.m.
3) Boosting to 24 °C from 1 a.m. to 5 a.m.
4) Boosting to 23 °C from 1 a.m. to 5 a.m.

For all four signals, the temperature set point was 22 °C outside the boosting period. The calibration period with NB signals was the first 16 days each month, and the validation period was the last 11 days each month. The same NB signal was used in the calibration and validation period. Furthermore, the models calibrated with a NB signal was also validated with a PRBS signal, as the PRBS signal is considered a more thorough test of calibrated models' capabilities.

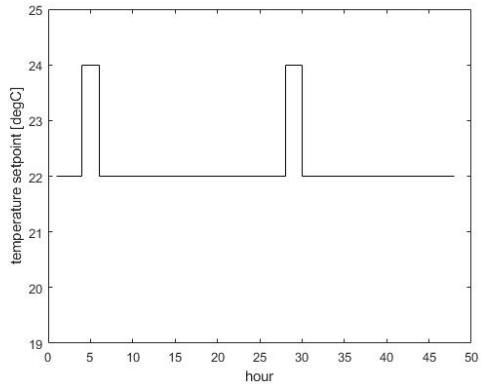

Fig. 3 – 48 hours of a NB signal.

2.4 Heat load data

We tested six different datasets of truncated heat consumption [kWh] to evaluate the impact on model performance:

1) 15-minute truncation for every 0.1 kWh (benchmark).
2) 15-minute truncation for every kWh.
3) 30-minute truncation for every 0.1 kWh.
4) 30-minut truncation for every kWh.
5) 1-hour truncation for every 0.1 kWh.
6) 1-hour truncation for every kWh (typical resolution in Danish district heat meters).

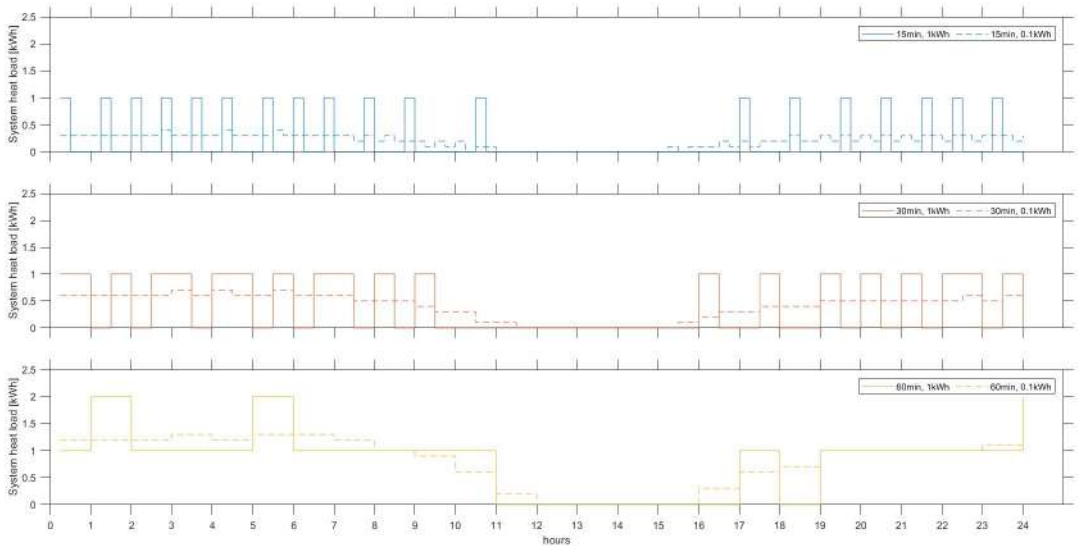

Fig. 4 – Example of the effect of truncation of the six evaluated datasets.

Fig. 4 illustrates how the six different precisions and resolutions varies using simulated one-minute consumption data from the case building on the last day of March. Temperature set point was kept constant at 22 °C. The datasets were created from the one-minute consumptions by summing all values within the given timestep and thereafter truncating the data, to recreate what the typical Danish heat meters would deliver.

3. Results

This section evaluates the performance of the black-box model described in section 2.2 when calibrating with a PRBS signal (see section 3.1) and with a NB signal (see section 3.2). The model performance is given by its ability to predict the indoor temperature 24 hours ahead in accordance with what would be appropriate for an MPC control. The model accuracy is described with the Root Mean Square Error (RMSE) [°C] and the Normalized Root Mean Square Error (NRMSE) [%]. The tables in this section show results from the six datasets described in section 2.4, when the models are calibrated and validated within the same month.

3.1 PRBS signals

Tab. 3 and Tab. 4 show the results for models calibrated and validated with a PRBS signal between 20 °C and 24 °C, and between 21 °C and 23 °C, respectively.

Tab. 3 – RMSE [°C] / NRMSE [%] with PRBS signal between 20 °C and 24 °C. Green: NRMSE > 70 %, yellow: NRMSE 70-50 %, and red: NRMSE < 50 %.

		Jan	Feb	Mar	Apr	May	Sep	Oct	Nov	Dec
1 hour	1 kWh	0.8 / 57	1.0 / 49	0.6 / 65	1.3 / 11	0.4 / 77	0.7 / 41	1.3 / -2	2.0 / 1	0.6 / 69
	0.1 kWh	0.4 / 79	0.7 / 64	0.4 / 80	0.9 / 40	0.3 / 84	0.6 / 48	0.6 / 56	0.8 / 60	0.2 / 89
30 min.	1 kWh	1.0 / 47	1.6 / 13	0.9 / 49	1.0 / 30	0.3 / 80	0.8 / 29	0.9 / 29	1.2 / 36	0.9 / 55
	0.1 kWh	0.5 / 75	0.7 / 65	0.4 / 79	0.7 / 49	0.3 / 84	0.6 / 49	0.6 / 53	1.0 / 50	0.3 / 85
15 min.	1 kWh	1.0 / 43	1.6 / 13	1.1 / 37	1.1 / 18	0.3 / 79	0.8 / 28	1.4 / -16	1.1 / 42	1.0 / 46
	0.1 kWh	0.7 / 61	0.6 / 64	0.4 / 78	0.6 / 57	0.3 / 81	0.7 / 38	0.6 / 54	0.9 / 51	0.3 / 83

Tab. 4 – RMSE [°C] / NRMSE [%] with PRBS signal between 21 °C and 23 °C Green: NRMSE > 70 %, yellow: NRMSE 70-50 %, and red: NRMSE < 50 %.

		Jan	Feb	Mar	Apr	May	Sep	Oct	Nov	Dec
1 hour	1 kWh	0.7 / 28	0.8 / 22	0.7 / 34	1.0 / 28	0.4 / 77	0.6 / 45	1.2 / -20	0.8 / 16	0.6 / 42
	0.1 kWh	0.3 / 69	0.5 / 47	0.3 / 68	0.7 / 50	0.3 / 84	0.6 / 46	0.5 / 48	0.5 / 50	0.2 / 84
30 min.	1 kWh	0.7 / 26	1.0 / -3	0.9 / 8	0.9 / 31	0.4 / 76	0.7 / 34	1.3 / -31	0.7 / 28	0.9 / 6
	0.1 kWh	0.3 / 67	0.5 / 49	0.3 / 66	0.5 / 61	0.3 / 84	0.6 / 43	0.6 / 45	0.5 / 52	0.2 / 80
15 min.	1 kWh	0.8 / 22	1.1 / -18	0.9 / 12	1.1 / 21	0.5 / 72	0.7 / 32	1.3 / -33	1.1 / -12	0.8 / 22
	0.1 kWh	0.6 / 43	0.5 / 47	0.4 / 64	0.5 / 61	0.3 / 84	0.7 / 30	0.6 / 44	0.6 / 42	0.2 / 76

Tab. 3 and Tab. 4 both show that the model accuracy is higher with truncation to 0.1 kWh compared to truncation to 1 kWh and nothing is gained from choosing a finer timestep than one hour. Furthermore, it is seen that a little higher accuracy is reached using a higher temperature fluctuation (Tab. 3) compared to the small temperature fluctuation (Tab. 4) when comparing NRMSE, while the RMSE is almost the same. The NRMSE indicate that the model accuracy is only appropriate for MPC (>70 %) in maximum four of the nine evaluated months.

3.2 Night boost signals

Tab. 5 and Tab. 6 show the results when then model is calibrated with a NB signal, boosting to 24 °C for two and four hours, respectively, and validated with a PRBS signal between 20 °C and 24 °C.

Tab. 5 – RMSE [°C] / NRMSE [%] when calibrating with NB signal; 2 hour boost to 24 °C and validating with PRBS signal between 20 °C and 24 °C . Green: NRMSE > 70 %, yellow: NRMSE 70-50 %, and red: NRMSE < 50 %.

		Jan	Feb	Mar	Apr	May	Sep	Oct	Nov	Dec
1 hour	1 kWh	1.2 / 35	1.4 / 27	1.3 / 31	1.1 / 26	0.3 / 81	0.9 / 19	0.8 / 40	1.4 / 31	3.0 / -54
	0.1 kWh	0.6 / 66	0.7 / 63	0.7 / 61	0.5 / 64	0.3 / 83	0.8 / 31	0.5 / 59	0.5 / 76	0.5 / 76
30 min.	1 kWh	1.8 / 2	1.5 / 17	2.0 / -12	1.6 / -15	0.3 / 82	1.0 / 11	1.0 / 20	1.7 / 10	2.4 / -28
	0.1 kWh	0.8 / 58	0.7 / 62	0.7 / 58	0.5 / 64	0.3 / 81	0.7 / 37	0.6 / 57	0.5 / 73	0.5 / 72
15 min.	1 kWh	1.4 / 21	1.5 / 15	1.4 / 17	1.2 / 15	0.3 / 81	1.0 / 11	1.0 / 21	2.0 / -7	1.5 / 17
	0.1 kWh	0.8 / 58	0.7 / 60	0.9 / 49	0.5 / 63	0.3 / 84	0.8 / 28	0.6 / 55	0.7 / 65	0.5 / 70

Tab. 6 – RMSE [°C] / NRMSE [%] when calibrating with NB signal; 4 hour boost to 24 °C and validating with PRBS signal between 20 °C and 24 °C . Green: NRMSE > 70 %, yellow: NRMSE 70-50 %, and red: NRMSE < 50 %.

		Jan	Feb	Mar	Apr	May	Sep	Oct	Nov	Dec
1 hour	1 kWh	1.1 / 40	1.5 / 20	1.3 / 28	1.1 / 22	0.3 / 80	0.8 / 31	0.8 / 41	1.9 / 2	1.1 / 42
	0.1 kWh	0.9 / 53	0.7 / 61	0.9 / 49	0.5 / 63	0.3 / 83	0.7 / 40	0.5 / 60	0.5 / 75	0.5 / 75
30 min.	1 kWh	1.6 / 14	1.6 / 14	1.5 / 14	1.1 / 18	0.4 / 79	0.9 / 23	1.0 / 21	2.8 / -43	1.4 / 25
	0.1 kWh	0.8 / 55	0.7 / 62	0.9 / 51	0.5 / 62	0.3 / 84	0.6 / 42	0.6 / 55	0.6 / 71	0.6 / 67
15 min.	1 kWh	1.4 / 24	1.5 / 17	1.4 / 21	1.3 / 9	0.3 / 81	0.8 / 29	1.0 / 17	3.3 / -74	1.5 / 18
	0.1 kWh	0.8 / 54	0.7 / 59	0.9 / 50	0.5 / 61	0.3 / 82	0.7 / 32	0.6 / 53	0.6 / 67	0.6 / 66

The same tendency as when calibrating with the PRBS signals can be observed: the models perform better with truncation to 0.1 kWh compared to 1 kWh while nothing is gained from choosing a finer timestep than one hour. The results of a smaller temperature fluctuation are not shown in a table, but the tendencies are the same: the mean and standard deviation of the RMSE/NRMSE across the nine months, when boosting for 2 hours to 23 °C and validating with a PRBS signal between 21 °C and 23 °C, is 0.8 ± 0.2 °C/ 27 ± 23 %, 0.8 ± 0.2 °C/ 24 ± 24 %, and 0.9 ± 0.3 °C/ 12 ± 34 % when truncating to 1 kWh with timestep 1 hour, 30 min., and 15 min., respectively. While the mean and standard deviation of the RMSE/NRMSE, when truncating to 0.1 kWh, is 0.5 ± 0.3 °C/ 52 ± 23 %, 0.5 ± 0.3 °C/ 50 ± 20 %, and 0.7 ± 0.4 °C/ 28 ± 41 %, respectively.

A comparison of the results in Tab. 5 to the results in Tab. 6 show that little to nothing is gained in relation to model accuracy from boosting the temperature for four hours (Tab. 6) instead of two hours (Tab. 5). Only in September (with a timestep of one hour and truncation to 0.1 kWh) do we see a little higher NRMSE.

Tab. 7 and Tab. 8 show the results for models calibrated and validated with a NB signal boosting to 24 °C for two and four hours, respectively. These results also show a tendency of the model accuracy being higher when truncating to 0.1 kWh compared to truncation to 1 kWh. The model accuracy does not increase when using a finer timestep than one hour. The results with a boost to 23 °C show the same tendencies as well; the mean and standard deviation of the RMSE/NRMSE across the nine months, when boosting for two hours, is 0.5 ± 0.2 °C/ 0 ± 54 %, 0.5 ± 0.2 °C/ -7 ±62 %, and 0.5 ± 0.4 °C/ -3 ± 93 when truncating to 1 kWh with timestep 1 hour, 30 min., and 15 min., respectively. The mean and standard deviation of the RMSE/NRMSE, when truncating to 0.1 kWh, is 0.5 ± 0.3 °C/ 9 ± 50 %, 0.4 ± 0.2 °C/23 ± 38 %, and 0.5 ± 0.3 °C/-9 ± 100 %, respectively.

A comparison of results from Tab. 7 and Tab. 8 to results from Tab. 3 and Tab. 4 show that models calibrated with a simple NB signal does not perform as good as models calibrated with the more fluctuating PRBS signal, not even when the validation signal is simple too.

Tab. 7 – RMSE [°C] / NRMSE [%] with NB signal; 2 hour boost to 24 °C. Green: NRMSE > 70 %, yellow: NRMSE 70-50 %, and red: NRMSE < 50 %.

		Jan	Feb	Mar	Apr	May	Sep	Oct	Nov	Dec
1 hour	1 kWh	0.4 / 23	0.8 / -42	0.6 / -3	0.9 / 33	0.3 / 81	0.6 / 40	0.7 / 12	1.0 / -76	0.6 / -9
	0.1 kWh	0.3 / 43	0.4 / 24	0.3 / 49	0.4 / 69	0.3 / 84	0.5 / 51	0.5 / 35	0.2 / 64	0.1 / 79
30 min.	1 kWh	0.7 / -21	0.8 / -37	0.7 / -8	1.2 / 9	0.3 / 82	0.7 / 30	1.2 / -54	1.2 / -111	0.5 / 1
	0.1 kWh	0.4 / 27	0.4 / 35	0.3 / 46	0.4 / 68	0.3 / 81	0.4 / 58	0.5 / 37	0.2 / 67	0.1 / 75
15 min.	1 kWh	0.5 / 12	0.7 / -26	0.6 / 7	1.0 / 24	0.3 / 81	0.8 / 29	1.1 / -40	1.4 / -152	0.5 / 2
	0.1 kWh	0.4 / 28	0.4 / 33	0.4 / 32	0.4 / 68	0.3 / 83	0.5 / 48	0.5 / 35	0.2 / 58	0.2 / 68

Tab. 8 – RMSE [°C] / NRMSE [%] with NB signal; 4 hour boost to 24 °C. Green: NRMSE > 70 %, yellow: NRMSE 70-50 %, and red: NRMSE < 50 %.

		Jan	Feb	Mar	Apr	May	Sep	Oct	Nov	Dec
1 hour	1 kWh	0.5 / 35	1.0 / -38	0.9 / -11	1.0 / 29	0.3 / 81	0.6 / 42	0.7 / 25	2.0 / -167	0.5 / 39
	0.1 kWh	0.5 / 36	0.5 / 33	0.5 / 43	0.5 / 67	0.3 / 83	0.5 / 53	0.5 / 46	0.2 / 69	0.1 / 83
30 min.	1 kWh	0.7 / 3	1.0 / -33	1.1 / -39	1.0 / 27	0.3 / 80	0.8 / 33	1.2 / -27	2.6 / -246	0.6 / 23
	0.1 kWh	0.4 / 40	0.4 / 46	0.4 / 48	0.5 / 67	0.3 / 84	0.4 / 60	0.5 / 45	0.2 / 73	0.1 / 80
15 min.	1 kWh	0.6 / 24	0.7 / 0	0.6 / 19	1.1 / 18	0.3 / 82	0.7 / 38	1.1 / -23	2.9 / -287	0.7 / 9
	0.1 kWh	0.4 / 41	0.4 / 44	0.4 / 45	0.5 / 66	0.3 / 82	0.5 / 51	0.5 / 43	0.2 / 71	0.2 / 77

4. Discussion

The results of 24-hours ahead predictions indicate that model accuracy increases significantly when heat load is truncated to 0.1 kWh instead of 1 kWh. This is also the case for 1-hour ahead prediction: Models calibrated and validated with a PRBS signal between 20 °C and 24 °C and truncation to 1 kWh led to a mean and standard deviation across the nine months of 35 ± 39 % while truncation to 0.1 kWh led to a mean and standard deviation across the nine months of 83 ± 9 %. The latter accuracy corresponds to other studies using 1-step ahead predictions, e.g. [4,5,10], where the NRMSE are between 80 % and 100 %. However, in [10], they have high performing models for one-step ahead as well as 24-step ahead predictions. This may be due to their choice of inputs. For example, they use the solar radiation on the window surface which highly correlates with the room temperature. In this study we chose the global solar radiation as this is easily measured compared to the solar radiation on the window surfaces.

In general, the models perform much better in some months (the heating season November-March) compared to other months (e.g. April and September). This could indicate that the models are not robust to changes in the input data; in the heating season the outdoor conditions do not change significantly. In May, the heat load is zero most of the month which can explain why the truncation does not have an effect here. In April and September, the outdoor conditions change from the calibration period to the validation period which is why the model accuracy may be reduced in these months. However, the RMSE is below 1 °C in most cases.

5. Conclusion

The purpose of this paper was twofold. First, it was to evaluate how the data resolution on the heating energy consumption affected the ability of a black-box model to predict the indoor temperature 24 hours ahead. The model accuracy is of high importance when performing MPC. The results showed that the resolution of the data itself had a larger effect than the time resolution of the data. Meaning that data changed from the commonly used resolution of 1 kWh to a resolution of 0.1 kWh led to a higher increase in NRMSE and reduction in RMSE compared to a change in timestep (comparing one hour, 30 min., and 15 min. timesteps). Therefore, a one-hour timestep with a 0.1 kWh data resolution seems appropriate for MPC. Furthermore, this means that the typically used data measurements in Denmark (one hour and 1 kWh resolution) does not have to be changed much for an MPC to be possible in Danish households.

The second purpose of the paper was to investigate whether sufficient black-box models could be obtained from data generated with an excitation signal which in theory does not lead to occupant discomfort (NB signal). This was done by comparing the performance of black-box models calibrated with an NB signal to black-box models calibrated with the commonly used and more fluctuating PRBS signal. The results showed that the model accuracy, in terms of NRMSE, was highest when calibrating and validating with a PRBS signal with a temperature span between 20 °C and 24 °C. However, the narrow temperature span (21-23 °C) gave similar results, in terms of RMSE. When calibrating with an NB signal, the model accuracy falls in terms of NRMSE, while the RMSE is kept below 1 °C for all cases with truncation to 0.1 kWh and one hour time step. Further investigation of simple excitation signals, which theoretically lead to less discomfort compared to the highly fluctuating PRBS signal, could be a potential next step.

6. Acknowledgement

The research was conducted as part of the project, HEAT 4.0 (Jour. No. 8090-00046B) and FED (Jour. No. 8090-00069B) both financed by Innovation Fund Denmark.

7. Data access

The datasets generated during and analysed during the current study are not publicly available due to practical reasons but will be available from contacting the authors.

8. References

[1] European Commission. 2050 long-term strategy [Internet]. [cited 2021 Sep 14]. Available from: https://ec.europa.eu/clima/policies/strategies/2050_en

[2] Eurostat. Energy consumption in households [Internet]. 2020 [cited 2020 Dec 9]. Available from: https://ec.europa.eu/eurostat/statistics-explained/index.php?title=Energy_consumption_in_households#Context

[3] Dahl Knudsen M, Petersen S. Demand response potential of model predictive control of space heating based on price and carbon dioxide intensity signals. Energy Build [Internet]. 2016;125:196–204. Available from: http://dx.doi.org/10.1016/j.enbuild.2016.04.053

[4] Pedersen TH, Hedegaard RE, Petersen S. Space heating demand response potential of retrofitted residential apartment blocks. Energy Build [Internet]. 2017;141:158–66. Available from: http://dx.doi.org/10.1016/j.enbuild.2017.02.035

[5] Avci M, Erkoc M, Rahmani A, Asfour S. Model predictive HVAC load control in buildings using real-time electricity pricing. Energy Build [Internet]. 2013;60:199–209. Available from: http://dx.doi.org/10.1016/j.enbuild.2013.01.008

[6] Prívara S, Široký J, Ferkl L, Cigler J. Model predictive control of a building heating system: The first experience. Energy Build. 2011;43(2–3):564–72.

[7] Cigler J, Gyalistras D, Siroky J, Tiet V-N, Ferkl L. Beyond Theory: the Challenge of Implementing Model Predictive Control in Buildings. 11th REHVA world Congr 8th Int Conf Energy Effic Smart Heal Build. 2013;1008–18.

[8] Yu X, Georges L, Imsland L. Data Pre-Processing and Optimization Techniques for Stochastic and Deterministic Low-Order Grey-box Models of Residential Buildings. Energy Build [Internet]. 2021;236:110775. Available from: https://doi.org/10.1016/j.enbuild.2021.110775

[9] Kristensen MH, Petersen S. District heating energy efficiency of Danish building typologies. Energy Build [Internet]. 2021;231:110602. Available from: https://doi.org/10.1016/j.enbuild.2020.110602

[10] Knudsen MD, Petersen S. Economic model predictive control of space heating and dynamic solar shading. Energy Build. 2020;209.

[11] Knudsen MD, Georges L, Skeie KS, Petersen S. Experimental test of a black-box economic model predictive control for residential space heating. Appl Energy [Internet]. 2021;298(May):117227. Available from: https://doi.org/10.1016/j.apenergy.2021.117227

[12] Hedegaard RE, Pedersen TH, Knudsen MD, Petersen S. Towards practical model predictive control of residential space heating: Eliminating the need for weather measurements. Energy Build. 2018;170:206–16.

[13] U. S. Department of Energy. No Title [Internet]. 2019. Available from: https://energyplus.net/

[14] Hauge Broholt T, Rævdal Lund Christensen L, Dahl Knudsen M, Elbæk Hedegaard R, Petersen S. The effect of seasonal weather changes on the performance of databased models of the thermodynamic behaviour of buildings. E3S Web Conf. 2020;172:1–8.

[15] Bolig- og planstyrelsen. Bygningsreglementet [Internet]. bygningsreglementet.dk. 2018 [cited 2021 May 19]. Available from: https://bygningsreglementet.dk/

[16] U. S. Department of Energy. Input Output Reference. 2021;579.

[17] Broholt TH, Petersen S. Vejrdata filer [Internet]. [cited 2021 Jun 22]. Available from: http://vejrdatafiler.dk/

[18] Ma J, Qin J, Salsbury T, Xu P. Demand reduction in building energy systems based on economic model predictive control. Chem Eng Sci [Internet]. 2012;67(1):92–100. Available from: http://dx.doi.org/10.1016/j.ces.2011.07.052

[19] Knudsen MD, Hedegaard RE, Pedersen TH, Petersen S. System identification of thermal building models for demand response - A practical approach. Energy Procedia [Internet]. 2017;122:937–42. Available from: https://doi.org/10.1016/j.egypro.2017.07.426

[20] Hedegaard RE, Pedersen TH, Dahl Knudsen M, Petersen S. Identifying a Comfortable Excitation Signal for Generating Building Models for Model Predictive Control : A Simulation Study. 2016;(May).

[21] Madsen H, Bacher P, Bauwens G, Deconinck A-H, Reynders G, Roels S, et al. Thermal Performance Characterization using Time Series Data – statistical guidelines. IEA EBC Annex 58 Guidel. 2016;

[22] Prívara S, Cigler J, Váňa Z, Oldewurtel F, Sagerschnig C, Žáčeková E. Building modeling as a crucial part for building predictive control. Energy Build. 2013;56:8–22.

Health monitoring: a machine learning approach for anomaly detection in multi-sensor networks

Bram Hajee [a], Kees Wisse [a], Peyman Mohajerin Esfahani [b]

[a] DWA, The Netherlands

[b] Delft Center for Systems and Control, Delft University of Technology

Abstract. Multi-sensor networks are becoming more and more popular in order to assess the post-occupancy performance of smart buildings, since they enable continuous monitoring with a high spatial resolution of the occupancy, thermal comfort and indoor air quality. An urgent, but poorly attended topic in this field is the automated detection of sensor anomalies. For example, CO_2-sensors can perform auto-calibration, during which the data is not reliable. Without identifying the poor reliability of this data, any analysis based on it may be misleading. Automated detection and diagnosis of multi-sensor anomalies is a challenging task due to the complex characteristics of each data point, the variety of data points and the sheer number of data points. As a result, rule-based algorithms require an extensive expert-based set of rules, which makes them sensitive to threshold values and case specific exceptions. Machine learning algorithms can overcome these issues, but they require datasets with labelled sensor anomalies to do diagnosis. Acquiring such labelled datasets is labour intensive and therefore expensive. In this paper we show the potential of a transition from an unsupervised to a supervised machine learning approach. The unsupervised algorithm is used to detect anomalies and to identify anomaly classes of interest. This enables for labelling such classes efficiently in order to train classifiers for multiple classes of anomalies. The unsupervised and supervised algorithms are employed in parallel during the transition, allowing for the simultaneous detection of unknown anomaly classes and diagnosis of known anomaly classes. The improved performance of the combined classifier compared to unsupervised detection is shown by the precision-recall curve. Though the presented approach is rather generic, it does have some limitations. Because a window-based approach is used, only time windows can be detected as being anomalous, not the exact time. Also, we focus on the detection of sudden anomalies and the approach does not allow for detecting stationary or trend anomalies.

Keywords. Multi-sensor networks, anomaly detection and diagnosis, machine learning, HVAC
DOI: https://doi.org/10.34641/clima.2022.262

1. Introduction

Health monitoring in buildings is, apart from Covid-19, an important topic as people spend a lot of hours in the indoor environment. Evaluation standards are commonly based on samples that are taken from a selection of rooms in a limited time (see for example [1]). Multi-sensor networks enable the possibility to assess thermal comfort (temperatures), indoor air quality (CO_2, TVOC, relative humidity), light and sound with a high spatial resolution using continuous monitoring. Together with occupancy measurements, it's becoming a standard within so-called smart buildings.

Continuous monitoring with a high spatial resolution also opens new perspectives for continuous commissioning instead of periodic commissioning or initial commissioning after the construction phase [2].

An urgent, but poorly attended topic in this field is the accuracy of the sensors and potential sensor anomalies. Applying sensors at such a large scale will lead to a preference for low-cost solutions with potential poor performance related to accuracy. The large scale applications also challenge the maintenance of the sensors.

Copyright ©2022 by the authors. This conference paper is published under a CC-BY-4.0 license.

Automated fault detection and diagnosis (FDD) for sensor networks is therefore inevitable. This is enhanced by the fact that sensors play also an important role in FDD on the HVAC system level. The consideration of sensor faults together with a component fault can increase the difficulty of FDD exponentially [3]. This can be the case especially for temperature, CO_2 and humidity measurements as they can be involved in control loops of room supply of heating and cooling by variable air volume terminal units, chilled beams, ceiling panels etc. Specific anomaly detection focussed on sensors will strongly improve the FDD on the component and system level.

1.1 Anomalies in multi-sensor networks

Anomalies in sensors occur due to different causes. Examples are inaccurate measurement position of the sensor, connection losses to the data acquisition, blocking of sensors by objects and calibration issues. CO_2 sensor calibrations degenerate over time and some CO_2 sensors perform auto-calibration procedures with a possible erroneous outcome.

To deal with the vast amounts of data, pre-processing is often performed in the local sensor unit, which makes the performance also sensible to software updates. New versions of the pre-processing software may for example not be compatible with the older versions of the hardware.

In order to reduce the data transfer from local to central data processing systems may also use the change-of-value (CoV) principle. The local sensor unit only provides a new sample to the central system when the measured value is changed related to the previous measured value. On the level of the central system, it is difficult to distinguish between the regular missing values due to the CoV principle and temporal connection losses of the multi-sensor unit. Fig. 1 shows connection losses in temperature measurements. As can be seen, the connections losses are hard to identify by looking at the single sensor in isolation. Alternatively, they are easily detected when looking at all sensors combined.

Anomalies in temporal data are often categorized as either point, contextual or collective anomalies [4, 5, 6]. A point anomaly is a single instance and a collective anomaly is a collection of instances that is anomalous as a whole (see Fig. 2). Furthermore, we can distinguish sudden, stationary and trend anomalies. Continuous blocking of a sensor for example will give a stationary error. Slowly degenerating CO_2 sensors will give a trend error, while a CO_2 sensor that performs auto calibration will give a sudden error. In this paper, we focus on sudden errors.

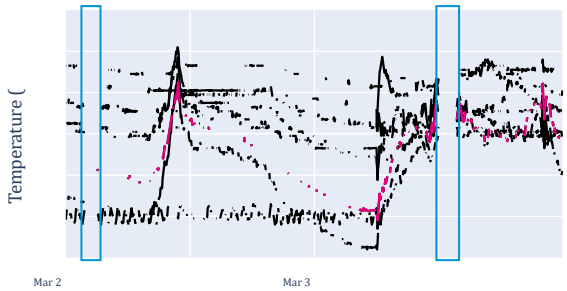

Fig. 1 - Analysis of a single sensor (pink) in relation to its neighbouring sensors (black) for the detection of connection losses (blue).

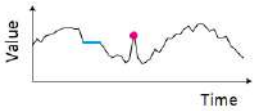

Fig. 2 - Point (pink) and collective anomalies (blue).

1.2 Related work

Fault detection and diagnosis for building systems and HVAC applications show a long history of techniques which already has been applied. Kim and Katipamula provide an overview of the different methods with their applications, from quantitative as well as qualitative model-based diagnostic methods and process history-based methods [7].

Process history-based and qualitative model-based methods are the most popular methods. Quantitative model-based methods desire an explicit mathematical expression of the system as well as accurate input parameters. For multi-sensors, this should include thermal models, air quality models, light models and sound models. From the qualitative model-based models the rule-based algorithms show the most extensive track record. However, they require an extensive expert-based set of rules, which makes them sensitive to threshold values and case-specific exceptions.

An overview of artificial intelligence-based FDD methods is given by Zhao, Li, Zhang et al. [3]. They divide the data-driven detection methods into classification based methods and unsupervised detection methods. From the unsupervised methods, principle component analysis is the most popular method, while from the classification based methods multi-class classification has received the most attention.

Related work from other disciplines than HVAC can be found in the field of wireless sensor networks, see for example Chen, Li and Huang [8].

1.3 State of the art and its limitations

One common problem for the application of artificial intelligence-based FDD is the lack of labelled datasets. Zhao, Li, Zhang et al. [3] indicate it as one of the main shortcomings of data-driven methods. The availability of normal data, separated from faulty data is often a prerequisite for applying the available methods which are described in the review [3]. However, in practical applications manufacturers of multi-sensors don't provide 'normal' datasets.

This problem is not limited to HVAC applications. Also, Chen, Li and Huang mention this problem for wireless sensor network datasets in general and use anomaly insertion methods to test their detection methods [8].

Acquiring labelled datasets is labour intensive and therefore expensive. Efficient labelling is a possible way out. Efficient labelling can be performed by starting with unsupervised learning followed by supervised learning for the most common faults or faults with a high impact.

In this paper, we show the potential of a transition from an unsupervised to a supervised machine learning approach. The main contribution of the paper is the development of a systematic framework for this transition and a proof of concept in the application domain of multi-sensors using a real-world dataset.

The unsupervised algorithm is used to detect anomalies and to identify anomaly classes of interest. This enables for labelling such classes efficiently in order to train classifiers for multiple classes of anomalies. The unsupervised and supervised algorithms are employed in parallel during the transition, allowing for the simultaneous detection of unknown anomaly classes and diagnosis of known anomaly classes.

It will be shown how parallel operation of supervised and unsupervised provides a way of efficient labelling compared to conventional querying and labelling of datasets. Efficient labelling, however, can still lead to extensive datasets which have to be queried and labelled. Therefore we also show how limited querying and labelling performs when unsupervised and supervised learning are used in parallel.

Results are shown for a real-world dataset from a case study: a Dutch office building utilized with multi-sensors.

2. Research methods

2.1 Case study

The case study comprises a Dutch office building in the Netherlands, which is utilized with BRT-35 ceiling multi-sensors [9]. The following parameters are measured: occupancy of the room (passive infrared detection), infrared temperature, CO_2 concentration, relative humidity, sound pressure level and light intensity. The data is processed by the local sensor unit, while the data is stored in the database of the building management system.

The storage uses the change-of-value (CoV) principle, i.e. a value is only stored when it has changed within a certain resolution. The results of this paper are based on the averaged values on a time grid of 3 minutes. In this case study, the results are presented for the infrared temperature sensors. Due to CoV principle, connection loss is an important anomaly that is challenging to detect. This is one of the labelled anomaly classes and it is used in this paper to demonstrate the transition from unsupervised detection to supervised classification.

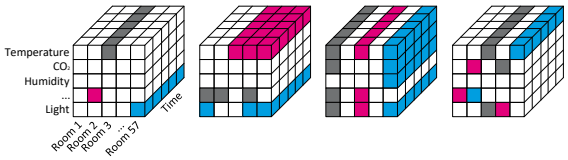

Fig. 3 - The four categories for analyzing the data in a multi-sensor network.

As illustrated by Fig. 3, the data analysis can be categorized into four categories. In the first category, each sensor at each location is analyzed in isolation on a purely temporal basis. In the second category, spatial relations are used as well, e.g. to compare a CO_2 sensor to neighbouring CO_2 sensors. In the third category, temporal and sensorial relations are used, e.g. to compare a CO_2 sensor to a temperature sensor at the same location. In the fourth category, temporal, spatial and sensorial relations are used, e.g. to compare a CO_2 sensor at a certain location to a temperature sensor at another location. For this paper, we mainly focus on the first category, but we also show the potential benefit of adding the second category. Starting with the temporal basis allows also the application of the concept for other HVAC-applications like flow, electricity consumption etc.

The dataset consists of data gathered from 57 multi-sensors from February 20, 2020 until July 10th, 2020 (139 days). Labelling is performed per day (see section 3.1), so we have 7923 day records available. With the manual labelling of the temperature sensors, the following numbers of labels apply: 5434 unlabelled, 2489 anomalies. Of these anomalies, 1653 are labelled as connection loss and 836 as other anomalies.

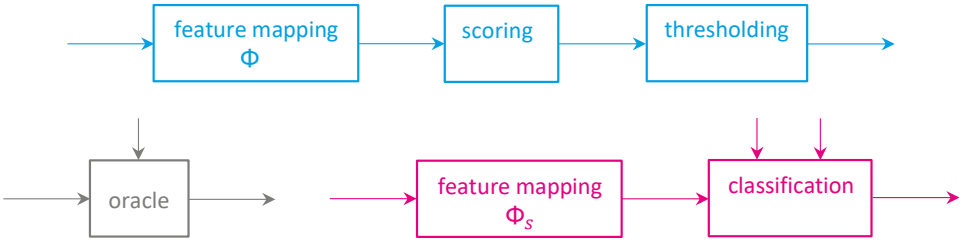

Fig. 4 - Framework for unsupervised querying (blue), manual labelling (grey) and supervised classification (pink).

Furthermore, the labelling was done by an expert. For each window of a day, visually deviating patterns in the entire dataset of 57 sensors were labelled as being anomalous. Note that the deviating pattern was judged in the temporal context of the sensor itself. This process was performed for temperature all temperature sensors.

2.2 Proposed framework

In this section, the proposed framework for learning and labelling is further discussed. We aim to detect and diagnose anomalies coming from the sensor network such that the results can be visualized in a dashboard. As illustrated in Fig. 4 together with Tab.1, the framework can be divided into three sections; unsupervised querying, manual labelling and supervised classification. Likewise, the framework can be summarized with one equation for each section:

$$l_u = \tau_\theta\left(h_u(\Phi_u(d))\right) \tag{2.1}$$

$$l_m = oracle(d, l_u) \tag{2.2}$$

$$l_s = h_s(\Phi_s(d), l_m, s) \tag{2.3}$$

Tab. 1 - Signal and function descriptions.

Notation	Name	Domain
d	Raw data	R^n
x_u, x_s	Unsupervised, supervised instances in feature space	R^o, R^p
l_u, l_m, l_s	Unsupervised, manual, supervised labels	$\{0,1\}, N, \{0,2,3,\dots\}$
s	Anomaly score	R_+
Φ_u, Φ_s	Unsupervised, supervised feature mapping	$R^n \to R^o$, $R^n \to R^p$
h_u	Scoring function	$R^o \to R_+$
h_s	Classifier	$R^p \times R_+ \times N \to \{0,2,3,\dots\}$
τ_θ	Thresholding function	$R_+ \to \{0,1\}$
oracle	Oracle	$R^n \times \{0,1\} \to N$

For the unsupervised querying, the raw data d is first mapped to x_u in the feature space using the feature mapping function $\Phi_u : R^n \to R^o$, with $o \ll n$ for dimensionality reduction. A scoring function h_u is then applied to x_u to generate an anomaly score s. Lastly, a threshold function τ_θ is applied to s for a given threshold θ to generate labels l_u, where $l_u = 0$ implies normal data and $l_u = 1$ implies anomalous data.

The manual labelling is performed by a human expert, who provides manual labels l_m for the instances where $l_u = 1$. Data selected by the query algorithm is presented to the human expert for a single sensor and for the corresponding day within the context of all other days of that sensor. Visually deviating patterns are labelled as being anomalous within their corresponding class ($l_m \in \{1,2,\dots\}$) and are labelled normal otherwise ($l_m = 0$).

For the supervised classification, the raw data d is first mapped to x_s in the feature space using the feature mapping function Φ_s. A classifier h_s is then applied to x_s using the anomaly scores s and manual labels l_m to generate supervised labels l_s. Where $l_s = 0$ implies normal data and other values imply a specific class of anomalies.

In practice, l_u is used for unsupervised anomaly detection, while l_s is used for supervised anomaly detection and diagnosis. The framework, therefore, allows us to transition from detection towards detection and diagnosis, by manually labelling instances where $l_u = 1$ and using those manual labels l_m for supervised classification.

Assuming that l_u is a good indication of anomalousness, the transition is more efficient compared to traditional querying. Additionally, the unsupervised nature of the querying allows us to query novelties. The latter is important as we need to label novelties to construct new supervised classification blocks for previously unknown anomalies. Note that once l_s is available (i.e. h_s is trained using l_m), it can be used in parallel with l_u to generate combined labels $l_c \in N$, see equation 2.4.

$$l_c = max(l_u, l_s) \tag{2.4}$$

2.3 Performance metrics

The performance of the proposed framework is evaluated in two ways. Firstly, the labelling efficiency is evaluated by comparing the fraction of anomalies queried with l_u-based querying to those queried with traditional querying. This is tested using the manually obtained labels for the entire dataset. As explained in section 2.1, these labels should not be confused with the labels obtained through l_u-based querying.

Because l_u depends on the chosen threshold θ, the performance should be measures as a function of θ. This is commonly done by ranking all instances by their anomaly score s and subsequently applying the varying threshold θ to convert the scores to labels l_u [4, 10].

Secondly, the detection performance is evaluated by comparing the combined labels l_c to the unsupervised labels l_u. But this can not be done directly, because $l_c \in N$ can be used for both detection and diagnosis while l_u can only be used for detection. Thus, compare the detection performance of the two by transforming l_c to combined detection labels $l_{cd} \in \{0,1\}$, see equation 2.5.

$$l_{cd} = \begin{cases} 0, & l_c = 0 \\ 1, & l_c \geq 1 \end{cases} \tag{2.5}$$

The labels are used to compute whether an instance is a true positive (TP), false positive (FP), true negative (TN) or false negative (FN) for each threshold. Subsequently, the precision ($PR = TP/TP + FP$) and recall ($RE = TP/TP + FN$) are computed to create a precision-recall curve. The area under the curve (AUC) is computed and used as a performance measure for detection. However, a downside to using the AUC is that it does not put emphasis on the precision. Precision is an important performance measure when addressing an important drawback of many rule-based systems: too many false positives, resulting in the loss of attention of users of the anomaly detection system. Therefore, the recall for a precision of 95% ($RE_{PR=95\%}$) and for a precision of 98% ($RE_{PR=98\%}$) are used as well.

3. Framework application

The main contribution of this paper is the proposed framework, which can be exercised with various functions for Φ_u, h_u, Φ_s and h_s. These functions can be adapted to the application at hand and the functions used here are described in this chapter. Furthermore, this chapter starts with a description of the window-based approach that is applied to the framework.

3.1 Window-based approach

Anomaly detection methods are either prediction-based or window-based [4, 5]. The window-based approach is applied in this paper. The main consideration for designing the window is that the raw data is periodic in nature, i.e. seasonal, weekly and daily. Daily windows are used because the number of seasonal and weekly cycles in the data is quite low and it allows for the detection of sudden anomalies, rather than trend or stationary anomalies.

Consequently, the data d is partitioned into non-overlapping, equally sized data windows d_{W_i} such that each day is represented by one window $W_i \subseteq t \in \{1, \dots, T\}$ with $1 \leq i \leq w$. This is done through the feature mapping functions Φ_u and Φ_s. These functions respectively generate a single o- and p-dimensional point in the feature space for each window.

3.2 Unsupervised querying

The unsupervised nature of the querying allows us to query novelties so that we can obtain manual labels for new anomaly classes and train a classifier on those labels. However, the unsupervised nature also makes automated feature learning and extraction challenging [4]. Therefore, Φ_u is constructed using expert domain knowledge only, i.e. without knowledge of the querying performance. Φ_u consists of a set of seven features $\varphi_{u,1:7}$ and thereby reduces the number of dimensions to seven. Tab. 2 gives mathematical descriptions of $\varphi_{u,1:7}$.

Tab. 2 - Feature mapping function Φ_u.

Feature	Description
$\varphi_{u,1:2}(W_i)$	$\min_{t \in W_i} d(t), \max_{t \in W_i} d(t)$
$\varphi_{u,3}(W_i)$	$\sum_{t \in W_i} d(t)/\lvert W_i \rvert$
$\varphi_{u,4}(W_i)$	$\min_{t \in W_i} d(t) - d(t-1)$
$\varphi_{u,5}(W_i)$	$\max_{t \in W_i} d(t) - d(t-1)$
$\varphi_{u,6}(W_i)$	$\lvert\{d(t) : t \in W_i\}\rvert$
$\varphi_{u,7}(W_i)$	$\sum_{t \in W_i} \left\lVert d(t) - \frac{1}{w}\sum_{j=1}^{w} d\left(t + j\frac{T}{w}\right)\right\rVert$

The textual descriptions of $\varphi_{u,1:7}$ are respectively the minimum, the maximum, the average, the minimum first order difference, the maximum first order difference, the number of unique values and the Euclidean distance to the average window of a window W_i.

As we are interested in the detection at the individual sensor level, Φ_u is applied to each sensor individually. However, the scoring function h_u and thresholding function τ_θ are applied to all sensors combined so that the detection at the sensor level is done with the knowledge of the behavior of the other sensors. Note that all sensors are treated equally here and no information (e.g. spatial information) is used to group them.

The unsupervised scoring function h_u: $R^o \rightarrow R_+$ first scales the feature space using median-MAD scaling, as it is robust to anomalies and it centers the data around the origin [11, 12]. The median-MAD scaling function is given by equation 3.1, where x is a vector containing a feature's values in the feature space and x' is the scaled version of that vector.

$$x' = \frac{x - median(x)}{median(\lvert x - median(x)\rvert)} \tag{3.1}$$

An unsupervised learning algorithm is then applied to the scaled feature space in order to generate scores s. Unsupervised learning algorithms for anomaly detection can broadly be categorized as statistical, proximity-based and information-theoretic [4, 5, 6]. Two of the most established algorithms are the kth nearest neighbour (k^{th}-NN)

and the local outlier factor (LOF) algorithms [4, 10, 13]. k^{th}-NN is better suited for finding global anomalies, while LOF is better suited for finding local anomalies [10]. Since we are mainly interested in global anomalies, we apply k^{th}-NN.

Please note that the unsupervised k^{th}-NN algorithm should not be confused with the supervised k-NN he k^{th}-NN algorithm finds the distance to an instances k^{th} nearest neighbour and we use that distance as anomaly score s. For k, we use half the size of the dataset [14].

3.3 Supervised classification

For the supervised classification, two sets of the feature mapping function Φ_s and the classifier h_s are constructed to demonstrate the transition from detection towards detection and diagnosis. Both sets aim to detect and diagnose detection losses.

Classification set 1: $\Phi_{s,1}$ computes the longest period during which the values do not change for each sensor individually. The classifier $h_{s,1}$ is then applied to all sensors combined.

Classification set 2: $\Phi_{s,2}$ computes the longest period during which the values of all sensors do not change. The classifier $h_{s,2}$ is then applied to the resulting feature space.

Two sets are constructed to demonstrate the strength of utilizing the sensor network for anomaly detection and diagnosis on a single sensor level for connection losses. Note that both $h_{s,1}$ and $h_{s,2}$ scale the feature space through median-MAD scaling, see equation 3.1.

Though the proposed framework allows us to efficiently obtain positive manual labels, only a small subset of the data is generally labelled as such. Additionally, very few or no negative labels are obtained. Given these constraints and the need to distinguish classes of anomalies from the normal data, we are limited to a specific case of binary classification called positive unlabeled (PU) learning [15]. In PU-learning, a learner only has access to positive and unlabeled instances.

In order to obtain a binary classification problem, both positive and negative labels are required to train the classifier. As the oracle provides mostly positive labels, there is a lack of negative labels in the training set. But since normal data is abundant, we can leverage the anomaly score s to select instances that are likely normal, i.e. instances with a low anomaly score. Those instances are then assumed to be normal and used to enrich the training set, see Fig. 5. This is done such that the normal of positive labels equals the number of negative labels.

For the resulting classification problem, we use a k-NN classifier, which is optimized with respect to the leave-one-out classification error. As described by equation 2.4, the output l_s of the classifier overrules the output l_u of the unsupervised detection.

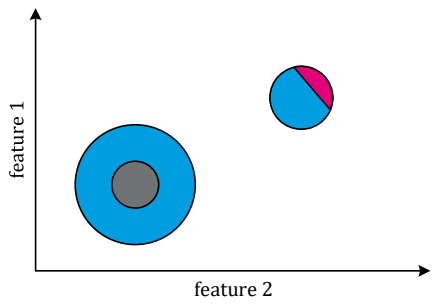

Fig. 5 - Selecting likely normal instances (grey) from unlabeled data (blue) to enrich the training set, which would otherwise consist of only manually labelled anomalous instances (pink).

4. Results

4.1 Labelling efficiency

As described in section 2.3, the labelling efficiency using l_u-based querying is compared to conventional querying. With conventional querying, a human annotator sequentially inspects the data day by day. The strategies are compared by comparing the percentage of anomalies labelled as a function of the percentage of instances queried for both query strategies, see Fig. 6.

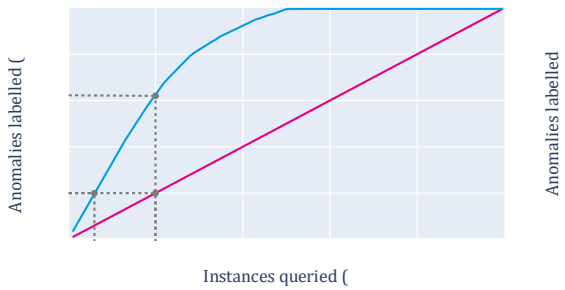

Fig. 6 - Labelling efficiency for anomalies using l_u-based (blue) and conventional querying (pink).

When querying 20% of all instances using conventional querying, 20% of all anomalies will be labelled. But when querying 20% of all instances using l_u-based querying, 62% of all anomalies will be labelled. Alternatively, to label 20% of all anomalies using l_u-based querying, only 6% of all instances need to be queried.

Because supervised labels l_s are generated for connection losses, as described in section 2.3, we also evaluate the labelling efficiency for this specific class of anomalies, see Fig. 7.

When querying 20% of all instances using conventional querying, 20% of all connection losses will be labelled. But when querying 20% of all instances using l_u-based querying, 69% of all connection losses will be labelled. Alternatively, to label 20% of all connection losses using l_u-based querying, only 7% of all instances need to be queried.

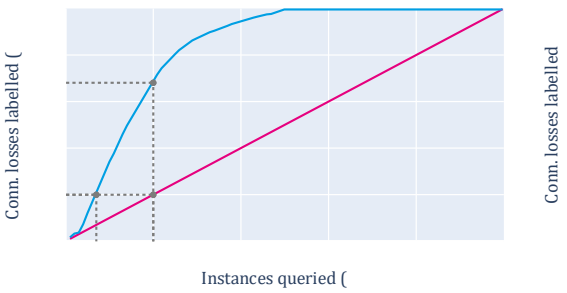

Fig. 7 - Labelling efficiency for connection losses using l_u-based (blue) and conventional querying (pink).

The results show the improved labelling efficiency for labelling anomalies and a specific anomaly class (i.e. connection losses) using l_u-based querying compared to conventional querying. The improved efficiency allows the oracle to label more anomalies for a given number of queries. Or alternatively, it allows the oracle to reduce the number of queries to label a given number of anomalies and thereby reduce the resources required for human annotation.

4.2 Detection performance

As described in section 2.3, the combined performance is evaluated by comparing the combined detection labels l_{cd} to the unsupervised labels l_u with precision-recall curves. Naturally, this performance is a function of the number of labelling instances. But though the labelling is done efficiently, the process could still be labour intensive if a large number of labels is required for classification.

In this section, we show the combined performance when only 1% of all instances are queried, i.e. those with the highest anomaly scores s. This provides us with 27 labelled connection losses. Additionally, the 27 instances with the lowest s are selected to complete the training set, while assuming they are normal.

For classification set 1, the feature mapping function $\Phi_{s,1}$ is applied to the raw data and classifier $h_{s,1}$ is trained on the training set. $h_{s,1}$ is then applied to the remaining instances, i.e. the test set, to generate supervised labels l_s. Fig. 8 shows the resulting performance when equation 2.4 and equation 2.5 are applied.

For classification set 2, we use the knowledge that connection losses often occur for all sensors simultaneously. So if we have a label for 1 sensor for a day, we assume all sensors have a connection loss and use that for training the classifier. Again, Fig. 8 shows the resulting performance when equation 2.4 and equation 2.5 are applied.

The performance can now be measured by the AUC of the precision-recall curves, see Tab. 3. Though as stated in section 2.3, this metric does not put emphasis on the precision, which is important for preventing false positives. Therefore, we also take into account $RE_{PR=95\%}$ and $RE_{PR=98\%}$.

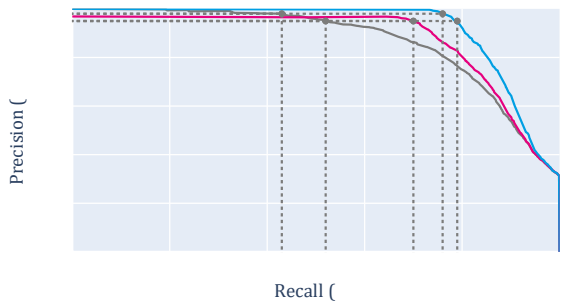

Fig. 8 - The precision-recall curve for unsupervised detection (grey), combined detection using classification set 1 (pink) and classification set 2 (blue).

Tab. 3 - AUC, $RE_{PR=95\%}$ and $RE_{PR=98\%}$ for the different configurations.

Configuration	AUC	$RE_{PR=95\%}$	$RE_{PR=98\%}$
Unsupervised detection	87%	52%	43%
Combined detection using class. set 1	88%	70%	-
Combined detection using class. set 2	90%	78%	76%

Clearly, the combined detection using classification set 2 performs the best, as it scores the highest on all metrics. Whether the unsupervised detection is preferred over the combined detection using classification set 1 is depends on the application though. The latter does have a higher AUC and $RE_{PR=95\%}$, but its main drawback is that it never achieves a precision higher than 97% (and therefore does not have a $RE_{PR=98\%}$). This is due to the false positives generated by the supervised classification, which overrule the output of the unsupervised detection.

5. Discussion and future direction

The proposed framework is rather generic in nature, but it does have two limitations resulting from the framework application. Firstly, the window-based approach results in the detection of anomalous windows. But if a short anomalous event occurs that renders the window anomalous, the detection is not able to single out the event itself within the window. Secondly, we focus on the detection of sudden anomalies and the approach does not allow for detecting stationary or trend anomalies.

Furthermore, we have shown that an improvement in labelling efficiency can be achieved by querying instances with a high anomaly score. Though a drawback of this strategy is that it does not allow us to target edge cases for querying. Future research could focus on utilizing active learning methods to query edge cases for partially labelled anomaly classes.

When instances are manually labelled by the oracle and they are used to train a classifier, we have seen that the false positives provided by the classifier limit the precision of the whole framework. This is a direct result of the supervised labels overruling the unsupervised labels through equation 2.4. It is therefore advised to use only supervised classifiers with high precision in combination with unsupervised detection. Furthermore, a specific feature mapping function and binary classifier need to be designed for each anomaly class. To reduce the required work associated with classifying multiple anomaly classes, it is worth investigating the usage of a multi-class classifier and automated feature extraction.

Note that the unsupervised/supervised approach not only improves anomaly detection but also provides diagnosis for labelled classes.

6. Conclusions

A common problem for the application of machine learning-based FDD is the lack of labelled data. In this paper, we have shown that the proposed framework allows us to efficiently obtain labels and use those labels to transition from unsupervised detection towards supervised diagnosis. This was shown using a real-world dataset of multi-sensors in an office building.

Additionally, we have shown that the (mostly positive) labels can be used in combination with the anomaly scores to train a classifier using PU-learning. This results in an improved precision-recall curve, and additionally allows us to generate supervised labels for diagnosis. This has been shown for connection losses of the multi-sensor, an urgent topic when multi-sensors operate according to the CoV principle with its frequently missing values in the time series.

7. Acknowledgements

The authors acknowledge the financial support of the Dutch RVO TKI Urban Energy through the project Brains for Buildings.

8. References

[1] Neumann C., Yoshida H, Choinière et al. (ed.) Commissioning tools for existing and low energy buildings, 2010, IEA Annex 47 report 2.

[2] The Well Performance Verification Guidebook Q3 2021. WELL Building Institute 20.

[3] Zhao Y., Li T., Zhang C., Artificial intelligence-based fault detection and diagnosis methods for building energy systems: Advantages, challenges and the future. Renewable and Sustainable Energy Reviews. 2019; 109: 85-101.

[4] Aggarwal C. C., Outlier Analysis. Springer; 2015.

[5] Chandola V., Banerjee A., Kumar V., Anomaly detection: A survey, ACM computing surveys (CSUR). 2009; 41(3): 1–58.

[6] Zhang Y., Meratnia N., Havinga, P., Outlier detection techniques for wireless sensor networks: A survey. IEEE communications surveys & tutorials. 2010; 12(2): 159–170.

[7] Kim W., Katipamula S. A review of fault detection and diagnostics methods for building systems. Science and Technology for the Built Environment. 2018; 24:1, 3-21.

[8] Chen L., Li G., Huang G., A hypergrid based adaptive learning method for detecting data faults in wireless sensor networks. Information Sciences. 2021; 553: 49-65.

[9] BR Controls, BRT-35 Plafond multi-sensor, V20200124. [Download 2020 Nov 2] Available from www.brcontrols.com.

[10] Goldstein M., Uchida S., A comparative evaluation of unsupervised anomaly detection algorithms for multivariate data. PloS one. 2016; 11(4), p. e0152173.

[11] Kandanaarachchi S., Muñoz M. A., Hyndman R. J., Smith-Miles K. On normalization and algorithm selection for unsupervised outlier detection. Data Mining and Knowledge Discovery, 2020; 34 (2): 309–354.

[12] Rousseeuw P.J., Hubert M., Anomaly detection by robust statistics. Wiley Interdisciplinary Reviews: Data Mining and Knowledge Discovery. 2018; 8(2), p. 1236.

[13] Breunig M.M., Kriegel H.-P., Ng R. T., Sander J., Lof: identifying density-based local outliers. In: Proceedings of the 2000 ACM SIGMOD international conference on Management of data, 2000, p. 93–104.

[14] Hajee B., Anomaly detection in multi-sensor networks: an active learning approach. Master Thesis Delft University of Technology. 2020; p.24.

[15] Bekker J., Davis J., Learning from positive and unlabeled data: a survey. Machine learning. 2020; 109:719-760.

Data Statement

The datasets generated during and/or analysed during the current study are not available due to commercial restrictions.

Assessment of energy and business performance of innovative technologies in SMEs

Pieter Proot [a], Ad Breukel [b], Jeroen Lippens [c], Hugo de Moor [d], Hilde Breesch [e]

[a] KU Leuven, Building Physics and Sustainable Design, Department of Civil Engineering, Ghent Technology Campus, Ghent, Belgium, pieterproot@telenet.be

[b] Avans University of Applied Science, Research Group Smart Energy, 's-Hertogenbosch, Netherlands, awv.breukel@avans.nl

[c] KU Leuven, Building Physics and Sustainable Design, Department of Civil Engineering, Ghent Technology Campus, Ghent, Belgium, jeroen.lippens@kuleuven.be

[d] Avans University of Applied Science, Research Group Smart Energy, 's-Hertogenbosch, Netherlands, hhc.demoor@avans.nl

[e] KU Leuven, Building Physics and Sustainable Design, Department of Civil Engineering, Ghent Technology Campus, Ghent, Belgium, hilde.breesch@kuleuven.be

Abstract. A major target of the European Green Deal is to raise the 2030 greenhouse gas emission reduction target to 55% compared to 1990. This high ambition includes an increase of the energy performance of buildings and additional generation of renewable energy in all sectors. The tertiary sector, including small and medium sized enterprises (SMEs) such as butchers, small food and non-food shops, restaurants and pubs, is one of the sectors that can contribute to this goal. While large companies in this sector are regularly in the news with iconic projects, for many SME owners "sustainability" is not a key issue. Reasons are that 1) they are not aware of interesting technologies or business cases specific for their company, 2) they are focused on their own business operation and 3) do not always own the building. That is why the Flemish-Dutch TERTS project strives for a transition in energy use and production by 1) demonstrating cutting-edge (innovative) technologies (e.g. circular isolation materials, heat pumps etc.) in SMEs and 2) by guiding these SMEs. This study assesses the impact of different (innovative) technologies specific for the target group 'barber shops'. A reference building is made by analysing 60 existing barber shops in Flanders. The energy use of the barber shop including the systems is calculated according to DIN V 18599 using the Energieberater 18 599 3D PLUS. Subsequently, the cost-benefit of various measures is calculated and compared. This provides us with an approach that not only includes financial measures but also takes metrics into account for CO_2 reduction and comfort. Several technologies, which only have moderate financial benefits, reach acceptable overall satisfaction due to the inclusive metrics. This approach is based on modern business model developments and offer SMEs a more qualitative and inclusive way of the return of innovative technologies to support their investment decision making.

Keywords. Energy assessment, inclusive business case, energy transition/innovation, SMEs (tertiary sector)
DOI: https://doi.org/10.34641/clima.2022.266

1. Introduction

A major target of the European Green Deal in September 2020 is to raise the 2030 greenhouse gas emission reduction target to 55% compared to 1990 (1). This is a very high ambition and includes an increase of the energy performance of buildings and additional generation of renewable energy in all sectors. In Flanders only 7,2% of the final energy consumption was renewable in 2019 (2). Looking at the Netherlands, only 8,8% of the final energy consumption was renewable in 2019 (3). The tertiary sector with many small and medium sized enterprises (SMEs) such as butchers, barbers, small food and non-food shops, restaurants and pubs is one of the sectors that can contribute to this end as SMEs in this sector have significant CO_2-emissions and energy use (4). While large companies are regularly in the news with iconic sustainable projects, for many SME owners the Green Deal is not a key issue. Most of the owners of SMEs attach more importance to investments in their business operation than to invest in energy performance of buildings. Reasons for this include that 1) they are not aware of interesting technologies or business cases specific for their type of company 2) they are not interested

Copyright ©2022 by the authors. This conference paper is published under a CC-BY-4.0 license.

in technologies that have presumably no relation with their core business and 3) they are not always the owners of the building.

Following actions are already taken by the governments to stimulate SMEs in this energy transition. The Flemish government will oblige SMEs to draw up a so-called 'energy balance', which mainly intends to gain insights into their energy consumption. SMEs will be required to implement measures that have a payback period shorter than three years. These measures are called the 'no-regret' measures and include roof and (cavity) wall insulation, relighting with LEDs etc. (5). In the Netherlands, if the energy use of SMEs exceeds 50.000 kWh for electricity or 25.000 m^3 for natural gas, SMEs are required to inform the authorities about their energy reduction investments with technologies with a pay-back period of less than five years. However, monitoring and verification of these measures is not yet deployed. Besides, more complex investments depend on the voluntarily attitude of the entrepreneurs with the assumption that investments (such as heat pumps) are cost effective within their technical lifetime. This is not always the case without subsidies (6).

The Flemish-Dutch Interreg TERTS project (7) focusses on this topic and aims for a transition of energy use by 1) demonstrating cutting-edge innovative energy technologies supported by subsidies and 2) guiding these SMEs. To make the sector more aware of the potential of innovative technologies, demonstration projects are established in Flanders and in the Netherlands. Moreover, the innovative technologies are listed in guidelines for each target group of SMEs. These innovative technologies include circular insulation materials (e.g. glass foam granulate), vacuum glazing, different HVAC-systems (e.g. heat pumps, cooling systems with heat recovery etc.), controllable (LED) lighting and collective energy management systems. The present study focuses on barber shops, which falls into the category of non-food shops.

The objective of this study consists of 1) the identification of the most cost-effective technologies to improve energy performance of SME buildings, represented by barber shops and 2) estimation of the returns of (innovative) technologies towards ecological and non-financial matters. First, the method to determine the reference building is presented, followed by the description of the energy calculations and the cost-benefit analysis. Here, the focus will lie on possible 'no-regret' measures and the implementation of technologies introduced by the TERTS project. Subsequently, this study also takes into account the importance of the society values toward ecological and non-financial matters, such as (thermal) comfort experiences of clients. Price models such as "true price" already take this into account (8). New business model approaches address the rewards of ecological and social values next to the traditional business case (9). These values offer SMEs a more qualitative way of the returns of renewable technologies that may support their renewable investment decision making.

2. Research method

2.1 Reference building

First, a reference building model of a barber shop is determined. In this case, the reference building model aims to represent each individual building within the analysed category 'barber shop'. The geometry and building envelop are based on an analysis of 60 existing barber shops located in the metropolitan area of Bruges (Flanders, Belgium) and the city of Gistel (Flanders, Belgium), which represents the more rural areas. Barber shops are usually located on the ground floor of a residential building. Since this trend is also noticeable in the sample, the building characteristics are based on the TABULA database for dwellings (10). By using this database, an estimation of the U-value of the building envelope is made based on the year of construction. The properties of domestic hot water and heating systems are also determined from this database.

2.2 Calculation final energy use

The energy use of the barber shop including the systems is calculated according to DIN V 18599 (11) using the Energieberater 18 599 3D PLUS software (12). As no specific electrical appliances (such as hairdryers) can be simulated in the Energieberater, the electricity consumption of this equipment is estimated based on a site visit of a (small) barber shop and combined with the energy use as output from the simulation model. Climate file of Düsseldorf (Germany), comparable to Uccle (Belgium) is used for calculating the final energy use.

2.3 Financial cost-benefit analysis

The Energieberater offers changes in energy use (in kWh and m^3) as a result of investment in (innovative) technologies. It also includes measurements of changes in energy costs, in CO_2 emission and offers the payback period of the investment. A cost-benefit model has been developed for the TERTS project that uses the energy quantities of the Energieberater as input for subsequent cost-benefit calculations. This model applies the Net Present Value (NPV) approach that sums the future cash flows from an investment while taking the life time of this investment into account. This economic approach is based on the assumption that money loses value over time because it could have been invested elsewhere. The benefits in the model are the decreased use of fossil energy (in kWh or m^3) during their lifetime as calculated by the Energieberater and based on average energy prices in Flanders. The costs are the total sum in investments and add annual costs such as maintenance and income tax. The present study includes the TERTS subsidy (50% of investment

costs) and possible other subsidies from the government. This data makes it possible to compute the Return-on-Investment (ROI) as the quotient of summated cashflows minus the investment divided by the investment. The Internal rate of return (IRR), which is the discount rate where the benefits are zero, and the pay-back period are also determined.

Following assumptions are made. Initial investment costs are gathered through surveys or are based on already performed research for the target group of butcher's shops (13). Current prices for electricity and natural gas are respectively 0.26 €/kWh and 0.05 €/kWh and subject to changes in the global energy market and due to tax changes (14).
Finally, the cost-benefit model has been checked by calculating the energy and cost effects independently from the Energieberater for two technologies without TERTS subsidy, namely the insulation of the cavity wall and heat pump for domestic hot water (DHW). Comparable outcomes in energy costs savings, CO_2 emission reduction and payback period have been found.

2.4 Non-financial benefits

Regular cost-benefits analyses often only apply financial parameters. The inclusion of ecological and social returns are needed to support a fundamental shift in business models of companies, in order to increase the level of sustainability (15). The Triple Layered Business Model Canvas offers possible metrics for sustainability-oriented business models, with attention to carbon reduction and the quality aspects for customer (9). This approach aligns with a contemporary idea of true prices that takes externalities, such as waste, into account in pricing.

Two parameters from this business model approach have been selected for the TERTS project to widen the regular cost-benefits calculations: 1) the decrease of CO_2 emission (in kg) and 2) the increase of non-financial returns such as comfort.

The CO_2 reduction is determined as 0,6 kg for each used kWh electricity and 1,9 kg for each used m^3 natural gas (16). Comfort is an important functional need that the physical environment of a company may offer to their clients (17). The comfort measurement method has been used as a starting point to address parameters that all refer to comfort and well-being. These parameters are: thermal comfort (air temperature, radiant temperature, drafts), air quality, lighting, acoustics, basic quality and appearance and supplements such as energy autonomy. These parameters will be individually assessed and then used as a basis for a joint comfort evaluation score (see an example in Tab. 1)

The expected ROI is based on the NPV calculation as described in section 2.3, the CO_2 decrease (in kg) is determined on the reduced amount of electricity & gas and the comfort points are the result of the expected improvement in comfort. The entrepreneurs related to the TERTS project will be interviewed about their expected satisfaction of these financial parameter (ROI), ecological (CO_2 emission reduction) and social returns (comfort evaluation). Next, these interview scores are summarized in one final satisfaction metric (maximum 5) based on the relative importance of the various return measures.

Tab. 1 offers an example of the ROI, CO_2 and comfort return data of investments in relighting technology followed by the satisfaction calculations.

Tab. 1– Satisfaction evaluation of relighting + control

Returns of innovative energy technology investment	Expected ROI	Expected CO2 reduction	Expected comfort increase	Overall investment satisfaction score
ROI (based on NPV calculation)	28,06%			
CO2 reduction as a result of less kWh electricity		991,2 kg		
CO2 reduction as a result of less m3 natural gas		-300,2kg		
Total CO2 reduction		691 kg		
Comfort increase (based on assessment of comfort parameters)			Positive	
Satisfaction with expectation (range 1-5)	3	5	3	
Relative importance of expectation	60%	10%	30%	
Satisfaction score (range 1-5)	1,8	0,5	0,9	3,2

During the present, first stage of the research, an estimation is made of the assessments of the entrepreneurs based on desk research and internal discussions. In the follow-up stage, the opinion of the SME entrepreneurs will be collected by means of interviews.

3. Reference building

3.1 Geometry and zoning

First, the building type (detached, semi-detached, terraced) is determined. Fig. 1 shows that a terraced building is the most common in the analysis of 60 existing barber shops. Second, boxplots are made of the width of the façade, floor area, building depth and window area. In Fig. 2 an example is shown of the façade width (6,8 m) and window area (5,94 m^2).

Results from the boxplots are used to design the reference model, most of the analysed barber shops are located on the ground floor of a residential building. For the present study, the residential part is not taken in consideration. The barber shop is divided into two different zones, namely zone 1 (barber shop) and zone 2 (storage + toilet). The properties of the zones are mentioned in Tab. 1. The floor plan and the 3D front view can be found on Fig. 3 and Fig. 4.

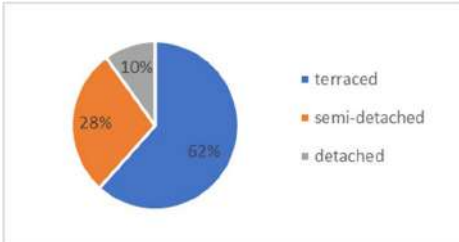

Fig. 1- Building type of studied buildings

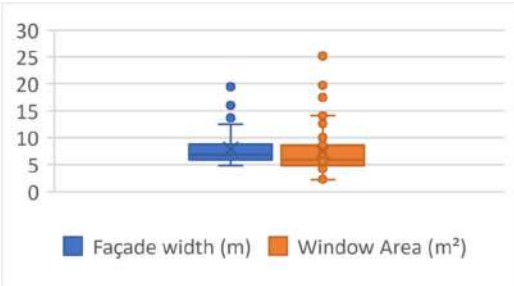

Fig. 2- Boxplots of façade width (m) and window area (m^2) of studied buildings

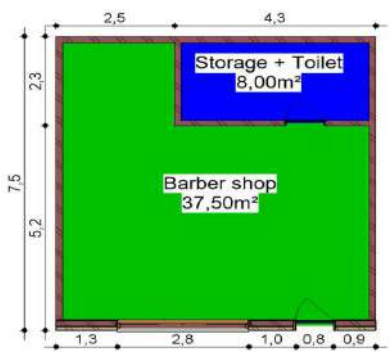

Fig. 3 - Floor plan of the reference building

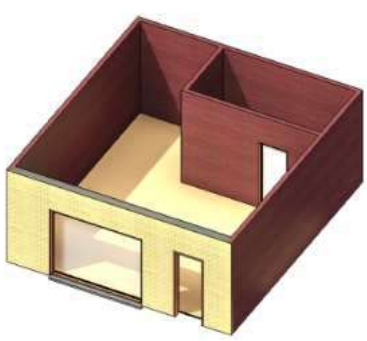

Fig. 4 - 3D front view (NW) of the reference building

Tab. 1 – Zoning of reference building

Zone	Floor area (m^2)	Temperature (°C)	Illuminance (Lx)
Barbershop	37,5	21	500
Storage + Toilet	8	-	200

3.2 Building characteristics and use

Based on the analysis of 60 barber shops, the year of construction is determined. The construction year of the reference building is assumed to be between 1946 and 1970 as shown on Fig. 5.

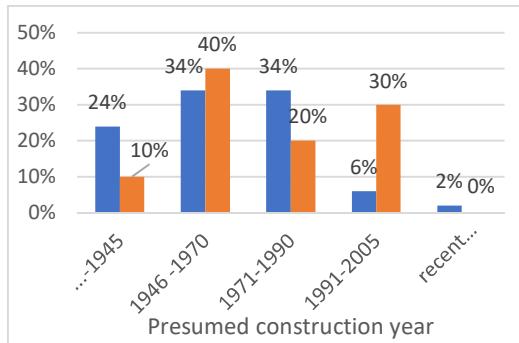

Fig. 5 - Analysis of presumed construction year (data in blue for Bruges and orange for Gistel)

After consulting the TABULA database, assumptions of the thermal transmittance U and building characteristics are mentioned in Tab. 2. For the air tightness (n_{50}) a value of 6 h^{-1} is assumed, based on previous research of the category 'butcher's shops' also no solar shading is assumed (13).

An occupancy of 250 days/year from 8 a.m. until 8 p.m. is assumed according to the Din V 18599. For the reference model, it is assumed that there are two people (fulltime) working in the barber shop.

Tab. 2 - Building characteristics and U-values

Component	Description	U (W/m^2K)
Façade	Non-insulated cavity wall	1,7
Ground floor	Non insulated	0,85
Window	Double glazing	3,5
Door	Double glazing	3,5

3.3 Systems

The barber shop includes a central heating system that is provided with a non-condensing gas boiler (from the year 2000), with radiators. The DHW is linked to the heating system with a consumption of 260 l/day (18). No ventilation system is provided in the reference simulation model. Fluorescent bulbs are provided in the barber shop (31,4 W/m^2) and technical room + toilet (32,4 W/m^2).

4. Results

4.1 Final energy use

The annual final energy use of the reference building, including heating, domestic hot water, lighting and other electrical equipment is listed in Tab. 3. The energy use of the electrical equipment is an

estimation based on a site visit of a (small) barber shop with 2 employees and takes hairdryers, curlers and straighteners into consideration.

Tab. 3 - Final annual energy use of the reference building

Final energy use (kWh)		(kWh/m²)
Total Gas:	11562	254,1
Heating	10789	237,1
DHW	3262	71,7
Total Electricity:	7540,5	165,7
Lighting	2918	64,1
Equipment	4622,5	101,6

4.2 Studied technologies

The following measures are studied regarding the building envelope:

- Insulation of the cavity wall (biofoam, d = 0.08m, λ = 0.034 W/mK)
- Insulation of floor (glass foam granulate, d = 0.15m, λ = 0.08 W/mK)
- Combination: cavity wall and floor
- Replacement of the glazing to vacuum glazing ($U_{glazing}$ = 0.7 W/m^{2}K)

The impact of relighting with controllable LED and adding PV-panels (4,2 kWp, NW, slope of 40°) is also studied. Regarding the HVAC systems, the following systems are studied:

- Condensing boiler (27 kW, efficiency = 94%)
- Solar collector ($V_{storage\ tank}$ = 300l)
- Heat pump DHW (27 kW, COP = 3.3, $V_{storage\ tank}$ = 300l)

4.3 Financial cost-benefit analysis

- ***Building envelope***

First, different individual measures concerning the building envelope are studied. Tab. 4 shows the final energy use, the initial investment cost, the IRR, the ROI and (discounted) payback period compared to the existing situation (benchmark). TERTS subsidies (50% of investment cost) and additional (local government) subsidies are taken into consideration for this analyses.

It can be concluded that concerning the building envelope, insulating the cavity wall is the best solution to increase the energy performance of this reference building. The payback period is only 2 years, so this measure can be an example of a 'no-regret' measure, as mentioned in the introduction. Insulating the floor or replacing the glazing both have higher investment costs, which results in a longer payback period. The combination of insulating floor and the cavity wall offers a business case with 6 year payback period. Without taking the TERTS subsidy in consideration this payback period rises to 18 years.

Tab. 4 - Cost-benefit of individual measures concerning the building envelope

	benchmark (chapter 3.2)	Façade insulation (8 cm)	Floor insulation (15 cm)	Façade & Floor	Vacuum glazing
Heating (gas, kWh)	10789	8677	8973	6885	8523
DHW (gas, kWh)	3262	3303	3301	3372	3316
Lighting (elec, kWh)	2918	2198	2918	2918	2918
Equipment (elec, kWh)	4622	4622	4622	4622	4622
Investment (€)	-	300	1657	1957	2072
ROI (%)		319	30	73	15
IRR (%)	-	44	11	17	7
Payback period	-	2	11	6	18

- ***Systems and lighting***

Second, the effect of the measures regarding the systems and lighting are studied and illustrated in Tab. 5. Relighting with controllable LEDs causes a reduction of the final electricity use of 1670 kWh per year. The payback period, also due to the TERTS subsidy, of this measure is 8 years. Without the TERTS subsidy no payback period can be realised. Concerning the HVAC systems, a condensing boiler (heating + DHW) and a heat pump for DHW are not cost-effective for this case study. As for the heat pump DHW, the gas consumption decreases but a higher electricity consumption is measured. Due to the high electricity prices in Flanders, the benefits will not exceed the costs. Only the solar collector is concluded to be a cost-effective system. This technology is currently not included in the list of innovative technologies for the TERTS project. However, the present study shows that this renewable technology can offer a good solution with a TERTS subsidy.

To obtain a better business-case with the heat pump for DHW, a combination with renewable energy production is investigated. As an example, 14 solar panels (4,2 kWp) are placed (NW) on the pitched roof (slope: 40°). The results of this combination (without TERTS subsidy for the solar panels) can be found in Tab. 5 and shows that a better business-case is realised.

Tab. 5- Cost-benefit of individual and combined measures concerning systems and lighting

	Relighting + control	Condensing boiler heating +DHW	Solar collector	Heat pump DHW	Heat pump DHW + Solar panels
Heating (gas, kWh)	12668	7213	7402	8523	8523
DHW (gas, kWh)	3228	3638	104	3316	3316
Lighting (elec, kWh)	1248	2918	2918	2918	2918
Equipment (elec, kWh)	4623	4622	4622	5760	3181
Investment (€)	5000	3850	5000	2072	7700
ROI (%)	28	- 18	29	- 40	4
IRR (%)	11	1	13	<0	6
Payback period	8	-	8	-	14

4.4 Non-financial benefits

This section includes the non-financial benefits. Tab. 6 and Tab. 7 start with the ROI scores, and several self-evaluations from the perspective of the entrepreneur.

Tab. 6- Satisfaction points on financial – ecological – social returns concerning the building envelope investments

	Façade insulation (8 cm)	Floor insulation (15 cm)	Façade & Floor	Vacuum glazing
ROI (%)	319,6	30,83	73,6	15,77
ROI points	5	3	4	2
CO_2 decrease (kg)	336,3	288,8	615,6	359,1
CO_2 points	4	3	4	3
Comfort score	Positive	Positive	Positive	Positive
Comfort evaluation	3	3	3	4
Overall satisfaction score	4,3	3	3,7	2,7

Insulation technologies earn positive reviews, especially when it comes to insulating the façade. CO_2 reduction and comfort follow, and in the case of vacuum glazing, even add to the ROI evaluation. Overall, only the insulation gets a positive evaluation mainly based on high ROI.

Tab. 7 - Satisfaction points on financial – ecological – social returns concerning systems and lighting investments

	Relighting + control	Condensing boiler heating +DHW	Solar collector	Heat pump DHW	Heat pump DHW + Solar panels
ROI (%)	28,06	-18,23	29,31	-40,02	4,03
ROI points	3	1	3	1	2
CO_2 decrease (kg)	691	524,1	1083	295,7	1843
CO_2 points	5	3	4	2	4
Comfort score	Positive	Neutral	Neutral	Neutral	Neutral
Comfort evaluation	3	3	3	3	5
Overall satisfaction score	3,2	1,8	3,3	1,7	3,1

The lighting energy systems and solar collector have acceptable overall assessments, also because of the CO2 reduction, but the boiler and heat pump DHW do not have a good business case even with reasonable comfort points. However, adding a combination of PV (without TERTS subsidy) to the heat pump DHW (with TERTS subsidy) creates an acceptable satisfaction value for the previously unprofitable energy heat pump technology.

5. Conclusions, limitations and further research

5.1 Conclusions

The present study aims to identify the most cost-optimal technologies to improve the energy performance of the building and estimate the returns of (innovative) technologies towards ecological and non-financial matters. This study focusses on the category of barber shops, with domestic hot water and electricity use as the main energy consumers.

It can be concluded that in several cases (relighting, façade and floor insulation) the application of 50% TERTS subsidies is effective to elevate several innovative energy technologies without an acceptable business case to cost-effective technologies with an acceptable business case. Although the solar collector is not on the list of innovative TERTS technologies, the same conclusion applies for this technology. The positive impact is especially seen in the case of the combination of technologies (façade and floor insulation; PV and heat pump DHW), in which separate technologies do not have a proper business case but where the combination shows acceptable results.

Moreover, the inclusion of CO_2 decrease and increase of comfort measurements demonstrate an added value of these technologies in the eye of the entrepreneurs. These indicators provide a link between energy technologies with the core business of the SME. This is even true in the case of the floor

insulation technology and the combination of solar panels + heat pump DHW, which have a long pay-back period but reach acceptable overall satisfaction levels.

5.2 Limitations and further research

This study argued that innovative energy technologies require subsidies to develop their economic potential and that they are not just commodities with a price tag, but also offer the entrepreneur an option to deliver sustainability, comfort and experience as unique selling points. There are three limitations concerning the conclusions.

First, this approach of inclusion requires more development and testing of the applied measurements, because the 1-5 scale of measurement for comparing the different benefits is less refined than traditional financial and ecological (LCA) measurement methods. Further research will focus on the measurement of comfort and experiences at SMEs (using Fanger's comfort equation to indicate how occupants assess the indoor climate) in order to reach a better comparison.

Second, several innovative technologies (such as façade insulation) are effective even without the TERTS subsidy. A recommendation to SME companies is to invest in one of this technologies as a no-regret measure.

Third, several other technologies (like heat pump, vacuum glazing) do not result in an acceptable business case even with a 50% subsidy. The positive ecological and comfort points are not sufficient to transform the business case in an overall satisfactory result. In order to support promising energy technologies without a proper business case for this tertiary sector, permanent governmental attention is suggested to develop appropriate support schemes for innovative energy technologies.

Next to that, further research will focus on different sales models (such as leasing constructions) as a solution to adopt such technologies. For these sales models, the concept of customer experiences will be included which is a fitting concept for the tertiary sector. Pine and Gilmore emphasize in "The Experience Economy" the focus shift for customers to pay for the experiences they receive instead of buying the product (19). This attention for experiences has led to a range of as-a-service leasing and performance contracts for sustainable technologies, which offers entrepreneurs the opportunity of using an innovative energy technology usage without the burden of high investments. This development, which has also been referred to as the concept of servitisation or Product Service Systems approach, offers a mix of products and services to fulfil customer demand with attention for environmentally and socio-ethically beneficial new solutions" (20).

Finally, a comparison of the findings of this study specific for barber shops with the results of other target groups (bakeries; butchers) will be made in order to generalize the conclusions to the SME sector of Flanders and the Netherlands as a whole.

Acknowledgements

TERTS is financed within the Interreg V Flanders-Netherlands program, the cross-border cooperation program with financial support from the European Regional Development Fund. The project also received funding from local actors.

Data access statement

The datasets generated during and analysed during the current study are not available but the authors will make every reasonable effort to publish them in near future.

References

1. European Commission. Green Paper - A 2030 framework for climate and energy policies. COM(2013) 169 Final [Internet]. 2013;1–16. Available from: http://ec.europa.eu/clima/policies/strategies/2030/documentation_en.htm
2. Hernieuwbare energie - Statistiek Vlaanderen [Internet]. Available from: https://www.statistiekvlaanderen.be/nl/hernieuwbare-energie#aandeel_zon-_en_windenergie_in_groene_stroomproductie_groeit
3. CBS. 11 Procent Energieverbruik in 2020 Afkomstig Uit Hernieuwbare Bronnen [Internet]. Cbs. 2021. Available from: https://www.cbs.nl/nl-nl/nieuws/2021/22/11-procent-energieverbruik-in-2020-afkomstig-uit-hernieuwbare-bronnen
4. Relatieve evolutie broeikasgasemissie per sector sinds 1990 (Vlaanderen, 1990-2018) — Milieurapport Vlaanderen (MIRA) [Internet]. Available from: https://www.milieurapport.be/milieuthemas/klimaatverandering/broeikasgassen/emissies-broeikasgassen-per-sector/relatieve-evolutie-bkg-sector
5. Flemish Government. Versterkte wetgeving voor niet energie-intensieve ondernemingen [Internet]. 2021 [cited 2022 Jan 12]. Available from: https://beslissingenvlaamseregering.vlaanderen.be/document-view/60B871BF364ED9000800064E
6. Planbureau voor de Leefomgeving. Klimaat- en Energieverkenning 2020. 2020;184.

7. TERTS. Transition in Energy via direction Role in the Tertiary Sector [Internet]. Available from: https://www.terts.org/
8. Eidelwein F, Collatto DC, Rodrigues LH, Lacerda DP, Piran FS. Internalization of environmental externalities: Development of a method for elaborating the statement of economic and environmental results. J Clean Prod. 2018;170:1316–27.
9. Joyce A, Paquin RL. The triple layered business model canvas: A tool to design more sustainable business models. J Clean Prod. 2016;135:1474–86.
10. TABULA WebTool [Internet]. Available from: https://webtool.building-typology.eu/#bm
11. DIN. DIN V 15899: energy efficiency of buildings. 2018.
12. Dimitroulopoulou C. Ventilation in European dwellings: A review. Build Environ. 2012;47(1):109–25.
13. Lippens J, Lokere S, Barbary W, Breesch H. Evaluation of the energy performance and cost-benefit of innovative technologies in butcher's shops. E3S Web Conf. 2021;246:1–6.
14. Evolutie energieprijzen en distributienettarieven | VREG.
15. Bocken NMP, Short SW, Rana P, Evans S. A literature and practice review to develop sustainable business model archetypes. J Clean Prod. 2014;65:42–56.
16. CO2-Calculator - CO2- en klimaatneutraal ondernemen voor energiebewuste MKB-bedrijven [Internet]. Available from: https://www.klimaatplein.com/gratis-co2-calculator/
17. Kastelein J-P. Space meets knowledge. impact Work Des knowlegde Shar. 2014;319.
18. Din V 18599. 2013. p. 11–3.
19. Pine BJ, Gilmore. JH. The Experience Economy | Semantic Scholar [Internet]. Available from: https://www.semanticscholar.org/paper/The-Experience-Economy-Pine-Gilmore/87ece758df9f27fd5d742c0f7405366bc830ad00
20. Reim W, Parida V, Örtqvist D. Product-Service Systems (PSS) business models and tactics - A systematic literature review. J Clean Prod. 2015;97:61–75.

Increasing the Energy Flexibility of Buildings controlled by Model Predictive Control

Christian Karczewski [a], Tobias Henzler [a], Konstantinos Stergiaropoulos [a]

[a] Institute for Building Energetics, Thermotechnology and Energy Storage (IGTE), University of Stuttgart, Stuttgart, Germany, christian.karczewski@igte.uni-stuttgart.de

Abstract. The growth of renewable energy sources in the electricity grid and the electrification of heat generation in buildings using heat pumps increase the necessity of flexible consumers who can change their electric load. Operating the building in a flexible way means that the building's load is adjusted, e.g. to an electricity price. Model Predictive Control (MPC) is seen as a key algorithm in building energy management systems to provide the requested flexibility. In most studies covering energy flexible buildings, the load shifting is achieved by an economic MPC that uses an objective function, which aims to minimize the building's operating costs, assuming a variable electricity tariff. However, the most economic operating point corresponds in the heating period to the lower limit and in the cooling period to the upper limit of the thermal comfort band. As a result, the available flexibility that a building can offer is limited. In this work, a novel formulation of the control law, aiming to increase the energy flexibility of buildings, is derived and evaluated. From the current operating point, the heat pump's load for reaching the upper and lower comfort limit in the building is estimated. These two demand curves are used to determine a control signal that balances the trade-off between thermal comfort and operating costs whilst increasing the building's available flexibility. The proposed control strategy is evaluated on lumped-element models of German single-family houses, which are equipped with heat pumps, using the day-ahead electricity price as an incentive. Different indicators (e.g. power shifting capability and flexibility factor) are evaluated showing increased flexibility but also increased operating costs compared to classical economic MPC. Providing flexibility to the grid through demand response will require to operate the building at a point that is not cost-optimal. Higher operating costs on the building side would need future electricity contracts to include a flexibility refund in order to increase the building operator's willingness to provide flexibility.

Keywords. Energy Flexibility, Model Predictive Control, Building Climate Control, Heat Pump
DOI: https://doi.org/10.34641/clima.2022.334

1. Introduction

The German electricity grid is subject to significant changes in both the generation and the consumption side. The generation side is affected by an increasing share of renewable energies, which is a result of the European Green Deal [1]. The hardly controllable and predictable nature of renewable energy sources, like solar radiation and wind, lead to a growing need for demand-side management. The building sector is a major consumer since it is responsible for approximately 40% of the primary energy use in the EU [1]. Most of the consumption is attributed to space heating, where heat is mainly generated through the combustion of fossil fuels. There is a rising share of heat pumps that is leading to an electrification of the heating sector and hence to increased stress on the electricity grid. As heat pumps couple the heating sector with the electricity grid, they will prospectively play a central role in demand-side management.

A high share of renewables in the energy system can only be reached if the installed capacity exceeds the consumption. However, this will result in a waste of electricity production [2]. Thus, additionally to energy efficiency, energy flexibility will be crucial [3]. The building's mass is capable of storing a high amount of energy, allowing to keep the indoor air temperature inside a comfort band for a certain period [4], while heat and cold supply systems are operated with an increased or decreased load. For instance, instead of curtailing wind parks, buildings equipped with heat pumps could increase their load and store thermal energy in the building's mass [5]. If Germany's single-family houses were equipped with heat pumps, an electrical load in the magnitude of up to 57 GW could be shifted through the

Copyright ©2022 by the authors. This conference paper is published under a CC-BY-4.0 license.

exploitation of the thermal capacity of the building mass [4]. This load shifting potential is immense, considering that currently, Germany's yearly mean electricity demand is around 60 GW.

To exploit the building's energy flexibility intelligent control algorithms are necessary. Model Predictive Control (MPC) is an advanced control algorithm that is suitable for building climate control, being able to achieve an optimized operation in terms of user comfort, energy efficiency or operational cost [6].

This contribution discusses the disadvantages of a commonly used formulation of MPC for load shifting while simultaneously introducing a new approach that aims to increase the grid-oriented energy flexibility of buildings.

2. State of the art

In this section, the use of MPC for advanced building control is introduced first. Then, the state of the art in using MPC to exploit the energy flexibility in buildings is presented. Finally, the research gap and the contribution of this paper are highlighted.

2.1 Advanced building control

Intelligent buildings are independent entities that operate in a way, which ensures the building users' comfort needs whilst energy consumption is minimized. Additionally, intelligent buildings communicate with the grid and contribute to grid stability through demand response [7]. The building's energy management system controls the heating, ventilation and air conditioning systems and plays a central role in achieving the above-mentioned properties. MPC is an advanced control algorithm, that can be incorporated as a supervisory control strategy into the building's hierarchical control structure [8].

Through MPC, the controlled system is steered into the desired state by solving an optimal control problem. A process model is used to determine the system's future reaction whilst considering future disturbances. The optimal control signal is attained through the minimization of an objective function. The objective function defines the control objective, which can be for instance reference tracking or an economic operation. Additionally, systems states and control inputs can be constrained. [9]

If MPC is used for building climate control, the actuated values are mostly the heat flows into the building zones and the controlled values are the zone temperatures. Due to the building's large thermal mass and the related long time constants, MPC can outperform reactive controllers like PID controllers [8]. For example, MPC can preheat a building before the outdoor air temperature falls, thus keeping the indoor air temperature inside the comfort band. Numerous studies prove the potential of MPC in reaching common control objectives, like the maximization of user comfort, energy efficiency [10] or monetary savings [11]. As these targets are partly opposing, they need to be weighted if several of these are considered [12]. For further information on MPC in building climate control, the reader is directed to the extensive review by Drgoňa et al. [6].

2.2 Energy flexibility in buildings

The growing need for exploiting the energy flexibility of buildings led to the launch of International Energy Agency Annex 67 "Energy Flexible Buildings" [13] and the subsequent Annex 82 [14]. Flexibility is the capability to adjust a building's load profile, e.g. through load shifting in response to a price signal [15]. In order to exploit the building's energy flexibility, a control strategy is necessary. The identified mainly used control strategies are Rule-Based Control (RBC) and MPC [16].

The control law for RBC can be expressed with if-then statements or time schedules. Set point changes according to schedules enable load shifting. An example, already applied in the 1950s, is the use of electric storage heaters in off-peak periods [17].

In MPC the optimization targets are formulated more clearly than in RBC [16]. In terms of economic operation, MPC can achieve lower operating costs compared to RBC [18]. A review of control strategies for enabling energy flexibility in buildings reveals, that the cost-optimal formulation of MPC is a promising approach and thus being most commonly evaluated in scientific studies [5]. An Economic MPC (EMPC) aims to minimize operating costs in the prediction horizon. The incorporation of future energy prices (e.g. the day-ahead electricity price [19]) into the optimization leads to an increased load in low price regions and a decrease in high price regions. Although the main objective is to minimize costs, a load shift is achieved as a side effect.

Depending on the objective of exploiting the building's energy flexibility different Key Performance Indicators (KPIs) are used for the assessment. These are, among others, increased self-sufficiency [18], peak power reduction [18], monetary cost reduction [19] or the reduction of greenhouse gas emissions [20].

2.3 Research Gap – Increasing the grid-oriented energy flexibility

Exploiting the building's energy flexibility through EMPC seems favourable from the building operator's point of view, as it yields an economic benefit. Obviously, the biggest savings are attained if the electrical heat or cold generators are operated with full load in low price regions and turned off in high price regions. An aggregation of economically controlled buildings will cause fluctuations in the grid, making this approach questionable from the grid operator's point of view. To ensure grid stability, the authors in [21] propose buildings to be grid-

friendly and grid-responsive. Thus, buildings should avoid putting additional stress on the grid and be able to change their demand according to the needs of the grid. The ability to change the demand requires buildings to provide grid-oriented flexibility which is composed of positive and negative flexibility, i.e. the demand can be increased and decreased.

EMPC can be used to exploit the building's flexibility in a grid-oriented way through adding optimization targets to the objective function like a load reference profile [22], [23]. In this way, a demand reduction is incentivised by the grid operator. An economical controller keeps the zone temperature at the lower limit in the heating period so that the zone needs to be preheated before the load can be reduced. However, the duration of the demand reduction is limited, as the indoor air temperature will fall quickly [22]. Operating a building in a way, where grid-oriented flexibility can be provided, results in increased operating costs [23].

To the knowledge of the authors, there is a lack of price-sensitive control approaches, which focus on increasing the building's available flexibility, both in the positive and negative direction. Therefore, the aim of this contribution is to introduce a novel, flexible control approach that enables the use of the building's flexibility according to a price signal.

3. Control law

In this section, the control law of the EMPC is introduced first. Next, a novel flexibility oriented control law based on MPC is presented.

3.1 Cost optimal control law

The general optimal control problem can be formulated in the following way [24]:

$$\begin{aligned} &u_{\text{opt}}(\cdot) = \arg\min_{x(\cdot),u(\cdot)} J(x,u) \\ &\dot{x}(t) = f\big(x(t),u(t)\big) \\ &x(0) = x_0 \\ &x(\cdot) \in \mathcal{X}, u(\cdot) \in \mathcal{U} \end{aligned} \tag{1}$$

The optimal control sequence $u_{\text{opt}}(\cdot)$ minimizes the objective function $J(x,u)$, that is dependent on the control signal u and the system's states x. The minimization is executed with respect to the system model f, the initial state x_0 and constraints for the control inputs and states $\mathcal{U}$ and $\mathcal{X}$.

For the ease of finding a solution to the optimal control problem, quadratic objective functions are favourable. In the case of an EMPC, the cost-optimal formulation of the objective function is chosen as

$$J_{eco} = \left(\sum_{i=0}^{N-1} c(i) \cdot u_{\text{el}}(i)\right)^2 \tag{2}$$

with $c(i)$ being the time-dependent electricity cost and u_{el} being the electrical load of the heat or cold generator.

3.2 Flexibility oriented control

The flexibility oriented control law consists of a two-step approach. From the current operating point, the demand for reaching the upper and lower comfort limit in the building is estimated. The approach is applicable for the heating and cooling case. In the following, it will be presented exemplarily for the heating case.

As a first step, the electrical demand is estimated that is needed to reach an energetic efficient operating point while simultaneously discharging a possibly present thermal energy storage through solving

$$\begin{aligned} u_{\min} = \arg\min_{u(\cdot)} \; &\alpha\left(\sum_{i=1}^{N} \left\|\vartheta_{s,min}(i) - \vartheta_s(i)\right\|^2\right) \\ &+ \sum_{i=0}^{N-1} \|u_{el}\|^2 \end{aligned} \tag{3}$$

under the condition, that the indoor air temperature stays within the comfort boundaries. The storage temperature at each prediction step i is denoted by $\vartheta_s(i)$. The objectives of discharging the storage and minimizing the control input are weighted through the weight α. In the heating period, the vector sequence $u_{\min}$ corresponds to the electrical load of the heat generator and to heat flows into the zones that keep the building at its lower temperature limit. In the cooling period, $u_{\min}$ corresponds to the electrical load of the air conditioning units required to keep the building at the upper comfort limit.

As a second step, the electrical demand needed to reach the upper temperature limit in the building's zones and thermal storage is estimated. This is performed by solving

$$u_{\max} = \arg\min_{u(\cdot)} \sum_{i=1}^{N} \|\vartheta_{set}(i) - \vartheta(i)\|_{\text{W}}^2 \tag{4}$$

with $\vartheta(i)$ as the temperature vector composed of all building zones and the thermal storage. The weight matrix W is used to define which set point ϑ_{set} is to be reached first. The left plot in figure 1 depicts the qualitative course of the zone temperature as a result of the input sequences according to equations (3) and (4). The two energy lines in the right plot span the range in which the building can be operated flexibly.

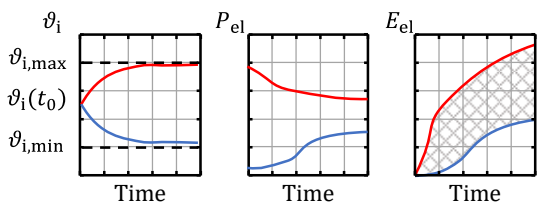

Fig. 1 – Schematic view of heating up (red lines) and cooling down (blue lines) the building. The plots show the indoor air temperature (ϑ_i), the electrical load of the heat generator (P_{el}) and the energy demand (E_{el}).

The current control signal, which keeps the buildings operating point inside the flexibility range is

calculated through the control law

$$u_{\text{Flex}} = (1-\rho)^2 \cdot (u_{\max} - u_{\min}) + u_{\min} \tag{5}$$

The flexible control input u_{Flex} is dependent on the normalized price signal ρ. A high price signal $\rho = 1$ causes the controller to keep the building in the energy efficient operating mode. A low price signal $\rho = 0$ results in an increased load. Thus, for the heating case, the room temperature will be increased and the thermal mass activated. The price is considered quadratically to dampen the increase of the load and to keep the building closer to the energy efficient operating point.

4. Case study

In this section, the thermal energetic building model is described, which is used to compare the operation of the flexible and the economic controller. The case study aims to show the negative flexibility of two exemplary German single-family houses that are equipped with heat pumps. The simulative model and setup are explained first. Then, the evaluation metrics used to quantify flexibility are presented.

4.1 Simulative model

A resistance capacitor network is able to describe the heat dynamics of a building adequately [25]. Two representative German single-family houses are considered, one equipped with a radiator for space heating and the second equipped with an underfloor heating system. The models are adapted from [4]. A second-order model with two temperature states describes the building with radiators:

$$\begin{aligned} C_i\dot{\vartheta}_i &= \frac{\vartheta_e-\vartheta_i}{R_{ei}} + \frac{\vartheta_a-\vartheta_i}{R_{ai}} + A_w\dot{Q}_{sol} + \dot{Q}_{Int} + \dot{Q}_h \\ C_e\dot{\vartheta}_e &= \frac{\vartheta_i-\vartheta_e}{R_{ei}} + \frac{\vartheta_a-\vartheta_e}{R_{ea}} \end{aligned} \tag{6}$$

The states are the indoor air temperature ϑ_i and the temperature of the building's envelope ϑ_e. Solar gains are denoted by $\dot{Q}_{sol}$, internal gains by $\dot{Q}_{Int}$, the outdoor air temperature by ϑ_a and the heat supplied by the heating system by $\dot{Q}_h$. The heat capacities of the states are denoted by C and the heat transfer resistances are denoted by R. The solar radiation enters the building through windows with the effective window area A_w.

Due to the high capacity of the heating system, the building with underfloor heating is described by

$$\begin{aligned} C_i\dot{\vartheta}_i &= \frac{\vartheta_e-\vartheta_i}{R_{ei}} + \frac{\vartheta_a-\vartheta_i}{R_{ai}} + \frac{\vartheta_f-\vartheta_i}{R_{fi}} + A_w\dot{Q}_{sol} + \dot{Q}_{Int} \\ C_e\dot{\vartheta}_e &= \frac{\vartheta_i-\vartheta_e}{R_{ei}} + \frac{\vartheta_a-\vartheta_h}{R_{ah}} \\ C_h\dot{\vartheta}_h &= \frac{\vartheta_i-\vartheta_h}{R_{hi}} + \dot{Q}_h \end{aligned} \tag{7}$$

The states in equation (7) are the temperatures of the indoor air ϑ_i, the building's envelope ϑ_e and the underfloor heating ϑ_h.

The building is equipped with an air-water heat pump with a continuously adjustable inverter. It is modelled as follows

$$\dot{Q}_{\text{HP}} = COP \cdot P_{\text{el}} \tag{8}$$

with COP being the coefficient of performance. This coefficient depends on the operating point of the heat pump. The COP is derived from [26] and can be expressed by

$$COP = COP_{\text{fl}} \cdot PLF \cdot DOF \tag{9}$$

with COP_{fl} being the COP under full load, PLF being the partial load ratio and DOF being the defrost operation factor. Defrost is neglected in this work, i.e $DOF = 1$. The COP_{fl} and PLF are derived from standard data available in [27]. The COP_{fl} is dependent on the outdoor air temperature and the supply temperature in the circuit. In addition, the building is equipped with a thermal storage. The energy balance for the storage is

$$C_w V_s \dot{\vartheta}_s = \dot{Q}_{HP} - \dot{Q}_h \tag{10}$$

with the temperature of the storage ϑ_s and the volume of the storage V_s. The storage is assumed to be ideally mixed. Through a three-way mixing valve, a constant supply flow temperature is achieved in the space heating circuit. The temperature of the supply flow in the heat pump's circuit is set to 5 K above the storage temperature ϑ_s. The modelled system is depicted in figure 1.

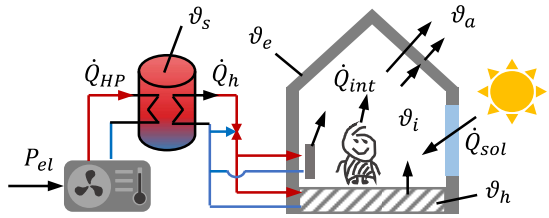

Fig. 1– Schematic view of the used model.

4.2 Simulative setup

Heat pumps are especially suitable for heating purposes if the supply temperature of the heating circuit is low. As the German stock of single-family houses is heterogeneous, two exemplary buildings are considered: The first is a retrofitted house, that has been built in the period between 1984 and 1994 and is equipped with radiators. The second building is constructed after the year 2016 and is equipped with an underfloor heating system. The lower storage temperature limit is set to the supply temperature of the heating system and the upper limit is set to 70°C. The heat pump is designed to meet the heating load of the building at an outdoor air temperature of -7°C for an indoor air temperature of 22°C. The model parameters are summarized in table 2 in the appendix. Weather data, namely solar radiation and ambient air temperature, is used for Stuttgart from the year 2019. The day-ahead

electricity price for 2019 is used as a price signal. The price is transformed through a logistics function to the range $0 \leq \rho \leq 1$. The simulations are implemented in *MATLAB* and the open-source framework *acados* [24] is used for solving the optimal control problems.

4.3 Evaluation metrics

The flexible control aims to operate the building at a point at which the available flexibility is increased. To characterize the flexibility the following definition, adapted from [23], is used

$$\begin{aligned} \Phi^{+} &= l_{\max}(t) - l_{\mathrm{ref}}(t) \geq 0 \\ \Phi^{-} &= l_{\mathrm{ref}}(t) - l_{\min}(t) \geq 0 \end{aligned} \tag{11}$$

with the reference load l_{ref}, the maximum and minimum load $l_{\max}$ and $l_{\min}$. The minimum and maximum load result from the operational limits of the heat or cold generators and the comfort band of the room temperature. For instance, if the room temperature is at the upper comfort limit in summer, the electrical load of an air conditioning unit cannot be decreased and the negative load change Φ^{-} equals zero. The energy, which can be shifted in an interval T is calculated by

$$\Psi_T^{+/-}(t) = \int_t^{t+T} \Phi^{+/-}(\tau) d\tau \tag{12}$$

The total shiftable load substantially depends on the heating and cooling demand of the building. Therefore, the relative load shifting capability

$$\varphi_{rel,T}^{-} = \frac{\bar{P}_{el}}{P_{el,max}} = \frac{\Psi_T^{-}}{T \cdot P_{el,max}} \tag{13}$$

is used. It describes the mean load that can be reduced in the flexibility interval T as a share of the maximum electrical load of the heat or cold generator $P_{el,max}$. To characterise the type of flexibility, the flexibility factor

$$FF = \frac{\Psi_T^{-}}{\Psi_T^{-} + \Psi_T^{+}} \tag{14}$$

will be used. The denominator is the sum of the available positive and negative flexibility. If FF equals zero, the system can only increase its demand in the predicted horizon. If FF equals one, the system is operated at a point, where the system can only decrease its load.

5. Results and discussion

In this chapter, the differences in the operation modes of the flexible and economic control approach will be presented and discussed.

5.1 Results

First, the closed-loop behaviour of the buildings, which is shown in figure 2, is inspected in detail. The top graph shows the input variables, i.e. the outdoor air temperature and the normalized price signal. The electrical power of the heat pump, the indoor air and storage temperature are depicted in the following graphs. The last graph shows the available flexibility for the next 12 hours that is calculated by equation (12). During the first days, the price signal gradually falls, while the outdoor air temperature is rising from -2 to 7 °C. The lines belonging to the flexible controller are in blue, the ones belonging to the economic controller are in red.

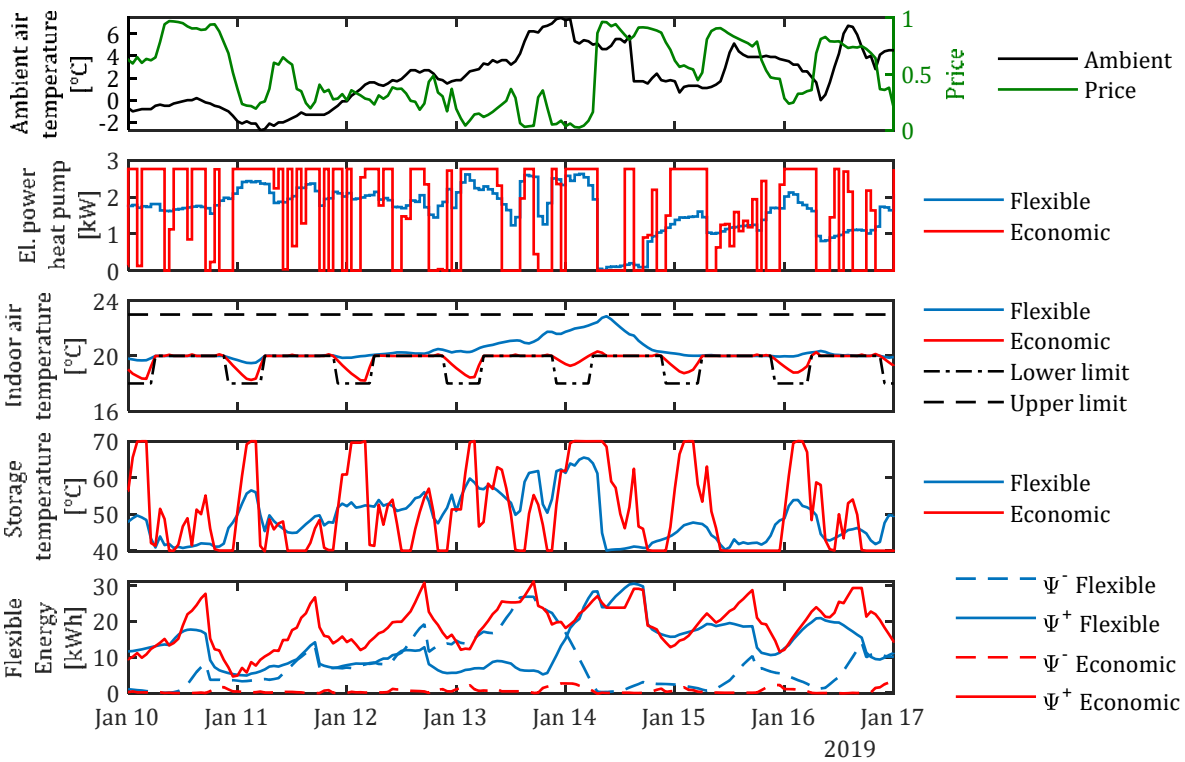

Fig. 2– Comparison of the closed-loop behaviour of a flexibly and an economically controlled building.

The economic controller keeps the indoor air temperature at the lower limit. The heat pump is primarily operated at full load during the local price minima, which causes an increase in the storage temperature. The heat buffered in the storage is drawn gradually to fulfil the building's heating demand. It is seen, that the economic controller mainly exploits the flexibility of the thermal storage. Due to the relatively large price step on the 14th of January, the heat pump is operated for a longer period. As soon as the storage is fully charged, the indoor air temperature is elevated, too. Due to the raise of the indoor air temperature, heat is stored in the thermal mass, which allows sustaining a higher temperature of the thermal storage for a longer time.

The flexible controller differs from the economic controller through a continuous operation of the heat pump. During the first days, while the price signal is falling, the storage temperature continuously rises. After the storage has reached a certain state of charge, the indoor air temperature is elevated additionally. At the time when the price step occurs, both the indoor air temperature and the storage temperature are close to the upper limit. After the price step, the storage is discharged first and then the indoor air temperature drops. It takes approximately two days for the indoor air temperature to reach the lower temperature limit again

The available flexibility differs in both cases. As the economic controller keeps the indoor air temperature at the lower comfort limit, the load of the heat pump cannot be lowered any further, without violating the users' comfort needs. This results in negative flexibility, that is close to zero throughout the depicted period. In return, the positive flexibility is significantly higher. The flexible controller operates the heat pump at a higher load than necessary, which allows storing heat in the thermal storage and the building mass. This can be seen especially during the night setbacks when the flexible controller does not let the building cool down completely. While the price is falling, the system is charged and positive flexibility is decreased, whereas negative flexibility is increased. When the price rises, the heat pump is operated at a significantly lower load for a longer time and the negative flexibility of the building is exploited. In the shown case, the flexible controller leads to a reduced operation of the heat pump for 11 hours after the price step, while the cost-optimal controller turns on the heat pump at full load after 6 hours again.

Next, the type of available flexibility for one year is analysed. Figure 3 shows the hourly distribution of the flexibility factor that is calculated through equation (14) for the heating period in dependence on the outdoor air temperature and the 12 hours mean value of the future price signal. The flexibly controlled building's flexibility factor reaches from 0 to 1 and is dependent on the price signal. As expected, the available flexibility for low future prices is of negative type (i.e. FF close to 1). The flexibility factor of the building controlled by an EMPC is mainly in a range from 0 to 0.25, which indicates that only a small fraction of the building's flexibility is negative.

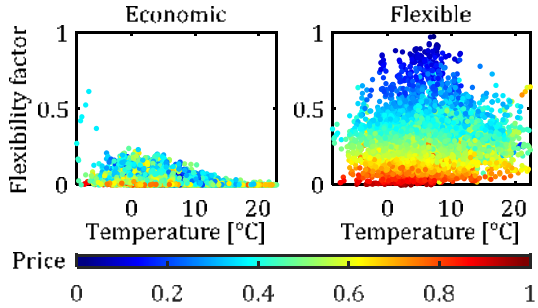

Fig. 3– Comparison of the flexibility factor for the two control approaches. Left plot: economic control, right plot: flexible control.

Figure 4 shows the mean total flexibility. The bars are divided into the type of flexibility. The building equipped with underfloor heating has a mean total flexibility of 21 kWh for the prediction horizon of 12 hours. The total flexibility of the economically controlled building is slightly higher than of the flexibly controlled building. The flexibly controlled building shows an increased share of negative flexibility.

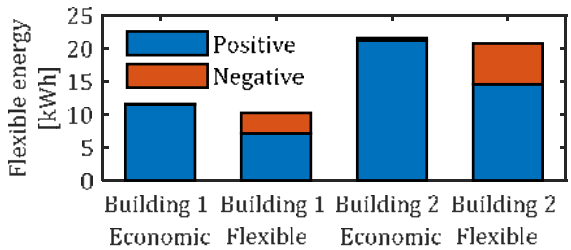

Fig. 4– Comparison of the yearly mean value for the 12 hours flexibility.

The results for the buildings are summarized in table 1. For both considered buildings, the economic controller shifts the loads to lower price regions, noticeable by the lower mean price. The heat pump's electrical demand for the flexibly operated buildings is 7 %, respectively 13 %, higher than for the economical operation. This leads to lower total operating costs. The mean load shifting capability of the flexibly operated buildings is increased, i.e. building 1 is able to reduce its load by 21.3 %. Both buildings show a flexibility factor of 0.3, whereas the factor is almost 0 for the economically controlled buildings.

5.2 Discussion

In the following section, the results are discussed briefly. The economic controller can shift loads to low price regions (figure 2). This happens through operating the heat pump at full load during local price minima and turning it off if possible. The indoor air temperature is kept close to the lower limit to avoid heat losses, this limits the available negative flexibility. In contrast, the proposed novel control approach greatly increases the available negative flexibility. Through a longer lasting low price the

Tab. 1 – Comparison of KPIs for the flexibly (Flex) and economically (Eco) controlled buildings. A bar indicates yearly mean values. The following KPIs are shown: Price ($\bar{\rho}$), electrical demand of heat pump ($E_{total,el}$), seasonal COP ($SCOP$), relative load shifting capability ($\overline{\varphi}^{-}_{rel,12h}$) and flexibility factor ($\overline{FF}$).

KPI	Unit	Building 1		Building 2	
		Eco	Flex	Eco	Flex
$\bar{\rho}$	$\frac{1}{kWh}$	0.37	0.39	0.40	0.42
$E_{total,el}$	$\frac{kWh}{m^2 \cdot a}$	18.6	21.0	40.5	43.2
$SCOP$	-	2.12	2.26	2.30	2.45
$\overline{\varphi}^{-}_{rel,12h}$	%	0.4	21.3	1.1	18.6
$\overline{FF}$	–	0.0	0.3	0.0	0.3

building is heated up, being able to perform load reduction for a longer duration.

As the load of a single building is too low to participate in the electricity market, buildings need to be aggregated. Aggregating flexibly controlled buildings, unlike cost optimally controlled buildings, yields several advantages from the grid's point of view. As the load smoothly follows the price signal, a load forecast can be performed more easily. Additionally, the proposed flexible controller only uses the current price as a control signal. This allows short term price increases while the flexibly controlled building can lower its load. These aspects are essential for a cost-effective operation of the grid, as deviations from the planned consumption can be balanced more easily.

Providing negative flexibility leads to higher electricity demand, as the indoor air temperature needs to be elevated. Thus, future electricity contracts should include a refund to increase the building operator's willingness to provide flexibility. Today's electricity tariffs are flat in many European countries. Building operators might agree to control their heat pumps flexibly and not cost optimally if they are offered a variable price, that is lower than the flat one.

6. Summary and conclusion

The growing share of renewables and the electrification of the heating sector increase the need for consumer flexibility. Due to the thermal capacity of buildings, heat pumps are suitable for flexible operation. Flexibility is the ability to change the demand following a price signal. Consequently, the cost-optimal formulation of Model Predictive Control (MPC) is the mainly used approach to exploit the building's energy flexibility. This work presents a new control algorithm, which aims to increase the building's energy flexibility. First, the available flexibility is determined through solving two optimal control problems. Next, the control input is calculated according to a price signal. A case study is conducted and the operation of an economic and a novel flexible controller are compared on a yearly basis. The economic controller usually keeps the building's temperature at the lower limit of the comfort band. The available negative flexibility is close to zero, as the possibility to decrease the load is prevented. In contrast, the flexible controller provides 30 % of the total flexibility as negative flexibility. This corresponds to the possibility to reduce the mean demand by around 20 % of the nominal load. Additionally, the new flexible controller shows a smoother load that follows the price signal. These characteristics qualify the flexible control approach for aggregation of buildings. The flexible operation is achieved through an elevated temperature. This goes along with increased consumption of around 7…13 %. As the electricity tariffs are flat in most European countries, the introduction of variable prices is a promising incentive for building operators to control their heat pumps flexibly.

7. Acknowledgement

The present contribution is a result of the research area "Flexibility" at the Graduate and Research School for Energy Efficiency Stuttgart (GREES). The authors thank GREES for the funding.

8. Appendix A

The parameters (table 2) used for the simulative model are adapted from [4]. The heat transfer coefficient R_{hi} for Building 2 was adjusted to meet design values in [27]. The window area A_w is an effective value including the transparent area and transmittance. The heated living area is denoted by A_h.

Tab. 2 – Model parameters.

Parameter	Unit	Building 1	Building 2
A_h	m^2	111	160
A_w	m^2	2.34	2.94
C_i	kJ/K	$5.11 \cdot 10^3$	$9.94 \cdot 10^3$
C_e	kJ/K	$4.15 \cdot 10^4$	$4.51 \cdot 10^4$
C_h	kJ/K	-	$9 \cdot 10^3$
C_s	kJ/K	$2.01 \cdot 10^3$	$2.01 \cdot 10^3$
R_{ea}	K/kW	15.73	10.28
R_{hi}	K/kW	-	1.0
R_{ia}	K/kW	34.48	7.12
R_{ie}	K/kW	1.04	0.46
$P_{el,max}$	kW	1.21	2.76

9. References

[1] European Commission, Stepping up Europe's 2030 climate ambition. COM(2020) 562 final, 2020.

[2] K. Hansen, B.V. Mathiesen, I.R. Skov, Full energy system transition towards 100% renewable energy in Germany in 2050, Renewable and Sustainable Energy Reviews 102 (2019) 1–13.

[3] W. Deason, Comparison of 100% renewable energy system scenarios with a focus on flexibility and cost, Renewable and Sustainable Energy Reviews 82 (2018) 3168–3178.

[4] E. Sperber, U. Frey, V. Bertsch, Reduced-order models for assessing demand response with heat pumps – Insights from the German energy system, Energy and Buildings 223 (2020) 110144.

[5] T.Q. Péan, J. Salom, R. Costa-Castelló, Review of control strategies for improving the energy flexibility provided by heat pump systems in buildings, Journal of Process Control 74 (2019) 35–49.

[6] J. Drgoňa, J. Arroyo, I. Cupeiro Figueroa, D. Blum, K. Arendt, D. Kim, E.P. Ollé, J. Oravec, M. Wetter, D.L. Vrabie, L. Helsen, All you need to know about model predictive control for buildings, Annual Reviews in Control 50 (2020) 190–232.

[7] F. Mofidi, H. Akbari, Intelligent buildings: An overview, Energy and Buildings 223 (2020) 110192.

[8] J. Al Dakheel, C. Del Pero, N. Aste, F. Leonforte, Smart buildings features and key performance indicators: A review, Sustainable Cities and Society 61 (2020) 102328.

[9] J.B. Rawlings, D.Q. Mayne, M. Diehl, Model predictive control: Theory, computation, and design, secondnd ed., paperback ed., Nob Hill Publishing, Santa Barbara (California), 2020.

[10] F. Oldewurtel, A. Parisio, C.N. Jones, D. Gyalistras, M. Gwerder, V. Stauch, B. Lehmann, M. Morari, Use of model predictive control and weather forecasts for energy efficient building climate control, Energy and Buildings 45 (2012) 15–27.

[11] R. Halvgaard, N.K. Poulsen, H. Madsen, J.B. Jorgensen, Economic Model Predictive Control for building climate control in a Smart Grid, in: 2012 IEEE PES Innovative Smart Grid Technologies (ISGT), Washington, DC, USA, IEEE, 16.01.2012 - 20.01.2012, pp. 1–6.

[12] G. Masy, E. Georges, C. Verhelst, V. Lemort, P. André, Smart grid energy flexible buildings through the use of heat pumps and building thermal mass as energy storage in the Belgian context, Science and Technology for the Built Environment 21 (2015) 800–811.

[13] S.Ø. Jensen, A. Marszal-Pomianowska, R. Lollini, W. Pasut, A. Knotzer, P. Engelmann, A. Stafford, G. Reynders, IEA EBC Annex 67 Energy Flexible Buildings, Energy and Buildings 155 (2017) 25–34.

[14] O.M. Jensen, Factsheet Energy Flexible Buildings towards Resilient Low Carbon Energy Systems: EBC Annex 82.

[15] M. Neukomm, V. Nubbe, R. Fares, Grid-Interactive Efficient Buildings Technical Report Series: Overview of Research Challenges and Gaps, 2019.

[16] International Energy Agency, Control strategies and algorithms for obtaining energy flexibility in buildings: Energy in Buildings and Communities Programme Annex 67 Energy Flexible Buildings, Teknologisk Institut, 2019.

[17] J. Burner, T. Braun, M. Gaus, M. Michl, J. Franke, Potential analysis of the use of electric storage heaters for demand side management applications, in: 2016 IEEE Smart Energy Grid Engineering (SEGE), Oshawa, ON, Canada, IEEE, 2016, pp. 284–291.

[18] J. Gasser, H. Cai, S. Karagiannopoulos, P. Heer, G. Hug, Predictive energy management of residential buildings while self-reporting flexibility envelope, Applied Energy 288 (2021) 116653.

[19] H. Golmohamadi, K. Guldstrand Larsen, P. Gjøl Jensen, I. Riaz Hasrat, Optimization of power-to-heat flexibility for residential buildings in response to day-ahead electricity price, Energy and Buildings 232 (2021) 110665.

[20] K. Leerbeck, P. Bacher, R.G. Junker, A. Tveit, O. Corradi, H. Madsen, R. Ebrahimy, Control of Heat Pumps with CO2 Emission Intensity Forecasts, Energies 13 (2020) 2851.

[21] H. Wang, S. Wang, R. Tang, Development of grid-responsive buildings: Opportunities, challenges, capabilities and applications of HVAC systems in non-residential buildings in providing ancillary services by fast demand responses to smart grids, Applied Energy 250 (2019) 697–712.

[22] R. El Geneidy, B. Howard, Contracted energy flexibility characteristics of communities: Analysis of a control strategy for demand response, Applied Energy 263 (2020) 114600.

[23] R. de Coninck, L. Helsen, Quantification of flexibility in buildings by cost curves – Methodology and application, Applied Energy 162 (2016) 653–665.

[24] R. Verschueren, G. Frison, D. Kouzoupis, N. van Duijkeren, A. Zanelli, B. Novoselnik, J. Frey, T. Albin, R. Quirynen, M. Diehl, acados: a modular open-source framework for fast embedded optimal control, 2019.

[25] P. Bacher, H. Madsen, Identifying suitable models for the heat dynamics of buildings, Energy and Buildings 43 (2011) 1511–1522.

[26] F. Madonna, F. Bazzocchi, Annual performances of reversible air-to-water heat pumps in small residential buildings, Energy and Buildings 65 (2013) 299–309.

[27] DIN V 18599-5:2018-09, Energy efficiency of buildings - Calculation of the net, final and primary energy demand for heating, cooling, ventilation, domestic hot water and lighting - Part 5, Beuth Verlag GmbH, Berlin.

Mapping of an abstract PLC information model into different fields of application

Björn Kämper [a], Maximilian Both [a], Nicolai Maisch [a], Jochen Müller [a]

[a] Institute of Building Services Engineering, TH Köln, University of Applied Sciences, Cologne, Germany, { bjoern_klaus.kaemper; maximilian_alexander.both; nicolai.maisch; jochen.mueller}@th-koeln.de.

Abstract. Collaborative working in BIM applications requires that different users have a common understanding of components such as pumps, valves or pipes. This common understanding is achieved by describing components through information models composed of defined properties. The different roles involved in the planning process (manufacturer, planner, operator) have different views of components. To avoid that different roles, develop specific information models, it makes sense to develop common information models describing the whole product life cycle (PLC). Besides BIM applications, information modeling of components is an area that is also used in industrial applications. An abstract modeling approach helps to ensure that information models are not developed in a technology-specific way.
This paper describes how a manufacturer- and technology-independent PLC information model for pumps and vacuum pumps was developed and subsequently integrated into industrial services and building services information standards. The integration is intended to serve as the basis for a continuous flow of information over the life cycle of pumps in building services applications. The challenges of this work include mapping an abstract modeling concept to existing semantics in different technologies and not creating duplicates in existing data standards.

Keywords. Industrie 4.0, cross-lifecycle information model, semantic description, BIM
DOI: https://doi.org/10.34641/clima.2022.341

1. Introduction

The term "Industry 4.0" describes the progressive digitization and networking of systems in value chains. The core idea of the fourth industrial revolution is that systems exchange information independently and networked, thereby optimizing processes. Even if the term "Industry 4.0" (I4.0) is today more associated with the manufacturing/production phase of assets, there are also approaches that assume that the concepts of I4.0 have an impact on the entire life cycle of an asset [1] [2].
An asset passes through different phases in its life cycle and comes into contact with a wide variety of systems and economic sectors. A pump, for example, already has information stored for integration into planning software as well as information for control in building automation. The different definitions of properties and functions make it difficult to implement self-organizing systems today. An example is given in Fig. 1. Assets from different manufcaturer should be integrated in an application for energy management. Different semantics (here namingconventions and physical unnit) lead to manual effort.

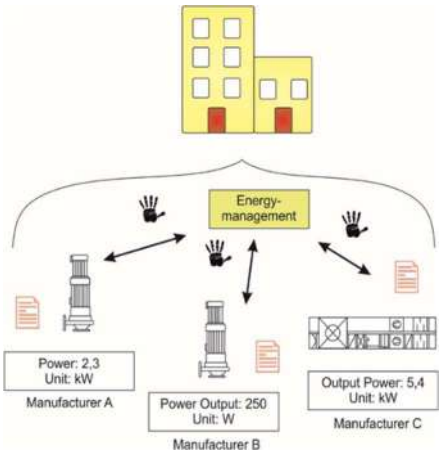

Fig. 1 - Different semantics complicate the integration effort of assets in applications (in this case an automation system).

In order for assets to be able to interact automatically and with minimal manual integration effort with the systems relevant for the respective lifecycle phases in the future, information for assets should be standardized. In order to be able to exchange information between systems in different lifecycle phases in the

Copyright ©2022 by the authors. This conference paper is published under a CC-BY-4.0 license.

future (e.g., between a BIM-based planning software and an energy management application), information should not be developed for a single technology or a single use case, but rather in an abstract and cross-lifecycle manner. Fig. 2 shows different life cycle phases of assets according to IEC 62890.

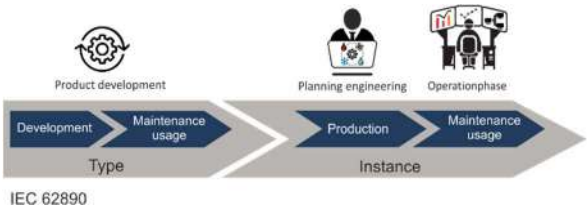

Fig. 2 - Assignment of life cycle processes according to IEC 62890 to application fields

In a common project between the Cologne University of Applied Sciences and the VDMA trade associations Pumps + Systems and Compressors, Compressed Air and Vacuum Technology, more than 500 pump-specific and lifecycle-describing properties were derived from national and international standards. These properties were summarized in process- and life-cycle-oriented *Submodels* and mapped onto the abstract information model of the *Asset Administration Shell* (AAS) [3]. In further projects, this developed information model was implemented in specific domains and areas of use (see Fig. 3). By defining this information model as an OPC UA Companion Specification, a communication connection to the OPC UA communication protocol was made possible [4]. OPC UA is considered to be the future standard for industrial communication. By integrating the properties into the online repository ECLASS, the properties are available in the "Language 4.0" [5, 6]. ECLASS is a data standard that classifies products and describes them using ISO-compliant properties [6]. In order to be able to use the properties in the process flows of building equipment programs, it is necessary to calculate the properties in a role- and user-specific manner. In order to integrate the information model into the planning phase of building services engineering, the properties are integrated into BIM as role-specific views.

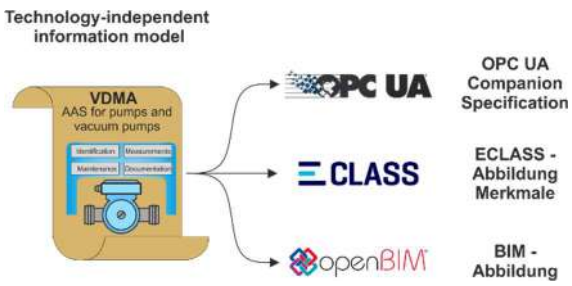

Fig. 3 - Derivation from abstract and independent information model into different domains / areas of use

The following chapters describe the path from the creation of an abstract information model to its implementation in the various technologies.

2. Asset Administration Shell for pumps and vacuum pumps

The "*Plattform Industrie 4.0*" was launched in 2013 by the German Federal Ministries for Economic Affairs and Energy and for Education and Research. A wide variety of companies and associations are organized in this platform with the aim of advancing the digital transformation in Germany. The *Plattform Industrie 4.0* develops technical solutions in various working groups, which are freely accessible via the platform [7]. The *Plattform Industrie 4.0* has defined the term *Industrie 4.0 Component* as a "globally uniquely identifiable participant with communication capability consisting of AAS and asset" [8]. Such an *AAS for pumps and vacuum pumps* was developed as an abstract information model.

2.1 Structure of Asset Administration Shells

The asset is defined by *Plattform Industrie 4.0* as "Everything that requires a *connection* for an Industry 4.0 solution: Machines and, if applicable, their components; supplier material and products; documents that are exchanged (plans, orders); contracts; purchase orders;..." [8]. Thus, an asset can be both a non-physical file and a physical product.

According to *Plattform Industrie 4.0*, the AAS is the implementation of the "digital twin" [7]. This digital image represents information and properties of an asset. AASs can contain information about the entire life cycle of an asset. Information is divided into *Submodels*. A *Submodels* can be described as a group of features that describes a particular aspect of an asset. Figure 4 shows an asset administration shell that has two *Submodels* "Measurements" and "Design" assigned to it. In the "Measurements" *Submodel* are properties that represent current measurements of the asset (e.g. speed or fluid temperature). *Submodels* can contain any number of properties.

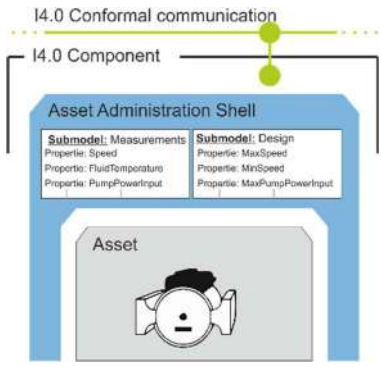

Fig. 4 - I4.0 - Component consisting of asset and AAS consisting of two Submodels with corresponding properties

2.2 Defining Submodels for pumps and vacuum pumps

The process of creating the *Submodels* for pumps and vacuum pumps can be described in three steps (see Fig. 5). First, use cases were defined together with the association companies that are to be realized with the *Submodels* to be developed. In the next step, properties were derived from national and international standards with which the corresponding use cases can be mapped. In the last step, the properties derived from the standards were divided into corresponding *Submodels*.

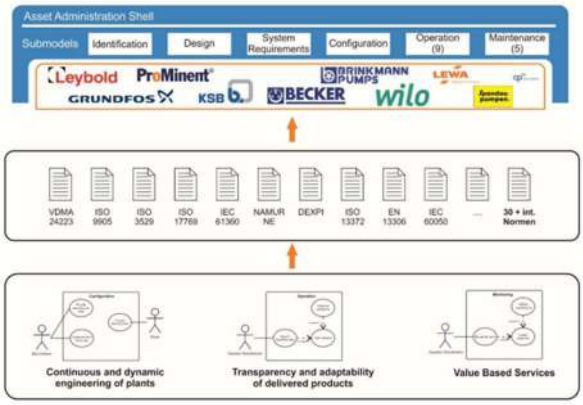

Fig. 5 - Procedure for deriving the Submodels for pumps and vacuum pumps

- ***Use-Case 1:***
  Continuous and dynamic engineering of plants (short form: Configuration)
  This use case is used to deliver a preconfigured device to the operator / integrator. The basis for this is the manufacturer data of the asset and the data of the operator / integrator about the process in which the asset is to be used. On this basis, a device is configured by the manufacturer so that the correct operating points are preset, and it can be put into operation.

- ***Use-Case 2:***
  Transparency and adaptability of delivered products (short form: Operation)
  An Operator / integrator should be able to measure and archive the operating data of the asset. It should also be possible to control the asset remotely.
  For the operator´s / integrator´s process monitoring, the device provides access to standardized alarms, warnings and events.
  In combination with the information of the use case configuration, the device operation can be analyzed and optimized. A subsequent reconfiguration of the device can be realized in order to adapt it optimally to the requirements of the operation.

- ***Use-Case 3:***
  Value based services (short form: Maintenance)
  For integrating a device in the operator´s Maintenance Management application, the device provides a common set of properties representing different maintenance strategies. Properties for breakdown, preventive and condition-based are available – depending on the maintenance strategy assigned to the asset within the operator´s maintenance process.

  Based on unique asset identification, an operator / integrator requires device related documents. Properties should contain a file or link to e.g. P&I diagrams, wiring diagrams, manuals or spare parts lists for the respective asset.
  The wear of the device is observed during operation and diagnostic information about the current state of the device is generated.

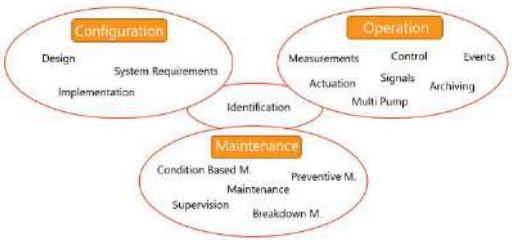

Fig. 6 - The derived Submodels with assignment to the corresponding use cases.

As shown in figure 6, a *Submodel* "Identification" has been defined. The *Submodel* Identification forms the basis for the operation of an asset and the operators Plant Asset Management, e.g. Documentation Management, Energy Management and Maintenance Management. Since this *Submodel* is so general, it was not assigned to a separate use case but as part of each use case.

In total, more than 500 life cycle describing properties for pumps and vacuum pumps were classified into 18 *Submodels*. As can be seen in table 1, the properties were defined according to IEC 61360 (Standard data element types with associated classification scheme – see table 1). The defined *Submodels* were deposited with the VDMA Association for Pumps and Vacuum Pumps for the following work as an interim report.

Tab. 1 - Exemplary representation of an IEC 61360 compliant attribute

Attribute	Pump power input
Identifier	0173-1#02-ABC172#001
Version number	-
Change number	-
Preferred name	Pump power input
Formula symbol	P_op
Definition	Measured power transmitted to the pump by its driver
Data type	REAL_MEASURE
Value format	NR2..3.3
Class of the properties	K27
Unit of measurement	Watt
Short name	P_{op}
Source document	DIN EN ISO 17769-1

3. Mapping in ECLASS

ECLASS is an ISO/IEC-compliant data standard that enables products and services to be described uniquely. This enables a standardized digital data exchange between different organizations even if they are located in different language areas. In ECLASS, more than 19,000 properties are organized in over 42500 classes. Each property is assigned a unique ID in ECLASS [9]. Such an identifier can be seen for example in table 1 in the first row.

The integration into ECLASS was done to have the developed properties defined globally unique in an online repository and to link them with a globally unique identifier.

3.1 Structure of ECLASS

The ECLASS data standard is based on a four-level hierarchy. At the lowest level (*Commodity classes*), ECLASS provides the property lists. In these properties lists, the product-specific properties can be assigned to the different classes. The four-level hierarchy is shown in Fig. 7.

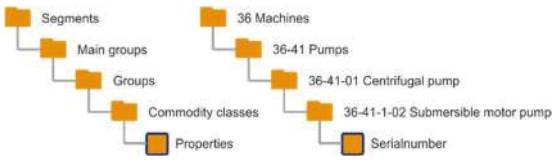

Fig. 7 - Structure of the hierarchy levels in ECLASS with representation of a submersible motor pump.

As can be seen in figure 7, in ECLASS properties are only added to the lowest hierarchy level. Properties that describe a pump in general (e.g. "pump type") cannot be assigned to the main group and thus inherited by the subordinate hierarchies.

In ECLASS there are two different modeling approaches: *Basic* and *Advanced*. In ECLASS *Basic*, properties can only be assigned to the corresponding *Commodity classes* as a flat list. ECLASS *Advanced* was integrated with Release 7.0 (currently ECLASS Release 12.0), providing extended modeling capabilities. Among other things the *Aspect* was introduced by ECLASS *Advanced*. An *Aspect* allows to bundle single properties and to assign these bundled *Aspects* to *Commodity classes*. Figure 8 shows this at the example of two properties "SerialNumber" and "MinmumSpeed". While the proeprties in ECLASS Basic are arranged as a flat list, in ECLASS Advanced it is possible to sort the properties according to their topic.

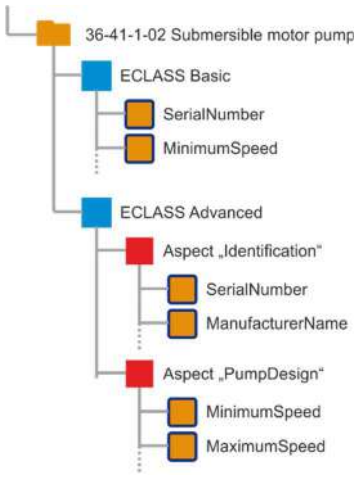

Fig. 8 - Comparison of ECLASS Basic to ECLASS Advanced.

Due to the possibility of assigning arbitrary properties to *Aspects* and then assigning these *Aspects* to any number of classification classes, this modeling approach is suitable for modeling *I4.0-Submodels* in ECLASS.

3.2 Modelling of ECLASS Aspects for Pumps & Vacuum pumps

In the first step of the integration of the *I4.0-Submodels* for pumps and vacuum pumps, all attributes contained in the *Submodels* had to be integrated into ECLASS. In ECLASS, each attribute may only occur once. Before a property from the *Submodels* was integrated into the ECLASS platform, it had to be checked whether this property was already described in ECLASS in order to avoid a duplicate.
After the integration of all properties, the properties were bundled into *Aspects* according to the *Submodels*. Again, it had to be considered that no existing *Aspect* is duplicated in ECLASS. This is especially true for the ECLASS *Aspect* "Identification". In ECLASS there are *Aspects* that are mandatory assigned to each *Commodity class*. These *Aspects* contain properties which are generally valid and not product specific. One of these mandatory *Aspects* is the *Aspect* "Identification". This *Aspect* contains properties of the manufacturer (e.g.: manufacturer name, article

number...) and properties of the supplier (e.g.: supplier name, delivery time). In this already existing ECLASS *Aspect* many properties are contained which are also contained in the Submodel "Identification". In order to avoid a duplicate, but still to be able to take over all properties from the *Submodels* in ECLASS, an ECLASS *Aspect* "PumpIdentification" was created. In this *Aspect* all properties are available which deal with identification properties but are not mapped in the general ECLASS *Aspect* "*Identification*".

The contents of the *Submodels* were developed for different pump types (liquid pumps, vacuum pumps...) and thus contain both pump-general properties and properties for specific pump types. To ensure that a liquid pump does not support the same properties as a vacuum pump when all *Submodels* are integrated, different *Aspects* had to be created for the different pump types.

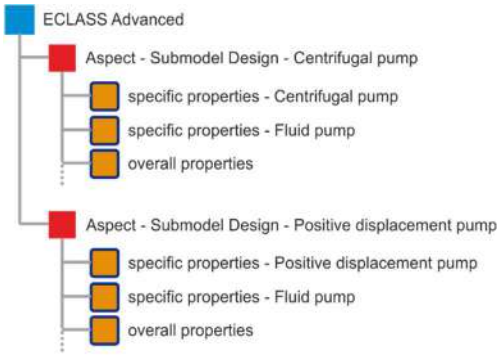

Fig. 9 - The Submodel Design divides into ECLASS-Aspects for centrifugal pumps and positive displacement pumps.

Figure 9 shows this type of modeling. For the "Design" submodel, two different *Aspects* were defined for centrifugal pumps and positive displacement pumps. In both *Aspects*, generally valid properties and properties for liquid pumps are stored. However, the two *Aspects* differ according to the specific properties for centrifugal pumps and positive displacement pumps.

4. Mapping in OPC UA

OPC UA (Open Platform Communications Unified Architecture) is a platform-independent communication protocol which is regarded as the new de facto standard in industrial automation [10]. Compared to the predecessor protocol of the OPC Foundation (OPC DA - Data Access), it is not only possible in OPC UA to transport machine data, but also to describe machine data semantically. Such semantic descriptions are developed as Companion Specifications by associations and made available by the OPC UA Foundation. In OPC UA servers, the objects, methods and attributes of the Companion Specifications can be mapped and instantiated in an object-oriented manner.

4.1 Structure of an OPC UA Server

OPC UA servers follow a layered structure (Figure 10).

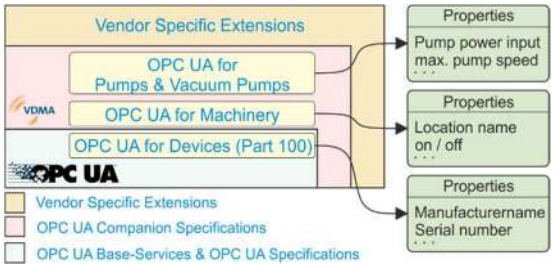

Fig. 10 - Graphical representation of an OPC UA server structure with consideration of different specifications

In the lowest layer, the basic services for information modeling and data exchange are organized. Thus, these services are available in every OPC UA server [11]. In addition to the basic services, the OPC Foundation Foundation also develops its own specifications that deal with general functions and attributes. Figure 10 shows *OPC UA for Devices (Part100)* as one such specification [12]. In this specification, general attributes of devices (e.g., manufacturer name or serial number) are organized. These generalized specifications enable client applications to program an OPC UA server in such a way that it can read out the manufacturer names and serial numbers of all devices, regardless of what kind of device they are. For this reason, it is recommended to base all companion specifications that represent devices on the general specification of the OPC Foundation [12].
In the middle layer of Figure 10, the semantic descriptions are stored in the form of OPC UA Companion Specifications that are drafted by professional associations (such as the VDMA in this example) for individual machine types. In addition to these machine-specific specifications, there are also specifications in this layer that deal with generalized functions and attributes. The specification *OPC UA for Machinery* [13] contains attributes and methods that extend the specification *OPC UA for Devices (Part 100).* The specification for pumps and vacuum pumps is also based on this specification and can also be seen in the middle level of Figure 10. More about the modeling in the next chapter.
The top level of Figure 10 shows the possibility for manufacturers and users to develop their own specifications independently or based on specifications drafted by trade associations.

4.1 Modelling of OPC UA Companion Specification for Pumps & Vacuum pumps

The designed *Submodels* of the *AAS for Pumps and Vacuum pumps* were converted into an OPC UA Companion Specification in a joint working group of the Cologne University of Applied Sciences and the VDMA trade association for Pumps + Vacuum pumps [4]. This comprehensive specification contains all attributes from the *Submodels*. The only attributes that

are mandatory are the attributes that are marked as mandatory by *OPC UA for Devices (Part 100)* and *OPC UA for Machiner.*

As a working group under the umbrella of the VDMA, the mapping was done considering the general VDMA specification *OPC UA for Machinery* and thus also the general OPC UA *specification OPC UA for Devices (Part 100).*
Figure 11 shows the modeling of the *Submodels* in an OPC UA server structure with consideration of the modeling rules and attributes from *OPC UA for Machinery* and *OPC UA for Devices (Part 100)*. In the figure, all objects are preceded by leading numbers that indicate the specification from which the corresponding objects originate.

- Leading 0: OPC UA Base-Services
- Leading 1: *OPC UA for Devices (Part 100)*
- Leading 2: *OPC UA for Machinery*
- Leading 3: *OPC UA for Pumps and Vacuum Pumps*

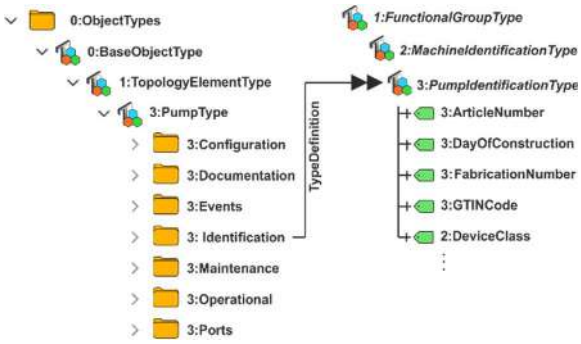

Fig. 11 - Nodestructure of OPC UA Companion Specification for Pumps and Vacuum pumps

As can be seen in the figure 12, the *Submodels* are arranged under a PumpType. The "Identification" Submodel shown here as an example in more detail shows how the modeling was implemented considering *OPC UA for Machinery* and *OPC UA for Devices (Part 100)*.

In *OPC UA for Machinery*, there is already a *MachineIdentificationType* that contains many attributes that are also contained in the *Submodel* "Identification" from the *AAS for Pumps and Vacuum Pumps*. Here, when transferring the attributes from the *Submodels* to the Companion Specification, it had to be considered which attributes are already available and which attributes have to be supplemented, just as with ECLASS. In the figure 12 this is to be recognized at the attribute "*2: DeviceClass*". This attribute was defined in the *Identifiaction* part model as well as in *OPC UA for Machinery*, which is why it was not defined again in the OPC UA Companion Specification for Pumps and Vacuum Pumps, but inherited (recognizable by the leading 2 instead of a leading 3).

All *Submodels* have been modeled in the OPC UA Companion Specification for Pumps and Vacuum Pumps as subtypes of the *FunctionalGroupType* defined in *OPC UA for Devices (Part 100).* The *FunctionalGroupType* is defined as: "*FunctionalGroups* are used to structure Nodes like Properties, Parameters and Methods according to their application such as configuration, diagnostics, asset management, condition monitoring and others.".

4.2 OPC UA Companion Specification referring to online dictionaries

In [14] it is defined that objects in OPC UA can reference online dictionaries as ECLASS. Each object can be assigned a reference in which the globally unique identifier is arranged that refers to the corresponding repository. This enables OPC UA client applications to search for attributes in OPC UA servers that are linked to corresponding entries in an online repository.
Since the attributes integrated in the online dictionary ECLASS are consistent with the attributes integrated in the OPC UA Companion Specification for Pumps and Vacuum Pumps, this referencing can be implemented in this Companion Specification. However, due to different release dates, this was not done in the first version of the OPC UA Companion Specification for Pumps and Vacuum Pumps.

5. Mapping in BIM

In technical building equipment, different actors/roles work integrally with each other in the planning and operating processes. Today, Building Information Modeling (BIM) is used as a planning method in large-scale projects.
Programs that supports BIM work with the standardized data format IFC, which is managed by BuildingSmart [15].

5.1 Structure of BIM

In order to be able to semantically describe attributes and products in an IFC-Model and to exchange them in a standardized way, the attributes that can be used in BIM are structured in the bSDD (building Smart Data Dictionary) and managed by the building Smart organization [15]. In order to make the contents of the *Submodels* accessible for BIM, the properties from the *Submodels* are integrated into the bSDD (see fig. 12). Just as in ECLASS and OPC UA, duplicates must be prevented here.

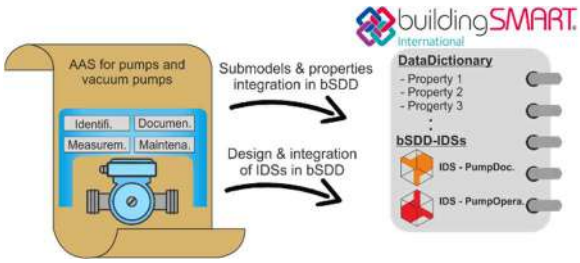

Fig. 12 - Transfer of the contents of Submodels into bSDD as attributes and Information Delivery Specifications

In addition to attributes, *Information Delivery*

Specifictaions (IDS) are also defined in the bSDD. IDS will find their way into the BIM world with the major release of IFC5.0.
With the help of an IDS, specific attributes can be retrieved from an existing and extensive IFC file (see fig. 13).

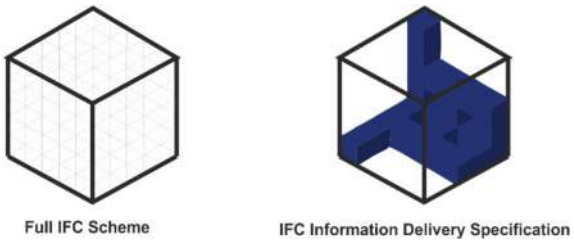

Fig. 13 - IDS allow to export a reduced set of attributes from an existing IFC Model for a common building.

IDSs thus define a role-specific perspective (view) on a building [16]. This prevents, for example, that role-specific applications have to process information that is not of interest for the specific application.

In BIM, a concept is already used in the current IFC versions to obtain role-specific information from a common IFC file. *Model View Definitions* (MVDs) allow the different actors/roles in the design and operation process (architects, building services engineers, etc.) to export a trade-specific model (architecture, HVAC) from the common IFC model and use it in specific software applications. IDS will replace MVDs and allow such specific views to be applied not only at the trade level, but also at the component level [17].

5.2 Role-specific expression of Submodels

Roles involved in building construction and operation processes are derived from existing HVAC design and operation processes. The *Submodels* for pumps and vacuum pumps are then assigned to the individual roles. The assigned *Submodels* are then transferred into IDSs and integrated into the bSDD.
By integrating machine-specific and role-specific IDSs into the world of BIM, it will be possible in the future to develop programs for building services engineering that deal with specific life cycle phases of a pump. The different roles from the planning and operating processes of building services engineering can have only those attributes specifically displayed from the entire IFC file that are of interest to the respective role (see fig. 14).

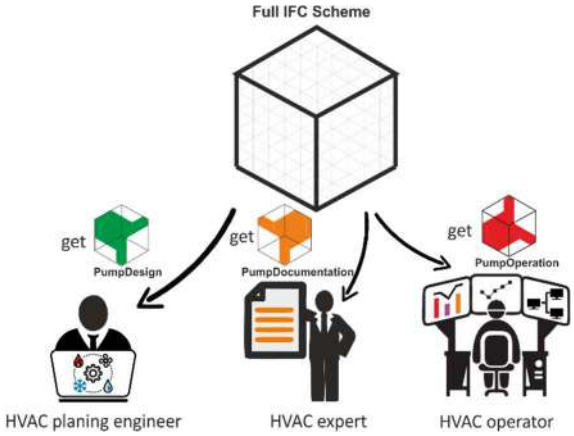

Fig. 14 - Different roles interacting with the IFC model over the life cycle of a building can export specific attributes for the respective use case through IDS.

6. Summary

This paper described how an abstract and cross-lifecycle information model was developed for an asset. This information model was mapped to the modeling rules of the *Asset Administration Shell* developed by *Plattform Industrie 4.0*. Even though there are different approaches to develop an executable technology from the AAS [18, 19], in this project the AAS was mainly used as a technology-independent and thus abstract information model for modeling. Based on this abstract information model, the content was transferred into three different application areas.
As a communication mapping, the contents were transferred into an OPC UA Companion Specificication, which was published in May 2021 [4]. In ECLASS, the content was published with MAJOR Release 12.0 in November 2021. The mapping of the content in the bSDD and the creation of the *Information Delivery Specifications* will be completed by September 2022.
When transferring the content to the different technologies, the biggest workload is to review the existing content to avoid duplicates. Another difficulty arises from the different modeling capabilities. While in OPC UA object-oriented modeling approaches can be used, in ECLASS only the classes on the lowest hierarchical level are provided with properties.
The goal of this work is to develop a cross-lifecycle and technology-independent understanding of the semantic description for a single component (in this case a pump). This semantically uniform description can enable applications to exchange information about the component with other applications outside their own value chain.

References

[1] *DIN SPEC 91345:2016-04, Reference Architecture Model Industrie 4.0 (RAMI4.0)*, Berlin.

[2] Federal Ministry for Economic Affairs and Energy (BMWi), *Mission Statement 2030 for Industry 4.0: Shaping digital ecosystems globally*.

[3] M. Both, J. Müller, B. Kämper, and D. Eichberger, ""Digitization of pumps: Industry 4.0 Sub-models for liquid and vacuum pumps,"", 4th International Rotating Equipment Con-ference 2019,, Wiesbaden,, 2019.

[4] *VDMA 40223: OPC UA for Pumps and Vacuum Pumps,,* VDMA, Apr. 2021.

[5] *Language for I4.0 Components - Structure of messages*, 2193-1, VDI/VDE, Apr. 2020.

[6] E. ECLASS e. V, *"WITH DATA AND SEMANICS ON THE WAY TO INDUSTRY 4.0: A Whitepaper from ECLASSe.V"*. Köln, 2018.

[7] *Background to the Industry 4.0 platform.* [Online]. Available: https://www.plattform-i40.de/PI40/Navigation/DE/Plattform/Hintergrund/hintergrund.html

[8] Plattform Industrie 4.0, *The Asset Administration Shell in detail: from the idea to the implementable concept [UPDATED VERSION].* [Online]. Available: https://www.plattform-i40.de/PI40/Redaktion/DE/Downloads/Publikation/verwaltungsschale-im-detail-pr%C3%A4sentation.html (accessed: Jan. 11 2022).

[9] ECLASS, *ECLASS Wiki.* [Online]. Available: https://wiki.eclass.eu/wiki/Main_Page (accessed: Jan. 13 2022).

[10] OPC Foundation, *OPC UA Roadmap.* [Online]. Available: https://opcfoundation.org/about/opc-technologies/opc-ua/opcua-roadmap/

[11] *OPC 10000: Part 1 - Part 22,* OPC Foundation.

[12] *OPC 10000-100: Devices: OPC Unified Architecture: Part 100: Devic-es,* OPC Foundation, Mar. 2021.

[13] *OPC 40001-1 - OPC UA for Machinery:: Part 1: Basic Building Blocks, VDMA 40001-1:2020-11,* VDMA, Apr. 2021.

[14] *OPC 10000-19 OPC Unified Architecture: Part 19: Dictionary Reference,* OPC Foundation, Apr. 2021.

[15] A. Borrmann, *Building Information Modeling: Technological foundations and industrial practice*. Wiesbaden: Springer Fachmedien Wiesbaden GmbH, 2015.

[16] E. industrial internet consortium, "The Industrial Internet of Things: Volume G1: Reference Architecture,: Version 1.9," Jun. 2019.

[17] buildingSMART International Ltd, Ed., "Technical Roadmap buildingSMART: Getting ready for the future," Apr. 2020.

[18] *BaSyx / WhatIsBasyx - Eclipsepedia.* [Online]. Available: https://wiki.eclipse.org/BaSyx_/_WhatIsBasyx (accessed: Aug. 7 2020).

[19] *BaSys 4.0 | Basissystem Industrie 4.0.* [Online]. Available: https://www.basys40.de/ (accessed: Aug. 7 2020).

Assessment of fouling in plate heat exchangers using classification machine learning algorithms

Seyit Ahmet Kuzucanlı [a], Ceren Vatansever [b], Alp Emre Yaşar [c], Ziya Haktan Karadeniz [d]

[a] Department of Hydraulic Module R&D, Bosch Thermotechnology, 45030, Manisa, Turkey, ahmet.kuzucanli@tr.bosch.com

[b] Department of Hydraulic Module R&D, Bosch Thermotechnology, 45030, Manisa, Turkey, ceren.vatansever@tr.bosch.com

[c] Department of Hydraulic Module R&D, Bosch Thermotechnology, 45030, Manisa, Turkey, alpemre.yasar@tr.bosch.com

[d] Department of Energy Systems Engineering, İzmir Institute of Technology, İzmir, Turkey, haktankaradeniz@iyte.edu.tr

Abstract. Plate heat exchangers (PHE) used in combi-boilers are continuously affected by small particles, both from the heating circuit and other components of the heating system. These particles can accumulate in the heat exchanger and create clogging that affect the performance of the heat exchanger over time by generating a insulating layer. To avoid unexpected blockage and other kinds of mechanical failure caused by unintended particles that originate from the pipeline and other components, it is crucial to design an effective predictive maintenance system for PHE used in the combi-boiler. In this study, the early stage of blockage in a PHE is investigated experimentally to minimize the field failure rate. The data is acquired from an experimental set-up in which just the PHEs are tested. The PHEs with the same plate pattern and different plate numbers are tested using varied flow rate and inlet temperatures as parameters. The overall heat transfer coefficient and fouling resistance are calculated to associate with the functionality of PHE. A comparison study of multi-classification algorithms has been investigated to present an algorithm which gives the most accurate model trained by experimental data. K-folds cross validation are studied using Naïve Bayes, k-nearest neighbours (kNN) and decision tree machine learning algorithms. As a result, the behaviour of overall heat transfer coefficient and fouling resistance in normalized time scale show the expected trends. The attempted models of machine learning algorithms result in Naïve Bayes predicting the classes of test data perfectly and it is followed by decision tree algorithm with an accuracy of 99.3% and kNN algorithm with 96.3%.

Keywords. Fouling, plate heat exchanger, machine learning, classification, Naïve Bayes, k-nearest neighbours, decision tree.
DOI: https://doi.org/10.34641/clima.2022.127

1. Introduction

Fouling is the process of continuous accumulation of deposited undesirable particles on heat transfer surface areas (1). In heating appliances, such as combi-boilers, a plate heat exchanger (PHE) is essential in heating up domestic water to the desired temperature. The primary heat exchanger provides heat transfer by combusting fuel (e.g natural gas) to central heating (CH) water which is used to transfer heat to the domestic water via PHE, which consists of two channels that guide two immiscible fluids, CH and domestic water. Both sides of the PHE are affected by dirt accumulation from the system components. In addition, domestic water channel of the PHE is also affected by calcification due to calcium compounds in sanitary water. Crystallization and calcification are investigated by Lee et al. (2) and Pääkkönen et al. (3,4) The CH side of the PHE is mostly affected by the particles coming from system components such as the primary heat exchanger. Due to continuous interaction with water, corrosion occurs on the surface of the aluminium primary heat exchanger. The corrosion of primary heat exchanger and particles from the pipe systems cause particulate type fouling on this side of the plates. The main particle that is seen, although in small amounts, is AI2O3, along with other calcium compounds. There are several published experimental and numerical investigations into particulate and composite fouling. (5–8)

In recent years, one of the trending research topics centered around fouling prevention is modelling and prediction algorithms. These algorithms have mostly been based on statistical methods and machine

Copyright ©2022 by the authors. This conference paper is published under a CC-BY-4.0 license.

learning techniques and include fouling prediction and detection algorithms based on support vector machines (SVM) (9,10), auto-associative kernel regression (AAKR) (11), autoregressive integrated moving average (ARIMA) (12) and artificial neural networks (ANN) (13–17). Model-based fouling prediction research have also been investigated by Kalman filter usage (18).

The predictive maintenance approach has also been looked at with an algorithm to predict fouling behaviour. The predictive maintenance techniques are designed based on mainly fault diagnostics using data analysis. The purpose of this algorithm determines the presence of anomalies and fault diagnostics generally focus on statistical approaches that provide classification and clustering. Most failure mechanisms can be associated with the degradation processes (19). The data acquisition process can be maintained by health system monitoring as in Ref. (20). The machine learning algorithms used for classification are Naïve Bayes, k-nearest neighbours (kNN), decision trees, random forests. In the Ref. (21) these algorithms are successfully studied to classify the faults of boilers by using simulated data. As a result, decision tree algorithm gave the best result with an accuracy of 97.8%. As can be seen from references, the machine learning techniques are generally used in HVAC industry especially in heat exchangers but when the open resources are considered the classification machine learning algorithms on PHEs have been investigated rarely ever.

In this study, a multi-classification study to determine fouling levels with the aim of generating a warning on combi-boiler appliances is carried out for compact brazed plate heat exchangers. The Naïve Bayes, kNN and decision tree machine learning algorithms are studied with cross-validation method for experimentally acquired data. A comparison of multi-classification machine learning algorithms, which are applied for detecting the fouling level of PHEs in the combi-boiler appliances, is provided as an introductory study.

2. Research methods

2.1 Experimental conditions

Algorithm development process starts with data acquiring regarding to get healthy and faulty conditions. To get a dataset for both conditions, just PHEs are tested. Two PHEs one having 30 and the other 32 plates are considered to examine the clogging status. Each PHE is designed for a specific combi-boiler heating capacity and dynamic system behaviour. The technical specifications that are generated from the design parameters, includes the working range information of CH and domestic water channel of PHEs. Specifications indicate that for the given inlet temperatures and flow rates, the outlet temperatures and flow rates of the PHE should be in the desired range. Investigated PHEs are already meeting these specifications therefore they are considered as the reference and their performance is considered as zero-hour performance.

The tests are conducted in the flow rates shown in Table 1. The domestic water inlet temperatures, i.e., domestic cold water (DCW), are kept constant as 10°C. The CH inlet temperatures are applied in a range of 72±1°C. The first conditions of both PHEs represent the technical specifications of 30 and 32 plates. Therefore, the results with respect to first test conditions are considered as the initial status (at t_0) of fouling process. Other test conditions are the technical specifications of PHEs with 28, 26, 24, 22, 20, 18 and 16 plates, respectively. By performing this test procedure, it is assumed that the effect of fouling on the performance of PHE is the same as the effect that would occur if the PHE with fewer plates was used instead of the designed one. Thus, a representation of the clogging behavior has been demonstrated. 50% clogged PHE as maximum clogging percentage is considered in test condition 8 (Tab. 1), technical specifications of 16 plate PHE that are implied to 32 plate PHE.

Tab. 1 – Experimental conditions applied to demonstrate the clogging behaviour of the PHEs.

	32 Plates		30 Plates	
	CH Flow Rate (l/min)	DHW Flow Rate (l/min)	CH Flow Rate (l/min)	DHW Flow Rate (l/min)
Test 1	29	18	26	10.3
Test 2	26	10.3	25.1	10.1
Test 3	25.1	10.1	21.5	8.5
Test 4	21.5	8.5	21.5	8.7
Test 5	21.5	8.7	17	6.9
Test 6	17	6.9	17.2	6.9
Test 7	17.2	6.9	17.6	6.9
Test 8	17.6	6.9		

2.2 Experimental set-up

The experimental setup contains two lines that represent CH (orange line) and DHW (green line) circuits (Fig.1). CH line is a closed circuit, and the demand of hot water is met with a combi-boiler. CH water is supplied from a tank, which is heated by the combi-boiler's system circuit with a heater coil. The static pressure of the closed circuit is 2 ± 0.1 bar which is measured inside the tank. A pump circulates water through the closed circuit. A flow control valve is located on the CH line, together with the pump that can be controlled manually to adjust the required flow rates. On the CH circuit, there is a bypass line that is used for heating the water without preheating the PHE. CH line is interacted with a cold- water

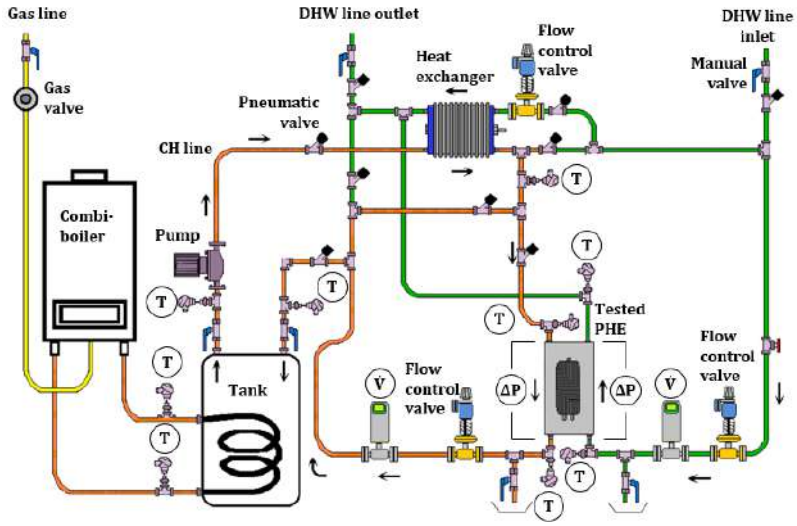

Fig. 1 – Schematic diagram of experiment set-up and its components

line to achieve the ability of necessary cooling with an additional plate heat exchanger. This cooling process control is carried out manually with the help of a flow control valve that is located on the cold-water line.

DHW line is supplied from a main chiller unit. The required flow rates are provided by a flow control valve manually. There are temperature sensors to measure the temperature of water at the inlets and outlets of the tested PHE beside the other important points such as tank inlet and outlet. The sensor locations can also be seen in Fig. 1. Flow sensors are located on both lines to measure the volume flow rate. Two differential pressure meters are placed to measure the pressure drop over the inlets and outlets of the tested PHE.

2.3 Data processing

The main effect of fouling in the PHEs is functional performance decreasing. The accumulated fouling particles creates a film layer on the plates, which pretends like an insulation layer that results in degression of heat transfer. This film layer can be represented as fouling resistance regarding to the thermal resistance concept. The logarithmic mean temperature difference (LMTD) method is used to calculate overall heat transfer coefficient (U) (Equation. (1)). Heat transfer rates of DHW and CH side are calculated by equation (2) and (3). The material properties are taken at the average temperatures of the inlets and outlets for both fluids. The total heat transfer rate is determined by taking th average of the heat transfer rates of CH and DHW sides. This overall heat transfer coefficient calculation method is also implied successfully by Zhang et al. (6).

$$\dot{Q}_{total} = U \cdot A \cdot LMTD \quad (1)$$
$$\dot{Q}_i = \dot{m}_i c_{p,i} \Delta T_i \quad (2)$$
$$\dot{Q}_j = \dot{m}_j c_{p,j} \Delta T_j \quad (3)$$
$$U = R_i + R_{wall} + R_j + R_f \quad (4)$$

Here, $\dot{Q}$ denotes heat transfer rate. DHW and CH are indicated as i and j, respectively. Specific heat is indicated as c_p, mass flow rate is $\dot{m}$, temperature

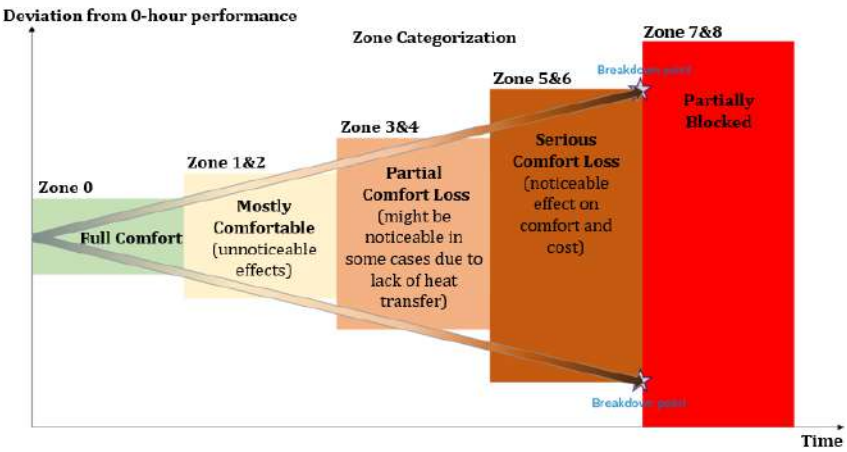

Fig. 2 – Zone categorization.

difference is ΔT. A denotes the heat transfer area. Fouling resistance (R_f) is obtained from equation (4), where R_i and R_j denote the convective thermal resistances of the DHW and CH sides, respectively. They are obtained from the CFD simulations generated by using the test conditions as boundary conditions. R_{wall} denotes conduction heat resistance which is neglected in this study.

2.4 Classification method

The used main algorithm development method is fault diagnosis to obtain the current fouling status of the PHE. There are several machine learning techniques that can be applied to diagnose faults and current situations. Classification, which is implied in this study, is a type of supervised machine learning in which an algorithm learns to classify the new data. The training data, from the experimental results is used in an algorithm to teach the zones to be predicted. The zones that are the fault labels (1 to 8) of the algorithm, represent the test conditions. Experimental conditions and measured parameters are predictors, while the zones are categorized responses in the classifier algorithm. While the deviation from 0-hour performance, initial status, is increasing, the deterioration of PHE will be increased also as expected. Zones represent the comfort loss and cost increase levels till the required maintenance time comes and finally when the PHE is required to be changed. (Fig. 2)

As there are more than one classes to be predicted, multi classification algorithms are used. Naïve Bayes, kNN (k-nearest neighbours) and decision tree algorithms are chosen due to their applicability to

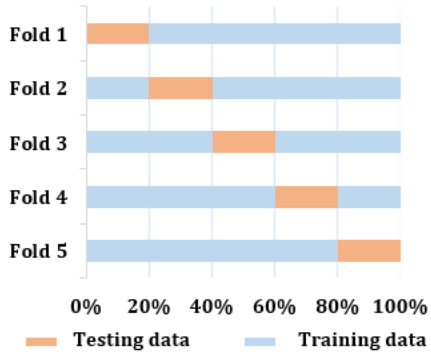

Fig. 3 – k-fold cross validation designation.

multi classification cases. The algorithms are applied to data using Classification Learner App in MATLAB. Before training of the algorithms, cross-validation is used in the process of creation the testing and training data. Cross-validation is a model assessment technique used to evaluate the algorithm's performance. Basically, this offers several techniques that split the data differently to be protected against overfitting. The k-fold cross-validation technique, which is used, partitions data into k randomly chosen subsets (or folds) of roughly equal in size as described in Fig. 3. One subset is used to validate the model that is trained using the remaining subsets (22). The average error across all k partitions is chosen to determine overall accuracy percentage. The k value is chosen as 5 in this study for all used algorithms.

Naïve Bayes is a classification algorithm that applies

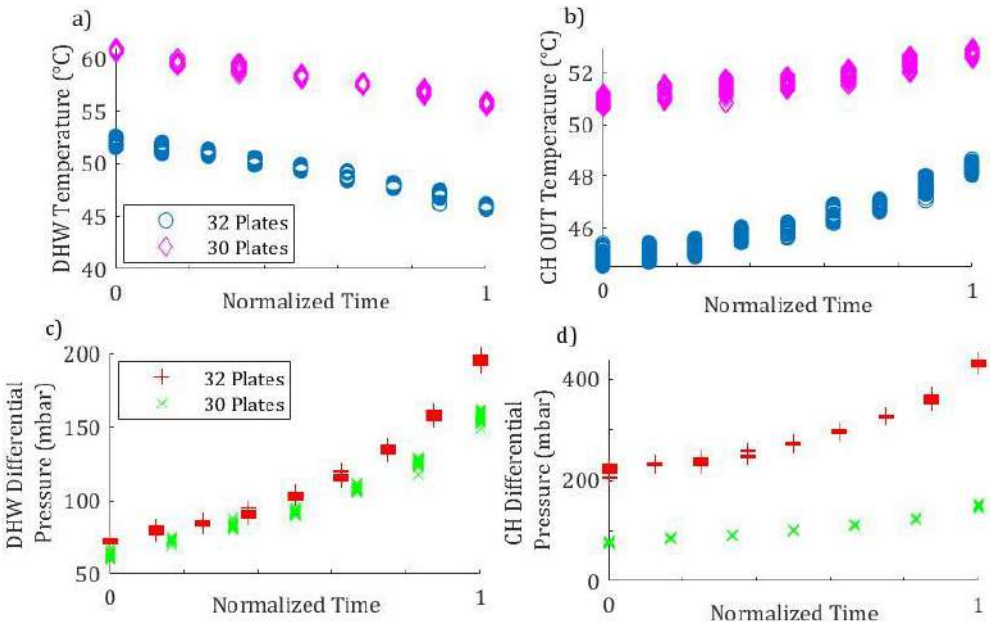

Fig. 4 - The performance trends for 32 and 30 plates a) DHW temperature behaviour b) CH outlet temperature behaviour c) Pressure drop behaviour of DHW d) Pressure drop behaviour of CH.

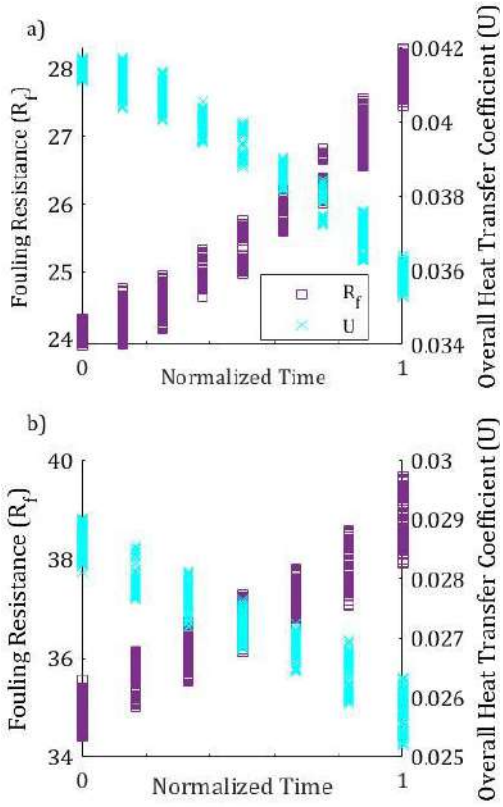

Fig. 5 – Fouling resistance and overall heat transfer coefficient behaviours a) for 32 plates b) for 30 plates.

density estimation to the data. The algorithm uses Bayes theorem, and assumes that the predictors are conditionally independent, given the class. Naive Bayes classifiers assign observations to the most probable class (23). Kernel distribution is used as a numerical predictor where the kernel width is automatically determined using an underlying fitting function via MATLAB (24).

Given data for n number of points and a distance function, k-nearest neighbours (kNN) algorithm finds the k closest points in data (25).

Number of nearest neighbours (k) to find for classifying each point when predicting, specified as 10 in this study while Euclidean distance is implied as a default in MATLAB Classification learner application. Decision trees create a hierarchical partitioning of the data, which relates the different partitions at the leaf level to the different classes (26). The hierarchical partitioning at each level is created using a split criterion. The Gini's diversity index is chosen as split criterion in this study while the maximum number of splits is implied as 100.

3. Results and discussion

The experimental results are processed as grouped to be predicted. The outlet temperatures of PHE and the differential pressure between inlets and outlets of the PHE of both CH and DHW lines are presented in scatter plot for 30 and 32 plates (Fig. 4). The results are presented in normalized time scale, here the normalized time axis represents the zones since they stand for the degradation of PHE from zone 0 to 8, respectively.

Since clogging of plates results in performance decrease in PHEs, trends of the DHW outlet temperature for both 30 and 32 plates decrease as shown in Fig. 4. In contrast, trends of the CH outlet temperature and the pressure drops of both CH and DHW lines for 30 and 32 plates increase as shown in Fig. 4. The calculated overall heat transfer coefficients for both 30 and 32 plates are shown in Fig. 5. The trends of overall heat transfer coefficient are decreasing as an expected statement of the decreasing performance.

The fouling resistance values also follow the expected trends in contrast to the overall heat transfer coefficient as shown in Fig. 5. In addition to that, the fouling resistance graphs show similar trends for particulate and composite fouling behaviours of four PHEs having different geometries studied by Zhang et al. (6).

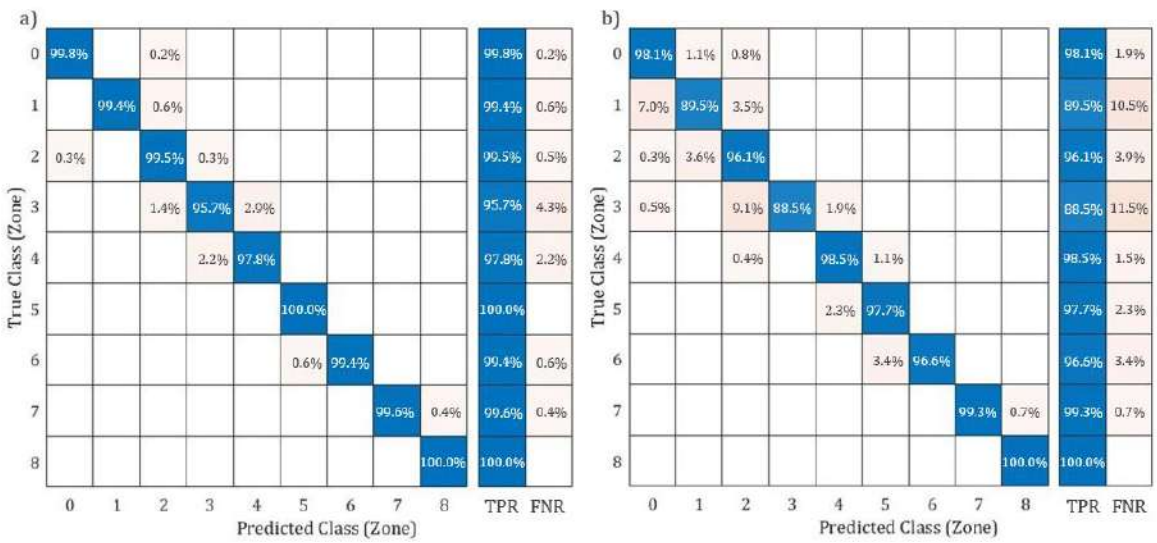

Fig. 6 – Confusion matrices of a) decision tree model b) kNN model.

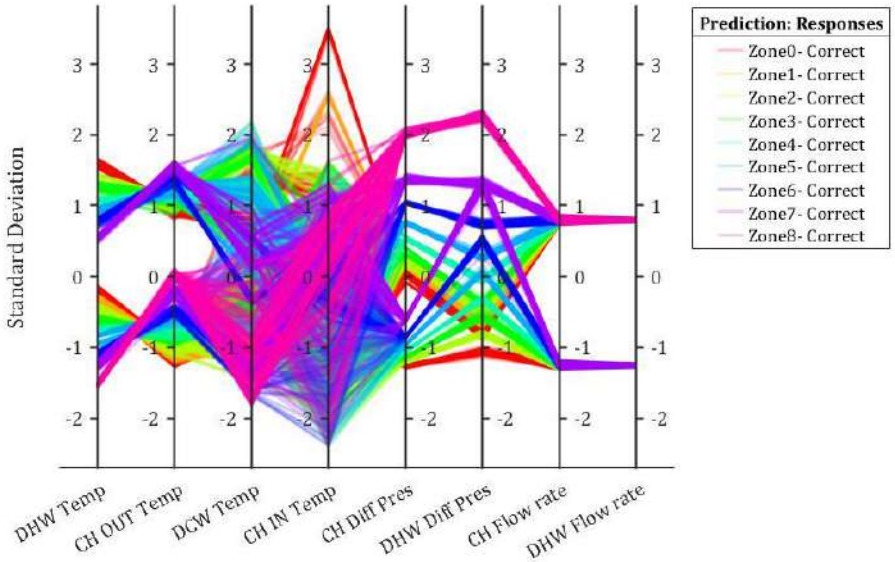

Fig. 7 – Parallel coordinates plot of experiment data shown in standard deviation scales for Naïve Bayes model.

The PHE indicated as 1st in reference study has similar geometric parameters with the ones used in this study. The Reynolds number range designated in the reference study is similar to the range in this study. As a result, trends of the calculated fouling resistance can be considered as a realistic representation of the fouling behaviour with the help of the experimental method implied in this study.

The confusion matrices of the decision tree and kNN algorithms as the results of the predicted performances of the trained models are shown in Fig. 6. Naïve Bayes is predicted the response classes perfectly with 100% accuracy. As the decision tree algorithm can predict fouling with an accuracy of 99.2%, it is followed by kNN algorithm with 96.7% accuracy. The true positive rates (TPR) and false negative rates (FNR) are designated in confusion matrices with the prediction accuracies portioned by classes. The standard deviation of the imported data can be seen in the parallel coordinates plot for Naïve Bayes trained model in Fig. 7. In the figure, the classes show more distinguishable distribution on the CH and DHW pressure difference data rather than CH inlet and DCW temperatures. This results in that the pressure difference is more convenient parameters to predict classes correctly rather than the other parameters. The DHW and CH outlet temperature data are also helpful to distinguish the classes according to the distribution shown in parallel coordinate plot (Fig. 7). With this representation of high dimensional experiment data as 2-dimensional visualization, the relation of standard deviation between the predictors can be seen.

4. Conclusion

In this study, an algorithm is developed to imply on combi-boiler appliances with the aim of generating a warning that indicates the fouling level of PHEs. Naïve Bayes, kNN and decision tree are used as the multi-classification machine learning algorithms.

The data is acquired from an experiment set-up for PHEs having 32 and 30 plates are tested. The experimental conditions are selected as the technical specifications of the PHEs. The experimental data is grouped by zones representing the fouling levels of PHE. During creation of zones, it is assumed that the effect of fouling on the performance of PHE is the same as the effect that would occur if the PHE with fewer plates was used instead of the designed. The behaviours of the overall heat transfer coefficient and the fouling resistance in normalized time scale show the expected trends. The attempted models of machine learning algorithms result in that Naïve Bayes has better accuracy compared to other models and it is followed by decision tree algorithm with an accuracy of 99.2% and kNN algorithm with 96.7% prediction accuracy. The results of trained models with tested data are shown in confusion matrices. The standard deviation of the data can be represented in parallel coordinates plot which results in the pressure drop values being seen to have the best distinguishing feature among the predictors.

Overall, this study demonstrates the possibility to generate a warning for current fouling level classification of PHEs in combi-boiler appliances by implying machine learning algorithms with high accuracy. Generation of fouling level warning results in the possibility to release a feature that can be the major effect of cost saving by retrenching on maintenance.

The framework of this study can be refined by taking time-dependent dataset into account to assess optimum time schedule of maintenance in future studies.

5. Acknowledgement

Sincere gratitude is expressed deeply to acknowledge the help provided by the technical and support staff in Bosch Thermotechnology.

6. References

1. T. Reg Bott, G. F. Hewitt, G. L. Shires. Process Heat Transfer. 1st ed. CRC-Press; 1994.

2. Lee E, Jeon J, Kang H, Kim Y. Thermal resistance in corrugated plate heat exchangers under crystallization fouling of calcium sulfate (CaSO4). International Journal of Heat and Mass Transfer. 2014 Nov 1;78:908–16.

3. Pääkkönen TM, Riihimäki M, Simonson CJ, Muurinen E, Keiski RL. Modeling CaCO3 crystallization fouling on a heat exchanger surface – Definition of fouling layer properties and model parameters. International Journal of Heat and Mass Transfer. 2015 Apr 1;83:84–98.

4. Pääkkönen TM, Riihimäki M, Simonson CJ, Muurinen E, Keiski RL. Crystallization fouling of CaCO3 – Analysis of experimental thermal resistance and its uncertainty. International Journal of Heat and Mass Transfer. 2012 Nov 1;55(23–24):6927–37.

5. Müller-Steinhagen HM, Middis J. Particulate fouling in plate heat exchangers. Heat Transfer Engineering. 1989;10(4):30–6.

6. Zhang GM, Li GQ, Li W, Zhang Z, Leng XL, Tian MC. Particulate fouling and composite fouling assessment in corrugated plate heat exchangers. International Journal of Heat and Mass Transfer. 2013 May 1;60(1):263–73.

7. Li W, Li HX, Li GQ, Yao SC. Numerical and experimental analysis of composite fouling in corrugated plate heat exchangers. International Journal of Heat and Mass Transfer. 2013 Aug 1;63:351–60.

8. Song KS, Lim J, Yun S, Kim D, Kim Y. Composite fouling characteristics of CaCO3 and CaSO4 in plate heat exchangers at various operating and geometric conditions. International Journal of Heat and Mass Transfer. 2019 Jun 1;136:555–62.

9. Sun L, Zhang Y, Saqi R. Research on the fouling prediction of heat exchanger based on Support Vector Machine optimized by Particle Swarm Optimization algorithm. In: 2009 International Conference on Mechatronics and Automation. IEEE; 2009. p. 2002–7.

10. Sun L, Zhang Y, Zheng X, Yang S, Qin Y. Research on the fouling prediction of heat exchanger based on support vector machine. In: Proceedings - International Conference on Intelligent Computation Technology and Automation, ICICTA 2008. 2008. p. 240–4.

11. Ardsomang T, Wesley Hines J, R. Upadhyaya B. Heat Exchanger Fouling and Estimation of Remaining Useful Life. Annual Conference of the PHM Society. 2021 May 29;5(1).

12. Nguyen H-P, Fauriat W, Zio E, Liu J. A Data-Driven Approach for Predicting the Remaining Useful Life of Steam Generators. In: 2018 3rd International Conference on System Reliability and Safety (ICSRS). IEEE; 2018. p. 255–60.

13. Riverol C, Napolitano V. Estimation of fouling in a plate heat exchanger through the application on neural networks. Journal of Chemical Technology and Biotechnology. 2005 May;80(5):594–600.

14. Mohanty DK, Singru PM. Fouling analysis of a shell and tube heat exchanger using local linear wavelet neural network. International Journal of Heat and Mass Transfer. 2014 Oct 1;77:946–55.

15. Wen X, Miao Q, Wang J, Ju Z. A multi-resolution wavelet neural network approach for fouling resistance forecasting of a plate heat exchanger. Applied Soft Computing. 2017 Aug 1;57:177–96.

16. Sundar S, Rajagopal MC, Zhao H, Kuntumalla G, Meng Y, Chang HC, et al. Fouling modeling and prediction approach for heat exchangers using deep learning. International Journal of Heat and Mass Transfer. 2020 Oct 1;159:120112.

17. Dheenamma M, Soman DP, Muthamizhi K, Kalaichelvi P. In pursuit of the best artificial neural network configuration for the prediction of output parameters of corrugated plate heat exchanger. Fuel. 2019 Mar 1;239:461–70.

18. Palsson OP, Jonsson GR, Desmet B, Lalot S, et al. Comparison of neural networks and Kalman filters performances for fouling detection in a heat exchanger [Internet]. Article in International Journal of Heat Exchangers. 2007. Available from: https://www.researchgate.net/publication/286315300

19. Wang W, Christer AH. Towards a general condition based maintenance model for a stochastic dynamic system. Journal of the

Operational Research Society. 2000;51(2):145–55.

20. SUN J, WANG F, NING S. Aircraft air conditioning system health state estimation and prediction for predictive maintenance. Chinese Journal of Aeronautics. 2020 Mar 1;33(3):947–55.

21. Shohet R, Kandil MS, McArthur JJ. Machine learning algorithms for classification of boiler faults using a simulated dataset. IOP Conference Series: Materials Science and Engineering. 2019 Sep 1;609(6):062007.

22. Cross-Validation - MATLAB & Simulink [Internet]. [cited 2022 Jan 3]. Available from: https://www.mathworks.com/discovery/cross-validation.html

23. Naive Bayes classification for multiclass classification - MATLAB [Internet]. [cited 2022 Jan 3]. Available from: https://www.mathworks.com/help/stats/classificationnaivebayes.html

24. Train Naive Bayes Classifiers Using Classification Learner App - MATLAB & Simulink [Internet]. [cited 2022 Jan 3]. Available from: https://www.mathworks.com/help/stats/Train-Naive-Bayes-Classifiers-Using-Classification-Learner-App.html

25. Classification Using Nearest Neighbors - MATLAB & Simulink [Internet]. [cited 2022 Jan 3]. Available from: https://www.mathworks.com/help/stats/classification-using-nearest-neighbors.html

26. Wang, Po-Wei C-JL. Data Classification: Algorithms and Applications [Internet]. Aggarwal CC, editor. C. Aggarwal eds. Data Classification: Algorithms and Applications,Data Mining and Knowledge Discovery Series. Chapman & Hall/CRC; 2014 [cited 2022 Jan 3]. 187–202. Available from: http://www.crcnetbase.com/doi/book/10.1201/b17320

Data Statement

The datasets generated during and/or analysed during the current study are not available due to company policy restrictions based on company profits.

Digital system interaction test: quality assurance of system functions through standardized tests

Rebekka Benfer [a], Ralf Ulmer [a], Eike Hinck [a], Jochen Müller [a], Samuel Rischmüller [b], Stefan Plesser [b]

[a] Institute of Building Services Engineering, Faculty of Process Engineering, Energy and Mechanical Systems, TH Köln - University of Applied Sciences, Cologne, Germany, rebekka.benfer@th-koeln.de, ralf.ulmer@th-koeln.de, eike.hinck@th-koeln.de, jochen.mueller@th-koeln.de.

[b] synavision GmbH, Bielefeld, Germany, rischmueller@synavision.de, plesser@synavision.de.

Abstract. Technical building systems are becoming increasingly complex, more diverse and more strongly networked through building automation systems. As a result, resource-saving and energy-efficient operation can be achieved. In practice, however, faults and deficiencies often exist in the systems that prevent the most efficient plant operation possible. The deficiencies include, for example, an incorrect parameterization of systems, controller settings that are not matched and optimized to the system, and inadequate cross-plant automation functions. In practice, various methods are used to identify these deficiencies and ensure the quality of automation functions. These include visual inspection of the plant to be tested by certified testing experts. In addition, applications of monitoring and commissioning as well as user-oriented test sequences can be used for fault detection and quality assurance of automation functions. However, the aforementioned procedures are associated with time and configuration effort, which result in costs for their usage and configuration. In addition, they are not based on any generally valid and standardized procedure. Based on these findings, this paper describes the conceptual development of digital system interaction tests that can be used to check different cross-plant automation functions. On the one hand, the focus of the process is on implementing the test procedure as automatically as possible. On the other hand, it should be standardized and generally applicable. Due to the low configuration effort, time and costs for the use of the procedure can be reduced. The standardization of the test procedure enables the application to be used in different technical building systems and creates a transparent form of testing.

Keywords. Energy efficiency, Quality assurance of building services, Automated and low configuration functional tests, Standardized test procedures.
DOI: https://doi.org/10.34641/clima.2022.292

1. Introduction

Technical building systems are becoming increasingly complex due to their networking. At the same time, the demands on installers and operators are increasing due to the requirement for demand-oriented and energy-efficient operation [1]. In 2019, the energy consumption of the building sector was 35% of the total global energy consumption [2]. [3] have shown that various deficiencies in building systems can be observed in operation. These deficiencies can result in energy not being used optimally and thus the possible energy savings potential not being fully exploited. Future remediation of these deficiencies can lead to increased efficiency and reduced energy consumption in the building sector.

The detection of deficiencies with the aim of quality assurance and optimization of technical building systems, is currently carried out using various methods. Examples are expert inspections, monitoring or commissioning processes and user-oriented test procedures, which are explained below.

Expert inspections

In Germany, expert inspections ensure the effectiveness and operational safety of systems subject to mandatory inspection, as well as the proper interaction of various systems. [4, 5] The inspection is carried out during commissioning, after major modifications and at specified intervals during operation. [4] Tests are executed on site at the plant and include visual inspections of the components, display of the operating states, but also defined functional tests of frost protection, damper control and flow monitoring for the example of an air handling unit (AHU). Building permits and functional descriptions of the systems serve as the basis for testing. [6].

Copyright ©2022 by the authors. This conference paper is published under a CC-BY-4.0 license.

A weakness of expert inspections is that tests take place on site, which creates expense. In addition, the selection of tests specified in the test principles does not include a review of plant efficiency, but only of the effectiveness of selected functions [6].

Monitoring

Plant monitoring aims at the recording and analysis of operating states for function control, operation optimization and analysis of fault conditions. For fault detection various methods can be used for example limit value monitoring, process models or plant simulations. [7]

Due to the fact that data from building automation can be used for plant monitoring [7], remote plant monitoring of analyzable data is possible. In addition, the detection of errors [8, 9] in the operating states enables to eliminate them and thus improve the energy efficiency of the systems. However, since the tests are based on the operating states of the plant, this prevents the verification of the chronological sequence of automation functions. Other disadvantages of the current monitoring systems are the manual integration of data points into test scenarios and that selection of test scenarios is not standardized. Test scenarios are usually created individually for each plant, which results in manual effort. In addition, monitoring is a process without intervention in the plants. If certain load situations do not occur within the monitoring period, they cannot be checked.

Commissioning

Commissioning is the process of ensuring components operate to code and planning. It also includes the optimization of plant parameters under real load conditions to achieve an optimal operating condition. Energy management and information systems or at the plant level building automation systems can be used as tools for this purpose. [10] Continuous or monitoring based commissioning represents the ongoing commissioning in building operation with recording of plant data and evaluation of performance [7]. In [11], due to the increasing complexity of BACS, the need for automated process for commissioning building automation systems is described but not the process itself.

Similar to plant monitoring, energy savings can also be achieved through commissioning [10, 12, 13] However, here too, no test procedures and test scopes are defined in advance.

User-oriented certification

The aim of user-oriented certification [14] is to test the correct functionality of user-specific efficiency programs for technical building services. The configuration effort for testing can be kept low, since test scenarios are adapted to the user requirements and can thus be used for testing all of his systems. In addition, the system is manipulated during the test sequence by means of synthetic values, which means that a check under simulation of different load conditions can be carried out in a short time.

An evaluation of efficiency programs in the municipal environment has shown that only 30% of the efficiency programs tested perform their required function. Identifying these deficiencies and correcting them can save energy, as with monitoring and commissioning. Nevertheless, the configuration effort cannot be completely avoided, since the selection of suitable data points and their integration into the testing process is done manually.

The possibilities for quality assurance and operational optimization of building automation have been described in the previous sections. However, all of the above-mentioned methods involve configuration efforts that are time-consuming. In addition, the test mechanisms differ depending on the system to be tested, which reduces both the transparency and the traceability of the test results. In comparison to the previously described methods, this paper presents a method that is intended to guarantee automated quality assurance and operational optimization of building automation by using uniform test methods and minimizing the manual configuration effort.

2. Research method

This section describes the concept of an automated, digital system interaction test. Its aim is a standardized and transparent testing and quality assurance of automation functions. The test procedure is structured in such a way that it runs uniformly and as automatically as possible. This results in the benefit of minimizing the manual configuration effort prior to the use of test methods such as those described in section 1. In addition, the procedure can be applied to various building services due to its standardized process. The sub-aspects of the test procedure considered are divided into:

- User inputs
- Exploration of the building automation and control network
- Generation of a BACnet [15] data point file for the edge device
- Design of an explorable MQTT [16] topic structure
- Component-based creation of a digital twin
- Generation of a MQTT data point file for the edge device
- Generation of a dispatch file for the edge device
- Component-based test configuration
- Execution of the test scenarios
- Evaluation of the test results

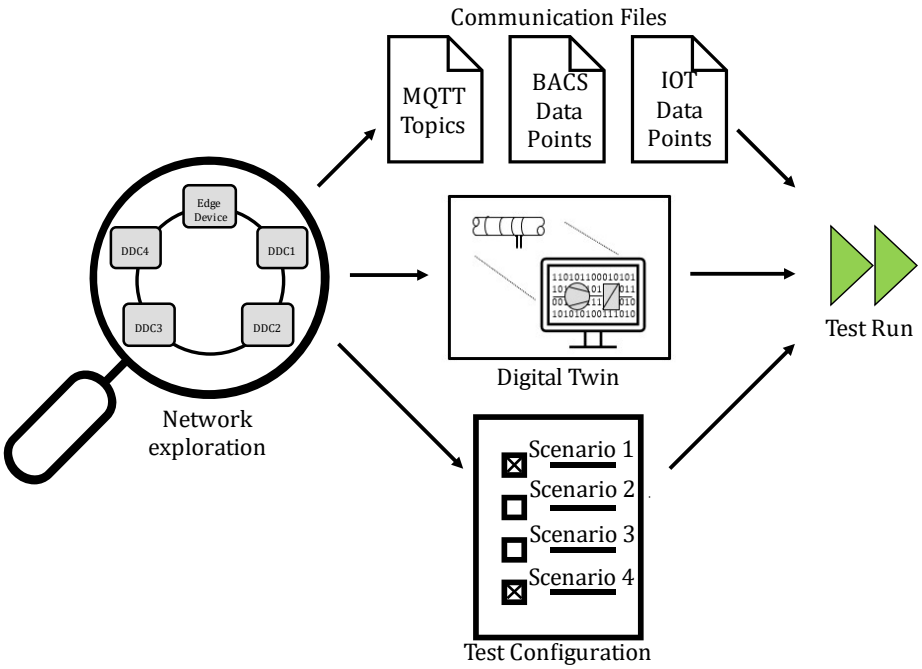

Fig. 1 - Overview of the sub-aspects of digital system interaction tests

In the following sections, the aforementioned sub-aspects of a digital system interaction test will be explained using an exemplary use case of building services. In the first part the general conditions for the use case are defined and followed by separate sections which explain the different aspects of the test procedure in more detail.

Use case assumptions

The scenario shown in Figure 2 is assumed as an example to describe the method of a digital system interaction test.

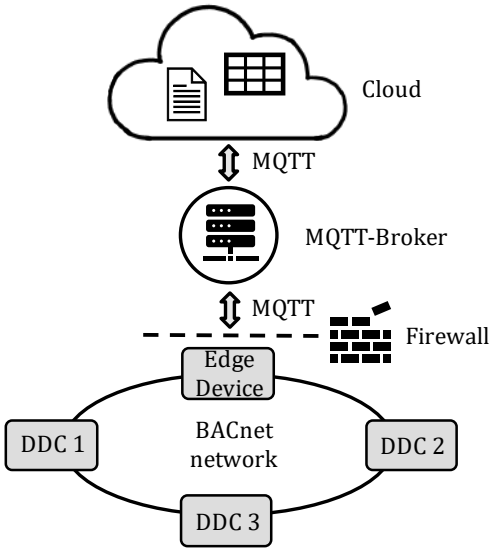

Fig. 2 - Implementation of the communication between protocols of BACS networks and the IoT on the example of BACnet and MQTT using an Edge-Device and an MQTT-Broker

The communication within the building automation and control systems (BACS) network of a property owner is realized via the BACnet protocol [15]. The automation and control of various plants, for example an AHU, is carried out by a programmed automation station (DDC). The existing data points of the plants were designated according to a standardized, defined user address system (UAS). In addition, an edge device has been installed in the same network. It is used to translate between different BACS protocols, explore BACS networks and communicate with IoT protocols. An often used messaging transport system for IoT communication is the Message Queuing Telemetry Transport protocol (MQTT) [16]. An established MQTT broker is used as an interface for a cloud connection. This enables the data transfer between a BACS network and a cloud platform. The data stored in the cloud is available for analysis and evaluation in IoT applications.

User inputs

The process is started by the inspector giving general information about the inspection. It is necessary to specify which plant is to be subjected to a test. This information is based on the plant designation according to the UAS. According to [17], the user input could be "FAC01" (full air-conditioning system). Furthermore, it is necessary to specify the Ida of the BACnet devices which contain information about the plant to be tested.

Exploration of the building automation and control network

The next step is the automated exploration of the BACnet network and data filtering. A BACnet scan is performed by the edge device. It is initiated by an MQTT topic that is published to the MQTT broker by

the application for digital system interaction test and subscribed by the edge device. The payload contains the IDs of the BACnet devices to be scanned. The results of the scan are published to the MQTT broker under an MQTT topic created specifically for each BACnet device, for example in XML or JSON format. [18]

After the BACnet scan, the application subscribes to the result topics of the scan using the device IDs in order to be able to further use the detected data points. The payloads of these topics are stored in a database. Since the results of the BACnet scan can be used to test multiple assets, the payload files are duplicated. In the process of the digital system interaction test, only the data points of the plant to be tested are required. To filter the required data, a comparison of the BACnet data point designations with the plant designation defined in section "User inputs" is performed using the duplicates for all BACnet objects from the scan result. All data points whose designation do not include the plant designation are deleted from the XML or JSON files.

Generation of a BACnet data point file for the edge device

Based on the explored and filtered data points described in the previous section, a BACnet data point file is generated. This file contains an entry with specific information from the BACnet scan for each BACnet object of the plant to be checked. This information includes the ID of the BACnet device on which the object was found, the object type and the object instance. This is used to ensure that each entry within the BACnet data point file can be uniquely assigned to a BACnet object. Depending on the structure used by the edge device, every data point looks as follows:

<deviceID>.<objectTyp>_<objectInstance>

If there is, for example a BACnet Object with the object type “binary-input” and the object instance 12 found on the BACnet device with device-ID 25001 the entry would look as follows:

25001.BI_12

In the further process of the digital system interaction test, the BACnet data point file is used as the basis for generating an MQTT data point file for communication with the IoT. BACnet and MQTT data point file are used in the context of this paper by the edge device for communication between protocols of the BACS network (here BACnet) and protocols of the IoT (here MQTT). The description of the implementation is given later in section "Generation of a dispatch file for the edge device".

Design of an explorable MQTT topic structure

In order to be able to implement the further steps of the digital system interaction test as automatically as possible, it is necessary to design an explorable MQTT topic structure. For this purpose, an MQTT topic is designed for each BACnet object based on its data point designation, which also uses the structure from the already defined UAS. This ensures that each MQTT topic is unique and can be assigned to the associated BACnet object.

Component-based creation of a digital twin

In the application, a digital twin is derived from the real plant. It is represented by the information model of the asset administration shell (AAS) [19] and is based on a predefined template depending on the plant type. In the use case "Digital system interaction test", the AAS contains the submodels "Components" and "Test descriptions" (Fig. 3). The submodel "Components" is used to identify the components of the real system. It consists of several SubmodelElementCollections (SMC) for all possible components of an AHU and their designs. In each SMC, properties (Prop) are defined whose values contain MQTT topics. These MQTT topics can be used to indicate the installation of the component described by the SMC in the real system under test. For example, with regard to the preheater of an AHU, the submodel „Components“ contains SMCs for a water preheater and an electric preheater. By matching the explorable MQTT topics of the real system with the values of the properties, it is possible to identify which component is installed in the system. The instance of the digital twin depends on the structure of the real system. For example, if a preheater pump (HEA/PUM) exists in the MQTT topics of the real system, it can be concluded that the preheater is a water preheater.

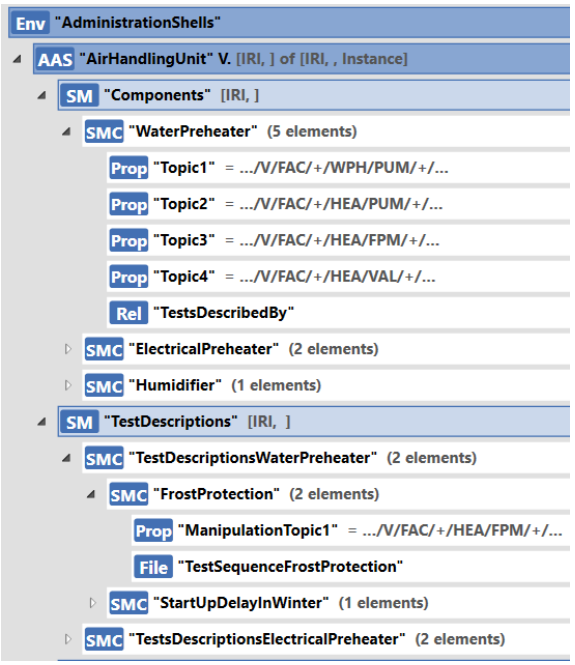

Fig. 3 - Excerpt of the template of an AHU for the instantiation of a digital twin based on a real system

Legend: V – ventilation, FAC – full air conditioning system, WPH – water preheater, PUM – pump, HEA – heater, FPM – frost protection monitor, EPH – electrical preheater, VAL - valve

As a result, only the SMC WaterPreheater of the submodel „Components“ and the SMC “TestDescriptionsWaterPreheater” of the submodel “TestDescriptions” are considered when instantiating the digital twin. In the SMCs of the submodel "Components", RelationshipElements (Rel) refer to the test descriptions associated with the components, which are contained in the SMC of the submodel "Test descriptions". This submodel describes the scope of the tests required to check the subcomponents of the AHU. For each test there is a separate SMC in which the associated test sequences are stored as files and the topics to be manipulated are described. Using the example of a water preheater, the test comprises the check of the frost protection and the winter start-up circuit as shown in Figure 3.

Generation of an MQTT data point file for the edge device

From the information of the instantiated AAS for the system under test described in the previous section, an MQTT data point file can be generated, analogous to the creation of the data point file of the BACS network. This file is used by the edge device for communication with the IoT.

For the purpose of time series data collection, an entry is created for each data point of the system under test, which contains the MQTT topic of the respective data point defined in section "Design of an explorable MQTT topic structure". This topic is supplemented by a suffix, e.g. “/measure”. The suffix is used to inform that the entry contains a data point with information from the BACS network. The edge device is used to send the BACS information to an MQTT broker that is part of the cloud platform. So the sent data can be used for evaluation in the IoT.

In addition, entries are created in the file for data points that have to be overwritten for checking purposes. These depend on the structure of the system under test and its components. The information which data points have to be manipulated are stored in the submodel “TestDescriptions” of the AAS. For each test the topics used for manipulation are stored in the values of the properties of the according SMC. To indicate that the MQTT topic is used for manipulating the system, it is supplemented with the suffix “manipulate”. This suffix informs that the entry contains a data point with information from the IoT that has to be subscribed from the MQTT broker by the edge device. After this step the information of the IoT is available in the BACS network.

Generation of a dispatch file for the edge device

In order to map the BACnet and MQTT data points to each other, a dispatch file is generated automatically using the described data point files of BACnet and MQTT. In the first step, the topic of each entry in the MQTT data point file is compared with the data point designations of the BACnet data point file. If the MQTT topic contains the BACnet data point designation, an entry for a data point mapping is created in the dispatch file. The structure of the entry, as shown in Figure 4, depends on whether it is an MQTT topic for time series data collection of the system from the BACS network or one for manipulating system data for testing purposes. An indication of this is the suffix of the MQTT topic under consideration described in the previous section.

In the case of an MQTT topic for time series data collection with the suffix "/measure", data from the BACS network has to be transmitted by the edge device to an MQTT broker and thus made available to the IoT. The entry in the dispatch file contains the entry from the BACnet data point file as the information source and the entry from the corresponding MQTT data point file as the destination (compare Figure 4).

In the case of an MQTT data point topic for manipulation of plant data with the suffix "/manipulate", test sequences have to be transmitted from the MQTT broker to the BACS network using the edge device. In the dispatch file, the entry from the MQTT data point file is used as the information source and the one from the BACnet data point file as the destination (compare Figure 4).

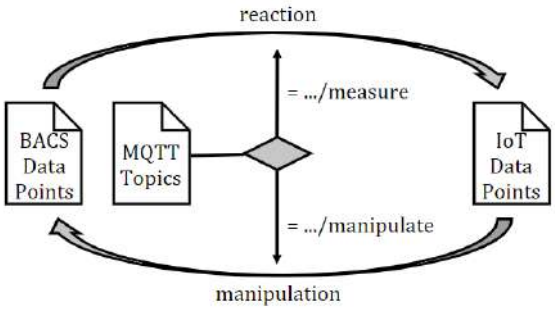

Fig. 4 - Dispatch mechanism for mapping BACnet data points and MQTT data points

Component-based test configuration

This section describes the automated configuration and compilation of test scenarios to be run through as part of the digital system interaction test. This depends on the plant and its components. The results of section "Component-based creation of a digital twin" can be used as a basis for the compilation. Each SubmodelElementCollection (SMC) of a component includes a RelationshipElement, that references to a SMC which contains information about the required tests. (Figure 3) For example the SMC “WaterPreheater” includes the RelationshipElement “TestsDescribedBy” that references to the SMC “TestDescriptionsWaterPreheater”. This SMC contains the required information for a test of frost

protection and start-up delay in winter for a water preheater. An excerpt of required tests for different components is shown in table 1. Column 1 contains the component to be tested. In the second column, the test is designated. The third column contains the components that have to be included in the test, depending on their availability. In table 1, the water preheater of an AHU is considered as an example. If a water preheater is available, the triggering of the frost protection monitor and the start-up delay in winter should be checked. These are used to protect the system in order to prevent the heater from being damaged by frost at low outdoor air temperatures. In addition to the preheater, it is also necessary to check the control of the dampers and fans of the system. If the preheater is an electric preheater instead of a water preheater, the triggering of the temperature monitor or the run-on time of the fans in case of system shutdown have to be checked to ensure system safety. By means of the principle presented, all necessary test mechanisms can be selected automatically, depending on the components recognized in section "Component-based creation of a digital twin".

Execution of the test scenarios

Based on the compilation of required tests described in the previous section, setpoints for schedules or indoor air temperatures, for example, are first transferred from the BACS network. These are required for a subsequent target-actual comparison. This is followed by the execution of the test sequences. They are called according to the functions under test together with the associated time series for data points that need to be overwritten during the test process of the function. This time series data are stored in the AAS of the plant under test. Every SMC of the submodel “TestDescriptions” that describes function tests of a component contains a File with the used time series data. Parameters such as climatic environmental influences, measured values or specified setpoints are changed and the reaction of the plant is observed.

In the following, the sequence for testing the frost protection function of a water preheater in an AHU will be explained as an example using table 2. For this purpose, the data point of the frost protection monitor is manipulated in such a way that the system is simulated to be triggered (column "manipulation"). In case of a correctly implemented frost protection function, the system should be switched off. This will cause the closing of outdoor and exhaust air dampers and the switching off of fans. In addition, the preheater should be heated up completely, for which purpose the preheater pump has to be switched on and the preheater valve has to be opened completely (columns "expected reaction"). The actual behavior of the components is recorded using time series data acquisition and published to an MQTT broker by the configured edge device. The data is stored in a cloud database and thus made available for evaluation in the IoT.

Evaluation of the test results

The test sequences defined in table 2 of section "Execution of the test scenarios" represent not only the required manipulation but also the target behavior of the system. Its actual behavior is captured by the records of the test-relevant data points that have been stored in a cloud database. Target and actual behavior are compared with each other. The tests are evaluated component-by-component. If, for example, the outdoor and exhaust air dampers in the example of the frost protection function only react after several minutes, the reaction of these is documented as not corresponding to the target behavior and thus represents a deficiency. For each test, a key performance indicator (KPI) is created that describes the fulfillment of the target state. It comprises a scale from one to ten. If the value of the KPI for the frost protection test is ten, this indicates that all components exhibited the expected target behavior at all times during the test. If the value of the KPI is three, this means that all components together have fulfilled their target behavior over a period of 30% of the tested time.

Tab. 1 - Excerpt of required test scenarios depending on existing plant components using the example of different heater types

Component	Test designation	Components to be tested (according to availability)
Water preheater	Frost protection control	Dampers, fans, heater
Water preheater	Start-up delay in winter	Dampers, fans, heater, control release
Electrical preheater	Overheating control	Heater, fans
Electrical preheater	Fan run-on during system shutdown	Fans

Tab. 2 - Example test sequence for testing the frost protection function of a water heater
t = time unit, *bef = expected plant behavior before test, *man = manipulation, *er = expected reaction, *af = expected plant behavior after test

Component	*bef	*man	*er			*man	*af		
	t = -1	t = 0	t = 1	t = 2	t = 3	t = 4	t = 5	t = 6	t = 7
Frost protection monitor	0	1	0	0	0	0	0	0	0
Outdoor and exhaust air damper	Min-100	-	0	0	0	-	Min-100	Min-100	Min-100
Fans	1	-	0	0	0	-	1	1	1
Heater pump	0/1	-	1	1	1	-	0/1	0/1	0/1
Heater valve	0-100	-	100	100	100	-	0-100	0-100	0-100
Acknowledgement	0	-	-	-	-	1	-	-	-

3. Discussion and conclusion

The possibilities for detecting deficiencies and saving energy have already been presented in the introduction by the methods of monitoring, commissioning and user-oriented certification. The advantages of the method presented in this paper primarily relate to the savings in configuration effort and the standardization of test procedures.

Savings in configuration effort

Compared to the described expert inspection, access to the building automation network reduces the effort for on-site inspections. By using a unified UAS and incorporating a gateway, building automation networks, in this case BACnet, can be explored automatically and the available data points can be transferred into a UAS oriented MQTT topic format. This reduces the configuration effort compared to monitoring applications, commissioning processes or user-oriented certification. With these methods, the data points still have to be explored and mapped to the test scenarios manually. The converted MQTT data points, described in this paper, are standardized by templates of the submodel "Components" of a digital twin and are used for configuration-free selection of test scenarios. This is based on the actual plant structure, its components and their subtypes mapped in the digital twin. The inspector-independent and component-dependent selection thus made possible is not considered in previous monitoring and commissioning applications.

Standardization

Standardization is achieved through component-based test selection and predefined test scenarios. The test scenarios contain synthetic data for triggering specific plant states, so that functions can be checked completely independent without being influenced by real load conditions.

Various stakeholder of the building benefit from the described process. Building owners benefit from time and associated construction cost savings due to increased productivity of executing companies during the commissioning phase. For inspectors of technical systems, the advantage is that inspections can be digitized and automated. Uniform, standardized testing procedures are available that can be used with little configuration effort.

During the operating phase, owners and tenants in particular benefit from the procedure, because detected deficiencies can be eliminated which contributes to energy savings and thus to the reduction of energy costs.

This could lead to a broader application of the described inspection procedure, which would reveal more operational faults and non-energy-saving plant operating conditions. The energy consumption of the building sector can be permanently reduced by eliminating the detected deficiencies and causes an increase in energy efficiency in the operation of technical equipment.

4. References

[1] Verein Deutscher Ingenieure e.V. Guideline VDI 6039. Facility Management – Managing of building commissioning – Methods and procedures for building-services installations. Berlin: Beuth-Verlag GmbH; Jun 2011.

[2] United Nations Environment programme. 2020 Global status report for buildings and construction – Towards a Zero-emission, Efficient and Resilient Buildings and Construction Sector. Nairobi: 2020. 80p.

[3] Mills E. Building commissioning: a golden opportunity for reducing energy costs and greenhouse gas emissions in the Unites States. Energy Effic. 2011 Feb 12; 4:145-173. doi: 10.1007/s12053-011-9116-8

[4] Verordnung über die Prüfung technischer Anlagen und wiederkehrende Prüfungen von Sonderbauten (PrüfVO NRW). 2009 Nov 24

[5] Verein Deutscher Ingenieure Guideline VDI 6010 Part 3. Technical safety installations for buildings – Integrated system test. Berlin: Beuth-Verlag GmbH; May 2020.

[6] Verordnung über die Prüfung technischer Anlagen und wiederkehrende Prüfungen von Sonderbauten (PrüfVO NRW). Anhang - Grundsätze für die Prüfung technischer Anlagen entsprechend der Prüfverordnung durch Prüfsachverständige. 2019 Jul 17.

[7] Verein Deutscher Ingenieure Guideline VDI 6041. Facility Management – Technical Monitoring of buildings and building services. Berlin: Beuth-Verlag GmbH; Jul 2017.

[8] Andriamamonjy A, Saelens D, Klein R. An auto-deployed model-based fault detection and diagnosis approach for AHU using BIM and Modelica. Autom Constr. 2018; 96: 508-526. doi: 10.1016/j.autcon.2018.09.016

[9] Reeve H, Jing B, Zhu Z, Chabukswar R, Ghosh A, Li Y. Field Demonstration of an Automated Building Comissioning Tool. ASHRAE Trans. 2019; 125:37-46.

[10] Kramer H, Lin G, Curtin C, Crowe E, Granderson J. Building analytics and monitoring-based commissioning - industry practice, costs, and saving. Energy Effic. 2019 May 03; 13: 537-549. doi: 10.1007/s12053-019-09-09790-2

[11] Muhyiddine J, Boel N, Madsen BE, Jacobsen J, Hooge JS, Kildelund L. BuildCOM: automated auditing and continuous commissioning of next generation building management systems. Energy Inform. 2021; 4:2. doi: 10.1186/s42162-020-00136-2

[12] Kim YK, Altan H. Analysis of Energy Reduction trough HVAC Comissioning. In: 2018 5th International Conference on Renewable Energy: Generation and Applications; 2018 Feb 26-28; United Arab Emirates: IEEE; 2018. p.216-4.

[13] Wang L, Greenberg S, Fiegel J, et al. Monitoring-based HVAC comissioning of an existing office building for energy efficiency. Appl Energy. 2012 Oct 18; 102: 1382-1390. doi: 10.1016/j.apenergy.2012.09.005

[14] Ulmer R, Müller J. User-oriented verification of automation stations. E3S Web of Conferences. 2019 Aug 13; 111. doi: 10.1051/e3sconf/201911105024.

[15] Deutsches Institut für Normung Standard DIN EN ISO 16484-5. Building automation and control systems (BACS) – Part 5: Data communication protocol. Berlin: Beuth-Verlag GmbH; Dec 2017.

[16] OASIS Message Queuing Telemetry Transport TC. MQTT Version 5.0. 2019 Mar 07 [cited 2022 Feb 24]. Available from: https://docs.oasis-open.org/mqtt/mqtt/v5.0/os/mqtt-v5.0-os.pdf

[17] Verein Deutscher Ingenieure Guideline VDI 3814 Part 4.1. Building automation and control systems – Methods and tools for planning, building, and acceptance tests – identification, addressing, and lists. Berlin: Beuth-Verlag GmbH; Jan 2019.

[18] Friesen J. Java XML and JSON: Document Processing for Java SE. 2nd ed. Dauphin (CA): Apress; 2019.

[19] Plattform Industrie 4.0. Details of the Asset Administration Shell. Berlin: Federal Ministry for Economic Affairs and Energy (BMWi); 2020 Nov. 523p.

Data Statement

Data sharing not applicable to this article as no datasets were generated or analysed during the current study.

Interoperable interactions of HVAC components based on a capability ontology

Nicolai Maisch [a], Maximilian Both [a], Ralf Ulmer [a], Prof. Dr. Jochen Müller [a]

[a] Institut für Technische Gebäudeausrüstung, Faculty of Process Engineering, Energy and Mechanical Systems, TH Köln – University of Applied Sciences, Cologne, Germany, nicolai.maisch@th-koeln.de, jochen.mueller@th-koeln.de.

Abstract. In today's building automation networks, automation functions of installed HVAC components are rigidly predefined. Increasingly hybrid HVAC systems combining different generators (e.g. heat pumps with fossil boilers) and different transmission options pose new challenges for the engineering of automation functions. Rigidly predefined automation functions lead to inflexible operating procedures and high engineering efforts when changing the system environment. The reason for this is the lack of availability of standardised digital twins and the lack of mutual informational explorability of their capabilities to enable interactions between assets without rigid automation functions. Yet if digital twins of technical assets are not semantically described in a uniform way, the semantics of their information and capabilities can be referenced to external ontologies. Semantically describing the capabilities is necessary for self-x interactions between assets to be able to take over joint functions. In the field of HVAC, there is no ontology for capabilities that can be referenced by digital twins of HVAC assets, for example, to semantically characterise their functionality within a power generation system. This paper describes the development of such an ontology and the method used to derive the key terms. The ontology also presents a framework to compose the higher-level functionalities from granular asset functions. This is to ensure that references to the respective functions of individual assets can be used to imply the functionality of their overall system. The usage of the presented ontology by digital twins of HVAC components can serve as a basis for flexible interactions between real world assets. This can help to reduce engineering effort and increase energy efficiency.

Keywords. Industrie 4.0, Capability-Based Engineering, Ontology, Semantic Interoperability
DOI: https://doi.org/10.34641/clima.2022.201

1. Introduction

The information model for digital twins of the Industrie 4.0 (I4.0) initiative - the *Asset Administration Shell (AAS)* - represents characteristics of assets in a standardised way. The information of an asset is collected within an AAS, structured according to the meta model and mapped in a machine-readable way in order to lay the foundation for self-x functions, i.e. the ability to independently explore their technical environment and interact with other assets. The central components of the AAS are *submodels*, which represent the properties and functionalities of the assets and their contents. Submodels, for their part, contain *submodel elements* that contain the actual information of the components [1].

Although the metamodel of the AAS is standardised, a semantically homogeneous environment is not guaranteed, as the submodel elements can be described in a manufacturer- or domain-specific way. Figure 1 shows the integration of semantically heterogeneously described assets into an application, which involves a lot of manual engineering because of the different semantic descriptions.

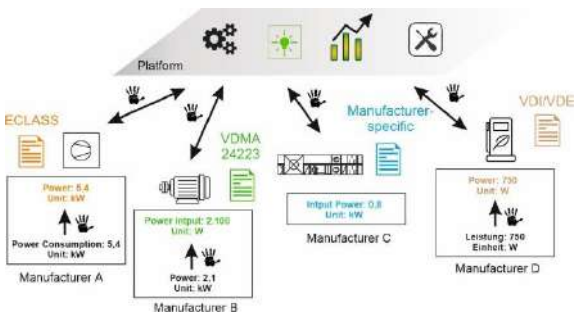

Fig. 1 - Example of manual engineering to integrate the power of semantically heterogeneously described assets

Copyright ©2022 by the authors. This conference paper is published under a CC-BY-4.0 license.

One approach to create a semantically homogeneous space is to provide a uniform standard for describing information that all producers use to describe their assets, e.g. ECLASS. ECLASS is a repository for the classification of products and their characteristics [2]. ECLASS entries can be referenced by a globally unique IRDI within AASs [1]. Another approach references submodel elements to online and generally accessible knowledge bases (*ontologies*). If a submodel element of an AAS is referenced to an item of an ontology, applications or other interacting assets can determine its description and the relationships of the item to other items [1, 3]. Linked Data is used to create links between different manufacturer- and industry-specific ontologies [4], enabling the exchange of information between semantically heterogeneously described AASs (Figure 2).

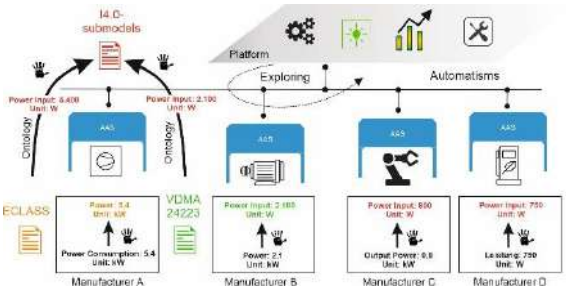

Fig. 2 - Interoperability by mapping semantically heterogeneous standards and feature descriptions to ontologies

The submodel element class *capability* describes a capability of an asset represented by the AAS [1]. Through references to ontologies, the capabilities are semantically distinguished so applications or other AASs can understand and classify them [3]. This forms the basis for the assumption of joint functions by several assets such as the heat supply of a building.

In the field of HVAC, there is a lack of an ontology that maps basic functionalities for the description of supply processes within buildings. In this paper, the development of an HVAC capabilities ontology is explained. The aim is that the ontology enables different HVAC systems within a building to interact in an interoperable and configuration-free way by exchanging their supply functions in order to reduce engineering effort.

2. Functionalities in HVAC Operation

A classification of the primary objectives in the operation of buildings is provided by [5]. The usage phase of buildings is divided into nine fields (Figure 3). In addition to administrative activities such as cost or space management, the activity of supplying and disposing of objects is particularly relevant for the area of HVAC and therefor also for building automation. *Supplying objects* is described as the supply of energy and media in an appropriate form [5].

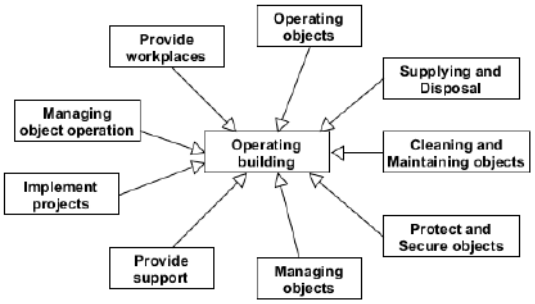

Fig. 3 - Tasks of the life cycle operating according to [5]

Consistent with [5], [6] divides building supply tasks into the energy and media usage (Figure 4). [7] divides the processes for fulfilling energy supply tasks within buildings into their basic components: Generation, distribution and transfer. The supply task with media can be subdivided analogously (Figure 4).

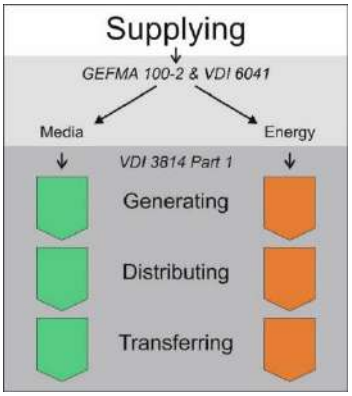

Fig. 4 - Derivation of the basic functions for supplying buildings with energy and media according to [5–7]

In addition to the primary utility functionalities within a building, there are granular functions of individual assets. [8] provides a pool of basic asset functions and describes a three-level classification and coding that defines and differentiates functional properties. Both the tasks to fulfil supply functions within buildings, such as heat generation, and the granular asset functions according to [8] can be described as capabilities in the context of I4.0 and thus assigned to assets in their AASs [1].

3. Capabilities in an AAS

The metamodel of the AAS is fundamental for the exchange of information between assets, as it provides a framework for the representation of submodel elements and thus asset information [1]. For "plug and produce" scenarios and flexible value networks in which assets independently take over common functions without configuration effort, the capabilities of assets must be represented in AASs in addition to descriptive submodel elements (*properties*) [3]. Through communication between AASs, required and existing capabilities can be matched to initiate actions. After a check of the

capabilities of an asset (*capability check*), a *feasibility check* is carried out for an interaction process on the basis of the specific conditions and properties [3]. Submodel elements that are semantically linked to the pre-matched capability with the relation attribute *CapabilityRealizedBy* within the AAS serve as the information basis for the feasibility check [9].

The concept is based on the *Process, Product and Resource (PPR)* model, according to which in certain technical areas (e.g. manufacturing industry) production lines are planned and automated in a modular way. This is based on the manufacturing capabilities of individual plants. This allows reacting to changing conditions and easily replacing modules of manufacturing if necessary. [3]. To do so, it is necessary to model the manufacturing operation as an interaction of resource, process, product and capabilities. In this case, a certain manufacturing process, through which a product is created, is fulfilled by a resource with the help of a capability. A sufficient condition for the realisation of the process by the resource is the matching of the functions of the resource with the functions necessary for the process [10–12].

The necessary functions of a process can be formalised and orchestrated in a structured way through ontologies. This also allows resources to be identified for more complicated processes that require more than one capability [13]. The C4I ontology [14] provides a method for assigning capabilities to resources. In addition, it provides the possibility to distinguish between *associatedWithCapability* for a general composition of capabilities and the relationship *hasCapability* for the necessary execution of a process by a single resource.

4. Ontologies as semantic basis of AASs

For different assets to take over common functions, it is necessary that the definitions of the capabilities are semantically aligned. Therefore, the definitions should be external to the AASs, which can be achieved by references to external ontologies [3]. An ontology is a set of axioms that describe relationships between entities explicitly and in a machine-readable way. Through the logic of formalisation languages for ontologies, further relationships and thus additional knowledge can be implied from the explicitly described knowledge [15]. With a reference to entries within an ontology, properties and capabilities of assets can be semantically described. The reference to a specific entry of an ontology can be achieved within an AAS using a semantic ID in the form of a unique URL [1]. Formalised knowledge in the ontology can thus be used to establish relationships between entities defined by semantic triples. With the W3C standards for languages to formalise triples "RDF" [16] and "RDFS" [17], relationships such as "heating by gas boiler *rdfs:subClassOf* heating" can be described. The "Web Ontology Language (OWL)" [18] extends the possibilities for defining axioms with further relationship descriptions. This also makes more complicated statements possible, such as that heating and cooling are always disjoint.

5. HVAC Ontologies

In the HVAC domain, submodel elements can be semantically specified by ontologies. Existing ontologies have different thematic focuses and approaches to the division of HVAC.

The Building Topology Ontology (BOT) is an ontology for the topological description of basic components of a building [19–21]. It divides buildings into *zones*, *elements* (physical components like walls, doors or sensors) and *interfaces* (transitions between zones and elements). The classes are not further subdivided, since for more detailed descriptions of the elements, reference is made to more domain-specific ontologies.

The BRICK ontology [22] can be used to virtually map a building and its HVAC assets as well as their metadata and relationships. In studies, between 96 and 99% of all data points of existing buildings could be covered by entries of the ontology.

The DogOnt ontology [23, 24] allows the mapping of the controls of SmartHome devices with the objective of semantically connecting systems from different manufacturers. For example, on-off signals can be referenced.

The Smart Applications REFerence Ontology (SAREF) [25] can be used to describe assets within buildings. The functions for controlling a device are described, but not the basic functionalities of building services components such as heating.

With ifcOWL [26, 27], *Building Information Models (BIM)* can be represented in the form of semantic triples. A definition of basic functions of the assets within an HVAC system is not part of BIM.

With the ontologies SSN (Semantic Sensor Network Ontology) and SOSA (Sensor, Observation, Sample and Actuator) [28, 29], concepts of sensors and actuators are abstracted. Concrete HVAC capabilities are not mentioned.

Existing ontologies in building services engineering map existing structures and functions within buildings. With none of the mentioned ontologies basic HVAC functionalities can be referenced by AASs in order to take over common tasks interoperably. In the following, the development of an ontology is described that provides a structured description of supply functionalities. This can also be used to infer primary HVAC functionalities from granular asset functions.

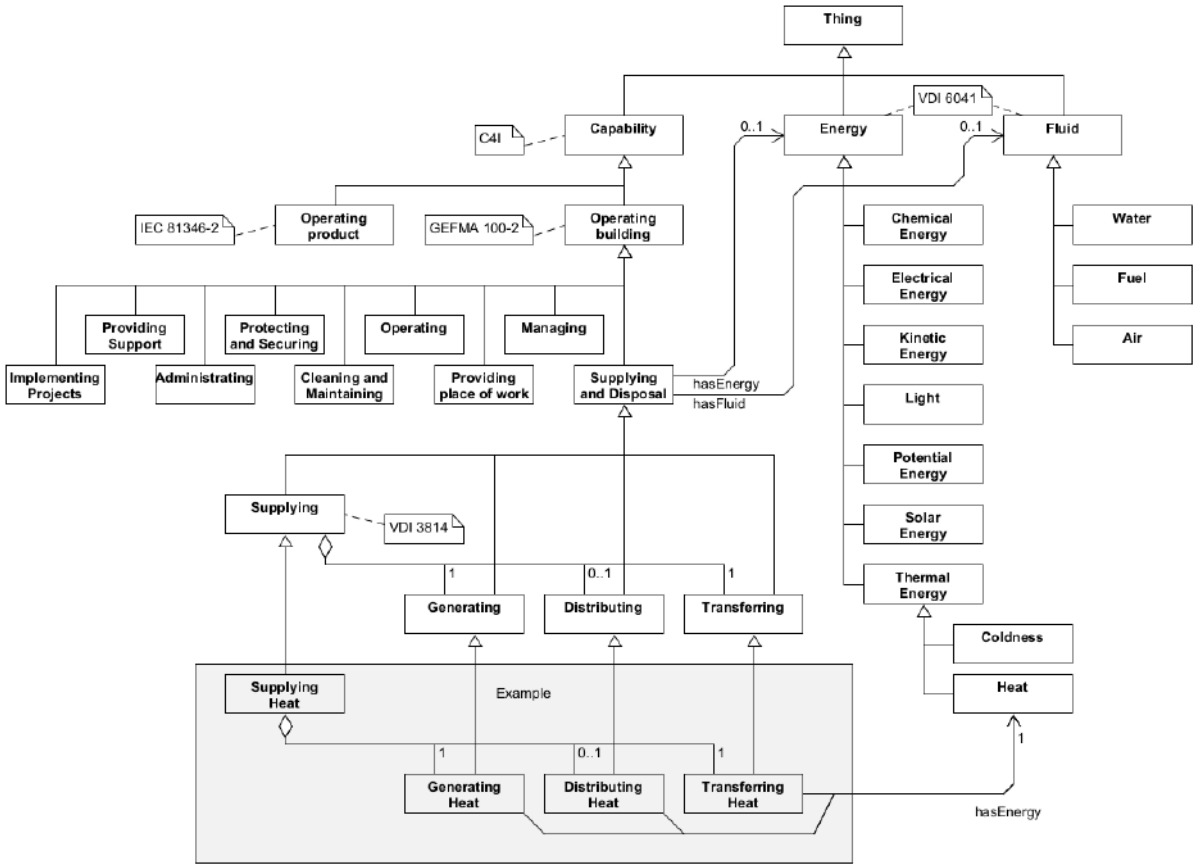

Fig. 5 - Structural design of the ontology for building technology capabilities and exemplary representation of the aggregation of heat supply

6. Derivation of fundamental HVAC functions and structure of the Ontology

For the development of the ontology, all capabilities were derived from the class *Capability* according to [14] in order to create a basis for interoperability of the ontology with other capability ontologies. The basic capability defined is *Operating_Building* and its subclasses according to [5]. Since the scope of the ontology is in building services, specifically in supplying buildings, the main focus of the ontology is on supplying and disposal of objects. Based on [7], the basic capabilities *Generating*, *Distributing* and *Transferring* were derived from this class. However, since a single asset cannot take over a complete supply task with only one of these three basic capabilities, the class *Supplying* was defined as a primary class that can be aggregated from the three fundamental functions (Figure 5). *Distributing* can be omitted in case a supply unit is both generating and transmitting in the sense of the relationship *hasCapability* according to [14], for example a stove.

Based on [6], the three fundamental capabilities were divided with an attribute into their area of activity for the supply type. For example, *Transferring* was divided into *Transferring_Energy* and *Transferring_Fluid*. For this purpose, the object properties *hasEnergy* and *hasFluid* were introduced, which assign one of the different classes of possible energies and fluids to a supplying capability.

By supplying air (*Supplying_Air*), an additional supply of heat or cold can also take place, which is why the supply of heat (*Supplying_Heat*), for example, can additionally be aggregated from the supply of air and the transfer of heat (Figure 6).

The presented ontology structure enables supply tasks within buildings to be composed modularly and according to the type of supply. The background is the possibility for supply systems in buildings to be able to reference capabilities in order to provide supply tasks and thus to be able to react flexibly to a specific need of the building.

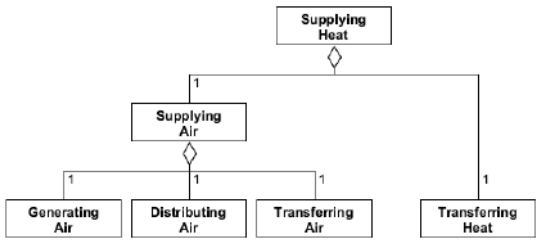

Fig. 6 - Aggregation of the heat supply by an air handling unit

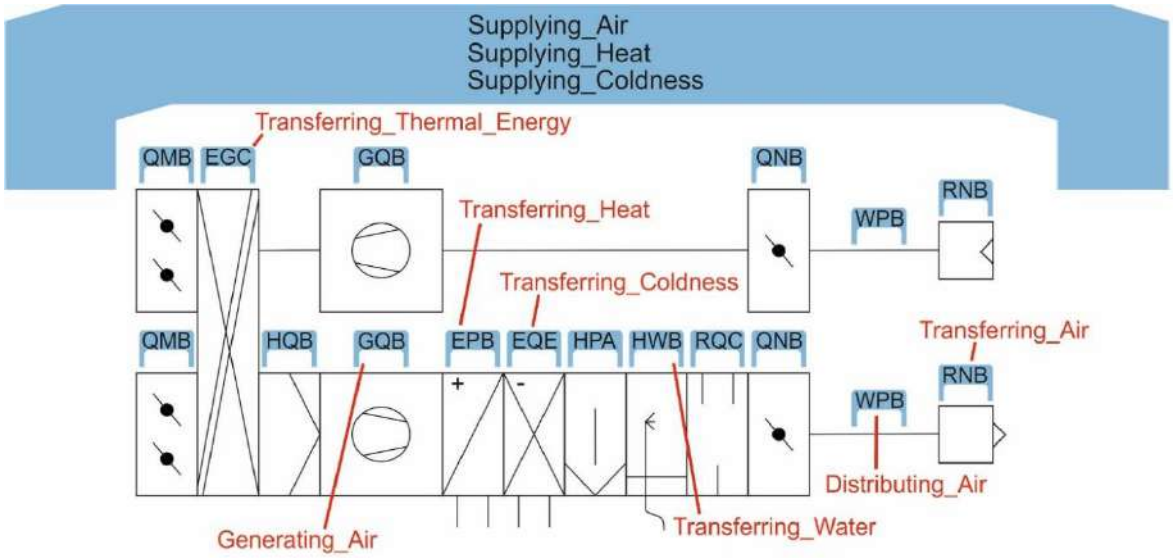

Fig. 7 - Elementary asset functions of the components of an air handling system according to [8] and their equivalent higher-level HVAC capabilities

7. Matching the supply functionalities with basic asset functions

Individual assets (e.g. fans) cannot fulfil entire supply tasks. Therefore, it must be ensured that the defined fundamental supply tasks can be implicitly inferred from various capabilities at the device level. Therefore, in addition to the ontology for building services capabilities, an ontology for asset-level capabilities has been created, which is modelled on [8]. By creating equivalences of subclasses of the basic functions Generating, Distributing and Transferring with capabilities from the ontology according to [8], both ontologies are linked so that the sum of granular asset capabilities can be used to imply higher-level HVAC functionalities. For example, a gas boiler with the capability *EM_Combustion_Heating* in a power generation system can be implied to have the higher-level HVAC functionality *Generating_Heat* without specifying this in the digital twin when developing the asset. Figure 7 shows an example of the components of a full air handling unit with all four thermodynamic air handling functions described individually at the functional level (with three-digit code). For the functions relevant to the fundamental supply functionality, the equivalent functions from the ontology are listed.

If an area within a building can be supplied with heat by more than one system, this can be determined by a capability check. A following feasibility check can be used to determine the most suitable participant, considering all asset-specific characteristics (Figure 8).

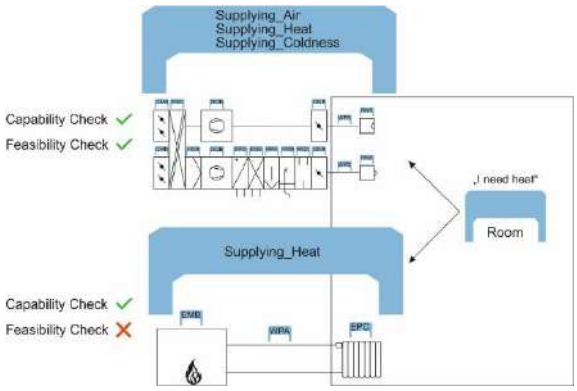

Fig. 8 - Exemplary capability and feasibility check of the heat supply of a room

8. Prototypical implementation of capability checks based on the HVAC capability ontology

In the next step, a script for querying and matching capabilities of AASs has been designed and prototypically implemented in an I4.0 environment. The developed ontologies, which can be accessed online, AASs of exemplary HVAC assets with semantic IDs to the ontologies and programmes for local hosting of the AASs are used as the basis for this.

For this purpose, both ontologies were first formalised and made available online [30]. The online access creates URLs for the respective classes of the ontologies, which can be used as semantic IDs for submodel elements of an AAS, see chapter 4.

Using [31], AASs of pumps, heat pumps and a gas boiler were designed. The AASs receive the corresponding capabilities (e.g. *Heating*) with the

respective semantic IDs from the ontology for capabilities at asset level according to [8].

Subsequently, using [32], the AASs were hosted on local HTTP servers to access their data enabling the capability check. In addition, a registry was implemented in which hosted AASs are listed and which thus serves as a directory of available AASs [33].

The capability check is implemented as a script that can be executed inside or outside of AASs. For example, if a heat demand is determined via a trigger, the script is executed. The required ontology class is used as input (Figure 9, step 1). Because of the availability online, the equivalent capabilities defined in the ontology can be determined (step 2). Subsequently, AASs available in the registry are determined (step 3). In the following step capabilities of the AASs get queried and the corresponding semantic IDs are matched with the required ones (step 4). If the classes of one of the required capabilities matches an available capability, information about the corresponding AAS and the submodel elements of an AAS that are linked to the capability by means of the *CapabilityRealizedBy* attribute are retrieved. These form the starting point for a downstream feasibility check. The labelling of the digital twins of HVAC assets with their capabilities through references to ontologies available online thus forms the basis for interactions between assets through a check-up of the existing capabilities.

9. Conclusion and outlook

With the ontology of HVAC capabilities, a foundation has been laid for the assumption of common functions of different assets within buildings and self-x functionalities. By defining the capabilities of individual assets, the ontology can imply which functionality an asset has within a supply system. Buildings can be operated more efficiently and demand-oriented through energy supply systems that can be activated flexibly, because they can be controlled on the basis of current operating and environmental data. Complex engineering of the systems is not necessary. In further research work, the developments presented will be combined with concepts in the area of self-organising interactions between AASs [34]. Capability and feasibility checks are integrated as executable algorithms in active AASs. The checks provide the basis for interactions between AASs.

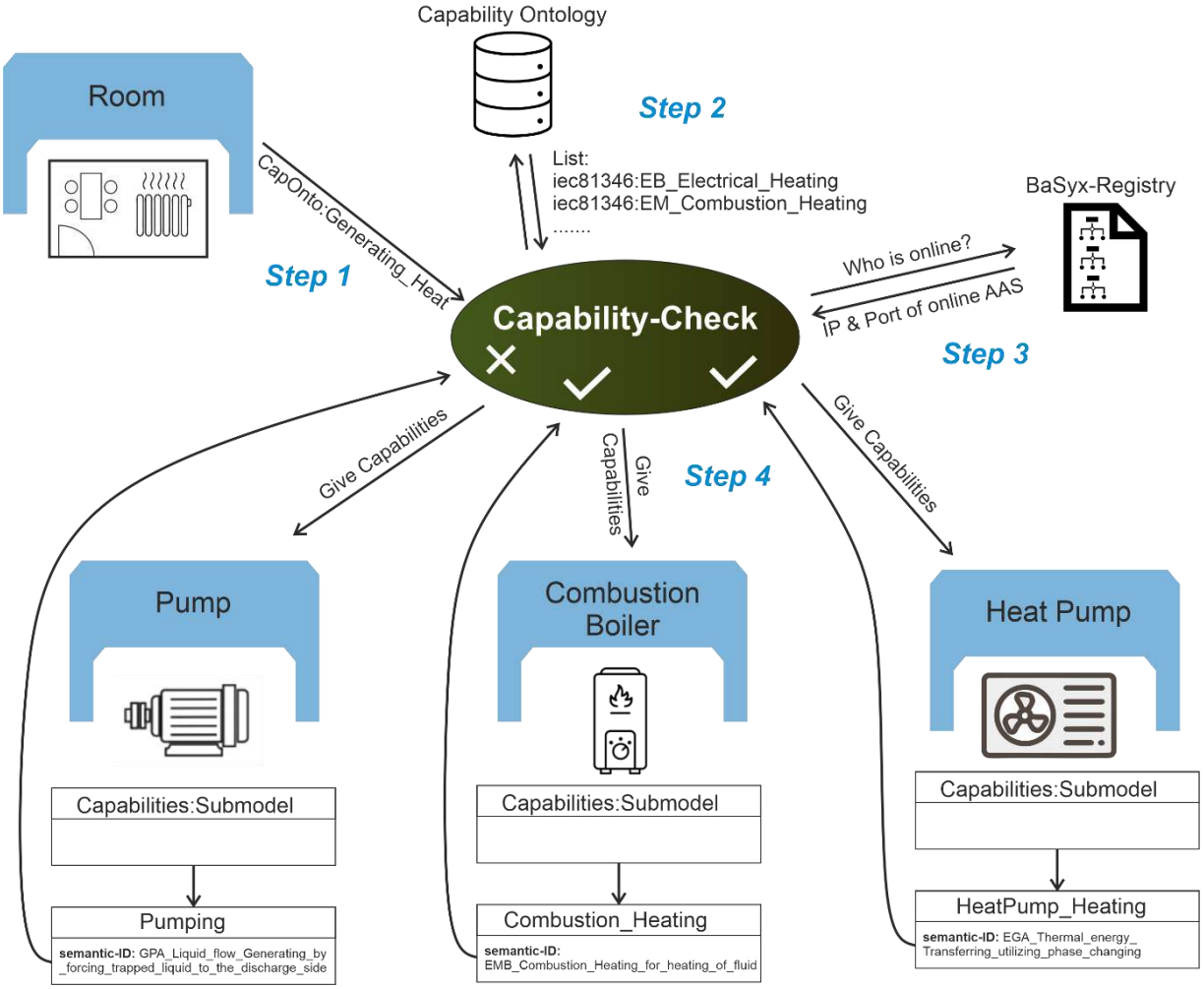

Fig. 9 - Exemplary scheme of implementing the Capability Check

The use of ontologies and the linking of different domain-specific ontologies is one way to achieve interoperability in semantically heterogeneous domains. Nevertheless, this approach involves a lot of manual effort: Ontologies must be built, linked and implemented. Results of investigations in the field of artificial intelligence (AI) show that an automated mapping of different ontologies and manufacturer- and domain-specific knowledge bases to each other is possible by means of natural language processing (NLP) [35].

10. Acknowledgement

The authors gratefully acknowledge financial support from the KSB Foundation in the project Automatic interaction of semantically heterogeneous Industrie 4.0 Asset Administration Shells by means of generic translation mechanisms based on methods of Natural Language Processing (1.1359.2020.1).

11. References

[1] Federal Ministry for Economic Affairs and Energy (BMWi). Details of the Administration Shell: Part 1 - The exchange of information between partners in the value chain of Industrie 4.0; Version 3.0. Berlin; 2020.

[2] ECLASS e.V. ECLASS: ECLASS - Standard für Stammdaten und Semantik für die Digitalisierung [cited 2020 November 17] Available from: URL: https://www.eclass.eu/index.html.

[3] Bayha A, Bock J, Boss B, Diedrich C, Malakuti S. Describing Capabilities of Industrie 4.0 Components: White Paper. Berlin; Nov 2020.

[4] McCrae JP. The Linked Open Data Cloud: Insight SFI Research Centre for Data Analytics. Available from: URL: https://lod-cloud.net/.

[5] GEFMA. GEFMA 100-2: Facility Management: Leistungsspektrum; 2004.

[6] VDI. VDI 6041, Facility-Management: Technical monitoring of buildings and building services; 2017.

[7] VDI. VDI 3814, Building automation and control systems (BACS): Part 1: Fundamentals; 2019.

[8] IEC. IEC 81346-2:2019-06, Industrial systems, installations and equipment and industrial products - Structuring principles and reference designations: Part 2: Classification of objects and codes for classes 2019.

[9] Diedrich C, Miny T, Schmitt S. D-2.11 Capability- und Feasiblity-Interaktion: BaSys 4.2; 2021 Oct 18.

[10] Backhaus J, Reinhart G. Digital description of products, processes and resources for task-oriented programming of assembly systems. J Intell Manuf 2017; 28(8): 1787–800 [https://doi.org/10.1007/s10845-015-1063-3]

[11] Pfrommer J, Stogl D, Aleksandrov K, Schubert V, Hein B. Modelling and orchestration of service-based manufacturing systems via skills. In: Modelling and orchestration of service-based manufacturing systems via skills; 2014 - 2014. IEEE.

[12] Malakuti S, Bock J, Weser M, *et al.* Challenges in Skill-based Engineering of Industrial Automation Systems *. In: Challenges in Skill-based Engineering of Industrial Automation Systems *; 2018 - 2018. IEEE; 67–74.

[13] Perzylo A, Grothoff J, Lucio L, *et al.* Capability-based semantic interoperability of manufacturing resources: A BaSys 4.0 perspective. IFAC-PapersOnLine 2019; 52(13): 1590–6 [https://doi.org/10.1016/j.ifacol.2019.11.427]

[14] Weser M, Bock J, Schmitt S, Perzylo A, Evers K. Ontology-based Metamodell for Capability Descriptions 2020.

[15] Hitzler P, Krötzsch, Markus, Rudolph, Sebastian, Sure Y. Semantic Web. Berlin, Heidelberg: Springer Berlin Heidelberg 2008.

[16] The RDF Concepts Vocabulary (RDF); 1999. Available from: URL: https://www.w3.org/1999/02/22-rdf-syntax-ns#.

[17] The RDF Schema vocabulary (RDFS); 2000. Available from: URL: https://www.w3.org/2000/01/rdf-schema#.

[18] The OWL 2 Schema vocabulary (OWL 2); 2002. Available from: URL: https://www.w3.org/2002/07/owl#.

[19] Rasmussen MH, Pauwels P, Hviid CA, Karlshøj J. Proposing a Central AEC Ontology That Allows for Domain Specific Extensions. LC3 2017: Volume I - Proceedings of th Joint Conference on Computing in Construction 2017: 237–44 [https://doi.org/10.24928/JC3-2017/0153]

[20] Schneider GF. Automated Ontology Matching in the Architecture, Engineering and Construction Domain - A Case Study. The 7th Linked Data in Architecture and Construction Workshop 2019.

[21] Rasmussen MH, Pauwels P, Lefrançois M, Schneider GF. The Building Topology Ontology (BOT); 2018 [cited 2021 April 25] Available from: URL: https://w3c-lbd-cg.github.io/bot/bot.ttl.

[22] Fierro GT. Design of an Effective Ontology and Query Processor Enabling Portable Building Applications. Technical Report No. UCB/EECS 2019; 2019-106.

[23] Bonino D, Russis L de. DogOnt: An Ontology for Intelligent Environments; 2013. Available from: URL: http://iot-ontologies.github.io/dogont/index.html#.

[24] Bonino D, Corno F. DogOnt - Ontology Modeling for Intelligent Domotic Environments. The Semantic Web - ISWC 2008 2008: 790–803.

[25] Daniele L, Hartog F den, Roes J. Created in

Close Interaction with the Industry: The Smart Appliances REFerence (SAREF) Ontology; 225: 100–12 [https://doi.org/10.1007/978-3-319-21545-7_9]
[26] Pauwels P, Terkaj W. EXPRESS to OWL for construction industry: Towards a recommendable and usable ifcOWL ontology. Automation in Construction 2016; 63: 100–33 [https://doi.org/10.1016/j.autcon.2015.12.003]
[27] buildingSMART International. ifcOWL; 2021 [cited 2021 April 25] Available from: URL: https://technical.buildingsmart.org/standards/ifc/ifc-formats/ifcowl/.
[28] Haller A, Janowicz K, Cox SJD, *et al.* The SOSA/SSN Ontology: A Joint W3C and OGC Standard Specifying the Semantics of Sensors, Observations, Actuation, and Sampling. Semantic Web X 2018.
[29] Haller A, Janowicz K, Cox SJD, Le Phuoc D, Taylor K, Lefrançois M. Semantic Sensor Network Ontology; 2020 [cited 2021 April 25] Available from: URL: https://w3c.github.io/sdw/ssn/.
[30] Maisch N. CapOnto: Describing the development and usage of an ontology for I4.0-Capabilities of HVAC-Assets: TH Köln – University of Applied Sciences; 2021 [cited 2022 January 12] Available from: URL: https://github.com/thcologne-gart/CapOnto.
[31] AASX Package Explorer. Festo AG & Co. KG; PHOENIX CONTACT GmbH & Co. KG; Fraunhofer IOSB-INA Lemgo; Schneider Electric Automation GmbH; SICK AG; KEB Automation KG; Lenze SE; 2021. Available from: URL: https://github.com/admin-shell-io/aasx-package-explorer.
[32] Fraunhofer-Institut für Experimentelles Software Engineering IESE. BaSyx [cited 2021 April 25] Available from: URL: https://www.eclipse.org/basyx/.
[33] Kuhn T, Schnicke F, Ziesche C. Gut verpackt: BaSys-Tutorial, Teil 2: Verwaltungsschalen und Teilmodelle mit der BaSyx-SDK definieren. ix 2019; (12): 132–42.
[34] VDI/VDE. VDI/VDE 2193, Language for I4.0 components: Part 1: Structure of messages; 2020.
[35] Both M, Müller J. Deep Learning in Industrie 4.0 Umgebungen als Wegbereiter für automatisierte Abbildungen von Ontologien. Automation 2020 2020: 675–86 [https://doi.org/10.51202/9783181023754-675]

Futureproofing and scaling machine learning for occupancy prediction

Davor Stjelja [a,b], Juha Jokisalo [a], Risto Kosonen [a,c]

[a] Department of Mechanical Engineering and Automation, Aalto University, 02150 Espoo, Finland; davor.stjelja@aalto.fi juha.jokisalo@aalto.fi; risto.kosonen@aalto.fi

[b] Innovations, Granlund Oy, 00701 Helsinki, Finland; davor.stjelja@granlund.fi

[c] College of Urban Construction, Nanjing Tech University, Nanjing 211800, China

Abstract. An important instrument for achieving smart and high-performance buildings is Machine Learning (ML). A lot of research was done in exploring the ML learning models for various applications in the built environment such as occupancy prediction. Nevertheless, this research focused mostly on analyzing the feasibility and performance of different supervised ML models but have rarely focused on practical applications and scalability of those models. In this study, we are proposing a transfer learning method as a solution to few typical problems with the practical application of ML in buildings. Such problems are scaling a model to another (different) building, collecting ground truth data necessary for training the supervised model and adapting the model when conditions change. The practical application examined in this work is a deep learning model used for predicting room occupancy using indoor air quality (IAQ) IoT sensors. The importance of occupancy prediction has risen in recent times of remote work and is especially important for futureproofing of the built environment. This work proves that it is possible to reduce significantly the need for ground truth data collection for deep learning based occupancy detection model. Additionally, the robustness of the transferred model was tested, where performance stayed on similar level if suitable normalization technique was used.

Keywords. Occupancy prediction, environmental sensors, deep learning, transfer learning, scalability, practical issues
DOI: https://doi.org/10.34641/clima.2022.95

1. Introduction

The CO_2 emissions of buildings in European Union are 36% and 28% on global scale [1], [2]. While HVAC systems in developed countries are responsible for 50% of building energy consumption alone [3]. To battle this problem, the EU has set the goal of developing a sustainable, competitive, secure and decarbonized energy system by the year 2050 [1].

One of the tools to achieve this goal is through the digitalization of energy systems and buildings and the EU has introduced a smart readiness indicator (SRI). The purpose of this indicator is to determine the capability of buildings in using information and communication technologies to adapt the building operation to the needs of the occupants and the grid while improving the overall performance of the buildings [1]. Recently, many research attempts have been made using advanced technologies in the field of computer science such as artificial intelligence (AI), machine learning (ML) and the internet of things (IoT) in building operations. Enabling use cases such as model predictive control, system fault detection and diagnosis, occupancy estimation and detection, demand response and in more general system integrator of different building subsystems and occupants [4], [5]. These technologies can help to significantly improve building performance, from higher indoor environment quality, lower energy consumption to better space efficiency.

Office building occupancy inefficiency is a significant potential for improvement, as in one British study from 2013 has concluded that regular offices had an average occupancy level between 60 and 70% [6]. The recent COVID-19 pandemic has fast tracked remote work making occupancy levels worse, where in one Israeli study more than 60% of interviewees expects to come to the office only two to three times a week after the end of pandemics [7]. If these claims come true, existing buildings and their HVAC systems can become even more inefficient, since the standard static occupancy profile, with which they were designed with, is not valid anymore.

This all leads to the expectation that information on building occupancy is going to become more valuable and needed than ever before as it is

Copyright ©2022 by the authors. This conference paper is published under a CC-BY-4.0 license.

important for optimizing the space and building's system operation. Fortunately, a considerable amount of literature has been published on the matter of building occupancy estimation and detection [8].

To infer and analyze the information on occupancy in a larger scale, the commonly available sensors in buildings should be utilized. Environmental sensors commonly available in buildings are CO_2, room air temperature, relative humidity and in some case total volatile organic compound (TVOC) of which CO_2 has highest correlation with occupants in a room [9], [10].

For occupancy prediction from room environmental data methods range from physical, gray-box, statistical, machine learning to deep learning models. Where in this work focus was on machine and deep learning methods. Machine learning methods, have shown good accuracy with occupancy prediction, but require a process which is called feature engineering [11]–[15]. This time-consuming process was solved using deep learning methods such as in [16], where proposed method has outperformed statistical and machine learning methods. However, for using the model in a different room, the authors have needed to collect new ground truth data and train the model from scratch. The collection of occupancy ground truth is challenging and has been identified in several works as costly and time consuming [5], [17], [18].

In this work solving the problem of deep learning method scalability for room occupancy prediction is attempted. This is done using transfer learning, which is a technique for extracting knowledge from extensive and known source dataset and using it to improve the learning of a model on the lesser-known target dataset [19]. A similar work was done by Weber et al. [20], but using the simulated data of the same room as a source model. Here, a model trained from one room's data is transferred to another room in a different building, for which much fewer training data is available. Additionally, transferred model robustness is tested with different ventilation setting as well.

2. Methodology

2.1 Overview of CDLSTM model

Deep learning model used for predicting occupancy from environmental variables in this work is Convolutional Deep Long Short-Term Memory (CDLSTM), inspired by Chen et al. [16]. The CDLSTM model uses combination of different layer's specific properties to classify occupancy state from raw data. Mainly convolutional operation (CD) is used for extracting features from raw data, while a DLSTM is used to understand the temporal dependence of the data.

The CDLSTM model functions in the following way. Windows of raw time-series data enter first the convolutional layer, which slides a filter window to extract the characteristics. Extracted features are then passed through the pooling operation, which compresses the features by removing less important local features. A Long Short-Term Memory (LSTM) belongs to Recurrent Neural Network (RNN), commonly used with sequential data processing, since RNNs are good in finding dependence of features over time sequence. LSTM are an improvement over regular RNN because of their ability to learn long-term dependencies. Chen et al. in their work used a Bidirectional LSTM (BLSTM), where the data flows from the past but also from the future through the model. In this work, unidirectional LSTM showed better performance than the proposed BLSTM. A Deep LSTM (DLSTM) model, consisting of more than one LSTM layer is used. After each LSTM layer, there is a dropout layer used for regularization.

Regularization is the name for a technique used to solve the overfitting problem. The problem of overfitting results in a model showing significantly better performance on training dataset then on testing, which is common with deep learning models. A dropout layer randomly drops out hidden nodes from the neural layer during the training time. In each loop, different nodes are dropped, making model to learn representations which are more robust to the noise in the data. While during the testing time, nodes are not dropped.

The following DLSTM layers in the framework of the neural model used in this research are fully connected dense layers, with their dropout layers as well. The fully connected part of the model is used to learn more abstract features in the data such as learning non-linear combinations of input features and preparing the features to their final representation. The final representation of the learned features from raw time-series data is then fed finally to the softmax classification layer. The softmax classification layer, translates given features into classes, which are in the case of this work occupancy states.

2.2 Proposed transfer method

Training a deep learning model such as the proposed CDLSTM requires significant amount of training data. Labelled training data is difficult to collect when it comes to room occupancy, especially the occupancy count or level. Therefore, in this work the transfer method of CDLSTM model is studied.

The principle behind transfer learning is that a model is trained on a labelled and extensive dataset, called source dataset. The acquired knowledge from training the source model can then be transferred to solve a similar problem on a target dataset. The

weights of the trained CDLSTM model have then been transferred to a target CDLSTM model which was fine-tuned on a target dataset.

2.3 Data acquisition

Source dataset for the initial training of the CDLSTM model was collected using temperature and CO_2 IoT sensor in a meeting room in one office building located in Helsinki, Finland. This room is named Source Room. The measurements were done in period from February and March 2020. The source room is rather small with seats for four persons and with approximate size of 6 m^2. It is located in the middle of the floor and surrounded by an open office area. Ventilation is with constant airflow of 15 l/s consisting of 100% fresh outdoor air. The environmental IoT sensor was placed on the desk in the room. Camera for collecting ground truth occupancy was installed on the ceiling, just above the door.

Ground truth for the source model was acquired using video camera recording (the image was blurred for privacy purposes), which was used for manual counting of people in the source room. Target for the transfer of occupancy prediction model in this work is a large meeting room located in a hospital building in Finland. The Target Room has a capacity for 12 people with area of 21 m^2 and by the design, its ventilation system is designed to be of variable airflow. Temperature and CO_2 were collected with IoT sensor. The sensor was placed on the conference desk. Ground truth for transfer dataset has been acquired using infrared time of flight based people counting sensors. Automatic counting using IR-based sensors has a known problem with missing counts [21] and therefore this count was manually corrected using the presence and noise sensor in the room.

The measurement was done in two periods. First period, or period with constant airflow ventilation was from March and April 2021. Second period with variable airflow was from May to July 2021. During the measurement, the problem with the ventilation setting was noticed, the room did not operate with the expected variable airflow, because the settings were overridden to constant maximum design airflow of 90 l/s (first measurement period). When this was noticed, the setting has been changed to a predefined variable airflow (second measurement period).

Variable airflow in the room is controlled by the signal from three BMS sensors; PIR, CO_2 and temperature. The airflow rate is possible to control between 30 and 90 l/s. With variable airflow operation, it was also noticed that it is not performed as expected. In reality, the airflow almost never dropped under ~50 l/s, even though the room was empty for days at times. The source of the problem was too high room temperature compared to the setpoint (user adjusted between 18.5 and 23.5°C) which BMS tried to decrease by increasing the airflow. On the other hand, the air supply temperature was too high (about 21°C), making it impossible to cool down the room and therefore keeping the airflow at least on the medium level. Therefore, there is no clear connection between airflow and occupancy as such, making it more difficult to use the occupancy prediction model, which is addressed later in this paper, where the robustness of the transferred model is tested.

Therefore, in this work we have two periods with different ventilation strategies in same room, during March and April there was constant airflow, while from May onwards the work is performed with variable airflow data.

2.4 Experimental setup

Data was gathered from IoT temperature and CO_2 sensors with a sampling rate of one minute, while ground truth for the source dataset was acquired in three-minute intervals. Therefore, all other measurements were resampled to three minutes.

Before it was used for the deep learning model, the raw sensor data was preprocessed. Missing values, caused by connection problems or other IoT sensor problems, were interpolated using polynomial interpolation of second order. Raw sensor data was noisy and through the experimentation we have noticed that using data as such, accuracy of model was lower and with longer computational time. Therefore, we decided to smooth the data before the model input. For this purpose, smoothing based on Kalman filtering with Python package *tsmoothie* [22] was used. Kalman smoothing was performed on time-series level components.

During the initial experimentation, it was noticed that partly balancing the classes in the dataset also improved the results. Imbalanced classes in the dataset means that certain class classes are overrepresented then the other classes. In this case, the occupancy class of zero or empty room makes large majority of the dataset, while occupied state makes smaller portion of the dataset. Training the deep learning model on the imbalanced dataset can lead to a model with lower sensitivity to classes which are underrepresented. In this study, this issue was reduced by removing the periods when occupancy is expected to be zero, such as during the nighttime or the weekend.

The last thing to do before using the data with neural model is to normalize it. Z-score normalization was used, where the values are normalized according to their mean and standard deviation. Data was normalized using the mean and standard deviation from the training data, while for the later use of the model with variable airflow, a sliding method was used as described in section 3.3.

Normalized and preprocessed data was then ready to be used with CDLSTM model. The model was created using the deep learning Python package *Tensorflow/Keras* [23] and was designed as follows. The convolutional layer was created with 100 output filters, a kernel size of three which specifies the 1D convolutional window and pooling size of two, with ReLU activation function. Following is deep LSTM model, consisting of three LSTM layers, with hidden sizes of 100, 150 and 200 respectively. After each layer there is a dropout layer served for regularization with masking probability of 0.5. Following LSTM layers, there are two fully connected dense layers with hidden size 200 and 300. Another dropout layer is placed between the fully connected layers with a probability of 0.3. At the end, there is a softmax layer classifying the model outputs to classes, in our cases occupancy classes.

Another important setting for the CDLSTM model is the batch size and window sequence length and this varies depending on the sampling rate of the data on which the model was trained. For example, when using the dataset with three-minute sampling rate, a batch size of 16 and a sequence length of four were used. This means that one window was a size of four timesteps or twelve minutes which were fed to the model in batches of 16 windows at a time. The exact size of batches and sequences were found with the trial-and-error method.

2.5 Performance metric

To evaluate the performance of the model, the main metric used was the Matthews correlation coefficient (MCC). Similar work on occupancy estimation used a more traditional accuracy score or an F1 score, which happens to show dangerously optimistic results on overly imbalanced datasets. Since the rooms in question are majority of the time vacant, the number of times a vacant class (zero) is present in the data set is much higher compared to the number of times the room is occupied. Which means that if a model would always predict the room is vacant, it would be awarded with a high accuracy score. The MCC score, on the other hand, gives more understandable accuracy metrics for those cases: to achieve a high quality score, the classifier (such as the occupancy prediction model) has to make a prediction in majority of positive and negative cases independently of their ratios in the overall dataset [24].

On the other hand, MCC score gives a very general metric, which is not straightforward for the potential use cases of this work. To make the results more understandable additional performance metrics were developed. Aside from the room occupancy in each timestep, from the perspective of optimizing HVAC system and space utilization, it is useful to know the following about the meeting room occupancy; the time of the first and last occupancy in the day and the duration of room occupancy. Therefore, the corresponding metrics were developed. The difference in the first or last occupancy of the day between the measured and predicted occupancy is shown as averaged throughout the period and in minutes. Duration of room occupancy is shown as a percentage of the average day being occupied.

3. Results

3.1 Source model training

The source model for occupancy estimation was trained with data from source room. Training of the model was done using 22 days (14 days occupied) and validation of the training was done with the following three days. The model was first trained using the raw sensor data in 30 epochs and then in the second iteration smoothed data was used. Using raw and smoothed version of the same data showed better performance during training and it served as an additional regularization technique, making model less prone to overfitting. Trained source model has shown MCC score of 0.85.

3.2 Transfer to the target room

Transfer learning of the source model for successful occupancy detection is analyzed from the point of minimum training data needed from the target room.

Process for re-training of CDLSTM model considers which layers of the model are frozen and which are retrained with the new data and in which way. If a particular layer is not frozen, it can be trained from scratch (weights are reinitialized) or the layer weights can be transferred and then retrained.

Models compared in this work are Model which was trained using training data from only target dataset is called Baseline model, while model which was not retrained at all is Pure source model. The Transfer model is a model with pre-trained weights for all layers, which were retrained.

Goodness of the models is first assessed with MCC score and then the best cases are further analyzed using the additional performance metrics. In **Tab. 1** MCC score of different models with different training data length is presented. Analyzing the results from the training length perspective, it can be seen that with already two days of ground-truth data with transfer learning it is possible to get high MCC score, as with longer training period and nearly as

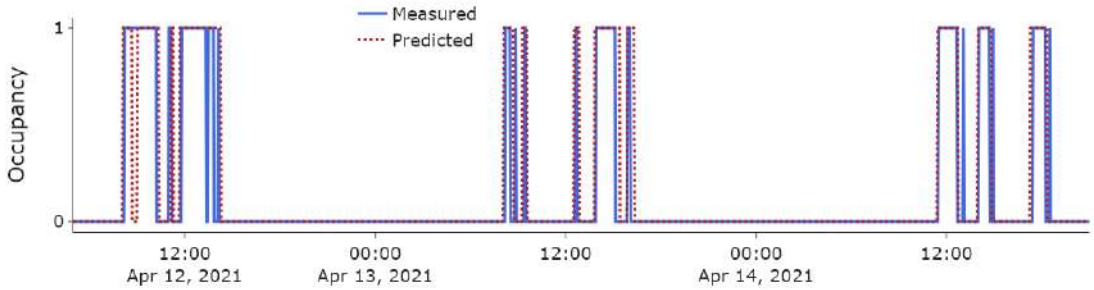

Fig. 1 - Three-day showcase of the selected target model performance and comparison with measured occupancy.

high as with source model. Without transfer method for two days training the best score would be 0.73, while for 5 days 0.80.

Tab. 1 – Comparison of different occupancy detection models performance with regards to the length of training data shown with MCC score

Model	1 day	2 day	3 day	5 day
Baseline model	0.67	0.73	0.79	0.80
Pure source model	0.71	0.71	0.71	0.71
Transfer model	0.77	0.82	0.82	0.82

Tab. 2 – Additional performance metrics for selected models of different training length and method, as daily average occupied time and average difference of first and last occupancy in a day

Model	MCC	Daily avg. occupied time [%]	First occ. avg. difference [min]	Last occ. avg. difference [min]
Ground truth	-	7.5	-	-
2 day - Baseline model	0.73	11	5	28
2 day - Transfer model	0.82	8.9	7	7
5 day – Baseline model	0.80	9.4	5	15

For further analysis, three interesting cases were chosen, which are made bold in **Tab. 1**. Selected cases are then further examined with additional performance metrics in order to understand what MCC score might mean for practical use and to select a final occupancy detection transfer model. This analysis can be seen in **Tab. 2**. Where the best result shows the case using two-day Transfer model. Having closest daily average occupied time to the ground truth of the shown cases and having only seven minutes average difference between the first and the last occupancy of the day. This case will be called the transferred occupancy detection model in the next sections. Transferred occupancy detection model's performance is visualized in **Fig. 1** where it is compared to the measured ground truth occupancy.

3.3 Robustness check - change in ventilation system operation

Robustness of ML models for predicting the room occupancy using environmental variables is important for using them commercially, as certain changes might happen in a building system operation. In this section the performance of the Transfer model is checked after a change in ventilation system operation occurs. In the target room, during the model transfer, ventilation operated with a constant airflow of about 90 l/s. Change in the operation was the demand-controlled variable air flow operation activation, where airflow was modulated between about 55 to 90 l/s, depending on the control logic described in section 2.3.

Robustness check on data from VAV operation was done using data measured during May 2021. During the process, it became clear that the way how z-score normalization is performed is important. In many time-series ML work the z-score normalization statistics derived from the training dataset is used also for the test data. This is suitable only for stationary time series, but not for non-stationary time series [25]. In this case introducing the variable airflow makes mean and standard deviation of CO_2 and temperature time series more susceptible to change over time. Therefore, a sliding window approach was used, where a normalization statistics was calculated on an arbitrarily chosen 14 days window prior to the day being predicted. More advanced approaches exist such as adaptive normalization [25], [26], but are out of the scope of this work.

Tab. 3 – Performance of previously transferred model after the room ventilation changed from CAV to VAV operation

Model	MCC	Daily avg. occupied time [%]	First occ. avg. difference [min]	Last occ. avg. difference [min]
Ground truth	-	5.7	-	-
Trans. model, norm. on training	0.71	8.4	-74	21
Trans. model, Sliding norm.	0.78	6.9	-27	2

Tab. 3 presents results from the robustness check of the transferred detection model with two normalization approaches. Results are presented using MCC for model accuracy and the additional performance metrics. The sliding window normalization produced significantly better results than using the normalization from the training phase. Using the sliding window normalization, detection performance of the model is close to the original performance of the detection model during ventilation operation in the CAV mode. Where largest difference in performance is in detection of the first daily occupancy.

4. Discussion

As mentioned in the literature review, plenty of studies were done exploring the accuracy of occupancy inferring methods from environmental variables. On the other hand, very little was done on scalability of those methods and therefore they have not found their way in the industry.

In this work, main obstacle was tried to be avoided or at least minimized by using transfer learning method. Having a previously trained model on large dataset and having a small amount of ground truth data (two days) from a different room, it is possible to get good occupancy detection accuracy.

Second obstacle, is what happens after certain conditions in the room change, how will the model perform? In this work, transferred model with the small amount of data from constant airflow conditions was tested after the conditions in room have changed to variable airflow. The test has shown that it is possible to keep the performance on same level, if normalization technique is improved.

For wider usage of similar models, probably even with this method, the problem is not solved. However, a further work should continue with removing the need for ground truth collection completely, if possible. Additionally, methods for monitoring drift of such models should be explored. Where the biggest issue is not having ground truth at all.

In this work, as a tool to increase robustness, a sliding version of z-score normalization was used. However, there are other state-of-the-art normalization methods for non-stationary time series, which should be explored.

Finally, occupancy detection is good, but much more valuable is knowing the number of people or at least the level of room occupancy. Minimizing the training data needed for this purpose is difficult, since machine learning models need to see enough examples of every class. This is an important issue for future research in this field.

5. Conclusion

The main goal of the presented study was to explore the scalability of deep learning-based method for inferring room occupancy information using environmental IoT sensor. Previous research has focused on testing different ML based methods in order to get as high accuracy as possible, but since it is difficult to collect labelled training data the methods were not used widely. In this study, a transfer learning method has been applied and it showed that it is possible to create occupancy detection model of good accuracy with only two days of ground truth data, instead of several weeks.

Furthermore, a robustness of the transferred model was tested in different airflow conditions and accuracy did not drop significantly when sliding normalization was used.

6. References

[1] European Union, “Directive 2018/844 of the European Parliament and of the Council of 30 May 2018 amending Directive 2010/31/EU on the energy performance of buildings and Directive 2012/27/EU on energy efficiency,” *Off. J. Eur. Union*, p. L 156/75-L 156/91, 2018.

[2] UN Environment and International Energy Agency, “Towards a zero-emission, efficient, and resilient buildings and construction sector,” 2017.

[3] L. Pérez-Lombard, J. Ortiz, and C. Pout, “A review on buildings energy consumption information,” *Energy Build.*, vol. 40, no. 3, pp. 394–398, 2008, doi: 10.1016/j.enbuild.2007.03.007.

[4] J.-H. Choi, B. Yang, and C. W. Yu, “Artificial intelligence as an agent to transform research paradigms in building science and technology,” *Indoor Built Environ.*, p. 1420326X2110176, Jun. 2021, doi: 10.1177/1420326X211017694.

[5] Z. Wang, J. Liu, Y. Zhang, H. Yuan, R. Zhang, and R. S. Srinivasan, “Practical issues in implementing machine-learning models for building energy efficiency: Moving beyond obstacles,” *Renew. Sustain. Energy Rev.*, vol. 143, no. February, p. 110929, 2021, doi: 10.1016/j.rser.2021.110929.

[6] M. Bedford, R. Harris, A. King, and A. Hawkeswood, “Occupier density study,” *Br. Counc. Off. BCO*, 2013.

[7] M. Naor, G. D. Pinto, A. I. Hakakian, and A. Jacobs, “The impact of COVID-19 on office space utilization and real-estate: a case study about teleworking in Israel as new normal,” *J. Facil. Manag.*, 2021, doi: 10.1108/JFM-12-2020-0096.

[8] Z. Chen, C. Jiang, and L. Xie, “Building occupancy estimation and detection: A review,” *Energy Build.*, vol. 169, pp. 260–270, 2018, doi: 10.1016/j.enbuild.2018.03.084.

[9] B. Dong *et al.*, “An information technology enabled sustainability test-bed (ITEST) for occupancy detection through an environmental sensing network,” *Energy Build.*, vol. 42, no. 7, pp. 1038–1046, 2010, doi: 10.1016/j.enbuild.2010.01.016.

[10] L. M. Candanedo, V. Feldheim, and D. Deramaix, “A methodology based on Hidden Markov Models for occupancy detection and a case study in a low energy residential building,” *Energy Build.*, vol. 148, pp. 327–341, 2017, doi: 10.1016/j.enbuild.2017.05.031.

[11] M. Amayri, A. Arora, S. Ploix, S. Bandhyopadyay, Q. D. Ngo, and V. R. Badarla, “Estimating occupancy in heterogeneous sensor environment,” *Energy Build.*, vol. 129, pp. 46–58, 2016, doi: 10.1016/j.enbuild.2016.07.026.

[12] Z. Chen, M. K. Masood, and Y. C. Soh, “A fusion framework for occupancy estimation in office buildings based on environmental sensor data,” *Energy Build.*, vol. 133, pp. 790–798, 2016, doi: 10.1016/j.enbuild.2016.10.030.

[13] M. S. Zuraimi, A. Pantazaras, K. A. Chaturvedi, J. J. Yang, K. W. Tham, and S. E. Lee, “Predicting occupancy counts using physical and statistical Co2-based modeling methodologies,” *Build. Environ.*, vol. 123, pp. 517–528, 2017, doi: 10.1016/j.buildenv.2017.07.027.

[14] M. K. Masood, Y. C. Soh, and V. W. C. Chang, “Real-time occupancy estimation using environmental parameters,” *Proc. Int. Jt. Conf. Neural Netw.*, vol. 2015-Septe, pp. 1–8, 2015, doi: 10.1109/IJCNN.2015.7280781.

[15] M. K. Masood, C. Jiang, and Y. C. Soh, “A novel feature selection framework with hybrid feature-scaled extreme learning machine (HFS-ELM) for indoor occupancy estimation,” *Energy Build.*, vol. 158, pp. 1139–1151, 2018, doi: 10.1016/j.enbuild.2017.08.087.

[16] Z. Chen, R. Zhao, Q. Zhu, M. K. Masood, Y. C. Soh, and K. Mao, “Building occupancy estimation with environmental sensors via CDBLSTM,” *IEEE Trans. Ind. Electron.*, vol. 64, no. 12, pp. 9549–9559, Dec. 2017, doi: 10.1109/TIE.2017.2711530.

[17] B. Dong *et al.*, “Sensing and data acquisition,” in *Exploring occupant behavior in buildings: Methods and challenges*, Springer International Publishing, 2017, pp. 77–105.

[18] B. Dong, D. Yan, Z. Li, Y. Jin, X. Feng, and H. Fontenot, “Modeling occupancy and behavior for better building design and operation—A critical review,” *Build. Simul.*, vol. 11, no. 5, pp. 899–921, 2018, doi: 10.1007/s12273-018-0452-x.

[19] S. J. Pan and Q. Yang, “A survey on transfer learning,” *IEEE Trans. Knowl. Data Eng.*, vol. 22, no. 10, pp. 1345–1359, Oct. 2010, doi: 10.1109/TKDE.2009.191.

[20] M. Weber, C. Doblander, and P. Mandl, “Towards the detection of building occupancy with synthetic environmental data,” 2020, [Online]. Available: http://arxiv.org/abs/2010.04209

[21] J. Kuutti, K. H. Blomqvist, and R. E. Sepponen, “Performance of commercial over-head camera sensors in recognizing patterns of two and three persons : A case study,” 2013.

[22] M. Cerliani, “tsmoothie.” 2020. [Online]. Available: https://github.com/cerlymarco/tsmoothie

[23] F. Chollet and others, “Keras.” 2015.

[24] D. Chicco and G. Jurman, “The advantages of the Matthews correlation coefficient (MCC) over F1 score and accuracy in binary classification evaluation,” *BMC Genomics*, vol. 21, no. 1, p. 6, Jan. 2020, doi: 10.1186/s12864-019-6413-7.

[25] E. Ogasawara, L. C. Martinez, D. De Oliveira, G. Zimbrão, G. L. Pappa, and M. Mattoso, “Adaptive normalization: A novel data normalization approach for non-stationary time series,” in *The 2010 International Joint Conference on Neural Networks (IJCNN)*, 2010, pp. 1–8.

[26] N. Passalis, A. Tefas, J. Kanniainen, M. Gabbouj, and A. Iosifidis, “Deep Adaptive Input Normalization for Time Series Forecasting,” *IEEE Trans. Neural Netw. Learn. Syst.*, vol. 31, no. 9, pp. 3760–3765, Sep. 2020, doi: 10.1109/TNNLS.2019.2944933.

Automated classification of HVAC systems through analysis of system behaviour

Björn Kämper [a], Maximilian Both [a], Nicolai Maisch [a], Jochen Müller [a]

[a] Institute of Building Services Engineering, TH Köln, University of Applied Sciences, Cologne, Germany, { bjoern_klaus.kaemper; maximilian_alexander.both; nicolai.maisch; jochen.mueller}@th-koeln.de.

Abstract. Technical monitoring applications support the operator in identifying potential improvements in plant operation and deriving recommendations for action. Today, the integration of building automation network data points into technical monitoring applications is complex and costly. The current state of the art is to manually integrate data points into dashboard applications. The decision which data point describes which HVAC component is made by engineers. The basis for the decision is usually identifiers or data point descriptions. An automated recognition of the structural information of the HVAC systems would help to automate the process and make the implementation of a technical monitoring in existing buildings and new buildings easier. One way to determine structural information from data points is to look at the behaviour of an HVAC system type.

Common HVAC systems follow known regularities in their construction and behaviour. By analysing the system behaviour, conclusions can be drawn about the heating circuit type (flow temperature controlled, outdoor temperature controlled, etc.). For example, an outdoor temperature-controlled heating circuit will behave differently than a flow temperature controlled heating circuit. Likewise, by analysing the system behaviour, it is possible to predict which data point is assigned to which system component. If two data points increase by a similar value with a short time offset, it is highly probable that they represent the supply and return temperature of a heating circuit. If the flow and return are heated up, it is likely that a pump has started up beforehand, which was represented by a binary switching command.

This paper describes an automated method to classify heating circuit data based on system behaviour. BACnet trend objects of heating circuits from different buildings, that are maintained by the building management of the city of Cologne, serve as data sets. This ensures that the developed method can be applied to a wide variety of heating circuit types. The automated classification of a heating circuit is intended to reduce the effort of manually assigning data points to specially created dashboards. Building operators can thus be supported in the creation and implementation of technical monitoring.

Keywords. Building Automation Systems, Building Control Systems, Classification of HVAC systems, Datapoint analysis, BACnet, reducing manual effort
DOI: https://doi.org/10.34641/clima.2022.169

1. Introduction

In buildings, technical monitoring (TMon) can serve as a central information platform for the operation of building services equipment. With the help of a TMon, the personnel responsible for building services engineering can identify potential for improvement in system operation and derive recommendations for action [1].

Operating information visualized in TMon applications originates from the automation level of the building. In this level the information is mapped to the data points of the communication protocols. Typical in the field of building automation are for example the communication protocols Building Automation and Control Networks (BACnet), Konnex-Bus (KNX) or Local Operating Network (LON). In these common communication protocols, it is not possible to store information about the system structure for individual data points. This means that a data point describing a temperature has no information about the fact that it is describing a temperature and whether the temperature is measured e.g. in a heating circuit or in a water boiler. State of the art is that information about the measured value, the system type or the measurement location is stored within the data

Copyright ©2022 by the authors. This conference paper is published under a CC-BY-4.0 license.

point in the form of textual descriptions that can be understood by humans [2].

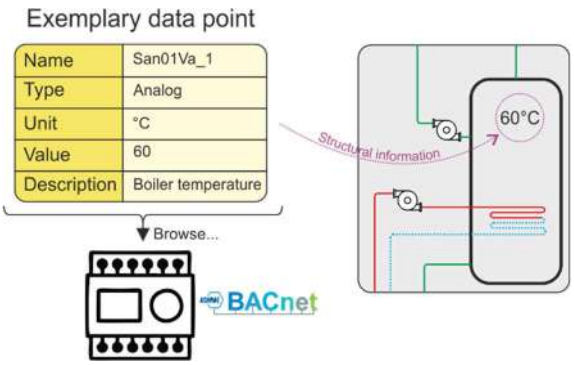

Fig. 1 - Exemplary datapoint which stands for the hot water temperature in a boiler. Structural information is only stored as text in the description.

For the creation of a TMon in existing buildings, it is necessary under today's conditions to consider these textual descriptions of the data points individually and to assign the data points manually to the corresponding applications and icons. Since such a manual assignment is associated with high effort and costs, TMon applications are not widespread in building technology, although they are indispensable for the energy- and cost-efficient operation of buildings [3].

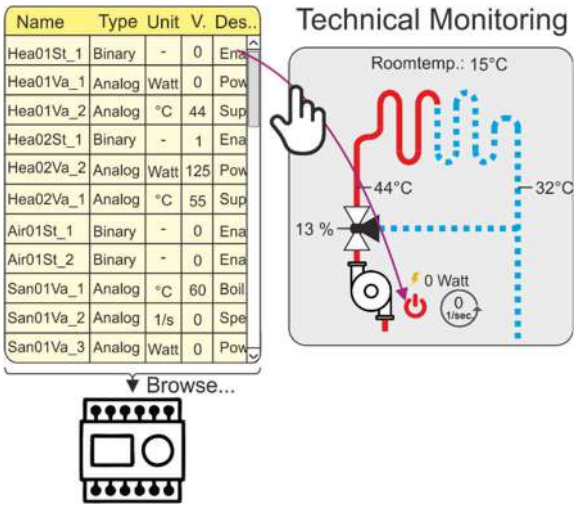

Fig. 2 - Manual assignment of a data point to a technical monitoring application.

By linking data points with corresponding structural information, the information content of a data point can be increased. This increased information content can be used to increase the degree of automation in the creation of TMon applications.

Since there are no mandatory attributes for meta-information, structural information, or textual descriptions in current HVAC communication protocols, there may not be enough information to derive structural information from.

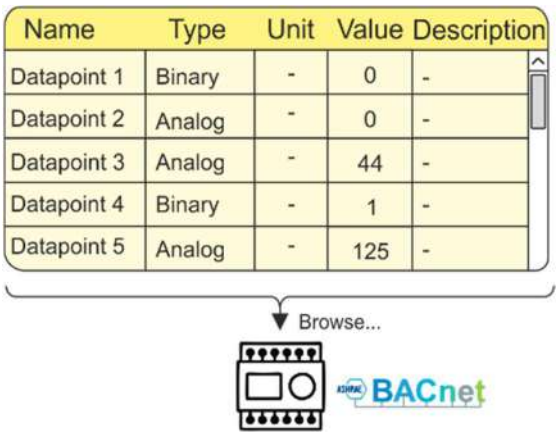

Name	Type	Unit	Value	Description
Datapoint 1	Binary	-	0	-
Datapoint 2	Analog	-	0	-
Datapoint 3	Analog	-	44	-
Datapoint 4	Binary	-	1	-
Datapoint 5	Analog	-	125	-

Fig. 3 - Example of data points that do not have information about physical units, descriptions, or meaningful labels.

This paper describes how behavioral rules can be derived from real, non-processed, building services engineering data. These behavioral rules are derived from the generally known laws of building services engineering. The goal is to be able to make predictions on the basis of the behavioral rules as to whether an individual data point is a setpoint, a measured temperature or a valve position, for example. In addition, it should be possible to recognize with the help of the behavior rules whether several data points can be assigned to a system component (e.g. a heating circuit).

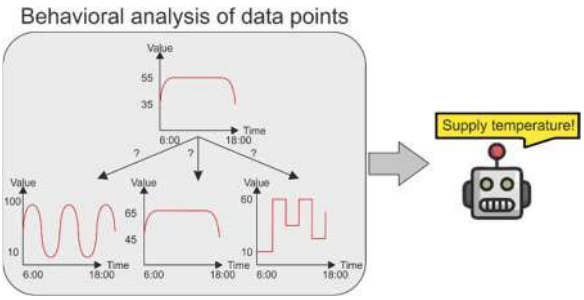

Fig. 4 - By the behaviour of a data point, conclusions should be made about structural information.

2. State of the art

Today, there are already different approaches how structural information of HVAC data points can be determined or provided:

[4] describes how textual descriptions of HVAC data points can be analyzed using Natural Language Processing (a subfield of artificial intelligence).

[5] extends and improves the previously described approach by considering meta-information such as physical units. Through this analysis, information about the component and/or the installation location can be derived.
Project Haystack is an open-source project that aims to develop a semantic data model for the

operational data in buildings. This semantic data model is primarily developed independently of a technology [6]. In the next steps, these semantic data models are to be mapped to the established communication technologies of building services engineering. The Haystack data model is to be implemented in BACnet, for example, by extending BACnet data points with tags in which additional structural information is stored [7]. Project Haystack thus offers a technological possibility to provide structure information about data points of the HVAC-Systems in the automation level. However, an automated generation and assignment of structure information to data points is not part of Project Haystack. In existing automation environments, these tags would also have to be linked manually.

[8] describes a process how data points from HVAC can be automatically mapped to standards like Project Haystack or Brick Schema. In this process, trend curves and labels of data points are evaluated and classified accordingly with the help of different machine learning algorithms. In the present paper a procedure is described which is similar in principle [8]. However, in this paper only the trend length (value over time) of single data points are considered for the analysis. [8] additionally includes textual descriptions in the analysis.

3. Procedure

In order to be able to make predictions about the structural information behind a data point, existing historical data (referred to as training data in the following) of different buildings were analyzed with a Java script. From this training data, commonalities and behavior rules for certain structural components (temperature sensor, valve, pump) were derived. For validation purposes, the commonalities and behavioral rules were tested against a further plant in a final step.

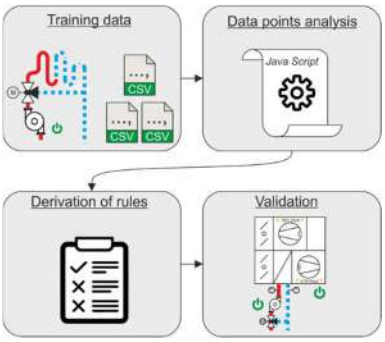

Fig. 5 – Procedure for deriving commonalities and behavior rules

3.1 Data basis

The rules were provided from existing and historicized data of buildings of the city of Cologne. The building management of the city of Cologne has connected a large number of buildings to the automation system and histories various building services systems in order to find potential for improvement or to document alarms.

The building management of the city of Cologne uses BACnet for communication and historization of HVAC data points. With BACnet, trend objects can be created for individual data points, which record the corresponding history of a data point [9]. The historization can be implemented with BACnet in two different ways. The values can either be recorded with the polling method and thus sampled at fixed intervals, or with the change-of-value (COV) method, in which a threshold value is defined that determines at which change of the value a recording of the data point should take place. Since COV leads to a smaller amount of data, the city of Cologne historizes the trend data with the COV method for reasons of efficiency.

The historized trend data can be exported by the building management the city of Cologne and made available as a CSV file.

Historic data from ten heating circuits from different buildings were used to derive the behavior rules. The heating circuits have different data points (some have recorded the supply temperature and others the return temperature) and different control strategies (supply temperature controlled, weather temperature controlled). The historized data points are from both summer and winter months. In total, over 700,000 recorded value pairs were considered.

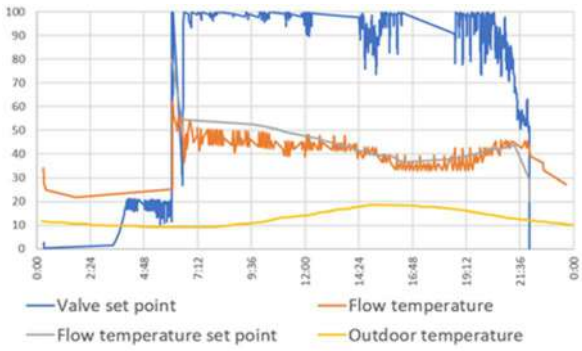

Fig. 6 - Exemplary trend curves of a heating circuit over a period of 24 hours.

Before the script examines the historized data points for commonalities and dependencies, the available data still had to be edited. During the historization of the data points, status messages are sometimes recorded instead of the value due to the system. These individual logs had to be removed from the historized data. This could be done with a simple function that deletes all logs that do not contain pure numerical values.

2.2 Analysis of training data and derivation of decision rules

The script examines each data point for certain aspects that help to assign structural information to the data point.

When looking at the data points, it is noticeable that

in individual cases incorrect and thus illogical values occur during the historization. In line 5338 of figure 7 such an illogical recording occurs when the value for the currently measured outdoor temperature for a short period of time is given as 151.5 °C.

5333	08.07.2021 10:02	20,73830032
5334	08.07.2021 10:14	20,93840027
5335	08.07.2021 10:34	21,13909912
5336	08.07.2021 10:41	24,31769943
5337	08.07.2021 10:41	21,2635994
5338	08.07.2021 10:42	151,5
5339	08.07.2021 10:42	21,3029995
5340	08.07.2021 10:58	21,50379944

Fig. 7 - System-related incorrect recording of a data point representing the outdoor temperature.

Due to such few erroneous recordings of the data points, the following rules are determined as percentages.

In the following, three exemplary functions are described which examine the logged values of a data point and classify this data point in a list on the basis of the trend.

Binary or analog:

The script finds out whether a data point describes a binary or analog value by checking whether a data point has assumed 0, 1 or another value over the entire period under consideration. If the value is exclusively 0 or 1 over 99% of the entire period, it is a binary data point. If the data point also takes other values, it is an analog data point. Based on this rule, the data points are placed in the corresponding list for binary or analog data points.

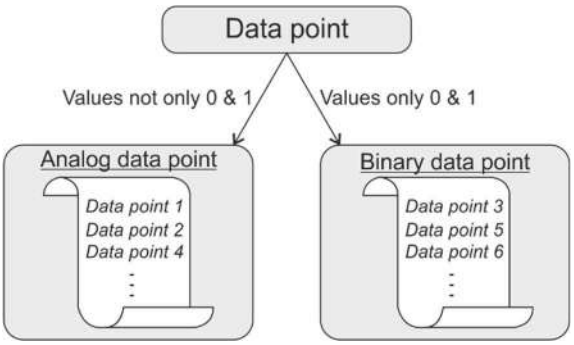

Fig. 8 - Binary or analog data point classification.

Based on this information, data points can be presorted in order to establish initial correlations in the further course. Binary data points rather represent operating messages such as pump switching commands to which analog values such as temperatures or positioning commands can react.

(The data used was provided with the help of the BACnet communication protocol. In BACnet, it is mandatory to specify whether a data point describes an analog or binary state. Therefore, it would not be necessary to determine this information with the help of a script. However, the approach taken in this paper is to consider data points independently of technology and to work only with the values provided and the associated timestamps).

Values over/under 100:

When checking whether a data point takes analog values above or below the value 100, the information taken before can already be used as support. For this information only, data points need to be considered which were sorted into the list for analog data points by the function *'Binary or analog'* described before.

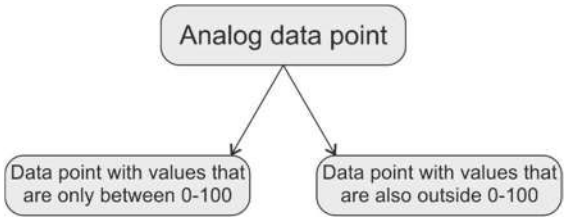

Fig. 9 - Data points with values that are only between 0-100 classification.

This information helps in the further course to give prognoses whether it is a data point which describes a valve position (0-100%). If the data point has values above 100 or below 0, it is most likely not a valve position.

Set points:

A measured value behaves differently from than an associated setpoint. A setpoint changes suddenly and abruptly in contrast to a measured temperature value.

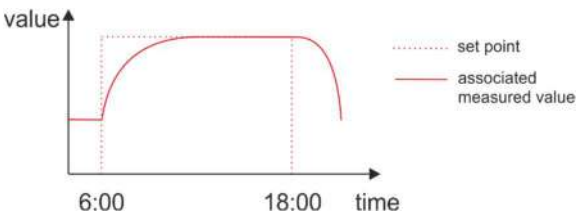

Fig. 10 - Qualitative representation of a setpoint and an associated measured value.

The data points were examined in terms of how often a data point executes a jump. A jump was declared as a 20% change of the value in a time window of less than one minute. As a percentage threshold value, it was found that every data point that makes these jumps (i.e. > 0%) can be declared as a control signal. Thus 18 of 22 setpoints were correctly recognized with two incorrect assignments. Thus, the data points were divided

into "jumping" and "not jumping" data points.

Room temperature:

To check whether a data point could be a room temperature, only data points that have already been classified as analog data points are considered. Then, for each data point, the percentage of all recorded values that are within a typical temperature range for room temperatures is checked. This temperature range was set to the range 17 - 27. Applying this rule to the training data, it was found that if 50% or more of the recorded values are within this range, all existing room temperatures are correctly assigned.

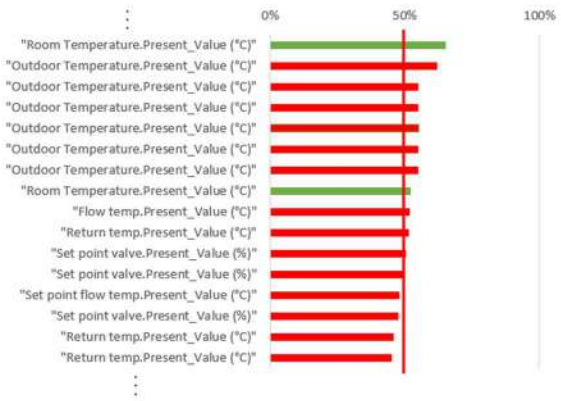

Fig. 11 - Evaluation for the classification of a room temperature.

In Fig. 11 it is to be seen that many data points (red bars which go beyond the boundary line of 50%) which do not represent room temperatures also fulfill the rule and thus would be classified as room temperature. Therefore, it is necessary to clean up the lists after the first classification with logical regularities. For example, if a data point was declared as a potential room temperature and as a potential outdoor temperature, the outdoor temperature can be removed from the list of potential room temperatures afterwards. For example, an outdoor temperature could be recognized more precisely by the typical day & night cycle, which is more pronounced than for a room temperature, and thus be removed from the list of room temperatures.

Heating temperature:

Another list in which data points can be sorted is a list containing all data points representing heating temperatures. For the time being, no distinction is made between setpoints / measured values or flow/return temperatures. The decisive criterion here is again a range of values which in this case was set to 25 to 65. As a percentage threshold value, whether a data point represents a heating temperature or not, 55% was chosen.

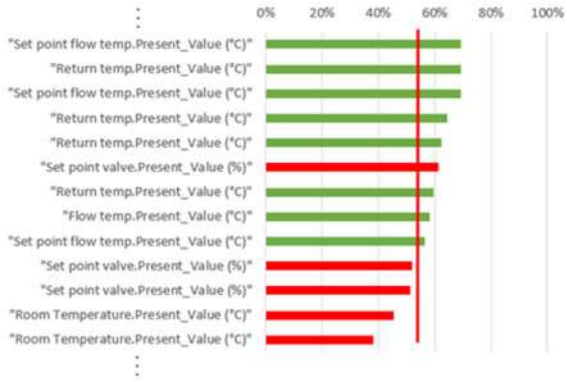

Fig. 12 - Evaluation for the classification of a heating temperature.

For the training data, this threshold detected all heating temperatures and assigned them to the list.

Outside temperature:

To detect outdoor temperatures, the percentage value was determined of how often the value of a data point corresponded to the historical monthly mean values (± 5 Kelvin) for the corresponding region (Greater Cologne-Germany). For the training data, a limit value of 40% resulted here.

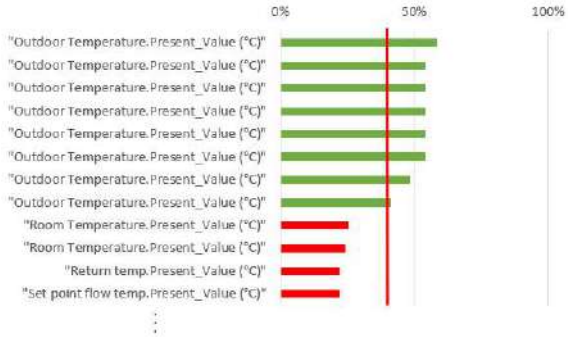

Fig. 13 - Evaluation for the classification of an outdoor temperature.

In this function, unlike the three rules presented previously, no incorrect data points were added to the list.

2.2 Finding relationships between data points

Data points in building technology often interact with each other in a generally known way. For example, if a valve position changes or the status of a pump changes from "off" to "on", this is often accompanied by a time-delayed change in temperature. Fig. 14 shows such a relationship between flow temperature, valve position and pump status.

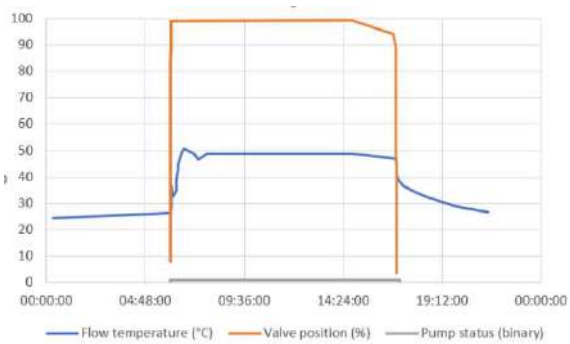

Fig. 14 - Relationship between flow temperature, valve position and pump status.

The data points were divided into individual lists using the rules applied in the previously described. These lists are used in the next steps to derive relationships between the individual data points, as explained in the previous section.

Temperature-pump dependencies:

To find out which of the temperatures is related to which pump switching command, the data points from the list for binary data points were first searched for state changes. If a state change was found in one of the data points, the timestamp of the state change was selected as a new search criterion. With this timestamp, each data point in the list 'Heating temperatures' was checked to see if there were values for this point in time that had changed significantly, but with a time delay. As a criterion how much a value must change, 10 Kelvin was defined. The time delay was chosen with 0-10 minutes.

The following graphic shows an exemplary result for a selected binary data point. By applying the rule described above, the correct data point (green bar) could be found. Compared to the other data points, it is by far the one that most frequently fulfills the search criterion.

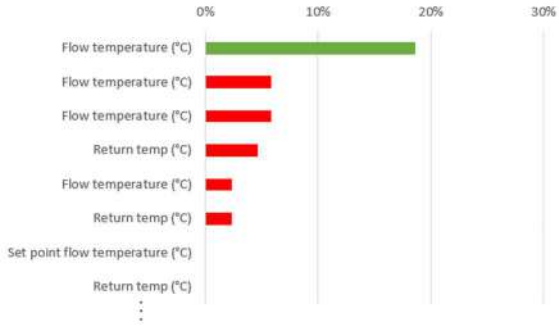

Fig. 15 - Evaluation for the relationship between a heating temperature and a pump status.

In 19% of the cases, this supply temperature met the condition of a change of 10 Kelvin within 0-10 minutes after a change of state of the binary data point. The low percentage value results from inconsistent training data. The historicized trend data for heating circuits do not have the same time records for all data points. In the training data it happens that binary pump switching commands are available for a period for which the corresponding temperatures of the heating circuit have not been historized. For this reason, it was decided not to declare a percentage as the limit for this rule, but to take the data point with the highest percentage as the decision criterion.
Further dependencies that are examined between the data points are, for example:

- How often a data point declared as temperature follows a data point declared as valve position.
- How often a data point declared as temperature or valve position follows a setpoint.

4. Validation

In order to validate the previously derived rules, the rules were applied to historized data from another building technology system. The data points of this system relate to a ventilation system with supply and exhaust air fans, heat recovery and a heater including the associated heating circuit. The data points were historicized over a period of one week in November.

Table 1 - Validation of the established rules based on data points of an air conditioning system. Cells with a green background mean that the respective data point has met the conditions of the respective rule.

Datapoint	Is binary	Is analog	values over 100	values under 0	Roomtemp.	Heatingtemp.	Percentage of jumps	Outsidetemp.
Exhaust air temperature ventilation (°C)	0%	100%	0%	0%	76%	0%	0,00%	75%
Supply air temperature ventilation (°C)	0%	100%	0%	0%	78%	2%	0,00%	62%
Outdoor air temperature ventilation (°C)	0%	100%	0%	0%	1%	0%	0,00%	85%
Control signal heat recovery ventilation (%)	63%	37%	0%	0%	0%	3%	0,23%	0%
Control signal heating valve ventilation (%)	22%	78%	0%	0%	7%	33%	0,08%	8%
Set point supply air temperature ventilation (°C)	0%	100%	0%	0%	100%	0%	0,00%	36%
Control signal supply air fan ventilation (%)	38%	62%	0%	0%	3%	34%	0,07%	3%
Control signal exhaust air fan ventilation (%)	40%	60%	0%	0%	3%	37%	0,07%	2%
Operating signal pump heater ventilation	100%	0%	-	-	-	-	-	-
Operating signal supply air fan ventilation	100%	0%	-	-	-	-	-	-
Operating signal exhaust air fan ventilation	100%	0%	-	-	-	-	-	-
Return temperature heater ventilation (°C)	0%	100%	0%	0%	19%	74%	0,00%	19%

- ***Binary or analog:***
  The rules that are supposed to distinguish whether a data point is a binary or analog data point work without error for this example. All three binary operating messages have been classified as such. A data point that has been classified as binary is no longer checked with the other rules.

- ***Values over/under 100:***
  The rules 'values over 100' and 'values under 100' should be used to distinguish data points that can take high/low numerical values (e.g. counters or high electrical power consumption) from data points that operate between 0-100 (e.g. system temperatures or valve positions). According to this rule, the historized data points of the ventilation system showed that each analog data point can be e.g. a system temperature or valve position and no data point could be excluded for the examination of the further rules.

- ***Room temperature:***
  The rule that checks a data point for a potential room temperature has detected three data points. The three detected data points are all related to the room temperature, but are not explicitly declared as such. Particularly From this example, potential for improvement of this rule can be derived. The data point "Setpoint room temperature" was declared 100% as potential room temperature, because it did not change over the entire period and was constantly in the defined number range. An addition to the rule stating that the data point must change by a defined value within a certain time period could act as an exclusion criterion here.

- ***Heating temperature:***
  The rule for detecting heating temperatures found the correct data point during validation. In this plant there was only one return temperature.

- ***Set points:***
  The recognition of the control signals also worked without errors. All four control signals were declared as such.

- ***Outside temperature:***
  The declaration of the outdoor temperature also worked well. Even though three data points were declared as potential outdoor temperature, the correct outdoor temperature has the highest percentage. This can also be improved by defining the rule in such a way that only the data point with the highest percentage is recognized as outdoor temperature.

Table 2 - Relationship between binary datapoints and heating temperatures.

Binary datapoint	Return temperature heater ventilation (°C)
Operating signal pump heater ventilation	0%
Operating signal supply air fan ventilation	0%
Operating signal exhaust air fan ventilation	0%

- ***Temperature-pump dependencies:***
  Table 2 shows the percentage values of the rule that is to find out which temperature follows which binary switching command. The only detected heating temperature could not be assigned to any of the three binary switching commands. The rule searches for a changing temperature after there has been a change of state of a binary signal. Figure 16 shows the recorded course of the heating temperature, the corresponding valve position and the operating message of the pump over a period of 24 hours. As can be seen, the control of the system is selected in such a way that the return temperature is controlled only by the valve position. The binary switching command of the pump is constant 1, so a dependence of the temperature to the pump cannot be found.

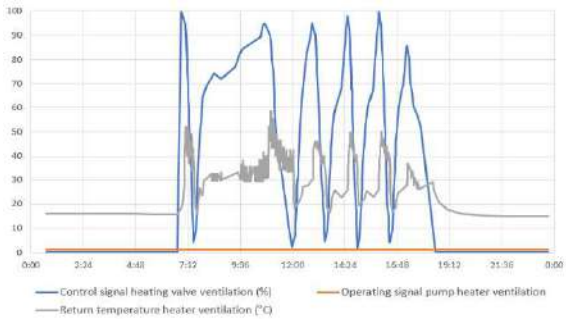

Fig. 16 - Relationship between return temperature, control signal valve position and pump status

But knowing that there is a heating temperature that follows a valve position and no associated pump switching command, predictions can be made about system behavior.

5. Problems and approaches

In the presented methodology, different problems due to inconsistent and incomplete data were identified. The goal must be to historize all data points of a building services system for a certain period of time. When recording a building's behavior, it is then important that the building's systems also operate accordingly. If valves do not move (e.g. because it is summer and no heating load is required), it is difficult to identify dependencies between data points.

6. Outlook and summary

This paper describes a first attempt to draw conclusions about the structural information of a data point from historized HVAC data points based only on the value and the corresponding timestamp.

Of course, HVAC-systems consists of larger and more complex systems than the systems taken as a basis in this paper. Nevertheless, with such simple rules, and knowledge of the known regularities of HVAC-systems, there is the possibility to generate information about the structure of a system.

The next steps in extending this method will be to further specify the rules for heating circuits and to define rules for other trades and components. The historization of the data can be done by a microcontroller which searches for the common communication protocols in a building automation network and historizes all data points in fixed intervals. These data can be used again as validation.

The rules described in chapter 3 can serve as a basis for one of the most widely used AI algorithms 'Decision Trees'. In 'Decision Trees', simple if-else relationships for data are also established and then interrelated using stochastic distribution in such a way that predictions can be made for data sets [10]. Whether the methodology presented in this paper can be used to automatically link HVAC data points with TMon applications could not be finally answered. In chapter 2 different methods were already presented which deal with similar questions. It will be interesting to investigate how far the methods can complement and support each other.

References

[1] Facility management - Technical monitoring of buildings and building services, 6041, Verein deutscher Ingenieure, 10772 Berlin, Jul. 2017.

[2] H. Merz, T. Hansemann, and C. Hübner, Building automation: Communication systems with EIB/KNX, LON and BACnet. München: Fachbuchverl. Leipzig im Carl Hanser Verl., 2007.

[3] J. Granderson and G. Lin, “Building energy information systems: synthesis of costs, savings, and best-practice uses,” Energy Efficiency, vol. 9, no. 6, pp. 1369–1384, 2016, doi: 10.1007/s12053-016-9428-9.

[4] M. Both, Maisch Nicolai, and Kämper Björn Prof. Dr. Müller, Jochen, “Automated performance monitoring of HVAC components by artificial intelligence,” Rotterdam, May. 2022.

[5] A. Cartus, M. Both, and J. Prof. Dr. Müller, “Interoperability of semantically heterogeneous digital twins through Natural Language Processing methods,” Rotterdam, May. 2022.

[6] John Petze, Unlocking the Value of Equipment System Data: Introduction to Project Haystack and Data Modeling for Equipment systems. [Online]. Available: https://project-haystack.org/download (accessed: Jan. 10 2022).

[7] B. I. John Petze, ASHRAE'S BACnet committee, Project Haystack and Brick schema collaborating to provide unified data semantic modelling solution [Online]. Available: https://www.ashrae.org/about/news/2018/ashrae-s-bacnet-committee-project-haystack-and-brick-schema-collaborating-to-provide-unified-data-semantic-modeling-solution (accessed: Jan. 10 2022).

[8] Sakshi Mishra, Andrew Glaws, Dylan Cutler, Stephen Frank, “Unified Architecture for Data-Driven Metadata Tagging of Building Automation Systems,” National Renewable Energy Laboratory, Golden, USA.

[9] H. R. Kranz, BACnet Building Automation 1.12: Basics in German language, 3rd ed. Karlsruhe, Baden: cci-Dialog, 2013.

[10] D. N. Sidorov, Ed., Machine Learning for Energy Systems. Basel, Switzerland: MDPI - Multidisciplinary Digital Publishing Institute, 2020. [Online]. Available: https://directory.doabooks.org/handle/20.500.12854/69401

Time Series Building Energy Systems Data Imputation

*Adrien Lucbert [a], Juliën van der Niet [b], Albert Corson [a], Michael Weij [b], Ramon Isaac van der Elst [b], Jesús Mª Martínez de Juan [c], Tadeo Baldiri Salcedo Rahola [b] **

[a] Epitech, France.
[b] The Hague University of Applied Sciences, The Netherlands.
[c] Francisco de Vitoria University, Spain.

Abstract: Completeness of data is vital for the decision making and forecasting on Building Management Systems (BMS) as missing data can result in biased decision making down the line. This study creates a guideline for imputing the gaps in BMS datasets by comparing four methods: K Nearest Neighbour algorithm (KNN), Recurrent Neural Network (RNN), Hot Deck (HD) and Last Observation Carried Forward (LOCF). The guideline contains the best method per gap size and scales of measurement. The four selected methods are from various backgrounds and are tested on a real BMS and metereological dataset. The focus of this paper is not to impute every cell as accurately as possible but to impute trends back into the missing data. The performance is characterised by a set of criteria in order to allow the user to choose the imputation method best suited for its needs. The criteria are: Variance Error (VE) and Root Mean Squared Error (RMSE). VE has been given more weight as its ability to evaluate the imputed trend is better than RMSE. From preliminary results, it was concluded that the best K-values for KNN are 5 for the smallest gap and 100 for the larger gaps. Using a genetic algorithm the best RNN architecture for the purpose of this paper was determined to be Gated Recurrent Units (GRU). The comparison was performed using a different training dataset than the imputation dataset. The results show no consistent link between the difference in Kurtosis or Skewness and imputation performance. The results of the experiment concluded that RNN is best for interval data and HD is best for both nominal and ratio data. There was no single method that was best for all gap sizes as it was dependent on the data to be imputed.

Keywords: Building Management System time series data, Imputation, KNN, RNN, Hot Deck, trend
DOI: https://doi.org/10.34641/clima.2022.302

1 Introduction

Missing data is a common occurrence in time series data, possible causes include faulty sensors or errors in data storage. Missing data can cause downstream applications to malfunction and can thus have serious consequences. Missing data in Building Management Systems (BMS) can cause underperforming building services e.g., lower comfort of living or higher power usage, or in worst-case scenarios building breakdown as system control decisions are based on the collected data.

Imputation methods evaluated in this paper are selected from previous research that has been done into the imputation of time series data. The methods that are selected for evaluation are: Last Observation Carried Forward (LOCF), K-Nearest Neighbour algorithm (KNN), Recurrent Neural Network (RNN) and Hot Deck (HD).

HD can be outperformed by machine learning as seen in (Sree Dhevi,2014)[1]] but it is applicable when there are similar units available for study. The time series imputation performance of different types of RNN's has been studied before in Che et al. (2018) [2]. The study concluded that when a Gated Recurrent Units (GRU) architecture is properly set up *"it pulled significantly ahead of non-deep learning methods"* [2].

Pazhoohesh et al.(2019) [3]found that for datasets where 10% to 30 % of the data is missing, the KNN algorithm does great compared to eight other methods. Poloczek et al. 2014 [4] analysed the use of KNN regression and LOCF and found that both did well for the study, but that KNN regression outperformed other methods.

There are limited studies to clarify how to deal with missing data in BMS datasets. Previous research has focused on lighting and occupancy [3] data or created a generic framework for imputing data from multiple sensors [5]. In the

Copyright ©2022 by the authors. This conference paper is published under a CC-BY-4.0 license.

case of (Zhang,2020) it is advised that a more generic plug-n-play framework is to be further studied. This study does not build on the framework created by (Zhang,2020) but tries to give a guideline on when to use what method. The research focused on imputing trends rather than accurately imputing data in a single moment in time.

This paper aims to evaluate and compare the imputation performance of the following methods: KNN algorithm, LOCF, RNN and Hot Deck. The imputation performance has been evaluated by making use of various criteria to facilitate the choice of the most suitable method for each scenario. Aside from the most suited scenario, the imputation method's ability to impute trends is also evaluated.

The method section contains a description of the datasets, description of the pipeline, imputation methods and the criteria used for evaluation. The result section presents the imputation results and a recommended action for each data measurement scale and gap size.

2 Methodology

2.1 Dataset description

BMS datasets store sensor data such as fluid temperature, power usage, flow rate, operational mode, solar radiation and outdoor temperature. Two datasets have been used: BMS data of hundred-twenty residential Net-Zero energy houses and data of twenty-five weather stations from the Royal Netherlands Meteorological Institute (KNMI) [6]. The NZEB BMS time series dataset contains data from 2019 and has a five-minute interval data measurements (105096 rows). The KNMI dataset contains data from 2018 to 2020 and it is measured at hourly intervals (17545 rows). The only change made to the original datasets was converting the timestamps to Python Date Time objects.

2.2 Columns selected for imputation

Seven columns have been selected from the two datasets to evaluate the imputation performance. The selected features from the BMS dataset are power usage (power), CO2 level measurements (CO2), heat pump flow temperature (flow_temp) and operational mode (op_mode). The features selected from the KNMI datasets are solar radiation (global radiation), temperature (temperature) and relative atmospheric humidity (Relative atmospheric humidity). The BMS features were selected for their data measurement scale. The KNMI columns were selected for the strong correlation between the features.

3 Pipeline

A pipeline has been developed to evaluate the performance of imputation methods under the same reproducible conditions. The pipeline performed the following tasks: loading the data, creating gaps, imputing the artificial gaps, calculating imputation performance, and storing the evaluation results. The pipeline code and trained models can be found in the references.

3.1 Gap creation

To evaluate the performance of each imputation method, artificial gaps have been created in both datasets. The gaps come in different sizes to evaluate the performance of each imputation method on different amounts of missing sequential data. The gaps have been created making use of the rules stated in Tables [2-3] and are generated using a set random seed. The set random seed is also used in order to determine gap location and the size of the gap. The gap sizes and locations are the same for every feature and method tested.

Tab. 2 - BMS artificial gap rules

Nr.	Min size	Max size	% of data
1	5 min	60 min	15%
2	1 hour	6 hours	5%
3	6 hours	24 hours	1.5%
4	24 hours	72 hours	0.5%
5	72 hours	168 hours	0.01%

Tab. 1 - Columns with the dataset of origin, device, unit of measurement and measurement

Column name	Dataset	Device	Unit of measurement	Measurement scale
Temperature	KNMI	-	C (in 0.1c)	Interval
Global Radiation	KNMI	-	j per cm^2	Ratio
Humidity	KNMI	-	%	Ratio
Flow_temp	BMS	Alklima Heat Pump	C	Interval
op_mode	BMS	Alklima Heat Pump	0-6 modes	Nominal
Power	BMS	Smartmeter	W	Ratio
C02	BMS	C02 Sensor	PPM	Ratio

Tab. 3 - KNMI artificial gap rules

Nr.	Min size	Max size	% of data
1	1 hour	6 hours	15%
2	6 hour	24 hours	5%
3	24 hours	72 hours	1.5%
4	72 hours	168 hours	0.005%

4 Imputation methods

Four imputation methods are compared in this paper: Hot Deck, Recurrent Neural Network (RNN), Last Observation Carried Forward (LOCF) and K-Nearest Neighbour algorithm (KNN). The methods have been selected from previous literature and aim to have a wide scope of imputation approaches to facilitate each method's characterizations, advantages and disadvantages.

4.1 KNN algorithm

KNN algorithm is a nonparametric imputation method that works by taking the average of a gap's K-number of neighbours. Treating every neighbouring value equally, simple KNN would make it more vulnerable to outliers. To mitigate this, KNN is set up to weigh the nearer neighbours of a gap heavier than further away values.

The K-values tested are: 1,5,10,15,20,100. The K-value selection has been done by evaluating the results gotten from imputation using the Variance Error. From the results of the evaluation, it can be concluded that K=5 is best for the gap size 1 and K=100 for gap sizes 2 to 5.

4.2 Last Observation Carried Forward

Last Observation Carried Forward works by filling in the gap with the last valid before the gap observation forwards. LOCF can introduce substantial bias in datasets that do have high volatility in values [7]. Columns such as power usage are most likely to suffer the most from this due to the unpredictability in data which is expected to worsen with larger gaps in the data. Nevertheless, LOCF is still in common use nowadays and has been compared before in time series imputation performance [3, 5].

4.3 Hot deck

Hot Deck imputation is a method for handling missing data in which each missing value from a recipient is replaced with an observed value from a similar unit (the donor). This method applies perfectly to this study since there are multiple units (different houses or different weather stations' data).
HD is a well-known method, but the theory behind the Hot Deck is not as well developed as the theory of other imputation methods, leaving researchers with limited guidance on how to apply it. The main challenge is selecting donors.
In some versions, the donor is selected randomly from a set of potential donors, which is called the donor pool. In other more deterministic versions, a single donor is identified, and values are imputed from that case usually, the "nearest neighbour" based on a dataset-dependent metric (i.e.: the mean when imputing temperature time series).

In the case of this research, the donor selection was based on pattern recognition. It works by taking an extract containing data before and after a series of missing values (a gap) found in the recipient. To find the best matching segment of data from a donor, the recipient's extract would then be compared to similarly-sized extracts from the same time period in a donor.

Using the difference in the mean of the donor's extracts and recipient's extract, the values from the donor's extracts can be shifted towards those of the recipient except when imputing categorical data. The sum of the absolute difference between the extracts can now be used to sort the comparisons: the smaller the sum is, the better the pattern matches. The operation can then be repeated throughout each donor of the donor pool, for each gap, to find the best possible match before finally importing data into the recipient.

4.4 Recurrent Neural Network

Recurrent Neural Networks have been proven to perform well when working with time series data [8] and in [2] it pulled significantly ahead of non-deep learning methods. RNN's benefits from having an internal memory, unlike other NNs, this helps them to preserve context which is useful with the imputation of BMS time series data. The internal memory of the RNN architecture is useful for the purpose of imputing time series data as the missing values are highly depend on the trend before and after a gap.

Two different architectures of RNN's were compared on performance in time series imputation: Long- Short term Memory (LSTM) and Gated Recurrent Units (GRU). Both architectures use long-short term memory, but the key difference is that LSTM uses three gates: forget, input and output, whilst GRU uses two: update and reset. Another difference between the two is that GRU exposes the entire memory including hidden layers whilst LSTM keeps them hidden.

Both architectures were compared using a genetic algorithm, random configurations are generated

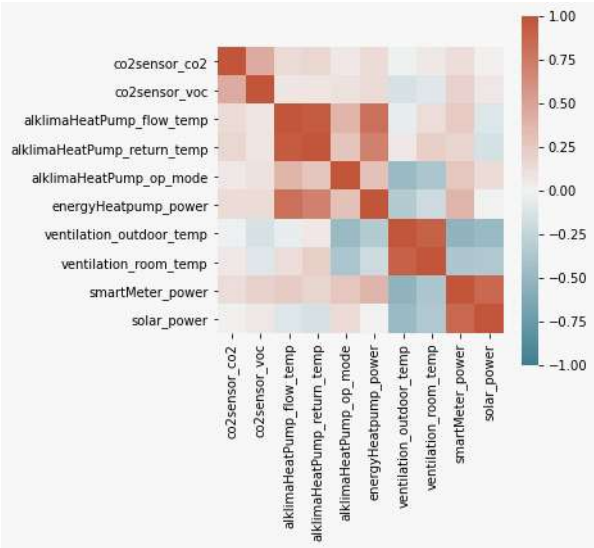

Fig.1 - Correlation matrix BMS data

by changing the GRU or LSTM. Architectural parts that were randomized are the number (1 – 5) and size (2 – 100) of hidden layers, input sequence size (2 – 12) and the loss-function (MSE or Huber).

The best architecture configuration found during testing was a GRU RNN configured with 1 hidden layer of size 95, input sequence length 12 and the using the MSE loss function. The final GRU was configured as listed before in addition a fully connected layer was added. This was done to transform the GRU layer output into prediction. The GRU-based RNN was trained for every column that was to be imputed.

RNN results are drastically improved when using multiple correlated columns as input. To select the most correlated columns a correlation matrix (Figure 1) is used to display both positive and negative correlations. From Figure 1 the best correlators were chosen to train each model with. The implementation of the current GRU-based model has two major limitations. First, it only imputes one value at a time based on the X-number of preceding values. This means that with a sufficiently large gap it uses its own values to impute further. Using previously imputed values can result in biases in the imputation since one imputation error impacts all following imputations. Another limitation is that the current GRU RNN version trained using Mean Squared Error (MSE) may not line up with the goal of imputing trends back into missing data.

4.5 Imputation evaluation criteria

The aim of this paper is to create a selection of the most suitable imputation methods for certain scenarios with measurement scales and gap sizes. To select the best method for each scenario evaluation criteria are required. In this paper the selected criteria are Variance Error (VE) and Root Mean Squared Error (RMSE).

VE is used to give insight into the imputation method's ability to impute trends back into the missing data since that is one of the focal points of this research. The VE is calculated by calculating the difference in variance between the original and imputed data for each gap and then averaging it out if multiple gaps are present. To get the difference in variance in a gap, the pandas method "pandas.var" has been used.

In previous literature [3, 8, 9] RMSE has been used to evaluate the performance of imputation on time series data. RMSE is calculated to give a comparison point for imputations done in this paper compared to results in previous research. The RMSE was calculated by taking the square root of the Mean Squared Error.

In this study normality testing of the datasets is done to measure the impact of a change in the distribution on imputation. Kurtosis and

Tab. 4 - List of methods included in this paper

Method	Abbreviation	Category	Description	Library used
Last Observation Carried Forward	LOCF	Simple	Use the last cell before the gap to fill a gap.	pandas.DataFrame.fillna
KNN regression	KNN	Simple	Take the weighted average K-number of nearest neighbours.	sklearn.impute.KNNImputer
GRU RNN	RNN	Neural Network	RNN considers past to impute missing data.	torch.nn.GRU
Hot deck	HD	Statistical	Take data from a different unit with a similar trend.	None

Skewness are used to test the normality of data because according to [9] it is significant to model development. According to the central limit theorem, the distribution of data can be ignored with hundreds of observations [10]. But according to [11] statistics such as Kurtosis and Skewness can be used to measure the normality of continuous data with sample sizes higher than 50.

5 Results and discussion

With the developed pipeline and datasets as described in the methodology, an experiment ran with the settings of Tables 2 and 3 to determine the best imputation method per gap size and measurement scale.

The imputation target for the experiment was unit 099 for BMS data and de Bilt weather station as KNMI climate data. To train the models RNN used unit 054 and Rotterdam KNMI weather station. RNN and KNN both imputed op_mode with decimal values and should thus be ignored. Whilst op_mode is numerical, the performance of RNN and KNN wouldn't represent the performance on other text-based data.

The pipeline evaluated each imputation method based on the evaluation metrics listed under the evaluation criteria per gap and feature. The imputation performance is mainly be evaluated based on the VE metric as mentioned in the evaluation criteria. RMSE is also calculated to evaluate imputation performance as seen in previous literature.

Based on the information in Tables 6 - 10, several conclusions can be made by comparing the performance of the imputation method over various gap sizes and measurement scale:

- The RMSE results show that the imputation performance as judged by traditional metrics is poor. However, since the focus of this paper is to impute trends the comparison point should be the VE between methods instead of the RMSE.
- HD tends to score better on the KNMI datasets, this might be due to the more similar previous trends found in the datasets. In both VE and RMSE, HD tends to outperform RNN in imputing temperature data across all gaps. This performance doesn't transition to other interval data such as flow_temp as HD's performance in both VE and RMSE is worse than expected in this column.
- RMSE and VE do not always align when it comes to trend prediction in imputed data. CO2 sensor data gap 3 and 4 have a relatively close RMSE while their VE scores further apart. When visualising the data in Figure 1 it can be seen that HD tries to impute a trend that matches relatively well according to

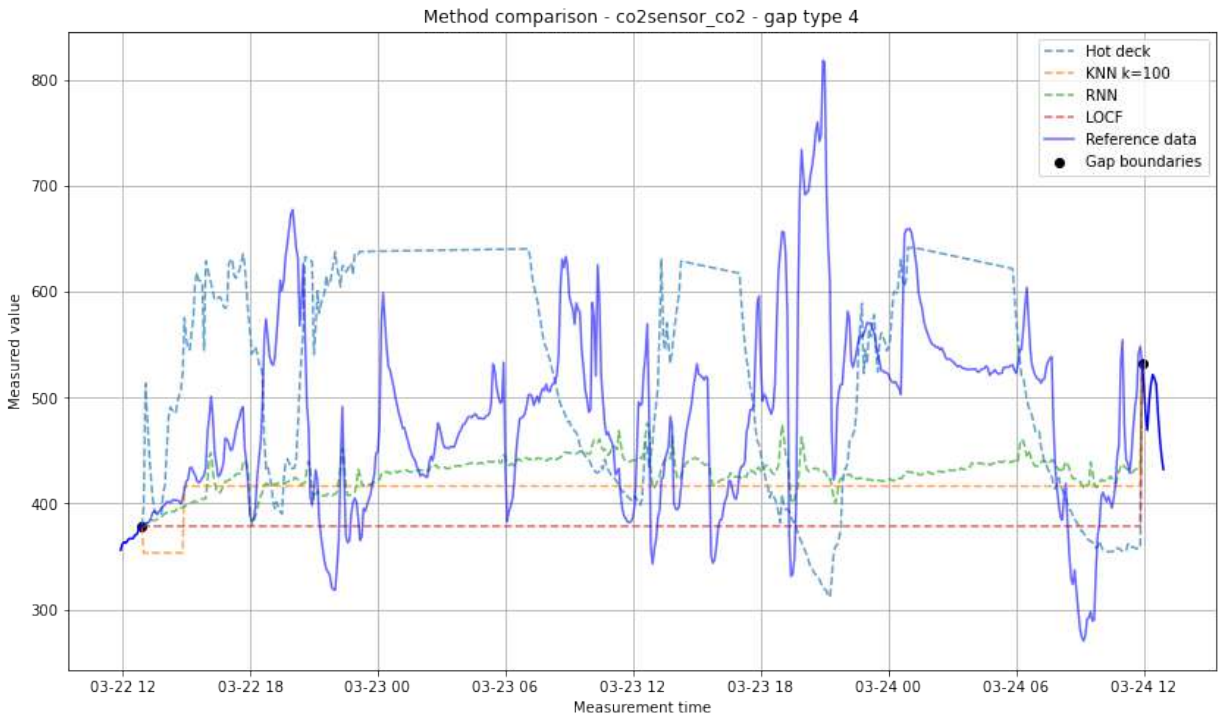

Fig. 2 - CO2 sensor trend imputation performance comparison

the VE. However, RNN has a more stable line without any big noticeable trends. In this case, RMSE seems to punish imputing trends and reward imputing a stable line of data without trends.

- As seen in Table 11, a high difference in Kurtosis was found between training and imputation target data. This might explain RNN's behaviour in the imputation results of the CO2 sensor data as seen in Figure 1 and Tables 6 -10. However, no consistent link has been found between Kurtosis and trend imputation performance. In Figure 2 the imputation of a flow_temp gap is shown, in the figure RNN tracing a trend is observed. RNN has a comparatively better performance in flow_temp than in power despite having a higher difference in both Kurtosis and Skewness. The normality of the distribution does not seem to explain the difference in RNN imputation performance from interval to ratio data.

- In the achieved results (Tables 6 - 10) no strong link can be found between having multiple strong correlators and a good RMSE or VE score. Flow_temp has two strong correlators in return temperature (0.94) and heat pump power usage (0.81) and gets good imputation results. Power and CO2 data seem to contrast these findings as power has two strong correlators (-0.56 and 0.86) and CO2 one decent correlator (0.44) but both get bad imputation results.

To sum up, the results as seen in Tables 6 - 10 and discussed before there is no single imputation method for all data measurement scales. Based on the results it can be concluded that there is no imputation method that works well for all gap sizes. HD tends to score better on KNMI data across measurement scales RNN does not do the same. VE and RMSE don't always align and VE is in some cases the better indicator for the ability of an imputation method to follow the trend displayed in Figures 1 & 2. The difference in Kurtosis was not as big of a factor as initially thought.

6 Conclusion

This paper proposes a guideline to impute BMS nZEB data based on gap size and different scales of measurement. The problem with missing data in BMS is becoming a bigger problem in an era where buildings depend on data. Previous research has been done about imputing BMS time series data; this paper tries to build on that by creating a comprehensive guideline to follow for

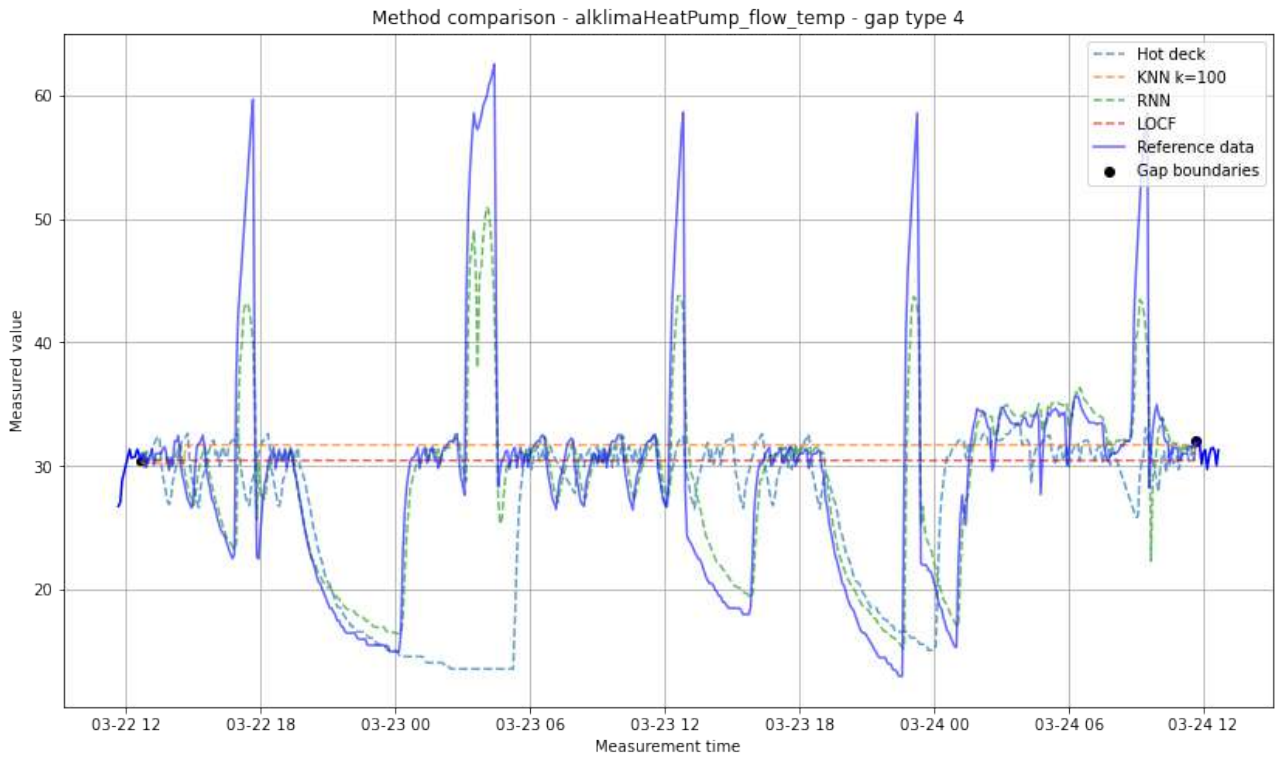

Fig. 3 - Trend performance RNN on interval flow_temp data

certain scenarios. To create a guideline 4 methods were chosen from previous literature: GRU RNN, Hot Deck, KNN algorithm and LOCF. During the research, imputing trends back into missing data became the focal point of this study which is why Variance Error (VE) was used instead of a more traditional metric like Root Mean Squared Error (RMSE). The guideline that resulted from this experiment is listed down below in Table 5. Performance was evaluated using both RMSE and VE but metrics concluded the same methods as best for each gap type and data measurement scale.

From the results of both VE and RMSE can be concluded that there is no single best imputation method for all gap sizes and measurement scales. The best method for a gap size is dependent on the measurement scale of the to be imputed data. No consistent crossover was found between the gap size and measurement scale as can be seen in Table 5.

Tab. 5 - Guideline for what method to use based on VE

	Gap type 1.	Gap type 2.	Gap type 3.	Gap type 4.	Gap type 5.
Nominal	HD	HD	HD	HD	HD
Ratio	HD	HD	HD	HD	HD
Interval	RNN	RNN	RNN	RNN	RNN

When comparing RMSE scores achieved in this paper to previous research it seems the imputation performance is poor. The focal point of this paper however was to impute trends back into data and seeing the VE score and visualisations a good starting point was made.

An important thing to note for this paper is the use of HD, due to this research having large amounts of similar data units HD was uniquely applicable. With no similar data HD will not be applicable and even with fewer external data sets HD might suffer a performance hit.

In future work, the focus of research should be less on evaluating imputation with metrics based on the error and more on the impact of forecasting using imputed data. The effect on forecasting performance ought to be evaluated as it can provide a more complete view of imputation performance.

The data sets used for this study contain only numerical data and no ordinal data. To get a full view of the imputation performance on text-based categorical data further research is required.

The GRU RNN architecture used in the research had clear limitations based on how it was set up. To evaluate the full potential of imputation using RNN the architecture should be changed to an encoder-decoder sequential based design. This would remove the potential bias of imputation using its own imputed values.

7 Appendix A

Tab. 6 - gap size 1

Field	Method	HD	RNN	KNN	LOCF
Temperature	**VE**	60.13	63.738	92.126	92.701
	RMSE	14.07	12.31	38.19	22.352
FLOW_TEMP	**VE**	8.67	7.20	10.76	10.76
	RMSE	5.29	3.21	5.34	6.79
op_mode	**VE**	0.08	0.08	0.08	0.08
	RMSE	0.49	0.45	0.45	0.56
Global Radiation	**VE**	337.621	369.87	620.279	620.85
	RMSE	25.16	29.84	66.47	53.02
Humidity	**VE**	15.38	15.45	20.71	20.80
	RMSE	6.78	6.19	14.52	9.88
Power	**VE**	137217	151494	158763	158763
	RMSE	686.24	798.725	632.54	800.01
C02	**VE**	372.92	393.49	420.02	420.02
	RMSE	44.41	40.34	35.29	43.03

Tab. 7 - gap size 2

Field	Method	HD	RNN	KNN	LOCF
Temperature	**VE**	264.83	290.36	604.13	609.78
	RMSE	17.61	17.19	38.72	45.14
FLOW_TEMP	**VE**	32.892	21.36	39.59	39.631
	RMSE	8.03	3.78	8.43	10.28
op_mode	**VE**	0.28	0.32	0.33	0.33
	RMSE	0.84	0.84	0.83	0.99
Global Radiation	**VE**	1086.88	1427.15	2902.85	2904.88
	RMSE	32.52	45.92	67.81	91.24
Humidity	**VE**	51.67	59.07	108.11	108.60
	RMSE	9.08	9.45	15.12	18.78
Power	**VE**	357663	425962	494539	504114
	RMSE	895.32	1258.1	1176.21	1181.55
C02	**VE**	1393.59	1587.98	1782.42	1747.18
	RMSE	53.07	66.71	78.15	74.81

Tab. 8 - gap size 3

Field	Method	HD	RNN	KNN	LOCF
Temperature	**VE**	328.88	381.24	901.32	912.82
	RMSE	14.39	17.19	37.874	45.98
FLOW_TEMP	**VE**	53	32.168	65.99	65.99
	RMSE	10.35	3.87	9.26	11.58
op_mode	**VE**	0.62	0.544	0.63	0.63
	RMSE	1.20	0.93	0.96	1.34
Global Radiation	**VE**	1138.15	2380.38	4392.39	4396.39
	RMSE	28.90	57.54	68.1	96.89
Humidity	**VE**	69.05	89.98	176.42	177.53
	RMSE	7.64	10.26	14.75	18.64
Power	**VE**	579467	1.15e+06	1.36e+06	1.36e+06
	RMSE	997.66	1516.92	1725.46	1906.12
C02	**VE**	3862.98	4608.09	5272.42	5282.86
	RMSE	109.88	100.2	113.50	115.28

Tab. 9 - gap size 4

Field	Method	HD	RNN	KNN	LOCF
Temperature	**VE**	415.57	407.244	1220.58	1228.37
	RMSE	14.67	18.23	42.08	52
FLOW_TEMP	**VE**	54.81	33.72	73.699	73.701
	RMSE	9.59	3.76	9.37	11.75
op_mode	**VE**	0.47	0.67	0.78	0.78
	RMSE	1.20	0.98	0.96	1.34
Global Radiation	**VE**	735.97	1715.78	4221.93	4222.48
	RMSE	22.94	64.08	65.86	97.46
Humidity	**VE**	67.07	95.86	187.31	187.40
	RMSE	7.12	11.46	15.21	19.94
Power	**VE**	760667	1.59e+06	1.96e+06	1.96+06
	RMSE	843.932	1744.81	1759.17	1992.42
C02	**VE**	6316.95	8492.07	9311.84	9315.94
	RMSE	115.84	116.52	123.39	142.02

Tab. 10 - gap size 5

Field	Method	HD	RNN	KNN	LOCF
FLOW_TEMP	**VE**	63.54	36.65	75.85	75.85
	RMSE	9.12	3.95	9.48	12.60
op_mode	**VE**	0.15	0.152	0.598	0.598
	RMSE	0.89	1.02	1.59	0.92
Power	**VE**	746953	1.81e+06	2.079e-6	2.079e-6
	RMSE	778.901	1594.85	1628.55	2218.56
C02	**VE**	5956.65	9086.66	9902.27	9902.33
	RMSE	105.32	122.10	114.78	131.26

Tab. 11 - kurtosis and skewness diference

Column	**Kurtosis difference**	**Skewness difference**
Temperature	0.04	0.03
Relative atmospheric humidity	0.28	0.04
Global radiation	0.09	0.02
alklimaHeatPump flow_temp	0.45	0.25
alklimaHeatPump op_mode	2.20	0.81
smartMeter power	0.31	0.07
co2sensor co2	5.41	0.57

[12]

References

[1] A.T. Sree Dhevi. "Imputing missing values using Inverse Distance Weighted Interpolation for time series data". In: *2014 Sixth International Conference on Advanced Computing (ICoAC)*. 2014, pp. 255–259. DOI: 10.1109/ICoAC.2014.7229721.

[2] Zhengping Che. "Recurrent Neural Networks for Multivariate Time Series with Missing Values". In: *Scientific Reports* (2018). DOI: 10.1038/s41598-018-24271-9.

[3] Mehdi Pazhoohesh, Zoya Pourmirza, and Sara Walker. "A Comparison of Methods for Missing Data Treatment in Building Sensor Data". In: *2019 IEEE 7th International Conference on Smart Energy Grid Engineering (SEGE)*. 2019, pp. 255–259. DOI: 10.1109/SEGE.2019.8859963.

[4] Kramer O. Poloczek J. Treiber N.A. "KNN Regression as Geo-Imputation Method for Spatio-Temporal Wind Data". In: 299 (2014). DOI: 10.1007/978-3-319-07995-0_19.

[5] Liang Zhang. "A Pattern-Recognition-Based Ensemble Data Imputation Framework for Sensors from Building Energy Systems". In: *Sensors* 20.20 (2020). ISSN: 1424-8220. DOI: 10.3390/s20205947.

[6] KNMI. *KNMI - Uurgegevens van het weer in Nederland. KNMI - Hourly weather data of Dutch climate.* URL: https://www.knmi.nl/nederland-nu/klimatologie/uurgegevens.

[7] Roderick Little and Linda Yau. "Intent-to-Treat Analysis for Longitudinal Studies with Drop-Outs". In: *Biometrics* 52.4 (1996), pp. 1324–1333. ISSN: 0006341X, 15410420.

[8] Jun Ma et al. "A bi-directional missing data imputation scheme based on LSTM and transfer learning for building energy data". In: *Energy and Buildings* 216 (2020), p. 109941. ISSN: 0378-7788. DOI: 10.1016/j.enbuild.2020.109941.

[9] Mel Keytingan M. Shapi, Nor Azuana Ramli, and Lilik J. Awalin. "Energy consumption prediction by using machine learning for smart building: Case study in Malaysia". In: *Developments in the Built Environment* 5 (2021), p. 100037. ISSN: 2666-1659. DOI: doi.org/10.1016/j.dibe.2020.100037.

[10] Douglas G Altman and J Martin Bland. "Statistics notes: The normal distribution". In: *BMJ* 310.6975 (1995), p. 298. ISSN: 0959-8138. DOI: 10.1136/bmj.310.6975.298.

[11] Singh U Mishra P Pandey CM. "Correlation between earlobe crease and coronary artery disease in Indian population- A multicentre experience". In: *Annals of Cardiac Anaesthesia* (2019). DOI: 10.4103/JCPC.JCPC_10_20.

[12] *Pipeline used in research(2021)[source code results].* URL: https://github.com/thuas-imp-2021/thuas-imp-2021.

One of the two datasets analysed during the current study is available in the KNMI repository, https://www.knmi.nl/nederland-nu/klimatologie/uurgegevens

Practical experiences from the implementation of extensive sensoring in a modern building

Ádám Bognár[a], Pieter-Jan Hoes[a], Twan van Hooff[a], Marcel G.L.C. Loomans[a]

[a] Department of the Built Environment, Eindhoven University of Technology, Eindhoven, the Netherlands, a.bognar@tue.nl, p.hoes@tue.nl, t.a.j.v.hooff@tue.nl, m.g.l.c.loomans@tue.nl;

Abstract. The extensive use of sensors is quickly becoming a standard feature of modern new buildings. Apart from the use of regular Building Management System (BMS) data, we see the addition of sensors that monitor in more detail the indoor environmental quality and the use and performance of innovative (and local) system solutions. This is also combined with integrated energy solutions at supra-building level. The assumption is that all these data are valuable to arrive at buildings that can optimize their operation towards indoor environmental and other sustainable performance indicators. In this research, data from a large modern building that combines office and educational rooms, features an innovative façade design and is connected to an aquifer thermal energy storage are considered. In order to perform detailed analyses, several sensor and data related issues had to be resolved first. In this paper we provide a procedure for structuring the data as was available for this specific building, originating from different sources. The outcomes provide a practical basis for other buildings to assess the correctness and quality of the sensor data and the analysis potential. An example of an analysis is presented. In addition, the paper demonstrates how the obtained measurement data can be used to calibrate a simulation model that is employed to analyse the ventilative cooling potential of the innovative façade in comparison to shading.

Keywords. Sensor data, Simulation, Model calibration, Ventilative cooling, Solar shading
DOI: https://doi.org/10.34641/clima.2022.308

1. Introduction

According to literature, in most buildings 14-50% thermal energy and 9-13% electrical energy use reduction can be achieved by improving building controls [1]. Apart from energy, monitoring and optimization of Indoor Environmental Quality (IEQ) is increasingly in the focus of research, especially in office or educational buildings [2,3]. Health, comfort and productivity for its occupants are regarded as important performance aspects of buildings. From a cost-perspective, investing in good IEQ is beneficial: literature indicates an order of magnitude cost ratio of 1:5:200, where for every Euro spent on building construction cost, five are spent on maintenance and building operating and 200 on staffing and business operating costs [4]. Therefore, rates on return can be high in this case, but this should be supported by thorough performance evaluation and control of the IEQ [5].

There are several platforms available for building energy management and control. Some are control hardware-independent, such as Strukton PULSE platform, Cloud Energy Optimizer, Spectral Smart Building Platform, Entronics facility analysis platform, and bGrid. Others are optimized for the hardware developed by the same company, such as control solutions of Priva, Schneider Electric, Siemens, Johnson Controls, and SAIA. Websites for further information on these platforms are provided in the reference list.

These efforts and the scientific community could benefit from further application of sensory data for real world performance analysis of innovative solutions being applied in buildings. In this paper, an example is shown of how different sensory data can be combined and analysed. However, not every building parameter can be measured, and to explore future scenarios one cannot rely merely on measured historical data. Therefore, in this paper we also present an example of using a calibrated building energy simulation model to investigate the ventilative cooling potential of an innovative façade system, decreasing the cooling energy demand.

2. Context

2.1 Building information

To aid the efforts of conducting new research about building energy, occupant comfort and building

Copyright ©2022 by the authors. This conference paper is published under a CC-BY-4.0 license.

control systems, the Eindhoven University of Technology (TU/e) started the Atlas Living Lab project. In this project, the recently renovated Atlas building serves as the source of measured building performance and occupant comfort data, thus providing input for new research. The Atlas building dates back to the 1960's. Since then, it served as the main building of the TU/e campus. A comprehensive renovation process started in 2016, when the building was equipped with a new façade with remotely openable windows, an automated shading system, new interior and building systems (see **Fig. 1**).

Fig. 1. Atlas building. Image source: TU/e.

As part of the renovation process, the building was equipped with sensors which can be categorized to three main sources of information about the building's performance and its boundary conditions:

Indoor environment: 474 air temperature, 460 occupancy and 126 CO_2 level sensors provide information about the indoor conditions in hourly resolution.
Energy: Heating, cooling and electric meter data with 5-minute resolution metered for each floor separately.
Weather: Ambient temperature, relative humidity, wind speed and solar irradiance components are measured on campus in minute resolution.

The sensor information from the three sources is stored in three different databases: the *indoor environment* data is extracted from the building management system (BMS), the *energy* data is extracted from the database of a campus-wide smart meter network, and the *weather* data for this study was extracted from a weather station on campus [6]. A new weather station on top of the Atlas building is operational now.

2.2 From data to information

To be able to assess the energy and IEQ performance of the building, and therefore retrieve more valuable information about a system, the three data sources need to be merged and cleaned. In order to do this, an automated process was developed in Python programming language with the following main steps:

Find the temporal overlap of the time series: The official opening of the Atlas building was on the 21st of March 2019, however, the commissioning process of certain data logging systems took longer, therefore all data sources are available simultaneously from 1st of November 2019.

Identify missing values: In case of a small gap (e.g. for metered heat < 1 hour) in one of the data sources the missing section can be replaced with linear interpolation. In case of a larger gap (e.g. > 1 h), the data for the same section is removed from the other data sources as well.

Identify erroneous values: Erroneous values can be negative or impossibly large metered values, which can occur due to clipping or resetting of heat meters. When detected, the erroneous values are removed and the process described for missing values is followed.

Enhance the dataset with derived parameters: Some useful parameters can be calculated from the measured ones. One such derived parameter is the total incident solar irradiation on the façade of the Atlas building, which is calculated from the façade areas and separately measured solar irradiance components (global horizontal, direct normal and diffuse horizontal irradiance).

Resample all time series to a common time resolution: The hourly, 5-minute and 1-minute datasets are resampled to hourly or daily resolution.

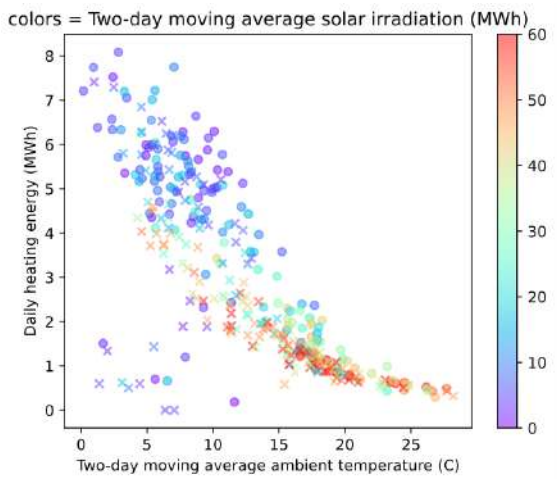

Fig. 2. Heating energy signature curve of the Atlas building for occupied (o) and unoccupied (x) periods and as function of the solar irradiation on the façade.

The cleaned and pre-processed time series are saved in a new database which is used for analysing the energy performance and IEQ of the building. One example (visualization) of the cleaned and merged sensor data is shown in **Fig. 2**. It presents the so-called heating energy signature curve. In this graph also information on the solar irradiation and occupancy is included.

With respect to the latter, the occupancy during the period shown was heavily influenced by the COVID restrictions that have been in place on and off during the last two years. Due to this situation, it was not possible to investigate the ventilative cooling potential of the façade from the available measured

data. Therefore, building simulation was used to answer the research question. The available data was used for calibrating the model. The following part of the paper will address the modeling and the outcomes of that investigation.

3. Building energy modeling

In order to virtually investigate different (ventilative cooling) control strategies for the Atlas building, a building energy model has been developed that can serve as a testbed to try out new control strategies.

3.1 Model considerations and tested strategies

In order to reduce the modeling effort, only the 10th floor of the Atlas building was selected for modeling. This is a fairly generic floor of the building and we assume that the effect of the tested modeling strategies would act similarly on the entire building and therefore expect that the conclusions of the study are applicable for the entire building.

The simulations were conducted using EnergyPlus [7], DesignBuilder [8] and Python. The model geometry and the construction materials were built in DesignBuilder (see **Fig. 3.**), then the model was exported to EnergyPlus, to perform the model fitting using Python. The model parameters from the best fit then were used as an input in the initial DesignBuilder model to perform the simulations for the different case studies (see **Fig. 4.**). This modeling process takes advantage of the convenient geometry editor of DesignBuilder and the easy automation of large numbers of EnergyPlus simulation runs with Python.

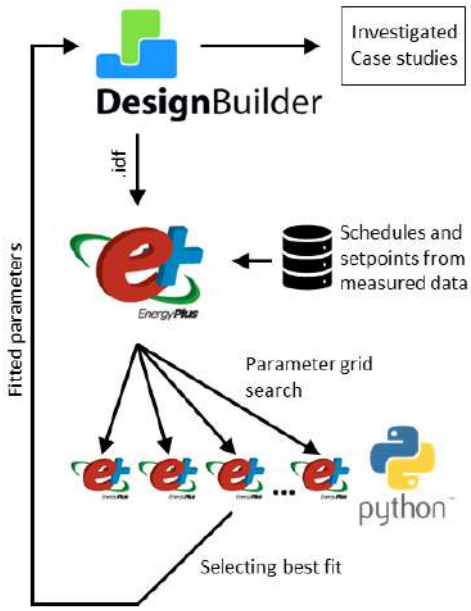

Fig. 4. Schema of the modeling process.

The tested cases investigate the effect of different control strategies for shading and natural ventilation (ventilative cooling). This is done by comparing the simulated heating and cooling demand of the following 7 cases to the measured heating and cooling demand of the 10th floor of the Atlas building:

1. A baseline case EnergyPlus model that was fitted to the measured data (*fitted_ep*).
2. A baseline case DesignBuilder model, that uses the fitted parameters from the EnergyPlus model (*baseline_db*).
3. A case without solar shading (*no_shade*).
4. A case with solar shading that is half-drawn every time it is activated (*half_shade*).
5. A case with temperature-controlled natural ventilation through the windows, with a control logic that turns of the HVAC systems in the zones while the windows are open (*nat_vent_opt*).
6. A case with temperature controlled natural ventilation, but without the above control logic (*nat_vent_unopt*).
7. A case that combines cases *nat_vent_opt* and *no_shade* (*nat_vent_opt_no_shade*).

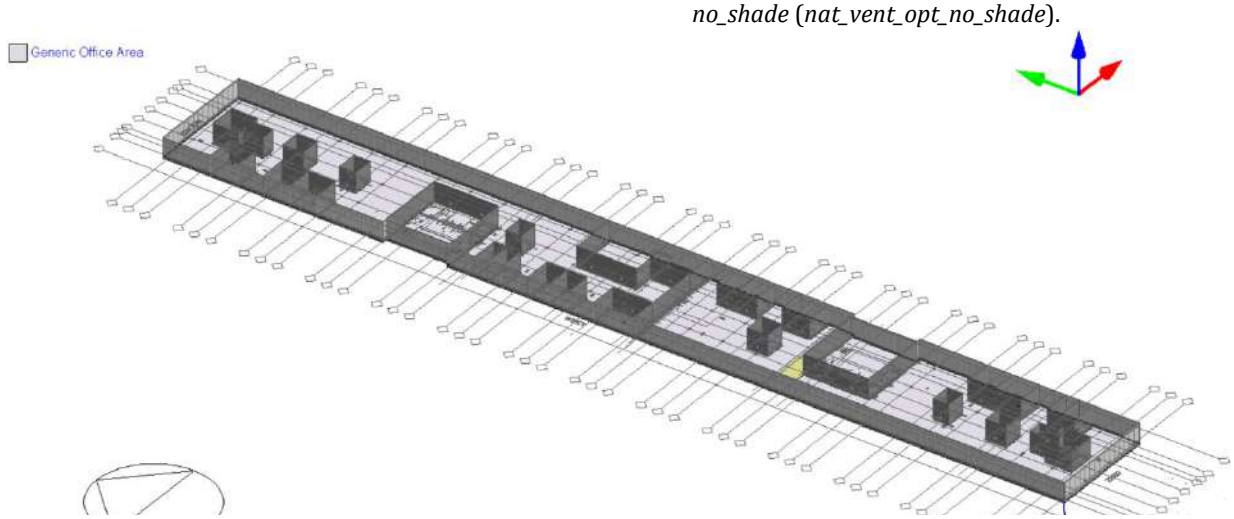

Fig. 3. DesignBuilder model geometry of the 10th floor of Atlas.

Table 1. contains the temperature setpoints that were used by the above listed cases.

Table 1. Temperature setpoints

Parameter	Value	Unit
Heating setpoint/setback	22/18	˚C
Cooling setpoint/setback	24/28	˚C
Ventilative cooling setpoint	23	˚C
Min/max outdoor temperature limit for ventilative cooling	14/23	˚C
Ventilative cooling setpoint	23	˚C
Solar transmittance of shading	0.1	-

3.2 Description of the fitting method

Though most building related information was available for the model, there is a need to fit (i.e. calibrate) the building energy model. In order to do that the following known model parameters are applied:

1. Actual weather in Eindhoven (prepared from measured weather data).
2. Floor electric energy use (historical measured electric energy use of the floor). The heat gain from this is evenly distributed in the building.
3. Hot and cold energy use of the floor from smart meter data export (this is used for checking goodness of the fit).
4. Zone temperatures (measured in every zone - the model has as many zones as measurement locations available).
5. Zone occupancy (measured in every zone).
6. Certain HVAC system parameters and schedules.

The HVAC system of the 10th floor of the Atlas building is modeled in EnergyPlus with two parallel systems that provide the fresh air and zone heating:

1. A Dedicated Outdoor Air System (DOAS) is providing constant air flow to the zones:
   - Inlet air temperature: 18 °C
   - Heat recovery sensible effectiveness: 70%
   - Outdoor air flow rate (this is a fitted variable)
   - Availability schedule: 07:00 h to 17:00 h on weekdays

2. A Packaged Terminal Air Conditioner (PTAC) for every zone, providing the local heating/cooling:
   - The heating/cooling availability schedule is prepared based on actual measured operation of the heating/cooling system of the building: when there was heating/cooling energy consumption on the floor, the heating/cooling system in the model is allowed to operate.
   - Heating/cooling setpoints are indicated in **Table 1.**

In the real building the zone heating/cooling is supplied with a heated/cooled ceiling. The lack of latency and heat storage in the PTAC system (as opposed to the heated/cooled ceiling system in the real building) is compensated by adding more internal thermal mass to the zones during model fitting.

Since not all building properties are known, the following building parameters are used as variable parameters during the model fitting:

- Minimum fresh airflow rate of the DOAS system
- Additional internal thermal mass in the building (mass and surface area)
- Infiltration
- Fraction of measured electric energy use dissipated as heat in the zones
- Global horizontal irradiance limit for activating the shading system.

Since it is difficult to implement the entire (unknown) control logic of the building systems, the aim is to achieve a thermal state of the building during the simulated year that is similar to the thermal state of the building in reality. This can be achieved by using measured weather data, and by giving the measured zone temperatures as heating/cooling setpoints for the model. This way, when the heating is on, the zone temperatures match closely in the model and in the real building. Via system availability schedules it is also enforced that the heating can only run in the model when it is running in the real world as well. Information for this is available from the collected smart meter data. Similarly to heating, the ventilation is also controlled with schedules and only running based on an availability schedule.

Thermal mass is added as a timber material in 4 cm sheets. The mass/floor area of the thermal mass is the fitted parameter, and the surface area is calculated from it. As mentioned above this thermal mass is added to compensate for the lack of latency of the PTAC air system used in the model.

The execution of the fitting is done with a grid search using Python. For each of the above listed fitted parameters there is a "multiplier" built in the EnergyPlus model, which at each simulation run changes the value of the corresponding parameter. The range of the tested multipliers is shown in **Table 2.**

Table 2. Model parameter multipliers

Parameter	Initial value	Multiplier range	Unit
Outdoor air	1	0.3 - 1.5	l/sm^2
Thermal mass	200	0.15 -2	kg/m^2
Infiltration	0.2	0.5 - 2	1/h
Electric equipment	3	0.15 - 1	W/m^2
Shading control	250	0.25 - 2	W/m^2

Choosing the best fit was done by first running 674 simulations while varying the above multipliers, then

calculating the daily and hourly Mean Absolute Error (MAE) of the heating and cooling energy demands for each simulation run. **Fig. 5** and **Fig. 6** show the hourly and daily MAE of heating and cooling demand, respectively. The combination of parameters that resulted in a good agreement for both the heating and cooling energy demand and both on an hourly and daily level was searched for. Therefore, in **Fig. 5** and **Fig. 6** the simulation runs were ordered by the hourly and daily MAE of the zone heating and cooling demand, and a simulation run was selected that ranked low in all four MAE orders (indicated with a green marker in both figures).

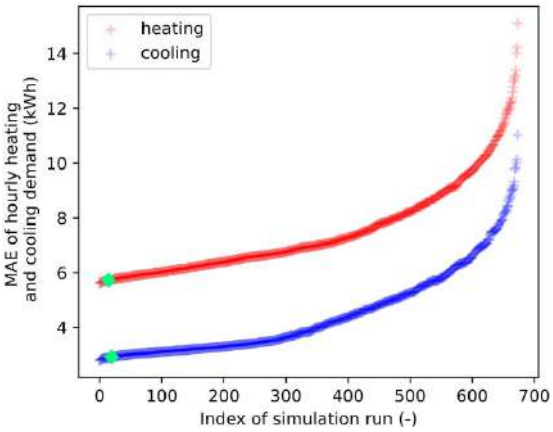

Fig. 5. MAE of hourly heating and cooling demand in ascending order with the best fit case marked in green.

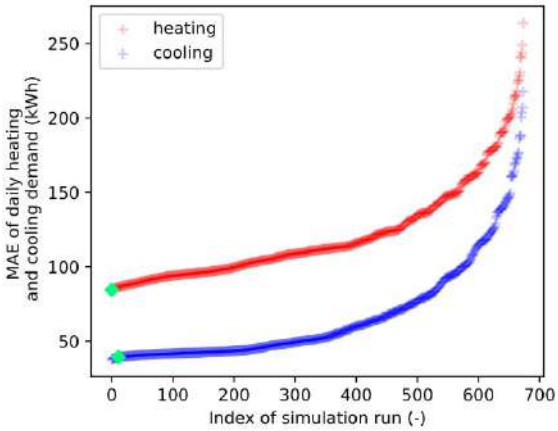

Fig. 6. MAE of daily heating and cooling demand in ascending order with the best fit case marked in green.

The multipliers of the best fit resulted in the simulation parameters as shown in **Table 3.**

With the above parameters the simulated mean zone temperatures were confirmed. **Fig. 7** shows the comparison between the measured and the simulated heating and cooling energy demands. The model fitting aimed to minimize the difference between the measured and simulated zone heating and cooling loads both on an hourly and daily level. Here we can observe that the fitting was fairly successful.

Table 3. Model parameter multipliers

Parameter	Value	Unit
Outdoor air	1 * 0.5 = 0.5	l/sm²
Thermal mass	200 * 0.15 = 30	kg/m²
Infiltration	0.2 * 0.75 = 0.15	1/h
Electric equipment	3 * 0.15 = 0.45	W/m²
Shading control	250 * 0.25 = 65	W/m²

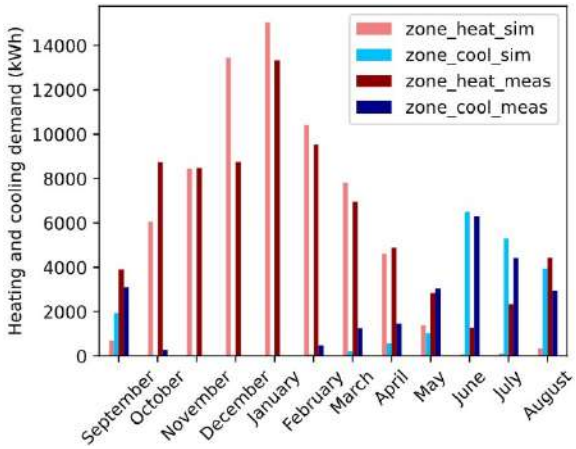

Fig. 7. Monthly measured heating and cooling demand of the 10th floor of Atlas.

The model fitting was done in EnergyPlus, by using a Python script to set the model parameters, run the simulations and interpret the results. However, we would also like to investigate the effect of natural ventilation on the building performance. In order to be able to conduct air flow network simulations conveniently, the above determined model parameters are used as an input for the DesignBuilder model that was used to create the initial model. This workflow facilitated a more convenient implementation of the air flow network with the control of openable windows in DesignBuilder as opposed to implementing it by hand in EnergyPlus.

4. Results and discussion

Fig. 8 shows the measured and simulated annual heating and cooling demand of the different cases (as defined in Section 3.1).

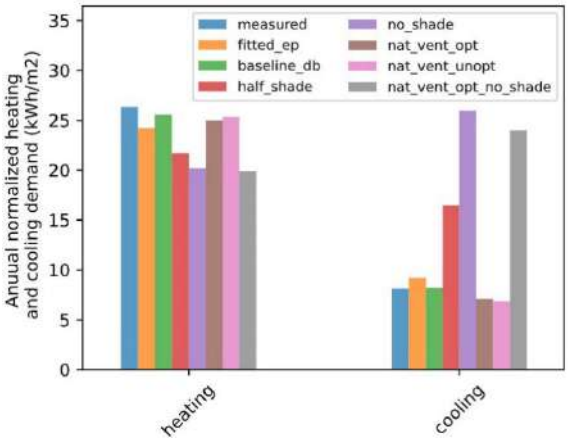

Fig. 8. Annual heating and cooling demand of the 10th floor of Atlas with different solar shading and natural ventilation controls.

The annual heating and cooling demand of the fitted EnergyPlus model (*fitted_ep*) deviates by 8% and 13% respectively from the measured heating and cooling demand. The DesignBuilder model (*baseline_db*) that is built using the fitted parameters deviates by 3% and 0.8% from the measured values. The difference between the best fit EnergyPlus model and the baseline DesignBuilder model is likely due to the slightly different way of setting model inputs in EnergyPlus and DesignBuilder and perhaps a difference between the EnergyPlus version used by DesignBuilder (8.9) and the version used for model fitting (9.5). Another source of difference is that in the DesignBuilder model it was not possible to take into account occupant interaction with the heating/cooling setpoints. It was assumed that the heating/cooling setpoint offset options of the room thermostats are not used by the occupants.

The *no_shade* case investigates the scenario when the shading system of the building is not active throughout the year. We learned that in the summer the automatic operation of the shading system was not active in the real building due to high cost of damage when various objects (e.g., backpacks) are left under the shade when it gets drawn. If this is the case throughout the year, then according to the simulation results, it would lead to a significant 24% decrease in heating demand. However, it also would lead to a more than three-fold increase in cooling energy demand. Therefore, it is recommended to strive for using shading in the summer months as much as possible.

If damage to the shading screens is a common problem, it could be considered to draw the shading only half way (if this is technically possible). This way the chance of damage to the shading screens would reduce, while still allowing for some protection from overheating. This hypothetical case is modeled with the *half_shade* scenario. In this case the cooling demand increase is only two-fold.

Another strategy is to use natural ventilation to reduce the cooling loads. With the *nat_vent_opt* model it is demonstrated that a 12 % reduction in cooling loads can be achieved, if the windows are opened when they can contribute to the cooling of the zones. In this model, the windows are opened if the outdoor temperature is between 12 °C and 23 °C and if the indoor temperature is higher than 23 °C. The mechanical cooling in this case turns on if the zone temperature increases over 24 °C and it never operates when the windows are open. Moreover, in this model the windows are closed in case of rain or high wind speeds. The *nat_vent_unopt* case, models a less sophisticated system that does not connect the operation of the HVAC systems to window opening, nor the wind speed or rain. In this case, contrary to the expectation the cooling savings are slightly higher. Perhaps this is due to the higher freedom in operation and the fact that simultaneous operation of natural ventilation and the HVAC system was not really an option in the *nat_vent_unopt* case either, as the setpoint for the HVAC cooling is higher than the cooling setpoint with natural ventilation.

When comparing the effect of natural ventilation and solar shading, it can be concluded, that for the Atlas building, solar shading seems to have higher potential to reduce cooling loads than natural ventilation. Therefore, restoring (at least partially) the functionality of automated solar shading would greatly reduce cooling loads, because the primary cause of overheating in the Dutch climate and in the case of such a highly glazed building is not the high outdoor temperatures, but the solar gains. The higher significance of shading can also be observed in the results of the last simulation case, *nat_vent_opt_no_shade*. This case clearly shows that natural ventilation cannot recover much from the increased cooling loads in the case of simultaneous application of no shading and openable windows.

The comparison between ventilative cooling and shading use, however, is not complete. In the model we did not yet include the possibility to apply night-time ventilation to precool the building during the cooling season. Moreover, one could experiment with further, different combinations of mechanical cooling and ventilative cooling setpoints in order to more efficiently utilize the potential in the latter. The results, nevertheless, clearly indicate that in daytime shading should be part of the strategy to reduce the cooling energy demand. Furthermore, in the analysis thus far we also did not include yet the connection to the large aquifer system that serves most buildings at the campus. For balancing reasons, the heating and cooling energy requirements may have different optimized values when only looking at the outcomes for the building instead of at the campus as a whole. The analysis does show that the availability of measured data adds to the quality of the analysis possible, as we now learn and are able to assess the building performance in reality.

5. Conclusions

The results show that availability of sensor data can support the performance evaluation of in-use buildings. In order to make full use of the data, for the case investigated, it required quite some effort to clean and combine the data. The assumption is that such effort is also needed in many other buildings where more extensive sensoring is applied. The added value of bringing all the data in one database is that it allows for much more detailed information than just performance indicator checking such as, e.g., temperature conditions.

For control strategy assessment the available data is also useful, as it can help in developing building simulation models that more closely resemble the building. In the example presented it is shown that the innovative façade does contribute to the daytime reduction in cooling energy demand, though a well operated shading system should be prioritized for the Dutch climate. The full potential of the façade, however, has not been exploited yet and is intended for further research.

6. Acknowledgement

This work was financed by OPZuid, province Noord-Brabant and Eindhoven University of Technology. The help of all those involved in the Atlas project to obtain all the necessary information is highly appreciated.

7. Data access statement

The datasets analyzed during the current study are not available, but the work performed is part of an effort to make the data (and databases) from the Atlas building usable for future researchers.

8. References

[1] Schneider, G.F., Kontes, G.D., Qiu, H., Silva, F.J., Bucur, M., Malanik, J., Schindler, Z., Andriopolous, P., de Agustin-Camacho, P., Romero-Amorrortu, A., Grün, G., Design of knowledge-based systems for automated deployment of building management services. Autom. Constr. 2020;119, 103402. https://doi.org/10.1016/j.autcon.2020.103402

[2] Van Kemenade, P., Loomans, G.L.C. Marcel, S. Opschoor, Hensen, J.L.M. Building comfort performance assessment using a monitoring tool, in: Y. Li (Ed.), Proc. 13th Int. Conf. Indoor Air Qual. Clim. (Indoor Air 2014), Hongkong, 2014, pp. 1–7

[3] Boerstra, A.C. New health & comfort promoting CEN standard, REHVA Journal. 2019; 4 pp. 6-7 https://www.rehva.eu/rehva-journal/chapter/new-health-comfort-promoting-cen-standard.

[4] Evans, R., Haryott, R., Haste, N., Jones A. The long-term costs of owning and using buildings. 1998. The Royal Academy of Engineering, London, United Kingdom.

[5] Thoen, H. M. J., Roelofsen, P., Mishra, A. K., Loomans, M. G. L. C., Hoes, P., & Hensen, J. L. M. Monitoren van werknemersproductiviteit in kantoren. TVVL Magazine. 2019 (01), pp.30-34.

[6] Valckenborg, R. M. E., Hensen, J. L. M., Folkerts, W. Vries A. de. Characterization of BIPV(T) applications in research facility 'SOLARBEAT. Proc. EU PVSEC 2015, 14-18 Sept. 2015, Hamburg, Germany, 2015.

[7] Crawley, D. B., Lawrie, L. K., Pedersen, C. O. , Winkelmann, F. C. EnergyPlus: Energy Simulation Program. ASHRAE Journal. 2000: 42, pp. 49–56.

[8] DesignBuilder. DesignBuilder Software Ltd, 2021.

Websites for the indicated monitoring platforms:

- https://www.struktonpulse.nl/energy
- https://www.cloudenergyoptimizer.com/en/Technique
- https://spectral.energy/solutions/sbp/
- https://entronix.io/
- https://bgridsolutions.com/#how
- https://www.priva.com/solutions/building-automation/priva-bi-metrics
- https://www.se.com/ww/en/product-range-presentation/62111-ecostruxure%E2%84%A2-building-operation/?parent-subcategory-id=1210#tabs-top
https://new.siemens.com/global/en/products/buildings/automation/desigo.html
- https://www.johnsoncontrols.com/en_gb/building-automation-and-controls/building-automation-systems/metasys
- https://www.saia-pcd.com/en-gb/solutions/energy/monitoring/

Automated energy performance diagnosis of HVAC systems by the 4S3F method

Arie Taal [a], *Laure Itard* [b]

[a] Department Mechanical Engineering, The Hague University od Applied Sciences, Delft, the Netherlands, actaal@hhs.nl.

[b] Faculty of Architecture and the Built Environment, Delft University of Technology, Delft, the Netherlands, l.c.m.itard@tudelft.nl.

Abstract. In practice, faults in building installations are seldom noticed because automated systems to diagnose such faults are not common use, despite many proposed methods: they are cumbersome to apply and not matching the way of thinking of HVAC engineers. Additionally, fault diagnosis and energy performance diagnosis are seldom combined, while energy wastage is mostly a consequence of component, sensors or control faults. In this paper new advances on the 4S3F diagnose framework for automated diagnostic of energy waste in HVAC systems are presented.

The architecture of HVAC systems can be derived from a process and instrumentation diagram (P&ID) usually set up by HVAC designers. The paper demonstrates how all possible faults and symptoms can be extracted on a very structured way from the P&ID, and classified in 4 types of symptoms (deviations from balance equations, operational states, energy performances or additional information) and 3 types of faults (component, control and model faults). Symptoms and faults are related to each other through Diagnostic Bayesian Networks (DBNs) which work as an expert system. During operation of the HVAC system the data from the BMS is converted to symptoms, which are fed to the DBN. The DBN analyses the symptoms and determines the probability of faults.

Generic indicators are proposed for the 4 types of symptoms. Standard DBN models for common components, controls and models are developed and it is demonstrated how to combine them in order to represent the complete HVAC system. Both the symptom and the fault identification parts are tested on historical BMS data of an ATES system including heat pump, boiler, solar panels, and hydronic systems. The energy savings resulting from fault corrections are estimated and amount 25%. Finally, the 4S3F method is extended to hard and soft sensor faults. Sensors are the core of any FDD system and any control system. Automated diagnostic of sensor faults is therefore essential. By considering hard sensors as components and soft sensors as models, they can be integrated into the 4S3F method.

Keywords. 4S3F, FDD, Energy performance, DBN, P&ID
DOI: https://doi.org/10.34641/clima.2022.183

1. Introduction

The Heating Ventilation and Air Conditioning (HVAC) sector is responsible for a large part of the total worldwide energy consumption, a significant part of which is caused by incorrect operation of controls and maintenance. HVAC systems are becoming increasingly complex, especially due to multi-commodity energy sources, and as a result, the chance of failures in systems and controls will increase. Therefore, systems that diagnose energy performance are of paramount importance. However, despite much research on Fault Detection and Diagnosis (FDD) methods for HVAC systems, they are rarely applied. One major reason is that proposed methods are different from the approaches taken by HVAC designers who employ process and instrumentation diagrams (P&IDs). This paper shows how P&IDs can be combined with data from Building Management Systems and Bayesian statistics to identify operation faults and diagnose energy performance.

2. FDD methods for energy performance evaluation of HVAC systems

Copyright ©2022 by the authors. This conference paper is published under a CC-BY-4.0 license.

2.1 Phases of an FDD process

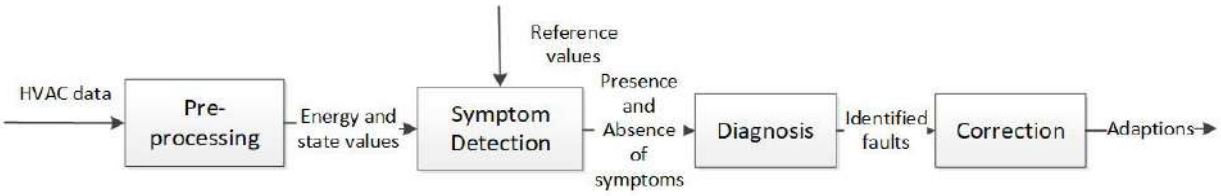

Fig. 1. Phases of an FDD process

In general, a fault analysis process consists of phases as shown **in Fig. 1**.

- Step 1: Pre-processing - Raw data from data loggers or from the building (energy) management system ((B(E)MS) is converted in processable format for FDD as energy data and other metrics. In this stage, incomplete and corrupted data is filtered. Furthermore, values derived from measurements are estimated.

Then, the FDD finds place:

- Step 2: Symptom detection – Presence or absence of symptoms indicating malfunction.
- Step 3: Diagnosis - Faults causing the detected symptoms are identified based on symptoms (see **Fig. 2**) and fault effects on energy performance and comfort are quantified.

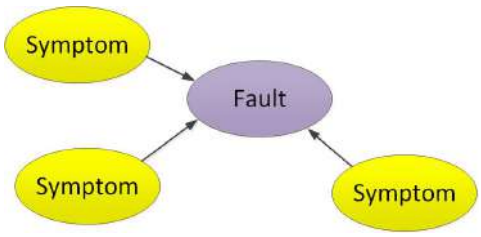

Fig. 2. Isolation of a fault from symptoms

End after diagnosis:

- Step 4: Correction – In this stage decisions are made for repair and adjustments.

The focus in the present paper is on the detection and diagnosis phases.

2.2 Symptom Detection methods

An overview of methods used in such applications is discussed below. First, the different generic types of FDD methods are discussed and **Fig. 3** presents an overview of these methods, derived from Yang [1].

- **Knowledge-driven based** which are based on physical models, e.g., from simulation models (could be detailed) or physical balances (simplified) and are also called **model-based** methods. See for instance [2]. Next to this, **rule-based** methods are applied, e.g., measured temperatures are compared to expected ones [3].
- **Data-driven based** methods have gained in popularity during the last decades. These methods are based on measured data from which patterns are identified. The pattern recognition leads to fault isolation. Several data-driven methods have been proposed. Commonly mentioned are supervised methods using black boxes in which physical output (e.g., energy usage) is calibrated against historical data (e.g., regression methods and artificial neural networks [4]). Next to this unsupervised methods are proposed, such as SVM (support vector machine) which divide a data set in faulty and unfaulty outcomes for the HVAC operation [5] and PCA (principal component analysis) methods [6] which reduce a higher dimensional space of variables into a lower dimensional space.

2.3 Fault Diagnosis methods

Most diagnosis methods are coupled to the applied detection method. For instance., from a PCA method for sensor fault detection the specific faulty sensor can be isolated directly. This lead to many FDD methods for different HVAC components.
All these methods diagnose faults on different levels: from component level to whole system level. When a multi-level approach is present, it is either top-down or bottom-up in sequences incorporating multiple types of methods [7]. It is also noticeable that the diagnosis approach often strongly depends on the detection method used.

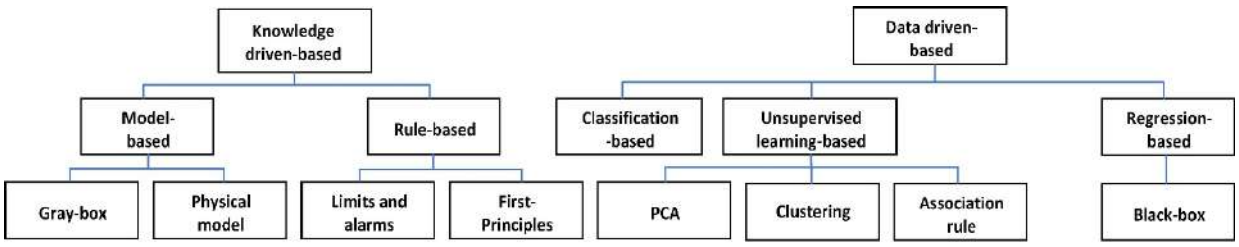

Fig. 3. Classification of FDD methods
(Derived from [1]).

They classify FDD methods into quantitative, qualitative, and process history-based methods:

For instance, when diagnosing sensor faults using PCA methods there is a one-on-one correlation

between symptoms and faults [6]. Hence, libraries with generic FDD models for all kind of HVAC systems are still missing.

Furthermore, most available FDD methods result in a binary outcome for (presence of) symptoms and faults leading to faulty outcomes by inaccuracies in measurement data and the applied FDD method. Therefore, studies over the past decade have focused on minimizing the false diagnosis results through adapted, complex FDD methods optimized for a specific HVAC component. To overcome this problem, the application of diagnosis methods based on probabilities is promising, like Bayesian statistics, which predict fault chances from presence and absence of symptoms. One of such method is the diagnostic Bayesian network (DBN) method, see [8-10]. The DBN method can also largely overcome the other above-mentioned problems because it can handle with simultaneous multi-level diagnosis, modularity, simple extension of symptoms or faults, little data points, different types of symptoms and faults, and even with contradictory and redundant symptoms.

All considered, most FDD methods are still complex, tens of different methods must be used at subsystem or component level for a specific (unique) building and there is no integration at system level. A reference architecture for HVAC FDD is missing which embeds different methods and structures of the FDD process. However, a DBN-based method seems to be able to overcome problems in other methods.

3. HVAC engineering practices

HVAC system design is based on first principles, like mass and energy balances, and from systems science telling that systems can be divided in subsystems. It is common use to apply schematics which grow from raw to detail (e.g., ASHRAE's handbook [11] and design manual [12]). In the design stage, HVAC designers determine the specifications of the components, sub-systems and systems and their control. They capture it into P&IDs (Process and instrumentation diagrams) in which the main HVAC and control components are represented with all their interconnections as well as all mass (fuel, water, air), electric energy and signal transfer channels, by which thermal energy flows can be easily computed. Guidelines for setting up HVAC modules are available.

Fig.4 shows such a P&ID diagram based on Dutch guidelines for measurement points [13] and hydronic hot water [14] modules. A P&ID contains components (presented as symbols) which are linked by pipes, ducts and signals, and contain sensors (depicted as transmitters) and actuators (e.g., electric motors of valves) which are coupled via controllers. Furthermore, the nominal power of components is often shown (see Pnom), and the controlled and designed temperatures and flow rates at design conditions on the P&IDs (T and qv in the figure). All-over, P&IDs contain information about components, controls and expected state values which are important for energy performance analysis.

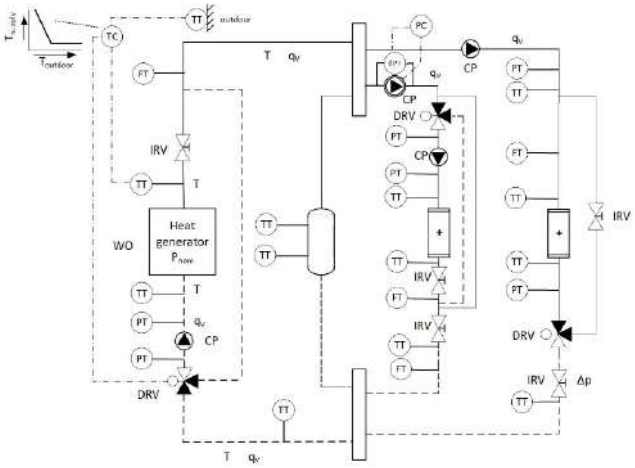

Fig. 4 – Example of a P&ID of a hot water system.

From the P&ID two types of faults can be distinguished: component faults (such as pumps, valves, boilers, sensors) and control faults (settings in controllers, such as TC and CC). Faults of this kind could lead to energy performance (EP) symptoms, such as low coefficients of performance (COPs). From the P&ID, the sensors needed to estimate the exchanged energy amounts for energy performance measures can be estimated. These faults also lead to symptoms such as unwanted temperatures (measured by de sensors TT, CT, PT in the presented P&IDs) or unexpected states of actuators (pumps, valves). These symptoms can be stated as operational state (OS) symptoms. Finally, for the diagnosis to take place with correct measurements, the idea is to use mass, energy, and pressure balance symptoms to rule out sensor errors.

The above types of symptoms and faults are generic, useful, and available for any multi-level HVAC installation and can be extracted from P&IDs.

4. The 4S3F method

Despite much research in this area, major shortcomings result in lack of applications of FDD. Set-up of FDD models is labour intensive because each HVAC system is unique and the set-up demands HVAC, information technology (IT), data analytics, or modelling expertise. IT and data analytics experts have generally little expertise in HVAC, and for them it is difficult to understand the physical meaning of the data they handle. HVAC and building modellers on the contrary lack knowledge on IT and data analytics methods. In addition, FDD methods lack the ability to integrate diagnosis simultaneously on different system levels: component to whole system level. Next to this, most methods are detection methods, which detect that a symptom but do not isolate its causes, the faults. All considered, the HVAC FDD methods are still complex and there is need for a structured approach to FDD, integrating

expertise, components, and methods.

From P&IDs, two types of faults can be extracted: **component and control faults** which lead to three types of symptoms: **energy performance, operational state and balance symptoms**. This was used as a starting point for the development of a novel FDD architecture for HVAC energy performance. The above types of symptoms and faults are generic and usable and available for any HVAC installation at multi-level.
In addition, other symptoms may be available, such as maintenance and inspection information, user complaints, and information from embedded component FDD. However, this information is not always available. It is proposed that this fall under the container term **additional symptom**.
Models have sometimes been drawn up for the symptoms, for example for soft sensors, to determine a value. This also makes faults possible. This is referred to as **model faults**. In [15] a case study is presented that applies this.

4.1 4S3F Architecture

As a result, 4 types of symptoms and 3 types of faults are identified which results in the so-called **4S3F** (4 symptoms and 3 faults) architecture. See **Fig. 5**.

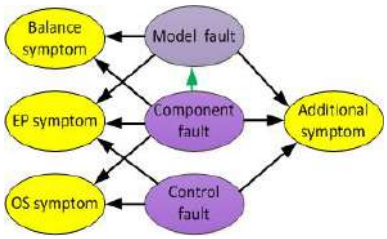

Fig. 5. The 4S3F architecture

This 4S3F architecture was discussed in [16].

4.1 Detection symptoms

In the 4S3F architecture four categories of symptoms are present which are elaborated in [17]. In this paper the symptom detection is applied in a case study.

a. Balance symptoms
   These symptoms are based on first principles and are divided in **energy**, **mass** and **pressure** balance. Therefore model-based detection methods are applied.
b. Energy performance symptoms
   Here, energy performance indicators are applied, such as coefficient of performance (**COP**) values, **efficiencies** and **capacities** which can be obtained from all types of model-based, rule based methods and data-driven methods.
c. Operational state symptoms
   Here, we distinguish for instance **control-based** symptoms, such as deviating supply temperatures and flow rate and **design-based** symptoms as return temperatures. Also included are the operational **states of components** such as an on-off state and a low or high energy exchange.
d. Additional symptoms
   In this container term, other kind of symptoms are present. For instance, **maintenance** or **inspection** information, **complaints** from building users and results from trade **component FDD** results.

4.2 Diagnostic Bayesian Networks

Strength of the 4S3F DBN is that it mimics the way HVAC experts diagnose.
From a P&ID a DBN model can be setup which has to done once. In this model the faults are linked to the symptoms. See **Fig. 6** which is based on [18] where diagnosis based on DBN's was discussed. In the showed blue nodes ,DBNs of subsystems are present which supports simultaneous diagnosis at multi system level.

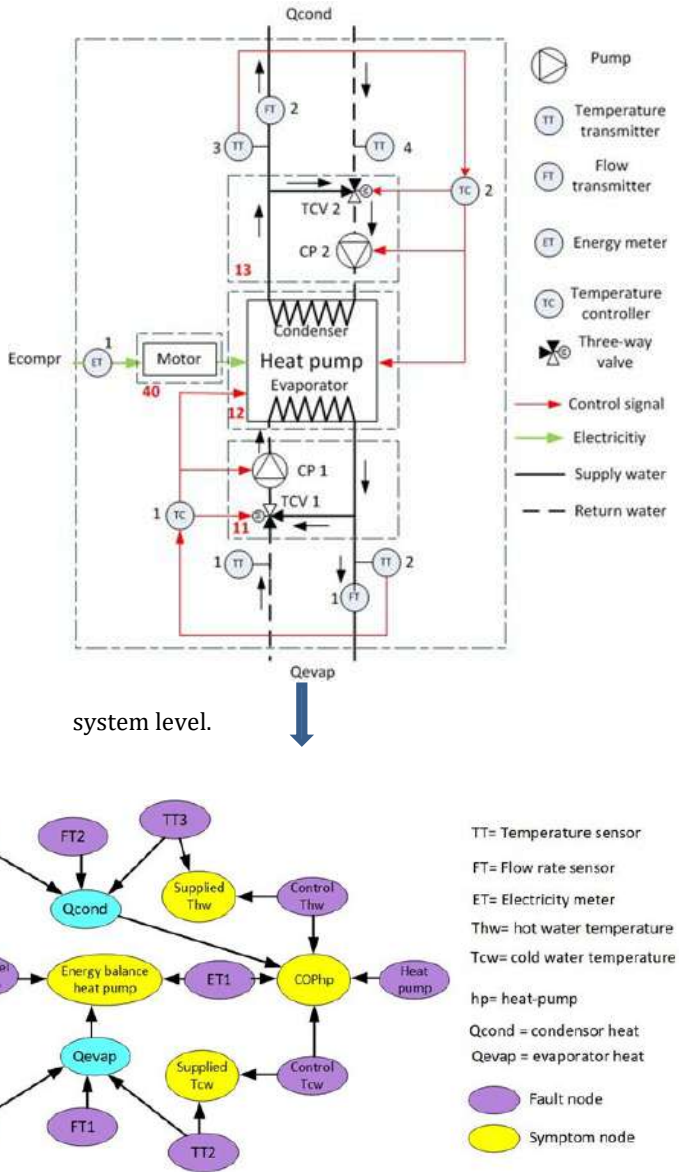

Fig. 6 DBN model extracted from the P&ID.

In de DBN fault nodes, a prior probability for the faults are set and in the DBN symptom nodes, conditional probabilities which means that when more than one fault is linked to a symptom a weighting factor can be assigned.
At operational stage, the DBN is fed by presence or absence of the symptoms. Then the DBN estimates the posterior probabilities of all faults. The HVAC engineer can take action then.

5. Case studies

Case studies were conducted on an actual HVAC system with real measurement data from The Hague University of Applied Sciences (THUAS) building in Delft.

5.1 The building of The Hague University in Delft

This building mainly contains classrooms, offices for lecturers and other staff members, and a restaurant. It was selected because it has a complex HVAC system with an advanced control system, and extensive measurement data is available for analysing energy consumption and indoor climate. In addition, it is an operational HVAC system with a reputation for working properly and apparently being energy efficient. In winter, heat is generated by a heat pump. When the heat loads are high, a gas boiler can deliver additional heat. The heat source of the heat pump is warm ground water delivered by the warm well of an ATES (Aquifer thermal energy storage) system. The ATES system can also deliver heat to the parking lanes on the roof to keep it free of ice. In the summer months, cold water from the cold well of the ATES system delivers cooling. When cooling loads are high, the heat pump produces additional cold at the evaporator side. During the summer, heat from the heat pump condenser and the roof collector can be used to regenerate the warm well of the ATES system, as the annual thermal energy extracted from and pumped into the wells has to be balanced under the Dutch regulations. Cold and heat are delivered to the rooms of the building by a thermal floor system which acts as a Thermally Activated Building System (TABS) and by ceiling radiation panels where hot or cold water is circulated. The hot and cold-water groups are divided in south and north groups which are further divided into sub-groups for the air handling in de air handling units, the ceiling and the floor equipment. A demand driven air ventilation system (DCV system) is present in which the air flow rates to the rooms are controlled by CO_2 concentration and occupancy.

5.2 Results

Studies were conducted on the thermal energy plant and the DCV system for a lecturer room. The 4S3F method was applied for energy performance purposes [17-18] as well for isolating soft and hard sensor faults. Additionally it was conducted on an air supply system for a room [19]. This three case studies showed that the 4S3F method isolated faults correctly. Furthermore, the studies were conducted as well on energy performance diagnosis as on component FDD and model FDD, for instance soft sensor faults, were elaborated.

As example we show the results from the 4S3F method for the energy plant (presented in [18)]. It is discussed by **Fig. 7**.

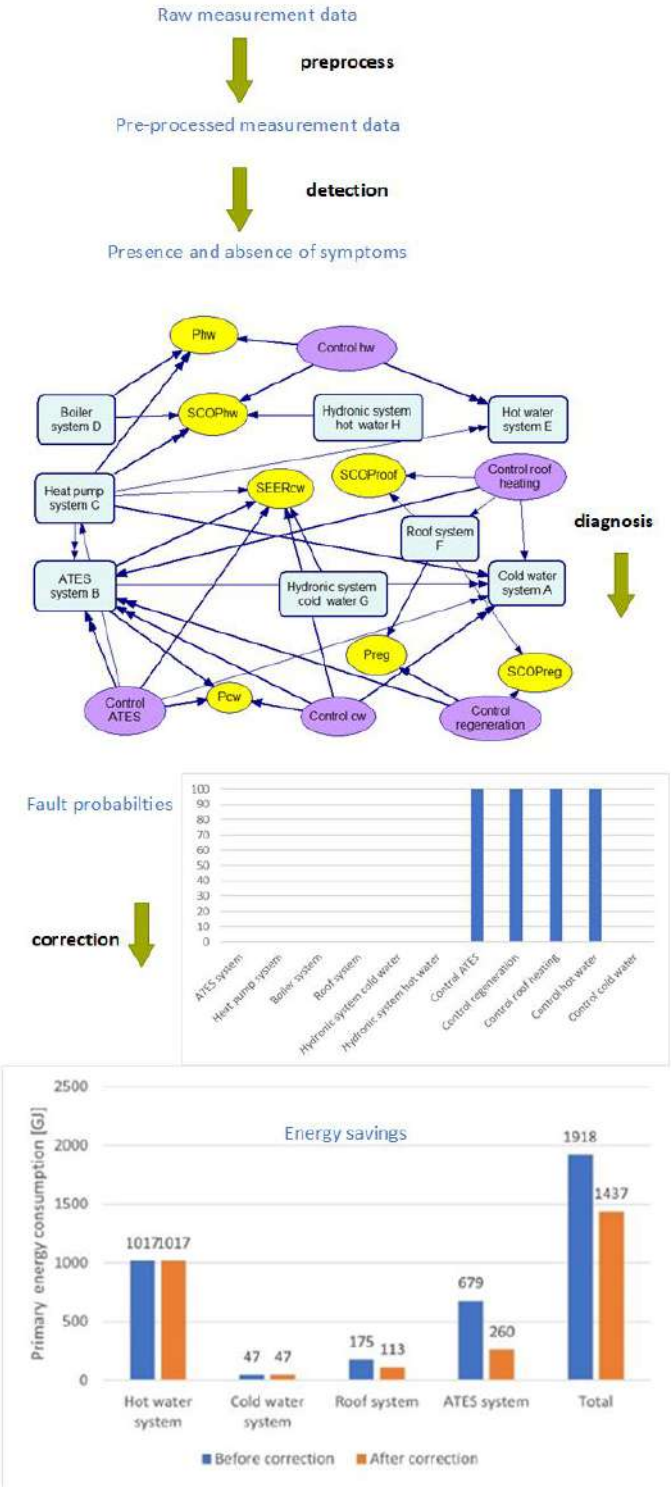

Fig. 7. The 4S3F method applied on the thermal energy plant of THUAS.

Raw measurement data were obtained from the building management system of THUAS. First, this this data was **pre-processed** in in the correct form for symptom detection. In the case studies, the data was labelled in the correct form (CSV-file), outliers were corrected and missing daily energy data were replaced by results from regression equations. This is common use for measurement data. For 4S3F purposes, soft sensors for missing measurement points (temperatures, flow rates and flow directions) were estimated and energy amounts were estimated. In the next step, the **detection** of balance, energy performance and operational state symptoms have taken place. The results of the detection is fed tot a DBN application (GeNie) which **diagnosed** (isolated) the posterior fault probabilities. In this case study it was shown that 4 control faults were present during the measurement period (1 year) with fault probabilities of 100%. Then a theoretical exercise has been conducted on the effect of correcting faulty controls. This is easy to do because the energy amounts were already available from the balance and energy performance symptoms. **Correction** of the control faults resulted in 25% primary energy savings (1437 instead of 1918 GJ).
In all studies, a sensitivity analysis was performed on the set probabilities in the DBN nodes. They showed that, although the resulting fault probabilities varies a bit, the fault identification results were unaffected over a wide range of set probabilities. Only relative differences between them (e.g. that some temperature sensors break more often than other ones etc..), generally known to HVAC experts, matter.

6. Conclusions from the case studies and recommendations

6.2 Conclusions

The main conclusions from the case studies were
a) P&IDs can be used as the starting point for setting up an energy performance diagnostic system.
b) Energy performance diagnosis can be conducted with DBNs.
c) The 4S3F DBN mimics the way HVAC experts diagnose.
d) It is possible to apply results from model-, rule- and data driven based FDD methods in the 4S3F DBN.
e) The simultaneous diagnosis at multi-level is supported by the 4S3F DBNs.
f) Many faults can be isolated at the same time.
g) The simultaneous redundant detection using balance symptoms on aggregated systems and associated subsystems improves the isolation of the faults.
h) The 4S3F architecture supports energy performance diagnosis of a thermal energy system as well a DCV system.
i) Integration of energy performance diagnosis with component FDD is new.
j) Uncertainties in the FDD method and inaccuracies in the measurement data can be processed in the 4S3F method.
k) Application of model faults, especially soft sensors, in an FDD method is new.
l) Absolute set probabilities of the fault and symptom nodes of the 4S3F DBN are less important than the relative ones.
m) A start to classify rules for energy performance, balance and operational state symptoms was made.

6.2 Recommendations

A start was made to automate the 4S3F method which resulted in the automation of the fault detection and diagnosis. However, automation of the pre-process and correction was not considered. Next to this the automatic set up of the DBN from a P&ID and the feed of symptom detection output were not elaborated. In the case studies libraries of symptoms and DBNs were presented which should be extended for HVAC systems which were not considered yet, such as air handling units, thermal emitter systems, solar energy systems and hydrogen installations.
In the Dutch project Brains for Buildings (B4B) [20] the 4S3F method will be elaborated further.

7. References

[1] Y. Zhao, T. Li, X. Zhang, C. Zhang, Artificial intelligence-based fault detection and diagnosis methods for building energy systems: Advantages, challenges and the future. Renewable and Sustainable Energy Reviews 109 (2019):85-101. https://doi.org/10.1016/j.rser.2019.04.021.

[2] J. Bynum, D. Claridge, J. Curtin, Development and testing of an Automated Building Commissioning Analysis Tool (ABCAT). Energy and Buildings 55 (2012):607-617. https://doi.org/10.1016/j.enbuild.2012.08.038.

[3] J. Schein, S.T. Bushby, A Hierarchical Rule-based Fault Detection Diagnostic Method for HVAC Systems, HVAC&R Research 12 (2006): 111-125. https://doi.org/10.1080/10789669.2006.10391170

[4] Z. Du, B. Fan, X. Jin, J. Chi, Fault detection and diagnosis for buildings and HVAC systems using combined neural networks and subtractive clustering analysis, Building and Environment 73 (2014):1-11, https://doi.org/10.1016/j.buildenv.2013.11.021

[5] K. Sun, G. Li, H. Chen, J. Liu, J. Li, W. Hu, A novel efficient SVM-based fault diagnosis method for multi-split air conditioning system's refrigerant charge fault amount, Applied Thermal Engineering 108 (2016): 989-998. https://doi.org/10.1016/j.applthermaleng.2016.07.109.

[6] F. Xiao, S. Wang, X. Xu, G. Ge, An isolation enhanced PCA method with expert-based multivariate decoupling for sensor FDD in air-conditioning systems. Applied Thermal Engineering 29 (2009): 712-722. https://doi.org/10.1016/j.applthermaleng.2008.

03.046

[7] D. Choiniere, DABOTM: A BEMS assisted on-going commissioning tool. Proceedings of the National Conference on Building Commissioning (2008).

[8] Y. Zhao, J.Wen , F. Xiao, X. Yang, S. Wang, Diagnostic Bayesian networks for diagnosing air handling units faults – part I: Faults in dampers, fans, filters and sensors. *Applied Thermal Engineering* 111 (2017): 1272-1286. https://doi.org/10.1016/j.applthermaleng.2015.09.121

[9] Y. Zhao, J. Wen, S. Wang, 'Diagnostic Bayesian networks for diagnosing air handling units faults – Part II: Faults in coils and sensors,' *Applied Thermal Engineering* 90 (2015): 145-157. https://doi.org/10.1016/j.applthermaleng.2015.07.001.

[10] Y. Zhao, S. Wang, An intelligent chiller fault detection and diagnosis methodology using Bayesian belief network. Energy and Buildings 57 (2013):278–288. https://doi.org/10.1016/j.enbuild.2012.11.007

[11] ASHRAE Handbook, HVAC Systems and Equipment. American Society of Heating, Refrigerating and Air Conditioning Engineers (2012). ASHRAE.

[12] Air-Conditioning System Design Manual, Second Edition (2007). ASHRAE Press.

[13] Meetpunten en meetmethoden voor klimaatinstallaties (2014), ISSO-publicatie 31, Stichting ISSO, Rotterdam, The Netherlands.

[14] Ontwerp van hydraulische schakelingen voor verwarmen (1998), ISSO-publicatie 44, Stichting ISSO, Rotterdam, The Netherlands.

[15] A. Taal. A new approach to automated energy performance and fault detection and diagnosis of HVAC systems. PhD thesis. Bouwstenen 325. Eindhoven University of Technology. November 2021. ISBN 978-90-386-5409-6.

[16] A. Taal, L. Itard, W. Zeiler, A reference architecture for the integration of automated energy performance fault diagnosis into HVAC systems, Energy & Buildings 179 (2018) 144-155. https://doi.org/10.1016/j.enbuild.2018.08.031

[17] A. Taal, L. Itard, P&ID-based symptom detection for automated energy performance diagnosis in HVAC systems. Automation in Construction 119 (2020),103344. https://doi.org/10.1016/j.autcon.2020.103344

[18] A. Taal, L. Itard, P&ID-based automated fault identification for energy performance diagnosis in HVAC systems: 4S3F method, development of DBN models and application to an ATES system. Energy and Buildings 224 (2020): 110289. https://doi.org/10.1016/j.enbuild.2020.110289

[19] A. Taal, L. Itard, Fault detection and diagnosis for indoor air quality in DCV systems: Application of 4S3F method and effects of DBN probabilities. Building and Environment 174 (2020),106632. https://doi.org/10.1016/j.buildenv.2019.106632

[20] Brains for building's energy systems (B4B). https://brains4buildings.org.

The datasets generated during and/or analyzed during the current study are not publicly available as explanations are needed to apply them, but are available after contacting the first author.

Interactive GUI for enhancing user awareness applying IoT-sensors and physics-assisted AI

Dietmar Siegele [a], Paola Penna [a], Alice Schweigkofler [a], Orjola Braholli [a], Michael Riedl [a], Dominik T. Matt [a,b]

[a] Fraunhofer Italia, Bolzano, Italy, dietmar.siegele@fraunhofer.it

[b] Free University of Bolzano, Bolzano, Italy

Abstract. Several studies proved that occupant behaviour has a significant impact on energy consumption and indoor comfort. Thus, monitoring data and Internet of Things solutions are used to address behavioural changes for promoting energy efficiency and increasing, at the same time, the comfort perception. The possibility of seeing invisible information, such as energy consumption or comfort parameters, on a digital support have been proved to be effective in increasing users' awareness and to encourage efficient behaviours. This paper presents a GUI developed for increasing the user awareness and involving them actively in addressing their actions and presents the back-end architecture for making prediction and sharing feedbacks with the users. By means of the interface user can: (1) Visualize information related to monitoring data, selecting, and filtering the data they would like to see. (2) Receive real time personalized feedbacks based on behavioural predictions defined by using Artificial Intelligence (AI) algorithm. The AI algorithms are based on a physics-assisted approach to achieve better results with less input. Missing (monitoring) data is calculated by applying physical models (building energy simulations) and only for the remaining parts machine learning models are used. Mainly we apply LSTM models. (3) Express personal comfort feedbacks based on comfort perception, for setting user-oriented feedbacks. The first part of the paper describes the architecture of the monitoring systems and presents the GUIs developed for two different case studies: a social housing building and a nursery school. The personalization of the GUIs based on user's typology has been done for enhancing the active participation and the involvement of the users in the project. The second part of the paper presents the back-end architecture of the GUI and the AI algorithms used for monitoring data analysis. The physis-assisted algorithm allows us to make predictions based on occupancy behaviour and to provide each occupant with tailored personalized feedback to promote energy-saving behaviours in real-time. We have placed more than 150 sensors in these two buildings that return us almost 1000 measured variables that can be used for the training of the AI models.

Keywords. IoT data, physics-assisted AI, health and comfort monitoring, user behaviour.
DOI: https://doi.org/10.34641/clima.2022.403

1. Introduction

Monitoring data and IoT solutions seems to be a promising strategy for driving the people's habits in taking effective actions for reducing the energy consumptions and, at the same time, increasing the indoor comfort perception of the users. Data from the Internet of Things (IoT) can be used by two main approaches:

- directly to optimize the control of the HVAC (Heating, Ventilation and Air Conditioning) systems and reducing the energy peak and the overall consumptions [1], and
- indirectly by communicating the monitoring data to the users in order to raise their awareness for adopting an energy efficient behaviour.

The development of user interfaces for communicating with users is highly investigated in recent literature [1]–[4] and by several European projects (The4Bees, EnerGAware, Klimakit, Sinfonia, OrbEEt, Entropy, GreenPlay). The studies proved that increasing the users' awareness, showing them

Copyright ©2022 by the authors. This conference paper is published under a CC-BY-4.0 license.

information related to their energy consumption and sending them targeted feedback, can reduce the energy consumption by 15% to 25% [3]. The information can be shown by simple dashboards or more effectively by advanced digital tools [5], [6] that allows an interactive communication with users and a customization of the data visualization. [7]–[9] highlight which are the most important aspects that should be considered for developing an effective communications tool. They stated that a key role is played by the way in which the information is presented to the users. Some of the main aspects that should be considered and integrated for the development of an effective digital interface are:

- Real time feedback on the actions that the user should adopt.
- Benchmark of virtuous users in order to incentivise the competition and to increase the gaming effect.
- Visualization of real time energy consumption measurement and past data for allowing a direct comparison of historical and current situation.

According to [10] and [11] receiving daily tips seems to be effective in reducing energy consumptions. [10] developed a mobile application where the users receive daily tips for reducing their electricity usage. [11] developed a more complex user interface based on gamification where the users receive tailored, interactive tips, information, and data-driven messages that can give users a clear view of how their actions impact on the amount of energy they waste and how they can improve their active participation. Moreover, the systems propose rewards for consumers by sending stimuli to change consumer behaviour. Moreover, [12] proved that the gamification is a good strategy for keeping the users motivated and involved in driving their behavioural changes. The work of [13] proposes an approach based on visualization of real time data based on dashboards, which to a large extent follow the idea of using dashboards in cars to inform drivers of the current state of their car. Another important aspect is stated by [14]. The authors highlight the importance of allowing the users to express their preference on their comfort perception, to actively consider their point of view and integrating this information in the heating system management.

This paper proposes the development of a digital interface that integrates all these aspects. The developed GUI allows to provide interactive and customized real time information, based on the users' profile. The backend of the system uses AI algorithms for analysing monitoring data and a physis-assisted algorithm allows to make predictions based on occupancy behaviour. It can provide each user with tailored personalized feedback for energy-saving and comfort recommendations in real-time. We developed two different interfaces for a residential and a non-residential building. Moreover, the software architecture is designed in a modular way and allows to adapt the interface according to the actual necessities. The AI algorithm is trained as a global model for each building type, and it is re-trained for each single unit by applying transfer learning using actual data.

2. Methodology

2.1 Case study

We chose two case studies to prove our approach: a residential and a non-residential building.

Fig. 1 shows a school building, that is used as a nursery school. With this non-residential building we want to show how our approach can be used in a comprehensive solution by applying it to the overall building and to all classrooms. At the same time each classroom is independent in the use of the application. In total we count ten classrooms with altogether five classes with alternating room use. Four classrooms are equipped with a mechanical ventilation system, which is not known to users. Huge parts of the building are not renovated and show a low quality of the building envelope. Due to this, and a high complexity of the heating system, energy consumption is not analysed in this case study.

Fig. 1 - School building.

Fig. 2 depicts a residential building. In the residential building two flats were chosen where we apply the application. With this case study we want to prove that the approach can also be used in small units like an apartment without the need to apply it to the overall building.

Fig. 2 - Residential building.

The residential building has a very high energy efficient standard and uses passive house components (U-value of walls lower than 0.15 W/m^2.K, of windows lower 0.85 W/m^2.K). However, there is no mechanical ventilation system installed.

2.2 Monitoring solution

Our approach depends on sensor data. Thus, a monitoring solution was developed and rolled out in the two case studies. Several IoT technologies are available on the market. However, only a small number has the capability to be power supplied by battery. This is essential in our case studies, as we want to install our system in an existing building structure. We think that our approach is mainly feasible in existing buildings and therefore a long battery runtime is essential. In practise this can be guaranteed only by applying one of the three communication protocols ZigBee, EnOcean or LoRaWAN.

We decided to go for LoRaWAN, as it shows two main advantages. First, it has the longest radio range of all protocols. The presented case studies are situated within a distance of 500 metres, and it is possible to gather the data with only one gateway (= device to collect the data and forward it to a server). We use two gateways to improve the battery lifetime of the sensors. This is also the second advantage of LoRaWAN: it uses a modern hardware and software architecture. Designed for security, it allows us to guarantee a fully encrypted data communication from sensor to database. Furthermore, we use features like adaptive data transfer rates, that improves the battery lifetime. We are gathering data each 10 minutes or when an event happens (like window opening). We expect a battery lifetime of almost 10 years for all devices, expect of the Ursalink AM102 that is equipped with an additional display. Here we expect 1 year of battery lifetime.

Fig. 3 and Tab. 1 show the sensors used in the case studies. In overall, almost 150 sensors are in use.

Fig. 3 - Sensors used in the case study, from left to right: Ursalink AM102, ELSYS DOOR, ELSYS ERS CO2, mcf88 Weather Station.

Tab. 1 - Used LoRaWAN sensors.

Manu-facturer	Name	Type
Ursalink	AM102	Temperature, humidity, CO_2, VOC, presence, display
ELSYS	ERS CO2	Temperature, humidity, CO_2, presence
ELSYS	ERS EYE	Temperature, humidity, presence, people detection
ELSYS	ERS DOOR	Opening/closing
mcf88	MCF-LWWS00	Weather station, temperature, humidity, global radiation, wind speed and direction, rain
MClimate	Vicki	Thermostatic valves

Fig. 4 shows the architecture of the monitoring solution. The sensors send the data wireless via LoRaWAN to a LoRaWAN server. A gateway is used as a physical device to forward the (encrypted) sensor data from LoRaWAN to WAN (internet). The gateways are connected to the LoRaWAN server via VPN and a cellular connection. As LoRaWAN server LORIOT is used.

On the LoRaWAN server sensor data is decrypted and is forwarded via encrypted MQTT to a timeseries database. Here we use InfluxDB as a database, but the design allows the use of any timeseries-based database. Data is then accessible by the application for further use (see next section).

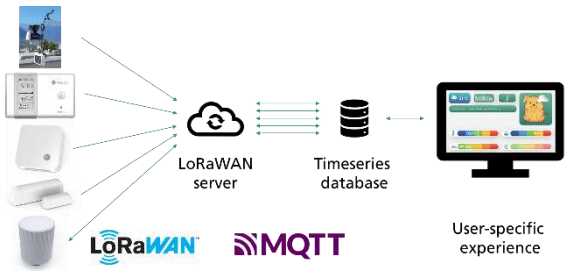

Fig. 4 - Architecture monitoring system.

2.3 Software architecture of the application

Fig. 5 depicts the (simplified) software architecture of the application. The application is based on web technology, namely HTML, CSS and JavaScript for the frontend, ASP.NET for the backend and Python for the micro services. Frontend, backend and micro services are separated from each other and are connected via a RESTful API. A full user authentication (from frontend, over backend to micro services) is implemented. That guarantees full data integrity. A sensor management is implemented by gathering data from the LORIOT LoRaWAN server by applying a RESTful API. The frontend (GUI) can be changed by applying different themes. AI-based recommendations and the handling

of user feedback are implemented by micro services based on Python. A specially developed AI-hub ensures the data exchange between micro services and backend. The application is multi-language compatible and at the moment English, German and Italian are implemented as languages.

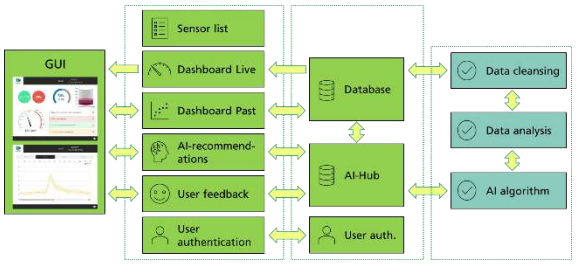

Fig. 5 - Software architecture.

The GUI itself was developed within a design thinking process. Fig. 6 depicts the results of the "ideate" part (prior step of rapid prototyping) of the GUI for the school building. Using the presented software architecture, specific themes can be developed and easily implemented.

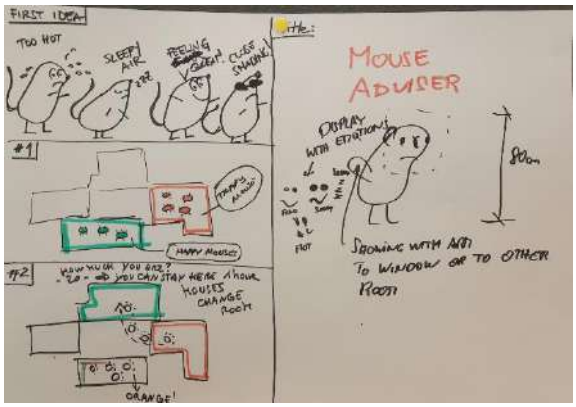

Fig. 6 - Design thinking process of the GUI (here for the school).

Within the design think process also possible advices for the users were developed. In total 64 different recommendations were rolled out in the first version of the application. Typical suggestions have a format similar to "The air quality here is not very good. But outside it is very hot, so let's wait a little bit before opening the windows.". The following categories for giving advices on the comfort are implemented in the first version: temperature, humidity, indoor air quality and illuminance.

2.4 AI-algorithm

We use two AI-algorithms that were implemented as Python micro services. The first AI algorithm is a classification tree that decides, either depending on actual real time monitoring data or on predicted data, if a recommendation (see section above) is useful for a user. The second algorithm is based on a long short-term memory (LSTM) time series forecasting and predicts the room states (temperature, humidity, CO_2, illuminance) in 15, 30, 45 and 60 minutes. This allows us to give advices already in advance. The prediction uses a semi-physical approach to achieve a higher accuracy of the LSTM network with less training data. The results of this predictions are again the input data for the beforementioned classification tree. If no advice based on the real time data is found (i.e., the comfort is optimal), recommendations for future conditions, based on the prediction can be displayed in the application.

The classification tree is generated by applying decision tree models from the *scikit-learn* toolbox. Training data is generated from measurement data and by manual labelling. As input data, data from Tab. 2 is used (same data as for the neural network, see below). As labels, the advices as described in the section above are used.

For the timeseries forecast a recurrent neural network (RNN) using the so-called LSTM architecture is implemented [15]. For each room (classroom) or each apartment an own model is used. However, all models use the same input and output vectors. This allows us to train once a model of a single room or apartment and then to apply transfer learning for other rooms. By this, we achieve faster training results, and, in the future, we will be able to use a shorter training period for similar building structures.

Our model uses 256 nodes that are based on LSTM with a forget gate. We use a multi-output model, so that it is possible to predict the future room states but also the future weather conditions by one model. This implicates that we need a high number of nodes. For training we allow a maximum of 100 epochs. The model sees an input data length of 7 days. Retraining is carried out for all different rooms based on previous models to reduce the necessary time for training.

Tab. 2 shows the input data vector that is used for the neural network. Apart from measurement data we also use physically calculated data for the solar radiation on the vertical surfaces (South, North, East, West), that is crucial for solar gains through the windows. The area of the windows is also introduced by using an accurate BIM (Building Information Modelling) model of the case studies. By applying data exchange via the file format gbXML this information is imported into the micro service that runs the neural network. In future we plan to implement even more sophisticated physical calculations based on building energy simulation, like air flow calculations.

Tab. 2 - Input data for the neural network.

Input data	Type
Hour of day as sine	Generated from timestamp
Hour of day as cosine	Generated from timestamp
Day of year as sine	Generated from timestamp
Day of year as cosine	Generated from timestamp
Day of week	Generated from timestamp
Hour of day	Generated from timestamp
Temperature	Measured value of temperature
Humidity	Measured value of humidity

CO_2	Measured value of CO_2
Pressure	Measured value of ambient absolute air pressure
Illumination	Measured value of illumination
Motion	Measured value of motion
Window South opening state	Measured opening state of South windows (summed up)
Window North opening state	Measured opening state of North windows (summed up)
Window East opening state	Measured opening state of East windows (summed up)
Window West opening state	Measured opening state of West windows (summed up)
Door opening state	Measured opening state of door against corridor
Ambient temperature	Measured ambient air temperature (weather station)
Ambient humidity	Measured ambient air humidity (weather station)
Ambient pressure	Measured ambient air pressure (weather station)
Wind speed x-direction	Measured wind speed (weather station)
Wind speed y-direction	Measured wind speed (weather station)
Solar radiation South orientation	Calculated solar radiation on vertical surface against South based on measured global radiation
Solar radiation North orientation	Calculated solar radiation on vertical surface against North based on measured global radiation
Solar radiation East orientation	Calculated solar radiation on vertical surface against East based on measured global radiation
Solar radiation West orientation	Calculated solar radiation on vertical surface against West based on measured global radiation
Window South area	Area of South windows (summed up)
Window North area	Area of North windows (summed up)
Window East area	Area of East windows (summed up)
Window West area	Area of West windows (summed up)

3. Results and Discussion

3.1 Graphical user interface

Two different graphical user interfaces (GUI) were developed for the case studies. Fig. 7 and 8 show the GUI for the school building. The teachers and the children can change the room where they are, in every moment (Fig. 8). All main rooms are equipped with tablets, that have installed the application. To simplify the use of the app for the children, almost no text was used on the main pages. Only when asking for the advice (here not visible), the textual advice will be accompanied with a picture of the action that the mouse should do (compare Fig. 9).

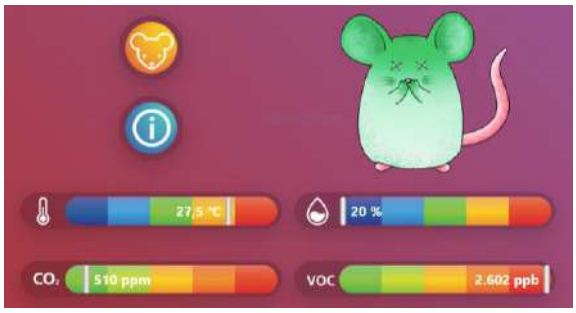

Fig. 7 - GUI of school building (adviser).

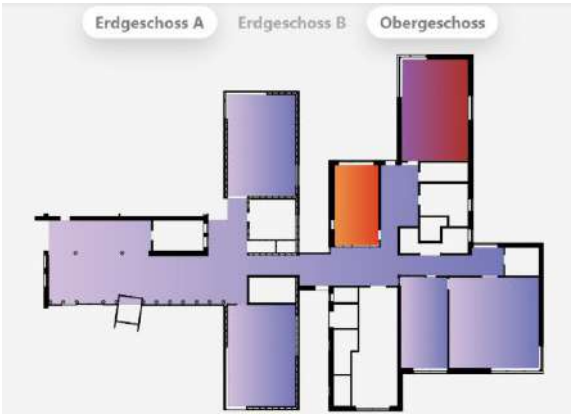

Fig. 8 - GUI of school building: room selection.

Fig. 9 - GUI of school building: different states & actions.

Fig. 10 shows the GUI used in the residential building. The occupant can see actual data of a central sensor, past data of sensors in each room, actual weather and the advices how to improve the IAQ and to reduce the energy consumption.

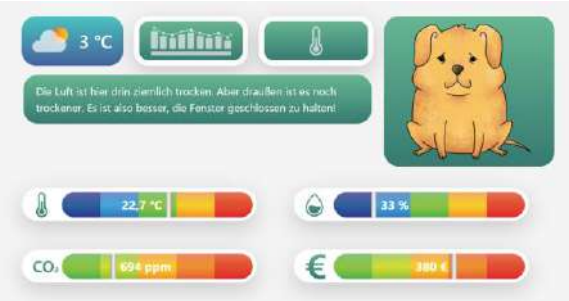

Fig. 10 - GUI of residential building.

In both GUIs the optimal temperature and humidity range is determined depending on the thermal comfort, mainly on the concept of predictive mean vote (PMV). The user has also the possibility to change the setpoint of the thermostatic valves in each room. Also this is realized by LoRaWAN and LoRaWAN compatible thermostatic valves.

3.2 AI-algorithm

Training of the decision tree was carried out by using the period between 2021/09/27 and 2021/10/31. The labelling was carried out for the whole period by applying a semi-automatic labelling routine. The advices described in the section above were used as labels and in addition a label for an "all okay" state. The first three weeks were used for training and the last two weeks for validation. In overall a prediction accuracy of around 90% was achieved.

The main advantage of this approach is that the overall decision tree does not have to be programmed. Programming a decision tree, considering room sensor data and weather information, as input and (at the moment) 64 different results leads to a very high effort in programming and a high number of errors can be introduced. Considering the actual result of 90% accuracy of prediction of the decision tree, in overall better results can be expected compared to traditional approaches. Further, when more data is available a re-training can be carried out. Also adding additional advices is very simple by applying this approach. However, the labelling takes quite a lot of time and needs expertise. It is not a trivial work and is at the same time very time-consuming. Moreover, due to the very time-limited training period (limited in particular to a specific season), not all available labels could be used. This means, that more time periods are necessary to ensure that all labels can be used and to achieve an even higher prediction accuracy.

Training of the RNN was carried out by using the period between 2021/09/27 and 2021/12/19. Here 70% of the data was used as training data, the rest as validation data. The batch size was data of 12 hours. We take a 10-minute interval for the data points. The prediction is carried out for 15, 30, 45 and 60 minutes. We train a model for each single room; however, we use the previously trained model as starting point. With this approach, we need for the further rooms only about 3 epochs to get a high accuracy. In overall, the accuracy of the prediction is very high. There is only a very little amount of time, where the prediction fails completely (< 1%). As quality criteria for failing of the prediction we set for the indoor temperature a range of 0,3 °C, for the humidity 3%, for the illumination 10 lux and for the CO_2 concentration 50 ppm. Highest failure rate can be seen in the illumination.

3.3 Preliminary monitoring results

We present here first preliminary monitoring results of the application impact. At the moment it is only feasible to evaluate the comfort parameters, as changes there can already be obtained after a very short time. For evaluating the impact of the advices that could reduce the energy consumption, a longer observation period is necessary.

For the indoor air quality in particular the CO_2 concentration was analysed. The period between 2021/10/04 and 2021/10/24 was taken for the reference values. The validation period of the application is between 2021/12/06 and 2021/12/19. Tab. 3 shows the number of total hours in the two weeks periods with CO_2 concentrations above 800 ppm for the school building. The use of the classrooms was in both periods the same. Also the number of children was unchanged. Independent of this study, teachers have been advised to open the windows regularly due to the COVID pandemic in both periods. In the validation period the ambient temperature was significantly lower than in the reference period (which usually leads to a reduced ventilation). The total hour of use in these periods is each about 70 hours.

Tab. 3 - Hours with CO_2 concentration above 800 ppm.

Room	Reference	Validation	Difference
G01a	16.83 h	2.17 h	-87%
G01b	16.17 h	11.50 h	-29%
G02a	4.33 h	3.83 h	-12%
G02b	35.33 h	51.33 h	+45%
G03a*	5.67 h	0.00 h	-100%
G03b*	4.17 h	3.83 h	-8%
G04a	8.17 h	10.83 h	+33%
G04b*	11.0 h	22.50 h	+105%
G05a*	1.00 h	0.00 h	-100%
G05b	4.25 h	3.17 h	-25%
TOTAL	**106.92 h**	**109.16 h**	**2%**

** Equipped with mechanical ventilation system.*

For the classrooms the hours of CO_2 concentration

could only be reduced by 2%. For the residential building we can obtain the same results in our first analysis. In terms of thermal comfort, no significant change was obtained so far, but the observation period is rather short for such analysis.

4. Conclusions and Outlook

We conclude that with a high number of sensor data available creating AI models is a relatively simple task. The decision tree approach allows to reduce the demand of necessary work to implement decision logics considerably. However, the labelling task is time-consuming and non-trivial. Here more sophisticated approaches are necessary to automate the labelling. Non-supervised machine learning models were not considered in this work. However, for decision trees they are not common, since the data is not labelled, there is no objective function to determine an optimum clustering. A prior unsupervised clustering of the data would be possible to reduce the amount of necessary labelling.

Short-time prediction by applying RNNs and the LSTM approach seems to be very convenient. In particular when combining it with physical calculated data, training time and prediction results can be improved. It seems that it can help to find the neural network more direct correlations in a shorter period of time. However, for training a significant amount of data is necessary to achieve good results. Combining it in a second step with the decision tree model seems to be convenient.

According to preliminary results the impact of the application in terms of indoor air quality seems to be modest. However, for a comprehensive validation a longer observation time is necessary. Also for evaluating the aspects linked to energy demand a longer observation time is needed. Therefore, the monitoring will be continued for the next months to gather data of an overall heating seasons. Comparison with energy demand data of previous heating seasons will be carried out.

5. Data Access Statement

The datasets generated during and/or analysed during the current study are not available because the project is still ongoing and results are preliminary, but the authors will make every reasonable effort to publish them in near future.

6. Acknowledgement

The research leading to these results has received funding within the project SINCRO from the European Regional Development Fund (Fondo Europeo di Sviluppo Regionale FESR Alto Adige 2014-2020) under the Grant Agreement n. FESR1141 CUP B54E20002030001. The authors would like to thank the school building supervisors as well as the building users for their contribution and participation in this project.

7. References

[1] A. Jáñez Morán, P. Profaizer, M. Herrando Zapater, M. Andérez Valdavida, and I. Zabalza Bribián, "Information and Communications Technologies (ICTs) for energy efficiency in buildings: Review and analysis of results from EU pilot projects," *Energy Build.*, vol. 127, pp. 128–137, 2016, doi: 10.1016/j.enbuild.2016.05.064.

[2] M. Casals, M. Gangolells, M. Macarulla, N. Forcada, A. Fuertes, and R. V. Jones, "Assessing the effectiveness of gamification in reducing domestic energy consumption: Lessons learned from the EnerGAware project," *Energy Build.*, vol. 210, p. 109753, 2020, doi: 10.1016/j.enbuild.2019.109753.

[3] A. Nilsson, M. Wester, D. Lazarevic, and N. Brandt, "Smart homes, home energy management systems and real-time feedback: Lessons for influencing household energy consumption from a Swedish field study," *Energy Build.*, vol. 179, pp. 15–25, 2018, doi: 10.1016/j.enbuild.2018.08.026.

[4] D. Pasini, F. Reda, and T. Häkkinen, "User engaging practices for energy saving in buildings: Critical review and new enhanced procedure," *Energy Build.*, vol. 148, pp. 74–88, 2017, doi: 10.1016/j.enbuild.2017.05.010.

[5] J. K. Day *et al.*, "A review of select human-building interfaces and their relationship to human behavior, energy use and occupant comfort," *Build. Environ.*, vol. 178, no. April, p. 106920, 2020, doi: 10.1016/j.buildenv.2020.106920.

[6] H. N. Rafsanjani, A. Ghahramani, and A. H. Nabizadeh, "iSEA: IoT-based smartphone energy assistant for prompting energy-aware behaviors in commercial buildings," *Appl. Energy*, vol. 266, no. January, p. 114892, 2020, doi: 10.1016/j.apenergy.2020.114892.

[7] D. Bonino, F. Corno, and L. De Russis, "Home energy consumption feedback: A user survey," *Energy Build.*, vol. 47, pp. 383–393, 2012, doi: 10.1016/j.enbuild.2011.12.017.

[8] A. Mäkivierikko, H. Shahrokni, and O. Kordas, "Designing energy feedback for a local social network," *Energy Build.*, vol. 199, pp. 88–101, 2019, doi: 10.1016/j.enbuild.2019.06.038.

[9] I. Vassileva, E. Dahlquist, F. Wallin, and J. Campillo, "Energy consumption feedback devices' impact evaluation on domestic energy use," *Appl. Energy*, vol. 106, pp. 314–320, 2013, doi: 10.1016/j.apenergy.2013.01.059.

[10] D. Oppong-Tawiah, J. Webster, S. Staples, A. F. Cameron, A. Ortiz de Guinea, and T. Y. Hung, "Developing a gamified mobile application to encourage sustainable energy use in the office," *J. Bus. Res.*, vol. 106, no. October 2018, pp. 388–405, 2020, doi: 10.1016/j.jbusres.2018.10.051.

[11] P. Ponce, A. Meier, J. I. Méndez, T. Peffer, A. Molina, and O. Mata, "Tailored gamification and serious game framework based on fuzzy logic for saving energy in connected thermostats," *J. Clean. Prod.*, vol. 262, 2020, doi: 10.1016/j.jclepro.2020.121167.

[12] I. C. Konstantakopoulos, A. R. Barkan, S. He, T. Veeravalli, H. Liu, and C. Spanos, "A deep learning and gamification approach to improving human-building interaction and energy efficiency in smart infrastructure," *Appl. Energy*, vol. 237, no. September 2018, pp. 810–821, 2019, doi: 10.1016/j.apenergy.2018.12.065.

[13] L. G. B. Ruiz, M. C. Pegalajar, M. Molina-Solana, and Y. K. Guo, "A case study on understanding energy consumption through prediction and visualization (VIMOEN)," *J. Build. Eng.*, vol. 30, no. February, p. 101315, 2020, doi: 10.1016/j.jobe.2020.101315.

[14] M. Monsberger, D. Koppelhuber, V. Sabol, H. Gursch, A. Spataru, and O. Prentner, "An innovative user feedback system for sustainable buildings," *IOP Conf. Ser. Earth Environ. Sci.*, vol. 323, no. 1, 2019, doi: 10.1088/1755-1315/323/1/012123.

[15] K. Greff, R. K. Srivastava, J. Koutnik, B. R. Steunebrink, and J. Schmidhuber, "LSTM: A Search Space Odyssey," *IEEE Trans. Neural Networks Learn. Syst.*, vol. 28, no. 10, pp. 2222–2232, Oct. 2017, doi: 10.1109/TNNLS.2016.2582924.

Response of low-cost environmental monitors to typical emission events in daycare centers

Hailin Zheng [a], Marcel Loomans [a], Shalika Walker [a], Wim Zeiler [a]

[a] Department of the Built Environment, Eindhoven University of Technology, Eindhoven, the Netherlands, h.zheng1@tue.nl

Abstract. Daycare centers (DCCs), the first program for the social development of young children (0-5 years old), are the most important place for young children besides their homes. Continuous indoor air quality (IAQ) monitoring in DCCs is a means to assess the IAQ and assure a healthy and comfortable environment for infants and toddlers. To date, an extensive array of low-cost air quality monitors (LCMs) is available on the commercial market. Still, only a limited number of these LCMs have been subjected to any research-based evaluation. Furthermore, performance evaluations of low-cost sensors in previous literature are mainly focused on residential emission activities. To the best of our knowledge, there is no research into simulating emission sources related to DCCs scenarios yet. Therefore, this study is aimed to evaluate the response of one type of LCM (2 units) to typical emissions events related to DCCs in detecting the IAQ parameters, that is, particulate matter (PM2.5, PM10), carbon dioxide (CO2), total volatile organic compounds (TVOC), temperature (T), and relative humidity (RH). The LCMs were compared to outcomes from research-grade instruments (RGIs). All the experiments were performed in a climate chamber, where 3 kinds of typical activities (Background test; Arts-and-crafts events; Cleaning events; in a total of 20 events) were simulated by recruited subjects in an indoor climate condition ([20±1 °C & 40±5% RH]). The IAQ parameters sensed by the LCM detected the majority of events, despite a difference in the magnitude of responses. Intra-sensor consistency was significantly strong for all IAQ parameters, with a mean coefficient of variation of 4.14%. The LCM particle sensor underestimated the reference concentrations, with a mean RMSE of 12.8 μg/m^3 for PM2.5 and 36.5 μg/m^3 for PM10. Although TVOC and CO2 sensors reported a weak quantitative response, both had a close correlation with RGIs' data, with R2 values in the range of 0.8-1.0 and 0.5-1.0, respectively. A good qualitative and quantitative agreement was observed in both T (within 1.1°C) and RH sensor (within 1%). In summary, this study reveals that the LCMs investigated are useful in providing IAQ-based monitoring in the specific application scenarios of daycare centers.

Keywords. Indoor air quality, Daycare center, Monitoring, Low-cost monitor
DOI: https://doi.org/10.34641/clima.2022.213

1. Introduction

Nowadays, a majority of young children around the world attend daycare centers (DCCs). This is an educational project before entry into the compulsory schooling system [1]. In the Netherlands, young children (generally aged 0-4 years old) spend most of their time at DCCs (up to 10 hours per day, 5 days per week, mostly indoors) [2]. Significant space-related contaminants, including diapers, arts-and-crafts supplies, cleaning agents, etc., can be present in DCCs. These typical emission sources result in such spaces being classified as Air Class 2 in ASHRAE 62.1 [3]. Considering the not-fully-developing organ systems of early life, ensuring a healthy indoor environment is of utmost importance to support the well-being of infants and children, as well as staff, in daycare centers.

Over the past two decades, remarkable advances in environmental sensor technologies have enabled the deployment and applications of low-cost air quality sensors for real-time and continuous indoor air quality (IAQ) monitoring and management [4]. Specifically, technological improvements in light scattering for the measurement of particulate matters [5], metal oxide semiconductor (MOS) sensors for the detection of various gases [6], and photoacoustic spectroscopy (PAS) and non-dispersive infrared (NDIR) based systems for the monitoring of carbon dioxide [7] allowed the development of low-cost air quality monitors (LCMs). Consequently, a large array of LCMs are available on the current commercial market, but very few of these monitors have been subjected to any research-based evaluation or data quality certificate. These LCMs normally integrate multiple sensors into one device, including temperature, relative humidity, particulate matters, carbon dioxide, total volatile organic compounds sensors, etc [8].

Copyright ©2022 by the authors. This conference paper is published under a CC-BY-4.0 license.

The recent existing literature on the performance evaluation of low-cost sensors and monitors is mainly focused on particulate matter compared to a reference instrument [9, 10], but very few studies examined other IAQ parameters, especially the TVOC and CO_2 parameters [8]. Additionally, the application scenarios where the low-cost sensors were tested and analyzed are primarily focused on residential emission activities [9-11]. To the best of our knowledge, there is no research into testing the response of LCMs to typical emission sources in daycare centers scenarios yet.

Therefore, in this paper, we present results fromone LCM which has not been tested in previous scientific literature and can detect multiple IAQ parameters, that is, $PM_{2.5}$, PM_{10}, CO_2, TVOC, T, and RH. It is part of a larger and more extensive research where multiple LCMs have been tested for application in DCCs. The research question we seek to answer in this paper is whether this specific LCM is able to reliably monitor IAQ performance in DCCs, given their specific exposure conditions.

2. Research Methods

Three typical main kinds of indoor emissions events related to the DCCs were simulated in a dedicated climate chamber. Performance comparison between the LCM and research-grade instruments (RGIs) was carried out under a typical climate condition: cool & dry.

2.1 climate chamber setup

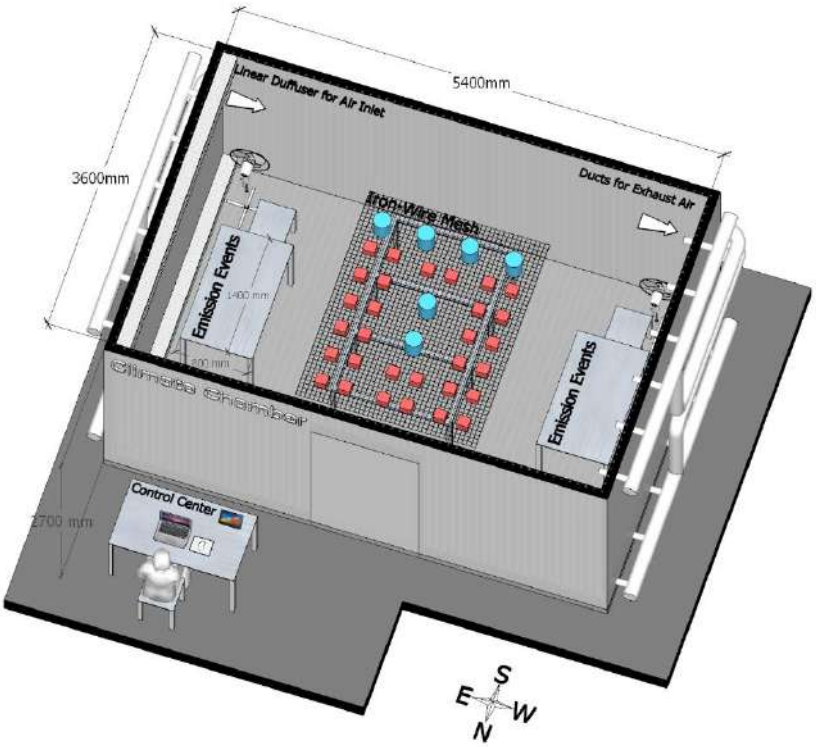

Fig. 1 - An interior axonometric view of the climate chamber set-up.

The experiments were performed in a 52.5 m^3 (W*L*H=3.6×5.4×2.7 m) climate chamber at the Eindhoven University of Technology, the Netherlands. An interior axonometric view of the measurement set-up in the climate chamber is shown in **Fig. 1**. Indoor environmental conditions, that is, temperature, relative humidity, and air exchange rate, are controlled by a dedicated HVAC unit via a proprietary software (LabVIEW2015, BPSCC, version 1.0) in a computer system (outside the chamber, see **Fig. 1**) with data acquisition and storage of historical records. The fresh outdoor air is supplied to the chamber through a 2-stages media filter, i.e., firstly using a coarse air filter, and then a HEPA box air filter (H13-Class with average performance efficiency up to 99.95% for larger than 0.3 μm particles according to EN779:2012). In order to minimize any emissions other than from the primary simulated events, the chamber was furnished with only four stainless-steel chairs, two stainless-steel tables (W*L*H=0.7x1.4x0.9 m), an iron-wire mesh table (W*L*H=2x2.5x0.9m), and four pedestal mechanical fans, as well as the instrumentation of LCMs and RGIs (**Fig. 1**). The iron-wire mesh panel setting is aimed to allow sufficient airflow to go along the sensors. Four mechanical fans were operated and pointed, respectively, towards interior surfaces (north and south wall) during the whole experiment, to ensure the homogeneous distribution of indoor air. Also, prior to the first experiment, a thorough cleaning and thermal treatment of the chamber interior were performed to remove all reactive compounds. All the LCMs and RGIs are co-located on the iron-wire mesh table in

the center of the climate chamber during the experiments and kept at least one-meter distance away from the emission sources.

2.2 selection and simulation of the typical IAQ emission sources in DCCs

The selection of simulated activities was based on the discussions and interviews with managers and pedagogical staff in two Dutch daycare centers during a preliminary field survey. Ultimately, considering the frequent occurrence in DCCs, three types of emissions activities were selected, that is, arts-and-crafts activities (4 art-painting tests, 4 plasticine-modeling tests, 4 gluing tests), cleaning activities (2 table-cleaning tests, 1 vacuum-cleaning test), and background activities (4 tests with subjects, 1 test without subjects). Briefly, four subjects were given one set of material-kit and performed each arts-and-crafts event test for one hour inside the chamber; two subjects use disinfectants or vacuum cleaners to perform clean activities; for the background test, four subjects sat inside the chamber and did reading work, except for one background test without any subject.

Regarding the experimental procedure, the first step is to ventilate the chamber room at the maximum rate (6.84/h) for at least 60 minutes to ensure indoor air quality comparable to outside conditions before the experiments. Then, the ventilation system was turned off, but an additional evaporative humidifier and two dehumidifiers with the filters removed were still kept working to make temperature and relative humidity achieve the desired values (20±1 ℃ & 40±10 ℃)). Once the equilibrium was achieved, four or two volunteers would enter the chamber. The subjects wore identical new lab coats and filter masks (OSHA & NIOSH N95 rating, Model 8210, 3MTM) and did not use any fragrance personal care products after taking a shower one night prior to the experiment to minimize any emissions from the researchers. After 10 min, they performed prescribed activities for a period of 60 min. This 60-min activity is indicated as one event test. After that, the subject exited the chamber, and at the same time, the ventilation system was turned on again to exhaust all of the pollutants. The next experiment was conducted when the values of contaminants (CO_2, PM, and TVOC) in the research-grade instruments showed background levels as before the emission events.

2.3 low-cost air quality monitors

Results from the AI-2003W (Edimax Technology Co., Ltd, Taipei City, Taiwan) are presented in this paper for the cool & dry conditions [20±1 ℃ & 40±10% ℃]. This LCM was selected due to the fact that it measures multiple IAQ parameters, that is, $PM_{2.5}$, PM_{10}, CO_2, TVOC, T, RH, and formaldehyde (HCHO). Its specifications are shown in **Tab. 1**. This monitor has not been tested in previous research. Two units of AI-2003W were purchased in the Netherlands in February of 2021. The two units take measurements at 5-min intervals.

Tab. 1 – manufacturer specifications for the Edimax AI-2003W.

Parameter	Sensor	Accuracy	Range
T	Sensirion SHT30	±1°C	0-80 °C
RH	Sensirion SHT30	±5%	0-100%
$PM_{2.5}$	Plantower PMS5003	±20% at 100-500 μg/m³; ±15μg/m³ at 0-100 μg/m³	0-500 μg/m³; 0.3-2.5μm
PM_{10}	Plantower PMS5003	-	0-500 μg/m³; 0.3-10μm
CO_2	Sensirion SCD30	±30ppm	0-5,000 ppm
TVOC	Sensirion SGP30	±15%	0-1,000 ppb
HCHO[a]	Winsen ZE08-CH2O	±10%	0-1 mg/m³

[a] Has the ability to detect HCHO, which was not tested and analyzed in this study.

2.4 research-grade instruments

For reference monitoring of time-resolved and size-resolved particulate matters level, Grimm Aerosol Spectrometer Model 11-D (abbreviated here as Grimm 11-D) detects the particles in 31 equidistant size channels from 0.253 to 35.15 μm. Three Grimm 11-D spectrometers were successfully calibrated with NIST certified PSL particles, and the calibration was verified on November 23rd, 2020, in GRIMM Aerosol Technik. Grimm 11-D measures particle mass concentration via light scattering technique and measures at an interval of 6 seconds. Grimm 11-D can output mass levels and the particle counts concentrations for all size channels. Although both are not regulatory-grade particles monitors, their portability and affordability, as well as high reliability, have made them widely used in previous and recent air-quality-related scientific research studies [12, 13].

A Photoacoustic Gas Monitor (INNOVA 1512, LumaSense Technologies A/S, Ballerup, Denmark) coupled with a Multipoint Sampler and Doser (INNOVA 1403, LumaSense Technologies A/S, Ballerup, Denmark) was used for the reference measurement of CO_2 gas. It was factory calibrated and compensated for temperature, pressure fluctuations, and water vapor by the manufacturer on December 21st, 2020, to ensure accuracy of the

measurement within 1.5% of the gas concentration. The detection limits given by the calibration chart of the manufacturer were 1.5 ppm for CO_2 and 0.006 ppm for SF_6. Five sampling points (four at the corners and one at the center of the sensor table) and one tracer-gas dosing point (in the bottom air inlet of the climate chamber) were selected. Those sampling and dosing points were connected by AISI-316 stainless steel polytetrafluoroethylene (PTFE) tubes to the respective channels on the devices of INNOVA 1403. The air was continuously and consecutively sampled from the five sampling points and analyzed at a ca. 42-second interval for each point. One measuring cycle lasted for ca. 3.5 minutes. We integrated the data of five sampling points into one INNOVA dataset after confirming the full mixing of the air inside the chamber. The INNOVA data were averaged at 5-min intervals.

As mentioned in a recent research article [8], there is no true reference instrument for monitoring time-resolved TVOCs due to limitations in the current technologies. Two Aeroqual Photoionization Detectors with a photon energy of 10.6 electron Volts (Aeroqual, Series 500 IAQ, Aeroqual Ltd., Auckland, New Zealand) were used as the research-grade TVOC measurement instrument. On December 17th, 2020, the two Aeroqual instruments were factory calibrated against a certified mixture of isobutene in synthetic air diluted with zero air using mass flow controllers with calibrations traceable to the National Institute of Standards and Technology (NIST). The Aeroqual has a working range of 0.01-30 ppm and accuracy of ±10%, storing data every minute.

For reference monitoring of room temperature and relative humidity, we deployed an EE08 series transmitter (E+E Elektronik® Ges.m.b.H., Engenwitzdorf, Austria) with a data logger (Squirrel 2040, Grant Instruments Ltd., Cambridge, UK) set at a 1-minute interval. The EE08 series is equipped with an NTC thermistor with interchangeable curves (Ø2.4mm) in the working range of -55 to +80°C, and reported accuracy of ±0.05°C from 0-50°C, and contains an HC101 high-end humidity sensor with a range of 0-100% RH and a factory accuracy of ±2% at 0-90% RH, ±3% at 90-100% RH.

2.5 data analysis and statistical methods

To understand the overall performance of the monitor, focus was put on two aspects: 1) Consistency; 2) Event detection. The first part is to compare the precision of the two units, which was characterized by two metrics: standard deviation and coefficient of variation (CV). In the second part, we computed the linear regression of each unit's and research-grade instrument data, where the coefficient of determination (R^2), slope, and intercept were calculated and compared. Also, the root mean square error, and the normalized root mean square error were used to help understand the error associated with each sensor measurement when compared with the research-grade instruments. All the aforementioned metrics and corresponding equations were suggested to evaluate the performance of low-cost sensors by U.S. EPA [14]. All the data processing and analysis were done by using python 3.8.

3. Results

3.1 Consistency

Tab. 2 and **Tab. 3** represent the results of the consistency (SD and CV) between the two similar LCM units in detecting all the IAQ parameters, that is, $PM_{2.5}$, PM_{10}, CO_2, TVOC, T, and RH. Lower SD and CV values mean better precision and less variation in trends. Considering the limit of paper pages, only the maximum, average, and minimum of SD and CV among 20 event tests are summarised in the table. Overall, for all the IAQ parameter-sensors tested in 20 events, the mean of SD is in the range of 0.1-13.8 (with specific unit) and the mean of CV is in the range of 0.31-10.53%, which exhibits strong consistency and supports the use of comparison for analysis. Specifically, when it comes to the CV metric, the temperature sensors showed the best precision among all the IAQ-parameter sensors, which reported 0.06-0.74% precision under 20 event tests. Also, the RH sensor and CO_2 sensors showed very good consistency with the CV in the range of 0.64-1.35% and 0.55-1.62%, respectively. It should be mentioned that $PM_{2.5}$ and PM_{10} sensors reported zero SD and CV values in some tests due to the very low emissions concentrations in these tests. In this case, all the output of sensors were close to the lower detection limit.

Tab. 2 – Standard deviation (SD) for different parameters between two similar LCM units under 20 tests.

Test	$PM_{2.5}$	PM_{10}	CO_2	tVOC	T	RH
Max	4.3	2.5	21.2	30.9	0.1	0.6
Mean	0.4	0.3	13.8	5.5	0.1	0.4
Min	0	0	2.6	1.7	0	0.3

Notes: the unit of $PM_{2.5}$ and PM_{10} is μg/m^3; the unit of CO is ppm; the unit of tVOC is ppb; the unit of T is °C; the unit of RH is %.

Tab. 3 – Coefficient of variation (CV) for different parameters between two similar LCM units under 20 tests (values in %).

Test	$PM_{2.5}$	PM_{10}	CO_2	tVOC	T	RH
Max	61.12	57.10	1.62	4.88	0.74	1.35
Mean	9.12	10.53	1.17	2.78	0.32	0.93
Min	0	0	0.55	0.93	0.06	0.64

3.2 Event detection

Fig. 2 shows the typical response of the two LCM units and research-grade instruments to 5 typical emissions events related to daycare centers, as illustrated by the time-series plot of the sensor logging. The highlighted region of each plot is the 60-min event test period. Correspondingly, **Fig. 3** shows the scatter plots and linear regression between RGIs and each unit, with slopes, intercept and R^2 for each 60-min event test. We describe the components of **Fig. 2** and **Fig. 3** in parallel by following the response of the sensed parameters, from $PM_{2.5}$, PM_{10}, CO_2, TVOC, T, to RH, to each event, from "Background test", "Gluing", "Painting", "Table cleaning", to "Vacuum cleaning".

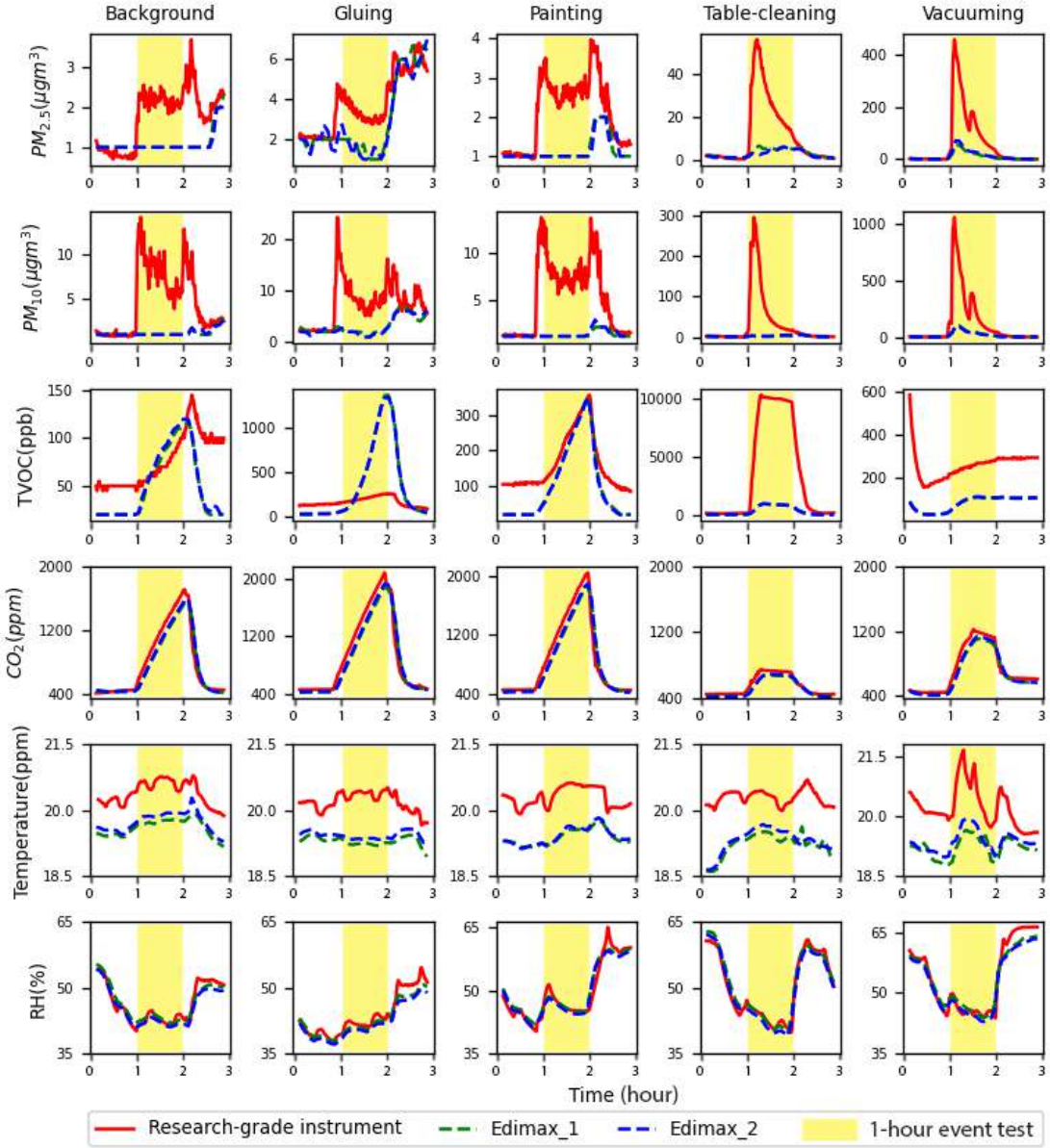

Fig. 2 – Time series plots of LCM and RGIs during Background test, Gluing, Painting, Table-cleaning, and Vacuuming events (the highlight region of the plot refers to the 60-min event test period).

In the first and second rows of **Fig. 2** and **Fig. 3**, $PM_{2.5}$ and PM_{10} sensors are compared with RGI (Grimm 11-D). When it comes to the Background test, during which four volunteers sat still inside the chamber and did reading work, the LCM $PM_{2.5}$ and PM_{10} sensors did not detect the event while the RGI (Grimm 11-D) monitored the variations in $PM_{2.5}$ concentrations from 0 to 3 μg/m^3, PM10 concentrations from 1 to 10 μg/m^3. Consequently, linear regression cannot be made during these two tests. During one of the arts-and-crafts events (Gluing), two units reported particle variations in $PM_{2.5}$ and PM_{10} and followed the trends similar to RGI (Grimm), with the correlation for $PM_{2.5}$: R_1=0.65, R_2=0.61; for PM_{10}: R_1=0.38, R_2=0.81, despite much lower mass concentrations emissions. Both under-reported the particle reference concentrations with a RMSE of 1.8 μg/m^3, and a NRMSE of 55.7% for

$PM_{2.5}$; with a RMSE of 7.0 μg/m^3 and a NRMSE of 82.1% for PM_{10}. However, similar to the Background test, both LCM units did not detect another arts-and-crafts event (Painting). In the cleaning activities (Table-cleaning and Vacuuming), both units reported slight variations while the RGI (Grimm) detected significant particle emissions concentrations in $PM_{2.5}$ and PM_{10}. Both units displayed weak quantitative response in Table-cleaning and Vacuuming, with a RMSE of 27.1 and 167.3 μg/m^3 and a NRMSE of 97.5% and 105.1% for $PM_{2.5}$; with a RMSE of 114.9 and 370.1μg/m^3 and a NRMSE of 137.9% and 121.2% for PM_{10}, respectively. When compared to the RGI (Grimm 11-D), good correlations for the two units were found in the Vacuum-cleaning event (for $PM_{2.5}$: R_1=0.59, R_2=0.66; for PM_{10}: R_1=0.58, R_2=0.66). Besides, both LCM units showed the ability to return to background levels after the emissions events.

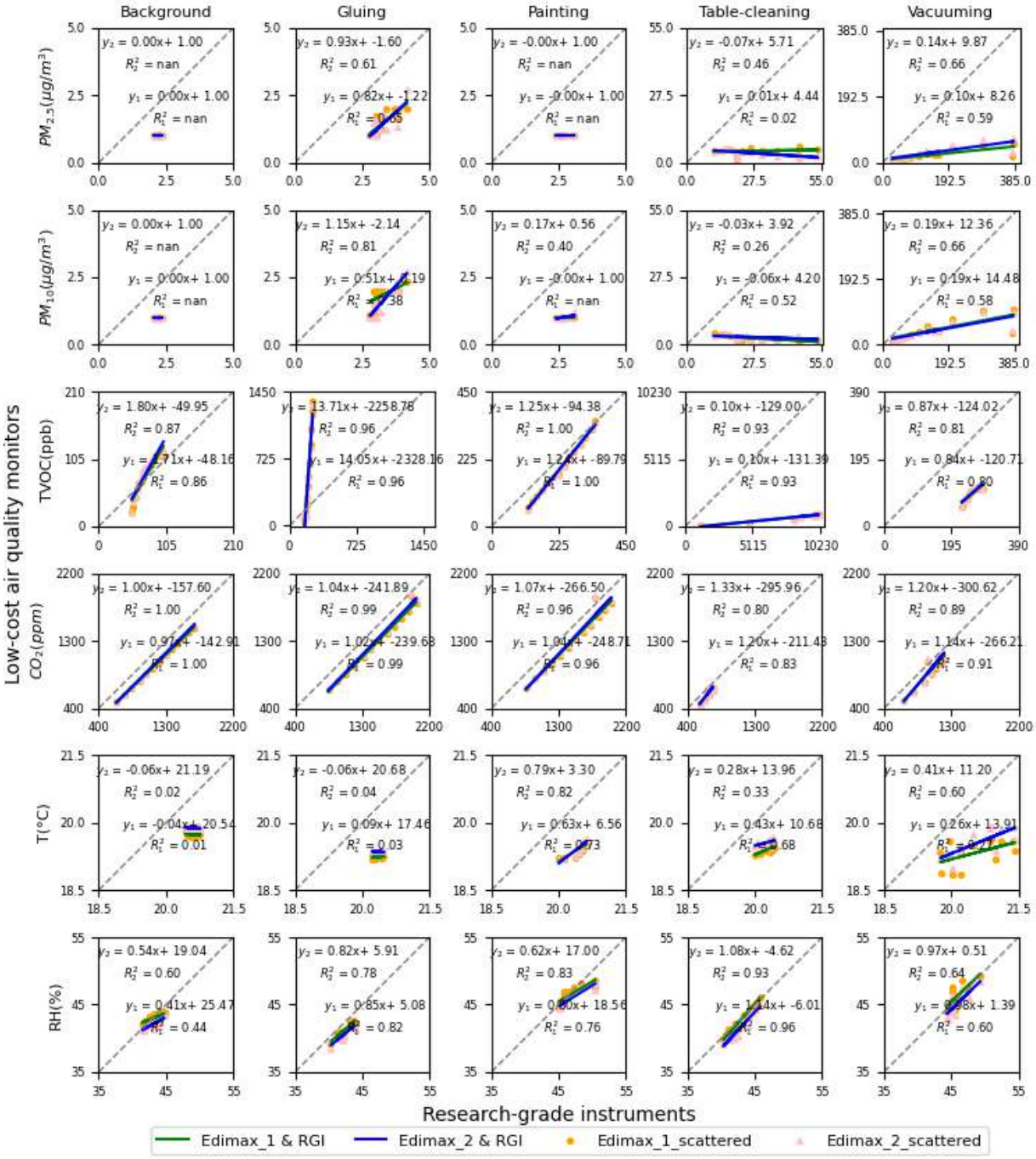

Fig. 3 – Scatter plots and linear regression of each unit with RGIs during Background test, Gluing, Painting, Table-cleaning, and Vacuuming events.

The third row of **Fig. 2** and **Fig. 3** presents the TVOC sensors comparison with RGI (Aeroqual-PID). Both LCM units detected all events, followed the consistent trends with the RGI (Aeroqual-PID), and showed a close correlation (R^2 in the range of 0.8-1.0). But the quantitative response varied up to 11 times depending on the emissions events, with a RMSE in the range of 16 to 8274 ppb, and a NRMSE

in the range of 23.0 to 257.3% when compared to the RGI (Aeroqual-PID).

In the fourth row of **Fig. 2** and **Fig. 3**, the CO_2 sensors are compared with RGI (Innova). It shows that the two units and RGI (Innova) were very closely correlated in their response to the CO_2 emissions events (R^2 in the range of 0.8-1.0). Considering the whole period of the 5 event tests, the LCM CO_2 sensors under-reported the reference CO_2 levels with a RMSE in the range of 74 to 199 ppm, and a NRMSE in the range of 10.6% to 14.2%.

In the fifth row of **Fig. 2** and **Fig. 3**, the air temperature sensors comparison with RGI (EE08) is shown. Throughout 20 events (under cool and dry conditions), the two LCM units detected the temperature variations despite a relatively narrow temperature span (19.8-21.4°C, mean=20.5°C) as registered by the RGI. unit 1 and unit 2 under-reported the air temperature on average by 1.1°C and 1.0°C, respectively, during the overall duration of these 20 events.

In the sixth row of **Fig. 2** and **Fig. 3**, the RH sensors are compared with RGI (EE08). Similar to temperature, the RH sensors displayed a consistent dynamic response to RH variations even though variations were limited (37-50%, mean=43%) during the 20 events.

4. Discussion

The precision (SD and CV) acquired in the event tests related to daycare centers revealed a significantly reliable consistency of two identical units of a low-cost air quality monitor in detecting the IAQ-parameters, that is, $PM_{2.5}$, PM_{10}, CO_2, TVOC, T, and RH. A similar outcome was obtained by Moreno-Rangel et al. [15], which assessed and compared five Foobot low-cost air quality monitors and research-grade instruments in measuring residential emissions events. Their results showed a very strong uniformity and low variability among five units in detecting IAQ-parameters including $PM_{2.5}$, CO_2, TVOC, T, and RH.

Regarding the performance of particle sensors, both units under-reported $PM_{2.5}$ and PM_{10} concentrations when compared to reference instruments for all events tested in this study. This aligns with the study of Zou et al. [16]; Also, in the study of Demanega et al. [8], which examined 8 LCMs and 8 low-cost single sensors in detecting residential PM_1, $PM_{2.5}$, PM_{10}, CO_2, TVOC, T, and RH, stated that the majority of tested devices underestimated reference values by up to 50%. The sensors showed the ability to return to baseline concentration after an event related to the daycare center. This was also found for residential events [16, 17]. In particular, it was shown that the qualitative and quantitative agreement varied depending on the emissions events, possibly because of the different particle composition, size distribution, and optical properties under certain events [17]. Besides, the differences might be caused by the limited detection bins of light scattering sensors [11, 18]. In general, the two LCM unit $PM_{2.5}$ sensors reported a mean RMSE of 12.8 μg/m^3 under 20 events tested in this study, which met the original equipment manufacturer (OEM) specification (±15μg/m^3), as outlined in **Tab. 1**.

In this study, due to the currently limited detection technology, we utilized the PID-based VOC instruments as a reference device, which could provide high temporal resolution and agreeable results of air monitoring, but were stated not as robust and accurate as a flame ionization detector (FID) [19]. The two units and RGI (Aeroqual-PID) displayed a different sensitivity toward the different events. The reason might be caused by the intrinsic properties of the devices [19, 20].

As reported in the study [8, 15], the results reported from the two LCM CO_2 sensors in this study re-confirmed that the non-dispersive infrared (NDIR) technology can result in measurable qualitative responses to all events. The two units do underestimate the reference values. For all 20 events tested in this study, the accuracy of two units produced a RMSE in the range of 25-227ppm (mean=168ppm), which did not meet the OEM specification (±30ppm). Regarding the air temperature and RH sensors, the results showed that both-parameters sensors were strongly correlated with reference measurements and produced quantitative responses to variations, which met the OEM specifications.

Additionally, when it comes to the comparison of the 3 different main events tested in this study, we found that the dominance of pollutants varied per event type. Specifically, in the Background tests, only CO_2 concentrations caused by the presence of occupants were dominant; in the arts-and-crafts events, TVOC concentrations, as well as CO_2 levels, became significant. Particularly, in the cleaning activities, PM concentrations were significantly dominant, in addition to CO_2 and TVOC levels.

Some limitations in this study design should be mentioned here. First, only the measurement performance aspect of the LCM was evaluated and compared, not the utility, portability, and cost. The particle reference instrument (Grimm 11-D) is an optical-based instrument. During the measurement, the density of the particle was not calibrated by the gravimetric-based source-specific measurement due to the constraints of the devices available. Instead, it was set in the device as 1.68 g/cm^3. Similarly, the TVOC reference (Aeroqual-PID) is not a reference instrument designated by national accreditation bodies.

5. Conclusions

The experimental design of this study is aimed to

evaluate the response of one type of low-cost air quality monitor (2 units) to 3 kinds of typical emissions events in the application scenario of a daycare center in detecting IAQ parameters ($PM_{2.5}$, PM_{10}, CO_2, TVOC, T, and RH). To summarize, the LCM displayed large variability as indicated by performance metrics suggested by U.S. EPA, including precision, bias, linearity, and error. The IAQ-parameters sensors, however, detected the majority of events simulated for the application scenarios in daycare centers, despite the different degree magnitude of response. This means that not for each IAQ parameter the absolute values can be trusted, but the LCM investigated is able to detect events, which could trigger mitigation actions to correct the situation.

6. Acknowledgment

The authors would like to thank Vinayak Krishnan for assisting in creating a preliminary framework of the python code. This study was sponsored by the fellowship provided by the Eindhoven University of Technology under the Department of Built Environment and the China Scholarship Council (CSC).

7. References

[1] OECD. Education at a Glance 2020. 2020.
[2] Offermans A, Zheng H, Zeiler W. Indoor Air Quality conditions within the baby bunk beds at Dutch daycare centers indicate the necessity for an improved ventilation design. 16th International Conference on Indoor Air Quality and Climate (INDOOR AIR 2020): International Society of Indoor Air Quality and Climate (ISIAQ); 2020. p. 1-6.
[3] ANSI/ASHRAE. ANSI/ASHRAE Standard 62.1-2019 -- Ventilation for Acceptable Indoor Air Quality. American Society of Heating, Refrigerating and Air-conditioning Engineers (ASHRAE); 2019.
[4] Kang Y, Aye L, Ngo TD, Zhou J. Performance evaluation of low-cost air quality sensors: A review. Sci Total Environ. 2021:151769.
[5] Morpurgo A, Pedersini F, Reina A, editors. A low-cost instrument for environmental particulate analysis based on optical scattering. 2012 IEEE International Instrumentation and Measurement Technology Conference Proceedings; 2012: IEEE.
[6] Liu X, Cheng S, Liu H, Hu S, Zhang D, Ning H. A survey on gas sensing technology. Sensors. 2012;12(7):9635-65.
[7] Kwon J, Ahn G, Kim G, Kim JC, Kim H, editors. A study on NDIR-based CO2 sensor to apply remote air quality monitoring system. 2009 Iccas-Sice; 2009: IEEE.
[8] Demanega I, Mujan I, Singer BC, Andelkovic AS, Babich F, Licina D. Performance assessment of low-cost environmental monitors and single sensors under variable indoor air quality and thermal conditions. Building and Environment. 2020:107415.
[9] Zou Y, Clark JD, May AA. A systematic investigation on the effects of temperature and relative humidity on the performance of eight low-cost particle sensors and devices. Journal of Aerosol Science. 2021;152:105715.
[10] Li J, Mattewal SK, Patel S, Biswas P. Evaluation of nine low-cost-sensor-based particulate matter monitors. Aerosol and Air Quality Research. 2020;20(2):254-70.
[11] Wang Z, Delp WW, Singer BC. Performance of low-cost indoor air quality monitors for PM2. 5 and PM10 from residential sources. Building and Environment. 2020;171:106654.
[12] Vasilatou K, Wälchli C, Koust S, Horender S, Iida K, Sakurai H, et al. Calibration of optical particle size spectrometers against a primary standard: Counting efficiency profile of the TSI Model 3330 OPS and Grimm 11-D monitor in the particle size range from 300 nm to 10 μm. Journal of Aerosol Science. 2021;157:105818.
[13] Masic A, Bibic D, Pikula B, Blazevic A, Huremovic J, Zero S. Evaluation of optical particulate matter sensors under realistic conditions of strong and mild urban pollution. Atmos Meas Tech. 2020;13(12):6427-43.
[14] Duvall R, Clements A, Hagler G, Kamal A, Kilaru V, Goodman L, et al. Performance Testing Protocols, Metrics, and Target Values for Fine Particulate Matter Air Sensors: Use in Ambient, Outdoor, Fixed Sites, Non-Regulatory Supplemental and Informational Monitoring Applications. US EPA Office of Research and Development. 2021.
[15] Moreno-Rangel A, Sharpe T, Musau F, McGill G. Field evaluation of a low-cost indoor air quality monitor to quantify exposure to pollutants in residential environments. Journal of Sensors and Sensor Systems. 2018;7(1):373-88.
[16] Zou Y, Young M, Wickey M, May A, Clark JD. Response of eight low-cost particle sensors and consumer devices to typical indoor emission events in a real home (ASHRAE 1756-RP). Science and Technology for the Built Environment. 2020;26(2):237-49.
[17] Singer BC, Delp WW. Response of consumer and research grade indoor air quality monitors to residential sources of fine particles. Indoor Air. 2018;28(4):624-39.
[18] Manikonda A, Zikova N, Hopke PK, Ferro AR. Laboratory assessment of low-cost PM monitors. Journal of Aerosol Science. 2016;102:29-40.
[19] Xu W, Cai Y, Gao S, Hou S, Yang Y, Duan Y, et al. New understanding of miniaturized VOCs monitoring device: PID-type sensors performance evaluations in ambient air. Sensors and Actuators B: Chemical. 2020:129285.
[20] Nirlo EL, Crain N, Corsi RL, Siegel JA. Field evaluation of five volatile organic compound measurement techniques: Implications for green building decision making. Science and Technology for the Built Environment. 2015;21(1):67-79.

Data Statement

The datasets generated during and/or analysed during the current study are not available because part of data is still being involved in another project un-published, but the authors will make every reasonable effort to publish them in near future.

Economic evaluation of properties based on consumption data

Rebekka Benfer [a], Jo Mathis Ihnenfeldt [b], Mathis Stange [c], Jan Manuel Westerkowski [d]

[a] Institute of Building Services Engineering, Faculty of Process Engineering, Energy and Mechanical Systems, TH Köln - University of Applied Sciences, Cologne, Germany, rebekka.benfer@th-koeln.de
[b] Institute of Building Services Engineering, Faculty of Process Engineering, Energy and Mechanical Systems, TH Köln - University of Applied Sciences, Cologne, Germany, jo_mathis.ihnenfeldt@smail.th-koeln.de
[c] Institute of Building Services Engineering, Faculty of Process Engineering, Energy and Mechanical Systems, TH Köln - University of Applied Sciences, Cologne, Germany, mathis.stange@smail.th-koeln.de
[d] Institute of Building Services Engineering, Faculty of Process Engineering, Energy and Mechanical Systems, TH Köln - University of Applied Sciences, Cologne, Germany, jan_manuel.westerkowski@smail.th-koeln.de

Abstract. The building stock is a major factor for achieving climate targets. By improving existing buildings, their efficiency can be significantly increased, thus reducing emissions. The economic evaluation of consumption data is an essential task for operators of properties in order to identify optimization potential. Here, the costs of heat transfer media, electricity and water are essential. The sole evaluation of building-specific consumption data does not fully allow for cross-building comparisons, since other aspects such as their type of use, size and intensity of use have a significant influence. It is necessary to develop a method that allows this comparison and at the same time can be applied with little effort. This paper presents a method for the economic evaluation of buildings taking into account the type of use, size and intensity of use. The innovative method allows the calculation of annuities for certain consumption categories such as electricity. These are combined into an overall performance indicator (PI) for each building. The scale of the PI is generated dynamically depending on the building data under consideration. Thus, a comparison of different buildings is easily and at the same time individually possible in consideration of the real estate portfolio. The results provide an overview of the potential need for optimization of the building as well as the installed plant technology. The effects of potential optimizations on the economic building performance are calculated based on the annuity method and are also included in the revaluation of the respective building. The method was tested in a study of school buildings in a major city in Germany. The method can be used to compare different combinations of measures and determine the optimal option. As a result, decisions regarding possible building optimization measures can be made transparently and scientifically in the future. This enables a more efficient use of resources.

Keywords. Performance Indicator, Annuity, Evaluation of optimizations, Calculation property evaluation.
DOI: https://doi.org/10.34641/clima.2022.186

1. Introduction

To achieve the climate targets, it is important to plan and construct buildings in an energy-optimized way. However, since the building stock is still responsible for 38% of global energy-related CO2 emissions [1], it should be operated optimally. According to [2], renovating the energy efficiency of buildings has resulted in multiple benefits in terms of energy consumption and environmental impact. To meet this requirement, property operators are regularly faced with economic as well as technical decisions regarding renovation measures of existing properties. Prioritizing which properties to renovate is a challenge. Possible evaluation criteria include, for example, social, moral, economic and other factors [3].

Investments for renovation measures are predominantly made due to economic motivations such as saving energy and repair costs. Less strong motivating factors represent, for example,

Copyright ©2022 by the authors. This conference paper is published under a CC-BY-4.0 license.

environmental benefits, efficiency gains, and peer influence. [3]

For this reason, the economic consideration of properties is based on their cost of use. Utilization costs consist of capital, administrative, operating and maintenance costs [4]. The operating costs are the easiest to influence by the operator. According to [5], in residential buildings, energy and water costs account for at least 51%. [6] shows that in the life cycle analysis of various residential buildings, about 44% of the energy consumption is due to the operating phase.

For the reasons mentioned above, it makes sense to consider operating costs when looking at economic optimization measures. However, in order to make recommendations for action on properties to be renovated based on operating costs, reference values or a framework is needed that allows properties to be evaluated economically.

From an energy point of view, the operation of existing residential and non-residential buildings can be assessed, for example, using characteristic values from [7]. However, the use of these characteristic values is hindered by the problem that they represent an outdated building stock from the years 2003 to 2005.

Operator/user-oriented standardized requirements in the building condition and the building technology are not documented there and thus not clearly comprehensible. In [8], energetic factors of building operation are mapped to a specific application. In this example, consumption data is related to supermarket customers.

However, these aforementioned energetic mappings do not allow for an evaluation of possible optimization measures, especially the resulting costs.

Existing tools for deciding on optimization measures so far only consider either the comparison of several optimization measures [9, 10, 11] or the evaluation of buildings [3]. In addition, they include, for example, methods of "machine learning" and can therefore only be used by appropriate experts [9]. Other tools consider the most effective measure under the consideration of different criteria. The focus is on calculating the impact of the different measures rather than making a decision for a property and a measure [10, 11, 12].

The aim of this work is therefore to create a low-threshold and simple tool that can be used to realize a first economic approximation regarding properties worth optimizing. This approximation is based exclusively on data that are reliably available and easy to collect. The evaluation scale is individually adapted to the property portfolio under consideration so that a ranking can be easily identified. The evaluation is carried out with the help of performance indicators, each of which takes into account criteria that are meaningful and individual to the user. The application is based on common spreadsheet programs, which means that investment costs are minimal. In addition to the aforementioned evaluation of the inventory data, an economic evaluation of possible optimization measures with regard to their effects is also planned.

In the following, therefore, section 2 describes the generally applicable calculation method. Section 3 explains the practical implementation of the method on the basis of an application example. Section 4 evaluates the method in terms of its usefulness and discusses its application limits. Finally, section 5 offers concluding remark.

2. Research Methods

In the following section, the method of economic evaluation of properties and suitable optimization measures is considered on the basis of the input parameters, the calculation formulas and the output parameters. In the first step of the method, a current property performance is determined. This is followed in the second step by a comparison of the economic effects of different optimization measures for one of the properties. The choice of the property to be considered is up to the user. It is recommended to investigate optimization possibilities for one of the properties that has a bad economic rating, since the potential for improvement is greater here.

2.1. Input parameters for property evaluation

The input parameters for the calculation are provided by the user. The input is done in list form line by line in given columns.

Object designation: For the identification of the considered objects of the property portfolio, a unique designation for the different objects has to be entered.

Comparison parameters: When creating the data set, care must be taken to ensure that the objects match in certain parameters and are thus comparable with each other in terms of consumption data. One column is provided for each parameter. This enables filtering the list.

Medium e: The following key figures each refer to a medium for which consumption data is available. Examples are water, fuels, or other consumption media.

Price medium p_e: The prices of the medium should be adjusted according to the energy supplier and location. For different energy suppliers and locations, other taxes and charges should be included in the price. Alternatively, an average price depending on the city can be used.

Consumption medium c_e: The consumption of the media heating energy, electricity and water should be stated in kWh/a or l/a. If the properties are located in different climatic zones, the consumption of the heating energy medium must be adjusted with regard to the weather. This can be done, for example, according to [7].

Reference parameter r_d: The key performance indicator can refer to various reference parameters. These reference parameters should reflect the use of the property in the best possible way. Examples of reference parameters include net floor area, number of users, usage times and revenues generated by the property. At least one reference parameter must be specified.

2.2. Calculation of property evaluation

The first step of the calculation includes the calculation of the annuity of the demand-related costs $A_{N,V}$. The calculation is performed per object according to the following formula:

$$A_{N,V,i} = \frac{\sum_{e=1}^{n} p_e * c_e}{\prod_{d=1}^{n} r_d} \quad (1)$$

$A_{N,V,i}$	*Annuity of the demand-related costs*
p_e	*Unit price per medium*
c_e	*Consumption per medium*
r_d	*Reference parameters*
i	*Index per property*

In order to generate a dynamic evaluation of all properties considered, the annuity $A_{N,V}$ of the individual properties is projected onto a performance indicator $PI_{ECO,tot}$. Here, the scale range is defined between the property with the highest annuity ($A_{N,V,max}$) and the property with the lowest annuity ($A_{N,V,min}$) and mapped to a scale from 1 (worst) to 10 (best).

$$PI_{ECO,tot,i} = 1 + \left(\frac{10-1}{(A_{N,V,min} - A_{N,V,max})}\right) * (A_{N,V,i} - A_{N,V,max}) \quad (2)$$

$PI_{ECO,tot,i}$	*Performance indicator economic*
$A_{N,V,i}$	*Annuity of the demand-related costs*
$A_{N,V,min}$	*minimum value of $A_{N,V,i}$*
$A_{N,V,max}$	*maximum value of $A_{N,V,i}$*
i	*Index per property*

2.3. Output of property evaluation

Performance indicator economic: The result represents a listing of all objects. Objects in particular need of optimization can be identified on the basis of $PI_{ECO,tot}$.

2.4. Input parameter for measure evaluation

In order to be able to compare different optimization measures for a specific property, information must be provided on the investments and savings that these measures entail. These optimization measures should be developed and quantified by a specialist planner in terms of their investment costs and consumption savings, depending on the property and the system technology used. In the case of an entry of optimization measures, the previously mentioned parameters of the calculation are adopted for the respective property. The object designation is supplemented by a designation of the respective optimization measure in order to enable a differentiation of the lines. The original object remains in the calculation.

Investment-linked annuity of the optimization measure (according to [13]): The optimization measures of a property are to be calculated on a matching observation period to maintain comparability.

Consumption savings of the optimization measure: This is to be subtracted from the consumption of the respective medium in the original unit.

2.5. Calculation of measure evaluation

The calculation of the effects of the individual optimization measures is analogous to the calculations described above. In addition to the annuity of the demand-related costs, the annuity of the capital-related costs (= investment) is also taken into account. The annuity of the operation-related costs is not included here.

$$A_{N,j} = A_{N,V,j} + A_{N,K,j} \quad (3)$$

$A_{N,j}$	*Total annuity optimization measure*
$A_{N,V,j}$	*Annuity of the demand-related costs*
$A_{N,K,j}$	*Annuity of capital-linked costs*
j	*Index per optimization measure*

The following parameters of [13] must be chosen sensibly according to the market situation and individual approach.

Tab. 1 - Parameters of the annuity method

variable	meaning
a	Annuity factor
b_i	Present value factors per cost type
r	Price change factor
T	Number of years of the period under review
T_N	Number of years of calculated useful life
q	Interest factor

The new performance indicator of profitability is calculated analogously to the formula of the

calculation of the property comparison according to the formula:

$$PI_{ECO,tot,i} = 1 + \left(\frac{10-1}{A_{N,min} - A_{N,max}}\right) * \left(A_{N,i} - A_{N,max}\right) \quad (4)$$

$PI_{ECO,tot}$	*Performance indicator economic*
$A_{N,i}$	*Total annuity*
$A_{N,min}$	*minimum value of* $A_{N,i}$
$A_{N,max}$	*maximum value of* $A_{N,i}$
i	*Index per property*

2.6. Output of measure evaluation

Performance indicator economic: The included optimization measures for a property in the calculation tool usually lead to an adjusted scale with a new scale range. Measures are economically meaningful if their $PI_{ECO,tot}$ is better than that of the property in its original state. The greater the deviation, the more worthwhile the measure. If $PI_{ECO,tot}$ is lower than that of the property in its original condition, the measure is not recommended from an economic point of view. However, social and ecological aspects can speak for the implementation of this measure.

3. Application example

The method presented in the Research Methods was tested for its effectiveness on the basis of a concrete application.

The basis of the examination is the characteristic data of 220 educational facilities of a municipal real estate operator, who strives for an optimized operational behavior of his real estate.

The focus is on a property selected by the operator. This property was first evaluated for its economic efficiency using the method presented here. After the property evaluation, predefined and elaborated optimization measures were prioritized. The example is based on data of the year 2018.

3.1. Input parameters for property evaluation

Object designation: Each educational institution is given a short designation. The property under consideration within the educational facilities is a vocational college and is designated "BK1".

Comparison parameters: The comparison parameters school type and time of use, ensure the comparability of the selected data.

Through these comparison parameters, the selection of 220 real estate objects was filtered to 14 different vocational colleges.

Media: The media electricity and water heat are considered. The medium heat is divided in the property portfolio into gas, district heating and heat supply by electrical energy. BK1 is supplied by gas as the heat energy carrier.

Price medium p_e (Tab. 2): The unit prices of the media are based on the assumption according to [14] and are shown in Tab. 2.

Consumption medium c_e (Tab. 2): The consumption values of the individual media were recorded by an energy monitoring of the property operator and subjected to a weather and area adjustment. The unit of these values is $\left[\frac{kWh}{m^2}\right]$.

Reference parameters r_d (Tab. 2): The reference parameter net floor area is already integrated in the available data.

The number of students was added as a reference parameter to best represent the use of the property. This results in the following unit:

$$\left[\frac{kWh}{m^2 * a}\right] * \left[\frac{1}{students}\right] = \left[\frac{kWh}{m^2 * students}\right]$$

Tab. 2 - Input parameters for demand-related annuity

variable	meaning	value	unit
p_{gas}	Unit price: gas	0.044	$\frac{€}{kWh * a}$
p_{elec}	Unit price: electricity	0.20	$\frac{€}{kWh * a}$
$p_{wat.}$	Unit price: water	3.9	$\frac{€}{m^3 * a}$
$r_{students}$	Number of students BK1	3,011	-
$c_{gas,BK1}$	Consumption BK1: gas	63	$\frac{kWh}{m^2 * a}$
$c_{elec,BK1}$	Consumption BK1: electricity	8	$\frac{kWh}{m^2 * a}$
$c_{wat,BK1}$	Consumption BK1: water	0.35	$\frac{m^3}{m^2 * a}$

3.2. Calculation of property evaluation

In the following section, the property evaluation described in the methods section is calculated for BK1 as an example. In the first step, the demand-related annuity $A_{N,V,BK1}$ is determined based on formula (1):

$$A_{N,V,BK1} = \frac{\sum_{e=1}^{n} p_e * c_e}{\prod_{d=1}^{n} r_d}$$

$$= 9.206 * 10^{-3} \left[\frac{€}{m^2 * students * a}\right]$$

Using the extrema, the $PI_{ECO,tot}$ for the BK1 is calculated based on formula (2) (shown in Fig. 1).

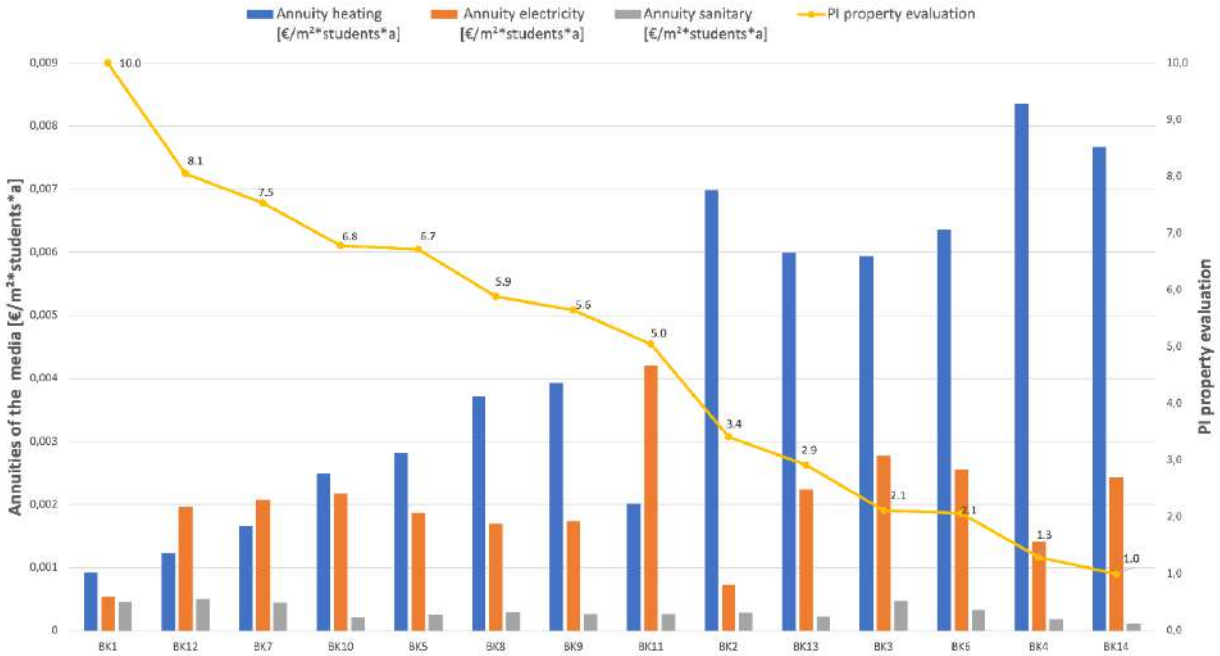

Fig. 1 - Annuities of heating, electricity and sanitary as well as the PI property evaluation for each property

3.3. Output of property evaluation

Performance indicator economic: The calculation of the demand-related annuity is carried out according to formula (1) for all 14 professional colleges considered. By looking at the maximum and minimum annuities, a mapping can be made to a scale of 1-10.

The analysis and the resulting $PI_{ECO,tot,BK1} = 10$ show that BK1 is the most economical vocational college out of all the participating vocational colleges in terms of demand-based efficiency.

Fig. 1 shows the state before the optimization measures were implied. The yellow line in the graph shows the course of the economic demand-based performance indicators of the economic efficiency of all 14 considered professional colleges. In addition, the medium-dependent absolute demand-based annuities are shown as columns. BK11 is striking here, as it has very high electricity costs. The reason for this is unclear due to the lack of detailed information on the installed systems.

The calculation of the medium-dependent annuities enables a detailed consideration and analysis of the demand-related costs, so that comparatively high medium-dependent annuities can be used as a reference point for extended investigations into optimization measures, but are not necessarily indicative of poor economic efficiency.

If the vocational college to be analyzed had been BK14, it would be appropriate to analyze the heating costs because it has a $PI_{ECO,tot,BK14}$ of 1 and a demand-based annuity for the medium heat of approx. $9.206*10^{-4}$ $\left[\frac{€}{m^2*students*a}\right]$, which is one of the highest.

This technical analysis of why medium-dependent demand-based annuities are high or low requires a technical understanding and therefore must be performed by a professional planner.

The evaluation result presented here shows the actual condition of the properties. Due to the dynamic scaling, the evaluation only applies exactly to the 14 vocational colleges analyzed here.

3.4. Input parameters for measure evaluation

Consumption savings of the optimization measure: The optimization measures were developed in advance and took technical aspects into account. On the one hand they arose from the analysis of the property described, and on the other hand from the wishes of the client. These wishes may have been influenced by aspects related to the social or ecological optimization of the property.

Investment-bound annuity of the optimization measure (according to [13]): In order to be able to keep the measures comparable, the period under consideration as well as the calculated useful life of the measure must be set equal. In addition to the new demand-related costs, the capital-related costs are also included in the calculation of the annuity.

The new annuity is made up of the following parameters:

- Period under review
- Service life
- Investment costs
- Medium-dependent consumption savings

The period under consideration was set at 10 years in order to keep the measures comparable with each

other. The remaining calculation parameters are listet in Tab. 3.

Tab. 3 - Parameters for calculating annuities of optimization measures

variable	value	unit
a	0.11	-
b_i	10.25	-
r	3	%
T	10	years
T_N	10	years
q	2	%

Using the parameters and the following investment costs and savings in different media (Tab. 4) the new annuities for choosen measures are calculated. The optimization measures include implementation of daylight control (M1), refactoring of heating curve (M2), optimization of supply air control for comfort (M3), expansion of energy supply through photovoltaics (M4) and hydraulic balancing of heating system (M5).

Tab. 4 - Investments and savings for choosen measures

measure	media	investment [€]	savings [kWh/m²*a]
M1	elec	2500	1,22
M2	gas	230	3,15
M3	-	2560	-
M4	elec	10000	5,39
M5	gas	870	2,05

Fig. 2 shows the converted annuities of the measures, which were multiplied by the area and the number of students. This results in the total costs or savings that the operator can expect from the respective measures in the period under consideration. The presentation of the total costs is intended to make the selected examples appear more comprehensible. In the end, they represent the calculated annuities.

The newly calculated annuity in each case results in the $PI_{ECO,tot,BK1}$.

The measure with the lowest annuity represents the new $PI_{ECO,tot,BK1}$ of ten. The measure with the highest has a $PI_{ECO,tot,BK1}$ of 9.7. The data for the property in its original state remains in the assessment to make the benefits of each measure visible.

In the case of this vocational college, the highest scoring measure is the adjustment of the heating curve (M2) in Fig. 2. The savings are 772€.

3.5. Output of measure evaluation

Performance indicator economic: The $PI_{ECO,tot}$ of the best measure causes the graph to shift. The school in the as-is state becomes a 9.96 from the original ten.

Thus, even though the client already has the best school in comparison, it is shown to the client that there is potential for optimization.

Since only economic considerations are dealt with here, the requirement of this elaboration is to give a reference point whether the investment is economically worthwhile or not. The other advantages of an optimization are not included in the evaluation here. The savings of an optimization measure can be identified by a better PI compared to the original property. In this application example, it follows that any measure that has a higher $PI_{ECO,tot}$ than 9.96 provides savings within the period under consideration. On the one hand, this allows ranking within the measures and relating the measures to other existing properties. On the other hand, it shows in an easily understandable way whether money is saved or not.

Fig. 2 shows the five measures selected. The columns indicate the annuities, the line in the graph the $PI_{ECO,tot,BK1}$. The results of the measure evaluation provide operators, on the one hand, with a benchmark of where their object stands economically and what potential is in it. On the other hand, it specifies which measures make economic sense and which do not. By projecting the annuities onto the performance indicators, no technical understanding of the individual measures is necessary.

Fig. 2 – Savings and new PI for each measure

4. Discussion

The method presented enables the operator of a real estate portfolio to perform an economic performance analysis for each of its properties.

It is divided into a property evaluation and a measure

evaluation. In the property evaluation, the properties are ranked by their annuity (formula (2)) on a dynamic scale. The basis for a comparability of the annuities is formed by the choice of reasonable comparison parameters.

This dynamic scale, which assigns each property a value on a scale from 1 - 10, means that reference values from standards, laws or empirical values are no longer necessary for the analysis of the building performance. Thus, in a real estate portfolio in which all properties already have a good economic performance, there will still be one property that represents the worst with a 1 on the scale created for this purpose. The purpose of this is to provide operators with a customized performance analysis within their property. The urgency of buildings in need of optimization becomes apparent through the ranking.

A high relevance in the real estate evaluation has also the data acquisition. Here, as in section 2.2, care must be taken to ensure that the various data are comparable with each other. Thus, the same boundary conditions must always apply (data quality, weather adjustment, meaningful reference parameters, observation period). The more reliable the data quality and boundary conditions are, the more accurate and meaningful the method is. Nevertheless, the method is only an approximation, which may also be subject to errors. It is based on consumption data only without taking into account further details like the HVAC-system installed.

If the operators have capital available, the evaluation can produce a suggestion as to which property can benefit most from optimization. Consequently, there will consistently be optimization potential within their property, which implies that the operators are constantly incentivized to optimize their facilities economically. The selection of the property to be optimized lies individually with the operator, despite the fact that the property has been evaluated.

The optimization proposals for the property should be prepared by persons with expertise in the respective trades, so that the measure evaluation can then be carried out according to section 2.5. The optimization proposals should only ever be compared with each other for one property. An improvement of the performance indicator always implies a cost saving, which makes the measure economically recommendable. The method then also enables a comparison of the optimization approaches. The performance indicator that generates the largest difference compared to the existing performance is then also the most economical.

This method only considers economic efficiency throughout. In the above example, saving economic resources always implies saving ecological resources. If an interdisciplinary evaluation (economic, ecological and social) of the optimization measures is to take place, a social as well as ecological analysis must be carried out in addition to the evaluation described.

5. Conclusion

In conclusion, this method provides the operator with a tool to evaluate the properties with regard to their economic performance and to identify properties worthy of optimization on the basis of this evaluation. Furthermore, the proposed optimizations for the property can be compared with each other, whereby the economically optimal measure can be filtered out. The property evaluation as well as the measure evaluation should also be understandable for laymen. This is achieved by the dynamic scale from one to ten. The operator does not need a deeper technical understanding for his decision making.

6. References

[1] United Nations Environment programme. 2020 Global status report for buildings and construction – Towards a Zero-emission, Efficient and Resilient Buildings and Construction Sector. Nairobi: 2020. 80p.

[2] Ardente F, Beccali M, Cellura M, Mistretta M. Energy and environmental benefits in public buildings as a result of retrofit actions. Renew Sustain Energy Rev. 2010 Sep 09; 15:460-470. doi: 10.1016/j.rser.2010.09.022.

[3] Kontokosta CE. Modeling the energy retrofit decision in commercial office buildings. Energy Build. 2016 Nov 01; 131:1-20. doi: 10.1016/j.enbuild.2016.08.062.

[4] DIN Deutsches Institut für Normung e.V. Norm DIN 18960. User costs of buildings. Berlin: Beuth Verlag GmbH; November 2020

[5] Madritsch T, Steixner D, Ostermann H, Staudinger R. Operation cost analysis of long-term care facilities. J Facil Manag. 2008 May 02 ; 6(2): 152-170. doi: 10.1108/14725960810872668

[6] Ramesh T, Prakash R, Shukla K. Life Cycle Energy Analysis of a Multifamily Residential House - A Case Study in Indian Context. Open J Energy Effic. 2013 Mar; 2: 34-41. doi: 10.4236/ojee.2013.21006.

[7] VDI Verband Deutscher Ingenieure e.V. Guideline VDI 3807 Part 2. Characteristic consumption values for buildings – Characteristic heating-energy, electrical-energy and water consumption values. Berlin: Beuth Verlag GmbH; Nov 2014.

[8] Timma L, Skudritis R, Blumberga D. Benchmarking Analysis of Energy Consumption in Supermarkets. Energy Procedia. 2016 Mar. 95:435-438. doi: 10.1016/j.egypro.2016.09.056

[9] Seyedzadeh A, Rahimian FP, Oliver S, Rodriguez S, Glesk I. Machine learning modelling for predicting non-domestic buildings energy performance: A model to support deep energy retrofit decision-making. Appl Energy. 2020 Sep 29; 279. doi: 10.1016/j.apenergy.2020.115908

[10] Ortiz J, Casas AF, Salom J, Soriano N, Casas PF. Cost-effective analysis for selecting energy efficiency measures for refurbishment of residentual buildings in Catalonia. Energy Build. 2016 Jun 28; 128: 442-457. doi: 10.1016/j.enbuild.2016.06.059

[11] Karmellos M, Kiprakis A, Mavrotas G. A multi-objective approach for optimal priorization of energy efficiency measures in buildings. Appl Energy. 2015 Feb 01. 139:131-150. doi: 10.1016/j.apenergy.2014.11.023

[12] Niemelä T, Kosonen R, Jokisalo J. Cost-optimal energy performance renovation measures of educational buildings in cold climate. Appl Energy. 2016 Sep 24; 183: 1005-1020. doi: 10.1016/j.apenergy.2016.09.044

[13] VDI Verband Deutscher Ingenieure e.V. Guideline VDI 2067 Part 1. Economic efficiency of building installations – Fundamentals and economic calculation. Berlin: Beuth Verlag GmbH; Sep 2012.

[14] Gebäudewirtschaft der Stadt Köln, Sachgebiet Energiemanagement. Energiebericht 2019. Köln: 2020 Mar. 54p.

Data Statement

The datasets generated during and/or analysed during the current study are not available because they are partially the property of third parties and may not be published but the authors will make every reasonable effort to publish them in near future.

Digital Twin as energy management tool through IoT and BIM data integration

Alice Schweigkofler [a], Orjola Braholli [a], Sylvia Akro [b], Dietmar Siegele [a], Paola Penna [a], Carmen Marcher [a], Lavinia Tagliabue [c], Dominik Matt [d]

[a] Fraunhofer Italia, Via A. Volta 13 A, 39100 Bolzano, Italy, alice.schweigkofler@fraunhofer.it

[b] Dipartimento ABC, Politecnico di Milano, Piazza Leonardo da Vinci, 32, 20133 Milano MI, Italy

[c] Dipartimento di Architettura, Ingegneria delle Costruzioni e Ambiente Costruito, University of Turin, Via G.Verdi, 8, 10124 Torino, Italy

[d] Free University of Bozen-Bolzano, Piazza Università 5, 39100 Bolzano, Italy

Abstract. Energy Management has gained increasing value in construction market. The spread of Building Information Modelling (BIM) as a methodology for the construction processes organization will bring progressively to a digitalized asset management. Taking a step further, the concept of Digital Twin (DT) is being used to integrate building's assets with digital technologies to allow real-time analysis, as well as to provide simulation capabilities. DT is expected to have high impact on facilitating sustainable transition through technological developments, according to the European Green Deal mission. Considering operation and maintenance phase in building lifecycle, one of the main problems is about data management. Energy managers and decision-makers use indeed text and spreadsheets to visualize and interpret data. The most recent software solutions in this field focus mostly on the collection of information in a systematic way and in document and deadlines management. This approach helps operators but makes it difficult to understand the real-time building's performance. Furthermore, the indoor environmental performance in dynamic use conditions is rarely considered in decision processes. Therefore, a more efficient and less error-prone method is needed for the real-time management of heterogeneous data. A new approach which combines BIM and Internet of Things (IoT) technology could create a shared data environment for crossed management energy aspects. Equipping the building with monitoring systems means that a large amount of collectible data needs to be managed. This paper describes an attempt to represent and visualize sensor data in BIM, in a user-friendly way to support complex decisions as a significantly improved alternative compared to the traditional ways. The proposed framework is tested and verified on the case study of a school building within the project "SINCRO". In the first part of the paper the use case, devices, and the proposed BIM-IoT integration workflow are described. In the second part the resulting cloud-based DT is explained together with its functionalities applied to a testing period. Feedbacks of the energy manager are collected to demonstrate how real-time performance information can lead to more responsive building management and improve energy efficiency.

Keywords. Digital Twin, BIM, IoT monitoring, Energy Management, Indoor thermal comfort.
DOI: https://doi.org/10.34641/clima.2022.46

1. Introduction

Real-time energy evaluation and management of a building is the key to achieve efficient and sustainable buildings [1]. Moreover, making available a high quantity of data on energy consumptions and indoor conditions of an existing building can have various positive impacts, i.e. it can drive the choice of energy retrofit interventions [2]. Considering public wellbeing, monitoring the Indoor Environment Quality (IEQ) in real-time is particularly beneficial for health-purposes. Indeed, indoor air pollution has been ranked among the top five environmental risks to public health [3] and from a survey conducted on US consumers, 76% would feel more comfortable entering buildings where IEQ is monitored and known.

Within the entire building lifecycle, the Operation and Maintenance (O&M) phase is the longest period [4] and thus it is also the most expensive phase. Therefore, efficiency and optimization in

Copyright ©2022 by the authors. This conference paper is published under a CC-BY-4.0 license.

information management during building utilization is becoming essential. It more and more helps managers and maintainers to have a clear picture of buildings health. A monitoring system established to check the internal environment can be very helpful and beneficial to ensure that buildings remain in good condition [5]. Moreover, it can be helpful for in-time decision-making or strategy changing that requires real-time data about building performances and energy management [6]. Despite this, at the moment the implementation of digital information management is not widespread [7].

To address this growing need, it is important to provide an appropriate method for sensor data visualization, as it may help building managers and/or users to intuitively understand and work with data faster and easier [2]. Technology such as the Internet of Things (IoT) is increasingly being deployed in the built environment to monitor building performance. Combining IoT with Building Information Modeling (BIM) methodology would make it possible to transform the interaction with the built environment. The integration of BIM with real-time data from the IoT devices result in the creation of Digital Twins (DT). This development is quite in an early stage, but it is already a powerful paradigm for numerous applications to increase construction and operational efficiencies, thanks to improving information availability. According to this, the overall purpose of this research is to integrate and visualize real-time and indoor monitoring sensor data during the building's lifecycle, with a special focus on energy management. The aim is to display a decision-making dashboard of indoor thermal comfort to support complex decisions, in a user-friendly and immediate way. Such a DT is presented as a significantly improved alternative compared to traditional ways for information management in O&M.

The paper is organized as follows. In section 2 it is presented the state of the art in the scientific field. Section 3 exposes the methodology and tools employed to integrate BIM and IoT and data within a unique and replicable workflow of the system. Moreover, a case study is presented. Results in terms of data visualization are presented in Section 4 and conclusions are presented in Section 5 and 6.

2. Background and state of art

During the O&M period of buildings the environment information should be constantly monitored to allow supervisors to take measures, deal with emergencies and improve energy efficiency. Nevertheless, building managers and decision-makers still face the need for solutions that allow to visualize, interpret, and utilize data [8]. They currently still use text or spreadsheets, which make it difficult to understand and to track the real-time building's performance, as well as this is a prone to errors way of work. [9].

Therefore a faster, more efficient and less error-prone method is needed for the real-time visualization and analysis of collected data. There should be a monitoring system, which can alert people under certain circumstances [5]. Our study shows how BIM-sensor integration can lead to more responsive building management and operation by making indoor condition data tangible and accessible for property managers, owners, and occupants within a user-friendly digital system.

2.1 BIM in Operation and Maintenance

Many studies have tried to review the status quo of BIM applications in building operation phase. Most studies were related to the design and construction stages, while few concern building maintenance, retrofitting, and demolition stages [10]. Generally, recent analyses [11] evaluated and summarized that BIM for O&M phase is still in its early stage. In particular, the use of BIM only as a three-dimensional model has no added value in the O&M phase and the need for interoperability, together with the lack of open systems, discourages its use. Moreover, the information contained in BIM models is static, while building maintenance requires dynamic data which include real time information. In the usual practice, a large amount of data can be provided, but these are not updated during the building life cycle. This lack of data and information in as-built digital models considerably limits the potential of BIM in building management [12]. Despite this, BIM is an important factor in improving decision making for buildings throughout their life cycle. For example, in [8] an exhaustive list of specific BIM functionalities in O&M is provided. It includes controlling lifecycle cost data and environmental data, locating building components effectively, facilitating retrieval of real time integrated building, improving maintainability studies and space management.

2.2 Digital Twin as BIM and IoT integration

BIM-IoT integration takes advantage of the geometric and parametric properties of BIM models and of the real-time streaming of environmental data (e.g., temperature, humidity, etc.) collected by IoT sensors, to create a DT for visualization monitoring data in real-time. This is a new approach, that integrates BIM data with sensors to create a shared database for improving the building's energy and indoor environmental performance, while reducing operational costs [9]. In this way, BIM technology can effectively cope with the complexity of the O&M of buildings, if it is coupled with monitoring data. In a BIM based building monitoring system, data can be classified into two categories: environmental data and BIM data [5]. The monitoring data are a kind of timeseries data produced by working sensors and the BIM data consists of a variety of information about building components. Indeed, the combination of BIM and IoT technology provides a comprehensive view of the building status and

improves the efficiency of information use [5]. However, research addressing the integration of these two technologies is still very limited and has focused exclusively on the automatic transmission of sensor information to BIM models [13], for example using Dynamo to accept sensor data as input and automatically redraw visualized information in BIM.

A DT has much more potential, since it represents the digital replica of the physical world, where components and processes can be aligned in real-time to achieve greater efficiency and generate a decision-making action. In recent times the application of DT has gained massive popularity in construction industry, while it is already utilized in manufacturing and Product Lifecycle Management. Its idea was already introduced three decades ago [14]. The *buildingSMART International* considers that the concept of DT can be achieved through alignment with common open digital solutions and standards [15].

Most of the definitions agreed on describing DT as the bidirectional data flow in real-time between physical and digital world [14]. In fact, DT is the digital copy of a physical object, and its main elements are the physical space, the digital space, and the bidirectional data flow between them. The evolving profile of a DT achieved from cumulative, real-time data helps to provide important better-decision-making insights on system performance, for example il [16] it has been demonstrated that the improved data management helps in finding some implicit logics among management tasks. What a DT requires is an information system to store building data. This is based on dynamic data, acquired real-time from the building, and on the information of the building itself, which is stored in the model [17].

2.3 Data visualization for energy management

Choosing an appropriate method for sensor data visualization is important as it may help users to intuitively understand and work with data faster and easier [2]. Several studies have been conducted in this direction. A prototype framework for the BIM and IoT-based integration for providing a comprehensive view of the general status of buildings was proposed in [5]. In [2] a tool that can provide building managers with real-time data and information about the energy consumption and the indoor conditions of buildings, but also allows for viewing of the historical sensor data was developed. Machado et al. A novel approach has been proposed in [18] that exploits IoT sensors using Wi-Fi, to evaluate the energy behavior of individuals, which can be applied to identify inefficiencies in individual´s actions and responding to them. In [19] an IoT framework to estimate indoor conditions and occupancy rates, which provided hints for energy-saving strategy by further understanding the indoor condition patterns was proposed. In further experiments, using a cloud-based service, building supervisors can remotely monitor the thermal condition of fan coils and can easily find the location of the faulty component on the building 3D model by room ID or room name [20].

Consequently, all the recent experimentations show that the usefulness of DT in the built environment can significantly increase through the automatic decision making and feedback loops by enabling real-time automated control. It is clear, that this integration method takes advantage of the geometric and parametric properties of BIM models and the real-time streaming of environmental data collected by IoT sensors to create a DT for visualization monitoring data in real-time. However, despite the emerging new data capturing technologies and advanced modelling systems, the process of DT modelling for existing buildings still lacks a systematic framework [21].

3. Methodology

Our research proposes a scalable and flexible workflow for creating a cloud-based and accessible solution, that enables BIM-IoT integration in a DT. A case study was used to test the framework implementation. The developed methodology for integrating the monitoring data with BIM was tested on an existing school building located in the South Tyrol province of Northern Italy. The building has a total area of approximative 1450 sqm, two floors and a vast number of spaces for different uses like teaching classes, playing areas, kitchen and offices.

3.1 Energy monitoring

For this study, there were two types of implementation domains: IEQ and indoor thermal comfort. IEQ refers to the quality of a building's environment relating to the health and wellbeing of users. IEQ parameters were measured such as temperature, humidity, CO_2 concentration, Total Volatile Organic Compound Concentration (TVOC) and illumination. Indoor thermal comfort is defined as "that condition of mind that expresses satisfaction with the thermal environment" [23]. This condition can be expressed by the Predicted Mean Vote (PMV) and the Predicted Percentage of Dissatisfied (PPD) indices, which are the most widely used thermal model for indoor environments [22], adopted by many international standards, such as ISO 7730, ASHRAE 55 [23].

Multiple market-available sensor devices were deployed in the indoor spaces of the school building to perform environmental data collection. The IEQ parameters (temperature, humidity, CO_2 concentration, TVOC and illumination) were measured for each room. Data are gathering each 10 minutes. The indoor thermal comfort parameters (PMV and PPD) are calculated for each classroom i.e., for each room for which advanced monitoring is planned. The sensor fleet is comprised of four

sensor types and of twenty-four instances placed in total in the building.

Figure 1 shows where the sensors are located on the ground floor and how the different areas are monitored. Except for one of the classrooms, where five sensors are installed measuring all the parameters mentioned before, all the classes have been equipped with a sensor which is integrated with an additional display. This is classified as advanced monitoring. All the other rooms i.e., two offices, one kitchen and the corridors are classified under basic monitoring, where one sensor is installed without a display. Service areas were not monitored. The first floor is composed about only one class, where advanced monitoring is performed.

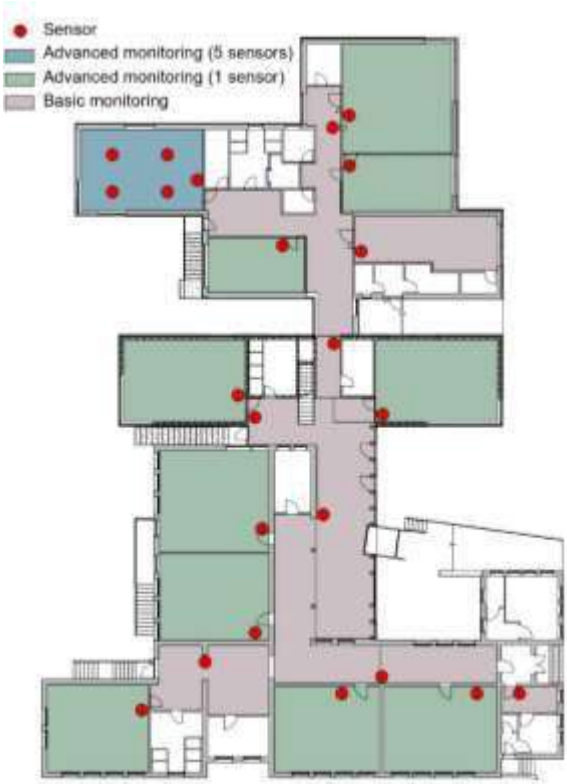

Fig. 1 – Monitoring system and sensor deployment on the ground floor.

3.2 BIM model

The BIM model of the school building is built within a BIM environment using all the information from the existing documentation. Revit 2020 software was used to develop the model throughout the whole modelling process. Figure 2 shows the general view of the BIM model. The level of information needed is such as to provide an accurate geometrical representation of the building's existing state and accurate positioning of the sensor families in the building. The geometrical information is represented mainly on a generic level with some elements represented in a more detailed level like sensors, walls and windows. The advantage of the BIM environment is that it provides the possibility to integrate different types of information in a single model. E.g., the sensor family contains information regarding the identification and environmental parameters that are mapped and connected to the real-time data in the DT.

Fig. 2 – Overview of the school building in the BIM model.

3.3 Integration of sensors in the BIM model

A unique family was created as a generic model to represent all the sensor devices. This sensor family was placed in the BIM model representing the real position of the asset in the physical building, as shown in Figure 3. The different sensor devices installed in the school building were created as types under the sensor family with varying type and instance properties. Two sets of parameters were created for the sensor family and grouped under Identity Data and Green Building Properties. The Identity Data is an existing section in the Type Properties window that contains identification parameters of the family type. In this case it contains parameters for the name, location and activation state of the sensor. Green Building Properties is a created section in the Type Properties Revit window that contains the environmental parameters measured by the sensors. Each virtual sensor placed in the model is defined as a unique alphanumeric ID which derives directly and corresponds to the location where it is placed, i.e., the ID contains the building zone, floor number and room number and it is automatically generated. In this way the sensors are correctly mapped in a unique way.

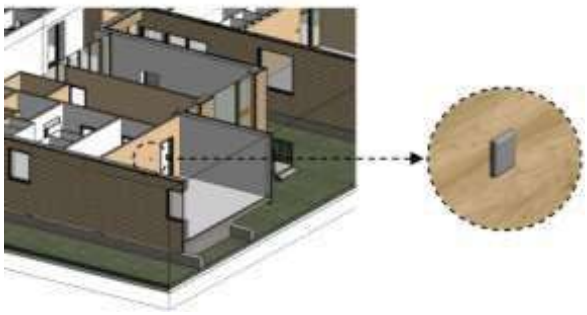

Fig. 3 - The sensor family.

The Green Building Properties represent all the environmental parameters that the sensor is measuring inside the building (Figure 4). Each of these parameters is mapped and connected within the DT with the respective sensor values.

Fig. 4 - Sensor type example ELSYS ERS-CO2.

3.4 BIM-DT workflow

This paragraph describes the detailed application of the proposed workflow from the data collection process to the output visualization in the DT. Figure 5 shows the workflow schema made up of four main layers starting from the physical asset to the digital asset. The four phases from data acquisition to data analysis are described below.

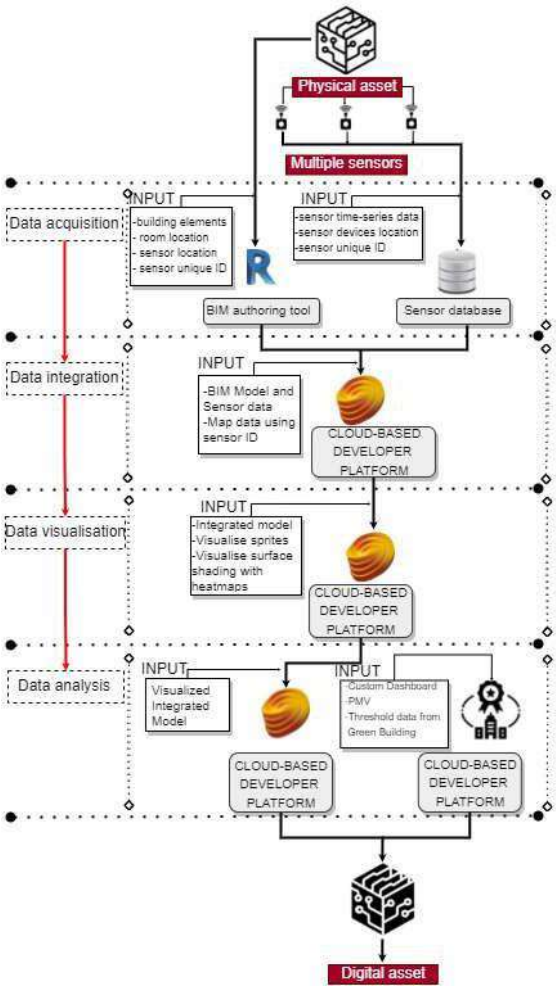

Fig. 5 - BIM-DT workflow process of implementation.

The first phase is about "data acquisition". The input data for the DT are obtained from two sources. The first source is the BIM model of the school building from which are obtained the geometrical information, the location of the virtual sensors accurately positioned in the model, their unique ID and their Green Building Parameters. The second source is the indoor environmental data retrieved from the IoT sensors in the building. The real-time data obtained from the sensors are stored using an InfluxDB database, a type of database developed specifically for storing time-series data.

The second phase is "data integration" and consists of matching the properties of the sensor data parameters with the sensor family parameters, previously created in the BIM model. A dynamic data integration process between BIM and IoT has been created, mapping and connecting the sensor data from the InfluxDB database to the sensor family in a cloud-based integrated model, using Autodesk Forge Platform. This is a cloud-based platform and provides Application Programming Interface (API) services that enables developing customized and scalable solutions to solve design, engineering, and manufacturing challenges. Forge APIs is partially and temporary available in open-source mode. It provides the necessary and sufficient services to create the customized application [20]. Most of the process to set up the DT was done in Visual Studio Code.

In the data visualization phase Autodesk Forge Platform is used to visualize the outputs that combine the BIM model and its data to the environmental data retrieved from the sensors. This is where the user interacts with the application. The platform itself is web-based and can be use in any web browser. It is obtained in this way, the visualization of contextual and spatial information in real-time. The resulting dashboard is further explained in section 4.

In the data analysis phase, the indoor environmental data retrieved from the IoT sensors are analyzed and compared with environmental data thresholds and ideal indoor thermal comfort conditions. Comfortable values have been defined according to Table 1 in concordance with green building benchmark standards.

Tab. 1 - Comfortable values for monitored parameters.

Temperature	Winter between 20 – 25°C, while summer between 23 – 26°C
Humidity	40 – 70% [24]
CO2	400 – 1000 ppm (CEN, EN 13779)
TVOC	300 – 500 ppb [27]
Illumination	100 – 500 lux (UNI EN

	12464:1:2004)
PMV	Between -0.5 and 0.5 (ISO 7730)
PPD	Below 10%

4. Results

The resulting application is a cloud-based dashboard where the user can interact with the DT of the school building. It is possible to deploy this DT to be viewed on the browser for easy accessibility from anywhere. The system is active since February 2020 and the project is still ongoing. In Figure 6 the dashboard is shown, and the functionalities are explained in this section.

Fig. 6 – Digital Twin and surface shading map.

BIM model: the BIM model can easily be explored and interrogated through the toolbar, including the parameters of single objects, such as walls, windows, doors, etc. The model is sectioned to allow internal view of the building.

Sensor visualization: grey dots as two-dimensional objects are overlaid onto the model to highlight and indicate sensors. This was done by using the location of the device family in the BIM model. A developed function checks the model and finds elements with the unique alphanumeric ID. It is possible to click on the dots to visualize every actual measured values. In the right side of the viewer the sensor list is placed, where every sensor can be found, and graphs on historic values can be checked.

Color map: every classroom is characterized by a colored surface shading, which is a graphical representation of the values measured in each room. Every monitored parameter (temperature, humidity, CO_2, TVOC and illumination) can be chosen from a drop-down menu, to be visualized in the DT. The calculated thermal comfort level (PMV and PPV) is visualized in the DT in the same way. To generate this map, based on the position and size of each classroom, a bounding box is obtained, and sensors have been linked to them. This step can be done automatically since room information and device position are available from the BIM model.

Gradient: the color assigned to the surface shading refers to the output of data analysis. The visualized color depends on minimum range and maximum range value and varies between a multi-colored gradient for each monitored parameter. The information about the device type is used together with the specific gradient for creating the surface shading of the classrooms. Moreover, to make sense of this data for the user, a legend has been added to compare measured values and map colors to green building benchmark standards.

Data: through the time slider placed in the upper part of the viewer, it is possible to not only display the real-time data from the building, but also to visualize data of the past. To add the sensor data from the InfluxDB in real-time, this is done creating a custom data adapter and gateway. It is possible to use a time-series data source for the visualization of historic data over a specific timeframe. This option has been explored using a CSV file for a timeframe from June to July to analyze in detail the summer season.

5. Discussion

In order to compare the proposed DT as new representation of data with the actual situation, the system has been presented to the supervisors and energy manager of the school building. Thanks to the received feedback it has been confirmed that the color map for the intuitive interpretation of data makes the DT more user-friendly. The end-user can easily evaluate the thermal comfort level in real-

time for decision making. Moreover, the proposed visualization dashboard can be used and understood by anyone with a less technical background. It allows users to interpret values immediately rather than the usual way, such as using bar diagrams, tables, and graphs. Moreover, this kind of representation induces user commitment and increases user engagement and participation in taking actions for comfort improvement. Since the energy manager is not usually the BIM model author and does not have access to BIM authoring software, it has been appreciated that the application is easily accessible through a browser. The proposed workflow is cloud-based and in addition it can integrate BIM models from open non-proprietary file formats such as IFC, gbXML, glTF as well as other industry proprietary file formats. However, the selected case study is a medium-small sized building and there are no historical data available about energy management of the building for a quantitative comparison after adoption of the system. Neither a BIM model of the building was utilized, and the detection of energetic anomalies and discomfort was previously not carried out. After a certain period of use of the DT it will be possible to estimate the usefulness of the system on the basis of the number of anomalies detected, with the aim to perform an evaluation of application of the technology.

A limitation in the proposed approach is that a small number of sensors were used to test the proposed framework in this study. As the system evolves and the amount of data increases, it will be necessary to implement a data analysis module to manage and detect data anomalies, possibly based on artificial intelligence. Moreover, only indoor environmental monitoring has been performed. This could be extended integrating information about building energy simulation and/or the monitoring of building facilities for evaluating energy consumptions. To view such kind of information could have high impact in improving energy manager´s work. For this study, it is planned to monitor the heating system, that is connected to district heating system, partially with traditional radiators and partially with underfloor heating. Except a mechanical ventilation system located only in four classrooms, the building is not equipped with other kind of plants or automation system. Further, the BIM model could be enriched with energy parameters of components. Through a cross-analysis of the proposed data collection the DT could suggest optimized management strategies and indicate limits beyond which renovation interventions would be suitable. Further research and improvement on the workflow implementation could focus on predictions and on automatic control feedbacks. Predictions can be performed through advanced data analysis to provide better insights and evaluation, allowing for predictive energy strategies. On the other hand, defining an alert system to notify unacceptable threshold of monitored parameters, could lead to quicker response and fast reactions.

6. Conclusion

The implemented framework integrates the indoor environment data collected by multiple sensors with a BIM-based model to automatically combine monitored data. The followed workflow is based on a four-layer methodology, which are data acquisition, data integration, data visualization and data analysis and can be adopted for further monitoring system implementation and extension. The real-time visualization of indoor environment conditions provides a better overview of the building status to supervisors. As a result, it plays an important role in increasing commitment in taking improvement actions for indoor comfort and in engaging users to accept building interventions. It has been confirmed by building energy supervisors, that BIM-IoT integration to apply the DT paradigm in the built environment improves the user's experience and better decision-making opportunity and provides useful information to monitor and maintain the building performance during the operational phase, which is the more expensive phase in the whole building lifecycle. To promote openness and interoperability between disciplines and different BIM authoring platforms used in the building industry, Autodesk Forge was used as cloud-based developer's platform to create the DT based on its capability to integrate models from open non-proprietary file formats as well as other industry proprietary file formats to visualize indoor monitoring data. Despite the acquired benefits, the application of the DT paradigm in the construction industry has still enormous potential. An advancement in research in this field, could lead to DTs that support automatic feedback and perform automatic control system in buildings, allowing to automatic actions on built environment according to specific objectives and energy strategies.

7. Acknowledgement

This paper has been supported by funding from the European Regional Development Fund ERDF 2014-2020 Südtirol/Alto Adige, in the project SINCRO - Sensible INteractive ContROl system for smarter buildings 1141 (CUP: B54E20002030001). The authors would like to thank the school building supervisors as well as the building users for their contribution and participation in this project.

8. References

[1] Deng, M., Menassa, C. C., & Kamat, V. R. (2021). From BIM to digital twins: A systematic review of the evolution of intelligent building representations in the AEC-FM industry. Journal of Information Technology in Construction, 26, 58–83 doi.org/10.36680/J.ITCON.2021.005

[2] Desogus, G., Quaquero, E., Rubiu, G., Gatto, G., & Perra, C. (2021). Bim and iot sensors integration: A framework for consumption and indoor conditions data monitoring of existing buildings.

Sustainability 13(8) doi:10.3390/su13084496

[3] Sun S., et al. Indoor Air-Quality Data-Monitoring System: Long-Term Monitoring Benefits. Sensors (2019). 19, 4157 doi: 10.3390/S19194157

[4] Peng, Y. et al. (2017). A hybrid data mining approach on BIM-based building operation and maintenance', Building and Environment, 126(October), pp. 483–495 doi: 10.1016/j.buildenv.2017.09.030

[5] Kang K., Lin J. and Zhang J. BIM- and IoT-based monitoring framework for building performance management. 2018; Journal of Structural Integrity and Maintenance, 3(4), 254–261 doi: 10.1080/24705314.2018.1536318

[6] Xu, X., Ma, L. and Ding, L. (2014) 'A Framework for BIM-Enabled Life-Cycle Information Management of Construction Project':, https://doi.org/10.5772/58445, 11(1). doi: 10.5772/58445.

[7] Parsanezhad P. A Lifecycle Approach towards Building Information Management: Technical and procedural implications for the facility management and operations sector. Stockholm; (2015)

[8] Guzman, G., & Ulloa, W. (2020). BIM application in the operation and maintenance management of a sports infrastructure. IGLC 28 - 28th Annual Conference of the International Group for Lean Construction 2020, July, 949–960. Doi: org/10.24928/2020/0015

[9] Kazado, D., Kavgic, M. and Eskicioglu, R. (2019) 'Integrating building information modeling (BIM) and sensor technology for facility management', Journal of Information Technology in Construction, 24(August), pp. 440–458. doi: 10.36680/j.itcon.2019.023.

[10] Dixit Manish, K., V. Venkatraj, M. Ostadalimakhmalbaf, F. Pariafsai and S. Lavy (2019). Integration of facility management and building information modeling (BIM): A review of key issues and challenges. 37(7/8): 455-483.

[11] Gao, X. and P. Pishdad-Bozorgi (2019). BIM-enabled facilities operation and maintenance: A review. Advanced Engineering Informatics.

[12] Mannino, A., & Dejaco, M. C. (2021). Building Information Modelling and Internet of Things Integration for Facility Management—Literature Review and Future Needs. Applied Sciences, 11(7), 3062 | 10.3390/app11073062

[13] Chang, K. M., Dzeng, R. J., & Wu, Y. J. (2018). An automated IoT visualization BIM platform for decision support in facilities management. Applied Sciences (Switzerland), 8(7). Doi: org/10.3390/app8071086

[14] Singh, M. et al. (2021) 'Digital twin: Origin to future', Applied System Innovation, 4(2), pp. 1–19. Doi: 10.3390/asi4020036.

[15] buildingSMART et al. (2020) 'Enabling an Ecosystem of Digital Twins', Enabling an Ecosystem of Digital Twins, p. 8.

[16] Parrott, A. and Warshaw, L. (2017) 'Industry 4.0 and the digital twin', Deloitte University Press, pp. 1–17

[17] Tagliabue, L. C., Re Cecconi, F., Rinaldi, S., & Ciribini, A. L. C. (2021). Data driven indoor air quality prediction in educational facilities based on IoT network. Energy and Buildings, 236, 110782doi: org/10.1016/j.enbuild.2021.110782

[18] Rafsanjani, H. N. and A. Ghahramani (2020). "Towards utilizing internet of things (IoT) devices for understanding individual occupants' energy usage of personal and shared appliances in office buildings." Journal of Building Engineering 27: 100948.

[19] Rinaldi, S., A. Flammini, L. C. Tagliabue and A. L. C. Ciribini (2019). "An IoT framework for the assessment of indoor conditions and estimation of occupancy rates: Results from a real case study." ACTA IMEKO 8(2): 70-79.

[20] Villa, V., Naticchia, B., Bruno, G., Aliev, K., Piantanida, P., & Antonelli, D. (2021). Iot open-source architecture for the maintenance of building facilities. Applied Sciences (Switzerland), 11(12). Doi: org/10.3390/app11125374

[21] Lu, Q.; Chen, L.; Li, S.; Pitt, M. Semi-automatic geometric digital twinning for existing buildings based on images and CAD drawings. Autom. Constr. (2020), 115, 103183

[22] Fanger, P. O. (1970). Thermal comfort. Analysis and applications in environmental engineering. Thermal comfort. Analysis and applications in environmental engineering.

[23] Zahid, H., Elmansoury, O. and Yaagoubi, R. (2021) Dynamic Predicted Mean Vote: An IoT-BIM integrated approach for indoor thermal comfort optimization. Automation in Construction, 129, p. 103805. doi: 10.1016/j.autcon.2021.103805.

[24] Mataloto, B. et al. (2021) 3D IoT System for Environmental and Energy Consumption Monitoring System. Sustainability 2021, Vol. 13, Page 1495, 13(3), p. 1495. doi: 10.3390/SU13031495.

Improving the Calibration on Building Stock Level method by Comparing objective functions and optimization algorithms

Paula van den Brom [a], Samuel Smets [b], Laure Itard [c]

[a] Faculty of Architecture and the Built Environment, Delft University of Technology, Delft, the Netherlands, P.I.vandenBrom@tudelft.nl

[b] Faculty of Architecture and the Built Environment, Delft University of Technology, Delft, the Netherlands, L.C.M.Itard@tudelft.nl

[c] Faculty of Architecture and the Built Environment, Delft University of Technology, Delft, the Netherlands, S.J.Smets@tudelft.nl

Abstract. Many researchers have indicated the energy performance gap (difference between actual and predicted energy used in buildings), not only on an individual building level, but also on a building stock level. For policy makers it is important that predictions are correct on an building stock level to make them a useful tool to predict the effect of their proposed energy saving policies. Often not all input parameters for building energy simulations are known (e.g. insulation rates are often only possible to determine with destructive inspection or extensive measurements), therefore assumptions are made (e.g. assumptions for insulation rates are often made based on construction year). It is expected that a large part of the energy performance gap on building stock level are caused by incorrect assumptions of the unknown parameters in the building simulations. Previous research has shown that automated calibration of the assumptions on building stock level seems a promising method to reduce the energy performance gap and therewith make building energy simulations on building stock level a more reliable tool for policy makers. The previous research about calibration on building stock level was a proof of concept and still needs some improvements before it can be applied in practice. One of the aspects to improve the method is to determine the most suitable objective function and the most suitable optimization algorithm. In this paper we compare different objective functions (e.g. Root Mean Square Error, Mean Absolute Error, Sum of Absolute Errors). Next to that we compare different optimization algorithms (e.g. Genetic Algorithm, Particle Swarm and simulated Annealing Algorithm). For the comparison of the objective functions and the algorithms the former Dutch calculation method to determine the energy label in dwellings is used, in combination with the SHAERE database and data from the Dutch Statistics. The SHAERE database contains all input information on individual dwelling level to calculate the energy label of a dwelling of almost 2 million dwellings. The Dutch Statistics database contains the individual annual energy use of all dwelling of the Netherlands and can be linked to the SHAERE database.

Keywords. Energy Performance Gap, Calibration on building stock level, Optimization algorithms, measured data, Energy performance
DOI: https://doi.org/10.34641/clima.2022.420

1. Introduction

Many researchers have indicated the energy performance gap (difference between actual and predicted energy used in buildings), not only on an individual building level, but also on a building stock level. For policy makers it is important that predictions are accurate on an building stock level to make them a useful tool to predict the effect of their proposed energy saving policies. Often not all input parameters for building energy simulations are known (e.g. insulation rates are often only possible to determine with destructive inspection or extensive measurements), therefore assumptions are made (e.g. assumptions for insulation rates are often made based on construction year). It is expected that a large portion of the energy performance gap on building stock level are caused by incorrect assumptions of the unknown parameters in the building simulations. Previous research has shown that automated calibration of the assumptions on building stock level seems a promising method to reduce the energy performance gap and therewith make building energy simulations

Copyright ©2022 by the authors. This conference paper is published under a CC-BY-4.0 license.

on building stock level a more reliable tool for policy makers.

The previous research about calibration on building stock level was a proof of concept and still requires some improvements before it can be applied in practice. One of the aspects to improve the method is to determine the most suitable objective function and the most suitable optimization algorithm. In this paper we compare different objective functions (e.g. Root Mean Square Error, Mean Absolute Error, Sum of Absolute Errors). Next to that we compare different optimization algorithms (e.g. Genetic Algorithm, Particle Swarm and simulated Annealing Algorithm). For the comparison of the objective functions and the algorithms the former Dutch calculation method to determine the energy label in dwellings is used, in combination with the SHAERE database and data from the Dutch Statistics. The SHAERE database contains all input information on individual dwelling level to calculate the energy label of a dwelling of almost 2 million dwellings. The Dutch Statistics database contains the individual annual energy use of all dwelling of the Netherlands and can be linked to the SHAERE database.

This paper will first introduce the Energy performance gap (section 2). After that the calibration on building stock level will be explained further (section 3). In section 4 the research methods are explained, followed by the results in section 5. Finally the results are discussed in section 6 and conclusion are drawn in section 7.

2. The Energy Peformance Gap

2.1 The Energy performance gap

Building energy simulation models are widely used to estimate the energy demand of a building. In Europe the EPBD (Energy Performance of Buildings Directive) demands all European countries to have a system that informs potential buyers and tenants of buildings about the energy performance of buildings. This is often done by an Energy Performance Certificate (or in for example the Netherlands also called Energy Label). The method used to calculate an Energy Performance Certificate is different per country but has to fulfil at least some minimal requirements as set by the European Union. Also important to mention is that the EPBD calculations use a standardized building use to make the results comparable. This makes that these calculation results are often not a realistic reflection of actual energy use in buildings, because all buildings are used differently. This means that there is a gap between actual and calculated energy use. However the gap is not only there on individual building level, but also on building stock level. This implies that there is a more structural problem. The gap between actual and calculated energy use in a building is called the Energy Performance Gap (EPG) and occurs on individual but also on building stock level.

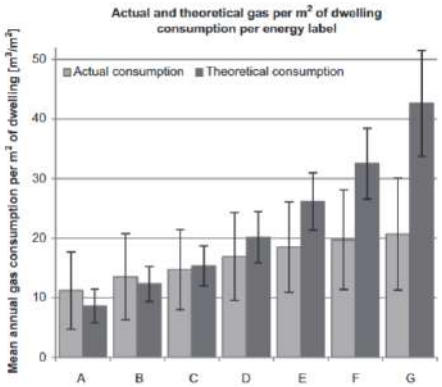

Fig. 0 – The energy performance gap source:[1]

2.2 National and international context

One of the first studies presented on the EPG on building stock level was presented based on Dutch data. Due to the strong increase on data availability also many other countries have found an EPG on building stock level e.g. Portugal [2], Switzerland [3, 4], Denmark [5], Ireland [6], United Kingdom [7], France [8], Germany [7]. This indicates that the EPG on building stock level is not just caused by the method used in the Netherlands, but there is a more structural cause of this gap. This is an issue because the Energy Performance Certificates (or Energy Labels) are increasingly used to develop Energy saving policies and to determine subsidies for Building Energy Renovation measures.

2.3 Causes of the Energy Performance Gap

The past years many researchers have studied the EPG and potential explanation of the EPG. Some of the explanations are:

1. Balance detail level simulation model and reliability of input parameters: If a simulation model is very detailed also many input parameters are required. The more input parameters are required the higher the probability that mistakes are made or assumptions have to be made because the input parameters are not known.

2. Occupant behaviour: on an individual level the occupant behaviour plays an important role. Every occupant uses her/his house differently. However we see also a gap on building stock level which might indicate that the assumptions we make for occupant behaviour (e.g. indoor temperature, ventilation rates) are not a realistic reflection of reality.

3. Mistakes in construction and/or installation process. In building energy simulation models we often assume that no construction or installation failures are present. However if something is not constructed properly or installed properly this could cause a difference between simulation and reality.

4. Difference in construction drawings and execution. Often construction drawings are used to make building energy simulation. If there is a difference

between the drawing and the real building this could cause a gap

5. Measurements are often considered as the solution for the energy performance gap. However if equipment is not calibrated or wrongly placed this could also provide wrong input.

3. Calibration on building stock level

Based on the previously presented findings an automatic calibration procedure on building stock level was developed aiming to reduce the EPG on building stock level. In this section the principle of the method is explained briefly. For a more detailed description of the method we refer to[9].
In section 2 we mentioned that many assumptions are made in Energy performance calculations which could be a cause of the EPG on a building stock level. The automated calibration method on building stock level aims to optimize the assumptions in such a way that the EPG will be reduced. The method makes use of existing data to optimize the assumptions. It is therefore only possible to execute this method if a representative dataset of buildings with actual energy use data is available including the input data for the energy calculation. Of which a significant part of the input should be measured and not be based on assumptions (we assume 30%, but more research should be done to determine the minimum required).

The method is based on a traditional calibration method. In a traditional calibration method the energy demand would be calculated and the unknown (assumed parameters) would be changed every optimization try until the optimal result is found (smallest gap between theoretical and actual energy use), see figure 1. Unfortunately this method won't be sufficient because the results will only be applicable for that individual building on which the occupant plays a very significant role. However, we have seen in the previous section that occupant behaviour should be averaged out if we look at the energy demand on a building stock level. Therefore the method suggest to optimize multiple buildings at the same time to find the smallest EPG on a building stock level. Since part of the buildings don't have assumed values but 'real' values the optimization could reduce the risk of assumed values 'compensating' for each other and therefore increase the probability of finding the 'real' assumed value. The results in the 'proof of concept study' have shown that this method has the potential to reduce the EPG significantly [9].
The parameters that are optimized are (see also appendix):

1. Rc-values (per construction period)
2. Air change rate ventilation
3. Indoor temperature settings
4. Domestic hot water consumption
5. Efficiency of heating system

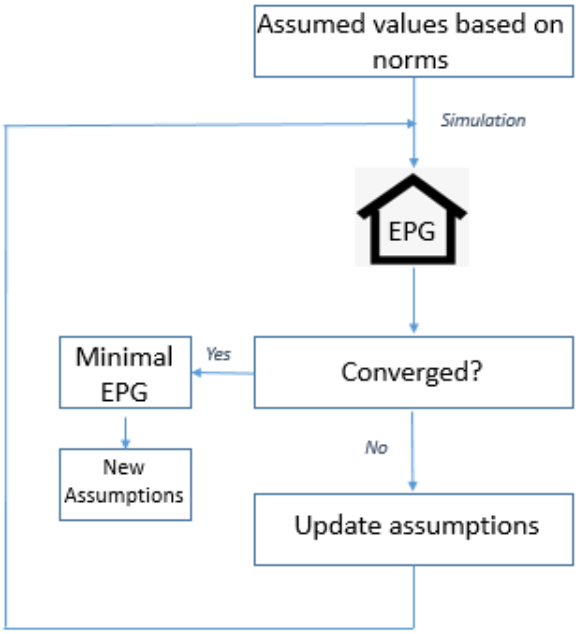

Fig. 1 – Calibration procedure

4. Method

This paper is based on the proof of concept method explained in section 3 and [9]. As written before the method is based on optimization. One of the remaining questions of the proof of concept paper was to determine which optimization method is the most suitable and which objective function is most suitable for this purpose. The three optimization algorithms that are applied are: Genetic Algorithm, Particle swarm optimization and Simulated Annealing. In this paper we compare also compare different objective functions (e.g. Root Mean Square Error, Mean Absolute Error, Sum of Absolute Errors). In this section we describe the different optimization algorithms, different objective functions and the data we use for the case study.

4.1 Optimization algorithms

There are many optimization algorithms, and therefore it is important to explore the optimization algorithms out there and make a selection of suitable algorithms for the problem at hand. The most reliable optimization algorithm would be to simulate all possible values for all parameters (brute-force method) [10]. However this method is practical often not feasible due to the high computational power that is required. Because the optimization problem is a non-linear and non-convex problem a global optimization algorithm is required (fig 2) and special attention should be paid to the barrier settings op the optimization. Figure 3 shows an overview of several optimization algorithms.

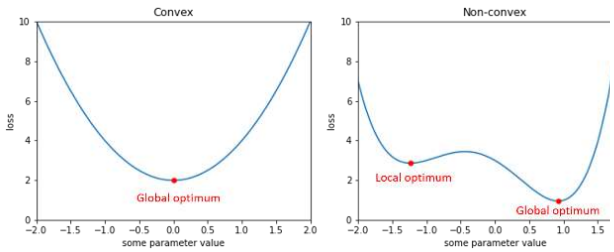

Fig. 2 - Examples of a convex and a non-convex problem. A non-convex problem has multiple sub-optima, of which the one with the lowest objective function loss (which is the objective function evaluation) is called the global optimum and the others local optima. (source: Thesis Samuel Smets)

The three algorithms indicated in orange (Simulated Annealing , Genetic Algorithm and Particle Swarm Optimization) are used for this paper. Only three algorithms are chosen due to time restrictions.

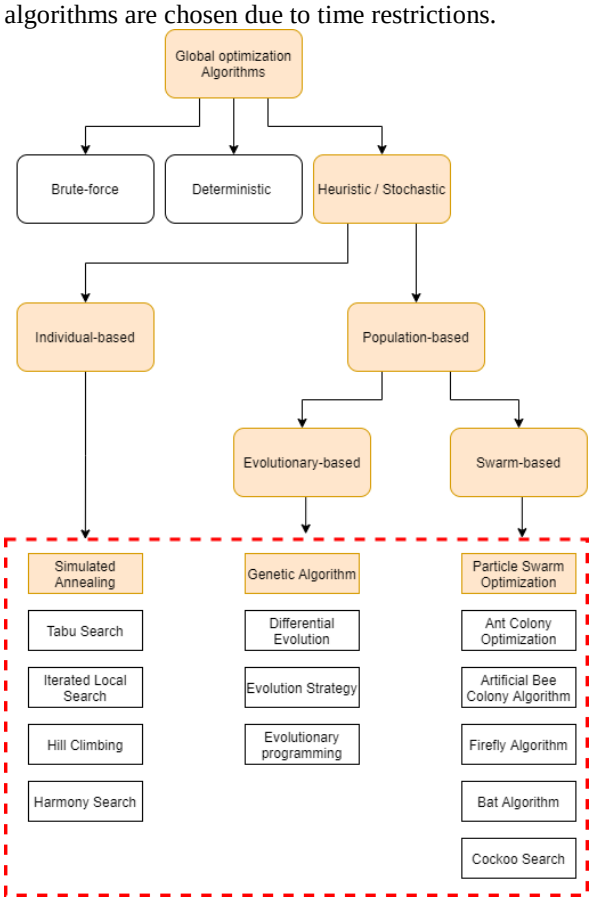

Fig. 3 - Overview of the most well-known global optimization algorithms. The ones indicated in orange are used in this project and further explained in the literature review. (source: Thesis Samuel Smets)

Figure 3 shows that the three chosen optimization algorithms are all stochastic optimization algorithms. Stochastic optimization algorithms have the advantage of being easy implementable and have better potential for complex problems compared to deterministic algorithms, they are also relatively fast in terms of function evaluation [11].
The first algorithm which will be applied is Simulated annealing. This is an individual-based algorithm. The advantage of individual-based algorithms is the lower number of computations per iteration, and therefore it usually has lower computation time until convergence. The disadvantage is that it is more prone to end up in local minima compared to population-based algorithms. Next to that, population-based algorithms usually explore the search space better, because multiple solution vectors are searching through the parameter space simultaneously [12].

Simulated Annealing (SA) is a global optimization algorithm that is inspired by the principles of the annealing process of metals. The annealing procedure of metals is defined as cooling down the matter slowly after being heated up to high temperatures, to get the optimal molecular arrangements of the metal particles, in which the energy of the system is minimized [13].

The second and the third optimization algorithms that will be applied are population-based algorithms. The principle of population-based optimization algorithms is that an initial set of parameter vectors are optimized every iteration until the global optimum is found. Population-based algorithms can be divided into evolutionary-based algorithms (also Evolutionary Algorithms) and swarm-based algorithms. The evolutionary-based algorithms use Darwinian evolution concepts and the swarm-based algorithms make use of specific movement patterns by the parameter solution vectors [12]. The genetic algorithm (evolutionary based) is the second algorithm that will be applied in this research The principles of the GA are based on the natural selection processes of life in which new solution vectors generations are created from the previous solution vector generations [14]. Like in natural selection, the 'genetic material' of solution vectors that are the fittest will survive. 'Genetic material' refers in this case to the solution values of the vectors. The last algorithm that will be applied is the Particle swarm optimization, which is a swarm-based algorithm. Swarm-based optimization algorithms are based on swarm intelligence, which is the collective behaviour of an organized group of animals or insects [15]. Swarm-based algorithms are increasing in popularity, while the algorithms are flexible, versatile, adaptable to external variations and they have self-learning capabilities [15].

4.2 Objective functions

In optimization the optimal solution can be found by minimizing op maximizing the objective function. It can be seen as a score that evaluates the goodness of fit. There are different objective function. There is no 'best' objective functions, since it is dependent on the optimization problem [16].

The main choice one has to make choosing an objective function is whether to use squared errors, absolute errors, absolute errors or normal errors.

Square errors penalize strongly for outliers. If one wants a model that does not predict values too far from reality, this is a good objective function to use. If one wants to treat all samples the same in terms of distance of the output to real data, and one is not concerned about outliers, then the absolute error will be a better choice. If one does not care about the errors of single data samples, but one is only interested in the summed error of the complete dataset (in which positive and negative errors can cancel each other out), then the normal error will be the better choice.

The objective functions that will be analysed in this paper are:
Root mean squared error (RMSE)

$$RMSE = \sqrt{\frac{\sum(S-O)^2}{n}}$$

Mean absolute error (MAE)

$$MAE = \frac{1}{n}\sum|S - O|$$

Percent bias (PBIAS)

$$PBIAS = \frac{\sum(O-S)}{\sum O}100(\%)$$

In these equations O stands for observations and $\overline{O}$ stands for the mean of all observations.
The S stands for simulations and $\overline{S}$ stands for the mean of all simulations. The n stands for number of samples.

4.3. Data

For this research we make use of the SHAERE database. This is a database from the Umbrella organisation of Dutch social housing companies (AEDES). They use this database to track the energy performance of their housing stock. In the database all input parameters to make the Energy performance calculation (based on ISO 82.3) are saved for all individual dwellings. This database is linked to the Dutch statistics database which has measured energy use data of almost every individual dwelling in the Netherlands. These data will be used to test the algorithms and the objective functions. The most important assumptions made in ISSO 82.3 are presented in the appendix.

5. Results

In this section the results are presented. The experiments were run on a system with the following processor specifications: Intel(R) Xeon(R) Gold 6146 CPU, @ 3.20GHz, 4 Cores.

5.1 Objective function

The three different objective functions that are compared are: RMSE, MAE and PBIAS. All three calibrations were run over 100 generations, with a population size of 100. The loss shown in the minimal objective function loss found by the population so far. The minima of all objective functions were found within the 100 generations. The calibration with the PBIAS objective function seemed to have reached the minima earlier than the RMSE and the MAE (~20 generations with respect to ~40 generations). The minimal objective function losses are not comparable between the different objective functions, so nothing can be said about that. The computation time is comparable for all of them, which is expected because the calibrations were run on the same dataset and the same algorithm with the same hyperparameters. Although PBIAS had its final drop in objective function loss at generation 98, the plot reveals that it was already close to this minimal objective function loss at around generation 20. Therefore the computation time at minimal objective function loss is also not very informative to look at. For the other model aspects these numbers will be important for determining which is the preferred option, but for selecting the objective function it is not of major importance for making a decision.

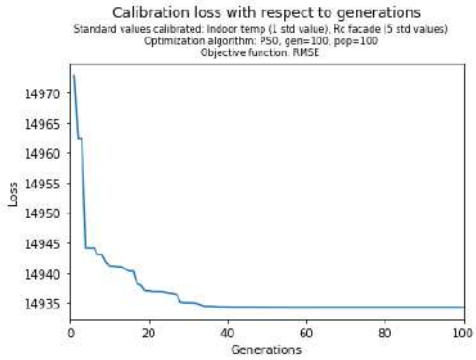

Fig. 4 - RMSE. (source: Thesis Samuel Smets)

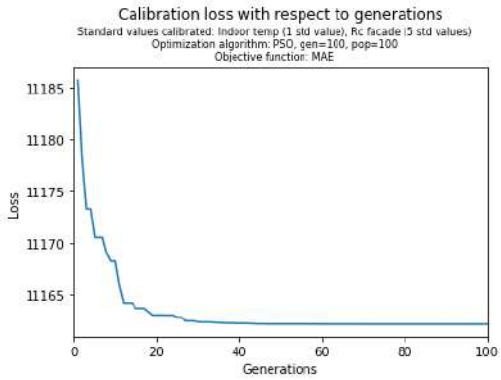

Fig. 5 - MAE. (source: Thesis Samuel Smets)

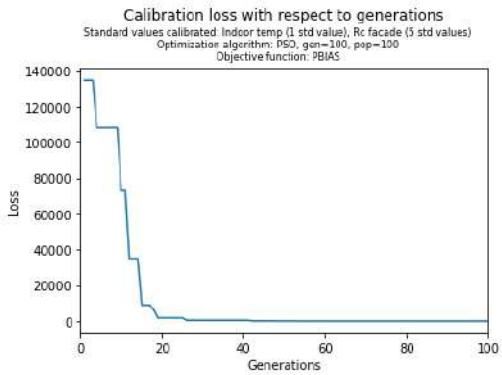

Fig. 6 - PBIAS. (source: Thesis Samuel Smets)

Table 1 shows the optimized standard values for the three different objective functions. However if we look at the results we see that in all three cases the EPG is reduced significantly (see fig 7)

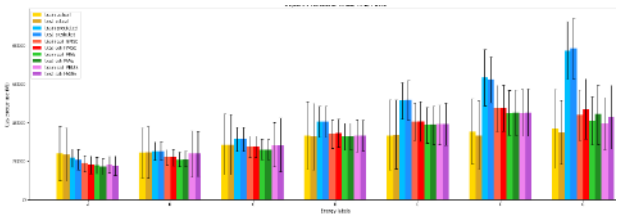

Fig. 7 - The average gas energy use (with standard deviation bars) for dwellings per energy label for both the training and the test dataset. In yellow one finds the actual energy use, in blue one finds the predicted energy use with the uncalibrated model, in red, green and purple one finds the predicted energy use with the calibrated model (with objective functions RMSE, MAE and PBIAS respectively).

If we look at the optimized variables (Table 1) we see that the ones calculated with the PBIAS are the least realistic (e.g. the lowest Rc value is 0, which is not possible) . Therefore it seems that this objective function is probably not suitable for this purpose. The differences between RMSE and MAE are only minimal and therefore we cannot conclude whether the RMSE or MAE is better.

Tab. 1 - Calibration results of the objective function analysis. Minimal objective function loss reached during optimization over 100 generations with a population size of 100; Generation count at which the minimal objective function loss was reached; Computation time at which minimal objective function loss was reached..

	Minimal subjective function loss	Computation time needed (hours)	Generations needed
RMSE	14934.32	9.44	58
MAE	11162.15	9.82	60
PBIAS	0.41	16.06	98

5.2 Optimization Algorithms

The figures below show the different optimization plots per optimization algorithm (using the RMSE objective function). The figures clearly show that the SA is an individual based algorithm and the other are population based algorithm. The individual based algorithm evaluates the function loss every single function evaluation.

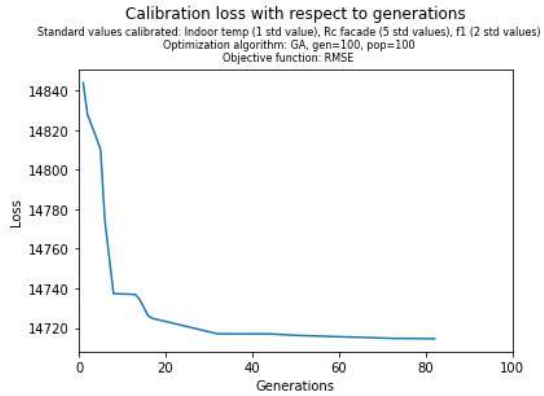

Fig. 8 - Genetic Algorithm with hyperparameter settings: mutation rate = 0.5, population size = 100, generations = 100

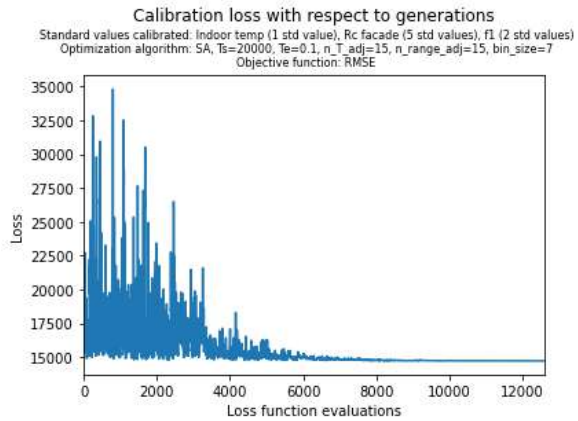

Fig. 9 - Simulated Annealing with hyperparameter settings: start temperature = 20000, end temperature = 0.1, temperature adjustments = 15, range adjustments = 15, number of cycles over all standard value solution dimensions per range = 7

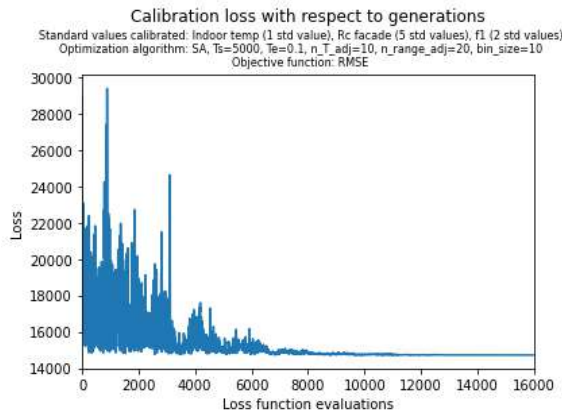

Fig. 10 - Simulated Annealing with hyperparameter settings: start temperature = 5000, end temperature = 0.1, temperature adjustments = 10, range adjustments = 20, number of cycles over all standard value solution dimensions per range = 10.

Table 2 shows the calibration results in numbers. The minimal objective function losses are similar to all

algorithms, as are the optimized values. One can also see that the Simulated Annealing algorithm has a longer computation time than the other two algorithms.

Tab. 2 - Calibration results of the optimization algorithm analysis. Minimal objective function loss reached during optimization; Generation count (PSO and GA) and iterations (SA) at which the minimal objective function loss was reached; Computation time at which minimal objective function loss was reached.

	Minimal subjective function loss	Computation time needed (hours)	Generations needed
PSO	14713.10	13.47	84
GA	14714.49	13.47	82
SA	0.14713.39	19.38	12067

If we look at the validation function we see that there is no significant difference between the training and the test datasets and therefore there was no overfitting for any of the algorithms.

It becomes clear that all of the algorithms perform equally. The only difference is de computation time, which is longer for SA. The reason for this might be that finding the optimal hyperparameters of SA is known to be difficult. Therefore PSO and GA are the most preferred ones.

6. Conclusion and discussion

This paper is a follow up on the calibration on building stock level method from which the proof of concept is published in: [9]. It aimed to answer some of the remaining questions which are important to transform the proof of concept into a practical applicable method.

Therefore we investigated in this paper which objective function and optimization algorithms are the most suited for calibration on building stock level. Based on the analysis we can conclude that from the three objective functions (RMSE, MAE and PBIAS) which we analysed the RMSE is the most preferred one in terms of performance.

If we look at the three optimization algorithms (PSO, GA and SA) no clear conclusion could be made. However we saw that the SA method required significant longer computation time.

The examples again showed that it is possible to reduce the energy performance gap using automated calibration on building stock level and the two findings from this paper bring the applicability of the method again a step closer. However there are still several aspects that have to be investigated before the method will be applicable in practice. This paper also shows the importance of solving the EPG and it showed that the EPG is an international problem.

7. Acknowledgement

This paper is based on the graduation thesis of Samuel Smets for the Master Industrial Ecology at Delft University of Technology.

8. Data access statement

The datasets used for this study are not public because they are owned by the umbrella organisation of the social housing companies in the Netherlands (Aedes) and are only allowed to be used with approval of Aedes.

9. References

[1] Majcen, D., L.C.M. Itard, and H. Visscher, *Theoretical vs. actual energy consumption of labelled dwellings in the Netherlands: Discrepancies and policy implications.* Energy Policy, 2013. **54**: p. 125-136.

[2] Palma, P., J.P. Gouveia, and S.G. Simoes, *Mapping the energy performance gap of dwelling stock at high-resolution scale: Implications for thermal comfort in Portuguese households.* Energy and Buildings, 2019. **190**: p. 246-261.

[3] Cozza, S., J. Chambers, and M.K. Patel, *Measuring the thermal energy performance gap of labelled residential buildings in Switzerland.* Energy Policy, 2020. **137**: p. 111085.

[4] Cozza, S., J. Chambers, C. Deb, J.-L. Scartezzini, A. Schlüter, and M.K. Patel, *Do energy performance certificates allow reliable predictions of actual energy consumption and savings? Learning from the Swiss national database.* Energy and Buildings, 2020. **224**: p. 110235.

[5] Gram-Hanssen, K., S. Georg, E.T. Christiansen, and P.K. Heiselberg, *How building regulations ignore the use of buildings, what that means for energy consumption and what to do about it*, in *ECEEE 2017 Summer Study on energy efficiency*. 2017, European Council for an Energy Efficient Economy, ECEEE: Presqu'île de Giens.

[6] Coyne, B. and E. Denny, *Mind the Energy Performance Gap: testing the accuracy of building Energy Performance Certificates in Ireland.* Energy Efficiency, 2021. **14**(6): p. 57.

[7] Laurent, M.H., B. Allibe, T. Oreszcyn, I. Hamilton, R. Galvin, and C. Tigchelaar, *Back to reality: How domestic energy efficiency policies in four European countries can be improved by using empirical data instead of normative calculation.*, in *eceee Summer Study*

proceedings, E.C.f.a.E.E.E. (ECEEE), Editor. 2013: Stockholm, Sweden.

[8] Cayre, E., B. Allibe, M.H. Laurent, and D. Osso, *There are people in the house! How the results of purely technical analysis of residential energy consumption are misleading for energy policies*, in *ECEEE 2011 summer studies - Energy efficiency first: the foundation of a low-carbon society*, ECEEE, Editor. 2011.

[9] Van den Brom, P., *Energy In Dwellings: A Comparison between Theory and Practice*, in *A+BE | Architecture and the Built Envornment*. 2020, Delft University of Technology: Delft.

[10] Lara, R.A., E. Naboni, G. Pernigotto, F. Cappelletti, Y. Zhang, F. Barzon, A. Gasparella, and P. Romagnoni, *Optimization Tools for Building Energy Model Calibration*. Energy Procedia, 2017. **111**: p. 1060-1069.

[11] Lin, M.-H., J.-F. Tsai, and C.-S. Yu, *A Review of Deterministic Optimization Methods in Engineering and Management.* Mathematical Problems in Engineering, 2012. **2012**: p. 756023.

[12] Mirjalili, S., *Genetic Algorithm*, in *Evolutionary Algorithms and Neural Networks: Theory and Applications*. 2019, Springer International Publishing: Cham. p. 43-55.

[13] Eren, Y., İ.B. Küçükdemiral, and İ. Üstoğlu, *Chapter 2 - Introduction to Optimization*, in *Optimization in Renewable Energy Systems*, O. Erdinç, Editor. 2017, Butterworth-Heinemann: Boston. p. 27-74.

[14] Arsenault, R., A. Poulin, P. Côté, and F. Brissette, *Comparison of Stochastic Optimization Algorithms in Hydrological Model Calibration.* Journal of Hydrologic Engineering, 2014. **19**(7): p. 1374-1384.

[15] Chakraborty, A. and A.K. Kar, *Swarm Intelligence: A Review of Algorithms*, in *Nature-Inspired Computing and Optimization: Theory and Applications*, S. Patnaik, X.-S. Yang, and K. Nakamatsu, Editors. 2017, Springer International Publishing: Cham. p. 475-494.

[16] Chai, T. and R.R. Draxler, *Root mean square error (RMSE) or mean absolute error (MAE)? – Arguments against avoiding RMSE in the literature.* Geosci. Model Dev., 2014. **7**(3): p. 1247-1250.

10. Appendix

Category	Assumptions
Façade insulation (Rc [m2K/W])	If the insulation is unknown and cannot be measured the assumed insulation level is based on construction year. ISSO 82.3 assumes the following values. Built before 1965 = 0.19 Built between 1965-1975 = 0.43 Built between 1975-1988 = 1.3 Built between 1998-1992 = 2 Built after 1992=2.3
Floor insulation (Rc [m2K/W])	If the insulation is unknown and cannot be measured the assumed insulation level is based on construction year. ISSO 82.3 assumes the following values.
Roof insulation (Rc [m2K/W])	If the insulation is unknown and cannot be measured the assumed insulation level is based on construction year. ISSO 82.3 assumes the following values.
Ventilation rate	Assumed ventilation rate is based on type of ventilation system (natural ventilation, mechanical exhaust ventilation, demand based mechanical exhaust ventilation, balanced ventilation with heat recovery) and minimum ventilation rate per m2 floor are. Natural ventilation q=0.47; mechanical exhaust ventilation q=0.47; demand based ventilation q=0.29; balanced ventilation=0.47. If a heat recovery system is present q is multiplied by 1-efficiency of heat recovery system.
Infiltration rate	Assumed infiltration rate is based on floor area and type of building (detached, semidetached, terraced house, common staircase and galleries, common staircase no galleries and maisonettes). f2= air permeable factor based on ventilation system (0.12 for demand based else 0.13); The exact values of qinf,10 can be found in table 10 of ISSO 82.3 (2011)
Indoor temperature	Assumed average constant indoor temperature of 18 °C
Domestic hot water consumption	Assumed amount for domestic hot water is based on number of occupants, which is based on floor area. Further it takes into account if a shower, bath and/or dishwasher is/are present and if water saving shower heads are installed.
Efficiency of heating system	The assumed efficiency of the heating system is based on the type of system, but also if the system is placed outside or within the thermal envelope of the building. Exact values can be found in table 19 ISSO 82.3 (2011)
Efficiency of domestic hot water system	The assumed efficiency of the domestic hot water system is based on the type of system, but also if the system is placed outside or within the thermal envelope of the build. The exact values can be found in table 24 of ISSO 82.3 (2011)

Development of a multi-criteria decision support tool for sustainable building retrofits

Zaid Romani [a], Abdeslam Draoui [b], Francis Allard [c]

[a] LaRAT, National School of Architecture of Tetouan, Morocco, z.romani@enatetouan.ac.ma.

[b] ETTE, Faculty of Sciences and Technology of Tangier, Abdelmalek Essaadi University, Morocco, adraoui@uae.ac.ma.

[c] LaSIE, La Rochelle University, France, francis.allard@univ-lr.fr.

Abstract. The existing building stock represents a major challenge for a successful energy transition and achieving zero carbon territories. Several thermal simulation tools have integrated optimization modules for building design and retrofit. However, in these tools there are problems of convergence towards local optimum and the unknown computation time. Indeed, we propose in this research work a tool allowing an optimal choice of building envelope to achieve a sustainable building retrofit by integrating 16 criteria representing the heating energy needs as well as economic and environmental criteria. This tool is based on thermo-aeraulic dynamic simulation using TRNSYS and CONTAM software, the metamodeling based on the design of experiments method and polynomial regression as well as three multicriteria analysis methods such as weighted sums, Min Max and Pareto optimality. Using this tool, the calculation time of the optimization process and the uncertainties of the results are known. Thermal comfort considered as a social criterion is studied in the post-processing. A real-life existing building located in La Rochelle city (France) was chosen as a case study. The results show that the tool developed allows a rapid choice of building envelope technical solutions and to get a compromise between all criteria studied.

Keywords. Building energy retrofits, Sustainable building, Multicriteria optimization tool.
DOI: https://doi.org/10.34641/clima.2022.136

1. Introduction

Currently, and in parallel with the health crisis of Covid 19 and the technological development that humanity is experiencing, the energy production and consumption are also at the center of public debates. They represent one of the essential subjects in international politics and societal discourses.

According to the International Energy Agency [1], the building and construction industry together represent actually the most energy-consuming and polluting sector in the world. Indeed, this sector is responsible for more than a third of final energy consumption and almost 38% of direct and indirect CO_2 emissions (this percentage represents the highest value of CO_2 emissions ever recorded) [1]. This consumption continues to increase due to the use of energy-intensive devices and the rapid growth of the buildings floor space [2]. It should be noted that to get involved in the mitigation of global warming, it will be necessary to achieve zero-carbon building stock by 2050 through the reduction of direct CO_2 emissions by 50% [3].

The implementation of energy efficiency strategies in buildings makes it possible to reduce a colossal share of the total expenditure of countries around the world [4], to mitigate the harmful impacts on the environment [5], to abolish energy poverty [6] and improve the comfort conditions of occupants [7]. Moreover, these strategies must be affordable by the population.

In this regard, we are faced with a multi-criteria problem (economic, social and environmental criteria). In addition, meeting these criteria must last over time to ensure climatic resilience. Therefore, a sustainable building implies considering, in the design process and during the rehabilitation, the life cycle of the building by evaluating these economic, social and environmental impacts from the extraction of the raw material to its deconstruction.

In the sketching stage of building retrofit, energy simulations with some parametric studies are insufficient to achieve an optimal choice among the technical solutions that exist on the market. To achieve this objective, research work proposes the coupling of optimization and multicriteria analysis methods with building energy simulation software [8, 9]. This coupling consists in the use of

Copyright ©2022 by the authors. This conference paper is published under a CC-BY-4.0 license.

programming languages (such as Matlab, Python, etc.) integrating mathematical optimization methods. To make this coupling more practical, recent tools have been developed with user-friendly interfaces to perform multi-criteria optimization [10, 11]. However, the large majority of optimization algorithms used in these tools presents several drawbacks such as the high computation time (in the case of several combinations) and the possibility of converging towards a local optimum.

To remedy these issues, in this research work, we present a multi-criteria decision support tool for sustainable building retrofit. It is based on the development of metamodels from the design of experiments method and polynomial regression as well as the TRNSYS and CONTAM software to predict the heating energy needs. Considering the fast calculation using these metamodels, they are then used in a combinatorial process by integrating environmental and economic criteria. The best compromise is obtained through three multicriteria analysis methods.

2. Calculation process

It is often difficult to find the best trade-off among the passive technical solutions that contribute to the sustainable building retrofit. The tool proposed in this work is based on a calculation process that we have already developed [12]. This calculation process integrates the development of the heating energy needs metamodel, the evaluation of the economic and environmental criteria on the building life cycle, the comparison between three multicriteria analysis methods as well as a post-processing to reduce indoor overheating in summer. The calculation process of this tool is presented in Figure 1.

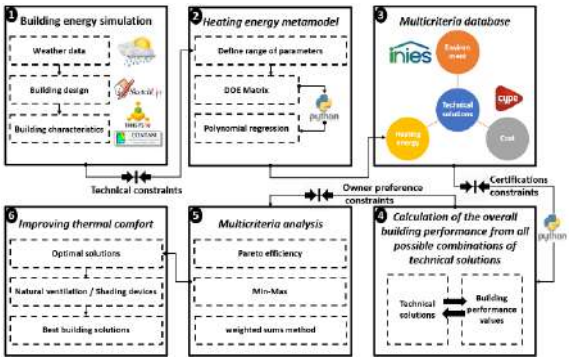

Fig. 1 - Calculation process proposed to get the best technical solutions for sustainable building retrofit [12].

In the first step of the calculation process, it is necessary to draw the building and define the characteristics of the building project which will be the object of the rehabilitation as well as the climatic data. In order to carried out the dynamic thermo-aeraulic simulations, the building modeling is achieved using the TRNSYS 3d and CONTAM coupling software. Technical constraints may exist and must be taken into account. For example, if it is not possible to change the coating of the exterior facade, the solar absorption coefficient will be fixed.

The passive building envelope parameters considered in our tool as variables are presented in Table 1. A variation interval of these parameters has been defined. The maximum values represent the envelope characteristics of the existing building which are generally the least efficient solutions. The minimum values represent effective solutions that exist in the construction market.

Tab. 1 - Passive building envelope parameters considered as variable in the tool developed [12]

Parameters	Symbol	Range	Unit
Transmission coefficient of external walls	U_{ew}	[0.15-EBV]	$Wm^{-2}\cdot K^{-1}$
Absorption coefficient of external walls	α_{ew}	[0.05-0.95]	-
Transmission coefficient of the roof	U_{rf}	[0.15-EBV]	$Wm^{-2}\cdot K^{-1}$
Absorption coefficient of the roof	α_{rf}	[0.05-0.95]	-
Transmission coefficient of the floor	U_{fl}	[0.15-EBV]	$Wm^{-2}\cdot K^{-1}$
Transmission coefficient of the windows	U_w	[0.4-EBV]	$Wm^{-2}\cdot K^{-1}$
Solar factor of the windows	g-value	[0.05-0.95]	-
Absorption coefficient of the frame	α_f	[0.05-0.95]	-
Infiltration rate (4 Pa)	$Q_{4\text{-}Pa}$	[0.1- EBV]	$m^3\cdot h^{-1}\cdot m^{-2}$
Transmission coefficient of the thermal bridge	ψ	[10^{-2}- EBV]	$Wm^{-1}\cdot K^{-1}$

EBV: Existing building value

In the second step, in order to reduce the computation time resulting from the dynamic thermo-aeraulic simulations in the optimization process, metamodels are developed to predict the heating energy needs. This is achieved with a limited number of simulations determined by the design of experiments method (D-optimal design) and a full quadratic polynomial regression [13]. Python programming language is used to automate the TRNSYS and CONTAM simulations. Thereafter, the

calculation of the building energy needs will be carried out from the metamodel developed without recourse to dynamic thermal simulation.

The next step is to generate a multi-criteria database of technical building solutions existing in the building market and their associated economic and environmental databases. The environmental criterion is made up of twelve indicators (Table 2) calculated over the life cycle of the building based on the French database (INIES) [14]. INIES database integrates the environmental characteristics of construction products available on the construction market in France. The economic criterion is a key element to assess the feasibility of construction projects. Three indicators used in our tool which are the initial investment cost, the payback time and the life cycle cost (Table 2). The cost of each technical solution is taken from the Cype software database [15].

Tab. 2 - Selected environmental and economic indicators

Parameters	Unit	Symbol
Climate Change	(kg CO_2 eq.)	CC
Depletion potential of the stratospheric ozone layer	(kg CFC-11 eq.)	OPD
Acidification potential of land and water	(kg SO_2 eq.)	APLW
Eutrophication	(kg $(PO_4)_3$ eq.)	ET
Photochemical ozone formation	(kg C_2H_4 eq.)	POF
Abiotic resource depletion potential for elements	(kg Sb eq.)	ADPE
Abiotic resource depletion potential of fossil fuels	(MJ)	ADPF
Air pollution	(m^3)	AP
Water pollution	(m^3)	WP
Total use of renewable primary energy resources	(MJ)	TRPER
Total use of non-renewable primary energy resources	(MJ)	TNRPER
Use of net fresh water	(m^3)	UNFW
Initial investment cost	(€ or €/m^2)	CINV
Payback period	(year)	PBP
Life cycle cost	(€ or €/m^2)	LCC

In the fourth step, using the Python programming language, the calculation of the set of criteria is performed for each combination of technical solutions. In this step, the user can give limit values not to be exceeded for each criterion in order to achieve a desired performance of the building (regulations, certification, etc.).

Three multi-criteria analysis methods are used and compared with the fifth step namely the weighted sums, the Min-Max and the Pareto optimality method [12]. In order to take into account user preferences, a weight is assigned to each criterion.

Once the choice of the optimal solution is made, the last step is to improve thermal comfort in summer. In our tool, a post-treatment was proposed to reduce the indoor temperature in the summer period. This objective will be achieved by the integration of two passive solutions such as natural ventilation and windows shading devices. The thermal comfort rate (TCR) is calculated as being the ratio of the hours of comfort (when the operating temperature exceeds the comfort temperature) and the hours of occupancy.

Thus, a package of optimal solutions allowing all the criteria to be met is obtained and which will guarantee the best compromise between all criteria studied and contributing to a sustainable building retrofit.

3. Tool application with a case study

The calculation process presented above has been transformed into a tool which can be used easily. The python code is linked through another VBA code embedded in an Excel file (Figure 2).

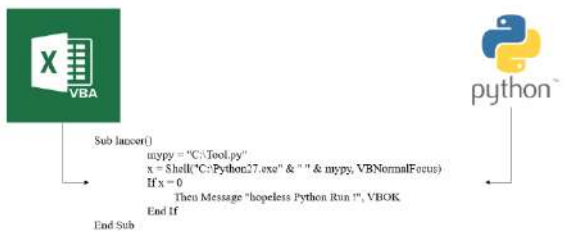

Fig. 2 – Python and Excel VBA code link.

The building case study is a real four-storey existing building with a total floor area of 960 m^2 (figure 3). It represents a typical French social housing built in 1954. It is located in La Rochelle city on the south-west Atlantic coast of France. This city is characterized by an oceanic climate.

Fig. 3 – Real building studied before rehabilitation.

Each floor consists of two T1 (one room) type apartments with a surface area of 26 m² and two T5 type apartments (4 rooms and one living room) with an area of 94 m². The ceiling height is 2.7 m. The large facades are oriented East-West and have large glass surfaces with a ratio of 30% and 20% respectively. This building is studied using the developed tool.

The different data entry steps are explained below:

The first window of the tool was devoted to introducing information about the project (Figure 4). A file name can be chosen according to the user. Then, it is possible to choose the climate data without going back to TRNSYS. In the TRNSYS/CONTAM file box, it will be necessary to put the link of modeling files. Users must enter the building lifespan to calculate the number of technical solutions replacements.

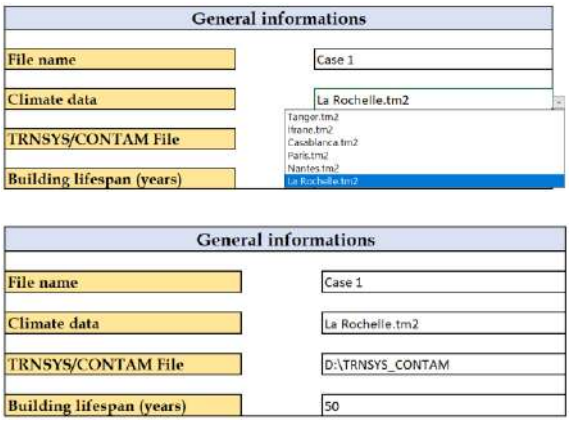

Fig. 4 – General information's windows of the tool.

The users can choose the metamodel type (linear, quadratic, linear with interactions, and full quadratic). In addition, the economic and environmental database has been fixed in this tool (Figure 5). There is also the possibility of integrating another database directly on another sheet of the same excel file.

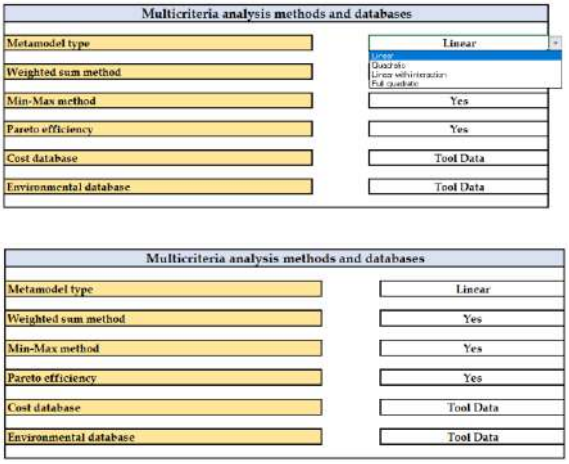

Fig. 5 – Second window of the tool concerning the metamodel type, multicriteria method used as well as the cost and environmental database.

The next window consists of introducing the minimum and maximum value as well as the construction constraints of each studied parameter (Figure 6). Depending on the location and orientation of the building studied, a number of windows with the same orientation must be fixed.

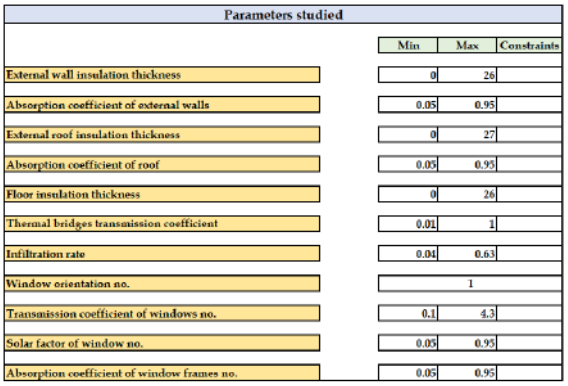

Fig. 5 - Third window for entering the value of the building envelope parameters.

The last entry step is the choice of criteria (Figure 6). If one of the criteria is included in the multicriteria study, the user must put Yes in the choice box and put his weight according to the preferences of decision makers. The sum of the weights of all the criteria must be equal to 1.

Criteria studied	Choice	Weight	Constraints
Heating energy needs	Yes	6.25	
Cooling energy needs	No	6.25	
The initial investment cost	Yes	6.25	
The payback period	Yes	6.25	
Life cycle cost	Yes	6.25	
Climate change	Yes	6.25	
Depletion potential of the stratospheric ozone layer	Yes	6.25	
Acidification potential of land and water	Yes	6.25	
Eutrophication	Yes	6.25	
Photochemical ozone formation	Yes	6.25	
Abiotic resource depletion potential for elements	Yes	6.25	
Abiotic resource depletion potential of fossil fuels	Yes	6.25	
Air pollution	Yes	6.25	
Water pollution	Yes	6.25	
Total use of renewable primary energy resources	Yes	6.25	
Total use of non-renewable primary energy resources	Yes	6.25	
Use of net fresh water	Yes	6.25	

Fig. 6 - Fourth window of the tool which concerns the choice of criteria, their weight and constraints.

Once the data entry is completed, it is therefore possible to start the calculations by pressing the Run button. The tool will therefore automatically start the simulations developing the metamodel of the building studied. Then, the optimization will be carried out using the three multi-criteria analysis methods. The optimal values of each criterion will be displayed in a radar diagram as shown in the Figure 7.

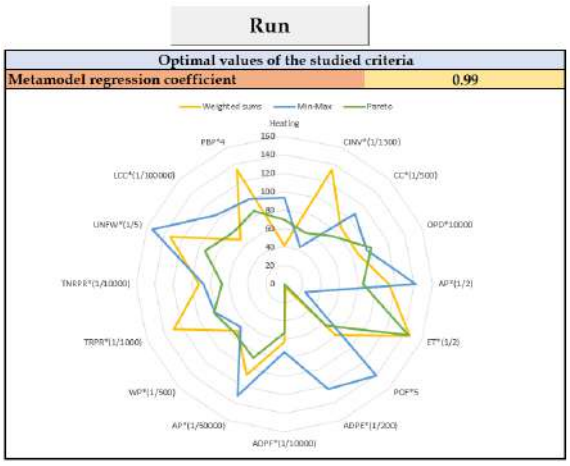

Fig. 7 - Display window of the results concerning the criteria and the precision of the metamodel.

The display of the optimal technical solutions for the rehabilitation of the building studied is shown in Figure 8. It indicates whether the value tends towards the maximum or the minimum depending on the range of variation chosen.

Optimal technical solutions	
External wall insulation thickness (cm)	18
Absorption coefficient of external walls (-)	0.5
External roof insulation thickness (cm)	14
Absorption coefficient of roof (-)	0.5
Floor insulation thickness (cm)	8
Thermal bridges transmission coefficient ($W.m^{-1}.K^{-1}$)	0.12
Infiltration rate ($m^3.h^{-1}.m^{-2}$)	0.5
Transmission coefficient of windows Ouest ($W.m^{-2}.K^{-1}$)	1.61
Solar factor of window Ouest (-)	0.56
Absorption coefficient of window frames Ouest (-)	0.5

Fig. 8 – Optimal building technical solutions obtained.

The last window (Figure 9) concerns a post processing in order to improve the indoor thermal comfort in summer and to avoid the overheating, especially in the case of the thermos flask.

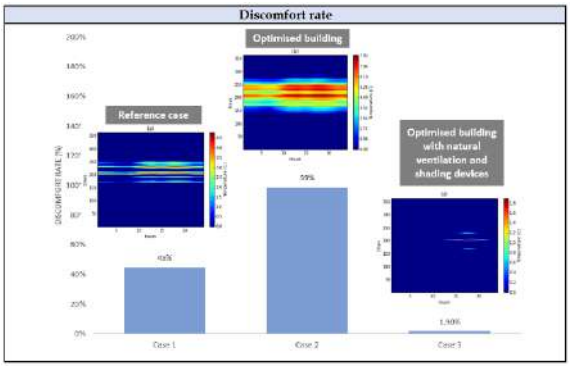

Fig. 9 – Display window of the post processing.

The tool displays the thermal discomfort rate and the difference between the interior temperature and a comfort temperature (26°C) with the discomfort rate which corresponds to 3 configurations: reference case (case 1), optimized building (case 2) and optimized building with natural ventilation and shading devices (case 3).

Using the tool developed, the time consumed to make 217728 combinations of technical solutions is approximately 8 minutes. By adding the time required to develop the metamodel, the total time is 326 minutes. If this combination study will be carried out only with TRNSYS and CONTAM software, the decision support becomes impractical because the calculation time of this combinatorial study is 303 days.

4. Conclusion

The energy transition must be accelerated in the building sector, which has significant potential in terms of saving and producing energy. However, this transition must be sustainable to protect the environment and future generations. In practice, builders need a multi-criteria decision support tools to get a sustainable technical solution instead of

intuitive and harmful choices for the environment.

France will adopt new environmental regulations, the RE 2020, which will replace the 2012 thermal regulations. Indeed, the choice of technical solutions will be more complex with the introduction of environmental indicators. The tool that we have developed and presented in this work will have a significant benefit in terms of computing time, the relevance of the results in the case of a sustainable approach. This tool has several advantages:

- Carrying out multi-criteria analyses (economic, environmental and social) with the allocation of weights for each criterion;
- Flexibility in terms of the choice of building envelope parameters, criteria and constraints according to user needs;
- The speed of calculations compared to classical parametric studies;
- The integration of life cycle analysis into the calculation process;
- The assurance of reaching the overall optimum with control of the results uncertainties.

An improvement of the tool can be envisaged in order to take into account other criteria such as visual, acoustic and indoor air quality criteria. In addition, it will be necessary to optimize the integration of renewable energies.

5. Acknowledgement

The contribution of TIPEE company (https://www.plateformetipee.com) is gratefully acknowledged for providing us the diagnosis information of the existing building studied.

6. References

[1] IEA. *World Energy Balances: Overview*. Paris, https://www.iea.org/reports/world-energy-balances-overview (2020).

[2] IEA. *Global Status Report for Buildings and Construction 2019*, https://www.iea.org/reports/global-status-report-for-buildings-and-construction-2019 (2019, accessed 19 January 2020).

[3] IEA. *Net Zero by 2050*. Paris, https://www.iea.org/reports/net-zero-by-2050 (2021).

[4] IEA. The Critical Role of Buildings, https://www.iea.org/reports/the-critical-role-of-buildings (2019, accessed 19 January 2020).

[5] UN Environment and International Energy Agency. Towards a zero-emission, efficient, and resilient buildings and construction sector. Global Status Report 2017, https://www.worldgbc.org/sites/default/files/UNEP 188_GABC_en %28web%29.pdf (2017, accessed 19 February 2020).

[6] Bouzarovski S, Petrova S. A global perspective on domestic energy deprivation: Overcoming the energy poverty-fuel poverty binary. *Energy Res Soc Sci* 2015; 10: 31–40.

[7] Ritchie H, Roser M. Access to Energy. *Our World Data*, https://ourworldindata.org/energy-access (2019).

[8] Nielsen AN, Jensen RL, Larsen TS, et al. Early stage decision support for sustainable building renovation - A review. *Building and Environment* 2016; 103: 165–181.

[9] Kheiri F. A review on optimization methods applied in energy-efficient building geometry and envelope design. *Renewable and Sustainable Energy Reviews* 2018; 92: 897–920.

[10] Longo S, Montana F, Riva Sanseverino E. A review on optimization and cost-optimal methodologies in low-energy buildings design and environmental considerations. *Sustainable Cities and Society* 2019; 45: 87–104.

[11] Machairas V, Tsangrassoulis A, Axarli K. Algorithms for optimization of building design: A review. *Renew Sustain Energy Rev* 2014; 31: 101–112.

[12] Romani Z, Draoui A, Allard F. Metamodeling and multicriteria analysis for sustainable and passive residential building refurbishment: A case study of French housing stock. *Build Simul 2021* 2021; 1–20.

[13] Romani Z, Draoui A, Allard F. Metamodeling the heating and cooling energy needs and simultaneous building envelope optimization for low energy

building design in Morocco. *Energy Build* 2015; 102: 139–148.

[14] INIES. Environmental and health reference data for building, https://www.inies.fr/accueil/ (2020, accessed 9 February 2020).

[15] Cype. Générateur de prix de la construction, http://www.prix-construction.info/ (2020, accessed 19 February 2020).

A Reference Architecture for Data-Driven Smart Buildings Using Brick and LBD Ontologies

Pieter Pauwels [a], *Gabe Fierro* [b]

[a] Department of the Built Environment, Eindhoven University of Technology, Eindhoven, the Netherlands, p.pauwels@tue.nl.

[b] Colorado School of Mines, Golden, CO 80401, United States of America, gtfierro@mines.edu.

Abstract. With the increasing adoption of sensors, actors and IoT devices in existing buildings, the real estate sector is becoming increasingly automated. Not only do these devices allow to monitor these buildings (energy use, occupancy, indoor air quality, etc), they also enable model predictive control (MPC) through building automation and control systems (BACS). A critical feature to enable these is the metadata associated to data streams obtained from the building. Such metadata allows building operators to assess what these data streams are, what they are measuring and how. This can be achieved using metadata schemes and vocabularies, such as Brick, Haystack, Linked Building Data, Industry Foundation Classes. Merging these model-based metadata schemas (semantics) with data-driven monitoring and control (machine learning) into a functional system architecture is a considerable challenge. In this paper, we review the mentioned technologies and propose a draft reference architecture based on state-of-the-art research. This reference architecture is evaluated using a set of predefined criteria.

Keywords. Smart buildings, Linked Data, Ontology, Metadata, Brick, FDD, MPC, Asset Management
DOI: https://doi.org/10.34641/clima.2022.425

1. Introduction

The built environment is rapidly digitizing. The design and engineering stages of projects are increasingly impacted by digital tools. The management and operation of facilities is also experiencing increasing use of IT technologies. This motivates the creation of smart buildings, many of which are primarily data-driven. A smart building is hereby understood as a building for which the operation is monitored, and in which the building can intervene itself in the operation, towards optimized use. Optimised use of a smart building hereby often targets either an optimised energy use [1], as energy is becoming increasingly expensive and scarce; or an optimisation towards the end user, in which case comfort stands central.

To optimize smart buildings using smart IT technologies, data monitored from these buildings is a primary source of information (temperature, electricity use, indoor air quality, etc.). Analytic techniques examine monitored data and retrieve patterns upon which actions can be taken [2,3]. Metadata schemas and annotations [1] can "tag" these data sources with contextual details that make analytics results more easily interpretable (e.g., needing to know which room an anomaly occurs in, and knowing the features of this room, such as presence of windows, specific devices, users, etc.) or potentially easier to configure and program [4]. While standardisation of these annotations is often sought, the majority of buildings rely on ad hoc labels and naming conventions to describe their data streams. A growing family of metadata ontologies and vocabularies for buildings aims to address these issues, but it is not always clear how these technologies complement or compete with one another, or how exactly they fit into a modern view of a data-driven building [1,3].

In this paper, we investigate available metadata schemas for data-driven smart buildings. We study how these metadata schemas can be combined with key data analytics technologies (monitored data), and we demonstrate a set of contemporary system architectures (e.g. [3]). Eventually, this paper presents an opinionated *reference architecture* that explicitly demonstrates how these metadata technologies can be combined with data monitoring equipment, support data-driven applications in buildings, and thus enable the development of smart data-driven buildings.

The rest of the paper proceeds as follows. Section 2 provides relevant background on existing smart

Copyright ©2022 by the authors. This conference paper is published under a CC-BY-4.0 license.

building ontologies and other relevant vocabularies in addition to a brief overview of the capabilities and features of existing data platforms. Section 3 applies a set of motivating applications to defining the design requirements for a representative platform architecture enabling data-driven applications. Section 4 presents the representative architecture built on the Brick [5] and Linked Building Data (LBD) ontologies [6], complemented with data monitoring devices and software as well as control algorithms aiming at model-predictive control (MPC).

2. Background

Before being able to build a reference architecture, a review is needed of the different components that are needed inside that architecture. In this Section, we investigate (1) available smart building ontologies, (2) existing data platforms, and (3) platform design patterns.

2.1 Smart Building Ontologies

In the last decade, plenty of ontologies and vocabularies have been created, investigated and proposed [7]. These ontologies cover diverse areas. For one, in the design and engineering domain, there is the long-standing IFC ontology or vocabulary [8] that is available in the Web Ontology Language since 2016 [9]. In parallel to that ontology, there exists the combination of Linked Building Data (LBD) ontologies [6], which are diverse combinations of building topology ontology (BOT – Fig. 1 – [10]), building element ontology (BEO) [11], Building Product Ontology (BPO) [12], MEP ontology [13], diverse props ontologies that provide specialised property sets, the Ontology for Property Management (OPM) [14], the File Ontology for Geometry Formats (FOG) [15,16], and the Ontology for Managing Geometry (OMG) [15,17]. With the modular approach towards the creation of these ontologies [6-7], it is fairly possible to create more ontologies and use those in combination. In that case, one needs to be careful of the overlap between multiple ontologies, and how a combination of two ontologies may best be used [7].

When considering also the asset management phase and existing buildings and infrastructure in general, diverse other ontologies can be of additional use, such as SAREF4BLDG [18], the Damage Topology Ontology (DOT) [19], Real Estate Core (REC) [20], and so forth. However, in the smart building area, and in the operational phase of the building, a different community of ontologies exists, that is much more focused on the data streams collected in the building as well as its systems and devices.

The most predominant ontology in this ecosystem is the Brick ontology [5, 21]. At its core, Brick consists of a class brick:Location, which groups the definition of Building, Space, Floor, Site, and Zone. These location classes are very similar to the core BOT classes (Fig. 1). They can be combined using the simpler hasPart and part of relations, thus enabling to build any building topology, in a less rigid manner compared to BOT (no domains or ranges in object properties). Further to the Location class, Brick also defines an Equipment class, System class and a Point class, each holding a considerable inheritance tree below to define specific subclasses of both. As such, the Brick ontology is very well capable of defining the system of a building, including those points of relevance for data monitoring.

The Project Haystack metadata model [22] differs substantially from other building ontologies in that it is not rooted in RDF technologies. Though similar in scope to Brick, Haystack instead describes the type, behavior and other properties of entities in the model using combinations of tags --- atomic terms with pre-defined meaning. Recent efforts have begun to standardize the choice of tags to ensure consistent and interpretable use, but the majority of Haystack usage is unrestricted and correspondingly irregular [23].

The Flow System Ontology (FSO) is aimed entirely at the flows, ports and interfaces in an HVAC system [24]. FSO allows to define systems, components and connections, including energy storage devices, supply units, and fluid and heat flows. As such, it is much closer to the design and engineering area compared to Brick and Haystack. The ontology can mainly be used to define and compute flows through a system, and design its dimensions accordingly to acquire an optimised HVAC system.

Existing ontologies such as QUDT, SSN/SOSA, O&M, Time, and others can easily be aligned and combined with the above mentioned ontologies, as is also commonly done.

2.2 Existing Data Platforms

In addition to the above ontologies and vocabularies, many data platforms have emerged to

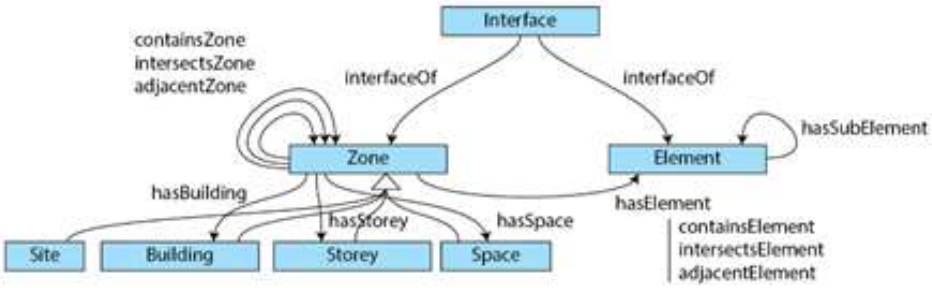

Fig. 1 – Main classes and properties in the BOT ontology.

help users organize, analyse and otherwise make sense of the data delivered by buildings. These include not only commercial platforms but also smaller open-source and community-driven efforts. The platforms examined below all make use of some sort of metadata to support data-driven smart buildings. The data itself is dominated by streams of time-series data collected from sensors and control networks, but also includes asset management data and static attributes of the building itself.

The SkySpark platform [25] ingests data from buildings using a variety of data adaptors and provides an API for constructing data-driven applications over that data. The results of these applications, like fault histories, are rendered in a web-based dashboard. SkySpark uses Haystack tags as the underlying metadata representation and defines a simple filter language over those tags to help users browse available data streams, and to allow applications to identify relevant data sources.

Google's Digital Buildings [26] effort defines an open-source ontology and schema for describing and reporting building data. The platform is not publicly documented; however, the ontology documentation demonstrates that it is possible to organize related data streams by the metadata provided by the ontology. If the ontology gets properly published in the future, this would make it easier for applications to discover relevant data because they only need to know the name of the collection containing the data they need.

The Azure Digital Twins platform [27] is another recent metadata-based data platform for smart buildings. The platform models properties of and interactions between data-producing entities in a cyber-physical environment (such as a building) as a graph using the RealEstateCore ontology [20] and a custom Digital Twin Description Language (DTDL). Applications query the graph to access live and historical data about the environment which is gathered using other data ingestion services.

Recent academic work highlights the importance of metadata in implementing and deploying data-driven applications [2,3,7,28-32]. The BOSS work develops a set of operating system-style services for executing portable and fault-tolerant applications [29]. Portable applications are those which require little to no adjustment to their implementation to execute in a variety of environments. BOSS achieves this through late-binding of resources discovered via a graph-oriented query mechanism. The Mortar work [28] further develops the notion of application portability through the construction of an analytics platform incorporating Brick-based graph models of buildings and a large public release of data. LBD reference architectures are different in style, also among each other. Malcolm et al. [30] defines a relatively standard web infrastructure in which multiple RDF triple stores are made available in combination with a web-based 3D viewer using the glTF data format. Ontological data integration happens in a modular fashion, similar to how it was described in Schneider et al. [32], but with the monitoring data outside the RDF graphs. This LBDServer namely also includes timeseries databases, and can then enable the joint access of building data together with monitoring data, within a state-of-practice web development framework. Werbrouck et al. [31] leverages this work and aims to make it available through the SOLID web data framework [33].

In the majority of the above systems, data is collected in state-of-the-art databases and amended with one or more metadata schemas to provide structure, standardisation and reference.

2.3 Platform Design Patterns

A critical question is exactly how metadata models can be used to build data-driven applications for buildings. We identify three representative design patterns, and identify later on in this section where these may be of more value and fit. In the first pattern, the metadata model is used as a reference for the programmer. A software developer may use certain representations --- such as building information models (BIM), one wire diagrams, blueprints and floor plans --- to help themselves understand the structure and composition of the building in its subsystems. Although this metadata is not consumed in an automated fashion, it helps the programmer understand what algorithms or approaches are appropriate, and which data sources and I/O points to consider when implementing the desired functionality.

The second design pattern uses the metadata model as an internal addressing and filtering system for manipulating data in a particular platform, as typified by Project Haystack. A data platform may contain the data and interfaces to those data sources and relevant I/O points. The programmer needs a way to identify which endpoints, API calls and parameters in the system are required to implement the desired functionality. This metadata may be added as an aftermarket feature, such as in a platform like SkySpark or the Google digital building stack, or it may consist of point names placed there by the installer of the building management system. An advantage of this second approach is that it is highly flexible. As no rigid ontology or standard is followed in annotating the data (no or hardly no metadata schema), the implementer or data engineer has a lot of freedom to work with the data collected from sensors and devices. These can simply be retrieved and used, provided that the implementer or user keeps track of how the data is actually structured. This last part is therefore also a weakness of this system: flexibility leads to many disagreements and confusion and then errors [23].

In the third design pattern, the metadata model is used to contextualize and further model resources that are contained in external, incumbent systems. In this context, metadata is implemented with linked data (specifically RDF graphs). This approach is like the second design pattern but is critically

different in that it includes formal or semi-formalized information that can be extended and validated. This semi-formalised information is enabled by the use of an OWL ontology in creating the RDF graphs. The scope of these metadata models is also not limited to the features provided by anyone ontology. Instead, the developer of this model can choose which elements, aspects or assets of the building are necessary for an intended suite of applications. An advantage of this third approach is that it normalizes the representation of metadata from various other systems, such as the metadata provided by the prior two patterns. Linked data decouples the meaning, or semantics, of metadata from its representation in a particular siloed system. Multiple ontologies can be used to represent the building [32] and thus provide an agreed upon representation and context of the data collected for the building.

Given the rising interest in developing ontologies based on linked data technologies (RDF graphs), we choose to examine data platforms of the third type. Metadata represented as linked data can be harder to integrate into existing data platforms for several reasons. First, the RDF format [34], describing a directed labelled multigraph, is quite abstract compared to the relational or object-oriented models many software developers are familiar with. Second, software supporting linked data is often quite generic due to the wide family of possible uses of linked data. It is not always obvious how to use a linked data system in conjunction with traditional aspects of a data system, such as a time series database [30]. Third, some ontologies such as SSN and QUDT formalize how to represent data and telemetry inside the RDF graph. However, this is far from the most intuitive or high-performing way of representing and accessing this data [32,35]. This can cause potential confusion for consumers or implementers of a linked data-based system.

2.4 Domains of Relevance

While this paper orients entirely towards data-driven smart buildings, there still exist several subdomains or areas of relevance. Each of these subdomains has a specific aim and corresponding business value. Depending on that business value, one or the other reference architecture may be more relevant.

A first domain of relevance is *asset management*. In a range of cases, primary relevance in building management is asset management. In such cases, the amount of monitored data is relatively small, and semantics play a much bigger role. As an example, a system or platform may be devised that has a semantic building model at its core, and additions are made using RDF graphs to further enrich the building model and its assets [30,31]. Enrichments then typically consist of annotations of damage and material wear (e.g. DOT in [19]). That damage can be represented using RDF graphs (e.g. using the DOT ontology [19]), and this often includes references to the collected measurements (e.g. element creep, cracks in concrete, photos, etc.). In this subdomain, the aim of the data-driven part in the data-driven smart building is mainly to collect data for analysis. The smart building is not self-repairing or self-cleaning, and therefore this can hardly be called a data-driven smart building.

A second domain of relevance is the systems and control domain. In this domain, a detailed view is required of the system inside the building, as well as how it is functioning (e.g. the purpose of the BACS [36] and FSO ontologies [24]). In many cases, this includes feedback loops and control models that allow to intervene in the building systems. Such subdomain typically relies on a Building Management System (BMS) that inhibits a detailed physical model of the building system (model-based), *and* provides access to monitoring data that is collected about those systems' operation. As such, the state of the system can at any given moment be tracked, and automated routines allow to intervene in the building (e.g. closing blinds, initiate heating, etc.). These systems tend to rely on two components, namely (1) a good physical model or simulation model that can compute at any time the expected performance and actions in the system, and (2) a live data-stream that logs the system status and can always be compared with the simulation model. If corresponding actions are taken, then this leads to Model-Predictive Control (MPC) [37].

Historically, semantics and metadata have had little to contribute to this specific target (MPC, systems and control) because of the reliance on detailed, hand-built, white-box models of the physics and dynamics of the system. However, recent work on grey-box and black-box models has heightened the need for systems which can organize the data required to fit these models. Both the FSO and BACS [24,36] ontologies aim to represent the system and all its components and flows using a semantic model. Models of the system's dynamics can then be determined by the structure of the related graph and historical telemetry of the system. The predictions from the model are used to implement MPC. MPC is the dominant control strategy studied in intelligent building research and has been demonstrated to provide thermal comfort to occupants while meeting energy consumption constraints, among other successes [37].

The last domain of relevance is data monitoring and prediction [2-3]. In this domain, the main purpose is to collect data for monitoring the building's function and predict its state over time, not limited to the state of the system and its devices. In this case, the focus lies heavily on data monitoring points (sensors) that provide access to monitored data. In this scenario, the focus lies a lot more on the actual time-series data that is collected, and a lot less on the definition of the system or its flow in full detail. A more commonly explored business opportunity in this case lies in the detection of patterns in the sensor data, to be able to detect and diagnose faults

over time (Fault Detection and Diagnosis – FDD). As there is much less need for a full representation of the system, this approach more often relies on the above outlined Approach 2, where data points are tagged and annotated, but mainly kept flexible and simple.

3. Platform Requirements

Those who would implement a platform for data-driven buildings must take into consideration the diversity enumerated above. Data-driven use cases in buildings consist of a variety of usage scenarios serving different goals. Implementation of these use cases may be facilitated through the incorporation of structured metadata. In this section, we examine the requirements that the above use cases -- model predictive control and fault detection – place upon a hypothetical data platform. These requirements will be incorporated into a representative architecture discussed in Section 4.

3.1 Requirements for an MPC application

Recall that MPC is an advanced control strategy which uses live and historical building telemetry to construct and refine a predictive model that allows a controller to implement an optimal policy. At its most essential, any MPC implementation requires three components. First, an MPC implementation needs a way of optimizing a control sequence relative to the predictions output by a model. The optimization itself is usually outsourced to an existing optimizer, but the MPC controller must be able to interface with that optimizer and use its results as part of the control process. Secondly, an MPC implementation requires a means of recording live observations about the state of the building. MPC controllers must constantly relay the feedback of their decisions to the optimizer to ensure they are making the best control decision at each opportunity. It is not always necessary for an MPC implementation to retain all historical data; often only the most recent data (e.g. one week) is required to update the model and inform the optimizer. Thirdly, an MPC implementation requires a means of actuating the environment with the control decisions reached by the optimizer. Depending on the deployment, it may be necessary to provide certain desirable properties for the actuation. As the BOSS work [29] details, transactional control can be beneficial in physical settings where having a building in an intermediate state can waste energy or even cause harm. Other deployments may be content with having an MPC controller write low-priority control signals that can be overridden by other safety software.

If the MPC implementation is using a white-box model to provide the predictions, then the supporting metadata only needs to describe the relevant data so it can be found by the controller. For grey-box and black-box models, the controller will require some knowledge about the structure and composition of the building in order to know what kinds of data sources would be relevant and what kind of model to train. While MPC applications may be less data-intensive, they generally are much more complicated on the systems and control side (signal processing and communication on the edge), which impacts software (and hardware) architecture significantly.

3.2 Requirements for an FDD application

FDD applications leverage a wide variety of computational models and algorithmic techniques. Some FDD approaches use equipment model- and manufacturer-specific information to identify errors in the equipment's operation (closer to FSO and BACS approaches – [24,36]). Others use timeseries analysis techniques to identify deviations from normal patterns, without having to know anything specific about the operation of a system [2,3]. Still others adopt an expert-system approach by evaluating rules over live telemetry from the building.

In contrast to MPC applications, which may require information about the composition and topology of an entire subsystem (usually HVAC), FDD applications typically require much more localized metadata. Many FDD rules are concerned with the operation of individual pieces of equipment. This means that the supporting metadata should capture the identification of equipment for FDD, and the properties of that equipment required to properly configure the FDD. These applications are therefore much more detailed and data-intensive, and are more likely needing multiple types of databases in their software architecture. Most FDD applications do not need the ability to actuate the building. This simplifies the platform requirements, especially compared with MPC. As with MPC, FDD application require the platform to provide a means of recording live observations about the state of equipment in the building.

4. A Representative Architecture

From a software architecture perspective, the requirements detailed above are nothing new. Many existing solutions --- building management systems, IoT platforms, SCADA systems, and so on --- incorporate a classic "three-layer cake" (Figure 2) above the hardware. A hardware abstraction layer interacts directly with deployed devices to provide standardized I/O interfaces to the rest of the platform. A system services layer provides storage, routing, scheduling and other essential functionality. Finally, an application layer on top presents an API and possibly an execution environment for software running on the platform.

This basic architecture is very flexible and leaves room for implementation choices such as which communication protocol and database to use. However, it is much less clear how metadata ontologies fit into this picture: what types of technologies should be used, and how do they interact with the other components of the

architecture? Furthermore, which metadata schemas should be used and to what extent? This particularly related to the two top layers in the given three-tier architecture in Fig. 2. Depending on the top-level application(s), database infrastructure and storage techniques can differ. Furthermore, application logic, e.g. computational models and black box prediction models, impact the stack further towards the two top tiers of the architecture.

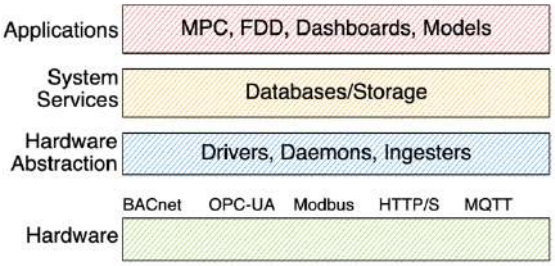

Fig. 2 – The three-layer architecture interacting with cyber-physical hardware (bottom) through a variety of protocols.

Based on the previous section, it is clear that the FDD case has the highest impact on the data infrastructure, as this has more challenging requirements on data infrastructure and prediction algorithms. The asset management case is less oriented towards live measurements, yet needs a similar semantic core to be managed for the building. The MPC case lastly is much more oriented towards the lower layers of the software stack and the devices (signal processing, communication and control). Hence we continue the construction of a reference architecture in this section with the FDD case primarily in mind, complemented with asset management features.

In the following sections, we first outline what the data infrastructure and computational setup might best be in the first and second tier of the 3-tier stack of Fig. 2. This includes a draft schema of how different databases and algorithms may best be combined and how all data can be interlinked without a too large data management overhead. Second, we elucidate in more detail how ontologies can support the software in the architecture. This is performed via the incorporation of a *metadata graph* that contains the relevant information to configure applications and enable them to discover important data sources and I/O points. The structure and content of the graph is informed by a family of RDF-based ontologies.

4.1 Computation-friendly Data Infrastructure

The first and second layer in the three-tier entire architecture of Fig. 2 are key in building a computation-friendly data infrastructure. As indicated before, the data infrastructure is highly required to include multiple types of databases (see Fig. 3). This cannot be a single database, not in RDF, not a relational database, not an object-oriented database (key-value store), because of the need for a very diverse set of data of different nature. Hence, the core of the reference system architecture needs to consist of a combination of these, as was also argued in many other places [2,3,7,30-32,35]. While flexibility may be useful in some cases, a highly interconnected network of data is better off with a defined and rigidly enough structure. Therefore,, it is highly recommended to adopt the more rigid ontologies for the management of the semantic data, in which case the LBD ontologies and the BRICK ontology and the IFC ontology are a better choice.

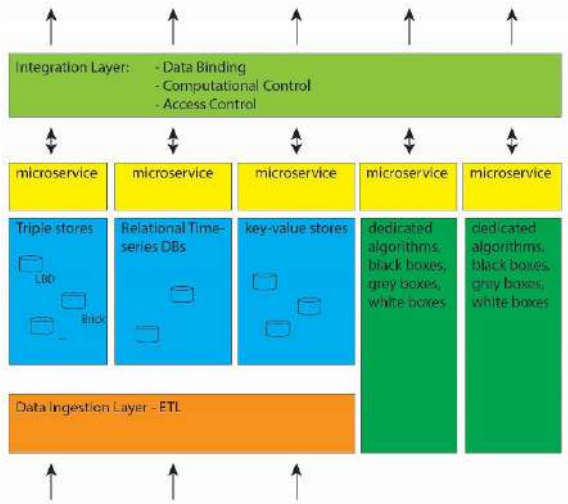

Fig. 3 – Core data infrastructure in combination with pre- and post-processing layers as well as computational components behind a microservice architecture.

To be able to connect to the upper and lower tiers, appropriate connectors are required, which can pre-process and post-process data coming in and going out of the system (top and bottom layers in Fig. 3). For example, in the case of asset management, a legacy IFC dataset needs to be transformed into the different core data models used in the system (not IFC). Similarly, timeseries data and the reference tags with which they are classified need to be put in correctly in the BRICK ontology as well as the corresponding timeseries databases. Furthermore, dedicated algorithms for FDD need to be provided in addition to the data, and these can be made accessible through microservices through the upper tier layer of the data infrastructure (Fig. 3).

4.2 Architecture of Supporting Ontologies

When considering more closely the metadata schemas and ontologies deployed in the proposed data infrastructure, we can clearly see how an "architecture" of ontologies is available that together forms the structure of a system metadata graph. In this case (FDD and asset management), we recommend here to adopt an entity-centric approach for the metadata supporting a data platform for buildings. Entities are the physical, virtual and logical "things" in a building which

produce and consume data. Examples of physical entities are sensors, equipment, devices, rooms and pipes. Examples of virtual entities are setpoints, commands, alarms and other digital registers. Examples of logical entities are zones, groups and other collections of entities. The identification of these entities constitutes the central part of the graph in Figure 4. The other parts of the graph contain different perspectives on those entities.

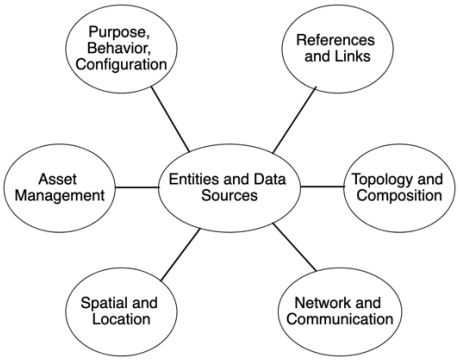

Fig. 4 – Categories of metadata required to support data-driven smart buildings. Circles represent ontology-based graphs.

Due to the diverse needs of applications [38], it is important that the graph provide multiple ways of identifying and understanding each entity. For example, FDD applications will require more *asset management* metadata to determine what kind of models and rules to use for each piece of equipment. FDD applications concerned with the health of the communication network will use *network and communication* metadata to diagnose connectivity issues. After faults are detected, an FDD application can leverage *spatial and location* metadata to tell a human operator where the broken device is. In contrast, MPC applications will require *topology and composition* and *purpose, behaviour and configuration* metadata to properly construct and configure the models of the system that allow optimal control sequences to be computed and executed. In each of these applications, *references and links* metadata (top layer in Fig. 3) provides the link between the representation of entities in the graph and how applications would interact with those entities: where historical data is, how to control the device's behaviour with an API, and so on.

5 Conclusion

The digital built environment transforms into a smart digital built environment. This leads to an abundance of data, algorithms and systems being commonly available for the creation of data-driven smart buildings. In recent years, several ontologies and metadata schemas have been proposed for supporting these smart buildings. In this paper, we reviewed mainstream approaches in that regard. While previous research focused a lot on schemas and vocabularies, this paper proceeded towards localising these ontologies in a draft reference system architecture. This draft architecture consists of three tiers (applications, systems and services, hardware abstraction). The systems and services layers has been detailed further in this paper, as a combination of different types of databases that is accompanied by a solid metadata infrastructure based on BRICK and LBD ontologies. The value of such a system lies primarily in FDD and asset management applications, yet, can be a solid basis also for MPC. Future work will focus on stress-testing the proposed architecture in multiple cases and examples internationally.

6. References

[1] Pritoni M, Paine D, Fierro G, Mosiman C, Poplawski M, Saha A, Bender J, Granderson J. Metadata Schemas and Ontologies for Building Energy Applications: A Critical Review and Use Case Analysis. Energies. 2021; 14(7):2024.

[2] Petrova E, Pauwels P. Semantic Enrichment of Association Rules Discovered in Operational Building Data for Reuse of Building Performance Patterns. In Proceedings of the 37th International Conference of CIB W78. Sao Paulo. 2020. p. 308-326.

[3] Xie X, Moretti N, Merino J, Chang J Y, Parlikad A K. Ontology-Based Spatial and System Hierarchies Federation for Fine-Grained Building Energy Analysis. Proceedings of the 38th International Conference of CIB W78, Luxembourg, 2021, pp 368-377.

[4] Pritoni M, Weyandt C, Carter D, Elliott J. Towards a Scalable Model for Smart Buildings. 2018. ACEEE Summer Study on Energy Efficiency in Buildings.

[5] Balaji B, Bhattacharya A, Fierro G, Gao J, Gluck J, Hong D, Johansen A, Koh J, Ploennigs J, Agarwal Y, Berges M, Culler D, Gupta R, Kjærgaard M B, Srivastava M, Whitehouse K. Brick: Towards a Unified Metadata Schema For Buildings. In Proceedings of the 3rd ACM International Conference on Systems for Energy-Efficient Built Environments (BuildSys 2016). Association for Computing Machinery, pp. 41–50.

[6] Linked Building Data Community Group. W3C Community Group Web Portal. https://www.w3.org/community/lbd/.

[7] Pauwels P, Costin A, Rasmussen M H. Knowledge Graphs and Linked Data for the Built Environment. 2022. Book Chapter in M. Bolpagni et al. (eds.), Industry 4.0 for the Built Environment, Structural Integrity 20. pp. 157-183.

[8] BuildingSMART. Industry Foundation Classes Specifications Database. https://technical.buildingsmart.org/standards/ifc/ifc-schema-specifications/.

[9] Pauwels P, Terkaj W. EXPRESS to OWL for construction industry: towards a recommendable and usable ifcOWL ontology. Automation in Construction. 2016;63:100-133.

[10] Rasmussen MH, Lefrançois M, Schneider GF,

Pauwels P. BOT: The building topology ontology of the W3C linked building data group. Semantic Web. 2021;12(1):143-161.
[11] BEO – Building Element Ontology. https://pi.pauwel.be/voc/buildingelement#.
[12] Wagner A, Rüppel U. BPO: The building product ontology for assembled products. In Proceedings of the 7th Linked Data in Architecture and Construction Workshop. 2019. CEUR Workshop Proceedings (Vol. 2389, pp. 106–119). https://ceur-ws.org/Vol-2389/08paper.pdf
[13] MEP – MEP ontology. https://pi.pauwel.be/voc/distributionelement#
[14] Rasmussen M H, Lefrancois M, Bonduel M, Hviid C A, Karlshoj J. OPM: An ontology for describing properties that evolve over time. In Proceedings of the 6th Linked Data in Architecture and Construction Workshop. 2018. CEUR Workshop Proceedings (Vol. 2159, pp. 24–33). https://ceur-ws.org/Vol-2159/03paper.pdf
[15] Bonduel M, Wagner A, Pauwels P, Vergauwen M, Klein R. Including widespread geometry formats in semantic graphs using RDF literals. In: Proceedings of the 2019 European Conference for Computing in Construction. European Council on Computing in Construction; 2019. p. 341–50.
[16] Bonduel M. The FOG ontology - File Ontology for Geometry formats. https://w3id.org/fog#
[17] Wagner A. Ontology for Managing Geometry (OMG). https://w3id.org/omg#.
[18] Garcia-Castro R, Poveda-Villalon M. SAREF extension for building (SAREF4BLDG). 2020. https://saref.etsi.org/saref4bldg/v1.1.2/
[19] Hamdan A-H, Bonduel M., Scherer R. An ontological model for the representation of damage to constructions. In Proceedings of the 7th Linked Data in Architecture and Construction Workshop. 2019. CEUR Workshop Proceedings (Vol. 2389, pp. 64–77). http://ceur-ws.org/Vol-2389/05paper.pdf
[20] RealEstateCore ontology. https://www.realestatecore.io/
[21] Brick consortium, Brick: a uniform metadata schema for buildings. https://brickschema.org/.
[22] Project Haystack. Ontology. https://project-haystack.org/doc/docHaystack/Ontology
[23] Fierro G, Koh J, Agarwal Y, Gupta R K, Culler D E. Beyond a House of Sticks: Formalizing Metadata Tags with Brick. In Proceedings of the 6th ACM International Conference on Systems for Energy-Efficient Buildings, Cities, and Transportation (BuildSys '19). Association for Computing Machinery, New York, NY, USA, 125–134.
[24] Kukkonen V, Kücükavci A, Seidenschnur M, Rasmussen M H, Smith K M, Hviid C A. An ontology to support flow system descriptions from design to operation of buildings. Automation in Construction. 2022; 134:104067.
[25] SkyFoundry. SkySpark. https://skyfoundry.com/
[26] Google. Google Digital Buildings. https://github.com/google/digitalbuildings
[27] Microsoft. What is Azure Digital Twins? 2021. https://docs.microsoft.com/en-us/azure/digital-twins/overview
[28] Fierro G, Pritoni M, Abdelbaky M, Lengyel D, Leyden J, Prakash A, Gupta P, Raftery P, Peffer T, Thomson G, Culler D E. Mortar: An Open Testbed for Portable Building Analytics. ACM Trans. Sen. Netw. 2020; 16(1); pp. 1-31.
[29] Dawson-Haggerty S, Krioukov A, Taneja J, Karandikar S, Fierro G, Kitaev N, Culler D E. BOSS: Building Operation System Services. In Proceedings of the 10th USENIX Symposium on Networked Systems Design and Implementation (NSDI 13). 2013. Pp. 443-457.
[30] Malcolm A, Werbrouck J, Pauwels P. LBD server: Visualising Building Graphs in web-based environments using semantic graphs and glTF-models. In Eloy S, Leite Viana D, Morais F, editors, Formal Methods in Architecture: Proceedings of the 5th International Symposium on Formal Methods in Architecture (5FMA), Lisbon 2020. Cham: Springer. 2021. p. 287-293.
[31] Werbrouck J, Pauwels P, Beetz J, van Berlo L. Towards a decentralised common data environment using linked building data and the solid ecosystem. In: Kumar B, Rahimian F, Greenwood D, Hartmann T, editors: Proceedings of the 36th CIB W78 2019 Conference. 2019. p. 113–23
[32] Schneider GF, Rasmussen MH, Bonsma P, Oraskari J, Pauwels P. Linked building data for modular building information modelling of a smart home. In: Karlshoj J, Scherer R, editors. eWork and eBusiness in Architecture, Engineering and Construction. CRC Press; 2018. p. 407–414.
[33] Solid. Solid: your data, your choice. https://solidproject.org/
[34] Manola F, Miller E, McBride B. RDF 1.1 Primer. W3C Working Group Note. 24 June 2014. http://www.w3.org/TR/rdf11-primer/
[35] Pauwels P, Terkaj W, Krijnen T F, Beetz J. Coping with lists in the ifcOWL ontology. In Proceedings of the 22nd EG-ICE Workshop 2015, Eindhoven, The Netherlands (pp. 111-120).
[36] Terkaj W, Schneider GF, Pauwels P. Reusing domain ontologies in linked building data : the case of building automation and control. In: Proceedings of the Joint Ontology Workshops 2017 Episode 3: The Tyrolean Autumn of Ontology. 2017.
[37] Drgoňa J, Arroyo J, Figueroa I C, Blum D, Arendt K, Kim D, Perarnau Ollé E, Oravec J, Wetter M, Vrabie D L, Helsen L. All you need to know about model predictive control for buildings. Annual Reviews in Control. 2020; 50; pp. 190-232.
[38] Bhattacharya A, Ploennigs J, Culler D E. 2015. Short Paper: Analyzing Metadata Schemas for Buildings: The Good, the Bad, and the Ugly. In Proceedings of the 2nd ACM International Conference on Embedded Systems for Energy-Efficient Built Environments (BuildSys '15). Association for Computing Machinery, New York, NY, USA, 33–34.

DEVELOPMENT OF AN OPTIMIZATION MODEL FOR DECISION MAKING IN BUILDING RETROFIT PROJECTS

Ehsan Asadi [a,b], *Manuel Gameiro da Silva* [b]

[a] MIT-Portugal program, Department of Mechanical Engineering, University of Coimbra, Portugal, ehsan.asadi@dem.uc.pt.

[b] ADAI – LAETA, Department of Mechanical Engineering, University of Coimbra, Portugal, manuel.gameiro@dem.uc.pt .

Abstract. Retrofitting of existing buildings offers significant opportunities for improving occupants' comfort and well-being, reducing global energy consumption and greenhouse gas emissions. This is being considered as one of the main approaches to achieve sustainability in the built environment at relatively low cost and high uptake rates. Although a wide range of retrofit technologies is readily available, methods to identify the most suitable set of retrofit actions for particular projects are still a major technical and methodological challenge. This study presents a simulation-based multi-objective optimization model to quantitatively assess technology choices in a building retrofit project (a combination of TRNSYS, and MOBO optimization freeware). This model is employed to assess a school building retrofit project as a case study to illustrate the practicability of the proposed approach, and therefore, the final decision (set of non-dominated solutions) for optimum building retrofit. The study starts with the individual optimization of objective functions focusing on building's characteristics and performance: primary energy consumption, global costs, and thermal discomfort hours. Then the proposed multi-objective optimization model is used to study the interaction between these conflicting objectives and assess their trade-offs.

Keywords. Energy, Indoor Environmental Quality for well-being in energy-efficient & retrofitted buildings.
DOI: https://doi.org/10.34641/clima.2022.435

1. Introduction

Buildings are among one of the major consumers of energy and therefore have a significant adverse impact on the environment. Although construction activities consume large amounts of energy, more than 80% of the energy consumed by a building during its life-cycle occurs when the building is in actual occupancy and use [1]. A building retrofit is the physical or operational change in a building, its energy consuming equipment, or its occupant's behavior to reduce the amount of energy to convert the building to a lower energy consuming facility [2]. Retrofitting of a building offers great opportunities for improving energy efficiency by reducing maintenance costs, reducing air emissions, creating job opportunities, enhancing human health, and improving thermal comfort [3, 4].

There are a number of models and methods developed to assess conditions and support decisions pertaining to building retrofit. These methodologies can be broadly categorized into two main approaches: the models in which alternative retrofit solutions are explicitly known a priori (see e.g. [6], [7], [8], [9]) and the models in which alternative retrofit solutions are implicitly defined in the setting of an optimization model (see e.g. [10], [5], [11], [12]).

The current study proposes an integrated MOO approach to develop a decision support model for building retrofit projects, based on the combination of TRNSYS, MATLAB and MOBO. The proposed methodology is used for the optimization of primary energy consumption, global costs, and thermal discomfort hours in a school building retrofit project. A wide decision space is considered,

Copyright ©2022 by the authors. This conference paper is published under a CC-BY-4.0 license.

including alternative materials for the external walls insulation, roof insulation, different window types, installation of a solar collector to the existing building, and a wide range of HVAC system types to meet heating and cooling requirements.

2. Methodology

The optimization framework is summarized in Figure 1. The scheme is a combination of TRNSYS 16, MOBO 0.3a and objective function calculator under MATLAB environment. TRNSYS [13] is a transient system simulation program with a modular structure that was designed to solve complex energy systems problems. MOBO is an optimization tool able to handle single and multi-objective optimization problems with continuous and discrete variables and constraint functions [14].

In this scheme first a model of the building before retrofit is created in TRNSYS. Then, using this model and MATLAB [15] as a post-processor of the objective functions, the combination is used within MOBO to evaluate the potential solutions.

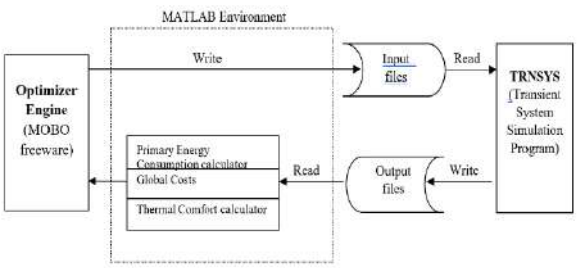

Figure 1 Optimization framework

2.1 Formulation of the optimization problem

This paper considers the multi-objective optimization (MOO) of buildings retrofit strategies. Therefore it requires the definition of appropriate decision variables, objective functions and constraints, and finally the selection of appropriate solution computation techniques.

2.1.1 Decision variables

The decision variables reflect the total set of alternative measures that are available for building retrofitting (e.g. windows, insulation materials, etc.). The set of retrofit actions concerns combinations of choices regarding external wall insulation material, roof insulation material, windows, installation of solar collector and different HVAC systems to the existing building. Five types of decision variables are defined concerning the alternative choices regarding:

- the external wall insulation materials;
- the roof insulation materials;
- the windows type;
- the solar collectors type;
- the HVAC systems.

For simplicity, it is assumed that only one retrofit action, from each one of the five sets of actions, may be selected for the building retrofit.

Assuming the availability of I alternative types of external wall insulation material, J alternative types of roof insulation material, K alternative types of windows, L alternative types of solar collector, and M alternative types of HVAC system, integer decision variables x^{EWAL}, x^{ROF}, x^{WIN}, x^{SC}, and x^{HVAC} are defined as follows:

x^{EWAL}: external wall insulation material type ident 1

x^{ROF}: roof insulation material type identifier 2

x^{WIN}: window type identifier 3

x^{SC}: solar collector type identifier 4

x^{HVAC}: HVAC system type identifier 5

A list of alternative retrofit actions applied in this study is based on a CYPE rehabilitation price generator database (CYPEingenieros 2010 [16]) and presented in Appendix A. This list includes 24 different external wall insulation materials, 18 roof insulation materials, 3 windows types, 4 solar collectors and 4 HVAC systems.

2.1.2 Objective functions

2.1.2.1 Primary Energy Consumption (PEC)

The primary energy consumption of the building is directly assessed by TRNSYS. The total primary energy consumption, PEC, consists in the sum of primary energy demands for space heating (QHEAT), space cooling (QCOOL) and sanitary hot water (QSHW) systems. SHW production by solar collector (QSC) is subtracted from the total primary energy consumption. Moreover, energy consumption for lighting is not included because this is not expected to significantly change as a result of the implementation of the considered retrofit actions.

2.1.2.2 Global Costs (GC)

The global costs for the building retrofit is defined as the NPV of all costs during the defined economic life cycle of the building, including investment costs (ReCost) and costs related to the use of the building. Investment costs include the initial costs for implementing the retrofit actions and also the NPV of the costs related to the replacement of building elements with a lifetime smaller than the defined economic life cycle of the building after the retrofit. Residual values for building elements with lifetimes longer than the economic life cycle are also taken

into account. Energy costs refer to the NPV of the energy bills for each year of the economic life cycle and maintenance costs refer to the NPV of annual costs with the maintenance of each building element and system.

ReCost(X), where (X denotes the vector of all decision variables) is calculated by adding individual retrofit action costs as follows:

$$ReCost(X) = A_{EWAL}.C^{EWAL}(X) + A_{ROF}.C^{ROF}(X) + A_{WIN}.C^{WIN}(X) + C^{SC}(X) + C^{HVAC}(X) \quad (6)$$

Where:

A_{EWAL} – exterior wall surface area [m²];

C^{EWAL} - cost in [€/m²] for selected external wall insulation material;

A_{ROF} - roof surface area [m²];

C^{ROF}- cost in [€/m²] for selected roof insulation material;

A_{WIN} - windows surface area [m²];

C^{WIN}– cost in [€/m²] for selected window;

C^{SC}- cost for selected solar collector [€];

C^{HVAC}- cost for selected HVAC system [€].

NPV of the costs are also calculated using the following formula:

$$NPV = -C_0 + \sum_{i=1}^{T} \frac{C_i}{(1+r)^i} \quad (7)$$

Where

$-C_0$: Initial Investment

C_i: Cash flow

r: Discount rate

T: Time

The retrofit actions (RAs) corresponding costs ($C^{EWAL}, C^{ROF}, C^{WIN}, C^{SC}, C^{HVAC}$) and the related maintenance costs are extracted from RAs characteristics that is estimated using CYPE software.

2.1.2.3 Total percentage of discomfort hours (TPMVD)

The metric used to assess thermal comfort is the predicted mean vote (PMV), based on Fanger's model [17]. PMV is representative of what, in average, a large population would think about a thermal environment, and is used to assess thermal comfort in standards such as ISO 7730 [18] and ASHRAE 55 [19]. It ranges from -3 (too cold) to +3 (too warm), and a PMV value of zero is expected to provide the lowest predicted percentage of dissatisfied people (PPD) among a population. In this study, an absolute value of 0.7 for PMV, the upper limit of category C, the less exigent comfort category in ISO 7730, is considered as the borderline of the comfort zone. Therefore, in order to maximize the thermal comfort, the total percentage of cumulative time with discomfort (|PMV| > 0.7) over the whole year during the occupancy period, TPMVD(X), should be minimized. The total percentage of discomfort hours is also predicted by TRNSYS. After processing this function in MATLAB, the MOBO uses the result to estimate TPMVD.

2.2 Multi-objective optimization

MOO models aim at capturing the multiple, conflicting and incommensurate aspects of evaluation of the merits of potential solutions, in order to identify their trade-offs and provide a sound technical basis to decision support. In general, due to the conflicting objective functions there is no unique solution to MOO but a set of non-dominated (Pareto optimal) solutions. In our model the simultaneous optimization of primary energy consumption, global costs and thermal discomfort hours is sought. This MOO model is of combinatorial nature because of its structure and decisions to be made, and it is nonlinear due to the building performance calculations. Therefore, an MOGA has been selected from MOBO library to characterize the non-dominated front.

In this work NSGA-II [20] is used from the library of MOBO optimization algorithms to tackle the multi-objective problem. Like any other GA, NSGA-II is based on the evolution of a population of individuals, each of which is a solution to the optimization problem. In this study, an individual represents a retrofit option (embodying different technologies and types of intervention) to be carried out in a building. To use a genetic analogy, each individual is represented by a chromosome whose genes correspond to a number of the individual's characteristics, as in Figure 2.

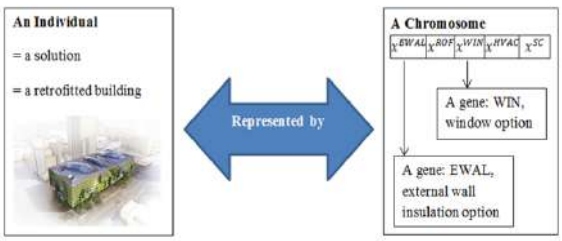

Figure 2 A solution to the retrofit optimization

problem, as presented by a chromosome

3. Model application on a school building

The school building is located in Coimbra, Portugal and serves some 800 students and 117 staff. The building consists of 6 blocks, the main block designed for administration purposes. 4 blocks (A, B, C and D), include classrooms and laboratories. These four blocks have similar architecture, with different number of stories. Blocks A and D have three stories and blocks B and C have 2 stories. The last block is the sport pavilion. Total occupied space floor area is 9,850 m2 and is divided between the 6 mentioned blocks.

In this project block A, one of the four identical blocks (Class rooms) is selected as a case study. The central zone in this block is a big atrium with visibility to all other sections in the building. This central zone uses natural lighting.

3.1 Building simulation

Table 2 presents summary of the set-up for the building. Based on this table, a building model is developed in TRNSYS. The type-56 multi-zone building is a reproduction of the reference building. The building model is divided into 5 zones: North zone, East zone, South zone, West zone, and Atrium zone. Heating is supplied locally in each room by electric resistance radiators; the buildings have no cooling system. However, as some of the considered HVAC retrofit actions include cooling systems, therefore, then an estimation of cooling needs was required. This has been taken into account by considering the recommended set point for cooling according to Portuguese national regulation RSECE [21] which is equal to 25˚C.The atrium is neither heated nor cooled. The TRNSYS model has been run using the existing building parameters described earlier, with one hour time step, using DOE typical meteorological year version 2 (TMY2) weather data.

To ensure accurate predictions of simulation, the base-case results were compared with monthly utility billing data. ASHRAE Guideline 14 [22] defines the standard for simulated data calibration. According to this guideline, simulation's degree of accuracy can be found by comparing the whole-building simulation data with actual building data using the two indicators that define error margins in comparison: CV_RMSE (Coefficient of variation of the root mean square error), and NMBE (Normalized mean bias error). For this case, CV_RMSE should be less than 15% per ASHRAE Guideline 14 while NMBE is suggested to be less than 5%. CV_RMSE and NMBE were found to be 12.81% and 3.26% respectively. Therefore, the base case model developed was considered acceptable for this case building.

Table 1 Brief description of the base building parameters for simulation

Location		*Coimbra, Portugal*
Building type		*School building*
Floor areas	*utility floor area*	*1,886 [m²]*
	conditioned floor area	*1,622 [m²]*
Dimension and Heights	*Average floor height*	*3.02 [m]*
	Window height	*2.7 [m]*
	Window-to-wall ratio	*65% , except South façade 59%*
Construction of building envelope	*External walls*	*2cm plaster + 11 cm Brick + 4cm air space + 11 cm brick + 2 cm plaster (U-value = 1.737 W/m²K)*
	Roof	*2cm plaster + 22cm concrete + 1cm bitumen + 4 cm cement (U-value = 2.654 W/m²K)*
	Windows	*Single-pane simple glass (U-value = 5.68 W/m²K, g-value = 0.855)*
Operating hours	*Monday to Friday*	*8:00 – 20:00*
	Weekend	*Closed*
HVAC parameters	*Total number of persons*	*200*
	Lighting + Equipment	*Lighting 10 W/m², Equipment 12 W/m²*
	Infiltration rate	*0.9 ACH*
	Cooling system	*None*
	Heating System	*electric resistance radiators*

Thermal set points	*20°C – No max.*

3.2 Multi-objective optimization

The final goal of the optimization problem in this phase is the simultaneous optimization of primary energy consumption, global costs, and total percentage of discomfort hours. The NSGA-II in MOBO is used to tackle this MOO problem and identify the set of non-dominated solutions. The MOO problem can be summarized as follows, using integer decision variables stated in (1) – (5):

$$Min\ Z_1(X) = PEC(X)$$

$$Min\ Z_2(X) = GC(X)$$

$$Min\ Z_3(X) = TPMVD(X)$$

$$S.t.$$

$$1 \leq x^{EWAL} \leq I, (I = 24) \qquad (8)$$

$$1 \leq x^{ROF} \leq J, (J = 18)$$

$$1 \leq x^{WIN} \leq K, (K = 3)$$

$$1 \leq x^{SC} \leq L, (L = 4)$$

$$1 \leq x^{HVAC} \leq M, (M = 4)$$

3.2.1 First set of optimization (single-objective)

In this first optimization set, the three objective functions (primary energy consumption, global costs, and total percentage of discomfort hours) have been individually minimized.

3.2.1.1 Single-objective minimization of primary Energy Consumption

The goal is to minimize primary energy consumption for heating, cooling and SHW purposes. The results are given in Table 3.

In the PEC optimized building, the insulation level is high with thick layers of insulating material with low U-values for external wall and roof. In addition, window type 3, which has the lowest thermal transmittance, is selected. Regarding the HVAC system, a natural gas boiler is recommended. Furthermore, the flat solar collector with highest area among all the systems considered is recommended. However, this set of retrofit actions resulted in a significant increase of the global costs with respect to the GC optimized building.

Table 2 Results of single-objective optimization (Refer to Appendix A for RAs characteristics)

Type of solution	*PEC [kWh/m²year]*	*GC [k€/m²]*	*TPMVD [%]*	*EWAL*
[min] PEC	***4.69***	*147.36*	*16.85*	*15*
[min] GC	*44.40*	***21.19***	*36.46*	*1*
[min] TPMVD	*18.40*	*101.13*	***16.7***	*16*

3.2.1.2 Single-objective minimization of global costs

The results of this optimization are given in Table 3. Minimizing global cost results in low insulation level of external wall insulation and single glazed window. In addition, the cheapest HVAC system (oil-based boiler without cooling system) and the cheapest solar collector are recommended. However, this results in a significant increase of the energy consumption and thermal discomfort hours compared to the EC and TPMVD optimized buildings.

3.2.1.3 Single-objective minimization of total percentage of discomfort hours

The aim is to minimize the total percentage of thermal discomfort hours in the building. There is no cooling system in the existing building, either active or passive. The results are given in Table 3.

Minimizing TPMVD results in high insulation level and double glazed windows, similarly to minimization of energy consumption. Regarding HVAC system, HVAC type 2 with natural gas boiler for heating and chiller for cooling is selected that leads to significantly better indoor comfort compared to the existing building.

As can be seen from Table 3, the results for minimization of global costs diverged significantly from the others. The solutions that minimizes primary energy consumption and thermal discomfort are comparable, which is due to the nature of retrofit actions considered and objective functions. This table can be used to shape the expectation of the DMs and help them to elicit appropriate bounds to objective function values to focus the search for new solutions in restricted regions of the search space.

3.2.2 Second set of optimization (two-objective)

In each of these multi-objective optimizations, two objectives were chosen from among primary energy consumption, global costs, and total percentage of discomfort hours.

3.2.2.1 Multi-objective optimization of primary energy consumption and global costs

The single-objective optimization suggests that these objectives are strongly opposed. The results are given in Figure 6. Each point on the Pareto front is a solution associated with a set of decision variables representing retrofit actions.

Wall and roof insulation material as well as windows and HVAC and solar collector systems vary in different non-dominated solutions. Also, it is worthwhile to mention that the solutions on the Pareto front are grouped according to the window types. This reveals that the window type has a stronger influence on the low PEC cost-effective solutions than the other decision variables.

To obtain the best solutions of GC, single glazed window (WIN=1), the lowest price window is found to be optimal with incrementally additional insulation. As the thickest insulation with lowest U-values for external wall and roof (EWAL= 24, ROF = 6) as well as the largest solar collector (SC=2) are selected, the optimization leads to double-glazed window (WIN=2). This leads to a significant reduction in the PEC, explaining the discontinuity in the Pareto front at 39 kWh/m^{2}year of PEC as illustrated in Figure 6. A similar gap happens at PEC = 27.8, where the optimization leads to window type 3 with lowest U-value resulting to a significant reduction in the PEC.

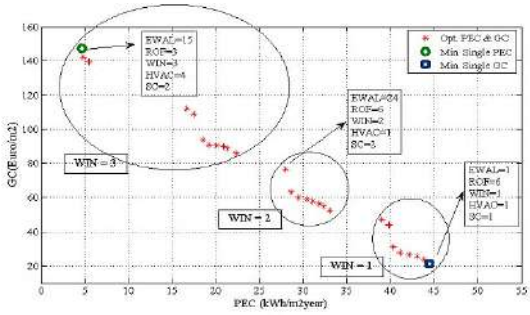

Figure 3 Multi-objective solutions for the building retrofit strategies (PEC - GC) (Refer to Appendix A for RAs characteristics

3.2.2.2 Multi-objective optimization of total percentage of discomfort hours and global costs

The results of this optimization are given in Figure 7. The different non-dominated solution all fall between two single-objective optima.

Regarding the solar collector, all the recommended solutions are equal: the cheapest solar collector is recommended. All the other retrofit actions vary in different non-dominated solutions. The optimization of TPMVD leads to using optimal combinations between the building envelope parameters (including external wall and roof insulation materials, and window type) and the HVAC system type. As in previous case, the solutions obtained on the Pareto front are grouped according to the window types. This again indicates that the window type has a stronger influence on the solutions than the other decision variables.

Double glazed window with lowest thermal transmittance, thick layer of insulation with low U-values for external wall insulation and roof, and the HVAC system type 2 with cooling option are selected giving the lowest TPMVD value. For a higher reduction in GC, HVAC system type 1 is used. Moreover, window type 2 and then type 1 is selected to reduce the GC. There is a large discontinuity in the Pareto front at 34.41% of TPMVD. This can be explained by changing the HVAC type 1 to 2 with cooling option.

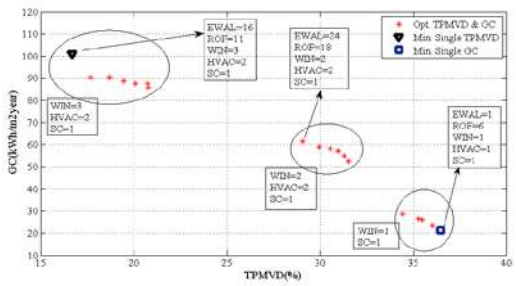

Figure 4 Multi-objective solutions for the building retrofit strategies (TPMVD - GC) (Refer to Appendix A for RAs characteristics)

3.2.2.3 Multi-objective optimization of primary energy consumption and total percentage of discomfort hours

The aim is to simultaneously minimize PEC and TMPVD. The optimization process generates just three solutions, which form the Pareto front. The single-objective optimization results for PEC and TPMVD are similar, with one major difference regarding the HVAC system. It is worthwhile also to mention that the small number of non-dominated solutions is due to the fact that the lower PEC values are mainly achieved with the HVAC system type 1 without cooling option (HVAC = 1) that leads to high TPMVD values. Therefore, a large number of potential solutions are dominated by the PEC optimal solution.

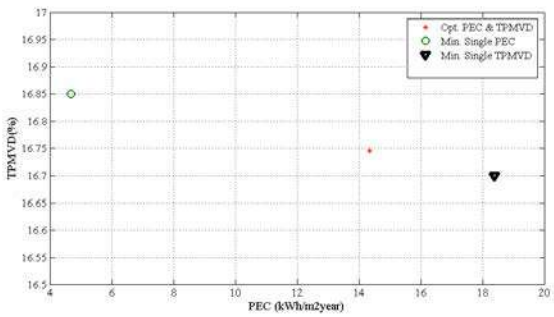

Figure 5 Multi-objective solutions for the building retrofit strategies (PEC – TPMVD) (Refer to Appendix A for RAs characteristics)

The three sets of optimization presented above results in the following conclusions:

- The number of non-dominated solutions for objectives with not much in conflict characteristics is lower than for those with dissimilar characteristics.
- The analysis of the results shows the physical characteristics of solutions and helps to understand the simultaneous influence of the decision variables on the PEC, GC, and TPMVD.
- Without considering a constraint on summer overheating, the influence of the window type on the results is more significant than the influence of the other decision variables.
- There are often discontinuities in the Pareto front where it is possible to gain a lot in one objective by sacrificing only a little in the other objective, so the trade-off analysis is essential for reaching a compromise solution.

4. Conclusions

This project proposed a multi-objective optimization model based on a combination of TRNSYS, MATLAB and MOBO. The proposed approach was applied to a school building case study, and the results demonstrate its practicability to provide decision support in an actual setting. In case an exhaustive-computation search method is implemented, then 20,736 simulation runs are needed to obtain all possible candidate solutions. The execution time of one simulation run is about 5.19 min. This means that 75 days would be required to get the result of an exhaustive search for this problem, which means the computation and analysis is only practical using an approach as the one herein proposed.

The single-objective optimization runs offered an overview of the impact of more "extreme" sets of retrofit actions, i.e. the ones individually optimizing each objective function, on the building's overall performance after retrofit. Then, the proposed multi-objective approach produced a wide range of non-dominated solutions embodying distinct trade-offs between the competing objectives. The model assessed the solution overall performance, while at the same time quantifying the impact of individual components. Furthermore, 2D graphical representation of non-dominated frontier unveils the trade-offs between the objectives.

Moreover, using the graphs, one can ascertain the impact on thermal comfort and global costs of any reduction or increase in the energy consumption. The final decision can therefore be based on a thorough understanding of the trade-offs, and the impact of primary energy consumption on thermal comfort and global costs. The search space, and therefore the set of non-dominated solutions, depends on the alternative retrofit actions considered and the constraints that may be imposed to their combination.

The proposed approach shows a great potential for the solution of multi-objective building retrofit problems, and can be used as an aid to decision-making in the context of a retrofit project. Knowing what can be feasibly achieved and what trade-offs are at stake, the DMs can progress towards the choice of the best compromise solutions by inserting additional bounds on the objective function values or look for solutions closer to their aspiration levels.

5. Acknowledgement

The project was funded by ADAI-LAETA, University of Coimbra: under the project RETROSIM—Multi-objective building retrofit, simulation and monitoring on-line optimization tool for improving energy efficiency in buildings with the reference PTDC/EME-SIS/32503/2017 and POCI-01-0145-FEDER-032503.

6. References

[1] Menassa, C.C. Evaluating sustainable retrofits in existing buildings under uncertainty. Energy and Buildings. 2011;43(12):3576-83.
[2] Jafari A, Valentin V. An optimization framework for building energy retrofits decision-making. Building and Environment. 2017;115:118-29.
[3] Ma Z, Cooper P, Daly D, Ledo L. Existing Building Retrofits: Methodology and state-of-the-art. Energy and Buildings. 2012;55:889-902.
[4] Pombo O, al. e. Sustainability assessment of energy saving measures: A multi-criteria approach for residential buildings retrofitting—A case study of the Spanish housing stock. Energy and Buildings. 2016;116:384-94.
[5] Diakaki C, Grigoroudis E, Kolokotsa D. Towards a multi-objective optimization approach for improving energy efficiency in buildings. Energy and Buildings. 2008;40(9):1747-54.
[6] Gero JS, Dcruz N, Radford AD. Energy in Context - a Multicriteria Model for Building Design. Building and Environment. 1983;18(3):99-107.
[7] Jaggs M, Palmer J. Energy performance indoor environmental quality retrofit — a European diagnosis and decision making method for building refurbishment. Energy and Buildings. 2000;31:97-101.
[8] Flourentzou F, Roulet CA. Elaboration of retrofit scenarios. Energy and Buildings. 2002;34:185-92.
[9] Rey E. Office building retrofitting strategies: multicriteria approach of an architectural and technical issue. Energy and Buildings. 2004;36:367-72.
[10] Asadi E, da Silva MG, Antunes CH, Dias L. A multi-objective optimization model for building retrofit strategies using TRNSYS simulations, GenOpt and MATLAB. Building and Environment. 2012;56:370-8.
[11] Asadi E, da Silva MG, Antunes CH, Dias L. Multi-objective optimization for building retrofit strategies: A model and an application. Energy and Buildings. 2012;44:81-7.

[12] Diakaki C, Grigoroudis E, Kabelis N, Kolokotsa D, Kalaitzakis K, Stavrakakis G. A multi-objective decision model for the improvement of energy efficiency in buildings. Energy. 2010;35(12):5483-96.

[13] TRNSYS. TRNSYS 16, A TRaNsient SYstems Simulation Program, version 16. USA: Solar Energy Laboratory, University of Wisconsin, 2009.
[14] Matti Palonen MH, Ala Hasan. MOBO Beta 0.3a Manual Version 1.3. 2014.
[15] Mathworks. MatLab Optimization Toolbox User's Guide. Natick, MA2010.
[16] CYPEingenieros. Software for Architecture, Engineering & Construction. 2010.
[17] Fanger P. Thermal Comfort. Danish Technical Press. 1970.
[18] ISO. Ergonomics of the thermal environment — Analytical determination and interpretation of thermal comfort using calculation of the PMV and PPD indices and local thermal comfort criteria. Geneva: ISO; 2005.
[19] ASHRAE. Thermal environment conditions for human occupancy. Atlanta: American Society of Heating, Refrigerating, and Air-Conditioning Engineers, Inc.; 2004.
[20] Deb K. Multi-objecvtive optimization using evolutionary algorithms. New York: John Wiley & Sons, 2001.
[21] Regulation for the energy and HVAC systems in buildings (in Portuguese: Regulamento dos Sistemas Energéticos de Climatização em Edifícios—RSECE). Decree-Law no 79/2006. Official Gazette of the Portuguese Republic2006.
[22] ASHRAE. Measurment of energy and demand savings. ASHRAE Guideline 14. US Standard2002.

From Data To Control: Learning an HVAC Control Policy

Bram de Wit [a], Lambert Schomaker [b], Jaap Broekhuizen [c]

[a] Advanced Climate Systems, Groningen, the Netherlands, b.dewit@acs-buildings.com

[b] Faculty of Science and Engineering, University of Groningen, Groningen, the Netherlands, l.r.b.schomaker@rug.nl

[c] Advanced Climate Systems, Groningen, the Netherlands, j.broekhuizen@acs-buildings.com

Abstract. This study introduced a framework for smart HVAC controllers that can be used at scale. The proposed controllers derive their control policy solely from data. First a simulator of the process is learned, which we call the Neural Twin. The results showed that the Neural Twin framework is able to simulate several distinct processes with an average absolute error close to 0.2 °C for all processes, even when predicting several hours ahead. Then, the Neural Twin was used to develop two different control algorithms. The first algorithm learned a control policy for a process using a neural network. The network was trained using Proximal Policy Optimization by gathering experience from the simulated environment provided by the Neural Twin. The second algorithm performed Model Predictive Control using the Neural Twin at real time during control. It used the Neural Twin to choose an optimal control sequence, given a set of possible control sequences. It selects the optimal control sequence based on a horizon, which is usually a few hours ahead. Both control algorithms were inspected in several environments and for one of those environments the best controller was tested on a physical room. The results show that the control algorithms were able to handle a wide variety of different processes, without manual tuning. The controllers achieved improved performance compared to the conventional control algorithms, which were manually tuned, mainly in terms of energy usage. It is estimated that the proposed controllers can lead to a 5% - 40% decrease in effective energy usage, while retaining the thermal comfort and stability. The controller trained using reinforcement learning showed the best performance. From the results it was concluded that the control methods pose an attractive alternative compared to conventional controllers.

Keywords. Deep Learning, Reinforcement Learning, HVAC control, system identification.
DOI: https://doi.org/10.34641/clima.2022.362

1. Introduction

Within a building the indoor climate is often actively regulated. This regulation is performed by Heating, Ventilating and Air Conditioning (HVAC) systems. There are various motivations for indoor climate regulation such as providing thermal comfort for occupants of the building, maintaining good conditions in greenhouses for growing crops or storing wares which require certain climate conditions.

According to the National Human Activity Pattern Survey, a person spends approximately 87% of their time indoors [1]. Furthermore, several studies have already shown the negative impact of poor indoor climate conditions, which can cause health issues and decreased productivity for occupants of the building, also known as the Sick Building Syndrome [2]. For these reasons, maximizing the quality of the indoor climate is desirable.

In general, regulating the indoor climate in buildings results in both energy costs and carbon dioxide emissions. Obviously it is desirable to reduce both of these as much as possible. The International Energy Agency claimed the following in their report of 2018: "The buildings and construction sector should be a primary target for greenhouse gases (GHG) emissions mitigation efforts, as it accounted for 36% of final energy use and 39% of energy- and process-related emissions in 2018." ([3] page 12). The same report showed that 30% of the process related energy is used by buildings alone and 28% of the energy-related carbon dioxide emissions come from buildings.

The goals above pose a conflict, as regulating the indoor climate always increases energy demand (compared to simply not regulating the indoor climate). This means that in the end a tradeoff has to be made between the quality of the indoor climate regulation and the energy consumption.

Copyright ©2022 by the authors. This conference paper is published under a CC-BY-4.0 license.

Much research has already been done with respect to machine learning and smart building controllers. An extensive survey of AI-assisted HVAC control is given in [4]. One of the difficult parts of HVAC control is that often the underlying dynamics of a building are unknown, and these dynamics can be very complex. When finding optimal HVAC control policies, it can be useful to try and understand the underlying dynamics of the system one is trying to control. This knowledge can then be exploited to create a good control policy. The process of using observed data of the process to build mathematical models of that dynamical system is called *system identification*.

An important part of system identification for building control is indoor temperature prediction. Many machine learning methods have been used for this purpose and have proven to be successful [5]. In [6], a Long Short-Term Memory-based (LSTM-based) sequence-to-sequence framework was proposed, achieving good results in predicting indoor temperatures 6 hours ahead at a 10 minute interval. The Neural Twin framework presented in this study was heavily based upon this work.

The recent developments in the field of Deep Reinforcement Learning (DRL) have also been applied to HVAC control. A recent survey showed the potential of these methods [7]. Although promising, the survey concluded that most DRL-based methods are studied within a simulation setting, and gives as reason that DRL-based agents require much time to train, making online deployment simply not desirable. Another survey showed that of the 77 articles that were studied [8]:

1. The majority of the DRL agents in the studies did not control the actuators of the building directly. Instead, they controlled for example the setpoint that a controller needs to regulate. Classic controllers were still needed to track the setpoints determined by the DRL agent;
2. 91% of the studies did not include previous states as inputs;
3. 90% of the studies used data simulated by simulation software such as EnergyPlus;
4. 83% of the studies did not include predictions as inputs;
5. Only 11% of the studies implemented and tested their approaches in an actual building.

Both surveys agree on the fact that no standardized benchmark exists for this problem, which have advanced the research in computer vision, speech recognition and reinforcement learning.

Reinforcement Learning has been applied onto many different parts of the building's control. In [9], the main supply temperature is determined and compared to the baseline as provided by ASHRAE, which is based on the outside air temperature. Another study trained different Q-networks for all zones in the building [10]. There, temperature violations were kept approximately constant but the cost of regulating was decreased significantly. In [11], 5% - 12% energy savings were achieved, also by controlling supply temperature setpoints. It made the action space discrete by letting the agent choose between five different supply temperatures. All three studies mentioned above used simulated data and evaluated the performance using a simulator.

To the best of the authors' knowledge, only one study tried learning a DRL using an environment based on a model which learned the system dynamics of the building [12] (hence, it did not need a simulator). In that study, an LSTM was used to approximate state transitions from state action pairs, on which an agent was trained. The agent learned to determine optimal setpoints for three air handling units (trained separately), decreasing the energy consumption with 27%-30% while retaining thermal comfort.

This study contributes to the literature presented above by:

1. Introducing a scalable approach for learning a HVAC control policy, solely using sensor data gathered from real buildings (instead of a simulated buildings);
2. Controlling the actuators of a building, rather than the setpoints. Therefore, it completely substitutes classical control methods;
3. Testing the approach on a variety of environments, with different physical properties and different HVAC controls, showing the scalability of the approach;
4. Testing the obtained controller on a real building, validating its performance in the physical world.

2. Research Methods

2.1 Data

In order to use the approach described in this study, a time series data set is needed which reveals the dynamics of the system at interest. A constant interval is assumed, which can and should be varied for different processes, i.e. for fast processes this interval can be 2 minutes, whereas for a slow process (regulating a swimming pool for example) the interval can be 10 minutes.

The data was retrieved from Climatics, the building management system of the buildings used in this study. Data from Climatics is always available at a 2 minute interval, hence it should be re-sampled when training for relatively slow processes.

At every timestep t, all sensor values are observed, which will be denoted as the observation vector $\mathbf{o}_t$.

From the day a building starts logging, up until now, it will collect these observation vectors at a fixed time interval (every 2 minutes), creating a sequence of observations $\{\mathbf{o}_0, \mathbf{o}_1, \ldots, \mathbf{o}_T\}$ where T is the current time. It is important to note that a single observation does not yield the full system state, as a state will consist of temperatures and values moving in a particular direction and this direction is not included in $\mathbf{o}_t$.

An observation at a specific time step consists of several components.

1. Values for all sensors of the building relevant for the specific process. These can be splitted into three types of sensors: the sensors to model (room temperatures), actuator sensors and remaining/external sensors that cannot be modelled or controlled, but are relevant for the process.
2. Values for weather data. In this study, weather data is retrieved using the DarkSky API, which provides hourly weather data. In the data set, weather data is padded (thus during an hour the weather data remains constant).
3. Encoded cyclic time information. Three cycles can be identified for a data set of a building: a day cycle, a week cycle and a year cycle. All cycles are mapped to a unit circle, and the corresponding x and y coordinates are fed to the network as input.

In general, the data was used to simulate short episodes of historical data. In order to do this, a certain start time t is considered. Then the input sequence will be several hours leading up to t. The target sequence will be several hours after time t. During real-time control, t will be the current time.

2.2 Environments

This study tested on four different environments. The environments all vary in some factor, either in size, geographic location or HVAC control system. The four environments are:

1. Sports hall, Slochteren. A relatively large room heated by a radiator. A schematic of the control system for this room is given in Figure 1.
2. Sports hall, Hoogezand. A comparable room heated by a radiator, located in Hoogezand.
3. Changing rooms, Hoogezand. A relatively small room, heated by a radiator.
4. Central hall, Kalckwijck. A large entry hall heated by an air handling unit.

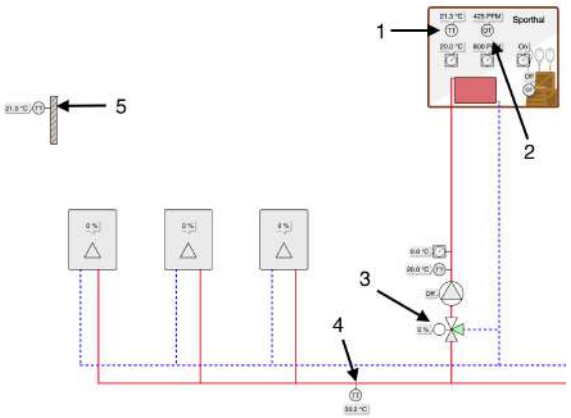

Fig. 1 - This figure was taken from Climatics. It shows the schematic for environment 1: the sports hall in Slochteren. The schematic shows the relevant sensors for this environment. Sensor 1: air temperature of the sports hall. Sensor 2: CO2 sensor, measuring parts per million (PPM), i.e. the concentration of the air. Sensor 3: valve position for the radiator. Sensor 4: central supply temperature. Sensor 5: outside air temperature.

2.3 Neural Twin

The Neural Twin is an Encoder-Decoder model based on Gated Recurrent Units (GRUs). A GRU retains its state over time, which is often called the hidden state. The sensor data fed to the network modifies this hidden state over time. In the context of control systems, Encoder-Decoder architectures can be interpreted as follows: Both the encoder and the decoder share the same memory structure (the GRUs have the same hidden size). The encoder will encode all past observations $\{\mathbf{o}_{t-h}, \ldots, \mathbf{o}_{t-2}, \mathbf{o}_{t-1}\}$ in order to yield a compact representation of the state of the process. The hidden state of the encoder is then used as the initial hidden state of the decoder. Then, when feeding a new observation to the decoder, it predicts the process values one timestep in the future. This can be realised by stacking a Multilayer Perceptron on the decoder, which interprets the hidden state at that time. However, as opposed to the encoder input, the input of the decoder might consist of only the process and control values of the system (excluding any external variables such as weather variables) depending on the use case of the Neural Twin. For Model-Predictive Control the latter is desirable because at inference time the model will not have access to the future values of external variables. When constructed like this, one can use the outputs of the decoder in combination with newly generated control values to simulate a trajectory over a short horizon. If, however, the goal of the model is to simulate the system as accurately as possible, one can choose to let the input of the decoder consist of the full observation. In this case, one can use historical data for these external variables concatenated with the output of the decoder and generated control values as input for the decoder. This might be desirable when one wants to train a Reinforcement Learning agent in a simulation

setting. Then, the Neural Twin will not be needed during inference, as in that case the trained agent will take over the control, which does not require future values of external variables.

A schematic view of an Encoder-Decoder network in the context of a control system is given in Figure 2. This figure shows the case where the decoder network omits external variables in its input. If this would be added, it would mean that at every timestep historical values for these external variables should be added.

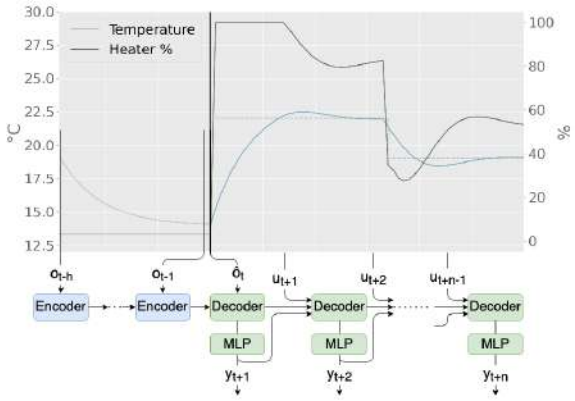

Figure 2 - A schematic view of a Neural Twin model where the decoder model expects a different number of inputs then the encoder model. The black vertical line represents the split between past observations and future observations. Past observations $\{\mathbf{o}_{t-h},\ldots,\mathbf{o}_{t-2},\mathbf{o}_{t-1}\}$ are fed into the encoder. Next, an initial observation $\mathbf{o}_t$ is fed to the decoder and from there the decoder simulates using its previous output $\mathbf{y}_{t+1}$ and newly generated control values $\mathbf{u}_{t+1}$ to generate output $\mathbf{y}_{t+2}$, and so on.

The Neural Twin is trained using gradient descent. It is trained for several epochs using mini batches. An important concept called teacher forcing is used during training. Teacher forcing means that during training the decoder receives the target value of the previous timestep as input, instead of its own output from the previous timestep. This helps speed up convergence at the beginning of training, as in the beginning it is likely that at the end of a target sequence the inputs for the decoder will be far from the realistic inputs when using its own outputs. During the course of training, less teacher forcing will be used and eventually the decoder will only use its own outputs. Then, when teacher forcing is no longer used, the learning rate is decreased exponentially over the remaining epochs. In order to enforce regularization, simple weight decay is used. This forces the weights to remain smaller, which helps against overfitting.

2.4 DRL Control Agent

The trained Neural Twin can be used as a simulator for a DRL agent that will try to learn an optimal control policy. In this case it is desirable to provide full input to the decoder of the Neural Twin, as it will only be used as a simulator. Historical data was used for the external variables during simulation.

In this study, a Multilayer Perceptron is used to parameterize the control policy learned by the agent. These types of networks expect only a single vector as input. However, giving only the current observation $\mathbf{o}_t$ as input for the network will not be enough, as the network will not be able to extract higher order movements of the system (for example is the temperature increasing or decreasing?). Inspired by [13], the past *n* observations will be concatenated. In addition to this, the agent will need to know the desired setpoint of the room. The setpoint will be concatenated to the past observations and these will serve as inputs for the policy network.

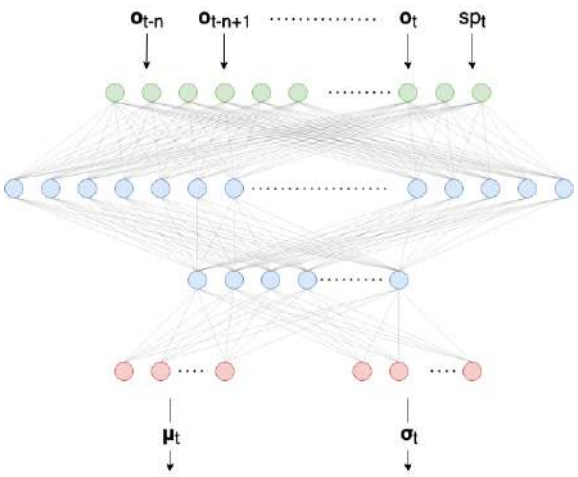

Figure 3 - A schematic view of the policy network used by the agent.

In order to perform exploration during training, the network is designed to output a mean and a standard deviation for every actuator of the control problem, i.e. $\boldsymbol{\mu}_t$ and $\boldsymbol{\sigma}_t$. During training, a value will be sampled from the distributions formed by these outputs, i.e. $\mathbf{a}_t \sim N(\boldsymbol{\mu}_t, \boldsymbol{\sigma}_t)$. During inference, the means will be used as actions. The action eventually produced by the agent will be offsets for the current control values. Hence, if there is a single actuator that has a current value of 50 and the output of the network is -2, the actuator's value will become 48. A schematic view of the policy network is given in Figure 3.

Proximal Policy Optimization [14] is used to train the agent. The Neural Twin of the environment is used to simulate episodes. It will take historical start moments, but then use the control values generated by the agent to simulate short episodes and gather experience to learn from.

Reinforcement Learning algorithms are designed to optimize a reward function. The reward function

describes quantitatively how 'good' the current state is. The reward function in this study consists of three weighted parts. The weights allow one to prioritize certain factors of control more compared to others. The reward function account for the following three factors:

1. Thermal comfort: the agent is rewarded by being close to the setpoint.
2. Stability: the agent is rewarded when its control is considered stable. The first order movements of the control values are used to measure this.
3. Energy consumption: the agent is rewarded more when using less energy.

This leads to the total reward:

$$R_{total} = R_{thermal} + \alpha R_{stability} + \beta R_{energy}$$

Here, α and β can be used to weigh the different parts of the reward. The aim of the agent is to find a policy that maximizes this reward function.

2.5 Model-Predictive Control

Another way to utilize a trained Neural Twin is by using it for Model-Predictive Control (MPC). Note that for MPC the decoder of the Neural Twin can only accept the control values and the values it predicts as input. At run time future values for other sensors will not be available.

In this study, the random-sampling shooting method was used for MPC. When applied to the process of controlling a room, it generates K random action sequences for a specific horizon h. The Neural Twin is now used to simulate many trajectories $\mathbf{y}$ for each of these control sequences. For all the trajectories a cost can be calculated, and the first action of the control sequence that yielded the lowest-cost trajectory will be executed. This is repeated at every timestep. Also here, the actions that are denote offsets for the current control value. The actions were within the range of -50% and 50%.

The cost function plays the key role in MPC, as it determines what is the best trajectory, and hence what will be the next control value. The cost function used will be the conjugate of the reward function used for DRL, hence both algorithms will optimize for the same objective: DRL optimizes the reward, whereas MPC minimizes the cost.

Note that after training a Neural Twin, no additional training is needed, and it can be used directly for MPC. The algorithm's performance is heavily dependent on the hyperparameters h and K. The horizon h must be long enough to be able control the process accurately, but short enough in order for the Neural Twin to remain accurate. The number of sequences K must be large enough in order to generate enough sequences such that a good control sequence will be found, but small enough such that it remains computationally feasible.

2.6 Experimental Setup

The ultimate goal of the study was to obtain a control policy that maximizes performance. Before such a policy is obtained, several steps need to be taken. For each of these steps, experiments were conducted for a total of 4 different environments. For every environment, the following experiments were performed:

1. One in which the validity of Neural Twins of an environment is verified. The error of the predictions of the Neural Twin was reported.
2. One in which the validity of training a DRL agent on a Neural Twin of an environment is verified. The reward of the trained agents was reported.
3. One that reveals the influence of the hyperparameters for MPC control. The cost of control was reported for various combinations of hyperparameters.
4. One in which the two control methods are compared, based on control on the Neural Twin. The cost/reward of the control algorithms were compared when controlling on the Neural Twin.
5. One in which the two control methods are verified by trying them out in a physical environment. This was done only for the sports hall in the Duurswoldhal, because testing on buildings can be costly and the authors got permission for this location.

3. Results

Figure 4 shows the result of the training of a Neural Twin for environment 1. The figure shows the mean and standard deviation of the training and validation loss over time for ten Neural Twins. As can be seen from the figure, the training and validation loss converge after approximately 25

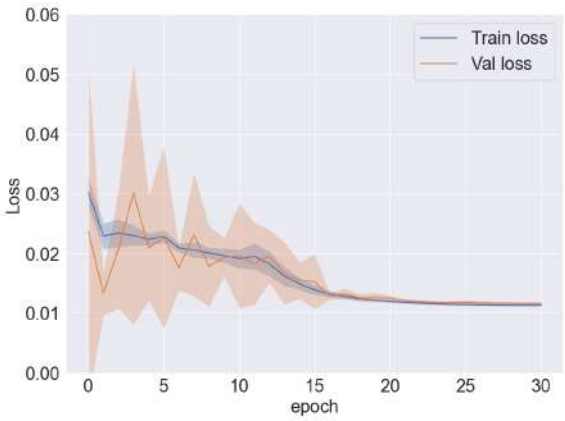

Figure 4 - Neural Twin training results for environment 1.

epochs around the same value, with low variance.

The same was observed for the other environments, but the graphs are excluded for brevity. Table 1 shows the error of the Neural Twins on the test set measured in ◦C for all environments.

Tab. 1 - Neural Twin results on the test data. The mean and the standard deviation of the ◦C error on the test data for the 10 training procedures are given.

Env	Error in ◦C
1	0.24 ± 0.21
2	0.23 ± 0.32
3	0.16 ± 0.13
4	0.20 ± 0.16

Figure 5 shows the results of training an DRL agent 10 times on the Neural Twin for environment 1. The graphs for the other environments are excluded for brevity. It can be observed that the training and validation reward converges over time, both to approximately the same value with low variance. Other environments showed the same behaviour.

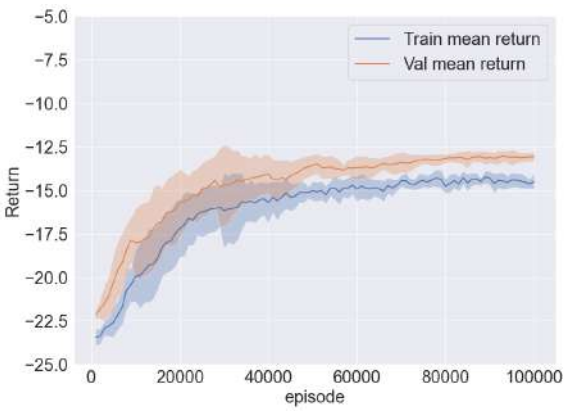

Figure 5 - DRL agent training results for environment 1.

Figure 6 shows the results for the hyperparameter experiment for environment 1. The graphs for the other environments are excluded for brevity. It is observed that the cost decreases for longer horizons and for a larger number of random sequences. The optimal combination of hyper parameters lies somewhere around the horizon of nine or ten timesteps ahead with at least 200 sequences, as there the cost is the lowest.

Table 2 shows the results when comparing the DRL agents to the conventional controller used when collecting the data, based on simulations with their corresponding Neural Twin. A negative percentage denotes an improvement, whereas a positive percentage denotes a decrease in performance. It can be observed that the DRL agents were able to decrease the energy usage for all environments while approximately retaining the same amount of comfort and stability. Table 3 shows the same but for the MPC algorithm.

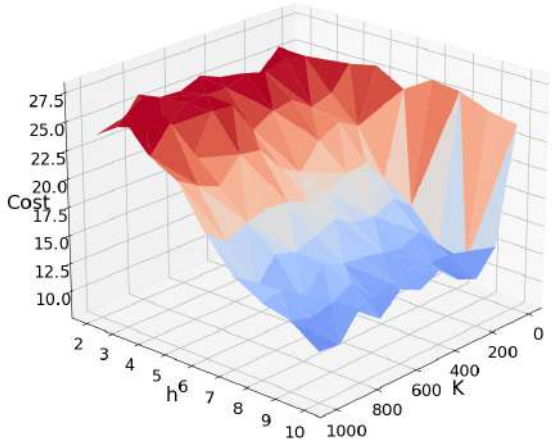

Figure 6 - MPC hyperparameter experiment results for environment 1.

Tab. 2 - Comparison of DRL control agent with the conventional controller. Negative values denote an increase in performance.

Env	Energy usage	Setpoint deviation	Roughness
1	-15.4%	-2.8%	-2.4%
2	-7.46%	-2.7%	-1.9%
3	-5.3%	-3.0%	+1.5%
4	-46.9%	-3.7%	+1.7%

Tab. 3 - Comparison of MPC algorithm with the conventional controller. Negative values denote an increase in performance.

Env	Energy usage	Setpoint deviation	Roughness
1	-17.5%	-3.3%	-2.5%
2	-5.7%	-3.2%	-2.4%
3	+25%	-4.8%	-1.0%
4	+37.2%	-6.1%	+2.3%

It was observed that in some cases the MPC algorithm decreased the energy usage, but in other cases also significantly increased the energy usage compared to the conventional controller. The deviation from the setpoint and the stability of the controller remained approximately equal.

Figure 7 shows the performance of the DRL agent on the physical room, i.e. the agent controlled the physical room in real time. It should be noted that the setpoint was enhanced by Climatics to warm up the room before the actual setpoint jump around

06:00 AM, which is not visible in the figure. This was done automatically to make sure the occupants did not enter a cold room in the morning.

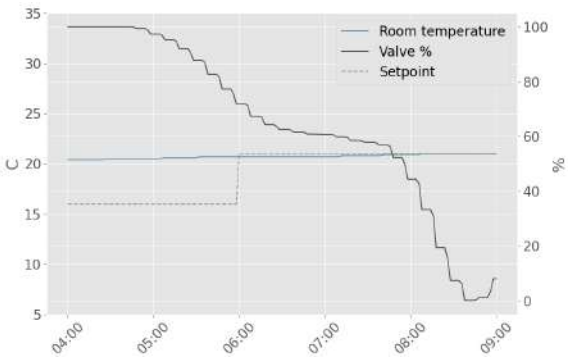

Figure 7 - Performance of the DRL agent controller on the physical room, i.e. the sports hall in Slochteren.

4. Discussion

The results of Table 1 show that all Neural Twins were able to converge to an error of approximately 0.2 ◦C. Furthermore it should be noted that there is some degree of variance in the error of the Neural Twins across environments. This can be explained due to the fact that all processes are different, and some can simply be more complex to model. The changing room environment consisted of a small room with almost no windows, making it easier to model. This is confirmed by the small error of 0.16◦C. Figure 4 shows how the loss converged over time when training the Neural Twin for environment 1. It can be observed that in the first 10 epochs the loss does not decrease much, and there is a high variance for the validation loss. This is because during these epochs teacher forcing was used with a decreasing chance the more epochs had passed. Hence, the training gradually became more difficult during these epochs. After 10 epochs, no teacher forcing was used and from there it can be seen that the training loss and validation loss converge to approximately the same value with low variance.

Figure 5 shows the learning scheme of the DRL agent on the Neural Twin of environment 1. It can be seen that the return converges over time. The return on the validation set is slightly higher than the return on the training set. This is because when validating the agent, the agent acted deterministically, whereas during training the agent acted stochastically. From the figure it can be concluded that a Neural Twin can serve as a valid simulator for a DRL agent to learn a policy on, and a DRL agent is able to control the simulator (note that it does not yet say anything about the validity of this policy on the physical process).

In Figure 6 the influence of the two hyperparameters for MPC can be clearly seen. It is observed that the cost decreases when the horizon is increased. This makes sense, as a large room like a sports hall often has a large time delay when reacting to changes in control. Hence, when taking a larger horizon into consideration when determining the optimal control values, it is expected that the MPC algorithm performs better. The number of random sequences generated at every time step does not seem to have a big influence on the cost, as long as it is larger than 100 sequences. This makes sense, as too few sequences will not cover the control space well enough to get good sequences to begin with, hence the algorithm will never be able to pick a good one. However, it seems that as soon as 200 or more sequences are generated, the cost does not decrease anymore, hence the extra sequences only introduce extra computational cost.

Table 2 and Table 3 compare the performance of the controllers with the conventional controller, i.e. the one that currently controls the process. This controller was manually tuned during the time it operated. From these results it can be concluded that the DRL agent improved upon the performance of the conventional controller for all four environments. It decreased the energy usage for all four environments while retaining the thermal comfort and stability of control. It also performed better compared to the MPC algorithm, which in 2 environments led to an increase in energy usage. For example in environment 4 the energy usage increased 37%. This can be explained by the fact that this environment was controlled by multiple control values, as opposed to the other environments. As the number of control values increases, the space of possible control values grows exponentially. This highlights an important bottleneck for the MPC algorithm, as a large number of control values means generating exponentially more sequences before the algorithm starts to work. The DRL agent decreased the energy usage for this environment with 47%. After consideration this is considered as optimistic, because this environment was controlled by an air handling unit, where the current controller controls for both the CO2 level and the temperature level. The DRL agent was only focussed on the temperature level, although this can be easily extended to other factors as well in future research. As a result, the comparison might not be completely valid. It *does* show that the DRL agent was able to control a more complex environment with an air handling unit and multiple control values. Furthermore, the reward function can easily be modified to include the CO2 level as well.

Figure 7 shows that the policy learned on the simulator transfers to the physical world as well. The figure shows how the process value reaches its setpoint and how the control value is adjusted correspondingly. Unfortunately, due to time constraints it was not possible to gather enough information about the comparison with the conventional controller, as the agent would have had to control the room for several weeks or months in order to obtain a quantitative measure. Hence, these

results only show that the gap from the simulator to the physical world is small enough to be able to train policies on the simulator, i.e. the Neural Twin.

5. Conclusion

To summarize:

- The Neural Twin framework can be used to accurately simulate the dynamic processes of various environments. The average prediction error was approximately 0.2 °C.
- The Neural Twin was used to train/develop two different control policies, one based on DRL and one based on MPC.
- The DRL agent showed the best control performance, outperforming the conventional controller in all four different environments. It was able to reduce the energy usage significantly between 5% and 40%, while retaining thermal comfort and stability.
- The policies learned on the Neural Twin transferred to the physical world, as the controller was able to control the physical process in real time as well.
- The simulators and policies were learned without manual tuning of hyperparameters, showing the scalability of the approach.
- Control using MPC degraded as the action space growed. DRL still handled this well, but it remains unknown whether the approach will work for large action spaces (i.e. a complex air handling unit with 7 actions).

6. Acknowledgements

The authors would like to thank Advanced Climate Systems (https://acs-buildings.com/en/) for letting us use their high resolution data and their platform: Climatics. Furthermore the authors would like to thank the building owners for allowing us to publish the results based on their data and letting us test the controller on the physical room.

The datasets generated during and/or analysed during the current study are not publicly available because the data is private but can be made available when requested in order to continue further research in cooperation with ACS. In that case, please contact the first author!

7. References

[1] Klepeis, Neil E., et al. The National Human Activity Pattern Survey (NHAPS): a resource for assessing exposure to environmental pollutants. Journal of Exposure Science & Environmental Epidemiology, 2001, 11(3): 231-252.

[2] Mayowa, M. O., Rowland, A. G., Babatunde, H. T., & Mumuni, A. Indoor air quality and perceived health effects experienced by occupants of an office complex in a typical tertiary institution in Nigeria. Science Journal of Public Health, 2015, 3(4): 552-558.

[3] IEA, I. E. A. Global status report for buildings and construction. 2019.

[4] Cheng, C. C.; Lee, D. Artificial intelligence assisted heating ventilation and air conditioning control and the unmet demand for sensors: Part 1. Problem formulation and the hypothesis. *Sensors*, 2019, 19(5): 1131.

[5] Alawadi, S., et al. A comparison of machine learning algorithms for forecasting indoor temperature in smart buildings. *Energy Systems*, 2020, 1-17.

[6] Mtibaa, F., et al. LSTM-based indoor air temperature prediction framework for HVAC systems in smart buildings. *Neural Computing and Applications*, 2020, 32(23): 17569-17585.

[7] Yu, L., et al. Deep reinforcement learning for smart building energy management: A survey. *arXiv preprint arXiv:2008.05074*, 2020.

[8] Wang, Z., Hong, T. Reinforcement learning for building controls: The opportunities and challenges. *Applied Energy*, 2020, 269: 115036.

[9] Jia, R., et al. Advanced building control via deep reinforcement learning. *Energy Procedia*, 2019, 158: 6158-6163.

[10] Wei, T., Wang, Y., Zhu, Q. Deep reinforcement learning for building HVAC control. *Proceedings of the 54th annual design automation conference 2017*. 2017. p. 1-6.

[11] Brandi, S., et al. Deep reinforcement learning to optimise indoor temperature control and heating energy consumption in buildings. *Energy and Buildings*, 2020, 224: 110225.

[12] Zou, Z., Yu, X., Ergan, S. Towards optimal control of air handling units using deep reinforcement learning and recurrent neural network. *Building and Environment*, 2020, 168: 106535.

[13] Mnih, V., et al. Playing atari with deep reinforcement learning. *arXiv preprint arXiv:1312.5602*, 2013.

[14] Schulman, J., Wolski, F., Dhariwal, P., Radford, A., & Klimov, O. Proximal policy optimization algorithms. *arXiv preprint arXiv:1707.06347*, 2017.

4S3F Diagnostic Bayesian Network method: discussion about application and technical design

Ziao Wang [a], *Arjen Meijer* [a], *Laure Itard* [a]
[a] Faculty of Architecture and the Built Environment, Delft University of Technology, Delft, the Netherlands, {Ziao. Wang, A.Meijer, L.C.M.Itard}@tudelft.nl

Abstract. In practice, automated energy performance fault diagnosis systems are seldom installed in HVAC systems. The main reason is that a specific Fault Detection and Diagnosis (FDD) setup is time-consuming and expensive because the existing methods are component-specific, not aligned with HVAC design practices, and not fully automated. 4S3F (four symptoms three faults) method, based on system engineering and Diagnostic Bayesian Networks (DBN), was proposed to decrease the gap between the design of HVAC systems for buildings and energy performance diagnosis, and proofs of concepts were tested on diverse parts of the HVAC system of one specific building. In order to test the further applicability potential of the method, it is necessary to expand these tests and to study possible problems arising in practice, like the lack of sensors installed in a specific system or practical difficulties in the construction of the 4S3F Bayesian network by HVAC or control. However, due to the small number of validations carried out on the environment, parameters, and installation process of this method still need further discussion and refinements. In this paper, we investigate how to construct the DBN for the quite generic AHU (Air Handling Unit) of a, with mechanical supply and exhaust, heating and cooling coils, and heat recovery. The paper describes the possible DBN's depending on the technical design and the measurement points. The diverse Bayesians networks are compared, and it is concluded that also, with a limited number of sensors, a diagnostic network can be set up. It is also concluded that step-by-step instructions would be needed to facilitate the work of HVAC engineers when setting up the diagnosis model.

Keywords. Bayesian network, building energy performance, building energy diagnostics
DOI: https://doi.org/10.34641/clima.2022.82

1. Introduction

10-30% of the energy used in buildings is wasted even in the most modern ones due to malfunctioning, degradation of the installed equipment, and suboptimal setpoints. The developments in the smart meter field, sensors, building management systems, and machine learning or artificial intelligence algorithms provide an opportunity to monitor real-time building performance, occupant behaviour, energy consumption and analyze the real-time data flow for building diagnosis and control. Taking the benefit of the development of these technologies, fault detection and diagnosis (FDD) technology for buildings has taken a big leap in recent years, and various amount of FDD methods for building energy systems have been proposed and developed, such as for HVAC level energy efficiency [1-3], chillers [4-6], air handling unit [7-10], sensors [11]. Effective FDD tools for building system is estimated to save 10-40% building energy consumption [12]. However, automated energy performance diagnosis is seldom applied in practice despite many proposed methods. Many researchers have recognized the major challenges in faults diagnosing of building energy systems in the last decade [13-16]. The first reason is that the setup of FDD methods is highly customized for each building because of different types of sensors, air handling unit, chillers, hot coils and available data. This condition makes standardization and a consistent approach for a broad application difficult. Second, It is very time-consuming to design and set up a FDD model. Third, when data-driven model are used, data about the correct functioning of the equipment is needed, but very difficult to obtain Fourth, when white-box models are used, they are difficult to set up for a complex system. Fifth, it is hard to apply the current methods to novel energy systems such as smart energy grids, thermally activated building systems, and adaptive façade, it. Sixth, an integrated approach for different HVAC components, controls, indoor environments and energy performance is lacking. Sevenths, energy performance FDD is far from being automated. In most scenarios, only data monitoring from BMS is automated, and HVAC engineers or energy experts need to diagnose the faults based on their experience.

In order to fill these gaps, the 4S3F (4 symptoms and

Copyright ©2022 by the authors. This conference paper is published under a CC-BY-4.0 license.

3 faults) method was proposed and proven by Taal [16]. This method separates the detection of symptoms and the diagnosis of faults. In the symptom detection part, the complete list of possible symptoms is generated from the HVAC diagrams and all possible components and their control systems. They are then checked constantly during operation. In the fault diagnosis and isolation part, all possible faults are identified from all possible components, models, and controls in the HVAC diagram. Then, symptoms and faults are connected through Diagnostic Bayesian Network (DBN). Using DBN models, the faults are identified based on the probability of observed symptoms, and the diagnosis runs simultaneously through all system levels. However, due to the small number of installations in practice so far, the possible problems that appeared in practice during the technical design are rarely studied and discussed, such as the lack of sensors or how to choose the system level of the Bayesian network model for certain HVAC components. In this paper, the 4S3F method is set up for the AHU (Air Handling Unit) of the HHS building, a generic type with mechanical supply, exhaust, heating and cooling coils, and heat recovery. This paper describes and compares diverse possibilities for the Bayesian network and discusses how the 4S3F method could be applied under different scenarios and conditions (e.g., limited number of data points and sensors). After an introduction of the 4S3S method in section 2 and a description of the air handling unit in section 3, the setup of the Bayesian network in the current sensor environment is researched in section 4, while the setup in a sensor-rich environment is explained in section 5 and the set up in a sensor-poor environment in section 6. Current AHU's may have few sensors, and it is relevant to show which diagnostics can still be done in this case. Sensor-rich environments, on the other side, are expected to become more common and to improve the quality of the diagnostic. They are compared in section 7and conclusions are drawn in section 8.

2. Introduction of 4S3F method

2.1 4S3F method

Symptom detection methods vary in FDD methods for energy performance. The detection is made by comparing actual and simulated energy performances in quantitative model-based methods, applying "operational state of systems, components, and controls" in rule-based methods, and tracing irregularities in the possibly correct operational patterns in data-driven methods. Frequently, further information obtained from maintenance and inspection data is also collected. In order to clarify the complicated symptoms in different methods, four categories are summarized by Taal [16]: "Balance symptoms," "Energy Performance (EP) symptom," "Operational State (OS) symptoms," and "Additional systems."

1. "Balance symptoms," based on energy balance deviations, belong to the quantitative model-based approach established from system theory and the first law of thermodynamics. Only balance equations are used, but not complex white-box models.
2. "Energy Performance (EP) symptom," based on deviations in energy performance metrics, like a deviation from an expected COP, is applicable for both quantitative and qualitative model-based approaches.
3. "Operational state (OS) symptoms," based on deviations of operating state from the expected conditions, e.g., a temperature or flow is not as it should be. This symptom could be either a qualitative model-based approach or a data-driven approach, and the outliers could be estimated through the historical data.
4. "Additional symptoms," based on additional information, are gathered either from historical and maintenance data or results from specific FDD included in trade components.

DBN diagnoses provide an effective solution in the HVAC fault diagnosis area because a DBN model is based on the probability theory in which the probability of faults is calculated according to the occurrence of symptoms. Therefore, the diagnosis process of DBN is very similar to the operation methods of HVAC experts. In the 4S3F approach [17, 18], all faults are divided into three general categories:

1. Component faults: Components faults include malfunction and degradation of the components, sensors, and incorrect installation or design.
2. Control faults: Control faults include incorrect setpoints, on-off control of components, and software faults.
3. Model faults: Model faults include models that are constructed to calculate missing and derived measurements or parameters. It also includes wrong assumptions (e.g., no heat loss in ducts).

The relationship between the Four types of symptoms and three types of faults is described in ***Fig. 1***.

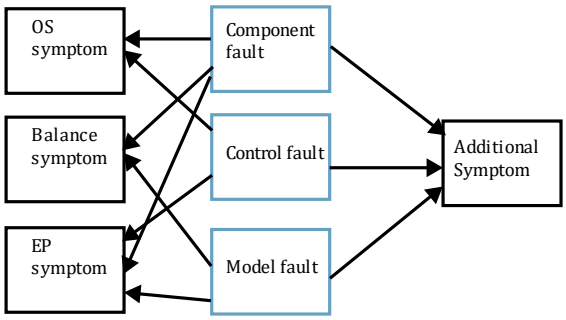

Fig. 1 – 4S3F DBN model faults and symptoms relationships from [16].

2.2 4S3F model setup

There are several steps to set up a 4S3F DBN model. Firstly, the object systems and subsystems should be selected. It is essential to choose a system or aggregated systems that have minimal necessary sensors—secondly, the presence and the absence of

symptoms should be determined. There are two steps for symptom detection. At first, all possible symptoms are listed once during the setup, based on the I&PD. Secondly, and not handled in this paper, symptoms are detected in certain time spans during operation (e.g., hours, day, week, month), and the automated comparison between the recorded value and expected value is processed, see [16, 17]. Thirdly, once the list of all possible symptoms has been determined during setup, the possible faults should also be identified the same way based on the system diagrams. Fourth, as one symptom can arise from many different faults, a fault can lead to various symptoms. Hence, the combination of all observed symptoms should be analyzed and linked to possible faults. Fifth, once all possible faults and symptoms are identified, the relationships between faults and symptoms are translated to a DBN, with which the probability of a specific fault can be estimated. The structure of the DBN is very similar to the structure of the HVAC diagrams. Therefore, the construction of this DBN model is expected to be straightforward for HVAC engineers.

3. Description of the Air Handling Unit (AHU)

3.1 Scheme of the AHU in HHS building

The Air handling unit (AHU) of the HHS building is quite a standard and generic one and is used to demonstrate the different ways of setting up the Bayesian network in the 4S3F method. The HVAC diagram of the AHU system (See ***Fig. 2***) is used.

The AHU provides ventilation and partial heating, cooling to the different building zones, and consumes a significant amount of energy. The AHU in HHS has a mechanical supply and exhaust and heat recovery. For the supply part (below in the diagram), it consists of an inlet damper (ID), filter (IFI), heat wheel (WW30-01), heating coil (HC), cooling coil (CC), fan (IF) and noise reduction damper (ND1). For the exhaust part (above in the diagram), it consists of an outlet damper (OD), filter (OFI), heat wheel (WW30-01), and fan (OF). The heat wheel recovers heat from the output air to the input air. CD30-02 and CD30-1 are motors to control the opening and closing of the inlet damper (ID) and outlet damper (OD). TV30-01 and AV30-01 are motors to control the speed of the fans. The fresh air is taken from the outside. The inlet flow rate sensor FT30-03 records the intake airflow. The inlet filter (IFI) will then remove the finer particles in the intake air. After air passes through the heat wheel, the heating coil (HC) would be switched on if the heating is needed. The cooling coil (CC) will be switched on if cooling is needed. When the heated or cooled air passes through the intake fan (IF), it will be accelerated. The noise reduction damper (ND1) will reduce the noise from the system. After the air passes through the noise reduction damper, it will be pushed to the building rooms. The exhaust air will be sucked into the output duct from the building rooms. The sucked air will pass the noise reduction damper (ND2) at first. The output filter (OFI) will remove the finer particles as the intake filter. The heat wheel will recover some heat from the exhaust air to the supply air through conduction heat transfer. The output fan (OF) will accelerate the speed of air. The output flow rate sensor FT30-04 records the exhaust airflow. After passing through the output damper, the exhaust air will be pushed to the exterior of the building. The available sensors are also shown in the diagrams (***Fig. 2***). FT30-03 and FT30-04 are flow sensors. PDT30-01 and PDT30-02 are pressure difference sensors. They can record the pressure difference of the filters. TA30-01 is a temperature sensor. It records air temperature after the heating coil. TT30-05/MT30-01 and TT10-06/MT30-02 are temperature sensors and moisture sensors. PT30-01 and PT30-02 are pressure sensors. They record pressure in the duct. It can detect smoke in the duct. The output air (OA) is measured by the temperature sensor TT30-10, and the input air (IA) is measured by the temperature sensor TT30-00.

In the zoom-in diagram (***Fig. 3***), FT31-01-65-1 and 64-6 are flow sensors. TT31-01-64-7 and 64-4 and TT31-02-64-8 and 64-5 are temperature sensors. They record water temperature before and after the heat exchange process. The heating coil is connected to a heat generator (e.g., boiler or the condenser of a heat pump). The cooling coil is connected to a cold generator (e.g., the evaporator of a chiller or a reversible heat pump, or an ATES system).

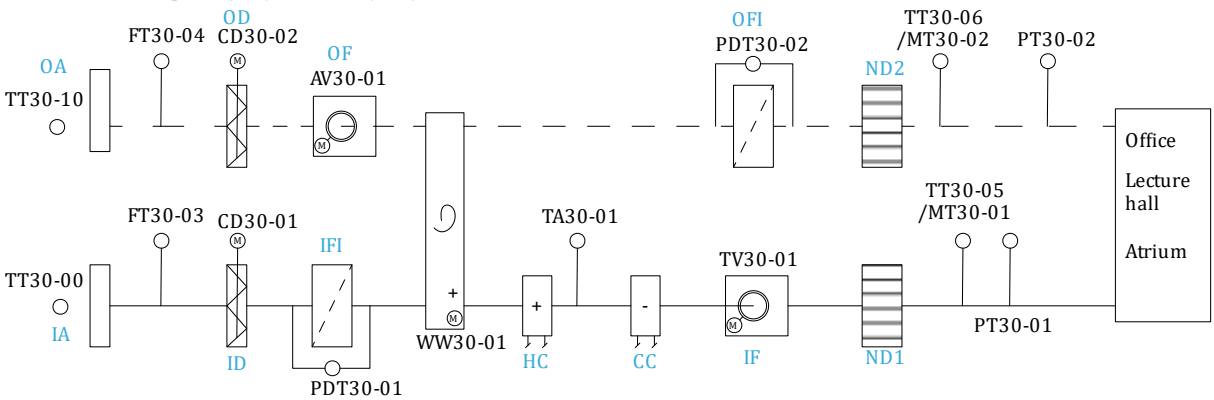

Fig. 2 – P&ID diagram of AHU in HSS

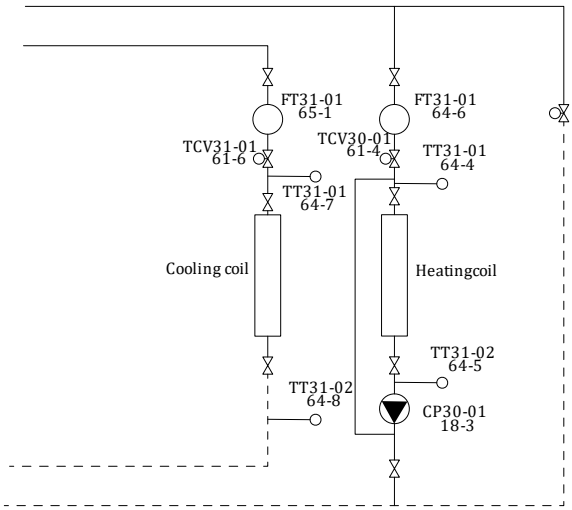

Fig. 3 – P&ID diagram of Heating and cooling coil

4. Case one: Setup in Actual environment

The AHU in the HHS building is quite generic. Once the DBN for this AHU has been constructed, it can be used in many other types of AHU systems with few modifications. In the actual setup environment, the symptoms of balance, Energy performance (EP), an operation state (OS) are considered. As described in the AHU scheme section, there are several possible balance symptoms. The heat losses in the diverse systems, components, and mechanical efficiencies are indicators for energy balance symptoms determination. These symptoms could be calculated from aggregated systems or subsystems. As shown in ***Fig. 2***, there are two levels of systems presented, which are the AHU system, including heating coil and cooling coil, and the heating coil and cooling coil as a subsystem shown in ***Fig. 3***. At the AHU system level, based on the information from the collected sensors, the following symptoms could be determined. Symptoms arise from information that can be measured and therefore relates strongly to sensors.

4.1 Energy balance symptoms

To identify energy balance symptoms, incoming energy and outcoming energy need to be calculated and measured, which means the measurement of flow rate and temperature from different components, systems, or subsystems are usually required. There are two observed energy balance symptoms. A first symptom will be if the energy balance on the heating coil is not zero. The water flow in the unit is recorded by FT30-01 (**Fig.3**). Temperature before the water goes into and after the heating coil is recorded by the temperature sensor TT30-01 and TT30-02 (**Fig.3**). By using this information, heat transfer could be calculated. The heat transferred from the heating coil to AHU can be calculated by using the total heat after the heating coil minus the heat generated before the heating coil. The total heat after the heating coil is derived from sensor TA30-01. The heat generated before the heating coil is calculated by TT30-00, FT30-03, and the recovered heat from the heat wheel. The recovered heat from the heat wheel was obtained by creating a "virtual sensor" by knowing the heat wheel efficiency, which will be introduced in 4.2. If the result of this balance is not zero, it will be considered unbalanced. Second, the energy balance on the cooling coil is not zero. Same as the heating coil, the water flow in the unit is recorded by FT30-01(**Fig.3**). Temperature before the water goes into and after the coiling coil is recorded by the temperature sensor TT30-01 and TT30-02(**Fig.3**). The heat generation of the cooling coil could be calculated through sensors information, and the total heat after the coiling coil is obtained by TT30-05. However, more symptoms may be identified if more temperature sensors were installed. This possibility will be discussed in case two.

4.2 Energy performance symptoms

The actual efficiency of the heat wheel (HW) being different from the efficiency rating listed by the heat wheel producer could be considered as a performance symptom. No other energy performance symptoms can be determined as the only specifications found from the supplier's information are the heat wheel's efficiency rating. In this AHU diagram, the intake flow rate (IFR), input air temperature (IA), Air temperature after heating coil (TAH), output air temperature in the duct(OAD), output air flowrate (OFR), and output air temperature (OA) are recorded by the various sensors. The heat generated from the heating coil (Qheat) is calculated through diagrams shown in ***Fig. 3***. Using these data, the heat recovered from the heat wheel could be estimated and compared with the efficiency rating provided by the supplier.

4.3 Operation state symptoms

The observable OS symptoms are as follows:

1. Difference between the AHU temperature setpoint and the recorded data from the temperature sensor TT30-05.
2. The cold-water supply temperature from TT31-01 is different from the specifications.
3. The hot water supply temperature from TT31-01 is different from the specifications.
4. The abnormal pressure difference of the inlet filter and outlet filter pressure sensors

These are all components being controlled. No other operational symptoms can be observed from the P&ID.

4.4 Identifiable faults

Basically, a fault is everything that can potentially ever be wrong. In the current case, all three types of possible faults can be identified as follows.

1. The control of the AHU temperature setting (TS) can be faulty.
2. The twenty-six components of the AHU can be faulty, including twenty sensors, a heating coil, cooling coil, heat wheel, fan motor, filter, and damper faults.
3. Three assumed models in 4.1 and 4.2 of heating coil heat balance, cooling coil heat balance, and the energy performance balance of heat wheel can be faulty.

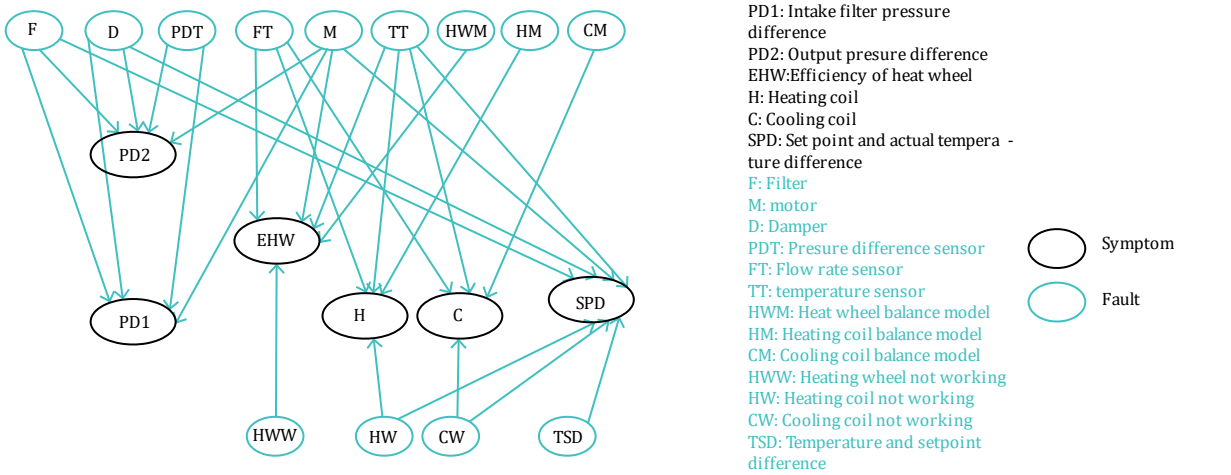

Fig. 4 – DBN model in actual scenarios

4.6 Relationship between faults and symptoms and DBN model

To decrease complexity a bit when explaining the relationships, we group together some faults and symptoms, as explained below, resulting in 6 possible symptoms and 13 fault nodes (instead of 26) To construct this DBN, six possible symptoms presented above are highlighted in black color (***Fig. 4***). Intake filter pressure difference (PD1) and output pressure difference (PD2), and setpoint and actual temperature difference (SPD) are OS symptoms. The energy efficiency of the heat wheel (EHW) is EP symptoms. Symptoms of heating and cooling coils are aggregated as heating (H) and cooling coils (C). Because faults that lead to these symptoms are almost identical, they could be isolated later. All listed faults are marked in blue color. All faults that come from the same sensor types are combined into one node for reducing the drawing complexity, such as Flow rate sensor (FT), pressure difference sensor (PDT), and Temperature sensor (TT), and they could be separated later for more accurate analysis. Three balance model fault heat wheel balance model (HWM), Heating coil balance model (HM), and cooling coil balance model (CM) are listed separately. All of these faults and symptoms are connected through the DBN (***Fig. 4***). The knowledge and experience of experts are needed to decide how to connect faults and symptoms. For example, motor broken (M), damper broken (D), polluted filter (F), Pressure difference sensor broken (PD) may lead to symptoms in output pressure difference (PD2) and intake filter pressure difference (PD1). Then these faults and symptoms should be connected. Moreover, flowrate sensor broken (FT), temperature sensor broken (TT), motor broken (M), Heat wheel not working (HWW), and Heat wheel balance model incorrect (HWM) may lead to symptoms of the inefficiency of the heat wheel. So, these symptoms and faults should be connected.

The description and explanation of the probability data and how to apply a conditional probability table to each node of the DBN model are not the purposes of this paper. Therefore, it will be discussed in future research. The DBN (***Fig. 4***) can be constructed and understood when compared with HVAC diagrams (***Fig. 2***, ***Fig. 3***).

5. Case two: sensor-rich environment

In this section, the case of an ideal environment will be discussed in which more sensors and information are available.

5.1 Energy balance symptoms

As described in the previous section, the heating and cooling coil's energy balance can be identified. In the ideal scenarios, if the connected or aggregated system information is available, more balance symptoms could be identified. Firstly, suppose the total amount of heat generated in the heat generator is known, as well as how this heat is distributed to separated systems, including the heating coil, via a hydronic system. In that case, the heat balance model for the efficiency of the aggregated system could be constructed. Secondly, with the measurement of heat distributed to AHU, the energy balance model of the heat generator system at the subsystem level can be made. Thirdly, the air pressure balance model could be constructed if there are air pressure sensors at the

inlet air duct, output air duct, and terminal rooms.

5.2 Performance symptoms

Unlike the previous section, the performance balance symptoms could be more accurate and substantial if only a few sensors were added. Suppose the temperature sensor (TT1) is installed between the heat wheel and the heating coil. In that case, it could record the intake air temperature before it passes through the heating coil. Then several new performance balances could be identified. At first, because this sensor was absent, the heat wheel efficiency calculation was based on the total heat balance equation in the previous section. Now, with this new sensor, the heat generated from the heating coil could be isolated. The extra heat obtained from the heat wheel could be calculated by deducting the reading from TT1 and the intake air temperature sensor TT30-00. Within this sensor, the calculation of the efficiency of the heat wheel can be done more quickly and directly. Secondly, the efficiency calculation of the heating coil and cooling coil becomes possible. The efficiency of the heating and cooling coil can be calculated by comparing the heat generated or removed from these two coils and the heat obtained between sensors TT30-05 and TT1.

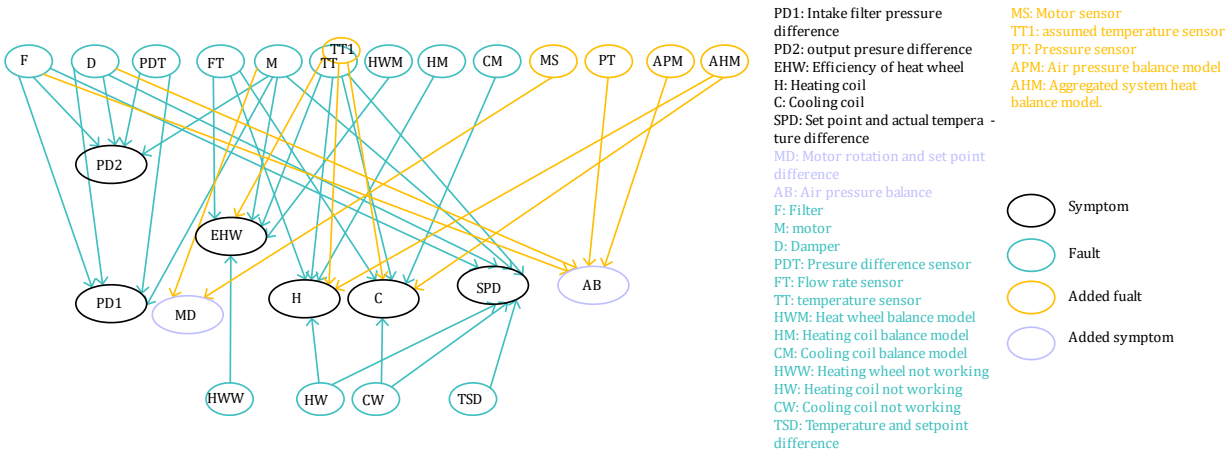

Fig. 5 – DBN model in expected scenarios

5.3 Operation state symptoms

The observable operation state symptoms will also be expanded if more information is added. At first, if the setpoint fan speed and the motor rotation data are recorded. Then the operation state symptoms of the fan will be identified by comparing this setpoint and rotation speed. Moreover, suppose the specific flow rate of the supply water in the heating and cooling coil is collected. In that case, symptoms of the cold-water supply and hot-water supply could be observed by comparing data in the flowrate sensor (FT30-01) and the specific parameter provided by the supplier.

5.4 Identifiable faults

The identified faults could also be expanded if more information is available. The new assumed sensors (e.g., TT1) will be additional potential sensor faults. Furthermore, several new model faults (e.g., the air pressure balance model) will be added as new balance symptoms are included. Additionally, the new control fault like fan speed difference between set speed and actual can be identified.

5.5 DBN model

The newly added symptoms, faults, and possibly are marked as purple and yellow ***(Fig. 5)***. The DBN model becomes more powerful and complex, with the possibility to identify more symptoms and faults at different levels. Several new energy balances and performance symptoms are added due to the information from the heat generator. It can be further analyzed if a more accurate diagnosis is needed. New added sensor fault TT1 is listed separately to compare with the previous DBN model that one added sensor could affect several components in the fault diagnosis. As presented in the DBN diagram, motor broken (M), motor speed sensor broken (MS) may lead to the symptoms of motor rotation and setpoint difference. Flowrate sensor broken (F), damper broken (D), pressure sensor broken (PT), and air pressure balance model incorrect (APM) may lead to air pressure balance difference (AB). Moreover, aggregated system heat balance model incorrect (AHM) is connected to heating coil and cooling coil symptoms. Here too, a specific DBN model could be constructed as another subsystem.

6. Case 3: sensor-poor environment

6.1 Balance symptoms

In the worst cases, necessary sensors for identifying balance symptoms may be unavailable because too few flow and temperature sensors have been placed; Therefore, no balance symptoms are detected.

6.2 Performance symptoms

It is still possible to have some basic performance information in sensor-poor environments. For example, the air is not heated or cooled, or no air comes through the AHU.

6.3 Operation state symptoms

Operation state symptoms are essential almost in all scenarios, as they are coupled to the control of the system, and there is always some kind of control. The setpoint's temperature difference and actual situation are observable in any case. The difference in water supply temperature in the heating coil and cooling coil between actual values and specifications may still be obtained.

6.4 Identified faults

The number of faults that can be identified decreases significantly in this scenario. The number of sensor faults is reduced because there are few available sensors. There are also no model faults since no balance model could be constructed. Only a few system faults and control faults are observable, such as incorrect setpoints or degradation of components.

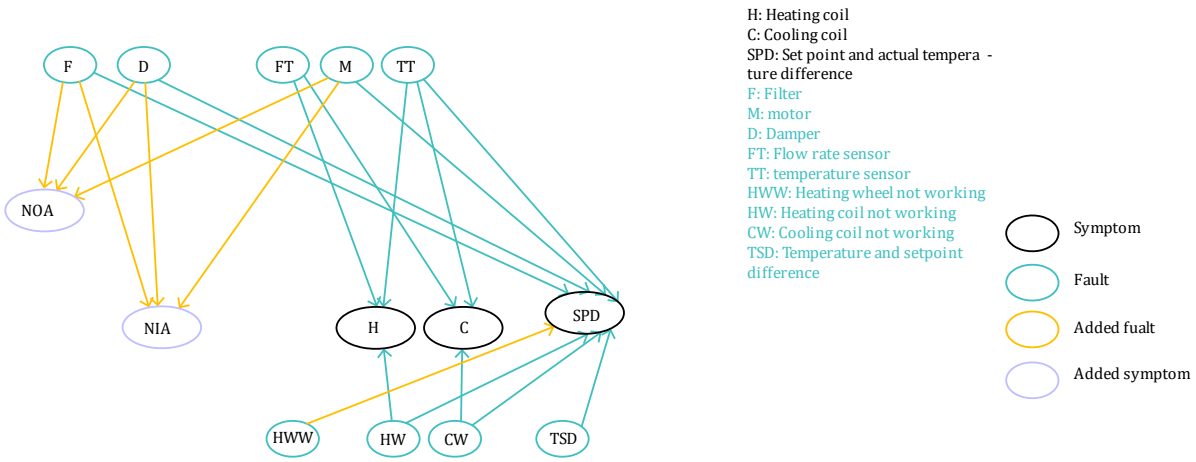

Fig. 6 – DBN model in sensor-poor scenario

6.5 DBN model

This leads to a relatively simple DBN model, constructed based on the available information (***Fig. 6)***. In the end, nine faults are identifiable. Due to the lack of sensors, almost all symptoms can lead to the set point and actual temperature difference fault (SPD). Therefore, this DBN model's fault detection and diagnosis ability have diminished a lot because of the limited data. If more sensors are placed later, more nodes can be added to this model and improve its fault detection and diagnosis ability.

7. Comparison of the three sensor environments

Three different DBN models were proposed based on different setup scenarios. It is apparent that a sensor-rich environment is an ideal condition to apply the 4S3F method. Multiple sensors will lead to more precise and effective fault diagnosis because of more identified symptoms and faults. The accuracy of the diagnosis may also increase because redundant information will lead to more precise fault probabilities. However, it also causes more complicated DBN models. It will increase the time needed for setup, computational time, and probability table requirements. Besides, it is very costly to install a large number of sensors. The 4S3F model set up in the actual environment is suitable for most practical situations where not all desired sensors cannot be placed. It can still perform specific fault-diagnosing tasks. In our example, twenty-six faults can still be identified (if happening). Many methods like virtual sensors could be applied in this situation to maximize the use of measured data. In a poor sensor environment, where many key sensors are lacking, the diagnosis ability of this method is lower due to limited information. However, the 4S3F method would still diagnose nine faults even in this situation. The accuracy of the diagnosis would be less than in the other environments. But the valuable faults and diagnosis could still be achieved. It may even be recommended for HVAC engineers to get acquainted with the 4S3F method in such a poor sensor environment, as it is easier to construct.

8. Conclusion and recommendation

This paper mainly discussed the engineering process of the proposed 4S3F method to an Air Handling Unit (AHU). Obviously, the application difficulty still exists with this recently proposed method. In general, more sensors mean a more precise model. However, it also increases the complexity of the model leading to higher computational time and time-consuming design. A solution for larger-scale complex systems needs to be explored in the future, but modular solutions will surely have a place herein. Moreover, standardization and library of module components have a great potential to accelerate the modeling setup process to avoid repetitive work.

Furthermore, we showed that by only adding one additional sensor, the accuracy and variety of the observed equations in symptoms is significantly increased, which indicates that there may be a possible economical solution for sensor installation if the places for placing sensors are well designed. In the end, step-to-step instructions would accelerate the model setup speed for HVAC engineers to avoid time-wasting of explorations of the setup method.

9. References

[1] Wang L, Greenberg S, Fiegel J, Rubalcava A, Earni S, Pang X, et al. Monitoring-based HVAC commissioning of an existing office building for energy efficiency. Applied Energy. 2013;102:1382-90.

[2] Wang L, Haves P. Monte Carlo analysis of the effect of uncertainties on model-based HVAC fault detection and diagnostics. HVAC&R Research. 2014;20(6):616-27.

[3] Zhang R, Hong T. Modeling of HVAC operational faults in building performance simulation. Applied Energy. 2017;202:178-88.

[4] Lee T-S, Lu W-C. An evaluation of empirically-based models for predicting energy performance of vapor-compression water chillers. Applied Energy. 2010;87(11):3486-93.

[5] Zhao Y, Xiao F, Wang S. An intelligent chiller fault detection and diagnosis methodology using Bayesian belief network. Energy and Buildings. 2013;57:278-88.

[6] Zhao X, Yang M, Li H. Field implementation and evaluation of a decoupling-based fault detection and diagnostic method for chillers. Energy and Buildings. 2014;72:419-30.

[7] Yu Y, Woradechjumroen D, Yu D. A review of fault detection and diagnosis methodologies on air-handling units. Energy and Buildings. 2014;82:550-62.

[8] Hosamo HH, Svennevig PR, Svidt K, Han D, Nielsen HK. A Digital Twin predictive maintenance framework of air handling units based on automatic fault detection and diagnostics. Energy and Buildings. 2022;261.

[9] Li T, Deng M, Zhao Y, Zhang X, Zhang C. An air handling unit fault isolation method by producing additional diagnostic information proactively. Sustainable Energy Technologies and Assessments. 2021;43.

[10] Najafi M, Auslander DM, Bartlett PL, Haves P, Sohn MD. Application of machine learning in the fault diagnostics of air handling units. Applied Energy. 2012;96:347-58.

[11] Zhang L, Leach M, Bae Y, Cui B, Bhattacharya S, Lee S, et al. Sensor impact evaluation and verification for fault detection and diagnostics in building energy systems: A review. Advances in Applied Energy. 2021;3.

[12] Schein J, Bushby ST, Castro NS, House JM. A rule-based fault detection method for air handling units. Energy and Buildings. 2006;38(12):1485-92.

[13] Katipamula S, Brambley MR. Methods for fault detection, diagnostics, and prognostics for building systems—a review, part I. Hvac&R Research. 2005;11(1):3-25.

[14] Kim W, Katipamula S. A review of fault detection and diagnostics methods for building systems. Science and Technology for the Built Environment. 2017;24(1):3-21.

[15] Zhao Y, Li T, Zhang X, Zhang C. Artificial intelligence-based fault detection and diagnosis methods for building energy systems: Advantages, challenges and the future. Renewable and Sustainable Energy Reviews. 2019;109:85-101.

[16] Taal A, Itard L, Zeiler W. A reference architecture for the integration of automated energy performance fault diagnosis into HVAC systems. Energy and Buildings. 2018;179:144-55.

[17] Taal A, Itard L. P&ID-based symptom detection for automated energy performance diagnosis in HVAC systems. Automation in Construction. 2020;119.

[18] Taal A, Itard L. P&ID-based automated fault identification for energy performance diagnosis in HVAC systems: 4S3F method, development of DBN models and application to an ATES system. Energy and Buildings. 2020;224.

Data Statement

Data sharing not applicable to this article as no datasets were generated or analysed during the current study.

From BIM databases to Modelica - Automated simulations of heating systems

Esben Visby Fjerbæk[a], Mikki Seidenschnur[a,b], Ali Kücükavci[a,c], Kevin Michael Smith[a], Christian Anker Hviid[a]

[a] Department of Civil Engineering, Technical University of Denmark, Kgs. Lyngby, Denmark, evifj@byg.dtu.dk, kevs@byg.dtu.dk, cah@byg.dtu.dk.

[b] Rambøll, Copenhagen, Denmark, msei@ramboll.dk

[c] Cowi, Kgs. Lyngby, Denmark, alkc@cowi.dk

Abstract. Detailed simulations of HVAC systems play a crucial role in creating 1:1 digital twins of buildings and their systems. In particular, detailed models of hydronic systems are essential for fault detection of building services and control optimization. However, modeling HVAC systems is labour intensive due to the components and connections that one must create based on drawings or models. Creating the HVAC simulation models from BIM data eases the modeling burden, simplifying the creation of digital twins. Straight-forward HVAC simulations can aid the design process. Instead of prescriptive design based on the worst-case conditions, simulations enable performance-based design with partial-loads and dynamic behaviour. This paper presents a preliminary tool using BIM data to create and simulate models of heating systems. The tool uses a central BIM data platform with a dedicated data format – defining components and their relations in a database. Python scripts apply model templates to create heating system models in the Modelica language. The tool simulates the models in Dymola, while Python scripts read and parse the results to the database for visualization and analysis. The tool efficiently simulated a small heating system and obtained results for the return temperatures of several loops.

Keywords. BIM, Modelica, HVAC, simulations
DOI: https://doi.org/10.34641/clima.2022.365

1. Introduction

There is a large discrepancy between the estimated energy consumptions of buildings and the one measured, often leading to underestimated energy consumption [1, 2]. The issue, known as the performance gap, has many causes. One significant cause is the precision of building energy performance simulations (BEPS) used to estimate energy consumption. BEPS tools rarely consider HVAC systems in detail [3] or simply assume ideal performance of components and controls [4]. This means that commonly occurring phenomena such as oscillation or system imbalance, that create disturbances, are not identified by the BEPS models.

Modeling HVAC systems in detail ensures that all non-ideal performance is considered in the BEPS simulations, which increases simulation precision. In the design phase, this can help to evolve the design process from a steady-state practice, where the design of HVAC systems is based on a worst-case full-capacity situation, to a dynamic design paradigm, where requirements for part-load conditions and dynamic behavior define the design. Additionally, it will be possible to check that the detail of the design is sufficient for actual operation under all conditions. Today, this is ensured through guidelines provided by component manufacturers and empirical knowledge of practitioners.

The combination of traditional BEPS models and detailed models of all HVAC systems can act as a digital twin if connected to live weather data. During operation, the digital twin estimates the expected/optimal operation of the building systems alongside the actual building. The expected operation can be used for fault detection and to test different control strategies continuously throughout the building's lifetime.

Modeling HVAC systems can, however, be a laborious task since the systems include many different elements that must be created manually. Often, the simulation models derive from diagrams of the systems, that the simulation engineer manually interprets and translates to the simulation model format. This error-prone process results in two separate models where changes to one does not affect the other.

Generating the HVAC simulation models from BIM

Copyright ©2022 by the authors. This conference paper is published under a CC-BY-4.0 license.

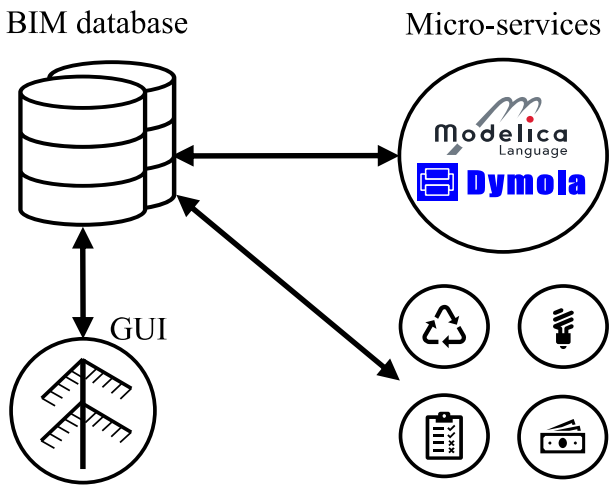

Fig. 1 - Several micro-services in addition to the Modelica service interface the BIM database platform.

data eases the burden of modeling. Integrating BIM and BEPS ensures that the BIM and simulation models share similar information. Both the BIM and BEPS industry work towards linking BIM and BEPS models. Tools such as IESVE [5] and IDA ICE [6] have functionalities to import geometry and construction parameters, whereas the BIM tool Revit contains some BEPS functionalities. Several tools for using BIM as a basis for models in the open-source Modelica language [7] exist [8–10], but all of these, including the traditional BEPS tools, have a primary focus on the envelope and thermal zone model. *IFC2Modelica* [10] includes an example for ventilation systems.

Common for all BIM to BEPS methodologies is the fact that they depend on file-based BIM information. Several critics argue that the use of file-based BIM models limits interoperability [11, 12]. A solution is to transfer from file-based to web-based collaboration, where information is exchanged through open data formats and stored in centralized databases [11, 12]. This corresponds to the BIM level 3 in the Bew-Richards BIM maturity model described in [13]. In the BIM maturity model, the information exchange on levels 0, 1, and 2 has different degrees of standardized data structures. In level 3, the information exchange is handled through standardized, open data formats for integration with various tools.

2. Cloud BIM platform

The toolchain, presented in the following sections, is implemented in a cloud platform that stores BIM models in a database to allow cross-platform access to the models. The platform is built with a micro-service structure, which means that several *micro-services* for design and evaluation of HVAC systems can utilize the data. Amongst these is the Modelica micro-service, which creates models in Modelica language and simulates them with Dymola. As seen in Fig. 1, the data flows back and forth between the micro-service and the database so that results are read and analyzed in the platform for analysis and visualization in the graphical user interface (GUI).

In the database, components and their relations are defined with the Flow Systems Ontology (FSO) [14, 15]. This ontology uses class hierarchies to define the type of component its relation to other components. E.g., a pipe supplying water to a radiator would have the class *Segment* and have the property *ConnectedWith* equal to the radiator's unique tag. Selected classes relevant to this project are listed in table Tab. 1, whereas the full list of classes and connections can be found online in [15].

Tab. 1 - Selected component classes

FSO class	Examples
Radiator	Radiators for heating
Segment	Pipe or duct segments
FlowController	Valves and dampers
FlowMovingDevice	Pumps and fans
HeatExchanger	Heating coils and heat recovery units

3. Toolchain

The toolchain automatically generates and simulates Modelica models of heating systems from BIM data. In fig. Fig. 2 the main processes of the toolchain are shown along with the flow of data. On the left side, the tool is connected through an API (see Fig. 3), that establishes an integration between the micro-service and the database. As seen in Fig. 3 the JSON format is used to parse data between the database and tool. As seen in Fig. 2 this is maintained throughout the tool, except for the last two steps, where the simulation environment needs a Modelica file and writes the results to a .mat file.

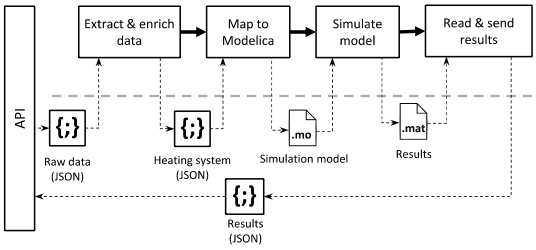

Fig. 2 - System architecture.

All functions are written with Python, since it is a straight-forward tool which is well suited for translation between data formats and since it is used in the BIM platform. Python does not carry out the simulations itself, but simply interfaces the simulation environment Dymola.

When the toolchain is activated, in the BIM platform, the platform sends a Post request, including BIM data for the desired system(s) to the service's API as seen in Fig. 3 where all data exchange between the database, the API and the toolchain is seen.

In the following sections, each step in the tool is described.

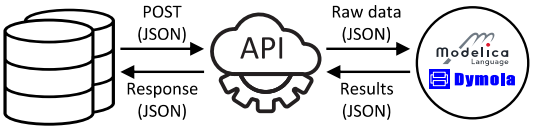

Fig. 3 - Interaction between the database and the toolchain through an API.

3.1. System extraction and data enrichment

When activating the tool, BIM data for the heating system is sent from the database, through the API to the tool. As a precaution and for future scenarios with several systems the tool extracts all components in the heating system from the data. To support the following mapping process, minor changes are made to the data by adding certain parameters based on the component classes. E.g., the length of pipe segments is calculated from the component's start and end coordinates. The enriched/manipulated data is then sent to the mapping process for model generation.

3.2. Mapping

In the mapping step, the Modelica models are generated. This is where the original data format and classes are translated to Modelica language and classes. This step is be divided into two separate processes; in the first, the program loops through all components and maps them to a corresponding Modelica class and instantiates it in the model code. In the second, all connections between the components are translated to Modelica connectors. To handle the lack of information on control, this is also where default control connections are established.

In the mapping process, seven FSO classes are mapped to 10 different Modelica classes. Some FSO classes have been mapped to multiple Modelica classes, depending on the value of certain attributes. The full mapping and the translated attributes are seen in Tab. 2. The parameters are all required in the BIM data; if not, the program will fail.

All Modelica classes, except the bend model, originate from the Buildings library [16] which includes models for most components in HVAC systems in addition to detailed models of thermal zones. To simplify the mapping process, a purpose-built library with models that combine component models from *Buildings* was created. The combined models simplify the mapping process, since several Modelica models would otherwise have to be instantiated for each database component. Examples are the radiator model, which combines a radiator model and a thermostat, acting as a proportional controller and the MotorValve class, which combines a motorized valve with a PI controller and a setpoint.

Tab. 2 - Mapping between classes in the database and their corresponding Modelica classes.

Component	Modelica
Segment	**model:** Pipe[a] **parameters:** nominal flow, insulation thickness, insulation lambda, diameter, length
FlowMoving-Device[d]	**model:** PumpConstantSpeed[b] **parameters:** speed, performance curve
FlowMoving-Device[d]	**model:** PumpConstantPressure[b] **parameters:** head, performance curve
Radiator	**model:** Radiator[b] **parameters:** nominal heat flux, nominal supply temp, nominal return temp, nominal room temp, nominal pressure loss
HeatExchanger	**model:** DryCoilCounterFlow[a] **parameters:** nominal air flow, nominal water flow, dp nominal air, dp nominal water, UA nominal
Bend	**model:** CurvedBend[c] **parameters:** angle, diameter, bend radius
Tee	**model:** Junction[a]
FlowControl-ler[d]	**model:** Valves.TwoWayLinear[a] **parameters:** nominal flow, Kv-value
FlowControl-ler[d]	**model:** CheckValve[a] **parameters:** nominal flow, Kvs-value
FlowControl-ler[d]	**model:** MotorValve[b] **parameters:** nominal flow, Kvs-value

[a] In Buildings.Fluid library

[b] In purpose-built library
[c] In Mocelica.Fluid library
[d] Mapping depends on component attributes

In the connection process, the connections between components are translated from the database format to Modelica language. In the database, the connection between components are described in *connectors*, in the *ConnectedWith* attribute, as seen in Fig. 4 that shows an example of two connected pipes. All components have at least 2 connectors. Each connector defines the expected direction of flow (in or out) and the connected component's tag, among other properties not relevant to this project.

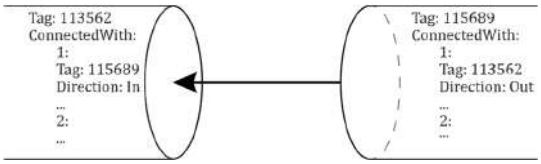

Fig. 4 - Example of connector definition.

The toolchain loops through all components and for every ingoing connector, a corresponding Modelica connector will be established. Only ingoing connections are considered to avoid duplicate connectors. In Modelica, components are connected through *ports*. The name of the ports vary, depending on the component class, and hence, they are stored in the components during data enrichment.

Since the BIM data does not support definition of control logics, default controls are assumed for the components that need control. E.g., all components mapped to the MotorValve class (see Tab. 2) are assumed to be controlling flow in a heating coil. Thus, these all take the measured ventilation supply temperature as an input for the processed variable for the PI controller.

For each component, a component model template is instantiated and added to a text string, containing the model information. After looping through all components, both for class mapping and connection establishment, the text string contains the entire model. The model is saved in a temporary model file for simulation.

3.3. Simulation and results reading

When simulating Modelica models, the models must first be compiled to a machine-readable executable and after that simulated. In the toolchain, this is done through *BuildingsPy* [17], which interfaces the commercial Modelica simulation environment Dymola. BuildingsPy takes the file path to the simulation file and simulation parameters, such as duration and solver, as parameters and parses these to Dymola. After simulation, the results are read through BuildingsPy, and the results are parsed to a JSON format and returned to the database. Since the simulations return many results for each component, the wanted results for each component class are defined in a specific file, and only these results are sent back to the database.

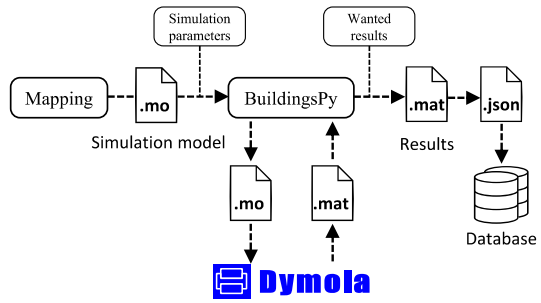

Fig. 5 - Simulation procedure.

4. Testing

To ensure that the tool is usable, it was tested on a small heating system model. The test did not focus on assessing the system's performance but merely to check whether the tool works, and the obtained results make sense and are of interest.

4.1. Test case description

The test case system, depicted in Fig. 6, consists of a heating coil and a radiator, each in separate loops. The main pump supplies flow to both loops, and a secondary pump is connected to the heating coil. To simulate the dynamic behavior, both the heating coil and the radiator are connected to a generic room with the parameters given in Tab. 3. For simplicity, only heat loss through the walls and window was considered.

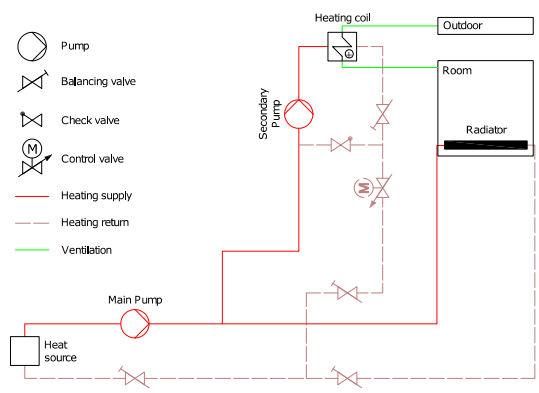

Fig. 6 - Heating system with one radiator and one heating coil used for testing the tool.

The radiator is controlled by a thermostatic radiator valve (TRV), connected to the room temperature. The TRV is not depicted in figure Fig. 6, since it is considered a part of the radiator. To control the heating output of the heating coil, a PI controller adjusts the control valve position to change the heating supply temperature. This is based on the ventilation supply temperature to the room, which has a constant setpoint. For simplicity, both pumps are operated with constant speed, although under normal circumstances, such pumps would either be controlled for constant or proportional pressure. The heat source is not considered, and it is assumed that

it supplies water at a fixed temperature of 70 °C.

Tab. 3 - Room parameters

Parameter	Value	
Floor area	30	m^2
Wall area	60	m^2
Window area (south)	4	m^2
Total envelope area	66	m^2
Wall U-value	0.27	$W/(m^2 K)$
Window U-value	1.31	$W/(m^2 K)$
Window g-value	0.73	[-]

4.2. Simulation setup

The simulation was done for the first five days of weather data for Chicago, USA. In this period, the temperature ranges between -15 °C and 0 °C. Hence, it is possible to see the dynamic effects in varying external temperatures, including maximum capacity conditions.

To initialize the solution, in addition to the Modelica initialization, one preceding day was simulated before the first day of the year.

4.3. Simulation results

By simulating the system through the toolchain, the overall temperature curves in Fig. 7 were achieved. Fig. 7 shows the temperature of the room and the ventilation supply air, compared to the external temperature. It is seen that the room temperature is stable, but that there is an offset from the setpoint. This offset is caused by the TRV, which in Modelica is modeled as a proportional controller, which will normally introduce an offset. Hence, this behavior is expected. The supply temperature is stable with no offset since it is controlled by a PI-controller.

In Fig. 8, the return temperature for both loops and the full system is seen. The return temperatures are stable around 30 °C, with a slight tendency to increase with lower external temperatures, as expected.

5. Discussion and gained experiences

The development process highlighted several points of attention during the mapping process. Most importantly, all needed data for the considered components must be available. If the parameters in Tab. 2 are not available for all components, the simulations will fail. This puts high demands on the level of information in BIM, but with tools for system dimensioning and component databases, the amount of information is not unrealistic. The possibility to perform detailed simulations of, e.g., return temperatures may even motivate designers to populate BIM models with more information on hydronic components.

In the presented work, controls were handled by applying a set of assumptions suitable for the specific test case. To work expand the work to larger systems, unambiguous control relations must be established in the database. This can be handled in two ways. Either the existing data format is extended with

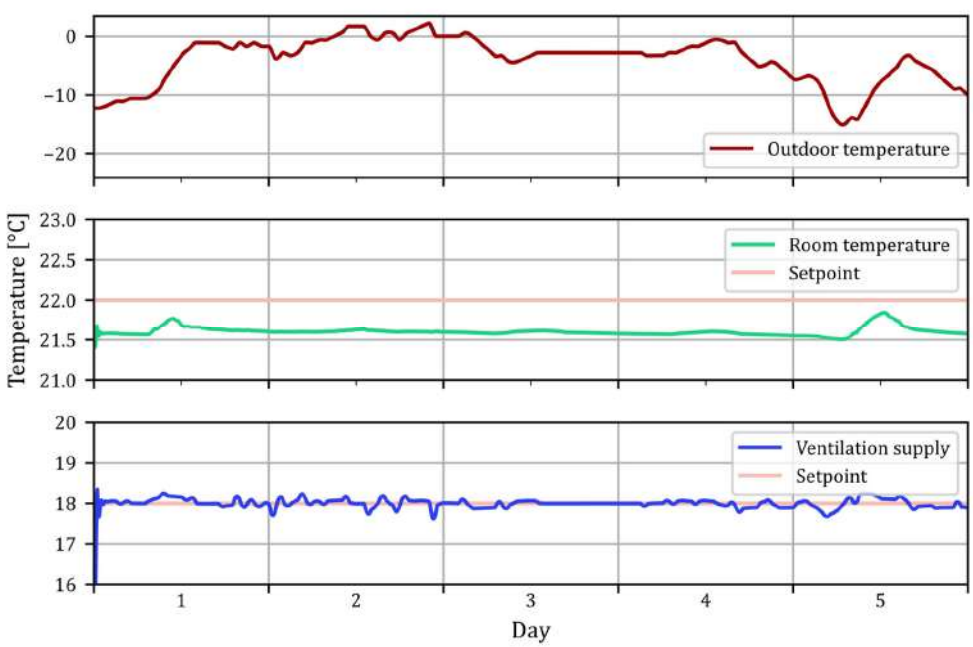

Fig. 7 - Results for the outdoor (t_{ext}), room (t_{room}) and ventilation supply (t_{vent}) temperature, including setpoints (SP).

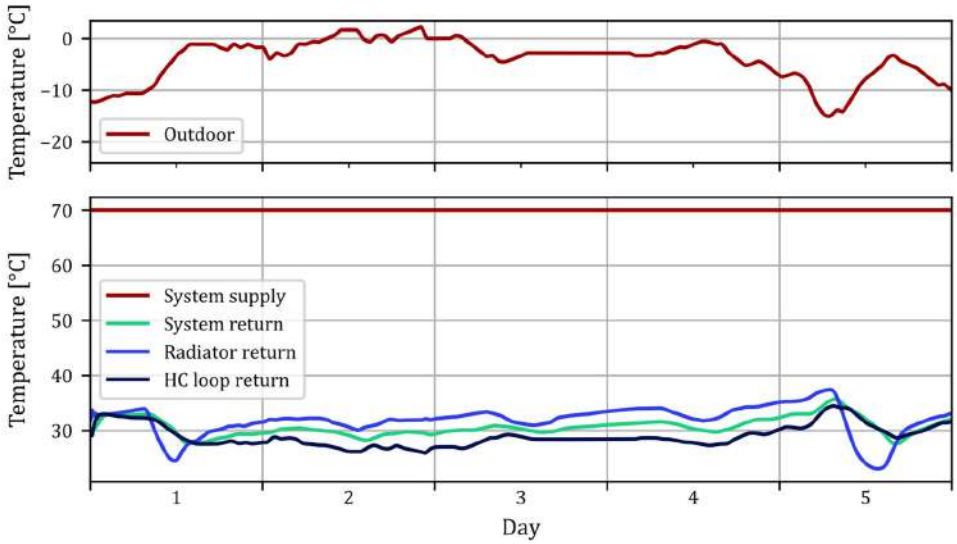

Fig. 8 – Return temperatures for heating coil loop (HC), radiator loop and for the entire system.

component parameters for controls, such as process variables, setpoints, etc., or a new data format for controls must be used. Work towards digitizing control information is in growth with several projects under development [11, 18]. Utilizing these existing frameworks to represent control logic in a database seems like a viable solution, but for simpler systems, the simple approach of added attributes may prove sufficient.

The connection between end units and rooms is a vital piece of information to correctly simulate the systems. Creating a link between end units and rooms may be a simple process in the BIM domain, but it requires additional mapping modules to include the rooms in the simulations.

6. Conclusion and future work

In this paper, it was proved that it is possible to create a tool for the simulation of heating systems based on BIM models. The simulations provided detailed and vital information on the performance of the individual components in the testing case. This showed the value of such simulations that are usually too time-consuming to be made. While the presented results may be trivial for a system as small as the test case, the same analysis for larger system will uncover results that are difficult for normal practitioners to quantify.

Several important attention points for a larger implementation were identified, the biggest being the lack of representation of controls in BIM models. These points resulted in several assumptions built into the tool, especially regarding control strategies. These assumptions mean that the tool is less flexible to different system configurations. By extending the data format to include the needed information on controls, the tool can easily be modified to simulate larger systems with both heating, ventilation, and cooling systems. When this work is done, the full models can be used in fault detection, detailed analysis of the dynamic effects of coupling the systems, etc.

7. Acknowledgement

This work was funded by the national IFD grant J.nr. 8090-00046B for the project “HEAT 4.0 - Digitally supported Smart District Heating”, Elforsk grant 352-042, IFD grant J.nr. 9065-00266A for the project “Virtual Commissioning in Building Services” and “Databaseret energistyring i offentlige bygninger”, EU Interreg-ÖKS 2020-2022.

8. References

[1] de Wilde P. The gap between predicted and measured energy performance of buildings: A framework for investigation. Automation in Construction. 2014;41:40–9.

[2] Menezes AC, Cripps A, Bouchlaghem D, Buswell R. Predicted vs. actual energy performance of non-domestic buildings: Using post-occupancy evaluation data to reduce the performance gap. Applied Energy [Internet]. 2012;97:355–64. Available from: http://dx.doi.org/10.1016/j.apenergy.2011.11.075

[3] Virta M. Initial Commissioning. In: HVAC Commissioning Guidebook [Internet]. REHVA; 2021. p. 13–42. Available from: https://app.knovel.com/hotlink/khtml/id:kt011ZBWH4/hvac-commissioning-process/initial-commissioning

[4] Wetter M. Modelica-based modelling and simulation to support research and development in building energy and control systems. Journal of Building Performance Simulation [Internet]. 2009 Jun 19;2(2):143–

61. Available from: https://www.tandfonline.com/doi/full/10.1080/19401490902818259

[5] Integrated Environmental Solutions | IES. Iesve 2021 [Internet]. Available from: https://www.iesve.com/ve2021

[6] EQUA Simulation Technology Group. IDA Indoor Climate and Energy [Internet]. 2014. Available from: http://www.equa-solutions.co.uk/de/software/idaice

[7] Mattsson SE, Elmqvist H. Modelica - An International Effort to Design the Next Generation Modeling Language. IFAC Proceedings Volumes [Internet]. 1997 Apr;30(4):151–5. Available from: https://linkinghub.elsevier.com/retrieve/pii/S1474667017436287

[8] Kim JB, Jeong W, Clayton MJ, Haberl JS, Yan W. Developing a physical BIM library for building thermal energy simulation. Automation in Construction. 2015;50(C):16–28.

[9] Nytsch-Geusen C, Inderfurth A, Kaul W, Mucha K, Rädler J, Thorade M, et al. Template based code generation of Modelica building energy simulation models. In: Proceedings of the 12th International Modelica Conference, Prague, Czech Republic, May 15-17, 2017. Linköping University Electronic Press; 2017. p. 199–207.

[10] Andriamamonjy A, Saelens D, Klein R. An automated IFC-based workflow for building energy performance simulation with Modelica. Automation in Construction. 2018;91(March):166–81.

[11] Terkaj W, Schneider GF, Pauwels P. Reusing domain ontologies in linked building data: The case of building automation and control. CEUR Workshop Proceedings. 2017;2050.

[12] Janowicz K, Rasmussen MH, Lefrançois M, Schneider GF, Pauwels P. BOT: The building topology ontology of the W3C linked building data group. Janowicz K, editor. Semantic Web [Internet]. 2020 Nov 19;12(1):143–61. Available from: https://www.medra.org/servlet/aliasResolver?alias=iospress&doi=10.3233/SW-200385

[13] Bew M, Richards M. BIM Maturity Model. Paper presented at the Construct IT Autumn 2008 Members' Meeting. 2008;

[14] Kukkonen V, Kücükavci A, Seidenschnur M, Rasmussen MH, Smith KM, Hviid CA. Proposing a Semantic Web Ontology to Support Flow System Descriptions from Design to Operation of Buildings. Automation in Construction. 2021;134.

[15] Flow Systems Ontology Web Page [Internet]. 2021. Available from: https://alikucukavci.github.io/FSO/

[16] Wetter M, Zuo W, Nouidui TS, Pang X. Modelica Buildings library. Journal of Building Performance Simulation [Internet]. 2014 Jul 4;7(4):253–70. Available from: http://www.tandfonline.com/doi/abs/10.1080/19401493.2013.765506

[17] Lawrence Berkeley National Laboratory - Simulation Research Group. BuildingsPy [Internet]. 2021 [cited 2021 May 4]. Available from: https://simulationresearch.lbl.gov/modelica/buildingspy/

[18] Wetter M, Ehrlich P, Gautier A, Grahovac M, Haves P, Hu J, et al. OpenBuildingControl: Digitizing the control delivery from building energy modeling to specification, implementation and formal verification. Energy [Internet]. 2022 Jan 1 [cited 2021 Sep 14];238:121501. Available from: https://doi.org/10.1016/j.energy.2021.121501

Data Statement

The datasets generated during and/or analysed during the current study are not publicly available because of ongoing development but are/will be available upon request.

Co-simulation studies of optimal control for natural refrigerant heat pumps

Thibault Péan [a], Daniel Ramón Lumbieres [a], Alba Colet [a], Ivan Bellanco [a], Martin Josef Neugebauer [b], Daniel Carbonell [b], Jon Iturralde Iñarga [c], Cristina Corchero García [a,d], Jaume Salom [a]

[a] Catalonia Institute for Energy Research (IREC), Sant Adrià de Besòs (Barcelona), Spain, tpean@irec.cat.

[b] SPF-OST Institut für Solartechnik, Rapperswil, Switzerland.

[c] Fundación Tecnalia Research and Innovation, Azpeitia (Gipuzkoa), Spain.

[d] Universitat Politècnica de Catalunya (UPC), Barcelona, Spain.

Abstract. The object of the present study is a natural refrigerant base (propane) heat pump system with a dual source/dual sink heat exchanger (air or ground-based) which is integrated into a centralized tri-generation system with PV and battery for a multi-family building located in Spain. To evaluate the performance of this complex system, a simulation environment was developed, connecting different software. The main program is TRNSYS, with the python package pytrnsys used to create the models and run the simulations, while a model predictive controller is externalized in a separate optimization software. The co-simulation environment enables to couple both software and operate the models in the simulation with the decisions made by the external controller. This environment was used to evaluate the considered system for three separate weeks of the year, each representative of the heating/cooling/DHW demands in winter, summer and intermediate seasons. For each of these weeks, the simulation was run once with a reference rule-based controller, and once with the advanced model predictive controller, to evaluate the additional benefits brought by the later strategy. The results were then extrapolated to the whole year, and revealed that the model predictive controller was able to provide cost savings of 12 to 20% (depending on the consideration or not of the cooling season which gave unexpectedly adverse results). This controller operated the heat pump more efficiently thanks to its prior knowledge of the best source to use at each moment (air or ground). It also managed the battery in a more economical way thanks to its prior knowledge of the time-varying electricity price, thus charging always at the cheaper hours of the day, and demonstrating the advantages of using forecasts and predictive optimization for HVAC control.

Keywords. Heat pumps, co-simulation, model predictive control, tri-generation systems
DOI: https://doi.org/10.34641/clima.2022.432

1. Introduction

Heat pumps have an important role in the decarbonisation of the building sector, thanks to their high efficiency and the possibility to operate them with renewable electricity. The corresponding market has been growing rapidly in the last years, with an increase from 893 k units sold in Europe in 2015 to 1.6 m in 2020 [1]. Furthermore, the Kigali amendment to the Montreal Protocol [2] will enforce a limit on the global warming potential of the refrigerants used in heat pumping systems, which will drive a shift towards natural refrigerants or less environmentally damaging substances.

Centralized heat pump installations for multi-family buildings present several advantages, including the economy of scale for the buffer storages in common spaces of the building. In this paper, a dual source/sink heat pump system adapted to mild Mediterranean climates is investigated. This heat pump includes a dual source heat exchanger that is able to transfer heat with either a geothermal or an air source/sink, and which can work as evaporator or condenser in heating or cooling modes respectively. Both sides can be switched depending on which is the most efficient heat source or sink at any moment. Such a system enables to downsize the length of the costly borehole by a factor of two, since part of the yearly load can be covered with the air source. Furthermore, the dual source/sink heat pump uses propane (R290) as a refrigerant, which has a much lower global warming potential than most refrigerants currently used in thermodynamic cycles, and therefore presents less potential impacts

Copyright ©2022 by the authors. This conference paper is published under a CC-BY-4.0 license.

in case of leakages.

To fully exploit the cost and carbon emission savings potential of heat pump systems, they must be controlled and operated in a smart manner. In this regard, model predictive controls (MPC) based on optimization and predictions of the future have proven to be a promising solution. It has been demonstrated that such strategies can provide savings of up to 30% in several cases [3].

The present study evaluates the benefits of the centralized dual source/sink system for a multi-family building. Through detailed simulations performed in co-simulation between different software, the complete studied system was evaluated under two different strategies: a reference rule-based control, and an advanced controller based on model predictive control. Selected representative weeks were chosen to perform these detailed simulations.

2. Methodology

The dynamic simulations performed for this study have been carried out in a software environment involving different interconnected programs. This simulation environment is first presented, then the study case is described with details of all the systems considered, and their control strategies. Finally, the weeks chosen for the analysis are presented.

2.1. Simulation environment

The simulation environment is based on the pytrnsys package [4], which is a complete framework to create, run and post-process TRNSYS simulation models in python. All the systems are represented with detailed models connected together with the pytrnsys interface. In the present case, two different control strategies have been used: a reference control, which was integrated directly in the TRNSYS models, and an advanced energy management (AEM) which is based on optimization and therefore has to be externalized.

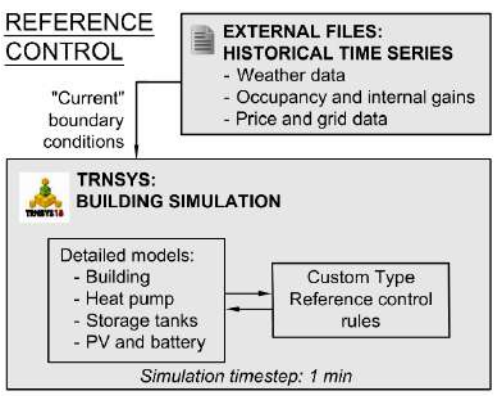

Fig. 1 – Architecture of the simulation environment in the reference control case.

The reference control schematic is presented in Fig. 1. In that case, the rules composing the reference control are implemented into a custom TRNSYS Type that manages the operation of the different systems.

The advanced control schematic is presented in Fig. 2. In that case, the controller (AEM) is written in an external GAMS code [5]. The simulation has a time step of 1 minute, and every 15 minutes, the AEM controller is called: first, a communication is established between a python script and TRNSYS (Type163) through read/write files. Afterwards the python script launches the GAMS model which performs its optimization calculations and returns its output to TRNSYS through python. In this way, the AEMS determines the optimal set-points for the next 15 minutes of simulation, which are then interpreted in TRNSYS by a custom Type and applied to the models of the different systems. This process is repeated after 15 minutes.

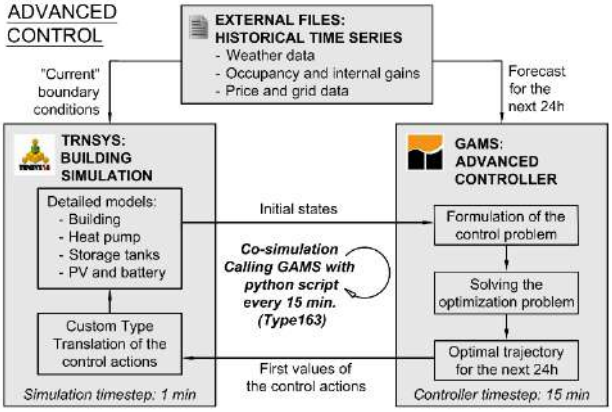

Fig. 2 – Architecture of the simulation environment in the advanced control case.

2.2. Characteristics of the study case

The study case presented in this paper is a multi-family building situated in Tarragona, Spain, with a total heated surface area of 2400 m^2. The heating and cooling systems are centralized and distribute the required power to the 38 flats that comprise the building.

The centralized systems consist of:

- A dual source/sink reversible heat pump with a dual source/sink heat exchanger (DSHX), capable of using either air or ground as sources (DSHX as evaporator) and sinks (DSHX as condenser).
- Two storage tanks, one for storing domestic hot water (DHW) and one for space conditioning including both space heating (SH) and cooling (SC).
- An electrical system composed of a photovoltaic field (PV) and an electrical battery that enables to store the surplus of electricity not directly consumed in the building.

Space heating is distributed to the flats through distribution pipes and a radiant floor system. Space cooling is distributed using fan coil units (FCU). The

DHW distribution system includes a recirculation loop to keep the piping to each apartment warm.
A conceptual schematic of the mechanical and electrical systems is presented in Fig. 3 and the list of subsystems and their respective sizes in the considered study case is presented in Tab. 1.

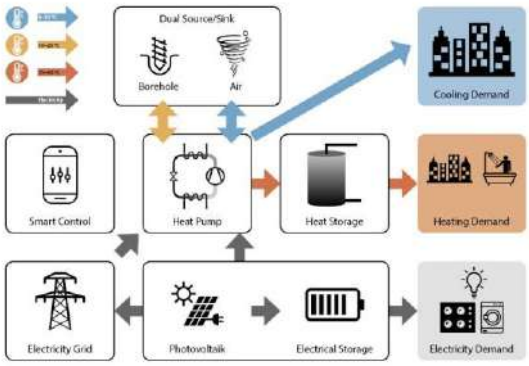

Fig. 3 – Conceptual view of the overall mechanical and electrical systems.

Tab. 1 – List and sizes of the considered systems for the study case of Tarragona.

Parameter	Unit	Value
Heat pump power	kW	44
DHW tank capacity	m^3	1.75
SH/SC tank capacity	m^3	1.5
PV peak power	kWp	62.5
Battery capacity	kWh	125
Heating demand	kWh/m^2	2.0
Cooling demand	kWh/m^2	7.0
Appliances elec. demand	kWh/m^2	31.5

2.3. Control strategies

The reference control for the dual source system consists in a set of rules that decide on the operation of its different components. The algorithm is split between heating and cooling modes. The temperatures in the two tanks and their associated set-points determine whether there is a demand for space heating, cooling or DHW. The demand is mainly covered by the heat pump with priority on DHW. The algorithm determines which is the most efficient source or sink (air or ground) for the DSHX at each moment, i.e. the warmest source is considered the most efficient in heating mode, while it is the coolest in heating mode. When both sources/sinks have the same temperature, the ground source is favoured. The room temperature demand is determined by a classic thermostatic control. In addition, in cooling mode, a free cooling operation is possible and prioritized: it consists in circulating water between the radiant floor circuit and the borehole to cool down the building. If this is not sufficient, cold water from the space conditioning tank is provided to the FCU to further cool down the rooms.

The advanced control presents a different approach based on model predictive control. It consists of an optimization problem that minimizes operational costs and discomfort. The optimization module uses reduced-order models of the system that enables it to project its operation into the future. It is also fed with weather forecasts, occupancy and energy prices. The optimization problem is solved every 15 minutes and sends the required set-points to the "real" (simulated) system, to which the set-points are applied in the TRNSYS simulation. The main configurational parameters of the model predictive control are presented in Tab. 2. The thermal systems are represented as RC models, as shown in Fig. 4. The heat pump is represented by a linear model which expresses its electrical consumption in function of the ambient temperature, the supply temperature and the thermal power delivered [6].

Tab. 2 – Configurational parameters of the model predictive controller.

Building model	R2C2
Tanks model	R1C1
HP model	Linear
Horizon length	24h
Time step	15 min
Optimization criteria	5% relative gap

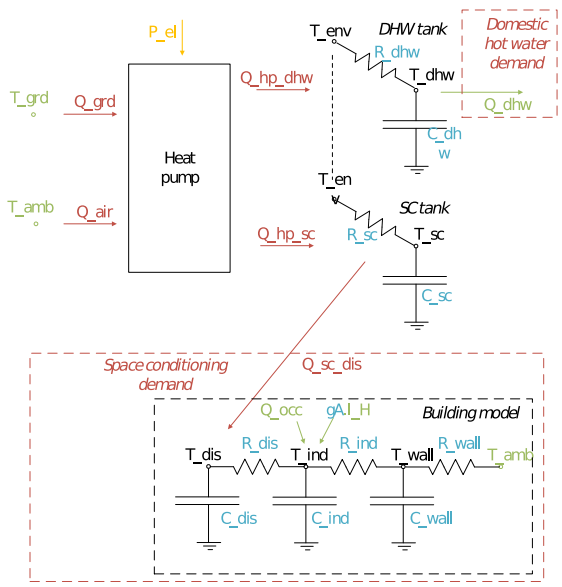

Fig. 4 – Simplified models of the considered systems (thermal part).

2.4. Simulated weeks

Three different weeks of the year have been simulated, covering the specific seasons encountered in the climate of Tarragona, Spain. These specific weeks were chosen as representative of their respective season, enabling an extrapolation to the whole year. The methodology for selecting the representative weeks followed these two main steps:

- Grouping all the weeks of the year into 4 different clusters using their average outdoor temperature and summed solar irradiation (using a k-means algorithm) [7],

- Within each cluster, choosing the week that is most representative of the cluster according to its space heating or cooling load (using a genetic algorithm) [7]

Following this process, one week was selected for the heating dominated cluster (January 18th to 24th) and one week for the cooling dominated cluster (July 4th to 10th). For the two remaining intermediate clusters with little to no space conditioning load, only one week was selected to represent both of them (April 10th to 16th), since they only have DHW load.

The weather conditions of the three selected weeks are represented in Fig. 5, with both the outdoor ambient temperature and the horizontal solar irradiation. In addition, the price signal for the first week has been plotted. This price signal represents one typical week, with high prices between 10:00 – 14:00 h and between 18:00 – 22:00 h in weekdays, while the weekends see low prices all day long. Here, the Saturday and Sunday are in the middle of the chosen 7 days (Jan. 20th and 21st). The price signal is the same for the other weeks, therefore they are not presented again, although the Saturday and Sunday fall to different positions.

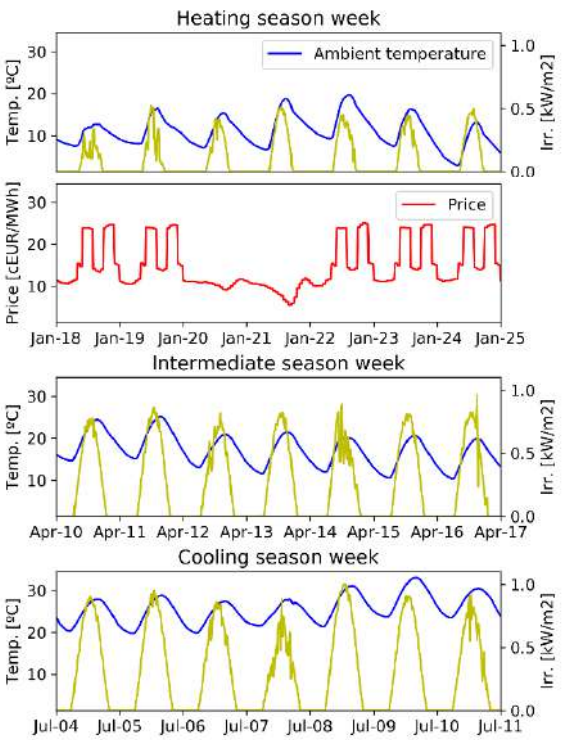

Fig. 5 – Representation of the three selected weeks.

Another important hypothesis is the impossibility to sell the excess electricity produced by the PV panels to the grid. Although the export is possible, it is not rewarded economically.

Regarding the interpretation of the results, several Key Performance Indicators (KPIs) have been calculated, among which the amount of electricity imported from the grid, the electricity from the PV that is exported to the grid, the average COP (averaged for COP and EER when operating for both DHW and SC in the cooling season), and the thermal energy produced by the heat pump for each use. Other KPIs are described in [8].

3. Results

3.1. Heating season week (winter)

The results are first analysed for the winter week in the heating season, which ranges from the 18th to the 24th of January. Fig. 6 presents the electricity imported from the grid in both the reference and the advanced control cases as well as the resulting energy cost. The periods of high prices have been represented in light red to highlight the moments of high penalty where the import of energy should be avoided.

Tab. 3 – Main KPIs computed for the reference and advanced control cases of the winter week, and the difference between both cases [8].

Parameter	Ref.	AEMS	Diff. (%)
Cost of imported electricity [EUR]	85.1	69.6	-15.5 (-18.2%)
Electricity import from grid [kWh]	646.9	670.8	+24.0 (+3.7%)
Electricity export to grid [kWh]	0	3.28	+3.27
Average COP [-]	3.23	3.50	+0.26 (+8%)
Thermal energy produced SH [kWh]	300.4	245.5	-54.9 (-18.3%)
Thermal energy produced DHW [kWh]	859.3	914.1	54.9 (+6.40%)
Comfort time in Cat. I [%]	83.2%	46.5%	-36.7%
Comfort time in Cat. II [%]	16.8%	53.5%	+36.7%
Average room temperature [ºC]	21.2	21.0	-0.23
Grid purchase ratio [%]	0.36	0.37	+0.02
PV generation ratio [%]	0.68	0.69	+0.01
Renewable primary energy [kWh]	2299	2321	+21.8 (+1.0%)
Total primary energy [kWh]	3563	3631	+68.7 (+1.90%)
Renewable Energy Ratio [%]	0.65	0.64	-0.01

It can first be observed that the reference control strategy actually performs well with regards to avoiding these high cost periods. In the hours of solar irradiation in the middle of the day, it charges the battery, and when the sun sets, it can use the charged energy: this moment coincides with the high price period of the night, and therefore the import of electricity is generally avoided at these times. The advanced control goes one step further by optimizing

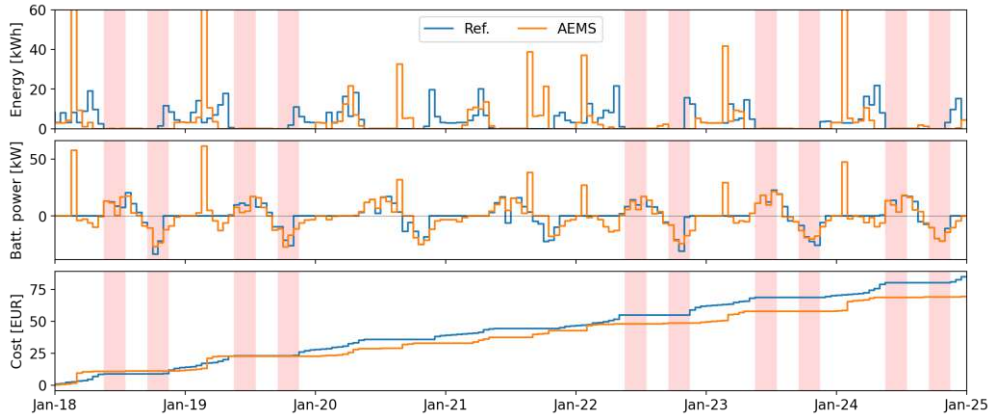

Fig. 6 – Hourly electricity import, battery power and cumulative energy cost compared for both the reference and advanced control cases in the winter week. Red shaded represents periods of high electricity prices.

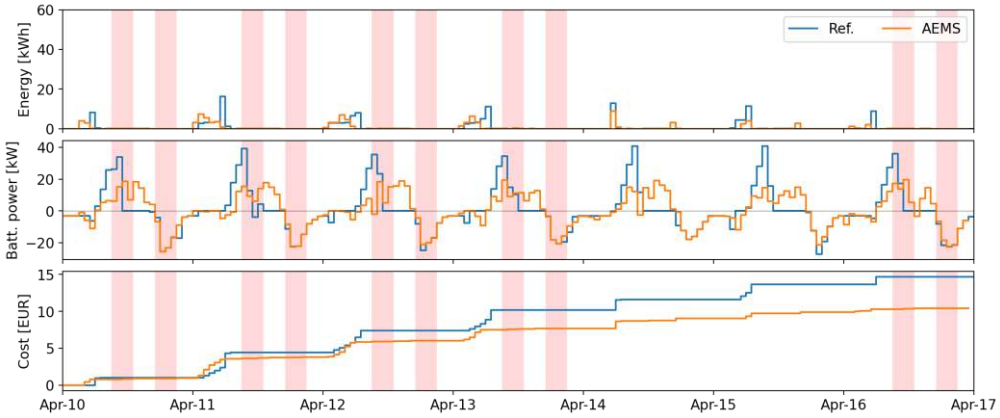

Fig. 7 – Hourly electricity import, battery power and cumulative energy cost compared for both the reference and advanced control cases in the intermediate week. Red shaded represents periods of high electricity prices.

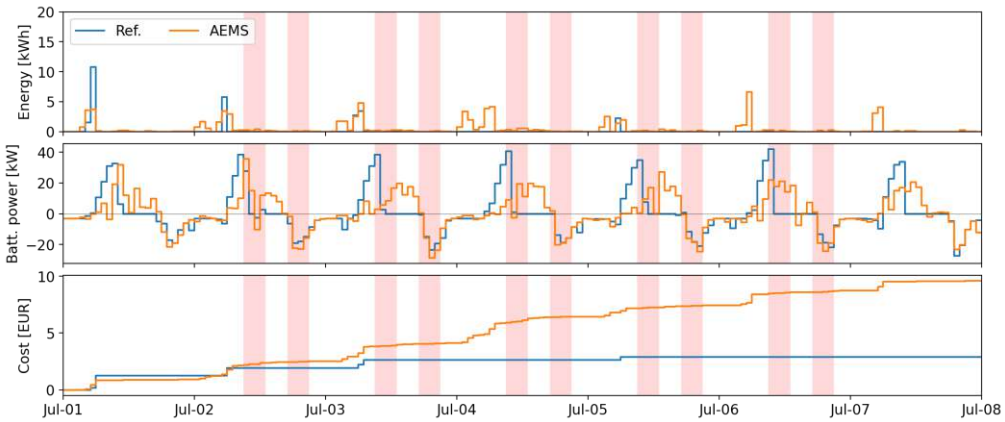

Fig. 8 – Hourly electricity import, battery power and cumulative energy cost compared for both the reference and advanced control cases in the summer week. Red shaded represents periods of high electricity prices.

the charging of the battery considering the energy price. A peak of energy import from the grid can be observed during certain nights: during this hour, the price is minimal over the rolling 24 hour horizon, therefore the advanced controller makes the most of it by fully charging the battery with the energy that will not anyways be available with solar power on the next day.

This operation enables to provide additional cost savings which is the final objective of the implemented control, as can be seen in Tab. 3 where the main KPIs that have been computed are presented. Although the amount of electricity imported from the grid slightly increases (+3.7%) due to this night charging operation, the energy operational costs decrease by 18%. It should be noted that the dual source heat pump operates at a higher efficiency with the advanced controller, since it knows the temperature evolution of both sources

and the resulting COP of the heat pump in those conditions in advance. The average COP for that week therefore increases from 3.23 to 3.50. Thermal comfort slightly decreases: the average room temperature is 21.2 °C in the reference case, while it is reduced to 21.0 °C with the advanced control. This slight difference is not considered to affect the occupants since thermal comfort always stays within the comfort categories I or II from the European standards on Indoor Environmental Quality [9].

3.2. Intermediate season week (spring)

The results of the intermediate season week are analysed next. For this case, it is a week with a mild climate which does not require active heating or cooling, and where thermal comfort can be achieved with passive strategies such as natural ventilation. The main thermal load is therefore DHW in this scenario. The imported electricity and cumulative cost in both control strategies are reported in Fig. 7.

In this scenario, both control strategies avoid the highest price periods to import electricity. However, the import peaks always happen at the lowest price hour for the advanced control, and a few hours later for the reference rule-based control. The main computed KPIs are presented in Tab. 4. The cost savings are lower in absolute values than in the heating case since the demand is also lower. However, in relative savings, the advanced control manages to reduce the electricity import from the grid by 28.5%, which then corresponds to cost savings of 29%, this despite a slight increase of the thermal energy produced for DHW (+5.5%). The heat pump is also operated at higher efficiency since the average COP increases from 3.44 to 3.96 thanks to the advanced control.

Tab. 4 – Main KPIs computed for the reference and advanced control cases of the intermediate week, and the difference between both cases.

Parameter	Ref.	AEMS	Diff (%)
Cost of imported electricity [EUR]	14.7	10.4	-4.3 (-29.0%)
Electricity import from grid [kWh]	132.1	94.5	-37.6 (-28.5%)
Electricity export to grid [kWh]	985.8	962.8	-23.0 (-2.3%)
Average COP [-]	3.44	3.94	+0.50
Thermal energy produced SH [kWh]	0.0	0.0	0.0
Thermal energy produced DHW [kWh]	747.9	788.9	+41.0 (+5.5%)
Grid purchase ratio [%]	0.08	0.06	-0.02
PV generation ratio [%]	1.59	1.61	+0.02
Renewable primary energy [kWh]	2198	2287	+88 (+4.0%)
Total primary energy [kWh]	2456	2471	+15 (+0.6%)
Renewable Energy Ratio [%]	0.89	0.93	+0.03

3.3. Cooling season week (summer)

Finally, we analyse the results of the week of the cooling season. In that case, the building can be cooled down using the borehole in a free cooling operation, or with active cooling using the cold water produced by the heat pump and stored in the space conditioning tank.

It should be noted that the cooling case with the advanced controller does not perform as expected. This is notably due to the higher complexity of the optimization problem with the additional free cooling variables, and the differences in the model parameters. For these reasons, the optimization fails to converge and to provide a solution within its allocated time (300 seconds for each optimization) for a significant number of instances. When such error occurs, the set-points are not updated, and thus it disturbs the strategy that had been planned until that moment, since local changes must be adapted to continue operating the systems.

Tab. 5 – Main KPIs computed for the reference and advanced control cases of the summer week, and the difference between both cases.

Parameter	Ref.	AEMS	Diff (%)
Cost of imported electricity [EUR]	2.89	9.59	+6.7 (+232%)
Electricity import from grid [kWh]	26.5	79.1	+52.6 (+198%)
Electricity export to grid [kWh]	1522	916	-606 (-40%)
Average COP [-]	3.82	3.86	+0.05 (+1.2%)
Thermal energy produced SC [kWh]	21.1	2318	+2297
Thermal energy produced DHW [kWh]	685	731	+46 (+6.8%)
Free cooling energy [kWh]	1980	568	-1411 (-71%)
Comfort time in Cat. I [%]	100%	100%	-
Average room temperature [ºC]	24.1	23.6	-0.48
Grid purchase ratio [%]	0.02	0.03	+0.02
PV generation ratio [%]	2.02	1.43	-0.59
Renewable primary energy [kWh]	2281	2325	+44 (+1.9%)
Total primary energy [kWh]	2333	2480	+147 (+6.3%)
Renewable Energy Ratio [%]	0.98	0.94	-0.04

The KPIs are presented in Tab. 5 and the time series (import, battery and cumulative cost) in Fig. 5. These results should be considered with caution because of the aforementioned faulty operation. In this considered summer week, the PV production is high and should suffice to cover almost all the electrical load of the building. The imported electricity is therefore small in both cases (26.5 and 79.1 kWh), although the advanced controller case actually imports more energy than the reference controller

case.

It can also be observed that the advanced controller performs worse than the reference one when it comes to the choice of the cooling strategy. Most of the cooling load is covered by free cooling with the reference controller, a strategy that has little to no cost (only circulation pumping). The advanced controller on the other hand resorts a lot to active cooling with the heat pump and the FCU. We suspect that the simplified model for the ground temperature used in the AEMS, which has large effects on the free cooling operation, is the main cause of such discrepancies and we are trying to solve this issue.

3.4. Yearly results extrapolation

The results of the separate weeks for each season have been presented in the previous section. An annual interpretation can then be carried out, by considering that the chosen weeks are representative of their respective seasons, and that the other weeks of their cluster will present similar levels of energy costs. The energy cost for each of the studied week and the extrapolation is reported in Tab. 6. Given the number of weeks in each cluster, the total cost for each season can be computed, which then gives the sum of the annual energy costs. In that case, the reference control would result in an annual cost of 1889 € against 1651 € for the advanced controller, hence the AEMS provides cost savings of 12.6%.

Given the uncertainty of the cooling week results, a separate sum considering only the heating and intermediate seasons has also been computed. In that case, the adverse effects of the cooling week performance are less notable, and therefore the cost savings reach a value close to 20% which complies with the 15% objective that had been envisioned for this type of system operated with the advanced controller.

Tab. 6 – Interpretation of yearly results.

	Number of weeks [-]	Cost Ref. week [EUR]	Cost AEMS week [EUR]	Season cost Ref. [EUR]	Season cost AEMS [EUR]	Savings [%]
Heating season	19	85.1	69.6	1616.9	1322.4	
Intermediate season	15	14.7	10.4	220.5	156	
Cooling season	18	2.89	9.59	52.0	172.6	
Yearly total	52			1889.4	1651.0	-12.6%
Yearly total (without cooling)	34			1837.4	1478.4	-19.5%

4. Conclusions

The study has first presented an innovative simulation framework including different interconnected software. This platform enables the testing of different controllers in an automated way, particularly of advanced controllers based on optimization which cannot be included in the main simulation software and must be externalized. It was shown that the communication between the different pieces of software functions correctly and that the overall simulation framework performs satisfactorily. This developed environment is an important outcome of the study that can be reused for further research.

In that simulation environment, a dual source/dual sink system adapted to a Mediterranean climate has been tested for three separate representative weeks. The overall HVAC system performs satisfactorily with a reference controller, but the advanced controller based on model predictive control enables to save an additional 12% to 19% on the energy costs annually. The advanced controller manages the heat pump in a more efficient way, benefitting from its knowledge in advance of the most efficient of the two available sources (air or ground) at every moment. The battery is also managed more efficiently according to the considered price signal, with charging hours coinciding with the lowest electricity prices.

As further research, the optimization problem of the advanced controller in cooling mode should be revised to obtain faster and more reliable results. Furthermore, a second system which includes additional elements will also be tested. This new system comprises a solar thermal collector and an ice slurry storage, hence the advanced controller will additionally manage these elements to optimize the operation of the whole system. This other system is a study case in another climate (Switzerland), thus enabling to have a better overview of the controller performance in a variety of climates and conditions.

5. Acknowledgement

The research conducted in this paper is funded by the European Union Horizon 2020 Research and Innovation program under grant agreement no. 814888 (TRI-HP).

6. References

[1] European Heat Pump Association. EHPA stats 2021. http://stats.ehpa.org

(accessed August 18, 2021).
[2] UN. Amendment to the Montreal Protocol on Substances that Deplete the Ozone Layer. Kigali: 2016.
[3] Péan T, Salom J, Costa-Castelló R. Review of control strategies for improving the energy flexibility provided by heat pump systems in buildings. J Process Control 2018;74:35–49. https://doi.org/10.1016/j.jprocont.2018.03.006.
[4] SPF-OST. pytrnsys 2021. https://pytrnsys.readthedocs.io/en/latest/.
[5] GAMS Development Corp. General Algebraic Modeling System (GAMS) 2021.
[6] Péan T. Heat pump controls to exploit the energy flexibility of building thermal loads. Universitat Politècnica de Catalunya, 2020.
[7] Haberl R, Schubert M, Péan T, Bellanco I, Belio F, Salom J. TRI-HP D7.1 - Concise Cycle Test (CCT) method definition. Rapperswil, Switzerland: 2021.
[8] Iturralde J, Alonso L, Pascual C, Hernandez P. TRI-HP D1.2 - Technical, economic and environmental performance KPIs definition. 2020.
[9] Mendoza-Serrano DI, Chmielewski DJ, Ieee. Controller and System Design for HVAC with Thermal Energy Storage. 2012 Am Control Conf 2012:3669–74. https://doi.org/10.1109/ACC.2012.6315658.

Data Statement

The datasets generated and analysed during the current study are not available because they require a prior work of processing, formatting and description of their metadata, but the authors will make every reasonable effort to publish them in near future.

FDD method for a variable-speed heat pump with natural refrigerants

Ivan Bellanco [a,b], Francisco Belío [a], Manel Vàlles [b], Raphael Gerber [c], Jaume Salom [a]

[a] Catalonia Institute for Energy Research (IREC), Jardins de les Dones de Negre 1, Sant Adrià del Besòs (Barcelona), 08930, Spain. ibellanco@irec.cat, jfbelio@irec.cat, jsalom@irec.cat

[b] Department of Mechanical Engineering, Unirversitat Rovira i Virgili, Av. Països Catalans No. 26, Tarragona, 43007, Spain. manel.valles@urv.cat

[c] Heim AG Heizsysteme, Wittenwilerstrasse 31, Aadorf, 8355, Switzerland. Raphael.Gerber@heim-ag.ch

Abstract. Heat pumps are one of the most efficient devices to provide heat and cool. The number of heat pumps sold in Europe increases every year as European Legislation moves towards the use of natural refrigerants that have negligible global warming potential compared to synthetic refrigerants. Variable-speed domestic heat pumps may have hard-to-detect faults that increase energy consumption while the demand is still covered. These faults could worsen and take down the equipment. Fault detection and diagnosis (FDD) systems aim to detect these types of soft faults, reducing operating and maintenance costs. The present study is the result of developing an FDD system for variable-speed heat pumps. The FDD system has been tested with a 10 kW water-to-water variable-speed heat pump charged with propane. Some of the most common faults were emulated for 10 kW and 12 kW heating loads. These faults were evaporator fouling, compressor valve leakage, liquid line restriction and refrigerant overcharge. The present paper presents the overall structure of the developed FDD, each of its different modules and the performance indicators during tests. The FDD developed consists of different modules: a steady-state detector, the input space module, the no-fault regression models and the diagnosis module. The steady-state detector filters the measurements to select only the steady-state data. The input space classifies the data in clusters defined by the heat pump driving variables. For each of these clusters, a regression model is trained. Once trained, the deviation between the models and the real data will indicate a fault occurrence. The diagnosis module analyses the trends of different features to diagnose the fault. The FDD was able to monitor in real time the heat pump performance during the fault tests. The results showed fault detection before 10 minutes with COP drifts above 7 %. Each fault could be diagnosed correctly, except evaporator fouling, which was detected as a fault but could not be distinguished from the others.

Keywords. FDD, variable speed heat pump, natural refrigerants
DOI: https://doi.org/10.34641/clima.2022.433

1. Introduction

In the European Union, a large part of the energy consumption in households is due to space heating, water heating and space cooling [1]. Heat pumps are one of the most efficient technologies for space heating and cooling and, coupled with renewable electricity sources they can reduce greenhouse emissions compared with classic solutions. However, the refrigerants used in heat pumps could have high global warming potential (GWP). These refrigerants could leak to the environment due to a leakage in the circuit or incorrect disposal at the end of life. For this reason, the restrictions to the use of refrigerants with high GWP are increasing, promoting the use of natural refrigerants, such as propane or carbon dioxide with lower GWP.

Despite their high performance, heat pumps could suffer fault conditions that can affect their optimal operation and reduce their energy efficiency [2]. There is a typology of faults called "soft faults" because they reduce the equipment efficiency while still covering the demand, making them difficult to detect [3]. These faults could remain undetected for long periods, increasing the energy consumption and could worsen and damage the heat pump. Fault Detection and Diagnosis (FDD) systems are used to detect soft faults or performance decreases [4].

Generally, the structure of an FDD is as follows: a learning phase where a model of the normal

Copyright ©2022 by the authors. This conference paper is published under a CC-BY-4.0 license.

operation of the heat pump is generated. The model could be trained with simulation, manufacturer or experimental data. Once trained, the measurements from the heat pump are compared with those coming from the models. If there is a difference, a fault is occurring. The diagnosis is usually performed by checking the trends of different features of the heat pump. Depending on the feature and if its trend is increasing or decreasing, the FDD could diagnose the fault. Machine learning could be used to avoid the need for expert knowledge about the fault effect, but it requires fault data to train the algorithms [5].
The present study describes the experimental evaluation of a new developed FDD. The general scheme of the FDD is explained and each part is described. A variable-speed heat pump charged with propane is used to emulate different faults. The tests data are used to train and validate the FDD algorithm.

2. Methodology

For this study, two different heating load conditions at steady state were tested, 10.2 kW and 12.3 kW. Table 1 shows the temperatures and water flows of the circuits for those conditions. The water flow was fixed. First, the heat pump with no fault was tested at those two conditions. Then, the faults evaporator fouling (EF), compressor valve leakage (CVL), liquid line restriction (LL) and refrigerant overcharge (OC) were tested for both conditions.

Tab. 1 – Steady-state test conditions. From the water side: condenser outlet temperature ($T_{cond,out}$), condenser inlet temperature ($T_{cond,in}$), evaporator inlet temperature ($T_{evap,in}$), condenser water flow ($\dot{V}_{cond}$) and evaporator water flow ($\dot{V}_{evap}$).

Heating load (kW)	$T_{cond,out}$ (ºC)	$T_{cond,in}$ (ºC)	$T_{evap,in}$ (ºC)	$\dot{V}_{cond}$ (lpm)	$\dot{V}_{evap}$ (lpm)
10.2	45	40	10	30	40
12.3	45	40	10	30	40

2.1 Evaporator fouling

In air heat pumps, the evaporator is normally located outdoors, where it is exposed to dirt and particles that can obstruct the heat exchanger. In water heat pumps, dirt could accumulate in the impeller of the pump [6]. In both heat pump typologies, mechanical faults as pump or fan malfunction can also appear. All these faults decrease the heat transfer coefficient and have been grouped in this paper under the term "Evaporator fouling". To emulate the fault, the water flow of the evaporator was decreased below the nominal value. Equation 1 describes the fault intensity (FI) related to this water flow decrease.

$$FI_{EF} = \frac{\dot{V}_{fault} - \dot{V}_{nom}}{\dot{V}_{nom}} \quad (1)$$

where $\dot{V}_{fault}$ is the evaporator water flow for the current fault level and $\dot{V}_{nom}$ is the water flow for the no-fault condition. The nominal water flow was 40 lpm.

2.2 Compressor valve leakage

The compressor valve leakage refers to a bypass between the high and low-pressure sides of the refrigerant circuit. This leakage could appear in the compressor or in the 4-way valves [6]. The fault was emulated by opening a valve that bypasses the discharge and suction sides of the compressor. Equation 2 describes the fault intensity related to the refrigerant mass flow.

$$FI_{CVL} = \frac{\dot{m}_{r_fault} - \dot{m}_{r_nom}}{\dot{m}_{r_nom}} \quad (2)$$

where $\dot{m}_{r_fault}$ is the refrigerant mass flow for the fault condition and $\dot{m}_{r_nom}$ is the refrigerant mass flow when no fault is present. As $\dot{m}_{r_nom}$ changes with the speed of the compressor, a correlation between speed and flow was obtained running the compressor at different speeds when no fault is present.

2.3 Liquid line restriction

The liquid line restriction appears when the filter placed in the liquid line gets fouled by debris in the refrigerant. This fouling increases the pressure drop of the liquid line [6]. The fault was emulated with a restriction valve placed in the liquid line. Equation 3 shows the fault intensity for this fault, which is related to the pressure drop variation in the liquid line.

$$FI_{LL} = \frac{\Delta P_{LL} - \Delta P_{nom}}{\Delta P_{nom}} \quad (3)$$

where ΔP_{LL} represents the liquid line pressure drop with fault and ΔP_{nom} the liquid line pressure drop without fault. The pressure drop was calculated as the difference between discharge and suction pressures.

2.4 Refrigerant overcharge

An overcharge of refrigerant occurs when more refrigerant than the nominal amount is charged during a commissioning or maintenance service [6]. The fault was emulated charging a 10% more refrigerant than the nominal. Equation 4 shows the fault intensity for OC.

$$FI_{OC} = \frac{m_{r_fault} - m_{r_nom}}{m_{r_nom}} \quad (4)$$

2.5 Equipment and validation procedure

A 10 kW variable-speed water-to-water heat pump was tested. The heat pump was a prototype developed in the framework of the *Trigeneration systems based on heat pumps with natural refrigerants and multiple renewable sources* (TRI-HP

project) [7] charged with 720 grams of propane as refrigerant. Figure 1 shows the heat pump scheme. More information about the heat pump architecture, the experimental procedure and the fault test results can be found in [8]. The no-fault data was used to train the FDD and the fault data was used to validate the FDD performance.

3. Fault detection and diagnosis algorithm

Despite the use of two steady state conditions, the development of the FDD algorithm has been focused on the use of different heat pumps at different conditions. Because of that, the algorithm counts with different modules to increase the detection accuracy. These modules are a steady state detector, an input space classifier, the regression model training and fault monitoring, and fault diagnosis. Figure 2 shows the operation flow scheme of the FDD.

3.1 Steady state detector

The objective of the steady-state detector (SSD) is to identify the stages where the heat pump is working at quasi-steady-state conditions to use the data for training and fault monitoring [9]. In statistics, a data series is in steady state when the slope of the mean and the variance is constant and there is no seasonality. When real-time data is used, sensor noise and variability due to variable speed operation will lead to a non-constant value of the mean and variance. Because of this, the detector will search for points with quasi-stationarity, where a percentage of change in variance and mean is allowed. A sliding window method [9] is applied for the calculation of the mean and variance slope. The mean and variance of the first window are used as a reference. Then, it is compared to the adjacent windows. If the mean and variance of all the windows are in inside the threshold then, the last point will be in steady state. The threshold was determined from an average of experimental data of previous tests with variable and fixed speed heat pumps

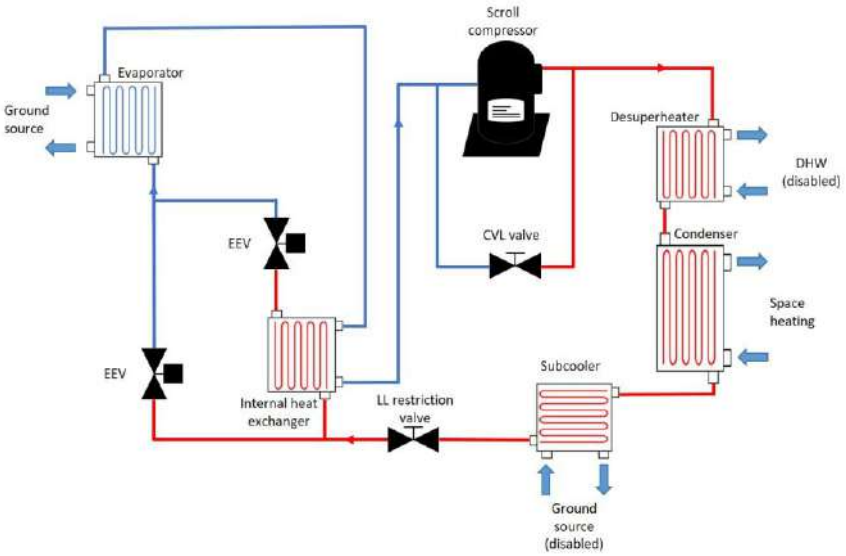

Fig. 1 – Heat pump architecture. The desuperheater and subcooler were not used during the tests.

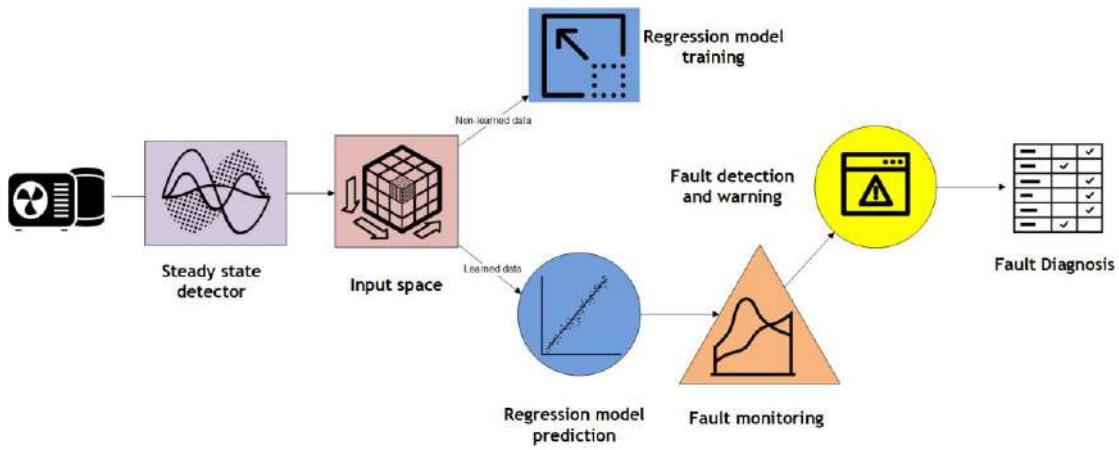

Fig. 2 – Software scheme of the FDD.

3.2 Input space classifier

Most of the FDD are developed to work under steady state conditions where the conditions do not change. Based on the work of Heo et al. [10], we used an input space classifier to allow the training of new data. The input space is the three-dimensional area defined by the independent or driving variables of the heat pump [11]. For a variable-speed heat pump, we choose the condenser outlet and inlet temperatures ($T_{cond,out}$ $T_{cond,in}$) and the evaporator inlet temperature ($T_{evap,in}$) as the driving variables. Figure 3 shows a representation of the input space division in groups. For each of these groups, a no-fault model could be trained.

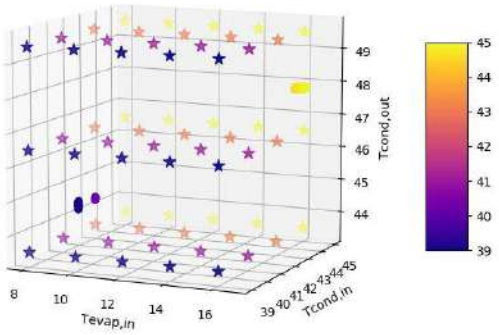

Fig. 3 – Input Space. The stars are the arithmetic center of each group. The points are the training data. The color scale is used in the $T_{cond,in}$ axis.

3.3 Regression model training and fault monitoring

For the generation of no-fault models, a stochastic gradient descent regression approach was selected for its good results and low requirement of computational power. During a defined period, while there is no fault present, the measurement data is stored. Once the period is over, the input space classifies the data into groups, and if there are enough data points (at least 50), a model will be trained for each group. This is the initial training period. When the current driving conditions are beyond those of the training period, the algorithm will store the data until there are enough data points to train that group. This gives the capability of self-training the algorithm.

After the initial training period, the data coming from the heat pump will be compared with the corresponding no-fault model. An uncertainty margin is applied to the original prediction of the FDD. This area is two times the maximum root-mean-square error (RMSE) of the cluster training. Figure 4 shows the uncertainty margin of a model of one of the clusters of the input space. If the coefficient of performance (COP) of the heat pump is outside this margin a fault could be happening. However, noise or outliers in the measurement could be outside this margin without an actual fault happening. Because of that, when there is a drift between the COP of the model and the COP measured, the algorithm starts a counter. A warning flag will be triggered if, for a period of ten minutes, the number of measurements outside the uncertainty margin represents more than 80% of the samples. Figure 5 shows an example of fault monitoring with a 30 minutes counter.

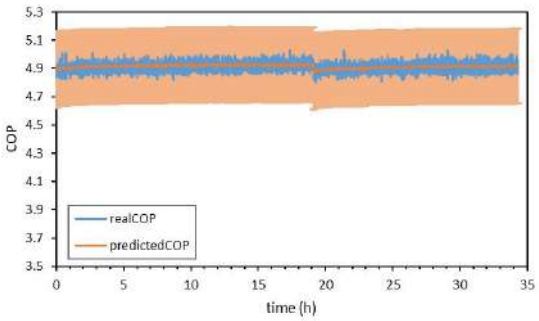

Fig. 4 – Training results of an Input Space cluster. The blue line is the real data. The orange one is the prediction of the algorithm. The shadowed area is the uncertainty margin.

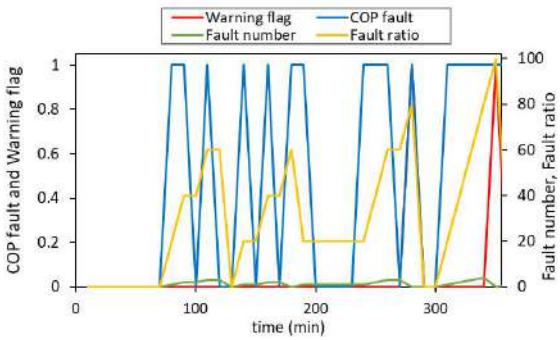

Fig. 5 – Fault monitoring example from a series with 10 minute frequency and 50 minutes of monitoring. COP flag is triggered when the COP measurements are outside the uncertainty range. Fault ratio is the percentage of measurements outside the uncertainty in the monitoring window. The warning flag is triggered when the fault ratio is above 80%.

3.4 Fault diagnosis

Once a fault warning is triggered, the algorithm will look at different trends of the heat pump features to diagnose the fault. In our case, we consider as valuable features the COP, the compressor electrical consumption (W_{comp}), the heat duty (Q_{heat}), the subcooling (T_{sc}), the superheating (T_{sh}), the evaporation temperature (T_{evap}), the condenser temperature (T_{cond}), the compressor outlet temperature (T_{co}), the liquid line refrigerant temperature (T_{ll}), the refrigerant mass flow (m_r) and the compressor frequency (f). For each of these features, a no-fault model is trained. The actual value is compared with the one from the models and three different trends are considered: increasing, decreasing or no change. The result is compared with a trend chart that serves to diagnose the fault.

Tab. 6 – Trend chart used to diagnose faults. ↓: decreasing trend, ↑: increasing trend.

Fault	COP	W_{comp}	Q_{heat}	T_{sc}	T_{sh}	T_{evap}	T_{cond}	T_{co}	T_{ll}	m_r	f
EF	↓	↑				↓					↑
CVL	↓	↑	↓	↑				↑	↓	↓	↑
LL	↓	↑		↑	↑	↓	↑	↑	↓	↓	↑
OC	↓	↑		↑		↑	↑	↑	↓		↓

Tab. 7 – Performance values for the FDD. "-": When the FDD did not reach any detection.

Code	FI	Accuracy (%)	COP drift (%)	Code	FI	Accuracy (%)	COP drift (%)
EF10.1	-0.100	-	0	CVL10.1	-0.042	-	2
EF10.2	-0.157	-	0	CVL10.2	-0.296	100	22
EF10.3	-0.214	-	1	CVL10.3	-0.372	100	29
EF10.4	-0.271	-	1	CVL10.4	-0.648	-	21
EF10.5	-0.328	-	2	CVL12.1	-0.131	100	11
EF10.6	-0.385	100	3	CVL12.2	-0.379	100	31
EF10.7	-0.442	100	4	CVL12.3	-0.608	100	47
EF10.8	-0.500	100	5	LL10.1	0.103	100	7
EF12.1	-0.100	-	1	LL10.2	0.181	100	14
EF12.2	-0.157	-	1	LL10.3	0.267	100	18
EF12.3	-0.214	-	2	LL10.4	0.418	100	26
EF12.4	-0.271	-	3	LL10.5	0.743	100	35
EF12.5	-0.328	-	3	LL12.1	0.055	-	2
EF12.6	-0.385	-	4	LL12.2	0.168	100	13
EF12.7	-0.442	-	6	LL12.3	0.281	100	19
EF12.8	-0.500	100	7	LL12.4	0.404	100	24
OC10.1	0.100	100	21	LL12.5	0.648	100	31
OC10.2	0.100	100	19				

4. Results and discussion

Table 6 summarizes the feature trends obtained in the fault tests [8]. This table serves to diagnose faults based on the trends of the different features. To evaluate the performance of the FDD, the indicators accuracy and COP drift were used.

The accuracy represents the fraction of correct fault warnings with respect to the total fault warnings given by the FDD system.

$$Accuracy = \frac{True\ \text{Positive}}{True\ Positive + False\ positive} \quad (5)$$

Equation 5 shows the Accuracy equation where a true positive means that the FDD detects a fault when it is actually happening and false positive when the FDD detects a fault when there is none.

The COP drift indicates the degree of COP deterioration as equation 6 shows. An ideal FDD should have a 100% accuracy and detect from 1% of COP drift.

$$COP\ drift = \frac{COP_{nominal} - COP_{fault}}{COP_{nominal}} * 100 \quad (6)$$

Table 7 shows the performance values for each fault level tested. The FDD detected COP drifts above 3% and 7%. A 100% accuracy was obtained when the FDD detected a fault. This means that the FDD did not give any false alarms. Figure 4 shows the training results of an input space cluster. Despite the use of an SSD, the uncertainty area is remarkable. The use of such a margin was to eliminate the possibility of false alarms and increase the reliability of the algorithm. The margin could be narrowed so the FDD could detect lower COP drifts in exchange for a higher probability of false alarms.

Table 8 shows the diagnosis results of the FDD. The indicator Misdiagnosis Rate (MR) was used to indicate the capability of the FDD for correctly

diagnose the faults detected. Equation 7 shows the calculation of MR, which is related to the number of incorrect diagnoses provided by the FDD.

$$MR = \frac{False\ Diagnosis}{False\ Diagnosis + True\ Diagnosis} \quad (7)$$

Except for EF, all the faults could be correctly diagnosed. EF had the lowest impact on the heat pump, which is the reason for not reaching a diagnosis. Nevertheless, the algorithm detects that there is a fault but cannot discern which.

Tab. 8 – MR values for the diagnosis module. "-": the algorithm does not reach a diagnose.

Code	MR (%)
EF10	-
EF12	-
CVL10	0
CVL12	0
LL10	0
LL12	0
OC10	0
OC12	0

5. Conclusions

A new FDD developed for variable-speed heat pumps has been validated with real equipment data. To do so, some of the most common faults on heat pumps has been emulated in a variable-speed heat pump charged with propane. The FDD is composed of different modules to ensure the efficiency of the algorithm. The use of an SSD and a fault monitoring module increases the accuracy of the algorithm and reduces the number of false alarms. However, this increases the time needed to detect a fault (less than 30 minutes). The use of regressions decreases the computational power needed to monitor the equipment and limits the training data needed. The self-training capability has not been needed for the experimental tests, as the same conditions were used for training and monitoring. But the use of self-training could be risky. The heat pump is considered with no fault when it has been installed and commissioned by a certified technician. After that, if the algorithm self-trains, it could do it when there is a fault on the equipment. The use of manufacturer data could help to tackle the problem, but more research is needed in this aspect.
With COP losses of as much as 47%, the use of FDD takes more relevance as the faults tested have not decreased the heat provided by the heat pump and therefore, the user does not detect the problem.

6. Acknowledgement

Ivan Bellanco acknowledges the Universities and Research Secretariat of the Catalan Government and the European Social Fund for the financial support of the predoctoral contract 2019FI_B 00928.

The research conducted in this paper is partially funded by the European Union's Horizon 2020 research and innovation program under grant agreement No.814888 (TRI-HP).

7. References

[1]Eurostat Statistic Explained. Energy consumption in households [Internet]. Online. 2019 [cited 2021 Dec 13]. Available from: https://ec.europa.eu/research/foresight/index.cfm

[2]Domanski P.A., Henderson H.I., Payne W.V., Domanski P.A., Henderson H.I., Payne W.V. Sensitivity Analysis of Installation Faults on Heat Pump Performance. NIST Technical Note 1848. 2014.

[3]Janecke A., Terrill T.J., Rasmussen B.P. A comparison of static and dynamic fault detection techniques for transcritical refrigeration. Int J Refrig [Internet]. 2017;80:212–24. Available from: http://dx.doi.org/10.1016/j.ijrefrig.2017.04.020

[4]Katipamula S., Brambley M.R. Review article: Methods for fault detection, diagnostics, and prognostics for building systems—a review, part I. HVAC R Res. 2005;11(1).

[5]Rogers A.P., Guo F., Rasmussen B.P. A review of fault detection and diagnosis methods for residential air conditioning systems. Build Environ [Internet]. 2019;161(July):106236. Available from: https://doi.org/10.1016/j.buildenv.2019.106236

[6]Bellanco I., Fuentes E., Vallès M., Salom J. A review of the fault behavior of heat pumps and measurements, detection and diagnosis methods including virtual sensors. J Build Eng. 2021;39(August 2020).

[7]TRI-HP project: Trigeneration systems based on heat pumps with natural refrigerants and multiple renewable sources [Internet]. [cited 2022 Jan 11]. Available from: https://www.tri-hp.eu/

[8]Bellanco I., Belío F., Vallés M., Gerber R., Salom J. Common fault effects on a natural refrigerant, variable-speed heat pump. Int J Refrig. 2022;133(January 2022):259–66.

[9]Kim M., Yoon S.H., Domanski P.A., Vance Payne W. Design of a steady-state detector for fault detection and diagnosis of a residential air conditioner. Int J Refrig. 2008;

[10]Heo J., Payne W.V., Domanski P.A., Du Z. Self Training of a Fault-Free Model for Residential Air Conditioner Fault Detection and Diagnostics. 2015.

[11]Kim M., Yoon S.H., Payne W.V., Domanski P.A. Development of the reference model for a residential heat pump system for cooling mode fault detection and diagnosis. J Mech Sci Technol. 2010;24(7):1481–9.

Data Statement

The data from the fault tests is accessible through the dataset Ivan Bellanco, Francisco Belío, Raphael Gerber, & Jaume Salom. (2021). Common faults tested on a variable-speed propane-charged heat pump on heating mode (Version 1). Zenodo. https://doi.org/10.5281/zenodo.5155136

Study on occupancy presence and heat use in a Norwegian office building

Lu Yan [a,b], Yuemin Ding [c], Natasa Nord [a], Meng Liu [b]

[a] Department of Energy and Process Engineering, Norwegian University of Science and Technology(NTNU), Trondheim, 7491, Norway

[b] School of Civil Engineering, Chongqing University, Chongqing, 400044, PR China

[c] Tecnun School of Engineering, University of Navarra, Manuel Lardizabal Ibilbidea, 13, San Sebastian, Spain 20018

Abstract. Energy management in buildings is facing a great challenge in Norway due to the COVID-19 pandemic. The largest difference between the pre-pandemic and post-pandemic period is the occupancy pattern in non-residential buildings. However, existing research only discussed the energy use change by longitudinal analysis, and no related research has been conducted based on the measured occupancy data in the post-pandemic period. Therefore, to fill this research gap, a case study with an office building in Trondheim, Norway, was conducted in our work to compare occupancy presence, heat use, and their relationship before and after the pandemic by using data-driven methods. For occupancy presence, on the one hand, occupants' presence rate was lower during the post-pandemic period compared with during the pre-pandemic period; on the other hand, occupants' absence rate in the lunchtime was decreased during the post-pandemic period compared with during the pre-pandemic period. In addition, two typical occupancy presence patterns in workdays were given in our study, the normal-working day pattern and half-working day pattern. The half-working day occupancy pattern appeared when Norway faced the second wave pandemic and the government implements more restrictive measures. In terms of heat use, the heat use increased markedly in the post-pandemic period, with the largest gap in hourly heat use between pre-pandemic and post-pandemic on workdays increasing around 21%, and increasing around 31% on holidays. The minimum daily heat demand of this building during the post-pandemic period was much higher than that in the pre-pandemic period, with increasing around 46% (on workdays and increasing around 86% on holidays. Regarding to their relationship, a more significant correlation between the daily heat use and the daily maximum occupancy rate during the post-pandemic period was observed compared with that during the pre-pandemic period. This study indicates that the operation of the heating system of the case building may be inefficient in the post-pandemic period, and findings of this study could help engineers to optimize the operation mode of the heating system according to the change of occupancy pattern and achieve better energy-efficiency management in the post-pandemic period for similar type of building.

Keywords. Occupancy, Heat use, Data-driven, COVID-19 pandemic.
DOI: https://doi.org/10.34641/clima.2022.116

1. Introduction

At the March of 2020, the World Health Organization declared that Coronavirus disease-19 (COVID-19) became a global pandemic [1]. To prevent virus spreading, many restrictions were taken by governments from all over the world. City lockdown, keeping social distance, and working at home were basic measures to prevent people from gathering and slow down the spread of COVID-19. Occupancy pattern is one of the most significant factors that affect energy demand of buildings [2–5]. Such restrictions caused by COVID-19 had a great effect on occupants' life habits and potentially affected energy demand of buildings due to the fact that working remotely would decrease occupancy presence in

Copyright ©2022 by the authors. This conference paper is published under a CC-BY-4.0 license.

non-residential buildings, while occupants spent more time at their home.

Building energy demand change related to COVID-19 is a new challenge in building energy management area and many publications discussed this issue. Some researchers focused on city-level electricity usage changes related to COVID-19. Investigation in [6] summarized the impact of pandemic on the power system all over the world and presented that power demand in many countries was reduced by around 8%~30% during the pandemic. A study that investigated electricity use among several European countries, showed that, in post-pandemic period, electricity use in countries (Spain, Italy, Belgium, and the UK) with severe restrictions was noticeably reduced, and their electricity usage pattern in weekdays presented similar profiles with weekend profiles in pre-pandemic period. However, lower decrease in electricity use was observed in countries with less restrictive measures, like Netherlands and Sweden [7]. Some researchers concentrated on the longitudinal comparison of energy use in residential buildings before and after the pandemic. For example, Rouleau and Gosselin [8] investigated the energy use difference before and after the lockdown in the Canadian social housing building, revealing that the electricity and hot water use increased obviously at the beginning of the city lockdown, and there was no evident change in space heating use during the lockdown period. Some researchers also conducted analysis only in non-residential buildings. For example, Geraldi et.al [9] conducted an analysis to explore the impact of the city lockdown on the electricity use in municipal buildings in Florianópolis, Brazil. Ivanko et.al [10] investigated how the city lockdown affected the heat use in Norwegian educational buildings. Ding et.al [11] analyzed how the city lockdown influenced the electricity use in Norwegians' educational buildings and residential buildings and discussed the energy saving potential in educational building by changing operation mode during the lockdown period.

Although the energy demand was declined in most countries during the pandemic period [12], the COVID-19 also adds many uncertainties for energy efficiency [13]. Improving the building energy efficiency in the post-pandemic period is a great challenge [14] and it varies on building type[11, 15]. However, on the one hand, the analysis of the pandemic impact on the energy use in office building is less. On the other hand, in the office building, one of the major differences between the pre-pandemic and post-pandemic period is the occupancy pattern due to the increasing trend of remote work, and as is well known that occupancy is also one of the most significant factors that affect building energy demand [2–5]. However, no related research has been conducted to investigate the difference in occupancy pattern of office building and how it influences on the energy use.

To fill the research gap, this study would focus on the impact of COVID-19 pandemic on occupancy pattern and heat use of an office building in Norway. An energy efficiency passive office building in Norway was conducted as the case study. The purposes of this study are composed of three parts:

1) Compare the occupancy pattern of this building in pre-pandemic period and post-pandemic period.

2) Compare the heat use of this building in pre-pandemic period and post-pandemic period.

3) Compare the relationship between the occupancy and heat use in pre-pandemic period and post-pandemic period.

2. Case introduction

2.1 Description of the case building

An office building located in Trondheim, Norway, was investigated in this study. Some details about this building are introduced as follows. The appearance of this building is shown in **Fig.1**. The building is composed of six floors. There are two floors underground, one of which is a parking area at the lowest floor, and another of which is used for cafeteria, office room, meeting rooms, and partially for the parking area. The other four floors above ground are composed of a mixture of meeting rooms, single-celled offices, miscellaneous rooms, and open-landscape working areas. The ventilation system in this building is a variable air volume (VAV) system. The heating ventilation system mode would adjust automatically according to the occupancy registered.

Fig. 1 - Body of this office building.

The thermal performance parameters of this building are summarized in **Tab 1**. The building was designed according to the Norwegian building code TEK17 [16]. The building code TEK17 is similar to the passive house standard. Although the parameters of the envelope of this building do not totally reach the passive house standard, it could be approximately seen as a passive building.

The heat demand of this building is caused by space heating (SH) and domestic hot water (DHW). An air-to-water heat pump with the rated heating capacity of 281 kW supplies the base heat demand for heating. The building is also connected to the district heating (DH) system, which offers the heat demand for the peak load demand. The heat pump would be turned off when the outdoor temperature is less than -10°C, and the SH heat

demand in this building would be totally covered by the DH system.

Tab. 1-Parameters of building envelope.

	U-value (W/m²·K)
Outer wall	0.18
Inner wall	0.15
Ground floor	0.13
Roof	0.13
Windows	0.8

2.2 Data collection

Building management system (BMS), including the indoor environment monitoring and energy monitoring system, is used in this building. Monitoring data can be acquired from this system. There are many sensors installed in this building to sample parameters including occupancy state, indoor and outdoor air temperature, energy use, etc. The sample interval of sensors in this building was 15 minutes. Occupancy data are key parameters used for analysis in this study. Regarding the occupancy sensors in this building, only the occupancy state within an area can be obtained, meaning that 0 or 1 would be recorded to represent whether an area is occupied by occupants, while occupant counts can't be known. To define the approximate occupancy level in this building, the hourly occupancy rate was calculated by dividing the sum of the occupancy status of all sensors in one hour by the total number of records of the occupancy status of all sensors in this hour.

2.3 Dataset selection and description used for this study

In our study, due to the limitation of data storage in the BMS system, the monitoring data in the BMS system can be only saved for a limited period, resulting in that the downloaded data didn't cover the whole year, leading that the data in the pre-pandemic period and post-pandemic period was not united in date. Therefore, different time period monitoring data was applied in different research purposes. For the first purpose, the comparison of occupancy pattern, data from January 1st to October 21st in 2019, from May 21st in 2020 to March 29th in 2021, was used for pre-pandemic period and post-pandemic period, respectively. For the second and third purpose, the comparison of heat use and the relationship between occupancy and heat use, considering that the heat use is influenced by the outdoor temperature, to eliminate the effects of the outdoor temperature on heat use profiles as much as possible, those days with their daily average outdoor temperature from -10 to 6°C during the same period (January 1st to March 27th) in 2019 and 2021, was chosen for the heat use comparison analysis. Finally, the data description for different research purposes is summarized in **Tab. 2**.

Tab.2- Dataset description for different research purposes.

	Research purpose	Data recording period	Number of days recorded in database	Number of hours recorded in database
pre-pandemic period	Comparison of occupancy pattern	January 1st to October 21st in 2019	294	7056
	Comparison of heat use and the relationship between occupancy and heat use	January 1st to March 27th in 2019	85	2040
post-pandemic period	Comparison of occupancy pattern	May 21st in 2020 to March 29th in 2021	313	7512
	Comparison of heat use and the relationship between occupancy and heat use	January 1st to March 27th in 2021	66	1584

3. Methodology and results

Next, a series of data-driven methods would be applied to achieve our research aims.

3.1 Comparison analysis of occupancy pattern

In this section, firstly, basic statistical analysis would be taken to explore the occupancy presence distribution difference in the pre-pandemic period and post-pandemic period. Then, clustering would be used for identifying typical occupancy patterns in these two periods and compare the clustering results.

Fig.2 shows that the distribution of daily maximum occupancy rate of workday both in the pre-pandemic and post-pandemic period. In order to obtain the most obvious impact of the pandemic on the occupancy pattern, the occupancy data of workdays was only used for this comparison analysis. As circled in red of **Fig.2**, in the post-pandemic period, a bimodal distribution was observed for the daily maximum occupancy rate, while that in the pre-pandemic presents a unimodal distribution. The most frequent values of the daily maximum occupancy rate in the pre-pandemic period was from 0.6 to 0.7, while the most possible daily maximum occupancy rate in the post- pandemic period

decreased to the range of 0.5 to 0.6, as can be noted in **Fig. 2**. Besides the most frequent daily maximum occupancy rate from 0.5 to 0.6, the daily maximum hourly occupancy rate from 0.25 to 0.30 also occurred frequently in the post- pandemic period, which indicated that there might be existed some particular occupancy scenarios in the post-pandemic period. Differences in the occurrence time point of the daily maximum hour occupancy rate could also be observed, as is shown in **Fig.3**. The most frequent time of the maximum occupancy rate of a day in the post-pandemic period was around 10 am to 11 am and 12 pm to 1 pm, while it was 1 pm to 2 pm in the pre-pandemic period. These observed differences in occupancy could give some references for the optimization of the operation mode in this building in the post-pandemic period.

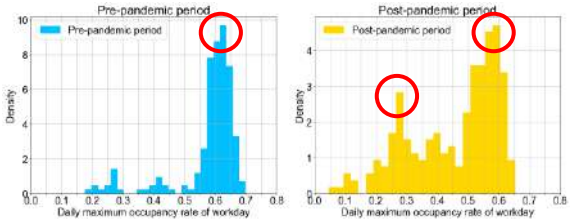

Fig. 2 - The distribution of daily maximum occupancy rate of workday in the pre-pandemic and post-pandemic period.

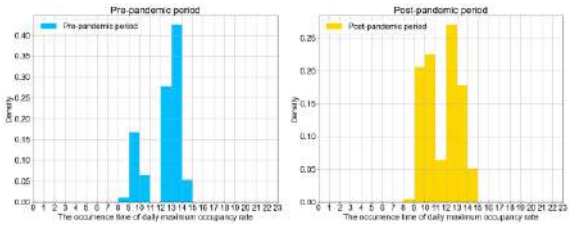

Fig. 3 - The distribution of the occurrence time point of the daily maximum occupancy rate for workday in the pre-pandemic and post-pandemic period.

To obtain the typical occupancy pattern, the fuzzy c-means was used in this study, which is considered as a best clustering method for occupancy pattern[17]. The Davies–Bouldin index (DBI) [18], a metric for evaluating clustering performance, was used to select the best cluster number for clustering. The smaller the DBI value, the better the clustering performance. From the results of DBI index, two was the best cluster number both for the pre-pandemic and the post-pandemic data set. Clustering results are shown in **Fig.4**. It can be seen that, no matter in the pre-pandemic or post-pandemic period, the two typical patterns of working days were identified. Pattern 1 was a normal-working day that accounted for the most of the days, accounting for 88% (178 of 202) in the pre-pandemic period and 64% (140 of 218) in the post-pandemic period of all investigated working days. Pattern 2 was the half-working day pattern when overall occupancy level was only about 50% of the normal-working day.

The differences of the typical occupancy patterns between the pre-pandemic and post-pandemic period could be explained from three aspects, as shown in **Fig.4**. Firstly, we could see that the occupied percentage for the half-working day pattern in the post-pandemic period was higher than that in the pre-pandemic period, from 12% increasing to 36%. Another difference was that the occupancy level was decreased in the post-pandemic period. For the normal-working day pattern, the occupancy rate decreased from 0.60 to 0.55, for the half-working day pattern, the occupancy rate decreased from 0.3 to 0.25. Lastly, occupants' absence rate in the lunch time was decreased during the post-pandemic period, no matter of the normal-working pattern or the half-working day pattern. This might be due to occupants' life habit change in the post-pandemic period, such as they did not tend to go to the common canteen to have lunch or there were rules which group of occupants could go to the common canteen to reduce the infection risk of COVID-19.

To observe the distribution of typical occupancy patterns on the timeline more clearly, we displayed the occupancy patterns distribution on the calendar, as shown in **Fig.5**. The calendar for 2019 presented the typical occupancy pattern distribution at the time axis in the pre-pandemic period. The calendar for 2020 and 2021 presented the typical occupancy pattern distribution in the post pandemic period. Due to the limitation of data access, we could not get the whole year data, so only a part of the year was presented. In this calendar, 0 presents the holiday occupancy pattern, 1 presents the normal-working day pattern, and 2 presents the half-working day pattern.

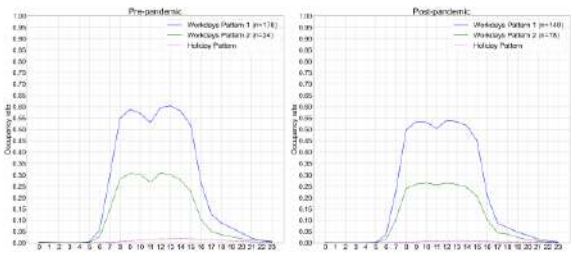

Fig. 4 - Clustering results of typical occupancy patterns in the pre-pandemic and post-pandemic period (The number in the bracket is the number of days belong to the pattern).

(a) In the pre-pandemic period

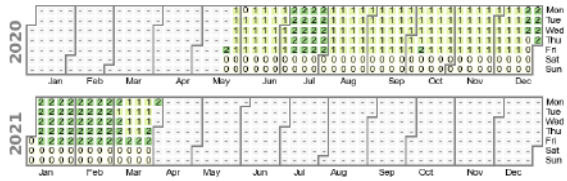

(b) In the post-pandemic period

Fig. 5 - The occupancy patterns' distribution in the pre-pandemic and post-pandemic period.

From the **Fig.4** and **Fig.5**, it can be seen that, the half-working day pattern would occur at three scenarios: 1) on Fridays; 2) on the days before a long national holiday such as the Easter; 3) in July, when many people take their annual vacation in Norway. However, in the post-pandemic period, we could see that, not only in previous mentioned scenarios, the half-working day would also occur in days at January, February, and some days on March in 2021, which might be due to the fact that Norway faced the second wave pandemic and the government implemented restrictive measures during that that days. Further, the results in **Figs. 4 and Figs. 5** could indicate that, when the pandemic rebounded, the occupancy presence pattern would show the half-working day occupancy pattern as it showed in July in the normal year.

3.2 Comparison analysis of heat use

In this section, we would take a comparison analysis of the heat use. Firstly, we would use the linear regression model to compare the relationship between the heat use and outdoor temperature in the pre-pandemic period and post-pandemic period. And then, the daily heat use profile in these two periods would be compared.

Due to the cold climate in Norway, the energy use for space heating and domestic hot water represents the main part of the total energy use. Accordingly, the outdoor temperature may be regarded as the key factor determining the heat demand. Therefore, this section would explore how the pandemic influences the relationship between heat use and outdoor temperature. To convince that our comparison analysis was conducted in a similar outdoor temperature distribution, before the comparison analysis, according to the research method in a similar analysis[19], the Kruskal-Wallis H-test [20] was used to test whether the distribution of the outdoor temperature before and after the pandemic was the same, showing that there were no statistically significant differences in the outdoor temperature distribution in these two data sets used for the comparison analysis. And then, we started to process the comparison analysis. First, the scatter plot of the daily heat use versus the daily outdoor temperature is shown in **Fig.6**. In **Fig. 6**, the daily heat use was the sum value of hourly heat use for 24 hours of a day, while the daily average outdoor temperature was the average value of hourly outdoor temperature for 24 hours of a day. The linear regression was used to describe the relationship between the daily heat use and the average outdoor temperature. In **Fig. 6**, it is possible to note that the linear relationship in the post-pandemic period was less steep than that in the pre-pandemic period, no matter on workdays or on holidays. However, the R^2 value was decreased more in holidays compared that in workdays. From this linear regression models in **Fig. 6**, it is also possible to note that when the outdoor temperature was above -4°C, the heat use in the post-pandemic period was higher than that in the pre-pandemic period.

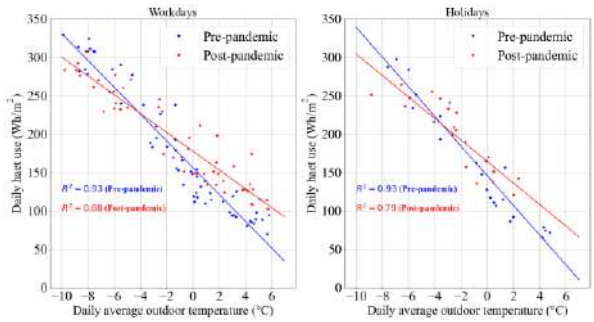

Fig. 6 - The relationship between daily heat use and daily outdoor temperature in the pre-pandemic and post-pandemic period.

The daily heat use profiles (24-dimensional curve) in the pre-pandemic and post-pandemic period are shown in **Fig.7**. Hourly heat use in the daily profile was the average value of the corresponding hourly value in all investigated days, as calculated as **Eq.(1)**, in which $HHU_{av,j}$ ($j \in [0,23]$) represents the daily average value in the daily profile, and i represents i^{th} day, and n represents the total number of investigated days.

$$HHU_{av,j} = \frac{\sum_{i=1}^{n} HHU_{i,j}}{n} \quad (1)$$

It can be observed that, on holidays, the daily heat use profile curve was higher in the post-pandemic period than that in the pre-pandemic period. On workdays, in most of hours, the hourly heat use is higher in the post-pandemic when compared with that in the pre-pandemic; however, in some particular hours, the hourly heat use is a little lower in the post-pandemic period than that in the pre-pandemic period, like the 2pm and 4am. Besides, the largest gap in the pre-pandemic and the post-pandemic on workdays occurred at 10 am (increasing around 21%, from 7.2 W/m² to 8.7 W/m²), and occurred at 2 am (increasing around 31%, from 7.0 W/m² to 9.1 W/m²) on holiday. Additionally, the peak demand time was also changed: on workdays, the peak load time was forward one hour during the post-pandemic period, shifted from 6 am to 5 am; on holidays, the two peak times could be seen in the post- pandemic period, 2

am and 7 am, while only one peak demand time, 6 am, can be observed in the pre-pandemic period.

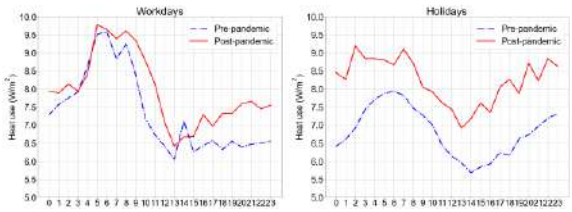

Fig. 7 - Heat use profile in the pre-pandemic and post-pandemic period.

From above analysis, we could see the heat use in the post-pandemic period seems to be higher than that in the pre-pandemic period. To explore how much the heat use increased due to the pandemic, the cumulative distribution function (CDF) curve of the daily heat use is plotted in **Fig.8**. From the curve in **Fig.8**, it can be obviously observed that the start point of the CDF curve was much higher in the post-pandemic period than in the pre-pandemic period, as summarized in **Tab.3**. The start point of the CDF could be considered as the minimum daily heat demand of this building. **Tab.3** indicates that the minimum daily heat demand was evidently increased in the post-pandemic period, especially on holidays, showing an increase of around 86%. It can be concluded from above heat use comparison analysis that, when outdoor temperature was in the similar situation, more heat use was observed in post-pandemic period than that in the pre-pandemic period, indicating that there may be inefficient operation mode in the post-pandemic period.

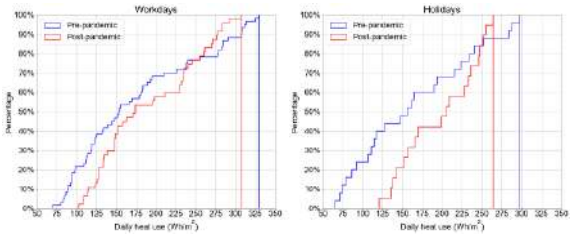

Fig. 8 - The cumulative distribution function curve of daily heat use in the pre-pandemic period and post-pandemic period.

Tab.3- Difference in the start value of CDF curve in the pre-pandemic period and the post-pandemic period.

	In the pre-pandemic (Wh/m^2)	In the post-pandemic (Wh/m^2)	Increase
Workdays	70	102	46%
Holidays	65	121	86%

3.3 Comparison of the correlation relationship of occupancy with heat use

As we addressed before, the heating ventilation system mode would adjust automatically according to the occupancy registered; also, this building is a passive building. Accordingly, the heat use may have some relevance with the occupancy rate. Therefore, in this section, we would like to explore how the pandemic has affected the relationship between the occupancy and the heat use. Firstly, the scatter plot of the daily heat use and the daily maximum occupancy rate is shown in **Fig.9**. As shown in **Fig.9**, a relatively dependence relationship between the heat use and the occupancy level could be observed (as the yellow arrow line) on workdays in the post-pandemic period. Therefore, to investigate their relationship more quantitatively, the Spearman correlation coefficient and Spearman correlation test was used to compare the relationship between the heat use and the occupancy level before and after the pandemic, as shown in **Tab.4**. The null hypothesis for the Spearman correlation test was that the two datasets were not correlated; as such, a p-value <0.05 indicated that these two datasets were correlated at a significance level of 0.05. Therefore, from the results of Spearman correlation test, a statistical significance negative correlation between the daily heat use and the daily maximum occupancy rate in the post-pandemic period was identified of the Spearman correlation coefficient of -0.63 (p-value<0.05), while their correlation relationship was not evident before the pandemic. The stronger relationship between the heat use and occupancy indicates that the inefficiency operation mode may be resulted from the occupancy pattern change in the post-pandemic period. Maybe due to the fact that the building performance is similar to the passive building, the internal heat gain of the building from the occupancy was decreased, resulting in that the increase of the heat use in the post-pandemic period was obviously, despite the outdoor temperature was similar. Above results indicate that it's an urgency to optimize the heating system operation mode to fit the occupancy pattern presented in the post-pandemic period.

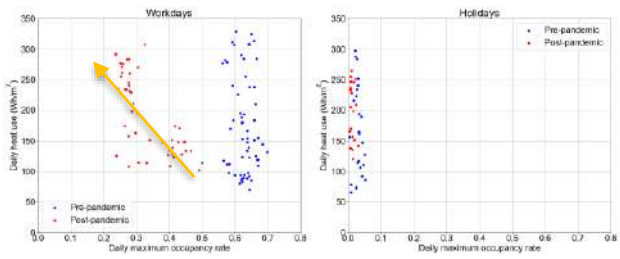

Fig. 9 - The scatter plot of daily heat use and daily maximum occupancy rate in the pre-pandemic and post-pandemic period.

Tab.4- Spearman correlation coefficient of daily heat use and daily occupancy rate on workdays in the pre-pandemic and post-pandemic period.

	Spearman correlation coefficient	p-value
In the pre-pandemic period	-0.05	0.7287
In the post-pandemic period	**-0.63**	**2.06E-06**

4. Conclusions

In this study, we applied a series of data-driven methods for the comparison analysis of the occupancy and heat use in the pre-pandemic and post-pandemic period. A passive office building located in Trondheim, Norway was taken as the case study. Firstly, the occupancy pattern in these two periods was compared. Then, the heat use in these two periods was compared. Finally, the relationship between the occupancy and heat use in these two periods was compared. The results show that, overall, due to the pandemic, some differences in these two periods can be obviously observed in this passive office building, which are summarized as follows:

1) The occupants' presence in this building in the post-pandemic period was lower than that in the pre-pandemic period. When Norway faced the second wave epidemic and the government implemented restrictive measures, the occupancy pattern in this case office building would show likes the half-working day pattern that would occur at some particular scenarios during the pre-pandemic period.

2) The heat use was increased markedly in the post-pandemic period. On the one hand, for hourly heat use, the largest gap in hourly heat use between these two periods on the workdays increased around 21% (from 7.2 W/m^2 to 8.7 W/m^2), and increased around 31% (from 7.0 W/m^2 to 9.1 W/m^2) on holidays. On the other hand, for daily heat use, the minimum daily heat use of this building during the post-pandemic period was much higher than that during the pre-pandemic period, with increasing around 46% (from 70 Wh/m^2 to 102 Wh/m^2) on workdays and increasing around 86% (from 65 Wh/m^2 to 121Wh/m^2) on holidays.

3) The relationship between occupancy rate and heat use presented a stronger negative correlation in the post-pandemic period than in the pre-pandemic period.

This study indicates that the operation of the heating system of the case building may be inefficient in the post-pandemic period, and the findings of this study could help engineers to optimize the operation mode of the heating system according to the change of occupancy pattern and achieve better energy efficiency management in the post-pandemic period for the similar type of building.

Acknowledgement

The authors are grateful to the company GK, https://www.gk.no/, department Indoor environment in Trondheim for allowing us to access the analyzed office building. GK made available their monitoring systems for our research. Specifically, the authors would like to thank to the colleagues that help in the analysis of the presented study, Rune Gjertsen and Knut-Ivar Grue.

References

[1] Coronavirus Disease (COVID-19) – events as they happen, https://www.who.int/emergencies/diseases/novel-coronavirus-2019/events-as-they-happen.

[2] Motuziene V, Vilutiene T. Modelling the Effect of the Domestic Occupancy Profiles on Predicted Energy Demand of the Energy Efficient House. *Procedia Engineering* 2013; 57: 798–807.

[3] Happle G, Fonseca JA, Schlueter A. Impacts of diversity in commercial building occupancy profiles on district energy demand and supply. *Applied Energy* 2020; 277: 115594.

[4] Gul MS, Patidar S. Understanding the energy consumption and occupancy of a multi-purpose academic building. *Energy and Buildings* 2015; 87: 155–165.

[5] Guerra Santin O, Itard L, Visscher H. The effect of occupancy and building characteristics on energy use for space and water heating in Dutch residential stock. *Energy and Buildings* 2009; 41: 1223–1232.

[6] Madurai Elavarasan R, Shafiullah G, Raju K, et al. COVID-19: Impact analysis and recommendations for power sector operation. *Applied Energy* 2020; 279: 115739.

[7] Bahmanyar A, Estebsari A, Ernst D. The impact of different COVID-19 containment measures on electricity consumption in Europe. *Energy Research & Social Science* 2020; 68: 101683.

[8] Rouleau J, Gosselin L. Impacts of the COVID-19 lockdown on energy consumption in a Canadian social housing building. *Applied Energy* 2021; 287: 116565.

[9] Geraldi MS, Bavaresco MV, Triana MA, et al. Addressing the impact of COVID-19 lockdown on energy use in municipal buildings: A case study in Florianópolis, Brazil. *Sustainable Cities and Society* 2021; 69: 102823.

[10] Ivanko D, Ding Y, Nord N. Analysis of heat use profiles in Norwegian educational institutions in conditions of COVID-lockdown. *Journal of Building Engineering* 2021; 102576.

[11] Ding Y, Ivanko D, Cao G, et al. Analysis of electricity use and economic impacts for buildings with electric heating under lockdown conditions: examples for educational buildings and residential buildings in Norway. *Sustainable Cities and Society* 2021; 74: 103253.

[12] Werth A, Gravino P, Prevedello G. Impact analysis of COVID-19 responses on energy grid dynamics in Europe. *Applied Energy* 2021; 281: 116045.

[13] Covid-19 and energy efficiency – Energy Efficiency 2020 – Analysis. *IEA*, https://www.iea.org/reports/energy-efficiency-2020/covid-19-and-energy-efficiency (accessed 27 May 2021).

[14] Jiang P, Fan YV, Klemeš JJ. Impacts of COVID-19 on energy demand and consumption: Challenges, lessons and emerging opportunities. *Applied Energy* 2021; 285: 116441.

[15] Kang H, An J, Kim H, et al. Changes in energy consumption according to building use type under COVID-19 pandemic in South Korea. *Renewable and Sustainable Energy Reviews* 2021; 148: 111294.

[16] Byggteknisk forskrift (TEK17).

[17] Vázquez FI, Kastner W. Clustering methods for occupancy prediction in smart home control. In: *2011 IEEE International Symposium on Industrial Electronics*. 2011, pp. 1321–1328.

[18] Davies DL, Bouldin DW. A Cluster Separation Measure. *IEEE Transactions on Pattern Analysis and Machine Intelligence* 1979; PAMI-1: 224–227.

[19] Yan L, Li J, Liu M, et al. Heating behavior using household air-conditioners during the COVID-19 lockdown in Wuhan: An exploratory and comparative study. *Building and Environment* 2021; 195: 107731.

[20] Kruskal WH, Wallis WA. Use of Ranks in One-Criterion Variance Analysis. *Journal of the American Statistical Association* 1952; 47: 583–621.

The role of simulation in design of high-performance buildings in Turkey

Gülsu Ulukavak Harputlugil [a], *Pieter De Wilde* [b]

[a] Department of Architecture, Çankaya University, Ankara, Türkiye, gharputlugil@cankaya.edu.tr

[b] Department of Architecture, University of Strathclyde, Glasgow, UK, pieter.dewilde@strath.ac.uk

Abstract. This paper reports on an exploration of the current role of building performance simulation tools in the building and HVAC design process. The focus of the study is on the design of high-performance buildings; our hypothesis is that this is the leading edge of building design, where simulation is most likely to be used to its full potential. The methodology underlying the paper consists of surveys with architects and engineers who carried out the design of a number of high-profile buildings. The paper adds to a small body of work that, over the years, has monitored the actual role of simulation in design. Whilst a lot of work is carried out to improve the role of simulation in design, especially the early phases, the real uptake and role of the technology may not always match our expectations. Critical review of the actual role of simulation tools remains necessary to assess progress and needs for further development. Results show that simulation is regularly used in building design projects, by a range of actors. However, the use of simulation efforts seems to be mainly the confirmation of expectations and the demonstration of meeting targets, especially those that are relevant for certification schemes. Building simulation still has unused potential in terms of selection of design alternatives from extensive search or option spaces. The use of more advanced techniques such as optimization in industry remains relatively low; work on uncertainty and sensitivity is not often undertaken in practice.

Keywords. high performance buildings, building performance simulation, integrated design, Turkiye
DOI: https://doi.org/10.34641/clima.2022.66

1. Introduction

Since the studies on the use of building simulation in building and HVAC design began to emerge, three important observations have been made in almost all contributions: i) Simulation is important for designers not only in testing current ideas, but also in developing and presenting new ideas; ii) Simulation is often used in the final stage of the design process as a "performance confirmation" [1-4]. However, in the early stages of design, it is possible to test many more options with easy returns, iii) Integrated design of buildings and systems must be carried out by an interdisciplinary team, and simulation should also be considered as a very important technology for ensuring communication between different disciplines [5-10].

However, from the perspective of practitioners, it cannot always be said that the approach to simulation-assisted design has met at the expectations of teamwork practice. Various studies were conducted to explore the professionals' practice and wishes in last 15-20 years [11-14). It can be said that most of the issues emphasized by those works are still valid after almost two decades.

This paper reports on an exploration of the current role of building performance simulation tools in the building design process in order to explore progress on the role of simulation. The focus of the study is on the design of high-performance buildings; our hypothesis is that this is the leading edge of building design, where simulation is most likely to be used to its full potential. The methodology underlying the paper consists of interviews with architects and engineers who carried out the design of a number of high-profile buildings. The research hones in on the situation Turkey, one of the MINT countries (Mexico, Indonesia, Nigeria, Turkey) who are seen as emerging economic powerhouses in the world economy [15].

2. Current Knowledge

In current Turkish literature, high building performance does not have a strict definition that can be compared to the international interpretations.

Copyright ©2022 by the authors. This conference paper is published under a CC-BY-4.0 license.

Instead, the prominent terminology used in the country refers to green buildings or sustainable buildings. When searching academic literature, internet and professional magazines for high performance buildings one can find buildings with some form of corresponding certificate such as LEED, BREEAM and similar. Generally, projects that have implemented some form of high-performance design strategies are driven by the need to meet the relevant performance requirements when applying for the required certificate. Since 2011, when Turkey first introduced LEED certification, and since 2012 when some buildings started to be BREEAM-certified, 514 buildings with a variety of functions and different sizes have been certified in total [16,17] (see Figure 1) There are 74 BREEAM certified buildings with several functions and 440 LEED certified buildings. When looking in detail at the statistics of the LEED certified buildings, 65% of these buildings are commercial, 22% are residential and the rest has several other functions such as hospital, hotel, education, mixed use, etc. Similarly, 65 % of BREEAM certified buildings are commercial, but BREEAM certified residential buildings are only 7 % of total certification in Turkey. The graph shows the state of art at Turkey in detail. Among LEED certified buildings, 66% are Gold, 14% are Silver and 12% are Platinum. The distribution of the certificate types of BREEAM buildings is more homogenous with 32% rated as Very good, 27% Excellent, 20% are Outstanding and 16% are Good.

According to the statistical reports and analysis efforts on current building stock presented by TUIK (Turkish Statistical Institute) [18] there are more than 11 million buildings in Turkey by 2020. From this point of view, the total number of certified buildings covers only 0.004% of the total stock. Over the last 10 years, especially in the "Terms of Refence (ToR)" of international construction consortia for major projects (for instance city hospitals, multinational company headquarters, or service buildings developed by foreign investors), several statements about building performance have been included, although legally they are not compulsory in Turkey. A wide body of literature, including dissertations, journal articles, conference papers and reports that address green buildings, sustainable architecture and energy efficiency of buildings in Turkey are available. Most of those studies have been focusing on energy efficiency which is still a hot topic for the region. The best cases and adaptation of regulations are usually referring to EU norms and applications. Technical reports and information documents have been prepared by the relevant units of the Ministry of Environment and Urbanization and the Ministry of Energy [19-21].

The background of the current knowledge of practice and professionals' perspective in Turkey is based on the evaluation of two previous studies [22, 23]. The first of these studies is the discussion of improved process management for the design of high-performance buildings through the use of design concepts in the pre-design stage in the paper prepared 13 years ago on this subject. The most important expectations of those was an opportunity to develop an environment that collects architectural idea and engineering idea in the same platform. This is an iterative process but at the end this platform helps to communicate the ideas in the same language. This attempt will also shift the program of requirement of the project to another specific or unique list based on the context of the project [22] (Figure-2).

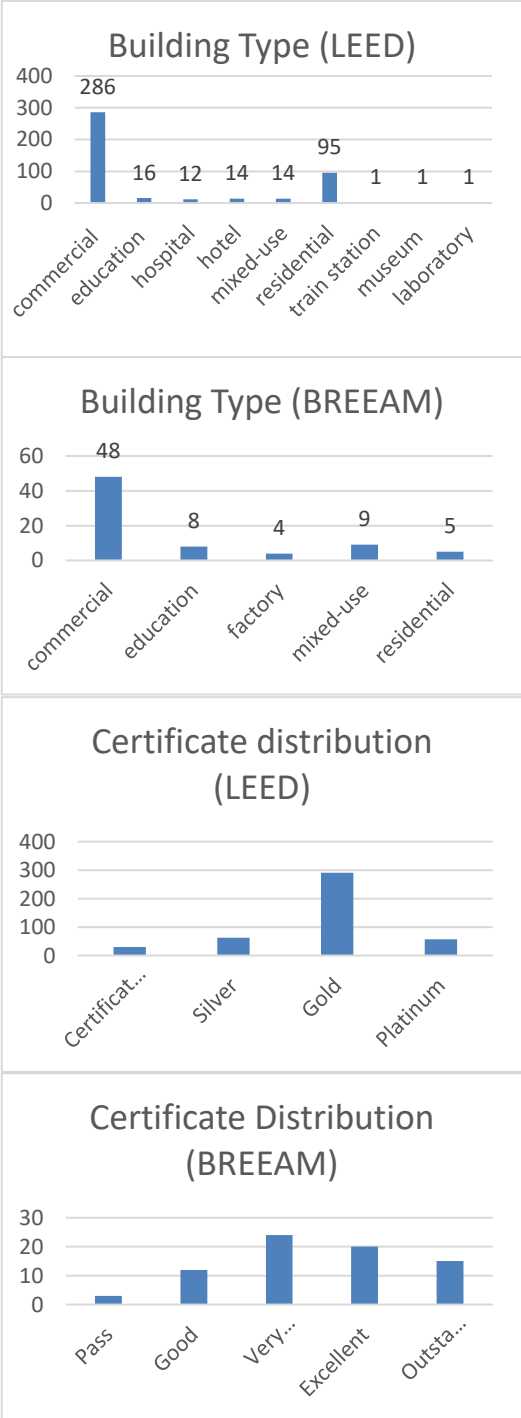

Fig.1- Statistics of LEED and BREEAM certified buildings in Turkey – distribution of building and certification types

Later, a paper presented in 2018 revealed the results of a survey conducted among professionals in Turkey [23]. In this study, 42 participants' views on building performance simulations were discussed under three titles: i) professional wishes, ii) barriers iii) future expectations. The brief of the responses to those three titles are at below.

The first collected responses for finding out professionals' wishes/expectations were mainly focus on the practical use of performance simulations. They were aware of the importance of the use of performance evaluation in any level of design process as long as the tools were easily accessible, user friendly, accurate enough and cost effective. On the other hand, the drawbacks they listed as barriers are;

- Software costs (buy, update, maintenance, etc.)
- Choosing right one among many options needs education and experience
- Lack of technological awareness
- Incompatibility with Turkish legislations
- No feedback to design process

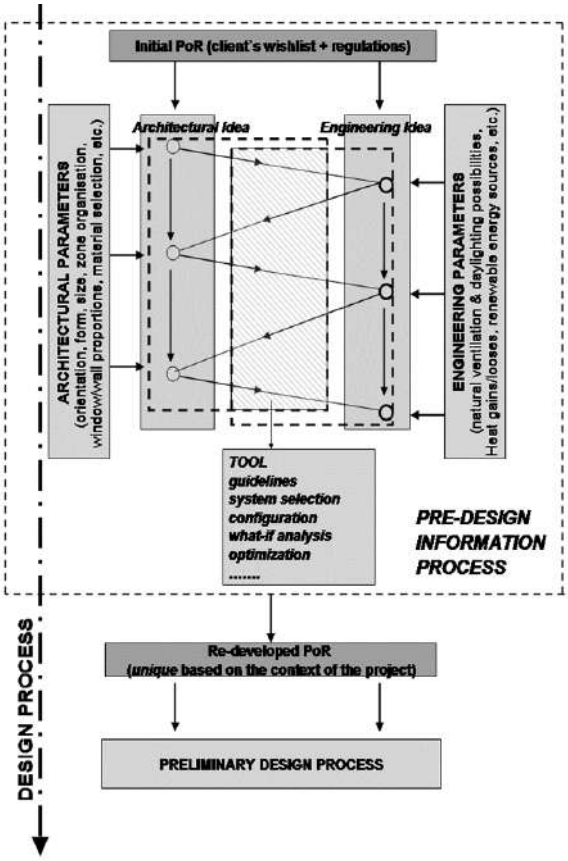

Fig.2- Pre-design information process flow chart [22]

The professionals had thoughts on dissemination of practically use of performance simulations in the future. The first expectation was enhancing undergraduate education and include courses on performance simulations. Those educations should continue after graduation as continuous professional development. Cost of the tools was a basic problem which needs to be solved in the near future. The support of government by encouraging the use of simulation by regulations and codes is another requirement stated by the professionals.

3. Methodology

In this paper, two specific further issues are evaluated. One of them is to understand the application practices of high performance building (HPB) design, and the second is to evaluate the role of simulation use in these applications. This study consists of compilations of interviews done with architects of large-scale and multifunctional buildings in Turkey and with engineers have taken part in similar projects. During the interview, local practices and approaches encountered in international projects were compared and evaluated. The interviews were done between January-March 2021 via an online platform (zoom). The interviewees were informed about the reason of the interview and the content was delivered before zoom meeting. Each of the zoom session was recorded. The questions are mainly open ended in order to make interviewees feel free to express their design practices.

3.1 Interviews

The interviews were done with six designer architects, five HVAC engineers and one engineer working at a ministry in a decision-making position (Picture 1). Thus, information was obtained not only about the routine design and application process but also about the way of execution and requirements of legal procedure which Turkish governmental bodies expect. Similar questions were asked during the interviews, and the answers received were grouped under four main headings.: i) high performance building experience ii) interdisciplinary team work and integrated design, iii) computer simulation applications iv) opportunities/challenges on designing HPB.

Picture.1- Screenshots of online interviews

4. Results

4.1 High performance buildings

In general all the interviewees have an opinion on High Performance Buildings but their definitions

vary significantly. The common consent on the definition is that such buildings should be energy efficient and sustainable. Architects with international experience provide broader definition than those working nationally. This wider definition includes user health, comfort and safety. Although there is no significant difference between the definitions of engineers and those of architects, it is easier for engineers to describe the technical approach.

While defining high performance buildings, it is seen that engineers' and architects' perspective were different. The comments of engineers and architects are listed separately here, in order to acquire the difference.

Engineers defined "high-performance buildings" as follows:

- A building which maximises energy and comfort,
- It is not only an energy efficient building, but also maximizes indoor air quality, acoustics, lighting, ventilation, selection of materials used, carbon footprint and lifetime cost analysis,
- Designed, built, operated and efficient use of resources in accordance with international standards,
- The buildings which their envelope is designed with specific consideration, and
- Buildings where electrical and mechanical systems are applied efficiently and comfortably

In addition, the engineers added the following to their thoughts on the high-performance building:

- High-performance building features should be legal and compulsory for all buildings,
- High performance buildings need to renew themselves with technology because today's high performance may be tomorrow's weak performance,
- It was also stated that occupants should feel the same comfort at the whole lifespan of high-performance buildings.

On the other hand, architects defined "high-performance buildings" as follows;

- Able to interact dynamically with its environment,
- The buildings that closest to nature,
- Being sustainable, functional, aesthetic, cost effective, easy to access, safe and giving importance to historical preservation,
- Self-sufficient buildings,
- It is described as a building where the right technology is used with the right consultants.

In addition, it was mentioned that high-performance building is a consciousness and should be defined as a sustainable and accessible goal.

Considering the interviewees' HPB design experience, it is understood that the building cases in which they have the experience are mostly projects produced abroad and dependent on international procedures, or projects carried out domestically but also carried out by international consortiums and subject to special specifications. It does not seem possible to talk about HPB principles in smaller scale projects that follow local procedures.

4.2 Interdisciplinary team-work and integrated design

When asked about the interdisciplinary work practice and frequency of the experts interviewed, they all mention the importance of interdisciplinary work. Here, it can be said that engineers attach more importance to collaboration with architects than architects themselves attach to working with engineers. However, in terms of implementation practice, it is understood that the process can be progressed in cooperation with all stakeholders from the beginning of the design process. This is not so often in local projects but mostly when an international consortium drives the process. Although the importance of integrated design is acknowledged by all participants, it is seen that engineers are more open here as well.

4.3. Computer simulation applications

The tools used in design process vary. Architects use computer applications throughout in the design process. However, with the widespread use of BIM, it was stated that commercial tools such as Autodesk REVIT and Rhino programs were preferred in most architectural offices. For energy analysis by engineering companies, it emerged that Energy Plus, EDSL Task, E-Quest, Design Builder and Carrier programs are preferred. For lighting analysis, the DiaLux program was generally used. Regarding to usage of these tools, mostly those are not seen as a 'design tool'. Frequently it is accepted that the concept design is under the responsibility of architects and energy analysis done by engineers seems as "next step" during which tools are used just for performance confirmation.

BIM applications are seen as an important platform that enables all the team in the consortium to work

together in international projects. However, it is understood that the possibilities provided by BIM are more effectively employed within engineering services, whilst in the architectural process possibilities beyond visualization are not yet used. No simulation software is used for performance evaluation in architectural offices in Turkey. However, expertise support is required when necessary. An architectural office, which has only established its own interdisciplinary teams, makes it possible to carry out the project with instant analysis and simulation support throughout the entire design process. In engineering offices, calculation tools are used to determine the capacity of the mechanical installation. It has been stated that international projects should benefit from various simulation applications when they are included in the process from the beginning as part of the design team.

The interviews generally focused on BIM. The advantages and disadvantages of BIM system were mentioned as follows:
Advantages:

- All disciplines are studied on the same model,
- Plan, section, elevation, etc. concurrently organized during the design phase,
- The problems previously encountered during the construction are solved during the design phase,
- Specifications of the materials and components can be loaded as library information and this information can be used in different phases later,
- The pre-concept stage and the final delivery file are usually in the same file,
- BIM allows to perform various analyses on the model if required.

Disadvantages:

- An expensive and complex system,
- There are still a few experienced people in the market
- A lot of time, people, costs and equipment are required,
- It is stated that the professional experience requirement of BIM will increase as the m^2 of the building grows

Regarding the opinions of the professionals listed above on BIM, it is obviously seen that, in practice, they usually use BIM in its basic level (up to LOD-300). Advanced usage is rarely a necessity, particularly if the process is proceeded by international consortium. On the other hand, BIM has a great potential on the passive and active measures identified by Krygiel and Nies [24]. The sustainable BIM approach has been reduced and listed in accordance with the possibilities that BIM can provide at the early design stage are; i) building orientation, ii) building massing, iii) solar and shadow analysis, iv) conceptual energy modelling and v) potential renewable energy analysis. However, none of the professional declares a plug-in that is used in BIM for performance evaluation in early design stage.

The professionals were also asked to compare practice of BIM in local applications and international projects. According to their opinions, in Turkey, there is high costs level for BIM applications that small and medium companies cannot afford easily. Becoming an expert needs time and extra effort which makes it difficult to get used to this system. The architecture and engineering offices that have started to implement 3D in BIM platform provides maximum benefit in terms of the quality, standard and time given to the design. On the other hand, if the collaborative offices do not use BIM models and provide only 2D drawings; it was stated that this causes to lost time and effort while converting the models into 3D models. It was mentioned that governmental bodies are not force public sector to use several software mandatorily as licensing of many of them are too expensive but supported/encouraged the use of programs such as BIM.

Professionals mentioned that during the international consortium projects, it is easier to switch to the BIM system due to such requirements/obligations in the tender. International marketing competitions also lead to use BIM platforms.

4.4. Opportunities and challenges when designing HPB

There are various opinions about the value of high performance buildings, and the process of designing them. Although there is a common view that there will be an important opportunity and that energy efficient and environmentally friendly buildings will increase, only a few participants made a value definition by taking into account user comfort, health and safety. To the question posed about the challenges and limitations of the design process of such buildings, all participants defined two issues as constraints: cost and legal procedure. In the case that the future user of the building is the client, the payback period of the initial investment cost that increases due to HPB applications can be significant and the client can be convinced. In terms of legal procedure, if the expected performance is not clearly defined in the tender files and specifications, it is stated that sufficient implementation cannot be made in this regard. On the other hand, the expert

who gave his opinion from the Ministry stated that the specifications for governmental structures were prepared very carefully and in detail, but they do not have control powers in special applications. Therefore, a comprehensive legal regulation is required.

5. Conclusions

In general, High Performance Buildings represent a category of buildings that are designed and engineered to be energy efficient, limit greenhouse gas emissions, and make efficient use of other resources such as water and materials. Typically these buildings benefit society, productivity, and the health and wellbeing of vulnerable members of the population [25].

The design of High Performance Buildings is based on a systematic exploration of design options, use of simulation tools to predict building behaviour, and rational decision making. Often the design process involves the concept of 'integral design'. System thinking and system engineering are seen as core contributors to success [26,27].

For more than two decades, performance-based evaluation of the design process, integration of building simulation programs into the process, the approach of professionals to this issue and what can be done in practice to improve the design process have been discussed. Although these requirements differ for each country and region, it is based on the understanding of the process by architects and engineers, who are two important members of the design team. In this study, it is questioned how the subject is still perceived by professionals in Turkey, and it is stated that nothing much has changed in practice, by referring to similar studies conducted in the past.

A new perspective to HPB will have a strong contribution to changing the lives of particularly vulnerable and low-income populations in Turkey. This part of society will be most strongly affected by climate change and scarcity of resources. The necessity for high performance buildings will address built environment challenges in terms of the need to cope with population growth, scarcity of resources (energy, water, material), climate change (global warming and extreme events), environmental protection and their side effects on economic fluctuation and social transformation.
A further study with more participants on high performance buildings' practice is going on. It is aimed to scrutinise a new perspective to the current understanding of practitioners by taking into consideration climate change adaptation and embodied carbon mitigation. By this study it is supposed that a step change shall be possible in thinking about building performance in Turkey and the wider region, changing building design, engineering and construction practice.

6. Acknowledgement

The research reported in this paper was funded through the British Council Newton Fund: Research Environments Links Turkey-UK Programme

7. References

[1] Struck, C., P. de Wilde, C. Hopfe and J. Hensen, 2009. An investigation of the option space in conceptual building design for advanced building simulation. Advanced Engineering Informatics, 23 (4), 386-395

[2] de Wilde, P. and D. Prickett, 2009. Preconditions for the use of simulation in M&E engineering. In: Strachan, Kelly and Kummert, eds. Building Simulation '09, 11th International IBPSA Conference, Glasgow, United Kingdom, July 27-30 2009, 414-419

[3] Augenbroe, G., 2011. The role of simulation in performance based building. In: Hensen, J. and R. Lamberts, eds. Building performance simulation for design and operation. Abingdon: Spon Press

[4] Struck, C., 2012. Uncertainty propagation and sensitivity analysis techniques in building performance simulation to support conceptual building and system design. PhD-thesis. Eindhoven: Eindhoven University Press

[5] de Wilde, P., 2004. Computational Support for the Selection of Energy Saving Building Components. PhD-thesis. Delft: Delft University Press

[6] Becker, R., 2008. Fundamentals of performance-based building design. Building Simulation, 1 (4), 356-371

[7] Harputlugil , G. U., 2009, An Assessment Model Addressed to Early Phases of Architectural Design Process Prioritised by Energy Performance, PhD dissertation, Gazi University Institute of science and Technology, Ankara, Turkiye.

[8] Bleil de Souza, C., 2013. Studies into the use of building thermal physics to inform design decision making. Automation in Construction, 30, 81-93

[9] Lin, S. and D. Gerber, 2014. Designing-in performance: a framework for evolutionary energy performance feedback in early stage design. Automation in Construction, 38, 59-73

[10] Negendahl, K., 2015. Building performance in the early design stage: an introduction to integrated dynamic models. Automation in Construction, 54, 39-53

[11] Morbitzer, C., 2003. Towards the Integration of

Simulation into the Building Design Process. PhD-thesis. Glasgow: University of Strathclyde

[12] Hopfe C., Stuck C., Ulukavak Harputlugil G., Hensen J. L. M. 2006. Computational tools for building services design - professionals' practices and wishes, 17th international air conditioning and ventilation conference proceedings, Prague-Czech Republic p. 297-302.

[13] McElroy, L., 2009. Embedding Integrated Building Performance Assessment in Design Practice. PhD-thesis. Glasgow: University of Strathclyde

[14] Bleil de Souza, C., 2012. Contrasting paradigms of design thinking: the building thermal simulation tool user vs the building designer. Automation in Construction, 22, 112-122

[15] Wright, C., 2014. "After The BRICS Are The MINTs, But Can You Make Any Money From Them?".https://www.forbes.com/sites/chriswright/2014/01/06/after-the-brics-the-mints-catchy-acronym-but-can-you-make-any-money-from-it/?sh=4441a7229a6c

[16] LEED, 2021, The list of certified buildings in Turkey,https://www.usgbc.org/projects?Country=%5B%22Turkey%22%5D

[17] BREEAM, 2021, The list of certified buildings in Turkey,https://tools.breeam.com/projects/explore/buildings.jsp

[18] TUIK, 2020, Turkish Statistical Institute Report, http://tuik.gov.tr

[19] MoEU, 2016a, "Energy Efficient Building Design Strategies", Ministry of Environment and Urbanism archive documents, https://webdosya.csb.gov.tr/csb/dokumanlar/mhgm0005.pdf

[20] MoEU, 2016b, "Integrated Building Design" Ministry of Environment and Urbanism archive documents, https://webdosya.csb.gov.tr/csb/dokumanlar/mhgm0003.pdf

[21] MoE, 2016c, "Energy Efficient Buildings and Turkish Legislation" Ministry of Environment and Urbanism archive documents, https://webdosya.csb.gov.tr/csb/dokumanlar/mhgm0002.pdf

[22] Ulukavak Harputlugil G., Harputlugil T., de Wilde P. (2008), Novel concepts for the design of high performance schools, 5th international conference AEC proceedings, 23-25 June, Antalya-Turkey.

[23] Ulukavak Harputlugil, G., (2018), Building Performance Simulation Applications in Turkey: Opportunities vs. Challenges, BEYOND ALL LIMITS 2018: International Congress on Sustainability in Architecture, Planning, and Design, 17-19 October 2018, Ankara, Turkey

[24] Krygiel, E. ve Nies, B. (2008). Green BIM-Successful Sustainable Design with Building Information Modelling, Wiley Publishing, Indianapolis, Indiana.

[25] de Wilde, P., 2018. Building Performance Analysis. Wiley.

[26] Evins, R., 2013. A review of computational optimisation methods applied to sustainable building design. Renewable and Sustainable Energy Reviews, 22, 230-245

[27] Zapata-Poveda, G. and C. Tweed, 2014. Official and informal tools to embed performance in the design of low carbon buildings. An ethnographic study in England and Wales. Automation in Construction, 37, 38-47

Data Statement

Data sharing not applicable to this article as no datasets were generated or analysed during the current study.

Development and evaluation of digital twins for district-level heating energy demand simulation

Twan Rovers [a], Christian Struck [a], Chris Gieling [a], Saleh Mohammadi[a], Olaf Slagmolen [a], André Dorée [b], Léon Olde Scholtenhuis [b], Karina Vink [b], Hans Poppe [c], Daniëlle Koopman [d], Herbert ter Maat [d], Berto Boeve [e]

[a] Chair of Sustainable Building Technology, School of Business, Building & Technology, Saxion University of Applied Sciences, Enschede, the Netherlands, t.j.h.rovers@saxion.nl

[b] Department of Construction Management and Engineering, Faculty Engineering Technology, University of Twente, Enschede, the Netherlands

[c] ROC van Twente, Hengelo, the Netherlands

[d] Municipality of Enschede, Enschede, the Netherlands

[e] Loohuis Energie & Installatie Advies, Almelo, the Netherlands

Abstract. To achieve the aim of a CO_2 neutral built environment in 2050, a large part of the existing housing stock will have to be energetically retrofitted. It has been noted that a neighbourhood-oriented approach will be necessary for the feasibility, affordability and timeliness of this aim. Considering that many different stakeholders are involved in renovations at the neighbourhood level, and that multiple neighbourhoods will have to be retrofitted at the same time, efficient working methods are imperative. To facilitate the design, construction and operation of the new energy infrastructure, a prototype for a digital environment (digital twin) is developed for four Dutch pilot neighbourhoods. In this contribution, the authors will describe a procedure to convert publicly available geo-information to a CityGML model, which is used to simulate the monthly and annual space heating energy demand using SimStadt. To assess model fidelity, the simulation results are compared with publicly available aggregated energy use data. A procedure will be described to split the measured natural gas use into gas usage for space heating, domestic hot water and cooking. It is found that the simulation tends to overestimate the energy demand for space heating by 4 - 125%. This difference is largely explained by the manner in which the thermal properties of the buildings are estimated. In addition, the homogeneity of the neighbourhood in terms of the different building functions present has an impact on the accuracy of the simulation. Finally, possible invalid assumptions concerning setpoint temperatures and internal heating loads are of interest. It is concluded that more accurate simulation results will be obtained through the use of current input data. Most importantly: (i) reliable information on the buildings' current thermal properties through e.g. energy audits, and (ii) reliable information on the buildings' setpoint temperatures and internal heating loads through on-board monitoring systems.

Keywords. Energy transition, digital twin, SimStadt, neighbourhood-oriented approach
DOI: https://doi.org/10.34641/clima.2022.399

1. Introduction

To achieve the aim of a CO_2 neutral built environment in 2050, a large part of the existing housing stock will have to be energetically retrofitted. It has been noted that a neighbourhood-oriented approach will be necessary for the feasibility, affordability and timeliness of this aim [1].

Considering that many different stakeholders are involved in renovations at the neighbourhood level, and that multiple neighbourhoods will have to be retrofitted at the same time, efficient working methods are imperative. To support the process, a Fieldlab Digitalization of the Energy Transition Twente (FiDETT) has been established, in which local and regional authorities, companies and educations and research institutions participate. Its focus is on collectively developing the necessary knowledge and skills to facilitate the neighbourhood-

Copyright ©2022 by the authors. This conference paper is published under a CC-BY-4.0 license.

oriented approach and to disseminate the knowledge into practice through educational programmes.

To facilitate the design, construction and operation of the new energy infrastructure, a prototype for a digital environment (digital twin) is developed for four Dutch pilot neighbourhoods. The idea is that different stakeholders involved in the energy transition of a neighbourhood could access such a digital environment, and extract relevant information for their activities.

In this contribution, the authors will focus on a specific aspect of the digital twin, namely heating energy demand simulation using the SimStadt [2] software.

2. Research Method

2.1 Description of model construction

To create a model which can be used for simulations in SimStadt, it is necessary to collect information on the geometry of the buildings within a neighbourhood, as well as their year of construction and function. In this project, this information has been retrieved from the BAG 3D dataset [3].

The geometrical information in the BAG 3D dataset is based on a point cloud. As a result, the dataset contains ground levels and roof heights at different percentiles. As a standard, the building height is estimated as the 75th percentile of the roof height, minus the zeroth percentile of the ground level.

The ArcGIS Pro software was then used to construct three-dimensional LOD1 models of the relevant neighbourhoods. It was found that post-processing of some building geometries is necessary, as some building heights are strongly overestimated (see Fig. 1). In addition, the building functions in the dataset are replaced by the relevant Alkis codes [4], which can be read by SimStadt.

The resulting model is exported as an ESRI Shapefile, and converted to a .gml file format through editing using the FME software. The CityGML file can be read by SimStadt.

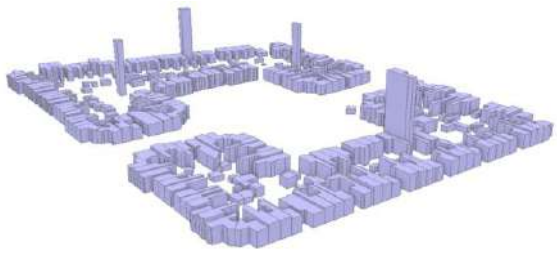

Fig. 1 – Overestimation of some building heights

2.2 Simulation using SimStadt

The SimStadt software (version 0.10.0) is used to simulate the monthly average heat demand of all buildings in the neighbourhood. This is done through the application of a monthly energy balance to each building in the neighbourhood, in which the relevant heat gains (i.e. internal and solar gains) and losses (i.e. transmission, infiltration and ventilation) are determined. When the total heat loss exceeds the total heat gains, this results in a monthly heating demand. In addition to the building geometry described in Section 2.1, the year of construction, building function and climate (year) are of importance.

In the PhysicsPreprocessor, thermal properties are assigned to the various buildings based on year of construction, building function and type of residential building, using a Physics Library. Four building physics libraries are available: A German one, one for New York City (NYC), a Dutch one developed by SimStadt, and a Dutch one developed by Saxion Chair of SBT. The two Dutch libraries are based on TABULA [5,6] and are used in the current project.

In the UsagePreprocessor, usage profiles are assigned to the various building functions using a Usage Library. This includes user density (persons m^{-2}), internal heat gains, setpoint temperatures (default 20 °C, night reduction to 16 °C) and use of hot tap water.

In the WeatherProcessor, weather data is used to calculate heat losses and gains, and the resulting energy consumption for heating.

2.3 Validation of simulation results

To validate the simulation results, these are compared with the actual heating energy consumption of the buildings for the districts under consideration.

The network operators in the Netherlands make data available with regard to the annual energy consumption of small-scale connections per postal code area [7]. Since most buildings in the Netherlands are currently heated with natural gas, the simulation results are compared with the natural gas consumption of the relevant postal code areas. The so-called standard annual consumption is reported, which includes the energy consumption of the buildings in the postal code area, corrected for gas quality and a normalized climate year [8].

Since natural gas is not only used for space heating, but also for domestic hot water (DHW) and cooking, the gas consumption must be split for these purposes (see Tab. 1). The gas used for space heating (SH) is then derived by subtracting the gas use for cooking and DHW from the total gas consumption.

Tab. 1 – Gas consumption for cooking and DHW

Use	Amount	Source
Cooking	37 m^3 per household	[9]
DHW	270 m^3 per household	[10]

For the conversion of m^3 of natural gas into kWh of heat, an average boiler efficiency of 104% on the net calorific value (31.65 MJ m^{-3}) is assumed.

2.4 Cases

Four Dutch neighbourhoods are simulated: Bruggenmors, Twekkelerveld, Bothoven and De Nijverheid. A sensitivity analysis (Section 3.1) is carried out on a part of Twekkelerveld, namely Bruggenmors. It consists exclusively of residential buildings. The median year of construction is 1930 (see Tab. 4).

3. Results

Firstly, a sensitivity analysis is carried out to assess the impact of varying building height, building physical properties and setpoint temperatures on the simulation results for Bruggenmors (Section 3.1). In Section 3.2, the heating energy demand is simulated for four neighbourhoods.

3.1 Sensitivity analyses

As discussed in Section 2.1, the building height is estimated as the 75th percentile of the point cloud, minus the ground level. Using this method, the building heights of several buildings are strongly overestimated (see Fig. 1). More realistic building heights are obtained through manual correction, see Tab. 2.

Tab. 2 – Building heights Bruggenmors

	Roof75	Roof75 corrected	Roof50
Min.	5.38	5.38	2.63
Mean	7.17	6.83	5.35
Median	6.84	6.82	5.51
Max.	36.81	8.20	6.98

Fig. 2 shows that the annual energy demand for space heating is overestimated for all three used building heights, compared to the data from the network operator (Enexis). The overestimation is the smallest when using the Roof50 data, as this simulates the smallest building volume to be conditioned.

As discussed in Section 2.2, several building physics libraries are available. Fig. 3 shows the simulated annual heating energy demand for two different Dutch building physics libraries (NL SimStadt and NL SBT). The energy demand for space heating is overestimated in both cases. The simulation results are almost the same, but the overestimation is slightly larger when using the NL SBT building physics library. This indicates that the NL SimStadt library uses slightly more favourable values for the physical properties of the buildings, such as thermal insulation and air permeability.

As discussed in Section 2.2, the standard usage profile in SimStadt assumes a setpoint temperature of 20 °C, with a night setback to 16 °C (hereafter referred to as 20 °C – 16 °C). Fig 4 shows the impact of using different setpoint temperatures on the simulated annual heating energy consumption. The space heating energy demand is overestimated in all cases. Naturally, the overestimation is smallest when using the lowest setpoint temperatures (18 °C – 15 °C).

It is concluded that both the building height and setpoint temperatures have a significant impact on the simulated energy use for space heating. The use of the two different building physics libraries has only a very small impact on the obtained results. In the next section, the datasets/values in Tab. 3 are used for the simulations.

Tab. 3 – Used datasets/values simulation Section 3.2

Variable	Dataset/value
Weather processor	Reference climate year NEN 5060:2018
Building height	Roof75 corrected
Building Physics Library	NL SimStadt
Setpoint temperature	20 °C – 16 °C

3.2 Heating demand of case neighbourhoods

Using the inputs as listed in Tab. 3, the results in Tab. 4 are obtained. The annual heating energy demand, comprising both space heating and domestic hot water, is overestimated in all cases, ranging from 3.6% for Bothoven to as much as 124.8% for Twekkelerveld.

Bothoven is a homogenous neighbourhood, comprising only residential buildings. In addition, the median year of construction of the buildings in this neighbourhood (1982) is relatively recent. As discussed in Section 2.2, the thermal properties of the buildings are estimated based on the year of construction. For older buildings, the estimation of the thermal properties is likely to be inaccurate, as these buildings have undergone retrofits, causing an improvement of the thermal envelope. More recent buildings, such as those in Bothoven, have generally not yet undergone (major) renovations, thus the estimated thermal properties will be closer to the actual values.

For the neighbourhoods with older buildings; Bruggenmors, Twekkelerveld and De Nijverheid, the overestimation of the heating energy demand is large. When comparing the two neighbourhoods with the same median year of construction (Twekkelerveld and De Nijverheid), it seems that the homogeneity of the neighbourhood also affects the accuracy of the simulated heating energy demand.

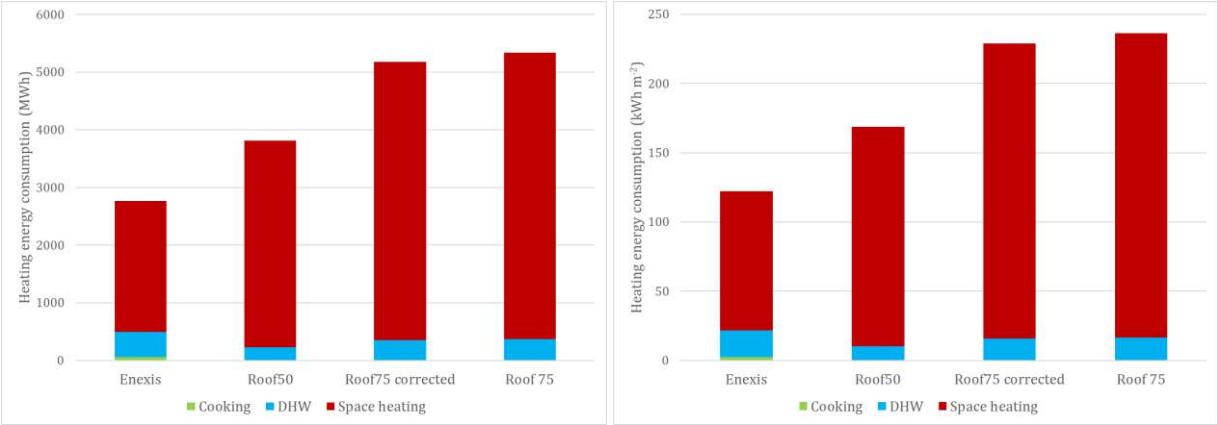

Fig. 2 –Impact of variation of building height on annual heating energy demand in MWh (left) and in kWh per m^2 heated floor area (right)

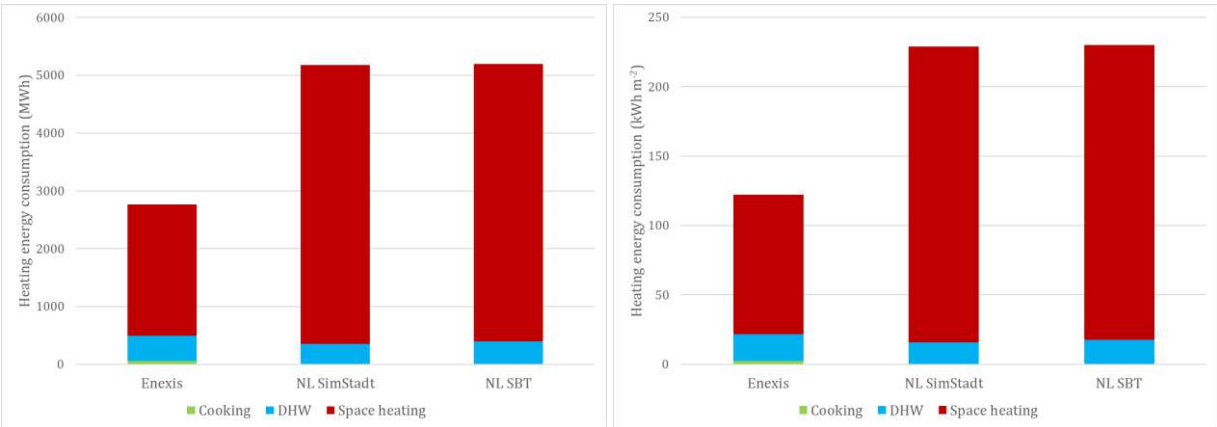

Fig. 3 – Impact of variation of building physics library on annual heating energy demand in MWh (left) and in kWh per m^2 heated floor area (right)

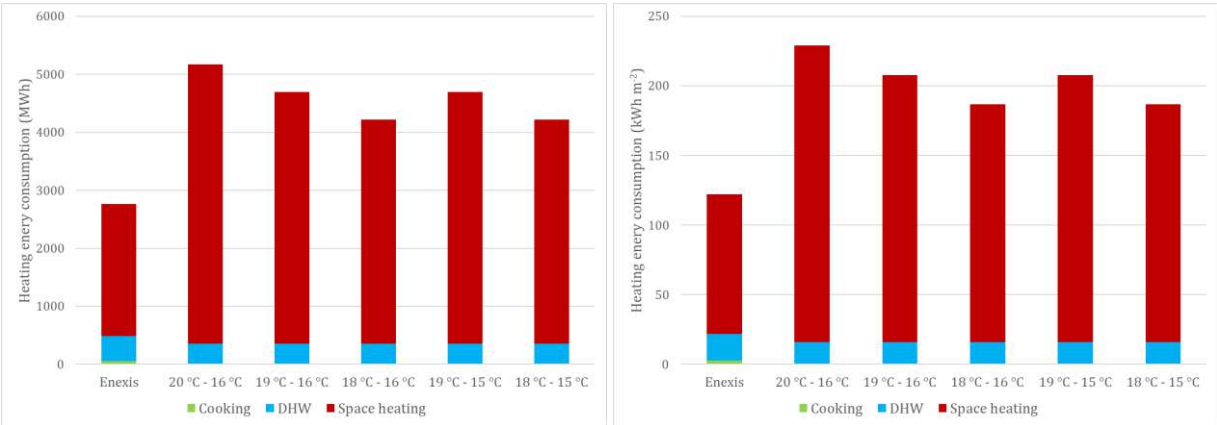

Fig. 4 – Impact of variation of setpoint temperature on annual heating energy demand in MWh (left) and in kWh per m^2 heated floor area (right)

The overestimation of the space heating energy demand (in kWh m^{-2} heated floor area) is even larger than the overestimation of the total heating energy demand (SH + DHW). It must be noted, however, that the approximate heated floor areas, which were derived from the SimStadt models, also contain inaccuracies. In particular in the case of Twekkelerverld, the heated floor area seems to be strongly overestimated, which leads to a lower space heating energy demand in kWh m^{-2} than would be expected based on the characteristics (i.e. year of construction and building functions) of the neighbourhood.

Tab. 4 – Summary of simulation results

	Bruggenmors, Enschede	Twekkelerveld, Enschede	Bothoven, Enschede	De Nijverheid, Hengelo
# simulated buildings	175	3 272 [a]	374	2 124 [a]
# gas connections	175	4 493	374	2 559
Approximate heated floor area (m^2)	22 597	921 732	35 475	374 158
Median year of construction	1930	1948	1982	1948
% residential	100.0%	95.6%	100.0%	98.4%
Measured heating demand (MWh)	2 703	59 580	3 830	36 757
Simulated heating demand (MWh)	5 175	133 922	3 969	62 240
Difference (%)	+91.5%	+124.8%	+3.6%	+69.3%
Measured space heating demand (kWh m^{-2})	100.5	52.6	81.9	81.4
Simulated space heating demand (kWh m^{-2})	213.2	123.1	96.1	149.1
Difference (%)	+112.1%	+134.0%	+17.2%	+83.3%

[a] The neighbourhoods Twekkelerveld and De Nijverheid contain fewer simulated buildings than gas connections, as these neighbourhoods contain apartment buildings. These are simulated as one building, though each apartment has its own gas connection.

4. Discussion

The previous section showed that the simulated heating energy demand of all case neighbourhoods was overestimated. Four limitations of the present study may explain some of these overestimations, both in terms of model construction (simulated heating demand) and validation (measured heating demand).

4.1 Limitations regarding the simulated heating demand

A first limitation of the current study is the use of LOD1 models. Recently, LOD2 models have become available [11]. The use thereof will result in more realistic building volumes, and therefore in more accurate simulations.

4.2 Limitations regarding the measured heating demand

For the validation of the simulation results, measured aggregated gas consumption figures from the network operator were used.

The so-called standard annual consumption is reported, which includes the energy consumption of the buildings in the postal code area, corrected for gas quality and a normalized climate year. The latter was accounted for by using the reference climate year from NEN 5060 in the simulations. However, the correction for gas quality has not been accounted for.

In addition, the total natural gas use was split into gas consumption for space heating, domestic hot water and cooking using standard figures. These do not necessarily represent the actual use in the considered neighbourhoods.

Finally, it was assumed that all buildings in the case neighbourhoods were heated by natural gas. Although this is the case for the majority of the buildings, some will be heated differently. As a result, the measured heating energy demand is actually underestimated, which means that the overestimation in the simulations is not as large.

5. Conclusions

The sensitivity analysis concluded that both the building height and the setpoint temperatures used have a significant influence on the simulated energy use for space heating. The use of the two different building physics libraries has only a very small impact on the obtained results.

By conducting simulations on four case neighbourhoods, it was found that the simulation tends to overestimate the total annual heating energy demand by 4 - 125%. This difference is largely explained by the manner in which the thermal properties of the buildings are estimated. In addition, the homogeneity of the neighbourhood in terms of the different building functions present affects the accuracy of the simulation. Finally, possible invalid assumptions with regard to setpoint temperatures and internal heating loads are of concern.

It is concluded that more accurate simulation results will be obtained through the use of current input data, with respect to: (i) the building geometry (use of LOD 2 models), (ii) reliable information on the buildings' current thermal properties through e.g. energy audits, and (iii) reliable information on the buildings' setpoint temperatures and internal heating loads through on-board monitoring systems.

6. Acknowledgement

The authors wish to acknowledge the financial support of the Nationaal Regieorgaan Praktijkgericht

Onderzoek SIA.

7. References

[1] Klimaatberaad. Klimaatakkoord. 2019. www.klimaatakkoord.nl

[2] HFT Stuttgart. SimStadt2. 2021 https://simstadt.hft-stuttgart.de/en/index.jsp

[3] ArcGIS. BAG 3D - Nederland. 2020. https://www.arcgis.com/home/item.html?id=abd5e3c4b173417f8c14f1283dee33c6

[4] Fitzky, M. Vergleichende Analyse verschiedener Methoden und Datensätze zur Berechnung von Energieausweisen von Gebäuden. 2018.

[5] Loga, T., Stein, B., Diefenbach, N. TABULA building typologies in 20 European countries—Making energy-related features of residential building stocks comparable. Energy and Buildings. 2000;132, 4–12.

[6] TABULA WebTool. https://webtool.build11]ing-typology.eu/?c=se

[7] Enexis. Open data. 2021. https://www.enexis.nl/over-ons/wat-bieden-we/andere-diensten/open-data

[8] Enexis. Toelichting bij dataset Kleinverbruiksgegevens. 2018. https://www.enexis.nl/over-ons/-/media/documenten/open-data/toelichting-kleinverbruiksgegevens-open-data-enexis-netbeheer.pdf?modified=00010101000000&la=nl-nl&hash=1A66620D8DBA0D55A55767B507C535BC218B0B14

[9] Milieu Centraal. Inductie kookplaat. 2020. https://www.milieucentraal.nl/energie-besparen/apparaten-in-huis/inductie-kookplaat/

[10] Milieu Centraal. Bespaartips warm water. 2020. https://www.milieucentraal.nl/energie-besparen/duurzaam-warm-water/bespaartips-warm-water/

[11] TU Delft. 2021. https://3dbag.nl/en/viewer

Data Statement

The datasets generated and analysed during the current study are not publicly available but can be made available upon request.

Real-time Model Predictive Control with Digital Twins and Edge Computing Technologies

Michael Berger [a], Filippo Bernardello [a], Craig Barry [a], Pravesh Badjoonauth [a], Shruthi Balaji [a], Michael Lakhdar [a]

[a] Conserve It, Melbourne, Australia, info@conserveitiot.com

Abstract. Buildings consume almost a quarter of Worlds Energy Consumption and hence are one of the major sources of emissions globally. In commercial buildings, HVAC is by far the most energy intensive system, accounting for close to half of the total energy consumption. For this reason every efficiency improvement in HVAC performance can significantly reduce the energy profile of the building, turning HVAC optimisation into a core requirement to deliver energy efficiency. Fundamental to optimising large energy consumers in today's modern buildings is the use of Machine Learning in order to dramatically improve the energy efficiency of modern central cooling and heating plants. This paper will demonstrate the techniques that have been implemented to deliver advanced Real-time Model Predictive Control on Edge Computing solutions that don't require Cloud connectivity or significant computing power. Through the use of deep domain knowledge and advances in Edge Computing, it is possible to 'learn' highly accurate models of how mechanical machines operate and apply those models to predict and then solve complex optimisation problems for advanced control and improvements in energy efficiency. The authors will show how, through the collection of real-time sensor data, our platform has successfully reduced energy consumption and electrical demand in real buildings without compromising space comfort in any way at all. The capability to generate self-adjusting control algorithms in an on-premises scenario not only delivers significant outcomes but lowers overall Total Cost of Ownership for the end client. The absence of ongoing subscription fees further improves the economic model and the case for on-premises, real-time, model predictive control. Furthermore, the paper will demonstrate how the same Digital Twins used for Model Predictive Control can be used for anomaly detection algorithms or Fault Detection and Diagnosis as well as Predictive Maintenance and that this will create new service opportunities and business models for smart companies of the future whilst continuing to deliver optimal performance of mechanical systems.

Keywords. Energy, Design of Innovative HVAC systems for optimized operational performances, Digitization, Digitization in HVAC control & Health Monitoring.
DOI: https://doi.org/10.34641/clima.2022.368

1. Introduction

Chilled water plants are widely used globally for air-conditioning and refrigeration applications, and account for a large proportion of commercial buildings' energy usage. As was highlighted again recently at the COP26 conference in Glasgow, curtailing CO2 emissions-driven global warming is one the biggest challenges of our time [1]. Reducing chilled water plants energy usage would contribute to this goal. Equipment efficiency has improved over the years, and variable speed drives (VSD) have been introduced to improve the part-load efficiency of the chillers, pumps, and cooling towers, and are now almost ubiquitous in new plants deployed around the world. However, those have also introduced many new variables to adjust by the supervisory control systems, such as the condenser water flow at each chiller for instance, and conventional controls solutions are not equipped to select the optimal setpoints in real-time as conditions vary throughout the days and seasons, and therefore do not allow these efficient machines to run together to their highest potential. Offline simulations have been carried out before to recommend some "rules-of-thumbs" that can be implemented in conventional control systems [2, 3], but those may not generalize well to every equipment sizing, performance, and systems design.

In this study, a deployable on-premises real-time model predictive control approach to address these

Copyright ©2022 by the authors. This conference paper is published under a CC-BY-4.0 license.

challenges and minimize the energy usage of the chilled water plant is presented and assessed with actual site data and operation. It is intended to operate on site on the edge on an embedded controls platform, as displayed on Fig. 1.

Fig. 1 – Embedded Edge hardware for real-time monitoring and controls of live equipment

2. Modelling approach

The setpoints of interest in this study are:

- The leaving chilled water temperature (LCHWT) at each chiller
- The condenser water (CW) flow at each chiller

The former will dictate the loading of each chiller, when keeping the overall plant LCHWT as per specifications, and allow to set each chiller at or near their most optimal part-load point or "sweet-spot". The latter will tackle the trade-off between CW pump power (lower flow will result in lower power) and chiller power (lower flow will result in higher refrigerant discharge pressure and therefore higher power).

It is important to note that neither of those would impact the chilled water production of the plant, as the chilled water flow and temperature leaving the plant are not affected, and therefore would not compromise comfort in the building.

2.1 Optimization Formulation

The optimization problem to solve as part of the Model Predictive Control approach is to minimize the power usage of the chillers and the CW pumps, as defined in Eq. (1).

$$\underset{Load_i,\ Flow_{CW,i}}{\text{Minimize}} \sum_{i=0}^{n} P_{chiller,i}(Load_i, Flow_{CW,i}) + P_{CW\ pump,i}(Flow_{CW,i})$$
$$\text{s.t.:} \sum_{i=0}^{n} Load_i = Load_{Plant,Target}$$
$$Load_{Min,i} \leq Load_i \leq Load_{Max,i}$$
$$Flow_{CW,Min,i} \leq Flow_{CW,i} \leq Flow_{CW,Max,i} \quad (1)$$

The decisions variables here are the cooling load and the CW Flow of each chiller. The LCHWT of each chiller can be derived from their load and the overall plant LCHWT target. The problem is treated as steady-state as it only selects setpoints that are then fed to lower-level control loops tasked to reach and maintain them, and also due to the absence of other time-dependent state variables such as storage-related for instance. As such, the optimization is carried out on a single point short-term horizon, with the target overall plant load being computed based on the measured and recorded cooling load and regression-based prediction of its future value in the near future. The computed optimum decision variables can then be fed to the lower-level systems: The LCHWT setpoint command is communicated to the chillers via high-level or low-level communication, and the CW flow setpoint can be passed to a PID controller with the CW pump speed as output command. The optimization is repeated on a regular basis, every 1 minute or less, to account for continuous changes of conditions on site.

Additionally, this mathematical program can be repeated for each number of chillers in the plant and used to select the most efficient number of chillers. It is also flexible and can be simplified to only include one set of decision variables, in case of site limitations, for instance if the CW pump speed is not equipped with VSD.

2.2 Equipment models

The power usage of a chiller is modelled as a 2nd order multivariate polynomial function of its cooling load; the difference between the entering condenser water temperature (ECWT) and the LCHWT; and the CW Flow, as per Eq. (2).

$$P_{chiller} = f(Load, T_{ECW} - T_{LCHW}, Flow_{CW}) \quad (2)$$

Chiller models have been proposed in [4, 5]. The selected model follows a similar direction with some modifications to further suit the requirements of live learning with potentially limited data, and of the optimization problem. Indeed, using the difference of water temperatures allow to capture the variation of power usage due to compression ratio without having to record significant data coverage of both chilled water and condenser water. Additionally, the use of the CW Flow and ECWT separately simplifies the optimization problem as they are both controllable variables, whereas LCWT is itself a function of the chiller power and would result in a recursive function that would add unnecessary complication to the downstream optimization algorithm. For air-cooled chillers, or water-cooled chillers with no CW Flow metering, the model can be simplified by omitting the CW Flow variable.

The efficiency of the chiller (and by extension the plant) is usually reported as Coefficient Of Performance (COP), following Eq. (3).

$$COP = \frac{Load}{Power} \tag{3}$$

The power usage of a CW pump is modelled as a 2nd order polynomial function of the CW Flow, as in Eq. (4)

$$P_{CW\ pump} = f(Flow_{\ CW}) \tag{4}$$

The above model is applicable to cases where there is a 1-to-1 relationship between chillers and pumps in the plant (often referred to as "dedicated" in the industry). Note that plants with 1-to-many chiller-pump relationship have been addressed by the authors separately but are not included in the present study.

2.3 Machine learning approach

The machine learning solution is intended to run autonomously on site and learn the performance of the site's equipment live, without human interaction. As such, one of the challenges is to handle cases where limited data is available, whether it is due to a small sample size or the dataset only spanning a small area of the operating range. After several previous site deployment reviews it was found that in numerous cases, the autonomously learnt model exhibited undesirable features, such as negative power values within the operating range in areas where little to no data had been available.

In addition to further data pre-processing, a solution that was investigated was to add constraints to the least-square learning of the model to further leverage the subject-matter experts' knowledge. Expected behaviours – for instance that the power usage of the equipment should always be positive in the operating range or that the power usage of a pump is expected to increase when the flow increases and all other values being equal – are embedded as linear constraints to the learning.

The resulting constrained least-square problem of a polynomial model with linear constraints is a standard convex Quadratic Program (QP) as defined in Eq. (5) and for the number of variables of the application (order of magnitude of 10 variables) can be solved in real-time well below 1 second on modern embedded hardware using state-of-the-art algorithms, such as an Interior Point method [6].

$$\begin{aligned} &\underset{x}{\text{Minimize}}\ \|Ax - b\|_2^2 \\ &\text{s.t.}: c\,.\,x\ \leq 0 \end{aligned} \tag{5}$$

In Eq. (5), the matrix A contains all the input data, the vector x the model coefficients, the vector b the output data (power usage in this case), and the vector c the linear constraints features.

2.4 Solving the optimization problem

The simplest but most computationally costly way to solve an optimization problem is an exhaustive search, a method that cycles through all the possible combinations of all the decisions variables. In the present application, the computational complexity grows exponentially with the number of variables, and even with a small number of chillers in the plant it quickly becomes impractical for real-time controls. For instance, with a 3 chillers plant, which results in 6 decision variables (3 loads and 3 CW flows), and assuming 100 points being checked for each variable, it would result in 100^6, or a trillion, iterations, each of which consists of several operations to compute the total power to be minimized. Even assuming each iteration can be computed within 1 micro-second, which is a generous assumption, this would result in 1 million seconds of computational time, which is obviously not acceptable for real-time supervisory controls that may require sub-minute or even sub-second decisions in some cases.

The proposed approach is to use an Interior-point method for non-linear optimization [7]. The optimization problem is a QP, with a quadratic objective as a sum of quadratic functions, and linear constraints. Provided that the objective function is convex, which is expected for the pump power and chiller power based on their affinity law, an Interior-point method can typically find the global minimum of a QP with dozens of variables within milliseconds on modest modern hardware [6]. Note that even if the objective function is not convex, a sequential quadratic program method [7] was found to provide a good local optimum in similar time for all cases tested. Additionally, specific constraints can be added to the models' learning to enforce their convexity.

3. Modelling results

3.1 Model learning results

The chiller power model learning results are reported for 2 separate anonymised sites, with roughly 1 year of 15 minutes interval data each. Site A is equipped with 2 multi-centrifugal-compressors chillers rated at 1,700 kW of refrigeration, and site B with 2 centrifugal-compressors chillers of 1,800 kW of refrigeration. Chillers on Site A and B are from different manufacturers. As shown on Tab. 1 the proposed chiller power model captures with a good accuracy the actual measured trend for all tested chillers, and therefore proves to be a suitable predictor for the application, for several separate sites and chillers.

Tab. 1 – Chiller model learning results with site data.

	Site A		Site B	
Chiller n°	1	2	1	2
MAE (kW)	7.1	4.5	6.3	6.4
MAE/Mean (%)	5.17	4.98	5.49	4.32
R-squared	0.962	0.978	0.957	0.961

For chiller 1 of Site A, the fit of the predicted power in regard to the actual power is displayed on Fig. 2 and shows a good fit. The predicted power is also displayed on Fig. 3 in regard to the Load, the temperature difference, and the CW Flow.

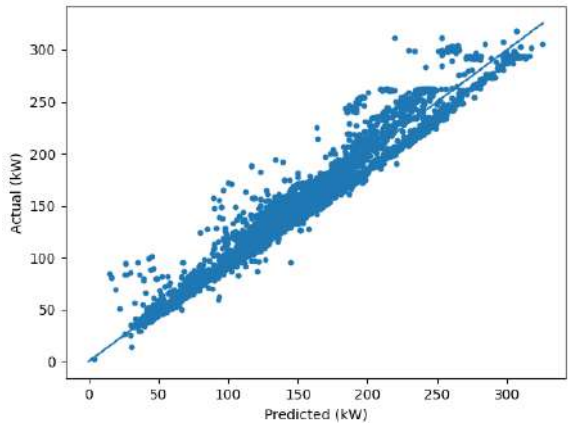

Fig. 2 – Site A, Chiller 1 predicted power compared to the actual measured power.

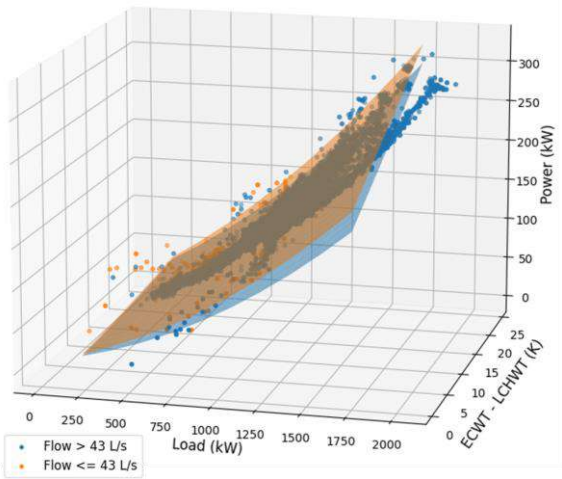

Fig. 3 – Site A, Chiller 1 predicted power in regard to the cooling load, difference of temperature and CW Flow. Surface plot: Predicted power. Scatter plot: Actual data.

The CW pumps power model was tested on the same sites, with the dedicated pump of each chiller. As shown on Tab. 2 the proposed pump power model performs well overall with low error and high correlation fit in all cases.

Tab. 2 – Pump model learning results with site data.

	Site A		Site B	
Pump n°	1	2	1	2
MAE (kW)	0.56	0.31	0.38	0.41
MAE/Mean (%)	4.78	3.47	3.57	3.66
R-squared	0.978	0.988	0.958	0.947

For pump 1 of Site A, the fit of the predicted power and actual power in regard to the flow is displayed on Fig.4.

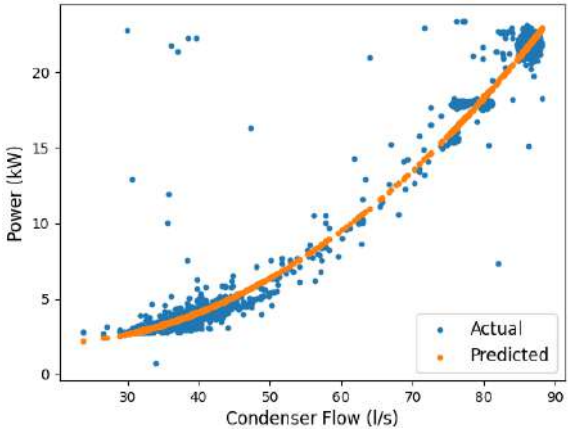

Fig. 4 – Site A, Pump 1 predicted and actual power in regard to the flow.

3.2 Optimization offline simulations

The optimization algorithms were initially run offline with models learnt from site data, to assess the validity of the premise as well as the savings potential.

As an example, the optimization of CW Flow setpoint was simulated for Site A's Chiller n°1 with its dedicated CW pump n°1. The rated data for this pair of equipment is a CW Flow of 86 L/s and a pump power of 22 kW. The power of each equipment individually and their sum is displayed on Fig. 5 and Fig. 6, for set conditions of LCHW and ECW temperatures, and respectively a low load of 30% and medium-high load of 70%. Those figures show the trade-off between pump power and chiller power and how at different conditions the optimal flow point is different. This illustrates the benefit of predictive modelling and continuous optimization to accurately assess the best CW Flow setpoint at all times under varying conditions.

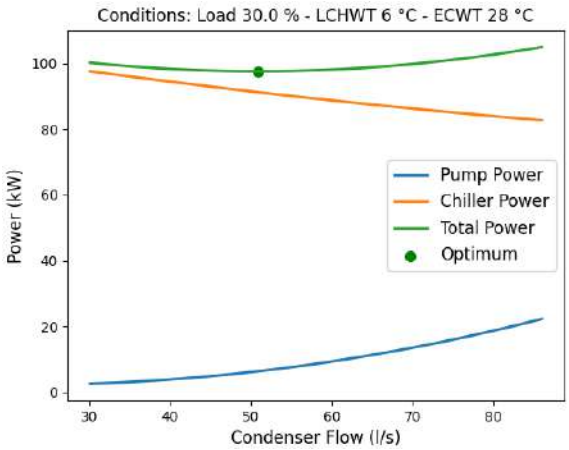

Fig. 5 – Site A, Chiller and Pump n°1 optimal CW Flow of 50 L/s (58% of design flow) under low load.

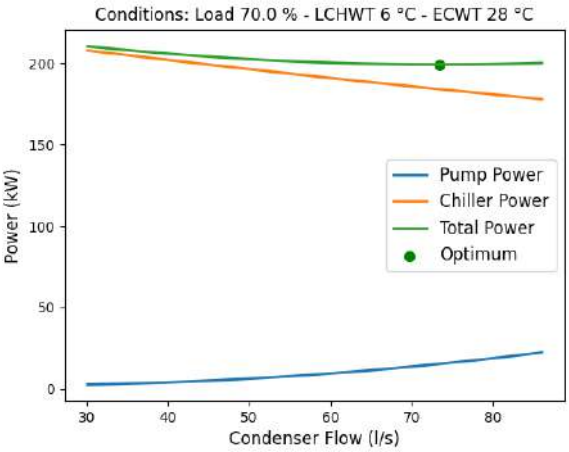

Fig. 6 – Site A, Chiller and Pump n°1 optimal CW Flow of 72 L/s (83% of design flow) under medium-high load.

At most sites, operators and conventional controls system typically maintain a constant CW Flow at all conditions, as the trade-off between the pump and chiller usage is not obvious. There is no clear rule-of-thumbs that can be followed. Indeed, as is shown on Fig.7, for a theoretical different pump sizing, at the same conditions and with the same chiller, the optimal CW Flow is very different.

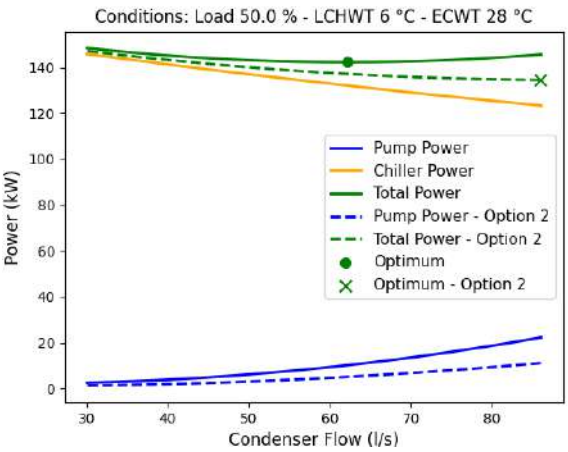

Fig. 7 – Optimal CW Flow comparison with a theoretical 2nd option of Pump sizing design.

Savings on Site A's Chiller and Pump n°1 power for the case of optimal CW Flow in comparison with the baseline case with constant CW Flow set at design value can be computed from the predictive models, as displayed on Fig. 8. The savings' opportunities are significant, at low and medium loads in particular, for this specific site.

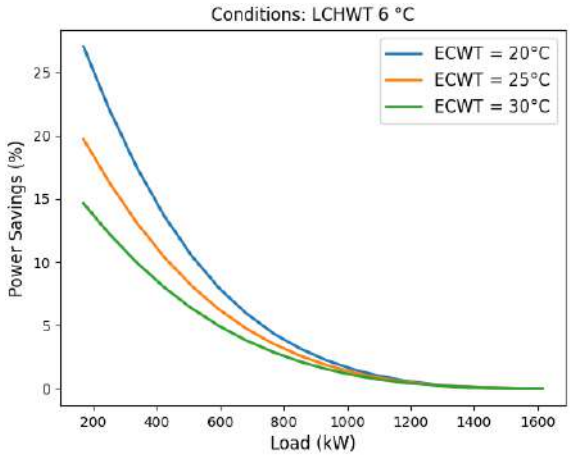

Fig. 8 – Site A, Chiller and Pump n°1 percentage savings for the optimal CW Flow setpoint, at different cooling loads and ECW temperatures.

On Site B, the combined impact of the optimal CW Flow and LCHWT is shown on Fig. 9, 10 and 11. The ECWT is configured to 28°C, the Plant LCHWT to 10°C, 2 chillers are running at the same time, and the simulation is run for plant cooling load points on their whole range of operation. The savings are computed by comparing with a case of constant CW Flows at each chiller and equal load distribution between the chillers.

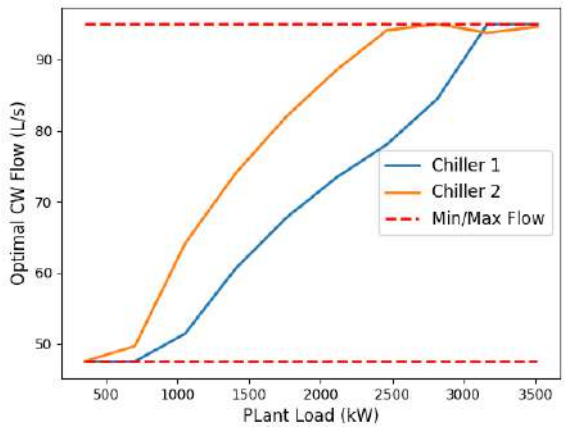

Fig. 9 – Site B, optimal CW Flow setpoints, at different plant cooling loads.

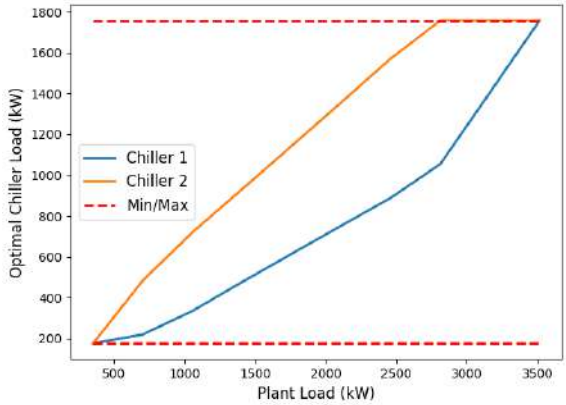

Fig. 10 – Site B, optimal chiller loads, at different plant cooling loads.

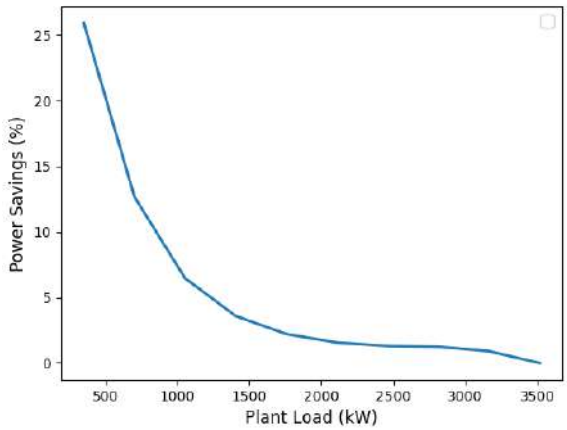

Fig. 11 – Site B, computed power savings at different plant cooling loads.

Due to the difference of part-load performance of the chillers, different optimal CW Flows and loads are found for each chiller, resulting in significant savings compared to the conventional case of maintaining constant CW Flow and equal loads on the chillers.

4. Real-time controls results

The approach has been implemented on site on embedded hardware for real-time direct controls of equipment via common high-level communication protocol such as Modbus or BACnet. This was integrated within the existing chiller plant controls hardware & software embedded solution PlantPRO®, which delivers a comprehensive on-premises controls solution that can fully manage the plant independently or in parallel with a Building Management System (BMS). The advantage of this implementation approach is that it does not rely on other control systems to manage the equipment, and contrarily to cloud-hosted solutions, it does not require a cloud subscription fee and removes downtime due to internet connection issues.

Two separate hardware platforms were used, initially a BeagleBone Black-based platform, with 1 core CPU and 500MB of RAM, and subsequently a Raspberry Pi 3+ compute module-based platform with a 4-core CPU and 1GB of RAM, as PlantPRO® transitioned to the latter. The solution was initially implemented as a prototype during the research phase with customizations on a site-by-site basis and has since then been implemented in the commercial product with full-suite of GUI and flexible configuration for various chiller plant configurations.

Resulting operational data further to deployments on Sites A, B & C were analysed. During operation on Site A, at a period of relatively constant conditions, the optimal CW Flow was overridden to the design CW Flow, to confirm that during actual operation the expected energy savings were indeed observed. As shown on Tab. 3, the optimal CW Flow brought savings of 10.4 kW of instantaneous power usage, or 22.6%. Albeit in a punctual scenario of low load, this site experiment does contribute to further validate the opportunities of optimizing over this variable in the plant.

Tab. 3 – Site A recorded site data comparison between optimal and standard CW Flow.

Case	Load (kW)	CW Flow (L/s)	Chiller Power (kW)	Pump Power (kW)	Total Power (kW)
Optimal	325	52.1	30.4	5.3	35.7
Standard	322	80.9	29.1	17.0	46.1

On Site C – which is equipped with 2 chillers of 3000 kW and 1 chiller of 1000 kW of refrigeration – the number of chillers and the loads were optimized but not the CW Flow due to sensor limitations at the condenser side. The overall plant COP was observed to increase noticeably at medium and high loads, which coincides with periods with more than 1 chiller enabled, when there are opportunities for varying the load proportion between chillers. This can be observed on Fig. 12. Note that periods with faulty equipment were removed.

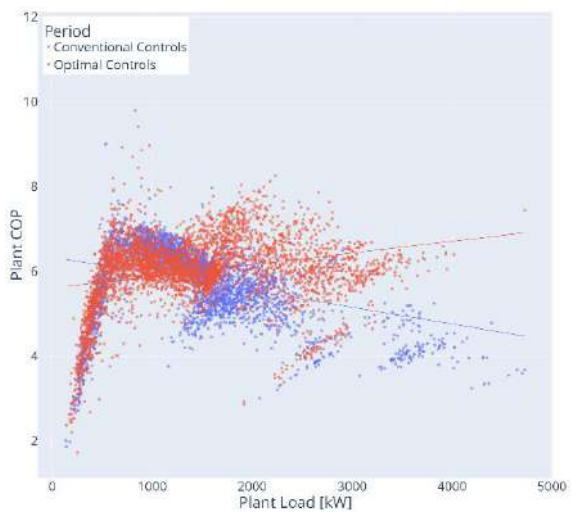

Fig. 12 – Instantaneous Plant COP at Site C with conventional controls period compared to optimal controls period, from measured data.

On Fig. 13 and 14, respectively the actual cooling and LCHWT of each enabled chiller is displayed during a few hours of operation, illustrating how – as a result of the optimal controls approach – the load is not distributed equally between each chiller as it would typically be with conventional controls, while still targeting to meet the plant level production requirement.

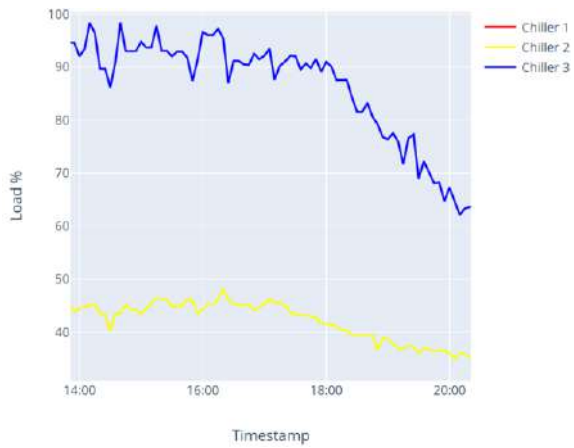

Fig. 13 – Cooling load distribution per chiller at Site C from measured data (with only chillers 2 and 3 running during that time period).

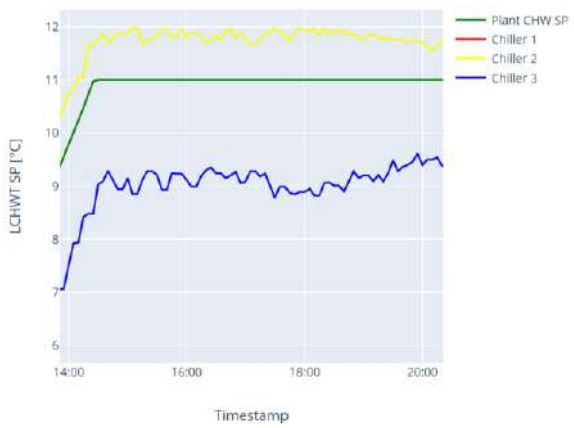

Fig. 14 – LCHWT distribution per chiller at Site C (with only chillers 2 and 3 running during that time period).

On Site B, both CW Flow and Loads were optimized. As shown on Fig. 15, the plant efficiency increased notably after deployment, compared to the previous conventional controls method.

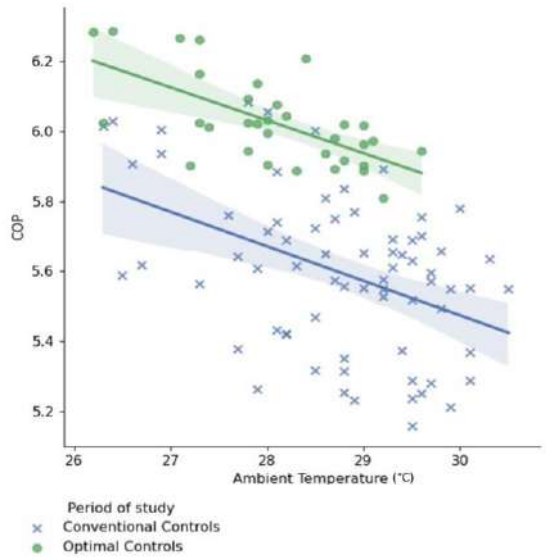

Fig. 15 – Daily Plant COP at Site B conventional controls period compared to optimal controls period, from measured data.

Measurement and verification (M&V) studies were carried out, following the guiding principles from the International Performance Measurement and Verification Protocol (IPMVP) [8], to assess the actual energy savings achieved while accounting for changes in conditions appropriately. For all 3 sites, a baseline was computed to represent the energy usage of the plant without optimal control and compared with the actual energy usage measured during the optimal controls period. For Site A, a calibrated simulation approach (IPMVP's option D) was used to simulate operation with constant CW flow, and the optimal controls period was of roughly 2 months. For Sites B and C, the measured energy usage of the plant prior to deployment was modelled as a function of the cooling load and outdoor air conditions (IPMVP's option B), and the optimal controls period was of roughly 1 month each. The savings are displayed on Tab. 4.

Tab. 4 – Energy savings.

Sites	Variables	Savings (kWh)	Savings (%)
Site A	CW Flows	15,948	3.6
Site B	CW Flows and Loads	7,358	7.1
Site C	Loads	4,056	5.1

The savings achieved in most cases are significant given that no mechanical equipment was replaced, and they are solely due to control strategies variations, moreover, only affecting 1 or 2 sets of setpoints (CW Flows and Loads) amongst all the variables in the plant. The efficiency of the plants prior to the implementation of the optimal controls features were already good in all cases, with conventional control strategies following best

practices in the field. Site A and C already had PlantPRO® installed and had had extensive manual tuning by experienced operators to extract as much savings as possible with conventional approaches. Note that for Site C, the LCHWT allowable range configuration for each chiller was extended to allow for the chillers' loads to be distributed as per the optimization live decisions. For Site B, a BMS was controlling the plant prior to deployment, and the plant COP was also reasonably high, as shown previously on Fig. 15, in particular given that it is located in a hot-and-humid climate. Note that for that site, the transition to optimal controls included the installation of PlantPRO®, and there could have been some minor additional changes in regard to other control strategies. Due to the solution being deployable within an existing controls solution providing additional benefits, on low-cost embedded hardware, the cost of adoption is expected to be relatively low, and the level of savings to provide adequate benefits to the stakeholders.

The computing time to solve the optimization problem on the embedded hardware was also measured for a few key cases, as displayed on Tab. 5, and were fast enough for real-time controls, as demonstrated by the successful site deployments.

Tab. 5 – Loads-only optimization algorithm computing time on Raspberry Pi 3+ based platform – Average of 1,000 runs.

2 Chillers	5 chillers	10 Chillers
46.1 ms	54.2 ms	64.4 ms

5. Further use: Predictive maintenance

The models to predict the power usage of the chillers and condenser pumps, that have been developed and validated in this study, can also be used to track and detect performance degradation of the equipment. Operators are often unable to properly assess this due to only limited data at full-load being available from the manufacturer. As seen above, chiller power usage and efficiency are affected by the cooling load, water temperatures, condenser flow, and it can be hard to discern if a lower efficiency than surmised is due to performance degradation or simply to the conditions. With the predictive models, performance of the equipment can be captured initially based on manufacturer data or initial operation. This baseline calibrated model can then be continuously compared in the plant management system with actual measured efficiency of the equipment based on the live conditions, to alert the operator if it has decreased over time.

This can be used as a predictive maintenance tool to address otherwise undetected issues that would increase the power usage of the plant and may be early signs of a potential future failure that may cost more to be fixed later on than if prevented.

6. Conclusions

A real-time model-based optimal controls approach was proposed, validated from site data, and deployed in actual chiller plants to demonstrate its resulting operation and benefits. The performance of the equipment was predicted using machine learning models that demonstrated generally high prediction accuracy. The optimization models were used to run offline simulations and showed notable potential energy savings. Finally, the solution was deployed on several sites, and demonstrated actual energy savings in the range of 3.6% to 7.1%, while maintaining both reliability of operation and comfort in the buildings. The solution was also designed to operate at low computing cost and be deployable on modern low-cost embedded controllers, eliminating the hurdles encountered with cloud-hosted approaches such as on-going maintenance fees and security and reliability concerns due to reliance on internet connection for equipment controls. The predictive models can also be applied to further use, such as predictive maintenance and fault detection, and deliver additional indirect benefits.

7. Acknowledgement

The authors would like to acknowledge John Wessel from Airmaster for sharing his invaluable advice and expert domain knowledge.

8. References

[1] UN, COP26 The Glasgow Climate Pact, 2021

[2] Hydeman M., Zhou G. Optimizing Chilled Water Plant Control. ASHRAE Journal. 2007;44-55.

[3] Taylor S. Optimizing Design & Control of Chilled Water Plants Part 5: Optimized Control Sequences. ASHRAE Journal. 2012;56-75.

[4] Supervisory control strategies and optimization. ASHRAE Handbook – HVAC Applications – Chapter 41. 2007

[5] Hydeman M., Gillespie K. Tools and Techniques to Calibrate Electric Chiller Component Models. ASHRAE Transactions. 2002

[6] Boyd S., Vandenberghe L. Convex Optimization. Cambridge University Press. 2004

[7] Wächter A., Biegler L. On the implementation of an interior-point filter line-search algorithm for large-scale nonlinear programming. Mathematical Programming. 2006;106:25-57

[8] Core Concepts – International Performance Measurement and Verification Protocol. EVO 10000. 2016

Data Statement

The datasets generated and/or analysed during the current study are not available due to commercial reasons but the authors will make every reasonable effort to publish them in the future.

Development of a remote refrigerant leakage detection system for chillers and VRFs

Shunsuke KIMURA [a], Michio MORIWAKI [b], Manabu YOSHIMI [c], Shohei YAMADA [d], Takeshi HIKAWA [e], Shinichi KASAHARA [f]

[a-f] Technology and Innovation Centre, Daikin Industries, Ltd., Nishi-Hitotsuya, Settsu, Osaka, 566-8585, Japan

[a] shunsuke.kimura@daikin.co.jp, [b] michio.moriwaki@daikin.co.jp, [c] manabu.yoshimi@daikin.co.jp

[d] shouhei.yamada@daikin.co.jp, [e] takeshi.hikawa@daikin.co.jp, [f] shinichi.kasahara@daikin.co.jp

Abstract. In Europe and Japan, owners of large refrigeration and air-conditioning equipment, such as chillers and VRFs, are required by law to carry out regular inspections for refrigerant leaks. There are two methods of regular inspection: the direct method, which uses visual inspection and leak detectors equipped with gas sensors; and the indirect method, which uses equipment operating data to estimate leaks. However, large equipment requires many inspection points and direct inspection is time-consuming and labor-intensive, placing a heavy burden on both the equipment owner and the inspector. On the other hand, the European F-gas regulation provides an incentive to halve the number of inspections if a permanent leakage detection system is installed, and similar incentives are being considered for other countries regulations. The authors developed a highly accurate refrigerant leakage detection system using machine learning techniques that can be used to meet incentive requirements. The details of the technology and the accuracy of the detection system tested on chillers and VRFs are discussed in this paper.

Keywords. refrigerant leakage detection, chiller, VRF, machine learning
DOI: https://doi.org/10.34641/clima.2022.373

1. Introduction

The F-Gas Regulation, which came into force in Europe in 2006, requires refrigeration and air-conditioning equipment with more than 3 kg of refrigerant to be tested for refrigerant leaks on a regular basis. However, it allows that the frequency of inspections to be halved if the equipment is provided with a leakage detection system. This led to a flurry of development of leakage detection systems.

A leakage detection system using remote monitoring data for VRF was also developed by one of the present authors and his colleagues [1]. However, the demand for leakage detection systems didn't grow because there were no specific penalties for non-compliance with regular inspection requirements.

The revision of the F-gas regulation in 2015, which has led to the implementation of penalties in many countries, has once again energised the development of leakage detection systems. In recent years, the development of big data analysis technology has led to numerous proposals of machine learning based refrigerant leakage detection systems.

According to Hosseini *et. al.* [2], 82 papers have been published worldwide on machine learning based air conditioner fault detection systems between 2016 and 2020, 10 of which are on leakage detection. Out of these 10 papers on leakage detection, 6 papers are on VRF. In Japan, Wakui *et. al*. [3] reported on the simulation of a leakage detection system for VRFs using machine learning.

However, most of these papers are validated using simulations or experimental data obtained in laboratories, and only few of them are validated using actual on-site operating data. Therefore, a leakage detection system for VRF equipment during cooling operation that uses machine learning operated on a remote monitoring system was developed, and its detection accuracy was validated using a large amount of on-site data [4-5]. Also, a leakage detection system for chillers was developed applying this technology [6], which has been launched in Europe. Leakage detection function in heating operation for VRFs has also been developed and validated using on-site data. In this paper, the leakage detection system for chillers and for cooling and heating of VRFs are discussed.

2. Methodology

2.1 Overview of the detection sysytem

The leakage detection system estimates the refrigerant charge amount from the operating data acquired from chiller and VRF equipment, and

Copyright ©2022 by the authors. This conference paper is published under a CC-BY-4.0 license.

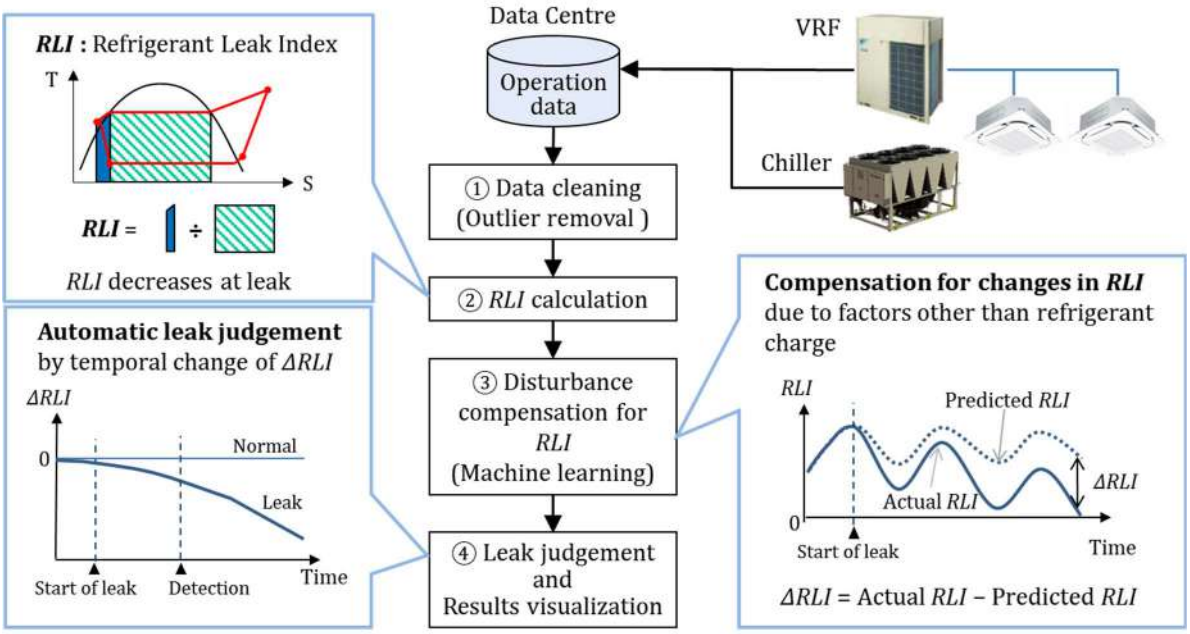

Fig. 1 – Overview of the leakage detection system

automatically detects leakages. Fig. 1 shows an overview of the developed system.

2.2 Refrigerant leak index (RLI)

The leakage detection system calculates the *RLI* (Refrigerant Leak Index), an index strongly correlated with the refrigerant charge amount, from the operating data and detects leakages based on changes in this value.

The *RLI* used in chiller and VRF cooling operations is a dimensionless value defined as the ratio of the area of the liquid region to the area of the saturated region on the T-S diagram, as shown in Fig. 1. As the refrigerant charge amount decreases due to leaks, the *RLI* also decreases.

During the heating operations of the VRF, the degree of superheat of the compressor discharge temperature (*DSH*) is used instead of the above *RLI*. When the refrigerant amount decreases due to leaks, the discharge temperature rises and so does the *DSH*.

The reason why *RLI* is not used during heating is that VRF operates multiple indoor units as condensers during heating, as shown in Fig. 2. The number and types of connected indoor units vary from one to another, and a machine learning model using the *RLI* obtained for each of these indoor units would make the logic very complicated. As a result, the amount of calculation increases, and implementation becomes difficult. Therefore, this VRF-specific challenge was solved by using *DSH* as an index for heating.

2.3 Disturbance compensation for RLI

The *RLI* changes not only due to the refrigerant amount, but also due to external disturbances such as outside temperature and compressor speed. Therefore, even though there is no refrigerant leak, the *RLI* may drop due to the disturbances and the detection algorithm may misjudge it as a leak.

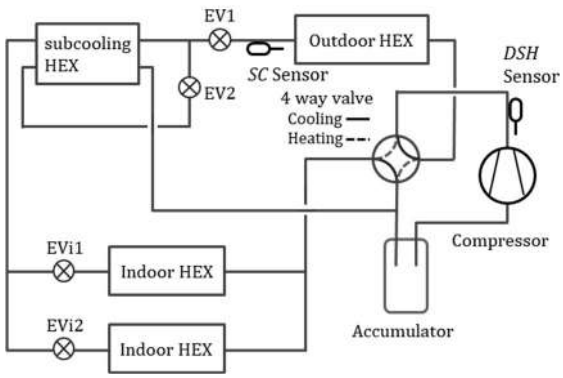

Fig. 2 – Example of VRF piping diagram

To prevent this, the disturbances from *RLI* is removed and the index *ΔRLI*, which represents only the variation of the refrigerant charge amount, is calculated. As shown in Fig. 1, *ΔRLI* is the difference between the actual *RLI* calculated directly from the operating data and the predicted *RLI* under normal conditions. This predicted *RLI* is calculated by a prediction model created using machine learning (ML) from past normal operating data. The disturbances for *DSH*, which is an index for heating, is removed in the same way as above, and *ΔDSH* is calculated as an index of the changes in only the refrigerant charge amount.

To create the *RLI* prediction model for the chillers and the *RLI* and the *DSH* prediction models for the VRFs, ML methods were used according to the characteristics of the respective training data. The specific ML methods and training data acquisition methods for each prediction model are described in the next section.

2.4 How to obtain training data for VRFs and create prediction models

Since VRFs have enough operating data stored in the data centre, it is possible to create an *RLI* prediction model for normal conditions using these as training data. However, the stored data contain both normal data and anomalous data. Normal data means that all functions are normal, and the refrigerant charge amount is appropriate. Anomalous data may be due to malfunctioning components or sensors, or insufficient or excessive refrigerant charge amount.

Therefore, in the process of data cleaning, only normal data were extracted from the stored data as training data for the creation of *RLI* prediction models. The extraction was carried out in the following two stages.

First, the data of equipment without failure records and equipment with completed failure repairs were extracted.

Next, the mean value of *RLI*, an index of refrigerant charge amount, was then calculated for each extracted equipment. The relative frequency distribution of these values is close to the black line of normal distribution curve shown in Fig. 3; the *RLI* value, in other words, the refrigerant charge amount, vary within the range not to be regarded as a failure shown in Fig. 3. This variation is caused by the refrigerant charging process during installation and the refrigerant recovery and recharging process before and after component replacement.

The equipment with a value near the centre of the distribution curve (the red area in the figure) is the equipment charged with the appropriate amount of refrigerant, and its operating data is determined to be available for training.

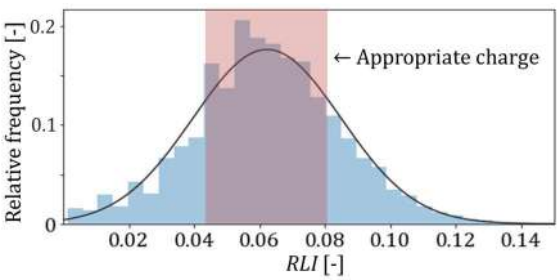

Fig. 3 – Distribution of *RLI*

Using the training data extracted in this way, a prediction model of normal *RLI* was created by LightGBM [7]. The explanatory variables used in the model were outdoor temperature, compressor speed, compressor current, and opening of the expansion valve for subcooling heat exchanger control ("EV2" in Fig. 2). For the training data, data obtained from several different units of the same type were used, instead of using only the data of the target VRF system itself. This is for reducing the operating cost. Therefore, the prediction model will be a common model for that type. The normal *DSH* prediction model for heating was also created in the same way: the explanatory variables in the case of the *DSH* prediction model were outdoor temperature, compressor speed, total capacity of indoor unit in operation and opening of the expansion valve for subcooling heat exchanger control.

The leaks found in the first process and the data during the failure period were labelled according to the failure and used as the anomaly data for the validation of leakage detection accuracy.

2.5 How to obtain training data for chillers and create prediction models

The prediction model for the chiller was created in a different way from that for the VRF. For chillers, the stored data could not be used as training data because there was almost no data of models equipped with a temperature sensor to measure the condenser outlet temperature used for *RLI* calculation. Therefore, a chiller equipped with a sensor for measuring the condenser outlet temperature was installed in a climate chamber, and tests were carried out under various conditions simulating actual operating conditions to obtain training data.

The four test conditions to be varied were outdoor temperature, compressor load ratio, leaving water temperature (*LWT*) and refrigerant charge amount as leak condition. For each condition, the range of variation and the test points within that range were investigated.

If the conditions are set to cover the entire variation range of all parameters uniformly, the number of test man-hours will be huge. Therefore, to create an accurate prediction model while reducing the number of test man-hours, the test conditions were chosen from the frequently occurring operating conditions from the on-site data stored in the data centre.

First, the variation range of the outdoor temperature was set to be between 5 and 35°C, taking into account the European climate. The compressor load ratio was set to vary between 33% and 100%, in line with the specifications of the chiller to be tested. The frequency distributions of the outdoor temperature and the compressor load ratio in the chiller in operation on-site are shown in Fig. 4.

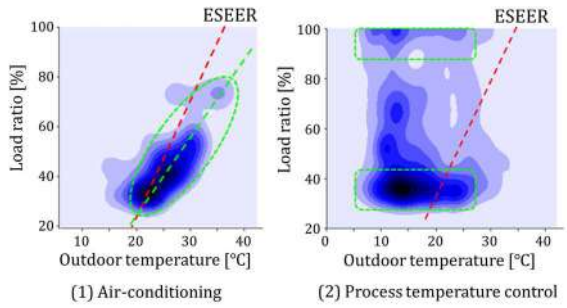

Fig. 4 – Distribution of the combination of outdoor temperature and compressor load ratio

Fig. 4(1) shows the distribution for the air-conditioning application. It shows a similar trend to the ESEER condition which the load ratio is proportional to the outdoor temperature. The centre of the distribution is slightly lower than that of the ESEER condition, which is thought to be due to the larger installed capacity compared to the actual load.

Fig. 4(2) shows the distribution for the process temperature control application in the factory, which is quite different from the distribution for the air-conditioning application: it operates more frequently around the maximum and minimum loads, regardless of the outdoor temperature.

Considering both characteristics, the combinations of test conditions set within the variation range of outdoor temperature and compressor load ratio are shown in Fig. 5. In the 27 conditions set, priority is given to the ESEER condition and the area below the ESEER condition (1), which has a high frequency of occurrence in air-conditioning applications, and to the area (2), which has a high frequency of occurrence in process temperature control applications.

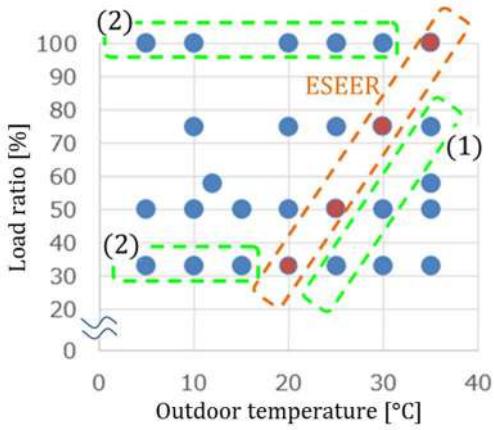

Fig. 5 – Combination of outdoor temperature and compressor load ratio set for the test

The relative frequency distribution of the stored *LWT* data is shown in Fig. 6. It is generally distributed in the range of 2 to 20°C because it is adjusted according to the application and load ratio. The four conditions of 5, 7, 11 and 13°C were chosen to focus on the areas with the highest frequency of occurrence.

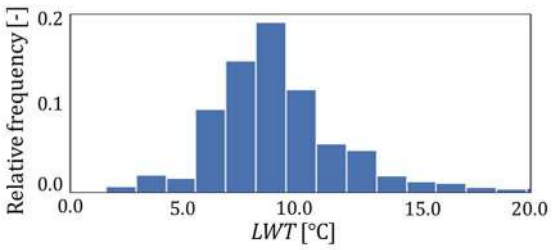

Fig. 6 – Distribution of leaving water temperature

The data obtained from the tests carried out based on the above test conditions were used as training data, and a normal *RLI* prediction model was developed using random forest regression. The six explanatory variables used in the prediction are outdoor temperature, compressor load ratio, *LWT*, main expansion valve opening ("main" in Fig. 7), economizer expansion valve opening ("ec" in Fig. 7) and compressor current.

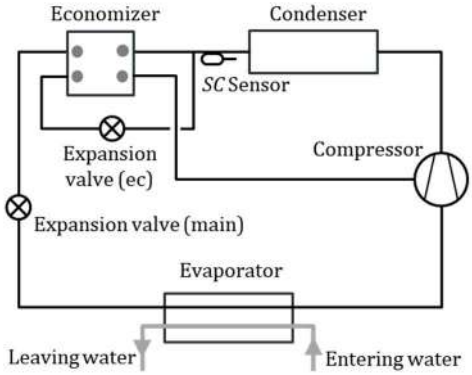

Fig. 7 – Piping diagram of the tested chiller

The training data for the prediction model are randomly selected from 70% of the data with 100% refrigerant charge amount. The remaining data with 100% refrigerant charge amount and the data with 120, 90, 85 and 80% refrigerant charge amount were used as the test data for the validation of leakage detection accuracy.

2.6 Automatic leakage detection logic

The automatic leakage detection logic outputs judgement results of leakage based on the decrease in *ΔRLI*. Fig. 8 shows an overview of the logic for the automatic judgement of refrigerant leakage based on the changes in *ΔRLI* time series data.

The detection logic consists of a moving window with *N* terms, a planar mapping section, an anomaly calculation section and a judgement section. The planar mapping section maps the points whose coordinates are two adjacent points *ΔRLI*(*t*-1) and *ΔRLI*(*t*) onto the plane whose axes are *ΔRLI*(*t*-1) and *ΔRLI*(*t*) at any given time.

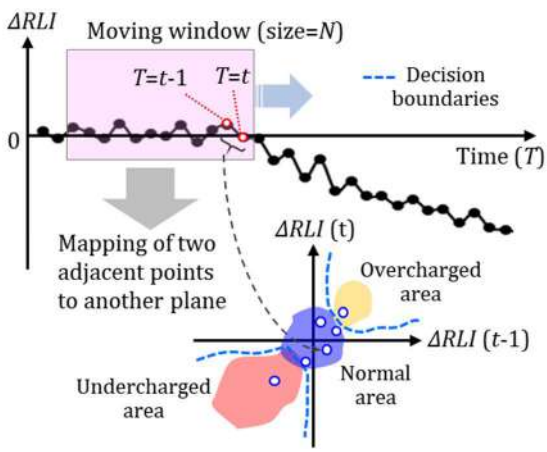

Fig. 8 – Overview of the automatic leakage detection logic

The mapping plane is pre-classified into normal, undercharged, and overcharged areas based on the decision boundaries plotted by machine learning. The undercharged area is in the third quadrant and the overcharged area is in the first quadrant. The anomaly calculation section calculates the anomaly score defined by the following equation (1) when the N-1 points created from the N data in the moving window have been mapped to another plane.

$$Anormaly\ score = \frac{Number\ of\ points\ in\ undercharged\ region}{N-1} \quad (1)$$

The anomaly score is the ratio of the number of N-1 points mapped from the moving window to the number of points mapped in the undercharged area. When this value exceeds a certain threshold, it is judged that there is a leak. If the distribution of points is mapped in the undercharged area from the beginning of operation, it is judged to be undercharged initially. If the distribution of points is mapped in the overcharged area from the beginning of operation, it is judged to be overcharged initially.

In the case of heating, the leakage index is ΔDSH, which increases opposite to ΔRLI during leakage, thus the undercharged area is distributed on the first quadrant.

3. Results and discussion

3.1 VRF data validation results

The responses of *ΔRLI* and *ΔDSH* in VRF equipment were evaluated. Fig. 9 shows the examples during cooling operation; the upper plot for normal equipment and the lower plot for equipment where 15% of the refrigerant charge amount was recovered during operation to simulate a leak.

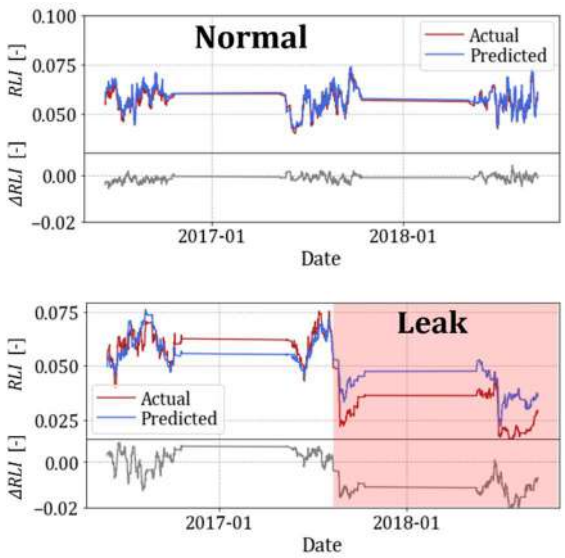

Fig. 9 – *RLI* and *ΔRLI* responses to normal and leak data during cooling operation

Fig. 10 shows the examples during heating operation, the upper plot for normal equipment and the lower plot for leaking equipment. In both Fig. 9 and 10, the red line represents the actual *RLI* and *DSH* calculated directly from the operating data, the blue line represents the *RLI* and *DSH* predicted by the normal prediction model and the grey line at the bottom represents their differences *ΔRLI* and *ΔDSH*, the red areas labelled "Leak" are the period during which the detection logic judged as a leak.

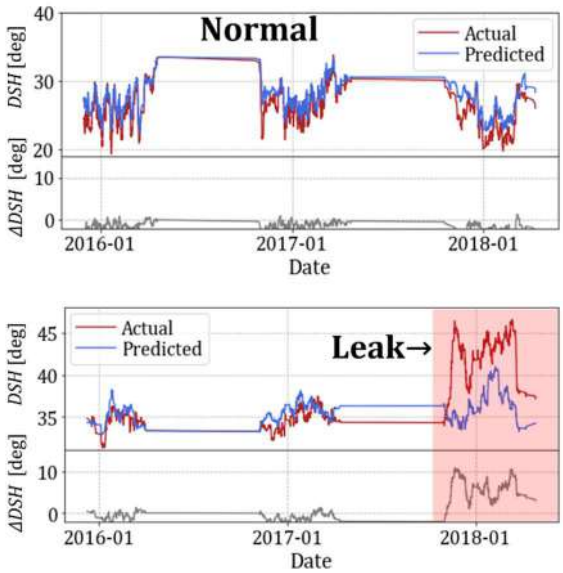

Fig. 10 – *DSH* and *ΔDSH* responses to normal and leak data during heating operation

In normal equipment, the actual values for both cooling and heating are close to the predicted values and the differences, *ΔRLI* and *ΔDSH* are almost 0. On the other hand, during the period when the refrigerant charge decreases in leaking equipment, the actual values for both cooling and heating differ significantly from the predicted values. Thus, the *ΔRLI* and *ΔDSH* values are sufficient for the automatic detection logic to detect the leak correctly.

Next, the leakage detection was carried out for several test data obtained from the stored data and the accuracy of the detection was evaluated from the confusion matrix of the detection results. The confusion matrix is a combination of the correct and incorrect judgment results for the actual equipment state (normal or leaking), and its definition is given in Tab. 1. The judgment performance was evaluated by two indices, accuracy and false discovery rate (*FDR*), as shown below.

$$Accuracy = \frac{TP + TN}{TP + TN + FP + FN} \quad (2)$$

$$False\ discovery\ rate\ (FDR) = \frac{FP}{TP + FP} \quad (3)$$

The accuracy is the ratio of correct predictions among the total number of test cases. The *FDR* is the proportion of normal equipment misclassified as leaks among the equipment classified as leaks.

Tab. 1 - Definition of confusion matrix

		Predicted	
		Normal	Leak
Actual	Normal	TN (True Negative)	FP (False Positive)
	Leak	FN (False Negative)	TP (True Positive)

When assuming the actual operation of a refrigerant leakage detection system, it is important to keep the *FDR* as low as possible. This is because misjudgement of normal equipment as leaking equipment not only increases operating costs due to the unnecessary dispatch of service personnel, but also leads to a loss of user confidence in the detection system. Considering these factors, the target accuracy and *FDR* of the current fault diagnosis by remote monitoring is set to be 80% or higher and 10% or lower, respectively. The detection sensitivity of the automatic leakage detection logic was adjusted to meet the above indices.

Tab. 2 - Confusion matrix of leakage detection evaluation results during cooling

Cooling		Predicted	
		Normal	Leak
Actual	Normal	93.7% (119)	6.3% (8)
	Leak	14.9% (7)	85.1% (40)

Tab. 3 - Confusion matrix of leakage detection evaluation results during heating

Heating		Predicted	
		Normal	Leak
Actual	Normal	98.8% (82)	1.2% (1)
	Leak	21.5% (6)	78.5% (22)

Tab. 2 and Tab. 3 show the confusion matrices for cooling and heating, respectively, that were calculated after adjusting the detection sensitivity. Each element of the confusion matrix in the table shows the incidence rate of normal and leakage detection against the actual number of normal and leak equipment. The number in () is the number of detections.

Equations (2) and (3) were used to obtain the accuracy and the *FDR* from the confusion matrices for cooling and heating, respectively. The accuracy of 80% or higher and the *FDR* of 10% or lower were achieved in both cooling and heating. The incidence rates in the tables were used for the calculations. The reason is that if there is a large difference between the number of normal equipment and the number of leaking equipment, the judgment result is affected by it. By using the incidence rates, this effect can be eliminated.

Tab. 4 – Accuracy and *FDR* in cooling and heating operation

Operation mode	Cooling	Heating
Accuracy	89.4%	88.7%
FDR	6.9%	1.5%

Finally, the sensitivity of leakage detection was evaluated by obtaining estimates of the leakage amount at the time when the automatic detection logic judged a leak for true positive (TP) equipment. In this paper, the definition of refrigerant leak rate is the ratio of leaked refrigerant amount to the initial charge amount, as commonly used in refrigerant regulations. To estimate the leakage amount at the time of the detection, the conversion coefficient of the changed refrigerant charge amount (% of total refrigerant amount) and *RLI* and *DSH* were determined first. To do this, the data of equipment for which the leakage amount could be identified from the repair records and equipment with intentionally adjusted refrigerant charge amount were used. The leakage amount at the time of the leak detection was calculated by multiplying the change in *RLI* and *DSH* by the conversion coefficient. The relative frequency distribution of the estimated leakage amounts obtained for all the true positive (TP) equipment is shown in Fig. 11. The distribution can be approximated by a normal distribution, and assuming that the mean value of the distribution is defined as the mean detection sensitivity, it was 12.3% for cooling and 13.9% for heating. Assuming a normal distribution as shown by the dotted line in Fig. 11, the worst detection sensitivity is defined as the value of μ+3σ, which is determined from the mean value μ and variance σ, and is estimated to be 19.3% for cooling and 20.3% for heating. Since the current detection logic for VRF has a detection sensitivity of more than 50%, this method improves the detection sensitivity by 30% over the conventional method.

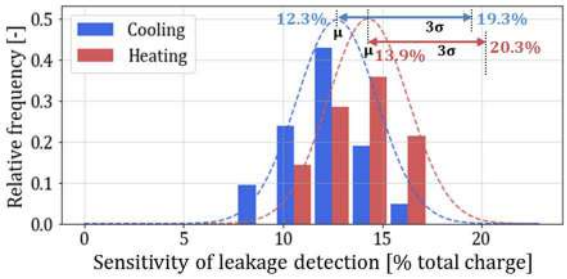

Fig. 11 – Sensitivity of leakage detection in cooling and heating operation

3.2 Chiller data validation results

ΔRLI was calculated using the *RLI* prediction model created with the training normal data obtained in the test chamber, and the responses of *ΔRLI* to normal and leak data were evaluated. Fig.12 shows the examples of measured *RLI,* predicted *RLI* and *ΔRLI*

responses to test data containing normal and leak cases. The test data was taken recovering the refrigerant from 100% to 80% in charge amount. The *ΔRLI*, which was zero at the start of the test, decreases as the refrigerant charge decreases, and the automatic leakage detection logic judges the refrigerant to be leaking around the middle of the transition from 100% to 80%.

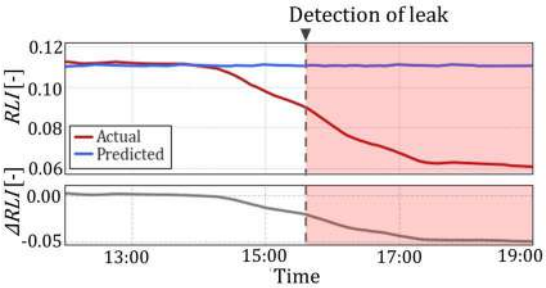

Fig. 12 – Response of *RLI* and *ΔRLI* to changes in refrigerant charge amount

Tab. 5 shows a confusion matrix of the results obtained by performing the same evaluation as above on test data for various operating conditions varying outdoor temperature, compressor load ratio, *LWT* and refrigerant charge amount. The breakdown of test conditions is 56 conditions of normal data with 100% refrigerant charge amount, and 52 conditions of leak data with 85% and 80% refrigerant charge amount. 86.5% of the accuracy and 0% of the *FDR* are calculated by the same method as VRF. However, all normal data are judged as normal, but 14 out of 52 leak data are judged as normal, which means that 26.9% of leak cases are overlooked. This is the reason why the accuracy is lower.

Tab. 5 - Confusion matrix of leakage detection results

		Predicted	
		Normal	Leak
Actual	Normal	56	0
	Leak	14	38

It was found that 12 out of 14 conditions where the leak was misjudged as normal had a compressor load ratio of 58% or less and a *LWT* of 10°C or more. Fig. 13 shows the correlation between refrigerant charge amount and *ΔRLI* when the outdoor temperature and *LWT* are fixed, and the compressor load ratio is varied. As the compressor load ratio decreases, the change in *ΔRLI* for the same change in refrigerant charge amount also decreases, thus reducing the detection sensitivity. Next, to confirm the effect of the *LWT* on the changes in *RLI* and *ΔRLI*, the occurrence rate of subcooling (*SC)* at different *LWT* was checked. Fig. 14 shows the relative frequency distribution of *SC* for 100% and 85% refrigerant charge amount under the conditions of 7°C and 13°C *LWT*. When the *LWT* is 7°C, the *SC* distributions for 100% and 85% of the refrigerant charge amount are separated by a boundary of *SC* =5, whereas when the *LWT* is 13°C, the *SC* distributions for each refrigerant charge overlap, making leakage detection difficult. Furthermore, the accuracy and the false negative rate (*FNR*), where a leak is overlooked and judged normal, were recalculated separately for cases with *LWT* below 10°C and the other above 10°C. As a result, the accuracy was 94.2% below 10°C and the *FNR* was 11.5%. On the contrary, for cases with *LWT* above 10°C, the accuracy was 78.8%, and the *FNR* was 42.3%.

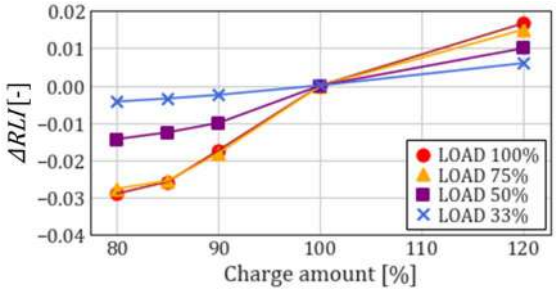

Fig. 13 – Effect of compressor load ratio on the correlation between refrigerant charge amount and *ΔRLI*

Thus, it was found that the chiller operated under the condition of low compressor load ratio and high *LWT* may increase the number of false judgments due to the decrease of leakage detection sensitivity. As a result of analysing the operating data of chillers in operation stored in the data centre, it was found that there are only a few chillers that are always operated at *LWT* of 10°C or higher. It was also found that even if the air-conditioning load decreases during the winter, the chiller operates at a high load and low *LWT* during start-up, so the chiller operates under conditions with high detection sensitivity at least once a day. Therefore, most of the chillers can be operated with this detection logic without any problems.

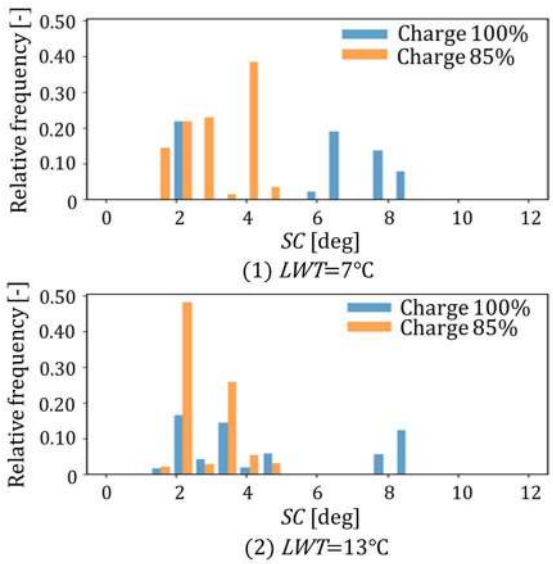

Fig. 14 – Effect of *LWT* on *SC* distribution for different refrigerant charge amount

3.3 Consideration of the limit of detection sensitivity by indirect method

To clarify the theoretical detection sensitivity limit and the feasible detection sensitivity of the indirect method of refrigerant leakage detection, a comparison was made between the simulation study and the results obtained in this study.

Wakui *et. al.* [3] evaluated the refrigerant leakage detection sensitivity of the VRF for several operating conditions using a steady-state refrigeration cycle simulator and a support vector machine classifier. They found that the leak from VRF becomes detectable under some conditions when the leakage amount exceeds 3% of the total charge amount, and when the leakage amount reaches 5%, the leak from VRF becomes detectable with a 100% positive response rate. Therefore, the worst value of the theoretical detection sensitivity characteristics ($\mu'+3\sigma'$) is assumed to be 5%.

On the other hand, as shown in Fig. 11, approximation of the estimated detection sensitivity of VRF during cooling proposed in this study using a normal distribution, the average sensitivity is 12.3% (μ) and the worst detection sensitivity ($\mu + 3\sigma$) is 19.3%. Fig. 15 shows a schematic diagram comparing these two leakage detection sensitivity distributions.

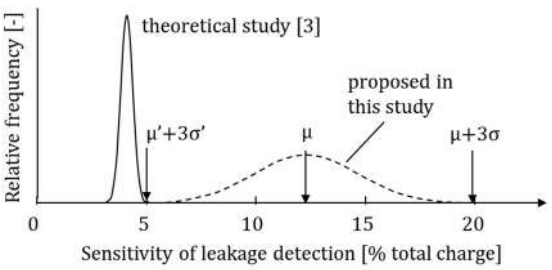

Fig. 15 – Comparison of theoretical and proposed sensitivity of leakage detection in VRF cooling mode

The detection sensitivity distribution by this method has a large variance compared to the theoretical detection sensitivity distribution by the simulation. This is because the machine learning model has not yet properly eliminated the disturbances that affect the detection sensitivity. As a result, when the decision threshold is adjusted so that the accuracy of the leakage detection is 80% or more and the *FDR* is 10% or less as the required level for operation, the detection sensitivity is significantly lower than the theoretical value. However, there is room to improve sensitivity by about 15% by improving the disturbance compensation.

There are two possible reasons for the lower disturbance compensation capability of the machine learning model used in this method compared to the simulation.

The first reason is that the simulation uses steady-state data with fixed compressor inlet pressure and superheat at the evaporator outlet and subcooling HEX outlet for both model training and leakage detection, whereas this method uses non-steady-state daily operating data for both. One possible countermeasure is to periodically set up operating conditions which are fixed to obtain steady-state operating data while VRF is in operation.

The second reason is that the simulation uses a dedicated prediction model for detection, which is created by learning the operating data of the target VRF system itself, while the present method uses a common prediction model as mentioned in chapter 2.4. If a dedicated model is used, sensitivity can be easily improved.

4. Conclusions

An indirect refrigerant leakage detection system based on machine learning was developed and its performance was validated on VRFs and chillers. The detection sensitivity was normally distributed according to the operating conditions and equipment characteristics and was able to detect leaks of 15% of the initial refrigerant charge amount on average and 20% at worst. There is room for improvement in accuracy by modifying the machine learning model and the training data. The next target is to improve the accuracy to detect 10% of leaks in the future.

5. References

[1] Yoshimi M., Yonemori T., Suko K., Yamaguchi T. Proc. The International Symposium on New Refrigerants and Environmental Technology 2010, (2010), pp. 169–172.

[2] Hosseini Gourabpasi A, Nik-Bakht M. Knowledge Discovery by Analyzing the State of the Art of Data-Driven Fault Detection and Diagnostics of Building HVAC. CivilEng. 2021;2(4):986-1008.

[3] Wakui T., Yokoyama R. Proc. of 2018 JSRAE Annual Conference, 2018; C222. (in Japanese)

[4] Yoshimi M., Hikawa T., Kasahara S. Proc. of 2019 JSRAE Annual Conference, 2019; C342. (in Japanese)

[5] Yamada S., Yoshimi M., Hikawa T., Kasahara S. Proc. of 2020 JSRAE Annual Conference, 2020; C323. (in Japanese)

[6] Yamada S., Kojiyama K., Yoshimi M., Kasahara S. Proc. of 2021 JSRAE Annual Conference, 2021; C312. (in Japanese)

[7] https://lightgbm.readthedocs.io/en/latest/

The datasets generated and analysed during the current study are not available due to commercial restrictions, but the authors will make every reasonable effort to publish them in near future.

Impact of Traditional Augmentation Methods on Window State Detection

Seunghyeon Wang[a], *Ivan Korolija*[a], *and Dimitrios Rovas*[a]

[a] Institute for Environmental Design and Engineering, University College London, London, UK,
E-mail: seung-hyun.wang@ucl.ac.uk, i.korolija@ucl.ac.uk, d.rovas@ucl.ac.uk.

Abstract. Window state information and changes can help understand ventilation patterns or be used as input in energy models. State identification can be achieved by capturing time-lapse images and processing these through a deep learning model. Deep learning methods have shown reliable performance in object detection tasks such as window and door detection, but have not been applied for window states detection. One of the challenges in setting up such models is to collect a large number of images of window states. In this case, image augmentation can be a critical pre-processing step to enhance the training dataset artificially. Image augmentation has been beneficial in similar contexts and applications. This paper investigates image augmentation methods, adjusting for brightness, scale, and weather. Windows images were used as the starting dataset to demonstrate the proposed methods, and augmented images were artificially generated from the original images. Using the expanded dataset, the Faster R-CNN (faster region-based convolutional neural network) trained a model to detect the binary window states. The augmented dataset model showed better performance than when the original dataset was used. The findings are a testament to the utility of image augmentation methods in the training model of window states detection using deep learning methods.

Keywords. Window states detection; Image augmentation methods; Deep learning
DOI: https://doi.org/10.34641/clima.2022.375

1. Introduction

In residential and non-residential buildings, indoor environments that meet high thermal and visual comfort standards are conducive to occupants' health and productivity. One way of controlling indoor environment parameters are manually openable windows. Operational patterns of each window, also called window states, can be very complex since they can be affected by many behavioural aspects driven by environmental or non-environmental factors (e.g. indoor conditions and personal characteristics) [1]. For example, when occupants feel uncomfortable with the indoor environment, windows may be partially opened, even during the cold season. On the other hand, other occupants may choose to fully close windows if they are sensitive to outside noise.

Knowing the window states and how they vary over time can be helpful in many applications. For example, window states are used as an influential input of energy, ventilation, and lighting simulations. There are two widely used methods for window state detection. One way is to monitor the windows' binary (open or closed) state through the magnetic contacts attached at the interface between the window frame and the wall. However, installing magnetic sensors' in large numbers requires high capital and installation cost, which diminishes the benefits from the available information [2]. Another approach to window state detection is to classify the window states after taking a picture of each building façade from places where window states can be recognisable accurately [3]. As photography can capture many windows simultaneously through a single camera, it is relatively inexpensive. However, time-lapse photography is limited when window states are recognisable using naked eyes, and such recordings can raise privacy concerns. For this reason, this method may be more appropriate in non-residential buildings such as offices and schools during occupied hours (generally 9 am to 5 pm) [4]. In addition, such manual classification of window states from images is time consuming and labour-intensive. In particular, this problem may become more serious when the sampling interval is short, and there are many windows on each façade.

Computer vision techniques can be introduced as an automatic method for analysing the images. While deep learning methods for computer vision have been proved in high generalisation ability to recognise different components such as window and door from building façade images [4], they have not been applied for window states detection yet. As

Copyright ©2022 by the authors. This conference paper is published under a CC-BY-4.0 license.

one of the data-driven methods, deep learning may have billons of parameters to be trained for high generalisation ability and requires a sufficiently large number of annotated datasets [5]. Curation of such large data sets for training the deep learning model can be time consuming and tedious. As an alternative, artificially expanding labelled training datasets from original data, known as image augmentation, could be introduced to address this data scarcity problem [6]. Image augmentation methods change the pixel values to produce artificial images based on original ones. However, computational time and generalisation ability may be increased and decreased, respectively if unrelated augmented data is trained. For this reason, appropriate augmentation methods based on a possible scenario in a real site needs to be applied. However, in previous studies, the data augmentation methods for window states detection have not been investigated yet.

Two image augmentation methods are often used in practice: traditional and elastic. Traditional methods involve various techniques such as rotation, flipping and brightness adjustment and take advantage of simple operations. While they are easy to apply and have low computational requirements [7], they often result in limited variation of the augmented images with regular change of pixel. On the other hand, elastic methods such as Generative Adversarial Network (GAN) generate artificial images using deep learning approaches. They make more substantial inconstant and irregular changes to the original image, but require significant computational resources and the augmented images that can be generated are limited by the available real data [8]. Although there is no doubt that both approaches may be useful for the augmentation of training data, traditional augmentation is considered in this research as a research scope.

In this paper, we propose image augmentation methods for improving the accuracy of the window states detection model based on deep learning. The developed model can detect the hinged and sliding window and its states with binary level (open, closed). The development of model with this binary level is still meaningful since existing automated research for sliding window states detection [9] manually performs localization of window and an automated method for hinged window states with reliable accuracy are not developed yet. Furthermore, given existing studies have still used a magnetic sensor and manual photographic method for 2-discretization level [10], binary window states detection can be utilized practically. To demonstrate the proposed methods, different datasets, which are original and augmented datasets, are created, respectively. Finally, the models with or without proposed augmentation methods are implemented and compared.

2. Image augmentation methods

As influential augmentation methods for window states in this research, the following traditional augmentation techniques: brightness, scale, and weather augmentation are selected. This chapter describes the reasons for selecting these methods with its predicted effectiveness.

2.1 Brightness augmentation

Since it is challenging to distinguish window states for dark lighting conditions, images with enough brightness should be collected. The brightness of each image can be ambient and different for reasons such as time of day and weather when picture of building facades from outdoor environment is taken. In general, images taken on a sunny day are likely to have a relatively higher intensity than those taken on a rainy day. Thus, various images with different lighting conditions are collected in real site. To effectively collect the dataset on this variation of the irregular lighting distribution, brightness augmentation can be applied. This one can artificially change original images into either brighter or darker by increasing or decreasing pixel intensity in original images [11], which is shown in equation 1:

$$I'(x) = I(x) + J(x); \tag{1}$$

where $I'(x)$ and $I(x)$ mean the augmented image that brightness is changed, and original image, respectively; $J(x)$ denotes a matrix having the brightness adjustment factor, which is a same matrix size as $I(x)$. By adding or subtracting $J(x)$ to current intensity of each pixel in original image $I(x)$, the augmented images with different lighting condition are generated. The acceptable intent of changed pixel by the brightness adjustment should be enough for recognition of window states. For example, suppose images of a sunny day with high illumination are collected mostly in whole dataset. In that case, dark day with low illumination is needed to be augmented by decreasing the pixel intensity with appropriate adjustment. However, if the pixel intensity of such a sunny day is highly increased, the visual information for recognising window states may be insufficient.

2.2 Scale augmentation

Various buildings have windows of different sizes. In addition, distance between building façade and photographic vantage point could be different due to visual obstacles such as cars and trees, even though similar buildings are recorded. By this reason, scale variation of building façade images is caused. To address this issue, scale augmentation, which is an affine transformation, can be utilised. The application process of scale augmentation is to first take an image and change its size along the coordinate axis relative to the original one. An

operation of this augmentation can be defined as followed in equation 2:

$$\begin{pmatrix} x' \\ y' \end{pmatrix} = \begin{pmatrix} S_x & 0 \\ 0 & S_y \end{pmatrix} * \begin{pmatrix} x \\ y \end{pmatrix} \quad (2)$$

where x' and y' denote the resized coordinates of x and y in a new image, respectively and, S_x and S_y are scaling factors for determining how much coordinates of original image are scaled by entering scaling factors into the matrix. And x and y denote the coordinates of the original image, respectively. Scaled images are newly generated by multiplying x and y by the scaling factors. Images are enlarged or reduced when scaling factors are more or less than 1, respectively. Moreover, the values of directions should be carefully adjusted. Too zoomed in or out images that unlikely to happen in real world observations should be not generated.

2.3 Weather augmentation

The window states detection model can be used for the investigation of different weather effects on window states. It may be possible for different weather such as sunny, cloudy, and rainy days except for the unrecognisable cases where visual information for identification of window states disappears (e.g., heavy fog and torrential rain). Therefore, weather-influenced scenarios should be considered to develop a model robust to variable weather conditions. However, collecting weather data can take a long time. Specifically, rainy days are not frequent in some countries, making assembling these images more difficult. Weather augmentation can help address this problem. The following simple operation, which is called an image blending technique, for making weather-related images can be formally written in equation 3:

$$g(x) = (1 - \alpha) * f_1(x) + \alpha * f_2(x) \quad (3)$$

With $g(x)$ an artificially weather-influenced image, $f_1(x)$ the original clear image, and $f_2(x)$ an image including weather information. Here a is a linear weighting factor. To obtain the image $g(x)$, transferring each source pixel's intensity value related to weather in the image $f_2(x)$ into a pixel position in the clear image $f_1(x)$. For weather image $f_2(x)$, according to the included information in pixels, different weather is represented. For example, a rainy image can be made with the following steps: Gaussian noise following gaussian distribution is created over a binary image, representing black (0) or white colour (1). And the motion blur filter that travels in a single direction horizontally is applied to the created binary image. This filter $h(x, y)$ can be in the form of equation (4) [12]:

$$h(x,y) = \begin{cases} \frac{1}{L}, if \sqrt{x^2 + y^2 \leq L/2}, y/x = \tan\theta \\ 0\,, otherwise \end{cases} \quad (4)$$

Two parameters govern the motion blur filter: length L and angle θ. Length affects the perceived distance that the pixels are moved from their original positions so that a more significant length value will result in more blurring. Angle describes the actual angle of the movement. A setting of $\alpha = 90^o$ will produce a vertical blur, and a setting of $\alpha = 0^o$ will produce a horizontal blur. Like other techniques, ranges of parameters should be properly adjusted for being more realistic rainy image. In addition, too strong weather effects over images make window states unrecognisable with naked eyes.

3. Methodology

This research aims to demonstrate the effectiveness of traditional augmentation techniques (brightness, scale, and weather augmentation) on window states detection. Fig. 1 shows an overview of the experimental process for the demonstration. The augmented datasets are generated by independently applying each augmentation method to original training data. After that, the original and augmented datasets are prepared to train a Faster R-CNN model for detecting the window states on building façade images. Finally, the models based on Faster R-CNN with or without proposed data augmentation methods are compared. In this chapter, the experimental process is described in detail.

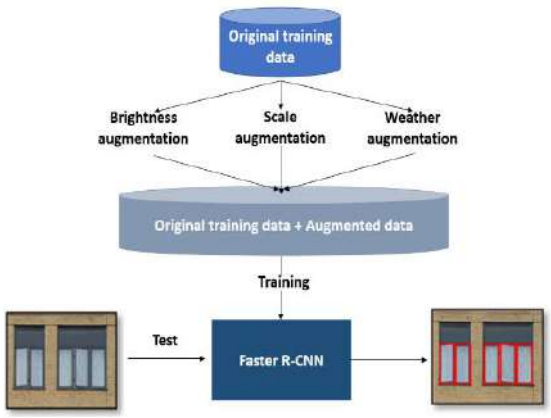

Fig. 1 – Experimental process using different augmentation techniques

3.1 Environmental settings

The simulations were performed on Windows 10 with an Intel Core i7-7700HQ CPU @ 2.80 GHz×8, an NVIDIA GeForce GTX 1080ti GPU and 32G RAM.

3.2 Dataset preparation

In this experiment, only non-residential buildings in the city of London, UK were captured as a case study. Various architectural designs including traditional (e.g. Victorian and Renaissance style)

and modern style (e.g. Sustainable and Postmodern architecture) were included in the dataset. Moreover, there exist different types of hinged and sliding windows including fixed window at the same time (e.g. awning, hopper window and, horizontal, and vertical sliding window). Concerning layout of window, while the most of windows are arranged as a symmetric structure, an unsymmetrical one was also contained. The detailed typology of building façade observed in this research can be downloaded here: (https://doi.org/10.5522/04/14993589)

The augmentation techniques may be ineffective for sample data collection if the collected dataset includes many variations enough for reliable accuracy. However, it is difficult to a priori define the required number of images. In this research, the used device for RGB camera was a smartphone with a polarising filter to reduce the veiling reflections. In total, 750 raw images of building façade with a resolution of 853×1440 pixels were collected, providing sufficient visual information for recognising the binary discretisation level. All images were taken during office hours (from 9am to 5pm) in the summer (from 21 April to 3 May). In addition, since photographs with different angles have severe angle variations, which can have an detrimental effect on the model accuracy [13]. For this reason, building facade images with the frontal view were collected as much as possible. In the case that tilted images were collected due to absence of photographic vantage points, they were rectified manually into frontal images, which is shown in Fig. 22. The manual rectification of building façade image is also time consuming and labour-intensive process.

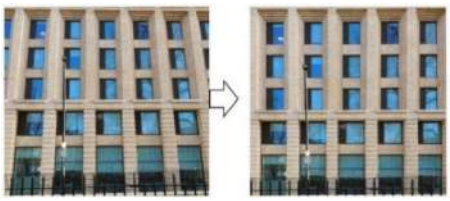

Fig. 2 - An example of rectified images (left: tilted images, right: rectified images)

After the rectification process, the collected whole images were randomly divided into the training (60%) and test (40%) set with 450 and 300 images respectively. Then, defined parameters, brightness, scale, and weather augmentation were applied to only training data. The used hyperparameters were selected after a trial-and-error process ensuring whether images were realistic or not. Created dataset with ranges of parameters is shown in Tab. 11. Firstly, for brightness parameters, pixel intensity between -30 and 30 randomly was added to the pixel intensity of original images. In scale augmentation, original images were randomly scaled up or down to a value of 80% to 120% in x and y-coordinates of their original size. This was performed independently per axis since there can exist a variety of window sizes according to buildings. In addition, the scaled-down images have void space. Since deep learning-based methods require fixed length vectors as input data, the augmented images should be the same size. Therefore, zero-value pixels were padded on the void space in the reduced image when scale is less than 1. In the case of weather augmentation, when images are taken, original images included only rainy images so that among weather, rainy effect was considered. To achieve this, two parameters length L and angle θ, which range from 3 to 7 and 45 to 60 randomly, respectively were selected. Based on 450 original training images, respective augmented image dataset (450 images) from each augmentation method using the described parameters were generated. Examples of the original and each augmented image is shown in Fig. 33. For demonstrating the effectiveness of augmented datasets, five different datasets were prepared: one original training dataset, four augmented datasets (original training dataset with brightness, scale, weather augmentation, and a sum of all augmentation techniques.

Tab. 1 - Created dataset with ranges of parameters

Dataset	Ranges of parameters	Number of images
Original	-	450
Brightness	[-30, 30]	450
Scale	[0.8, 1.2]	450
Rainy	L = [3, 7], θ = [45, 60]	450
Total	-	1,800

The subsequent process is to annotate the window states with binary discretisation level. As a result, localisation of each window as bounding box and binary state of corresponding window as each bounding box's class, which is "background", "opened", or "closed" were annotated. LabelImg [14] was used for this annotation process of ground-truth labels, which generates XML files containing information on the class of each object and the corresponding bounding boxes. In addition, when openable windows are together with fixed window, fixed window needs to be regarded as background since it is not openable, which is always closed states. However, especially distinguishing fixed and hinged window is difficult in certain case. For this reason, fixed windows were annotated as closed window. In addition, to effectively label a lot of augmented images, the following method was applied. In the case of the two methods (brightness and weather), we used the same label information as that of original images because the bounding box position of objects in augmented images does not change. On the other hand, scale transformation is a method to augment images by changing aspect ratio of original images at 2D axis. Thus, the label information representing the bounding box position

of windows were adjusted in accordance with the scale change of corresponding images.

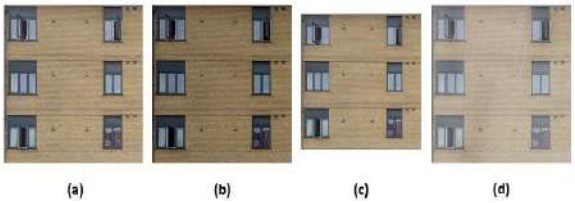

Fig. 3 - Examples of images: (a) original image, (b) brightness augmentation, (c) scale augmentation, (d) rainy augmentation

3.3 Faster R-CNN

To perform the binary window-state detection, window data with localisation and state information is required. To achieve this, object detection, which creates a bounding box for localisation and classification, can be applied. Faster R-CNN [15] has been widely used as an object detection method based on deep learning due to its high generalisation ability in computer vision tasks [16]. In particular, Faster R-CNN has shown reliable accuracy in window detection tasks [17], similar to window states detection. Therefore, Faster R-CNN was selected as a method for the object detection in this research. We used Detectron2 [18], which is a Facebook AI Research's next-generation software system for the implementation of Faster R-CNN.

3.3.1 Architecture

The Faster R-CNN model mainly comprises three components: (1) feature extractor, (2) RPN (Region Proposal Network), and (3) classifier and regressor. The feature extractor extracts features related to a task of window states detection from building façade images using CNN (Convolutional Neural Network). The function of RPN is to generate possible region proposals containing objects with a wide range of aspect ratios and scales using anchors. The classifier and regressor components compute the class probability of identified objects, and each such thing is localised.

The components of Faster R-CNN can have various architectures for specific tasks by modifying the original Faster R-CNN [15]. In deep learning, deeper architectures often have an advantage over shallow ones since the stacking of multiple layers can improve the representational capacity of model [19]. In this research, ResNet-101 was used as an architecture of feature extractor. One main reason is that deeper neural networks in deep learning have a limitation: with the network depth increasing, the accuracy becomes saturated and then degrades rapidly. This issue is called gradient vanishing. During training the model through backpropagation, the gradient of earlier layers is calculated by multiplying the gradients of later layers. When the gradient of later layers is less than one, the gradients in earlier layers close to almost zero. To overcome this problem, ResNet-101 preserves the information of prior layers by adding the output of the last layer to the next, thus allowing the network to remember the previous layer's information [20]. Faster R-CNN models with ResNet-101 developed for many tasks have shown a faster convergence early and a good trade-off relationship between the network speed and accuracy in many research [21]. For classifier, as an objective of this research is to detect binary classifications (open/closed) of window states, the number of output neurons in the last layer were modified into three neurons, including background class. The rest of the architectures including RPN and regressor followed the same original paper [15].

Meanwhile, generally training deep learning architecture, including ResNet-101, requires a lot of data and takes a long time to train a model from scratch. As an alternative, a pre-trained model can be utilised by using a model developed in advance. In other words, once trained using another dataset, the model can use the learned features to perform many other tasks. Moreover, its effectiveness can be more increased when different but more related data is pre-trained to target model tasks [22]. ImageNet [23], which was designed for the academic purpose of computer vision research, could be a pre-trained model. ImageNet is a large database of over 14 million images with many categories, including building façade images. Therefore, in this research, the feature extractor based on ResNet-101 was initialised using pre-training with ImageNet.

3.3.2 Hyperparameter settings

The training process aims to minimise the overall loss in Faster R-CNN. There are many tuneable hyperparameters (e.g. batch size, momentum, and epochs) for training the model. Since hyperparameters have a great impact on the model's performance, their combinations are carefully optimised through experiments. However, the main aim of this research is not to achieve reliable accuracy through careful optimisation but to demonstrate the impact of traditional augmentation techniques on window states detection. In this research, setting the hyper parameters were achieved by modifying the Detectron2 configuration. Expressly, the possible value for the batch size is limited by the available GPU memory. It was set to 2, considering the capabilities of the hardware system used. In the case of epochs, it can significantly affect our research question. Although the training time is shortened with fewer epochs, the original and augmented dataset may be less trained. Thus, 20,000 epochs were considered enough value for demonstrating the proposed method. All other configurations were kept as the default settings from Detectron2. Interested readers can refer to here [18] for detailed configurations.

Tab. 2 – Model performance with different training dataset

Rank	Training Dataset	Final training loss	AP: opened window	AP: closed window	mAP
5	Original images	0.21	0.875	0.905	0.89
3	Original + Brightness	0.19	0.91	0.94	0.925
4	Original + Scale	0.20	0.896	0.93	0.913
2	Original + Rainy	0.17	0.924	0.94	0.932
1	Original + All techniques	0.18	0.94	0.96	0.95

4. Results

To evaluate the performance of proposed augmentation techniques, the overall loss of training set, AP50 (Average Precision), and mAP (mean Average Precision), of test set were used as metrics. These metrics have been used generally in academia to measure object detection performance. Detailed descriptions of each metric can be found in the paper [24]. Tab 2. shows the experimental results. All models were trained enough until reaching the described training loss. A model using only original training data showed reliable accuracy with 0.89 in mAP to some extents. In addition, all augmentation methods improved the detection accuracy of Faster R-CNN. In independent applications of each augmentation method, while weather augmentation relatively more increased the model performance, brightness and scale augmentation relatively less increased one. The most effective method was using original images with brightness, scale, and weather augmentation simultaneously. Compared to only using the original dataset, the model performance in mAP of such method increased from 0.89 to 0.95. Fig. 4 shows the examples of visually detected results in the same scenes of testset using Faster R-CNN with original images (left) and images with all techniques (right). In Fig. 4 (the first row), both models detected all window states correctly with 100% accuracy. As shown from Fig. 4 (the second middle), only a model using all augmentation techniques had 100% accuracy, but the original model regarded opened window states as closed ones. Although a model with all augmentation techniques showed better accuracy than the original one, wrong results were still observed. In Fig. 4 (the third row), while both models incorrectly detected door parts as a closed window, a model using the augmented dataset was less frequently wrong. This result may be caused by one possible reason that images including such similar objects to windows are not included enough in the training dataset.

While augmentation techniques showed better accuracy than the original one, the extent of effectiveness for real applications of proposed

Fig. 4 - Comparison of the visual results using the models trained with different datasets: original images (left), images with all techniques (right)

methods may differ from the collected dataset on window states detection. In the case where a data distribution of train and test dataset in variations is bigger, the certain augmentation may be more effective. For example, weather augmentation may be not useful if the weather condition of application sites is constant (e.g., only summer or winter). Besides, a Faster R-CNN model with all augmentation techniques could achieve a good detection result in most complex scenarios included in an experimental dataset (e.g. intensive lighting conditions, different scales). However, a low generalisation ability was observed in one scenario where similar objects such as doors exist. For practical applications, the generated model may be used practically to investigate window states except for one scenario of similar objects. In addition, although incorrectly detected closed window will always be closed states and its implication on indoor environment might be negligible, the improvement of model in this scenario is required in the future research.

The proposed methods can be reproduced with the following guideline. Deep learning-based models typically are initialised with a random sampling approach before training the weights in trainable layers. For this reason, even with the exact same dataset, different and uncontrolled weight initialisation may yield different models with each performance. However, even if the exact same initialisation for the weights is applied, a lack of reproducibility may still be observed with many reasons such as software versions, implementation variations, and hardware differences.

5. Conclusion

This study described the impact of traditional augmentation techniques (brightness scale and rainy augmentation) on window states detection using deep learning. For demonstrating the proposed methods, window states detection with binary discretisation level was performed using Faster R-CNN. Building façade images (750 images) acquired by the RGB camera were spilt into two sets: a training set (450 images) and a test set (300 images). By applying each augmentation method to only train datasets, five datasets were prepared: the original dataset, and four augmented datasets with brightness, scale, rainy technique, and a combination of all methods. Each augmentation technique showed better accuracy than only using original images. The most effective augmentation method was simultaneously utilising original images with brightness, scale, and weather augmentation. It could improve the accuracy of detection in mAP by 95%, which was higher than a model accuracy of 89% when only the original dataset was used. The result shows that proposed augmentation techniques can be used for simply and quickly creating a large size dataset without much effort of collecting the data in the real sites.

Although the effectiveness of augmentation methods was demonstrated to window states detection, such ways may also be practical for other similar applications such as building age classification and window detection as potential applications. Furthermore, the generated model can be used as a pre-trained model for subsequent future research of window states detection. And, when the annotation of images of window states is required, the generated model can make pre-annotated boxes.

In this research, 95% accuracy was finally achieved through the used dataset and proposed method with defined hyperparameters. More datasets with careful optimisation should be performed to reach more reliable accuracy. As a limitation of this study, elastic augmentation methods such as techniques based on GAN are not considered. It may generate realistically visual information such as texture or colour for window states detection. Through such augmentation methods, further research is needed to demonstrate that window states detection models with more discretised levels (e.g., three or percentage states level).

6. References

[1] S. Wei, R. Buswell, D. Loveday, Factors affecting "end-of-day" window position in a non-air-conditioned office building, Energy Build.2013;62: 87-96. https://doi.org/10.1016/j.enbuild.2013.02.060.

[2] S. Gilani, W. O'Brien, Review of current methods, opportunities, and challenges for in-situ monitoring to support occupant modelling in office spaces, J. Build. Perform. Simul.2017;10:444–470. https://doi.org/10.1080/19401493.2016.1255258.

[3] A. Wagner, W. O'Brien, B. Dong, Exploring occupant behavior in buildings: Methods and challenges, 2017. https://doi.org/10.1007/978-3-319-61464-9.

[4] H. Hu, L. Wang, M. Zhang, Y. Ding, Q. Zhu, Fast and Regularized Reconstruction of Building Fac Ades from Street-View Images Using Binary Integer Programming, in: ISPRS Ann. Photogramm. Remote Sens. Spat. Inf. Sci., 2020;365–371. https://doi.org/10.5194/ isprs-annals-V-2-2020-365-2020.

[5] C. Shorten, T.M. Khoshgoftaar, A survey on Image Data Augmentation for Deep Learning, J. Big Data. 2019;6. https://doi.org/10.1186/s40537-019-0197-0.

[6] E.D. Cubuk, B. Zoph, D. Mane, V. Vasudevan, Q. V. Le, Autoaugment: Learning augmentation strategies from data, in: Proc. IEEE Comput. Soc. Conf. Comput.

Vis. Pattern Recognit., 2019;113-123, https://doi.org/10.1109/CVPR.2019.00020.

[7] S.C. Wong, A. Gatt, V. Stamatescu, M.D. McDonnell, Understanding Data Augmentation for Classification: When to Warp?, in: 2016 Int. Conf. Digit. Image Comput. Tech. Appl. DICTA 2016, 2016;1-6 https://doi.org/ 10.1109/DICTA.2016.7797091.

[8] A. Mikołajczyk, M. Grochowski, Data augmentation for improving deep learning in image classification problem, in: 2018 Int. Interdiscip. PhD Work. IIPhDW 2018, 2018;117-122. https://doi.org/10.1109/IIPHDW.2018.8388338.

[9] H. Zheng, F. Li, H. Cai, K. Zhang, Non-intrusive measurement method for the window opening behavior, Energy Build. 2019;197:171–176. https://doi.org/10.1016/j.enbuild.2019.05.052.

[10] H.B. Gunay, W. O'Brien, I. Beausoleil-Morrison, A critical review of observation studies, modeling, and simulation of adaptive occupant behaviors in offices, Build. Environ. 2013;70:31–47. https://doi.org/10.1016/j.buildenv.2013.07.020.

[11] Q. Zheng, M. Yang, X. Tian, N. Jiang, D. Wang, A full stage data augmentation method in deep convolutional neural network for natural image classification, Discret. Dyn. Nat. Soc. 2020. https://doi.org/10.1155/2020/4706576.

[12] S. Jana, Y. Tian, K. Pei, B. Ray, DeepTest: Automated testing of deep-neural-network-driven autonomous cars, in: Proc. - Int. Conf. Softw. Eng., 2018;303-314. https://doi.org/ 10.1145/3180155.3180220.

[13] M. Neuhausen, A. Martin, M. Obel, P. Mark, M. König, A cascaded classifier approach to window detection in facade images, in: ISARC 2017 - Proc. 34th Int. Symp. Autom. Robot. Constr., 2017;690-697. https://doi.org/10.22260/isarc2017/0096.

[14] Tzutalin, LabelImg, Git code (2015). https://github.com/tzutalin/labelImg

[15] S. Ren, K. He, R. Girshick, J. Sun, Faster R-CNN: Towards real-time object detection with region proposal networks, in: Adv. Neural Inf. Process. Syst., 2015;1:91-99

[16] J.C.P. Cheng, M. Wang, Automated detection of sewer pipe defects in closed-circuit television images using deep learning techniques, Autom. Constr. 2018;95:155-171 https://doi.org/ 10.1016/j.autcon. 2018.08.006.

[17] S. Hensel, S. Goebbels, M. Kada, FACADE RECONSTRUCTION for TEXTURED LOD2 CITYGML MODELS BASED on DEEP LEARNING and MIXED INTEGER LINEAR PROGRAMMING, in: ISPRS Ann. Photogramm. Remote Sens. Spat. Inf. Sci., 2019;37–44. https://doi.org/10.5194/isprs-annals-IV-2-W5-37-2019.

[18] Y. Wu, A. Kirillov, F. Massa, W.-Y. Lo, R. Girshick, Detectron2, (2019). https://Github.Com/Facebookresearch/Detectron2.

[19] D. Rolnick, M. Tegmark, The power of deeper networks for expressing natural functions, in: 6th Int. Conf. Learn. Represent. ICLR 2018 - Conf. Track Proc., 2018.

[20] K. He, X. Zhang, S. Ren, J. Sun, Deep residual learning for image recognition, in: Proc. IEEE Comput. Soc. Conf. Comput. Vis. Pattern Recognit., 2016. https://doi.org/10.1109/CVPR.2016.90.

[21] S. Srivastava, A.V. Divekar, C. Anilkumar, I. Naik, V. Kulkarni, V. Pattabiraman, Comparative analysis of deep learning image detection algorithms, J. Big Data. Volume 8, 66, (2021). https://doi.org/10.1186/s40537-021-00434-w.

[22] L. Torrey, J. Shavlik, Transfer learning, in: Handb. Res. Mach. Learn. Appl. Trends Algorithms, Methods, Tech., 2009;242-264 https://doi.org/10.4018/978-1-60566-766-9.ch011.

[23] A. Krizhevsky, I. Sutskever, G.E. Hinton, ImageNet classification with deep convolutional neural networks, Commun. ACM. 2017. https://doi.org/10.1145/3065386.

[24] P. Martinez, B. Barkokebas, F. Hamzeh, M. Al-Hussein, R. Ahmad, A vision-based approach for automatic progress tracking of floor paneling in offsite construction facilities, Autom. Constr. 2021;125.https://doi.org/10.1016/j.autcon.2021.103620

Data Statement

The datasets generated and analysed in the current study are available in the repository (https://doi.org/10.5522/04/14993589).

Fault detection in district heating substations: a cluster-based and an instance-based approach

Jad Al Koussa [a,b], *Sara Månsson* [a,b,c,d]

[a] Unit Energy Technology, VITO, Boeretang 200, BE-2400 MOL, Belgium, jad.alkoussa@vito.be

[b] EnergyVille, Thor Park 8310, BE-3600, Genk

[c] Department of Energy Sciences, Faculty of Engineering, Lund University, P.O. Box 118, SE-221 00 Lund

[d] current affiliation: Utilifeed, Stora Badhusgatan 18-20 - 411 21 Gothenburg – Sweden, sara@utilifeed.com

Abstract. In district heating or collective heating substations, components can fail or can be inappropriately installed or configured (e.g. valves get broken, heat exchangers get fouled, controller parameters are inappropriately chosen, heat exchanger wrongly connected, internal heating system problems, etc.). The result of these faults is a reduced cooling of the supply water, and as such higher than necessary return temperatures to the grid and higher volume flows (to deliver the same needed power) occur, leading to higher OPEX for all stakeholders. In this work, two approaches for a fault detection routine for district heating substations are introduced, based solely on the energy meter data, with an application on a real-life district heating network in Sweden. The first approach is a cluster-based approach in which substations within the district heating are compared to each other using the overflow method and performance signatures to flag substations with sub-optimal performance compared to other substations in the network. The second method is an instance-based approach using a black-box model to predict the behaviour of the substation using an extended set of input variables and comparing the predictions to the measurements. The results from the two fault detection approaches show that both the cluster-based and the instance-based methods can detect deviating behaviours in DH customer installations.

Keywords. Fault detection and diagnosis, District heating, District heating substations
DOI: https://doi.org/10.34641/clima.2022.45

1. Introduction

District heating (DH) is a collective heating system in which heat is produced in one (or multiple) locations to meet the heat demand, usually of multiple customers at other locations. The heat is transferred using water circulating in a pressurized piping system. The heat demand consists of Space Heating (SH) demand as well as Domestic Hot Water (DHW) demand for sanitary purposes for residential and commercial buildings. A simplified illustration of a district heating system is shown in Fig. 1: the main components are the heat production where heat is produced, the heat distribution that transports the heat, the customer substation that transfers the heat from the heat distribution pipes to the internal heating system, and the internal heating system that consists of the SH and the DHW circuits.

Due to the inherent energy efficiency, heat source flexibility and the capability of utilizing residual heat, district heating has been identified by the European Union as an essential solution in future energy

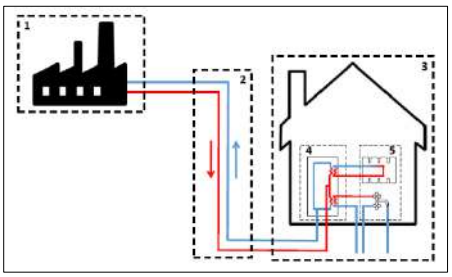

Fig. 1 - A simplified illustration of a district heating system, where 1 represents production, 2 represents distribution, 3 represents the customer installations, 4 represents the customer substation, and 5 represents the internal heating system.

systems to help decarbonizing Europe [1,2]. The district heating network can be supplied by a multitude of sources such as fossil fuel based boilers

Copyright ©2022 by the authors. This conference paper is published under a CC-BY-4.0 license.

as well as more sustainable sources such as excess heat from industrial processes and Combined Heat and Power plants (CHPs) based on biomass or waste incineration, geothermal heat and solar thermal heat [1]. Moreover, large-scale heat pumps can be used as a heat source providing the possibility to increase the flexibility of the energy system by integrating the heating and electricity sectors [3].

In existing DH systems, multiple components can perform sub-optimally leading to inefficiency in the operation of the system due to an increase in the system's temperatures. Customers' installations (component 3 in Fig-1) is one of the major components that can perform sub-optimally, causing increased return temperatures in the DH system and consequently either the flow or the supply temperature need to be increased to provide the needed heat [4,5]. The customer's installation consists of: 1) the substation, which is a combination of heat exchangers, valves, sensors, actuators, control and a heat meter, as well as 2) the SH and DHW system that contains a number of valves, radiators and heat exchanger. The issues, or faults, in the customer installations may occur in a number of different components and include faults and problems such as fouling of heat exchangers, broken temperature sensors, control valves stuck in an open position, temperature sensors placed on the wrong pipe, DHW circulation connected before the pre-heater, high return temperatures from the customer's internal heating system, and high set point values in the customer system [7-9]. All of these faults may not be seen as an actual fault where something is broken, but they still lead to high return temperatures.

Previous studies have shown that a large share of the substations in different DH systems are not performing well [6,7], indicating that substations have a large impact on the DH system's temperature and its efficiency. With the district heating utilites aiming at decreasing their system's temperatures to increase their efficiency and integrate low temperature renewable heat sources, and the emergence of the 4th generation district heating networks, it becomes increasingly important that faulty installations are detected and corrected. Traditionally, the poorly performing installations have been detected using manual analysis methods [10]. However, given the large number of substations that might be present in a DH network, the manual approach can be very time consuming and costly. For this reason, there is a need for more automated methods to help in the fault detection process.

In this paper, two methods to detect sub-optimally performing substations are presented: the first approach is a cluster-based approach in which substations are compared to each other based on their historical data and the second approach is an instance-based approach in which a substation is modelled using a black box and a deviation is detected by comparing the outcome of the model to the field measurements. In what follows, a review of exisiting methods for Fault Detection is presented followed by the explanation of the implemented methods and after that the results are presented. The paper finishes by a discussion on the implemented methods followed by concluding remarks and the prospect of future work.

2. Fault detection in district heating substations

Fault detection and diagnosis (FDD) is a collection of methods to monitor a system's behaviour, to determine if a fault is present in the system, and to determine the characteristics and root cause of the detected fault(s) [11]. FDD is applied in a variety of domains for fault detection and predictive maintenance.

The application of fault detection on DH customer installations is gaining momentum in recent years. The European Energy Efficiency Directive which became effective in 2012 states that all energy customers should be billed according to their actual energy consumption[12]. In order to do that, energy meters need to be placed at the primary side of the customer's district heating substation. With this data being available, the utilities have the chance to perform analysis for different purposes, such as FDD. Literature regarding this topic shows that different types of data analysis methods are applicable for the detection of faults in DH substations. The literature includes aproaches based on cluster-based fault detection techniques as well as instance-based techniques. Sandin et al in [13] provided an overview of different statistical and probabilistic methods for fault detection in substations, such as linear regression modeling, limit checking, correlation analysis and outlier detection, and provided examples of their application on hourly based data. Gadd and Werner in [5] used the overflow method, a common method that compares the actual flow over a period of time to an ideal flow derived from an ideal value of the primary temperature difference. The authors also use temperature difference signatures to detect faults. In [14], Calikus et al. use heat power signatures and their degree of abnormality to rank individual buildings. Farouq et al. present in [15] a reference-group based approach for detecting customer installations that display a deviating behaviour. The reference groups were based on a k-nearest neighbour approach, utilizing the return temperatures from the investigated installations to identify the reference groups for each installation in the data set. If an installation deviates significantly from its reference group, it is considered faulty.

Machine learning (ML) and instance-based methods have also been explored in the literature. In [16], Ingvarsson et al. explored the possibilities to use models for fault detection and to track slow drifts in the substations' performance. The results show that the best suited model is a SARIMAX (0, 1, 1)x(0, 1, 1)24, for any combination of variables. In the project

RELaTED [18], two tools have been developed for automatic fault detection in DH substations based on ML algorithms: DH doctor and DH Autotune. The first one exploits clustering in which anomalies can be detected by measuring the distance among the clusters and following the evolution of the centroids related to a particular variable over time. The second tool is based on hourly averaged readings and allows the prediction of the load. Alarms are activated if some KPIs exceed a threshold. The work done by Guelpa et al. in [17] focused on the detection of fouling in district heating substations. An automatic method using the most commonly collected metering variables, such as volumetric flow and temperatures in the substation primary and secondary circuits, has been developed.

The literature shows that there is a variety of successfully implemented methods for fault detection. However, many of the presented methods require an amount of manual handling and/or interpretation. Some of the methods also require a certain amount of understanding for more advanced computer science and data handling methods. In this study, the aim is to show two simple methods that help eliminating a lot of manual stages in the data analysis, which can be used by the DH industry without the need for prior advanced knowledge in computer science and data handling.

In the next two sections, the two approaches are presented.

3. Cluster-based approach

3.1 data used

The data used in this study was gathered from the business system of a DH utility in Sweden between April 2015 and March 2016, and it includes data from the 3 000 installations that had the largest energy consumption in the system. The data set contained typical energy meter data, such as the accumulated energy consumption, the accumulated volume passing through the installation, the primary return temperature, and the primary supply temperature for each of the 3 000 installations. Moreover, the installation ID, the postal code of the installation, and the outdoor temperatures were collected.

3.2 Method

The cluster-based method compares substations within a group or a cluster of substations to find faulty or poorly performing substations. A schematic of this method is shown in Figure 2.

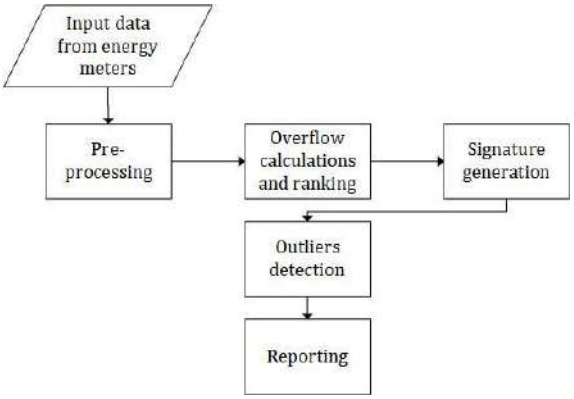

Fig. 2 – Schematic view of the cluster-based fault detection method.

First, a pre-processing and data handling is performed on the input data. During this step, the data is prepared and transformed into a suitable format for the data analysis step. Data processing may include several tasks, such as removal of duplicate values, feature extraction, and removal of outliers. In this first step, faults in sensors readings, communications and data logging can be detected. After that, data analysis is performed. Here, for each substation, an overflow value is calculated. The overflow represents the extra volume of water that passed on the primary side of the substation during a certain period compared to an ideal calculated volume. This ideal volume is calculated based on an ideal cooling value of the primary temperature. The overflow can be calculated using equation (1):

$$V_{overflow} = V_{actual} - V_{ideal} = V_{actual} - \frac{E_{actual}}{\rho . c_p . \Delta T_{ideal}} \text{ (m}^3\text{)} \quad (1)$$

Where

$V_{overflow}$ = overflow volume (m³)

V_{actual} = actual measured volume (m³)

V_{ideal} = ideal volume (m³)

E_{actual} = actual energy (J)

ρ = fluid density (kg/m³)

Cp = specific heat capacity (J/kg.K)

ΔT_{ideal} = ideal temperature difference between the primary supply and return (K)

The ΔT_{ideal} value varies depending on which DH system is being investigated. In this study, it was chosen to be 45 °C, in accordance with [3]. As equation (1) shows, the lower the primary ΔT, the higher the overflow. This is an indication that the customer's installation doesn't function optimally.

After the calculation of the overflow, a set of the substations with the lowest overflow values is picked and considered as the reference case: a representative set of the best performing substations. In this case, the top 25 % are considered for the reference case. Then, to determine from the remaining substations the poorly performing ones, three different criteria were used: the cooling performance, the return temperature level, and the energy consumed in the building. Two criteria were used to create two signatures: one cooling signature and one return temperature signature. The signatures consisted of a reference case and threshold values which were used for outlier detection. For each of the signatures, the reference case is determined by performing a piecewise linear regression on the reference substations chosen based on the overflow method. The mathematical relationship for a piecewise linear regression model with one breakpoint H is defined as follows [19]:

$$Y_i = \beta_0 + \beta_1 X_i + \beta_2 (X_i - H)\, I(X_i, H) + \varepsilon_i\,, \qquad (2)$$
$$where\ I(X_i, H) \begin{cases} 1, & X_i > H, \\ 0, & X_i \leq H. \end{cases}$$

In the equation, β_n, n = 0, 1, 2 are the parameters of the regression model, Y_i is the dependent variable being modelled, X_i is the independent variable which is used to model the dependent variable, and ε_i is the model error. In the cooling signature, the cooling of the substation was modelled as a function of the outdoor temperature. The breakpoint for the piecewise linear regression was determined by visually inspecting the data set.

Once the piecewise linear regression for the reference case is determined, the deviating, or outlier, values can be identified. The outliers were identified using the mean and the standard deviations of the reference case values. Values located at a distance larger than 3 standard deviations from the mean are considered as outliers [13]. For the cooling, piecewise linear regression was used to model the mean of the reference case and so the thresholds were also linear. For the return temperature signature, the mean was modelled using a constant value, resulting in constant thresholds.

3.3 Results

Figures 3 and 4 show the cooling and return temperature signatures with one well performing and one poorly performing customer installation visually represented. In both Figures, the well performing installation is represented by the blue circles, while the poorly performing installation is represented by the red circles. As may be seen in the figures, the well performing installation has all its values located *inside* the thresholds, while the poorly performing installation has the main share of the values located *outside* of the thresholds.

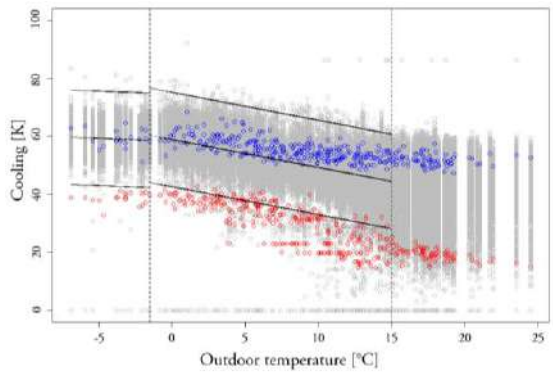

Fig. 3 – Cooling signature with one well performing (blue circles) and one poorly performing (red circles) installation represented.

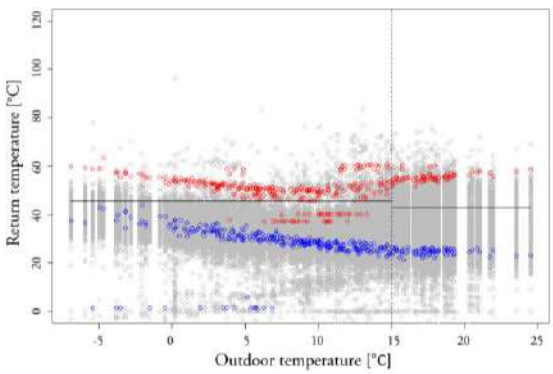

Fig. 4 – Return temperature signature with one well performing (blue circles) and one poorly performing (red circles) installation represented.

The developed fault detection approach identified 1 273 installations as being poorly performing, which corresponds to approximately 43 % of the investigated installations. Tab.1 presents the five installations that were identified as the substations that deviated the most from the expected behaviour.

Tab. 1 - The five substations with the highest overflows, and with outliers for both cooling and return temperature signatures.

Subs #	6	7	8	9	10
ID	X54	X93	X45	X41	X21
# of dT Outliers	277	277	169	201	277
# of Tr Outliers	366	366	316	363	366
$V_{overflow}$ (m³)	124 581	102 885	64 824	57 121	55 927

4. Instance-based approach

4.1 data used

The dataset used in this study consisted of hourly values for one year (November-November) from the energy meter of one DH substation in a DH system in Sweden. The variables, or features, that were included in the dataset are: substation ID, average hourly outdoor temperature, hourly measurements of heat power consumption, mass flow, supply and return temperatures, as well as the average value of the outdoor temperature during the previous 24 hours.

4.2 Method

In this method, a well-performing substation is modelled and then its performance is predicted based on subsequent input data. Any faults are then detected as deviations from the normal behaviour in the model predictions. The installation was selected from a data set of approximately 1 000 customer installations. First the overflows (Section 3.2) for all installations were calculated and then 10 installations with the lowest values of overflow were visually inspected to identify the best performing one.

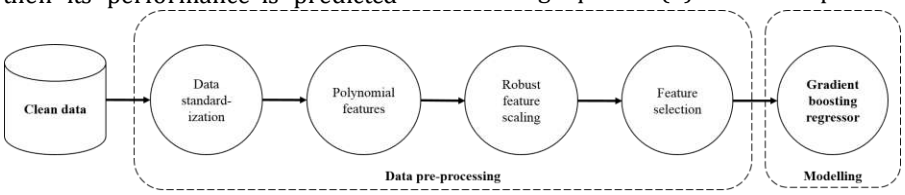

Fig. 5 – The TPOT pipeline used in the study

The fault detection method was developed in Python using the Tree-based Pipeline Optimization Tool (TPOT), an automated machine learning tool that creates combinations, or pipelines, of data transformations and machine learning models using genetic programming. This tool helps simplifying some of the requirements of ML methods regarding the data quality: the variables (or features) may have to be modified in some way, e.g., scaling or introduction of polynomial features, and a well-performing predictor must be chosen [20]. Given a set of data without missing or mislabelled values, the TPOT automatically optimizes feature selection, feature pre-processing, feature construction, model selection, and parameter optimization. The last step of the ML process, the model validation, is carried out by the user.

To choose the best TPOT pipeline to be used, 16 different training sets and 16 different test sets were used to produce 16 different pipelines. These pipelines were then introduced to the same training set, to evaluate which pipeline to further test and evaluate in the study. Training sets and tests set are subsets of the input data, with the ration training over test set equal to 80/20. To evaluate the performance of the TPOT pipeline, the coefficient of determination (R^2) and the Mean Absolute Error (MAE) were used. Equation (3) shows how R^2 is calculated. The closer R^2 is to one, the better is the performance of the model.

$$R^2 = 1 - \frac{SS_{res}}{SS_{tot}} \tag{3}$$

Where:

SS_{res} = the sum of squares of the residuals

SS_{tot} = the total sum of squares, which is proportional to the variance of the data

The mean absolute error, MAE, is the averaged sum of the absolute value of the residuals between actual values and predicted values, and can be calculated using equation (4). For a well performing model the MAE is expected to be as close to zero as possible.

$$MAE = \frac{1}{n}\sum_{i=1}^{n} |(actual\ value)_i - (predicted\ value)_i| \tag{4}$$

By investigating the values of MAE and R^2 the most accurate TPOT pipeline, shown in Figure 5, was chosen.

After choosing the TPOT pipeline, a choice of the parameter to be predicted using the substation model must be made. For that, different combinations of input/output variables were tested. The performance of the models was evaluated using the R2 and MAE values. The results are shown in Tab.2.

Tab. 2 - Parameter combinations that were tested with the model. Combination number 5, highlighted in grey, obtained the best R^2 and MAE value.

comb	Input	Output	R^2	MAE
1	T_{out}, T_r, T_s, t	$\dot{m}$	0.9703	0.1337
2	$T_{out,24}$, Tr, Ts, t	$\dot{m}$	0.9555	0.2027
3	T_{out}, T_s, t, $\dot{m}$	T_r	0.8839	1.1091
4	$T_{out,24}$, $\dot{m}$, T_s, t	T_r	0.8903	1.10348
5	$T_{out,24}$, T_s, t, T_{out}	$\dot{m}$	0.9740	0.1301
6	$T_{out,24}$, T_s, t, T_{out}	T_r	0.8841	1.0555

7	$T_{out,24}$, T_s, t, T_r, $\dot{m}$ T_{out}	0.9296	0.5857

To test the fault detection capability of the model, artificial faults were introduced to the data set. The model outputs for the faulty data sets were then compared to the outputs for the well-performing, original data set by calculating the hourly and accumulated residuals (rolling window of the previous 24 hours) between the model outputs and the actual measurements from the customer installation. By comparing these residuals to each other, it was possible to investigate whether the model performance changed when introduced to a data set containing faults.

Two faults were induced in the dataset. The first one represents a loss of communication between the energy meter and the database of the DH utility. To handle this type of fault, the utilities usually replace the missing values by a constant value. In this case, a value of 60 °C was chosen and inserted randomly in the data set for the supply temperature. Since this was an extremely low value compared to the original dataset, another fault was also induced where the original value of the supply temperature was decreased by 10 %. The second type of fault was induced as a gradual change in output over a time period, representing a drifting meter. This was done for the outdoor temperature sensor as well as the supply temperature sensor. These two faults are a common occurrence in DH metering data. In what follows only the results for a drifting meter will be presented.

4.3 Results

Figures 6 and 7 shows two different residual plots for two of the faults investigated in the study: the drifting outdoor temperature sensor (Figure 6) and the drifting supply temperature sensor (Figure 7). The residuals for the data sets containing a fault are represented by the red line in the figures. The blue line in both figures represents the residuals between the real and the predicted values for the data set that did not contain a fault.

Figure 6.a) shows the residuals between the real values and the values that were predicted by the model. Figure 6.b) shows the cumulative sum over a 24 h interval of the same residual values. As may be seen in Figure 6.a), the model prediction changes when this fault is present in the data set, but the deviation is not clearly distinguishable. The cumulative sum of residuals in Figure 6.b) displays a clear deviation approximately one month after the fault was induced in the data, indicating that this method may be well suited for automated detection of a drifting outdoor temperature meter.

Figure 7.a) shows the residuals between the real values and the values that were predicted by the model. Figure 7.b) shows the cumulative sum over a 24 h interval of the same residual values. As may be seen in Figure 7.a), the model prediction does not change significantly when this type of fault is present in the data set. This may also be seen in Figure 7.b).

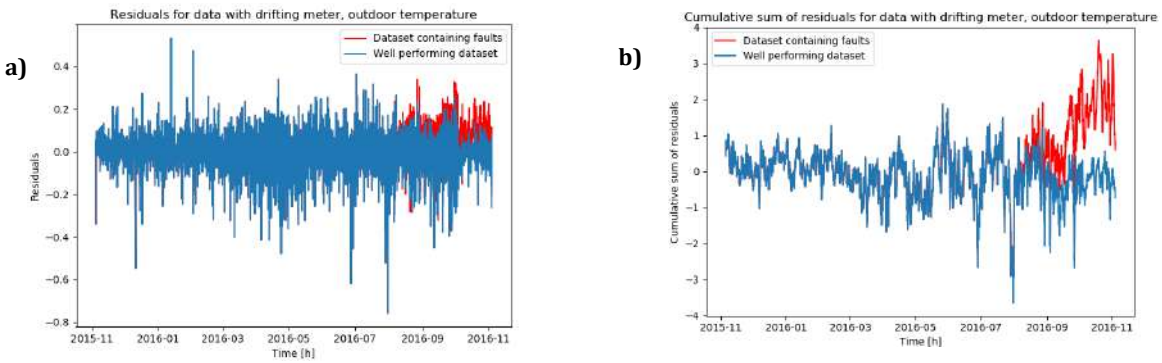

Fig. 6 – Analysis of the residuals between the real and the predicted values for the data set without a fault (blue line) and the data set with a drifting outdoor temperature meter (red line). **a)** Residuals between real and predicted values as a function of time. **b)** Cumulative sum of residuals as a funcion of time.

4. Discussions and conclusions

The results from the two fault detection approaches show that both can detect deviating behaviours in DH customer installations. The cluster-based method

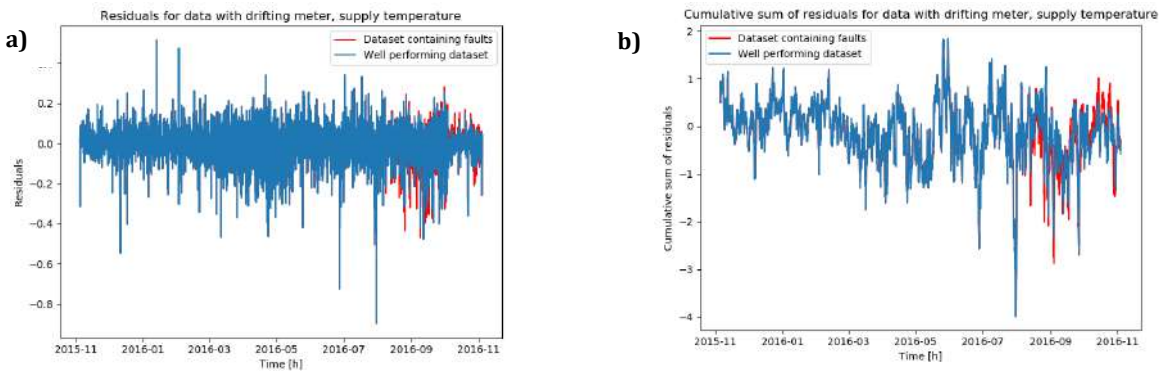

Fig. 7 – Analysis of the residuals between the real and the predicted values for the data set without a fault (blue line) and the data set with a drifting supply temperature meter (red line). **a)** Residuals between real and predicted values as a function of time. **b)** Cumulative sum of residuals as a function of time.

rapidly detects several installations that have a high overflow. Since a high overflow is an indication that the installation is not working as it should, this further implies that the cluster-based approach detects poorly performing installations.

For the instance-based approach, the model behaviour changes when a fault is present in the data, as may be seen in Figures 6 and 7. This indicates that the method can detect the deviations induced in the data set. However, when analysing the results, it can be concluded that different faults have different impacts on the model performance. This is especially clear for the two faults that are related to drifting meters. Although the fault is the same (a gradual increase of the meter readings over time), a drifting outdoor temperature sensor in the meter readings has a much larger impact on the model performance than when a drifting supply temperature sensor is present. This may be seen in Figures 6 and 7. In Figure 6.b), the drifting outdoor temperature sensor causes the cumulative sum of residuals for the data set known to contain a fault (red line) to deviate from the expected behaviour (blue line) soon after the fault has been induced in the data set. This shows that the model predictions have changed, thus indicating that a fault is present in the data set. When investigating the cumulative sum of residuals for the predictions of the drifting supply temperature sensor (Figure7.b)), it can be noticed that the deviation from the expected behaviour is not as large as for the data set in Figure 6. This indicates that the model used in the instance-based fault detection approach may not be able to detect *all* faults that are present in DH customer installations. However, this also indicates that the method may be suitable for fault diagnosis as it seems to be capable of distinguishing between different faults.

The two methods are based on two different fault detection approaches. The cluster-based approach is based on a reference case of several installations, to which the behaviour of each individual installations is compared. This means that the method can be generalized between different installations and different DH systems rather easily. The change that must be made when investigating a new DH system is to change the reference case that the fault detection signatures are based on. However, the generality of the method may be a problem since the current method does not differentiate between different types of customer installations which may have a wide variety of different behaviours in terms of heat use, e.g., if comparing a school building to a single-family household. One way to solve this problem is to introduce another, initial step in the fault detection method, right after the data validation step. In this step, the buildings would be divided into smaller groups or clusters, representing different types of buildings (in terms of heat use). The fault detection method would then be applied to each of these groups. Another improvement on the method would be to introduce extra Key Performance Indicators (KPIs) in addition to the absolute overflow calculated. For example, using a relative or an energy weighted overflow can enhance the accuracy of the method.

The instance-based approach uses the model of *one* installation. This means that one model for each installation in the DH system should be developed to obtain a well-performing fault detection method. However, this may be a very time-consuming task that would have to be repeated each time a new customer installation is installed in the DH system. One way to reduce the number of models needed could be to implement the same type of grouping of installation types as suggested for the cluster-based fault detection approach. The behaviour of each group would then be modelled in the way suggested in this paper. This approach would probably reduce the accuracy of the fault detection model, since the model of a *group* of installations will be less accurate for *individual* installations.

A natural step in the process of developing a fault detection method is to validate the results. However, obtaining such data sets from DH industry has been a challenge. Most DH utilities do not log when a fault has occurred in their systems, only when they have corrected a fault. Neither do they connect the records of the corrected faults to deviations in customer data. This may be referred to as the lack of labelled data. Labelled data may in this case be described as data where a specific fault is known to have occurred at a specific time, in a specific customer installation. The lack of labelled data has made it challenging to validate the developed fault detection methods properly. The lack of labelled data also introduced a problem that may be present for both the cluster-based and the instance-based approach: how to know that the data from the installations represent a well performing installation that can be either modelled or included in the reference case? Since no labelled data is available, it may be that some installations that contain a fault today are included in the reference case for the cluster-based approach. It is also possible that some installations seem to be well performing since no larger deviations are present in the data set. However, they may in fact contain a fault that has been present during a long time, which makes it look like their "faulty" behaviour is their normal behaviour. Using the instance-based approach on such data sets would generate an incorrect model of the expected behaviour of the installation.

Therefore, an important initial step to further improve the fault detection methods developed would be to identify several installations where specific faults are known to have occurred, at a specific time. It is also important to identify several installations that are known to *not* have had any faults during the same time. This would provide the possibility to validate the methods, and to make sure that they detect the installations that *actually* contained a fault during the investigated period of time. To also overcome the lack of labelled data, both

methods can be used simultaneously by the district heating utility. Starting from historical data, the cluster-based approach can be used to gradually detect malfunctioning substations. It can be re-evaluated on a periodic basis, for instance monthly. The instance-based approach can be used in parallel. Given that the instance-based method uses historical data, it would not be known from the start if the behaviour modelled is for the well-behaving or faulty substation. For that, the cluster-based method can help. As a faulty substation is corrected, the model is recalibrated, and any further deviations can be an indication of a fault in the substation. Another point of improvement is how the deviating behaviours are detected for the instance-based approach. Currently, this is done by visual inspection of the residuals. To be able to use the instance-based approach on a larger scale, the identification of deviating residuals must be automated. This could be done by introducing, e.g., threshold values that the deviations may not exceed (in similarity to the threshold values used in the cluster-based approach). Overall, the two approaches show great promise for fault detection. The next steps include testing the methods on labelled data sets, and to develop a solution for fully automating the fault detection methods.

5. Acknowledgement

This work is part of the TEMPO project which is funded by the European Union's Horizon 2020 Programme under Grant Agreement no. 768936.

6. Data access statement

The datasets analysed during the current study are not publicly available because of privacy requirements.

7. References

[1] Lund H. et al. "4th Generation District Heating (4GDH) - Integrating smart thermal grids into future sustainable energy systems". Energy.2014;68:1–11.

[2] Kavvadias K., Jiménez-Navarro J., Thomassen G. Decarbonising the EU heating sector -Integration of the power and heating sector. EUR 29772 EN. Luxembourg: European Union, 2019.

[3] Lund H. et al. "Smart energy and smart energy systems". Energy.2017;137:556–565.

[4] Sandin F., Gustafsson J., Delsing J. Fault Detection with Hourly District Energy Data; Research Report 2013;27.

[5] Gadd H., Werner S. Achieving Low Return Temperature from District Heating Substations. Appl. Energy. 2014;136:59–67.

[6] Gadd H., Werner S. Fault Detection in District Heating Substations. Appl. Energy. 2015;157:51–59.

[7] Werner S. Feltyper i fjärrvärmecentraler strukturerade (Types of Faults in District Heating Substations Structured); Halmstad Högskola: Halmstad.2013. (In Swedish)

[8] Yliniemi K. Fault Detection in District Heating Substations. Licentiate Thesis, Luleå University of Technology, Luleå, Sweden.2005.

[9] Alsbjer M., Wahlgren P. Fjärrvärmecentraler 10 år—Håller de måttet? (District Heating Substations 10 Years—Do They Measure up?); Research Report 2011;9. (In Swedish)

[10] Frederiksen, S.,Werner S. District Heating and Cooling; Studentlitteratur: Lund, Sweden, 2014.

[11] Park YJ., Shu-Kai F., Chia-yu H. "A Review on Fault Detection and Process Diagnostics in Industrial Processes". Processes.2020.

[12] The European Commission. Annex to the Commission recommendation on the implementation of the new metering and billing provisions of the Energy Efficiency Directive 2012/27/EU no C(2019) 6631 final. 2019.

[13] Sandin F., Gustafsson J., Delsing J. Fault detection with hourly district data. 2013.

[14] Calikus E et al. "Ranking Abnormal Substations by Power Signature Dispersion". Energy Procedia.2018; 149: 345–353.

[15] Farouq S. et al. "Large-scale monitoring of operationally diverse district heating substations: A reference-group based approach". Engineering Applications of Artificial Intelligence 2020.

[16] Ingvarsson S. Statistical Modelling of Individual Substations in a District Heating System. 2018.

[17] Guelpa E., Verda V. Automatic fouling detection in district heating substations: Methodology and tests. Applied Energy, 2020;258.

[18] Garay R., Fester J., Mugaguren, L., Martinez R. RELaTED D2.4 – Energy flexibility and DH Control. 2019.

[19] Cogger K.O. Piecewise linear modeling: Theory, guidelines, and applications. In Management Science & Technology Symposium. 2006.

[20] Olson R., Urbanowicz R., Andrews P., Lavender N., Kidd L., Moore J. "Automating Biomedical Data Science Through Tree-Based Pipeline Optimization," European conference on the Applications of evolutionary computation. 2016.

Enhanced building energy flexibility using passive PCM envelope and HVAC control automation

Mohammad Saffari [a], *Conor Roe* [b], *Donal P. Finn* [b, c]

[a] School of Mechanical and Manufacturing Engineering, Dublin City University, Dublin 9, Ireland, mohammad.saffari@dcu.ie

[b] School of Mechanical and Materials Engineering, University College Dublin, Dublin 4, Ireland, conor.roe.1@ucdconnect.ie

[c] School of Mechanical and Materials Engineering and UCD Energy Institute, University College Dublin, Dublin 4, Ireland, donal.finn@ucd.ie

Abstract. One solution for improving the thermal performance of existing building envelopes is the use of pre-formed internal insulative panels that incorporate impregnated phase change materials (PCM). Such measures have the potential to enhance the energy flexibility of buildings when combined with HVAC control automation and digitalisation techniques, thereby offering the possibility of participation in demand side management measures such as demand response programmes. The current literature on building envelope physics lacks research on the integration of such PCMs in building envelopes and advanced HVAC control automation, especially in the context of research into the energy flexibility and demand response nature under heating and cooling scenarios. The aim of the current study is to evaluate how the addition of PCM impregnated internal wall panels and HVAC thermostat control automation affect both the thermal performance of the building envelope, as well as the wider building energy characteristics, when subject to different demand response events. The reference building is a detached residential house which has a floor area of 160 m^2 and a south-easterly facing aspect. This study presents a building energy management methodology to develop new energy flexibility indicators for HVAC thermostat control automation taking into consideration a pre-cooling period prior to the demand response event as well as evaluating the thermal energy storage capacity and peak power curtailment. Four different demand response scenarios are examined. Simulation results show that shorter envelope pre-cooling periods in association with longer demand response periods are preferable for all envelopes to achieve the maximum power curtailment for cooling. Gypsum boards enhanced with PCM were retrofitted as part of lightweight thermal mass and medium weight thermal mass envelopes and are shown to give best cooling demand shifting and performance. It is concluded that for energy flexibility scenarios, the pre-cooling length should be always less than the length of the demand response event to ensure higher cooling efficiencies.

Keywords. PCM thermal storage, demand response, energy flexibility, HVAC control automation, energy-efficient envelopes
DOI: https://doi.org/10.34641/clima.2022.380

1. Introduction

Thermal energy storage (TES) is a practical solution to give flexibility to the energy demands and hence allows for a building to perform efficiently in times of high peak energy demands while also remaining comfortable for the occupants. TES is a storage arrangement that can store thermal energy by heating, cooling, melting, solidifying, or vaporizing a material [1].

The TES of a building is influenced by the building thermal mass and can be controlled by the building envelope material characteristics. The thermal mass will absorb heat and release it when the ambient temperature around it drops resulting with a relatively stable indoor temperature being maintained. When considering thermal energy storage, it can be called sensible heat storage when the material temperature rises or falls to store heat energy or latent heat storage when a material phase change occurs with little to no change in temperature.

Copyright ©2022 by the authors. This conference paper is published under a CC-BY-4.0 license.

Sensible heat storage materials are heavy, dense and a good heat conductor which heat up or cool down in order to store energy. Phase change materials (PCM) is a latent heat storage technology which can store large amounts of heat energy at mostly isothermal conditions or in a very narrow temperature range.

There is an increasing number of studies emerging which are working on smart thermal energy storage such as PCM to facilitate demand response and improving the energy performance of buildings. For example, a numerical study carried out by Rahimpour et al. [2] on buildings in five Australian cities showed that the retrofitting of PCM on ceilings, walls and floors had an influence on the HVAC demand. HVAC demands were reduced Hobart and Melbourne by 7.3% and 11.4%, respectively, but in the other cities were not affected due to climatic conditions.

Arıcı et al. [3] numerically investigated the effect on heating and cooling loads due to the integration of 100% concentrated PCM (with a range of temperatures) on an external wall of a building. It was concluded that the optimum melting temperature for maximum latent heat storage depends on the climatic conditions and on the location of the PCM in the external wall. Another significant finding from this research is that the optimum thickness for PCM for all climatic conditions and PCM locations was 20 mm and that the maximum delays in the peak heat fluxes ranged from 10.3 hours in August to 13.3 hours in July. This change in time lag by means of activating latent heat storage compared to a reference solution is significant when studying the retrofitting of PCM to enhance the TES of a building for demand response events. However, the effect of different building typologies was not studied.

A study done by Chen et al. [4] which had similar conclusions for sensible heat storage, showed that thinner thermal masses can contribute more to electricity flexibility at peak demand times in a demand response event due to its higher heat release ratio of the stored sensible energy. However, thicker thermal masses have a low heat-release ratio and are therefore not as effective during a demand response event. The heat release ratio is defined by thickness and thermal characteristics of the thermal mass.

Markarian and Fazelpour [5] showed how PCM integration into building envelopes can reduce the need for the air conditioning system to be running in high demand times. However, the authors did not take into consideration, the pre-charging of the buildings sensible and latent TES elements. With these results considered, a pre-charging (pre-cooling) event could be implemented before a demand response event which would offer greater flexibility as the air conditioning system load requirement would be further reduced.

Devaux and Farid [6] performed a numerical and experimental study in Tamaki New Zealand where they compared two huts and validated an Energy Plus model. Hut 1 was a standard reference hut, while hut 2 had PCM fitted on the walls and ceilings along with PCM underfloor heating all with a melting temperature between 27 – 29 °C. During high power demand periods (4 hours long) the setpoint temperature was set to 18°C, whereas during low demand periods the setpoint temperature was at 20.2°C. Turning the underfloor heating off at 5:00 hrs and at 19:00 hrs was shown to be the best time to give optimum peak load shifting along it reduced energy consumption. Devaux and Farid [6] also examined peak load shifting for demand response events, however, pre-charging of the PCM prior to a demand response event to a higher setpoint temperature was not considered.

A gap in knowledge has been identified in field of demand response and PCM technology, and few studies have been published on the effect of PCMs for both heating and cooling scenarios in buildings while taking into consideration various demand response events with different enhanced building envelope typologies.

The current study proposes a new demand response indicator and investigates the pre-charging (pre-cooling) temperature by modulating the thermostat and the duration of this pre-charging period prior to a demand response event for power curtailment and peak load shifting. In addition, a digital design tool for building envelope energy flexibility assessment is developed in EnergyPlus using the in-built Runtime Language and a Python post-processing script.

2. Methodology

2.1 Overview

To simulate a demand response event a pre-charging timeframe was considered, where the building envelopes thermal mass was charged by increasing the thermostat setpoint temperature. This is known as an upward flexibility event. Immediately after such an upward flexibility event, the proposed demand response event took place. The demand response event was simulated for each timeframe of the day to determine the most efficient time of day for the upward flexibility event to take place for the activation of the TES. The energy flexibility for each building envelope considered was evaluated and analysed. The building envelopes were numerically modelled for both an upward and a downward flexibility event for cooling. The retrofitting of 100% concentrated PCM (**PCM-1**) [7] and PCM-enhanced gypsum wallboard (**PCM-2**) [8] to the building envelope was also considered in the analysis to determine the influence of PCM concentration on the TES of the building and thus its contribution to a demand response scenario when envelope pre-charging (pre-cooling) occurs.

2.2 Case study building

The reference building is a residential detached house constructed in 1999. The construction geometry considered for analysis can be seen in Fig. 1. The building has a floor area of 160 m^2 and an easterly facing aspect. The ground floor consists of four communal living spaces and a bathroom, while the first floor contains four bedrooms and a bathroom. The building has ceiling to floor height of 2.5 metres and a total external wall surface area of 139 m^2. The windows are double-glazed units, with a window to wall ratio of 0.22 and a total glazed area of 30.5 m^2, with a majority of the glazing on the ground floor. A typical dwelling house construction and geometry was considered for the thermal analysis in EnergyPlus. The digital energy model of this building was validated by the authors of this study elsewhere [9].

Fig. 1 - Digital CAD model of the building.

EnergyPlus [10] software was used to develop and analyse the building models. The software used for the data analysis and data post-processing was Python [11]. A Python code was developed to analyse the data efficiently and apply demand response indicators to evaluate the potential for an energy flexibility event. In the simulation setup, three-minute timestep intervals for a run period of three days were considered.

A packaged terminal heat pump with constant volume fan control, direction expansion cooling coil and electric heat pump according to baseline building HVAC system types of recommendations of ANSI/ASHRAE/IES Standard 90.1-2013 [12] was selected. HVAC system schedules were matched to the occupancy schedules, and according to the recommended indoor temperatures for energy calculations of (BS EN 16798:2019 2019 [13]. The simulation model uses climatic data made available by EnergyPlus [14]. In this study, the climatic region of Madrid, Spain was used as the geographical region which has a Mediterranean climate (Köppen Climate Classification subtype "Csa") [15]. For the analysis of the cooling period, the design day was 21st of July. For the analysis of influence of different building envelopes on the potential of energy flexibility and demand response events, two different construction envelopes were chosen; a lightweight (LW) building typology and a mediumweight (MW) building typology, which differ in thermal mass and are shown in Table 1. The window U-value was constant for both building constructions with a value of 2.46 W.m^{-2}.K^{-1}.

Tab. 1 - LW and MW construction components.

Construction Envelope	LW Building U-value (W.m^{-2}.K^{-1})	MW Building U-value (W.m^{-2}.K^{-1})
External Walls	0.473	0.449
Ceiling	0.66	0.79
Floor	0.38	0.45

2.3 Phase change materials

To investigate different concentrations of PCM on the TES potential of a building envelope, the original gypsum board construction material of the external walls was replaced with PCM. The PCM types chosen were 100% concentrated PCM (with thickness of 10mm, PCM concentration of 100%, specific heat capacity of 2000 J.kg^{-1}.K^{-1}, and melting point of 25°C) (**PCM-1**) [16]; and PCM-enhanced gypsum wallboard (with thickness of 12.5 mm, PCM concentration of 30%, specific heat capacity of 2000 J.kg^{-1}.K^{-1}, and melting point of 25°C) (**PCM-2**) [8].

2.4 Building Energy Flexibility Scenarios

The numerical model was developed with the capability of simulating an energy flexibility event for each hour of the day by varying the room setpoint temperature. To simulate a demand response event, a pre-charging timeframe was considered, where the building envelope thermal mass was pre-cooled by decreasing the thermostat setpoint temperature. This is considered to be an upward flexibility event. Immediately after the upward flexibility event, the proposed demand response event takes place. Fig. 2 shows an example energy flexibility event programmed for the HVAC thermostat for a cooling event. The demand response event was simulated for each timeframe of the day to determine the most efficient time of day for the upward flexibility event. The energy flexibility for each building envelope considered was evaluated and analysed. The building envelopes were numerically modelled for both an upward and a downward flexibility event for cooling.

In Fig. 2, for pre-cooling of the building envelope, the thermostat setpoint temperature is decreased from 25 °C to 23 °C for either 0.5 hours, 1 hour or 2 hours for the pre-cooling stage followed immediately by a demand response event which sees the setpoint temperature increased to 27 °C for either 1 hour, 2 hours or 4 hours before returning to the normal operating temperature of 25 °C.

Simulation results of this study show that all temperature changes of the indoor environment due to demand response events are within the recommended ranges and comply with ASHRAE Standard 55-2013 [17].

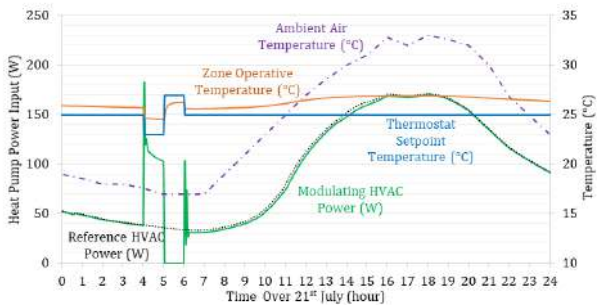

Fig. 2 – Energy flexibility event example, pre-cooling at 23°C for 1 hr, demand response at 27°C for 1 hr.

In this study, six different building envelopes were considered for cooling energy flexibility assessment:

1- LW Building with gypsum board (LW gypsum board),

2- LW Building with concentrated PCM panel (LW PCM-1),

3- LW Building with PCM-enhanced gypsum board (LW PCM-2),

4- MW Building with gypsum board (LW gypsum board),

5- MW Building with concentrated PCM panel (LW PCM-1), and

6- MW Building with PCM-enhanced gypsum board (LW PCM-2). Fig. 2 summarises the simulation scenarios.

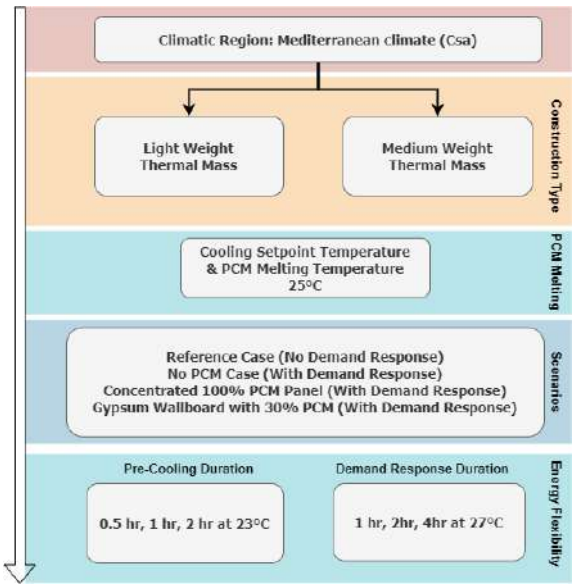

Fig. 3 - Simulation cases for a cooling energy flexibility scenario.

2.5 HVAC thermostat algorithm and data analysis

A sensitivity analysis algorithm has been programmed in EnergyPlus Energy Management System (EMS) using EnergyPlus Runtime Language [18]. This helps to automatically create various demand response events by thermostat modulating the thermostat temperature and schedule. The modulating process was repeated for each time interval of the day to numerically investigate what is the optimum pre-charging time of the day, as well as demand response duration for each building envelope. To post-process this wide array of data, Python scripts were developed which allowed for demand response indicators to be programmed and applied to the data. Currently, EnergyPlus software does not have any specific energy flexibility class, and the developed demand response and energy flexibility algorithm in this study can be integrated into EnergyPlus to further improve its capability to implement and analyse energy flexibility in buildings.

2.6 Demand Response Indicators

Reynders et al. [19] defined three indicators for quantifying energy flexibility in a DR event. These are: storage capacity (CADR), rebound effect (RE_{ADR}) and storage efficiency (η_{ADR}). To apply these performance indicators, the difference in HVAC power usage between the modulating building zone and reference building zone is calculated using equation 1:

$$P_{diff} = P_{mod} - P_{ref} \quad (1)$$

Where P_{diff} = Difference in HVAC power consumption (W), P_{mod} = Modulating HVAC power consumption (W), and P_{ref} = Reference HVAC power consumption (W).

The capacity available for energy storage (SC) is defined as the amount of energy that can be stored during the pre-charging phase (pre-cooling) prior to the demand response event, without interfering with internal thermal comfort of the building zone as shown in Fig. 4 and can be calculated using equation 2.

$$SC = \int_0^{DR} |P_{diff}|\, dt \quad (2)$$

Where SC = Storage Capacity (kWh).

The rebound effect indicator (RE) is defined as the amount of energy which is required by the HVAC system to restore the internal dwelling conditions to the ordinal setpoint temperature after the demand response event has passed and is given by equation 3.

$$RE = \int_{Post-DR}^{\infty} |P_{diff}|\, dt \quad (3)$$

Where RE = Rebound Effect (kWh).

In this study, the rebound effect for six hours after the demand response event was considered. An indicator that is not considered by Reynders et al. [19] is the power curtailed during the demand response event. This is an indicator needed to define the amount of energy that can potentially be curtailed during the demand response event and is shown in Fig. 4. It is also needed to define the storage efficiency of the building and can be calculated using equation 4.

$$PC = \int_{DR}^{\text{Post-DR}} |P_{diff}|\, dt \quad (4)$$

Where PC = Power Curtailment (kWh)

According to Reynders, Diriken, and Saelens [19], the storage efficiency (η) is described as the fraction of stored heat prior to the demand response event compared to the heat released to maintain the internal comfort temperature during the demand response event and is given by equations 5 and 6.

$$\eta_{DF} = 1 - \frac{RE}{SC} \quad (5)$$

$$\eta_{UF} = \frac{RE}{SC} \quad (6)$$

Where η_{DF} = Efficiency of a downward flexibility event, and η_{UF} = Efficiency of an upward flexibility event.

However, indicators defined by Reynders et al. [19], do not take into account an event where both a pre-charging phase and a demand response event are considered. Therefore, in the current study, the storage efficiency indicator was further improved to consider the pre-cooling thermal energy storage event as shown in equation 7 and Fig. 4.

$$\eta = \frac{PC}{SC + RE} \quad (7)$$

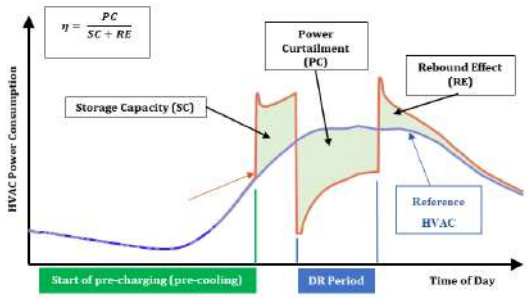

Fig. 4 – Energy flexibility indicators and schematic.

3. Results

3.1 Peak power and cooling energy analysis

When studying the building envelope to investigate power curtailment, it can be seen that the energy flexibility event which has a 2-hour pre-charging (pre-cooling) time and a 4-hour demand response time offers the highest power curtailment. For example, Fig. 5 shows the power curtailment for MW thermal mass envelope with 100% concentrated PCM for all flexibility events and it can be observed that 2-hour, and 0.5-hour pre-cooling, followed by a 4-hour demand response event, offer the highest power curtailment and energy flexibility for cooling.

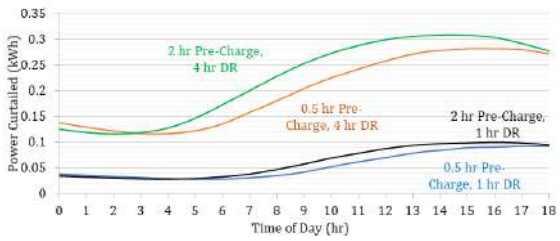

Fig. 5 - Power curtailment for MW PCM-1 envelope across each energy flexibility event.

From the results achieved in this study, it can be concluded that for energy flexibility scenarios, the pre-charge length should be always less than the length of the demand response event to ensure higher efficiencies. A pre-charging event which is the same length or longer than the demand response event is the least efficient type of energy flexibility event and should be avoided when participating in an energy flexibility scenario.

It can be observed that in the 0.5-hour pre-charging event and the 4-hour demand response, power curtailment is highest in the LW envelopes for each class of material, however, the MW buildings have a higher efficiency for each class.

By considering Fig. 5, it can be seen that the highest power curtailment for each energy flexibility event in a MW 100% concentrated is achieved around 14:00 hrs. The energy flexibility event start time of 14:00 hrs sees the highest power curtailment (0.31 kWh) due to the highest ambient air temperature occurring during the demand response period, with the 2-hour pre-charge and 4-hour demand response. The lowest power curtailment value is seen for 0.5-hour pre-charge and the 1-hour demand response with a value of 0.09 kWh.

However, to achieve the highest efficiency, the energy flexibility event should start later in the day at a time of 18:00 hrs. The maximum efficiency is seen later in the day due to the reduced rebound effect. Taking this into consideration when applying an energy flexibility scenario to a dwelling house, it is important to consider the purpose of the energy flexibility event and is it essential to curtail power or essential to have an efficient event. Similar trends are seen for LW building envelopes across all energy flexibility events.

Another observation is that the length of the demand response event is the most influential variable on power curtailment and efficiency, compared to the pre-charging length and therefore, the length of demand response event should be considered the most when implementing an energy flexibility event.

The data shown in Tab. 2, Tab. 3, and Tab. 4, is the mean value for each energy flexibility event across the whole design day for storage capacity, power curtailment and flexibility efficiency, respectively. Tab. 2 shows that the LW and MW PCM-1 envelopes have the highest average storage capacity across all events. The LW and MW are shown to have the lowest average storage capacity for each day which shows that the building envelopes storage capacity performance can be enhanced by PCMs. It can also be concluded that the percentage of PCM retrofitted to the wall has an influence on the storage capacity.

Tab. 2 - Average value for storage capacity across the cooling design day.

	Storage Capacity (kWh)								
Pre-charging length	**0.5 hr**			**1 hr**			**2 hr**		
DR length	**1 hr**	**2 hr**	**4 hr**	**1 hr**	**2 hr**	**4 hr**	**1 hr**	**2 hr**	**4 hr**
LW Gypsum	0.04	0.04	0.04	0.08	0.08	0.08	0.14	0.14	0.13
MW Gypsum	0.04	0.04	0.04	0.08	0.08	0.08	0.14	0.14	0.14
LW PCM-1	0.05	0.05	0.05	0.09	0.09	0.09	0.15	0.16	0.15
MW PCM-1	0.05	0.05	0.05	0.09	0.09	0.09	0.16	0.16	0.16
LW PCM-2	0.05	0.05	0.05	0.08	0.08	0.08	0.15	0.15	0.15
MW PCM-2	0.05	0.05	0.05	0.09	0.09	0.09	0.16	0.16	0.16

For the daily average values of power curtailment shown in Tab. 3, it can be observed that the LW PCM-2 and the LW PCM-1 offer the greatest amount of power curtailment across each energy flexibility event. It can be noticed that the LW gypsum envelope has only a marginal difference in the power curtailment values.

Tab. 3 - Average value for power curtailment across the cooling design day.

	Power Curtailed (kWh)								
Pre-charging length	**0.5 hr**			**1 hr**			**2 hr**		
DR length	**1 hr**	**2 hr**	**4 hr**	**1 hr**	**2 hr**	**4 hr**	**1 hr**	**2 hr**	**4 hr**
LW Gypsum	0.07	0.12	0.20	0.07	0.12	0.21	0.07	0.13	0.22
MW Gypsum	0.06	0.11	0.19	0.06	0.11	0.20	0.06	0.12	0.21
LW PCM-1	0.07	0.13	0.22	0.07	0.13	0.23	0.08	0.14	0.25
MW PCM-1	0.06	0.11	0.21	0.06	0.11	0.21	0.06	0.12	0.22
LW PCM-2	0.07	0.12	0.21	0.07	0.13	0.22	0.08	0.14	0.24
MW PCM-2	0.06	0.11	0.21	0.06	0.12	0.21	0.07	0.12	0.23

The MW envelopes are shown to have the worst power curtailment potential, however, in general MW buildings require the least amount of reference HVAC energy consumption and are overall more favourable at reducing energy consumption during demand response events.

Looking at the average flexibility efficiency values in Tab. 4, the MW PCM envelopes have the highest efficiency when they are involved in short pre-charging events and long demand response events. However, when short pre-charge lengths are combined with short demand response events, the LW PCM buildings are better performers. The MW gypsum building has overall worst performance for the short pre-charging events.

Tab. 4 - Average value for flexibility efficiency across the cooling design day.

	Flexibility Efficiency (%)								
Pre-charging length	**0.5 hr**			**1 hr**			**2 hr**		
DR length	**1 hr**	**2 hr**	**4 hr**	**1 hr**	**2 hr**	**4 hr**	**1 hr**	**2 hr**	**4 hr**
LW Gypsum	96	130	169	66	100	138	47	75	112
MW Gypsum	91	134	188	62	98	147	41	69	112
LW PCM-1	104	141	181	69	106	147	45	75	117
MW PCM-1	99	145	203	62	103	156	35	68	115
LW PCM-2	102	139	180	67	104	145	46	74	115
MW PCM-2	99	144	202	65	105	156	39	70	116

When the pre-charging events increase towards 2 hours, the LW envelopes are seen to outperform the MW buildings. For a combination of long pre-charging phases and short demand response phase, the MW PCM-1 envelope is seen to be overall the worst performer. This is due to a large quantity of energy that can be stored in the thermal inertia, however, cannot be released in the short demand response period.

4. Conclusions

This study gives important data on how the building envelope can provide energy flexibility for the grid and how innovative design of building envelope using PCM can increase the overall energy performance of the building and more importantly offer energy-resilient buildings. Demand response strategies presented here for building envelope design could be used in energy retrofit policies and demand response strategies. A building sensitivity assessment to show the characterisation and performance of each TES building envelope in a cooling condition was carried out. A detailed assessment of the power curtailment performance of four different energy flexibility scenarios were looked at and discussed in detail.

- It was clear for the cooling scenario that, the short pre-charging period and long demand response period is the most preferable event across all envelopes for maximum power curtailment and efficiency.

- PCM-impregnated gypsum board retrofitted on the LW, and MW envelopes are shown to give an overall good performance in flexibility efficiency and in power curtailment.

- The MW envelopes showed to be resistant to the effects of the external environment due to the heavier sensible thermal inertia that is involved with it.

- For shorter demand response events, the LW sensible TES is shown to be most effective as the storage capacity can discharge faster over the short demand response period. The PCM enhanced envelopes are marginally better than the Gypsum envelope when the pre-charging period is shorter.

- Overall, the thermostat modulation from 25 °C to 23 °C in the pre-charging phase is less effective than changing the thermostat from 23 °C to 27 °C in the demand response phase.

5. Acknowledgement

This publication has emanated from research supported (in part) by Science Foundation Ireland (SFI) under the SFI Strategic Partnership Programme Grant Number SFI/15/SPP/E3125. The opinions, findings and conclusions or recommendations expressed in this material are those of the author(s) and do not necessarily reflect the views of the Science Foundation Ireland. The authors also acknowledge the framework of IEA EBC Annex 67 Energy Flexible Buildings and Annex 82 Energy Flexible Buildings Towards Resilient Low Carbon Energy Systems.

6. References

[1] Navarro L, de Gracia A, Colclough S, Browne M, McCormack SJ, Griffiths P, et al. Thermal energy storage in building integrated thermal systems: A review. Renew Energy 2016;88:526–47. https://doi.org/10.1016/j.renene.2015.11.040.

[2] Rahimpour Z, Faccani A, Azuatalam D, Chapman A, Verbič G. Using Thermal Inertia of Buildings with PCM for Demand Response. Energy Procedia, 2017. https://doi.org/10.1016/j.egypro.2017.07.483.

[3] Arıcı M, Bilgin F, Nižetić S, Karabay H. PCM integrated to external building walls: An optimization study on maximum activation of latent heat. Appl Therm Eng 2020. https://doi.org/10.1016/j.applthermaleng.2019.114560.

[4] Chen Y, Chen Z, Xu P, Li W, Sha H, Yang Z, et al. Quantification of electricity flexibility in demand response: Office building case study. Energy 2019;188:116054. https://doi.org/10.1016/j.energy.2019.116054.

[5] Markarian E, Fazelpour F. Multi-objective optimization of energy performance of a building considering different configurations and types of PCM. Sol Energy 2019;191:481–96. https://doi.org/10.1016/J.SOLENER.2019.09.003.

[6] Devaux P, Farid MM. Benefits of PCM underfloor heating with PCM wallboards for space heating. Appl Energy 2017. https://doi.org/10.1016/j.apenergy.2017.01.060.

[7] RUBITHERM. Rubitherm® Technologies GmbH 2022. http://www.rubitherm.de/ (accessed January 1, 2022).

[8] Knauf Comfortboard 2022. http://www.knauf.de/wmv/?id=13825 (accessed January 1, 2022).

[9] Keogh D, Saffari M, De Rosa M, Finn DP. Energy assessment of hybrid heat pump systems as a retrofit measure in residential housing stock. E3S Web Conf., vol. 111, 2019. https://doi.org/10.1051/e3sconf/201911101064.

[10] US Department of Energy. EnergyPlus. Energy Effic Renew Energy 2017. http://apps1.eere.energy.gov/buildings/energyplus/energyplus_about.cfm (accessed July 31, 2017).

[11] Python 2019. https://www.python.org/ (accessed January 30, 2019).

[12] ANSI/ASHRAE/IES Standard 90.1-2013 - Energy Standard for Buildings. ASHRAE; 2013.

[13] 16798-1:2019 BE. BS EN 16798-1:2019 Energy performance of buildings - ventilation for buildings. Indoor environmental input parameters for design and assessment of energy performance of buildings addressing indoor air quality, thermal environment, lighting and acoustics - 2019.

[14] EnergyPlus Weather Data Sources. Energy Plus Weather (EPW) Data Sources 2021. https://energyplus.net/weather/sources (accessed January 1, 2021).

[15] Kottek M, Grieser J, Beck C, Rudolf B, Rubel F. World map of the Köppen-Geiger climate classification updated. Meteorol Zeitschrift 2006;15:259–63. https://doi.org/10.1127/0941-2948/2006/0130.

[16] Rubitherm® Technologies GmbH- CSM modules 2017. http://www.rubitherm.de/english/pages/02h_air_heating_systems.htm (accessed August 16, 2017).

[17] ANSI/ASHRAE Standard 55-2013. ANSI/ASHRAE Standard 55-2013 Thermal Environmental Conditions for Human Occupancy. Atlanta, GA: 2013.

[18] Ellis PG, Torcellini PA, Crawley DB. Simulation of Energy Management Systems in EnergyPlus. Build. Simul. 2007, U.S. Department of Commerce National Technical Information Service; 2007, p. 1346–53.

[19] Reynders G, Diriken J, Saelens D. Generic characterization method for energy flexibility: Applied to structural thermal storage in residential buildings. Appl Energy 2017;198:192–202. https://doi.org/10.1016/j.apenergy.2017.04.061.

Data Statement

The authors confirm that the data supporting the findings of this study are available within the article. Currently, the CAD files used by the simulation models are not available to be shared publicly.

Data driven energy efficiency in an air heated office building in Norway

Natasa Nord[a], Ingrid Jæger Landsnes[b], Yuemin Ding[c]

[a] Department of Energy and Process Engineering, Faculty of Engineering, Norwegian University of Science and Technology, Trondheim, Norway, natasa.nord@ntnu.no.

[b] Enterprise ventilation, Gunnar Karlsen, Trondheim, Trondheim, ingrid_landsnes@msn.com.

[c] Department of Electrical and Electronic Engineering, Tecnun School of Engineering, University of Navarra, San Sebastián, Gipuzkoa, Spain, yueminding@ceit.es.

Abstract. There are lots of data stored about buildings that could be better used to improve the operation of existing and new buildings. In the long run, this means that building data can be used much more efficiently for energy, heat rate, and electricity reduction based on price and load. However, building data are only stored and the knowledge that may be found in this data is not fully utilized. The aim of the study was to evaluate potentials and opportunities with continuous energy, heat rate, and power reduction in an all-air heated office building in Trondheim, Norway. The observed building has an area of 14 000 m^2 and the building was built according to the passive house standard. The background for the work was that high peak loads in electricity and heat are challenging for both the district heating and power grid. By reducing or moving the energy use of the ventilation heat to periods with low grid loads, cost savings can be achieved through a reduced rate in district heating and electricity. In this study, a model of the building was created in the simulation program IDA-ICE, where data about building body, outdoor climate, energy supply, energy distribution, set points for room control, operation and schedules were used from a real building. This included measurements of the outdoor temperature, supply temperature, internal loads, electricity use, district heating, and hot water, as well as indoor temperatures and air flow rates. Various scenarios were developed to reduce peak loads in heating and electricity with the focus on controlling the ventilation system. The results for the annual simulation showed a reduction in ventilation heat rate from 12% to 33%. Further, the results showed a cost saving for heat and electricity from of 10% to 16%. The study may be useful for facility managers, operators, and end users of office buildings that want cost-effective building performance improvement.

Keywords. Peak load, ventilation, BEMS, building simulations, demand response.
DOI: https://doi.org/10.34641/clima.2022.352

1. Introduction

Energy efficiency measures in buildings imply reduction of demand load and energy requirements in buildings, without sacrificing indoor thermal comfort. These measures may range from good building insulations, efficient building service systems, effective operation and maintenance, and expert-based utilization of building energy monitoring [1]. An example of energy efficiency measures is implementation of improved control strategies on a single building service system or on different systems such as heating, ventilation, and domestic hot water use. The work flow for identification of potentials for energy efficiency measures may be defined by following steps: 1) identify real energy use in buildings [2] by performing energy auditing; 2) suggest and introduce energy efficiency measures; 3) perform measurement and verification of the introduced measures; 4) perform economic analysis. Depending on the performed study, evaluation of the energy efficiency measure impacts may be theoretical or real. In this study, potentials and opportunities with continuous energy, heat rate, and power reduction in an all-air heated office building in Trondheim, Norway, were evaluated by utilizing the building energy and management system (BEMS) data and a building simulation tool. An economic analysis was also performed to estimate the economic benefits of the suggested measures.

Modern buildings have usually a well instrumented energy and indoor environment monitoring system

Copyright ©2022 by the authors. This conference paper is published under a CC-BY-4.0 license.

such as BEMS. Due to development of the communication technologies, these systems are getting improved. However, their full potential to operate buildings efficiently and to work together with the energy system is not yet well developed. These systems may produce lots of monitoring data, but their full potential to develop real building knowledge for continual building energy efficiency improvement is not yet achieved. In a review paper where 30,000 full-text building-related articles have been extracted for text mining, it was found that data science techniques are applied more for operation phase applications such as fault detection and diagnosis (FDD), while being under-explored in design and commissioning phases [3]. Specifically, when it comes to use of building data to development of control strategies in buildings, the application is on an average level. A survey study on data-driven predictive control strategies for energy efficiency in buildings led to 10 insights considering improvement of building energy performance. Among else two insights are very interesting: 1) minority of studies addresses the aspect of BEMS integration and 2) systemic interdependencies or conflicting control commands are rarely studied [4]. An approach for data-driven building energy modelling with feature selection and active learning for data predictive control was proposed in [5], where a detail workflow for calibration of the building simulation model was proposed. Based on the above mentioned, there is a huge need to make better utilization of the BEMS data to develop building knowledge for continual building energy efficiency improvement Therefore, in our study, methods to actively utilized BEMS data for building simulation model calibration and control improvements for energy efficiency were suggested. Further, a systematic approach to avoid conflicting control outputs was suggested. The last was possible, because the observed case building is an all-air heated building [6].

A data-driven methodology for enhanced measurement and verification of energy efficiency savings in commercial buildings where an innovative technique to evaluate the building's weather dependency to design a model able to provide accurate dynamic estimations of the achieved energy savings and the building energy simulation software EnergyPlus, as well as monitoring data from real-world buildings was suggested in [7]. This study is an excellent example how to combine real measurements, building simulation tools, and data mining techniques for measurement and verification of energy efficiency savings in buildings. To evaluate the building's weather dependency, energy signature curves were firstly developed and analyzed in [7]. Similarly, in our study, real measurements and a building simulation tool were combined, while to develop simple yet effective energy savings measures, energy signature curves were firstly analyzed.

Demand response will play an important role in the smart buildings and energy systems of the future. Today, there are many studies that have gone into depth on Demand Response for the power grid, but a similar progress has not yet been made for the district heating systems and building service systems [8, 9]. Demand controlled ventilation with temperature dependent flow rate control [10] implemented in an all-air heated building gives a huge potential to implement demand response in a reliable way in buildings for energy efficiency and decreasing of the demand load. Optimization and implementation of cost-effective energy efficiency measures in an all-air heated building in Norway has been presented in detail in [11, 12]. However, thorough analyses on both decreasing heat and electricity demand load in buildings through data-driven control strategies is still missing. Therefore, in this study different data-driven strategies were developed to intensify energy efficiency and decrease the demand load for heating and electricity.

The aim of the paper was to use the building simulation tool combined with the BEMS data to identify potentials for demand load reduction in an all-air heated office building. Reduction of peaks for ventilation heating, would affect fan power, indoor climate, and could lead to cost savings for heating and electricity. In this study, an office building located in Trondheim, Norway, was analyzed. The building is all-air heated. This allowed possibility to utilize the ventilation parameters for the peak load reduction in both heating and electricity use. Temperature measurements, schedules for internal loads, and district heating use were used to calibrate the model. Further, consequent simulation-based analyses were developed for various scenarios to identify potential for load reduction. The aim of this analysis was to estimate whether the building might have the potential for reduction of peak loads through data-driven control strategies.

Innovations in the study are extensive utilization of the BEMS data and simulation results to identify improvement scenarios for energy efficiency and the peak load reduction. For example, a thorough analysis of the energy signature curves showed the time delay between the supply air temperature in ventilation and the highest demand.

The rest of the paper is organized as the following. Method consisting of the model presentation, calibration, and scenarios is presented. Results are given by firstly showing daily analysis and then annual results.

2. Methods

In this section, methods used in the study are presented. To perform this study, combination of building simulation and real building data were used. BEMS data were used for two purposes: 1) to calibrate the simulation model and 2) to suggest new control strategies in ventilation. Finally, the improvement scenarios to decrease the peak loads

were suggested based on a combination between the BEMS data and consequently produced, organized, and analyzed building simulation results.

Based on the building data, the building model was developed using the dynamic simulation tool IDA ICE 4.8 [13].

Since most of the BEMS data were collected for 2019, the boundary conditions considering indoor and outdoor temperature were the respective data for 2019. Considering the economic analysis, the current energy price models in Norway were used.s

2.1 Model calibration

To calibrate the model, monitoring data on internal loads, occupancy presence, and supply air temperature were used. In this study, data from 2019 were available.

To calibrate the building simulation model, the simulated space heating (SH) demand was compared with the real building SH demand. The domestic hot water (DHW) use was used as an input because it was separately measured. Consequently, it was enough to compare the simulated and the measured SH demand to calibrate the model. Comparison of the hourly values was performed to calibrate the model properly. This means that it was assumed that the simulated duration curve for the SH corresponds to the measured duration curve for SH. It was assumed that there was enough available heat, so that the set point for the supply air temperature in ventilation was reached in the simulations.

Considering the indoor environment in the model calibration process, it was observed that the CO_2 level in the simulations were below the maximum setpoint for the CO_2 level. This meant that it was reasonable to allow modulation on the air volume rates that were controlled according to the indoor temperature and the CO_2 level in the further scenarios without negative consequences on indoor environment.

2.2 Case building and building model

An office building located in Trondheim, Norway, was investigated in this study. The building area is 14 000 m^2. Some details about this building are introduced as follows. The appearance of this building is shown in **Fig. 1**. The building is composed of six floors. There are two floors underground, the lower one is completely used for paring area, while the higher one is used for cafeteria, office room, meeting rooms, and partially for the parking area. The other four floors above the ground are composed of a mixture of meeting rooms, single-celled offices, miscellaneous rooms, and open-landscape working areas. The heat demand of this building is caused by SH and DHW. The heating supply is provided by district heating. The ventilation system in this building is a variable air volume (VAV) system. The heating system in this building is an all-air heating system [6]. This means that all space heating is delivered by ventilation.

Fig. 1 - Observed office building.

The thermal parameters of the observed building are summarized in **Tab 1**. The building was designed according to the Norwegian building code TEK17 [14]. The building code TEK17 is similar to the passive house standard.

Tab. 1-Parameters of building envelope.

	U-value (W/m^{2}K)
Outer wall	0.18
Inner wall	0.15
Ground floor	0.13
Roof	0.13
Windows	0.8
Doors/openings	1.2

BEMS consists of two systems: 1) the indoor environment monitoring and 2) energy monitoring system. These two systems were used to retrieve building operation data. There are many sensors installed in this building to sample parameters including occupancy state, indoor and outdoor air temperature, energy use, etc.

The building model in IDA-ICE is shown in **Fig. 2**. In total the building was modeled with 425 zones. All the zones are grouped as internal offices, external offices, meeting rooms, toilets, cafeteria, and the parking areas.

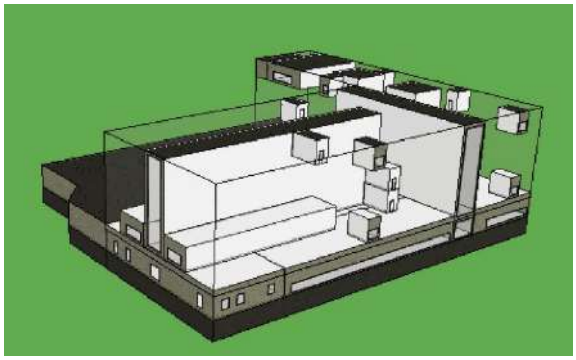

Fig. 2 – Building model in IDA-ICE.

The internal loads used as the simulation input are given in **Fig. 3**. These profiles were obtained by statistical analysis of the monitoring data from the indoor environment monitoring system.

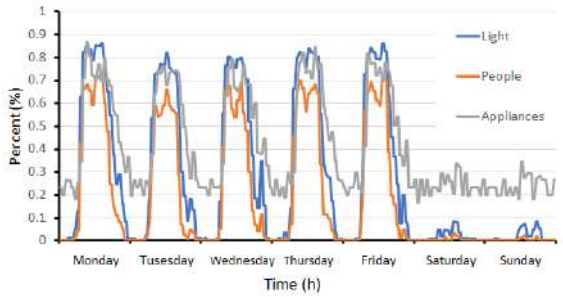

Fig. 3 – Weekly profile for internal loads

2.3 Scenarios for decreasing peak loads

Scenarios for decreasing the building loads focused primary on decreasing of the heat load, while decrease of the electricity load was a by-product. Decrease of the heat loads would also influence the electricity loads, because the building is all-air heated. Four scenarios were defined to decrease the peak loads. The scenarios are based on control of the supply air temperature and air amount in the ventilation system.

To formulate the scenarios for decreasing the heat load, detail analyses of the measured and simulated data were performed. **Fig. 4** shows a summary and influence of the supply air temperature and the ventilation heat rate. The results in **Fig. 4** were obtained based on simulation. The supply temperature was successively moved for each hour and a new simulation was generated. Based on all these results, **Fig. 4** was organized.

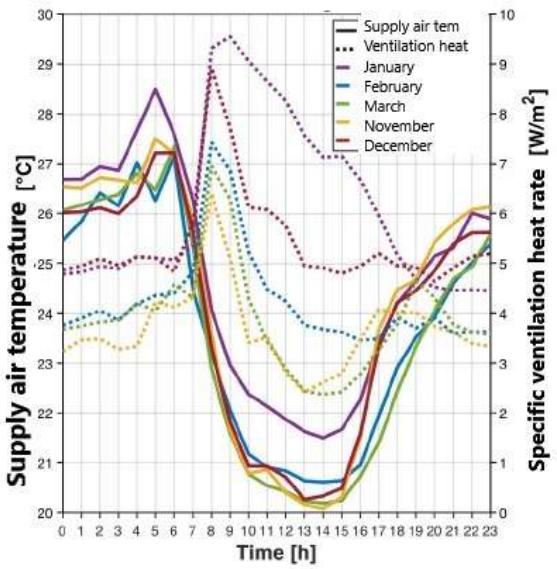

Fig. 4 – Daily average months of the supply air temperature and ventilation heat rate in heating months

The analyses included thorough analyses of energy signature curves on hourly level. Ventilation heat demand was compared to the outdoor temperature and the supply air temperature for different months and working and non-working hours. The analysis showed a clear dependency of the ventilation heat demand on the outdoor temperature in the heating period from November to March. In addition, a linear relationship between the ventilation heat rate and the temperature difference between the supply ventilation air and the outdoor temperature was noted. All these gave the motivation to introduce different control scenarios on the supply air temperature to decrease the heating peak loads.

Fig. 4 shows a clear time delay in the peaks between the highest supply air temperature and ventilation heat for working days. Therefore, this delay was studied further and utilized to develop the peak load decreasing scenarios. The time delay between the highest supply air temperature and the highest ventilation heat rate was from 4 hours in January to 2 hours in December, March, and February. In general, the higher temperature delay was noted in colder months.

Based on the analysis of the time delay between the highest supply temperature and the aim to decrease the heat demand load to estimate the potential for the demand response, the following four scenarios were tested as shown in **Tab. 1**.

Tab. 1 – Scenarios for decreasing heat load

Scenario	Description
Scenario 1	Moved the highest supply temperature until the lowest peak was achieved
Scenario 2	Supply air temperature was increased or decreased for the coldest or warmest days in periods for 1 – 2 K
Scenario 3	Set point for the supply air temperature was set between 21 - 24°C
Scenario 4	The set point for the air flow rate for the VAV system was to 0.7 to 3 L/s/m²

The first two scenarios in **Tab. 1** were suggested by detail analyses of the time delays between the highest peak load and the highest supply air temperature. The idea behind Scenario 1 was developed by a successive moving of the supply ventilation air temperatures given in **Fig. 4** for one hour and analyzing the achieved peaks. For each moved supply temperature profile, the heat loads were produced by the simulation and compared. It was observed that if the supply air temperature with the highest value at 5 AM as shown in **Fig. 4** was moved to 4 PM, the lowest heat peak load was achieved. The indoor temperature was also followed all the time and satisfactory values were also obtained. Scenario 2 was reached in a similar way as Scenario 1, except that it was noted that it would be worth just to increase or decrease the supply air

temperature for 1 – 2 K in the case when the outdoor temperature was lower or higher, respectively. In general, in the heating period, the supply temperature was increased by 1 – 2 K. Scenario 3 was reached by allowing a wider range for the indoor air temperature to variate. Finally, Scenario 4 was suggested by decreasing the limit for the maximum air flow rate.

2.3 Energy cost models

To calculate the impact of the suggested scenarios for peak load decreasing, energy cost for the observed building were calculated. The energy costs were calculated both for heating and electricity based on the current pricing models in Norway.

Electricity cost was calculated as:

$$C_{el} = C_{gf} + C_{ee} =$$

$$(C_{fix} + C_{gen} + C_{gp})_{fg} + (C_{en} + C_{add})_{en} \qquad (1)$$

In Equation (1) there are two main items to be considered, grid fee, C_{gf}, and energy cost, C_{gf}. The grid fee part consists of three parts, fixed part, C_{fix}, that is the same for all the costumers in the same group, energy part, C_{gen}, calculated based on the energy use, and the grid fee part due to power extraction, C_{gp}, calculated based on the maximum power taken during a month.

Heating cost was calculated in the same way as the electricity cost in Equation (1), except that there is no fixed part, C_{fix}, in the calculation of the heat cost.

The specific values used to calculate the heat and electricity cost are given in **Tab. 2**. The cost data in **Tab. 2** are given in Norwegian Kroner (NOK) and the current valuta ration is about 10 NOK = 1 EUR.

Tab. 2 – Energy cost data

Type of cost	Price	Electricity	District heating
Grid fee	Fixed (NOK/year)	8800	
	Energy (NOK/kWh)	0.05	0.05
	Consumption tax (NOK/kWh)	0.158	0.158
	Power rate (NOK/kW/month)	40 - 60	40 - 60
Energy	Energy (NOK/kWh)	NordPool hourly marked	0.3– 0.5
	Addition (NOK/kWh)	0.03	0.03

The presented results and influence of the peak load decrease on the cost saving are very dependent on the energy pricing models. However, for the purpose of this study, only the current model and the values given in **Tab. 2** were used.

3. Results

In this section, firstly the results on the model calibration are given. Further, a simple example how change in the supply ventilation air temperature influenced the heating demand for one cold day is given. Finally, annual analysis for the heating load and cost is given.

3.1 Calibrated model

To calibrate the model, the input values on the occupancy, internal loads, and ventilation control were used. To recall, DHW use was used as an input, because it was separately measured. Therefore, to check the model quality, the SH demand was checked, and the results are given in **Fig. 5**.

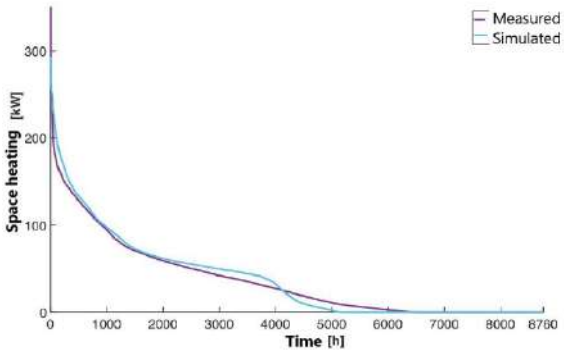

Fig. 5 – Model calibration

The results in **Fig. 5** showed that the SH total heat demand of the calibrated model was 3.4 % higher and the maximum peak demand was lower for 16.3 %. Based on the other parameters and the result analysis, the model was considered reliable for further use.

3.2 Daily energy use analysis

To illustrate importance of decreasing the total energy demand and importance of the supply air temperature in ventilation, the results in **Fig. 6** are shown. The results are given for one cold day when the outdoor temperature was – 10.5°C. The results are given for the calibrated model and three different control strategies.

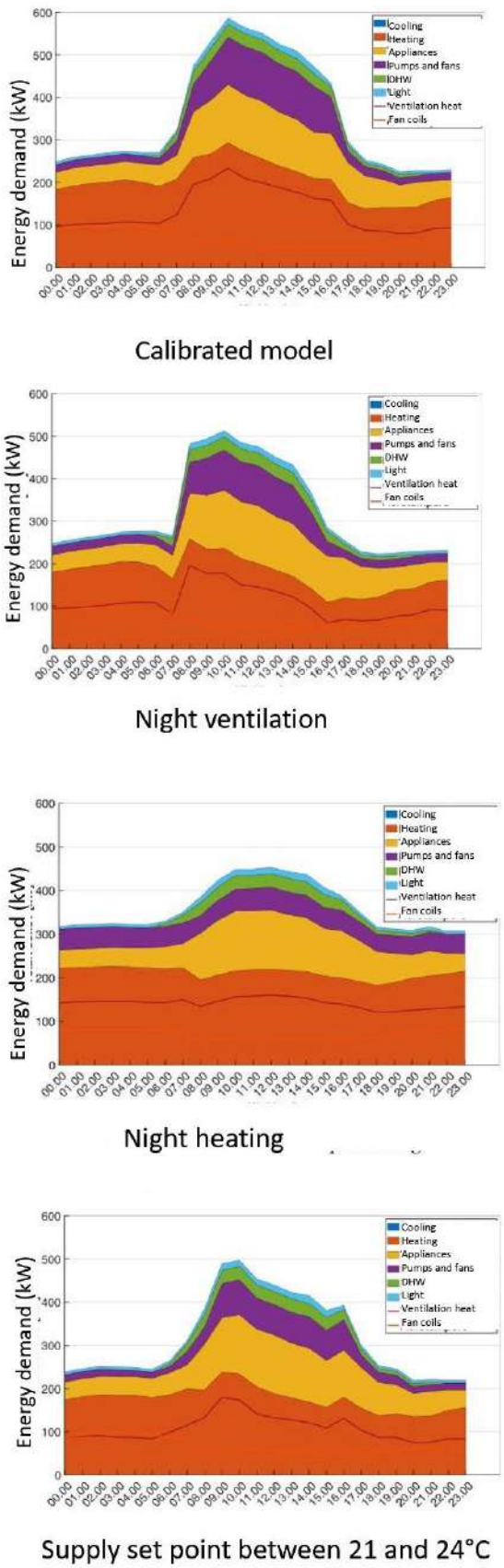

Fig. 6 – Daily analysis of the heat load reduction due to different ventilation control

From **Fig. 6**, it is possible to identify how small changes in control might reduce the peak heating demand up to 23%. To identify this decrease in **Fig. 6**, consider the horizontal line at 500 kW heating demand. For the Calibrated model, the highest peak was above that value, while for the other scenarios the highest heating demand was lower. It is very interesting to notice that the control strategy Night heating when the office was heated up to certain level gave the lowest variation in the heating demand. Electricity use for fans and pumps was decreased by 26%, when comparing the calibrated model and the model when the indoor temperature variated from 21 - 24°C. To follow the decrease in the electricity use for fans and pumps, follow the pink area in **Fig. 6**. Based on the results in **Fig. 6**, it is obvious that the different control in ventilation reshaped much electricity demand for fans and pumps. In the control strategy with the night heating, the electricity demand for fans and pumps seems to be constant over the day. This result is very good, meaning that only electric appliances and DHW, or occupancy related energy use, were changing the building demand.

4.2 Annual energy use analysis

To present results on annual energy use, firstly duration curves for the scenarios given in **Tab. 1** are given in **Fig. 7**.

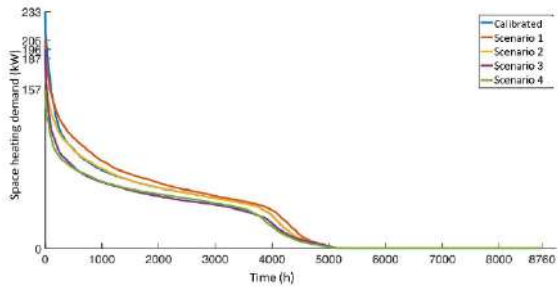

Fig. 7 – Duration curves for different control scenarios

In **Fig. 7**, it is possible to notice decrease in the peak load for SH and in the total SH demand due to the implemented control strategies. As a summary, the peak load was mostly decreased when the range for the maximum air flow rate was decreased, Scenario 4. In that case, the peak load was decreased for 33 %. The total heat use was mostly decreased when the temperature range and the air flow rate range were changed. The decrease in SH was about 17%.

Finally, the total annual cost for electricity and heat are given in **Fig. 8** for the different scenarios introduced in **Tab. 1**. As a summary, the cost results in **Fig. 8** show that the highest cost reduction were achieved in Scenarios 3 and 4. The results for Scenario 4 are not given directly in **Fig. 8**, because they are similar as for Scenario 3. In Scenario 1, even an increase in the heating cost was achieved, because the resulting cost effect of the decreased peak load was lower than a small increase in heating energy demand.

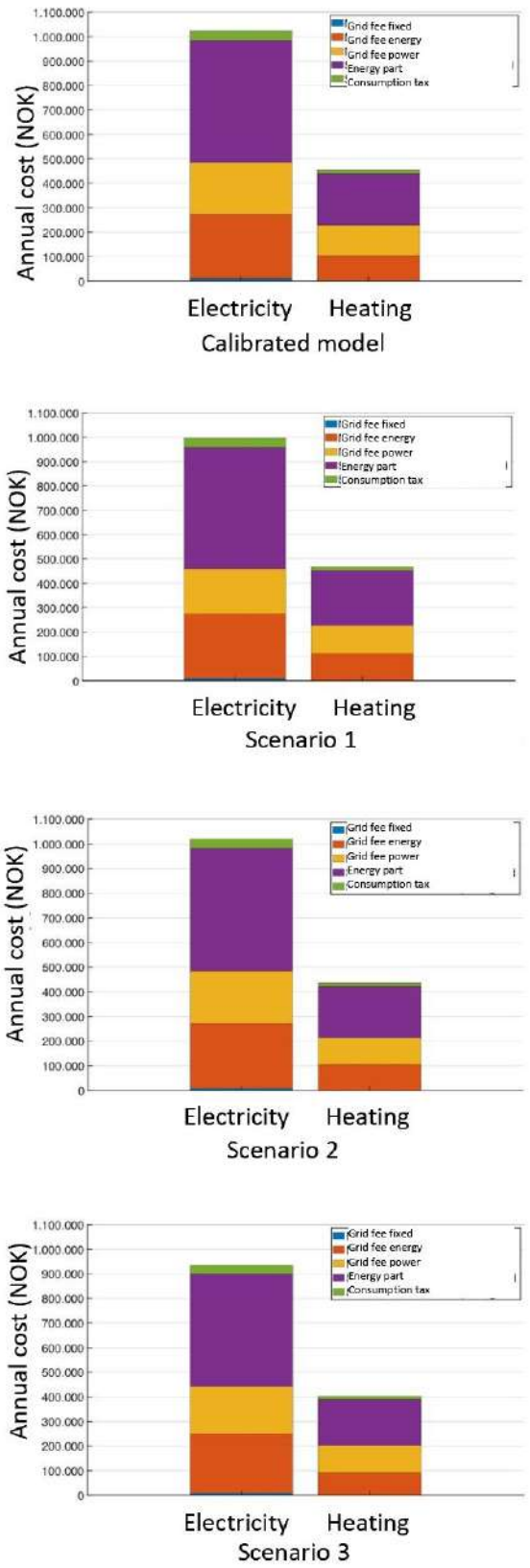

Fig. 8 – Annual cost for different control strategies

The best cost savings achieved in Scenario 3 and 4 are due to decrease in the peak loads and energy use. These decreases were achieved due to limited possibility for modulation of the air flow rates. By analyzing the results in **Fig. 8**, it is possible to notice that modulation of the air flow rates may be used as a demand response measure to decrease the energy cost. Scenario 1 that was suggested based on the data analysis and is simple to implement, just by moving the highest temperature might give some saving results specifically on the peak demand, while the final economic results depended highly on the energy pricing model and weighing between energy and heat rate in the pricing model. In general, all the results in **Fig. 8** showed potentials and opportunities with continuous energy, heat rate, and power reduction in an all-air heated office building. Thereby, it may be concluded that all the suggested scenarios may be considered as possible demand response measures. However, the final economic benefits are dependent on valid pricing models. The results in **Fig. 8** are valid for the energy price models and values given in **Tab. 2**. Therefore, a further analysis on the price models may show different results.

4. Conclusions

In this study, various scenarios were studied to reduce peak demand for the ventilation heat in an office building with all-air heating. The simulation program IDA-ICE was used to perform the analysis. Different scenarios were simulated for a specific cold day and for the whole year to analyze how demand reduction might affect the ventilation heat, fan power, indoor climate, and costs for thermal and electrical energy. Detailed monitoring data including indoor environment, ventilation parameters, and energy use were used to calibrate the model and to develop the scenarios.

To develop control scenarios for decreasing peak load, detail analysis of the simulation results was performed. The idea of the analysis was to identify time delay between the highest supply temperature and the highest peak load for heating. This approach may be useful for practical applications when supply temperature may be moved to decrease the peak load.

The results show that the different scenarios give different changes in the peak load both when it comes to heating and electricity. The best results were achieved then the temperature range for the allowed indoor air temperature was bigger and when the range for the maximum air amount was lower.

Future research should include the following. Influence of different energy pricing models that would motivate higher peak load reduction. In this work, the focus was solely on the heat load decrease. However, further study on different control strategies in ventilation such as the return air compensation control may be be tested.

5. Acknowledgement

The authors are grateful to the company GK, https://www.gk.no/, department Indoor

environment in Trondheim for allowing us to access the analyzed office building. GK made available their monitoring systems for our research. Specifically, the authors would like to thank to the colleagues that help in the analysis of the presented study, Rune Gjertsen and Knut-Ivar Grue.

6. References

[1] Nord N. Building Energy Efficiency in Cold Climates A2 - Abraham, Martin A. Encyclopedia of Sustainable Technologies. Oxford: Elsevier; 2017. p. 149-57.
[2] Yoshino H, Hong T, Nord N. IEA EBC annex 53: Total energy use in buildings—Analysis and evaluation methods. Energy and Buildings. 2017;152:124-36.
[3] Abdelrahman MM, Zhan S, Miller C, Chong A. Data science for building energy efficiency: A comprehensive text-mining driven review of scientific literature. Energy and Buildings. 2021;242:110885.
[4] Schmidt M, Åhlund C. Smart buildings as Cyber-Physical Systems: Data-driven predictive control strategies for energy efficiency. Renewable and Sustainable Energy Reviews. 2018;90:742-56.
[5] Zhang L. Data-driven building energy modeling with feature selection and active learning for data predictive control. Energy and Buildings. 2021;252:111436.
[6] Rabani M, Madessa HB, Nord N, Schild P, Mysen M. Performance assessment of all-air heating in an office cubicle equipped with an active supply diffuser in a cold climate. Building and Environment. 2019;156:123-36.
[7] Grillone B, Mor G, Danov S, Cipriano J, Sumper A. A data-driven methodology for enhanced measurement and verification of energy efficiency savings in commercial buildings. Applied Energy. 2021;301:117502.
[8] Mishra AK, Jokisalo J, Kosonen R, Kinnunen T, Ekkerhaugen M, Ihasalo H, et al. Demand response events in district heating: Results from field tests in a university building. Sustainable Cities and Society. 2019;47:101481.
[9] Ju Y, Lindholm J, Verbeck M, Jokisalo J, Kosonen R, Janßen P, et al. Cost savings and CO2 emissions reduction potential in the German district heating system with demand response. Science and Technology for the Built Environment. 2022;28(2):255-74.
[10] Yang A, Holøs SB, Resvoll MO, Mysen M, Fjellheim Ø. Temperature-dependent ventilation rates might improve perceived air quality in a demand-controlled ventilation strategy. Building and Environment. 2021;205:108180.
[11] Rabani M, Bayera Madessa H, Mohseni O, Nord N. Minimizing delivered energy and life cycle cost using Graphical script: An office building retrofitting case. Applied Energy. 2020;268.
[12] Rabani M, Bayera Madessa H, Nord N. Achieving zero-energy building performance with thermal and visual comfort enhancement through optimization of fenestration, envelope, shading device, and energy supply system. Sustainable Energy Technologies and Assessments. 2021;44.
[13] IDA-ICE 4.8. EQUA; 2019.
[14] Building directorate. Norwegian building code. 2020.

An ontology-based approach for building automation data analysis

Eunju Park [a], Sumee Park [b], Sebastian Stratbücker [c]

[a] Thermal Comfort, Models and Simulation, Department Energy Efficiency and Indoor Climate, Fraunhofer Institute for Building Physics IBP, Valley, Germany, eunju.park@ibp.fraunhofer.de

[b] Thermal Comfort, Models and Simulation, Department Energy Efficiency and Indoor Climate, Fraunhofer Institute for Building Physics IBP, Valley, Germany, sumee.park@ibp.frauhnhofer.de

[c] Thermal Comfort, Models and Simulation, Department Energy Efficiency and Indoor Climate, Fraunhofer Institute for Building Physics IBP, Valley, Germany, sebastian.stratbuecker@ibp.fraunhofer.de

Abstract. For the efficient and sustainable operation of building automation systems, it is critical to consider various aspects such as users' comfort requirements and energy consumption. The successful application is associated with the integration of multiple and heterogeneous data sources. However, the high complexity of the data poses a challenge. To address this problem, various ontologies have become popular with many applications for data modelling, management and analysis through harmonizing different data sources, as well as efficient querying. In this work, the design, implementation and usage of semantic approaches is investigated to exploit building automation data for customized room automation. As a main contribution, a building automation ontology focusing on room automation is proposed, which is represented in the Resource Description Framework (RDF). Furthermore, several scenarios with the proposed model are demonstrated in-situ, showing easier access to various data sources using a query language like SPARQL. Based on the ontology in RDF format, building data from different sources such as commercial building automation system (e.g. KNX), weather station and room monitoring sensors (e.g. temperature, humidity) are considered for multiple scenarios: (a) anomaly detection of shading automation systems, (b) monitoring user's shading controls in automatic and manual mode, (c) identifying influential factors affecting user's preference. The ontology-based approaches have benefits especially in multiple and heterogeneous data environments using a standardized common and controlled vocabulary. It allows engineers and researchers to enrich and interlink with various databases. Additionally, it explicitly describes the relationships between variables that make data understandable for both humans and machines.

Keywords. Ontology, Semantic model, Anomalies detection, Data mining,
DOI: https://doi.org/10.34641/clima.2022.351

1. Introduction

There is increasing demand for building automation systems. These play an important role in solving existing global warming challenges. Simultaneously, they need to meet user expectations for comfort and usability. The successful application of efficient and sustainable building operation is associated with integration of multiple and heterogeneous data sources. However, the high complexity of the data remains a big challenge. To address these problems, the application of ontologies has become popular in data modelling, management and analysis by harmonizing different data sources, as well as efficient querying. Successful application requires appropriate ontologies to create and accumulate building data through standardized metadata schemas.

Numerous ontologies have been introduced provide the standardized metadata to represent knowledge of buildings with terms in formal and shared conceptualization. As discussed in Pritoni et al. [1], several communities use individual terms, resulting in 40 metadata schemas that adopted different standards. Building Topology Ontology (BOT) [2] provides topological concepts of building components by defining relationships between subcomponents: Site, Building, Storage, Space and Element. The Smart Applications REFerence (SAREF) [3] was intended to capture generic sensors and smart devices, which allows the interoperability among IoT solutions developed by different manufacturers. However, it does not effectively

Copyright ©2022 by the authors. This conference paper is published under a CC-BY-4.0 license.

cover the diversity of devices and equipment in buildings. Brick [4] aims to provide a standardized ontology for physical, logical, and virtual assets in buildings and the relationships between them. Frequently utilized, it shows extensibility and interoperability with other existing schemas. Existing schemas are strong candidates to digitalize building data. However, they are limited to describing building concepts, ignoring logics (e.g. rule-based automation).

To propose a building automation ontology focusing on room automation: (a) the existing schemas are reused, (b) a new schema is created to represent motions triggered by automation systems and user's commands, and (c) these schemas are integrated. With the ontology model investigates the design, implementation and usage of semantic approach to exploit building automation data.

The motivation of this work is to convert existing data sources from a relational database to a model based on the Resource Description Framework (RDF). This allows engineers and researchers to engage with multiple databases, enabling further analysis. Once the data in a RDF format is stored in a graph database, it can be easily accessed on the web using a query language (e.g., SPARQL). In order to demonstrate the application of the RDF data model, building data such as commercial building automation system (e.g. KNX), weather station and room monitoring sensors (e.g. temperature, humidity) are considered in several scenarios: (a) detecting anomalies of shading automation system based rules by monitoring whether the automation system works properly, (b) monitoring user's activities in shading controls when it is in automatic and manual mode, (c) identifying influential factors influencing user preference.

The proposed ontology is illustrated in detail and the usefulness of the proposed model is evaluated in case scenarios.

2. Ontology

The proposed ontology aims at combining the following information:

- Topological concepts of a building
- Equipment, devices and their physical location in a building as well as logical relationships between them
- Rule-based logics of automation systems and actual motions
- Data sources

According to the ontology development guide [5], reusing existing ontologies was considered. The scope includes motions triggered by automation systems and users' commands. The prefixes of the reused ontologies are in Tab. 1.

Tab. 1 – Prefixes and namespaces

Prefix	Namespace
brick	https://brickschema.org/schema/Brick#
bot	https :// w3id .org/bot#
owl	http://www.w3.org/2002/07/owl#
qudt	http://qudt.org/schema/qudt/
rdf	http://www.w3.org/1999/02/22-rdf-syntax-ns#
rdfs	http://www.w3.org/2000/01/rdf-schema#
skos	http://www.w3.org/2004/02/skos/core#
tag	https://brickschema.org/schema/BrickTag#
unit	http://qudt.org/vocab/unit/
xsd	http://www.w3.org/2001/XMLSchema#

2.1 Building structure

In the proposed ontology, well-known concepts such as basement, rooftop and floor form the basic building structure. Several spaces belong to each floor to describe building indoor parts. Spaces are specified into subclasses (e.g. Office). For example, a floor in a building has East and South zones and offices in the East zone. The elements are linked to form the hierarchical building structure by using relationships bot:hasStorey, bot:containsZone or bot:hasSpace. Devices and equipment can be assigned directly to basement, rooftop, floor, zone and space by using relationships brick:hasLocation or brick:isLocationOf. Then, the devices and equipment in the same location can be easily inferred.

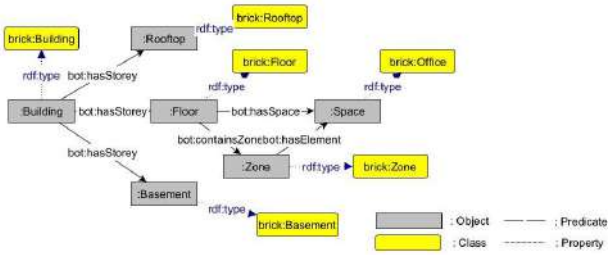

Fig. 1 – Structural modelling of a building.

2.2 Equipment and devices

Equipment and devices are assigned to target locations. Each office has 4 systems: shading, lighting, HVAC and occupancy. Each system except for occupancy consists of 4 components.

- Target object: when an actuator receives a command, it produces a motion to the target object (e.g. blind, light).
- Sensor: to measure the indoor climate. Each sensor belongs to a corresponding system.
- Manual control: input produced by a user manually through a manual object (e.g. switch).
- Remote control: input produced remotely

from a remote device (e.g. PC, mobile devices).

- Motion: actual motion triggered by rules or commands by users. Motion classes are explained in section 2.3 in detail.

Fig. 2 – A room with indoor climate monitoring devices

Each room has a light, blind and radiator as a target object (Fig. 2). The status of target objects are monitored: light (light power), blind (blind position, blind angle), radiator (temperature measured via thermostat, valve position). Sensors to measure indoor climate are located in each room.

- Lighting: Illuminance sensors on desk and ceiling
- HVAC: Temperature, CO2, humidity sensors
- Presence: Occupancy sensors

Commands issued by a user are monitored separately depending on device types (physical switch or remote interface such as PC, app, etc.). A setpoint (e.g. desired radiator temperature) is considered as commands.

- Lighting: Light on/off, dimming
- Shading: Blind up/down, angle position
- HVAC: Desired radiator temperature

A real room in Fig. 2 is described as an ontology as illustrated in Fig. 3.

The weather station located on the rooftop consists of several types of sensors as illustrated in Fig. 4. Temperature, illuminance and wind speed sensors are included in the ontology. Other sensors (e.g. wind direction, air pressure) could increase flexibly. As systems and devices differ, other concepts can be added if additional characteristics are desired.

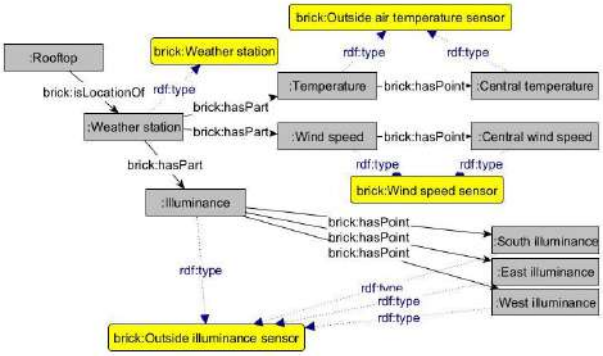

Fig. 4 – Weather station on the rooftop

2.3 Motion

Although there have been several attempts to describe rule-based algorithms in building automation [8], [12], no ontology exists to define motions of an actuator. An ontology is created to express lighting, shading and HVAC system motions. Two factors initiate a trigger to an actuator: rule and command. An object defined as motion class refers to motions triggered by rules of automation systems or commands by users. Similarly to existing ontologies, it has a hierarchical structure. As shown in Fig. 5, the Motion is defined as the top class with subclasses defining specific types of motions: shading, lighting and air control motions.

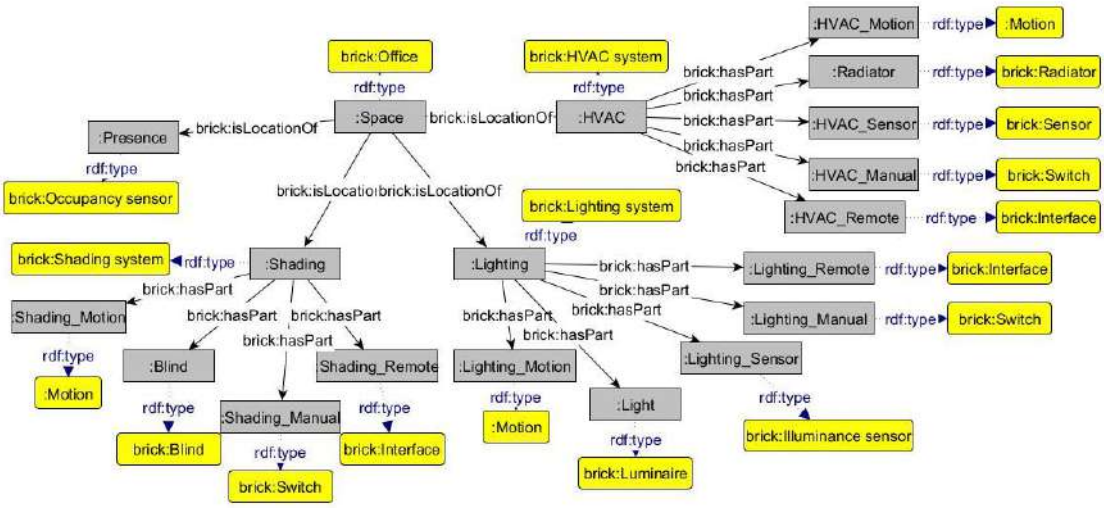

Fig. 3 – Indoor climate monitoring systems

By using the motion ontology and existing ontologies, relationships between motion and rule or command in a room are represented. An example of relationships is presented in section 2.5.

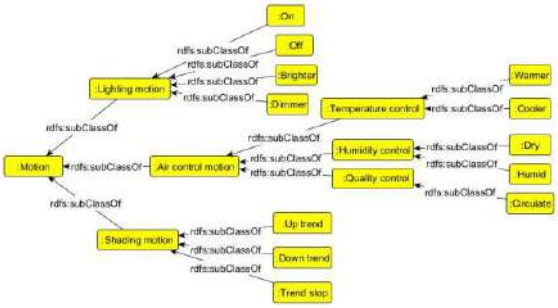

Fig. 5 – Motion ontology

2.4 Data sources

Since the intention was to design an ontology for easier access to relational databases, the data source information is represented in the ontology. As time series data, each data point has at minimum, a timestamp and attribute. If data of an object is available in a relational database, the object includes data source information: database name and primary key. For data description, the unit type information (e.g. Celsius, LUX) is added. For instance as seen in Fig. 7, outdoor illuminance data is collected from a weather station. It is stored in a database called *wetterturm*. The illuminance sensor has the data source and unit (LUX) information as properties.

Although the source information is simplified with database name, primary key and unit type, low-level description such as IP address can be included as well.

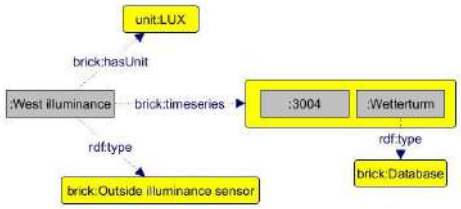

Fig. 7 – Data source information of illuminance sensor

2.5 Example: Shading system

In this section, relationships in up-trend motion in shading systems are described. As shown in Fig. 8, Up-trend of a shading system in a room receives inputs from commands (:Push button up) and an illuminance sensor located on the rooftop. It is configured to trigger the motion depending on the outside illuminance level.

When the conditions are satisfied, the automation system opens the blind. Simultaneously, commands are considered as inputs. A single command input changes the position of the blind. It means that a user can not only trigger a motion by using a manual switch or a remote interface, but also interrupt Up-trend motion triggered by the automation system. As the motion is triggered, it is transferred to the target object (blind). At the same time, the physical position or status of the target object is monitored. If an object has data, it has a property brick:timeseries to refer the database and unique key used in a relational database the database and unique key used in a relational database. The data related to shading system in a room is stored at two different databases: :imedas and :Wetterturm at the investigated building.

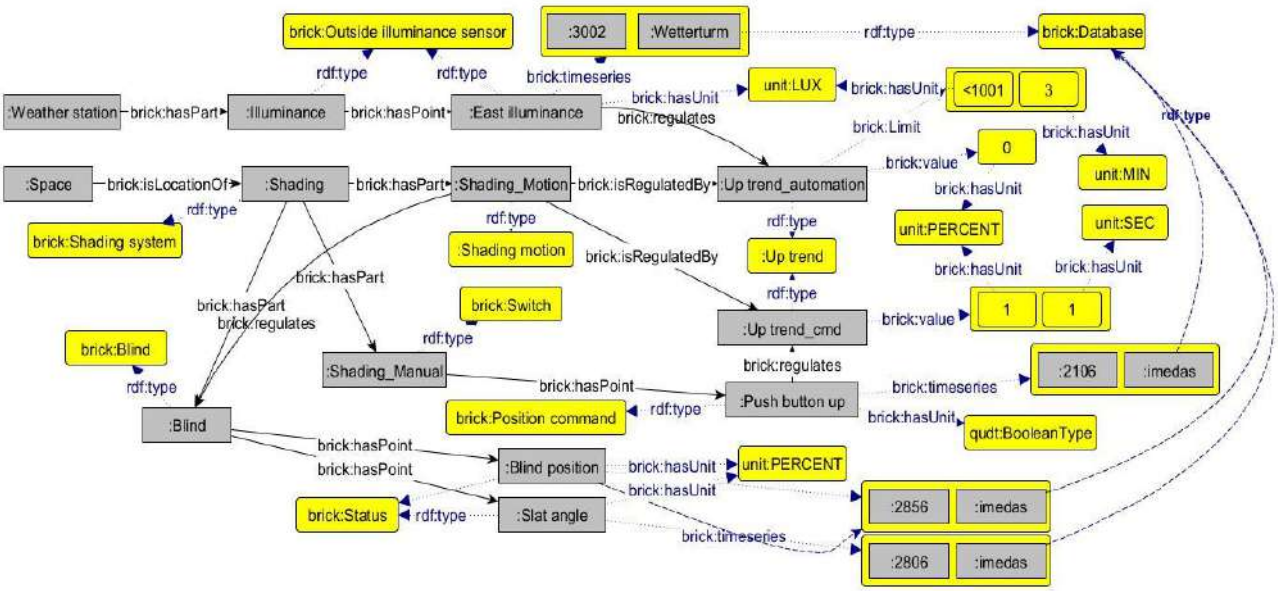

Fig. 8 – Up-trend motion in shading system trigged by automation system (outside illuminance level) or user (manual switch)

3. Application

In the following section, several useful applications are introduced based on the proposed ontology in shading automation systems. Since a user is not regularly present at work, different target offices and periods are used in each application.

3.1 Current building & Shading automation

Twenty offices located on first or second floor in the same building are monitored. Each office has 40 or 41 channels (e.g. sensors, commands) for real-time monitoring. Each office has different numbers of channels monitored. Regardless of the different numbers, the data is easily accessible based on the ontology.

The outside illuminance level and wind speed are only used as the configuration values in shading automation systems. When the outside illuminance level is smaller than 1001 Lux or wind speed is over 10 m/s, the automation system changes the blind position to 0(open). Likewise, it changes the blind position to 100(close) when the outside illuminance level is bigger than 25000 Lux.

3.2 Anomaly detection of shading automation system

From July 2nd to 6th July, two offices (E2, E3) facing the east direction and 2 offices (S2, S3) facing the south direction were monitored. If the configuration condition is satisfied, the position of a blind is changed by the automation system. Since there was no strong wind, only outside illuminance level was influential. Here anomalies are defined as irregular behaviours of shading automation systems, although the configuration conditions are satisfied in automation mode.

The actions triggered by automation systems in office E2 and E3 were identical. Likewise, office S2 and S3 reported identical automation operations. While the Down-trend motion (blind closing) was configured in east-facing offices at 25000 Lux, the blinds were closed in south-facing offices when the outside illuminance level was higher than 35000 Lux. The opening trigger illuminance level was identical with 1000 Lux for both façade.

It took the same time to deliver the operation to south and east-facing offices. Except 5th and 6th July in office E2 and E3 between 5:21 A.M. and 5:25 A.M., approximately 5 minutes delay existed in general. In spite of the delay, it means that the automation system works properly as it is configured.

As the ontology has descriptive information including relevant elements, data source information and configuration values in each office, it is easily retrieved by using a SPARQL as written in Frag. 1 and Frag. 2. Fig. 10 illustrates the filtered sample offices E2 and S2 in shading automation system.

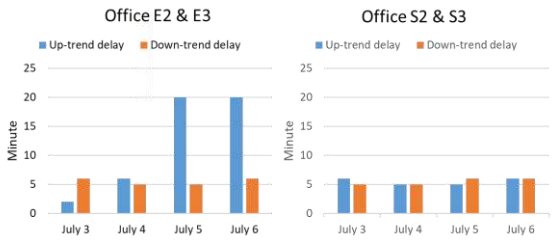

Fig. 9 – Observed command passing delay during 2nd to 6th July.

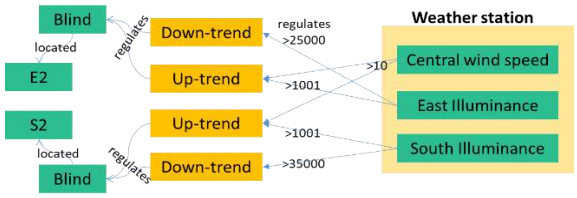

Fig. 10 – Retrieved results of E2 and S2.

Frag. 1 – SPARQL query to get the status of blinds and their data source information.

```
SELECT ?office ?stat ?db ?key
WHERE {
?office rdf:type/rdfs:subClassOf*
brick:Office .
?blind a brick:Blind .
?blind brick:hasLocatoin ?office .
?blind brick:hasPoint ?stat .
?stat a brick:Status .
?stat brick:timeseries ?uid .
?uid brick:hasTimeseriesId ?key  .
?uid brick:storedAt ?db . }
```

Frag. 2 – SPARQL query to get configuration parameters and related data source information.

```
SELECT DISTINCT
        ?office ?motion ?point ?db ?key ?val
WHERE {
?sys brick:hasLocation ?office .
?sys brick:hasPart ?elem .
?elem a mo:Shading_Motion .
?elem brick:isRegulatedBy ?motion .
?motion brick:isRegulatedBy ?point .
?point brick:timeseries ?timeseriesid .
? timeseriesid brick:hasTimeseriesId ?key .
? timeseriesid brick:storedAt ?db .
?point brick:hasUnit ?punit .
?motion brick:Limit ?limit .
?limit brick:hasUnit ?lunit .
?limit brick:value ?val .
FILTER (?punit = ?lunit)
}
```

3.3 Shading control in automatic and manual mode

The indoor climate and user's behaviours were monitored during July (10 days). In this section, two users from east-facing office E1 and south-facing office S1 and their offices are described in shading systems. While the shading automation in E1 was

active and the position of the blind was controlled by the automation system as it is configured during the observed period, the shading system in office S1 was inactive (manual mode), such that the shading automation system did not change the position of a blind and slat angle regardless of the configuration. Both users were present often at work and spent more than 4 hours on average at work. They changed the position of a blind in their offices when they were present.

As already discussed in [9] and [10], there are several possible reasons why the automation systems fail: (a) sensor failures, (b) control logic problem and (c) longer notification time and delay issues. The data could not identify whether a sensor failure did occur, only capturing the control logic and the delay issues.

On July 3rd, the automation system changed the position of the blind and slat angle when the outside illuminance level measured was higher than 25000 Lux at 13:12 P.M. by the configuration. Likewise, it was changed when the outside illuminance level was lower than 1001 at 19:40 P.M. as it is configured. It seems that the control logic works properly. Regarding the delay issue, it took 2 minutes to deliver Down-trend motion and 6 minutes for Up-trend motion by the automation system. The details of office E1 on 3rd July is illustrated in Fig. 11. Additionally, the light was off and there was not strong wind on the day.

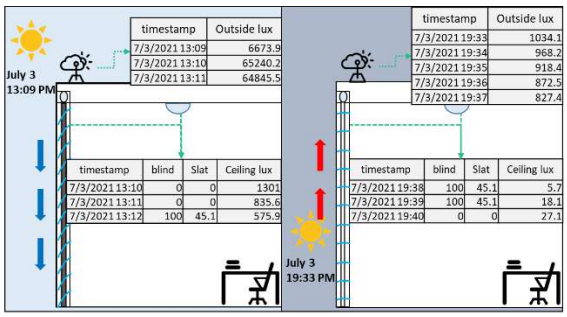

Fig. 11 – Shading automation monitoring in office E1.

The user in office S1 pressed the blind button to open and close the blind on 1st July because the automation system was inactive. A command message generated from a physical button was directly delivered to the blind actuator without delays.

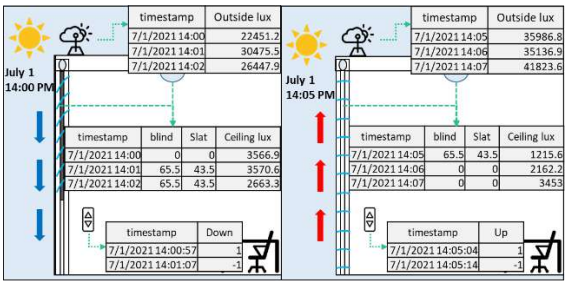

Fig. 12 – Occupant behaviours monitored in office S1.

Both users were in their offices on July 1st, 5th, 6th, 7th and 9th. Comparing the indoor illuminance level measured on the ceiling when both users were in their offices, the user S1 preferred the brighter indoor environment than given by the settings of the automatic system. During 5 days, the average was 759 lux in office E1 and 2409 lux in office S1. Except July 9th as shown in Fig. 13, there is a distinct difference between office E1 and S1. If the automation system in office S1 was active, it would not meet the user's expectations.

Results suggest:

- Control logics of the automation works properly.
- The delay of message delivery exists in automation.
- Centralized automation systems could not meet user's comfort requirements.

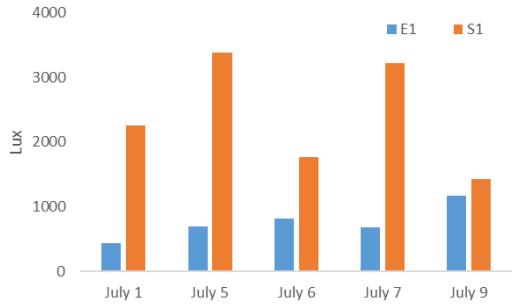

Fig. 13 – Monitored indoor illuminance level on average in office E1 (with automatic mode) and S1 (with manual mode).

3.4 Identifying influential factors affecting user's preference

As mentioned in previous section, the automation system in the south-facing office S1 was inactive and the user changed the position of the blind depending on his comfort preference. An empirical analysis investigates the other associated factors to the user's preference.

Although the shading automation system is configured with outdoor factors (illuminance level and wind speed), it is assumed that indoor climate related factors are the determinants of a user's preference since a user determine whether to open or close a blind according to the indoor climate not outdoor climate. To discover influential factors in office S1, indoor climate related data (e.g. Illuminance level on desk or ceiling) is extracted. By using SPARQL to retrieve related elements and data source information as shown in Frag. 3, sensors and statuses of objects data are easily accessible. Afterwards, the data is filtered based on user's presence at work in order to infer the user's personal indoor climate comfort preference.

Frag. 3 – SPARQL query to get indoor climate related elements and their data source information.

```
SELECT ?system ?elem ?db ?key
WHERE {
```

```
?system brick:hasLocation :S1 .
?system brick:hasPart ?part .
?part brick:hasPoint ?elem .
?elem brick:timeseries ?uid .
?uid brick:storedAt ?db .
?uid brick:hasTimeseriesId ?key .
{?elem rdf:type/rdfs:subClassOf* brick:Sensor}
UNION
{?elem rdf:type/rdfs:subClassOf* brick:Status}
}
```

The indoor climate of office S1 in July was monitored when the user was at work. The total length of the observed period (timestamps) is 9218 based on the measurement in every minute. During his presence, he sent Up-trend command 21 times and Down-trend command 20 times to the blind in his office. These 41 commands include interruptions of the automation system and commands after the interruption. The indoor climate data is labelled as Up-trend when he initiated the Up-trend motion. When he initiated the Down-trend motion, the data are labelled as Down-trend. The remaining 9177 time stamps are labelled as "None". Before training a model to identify influential indoor factors, pre-processing is required to address data imbalanced. Many techniques [11] to handle this issue have been introduced such as over/under-sampling. Among them, the over-sampling technique is applied to increase the size of the minority class (labelled as Up-trend, Down-trend) to balance the majority class (labelled as "None"). The data with Up-trend and Down-trend labels were duplicated to fit the same numbers of data in each label. After pre-processing, the manipulated length of the timestamps is 18354(9177 labelled as None, 9177 labelled as Up-trend or Down-trend). Based on the processed data, a logistic regression model is applied to predict when the user sends a command.

First, two separate models for Up-trend and Down-trend classifications are trained. To find out whether outdoor climate or indoor climate is more influential to user's behaviours, the models only with outdoor or indoor climate factors are trained. For evaluation, 70% of the data is randomly selected into a training set and the remaining 30% into a testing set. The illuminance level and wind speed are used for outdoor climate models. The result only with outside factors is in Tab. 3. Although the outdoor climate factors are used in the shading automation system as configuration values, it does not explain the behaviours of the user effectively.

Tab. 3 – Experiment results with outdoor factors

Model		Up-trend	Down-trend
Coefficient	Wind	-0.0052	0
	Illum.	-0.0004	-0.0003
Accuracy	Training	0.57	0.49
	Testing	0.57	0.49

The office S1 has 12 indoor climate factors available. In order to find the important variables, a feature selection technique is applied. In Up-trend motion, illuminance level measured on a desk and the slat angle of a blind are the influential factors among 12 indoor climate factors. In down-trend motion, illuminance level measured on a desk and ceiling and the position of a blind are important. The results of the best models are listed in Tab. 4.

From empirical analysis, the following is inferred for the user in office S1: in Up-trend (blind opening) and Down-trend(blind closing), indoor illuminance level and the status of blind(positon and slat angle) are highly related to his comfort requirements rather than other indoor factors.

Tab. 4 – Results with different indoor factors

Model		Up-trend	Down-trend
Coefficient	Lux(desk)	-0.0172	-0.0001
	Lux(ceiling)	-	-0.0021
	Blind pos.	-	-1.1478
	Slat angle	-0.0018	-
Accuracy	Training	0.85	0.78
	Testing	0.86	0.79

4. Conclusion

In order to integrate multiple and heterogeneous data environments, we built an ontology for building automation data analysis. It explicitly describes the relationships between variables which makes data understandable for both humans and machines. Although each room has a different number of channels monitored and configuration descriptions, the data and relevant information were efficiently retrieved based on the ontology without changing a SPARQL query. In this paper, we focus on convenient access to different data sources for further research with several possible use scenarios. In terms of data engineering, an ontology-based approach provides efficient data handling. This study is limited by the small number of observed data of user's activities (e.g. blind closing, opening) due to occupants working from home due to COVID-19. Future work will build a scalable model based on the proposed ontology containing a set of evaluated methods and comparisons between them.

5. References

[1] Pritoni M, Paine D, Fierro G, Mosiman C, Poplawski M, Saha A, Bender J, Granderson J. Metadata Schemas and Ontologies for Building Energy Applications: A Critical Review and Use Case Analysis. Energies. 2021 Jan;14(7):2024.

[2] Rasmussen M, Pauwels P, Lefrançois M, Schneider

GF, Hviid C, Karlshøj J. Recent changes in the building topology ontology. InLDAC2017-5th linked data in architecture and construction workshop 2017 Nov 13.

[3] Daniele L, den Hartog F, Roes J. Created in close interaction with the industry: the smart appliances reference (SAREF) ontology. InInternational Workshop Formal Ontologies Meet Industries 2015 Aug 5 (pp. 100-112). Springer, Cham.

[4] Balaji B, Bhattacharya A, Fierro G, Gao J, Gluck J, Hong D, Johansen A, Koh J, Ploennigs J, Agarwal Y, Bergés M. Brick: Metadata schema for portable smart building applications. Applied energy. 2018 Sep 15;226:1273-92.

[5] Noy NF, McGuinness DL. Ontology development 101: A guide to creating your first ontology.

[6] Mahdavi A, Taheri M. An ontology for building monitoring. Journal of Building Performance Simulation. 2017 Nov 2;10(5-6):499-508.

[7] Fierro G. Design of an effective ontology and query processor enabling portable building applications. University of California, Berkeley. 2019 May 10.

[8] Terkaj W, Schneider GF, Pauwels P. Reusing domain ontologies in linked building data: the case of building automation and control. In8th International Workshop on Formal Ontologies meet Industry 2017 (Vol. 2050).

[9] Daissaoui A, Boulmakoul A, Karim L, Lbath A. IoT and big data analytics for smart buildings: a survey. Procedia Computer Science. 2020 Jan 1;170:161-8.

[10] Giraldo-Soto C, Erkoreka A, Mora L, Uriarte I, Del Portillo LA. Monitoring system Analysis for evaluating a building's envelope energy performance through estimation of its heat loss coefficient. Sensors. 2018 Jul;18(7):2360.

[11] Hasib KM, Iqbal M, Shah FM, Mahmud JA, Popel MH, Showrov M, Hossain I, Ahmed S, Rahman O. A survey of methods for managing the classification and solution of data imbalance problem. arXiv preprint arXiv:2012.11870. 2020 Dec 22.

[12] Schneider GF, Pauwels P, Steiger S. Ontology-based modeling of control logic in building automation systems. IEEE Transactions on Industrial Informatics. 2017 Aug 23;13(6):3350-60.

[13] Petrova-Antonova D, Ilieva S. Digital twin modeling of smart cities. InInternational Conference on Human Interaction and Emerging Technologies 2020 Aug 27 (pp. 384-390). Springer, Cham.

[14] Mavrokapnidis D, Katsigarakis K, Pauwels P, Petrova E, Korolija I, Rovas D. A linked-data paradigm for the integration of static and dynamic building data in Digital Twins. InProceedings of the 8th ACM International Conference on Systems for Energy-Efficient Buildings, Cities, and Transportation 2021 Nov 17 (pp. 369-372).

Control device for pumping one-pipe hydronic systems

Jiří Dostál [*], *Tomáš Bäumelt, Jiří Cvrček*

University Centre for Energy Efficient Buildings, Czech Technical University in Prague, Buštěhrad, The Czech Republic.
[*] corresponding author, jiri.dostal@cvut.cz

Abstract. The article presents the development and algorithms behind an active control device for pumping one-pipe (or primary-secondary pumping) systems. The main feature of such a system is the series connection of thermal loads/sources and a small pump by each load/source, as opposed to classical two-pipe systems with a parallel connection and throttling valves. Our main contribution is an integration of all necessary components into one device and the ability to infer mass flow in a secondary circuit without a flowmeter. By also measuring a temperature drop, we can estimate and control a heat flow and provide remote thermal and hydraulic diagnostics of a connected heat terminal via the device. It is powered and communicates through the Ethernet and contains a wet-rotor BLDC pump controlled by the field-oriented control method. A Kalman filter provides a mass flow estimate, and a robust distributed parameter system controller regulates the heat flow.

Keywords. One-pipe, single-pipe, primary-secondary pumping, heat flow control, iQ-pump
DOI: https://doi.org/10.34641/clima.2022.349

1. Introduction

This article focuses on one-pipe hydronic networks, also called single-pipe or referred to as primary-secondary pumping systems. Nowadays, however, mostly two-pipe hydronic heating systems are used. The most widespread is quantitative regulation, where varying hydraulic resistance in a branch regulates flow through a heat terminal. The easiest quantitative regulation actuator is a manual valve; however, nowadays, legislative norms (e.g. [1] in Czech Rep.) no longer allow its use – at least automatic thermostatic valves have to be utilised. A thermostatic valve controls its opening mechanically, depending on the room temperature. A more up-to-date solution is the use of Pressure Independent

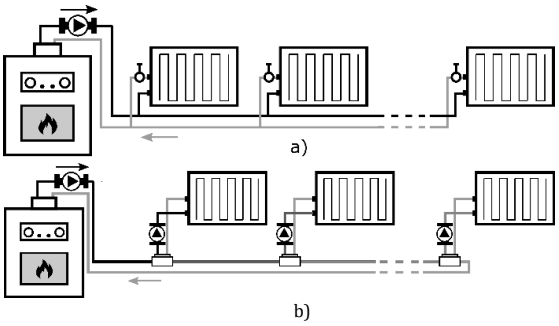

Fig. 1 – Hydronic system topologies: a) two-pipe throttling system, b) pumping one-pipe system.

Control Valves (PICV, [1]), which are utilised mostly in fan-coil unit (FCU) applications. A PICV contains a spring mechanism for maintaining a constant pressure drop across an adjacent control valve; the flow, therefore, depends only on the valve opening and not on any pressure variations [1].

Another way to control a hydronic system is to pump heat transfer liquid where needed instead of throttling it where not required. This solution is already available on the market [2,3] and uses a small pump for each heat terminal. Let us call systems with throttling valves "passive" or "throttling" and systems using the pumps "active" or "pumping". Wilo AG has also established a terminology where throttling systems are called "supply oriented" and those with pumps "demand oriented". It is possible to meet also the term "centralised" for systems with a central pump and "decentralised" for decentralised pumping systems.

Although there is also a two-pipe variant of a decentralised pumping system [2,4], this article expands only on the one-pipe pumping hydronic network and the control device designated.

The article will present the one-pipe network, the control device development, and algorithms, finished by its real-life validation.

Copyright ©2022 by the authors. This conference paper is published under a CC-BY-4.0 license.

1.1 Pumping one-pipe hydronic network

Pumping one-pipe systems, also referred to as "primary-secondary pumping" [5], are mostly used to connect heat sources, but can also be utilised on the load side. In short, from the main pipe in the circuit branch out two closely-spaced T-fitting, where a secondary (the "small") pump with a heat source/terminal is looped around. The heat sources/terminals are connected in series on the main (primary) piping, that loops back to the main circulator and a heat load/source side, respectively. See Fig. 1 for a schematic depiction.

The advantages of the pumping one-pipe hydronic system are:

- the system generally contains only two pipe diameters (primary and secondary),
- time and material savings (fewer pipes, connections, valves and plumber's work),
- one type of pump in the secondary loop can control a wide range of load capacities; i.e. the system is robust against design inaccuracies/changes,
- the amount of the overall dissipated pumping energy is the lowest of all possible topologies,
- one-pipe system contains less heat transfer liquid (water, glycol) than a comparable two-pipe system.

The disadvantages are:

- practitioners hold on the impression that one-pipe systems are inefficient and problematic. This is based on the long-surpassed throttling one-pipe heating variant with its real higher operational cost and low comfort [5]. It harms, beforehand, the reputation of the pumping one-pipe systems,
- temperature relations among secondary loops shall be considered during system design. However, there is a one-pipe network design and validation tool [8,9] available,
- this solution became feasible only recently as canned wet rotor pumps, and electronically commutated motor became available. There are not many installations proving the performance of this system. However, dozens of pumping one-pipe systems are in service in the US, e.g. [3].

For more hydronic network topologies details and a one-pipe network design tool description, resort to [6].

2. One-pipe control pump device

The thermal power of a heat terminal in a pumping one-pipe network is controlled by the speed of the secondary pump impeller. And as there is no variable hydraulic resistance in the secondary circuit, the secondary flow is governed solely by the pump speed.

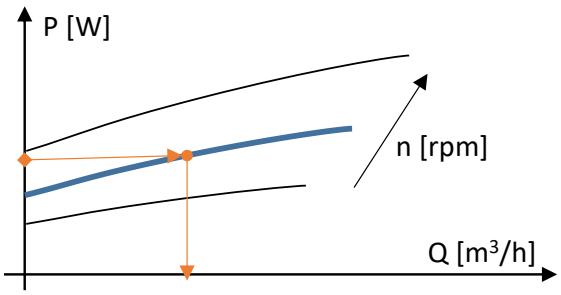

Fig. 2 – The basic principle of inferring flow from a pump electrical power reading.

This scenario makes it possible to infer flow from pump power readings, as Fig. 2 suggests. Knowing the pump speed, power, and power-flow characteristics is enough to estimate the absolute volumetric/mass flow through the pump and consequently through the whole secondary circuit. A heating/cooling power can be calculated by adding a pair of temperature sensors on a supply and return line.

Our patented invention [7,8], with the business name iQ-pump (IQP), bundles the two closely-spaced T-fittings, a pump housing, check-valve and a pair of temperature sensors together into one device. Such a device connects a heat source/terminal directly to the main pipe. See Fig. 3 for schematic depiction.

Note: Although the same principles generally apply to heat sources, the one-pipe control pump devices will only be depicted in the heat distribution to the heat terminals. Also, even though only heating will be addressed further, similar principles apply to the distribution of cooling power.

2.1 Design and Manufacturing

The EU directive [9] recommends designing heat sources for a typical building load (instead of a maximal load), with a complimentary heat source for extreme conditions. Applying the same principle to heat distribution, the main pipe has been chosen DN32 with G5/4 threads, which renders an economic pressure drop [10] for supplying one floor of 75% of commercial buildings in the EU [11]. The other 25% of establishments with higher loads shall, but only for 6% of operation time [12], experience higher main pipe velocities than 1.2 m/s and higher pressure losses.

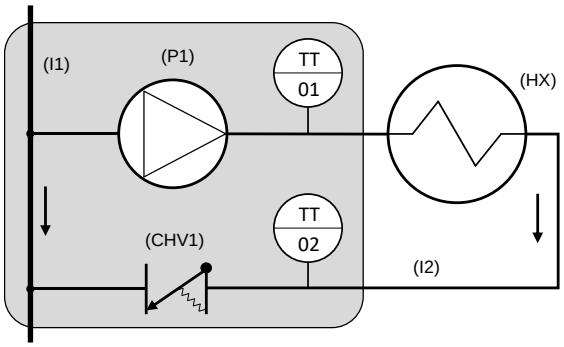

Fig. 3 – One-pipe control pump device scheme. HX – heat exchanger, CHV – check-valve, I – pipe, P – pump, TT – temperature sensor.

The device's secondary pipe and pump are sized for a load of 10 kW with an average weighted hydraulic conductivity of 0.8 bar/m³/h. The secondary ports are DN15 with G1/2 threads, the standard connection for most heat terminals. See Fig. 4 for results from the research on typical design operation conditions (normalised using EN 442-1:1995) and typical loads.

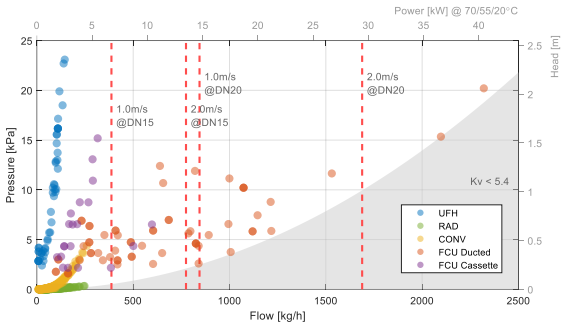

Fig. 4 – Typical design operation conditions for underfloor heating (UHF), radiators (RAD), convectors (CONV) and fan-coil units (FCU). All datasheet values normalised to conditions 70/55/20°C using the norm EN 442-1:1995

A D5-sized pump [13] (used in solar-thermic installation) serves as the secondary pump. It is a spherical-shaped wet-rotor electronically commutated pump with four rotor poles and six stator coils on a magnetic core ring.

The IQP body (Fig. 5) consists of the main pipe, from which a pump housing extends with its suction hole. The pump outlet directs perpendicularly away from the main pipe axis. The secondary outlet port houses a spring check valve and a secondary supply temperature sensor. From the same direction comes the secondary inlet, where the secondary return temperature sensor is housed and which connects back to the main pipe.

The IQP body was made as symmetrical as possible from the primary-pipe point of view to enable directing the secondary ports to the right or left regardless of the flow direction in the main pipe. I.e. the direction of flow in the main pipe does not alter hydraulic conditions in the secondary piping.

The first prototypes were manufactured using additive 3D printing from ABS and were waterproofed by curing in a solvent. This technique sufficed for all tests not involving elevated temperatures (> 50°C). Later prototypes were manufactured by selective laser sintering using high-temperature resins. These prototypes were waterproof from the beginning but were found to be very brittle and had to be later reinforced with a polymer resin armour. Later prototypes were manufactured using selective heat sintering using PA12 nylon material. These prototypes were found indestructible for all our relevant tests. The final prototypes were cast from brass using ceramic moulds (created on top of 3D printed masters). The final design is brass-castable and machinable by standard industrial methods.

The electronics cover is designed to be injection-moulded without special cores. It is designed to comply with IP44 and cable-pull protection.

3. Electronics and software

The first electronics prototype was built on the Arduino platform, mainly as a relay between the peripheries and Matlab. Afterwards, a custom-built PCB empowered by a Raspberry Pi 3 Compute Module was used. In-line motor phase measurements were performed using shunt resistors. Several Raspbian kernel modules operating the ADC over SPI were built to quickly and precisely sample the phase voltages and currents and calculate power from the asymmetric readings. Reliable measurement of the phase between voltage and current, however, remained a problem, which only was solved by a power acquisition directly by a microchip later on. The EC motor was driven by a 6-step control on-chip driver TI DRV10987.

The final electronics utilises an NXP i.MX-RT microcontroller with built-in motor control features. The pump speed control and electrical power acquisition are performed by vector control methods (FOC) [14], allowing for efficient device control in the whole range from zero to maximal flow.

The powerful ARM Cortex-M7 processor, running FreeRTOS, also allows for broadband communication, temperature readings and heat estimation and control computations.

Fig. 5 – One-pipe control pump device. Early design at the top (3D print manufacturing); brass-casted and machined final design with injection-mould-manufacturable electronics cover on the bottom.

2.2 Mass flow estimation

Mass flow estimation is the key component of the one-pipe control pump device. Being able to determine flow without the use of a flow meter enables cost-effective implementation of the following features:

- Heat flow estimation
- Heat flow control
- Heat metering
- Thermal diagnostics

Looking at the schematic of the secondary circuit (Fig. 3), there are three main features from the hydraulic point of view: the double T-fitting (connection to the primary circuit), the pump body with a check-valve and the hydraulic load, i.e. the heat terminal with its piping. The T-fittings are spaced closely together to not to create a pressure source for the secondary circuit. Changes in the primary flow do not influence the secondary flow (verified by measurement, variation less than 5 l/h per 1000 l/h change in the primary flow) – hence the two circuits are hydraulically separated. It simplifies the secondary hydraulic circuit to just two components: the pump and the load.

The IQP device sizes neither up nor down with the capacity of the load; the control authority is always full, as we control the flow directly. Precision speed control of the pump means sufficient flow control precision for any load capacity. Therefore, the IQP body with its pump housing, check-valve and ports is of a fixed size and can be described precisely by its head-flow (HQ) and power-flow (PQ) characteristics. Fig. 6 presents the measured data and their fitted polynomial model. Fitting in L1 norm under shape constraints [15] was used.

The hydraulic conductivity of the load is considered fixed but unknown.

A dynamical model of the pump (Fig. 7) will be described now. The inputs to the model are: speed reference S_{REF}[rpm], volumetric flow Q [l/h] and inlet water temperature T_{wi}[°C]. The dynamic states are: pump speed S [rpm] and coil temperature T_c[°C].

The model's outputs are: pump head H [m], pump electrical power P [W] and pump speed

$$\begin{aligned} u &= [S_{REF}, Q, T_{wi}]^T, \\ x &= [S, T_c]^T, \\ y &= [H, P, S], \theta = [\tau_S, C_c, h_c]^T. \end{aligned} \tag{1}$$

The state equation for speed is governed mainly by the speed controller, impeller inertia and flow, but the dynamics are fast enough to enable coarse approximation by first-order dynamics

$$\begin{aligned} \dot{S} &= \tau_S^{-1}(S_{REF} - S) \\ \dot{T}_c &= C_c^{-1}\left(h_c(T_{wi} - T_c) + \mathrm{pol}_{PQ}(Q, S)\right), \end{aligned} \tag{2}$$

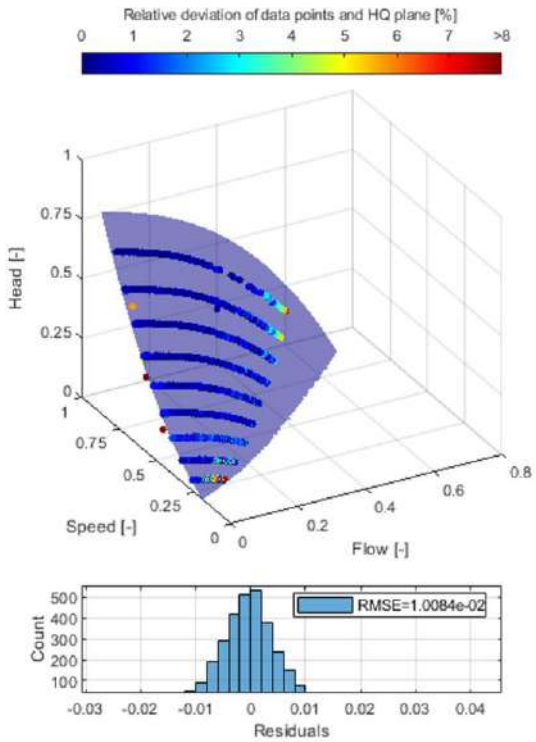

a)

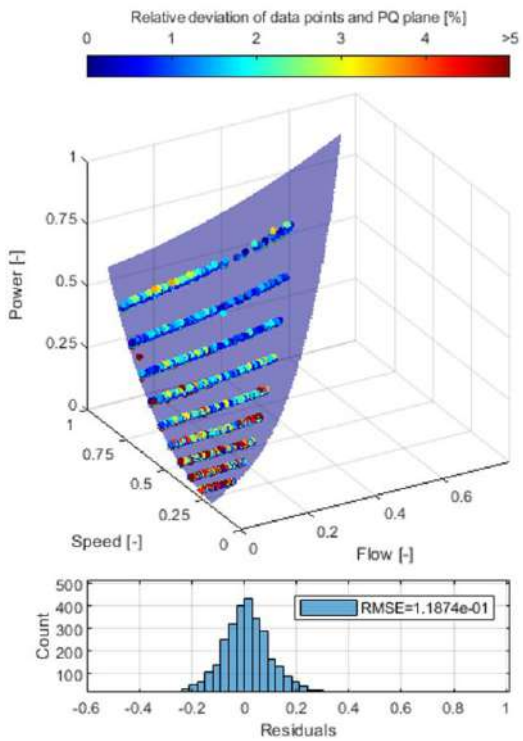

b)

Fig. 6 – IQP device characteristics fitting: a) HQ plane, b) PQ plane.

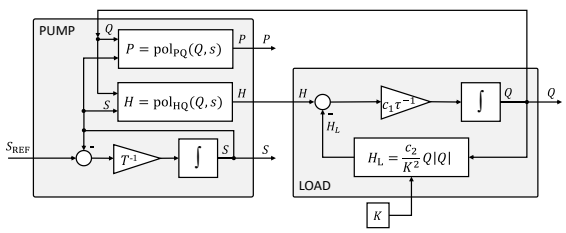

Fig. 7 – Simplified scheme of the dynamical model used for mass flow estimation.

where τ_S [s] is a time constant. The coil temperature has been identified to affect the power consumption. There is a heat transfer to the pumped water of the supply temperature, where the heat transfer coefficient is h_c[W/K] and the electrical power is represented by a polynomial model (eq. (3)). The heat capacity of the coil is denoted C_c [J/kg · K].

The outputs are defined by the steady-state polynomial maps (Fig. 6)

$$\begin{aligned} H &= \mathrm{pol}_{HQ}(Q,S) = \\ &= a_3Q^3 + a_2Q^2 + a_1Q + c_{11}Qs + \\ &\quad + b_2s^2 + b_1s + a_0 \\ P &= \mathrm{pol}_{PQ}(Q,S) = \\ &= \bar{c}_{13}Qs^3 + \bar{c}_{12}Qs^2 + \bar{a}_1Q + \bar{c}_{11}Qs + \\ &\quad + \bar{b}_3s^3 + \bar{b}_2s^2 + \bar{b}_1s + \bar{a}_0, \end{aligned} \tag{3}$$

with coefficients $a, b, c, \bar{a}, \bar{b}, \bar{c}$ fitted to measured data.

A dynamical model of the load (Fig. 7) has three inputs: head difference across the load H [m], inlet water temperature T_{wi}[°C], outlet water temperature T_{wo}[°C]. The only dynamical state is the flow Q [l/h], which is also the only output. The parameters θ are described below

$$\begin{aligned} u &= [H, T_{wi}, T_{wo}]^T, \\ x &= Q, \\ y &= Q, \\ \theta &= [K, \tau]^T. \end{aligned} \tag{4}$$

The dynamical flow model is derived from an inertance model, where the difference between input head H and load head H_L [m] is the change driving potential,

$$\dot{Q} = 3.6 \cdot 10^6 \cdot g \cdot \tau \cdot (H - H_L). \tag{5}$$

The load head follows from the Darcy-Weisbach law, where K [bar → m^3/h] is the hydraulic conductivity factor of the load, gravity is denoted g [m/s^2],

$$H_L = \frac{10^{-4}}{K^2 g} Q|Q|. \tag{6}$$

Inertial constant τ[m] is the ratio of the pipe cross-section A_c[m^2] and total pipe length L [m],

$$\tau = \frac{A_c}{L}. \tag{7}$$

The hydraulic conductivity is mildly dependent on mean water temperature by a multiplication factor k_K. The hydraulic conductance at nominal temperature $K_{nom} = K|_{T=T_{nom}}$ is a parameter estimated by a Kalman filter,

$$K = K_{nom} + k_K \left(T_{nom} - \frac{T_{wi} + T_{wo}}{2} \right). \tag{8}$$

The dynamical model is non-linear, with one parameter to be estimated. The states of the system – pump speed S [rpm] and most importantly the flow Q [l/h] – all together with the hyd. conductance of the load K_{nom} are estimated by an extended Kalman filter (EKF). The resulting flow estimate Q is denoted $\widehat{\dot{m}_w}$.

2.3 Heat flow control

A heat terminal, e.g. FCU, is generally a distributed parameter, distributed time-delay system governed, when simplified, by a one-dimensional hyperbolic PDE [16]. Additionally, temperature measurements are situated at the IQP device, so there is also a, possibly significant, transport delay present due to secondary piping lenght.

Standard PID feedback control is not suitable for such systems. But a controller by Sandoval [17] is specifically designed for robust velocity control of convective spatially distributed systems, e.g. heat terminals.

The control problem statement is to find a controller of a form

$$\begin{aligned} \dot{\zeta} &= g(\zeta, e) \\ u(t) &= \phi(\zeta, \mathrm{e}), \end{aligned} \tag{9}$$

where $u(t)$ is the manipulated variable (the pump speed reference S_{REF} in our case), $e = y - r$ is the control error (heat flow error in our case) and ζ is the integrator state of the controller. The goal is to find functions g, ϕ such that the control error vanishes in time. Let the function $\phi(\zeta, e) = \zeta + \theta\psi(e)$ be such that $e\psi(e) > 0$ with $\theta = \mathrm{sign}(L_f h) = \mathrm{const.}$ being the sign of the Lie derivative of the problem (either 1 or -1). Then for an input function

$$u = u(t - \tau) + \theta\psi(e), \tag{10}$$

the error dynamics is asymptotically stable [17].

The stabilising control law is defined exactly as

$$\begin{aligned} \dot{\zeta} &= k_I \mathrm{sg}(e)\theta(|(u - \zeta)\zeta| + |\dot{e}|) \\ u &= \zeta + \theta\psi(e), \end{aligned} \tag{11}$$

where $\psi(e) = k_P e$ and $\mathrm{sg}(e) = 1$ for $e \geq 0$ and -1 otherwise.

The two constants k_P and k_I are tuning parameters for proportional and integral action, respectively. The controller can be considered a PI controller with a variable integral gain. An anti-windup clamping modification has been utilised to prevent wind-up situations.

In our scenario, the controlled output is a calculated heat output of the heat terminal

$$\begin{aligned} y &= \hat{Q}_H = \widehat{\dot{m}_w} c_\mathrm{p}(T_{wi} - T_{wo}) \\ r &= Q_{REF}, \end{aligned} \tag{12}$$

where c_p[J/kg/K] is the specific heat capacity of the heat transport fluid (assumed water, a statistical test for the presence of water can be performed), T_{wi}, T_{wo} [°C] are supply and return temperature measurements in the IQP device. Heat flow reference

Q_{REF} [W] is given by a supervisory temperature controller – a wall module or a zone temperature MPC [18].

3. Validation

The development of the IQP device would not be possible without a precise and multifunction measurement and validation testbed. Flow estimation and heat control precision will be presented in this section.

3.1 Testbed

A hydronic testbed for temperature feedback hydronic control devices (Fig. 8) contains three main circuits: the main hydronic circuit starting with the main pump, passing through a hot-water tank, the IQP device, set of PT1000 temp. sensors and electromagnetic flowmeter back to the primary pump. The secondary circuit starts at the IQP device, passes through an actuated valve, a Coriolis flowmeter, a set of PT1000 temp. sensors to a water-to-air heat exchanger and back to the IQP device. A precise differential pressure sensor can be connected to IQP device ports on the secondary and the primary side. The airstream starts with a straight duct with a Wilson grid flowmeter, continues through a controlled fan and a set of PT1000 temp. sensors into the heat exchanger, from where it leaves the testbed.

The testbed also contains a small (cold) tank to realise sharp temperature changes. The cold tank is connected to the main-primary circuit using a one-pipe connection via an old IQP prototype. The heating tank is controlled by an ADRC controller, airflow and primary water flow by regular PI controllers. All controllers are embedded from Matlab into the main Unipi Neuron PLC. See Fig. 8 for a depiction of the testbed.

Two-pipe throttling actuators with temperature feedback may also be developed and tested on the testbed.

3.2 Results

Fig. 9 presents flow estimation precision. The data were obtained by ramping the pump speed up and down, preceded by three load steps, where identification (by the KF) of the hydraulic load occurred. The actuated valve connected to the secondary circuit was set to a random position to represent an unknown hydraulic load. The standard deviation in the whole range for the actual hydraulic load is 3.91 l/h; however, the estimation in the low-flow region is inaccurate due to the lack of feedback from the pump's electrical power reading; the PQ characteristics is flat here.

Fig. 10 presents results on the heat flow control of the water-to-air heat exchanger present at the testbed. The results were obtained by slowly ramping up and down the absolute heat reference value. The standard deviation over the whole range

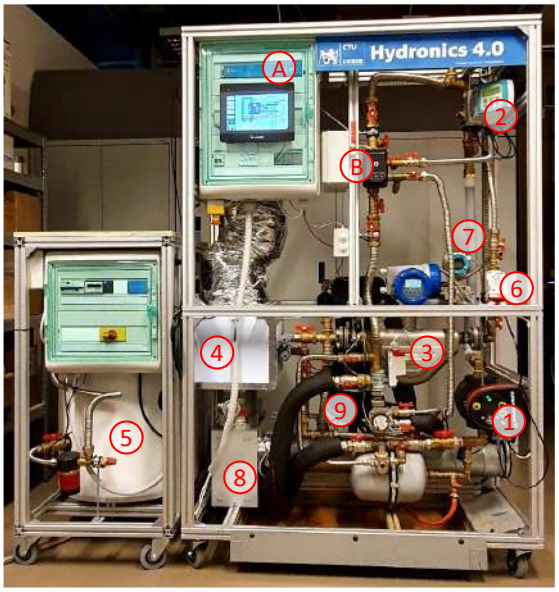

Fig. 8 - Hydronic Testbed. A) Testbed controller, B) One-pipe control pump device, 1) Primary pump, 2) Primary induction flowmeter, 3) Secondary Coriolis flowmeter, 4) Water-to-air heat exchanger, 5) Main tank, 6) Actuated valve, 7) Differential pressure sensor, 8) Controlled fan, 9) Second tank for sudden temperature steps.

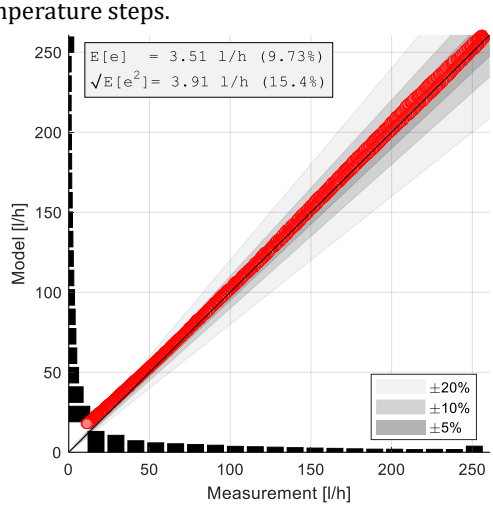

Fig. 9 – Flow estimation precision for a random fixed position of the actuated valve in the secondary circuit.

of the heat terminal was 158 W. However, the tracking precision at low heat flows is unsatisfactory due to multiple factors. First and foremost, the error in mass flow estimation is to be blamed; secondary, the delivered (real) heat is calculated from the wet water temperature sensors positioned directly on the heat exchanger inlet and outlet, whereas the estimated power is calculated from the temperature sensors on-board the IQP device, and there is a good portion of uninsulated piping between them. Note that the heat flow controller tracks the heat reference closely without any error, but the estimated power differs from the real one. Therefore, the power control error is likely accountable to the heat dissipated by secondary piping (not well insulated) and other errors in temperature measurements, but the flow estimation error also participates.

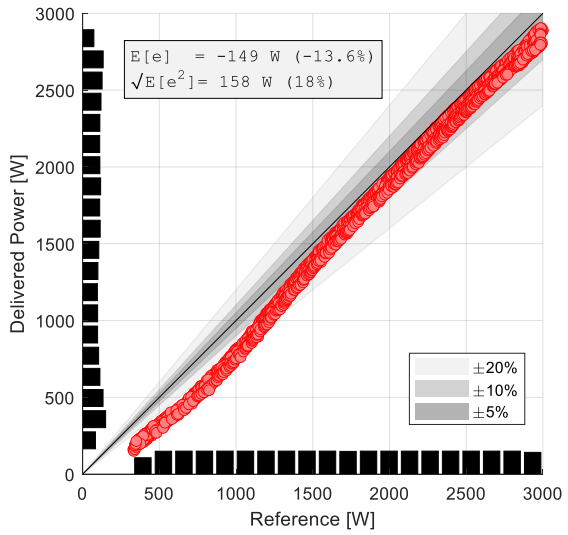

Fig. 10 – Steady-state heat flow control precision for the heat terminal present at the hydronic testbed.

4. Conclusion

This paper presents the results of a three-year-long development of the one-pipe control pump device (iQ-pump). We have built a well working testbed suitable for developing temperature feedback hydronic actuators (valves, pumps) and have designed and built the IQP device according to the patented ideas. The paper presents the mechanical development process and the core working principle from the estimation and control point of view. Measurements validate the method to be sound, although there is still room for improvement in details. Future development will be directed towards thermal diagnostics, mainly detecting diminishing heat transfer due to dust build-up in an FCU.

Acknowledgement

This research was funded by the Technology Agency of the Czech Republic, grant number TK01020024.

References

[1] Pressure Independent Control Valve: Quick Selection Guide. Honeywell; 2014.
[2] Wilo-Geniax: Der Komfort-Manager für die Heizung. Wilo SE; 2014.
[3] Taco LoadMatch System 2021.
[4] Dostál J, Havlena V. Modeling, optimization and analysis of hydronic networks with decentralized pumping. CACS 2014 - 2014 International Automatic Control Conference, Conference Digest, 2014, p. 269–274.
[5] Einrohrheizungen: Neues System für die Sanierung. HeizungsJournal 2016.
[6] Zlevor O, Dostál J. Demand-oriented Hydronic Heating System and the Active One-pipe System Design Tool. E3S Web of Conferences, vol. 111, EDP Sciences; 2019, p. 01091.
[7] Dostal J. Heat Exchanger Control and Diagnostic Apparatus. US15/577.882, 2018.
[8] Dostal J, Baumelt T, Hauser J, Kubes J, Valtr J, Zlevor O. One-pipe Hydronic Heating Control Device. US2021088230A1, 2021.
[9] Directive (EU) 2018/844 of the European Parliament and of the Council of 30 May 2018. European Commission; 2018.
[10] Siegenthaler J. Modern Hydronic Heating: For Residential and Light Commercial Buildings. Course Technology; 2011.
[11] Kemma R. Average EU building heat load for HVAC equipment. European Commission; 2014.
[12] Europump: Energy Efficiency of Circulators. European Association of Pump Manufacturers; 2011.
[13] Ecocirc D5vario DC pumps. Xylem; 2020.
[14] Application Note:s 3-Phase Sensorless PMSM Motor Control Kit with S32K144. NXP Semiconductors; 2020.
[15] Wahl F, Espinasse T. Polynomial regression under shape constraints. 2014.
[16] Dostál J, Havlena V. Mixed Mesh Finite Volume Method for 1D Hyperbolic Systems with Application to Plug-flow Heat Exchangers. Mathematics 2021;9:2609.
[17] García-Sandoval JP, González-Álvarez V, Pelayo-Ortiz C. Robust continuous velocity control of convective spatially distributed systems. ChemicalEngineeringScience 2008;63:4373–4385.
[18] Dostal J, Baumelt T. Model Predictive Control for Buildings with Active One-pipe Hydronic Heating. E3S Web of Conferences, vol. 111, EDP Sciences; 2019, p. 04050.

De-Risking Building Performance Investments by Certified Quality Management Services (QUEST)

Ivo Martinac[a], Han-Suck-Song[b], Stefan Plesser[c], Cormac Ryan[d], Ole Teisen[e], Jin Wen[f]

[a]Division of Sustainable Buildings, KTH Royal Institute of Technology, Stockholm, Sweden, im@kth.se

[b]Division of Real Estate Economics and Finance, KTH Royal Institute of Technology, Stockholm, Sweden, han-suck.song@abe.kth.se

[c]synavision GmbH, Bielefeld, Germany, plesser@synavision.net

[d]COPILOT Building Commissioning Certification, Paris, France, c.ryan@copilot-building.com

[e]Sweco Denmark A/S, Copenhagen, Denmark, ole.teisen@sweco.dk

[f]Civil, Architectural and Environmental Engineering, Drexel University, Philadelphia, PA, USA, jinwen@drexel.edu

Abstract. Non-compliance with predicted, contracted or otherwise required aspects and levels of building performance can result in a wide range of problems. This includes sub-par quality of building functions and services, unsatisfactory indoor environmental quality, disappointing end-user experience, excessive energy use, excessive environmental emissions, increased maintenance and operational costs, operational start-up loss, component and system faults, difficulties in achieving targeted building certification levels, mismatch with business case, lack of adaptability and flexibility, expenses changed from capital expenditure to operational expenditure, facility not meeting regulatory requirements, as well as increased risk and liability. This is often referred to as the building performance gap.

Compliance with ambitious levels of resource efficiency, energy performance, decarbonisation and circularity goals, as well as other key objectives defined by the EU Taxonomy for sustainable activities will be essential criteria for the sustained future success of businesses throughout the building sector.

Building performance investments, including investments in energy efficiency, can generate significant environmental benefits, while also increasing financial returns. The key goal of the EU-funded project Quality Management Investments for Energy Efficiency (QUEST) is to promote private investments and financing in quality management services to ensure sustainability and energy-efficiency of building projects. To that end, a toolkit, with the QUEST data engine as the core data source, has been developed that will enable financial institutions to determine key factors influencing risk in the design, development and operations of energy-efficiency and sustainability projects, as well as the impact of quality management services. This will allow them to reduce risk, increase financial performance and therefore significantly increase investment volumes.

Keywords. QUEST Model, QUEST Tool, Quest Engine, Certified Quality Management Services, De-risking, Investments, EU Taxonomy, Buildings, Building Performance, Real Assets, Financial Performance
DOI: https://doi.org/10.34641/clima.2022.343

1. Introduction

Non-compliance with predicted, contracted or otherwise required aspects and levels of building performance can result in a wide range of problems, including excessive energy use, excessive emissions of carbon and other green-house-gases, increased maintenance and operational costs, operation start-up loss, sub-par quality of building functions and services, unsatisfactory indoor environmental quality, component and system faults, difficulties in achieving targeted building certification levels, disappointing end-user experience, mismatch with business case, lack of adaptability and flexibility, expenses changed from capital expenditure (CAPEX) to operational expenditure (OPEX), facility not meeting regulatory requirements, as well as increased risk and liability. This is often referred to as "The Performance Gap, see Figure 1, [1].

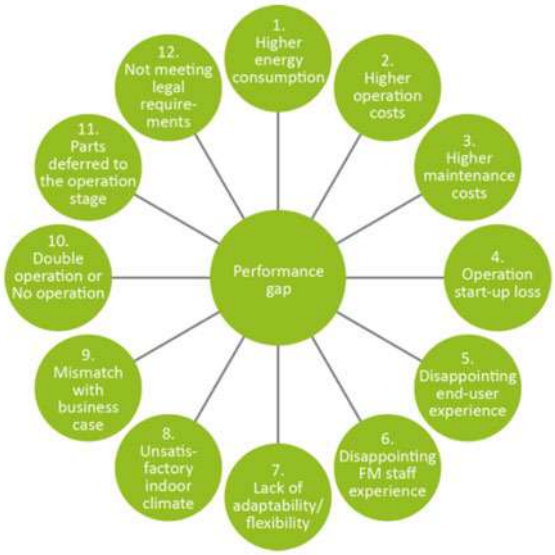

Fig. 1. A facilities manager's typology of performance gaps in new buildings, [1]

Recent studies indicate that only about 25% of new Swedish multifamily buildings (including those designed for high-energy-performance) comply with predicted energy use ([2], [3]).

Similar examples of non-compliance with predicted performance have been extensively documented by previous research ([4], [5], [6], [7], [8], [9], [10], [11], [12]).

Compliance with ambitious levels of resource efficiency, energy performance, decarbonisation and circularity goals, as well as other key objectives defined by the EU Taxonomy for sustainable activities, [13], will be essential criteria for the sustained future success of businesses throughout the building sector.

In the last decade, much research has focused on the impact of various sustainability characteristics such as green certifications on real estate values and other key real estate economic performance variables. In a review study, green certificates were found to have the potential to increase the rental income and decrease the operating expenses, vacancy, and risks of a property, resulting in higher net operating income growth rates and lower risk premiums, altogether resulting in increases in property values [14].

2. Quality Management in Buildings

Colloquially, *quality* is often used as a synonym for "good" or "high" quality. In the field of engineering or business, however, *quality* also refers to the degree to which a unit, e.g. a product or a service, meets the requirements placed on it. Quality management is a process to support the fulfillment of requirements. In addition to the definition of requirements, the process of testing the degree of fulfillment - consisting of the definition and application of the testing methodology - is a central component of the quality management process.

In the construction and real estate industry, the first Quality Management Services (QMS) have been established on this basis in recent years. And to varying degrees, they are taking advantage of the opportunities offered by digitization, making them technically and economically feasible on a larger scale.

2.1 The objective of the QUEST project

The objective of the QUEST project, [15], is to support the understanding of QMS and of their value-add and to support their application in real estate projects. The QUEST project developed tools to easily calculate a prognosis for cost and financial value add of QMS thus supporting early investment decisions into QMS as an essential part of the green transformation of the European building stock.

2.2 Quality management, technical monitoring, and commissioning

"Quality management" is thus a process of supporting the fulfilment of specified requirements. In the building sector, Technical Monitoring and Commissioning have evolved as reliable quality management services for buildings and are becoming increasingly popular. Technical

Monitoring (TMon) applies procedures to compare measured values from building operation versus design target values providing a transparent result to the owner. TMon can predominantly be carried out digitally. Commissioning (Cx) allows the owner to check in detail whether the building delivered complies with the Owners' Project Requirements. Cx requires to a significant extent skilled expert work. Since quality management starts with the definition of requirements, it obviously should start in the earliest stages of any project. Although quality management can be applied even after a building is completed, building owners should not wait until they incur the problems and costs of a failing project. Both TMon and Cx are most powerful and cost effective when initiated in the very beginning of a project, ([16], [17]).

3. The QUEST Model and its impact on real estate financial performance

An increase in the financial profitability of real estate investments is a key financial motivation for implementing the QUEST model. Due to the large size of the real estate assets, and the many important economic and sustainable finance linkages between the real estate markets, the debt and financial markets, and the wider society, the importance of accurate assessments of the linkage between buildings' technical and financial performance are key for increasing the flow of funds and other resources necessary for the sustainable development of real estate and financial markets.

3.1 Quality management reduces technical risks

The real estate investment community has difficulty statistically evaluating technical risk on specific construction and real estate investments. In this context, the term "technical risk" refers to technical building services like heating or ventilation. Malfunction or failure of these technical systems negatively impact building performance, increase CO_2-emissions, and thus become a risk for real estate investments.
Lower technical risk should be transmitted to improved financial performance of real estate investments. Therefore, real estate stakeholders who have successfully implemented quality management activities that de-risk a building's technical performance should also be rewarded by decreased financial risks and improved financial performance.

The QUEST model contributes with transparency in relation to what it costs to handle the technical risks through quality management on the individual construction project and on the return on investment of this investment.

4. QUEST Tool: Value-add Impact of Certified Quality Management Services

Within the context of the QUEST Project, the QUEST Tool was created to evaluate the quantitative impact of certified quality management services on value-add of real estate financial performance. While a particular situation may have an innate level of technical risk, that risk can be reduced by application of standardized and verifiable processes.

To achieve internationally replicable, scalable and trusted technical risk modulation via Quality Management, QUEST relies on Certified Quality Management Services.

- *Certified Technical Monitoring* verifies the correct functioning and operation of installed technical systems
- *Certified Building Commissioning* verifies compliance with Client Project Requirements through planning, design, construction/renovation & installation, and initial operation of a new or existing building.
- Certified Sustainable (or Green) Building Certification verifies compliance with specific schemes of environmental and related standards with some degree of commissioning involved.

Certified QMS are international third-party building certification processes (conforming with e.g. EN ISO 17065) that can impact buildings' net operating incomes, capitalization rates and ultimately their market values.

4.1 QUEST Tool algorithm

The QUEST Tool applies an algorithm to technical and financial data of investments into these Certified Quality Management Services. Investors can risk-grade investments and select the most profitable quality management services to de-risk projects.

Figure 2 shows a schematic illustration of the algorithm. A main feature and important contribution of the QUEST Tool is to integrate detailed information about how different levels of technical risk, which typically is excluded from real estate financial analysis calculations.

Even when technical risk is considered, it is often limited to aggregated and standard figures, and thus does not reflect the true technical risks and how they should be translated into the financial performance or real estate investments.

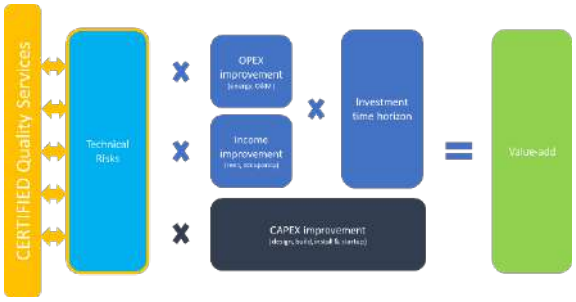

Fig. 2. Schematic illustration of the algorithm(s) applied to technical and financial data of investments into Certified Quality Management Services.

As shown in Figure 2, QMS investments result in positive value-add effects through lowering technical risks, which in turn result in lower and more stable annual operating expenses (in the figure denoted OPEX Improvement), higher and more stable annual revenues (in the figure denoted Income Improvement) and finally lower and more stable construction and renovation costs (in the figure denoted CAPEX Improvement). The investment time horizon is time factor in year units that is multiplied with the OPEX and Income effects. This time factor takes into account the fact that an initial certified quality service investment might have effects on revenues and costs, and ultimately on market values for several years ahead.

4.2 Technical risk indicators

A key innovation of the QUEST methodology is to include numerical figures of technical risk indicators. Initially the risk inputs relied on self-assessment of different technical risks in a building or building project:

- Technical risk impact on energy consumption and costs
- Technical risk impact on operation & maintenance work and costs
- Technical risk impact rental income
- Technical risk impact on occupancy rate

In order to reduce variability of this self-assessment, QUEST has decided to propose technical risk profiles which depend on user feedback regarding:

- Building type (ex. laboratory deemed higher risk profile than residential property)
- User confidence/experience in the technical teams managing the project.

QUEST is designing a solution for financial stakeholders who do not have the expertise to directly assess building technical risk. However, they can evaluate their risk perception of technical management teams based on their experience and/or confidence in these teams. Work together on, and results from, past projects can contribute to this assessment.

4.3 Inputs to QUEST Tool

The QUEST Tool ask users to input six project characteristics (see figure 3):

- Building type
- Experience/confidence in the technical teams
- Project build cost ➔ Capital saving calculation
- Building systems operating cost ➔ Cost improvement calculation
- Rental income ➔ Income improvement calculation integrating rent and occupancy impacts
- Time horizon of investment ➔ Capital saving calculation

The QUEST Tool proposes default values for each element in case the user fails to enter their values.

Your building project	
DE-RISK INVESTMENTS IN CONSTRUCTION & SUSTAINABLE BUILDINGS	**Input values**
What is the type of building?	Office
How do you rate the experience in the technical teams managing the project?	Medium confidence
What is the estimated project cost (per m²)? (Build/renovation/refurbishment/technical installation including design work)	1 000 €
What are the expected operating expenses per m² per year (OPEX/ m²/ year)? (Energy, operation & maintenance)	20 €
What is the expected rental income (per m² per year) If there is no rent value (ex. hospital or public building), use local Office rent values and adjust upwards to reflect sophistication of the building	400 €
Define the time horizon that the rating should consider for your QM-investment (5 to 20 years; the value is used to capitalise annual savings)	10

Fig 3. Inputs to QUEST Tool

4.4 Output of QUEST Tool Output

Based on the inputs, the QUEST Tool predicts value-add of different Certified Quality Services (see figure 4). The following value-add forecasts are available:

- Value-add prediction based on OPEX improvement from energy and operation & maintenance savings;
- Value-add prediction based on rental income and occupancy rate improvements from better buildings;
- Value-add prediction based on all cost and revenue improvements in 1 and 2 above.

The QUEST Tool also provides indicative investment costs for Certified Quality Services including expert audit costs and certification fees.

De-risking solutions		Value-add (per m²) over investment lifetime of 10 years		
CERTIFIED SERVICES*	Investment cost**	OPEX improvement	Rent & Occupancy improvement	TOTAL: OPEX + Rent & Occupancy improvement
Certified Technical Monitoring (ex. COPILOT)	1 €	4 €	52 €	**57 €**
Certified Building Commissioning (ex. COPILOT)	10 €	36 €	139 €	**175 €**
Certified Green Buildings (ex. LEED)	20 €	4 €	157 €	**161 €**

* Certified quality services provided by independent third parties to approved certification rules

** Indicative costs (verification by accredited expert + certification fees) based on Building > 2000 m² with significant project cost

Fig. 4. Outputs from Quest Tool

5 The QUEST data engine

In 2021, the European Commission adopted a package of measures to increase the flow of financial capital towards sustainable activities across the European Union, [18]. One of the packages is the (proposal for a) Corporate Sustainability Reporting Directive (CSRD), which will amend the existing Non-Financial Reporting Directive (NFRD). According to the European Commission, the CSRD "aims to improve the flow of sustainability information in the corporate world. It will make sustainability reporting by companies more consistent, so that financial firms, investors and the broader public can use comparable and reliable sustainability information."

The QUEST data engine provides an iterative loop to collect building data on a large number of characteristics regularly. It is intended to collect data from a large number of buildings monitored over time. Thus, the quest data engine will create a panel data set that can be used for deeper empirical analysis of the main drivers (such as QMS) of technical, financial, and sustainable performance of buildings.

The QUEST data engine adapts to CSRD to support the European Union's sustainability goals, in which property owners and its equity and debt investors need comparable and standardized data from the real estate industry. The QUEST data engine aims to be the industry standard in its field with standardized vocabulary and definitions of data variables.

5.1 Benchmarking analysis with QUEST data engine

The QUEST data engine can be used for internal and external benchmarking across buildings. By performing internal benchmarking, property owners can analyze and compare the performance of each of their buildings' performance over time. The internal benchmarking analysis can give answers to questions such as how and why various degrees of investments in QMS affect the financial and technical performance of its buildings.

With external benchmarking analysis, property owners make comparisons of the performance of their buildings with competitors.

5.2 QUEST data engine and effect of QMS

A key scientific research question is to quantify the effect of certain QMS activities on buildings' financial and technical performance. By studying how the QMS evaluation variables affect the QMS impact evaluation variables, important knowledge of the impact of QMS is obtained. The QUEST data engine can be used to analyze how large effects QMS activities have on technical and financial risk and performance variables. The financial variables that various QMS activities might impact on include

- Annual energy costs
- Annual Q&M costs
- Rent levels
- Occupancy level
- Handover time
- Legal claims
- User acceptance.

There are many other variables that also affect a building's technical and financial performance. Therefore, it is important to also include so-called control variables to mitigate problems with selection bias and omitted variable bias. The goal is to statistically obtain unbiased and/or consistent estimation of the QMS implementation effects. For instance, if the implementation effect analysis yields that buildings in which a certain QMS has been applied on average generate 10% higher annual financial performance (or value-add) compared to buildings where no QMS were applied, it is essential that the extent of the positive financial effect (10% here) can be trusted.

Relevant control variables can be building specific (property type such as hotel, office, residential, shopping mall, age, design, levels), location, neighborhood, and city characteristics (CBD, attractive area), urban economic, regional economic and macroeconomic variables. The economic variables are important to consider when the data set includes buildings located in different cities across different countries.

Location variables are also important since the changes in energy cost savings from one year to another may be highly related to annual local climate conditions. Therefore, certain climate variables should also be included as key control variables. For instance, if a building has received QMS that indeed has resulted in considerably more efficient energy usage, the building's energy costs may still have increased since if average outdoor temperature was significantly lower the year the QMS was applied. By adding local climate control variables, more accurate estimates of the impact of QMS on energy savings will be obtained.

6 On-going data analysis to improve QUEST model's financial impact and QUEST Tool

Once enough QUEST data for several buildings have been collected, the QUEST data engine can be used to build statistical (econometric) treatment effect models using panel data to scientifically estimate the size of QMS activities on buildings' financial and technical performance.

Currently there is a great need to develop the transparency in the commercial real estate market based on data. The QUEST data engine has therefore been created as an additional tool to gather more and precise data to overcome this deficit. The QUEST tool is therefore only a starting point.

6.2 Simple simulation to demonstrate QUEST data engine use

With the data of several buildings gathered using the QUEST data engine, empirical hedonic panel data models can be built and estimated, [19] . That is, in hedonic models, the variation in market values is determined by several property characteristics including if they have been subject to various QMS treatments.

The panel data approach to analyse the effect of various quality management services on a buildings' technical and financial performance requires many repeated observations on buildings. This is an on-going work.

The very simple simulation presented here aims at demonstrating an example of how panel data, building on longitudinal (in this case several years) observation of a chosen set of buildings, can be used to show the value-add financial impact of QMS.

To demonstrate a key usage of the QUEST data engine, such as quantifying the effect of various QMS services on buildings financial performance, e.g., the value add of certified QMS, the simulation is based on following simplified assumptions.

- 10 office buildings in a certain location.
- Data on the buildings have been observed over 5 years.
- 5 of the buildings have been subject to the identical measure of improvement (e.g. total (deep) refurbishment) when entering year 1 in the data collection process; they have identical technical characteristics.
- 5 of the buildings have not been subject to any measure of improvement when entering year 1 in the data collection process; they have identical technical characteristics.
- All buildings start (year 1) with identical rental situation (tenants, rental contracts): 300 €/(m^2a).
- All buildings start (year 1) with identical OPEX: 60 €/(m^2a).
- All buildings start (year 1) with same net operation income: 240 €/(m^2a).
- For year 2 – 5, the 5 buildings that have been subject to some measure of improvement, the Net Operating Income (NOI) will grow faster relative to the 5 buildings that have not been subject to a measure of improvement. This is assumed to be a result of lower Operating Expenses (OPEX) (e.g., due to improved energy efficiency) and higher rental incomes (e.g., due to higher occupancy rates and lower vacancies).
- For year 2 – 5, the 5 buildings that have been subject to some measure of improvement will have (relatively) lower financial risk premium and higher net operating income growth rates implying lower capitalization rates and therefore higher market valuations.
- For year 2 – 5, an identical type of QMS has been applied to 3 of the 5 buildings that have been subject to some measure of improvement. The other 7 (2 + 5) have not received any QMS at all.
- For those 3 buildings that have received QMS, the NOI growth rate is higher than all other buildings. Furthermore, the risk premium and the capitalization rates are the lowest for these 3 buildings.
- NOI growth rate for the 5 buildings that have not received any measure of improvement: 1.5% per annum.
- NOI growth rate for the 2 buildings that have received measure of improvement but not received QMS: 3.0 % per annum.
- NOI growth rate for the 2 buildings that have received both measure of improvement and QMS: 4.5 % per annum.
- Capitalization rate year 4 for buildings that have not received any measure of improvement: 7%.
- Capitalization rate year 4 for the 2 buildings that have received measure of improvement but not received QMS: 5.5 % per annum.

- Capitalization rate year 4 for the 2 buildings that have received both measure of improvement and QMS: 4.0 %.

Given the above assumptions, the valuations obtained, and above all, the quantified value-add of measure of improvement and QMS are:

- Market value year 4 for 5 buildings not subject to any measure of improvement = NOI year 5 / cap rate year 4 = 254.54/7.0% = 3 636 €/m^2.

- Market value year 4 for 2 buildings that are subject to a measure of improvement but not received QMS= NOI year 5 / cap rate year 4 = 270.12/5.5% = 4 911 €/m^2.

- Market value year 4 for 3 buildings that are subject to a measure of improvement and have received QMS= NOI year 5 / cap rate year 4 = 286.01/4.0% = 7 150 €/m^2.

Although the above calculations are very simplified, they show what type of final results that the QUEST data engine can yield. The QUEST data engine can not only to empirically establish the value-add of various measures of improvements. In more realistic settings, the buildings included in the QUEST data engine will be heterogenous in many different aspects. With detailed information on the different characteristics of the buildings, sophisticated hedonic panel data regression analysis can be conducted to empirically establish the size of QMS on buildings financial and technical performance, while controlling the differences among the buildings' characteristics.

Conclusions

Investments in building performance, including energy efficiency, can generate substantial economic and environmental benefits, while also increasing financial returns. The main goal of the EU-funded QUEST project is to promote private investments and financing in sustainability and energy-efficiency projects. To that end, a simple toolkit was developed that enables financial stakeholders and institutions to determine relevant factors that influence risk in the design, construction and operations of energy-efficiency and sustainability projects. This allows them to reduce risk and increase investment levels, while supporting compliance with EU Taxonomy requirements.

Acknowledgement: This article is prepared within the scope of the QUEST project, which has received funding from the European Union's Horizon 2020 research and innovation programme under the Grant Agreement number 846739. The European Union is not liable for any use that may be made of the information contained in this document, which is merely representing the authors' views.

References

[1] Rasmussen H.L. and Jensen P.A. (2020), "A facilities manager's typology of performance gaps in new buildings", Journal of Facilities Management, Vol. 18 No. 1, pp. 71-87. https://doi.org/10.1108/JFM-06-2019-0024.

[2] Martinac I. et al. (2017): Brukaranpassad, hållbar byggnadsdrift med fokus på inneklimat och energiprestanda i kontorsbyggnader – en kunskapssyntes (User-adapted, sustainable building performance management with focus on indoor environment end energy performance in office buildings – a knowledge synthesis. In Swedish). Final Report, Energimyndigheten (Pnr 42639-) & SBUF (Pnr 13293). Stockholm.

[3] Kempe P. (2020): Förstudie: Stegvis verifiering av delsystem - Exempel VVC-system. Lågan Rapport.

[4] Månsson L-G et al (1997): IEA Annex 17: Building Energy Management Systems – Evaluation and Emulation Techniques.

[5] Fisch M. N. et al. (2007): EVA - Evaluierung von Energiekonzepten für Bürogebäude: (Gesamt-) Abschlussbericht. Braunschweig / Hannover, Technische Informationsbibliothek u. Universitäts-bibliothek.

[6] Fraunhofer ISE (2011), ModBen – Endbericht: Modellbasierte Methoden für die Fehlererkennung und Optimierung im Gebäudebetrieb. Freiburg.

[7] Baumann O. (2005): OASE – Optimierung der Automationsfunktionen betriebstechnischer Anlagen mit Hilfe der dynamischen Simulation als Energie-Management-System. Abschlussbericht zum Vorhaben OASE, Förderkennzeichen 0327246D. München.

[8] Plesser S., Gräff S., Rozynski M. and Fisch M. N. (2012): www.EnBop.info - Netzwerk für Betriebsoptimierung. Intelligente Architektur XIA 04-06 2012, Seite 066-071, Leinfelden-Echterdingen. 2012.

[9] Franzke U. and Schiller H. (2011): Untersuchungen zum energieeinsparpotenzial der Raumlufttechnik in Deutschland. ILK Dresden, Fachbericht ILK-B-31-11-3667, Dresden.

[10] Crowe E. et al (2020): Building Commissioning Costs and Savings Across Three Decades and 1,500 North American Buildings. LBNL, Energy Technologies Area.

[11] Coyner R., Kramer S. (2017): Long Term Benefits of Building Commissioning: Should Owners Pay the Price?, Creative Construction Conference, Primosten, Croatia.

[12] Wen J., Chen Y., Regnier A. (2020) Building Fault Detection and Diagnostics. In: Baillieul J., Samad T. (eds) Encyclopedia of Systems and Control. Springer, London. https://doi.org/10.1007/978-1-4471-5102-9_100080-1.

[13] European Commission (2021): EU Taxonomy for Sustainable Activities. https://ec.europa.eu/info/business-economy-euro/banking-and-finance/sustainable-finance/eu-taxonomy-sustainable-activities_en, as accessed 21/5/2021.

[14] Leskinen, N., Vimpari, J. and Junnila, S. (2020). A Review of the Impact of Green Building Certification on the Cash Flows and Values of Commercial Properties, Sustainability.

[15] European Commission (2019): Quality Management Investments for Energy Efficiency (QUEST). Horizon 2020 Grant Agreement ID 846739, https://cordis.europa.eu/project/id/846739, as accessed 21/5/2021.

[16] Federation of European Heating Ventilation and Air Conditioning Associations: HVAC Commissioning Process. Guidebook No. 27, Brussels.

[17] Federation of European Heating Ventilation and Air Conditioning Associations: Quality Management for Buildings. Guidebook No. 29, Brussels.

[18] European Commission (2021): Sustainable Finance Package, Proposal for a Corporate Sustainability Reporting Directive (CSRD). https://ec.europa.eu/info/publications/210421-sustainable-finance-communication_en#csrd, as accessed 21/5/2021.

[19] Fuerst, F. (2008): Office Rent Determinants: A Hedonic Panel Analysis. SSRN Working Paper Series, DOI:10.2139/ssrn.1022828.

Floor heating pre-on/off parameters based on Model Predictive Control feature extrapolation

Ettore Zanetti[a], Rossella Alesci[b], Rossano Scoccia[c], Marcello Aprile[d]

[a] Department of Energy, Politecnico di Milano, Milano, Italy, ettore.zanetti@polimi.it

[b] Department of Energy, Politecnico di Milano, Milano, Italy, rossella.alesci@polimi.it

[c] Department of Energy, Politecnico di Milano, Milano, Italy, rossano.scoccia@polimi.it

[d] Department of Energy, Politecnico di Milano, Milano, Italy, marcello.aprile@polimi.it

Abstract. Floor heating systems are typically characterized by a relatively high thermal inertia, thus they react slowly to setpoint changes. When the system turns on, an under-heating period could occur for a relative long period, vice versa when the setpoint is decreased the floor thermal inertia could lead to overheating. In residential applications, the users try to avoid these discomfort problems by using a constant setpoint, higher than the setback. In this way the average energy consumption as well as the user's bill increases. A smarter solution to mitigate this problem is to include a pre-on period parameter, so that the system will turn on a certain time before the increase in setpoint to avoid the under-heating period and a pre-off period so that it will switch off before overheating. Predictive controllers can be a solution to compensate the slow response of the radiant floor system. However, besides the need for more data, the computational power goes beyond what is available in heating systems micro controllers for residential cases. To avoid these issues, in this paper the optimal control trajectory obtained using a Model Predictive Control (MPC) approach is used to identify the pre-on and pre-off parameters to be periodically updated in the micro controller (e.g. monthly). A simulation work was carried out to compare the performance between a baseline Rule Based Controller (RBC), an improved RBC and a MPC in terms of comfort and energy use. The result is a reduction from an average of 1.1°C to 0.2°C for the worst thermal zone meaning 80% reduction of the discomfort with respect to the baseline and a slight increase of the electrical consumption of the heat pump (less than 5%).

Keywords. Radiant floor, model predictive control, feature extrapolation, pre-heating, KPI.
DOI: https://doi.org/10.34641/clima.2022.331

1. Introduction

HVAC systems account for 20% of the primary energy consumption in MEF countries [1]. Within the perspective of reducing energy consumption and fight climate changes, radiant floor heating applications are becoming more and more used [2]. An important characteristic of standard radiant floor systems is the high thermal inertia which causes a delay between the heat supply and the response in the internal air temperature. For concrete core radiant floors this has been estimated to be 1 to 3 hours [3]. This slow response can create underheating or overheating issues and consequent discomfort and/or waste of energy. In order to assess which are effectively the discomfort periods, the standard EN 12098-1:2017 [4] defines the time and temperature tolerances to guarantee the comfort levels inside the thermal zone.

A solution to compensate the slow response of the radiant floor system and reduce the consequent discomfort could be the use of advanced control strategies such as Model Predictive Control (MPC). The benefit of predictive controllers is that the heat supply can be adjusted in advance thanks to heat demand forecasts [5]. Even if it was proven that MPC can be a good solution to reduce the energy consumption of the HVAC systems, as reported in [6] most buildings today use rule-based controllers to manage the indoor conditions. This is related to the fact that there are different challenges that must be faced to implement MPC in buildings [7] and one of this is the availability of the proper hardware and software infrastructure. For example, model predictive control requires a high computational power that is not available in standard heating systems micro controllers for residential buildings. As reported in [8], MPC can be adopted for complex new commercial buildings while it may not be as

Copyright ©2022 by the authors. This conference paper is published under a CC-BY-4.0 license.

solution for residential buildings because it could be too expensive.

This paper proposes a methodology to extrapolate the monthly pre-on and pre-off parameters to be implemented on a micro controller, starting from the results of an optimization problem. This methodology can be deployed as a cloud service, where the pre-on and pre-off parameters can be updated remotely on the micro controller.

This work is part of the Merezzate+ project co-founded by EIT Climate-KIC. The project focuses on sustainability issues from a social, environmental, and economic point of view, adopting measures in the sectors of energy, mobility and circular economy that are the ones with the highest impact on climate change. The project included the construction of around 800 apartments, one of them was chosen as a simulation case study for this work. It is in Milan and is characterized by two rooms and a bathroom. The detailed description is reported in Section 3.

2. Method

An optimal control problem was formulated to obtain the floor heating pre-on and pre-off parameters. In this case, the objective of the optimization problem was to find the control strategy that allows to maximize the comfort of the considered thermal zones.

Starting from the resulting optimal control trajectory, the pre-on and pre-off parameters can be estimated and included in the rule-based controller.

In order to couple the optimization problem with the detailed apartment model at the base of this study, the BOPTEST framework [9] was chosen. It allows to create an API interface between the detailed physics-based model we created using the Modelica Buildings [10] and IBPSA [11] libraries and the optimization problem implemented in a Python code using the Pyomo toolbox [12].

This Section is structured in two sub-sections. In Section 2.1 it has been described the optimization problem and the feature extrapolation. In Section 2.2 it is described the co-simulation environment

2.1 Optimization problem and feature extrapolation

The model predictive control scheme is reported in **Fig. 1**.

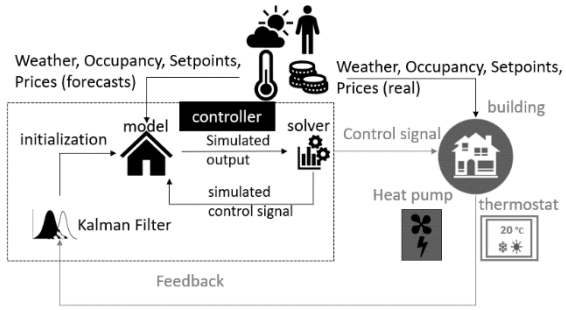

Fig. 1 – Model predictive control scheme.

In order to find the control strategy that allows to achieve the goal, it is necessary to create a simplified model that can capture the correct dynamics of the system. Then, starting from the response of this simplified model subjected to various disturbances (e.g. weather, setpoints, occupation and prices forecasts), the solver calculates the best control trajectory to achieve the "objective function", which is shown in eq. 1. In this case, the forecast is assumed to be deterministic, which means that the forecast adopted during the optimization process is identical to the input of the detailed model of the building. The optimization horizon is 24h and the control signal obtained solving the optimization problem is updated in the detailed model every 15 minutes.

The general form of the objective function can be:

$$\boldsymbol{min\, J_{tot}\,(t)} = \int_{t_0}^{t_f} \sum_{i=1}^{N} k_i J_i(t)\, \boldsymbol{dt} \quad 0 \le k_i \le 1 \qquad (1)$$

Where $J_i(t)$ represents the various objectives and k_i the weighting factor associated with the i-th objective.
In this work, the following combination of objective functions has been adopted:

$$\min \int_{t_0}^{t_f} (k_1\, J_1(t) + k_2\, J_2(t))\, \boldsymbol{dt} \qquad (2)$$

$$J_1(t) = \left(\left[T_r(t) - \left(T_{setpoint} + \delta\right)\right]^{-}\right)^2 \qquad (3)$$

$$J_2(t) = \frac{\dot{Q}_{hp}(t)}{COP(t)} \qquad (4)$$

Where $J_1(t)$ represents the squared difference between the room air temperature and its setpoint, only in case of under heating. Furthermore, a constant offset δ is added to the setpoint to give a more robust result that will make the parameters work even in a particularly cold day. The value of δ is a tuning parameter that depends on how frequently the pre-on/off parameters will be updated. The solver will try to minimize the differences between these two temperatures to improve the thermal comfort of the users. $J_2(t)$ represents the main electric power needed by the heating system, in this case study represented by a heat pump. In order to minimize this objective, the solver will try to minimize the thermal power $\dot{Q}_{hp}(t)$ but also to maximize the heat pump Coefficient of Performance ($COP(t)$) shifting the

heat demand from colder to warmer periods and working at partial load with a lower supply temperature.

The control strategy adopted in this paper tries to maximize the comfort in a specific time interval and to extrapolate some simplified rules to be applied on the energy management system installed in field. The weighting factors adopted in the objective function are $k_1 = 1$ and $k_2 = 0.05$.

The result of the optimization problem described above will be a control that switches on and off the heat pump to guarantee the thermal comfort of the users. Starting from the results of the optimized simulation it is possible to extrapolate some simplified rules that allow to find the pre-on and pre-off parameters to be implemented on a rule-based controller in field. In particular, the pre-on and pre-off parameters are monthly averages. For the months of April and October they take the average only of the days that belong to the heating season, which are respectively the period from the 1st to the 15th for April and the days from the 15th to the 31st for October. They have been obtained starting from the calculation of the supplied energy to the radiant floor distinguishing between the pre-on phase and the normal operation. These two values ($Q_{preheaOPT}$ and Q_{heaOPT}) correspond to the orange and red areas in **Fig. 2**. Then the mean supply heat rate was estimated for the two phases ($\dot{Q}_{meanOn}$ and $\dot{Q}_{meanOff}$). The two areas (orange and red), underneath the thermal power curve, are respectively equal to the areas of the two rectangles, in which the two heights are $\dot{Q}_{meanOn}$ and $\dot{Q}_{meanOff}$ and the two widths are Δt_{On} and $\Delta t_{tot} - \Delta t_{Off}$. Thus, inverting the following formulas, it is possible to obtain the two parameters Δt_{On} and Δt_{Off}:

$$\dot{Q}_{meanOn} = \frac{Q_{preheaOPT}}{\Delta t_{On}} \quad (5)$$

$$\dot{Q}_{meanOff} = \frac{Q_{heaOPT}}{\Delta t_{tot} - \Delta t_{Off}} \quad (6)$$

where Δt_{tot} is the difference of time between the setpoint changes and Δt_{off} is the time difference between the time at which the power goes below a threshold and the lower setpoint change.

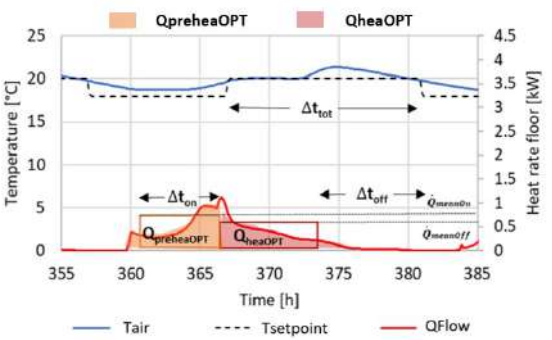

Fig. 2 – Visualization of Δt_{On} and Δt_{Off} calculation procedure.

In this way, starting from the control trajectory it is possible to obtain the two values of Δt_{On} and Δt_{Off} for each pre-on and pre-off and finally calculate the average of these values for each month.

2.2 Implementation

For this work, the Modelica "Buildings" and "IBPSA" libraries were used to develop the detailed model of a three-zone apartment with radiant floor described in Chapter 3.

In particular, for the floor heating modelling, the model called "SingleCircuitSlab" of the "Buildings" library [10] was adopted. It models the radiant slab as a thermal resistance network and uses a fictitious resistance to compute the temperature of the plane that contains the pipes. The same method is implemented in TRNSYS 17 [13]. The rule-based controller used is a tuned PI controller with 0.4 °C hysteresis on the setpoint and a tuned climatic curve on the heat pump supply temperature.
From the detailed model of the building - HVAC system a simplified model was derived through an identification process performed with the MATLAB Identification Toolbox. The simplified model is a grey box, where a thermal electrical analogy is used. This allows to identify a circuit of resistances and thermal capacities (R-C network) to represent the most significant temperatures of the building and HVAC system (**Fig. 3**), starting the identification from the data contained in the detailed model. The methodology followed for the model identification is described in [14]. In summary each thermal zone has a 7R3C circuit and they are all connected to each other.

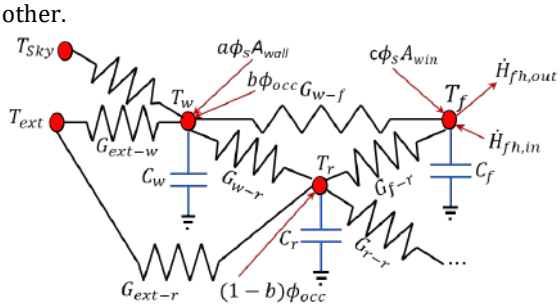

Fig. 3 – R-C network - in red are the temperature nodes T, G_i are the conductances, $\emptyset_i$ are the disturbances (solar, appliances), A_i are the wall and windows area, $\dot{H}$ are the inlet and outlet heat flow rate in the floor and *a,b,c* are the tuning constants.

After this phase, the simplified model and the optimization problem were implemented in Python using the Pyomo toolbox.

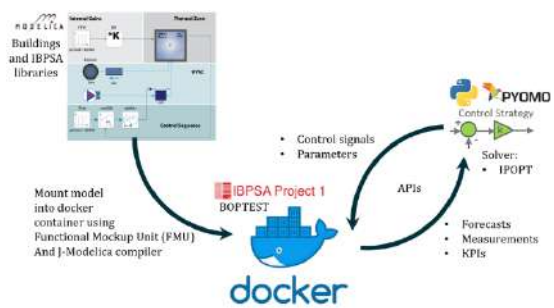

Fig. 4 – Co-simulation environment, on the left the Modelica detailed model and on the right the optimization environment in Python-Pyomo. In between the BOPTEST software is used as a wrapper for the detailed model allowing an API input/output exchange with Python

Finally, the detailed model developed in Modelica interfaces with the optimization problem through the BOPTEST framework. The BOPTEST framework allows a way to easily compile the detailed Modelica model and wrap it around a Docker container. In this way the model can freely run through an easy-to-use API interface, that can be used to obtain sensor signals from the detailed model and provide control trajectories from the optimization routine in Python through APIs.

All these steps are summarized in **Fig. 4.**

3. Case study

The case study chosen for this work is a two rooms one bathroom apartment reported in **Fig. 5**. It is in Milan (Italy) and shares two walls with two adjacent apartments (in green), a wall with the landing (in red) while the rest faces towards outside (in yellow).

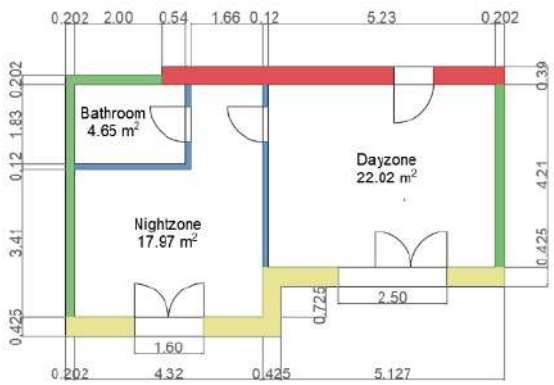

Fig. 5 – Floor Plan of apartment

It is equipped with an air source heat pump, a radiant floor, a DHW tank and PV panels installed on the roof of the building. The heat is used for both space heating and DHW production, giving priority to the latter. The most important characteristics of the above-mentioned system are reported in **Tab. 1**.

Tab. 1 – Characteristics of the system.

Parameter	Value and unit of measurement
Floor area	44.45 m²
Zones height	2.7 m
Number of occupants	1
HP nominal electrical power	1.33 kW*
HP nominal thermal power	4 kW*
PV panels area	5.5 m²
PV panels peak power	0.8 kWp

*Nominal conditions (-7°C, 35°C)

For the simulation of the considered apartment, the occupation profiles were arranged as shown in **Fig. 6** and **Fig. 7**. The first one is used for all the weekdays, while the other is used to simulate the weekends.

The other input data chosen for these simulations are function of the above-described occupation profiles. In particular, a setpoint temperature of 20°C has been chosen for occupied periods, while a setback temperature of 18°C is applied for the rest of the considered day. In the same way the shading systems of each room are fully closed when it is unoccupied while they are half opened when the considered room is occupied.

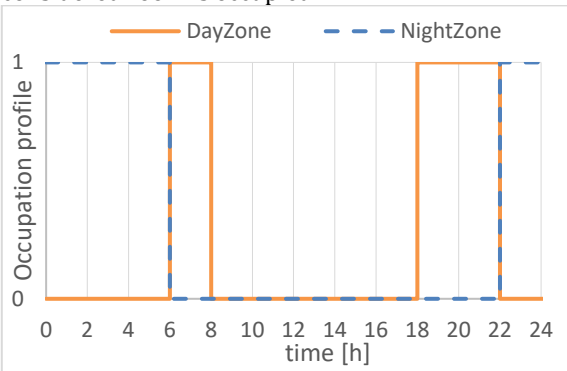

Fig. 6 – Occupation profile weekdays

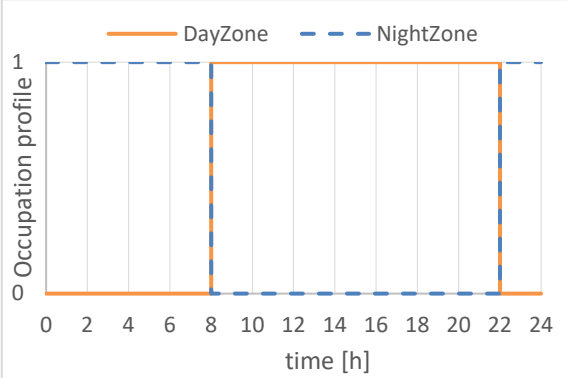

Fig. 7 – Occupation profile weekend

In addition, there are the internal gains related to the presence of people, appliances, and lighting.

Specifically, the sensible internal gain due to the presence of people is defined per person while the others are defined per unit area.

In this case study the following values have been chosen:

$$\dot{Q}_{sens} = 60\frac{W}{pers} \quad (7)$$

$$\dot{Q}_{appliances} = 2.5\frac{W}{m^2} \quad (8)$$

$$\dot{Q}_{lighting} = 4\frac{W}{m^2} \quad (9)$$

In particular, the sensible heat produced by a person respects the standard UNI EN 13779 [15] while the other two values are due to specific assumptions. In fact, since the apartment is small and new, the authors considered to have few and efficient appliances. In addition, they chose led lamps that emit a thermal power of about 80 W for each thermal zone.

In this case, only one user is present inside the apartment as reported in **Fig. 6** and **Fig. 7**.

All these contributions are different than zero only when the considered thermal zone is occupied. In addition, the lighting contribution is set to zero from 8 a.m. to 5 p.m. thanks to daylight availability.

Finally, the parameters related to the mass exchange with the external environment are summarized in **Tab. 2**. In particular, the value of the air changes related to infiltrations has been chosen considering high quality windows while the value related to mechanical ventilation takes into account the sanitary regulation of the Municipality of Milan [16] which imposes at least 20 m3/h/pers. In this case it was chosen to apply 30 m3/h/pers and 24 m3/h/pers respectively for the DayZone and the NightZone.

Tab. 2 – Infiltration and mechanical ventilation

Air changes	DayZone	NightZone
Infiltrations [1/h]	0.05	0.05
Mechanical ventilation [1/h]	0.5	0.5

4. Results

For this work, three different simulations were performed: a first simulation with a normal rule-based control (baseline), a second simulation based on model predictive control and a final simulation with a rule-based control with pre-on and pre-off parameters obtained averaging the results of the second simulation.

In Section 4.1 are reported the pre-on and pre-off parameters obtained from the calculations described in Section 2.1. In section 4.2 it is possible to observe which are the effects of the activation of the pre-on and pre-off strategies on the air temperature and the thermal power delivered by the heat pump in the three cases, while in Section 4.3 are summarized the Key Performance Indicators (KPI) of the three simulations.

4.1 Monthly pre-on and pre-off parameters

The results of the calculation reported in detail in section 2.1 are summarized in **Tab. 3** and **Tab. 4**. In particular, in the DayZone (**Tab. 3**), the pre-on is not required for the periods that go respectively from the 1st to the 15th of April and from the 15th to the 31st of October.

Tab. 3 – Average values for pre-on and pre-off parameters in the DayZone

Period	Pre-on [h]	Pre-off [h]
1st-31st Jan	1.56	0.00
1st-28th Feb	1.22	0.00
1st -31st Mar	0.20	0.20
1st-15th Apr	0.00	1.30
15th-31st Oct	0.00	0.60
1st-30th Nov	0.80	0.10
1st-31st Dec	1.40	0.10

Tab. 4 – Average values for pre-on and pre-off parameters in the NightZone

Period	Pre-on [h]	Pre-off [h]
1st-31st Jan	4.00	0.20
1st-28th Feb	3.60	0.30
1st -31st Mar	3.00	1.70
1st-15th Apr	2.20	2.20
15th-31st Oct	1.00	1.90
1st-30th Nov	2.60	0.80
1st-31st Dec	3.40	0.20

4.2 Time series analysis

To understand the benefits related to the application of the pre-on and pre-off strategies, in this section a detailed analysis of two days is shown (Friday, 19th of January and Saturday, 20th of January).

In **Fig. 8** and **Fig. 9** are represented the trend of the air temperature with respect to the setpoint respectively in the DayZone and NightZone, while in **Fig. 10** is reported the trend of the thermal power provided by the heat pump to heat up the two thermal zones.

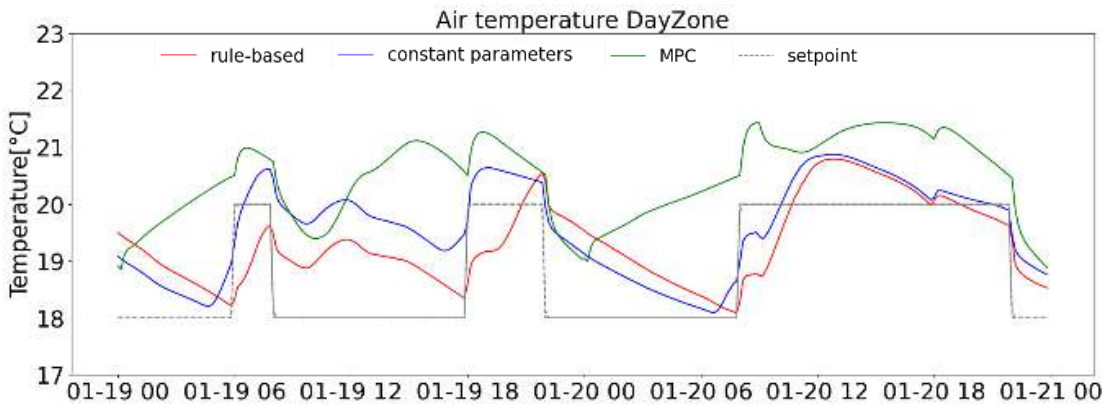

Fig. 8 – DayZone air temperature trend for sample days including weekend

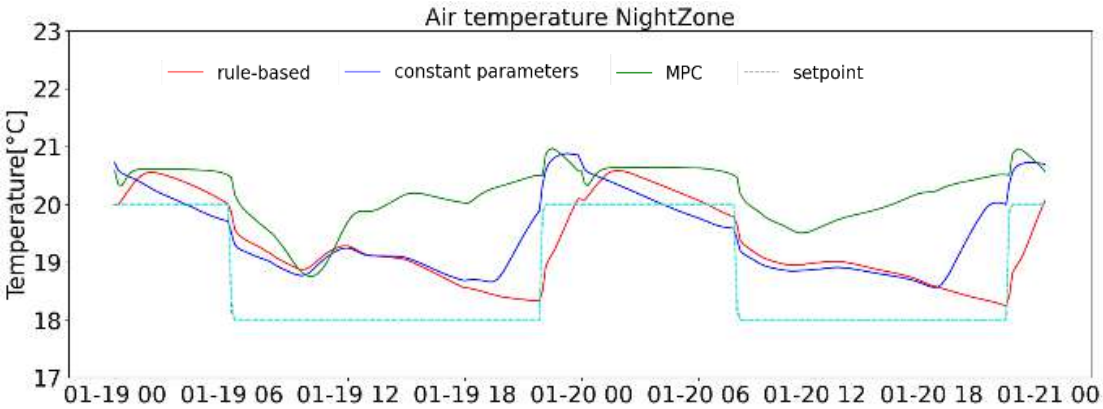

Fig. 9 – NightZone air temperature trend for sample days including weekend

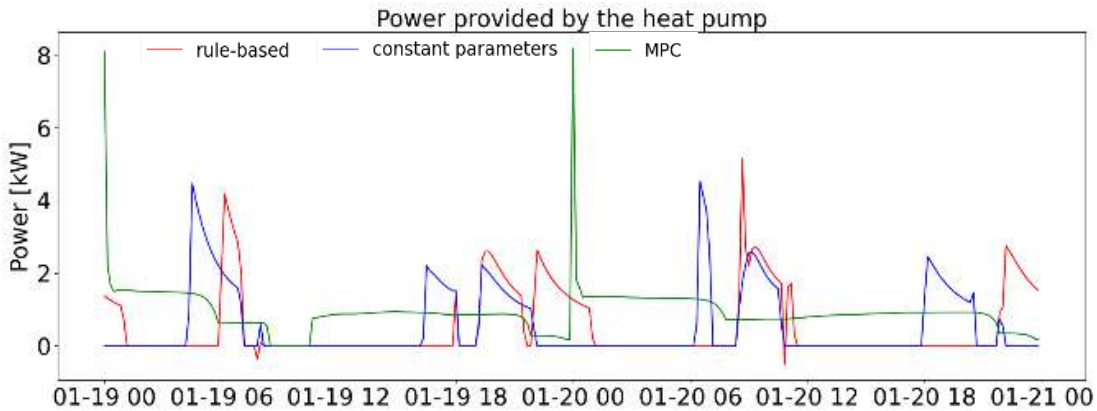

Fig. 10 – Thermal power provided by the heat pump for sample days including weekend

From the first two figures (**Fig. 8** and **Fig. 9**) it can be seen that, while with the normal rule-based control (represented by the red line) the temperature reaches the desired setpoint after about 3 hours, the rule-based control with the pre-on and pre-off parameters (blue curves) is able to follow the change of the setpoint, reducing a lot the periods of discomfort that occur in the baseline case. Finally, from the same graphs it is visible that the temperature obtained with the model predictive control strategies is consistently higher than the setpoint. This is done because the MPC is targeting the setpoint temperature plus δ °C to have a more conservative result when finding the pre-on and pre-off parameters. The big gap between the rule-based and the other controllers can be explained by the fact that in this simulation the baseline rule-based controller turns on the heat pump when the difference between the room and setpoint temperature is lower than minus the hysteresis value. This control strategy will inevitably lead to underheating. So, what expert users usually do is manually insert a pre-on / pre-off parameter based on experience. Less expert users instead will keep the systems always on, leading to a big waste of energy.

Then, from **Fig. 10**, it is clearly visible that the thermal power provided by the heat pump, in the case of application of the pre-on and pre-off strategy (blue line), has been anticipated (shifted towards left) with respect to the normal rule-based control (red line), while MPC keeps the system on for a longer period at a lower mean power. This is due to the fact that, as reported in eq. 1, the objective function not only promote the thermal comfort achievement but also tries to reduce the electric power consumption.

4.3 KPIs analysis

Finally, some Key Performance Indicators (KPI) were defined with the aim of evaluating the overall performance of the advanced control strategies.

In particular, the KPI related to the discomfort of the i-th thermal zone (Dis_{TZi}) is defined as the integral of the difference between the setpoint ($T_{set,i,TZi}$) and the room air temperature ($T_{air,i,TZi}$) for the heating season (from the 15th of October to the 15th of April), subdivided for the number of occupied hours ($n_{occ\ hours}$) in the same period. The integral at the numerator is calculated only in the occupied hours of each day and only when the indoor air temperature is lower than the setpoint temperature minus the hysteresis ($hys = 0.4°C$), as reported below:

$$Dis_{TZi} = \frac{\int_{t_0}^{t_f} \left| T_{set,i,TZi} - hys - T_{air,i,TZi} \right|^{+} dt}{n_{occ\ hours}} \quad (10)$$

Then it is reported the average air temperature ($T_{airAvg,TZi}$) of each thermal zone calculated considering the entire heating season and the related thermal energy need ($E_{th,SH}$) that has to be provided by the heat pump in order to maintain those conditions inside the various thermal zones. They are mathematically expressed as:

$$T_{airAvg,TZi} = \frac{\sum_{j=1}^{N} T_{air,j,TZi}}{N} \quad (11)$$

$$E_{th,SH} = \int_{t_0}^{t_f} \dot{Q}_{th,SH}(t)\, dt \quad (12)$$

Where:

- $T_{air,j,TZi}$ is the air temperature of the thermal zone TZi registered at the j-th time;
- N is the number of elements of the temperature vector during the heating season;
- $\dot{Q}_{th}$ is the thermal power provided by the heat pump for space heating at a specific time.

Finally, it is introduced a KPI which describes the electrical energy consumption of the heat pump ($E_{el,SH}$) for providing heat to the radiant floor (space heating), that is equal to:

$$E_{El,SH} = \int_{t_0}^{t_f} \dot{P}_{el,SH}(t)\, dt \quad (13)$$

Where:

- $P_{el,SH}$ is the electrical power consumption of the heat pump for space heating at a specific time.

The summary of these KPIs is reported in **Tab. 5**.

Analysing the values reported in **Tab. 5** it appears that the value of the discomfort related to the DayZone in the Baseline case is equal to 1.104 K, which is already a low value, but it is still higher than the temperature tolerance, which is fixed to $\pm 0.5K$, as reported in the standard EN 12098-1:2017 [4]. Thus, with the use of the optimized control (PreOnOff Const and PreOnOff Var), the authors were able to respect this tolerance and to obtain a strong percentage reduction of the discomfort, higher than the 80%. For the NightZone, as it is possible to observe from **Tab. 5** the Baseline was already able to respect the above-mentioned tolerance, but the percentage reduction of the discomfort is still important.

In addition, the results in **Tab. 5** show that the optimized rule-based controller, with constant pre-on and pre-off parameters (PreOnOff Const), has comparable performance with respect to the results of the model predictive control (PreOnOff Var).

Tab. 5 – KPI comparison.

KPI	Baseline	PreOnOff Const	PreOnOff Var
$Dis_{DayZone}$ [K]	1.104	0.191 (-83%)	0.006 (-99%)
$Dis_{NigZone}$ [K]	0.155	0.006 (-96%)	0.011 (-93%)
$T_{airAvg,DayZone}$ [°C]	19.7	20.0 (+1.5%)	20.9 (+6.1%)
$T_{airAvg,NigZone}$ [°C]	19.6	19.8 (+1.0%)	20.4 (+4.1%)
$E_{th,SH}$ [kWh]	1758	1808 (+2.8%)	2874 (+63.5%)
$E_{El,SH}$ [kWh]	437	455 (+4.0%)	672 (+53.6%)

The average air temperature increases of the 1-1.5% in the case with monthly constant parameters and of the 4-6% in the case of variable parameters (MPC). The increase of temperature obviously leads to an increase of the thermal energy needs and consequently of the electrical consumptions of the heat pump.

This methodology can be deployed as a cloud service, where the pre-on and pre-off parameters can be updated remotely. In the Merezzate+ project some apartments could be used for testing the methodology. In terms of economic feasibility, it can be used for large residential complexes where the building envelope and HVAC systems can be modelled once and tweaked using data, introducing an economy of scale. For smaller residential buildings archetypes can be built and modelled, where the solution may not be optimal but still better than the baseline.

5. Conclusions

In this paper it is proposed a methodology to extract pre-on and pre-off parameters that can be implemented in micro-controllers of residential buildings. This could help managing the radiant floor heating system and solve the problems of discomfort that could be caused by its slow response.

From the control trajectory obtained solving the optimization problem, some simplified rules were extrapolated. They allow to obtain the monthly pre-on and pre-off parameters to be implemented in the energy management system installed in field thanks to a cloud service.

Then, three simulation that consider respectively a normal rule-based control, model predictive control and a rule-based control with monthly pre-on and pre-off parameters have been performed. Comparing the results of the three simulations it is possible to observe that with both the constant and variable (MPC) pre-on and pre-off parameters, the time in which the air temperature is below the setpoint is strongly reduced and this is also confirmed by the KPI of the discomfort, that undergoes a reduction higher than the 80%. For the future development of this work, the authors will consider different feature extrapolation methods. Instead of monthly, the pre-on/pre-off parameters could be updated with a different frequency. Furthermore, depending on the sensors available locally or cloud forecast different heuristic metrics will be developed.

6. Acknowledgement

The research work presented in this paper receives the support of EIT Climate-KIC through the project "Merezzate+" and REDO sgr spa.

7. References

[1] I. E. A. B. E. P. Metrics. Supporting Energy Efficiency Progress in Major Economies. Int. Energy Agency Paris, Fr., 2015.

[2] Olesen B. W. Radiant Floor Heating In Theory and Practice. no. July, pp. 19–24, 2002.

[3] Zhao K., Liu X., and Jiang Y. Dynamic performance of water-based radiant floors during start-up and high-intensity solar radiation. Sol. Energy, vol. 101, pp. 232–244, 2014.

[4] EN 12098-1:2017 Energy Performance of Buildings - Controls for heating systems Part 1: Control equipment for hot water heating systems - Modules M3-5, 6, 7, 8

[5] Karlsson H. and Hagentoft C. Application of model based predictive control for water-based floor heating in low energy residential buildings. Build Environ, vol. 46, pp. 556–569, 2011.

[6] Drgoňa J. et al. All you need to know about model predictive control for buildings. Annual Reviews in Control, vol 50, pp 190-232, 2020.

[7] Cigler J. et al. Beyond theory: the challenge of implementing Model Predictive Control in buildings. Proceedings of 11th rehva world congress, Clima, Prague, Czech Republic.

[8] Thieblemont H. et al. Predictive control strategies based on weather forecast in buildings with energy storage system: A review of the state-of-the art Energy and Buildings, vol. 153, pp. 485–500, 2017.

[9] Blum D. et al. Building optimization testing framework (BOPTEST) for simulation-based benchmarking of control strategies in buildings. J. Build. Perform. Simul., vol. 14, no. 5, pp. 586–610, 2021.

[10] Wetter M., Zuo W., Nouidui T. S., and Pang X. Modelica Buildings library," J. Build. Perform. Simul., vol. 7, no. 4, pp. 253–270, 2014.

[11] M. Wetter M., D. Blum D., J. Hu J., and USDOE, "Modelica IBPSA Library v1," 2019.

[12] Bynum M. L. et al. Pyomo--optimization modeling in python. Third., vol. 67. Springer Science \& Business Media, 2021.

[13] Thermal Energy System Specialists, LLC. TRNSYS 17 a TRaNsient SYstem Simulation program Multizone Building modeling with Type56 and TRNBuild Vol. 5, Madison USA.

[14] Zavaglio E., Scoccia R., and Motta M. RC Building Modelling for Control Purposes: A Case Study. Build. Simul. Appl. BSA 2017, 2017.

[15] UNI EN 13779 Requisiti di prestazione per i sistemi di ventilazione e di climatizzazione

[16] "Regolamento locale d'igiene, Comune di Milano", December 2012.

8. Data access statement

The datasets generated and analysed during the current study are available in the Zenodo repository, https://zenodo.org/record/6398238#.YkVWfOdByUl

Interoperability as a driver or barrier of smart building technologies?

Stijn Verbeke [a,b], Karine Laffont [c], David Rua [d]

[a] Unit Smart Energy and Built Environment, VITO, Belgium. stijn.verbeke@vito.be

[b] Energy and Materials in Infrastructure and Buildings, Faculty of Applied Engineering, University of Antwerp, Antwerp, Belgium.

[c] Dowel innovation, Valbonne, France

[d] Centre for Power and Energy Systems, INESC TEC, Porto, Portugal

Abstract. Smart building solutions are a strong leverage for increased energy efficiency in buildings, improved quality of life for occupants and added value for work performance. However, the degree of interoperability of technical building systems (and analysis / software tools that use data from these systems) can be a limiting factor affecting the smart services and impacts that can be delivered within a building since several ways of representing components and systems exist and inherently means a comprehensive knowledge not easily reachable. Interoperability is essential for allowing technical building systems to interact with the energy grids, can avoid duplication of efforts and is desirable in the light of future upgrades of the building. On the downside, it can increase the risk for malfunctioning and introduce cybersecurity and liability risks. This paper presents an overview of the various layers of interoperability in smart buildings and related standards and ontologies. Experts from industry and academia were surveyed and mapped the barriers and drivers related to interoperability of smart building systems, followed by further prioritisation of key actions to strengthen the market uptake of smart building technologies.

Keywords. interoperability, smart buildings, protocol
DOI: https://doi.org/10.34641/clima.2022.327

1. Introduction

Smart building solutions are a strong leverage for increased energy efficiency in buildings, improved quality of life for occupants and added value for work performance. Smart digital technologies in buildings are an important infrastructure requirement to explore flexible assets in the provision of energy and non-energy services.

The degree of interoperability of technical building systems (and analysis / software tools that use data from these systems) can be a limiting factor affecting the smart services and impacts that can be delivered within a building. Interoperability of systems can avoid duplication of efforts (e.g. investment for occupancy detection systems and monitoring displays for lighting, for space heating and cooling and ventilation systems) and optimise the control and maintenance of technical building systems (e.g. single interface for controlling heating and cooling facilitates the operation of the building and prevents spilling energy through uncoordinated simultaneous heating and cooling in building zones). Furthermore, interoperability is essential for allowing technical building systems to interact with the energy grids. Finally, interoperable systems are desirable in the light of future upgrades of the building as they can avoid proprietary lock-in and facilitate innovative solutions.

There can, however, also be a downside to interoperability. Exploiting interoperability through connecting various systems – potentially stemming from multiple manufacturers – can increase the risk for malfunctioning compared to proprietary systems and protocols. Fault diagnosis in a system of interconnected technical building systems can also be more intricate compared to a set of stand-alone systems. Finally, the delineation of responsibility for the provision of the service can become blurred in case of interoperable and interconnected systems. This can introduce cybersecurity risks and the risk that an end user is unable to establish who is responsible for the service and hence cannot legally seek recourse if a

Copyright ©2022 by the authors. This conference paper is published under a CC-BY-4.0 license.

service they have paid for is not functioning as intended.

The topic of interoperability has been identified as one of the key topics to be investigated by the "SmartBuilt4EU" project, a Coordination and Support Action funded by the European Commission to bring together the research and innovation community on smart buildings.

2. Research Methods

2.1 Set up of Task Forces

The SmartBuilt4EU project has set up four task forces investigating issues related to smart buildings: their objective is to identify the remaining challenges and barriers to smart building deployment, and the associated research and innovation activities that should be carried out in the near future to address those.

The participation to Task Forces is open and on a voluntary basis: members are welcomed to join by applying to SmartBuilt4EU Smart Building Innovation Community (SBIC). Most members are currently involved in Smart Building projects funded by the European Commission., while others are involved in European sector organisations, standardisation bodies, academia, or private companies.

The Task force No 2 of SmartBuilt4EU focuses on the optimal integration and use of smart solutions to allow an efficient building operation. The Task Force investigates what are the interoperability requirements to ensure a seamless operation, as well as the optimisation in terms of building costs and reduction of environmental impacts, over the full life cycle. The first topic addressed by this task force and presented in this paper was on interoperability of smart building systems and services.

2.2 Process to collect inputs, package results and validate through consultation

The process developed by SmartBuilt4EU started at the end of February 2021 with a workshop officially launching all Task Forces and attended by close to 50 participants. Preliminary feedback on the scope of the topics to be investigated from March to September 2021 was gathered through the online interactive tool Conceptboard. Three online meetings were then organised on a monthly basis with the members of Task Force 2 to collect inputs on the State of the Art (SoA) related to the interoperability topic, to identify barriers to the market uptake of smart buildings related to interoperability of building components and systems (as well as drivers); and finally propose activities to overcome the barriers and leverage the drivers. All the inputs provided through Conceptboard were then consolidated in a White Paper, which went through an internal quality review followed by a peer-review open to all members of SmartBuiltEU SBIC. The final White Paper was officially released during the Sustainable Places Conference in Rome, in September 2021, and published on SmartBuit4EU website [1].

3. Results of the screening and surveying tasks

3.1 Definition of interoperability

Various definitions of interoperability are being used in practice, e.g. proposed by the **European Interoperability Framework** (EIF) and **ISO/IEC 2382-017** [2]**.** In the work carried out by the task force members, it was opted for using the definition proposed by ETSI: "*Interoperability can be considered to be the ability of two or more systems or components to exchange data and use information*' [3]. ETSI also defined different levels of interoperability:

- technical interoperability (Systems and components that should work seamlessly together: sensors, actuators, central controllers and displays, etc.): addresses the aspects related with connectivity, network, and device representation;
- syntactical interoperability: addresses packing and transmission of data;
- semantic interoperability: addresses the representation and knowledge description;
- organisational Interoperability: addresses the aspects related to business objectives and regulatory frameworks

Other organisations or authors have proposed slightly different taxonomies, e.g. the interoperability stack by GridWise Architecture Council (GWAC) [4].

The semantic interoperability is an important research challenge tightly related with the purpose of allowing computer-based systems to exchange data and more importantly to infer on that data and allows the exchange of knowledge [5]. Ontologies, such as SAREF [6], are being developed based on graph patterns to set understandable and interpretable definitions of components related to devices, systems and buildings.

3.2 Landscape of standards, protocols and taxonomies

Interoperability can be relevant in multiple stages of the life cycle of a building; e.g. exchanging information between various building professions during the planning stage benefits greatly from interoperable models such as BIM (Building Information Models) data based on Industry Foundation Classes (IFC) standards [7]. Following

this standard, various participants in a building construction or facility management project can collaborate on a same data model; irrespective of the specific software tools they need for their activities. The desired IFC data can be encoded in various formats, such as XML, JSON, and STEP.

For smart buildings, interoperability during the operational phase becomes specifically important. Building management systems (BMSs) have evolved in recent years to support and efficiently operate diverse systems and appliances through technologies and ICT solutions; however, comprehensive multi-system management using one all-inclusive BMS and standardization of data flows, data analysis, and actuation remains an unattained goal [8]. A very broad range of IoT communication protocols is currently available. Besides proprietary protocols used by a single manufacturer, a large number of open protocols are being used including BACnet, LoraWan, ZigBee, KNX, DACI, EnOcean, Sigfox, Z-Wave, etc. [9,10]. Some of these are described in international standards, other are maintained by private initiatives supported by an ecosystem of multiple vendors. Given this multitude of protocols, using an 'open' protocol is not sufficient to guarantee interoperability. Furthermore, some of these protocols focus mainly on the communication layer, but do not extensively define the content and structure of the data exchange, thus still resulting in products of multiple vendors to not seamlessly integrate. One of the solutions to overcome this is making use of semantic taxonomies and standardised ontologies, which act as a common dictionary to map similar contents and data points across various protocols. This is especially relevant when the scope is widened from the single building to the interaction of the building and the connected energy grids. Irrespective of the building energy management system or smart appliances used at the building level, grid operators want to use a common approach to allow data exchange, e.g., when unlocking the flexibility offered by buildings to shift energy needs in time in response of fluctuating availability of renewable energy sources on the grid. Common ontologies such as SAREF allow to operate such an intricate system of buildings connected with an energy grid without forcibly imposing common hardware or communication protocols withing the buildings.

Two important initiatives in this regard are SMARTM2M and S2 interface. The SmartM2M initiative is supported by ETSI and focuses on creating the grounds for semantic interoperability in several sectors like the industry that led to IoT based ontology definitions [11]. SAREF is one of the related outputs concerning the smart appliances domain. The S2 Interface is initiated by a group of stakeholders and sponsored by IEC [12]. It aims developing a standardized way to exchange information to support energy flexibility services between for the grid side, making use of data representation of flexible assets within buildings under the resource manager designation.

One of the approaches being considered by several EU projects is the focus on the semantic interoperability and the ability to create decoupled representations of assets and entities that allow the development of new services for buildings. The InterConnect project has set an approach based on an interoperability framework (IF) to which adapters are used to ensure that different strategies or implementation approaches can be followed. The manufacturer, system integrator or service provider is responsible for developing software adapters to ensure the interaction with the IF based on graph patterns that exposes specific features based on SAREF extensions. The ability to ensure the interaction with other ontologies allows new generation of services to be exploited in the context of buildings, such as energy flexibility, energy forecasting, etc.

3.3 Main barriers identified by the Task force

Barriers to the market uptake of smart buildings related to interoperability of building components and systems were discussed by the Task Force.

Tab. 1 – Barriers related to interoperability.

Type	Barrier
Value Chain barriers	- **Vendor Lock-in (e.g. in the case of solutions sold with support & maintenance)** - Readiness of industrial players and complexity of value chain
Regulatory barriers	- Lack of industrial standards for homogenous interoperability - Data integration issues related to GDPR (General Data Protection Regulation) - Lack of regulation preventing or discouraging vendor lock-in
Social barriers	- **User acceptance / Final users' awareness and user friendliness** - Complex inclusiveness, lack of human-centric solutions for non-expert users
Economic barriers	- Reluctancy to adopt interoperability by manufacturers as it might affect market share / profit - Reluctancy to adopt interoperability by service providers / integrators who generate business on tailor made integrations - Cost related to IoT investment or semantic modelling (i.e. BIM)
Technical barriers	- **Cybersecurity of open systems** - Low "Smartness" of the building stock/ legacy equipment

Based on these extensive discussions, 12 main barriers were identified, which are displayed in Tab. 1. An attempt to further prioritise these barriers was undertaken by the Task Force, leading to highlighting the three top priority barriers – indicated in bold in Table 1. A first key barrier is related to vendor lock-in effects. A conventional example is a market offering of products of a specific vendor which are not interoperable with other products of different vendors. Many market actors are evolving into new business models relying on servitisation [13,14]. This might enhance lock-in effects, where not only products but also supporting services such as maintenance are closely tied to a specific vendor. While potentially beneficial for specific market actors, the proliferation of models relaying on vendor lock-in might hamper the overall market uptake of smart building solutions. A second key barrier to the uptake of smart building solutions is related to social aspects, namely the lack of user awareness and user-friendliness. Interoperability is a highly intricate field, even for experts working on this very topic. The complex technical concepts and terminology, e.g., related to various protocols used by smart building products, can cause confusion and lack of trust for many individuals. This barrier can become more crucial as the market is maturing and moving from frontrunners to a more general public uptake of smart building solutions. The third key barrier relates to cybersecurity of smart digital systems. Increased uptake of smart technologies and services relies on larger numbers of connected devices (sensors, actuators, controllers, etc.) which can mutually communicate and interact. Such intricate digital systems inherently raise the importance of cybersecurity aspects, especially compared to conventional buildings which rely on . In this regard, the role of interoperability can be ambiguous, as the possibility of connecting multiple systems of multiple vendors could also increase the risk for vulnerabilities. Typically, the risk for cybersecurity infringements will depend on the 'weakest' part of the system, and this harder to manage and maintain in an open system with multiple interoperable parts compared to a closed ecosystem for which roles and responsibilities are much more clear.

3.4 Main drivers identified by the Task Force

The Task Force also set out to define the main drivers for the uptake of smart building solutions related to interoperability. In total, 14 main drivers were defined, as listed in Table 2.

Two drivers were identified to be most critical. At first this is the market push, in which the market uptake of technologies clearly favours open standards and technologies. This is in clear contrast with the barrier of potential lock-in effects. Next, an important driver related to regulatory initiatives. Legislation such as the European Energy Performance of buildings directive and policy initiatives such as the Smart Readiness Indicator, Digital Logbooks for buildings and building renovation passports are perceived as important instruments to further drive the market towards interoperable smart building solutions.

Tab. 2 – Drivers for smart buildings related to interoperability.

Type	Drivers
Value Chain drivers	- **Market push** Initiatives from market actors providing energy and non-energy services - Democratisation of data assets/ strong push to make all the data available to all market players in the value chain
Regulatory drivers	- **EU Regulation: Energy Performance of Buildings Directive, Smart Readiness Indicator, Digital Logbooks and renovation passports** Renovation Wave - Development of (open) standards
Social drivers	- New trends in health care (tele-assistance - Customers requesting more plug-&-play solutions, democratisation of smart devices - Buildings becoming active in energy market: occupants require interoperability - Inclusiveness: a building should be as simple as a smart phone
Economic drivers	- Reduced development costs for new services thanks to interoperability
Technical drivers	- Cybersecurity: push to have a more interoperable system providing increased shared resistance to cyberattacks - Enhancement of potential synergies among devices - Crowd-evaluation of protocols

3.5 'Gaps'

Various activities required to overcome the barriers and leverage the drivers related to interoperability were suggested and prioritised by the Task Force members and are presented in Table 3. The priority ones according to the Task Force are indicated in bold.

Tab. 3 – Required R&I activities identified by the Task Force.

Type	Activities
R&I	- **Develop a unified and shared EU ontology & semantics for devices, equipment and assets (e.g. "Dictionary" bringing together all relevant semantics and ontologies, with shared definitions)** - Develop interoperable software tools allowing building operators to select their monitoring/actuation/analysis packages as a "kit of Parts" type approach - Develop Plug and Play hassle-free solutions specifically targeted at existing buildings.
Demo	- Build a marketplace for the manufacturing industry to respond to interoperability-related services - Set up exemplary projects showcasing the added value of interoperable equipment
Regulation & legal framework	- **Set up a central registry to give users a personal unique interface for filling, updating and sharing (give access to) information, in a just and safe way**. - Integrate interoperability into digital logbook / building passport - Develop regulations to demand open standards, create an imperative for strategic data flexibility - Set up minimum levels of interoperability/ smartness of buildings to maintain energy certificates validity - Define open and modular end-to-end interoperability and data management frameworks that enable open standards-based communication along the demand response value chain
Certification & standardisation	- Develop an interoperability label (with cybersecurity certification) at device scale - Standardization of semantic data tags for linked data in buildings - Set up exemplary projects showcasing the added value of smart building certification assessing the level of interoperability (e.g., Ready2Service certification, Smart Score, WiredScore)
Scaling up & industrialisation	- Develop approaches to facilitate the uptake of smart and interoperable solutions: start with the safety/security equipment - Develop data processing agreements with different stakeholders - Implement naming and tagging on devices
Upskilling & awareness raising	- Public acceptance/ awareness of interoperability: better educate or target the right market segment - Upskilling of practitioners in the field to fully take advantage of smart building and smart construction technologies

In next stages of the SmartBuilt4EU project, insights on identified gaps in knowledge, standards, industry uptake, etc. will feed into the development of a proposal for a strategic research and innovation agenda for European Commission services and the wider research and innovation community.

4. Discussion

The work carried out by the Task Force identified important barriers and drivers related to the interoperability of smart building products and services. Interestingly, some of these barriers and drivers can be in conflict. As an example, cybersecurity is definitively identified as an important issue, and like any digital technology, smart building solutions can bring about security risks, e.g. related to system hacking, fraud, data theft, etc. The role of interoperability is however ambiguous. Interoperable systems might be perceived as causing additional risks. Open systems can increase the risk for malfunctioning compared to proprietary systems and protocols and complicate fault diagnosis compared to stand-alone solutions. On the other hand, open protocols can often rely on a much larger user group and much more scrutiny in peer review of potential risks. An active community of multiple private companies, academics or individual software developers who review code and protocols and keep them up to date might result in lower overall risks compared to closed ecosystems.

Many of the other identified barriers and drivers relate to the complexity of interoperability: the large amount of stakeholders with divergent backgrounds, vested interests, competing protocols, etc. result in a highly intricate domain. While many demonstration projects have showcased the potential of fully interoperable solutions, a more seamless integration is needed to enhance a better uptake of such solutions.

One important aspect of interoperability in the building domain is the underlying goal of ensuring the necessary openness to allow the evolution of different representations devices, systems, services, among others. This is highly related with the barriers that have been addressed in several EU initiatives, including EU projects like SmartBuilt4EU, where contributions sought after by several groups of stakeholders are brought into standardization bodies where the discussion on contributions should be made to ensure that independent assessment is carried out, integration is made on existing standard and adoption is guaranteed. Aspects such as openness, modularity, and extensibility in interoperability strategies

prevent lock-in strategies or closed innovation ecosystems thus ensuring an evolving and long-term lifecycle of interoperability standards and initiatives.

The use of open protocols may be a good starting point in the ability to provide ground for participatory engagement on creating solutions towards generalized adoption, whilst allows contributions to be made on several levels, the fact remains that currently that is not sufficient. The focus on modular and extensibility of standards supported by appropriate annotation schemes allows the creation of complex representation of graph-based information that intrinsically provide automated ways support knowledge-based information exchange.

Given the importance of interoperability in designing and operating smart buildings, providing trustworthy and up-to-date information on the interoperability of technical building systems could raise awareness and facilitate operational management. At present, assessment and certification programmes however rarely take into account these aspects. Technical interoperability can be already assessed in some certification schemes. The Ready2Service label of Smart Building Alliance in France includes a theme "Equipment and interfaces", which deals with elements of interoperability such as the presence or absence of documented APIs (application programming interfaces), modalities for data access, etc. SmartScore by WiredScore evaluates some of the wired and wireless infrastructure implemented for building systems, and for example promotes the use of a single platform for analysing building performance data, irrespective of the underlying protocols or technology.

A similar approach is advocated by the Smart Readiness Indicator (SRI) for buildings, a scheme under the framework of the European Energy Performance of Buildings Directive that establish a common EU method for assessing smart buildings [15]. The SRI uses a twofold approach to include aspects of interoperability in the evaluation.

The implicit approach entails that interoperable systems are not explicitly assessed in the SRI method, but still will influence the scoring as some of the higher service levels and related impacts implicitly require interoperability. For example, the SRI score will improve for buildings with provisions to avoid simultaneous heating and cooling. Implicitly, this will require some level of interoperability of these systems (either directly or through other gateways).

Next to the inherent inclusion of some interoperability aspects in the scoring method of the SRI, there are also provisions to enhance the SRI label and supporting documents with additional information provisions, e.g. explicitly referencing the various technical systems and their corresponding protocols. This however is a voluntary add-on, and EU Member States implementing the SRI can further define this approach. There are significant challenges to overcome to make this an actionable feature of the SRI. Information on interoperability is usually not readily available to an assessor such as a certifier issuing Energy Performance Certificates and would require additional investigations. Especially in the case of legacy equipment it might be very hard or even impossible to retrieve sufficiently detailed information. Furthermore, such an assessment would need to be performed for many of the technical building systems present in a building (heating, cooling, lighting, ventilation, BMS…), requiring a large amount of time and effort which would have important repercussions on the cost of an SRI assessment. Furthermore, the SRI would in any case only provide a snapshot of the current status of the interoperability features of the technical building systems. This is a fast-moving field, and many software and hardware solutions emerge which allow interoperability despite using different technologies and protocols. Finally, this approach would require further efforts to generate a broad consensus on standards and protocols that would be included in this assessment. Open standards are not necessarily mutually interoperable. Nevertheless, their openness allows for developing gateways which can indeed facilitate communication between two distinct protocols; a practice which is very common in the current market. From this perspective, the use of open protocols does not guarantee interoperability, but it would indeed create a form of "readiness" to allow interoperability now or in the future.

Finally, a key lesson learned from the work of the Task Force is the importance of interoperability on a larger scale than just interaction within a building. In a context of intermittent renewable energy sources and smart grids, two-way communication between buildings and the grid (or peer-to-peer communication between buildings) becomes essential. Interoperability should not necessarily be attained through standardisation of all systems, components and protocols; rather ontologies and semantic models are proposed as the way forward to practically achieve interoperability in a context where various systems and protocols can still co-exist at the individual building level. Industry, policy actors and academia need to closely collaborate to further develop and implement such common ontologies and semantic models.

5. Conclusion

Interoperability is a key issue for smart building technologies. In an open collaboration process, a task force initiated by the SmartBuilt4EU coordination and support action has revied barriers, drivers and gaps related to interoperability of smart building technologies. Several demonstrations will take place to demonstrate the advantages of an interoperability approach to different technologies and digital platforms ecosystems to foster open and innovative services and solutions. In a next phase, draft for a European strategic research and innovation plan will be developed, highlighting the various actions needed for long-term and continuous support to enhancing interoperable implementations of smart building technologies, and the corresponding expected benefits, e.g. with regard to the active integration of smart buildings in a low carbon energy system.

6. Acknowledgement

The authors would like to acknowledge the active contributors of the Task Force No 2 of the SmartBuilt4EU project. This project has received funding from the European Union's Horizon 2020 research and innovation programme under grant agreement N° 956936.

7. Data access statement

Data sharing not applicable to this article as no datasets were generated or analysed during the current study.

8. References

[1] Interoperability for efficient operation of smart buildings; SmartBuilt4EU White Paper Task Force 2 topic A. 2021. Published online at https://smartbuilt4eu.eu/publications/

[2] ISO/IEC 2382:2015 - Information technology — Vocabulary. 2015

[3] Van der Veer H, Wiles A. ETSI White Paper 3 – Achieving technical interoperability, the Etsi approach. European Telecommunications Standards Institute.2008 ; 30p

[4] Knight M, Widergren S, Mater J, Montgomery A. Maturity model for advancing smart grid interoperability 2013 IEEE PES Innovative Smart Grid Technologies Conference (ISGT), 2013, pp. 1-6

[5] Bonino D, Corno F, De Russis L. A Semantics-Rich Information Technology Architecture for Smart Buildings. Build 2014, Vol 4, Pages 880-910

[6] ETSI TS 103 410 (parts 1 to 11): SAREF Technical Specification series

[7] ISO 16739-1:2018 Industry Foundation Classes (IFC) for data sharing in the construction and facility management industries — Part 1: Data schema. 2018

[8] Minoli D, Sohraby K, Occhiogrosso B. IoT Considerations, Requirements, and Architectures for Smart Buildings – Energy Optimization and Next Generation Building Management Systems, IEEE Internet Things J., vol. 4, no. 1; 2017

[9] Lohia K, Jain Y, Patel C, Doshi N. Open Communication Protocols for Building Automation Systems. Procedia Comput Sci. 2019 Jan 1;160:723–7

[10] Domingues P, Carreira P, Vieira R, Kastner W. Building automation systems: Concepts and technology review. Comput Stand Interfaces. 2016;45:1–12.

[11] ETSI TS 103 264: "SmartM2M; Smart Applications; Reference Ontology and oneM2M Mapping". 2017

[12] EN 50491-12-2 - General requirements for Home and Building Electronic Systems (HBES) and Building Automation and Control Systems (BACS) - Part 12-2: Smart grid - Application specification - Interface and framework for customer - Interface between the Home / Building CEM and Resource manager(s) - Data model and messaging. 2020

[13] Zhang W, Banerji S. Challenges of servitization: A systematic literature review. Ind Mark Manag. 2017 Aug 1;65:217–27

[14] Liu D, Wang H, Zhong B, Ding L. Servitization in Construction and its Transformation Pathway: A Value-Adding Perspective. Engineering. 2021

[15] Commission Delegated Regulation (EU) 2020/2155 of 14 October 2020 supplementing Directive (EU) 2010/31/EU of the European Parliament and of the Council by establishing an optional common European Union scheme for rating the smart readiness of buildings

A novel machine learning approach to predict short-term energy load for future low-temperature district heating

Thomas Ohlson Timoudas [a], *Yiyu Ding* [b], *Qian Wang* *[c, d]

[a] RISE Research Institutes of Sweden, Sweden, thomas.ohlson.timoudas@ri.se

[b] Department of Energy and Process Engineering, Norwegian University of Science and Technology (NTNU), Trondheim, Norway, yiyu.ding@ntnu.no

[c] Department of Civil and Architectural Engineering, KTH Royal Institute of Technology, Brinellvägen 23, Stockholm, Sweden, qianwang@kth.se

[d] Uponor AB, Hackstavägen 1, Västerås, 721 32, Sweden

Abstract.
In this work, we develop machine learning methods to forecast the day-ahead heating energy demand of district heating (DH) end-users in hourly resolution, using existing metering data for DH end-users and weather data. The focus of the study is a detailed analysis of the accuracy levels of short-term load prediction methods. In particular, accuracy levels are quantified for Artificial Neural Network (ANN) models with variations in the input parameters. The importance of historical data is investigated – in particular the importance of including historical hourly heating loads as input to the forecasting model. Additionally, the impact of different lengths of the historical input data is studied. Our methods are evaluated and validated using metering data from a live use-case in a Scandinavian environment, collected from 20 DH-supplied nursing homes through the years of 2016 to 2019. This study demonstrates that, although there is a strong linear relationship between outdoor temperature and heating load, it is still important to include historical heating loads as an input for prediction of future heating loads. Furthermore, the results show that it is important to include historical data from at least the preceding 24 hours, but suggest diminishing returns of including data much further back than that. The resulting models demonstrate the practical feasibility of such prediction models in a live use-case.

Keywords. Low-temperature district heating, short-term load prediction, machine learning, Scandinavian climate.
DOI: https://doi.org/10.34641/clima.2022.319

Copyright ©2022 by the authors. This conference paper is published under a CC-BY-4.0 license.

1. Introduction

District heating (DH) plays a vital role for the operation of building energy supply systems, which accounted for 35% of global final energy use and 38% of energy-related CO_2 emissions [1]. However, existing DH networks in many cold climates still use rather high supply temperatures, such as 75 °C or above [2]. In the face of green energy initiatives, increasing shares of low-energy buildings, and case examples in mild climates, there is a pressing need to transform the existing DH networks toward low-temperature DH (LTDH). Moreover, digitalization and the overall transition towards smart energy systems and cities are placing higher requirements on integration, communication, and cooperation with end-users (buildings) connected to such LTDH networks. As a result, future generations (4th and 5th) of LTDH networks will feature low operating temperatures, and greater integration with the end-users (buildings) and building-sized renewables. However, how to operate such integrations still rely fundamentally on a thorough understandings of heating loads.

On the other hand, digital solutions for measuring and controlling the network will allow for higher degrees of system optimization with intermittent renewables and heat pumps. This means that short-term predictions of heating loads are essential. But updating all the legacy monitoring facilities is a very costly and lengthy process. There is still a pressing need for more knowledge about what tools are available, and how well these methods can be utilized for load predictions in LTDH applications. At the same time, there is still room for improvement and solutions that can work on top of the existing DH systems, using existing metering data, during this transition period.

Large amounts of studies have developed different types of models to predict short-term energy demand in buildings in general. However, most of them are oriented towards electricity load predictions. For those reports that have been investigating DH load predictions, a great amount of methods are based on linear regression models, due to the strong linear relationships of heating load with respect to outdoor temperature. These existing methods commonly have not taken full advantage of using data-driven approaches, such as emerging machine learning (ML) models to perform such predictions. Even within those limited publications in the respective areas, it is still not clear what are the key advantages of using such ML approaches, and to what extent the accuracy levels can be quantified, given limited dataset inputs. This study provides a practice of the above raised challenges.

1.1 Previous studies

As mentioned, great amounts of studies exist with respect to building load predictions. These studies commonly utilize knowledge and experience gained from buildings' electricity demand data research, and transferable to heating demand analysis and uncertainties (i.e., weather forecasting) [3]. Among them, two types of models, namely, autoregressive multiple linear regression (MLR) and autoregressive multiple non-linear regression (MNLR), were firstly built to predict the DH load profiles, which can further aggregate them into district levels [4]. The Artificial Neural Network (ANN)-based MNLR shows better performance than MLR in the application of high load variations within 1-day time series [4]. Additionally, three supervised learning methods, namely, Support Vector Machine (SVM), deep neural network (DNN, ANN with two or more hidden layers), and extreme gradient boosting (XGBoost), were exercise to predict loads on a multi-step basis. These methods were also practiced with direct and recursive strategy [5]. By feeding day-before influential factors, all the above methods yield rather accurate forecasting for the day-ahead DH load at the given climate. However, how to use these heating load forecasting to optimize operation for DH system were not explored [5]. Some studies applied Gaussian mixture model (GMM) clustering enables defining four typical DH operation patterns in office buildings in a semi-arid climate (with cold and dry winters) [6]. Both outdoor temperature and occupant behavior data were considered. It is reported that by combining the clustering with regression and ANN models, the qualities of hourly heating load forecasting are improved by 38.7-75.7% in the given climate. However, it showed challenges to predict the peak heating loads during night-to-daytime periods, which can highly reply on random operation behaviors [6]. Forecasting model based on convolutional neural network long-short term memory (CNN-LSTM) outperformed other data-driven methods when solving thermal inertia problems in DH networks. This is reasoned by mainly owing to its integration of CNN's feature extraction ability and LSTM's two-dimensional space ability [7]. But this model requires large amounts of sensors, large data storage, and daily retraining, which place high pressure on the data management infrastructure [7]. Some other studies compared different data-driven methods, such as SVM and nonlinear autoregressive exogenous recurrent neural network (NARX-RNN) in the content of DH applications [8]. It was found that the NARX-RNN exceeds the SVM regarding the quality indicators and computation time. However, the overfitting tendency of NARX-RNN needs further study [8].

1.2 Objective

In this work, we develop ML methods to forecast the day-ahead heating energy demand of DH end-users in hourly resolution, by using existing metering data for DH end-users and weather data. The importance of historical data is investigated – in particular the importance of including historical hourly heating loads as input to the forecasting model. Additionally, the impact of different lengths of the historical input data is studied. The feasibility of such models, and their accuracy, are evaluated using data from a live

use-case in Scandinavian environment. A detailed analysis of the accuracy levels of short-term load prediction methods are in focus.

2. Methodology

The study applies combinations of a two-step approach:

Step 1. A thorough understanding of the DH network and building load on annual basis, namely load profiles. This provides an overall view and boundary conditions of DH networks.

Step 2. Based on the definitions of DH load profile, day-ahead prediction models are developed. The model is rooted as an Artificial Neural Network (ANN) model, varying the input parameters, and trained and evaluated using the DH dataset.

To measure and evaluate the performance of the models, the mean squared error (MSE), and the mean absolute error (MAE), were both recorded for each model after training had been completed, using the 2019 test data (that had not been seen by the models during training).

2.1 Data inventory

The heating load was measured and collected for 20 separate nursing homes in Scandinavian climate, all located in the city of Trondheim, Norway. All of these buildings are connected to the same DH network, and the measurements were obtained directly from the measuring equipment of the network operator. The data contains the hourly heating loads for each of the buildings, spanning the entire time period from January 1, 2016 to December 31, 2019, obtained from the energy monitoring platform of Trondheim Municipality [9].

For the model construction and evaluation, the average heating load per square meter (W/m^2) was calculated across the 20 buildings for each hour. The data were supplemented with hourly outdoor temperature measurements obtained from the Norwegian meteorological station [10] in Trondheim, for the corresponding period.

2.2 Load profile development

The load profile was identified using an energy signature (ES) curve in the study. This method has been widely employed for planning and sizing purposes. An ES curve consists of a temperature dependent part, and a temperature independent part, which are divided by changing point temperature (CPT) or heating effective temperature, defined as:

If $T_t \leq$ CPT, $$P(T_t) = p_1 \cdot T_t + p_2 + \varepsilon \quad (1)$$

If $T_t >$ CPT, $$P(T_t) = p_1 \cdot T_t + p_2 + \varepsilon \approx p_2 \quad (2)$$

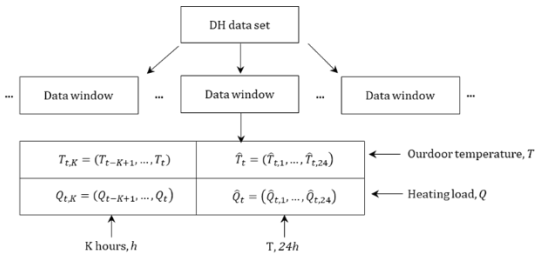

Fig. 1 The logic of short-term prediction model

where T_t is the outdoor temperature at time t, p_1 and p_2 are the coefficients of each ES curve model, and ε is the residual error. The heating demand follows the linear growth under the slope of p_1. Below the changing point temperature, it is the outdoor temperature dependent part and above the changing point temperature, it is the outdoor temperature independent part, when most of the heating needs go to domestic hot water (DHW) use.

For DH network monitoring, the load data are commonly aggregated as a combination of space heating and domestic hot water usage. Therefore, in the energy signature analysis, DHW load is extrapolated based on the existing studies [11], which has reported as a representative DHW profile for the given climate and resident types.

For modeling boundary conditions, daily heating degree hours (HDH) is calculated as the daily summation of the difference between balance temperature and hourly outdoor temperature, see below:

$$HDH = \sum_{t=t_0}^{t_0+23} \max(0, T_{bal} - T_t) \quad (3)$$

where t_0 is the first hour of the day, the heating balance temperature T_{bal} is assumed at 15°C and negative summands are set to zero. From this, high-heating season, mild-heating seasons and non-heating seasons can be identified in the ES curve.

2.3 The day-ahead prediction models

In this study, short-term prediction is defined as 24-hours (day-ahead) time horizon. ANN-based models were developed to predict the short-term heating load, starting from a given hour, for each hour of the following 24-hour period. As mentioned, this serves as a decision-supporting tool for the operation purposes in future LTDH transitions. All of these models used as input the forecasted outdoor temperature for the corresponding 24-hour period. To study the importance of historical data, and the performance impact of different measuring scenarios, nine differentiated ANN models were created and compared.

The models differed in what additional input data were used. One of them used no additional inputs, i.e., only the forecasted outdoor temperature. The other eight models were split into two main categories:

- Half of them were additionally supplied with the historical outdoor temperature,

- The other half were supplied, in addition to that, with the historical measured heating load.

For both cases, the historical data were given in the same hourly resolution. Within each category, the models were further differentiated based on the number of hours of historical data stretched back: 12, 24, 48, or 72 hours.

All of these models had one input layer (the number of inputs varied between the models), one hidden Rectified Linear Unit (ReLU) layer with 64 nodes (this number was determined through hyperparameter search), and one output layer. All the layers were densely connected. Mean squared error (MSE) was used as the loss function, and Adam was used for the parameter optimization, with the maximum number of epochs set to 100.

2.4 Mathematical description of the models

The logic of the developed model is presented in Figure 1. Let Q_t and T_t represent the measured heating load, and the measured outdoor temperature, at hour t, respectively; and let $\hat{Q}_{t,s}$ and $\hat{T}_{t,s}$ represent the predicted heating load, and the forecasted outdoor temperature, made at hour t for hour $t+s$ (defined for $s = 1, \dots, 24$), respectively. Let K be a parameter representing the number of hours of historical measured data to be used as input for the model. Introduce the shorthand notation as,

$$\hat{Q}_t = (\hat{Q}_{t,1}, \dots, \hat{Q}_{t,24}), \tag{4}$$

$$\hat{T}_t = (\hat{T}_{t,1}, \dots, \hat{T}_{t,24}), \tag{5}$$

$$Q_{t,K} = (Q_{t-K+1}, \dots, Q_t), \text{and} \tag{6}$$

$$T_{t,K} = (T_{t-K+1}, \dots, T_t). \tag{7}$$

That is, $\hat{Q}_t$, $Q_{t,K}$, $\hat{T}_t$, and $T_{t,K}$ represent, at the time instance t, the predicted heating load for the following 24 hours, the historical heating load for the preceding K hours (including t), the forecasted outdoor temperature for the following 24 hours, and the historical outdoor temperature for the preceding T hours (including t), respectively.

Each ANN model can then be expressed as either the function

$$\hat{Q}_t = f_K(\hat{T}_t, T_{t,K}), \tag{8}$$

if historical heating load is not an input to the model, or as

$$\hat{Q}_t = g_K(\hat{T}_t, T_{t,K}, Q_{t,K}), \tag{9}$$

if historical heating load is supplied, where f_K and g_K are abstract representations of our ANN models, and the parameter K takes either of the values 0, 12, 24, 48, and 72 (hours).

2.5 Training and evaluation of the models

As mentioned above, the different models were all trained and evaluated using the same dataset, introduced in Section 2.1. The dataset was created from the original data by first considering every possible consecutive 24-hour window of both the outdoor temperature and the heating loads, and then appending the preceding K-hour window to it, both for the outdoor temperature and the heating loads. In the cases that did not consider the historical heating load, that part of the window was simply discarded. Each window is therefore split into input and output, according to Fig. 1.

The data for the years 2016 and 2017 was used as the training set for the ANN, while the data for 2018 was used as the validation dataset, for the stopping criterion of the training. The resulting models were evaluated using the data for the entire year of 2019, the testing set, to ensure that the models were evaluated on a whole year of data.

Note that the model was evaluated using the actual measured outdoor temperature as the outdoor temperature forecast input. To improve statistical reliability, each model was trained from scratch ten times (using the same training data, but randomly initializing the weights each time), and the averages of these performance measures across the ten iterations were recorded.

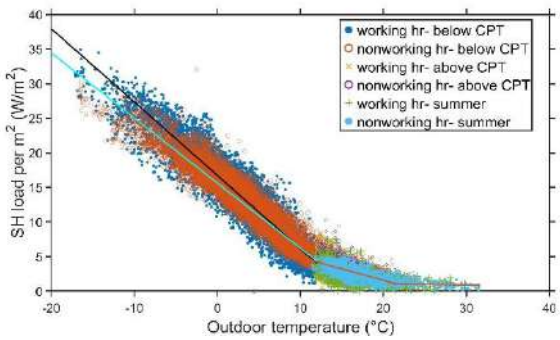

Fig. 2 – Energy signature (ES) curve for the district heating (DH) load profile

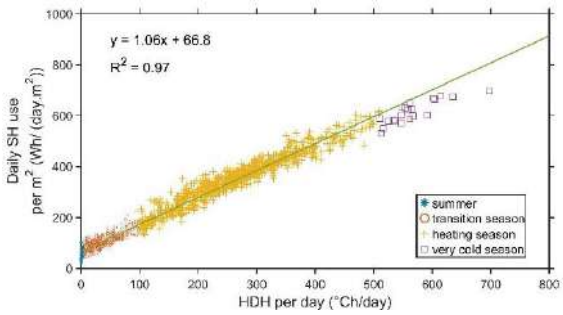

Fig. 3 – Load characteristics given the whole heating season, presented by heating degree hours (HDH)

3. Results

3.1 ES and load profile characteristics

Fig. 2 shows the ES of the DH network. Around 12°C was found as the changing point temperature for providing a proper piece-wise approximation. It is found that outdoor temperature that are above the changing point temperature consists of 22.4% of heating seasons. Fig. 2 also shows that space heating loads are less temperature dependent at the mild-heating season (constant slope), and these small loads can be described by one regression line regardless of working hours and non-working hours. The rest 77.6% of the time the outdoor temperature was below the changing point temperature, falls into high-heating season. Along the regression lines below the changing point temperature, there is a small region where non-working hour may need slightly higher space heating load than working hour under the same outdoor temperature (c.a. 10 - 12°C).

From the linear relationship between specific daily space heating and heating degree hours, as displayed in Fig. 3, it shows the daily space heating operation follows the daily heating degree hours, without influences from day types or manual false operation/intervention. These results are expected, given the rather high-temperature/conventional DH networks in the study. This also provides the boundary conditions that the day-ahead predictions will be constrained by the operation scenarios, instead of allowing the network temperature drift freely with load variations.

3.2 Accuracy levels of day-ahead prediction

Tab. 1 – Performance measures for the models, evaluated on the testing set of 2019

Model parameter	Mean squared error (MSE)	Mean absolute error (MAE)
No historical data, i.e., f_0		
K = 0	0.0824	0.2275
Only historical outdoor temperature, i.e., f_K		
K = 12	0.0790	0.2213
K = 24	0.0770	0.2183
K = 48	0.0753	0.2161
K = 72	0.0698	0.2086
Including historical heating load, i.e., g_K		
K = 12	0.0307	0.1299
K = 24	0.0219	0.1106
K = 48	0.0231	0.1133
K = 72	0.0221	0.1112

The evaluation error of the models are shown in Table 1. Recall that the evaluation of the models was performed on the dataset covering the entire year of 2019, and that this data had not been previously seen by the model (during the training stage). The results show a clear difference between the models g_K that use the historical load data, and the models f_K that do not. In particular, the impact of *only* including historical outdoor temperature data as input to the model is relatively small, even when longer periods of historical data are used, compared to also including the historical load data.

3.3 Example prediction results

The prediction performance of the two models f_{72}, g_{72}, and the models using 72 hours of historical data as input, are compared in both Fig. 4 and Fig. 5, showing results for different heating seasons. Recall that the model f_{72} does not consider the historical heating load as input, whereas g_{72} does. The top row shows the prediction results for f_{72}, and the bottom row the results for g_{72}. Each column shows the prediction for the 24-hour period following the time indicated above it, i.e., the prediction of the heating load $\hat{Q}_t = (\hat{Q}_{t,1}, \dots, \hat{Q}_{t,24})$ is plotted for the time instance t equal to the given date. Therefore, the performance of the two different models can be easily compared for the same time instant, by looking at each column.

The red crosses show the predicted heating load made by the model, while the blue boxes indicate the actual measured heating load. The dashed black line shows the forecasted outdoor temperature for the corresponding 24-hour period – in this case the actual outdoor temperature for evaluation purposes.

The three dates in Fig. 4 were randomly sampled from the 2019 testing data, to ensure statistical reliability. Since the first random sample did not cover the high-heating season (the period with the highest heating demand), we sampled and plotted the predictions for three additional dates from the months of December, January, and February, shown in Fig. 5, which falls in the high-heating season.

4. Discussion

A significant difference can be observed between the models those use both historical heating loads and outdoor temperature as inputs and the models those only use historical outdoor temperature. This difference is especially significant during the mild-heating season, when the heating load is dominated by domestic hot water, as evidenced by Fig. 4. This is likely due to the relatively weak relationship between outdoor temperature and the total heating load during that period, compared to the high-heating season, when space heating demand is the dominant component. Another reason could be due to thermal inertia and storage effects of the buildings, as well as suboptimal control of the heating loads, in which case the historical heating loads could be useful to model. This evidence provides a basis for how future LTDH should be transferred under different climate conditions, when heating loads fall more into the mild-heating season regime, with

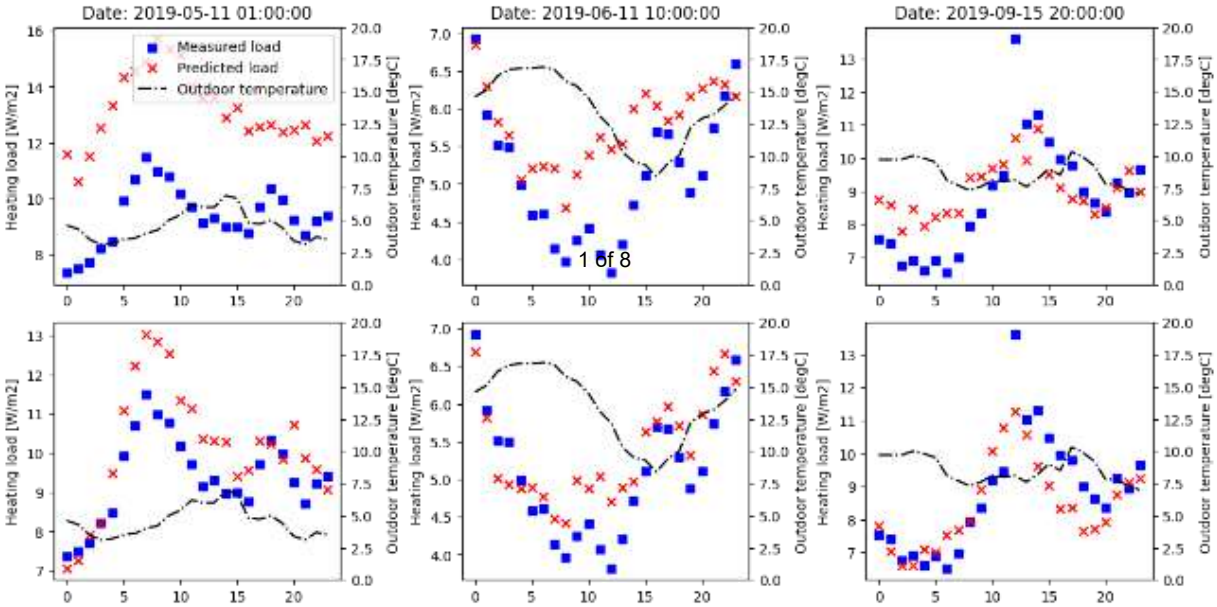

Fig. 4 – Plotted predicted heating load for the 24-hour period following the date indicated above each column, for the model f_{72} (top row), and the model g_{72} (bottom row). The dashed black line shows the outdoor temperature for the corresponding 24-hour period, the red crosses the predicted heating load for each hour, and the blue squares the measured (actual) heating load. Randomly sampled dates in mild-heating season.

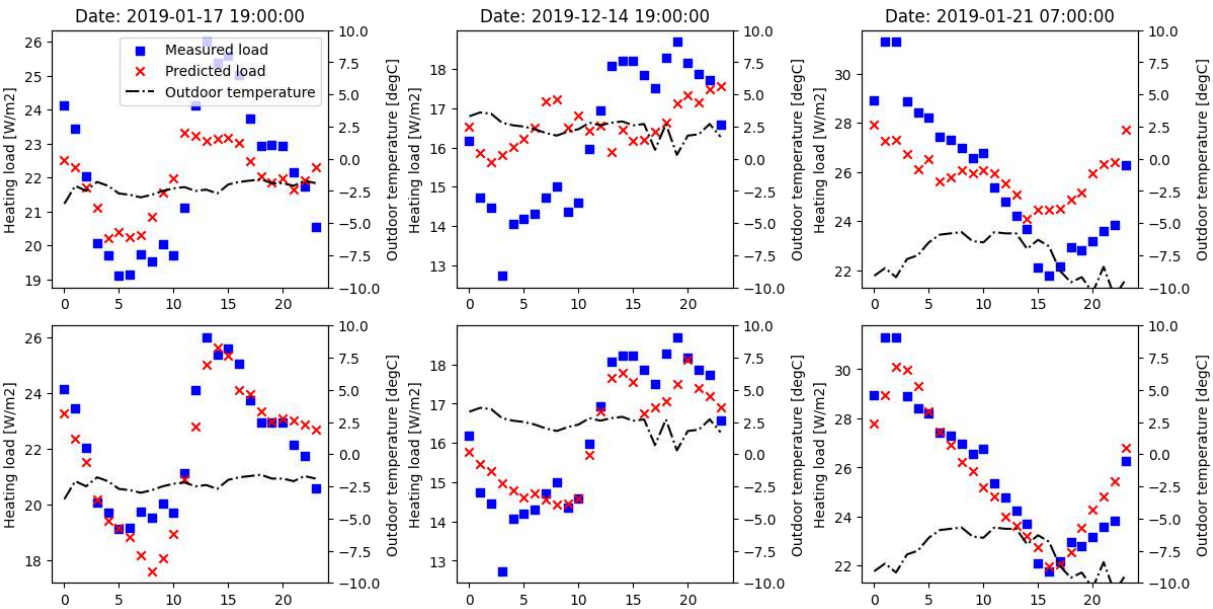

Fig. 5 – Plotted predicted heating load for the 24-hour period following the date indicated above each column, for the model f_{72} (top row), and the model g_{72} (bottom row). The dashed black line shows the outdoor temperature for the corresponding 24-hour period, the red crosses the predicted heating load for each hour, and the blue squares the measured (actual) heating load. Randomly sampled dates from December, January, and February, high-heating season.

perhaps only peaks fall into the high-heating season regime. These differences are also evident in the Table 1, which shows the average performance over the whole-year period. The results demonstrate the importance of making historical heating load available to heating load prediction models. Yet, while historical hourly outdoor temperature is often publicly available, historical heating loads are in many cases only available with large delays or low temporal resolution, if at all. The results additionally demonstrate the importance of using historical data from longer time periods, although they seem to suggest diminishing returns beyond the data for the previous 24 hours. This optimal cut-off period will likely differ between different building types, due to differences in thermal inertia.

It should be noted that the performance of the models was evaluated using the actual measured outdoor temperature as the forecasted outdoor

temperature for the following 24-hour prediction. In practical applications, this forecast would typically be inaccurate. Such inaccuracies would lead to lower performance than observed in this study. As such, it is important that the base model is as accurate as possible, to reduce the propagation of such inaccuracies within the model. Moreover, further studies are needed to understand and quantify the effects of inaccurate forecasts, to ensure practical applications of these prediction models. Since thermal storage and intermittent renewables have own inaccuracies and uncertainties, it is especially important when they are integrated into the LTDH network perspective and optimized as a whole.

The mean average percentage error (MAPE), another common evaluation metric in the literature, was left out since the average heating load per square meter was close to 0 during certain times of the year (division by zero).

The limitation of this study is that it only considered a single type of model, an ANN, and that we did not perform a wide hyperparameter search (although we tried several different numbers of nodes and hidden layers, that all produced similar results). A further study should investigate if the results hold also for other types of prediction models and ANN architectures.

Moreover, we only considered two parameters: outdoor temperature (provided by a meteorological institute), and measured heating loads (provided by a municipality monitoring platform). It would be interesting to study the impact of additional variables, such as the integrated heat pumps and short-to-medium term thermal storage in such networks.

5. Conclusions

This study demonstrates that, although there is a strong linear relationship between outdoor temperature and heating load, it is still important to include historical heating loads as an input for prediction of future heating loads. Accuracy levels are quantified by using ANN models with input parameter variations. Furthermore, the results show that it is important to include historical data from at least the preceding 24 hours, but suggest diminishing returns of including data much further back than that. The models developed in this study were evaluated on actual measured data from a live use-case, demonstrating the practical feasibility of such prediction models.

6. Acknowledgement

This work is financially supported by Swedish Energy Agency with project No. 51544-1 and EU H2020 programme under Grant Agreement No. 101036656. Special thanks to Trondheim municipality, Norway, for providing data and user information.

7. References

[1] U. N. Environment, "2020 Global Status Report for Buildings and Construction." https://globalabc.org/news/launched-2020-global-status-report-buildings-and-construction (accessed Nov. 15, 2021).

[2] K. Lygnerud, S. Werner, and etc., "Low-Temperature District Heating Implementation Guidebook. IEA DHC Report; 2021," p. 206.

[3] M. Lumbreras *et al.*, "Data driven model for heat load prediction in buildings connected to District Heating by using smart heat meters," *Energy*, vol. 239, p. 122318, Jan. 2022, doi: 10.1016/j.energy.2021.122318.

[4] B. Talebi, F. Haghighat, and P. A. Mirzaei, "Simplified model to predict the thermal demand profile of districts," *Energy and Buildings*, vol. 145, pp. 213–225, Jun. 2017, doi: 10.1016/j.enbuild.2017.03.062.

[5] P. Xue, Y. Jiang, Z. Zhou, X. Chen, X. Fang, and J. Liu, "Multi-step ahead forecasting of heat load in district heating systems using machine learning algorithms," *Energy*, vol. 188, p. 116085, Dec. 2019, doi: 10.1016/j.energy.2019.116085.

[6] Y. Lu, Z. Tian, P. Peng, J. Niu, W. Li, and H. Zhang, "GMM clustering for heating load patterns in-depth identification and prediction model accuracy improvement of district heating system," *Energy and Buildings*, vol. 190, pp. 49–60, May 2019, doi: 10.1016/j.enbuild.2019.02.014.

[7] J. Song, L. Zhang, G. Xue, Y. Ma, S. Gao, and Q. Jiang, "Predicting hourly heating load in a district heating system based on a hybrid CNN-LSTM model," *Energy and Buildings*, vol. 243, p. 110998, Jul. 2021, doi: 10.1016/j.enbuild.2021.110998.

[8] D. Koschwitz, J. Frisch, and C. van Treeck, "Data-driven heating and cooling load predictions for non-residential buildings based on support vector machine regression and NARX Recurrent Neural Network: A comparative study on district scale," *Energy*, vol. 165, pp. 134–142, Dec. 2018, doi: 10.1016/j.energy.2018.09.068.

[9] "iEOS - Planning." https://www2.esave.no/Esave.nsf/iEOS_Hovedbilde.xsp (accessed Feb. 24, 2021).

[10] "Norsk Klimaservicesenter." https://seklima.met.no/observations/ (accessed Feb. 24, 2021).

[11] D. Ivanko, H. T. Walnum, and N. Nord, "Development and analysis of hourly DHW heat use profiles in nursing homes in Norway," *Energy and Buildings*, vol. 222, p. 110070, Sep. 2020, doi:

10.1016/j.enbuild.2020.11007

8. Data access statement

The datasets generated during and/or analysed during the current study are not publicly available because the Municipality holds the right of the datasets but the authors will make every reasonable effort to publish them in near future.

Co-benefits of building automation and control systems: an analysis of smart office buildings

Federico Garzia [a, b], Lotte Van Thillo [b], Stijn Verbeke [b, c], Cristian Pozza [a], Amaryllis Audenaert [b]

[a] Institute for Renewable Energy, EURAC Research, Viale Druso 1, I-39100 Bolzano, Italy, federico.garzia@eurac.edu.

[b] Energy and Materials in Infrastructure and Buildings, University of Antwerp, Faculty of Applied Engineering, Groenenborgerlaan 171, 2020, Antwerp, Belgium.

[c] Unit Smart Energy and Built Environment, VITO, Boeretang 200, 2400, Mol, Belgium.

Abstract. The more and more widespread availability and implementation of building automation and control systems (BACS) is revealing how building monitoring, control, and real-time data, can support building users' well-being, providing additional co-benefits, besides the positive energetic impacts. Therefore, these technologies will play an important role in the transition towards a smart built environment, reducing energy consumption, enhancing comfort and interacting with a smart grid and building users. The Standard EN15232 with the BAC factor method introduces smart control efficiency classes and provides quantitative data for estimating the energy savings associated with the installation of smart controls. Although this method is not very detailed, it aims to provide a rough estimation in the early design stages. Assessment methods for BACS (such as the European Smart Readiness Indicator, the French SBA 'Ready to Service label') also stress the importance of non-energetic impacts of BACS. At present, these methods mostly rely on qualitative assessments or use ordinal scores, since investigation on non-energetic benefits and quantitative data are largely lacking. This paper analyses the multiple co-benefits of smart controls in office buildings in greater detail. By means of data reported in literature and building simulations, the most important co-benefits are identified and to the extent possible also quantified. A contemporary office building is used as case study to apply and demonstrate the proposed analysis framework.

Keywords. Smart buildings, BACS, co-benefits.
DOI: https://doi.org/10.34641/clima.2022.316

1. Introduction

In 2019, commercial building sector accounted for 12% of the energy consumption in the United States [1]. In Europe office buildings represent 25% of the non-residential floor space and 26% of the energy consumed in tertiary sector [2]. The European energy performance of buildings directive (EPBD) and the directive 2012/27/EU on energy efficiency are the main policy instruments to promote a phase-out of inefficient buildings. In particular, the 2018 amendment of the EPBD (directive 2018/844 of the European Parliament and of the Council of 30 May 2018 [3]) promotes the implementation of building automation and electronic monitoring of technical building systems to support building digitalization and the improvement of energy efficiency. Real estate industry lags behind in adopting new technologies compared to other sectors, nevertheless according to a recent market report, the global smart buildings market is expected to grow with a compound annual growth rate (CAGR) of 32%, reaching $43 billion USD by 2022 [4]. A wider implementation of Building Automation and Control Systems (BACS) which can provide technical management and monitoring is expected to produce energy savings in a cost-effective way and to improve comfort and indoor air quality (IAQ), adjusting the indoor environmental conditions to occupant needs. Furthermore, in a future energy system with a large share of distributed renewable energy generation, smart buildings will be the cornerstone for an efficient demand-side energy flexibility and an optimized self-consumption [5, 6], with BACS being key enablers of the building integration within the so-called "Smart Grid" [7].

Despite the growing attention on BACS multiple benefits, a review and meta-analysis performed by O'Grady et al. (2021) [8] highlighted that the most investigated trend by far in this field is the impact on energy reduction (92% of the reviewed publications). The European standard EN 15232:2017 [9] focuses on this aspect by providing an estimation of the impact that these systems have on energy performance and introducing a

Copyright ©2022 by the authors. This conference paper is published under a CC-BY-4.0 license.

classification of the building control systems and functionalities. However, further co-benefits of smart technologies are for many actors and stakeholders within the construction sector still unclear or unknown, therefore, the 2018/844 directive introduced the Smart Readiness Indicator (SRI), a voluntary EU scheme for rating building smartness and the ability to interact with the occupants and the grid [10]. The SRI tackles the lack of awareness of the benefits associated with smart building technologies and functionalities, aiming at making these benefits more tangible for building users, owners, tenants, and smart service providers. Another example is the Ready2Services (R2S) label set up by the French Smart Building Alliance (SBA) with the Certivéa certifier for non-residential buildings. The R2S reference framework describes the key requirements for communication between the building systems and services with the objecting of providing more services, optimizing operating costs, improving flexibility and scalability and enhancing attractiveness. Nevertheless, the SRI scheme as well as the R2S are qualitative appraisals which aim at raising awareness of possible smart technologies implications and co-benefits beyond energy savings without providing insights on the real entity of these co-benefits. For this reason, more mixed method (qualitative and quantitative) insights to capture the human experience are needed [8], as well as quantitative approaches that can be implemented as early design stage assessments [11].

This paper proposes an approach which considers the energetic and non-energetic benefits of BACS, focusing on office buildings. This building typology was chosen due to the higher permeability to smart technologies and the relevant impacts that these promise to achieve [12]. Major market players highlight how a smart office can leverage BACS to deliver a better user experience of the workplace, meeting in this way evolving employees' needs as recorded for instance during COVID-19 pandemic. Employees are increasingly aware of the importance of having a better work environment in terms of comfort and health aspects. These systems, combining several data-driven and digitally-enabled services, have an impact on employee well-being and performances by managing lighting, heating, ventilation, and air conditioning systems, office desks, and elevators, up to whole office spaces. Defining and quantifying the benefits of BACS in office buildings will allow to decrease the risk perception associated to the adoption of smart technologies. The proposed approach collects and analyzes main smart office co-benefits and presents an application on a case study. A reference office building was modeled within EnergyPlus simulation engine and a shading control has been selected for the assessment of energy savings in combination with co-benefits. A proper adjustment of daylight not only has a direct impact on building internal gains, which in turn influence the heating and cooling consumption, but also on thermal and visual comfort, attention restoration, and stress reduction.

2. Smart office building co-benefits

Nowadays, considering not only energy efficiency, but also co-benefits is gaining more and more relevance when it comes to evaluating innovative solutions for built environment. Smart building technologies are no exception as demonstrated by the SRI scheme, which assesses the impacts that a smart ready service can provide to the building, its users, and the energy grid by defining a set of seven categories: energy efficiency, comfort, health, well-being and accessibility, maintenance and fault prediction, convenience, information to occupants and energy flexibility and storage.

Co-benefits in the field of comfort, health and well-being, are the second most investigated topic in BACS sector after energy efficiency, with 34% of the publications that are related to the impacts of perceived human comfort in the built environment, and the effects of IAQ on health and productivity of building occupants [8]. Nevertheless, there are still many questions on how to effectively measure and quantify impact of BACS on occupant comfort and in general on indoor environmental quality (IEQ); aspects that play a key role in improving the conditions of an office environment. Smart technologies can manage heating or cooling generation and emission systems to influence thermal comfort sensation. Controls managing shading devices can influence internal gains and visual comfort. To quantify those impacts common metrics such as indoor temperature, daylight factor and illuminance need to be taken into account [13]. In case of IAQ, BACS can manage the control of ventilation systems based on sensors such as CO_2 sensors which connect the environment variables with building systems. A systemic review of their influence in managing energy savings, thermal comfort, visual comfort, and IAQ in the built environment is reported by Dong et al. (2019) [14]. Visual contact to nature was investigated due to its positive effects on concentration, stress, and cognitive performance [15]. Some studies tried to link IEQ with higher occupant satisfaction [16] or with employee health and productivity [17, 18] in green rated buildings. Others focused on indicators specific for office buildings and related to co-benefits such as increased productivity, reduced sick leaves, reduced employee turnover [19–21]. The opposite perspective can be found as well, linking negative impacts of poor IEQ with direct medical costs or indirect costs related to poor employee performance, which could either cause higher absenteeism, reduce work effectiveness and employee recruiting and retention. The benefits of an improved IEQ are related to containing the mentioned negative effects [22]. One of the main barriers that makes these benefits hard to calculate, is that the figures required should be obtained from the accountability and human resources departments of the companies.

Smart functions such as automated fault detection and diagnosis of building equipment operation are

strongly connected to an optimized building functioning as well. Article 2 of the 2018 EPBD amendment places the focus on the functionalities of continuous monitoring of energy use, efficiency benchmarking and communication which have the potential to improve operation and maintenance activities of technical building systems, as performances, and device failures are monitored in all systems. In this way, the directive recognizes that a good design only, cannot avoid a performance decrease over the building operating life. Building operation presents several inefficiencies compared to project conditions. The performance gap caused by these inefficiencies can be reduced by installing monitoring and diagnosis systems. For instance, in case of heat pumps, an energy performance gap can be identified with the system performance degradation over time [23] or in case of controlled ventilation, filters fouling is responsible for an increased energy consumption. A second benefit in this area is related to lower maintenance and replacement costs [24, 25].

Finally, another set of benefits is related to the ability of BACS to provide information on building operation, such as IEQ parameters, electricity production from renewable sources, storage capacity, services availability and other building performances to occupants or to facility managers. This information can positively influence user interaction with the building, as occupant behavior is one of six influencing factors of building energy performance [26]. In case of commercial buildings, approaches have been proposed to decrease energy demand by improving occupants' energy-consuming behaviors [27]. In addition, an informed user is key for the acceptance of BACS. A study showed that occupants' comfort feeling was correlated to control perception over the indoor environment, as they were not satisfied with the implemented automation, and wanted a more direct control [28]. Inkarojrit (2005) [29], for instance, carried out a study among 25 office users in Berkeley, finding that more than half of the participants preferred either a manual window blind control or a smart one with the override possibility. Similar results were found in a more recent study [30], also focused on comparing manual and automated blind control strategies in office buildings.

3. Methods

The present study proposes an approach which includes both energetic and non-energetic benefits in the assessment of BACS impacts in an office environment. The approach is illustrated using a reference office building model set up using the dynamic simulation engine EnergyPlus. This tool, further than performing a building energy simulation, allows including thermal comfort modeling and simplified control strategies. As a case study for the analysis of BACS impacts on the selected reference building, two different control strategies of a sun shading system have been modeled: a manual control versus an automated control.

3.1 Building model description

The selected building model is the office division of the Flemish research organization VITO in Berchem, Belgium (Fig. 1). This model was chosen as representative of office buildings at European level. In order to simplify the analysis, out of the whole model, one floor located in the middle of the building was considered.

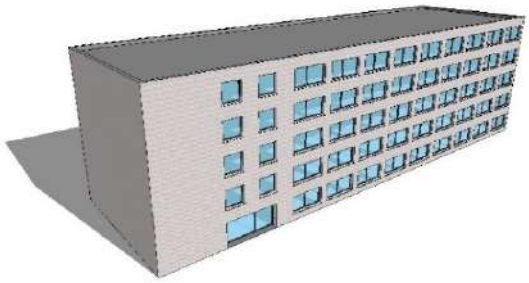

Fig. 1 – Model of Berchem office division.

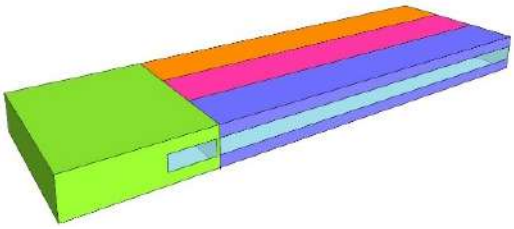

Fig. 2 – Model of the middle floor.

Its interior dimensions are 60x18x3.4 m and it is divided in four zones (Fig. 2):

1. Right zone (45x6 m - purple): office area
2. Left zone (45x6 m - orange): office area
3. Corridor (45x6 m – pink)
4. Auxiliary zone (15x18 m - green)

Floor and ceiling are considered to have identical thermal conditions, therefore adiabatic. The surfaces in contact with the external environment are the south facing façade (right and auxiliary zones), the north facing façade (left and auxiliary zones) and the two side surfaces which have no windows. Shading on the façade caused by obstacles is not considered. Tab. 1 reports main characteristics and relative U-values of the construction elements such as ceiling, floor, external and internal walls. Tab. 2 reports the characteristics of the windows such as U-values and g-value. An internal mass due to walls and furniture is also considered (left zone and corridor: 100 m^2; auxiliary zone and right zone: 50 m^2).

Tab. 1 – Construction materials.

	Ceiling/Floor	Int. wall	Ext. wall
Materials	Carpet Pad	Gypsum board	Façade brick
	Air	Air	Air
	Concrete	Gypsum board	Insulation
	Gypsum board		Brick
			Plaster
U-value [W/m²K]	1.53	2.58	0.21

Tab. 2 – Windows properties.

	Values
U-value window [W/m²K]	1.2
U-value frame [W/m²K]	1.8
g-value	0.39

A gas boiler feeds a hot water loop. All zones are heated by fan coil units and a controlled ventilation system provides the air change. The outdoor air flow rate is 0.000944 m^3/s (per floor area). The natural infiltration rate was assumed to be constant to 0.0001111 m^3/s (per exterior surface area). Moreover, air mixing between zones is also taken into account: 0.000315 m^3/s between offices and corridor, 0.00009 m^3/s between corridor and auxiliary zone. User behavior and system schedules are reported in Tab. 3. Occupancy schedule does not take into consideration intermediate steps between no employees at workplace and full occupancy.

Tab. 3 – User behavior and system schedules.

Typology	Schedule
Occupancy	100% weekdays between 8:00 a.m. and 12:00 p.m. and 2:00 p.m. and 5:00 p.m.
Ventilation	Weekdays at 100% (=0.001389 m^3/s per floor area) from 6:00 a.m. to 8:00 p.m., else 25%
Heating setpoint	21°C from 6:00 a.m. and 5:00 p.m. on weekdays, else 15.6°C

Internal loads associated with lights and electric equipment follow the occupancy schedule and are reported in Tab. 4. Although, it is important to underline that daylight is the only responsible for office illuminance levels, since no artificial lighting is simulated. A typical metabolic rate of 120W per person has been selected for office activities.

Tab. 4 – Internal loads.

Typology	Values
People [m^2/person]	10
Activity level [W/person]	120
Lights [W/m^2]	10
Electric equipment [W/m^2]	7.5

3.2 BACS model description

Control of solar protection shadings has been chosen to be modeled and investigated within the proposed approach. The solution implemented is an external shading system which main characteristics are reported in Tab. 5.

Tab. 5 – Shading characteristics.

	Shading
Thickness [mm]	5
Solar transmittance	0.21
Solar reflectance	0.43
Visible transmittance	0.14
Visible reflectance	0.8

Two control strategies have been compared to determine their impact on the building: on the one side a basic manual control, on the other side an automatic control. Manual control means that employees can open or close the shadings according to the circumstances: glare, thermal discomfort, need for more light, etc. This control has been approximated by making the assumptions that employees close the blinds whenever the illuminance exceeds 2000 lux for at least 20 minutes or the indoor temperature is above 26°C (thermal discomfort sensation). Work plane illuminance is the most cited and studied parameter when it comes to visual comfort [31] and 2000 lux is considered a limit value above which visual discomfort perception arise (glare or scarce visibility of computer screens) [32]. Besides, the assumption that shadings are forgotten close for the rest of the day and opened again the next working day (if temperature is below 24°C and illuminance below 2000 lux) has been made. The automatic control is based on sensors which take into account irradiance, illuminance and temperature levels [33, 34]. Opening and closing strategies are displayed in detail in Fig. 3 and Fig. 4. The displayed control strategies have been modeled within the Energy Management System (EMS) feature of EnergyPlus, which allows implementation of custom control strategies and calculation routines that go beyond standard modeling processes provided by EnergyPlus.

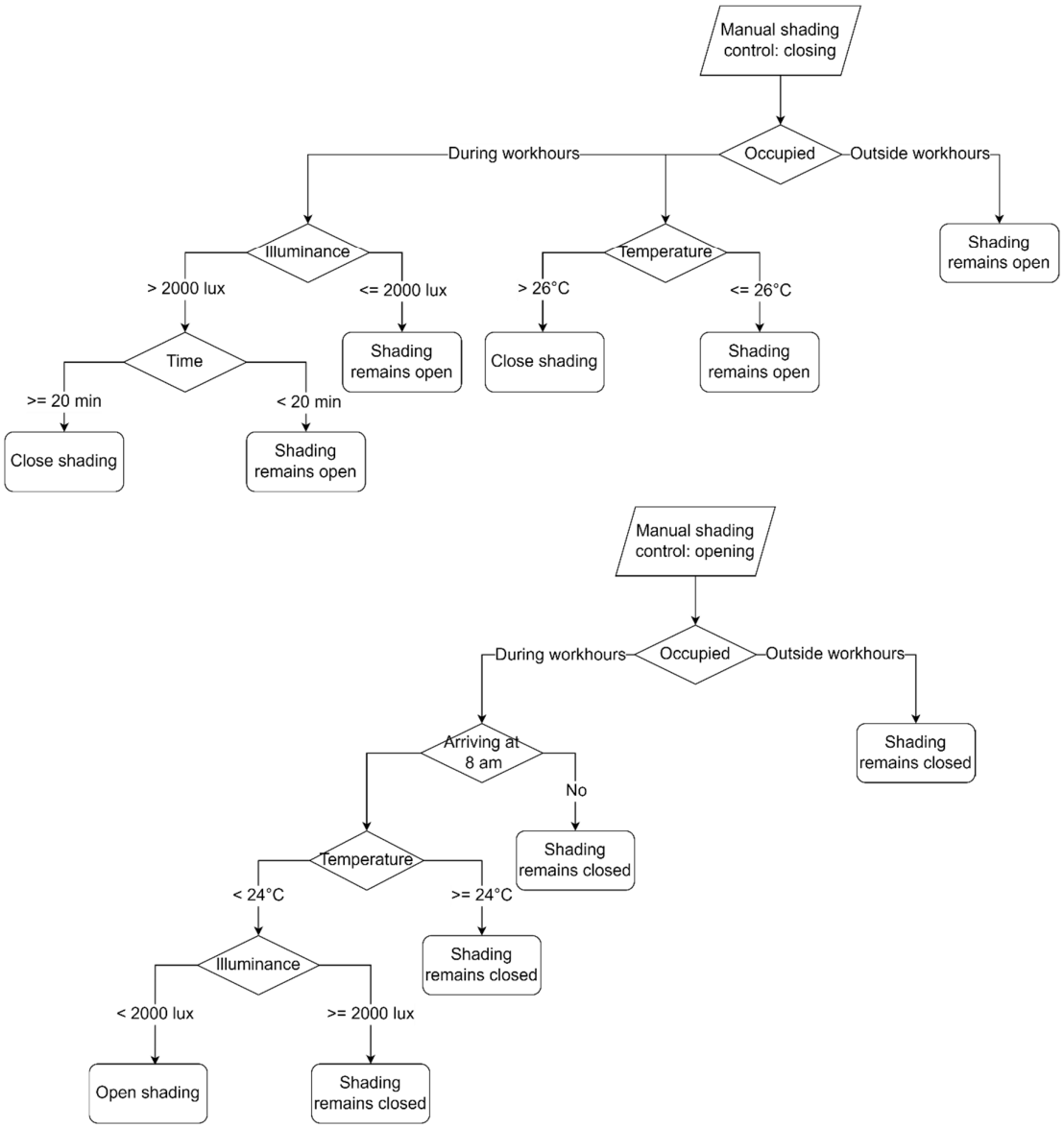

Fig. 3 – Overview of the manual shading control: closing and opening strategy.

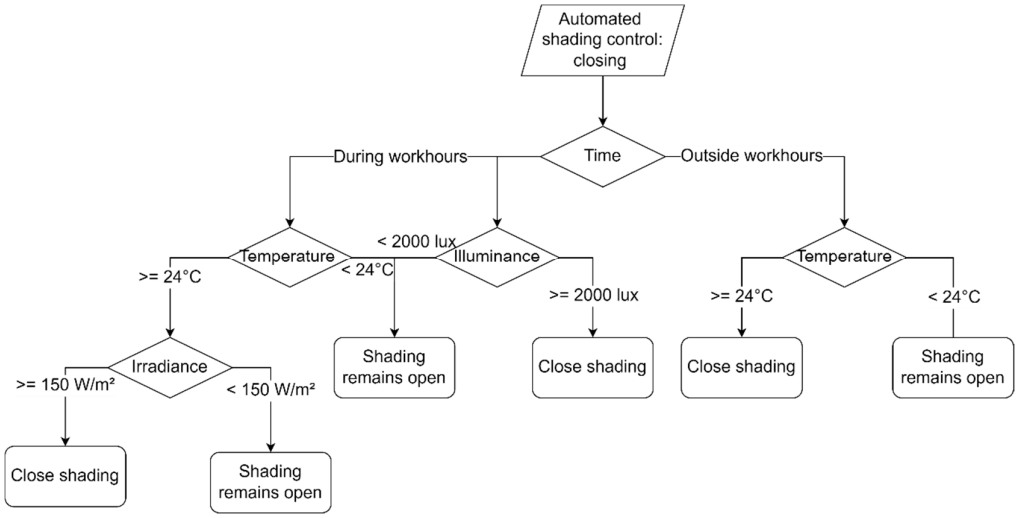

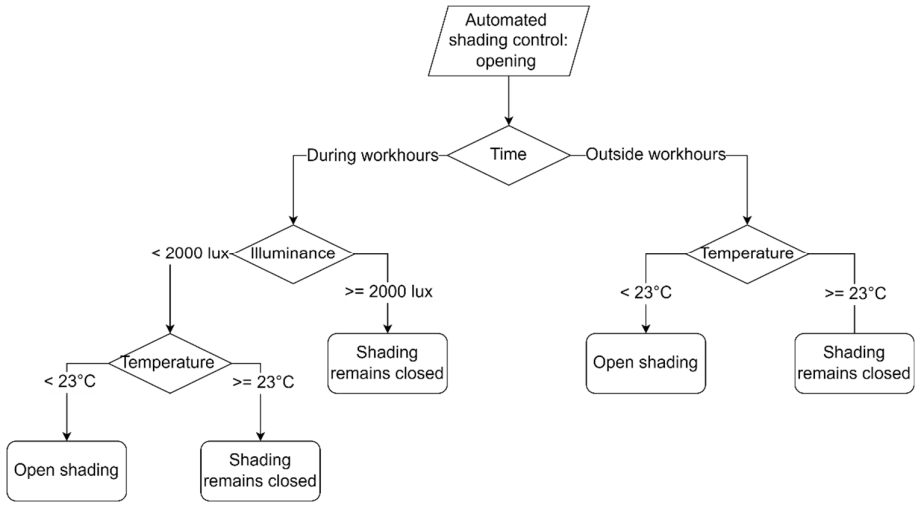

Fig. 4 - Overview of the automated shading control: closing and opening strategy.

4. Results and discussion

Main output parameters resulting from the simulation are:

- Heating energy consumption: the yearly energy use associated to heating gas boiler.
- Zone operative temperature (OT): is the average of the Zone Mean Air Temperature (MAT) and Zone Mean Radiant Temperature (MRT). In particular the total number of working hours where the OT is above 26 °C was computed in order to highlight discomfort conditions. The EN 16798-1:2019 sets IEQ criteria divided in 3 categories. In case of office buildings in summer, the comfort range corresponding to category II is 23-26 °C.
- Zone reference point illuminance: the measurement point is placed at desk height (0.8 m) located 1 m away from the window. In this case the cumulated number of working hours for different illuminance ranges was computed.

The results in Tab. 6 show that the implementation of both control strategies leads to a similar heating consumption (1.4% difference). The number of working hours where the OT reports values above 26 °C do not show significant differences either, being 6% higher for the automatic control strategy.

Tab. 6 – Results.

	Auto	Manual
Heating energy consumption [kWh/m²a]	71.6	72.6
OT > 26°C, cumulated hours	350	330
illuminance > 2000 lux, cumulated hours	53.5	93.2

Finally, the illuminance parameter highlights the impact of the automated control strategy on the visual comfort. In this case, employees are exposed to an illuminance level higher than 2000 lux for 53.5 hours only, 43% less than manual control. This is visible in Fig. 5, where histograms represent the cumulative working time (hours) of illuminance levels binned per 500 lux intervals. In addition, under the premise that no artificial lighting is simulated, manual control leads to spend more hours in the interval 0-500 lux (scarce illuminance). EN 16768-1:2019 and EN16464-1 defines 500 lux as minimum illuminance level for office buildings.

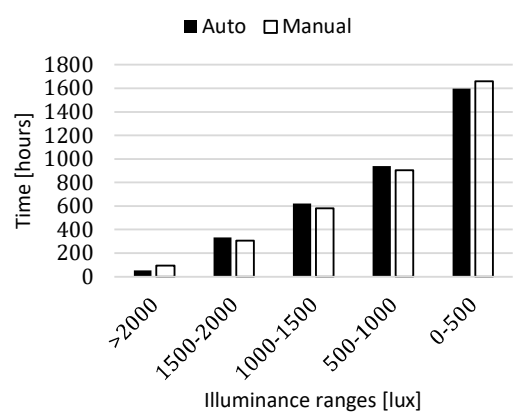

Fig. 5 - Cumulated working hours for different illuminance ranges.

Under the conditions defined in this simplified approach, the automated shading control does not provide appreciable benefits in terms of energy efficiency, although it is important to underline the positive impact on visual comfort. As pointed out in paragraph 2, visual comfort is directly related to attention restoration, stress reduction, and a better cognitive performance, which in turn impact on employee's productivity and the amount of sick leave each year. Furthermore, an automated control that provides detailed information to the occupants as

well, giving the possibility to be aware of the current environmental conditions and to interact with them if needed, is proven to further enhance thermal and visual comfort sensation of the occupants.

5. Conclusions

To facilitate the transition to smart buildings, the multiple advantages that BACS offer need to be made more visible and to be considered altogether. An analysis framework for the evaluation of BACS co-benefits in office buildings has been introduced, outlining main benefits of automation systems for this building typology. Furthermore, a contemporary office building case study has been modeled within EnergyPlus to quantify the improved benefits associated to building automation, focusing on the analysis of a shading automated control system compared to a manual one. Control of movable elements such as openings, blinds and other sun shading solutions has a specific domain within the SRI scheme which is called "dynamic building envelope". Improving the control level of a shading system can not only reduce heating and/or cooling needs but also improve thermal and visual comfort of employees, enhancing the office experience. In turn, this has an impact on health related aspects such as stress reduction and productivity.

An approach that considers all the impact spectrum, highlights how often building design should put together competing interests. Minimizing energy consumption, can be in contrast with enhancing visual comfort or indoor air quality, nevertheless BACS can provide a solution to this issue, as these can be the cornerstone of a multi-objective optimization process, aiming at an optimal trade-off between opposite targets. Main limitations of this study are due to the reduced building model, the control strategies simplification, and the limited possibilities offered by the EnergyPlus EMS to model real controls. The aim of this analysis was to approach the evaluation of added values and benefits associated with an improved control level in office buildings. More research should be carried out to further develop this approach and test it on more BACS.

Acknowledgement

The work was carried out as part of the project SmartBuilt4EU – Grant Agreement No. 956936 (www.smartbuilt4eu.eu) financed by the European Commission in the Horizon 2020 Framework Programme of the European Union.

References

1. Energy Information Administration, Energy Department. Annual Energy Review: Primary energy consumption by source and sector: Government Printing Office; 2019.
2. Lapillonne B, Sebi C, Pollier K, Mairet N. Energy Efficiency Trends in Buildings in the EU—Lessons from the ODYSSEE MURE project. ADEME. Retrieved December. 2012;30:2014.
3. Directive (EU) 2018844 of the European Parliament and of the Council of 30 May 2018 amending Directive 201031EU on the energy performance of buildings and Directive 201227EU on energy efficiency.
4. Smart Building Market. 2018 Global Trends, Market Share, Industry Size, Growth, Opportunities and Forecast to 2023. 2018.
5. Martirano L, Habib E, Parise G, Greco G, Manganelli M, Massarella F, Parise L. Demand Side Management in Microgrids for Load Control in Nearly Zero Energy Buildings. IEEE Transactions on Industry Applications. 2017;53:1769–79. doi:10.1109/TIA.2017.2672918.
6. Ożadowicz A. A New Concept of Active Demand Side Management for Energy Efficient Prosumer Microgrids with Smart Building Technologies. Energies 2017. doi:10.3390/en10111771.
7. Fan Z, Kulkarni P, Gormus S, Efthymiou C, Kalogridis G, Sooriyabandara M, et al. Smart Grid Communications: Overview of Research Challenges, Solutions, and Standardization Activities. IEEE Communications Surveys Tutorials. 2013;15:21–38. doi:10.1109/SURV.2011.122211.00021.
8. O'Grady T, Chong H-Y, Morrison GM. A systematic review and meta-analysis of building automation systems. Building and Environment. 2021;195:107770. doi:10.1016/j.buildenv.2021.107770.
9. European Technical Standard. EN 15232 Energy Performance of Buildings: Impact of Building Automation, Control, and Building Management 2012. Brussels.
10. Verbeke S, Dorien A, Reynders G, Ma Y, Waide P. Final report on the technical support to the development of a Smart Readiness Indicator for buildings; 06/2020.
11. Märzinger T, Österreicher D. Extending the Application of the Smart Readiness Indicator—A Methodology for the Quantitative Assessment of the Load Shifting Potential of Smart Districts. Energies 2020. doi:10.3390/en13133507.
12. Billanes JD, Ma Z, Jørgensen BN. Consumer central energy flexibility in office buildings. Journal of Energy and Power Engineering. 2017;11.
13. Zhang W, Liu F, Fan R. Improved thermal comfort modeling for smart buildings: A data analytics study. International Journal of Electrical Power & Energy Systems. 2018;103:634–43. doi:10.1016/j.ijepes.2018.06.026.
14. Dong B, Prakash V, Feng F, O'Neill Z. A review of smart building sensing system for better indoor environment control. Energy and Buildings. 2019;199:29–46.

doi:10.1016/j.enbuild.2019.06.025.
15. Ko WH, Schiavon S, Zhang H, Graham LT, Brager G, Mauss I, Lin Y-W. The impact of a view from a window on thermal comfort, emotion, and cognitive performance. Building and Environment. 2020;175:106779. doi:10.1016/j.buildenv.2020.106779.
16. Altomonte S, Schiavon S, Kent MG, Brager G. Indoor environmental quality and occupant satisfaction in green-certified buildings. Building Research & Information. 2019;47:255–74.
17. Singh A, Syal M, Grady SC, Korkmaz S. Effects of Green Buildings on Employee Health and Productivity. American Journal of Public Health. 2010;100:1665–8. doi:10.2105/AJPH.2009.180687.
18. Purdey B. GREEN BUILDINGS AND PRODUCTIVITY. Environment Design Guide. 2005:1–9.
19. Berggren B, Wall M, Weiss T, Garzia F, Pernetti R, editors. LCC analysis of a Swedish net zero energy building–including co-benefits; 2018.
20. Bleyl J, Bareit M, Casas M, Coolen J, Bruyn BD, Hulshoff A, Robertson M, editors. Building deep energy retrofit: Using dynamic cash flow analysis and multiple benefits to convince investors; 2017.
21. Brew JS, editor. Finding the Value in Deep Energy Retrofits; 2017.
22. Brager GS, editor. Benefits of improving occupant comfort and well-being in buildings; 2013.
23. Yoon SH, Payne WV, Domanski PA. Residential heat pump heating performance with single faults imposed. Applied thermal engineering. 2011;31:765–71.
24. Loureiro T, Gil M, Desmaris R, Andaloro A, Karakosta C, Plesser S, editors. De-Risking Energy Efficiency Investments through Innovation; 2020.
25. Dobson DW, Sourani A, Sertyesilisik B, Tunstall A. Sustainable Construction: Analysis of Its Costs and Benefits. American Journal of Civil Engineering and Architecture. 2013;1:32–8. doi:10.12691/ajcea-1-2-2.
26. Bastida L, Cohen JJ, Kollmann A, Moya A, Reichl J. Exploring the role of ICT on household behavioural energy efficiency to mitigate global warming. Renewable and Sustainable Energy Reviews. 2019;103:455–62. doi:10.1016/j.rser.2019.01.004.
27. Rafsanjani HN, Ahn CR, Alahmad M. A Review of Approaches for Sensing, Understanding, and Improving Occupancy-Related Energy-Use Behaviors in Commercial Buildings. Energies. 2015;8:10996–1029. doi:10.3390/en81010996.
28. Tamas R, Ouf MM, O'Brien W. A field study on the effect of building automation on perceived comfort and control in institutional buildings. Architectural Science Review. 2020;63:74–86. doi:10.1080/00038628.2019.1695573.
29. Inkarojrit V. Balancing comfort: occupants' control of window blinds in private offices: University of California, Berkeley; 2005.
30. Sadeghi SA, Karava P, Konstantzos I, Tzempelikos A. Occupant interactions with shading and lighting systems using different control interfaces: A pilot field study. Building and Environment. 2016;97:177–95. doi:10.1016/j.buildenv.2015.12.008.
31. Correia da Silva P, Leal V, Andersen M. Influence of shading control patterns on the energy assessment of office spaces. Energy and Buildings. 2012;50:35–48. doi:10.1016/j.enbuild.2012.03.019.
32. Reinhart CF, Mardaljevic J, Rogers Z. Dynamic Daylight Performance Metrics for Sustainable Building Design. LEUKOS. 2006;3:7–31. doi:10.1582/LEUKOS.2006.03.01.001.
33. Karlsen L, Heiselberg P, Bryn I, Johra H. Solar shading control strategy for office buildings in cold climate. Energy and Buildings. 2016;118:316–28. doi:10.1016/j.enbuild.2016.03.014.
34. Thalfeldt M, Kurnitski J. External shading optimal control macros for 1- and 2-piece automated blinds in European climates. Building Simulation. 2015;8:13–25. doi:10.1007/s12273-014-0194-3.

Data Statement

Data sharing not applicable to this article as no datasets were generated or analysed during the current study.

Reinforcement learning for occupant-centric operation of residential energy system: Evaluating the adaptation potential to the unusual occupants´ behavior during COVID-19 pandemic

Amirreza Heidari, François Maréchal, Dolaana Khovalyg

School of Architecture, Civil and Environmental Engineering (ENAC), Ecole Polytechnique Fdérale de Lausanne (EPFL), Lausanne, Switzerland, amirreza.heidari@epfl.ch

Abstract. Occupant behavior is a highly stochastic phenomenon, which is known as a key challenge for the optimal control of residential energy systems. With the increasing share of renewable energy in the building sector, the volatile nature of renewable energy is also another key challenge for optimal control. It is challenging and time-consuming to develop a rule-based or model-based control algorithm that can properly take into account these stochastic parameters and ensure an optimal operation. Rather, a learning ability can be provided for the controller to learn these parameters in each specific house, without the need for any model. This research aims to develop a model-free control framework, based on Reinforcement Learning, which takes into account the stochastic occupants' behavior and PV power production and tries to minimize energy use while ensuring occupants' comfort and water hygiene. This research, for the first time, integrates a model of Legionella growth to ensure that energy saving is not with the cost of occupants' health. Hot water use data of three different residential houses are measured to evaluate the performance of the proposed framework on realistic occupants' behavior. The measurement campaign was during the COVID-19 pandemic, which would further highlight the adaptability of the Reinforcement Learning framework to the unusual situation when the prediction of occupants' behavior is even more challenging. Results indicate that the proposed framework can successfully learn and predict occupants' behavior and PV power production, and significantly reduce energy use without violating comfort and hygiene aspects.

Keywords. Reinforcement Learning, Space heating, Hot water, Occupant behavior, Solar energy, Machine Learning
DOI: https://doi.org/10.34641/clima.2022.286

1. Introduction

Optimal operation of building energy systems is challenging as there are several stochastic and time-varying parameters that affect building energy use. One of these parameters is occupant behaviour, which is highly stochastic, can change from day to day, and therefore is very hard to predict [1]. The occupant behaviour of each building is unique, and thus there is no universal model which can be embedded in the control system of various buildings at their design phase. To cope with this highly stochastic parameter, current control approaches are usually too conservative to ensure the comfort of occupants regardless of their behaviour. An example is hot water production, where huge volume of hot water with high temperature is produced in advance and stored in a tank to make sure enough hot water is available whenever it is demanded [2,3].

Another stochastic parameter affecting building operation is renewable energy. The share of renewable energy in the building sector is increasing, and is expected to get doubled by 2030 [4]. Due to the volatile nature of renewable energy sources, it will also increase the complexity of optimal energy management in buildings [5]. There are several other stochastic parameters, such as weather condition or electric vehicles charging that all affect the building energy use. The control logic of buildings should properly take into account these stochastic parameters to guarantee an optimal operation.

To integrate these stochastic parameters, a possible option is Model Predictive Control (MPC) that uses a model of the system, together with the predictions of stochastic parameters, to determine the optimal control actions for an upcoming horizon. Despite its potential benefits, MPC relies on a model of the system. However, developing an accurate model for

Copyright ©2022 by the authors. This conference paper is published under a CC-BY-4.0 license.

the building is extremely time-consuming, and therefore, not practical in most cases. Moreover, even if an accurate model of the system is developed, it can become fairly inaccurate over time due to, for instance, renovation or aging of the system. Furthermore, similar to the other model-based approaches, MPC requires a high computational power to optimize the model of the system. Last but not least, as MPC is based on a model of the building and the prediction of stochastic parameters, it is building-specific and not easily transferrable to other buildings [6].

Uniqueness of occupant behaviour in each building makes it challenging to program a rule-based or model-based control logic that can be easily transferred to many other buildings. Rather than hard programming a rule-based or model-based control method, a learning ability can be provided to the controller such that it can learn and adapt to the specifications of that building and maintain an optimal operation. Reinforcement Learning (RL) is a method of Machine Learning that can provide this learning ability to the controller. In RL, a learning agent interacts with its environment, and uses feedback from the environment to determine the best possible action to maximize a pre-defined metric called reward [7]. RL provides two main benefits over the rule-based and model-based control methods. First of all, RL does not require a complex thermodynamic model of the system, as agent can learn the system model only by interacting with the system [8]. This is a great advantage over MPC, especially in case of complex systems that require a lot of time and effort for modelling [9]. Secondly, RL can continuously learn and adapt to the changes in system such as variating weather conditions, volatile renewable energy, or stochastic occupants behaviour [9]. These two benefits can ensure the transferability of RL to several buildings and provide the potential of a wide-spread implementation.

Recent studies evaluated RL on different aspects of buildings, such as joint control of thermal comfort and air quality [10], thermal comfort and electric vehicle charging [11] or lighting system [12]. Several studies have evaluated RL to provide a balance between occupants comfort and energy use in air conditioning systems. In these studies, RL agent is usually supposed to learn how to minimize the energy use while maintaining occupants comfort. For instance, Brandi et al. [13] investigated the application of RL to make a balance between energy use and comfort by a water-based space heating system in an office building. It was indicated that RL-based control provides 5% to 12% energy saving with an enhanced indoor temperature compared to the rule-based control. Considering that highly stochastic occupants behavior is a key challenge for efficient hot water production [3], few studies have evaluated model-based [14] and model-free RL [2] for occupant-centric hot water production. These studies indicated that while hot water use behavior of occupants is highly stochastic, RL can continuously learn and adapt the control strategy to the occupants' behavior and provide a significant energy saving. Although space heating and hot water production are usually combined, only few studies have evaluated RL for their combination. Lissa et al. [15] proposed a framework for optimal control of space heating and hot water system integrated to the PV solar panels. The proposed framework aimed to reduce the energy consumption by optimizing the operation of heat pump and maximizing the PV self-consumption, while keeping the occupants comfort. However, hot water use profiles were not used in this work and only random temperature drops for the tank were used to simulate a hot water demand.

Another key challenge in hot water systems is Legionella, which is a water-born bacteria that grows in the hot water with a temperature between 20 °C and 50 °C [16]. It be transferred to occupants by breathing in the contaminated water droplets and cause a respiratory disease [16]. To prevent the growth of this bacteria in the tank, conventional control methods usually maintain the tank temperature above 60 °C, which results in higher energy consumption [17]. To propose a realistic control method the hygiene aspect of hot water tank is very important to be considered. However, based on the literature review performed in this study, this aspect has been neglected in the previous studies on RL for hot water systems. Only a recent study by authors included the hygiene aspect in an RL framework for hot water production systems [2]. The hygiene aspect in this recent study was considered by following a simple rule stating that the hot water tank should be heated to 60 °C at least once a day [17].

The aim of this research is to develop an intelligent control framework that takes into account the stochastic hot water use behavior of occupants, and variating solar power production, and learns how to optimally operate the system to minimize energy usage while preserving the comfort and hygiene aspects. Case study energy system is the combined space heating and hot water production, assisted by Photovoltaic (PV) panels.

The main novelties of the proposed framework are:

Integration of water hygiene: While the pervious study by authors [2] followed a simple rule to respect hygiene aspect, this study for the first time integrates a temperature-based model that estimates the concentration of Legionella in hot water tank at each time step. Estimation of Legionella concentration in real-time enables the agent to spend as minimum energy as required for maintaining the hygiene aspect.

Investigation on real-world hot water use behavior: In this research, hot water demand of 3 residential houses is monitored to assess the performance of agent on real-world hot water use

behavior of occupants.

Stochastic offline training to ensure occupants comfort and health: An RL control framework always starts with a training process, in which the agent starts a learning curve by interacting with the environment. As during this phase the agent is not experienced enough, and even has to perform random actions to explore the environment, it is very probable that it perform non-optimal actions that violates the comfort of occupants, or endanger their health by not maintaining the hygiene aspect of hot water. In practice, a control strategy that endangers the health of occupants would never be acceptable. Frequent violations of comfort aspect at the training phase also can reduce the satisfaction of occupants and their willingness to use the intelligent controller. To ensure that agent would quickly learn the optimal behavior with a minimum risk of violating comfort and hygiene aspects, an offline training phase is designed in this study. This offline phase integrates a stochastic hot water use model to emulate the realistic occupants' behavior. Also it includes a variety of climatic conditions and system sizes to provide a comprehensive experience to the agent.

The remainder of this paper is organized into four sections: Section 2 describes the research methodology, ssection 3 presents the results, and Section 4 concludes the paper.

2. Methodology

Fig. 1 shows the interactions of agent and environment in an RL problem. In RL, agent observes the current state (s_t) of the environment. According to the observed state, it selects an action and performs it on the environment (a_t). Due to this action, environment would transit to the next state (s_{t+1}), and agent would receive a reward (r_{t+1}) that quantifies how good was the performed action. The goal of agent is then to maximize the cumulative rewards during an entire episode. Therefore, different from Supervised Learning where a labelled dataset is required to train a model, in RL an interaction between agent and environment should be provided to enable the agent to learn optimal control strategy. In this section, the design of environment and agent are first explained. Then, the design of state, action, and reward space is described. Finally the monitoring campaign and training procedure are presented.

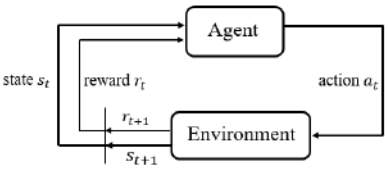

Fig. 1: Interaction of agent and environment in Reinforcement Learning [18]

2.1 Environment design

Layout of residential energy system in this study is shown in **Fig. 2**. This system uses an air-source heat pump to provide hot water in a tank, which is used for both hot water production and space heating through radiators. PV panels are also connected to the heat pump. PV panels are grid-connected, so the surplus power can be supplied to the grid. A dynamic model of the system is developed in TRNSYS.

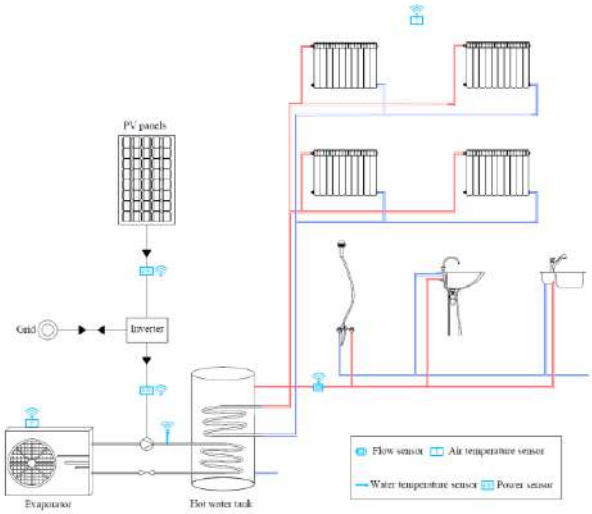

Fig. 2: Layout of solar-assisted space heating and hot water production system

2.2 Agent design

The agent is developed in Python using Tensorforce library [19]. An improved version of Deep Q-Network (DQN), known as Double DQN is used as it is proved to solve the issue of overestimation by typical DQN. Specifications of agent are provided in **Tab. 1**.

Tab. 1: Selected parameters for the agent

Parameter	Value
Learning rate	0.003
Batch size	24
Update frequency	4
Memory	48×168
Discount factor	0.9

2.3 State, action and reward space

Proper design of state, action and reward space is very important to obtain a good performance by RL framework. Parameters included in the state are presented in **Tab. 2**. Each parameter is a vector including the value of that parameter during one or multiple previous hours. The demand ratio is the ratio of total hot water demand of the current day until the current hour, to the total demand of the previous day. Hour of day is a value between 1-24 indicating what is the upcomming hour of day. Day of week, similarly, indicates the current day as a value between 1-7, where 1 represents Monday. The values are normalized to a vlue between 0 to 1.

Tab. 2: Parameters included in the state vector

Parameter	Length of look-back vector
Hot water demand	6
Demand ratio	-
Outdoor air temperature (°C)	1
Indoor air temperature (°C)	3
PV power (kW)	6
Heat pump outlet temperature (°C)	1
Legionella concentration (CFU/L)	1
Tank temperature (°C)	1
Hour of day	-
Day of week	-

Possible actions should allow the agent to exploit the possibility of energy storage in hot water tank and in thermal mass of building, by regulating the tank and indoor air temperatures. To this aim, at each hour agent can select between four possible actions: Turning ON the heat pump, Turning OFF the heat pump, selectig the indoor air temperature setpoint of 21 °C (as an energy-saving setpoint) or 23 °C (as an energy-storing setpoint). Based on the selected indoor air temperature setpoint by the agent, a two-point controller with a dead-band of 2 °C tries to maintain the specified setpoint during the next hour.

Reward function includes 4 different terms. An energy term to penalize the agent for net energy use, hot water comfort term to penalize the agent if a hot water demand is supplied with a temperature less than 40 °C, which is considered as the lower limit of comfort for hot water uses [2], space heating comfort term to penalize the agent if the indoor air temperature is out of the comfort region of 20 °C-24 °C, and a hygiene term if the estimated concentration of Legionella is above the maximum threshold of 500×10^3 CFU/L recommended for residential houses [20]. Equations 1-4 shows the formulation of energy, hot water comfort, space heating comfort, and hygiene terms.

$$R_{energy} = -a \times \left|HP_{power} - PV_{power}\right| \quad (1)$$

$$if\ T_{tank} \geq 40\text{:}\ R_{DHWcomfort} = 0\ else - b \quad (2)$$

$$if\ 20 \leq T_{indoor} \leq 24\text{:}\ R_{Indoorcomfort} = 0\ else - c \quad (3)$$

$$if\ Conc \leq Conc_{max}, R_{Hygiene} = 0\ else - d \quad (4)$$

Where HP_{power} and PV_{power} are the power use of heat pump and power production of PV panels (kW), T_{tank} and T_{indoor} are the tank and indoor air temperature, $Conc$ and $Conc_{max}$ are the current and maximum concentration of Legionella in the tank (CFU/L), R_{energy}, $R_{DHWcomfort}$, $R_{Indoorcomfort}$ and $R_{Hygiene}$. a, b, c and d are set to 1, 12, 10 and 10 determined by a sensitivity analysis. The total reward is therefore the summation of all these terms.

2.4 Monitoring campaign

It is challenging to directly test the performance of the proposed RL controller on a real-world residential building because if it fails to learn the behavior of occupants it can violate their comfort. On the other hand, it is important to investigate its performance on the realistic behavior of occupants. To perform a realistic test without disturbing the occupants, hot water use behavior of people is monitored and the collected data are used in TRNSYS model to emulate the real hot water demand. For the current framework, as shown in **Fig. 2**, only one single sensor at the tank outlet is enough to measure the hot water demand. In this study, to collect a comprehensive dataset which can be used also for future research, the hot and cold water demand is monitored at all the end uses in the case study buildings. The hourly hot water use data are then summed to represent the total hourly demand. **Fig. 3** shows the example of sensor installation on a faucet and a shower. LoRaWAN-based low power IoT flow sensors (with an integrated temperature sensor) are used to enable monitoring for a long duration (several months) with a single battery.

Fig. 3: Example of IoT flow and temperature sensor installation on a faucet

2.5 Training procedure

Interaction of agent and environment is provided by integrating Python and TRNSYS software. A Python code calls the TRNSYS simulation with the desired control actions, runs the simulation for a timestep, and reads the desired outputs to form the state and reward functions. Training and deployment stages are shown in **Fig. 4**. To ensure occupants' comfort and health, first, the agent is trained on an offline training process. In this stage, a virtual environment is provided to enable the agent to gain enough experience before being implemented on the target house. In this stage, a hot water use model [21] is used to emulate the hot water use behavior of occupants. This model is developed based on data from 77 residential buildings, and therefore is a great tool to provide a prior experience to the agent. In this stage, it is desired that the agent also experience a good variety which can help it to generalize its knowledge and quickly adapt to new cases. To this aim, the offline training phase is repeated for 10

years, and at each year the agent is interacting with a different size of the system (heat pump, tank, building area, etc), the weather condition of a different city, and a different hot water use profile generated by the stochastic model. After these 10 years, the agent is then trained on the target house for 16 weeks. The aim of training on the target house is to let the agent adapt to the specific characteristics of the target house, such as occupants' behavior, systems sizes, or weather conditions. To simulate the target house, in online training stage the collected hot water use data, and also the weather data collected from a weather station near the case study is used. After the online training on the target house, the training process can be stopped and the agent starts the deployment stage, in which agent is no longer learning but only controlling the system. Although to take the full power of RL the training process should be always continued, it makes it computationally expensive and agent should be always on the cloud. But once the training is stopped, the saved agent can be uploaded on a cheap hardware and control the system locally. Duration of deployment phase is 4 weeks.

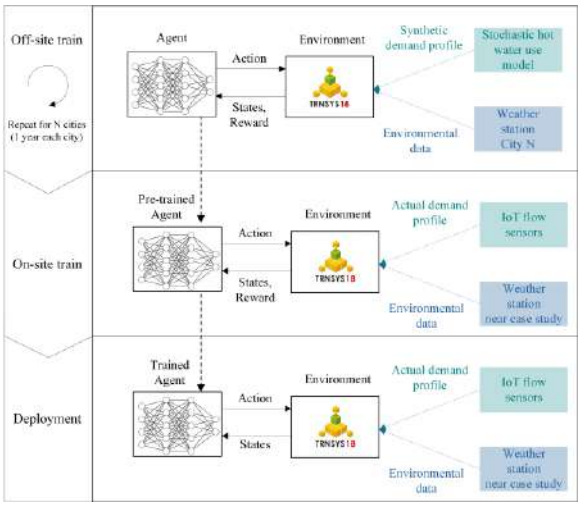

Fig. 4: Training and deployment process

3. Results

The stability of the reward function indicates that the agent is converged to an optimal control policy. **Fig. 5** shows the evolution of reward function during the offline training phase, and also online training on each of the case studies. $\varepsilon - greedy$ method with a linear decay is used to impose exploration at the 12 first weeks of the offline training phase. During the last 90 weeks of the offline training stage, the reward function is almost stable. During the online training on the target houses, the reward function is stable since the very first week. The existing variations compared to the potential variations of reward function are very small and mainly due to the energy use, which is not avoidable. It shows that the offline training stage has provided a generalizable experience for the agent, and since the beginning of implementation on the target houses, the agent can provide energy saving while maintaining comfort and hygiene aspects.

Fig. 6 shows the control signal, PV power production, and tank temperature over the deployment stage on three case studies. The deployment stage of houses 1 and 2 is during December, while the deployment stage of house 3 is during July. Therefore the PV power production of the third case study is higher than others. In all of the case studies, it can be seen that the agent is trying to adapt the control signal to the PV power production and reduce the power use from the grid, by turning ON the heat pump more frequently during the hours of PV power production. This adaptation can be seen very well on house 3, where PV power production is significantly higher and the agent tries to turn ON heat pump only when there is a PV power production. In all of the case studies, the agent has learned how to keep tank temperature above 40 °C to respect the comfort of occupants. It shows that agent could successfully learn and adapt to the occupants behavior, because none of the demands reduced the tank temperature below 40 °C.

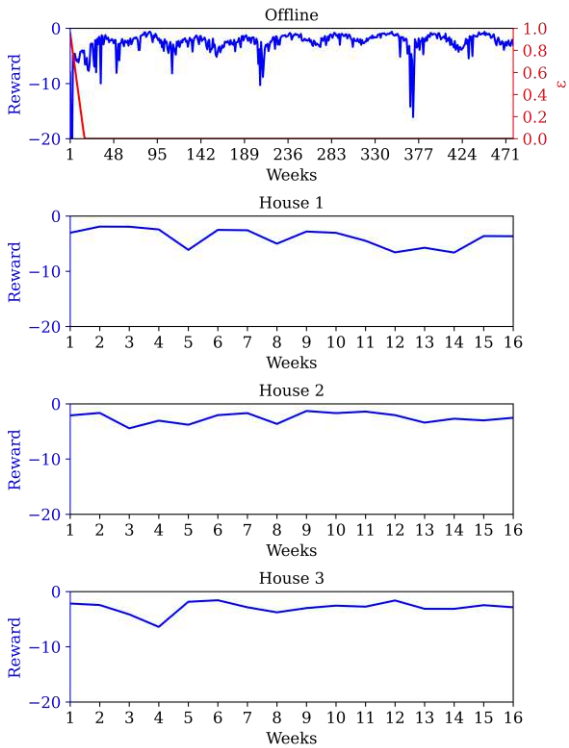

Fig. 5: Evolution of reward function over the offline training phase and case studies

To compare the performance of the proposed framework with the conventional methods, two conventional scenarios are modeled. The first method is Rule-based Conventional control (RC), where the tank temperature setpoint is 60 °C with a dead-band of 10 °C. The second scenario is Rule-based Energy-saving control (RE), in which with the aim of reducing energy usage the tank temperature setpoint is considered as 50 °C. This method might not be practical because a constant setpoint of 50 °C for the tank can still impose the risk of Legionella growth. But this method is included in comparison to represent an extreme case of energy-saving by a rule-

based method and to prove that the better performance of RL is not only due to a lower tank temperature. Main performance metrics over the deployment stage are shown in **Tab. 3**. In all the houses, RL has provided energy saving compared to the RC and RE methods. As expected, energy saving compared to the RC is higher than RE, because heat pump COP is RC is lower than RE. The energy saving in the houses 2 and 3 are around 7% and 8%, which represent the order of potential energy saving by RL method duirng the cold season. Energy savings in house 3 are much more, because PV power production in the hot season is much more an agent learns how to get the best use of PV power production to cover space heating and hot water energy use. This is a great example to highlight the importance of a controller that can learn and adapt to the changes, over a static and rigid controller. As expected, the comfort of occupants in case of space heating is always preserved because the possible choices for agent has been in the comfort range, and the tank temperature has been always high enough to provide the specified setpoint. The hygiene aspect is also preserved in all the houses because the maximum Legionella concentration in the tank in all the cases is below 5×10^5 CFU/L.

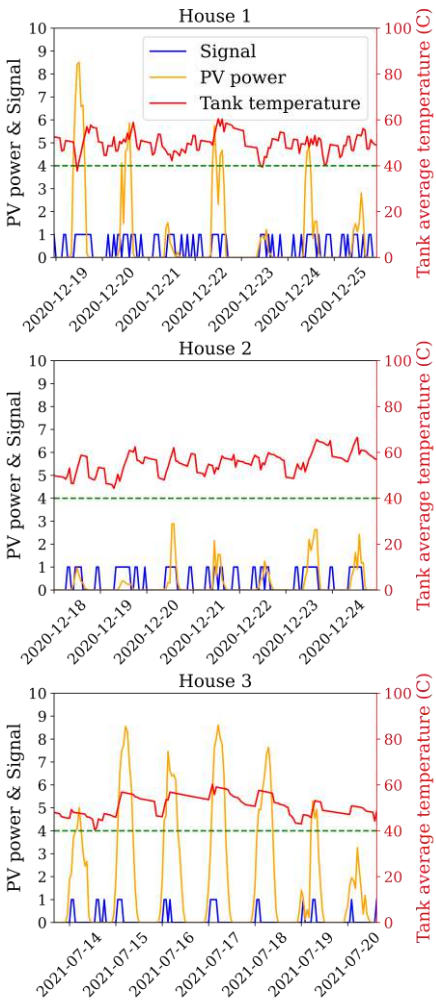

Fig. 6: Control signal versus PV power production and tank temperature

Tab. 3: Main performance metrics over different case studies

	House 1	House 2	House 3
Energy saving to RC (%)	28.9	40.4	75.7
Energy saving to RE (%)	7.2	8.7	61.6
Violated DHW comfort (%)	8.1	5	1.7
Average temperature of DHW comfort violations (°C)	38.8	39	37.98
Maximum Legionella concentration (CFU/L)	2060	49704	6764

To better highlight how RL could better exploit solar power production, the contribution of PV power production in the total power use of the heat pump is shown in **Fig. 7**. As can be seen, in all the case studies RL has used a higher contribution of PV power, compared to the RC and RE. In case of house 3, the contribution of PV power production is much higher than RC and RE, which is the why in this house the energy saving is much higher than other houses. It shows that a significant advantage of the proposed RL framework is to learn how to adapt the operation to the PV power production, and therefore potential energy-saving increases in regions with higher solar radiation.

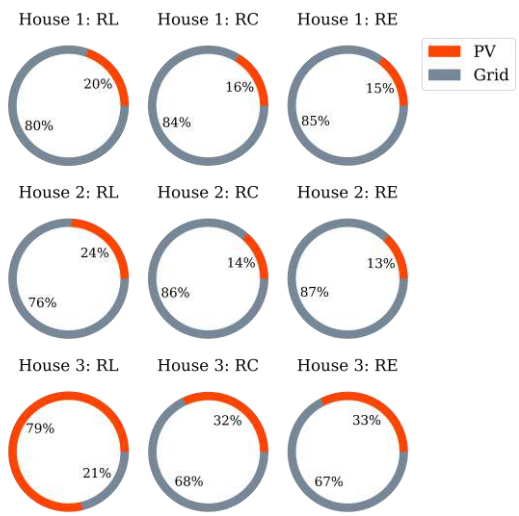

Fig. 7: Contribution of PV power production in power consumption of heat pump

4. Conclusion

Optimal energy management in the buildings is affected by several stochastic parameters, such as weather conditions, occupants' behavior, or solar energy, that vary by time and are hard to predict. It is therefore challenging and time-consuming to develop a rule-based or model-based control logic that can properly take into account all these parameters and maintain an optimal operation. Rather, a learning ability can be provided to the

controller, so in each specific building, it can learn these stochastic parameters and continuously adapt the system operation to their variations.

This research proposed a model-free RL control framework that can learn the hot water use behavior of occupants and PV power production, and accordingly adapt the system operation to meet the comfort requirements with minimum energy use. Different from previous studies, where RL is supposed to make a balance between energy use and comfort, in this study RL tries to make a balance between energy use, comfort, and hygiene. Inclusion of hygiene aspect is very crucial to ensure the health of occupants. Real-world hot water use data is monitored in three residential case studies and used to evaluate the performance of the proposed framework over the realistic behavior of occupants. The RL framework is compared with two rule-based scenarios of RC and RE.

Results indicate the proposed framework could provide a significant energy saving, mainly by learning how to get the best use of PV power production. Therefore the energy-saving potential is expected to be even more in regions with higher solar radiation than Switzerland. Also, the agent has successfully learned how to respect the comfort of occupants and water hygiene, so the potential energy saving is not with the cost of violating occupants' comfort or health.

Data statement

The datasets measured during the current study are not publicly available but can be shared based on request.

5. References

[1] Esrafilian-Najafabadi M, Haghighat F. Occupancy based HVAC control systems in buildings: A state-of-the-art review. Build Environ2021;197:107810.

[2] Heidari A, Marechal F, Khovalyg D. An adaptive control framework based on Reinforcement learning to balance energy, comfort and hygiene in heat pump water heating systems. J Phys Conf Ser 2021;2042:012006.

[3] Heidari A, Olsen N, Mermod P, Alahi A, Khovalyg D. Adaptive hot water production based on Supervised Learning. Sustain Cities Soc2021;66:102625.

[4] International Renewable Energy Agency. REmap 2030 Full Report. 2014.

[5] Mohammed NA, Baghdad-Iraq M. Modelling and Optimisation Planning of the Dynamic System of Energy Supply-Integrating Demand-Side Management and Forecasting. Opus4KobvDe 2019:xvi, 188 Seiten.

[6] Haji Hosseinloo A, Ryzhov A, Bischi A, Ouerdane H, Turitsyn K, Dahleh MA. Data-driven control of micro-climate in buildings: An event-triggered reinforcement learning approach. Appl Energy 2020;277:115451.

[7] Sutton R, Brato A. Reinforcement learning: an introduction. Robotica 1999;17.

[8] Zou Z, Yu X, Ergan S. Towards optimal control of air handling units using deep reinforcement learning and recurrent neural network. Build Environ 2020;168:106535.

[9] Schreiber T, Eschweiler S, Baranski M, Müller D. Application of two promising Reinforcement Learning algorithms for load shifting in a cooling supply system. Energy Build 2020;229:110490.

[10] Valladares W, Galindo M, Gutiérrez J, Wu WC, Liao KK, Liao JC, et al. Energy optimization associated with thermal comfort and indoor air control via a deep reinforcement learning algorithm. Build Environ 2019;155:105–17.

[11] Svetozarevic B, Baumann C, Muntwiler S, Di Natale L, Zeilinger MN, Heer P. Data-driven control of room temperature and bidirectional EV charging using deep reinforcement learning: Simulations and experiments. Appl Energy 2021:118127.

[12] Park JY, Dougherty T, Fritz H, Nagy Z. LightLearn: An adaptive and occupant centered controller for lighting based on reinforcement learning. Build Environ 2019;147:397–414.

[13] Brandi S, Piscitelli MS, Martellacci M, Capozzoli A. Deep reinforcement learning to optimise indoor temperature control and heating energy consumption in buildings. Energy Build 2020;224:110225.

[14] Kazmi H, Mehmood F, Lodeweyckx S, Driesen J. Gigawatt-hour scale savings on a budget of zero: Deep reinforcement learning based optimal control of hot water systems. Energy 2018;144:159–68.

[15] Lissa P, Deane C, Schukat M, Seri F, Keane M, Barrett E. Deep reinforcement learning for home energy management system control. Energy AI 2021;3:100043.

[16] Springston JP, Yocavitch L. Existence and control of Legionella bacteria in building water systems: A review. J Occup Environ Hyg2017;14:124–34.

[17] Booysen MJ, Engelbrecht JAA, Ritchie MJ, Apperley M, Cloete AH. How much energy can optimal control of domestic water heating save? Energy Sustain Dev 2019;51:73–85..

[18] QU X, Chang Q, Arinez J, Zou J. Knowledge-guided Reinforcement Learning for Gantry Work Cell Scheduling. IEEE Access 2018.

[19] Tensorforce: a TensorFlow library for applied reinforcement learning n.d.

[20] Standard SIA 385/1. n.d.

[21] Ritchie MJ, Engelbrecht JAA, Booysen MJ. A probabilistic hot water usage model and simulator for use in residential energy management. Energy Build 2021;235:110727. 10727.

Data Integrity Checks for Building Automation and Control Systems

Markus Gwerder [a], Reto Marek [b], Andreas Melillo [c], Maria Husmann [a]

[a] Smart infrastructure, Siemens Switzerland Ltd., Zug, Switzerland, markus.gwerder@siemens.com.

[b] Center for integrated building technology, Lucerne school of engineering and architecture, Horw, Switzerland, reto.marek@hslu.ch.

[c] Institute of mechanical engineering and energy technology, Lucerne school of engineering and architecture, Horw, Switzerland, andreas.melillo@hslu.ch.

Abstract. Data from building automation and control systems are becoming more and more important, since they are used in a growing number of (novel and established) analytics applications such as fault detection & diagnostics (FDD), smart maintenance and optimization. However, the quality of such data is often poor due to erroneous installation, commissioning, data recording or meta-information. In addition, building automation engineering and service departments usually focus on implementing and maintaining basic control functionality – data acquisition, tagging quality, and analytics do often not take priority. Due to these data quality issues, a first important step in any data analytics operation is to ensure data integrity. One main goal of data integrity checks is to increase data reliability. The paper presents such checks for building automation applications, in particular three different types of plausibility checks for time series data: single signal tests, similarity tests, and reaction tests. Examples using data recorded from real building automation project are presented for each of the three check types, demonstrating the usefulness of these checks. Data integrity checks are set up and configured using the available metadata which – in our case – comes in the form of semantic models that are automatically generated from building automation engineering data. Many data integrity checks have been identified that are potentially of great benefit in practice – both as a stand-alone application or as first part in a data analytics process. The major prerequisite for successful data integrity checking is that the checks can be set up with minimal effort and executed periodically. To achieve a high degree of automation, semantic data is of great importance, because it is through them that the recorded time series are provided with context and meaning. The automatically generated semantic models from building automation engineering proved to be already rich in automation information and are sufficient for many of the checks investigated.

Keywords. Building automation, analytics, data integrity, data plausibility, semantic modeling.
DOI: https://doi.org/10.34641/clima.2022.271

1. Introduction

Data analytics and fault detection & diagnostics (FDD) methods are essential for the energy-efficient and comfortable operation of buildings. The objectives are manifold: Create transparency regarding optimizations in planning and operation, determine the origin of performance gaps, ensure and maintain the desired building performance, check the success of energy optimization measures, create reliable foundations for further optimization steps. However, these goals can only be achieved based on reliable and trustworthy data. The challenge here lies in the frequently poor quality of the data: incomplete, erroneous, unstandardized, or non-normalized data are quite common. Reasons for poor data quality originate from all different processes in building automation. Below, examples for such reasons per phase are given:

- Installation: faults in hardware, bad sensor placement, wiring errors
- Engineering: faults in control program, including faults in system integration; wrong or misleading names, tags, units
- Commissioning: point test not done properly, system test not done (e.g., hydraulic balancing)
- Operation: interruptions in connectivity or recording; gateway config.; neglected maintenance of building automation; changes in building automation software without re-commissioning and/or adaptation of management layer

Copyright ©2022 by the authors. This conference paper is published under a CC-BY-4.0 license.

Thus, ensuring data integrity is the first important step in data analytics and FDD. Data analytics – including the verification of data integrity – and its setup process can be significantly improved by combining measurement data (i.e., time series data) with semantic models, e.g., metadata about building geometries, building automation systems, components. Based on the knowledge contained within semantic models, data can be automatically checked for integrity, similar to what a human expert would do.

There are two key questions when assessing data integrity checks: (i) To what extent are the available semantic models applicable to set up and configure data integrity checks – both conceptually and in real-world project settings? (ii) Which data integrity check methods qualify through their broad applicability, high reliability and manageable computational needs for an implementation in practice.

There is a functional overlap between the data integrity checks investigated and widespread analytic solutions such as rule based FDD. However, the investigated methods are intended for specific tasks and strictly limited to data integrity verification, i.e., checking plausibility only. Checking for plausibility only has the distinct advantage that no prior knowledge is required about the building's usage and the correct design of its plants. This facilitates automatic testing – ideally, this can take place without any building- or plant-specific tuning. The main disadvantage of this approach is that the checks will not detect faults other than implausible behavior: the checks do not verify whether the systems operation is reasonable (e.g., inefficient system operation, unreasonable comfort setpoints, …).

Figure 1 shows a high-level overview of a data analytics workflow from «data collection», «merging» (unification and central storage), data pre-processing and data cleaning to subsequent checks. The checks considered in this paper are clearly distinguished from preceding classical checks regarding data acquisition, detection of data gaps and associated imputation, pre-processing, outlier detections and data cleaning. On the other hand, a separation shall be made to subsequent checks like e.g., checking design/dimensioning or comfort end energy by methods such as classical rule based FDD checks.

2. Methods

2.1 Processing and storing time series data

Dealing with data from multiple sources can become complicated. Understanding the data, extracting, and transferring it to a central storage location is the first step in a data warehouse architecture [1]. Figure 2 represents a simplified representation of such a data workflow which includes as first steps the «data collection», «merging» and «pre-processing/data cleaning» of the data. Although the scope of this paper lies in the subsequent «data integrity checks», these first three steps are essential because each data integrity check as well as other subsequent checks such as e.g., FDD requires dedicated pre-processed data: Some methods rely on raw data, others rely on «resampled data» or «cleaned data» and further methods on «resampled and cleaned data».

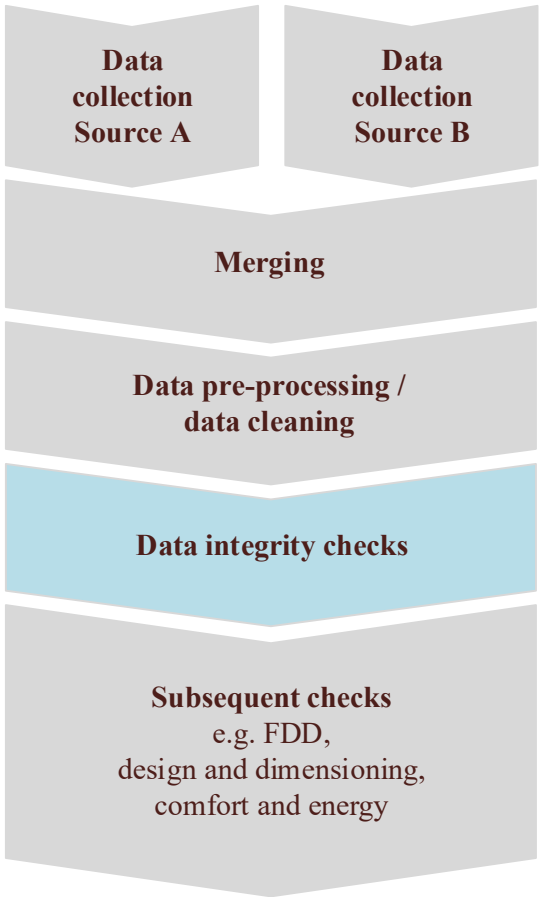

Fig. 1 - High-level overview of a data analytics workflow with incorporated data integrity checks.

Time series data processing steps such as correction/flagging of bad quality data or data resampling may profoundly affect the results of data integrity checks. Therefore, it is important to outline the different states of the data and the preprocessing steps that take place in between. Based on [1] and [2], a general data processing procedure is outlined in Figure 2, where each bucket represents a storage containing data in a particular state. The rectangular boxes in between represent the processing steps, including the activities required to transform the data.

2.2 Data check workflow

Following the general data analytics workflow introduced above, data integrity checks as well as other checks can be performed using different kind of processed data (buckets). Figure 2 shows a possible data processing pipeline including checks of several types. Data integrity checks are colored blue, checks outside the paper's scope have a grey background. The data integrity checks investigated focus on plausibility using semantic information. The required semantic data is indicated in the yellow boxes.

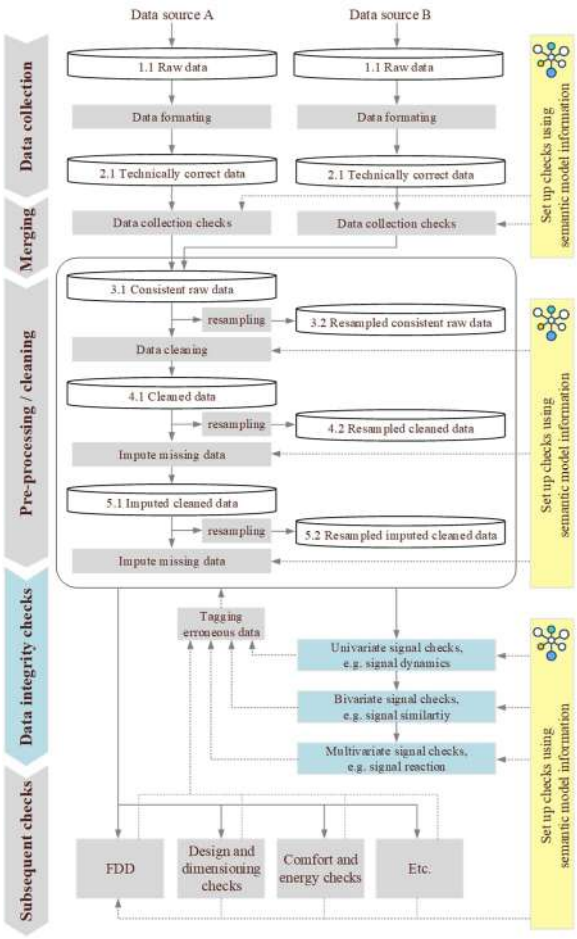

Fig. 2 - Data check workflow (blue boxes: checks considered in the paper, yellow boxes: semantic model information, grey boxes: checks outside the paper's scope, white buckets: data storages).

If a data integrity check fails, further analyses such as FDD do not make sense in general, as they would produce erroneous results. Failed data integrity checks should therefore tag erroneous data and subsequent checks should consequently evaluate such quality tags.

2.3 Development environment

For prototyping and evaluation of data integrity check algorithms, a software test environment was designed and used for preprocessing and storing time series data, corresponding semantic model data access, and automated execution of data integrity checks. The software development environment consists of three main parts:

- Time series database: InfluxDB
- Graph database to store semantic information, also known as metadata: GraphDB
- Data workflow management platform to automate checks: Apache Airflow

Both databases and the data workflow management platform used to automate were put into operation on an Amazon Web Services (AWS). Time series data is exported daily from building automation and control systems (BACS) and stored in an AWS data lake. A script (run on an AWS server) processes and stores the pre-processed data. The pre-processed data corresponds to the bucket «4.2 Resampled cleaned data» in Figure 2. Another script ingests the data finally to the time series database.

The main hub is the workflow management platform. It performs periodic checks and stores and visualizes the results. The data for the checks are obtained directly from the two databases. The platform executes a chain of operations and analysis steps (data pipeline), where the output of an operation becomes the input to another [5].

2.4 Data sets

Two different data sets representing building automation data from two buildings in Vienna were used for the project. These buildings are part of the ongoing research project «Aspern Smart City Research» (https://www.ascr.at/en/).

- Student home for 300 students
  The BACS includes room control, heat distribution (from district heating), ventilation as well as the electrical energy management of photovoltaic power plant and electric battery.
- Office building, ca. 8'000 square meters
  The BACS includes room control, heat and cold distribution and storage using a thermally activated building system, heat and cold generation using a heat pump, ventilation as well as the electrical and thermal energy management.

Since the buildings have been used in a large-scale research project already, a lot of data, knowledge, and information are available – much more than what is typically available in regular building automation projects. Therefore, data integrity check results can be applied and evaluated using multiple years of operational data and assessed in more detail based on the knowledge previously gathered.

2.5 Data integrity checks

Most of the investigated data integrity tests were relatively simple rule-based methods based on statistical properties of the time series data, tailored to the considered application. All checks as well as data base access and basic visualization were implemented in Python. A statistical feature framework was developed for flexible and broad application of signal comparison operations. With customizable and extendable sets of conditions, statistical features, and actual tests, it is possible to design a custom data integrity check using the developed framework. The suggested procedure is divided in 4 steps which are summarized as follows:

1. Define conditions on data: Multiple conditions on multiple time series can be combined such that the timestamps, where all conditions are fulfilled, are flagged as valid. Consecutive valid

timestamps are forming valid ranges.

2. Calculate a list of selectable statistical features such as mean, standard deviation, polynomial fit parameters representing the valid time ranges (either calculate the features for each entire valid range or using a moving window within each valid range).
3. Use a methods collection to execute the appropriate test on the calculated features representation.
4. Visualize the outcome with the help of dedicated visualization methods.

2.6 Semantic Modeling of Building Technology and Automation

Time series data can only be evaluated and analyzed if they are used in the context of the real plant. The data only becomes meaningful, understandable, and usable with so-called metadata. The goal is for the data to be self-describing, so that it can be used to add value without a great deal of manual effort. The intent of a semantic models for building automation and technology is to provide such information in a defined structured form so that it can be processed automatically by machines. The data check workflow presented in Figure 2 is an example of where semantic information can be used. Today, most building analytics applications are still mapped to the time series data (at least in part) manually, which is time consuming and error prone. Sematic models have the potential to improve this situation radically. Particularly important semantic model content for analytics applications is relational information such as supply chains, zones/command groups, locations, or control functional interactions (e.g., relations between controllers, control variables, setpoints, manipulated variables).

One approach to describe semantic information is to create ontologies (schemas) and describe instance data using these schemas. W3C provides standardized technologies such as RDF and OWL for that purpose and SPARQL for querying RDF data. There is no standardized ontology for the building automation domain, though several ontologies have been published by academia and various community groups [6, 7, 8]. We used our own ontology that – unlike the ones referenced – focuses on a functional description of the building automation system. The instance data can be exported from a building automation engineering tool or automatically generated from BACnet scans of systems that have been engineered with that tool. The building automation control application contains a lot of information relevant for data analytics (including data integrity checks). It is obvious that making this knowledge machine-readable and using it for analytics is highly advantageous compared to an analytics mapping process as described above.

Figure 3 shows a simple example of the functional model representing one part of a room thermostat (knowledge graph containing points, functions, locations, and relationships between them).

3. Results

In this section, a small extract of potential data integrity checks is given, as well as one concrete example check result for the three investigated test types.

3.1 Data integrity check collection

Data integrity checks are preferably based on semantic models. While a comprehensive analysis of semantic data models is beyond the scope of this paper, the proposed approach is bottom-up: First, potential checks are considered which are meaningful and profitable. In a further step, it is analyzed which metadata are necessary for the check. Thus, a statement is then possible as to which data is missing in the available semantic models and which data is most important to be added from a practical point of view.

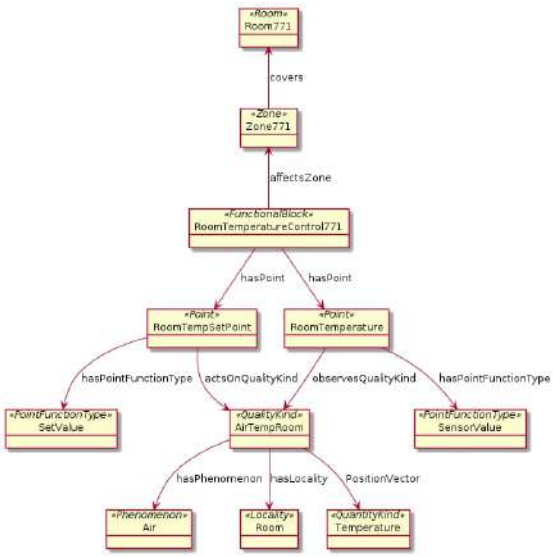

Fig. 3 – Functional semantic model instance example.

Different data integrity checks for building automation data have been derived from literature (see [3], [4]) and developed by our own. Here, we provide a small extract of the collection in Table 1.

Tab. 1 - Extract of the data integrity check collection.

Test type	Test description
Signal dynamic property	Minimal room air quality measurement over longer time periods should be close to outside air concentration.
Signal dynamic property	Room air quality measurements should exhibit a daily cycle when observed for a longer period of time.
Signal reaction	Room temperature measurement reacts on radiator valve position change when heat is provided by associated heat group.
Signal reaction	Room brightness sensor measurement reacts on light command/modulation change.
Signal reaction	Supply air temperature measurement reacts on heating coil valve position change when heat is provided by the associated

	heat group and air flow is provided by the associated air handling unit.
Signal similarity	Time series temperature measurements before and after air treatment steps in air handling units must be similar when air treatment is turned off and fan is running.

3.4 Single signal check example

Single signal checks are applied to one single measured / recorded time series. Additional information might be used such as geographical location and local time (e.g., to calculate solar position).

Example: Finding convenient locations for room temperature sensors is often not easy. The measurements might be influenced in an undesired way by internal or external heat gains. Single signal checks for room temperature measurements can detect such cases by assessing dynamic properties of the time series. For room temperatures, checking for unreasonable spikes is an adequate test.

Application of such tests to room temperature measurements of the office building introduced in 2.4 resulted in mostly passed checks. However, there were rooms which showed short positive spikes during 7-8pm local time in summer. An example time series of such a room temperature is given in Figure 4. Such spikes can lead – depending on the HVAC control – to unnecessary heavy cooling activity. To prevent this, either the sensor can be relocated, or the control program can be changed.

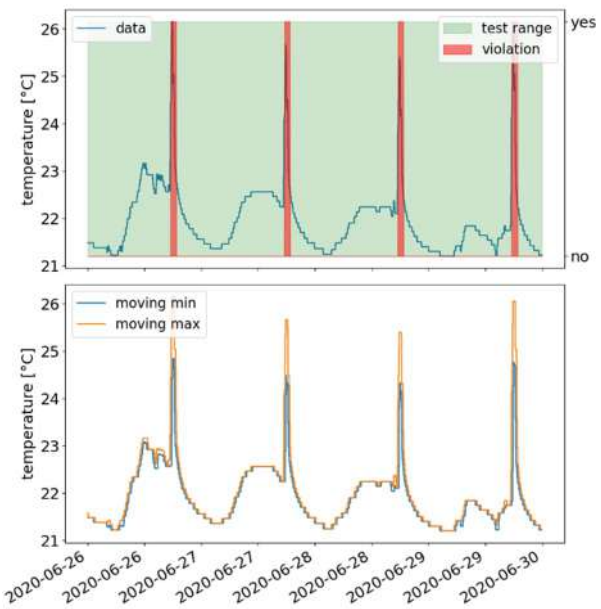

Fig. 4 – Example of failed room temperature single signal check. The difference between moving window minima and moving window maxima are used to identify peaks in the time series.

The assumed reason for the spikes (which was confirmed later) was exposure of the sensors to direct sunlight (because the blinds would have been controlled open in the evening). Using the semantic information of the room façade orientation, the assumption could also be consolidated (all the concerned rooms had western orientation). Even further consolidation is possible when additional measurements such as solar radiation or brightness is incorporated in the test (which of course makes the check no longer a single signal test).

3.3 Signal similarity check example

Signal similarity tests check whether two time series are similar at certain points/ranges in time. They can be used to test signal similarities. In the simplest case, there are several sensors with which the same variable is measured. It can then be checked whether the signals are similar. In building automation, however, this case is typically rare, since redundancy is associated with additional costs. An example of such test methods is that of heat or cold meters, where the flow and return temperatures are measured by the meter as well as by separate sensors for control. In this case, the similarity only should be checked when the heat/cold fluid is circulating. Additional conditions for checking depend on the installation setup (e.g., heat meter on primary or secondary side).

In most cases, two signals are similar under specific conditions only, e.g., flow and return temperatures of a heat exchanger when no heat is transferred, or air temperature / humidity measurements before and after an inactive air treatment aggregate, such as temperature measurements before and after the heating coil.

Example: Redundant temperature measurements (heat meter & control temperature reading) in various heating circuits have been investigated based on data from the buildings introduced in 2.4. Figure 5 shows an example result for a flow temperature similarity test: The heat meter flow temperature measurement has a low resolution of 1 K and a relatively low sampling rate compared to the sensor used for control. Time periods where the similarity test passed are colored green, periods where the test failed are colored red. During all other time periods, the test was not applicable (i.e., conditions were not met). As can be seen, the example shows a high degree of similarity.

In practice, it can happen that heat meters are configured wrongly, e.g., the addresses of two heat meters are mixed up. Similarity tests can detect such misconfigurations. In the heating system of the school building (see 2.4), there are five main heat groups which are operated using similar schedules and setpoints. Nevertheless, the presented similarity test proved to be able to detect (artificially) misconfigured meters in all cases.

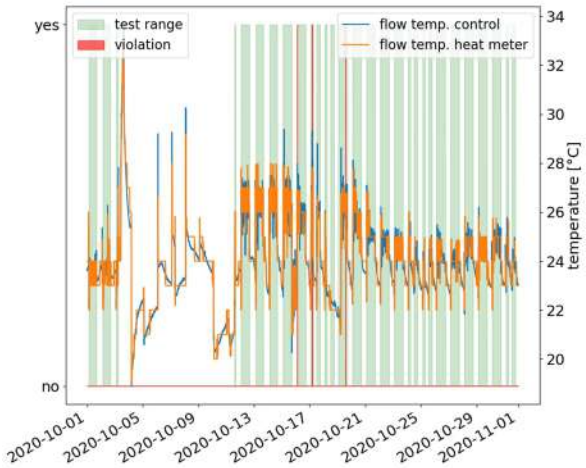

Fig. 5 – Example of passed heating circuit flow temperature similarity check. The test fails if the difference in the two signals is too large for a minimal amount of consecutive timesteps.

3.2 Reaction check example

Signal reaction tests check whether a time series provides an expected response due to an event.

Example: A valve operation reaction test checks for plausible behavior regarding the operation of a temperature control valve / valve actuator in building automation. The checks are based on time series data of the valve command, temperature readings and the operating state of the associated pump. The check passes if the signals correspond to what is defined as plausible; it fails if this is not the case. Reasons for the check to fail:

- The valve is stuck (open, close, mid position)
- There is a fault in one of the sensors or sensor installation used to measure the required data
- There is a fault in the pump associated to the valve
- There is a fault in the measurement processing chain (including data recording)
- There is a fault in the mapping or labeling of the data

The checks are assumed to be particularly helpful for valves/valve actuators without position feedback signal. Ideally, the check can be applied broadly to different types of valves and applications using typically available time series data. Very common applications are heating or cooling mixing circuits, but also room temperature control valves.

A practical room automation example of a failed test is shown in Figure 6. In this case, a concrete core conditioning system is operated by opening and closing heating and cooling valves – the data comes from the office building, see 2.4. The figure shows a few days in August 2020 (cooling season). Time periods with opened cooling valve are indicated by green areas. The cooling command marked by dashed red lines was identified as failed by the applied reaction test: Despite the opening command of the valve (and flow temperature provided by the cooling circuit sufficiently low), there is no reaction visible in the concrete core temperature. The test result proved to be correct. The reason was found to be a fault in the commanding of the valve actuator by the room controller leading to sporadically non-executed commands. The fault could be fixed by a software update of the room controller.

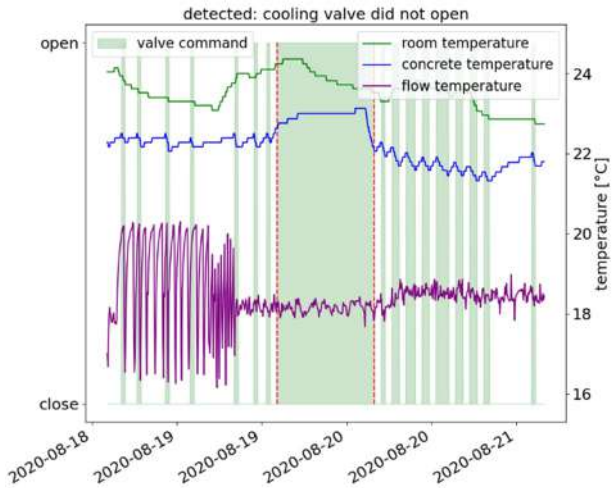

Fig. 6 – Example of failed cooling valve reaction check.

4. Conclusions

Data integrity checks are of great benefit to enhance the quality of subsequent data analyses and increase confidence in the data (as well as the plant operation the data reflects). These checks can be considered as the first part in a data analytics process. But they can even be beneficial as stand-alone tests.

There are several data integrity checks that are considered promising in practice. However, a thorough evaluation of their performance would require applying the checks to many more (labeled) data sets than has been possible. Most of the investigated / developed methods are potentially broadly applicable (different buildings, control application, ...) and can be performed from the beginning of building operation, which means they can be useful already in the commissioning phase. No training with historical data is needed. The challenges in the practical application of the checks lie mostly in the robust and broadly applicable design of the test methods. Currently, e.g., a reaction test must be configured for the expected reaction speed (which cannot be easily derived from semantic information).

The main prerequisite for successful application of data integrity checks is that they can be set up with minimal effort and executed periodically. In order to achieve a high degree of automation in setting up the checks, semantic data is of great importance, because it is only through them that the recorded time series data are given context and meaning. The semantic models we used were automatically generated from

the building automation control solution. Therefore, these models are already rich in automation information. Currently not yet contained aspects in these models are some cross-plant relationships, particularly supply chain relationships, which are used in many of the data integrity checks studied. Fortunately, in many cases, such relationships are contained in the control program to implement demand-driven control, which means this information can be added to the semantic models. Other missing aspects such as hydraulic topology or equipment specification typically are not needed for control and therefore would have to be incorporated using other data sources such as BIM. However, many of the checks studied can be set up and executed without this additional information. Furthermore, semantic models that include control functions are also useful for subsequent analytics applications [9].

5. Outlook

The results stimulate the development and application of «plausibility check» type data integrity tests. With the valuable knowledge and experience gained, a systematic process will be followed in the future: Based on the complemented and evaluated integrity checks collection, checks with the highest potential benefits will be selected for further analysis. The development of the selected checks will then focus on broad and robust application. Automation, reporting and visualization of the checks are then prototyped, and successful methods will be applied outside of limited test data sets.

6. Acknowledgement

The authors would like to gratefully acknowledge the funding by Siemens Switzerland Ltd. The authors would also like to thank Prof. Olivier Steiner and Prof. Philipp Schütz (both Lucerne school of engineering and architecture) for their support.

7. References

[1] Kimball R., Ross, M. The data warehouse toolkit: the definitive guide to dimensional modeling. 3rd Edition. John Wiley & Sons. 2013.

[2] De Jonge, E., van der Loo, M. An introduction to data cleaning with R. The Hague: Statistics Netherlands. 2013.

[3] Brady, N., Lloyd, R. Trust the raw data? The importance of applying data integrity. CLIMA 2016, 22-25 May 2016, Aalborg, Denmark.

[4] Gitzel, R. Data quality in time series data: An experience report. CBI 2016, 29 Aug - 1 Sep 2016, Paris, France.

[5] Wang, E., Cook, D., Hyndman, R. J. A new tidy data structure to support exploration and modeling of temporal data. Journal of Computational and Graphical Statistics. 2020;29(3):466–478.

[6] Balaji, B., Bhattacharya, A., Fierro, G., Gao, J., Gluck, J., Hong, D., Johansen, A., Koh, J., Ploennigs, J., Agarwal, Y., Berges, M., Culler, D., Gupta, R., Kjærgaard, M.B., Srivastava, M., Whitehouse, K. Brick: Towards a Unified Metadata Schema for Buildings. BuildSys '16. Proceedings of the 3rd ACM International Conference on Systems for Energy-Efficient Built Environments. 2016.

[7] Hammar, K., Wallin, E.O., Karlberg, P., Hälleberg, D. The RealEstateCore Ontology. In: Ghidini C. et al. (eds) The Semantic Web – ISWC 2019. ISWC 2019. Lecture Notes in Computer Science, vol 11779. Springer, Cham. 2019.

[8] Project Haystack. http://project-haystack.org/. 2021.

[9] Ramanathan, G., Husmann, M., Niedermeier, C., Vicari, N., Garcia, K., Mayer, S. Assisting automated fault detection and diagnostics in building automation through semantic description of functions and process data. BuildSys '21: Proceedings of the 8th ACM International Conference on Systems for Energy-Efficient Buildings, Cities, and Transportation. 2021.

Data Statement

The datasets generated during and/or analysed during the current study are not available due to confidentiality agreements, but the authors will make every reasonable effort to publish them in near future.

Predict the remaining useful life in HVAC filters using a hybrid strategy

Hossein Alimohammadi [a], kristina Vassiljeva [b], Eduard Petlenkov [c], Tuule Mall Kull [e], Martin Thalfeldt [d]

[a,b,c] Centre for Intelligent Systems, Department of Computer Systems, Tallinn University of Technology, Tallinn, Estonia, hossein.alimohammadi@taltech.ee.

[d,e] Centre for Intelligent Systems, Department of Civil Engineering and Architecture, Tallinn University of Technology, Tallinn, Estonia, tuule.parts@taltech.ee.

Abstract.

Introduction: This article discusses an engineering prediction-oriented method to monitor and predict the healthy conditions of air filters in heating, ventilation and air conditioning (HVAC) installations in the construction industry.

Background: In the literature, many researchers have studied hybrid prognostic methods for monitoring and predicting filter clogging, and experimental studies have been conducted to develop degradation models to demonstrate the mechanism of filter clogging. The common methods usually predict residual useful life based on a physics-based degradation model along with a prognostic model based on measured data. However, if there is not run-to-fail data or it is costly to prepare, another method is needed. The method used in the present work is useful when the data of entire operating period is not available, instead part of the operational range is obtained during the operation of the air handling unit (AHU).

Methods: The method described in this article includes a combination of physically-based models and acquired operational data. An appropriate health indicator (HI) is calculated based on measurements. Learning algorithms are used to calibrate a carefully designed filter degradation model. The remaining useful life (RUL) of the filter is estimated using the dimensional reduction method, in particular principal component analysis (PCA) technique. The proposed method has been tested on a real air conditioning unit installed in a building located in Tallinn.

Results: The results show that the selected degradation model provides the best fit based on the data observed from the field. In addition, using dimensional reduction methods to estimate remaining useful life is feasible for HVAC filter clogging prediction. This is based on a comparison between an acceptable remaining useful life estimate and experimental data. The performance analysis results show that predictive maintenance methods can provide accurate prognostic indications.

Conclusion: The application of a hybrid prediction model allows accurate estimation of the characteristics of the remaining useful life of the target component. It should be noted that the use of predictive maintenance strategies in this situation has increased the life of filters in buildings by a significant amount compared to replacement time schedule.

Keywords. predictive health maintenance HVAC filter prognosis, remaining useful life.
DOI: https://doi.org/10.34641/clima.2022.273

1. Introduction

The building industry needs to focus most on optimizing current maintenance practices, avoiding services that affect failures and reducing related costs. Given recent advances in data technology and science, many companies have made unprecedented efforts to use advanced analytics to improve the operational efficiency of their products and services. Especially in the field of HVAC industry, it is particularly important to develop predictive maintenance (PM) strategies. Many researchers from academia collaborate with industry ones to explore various methods to better plan and manage the maintenance of construction and transportation assets. The development of predictive health maintenance (PHM) solutions for HVAC has been the focus of industrial research [1]. Effective HVAC equipment can lead to increased energy consumption, increased equipment failure, and decreased thermal comfort for occupants, and leading to higher maintenance costs. When ventilation system is affected by faults, the health of the occupants may also be endangered due to the increased possibility of exposure to indoor pollutants. Therefore, PHM is an important tool to

Copyright ©2022 by the authors. This conference paper is published under a CC-BY-4.0 license.

ensure efficient operation of HVAC equipment so that air-conditioning assets can achieve their best optimal energy consumption and performance. The health indicator (HI) which is calculated based on a combination of physic-based and data-driven models has been used in this article. This approach leads to the development of degradation model in order to calculate the RUL prediction of working HVAC unit. RUL prediction of degradation is not set explicitly and can be linear, exponential, polynomial or logarithmic, and it depends on the object being studied. In different research cases, the deterioration behaviour of component life may be different. The RUL prediction depends on case study since first, despite the fact that exponential prediction model is used frequently, there are other case studies which concluded that above mentioned model is not appropriate for their systems. For example, Kang et al. [2] used the training datasets which RUL was not provided. They applied a polynomial degradation model and the intersection between the polynomial and the axis of the cycle was calculated as the failure point. Coble et al. [3] implemented the second-order polynomial to model the degradation parameter. While an exponential model may be more physically appropriate, the quadratic model is more resistant to noise and better describes the relevant data for the selected prognostic parameter. Zheng et al. [4] present a RUL of bearing as case study using Hilbert–Huang entropy prediction method with linear degradation model. Second, the exponential degradation model will increase dramatically for predicting over a larger period of time. This is due to the mathematical nature of the exponential function compared to other functions. The third reason is the uncertainty in the RUL models. Celaya et al. [5] discussed the importance and interpretation of uncertainty in RUL prediction of components used in several types of engineering applications and explained why RUL prediction is uncertain. Another influential reason is the existence of unexpected conditions like covid-19 crisis. The main problem is that in the majority of research, the filter behaviour and its pressure drop are based on changes in volumetric or mass flow rate. Those can be described on laboratory conditions. On the contrary, in real conditions, the flow rate is controlled by the controller on a fixed value. These measurements lead to the acquisition of a set of run-to-fail data, which is suitable for use in the survival and similarity based methods. However, this can lead to high costs for laboratory equipment. Another problem is that measuring and having a set of run-to-fail data takes a lot of time. At the same time, run-to-fail data set are sometimes very non-linear with high variations and reduce the prediction accuracy. In the present work, these limitations have been resolved and the measured values from AHU have been used directly.

The organization structure of this article is as follows: The Section 2 provides related work and problem descriptions. Section 3 focuses on the formulation of health indicators and prognostic strategies, and outlines the proposed methods. Section 4 discusses the results of the proposed method to the case study. Finally, conclusions in the Section 5 provide suggestions for future research directions.

2. Background

In many industrial systems, filtration is a key process to achieve the required level of purification of liquids. Filter clogging and pressure drop are the main failure mechanisms that lead to filter replacement or adverse consequences such as reduced performance and efficiency. For HVAC applications, filters are installed to purify the air from particles such as dust, pollen and other airborne materials from windows, kitchens, etc. This accumulates in the filters and can leads to clogging or even blocking, (Figure 1). A clogged air filter will adversely affect the performance of the HVAC system and may cause damage, such as extended compressor running time, reduced energy efficiency, freezing of the evaporator coil, and ultimately damage to the air conditioning system.

Fig. 1 - Samples of new filter (right) and clogged filter (left), [Theengineeringmindset.com]

It is expected that there will be a large amount of articles on HVAC systems. The focus of this paper is to use hybrid methods to detect and predict the pressure drop of air filters in HVAC systems. In the literature, many researchers have studied methods of controlling and predicting filter pressure drop, and conducted experimental studies to establish degradation models to show the mechanism of filter clogging. The authors proposed a simple model-based model for filter clogging by using the Markov model to calculate the remaining useful life in [6]. In the maintenance strategy, three terms are usually used: preventive maintenance, predictive maintenance and reactive (corrective) maintenance, depending on the type and degree of safety of the system. Preventive maintenance usually used on high-precision equipment such as airplanes. The predictive maintenance is usually selected based on the comfort or cost of the residents such as building HVAC. Reactive maintenance is mainly used for consumables such as vehicle parts. Two predicted maintenance cases were found in the literature: Condition-Based Maintenance (CBM) and Prognostics and Health management (PHM). In predictive maintenance, if we are looking for a general strategy, we can use condition-based maintenance to disable component data with the help of a set of executions, and if we only want to maintain components that contain only one data set, we usually use PHM for health prediction. In the process of diagnosis and prognosis, two main approaches can be extracted in the prediction: single

model approaches and multiple model approaches. For the single-model approach, there are three types of models are called «knowledge-based models, data-driven models, and physics-based models». The multi-model approach combines at least two of the above three models. Multi-model methods are sometimes referred to as hybrid models, and may have different configurations. In data driven approach, classification and regression algorithms are commonly used for supervised learning. Unsupervised learning algorithms usually use clustering and dimensionality. The third type is reinforcement learning which is used in the absence of training data sets, and learns from its experience. Authors in [7] covered the most complete reviews of predictive maintenance models in 2017 and 2018, respectively. Authors in [8], made studies the comprehensive systematic review in 2019. The main topic was devoted to data-driven methods for prediction work, especially methods related to machine learning and deep learning. Most consulting studies have limited case studies, with few failures (sometimes only one), which is a challenge for extrapolating single-model methods to complex applications of systems. Multi-models usually are used to overcome the complexity of the maintenance predictive task. The author in [9] divided them into 5 specific groups with admirable details. For the research described in this article, a predictive maintenance strategy based on a health indicator has been developed. The health indicator is calculated based on a combination of physics-based models and sensor data collected from working HVAC units, resulting in RUL predictions. Using dimensional reduction methods, it is possible to simulate the future development of the health indicator related to the development of pressure drop due to the clogging. Among dimensionality reduction methods, the PCA is one of the methods that is used for faster and more cost-effective prediction purposes. The reason to use PCA is that in the present case study, the entire execution run-to-fail data is not available, instead a part of the operating range is acquired during the operation of AHU. Lack of information about the final output of failure leads us to used unsupervised learning. The values from the sensors are divided into different parts. This is good idea, especially if we want to upload the new data periodically to the PM algorithm. Each data set can be clustered and extracted based on its own feature.

2.1 case study

The case presented in this paper is based on a real HVAC unit installed on a AHU in the city of Tallinn. Typically, or at least for existing AHUs for current work, filters are replaced periodically based on manufacturer's suggestion. Replacement is often done without assessing the actual retention life of the filter. In addition, inspecting air filters usually requires stopping the building's air conditioning system. Unnecessary filter replacement is costly, time consuming and therefore undesirable. Thus, having the platform that predicts the time of filter replacement is the main idea of doing this work. The proposed method should be easier to implement and also has an acceptable reliability and faster processing speed. The system is equipped with a variable frequency drive, which can adapt the fan motor to the thermal load. In fact, understanding background information is essential to ensure that health indicator is properly assessed. For this reason, it is necessary to consider factors that affect the performance of HVAC components. For the expected situation, it is necessary to control variables such as external temperature, humidity level, fresh air damper position, and HVAC power supply voltage. These factors may affect the failure mechanism.

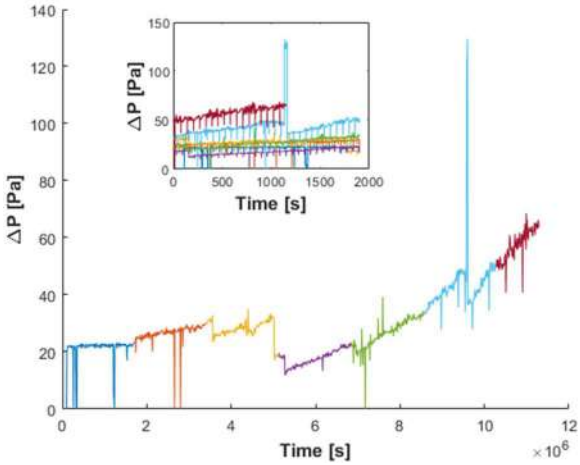

Fig. 2 - Pressure drop measured across the air filter, (top) monthly acquired data, (bottom) assembly of them.

The main health variable that helps to establish health indicators is the pressure difference across the filter. That parameter is not affected by the air flow rate associated with it, because it is controlled by a constant setting point. Figure 2 shows the pressure drop ΔP obtained from BIM from 10th July 2019 to 27th February 2020. The requirement of the original data pre-processing is set, in order to eliminate the influence of the noisy and misprinting data, integrating the pre-processed signal with a time series generated using the most important data features. These feature are the combination of time or frequency features (mainly useful for rotating parts). After processing and filtering, the algorithm will find the most important features. Figure 3 shows the framework used in this work.

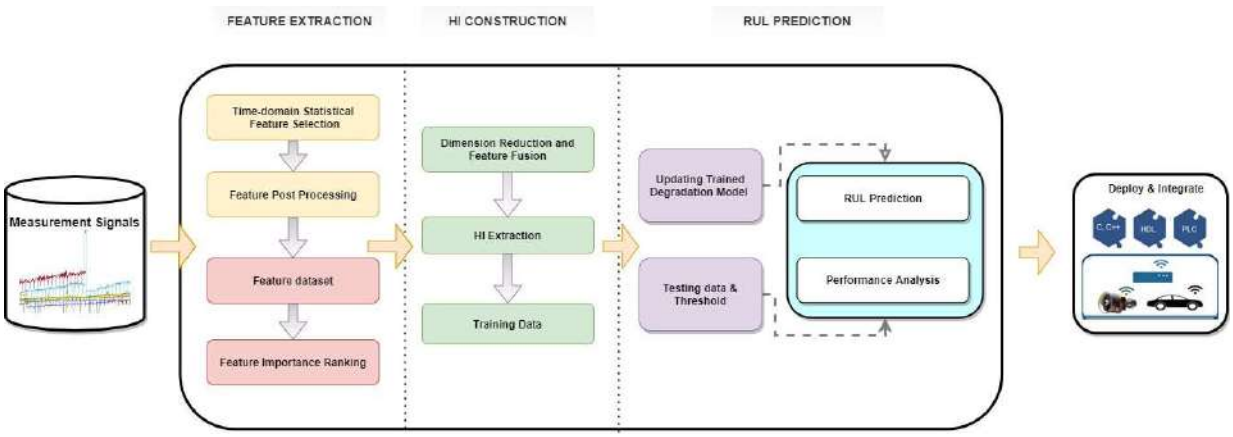

Fig. 3 - The framework of the prediction

The next step is to reduce the dimension of important selected features and extracting the health indicator. Therefore, the proposed method and dimension reduction applied as a hybrid PHM model (with a data-driven model based on a physical model) that relies on a combination of measured data and simulated data. The development of the method is described in the next section. The physic-based model will update with validation data and then will be verified using testing data. The obtained model is used for prediction.

3. Method

This section introduces methods designed for predictive maintenance of HVAC filter. First, a method of extracting relevant information from the original data is proposed. The purpose of this step is to realize the features properly that reflect the filter performance status. Then, the construction of health indicator and the description of related fault threshold are discussed. Finally, a prognostic strategy is described, which involves the use of dimensionality reduction.

3.1 data Preparation and features extraction

As in the majority of machine learning programs, the quality of input data is a key factor in building high-performance predictive models. For not rotating/vibration components usually the time series analysis is performed to extract potentially relevant time series features. In order to eliminate the effect of noise, we can calculate the moving average in a specific attribute window to add them into the feature set. As shown in Figure 2, the raw data collected from this field fluctuates sharply, which makes it difficult to obtain directly the health indicator of the filter from the sensor measurements. For the study carried out in this paper, the following approaches are used to extract the features needed to construct a health indicator: First, pre-processing the original data to eliminate the influence of disturbing variables. Second, extraction of feature importance ranking from the pre-processed signals. Third, generation of PCA based on dimensional reduction of data. Forth, defining the more important principal component for subsequent construction of the health indicator. When the pre-processed pressure drop ΔP is obtained, several features can be calculated including the mean value, the standard deviation, the slope, the maximum/minimum value, the mean square root value, skewness, SNR, and band power. Taking into account the slow changes in the clogging process, in this case, a monthly health assessment can be performed. Therefore, features can be extracted within a time frame of one month. For current case study, seven out of twenty features were found to be sufficient to establish an effective health indicator. There are basically three criteria for extracting the most important features, monotonicity (uniformity), trendability (machinability) and prognosability. Monotonicity is used to quantify whether the features is suitable for prognosis. The monotonicity is obtained using the following equation:

$$Mon(x_i) = \frac{1}{m}\sum_{j=1}^{m}\left|\sum_{k=1}^{n_j-1}\frac{sgn(x_j(k+1)-x_j(k))}{n_j-1}\right| \quad (1)$$

Where x_j represents the measurement vector of a feature on the *jth* system, m is the number of monitored systems, and n_j is the number of measurements in system j. The mean and skewness of the signal is the top feature based on monotonicity.

3.2 dimension reduction

The next step is to reduce the dimension of the selected important features and extract the health indicator. The physics-based model is then updated with validation data and then verify with testing data. The obtained model is used for prediction. Our goal is to build a predictive model for clustering task and reduce its dimension. Due to time constraints in massive data processing, longer computation time, and high storage, dimensional reductions are essential, especially in real-time applications. Feature selection is the first step to reducing dimensions. Many other dimensional algorithms are available through machine learning research, including T-SNE, MDS, multidimensional scaling, missing value ratio, low variance filter, high correlation filter, random forests / ensemble trees, PCA, backward features Elimination, and forward

features Construction. The main reasons for selecting the dimension reduction, in particular PCA are: 1) In the modern computer era, large high-dimensional data sets are common; 2) Data visualization is impossible in higher dimensions. As a result, pattern recognition, data pre-processing and model selection must rely heavily on numerical methods; 3) In larger dimensions, the data shows too many edges of the sample distribution, because areas with larger spaces have the largest volume near the surface; 4) In high dimensions, the sampling frequency of internal data points (distribution) is low; 5) The features of high-dimensional data may be irrelevant or redundant; 6) The regression, classification, and clustering algorithms used to process raw data may require a lot of computation time and storage, and even if the algorithm is successful, the resulting model may contain a number of unclear terms. The algorithm provides a linear combination of important features on its first principle axes and the idea is to use these main axes as an important indicator or health indicator for use in training purposes to find a proper physical based model. Its advantages include useful items for the high input dimension (in our case 47 dimensional, 7 month times 7 important features). It also improved algorithm solving speed.

3.3 health assessment

The calculation of the appropriate health indicator (HI) is necessary to establish the relationship between the degradation or deviation of a case and its RUL. Therefore, an accurate HI is a key to more accurate prediction. In this paper, the first component of PCA coordinates is selected as a health indicator. To assess the health status of the filter, it is necessary to select the threshold for the health indicator. For current case study, the failure threshold is $\Delta P = 300$ Pa equal to $HI_{thr} = 30$. Health indicators has been matched on PCA in terms of experimental data, and to mathematical degradation model in terms of prediction.

3.4 prognostics: degradation model and RUL

Once the filter health indictor is determined, the parameters of mathematical prognostic model is updated and is implemented to predict RUL. First, a physics-based mathematical degradation model is used to express the evolution of pressure drop in the filter. Approximately, it is assumed that the filter clogging behaviour is exponential, although it should be noted that the degradation curve can vary or be different depending on the type of machines. For example, Zhao et al. [10] explained that regarding the determination of the empirical data, the different model can be used like exponential model (Table 1).

Tab. 1 - Different mathematical models according to the physical nature of the degradation.

Degradation model	Formula
exponential	$a.exp(b.t)$
quadratic polynomial	$a.t^2+b.t+c$
hybrid	$a.exp(b.t)+ c.t^2+d.t+e$
hybrid	$C=(a/b)/(1+(a/(b.C(t_0))-1). exp(-a.(t-t_0)))+ c.exp(d.t)$
Chaos	*due to abnormal conditions such as the Covid period, unintended and sudden breakdown of a part or machine, etc.*

The authors chose the exponential function because due to the fact that in the authors' previous research [5], it was found that the exponential equation gives acceptable results for clogging prediction among existing filters studied. The exponential degradation model for the health index, h (t) is defined as [11].

$$h(t) = \phi + \theta e^{(\beta t+\epsilon-\frac{\sigma^2}{2})} \quad (2)$$

where Φ is a constant deterministic parameter, $\boldsymbol{\theta}$ and β are random variables. These parameters are determining the slope of the model. At each time step t, the distribution of $\boldsymbol{\theta}$ and β is updated to the posterior based on the latest observation of h(t). ε is a Gaussian white noise or a normally distributed random error term with mean 0 and variance σ^2. The variance $\sigma^2/2$ in the exponential is to meet expectation. The model will find the closest training data set in the validation data, fit the probability distribution, and use the median of the distribution as the estimated value of RUL. Using the degradation model in (2), the evolution of health indicators can be obtained. In order to estimate the RUL of the air filter, based on the degradation model, we performed a two-step process: 1) Training phase: Perform model fitting to calibrate and update the degraded model based on pressure drop measurement data collected from the field. 2) Prognosis stage: Use a trained model to simulate changes in pressure drop over time until the air filter's service life is achieved. After finding and updating the model, the future, in particular RUL can be predicted, which could be failure or replacement time. RUL of a machine is the expected life or usage time (cycles, miles, etc) remaining before the machine requires repair or replacement. RUL prediction here is the main purpose of prediction maintenance algorithms.

$$RUL = t_f - t_c \quad (3)$$

Where t_f is a random variable for the time of failure or replacement, and t_c is the current time.

3.5 prognostic performance analysis

In order to prove the performance of the proposed method, the performance algorithm is applied to predict RUL. There is uncertainty in the prediction, which can be represented by a probability density

function (PDF). The type of data and the method of predicting RUL based on data are crucial. This uncertainty may occur due to the following reasons: insufficient data, lack of clean data (noise, mispointing, etc), lack of failure data. Therefore, using the set of standards for analysing RUL's predictive performance is required. In these years, many indicators for predictive maintenance performance analysis have been provided. Recently, high robustness metrics for predictive maintenance have been proposed, and four of them have been used in this work, including prognostic Horizon, alpha-lambda performance, relative accuracy, and convergence metrics. The horizon prognosis is obtained from the difference between the end of life (EOL) and the predicted time, *i*. The best result is when the PH(i) reaches zero. We prefer to present the PH results as a percentage of the actual life of the test specimens.

$$PH = EOL - i \tag{4}$$

Obviously, given that we are using a threshold, we must have a real RUL here, so we can use this metric (the point is that our threshold is a health indicator equal to the 300 pa, filter pressure drop). The alpha-lambda diagram is used to analyze the prognostic effect, in which the bound is set to 25%. Alpha-lambda performance evaluates the performance of the prediction inside a shrinking accuracy cone defined by α [12].

$$[1-\alpha].r^*(t_\lambda) \leq r(t_\lambda) \leq [1+\alpha].r^*(t_\lambda) \tag{5}$$

$$where\ \ t_\lambda = P + \lambda(EOL - P)$$

where λ is windows modifier, r is the estimated RUL at time t, r^* is the true RUL at time t, P is prediction time, t_λ as current time is between conical range of actual RUL. Observing the accuracy of the algorithm with the help of relative accuracy (RA) is another performance evaluation. As shown in the equation, the actual RUL is equal to the predicted RUL if RA tends to 1.

$$RA = 1 - \frac{|r^*(t_\lambda) - r(t_\lambda)|}{r^*(t_\lambda)} \tag{6}$$

Finally, convergence is the ultimate metric that is confirmed. Previously, the algorithm determines whether the accuracy or precise measurement improves over time for true RUL path convergence [13]. The idea of convergence metric is to calculate the center of mass or area of an M which defines as predicted RUL curve. The perfect score for convergence performance metrics is when convergence (CM) tends to zero.

$$CM = \sqrt{(x_c - t_p)^2 + {y_c}^2} \tag{7}$$

$$x_c = \frac{\frac{1}{2}\sum_{t=P}^{EOP}({t_{i+1}}^2 - {t_i}^2)\, M(i)}{\sum_{t=P}^{EOP}(t_{i+1} - t_i)\, M(i)} \tag{8}$$

$$y_c = \frac{\frac{1}{2}\sum_{t=P}^{EOP}(t_{i+1} - t_i)\, M(i)^2}{\sum_{t=P}^{EOP}(t_{i+1} - t_i)\, M(i)} \tag{9}$$

Where (x_c, y_c) is center of area of prediction error accuracy curve *M(i)*, *EOP* is end of prediction and *P* is prediction time.

4. Results and discussion

The predicted maintenance approach is implemented on a filter installed at one of Tallinn's sites. According to the scheduled preventive maintenance plan, the interval for replacing the fresh air filter was 7 months. With new data from this field, the RUL forecast is updated based on new measurements collected from the HVAC unit. Sufficient additional time must be taken to ensure the availability of spare parts and of personnel to operate the replacement as well as to prepare a suitable schedule plan. The results of the application of the proposed algorithm are shown from Figure 4 to Figure 6. The number of months in figures is counted starting from the first prediction date, 10th July 2019. The measured data includes seven data sets due to seven months' data set that contain a combination of the most important features. The selected features were about seven features (mean, skewness, peak2peak, RMS, shape factor, energy and band power), so each of these points is a set of clusters. In fact, there is a 49-dimensional data space that includes seven sets of seven most important features. As mentioned earlier, the main constituent component, PCA_1, is the most important component and is selected as an indicator of health. Bottom plot in Figure 4 shows the results of principal component analysis, which indicates the virtual conversion from multi-dimensional to two-dimensional graph. Each point represents a data set (7 sets) based on the selected important features. From this graph it can be seen that the HVAC filter data of sixth and seventh months is strictly separated from other data sets. So it is quite characteristic that the filter goes to its threshold. The plot indicates that the first principal component is increasing as the machine approaches to failure. Therefore, the first principal component (PCA_1) is a promising candidate for health indicator. In other words, PCA_1 shows that the most important features of filter clogging index approaches the defined critical pressure drop value. The critical pressure drop value is already found in BMS, and is usually calculated based on filter type, manufacturer's data sheet, and etc.

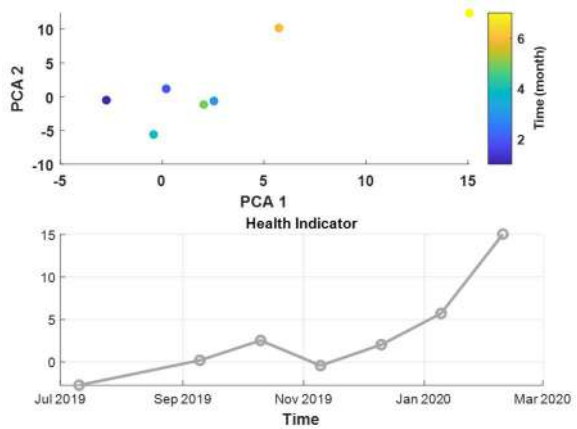

Fig. 4 - The process of filter destruction (up), and Filter health indicator (down)

The health indicator for the monitored filter is shown in Figure 4. If smoothing is needed, the moving average and low pass filter can be used. Possibly using filter can make lag or delay on the signals. The calculated threshold is 30 and it can be seen that the health indicator is still below the threshold. This demonstrates that the preventive schedule to be used in this situation will lead to premature replacement of the filter. In fact, the health indicator clearly shows that the load on the filter pressure drop level is close to the maximum after 7 months. Once the health status of the filter is evaluated, the RUL can be estimated based on the exponential degradation model. Exponential degradation model is fit to the considered health indicator and the model is able to predict the RUL. First, the degradation model (2) is trained to estimate the rate of the pressure drop, so as to minimize the error between the output of the degradation model and the observations collected from the filter. The best degradation model over time related to the health indicator is shown in Figure 5. It should be noted that the hybrid model actually reflects the exponential growth of the health indicator. Using the described method in this article, the RUL shown in upper plot of Figure 5 can be calculated. For each simulation, RUL can be easily predicted and obtained as the difference between end of life and the prediction time. Figure 5 (down) shows the probability density function (PDF) of the predicted results. When the data is updated every month, the PDF will decrease. The confidence interval represents the maximum probability of failure. There will be a lot of variation at the beginning of the prediction, but the more months of training, the more PDFs is obtained. This is advantage since in similarity models, most similar curves are close at the beginning, but when they are close to the breakdown state (threshold), they split and create approximately two states in the RUL distribution. The final RUL estimation is 0.8787 month or 26 days, when the actual life for filter based on measured data was 0.9861 or 29 days.

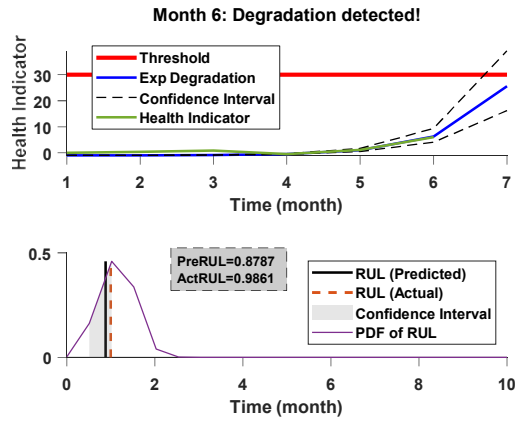

Fig. 5 - Model fitting for degradation model parameters estimation (up); and the probability value of prediction accuracy and final predicted RUL (down)

In order to evaluate the accuracy of the predictions, the prognostic horizon, relative accuracy, alpha-metric and conversion performance analysis has been applied. The alpha performance compares the actual RUL against the predicted RUL, which in Figure 6 (bottom) are indicated as actual RUL and predicted RUL, respectively. For the case illustrated in the figure, considering the slow dynamics of the pressure drop process, the value of alpha has been set to 25%.

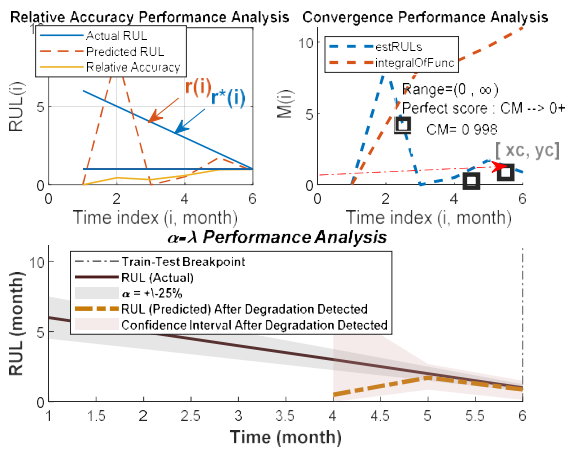

Fig. 6 – Top left: relative accuracy of final prediction, top right: convergence metric of prediction performance, bottom, the α-λ Accuracy metric determines whether predictions are within the cone of desired accuracy levels at a given time instant (t_λ).

It can be seen that after the degradation is detected, the predicted RUL is placed in the safe prediction cone, and the prediction is correct. This means that the relative accuracy of the proposed PHM algorithm (Figure 6, top left) is 100% within the desired prediction range. The convergence metrics is shown in Figure 6 (top right) indicates that the center of mass is shrinking to zero, but due to the type of data, the health indicator rises again over a period of time. As a result, the center of mass is a bit far from ideal, but tended to zero as the prediction continues. Finally, it should be noted that the use of predictive

maintenance strategies in this situation has increased the life of filters in buildings by more than 90% compared to replacement time schedule.

5. Conclusions

This article describes the use of maintenance predictive strategies to improve the maintenance of air filters in HVAC systems. First, the appropriate health index is calculated based on the pressure difference measured on the filter. The health indicator can evaluate the actual condition of the filter based on the increase in clogging and pressure drop. Subsequently, a hybrid prognostics method was developed to predict the failure time (time to replace) of the filter on the AHU. The hybrid prediction strategy relies on a physics-based degradation model that uses real data collected from the field. The physics-based model quantitatively describes the degradation process that affects the air filter. The optimization plan is used to determine the parameters of the degradation model, which best matches the observation data in the field. The RUL is then estimated using dimensional reduction approach. This allows to speed up the implementation of algorithms, to help overcome overfitting, and to improves visualization. Finally, the results of performance analysis also show that predictive maintenance methods can provide accurate and accurate prognostic signs.

Future work can be the implementation to all AHUs with the aim of extending the proposed approach as well as different types of inventory and examining the application of health indicators in different situations. Next step is to applying other degradation models. The reason for using other degradation models is that, at least during the Covid crisis period, we realized that the degradation process is not exponential or even linear. However, in practical applications, there are other extras, such as decision time and retention time, which are not usually considered in article prediction calculations.

6. Acknowledgement

This work has been partially conducted in the project "ICT programme" which was supported by the European Union through the European Social Fund. It was also supported by the Estonian Research Council grant PRG658.

7. References

[1] R. Ghimire, K. R. Pattipati and P. B. Luh, "Fault diagnosis and augmented reality-based troubleshooting of HVAC systems," in 2016 Ieee Autotestcon, 2016.

[2] Z. Kang, C. Catal and B. Tekinerdogan, "Remaining useful life (Rul) prediction of equipment in production lines using artificial neural networks," Sensors, vol. 21, p. 932, 2021.

[3] J. Coble and J. W. Hines, "Applying the general path model to estimation of remaining useful life," International Journal of Prognostics and Health Management, vol. 2, p. 71–82, 2011.

[4] Y. Zheng, "Predicting remaining useful life based on Hilbert–Huang entropy with degradation model," Journal of Electrical and Computer Engineering, vol. 2019, 2019.

[5] J. R. Celaya, A. Saxena and K. Goebel, "Uncertainty representation and interpretation in model-based prognostics algorithms based on kalman filter estimation," 2012.

[6] Z. Skaf, O. F. Eker and I. K. Jennions, "A simple state-based prognostic model for filter clogging," Procedia CIRP, vol. 38, p. 177–182, 2015.

[7] V. Atamuradov, K. Medjaher, P. Dersin, B. Lamoureux and N. Zerhouni, "Prognostics and health management for maintenance practitioners-review, implementation and tools evaluation," International Journal of Prognostics and Health Management, vol. 8, p. 1–31, 2017.

[8] W. Zhang, D. Yang and H. Wang, "Data-driven methods for predictive maintenance of industrial equipment: a survey," IEEE Systems Journal, vol. 13, p. 2213–2227, 2019.

[9] L. Liao and F. Köttig, "Review of hybrid prognostics approaches for remaining useful life prediction of engineered systems, and an application to battery life prediction," IEEE Transactions on Reliability, vol. 63, p. 191–207, 2014.

[10] Q. Qin, S. Zhao, S. Chen, D. Huang, and J. Liang, "Adaptive and robust prediction for the remaining useful life of electrolytic capacitors," Microelectron. Reliab., vol. 87, 2018.

[11] N. Gebraeel, "Sensory-updated residual life distributions for components with exponential degradation patterns," IEEE Transactions on Automation Science and Engineering, vol. 3, p. 382–393, 2006.

[12] A. Saxena, J. Celaya, E. Balaban, K. Goebel, B. Saha, S. Saha and M. Schwabacher, "Metrics for evaluating performance of prognostic techniques," in 2008 international conference on prognostics and health management, 2008.

[13] G. Vachtsevanos and P. Wang, "Fault prognosis using dynamic wavelet neural networks," in 2001 IEEE Autotestcon Proceedings. IEEE Systems Readiness Technology Conference. (Cat. No. 01CH37237), 2001.

Energy consumption characteristics based on monitored data: a school case study

Kristina Vassiljeva [ac], Margarita Matson [bc], Eduard Petlenkov [ac], Juri Belikov [bc], Matrin Thalfeldt [dc], Jarek Kurnitski [dc]

[a] Department of Computer Systems, Tallinn University of Technology, Tallinn, Estonia, {kristina.vassiljeva, eduard.petlenkov}@taltech.ee.

[b] Department of Software Science, Tallinn University of Technology, Tallinn, Estonia, {margarita.matson, juri.belikov}@taltech.ee.

[c] Smart City Centre of Excellence (Finest Twins).

[d] Department of Civil Engineering and Architecture, Tallinn University of Technology, Tallinn, Estonia, {martin.thalfeldt, jarek.kurnitski}@taltech.ee.

Abstract. This study is an initial step for a creation of smart platform for schools in Estonia which will model, analyze, and evaluate the real energy performance of school buildings. Energy meters provide electricity consumption data which can be used to understand energy usage patterns and finally improve building energy management. First, data preparation is made. On the following step hierarchical clustering is applied to identify the outliers of weekly electricity load profiles. Finally, daily electrical load patters are clustered and similar profiles are grouped using K-means centroids.

Keywords. Electricity consumption, school building, occupants' behavior, COVID, energy efficiency analysis, profiling.
DOI: https://doi.org/10.34641/clima.2022.274

1. Introduction

The building sector is crucial for achieving the EU's energy and environmental goals. In general, buildings are responsible for approximately 40% of final energy consumption [1]. The first step towards sustainable transformations is understanding of the underlying factors influencing energy demand. Beside formal information above mentioned documents do not provide information how to support a sustainable change in the end-user behavior. Influence of occupants' behavior on energy consumption is getting more and more significant as the overall energy demand of the new or renovated buildings is substantially decreasing [2]. Development of the smart technologies and metering devices together with a concept of Industry 4.0 has opened new perspectives in monitoring occupants' behavior. Obtained data can be used for different purposes such as end-user behavioral modelling, fine tuning of certain values or load forecasting. Moreover, clear understanding of energy consumption is the key for timely decisions to reduce energy consumption. In addition, improvement of energy efficiency of public buildings promotes significance of culture of energy efficiency to the local society [3], [4].

Several studies related to energy consumption and efficiency of school buildings have been conducted [5]–[7]. Advanced metering infrastructure measures and collects electricity consumption data. Readings help to understand the characteristics of energy use behaviors and potentially prevent energy waste. Energy consumption of the buildings can be influenced by the various parameters: building characteristics, energy use profile and occupants' behavior. Energy use includes space heating/cooling, lighting, ventilation and plug loads. Occupants' behavior consists of turning off the lights, air conditioners and other equipment then not in use.

The aim of this work is to find out what is the occupants' behavior and what are the consumption profiles of air handling units. This is preliminary step for creation of a smart platform for schools which further will automatically classify current consumption and forecast it based on already known. The difficulties for the automation of the profiles clustering based on available data caused by the fact that non-classical behavior during so-called COVID-19 periods should be considered. Pattern differences are caused by the fact that legislation for handling ventilation units has been changed. Secondly, occupation of the schools during those times is changing drastically [8], [9].

Copyright ©2022 by the authors. This conference paper is published under a CC-BY-4.0 license.

2. Methodology and data

2.1 The case study building

Metered data was retrieved from one of the schools in Tartu, Estonia, which renovation have been finished by August 2020.

2.2 Data preparation

The data is gathered from the following measurement points: kitchen, air-conditioning and main meter. The school facility management collects energy data with hourly resolution. Non-air-conditioning loads (plugs and lighting) were found by subtracting sum of all HVAC systems from the readings of main meter.

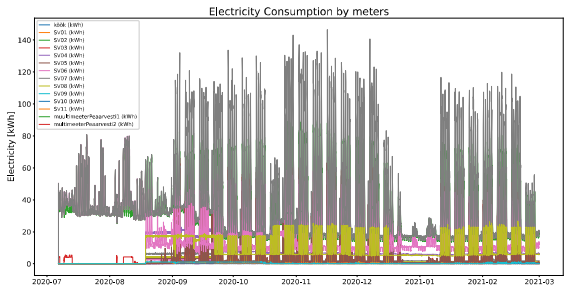

Fig. 1 - General consumption of the school: air-conditioning plus plugs and lighting consumptions

First, electricity meter data was transformed into the electricity consumption time series, shown in Fig. 1. Additional data engineering and analysis are needed, since smart meter data from buildings can be very noisy with gaps of missing values and typically contains outliers. In general case, where a lot of different objects are studied, obtained values should be normalized since we mostly interested in capturing of temporal variation rather than absolute values of magnitudes [10]. Here we are focused on a single building and therefore normalization step can be skipped.

We reshape raw time series to be used by data segmentation. To identify Typical Electricity Load Patterns (TELPs) available data was segmented using weekly cycles. Tracking changes in energy performance by week may help to understand is there some specifics in days-of-the-week and how does the electricity usage behavior differ during weekends [11].

Consumption calculated from the readings of the "Main meter" is shown in Fig. 2. Consequent weeks have close colors, after one-year colors repeat. Such an approach gives possibility to see common patterns of the subsequent weeks and observe if behavior repeats at the same week in the next year. Additionally, this helps during validation stage when clusters found with machine learning techniques are approved. Fig. 2 shows that several behavioral patterns can be extracted from the obtained results.

For better understanding of the energy use and its correlation with occupants' behavior, the following analysis is made separately for air-conditioning and non-air-conditioning units.

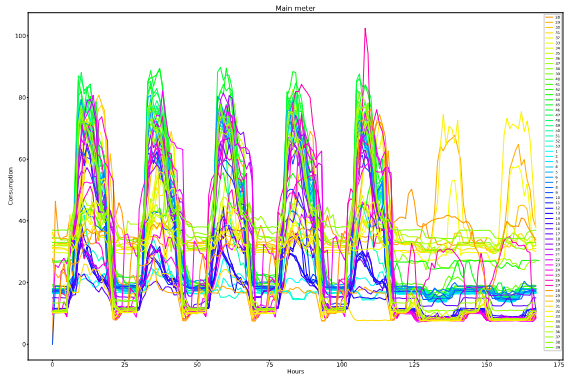

Fig. 2 - Main meter with weekly segmentation

2.3 Extraction of typical electricity patterns

To find typical electricity patterns hierarchical clustering was applied. Namely, Agglomerative Clustering with bottom-up approach, where separate clusters are merge using the minimization of the maximum distance between all observations of pairs of clusters with Euclidian metrics.

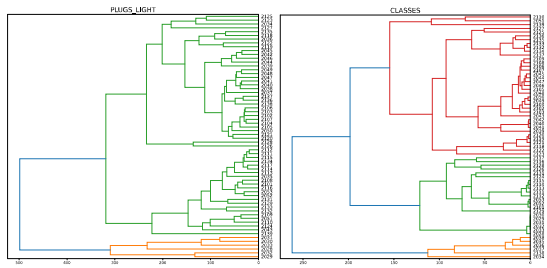

Fig. 3 - Dendrograms, where numbers on the right site represent 'yyww': week ('w') of a year ('y'). Left plot shows all plugs and lighting consumption at school. Right plot represents ventilation units of all classes

Fig. 3 illustrates that in every case weeks 28-33 from the year 2020 are separated to independent cluster and considered as outliers: baseline of those signals is higher than others. Additionally, there is a high consumption at the weekends (see Fig. 2 yellow and orange lines after 125 hours). On the other hand, lines of the same color which represent exactly the same time period from the next year, have different pattern. This is caused by the fact that data obtained during first six weeks should be removed from further analysis since ventilation worked in a test or special mode caused by the completion of repair works and school preparation for a new academic year.

On the next step Nearest Centroid or K-Means Clustering proposes centroids for each group of clusters and typical representatives of behavioral patterns are found (see Fig. 4). First, it is seen that there is no difference in ventilation behavior during

the working days. It is working according to the schedule and does not depend on the occupancy of the room, in other words, ventilation is not controlled by CO_2 level measurements.

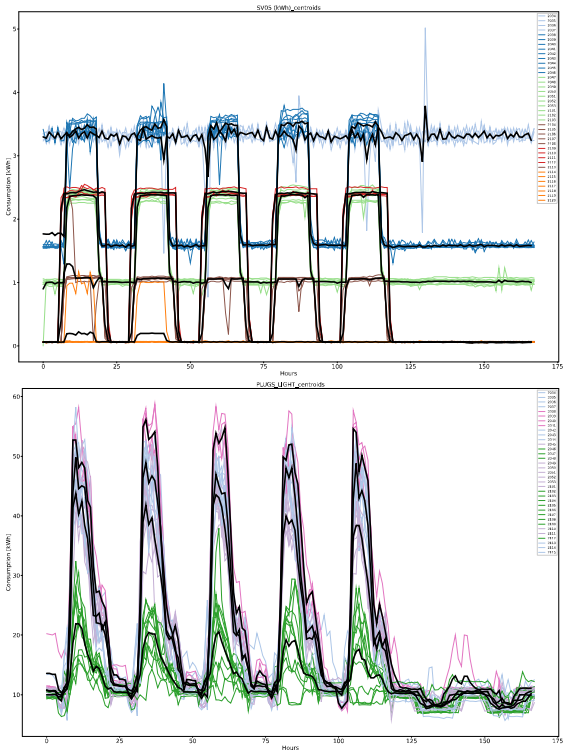

Fig. 4 - Weekly Clustering of a) a typical ventilation unit on example of "Teachers' room" and b) "Plugs and Lighting" for the whole period

Moreover, through the year behavior of the system has changed a lot. Some patterns were valid for a longer period, others – not. Additionally, it is set that clusters having less than three weeks are not taken into account. In general, clustering procedure should be automated, thus other additional parameters and conditions should be considered.

First, unlike other (for example office) buildings on business days schools may have vacations. At those times some patterns are close to non-working days, but since school workers are visiting buildings, have meetings, consultations with some students, etc. those patterns make separate class. Occupancy of the building is lower, that should as well decrease the consumption and ventilation loads.

All above mentioned leads to the conclusion that Daily Electricity Load Patterns (DELPs) can be studied. Initially data was split into three periods: business days, business days on vacations and weekends with holidays. Unfortunately, behavioral patterns during business days differ too much and automatic clustering procedure cannot guarantee satisfying result. Thus, it was suggested to split working days into two categories: normal working days then school has original occupational load and so-called COVID period, where occupation can vary from fully closed, occupied by some personnel, elementary school and graduation students. In addition, other legislation procedures were applied to control of ventilation units (working hours and loads). This explains why there are several base lines for electricity consumption.

Finally, four different time periods were studied for clustering: normal working days (see Fig. 5, Fig. 9), vacations working days (see Fig. 6 and Fig. 10), weekends plus holidays (Fig. 7 and Fig. 11) and COVID-19 working days (Fig. 7 and Fig. 12).

3. Results

Once profiles are set the following analysis was made. At the beginning of a school year rooms are ventilated with high constant air flow ("light blue line" in Fig. 5).

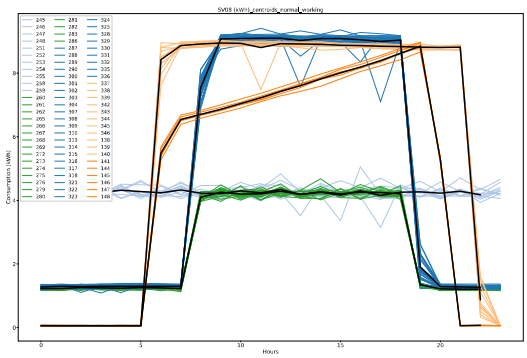

Fig. 5 - DELPs of ventilation unit for A-building Westside classes in normal working conditions

After that scheduled technique is applied: all air units are starting from 7.00 and reaching its highest load by 8.00. At 18.00 ventilation is turned off and reaches its base line after one hour. In some classes after beginning of the heating season high load was increased (see "green and blue lines" in Fig. 5). Rise of the top load mostly depends on the fact if this part of the building belongs to "sunny side" or not.

At the beginning of December 2020 COVID situation in Estonia became worser, thus ventilation schedule was changed from 5.00 till 21.00. In second part of May 2021 when all students returned to schools, gradual increase of the ventilation load was applied. Such an approach was used only in this part of the building and, most probably, caused by the fact that it belongs to the "sunny side" where through the day temperature increases drastically.

During weekends common situation can be described as: preparation for a new academic year, low season base line, high season base line.

In general, ventilation levels are set to minimal during the vacations, but during hot summer of 2021 it was working on high load from 5.00-20.00 (Fig. 6).

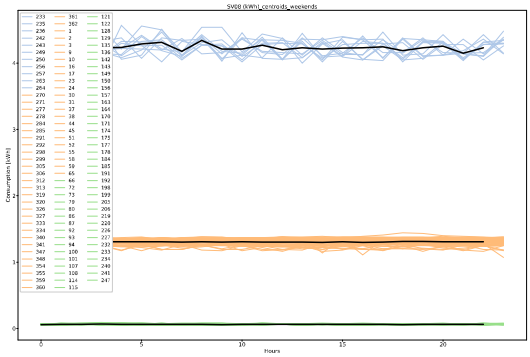

Fig. 6 - DELPs of ventilation unit for A-building Westside classes on weekends and holidays

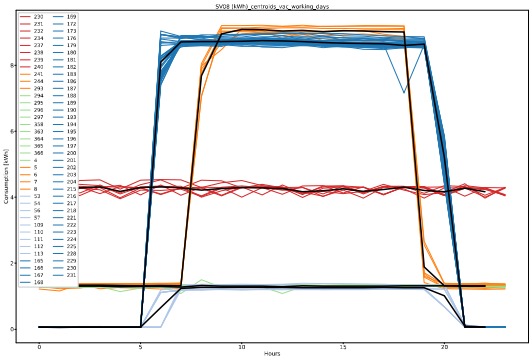

Fig. 7 - DELPs of ventilation unit for A-building Westside classes during vacations (working days only).

On 14.12.2020 schools were closed for all students; thus, ventilation was switched back for shorter working hours ("light blue line" Fig. 8). Then only elementary school studied, or building was closed, ventilation worked at minimum level. When graduation classes returned, ventilation worked with maximum load 5.00-21.00.

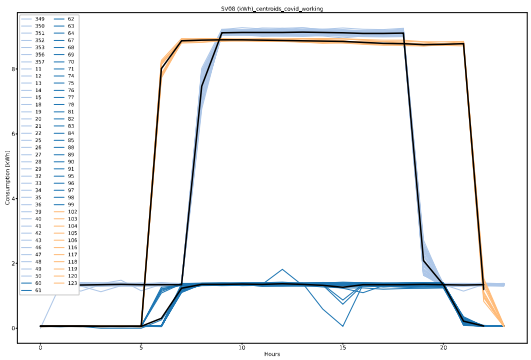

Fig. 8 - DELPs of ventilation unit for A-building Westside classes under COVID-19 working conditions

Plug and Lighting consumption strictly corresponds to the occupancy of the school and daylight period. This can be seen from most of the figures: during high season outside lighting works for a longer period and then electricity consumption drops to a lower level. This can be explicitly seen during weekends and holidays in Fig. 11. During normal working days level drops near by 5 o'clock in the morning before people come to school and after that plugs loads drastically rise. It can be observed in Fig. 9.

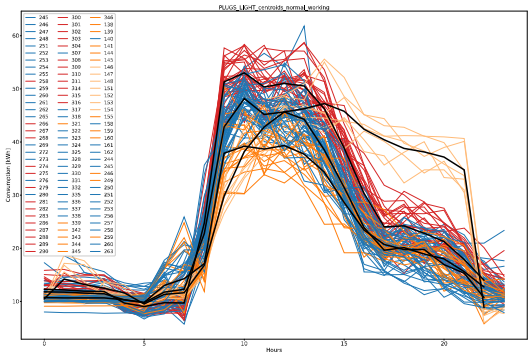

Fig. 9 - DELPs of Plugs and Lighting in normal working conditions

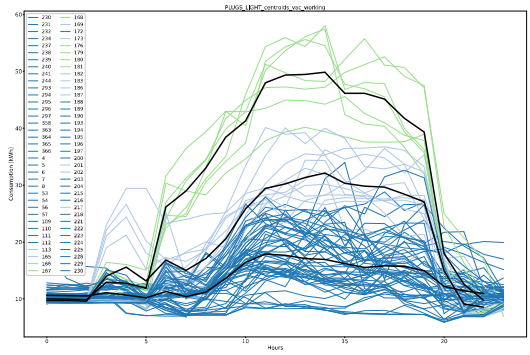

Fig. 10 - DELPs of Plugs and Lighting during vacations (working days)

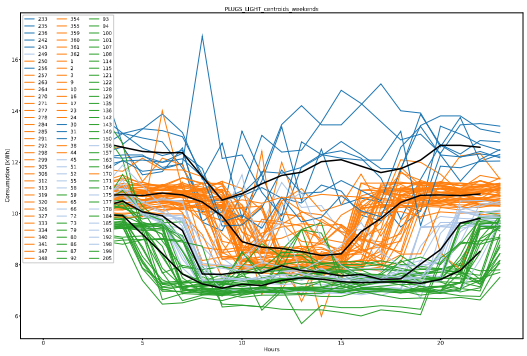

Fig. 11 - DELPs of Plugs and Lighting weekends and holidays

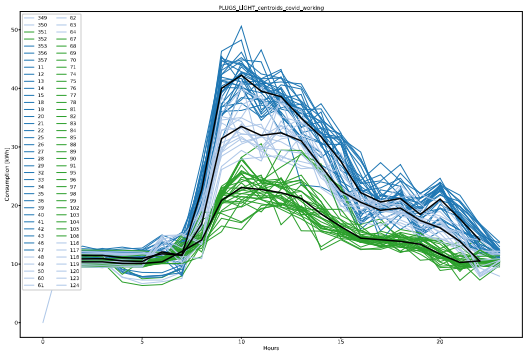

Fig. 12 - DELPs of Plugs and Lighting under COVID-19 working conditions

Occupancy of the building during COVID period can be derived from patterns presented in Fig. 12. By comparing with Fig. *9* one can observe a significant decrease of occupancy level of the building during this period.

Another point that should be mentioned, starting from 02.04.20 (with amendments on 29.11.20) ventilation with normal occupancy of the building must be turned on full power 2 hours before occupational hours and turned off 2 hours after those (if occupancy is less than 50%, then with the above-mentioned timing ventilation load allowed to be 50% of full power).

In Fig. 13 Plug and lighting profiles, which are presented by red lines, are overlaid on ventilation profiles. Assuming that plug loads to some extend represent occupancy of the building, it can be observed from timing comparison that sometimes air handling units' schedules were not set according to the new standards.

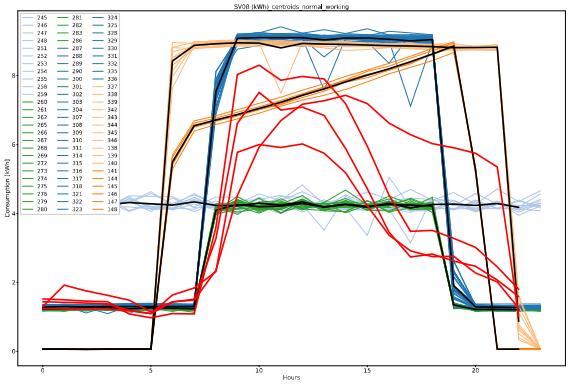

Fig. 13 – Plug and Lighting profiles correspondence to ventilation schedules in normal working period

4. Conclusions

Initial step for creation of smart platform for schools has been made. Automatic finding DELPs at schools differs from other buildings profiles. Instead of business days and weekends for high and low seasons, school vacations should be considered as well. Additionally, COVID-19 brought variety of settings for air handling units' schedules. The effectiveness was demonstrated by comparison of found clusters and timing of events happened in Estonia.

5. Acknowledgement

This work has been supported by the Estonian Ministry of Education and Research and European Regional Fund (grant 2014-2020.4.01.20-0289) and partially supported by the Estonian Research Council grants no. PRG1463, PRG658 and PSG409.

6. References

[1] The European Parliament and of The Council of the European Union, "Directive (EU) 2018/844 of the European Parliament and of the Council of 30 May 2018 amending Directive 2010/31/EU on the energy performance of buildings and Directive 2012/27/EU on energy efficiency (Text with EEA relevance)," Jun. 19, 2018. http://data.europa.eu/eli/dir/2018/844/oj (accessed Jan. 12, 2022).

[2] N. Kampelis *et al.*, "Evaluation of the performance gap in industrial, residential & tertiary near-Zero energy buildings," *Energy and Buildings*, vol. 148, pp. 58–73, Aug. 2017, doi: 10.1016/J.ENBUILD.2017.03.057.

[3] Y. Zhao, C. Zhang, Y. Zhang, Z. Wang, and J. Li, "A review of data mining technologies in building energy systems: Load prediction, pattern identification, fault detection and diagnosis," *Energy and Built Environment*, vol. 1, no. 2, pp. 149–164, Apr. 2020, doi: 10.1016/j.enbenv.2019.11.003.

[4] B. Yildiz, J. I. Bilbao, J. Dore, and A. B. Sproul, "Recent advances in the analysis of residential electricity consumption and applications of smart meter data," *Applied Energy*, vol. 208, pp. 402–427, Dec. 2017, doi: 10.1016/J.APENERGY.2017.10.014.

[5] B. Simanic, B. Nordquist, H. Bagge, and D. Johansson, "Predicted and measured user-related energy usage in newly built low-energy schools in Sweden," *Journal of Building Engineering*, vol. 29, p. 101142, May 2020, doi: 10.1016/J.JOBE.2019.101142.

[6] Y. Ding, H. Brattebø, and N. Nord, "A systematic approach for data analysis and prediction methods for annual energy profiles: An example for school buildings in Norway," *Energy and Buildings*, vol. 247, Sep. 2021, doi: 10.1016/j.enbuild.2021.111160.

[7] M. M. Ouf and M. H. Issa, "Energy consumption analysis of school buildings in Manitoba, Canada," *International Journal of Sustainable Built Environment*, vol. 6, no. 2, pp. 359–371, Dec. 2017, doi: 10.1016/J.IJSBE.2017.05.003.

[8] M. Chihib, E. Salmerón-Manzano, M. Chourak, A. J. Perea-Moreno, and F. Manzano-Agugliaro, "Impact of the COVID-19 pandemic on the energy use at the university of almeria (Spain)," *Sustainability (Switzerland)*, vol. 13, no. 11, Jun. 2021, doi: 10.3390/SU13115843.

[9] X. Gui, Z. Gou, F. Zhang, and R. Yu, "The impact of COVID-19 on higher education building energy use and implications for future education building energy studies," *Energy and Buildings*, vol. 251, p. 111346, Nov. 2021, doi: 10.1016/J.ENBUILD.2021.111346.

[10] X. Liu, Y. Ding, H. Tang, and F. Xiao, "A data mining-based framework for the identification of daily electricity usage patterns and anomaly detection in building electricity consumption data," *Energy and Buildings*, vol. 231, p. 110601, Jan. 2021, doi: 10.1016/J.ENBUILD.2020.110601.

[11] C. Fan, F. Xiao, Z. Li, and J. Wang, "Unsupervised data analytics in mining big building operational data for energy efficiency enhancement: A review," *Energy and Buildings*, vol. 159, pp. 296–308, Jan. 2018, doi: 10.1016/j.enbuild.2017.11.008.

domOS: an "Operating System" for Smart Buildings

Junior Dongo[a], Dominique Gabioud[b], Amir Laadhar[a], Martin Meyer[b], Brian Nielsen[a], Frédéric Revaz[b], Christian Thomsen[a]

[a] Department of Computer Science, Aalborg University, Aalborg, Denmark. {juniord, amirl, bnielsen, chr}@cs.aau.dk

[b] Institute of Sustainable Energy, School of Engineering, University of Applied Sciences Western Switzerland Valais, Sion, Switzerland. {dominique.gabioud, martin.meyer, frederic.revaz}@hevs.ch

Abstract. Smart energy services deployed in buildings have the potential to increase their energy efficiency and to turn them into active nodes of energy grids, with limited costs and in the short term. Today, smart services are deployed by manufacturers of energy appliances as independent silo solutions. The lack of a common approach prevents the deployment of unified multi-appliance, multi-service solutions.

This paper presents the domOS ecosystem specification, a guideline for a unified organisation of energy services where multiple applications can access multiple on-line appliances and devices, if permitted. The specification leverages legacy IoT technologies and can be implemented with a limited effort on any existing IoT platform. A compliant IoT platform acts as an "operating system" for the building, effectively decoupling the application plane and the building infrastructure plane.

The domOS ecosystem specification builds upon the Web of Things (WoT) architecture defined by W3C. Compliant buildings feature a digital nameplate called Building Description (BD). The BD is a document readable by machines and humans that contains relevant metadata (e.g., construction type, size, energy system…) and provides handles to monitor and control local energy processes. The domOS ecosystem specification leads to a unified and standardised approach of energy services in buildings.

Keywords. smart building, IoT, ontologies, WoT, interoperability.

DOI: https://doi.org/10.34641/clima.2022.437

1. Introduction

Over the last two decades, digitalisation has penetrated almost all activity domains. The digitalisation in buildings can be assessed as late compared to other sectors. Buildings, and more specifically energy appliances in buildings, have a life duration of several decades. Hence, many date from the pre-digital era. Admittedly, recently installed appliances – from coffee machines to heat pumps – feature a digital interface and can be monitored and controlled remotely. However, each appliance features its own solution, which is generally proprietary and closed. Hence, the user experience is not optimal (users must cope with several apps, each one with its access control and presentation logic), and the deployment of multi-appliance solutions is complicated – if possible at all.

To overcome these limitations, the domOS project [1] designs and prototypes a mediating platform ("Platform") enabling:

- the integration of all connectible in-building appliances and devices ("Things"), and
- the deployment of applications for monitoring, visualisation, optimisation, or control ("Applications") to access any in-building infrastructure, if permitted by the owner.

In a computer, the operating system provides the hosted applications with an abstraction layer for the peripheral devices. The Platform offers a similar function for buildings.

The rest of this paper is organised as follows: In Section 2, the background context for energy and IoT is presented. Section 3 summarises the functional and non-functional requirements for the domOS ecosystem. Section 4 presents an overview of the WoT architecture, a main component of the domOS ecosystem. The ecosystem specification is detailed in Section 5. Section 6 illustrates the ecosystem with an example. Section 7 concludes the paper with an outline of future work.

Copyright ©2022 by the authors. This conference paper is published under a CC-BY-4.0 license.

2. Background

2.1 Energy and buildings

To limit global warming, countries have set ambitious objectives for the reduction of greenhouse gas emissions. Reaching these goals requires a radical transformation of the energy sector. Buildings, which are responsible for 40% of the total energy consumption, can make their contribution to the energy transition in two complementary ways: firstly, the energy infrastructure of the building can be upgraded (better isolated envelope, renewable energy prodution, CO2-free heat and cold generation…), and secondly smart services can optimize the operation of the existing energy infrastructure. The second approach requires less investment and can be deployed in the short term.

Research projects have shown that smart services can bring significant contributions to achieve more efficiency and more flexibility. A few examples are listed below:

- Closed-loop control of the heat system can lead to 8%-18% average energy savings [2].
- Providing feedback to consumers on their own energy consumption leads to reduction of the final energy consumption in the range from 5% to 10% [3].
- The available flexibility of space heating, domestic hot water preparation and electrical vehicle charging can be used to turn buildings into active nodes of the grids they are connected to [4] [5].

As of today, a wide cluster of smart services are available [6]. The two most common implementation patterns are:

- frameworks operated by appliance manufacturers, with a scope limited to the concerned appliances, and
- single-service frameworks (e.g., demand-response [7]).

It is not uncommon to find buildings equipped with multiple parallel and independent frameworks. However, the energy issue in buildings is essentially one, as illustrated by the following example: an Energy Management System (EMS) must orchestrate the heat pump, the electrical vehicle charging station, based on local production by the photovoltaic inverter and on the grid status.

The vision is to equip buildings with a mediating Platform, on which all Things are connected. Then a cluster of services ("Services") could arise from the interplay of Applications and Things, as illustrated in Fig. 1.

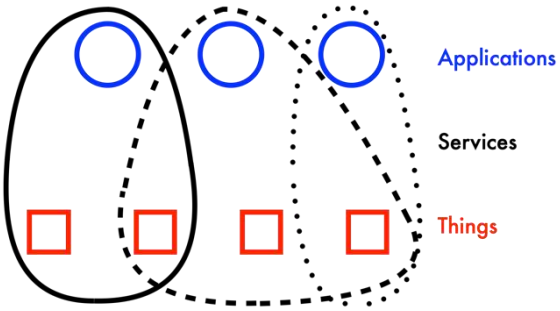

Fig. 1 - Things, Applications, and services

2.2 IoT and semantics

Today's IoT technologies allow to connect Things with investment and operation costs tending towards zero. New Things feature a communication interface, but each of them has its own IoT solution (Fig. 2 (a)). A unified solution (Fig. 2 (b)) is necessary to address the energy requirements.

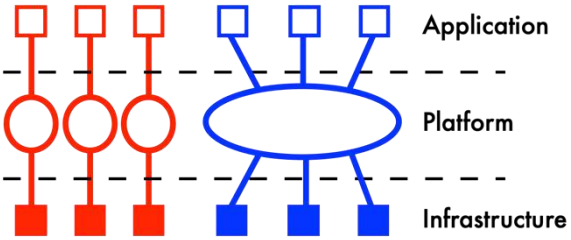

Fig. 2 - IoT in buildings: (a) current silo organisation, and (b) target unified organisation

Platforms take over auxiliary functions like provisioning, security management, privacy management, and supervision and can also work as proxies for Things. Platform functions can be implemented in a dedicated component hosted in the cloud or at the edge in a building gateway.

From a networking perspective, Things feature three layers:

- **Protocols ("*Language*")**: The platform and the Things must share a common set of protocols, including security mechanisms.
- **Interaction model ("*Verbs*")**: The set of operations that can be remotely triggered on a Thing forms its interaction model.
- **Semantic annotations ("*Nouns*")**: Semantics refers to the assignment of meaning (e.g., "instantaneous electrical power") to addressable entities within a Thing (e.g., "MQTT topic "@update/a3b61480/el_power").

It should be noted that the above description does not deal with semantics in general, but rather with semantics within Things.

In a unified organisation, Things must share:

- a set of protocols with their Platforms, and
- an interaction model and semantic annotations with Applications interacting with them.

One of the main challenges in the IoT landscape is achieving semantic interoperability between Things and Applications. To this end, standardised vocabularies have been defined by associations of manufacturers [8], by professional associations [9], by academics [10], and by legacy standardisation bodies [11]. They can take different forms: assignment of meanings to register numbers or message topics, or UML class diagrams

3. Requirements

We want to elaborate a specification called "domOS ecosystem specification" allowing the interplay of multiple Things and multiple Applications, according to a unified organisation as illustrated on Fig. 2.

3.1 Functional requirements

We assume the following situation:

- Things of different types (e.g., "heat pump") are deployed in buildings. There can be many Thing models (e.g., from different manufacturers) for a given Thing type.
- A cluster of generic (i.e., not building-specific) Applications is available.

The objective is to automate the deployment of Services on buildings featuring the required infrastructure.

Realising the objective requires that:

1. Applications can access building metadata, to learn relevant information regarding the building and to check whether the in-building topology is appropriate.
2. Applications can find addresses to access monitoring and control points in Things. An address includes all relevant parameters required to access an element within a Thing.
3. Applications can interact with Things, in a model-independent way, by making use of the interaction model and of addresses.

3.2 Non-functional requirements

It should be possible to integrate Things in their current state. Neither firmware upgrades nor adaptation gateways should be required.

The domOS ecosystem specification should leverage legacy IoT tools and processes. The technological threshold to implement the specification must be kept low, so that implementation requests a limited effort.

4. Introduction to the WoT Architecture

The W3C's Web of Things (WoT) architecture [12] is a key component of the domOS ecosystem specification. It is briefly introduced in this section.

4.1Model

In WoT, Consumers are software components interacting with Things (Fig. 3). To cope with the heterogeneity, each Thing must feature a formal description document called a Thing Description (TD) [13].

Fig. 3 - WoT Model [12].

4.2 The WoT interaction model

WoT introduces a simple interaction abstraction based on properties, events, and actions. This interaction model is generic enough to be applicable to all Things.

If permitted, Applications working as Consumers can (see Fig. 4):

- read or write properties, possibly also observe them and receive updates,
- subscribe to events and get notified of occurrences, and
- request the execution of actions.

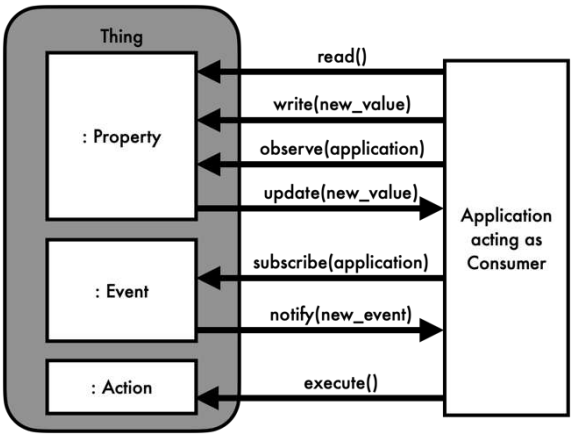

Fig. 4 - The WoT interaction model.

A unitary operation on a property, an event or an action is named an "interaction affordance".

4.3 Protocol bindings

In a real Thing, an interaction affordance is performed through the exchange of messages compliant with Things specific protocols.

A TD contains so-called protocol bindings describing how abstract interaction affordances are mapped to concrete protocol-level messages.

4.4 The WoT scripting API

Through the WoT scripting API, a Consumer can handle interaction affordances (i.e., operations on properties, events, and actions) independently of protocol bindings.

The structure of a WoT compliant system is presented on Fig. 5:

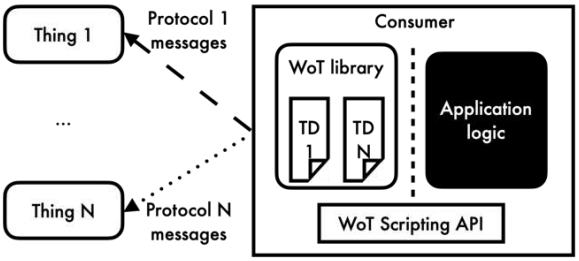

Fig. 5 - Structure of a WoT compliant system.

The WoT scripting API is implemented by WoT libraries [14].

The WoT architecture has been implemented in the Arrowhead IoT framework, which is used in two domOS demonstration sites [15].

5. The domOS Ecosystem Specification

The domOS ecosystem specification is made up of the four key components introduced in this section: the Thing Descriptions (TDs), the Building Description (BD), the domOS Common Ontology (dCO) and the Platform.

5.1 Thing Descriptions (TDs)

Energy appliances like photovoltaic inverters, electrical vehicle charging stations, heat pumps, meters and other monitoring devices are considered as Things.

TDs are elaborated by customising Thing-type specific documents that could be made available by manufacturers or by a user community.

5.2 Building Descriptions (BDs)

The Building Description (BD) is a machine and human-readable document containing a description of the building as an energy system. It contains for instance the following metadata (Fig. 6):

- energy flows within the building and between the building and the grids it is connected to,
- processes to consume, generate or transform energy including description of the corresponding appliances and monitoring devices, and
- links to interaction affordances in Things, to enable real-time monitoring and control.

The domOS ecosystem specification contains schemas for BDs. The semantics in BDs is provided by the dCO.

The BD is stored in a semantic knowledge base. By querying the BD, an Application can:

- determine if the building energy infrastructure is appropriate for its operation,
- understand the building's energy organisation, and
- associate meaning to interaction affordances in Things.

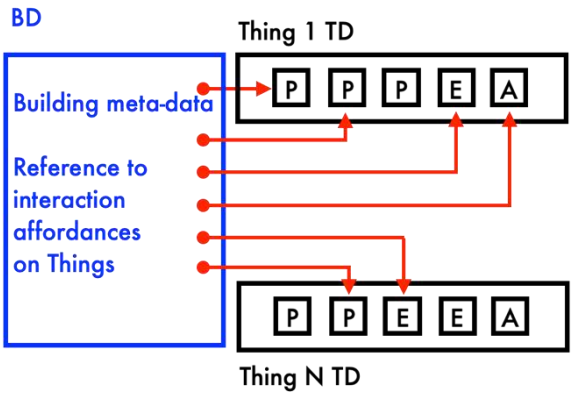

Fig. 6 - Building Description (BD) structure.

5.3 The domOS Common Ontology (dCO)

The domOS Common Ontology (dCO) is an information model for the domOS project [1] that allows a common understanding of the building as an energy system by humans and machines. dCO is available online [16] and is considered as the unique source of truth. The dCO has been designed by analysing the needs of the five demonstration sites of the domOS project, which cover a broad spectrum of uses cases. The dCO reuses existing ontologies whenever possible.

The following use cases of the dCO have been identified:

- **Semantic annotations of TDs**: TDs should be annotated using the entities of the dCO to correctly express the meaning of the Things' metadata. According to the WoT Thing Description recommendation [13], TDs can be annotated using the "@type" field (e.g., "@type": "dco:temperatureProperty"). Measurements can also be annotated with their unit using the dCO (e.g., "unit": "dco:Celsius").

- **Elaboration of BDs**: BDs are dCO compliant RDF documents.

- **Semantic validation of TDs and BDs**.

- **Semantic search of TDs and BDs**: Using semantic search queries, Applications can learn relevant features of buildings and of their Things without any prior knowledge.

- **Compliance check for Applications.** This process allows an application to formally verify before deployment that the building infrastructure is appropriate for its operation.

5.4 The Platform

Mediating Platforms are legacy IoT frameworks upgraded according to the domOS ecosystem specification.

Using appropriate interfaces, Platforms let facility operators register their buildings and upload their BDs, manage the life cycle (install, replace, decommission) of local Things, and subscribe to validated Services.

Platform administrators can register buildings and Applications.

Platforms are also in charge of privacy and safety rules enforcement: building facility operators should formally permit Applications to access Things monitoring and control points.

Applications can query the BD to check that the needed set of Things are installed. However, to support strong privacy rules, Platforms are designed to reveal only the parts of the BD required for the operation of Applications.

Platforms should monitor the health status of the Things and Applications, and trigger alerts when failures are detected, to ensure a reliably working distributed system.

Depending on the design, Platforms can work as proxies between Things and Applications, or only provide a directory service to Applications, which then communicate directly with Things.

The domOS ecosystem specification leaves a high degree of freedom to Platform developers: implementations on home gateways, in clouds, or a mix thereof are possible.

6. Example

Let us consider the sample single-family house "dco:b-001" illustrated on Fig. 7. Devices represented in orange are WoT Things and dispose therefore of TDs. Three Services will be deployed: a web-based energy dashboard for occupants, an electricity flexibility management service for space and domestic hot water heating, and a performance assessment service for heating.

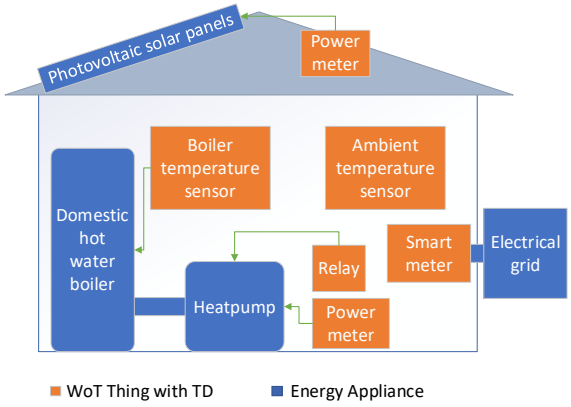

Fig. 7 – Topology of the sample building "dco:b-001".

Some of the RDF triples of the BD for the building "dco:b-001" are represented graphically in Fig. 8. One can recognise the metadata describing the building energy infrastructure as well as references to WoT properties.

A BD refers to a particular interaction affordance in two steps:

1. An instance of the classes dco:Property, dco:Event, dco:Action or of subclasses thereof is inserted in the BD (e.g., "dco:Temperature01").

2. This instance is linked to an interaction affordance of a Thing by two RDF properties: the property "dco:hasTD" refers to the URL of the Thing's TD ("https://domos.oiken.ch/b-001/pm1"), whereas the property "dco:hasInteractionName" refers to the name of a property, action or event in the TD ("Temperature01").

TDs can be instantiated in RDF and stored in a semantic knowledge base along with the BD. Therefore, semantic search queries are possible as the TDs and the BD are semantically integrated.

Using semantic queries, an Application can determine that the building envelope is heated by the heat pump. An Application can also find how to read the real-time values for the ambient temperature and for the heat pump active power, and how to control the heat pump operation by a relay property

associated to the heat pump (not represented on Fig. 8).

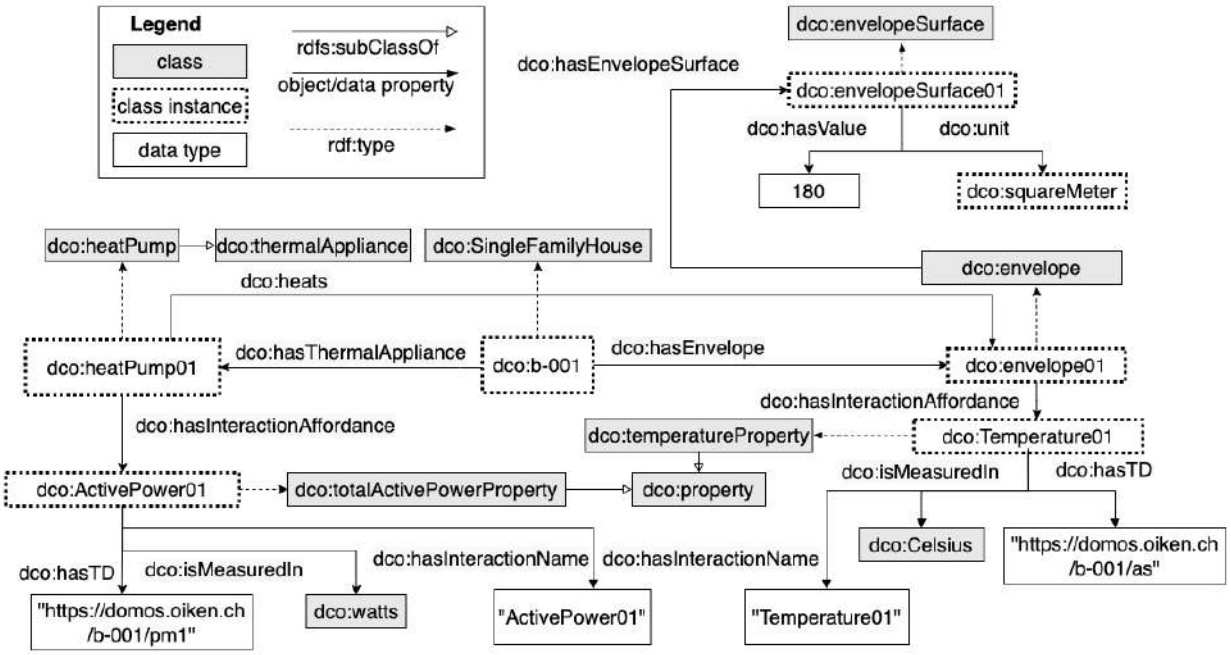

Fig. 8 - Building Description (BD) for the building "dco:b-001" (excerpt).

An excerpt of the TD for the ambient temperature sensor is presented on Fig. 9. It states that the "Temperature01" property can be read with a HTTP GET operation at the URL https://domos.oiken.ch/temperature/datapoint and that the response body contains the current temperature in Celsius as a character string.

```
{ "id": "21cf7981-59fb-4a0d-85e9-3f101c1aa633",
  "@context": [
    "https://www.w3.org/2019/wot/td/v1",
    {"dco": "https://w3id.org/dco/"}],
  "title": "Ambient sensor",
  "base": "https://domos.oiken.ch",
  "@type": "dco:ambientSensor",
  "properties": {
    "Temperature01": {
      "@type": "dco:temperatureProperty",
      "type": "number",
      "unit": "dco:Celsius",
      "forms": [{"href": "/temperature/datapoint
      "op":"readProperty"}]},
  "actions": {},
  "events": {}
}
```

Fig. 9 - Thing Description (TD) for the ambient temperature sensor (excerpt).

7. Conclusion

Thanks to the proposed domOS ecosystem specification, existing IoT frameworks can be upgraded to become Platforms supporting the integration of energy appliances and devices in buildings. A cluster of generic Applications can be deployed on buildings without a priori knowledge of the building configuration. This approach allows the industrialisation of the deployment of energy services without putting constraints on the field infrastructure inside buildings.

However, many challenges must be addressed to enable a large-scale deployment of compliant Platforms: WoT must become an established standard; the dCO must provide at the same time flexibility to deal with various building topologies and conciseness to ease Application development; privacy, cyber-security and liability issues require sound answers; Platform operator is a new role for which viable business models must be elaborated.

Data sharing is not applicable to this article as no datasets were generated or analysed during the current study.

8. Acknowledgements

The domOS project leading to this research has received funding from the European Union's Horizon 2020 research and innovation program under grant no. 894240.

9. Bibliography

[1] domOS project team, "domOS project web site," [Online]. Available: https://www.domos-project.eu/.

[2] D. Grivon, P. Riederer, Y. Stauffer and A. Hutter, "Smart Control Strategy For The Reduction Of Energy," in *Building Simulation*, 2019.

[3] P. Zangheri, T. Serrenho and P. Bertoldi, "Energy Savings from Feedback Systems: A Meta-Studies' Review," *Energies,* vol. 12, no. 19, p. 3788, 2019.

[4] C. Hanmin, A. Hutter, E. Olivero, P. Roduit and P. Ferrez, "Load shifting for tertiary control power provision," in *2015 IEEE 5th International Conference on Power Engineering, Energy and Electrical Drives (POWERENG)*, Riga, 2015.

[5] A. Karpenko, T. Kinnunen, K. Främling and B. Dave, "Open IoT ecosystem for smart EV charging," in *2018 Global Internet of Things Summit (GIoTS)*, Bilbao, 2018.

[6] A. Verma, S. Prakash, V. Srivastava, A. Kumar and S. C. Mukhopadhyay, "Sensing, Controlling, and IoT Infrastructure in Smart Building: A Review," *IEEE Sensors Journal,* vol. 19, no. 20, pp. 9036-9046, 2019.

[7] Sidqi, Y.; Ferrez, P.; Gabioud, D.; Roduit, P., "GOFLEX: Towards a New Integrated Solution for a Cost-Effective Use of Demand Response in Distribution Grids," in *CIRED 2020 Berlin Workshop*, Berlin, 2020.

[8] SunSpec Alliance, "The SunSpec Alliance," [Online]. Available: https://sunspec.org/.

[9] SmartGrid ready Assocation, "The SmartGrid ready Assocation," [Online]. Available: https://www.smartgridready.ch/.

[10] daisy (Center for Data-intensive Systems), "Flex-Offers: Unified generalized modelling and management of flexibility in electricity demand and supply," University of Aalborg, [Online]. Available: https://www.daisy.aau.dk/projects/flexoffers/.

[11] SAREF, "Smart Applications REFerence Ontology, and extensions," ETSI, [Online]. Available: https://saref.etsi.org/.

[12] W3C WoT – Architecture Task Force, "Web of Things (WoT) Architecture 1.1 - W3C First Public Working Draft 24 November 2020," World Wide Web Consortium (W3C), [Online]. Available: https://www.w3.org/TR/wot-architecture/.

[13] W3C WoT – Thing Description Task Force, "Web of Things (WoT) Thing Description 1.1 - W3C Working Draft 7 June 2021," [Online]. Available: https://www.w3.org/TR/wot-thing-description11/.

[14] Eclipse Foundation, "Thingweb: A Web of Things Implementation," [Online]. Available: http://www.thingweb.io/.

[15] J. Dongo, M. Albano, A. Skou and B. Nielsen, "Web of Things Interoperability for the Arrowhead Framework," in *IECON 2021 – 47th Annual Conference of the IEEE Industrial Electronics Society*, 2021.

[16] A. Laadhar and C. Thomsen, "domOS Common Ontology," University of Aalborg, [Online]. Available: https://www.dco.domos-project.eu/.

A web-based approach to BMS, BIM and IoT integration: a case study

Lasitha Chamari, Ekaterina Petrova, Pieter Pauwels

Department of the Built Environment, Eindhoven University of Technology, Eindhoven, the Netherlands, l.c.rathnayaka.mudiyanselage@tue.nl, e.petrova@tue.nl, p.pauwels@tue.nl.

Abstract. Buildings are complex cyber-physical systems that rely on a combination of heterogeneous systems to provide smooth operation, energy efficiency, occupant comfort, well-being and safety. Building Management Systems (BMS) are central to these operations and generate a huge amount of data. Traditionally operated in a local server in a building, state-of-art BMS solutions are now moving towards the cloud. Internet of Things (IoT) meters and sensors are also increasingly used in buildings and hold tremendous potential for smart building monitoring and control. Another valuable data source is a properly developed and managed Building Information Model (BIM). BIM itself is moving towards Level 3, which is web-based and data-driven, as opposed to the file-based BIM of today. Improving building performance (e.g., energy, comfort, operational cost) relies on data from all the above systems. However, these data usually remain siloed within their own environment and do not provide an opportunity to perform evaluations across multiple systems. Moreover, valuable information about geometry, spatial location, and metadata about the building objects that the BIM models already contain remains unusable for building performance monitoring and reporting tools. Integrating these heterogeneous data sources will provide ample opportunities to improve building performance. Even though some commercial tools enable the integration of sensor data with BIM models, such tools remain largely proprietary and are not compatible with other applications. This study presents a methodology to integrate multiple information sources at their system level in a distributed manner. The Industry Foundation Class (IFC) model of the building is used as the primary source of information for creating a semantic building graph. Since the semantics of BMS sensors was not originally available in the IFC model, the Brick ontology is used to semantically describe BMS sensors in the graph. Sensor data related to spaces in the BIM model is visualized by selecting a space from the 3D model via the web application. Each data stream remains in its optimum environment and the connections are made via an Application Programming Interface (API).

Keywords. Data integration, BMS, IoT, BIM, Semantic Web, Brick
DOI: https://doi.org/10.34641/clima.2022.228

1 Introduction

Buildings are equipped with many systems such as HVAC, lighting, security, water, energy, etc. A building Management System (BMS) is used to centralize, automate and make the management of the above systems more efficient. By doing so, more efficient building operation is achieved at a reduced labour and energy cost, while ensuring a safe and comfortable environment [1]. Internet of Things (IoT) devices are also extensively used in many new buildings [2], giving rise to a large volume of real-time data about energy usage, ambient conditions (temperature, humidity, illuminance), as well as machine and equipment related parameters such as vibration, faults, alarms, etc. This data is used for reporting, monitoring, dashboards, fault detection, energy forecasting, etc. Smart buildings produce an abundance of such data, forming a virtual representation of the physical building, known today as a "Digital Twin" [3]. Other than the time series data, another invaluable source of information is the Building Information Model (BIM) [4] which is an essential component of the Architecture, Engineering and Construction (AEC) industry. A BIM model can be defined as the digital

Copyright ©2022 by the authors. This conference paper is published under a CC-BY-4.0 license.

representation of a building that contains semantic information about the objects [5]. A properly developed and managed BIM model is a data source of high fidelity. It includes geometry, spatial location, and a broad representation of metadata about the properties of the building, its subsystems, devices, Mechanical, Electrical and Plumbing (MEP) equipment, etc. [6].

1.1 Data integration for smart buildings

To manage a building holistically and leverage the benefits of smart operation, various domains such as Supervisory Control and Data Acquisition (SCADA) systems, floor plans, IoT devices, 3D models need to be integrated. With the ever-increasing demand for smart building applications (Digital Twins, real-time monitoring, energy flexibility), there is a need to develop applications that depend on data available across multiple decentralized systems. This is where the importance of data integration arises. However, this integration is far from easy. There is no straightforward way, for example, to integrate a Honeywell BMS with a BIM model developed in Autodesk Revit, because they are incompatible by definition and rely on different modelling approaches, languages and protocols.

Therefore, a significant body of research in the AEC industry focuses on how to exchange and integrate data [3]. Many such attempts are revolving around Industry Foundation Classes (IFC), which is a vendor-neutral data model for exchange of AEC data [3] relying on the EXPRESS schema language. IFC is an open international standard for BIM data that is exchanged and shared among software applications used by the various participants in the construction and facility management sectors [7]. However, not all aspects of the built environment can be modelled in IFC. For example, a crucial part of the operational phase of a building is the dynamic sensor data, which cannot be easily represented using IFC. Even though the IFC standard describes many common Heating Ventilation & Air Conditioning (HVAC), lighting, and sensor devices, they are not capable of representing the context of the devices contained within [8].

1.2 Semantic web technologies

Semantic technologies and linked data have gained traction in the built environment. IFC itself is also available as ifcOWL ontology [9]. Linked data models are built using formal ontologies and thereby provide the opportunity for extending and linking with other domain-specific ontologies, exchanging heterogeneous information [10], and deriving new information based on the semantic graph [8]. Semantic graphs, also referred to as knowledge graphs, can also be queried using various query languages [9]. Linked Building Data (LBD) is an initiative with a focus on making building data web-ready [11]. A number of vocabularies and ontologies such as BOT, PRODUCT, and PROPS have been developed using a linked data approach [12]. Many other ontologies, such as SSN [13], RealEstateCore [14], Haystack [15], Brick [16], etc., have also emerged to fulfil various information requirements throughout the building lifecycle.

1.3 Current status of data integration in buildings

With such technologies available, one might anticipate a connected building with readily available data from multiple systems co-exising in a common platform. However, this is far from reality. Data is maintained in isolated silos and there is little interaction between different datasets. For example, BIM models developed in the design phase often remain disconnected from the operational data. Most of the sensors and devices are also not included in the BIM models at the design stage. Again, although the spatial information is already available in the BIM model, this information is duplicated in the BMS due to the lack of interoperability. Therefore, despite the number of systems or amount of data being collected, it is difficult to interpret information across domains due to little interaction between islands of data [17]. Available data, their formats, naming conventions, and standards also differ significantly among each building and vendor [18]. This absence of a common data collection structure leads to unstructured data that is difficult to discover, integrate, process and use. This has made the integration of data siloes an essential requirement in the built environment.

According to the literature [13, 14], a common use case is integrating sensor data into the BIM model using commercial BIM authoring tools like Revit or Navisworks. Although they may serve as appropriate tools for visualizing sensor data in a 2D or 3D environment, such approaches rely on vendor-specific software and do not provide reusable components for other applications. Alternative approaches rely on integrating datasets including building geometry, the relationship between spaces, sensors and actuators, and time series data into a single semantic graph in Resource Description Framework (RDF) using semantic web approaches [21]. Sensor data is further retrieved for visualization in charts and colour-coded maps in 2D plans. Other studies [16, 17] suggest that retaining sensor data in a database that is optimized to store time series data is more efficient. Apart from BIM and sensor data integration, another path is integrating BIM with Linked Building Data. Visualizing BIM models on the web provides a vendor-neutral platform for collaboration and exchange of data, as well as means to integrate data across domains [11]. As such, a web-based server is proposed in [11], which allows users to upload BIM models in IFC format, and visualise it in a graphical user interface. Attaching Linked Building Data (as graphs) to the project allows querying the BIM model based on the graph.

However, implementations integrating systems, BIM, sensor data, and semantic graphs in a decentralized manner are still in their infancy. Also, the built environment is not static. More and more energy-efficient buildings are demanded, and various sensors, devices and systems are continuously added to buildings. Therefore, the building information models also evolve. Data-driven smart building applications such as forecasting, fault detection and diagnosis, energy balancing, etc., are also increasingly deployed, and the output from these algorithms needs to be communicated to level building controllers, making the information flow bidirectional. Therefore, other essential components for future integration are the building controllers.

1.4 Objective and scope

This paper presents the first step towards integrating heterogeneous systems in a building. The study approaches multiple information sources at their system-level and demonstrates how to integrate them in a distributed manner. The proposed approach uses an IFC file to create the initial graph, followed by another graph to represent the semantics of BMS sensors. Each data stream remains in its optimum environment and the connections are made via Application Programming Interface (API), rather than file-based transfers. The developed platform can be used to collectively view and query the building data in its entirety. It also provides the opportunity for visualizing sensor data. Future work will address the integration of real-time data and bi-directional communication with building controllers.

2 Case study building

The use case building is a 12-storey renovated university building consisting of offices, study, and lecture rooms. It has been renovated in 2019 and contains a BMS, Energy Management System (EMS), and a Lighting Management system. The 4th to 11th floor of the building are considered a Living Lab and are used for research regarding indoor environmental quality, energy efficiency, lighting, Digital Twin implementation, etc.

2.1 BMS time series data

The campus building has a Honeywell BMS. A data dump from the BMS containing occupancy, temperature, and CO_2 data is used for this study. They constitute 1,314,720 data points per month. Measurements are stored on an hourly basis and the extracted data from the BMS is stored in xlsx format (**Tab. 1**). The table columns contain the timestamps and the sensor IDs. Mapping sensor IDs and their description are available as shown in **Tab. 2.** In **Tab. 2**, sensor location is included in the description. For example, sensor 11NR008TE-001TRL is in room no.128 of the 8th floor.

2.2 IoT time series data

Envision Manager is the API available to interact with the Lighting Management System for monitoring and controlling dimming levels and colour temperature. Furthermore, an ESP32-based IoT sensor network is in development to collect and display real-time temperature, humidity and illumination data. In this study, this sensor network is used to demonstrate how real-time sensor data can be integrated into the platform.

Tab. 1 – BMS data extraction.

Timestamp	11NR008TE-001TRL	11NR008TE-003TRL
28-02-2021 00:02:00	22.1	21.1
28-02-2021 01:02:00	22.0	20.9
28-02-2021 02:02:00	21.9	20.8
28-02-2021 03:02:00	21.7	21.2

Tab. 2 – BMS data point mapping table.

Item name	Description
11NR008TE-001TRL	Room temperature 8_128
11NR008QT-040CO2	*CO2 measurement 8_323
11NR008LT-001PIRTM	Presence 8_128

2.3 BIM model

The BIM model used for this study contains the 8th and 9th floors of the case study building. It is developed in Autodesk Revit and includes space-related information (room name, room number, and the floor) and equipment-related information (sensors and lighting fixtures) as shown in **Fig. 1.**

Fig. 1– BIM model developed in Revit

3 Implementation

This section describes the approach on how to integrate the various data sources identified above. In brief, that includes how to,

1. Use the IFC file as the data source for the 3D viewer, as well as the main source of building information (geometry, spatial information).
2. Convert the IFC file into a web browser compatible format.
3. Generate the semantic graph of the building using the IFC file. This carries information about different spaces and sensors/equipment contained within each space.
4. Use the BMS sensor mapping table to populate the graph about sensors.
5. Choose appropriate databases to store 3D models, time series data, and graph data.
6. Provide a web application for the user to interact with the BIM model and time series data of the building.
7. Visualize real-time and historical data in the front-end web app.

The underlying data conversion and storage infrastructure are shown in **Fig. 2**.

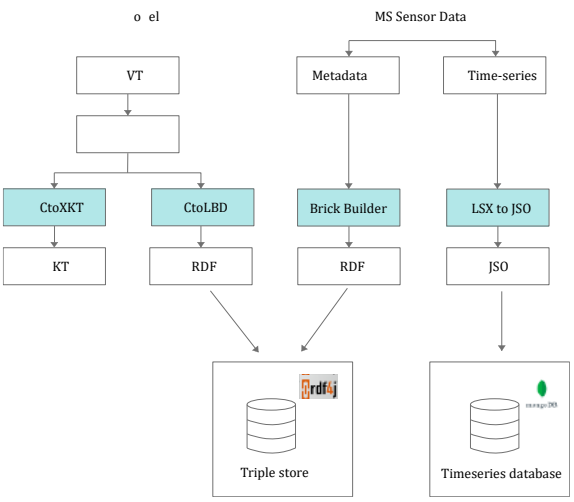

Fig. 2 – Data conversion and storage infrastructure.

3.1 Creating the semantic graph

A number of metadata representations are available that are useful in different phases of the building's lifecycle. IFC is an industry-wide standard data schema for BIM and covers many aspects in the design and construction phases of a building [3]. Geometry, building elements, and product properties are represented in IFC. IFCtoLBD converter [24] is a tool used to generate RDF triples using an IFC STEP file. It makes use of BOT, RDFS, and PROPS ontologies. The tool presented in [24] is used in this study to generate the RDF model of the building. Part of the IFC file containing information about the room "test 1 area" is shown in **Fig. 3.** In IFC, there is a Globally Unique Identifier (GUID) for every element and "0KLkXPBfvES9D1y7EjijkE' is the GUID of the space.

```
1.  #1266=
    IFCSPACE('0KLkXPBfvES9D1y7EjijkE',#42,'9',$
    ,$,#1245,#1263,'test 1
    area',.ELEMENT.,.SPACE.,$);
2.  #1269=
    IFCSPACETYPE('0H12gSHLX9KAhW1PyBN1jS',#42,'
    test 1 area
    9:543779',$,$,$,$,'543779',$,.NOTDEFINED.,$
    );
3.  #1270=
    IFCPROPERTYSINGLEVALUE('Name',$,IFCLABEL('t
    est 1 area'),$);
4.  #1271=
    IFCPROPERTYSET('2b$cWxcoTB9AhqrEJK8Q2s',#42
    ,'Pset_AirSideSystemInformation',$,(#1270))
    ;
```

Fig. 3 – Part of the IFC file containing IFCSPACE info.

The above IFC file, when converted to RDF, is shown in **Fig. 4.** "Space_1266" is a *bot:Space*, in which the number 1266 is related to the line number of the IFC file. The room can be uniquely identified by its GUID represented using *props:hasCompressedGuid* relationship.

```
1.  inst:space_1266 a bot:Space ;
2.  bot:containsElement
    inst:lightFixture_241729,
3.        inst:lightFixture_241879,
4.        inst:sensor_239793 ;
5.     props:hasCompressedGuid
    "0KLkXPBfvES9D1y7EjijkE"^^xsd:string ;
6.     bot:hasGuid "1456e859-2e9e-4e70-9341-
    f073adb2db8e"^^xsd:string ;
```

Fig. 4 - Part of the graph generated by the IFCtoLBD converter.

The Revit model of the building does not contain the BMS sensors, and, therefore, they are not available in the above graph. Compared to other structured representations of other building elements, the only source of metadata of the sensors is the mapping table shown in **Tab. 2** . However, the type of sensor and its location is available in this table. Other information such as their units and parent components were unavailable. To represent the BMS data points, this study relies on the Brick Ontology. Brick is built with a focus on supporting energy applications based on BMS in commercial buildings. It can represent metadata information of a sensor such as its location, function, and type. It also captures the relationships between those entities.

The RDF graph is created using the Brick-builder [25] tool. It is a simple method to generate a graph by providing the entities and their relationships.. A CSV file containing all the entities (shown in **Fig. 5**) and a text file defining the relationships, (shown in **Fig. 6**) form the inputs to the Brick-builder tool to generate the graph. Sensor ID, description, room

number, room GUID, space ID, room name and the Brick sensor tags are included in this file. This CSV file is generated by joining the extracted spaces and GUID relationships from the graph generated from IFCtoLBD converter, and the BMS mapping table. By having the space identifier (e.g. space_1266) included in the graph, this identifier can be used to merge the two graphs.

```
1.  11NR008QT-301CO2,"*CO2 MEASUREMENT
    8_140",8.140,0KLkXPBfvES9D1y7EjijkE,space_1
    266,"test 1 area",CO2_Sensor
2.  11NR008LT-302PIRTM,"PRESENCE
    8_445",8.445,0LnrpxIav0Ju4gTy7JmW7k,space_6
    846,"Zone4- R9",Occupancy_Sensor
3.  11NR008TE-302TRL,"ROOM TEMPERATURE
    8_445",8.445,0LnrpxIav0Ju4gTy7JmW7k,space_6
    846,"Zone4- R9",Temperature_Sensor
```

Fig. 5 – Part of the CSV file.

```
1.  inst:$5 rdf:type brick:Room
2.  inst:$1 rdf:type brick:$7
3.  inst:$1 brick:hasLocation inst:$5
4.  inst:$1 rdfs:label $2
```

Fig. 6 – Relationships defined among columns of the CSV file.

This results in a graph with the relationships as shown in **Fig. 7**.

```
1.  inst:11NR008QT-301CO2 a brick:CO2_Sensor ;
2.      rdfs:label
    "*CO2_MEASUREMENT_8_140"^^xsd:string ;
3.      brick:hasLocation inst:space_1266 .
4.
5.  inst:11NR008LT-302PIRTM a
    brick:Occupancy_Sensor ;
6.      rdfs:label"PRESENCE_8_445"^^xsd:string;
7.      brick:hasLocation inst:space_6846 .
8.
9.  inst:11NR008TE-302TRL a
    brick:Temperature_Sensor ;
10.     rdfs:label
    "ROOM_TEMPERATURE_8_445"^^xsd:string ;
11.     brick:hasLocation inst:space_6846 .
```

Fig. 7 – Relationships defined among columns of the CSV file

The first RDF graph (**Fig. 4**) semantically describes the context of the building and the second graph (**Fig. 7**) describes BMS sensors. These two graphs are stored in RDF4J database [26] as two separate graphs. RDF4J is a native Triplestore. An instance of the resulting visual graph using GraphDB is shown in **Fig. 8**. GraphDB [27] is another Triplestore that also provides visual representation of a graph.

3.2 Time series data

As stated, time series data from BMS sensors including temperature, occupancy and CO_2 are available as records in xlxs format as shown in **Tab. 1**. This data type fits well in a time series database. Therefore, MongoDB Timeseries Collection is used. Time series collection has the advantage of improved query efficiency and reduced disk usage for time series data, compared to normal document collections [28]. Before uploading to MongoDB, the timestamp was converted into Coordinated Universal Time (UTC) and data were formatted to JavaScript Object Notation (JSON) with the timestamp, sensor ID, and the value. A sample MongoDB document is shown in **Fig. 9.**

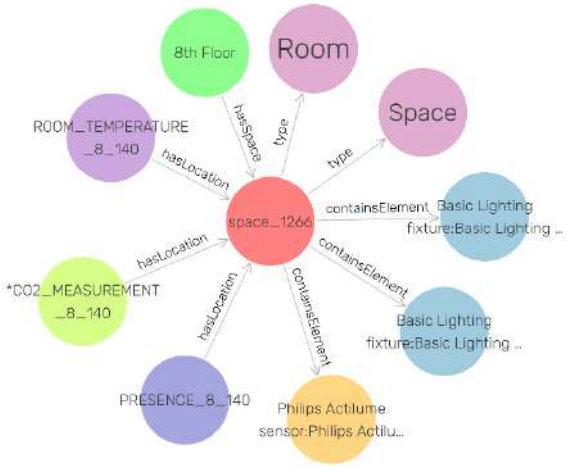

Fig. 8 – Graph representation of space_1266 using GraphDB.

```
1.  {"timestamp":{"$date":"2021-03-
    31T22:02:00.000Z"},"sensor_id":"11NR008QT-
    301CO2","_id":{"$oid":"61bfcef2c72be614e6cd
    a971"},"value":425}
2.  {"timestamp":{"$date":"2021-03-
    31T22:02:00.000Z"},"sensor_id":"11NR008LT-
    302PIRTM","_id":{"$oid":"61bfceeac72be614e6
    caf861"},"value":2}
3.  {"timestamp":{"$date":"2021-03-
    31T22:02:00.000Z"},"sensor_id":"11NR008TE-
    302TRL","_id":{"$oid":"61bfcec8c72be614e6c0
    d471"},"value":20.1}
```

Fig. 9 – Sensor data in MongoDB time series collection.

3.3 BIM-SIM web application

BIM-SIM is the web application developed to support the above tasks. The front end is built using React, a JavaScript framework. One intended functionality of the application is to view the building geometry in 3D using a web browser. The proposed approach utilises xeokit, an open-source JavaScript 3D graphics Software Development Kit (SDK) from xeolabs [29] [30] to render the 3D file in the browser. It provides functionalities like tree view, filtering elements by type, user event such as pick elements, etc. We used XKT format to view the 3D BIM model in the browser. XKT is a binary format and allows fast rendering. When converting, it preserves metadata in the IFC including the GUID. This GUID is used to uniquely identify the spaces in this application. The IFC model can be transformed into XKT, using several open-source command-line tools as described in [31]. The conversion flow is shown in **Fig. 10,** which is adapted from [31]. This conversion is implemented as a separate entity and is not a part of the web application. After the conversion process, the XKT file can be imported to

the web application. **Fig. 11** shows the XKT file loaded in the web app. Plotly.js, a JavaScript graphing library, is utilised for charts. The NestJS framework is used to develop the API with Mongoose Object Data Modeling (ODM).

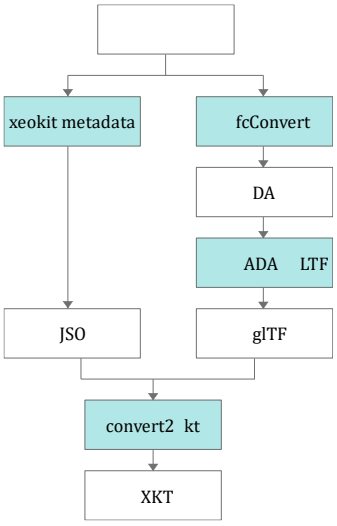

Fig. 10 - IFC to XKT conversion procedure [20].

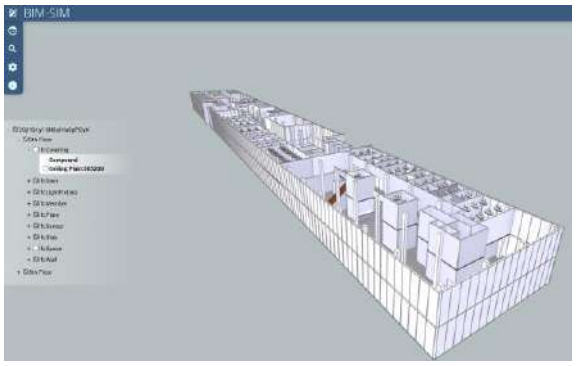

Fig. 11 - XKT file loaded in the web app.

3.4 Functionality

When a particular space is selected from the 3D model, the front end application picks the element's GUID, which is used to call the API, where a SPARQL query is executed to find all sensors contained in that space. A SPARQL query is sent in the request body in a POST request to the RDF4J server. Then the "Info window" is populated by the sensors contained in that space. These sensors are extracted from the RDF graph using the query shown in **Fig. 12.**

```
PREFIX brick: <https://brickschema.org/schema/Brick#>
PREFIX inst: <http://linkedbuildingdata.net/ifc/resources20201208_005325/>
PREFIX props: <https://w3id.org/props#>
PREFIX rdf: <http://www.w3.org/1999/02/22-rdf-syntax-ns#>
select * where {
    ?space props:hasCompressedGuid '0KLkXPBfvES9D1y7EjijkE' .
    ?sensors brick:hasLocation ?space .
    ?sensors rdf:type ?sensor_type .
}
```

Fig. 12 - SPARQL query that runs in the API.

This query results three sensors that are contained in that space as shown in **Tab. 3**.

Tab. 3 – SPARQL query results.

	space	sensors	sensor_type
1	inst:space_1266	inst:11NR008 LT-301PIRTM	brick:Occupancy_Sensor
2	inst:space_1266	inst:11NR008 QT-301CO2	brick:CO2_Sensor
3	inst:space_1266	inst:11NR008 TE-301TRL	brick:Temperature_Sensor

These results are available via the web application un er "3 sensors" as shown in **Fig. 13** – Info window populated with sensors from SPARQL query.

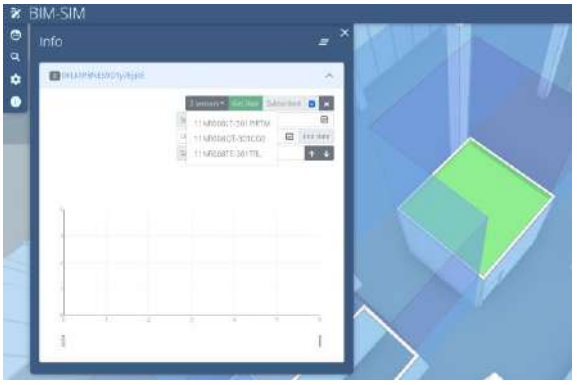

Fig. 13 – Info window populated with sensors from SPARQL query.

Then, selecting a particular sensor calls the API which sends a query to the MongoDB database using the sensor ID to retrieve historical data, and the returned data is displayed in a chart as shown in **Fig. 14**. The user can adjust the time interval and the sample size of data as well. When displaying sensor data, its metadata is also displayed. In this example, it is limited to the type of sensor (Brick CO2 Sensor), but this can be extended to display the location and other relationships as well, when available. This is particularly important as opposed to extracting time series data from a database, without knowing its provenance. Usually, naming conventions of BMS data points are ambiguous and do not provide much information about the sensor.

4 Discussion and conclusion

A large volume of data is produced in each phase of a building. In its operational phase, these data

become highly valuable for many applications. This paper demonstrates how various data sources in a building can be integrated in a distributed manner.

Compared to using commercially available BIM tools for visualizing sensor data, this paper provides a vendor-neutral method. Furthermore, as opposed to creating one central information model, we acknowledge the fact that it is more efficient to retain time series data in their optimum environment. Since there are 1,314,720 records per month, if all the sensor observations were included in the graph, this will add $1{,}314{,}720 \times 12 \cong 15M$ additional triples to the graph, without any value addition.

Fig. 14 – CO_2 Sensor data visualization.

The BIM model is used as the main information source to develop the knowledge graph of the building. Secondly, BMS sensor semantics were introduced as another graph, using the Brick ontology. The IFC file is also used as the 3D model of the building, but it is limited to the XKT format to which it is translated, thereby preserving the geometry information in an industry standard. The web application provides the opportunity to interact with the knowledge graph, the 3D model, and the BMS sensor data. This integration was achieved by leveraging semantic web technologies, an open-source 3D graphics SDK, an API, and state-of-art web tools. Although the demonstration was done for an interactive monitoring application, other similar applications like reporting on energy usage and indoor climate are also possible via the same resources. Visualizing real-time data through the web application is possible using the MQTT JavaScript client with WebSocket. This is planned as a future implementation. Most importantly, this platform will further be extended to introduce building controllers and will be implemented on top of the existing BMS infrastructure. Although basic semantics (location, type) were used to describe BMS sensor data, more metadata such as unit, mounting height, accuracy, shall be described as required by applications in the future.

5 Acknowledgement

This project received funding from the Dutch Ministry of Economic Affairs and Climate Policy and Ministry of the Interior and Kingdom Relations under the MOOI program.

References

[1] Honeywell. Engineering Manual of Automatic Control for Commercial Buildings. 1997;

[2] Bilal M, Oyedele LO, Qadir J, Munir K, Ajayi SO, Akinade OO, et al. Big Data in the construction industry: A review of present status, opportunities, and future trends. Adv Eng Informatics [Internet]. 2016;30(3):500–21. Available from: http://dx.doi.org/10.1016/j.aei.2016.07.001

[3] Pauwels P, Costin A, Rasmussen MH. Knowledge Graphs and Linked Data for the Built Environment [Internet]. Springer International Publishing; 2022. 157–183 p. Available from: http://dx.doi.org/10.1007/978-3-030-82430-3_7

[4] Tang S, Shelden DR, Eastman CM, Pishdad-Bozorgi P, Gao X. A review of building information modeling (BIM) and the internet of things (IoT) devices integration: Present status and future trends. Autom Constr [Internet]. 2019 May 1 [cited 2022 Mar 15];101(June 2018):127–39. Available from: https://linkinghub.elsevier.com/retrieve/pii/S0926580518305764

[5] Pauwels P, Petrova E. Information in Construction. 2020.

[6] Eastman C, Teicholz P, Sacks R, Liston K. BIM Handbook, a Guide to Building Information Modelling 2nd ed. John Wiley & Sons, Inc, Hoboken. 2011.

[7] ISO - ISO 16739-1:2018 - Industry Foundation Classes (IFC) for data sharing in the construction and facility management industries — Part 1: Data schema [Internet]. [cited 2022 Jan 6]. Available from: https://www.iso.org/standard/70303.html

[8] Fierro G. Self-Adapting Software for Cyberphysical Systems. 2021; Available from: http://www2.eecs.berkeley.edu/Pubs/TechRpts/2021/EECS-2021-159.html

[9] Pauwels P, Terkaj W. EXPRESS to OWL for construction industry: Towards a recommendable and usable ifcOWL ontology. Autom Constr. 2016 Mar 1;63:100–33.

[10] Gruber TR. A Translation Approach to Portable Ontology Specifications. Knowl Aquis. 1993;5(2).

[11] Malcolm A, Werbrouck J, Pauwels P. LBD Server: Visualising Building Graphs in Web-Based Environments Using Semantic Graphs and GlTF-Models. Adv Sci Technol Innov. 2021;(2020):287–93.

[12] Bonduel M, Oraskari J, Pauwels P, Vergauwen M, Klein R. The IFC to linked building data converter - Current status. CEUR Workshop Proc. 2018;2159:34–43.

[13] Haller A, Janowicz K, Cox SJD, Lefrançois M, Taylor K, Le Phuoc D, et al. The modular SSN ontology: A joint W3C and OGC standard specifying the semantics of sensors, observations, sampling, and actuation. Semant Web. 2018;10(1):9–32.

[14] Hammar K, Wallin EO, Karlberg P, Hälleberg D. The RealEstateCore Ontology. In: Lecture Notes in Computer Science (including subseries Lecture Notes in Artificial Intelligence and Lecture Notes in Bioinformatics). 2019.

[15] Project Haystack - Tags [Internet]. 2020 [cited 2021 Aug 22]. p. 2016. Available from: https://project-haystack.org/tag.

[16] Balaji B, Bhattacharya A, Fierro G, Gao J, Gluck J, Hong D, et al. Brick: Metadata schema for portable smart building applications. Appl Energy [Internet]. 2018;226(February):1273–92. Available from: https://doi.org/10.1016/j.apenergy.2018.02.091

[17] Suzuki LR. Data integration approaches for smarter operation of large commercial buildings. 2015;

[18] Bhattacharya AA, Hong D, Culler D, Ortiz J, Whitehouse K, Wu E. Automated metadata construction to support portable building applications. BuildSys 2015 - Proc 2nd ACM Int Conf Embed Syst Energy-Efficient Built. 2015;3–12.

[19] Desogus G, Quaquero E, Rubiu G, Gatto G, Perra C. Bim and iot sensors integration: A framework for consumption and indoor conditions data monitoring of existing buildings. Sustain. 2021;13(8).

[20] Oti AH, Kurul E, Cheung F, Tah JHM. A framework for the utilization of Building Management System data in building information models for building design and operation. Autom Constr [Internet]. 2016;72:195–210. Available from: http://dx.doi.org/10.1016/j.autcon.2016.08.043

[21] Rasmussen MH, Frausing CA, Hviid CA, Karlshoj J. Demo: Integrating building information modeling and sensor observations using semantic web. CEUR Workshop Proc. 2018;2213(1):48–55.

[22] Donkers A, Yang D, De Vries B, Baken N. Real-Time Building Performance Monitoring using Semantic Digital Twins. Proc 9th Linked Data Archit Constr Work [Internet]. :12. Available from: http://ceur-ws.org/Vol-3081/05paper.pdf

[23] Hu S, Corry E, Curry E, Turner WJN, O'Donnell J. Building performance optimisation: A hybrid architecture for the integration of contextual information and time-series data. Autom Constr [Internet]. 2016;70:51–61. Available from: http://dx.doi.org/10.1016/j.autcon.2016.05.018

[24] pipauwel/IFCtoLBD: IFCtoLBD converts IFC (Industry Foundation Classes STEP formatted files into the Linked Building Data ontologies. (github.com) [Internet]. Available from: https://github.com/pipauwel/IFCtoLBD

[25] gtfierro/brick-builder (github.com). Available from: https://github.com/gtfierro/brick-builder

[26] Eclipse RDF4J™ | The Eclipse Foundation [Internet]. [cited 2022 Jan 11]. Available from: https://rdf4j.org/

[27] GraphDB Downloads and Resources (ontotext.com) [Internet]. [cited 2022 Jan 11]. Available from: https://graphdb.ontotext.com/

[28] Time Series Collections — MongoDB Manual [Internet]. [cited 2022 Jan 7]. Available from: https://docs.mongodb.com/manual/core/timeseries-collections/

[29] xeokit - 3D Web Programming Toolkit for BIM and Engineering Visualization [Internet]. [cited 2022 Jan 6]. Available from: https://xeokit.io/

[30] xeokit/xeokit-sdk: Open source JavaScript SDK for viewing high-detail, full-precision 3D BIM and AEC models in the Web browser. (github.com) [Internet]. Available from: https://github.com/xeokit/xeokit-sdk

[31] Converting IFC Models to XKT using 3rd-Party Open Source Tools (notion.so) [Internet]. [cited 2022 Jan 6]. Available from: https://www.notion.so/Converting-IFC-Models-to-XKT-using-3rd-Party-Open-Source-Tools-c373e48bc4094ff5b6e5c5700ff580ee

The datasets generated during and/or analysed during the current study are not available because of the privacy policy, but the authors will make every reasonable effort to publish them in near future.

LEARNING & EDUCATION

Integral design a necessity for sustainable building design

Wim Zeiler

Faculty of Architecture and the Built Environment, Eindhoven University of Technology, Eindhoven, the Netherlands, w.zeiler@bwk.tue.nl.

Abstract. Due to the rising demand for more sustainable buildings it is essential to make optimal use of the natural resources of sun, earth, water and wind. There is a urgent need saving energy and the necessity of zero or even energy positive buildings in the near future. However, therefor it is necessary to end the dichotomy between architecture and technology. This dichotomy leading to far from optimal functional buildings with poor indoor comfort and health conditions and also being responsible for high operational and failure costs. To close the gap between technology and architecture, between science and art, it is important to no longer subordinate to architecture but part of architecture itself. Instead of integrated design it is time for integral design. Architect and engineer working really together within the conceptual design phase of a building. It seems so easy however, it take an enormous mind shift for the engineers to become designers. The necessity for this was recognized by the Dutch Royal society of Architects, BNA, as well as the society of Dutch consulting engineers, NL Engineers. As a result the combined research project Integral Design was started together with the Dutch Building Services society, TVVL, in 2000. As a result of this project a design methodology was developed and implemented in the education curriculum of the Technical University of Eindhoven. In this paper the method and experiences of the application and testing of the method by organizing workshop between professionals and students will be presented

Keywords: Integral Design, Architect, Engineer
DOI: https://doi.org/10.34641/clima.2022.122

1. Introduction.

"*Until the mechanization of building is in service of creative architects and not creative architecture in service of mechanization we will have no great architecture.*" [Frank Lloyd Wright 1953]

People need buildings to protect them against the environmental conditions to be able to work and live in comfortable and healthy indoor air conditions. Architects shaped the built environment since the early beginning of civilization. Building Services make it possible to provide comfort and an acceptable indoor Air Quality for building occupants.

In the last 50 years the world has changed enormously: instead of 3.5 billion there are now living more than 7 billion people on earth with more than 50% in cities with an enormous increased standard of living. However, with 35% of the energy use the built environment is one of the most important areas for sustainable development [RVO 2020]. Collectively, buildings in the EU are responsible for 40% of our energy consumption and 36% of greenhouse gas emissions, which mainly stem from construction, usage, renovation and demolition [EU 2020]. There is a need to change the way how architects think about their role in the building design process, we cannot try to solve the problems using the same kind of approach that caused them. Traditionally a designer of HVAC systems was based on known mechanical systems and techniques. This has consequences for the direction in which architecture has to move towards a more sustainable future; a direction in which technology is used to guide architecture. However, there is a gap between technology and architecture and the research as the architect still takes a major leading role in designing both the indoor environment and the energy efficiency of buildings. With the role of the HVAC engineer as a traditional supporting role of the other consulting engineers during the process. The concept, the basic design, is conceived by the architect first, then there is room for other disciplines. However, the design of a highly sustainable building, due to the increased complexity of building design [van der Linder et al 2016], inevitably calls for more design collaboration in the

Copyright ©2022 by the authors. This conference paper is published under a CC-BY-4.0 license.

conceptual design phase as well. Only the early open collaboration of architects and engineers can facilitate the creation of the necessary new knowledge and solutions beyond the specific scope of each individual discipline [Kovacic and Fitzmoser 2014]. According to the Royal Institute of British Architects (RIBA) president Jane Duncan, architects, engineers and builders must collaborate [CIBSE 2016]. To fulfil the demand for Zero Energy Buildings there is a urgent need for synergy between the architectural and engineering domain.

Norman Foster and the design board at Foster + Partners are strong supporters of sustainable design and are keen to interpret and integrate engineering principles within design concepts [Smith 2019]. Their philosophy is that the best projects arise from a totally integrated approach to the design process, where the core disciplines work together to conceive and design a project from its earliest inception [Jackson and Heywood 2019]. Clearly Building Design is a team effort, team work is key therefor it is necessary to create a place for the needed innovation. The benefits of integrated design are: better decisions, higher speed of response, improved ability to iterate and thus reduce the complexity. Early engagement is essential within building design teams. In line with these developments in practice building design education has moved towards a collaborative practice where designers work in teams [Kiernan et al 2017] and with other disciplines to solve the unstructured problems of design [Kiernan et al 2019]. However, just putting all disciplines together is not enough, there is a clear need for design support to facilitate collaboration between the various design team members from different disciplines.

To cope with this complexity architects need more support from specialized engineers. The different expertise of engineers must be used more effectively especially in the conceptual design phase to reach for new solutions. This has consequences for the role of the engineers involved; they have to operate early in the conceptual building design process and act more as designers and less as traditional calculating engineers. As a consequence engineers have to develop new skills. Also the architect has to learn to not only share his ideas in the conceptual design phase but to really open up his mind and to truly design together with the engineers. Important is that no longer the architect is the one that leads the design process but that the team of architect and engineers leads the design process: Designing becomes a team effort already in the conceptual phase of design.

In section 2, details of the developed methodology is described. In session 3 the different interventions are provided to improve the design process and descriptions of the experiments for testing the method and interventions with professionals and with students. In section 4, the results of the different experiments are provided, in section 5 the analysis of the results followed with a discussion of the results in section 6. Finally in section 7 provides the conclusions about the added value of the design approach as an educational support tool and research tool as well as some remaining needs for further research and developments in relation to the morphological aspects of the developed design tools. This article is an up-dated overview of earlier published papers [Zeiler 2016-2020] and represents the result of research on Integral design that started in 1999 up to now.

2. Methodology

"*You never change things by fighting the existing reality. To change something build a new model that makes the existing model obsolete.*" [Buckminster Fuller]

Design problems are wicked as the information to start with is often very limited and there may be many ways of solving them [Kiernan et al 2017]. This poses difficulties for design teams and highlights the requirement to reach consensus on a variety of matters. Arriving at consensus can be challenging for teams and is affected by cognitive diversity [Kiernan et al 2017]. Due to problems resulting from the lack of quality of products and projects, in the early 1960's researchers and practitioners began to investigate new design methods as a way to improve the outcome of design processes [Cross 2007]. Since then, there has been a period of expansion through the 1990's right up to the present day [Le Masson et al 2012, Atkinson & Oppenheimer 2016]. Moreover, many of the design methodologies were developed at universities, and are rarely applied in industrial applications [Dorst 2016].

In 1999, the professional Dutch organization for architects and consulting engineers together with the University of Technology Delft and the Building Services Society started a research to develop an Integral design method to improve the conceptual building design process. Since 2003 this research has continued at the University of Technology Eindhoven and led to a design method based on intensive use of morphological charts [van den Kroonenberg 1988] and its outcome was evaluated in a situation as close as possible to practice amongst professionals, see section 3. The design method has a distinctive feature, the step pattern of activities (generating, synthesizing, selecting and shaping, that occurs within the design process, see Fig. 1.

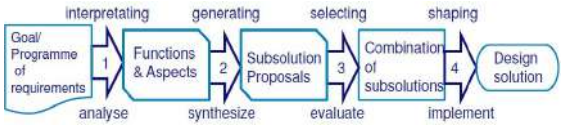

Fig. 1 - The four-step pattern of Integral Design.

A morphological chart is a kind of matrix with columns and rows which contain the aspects and functions to be fulfilled, see Fig. 2 step 1 and the possible solutions connected to them, see Fig. 2 step

2. These functions and aspects are derived from the program of demands. In principle, overall solutions can be created by combining various sub-solutions to form a complete system solution combination [Ölvander et al 2008]. Morphological chart structures the solution space and encourage creativity. Morphological charts are essentially tools for information processing, it is not confined to technical problems but can also be used in the development of management systems and in other fields [Pahl et al 2006]. The use of the morphological charts and morphological overview is an excellent way to improve the design process communication procedure. It makes it possible to record information about the solutions for the relevant functions and aids the cognitive process of understanding, sharing and collaboration [Ritchey 2010, Zeiler 2017].

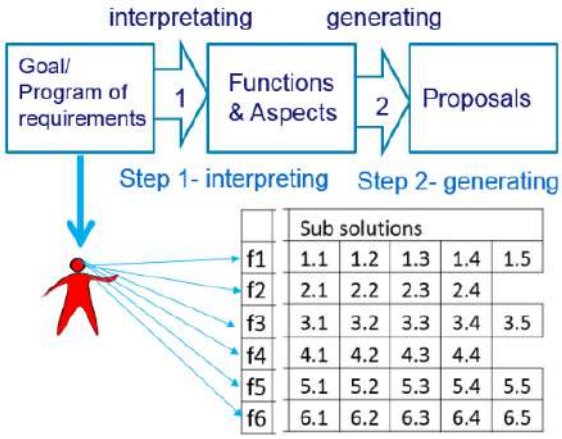

Fig. 2 - Concept of a morphological chart: Step 1 Functions and aspects to be fulfilled and step 2 related sub-solutions to the functions and aspects

In the first step of the integral design method, the individual designer has to make a list of what he thinks are the most important functions that has to be fulfilled based on the design brief. This is derived from their own specialist perspective. The morphological charts are formed as each designer translates the main goals of the design task, derived from the program of demands, into functions and aspects and is then put into the first column of the morphological chart, see Fig. 3 step 3. In the second step of the process, the designers add the possible part solutions to the related rows of the functions/aspects of the first column. Based on the given design task, each design team member perceives reality due to his/her active perception, memory, knowledge, and needs. The morphological charts represent the individual interpretation of reality, leading to active perception, stimulation of memory, activation of knowledge and definition of needs. These individual morphological charts can be combined by the design team to form one morphological overview, see Fig. 3 step 4. Putting the morphological charts together enables 'the individual perspectives from each discipline to be put on the table', which in turn highlights the implications of design choices for each discipline.

This approach supports and stimulates the discussion on and the selection of functions and aspects of importance for the specific design task. Important is the keeping of a phase of individual creativity during the morphological chart.

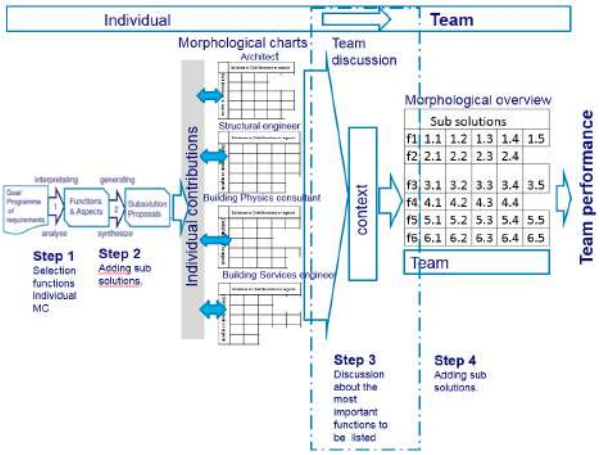

Fig. 3 - The first two design steps of the design team's process cycle, interpreting the design brief and list the functions in the first column of the individual morphological chart and add the related sub-solutions.

By structuring design (activities) with morphological overviews as the basis for reflection on the design results, stimulates communication between design team members and helps the understanding within design teams. It stimulates collaboration as it makes it easier to come forward with new design propositions. Through visualizing the contributions morphological overviews stimulate the understanding of the different perspectives among design team members. Unfortunately in the conceptual phase of the design it is not possible to accurately evaluate the quality of the mentioned functions/aspects or sub –solution. Only a quantitative analysis is possible by counting the number of mentioned functions/aspects and sub solutions. The number of functions and sub-solutions mentioned by the designers in their morphological charts and the design team's morphological overview were counted, for an example see Fig. 4 [Zeiler 2018].

3. Experiments

Since the year 2000 we, together with the Royal society of architects (BNA), the Association of Consulting Engineers (NLIngenieurs) and the Society of Building Services Engineers, organized a series of workshops in the Netherlands. More than two hundred professionals, with at least 12 years' experience, from different professional organisations voluntarily participated in these workshops. After extensively experimenting with different setups for the workshop, a 2-day workshop setting was selected [Savanovic 2009]. The two days' workshop was organised as part of a professional training program for architects and consulting engineers (structural engineers, building services engineers and building physics engineers)

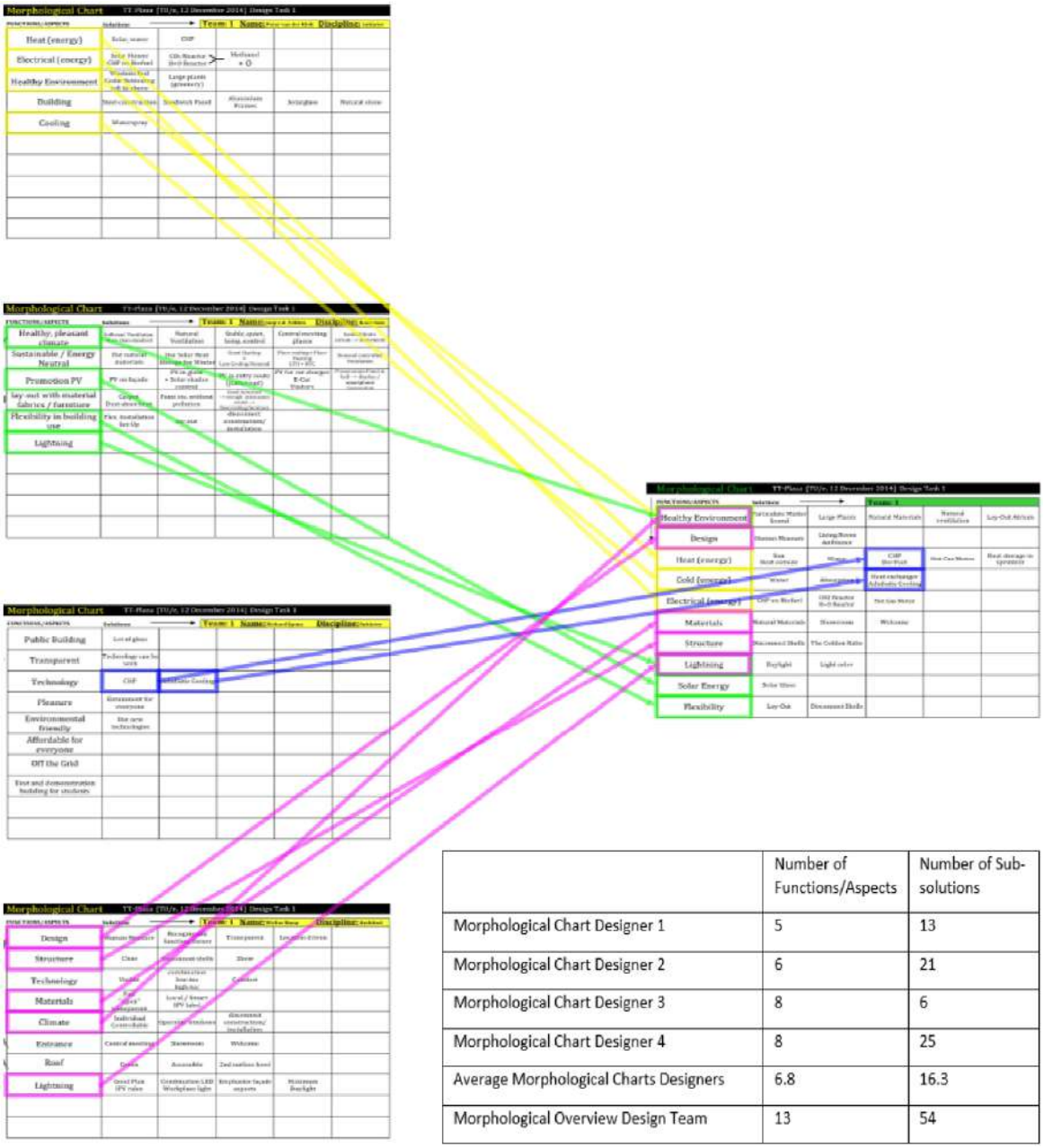

	Number of Functions/Aspects	Number of Sub-solutions
Morphological Chart Designer 1	5	13
Morphological Chart Designer 2	6	21
Morphological Chart Designer 3	8	6
Morphological Chart Designer 4	8	25
Average Morphological Charts Designers	6.8	16.3
Morphological Overview Design Team	13	54

Fig. 4 - An example of the transformation of the individual morphological charts into a morphological overview, indicate the functions/aspect in the morphological overview and where they came from [Zeiler 2018].

3.1 Workshops for professionals & students

In connection with the Integral design research project for professional in the Dutch building industry, we developed an educational project, the master project Integral Design. The concept of the integral design workshop for professionals was implemented within the start-up workshop of our multidisciplinary masters' project. The different design assignment all were related to the design of zero energy buildings. These complex tasks require early collaboration of all design disciplines involved in the conceptual building design and as such let the students experience the added value of the design method. Master students from architecture, building physics, building services, building technology and structural engineering participated in these projects. The basis of this project, which serves as a learning-by-doing start-up workshop for master students, is a method with extensive use of morphological charts combined to a morphological overview of the design team. The master project Integral design was initiated by the chair of Building Services in the 2005/06 academic year. During the start-up workshop professionals participated in the student's design teams and this specific intervention within the design process has been investigated. Having a tested framework for introducing the design method allowed us to investigate the effects of different interventions as well as the analysis of several aspects, such as the effectiveness of different designers or the effect of communication in words or sketches [Zeiler 2014]. The frame work of the approach is presented in Fig. 5, the program and setup of the workshop.

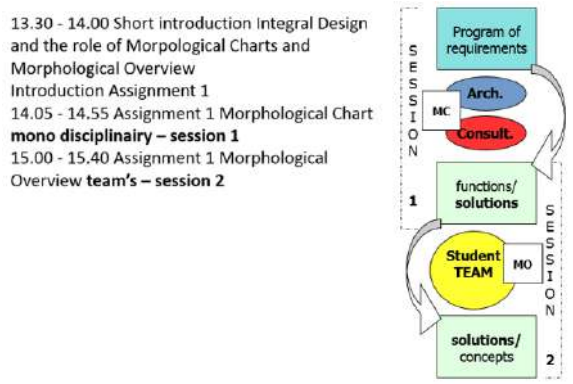

Fig. 5 - Program and set-up of start-up workshop

All the assignments had a similar level of complexity which made the results comparable. To investigate the effect of the morphological tools of the Integral design approach they were used in similar workshops setting for different types of students, professionals and practitioners, in brackets the number of particpants;

- Bachelor students (168) 2015-2021

The students of the course in which the workshop was held were 2nd and 3th year bachelor students, age around 20-22, all Dutch. The students were from the Faculty of the Built Environment and of the Faculty of Psychology and Technology.

- Master students (150) 2011-2018

These were 4th year students (architectural, structural, building physics and building services) all from the Faculty of the Built Environment, age around 22-24.

- Architectural Master students (11) 2017

One workshop was held for students of architecture all working in a Master thesis project design atelier as part of their MSc graduation project. So they were 5th year students who nearly had finished their studies, age around 23-25. This was the only mono disciplinary group in the comparison.

- PDEng students (18) 2012-2013

The students from the Post Doctoral Engineering (PDEng) program Smart Energy Buildings and Cities (SEB&C) were from all different International MSc discipline backgrounds, age 24-26.

- Professionals (24) 2009

In the research of Savanovic [2009] the concept of working with morphological overviews was tested in different series of workshops for professionals, with at least 12 years of experience. There were 4 series of workshops with in total 96 participants for testing different set-ups. Here only the results of the 4th workshop are included.

- Professionals (8) 2015

In 2015, the researchers participated in the start-up of a real professional project for the design of a nearly Zero Energy Building [de Bont et al. 2016]. The professionals had around 20 year experience.

- Practitioners (19) 2019

The Dutch society for Building Services Engineers TVVL, together with the TU Eindhoven organized a master call. There were to restriction towards the participants, unlike the workshops for professionals in the research of Savanovic [2009] where the participants should have a least 12 years of experience.

4. Results

4.1 From Morphological Chart towards Morphological Overview

Central element of the Integral Design process is the use of Morphological Charts by individual designers which were combined into one Morphological Overview by the design team. During all experiments the design teams existed of different disciplines. The average numbers of functions and solutions as mentioned by the design teams in their Morphological Charts and Morphological Overview as well as the relative increase are represented in Fig. 6, 7 and Fig. 8 based on Zeiler [2019] updated.

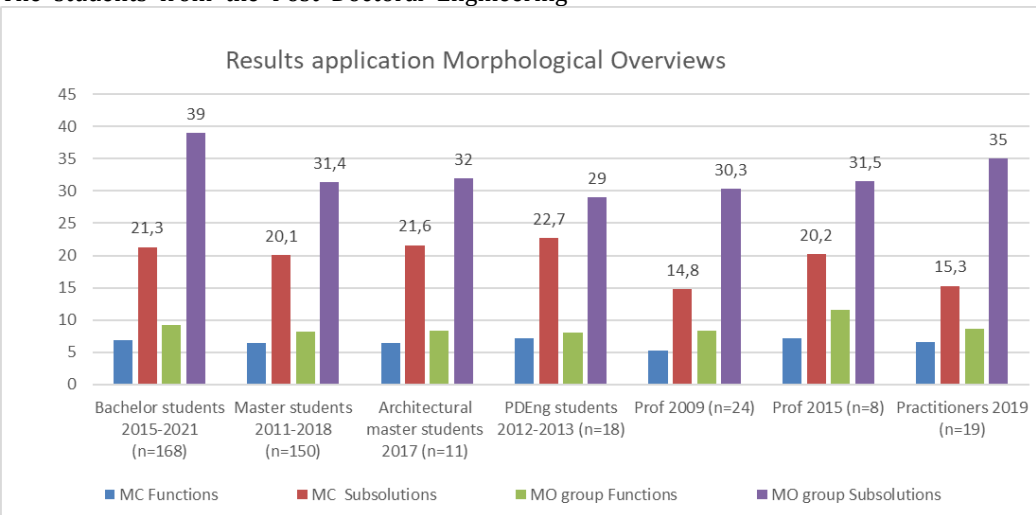

Fig. 6 - The average scores in Morphological Charts & Morphological Overview by individual students, professionals and practitioners for the different groups, based on Zeiler [2019] updated

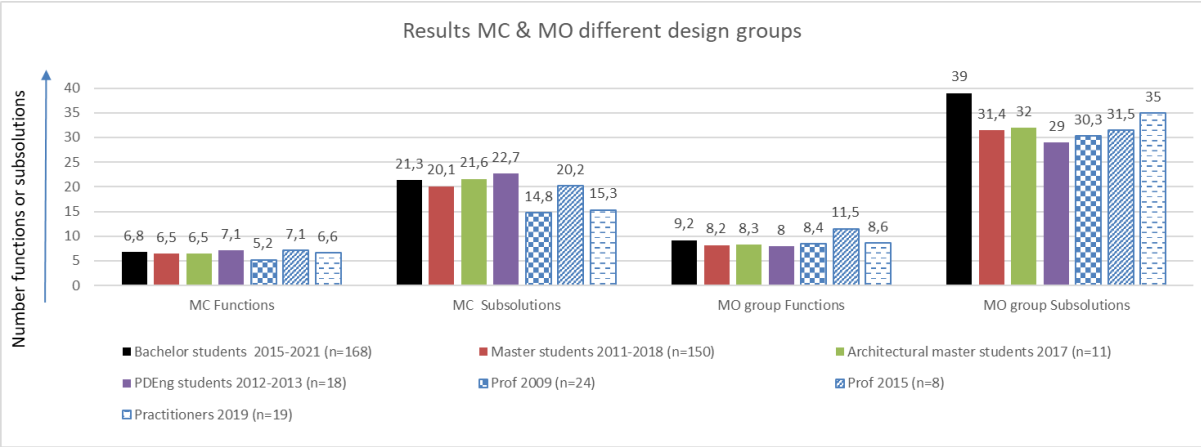

Fig. 7 - Comparison of the average scores in Morphological Charts & Morphological Overview by individual students, professionals and practitioners, based on Zeiler [2019] updated

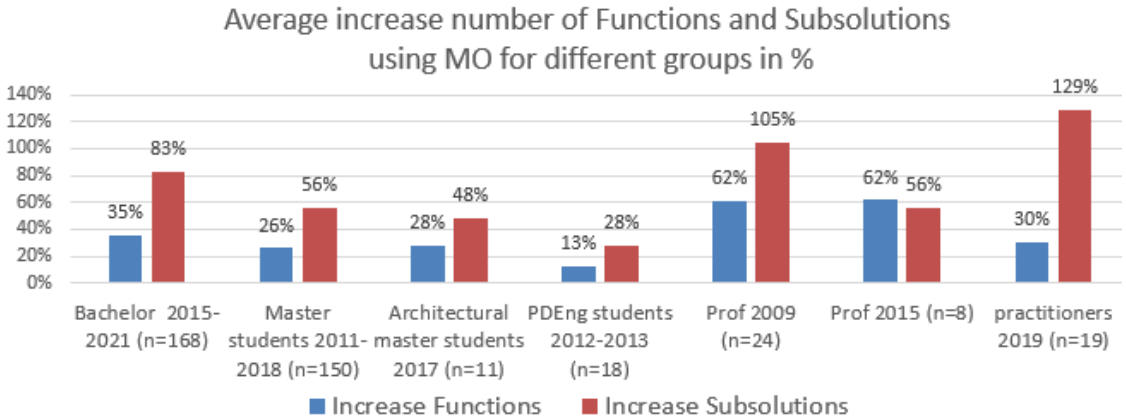

Fig. 8 - Comparison of the average relative increase in number of functions and sub solutions in their Morphological Overviews compared to the average results from the individual Morphological Charts, based on Zeiler[2019] updated

Using morphological charts during a conceptual design phase is not new, but adding the morphological overview after a team discussion makes it a new innovative team design approach. The group interaction is of great importance during the conceptual design phase and has a clear positive effect on the number of functions and aspects discussed as well as on the number of generated sub solutions. This was found by the original research with professionals [Savanovic 2009] as well as in the educational setting with different types of students, as well as in experiments in real projects and professional settings. Given the number of involved design teams in the series of workshops, with 347 students and 123 professionals as participants, there is a sound quantitative basis to the conclusion that it really helps to integrate the different design disciplines and create synergy..

6. Discussion

"*Under the symbolic composition I have placed two clasped hands, the fingers enlaced horizontally, demonstrating the friendly solidarity of both architect and engineer engaged, on the same level, in building the civilization of the machine age*"

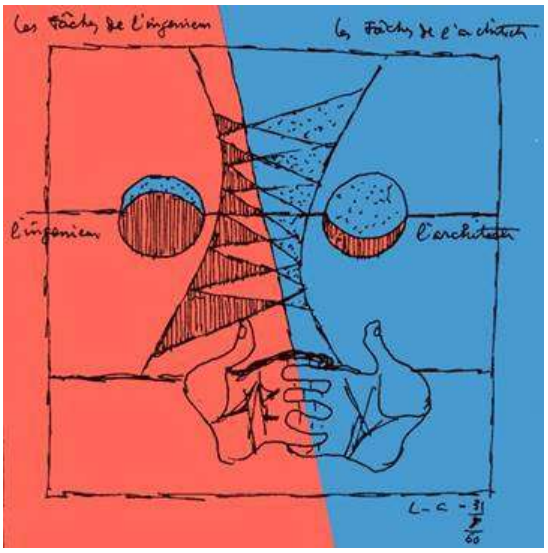

[Le Corbusier, 1960, Science et Vie].

The workshop setting of a design team in the conceptual phase of design is getting a more common situation in Dutch building design practice. Schön (1987) has proposed a practicum as a means to 'test' design(ing). A practicum can assess a design method and the degree to which it fits human cognitive and psychological attributes (Frey and Dym 2006). A workshop can be seen as a specific kind of practicum. It is a self-evident way of working for designers that

occurs both in practice as during their education. As such a workshop provides a suitable environment for testing and validating the added value of the design approach. Workshops make it possible to gather a large number of students and professionals in a relatively short time, repetition of the same assignment and comparison of different design teams and their results.

There is discussion whether the morphological approach is significantly subjective however, each design team member brings forward their own interpretation of the most important aspects of the design brief and discuss about it as a team. This team discussion leads to the agreed morphological overview which makes the design process transparent. It gives also clients and project managers a possibility to react on specific contributions of architects and engineers and there makes it significantly objective.

7. Conclusions

"*Architecture will become more informed by the wind, by the sun, by the earth, by the water, and so on. This does not mean that we will not use technology. On the contrary, we will use technology even more because technology is the way to optimize and minimize the use of natural resources*" [Richard Rogers]

Integral design is a necessity for nature assisted Air-conditioning where architect and consulting engineers have to truly collaborate in the conceptual phase of building design process. What is needed is an optimal exchange of interpretations of the design brief as well as an exchange of ideas on possible solutions, see Fig. 9.

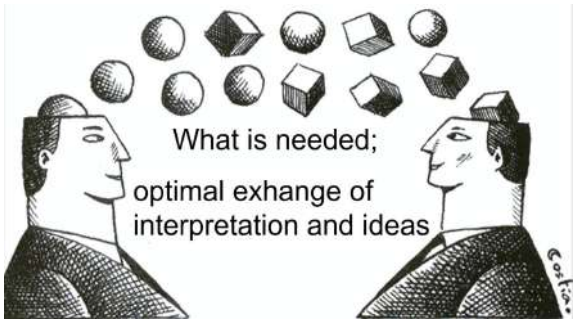

Fig. 9 - The needs with the conceptual design phase

However, a break with the traditional line of thoughts of architects as well as consulting engineers is there for needed. A new design model, Integral Design, was developed to support interaction between all the disciplines involved in the conceptual building design process by structuring the communication and solution generation process in steps. By structuring the information flow about the tasks and solutions of the other disciplines the method forms a design within the design process and enables a structured approach even in the conceptual design phase. The use of the morphological overview based on the individual morphological charts creates a way to share interpretations and ideas for solutions forming a basis for synergy leading to more and innovative designs, see fig. 10.

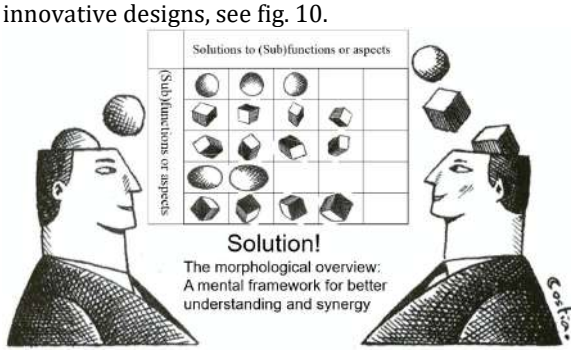

Fig. 10 – The morphological overview to connect the minds of the design team

The main lessons from the paper are that Integral Design with its use of morphological overviews stimulates collaboration and exchange of ideas and perspectives between architects and engineers. It helps them with their communication. As such it is a good method for supporting the education of a new generation of architects and engineers, who each have new roles in the highly complex tasks of designing sustainable nearly Zero Energy Buildings. The educational setting allowed us to investigate interventions in the design process of students and professionals. The results were presented and clearly showed the possibilities to stimulate the creativity of design teams by applying the integral design method with its use of morphological overview.

The design method had a major positive effect on the number of proposed sub-solutions and also on the amount of functions and aspects considered in the conceptual phase of the design process by the design team members. This indicates that the effectiveness and productivity of design teams was large improved by adding structure to the process. The role of the morphological charts and morphological overview is in structuring the process as well as it enables analysing the conceptual design process in more detail. As such is it a valuable approach to invent the necessary new more sustainable solutions for the future. We see Integral design as a necessity for truly sustainable buildings and as such a prerequisite for the energy transition towards 2050 .

8. Acknowledgement

This research was done in cooperation with the Dutch engineering consulting companies: Deerns, Smits van Burgst, Valstar Simonis, RHDHV and Nieman. The project was financially supported by the professional organisations Techniek Nederland (formerly UNETO-VNI) and Wij Techniek (formerly OTIB] as well as the foundations WOI and PIT. The earlier research which formed the basis was supported by the Dutch Society of Architects BNA, the Dutch Society for Consulting Engineers NL Ingenieurs and the Dutch Society for Building Services Engineers TVVL.

9. References

Atkinson H., Opperheimer M.R., 2016, Design Research – History, theory, practice: histories for future-focussed thinking, Proceedings DRS 2016, Brighton, UK

Bell B. S., Kozolowski S.W.J., 2002. A Typology of Virtual Teams, Implications for Effective Leadership. Group and Organization Managment 27(1), 14-49.

Bont K. de, Zeiler W., Velden J. van der, 2016, Integral Design method to support nZEB design: a real project experiment, Proceedings Clima 2016, Aalborg, Denmark

CIBSE, 2016, RIBA president wants 'frank debate' on supply chain conflict, CIBSE Journal January 2016

Cross N., 2007, Editorial Forty years of design research, Design Studies 28(1): 1-4

Dorst K., Design practice and design research: finally together? Proceedings DRS 2016, Brighton, UK

EU, 2020, Energy efficiency in buildings, https://ec.europa.eu/info/news/focus-energy-efficiency-buildings-2020-feb-17_en

Frey D.D., Dym C.L., 2006, Validation of design methods: lessons from medicine, Research in Engineering Design 17: 45-57

Jackon A., Heywood M., 2019, Development of Integrated Design , CIBSE-ASHRAE Group seminar and webinar, Foster+Partners, London, 18 September 2019

Jonassen, D., Strobel J., and Lee C., Everyday problem solving in engineering: Lessons for engineering educators. Journal of Engineering Education 2006. 95(2): p. 139.

Kanters J., Horvat M., Dubois M., 2014, Tools and methods used by architects for solar design, Energy Buildings 68(part C): 721-731

Kiernan L., Ledwith A., Lynch R., 2017, How design education can support collaboration in teams, Proceedings E&PDE, Oslo, Norway

Kiernan L., Ledwith A., Lynch R., 2019, Comparing the dialogue of experts and novices in interdisciplinary teams to inform design education, international Journal of Technology and Design Education, published online January 23th 2019, https://doi.org/10.1007/s10798-019-089495-8

King D., 2012, Holistic Approach, CIBSE Journal January 47-49

Kovacic I., Filzmoser M., 2014, Designing and Evaluation Procedures for Interdisciplinary BIM Use – An Explorative Study, Engineering Project Organization Conference Devil's Thumb Ranch, Colorado July 29-31

Kroonenberg H.H. van den, 1988, Stimulating creativity and innovations by methodical design, In Creativity and Innovation: towards a European Network, Springer Netherlands

Le Masson P., Hatchuel A., Weil B., 2012, How design theories support creativity – an historical perspective, Proceedings 2nd International Conference on Design Creativity, ICDC2012, Glasgow

Linder V. van der, Dong H., Heylighen A., 2016, Capturing architect's designerly ways of knowing about users: Exploring an ethnographic approach, Proceedings DS 2016, Brighton, UK

Ölvander J., Lundén B., Gavel H., 2008, A computerized optimization framework for the morphological matrix applied to aircraft conceptual design, Computer Aided Design 41(2): 187-196

Pahl G., Beitz W., Feldhusen J., Grote K.H., 2006, Engineering Design, A Systematic Approach, 3th edition, Ken Wallace K. and Blessing L. translators, Springer

Ritchey T., 2010, Wicked problems Social messes, Decision Support Modelling with Morphological Analysis, Swedish Morphological Society , Stockholm

RVO, 2020, monitor-energiebesparing-gebouwde-omgeving 2019
https://www.rvo.nl/sites/default/files/2021/01/monitor-energiebesparing-gebouwde-omgeving-2019.pdf

Savanović P., 2009, Integral design method in the context of sustainable building design, PhD thesis, Technische Universiteit Eindhoven, Eindhoven, Netherlands

Schön D. A., 1987, Educating the Reflective Practitioner: Towards a New Design for Teaching and Learning in the Professions, Jossy-Bass, San Francisco.

Smith A., 2019, Piers'Review, Integrated design at Foster+Partners, CIBSE Journal, September, 40-42, https://www.cibsejournal.com/general/piers-review-integrated-design-at-foster-partners/

Wright F.L., 1953, The language of organic architecture, The Magazine of Building, Architectural Forum, May 1953 106-107

Young L., 2014, I cannot think of a better career than services engineering, Interview with Mike Davis, CIBSE Journal April: 29-31

Zeiler W., 2016, Integral Design to improve communication and sub solution generation in building design collaboration, CIBSE Technical Symposium, Edinburgh, UK

Zeiler W., 2017, Design Handbook, A methodical framework, Noordhoff Uitgevers, Groningen, Netherlands

Zeiler W., 2018, Forming design teams for improved performances, Proceedings ASHRAE Annual conference, June 23-27, 2018, Houston, TX,, USA

Zeiler W., 2019, An Integral Design framework for Multi-Disciplinary Design, Proceedings ICED19, International Conference on Engineering Design, 5-8 August 2019, Delft, Netherlands

Zeiler W., 2020, De invloed van de morfologische aanpak op de oplossingsruimte , TVVL magazine 4: 52-57

Reflections on flipped classroom and digitized laboratory concept in building automation courses

Jochen Müller, Wilfried Huthmacher

Faculty of Process Engineering, Energy and Mechanical Systems, TH Köln, Germany, jochen.mueller@th-koeln.de, wilfried.huthmacher@th-koeln.de

Abstract. In the last decade, innovative digitized teaching concepts were developed to improve the learning environment of students. Also due to actual restrictions concerning classroom teaching during the corona pandemic, these concepts are increasingly spreading in daily university life.
This article describes our experience of the last five years with digitized lecture and laboratory based on the flipped classroom concept. A comparison to the classic teaching form is difficult to achieve in daily university practice. Thus, the paper reflects the applicability of flipped classroom format for control engineering and building automation based on subjective experiences of students and tutors, as well as lecturers.
Keywords. Digital education, flipped-classroom, blended learning
DOI: https://doi.org/10.34641/clima.2022.287

1. Introduction

Many of us can still remember the following scenes from a basic lecture: a crowded lecture hall, a seat on the stairs, the professor writes formulas on one of the three blackboards at an incredible speed, while his assistant is already cleaning the blackboard just described. Questions are not asked, only a few dares to interrupt this process - or have time, because the next board threatens to be cleaned.

To the advantage of today's students, the number of such lecture formats has decreased significantly, also due to increasing didactic training of professors. In addition, many innovative teaching concepts to improve the learning environment of students have been developed in the last decade, which - also due to the restrictions on classroom teaching during the Corona pandemic - are increasingly spreading in everyday university life.

2. Flipped Classroom

In lectures based on the flipped classroom concept [1,2], students independently develop teaching topics or competences that they apply and deepen during presence phases in small groups under close guidance of lecturers. This format is particularly widespread in basic lectures with a large number of students in order to counteract attitudes of students towards reception, to activate them for teaching content and to extend the learning process to the entire semester.

Flipped classroom goes hand in hand with a competency orientation in teaching, i.e. sub-competencies of a teaching module must be identified and their achievement over the semester must be timed. The application and deepening of these sub-competencies take place in presence phases, which are characterized by intensive supervision of the students.

In the self-study phase, students are provided with teaching materials via online media. These are videos for lectures and exercises, but also introductions to laboratory experiments and instructions for the operation of laboratory hardware and software can be offered digitally in preparation for lab experiments or projects. Even during the self-study phase, the students are closely supervised by lecturers and tutors, who discuss exercises or problems that arise in office hours or forums.

A flipped classroom format combines different learning processes of students: an individually shaped self-study process, a peer learning process during tutorials, and group work process during presence phase. To check the preparation and performance of the working groups, a test before starting the presence phase is a good idea.

3. Building automation courses

3.1 Principles of control engineering

The lecture principles of control engineering are offered to students of the Renewable Energies and Energy and Building Technology courses in the 3rd semester (about 350 students) – in combination with

Copyright ©2022 by the authors. This conference paper is published under a CC-BY-4.0 license.

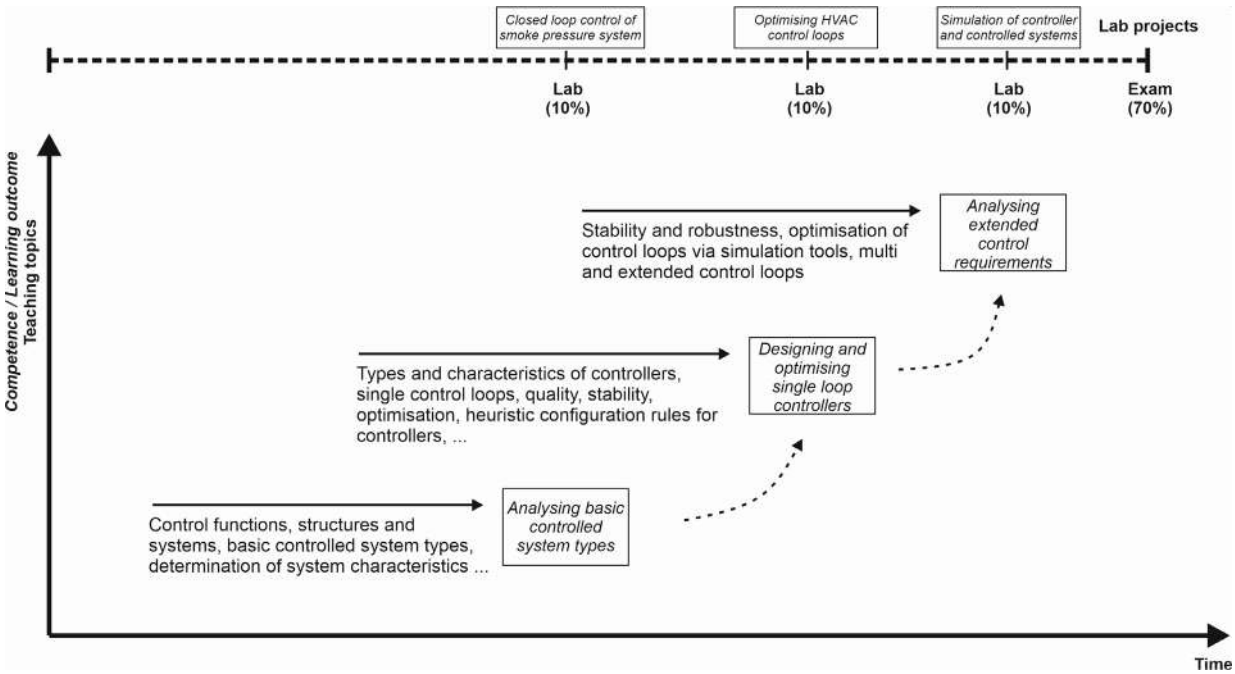

Fig. 1 – Learning outcomes and structure of control engineering

the basics of measurement technology in one module. The measurement part of the module follows a classic teaching format, 2017 the flipped classroom concept has been implemented for the control engineering part. The final competence in control engineering is the analysis of a building technology system from a control engineering perspective and the design and commissioning of a stable and optimized control. For this purpose, the students understand the means of describing control engineering tasks, characteristic curves, variables and behavior of control circuit components, properties and behavior of continuous and discontinuous controllers, control circuits and their stationary and dynamic behavior (Figure 1).

In control engineering, the aim is to achieve the expected final competence in three steps. Focus of the first learning phase is an introduction to controlled systems and the ability to analyze those. Building on this, the students develop competences to design and optimize a simple control task based on heuristic setting rules. This competence is deepened in the third learning phase through stability analyzes of control circuits and the use of simulation programs to optimize them.

The preparation for the presence phases is checked by means of a certificate by means of Ilias E-Assessment. After successful implementation, submission and debriefing of a laboratory report by the working groups, its result contributes to the overall result (10% each). An individual examination of the final competence is also carried out by means of a written exam (70%).

3.2 Principles of building automation

The desired final competence of the lecture principles of building automation (5th semester of Energy and Building Technology course, 100 students) follows a basic workflow of automation technology practice. It consists of the design, planning, implementation, commissioning and operation of an automation function in building technology. For this purpose, the students understand the means of description of building automation functions, function and functionality of the fundamental system components in the field, an at automation and management level, as well as methods for programming automation functions and apply this knowledge to their implementation. The students analyze basic problems and aspects of building automation and independently design solutions in terms of sustainable and optimized building operation. Prerequisites for the module are competences acquired in the modules plant hydraulics, control engineering and building system technology, basic system engineering (heating and cooling systems, air conditioning and sanitary technology), as well as the introduction to digital data transmission and information technologies.

The teaching of the topics in the self-study phases currently follows the classic teaching format for lectures and exercises (a flip is planned for the upcoming winter semester). Introductions to laboratory experiments and instructions for handling laboratory hardware and software are available in the form of instructional videos. The

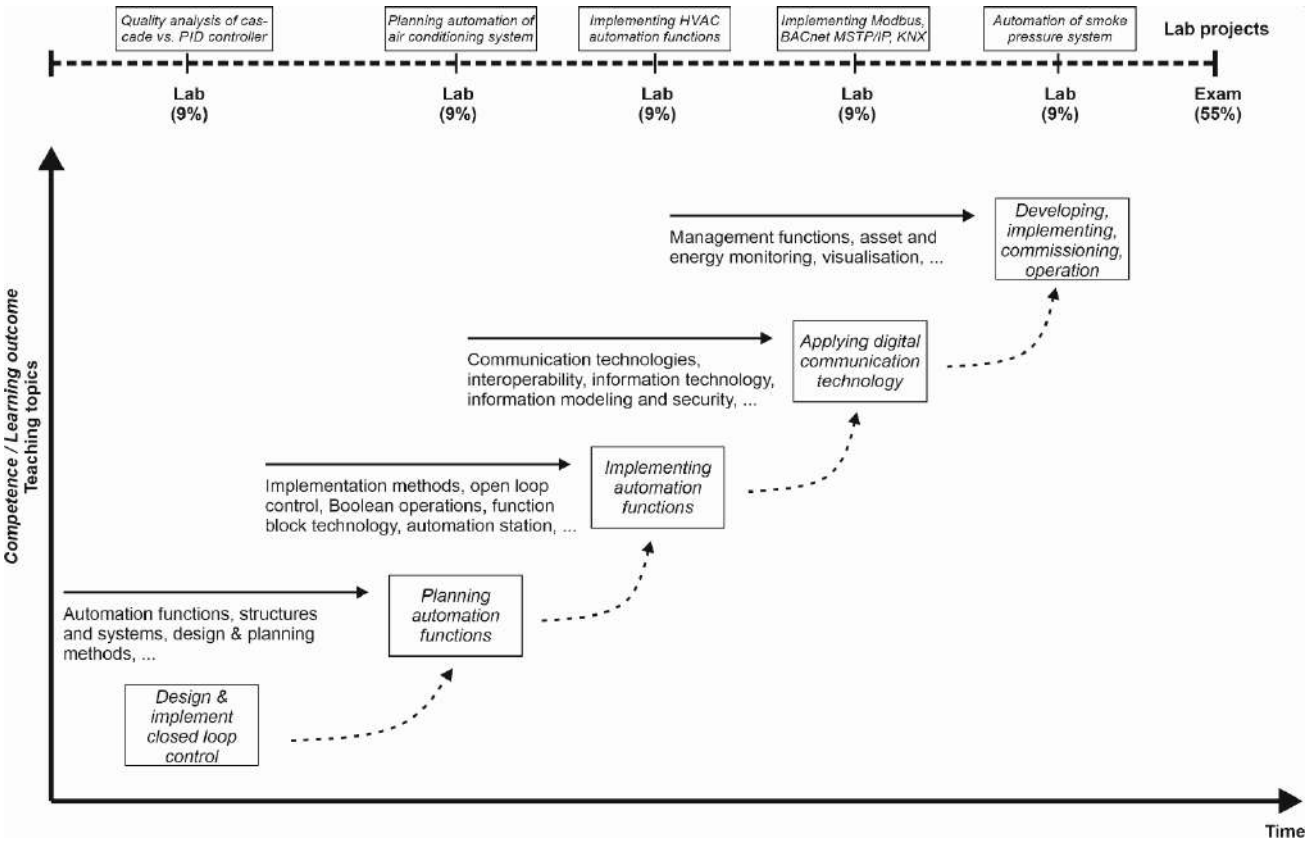

Fig. 2 – *Learning outcomes and structure of building automation*

competency orientation of the module, the application and deepening of partial competencies in presence phases, as well as the structure and sequence of the presence phases correspond to the flipped classroom concept (Figure 2). As in control engineering, lecture content and exercises are discussed individually by students and tutors during office hours. The teaching content developed in preparation for the presence phases is also checked in building automation in the form of certificate (9% each), and achievement of the final competence is assessed in a final examination (55%).

The final competence of principles of building automation is achieved in five steps. At the beginning of the module, control engineering skills are checked in a first presence phase, the subsequent step generates competences for the creation of planning documents of a HVAC system. These serve as the basis for the configuration of an automation station and the implementation of function block networks for the automated operation of the HVAC system. A deepening of skills for the use of digital communication technologies and the analysis of interoperability is the focus of the fourth competence step, the final level brings together all previous competences for the automation of a smoke pressure system and adds the skill for design and implementation of technical building management applications.

3.3 Teaching infrastructure, laboratory facilities

Teaching videos on YouTube are available for the self-study phases of the students [3].

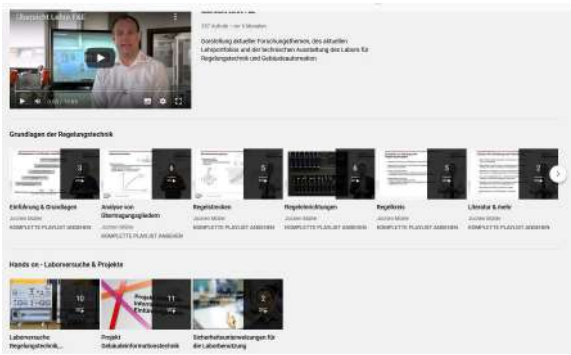

Fig. 3 – YouTube channel with teaching videos for lecture and laboratory experiments

Teaching videos are provided in a structured way for the self-study phases via links in the central teaching platform Ilias. To deepen the teaching topics, interactive exercises are integrated into the teaching videos via an Ilias-H5P [4] integration (Figure 4). An individual discussion of the exercises takes place in daily office hours, its content is individually designed by the students via forum contributions.

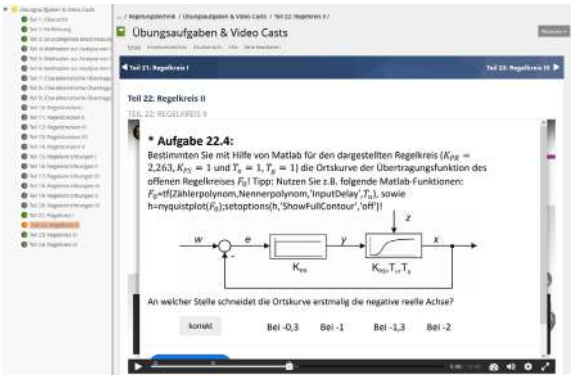

Fig. 4 – Teaching videos with embedded exercises in Ilias-H5P

Focus of the technical facilities [5] of the laboratory are in the areas of control engineering, digital communication technologies, automation of building systems and optimization of operational processes in technical building management. The automation of technical building facilities in the laboratory is integrated into lab experiments, in addition training systems are also available. Around twenty automation stations from different manufacturers are currently in use. Widespread digital communication technologies of building technology are used for information technology networking. Local and cloud-based solutions are available for the visualization of plant information in technical building management applications (Figure 5).

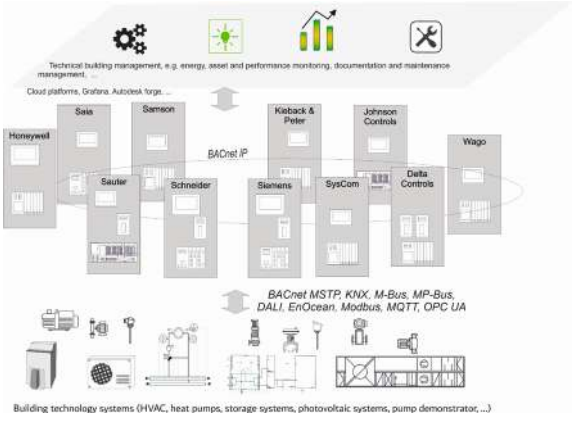

Fig. 5 – Technical facilities of the laboratory

Laboratory experiments within the principles of control engineering and principles of building automation are carried out simultaneously on six experiment facilities. The working groups of up to maximum five students are led by three lecturers resp. tutors. Under corona conditions, laboratory experiments take place via a zoom conference or in a hybrid form - by sending one student to the laboratory and a parallel zoom connection of the remaining group members.

A virtualized 360° laboratory [6] (Figure 6) serves as a central access point to laboratory experiments and the experimental rigs.

Fig. 6 – Tour in the virtualized 360° laboratory for building automation

Students enter the virtual laboratory, explore it, determine at the experimental setup (Figure 7) and receive videos explaining tasks and implementation of the experiment, as well as how to operate the hardware and software used.

Fig. 7 –Virtual exploration of laboratory experiments

In addition, direct access to teaching materials in Ilias is possible via links in the virtualized laboratory (Figure 8).

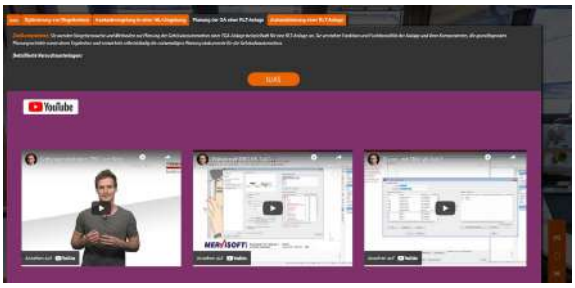

Fig. 8 – Central access to teaching materials via virtualized laboratory

4. Reflections

An objective comparison of courses in different teaching formats is not possible at this point. Conclusions about the performance of a course, analyzes of teaching quality, the desired target competences vs. the feasibility of the module etc. are affected by the individual characteristics of students and their annually changing composition. Analyzes based on a targeted compilation of comparable students and a parallel implementation of a teaching module in different teaching formats are not

available. Therefore, the following reflection on the applicability of the flipped classroom teaching format in modules of control engineering and building automation is based on the subjective experiences and feedback of the students and tutors as well as the lecturers in comparison to the classic teaching format.

The flipped classroom concept is suitable for activating students in courses. Working in small groups during the presence phases reduces the inhibition threshold with regard to questions about problems of understanding. The peer learning process through tutoring also lowers this inhibition threshold. Many difficulties or ambiguities can thus be clarified before the presence phases. The concept is therefore particularly useful for courses with a variety of students, e.g. for basic lectures. For elective modules with a small number of students, the great effort involved in creating teaching materials must be weighed against the benefit. This analysis should also include the stability of the teaching content, e.g. in the case of special elective modules related to research.

The self-study phase considers the individual learning characteristics and capacities of students. They can fix the scope, but also the time and place of acquiring teaching content themselves. The distribution of the presence phases over the semester, as well as the verification of the required teaching content and competences through certificates, extends the learning process of the students to almost the entire semester. This is also reflected in increased efficiency in the implementation of laboratory experiments or projects.

Overall, the failure rate has fallen in both modules in recent years (with stable learning outcomes), which is attributed to improved activation of the students and an expansion of the learning and examination process.

Critical to the successful implementation of the flipped classroom teaching format is a sufficient number of face-to-face phases and an intensive supervision of the students by lecturers. For example, three presence phases are to be regarded as insufficient for the desired final competence in control engineering. Close tutoring of the students during the self-study phase is also very important. Communication channels must be established for the short-term solution of problems of understanding. Fundamental to the success of a flipped classroom teaching format is the quality of teaching videos. They should always have a clear reference to the desired competence of the following presence phase. By embedding exercises in teaching videos, a sense of achievement is created, which additionally motivates students during the self-study phase. The participation of students in teaching videos or the creation of videos by tutors also resulted in positive feedback.

5. Conclusions

Are universities still needed when teaching materials are available via YouTube? Sure, because the key to flipped classroom is the teaching and deepening of subject-specific competences through intensive support of the students during the presence phases. Flipped Classroom does not replace lecturers or save staff, the use of resources remains the same or is increased. The improvements in the quality of teaching justify these investments.

The high effort involved in creating attractive teaching materials motivates closer cross-university cooperation between professors. Because a legitimate question is certainly whether a large number of these experts should devote a similar amount of effort to creating similar instructional videos, e.g. about common function block technology.

Data sharing not applicable to this article as no datasets were generated or analyzed during the current study.

6. References

[1] Bishop, J. L., The Flipped Classroom: A Survey of the Research. American Society for Engineering Education, 120th ASEE Annual Conference & Exposition, 2013

[2] Jonathan Bergmann and Aaron Sams, Flipped Learning: Gateway to Student Engagement, International Society for Technology in Education: Eugene, Oregon and Washington, DC, 2014

[3]https://www.youtube.com/channel/UC_sTSOiieIi2wCffZvL6D6A

[4] https://h5p.org/

[5]https://www.youtube.com/watch?v=noDJfj_ASbQ

[6] https://gart.web.th-koeln.de/

From insight into energy transition maturity to powerful task-based cross-sectoral upskilling

Jan Cromwijk [a], Carmen Poort[b], Tomo Cerovšek [c], Andrea Moro [d], Martin Breen[e]

[a] ISSO, Rotterdam, the Netherlands, j.cromwijk@isso.nl.

[b] ISSO, Rotterdam, the Netherlands, c.poort@isso.nl.

[c] Faculty of Civil and Geodetic Engineering, University of Ljubljana, Ljubljana, Slovenia, tomo.cerovsek@fgg.uni-lj.si.

[d] iiSBE, Turin, Italy, andrea.moro@iisbeitalia.org.

[e] Technological University of the Shannon, Thurles, Ireland, martin.breen@tus.ie.

Abstract. To make advancements in energy transition and creating a future proof built environment, professionals and workers who possess required skills are crucial. This paper proposes a model that can be flexibly adopted to reach an acceleration of upskilling opportunities and outcomes. The paper outlines the Technological Innovation Systems approach for delivering cross-sectoral knowledge and skill development agendas, as well as a method to develop and apply skills mappings and task-based qualifications. The combined approach is a stepping stone to enable digital support for learning on the job, learning transaction based recognition of successfully acquired knowledge and skills, as well as skills passports and micro-credentials. The approach has proven to be useful for sectors where technological innovations heavily influence ways of working, and it enables a common reference methodology in Europe. In order for the approach to be utilised optimally, key requirements should be taken into account, indicating that the taxonomy, toolkits and context of skills should be well aligned. The paper suggests future developments to address the transorganisational implementation of the approach, and the transitional management of skills gaps.

Keywords. Technical Innovation Systems, skill development, skill-levels, recognition, lifelong learning, micro-learning credentials, learning on the job
DOI: https://doi.org/10.34641/clima.2022.180

1. Introduction

The energy transition is moving currently from take-off phase into acceleration phase. Sustaining the built environment is one of the urgent challenges in play. To realise the transition towards a people centred, energy-efficient, circular, digitised, climate adaptive and healthy built environment, acceleration is urgently needed. Although, without a proper set of mastered knowledge and skills, participation in multidisciplinary design teams and cross-craft collaborations on-site prove to be difficult, thus hindering the needed acceleration.

By applying the Technological Innovation Systems approach (TIS) [1] in Horizon 2020 projects for improved energy innovation and skills, a method has been developed and applied to pinpoint where training and course development is needed in the short, intermediate and long term. This is in order to underpin when and for which occupations dissemination of technical innovations and related knowledge and skills is needed. The resulting skills-mappings prove to be of practical value in exploration and decision making processes by reducing the number of choices and providing a clear view on skill-levels needed.

As the building services sector also acts as an innovator and is the axis between the construction, energy, IT and health sectors, integrating knowledge from these fields into training and course development is not an easy challenge. Large scale projects about BIM integration and nZEB tackled this by developing an application of a task-based qualification framework. This framework enables intersectoral teams to create task-based qualifications and corresponding Unit of Learning Outcomes that cover all occupations and sectors involved.

Resulting curricula are cross-sectoral, highlighting roles and responsibilities and the minimal set of knowledge and skills needed for assessing the

Copyright ©2022 by the authors. This conference paper is published under a CC-BY-4.0 license.

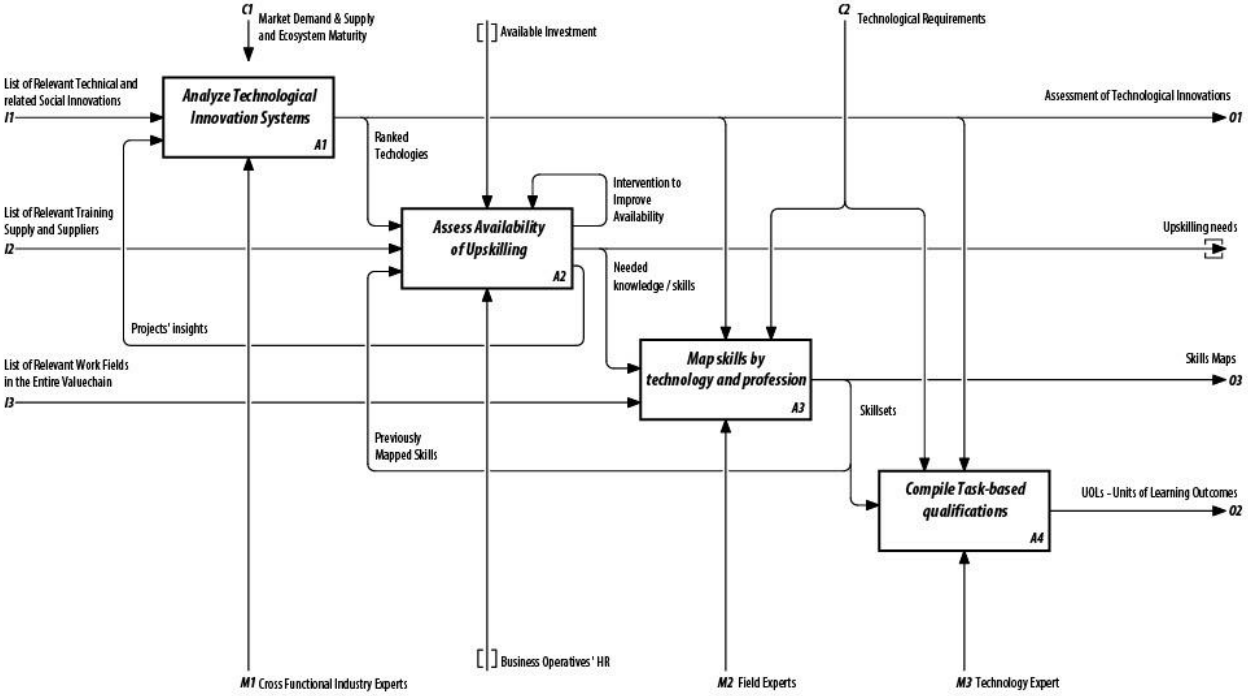

Fig 1 - Model of the main steps proposed to increase and improve upskilling opportunities, connected to their inputs and outcomes.

applied value of a specific innovation or theme. It also enables sectoral and intersectoral skills-registers / skills-passports to take task based knowledge and skill development into account. Furthermore, the development of transparent micro-learnings and micro-credentials is facilitated.

The purpose of this paper is to provide insight into methods that contribute to the establishment of upskilling, as well as propose a common language for the upskilling process. It is relevant to note that the methodology presented is hardly linear; it is dynamic for the sake of design thinking, which will allow the components to feed into one another. This can create a constant feedback loop, promoting innovation and exploration within the system. In order to make the system work optimally, the paper proposes several key requirements to consider.

2. Method

For this paper, outcomes of various large scale EU funded projects about energy technologies and upskilling have been used as input. The methodology is presented in the form of an IDEF0 diagram (Figure 1) with its main activities connected through outputs and inputs. A detailed description of individual activities is given in the follow-up sub-sections. The findings derived from the described activities are based on surveys, systematic action research, and iterative frameworking from the projects, which collectively lead to a well-informed synthesis.

3. Technological Innovation Systems approach

It is imperative that availability of upskilling supplies corresponds with the market adaptation stage and related TIS-maturity of upcoming technologies. When technologies advance, upskilling should be scalable at a fast pace. The Technological Innovation Systems (TIS) approach addresses these challenges by analysing the expected need and supply of upskilling.

The TIS model approach functions as a first step in the upskilling process that is needed to diffuse knowledge around critical innovations. The purpose of this step is to prevent knowledge gaps, allowing for new technologies to further penetrate the market. This can be achieved by providing pro-active upskilling possibilities to the workforce delivered through adapting the innovative means.

The analysis model developed applies the TIS-model and adds several additional knowledge dissemination indicators. It comprises an easy to use five-point scale ranking. The results of this ranking display to what extent the development of new training material is needed for a certain technology and in what period of time the training means should be established. Additionally, the model scores existing technologies for how well they are represented in upskilling and training at the time of investigation.

By combining the ranking of the maturity of an innovation, expected speed of development, and available upskilling, it becomes possible to make statements about what training topics and means should be developed in the short, intermediate and long term. This process enables prioritising for

annual development plans and budgets. The model allows many potential other forms of use. An example is elaborated upon in paragraph 2.2.

The applied TIS model is based on existing theories of market penetration and phases of innovation systems [2]. Firstly, innovations are rated on a scale between incremental and radical innovation (See Table 1) [3]. Secondly, it is rated whether the innovation demands a more modular or system-level change. Thirdly, seven criteria have been devised based on research about learning for innovation by Hekkert and Ossebaard [5]: entrepreneurial activity, knowledge development, knowledge transfer (Table 2), steering the search process, stimulating market demand, sources of innovation and dealing with resistance. As to the scoring of the representation of the innovation in present upskilling, four availability levels for schooling are introduced: custom knowledge transfer, on-request training, widely available training, and upskilling as part of regular education.

Tab. 1 – Example criterium 'incremental/radical innovation'. Each scoring table comes with 'gaps' (score 2 and 4), because of the subjectivity of the ranking.

Score	Description	Example
1	No adjustment required for application of the product	New type of boiler, new type of petrol car
2		
3	Small or medium adjustments required for application of the product	Building management system, hybrid car
4		
5	New product that is not comparable to other products in the market	Fuel cell, electric car

Tab. 2 – Example criterion 'knowledge transfer'.

Score	Description
1	Little to no knowledge available.
2	
3	Limited availability of knowledge for individual study and education. Producers and users start learning more and more from each other.
4	
5	Wide availability of knowledge for individual study and education. Producers make use of user experience to further develop their innovation.

2.2 Application of the TIS approach for mapping of innovations

In Dutch research, the model has been applied to energy transition in the installation sector by ranking and mapping the innovations tied to mapped insights from projects sustaining the built environment. Researchers made use of a spreadsheet to rank each technology as independently as possible in order to reach objective results. Ranking of criteria were eventually displayed with qualitative descriptions, in order to further substantiate the choices that were made.

A combined analysis of the ranking of technological innovations and the availability of upskilling was conducted (see Table 3). For example, airtightness as a technology is in its acceleration phase on the market, there is no wide availability of training, and knowledge transfer is ranked at level 3. Informed by the model, it can be concluded that development of airtightness schooling should be set in motion in the short term.

Tab. 3 – Relationships between criteria for determining the investment period.

Phase innovation system	Wide availability of upskilling	Knowledge transfer	Investment in upskilling needed
Acceleration or stabilisation	No	≤3	Short term
Take-off	No	≤3	Intermediate term
Exploration	No	≤3	Long term

The use of this model resulted in an overview of technologies and skills for which a sufficient amount of upskilling needs to be realised to prevent knowledge gaps in the (near) future. In this research example, outcomes were used to devise an agenda for the Dutch installation sector development fund in order to underpin investments in training development.

2.3 Practical value of innovation mapping with the TIS approach

The TIS model provides an integral view on the need for upskilling, taking into account different actors and processes across the value chain. In addition, the model allows for required soft skills and specifically interdisciplinary skills (which are critical in technological innovations), to be mapped and gain visibility.

On the one hand, results of applying the model can be used in an isolated manner to devise agendas and budgeting for educational developments. Results can also form the basis for further skills-mapping and the creation of a task-based qualification, which will be discussed in the following paragraphs. Figure 1 shows an example of a first mapping of technologies, to be used as input for further steps in the process. The TIS model constitutes the point of departure in

the journey towards powerful cross-sectoral upskilling: insight into energy transition maturity.

3. Skills mapping

Building on the list of technologies and innovations that result from applying the TIS model, one can execute a mapping of skills tied to the innovations. This skills mapping methodology was developed to support EU member states in finding a fast and practical manner to perform skills mappings with multiple stakeholders.

First, work fields relevant to the technologies should be considered in consultation with experts. By using expert knowledge, it can also be decided to what skill level a certain technology should be developed by a professional in a certain work field. After all, not all professions are expected to have the same skills for all the identified technologies. An example could be when a civil engineering professional is expected to reach skill level 4 for the subject of envelope systems (technology identified in Figure 2).

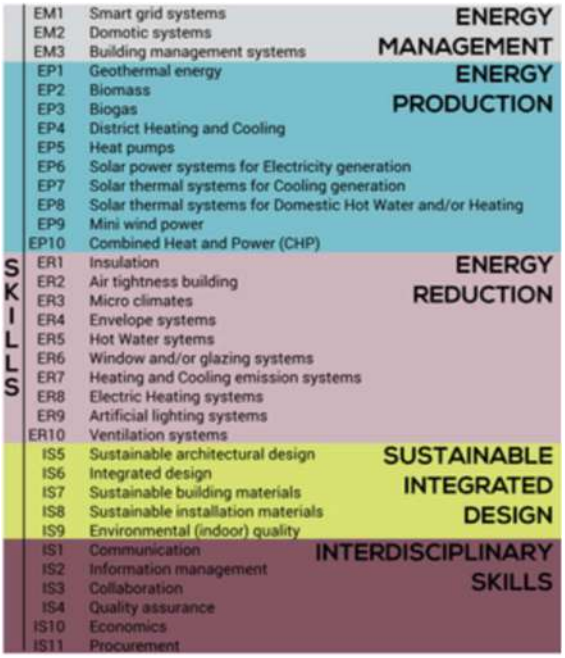

Fig. 2 - Example of an outcome of the TIS approach for energy innovations, where each technology is categorised and accompanied with a code.

The methodology contains 5 skill levels. See Figure 3 for a description of levels, which was based on EU terms and the Bologna declaration of 2010 (Cromwijk et al., 2017). A potential complete skills mapping outcome for the civil engineering professional mentioned in the previous example is shown in Figure 4. Visualisations like these that come with the methodology can be helpful for communication and collaborative application.

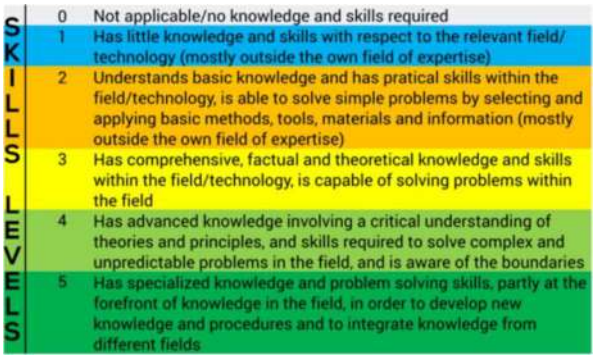

Fig. 3 - Skills mapping levels and descriptions.

Additional to skills mapping is that the methodology enables the mapping of current skills gaps, using the same skill levels. This way, it can be further decided what technologies and skills require upskilling in the (near) future.

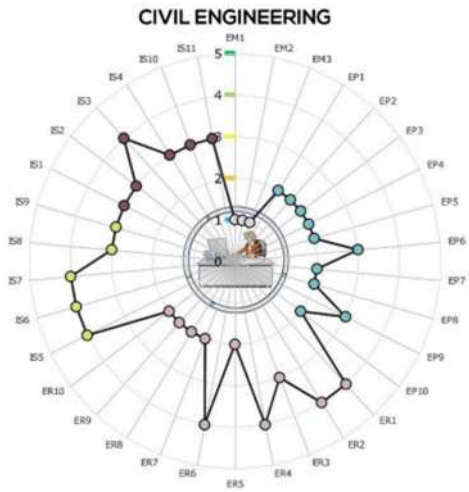

Fig. 4 - Example of a visualised skills mapping for the work field of civil engineering in nZEB. Each coloured circle marks the required skill level of the professional for that technology.

3.2 Application of skills mapping

In PROF/TRAC an H2020 funded project, the skills mapping methodology has been applied to white-collar professions in nearly-Zero Energy Building (nZEB). Execution of the method was organised with small groups of experts in work fields defined as relevant. They had all been working with nZEB skills before. The experts were trained in using the method, after which they executed the skills mapping in their own countries. As a validation, the results delivered by the expert groups were reviewed by consortium partners.

The outcome of the above mentioned process was a complete mapping of all the technologies and skills mentioned in Figure 1, for seven different work fields. Figure 5 shows one component of this

	Work field	Architecture	Civil Engineering	Electrical Engineering	Mechanical Engineering	Building Management	Construction Management	Financing and Procurement
	Reference professions	Architect	Civil Engineer	Electrical Engineer	Mechanical Engineer	Facility Manager	Project Manager	Procurer
			Construction engineer	ICT engineer	Building automation eng.	technical energy engineer	Cost engineer	project developer
			structural engineer		Energy engineer	operator	Quality assurance	
	TECHNOLOGY, INTERDISCIPLINARY SKILLS AND PROFESSIONS							
EM	ENERGY MANAGEMENT							
EM1	Smart grid systems	2	1	5	3	3	2	1
EM2	Domotic systems	2	1	4	4	3	2	1
EM3	Building management systems	2	1	4	5	3	2	1

Fig. 5 - Example of a skills mapping for energy management skills. Coloured cells represent applicable skill levels per technology for each profession.

project. The results, in turn, functioned as the origin for the development of a task-based qualification scheme, which will be elaborated upon in chapter 4.

3.3 Practical value of skills mapping

A practical experience from work in an additional H2020 funded project described the challenge of finding the right scope for establishing professions and specialisms in circular construction projects. This challenge simultaneously illustrates the flexibility and potential for wide applicability of the method. Project members found that the use of (guided) examples and collaboration helped in finding the right scope.

The skills mapping methodology can bring about a useful overview for each work field. From an EU perspective, broad work fields are considered for the mapping process to account for differences between job descriptions across countries. Results are mostly generalizable. Furthermore, the ability to use this method as a mapping of skills gaps between current and desired skill outcomes is a valuable addition to the applied TIS approach.

4. Task-based qualification framework

To create a task-based qualification framework with the input collected in executing the previous methods, more detailed competences and descriptions should be collected for each technology or interdisciplinary skill. Doing so will result in a set of specific competences. These are the so-called minimum qualifications per skill level. Here, it is decided what specific tasks and subtasks a professional should tend to and how. It focuses on the required knowledge, skills and behaviour.

For this methodology, expert consultation is a key aspect. Professionals with expertise in a specific technology or innovation are to be interviewed about the exact steps to be conducted and the skills needed to become proficient within the subject. Each qualification is linked to a unique Unit of Learning Outcome (ULO) [4]. All ULO's are stored in a database. With the help of this method, ULO's can be easily labelled with locations of existing learning content.

Additionally, if a certain skill is applied to multiple tasks, the ULO has to be written only once. Eventually, all processed information will be revised by the experts who were interviewed at the beginning of the process. See Figure 5 and 6 for examples of tasks and subtasks and corresponding ULO's. Devising a task-based qualification framework enables decisions about what exact profile professionals should possess. It also provides input for training and upskilling programmes. Together with TIS and the skills mapping methodology, this is a stepping stone for learning on the job and recognition of skills.

Check location of ventilation unit(s)		
	Determine optimal location of the ventilation unit(s)	45
	Prevent noise pollution	3
Check location of air supply and discharge in each room		
	Ensure air circulation through the room	5
	Prevent draft complaints	2
	Check location of the external air intake	13
	Check location of the air exhaust	14
	Check proper integration of cooker hoods	80

Fig. 5 - Example of two tasks and related subtasks

ULO Nr.		
1	**Competence**	Determine supply airflow rate
	Skills	Describe air quality; Classify air quality parameters
	Knowledge	Airflow requirements concerning health; Air quality parameters (CO2, VOC, PM2.5, odour) and their relationships
2	**Competence**	Prevent draft complaints
	Skills	Explain when draft occurs
	Knowledge	Draft in relation with pre-heating; When draft occurs; Draft in relation with air velocity

Fig. 6 - Example of two detailed Unit of Learning Outcomes. Note that ULO 2 is applied to one of the subtasks in Fig 5.

4.2 Application of task-based qualifications

In a practical application, ULO's may be tied to ambitions that were set for each profession during the skills mapping. For instance, if a work field has received a required skill level 2 for the technology of micro climates, this could mean a professional is recommended to acquire fewer ULO's than someone who has a required skill level 4.

Final results of the skills mapping and qualifications from several projects were used for the *BUILD UP Skills Advisor app*. This application is being used by professionals to visualise their skills development possibilities and to gain new skills by taking part in e-learnings that are tailored to the professional profile they are recommended to acquire. In this manner, earning and recognition of skills is further stimulated digitally.

4.3 Practical value of task-based qualifications

Task-based descriptions help steer users' focus towards the actual competences of professionals, without being restrained by differences in professional titles between countries. Furthermore, the opportunity for recognition of skills can be connected to micro-learning and micro-credentials. Micro-credentials certify the outcomes of short learning experiences and address the skills gap between initial qualifications and emerging skills needs in the market [6]. Task-based qualifications can further facilitate development of micro-credentials and enhance transparency in terms of what they represent.

5. Enforcing recognition of skills

This chapter provides an overview of minimum requirements for the levelling of skills and implementation in architecture, engineering and construction (AEC) processes. The premise is that the management of skills requires that the information on the skills must be first made available, accessible, and usable. To make descriptors of skills usable to the desired extent, the following requirements are identified as essential. Descriptors should be a) easy to understand; b) applicable in a specific context; c) consistent in semantics and granularity; d) comparable across above given criteria and; e) transferable within and across domains. In the follow-up sub-sections, key requirements for levelling the skills and the usefulness of the mapping of the skills are identified.

5.1 Key requirements for levelling of skills

For the definition of minimum requirements for the levelling of the skills it is important to align three important concepts: taxonomy, toolkit and context.

In this paper, taxonomy is understood as a principle of classification that allows for items to be characterised into types. In our case, we are interested in the characteristics of the skills. Bloom's taxonomy [7] is a well-known taxonomy of knowledge types that uses principles of classifications by the characteristic of directionally chained levelled states of knowledge. These levels are as follows: remember, understand, apply, analyse, evaluate, and create. This approach is an easy-to-understand levelling of knowledge that can be further elaborated upon in the context of skills management.

Toolkits are used to facilitate management. Skills toolkits may include a set of tools, frameworks, templates and real-life examples and best practices [8]. There are no well-established toolkits that could facilitate targeted transition addressed in this paper.

The skills management context is defined by the market, by jobs meeting the market needs and by job performance. The EU building services market is heavily affected by EU policies, which require job profiles that possess specific knowledge and technical skills for the processing of information and material. Related job performance may often only be objectively assessed through the performance appraisal.

In the context of building services we would like to define a framework that allows for context specific skill levelling as depicted in Figure 9.

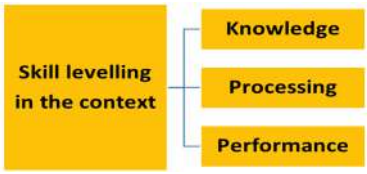

Fig. 9 - Skill levelling in the context

In a given context of levelling skills a number of factors should be addressed: supply chain, standardisation, unified granularity, process quality criteria, and feedback-loop assessment.

Regarding the supply chain, skills management should ensure that inter-organisational interoperability is more easily achieved in terms of the scope, required technical skills, objectives, performance and inter-task dependencies. In the context of building services and projects in the built environment, it is very important to control the supply chain across project stages, components and project-specifics.

Standardisation of the levelling should include the interplay of two critical contributing maturities with varying weight across project processes and results: (1) objectives of the technical skills, (2) and behavioural performance of individuals, teams and companies.

As we can see from the previous two items, there is a varying granularity in terms of the breakdown of processes, process results, subsystems, costs and more. Therefore, unification of granularity is important from several viewpoints, including, but not limited to the tasks.

The process quality criteria should be the base for the levelling of activities. Process quality criteria should include both process and process outcome assessment and how component and project-specific requirements are being met in the context of building or building services projects. This should include generic assessment, and component and project specific evaluation throughout project phases.

Regarding feedback-loop assessment, there are two essential intra and inter-related feedback loops: for individuals and for systems. The individual shall be assessed according to the job objectives (the difference between the targeted and actual objectives) and performance (the difference between the targeted and actual behaviour at job).

5.2 Usefulness of skill-level definitions for skills mapping

The task-based qualification scheme elaborated in the previous chapter project has been applied and further developed into a Competence Quality Standard (CQS) by the H2020 Train4Sustain project. The CQS allows to evaluate, score, and report the level of competence of professionals (white collars) and workers (blue collars) in sustainable building, expanding the original scope of the framework.

The CQS is formed by more than 100 Areas of Expertise, defined in relation to the most relevant innovations (as through the application of the TIS model), the main frameworks of sustainability indicators (e.g. Level(s), EN/ISO standards) and the most important assessment systems (e.g. DGNB, HQE, BREEAM).

In the CQS, the Areas of Expertise are organised in a hierarchic (5-levels: dimensions, thematic fields, macro areas of expertise, areas of expertise, learning outcomes) and modular (4 dimensions: environment, society, economy, and process) structure.

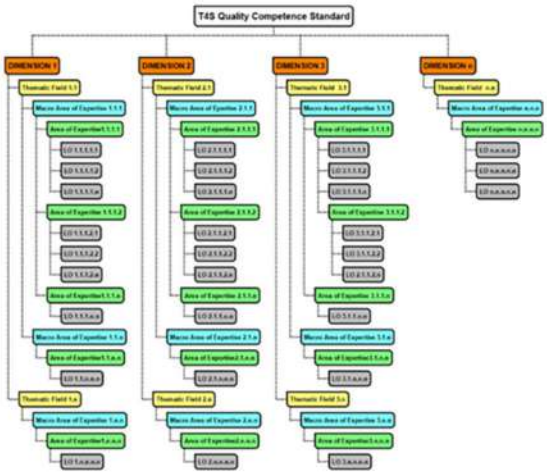

Fig. 10 - Structure of the Train4Sustain CQS, consisting of five levels and four dimensions. Areas of Expertise are represented by green boxes.

Each Area of Expertise is composed of a set of Learning Outcomes, described in terms of skill and knowledge. Each Learning Outcome is associated with a competence level using the same scoring scale adopted in the skills mapping, from 1 to 5, where 5 is the highest degree of competence.

To put this in a wider context, level 1 of the CQS requires learning outcomes similar to EQF 4. Level 2 and 3 correspond to learning outcomes of EQF 5 or 6, level 4 calls for learning outcomes comparable to EQF 6 or 7 and level 5 corresponds to EQF 7 or 8. The Train4Sustain competence levels are not related to the EHEA (European Higher Education Area) qualification or to vocational training qualification, meaning that each building professional has an official EQF level from 5 to 8 (i.e., the EQF range of white collars in terms of education). To their EQF, a Train4Sustain CQS level ranging from 1-5 can then be added. For instance, a professional with EQF level 7 on architecture without competences on renewable energy systems could achieve, through a training course, a CQS level 2 which is additional to the already present competence in architecture. Similarly, a blue-collar worker having a generic vocational qualification diploma (EQF level 3 or 4), can reach a CQS level 5 on a specific area of expertise (i.e. installation of insulation components) through participation in specific skills upgrading training courses or through work experiences.

Proven ability can be acquired by professionals and workers through training courses, and outside the formal learning context through work experience and independent study, provided that these learning outcomes satisfy the requirements of their qualifications. As in the skills mapping and task-based qualifications, the Areas of Expertise have been associated with different work fields for both professionals and workers. Depending on the Learning Outcomes acquired, a building professional receives a score for each Area of Expertise that is relevant to their work field. To reach a certain level of competence in an Area of Expertise, a professional has to be competent at all the necessary Learning Outcomes. For instance, if a professional wants to reach the competence level 4 in “ER1 Insulation”, he must acquire all the Learning Outcomes associated to level 4 and lower. The task-based qualification framework can be used to improve the quality and the applicability (in several contexts) of the Unit of Learning Outcomes.

The competence scores are reported in the Train4Sustain Skill Passport, which makes it possible to compare the level of competencies of building professionals through Europe, establishing a common reference methodology.

The CQS has been studied to support public authorities in the selection of competent professionals and craftsmen. Use of the CQS allows to integrate objective and measurable competence requirements in public tenders (GPP). Through the Skill Passport, professionals and craftsmen can easily demonstrate the fulfilment of requirements.

Any existing qualification scheme can be mapped using the CQS. The scoring system is useful to inform professionals of what level of competency is being provided by each qualification scheme and its relative level.

Train4Sustain CQS intends to be a tool to facilitate the request of qualified professionals and blue collar workers by public administrations and private clients. This will valorise, with a transparent common "reporting" system, the competences acquired through training courses and experience in the field. Train4Sustain CQS is an open and living system that will progress over time following the evolution of innovation, standards, and professional qualification schemes.

6. Conclusion and discussion

This paper demonstrated a structured approach for the cross-sectoral definition of skills registries applicable to the development of technical skills that could target specific key results areas and key performance indicators that allow for systematic definition of job objectives, target performances and appraisals.

Curricula resulting from the methodology mentioned in the current article are cross-sectoral, highlighting roles and responsibilities and the minimal set of knowledge and skills needed for assessing the applied value of a specific innovation or theme. The modularity of the methodology adds value. A lot of detail can be embedded, but the parts can also be isolated from the whole, and still be of practical value.

Furthermore, the method of task-based qualifications facilitates digital support for learning on the job and learning transaction-based recognition of successfully acquired knowledge and skills. It also enables sectoral and intersectoral skills registers or skills passports to take task-based knowledge and skill development into account.

Some limitations of this paper may be mentioned. The first is in terms of coverage of types of technical skills and applicability to particular job performance aspects. The depth of application of technical skills and behavioural competencies in the construction building projects, and in particular for the mechanical, electrical and plumbing systems, has several specifics that could not be covered holistically in the scope of the paper.

Second, the paper does not address the implementation of the presented approach in an organisational context in terms of jobs, their organisation, evaluation, importance for the specific market needs, key result areas, indicators and key performance indicators, nor does the paper address how specific skills collectively contribute to the overall target job objectives and specific job performance targets, achievements and appraisals.

Future developments should address the transorganisational implementation of the approach in the context of process performance standards and particular assessments. In addition, there is a potential to apply the approach to develop and advance transitional management of gaps in skills with evolving digital transition of the companies supporting next generation systems engineering AEC companies.

7. Acknowledgement

This paper reflects methodologies and lessons learned in several H2020 projects. BUStoB, PROF/TRAC, BIMplement, NEWCOM, SEEtheSkills and Train4Sustain. The projects have received funding from the European Commission.

8. References

[1] Hekkert, M.P., Suurs, R.A.A., Negro, S.O., Kuhlmann, S., Smits, R.E.H.M. Functions of innovation systems: A new approach to analysing technological change. Technological Forecasting & Social Change. 2007 May; 74(4): 413-432.

[2] Rogers, E.M. Diffusion of Innovations. Simon and Schuster, 4th edition. 2010, July 16th.

[3] Banbury, C. M., Mitchell, W. The Effect of Introducing Important Incremental Innovations on Market Share and Business Survival. Strategic management Journal. 1995;16(1):161-182.

[4] European Centre for the Development of Vocational Training. 2009: 1-176.

[5] Hekkert, M., Ossebaard, M. The Innovation Motor. Acceleration of pioneering innovations. Koninklijke Van Gorcum. 2010, July 1st.

[6] European Commission. Final Report: A European Approach to Micro-Credentials. Eds. H.S. Futures, T. Andersen and K.N. Larsen. Danish Technological Institute. 2020.

[7] Bloom, B. S. Taxonomy of educational objectives. Vol. 1: Cognitive domain. New York: McKay. 1956;20(24).

[8]Boston Consulting Group's Digital Transformation Change Management

Learning and Knowledge Transfer of Professionals within the Building Services Sector

Mohammad Samir Ahmed [a], Joep van der Velden [b], Ali Soleymani [c], Paula van den Brom [d], Maaike Konings [e], Laure Itard [f], Marcus Specht [g], Ellen Sjoer [h], Wim Zeiler [i]

[a] PDEng trainee, Department of the Built Environment, Eindhoven University of Technology, Eindhoven, the Netherlands, m.s.ahmed@tue.nl

[b] Director, Building Automation, Kropman Installatietechniek, Nijmegen, the Netherlands, joep.van.der.velden@kropman.nl

[c] PhD Researcher, Centre for Education and Learning (CEL), Delft University of Technology, Delft, the Netherlands, a.soleymani@tudelft.nl

[d] Postdoc Researcher, Faculty of Architecture and the Built Environment, Delft University of Technology, Delft, the Netherlands, p.i.vandenBrom@tudelft.nl

[e] Researcher at Sustainable Talent Development Research Group, and Advisor Quality & Accreditation, The Hague University of Applied Sciences, the Hague, the Netherlands, m.konings@hhs.nl

[f] Professor, Faculty of Architecture and the Built Environment, Delft University of Technology, Delft, the Netherlands, l.c.m.itard@tudelft.nl

[g] Professor, Centre for Education and Learning (CEL), Delft University of Technology, Delft, the Netherlands, m.m.specht@tudelft.nl

[h] Professor, Sustainable Talent Development, The Hague University of Applied Sciences, the Hague, the Netherlands, e.sjoer@hhs.nl

[i] Professor, Department of the Built Environment, Eindhoven University of Technology, Eindhoven, the Netherlands, w.zeiler@tue.nl

Abstract. Buildings need to be carefully operated and maintained for optimum health, comfort, energy performance, and utility costs. The increasing use of Machine Learning combined with Big Data in the building services sector has shown the potential to bring energy efficiency and cost-effectiveness. Therefore, upskilling and reskilling the current workforce is required to realize new possibilities. In addition, sharing and preserving knowledge are also required for the sustainable growth of professionals and companies. This formed the basis for the Dutch Research Council funded TransAct project.

To increase access to education on the job, online learning is experiencing phenomenal growth. A study was conducted with two focus groups - professionals of a building service company and university researchers - to understand the existing challenges and the ways to improve knowledge sharing and upskilling through learning on the job. This study introduced an Enterprise Social Network platform that connects members and may facilitate knowledge sharing. As a community forum, Yammer from office 365 was used. For hosting project files, a SharePoint page was created. For online courses, the company's online learning site was utilized.

The log data from the online tools were analysed, semi-structured interviews and webinars were conducted and feedback was collected with google forms. Incentive models like social recognition and innovative project results were used to motivate the professionals for online activities. This paper distinguishes the impacts of initiatives on the behaviour of university researchers vs company employees.

Keywords. Lifelong learning, knowledge sharing, building services professionals, learning communities.
DOI: https://doi.org/10.34641/clima.2022.142

1. Introduction

For a comfortable healthy indoor climate with an efficient amount of energy, buildings need to be carefully operated and maintained. With recent developments in sensor and communication technologies, modern buildings accumulate a large amount of operational data at small time intervals. These data provide the opportunity for in-depth investigation and assessment of the operational performance of buildings [1]. The increasing use of Machine Learning (ML) combined with Big Data in

Copyright ©2022 by the authors. This conference paper is published under a CC-BY-4.0 license.

the building services sector has shown the potential to bring energy efficiency and cost-effectiveness [2–4]. This field needs cohesive knowledge of engineers/Scientists from different backgrounds (i.e., electrical, mechanical, civil, computer etc.) and data engineering. Governments have recognized the need for building the capability of the future workforce [5], and accordingly, new courses have been introduced to the education system. However, that will take decades before undergraduate education influences energy efficiency performance in the workplace [6]. Upskilling and reskilling the current workforce can provide sufficient professionals to realize the use of new technologies [7].

To facilitate the personal development of professionals through training, online learning is experiencing phenomenal growth [8]. Due to the COVID pandemic, formal education practices have become reliant on technology which accelerated online learning enormously [9]. However, Weller M. [10] showed that no or limited face-to-face interaction in such programs, the associated feelings of isolation which, in turn, can lead to displeasure, poor performance, and high drop-out. Weller M. also found that learners' feelings about the community significantly affect the performance of e-learning. Hung DWL et al. [11] defined situatedness, commonality, and interdependency as fundamentals of an online community. Along with learning, sharing expert knowledge is also important for developing new skills and competencies. Hall H. [12] mentioned that anticipated exchange, reputation in the community, altruism, and tangible rewards as four main reasons that could motivate community members to share knowledge.

The rapid change in technology use and required competencies made learning an essential requirement on the job. In companies of building services, not all professionals are comfortable with online courses. Along with formal learning networks like online training and physical workshops, informal learning occurs through communication over the phone, email or physical interaction. Considering these factors and by reviewing the current literature, a lack of experimental research was identified for understanding the learning and sharing knowledge of professionals in the building services sector.

Therefore, this research aims to i) understand the obstacles and motivation of professional development in data analytics and ML applications in the building services sector and ii) develop a digital collaborative tool to explore incentives for sharing expert knowledge and experiences among professionals. The research project is called "TransAct" to research and develop a lifelong learning network model. The project will also identify the main motivation and barriers to knowledge adoption, transfer and exchange between different stakeholders ranging from producers, installers, to maintenance [13].

To achieve these aims, in this paper, the findings of a study on a group of professionals are discussed. The target group are professionals who have access to building data to optimize the energy performance and Fault Detection and Diagnosis (FDD) in building equipment. Despite the availability of different methods, FDD tools are not applied in practice, especially not when it comes to their application to energy performance diagnosis. There are two main categories of FDD methods; knowledge-driven-based methods and data-driven-based methods [14]. Zhao et al. [12] pointed out that, in reality, the combination of information (data-driven) and experience (knowledge-driven) is important for the learning processes within a company.

Russell and Ginsburg [15] defined an Online Learning Community (OLC) as an extension of the physical learning community to the electronic one. In addition, the definition of a learning community can include different contexts like a group of people with a shared will to learn [16] or an instructional design model for e-learning [17]. Throughout the study, a suitable method of establishing an OLC within organizations is identified. In this paper, OLC was considered as a developed activity system in which a group of learners, unified by a common cause and empowered by a supportive virtual environment, engage in collaborative learning within an atmosphere of trust and commitment [18].

In this paper, first, the research methodology is presented followed by an introduction to the study design. Then, the key points obtained from the study are mentioned. Later the insights from the learning and knowledge sharing tools are presented. The paper ends with a discussion on the results and limitations and prospects for future works.

2. Research methodology

Professionals in the building services sector have limited or no knowledge to analyse data and apply ML techniques. Interviews have been used to understand the learning and knowledge sharing practices within and among learning communities. How technology is used in the current setting was also explored. Learning Analytics was used to understand the interactions as also the effect of the technology tooling introduced.

An intervention study was planned to identify the potential added value of technology in this context. The following sections explain the steps followed and the assessment of methodologies utilized.

2.1 Step 1: Selection of learning communities

For the study, professionals from the building installation and services sector are required. Employees, trainees, and researchers working at companies, universities, or research institutes can be considered. Moreover, professionals with a background in smart buildings and cities can also be considered for the study. All the participants should

have access to data generated from buildings and energy systems.

2.2 Step 2: Developing a learning community through digital collaborative platforms

As the knowledge to be developed is around data analytics and ML applications, an online learning community can serve the learning and knowledge sharing requirements. Therefore, at first, a directory of professionals are needed where individuals can look for experts and feel the existence of such a community. They should be able to communicate on a community level and a personal level. It was revealed from 28 relevant articles that social media-enabled professional development allows professionals to connect with like-minded individuals [19]. The possibility to explore ongoing projects and previous projects is mandatory for gaining knowledge from the projects done by others. In addition, preserving the knowledge in an accessible and structured way will transform the central database into a knowledge base. A collaborative digital tool can support a learning community within organizations for a lifelong learning experience. An E-learning platform along with the communication tools can be a good option to track the learning progress and appoint new courses to the community members.

2.3 Step 3: Assessment methodologies

To understand the ability of professionals in data analytics and ML applications, a series of interviews need to be conducted. The focus of the interviews can be the incentives and motivations behind sharing and gaining knowledge, main challenges, and future development plans. Direct feedback can also be received through webinars. Other than that, the number of new courses followed by the professionals, innovative data-driven projects delivered, and the online activities within the community-based platform can represent the acceptance and the effectiveness of the digital collaborative platforms.

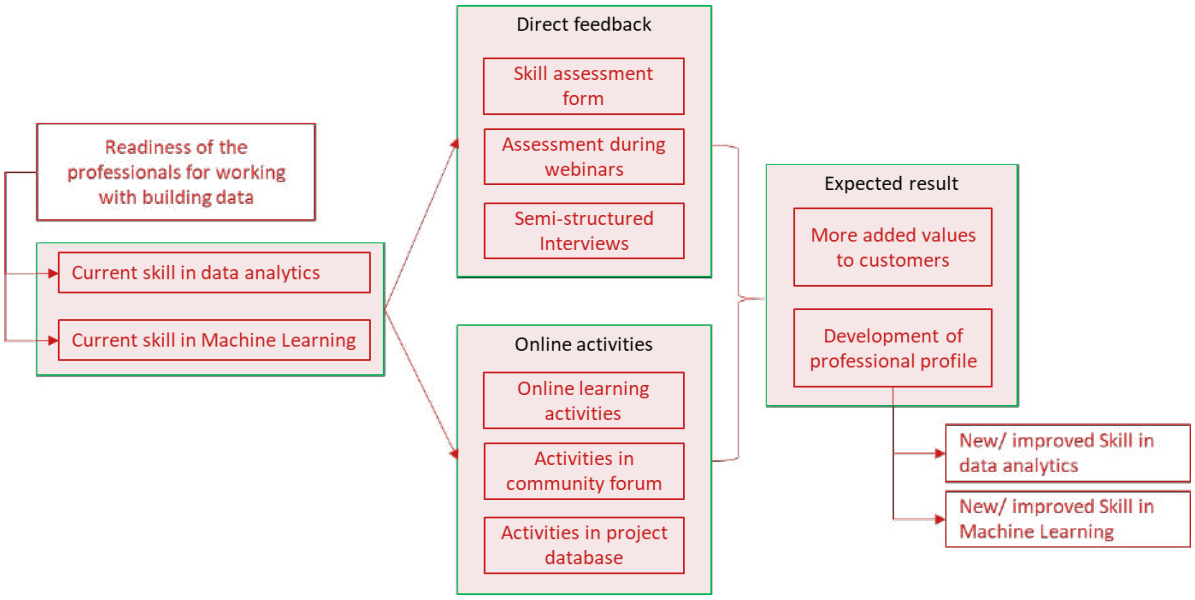

Fig. 1 - Tools used for the exploration of learning community

3. Study design and related work

This section discusses the methodology described in Section 2 with studies conducted on professionals who are working in the building services sector.

3.1 Exploring different similar communities

Seven innovative learning communities within the Netherlands that are working on projects related to data analytics and ML were contacted. Some of the key findings are as follows:

1. Regular group meetings are the most common form of knowledge dissemination.
2. Annual assessment of employees includes learning goals for the following year and assessment of the last year's learning and development activities.
3. The skills matrix is maintained for members.
4. Some companies have an internal learning management system to track the learning progress of employees on company-specific knowledge and new competencies.
5. Maintain formal and informal communication through MS Teams channels or WhatsApp groups.
6. Get recommendations from peers about courses on data analytics and ML applications.
7. Attend conferences, conduct literature reviews and follow blogs to remain updated with the latest development in the field.
8. One community rewards points to its members for sharing their knowledge gained from projects. The annual target of points is regularly fulfilled which is a part of the annual assessment meeting.

9. A central location for data depending on the type of information (i.e., MS SharePoint, OneDrive etc.) is maintained where project summaries, meeting minutes and other learning points are preserved.
10. At the age of 66, one engineer wants to learn ML applications. The purpose is to get an overview of the latest possibilities and to lead engineers who can code. The motivation is not to get outdated in the field as an old fashioned old grumpy man.

One of the challenges in the growth of knowledge is the lack of innovative projects for companies. That shows the knowledge of the community can be driven by customer projects.

3.2 Selection of learning community to study

A company in the Netherlands from the building services sector was selected for the study. Nineteen employees attended from different departments. Nine employees were from the building automation department, six employees were from the design and engineering department, and four employees were from the ICT department.

A group of trainees and researchers joined the study from the built environment department of a technical university in the Netherlands. All the trainees are working on projects from the same company of the study to ensure data privacy and smooth access to the company database.

3.3 Developing the learning community

To get insights into the company culture of learning and knowledge sharing, a series of semi-structured interviews were conducted. In addition, google survey forms were used to assess the level of data analytics and ML skills of the participants. Then, a series of webinars were conducted according to the requirements of the learning community. Before and after webinars, the preference for learning media, the skills level of the participants on the topic and feedback on the webinars were asked to improve the experience of the professionals. Learning activities of the professionals were tracked to assess the new competencies. The tools used to explore the communities are shown in Fig. 1.

3.4 Development of a digital collaborative platform and implementation

In order to develop a collaborative platform, first, the e-learning and the communication tools of the company were explored. Accordingly, a digital collaborative environment was developed with the existing Microsoft (MS) tools of the organization. The tools altogether are named using the project name *TransAct*. To explore communication beyond the boundary of the organization, an external community of ten trainees was also introduced who are working on different projects of the company. Therefore, data privacy was maintained without any conflict of interest. The overall structure of the digital environment is shown in Fig. 2.

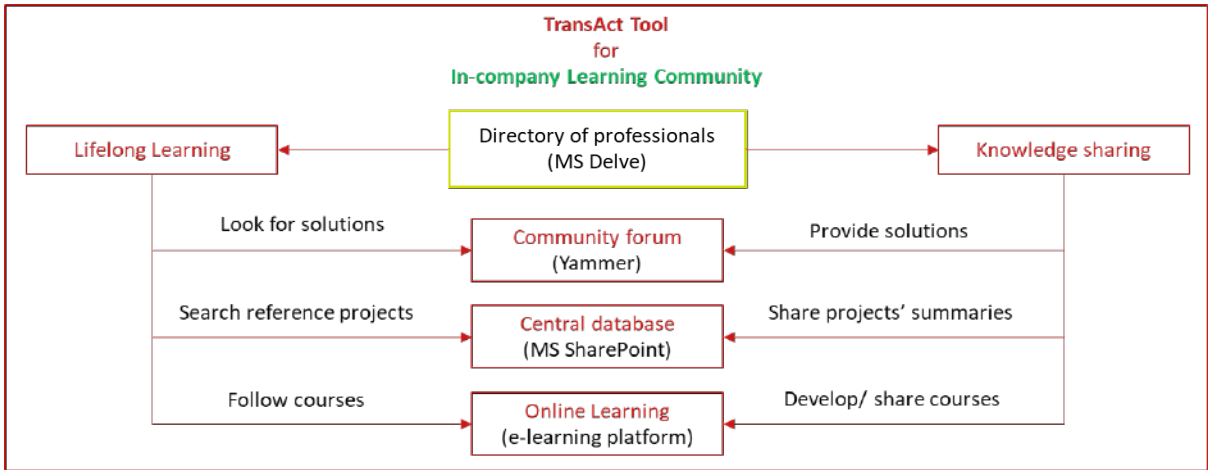

Fig. 2 - Overview of the digital collaborative learning and knowledge sharing platform

The community members have individual profiles in the ***MS Delve*** environment which is the directory of professionals. In this environment, current projects, existing skills, expertise on which others can inquire can be recorded by making an individual profile. As a result, other professionals can search for skilled colleagues and can approach them for support.

The two main focuses of the community are learning and sharing knowledge. Both are interconnected to the community forum at ***Yammer*** where employees will look for solutions and experts will provide solutions based on their experience and knowledge. The latest and the best possible solutions can be received from experts working at different parts and locations of the company. Yammer at a foundational level is gamified with basic game elements. i.e., like, comment, share, tag, mention, follow etc. [20]. Then a central database at ***SharePoint*** was introduced where employees will look for reference projects and project engineers will share summaries and learning points from different projects. This can convert a database into a knowledge base by preserving different resources. A smart search engine with different functionality to look into the contents within files made this tool convenient to look for

necessary information. In addition, the version control made this location suitable for sustainable knowledgebase with the possibility of integrating the latest information on the old data. Finally, the online learning platform of the company was used where employees will follow courses and experts can develop or recommend courses for their colleagues. The admin can appoint courses to employees or keep courses optional for self-development during personal time. Some of the mandatory courses can be followed during office hours. The methodology was followed to identify the motivation for learning and incentives for sharing knowledge.

At the beginning of the study, a SharePoint page was introduced on the existing intranet of the company. The page hosts the Yammer community page, the company's e-learning platform, a news board and the directory of the professionals. The page can be accessed from the homepage of the intranet environment. The MS tools generate the usage report. In addition, the office 365 admin account was used to generate reports of the usage by the participants.

4. Results

To measure the effectiveness of the learning community, the digital platform was introduced among the professionals to stimulate community building and knowledge exchange. The usage was analysed to find the added value and presented below.

4.1 Community forum - Yammer

The purpose of an in-company learning community discussion board is to find solutions to problems that are new or have been faced by others earlier. Networking with peers is another purpose of the community. The selected group of employees were added to a Yammer community. The focus of the community discussion forum was data analytics and ML applications in the building services sector. Initially, several posts were shared among the employees about the purpose of the discussion forum. It was found that employees mostly read messages posted by others. Very few messages (monthly overall average posts) and reactions to messages (monthly overall average likes) were found. Posts from employees attract more responses than posts from external trainees. The result shows the activities based on six consecutive months.

Within the community page of researchers, the activities are comparatively higher than in the community of employees. As learning and gathering information is part of the job for researchers, it is important to have responses from team members and supervisors. The community platform in that case is a convenient place to preserve information for newcomers and existing researchers. The data was collected based on activities over four months. The overall status is shown in **Tab. 1**.

Tab. 1 - Usage of the discussion forum

Title	Usage	Company	University
Average total monthly use by members	Read	268	762
	Posts	8	15.67
	Reactions to messages	3.63	18.33

4.2 Central database - SharePoint

For the analysed period of 6 months, in the company case, the total data stored is 10.8 GB. That means much of the project data was stored in the personal drives or the personal folders in the central server which is now accessible by other employees who are working on similar projects.

Within the community of the university, around 600 MB of reports and presentations were shared among the trainees and researchers to support their research and project activities. As the community members work in the same field, there are a lot of similarities among them. The summary of the usage is shown in **Tab. 2**.

Tab. 2 - Usage of the database

Title	Usage	Company	University
Average total monthly use of Sharepoint	Total data shared	10.8 GB	600 MB
	Site visit	189.17	111
	Unique viewers	51.17	32.67

4.3 Company's e-learning platform

An external e-learning platform provider along with more than two hundred online courses on different competencies was contracted by the company. In addition, expert employees of the company can produce and share online courses within the platform. It was found from the number of participants that, short videos of less than fifteen minutes have a better chance to be followed by the employees. Long videos or articles have a lower or no participation rate. The participation rate increases by the employees if courses are appointed from the platform by the admin with a deadline. This helps the employees to decide on more relevant courses among more than two hundred learning materials. In addition, the courses are free to follow and can be a part of the annual assessment session for the employees.

4.4 Directory of professionals - MS Delve Environment

During the study, all the participants were informed about the existence and benefits of the MS delve directory. The tool supports searching for experts within the community. It was found that not all the employees updated their information. Only the basic data are available from the human resources department. However, based on practices from other communities, considering the profile update during the annual review session may realize updated professional information in the central directory. As a result, newcomers will be able to find experts to approach for solutions.

4.5 Knowledge sharing media

In addition to the online tools, live webinars were conducted for the interested participants both the company employees and the researchers from the university. Before and after webinars, survey forms were circulated and feedback from five participants was analysed. On the Likert chart, the satisfaction level of the professionals on the content of the webinar was 3.3 on a scale of 4 with a standard error of 0.119. The satisfaction score on the delivery method was found 3.4 on the same scale with a standard error of 0.114. Therefore, it was found satisfactory and promising to continue hosting webinars on the topics of data analytics and applications of ML. The skill level of the participants was also asked and the mean value that we found was 2.3 on a scale of 4 (from no experience at 0 to an expert at 4) for the overall proficiency with a standard error of 0.019. The level of skill on the webinar topic was also measured and found a mean value of 2.33 with a standard error of 0.35. Short videos and live webinars were found as the preferred learning media from the feedback of participants. On the other hand, text files were found as the least preferred media for learning. In addition, some recommendations were also received from the respondents with a high impact on improving the upcoming webinars. Some of the key points were, brief and to the point discussion, demonstrating the practical implementations of the use cases, connecting with the daily activities of the professionals.

5. Discussion and limitations

During the study, some key points were observed and identified. These findings are discussed below.

5.1 Exploring in-company learning and knowledge-sharing culture

At first, the company culture was explored through semi-structured interviews. The key findings on learning barriers are as follows:

1. Project documentation is a challenge, because;
   - For smaller projects (project cost below Euro 500,000), no budget is appointed for the hours required to document learning points and project summaries.
   - No central location to preserve summaries of different projects.
   - To ensure the data privacy of a customer, the company limits access to some project folders in the central server only for the respective project employees.
   - Summarizing project results is not a mandatory task in most projects.
   - The regular project documents are saved on the central server. Annually the folders are archived. To access the old project files, permission is required from the ICT department.
2. In case of any problem, employees generally know, whom to communicate with for what kind of information. Accordingly, they send emails and speak over the phone. As a result, the solution remains with individuals and is not preserved within the organization.
3. Several senior employees are working for more than ten years. They are highly experienced and knowledgeable and intended to share their project's experiences through personal interaction. Because they believe most of the experiences are hard to explain through a written document. Webinars or short videos could be a solution which is an additional job on top of their regular responsibilities. Therefore, it is a challenge to document the knowledge of experts.
4. Except for some young employees, most of the employees still prefer physical training or workshop. They find it as an opportunity to interact with other colleagues and learn effectively. During those training, employees do not work on their projects. On the other hand, most of the online courses need to be followed outside of office time. Therefore, online courses became less of a motivating for them. However, management is promoting online learning through the company-owned e-learning platform. Some mandatory courses can be followed during office hours.
5. Generally, supervisors or managers suggest employees for physical training or online courses. During the annual assessment, the course plan can be defined for developing different skills and competencies. In some cases, professionals take online courses of their interest for personal development.

5.2 Handling projects with data analytics and ML applications

For any requirements related to data analytics or ML, experts from the building automation department support the project's engineers. Sometimes, trainees

are employed by universities to work on specific projects. Hence, existing employees are not gaining the skills to work with new tools for data analytics apart from MS excel. Employees also do not need to code ML algorithms. Instead, they depend on the software developed by the company to collect data from buildings and create graphs for analysis. This data analytics tool can perform some predictions based on historical data. By integrating advanced ML algorithms, the tool is getting upgraded from time to time. Hence, all the existing employees don't need to learn how the software works. Instead, what can be done is more interesting for them.

5.3 Limitations

There are several limitations to this study worth noting. First, the small group size greatly hinders the generalizability of the results. Second, the company-owned data analytics tool enables employees to generate results. So, they don't need to understand the underneath mechanism in the analytical tools and hence, limiting the courage to learn to code, algorithms for predicting the building energy demand or other ML applications. However, instead of how ML works, focusing on what can be done with ML can bring more benefits to the learning communities. This study did not consider the final state of the competence level of the participants. Future studies may address new competencies added to the profiles of the professionals and might look for different motivations and challenges in addition to the current study.

6. Conclusion and Recommendations

This research identified that, for the in-company learning community, the main motivation for learning was personal interest and the possibility to satisfy customers with new skills. In addition, the incentives discovered for sharing knowledge was the appreciation by colleagues and implementation of the knowledge in the regular project work.

Developing a sustainable knowledge base will facilitate the project participants to build on their existing knowledge and expertise [21]. Information can be stored and it can be prevented from becoming outdated. Onboarding of new professionals will then be efficient and effective. The shared documents should not contain any confidential content of specific clients. Standard templates are beneficial to make information better findable and can be used for project reports. Large projects should have project documentation as a mandatory task. Learnings from multiple small projects can be gathered through short collaborative sessions. During the study, a SharePoint location for storing project data according to the project type was introduced. Managers can continue storing project information as per project categories. Yammer was introduced as a community discussion forum. Employees can continue discussing problems/ ideas with multiple expert employees on this platform.

Annual review sessions can include learning and knowledge sharing goals for the following year by the managers. Assessment of the learning can also be done to follow up on progress.

For the future, three key performance indicators 1) the number of innovative projects delivered by the community, 2) the skills developed by the professionals in data analytics, and 3) ML applications can be used as a measure of the success of the TransAct tool. In addition, the amount of information shared among professionals can also be used for measuring the growth of community knowledge.

7. Acknowledgement

The research was funded by the Dutch Research Council (NWO) as a part of the project named "TransAct" to research and develop a lifelong learning network model and develop approaches to empower individuals in the exploration, monitoring, and planning of personal knowledge and competencies in learning communities. The following companies and organizations supported the project: Kropman Installatietechniek, TU Delft, TU Eindhoven, The Hague University of Applied Science, Halmos Adviseurs BV, Stichting ISSO, Caleffi International BV, Wij Techniek, Platform voor Mens en Techniek TVVL, Kennis & Praktijkcentrum Energie transitie – ROC Mondriaan and Bouw en Techniek Innovatiecentrum – TNO BITC.

8. References

[1] Yu Z, Haghighat F, Fung BCM. Advances and challenges in building engineering and data mining applications for energy-efficient communities. Sustain Cities Soc 2016;25:33–8. https://doi.org/10.1016/j.scs.2015.12.001.

[2] Linder L, Vionnet D, Bacher JP, Hennebert J. Big Building Data-a Big Data Platform for Smart Buildings. Energy Procedia, 2017. https://doi.org/10.1016/j.egypro.2017.07.354.

[3] Mehmood MU, Chun D, Zeeshan, Han H, Jeon G, Chen K. A review of the applications of artificial intelligence and big data to buildings for energy-efficiency and a comfortable indoor living environment. Energy Build 2019. https://doi.org/10.1016/j.enbuild.2019.109383.

[4] Marinakis V. Big Data for Energy Management and Energy-Efficient Buildings. Energies 2020;13:1555. https://doi.org/10.3390/en13071555.

[5] Fernández-Viñé MB, Gómez-Navarro T, Capuz-Rizo SF. Assessment of the public administration tools for the improvement of the eco-efficiency of Small and Medium Sized Enterprises. J Clean Prod 2013;47:265–73. https://doi.org/10.1016/J.JCLEPRO.2012.08.026.

[6] Desha CJ KH. Surveying the state of higher education in energy efficiency, in Australian engineering curriculum. J Clean Prod Elsevier 2010.

[7] Gowrie Vinayan, Harikirishanan D, Siow May Ling. Upskilling and Reskilling the Workforce via Industry Driven Technical and Vocational Education and Training: Strategies to Initiate Industry/Institution Partnership in Malaysia. J Econ Info 2020;7:94–103. https://doi.org/10.31580/jei.v7i2.1438.

[8] Meyer KA. Student Engagement in Online Learning: What Works and Why. ASHE High Educ Rep 2014;40:1–114. https://doi.org/10.1002/aehe.20018.

[9] Poquet O, de Laat M. Developing capabilities: Lifelong learning in the age of AI. Br J Educ Technol 2021;52:1695–708. https://doi.org/10.1111/BJET.13123.

[10] Weller M. The distance from isolation. Why communities are the logical conclusion in e-learning. Comput Educ 2007;49:148–59. https://doi.org/10.1016/j.compedu.2005.04.015.

[11] Hung DWL, Chen DT. Situated cognition, vygotskian thought and learning from the communities of practice perspective: Implications for the design of web-based e-learning. Int J Phytoremediation 2001;21:3–12. https://doi.org/10.1080/09523980121818.

[12] Hall H. (3) (PDF) Social exchange for knowledge exchange 2001. https://www.researchgate.net/publication/228359956_Social_exchange_for_knowledge_exchange (accessed September 20, 2020).

[13] Human Capital: Learning in Learning Communities n.d.

[14] Zhao Y, Li T, Zhang X, Zhang C. Artificial intelligence-based fault detection and diagnosis methods for building energy systems: Advantages, challenges and the future. Renew Sustain Energy Rev 2019;109:85–101. https://doi.org/10.1016/j.rser.2019.04.021.

[15] Russell ML. Learning Online: Extending the Meaning of Community. A Review of Three Programs from the Southeastern United States. 1999.

[16] Kowch E, Kowch E, Schwier R. Considerations in the Construction of Technology-Based Virtual Learning... Can J Educ Commun 1997;26:1–12.

[17] Wilhelmina C. Savenye, Rhonda S. Robinson. Computer-mediated Communication. Handb Res Educ Commun Technol 2013:402–36. https://doi.org/10.4324/9781410609519-23.

[18] Engeström Y. Developmental studies of work as a testbench of activity theory: The case of primary care medical practice. Underst Pract 2010:64–103. https://doi.org/10.1017/CBO9780511625510.004.

[19] Acuyo A. Reviewing the Literature on Professional Development for Higher Education Tutors in the Work-From-Home Era: Is it Time to Reconsider the Integration of Social Media? Educ Inf Technol 2022;27:89–113. https://doi.org/10.1007/S10639-021-10603-2.

[20] Does Yammer have gamification tools such as badges , points etc ? - Microsoft Tech Community n.d. https://techcommunity.microsoft.com/t5/yammer/does-yammer-have-gamification-tools-such-as-badges-points-etc/m-p/44941 (accessed October 19, 2021).

[21] Badii A, Sharif A. Information management and knowledge integration for enterprise innovation. Logist Inf Manag 2003;16:145–55. https://doi.org/10.1108/09576050310467287.

Data access statement

The datasets generated during the current study are not publicly available because of data privacy.

Flipped Classroom Concept for Industry 4.0 Pump Monitoring in Building Information Technology

Daniel Eichberger

Institute of Building Services Engineering, Faculty of Process Engineering, Energy and Mechanical Systems, TH Köln – University of Applied Sciences, Cologne, Germany, daniel.eichberger@gmx.de

Abstract. The Flipped Classroom teaching concept has already proven itself in regular school and university teaching for some time. It is already regularly used for frontal teaching, lectures, seminars, and exercises at many universities. For some time now, practical laboratory courses and projects have become the focus of digitalization. Considering distance learning in particular, solutions must be found in this field. This paper describes the didactic concept, the technical background as well as the implementation of a flipped project in the master course Building Automation. It answers the research question: "How to design didactics and implementation of a practical laboratory project on the topics of information modeling, OPC UA and Self-X capabilities using the example of pump monitoring for realizing it as a flipped classroom teaching concept for master students of Building Automation?" To answer the research question, established concepts of didactics were combined with established and new technologies. On the didactic aspect, resources and methods such as explanatory videos in the form of screencasts, competency-oriented learning objectives of different taxonomy levels and group work according to the partner-ship model are used. Combining this with technological tools and concepts, such as a GitHub Repository as reader, task collection and forum, Node-RED as low-code environment, OPC UA, information modeling and Self-X as challenging content emphasis, results in a modern and demanding Flipped Classroom teaching concept. Evaluation, student feedback and conclusion show that even high complexity practical projects can be realized as a Flipped Classroom concept on the level of a master's program. Furthermore, the project can be replicated at any time and, thanks to the manual, can in principle be carried out by any teaching staff or even other laboratories. Further work must primarily address the potential for optimization in terms of organization and content, yet the abstraction of the described project to a meta-level is also conceivable.

Keywords. flipped classroom, project oriented, explanatory videos, competence orientation, OPC UA, information modelling, monitoring, dashboards, self-x
DOI: https://doi.org/10.34641/clima.2022.100

1. Introduction

1.1 Initial Situation and Motivation

As part of the project phase of the Building Information Technology module of the part-time master's degree programme in Building Automation at FH Münster University of Applied Sciences and Biberach University of Applied Sciences, students develop requirement criteria for information technologies from an application perspective and can apply these independently to the technologies studied and document the main results. [2, p. 28]

To achieve this qualification goal, students carry out several supervised projects. However, the coronavirus pandemic from 2020 onwards has virtually disrupted the daily work and teaching routine at colleges and universities around the world. Classroom-based events have become rare and digital alternatives are being successively expanded. At the same time, however, teaching must not stand still, but must continue to be measured against technological developments.

New business models and integrated applications in industry are driving the use of information models and information modelling. Where data was previously seen as available anyway and not as a strategic business asset, there is now a paradigm shift towards valuing the information that is available. [3]

Copyright ©2022 by the authors. This conference paper is published under a CC-BY-4.0 license.

Industrial companies started to develop standardised information models a few years ago. This is often done in cooperation with or under the auspices of organisations such as the VDMA. The increase in standardised information models is particularly noticeable in the field of OPC UA. The VDMA now accompanies more than 30 working groups for the development of OPC UA Companion Specifications [4]. In 2020 and 2021, more than 20 companion specifications with concrete information models were published [5]. Currently, 13 more OPC UA Information Models are in their review phase as Release Candidates [6].

The developments in the fields of OPC UA and information modelling have not yet become part of building automation practice, but it is only a matter of when and not if. The integration of building technology into the process technology is already common practice, and the widespread use of information models and OPC UA will increase the demands on building automation accordingly.

The project described in this paper is the result of the circumstances previously outlined. Within the framework of a flipped classroom teaching concept, the building automation specialists of tomorrow learn important skills in forward-looking concepts such as information modelling and OPC UA. The merging of industrial and building technology is progressing inexorably. Engineers in building automation must be prepared for this.

2.1 Purpose

The project is intended to provide engineers within their master's degree programme with extended competences in the use of information models, OPC UA and the development of monitoring applications.

The paper describes the didactic concept and the technical implementation of the project as a flipped classroom teaching concept. It is intended to serve as an example for committed teaching staff in higher education to develop their own flipped projects for students. In addition, the project can also be implemented at other universities in other degree programmes if the technical requirements are met.

2. Research Methods

One of the defining methods of the project is the Flipped Classroom teaching concept. In preparation for the project work, the students work on basic competences with the help of explanatory videos and accompanying tasks.

However, it is common pedagogical knowledge that it is not enough to simply play films. [6, p. 138]

This method allows the brief attendance time to be put entirely at the disposal of practising and helping. In addition, small groups can emerge in advance, which support each other and thus strengthen the weaker students in particular [7, p. 117] - virtually integrated internal differentiation.

In practice, the combination of explanatory videos on YouTube and flipped lessons has proved particularly successful. The students are usually on the platform anyway, which eliminates the technological hurdle and the technical requirements for implementation are manageable, since perfectly produced, professionally edited, and brilliantly set to music content is not necessarily expected on a platform like YouTube [8, pp. 127-128].

The project work takes place in the partnership model and in small groups. The group work basically consists of additive and disjunctive tasks. The students come together independently in small groups of five people each. Although this procedure involves social risks, it can be carried out quickly and is feasible with a socially balanced group that is appropriate to the level of proficiency. [9, p. 85]

The group methods used are discussion in the whole group format and short presentations. At the beginning of the second day of the project, the students must decide together in a fixed time frame which data will be uploaded to the database and in which format. For this, a consensus must be reached, and a common understanding must be developed. The task sheet for the second part and instructions from the supervisor on the first day are used for preparation. [9, p. 96]

The short presentations serve as a form of examination. Students are given sufficient time on the second day of the project work to prepare for a 10-minute presentation without formal requirements. The structure of these short presentations should already be explained during the kick-off presentation by the supervisor, so that the students have sufficient opportunity to prepare. [9, pp. 98-99]

In addition to the integrated murmur phases [9, pp. 88-89], the method of the presentation [9, p. 87] by the supervisor is used at the very beginning of the project work. In this kick-off presentation, all details of the information model used, and the process of the project work are explained. In addition, an outlook on the expected result is given.

A specific survey via an online tool and a personal feedback round with the students are used to evaluate the success of the project.

To teach in a competence-oriented way, entry and target competences must first be defined. The entry competencies can be used to determine which skills the students need to bring to the project in order not to be overwhelmed by the entry tasks. This is because the use of didactic reduction is also limited and must not jeopardise the level of the course [9, p. 54].

The target competences are presented here in the form of the "Taxonomy Table" according to Anderson et al [10]. Thus, the learning objectives are classified in the taxonomy levels and the knowledge dimensions.

Since some topics are close to computer science, in addition to the usual operators, some of the operators defined by the Ministry for School and Further Education of the state of North Rhine-Westphalia for the subject of computer science [11] are also used.

3. Project Description

3.1 Required Skills

Since the target group is master's students in the second half of their programme, the entry-level competences can be set on a high level. It should be noted, however, that the content of the project was not necessarily part of the students' previous education and thus differentiation is required depending on the topic.

Generally, the competences in the following section are expressed as learning objectives.

Before the start of the preparatory phase of the project, the students must already possess the following skills:

The students ...

... know the monitoring application Grafana, name the basic functions and navigate the user interface.

... explain the HTTP REST methods GET and PUT, dissect and modify complex requests and construct simple requests themselves.

... analyse XML files and complete their content with further elements and values.

... explain the concept of the asset administration shell and model simple information models, both technology-neutral and according to the meta-model of the asset administration shell.

... analyse the OPC UA meta-model and name the function of the OPC UA namespaces.

... describe the principles of object-oriented programming and evaluate the benefits for automation technology.

... describe how Modbus RTU works and create any queries of the Modbus register.

Due to the internal differentiation and the possibility of mutual exchange, it is not mandatory that all students already have these competences at the beginning of the project - developing these competences during the project, however, is essential.

3.2 Goals

As mentioned at the beginning, the target competences are mapped in the form of the taxonomy table. For the learning objectives, tasks and examinations, a coding of designation and number is used in order not to overload the table and thus keep it clear.

The students ...

Goal 1: ... explain the context of the tools used.

Goal 2: ... use the AASX Package Explorer to model an asset administration shell with sub models and sub model elements.

Goal 3: ... parameterise a BaSyx AAS Server.

Goal 4: ... explain the data flow from Modbus to AAS Server.

Goal 5: ... design a Node-RED flow to read data from an XML file and write it to a BaSyx AAS Server.

Goal 6: ... conceptualise a cyclic query/write routine in Node-RED.

Goal 7: ... apply NodeOPCUA to create a simple OPC UA server.

Goal 8: ... modify an OPC UA server and extend it with additional data types.

Goal 9: ... model OPC UA models with the UaModeler program.

Goal 10: ... construct OPC UA namespaces.

Goal 11: ... parameterise the OPC UA Logger to load data into an InfluxDB database.

Goal 12: ... evaluate data regarding their usefulness in monitoring applications.

Goal 13: ... design a monitoring application based on a common data set.

Goal 14: ... define the requirements for a smart pump.

Goal 15: ... compare OPC UA with similar technologies.

Goal 16: ... assess the self-x capabilities of the components used.

3.3 Taxonomy Table

The competence levels of the individual project elements can be clearly identified using the taxonomy table shown here. The focus in the cognitive process dimension is clearly on 6. Create. In the knowledge dimension, there is an even spread across conceptual and action knowledge. Only one learning objective is allotted to metacognitive knowledge.

Tab. 1 – Taxonomy Table referencing the project goals

	1	2	3	4	5	6
A		4	7		14	13
B		1	11	8 1	12 16	5 10 13
C			2 3			6 9
D					16	

3.4 Teaching Material

All tasks of the teaching material are designed according to the quality criteria that they are challenging, solvable and authentic [9, p. 70]. In particular, the tasks accompanying the explanatory videos are demanding and often expect the students to transfer their knowledge. In addition, in terms of internal differentiation, some tasks can only be solved through the students' commitment and willingness to research.

For the preparation, students have nine explanatory videos at their disposal, which they can replay, pause, watch faster or slower, depending on their personal needs [12, p. 17].

All the explanatory videos belong to the screencast category. As they are mainly demonstrations of software products and web applications, with accompanying explanations, this is the common style [13, p. 13]. Generally, they are simple and quickly produced and give precise instructions for otherwise complex actions [12, p. 26]. To get started, the technical requirements are manageable and can be easily and inexpensively extended to produce professional-looking screencasts [8, pp. 128-129].

Christian [14] also describes that flipped classroom concepts with explanatory videos and accompanying tasks work well and can even put learners in a "learning-by-teaching" [14, p. 132] situation.

In addition, a GitHub repository is available to the students, which assumes the role of a Reader in the didactic context. After the effort of creating such a compendium, all information about the project is available to the students in a central and well-organised place. This makes it clear what the contents of the project are, what is expected in the preparation and how the students can prepare. [9, p. 68]

To achieve an internal differentiation already in the preparation, all tasks have a Hints and a Tips section. The hints are mainly technical or organisational hints, whereas the tips are intended for students who need help to solve the tasks.

The Issues section allows students to use the repository as a forum. Students are encouraged to help each other and ask questions if they encounter problems. [9, p. 69]

After the kick-off presentation, during the project work, students are given two worksheets. Basically, each of the two parts consists of only one task, which is specified by mandatory characteristics. In addition, both task sheets contain technical and organisational hints. The students will have to do without tips here, since the internal differentiation during the project work is exclusively achieved through the group dynamics as well as assistance from the supervisor.

Task 1: Create an OPC UA server with static and process data based on the information model provided and the data of your pump.

Task 2: Create a dynamic dashboard in Grafana and visualise static and process data of all pumps.

The project result of the individual groups is primarily examined in the form of a short presentation. The students must summarise their project in a maximum of 10 minutes and present the final dashboard. The presentation is followed by a question-and-answer session and discussion. In addition, the technical execution of the tasks will be assessed. During the students' presentation, a simple evaluation grid is used [9, p. 141]. This is then translated into points.

3.5 Technical Implementation

Currently, the test stand is equipped with four liquid pumps, manufactured by KSB, Grundfos, Wilo, and Spandau Pumpen, as well as a vacuum pump by Gebr. Becker, and a turbo vacuum pump by Leybold. The pumps are not connected to any media circuit and therefore cannot be operated normally. The pumps and the corresponding accessories were kindly provided by the respective manufacturer for the test stand. Figure 1 shows the layout of the pumps on display.

Fig. 1 – test stand front view

The cabinet below contains a router, a switch, and six Raspberry Pis. The router connects to the external (university) network or the internet, while the switch connects to the internal demonstrator

network. For each pump, a Raspberry Pi is provided, which serves as an extended embedded controller. Node-RED, an AAS Server, an OPC UA Server, and the OPC UA Logger all run here. Together, the Raspberry Pi and the pump form the industry 4.0 component.

3.6 Guide

The project is essentially divided into two parts - preparation and project work. The preparation should be carried out by the students in the run-up to the presence part, the project work. Whether this is done at home or at the university is up to the person carrying out the project.

A GitHub repository with tasks, explanations and explanatory videos on YouTube serves as preparation for the students. The tasks are intended to help develop the necessary competences for the project work. Four tasks with the focus on Node-RED, AAS, REST, OPC UA, InfluxDB, Grafana and dynamic dashboards are to be completed. There is no performance review or submission of the preparation. It must be made clear to the students that preparation is essential for the project work and that successful completion is not possible without sufficient preparation.

The explanatory videos are intended to illustrate the steps necessary to solve the tasks by means of an example. They do not represent a sample solution for the tasks. The students must be aware that simply working through the videos does not lead to the necessary acquisition of competences. Students should be encouraged not to write project-related questions or comments in the comments under the YouTube videos and instead use the Issues section of the GitHub repository. The comments section can be used if the comments are related to the video only.

The explanatory videos use an example to illustrate the necessary steps to solve the tasks, but do not provide the complete solution for the tasks. Students must be aware that simply watching the videos does not lead to the necessary acquisition of competences.

The project work takes place in the laboratory and uses the test stand, several laptops, and an external server as work equipment. Through the preparation, the students have acquired all the necessary competences for carrying out the project work and are able to perform the project work independently. In this scenario, the teacher is responsible for responding to the students' questions and giving decisive advice on how to solve the respective work step.

In principle, all project steps build on each other and deviations are only possible in specific cases. The person carrying out the project should make sure that no group falls too far behind and, if necessary, provide targeted support. However, except for selected moments, individual steps should not be completely prescribed, or the standard solution should not be provided.

3.7 Scoring

The scoring of the results should be based on the three core elements presentation, dashboard, and technical realisation. Furthermore, the assistance provided should be considered. The teacher does not have to keep a tally of the assistance provided but should bear in mind how extensive the assistance was for individual groups and take this into account in relation to the result. In this context, (partial) model solutions should be considered severely. Thorough preparation enables all students to work on the project without a model solution; accordingly, the need to provide model solutions suggests that no thorough preparation has taken place.

The teacher should also make sure that the whole group works together and that individual group members do not just float along. In case of doubt, this can also be clarified through dedicated group discussions. Under certain circumstances, a devaluation of individual group members may come into question. However, this should be treated with caution, as it can be difficult to evaluate the group dynamics from the outside.

4. Discussion

The project has already been carried out in real operation and evaluated. From the evaluation, the direct feedback of the students and the achieved results, some aspects for improvement could also be identified.

The aim of developing a project that is suitable for familiarising students with the practical application of information modelling, OPC UA, and dynamic dashboards with the self-x concept can be regarded as fulfilled. Thanks to the methods used, the flipped classroom teaching concept made it possible to develop and implement a challenging but also supportive project. Based on the evaluation and direct feedback, the students are subjectively satisfied with the competences they have acquired and have been able to expand their knowledge in these forward-looking areas.

Many planned aspects and processes could be implemented accordingly in practice. For example, the GitHub repository and YouTube videos were used intensively for preparation. The Issues section of the GitHub repository was also used by the students to clarify open questions. However, mutual support between students could not be observed here.

Thanks to the preparation, the students were able to complete the project work largely independently in their groups. Assistance was required mainly because of certain technical issues in the concrete implementation and the difference between the setup at home and the test stand.

The final presentations of the students made it clear, that the topics were largely understood, and most of the goals (see 3.2) were reached. In this first run of the project, only the aspect of self-x capabilities was not fully understood by the students and could therefore only be presented in its broad outlines.

Additionally, through process-oriented assessment during the project work, the person carrying out the project can objectively assess the individual progress and goal fulfilment of each learner.

To evaluate the results objectively during the project work and final presentations, the examiner can use an assessment form like the one shown in chapter 7.

Even though a high workload was basically intended, certain aspects took up more time and prominence than originally planned. Accordingly, the greatest potential for improvement lies in optimising the time schedule.

In summary, the resulting project represents a solid foundation for further development. Some elements need to be revised or refined, but the basic concepts, the methods used, and most of the technical solutions can be retained.

To further verify the projects effectiveness, case studies from its implementation must be conducted.

5. Conclusion

The project demonstrates that the well-tested flipped classroom teaching concept can be used for project-based work in addition to the usual application for lectures or traditional frontal teaching.

However, it is important that the learners are supported in their competence development through an intensive preparation phase with explanatory videos, tasks, and on-demand support from the teacher.

The project also shows that even complex and partly foreign subjects can be successfully dealt with in such a concept.

The results of the first run of the project have shown, that even during times of distance learning, and for distributed programs such as the Building Automation program in particular, the flipped-classroom teaching concept is an effective alternative to more conventional methods – even for project-oriented courses.

6. Acknowledgements

I thank Prof. Dr. Jochen Müller (TH Köln - University of Applied Sciences, Cologne) for mentoring me in the past and giving me the opportunity to develop this project, and for providing the test stand as well as the laboratory in which the project was carried out; I thank Prof. Dr.-Ing. Matthias Kloas (Berliner Hochschule für Technik, Berlin) for comments on my work and providing the Server as well as the IT infrastructure at the BHT; I thank Björn Kämper (TH Cologne – University of Applied Sciences, Cologne), Maximilian Both (TH Cologne – University of Applied Sciences, Cologne), and Julia Eichberger (University of Cologne) for useful discussions; I thank all the students who eagerly participated in the first iteration of this project.

7. Assessment Form

This assessment form can be used by the examiner for scoring during the process-oriented assessment, and the final presentations. Most indicator complete the sentence "The learners …".

Goal	Indicators	not met	partially met	fully met	exceeded
#1	… showcase the used tools and how they interact with one another.	0	1	2	3
#2	… use the AASX Package Explorer to model an asset administration shell.	0	0.5	1	1.5
	… showcase their asset administration shell and its sub models.	0	0.5	1	1.5
#3	… achieve a working BaSyx AAS Server.	0	1	2	3
#4	… show the data flow from Modbus to AAS either exemplary or using a concrete value.	0	1	2	3
#5	… achieve a working Node-RED flow.	0	0.5	1	1.5
	… describe their flow and what design decisions they made to accomplish the goal.	0	0.5	1	1.5
#6	… show live data from the pump at the output of Node-RED or in the final dashboard, without manual refreshing the flow or data.	0	1	2	3
#7	… show a working OPC UA Server.	0	1	2	3
#8	… use the provided tools to customize the OPC UA servers source code.	0	0.5	1	1.5
	… showcase challenges they faced during the implementation of all required data and how these challenges were overcome.	0	0.5	1	1.5
#9	… use UaModeler to model an OPC UA information model.	0	0.5	1	1.5
	… showcase their OPC UA information model in UaModeler or by using screenshots of the software.	0	0.5	1	1.5
#10	… show their used namespaces and have created at least one additional namespace for their information model.	0	1	2	3
#11	… use the provided tools to customize the OPC UA Logger source code.	0	0.5	1	1.5
	… show live data in the dashboard and explain the usage of OPC UA Logger.	0	0.5	1	1.5
#12	… showcase the final dashboard and account for used and unused variables during the project work or Q&A portion of their presentation.	0	1	2	3
#13	… showcase the monitoring applications of their dashboard.	0	0.5	1	1.5
	… account for the data points collected in the common data set.	0	0.5	1	1.5
#14	… list common properties of smart pumps and describe delimiting properties to pumps.	0	1	2	3
#15	… state similar technologies and describe common as well as distinctive features of the selected technologies.	0	1	2	3
#16	… define self-x as a concept.	0	0.3	0.6	1
	… list and describe self-x capabilities.	0	0.3	0.6	1
	… assess if and to what degree the used components can be described as self-x (capable) components.	0	0.3	0.6	1
The learners required no additional assistance.		-10	-5	0	0
Completeness		0	2	4	6
Comprehensibility, technical terms, factual accuracy		0	3	8	13
Eye contact, body language, speaking loudly and clearly, pace		0	1	2	3

Total score:

Score	70-68	67-64	63-61	60-57	56-54	53-50	49-47	46-43	42-40	39-35	34-0
Grade	1.0	1.3	1.7	2.0	2.3	2.7	3.0	3.3	3.7	4.0	5.0

Grade:

8. References

[1] Höttecke M., Becker M., Bollin E., Liebler K., Hahn H., Jensch W., Karbach A., Müller J., Rieke T. Weiterbildungs-Master Gebäudeautomation: Modulhandbuch. 2020(3):28-29.

[2] Weber H. Data Engineering 4.0: Kompositionale Informationsmodelle für industrielle Anwendungen. 2021;1:1-7.

[3] Herden H. Die OPC UA Arbeitskreise im Überblick [Internet]. 2021 [cited 2021 Jul 24]. Available from: https://www.vdma.org/viewer/-/v2article/render/1248676

[4] OPC Foundation. OPC UA Online Reference [Internet]. [updated 2021 Jul 23; cited 2021 Jul 24]. Available from: https://reference.opcfoundation.org

[5] OPC Foundation. OPC UA Information Models [Internet]. 2021 [cited 2021 Jul 24] Available from: https://opcfoundation.org/developer-tools/specifications-opc-ua-information-models/information-model-release-candidates-for-review

[6] Dorgerloh S. Wie Erklärvideos und Lehrfilme bereitstellen? - Eine Vorstellung aktueller Angebote. In: Dorgerloh S - Lehren und Lernen mit Tutorials und Erklärvideos. 2020:138-139.

[7] Dorgerloh S. Mehr Zeit für den Unterricht gewinnen? - Videoeinsatz am Beispiel des Flipped-Classroom-Konzepts. In: Dorgerloh S - Lehren und Lernen mit Tutorials und Erklärvideos. 2020:117-118.

[8] Schmidt S. Aus der Praxis: Beispiele für funktionierendes Flippen mit Erklärvideos. In: Dorgerloh S - Lehren und Lernen mit Tutorials und Erklärvideos. 2020:127-130.

[9] Osterroth A. Basiswissen Hochschullehre: Methodik – Didaktik – Evaluation. 2021.

[10] Anderson L., Krathwohl D., Airasian P., Cruikshank K., Mayer R. A Taxonomy for Learning, Teaching, and Assessing: Pearson New International Edition. 2014.

[11] Ministerium für Schule und Weiterbildung des Landes Nordrhein-Westfalen. Informatik: Übersicht über die Operatoren. 2015.

[12] Arnold S., Zech J. Kleine Didaktik des Erklärvideos. 2019.

[13] Schön S., Ebner M. Gute Lernvideos ... so gelingen Web-Videos zum Lernen!. 2013.

[14] Christian M. Den Unterricht auf den Kopf stellen? Mit Flipped Classroom Zeit gewinnen und gelehrtes vertiefen. In: Dorgerloh S - Lehren und Lernen mit Tutorials und Erklärvideos. 2020:130-132.

Data encounters in renovated homes: Sense-making beyond displays

Evert van Beek [a], Stella Boess [b]

[a] Faculty of Industrial Design Engineering, Delft University of Technology, Delft, the Netherlands, e.vanbeek@tudelft.nl

[b] Faculty of Industrial Design Engineering, Delft University of Technology, Delft, the Netherlands, s.u.boess@tudelft.nl

Abstract. There is an increasing acknowledgement of the role of residents in the success of low- or zero-energy renovations. One of the approaches to improve this factor is by influencing resident behaviour by means of devices for feedback on consumption. The goal of these systems is to help residents make sense of the relation between their actions and choices, and their energy consumption, indoor environmental conditions and comfort. In this paper we describe interactions with these devices as one form of data encounter. We then suggest that there are other forms of data encounters already happening in renovated homes by which residents make sense. These data encounters are useful to understand if we want to understand the interactions between residents and buildings. We introduce the concepts of sense-making and interactive adaptation to better understand these data encounters. In this study we show data encounters in various forms as they happen in four renovated homes in the same building in the Netherlands. We use interviews and video-recorded walkthroughs to identify data encounters related to indoor climate and energy consumption within these homes. We find data encounters that involve more than displays and technical devices. Residents use bodily senses, information from other people, and complex contextual information to understand indoor climate and energy consumption. We also find that data encounters relate to, and are embedded in everyday practices and routines. Finally, we find that data encounters involve active sense-making rather than passive consumption of information. We discuss these findings and conclude by suggesting that existing data encounters could serve as a starting point for the improved design of buildings, renovation processes, and the selection, design and implementation of new data encounters.

Keywords. Occupant behaviour, data, feedback, renovation, sense-making, design, home energy management systems
DOI: https://doi.org/10.34641/clima.2022.101

1. Introduction

There are a lot of unknowns concerning the interactions between residents and buildings, including about how resident behaviours change in response to feedback.

Although measures to improve the efficiency of buildings (e.g., renovations with heat pumps and improved insulation) have made great progress, a performance gap remains between expected and actual energy performance. Increasingly there has been an acknowledgement of the role of residents themselves in the performance of buildings and achieving actual energy savings [1]. The impact of occupant behaviour is significant, with potential energy savings of 62-86% in residential buildings [2].

This realization of the role of residents has spurred a wide variety of approaches to better understand this behaviour, including profiling of households, and the recording and modelling of this factor [3,4].

In addition, attempts are made to influence resident behaviour. This includes instruction of residents after the renovation by means of a manual, energy advise by professional energy advisors, and behavioural change programs [5].

1.1 Feedback on consumption

An increasingly popular way of influencing resident behaviour is by means of feedback on consumption within the home. This includes various forms and guises of eco-feedback: smart meters, smart thermostats, home energy management systems (HEMS), and in-home displays (IHD's), feedback

Copyright ©2022 by the authors. This conference paper is published under a CC-BY-4.0 license.

communicated to the user, e.g., by SMS or email, or made available on website. Sometimes these eco-feedback solutions go under the name of energy monitors, dashboards, or are embedded in smartphone applications. This eco-feedback is sometimes enriched with various forms of visualization, enables the setting of goals, or employs gamification approaches to achieve energy saving goals [6,7]. Finally, they sometimes include a component of social interaction, by e.g., ranking and comparing consumption within a neighbourhood [8].

The goal of these systems that are introduced is to help residents *make sense* of what is going on. This sense-making is expected to *relate energy consumption, indoor environmental conditions and comfort* to *choices or actions*. The expectation is that residents use some form of data or feedback, visualized or presented, to 'gain insight into, and control over, a household's energy consumption'[6]. Underlying assumptions are that households as end consumers of energy, make informed choices in everyday life, ultimately with the goal of reducing energy consumption. These systems often envisage householders as managers of resources [9] who, with the right information might be persuaded towards sustainable behaviour [10].

These interventions have reached varying degrees of success [11]. In particular in the long term, sustained energy savings are not guaranteed, and users may react in unexpected ways, generating undesired consequences such as cold homes or increasing levels of consumption[12]. The disappointing results of in-home displays even led researchers to urge the UK government to reconsider introduction of in-home displays [12].

Several reasons have been given for this lack of consistent success. Authors point to a lack of understanding, and design for, user engagement with these systems [12], and a lack of understanding why people would be interested in the feedback in the first place [13].

Despite the lack of consistent results, authors agree that, if well designed and implemented, there is a high potential in feedback on consumption to lead to changes in resident building interaction which improves comfort and energy savings in homes. This potential stems from observations that energy end-users are able to and willing to change behaviour (such as operating windows) if it is convenient and makes sense to them in everyday life [14].

1.2 Feedback as data encounters

Interactions with feedback systems are an encounter between residents and one very specific type of data: numbers or graphs indicating consumption of resources. However, in everyday life, residents encounter a lot of different forms and types of data or information. Some of these encounters have an impact on everyday practices: Looking out of the window to see the weather might influence one's decision to bike to work. And, less consciously, one might encounter the smell of a nearby restaurant, have increased appetite, and have lunch earlier. Some of these encounters do not give feedback on consumption of resources, yet have a significant influence on the consumption of resources and on indoor climate. One can think of opening windows as a response to smell, changing clothes in response to weather forecasts. We will call these moments of feedback related to indoor climate and energy consumption: *data encounters.*

The research question of the study reported here is: What data encounters related to indoor climate and energy consumption are currently happening? The aim of the study is to show data encounters in various forms as they happen in renovated homes, without the intervention of newly introduced interventions such as HEMS. This contributes to a better understanding of interactions between buildings and residents, which is a crucial aspect of the energy performance of the built environment.

A better knowledge of data encounters could impact the design of renovated homes by finetuning our expectations of resident behaviour in response to various design decisions (e.g., making the state of a ventilation system audible). In addition, this knowledge allows us to better select, design and implement new data encounters; both by designing essential ones (e.g., on thermostats or maintenance) and by introducing additional systems such as HEMS, smart meters or otherwise.

To answer the research question, we select some concepts pertinent to interactions between buildings and residents. We use these concepts to analyse interview data from four zero-energy renovated households. The results will show that data encounters are diverse, are embedded in everyday life and routines, and are active

1.3 Sense-making and interactive adaptation

Sense-making and interactive adaptation are two concepts that are presented and have been used in the past to understand interactions between residents and buildings, in particular data encounters.

The concept of sense-making has been used to understand how residents respond to information such as energy use feedback on HEMS [15]. Sense-making concerns how meaning and understanding is gained in action and interpretation, while also incorporating existing knowledge gained in the course of everyday life [16]. Three interrelated processes have been identified in literature, that together constitute sense-making. *Noticing:* something that interrupts ongoing activities and habits and triggers the need for further interpretation. *Interpreting:* The active process of drawing on different sources to form a more

complete sense of the situation. And *enacting*: acting on this more complete understanding. In this study, we use this framework to identify sense and categorize sense-making activities.

Interactive adaptation is a concept that has been used to understand occupants behaviour and perceptions regarding comfort and control [17,18]. The framework sees comfort as something that residents *achieve* in interplay with heating and cooling systems, and as part of other household practices such as cooking, washing and cleaning [19,20]. For this study, this means that we will look beyond system control actions of residents (e.g. turning up the thermostat), and pay attention to other daily practices that relate to and have an impact on indoor climate (e.g., cleaning or letting pets out).

2. Research methods

In this study we take a qualitative and ethnographic research approach to answer our research question: What data encounters related to indoor climate and energy consumption are currently happening within renovated homes?

2.1 Building and participating households

The building is located in the South-West of the Netherlands. The post-war industrialised housing is renovated around 5 years prior to this study, according to a zero-energy scheme, with solar panels powering electric heating. The building is social rented housing, and contains 12 apartments. This study includes four of the households within this building. Three of these households are single person households of age between 22 and 65, and one four-person household, all living in similar apartments of approximately 55 sqm.

The building is outfitted with a geothermal heat pump in a cascade-setup. Heating is delivered using a low temperature scheme, manageable by a simple thermostat, without clock-functionality. A generic ventilation control panel controls the mechanical heat recovery ventilation system. The building is highly insulated using triple glazing.

Some problems of the building are known: it tends to overheat on hot days, some of the households were unsatisfied with the heating performance of the low temperature heating, the installed climate management systems had small and bigger technical issues, and some households experienced general problems after the renovation such as leakage.

2.2 2.1 Data collection

We conducted semi-structured interviews (with the initial goal to explore occupant experiences and practices, and in relation to a larger study that monitors building performances). The interview included a walkthrough. A walkthrough is a method where residents guide the researcher through their house and provide descriptions and re-enactments of actions and practices related to indoor climate management and consumption. This technique has been introduced as a situated and embodied activity that enables users to participate in understanding and communicating their daily practices [14,21]. All interviews and walkthroughs were digitally recorded and transcribed for analysis.

2.3 Data analysis

Transcripts and video recordings were analysed by the authors, with the aid of Atlas.TI software. We identified data encounters by verbal mention of, and photographic evidence of sources of information that played a role in *noticing, interpreting* and *enacting*. We paid special attention to information related to indoor climate and energy use, commonly found in HEMS (like electricity usage, temperature and indoor climate) but were also attentive to secondary factors that might directly influence these (e.g., air flows). This would also include aspects like maintenance (of filters, e.g.,) as these aspects influence energy consumption, and might be concluded from HEMS as well. The authors listed, and clustered the data encounters using a bottom-up clustering approach. This resulted in 103 data points, with some overlap. The results section describes the most illustrative data encounters, after which we illustrate key findings with participants quotes and pictures.

3. Results

We have introduced the concepts of sense-making and interactive adaptation. In line with these concepts, we analysed the data and present it below. Sense-making includes processes of *noticing, interpreting* and *enacting* [15,16], which we identify in the data. In line with interactive adaptation [19], we look at how these data encounters relate to *daily practices*. This relation to daily practices is particularly present as a consequence of sense-making, and thus found in the process of *enacting.*

Below we present a selection of illustrative data encounters. We also identify possible effects of changes in daily practices in terms of their effects on indoor climate, comfort and energy consumption.

Tab. 1 – Data encounters involving technical devices.

Noticing	Data involved	Interpreting	Enacting	Effects
Turning the thermostat up to 21, each time before the grandchildren arrive for their weekly visit.	Temperature displayed on thermostat in the day that follows the action.	The heating system isn't able to heat the apartment to 21 degrees.	Leave the thermostat to 20 degrees	No change in energy consumption (if it does not reach 21 degrees), dissatisfaction with renovation
Opening cupboard door to view energy meter. Temporarily disabling Christmas lights	Energy consumption numbers on smart meter	Christmas lights consume more energy than expected	Turn off Christmas lights when resident is not present in living room	Reduction in energy consumption

3.1 Technical devices

Data encounters involving technical devices, like displays and thermostats, played a significant role in sense-making processes. (Table 1) shows some examples and their effects. One of the residents explained how she wasn't able to provide her grandchildren with the indoor climate she thought they needed. *'The thermostat just doesn't get to 21'.* In this case, the thermostat was particularly present as a display that shows current temperature in relation to set temperature. For this household, the data encounter was *noticed* as it was part of her preparation for the arrival of her grandchildren. It was particularly meaningful as it related to her frustration of not being able to have variable indoor temperatures (lower when she is alone, higher when her grandchildren are present).

Another data encounter was between a resident and the numbers on the energy meter. She explained how she went actively investigating to reduce the consumption of her Christmas lights. In this case her *noticing* followed from her own investigations. *"And then I thought "what the hell?" and then I'll go and see what's going on that I don't need. You know what I mean? Then I'll go and investigate."*

The insight from these data encounters with technical devices is that they enabled sense-making if people actively engaged with them (by opening a cupboard door and turning lights temporarily off), or if they disturbed *practices* related to values important to the resident (caring for her relatives).

3.2 Bodily senses

Data encounters that involved bodily senses featured prominently in the data (Table 2). Sometimes residents directly sensed the state of the indoor climate, such as temperature. Other data encounters that we found included *noticed* sound. One of the residents explained why he *interpreted* the mechanical ventilation system to be not working properly, and why he thought this led to his occasional shortness of breath. He referred to the sound it makes at different locations in his home. *"It is set to only properly extract in the bathroom. You hear nothing in here [the living room]"*.

Another resident noticed how she couldn't sleep with the traffic sound from a neighbouring street and therefore *enacted* her sense-making by closing the windows at night: *"It's quite a busy street, so that's something I hear".*

When asked about how she deals with hot days, one resident explained how she moved her hands across

Tab. 2 – Data encounters involving bodily senses.

Noticing	Data involved	Interpreting	Enacting	Effects
Sound from outside disturbs sleep with windows that are open for fresh air	Sound from outside (traffic)	Sound level is too high to fall asleep	Closing the window at night	Reduced thermal comfort (less 'fresh air')
There is a difference between sound levels in bathroom and living room	Sound levels emitted from air valves	The mechanical ventilation system only properly works in the bathroom	None	Reduced resident satisfaction
Dry throat	Waking up with a dry throat	The air is dry	Opening more windows during the day	Possibly increased in consumption because of heat loss through window
Felt airflows	Airflow on hands when put above convector	Convector fans are cooling	Turn the convector fans on when feeling hot	Slight increase in thermal comfort, negligible energy consumption of fans

Tab. 3 – Data encounters involving extended periods of time

Noticing	Data involved	Interpreting	Enacting	Effects
Clothes dry quicker than expected	Drying clothes feel dry to the touch	The air in this apartment has low humidity	None	None
Temperature does not increase while thermostat is set to 24 degrees for multiple days or weeks	Bodily sensed temperature and reading on thermostat over extended periods	This apartment is not heating as expected, it cannot reach the set temperature	Thermostat set to 24 degrees permanently, managing climate by electric heater & operating windows	Increased energy consumption, lack of thermal comfort

the convector panel and thereby *interpreted* the convector fans to bring some cooling (Figure 1).

Fig. 1 – Residents notices air flow with hands.

In addition, some residents *interpreted* dry throats and headaches as results of bad indoor air quality. Multiple residents explained how they opened windows to counter these effects.

The insight these data encounters bring, is that bodily senses were found by residents to result in highly trustworthy data, both to evaluate indoor climate, and to actively investigate the working of systems.

3.3 Extended periods of time

Sense-making doesn't just happen at one point in time. Often residents *noticed* data for extended periods of time (Table 3).

Residents were involved in data encounters that required repeated checking (of e.g., how dry clothes feel) and thereby *interpreted* the air quality in the apartment. This data encounter was significant to household practices as it reconfigured existing routines of clothes drying (drying for shorter periods).

Other times, the sense-making started with *enacting* change (setting the thermostat to 24) and not getting the expected response. *"When I sit down it's cold. When I work it's also cold.".* This required the family to keep an eye on the thermostat for longer periods of time and repeatedly *enact* their sense-making by turning the thermostat wheel to *notice* the set point.

The resulting insight from these observations is that sense-making can be intensive in terms of cognitive requirements. Residents rely on their memory of data encounters over extended periods of time to make sense of the state of their home. Another insight concerns the *effects* of sense-making over extended periods of time. With longer periods of *enacting* change (e.g., keeping the thermostat to 24), the effects on aggregate energy consumption increases. Additionally, when resorting to managing indoor climate by windows, the thermostat as a control device might well be forgotten and remain on a high setting, even when no heat is required.

3.4 Social situations

Interviews with the residents reveal that sense-making often involves other people and social dynamics (Table 4). The parents within the four-person household were increasingly worried about the health of their kids, when they *noticed* their coughing, and *interpreted* this as underheating of the apartment. *"I always think: are they cold or not? So they don't get sick."*.

Another resident knew about herself that she preferred lower temperatures, but *noticed* her guests mentioning they were cold. The small size of her apartment, and the slow cooling due to the high insulation values, motivated her to not immediately change her *practice* of keeping windows open. She

Tab. 4 – Data encounters involving social situations.

Noticing	Data involved	Interpreting	Enacting	Effects
Kids cough	Coughing repeatedly	The apartment is too cold for the health of the children	Getting and using an electric heater	Increased energy consumption
Visitors mention they're cold	What visitors say, thermostat setting and temperature.	The apartment is cold for others	Offer a blanket, and close windows if repeated	None, thermostat set point is not raised.

Tab. 5 – Data encounters involving complex contextual sense-making

Noticing	Data involved	Interpreting	Enacting	Effects
Cat sits on convector when convector fans are on	Position of cat	The convector fans are providing some cooling	Keeping the fans on hot days	Slight increase in thermal comfort, negligible increase of consumption by fans
Discolouration of interior	Colour of interior items	Keeping the sun out keeps things looking nice	Keeping curtains closed when away during the day	Reduces chance of overheating
Mechanical ventilation valves have changed colour	Colour of valves when inspected	The ventilation system is working, and the air is unclean	Cleaning the valves at regular moments	Possibly a slight increase in ventilation performance

would first act on guests' discontent by offering them a blanket.

Social sense-making reveals that sense-making, and in particular *enacting* change in *practices* is situated within social situations. Something might not be noticed if other people don't point it out. In addition, this category reveals that divergence from social norms and expectations ('having a cold apartment') triggers *noticing* and further sense-making.

3.5 Complex contextual sense-making

As already noted in some examples above, sense-making is often not a one-stop data encounter. It can involve drawing on multiple types of data and active investigations. We have clustered these data encounters as complex contextual sense-making (Table 5).

Fig. 2 – The cat on its way to jump on the convector.

One participant told a surprising story about how she was able to *interpret* the status and effect of convector fans from *noticing* the position of her cats on hot days (Figure 2). They would jump on the convector when the fans were displacing air. Not only did this require empathy with, and understanding of her pets, she was also able to corroborate this interpretation with her own senses as described above (3.2).

This participant also explained how she gained multiple *interpretations* from one data encounter with the colour of valves. *"It's been a while. So they are not really dirty. But when I moved in, they were pitch black."* She explained that they informed her of the unclean state of the air, and of the status of the mechanical ventilation system (Figure 3).

Fig. 3 – A slightly visible change in colour of valves.

The insight from these two examples of data encounters is that sense-making can happen by drawing on multiple complex data encounters, and result in multiple interpretations with possibly diverse effects on consumption and resident satisfaction.

4. Discussion

This research has shown data encounters in renovated homes and how sense-making happens. We have used the concepts of sense-making and interactive adaptation to analyse these data encounters. We have shown how data encounters are already happening in renovated homes, even when no newly introduced systems for feedback on consumption are present.

The data encounters we discovered *involve more than displays*: Although technical devices and displays (e.g., thermostats) were certainly present, other types of data were also encountered and sometimes found to be more trustworthy. Existing literature has described the goal of HEMS and other feedback devices as contributing to resident insight into, and control over, indoor climate and energy consumption [6]. The results show that there is a wide range of other data already present residents use to gain this insight. Residents use their bodily senses, information from other people, and complex contextual information such as the changing colour of ventilation valves to gain insight.

The data encounters we have shown are not solitary moments of insight. Instead, they *relate to, and are embedded in everyday practices and routines*. Sometimes these routines are disturbed, e.g., when traffic noise forces residents to close windows they had open during nights. Sense-making is not separate from, but embedded within practices of heating: When the apartment does not get to the set temperature, residents gain insight into the limited power of the heat pump. This research also confirms insights from studies of heating practices [22] by showing how practices are altered by sense-making and are interlocked with one another: The solution of using an electric heater daily will reduce the frequency of looking at the thermostat.

This research has also shown that data encounters involve *active sense-making*, rather than just a passive consumption of information. Residents *enact* a change of thermostat set point and gain insight from that, or engage in an experiment to ascertain the energy consumption of Christmas lights. This confirms the action-oriented dimension of sense-making found in literature [15].

Future analysis would be needed to further investigate and quantify the effects on energy consumption of the described data encounters. Future research also needs to collect more insights to develop a coherent framework for the development and evaluation of effective data encounters that contribute to energy efficiency.

4.1 Implications for design

The findings from this paper can be used to advance the field of indoor climate management by informing requirements and guidelines for the design of buildings and renovations, and guidelines for the design and implementation of data encounters, as part of a renovation or introduced later.

This improved understanding of the interactions between building and residents has several implications for the design of buildings, and the design of new data encounters such as HEMS.

In order to improve the design of housing and renovations, we can design for and build on existing data encounters and forms of sense-making. This could include e.g., enhancing rather than hiding the dirty state of ventilation valves.

In addition, the disturbance in daily practices introduced by renovations might be used as an opportunity to change everyday practices towards less resource intensive ones. This can be done using consumption feedback and efforts in communication in tandem, addressing e.g., window opening practices.

Finally, we have sought to bring attention to the active dimension of sense-making. Designing encounters with data could develop this active dimension more by making insights actionable for residents (e.g., suggesting to check the status of windows when lowering the thermostat for the night).

5. Conclusions

Currently, interventions that give feedback on consumption such as HEMS are focussed on one specific form of data on a display. In this paper, we have explored how other types of heterogenous data are encountered in the home. This has provided novel insights into how data is encountered and how these encounters relate to sense-making processes. We have shown how data encounters are diverse, are embedded in everyday life and routines, and are active. This paper has also suggested that existing data encounters could serve as a starting point for the improved design of buildings, renovation processes, and the design of new data encounters. Future research is needed to analyse the effects of these encounters and develop a framework for development and evaluation.

6. Acknowledgements

This project is implemented with support from the MMIP 3&4 scheme of the Ministry of Economic Affairs & Climate Change and the Ministry of the Interior & Kingdom Relations.

This research was funded by RVO, as part of the BTIC programme Integrale Energietransitie Bestaande Bouw. The authors want to thank the participants for their generous sharing of input during the interviews and walkthroughs.

Data access statement

The datasets generated and analysed during the current study are not publicly available because of the time and effort required for anonymization of video recordings that include personal details and faces, but requested portions of the data will be made available upon request to the corresponding author.

7. References

[1] Guerra Santin, O., Itard, L., Visscher, H. The effect of occupancy and building characteristics on energy use for space and water heating in Dutch residential stock. Energy and Buildings. 2009;41(11):1223–32.

[2] Ben, H., Steemers, K. Energy retrofit and occupant behaviour in protected housing: A case study of the Brunswick Centre in London. Energy and Buildings. 2014 Sep;80:120–30.

[3] Fabi, V., Andersen, R. V., Corgnati, S., Olesen, B. W. Occupants' window opening behaviour: A literature review of factors influencing occupant behaviour and models. Building and Environment. 2012 Dec;58:188–98.

[4] van den Brom, P., Meijer, A., Visscher, H. Performance gaps in energy consumption: household groups and building characteristics. Building Research and Information. 2018;46(1):54–70.

[5] Fischer, J., Crabtree, A., Rodden, T., Colley, J., Costanza, E., Jewell, M., et al. Just whack it on until it gets hot. In: Proceedings of the 2016 CHI Conference on Human Factors in Computing Systems [Internet]. New York, NY, USA: ACM; 2016. p. 5933–44. Available from: https://dl.acm.org/doi/10.1145/2858036.2858518

[6] Geelen, D. V. Empowering end users in the energy transition: An exploration of products and services to support changes in household energy management. Ph.D. Thesis. 2014.

[7] Kobus, C. B. A., Mugge, R., Schoormans, J. P. L. Washing when the sun is shining! How users interact with a household energy management system. Ergonomics. 2013 Mar;56(3):451–62.

[8] Pierce, J., Paulos, E. Beyond energy monitors: Interaction, energy, and emerging energy systems. Conference on Human Factors in Computing Systems - Proceedings. 2012;665–74.

[9] Strengers, Y. Smart energy in everyday life: Are You Designing for Resource Man? Interactions. 2014 Jul;21(4):24–31.

[10] Brynjarsdóttir, H., Håkansson, M., Pierce, J., Baumer, E. P. S., DiSalvo, C., Sengers, P. Sustainably unpersuaded: How persuasion narrows our vision of sustainability. Conference on Human Factors in Computing Systems - Proceedings. 2012;947–56.

[11] Paone, A., Bacher, J. P. The impact of building occupant behavior on energy efficiency and methods to influence it: A review of the state of the art. Energies. 2018;11(4).

[12] Buchanan, K., Russo, R., Anderson, B. The question of energy reduction: The problem(s) with feedback. Energy Policy. 2015 Feb 1;77:89–96.

[13] Strengers, Y. Designing eco-feedback systems for everyday life. Conference on Human Factors in Computing Systems - Proceedings. 2011;2135–44.

[14] Boess, S., Silvester, S. Behaviour change in home ventilation. Tijdschrift voor Human Factors. 2020;45(3):4–8.

[15] Wood, G., Day, R., Creamer, E., van der Horst, D., Hussain, A., Liu, S., et al. Sensors, sense-making and sensitivities: UK household experiences with a feedback display on energy consumption and indoor environmental conditions. Energy Research & Social Science. 2019 Sep;55:93–105.

[16] Weick, K. E., Sutcliffe, K. M., Obstfeld, D. Organizing and the process of sensemaking. Organization science. 2005;16(4):409–21.

[17] Stevenson, F., Rijal, H. B. Developing occupancy feedback from a prototype to improve housing production. Building Research & Information. 2010 Oct;38(5):549–63.

[18] Cole, R. J., Robinson, J., Brown, Z., O'Shea, M. Re-contextualizing the notion of comfort. Building Research and Information. 2008;36(4):323–36.

[19] Chiu, L. F., Lowe, R., Raslan, R., Altamirano-Medina, H., Wingfield, J. A socio-technical approach to post-occupancy evaluation: Interactive adaptability in domestic retrofit. Building Research and Information. 2014;42(5):574–90.

[20] Shove, E. Comfort, Cleanliness and Convenience: The Social Organization of Normality. Berg; 2003.

[21] Guerra-Santin, O., Bosch, H., Budde, P., Konstantinou, T., Boess, S., Klein, T., et al. Considering user profiles and occupants' behaviour on a zero energy renovation strategy for multi-family housing in the Netherlands. Energy Efficiency. 2018;11(7):1847–70.

[22] Kuijer, L., Watson, M. 'That's when we started using the living room': Lessons from a local history of domestic heating in the United Kingdom. Energy Research and Social Science. 2017;28(April):77–85.

Integrating technology, education and practice to change energy behaviours in schools

Edelle Doherty [a], Dmitry Brychkov [b], Natalia Romero Herrera [c], Eilish McLoughlin [d], Nadine Roudil [e], Sander Smit [f], Stefan Maas [g], Branca Arthur Delmonte [g], Florence Gauthier [h], Eoghan Clifford [i]

[a] National University of Ireland, Galway, Ireland, edelle.doherty@nuigalway.ie.

[b] National University of Ireland, Galway, Ireland, dzmitry.brychkov@nuigalway.ie.

[c] Delft University of Technology, Delft, the Netherlands, N.A.Romero@tudelft.nl.

[d] Centre for the Advancement of STEM Teaching & Learning, Dublin City University, Ireland, eilish.mcloughlin@dcu.ie.

[e] École Nationale Supérieure d'Architecture de Paris Val de Seine, France, nadine.roudil@paris-valdeseine.archi.fr.

[f] R2M Solution, London, UK, sander.smit@r2msolution.com.

[g] University of Luxembourg, Luxembourg, stefan.maas@uni.lu.

[h] Regional Council of Center-Val de Loire, Orleans, France, florence.gauthier@centrevaldeloire.fr.

[i] National University of Ireland, Galway, Ireland, eoghan.clifford@nuigalway.ie.

Abstract. Schools are learning communities where multiple stakeholders can collaborate to learn about energy efficiency, including via formal curricula, non-formal learning and day-to-day practices. Furthermore, by improving energy literacy among building occupants, the energy efficiency of schools can be improved. However, turning schools into learning communities rather than learning organizations is still problematic. This article details a case study realised in the form of the ENERGE project, which integrates technological, educational and practical activities in 13 post-primary schools from 6 European countries. Owing to an extensive collaboration of diverse stakeholders, the ENERGE project resulted in the origination of a learning community around energy efficiency in the schools. The outcomes of building a learning community within the ENERGE project included: capacity building (in the form of the ENERGE Committees and Teacher Network), the introduction of digital education (via the ENERGE digital platform), development of curriculum-based modules to raise energy literacy, and the establishment of a viable model for expanding ENERGE experience to other schools. The article concludes by explaining the benefits of the ENERGE approach for stakeholders.

Keywords. Business model, energy, energy literacy, digital platform, learning community
DOI: https://doi.org/10.34641/clima.2022.166

1. Introduction

The transition to nearly zero-energy buildings (NZEB) requires holistic efforts in all segments of energy generation and usage, as well as active engagement of multiple stakeholders, including, policy and decision makers, engineers, architects and designers, academia representatives, building owners, energy-related product/service suppliers, and last, but not least, building occupants [1]. As part of these holistic efforts, educational opportunities for building occupants regarding energy and the implications of its use should be developed. This can help create energy-centred learning communities to enable communities to take action to reduce energy consumption or advocate for changes that can do so. Energy-centred learning communities are places of extensive interpersonal collaboration between different stakeholders (e.g. educators, students, engineers, sociologists, businesses etc.) that can drive responsible energy use learning, teaching and practicing. The implementation of a learning community approach can turn schools, (regarded as primary educational units and key staging points for promoting responsible energy use in public and private environments), into leaning communities, rather than learning organizations, thus prioritising collaborative forms of learning for personal development [2].

There are various projects and programmes aimed at improving energy efficiency in schools [3-5]. However, such projects can underperform with respect to several important elements of building energy efficiency learning communities in schools [4]. These elements include the following:

Copyright ©2022 by the authors. This conference paper is published under a CC-BY-4.0 license.

(a) extensive multi-stakeholder collaboration (e.g. via energy efficiency-focused intra-school and inter-school groups),

(b) introduction of multi-purpose digital platforms (e.g. where energy-monitoring technology can be combined with educational activities),

(c) development of curriculum-based modules to raise energy literacy (e.g. via systemic and collaborative approach to energy module development), and

(d) the establishment of a viable business model to expand knowledge and experience obtained in such projects to other schools.

Thus, an interdisciplinary and longitudinal study within the Interreg ENERGE project, which stands for "Energizing education to reduce greenhouse gas emissions", is being undertaken to address these elements using 13 post-primary schools in 6 countries of North-Western Europe (France, Germany, Luxembourg Ireland, Northern Ireland, and The Netherlands) as pilot schools. The project follows a multiphase mixed methods research design. This article describes the ENERGE project as a case study to present its vision of building a learning community with the aim of improving energy efficiency in the schools, and also in their private homes from the lessons learned.

2. Research methods

2.1 Context analysis

In order to realise the learning community approach, the ENERGE project recruited diverse partners from various domains, including professional engineers and sociologists, energy service contractors, business innovators, decision makers, etc. These partners selected 13 post-primary schools in various North-Western European locations to be part of the learning community. **Appendix A** (**Tab. 1 to Tab. 4**) contains the profiles of the ENERGE project schools, including information on school location (with some climatic conditions), school type, construction/extension years, school building ownership, curriculum orientation, student/staff numbers and space heating fuel type. The appendix demonstrates a certain level of diversity of the project schools. The diversity of the partners and the schools is vital to build a rich and vibrant learning community, in which all entities could share varied knowledge, skills and experience.

2.2 Capacity building and social networking

Two key methodological tools of building an effective learning community included the formation of the school-based ENERGE Committees and Teacher Network [6]. The ENERGE Committees were formed in all project schools (one per project school) by attracting those students and staff that were primarily interested in energy saving and sustainability. Each committee comprised several students headed by a teacher. The committees served as testing grounds for various ENERGE-related activities, including, for instance, piloting energy literacy modules (see below in this section). An "ENERGE Teacher Network" (19 teachers from 11 project schools) was established to serve as a platform for sharing ideas, knowledge, skills and experience related to teaching and learning about energy and its saving. The prime concern of the Teacher Network was to develop and pilot energy literacy modules.

2.3 Energy literacy modules

As part of forming an effective learning community, the ENERGE project aimed to collaboratively create proprietary energy literacy content in the form of energy-related modules, (represented via separate units and activities). The methodology of this element of building a learning community was as follows. The partners developed an ENERGE energy literacy framework, which contained basic parameters of energy literacy [7]. Then, the partners, via a systematic literature review [8] (full specification of the literature review is provided in the Supporting Materials), created a shared database of energy-related teaching/learning modules. Each unit is divided into topic units with a range of 5-10 activities in each module. Furthermore, in cooperation with the members of the Teacher Network, the partners developed the ENERGE module design process and uploaded relevant energy literacy modules into this database. Specifically, the members of the Teachers Network provided their feedback on the compatibility of the designed modules with existing school curricula. After the design and content of the modules was agreed, the members of the Teacher Network piloted these modules among their students, including members of the ENERGE Committees. Following piloting, and further collaboration with all 13 project schools, the design and content of modules was finalised, while further suggestions on their compatibility with the school curricula were made.

2.4 ENERGE digital platform

Another vital tool for creating an innovative learning community was the development of an "ENERGE digital platform". The ENERGE Digital Platform was developed to monitor electrical energy consumption and indoor climate quality (specifically, temperature, humidity, carbon dioxide, lighting and noise levels) at specific locations in each of the 13 project schools. The platform included: (a) devices for energy use monitoring, i.e. nine-channel electrical meters and a Sigfox Modbus data collector; and (b) devices for indoor climate monitoring, i.e. Elsys wireless sensor boxes, together with a LoRa gateway and a router (the specifications of the installed devices are available upon request). The selection of relevant sensor/meter installation points was guided by the following considerations: (1) identification of significant energy users and/or energy/comfort-

related issues; (2) occupancy levels in the monitored areas; (3) the capacity of these points to be subject to energy-related interventions (e.g. behaviour change, etc.) that might lead to tangible energy-saving outcomes; and (4) the feasibility of installing monitoring equipment at these specific locations.

From the time the devices started to generate datasets on energy consumption and indoor climate conditions, the data has been processed and monitored via user-friendly proprietary interfaces. The available datasets are employed as a tool of collaborative learning by all stakeholders to monitor energy usage and comfort parameters to understand and implement various interventions and behaviour change measures. Collaborative learning opportunities have been harnessed in workshops in addition to the ENERGE Digital Platform co-design sessions, which were carried out with multiple stakeholders, including the members of the ENERGE Committees and Teacher Network in each of the project schools. Therefore, the ENERGE Digital Platform performs two roles: (a) it acts as a data hub, with a user-friendly interface, for analysing school built environment via a network of electrical energy meters and indoor climate sensors installed in the project schools, and (b) it acts as a teaching/learning tool to educate school stakeholders in energy-related interactions and strategies. Since the ENERGE project is a long-lasting initiative, which is intended to continue even after project finalization, the development of the Digital Platform is an ongoing process, subject to its adaptation for stakeholder needs based on received feedback.

2.5 ENERGE business model

The actions and outputs of the ENERGE project are somewhat wasted without a means of ensuring that the methodology in the project can be applied long after the project itself has ended. To ensure this, an ENERGE business model is being developed that allows for the exploitation of the ENERGE results across the six target countries in a viable manner. An important element of the ENERGE business model is that it should overcome differences in governance, administrative and financial structures for post primary schools in the different countries. The relevant business model for the ENERGE project is being developed with the help of a business model canvas, value network and five-stage business model generation process [9]. This work includes the following stages:

1) Mobilise: This meant mobilizing key ENERGE stakeholders to define the initial business model.

2) Understand: This included a good understanding of the context in which the business model will evolve (by preparing a special report on the project schools and running several surveys among the school population) and the collection of ideas of relevant stakeholders on the development of business model workshops.

3) Design: This included the exploration of the business model options. To select the most promising business model, a workshop among the project partners was carried out. This was enhanced by a series of key informant interviews with the project school administration and teachers. The key objective of the interviews was to clarify the focus of the project and expectations related to it.

4) Implement: The ENERGE business model will be implemented and executed first at the project schools. Based on the results and experiences from the project schools, the ENERGE business model will be adapted or adjusted. Once finalised, the ENERGE business model will be made available for implementation in a broader context.

5) Manage: Once implemented, the performance of the ENERGE business model will be monitored. If needed, the business model will be modified (the last two stages will be realised in the future as the ENERGE project is ongoing).

3. Results and Discussion

3.1 Establishment of the ENERGE Committees and the Teacher Network

The ENERGE Committees formed in each project school and the Teacher Network established a community of like-minded and active students and staff that are interested to learn how they can assist in improving energy efficiency in their schools. To some extent, these groups can be viewed as drivers of change and the project ambassadors, but they also can act as voluntary participants in multiple activities related to raising energy efficiency in the schools. They demonstrated their readiness to learn and share their own knowledge and experience, thus creating a much-needed atmosphere of reciprocity and collaboration. In general, joining the ENERGE Committee is an instrument of behaviour change in itself [10], as in accordance with self-perception theory, our attitudes, including pro-environmental, are formed when we observe our own overt behaviours and the circumstances in which these behaviours occur [11]. To this extent, the ENERGE Committee membership can be regarded as a commitment to community-based behaviour change [12]. In addition, the linking of the ENERGE Committees from different countries brings a cross-country element to the learning community and creates transnational cooperation between students when sharing ideas and experiences.

In a similar fashion, the work of the established Teacher Network resulted in extensive collaboration between the project school teachers engaged in the exchange of their knowledge, skills and experiences with respect to energy-related issues and initiatives, including teaching energy-related topics and piloting energy literacy modules. All members of the Teacher Network stressed a current lack of energy-related curriculum-supporting classroom modules

(including activities). They also suggested that there is a need for a series of activity-based modules on energy themes. As for energy literacy, low levels of energy literacy was also indicated by the Teacher Network members, which is substantiated by various studies looking at both student populations as well as the wider public [13,14].

3.2 Improvement of Energy Literacy

As a working definition of energy literacy, the members of the Teacher Network, in cooperation with the project partners, adopted the characteristics of an energy literate student defined by DeWaters and Powers [7]. These are as follows: (a) a basic understanding of energy science and its usage in everyday life; (b) understanding of how energy production and consumption affects environment; (c) recognition of the need to conserve energy to develop alternatives to fossil fuels; (d) recognition that personal energy-related decisions and actions matter; and (e) efforts to make pro-environmental choices and decisions with respect to energy consumption. As such, the concept of energy literacy has three interlinked dimensions – cognitive (skills and knowledge), affective (e.g. attitudes, commitments, motivations, responsibility, values etc.) and behavioural (e.g. participation, consumer actions, legal actions etc.). These dimensions are all reflected in the ENERGE energy literacy framework created by the project partners in cooperation with the Teacher Network members.

While co-developing energy literacy modules, the teachers, who represented different disciplines (geography, physics, information technology/ computer science and social sciences), expressed their views on the characteristics and the potential of these modules. In general, all teachers shared the view that, despite the fact that energy is taught as an interdisciplinary topic across various STEM and non-STEM disciplines, there is a lack of cohesion across the formal curricula. In addition, the teachers believe that the strongest benefit of the ENERGE educational materials is their alignment with the existing curricula. Geography teachers reported that energy literacy themes are present in the social and ecological dimensions of the subject. ENERGE-based modules are designed to support existing geography curricula by developing practical activities and lesson plans that are relevant to the modern students and able to stimulate behaviour change. The incorporation of local case studies based on geographic information system (GIS) technology would be beneficial. Physics teachers argued that current curricula in this discipline could offer little room for the affective and behavioural dimensions of energy literacy. To account for this, ENERGE modules can supplement the existing curricula by balancing the present tilt towards the cognitive dimension of energy literacy. Disciplines focusing on IT and data analytics could significantly benefit from the ENERGE modules that rely on the use of smart metering systems that monitor energy consumption and indoor climate quality (e.g. the ENERGE Digital Platform). Social science teachers also expressed their enthusiasm about the supplementary character of the ENERGE modules, which could provide depth to the existing curricula.

The profound collaborative efforts undertaken by the project partners, members of the Teacher Network and students who participated in the module piloting, resulted in the preparation of the final list of the selected designed modules. This list is available online for the open access (link: https://cutt.ly/3U6Vm0G) and the authors of this publication welcome any contribution from all interested parties/schools to review the presented modules. The piloting stage also resulted in several recommendations regarding the applicability of these modules. Firstly, the application of these modules should take into consideration interregional differences that exist between educational models of different countries (e.g. countries with common-core curricula vs. countries with highly differentiated curricula; [15]). Secondly, the module application should take into consideration variability of students between 12 and 18 years with respect to cognitive, affective and behavioural capacities. Thirdly, language may be a significant barrier so the modules need to consider the linguistic capacity of the targeted audience. Fourthly, informal opportunities for teaching energy literacy modules are underrepresented in the curriculum but can potentially offer the teachers the flexibility they need to accommodate for the needs of all students.

3.3 Origination of the ENERGE Digital Platform

Digital learning tools use a combination of text, graphics, simulation and multimedia to enhance the learning process [16]. In the context of energy education, digital learning has been used to present instructional materials as well as to monitor the learning that takes place. Numerous programmes report about the application of different digital learning tools. For example, computer-assisted instructional materials in the teaching of the process of photosynthesis can be employed [16]. Researchers can use simulations as tools for students in physics education to investigate energy concepts such as energy forms, transformation and conservation [17]. Digital game-based learning is widely used by educators in different fields [18]. Petra et al. [19] utilised Web-based Inquiry Science Environment (WISE) as a teaching aid on energy topics in biology. In their totality, digital learning tools engage students and develop knowledge as well as a variety of skills, including problem solving, inquiry, reasoning, argumentation, communication, and collaboration. The latter is a particularly important outcome of the digital tool application. To this extent, the ENERGE Digital Platform is key to building a collaborative learning community by incorporating such elements as data-based analysis, environment simulations, and decision-making

processes.

The ENERGE Digital Platform is an interactive interface, which displays the information on energy consumption and indoor climate quality in the project schools. As alluded before, the platform allows occupants to be involved in two interlinked tasks: energy management and energy-related learning (Fig. 1). Such diverse functionality was welcomed by all personnel of the project schools, which was confirmed by the key informant interviews.

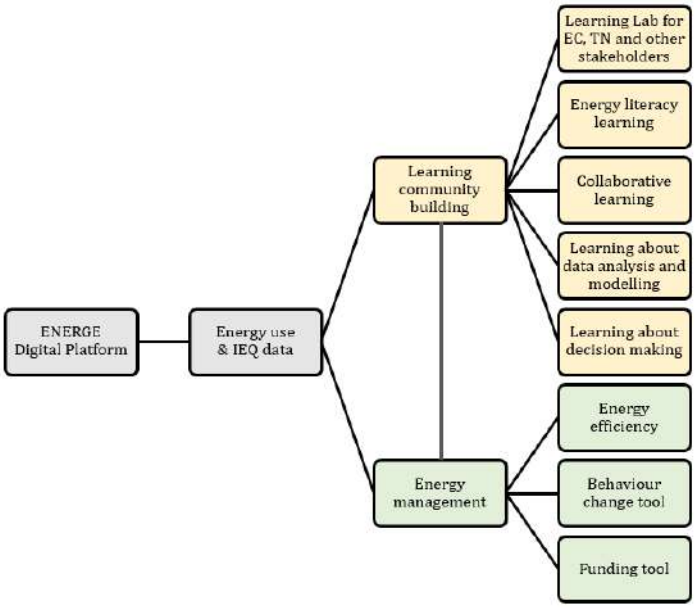

Fig. 1 - Energy Digital Platform multi-functionality. IEQ = indoor environmental quality, EC = ENERGE Committee, TN = Teacher Network.

The role of the ENERGE Digital Platform (**Fig. 2**) in building learning communities is clear. By using this tool, students, teachers and other stakeholders were able to collaboratively analyse data on the built environment, execute exercises in modelling and make certain decisions on the basis of the obtained energy/comfort data. It may serve as a learning lab for members of the ENERGE Committees, the Teacher Network and all other interested stakeholders. A "learning lab" metaphor here means that the interested persons could understand the essence of various parameters of their built environment, identify interdependences about these parameters and potentially be more driven to address challenges related to their environment. Of course, the ENERGE Digital Platform can also assist in energy management of the project schools, by acting as a tool for monitoring and displaying energy efficiency and changes in behaviour.

Fig. 2 - ENERGE Digital Platform mock-up

It is interesting to note that the platform could be also an instrument for attracting financial resources for the schools since it could provide substantiation for allocating funds to the schools, since the platform can generate data on energy usage and indoor environmental quality. One of the participants of the key informant interviews mentioned that "Funding [for energy efficiency] can be sought from a minor works application, but these are generally focused on Health and Safety (H&S) needs rather than energy etc., as H&S is the best way to try to get funding." The ability to link energy usage and the health of occupants due to indoor environmental quality offers a new perspective on seeking funding for projects such as lighting and building fabric upgrades, which are known to result in significant energy savings whilst also improving comfort levels for building occupants.

3.4 Formulation of the ENERGE business model

It was a consensus among all the ENERGE stakeholders (incl. the project partners, school personnel and students) that the best way to develop the ENERGE business model is to merge educational aspects of the ENERGE Project with its objectives to improve energy efficiency and energy management of educational facilities. As such, the core value proposition of the ENERGE project is twofold, i.e. (a) to build learning community around the issue of energy efficiency in the schools and (b) to improve their energy and indoor environmental quality. This duality of the business model is evident in its multiple dimensions, including key partners, activities, or resources, targeted customer segments, distribution channels and financials.

It is important to mention that the design of the ENERGE products and services needs to consider the context in which the ENERGE business model will be deployed. Three important factors that define how to shape the ENERGE value proposition are:

(1) The character of the targeted schools in terms of a region and type: general or vocational education and lower or upper secondary education;
(2) The level of digitalization of the ENERGE proposition: available infrastructure at the schools and digital literacy of teachers and

students; and

(3) The scope of the educational materials: Focus on energy efficiency only or the inclusion of other sustainability-related topics.

It is obvious that educational materials need to match the skills and competences of each specific age group. In addition to age, the education level needs to be taken into account when designing the ENERGE proposition. General education and vocational education have different needs in educational materials. In addition, the ENERGE proposition needs to be in line with the national curriculum. For the level of digitalization, two elements are relevant for the ENERGE proposition: the level of school building automation and the use of digital material and devices in lessons. Differences in degree of autonomy to schools for managing financial resources impacts the financial structure of the ENERGE business model. Schools in Ireland, U and the Netherlands generally have more autonomy for managing their financial resources, while schools in Germany, France and Luxembourg have very limited or no freedom in this area [20], while school budgets for educational materials and sensors and building automation are often allocated at different levels of authorities. The ENERGE project primarily focusses on energy efficiency and indoor climate quality. However, the key informant interviews with the project schools' principals and teachers showed that there is a preference for bundling multiple related topics. The overarching theme could be "sustainability", which is broader than energy and health.

3.5 General framework for the ENERGE learning community building

To summarise the above-mentioned contributions, **Fig. 3** provides a general framework for building a learning community around the issue of energy efficiency in schools, which is addressed in the course of the ENERGE project.

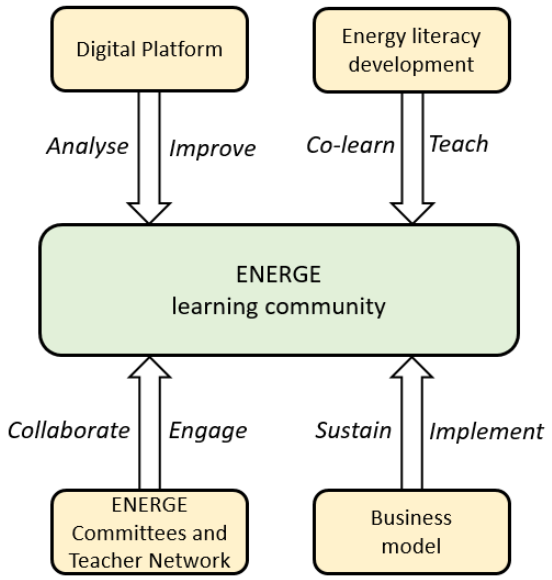

Fig. 3 - General ENERGE framework for learning community building.

The framework's four key components, i.e. the multi-functional Digital Platform, curriculum-based energy literacy development programme, networking opportunities (in the form of the ENERGE Committees and the Teacher Network), and a viable business model for the post-project exploitation of the ENERGE solutions, integrate both technological and educational approaches, which can be put into practice.

Within these four contributions, the realization of the ENERGE framework can lead to improved energy-efficient behaviours in schools **(Fig. 2**). The Digital Platform may stimulate data analysis-based improvement of energy management in schools. The suggested form of energy literacy development is a way to organise co-learning practices. Networking and collaboration, involving the ENERGE Committees, the Teacher Network and other stakeholders, are instrumental in originating a co-designed behavioural change, while an effective business model can help in implementing and sustaining energy efficiency activities in schools.

4. Conclusions

The suggested ENERGE framework for building a learning community can offer tangible benefits to various stakeholders, including school personnel, students, educators, policymakers, to name only a few. By educating young adults about energy-efficiency in their own school environment, we can influence their behaviours in school, but also their behaviours at home, and their behaviours as they move through life.

From an engineering perspective, building occupants who are aware of their energy-related behaviours can positively impact a building's energy consumption via their day-to-day actions. The ENERGE framework enables building occupants, in this instance school students, to gain a better understanding of how they actions can affect the energy-efficiency of a building and work together as part of a learning community to improve sustainability.

5. Acknowledgement

The ENERGE Project is funded by the Interreg North-West Europe Programme, which is financed through the European Regional Development Fund (Grant Number NWE-827).

6. Appendices

Appendix A

Tab. 1 – Profile of the ENERGE project schools (France and Germany).

School	France 1	France 2	Germany 1	Germany 2
Location	Orléans	Centre-Val de Loire region	Trier	Prüm (Trier)
School Type	Professional training	Agro college	Post-primary	Rural, vocational
Year of construction (extensions)	1953 (1960 / 1996)	2009	1914 (1965 / 2002)	1954 (1966 / 1974)
Building ownership	Regional Council	Regional Council	City of Trier	District admin.
Curriculum orientation	Engineering, crafts	Agricultural	Science and Maths	Technical
Student / staff number	791 / 150	493 / 90	1027 / 90	950 / 75
Space heating fuel type	Natural gas	Woodchips / natural gas (80/20%)	Natural gas	Natural gas
*Av. monthly temperature in Jan/Jul, °C **	5 / 19	5 / 19	2 / 18	0 / 17
*Av. monthly rainfall in Jan/Jul, mm **	52 / 59	52 / 59	79 / 70	79 / 70

Tab. 2 – Profile of the ENERGE project schools (Ireland and Northern Ireland).

School	Ireland 1	Ireland 2	Northern Ireland 1	Northern Ireland 2
Location	Galway	Galway region	Down Co.	Tyrone Co.
School Type	Post-primary	Rural, post-primary	Post-primary	Post-primary
Year of construction (extensions)	1919 (2009)	1830 (1930 / 1960 / 2013)	1970 (2015)	1954
Building ownership	Diocese of Galway	Dept. of Education	Dept. of Education	Dept. of Education
Curriculum orientation	General / classic	General / classic	General / classic	General / classic
Student / staff number	780 / 80	490 / 44	876 / 85	796 / 65
Space heating fuel type	Natural gas	Kerosene	Natural gas	Natural gas
*Av. monthly temperature in Jan/Jul, °C **	6 / 16	6 / 16	4 / 15	4 / 15
*Av. monthly rainfall in Jan/Jul, mm **	84 / 71	84 / 71	109 / 75	80 / 71

Tab. 3 – Profile of the ENERGE project schools (Luxembourg).

School	Luxembourg 1	Luxembourg 2	Luxembourg 3
Location	Luxembourg city	Luxembourg city	Luxembourg city
School Type	Post-primary, vocational	Post-primary	General secondary and vocational school
Year of construction (extensions)	1965 (1985)	1989	1972 (1998)
Building ownership	Public building administrat	Public building administrat	Public building administrat
Curriculum orientation	Technical	Technical	Technical
Student / staff number	4400 / 340	2500 / 200	1400/140
Space heating fuel type	Natural gas	Natural gas	Local district heating (gas-fired CHP) plant
*Av. monthly temperature in Jan/Jul, °C **	2 / 18	2 / 18	2 / 18
*Av. monthly rainfall in Jan/Jul, mm **	77 / 71	77 / 71	77 / 71

Tab. 4 – Profile of the ENERGE project schools (The Netherlands).

School	Netherlands 1	Netherlands 2
Location	Hague	Rotterdam
School Type	Gymnasium	Post-primary
Year of construction (extensions)	1907 (2011)	1950 (1999)
Building ownership	Secondary edu. office of Hague district	Edu. office & Municipaplity of Rotterdam
Curriculum orientation	General / classic	General / classic
Student / staff number	810 / 75	724 / 70
Space heating fuel type	Natural gas	Natural gas
*Av. monthly temperature in Jan/Jul, °C **	4 / 17	4 / 16
*Av. monthly rainfall in Jan/Jul, mm **	68 / 73	69 / 74

* Note: 2019 was used as a reference year

7. References

[1] Karlessi T, Kampelis N, Kolokotsa D, Santamouris M, Standardi L, Isidori D et al. The concept of smart and NZEB buildings and the integrated design approach. International High-Performance Built Environment Conference – A Sustainable Built Environment Conference 2016 Series (SBE16), iHBE 2016. Procedia Eng. 2017;180:1316-25.

[2] Mitchell C, Sackney L. Profound improvement: Building capacity for a learning community. 2nd ed. London: Routledge; 2011.

[3] Rijksdienst voor Ondernemend Nederland. Programma van Eisen Frisse Scholen 2015. Available from: https://www.rvo.nl/sites/default/files/2016/01/Programma%20van%20Eisen%20Frisse%20Scholen%20-%20September%202015%20v3.pdf. Dutch.

[4] Pietrapertosa F, Tancredi M, Salvia M, Proto M, Pepe A, Giordano M et al. An educational awareness program to reduce energy consumption in schools. J Clean Prod. 2021;(278):123949.

[5] Purnell K, Sinclair M, Gralton A. Sustainable schools: Making energy efficiency a lifestyle priority. Aust J Environ Educ. 2004;20(2):81-91.

[6] Camilleri AF, Barak N, Burgos D, Ullmann TD. Engaging the community in multidisciplinary TEL research: A case-study from networking in Europe. In: EDEN 2010 Annual Conference: Media Inspirations for Learning. What Makes the Impact?, 2010 Jun 9-12, Valencia, Spain.

[7] DeWaters JE, Powers SE. Establishing measurement criteria for an energy literacy questionnaire. J Environ Educ. 2013;44(1):38-55.

[8] Xiao Y, Watson M. Guidance on conducting a systematic literature review. J Plan Educ Res. 2019;39(1):93-112.

[9] Osterwalder AO, Pigneur Y. Business model generation: A handbook for visionaries, game changers, and challengers. 1st ed. Hoboken, New Jersey: John Wiley & Sons Inc.; 2010. (The Strategyzer Series).

[10] McKenzie-Mohr D. Introductory workshop in community-based social marketing. Online Zoom-based workshop. 2020 Jun 24-25 and Jun 29-30.

[11] Bem DJ. Self-Perception theory. In: Berkowitz L, editor. Advances in experimental social psychology (Vol. 6). New York: Academic Press; 1972, p. 1-62.

[12] McKenzie-Mohr D. Fostering sustainable behavior: An introduction to community-based social marketing. Gabriola Island, BC, Canada: New Society Publishers; 2011.

[13] Blasch J, Boogen N, Daminato C, Filippini M. Empower the consumer! Energy-related financial literacy and its socioeconomic determinants. CER-ETH – Center of Economic Research at ETH Zurich, Working Paper 18/289. SSRN Journal. 2018.

[14] Chen S-J, Chou Y-C, Yen H-Y, Chao Y-L. Investigating and structural modeling energy literacy of high school students in Taiwan. Energy Effic. 2015;8(4):791-808.

[15] European Commission/ Education, Audiovisual and Culture Executive Agency/Eurydice. The structure of the European education systems 2019/20: Schematic diagrams. Eurydice facts and figures. Luxembourg: Publications Office of the European Union. 2019. Available from: http://www.eurydice.si/publikacije/The-Structure-of-the-European-Education-Systems-2019-20_Schematic-Diagrams-EN.pdf.

[16] Cepni S, Tas E, Kose S. The effects of computer-assisted material on students' cognitive levels, misconceptions and attitudes towards science. Comput Educ. 2006;46(2):192-205.

[17] Choi E, Park J. Conditions for the effective use of simulation and its application to middle-school physics inquiry activities. J Korean Phys Soc. 2003;42(3):318-24.

[18] Chen S-W, Yang C-H, Huang K-S, Fu S-L. Digital games for learning energy conservation: A study of impacts on motivation, attention, and learning outcomes. Innov Educ Teach Int. 2019;56(1):66-76.

[19] Petra SF, Jaidin JH, Perera QJSH, Linn M. Supporting students to become autonomous learners: the role of web-based learning. Int J Inf Learn Technol. 2016;33(4):263-75.

[20] OECD. Education at a Glance 2018: OECD Indicators. Paris: OECD Publishing. 2018. Available from:https://www.oecd-ilibrary.org/education/education-at-a-glance-2018_eag-2018-en.

Using Social Network Analysis to explore Learning networks in MOOCs discussion forums

Ali Soleymani [a], Laure Itard [b], Maarten de Laat [c], Manuel Valle Torre [d], Marcus Specht [e]

[a] Center of Education and Learning, Delft University of Technology, Delft, the Netherlands, A.Soleymani@tudelft.nl.

[b] Department of Management in the Built Environment, Faculty of Architecture and the Built Environment, Delft University of Technology, Delft, the Netherlands, L.C.M.Itard@tudelft.nl.

[c] Center for Change and Complexity in Learning, University of South Australia, Australia, Maarten.DeLaat@unisa.edu.au.

[d] Center of Education and Learning, Delft University of Technology, Delft, the Netherlands, M.ValleTorre@tudelft.nl.

[e] Center of Education and Learning, Delft University of Technology, Delft, the Netherlands, M.M. Specht@tudelft.nl.

Abstract. Learning and educational challenges in the field of indoor climate and building services like energy systems are mainly due to the transformation of professional practices and learning networks, a big shift in the way in which people work, communicate, and share their knowledge and the need for additional workforce, either juniors or coming from other disciplines. One of the most important factors that highly influence professional development and workplace learning is networked learning. Our goal in this study, is understanding the learning networks characteristics and patterns of interaction using Social Network Analysis techniques in three MOOCs discussion forums. The result of this study shows not only the importance of Learning networks and peer support on professionalization of learners, but also how pedagogical approach of instructors in MOOCs can foster learning networks. This novel approach in developing learning networks and communities is not only able to help connect young professionals and experienced practitioners digitally, but also it can promote professional development and innovation in the energy installation sector.

Keywords. Professional learning networks, social network analysis, lifelong learning, Massive Online Open Courses.
DOI: https://doi.org/10.34641/clima.2022.300

1. Introduction

Massive Open Online Courses (MOOCs) have received a great amount of attention in the last few years. MOOCs provide an opportunity for students and professionals to educate or up-skill themself, learn new skills and communicate and build a professional network. Through MOOCs, several thousand learners, actively engage in a learning process with self-organized participation and with different goals, backgrounds, knowledge, and skills but with a common interest [1]. Many MOOCs users, use this learning opportunity for continued education and professional development for different reasons, from satisfying personal and intellectual curiosity to enhancing workplace or professional skills.

Learning and educational challenges in the field of indoor climate and building services like energy systems are mainly due to the transformation of professional practices and learning networks, a big shift in the way in which people work, and the need for an additional workforce, either juniors or coming from other disciplines. Therefore, we believe that MOOCs and the learning opportunities that they provide can tackle many educational challenges and help professional development in the field. Besides the above-mentioned benefits of MOOCs for professional development, they also provide a great opportunity for learners to communicate with their peers and shape a learning community or network. As also mentioned by [1], MOOCs can "model and build collaborative networks of unprecedented size that transcend time and space" and the "network ties created between people during a MOOC have the potential to continue as sustainable and relevant personal and professional connections beyond the boundaries of the course itself" (p. 35). Therefore, there is a big need to understand the learner's behavior and learning networks in MOOCs.

To build knowledge about how professional learning in MOOCs can serve as a catalyst for the development of learning networks and foster

Copyright ©2022 by the authors. This conference paper is published under a CC-BY-4.0 license.

continued networked learning amongst peers driven by workplace challenges as experienced in daily practice, in this research we investigate peer interaction and support in MOOCs developed for Buildings as Sustainable Energy Systems (BSES) professional certificate program in EdX platform by researchers at TU Delft, the Netherlands.

In the last 15 years, online social networks have grown dramatically and enabled companies like Facebook, Twitter, and Linked-In to collect and analyze users' data in detail. These social network technologies have also been used to support and develop Learning Networks (LN). Social Network Analysis (SNA) can be used to understand and help educational communities and learning networks to identify structures and important topics and links to enhance the learning outcomes and professional exchange [2, 3, 4, 5].

Siemens [6] in explaining the theory of connectivism mentioned that learning is a process of network formation and connections are the key to networked learning. And reviewing literatures have shown that the use of learning communities and learning networks can improve the capability of individuals and organizations to learn [7,8]. As Lave and Wenger (1991) [9] describe, learning communities have been used for a group of people who interact regularly, share the same concern or passion for something, and aim to improve their knowledge and practice. Networks of Practice (NoP) or learning networks [10] have been used to describe a more informal and developing social network that encourages and supports the sharing of knowledge and information between a group of people who gather around the same practice and profession. Social Network theory claim that the structure of social relations cannot only explain the different variables in social science but also, they can facilitate or hinder the results for individuals [11]. Reviewing the literature in online learning settings show the correlation between network structure and measures and academic achievements like academic performance [12, 13], knowledge construction [14; 15], and a more positive attitude toward the learning experience [16, 17].

Therefore, there is a need for conducting more research in network learning in the online learning environment. Also, exploring the mechanisms that are involved in shaping networks and having knowledge about the structure of learning networks, and in general, network thinking can expand our knowledge of the learning process as a social phenomenon. Given these questions this case study tries to address the important aspects of the social learning process and professional development in the MOOC using Social Network Analysis (SNA) techniques.

2. Research Methods

For this study, we use the discussion forum posts of participants who engaged in three MOOCs. Course 1: Energy Demand in Buildings (EDB), course 2; Energy Supply Systems for Buildings (ESSB), and course 3: Comfort and Health in Buildings (CHB). These online courses are part of the "Buildings as Sustainable Energy Systems professional certificate program" on the EdX platform provided by researchers at TU Delft, the Netherlands. The MOOCs are freely available, and students pay only if they want a certificate and are described in another paper in this conference. MOOC's discussion forum data was arranged in a MongoDB database. A Python script was used to extract three variables, discussion id, discussion creator, and discussion poster. Each thread created in the forum is a discussion id. The discussion creator refers to the user id that initially created the thread the participants who participate in that thread named discussion poster.

Course one Energy Demand in Buildings (EDB) was the biggest course by over 6500 participants and courses 2 and 3 were smaller by around 5000 participants. As we mentioned earlier, these courses were freely available to everyone, but the participants also had a chance of receiving the certificate by doing the courses' assignments and paying for the course and we called this group the "Certified" participants. Therefore, only 7-10 percent of participants were certified. In the result section, we will explore if there is any difference between these two groups of participants. Also, three tutors and moderators were also involved in discussion forums to mediate the discussions and answer participants' questions. Participants of these MOOCs include a range of people; from high school students who are interested in indoor energy systems to senior HVAC designers who want to update or upscale their knowledge.

In our Analysis, we entered all the posts in each course discussion forum. These courses were presented for the first time, and we analyzed the first round of data from these courses. This series of courses were designed in a way that promote learning through social interaction and focused more on student-centered structure instead of only teacher-centered interaction (for example, students were expected to answer questions from teachers and address learning tasks based on video lectures).

3. Results

Social Network Analysis allows us to have a descriptive overview of our network structure and identify patterns. We summarized the descriptive overview of the network of forum interaction in table 1.

As it is shown in the table, the number of replies to peer posting (edges) increases with the number of participants in the forum (vertices). Graph density measures how many ties or connections exist

between learners, compared to how many connections or ties between learners are possible. Evaluating the network's density can help us understand how connected the networks are in comparison with how connected they might be and in this research, it can also reveal the difference between networks. In This case, our graph density which is the number of unique edges (replies to peer posting) out of all possible edges decreased in the MOOC one, which had a higher number of participants (the number of possible replies to peer posting increased steadily with the number of vertices (participants) in the network).

Tab. 1 - Network measures

Network Metrics	CHB MOOC 3	ESSB MOOC 2	EDB MOOC 1
Vertices	100	98	278
Unique edges	161	156	503
Edges with Duplicates	112	128	274
Total edges	273	284	777
Edge weight avg.	2.69	1.93	2.92
Reciprocated vertex pair ratio	0.02	0.03	0.04
Reciprocated edge ratio	0.04	0.06	0.09
Graph density	0.03	0.01	0.006
In/outdegree avg.	1.98	2.07	2.12
In/outdegree median	1	1	1
Indegree range	0-14	0-12	0-89
Outdegree range	0-30	0-30	0-57

We can define the Reciprocated vertex pair ratio as the ratio between ingoing and outgoing connections. The higher ratio can show that a person engages in more two-way interaction or exchange. Our first MOOC, with the higher number of active participants in the forum, had a higher Reciprocated vertex pair ratio in comparison with MOOCs 2 and 3. The percentage of replies to peer posting that has a reciprocal relationship (mutual interchange) can be defined as Reciprocated edge ratio. Again, our first course had a higher score which replicates the higher number of mutual interactions in peer replies.

In an Edge-Weighted network, weight may represent the length of the edges (in this case, replies to peer posting). Therefore, considering the average edge weight in our MOOCs, they show that participants in course two (Energy Supply Systems for Buildings (ESSB)), were less interested to communicate with their peers in comparison with courses 1 and 3. Furthermore, although the number of participants in course one was around 20 percent more than the two other courses, the total number of vertices and edges in this course are significantly higher.

But when we categorize the participants into certified and not certified participants, we can see that certified participants were more active in the discussion forums. They tried to shape more mutual relationships with their peer and interact more. In table 2, more information about the networked measures of these two groups of participants is presented.

Tab. 2 – Network measures for Certified and Not certified

Network Metrics	MOOC 3		MOOC 2		MOOC 1	
	Not certified	Certified	Not certified	Certified	Not certified	Certified
Vertices	9	52	24	55	35	140
Unique edges	8	68	18	85	38	218
Edges with Duplicates	2	23	23	48	64	184
Total edges	10	91	41	133	102	402
Edge weight avg.	1.2	1.37	8.90	1.73	7.84	3.73
Graph density	0.11	0.02	0.03	0.02	0.03	0.01

But besides the differences between these three networks, we can detect some basic patterns. In directed networks, like discussion forums (someone answers someone else post and receive an answer), we have two measures of the connections linked to a vertex. In-degree is considered as the total number of connections that point inward at a vertex (In our case, the number of replies that someone receives for the post) and out-degree is the total number of connections originated from a vertex (number of replies that someone gives to someone else post) [18]. Here in our sample, all three networks show a similar pattern in the distribution of in/outdegree average. As you can see in figure 1. A big part of network actors had support ties with around two other peers which we considered as "core" participants. Also, edge weights show that most ties between participants are not just a single communication, but they tend to have more responses. This can represent the depth of

discussions which is necessary for shaping the productive learning network.

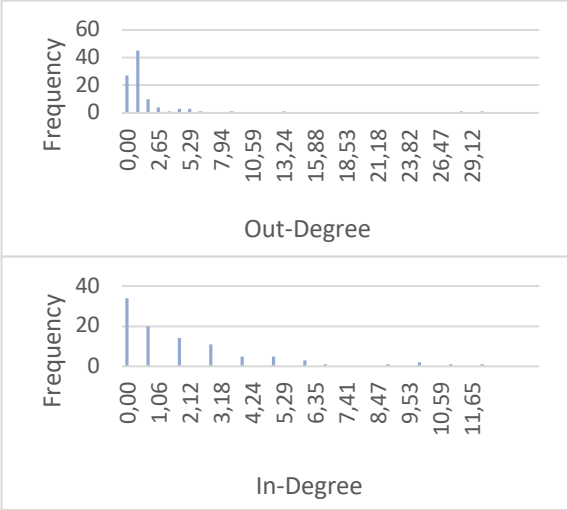

Fig.1- Proportion of out and in-degree distribution in MOOC 2

4. Discussion

Social Networks can be considered as "a set of relations, interactions, and connection with affordances for learning, such as information flows helpful linkages, joint problem solving, and knowledge creation" [19, p. 9]. In this research, we investigated the role of the discussion forums in facilitating professional networks and networked learning in MOOCs. Understanding learners' behavior in learning networks in MOOCs, the structure of these networks, and patterns can help us understand the fundamental of professional development.

In agreement with current findings [20], our results show the fundamental role of MOOCs design and pedagogical approach of MOOCs' instructors in gaining the desired out of these new online learning opportunities. Social network measures can help the energy sector on how to go forward with a networked learning-based approach to promote network community-based peer learning given challenges experienced in their workplace. Professional networks allow for raising challenges from a variety of workplaces and promote learning and problem solving based on a rich and diverse context of professional experiences. Based on our results of Social Network Analysis, we can suggest several design elements for future MOOCs in the technical field like energy management systems in the buildings. Building successful online communities have been studied and extensively discussed in Kraut & Resnick [21] and introduced designs that can encourage learners to share and exchange knowledge in online communities. First, it is suggested that a simple contribution request can raise greater compliance among learners in comparison with lengthy and complicated requests. Second, in agreement with the previous findings [22], mediators can play an important role in facilitating the discussions, providing quick and practical information about the course contents, solving the learners' challenges during the course. In our MOOCs mediators and tutors were actively engaged in discussion and our networks measures show their effects. Thirds, along with the findings in the medical professional development field [23], participants are more interested to share their knowledge and experience through online discussion forums when their peers have more similar professional roles, work contexts, or experience. For example, in this series of MOOCs, tutors simply asked participants to share their background and personal experiences with others. And we believe that it could increase the interactions (e.g., Measured using in and out-degree in our networks). Finally, we need to focus on not only the quantity of interactions but also the quality of exchanges that can play a significant role in a productive discussion forum [24, 25]. High quality and meaningful interaction can be considered as an exchange that stimulates the intellectual curiosity of learners [26]. Exchanging the information which is directly relevant to the learners' real-life situation and applied to similar culture or applied setting [27], providing clear guidelines for discussions and interactions [26], and setting or defining the expectations of learners, both in formal and informal learning context [28] are the most key strategies to have a successful and a high-quality online discussion forum. Future research can investigate the quality of exchanges in online learning forums using modern content analysis methods to better understand the social learning process and empower the potential of learning networks and communities.

5. Conclusion

Massive Open Online Courses (MOOCs) have been grown very fast in the last few years and the role of this new form of education and learning in professional development is undeniable. In this research, we tried to investigate peer interaction and support in the discussion forums of three MOOCs. We investigated the characteristic of these learning networks and their patterns of interactions to see how our pedagogical approach can affect this learning process.

6. Acknowledgement

The authors would like to express their sincere gratitude to all colleagues in TransAct project, Dr. Ellen Sjoer, Maaike Konings, Dr. Paula van den Brom, Prof. Wim Zeiler, and Samir Ahmed, for their extensive support and feedback during the preparation of this research. We also want to thank our colleagues at the Center of Education and Learning for their feedback on our manuscript. The authors would like to acknowledge Selma van Esveld and Nardo de Vries of the TU Delft Extension

School for their help in providing them with the data.

7. References

[1] Mcauley A, Stewart B, Siemens G, Cormier D. The MOOC Model for Digital Practice. Retrieved from http://www.elearnspace.org/Articles/MOOC_Final.pdf; 2010.

[2] De Laat M, Lally V, Lipponen L, Simons R-J. Investigating patterns of interaction in networked learning and computer-supported collaborative learning: A role for Social Network Analysis. Int J Comput Support Collab Learn [Internet].2007;2(1):87–103. http://dx.doi.org/10.1007/s11412-007-9006-4

[3] Haythornthwaite C, De Laat M. Social networks and learning networks: Using social network perspectives to understand social learning. In Proceedings of the 7th international conference on networked learning. 2010;183–90.

[4] Schreurs B, Cornelissen F, De Laat M. How do Online Learning Networks Emerge? A Review Study of Self-Organizing Network Effects in the Field of Networked Learning. Education Sciences [Internet]. MDPI AG; 2019 Dec 6;9(4):289. Available from: http://dx.doi.org/10.3390/educsci9040289

[5] Schreurs B, Van den Beemt A, Moolenaar N, De Laat M. Networked individualism and learning in organizations: An ego-network perspective on informal learning ties. J Workplace Learn 2019;31(2):95-115.

[6] Siemens G. Connectivism: Learning as network-creation. ASTD Learning News. 2005 Nov;10(1):1-28.

[7] Topsectoren (2019). Samen aan de slag: Roadmap Human Capital Topsectoren 2020-2023.https://www.topsectoren.nl/publicaties/kamerstukken/2019/november/12-11-19/roadmap-hc-topsectoren

[8] Topsectoren & PBT (2017a). Learning communities: Samen zetten we de volgende stap. Onderdeel van het publicatievierluik Learning communities 2018-2024. https://ptvt.nl/wp-content/uploads/2019/07/061217_PBT_LLO_Investeringsagenda_Binnenwerk_170x240_CMYK_LR.pdf

[9] Lave J, Wenger E. Situated learning: Legitimate peripheral participation. Cambridge university press; 1991 Sep 27.

[10] Brown JS, Duguid P. Knowledge and organization: A social-practice perspective. Organization science. 2001 Apr;12(2):198-213.

[11] Borgatti SP, Mehra A, Brass DJ, Labianca G. Network analysis in the social sciences. science. 2009 Feb 13;323(5916):892-5.

[12] Cho H, Gay G, Davidson B, Ingraffea A. Social networks, communication styles, and learning performance in a CSCL community. Computers & education. 2007 Sep 1;49(2):309-29.

[13] Russo TC, Koesten J. Prestige, centrality, and learning: A social network analysis of an online class. Communication Education. 2005 Jul 1;54(3):254-61.

[14] Aviv R, Erlich Z, Ravid G, Geva A. Network analysis of knowledge construction in asynchronous learning networks. Journal of Asynchronous Learning Networks. 2003 Sep 3;7(3):1-23.

[15] Rossi D. Learning relationships in online contexts: An educational response to declining rates of participation and a means of support for undergraduate students. Studies in Learning, Evaluation, Innovation & Development. 2010 Dec 1;7(3).

[16] Dawson TL. Metacognition and learning in adulthood. Prepared in response to tasking from ODNI/CHCO/IC Leadership Development Office, Developmental Testing Service, LLC. 2008 Oct 15.

[17] Lowes S, Lin P, Wang Y. Studying the effectiveness of the discussion forum in online professional development courses. Journal of Interactive Online Learning. 2007 Dec 1;6(3):181-210.

[18] Hansen DL, Shneiderman B, Smith MA, Himelboim I. Social network analysis: measuring, mapping, and modeling collections of connections. Analyzing social media networks with NodeXL. 2020:31-51.

[19] Wenger E, Trayner B, De Laat M. Promoting and assessing value creation in communities and networks: A conceptual framework.

[20] Pampouri A, Kostelidou S, Sionta E, Souitsme M, Mavropoulos A. MASSIVE OPEN ONLINE COURSES (MOOCs): A REVIEW. In Proceedings of INTED2021 Conference, 2021 Mar (Vol. 8, p. 9th).

[21] Kraut RE, Resnick P. Building successful online communities: Evidence-based social design. Mit Press; 2012 Mar 23.

[22] de Lima DP, Gerosa MA, Conte TU, Netto JF. What to expect, and how to improve online discussion forums: the instructors' perspective. Journal of Internet Services and Applications. 2019 Dec;10(1):1-5.

[23] Lin TC, Lai MC, Yang SW. Factors influencing physicians' knowledge sharing on web medical forums. Health Informatics Journal. 2016 Sep;22(3):594-607.

[24] Tibi MH. ESSENTIAL COMPONENTS IN STRUCTURING ASYNCHRONOUS DISCUSSION FORUMS. Turkish Online Journal of Distance Education (TOJDE). 2016 Apr 1;17(2).

[25] Woo Y, Reeves TC. Interaction in Asynchronous Web-Based Learning Environments. Journal of Asynchronous Learning Networks. 2008 Dec; 12:179-94.

[26] Pear J.J, Crone-Todd DE. A social constructivist approach to computer-mediated instruction. Computers & Education. 2002 Jan 1;38(1-3):221-31.

[27] Brown JS, Collins A, Duguid P. Situated cognition and the culture of learning. Educational researcher. 1989 Jan;18(1):32-42.

[28] Rovai AP. Building classroom community at a distance: A case study. Educational technology research and development. 2001 Dec;49(4):33-48.

Data Statement

The datasets generated during and/or analyzed during the current study are not publicly available because of the data privacy agreement between researchers and data provider but will be available under request.

A structured approach to online education of future HVAC and energy professionals

Laure Itard[a], Philomena Bluyssen[a] ,Paula van den Brom[a]

[a] Faculty of Architecture and the Built Environment, Delft University of Technology, Delft, the Netherlands, L.C.M.Itard@tudelft.nl; P.M.Bluyssen@tudelft.nl; P.I.vandenBrom@tudelft,nl

Abstract. The HVAC sector is essential to realize the energy transition and is facing numerous challenges like educating enough HVAC engineers to carry out the task and being able to integrate knowledge from the construction, energy, IT and health sectors and to cope with rapid technological changes. The availability of structured and easy-to-follow courses on HVAC and energy systems for buildings at higher education level could help to motivate (future) engineers to contribute to the HVAC sector, and to understand how challenging and high-tech it is. Such a course program would ideally also bring a basic understanding of the field to architects and building engineers, in such a way that a better common ground is created for collaboration and integrated design. It would also be useful to Machine Learning and Artificial Intelligence experts joining the HVAC sector. Last but not least, it could help bridging the gap between engineering and policy making, by here too, offering common views on primary energy, resource depletion and CO2 emissions relating to HVAC systems. The paper describes the structure and content of such an on-line course program. It was developed based on years of teaching experience with international master students of Mechanical Engineering, Civil Engineering, Architecture, Technical Management and Policy, Electrical Engineering and with professionals from housing associations, ministries and municipalities. The choices for the program structure, based on systems engineering, are underpinned and explained, as well as the choices for specific contents. Additionally, experience with the development of self-assessment tools for students, and self-paced courses is shared, as well as the feed-back from students. A first version of the course program was tested on the edX platform with more than 5000 students participating in each module and is publicly available.

Keywords. On-line education; HVAC; Building services; Professional program; MOOC.
DOI: https://doi.org/10.34641/clima.2022.401

1. Introduction

The Heating, Ventilation and Air Conditioning (HVAC) sector is essential to realize the energy transition and is facing numerous challenges like educating enough HVAC engineers to carry out the task and being able to integrate knowledge from the construction, energy, IT and health sectors and to cope with rapid technological changes. However, the building services sector is facing huge challenges. These challenges have been identified in studies in the Netherlands [1], or in the European BuildUpSkills project [2]. Dealing with these challenges have become even more important because they are decisive in realizing the targets of the energy transition. In detail the challenges relevant to this study include the following:

1.Need for a fast-growing professional workforce: There are too few people working in the sector to realize the transition. According to TechniekNL [1] , there is a shortage of 3000 workers per year in the Dutch sector. This has two implications related to education considering a) the continuous professional development of the current workforce as also b) the education of new employees, mainly having no background in building or energy engineering services.

2. Rapid change of technologies as also related competences: The sector is facing rapid changes in energy techniques (e.g. all electric instead of gas-driven; low temperature heating networks, integration of heating and electrical networks, NZEB buildings); engineering methods (e.g. digitization, circularity, design for maintenance); types of contracts (e.g. performance contracts including maintenance; lease); and processes (e.g. industrialization, prefab, turnkey). These changes are driven by societal needs while only a few innovators and early adaptors develop and start mastering these issues, leaving the question open how to accelerate fostering the maturity of the early majority.

3. Uptake of basic and integrated knowledge:

Copyright ©2022 by the authors. This conference paper is published under a CC-BY-4.0 license.

the main questions here are how to increase and improve the uptake of knowledge inside the company (from senior to junior and vice-versa; cross-specialism (e.g. from electrical to mechanical. From design departments to maintenance department)) balancing between innovation, risk management, lack of time and workforce

The availability of structured and easy-to-follow courses on HVAC and energy systems for buildings at higher education level could help to motivate (future) engineers to contribute to the HVAC sector, and to understand how challenging and high-tech it is. Such a course program would ideally also bring a basic understanding of the field to architects and building engineers, in such a way that a better common ground is created for collaboration and integrated design. It would also be useful to Machine Learning and AI experts joining the HVAC sector. Last but not least, it could help bridging the gap between engineering and policy making, by here too, offering common views on primary energy, resource depletion and CO2 emissions relating to HVAC systems.

This paper describes the contents of an online program of four courses, and the choices that were made in terms of structure and premise (section 2) and learning objectives and contents of each of the four courses (section 3-6), In section 7 we finally reflect briefly on the experience with the first run.

2. Structure of the course

2.1 Target Groups

Three target groups were defined, based on the challenges described in Section 1:

1. Starting professionals with a technical background like mechanical engineering, architecture industrial design or electrical engineering who want or need to get acquainted with indoor climate systems, including sustainable energy systems.

2. Traditional HVAC engineers used to piping and sizing calculations of conventional systems who want to broaden their view towards sustainable and renewable systems.

3. Technology-minded policy makers who want to be introduced to the basics of energy usage in buildings.

To match the target groups it was decided that the level of Maths and Physics should be kept limited to high school level in natural/economics sciences.

2.2 Overall structure of the course program

An analysis of the knowledge needed to understand and make basic designs of sustainable, renewable-based and low carbon-emission indoor climates and energy systems was conducted, based on multiple discussions and collaborations between the university and companies working in the field of indoor climate, energy and HVAC design. To the authors' opinion, the premise can be categorized as follows:

1. Because of the importance of energy use in new regulations, conventional maximum load calculation is not sufficient anymore and should be complemented by energy usage estimation on yearly basis. So, a part of the course program should address this.

2. If in the past it was sufficient to know how to size a boiler, multiple options for sustainable energy conversion are present nowadays, and often need to be combined. So a part of the course should address these possibilities and make sure learners do not focus on the one specific solution they know, but are aware of all others and can make an informed choice, accounting for primary energy use and CO2-emissions.

3. In comparison to industrial applications of energy, applications in buildings strongly relate to indoor health and comfort, which is a point acknowledged very well by professionals, but completely overlooked by engineers/students from other disciplines, although the COVID-19 pandemic may have change this a bit. So health and comfort should certainly have a place in the curriculum.

4. Modern HVAC design should include and integrate the three perspectives above. With regards to the target group, the focus should not be on detailed engineering but rather on the principles leading to efficient design of HVAC systems.

The proposed course structure is therefore as described in **Fig.1**. The courses Energy demand, Energy Supply Systems and Health & Comfort can be followed independently and in a random order. However, the dotted lines in the graphic indicate that some basic principles like conservation of energy and the related energy balances are explained in Energy Demand, but not in Energy Supply Systems. The course Health & Comfort makes use of a few concepts explained in the precedent courses (like insulation or emissions by burning fuels) and introduces some HVAC systems already. So, depending on the level of the learner, it can be better to follow them in the order.

The fourth course integrates the 3 domains and build up on them, introducing specific HVAC-related knowledge.

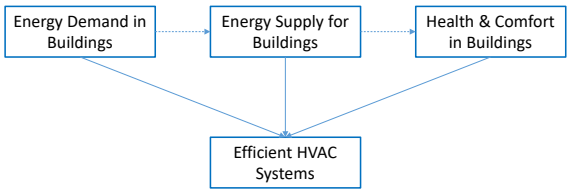

Fig. 1 – Structure of the course program Buildings as Sustainable Energy Systems

In sections 3 to 6 each of these courses is explained in terms of leaning objectives, learning contents and activities.

2.2 Cognitive Levels & Constructive Alignment

The effectiveness of teaching is known (e.g. [3]) to depend strongly on the appropriate correspondence between learning activities and the desired cognitive level, which is called constructive alignment. As for the cognitive levels, we used the ones from the widely applied Bloom's taxonomy [4], as represented in **Fig. 2**.

Fig. 2 – Cognitive levels in Bloom's taxonomy [5]

The course is an organized mix of the 5 highest level. Lectures and simple quizzes provide understanding and direct application of the knowledge. More elaborated quizzes vary in level from 'applying' to 'evaluating'. Finally a 'creating' level was introduced in the course 'Energy Demand' in which the students have to create an own design, reviewed by their peers.

Specific for online courses Salmon introduced an additional 5 stage scale [6] stating that knowledge construction by a learner is only one of the phases of learning. In addition to this 4th stage, much attention must be put to: motivating students through efficient access, welcoming and encouraging (stage 1); Online socialization (stage 2); Information exchange like facilitating tasks and supporting the use of learning materials (stage 3); and finally facilitating further development (e.g. links to external sites, stage 5).

In the development of the program stages 1 and 2 are offered by discussion groups moderated from Edx and TU Delft and by putting much attention to the introductions of each week, explanations and activation of the learners by asking about their expectations or sharing their experience in their own countries. In this paper we address only stages 2 and 3, which relate to the contents. In the first version of the course stage 5 was somehow neglected due to time constraints.

Each course consists of 4 to 5 weeks of lessons, organized thematically. Each week consists of 6 to 8 lectures of 10-15 minutes, coupled to many exercises in the form of quizzes to help the learners to understand and apply their knowledge. Much attention was put to make the course suitable for all types of climates over the world and to build understanding of the specific challenges in warm, cold, moderate, dry or humid climates. The course can be used for both new buildings and renovation projects. Learners are expected to study 6-7 hours a week.

3. Energy Demand in Buildings

The main objective of this course is to discover how building design and occupancy determine the energy demand in buildings and to learn how to (re)design buildings with a low energy demand. This course relates therefore to building design. It is based on the extension of the approach proposed in [7].

3.1 Learning Objectives and Subjects

As building design strongly influences the quantity of heating, cooling and electricity needed during building operation, a correct thermal design is essential to achieve low energy and low carbon buildings, with good indoor air quality.

The first objective of the course is to enable learners to understand the basic principles of the energy chain: demand, supply and distribution; and how they relate to design principles for sustainable and energy-efficient buildings. This is handled in week 1, in which the following subjects are addressed:

1. The importance of energy use in Buildings (e.g. climate, resources, comfort), relation with EPBD and with other sectors
2. The energy chain: from demand to supply
3. Design strategies (e.g 3- steps strategy; Reduce; Renewable; Efficiency)
4. Energy Efficient Building concepts (e.g. passive, (N)ZEB)
5. The basics of indoor comfort

The second objective is to discover what type of heat losses and gains take place in buildings and to learn how to estimate these heat flows using simple meteorological data and building materials properties. This way, steady-state heat transfer by transmission, ventilation, solar radiation or caused by internal sources are estimated.
This is combined with the third learning objective which is to learn to make estimates of space heating

and cooling loads on an hourly basis by using simple static energy balances. Week 2 therefore includes the following:

1. Principle and components of the energy balance in buildings
2. Heat transfer by transmission
3. Heat transfer by ventilation and infiltration
4. Solar gains
5. Internal Heat gains
6. Guided example heating & cooling loads

The fourth objective is to discover and apply diverse methods how to extend load estimates to yearly energy demand, which is essential to make sure that a building is energy efficient and to estimate energy savings and energy costs. The following subjects are handled in week 3:

1. The difference between energy use and loads (kWh and kW)
2. Nominal loads and size of heating and cooling equipment
3. Annual energy demand for space heating and cooling (full load hours, degree days and hourly simulations over a year)
4. Annual energy demand and loads for hot tap water
5. Annual energy demand for electricity (appliances and lighting)
6. Introduction to hourly based steady-state annual energy simulation with Excel

The fifth and final objective is to learn how to optimize building's thermal design and to determine (for instance) the optimal window size or the optimum insulation thickness, and more generally to understand and be able to make simple calculations on thermal interactions between building components and to make informed decisions on how to increase the energy efficiency of new and existing buildings. The setup of this week is different as the students have to actively use the excel simulation sheet to come to insights and answers. They had to do this using both a climate year in a moderate climate (de Bilt in the Netherlands) and in a hot climate (Mumbai, India). Sample answers were given after each exercise for both climates. The case study was a large office building, the geometry and thermal characteristics of which were given.

1. Determine cooling, heating & electricity demands and loads
2. Effect of varying occupancy and various ventilation systems (including passive cooling)
3. Effect of diverse levels of facade/roof/floor insulation
4. Effect of type, size, orientation of windows and solar blinds
5. Combine all knowledge to design a low energy building in NL and Mumbai.

Finally a final video recaps what students have learned and put much attention to the *limitations* of the approach (e.g. steady state modelling, neglecting thermal bridges) and what they still could learn in other courses.

3.2 Example of Self-Assessment after a Lecture

As the course is self-paced, and therefore teachers are not available to correct exercises, self-assessment is essential. If self-assessment using quizzes may seem too simple or boring, they also can be made exciting if they are correctly designed, accounting on beforehand for most types of misunderstandings learners can come through. They should include guidance about these faults.

In the following example, a picture of a mineral wool package (**Fig. 3)** is shown to the students and they have to choose the right answer from 5 possibilities. They cannot find the right answer without making the complete calculation, so they are forced to exercise. Alternatively, they can try all answers and learn from the feedback and hints included after choosing any of the answers.

Fig. 3 – Picture of a mineral wool packaging for a quiz

Question: 'You see on the picture a label of mineral wool (λ=0.035W/mK; thickness=120 mm, αi=7.5 W/m²K, αo=25 W/m²K), What is the Rc value [m²K/W] of this mineral wool?

Possible answers: a) 0.29; b) 3.43; c) 3.60; d) 0.28; e) 3429

If learners choose for b (which is the right answer), they are congratulated and also see the right calculation procedure. If they choose a wrong answer, they get a hint, e.g. if they have answered a) or d): ' you are probably confused between U and Rc (U=1/Rc)'; Or, if they have answered c): 'You have added to the resistance the αi and αo heat transfer coefficients, but that is not the definition of Rc'.; Or, if they answered e): ' you have forgotten to convert the mm into meters'.

4. Energy Supply Systems

The main objective of this second course is to discover how to convert natural resources into heat, cold and electricity, what the capabilities of renewable systems are, how to simply match energy supply with buildings' energy demand (the preceding course), and what that means for energy efficiency and carbon emissions. The working principles of the diverse systems are explained without going too much into the details of all components, with as less as possible formula's, except when it comes to efficiencies and CO2-emissions. Here too, the course is(partly based on the approach proposed in [7].

3.1 Learning Objectives and Subjects

The first step is to consider how to convert natural resources into the energy needed by buildings: what are the options to create heat, cold and electricity? Students will also learn about efficiency and use this concept to estimate building's primary energy use and carbon emissions. This methods are widely used in many national and international policies and building regulations, and are essential to counteract climate change.

The second objective of the course is to understand the performances of *single heating systems* like electrical heating, gas, or renewables like biomass, solar boilers and geothermal heat, followed by *single cooling systems* like evaporative cooling and environmental cold. For each of these systems, working principles, efficiencies , primary energy and resources used are studied as well as CO2-emissions. An additional lecture on heat exchangers was added, as many students appeared not to be familiar with it. Although gas is a fossil fuel, it has been included in the course as a reference, and because many countries consider gas as a transition fuel.

A third objective is to understand systems that *concurrently produce heat and cold* (heat pumps & chillers; Aquifer Thermal Storage systems). These three objectives are divided over the two first weeks of the course. Electrical and fuel burning boilers are handled in the first week, as easy-to-understand illustration of efficiency and carbon emissions.

Week 1:

1. Recap on energy demand (energy vs power, principle of energy balance)
2. Overview of supply systems for heating (resistance, fuel burning, heat pumps, waste heat, geothermal, solar), cooling (chillers, evaporative, geothermal cold) and electricity
3. Efficiency of systems and Primary Energy
4. CO2 and CO2-eq emissions, calculation principles
5. Electrical Resistance Heating and grid efficiency
6. Fuel burning in boilers
7. Guided boiler example with annual primary energy, resources used, CO2-emissions, investments costs and energy costs

Week 2

1. Heat Exchangers
2. Heat pumps and chillers: working principle
3. (Seasonal) Efficiency of heat pumps ((S)COP)
4. Geothermal Systems
5. Chillers and their efficiency ((S)EER)
6. Evaporative cooling and Environmental cold
7. Guided example on a reversible heat pump (same setup as in week 1)

The objective of the third week is to understand *electricity generation* methods using turbines (fuel-burning and nuclear based, wind, hydro), photovoltaics and hydrogen fuel cells. It is often left out from courses on buildings' energy use. It is however essential to fully understand primary energy use and CO2-emissions of buildings, and their relation to the electrical grid. This week is also meant to learn how *cogeneration of heat and power* works and relates to smart heating and cooling grids, and why this is important for the rational use of energy resources.

1. Combustion based electricity generation (generator with (combined) gas turbine, steam turbine (including nuclear))
2. Waste heat, cogeneration and rational use of energy
3. Electricity from geothermal heat, hydropower and wind
4. Hydrogen Technology and smart grids

Finally, the last two objectives of the course, handled in week 4, are to understand *solar systems*, and to apply the knowledge gained during the course to *design efficient building concepts* in order to match buildings' energy demand while keeping costs acceptable, using a minimum of natural resources and producing a minimum of carbon emissions. Week 4 is shorter than others to allow time for the final assessment for certified learners.

1. Solar heat
2. Solar electric (photovoltaic)
3. Guided example NZEB and energy positive buildings.

5. Health & Comfort in Buildings

The main objectives of this course are to raise awareness about the determinants and importance of a healthy indoor environment and to enable the learners to apply the basics of thermal comfort and indoor health theories when designing buildings and their energy systems. People spend more than 80% of their time in buildings. Therefore a good thermal comfort and quality of the indoor environment are essential for their wellbeing,

health and productivity. Part of the course is based on [8, 9,10].

Prior to the first week, learners were invited-if they wanted to, to fill in an anonymous survey about their health and comfort at home. This survey is described in [11] and is repeatedly used to collect new data. Next to activate the students, it is also useful for research purposes.

The objective of week 1 is to understand what is Indoor Environmental Quality (IEQ), what are its parameters and how it impacts health. After IEQ has been defined, two aspects of it, lighting and acoustical qualities are handled briefly. In Bloom's taxonomy we are working here at the level of remembering and understanding. As the focus of the course program is on thermal energy systems we have chosen to address these 2 aspects only lightly in order to put the focus on indoor air quality and thermal comfort, who are both affected greatly by thermal systems (including ventilation).

1. Why is environmental quality important (links with diseases and disorders)?
2. What is environmental quality (lighting, acoustical, thermal and air qualities)?
3. Lighting Quality: relation with health
4. Lighting quality: parameters of light indoors
5. Acoustical quality: relation with health
6. Acoustical quality: parameters of sound indoors

The second week of the course is devoted to thermal comfort with the objectives to familiarize the learners with the two main theories currently in use and to apply them to assess simple building designs.

1. Thermal quality and homeostatis (link with energy balance of human body and the 6 thermal comfort parameters, consequently handled in the following lectures)
2. Metabolism and Clothing
3. Air Temperature and Velocity; comfort diagrams
4. Relative Air Humidity, simple definition and comfort diagrams
5. Mean Radiant Temperature, definition, relation with insulation and comfort diagrams
6. Fanger's Comfort Model (PMV and PPD)
7. Local Discomfort
8. Adaptive Comfort Model

The third week is entirely devoted to indoor air quality (IAQ), with the objective of the learners becoming aware of all parameters of IAQ and being aware of efficient control strategies in the design of ventilation systems. A special lecture was devoted to the COVID pandemic and aerosols.

1. Reception of air and Health Effects
2. Parameters of Indoor Air (particles; gaseous pollutant and humidity)
3. Pollutants and Sources: Particles (sizes; biological and chemical; health effects)
4. Pollutants and Sources: Gaseous pollutants (inorganic; VOCs; health effects)
5. SARS Cov-2 (particle; droplets and aerosols)
6. Control strategies (low emitting materials; filtering of air and cleaning of ventilation systems; appropriate ventilation strategies)

To close this third week, the general results of the home survey like held in week 1 are discussed.

The objective of the last week of the course is that the students learn to apply their knowledge on the design of healthy buildings and to assess and analyse practices in building design and HVAC systems. All concepts learned before are translated to engineering aspects. In this sense week 4 is also an introduction to HVAC systems. The subjects handled are the following:

1. What is a healthy building? (summary or preceding weeks, with much attention to control possibilities, which are worked out in next lectures)
2. Introduction to healthy HVAC systems (basic description of air handling units, needs for filtering, clean components and piping and avoid recirculation)
3. Clean components for ventilation systems (characteristics of filters, humidifiers, heat exchangers and location air supply)
4. Healthy air supply (clean ducts, noise prevention, draught in supply grilles)
5. Façade & Ventilation: design of ventilation openings, acoustical and thermal insulation of openings, façade heat recovery, outdoor air quality, double skin facades.
6. Window design: thermal and lighting qualities and control in cold and warm climates, outside view
7. Energy efficient artificial lighting control (needed light levels, electricity use of diverse types of lighting, configurations and zoning)
8. Room heaters and coolers: energy efficiency and comfort (air-based & water based heaters and coolers, their temperatures and relation to mean radiant temperature, noise and draught and to energy use)

6. Efficient HVAC systems

All three previous courses are integrated into this last one, with as main learning objective to apply the knowledge in HVAC design practices at the level of basic and preliminary designs. In the design of the course we aimed at linking with more conventional HVAC design courses –generally focused on air handling units (AHU) and to complete the

understanding of learners with essential subjects that were not covered before, like dealing with humidification and de-humidification. The course is based for a part on [10], [12], [13].

The first week of the course is therefore a recap of all three previous courses, presenting the essentials of energy demand, energy supply and health & comfort, to which an additional lecture on the basics of heat exchangers was added.

The second week handles humid air, humidification and dehumidification processes and processes in air handling units. The students should be able to describe related processes and to make simple calculations of energy use and humidity contents. They learn to do so using either Mollier diagrams, psychrometrics charts or equations, to fit with habits in their own country. Learners can test their knowledge about equations if they want, but the attention is put to the use of diagrams and charts, as it fits better with the lower mathematical background of many students. Week 2 is organized as follows:

1. Introduction to properties of humid air
2. Psychrometric charts and humidity
3. Dew point: condensation, cooling & de-humidification processes
4. Enthalpy of humid air; Heating and cooling processes
5. Wet bulb temperature and humidification processes
6. Handling of humid air: summary of the possible processes.

The third week has been designed to familiarize the students with the diverse types of air, heat and cold distribution systems in buildings. We know from previous courses that knowledge is very local and it may be difficult for students to realize that there are diverse options. For instance learners from hot climates are not aware of water-based heat distribution systems, while learners from cold climates may not realize the problems water-based cold distribution systems would cause. In each presentation calculation examples are given and systems are visualized. The contents of week 3 are:

1. Overview of possibilities to transport hygienic air, heat and cold and their possible interactions; Advantages and disadvantages; Duct sizes)
2. Air handling units: the theoretical processes described in week 1 are applied in AHUs
3. Transport of air in ducts (location of supply, velocity & noise, sizing and efficient routing of ducts)
4. Pressure drop in ducts en fan energy
5. Transport of heat by water systems: hydronic heating (location of generation system; design of hydronic networks; sizing of convective/radiant emitters)
6. High and low temperature heating (advantages and disadvantages in relation to comfort, energy use and use of renewable sources)
7. Hydronic cooling (location of generation system; design of hydronic networks; options and sizing of emitters, low and high temperature cooling; dew point control)

In week 4, the students are familiarized with the basic principles of sizing and controlling simple systems. In view of the target audience, we've deliberately avoided to go into the details of control engineering (which is still handled in the last lecture), but rather focus on designs enabling control.

1. Enabling control (sizing, zoning, readjusting, combining, buffering)
2. Design for control: zoned HVAC systems (zoning of distribution ducts for flexibility in use and maximum efficiency; Introduction to Process and instrumentation diagrams (P&IDs)
3. Readjustments systems at room level (mixed air/water systems; central and decentral control; graphical review of possible configurations, for instance like in shown in **fig. 4**)
4. Load duration curves and generator combinations; relation to investment costs and energy use
5. Buffers for peak shaving, renewable energy and match between supply and demand; Design of buffers
6. HVAC operation control: basics of control (sensors, actuators, controllers) and application to temperature, pressure, flow rate and humidity control, using P&IDs.

The last week of the course handles design and control of integrated systems for Net Zero Energy Buildings. It starts with a lecture about the design process itself, before digging into the aspects of technical design. This includes 2 subjects on specific designs for moderate and cold climates, 2 subjects specific to hot climates, and stresses finally the importance of aquifer thermal storage systems (ATES).

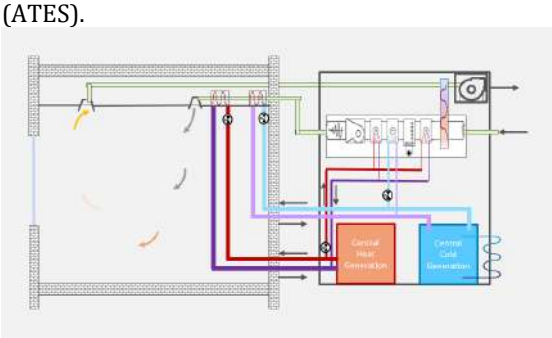

Fig. 4 - A configuration for central & decentral control

1. Design process for efficient HVAC systems (aims, collaboration with other experts,

process from program of requirement to maintenance, commissioning)
2. Efficient control of conditioned air from AHUS (CAV & VAV; energy efficient set point temperature control; flow patterns in rooms)
3. Efficient buildings and HVAC systems for moderate and cold climates (reduced heating demand; high quality ventilation, emitters, generators; solar electricity; NZEB)
4. Heat sources for heat pumps (ground, solar, (ventilation) air, working modes and control, collective systems)
5. Efficient buildings and HVAC systems for hot climates (reduced cooling demand, ventilation strategies, generators; solar electricity; NZEB)
6. Heat sinks for chillers and environmental cold (air, water, ground, collective systems; absorption systems)
7. ATES systems for heating and cooling (working modes explained in words and P&IDs)

7. Reflections

The first run of the complete program took place between September 2020 and November 2021. The four courses were offered in the same order as described in the paper. More than 5000 learners subscribed to each of them and 8-10% of them were following it on an active way, which is quite standard on the edX platform. Course 4 (Efficient HVAC systems)ended in the shortlist of 100 most popular online courses 2021 (out of 2900) [14], indicating a wide and worldwide interest for sustainable HVAC systems.

Although the detailed analysis of the students reviews still has to be done, it can be noted that the courses were highly rated with grades between 8 and 9, except for course 2, what was rated a little bit lower. About half of the students were junior HVAC professionals, many of them from India and US. It is not completely clear yet in how far policy makers have followed and/or appreciated the course.

In general the technical/theoretical level of course 1 (Energy demand) was found to be right, while the level of course 2 (Energy supply) was too high (mainly because of mismatch with background on heat transfer and heat exchangers). Course 2 was also less well-balanced between the levels of explanations on diverse technologies (e.g. too less solar in comparison to heat pumps). The last of week of course 1 (the only one at 'create' level, see **Fig. 1**) was appreciated a lot. Leaners found it 'fun'.

The first lecture in course 4 (design process and stakeholders) was highly appreciated and students asked for similar lectures in the other courses, as this helps to place the activities of the course in their context. Finally it was noted that there is very little literature or handbooks addressing the subject of design for control (e.g. zoning, readjustment, multiple generators) on a structured way. This is also true for reading and understanding P&IDs.

8. Acknowledgements

We thank Delft Extension School, and in particular Bertien Broekhans, Eloïse Ruby and Rins Lindeman for their support and help with financing, organizing and moderating the program. The development of this professional course program was partly founded by Climate-Kic City Retrofit Ecosystem Build Benelux and Delft University of technology.

9. References

[1] Interview Terpstra D., Techniek NL https://www.nu.nl/ondernemen/4476618/installatiebranche-tekort-15000-vakmensen-komende-vier-jaar.html
[2] https://buildupskills.eu/,access23-01-2022
[3] Duffy, T. M., Jonassen, D. H. (2013). Constructivism and the technology of instruction: A conversation. Routledge
[4] Bloom, B. S. (1956). Taxonomy of educational objectives. Vol. 1: Cognitive domain. New York: McKay, 20-24.
[5] Hernandez, A, access 21-01-2022, https://www.flickr.com/photos/21847073@N05/5857112597,\, License CCBY-SA2.0
[6] Salmon, G (2002) E-tivities. London. Kogan Page Ltd..
[7] van Bueren E., van Bohemen H., Itard L., Visscher H. (2012) Sustainable urban environments, Chapt. 5, Springer.
[8] Bluyssen, P.M. (2015) All you need to know about indoor air, Delft Academic Press, NL.
[9] Bluyssen, P.M. (2019) All you need to know about air conditioning, Delft Academic Press
[10] van Paassen A.H.C. (2004), 'Fundamentals: Thermo-dynamic aspects of humid air and comfort', course WB4426 (ME45111) Indoor Climate Control Fundamentals, TU Delft.
[11] Bluyssen, P.M., Zhang, D., Ortiz-Sanchez, M. (2021) Self-reported rhinitis and headaches of students from universities in Taiwan, Chile, Suriname, China and the Netherlands, and its association with their home environment, *Intelligent Buildings International*: 1964424. https://doi.org/10.1080/17508975.2021.1964424.
[12] ASHRAE handbook Fundamentals
[13] ISSO-TVVL Handboek Installatietechniek (2002), the Netherlands
[14] https://www.freecodecamp.org/news/most-popular-free-online-courses/, access 23-1-2022

Interactive worksheets as a resource for teaching building performance and energy systems simulation

Roel Loonen [a]

[a] Department of the Built Environment, Eindhoven University of Technology, Eindhoven, the Netherlands, r.c.g.m.loonen@tue.nl

Abstract. This paper describes the development, implementation and evaluation of Jupyter Notebooks as a digital tool to promote (i) self-directed learning of theory concepts and (ii) active engagement with practical assignments in a graduate-level course on building performance and energy systems simulation. Jupyter Notebooks are gaining popularity as an educational tool for their ability to accommodate digital documents that weave together executable code, equations, data visualizations, and narrative text, without the need for dedicated software environments or advanced programming skills. Specifically, Jupyter Notebooks allow the user - in this case both the lecturer and the student - to bring together data, code, and prose, to tell an interactive, computational story. In our case, the Jupyter Notebooks are used as a teaching resource to foster individualized place and time-independent learning as part of a regular on-campus course, with particular emphasis on homologation of students with heterogeneous backgrounds and for proactive engagement with theoretical subjects.
This paper follows the principles of 'constructive alignment' to highlight various aspects of the use of Jupyter Notebooks in this engineering education context. After a general discussion of the course set-up and key learning objectives, the implementation part of the paper showcases a number of concrete examples of the interactive worksheets on the subjects of thermal comfort assessment, building-integrated renewable energy systems and smart grid interaction. These example assignments illustrate a variety of tasks and functions, including dataset manipulation, scripting assignments, click-and-learn apps and explanatory video clips. An evaluation of the approach is presented on the basis of student questionnaires and informal evidence collected during two years of running the course. The paper finishes by providing a critical reflection of opportunities and caveats and suggested directions for further development.

Keywords. Engineering education, blended learning, Jupyter Notebooks, building performance simulation
DOI: https://doi.org/10.34641/clima.2022.209

1. Introduction

There is increasing awareness of the opportunities provided by digital and blended teaching methods to enable place-and-time independent learning in conjunction with on-campus teaching. Studies have shown that such approaches can effectively accomplish intended learning outcomes [1] with efficient use of resources, while accommodating diverse learning styles [2]. The COVID-19 pandemic has necessitated an almost unimaginable acceleration in the uptake of novel self-directed learning formats in higher education, and it is expected that the positive elements of this transition will prevail, also in the post-pandemic world [3]. Community-wide sharing of examples and lessons learned, to ultimately develop a repertoire of best-practices, is therefore of great international interest, especially also considering the need for educating the next generation of engineers who is entrusted with the challenge of realizing the transition towards an energy-efficient, circular, digitized and healthy built environment.

This paper contributes to these developments by reporting on the development, implementation and evaluation of interactive worksheets based on Jupyter Notebooks as a resource for promoting place-and-time independent learning in a graduate-level course on building performance and energy systems simulation at Eindhoven University of Technology, the Netherlands.

The course context and challenges that have led to the development of these interactive worksheets are described in Section 2. Section 3 then provides more

Copyright ©2022 by the authors. This conference paper is published under a CC-BY-4.0 license.

information about the developed solution direction and its key characteristics. Notes about the actual implementation together with a selection of illustrative examples of the Jupyter Notebooks are presented in Section 4, followed by an evaluation and reflection in Section 5. Finally, the paper concludes by providing a general discussion and future outlook in Section 6.

2. Context and motivation

2.1 course outline

Building Performance and Energy System Simulation is a 5 ECTS core course in the master track Building Physics and Services and in the master programme Sustainable Energy Technology at Eindhoven University of Technology, the Netherlands. The objectives of the course are to:

- Present the underlying theoretical and operational principles of building-integrated sustainable energy systems from component/system-level to district-scale.
- Introduce performance-based analysis as a useful tool for assessing the trade-offs between indoor climate, cost-effectiveness and environmental performance.
- Highlight the opportunities and challenges of state-of-the-art building performance simulation and to provide hands-on training in the use of such software.

Following the principles of constructive alignment [4], the weekly teaching activities (Figure 1) consist of a mix (i) oral lectures, (ii) self-guided learning using a combination of theory assignments based on the enriched skeleton concept mapping approach [5] and interactive videoclips on the FeedbackFruits platform [6], and (iii) hands-on tutorials for simulation-aided design assignments.

It is widely understood that learning to become proficient in building performance simulation entails much more than being able to generate results with a specific software tool [7]. The practical work in the course is therefore designed to demonstrate and reflect on the importance of underlying theoretical concepts in an applied context, and to gain practical hands-on experience in using state-of-the-art building performance simulation software for design of integrated building and energy system concepts. As such, the course set-up is well-aligned with the principles of experiential learning in building performance simulation [8] as it has evolved from the fundamentals of quality assurance as described in [9].

2.2 issues and challenges

Due to continuous shifts in student population and because of the desire to integrate more 21st century skills in the classroom, a number of issues and challenges were identified to further enhance the course:

1. Students in this first-year MSc course come in with very heterogeneous backgrounds from different (international) bachelor programs. The range of topics that is covered is quite broad. Only a small group of students (~25%) possesses all the required background knowledge, whereas for most of the others, something is lacking (e.g. either related to buildings and indoor comfort, or to energy (thermal or electrical) issues). Due to the compact scheduling, the course allows for very limited time for brushing up background knowledge, which increases chances that students get lost. Before the intervention, deficiencies were addressed in an ad-hoc way, by suggesting extra reading and practice material on an individual basis. A more systematic and integrated solution for homologation would likely lead to significant enhancements in the learning experience.

2. Intentionally, most of learning objectives in this course are approached from a rather application-oriented perspective in terms of subjects that are covered. A consequence of this is that there is less time to explain the more basic theoretical concepts (which would anyhow be a repetition for roughly half of the students). It is also believed that broadcasting this information in extended oral lectures is not the most efficient way of learning, for the material at hand. Instead, it would be desirable if

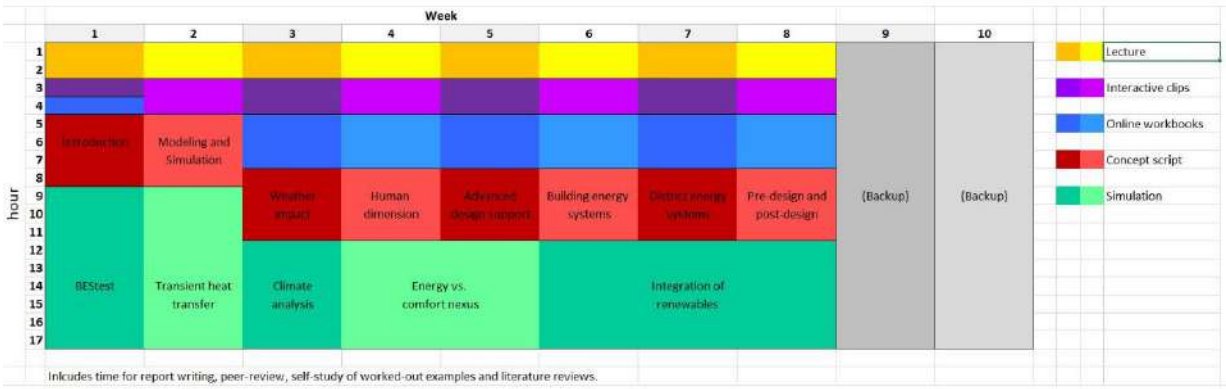

Fig. 1 – Outline of various teaching activities in the course Building Performance and Energy Systems Simulation at Eindhoven University of Technology, the Netherlands

students had access to a curated set of interactive explanatory and practice material (video, text, animations, small scripting exercises and app-like click-and-learn case studies for formative feedback), so they can revisit the theory if and when needed.

3. The course works with a series of weekly assignments. Before the intervention, the students would perform simulations and write separate reports. It would be desired to evolve these traditional written reports into a more interactive solution in which simple programming, visualizations, plots and explanatory text are all integrated in online worksheets. The intention is that students can submit these worked-out sheets as their report for the assignment. Integrating it in this interactive and updateable format will also allow the lecturer to embed the latest research findings as case study examples in the course.

2.3 proposed solution

To address the abovementioned challenges, an education innovation project was initiated, with the intention to develop, implement and evaluate Jupyter Notebooks to promote self-directed learning of theory concepts and active engagement with simulation assignments based on interactive worksheets.

3. Jupyter Notebooks

3.1 what are Jupyter Notebooks?

A Jupyter Notebook is a digital document that weaves together executable code, equations, data visualizations, and narrative text [10, 11]. Specifically, Jupyter Notebooks allow the user (in this case both the lecturer and the student) to bring together data, code, and prose, to tell an interactive, computational story in a web-based environment. Jupyter Notebooks are part of the Project Jupyter ecosystem, a large international community that promotes the development of open-source software and services for interactive computing across a large range of programming languages.

Popular applications of Jupyter Notebooks in the research domain include its use as (i) an interactive scripting and data analysis environment for individual researchers and research teams, and (ii) deployment platform for shareable web apps based on plug-ins such as Voilà, Bokeh and Dash. Jupyter Notebooks also form an important part of BESOS, the Building and Energy Simulation, Optimization and Surrogate Modelling framework, developed at the University of Victoria, Canada [12, 13].

3.2 Jupyter Notebooks in engineering education

Jupyter Notebooks have recently also gained popularity as an educational resource [14]. Its use is said to enhance: engagement, participation, increased understanding (e.g. guiding learners at their own pace) and student's performance [15]. Notable examples of Jupyter Notebook based teaching material related to the themes of the CLIMA 2022 conference that have served as inspiration for the present project include:

- CFD Python, a course developed by prof. Barba at Boston University [16].
- Data Science for Construction, Architecture and Engineering, an edX course developed by the BUDS lab at the National University of Singapore [17].

In particular, the following capabilities of Jupyter Notebooks are targeted in the present development:

- Deployment of click-and-learn apps, so students can explore relationships between variables in various complex energy systems on the basis of pre-loaded datasets.
- Empowerment of students without former training in programming to execute simple python scripting tasks. Students will receive simple snippets of code and are encouraged to develop this further.
- Code and real-time visualizations are executable from within a browser. There is no need for time-consuming installation procedures and accompanying troubleshooting efforts.
- Students have the possibility to combine code with text and tables and figures to develop stand-alone interactive reports.

4. Implementation and examples

4.1 overview

The developed Interactive Worksheets and supporting datasets are provided to the students via the Canvas learning management system that provides the online portal for all courses at TU/e. The Notebooks themselves are hosted using the Google Colab service, which allows students to execute their tasks in the internet browser of their choice, without the need for installing any additional software.

At present, eight Jupyter Notebooks have been developed, dedicated to the following topics: (i) Notebook basics, (ii) Weather data analysis, (iii) Thermal comfort, (iv) Occupant behaviour, (v) Multi-criteria decision making, (vi) Solar thermal collectors, (vii) On-site energy matching, and (viii) Energy signatures.

Each Notebook makes use of different combinations of text, video clips, data tables, figures, equations, interactive scripting widgets and executable code.

While working their way through the Notebooks, students are requested to complete a series of tasks and assignments. Dedicated answer sheets in pdf format have been developed in which students can note their solutions. These answer sheets are then uploaded for feedback and/or assessment. The time required to complete the tasks in each workbook range from approximately 15 minutes to 1.5 hour.

The developed Jupyter Notebooks are available for download via [18]. In the following sub-sections, a selection of Notebook snippets is presented to highlight specific features and thereby illustrate their potential added value in an education context.

4.2 example A: multimodal information

A typical example that makes use of the multiple modalities of information exchange offered by Jupyter Notebooks, is presented in Figure 2. On the topic of energy signatures, this worksheet fragment contains a combination of explanatory text, equations, hyperlinks, python code and figures. Here, the figures are based on a dataset with actual measurements from many buildings, leading to the possibility for each student to work with an individualized set of buildings.

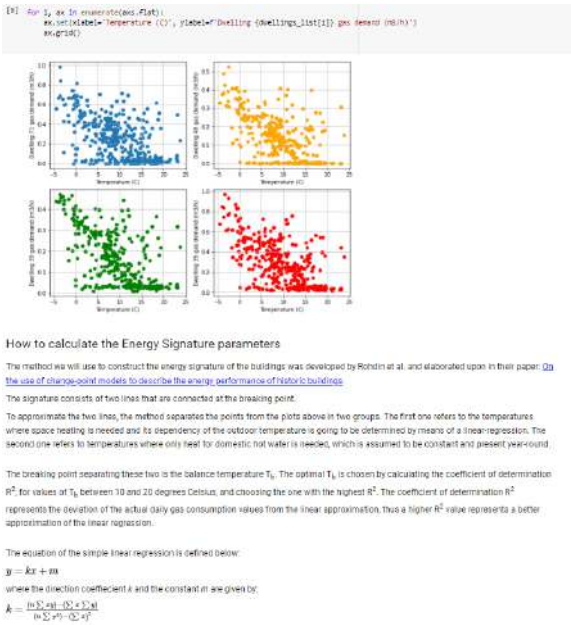

Fig. 2 – Typical Jupyter Notebook fragment, showing different types of information exchange

In addition to the type of information presented in Figure 2, the developed Jupyter Notebooks also take advantage of the possibility to embed video clips. For example, Figure 3 shows a case where a video is used to explain the working principles of solar domestic water systems. Videos from different (external) sources can be integrated. In this example, the embedded YouTube functionality has been used, but it is also possible to include self-recorded clips.

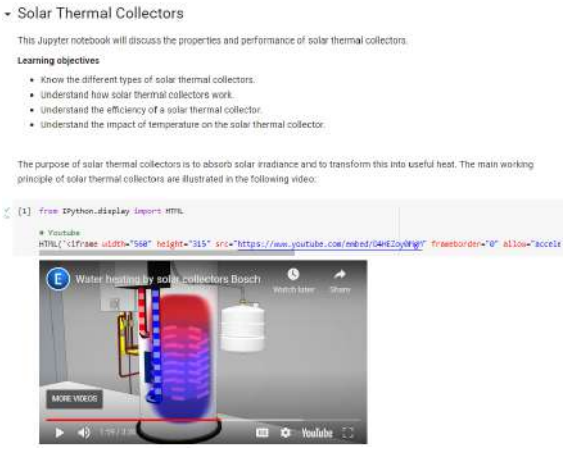

Fig. 3 – Integration of YouTube videos in the Notebook

4.3 example B: interactive widget

Figure 4 shows an example of an interactive widget that was developed to allow students to explore the multi-variate relationships in a thermal energy system. Specifically, in this case, the combined influence of temperature difference and irradiance conditions on the efficiency of various types of solar thermal collectors (flat-plate vs. vacuum) are visualized. By simply adjusting the slider to vary solar irradiance, the lines in the figure update automatically, aiding in the understanding of the complex relationships between variables. In a previous part of the Notebook, the students are presented with the theory and conventional equations for understanding the performance of solar thermal collector. Students can also inspect and adjust the code that is needed to build the widget, for example to observe what happens when different heat loss correction factors are assumed.

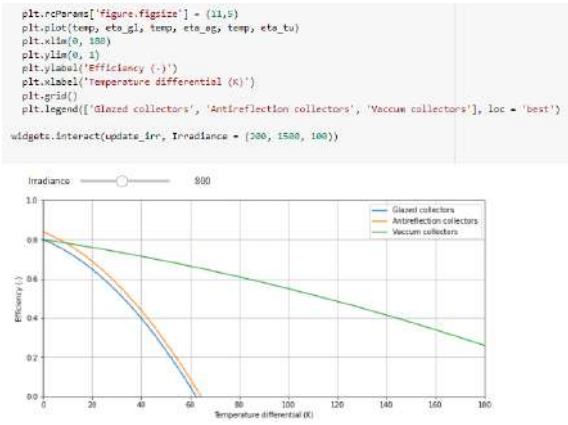

Fig. 4 – Example of an interactive widget

Another example of interactivity, this time related to the subject of variability in occupant behaviour and its influence on load coincidence factors, is presented in Figure 5. In this case, an interactive data visualization is shown, allowing the user to intuitively make the connection between input parameters and resulting output. Figure 5 also showcases an example of how the short assignments are an integral part of the Jupyter Notebooks.

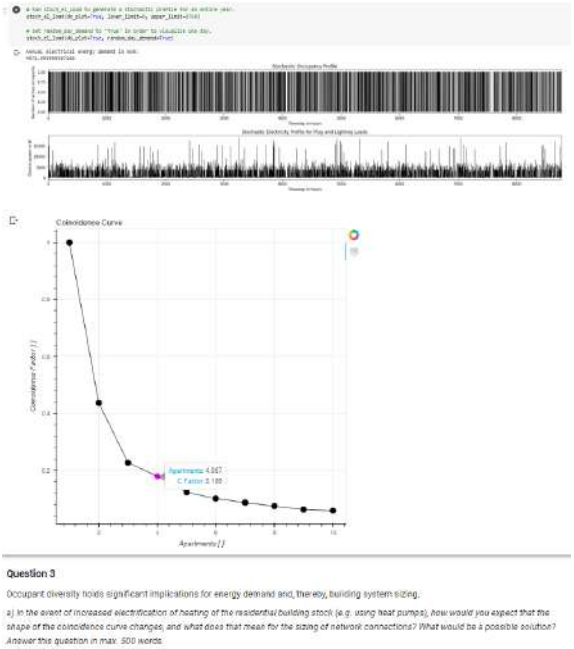

Fig. 5 – Interactive data visualization

4.4 example C: assisted data analysis

The Notebook snippet in Figure 6 is developed to give students a hands-on understanding of energy matching indices On-site Energy Matching (OEM) and On-site Energy Fraction (OEF). These relatively abstract concepts are made more tangible by letting students interact with a pre-loaded dataset that contains monitoring data from 20 houses. Preparatory tasks such as pre-processing, data cleaning etc. are all taken care of by the Jupyter Notebook, so students can immediately start exploring the data itself. In this case, an interactive date selection widget is added to further speed up the learning curve. The question the students are asked to answer in this Notebook is to quantify the effectiveness of rooftop PV by calculating energy matching indices in different seasons.

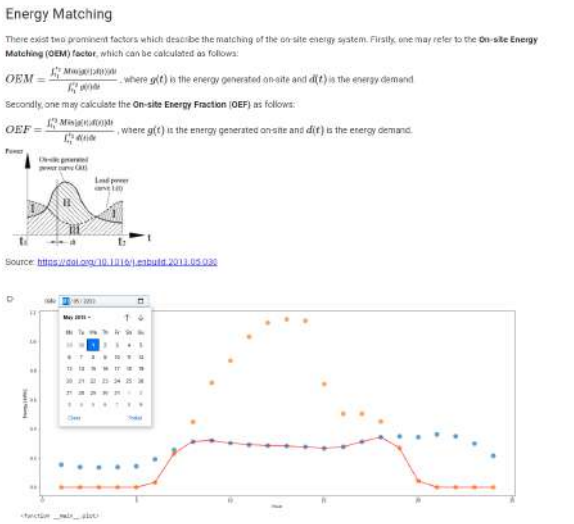

Fig. 5 – Exploring data with the help of a Notebook

5. Reflection

5.1 teacher's perspective

From a teacher's perspective, the experience with the integration of Jupyter Notebooks has been largely positive. No major obstacles were encountered in the practical workflow – all students with different personal laptops and operating systems were able to complete the tasks. It gives peace of mind to know that students have access to a curated set of explanatory documents, and relieves the task of recommending such sources to individual students on a case-by-case basis. One cannot ignore the time it takes to collect and process the material into engaging interactive worksheets, but it was found that teaching assistants are perfectly able to contribute to this effort. Moreover, it is believed that the developed workbooks remain relevant for years to come, which brings opportunities for gradually extending the library of Notebooks over time with new content. Ideally, such a development becomes part of a crowd-sourced open-access database for sharing within the global community.

One of the key benefits of the selected teaching approach is that it provides unprecedented opportunities to introduce bits and pieces of the latest academic research in the classroom. For example, one of the presented Notebooks makes use of functions in the `pythermalcomfort` library [19] to let students experience the differences and similarities between Fanger-based and adaptive thermal comfort models, while another Notebook takes advantage of `richardsonpy` [20] in an assignment were students use stochastic occupancy and electric load profiles based on the Richardson model [21]. Coincident with the transition towards Open Science, it is expected that many more of such developments can be integrated in the near future.

A drawback of the extra assignments is the increase in workload for checking and/or grading of submitted assignments. Until now, this formative and summative assessment was done manually. It would be worth to explore if peer review or automated assessment approaches could take over part of these tasks.

5.2 students' perspective

Questionnaire-based student feedback administered through the Evasys system after the end of the course, indicates that students were moderately satisfied with the interactive worksheets as a learning method. Figure 6 shows responses to the question "the Jupyter Notebook assignments help me to better understand the theoretical concepts covered in this course" for the academic years 20/21 and 21/22, respectively. These results show a fairly wide distribution with an overall positive impression.

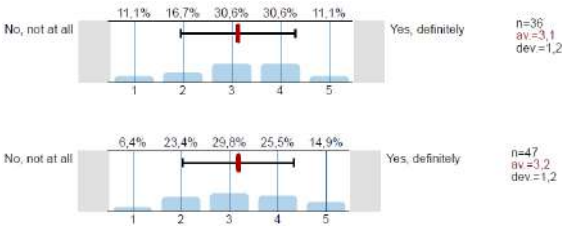

Fig. 6 – Distribution of student responses to the question "the Jupyter Notebook assignments help me to better understand the theoretical concepts covered in this course" for the academic years 20/21 (top) and 21/22 (bottom).

Remarkable results to the follow-up question "the use of Jupyter Notebooks makes the learning process more enjoyable" were found, with shifts towards both extremes indicating stronger feelings of (dis)liking. Answers to the open feedback section of the questionnaire helped in interpreting this observation, particularly relating to a perceived lack of clarity in terms of structure and to what extent the assignments counted toward the final grade.

Additional feedback obtained through informal sessions with student representatives halfway during the course, generally agreed with the findings from the questionnaire. What these sessions revealed, though, is that students without prior experience in the use of scripting languages (e.g. python or Matlab), found it difficult to get going with the assignments, especially in case the Notebook returned generic error messages without concrete indications that novice users could use for troubleshooting. Even though efforts were made to make the entry requirements regarding scripting/programming knowledge as low as possible, this finding highlights the need to be very thoughtful about expected prior knowledge and the possible usefulness of Frequently Asked Question overviews and peer support methods.

6. Concluding remarks

This paper has described the development of Jupyter Notebooks to support self-propelled learning in a graduate course on Building Performance and Energy Systems Simulation. A series of examples was given to illustrate the unique features of Jupyter Notebooks and its potential to deliver an engaging learning experience. Although the evaluation from both teacher's and students' perspective shows positive signs, it is still early to make conclusive statements about the success of this implementation.

Plans for further development in the near future include the development of additional Notebooks to cover more topics in the domain of building performance and energy system simulation. By having these Notebooks available in the public domain, it would be great if this could become the starting point of a joint international effort to make a library of Notebooks available for different types of learners. Within the context of a single course, the challenge will be in finding a right balance between giving students access to more material without creating an overshoot in the workload.

Another direction for further development is a more seamless integration between the task description and the way the responses are collected. At present, these two parts are disconnected, but it would be interesting to explore options for having students submit Notebook files instead of pdfs. The intention is that students would spend less time on writing reports and thus more time on the main learning objectives of this course. In addition, it is also anticipated that this use of the worksheets will reduce that amount of time that is needed to grade the assignments and hence it will increase opportunities for giving timely feedback. In this context, it is expected that much inspiration can be taken from efforts towards the development of "executable research papers", which are also largely driven by the Project Jupyter movement [22].

7. Acknowledgement

The author gratefully acknowledges the support received from the BOOST! TU/e Education Innovation programme: https://boost.tue.nl/

8. References

[1] Freeman, S., Eddy, S. L., McDonough, M., Smith, M. K., Okoroafor, N., Jordt, H., & Wenderoth, M. P. (2014). Active learning increases student performance in science, engineering, and mathematics. *Proceedings of the National Academy of Sciences*, *111*(23), 8410–8415.

[2] Cheng, G., & Chau, J. (2016). Exploring the relationships between learning styles, online participation, learning achievement and course satisfaction: An empirical study of a blended learning course. British Journal of Educational Technology, 47(2), 257-278.

[3] Rapanta, C., Botturi, L., Goodyear, P., Guàrdia, L., & Koole, M. (2021). Balancing technology, pedagogy and the new normal: Post-pandemic challenges for higher education. Postdigital Science and Education, 3(3), 715-742.

[4] Biggs J. Enhancing teaching through constructive alignment. Higher education. 1996 Oct;32(3):347-64.

[5] Marée TJ, van Bruggen JM, Jochems WM. Effective self-regulated science learning through multimedia-enriched skeleton concept maps. Research in Science & Technological Education. 2013 Apr 1;31(1):16-30.

[6] Campbell C, Borer L, McCarthy S. Using FeedbackFruits to enhance student learning: Scaling for transformative implementation.

[7] Gentile N, Kanters J, Davidsson H. A method to introduce building performance simulation to beginners. Energies. 2020 Jan;13(8):1941.

[8] Beausoleil-Morrison, I., 2019. Learning the fundamentals of building performance simulation through an experiential teaching approach. Journal of Building Performance Simulation, 12(3), pp.308-325.

[9] Hensen JLM, Radošević M. Teaching building performance simulation - some quality assurance issues and experiences. In: Proc. Int. Conference on Passive and Low-energy Architecture–PLEA 2004 Sep.

[10] Project Jupyter: https://jupyter.org/

[11] Perez, F. (2017) The course of the future – and the technology behind it: https://data.berkeley.edu/news/coursefuture

[12] Westermann P, Christiaanse TV, Beckett W, Kovacs P, Evins R. BESOS: Building and Energy Simulation, Optimization and Surrogate Modelling. Journal of Open Source Software. 2021 Apr 6;6(60):2677.

[13] BESOS Platform - Building and Energy Simulation, Optimization and Surrogate-modelling https://besos.uvic.ca/

[14] SURF - Jupyter Notebook: accessible and interactive data analysis for research and education https://www.surf.nl/en/jupyter-notebook-accessible-and-interactive-data-analysis-for-research-and-education

[15] Barba LA. Engineers Code: reusable open learning modules for engineering computations. Computing in Science & Engineering. 2020 Feb 24;22(4):26-35.

[16] Barba LA. CFD Python: https://github.com/barbagroup/CFDPython

[17] BUDS lab. Data Science for Construction, Architecture and Engineering https://github.com/buds-lab/data-science-for-construction-edx-course-notebooks

[18] Loonen, RCGM. Jupyter Notebooks for Interactive worksheets as a resource for teaching building performance and energy systems simulation: https://gitlab.tue.nl/bp-tue/clima2022_jupyter

[19] Tartarini F, Schiavon S. pythermalcomfort: A Python package for thermal comfort research. SoftwareX. 2020 Jul 1;12:100578.

[20] richardsonpy: https://github.com/RWTH-EBC/richardsonpy

[21] Richardson I, Thomson M, Infield D. A high-resolution domestic building occupancy model for energy demand simulations. Energy and buildings. 2008 Jan 1;40(8):1560-6.

[22] Lasser, J., 2020. Creating an executable paper is a journey through Open Science. Science. *Communications Physics*, *3*(1), pp.1-5.

9. Data statement

The datasets generated during and/or analysed during the current study are available in the Gitlab repository of the Building Performance group at Eindhoven University of Technology, https://gitlab.tue.nl/bp-tue/clima2022_jupyter.

Digital Erasmus – a pan-European approach to teaching building performance and resilient design

Christina J. Hopfe [a], Eleonora Brembilla [b], Lori B. McElroy [c], Robert S. McLeod [a], Matej Gustin [a], Daniel Costola [c]

[a] Institute of building physics, services and construction (IBPSC), Graz University of Technology, Graz, Austria, c.j.hopfe@tugraz.at, mcleod@tugraz.at, m.gustin@tugraz.at

[b] Faculty of Architecture and the Built Environment, Delft University of Technology, Delft, the Netherlands, e.brembilla@tudelft.nl

[c] Faculty of Engineering, University of Strathclyde, Scotland, lori.mcelroy@strath.ac.uk

Abstract. The global COVID-19 pandemic in 2020 has forced universities to completely re-think their teaching concepts to provide safe, remote teaching of students off-campus. One of the challenges of this rapid transition is ensuring that the quality of the learning experience remains high and that students are able to engage and thrive in this new and predominantly digital environment. This project, entitled 'Digital Erasmus - a roadmap to using building performance simulation to achieve resilient design', responds to this context by seeking to transform the learning experience of students in built environment disciplines using a continuous digital learning cycle. This paper outlines the concept of the program and the learning objectives that it responds to, as well as some initial results highlighting the programs opportunity for students to work collaboratively and transnationally. The program is still in its infancy but it is hoped that it can serve as a template for similar future online courses that will promote safe, interdisciplinary and engaging collaboration amongst students from different universities.

Keywords. Erasmus, digital learning & education, energy, building simulation, thermal comfort.
DOI: https://doi.org/10.34641/clima.2022.129

1. Introduction

Our pan-European approach to teaching building performance and resilient design is proposed in the context of the general restrictions on travel imposed by the COVID-19 pandemic. The restrictions that the entire Global population is facing considerably impact traditional mobility programmes offered to Higher Education students in Europe and hinder the acquisition of important interpersonal and research skills that these programmes usually promote.

At the same time, this situation has sparked a reflection about segments of the population that have often been excluded from participating in exchange and mobility activities, due to socio-economical, cultural or physical disadvantages. Moreover, the architecture, engineering and construction (AEC) sector is known for its widespread discrimination against atypical professional figures, e.g. women, minority groups and people with a wide range of disabilities [1]. We aim to tackle these issues (reduced international mobility and barriers to access in AEC professions) by taking advantage of the current re-thinking of how university lectures are structured and delivered, with a particular focus on the field of Building Performance Simulation (BPS) and resilient design.

Our objective is to develop a dynamic, experiential (see Figure 1, i.e. using both experience and observation) methodology to maximize student engagement and learning opportunities in a digital and transnational environment. With this we want to create an environment that encourages cooperation, diversity and equality. To achieve this, we started to create a safe yet challenging learning environment that exposes students to new ways of thinking and working, one which provides a framework for likeminded people to get to know each other, to collaborate and to learn with and from each other, independently of their geographical location. Building performance and the future resilience of the built environment are the core themes of this program, which responds to the rapid and well documented transitions occurring in the Earth's climatic, environmental and social conditions. Measurement, modelling and simulation are tools that can be used to futureproof our response to these challenges in the built environment. We aim to develop these skills by creating virtual test beds (linked to data from real buildings) so that students can explore existing designs and evaluate the impact of their design decisions in relation to key performance indicators including: health and wellbeing (TU Delft), energy and indoor air quality (TU Graz), and moisture and future resilience (University of Strathclyde). This paper outlines the concept of the program and its learning objectives that it is responding to, as well as some information on the different modules (in particular the workshops).

Copyright ©2022 by the authors. This conference paper is published under a CC-BY-4.0 license.

2. Context

Building simulation is traditionally taught in a classroom setting with access to computer labs, where students learn how to use the software in direct contact with staff [2,3]. In times of COVID-19 this is no longer possible. We are therefore targeting students who are enrolled in MSc programmes that include courses on building performance and resilience, but who are no longer able to participate in live classrooms activities. By doing so, we are taking into account both the current circumstances and the personal obstacles that students with disabilities might face in normal classroom settings as well as the barriers faced by those who cannot attend conventional classes (for a variety of other reasons).

In this context we propose a new pedagogical methodology that addresses the challenges of digital teaching but at the same time provides a platform for students to acquire the skills needed for a successful career. (see Figure 1)

There are a number of reasons why we have chosen to focus on innovative practices in a digital era. Building Performance Simulation (BPS) and its application in enhancing the resilience of the built Environment is by nature a digital activity. Paradoxically however, it is commonly taught in a traditional didactic manner, with students receiving direct instruction and experiencing little peer-to-peer interaction. Unsurprisingly pedagogic theory, including specific studies focused on the teaching of BPS in higher education have highlighted how such approaches have delivered exceptionally poor learning outcomes [2; 3]. This means that there is an urgent need to evolve new and innovative teaching practices, that better engage students whilst yielding more robust learning outcomes [4]. In the midst of a global pandemic, with greater than ever demand for online learning, there has never been a more appropriate moment to make this change. What we are proposing is rooted in the constructivists theory that learning occurs most profoundly when learners are actively involved in a process of meaning and knowledge construction.

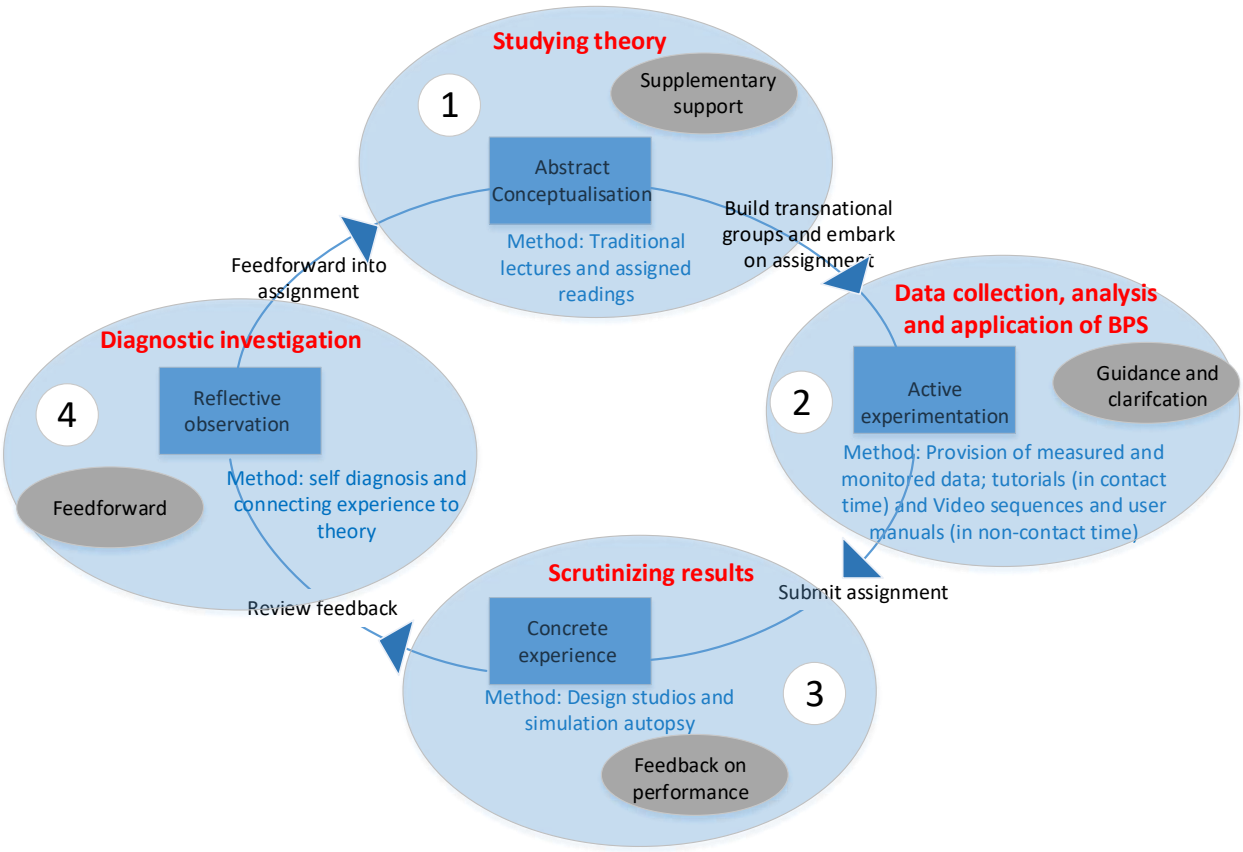

Fig. 1 – Framework continuous learning cycle. Adapted after Kolb

We believe that digital learning can be enhanced by incorporating experiential learning methods where learning is an iterative process which takes place through reflection on doing [5;6; 7]. Thus, we have designed an innovative learning cycle (see Fig 1-learning cycle) using digital practices to teach BPS in an experiential and reflective manner.

The four modes are briefly described as follows:

- **Concrete experience (CE)** involves learning how to scrutinize results and diagnose issues with measurements, monitoring and modelling of buildings. This can happen through direct feedback and through the examination and autopsy of simulation results in a group setting. The objective is to impact a certain degree of

scepticism in data and tools and to encourage greater scrutiny of simulation predictions.

- **Reflective observation (RO)** involves self-diagnosis and reviewing and connecting experience to theory. Through these activities students strengthen their understanding of building physics, models and simulation methods.
- **Abstract conceptualization (AC)** involves the study of data handling/ management, models and simulation methods through lectures, assigned readings, and group discussions. The objective is for the students to understand the theoretical implications of their choices of tools or alternate modelling methods, and to appreciate the uncertainties associated with analyses so that they can contextualize their findings.
- **Active experimentation (AE)** involves the application of methods and tools in workshops. This allows students to explore tools and alternate modelling methods to reinforce the theoretical studies.

To achieve our aim of the digital learning cycle, we have bridged the gap between BPS models (which act as a 'digital twin') and the real building by creating an interactive learning platform where students can access monitored data streamed live from the case-study buildings. This innovative shared learning platform helps to bring the three taught modules to life by allowing the students to better visualize real-world building performance data and then use this data to create accurate calibrated BPS models (which can then be compared to the real buildings). As such this process brings the digital realm closer to the reality which it seeks to model. This is an essential requisite in closing the 'performance gap' between BPS model predictions and real buildings [8]. In uniting these concepts (i.e. real-world building data with digital models) and placing them at the centre of our teaching approach we are facilitating a dialogue which seeks to embed state-of-the-art BPS practice with critical and testable thinking. This allows the students to learn experientially by developing virtual design experiments (using validated BPS models) to evaluate and inform complex design problems. Thus, we are able to use the same digital platform (and methodology) with buildings of different typologies, located in different geographic and climatic zones to focus our teaching on specific aspects of resilience (i.e. overheating, indoor air quality, daylight design, moisture control) (Fig 2-4 building case studies). Kolb's original learning cycle is therefore not only adapted to the context of teaching resilience and building performance simulation. It is also translated into a digital pan European teaching context, an approach that has not previously been investigated to the authors knowledge. The innovation here lies with the application of this method to diverse groups of students that are physically located in different universities and that are encouraged to follow this cycle together, remotely, whilst being solely reliant upon digital learning and communication tools.

2.1 Objectives

An understanding of the theory of thermodynamics underpins the application of simulation, and while it is possible through experiential learning to gain a deeper understanding of the subject, it is challenging (even for experienced users) to produce results that are transferable to the built environment. In fact, the user often becomes the greatest source of uncertainty in this process [9; 10]. To make the connection between simulation and reality clearer to students, one of the strategies adopted of late in building simulation teaching activities has been to couple simulation and on-site measurement assignments [11]. This approach has been beneficial in helping students to become familiar with uncertainty and risk in decision-making when building models and with the practicalities of the construction sector. However, as a result of COVID-19 restrictions, such measurement activities and field study work has now had to come to a halt, effectively breaking the learning cycle that had been built into building simulation teaching methods.

The objectives of our approach are as follows:

- to develop a digital Erasmus Programme to (i) address the continuing COVID-19 restrictions and limitations and (ii) to include those currently excluded and discouraged from participation in built environment disciplines for a variety of reasons;
- to provide a learning platform for Master students to complete a digital learning cycle in building performance and resilience;
- to offer a working environment in which students from multi-cultural and under-represented backgrounds can thrive, and one which enhances diversity, equality and inclusion opportunities;
- to challenge students to work in interdisciplinary and transnational teams to improve their social, communication and interpersonal skills;
- to learn from each other (through peer-to-peer and scaffolded learning) by being part of the assessment process and learning to constructively critique their peers' work.

2.2 Studio teaching

To challenge students to work in interdisciplinary and transnational teams to improve their social, communication and interpersonal skills we adopt the concept of studio teaching. Integrating the concepts of low carbon buildings, health and well-being and resilience, as well as the use of building performance simulation within the context of digital studio teaching allows a greater focus on project based work (compared with didactic lecturing). Experiential learning via project based work enhances the opportunity for communication between diverse groups of team members and with those outside one's own team. This concept is further strengthened by the use of interim team presentations (on work in progress) as well as via

peer-to-peer-critiquing of student work. In the past years, all these activities have been de-facto moved online, removing geographical constraints. The emphasis has shifted to the need to keep students actively engaged with their courses and with their peers. The use of whole building simulation in the context of an integrated design project demands input from interdisciplinary teams comprising diverse skillsets and perspectives. Thus, the design of the learning tasks and the way in which they are structured promotes both interdisciplinary and transnational participation with a significant emphasis on peer to peer learning.

3. The Learning Cycle

In the context of the digital Erasmus scheme, five different learning phases are incorporated in our pedagogical methodology following the four modes of learning (CE, RO, AC, AE) to accomplish the objectives (see Fig 1):

1. Study of theoretical underpinning concepts (AC).
2. Collection of data and creation of validated building performance models (AE).
3. Design of experimental studies to assess specific building performance problems (CE).
4. Analysis and interpretation of simulation predictions, including their scrutiny and verification (CE).
5. Interpretation and acting upon the information that has been generated through the previous phases of the process. Here students will be expected to consider both the building specific implications as well as the wider (policy and praxis) implications of their findings (RO).

For 1, we use modern flipped learning techniques using pre-recorded lectures and guiding students through assigned readings from the literature. These are supported by live tutorial sessions and study groups. Self-learning is supported through the reading of user manuals and the examination of exemplars, as well as video sequences illustrating certain aspects of measuring and monitoring data, as well as BPS tool operation.

For 2, the student teams collect key data that describe a case-study buildings performance including, measurement and monitoring data, occupant behaviour, and operational characteristics and learn to making decisions about which inputs should be provided to their models and which program defaults can be accepted.

For 3, the students need to assess different experimental methods which could be used to test their research hypothesis, such as the use of parametric studies to test and evaluate different design interventions. They also choose and apply specific tools relevant to their chosen investigation and will make choices between alternative modelling methods (e.g. methods to predict air infiltration or convective heat transfer coefficients) and simulation options (e.g. choice of time-step or methods for coupling calculation domains) to gain an awareness of model simplifications and the impacts of uncertainty.

For 4, student teams have to present their results in a (virtual) studio-based environment and demonstrate how they have made critical decisions and interpreted their results and relate this back to their understanding of the theory learned during the theoretical part.

For 5, we encourage the students to individually reflect on what they have learnt and then to share their experiences with the other students. This is an important step in the learning process and involves reflection upon what has been learnt. Here the students place their findings in a wider context (through considering a range of international contexts presented by other participants) and explore the wider implications of their findings in relation to national and international policy and praxis. Feedback is a critical input to support this experiential learning cycle. This is provided throughout the program via peer-to-peer interaction and also with the instructor or teacher. To this end, feedback (also known as formative assessment) is provided during each learning phase and at each iteration of the learning-cycle, as this provides the students with the opportunity to identify how they are progressing and where they may need to focus their attention in order to improve. Through this approach the students gain valuable additional experience in interdisciplinary team working and critical thinking, which are requisite skills for employment and further study in this field.

4. Different modules

Following the context of the project and its objectives and in line with the teaching framework, three new modules (each taught by one of the partnering universities) are proposed to challenge students to work in interdisciplinary transnational teams, in a digital manner, across borders thereby offering some of the benefits of the classical Erasmus 'year abroad' experience. This approach is designed to facilitate experiential and peer-to-peer learning by promoting collaboration and cooperation on live projects beyond conventional barriers. The learning format combines live data-streams from real buildings, with the use of validated simulation models of the same buildings in order to create a highly realistic and interactive learning environment. This concept helps to overcome the barriers imposed by the absence of site-visits and studio tutorials, which have been a common feature of experiential learning in the built environment. This learning format is designed to immerse the students in real-world problem solving and experimentation, commensurate with the attainment outcomes of master's level programs.

Through our Digital Erasmus approach, the students gain valuable additional experience in interdisciplinary working and critical thinking.

The three MSc level modules that were developed by the three institutions target their specific areas of expertise, focusing on the importance of the indoor environment, energy monitoring, and building simulation. This set of modules is considered crucial to the delivery of this integrated course. The modules

are targeted at master students in Architecture, Civil and Mechanical Engineering.

4.1 TU Delft (TUD)

The TUD "Technoledge Climate" module focuses on indoor comfort and associated physiological concepts. An important part of the teaching activities is traditionally dedicated to building surveys, where the students can collect spot measurements of comfort indicators, such as temperature, relative humidity, and illuminance. Due to the COVID-19 related restriction, the module was largely re-designed, and new innovative approaches were implemented so that students were able to engage with the experience of environmental surveys in existing buildings. Furthermore, existing content dedicated to daylight measurements and modelling required a substantial update which were implemented by staff participating in the project. Teaching concepts for visual comfort and advanced daylight modelling are essential for students to understand the importance of well-designed windows and shading systems. As complex technology advances in this field, students need to learn how to master the appropriate design tools to assess existing spaces accurately, using cutting-edge simulation methods delivered through appropriately scaffolded strategies.

Fig. 2 – Co-Creation Center Building, located in the TUD Green Village, The Netherlands

Tab. 1– Workshop and learning objectives (LO) for the Active Experimentation (AE) mode of learning at TUD

Workshop Topics Nr and title	Measurement rel. LO	IEQ rel. LO	BPS rel. LO
1.Indoor environmental quality survey	a,b,c	a,b,d	b
2.Design improvements and assessment	g	e	f,g

a, Refine how the indoor environment is experienced, looking at the existing building technology solutions with a critical mindset and identifying their shortcomings;
b. Relate changes in outdoor weather conditions to changes in the indoor environment and understand how this relationship is influenced by the building fabric and building systems;
c, Appreciate the differences in accuracy, precision and sensitivity between measuring instruments and sensors used for research/commercial purposes, and for spot-measures/continuous monitoring;
d, Appreciate the uncertainty in subjective evaluations of IEQ due to personal, seasonal, and daily variations;
e, Interpret IEQ questionnaire answers and extrapolate meaningful and representative results;
f, Recognise assumptions and model limitations that are embedded in BPS software and how they affect the virtual representation of the real building;
g, Propose improvements and/or alternative solutions to existing ones and assess their effectiveness using BPS

The two workshops organised within the module are an integral part of the module's structure and content. The students' progress is guided by expert tutors, and it is presented and shared with the class at multiple stages. During the module, the focus gradually shifts from the analysis of the case study building to the critical proposal of new design solutions. In this continuous framework, the two workshops act as catalysts for these two key learning phases. Most of the European building stock has already been built. Circular and sustainable building paradigms call for a well-planned re-use and refurbishment of existing buildings. In such a context, it is essential that students learn to critically assess building indoor performance and to think of creative and effective solutions that can reduce energy consumption while maintaining optimal indoor comfort conditions.

4.2 TU Graz (TUG*)*

TUG offers a module on Energy Monitoring and the Effects of Indoor Climate. In this module, students complement their existing knowledge in the field of energy-efficient construction with respect to the topics of energy monitoring and the impacts of indoor climate. Students get to know metrological concepts, to record the important thermal, hygric and energetic properties of the building envelope. They learn about the effect of the building's services and envelope on the indoor environmental performance and its interaction with user behaviour. This understanding of interconnected design factors allows them to better evaluate and interpret data that is captured as part of this module and accessible to students via the platform. The theoretical teaching uses the monitored operational data from the building to show the high potential for optimization of the built infrastructure. Students also learn how the indoor climate in buildings can be assessed in connection with building and ventilation systems using methods of comfort assessment. Measurement methods are introduced, to demonstrate how the room climate in real-buildings can be determined and evaluated experimentally, which can in turn be used to validate simulation models.
Researchers in academia are dealing with increasingly larger amounts of data. For this reason, students must learn to use the most appropriate

tools and understand various statistical and visualisation methods that allow them to examine and exploit large data sets to support their research projects and findings (Tab. 2).

Fig. 3 – TUG- Institute for building physics, services and construction (outside left and inside institute right), Austria

Tab. 2 – Workshop and learning objectives (LO) for the Active Experimentation (AE) mode of learning at TUG

Workshop Topics Nr and title	Measurement rel. LO	Resilience rel. LO	BPS rel. LO
1.Thermal comfort survey (Tableau)	a,b	a,b	b
2.Working with large data sets	d	c,d	c,d
3.Statistical analyses (R) of data sets	e,f	e.f,g	f,g

a. Understand sensitivity of thermal comfort survey data with respect to individuals, countries, continents and seasons;
b, Understand the differences between operative temperature, calculate using different equations and understand uncertainty when comparing to recorded data;
c, Understand and compile different weather formats for use in BPS;
d, Appreciate complexity of large data sets and understand how to identify, handle, reshape and clean incomplete data sets;
e, Understand various statistical and visualisation methods to examine, summarise and analyse environmental, climate and energy data;
f. Understand forecasting of indoor temperatures based on gas consumption, climate and environmental variables using linear regression;
g, Understand various error metrics of forecasting accuracy and model bias and understand their impact on predicted building performance.

The workshops at TUG have the objective of providing to students an overview and introduction to some commonly used tools that are used in academia and industry to work with data, identify some common pitfalls in data analysis and outline various methods to draw some meaningful insight from data. The workshops are structured into three parts: 1. Thermal comfort survey in Tableau; 2. Working with large data sets in R; and 3. Statistical Analysis of data sets in R.

In the first workshop, the student familiarises themselves with the use of Tableau which is an analytics software that is widely used in business intelligence. Due to its user-friendly drag-and-drop functionality, Tableau can be rapidly learned by students and allows them to create quick analyses and visualisations of existing data sets. The workshop allows the students to draw on knowledge of thermal comfort concept learned in the module's lectures and investigate the available data sets of the institute as well as one of the largest publicly available data sets on the subject, i.e. the ASHRAE Global Thermal Comfort Database II [12]. The latter contains thermal comfort data of various individuals that was gathered independently in many countries and continents in different seasons and buildings. This makes it an excellent exercise to test the capabilities of the software to produce quick dynamic visualisations and maps to get insights from the data set. In addition to the thermal comfort data, the students learn various approaches to derive the operative temperature from the observed environmental data.

In the second workshop, the students get an introduction to programming in RStudio to explore and analyse a large-scale monitoring data set. Learning to work efficiently with large data sets is becoming a necessity for young researchers. Spreadsheet programs (e.g. MS Excel) may be relatively easy to use, however, they have many limitations that are quickly becoming evident as soon as one attempts to open and analyse a large data set. In the second workshop, students learn the basics of programming in R/RStudio and how to load, clean and reshape a large data set which contains climate, environmental, and energy data. The exercise allows the students to experiment and exploit the power of R in handling, cleaning and reshaping massive amounts of data, exporting the findings with ease and compiling weather files for BPS.

The third and final workshop in this module builds upon the second one. In order to make sense of the large data sets and their analyses, the use of statistics and the creation of various plots is imperative to summarise the data and get some meaningful insights from it. This workshop teaches students some basic descriptive statistics, data analysis and how to exploit various types of plots to examine the data. Creating useful plots and communicating the findings is a necessary skill for every researcher and a prerequisite for most reports and publications. The workshop introduces the students to statistical data modelling and forecasting with the use of linear regression and various error metrics to evaluate the forecasting accuracy and bias of the developed models. Ultimately, the workshop allows students to understand the impact of model bias on the predicted building performance.

4.3 University of Strathclyde (UoS)

Building on existing knowledge in relation to static energy balancing methods, students at UoS acquire the necessary knowledge to carry out dynamic building simulations and to assess uncertainties. For this purpose, students gain knowledge about what is important at key points in the design process, depending on what the user wants to know when undertaking a building simulation (environment, building, plant, user). They will learn appropriate modelling approaches for the mathematical description of the corresponding heat and mass transfer processes. This includes a deeper insight into individual simulation modules, which students develop on their own by means of didactically suitable programming tools. Students implement their theoretical knowledge by modelling and simulating a reference building and calibrating it with the monitored data set from the UoS.

Fig. 4 – Test house, UoS; UK

Tab. 3 – Workshop and learning objectives (LO) for the Active Experimentation (AE) mode of learning at UoS

Workshop Topics Nr and title	Resilience rel. LO	BPS rel. LO
1.Building physics	f	a,b,c
2.Problem representation	d	a,b,c,e
3.Information management and analysis (R)	b,e,f	b,c,f

a, Understanding of heat and mass transfer processes occurring within energy supply and demand systems in the context of building performance modelling;
b, Understanding of simulation principles: problem representation, treatment of time and space, numerical methods, validation, use in practice;
c, Understanding of simulation practice: problem description, modelling methodology, results interpretation, case studies;
d, Understanding of built environment: energy demand, passive and active energy systems, options for intervention, performance assessment methods.; e, Understanding of renewable energy system modelling, focusing on supply-demand matching.,
f, Understanding of information systems: energy management, monitoring and targeting, classification techniques, trend analysis, smart metering and the role of these in calibrating simulation models.

5. Preliminary results

The project is at an early stage, but thus far with our pan-European approach to teaching building performance and resilient design we have produce the following results:

- an innovative knowledge exchange programme format, which will hopefully become a permanent offer of the partner universities (TUD, TUG, UoS), especially aimed at students who are not able to participate in traditional mobility programmes;
- an administrative procedure to enrol remote students from partner universities and to formally recognise their participation in courses in the form of the European Credit Transfer and Accumulation System (ECTS);
- the development of new, integrated digital procedures/ approaches and methodologies to facilitate the teaching of resilience and building simulation in the built environment;
- networking and learning about digital teaching methodologies and best-practice from colleagues in different institutions across Europe;
- construction of a shared web- and teaching platform and database with environmental data available for teaching purposes;
- building models that facilitate the analysis of outcomes on indoor environmental quality, energy, behaviour and future resilience;
- feedback from student and staff participants to further enhance existing programmes;
- action based pedagogic research leading to journal and/or conference publications, project report and brochure.

Additionally, we are actively working towards the sustainability and retention of the project's outcome for future use, so that it will be easier for institutions outside the partnership to embed the Digital Erasmus format in their permanent offer.

6. Conclusions

The presented pan-European approach to teaching building performance and resilient design creates a pedagogic framework for a digital Erasmus learning experience which can be used as a roadmap for other programmes in the STEM sector to follow.
Beyond the innovative methodological aspects of our program there are several wider reasons that this approach provides in breaking down conventional barriers to higher education in the construction and built environment sectors, which to date have been heavily male dominated disciplines.
Because of the partial anonymity and enhanced flexibility provided by digital learning we hope to break down many of the barriers which have hitherto prevented under-represented groups from engaging in higher education, particularly in this subject area.

We expect that the opportunity to undertake transnational studies using an interactive approach will appeal to those who might not have had the opportunity to consider this in the past and that the project will provide them with as close to an immersive experience as is possible in a digital realm. This new set of modules will provide opportunities to analyse buildings in a high level of detail - both theoretically, and from an end user perspective whilst focusing on three different aspects of resilient design. The project provides an opportunity for students to work collaboratively and transnationally, whilst exploring solutions in a supportive risk-free environment. This enables them to develop a deep knowledge of building performance and resilience, scaffolded by world-class facilities and expert knowledge.

7. Future work

We aim to target the following three steps in the future:

1. With the Covid pandemic hopefully coming to an end, it is apparent that in-class teaching will once again be prioritised in the future. This means that students will be back in attendance mode with the possibility to conduct measurements and make site visits in person. In order to maintain the flavour of the pan-European digital Erasmus year under these new circumstances we will look to new ways of incorporating hybrid teaching modes that will allow students to continue collaborating between the different partner countries, without losing the richness and diversity provided by the Erasmus+ experience.

2. At UoS we found out that despite the availability of some of the teaching materials to architecture students there has been a lack of uptake in comparison to students with a background in mechanical engineering. We would like to explore why that might be in the future and to broaden the appeal by linking the teaching of tools with some of the practical issues that the students might be faced within the real world. While we are hoping for uptake from existing student cohorts we also expect to see interest from qualified architects and engineers in the future.

3. In the near future, we aim to create close links to the professional body of the International Building Performance Simulation Association (IBPSA) to support the impact of this project by linking the IBPSA-academy and various other organisational activities to the work that is carried out within the student teams.

7. Acknowledgment

The Digital Erasmus project has been funded with the support of the Erasmus+ Programme (grant agreement no.: 2020-1-AT01-KA226-HE-092643) of the European Union. This publication reflects the views of its author(s) only and the European Commission cannot be held responsible for any use that may be made of the information contained herein. Dr Brembilla would like to acknowledge the TU Delft coordinator of the "Technoledge Climate" module, Dr Regina Bokel, and other colleagues involved in the module teaching.

References

[1] Guardian, Focus on sustainable change': tackling sexism in civil engineering, 2019 https://www.theguardian.com/careers/2019/jun/25/focus-on-sustainable-change-tackling-sexism-in-civil-engineerin

[2] Beausoleil-Morrison, I. and Hopfe, C. J. 2016. Teaching building performance simulation: ever done an autopsy? IN:The 3rd Building Simulation and Optimization 2016 (BSO2016), Newcastle University,Sept12-14th.

[3] Hopfe, CJ, Soebarto, V, Crawley, D., Rawal, R. Understanding the differences of integrating building performance simulation in the architectural education system. IBPSA conference San Francisco, 2017, www.ibpsa.org

[4] McLeod, RS, Hopfe, CJ. Experiential learning in Building Physics- the icebox challenge, Journal of Building Physics. Volume: 45 issue: 3, page(s): 391-401, 2021.

[5] Kolb, D. Experiential Learning: Experience as the Source of Learning and Development. second. Pearson FT Press, 2015, Available at: https://www.pearson.com/us/higher-education/program/Kolb-

[6] Felicia, P. Handbook of research on improving learning and motivation through educational games: multidisciplinary approaches. IGI Global (701 E. Chocolate Avenue, Hershey, Pennsylvania, 17033, USA), 2011.

[7] Kolb, D. Experiential Learning: Experience as the Source of Learning and Development. 2014, Pearson FT Press, 2nd edition.

[8] DeWilde, P. Understanding the differences of integrating The gap between predicted and measured energy performance of buildings: A framework for investigation, 2014. Automation in construction 41, 40-49

[9] Beausoleil-Morrison, I. and Hopfe, C. J. 2015. Teaching building performance simulation through a continuous learning cycle. In Proc. Building Simulation 2015, pages 2757–2764, Hyderabad, India.

[10] Mantesi, M., Hopfe, CJ, Cook, MJ, Glass. J, Strachan, P., The modelling gap: Quantifying the discrepancy in the representation of thermal mass in building simulation - Building and Environment, 2018

[11] Beausoleil-Morrison, I. and Hopfe, C. J. 2016. Developing and testing a new course for teaching the fundamentals of building performance simulation. InProc. eSim 2016, Hamilton, Canada.

[12] Földváry Ličina, Veronika et al. (2018), ASHRAE Global Thermal Comfort Database II, Dryad, Dataset, DOI: https://doi.org/10.6078/D1F671. *Data sharing not applicable to this article as no datasets were generated or analysed during the current study*.

Closing the Knowledge Gap on Circularity: the CBE Hub Lifelong Education Programmes

Olga Ioannou [a], Tillmann Klein [b]

[a] Assistant Professor, Chair of Building Product Innovation, Department of Architectural Engineering and Technology, Faculty of Architecture and the Built Environment, Delft University of Technology, Delft, the Netherlands, o.ioannou@tudelft.nl

[b] Professor Chair of Building Product Innovation, Department of Architectural Engineering and Technology, Faculty of Architecture and the Built Environment, Delft University of Technology, Delft, the Netherlands, t.klein@tudelft.nl

Abstract. This paper discusses the relevance of academia in addressing complex contemporary issues and more specifically, its potential to help society transition to a circular built environment. Can academia provide society with a safe space for developing imaginaries and socially performing alternative political futures? Can it help reconnect the many knowledge domains that appear now to be dispersed and fragmented? And what is the role of adult learning in achieving this transition and in dealing with complex issues such as sustainability? The typology and goals of adult educational modules developed by the Faculty of Architecture and the Built Environment of TU Delft and in particular the Circular Built Environment (CBE) Hub are presented here as a response to the growing need of creating synergistic alliances between academia and the rest of society. Three different typologies are examined in this chapter for their specific contribution in raising awareness; inspiring professionals and instigating change in attitudes as well as contributing to the training of selected groups of stakeholders respectively. Authors reflect on the benefits of such interaction, its limitations as well as its future potential. Promoting the benefits of transitioning to a circular built environment and reaching the widest audience possible to assist with the transition requires that academia develops new educational formats. Attention should therefore be given not only to the content produced, but also to the modes of delivery; the effectiveness of the message that is ultimately delivered as well as the establishment of a continuous presence where different individuals or groups can return to when challenged by complex issues. Consolidating this relation can close the knowledge gap between the two: on the one hand society directly benefits from academic research, on the other hand, academia becomes more relevant for society.

Keywords. Circularity in the built environment, adult education, lifelong learning, TU Delft
DOI: https://doi.org/10.34641/clima.2022.215

1. Introduction

One of the major contemporary challenges is addressing the discrepancy between the societal desire for economic growth and the ecological repercussions of growth. The complexity of the task at hand is further accentuated by the perseverance of the objectivist fragmentation of the world into isolated objects that become understandable only when abstracted from context: the usefulness of the vast amount and various forms of knowledge modernity generated, has been compromised by quarantining it into specialist silos (1). This extreme compartmentalisation of knowledge, keeps most people from understanding the basics of how the world works rendering the overhauling of educational systems a necessary condition for obtaining a wider cross-disciplinary perspective (2). However, as the relevance of the role of education increases, academia faces a challenge of its own: that of carrying out research that can induce change with a wider societal input (3).

In this context, the re-emergence of circularity and in particular, circular economy as an organizing principle for managing the constraints of the assimilative capacity of the environment holds a fair promise: founded on both theoretical and technical background knowledge, circularity has a highly interdisciplinary character (4) marking the need to consider them in a systemic manner. Furthermore, it requires that the technical knowledge base produced

Copyright ©2022 by the authors. This conference paper is published under a CC-BY-4.0 license.

will be connected to business, organization and management study research communities further highlighting its social character (5). However, despite its premise and its increasing popularity, it is still a concept in-the-making and thus it needs to be dealt with caution; otherwise, any attempt to approach it risks being superficial.

For architecture schools in particular, the question now becomes whether they can provide with a safe space to facilitate the transition to a circular built environment. If so, how can architectural education and also adult, professional education, contribute to the better understanding of circularity and its wider dissemination across individuals and organizations? Can it help enhance the relevance of academia within society by establishing a new cooperative ethos? This paper argues for the potential of circularity to constitute a future vision and the socially performative role of academia in assisting this vision to materialize. It also describes how CBE Hub has conceptualized and organized its life-long learning programs in order to address the needs of multiple different learners' communities and to also benefit from this interaction.

2. Circularity: a concept promoted, contested, and imagined

What it is, what is the scale of it | Circularity "conceptualizes the integration of economic activity and environmental wellbeing in a sustainable way" (6). Circular principles have been fully embraced by China since the 1970's as their official state-led development goal (7). Western economies reflexes have been slower to catch up, however, nowadays, EU policies cannot afford not to mention circular economy (CE) (8). Circularity and CE are often used interchangeably, but how do they specifically relate to the built environment? CBE Hub members describe the Circular Built Environment (CBE) is a system designed for closing resource loops at different spatial-temporal levels by transitioning cultural, environmental, economic & social values towards a sustainable way of living. Alongside this definition, CBE Hub members claim that circularity pervades the built environment across (at least) six scales: from materials and components, to buildings and neighbourhoods, all the way to cities and regions (9).

Challenges | Despite its wide dissemination, circularity still remains a relatively young field of research and therefore it is often scrutinized for its conceptual fragmentation and lack of clarity in implementation, whereas circular innovations are considered to be hard to scale up (10). Circular economy in particular, is heavily criticized for rebooting and reforming capitalism where citizens are still considered predominantly as consumers and whose civic duties are performed primarily via consumption (11).

The technical and social divide | In this light, one of the major challenges lies in determining how circularity impacts society. In policy and business development, for example, CE is expected to provide high value materials cycles and therefore current research focuses more on the practical and technical levels; however, from a scholarly position, values and societal structures and the paradigmatic potential of CE remain largely unexplored (10). Marin & de Meulder (12) distinguish between what they call the 'objectivist' and 'constructivist' frameworks of circular economy: whereas in the first case they foreground technology and entrepreneurship, in the latter, they drive attention to practices of sharing, re-using and collaborating leading to either technocratic or political positions respectively.

The potential of circularity as a future vision | Casson and Welch (13) call circular economy an "imagined future" that informs and motivates different areas of the social world through "a range of rhetorical, representational, organizational and material activities". But in order for these imaginaries to materialize, claim Volker et al. (8), they need to be collectively held, institutionalized and publicly performed.

3. The socially performative role of academia and the importance of adult education

Academia provides a framework for such imaginaries to be discussed not only as managerial or technocratic issues, but also as "politics of the future" and thus focus on the social processes and practices that allow imaginaries to become socially performative (14). "Our academic profession," Gümüsay & Reinecke argue (15), "is uniquely placed to do so because of our distinct ethos that is not driven by profit objectives but rather by scientific and societal norms."

A safe place to do dangerous things | School educates, say Hughes and Lokko (16), but training is a lifelong process happening after that. The two women, however, go beyond this statement; "inverting growth and our relationship to waste," they argue, highlight our need to have "safe places to do dangerous things" (ibid). On a similar line of thinking, Callan (17) claims that a good education challenges settled beliefs and values and subjects them to critique ultimately making learners intellectually unsafe.

Sustainability in education | Considering academia as a safe space to experiment becomes even more relevant for matters of high complexity such as climate change or resource depletion that require out-of-the-box approaches. Sustainability is already tied to education via the SDG goals; target 4.7 in particular stipulates that by 2030, Member States should ensure that:

all learners acquire the knowledge and skills needed to promote sustainable development, including, among others, through education for sustainable development and sustainable lifestyles, human rights, gender equality, promotion of a culture of peace and non-violence, global citizenship and appreciation of cultural diversity and of culture's contribution to sustainable development (18).

Combines practical and social benefits | Adult education research shows an immense potential of adult learning programs in achieving higher outcomes and has a range of non-economic benefits: there is strong evidence that adult learning contributes to changes in attitudes and behaviours that promote social capital and, possibly, social cohesion (19). Adult learning, say Abedini et al., (20) is a lifelong process whereby knowledge is formed through the transformation of adults' experience. The strength of adult education in particular, is its dual epistemological mandate to meet practical learning needs of individuals, groups, and systems while also attending to inclusion, representation, participation, critical reflectivity, and diversity amid unity (21).

4. The CBE Hub life-long learning programmes

Ever since its establishment in 2017, Circular Built Environment (CBE) Hub is focused -just like its name implies- on exploring the impact of circularity to the built environment. Counting more than sixty members from different departments and knowledge domains, CBE Hub has been able to collect significant evidence and to consolidate a body of knowledge on how circularity manifests across scales and across different aspects. Building on this experience, the Hub has been involved in a series of key activities, all aimed at promoting research and education both for on-campus students, as well as for professionals and adults.

Lifelong education holds a central position in CBE Hub activities developing different types of educational formats in this direction. Although the term was introduced as early as 1929 by Yeaxlee, it has only become more pertinent as late as the 1970's when learning became responsive to the demands of globalization and the transition of the industrial society to the knowledge society (22). Lifelong education now signals every institutionalized learning opportunity that has a humanistic basis and can occur at any stage in the life span (ibid).

For CBE Hub, lifelong learning programs regard different audiences both in kind and in number as well as multiple mediums of communication and with varied impact. Below, follows a taxonomy of the main online learning offerings of TU Delft's Faculty of Architecture and the Built Environment. These range from the more standard modules such as Massive Open Online Courses (MOOCs) to more tailor-made learning settings that target specific communities. Collective learning is key to enhancing the transformative capacity of cities: this requires transdisciplinary approaches, in which universities interact with societal stakeholders also in defining their research questions (23). It is also key for closing the knowledge gap between different stakeholders thus enabling the implementation of EU circular objectives as these are expressed in the new CE 2020 action plan. Afterall, imaginaries are more likely to emerge as collectively performed ideas of desirable futures if actors are brought together in new settings for that repositioning allows them to break out of the 'scene-act-ratio' of their institutional routines (24).

4.1 Typology of interaction

Massive Open Online Courses (MOOCs) | Ever since their original appearance almost a decade ago, MOOCs have presented institutions with numerous opportunities to broaden their audience and to help them rethink and redesign their pedagogical approach (25). A series of MOOCs that focus on circularity in the built environment have been launched by the Faculty of Architecture and the Built Environment since 2019, such as the "Circular Economy for a Sustainable Built Environment" MOOC. These modules were designed to appeal to a large international audience consisting of individuals interested in learning more about circularity across different scales: all the way from products to buildings, to cities, and regions. In this regard, their premise lies mainly in raising awareness on the subject, while also allowing for an informal exchange between learners that in turn helps them identify how circularity manifests around the globe.

Fig. 1 – First MOOC in collaboration with the Faculty of Industrial Design and Engineering at TU Delft (left) and perhaps the most popular MOOC on circularity in the built environment with more than 12,500 viewers worldwide (right).

Professional Education Courses | Members of the CBE Hub have also been experimenting with yet another online learning format: that of Professional Education courses (ProfEds). These modules are more focused on a specific scale and have been developed around the idea of addressing

professional cohorts exclusively. Therefore, they are more effective in providing customized frameworks per sector or per industry. CBE Hub is currently running one ProfEd course for the product scale and another one for the regional scale. Whilst the first targets professionals from the building products' industry, the latter focuses more on individuals or groups involved in administration bodies. ProfEd cohorts are designed to be limited in number; thus, learners' exchange is more direct and feedback is more precise and systematic.

Fig. 2 – There are two Professional Education courses available by the Faculty of Architecture and the Built Environment: the first focuses on the product scale (left) and the second on the regional one (right)

Planned Collaboration Programmes (PCPs) | Based on the experience of Professional Education courses and the increasing needs of companies to stay up-to-date with the latest developments in circular thinking and practice, the Hub has also engaged in what is called Planned Collaboration Programmes (PCPs). PCPs are based on direct interaction and exchange between academia and industry partners while focusing on one topic only. They can be held either online or in live meetings and they mainly consist of one-day long structured sessions that alternate between workshops and short lectures. Their strength lies in contextualizing the circular discourse around the participating companies' challenges, thus enabling the creation of more nuanced, individual approaches for each one of them respectively. CBE Hub has already run two PCPs: one on remanufacturing and another on reverse logistics for facades.

Fig. 3 – Planned collaboration programmes that have been implemented and funded by the EIT Raw Materials include one on Reverse Logistics for Façades (left) and another on Remanufacturing (right).

4.2 Aims and goals

TU Delft has a long-standing tradition of online learning. However, there are several reasons why the CBE hub has engaged in trying out new educational formats. Each new type represents an attempt to reach a different audience, but also to increase the efficiency of the mutual exchange. Here are some of the key motives behind the Hub's educational initiatives.

Integration of design and engineering knowledge into decision-making processes | Engineering studies are said to constitute the biggest body of knowledge behind CE, however, they are not related to studies typical for social sciences and thus cannot lead to a paradigm shift (5). Circularity asks for systemic change and therefore also requires political intervention to some degree. This is why rethinking how knowledge gets mobilized for politics in an effective manner is essential and there is a need to engage people more viscerally in conversations about the future (24). Educational modules such as the ones described earlier provide with a means to openly communicate knowledge to a large audience thus raising awareness, but also -and most importantly- to specific individuals in key positions with the operational capacity to apply the knowledge in more strategic decision-making processes.

Create shared understanding, identify barriers, provide alternatives | All content included in the educational modules developed by the CBE Hub feeds directly from the Hub members' ongoing research. One of the Hub's main task then becomes systemizing those findings according to its own modelling of circularity in the built environment in a consistent narrative. What comes out of this process is later integrated in the various educational modules and the school curricula and even adapted depending on the type of the module. This is one critical point for making meaning, but still largely dependent on academic validation only.

Communicating the Hub's academic research to professionals in educational environments helps disseminate this knowledge to a bigger audience. But it can also provide with significant input as academic knowledge gets contested by the participants' experiential knowledge. Testing academic research against real-life examples through learners' interaction, helps identify its weaknesses, or shed light to various points for improvement. Furthermore, sharing notions of circularity across a wide array of stakeholders can help identify potential implementation barriers at multiple levels. At times, it can also lead to novel ideas.

In this light, academia informs practice of the ongoing research, and practice reciprocates the input

by contextualizing and situating this research in real case scenarios. This is why it is important that educational modules content meet the requirements of specific learning groups. This ensures that: a. the information is properly communicated to the designated audience; b. what is exchanged is pertinent to the participants' interests and abilities in so far as they can assess the validity of information exchanged and constructively contribute to any further discussion about it and thus, c. the relevance of exchange remains high throughout the duration of the course.

Creating a community and a new cooperative ethos | The social nature of cognition is seen as influential to adult learners' construction of knowledge (26,27,28) whereas dialogue is considered to be key to meaning-making processes (29). In the early 1980's Wenger's "Communities of Practice" and Lave's "Situated Learning" theories further promoted that learning takes place "through the communication and participation of members within a community" (ibid). The notion of community persists: in recent years, internet and the proliferation of digital technologies for learning caused learning communities to expand to the online realm. One of the major repercussions of this is that learning in the online environment has consistently challenged traditional modes of delivery and exchange giving way to multiple formats for fostering meaningful community interaction online. In that regard, CBE Hub learning offerings do not solely focus on delivering the technical knowledge produced within the Faculty, but also on creating different types of active learning communities at different scales.

Besides sharing educational content on circularity, CBE Hub programmes' set ups seek to implicitly establish active learning communities and ultimately distil the practice of working together with societal agents as a means for understanding and managing complexity. Participants in ProfEd courses for example are invited to check out their peers' projects and to also carry out live discussions on topics related to the learning objectives of the course during live webinars. This is why the experience of running this type of courses, is completely different every time largely depending on the profiles of the members of the cohort. Courses of this type that are addressed to either industry or administration professionals not only are built to allow direct exchange but they actually rely on it in order to provide learners with an opportunity to benefit from each other's knowledge.

5. Discussion: what we've learned so far, what we need to tend to in the future

Change is possible | Integrating circularity in educational modules such as the ones discussed in this paper can lead to both formal and informal meaningful exchanges, contribute to a deeper understanding of circularity and even instigate change. Whereas audiences that only have a general interest in the subject can reflect on the implications of circularity on a more personal level, companies or organizations can significantly alter their status quo once exposed to academic research that is relevant to their scope. Planned collaboration programmes and to a certain extent ProfEd courses attest to that.

Limitations | There are, however, aspects that require special attention: one is assuring that all parties in the conversation are fairly represented: Schreiber-Barsch & Mauch (30) call this, "not only raising but also hearing voices as part of a dialogue in equal terms." Furthermore, in order to engage in conversation with an outside audience, academia needs to translate its work accordingly. Thus, every different type of module requires a revisiting of the format and the language to match the audience it addresses. Lastly, modules should always be susceptible to change themselves; their makers need to continuously evaluate the effectiveness of communication as well as the quality of exchange. As not all modules are efficient for all audiences, the weight falls primarily on academia to experiment with innovative formats and to determine new pedagogies for learning.

Future challenges | MOOCs as well as other online learning formats have enabled a free flow of information on different knowledge domains, however, as Barber et al., (31) argue, "current innovation and emergent thinking are taking place at the boundaries of disciplines, making traditional departmental silos a barrier to progress." In that regard, the task of academia needs to provide with innovative models that include and transcend traditional boundaries. CBE Hub learning communities of the future should be able to become more diverse and open up to an even wider spectrum of domains of expertise.

6. Conclusion

The understanding of circularity as well as its further development and integration are highly reliant on open cooperation between involved parties. CBE Hub has been trying to provide with different types of safe learning spaces that allow this concept to be socially performed. By proliferating courses in number, in kind and across different topics these courses also aspire to establish a continuous presence for academia and by that to rally different individuals or groups around the act of learning and working together with others as a means of tackling today's complexity and uncertainty. This is a time that challenges academia to reimagine its own future role and to explore its own potential in assisting the transition to a circular built environment. In that regard, CBE Hub efforts focus on transcending the traditional academic role of producing technical knowledge and strengthening circuits of capital towards also establishing new circuits of meaning

and values amongst affected stakeholders and society in general.

7. References

1. Buchanan, P. (2018). Reweaving Webs of Relationships. e-flux Architecture, overgrowth. Available from: https://www.e-flux.com/architecture/overgrowth/221630/reweaving-webs-of-relationships/
2. Ehrlich PR, Ehrlich AH. Solving the human predicament. Int J Environ Stud. 2012 Aug;69(4):557–65.
3. LERU Position Paper. Productive Interactions: Societal Impact of Academic Research in the Knowledge Society. 2017 March. Available from: https://www.leru.org/publications/productive-interactions-societal-impact-of-academic-research-in-the-knowledge-society.
4. Wiesmeth H. The circular economy – Understanding the concept. In: Implementing the Circular Economy for Sustainable Development [Internet]. Elsevier; 2021 [cited 2021 Dec 13]. p. 11–8. Available from: https://linkinghub.elsevier.com/retrieve/pii/B9780128217986000028
5. Korhonen J, Nuur C, Feldmann A, Birkie SE. Circular economy as an essentially contested concept. J Clean Prod. 2018 Feb;175:544–52.
6. Murray A, Skene K, Haynes K. The Circular Economy: An Interdisciplinary Exploration of the Concept and Application in a Global Context. J Bus Ethics. 2017 Feb;140(3):369–80.
7. Mathews JA, Tan H. Progress Toward a Circular Economy in China: The Drivers (and Inhibitors) of Eco-industrial Initiative. J Ind Ecol. 2011 Jun;15(3):435–57.
8. Völker T, Kovacic Z, Strand R. Indicator development as a site of collective imagination? The case of European Commission policies on the circular economy. Cult Organ. 2020 Mar 3;26(2):103–20.
9. Ioannou O, Geldermans B, Klein T, Konstantinou T, Overschie M, Wandl A. Integrating Circularity in Education: the CBE Hub Approach at the Faculty of Architecture and the Built Environment, Delft University of Technology. BK Books.
10. Corvellec H, Stowell AF, Johansson N. Critiques of the circular economy. J Ind Ecol. 2021 Aug 17;jiec.13187.
11. Hobson K, Lynch N. Diversifying and de-growing the circular economy: Radical social transformation in a resource-scarce world. Futures. 2016 Sep;82:15–25.
12. Marin J, De Meulder B. Interpreting Circularity. Circular City Representations Concealing Transition Drivers. Sustainability. 2018 Apr 24;10(5):1310.
13. Casson C, Welch D. Histories and Futures of Circular Economy. In: Bali Swain R, Sweet S, editors. Sustainable Consumption and Production, Volume II [Internet]. Cham: Springer International Publishing; 2021 [cited 2021 Dec 6]. p. 35–54. Available from: https://link.springer.com/10.1007/978-3-030-55285-5_3
14. Oomen J, Hoffman J, Hajer MA. Techniques of futuring: On how imagined futures become socially performative. Eur J Soc Theory. 2021 Jan 27;136843102098882.
15. Gümüsay AA, Reinecke J. Researching for Desirable Futures: From Real Utopias to Imagining Alternatives. J Manag Stud. 2021 May 6;joms.12709.
16. Hughes F, Lokko L. A school willing to take risks. Architectural Review 2021.
17. Callan E. Education in Safe and Unsafe Spaces. Philos Inq Educ. 2020 Jul 15;24(1):64–78.
18. UN General Assembly, Transforming our world : the 2030 Agenda for Sustainable Development, 21 October 2015, A/RES/70/1, available at: https://www.refworld.org/docid/57b6e3e44.html [accessed 4 January 2022]
19. Feinstein L, Centre for Research on the Wider Benefits of Learning (London E. The contribution of adult learning to health and social capital. London: Centre for Research on the Wider Benefits of Learning; 2003.
20. Abedini A, Abedin B, Zowghi D. Adult learning in online communities of practice: A systematic review. Br J Educ Technol. 2021 Jul;52(4):1663–94.
21. Nicolaides A, Marsick VJ. Understanding Adult Learning in the Midst of Complex Social "Liquid Modernity": Understanding Adult Learning in the Midst of Complex Social "Liquid Modernity". New Dir Adult Contin Educ. 2016 Mar;2016(149):9–20.
22. Jarvis P, Jarvis P. Adult education and lifelong learning theory and practice. London: RoutledgeFalmer; 2004.
23. Dirth E. Imagining Urban Futures: Inaugural Festival of the Urban Futures Studio. Universiteit Utrecht, March 16-17, 2017. Available from:
24. Hajer MA, Pelzer P. 2050—An Energetic Odyssey: Understanding 'Techniques of Futuring' in the transition towards renewable energy. Energy Res Soc Sci. 2018 Oct;44:222–31.
25. Hollands F M, Tirthali D. MOOCs: expectations and reality. Full report. Center for BenefitCost Studies of Education, Teachers College, Columbia University, NY; 2014.
26. Vygotzky L. Thought and Language (revised edition). Cambridge, MA: MIT Press; 1986.
27. Bandura A. Social Learning Theory. New York: General Learning Press; 1971.
28. Zimmerman BJ. A social cognitive view of self-regulated academic learning. J Educ Psychol. 1989;81(3):329–39.
29. Stacey E, Smith PJ, Barty K. Adult learners in the workplace: online learning and communities of practice. Distance Educ. 2004 May;25(1):107–23.
30. Schreiber-Barsch S, Mauch W. Adult learning and education as a response to global challenges: Fostering agents of social transformation and sustainability. Int Rev Educ. 2019 Aug;65(4):515–36.
31. Barber M, Donnelly K, Rizvi S. (2013). An Avalanche is coming: Higher Education and the Revolution Ahead. Available from IPPR, Institute for Public Policy Research Report. https://www.ippr.org/publications/an-avalanche-is-coming-higher-education-and-the-revolution-

ahead

Data sharing not applicable to this article as no datasets were generated or analysed during the current study.

A New Learning Programme to Facilitate nZEB Implementation

Florin Bode [a,b], Ilinca Nastase [a], Mihnea Sandu [a],Cristiana Croitoru [a] ,Horia Petran[c]

[a] CAMBI Research Center, Building Services Faculty, Technical University of Civil Engineering of Bucharest, Bucharest, Romania, Mihnea.sandu@utcb.ro

[b.] Department of Mechanical Engineering, Technical University of Cluj Napoca Cluj, Napoca, Romania florin.bode@termo.utcluj.ro

[c] National Institute for Research & Development URBAN-INCERC, hp@incerc2004.ro.

Abstract. The goal of nearly zero-energy can be achieved nowadays with existing technologies and practices, but the concept is still unfamiliar and elusive in most of the European countries, considering the whole process chain, despite all previous initiatives in this direction. At this moment there are still barriers in the value chain, making the nZEB concept difficult to arrive at the final users. The nZEB market analysis at European level reveals a significant gap between the countries with a high level of implementation and those which are not so well performing, and which remain more and more behind. To overcome this, a new learning programme to facilitate the nZEB implementation, has been launched in 2021 with the main objective to create support mechanisms and stimulating the development of skills frameworks by new market driven mutual recognition training and certification scheme for nZEB deployment that will facilitate the necessary legislative changes.

Keywords. nZEB, nZEB learning programme, nZEB implementation
DOI: https://doi.org/10.34641/clima.2022.430

1. Introduction

Buildings account for 40% of total energy consumption in the EU and generate 36% of the greenhouse gases in Europe (1). These are resulted from construction, usage, renovation and demolition of these buildings.

According to the European Energy Efficiency Plan 2011 (2), the greatest energy saving potential in order to lower the energy consumption lies in buildings. This is because 75% of the EU's building stock is still energy inefficient and the rate of building renovation remains very low at around 0.4% to 1.2% per year. To meet EU climate and energy objectives, the current rates of renovations should at least double. Also, the annual new buildings growth rate is assessed at around 1% in the European residential sector (3). The decrease in the rate of new constructions in the last decade is mainly due to the financial crisis of the construction sector.

The Energy Performance of Buildings Directive (4) (EPBD)'s specific concept, "nearly Zero Energy Buildings" (nZEBs), has now become a critical requirement for the building sector, along with the challenge for the architects and designers who are divided between keeping up with indoor environment quality standards and solutions for decreasing energy consumption (e.g. airtight buildings). New harmonizing solutions are thus required. Optimising indoor environmental quality with energy reduction is essential for the new buildings and in solving the problem for the existing buildings that are not meeting the expected performance. These buildings can drive occupants to take actions that may compromise the energy economy of the building. In the new context, occupant's comfort and health is one of the key drivers to stimulate the renovation and quality new construction market.

The goal of nearly zero-energy can be achieved nowadays with existing technologies and practices, but the concept is still unfamiliar and elusive considering the whole process chain, despite all previous initiatives massively financed by European Union. There are still barriers in the value chain, making the nZEB concept difficult to arrive at the final users. This discrepancy is even higher when compared within different countries.

A significant problem in the nZEB process is the performance gap between the designed and actual

Copyright ©2022 by the authors. This conference paper is published under a CC-BY-4.0 license.

energy performance in buildings. Main reasons behind that are: inadequate design, bad quality of the construction work, lack of soft landings, lack of continuous commissioning after the installation has been handed over, lack of proper use of systems and implemented technology, lack of understanding of how the technologies work, too general information in O&M manual, difficulties in changing users' previous behaviour etc. Even if, due to EPBD implementation, the public buildings should already be nZEB, the designers still do not know how to apply the nZEB requirements as indicated in the legislation because these are still not clearly linked to the current construction laws.

Results show that feasibility studies will not be focused on nZEB criteria but rather on the classical building functionality. Moreover, based on the feasibility study, tender specifications are further created for design and execution contracts, but usually the design is considered only based on classical construction requirements. Thus, the result is a technical design which is not for nZEB, even if it should be, and being at high risk during execution phase to be blocked by the beneficiary consultant or inspector. This is a classical story of the construction market in Romania. Bulgaria encounters same problems. It could have another version in Poland or Portugal. In Poland for example, the nZEB legislation is not really challenging. The nZEB uptake is driven by bottom-up initiatives, which however are not very frequent due to the lack of tender specifications with higher energy performance. On the other hand, some more advanced countries demonstrate a higher degree of nZEB level, despite of the existing specific barriers. These stories show how a two-speed Europe is represented in the nZEB and energy efficient construction field, leading to gaps and an unharmonized market.

Moreover, these barriers are considerably more important in the residential field, where the concerned end users do not have the information on materials, construction technologies (or renovation packages) and available funding opportunities. Thus, the market is missing important pieces from the nZEB puzzle, like skilled building professionals, across the whole building design, operation and maintenance value chain, ready to implement nZEB concept.

Although legal obligations are provided in the National legal framework by transposing the provisions of the 2010/31/EU Directive, the Nearly Zero Energy Building (nZEB) concept does not seem to be easily applicable yet in many countries from EU. Previous research showed that defining the cost-feasible optimal integration of the technologies suitable for nZEB and the skills gaps experienced by the building sector are among the most important barriers. While the current qualification courses and training schemes are still generally, there are still at a level of not satisfactory and underdeveloped to face the challenge of effective nZEB implementation, the requalification to skilled professionals for renovations and the new constructions of buildings. Despite strong political push towards nZEB and deep energy renovation, the traditionally conservative real estate market is still slow in the uptake of the new building standards and practices, especially in the residential sector. Considering our built environment, the policy efforts are hardly being transposed to more sustainable and environment-friendly lifestyles, and the benefits of nearly zero-energy buildings in terms of comfort, health and well-being are still widely unknown for the broader audiences, being left out of the media attention.

It can be observed that there are several causes that contribute to the difficult application of nZEB criteria in buildings in EU member states. The need to address these issues has become a necessity to increase the level of application of nZEB. For this, a new programme to facilitate the nZEB implementation, has been launched and financed from 2021, in the frame of a H2020 project (5). The main goal of the project is to support the increase of the market readiness for an effective nZEB implementation and to stimulate the demand for energy related skills and is oriented toward three different pillars: awareness, training, and support, responding to the critical points of market barriers, as identified in most European countries.

The aim of nZEB Ready project is to leverage the market drive by responding to 3 key questions: "Why nZEB?"; "Who can provide nZEB?"; and "How to reach nZEB". Thus, the nZEB Ready project will prepare ready to use frameworks to answer the needs related to lack of awareness, lack of skilled professionals and lack of support instruments, implementing the nZEB ready labelled procedures in 5 pilot countries in order to obtain a broader range of results, representative at European level. The frameworks obtained will be validated by specific stakeholders which are already part of the advisory board of the consortium and will be the starting point for the nZEB readiness roadmap for further replication in a wider use at the European level.

2. Objectives of the learning programme

Usually, improvements in energy efficiency planning and investments can decrease the energy consumption in the construction sector and unlock the nZEB market, but the reality shows us that it is not enough. The nZEB market analysis at European level reveals a significant gap between the countries with a high level of implementation and those which are not so well performing and which remain more and more behind (6). For these countries, energy efficiency is still an area with great potential to reduce greenhouse gas emissions.

Concerning this aspect, the countries like Bulgaria and Romania are consistently underperforming.

Related to the nZEB market it can be seen the problems related to jobs and qualifications needed. Through the market sustainable initiatives, countries like Croatia and Poland would preserve jobs in the construction sector, create new jobs and stimulate both public and private investments, thus contributing to the green recovery which will further contribute to other sectors like innovation and the development of new technologies, the production of new sustainable materials, new systems based on renewable energy sources. Moreover, some countries such as Bulgaria, Poland and not long-ago Romania, have low levels of ambition for tackling the energy transition, being still highly dependent on fossil fuel.

As previously stated, an nZEB building is a very high energy performance building with nearly zero or very low amount of energy use that should be covered to a very significant extent by on-site or nearby energy production from renewable sources. On one hand, reaching the nZEB target is very complex in new buildings and the level of difficulty rises in case of energy renovation of existing buildings, where the implementation of the renovation measures is limited. The renovation process to high energy performance, or even new construction process, is reduced by social (lack of reliable information or doubts on the potential benefits), technical (lack of skilled workers and proper support tools) economic (energy savings are not clear and the investment results reduced), and financial (scarce capital or limited financing scheme available or knowledge) barriers.

We are proposing in this paper a new learning programme to facilitate the nZEB implementation, which its main objective is to create support mechanisms and to stimulate the development of skills frameworks by new market driven mutual recognition training and certification scheme for nZEB deployment that will facilitate the necessary legislative changes. It can be observed that the lack of skilled professionals is one necessary step to break the vicious cycle of a blocked nZEB market (Fig.1).

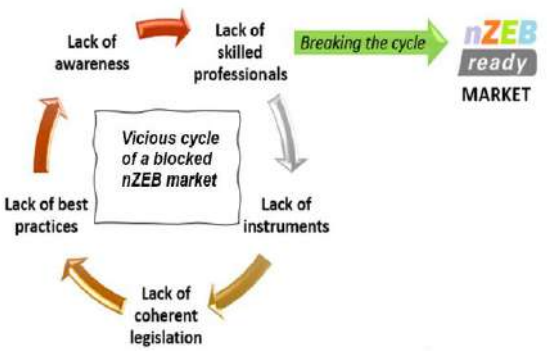

Fig. 1 – Breaking the vicious cycle of a blocked nZEB market (5)

Thus, the objective of the learning programme, namely the increasing the number of the skilled nZEB professionals is responding to the market barriers and needs, generated by the lack of skilled professionals which are essential in the nZEB construction chain, by expanding the pool of nZEB specialists for the design, execution, evaluation and validation of nZEB projects through dedicated training modules and replication activities. This will facilitate the increase of the available pool of skilled persons to be requested in nZEB tendering documentation.

The objective to increase the number of skilled nZEB professionals is referring at both "blue collar" and "white collar" professions across the building design, operation and maintenance value chain (designers, architects, engineers and other building professionals). In the frame of this objective, an important goal is to achieve and to implement mutual recognition procedures. The lack of skilled professionals is a problem extended to European level, but more critical on several markets. Among these critical markets, the 5 pilot countries that are partners in the nZEB Ready project encounter different concerns related to market labour for the nZEB specialists (5).

3. Approach of the learning programme

The nZEB Ready programme will provide a complex set of learning/training frameworks for nZEB concept, design, evaluation, execution, and exploitation by gathering together the already existing courses from previous European initiatives with new courses addressing domains not covered yet, to fully complete an nZEB approach.

Iven the discrepancies in the nZEB application between European countries, the approach will be specific for each state depending on the needs identified for each of them but the whole courses/training framework will facilitate the mutual recognition of energy skills and qualifications in the building sector. Based on the common learning results obtained from the training programs it will be possible to develop nZEB ready energy skills passports/registers for building professionals at regional/national level and support for their take up at European level.

One of the sensitive points regarding the actual nZEB market and the real demand for nZEB skills is that even if regulations requesting nZEB construction already exist, they are not applicable because of the lack of methodologies or lack of nZEB professionals even at the public authority level. This learning programme will support the public authorities for the requirements for skilled professionals in public procurement by providing guidelines for tender documents oriented towards nZEB skilled professionals. There will be also provisioned training programmes dedicated to public authorities, especially in Romania and Bulgaria, to help the administration to better understand the need to properly enforce the nZEB regulation.

To increase the number of skilled building professionals and/or blue-collar workers the learning programme will contribute to substantially increase the number of

nZEB professionals. Modules dedicated to white collars (e. g. architects, auditors, or engineers) and modules dedicated to blue collars related to nZEB buildings are considered. This a critical issue of the nZEB application in European countries because it will produce nZEB skilled professionals available on the market. The implementation of a mutual recognition procedure of the skilled nZEB professionals will be possible relying on the competences validated by the specific training programs.

4. Implementation of the learning programme

The learning programme to facilitate nZEB implementation will be implemented and tested on different layers in the 5 pilot countries (Romania, Bulgaria, Croatia, Poland, and Portugal) considering the needs addressed locally. This will guarantee the replicability success of the solutions.

According to the study (7), most of the countries from the European Union already introduced concepts regarding the implementation of nZEB buildings in their regulations and national plans. From the Fig.2, we can observe that in practice no country implemented the principles 100%.

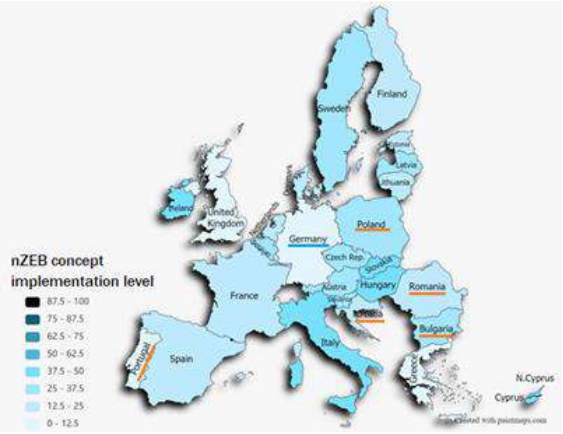

Fig. 2 – nZEB concept implementation across EU (5)

The project outcomes will be easily scalable to all member countries and easy to implement in any other country, regardless of the nZEB implementation level and knowledge. This is why the nZEB ready project has a key role in developing the nZEB market needs and skills all around Europe.

The 5 pilot countries were chosen based on a nZEB implementation questionnaire which revealed different needs and different problems on the local market, each indicating a certain level below the nZEB readiness level. Romania has a fair legislation, but it is not enforced accordingly. Moreover, there is an obvious need for new skills for the building designers and the nZEB concepts awareness must be increased to be properly implemented on a wider scale. Croatia has a good level of nZEB awareness and acceptance but needs to improve continuous learning programs regarding the nZEB design and construction skills. Portugal has nZEB regulation with specific requirements although still unclear, while the awareness level is moderate. Poland has fair regulations regarding the nZEB principles, but technical nZEB requirements are not ambitious and can be easily achieved.

There will be learning and training programmes dedicated to white collars especially for designers, architects or engineers but also to execution engineers, programmes that will cover specific skills characteristic to nZEB buildings like blower-door testers or thermal bridge evaluators and programmes for public authorities represented mainly by local administration. These ones will be trained and will get access to specific procedures and know-how relevant for nZEB market helping them to decide correctly regarding building permits authorisation. The circle of learning programmes will be closed by the modules dedicated to blue collars regarding nZEB Ready competences. It is particularly important to outline that the level of knowledge is not the same in each country part of the consortium. The existing successful learning modules from some countries will serve to adapt new modules in the countries where they are partially or completely missing. There will be new learning modules provided where they are totally missing or where the existing learning programmes are not valuable or applicable anymore. Each of the five countries participating in the program will make an analysis of critical categories to be trained and their training needs. Each country will organise pilot learning modules for the selected target categories and regarding the selected training programs to prove the feasibility of the whole nZEB Ready curriculum. The learning results from the whole learning modules will cover the competences needed to be nZEB Ready recognised and to have the "nZEB Ready passport". Finally, the nZEB Ready curriculum will be integrated in the nZEB Ready platform web-development to ensure the content dedicated to continuous learning training and certification program for mutual recognition.

Two main learning programs categories will be defined here based on the needs identified. The first program is dedicated to the nZEB auditors and to the nZEB designers, architects or engineers. The training program is addressed to architects and engineers which are already energy auditors, and the learning outcomes will allow the graduates to assess an existing building and, in addition to the energy audit of the building, will provide technical solutions to increase the energy efficiency of the house toward nZEB. The program is dedicated also to the design of nZEB addressing the three professionals' categories involved in achieving the nZEB target: architects, civil engineers and MEP engineers. The purpose of this learning program is to cover the gap of knowledge between nZEB concept principles and normal building principles, which is designed on a daily basis in each country. The designers will need to focus on a new integrated design concept and to unify their knowledge to design nZEB buildings. There will be six course modules: Thermal bridges calculation, Mechanical ventilation system with heat recovery, Building air tightness evaluation, Solar Shading systems, Bioclimatic Design Renewable energy sources. Romania and Bulgaria will implement most of the training programs because the competences are missing there. Croatia and Poland are better covered in current practice. Portugal will also develop learning

programs for the missing competences identified. The second learning program is dedicated to execution civil engineers and MEP engineers, and it will be divided in two learning modules, one for each category. This program will provide learning outcomes for the stakeholders involved directly in the on-site execution: workers, site managers, site coordinators, site professionals, contractors etc..

Two dedicated specific modules for key specialists in the market needed for nZEB certifying will be developed: blower-door testers and thermal bridges evaluator - infrared evaluator. These very specific skills are needed to sustain the nZEB assessor to complete the building certificate. Not only engineers or architects but also skilled workers could be integrated within these modules. The learning outcomes will be strictly related to practical methods used to measure technical parameters. This kind of learning programs will be developed mainly in Bulgaria where they are rather missing and in Croatia where some adult learning programs or university learning programs exist but are not enough. In Romania and Portugal there are already developed continuous learning programs dedicated to the above professional skills, which needs however to be significantly improved. Even so, each partner from the consortium will develop pilot modules in its own country for blower-door testers and thermal bridge evaluators as it is outlined in the table below.

Specialized training programs for blue collars professionals to integrate the learning outcomes regarding the nZEB buildings corresponding to the appropriate level of knowledge. The learning program related to this task will be split in two modules: 1. Construction skills related to nZEB; 2. Mechanical, electrical and plumbing (MEP) skills related to nZEB. They will attend either the Construction skills module, or the MEP skills module depending on their specialization.

Not the least, Public Authorities Staff and other decision makers will gain a deep understanding of the impact of policy instruments for supporting nZEB initiatives and support their specific design. The decision makers involved will get access to specific procedures and know-how relevant for nZEB market. This participation can provide transparency and confidence in the long-term perspective of this sector. In particular, this learning program is dedicated to people working mainly in local or central administration services who are generally responsible for the building permit authorisation.

The last part of the learning programme consists in creating and developing content dedicated to continuous learning training and certification programs for mutual recognition. The learning programs curriculum will be integrated to an online platform locally by each participant.

5. Conclusions

A new learning programme to facilitate the nZEB implementation, has been launched in 2021 with the objective of increasing the number of the skilled nZEB professionals is responding to the market barriers and needs, generated by the lack of skilled professionals which are essential in the nZEB construction chain, by expanding the pool of nZEB specialists for the design, execution, evaluation and validation of nZEB projects through dedicated training modules and replication activities.

Modules dedicated to white collars and modules dedicated to blue collars related to nZEB buildings are considered as well as the modules dedicated to Public Authorities Staff in order to gain a deep understanding of the impact of policy instruments for supporting nZEB initiatives and support their specific design.

6. Acknowledgement

The acknowledgement can be used to mention support from a funding organisation or from people who are not named as co-author. If the research presented received an in cash or in-kind contribution from a funding agency, government, companies or anyone else, please mention that here.

7. References

[1] World GBC. Global Status Report 2017 [Internet]. 2017. Available from: https://www.worldgbc.org/sites/default/files/UNEP188_GABC_en %28web%29.pdf

[2] European Council for an Energy Efficient Economy. European Energy Efficiency Plan [Internet]. 2011. Available from: https://www.eceee.org/policy-areas/energy-efficiency-policy/eep_2011/

[3] Buildings_Performance_Institute_Europe. Europe's buildings under the microscope. 2011; Available from: http://bpie.eu/publication/europes-buildings-under-the-microscope/

[4] European_Commission. Energy Performance Buildings Directive [Internet]. Available from: https://ec.europa.eu/energy/topics/energy-efficiency/energy-efficient-buildings/energy-performance-buildings-directive_en

[5] H2020_Project. Enhancing market readiness for nZEB implementation - nZEB Ready , call: H2020-LC-SC3-EE-2020-2, proiect: 101033733, Sep 2021 - Aug 2024.

[6] Attia S, Eleftheriou P, Xeni F, Morlot R, Ménézo C, Kostopoulos V, et al. Overview and future challenges of nearly zero energy buildings (nZEB) design in Southern Europe. Energy Build. 2017 Nov 15;155:439–58.

[7] Buildings_Performance_Institute_Europe. nZEB definitions across Europe. 2016; Available from: http://bpie.eu/uploads/lib/document/attachment/128/BPIE_factsheet_nZEB_definitions_across_Europe.pdf

A first attempt in shaping learning communities for the energy transition

Margot van Rees[a], Mirte Disberg - van Geloven[a], Amber Kornet[a], Stephan Corporaal[a], Maaike Endedijk[b]

[a] Saxion Research Group Employability Transition, Saxion University of Applied Sciences, Enschede, the Netherlands, m.r.vanrees@saxion.

[b] Faculty of Behavioural, Management, and Social Sciences, University of Twente, Enschede, the Netherlands, m.d.endedijk@utwente.nl.

Abstract. Learning communities (LCs) can be seen as an promising concept to shape professional development and thereby enhance innovation for the energy transition. However, as the design of an LC is dependent on the needs of the participating organizations and the problems they want to solve, no general blue prints are available for shaping an LC. Therefore, this study aims to find an answer to the question: *How should LCs for the energy transition be designed to support participants' professional development and stimulate innovation?* First, a literature study and needs assessment was conducted at eight SMEs in the installation sector, which led to an LC prototype. The LC prototype was then tested in four different SME's which eventually provided an LC prototype for the installation sector that stimulates professional development and innovation.

Keywords. Learning communities, installation sector, energy transition, professional development.
DOI: https://doi.org/10.34641/clima.2022.xx

1. Introduction

The energy transition is leading to significant changes in the work of installation technology professionals. These changes call for new technologies and sustainable energy sources, which requires continuous professional development [1,2]. This is one of the reasons that the Dutch installation sector embraced the concept of learning communities (LCs) to support the professional development of employees [3]. LCs refer to public-private partnerships in which learning, working and innovating come together in hybrid learning environments [3,4]. They are a powerful alternative to formal training programmes, which are often expensive, ineffective and unattractive for keeping up with the energy transition [5]. On the other hand, informal learning activities in the workplace are often too fragmented and unsupported [6]. To date, LCs are seen as promising to increase innovation [4,7]. However, designing LCs still needs attention. Evidence of how an LC can contribute to professional development and stimulate innovation is lacking [8,3]. Therefore, this paper aims to find an answer on the question: *How should LCs for the energy transition be designed to support participants' professional development and stimulate innovation?*

1.1 Theoretical framework

Although the term LC is frequently used, there is no universal definition of an LC. This is due to a variety in, for example, group size, subject and duration [9]. Nevertheless, the Topsectoren identified some key characteristics of an LC, based on extensive field consultation: LCs are (1) designed as a public-private partnership; (2) accessible to employees and students and employees of (higher) vocational education and training institutions; (3) focused on return on investment for all parties involved; (4) combining physical and virtual (learning) environments; (5) focused on connecting research, working, learning and innovation. Participants in a LC work together collectively on a meaningful challenge to build on already existing knowledge, and thus learn at the individual and group level [10,11]. However, this definition is more a description on what an LC is, than a description of how it works. Therefore, this study explored literature on professional learning, team learning, and work design to come up with important mechanisms that an LC needs to support. Subsequently, an effective LC should be based on the following principles: collaboration, the integration in daily work practice and the integration of formal and

Copyright ©2022 by the authors. This conference paper is published under a CC-BY-4.0 license.

informal learning, all of which are further discussed below.

1.2 Learning in an LC is a shared process

Interdisciplinary collaboration is important as it generates a deeper level of knowledge of different subjects and each other's expertise, increases critical thinking and initiative taking and develops a common purpose [12,13,14]. Sharing knowledge starts with the creation of shared goals, a shared identity that encourages engagement or a shared language that improves mutual understanding [15]. Palloff and Pratt[16] state that working towards a shared goal is not only the first step towards collaboration, but also the basis for an LC. If it is clear in advance that the participants are working towards a common goal, it is also easier for participants to engage in collaborative tasks [16,17]. By linking common learning goals to societal needs - such as the energy transition - LC participants are challenged to immerse themselves in new knowledge, integrate it with practice, reflect critically on themselves, solve problems creatively, collaborate, and understand the complex causes of societal problems [18]. When working towards a common learning goal, individual learning goals can also arise [19].

1.3 Learning and working is situated and integrated in daily practice

The LC is organised directly in, or next to, the working practice of participants, which requires a learning environment in which certain requirements are met. Complexities in work stimulate learning, initiative-taking, creativity, and problem-solving skills [20], but it also requires a context that offers room for autonomy [21]. Participants should be given the space to work on and come up with suitable tasks, both outside and within the LC. Therefore, both formal and informal learning activities should be set up [22]. This depends on the implicit ('know-how') and/or explicit knowledge ('know-that') of the LCs participants. This can be experimenting with new products, materials and services; reflecting on one's own work performance; looking up information; observing or attending presentations. The activities can take place at the physical workplace, in collaboration with colleagues or students or in contact with clients. The choice for a particular learning activity depends on the LCs learning goal [6]. The learning goal is linked to daily practice, as it is designed around a current, innovative issue. In that way, the LC and learning activities are situated and integrated in daily practice.

1.4 Learning in an LC is self-directed, but also guided

An important motor for professional learning is self-directedness. Participants learn if they experience certain challenges; performing motivating tasks, tasks that give a certain amount of uncertainty or risk [23]. By reflecting on one's own contribution to work experiences, uncertainties and success, participants will increasingly steer their own learning process, which will lead to self-monitoring and self-directed learning [24,25,26]. This is an ongoing process, in which actions are aimed at achieving goals. These goals are chosen and aligned with one's own vision [25,27]. In the LC, this means that both the LC as a whole, and the individual participants set their own goals, select necessary learning activities and evaluate [28].

Since self-directed learning does not automatically occur, a facilitator should be appointed to guide the process [27,29]. Literature also shows the importance of a facilitator in the creation of a safe learning climate, in which they can address important, but undiscussed, issues (e.g., values within the LC and mutual relationships) [30,31,32]. In addition, they can support and monitor the design process [33]. Also, participants need support in the transfer of what has been learned in the LC to daily working practice. A facilitator should coach participants in setting goals, practising new tasks and giving (individual) feedback [34]. Scaffolding is a way to support learning, which is the provision of support by, for example, asking questions, eliciting certain behaviour and modelling, which is adapted to the needs and progress of the participants and gradually fades away [35]. This increases the participants' self-confidence and sense of competence, which are important conditions for learning [35,36,37].

Following, the study examines whether the aforementioned conditions are present in the technical companies' current day-to-day practice, which is used to make the LC prototype suitable for their context.

2. Research methods

2.1 Method

This exploratory study has used a design research approach to arrive at three prerequisites for an LC prototype, which includes three iterative, flexible phases [38]. Figure 1 shows these different phases and used methods, corresponding the design research approach by McKenney and Reeves[41]. The

phases have been undertaken sequentially such that the findings from each phase will inform the next phase, and the final phase will involve reviewing the findings from phase two to confirm or modify the prerequisites for the prototype.

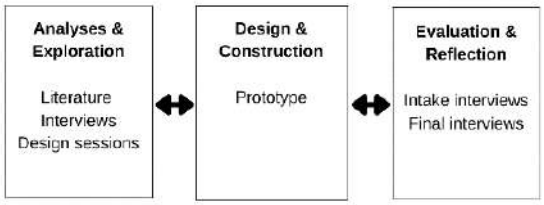

Fig. 1 – Research methods in a design research approach.

This research first looked at how LCs should be designed in the installation sector (literature and needs assessment through interviews and design sessions). In the second phase, the prerequisites resulting from the needs assessment were translated into an LC prototype. The prototype was tested and evaluated through intake and final interviews with participants during pilot studies. Goals of all measurements instruments are shown in Table 1.

Tab. 1 – Measurement instruments.

Phase	Instrument	Goal
Analyse	Interviews	Explore participants' perceptions of an LC and align prerequisites with the target group.
	Design sessions	Concretise the initial prerequisites and modify them to suit the context.
Design	Prototype	
Evaluate	Intake interviews	Establish a baseline; gauge expectations and current working methods.
	Observations	Observe whether the form of the LC is also carried out as described in the prerequisites, and whether this fits with the employees.
	Final interviews	Explore participants' opinions and experiences regarding (design of an) LC and the impact the LC has had on their daily work practice.

2.2 Respondents

Within all phases, the participants were employees of four installation companies. The participating installation companies were selected based on the following criteria: (1) small and medium-sized enterprises, (< 500 employees); (2) located in the Eastern part of the Netherlands; (3) active with energy transition-related innovations. In addition, teachers from four educational institutions participated in the study. The participating educational institutions consist of a post-secondary vocational education (ROC van Twente), two universities of applied sciences (Saxion and Windesheim Universities of Applied Sciences) and one university (University of Twente).

2.2 Phase 1: Analyses and exploration

Eight in-depth interviews were held with managers and employees with a leadership role, and six interviews with training coordinators and lecturers from two educational institutions. During the interviews, 1) the short- and long-term challenges in work and the energy transition, 2) reason(s) for participating in an LC and 3) expectations of the design were discussed.

Based on the outcomes of the exploratory interviews and the literature study, two LC design sessions were held to supplement the theoretically formatted principles with requirements for practical usability. This was done in the two sessions, one with directors and managers, and one with mechanics and operational staff. The participants worked together in groups of four with lecturers from educational institutions, under the guidance of a researcher, to complete a worksheet. The accompanying researcher ensured that every participant gave input from their own experiences, and that the considerations and answers were correctly noted on the worksheet. The complemented worksheets contained information about 1) appropriate LC goals, 2) suitable participants that can participate in the LC based on the LC goals, 3) required resources and/or learning activities, 4) possible presence of experts and 5) which preconditions are needed for the LC to succeed. Eventually, the researchers shared results between the two groups to reach consensus about the prerequisites.

Data analyses

The interviews were recorded, transcribed and then coded according to the previously mentioned topics of the in-depth interviews; 1) the short- and long-term challenges in work and the energy transition, 2) reason(s) for participating in an LC and 3)

Tab. 2 – Prerequisites resulting from the first phase.

Prerequisites	Substantive points
Learning in an LC is a shared process	- A shared purpose, task interdependence and joint responsibility for the final product creates team learning. - Participants have complementary expertise, which is made explicit and respected. - The three main facilitating team learning processes are supported by a facilitator (team activity, team reflexivity, boundary crossing). - Team learning is connected to individual learning. - The collaborative process is socially regulated - LC has a clear identity, participants feel connected to the group, and can identify with it (connectedness).
Learning and working in an LC is situated and integrated in daily practice.	- Learning outcomes are relevant and can be applied in work - The issue of the LC is within the domain of influence of the participants. - The issue of the LC is possible to address in the chosen time frame. - Learning activities are designed in line with work - The learning outcomes are integrated into the daily actions of employees and managers. At the organisational level, the learning outcomes are integrated into the 'way-of working' (way of scheduling jobs, evaluation strategies, stimulating knowledge sharing, etc.). - Working through LCs is integrated into the way of working of the company.
Learning in an LC is self-directed, but guided	- An agile rather than traditional plan-based system is used. - The individual process is self-directed, possibly through co-regulation. - Support and tools are developed, for both the collaborative and individual processes, according to principles of scaffolding - Participants have a say in designing work and learning goal(s) and how to reach them (autonomy, self-direction). - Participants feel confident (self efficacy / team efficacy) and competent, both through the support of the organisation and through the facilitation offered.

expectations of the design were discussed. These answers were then compared to each other in order to arrive at prerequisites (Table 2).

2.3 Phase 2: Design and construction

An LC prototype was designed on the basis of the prerequisites (Table 2) and shown in Table 3.

Subsequently, four LCs at four different companies were implemented based on the prototype. These LCs were held between December 2020 to October 2021 and supervised by an external facilitator. For each LC, one researcher was directly involved during the intake and final interviews, and at all LC meetings as a direct observer.

2.4 Phase 3: Evaluation and reflection

In order to confirm or modify the LC prototype, intake and final interviews were held with the participants to access the prerequisites. The meetings were also directly observed by a researcher to receive more information on the prerequisites.

The facilitator and researcher conducted intake interviews among all LC participants (N=36) before the LC sessions started. The intake interviews took

Tab. 3 – Connection prerequisites to prototype.

Prerequisites	In prototype
Learning in an LC is a shared process	Participants from different parts of the organisation are brought together around the intended goal. Everyone participates to find an answer to the common problem
Learning and working is situated and integrated with daily practice.	The LC is formed around a concrete, practical and innovative issue that is relevant to all participants and addressed in ten weekly meetings. During, and between, the meetings, different types of learning activities are undertaken, formal (presentation) and informal in the workplace (watching someone). This depends on the purpose of the LC.
Learning in an LC is self-directed, but guided	All participants set individual learning goals at the beginning of the LC, linked to the common goal. The LC is supervised by an external facilitator who facilitates the learning process at both the individual and team level.

approximately 45 minutes and asked the participants about background information, current work activities, their experience with the LC topic, expectations of the LC and preferences for learning and collaboration during work.

All LC meetings (N=35) were recorded and observed by a researcher using an observation scheme. This schedule was based on the established LC prerequisites. The observations looked at how, and if, the corresponding behaviours were visible during the LC meetings.

The same participants (N=36) were invited to final interviews after all the LC meetings to discuss 1) their experiences of the LC results, 2) the content and (learning) activities during and between the LC meetings, 3) the experienced effects of the LC in their own daily work practice, 4) the collaboration and knowledge sharing (among themselves) with the participants, and 5) the role of the facilitator during the LC. The facilitators (N=3) were asked about the 1) the interpretation of the prerequisites in the LC and how they steered this as facilitators, 2) their role as facilitators in stimulating knowledge sharing and collaboration between the participants, and 3) other remarks concerning the LC meetings and points of attention for follow-up.

Data analyses
The researchers made summaries of all intake and final interviews and observations. These summaries were used in debrief sessions, in which similarities and differences were explored and debated by two researchers.

3. Results

The first phase resulted in prerequisites, which were then translated into a prototype (Table 3). Finally, the prototype was tested in the third phase.

Prerequisite 1: Learning in an LC is a shared process.
The LC consisted of participants with different backgrounds and perspectives. Therefore, participants needed to share their expertise and knowledge explicitly, so that everybody understood each other. The facilitator enhanced this collective process by asking questions and connecting all individual perspectives to the collective goal. This made the participants feel connected to the group. However, the feeling of belonging reduced when the LC finished or the link between the LC theme and participants' daily working practice diminished (because of differences in individual goals or a change in job activities). As a result, participants were more inclined to become absent or did not actively participate during the meetings. All LCs started with a kick-off meeting to discuss the collective goal and the individual contributions. If these goals were clear in the beginning, the subsequent meetings also proceeded more easily.
This is also important, as participants found it difficult to define their individual learning goal. They found it hard to come up with things they wanted to 'learn'. Using language that matches the language used by the participants in the workplace (e.g., what are your struggles while working with X), stimulated participants to come up with suggestions and ideas for learning goals.

Prerequisite 2: Learning and working is situated and integrated in daily practice.
Participants felt connected and that they added value to the learning process if the collective goal/LC issue was relevant to their daily work practice. The LC issue needed to be closely linked to their own work activities and participants needed to be able to implement the outcomes of the LC directly into participants' work. For example, one LC was built around the issue of working with a digital, technical programme, which was not directly relevant to all participants' daily work practice. Participants became distant and cancelled the meetings.

The learning activities during the LC consisted of trying out a certain object, experimenting with technology in practice, or looking up information. The facilitator supported the participants to transform their ideas into learning activities. Participants indicated that carrying out tasks that take up a lot of time outside of meetings and which are not directly linked to their work activities, is not desirable, mainly due to increased work pressure.

Prerequisite 3: Learning in an LC is self-directed, but guided.
The participants often had a wait-and-see attitude when starting the LC, because they had never experienced such a way of learning and working before.
During the meetings, it was experienced as pleasant that the facilitator explored and showed the (learning) benefits of the meetings, because the participants indicated to be less aware of this.
Reflecting on, and evaluating, one's own contribution to work experiences, the uncertainties and successes, strengthens learning and self-directed learning. The facilitator is very decisive in the extent to which, and how, this happens.
The facilitator has no substantive knowledge of the subject, which is experienced as pleasant by the

participants, as they become induced to explain and argue everything. The facilitator helps to make implicit knowledge explicit by asking questions and making the results visible during the process. He/she is also important for creating a safe learning climate, and discusses issues that are somewhat more below the surface.

4. Discussion

The aim of this paper was to create an applicable model for LCs in the installation industry, by establishing prerequisites. These conditions were constructed into a prototype, which was then tested and evaluated in four pilot studies.

1. Participants will only demonstrate learning behaviour if they are given the room to make mistakes outside of the meetings and feel trusted by the organisation.

LC participants only share knowledge, evaluate and combine different perspectives and knowledge if they feel that they are allowed to do so [30,39]. Such psychological safe environment is important in and outside the LC meetings to enhance team learning behaviour (e.g., share knowledge, evaluate, combine different perspectives). A psychologically safe environment during the LC meetings does not guarantee that participants will show team learning behaviour outside the LC meetings. This research even shows that if the participants feel as if they can't make mistakes, this will influence their contribution to the LC meetings, because they are more reluctant in sharing knowledge and trying out new things.

2. Participants are more motivated to actively share their knowledge and skills during the meetings when the LC topic has a direct connection to participants' daily work

For participants to actively exchange knowledge and skills, they must be motivated to join the LC meetings. Therefore, it is important to align the (joint and individual) goals with participants' daily work practice. At least three meetings are necessary to align these goals. During those three meetings, the learning objectives can be tailored to the participants. As a result, participants come up with more practical examples that they can share with each other. Furthermore, a facilitator is needed to guide and support this process extensively [41], as participants find it difficult to do this themselves.

3. More than guidance and setting individual learning goals is needed to stimulate self-directed learning.

In line with research [26], participants find it hard to direct their learning, as 'learning' as a phenomenon is hard to understand and define. Therefore, different use of language to explain learning and intensive support from a facilitator is needed [27,41]. A facilitator should stimulate reflection during the meetings, by ensuring that the content is in line with the collective and individual goal and ask questions about the presented knowledge. The facilitator has no knowledge of the issue that is being raised, which makes the facilitator question the knowledge being shared [41]. Participants then share more knowledge and implicit knowledge is made explicit. In that way, the facilitator can steer self-directed learning.

4.1 Limitations and further research

As mentioned before, the facilitator is a crucial factor during the LC meetings. However, every facilitator has its own way of guidance, which results in LCs being facilitated differently every time. This affects LC outcomes. Further research should create a baseline for guidance by developing training for facilitators.

As this was a first attempt in shaping LCs for the energy transition, the prerequisites were only tested in four LCs. To receive more detailed results, further research should test the prerequisites and corresponding prototype more extensive in multiple LCs.

4.2 Practical implications

This research shows how LCs for the energy transition can be designed. Some implications for companies can be given to stimulate innovation among technical employees.

1. LCs are a promising concept for lifelong learning around the changes resulting from the energy transition. Through participation in LCs, employees can be trained on the job and during current work activities. This can be a solution to the labour shortage in SMEs.
2. Companies should stimulate innovation and professional development by creating a psychological safe environment [33]. In such context it is in allowed to make mistakes and employees feel trusted and respected.
3. Companies should implement the LC to stimulate professional development around innovation. As the role of a facilitator is important, companies should look at HR as a possible facilitator. He/she stands apart from the LC subject and has knowledge of professional development.
3. Organise LCs around a concrete project or challenge within the company. Make sure that the participants of the LC are also closely involved in this

project or challenge, so that they can immediately implement the knowledge from the meetings in their daily work.
4. Ask employees how they develop their knowledge and skills in their daily work practice. Make sure that the LC is connected to this.

5. Acknowledgements

This research is funded by the NWO (funding reference number: 055.19.001) and conducted under the direction of the University of Twente, together with ROC van Twente and Windesheim University of Applied Sciences. This paper is part of the overarching research project 'Hit the Gas', in which this research in conducted with the help of Mireille Post-Hubers, Tijmen Schipper, Victoria Bolotina, Loes de Jong, Natalie Greb-Sempel and Lodewijk Witteveen.

The datasets generated during and/or analysed during the current study are not available because follow-up research is ongoing, so the data is still being used. The authors will make every reasonable effort to publish them in near future.

6. References

1. Eilander M. De techniekprofessional en de energietransitie. Installatiejournaal. [internet] 2019. [cited 2020 Jun 1]. Available from https://www.installatiejournaal.nl/energie/nieuws/2019/08/de-techniekprofessional-en-de-energietransitie-1019926?_ga=2.143906802.695365027.1591867052-1224732855.15918670
2.Noorman KJ. Over Energiestransitie en nog zoveel meer. Groningen (NL): Hanze University of Applied Sciences; 2018.
3. Topsectoren. Advies Meerjarig Onderzoeksprogramma Learning Communities. [internet] 2019. [cited 2020 june]. Available from https://www.topsectorenergie.nl/sites/default/files/uploads/Algemeen/Advies meerjarig onderzoeksprogramma Learning Communities.pdf
4. Dingyloudi F, & Strijbos JW. Community Representations in Learning Communities. Scandinavian Journal of Educational Research. 2019;64(7):1052-1070. Available from: doi: 10.1080/00313831.2019.1640788
5. Bersin J. A new paradigm for corporate training: Learning in the flow of work. [internet] 2018. [cited 2020 Jun]. Available from https://joshbersin.com/2018/06/a-new-paradigm-for-corporate-training-learning-in-the-flow-of-work/
6. Eraut M. Non-formal learning and tacit knowledge in professional work. British Journal of Educational Psychology. 2000;70:113–136. Available from: http://www.ingentaconnect.com/content/bpsoc/bjep/2000/00000070/00000001/art00008
7. Gebauer R, Wade ME, Muller T, Kramer S, Leary M, & Sopper J. Unique Strategies to Foster Integrative Learning in Residential Learning Communities. Learning Communities Research and Practice. 2020;8(1).
8. Ke F, & Hoadley C. Evaluating online learning communities. Educational Technology Research and Development. 2009;57(4):487–510. Available from doi:10.1007/s11423-009-9120-2
9. Knol E, & Velzing E. Learning communities voor MMIP ' s : een schakel voor versnelling en opschaling. Verkenning op verzoek Topsector Energie en in opdracht van RVO. 2019. Available from doi:10.13140/RG.2.2.24965.81128
10. Blackshaw T. Key concepts in community studies. Thousand Ouks (US): Sage; 2010.
11. Scardamalia M, & Bereiter C. Computer Support for Knowledge-Building Communities. The journal of learning sciences. 1994;3:265-283. Available from doi:10.1207/s15327809jls0303_3
12. Brookfield SD. Becoming a critically reflective teacher. San Francisco (US): Jossey-Bass; 2017.
13. Edmondson AC, Dillon JR, & Roloff KS. 6 Three Perspectives on Team Learning. The Academy of Management Annals. 2017;1P:269-314. Available from doi: 10.1080/078559811
14. Kilpatrick S, Jones T, & Barrett M. Defining learning communities. Launceston (Tasmania): Centre for Research and Learning in Regional Australia; 2003.
15. Vollenbroek WB. Communities of Practice: Beyond the Hype: Analysing the Developments in Communities of Practice at Work. Enschede (NL): University of Twente; 2019.
16. Palloff RM, & Pratt K. Collaborating online: Learning together in community. New York (US): John Wiley & Sons; 2010.
17. Hord SM. Professional learning communities. Journal of staff development. 2009;30(1):40-43.
18. Jacoby B. Partnerships for service learning. New Directions for student services. 1999;(87):19-35.
19. Janssen S, Jansen F, Schaepkens H, & De Groot M. Van teamontwikkeling naar persoonlijke ontwikkeling en omgekeerd. Amsterdam (NL): Open Universiteit; 2011.
20. Chae H, & Choi JN. Contextualizing the effects of job complexity on creativity and task performance: Extending job design theory with social and contextual contingencies. Journal of Occupational and Organizational Psychology.

2018;91(2):316–339. Available from doi:10.1111/joop.12204
21. Van Ruysseveldt J, & Van Dijke MH. Wanneer bevordert en wanneer hindert werkdruk het werkplekleren? Gedrag En Organisatie. 2012;25(1):28–44. Available from doi:10.5117/2012.025.001.028
22. Tynjälä P. Toward a 3-P Model of Workplace Learning: a Literature Review. Vocations and Learning. 2013;6:11–36. Available from doi:10.1007/s12186-012-9091-z
23. Preenen PTY, Van Vianen AEM, De Pater IE, & Geerling R. Ervaren Uitdaging op het Werk. Gedrag & Organisatie. 2011;24(1):64-83. Available from doi:10.5117/2011.024.001.064
24. Knowles M. Self-Directed Learning: A Guide for Learners and Teachers. Chicago Self-Directed Learning: A Guide for Learners and Teachers. Chicago (US): Follett Publishing Company; 1975.
25. Luken T. De (on)mogelijkheid van nieuw leren en zelfsturing. In Kuijpers M. & Meijers F, editors. Loopbaanleren: Onderzoek en praktijk in het onderwijs. Antwerpen (BE): Garant; 2008. p. 127-151.
26. Margaryan A, Littlejohn A, & Milligan C. Self-regulated learning in the workplace: Strategies and factors in the attainment of learning goals. International Journal of Training and Development. 2013;17(4):245–259. Available from doi:10.1111/ijtd.12013
27. Harms GJ. Zelfsturing meetbaar maken. Groningen (NL): University of Groningen; 2010.
28. Siadaty M, Gašević D, Jovanović J, Pata K., Milikić N, Holocher-Ertl T, Jeremić Z., Ali L, Giljanović A, & Hatala M. Self-regulated workplace learning: A pedagogical framework and semantic web-based environment. Educational Technology and Society. 2012;15(4):75–88.
29. Hmelo-Silver CE, Chinn CA, Chan CKK, & O'Donnell AM. (2013). The International Handbook of Collaborative Learning. New York (US): Routledge; 2013. Available from doi:10.4324/9780203837290
30. Edmondson AC. Psychological safety and learning behavior in work teams. Administrative Science Quarterly. 1999;44:350-383
31. Pereles L, Lockyer J, & Fidler, H. Permanent small groups: group dynamics learning and
change. Journal of Continuing Education in the Health Professions. 2002;22(4):205-13. doi: 10.1002/chp.1340220404.
32. Wenger E, McDermott R, & Snyder, W. Cultivating Communities of Practice. Massachusetts (US); Harvard Business School Press; 2002.
33. Becuwe H, Tondeur J, Pareja Roblin N, Thys J, & Castelein E. Teacher design teams as a strategy for professional development: the role of the facilitator. Educational Research and Evaluation. 2016;22(3–4):141–154. Available from doi:10.1080/13803611.2016.1247724
34. Dochy F, & Segers M. Creating Impact Through Future Learning. Londen (UK): Routledge; 2018.
35. Van de Pol J, Volman M, & Beishuizen J. Scaffolding in teacher-student interaction: A decade of research. Educational Psychology Review. 2010;22(3):271–296. Available from doi:10.1007/s10648-010-9127-6
36. Parker SK, & Wang Y. Helping people to 'make things happen': A framework for proactivity at work. International Coaching Psychology Review. International Coaching Psychology Review. 2015;10(1):62-75.
37. Ryan RM, & Deci EL. Self-Determination Theory. New York (US): The Guilford Press; 2017.
38. McKenney S, & Reeves TC. Conducting Educational Design Research. New York (US): Routledge; 2019.
39. Van Veelen R, & Ufkes EG. Teaming Up or Down? A Multisource Study on the Role of Team Identification and Learning in the Team Diversity–Performance Link. Group and Organization Management. 2019;44(1):38-71. Available from doi:10.1177/1059601117750532
40. West RE, & Williams GS. "I don't think that word means what you think it means": A proposed framework for defining learning communities. Educational Technology Research and Development. 2017;65:1569–1582. Available from doi:10.1007/s11423-017-9535-0
41. Sessums C. Learning Communities and Support; transformation framework. Redmond (US): Microsoft Corporation; 2014.

CLIMA 2022

EYE ON 2030

Towards digitalized, healthy, circular and energy efficient HVAC

CLIMA 2022 is organised by

REHVA

TVVL

TU Delft

TU/e EINDHOVEN UNIVERSITY OF TECHNOLOGY

TU Delft OPEN

TU Delft OPEN Publishing
https://doi.org/10.34641/mg.33
ISBN: 978-94-6366-564-3

BOOKS.OPEN.TUDELFT.NL

9 789463 665643 >